Can. J. Chem. Downloaded from www.nrcresearchpress.com by 210.87.254.105 on 09/05/12
For personal use only.

Canadian Journal of Chemistry

Published by
THE NATIONAL RESEARCH COUNCIL OF CANADA

Journal canadien de chimie

Publié par
LE CONSEIL NATIONAL DE RECHERCHES DU CANADA

Volume 52 Number 1 January 1, 1974 Volume 52 numéro 1 1 janvier 1974

Kinetic Studies of the Reactions of Cyanide Ion and 1,3,5-Trinitrobenzene in Ethanol, *n*-Propanol, Isopropanol, and *t*-Butanol at 25.0 °C

LEONG HUAT GAN AND ALBERT RICHARD NORRIS
Department of Chemistry, Queen's University, Kingston, Ontario

Received July 3, 1973

The specific rate constants for the formation of the 1:1 1,3,5-trinitrobenzene – cyanide ion σ-complex in ethanol, *n*-propanol, isopropanol, and *t*-butanol are 442 ± 14, 932 ± 30, 2.45 ± 0.10 × 10^3 and 1.06 ± 0.05 × 10^5 M^{-1} s^{-1}, respectively. A plot of log *k vs.* Dimroth's solvent parameter E_t is linear with slope −0.25. The kinetics of the reactions of cyanide ion and 1,3,5-trinitrobenzene in ethanol and *n*-propanol are complicated by alcoholysis of cyanide ion which yields the corresponding alkoxide ion and the 1:1 1,3,5-trinitrobenzene – alkoxide ion σ-complex.

Les constantes spécifiques de vitesse pour la formation du complexe-σ 1:1 trinitro-1,3,5 benzène – ion cyanure dans l'éthanol, le *n*-propanol, isopropanol et le *t*-butanol sont respectivement égales à 442 ± 14, 932 ± 30, 2.45 ± 0.10 × 10^3 et 1.06 ± 0.05 × 10^5 M^{-1} s^{-1}. Un graphique de log *K vs.* le paramètre de Dimroth (solvant) E_t, révèle une ligne droite dont la pente est égale à −0.25. La cinétique des réactions de l'ion cyanure avec le trinitro-1,3,5 benzène dans l'éthanol et le *n*-propanol est perturbée par l'alcoolyse de l'ion cyanure qui conduit à l'ion alcoolate correspondant et au complexe-σ 1:1 trinitro-1,3,5 benzène – ion alcoolate. [Traduit par le journal]

Can. J. Chem., **52**, 1 (1974)

Introduction

Cyanide ion is known to react with 1,3,5-trinitrobenzene and related nitroaromatic compounds in a wide variety of solvents to form σ-complexes (1–4). The visible absorption characteristics of σ-complex **1** (X = CN), together with equilibrium constants and thermodynamic parameters associated with its formation, in a number of alcohols have been reported (5). The thermodynamic results were interpreted in terms of desolvation of the cyanide ion as being the primary factor affecting the enthalpies and entropies of formation (5).

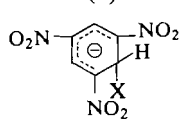

1

As part of a series of kinetic studies of the reactions of sulfite, cyanide, and various alkoxide ions with a number of 1-X-2,4,6-trinitrobenzenes (X = H, CH_3O, CH_3, CHO, NH_2, $NHCH_3$, and $N(CH_3)_2$) (6, 7) and, as an extension to earlier equilibrium studies, we have investigated the kinetics of reaction of 1,3,5-trinitrobenzene and cyanide ion in several alcohols.

Specific rate constants for the formation of **1** (X = CN) at 25.0 °C in ethanol, *n*-propanol, isopropanol, and *t*-butanol have been determined. Results are presented to show that in ethanol and *n*-propanol alcoholysis of cyanide ion is a significant side reaction and leads to the initial formation of **1** (X = RO) in these solvents.

Experimental

Reagents

Eastman 1,3,5-trinitrobenzene was purified and dried as previously described (8), m.p., 122 °C (lit., m.p. 122.5 °C (9)).

Eastman 1-(*p*-hydroxyphenol)-2,4,6-triphenylpyridinium betaine was converted to the perchlorate salt as described by Dimroth *et al.* (10) and recrystallized from

Can. J. Chem. Downloaded from www.nrcresearchpress.com by 210.87.254.105 on 09/05/12
For personal use only.

anhydrous methanol. After drying *in vacuo* over silica gel the pale yellow needle-shaped crystals had m.p. 250 °C.

Tetraphenylarsonium cyanide was prepared as described previously (5) and dried to constant weight *in vacuo* over phosphorus(V) pentoxide.

Absolute ethanol was distilled from magnesium and iodine according to the procedure described by Vogel (11). The remaining alcohols were dried by refluxing over Linde 4A Molecular Sieve overnight and then distilled under a dry nitrogen atmosphere. Only the middle portion of the distillate was retained in each case.

Stock solutions of 1,3,5-trinitrobenzene and tetraphenylarsonium cyanide were prepared by dissolving weighed quantities of each reagent in known volumes of the alcohol.

Instruments

Optical measurements in the equilibrium studies were carried out on a Cary 14 recording spectrophotometer using matched silica cells of 1.0-cm path length. The temperature in the cells was maintained constant to ± 0.1 °C by circulating water from a constant temperature bath through a specially designed cell holder in the spectrophotometer.

Kinetic measurements were carried out on a Durrum-Gibson stopped-flow spectrophotometer.[1] A closed circuit temperature control system utilizing an Ultra Kryomat TK 30D constant temperature bath kept the temperature in the valve-block, drive syringes, and observation cell constant to ± 0.1 °C. Temperature-jump or conventional stopped-flow cells of 2.0-cm path length were used. Minimum "dead times" of the two cells were 10 and 2 ms, respectively. For some of the kinetic runs the normal mode of operation of the spectrophotometer was modified so as to yield an oscilloscope trace of absorbance as a function of time rather than % transmittance as a function of time (12). Standard solutions of potassium permanganate, whose absorbances at several different wavelengths had been determined on the Cary 14, were used to establish that the input signal to the vertical axis of the storage oscilloscope was directly proportional to absorbance over the range 0–0.10 absorbance units. One advantage of this method of operation was that over the range indicated absorbances could be accurately determined at very low noise to signal ratios.

Procedures

Solutions containing 1,3,5-trinitrobenzene ($\sim 10^{-5}$ *M*) and tetraphenylarsonium cyanide (10^{-4}–10^{-2} *M*) were prepared immediately prior to each run by dilution of known volumes of the corresponding stock solutions with alcohol. Before each run each drive syringe was rinsed three times with the appropriate solution, filled to capacity, and allowed to stand for 20 min in order to reach thermal equilibrium with the bath. In the course of the kinetic studies the concentration of 1,3,5-trinitrobenzene was kept constant and only the solutions containing tetraphenylarsonium cyanide were changed. Each time this was done the drive syringe was thoroughly flushed with the new tetraphenylarsonium cyanide solution before being filled for the kinetic run.

[1]Durrum Instrument Corporation. Palo Alto, Calif.

The stopped-flow spectrophotometer was used in the conventional way to obtain values of absorbance at infinite time (A_∞) associated with the fast initial reactions in ethanol and *n*-propanol. The absorption characteristics of the species formed in the slow reactions were determined by running the reactions under the same experimental conditions used in the kinetic runs and recording the resulting spectra of the solutions on the Cary 14.

Traces on the storage oscilloscope of absorbance or % transmittance *vs.* time were recorded photographically when at least two consecutive runs gave identical traces. Absorbances or % transmittances at various times were read directly from the photographs and used to calculate values of $\ln (A_\infty - A_t)$ as a function of time. A_∞ and A_t refer to absorbances at a specified wavelength at times infinity and *t*, respectively.

Results and Discussion

When solutions containing 1,3,5-trinitrobenzene (TNB) in ethanol and tetraphenylarsonium cyanide in ethanol (in large excess) were mixed, the % transmittance *vs.* time trace recorded on the oscilloscope showed two distinct parts. The first portion of the trace rapidly reached a limiting absorbance value (A_∞); there was then a further slow increase in absorbance. As the concentration of tetraphenylarsonium cyanide was reduced, separation of the trace into two distinct portions became less distinct.

The visible spectrum of the species formed in the first reaction was determined by recording, for solutions of constant TNB and tetraphenylarsonium cyanide concentration, infinite absorbance values as a function of wavelength. The resulting absorption spectrum (Fig. 1) showed

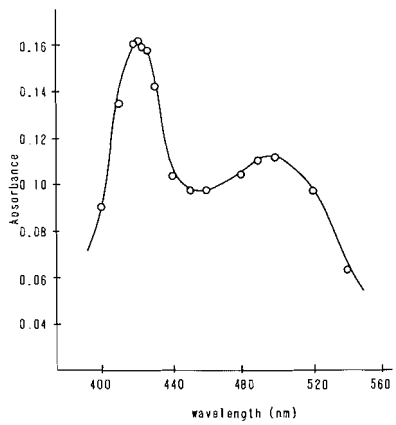

FIG. 1. Visible absorption spectrum (derived from A_∞ values) of the colored species formed in the "fast" reaction observed in ethanol solutions containing 1,3,5-trinitrobenzene and tetraphenylarsonium cyanide: $[TNB]_0 = 1.02 \times 10^{-5}$ *M*; $[\phi_4AsCN]_0 = 1.15 \times 10^{-2}$ *M*; $T = 25.0$ °C; $l = 2.0$ cm.

Can. J. Chem. Downloaded from www.nrcresearchpress.com by 210.87.254.105 on 09/05/12
For personal use only.

absorption maxima at 498 and 422 nm with $\varepsilon_{422}/\varepsilon_{498} = 1.45$. These absorption characteristics are very similar to those recorded for σ-complex **1** (X = C_2H_5O) (λ_{max} 497 and 424, $\varepsilon_{424}/\varepsilon_{497} = 1.49$) using the Cary 14 spectrophotometer (4, 6).

The progress of the fast reaction was followed at 480 nm. Plots of ln $(A_\infty - A_t)$ *vs.* time were linear to at least 80% completion of reaction. If this first reaction involves the reversible formation of **1** (X = C_2H_5O) according to the equation

$$[1] \quad TNB + C_2H_5O^- \underset{k_{-1}}{\overset{k_1}{\rightleftharpoons}} \mathbf{1}\ (X = C_2H_5O)$$

and the concentration of ethoxide ion in solution ($[C_2H_5O^-]$) is much greater than the total concentration of 1,3,5-trinitrobenzene ($[TNB]_0$), the slope of the ln $(A_\infty - A_t)$ *vs.* time plot (k_{obs}) should be related to the specific rate constants k_1 and k_{-1} and $[C_2H_5O^-]$ as follows:

$$[2] \quad k_{obs} = k_1[C_2H_5O^-] + k_{-1}$$

The $[C_2H_5O^-]$ in the system was calculated using the equation[2]

$$[3] \quad [C_2H_5O^-] = \frac{[\mathbf{1}\ (X = C_2H_5O)]}{K\{[TNB]_0 - [\mathbf{1}\ (X = C_2H_5O)]\}} = \frac{\frac{A_\infty}{l\varepsilon_{480}}}{K\left\{[TNB]_0 - \frac{A_\infty}{l\varepsilon_{480}}\right\}}$$

where A_∞ is the absorbance at infinite time associated with the fast reaction, l is the path length of the cell (2.0 cm), ε is the molar extinction coefficient of the complex at 480 nm ($1.65 \times 10^4\ M^{-1}\ cm^{-1}$) and $K(k_1/k_{-1})$ is the equilibrium constant for complex formation. A K value equal to 2020 M^{-1} was used in the calculations (6). A typical set of data is given in Table 1.

The plot of k_{obs} for the fast reaction *vs.* $[C_2H_5O^-]$ was linear with slope (k_1) equal to $37\,000 \pm 8000\ M^{-1}\ s^{-1}$ and intercept (k_{-1}) of $11.9 \pm 1.7\ s^{-1}$, respectively. (Errors in k_1 and k_{-1} are based on the errors associated with the "least-squares" slopes and intercepts of the k_{obs} *vs.* $[C_2H_5O^-]$ plots.) Values of k_1 and k_{-1} for the interaction of sodium ethoxide with TNB in ethanol have been reported as $33\,400\ M^{-1}\ s^{-1}$ and $27.5\ s^{-1}$ (13) and $49\,500 \pm 1500\ M^{-1}\ s^{-1}$ and $15.4 \pm 2.0\ s^{-1}$ (6), respectively. The good agreement in the k_1 and k_{-1} values and the observed absorption characteristics of the species first formed leave little doubt that the fast initial reaction involves formation of σ-complex **1** (X = C_2H_5O).

The visible absorption spectrum of the species formed at the termination of the slower second reaction showed absorption maxima at 435 and 544 nm. The spectrum is consistent with the formulation of this species as the 1:1 1,3,5-trinitrobenzene – cyanide ion σ-complex (1, 5).

The rate of formation of this species was followed at 580 nm where σ-complex **1** (X = C_2H_5O) has a negligible molar extinction coefficient (Fig. 2). Plots of ln $(A_\infty - A_t)$ *vs.* time for this second reaction were linear to at least 90% completion of reaction. For the reversible formation of σ-complex **1** (X = CN) in ethanol according to eq. 4 the k_{obs} obtained from the

$$[4] \quad TNB + CN^- \underset{k_{-2}}{\overset{k_2}{\rightleftharpoons}} \mathbf{1}\ (X = CN)$$

slope of the ln $(A_\infty - A_t)$ *vs.* time plot is related to k_2, k_{-2}, K, $[TNB]_0$ and the total concentration of cyanide ion in solution $[CN^-]_0$ as shown in eq. 5.[3]

$$[5] \quad k_{obs} = k_2\left\{\frac{[CN^-]_0 - [C_2H_5O^-] + [TNB]_0}{1 + K[C_2H_5O^-]}\right\} + k_{-2}$$

Values of k_{obs}, $[C_2H_5O^-]$ and the term $([CN^-]_0 - [C_2H_5O^-] + [TNB]_0)/(1 + K[C_2H_5O^-]$ for a series of runs at different tetraphenylarsonium

[2]The equilibrium concentrations of $C_2H_5O^-$ can be used to calculate an alcoholysis constant K' associated with the reaction

$$CN^- + C_2H_5OH \rightleftharpoons C_2H_5O^- + HCN$$

where $K' = [HCN]\,[C_2H_5O^-]/[CN^-]\,[C_2H_5OH] = [C_2H_5O^-]^2/\{[CN^-]_0 - [C_2H_5O^-]\}\,[C_2H_5OH]$

The mean value of K' at 25.0 °C was $1.33 \pm 0.03 \times 10^{-6}$. The error limits on K' represent the standard deviation of the mean for eight determinations over a range of ϕ_4AsCN concentrations 2.0×10^{-3} to $5.48 \times 10^{-3}\ M$.

[3]It is assumed in this deviation that the alcoholysis reaction is rapid and that the $[C_2H_5O^-]$ is maintained constant throughout the course of the TNB – cyanide ion reaction. Also $[C_2H_5O^-] \gg [TNB]_0$.

TABLE 1. Pseudo first-order rate constants (k_{obs}) for the "fast reaction" observed in ethanol solutions containing 1,3,5-trinitrobenzene and tetraphenylarsonium cyanide: $T = 25.0$ °C; $[TNB]_0 = 3.04 \times 10^{-5}$ M

$[\phi_4AsCN] \times 10^3$ (M)	$[C_2H_5O^-] \times 10^4$ (M)[a]	k_{obs} (s^{-1})[b]
0.665	1.12	16.0 ± 0.8
0.960	1.45	17.4 ± 0.9
2.007	2.01	19.6 ± 1.0
2.194	2.08	19.4 ± 1.0
2.803	2.38	20.0 ± 1.0
3.513	2.80	22.7 ± 1.1
4.876	3.19	24.0 ± 1.2
5.485	3.39	24.1 ± 1.2

[a] $[C_2H_5O^-]$ calculated using eq. 3 with $K = 2020$ M^{-1} and $\varepsilon_{480} = 1.65 \times 10^4$ M^{-1} cm^{-1}. It is assumed that rapid alcoholysis of cyanide ion maintains the $[C_2H_5O^-]$ constant throughout the course of reaction.
[b] k_{obs} values from the slopes of the ln $(A_\infty - A_t)$ *vs.* time plots. Errors in k_{obs} are based on the "least-squares" slopes of the plots.

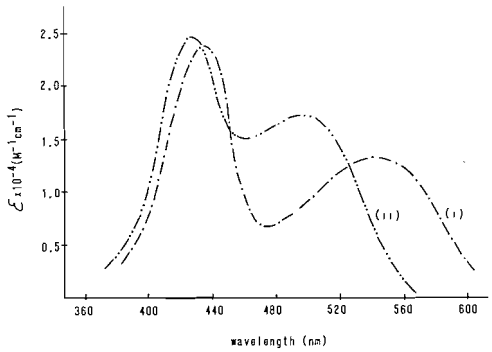

FIG. 2. Visible absorption spectra in ethanol at 25.0 °C of (*i*) the 1:1 1,3,5-trinitrobenzene – cyanide ion σ-complex and (*ii*) the 1:1 1,3,5-trinitrobenzene – ethoxide ion σ-complex.

cyanide concentrations are given in Table 2. The plot of k_{obs} *vs.* $([CN^-]_0 - [C_2H_5O^-] + [TNB]_0)/(1 + K[C_2H_5O^-])$ was linear with "least-squares" slope (k_2) and intercept (k_{-2}) of 442 ± 14 M^{-1} s^{-1} and 0.042 ± 0.033 s^{-1}, respectively.

When solutions of tetraphenylarsonium cyanide in *n*-propanol and 1,3,5-trinitrobenzene in *n*-propanol were mixed the % transmittance *vs.* time traces on the oscilloscope again indicated that "fast" and "slow" reactions were taking place in solution. By analogy to what was found to occur in the ethanol system, the fast reaction in *n*-propanol was considered to be associated with the formation of σ-complex **1** (X = *n*-C_3H_7O).

The progress of the fast reaction was followed at 505 nm. Plots of ln $(A_\infty - A_t)$ *vs.* time were linear to about 80% completion of reaction. Values of k_{obs} were not as reproducible in this system as for the fast reaction in ethanol, average reproducibility in k_{obs} being ±13% in *n*-propanol as compared to ±5% in ethanol. The $[n\text{-}C_3H_7O^-]$ was calculated as in eq. 3 using a K for σ-complex formation of 7.8×10^3 M^{-1} (6) and a molar extinction coefficient (ε) of the σ-complex at 505 nm of $1.74\ 10^4$ M^{-1} cm^{-1}. The plot of k_{obs} *vs.* $[n\text{-}C_3H_7O^-]$ was linear with slope (k_1) equal to $7.3 \pm 3.0 \times 10^4$ M^{-1} s^{-1} and intercept (k_{-1}) equal to 5.8 ± 3.6 s^{-1}. The agreement between these values of k_1 and k_{-1} and the k_1 of $9.26 \pm 0.17 \times 10^4$ M^{-1} s^{-1} and k_1 of 11.9 ± 1.1 s^{-1} determined from a study of the interaction of 1,3,5-trinitrobenzene and *n*-propoxide ion in *n*-propanol (6) is reasonable and confirms that the fast reaction involves the formation of σ-complex **1** (X = *n*-C_3H_7O).

The alcoholysis constant K' for the reaction of cyanide ion and *n*-propanol at 25.0 °C was determined to be $1.56 \pm 0.05 \times 10^{-6}$. The error limits on K' represent the standard deviation of the mean of nine determinations carried out over the tetraphenylarsonium cyanide concentration range 1.24×10^{-3} to 8.28×10^{-3} M.

The species present at the completion of the slow reaction in *n*-propanol possessed absorption maxima at 435 and 542 nm. This is consistent with the formulation of this species as σ-complex **1** (X = CN) (5). The rate of formation of this complex was followed at 580 nm since at this wavelength σ-complex **1** (X = *n*-C_3H_7O) has negligible absorption. Treatment of the rate data was identical to that employed for the reaction of cyanide ion and TNB in ethanol. A linear k_{obs} *vs.* $([CN^-] - [n\text{-}C_3H_7O^-]$

Can. J. Chem. Downloaded from www.nrcresearchpress.com by 210.87.254.105 on 09/05/12
For personal use only.

TABLE 2. Pseudo first-order rate constants (k_{obs}) for the 1,3,5-trinitrobenzene – cyanide ion reaction in ethanol: $T = 25.0$ °C; $[TNB]_0 = 8.03 \times 10^{-6}$ M

$[\phi_4AsCN] \times 10^3$ (M^{-1})	$[C_2H_5O^-] \times 10^4$ (M)[a]	$\frac{[CN^-]_0 - [C_2H_5O^-] + [TNB]_0}{1 + K[C_2H_5O^-]} \times 10^3$	k_{obs} (s^{-1})[b]
0.966	1.40	0.663	0.347 ± 0.005
1.38	1.66	0.197	0.404 ± 0.006
2.76	2.39	1.71	0.796 ± 0.006
3.45	2.68	2.08	0.969 ± 0.014
4.14	2.95	2.42	1.15 ± 0.01
5.52	3.42	3.08	1.44 ± 0.03
7.00	3.87	3.73	1.64 ± 0.04

[a]$[C_2H_5O^-]$ calculated using eq. 3 and the experimentally determined A_∞ associated with the first (fast) reaction. Alternatively, $[C_2H_5O^-]$ was calculated using K' for the alcoholysis of CN^- ion in ethanol.
[b]Slope of the ln $(A_\infty - A_t)$ *vs.* time plot. Error in k_{obs} based on the error associated with the "least-squares" slope of the plot.

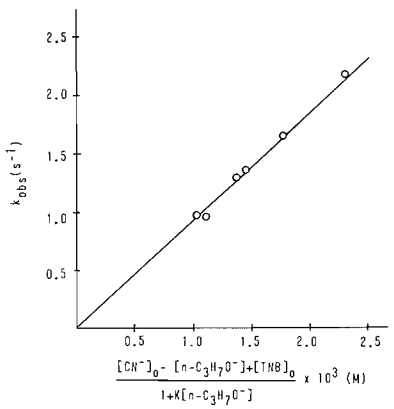

FIG. 3. Values of k_{obs} for the formation of the 1:1 1,3,5-trinitrobenzene – cyanide ion σ-complex in *n*-propanol as a function of $([CN^-]_0 - [n\text{-}C_3H_7O^-] + [TNB]_0)/(1 + K[n\text{-}C_3H_7O^-])$: $T = 25.0$ °C; $[TNB]_0 = 9.62 \times 10^{-6}$ M; $[\phi_4AsCN]_0 = 1.78 \times 10^{-3}$ to 1.10×10^{-2} M.

+ $[TNB]_0)/(1 + K[n\text{-}C_3H_7O^-])$ plot was obtained (Fig. 3) whose slope (k_2) was 932 ± 30 M^{-1} s^{-1}. The intercept of the plot was too small (<0.01) to be assessed with any real accuracy by this method.

When solutions of 1,3,5-trinitrobenzene in isopropanol and tetraphenylarsonium cyanide in isopropanol were mixed only a single reaction trace of % transmittance *vs.* time was observed. The resulting solutions possessed absorption maxima at 436 and 546 nm consistent with the formulation of the species in solution as σ-complex **1** (X = CN) (5).

The progress of the reaction was followed at 540 nm. Plots of ln $(A_\infty - A_t)$ *vs.* time were linear to greater than 90% completion of reaction over the entire range of cyanide ion concentrations employed. Plots of k_{obs} *vs.* $[CN^-]_0$ were linear in the range 2.0×10^{-4} M to 3.0×10^{-3} M but curved slightly upward between 3.0×10^{-3} and 7.0×10^{-3} M $[CN^-]_0$.[4] The value of k_2 at 25.0 °C obtained from the slope of the k_{obs} *vs.* $[CN^-]_0$ plot, for runs carried out at low concentrations of cyanide ion, was 2.45 ± 0.10×10^3 M^{-1} s^{-1}. The value of k_{-2} was too small to be accurately estimated from the intercept of the plot. Using the reported K (k_2/k_{-2}) for complex formation of $10.0 \pm 0.3 \times 10^3$ M^{-1} at 25.0 °C (5), k_{-2} is calculated to be 0.25 s^{-1}.

The reaction of 1,3,5-trinitrobenzene and cyanide ion in *t*-butanol also gave rise to only a single reaction trace of % transmittance *vs.* time. The species formed in solution possessed absorption maxima at 437 and 539 nm consistent with its formulation as σ-complex **1** (X = CN)(5).

The progress of the reaction was followed at 545 nm. Plots of ln $(A_\infty - A_t)$ *vs.* time were linear to greater than 90% completion of reaction at all cyanide ion concentrations employed. A plot of k_{obs} *vs.* $[CN^-]_0$ was linear over the range 2.0×10^{-4} to 5.0×10^{-4} M but curved slightly upward between 5.0×10^{-4} and 7.0×10^{-4} M $[CN^-]_0$. From the linear portion of the plot at low $[CN^-]_0$, k_2 and k_{-2} were found to be $1.06 \pm 0.05 \times 10^5$ M^{-1} s^{-1} and 2.5 ± 1.2 s^{-1}, respectively.

Specific rate constants for the formation of **1** (X = CN) decrease in the order k_2(*t*-C_4H_5OH) > k_2(iso-C_3H_7OH) > k_2(*n*-C_3H_7OH) > k_2-(C_2H_5OH). A plot of log k_2 *vs.* the solvent parameter E_t (10) is linear with slope −0.25.

[4]Over a comparable range of tetraphenylarsonium cyanide concentrations the curvature in the k_{obs} *vs.* $[CN^-]_0$ plots was more pronounced the higher the temperature. A study of this phenomenon is reported in the following paper.

Can. J. Chem. Downloaded from www.nrcresearchpress.com by 210.87.254.105 on 09/05/12
For personal use only.

Can. J. Chem. Downloaded from www.nrcresearchpress.com by 210.87.254.105 on 09/05/12
For personal use only.

Linear log k *vs.* E_t plots of comparable slopes have also been reported for the formation of **1** (X = RO) in ROH, where R = CH_3, C_2H_5, *n*- and iso-C_3H_7, and *n*-C_4H_9 (6), and for the formation of the 2,4,6-trinitrobenzyl anion (**2**) by reaction of 2,4,6-trinitrotoluene with RO^- in the corresponding alcohol (R = C_2H_5, *n*- and iso-C_3H_7) (14).

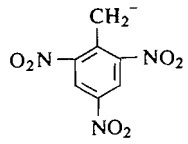

2

It has been argued that for the formation of **1** (X = OR) free energy changes associated with the desolvation of the anion play a critical role in determining the magnitudes of the specific rate constants (15, 6). The similarity in the slopes of the above log k *vs.* E_t plots suggests that, for the limited range of alcohols studied, cyanide ion and RO^- respond similarly to the changing solvation characteristics of the different alcohols.

Little can be said on the basis of our results concerning trends in k_{-2} for decomposition of **1** (X = CN), k_{-2} values in ethanol and *n*-propanol are both small ($<0.05\ s^{-1}$) and cannot be determined with any accuracy using the method described; k_{-2} values in isopropanol and *t*-butanol are approximately 0.3 and $2.5\ s^{-1}$, respectively. The trend in k_{-2} values is opposite to that which is observed for the decompositions of **1** (X = RO) in the alcohols where the higher values of k_{-2} are associated with the ethanol and *n*-propanol systems.

The ratios of the rate constants for formation of **1** (X = OR) and **1** (X = CN) in ethanol, *n*-propanol, isopropanol, and *t*-butanol are 116, 112, 43, and 0.27, respectively. The straight chain alkoxides are about 100 times more reactive than cyanide ion in the corresponding alcohol whereas isopropoxide is only about 40 times as reactive. A steric hindrance associated with a methyl group in isopropoxide would account for its lower reactivity compared to *n*-propoxide. This steric effect is sufficiently pronounced that in *t*-butanol cyanide is a better nucleophile towards the aromatic carbon center than is *t*-butoxide ion.

A comparison of the autopyrolysis constant of ethanol ($pK_a = 18.88$) (16) with the dissociation of hydrocyanic acid in ethanol ($pK_d \simeq 13$) determined above indicates that in ethanol ethoxide ion is about 10^6 times more basic than is cyanide ion. Comparable differences in hydrogen basicity may be expected to operate in the other alcohols. However, based on the reported equilibrium constants for formation of **1** (X = OR) and **1** (X = CN), carbon basicity towards the aromatic carbon center favors the alkoxide over the cyanide by less than a factor of 10 for R = C_2H_5, *n*- and iso-C_3H_7, and *n*-C_4H_9 (5, 6, 13).

Alcoholysis of cyanide ion was observed in ethanol and *n*-propanol but not in isopropanol and *t*-butanol. Combining the alcoholysis constants K' obtained in this study with the reported autopyrolysis constants of ethanol and *n*-propanol (16) one can calculate the dissociation constants (K_d) of HCN in ethanol and *n*-propanol at 25.0 °C as 9.92×10^{-14} and 1.72×10^{-14}, respectively. The constant (K_d) of HCN in water at 25.0 °C is 8.82×10^{-12} (17). This order of dissociation constants K_d (H_2O) > K_d (C_2H_5OH) > K_d (*n*-C_3H_7OH) is in qualitative agreement with the calculated pK_{BH^+} values of water (−3.43), ethanol (−1.93), and *n*-propanol (−1.91) reported by Levitt and Levitt (18). Isopropanol and *t*-butanol (pK_{BH^+} value −1.70 and −1.49, respectively) are too weakly acidic to undergo any substantial alcoholysis reaction. Although kinetic studies in methanol and *n*-butanol were not investigated, the pK_{BH^+} values of these alcohols (−2.17 and −1.90, respectively) suggest that complications due to cyanide ion alcoholysis would also be observed in these solvents.

The alcoholysis reactions of cyanide ion in methanol and ethanol may have been responsible in part for the experimental difficulties which lead to the placing of high error limits on the equilibrium constants for formation of **1** (X = CN) in methanol and the difficulties experienced in obtaining a good ΔH_{cal} for the formation of **1** (X = CN) in ethanol (5). In fact since the reaction to form **1** (X = OR) is always significantly faster than the reaction to form **1** (X = CN) in the same ROH, the slow secondary reactions referred to by Buncel *et al.* (5) may, in part, have been associated with the formation of the desired TNB – cyanide ion σ-complexes. More accurate values of k_{-2} for the decomposition of **1** (X = CN) in ethanol and *n*-propanol are required before any definitive statements can be made regarding possible errors in the re-

ported K and ΔH° for the formation of **1** (X = CN) in ethanol and *n*-propanol introduced through neglect of the alcoholysis reactions in these solvents.

Financial support by the National Research Council of Canada is gratefully acknowledged.

1. A. R. NORRIS. Can. J. Chem. **45**, 2703 (1967).
2. A. R. NORRIS. Can. J. Chem. **47**, 2895 (1969).
3. E. BUNCEL, A. R. NORRIS, and W. PROUDLOCK. Can. J. Chem. **46**, 2759 (1968).
4. E. BUNCEL, A. R. NORRIS, and K. E. RUSSELL. Q. Rev. Lond. **22**, 123 (1968).
5. E. BUNCEL, A. R. NORRIS, W. PROUDLOCK, and K. E. RUSSELL. Can. J. Chem. **47**, 4129 (1969).
6. L. H. GAN and A. R. NORRIS. Can. J. Chem. **49**, 2490 (1971).
7. E. BUNCEL, A. R. NORRIS, K. E. RUSSELL, and R. TUCKER. J. Am. Chem. Soc. **94**, 1646 (1972).
8. A. R. NORRIS. Can. J. Chem. **45**, 175 (1967).
9. J. R. A. POLLOCK and R. STEVENS (*Editors*). Dictionary of organic compounds. 4th Ed. Eyre and Spottiswoode Ltd., London. 1965.
10. K. DIMROTH, C. REICHARDT, T. SIEPMANN, and F. BOHEMANN. Liebigs Ann. Chem. **661**, 1 (1963).
11. A. I. VOGEL. A textbook of practical organic chemistry. 3rd Ed. Longmans, Green, London. 1956. p. 169.
12. P. G. ASHMORE, B. P. LEVITT, and B. A. THRUSH. Trans. Faraday Soc. **52**, 530 (1956).
13. C. F. BERNASCONI. J. Am. Chem. Soc. **92**, 4682 (1970).
14. E. BUNCEL, A. R. NORRIS, and K. E. RUSSELL. International conference on the mechanisms of reaction in solution, Canterbury, England. Paper B-11 (1970).
15. E. F. CALDIN. J. Chem. Soc. 3345 (1959).
16. R. SCHAAL and A. TEZE. Bull. Soc. Chim. Fr. 1783 (1961).
17. Handbook of chemistry and physics. 51st Ed. Chemical Rubber Publishing Co., Cleveland, Ohio.
18. L. S. LEVITT and B. W. LEVITT. J. Phys. Chem. **74**, 1812 (1970).

Can. J. Chem. Downloaded from www.nrcresearchpress.com by 210.87.254.105 on 09/05/12
For personal use only.

Kinetic and Equilibrium Studies of the Reactions of Cyanide Ion with 1,3,5-Trinitrobenzene, 2,4,6-Trinitroanisole, and 2,4,6-Trinitrotoluene in Isopropanol

LEONG HUAT GAN AND ALBERT RICHARD NORRIS
Department of Chemistry, Queen's University, Kingston, Ontario

Received July 10, 1973

Equilibrium constants for the formation of 1:1 cyanide ion σ-complexes with 1,3,5-trinitrobenzene, 2,4,6-trinitroanisole, and 2,4,6-trinitrotoluene have been determined spectrophotometrically over a range of temperatures. Standard enthalpy (ΔH^0) and entropy (ΔS^0) changes associated with each reaction have been evaluated. The kinetics of formation of the σ-complexes have been investigated by means of a stopped-flow technique and the activation parameters characterizing the formation of each complex have been determined. Evidence is presented which indicates the cyanide ion – 2,4,6-trinitroanisole σ-complex formed in isopropanol contains the cyanide ion bonded exclusively at the C-3 position.

Les constantes d'équilibres pour la formation d'un complexe-σ 1:1 ion cyanure – trinitro-1,3,5 benzène, trinitro-2,4,6 anisole et trinitro-2,4,6 toluène ont été déterminées dans un intervalle de températures à l'aide de la spectrophotométrie. Les changements d'enthalpie standard (ΔH^0) et d'entropie (ΔS^0) associés à chaque réaction ont été évalués. La cinétique de formation des complexes-σ a été étudiée à l'aide de la technique à débit interrompu et les paramètres d'activation se rattachant à la formation de chaque complexe ont été déterminés. On apporte des preuves pour montrer que le complexe-σ ion cyanure – trinitro-2,4,6 anisole formé dans l'isopropanol contient l'ion cyanure lié exclusivement à la position C-3.
[Traduit par le journal]

Can. J. Chem., **52**, 8 (1974)

Introduction

Cyanide ion is known to react with 1,3,5-trinitrobenzene and a number of related 1-X-2,4,6-trinitrobenzenes (X = CH_3, OCH_3, and CHO) in acetone, chloroform, and various alcohols to form σ-complexes of 1:1 stoichiometry (1–6). For X = CHO, addition of cyanide ion occurs exclusively at the C-1 position to yield **1** while with 2,4,6-trinitrotoluene, addition seems to occur exclusively at the C-3 position to yield σ-complex **2** (2). With 2,4,6-trinitroanisole

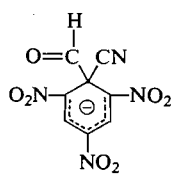

1

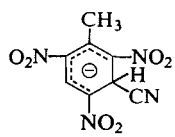

2

both the C-1 and the C-3 adducts **3** (X = CN) and **4** (X = CN) are formed in deuterochloroform (3). Studies over a range of temperatures suggest that **4** (X = CN) is the thermodynamically more stable species (3). In the reactions of 2,4,6-trinitroanisole with methoxide ion in methanol both the C-1 and C-3 adducts **3** (X = OCH_3) and **4** (X = OCH_3) are also formed

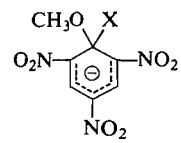

3

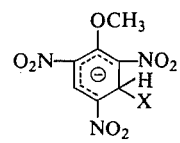

4

but the thermodynamically more stable σ-complex in this system is **3** (X = OCH_3) (7–11). The influence of the nature of the solvent and the properties of the group X on the relative stabilities of isomeric 1:1 σ-complexes of this type is still largely unknown.

As part of a series of kinetic studies of the reactions of bases and nitroaromatic compounds (12, 13), and as an extension of previously reported equilibrium studies of the reactions of cyanide with 1,3,5-trinitrobenzene in a number of alcohols (14), we have investigated the kinetics of σ-complex formation between cyanide ion and 1,3,5-trinitrobenzene, 2,4,6-trinitroanisole, and 2,4,6-trinitrotoluene in isopropanol.

Evidence is presented to show that the only σ-complex formed between cyanide ion and 2,4,6-trinitroanisole in isopropanol is the C-3 adduct **4** (X = CN). Specific rate constants and activation parameters for the formation of **2**, **4** (X = CN), and **5** (X = CN) have been deter-

Can. J. Chem. Downloaded from www.nrcresearchpress.com by 210.87.254.5 on 09/05/12
For personal use only.

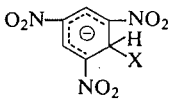

5

mined together with the standard enthalpy (ΔH^0) and entropy (ΔS^0) changes associated with their formation.

Experimental

Reagents

Eastman 1,3,5-trinitrobenzene was recrystallized twice from an ethanol–water mixture and dried to constant weight *in vacuo* over phosphorus(V) pentoxide, m.p. 122 °C, (lit. m.p. 122.5 °C (15)).

Eastman 2,4,6-trinitrotoluene was recrystallized twice from absolute ethanol and dried *in vacuo* over phosphorus(V) pentoxide, m.p. 89–82 °C, (lit. m.p. 82 °C (15)).

Eastman 2,4,6-trinitroanisole was recrystallized twice from carbon tetrachloride and dried *in vacuo* over phosphorus(V) pentoxide, m.p. 68–69 °C, (lit. m.p. 68 °C (15)).

Eastman tetraphenylarsonium chloride was dried to constant weight *in vacuo* over phosphorus(V) pentoxide.

Tetraphenylarsonium cyanide was prepared as previously described (14) and dried to constant weight *in vacuo* over phosphorus(V) pentoxide. Tetraphenylarsonium nitrite was prepared in a similar fashion but using sodium nitrite in place of sodium cyanide in both the initial preparation and the recrystallization procedures. After two recrystallizations the compound was dried to constant weight *in vacuo* over phosphorus(V) pentoxide.

All other reagents used in the study were A.R. grade or better.

Isopropanol was dried by refluxing over Linde 4A Molecular Sieve overnight and then distilled under a dry nitrogen atmosphere. Only the middle portion of the distillate was retained.

Stock solutions of the nitroaromatic compounds and the tetraphenylarsonium salts were prepared by dissolving weighed quantities of each reagent in a known volume of isopropanol. Solutions of lower concentrations used in the kinetic and equilibrium studies were prepared by dilution.

Instruments

The instruments used to record absorption spectra and to carry out kinetic studies using the stopped-flow technique have been described previously (16). For virtually all of the kinetic runs the normal mode of operation of the stopped-flow spectrophotometer was modified, as described previously (16), so as to yield an oscilloscope trace of absorbance as a function of time rather than % transmittance as a function of time (17).

Procedures

(a) Determination of Molar Extinction Coefficients (ε)

An empty 0.10-cm cell and a 1.0-cm cell filled with 2–3 ml of a concentrated solution of one of the reactants were placed in the sample cell compartment for thermostatting (about 20 min was required). A small volume (usually less than 0.20 ml) of solution containing the second reactant was then introduced by means of a Micrometer syringe[1] into the contents of the 1.0-cm cell. The resulting solution was quickly mixed, a portion of it transferred to the 0.10-cm cell and the absorbances of the solution recorded at a number of wavelengths. A matched 0.10-cm cell filled with isopropanol was used as a reference.

In all the systems the basic reagent was present in excess in order to minimize any neutralization effects due to absorbed carbon dioxide. At the highest concentrations of cyanide ion employed a slow decrease in absorbance was sometimes found to occur after the maximum absorbance had been reached. In these cases the absorbance was corrected by extrapolating the absorbance *vs.* time curve back to the time of mixing. The correction in most cases was small; less than 4% of the total absorbance.

Because of the high equilibrium constants associated with these reactions greater than 99% of the nitroaromatic compound was converted to complex under the reaction conditions employed. The molar extinction coefficient of the complex (ε) was therefore evaluated from the slope of the plot of absorbance *vs.* initial concentration of nitroaromatic compound. For all the systems studied molar extinction coefficients at the absorption maxima were found to be temperature independent over the temperature range studied (5–50 °C).

(b) Determination of Equilibrium Constants (K)

The experimental procedure was identical to that used in determining the molar extinction coefficients except that all solutions contained nearly equimolar amounts of tetraphenylarsonium cyanide and nitroaromatic compound. Equilibrium constants were calculated using the expression shown in eq. 1 where A is the measured

$$[1]\quad K = \frac{A/\varepsilon l}{\{[CN^-]_0 - A/\varepsilon l\}\{[N]_0 - A/\varepsilon l\}}$$

absorbance at equilibrium, ε is the molar extinction coefficient of the complex at the wavelength at which the absorbance was measured, l is the path length of the cell (0.1 cm), and $[CN^-]_0$ and $[N]_0$ represent the total concentrations of cyanide ion and nitroaromatic compound in solution.

(c) Determination of Pseudo First-order Rate Constants (k_{obs})

Solutions of the nitroaromatic compound in isopropanol ($\sim 10^{-5}$ M) and tetraphenylarsonium cyanide in isopropanol (10^{-4}–10^{-2} M) were prepared immediately prior to each run by dilution of known volumes of the corresponding stock solutions with isopropanol. The drive syringes were filled and traces of absorbance (A) *vs.* time and k_{obs} obtained as described previously (16).

The reactions of cyanide ion with 1,3,5-trinitrobenzene, 2,4,6-trinitroanisole, and 2,4,6-trinitrotoluene were monitored by following changes in absorbance at 540, 518, and 535 nm, respectively.

(d) Determination of Activity Coefficients at 25.0 °C

The activity coefficients of 1,3,5-trinitrobenzene and 2,4,6-trinitrotoluene in isopropanol solutions containing

[1]Roger Gilmont Instruments, Inc., Great Neck, N.Y.

Can. J. Chem. Downloaded from www.nrcresearchpress.com by 210.87.254.5 on 09/05/12
For personal use only.

TABLE 1. Spectral properties of some 1:1 cyanide ion σ-complexes in isopropanol at 25.0 °C

Nitroaromatic compound	Wavelengths of maximum absorption (nm)		Molar extinction coefficients at the absorption maxima[a] $\times 10^{-4}$ (M^{-1} cm^{-1})	
	λ_1	λ_2	ε_1	ε_2
1,3,5-Trinitrobenzene	436	546	2.67±0.02	1.47±0.02
2,4,6-Trinitroanisole	422	518	2.09±0.02	1.19±0.02
2,4,6-Trinitrotoluene	437	535	1.69±0.03	1.11±0.03

[a]Error limits are standard errors of the mean based on at least four determinations.

tetraphenylarsonium chloride were determined by a solubility method (18, 19).

Volumetric flasks (25 ml) containing solid 1,3,5-trinitrobenzene or 2,4,6-trinitrotoluene and a known amount of tetraphenylarsonium chloride in isopropanol were attached to a shaker. The shaker was immersed in a water bath thermostatted at 25.0 °C and the flasks shaken vigorously for 3 days. The saturated solution was then decanted into a test tube and centrifuged. A portion of the clear supernatant solution was withdrawn by means of a 2.0-ml Micrometer syringe[1] and diluted to the desired concentration for absorbance measurements on the Cary 14. To ensure the solution was saturated the measurement for each solution was repeated after 24 h. The amount of 1,3,5-trinitrobenzene or 2,4,6-trinitrotoluene in solution was determined from its absorbances at 300 and 310 nm.

Attempts to determine the solubility of 2,4,6-trinitroanisole in a similar fashion were unsuccessful because of the very slow precipitation of tetraphenylarsonium picrate from the solution.

Results and Discussion

When isopropanol solutions containing tetraphenylarsonium cyanide and 1,3,5-trinitrobenzene (TNB), 2,4,6-trinitroanisole (TNA), or 2,4,6-trinitrotoluene (TNT) were mixed, deep red-colored solutions resulted. The visible absorption spectra of the solutions suggested that the colored species present were 1:1 cyanide ion σ-complexes of the 1-X-2,4,6-trinitrobenzenes (X = H, OCH_3, CH_3) (1–4). The results of the equilibrium and kinetic studies were fully consistent with this formulation for the stoichiometry of the colored species. The wavelengths of maximum absorption and the molar extinction coefficients at the absorption maxima of the 1:1 cyanide ion σ-complexes of 1,3,5-trinitrobenzene, 2,4,6-trinitroanisole, and 2,4,6-trinitrotoluene in isopropanol at 25.0 °C are given in Table 1. The visible absorption curves of the three complexes are shown in Fig. 1.

An equilibrium constant of 10.0 ± 0.3 × 10^3 M^{-1} has been reported for the formation of the cyanide ion – 1,3,5-trinitrobenzene σ-complex

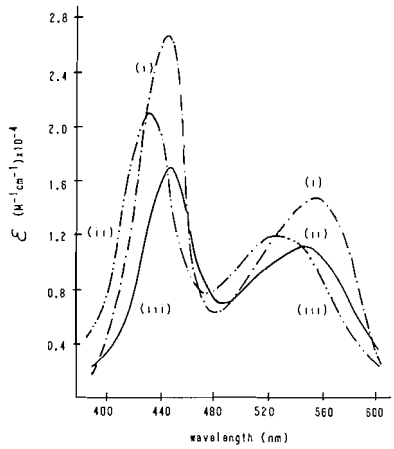

FIG. 1. Visible absorption spectra in isopropanol at 25.0 °C of 1:1 cyanide ion σ-complexes of (*i*) 1,3,5-trinitrobenzene (—·—·), (*ii*) 2,4,6-trinitrotoluene (—), and (*iii*) 2,4,6-trinitroanisole (—··—).

at 25.0 °C (14). The same authors report an enthalpy of reaction based on calorimetric measurements (ΔH_{cal}), of −7.1 ± 0.6 kcal mol^{-1} and a ΔS^0 of 5.5 ± 3.0 cal deg^{-1} mol^{-1}. Our studies have yielded an average equilibrium constant for formation of **5** (X = CN) at 25.0 °C of 5.1 ± 0.1 × 10^4 M^{-1}. Employing the reported ΔH_{cal} of −7.1 ± 0.6 kcal mol^{-1} we obtain a ΔS^0 of 2.5 ± 3.0 cal deg^{-1} mol^{-1}. There is no obvious reason why the equilibrium constants should differ. Fading reactions and complications due to alcoholysis of the cyanide ion are not problems in this system (16). Perhaps at the high ratio of concentration of cyanide ion to concentration of 1,3,5-trinitrobenzene used in earlier studies some degree of 2:1 σ-complex formation resulted. This complication would be reflected in lower values of ε_1 and ε_2. We note though that our ε_1 value (Table 1) is not significantly greater than the value of ε_1 previously reported (14).

Can. J. Chem. Downloaded from www.nrcresearchpress.com by 210.87.254.5 on 09/05/12
For personal use only.

Can. J. Chem. Downloaded from www.nrcresearchpress.com by 210.87.254.5 on 09/05/12
For personal use only.

The equilibrium constants for the formation of the cyanide ion – 2,4,6-trinitroanisole σ-complex were found to be $1.24 \pm 0.03 \times 10^4$, $1.18 \pm 0.04 \times 10^4$, and $1.12 \pm 0.05 \times 10^4$ M^{-1} at 4.6, 15.0, and 25.0 °C, respectively.[2] Based on the variation of the equilibrium constants with temperature ΔH^0 was calculated to be -0.81 ± 0.55 kcal mol^{-1}. ΔS^0 for the reaction was 15.8 ± 2.0 cal deg^{-1} mol^{-1}.

The equilibrium constants for formation of the cyanide ion – 2,4,6-trinitrotoluene σ-complex were determined to be $3.11 \pm 0.16 \times 10^4$, $2.01 \pm 0.09 \times 10^4$, and $1.50 \pm 0.01 \times 10^4$ M^{-1} at 9.1, 25.0, and 34.9 °C. The resulting ΔH^0 and ΔS^0 associated with the complex formation reaction were calculated to be -4.90 ± 0.30 kcal mol^{-1} and 3.4 ± 1.1 cal deg^{-1} mol^{-1}, respectively.

Equilibrium constants for 1:1 σ-complex formation with cyanide ion at 25.0 °C increase in the order TNA < TNT < TNB.

The variation in K is, however, very small. A far greater variation in K for complex formation is found for the sulfite ion complexes of TNA, TNB, and TNT in aqueous solution where the order of the equilibrium constants is TNT < TNA < TNB and the maximum K is a factor of about 40 times larger than the minimum K (20, 21). For the formation of ethoxide, *n*-propoxide, and isopropoxide σ-complexes of TNB and TNT in the corresponding alcohols, the equilibrium constants for complex formation with TNB are uniformly a factor of about 10^2 times larger than the equilibrium constants for σ-complex formation with TNT (22). For the methoxide ion complexes of TNB and TNA (**4**, X = OCH_3) in methanol at 25.0 °C, the equilibrium constants favor the formation of the TNB complex by a factor of approximately 6 (12, 23).

For the three complex formation reactions studied more negative ΔH^0 values are accompanied by more negative ΔS^0 values and a plot of ΔH^0 *vs.* ΔS^0 is reasonably linear. The least negative values of both ΔH^0 and ΔS^0 are associated with the formation of the cyanide ion – TNA σ-complex. It has been argued that for the reaction of sulfite ion with a number of 1-X-2,4,6-trinitrobenzenes (X = CHO, NH_2, $NHCH_3$, and $N(CH_3)_2$) decreasing ΔH^0 and ΔS^0 reflect decreasing solvation of the resulting 1:1 σ-complex (24). By analogy we might expect that of the three complexes under consideration here the cyanide ion – 2,4,6-trinitroanisole complex is least strongly solvated by isopropanol. This is a surprising result since the steric effects associated with the methoxyl group might have been expected to lead to greater rotation of the *ortho* nitro groups out of the plane of the ring and hence greater overall solvation of the σ-complex in this case. There are two reasons perhaps why analogies cannot be so simply drawn. First, because of its size isopropanol, unlike water, may be no more effective in solvating a nitro group rotated out of the plane of the ring than a nitro group in the plane of the ring. Second, the interpretation of trends in ΔH^0 and ΔS^0 in terms of trends in solvation effects of the resulting σ-complexes assumes that the starting nitroaromatic compounds have comparable properties. 2,4,6-Trinitroanisole has been estimated to be about 4 kcal mol^{-1} more stable than 1,3,5-trinitrobenzene as a result of ground state stabilization through resonance structures such as **6***a* and **6***b* (23).

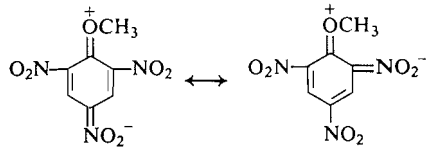

6a *6b*

In methanol, ΔS^0 for the formation of **5** (X = OCH_3) and **4** (X = OCH_3) are the same within experimental error while the ΔH^0 values are 1.0 ± 1.6 and 2.2 ± 1.5 kcal mol^{-1}, respectively (11, 12, 23).

For the three cyanide ion – 1-X-2,4,6-trinitrobenzene interactions studied, plots of ln ($A_\infty - A_t$) *vs.* time were linear to greater than 90% of reaction at all cyanide ion concentrations. At the high concentrations of cyanide ion to concentration of nitroaromatic compound used in the kinetic studies a slight fading reaction was observed in the TNT – cyanide ion system.[3] On the time scale involved in the kinetic study this

[2]Errors in K are standard deviations of the mean based on at least four determinations.

[3]This "fading reaction" was probably due to the slow formation of a 2:1 σ-complex as only one absorption maximum in the visible region, characteristic of a 2:1 σ-complex of this type (4, 6), remained after approximately 10 min. The nature of the species formed is under investigation.

Can. J. Chem. Downloaded from www.nrcresearchpress.com by 210.87.254.5 on 09/05/12
For personal use only.

fading reaction did not appear to interfere to any appreciable extent with the formation of the 1:1 σ-complex. In some instances a small correction to the infinite absorbance value (A_∞) was made by extrapolating the linear portion of the absorbance *vs.* time portion of the fading reaction plot back to the time of mixing. By analogy to the reaction of 2,4,6-trinitroanisole with methoxide ion in methanol (11), two reaction traces of absorbance *vs.* time might have been expected in the reaction of 2,4,6-trinitroanisole with cyanide ion. The faster of the two reactions would correspond to formation of σ-complex **4** (X = CN) while the slower reaction would be associated with the formation of σ-complex **3** (X = CN). A careful check of absorbance *vs.* time traces at different wavelengths and over a range of cyanide ion concentrations showed that only one reaction was occurring in the solutions containing 2,4,6-trinitroanisole and cyanide ion. The rapidity of the reaction suggests that the σ-complex formed is **4** (X = CN).

For the reversible formation of 1:1 σ-complex according to eq. 2 (where X = H, OCH_3, and

[2] 1-X-2,4,6-trinitrobenzene + $CN^- \underset{k_{-1}}{\overset{k_1}{\rightleftharpoons}}$ σ-Complex

CH_3) carried out under reaction conditions such that $[CN^-]_0 \gg$ [1-X-2,4,6-trinitrobenzene]$_0$ ([ ]$_0$ represents the total concentration), the k_{obs} obtained from the slope of the ln $(A_\infty - A_t)$ *vs.* time plot is related to the specific rate constants k_1 and k_{-1} and the $[CN^-]_0$ as shown in eq. 3.

$$[3] \qquad k_{obs} = k_1[CN^-]_0 + k_{-1}$$

Plots of k_{obs} *vs.* $[CN^-]_0$ were strictly linear for the reaction of cyanide ion and 2,4,6-trinitroanisole up to a $[CN^-]_0$ of 1.20×10^{-2} *M* (Fig. 2). However for both the 1,3,5-trinitrobenzene – and 2,4,6-trinitrotoluene – cyanide ion reactions, where the maximum $[CN^-]_0$ was much less than 1.2×10^{-2} *M*, k_{obs} *vs.* $[CN^-]_0$ plots were linear at low concentrations of cyanide ion but curved slightly upward at higher concentrations of cyanide ion (Figs. 3 and 4). In both systems curvature of the k_{obs} *vs.* $[CN^-]_0$ plots seemed to become more pronounced the higher the temperature.

The slopes (k_1) and intercepts (k_{-1}) of the k_{obs} *vs.* $[CN^-]_0$ plots for the reaction of cyanide ion and 2,4,6-trinitroanisole and the slopes (k_1) of the k_{obs} *vs.* $[CN^-]_0$ plots (obtained at low

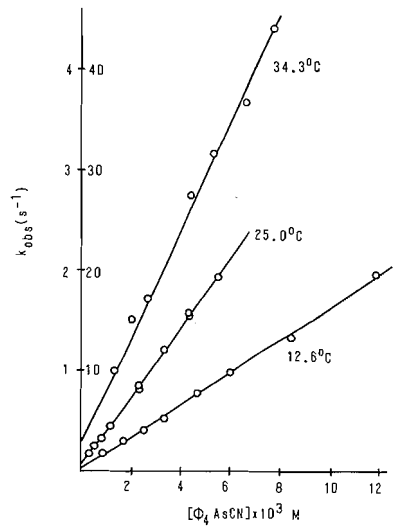

FIG. 2. k_{obs} as a function of the $[\phi_4AsCN]$ for the reactions of 2,4,6-trinitroanisole with cyanide ion in isopropanol at a number of temperatures.

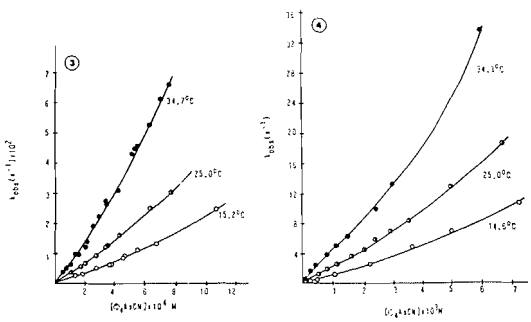

FIG. 3. k_{obs} as a function of the $[\phi_4AsCN]$ for the reactions of 1,3,5-trinitrobenzene with cyanide ion in isopropanol at a number of temperatures.

FIG. 4. k_{obs} as a function of the $[\phi_4AsCN]$ for the reactions of 2,4,6-trinitrotoluene with cyanide ion in isopropanol at a number of temperatures.

concentrations of cyanide ion) for the reactions of cyanide and 1,3,5-trinitrobenzene and 2,4,6-trinitrotoluene, are listed in Table 2. Values of the intercepts of the k_{obs} *vs.* $[CN^-]_0$ plots for the reactions of cyanide ion with 1,3,5-trinitrobenzene and 2,4,6-trinitrotoluene were too small to permit an accurate evaluation of k_{-1} values in these systems. Values of k_{-1} at 25.0 °C, calculated from the known values of *K* and k_1 at 25.0 °C, are given in Table 3.

Equilibrium constants (K_1) and specific rate constants k_1 and k_{-1} associated with the formation of a number of 2,4,6-trinitroanisole and

TABLE 2. Specific rate constants for the reactions of 1,3,5-trinitrobenzene, 2,4,6-trinitroanisole, and 2,4,6-trinitrotoluene with cyanide ion in isopropanol[a]

	$k_1(M^{-1}\ s^{-1})$			$k_{-1}(s^{-1})$
T(°C)	1,3,5-Trinitrobenzene	2,4,6-Trinitroanisole	2,4,6-Trinitrotoluene	2,4,6-Trinitroanisole
12.6		163 ± 3		0.003 ± 0.002
14.6	1205 ± 30			
15.2			18.0 ± 1.5	
25.0	2450 ± 100	344 ± 3	33.6 ± 1.6	0.044 ± 0.009
34.0		554 ± 15		0.258 ± 0.093
34.7			66.0 ± 3.0	
34.9	4400 ± 200			

[a]Error limits on k_1 and k_{-1} are based on the errors associated with the "least-squares" slopes and intercepts of the k_{obs} *vs.* $[CN^-]_0$ plots. In the 1,3,5-trinitrobenzene – cyanide ion and 2,4,6-trinitrotoluene – cyanide ion systems only points at low $[CN^-]_0$ were used in evaluating the slopes and intercepts.

1,3,5-trinitrobenzene σ-complexes at 25.0 °C are given in Table 4. For the formation of σ-complexes **5** (X = OCH_3) and **4** (X = OCH_3) in methanol values of K_1 differ by a factor of about 6, values of k_{-1} differ by a factor of about 7 and values of k_{-1} are approximately the same. For the formation of σ-complexes **5** (X = OCH_3) and **3** (X = OCH_3) in methanol the latter σ-complex is seen to be more stable but k_1 for its formation is a factor of about 500 times smaller and k_{-1} for its reversion to reactants about 10^5 times smaller than the corresponding values associated with the formation and decomposition of **5** (X = OCH_3) (6, 10, 12). For the formation of the cyanide ion σ-complex of 1,3,5-trinitrobenzene **5** (X = CN) and the cyanide ion complex of 2,4,6-trinitroanisole in isopropanol, values of K_1 differ by a factor of about 5, values of k_1 differ by a factor of about 6, and values of k_{-1} are approximately the same. The similarity in the pattern to that observed in the case of formation of **5** (X = OCH_3) and **4** (X = OCH_3) is strong evidence for the formulation of the cyanide ion – 2,4,6-trinitroanisole complex as the C-3 adduct (**4**, X = CN).

The question arises as to why **4** (X = CN) should be more stable than **3** (X = CN). Bernasconi (23) has argued that **3** (X = OCH_3) is more stable than **4** (X = OCH_3) by virtue of a stabilizing effect due to double bond – no bond resonance associated with the geminal alkoxy groups attached to the sp^3 carbon in the complex. No equivalent double bond – no bond resonance structures can be drawn when methoxide ion is replaced by cyanide ion hence such a stabilizing effect does not operate in **3** (X = CN). On the other hand, as has been pointed out by Bernasconi (23), the C-3 complex formed by TNA can benefit from resonance stabilization involving the methoxyl group {**4***a* ↔ **4***b* (X = CN}, therefore **4** (X = CN) could be more stable on this account.

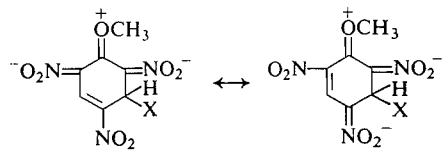

4*a* **4***b*

Solvation effects must also play a major role in determining relative stabilities. The energies associated with solvation effects are evidently comparable to those associated with the resonance energies discussed above since in deuterochloroform both **3** (X = CN) and **4** (X = CN) exist with the evidence being that **4** (X = CN) is the thermodynamically more stable species in this solvent (3).

Plots of ln k_1 *vs.* $1/T$ yielded the activation parameters $\Delta H^{\ddagger}$ and $\Delta S^{\ddagger}$ listed in Table 3.[4] Enthalpies of activation are, within experimental error, the same for the reactions of cyanide ion with 1,3,5-trinitrobenzene and 2,4,6-trinitrotoluene. The lower $\Delta H^{\ddagger}$ for the reaction of cyanide ion and 2,4,6-trinitroanisole seems to support Bernasconi's suggestion that the C-3 complex formed from 2,4,6-trinitroanisole can benefit from resonance stabilization **4***a* ↔ **4***b* (X = CN). Values of $\Delta S^{\ddagger}$ for the reactions of cyanide ion with 2,4,6-trinitrotoluene and 2,4,6-trinitroanisole are more negative by about 10 cal deg^{-1}

[4]There is no apparent curvature in the ln k *vs.* $1/T$ plot for the data from the cyanide ion – 2,4,6-trinitroanisole reaction. Curvature might have been expected if the formations of **3** (X = CN) and **4** (X = CN) were taking place at roughly comparable rates.

Can. J. Chem. Downloaded from www.nrcresearchpress.com by 210.87.254.5 on 09/05/12
For personal use only.

Can. J. Chem. Downloaded from www.nrcresearchpress.com by 210.87.254.5 on 09/05/12
For personal use only.

TABLE 3. Kinetic and thermodynamic parameters for the formation of some 1-X-2,4,6-trinitrobenzene–cyanide ion σ-complexes in isopropanol at 25.0 °C

σ-Complex	k_1 (M^{-1} s^{-1})	k_{-1}[a] (s^{-1})	$K \times 10^{-4}$ (M^{-1})	$\Delta H_1^{\ddagger}$[b] (kcal mol^{-1})	$\Delta H_{-1}^{\ddagger}$[c] (kcal mol^{-1})	ΔH^0 (kcal mol^{-1})	$\Delta S_1^{\ddagger}$[d] (cal deg^{-1} mol^{-1})	$\Delta S_{-1}^{\ddagger}$[e] (cal deg^{-1} mol^{-1})	ΔS^0 (cal deg^{-1} mol^{-1})	ΔG^0[f] (kcal mol^{-1})
5 (X = CN)	2450	0.048	5.1	11.7±0.5	18.8±1.3	−7.1±0.6[g]	−1.2±1.4	2.8±3.4	2.3±3.0	−6.43±0.02
4 (X = CN)	344	0.031	1.12	9.3±0.3	10.1±0.8	−0.81±0.55	−11.4±0.9	−27.2±2.9	15.8±2.0	−5.53±0.03
2	32.6	0.002	2.01	11.8±1.0	16.7±0.7	−4.9±0.3	−9.4±1.4	−12.8±2.5	3.4±1.1	−5.87±0.03

[a]Calculated from k_1/K.
[b]Error limits for $\Delta H_1^{\ddagger}$ are based on "least-squares" slopes obtained in plots of log k_1 *vs.* $1/T$.
[c]$\Delta H_{-1}^{\ddagger} = \Delta H_1^{\ddagger} - \Delta H^0$.
[d]Error limits for $\Delta S_1^{\ddagger}$ are based on "least-squares" intercepts, obtained at $1/T = 0$, in plots of log k_1 *vs.* $1/T$.
[e]$\Delta S_{-1}^{\ddagger} = \Delta S_1^{\ddagger} - \Delta S^0$.
[f]$\Delta G^0 = -RT \ln K$.
[g]From ref. 2.

TABLE 4. Kinetic and equilibrium data for the formation of some 1:1 σ-complexes of 1,3,5-trinitrobenzene and 2,4,6-trinitroanisole at 25.0 °C

σ-Complex	Solvent	K (M^{-1})	k_1 (M^{-1} s^{-1})	k_{-1} (s^{-1})
5 (X = OCH_3)	Methanol	16.6	7700[a] (7070)[b]	357[a] (305)[b]
5 (X = CN)	Isopropanol	51 000	2450	344
4 (X = OCH_3)	Methanol	2.71[c]	950	350
4 (X = CN)	Isopropanol	11 200	344	0.031
3 (X = OCH_3)	Methanol	17 000[d]	17.3	1×10^{-3}

[a]Reference 12.
[b]Reference 23.
[c]Reference 11.
[d]Reference 10.

mol^{-1} than the $\Delta S^{\neq}$ for the reaction of cyanide ion with 1,3,5-trinitrobenzene. This is the opposite trend to that observed for the ΔS^0 values. For the formation of **4** (X = OCH_3) and **5** (X = OCH_3) in methanol the value of $\Delta S^{\neq}$ was found to be 5 cal deg^{-1} mol^{-1} smaller in the former case.

There was no curvature in the k_{obs} *vs.* $[CN^-]_0$ plots for the cyanide ion – 1,3,5-trinitrobenzene reaction when the reactions were carried out in solutions maintained at a constant ionic strength (μ) of 0.007 *M* with tetraphenylarsonium nitrite. From the slopes of the k_{obs} *vs.* $[CN^-]_0$ plots, values of k_1 were determined to be $1.30 \pm 0.08 \times 10^3$, $2.75 \pm 0.10 \times 10^3$, and $5.46 \pm 0.10 \times 10^3$ M^{-1} s^{-1} at 14.6, 25.0, and 34.9 °C, respectively. At a constant $[CN^-]_0$ but varying concentration of total salt in the system the k_{obs} *vs.* [total salt] was found to increase linearly at low [total salt] then become independent of [total salt] at high concentrations of total salt. The variation in k_{obs} is not large: at $[CN^-]_0 = 1.96 \times 10^{-3}$ *M* and over the range of added salt 0 to 2.8×10^{-2} *M*, k_{obs} increased from 4.4 to 6.7 s^{-1}, *i.e.* a maximum increase of roughly 50%. Within experimental error, tetraphenylarsonium chloride and tetraphenylarsonium nitrite had the same effect on the variation of k_{obs} with [total salt]. The experimental results indicate therefore that the upward curvature in the k_{obs} *vs.* $[CN^-]_0$ plots at high $[CN^-]_0$ is not due to ion-pair effects involving the association of tetraphenylarsonium ion and cyanide ion and that effects associated with the presence of the counter anion in solution are not important. The observed rate increases seem to be due to a specific effect involving the tetraphenylarsonium cation.

Electrolyte effects on rate constants have been observed for several S_N2 reactions involving anionic nucleophiles reacting with alkyl or aryl halides (18, 25, 26) and with activated aromatic compounds to form σ-complexes (28, 29). The observed salt effects cannot generally be interpreted by using qualitative extensions of the Debye–Huckel theory since the theory predicts that the salt effects should be small and negative for the anion–molecule reactions (18, 25).

The kinetic salt effect may be best described by the Brønsted–Bjerrum equation (29). For the interaction of TNB and cyanide ion the equation gives [4], where k_2^S is the second-order rate con-

$$[4] \qquad k_2^S = k_2^0 \gamma_{TNB} \gamma_{CN^-} / \gamma^{\neq}$$

stant at a given salt concentration, k_2^0 is the limiting value of the second-order rate constant for zero value of all ion concentrations and γ_{TNB}, γ_{CN^-}, and $\gamma^{\neq}$ are the activity coefficients of TNB, cyanide ion, and the transition state, respectively. It is evident from eq. 4 that rate enhancement in the presence of salt is due to an increase in the activity coefficient ratio $\gamma_{TNB}\gamma_{CN^-}/\gamma^{\neq}$. The effect of salts on the activity coefficients of nonelectrolyte solutes has been discussed in detail in a review by Long and McDevitt (19).

The results of solubility studies of TNB and TNT in isopropanol at 25.0 °C are given in Fig. 5 in the form of a plot of $1 + \log S/S_0$ *vs.* the concentration of tetraphenylarsonium chloride. The salt is found to "salt in" both substrates, *i.e.* it decreases γ_{TNB}. The overall increase in rate of the cyanide ion – 1,3,5-trinitrobenzene reaction in the presence of added tetraphenylarsonium ion is therefore the result of an increase in the $\gamma_{CN^-}/\gamma^{\neq}$ ratio.

Can. J. Chem. Downloaded from www.nrcresearchpress.com by 210.87.254.5 on 09/05/12
For personal use only.

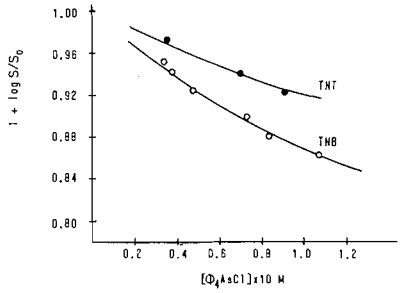

FIG. 5. Solubilities of 1,3,5-trinitrobenzene and 2,4,6-trinitrotoluene in isopropanol at 25.0 °C as a function of the concentration of tetraphenylarsonium chloride in solution. S and S_0 represent solubilities at a given concentration of salt and zero concentration of salt respectively. ($1 + \log S/S_0 = 1 + \log \gamma/\gamma_0$ where γ refers to the activity coefficient of the nitroaromatic compound).

In the course of a study of the reactions of 1-X-2,4-dinitrobenzene (X = Cl, F) with hydroxide ion, Bunton and Robinson (18, 25) found that an ion of low charge density such as tetramethylammonium ion "salted in" the substrates but nevertheless increased the rate of the reactions. The overall rate enhancement was attributed to a large increase in the $\gamma_{OH^-}/\gamma^{\pm}$ ratio. The increase in $\gamma_{OH^-}/\gamma^{\pm}$ was taken to imply that the major effect of tetramethylammonium chloride was to stabilize the large anionic transition state relative to the small hydroxide ion. Hostetler and Reinheimer (26) have attributed the rate enhancement for the reaction of benzyltrimethylammonium methoxide and activated aromatic halides to the association of the R_4N^+ with the nitro group or with the π-electron system of the activated halide in the transition state (**7** and **8**).

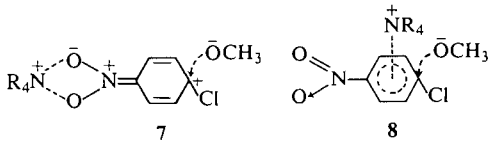

7 **8**

In the case of the tetraphenylarsonium cation, the transition state for the formation of σ-complex **4** (X = CN) may be stabilized by a weak interaction of the type proposed by Hostetler and Reinheimer. That an interaction of some type does exist is suggested by the observation that in deuterochloroform at 22 °C there is a linear relationship between the chemical shift of the TNB ring protons and the mol % of tetraphenylarsonium nitrite in solution. More detailed studies of this interaction are planned.

The nonlinear plot of k_{obs} *vs.* $[CN^-]_0$ for the reaction of 2,4,6-trinitrotoluene and cyanide ion is intelligible in terms of the same type of salt effect operating as in the TNB – cyanide ion reaction. Linear plots of k_{obs} *vs.* $[CN^-]_0$ for the cyanide ion 2,4,6-trinitroanisole reaction indicate that the term $\gamma_{TNA}\gamma_{CN^-}/\gamma^{\pm}$ is approximately unity. This may arise either because of a negligible effect of the cation on both γ_{TNA} and the ratio $\gamma_{CN^-}/\gamma^{\pm}$ or because the effects of the cation on γ_{TNA} and $\gamma_{CN^-}/\gamma^{\pm}$ are almost equal and cancel each other out. In the absence of solubility data for 2,4,6-trinitroanisole in isopropanol in the presence of tetraphenylarsonium chloride, a clear choice between these two possibilities cannot be made. However, steric considerations suggest that the former possibility is much more likely. The size of the substituents X in our series of 1-X-2,4,6-trinitrobenzenes decrease in the order $CH_3O > CH_3 > H$. By analogy to what occurs in 2,4,6-trinitrophenetole (X = C_2H_5O) where the *ortho* nitro groups are extensively twisted out of the plane of the ring (30) the methoxyl group would also be expected to lead to rotation of the *ortho* nitro groups out of the plane of the ring. This could lead to a much larger distance of closest approach of the tetraphenylarsonium cation and the nitroaromatic compound and hence a much smaller stabilization effect in both the ground state and the activated complex leading to **4** (X = CN).

Financial support by the National Research Council of Canada is gratefully acknowledged.

1. A. R. NORRIS. Can. J. Chem. **45**, 2703 (1967).
2. E. BUNCEL, A. R. NORRIS, and W. PROUDLOCK. Can. J. Chem. **46**, 2759 (1968).
3. A. R. NORRIS. Can. J. Chem. **47**, 2895 (1969).
4. E. BUNCEL, A. R. NORRIS, and K. E. RUSSELL. Q. Rev. Lond. **22**, 123 (1968).
5. M. R. CRAMPTON. Adv. Phys. Org. Chem. **7**, 211 (1969).
6. M. J. STRAUSS. Chem. Rev. **70**, 667 (1970).
7. V. GOLD and C. H. ROCHESTER. J. Chem. Soc. (B), 1692 (1964).
8. K. L. SERVIS. J. Am. Chem. Soc. **87**, 5495 (1965).
9. M. R. CRAMPTON and V. GOLD. J. Chem. Soc. (B), 893 (1966).
10. J. H. FENDLER, E. J. FENDLER, and C. E. GRIFFIN. J. Org. Chem. **34**, 689 (1969).
11. C. F. BERNASCONI. J. Am. Chem. Soc. **93**, 6975 (1971).

Can. J. Chem. Downloaded from www.nrcresearchpress.com by 210.87.254.5 on 09/05/12
For personal use only.

12. L. H. GAN and A. R. NORRIS. Can. J. Chem. **49**, 2490 (1971).
13. E. BUNCEL, A. R. NORRIS, K. E. RUSSELL, and R. TUCKER. J. Am. Chem. Soc. **94**, 1646 (1972).
14. E. BUNCEL, A. R. NORRIS, K. E. RUSSELL, and W. PROUDLOCK. Can. J. Chem. **47**, 4129 (1969).
15. J. R. A. POLLOCK and R. STEVENS (*Editors*). Dictionary of organic compounds. 4th Ed. Eyre and Spottiswoode Ltd., London. 1965.
16. L. H. GAN and A. R. NORRIS. Can. J. Chem. **52**, 1 (1974).
17. P. G. ASHMORE, B. P. LEVITT, and B. A. THRUSH. Trans. Faraday Soc. **52**, 530 (1956).
18. C. A. BUNTON and L. ROBINSON. J. Am. Chem. Soc. **90**, 5965 (1968).
19. F. A. LONG and W. F. MCDEVITT. Chem. Rev. **51**, 119 (1952).
20. A. R. NORRIS. Can. J. Chem. **45**, 175 (1967).
21. M. R. CRAMPTON. J. Chem. Soc. (B), 1341 (1967).
22. E. BUNCEL, A. R. NORRIS, and K. E. RUSSELL. International conference on the mechanisms of reactions in solution. Canterbury, England. Paper B-11. 1970.
23. C. F. BERNASCONI. J. Am. Chem. Soc. **92**, 4682 (1970).
24. E. BUNCEL, A. R. NORRIS, K. E. RUSSELL, and P. J. SHERIDAN. Can. J. Chem.
25. C. A. BUNTON and L. ROBINSON. J. Org. Chem. **34**, 780 (1969).
26. W. HOSTETLER and J. D. REINHEIMER. J. Org. Chem. **33**, 3510 (1968).
27. J. B. AINSCOUGH and E. F. CALDIN. J. Chem. Soc. 2528 (1956).
28. C. F. BERNASCONI and R. G. BERGSTROM. J. Org. Chem. **36**, 1325 (1971).
29. A. FROST and R. G. PEARSON. Kinetics and mechanism. 2nd Ed. John Wiley and Sons, Inc., New York. 1953.
30. C. M. GRAMACCIOLI, R. DESTRO, and M. SIMONETTA. Acta Crystallogr. **24**, 129 (1968).

Can. J. Chem. Downloaded from www.nrcresearchpress.com by 210.87.254.5 on 09/05/12
For personal use only.

Kinetic Studies of the Reaction of Picryl Chloride with Sodium Methoxide in Methanol

LEONG HUAT GAN AND ALBERT RICHARD NORRIS
Department of Chemistry, Queen's University, Kingston, Ontario

Received June 20, 1973

Picryl chloride reacts rapidly with methoxide ion in methanol to form a σ-complex containing methoxide ion attached to the C-3 position of the picryl chloride. Thermodynamic and kinetic parameters characterizing this reaction are presented and compared with corresponding parameters for the analogous reaction of methoxide ion and 2,4,6-trinitroanisole in methanol. Details concerning the much slower formation of the σ-complex containing methoxide ion added to the C-1 position of picryl chloride are also presented.

Le chlorure de picryle réagit rapidement avec l'ion méthoxyde dans le méthanol pour conduire à un complexe-σ contenant l'ion méthoxyde relié à la position C-3 du chlorure de picryle. On présente les paramètres thermodynamiques et cinétiques caractérisant cette réaction et on les compare avec ceux de la réaction analogue de l'ion méthoxyde avec le trinitro-2,4,6 anisole dans le méthanol. On présente aussi les détails se rattachant à la formation beaucoup plus lente du complexe-σ qui contient l'ion méthoxyde relié à la position C-1 du chlorure de picryle. [Traduit par le journal]

Can. J. Chem., **52**, 18 (1974)

Introduction

The substitution of chloride ion in picryl chloride by hydroxide or alkoxide ion is postulated to involve the intermediate σ-complex **1** (1). There are questions, however, concerning the relative stability of this σ-complex and whether the initial color observed in these systems is due to **1** or the presence of small amounts of the isomeric σ-complex **2** (2, 3).

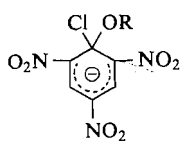

1

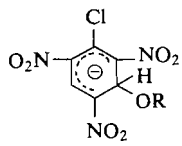

2

Gaboriaud and Schaal (4) interpreted their kinetic results from a study of the reaction of picryl chloride with hydroxide ion in aqueous solution in terms of a rapid preequilibrium formation of **1** (R = H) followed by the slow release of chloride from **1** to yield picric acid. The color observed in solution was attributed to the presence of small amounts of **1** (R = H). One problem with this interpretation is that it requires the hydroxide ion to be a better leaving group than the chloride ion. This seems unlikely (1, 3).

We have investigated the reaction of picryl chloride with methoxide ion in methanol in an attempt to obtain more detailed information on the sequence of steps in the substitution process. The results obtained implicate **2** rather than **1** (R = CH_3) as the color producing species early in the reaction and shed some light on the validity of the reaction sequence proposed by Gaboriaud and Schaal for the picryl chloride – hydroxide ion reaction.

Experimental

Reagents

Eastman 2,4,6-trinitrochlorobenzene (picryl chloride) was recrystallized twice from absolute ethanol and dried *in vacuo* over phosphorus(V) pentoxide, m.p., 83.0 °C (lit. m.p., 83.0 °C (5)).

Analytical grade sodium chloride (Fisher Scientific) was recrystallized from water and dried to constant weight *in vacuo* at 100 °C over silica gel.

Reagent grade methanol (Fisher Scientific) was distilled under nitrogen from magnesium and iodine according to the procedure described by Vogel (6). The middle portion of the distillate was collected and stored under a dry nitrogen atmosphere.

All other reagents used were A.R. grade or better.

Stock solutions of picryl chloride ($\sim 10^{-2}$ *M*) were prepared by dissolving an accurately weighed amount of the compound in 25.0 ml of methanol.

Stock solutions of sodium methoxide were prepared by adding freshly cut sodium metal, prewashed in a separate portion of dry methanol, to pure methanol maintained in an atmosphere of dry nitrogen. Solutions thus prepared were standardized by titration with 0.1 *N* HCl to the phenolphthalein end point. The concentration of sodium methoxide in the stock solution was usually 0.05 to 0.10 *M*. Exposure of the solutions to air was kept to a minimum to prevent the absorption of water and carbon dioxide.

Instruments

The instruments used to record absorption spectra

Can. J. Chem. Downloaded from www.nrcresearchpress.com by 210.87.254.40 on 09/05/12
For personal use only.

Can. J. Chem. Downloaded from www.nrcresearchpress.com by 210.87.254.40 on 09/05/12
For personal use only.

and to carry out kinetic studies, using the stopped-flow technique, have been described previously (7).

An Orion[1] solid state chloride ion selective electrode was used in conjunction with an Orion Ionanalyzer double-junction reference electrode and an Orion Model 801 digital p*H*/mV meter to determine the concentration of chloride ion in solution. A Moseley strip chart recorder (Model 7100B) connected to the meter was used to record e.m.f. as a function of time.

Calibration of the chloride ion selective electrode with solutions of recrystallized sodium chloride in methanol showed that, at 3.7 °C, the cell e.m.f. could be related to the concentration of chloride ion in solution by eq. 1.

$$[1] \qquad E(\text{mV}) = \text{constant} - 53.0 \log [\text{Cl}^-]$$

The concentration range covered in the calibration procedure was from 1×10^{-4} to 12×10^{-4} *M* in sodium chloride.

Procedures

Equilibrium and Kinetic Studies Using the Durrum–Gibson Stopped-flow Spectrophotometer

Solutions containing picryl chloride (approximately 10^{-5} *M*) and sodium methoxide (10^{-3} to 10^{-2} *M*) were prepared immediately prior to each run by dilution of known volumes of the corresponding stock solutions with distilled methanol. Before each run the drive syringes were each rinsed three times with the appropriate solution, filled to capacity, and allowed to stand for 20 min in order to reach thermal equilibrium with the bath. In the course of the kinetic and equilibrium studies the concentration of picryl chloride generally was kept constant and therefore only the sodium methoxide solutions were changed. Each time this was done the drive syringe was flushed thoroughly with the new sodium methoxide solution before being filled for the kinetic run.

For the equilibrium studies the spectrophotometer was used in the conventional way to obtain values of absorbance at infinite time (A_∞) associated with both the fast initial reaction and the slower secondary reaction. Values of A_∞ associated with the second reaction were checked by running the reaction under the same experimental conditions and recording the A_∞ value and the spectrum of the solution on the Cary 14; A_∞ values agreed in all cases to within experimental error.

For most of the kinetic runs the normal mode of operation of the spectrophotometer was modified, as described previously (7), so as to yield an oscilloscope trace of absorbance as a function of time rather than % transmittance as a function of time (8). Traces on the storage oscilloscope of absorbance *vs.* time were recorded photographically when at least two consecutive runs gave identical traces. In the case of the fast reaction an epidiascope was used to magnify the photograph so that absorbances at different times could be measured more accurately. For the slower second reaction absorbances at different times were read directly from the photographs. All kinetic runs were carried out with sodium methoxide concentrations much greater than the concentration of picryl chloride.

Kinetic Studies of Chloride Ion Release

A 150-ml beaker containing about 80 ml of a solution of picryl chloride in methanol was put in a thermostatted bath kept at 3.7 ± 0.1 °C. The reference and chloride ion selective electrodes were immersed in the solution, which was stirred by means of a mechanical stirrer, and the system allowed to reach thermal equilibrium. A small volume (1–3 ml) of sodium methoxide solution prethermostatted at 3.7 °C was quickly added and the cell e.m.f. recorded as a function of time on the strip chart recorder.

[1]Orion Research Incorporated, Cambridge, Mass.

Results and Discussion

When sodium methoxide in methanol (10^{-4} to 10^{-2} *M*) was added to a dilute solution of picryl chloride ($\sim 10^{-5}$ *M*) in methanol a red color resulted. At any wavelength in the region 350–525 nm the absorbance of the solution was seen to increase rapidly after mixing of the two components, reach a maximum absorbance within 1 min and then remain constant for at least 20 min. A very slow decrease in absorbance was observed after that time; this fading reaction was more rapid at higher temperatures and at higher base concentrations. The species in solution in the time interval between 1 and 20 min after mixing had absorption maxima and molar extinction coefficients identical to those reported for the 1,1-dimethoxy-2,4,6-trinitrocyclohexadienate anion (**3**) (9, 10)

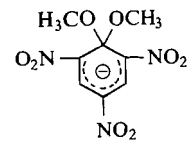

3

When the interaction of picryl chloride (P) with sodium methoxide (in excess) was studied using the stopped-flow spectrophotometer, two distinct reaction traces were observed on the oscilloscope. The rates of the two reactions were sufficiently different ($t_{1/2}$ values of approximately 5 ms and 10 s, respectively, at 25.0 °C) that separate studies of each reaction could be made.

For a series of solutions of fixed picryl chloride ($\sim 3 \times 10^{-4}$ *M*) and varying sodium methoxide concentration (1×10^{-2} to 7×10^{-2} *M*) values of A_∞ at 480 nm were recorded from the absorbance *vs.* time traces associated with the first reaction. If the reaction taking place in solution at this stage is represented by eq. 2

$$[2] \qquad \text{P} + \text{CH}_3\text{O}^- \underset{k_{-1}}{\overset{k_1}{\rightleftharpoons}} \text{1:1 } \sigma\text{-Complex}$$

and the absorbance at 480 nm is due solely to

absorption by the 1:1 σ-complex then plots of the experimental data in the form $[P]_0/A_\infty$ *vs.* $1/[CH_3O^-]_0$ should be linear with intercepts equal to $1/\varepsilon$ and slopes equal to $1/K\varepsilon$ (11). K represents the equilibrium constant for complex formation ($K = k_1/k_{-1}$), ε represents the molar extinction coefficient of the complex at 480 nm and $[P]_0$ and $[CH_3O^-]_0$ represent the total concentrations of picryl chloride and methoxide ion respectively. Plots of $[P]_0/A_\infty$ *vs.* $1/[CH_3O^-]_0$ for this system were linear in all cases. However, because K associated with this reaction is small, and large ratios of $[CH_3O^-]_0/[P]_0$ could not be used in the experimental runs, fairly large errors are associated with both the K and ε determined in this way (12).

As a result ε was chosen as $1.50 \times 10^4\ M^{-1}\ cm^{-1}$ over the temperature range studied[2] and K calculated for each run using the expression shown in eq. 3. The calculated K was constant

$$[3] \qquad K = \frac{A_\infty/2\varepsilon}{\left\{[P]_0 - \frac{A_\infty}{2\varepsilon}\right\}[CH_3O^-]_0}$$

over a wide range of sodium methoxide concentrations. This is further confirmation that the colored species has a 1:1 stoichiometry. The equilibrium constants associated with the formation of this 1:1 species were found to be 1.53 ± 0.03, 2.03 ± 0.03, and 2.66 ± 0.05 M^{-1} at 7.5, 15.4, and 25.0 °C respectively. The error limits on K represent the standard deviations of the mean of at least 10 determinations.

The visible absorption spectrum of the species formed in the first reaction was obtained by measuring at different wavelengths in the 350 to 550 nm region A_∞ values associated with the first reaction. Since picryl chloride absorbs to some extent below 450 nm, the absorption curve so obtained had to be corrected for residual absorption due to unreacted picryl chloride. This was done with the aid of separately determined values of ε for picryl chloride and use of the known K for this reaction to calculate the concentration of unreacted picryl chloride at equilibrium. A typical absorption curve obtained

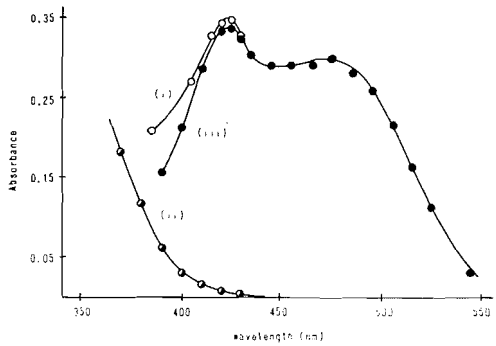

FIG. 1. (*i*) Absorption curve (as measured from A_∞ values) resulting from the fast reaction between picryl chloride and sodium methoxide in methanol at 10 °C: $[\text{picryl chloride}]_0 = 3.97 \times 10^{-4} M$; $[NaOCH_3]_0 = 1.33 \times 10^{-2} M$; $l = 2.0$ cm. (*ii*) Absorption curve due to unreacted picryl chloride in solution. (*iii*) Absorption curve due to the species formed by methoxide ion addition at the C-3 position of picryl chloride (σ-complex **2**).

from the A_∞ values and the curve obtained after correction for absorption by picryl chloride are shown in Fig. 1. The positions of the absorption maxima (424 and 475 nm) were independent of temperature and of the concentration of sodium methoxide used in the experiment. While the absorption spectrum is characteristic of the 1:1 σ-complex it is not diagnostic of C-1 or C-3 methoxide ion addition (2, 3). Crampton *et al.* (13) have reported however that the C-3 adduct of methoxide ion and picryl chloride in methanol–dimethylsulfoxide has an absorption maximum at 424 nm and a shoulder at 480 nm. The similarity of the two absorption spectra strongly suggests that our fast reaction in methanol involves addition of methoxide at the C-3 position in picryl chloride to form **2** (R = CH_3).

For the fast reaction traces of absorbance *vs.* time gave rise to linear $\ln(A_\infty - A_t)$ *vs.* time plots to greater than 90% completion of reaction. For the reversible formation of 1:1 σ-complex according to eq. 2, the slope of the $\ln(A_\infty - A_t)$ *vs.* time plot (k_{obs}) is related to the specific rate constants k_1 and k_{-1} and the concentration of methoxide ion by the relation

$$[4] \qquad k_{obs} = k_1[CH_3O^-]_0 + k_{-1}$$

Plots of k_{obs} *vs.* $[CH_3O^-]_0$ were linear over the methoxide ion concentration range 5×10^{-3} to $7 \times 10^{-2}\ M$. Since k_{-1} values for this reaction were large and the term $k_1[CH_3O^-]_0$ small in comparison to k_{-1} in all cases the slopes of the k_{obs} *vs.* $[CH_3O^-]_0$ plots were small. Conse-

[2]This choice of ε was based on the mean values of ε obtained from the $[P]/A_\infty$ *vs.* $1/[CH_3O^-]_0$ plots. The value of ε at 480 nm for **3** is $1.63 \times 10^4\ M^{-1}\ cm^{-1}$ (9). Molar extinction coefficients are generally found to be temperature independent over the temperature range studied (2).

Can. J. Chem. Downloaded from www.nrcresearchpress.com by 210.87.254.40 on 09/05/12
For personal use only.

Can. J. Chem. Downloaded from www.nrcresearchpress.com by 210.87.254.40 on 09/05/12
For personal use only.

quently k_{-1} was obtained fairly accurately from such a plot but k_1 (obtained from the slope) had a larger error limit associated with it. More reliable values of k_1 could be obtained from the expression $K = k_1/k_{-1}$. Values of k_1 and k_{-1} at 25.0 °C and thermodynamic and kinetic parameters associated with the first reaction are presented in Table 1 together with the corresponding data for the formation of **4**, the C-3 complex of methoxide ion and 2,4,6-trinitroanisole (14). Detailed comparisons strongly

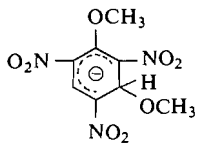

4

support the conclusion, arrived at on the basis of spectral studies, that the 1:1 σ-complex first formed in this system is **2**. The smaller ΔH^0 associated with the formation of **4** may be due in part to resonance stabilization involving the methoxy group (**5***a* ↔ **5***b*) as suggested by Bernasconi (14). A greater steric effect

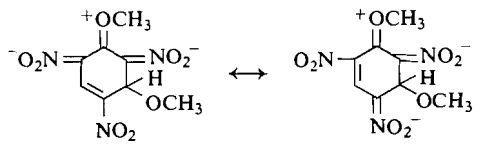

5*a* **5***b*

associated with the methoxy group could also lead to increased solvation of **4**, as compared to **2**, and thus a smaller ΔH^0 for the formation of **4**. The more positive ΔS^0 for formation of **2** is consistent with this possibility.

The second reaction trace observed on the stopped-flow spectrophotometer did not give rise to linear ln $(A_\infty - A_t)$ *vs.* time plots. In addition there was associated with this part of the reaction the appearance of chloride ion in solution.

The liberation of chloride ion was followed at 3.7 °C as described in the Experimental section. If one assumes the following sequence of reactions shown in eqs. 2, 5, and 6

[2] $\mathrm{P} + \mathrm{CH_3O^-} \underset{k_{-1}}{\overset{k_1}{\rightleftharpoons}}$ 1:1 σ-Complex (**2**)

[5] $\mathrm{P} + \mathrm{CH_3O^-} \xrightarrow{k_2}$ 1:1 σ-Complex (**1**)

[6] $\mathbf{1} \underset{\text{(fast)}}{\xrightarrow{k_2^1}}$ 2,4,6-Trinitroanisole + $\mathrm{Cl^-}$

with the step involving the formation of **1** being rate determining, then the rate of appearance of chloride ion in solution can be expressed by the equation

$$[7]\quad \log\{[\mathrm{P}]_0 - [\mathrm{Cl^-}]_t\} = \left\{\frac{k_1[\mathrm{CH_3O^-}]_0}{1 + K[\mathrm{CH_3O^-}]_0}\right\}\frac{t}{2.303} + \log[\mathrm{P}]_0$$

For a series of runs with different $[\mathrm{P}]_0$ and $[\mathrm{CH_3O^-}]_0$ the experimental traces of cell e.m.f. as a function of time were used in conjunction with eq. 1 to calculate values of $\log\{[\mathrm{P}]_0 - [\mathrm{Cl^-}]_t\}$ as a function of time. Based on the slopes of the $\log\{[\mathrm{P}]_0 - [\mathrm{Cl^-}]_t\}$ *vs.* time plots and a value of K of 1.41 M^{-1} at 3.7 °C, the average value of k_2 at 3.7 °C, for a series of runs in which $[\mathrm{CH_3O^-}]_0$ covered the range 3.6×10^{-3} to 5.4×10^{-3} M, was 3.7 ± 0.3 $M^{-1}\,s^{-1}$; k_2 was independent of $[\mathrm{P}]_0$ over the range 3.39×10^{-4} M to 6.70×10^{-4} M. The rapidity of chloride ion formation limited detailed studies to this low temperature. Studies at higher temperature indicated that, under typical reaction conditions, >90% of the chloride ion was released within about 1 min of mixing of the reagents.

The final spectrum of the solution indicates that all the picryl chloride initially present has been converted to σ-complex **3**. If one assumes, as above, that reactions 2, 5, and 6 are occurring together with reaction 8 to form **3**

[8] 2,4,6-Trinitroanisole + $\mathrm{CH_3O^-} \underset{k_{-3}}{\overset{k_3}{\rightleftharpoons}}$ **3**

then

$$[9]\quad [\mathbf{3}]_t = [\mathrm{P}]_0\left\{1 - \left[\frac{k_3}{k_3 - k_2}(1 + KB_0)\right] \times [e^{-k_2B_0t} - e^{-k_3B_0t}] - e^{-k_3B_0t}\right\}$$

where $B = [\mathrm{CH_3O^-}]$. If negligible amounts of **1** and **4** are present in solution then **2** and **3** are the only species absorbing at 480 nm. The absorbance due to **3** at any time t can be expressed as

$$[10]\quad (A_3)_t = \frac{A_t - \dfrac{KP_0B_0}{1 + KB_0}\varepsilon_2 l}{1 - \dfrac{KB_0\varepsilon_2}{(1 + KB_0)\varepsilon_3}}$$

Since reaction 8 goes to completion (K = 7700

Can. J. Chem. Downloaded from www.nrcresearchpress.com by 210.87.254.40 on 09/05/12
For personal use only.

TABLE 1. Specific rate constants and kinetic and thermodynamic parameters for the formation and decomposition of **2** and **4** in methanol

σ-Complex	k_1 at 25.0 °C (M^{-1} s^{-1})[b]	k_{-1} at 25.0 °C (s^{-1})[c]	K (M^{-1})[d]	$\Delta H_1^{\neq}$ (kcal mol^{-1})[e]	ΔH_{-1} (kcal mol^{-1})[f]	ΔH^0 (kcal mol^{-1})[f]	$\Delta S_1^{\neq}$ (cal deg^{-1} mol^{-1})[g]	ΔS_{-1} (cal deg^{-1} mol^{-1})[h]	ΔS^0 (cal deg^{-1} mol^{-1})[h]
2	912±100	303±38	2.58±0.06	12.90±2.2	8.2±1.8	4.66±0.42	2.6±8.4	−14.9±6.9	17.5±1.5
4[a]	950±100	350±20	2.71±0.45	10.4 ±1.0	8.2±0.5	2.2 ±1.5	−10.8±3.4	−19.3±1.7	8.5±5.1

[a]Data from ref. 14.
[b]k_1 obtained from Kk_{-1}.
[c]Error limit for k_{-1} is based on the maximum and minimum intercepts obtained in plot of k_{obs} *vs.* [$NaOCH_3$].
[d]Error limit for K is the standard deviation of the mean calculated from 10 determinations.
[e]$\Delta H_1^{\neq}$ is calculated from $\Delta H_1^{\neq} = \Delta H^0 + \Delta H_{-1}^{\neq}$.
[f]Error limits for $\Delta H_{-1}^{\neq}$ and ΔH^0 are based on the maximum and minimum slopes obtained in plots of log k_{-1} and log K against $1/T$, respectively.
[g]$\Delta S_1^{\neq}$ is calculated from $\Delta S_1^{\neq} = \Delta S^0 + \Delta S_{-1}^{\neq}$.
[h]Error limits for $\Delta S_{-1}^{\neq}$ and ΔS^0 are based on the maximum and minimum intercepts obtained at $1/T = 0$, in plots of log k_{-1} and log K against $1/T$, respectively.

Can. J. Chem. Downloaded from www.nrcresearchpress.com by 210.87.254.40 on 09/05/12
For personal use only.

M^{-1} at 25.0 °C (9)) $[3]_t/[P]_0 = (A_3)_t/(A_3)_\infty$ and eq. 9 can be written in the form

$$[11]\quad [P] = 1 - \frac{(A_3)_t}{(A_3)_\infty} = \frac{k_3}{k_3 - k_2}(1 + KB_0)e^{-k_2B_0t} - \frac{k_3}{k_3 - k_2}(1 + KB_0)e^{-k_3B_0t} + e^{-k_3B_0t}$$

For each kinetic run 7 to 10 experimental absorbance readings (A_t) covering from 25 to 75% completion of the reaction were taken to calculate $(A_3)_t$. A nonlinear "least-squares" program was used together with the known $(A_3)_t$, $(A_3)_\infty$, K, and B_0 values to fit eq. 11. Approximate values of k_2 and k_3 were supplied initially and the program executed to yield values of k_2 and k_3 which gave the least sum of squares of the residuals among these points. Typical calculated values of k_2 and k_3 over a range of sodium methoxide concentrations at 25.0 °C are given in Table 2. Mean values of k_2 and k_3 determined at different temperatures are given in Table 3.

From the data in Table 3 the value of k_2 at 3.7 °C is calculated to be 3.90 M^{-1} s^{-1}. This is in excellent agreement with the k_2 value of 3.7 ± 0.3 M^{-1} s^{-1} determined by following the rate of chloride ion release at 3.7 °C. The closeness of the k_2 values determined by the two different methods offers support for the formulated mechanistic scheme (reactions 2, 5, 6, and 8) and the assumptions made in the derivations of eqs. 10 and 11. The enthalpy and entropy of activation associated with reaction 5 are 14.0 ± 1.3 kcal mol^{-1} and −0.7 ± 4.4 cal deg^{-1} mol^{-1}, respectively. Miller (15) has predicted a $\Delta H^\ddagger$ of 12.9 kcal mol^{-1} for this reaction.

A further indication that the formulated mechanistic scheme is correct comes from the observed value of k_3 which, based on the above method of analysis, is found to be 14.0 ± 1.2 M^{-1} s^{-1} at 25.0 °C. From a study of the direct reaction of methoxide ion and 2,4,6-trinitroanisole to form **3**, Fendler *et al.* (9) reported a k_3 of 17.3 M^{-1} s^{-1} at 25.0 °C, a $\Delta H^\ddagger$ of 12.9 ± 1.0 kcal mol^{-1}, and a $\Delta S^\ddagger$ of −9.4 ± 2.0 cal deg^{-1} mol^{-1}. Our values of $\Delta H^\ddagger$ and $\Delta S^\ddagger$ for formation of **3** (reaction 8) were 10.7 ± 1.5 kcal mol^{-1} and −12.8 ± 3.6 cal deg^{-1} mol^{-1}, respectively. The agreement is well within experimental error.

All the experimental results are consistent with the methoxide ion substitution of chloride ion in picryl chloride proceeding via reactions 2, 5, 6, and 8. The specific rate constants k_1 and k_{-1} for formation and decomposition of the C-3 adducts **2** (R = CH_3) and **4** are very similar, while the specific rate constants for formation of the C-1 adducts **1** (R = CH_3) and **3** differ by at least a factor of 2 at 25.0 °C. The similarity in the specific rate constants k_1 and k_{-1} for the reactions of hydroxide ion with picryl chloride and 2,4,6-trinitroanisole in aqueous solution (4) strongly suggests that these constants are associated with the formation of **2** (R = H) and **6** respectively rather than **1** (R = H) and **7**.

TABLE 2. Specific rate constants k_2 and k_3 for the interaction of picryl chloride with sodium methoxide at 25.0 °C

$[NaOCH_3] \times 10^2 (M)$	$k_1 (M^{-1}s^{-1})$	$k_2 (M^{-1}s^{-1})$
1.560	31.0±1.0	13.4±0.2
1.950	33.3±2.9	12.8±0.6
2.145	27.3±2.8	13.1±0.9
2.438	25.0±3.4	14.3±1.4
2.730	22.6±2.5	15.6±1.4
3.413	29.0±1.8	13.1±0.5
3.423	30.5±1.7	13.7±0.5
3.900	24.9±2.2	14.6±1.0
5.202	28.4±3.5	14.0±1.2

TABLE 3. Average specific rate constants k_2 and k_3 for the interaction of picryl chloride with sodium methoxide in methanol

T(°C)	$k_2 (M^{-1}s^{-1})$	$k_3 (M^{-1}s^{-1})$
18.1	14.1± 0.64	9.46±0.36
25.0	27.4± 2.0	14.0 ±1.2
34.5	48.8± 2.1	24.8 ±0.8
39.5	83.2± 5.2	34.5 ±1.2
42.6	104.5±16.3	42.8 ±3.9

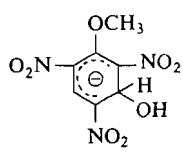

6

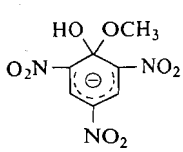

7

Financial support by the National Research Council of Canada is gratefully acknowledged.

1. J. MILLER. Aromatic nucleophilic substitution. Elsevier, Barking, Essex, England. 1968.
2. E. BUNCEL, A. R. NORRIS, and K. E. RUSSELL. Q. Rev. Lond. **22**, 123 (1968).
3. M. J. STRAUSS. Chem. Rev. **70**, 667 (1970).
4. R. GABORIAUD and R. SCHAAL. Bull. Soc. Chim. Fr. 2683 (1969).
5. J. R. A. POLLOCK and R. STEVENS (*Editors*). Dictionary of organic compounds. 4th ed. Eyre and Spottiswoode Ltd., London. 1965.
6. A. I. VOGEL. A textbook of practical organic chemistry. 3rd ed. Longmans, Green, London. 1968. p. 169.
7. L. H. GAN and A. E. NORRIS. Can. J. Chem. **52**, 1 (1974).
8. P. G. ASHMORE, B. P. LEVITT, and B. A. THRUSH. Trans. Faraday Soc. **52**, 530 (1956).
9. J. H. FENDLER, E. J. FENDLER, and C. E. GRIFFIN. J. Org. Chem. **34**, 689 (1969).
10. T. ABE, T. KUMAI, and H. ARAI. Bull. Chem. Soc. Jap. **38**, 1526 (1965).
11. H. BENESI and J. HILDEBRAND. J. Am. Chem. Soc. **71**, 2703 (1949).
12. D. A. DERANLEAU. J. Am. Chem. Soc. **91**, 4050 (1969).
13. M. R. CRAMPTON, M. A. EL GHARIANI, and H. A. KHAN. Chem. Commun. 834 (1971).
14. C. F. BERNASCONI. J. Am. Chem. Soc. **93**, 6975 (1971).
15. J. MILLER. J. Am. Chem. Soc. **85**, 1628 (1963).

Can. J. Chem. Downloaded from www.nrcresearchpress.com by 210.87.254.40 on 09/05/12
For personal use only.

Kinetic and Thermodynamic Studies of the Reactions of Sulfite Ion with Picramide, *N*-Methylpicramide, and *N*,*N*-Dimethylpicramide in Aqueous Solution

ERWIN BUNCEL, ALBERT RICHARD NORRIS,[1] KENNETH EDWIN RUSSELL, AND PETER JURA SHERIDAN

Department of Chemistry, Queen's University, Kingston, Ontario

Received July 4, 1973

The kinetics of the reactions between sulfite ion and picramide, *N*-methylpicramide, and *N*,*N*-dimethylpicramide, to form 1:1 σ-complexes in aqueous solutions of constant ionic strength 0.14 *M*, have been investigated using a stopped-flow spectrophotometer. Specific rate constants for the formation and decomposition of these three complexes at 25.0 °C are $5.7 \pm 0.2 \times 10^4\ M^{-1}\ s^{-1}$ and $7 \pm 1\ s^{-1}$, $1.4 \pm 0.1 \times 10^4\ M^{-1}\ s^{-1}$ and $0.20 \pm 0.02\ s^{-1}$, and $4.1 \pm 0.2 \times 10^3\ M^{-1}\ s^{-1}$ and $0.14 \pm 0.04\ s^{-1}$, respectively. Enthalpies and entropies of activation characterizing the formation of the 1:1 σ-complexes have been determined. Equilibrium constants, determined spectrophotometrically at a number of temperatures, have been used to calculate the enthalpy (ΔH^0) and entropy (ΔS^0) changes associated with 1:1 and 2:1 σ-complex formation. These values are compared with corresponding ones for complex formation of sulfite ion with 1,3,5-trinitrobenzene and 2,4,6-trinitrobenzaldehyde. The extent of solvation of the σ-complexes is considered to play a primary role in determining the observed trends in the enthalpies and entropies of reaction.

On a étudié à l'aide d'un spectrophotomètre à débit interrompu la cinétique des réactions entre l'ion sulfite et la picramide, la *N*-méthylpicramide et la *N*,*N*-diméthylpicramide; ces réactions conduisent à des complexes-σ 1:1 dans des solutions aqueuses de force ionique constante 0.14 *M*. Les constantes spécifiques de vitesse pour la formation et la décomposition de ces troix complexes à 25.0 °C sont respectivement égales à $5.7 \pm 0.2 \times 10^{-4}\ M^{-1}\ s^{-1}$ et $7 \pm 1\ s^{-1}$, $14 \pm 0.1 \times 10^4\ M^{-1}\ s^{-1}$ et $0.20 \pm 0.02\ s^{-1}$, $4.1 \pm 0.2 \times 10^3\ M^{-1}\ s^{-1}$ et $0.14 \pm 0.04\ s^{-1}$. On a déterminé les enthalpies d'activation caractérisant la formation des complexes-σ 1:1. Les constantes d'équilibre, déterminées spectrophotométriquement à différentes températures, ont été utilisées afin de calculer les changements d'enthalpie (ΔH^0) et d'entropie (ΔS^0) associés à la formation des complexes-σ 1:1 et 2:1. Ces valeurs sont comparées à celles obtenues lors de la formation des complexes de l'ion sulfite avec le trinitro-1,3,5 benzène et le trinitro-2,4,6 benzaldéhyde. On considère que le degré de solvatation des complexes-σ joue un rôle important dans la détermination des tendances observées dans les enthalpies et les entropies de réaction.

[Traduit par le journal]

Can. J. Chem., 52, 25 (1974)

Introduction

The formation of colored species as a result of the reactions of aqueous sodium sulfite solutions with nitroaromatic compounds has been known for some time (1). Early studies of the 1,3,5-trinitrobenzene – sulfite ion interaction were concerned with ascertaining the nature, the composition(s), and spectral properties of the colored species and determining the equilibrium constants and thermodynamic parameters associated with their formation (2–5). Proton magnetic resonance studies of the reactions of sulfite ion with a number of 1-X-2,4,6-trinitrobenzenes {X = H, OH, OCH_3, NH_2, $NHCH_3$, $N(CH_3)_2$, NHC_6H_5, and $NCH_3(C_6H_5)$} in water and aqueous dimethylsulfoxide solutions clearly established the colored species as σ-complexes (5–8). The complexes of 1:1 stoichiometry were found to have structure **1** whereas those of 2:1 stoichiometry were found to have structure **2**.

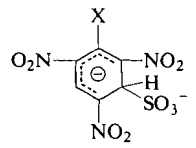

1

X = H, OCH_3, NH_2, $NHCH_3$, $N(CH_3)_2$, $NH(C_6H_5)$, $NCH_3(C_6H_5)$

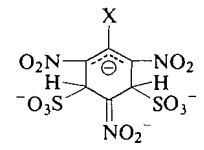

2

X = H, O^-, OCH_3, NH_2, $NHCH_3$, $N(CH_3)_2$, $NH(C_6H_5)$, $NCH_3(C_6H_5)$

[1]Author to whom correspondence should be addressed.

Can. J. Chem. Downloaded from www.nrcresearchpress.com by 210.87.254.42 on 09/05/12
For personal use only.

For X ≠ H, there was no evidence for the existence of either 1:1 or 2:1 σ-complexes containing the sulfite ion bonded at the C-1 position. Recent studies have shown that σ-complexes with structures **3** and **4** exist when X = CHO (9).

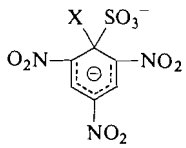

3

X = CHO

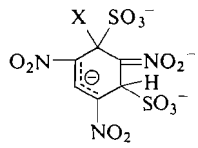

4

X = CHO

As part of a series of kinetic and equilibrium studies of the reactions of nitroaromatic compounds and bases (9–11) we have investigated the reactions of sulfite ion with picramide, *N*-methylpicramide, and *N*,*N*-dimethylpicramide. We have determined the specific rate constants and activation parameters for the formation of the 1:1 σ-complexes as well as the thermodynamic parameters associated with 1:1 and 2:1 σ-complex formation in these systems.

Experimental

Reagents

Sodium sulfite and potassium nitrate were both A.R. grade reagents (Fisher Scientific) and were used as received. Picramide (K & K Laboratories) was recrystallized from absolute ethanol and dried to constant weight *in vacuo* over phosphorus(V) pentoxide, melting point, 192–195 °C (12). *N*-Methylpicramide was prepared by adding an excess of methylamine in ethanol to a 5% solution of picryl chloride in ethanol and evaporating the resulting solution to dryness. The solution formed by extraction of the residue with acetone was filtered to remove the insoluble methylammonium chloride and evaporated to dryness. The resulting solid was recrystallized to constant melting point from absolute alcohol. After drying *in vacuo* over phosphorus(V) pentoxide, the product had a melting point 114–115 °C (13). *N*,*N*-Dimethylpicramide was prepared in exactly the same manner as *N*-methylpicramide but using dimethylamine as the base. The product, after repeated recrystallization from absolute ethanol and drying to constant weight *in vacuo* over phosphorus(V) pentoxide, had a melting point of 138 °C (13). All other reagents used were A.R. grade or better.

Doubly distilled and deionized water was boiled for approximately 30 min to remove dissolved gases, then allowed to cool to room temperature and stored under a nitrogen atmosphere.

Stock solutions of picramide, *N*-methylpicramide, and *N*,*N*-dimethylpicramide ($\sim 2 \times 10^{-2}$ *M*) were prepared by dissolving a weighed amount of the dried compound in a known volume of acetone. Solutions used in the kinetics and equilibrium studies were freshly prepared prior to use by appropriate dilution (usually 0.10 to 100 ml) of an aliquot of the stock solution with 0.14 *M* aqueous potassium nitrate solution.

Sodium sulfite and potassium nitrate stock solutions were prepared by dissolving weighed quantities of each reagent in known volumes of water. Both stock solutions were always prepared immediately prior to use. The composition of the stock sodium sulfite solution was determined by iodimetric titration (14). Sodium sulfite solutions used in the kinetic and equilibrium studies were prepared by dilution of the stock solution with 0.14 *M* potassium nitrate solution. The p*H* values of the stock solutions and the solutions used in the equilibrium and kinetic studies were checked with a p*H* meter, and if required adjusted to p*H* 9.00 by the addition of 2×10^{-3} *M* sodium hydroxide. The amount of base added was generally so small that neither the concentration nor the ionic strength of the solution was affected by this procedure.

Instruments

Kinetic measurements were carried out on a Durrum–Gibson stopped-flow spectrophotometer.[2] A closed circuit temperature control system utilizing an Ultra Kryomat TK30D constant temperature bath kept the temperature in the valve-block, drive syringes, and observation cell constant to within ±0.1 °C. Temperature-jump or conventional stopped-flow cells of 2.0 cm path length were used. Minimum "dead times" of the two cells were 10 and 2 ms, respectively. For most of the kinetic runs the normal mode of operation of the stopped-flow spectrophotometer was modified so as to yield an oscilloscope trace of absorbance as a function of time rather than % transmittance as a function of time (15). Standard solutions of potassium permanganate, whose absorbances at several different wavelengths had been determined on the Cary 14, were used to establish that the input signal to the vertical axis of the storage oscilloscope was directly related to absorbance over the range 0 to 0.10 absorbance units. One advantage of this method of operation was that, over the range indicated, absorbances could be determined accurately at very low noise to signal ratios.

In the equilibrium studies optical measurements were carried out on a Beckman DU and a Cary 14 recording spectrophotometer using matched silica cells of 1.0 cm path length. In both cases the temperature in the cells was maintained constant to ±0.1 °C by circulating water from a constant temperature bath through a specially designed cell holder in the spectrophotometer.

Measurements of p*H* were carried out with an EIL Model 23A p*H* meter. Calibration of the p*H* meter with standard buffer solutions of p*H* 7.40 ± 0.02 and p*H* 10.00 ± 0.02 at 25 °C was performed prior to each measurement.

Procedures

Kinetic Studies

Solutions containing the nitroaromatic compound at approximately 2×10^{-5} *M* and sodium sulfite were prepared immediately prior to the kinetic run by dilution of known volumes of the corresponding stock solutions with 0.14 *M* potassium nitrate solution. Prior to each run the drive syringes were rinsed three times with the appropriate solution, filled to capacity and allowed to stand 20 min to reach thermal equilibrium with the bath. In the course of the kinetic measurements the concentration of the nitroaromatic compound was generally kept constant, and therefore only the sodium sulfite solutions

[2]Durrum Instrument Corporation, Palo Alto, Calif.

Can. J. Chem. Downloaded from www.nrcresearchpress.com by 210.87.254.42 on 09/05/12
For personal use only.

Can. J. Chem. Downloaded from www.nrcresearchpress.com by 210.87.254.42 on 09/05/12
For personal use only.

were changed. Each time this was done the appropriate drive syringe was flushed thoroughly with the new sodium sulfite solution before being filled for the kinetic run.

Kinetic runs were monitored by following changes in absorbance at a number of wavelengths. Traces on the storage oscilloscope of absorbance *vs.* time were recorded photographically when at least two consecutive runs gave identical traces. The kinetic curves were then transferred from the photographs to centimeter graph paper. Absorbances at different times, taken from the graph paper, were used to construct plots of ln $(A_\infty - A_t)$ *vs.* time (A_∞ and A_t refer to absorbances at times infinity and t, respectively). The slopes of these plots yielded pseudo first-order rate constants k_{obs}. Within experimental error k_{obs} values, calculated using absorbance data collected at a number of different wavelengths, were equal.

Equilibrium Studies

A 1.0-cm cell containing 3.00 ml of 0.14 *M* potassium nitrate solution was placed in the thermostatted cell compartment of the spectrophotometer and allowed to come to thermal equilibrium with the compartment. Stock solutions of sodium sulfite and the nitroaromatic compound were added by means of Micrometer syringes,[3] the solution thoroughly mixed, and the values of absorbance measured at a number of preselected wavelengths. Absorbances were always checked as a function of time to ensure that equilibrium absorbance values were being measured. (Fading reactions can occur in these systems particularly at high temperatures and at high sulfite ion concentrations.)

Treatment of Data Obtained in the Equilibrium Studies

For the systems under investigation both 1:1 and 2:1 σ-complexes are formed in aqueous solution (5). The formation reactions can be written as follows:

$$\text{[1]}\quad \text{Nitroaromatic} + SO_3^{2-} \overset{K_1}{\rightleftharpoons} \text{1:1 σ-Complex (C)}$$

$$\text{[2]}\quad \text{C} + SO_3^{2-} \overset{K_2}{\rightleftharpoons} \text{2:1 σ-Complex (D)}$$

The equilibrium expressions associated with the formation of C and D are

$$\text{[3]}\quad K_1 = \frac{[C]}{[N][S]} = \frac{[C]}{\{[N]_0 - [C] - [D]\}\{[S]_0 - [C] - 2[D]\}}$$

and

$$\text{[4]}\quad K_2 = \frac{[D]}{[C][S]} = \frac{[D]}{[C]\{[S]_0 - [C] - 2[D]\}}$$

where [C], [D], [N], and [S] represent the equilibrium concentrations of 1:1 σ-complex, 2:1 σ-complex, uncomplexed nitroaromatic, and uncomplexed sulfite ion, respectively. $[N]_0$ and $[S]_0$ represent the total concentrations of nitroaromatic compound and sodium sulfite in solution.

The experimental approach best suited to obtaining the most reliable values of K_1, K_2, and the molar extinction coefficients ε_C and ε_D is dictated by the magnitudes of K_1 and K_2, the ratio of K_2 to K_1, and the absorption characteristics of the nitroaromatic compound and the 1:1 and 2:1 σ-complexes that it forms. Because the procedures used in the study of the three systems were different they are briefly outlined.

(i) Picramide (P) – Sulfite Ion System

For this system K_1 is large, the ratio K_2 to K_1 is very small, and only C absorbs at 480 nm.

A series of solutions were prepared containing a fixed concentration of picramide ($\sim 1 \times 10^{-5}$ *M*) and a range of sodium sulfite concentrations such that the ratio [C]/[N] was always greater than 100. The absorbance (A) of each solution was measured at 480 nm and this value of A used in an iterative procedure, based on eq. 5 to calculate the best values of both K_1 and ε_C.

$$\text{[5]}\quad \varepsilon_C = \frac{A}{[N]_0}\left(1 + \frac{[N]}{[C]}\right)$$

Alternatively K and ε_C could be obtained from Benesi–Hildebrand type plots of $[N]_0/A$ *vs.* $1/[S]_0$ (16). The above process was repeated using solutions of different initial concentrations of picramide. In all cases the range of sodium sulfite concentrations was chosen so as to keep the maximum conversion of 1:1 σ-complex to 2:1 σ-complex at less than 0.2% (*e.g.*, the maximum $[SO_3^{2-}]_0$ was 4.9×10^{-3} *M* at $T = 50.1$ °C).

Attempts to operate at high $[N]_0$ to $[S]_0$ ratios in order to effect a complete conversion of sulfite ion to the 1:1 σ-complex were unsuccessful due to the low solubility of picramide in aqueous solution.

(ii) N-Methylpicramide (NMP) – Sulfite Ion System

For this system both K_1 and K_2 are large and the ratio of K_2 to K_1 is ~0.02. *N*-Methylpicramide and both σ-complexes absorb at 480 nm.

In solutions of constant NMP concentration ($\sim 1 \times 10^{-4}$ *M*) there was no observable effect on the visible absorption spectrum when the sulfite ion concentration was increased from 0.10 to 0.50 *M*. Therefore the molar extinction coefficient of the 2:1 σ-complex (ε_D) was determined by measuring the absorbances at different wavelengths of a series of solutions of fixed sodium sulfite concentration (0.50 *M*) and varying NMP concentrations over the range 7×10^{-5} to 3×10^{-4} *M*.

To measure ε_C, the absorbances at 480 nm were measured for a series of solutions containing a fixed NMP concentration ($\sim 6 \times 10^{-5}$ *M*) and varying sodium sulfite concentrations in the range 1×10^{-5} to 2×10^{-4} *M*. Under these reaction conditions the measured absorbance (A) is the sum of the absorbances due to C (A_C) and unreacted NMP $\{A_{NMP} = \varepsilon_{NMP}[NMP]\}$. The value of A_C was calculated and plotted against [S]. Based on the equilibrium expressions [3] and [4] it can be shown that the maximum absorbance in such a plot is related to K_1, K_2, $[N]_0$, and ε_C as follows:

$$\text{[6]}\quad \varepsilon_C = \frac{(A_C)_{max}}{X_{max}[N]_0}$$

where

$$\text{[7]}\quad X_{max} = \frac{\sqrt{K_1/K_2}}{2 + \sqrt{K_1/K_2}} = \frac{[C]_{max}}{[N]_0}$$

In order to determine K_2, absorbances at 480 nm were determined for a series of solutions containing different

[3]Roger Gilmont Instruments, Inc., Great Neck, N.Y.

Can. J. Chem. Downloaded from www.nrcresearchpress.com by 210.87.254.42 on 09/05/12
For personal use only.

NMP concentrations ($\sim 1 \times 10^{-4}$ *M*) and sodium sulfite concentrations over the range 1×10^{-3} to 3×10^{-2} *M*. The concentration of NMP was chosen to give a range of absorbance values from 0.10 to 0.50. K_2 was calculated using the expression

$$[8] \quad \frac{1}{A - \{[C] + [D]\}\varepsilon_D} = \frac{1}{[N]_0(\varepsilon_C - \varepsilon_D)} \{K_2[S] + 1\}$$

Under the experimental conditions $[C] + [D] \simeq [N]_0$ and $[S] = [S]_0 - [N]_0$. An iterative procedure using a "least-squares" computer program was utilized to obtain the best values of K_2 consistent with the known ε_C and ε_D values and the measured values of *A*.

In order to determine K_1, absorbances at 480 nm were measured for a series of solutions containing NMP (5×10^{-5} to 1.1×10^{-4} *M*) and various sulfite ion concentrations over the range 5×10^{-5} to 1.5×10^{-4} *M*. Under these reaction conditions the measured absorbance (*A*) is due to absorbance by both C and unreacted NMP, *i.e.*,

$$[9] \quad A_C = A - \varepsilon_N[N]$$

An approximate value of [C] was obtained from the relation

$$[10] \quad [C] = A/\varepsilon_C$$

while the [D] was calculated using the expression

$$[11] \quad [D] = \frac{K_2[C][S]_0 - K_2[C]^2}{2K_2[C] + 1}$$

and approximate values of [N] and [S] evaluated. Equations 9, 10, and 11 were then used iteratively to obtain the best values of ε_C, A_C, [N], [C], and [D]. K_1 was then calculated using eq. 3.

(iii) N,N-Dimethylpicramide (DMP) -- Sulfite Ion System

For this system K_1 and K_2 are both large and the ratio K_2/K_1 is > 2 over the temperature range 0 to 50 °C. As a result all three species DMP, C, and D are present in appreciable amounts over most of the workable sodium sulfite and DMP concentration ranges.

The molar extinction coefficients of DMP at 350, 420, and 490 nm were measured in aqueous solutions of constant ionic strength 0.14 *M* (KNO_3).

The molar extinction coefficients of D at 350, 420, and 490 nm were obtained from absorbance measurements on solutions containing a range of DMP concentrations (3×10^{-5} to 1.4×10^{-4} *M*) and 0.10 *M* in sulfite ion. There was no observable effect on the recorded absorbances in the visible region when the sulfite ion concentration was increased beyond 0.10 *M*.

Molar extinctions of C at 350, 420, and 490 nm were obtained from stopped-flow traces of % transmittance *vs.* time for solutions containing $\sim 1 \times 10^{-5}$ *M* DMP and 2×10^{-2} *M* sodium sulfite. The sulfite concentration was sufficiently large that, in the absence of reaction to form D, all the added DMP would be converted to C. Experimentally the rate of the reaction DMP + $SO_3^{2-} \rightarrow$ C is very much faster than the conversion of C to D. As a result the absorbance value at infinite time recorded for the first reaction taking place in solution could be attributed exclusively to absorbance by C. Because of the method of determining ε_C the error limits on ε_C are higher than the error limits on ε_N and ε_D at the same wavelength.

Absorbance measurements at 350, 420, and 490 nm were then carried out on solutions of varying sodium sulfite and DMP concentration. At a given wavelength the absorbance *A* is given by the expression

$$[12] \quad A = \varepsilon_N[N] + [C]\varepsilon_C + [D]\varepsilon_D$$

With three absorbance values at three wavelengths and known values of ε_N, ε_C, and ε_D at these wavelengths, the three quantities [N], [C], and [D] could be calculated. K_1 and K_2 were then evaluated using eqs. 3 and 4.

Results and Discussion

Kinetics of σ-Complex Formation

Under the conditions employed in our studies, sulfite ion reacts reversibly with the nitroaromatic compounds (N) being discussed to form 1:1 and 2:1 σ-complexes according to eqs. 1 and 2. In all the systems the reaction to form the 2:1 σ-complex (D) was very slow compared to the reaction leading to the formation of the 1:1 σ-complex (C). As a result reliable values of A_∞ could be obtained even at very high sulfite ion concentrations where the 2:1 σ-complex D would be the predominant species at equilibrium. Over the entire range of sulfite ion concentrations employed, plots of $\ln(A_\infty - A_t)$ *vs.* time were linear to at least 90% completion of the reaction.

For the reversible formation of C according to eq. 1, studied under conditions such that $[SO_3^{2-}]_0 \gg [N]_0$, k_{obs} is related to the specific rate constants k_f and k_b as follows:

$$[13] \quad k_{obs} = k_f[SO_3^{2-}]_0 + k_b$$

where $K_1 = k_f/k_b$. In all systems values of k_{obs} were independent of $[N]_0$ and k_{obs} *vs.* $[SO_3^{2-}]_0$ plots were linear over the entire range of sodium sulfite concentrations used in the experiments. Values of k_f, obtained from the slopes of the k_{obs} *vs.* $[SO_3^{2-}]_0$ plots, are presented for the three systems in Tables 1, 2, and 3. In all cases the intercepts of the k_{obs} *vs.* $[SO_3^{2-}]_0$ plots were small. As a result k_b could not be determined in this way with a high degree of accuracy. The largest values of k_b were observed in the picramide–sulfite system. For purposes of comparison k_{obs} values, obtained from the intercepts and values of k_f/K_1 for this system, are given in Table 1. Clearly the ratio k_f/K_1 yields a much more reliable value of k_b. In the *N*-methylpicramide – sulfite and *N*,*N*-dimethylpicramide – sul-

Can. J. Chem. Downloaded from www.nrcresearchpress.com by 210.87.254.42 on 09/05/12
For personal use only.

TABLE 1. Specific rate constants for the formation (k_f) and decomposition (k_b) of the 1:1 picramide – sulfite ion σ-complex in aqueous solutions of constant ionic strength 0.14 M (KNO_3)[a]

T(°C)	$k_f \times 10^{-4}$ (M^{-1} s^{-1})	k_b (s^{-1})	k_f/K (s^{-1})
1.6	2.0±0.1	0±1	1.2±0.2
6.7	2.5±0.2	1±1	1.8±0.2
13.7	3.5±0.2	3±1	3.0±0.3
21.5	5.1±0.3	5±1	5.3±0.5
28.8	6.9±0.4	8±2	8.5±1.0
35.5	8.7±0.4	12±2	13.0±1.0

[a]Error limits on k_f and k_b are based on the errors associated with the "least-squares" slopes and intercepts of the k_{obs} *vs.* $[SO_3^{2-}]_0$ plots.

TABLE 2. Specific rate constants for the formation (k_f) and decomposition (k_b) of the 1:1 *N*-methylpicramide – sulfite ion σ-complex in aqueous solutions of constant ionic strength 0.14 M (KNO_3)[a]

T(°C)	$k_f \times 10^{-4}$ (M^{-1}s^{-1})	$k_b(=k_f/K_1)$ (s^{-1})
9.5	0.69±0.03	0.06±0.01
20.4	1.06±0.05	0.13±0.02
29.5	1.7±0.1	0.28±0.03
39.4	2.6±0.2	0.63±0.06
49.1	3.8±0.2	1.4±0.1

[a]Errors in k_f based on the errors associated with the "least-squares" slopes of plots of k_{obs} *vs.* $[SO_3^{2-}]_0$.

TABLE 3. Specific rate constants for the formation (k_f) and decomposition (k_b) of the 1:1 *N,N*-dimethylpicramide – sulfite ion σ-complex in aqueous solutions of constant ionic strength 0.14 M (KNO_3)[a]

T(°C)	$k_f \times 10^{-3}$ (M^{-1}s^{-1})	$k_b(=k_f/k_1)$ (s^{-1})
9.7	2.2±0.1	0.04±0.01
19.7	3.4±0.2	0.10±0.02
30.8	5.2±0.3	0.20±0.04
39.5	7.3±0.3	0.45±0.10
49.7	10.3±0.5	0.90±0.20

[a]Error limits on k_f are based on the errors associated with the "least-squares" slopes of the k_{obs} *vs.* $[SO_3^{2-}]_0$ plots.

fite systems k_b values were so small they could not be accurately obtained from the intercepts. Therefore Tables 2 and 3 list only values of k_f/K_1 for these systems.

Values of $\Delta H_1^{\ddagger}$ and $\Delta S_1^{\ddagger}$ obtained from plots of log k_f *vs.* $1/T$ are tabulated in Table 4. Errors in $\Delta H_1^{\ddagger}$ and $\Delta S_1^{\ddagger}$ are based on the errors in the "least-squares" slopes and intercepts of these plots.

Values of k_f at 25.0 °C decrease by a factor of four in going from the picramide–sulfite system to the *N*-methylpicramide – sulfite system and decrease by a factor of four again in going from the *N*-methylpicramide to the *N,N*-dimethylpicramide – sulfite system. Trends in k_b are far less regular; k_b decreases by a factor of 35 in going from the picramide–sulfite system to the *N*-methylpicramide – sulfite system whereas k_b for the *N*-methylpicramide – sulfite system is only slightly smaller than k_b for the *N,N*-dimethylpicramide – sulfite system.

Specific rate constants for the formation and decomposition at 25.0 °C of the 1,3,5-trinitrobenzene – sulfite ion complex are 3.54×10^4 M^{-1} s^{-1} and 125 ± 10 s^{-1}, respectively (17). In the 2,4,6-trinitrobenzaldehyde – sulfite ion system values of k_f and k_b at 25.0 °C are approximately 9×10^4 M^{-1} s^{-1} and 8 s^{-1}, respectively.[4] Over the range of X groups studied the effect of X is much greater on k_b than on k_f. The primary role of X in determining the stability of the 1:1 σ-complex may be related more to the extent to which the group X influences the solvation of the 1:1 σ-complex than to its electronic properties. Unfortunately the $\Delta H^{\ddagger}$ and $\Delta S^{\ddagger}$ values for the formation and decomposition of a wide range of 1-X-2,4,6-trinitrobenzene – sulfite ion complexes, necessary in order to support or refute this suggestion, are not yet available. In the case of the picramide–sulfite and *N*-methylpicramide – sulfite reactions there are no clear trends in the $\Delta H_1^{\ddagger}$ and $\Delta S_1^{\ddagger}$ values. $\Delta S_1^{\ddagger}$ is significantly more negative for the *N,N*-dimethylpicramide – sulfite ion reaction. This observation is consistent with the argument (presented later) that this complex is more strongly solvated than the other 1:1 σ-complexes in this series.

Thermodynamics of σ-Complex Formation

Equilibrium constants for the formation of the 1:1 sulfite ion – picramide σ-complex and molar extinction coefficients of this complex at a number of temperatures are listed in Table 5. Values of ε_C at 480 nm increase slightly over the temperature range studied, possibly as a result of some broadening of the absorption band as the temperature is increased. Studies carried out at sulfite ion concentrations greater than 4.9×10^{-3} M yielded a molar extinction coefficient (ε_D) for the 2:1 species at 421 nm of $2.80 \pm 0.03 \times 10^4$ M^{-1} cm^{-1}. Values of the equilibrium constant for 2:1 σ-complex formation (K_2) were found to decrease from 20 M^{-1} at 9.7 °C to 10 M^{-1} at 19.7 °C to 2.6 M^{-1} at 50.1 °C.

[4]A. R. Norris and N. Marendic. Unpublished results.

Can. J. Chem. Downloaded from www.nrcresearchpress.com by 210.87.254.42 on 09/05/12
For personal use only.

TABLE 4. Thermodynamic and kinetic parameters associated with 1:1 sulfite ion σ-complex formation with picramide (P), *N*-methylpicramide (NMP), and *N*,*N*-dimethylpicramide (DMP) in aqueous solutions of ionic strength 0.14 *M* (KNO_3)

Compound	K (at 25.0 °C) (M^{-1})	ΔH^0 (kcal mol^{-1})[a]	ΔS^0 (cal deg^{-1} mol^{-1})	k_f (at 25.0 °C) (M^{-1} s^{-1})[b]	k_b (at 25.0 °C) (s^{-1})	$\Delta H_1^{\neq}$ (kcal mol^{-1})[c]	$\Delta S_1^{\neq}$ (cal $deg^{-1}mol^{-1}$)[c]
P	$8.6\pm0.4\times10^3$	-4.3 ± 0.1	3.5 ± 0.4	$5.7\pm0.2\times10^4$	7 ± 1	6.8 ± 0.1	-14.0 ± 0.6
NMP	$6.8\pm0.4\times10^4$	-6.1 ± 0.2	1.5 ± 0.6	$1.4\pm0.1\times10^4$	0.20 ± 0.02	7.3 ± 0.2	-14.7 ± 0.6
DMP	$3.0\pm0.3\times10^4$	-7.4 ± 0.4	-4.0 ± 0.1	$4.1\pm0.2\times10^3$	0.14 ± 0.04	6.4 ± 0.1	-20.4 ± 0.6

[a]Errors in ΔH^0 based on errors in the "least-squares" slopes of the log K_1 *vs.* $1/T$ plots.
[b]Errors in k_f based on errors associated with $\Delta H_1^{\neq}$ and $\Delta S_1^{\neq}$.
[c]Errors in $\Delta H_1^{\neq}$ and $\Delta S_1^{\neq}$ based on errors in the "least-squares" slopes and intercepts (at $1/T$ equal to 0) of the log k_f *vs.* $1/T$.

Can. J. Chem. Downloaded from www.nrcresearchpress.com by 210.87.254.42 on 09/05/12
For personal use only.

TABLE 5. Picramide – sulfite ion interaction in aqueous solutions of constant ionic strength 0.14 M (KNO_3), pH 9.00. Equilibrium constants for 1:1 σ-complex formation and molar extinction coefficients of the 1:1 σ-complex at 480 nm[a]

T(°C)	$\varepsilon \times 10^{-4}$ (M^{-1} cm^{-1})[b]	$K_1 \times 10^3$ (M^{-1})
9.7	1.09±0.02	12.7±0.3
19.7	1.13±0.02	10.2±0.7
31.3	1.18±0.02	7.5±0.3
40.4	1.19±0.02	6.2±0.2
50.1	1.20±0.02	4.9±0.2

[a]Errors in K_1 and ε are based on the observed range of experimental values of K_1 and ε calculated using different initial picramide and sodium sulfite concentrations.
[b]The absorption maximum for the 1:1 σ-complex appears at 424 nm. At this wavelength ε is calculated to be 2.73 ± 0.02 × 10^4 M^{-1} cm^{-1} at all temperatures.

The equilibrium constants for 1:1 and 2:1 sulfite ion – *N*-methylpicramide σ-complex formation, and the molar extinction coefficients at 480 nm of *N*-methylpicramide and the two complexes at a number of temperatures are presented in Table 6. At 480 nm values of ε_C for the *N*-methylpicramide – sulfite ion complex are somewhat lower than ε_C values for the picramide – sulfite ion complex.

In Table 7 are listed the molar extinction coefficients at several different wavelengths of *N*,*N*-dimethylpicramide and its 1:1 and 2:1 σ-complexes with sulfite ion. The values of ε_N, ε_C, and ε_D were, within experimental error, independent of temperature. Table 8 contains the equilibrium constants for the formation of C and D in the *N*,*N*-dimethylpicramide – sulfite ion system over a range of temperatures.

In general Crampton's values of K_1 and K_2, at 20 ± 2 °C and μ = 0.14 M (Na_2SO_4),[5] agree reasonably well with our values of K_1 and K_2 at 20.0 °C and μ = 0.14 M (KNO_3). We find that K_1, for formation of the *N*,*N*-dimethylpicramide – sulfite ion complex, is less however than K_1 for the formation of the *N*-methylpicramide – sulfite ion complex, whereas Crampton reports equal values of K_1 for these two systems.

Equilibrium constants for formation of the 1:1 and 2:1 sulfite ion σ-complexes show that at 20.0 °C K_1 varies in the order

TNT < TNA < TNB < P < TNBA < DMP < NMP

while K_2, at 20.0 °C and μ = 0.14 M, varies in the order

TNB < P < TNBA < TNA < NMP < DMP

For the formation of 1:1 hydroxide ion σ-complexes at 25.0 °C K_1 varies in the order

TNB < P < TNBA

(TNT, TNA, TNB, and TNBA are 2,4,6-trinitrotoluene, 2,4,6-trinitroanisole, 1,3,5-trinitrobenzene, and 2,4,6-trinitrobenzaldehyde respectively).

A consideration of the K_1 values in the light of the k_f and k_b values (Table 4) indicates that the increased stabilities of the 1:1 *N*,*N*-dimethylpicramide – sulfite ion and *N*-methylpicramide – sulfite ion complexes compared to the 1:1 picramide – sulfite ion complex are more the result of lower rates of decomposition of the former 1:1 σ-complexes rather than, as suggested by Crampton (5), more favorable k_f values for formation of the former 1:1 σ-complexes.

Values of ΔH^0 and ΔS^0 for 1:1 σ-complex formation in the picramide –, *N*-methylpicramide –, and *N*,*N*-dimethylpicramide – sulfite ion systems are presented in Table 5. In the 1,3,5-trinitrobenzene – sulfite ion system ΔH^0 and ΔS^0 values for 1:1 σ-complex formation are reported to be −4.0 ± 0.1 kcal mol^{-1} and −2.3 ± 0.5 cal deg^{-1} mol^{-1}, respectively (4). In the 2,4,6-trinitrobenzaldehyde – sulfite ion system ΔH^0 and ΔS^0 are −2.41 ± 0.16 kcal mol^{-1} and 11.4 ± 1.1 cal deg^{-1} mol^{-1}, respectively (9).

For the process of 1:1 σ-complex formation we can consider, to a first approximation, that ΔH^0 represents the sum of the enthalpy change associated with formation of the C—SO_3^- bond (ΔH_a), the enthalpy change associated with desolvation of sulfite ion in going from free sulfite in solution to sulfite bonded to carbon (ΔH_b), and the enthalpy change associated with solvation of the negatively charged σ-complex (ΔH_c). In the same way ΔS^0 is the sum of the entropy change associated with the sulfite ion and the nitroaromatic compound coming together to form the complex (ΔS_a), the entropy change associated with desolvation of sulfite ion in going from free sulfite to sulfite in the complex (ΔS_b) and the entropy change associated with solvation of the negatively charged complex (ΔS_c). For a series of comparably solvated nitro-

[5]Crampton's values for K_2 at μ = 0 and T = 20 ± 2 °C were used in conjunction with his reported relationship (5)

$$\log_{10}(K_2)_\mu = \frac{\sqrt{\mu}}{1 + 1.2\sqrt{\mu}}(4.06) + \log_{10}(K_2)_{\mu=0}$$

to calculate values of K_2 at μ = 0.14 M and T = 20 ± 2 °C.

TABLE 6. *N*-Methylpicramide – sulfite ion interaction in aqueous solutions of constant ionic strength 0.14 *M* (KNO_3), p*H* = 9.00. Equilibrium constants for 1:1 and 2:1 σ-complex formation and molar extinction coefficients of *N*-methylpicramide and the two σ-complexes C and D at 480 nm

T(°C)	$\varepsilon_N \times 10^{-2}$ (M^{-1} cm^{-1})	$\varepsilon_C \times 10^{-3}$ (M^{-1} cm^{-1})	$\varepsilon_D \times 10^{-2}$ (M^{-1} cm^{-1})	$K_1 \times 10^{-4}$ (M^{-1})	$K_2 \times 10^{-2}$ (M^{-1})
20.1	4.4±0.1	9.0±0.3	1.3±0.1	7.9±0.8	18±2
29.9	4.4±0.1	9.2±0.3	1.3±0.1	5.8±0.6	10±1
39.0	4.4±0.1	9.0±0.3	1.3±0.1	4.2±0.4	6.0±0.6
48.1	4.4±0.1	8.8±0.3	1.3±0.1	3.2±0.3	3.5±0.4

TABLE 7. *N,N*-Dimethylpicramide – sulfite ion interaction in aqueous solutions of constant ionic strength 0.14 *M* (KNO_3), p*H* = 9.00. Molar extinction coefficients of *N,N*-dimethylpicramide (DMP) and the 1:1 and 2:1 σ-complexes C and D

	$\varepsilon \times 10^{-3}$ (M^{-1} cm^{-1})		
Compound	350 nm	420 nm	490 nm
DMP	9.4±0.2	6.4±0.1	0.33±0.01
1:1 σ-complex (C)	5.0±0.2	20±2	8.0±1.0
2:1 σ-complex (D)	4.3±0.1	20.0±0.5	0.285±0.005

TABLE 8. *N,N*-Dimethylpicramide – sulfite interaction in aqueous solutions of constant ionic strength 0.14 *M* (KNO_3), p*H* = 9.00. Equilibrium constants for formation of the 1:1 and 2:1 sulfite ion – *N,N*-dimethylpicramide σ-complexes C and D

T(°C)	$K_1 \times 10^{-4}$ (M^{-1})	$K_2 \times 10^{-4}$ (M^{-1})
11.8	4.8±0.4	7.0±1.0
20.5	3.8±0.4	3.8±0.7
30.7	2.4±0.2	1.8±0.3
40.6	1.6±0.2	0.80±0.10
49.2	1.1±0.1	0.35±0.05

aromatic compounds forming a series of structurally similar 1:1 σ-complexes, ΔH_1, ΔH_2, ΔS_1, and ΔS_2 should each remain reasonably constant. Trends in ΔH^0 and ΔS^0 should therefore mainly reflect trends in the overall solvation of the 1:1 σ-complex with a greater degree of solvation of the complex implying more negative values of both ΔH^0 and ΔS^0.

For the 1:1 1-X-2,4,6-trinitrobenzene – sulfite ion σ-complexes in which X = CHO, NH_2, $NHCH_3$, and $N(CH_3)_2$, more negative ΔH^0 values are in fact associated with more negative ΔS^0 values. For the four X groups mentioned a reasonably linear ΔH^0 *vs.* ΔS^0 plot is obtained (18). For the 2:1 1-X-2,4,6-trinitrobenzene – sulfite ion σ-complexes, where X = NH_2, $NHCH_3$, $N(CH_3)_2$, and CHO, more negative values of ΔH^0 (−9, −11, −14, and −8.53 kcal mol^{-1}, respectively) are also accompanied by more negative ΔS^0 values (−12, −22, −28, and −21.8 cal deg^{-1} mol^{-1}, respectively). However, a plot of ΔH^0 *vs.* ΔS^0 is not linear in this case. A complicating factor in 2:1 σ-complex formation is the steric strain associated with addition of the second sulfite ion. This steric strain would be expected to be least in the picramide–sulfite 2:1 σ-complex and it is for this system that the ΔH^0 term is accompanied by a higher than expected ΔS^0 term.

In the picramide – and *N*-methylpicramide – sulfite σ-complexes a smaller degree of solvation might be required as a result of intramolecular N—O$^-$.....H—N bonding serving to compensate, in part, the partial negative charge on the oxygens of the ortho nitro groups in the complex. Trends in the ΔS^0 values associated with the formation of the picramide–sulfite, *N*-methylpicramide – sulfite, and 1,3,5-trinitrobenzene – sulfite complexes are certainly in accord with this idea. The ΔS^0 value is highest in the picramide complex (two hydrogen bonds) and becomes progressively more negative the greater the requirement for solvation of the nitro groups by water. That factors other than hydrogen bonding are important is seen by comparing

Can. J. Chem. Downloaded from www.nrcresearchpress.com by 210.87.254.42 on 09/05/12
For personal use only.

ΔS^0 data in the *N*-methylpicramide – and 2,4,6-trinitrobenzaldehyde – sulfite systems. Both substrates have a single hydrogen available for hydrogen bonding but both ΔS^0 and ΔH^0 for the latter system are far more positive. This may arise because of some degree of delocalization of negative charge onto the aldehyde group in the complex which thereby renders solvation of the nitro groups less extensive.[6] Alternatively 2,4,6-trinitrobenzaldehyde may be more strongly solvated in its initial state. Extensive heats of solvation data for these nitroaromatic compounds in water would be needed in order to solve this problem.

Financial support by the National Research Council of Canada is gratefully acknowledged.

[6]If the magnitudes of $\varepsilon(\lambda_{max})$ reflect the degree to which the nitro groups ortho to X are rotated out of the plane of the ring in the complex, and solvation of the nitro groups is more extensive the greater their degree of rotation out of the plane, then the order of solvation of the nitro groups (based on ε_C) is

$$P < NMP \sim TNB < TNBA < DMP < TNA < TNT$$

and (based on ε_D) is

$$P < NMP < DMP < TNB < TNA$$

1. H. MURAOUR. Bull Soc. Chim. Fr. **35**, 367 (1927).
2. F. ČŮTA and E. BERÁNEK. Coll. Czech. Chem. Commun. **23**, 1501 (1958).
3. R. A. HENRY. J. Org. Chem. **27**, 2637 (1962).
4. A. R. NORRIS. Can. J. Chem. **45**, 175 (1967).
5. M. R. CRAMPTON. J. Chem. Soc. (B), 1341 (1967).
6. E. BUNCEL, A. R. NORRIS, and K. E. RUSSELL. Q. Rev. Lond. **22**, 123 (1968).
7. M. R. CRAMPTON. Adv. Phys. Org. Chem. **7**, 211 (1969).
8. M. J. STRAUSS. Chem. Rev. **70**, 667 (1970).
9. A. R. NORRIS and N. MARENDIC. Can. J. Chem. **51**, 3927 (1973).
10. L. H. GAN and A. R. NORRIS. Can. J. Chem. **49**, 2490 (1971).
11. E. BUNCEL, A. R. NORRIS, K. E. RUSSELL, and R. TUCKER. J. Am. Chem. Soc. **94**, 1646 (1972).
12. J. R. A. POLLOCK and R. STEVENS (*Editors*). Dictionary of organic compounds. 4th ed. Eyre and Spottiswoode, Ltd., London. 1965.
13. J. GLAZER, E. D. HUGHES, C. K. INGOLD, A. T. JAMES, G. T. JAMES, and E. ROBERTS. J. Chem. Soc. 2674 (1950).
14. A. I. VOGEL. A textbook of quantitative inorganic analysis. 3rd ed. Longmans, Green, London. 1968. p. 343.
15. P. G. ASHMORE, B. P. LEVITT, and B. A. THRUSH. Trans. Faraday Soc. **52**, 530 (1956).
16. H. BENESI and J. HILDEBRAND. J. Am. Chem. Soc. **71**, 2703 (1949).
17. C. F. BERNASCONI and R. G. BERGSTROM. J. Am. Chem. Soc. **95**, 3603 (1973).
18. J. E. LEFFLER and E. GRUNWALD. Rates and equilibria of organic reactions. J. Wiley and Sons, Inc., New York. 1963.

Can. J. Chem. Downloaded from www.nrcresearchpress.com by 210.87.254.42 on 09/05/12
For personal use only.

Vacuum Ultraviolet Photolysis of Trimethylethylene

GUY J. COLLIN AND CHRISTIAN M. GAUCHER

Département des Sciences Pures, Université du Québec à Chicoutimi, Chicoutimi, Québec

Received June 28, 1973

The vacuum u.v. photolysis of trimethylethylene (2-methyl-2-butene) was carried out in a static system using rare gas resonance lamps: xenon (147.0 nm) and krypton (123.6 nm). The main hydrocarbon products were isoprene, 1,3-butadiene, propyne, allene, ethylene, and other minor products. Identification and measurements of the yields of hydrogen atoms, methyl, and ethyl radicals were carried out quantitatively by the use of radical–radical reactions. Because of the high yield of isoprene, the effect of conversion was studied. At a high conversion (*i.e.* 0.1%) the isoprene quantum yield decreases. Hydrogen atoms add mainly to the secondary carbon of the monomer (≥90%). The $\Delta(CH_3,tert\text{-}C_5H_{11})$ value was calculated to be 1.32 ± 0.14. With the krypton line (10.0 eV) no evidence was found for the participation of ionic reactions in the formation of the measured products except for the formation of 2-methyl-1-butene in a low yield. At this wavelength the ion quantum yield is $0.22_4 \pm 0.00_5$.

Nous avons étudié la photolyse dans l'ultraviolet à vide et en système fermé du triméthyléthylène (méthyl-2-butène-2). Nous avons utilisé les lampes de résonnance à gaz rare: xénon (147.0 nm) et krypton (123.6 nm). Les principaux produits formés sont l'isoprène, le butadiène-1,3, le propyne, l'allène, l'éthylène ainsi que d'autres produits formés en quantités mineures. L'identification et la mesure des rendements des atomes d'hydrogène, des radicaux méthyles et éthyles ont été faites à travers les réactions du type radical–radical. Nous avons également étudié l'influence du taux de conversion étant donné le rendement important en isoprène. Le rendement quantique de ce produit décroît à haut taux de conversion (≥0.1%). Les atomes d'hydrogène s'additionnent principalement sur le carbone secondaire de la double liaison (≥90%). Le rapport dismutation/combinaison des radicaux méthyles–$tert\text{-}C_5H_{11}$ obtenu est de 1.32 ± 0.14. A 10.0 eV (raie de résonnance du krypton), il ne semble pas que l'ion parent formé interfère avec la formation des produits mesurés sauf en ce qui concerne une formation mineure de méthyl-2-butène-1. Le rendement quantique ionique est alors de $0.22_4 \pm 0.00_5$.

Can. J. Chem., **52**, 34 (1974)

Introduction

Recently, we studied the vacuum u.v. photolysis of 2-methyl-1-butene (1*a*) and 3-methyl-1-butene (1*b*) to compare the fragmentation of excited isomeric molecules at 8.4 eV and the ionic reactions occurring at 10.0 eV, *i.e.* above the ionization energy. Very little work has been reported on the photolysis of trimethylethylene (TME) (2). The present work was done to elucidate the mechanism of the chemistry of excited and superexcited trimethylethylene molecules.

Experimental

Materials

Trimethylethylene was an API product (impurity 0.06 ± 0.04%) and was used without further purification. Analysis of the starting material revealed the presence of 2-methyl-1-butene (0.024%). Other materials used have been described in previous studies (3–5). The xenon and the krypton resonance lamps were also described in the literature (6); actinometry was done by comparing product yields with those from the vacuum u.v. photolysis of isobutene in similar conditions (7, 8). Above the ionization potential, (*i.e.* at 10.0 eV), the ion current was recorded at various pressures between 0.5 and 3 Torr to measure the ion quantum yield. Analytical procedures were also described previously (1, 3).

Mercury sensitized photolyses were carried out in a quartz bulb with a low pressure Hanovia lamp equipped with a Vycor filter (9).

Results

At 8.4 eV, typical quantum yields of products are reported in Table 1. In the presence of oxygen (5–7%) quantum yields are independent of the total pressure of the reactants except that of isobutene which increases sharply at lower pressures. The presence of 5% oxygen completely eliminates the formation of propane, isopentane, 3-methyl-1-butene, and all the measured C_6H_{12} and C_6H_{14} products. With 10% oxygen, the ethane quantum yield is zero and the 2-methyl-1-butene quantum yield is lower than 0.01 (see Table 1).

At 10.0 eV, the results are similar to those reported at 8.4 eV (Table 1). Figures 1 and 2 show that the absolute quantum yields of all products are independent of irradiation time provided that the concentrations of isoprene and 1,3-butadiene in the sample were lower than 0.1%. The ion current recorded at this wavelength shows that the photochemically excited

Can. J. Chem. Downloaded from www.nrcresearchpress.com by 210.87.254.40 on 09/05/12
For personal use only.

TABLE 1. Quantum yields in the photolysis of trimethylethylene at 8.4 and 10.0 eV

	Incident energy 8.4 eV				Incident energy 10.0 eV			
C_5H_{10}[a]	12.0[b]	10.0	0.18	0.10	10.0[b]	1.0	1.0	0.05
O_2[a]	0.84	—	—	—	—	0.1	—	—
$C_5H_8 \times 10^3/C_5H_{10}$[c]	1.6	0.6	33.0	12.3	0.05	2.0	4.4	25.0
Methane	0.04	0.26	0.14_5	0.08	0.23	0.03	0.13_5	0.13
Acetylene	0.00_5	0.00_5	0.01_5	0.00_7	0.00_4	0.00_5	0.00_5	0.01
Ethylene	0.03_5	0.03_2	0.04	0.10	0.03_5	0.05	0.03_7	0.06
Ethane	0.00	0.26	0.27_5	[f]	0.22_5	0.0	[f]	[f]
Propene	0.01_2	0.01_6	0.01_8	0.02_1	0.01_5	0.01_7	0.01_9	0.03
Propane	0.00	0.00_8	[f]	[f]	0.00_8	0.00	[f]	[f]
Propyne	0.22	0.22	[f]	[f]	0.15_5	0.15_5	[f]	0.12
Allene	0.05_2	0.05_5	0.05_5	0.05_5	0.05	0.05	0.05	0.05
Isobutene[d]	0.13	0.01	0.05	0.09	0.09_2	0.09_8	0.11_8	0.20_6
1,3-Butadiene		0.13	0.13	0.13				
1,2-Butadiene	0.02_1	0.02_7	0.02_2	0.02	0.02_8	0.02_4	0.02_4	0.02_3
Unknown (C_5?)[e]	0.02_5	[f]	[f]	0.02	[f]	0.02_2	[f]	[f]
Isoprene	0.31	0.33	0.15	0.26_5	0.28	0.27_6	0.23_3	0.19
2-Methyl-1-butene	0.00_8	0.31	0.10	0.03	0.27_6	0.01_7	[f]	0.09_7
Isopentane	0.00	0.19	0.07_8	[f]	0.19	0.00	0.08_2	[f]
3-Methyl-1-butene	0.00	0.02	0.00_7	[f]	0.01_5	0.00	0.00_6	[f]
3,3-Dimethyl-1-butene	0.00	0.03_4	[f]	[f]	0.03_7	0.00	[f]	[f]
2,2-Dimethylbutane	0.00	0.17_5	0.11_2	[f]	0.15_3	0.00	0.06	[f]
1,1,2-Trimethyl cyclopropane	0.00	0.00_1	[f]	[f]	0.00_1	0.00	0.00	[f]
2,3-Dimethyl-1-butene	0.00	0.03_9	0.01_5	[f]	0.03_1	0.00	[f]	[f]
2,3-Dimethylbutane	0.00	0.01_7	0.01	[f]	0.01_5	0.00	[f]	[f]
2-Methyl-2-pentene	0.00	0.05_7	[f]	[f]	0.04	0.00	[f]	[f]
3-Methyl-2-pentene (*cis* + *trans*)	0.00	0.07	[f]	[f]	0.05_7	[f]	[f]	[f]

[a]Pressure in Torr.
[b]Addition of helium (150 Torr) does not change the quantum yields.
[c]Final ratio.
[d]Φ(1-butene) = 0.00.
[e]Retention time close to that of isopentane on the squalane column.
[f]Not measured.

molecules autoionize (Fig. 3). In the presence of ammonia, toluene, and methylcyclopentane (5–10%) there is a decrease of the 2-methyl-1-butene quantum yield from 0.01_7 to 0.00_5. This effect is not observed at 8.4 eV.

Discussion

A. Effect of Conversion

In order to verify the importance of conversion on the product yields, a series of experiments was carried out by varying the irradiation time at constant lamp intensity (Figs. 1 and 2). Whereas the quantum yields of allene, ethylene, acetylene, 1,2-butadiene, and other products are constant and their absolute yields are directly proportional to the irradiation time, anomalies in the curves of the absolute yields of isoprene and of propene were noted. Isoprene is the major product in the photolysis of trimethylethylene. *A priori*, this product is expected to be very reactive towards radicals although no data seem to be available; we shall consider that its reactivity is similar to that of 1,3-butadiene. Hydrogen atoms (10), and methyl (11) and triplet and singlet methylene radicals (12) react faster with 1,3-butadiene than with trimethylethylene. In these circumstances it is interesting to note the behavior of isoprene and of 1,3-butadiene produced in the photolysis of trimethylethylene. Their quantum yields decrease with an increase in conversion. In the case of isoprene, this effect can be explained partially by direct absorption of light, especially at high conversion of the monomer. A radical scavenging effect, or the absorption of light or other unknown processes could explain that propene is a secondary product formed via an intermediate isoprene molecule (Fig. 2). Because the quantum yield of hydrogen atoms is high (see later), the mercury sensitized photolysis of a hydrogen–isoprene

Can. J. Chem. Downloaded from www.nrcresearchpress.com by 210.87.254.40 on 09/05/12
For personal use only.

Can. J. Chem. Downloaded from www.nrcresearchpress.com by 210.87.254.40 on 09/05/12
For personal use only.

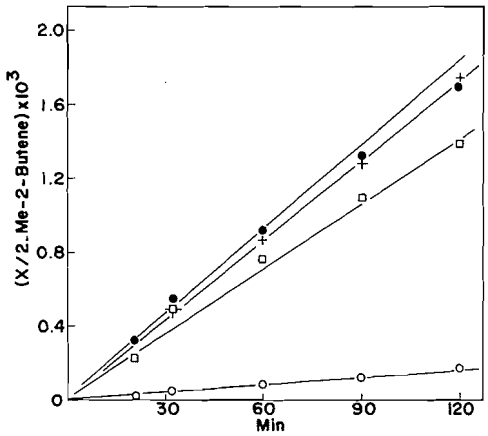

FIG. 1. Absolute yields of decomposition products *vs.* irradiation time: ○, acetylene; □, ethylene; +, methylacetylene; ●, 1,3-butadiene+isobutene; λ = 123.6 nm.

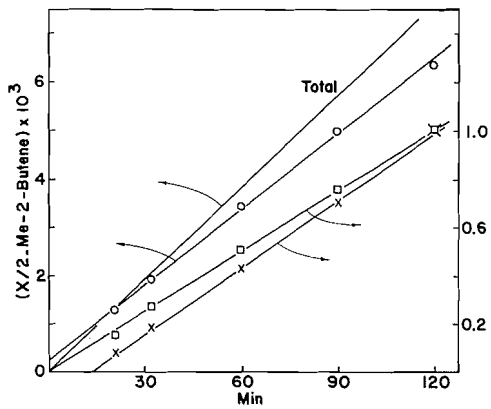

FIG. 2. Absolute yields of decomposition products *vs.* irradiation time: X, Propene; □, 1,2-butadiene; ○, isoprene; λ = 123.6 nm. Total = propene + isoprene.

mixture (12:0.2 Torr) was studied. In contrast to the 1-butyne system (9), we do not observe the fragmentation of a C_5H_9 intermediate radical into a C_3 product. This radical is probably stabilized by allylic resonance.

B. Radical Reactions

The results in the absence and in the presence of a small amount of oxygen are very different. Because oxygen acts as a good radical scavenger, it can be thought that all products which disappear in the presence of oxygen are formed through radical reactions. Thus, as the formation of *n*-butane was not observed ($\Phi(n\text{-}C_4H_{10}) < 0.005$), ethane is essentially formed by the combination of two methyl radicals. Since the propane yield is very low, one can calculate an upper

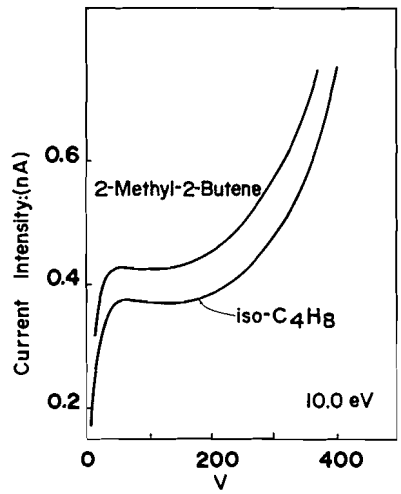

FIG. 3. Saturation current *vs.* voltage, obtained during irradiation of isobutene and trimethylethylene at 123.6 nm. The intensity of the krypton lamp was kept constant.

limit to the ethyl radical quantum yield of the order of 0.02. The structure of the main products suggests that they are produced from C_5H_{11} radicals (Table 1). Although the ratios of the

[1*a*] $H + TME \rightarrow (C_2H_5C(CH_3)_2)^*$

[1*b*] $H + TME \rightarrow (CH_3CHCH(CH_3)_2)^*$

[1*c*] $H + TME \rightarrow H_2 + C_5H_9$

rate constants are not known for reactions 1*a–c* (10), from what is known about the interaction of hydrogen atoms with butenes (13), the k_{1c}/k_1 ratio must be less than 0.05, provided that the hydrogen atoms can be considered as thermal. Thus as a first approximation, the abstraction reaction can be ignored. One can approximate the ratio k_{1a}/k_{1b} by the 2,2-dimethylbutane/2,3-dimethylbutane ratio since these two products are formed by the combination of the methyl and the implied pentyl radicals. Then, if the disproportionation–combination ratios are the same for the two planned reaction systems, the k_{1a}/k_{1b} ratio is of the order of 11. At low pressures, the pentyl radicals decompose before being stabilized by collision (14). This reaction explains the increase in the yield of isobutene at lower pressures. The excited $CH_3CHCH(CH_3)_2$* radical has a stabilization/decomposition (S/D)

[2] $(C_5H_{11})^* + M \rightarrow C_5H_{11} + M$

[3] $(C_2H_5C(CH_3)_2)^* \rightarrow CH_3 + \text{iso-}C_4H_8$

[4] $(CH_3CHCH(CH_3)_2)^* \rightarrow 2\text{-}C_4H_8 + CH_3$

Can. J. Chem. Downloaded from www.nrcresearchpress.com by 210.87.254.40 on 09/05/12
For personal use only.

ratio closed to unity at pressures about 0.2 Torr. Since even at a pressure of 0.04 Torr no appreciable increase of *cis*- and *trans*-2-butene was observed, the addition of the hydrogen atom to the tertiary carbon is not favored over that to the secondary carbon atom of the monomer.

The formation of the C_6 olefins in the absence of oxygen is the result of at least two reaction pathways (Table 1). First, they are produced by the combination of methyl and pentenyl (C_5H_9) radicals. These latter radicals are produced either directly by fragmentation of the excited molecule (this process should be a relatively minor one because of the initial energies) or by the abstraction of a hydrogen atom from the parent molecule by radical, *e.g.*, reaction 1*c*. Secondly, these products can be formed by the insertion of the singlet methylene radical into the monomer. However, the low yield of 1,1,2-trimethylcyclopropane suggests that this reaction is of limited importance (15). Moreover, it has been shown (5, 7) that at 8.4 and 10.0 eV the formation of the methylene radical has a small quantum yield, of the order of 0.02–0.04. Consequently, the formation of the C_6 olefins via methylene reactions is of little importance. Because the system contains mainly methyl and *tert*-pentyl radicals (Table 2), the $\Delta(CH_3,tert\text{-}C_5H_{11})$ ratio can be determined:

[5] $CH_3 + CH_3 \rightarrow C_2H_6$

[6] $CH_3 + tert\text{-}C_5H_{11} \rightarrow CH_4 + C_5H_{10}$

[7] $CH_3 + tert\text{-}C_5H_{11} \rightarrow$ 2,2-Dimethylbutane (DMB)

[8] $2\ tert\text{-}C_5H_{11} \rightarrow$ Products

The methane/DMB ratio is equal to 1.32 ± 0.14.[1] Methane is probably formed by other chemical pathways than reaction 6 and the $\Delta(CH_3,tert\text{-}C_5H_{11})$ value may be less than the preceding value.

Finally, from the effect of oxygen on the formation of the products one can derive the radical yields at the two wavelengths (Table 2). In contrast to the results from the study of other methylbutenes (1), the high yield of the C_5H_9 radical should be noted. This may be the result of the presence of nine allylic hydrogen atoms in the monomer. Hydrogen atom scavenging by isoprene may also contribute to the formation of this radical. In addition, it should be noted that the total quantum yield of the radicals is calculated to be of the order of 2.

TABLE 2. Radical yields in the photolysis of trimethylethylene

	Incident energy	
Product	8.4 eV	10.0 eV
H	0.80 ± 0.10	0.73 ± 0.08
CH_3[a]	1.10 ± 0.10	0.99 ± 0.1
C_2H_5	< 0.02	< 0.02
C_5H_9[b]	0.35 ± 0.1	0.33 ± 0.1
Total[c]	$2.2_5 \pm 0.3$	$2.0_6 \pm 0.3$

[a]Does not include methyl radicals formed by the fragmentation of *tert*-pentyl radicals (reactions 3 and 4).
[b]An important fraction of the yield of this radical may be formed by secondary processes and not directly by the fragmentation of excited molecules.
[c]Other minor radicals or unmeasured radicals can increase this total yield.

C. Fragmentation of Excited Trimethylethylene Molecules

The ionization potential of trimethylethylene is reported to be 8.67 eV (16). With the xenon lamp (8.4 eV) no ionization occurs and the excited molecule may be stabilized by collision, or may decompose.

[9] $TME + h\nu \rightarrow (TME)^{**}$

[10*a*] $(TME)^{**} + M \rightarrow TME$ or other C_5H_{10}

[10*b*] $(TME)^{**} \rightarrow$ Products

The absence, or the very low quantum yield ($\Phi < 0.01$), of isomeric compounds shows that if the isomerization of the 8.4 eV excited molecule occurs, these excited molecules are not stabilized by collision, at least in the range of pressure studied, and they decompose. The products from the fragmentation of the 8.4 eV photolysis of 1-pentene (17), 2-methyl-1-butene (1*a*), and 3-methyl-1-butene (1*b*), are similar, but their relative yields are very different. The fragmentation of photochemically excited molecules can then be considered to be very fast and, if isomerization does occur, it is of little importance. Reaction 10*b* must be the most important reaction.

The isoprene quantum yield is constant with pressure provided the percentage of conversion is kept very low. The same result is observed for all products measured in the presence of oxygen, except for the isobutene quantum yield. Then there is no apparent pressure stabilization, and fragmentation prevails over the stabilization

[1]This ratio is in accord with the formation of C_5H_{10} (see ref. 18) and with the ratio (reaction 6 + 7)/[(reaction 5)$^{1/2}$ × (reaction 8)$^{1/2}$] = 1.92 ± 0.10. Both values are the mean of seven independent measurements.

reaction, even in the presence of 200 Torr of helium.

[11] $(TME)^{**} \rightarrow C_4H_6 + H_2$ (or 2 H); $\Delta H = 1.2$ eV (or 5.65 eV)

[12] $(TME)^{**} \rightarrow C_3H_4 + 2\,CH_3$; $\Delta H = 5.2$ eV

[13] $(TME)^{**} \rightarrow C_3H_4 + C_2H_6$; $\Delta H = 1.5$ eV

[14] $(TME)^{**} \rightarrow C_3H_4 + C_2H_5 + H$; $\Delta H = 5.7$ eV

Although thermally possible, these reactions do not have the same importance. Because of the low yield of molecular ethane, (*i.e.* formed in the presence of oxygen, the $\Phi(13)/\Phi(12 + 13 + 14)$ ratio is lower than, or at the most, equal to 0.02 at the two wavelengths used, thus showing that the fragmentation of the excited species will preferentially give a stable molecular product and two radical fragments (5, 7). Reactions 12 and 14 are not of the same importance. The yields of ethyl and of methyl radicals previously reported confirm the preponderance of reaction 12: $\Phi(14)/\Phi(12) \leqslant 0.03$. The formation of 1,3- and 1,2-butadienes can also be explained by the fragmentation of the excited molecule:

[15] $(TME)^{**} \rightarrow C_4H_6 + CH_3 + H$ (or CH_4); $\Delta H = 6.10$ (or 1.6) eV

Ethylene and acetylene are also formed in the same manner. It is impossible to discuss all conceivable reactions here.

Finally, one must notice the similarity of the fragmentation products obtained at the two wavelengths. As we have already mentioned (5), a variation on the wavelength has little effect on the fragmentation of the excited molecule, except in the case of the formation of the parent ion at 10.0 eV. In addition, it is concluded (Table 3) that the sum of the yields of the primary processes is about unity. It appears that stabilization of the photochemically excited molecule is very unimportant relative to its decomposition.

D. Ionic Reactions

Since the ionization of trimethylethylene is 8.67 eV, the absorption of 10.0 eV photons may lead to the formation of the excited parent ions. The recorded ion current (Fig. 3) gives a Φ(ion) value about $0.22_4 \pm 0.00_5$. Nothing can be said

[16] $(TME)^{**} \rightarrow [(CH_3CH{=}C(CH_3)_2)^+]^* + e^-$

about the fate of this ion on the basis of the present data. In contrast to the 8.4 photolysis, the 2-methyl-1-butene produced at 10.0 eV in the presence of oxygen is sensitive to the presence of scavengers such as ammonia, toluene, methylcyclopentane (see Results). The ionic origin of part of this product cannot be ruled out, but the mechanism is not clear.

TABLE 3. Fragmentation of excited trimethylethylene molecules, $(C_5H_{10})^{**}$

Products	Incident energy 8.4 eV	Incident energy 10.0 eV
$C_5H_8 + 2H$ (H_2)	0.33 ± 0.02	0.28
$C_3H_4 + 2\,CH_3$	$0.27_5 \pm 0.02$	0.20
$C_4H_6 + CH_3 + H$ (CH_4)	$0.15_5 \pm 0.01$	0.10
$[C_5H_{10}^+]^* + e^-$	0.00	0.22_4
$C_5H_9 + H$	0.15 ± 0.1	0.12
Others	0.09 ± 0.02	0.08

We wish to thank the National Research Council of Canada and l'Université du Québec à Chicoutimi for their support.

1. (*a*) H. GAGNON, G. J. COLLIN, and C. BERTRAND. J. Phys. Chem. In press. (*b*) G. J. COLLIN and C. BERTRAND. J. Photochem. In press.
2. A. B. CALLEAR and H. K. LEE. Trans. Faraday Soc. **64**, 2017 (1968).
3. G. J. COLLIN, P. M. PERRIN, and C. M. GAUCHER. Can. J. Chem. **50**, 2391 (1972).
4. G. J. COLLIN and P. M. PERRIN. Can. J. Chem. **50**, 2400 (1972).
5. G. J. COLLIN and P. M. PERRIN. Can. J. Chem. **50**, 2823 (1972).
6. R. GORDEN, JR., R. E. REBBERT, and P. AUSLOOS. Natl. Bur. Stand. Technical note 496. 1969.
7. J. HERMAN, K. HERMAN, and P. AUSLOOS. J. Chem. Phys. **52**, 28 (1970).
8. A. A. SIDDIQI, C. T. CHEN, G. G. MEISELS, and R. GORDEN, JR. J. Chem. Phys. **57**, 4506 (1972).
9. K. L. HILL and R. D. DOEPKER. J. Phys. Chem. **76**, 1112 (1972).
10. R. J. CVETANOVIĆ and L. C. DOYLE. J. Chem. Phys. **50**, 4705 (1969).
11. R. J. CVETANOVIĆ and R. S. IRWIN. J. Chem. Phys. **46**, 1694 (1967).
12. S. KRZYSANOWSKI and R. J. CVETANOVIĆ. Can. J. Chem. **45**, 665 (1967).
13. W. E. FALCONER and W. A. SUNDER. Int. J. Chem. Kinet. **4**, 315 (1972).
14. C. W. LARSON, B. S. RABINOVITCH, and D. C. TARDY. J. Chem. Phys. **47**, 4570 (1967).
15. F. H. DORER and B. S. RABINOVITCH. J. Chem. Phys. **69**, 1952 (1965).
16. J. L. FRANKLIN, *et al.* Natl. Stand. Ref. Data Syst. N.B.S. 26 (1969).
17. P. M. PERRIN and G. J. COLLIN. Can. J. Chem. **51**, 724 (1973).
18. J. H. GEORGAKAKOS, B. S. RABINOVITCH, and C. W. LARSON. Int. J. Chem. Kinet. **3**, 535 (1971).

Can. J. Chem. Downloaded from www.nrcresearchpress.com by 210.87.254.40 on 09/05/12
For personal use only.

A Reconsideration of the Validity of Correlating Substituent-induced Proton Chemical Shifts in Aromatic Derivatives with Reactivity Parameters

DANIEL A. DAWSON,[1] GORDON K. HAMER,[2] AND WILLIAM F. REYNOLDS

Department of Chemistry, University of Toronto, Toronto, Ontario M5S 1A1

Received November 10, 1972[3]

Comparisons of ^1H chemical shifts and charge densities (determined by CNDO/2 MO calculations) for 4-substituted derivatives of styrene, toluene, benzylchloride, and *N,N,N*-trimethylphenylammonium ion indicate that the chemical shifts primarily reflect intramolecular electronic effects. These effects are reflected by correlations of ^1H chemical shifts with the *F* and *R* reactivity parameters of Swain and Lupton. It is concluded that it is valid to correlate substituent-induced chemical shifts for aromatic derivatives with divided reactivity parameters provided that (*1*) chemical shifts are measured at infinite dilution in a non-polar medium and (*2*) at least ten derivatives of each family are investigated.

Calculations for 4-substituted toluenes indicate that there will be a small conformational dependence for substituent-induced benzylic proton chemical shifts.

La comparaison des déplacements chimiques ^1H et des densités de charge (déterminées par la méthode CNDO/2 MO) pour des dérivés substitués en position 4 du styrène, du toluène, du chlorure de benzyle et de l'ion *N,N,N*-triméthylphényl ammonium indiquent que les déplacements chimiques reflètent principalement les effets électroniques intramoléculaires. Ces effets apparaissent sous forme de corrélation entre les déplacements chimiques ^1H avec les paramètres de réactivité *F* et *R* de Swain et Lupton. On en conclut qu'il est valide de faire une corrélation entre le substituant et les déplacements chimiques induits dans les dérivés aromatiques possédant des paramètres de réactivité divisés pourvu (*1*) que les déplacements chimiques soient mesurés à dilution infinie dans un solvant non-polaire et (*2*) qu'au moins dix dérivés de la famille soient étudiés.

Les calculs pour les toluènes substitués en position 4 indiquent qu'il y a une petite dépendance conformationnelle pour les déplacements chimiques des protons benzyliques qui ont été induits par les substituants. [Traduit par le journal]

Can. J. Chem., **51**, 39 (1973)

Introduction

Miller and co-workers summarized the results of nearly one hundred correlations of substituent-induced ^1H chemical shifts (s.c.s.) in aromatic derivatives against Hammett σ constants (1)

$$[1] \qquad \delta = \rho\sigma + \delta_0$$

Many of the correlations were poor and they detected no pattern of slopes, ρ, which could be related to mechanisms of transmission of substituent effects. More recently (2) they investigated correlations of s.c.s. with the Swain–Lupton divided reactivity (*F* and *R*) parameters (3)

$$[2] \qquad \delta = fF + rR + \delta_0$$

While much better correlations were obtained, they concluded that the *f* and *r* values were unrealistic. In particular, they believed that it was unreasonable that s.c.s. for $N(CH_3)_3^+$ protons of 3- and 4-substituted *N,N,N*-trimethylphenylammonium derivatives (henceforth referred to as trimethylanilinium or TMA derivatives) should reflect resonance effects since $R = 0$ for the $N(CH_3)_3^+$ group (3). They also found it inexplicable that 3- and 4-substituted derivatives of the same family should often have nearly identical *r* values. The above observations led them to conclude that reactivity parameters are inherently unsuitable for interpreting s.c.s. In addition, they concluded that their failure to observe linear relationships when plotting s.c.s. for one family against another (δ–δ plots) confirmed that s.c.s. are, in general, strongly influenced by factors other than intramolecular electronic effects.

We recently measured ^1H and ^{13}C chemical shifts for over forty 4-substituted styrenes under inert conditions and compared these with charge densities estimated by CNDO/2 calculations (4). By contrast with the above-outlined pessimistic conclusions, correlations of ^1H and ^{13}C s.c.s.

[1]NRCC Scholarship holder 1970–1972.
[2]NRCC Scholarship holder 1967–1970.
[3]Revision received May 31, 1973.

Can. J. Chem. Downloaded from www.nrcresearchpress.com by 210.87.254.40 on 09/05/12
For personal use only.

Can. J. Chem. Downloaded from www.nrcresearchpress.com by 210.87.254.40 on 09/05/12
For personal use only.

and charge densities with F and R gave a self-consistent picture of electronic effects which could be rationalized by a simple model for transmission of substituent effects. We concluded that the correlations were meaningful and that s.c.s. for styrene primarily reflected intramolecular electronic effects.

In view of this difference of opinion, we decided to attempt to estimate the importance of intramolecular electronic effects upon s.c.s. for some of the systems investigated by Wiley and Miller (2), using CNDO/2 MO calculations. A comparison of f and r values obtained for correlations of charge densities and s.c.s. with F and R should show how closely s.c.s. reflect intramolecular electronic effects.[4]

Calculations were performed for 3- and 4-substituted TMA derivatives and 4-substituted toluenes. The latter compounds were chosen not only because benzyl derivatives were included in ref. 2 but also because the conformational dependence of benzylic proton s.c.s. has recently aroused considerable interest (1, 5–7) (toluenes were chosen in place of benzyl derivatives to economize on computer usage).

Results of the calculations are presented below along with a discussion of the reasons advanced by Miller and Wiley for rejecting s.c.s. – reactivity parameter correlations.

Results and Discussion

CNDO/2 calculations were performed with a standard program (8) and standard geometries (9). Calculations for TMA derivatives had one N—CH_3 bond at right angles to the phenyl group (Fig. 1). Calculations were performed for two conformations of the methyl group in toluene, yielding charge densities at dihedral angles, ϕ, of 0, 30, 60, and 90°. Calculations were performed for all reasonable substituent conformations and averaged.

Averaged charge densities for $N(CH_3)_3^+$ hydrogens of TMA derivatives are given in Table 1 while methyl hydrogen charge densities and dipole moments of toluene derivatives are given in Table 2. Correlations of charge densities and s.c.s. with F and R are given in Table 3. The s.c.s. correlation for 4-TMA derivatives (2) was repeated to include the $N(CH_3)_2$ derivative,

[4]Charge densities and s.c.s. could be directly compared, but this provides little information about mechanisms of transmission of substituent effects.

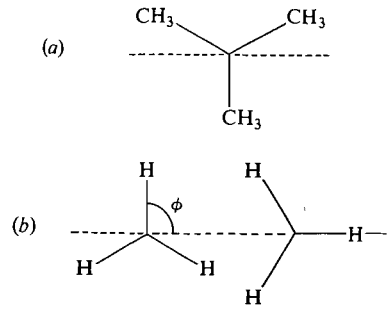

FIG. 1. (*a*) Conformation of $N(CH_3)_3^+$ group for which calculations were performed (with methyl groups oriented so that one C—H bond for each methyl group is *anti* to the N—C(1) bond, *i.e.* at 90° to the plane of the diagram). Dotted line indicates the plane of the phenyl group. (*b*) Two conformations for CH_3 group for which calculations were performed.

TABLE 1. Methyl hydrogen charge densities for 3-substituted and 4-substituted trimethylphenylammonium ions (TMA)

	Charge density (q_H)* × 10^4	
Substituent	3-TMA	4-TMA
H	+504	+504
CN	+512	+510
NO_2	+531	+531
OCH_3	+503†	+493
CH_3	+499	+496
F	+518	+509
Cl	+513	+509
SCH_3	+500†	+495
CO_2CH_3	+510†	+510
$N(CH_3)_2$	+494	+481
NH_2	+500	+495

*q_H = (1.000 − valence electron density).
†Average of *syn* and *anti* planar conformations.

using recently estimated F and R values. It was found that the CO_2^- derivative showed a large deviation. This derivative was generated in *situ* by addition of small amounts of base (2). Since we have found that similar procedures often yield unreliable results, correlations were repeated for both sets of TMA derivatives with CO_2^- derivatives omitted. Significantly improved correlations were obtained in both cases. The new correlations are given in Table 3.

Consideration of the Validity of s.c.s. – Reactivity Parameter Correlations

4-Substituted derivatives will be considered first since there are more results for these compounds. We previously noted a good correlation between the chemical shift difference,

TABLE 2. Methyl hydrogen charge densities ($\times 10^4$) and calculated and experimental dipole moments for toluene and 4-substituted toluenes

	q_H* for ϕ =						Δq_H†			
Substituent	90°	60°	30°	0°	Ave.	$q_H(90°) - q_H(0°)$	90°	0°	$\mu_{calcd.}$	$\mu_{exptl.}$‡
H	+109	+78	+14	−19	+46	+128	—	—	0.20	0.43
CH_3	+91	+61	+2	−28	+31	+119	−18	−9	0	0
NH_2	+59	+31	−19	−44	+6	+103	−50	−25	1.50	1.64
$N(CH_3)_2$	+42	+19	−29	−52	−5	+94	−67	−33	0.75	1.30
OCH_3	+69	+43	−10	−36	+16	+105	−40	−17	1.55	1.21
F	+108	+79	+21	−9	+50	+117	−1	+10	1.83	1.81
CF_3	+178	+141	+67	+29	+104	+149	+69	+48	2.90	3.07§
CN	+145	+111	+42	+8	+76	+137	+36	+27	3.53	4.41
NO_2	+213	+173	+93	+53	+133	+160	+104	+72	5.38	4.39
NH_3^+	+421	+372	+276	+227	+324	+194	+312	+246	3.33	—

*q_H = (1.0000 − valence electron density).
†$\Delta q_H = q_H(YC_6H_4CH_3) - q_H(C_6H_5CH_3)$.
‡Recommended values where quoted (32) or average of experimental values (32).
§Sum of dipole moments for toluene and α,α,α-trifluorotoluene (32).

TABLE 3. Correlations of s.c.s. and hydrogen charge densities with field (F) and resonance (R) substituent constants and ratios of f values and r values for the two correlations

(*a*) ^1H chemical shifts (in p.p.m.)

Family	f	r	%R	Reference
3-TMA	0.055(0.077)*	0.103(0.115)	54(48)	2†
4-TMA	0.035(0.051)	0.097(0.105)	63(56)	2†
Toluene	0.108	0.209	55	33
Benzylchloride	0.063	0.148	59	2

(*b*) ^1H charge densities

Family	f ($\times 10^{-3}$)	r ($\times 10^{-3}$)	%R
3-TMA	2.27	0.89	20
4-TMA	1.83	2.21	43
Toluene(ρ = 0°)	4.3	6.1	47
Toluene(ρ = 30°)	4.7	7.5	50
Toluene(ρ = 60°)	5.4	10.3	54
Toluene(ρ = 90°)	5.7	11.6	56
Toluene(ave)‡	5.0	8.9	52

(*c*) Ratios of f values and r values (from parts (*a*) and (*b*) in p.p.m./unit charge density)

Family	f/f	r/r
3-TMA	24(34)	116(129)
4-TMA	19(28)	44(48)
Toluene(ave)	22	23
Benzylchloride (ρ = 30°)§	14	20
Benzylchloride (ρ = 60°)§	12	14

*Values for CH_3CN and (in parentheses) D_2O solutions.
†See text concerning these correlations.
‡For ρ = 45°, corresponding to $\langle \sin^2 \rho \rangle = 0.5$.
§ρ = 30° and ρ = 60° correspond to the limiting averaged values for $\sin^2 \rho$ (respectively 0.25 and 0.75) for a CH_2X group.

Can. J. Chem. Downloaded from www.nrcresearchpress.com by 210.87.254.40 on 09/05/12
For personal use only.

Can. J. Chem. Downloaded from www.nrcresearchpress.com by 210.87.254.40 on 09/05/12
For personal use only.

$\Delta\delta$(B—C), and the charge density difference, Δq(B—C), for the β vinyl protons of 4-substituted styrenes (4). The slope for this correlation was 18–23 p.p.m./hydrogen 1s electron, in excellent agreement with previously suggested scaling factors of 18–27 p.p.m./electron (10, 11). The variation of $\Delta\delta$(B—C) was due to an electric field effect (4, 12) while correlations of ^1H and ^{13}C s.c.s. and charge densities gave a consistent pattern of results which could be accounted for by field, π inductive, and resonance effects (4).[5]

In the case of 4-substituted toluenes ratios of f values and r values from s.c.s. and charge density correlations (Table 3) are also in quantitative agreement with previously accepted values for this scaling factor. In addition, chemical shifts calculated from charge densities are in satisfactory agreement with experimental values (Table 4), as are calculated and experimental dipole moments (Table 2). These observations indicate that the calculations reproduce charge densities for 4-substituted toluenes with reasonable accuracy. They also suggest that s.c.s. for these compounds are dominated by intramolecular effects and that these effects are reflected by the F and R correlations. Similar agreement is noted for the benzyl chlorides, assuming ϕ = 30°, corresponding to the C—Cl bond at right angles to the phenyl group (the calculations are relatively insensitive to ϕ in the allowed range 30–60°). The f/f value is slightly smaller than for toluene, but this may not be statistically significant in view of the small number of data points (seven) for the s.c.s. correlation.

TABLE 4. Calculated and experimental chemical shifts for methyl protons of 4-substituted toluenes, relative to toluene

	Chemical shift (p.p.m.)	
Group	Calculated*	Experimental†
NH_2	−0.09	−0.16
OCH_3	−0.07	−0.08
CH_3	−0.03	−0.06
F	+0.01	−0.03
CN	+0.07	+0.09
NO_2	+0.19	+0.15

*Reference 33.
†$(\langle q_H\rangle - \langle q_H\rangle_{C_6H_5CH_3}) \times 22$.

[5]Preliminary results of a similar investigation for 4-substituted phenylacetylenes also show a consistent pattern of ^1H and ^{13}C s.c.s. and charge densities with f and r values consistent with those for styrene (13).

The s.c.s. and charge density correlations for 4-TMA derivatives also show similar patterns of f and r values, but the ratios f/f and r/r are larger than normal (particularly the latter). However, s.c.s. for phenolic and amino protons are enhanced by a factor of 2–3 on going from non-polar to polar solvents (1). A similar enhancement could occur for TMA derivatives since the $N(CH_3)_3^+$ hydrogens bear considerable positive charge and should be susceptible to hydrogen bonding (the larger f and r values in D_2O than in CH_3CN support this). This would account for the larger than normal scaling factors for these correlations.

The calculations indicate that the $N(CH_3)_3^+$ group has a very small resonance interaction with the phenyl group, although possibly not precisely zero as postulated by Swain and Lupton (3). For example, for the $N(CH_3)_2$ derivative, the charge density (relative to unsubstituted TMA) is -26×10^{-4} for the CH_3 group at $\phi = 90°$ and -22×10^{-4} for the CH_3 group at $\phi = 30°$. If charge density changes were dominated by a direct resonance interaction, then one would have expected a much greater change with ϕ (see below). We believe that the resonance dependence of $N(CH_3)_3^+$ hydrogens arises indirectly; *i.e.* it is primarily due to changes in π electron density at C(1). This in turn alters the hydrogen electron density by through-space polarization of the C—H bonds.[6] A similar effect has been noted for the α-vinyl protons of 4-substituted styrenes (4). Therefore, there is no inconsistency between the assumption that R = 0 for the $N(CH_3)_3^+$ group and the observation of a resonance dependence in s.c.s. of TMA derivatives since the latter can arise indirectly.

Thus comparisons of correlations of s.c.s. and charge densities with F and R for four families of 4-substituted derivatives (styrenes, toluenes, benzyl chlorides, and TMA derivatives) have shown in all cases similar patterns of s.c.s. and charge densities. Furthermore, the ratios of s.c.s. to charge densities are in good agreement with previously accepted values for this scaling factor (10, 11), except for TMA derivatives where s.c.s. are apparently enhanced by polar solvents. Therefore, it is concluded that for these derivatives (*1*) s.c.s. are dominated by intramolecular electronic effects and (*2*) these effects are reflected

[6]A similar conclusion has been reached by B. M. Lynch (14).

Can. J. Chem. Downloaded from www.nrcresearchpress.com by 210.87.254.40 on 09/05/12
For personal use only.

with reasonable accuracy by the F and R correlations.

Correlations for phenyl and 4-substituted phenol derivatives (2) will not be considered in detail since the former involved only five data points while the latter measurements were carried out in DMSO. However, neither set of f and r values seems obviously unreasonable, particularly allowing for both solvent enhancement of s.c.s. (2) and the strong resonance interaction between hydroxyl and phenyl groups (3) for the phenol derivatives.

While Wiley and Miller felt that it was inexplicable that 3- and 4-substituted derivatives of the same family could give nearly identical r values (2), this seems much less unreasonable, if one allows for through-space transmission of substituent effects. In toluene derivatives $\langle r^2_{H-C(2,6)}\rangle/\langle r^2_{H-C(1)}\rangle = 2.0$, where $\langle r^2_{H-C}\rangle$ is the average squared distance of a methyl proton from a particular ring carbon. A slightly smaller ratio is found for $N(CH_3)_3^+$ protons. Since the field effect of a point charge should vary approximately as $1/r^2$ (ignoring the cos θ term for the angular dependence of the C—H bond) (15), s.c.s. should be approximately only twice as sensitive to π charge density changes at C(1) than at C(2) or C(6). Assuming that a substituent induces large changes in π electron density proportional to $+R$ at *ortho* and *para* carbons and a relatively smaller change proportional to $-R$ at *meta* carbons, similar r values for 3- and 4-substituent derivatives are not unreasonable (assuming the factor of two given above, r values should be approximately equal when magnitudes of resonance-induced changes in π electron density at *meta* carbons are *ca.* 1/3 of those at *ortho* and *para* carbons).

CNDO/2 calculations were carried out for 3-TMA derivatives in an attempt to confirm this point. Unfortunately, the agreement between s.c.s. and charge density correlations is much worse than for 4-TMA derivatives. In particular, the r/r value is much too high, even allowing for solvent enhancement, although the calculations correctly predict the positive r value. However, we believe that the discrepancy is not due to any lack of validity of the s.c.s. correlation but rather due to a fault in the calculations. Specifically, we have noted excellent agreement between ^{13}C s.c.s. and carbon charge densities for C(1) and C(β) of 4-substituted styrenes (4, 16). However, the agreement is much worse for C(2,6) and C(α), apparently because the CNDO/2 calculations significantly over-estimated the $-R$ dependence for these carbons. A similar error for the 3-TMA derivatives would lead to an over-estimated $-R$ dependence for C(1) charge density and consequently an overall $+R$ dependence which is too small (leading to the anomalously large r/r value). Presumably, more rigorous m.o. calculations (such as the *ab initio* STOG-3G calculations of Pople and co-workers (17)) would lead to better agreement with experiment.[7]

With respect to δ–δ plots (2), it is important to realize that these plots are *inherently* non-linear, even for pairs of families where s.c.s. are completely dominated by intramolecular electronic effects. This occurs because, in general, the two families will have different relative sensitivities to field and resonance effects. To illustrate this point, we have prepared a δ–δ plot for two hypothetical families of compounds whose s.c.s. due to intramolecular electronic effects exactly fit the following correlation equations

$$[3] \qquad \delta(1) = 0.10F + 0.40R \quad (71\%\ R)$$

$$[4] \qquad \delta(2) = 0.30F + 0.20R \quad (29\%\ R)$$

(The respective f and r coefficients closely correspond to those for the β-*cis* proton of 4-substituted styrenes and the *meta* proton of substituted benzenes (2).) For a representative set of derivatives the correlation is mediocre (see Fig. 2). Thus, δ–δ plots such as those given in Table 3 of ref. 2 provide no conclusive evidence whether or not s.c.s. are dominated by intramolecular electronic effects. Similar objections can be made concerning correlations of s.c.s. with a single Hammett σ constant since the σ constant may also reflect a different proportion of field and resonance effects than the system under investigation. For this reason, it is essential to use divided σ constants (such as F and $R(3)$) in investigations of s.c.s.

Thus we conclude that the correlations of s.c.s. with F and R reported by Wiley and Miller (2) reflect intramolecular electronic effects to a

[7]Correlations of π charge densities for benzene derivatives estimated by STOG-3G calculations (17) and for styrene derivatives estimated by CNDO/2 calculations (4) with F and R show nearly identical f and r values for carbons *para* to the substituent but a much smaller r value for *meta* carbons by STOG-3G calculations than by CNDO/2 calculations (18).

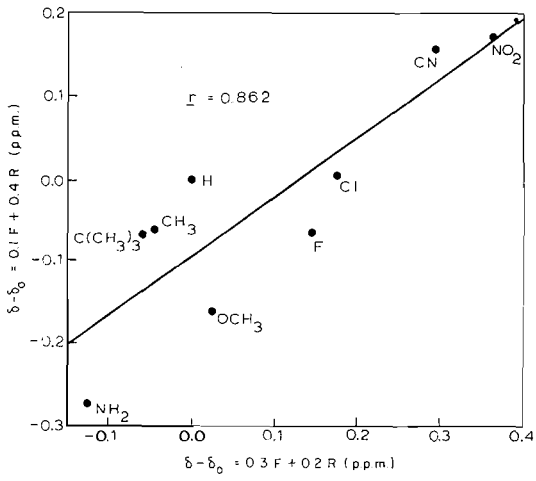

FIG. 2. Plot of chemical shifts for two hypothetical sets of compounds whose chemical shifts due to intramolecular electronic effects are exactly determined by the correlation equations shown along x and y axes (r = correlation coefficient for δ–δ plot).

much greater extent than they believed. It might be argued that this conclusion is inconsistent with the failure of Miller and co-workers (1) to find any consistent pattern of ρ values in many correlations of the type represented by eq. 1. However, there are at least two possible reasons for this discrepancy. The first, minor, reason involves the use of a single σ constant (see above). The second, more important, reason is that few previous investigations have satisfied the minimum conditions specified by Wiley and Miller (2), *i.e.* that ^{1}H s.c.s. must be measured at infinite dilution in an inert medium[8] and that a given family must contain at least ten derivatives. Failure to meet these two conditions can respectively introduce significant errors due to solute–solute and solute–solvent interactions and due to magnetic anisotropic effects of substituents. The latter effects are unrelated to electronic effects and will not obscure the overall pattern of electronic effects, *provided that a large number of substituents are investigated* (4). Alternatively, s.c.s. measurements can be carried out in a highly polar medium to enhance electronic effects relative to magnetic effects (2, 20), although this introduces an uncertain solvent enhancement factor. In either case, it is useful to compare ^{1}H s.c.s. with ^{13}C s.c.s. and calculated charge densities for the same derivatives. On the basis of the above discussion, many previous investigations of ^{1}H s.c.s. must be regarded as of dubious reliability. This, rather than any inherent unsoundness in s.c.s. – reactivity parameter correlations, may account for many of the discrepancies pointed out by Wiley and Miller (2).

Conformational Dependence of Benzylic Proton s.c.s.

For all of the toluenes, methyl hydrogen charge density, q_H, varies as $\sin^2 \phi$, attaining a maximum for $\phi = 90°$. q_H at 30 and 60° can be predicted (within 1×10^{-4}) by equations of the type

$$[5] \quad q_H(\phi) = q_H(0°) + (q_H(90°) - q_H(0°)) \sin^2 \phi$$

This conformational dependence agrees with results of STOG-3G m.o. calculations (21) and with measurements of hyperfine e.p.r. coupling constants (22, 23) and proton–proton coupling constants (24–29). It is entirely consistent with a hyperconjugative donation of electrons to the phenyl π electron system by the methyl group (π electron density for toluene is greater than for benzene by 132×10^{-4}), in agreement with previous conclusions (22, 24–27, 30).

The methyl hydrogen charge density correlations in Table 3 indicate that there is also a significant conformational dependence for s.c.s. The increase in r with ϕ apparently reflects enhancement or inhibition of the hyperconjugative effect of the methyl group by the substituent. This is confirmed by the magnitudes of ($q_H(90°) - q_H(0°)$) for individual derivatives (Table 2). This parameter is largest for $+R$ groups (NO_2, CF_3, CN) and smallest for $-R$ groups (CH_3, F, OCH_3, NH_2, $N(CH_3)_2$), indicating respective enhancement and inhibition of hyperconjugative donation of electrons by the methyl group. The variation of f with ϕ probably arises from π charge density changes at C(1) due to π polarization effects (4, 31).

A plot of $q_H(90°)$ *vs.* $q_H(0°)$ (not shown) has a slope of 1.6. This defines the theoretical maximum range of ρ values for benzylic protons, assuming s.c.s. are dominated by intramolecular electronic effects. The range is even smaller (*ca.* 1.15) for systems in which benzylic protons are not locked in a single conformation since in this case $\langle\phi\rangle$ must lie between 30 and 60°. Although many experimental ρ values are in at least qualitative agreement with the predictions given above (1, 6, 7), others differ markedly (*e.g.* $\rho_{C_6H_5CH_3} = 0.21$ (32), $\rho_{C_6H_5CH_2Br} = 0.0$ (6)). Con-

[8]Carbon tetrachloride cannot be regarded as an inert medium for ^{1}H s.c.s. measurements (19).

Can. J. Chem. Downloaded from www.nrcresearchpress.com by 210.87.254.40 on 09/05/12
For personal use only.

Can. J. Chem. Downloaded from www.nrcresearchpress.com by 210.87.254.40 on 09/05/12
For personal use only.

sequently, the conclusion that experimental ρ values are dominated by factors other than conformational electronic effects (7) appears to be valid for at least some of the systems investigated. This is not surprising since, in most cases, s.c.s. were measured for a limited number of substituents under less than ideal conditions.

Summary and Conclusions

The three main reasons advanced by Wiley and Miller for rejecting the validity of correlations of ^{1}H s.c.s. with divided reactivity parameters, *i.e.* the observation of non-zero r values for TMA derivatives, the apparently unreasonable f and r values for other systems (particularly the similarity of r values for 3- and 4-substituted derivatives of the same family), and the observation of non-linear δ–δ plots, have been examined. It is concluded that none of these represents a valid reason for rejecting these correlations.

Substituent-induced ^{1}H chemical shifts and charge densities have been compared for four sets of 4-substituted derivatives. It is concluded that s.c.s. for these systems are dominated by intramolecular electronic effects and that these effects are reflected by F and R correlations. However, it cannot be stressed too strongly that these conclusions will not necessarily be valid for other systems unless s.c.s. are determined under carefully controlled conditions similar to those outlined by Wiley and Miller (2). Specifically, it is essential to carry out measurements at infinite dilution in as inert a solvent as possible (preferably cyclohexane for ^{1}H s.c.s. measurements) and to include a minimum of ten substituents. It is also useful to compare ^{1}H s.c.s. with ^{13}C s.c.s. and/or calculated charge densities for the same compounds. Failure to meet these conditions may account for many of the apparent discrepancies which have been pointed out (1, 2).

CNDO/2 calculations for 4-substituted toluenes indicate a small conformational dependence of benzylic proton s.c.s. which can be attributed to enhancement or inhibition of the hyperconjugative effect of the methyl (or methylene) group by the substituent.

Financial support from the National Research Council of Canada is gratefully acknowledged. We thank Professors B. M. Lynch and S. I. Miller for providing preprints of papers.

1. T. Yokoyama, G. R. Wiley, and S. I. Miller. J. Org. Chem. **34**, 1859 (1969).
2. G. R. Wiley and S. I. Miller. J. Org. Chem. **37**, 767 (1972).
3. C. G. Swain and E. C. Lupton. J. Am. Chem. Soc. **90**, 4328 (1968).
4. G. K. Hamer, I. R. Peat, and W. F. Reynolds. Can. J. Chem. **51**, 897, 915 (1973).
5. M. D. Bentley and M. J. S. Dewar. J. Org. Chem. **35**, 2797 (1970).
6. R. R. Fraser, Gurudata, R. N. Renaud, C. Reyes-Zamora, and R. B. Swingle. Can. J. Chem. **47**, 2767 (1969).
7. R. R. Fraser and R. N. Renaud. Can. J. Chem. **49**, 800 (1971).
8. Quantum Chemistry Program Exchange Program 141.
9. D. L. Beveridge and J. A. Pople. Approximate molecular orbital theory. McGraw-Hill, New York. 1970.
10. J. A. Pople, W. G. Schneider, and H. J. Bernstein. High resolution n.m.r. McGraw-Hill, New York. 1959. Ch. 7.
11. J. I. Musher. *In* Advances in magnetic resonance. Vol. 2. *Edited by* J. S. Waugh. Academic Press, New York. 1966. P. 177.
12. G. K. Hamer and W. F. Reynolds. Chem. Commun. 1218 (1971).
13. D. A. Dawson, I. R. Peat, and W. F. Reynolds. To be published.
14. B. M. Lynch. Private communication.
15. A. D. Buckingham. Can. J. Chem. **38**, 300 (1960).
16. I. R. Peat. Ph.D. Thesis, University of Toronto, Toronto, Ontario. 1973.
17. W. J. Hehre, L. Radom, and J. A. Pople. J. Am. Chem. Soc. **94**, 1496 (1972).
18. W. F. Reynolds. Unpublished results.
19. P. Laszlo. *In* Progress in n.m.r. spectroscopy. Vol. 3. *Edited by* J. W. Emsley, J. Feeney, and L. H. Sutcliffe. Pergamon Press, Oxford. 1967. Chapt. 6.
20. B. M. Lynch, B. C. MacDonald, and J. G. K. Webb. Tetrahedron, **24**, 3595 (1968).
21. W. J. Hehre and J. A. Pople. J. Am. Chem. Soc. **92**, 2191 (1970).
22. J. L. Colpa and E. de Boer. Mol. Phys. **1**, 333 (1964).
23. M. C. R. Symons. *In* Advances in physical organic chemistry. Vol. 1. *Edited by* E. Gold. Academic Press, New York. 1963.
24. M. J. S. Dewar and R. C. Fahey. J. Am. Chem. Soc. **85**, 2704 (1963).
25. D. J. Blears, S. S. Danyluk, and T. Schaefer. J. Chem. Phys. **47**, 5037 (1967).
26. M. P. Williamson, R. J. Kostelnik, and S. M. Castellano. J. Chem. Phys. **49**, 2218 (1968).
27. C. J. MacDonald and W. F. Reynolds. Can. J. Chem. **48**, 1002 (1970).
28. C. L. Bell, S. S. Danyluk, and T. Schaefer. Can. J. Chem. **47**, 3529 (1969).
29. M. Barfield, C. J. MacDonald, I. R. Peat, and W. F. Reynolds. J. Am. Chem. Soc. **93**, 4195 (1971).
30. E. T. McBee, I. Serfaty, and T. Hodgins. J. Am. Chem. Soc. **93**, 5711 (1971).
31. W. F. Reynolds, I. R. Peat, M. H. Freedman, and J. R. Lyerla. Can. J. Chem. **51**, 1857 (1973).
32. Tables of experimental dipole moments. A. L. McClellan, W. H. Freeman and Co., San Francisco. 1963.
33. S. H. Marcus, W. F. Reynolds, and S. I. Miller. J. Org. Chem. **31**, 1872 (1966).

Crystallographic Studies of Cobalt Arsenate. III. Crystal Structure of $Co_{6.95}As_{3.62}O_{16}$

NARASIMHAN KRISHNAMACHARI AND CRISPIN CALVO

Department of Chemistry and Institute for Materials Research, McMaster University, Hamilton, Ontario

Received January 12, 1972[1]

Crystals of $Co_{7.0}As_{3.6}O_{16}$ (1.8×3.84 $CoO.As_2O_5$) are orthorhombic with unit cell parameters $a = 10.526(5)$, $b = 5.985(2)$, and $c = 4.871(2)$ Å. The space group is *Pnma* with $Z = 1$ and, except for fractionally occupied cation sites, the crystals have a structure closely related to that of the mineral olivine. The structure was refined by full-matrix least-squares with isotropic thermal parameters, using 1175 independent reflections measured with MoKα radiation, to a final R value of 0.075. The composition was determined by site population analysis. The structure is based upon a hexagonally close-packed arrangement of oxygen layers with As in tetrahedrally and Co in octahedrally coordinated interstices. The mean As—O bond length is 1.676 Å and the mean Co—O bond lengths are 2.139 Å for the site with *m* symmetry and 2.174 Å for the site showing inversion symmetry. These bond lengths are uncorrected for the effects of fractional occupancy of some of the cation sites.

Les cristaux de $Co_{7.0}As_{3.6}O_{16}$ (1.8×3.84 $CoO.As_2O_5$) sont orthorhombiques et les paramètres de la maille sont $a = 10.526(5)$, $b = 5.985(2)$ et $c = 4.871(2)$ Å. Le groupe d'espace est *Pnma* avec $Z = 1$ et, sauf pour les sites cationiques partiellement occupés les cristaux ont une structure étroitement liée à celle du minéral olivine. L'affinement de la structure a été effectué par moindres carrés (matrice entière), l'agitation thermique étant considérée isotrope, et a porté sur 1175 réflections indépendantes mesurés avec la radiation MoKα. Il a été poursuivi jusqu'à un R final de 0.075. La composition a été déterminée par l'analyse de population des sites. La structure est établie sur un arrangement hexagonal compact des couches des atomes d'oxygène avec les atomes d'As dans les interstices tétraédriques et les atomes de Co dans les interstices octaédriques. La longueur moyenne de la liaison As—O est de 1.676 Å et les largeurs moyennes des liaisons Co—O sont 2.139 Å pour les sites présentant la symétrie *m* et 2.174 Å pour les sites présentant une inversion de symétrie. Ces longueurs de liaisons n'ont pas été corrigées des effets dû à l'occupation partielle de quelques sites cationiques. [Traduit par le journal]

Can. J. Chem., **51**, 46 (1973)

Introduction

Studies of the nCoO.As_2O_5 system have indicated that compounds corresponding to $n = 1/2$, 1, 2, 3, and 6 can be prepared (1, 2). Masson and co-workers (2) have studied the thermal stability of compounds obtained by the pyrolysis of $CoO.As_2O_5.5H_2O$. They observed that in air, water and successive amounts of As_2O_5 were lost, yielding $3CoO.As_2O_5$ as the final product stable up to at least 1000 °C. However, on prolonged heating in vacuum at 850 °C, this compound decomposed yielding first $6CoO.As_2O_5$, which further decomposed at 1000 °C to CoO. Stable compounds corresponding to compositions near $4CoO.As_2O_5$ were unknown prior to this study, although the compositions $4MO.As_2O_5$(M = Cu, Sr, Ba) and $5MO.As_2O_5$(M = Cu) have been reported (3–6).

The structure of all previously reported members of the nCoO.As_2O_5 series, except for $n = 1/2$, have been characterized. Taylor *et al.* (1) concluded from an indexed powder pattern that $CoO.As_2O_5$ had the $PbSb_2O_6$ structure (7). This structure consists of hexagonally stacked layers of oxygen atoms with both As and Co ions in sites coordinated octahedrally to oxygen atoms. The AsO_6 group forms two dimensional infinite arrays by sharing three O—O edges. The Co ions lie in planes between two such sheets with the Co ions between empty sites in the $(AsO_6)_\infty$ sheets. The structure of $2CoO.As_2O_5$ (8) can be derived from that of $CoO.As_2O_5$ by replacing the As ions with Co and the Co ions with the As—O—As moiety. This latter substitution in fact generates tetrahedrally coordinated As ions. Both $3CoO.As_2O_5$ (9) and the so-called $6CoO.As_2O_5$ (10) form structures based upon close-packed layers of oxygen atoms with Co ions in octahedrally coordinated sites. In the former case oxygen atom layers show ABAC stacking while ABC stacking is featured in the latter case. The As ion is also tetrahedrally coordinated in $Co_3(AsO_4)_2$ while 1/3 of the As ions are octahedrally coordinated to oxygen

[1]Revision received August 27, 1973.

Can. J. Chem. Downloaded from www.nrcresearchpress.com by 210.87.254.6 on 09/05/12
For personal use only.

Can. J. Chem. Downloaded from www.nrcresearchpress.com by 210.87.254.6 on 09/05/12
For personal use only.

atoms in "$6CoO.As_2O_5$". A recent refinement of "$6MgO.As_2O_5$" showed it to be $5.44MgO.As_2O_5$ and isotypic to "$6CoO.As_2O_5$" (11) thus it is likely that the latter also has this composition without the oxidation of Co or the reduction of As previously suggested. A second form of $3CoO.As_2O_5$ is isotypic with $3MgO.As_2O_5$ (12), a tetragonal phase, but the latter structure is not based upon a close packed arrangement of oxygen atoms. Non-stoichiometry, in the sense that sites in the unit cell are on the average fractionally occupied, has been found in $5.44CoO.As_2O_5$, $3MgO.As_2O_5$, the tetragonal form of $3CoO.As_2O_5$, and in the present compound.

Experiments

The crystals used in this study were prepared by the reaction of $2CoCO_3.3Co(OH)_2$ (Fisher Scientific Co.) and As_2O_5 (Mallinckrodt Chemical Works) in proportions so as to yield $CoAs_2O_6$ upon the loss of CO_2 and H_2O. The mixture was heated to about 950 °C in an open Vycor tube and slowly cooled. The Vycor tube showed no indication of having been attacked. A small number of dark purple single crystals were extracted from the sample. Attempts at microprobe analysis were completely unsuccessful.

These crystals were orthorhombic with space group $Pn2_1a$ or $Pnma$ since the systematic absences corresponded to those $0kl$ reflections with $k + l$ odd and those $hk0$ reflections with h odd. Accurate cell parameters were obtained from a least-squares refinement of the 2θ values measured for 15 reflections with a Syntex automatic diffractometer at 20 °C utilizing graphite monochromatized MoKα radiation (0.71069 Å). Crystal data are as follows.

$Co_{6.95}As_{3.62}O_{16}$ f.w. = 932.5

a = 10.526(5), b = 5.985(2), c = 4.871(2) Å, V = 308.9 Å^3, T = 20 °C, Space group: $Pnma$, $\rho_{calcd.}$ = 5.01 g/cm^3, Z = 1.

The small number of crystals prevented an estimation of the density. These unit cell parameters and space group were reminiscent of those of olivine (13). The composition was initially assumed to be $Co_3(AsO_4)_2$ with Z, the number of formula units per cell, equal to 2.

MoKα radiation was used to collect all the data. A crystal with the dimensions of 0.15 × 0.06 × 0.45 mm was used to collect data with an integrating precession camera and a manually set scintillation counter employing equi-inclination Weissenberg geometry and an ω-scan of 2°. The former data sets were of type hkn, n = 0, 1, 2 and mkl, m = 0, 1, ..., 4 while the latter set were of type hsl, s = 0, 1, ..., 4. These data were combined with a set obtained with a Syntex P$\bar{1}$ automatic diffractometer from a crystal whose dimensions were 0.02 × 0.04 × 0.04 mm. Background counts on either side of each peak were determined for the same time period as used to scan the peak. The scan ranged from 1° below the α_1 peak to 1° above the α_2 peak. Graphite monochromatized MoKα radiation was used. Those reflections whose intensity was less than 3σ were treated as unobserved and assigned a maximum possible intensity of 3σ. The average deviation in intensity between the two sets was less than 4%. These data were corrected for Lorentz and polarization effects. Absorption corrections were made near the final refinement stage after the approximate composition had been ascertained.

The parameters of $LiMnPO_4$ (14) were used as the trial model assuming that the crystal was an orthorhombic analog of the mineral sarcopside, $(Fe, Mn, Mg)_3(PO_4)_2$ (15), with the cation site at the inversion centers. Full-matrix least-squares refinement was carried out with a program written by J. S. Stephens for the CDC-6400. Atomic scattering curves for Co^{2+} and As^{3+} (16) were corrected for dispersion (17) while that for O^- was taken from the International tables for X-ray crystallography (18). Weights, ω, were chosen so that $\omega(\Delta F)^2$ would be independent, on a local average, of the magnitude of the observed structure factor. Those observed structure factors whose calculated value exceeded the assigned minimum observed value were included in the refinement while the other unobserved were given ω = 0. The population parameters were varied separately under the restriction of electrical neutrality for the cell and with independent isotropic thermal parameters. These refinements suggested that the Co(1) site was completely occupied and therefore this further restriction was applied. A total of 1175 unique reflections of which 787 were observed was then used to obtain the final parameters listed in Table 1. The R value when the shifts were less than 0.3σ was 0.075. The weighted residual

$$(\Sigma\omega||F_o| - |F_c||^2/\Sigma\omega|F_o|^2)^{1/2}$$

is 0.09. The average deviation of a reflection of unit weight was 1.08. Table 2[2] contains the final calculated and observed structure factors.

Description of the Structure

The composition of the crystals, as determined from the site populations, is $nCoO.As_2O_5$, with n = 3.84(8). The oxygen atoms and Co(1) ion sites are completely occupied but only 0.90 and 0.72 of the As and Co(2) sites, respectively, are filled. If all the sites were filled the composition would be $Co_8As_4O_{16}$ with each oxygen atom shared between three Co ions and one As ion.

The structure, except for the fractional occupation of some cation sites, is essentially the same as olivine. The oxygen atoms are in hexagonally close-packed layers with cobalt ions in two types of octahedrally coordinated sites and the As in tetrahedral sites as is shown in Fig. 1. The $Co(2)O_6$ groups, with the cobalt ion on a center of inversion, share edges forming chains, running parallel to the b axis, at the corners and center of the cell. The $Co(1)O_6$ groups, with the

[2]Photocopies of Table 2 may be obtained, at a nominal charge, from the Depository of Unpublished Data, National Research Council of Canada, Ottawa, Canada K1A 0S2.

TABLE 1. Atomic and thermal parameters for $Co_{6.95}As_{3.62}O_{16}$ with estimated standard deviations in parenthesis

Atom	Site	Number of atoms	x	y	z	U (Å^2)
Co(2)	4*a*	2.91(3)	0	0	0	0.0107(2)
Co(1)	4*c*	4	0.2753(1)	¼	0.9892(2)	0.0075(2)
As	4*c*	3.60(4)	0.0946(1)	¼	0.4284(2)	0.0104(2)
O(1)	4*c*	4	0.0967(6)	¼	0.7706(13)	0.0090(8)
O(2)	4*c*	4	0.4477(6)	¼	0.2022(12)	0.0077(8)
O(3)	8*d*	8	0.1680(4)	0.0320(9)	0.2791(9)	0.0103(6)

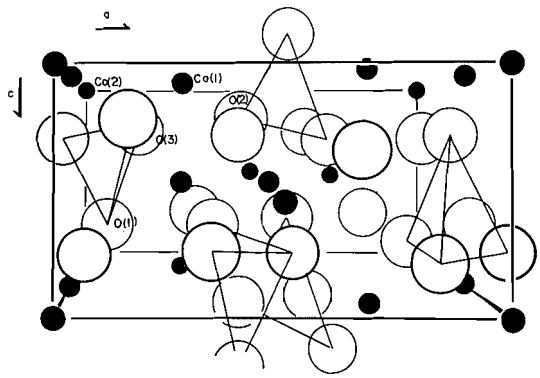

FIG. 1. The structure of $Co_{6.95}As_{3.61}O_{16}$ viewed parallel to the *b* axis. Oxygen atoms are indicated by open circles and the cobalt ions as full circles. The AsO_4 tetrahedra are outlined.

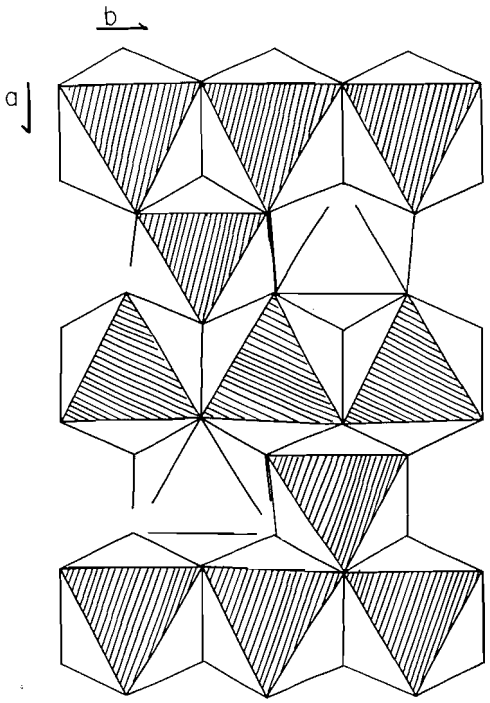

FIG. 2. The CoO_6 octahedral network in $Co_{6.95}As_{3.62}O_{16}$ projected onto the *ac* plane. Co(2) lie in a row of octahedra parallel to *b* at $x = 0$, 1/2 and Co(1) lie in those at $x = \pm 1/4$.

Co(1) lying on a mirror plane, share oxygen atoms with three separate chains of $Co(2)O_6$ groups as seen in Fig. 2. The AsO_4 groups have three oxygen atoms in close-packed layers of oxygen atoms, sharing each of three edges formed by these oxygen atoms, with three separate CoO_6 groups.

The pertinent bond lengths and angles are listed in Table 3. The average Co(1)—O bond length is 2.139 Å while the apparent average Co(2)—O bond length for the fractionally occupied cation site is 2.174 Å. The individual As—O bond lengths do not deviate significantly from their mean value of 1.676 Å, but the O—As—O angles, ranging from 101.8 to 115.2°, do suggest substantial deviations from regularity. Those angles subtending edges shared between AsO_4 and CoO_6 groups are contracted, presumably because of cation–cation repulsion. For example, Co(2) shares two edges, one with each of a pair of AsO_4 groups and the angles subtending these edges, O(2)*b*—As—O(3)*a* and O(2)*b*—Co(2)—O(3)*a*, are 105.1 and 74.6°, respectively. On the other hand, the edge between $Co(2)O_6$ groups does not suggest much cationic repulsion. The angle subtended by this edge is smaller in olivine (13), with a value of 87.5°, suggesting that the repulsion is reduced by the partial occupancy in $3.84CoO.As_2O_5$.

Conclusions

The average Co—O bond lengths in the series of $nCoO.As_2O_5$ show bond lengths ranging from 2.12 to 2.17 Å. The average As—O bond lengths in turn vary between 1.67 and 1.70 Å. The present compound shows the largest Co—O bond length in the series but this is not easily attributable to the fractional occupancy, since in "$6CoO.As_2O_5$" (10), where the cation sites are

Can. J. Chem. Downloaded from www.nrcresearchpress.com by 210.87.254.6 on 09/05/12
For personal use only.

TABLE 3. Bond lengths and angles in $Co_{6.95}As_{3.62}O_{16}$ (transformations as in footnotes)

Bond	Distance (Å)	Bonds	Angle (deg)	Bonds	Angle (deg)
As O4 group					
As—O(1)[a]	1.667(6)	O(1)[a]—As—O(2)[b]	113.2(3)	O(2)[b]—As(2)—O(3)[a] 2×	105.1(2)
—O(2)[b]	1.672(6)	—O(3)[a] 2×	115.2(2)	O(3)[a]—As(2)—O(3)[g]	101.8(2)
—O(3)[a] 2×	1.682(5)				
Co(1)—O_6 group					
Co(1)—O(1)[a]	2.161(7)	O(1)[a]—Co(1)—O(2)[a]	179.8(2)	O(2)[a]—Co(1)—O(3)[a] 2×	97.2(2)
—O(2)[a]	2.090(6)	—O(3)[a] 2×	82.6(2)	—O(3)[d] 2×	89.7(2)
—O(3)[a] 2×	2.230(5)	—O(3)[d] 2×	90.4(2)	O(3)[a]—Co(1)—O(3)[d] 2×	89.0(2)
—O(3)[d] 2×	2.062(5)	O(3)[d]—Co(1)—O(3)[f] 2×	109.9(2)	—O(3)[f]	160.0(2)
		—O(3)[g]	160.0(2)	—O(3)[g] 2×	71.6(2)
Co(2)—O_6 group					
Co(2)—O(1)[a] 2×	2.127(5)	O(1)[a]—Co(2)—O(1)[c]	180.0(3)	O(2)[a]—Co(2)—O(3)[a]	74.6(2)
—O(2)[b] 2×	2.155(4)	—O(2)[b]	89.3(2)	—O(2)[d]	180.0
—O(3)[a] 2×	2.239(4)	—O(3)[a]	83.2(2)	O(3)[a]—Co(2)—O(3)[e]	180.0

[a] x, y, z.
[b] $1/2 + x, 1/2 - y, 1/2 - z$.
[c] $-x, 1/2 + y, -z$.
[d] $1/2 - x, -y, 1/2 + z$.
[e] $-x, -y, -z$.
[f] $1/2 - x, 1/2 + y, 1/2 + z$.
[g] $x, 1/2 - y, z$.

only partially filled, this bond length is 2.12 Å on the average.

Baur (19) has shown that individual X—O bond lengths, d(X—O), in silicates and phosphates depend upon the charge environment of the atom through

$$d(\text{X—O}) = a + bp_0$$

where d(X—O) is the predicted bond length and p_0 is the electrostatic valency defined as $\sum_i$ (formal charge of X_i/coordination number of X_i) where X_i represents all neighboring cations to the oxygen atom respectively. In $3.84CoO.As_2O_5$, if partial occupancy is ignored, all As—O bond lengths are predicted to be 1.715 Å. On the other hand if the individual contributions to p_0 are weighted in direct proportion to the site occupancy the predicted As—O(n) bond lengths are 1.68 Å for $n = 1$ and 2, and 1.69 Å for $n = 3$. In this structure and that of sarcopside (14) it is the site analogous to that at the center of symmetry in olivine that is vacated. Although the edge shared between As and Co(1) indicates the greatest cationic repulsion, emptying a Co(2) site removes the repulsion of that ion and the two As ions with which it shares O—O edges.

All the $n CoO.As_2O_5$ with $n = 1$ through 3.84 which show close-packed arrays of oxygen atoms are hexagonal close-packed, but become cubic close-packed for $n = 5.44$. This may be related to a generalization of Kamb's (20) conclusion that in the spinel–olivine system cubic close-packing is favored when the ratio, η, of bond lengths of the octahedrally coordinated ion lies below an ideal value of 1.155. Hexagonal close-packing results when the ratio increases beyond this ideal value. All these $n CoO.As_2O_5$ are in agreement with a boundary between these packing motifs at $\eta = 1.24$, as shown in Table 4.

TABLE 4. Ratio of the octahedrally to tetrahedrally coordinated cation oxygen atom bond lengths

Compound	η	Packing sequence of oxygen atom layers
$Ni_3V_2O_8$	1.18	ABC
$Mg_3V_2O_8$	1.21	ABC
$Co_3V_2O_8$	1.21	ABC
$Zn_3V_2O_8$	1.23	ABC
$5.44MgO.As_2O_5$	1.23	ABC
$5.44CoO.As_2O_5$	1.24	ABC
$Co_3As_2O_8$	1.25	ABAC
$3.84CoO.As_2O_5$	1.29	AB

Ideally the composition of these crystals can vary between $3CoO.As_2O_5$, where all the vacancies are on Co^{2+} sites, to $5CoO.As_2O_5$, where all the vacancies are on As^{5+} sites. In this context it is of some interest to note that recent studies (21) have shown that both defect spinel-like and olivine-like structures having the stoichiometry $M_3(XO_4)_2$ can be prepared. Those with large ions in the tetrahedral sites form spinel structures while those with small ions are iso-

Can. J. Chem. Downloaded from www.nrcresearchpress.com by 210.87.254.6 on 09/05/12
For personal use only.

typic with sarcopside. In the former case the vacancies disorder upon increasing the temperature. A comparable ordered arrangement has not been reported in defect olivines nor has an order olivine-like phase been seen among the cobalt arsenates.

This research is supported by a grant from the National Research Council of Canada.

1. J. B. TAYLOR and R. D. HEYDING. Can. J. Chem. **36**, 597 (1958).
2. J. MASSON, B. CHARLES-MESSANCE, M. BASTICK, and H. GUERIN. C. R. Acad. Sci. Fr., Ser. C, **250**, 859 (1960).
3. H. GUERIN and R. MAS. C. R. Acad. Sci. Fr. Ser. C, **227**, 973 (1948).
4. H. BAUER and W. BALZ. Z. Anorg. Allg. Chem. **340**, 225 (1965).
5. H. GUERIN and C. DUC-MAUGE. Bull. Soc. Chem. Fr. 518 (1952).
6. H. GUERIN, J. MASSON, P. MATTRAT, R. BOULITROP, C. DUE-MANGE, R. MARTIN, and R. MAS. Bull. Soc. Chim. Fr. 440 (1953).
7. A. MAGNELI. Ark. Kem. Miner. Geol. **17B** (1941).
8. J. OZOG, N. KRISHNAMACHARI, and C. CALVO. Can. J. Chem. **48**, 388 (1970).
9. N. KRISHNAMACHARI and C. CALVO. Can. J. Chem. **48**, 881 (1970).
10. N. KRISHNAMACHARI and C. CALVO. Can. J. Chem. **48**, 3124 (1970).
11. P. W. BLESS and E. KOSTINER. J. Solid State Chem. **6**, 80 (1973).
12. N. KRISHNAMACHARI and C. CALVO. Acta Cryst. To be published.
13. L. W. FINGER. Am. Cryst. Assoc. Summer Meeting. Carleton University, Ottawa, Canada, 66 (1970).
14. W. MOORE. Am. Mineral. **57**, 24 (1972).
15. S. GELLER and J. L. DURAND. Acta Cryst. **13**, 325 (1960).
16. L. H. THOMAS and K. UMEDA. J. Chem. Phys. **26**, 293 (1957).
17. D. T. CROMER. Acta Cryst. **18**, 17 (1955).
18. International tables for X-ray crystallography. Vol. III. Kynoch Press, Birmingham. 1962.
19. W. H. BAUR. Trans. Am. Cryst. Assoc. **6**, 129 (1970).
20. B. KAMB. Am Mineral. **53**, 1439 (1968).
21. G. BERTHET, J. C. JOUBERT, and E. F. BERTANT. Z. fur Kristallogr. **136**, 98 (1972).

Can. J. Chem. Downloaded from www.nrcresearchpress.com by 210.87.254.6 on 09/05/12
For personal use only.

New Route to Branched-chain Aminodeoxy Sugars by Reaction of Ketoses with Acetonitrile. Synthesis of Methyl 3-*C*-2′-Aminoethyl-2-deoxy-α-D-*arabino*-hexopyranoside

ALEX ROSENTHAL AND G. SCHÖLLNHAMMER

Department of Chemistry, The University of British Columbia, Vancouver 8, British Columbia

Received July 14, 1972[1]

Addition of methyl 4,6-*O*-benzylidene-2-deoxy-α-D-*erythro*-hexopyranosid-3-ulose (**1**) to acetonitrile in liquid ammonia at −50 to −60° in the presence of lithium amide gave, in high yield, crystalline methyl 4,6-*O*-benzylidene-3-*C*-cyanomethyl-2-deoxy-α-D-*arabino*-hexopyranoside (**2**) exclusively. The proof of structure **2** is described. Debenzylidenation of **2** afforded the branched-chain cyano glycoside **3**. Compound **3** was converted into its 3,4,6-tri-*O*-acetate (**8**) and 4,6-di-*O*-*p*-nitrobenzoate (**9**) derivatives. Catalytic hydrogenation of **3** over rhodium on alumina yielded methyl 3-*C*-2′-aminoethyl-2-deoxy-α-D-*arabino*-hexopyranoside which was characterized as its *N*-2,4-dinitrophenyl derivative (**7**).

L'addition de *O*-benzylidène-4,6-déoxy-2-α-D-*èrythro*-hexopyranoside-ulose-3 de méthyle (**1**) à l'acétonitrile, dans l'ammoniaque liquide entre −50 et −60°, en présence d'amidure de lithium, conduit exclusivement, avec un haut rendement, au *O*-benzylidène-4,6-*O*-cyanométhyl-3-déoxy-2-α-D-*arabino*-hexopyranoside de méthyle (**2**). Les preuves de la structure **2** sont décrites. La débenzylidénation de **2** conduit au cyanoglycoside **3**. Ce composé **3** a été converti en ses dérivés tri-*O*-acétate-3,4,6 (**8**) et di-*O*-*p*-nitrobenzoate-4,6 (**9**). L'hydrogénation catalytique de **3** en présence de rhodium sur alumine conduit à l'aminoéthyl-3-*C*-2′-déoxy-2-α-D-*arabino*-hexopyranoside de méthyle qui est caractérisé par son dérivé *N*-dinitro-2,4-phényl (**7**). [Traduit par le journal]

Can. J. Chem., **52**, 51 (1974)

In a preliminary communication (1) we have reported the synthesis of a branched-chain cyanomethyl sugar by a base catalyzed condensation of acetonitrile to methyl 4,6-*O*-benzylidene-2-deoxy-α-D-*erythro*-hexopyranosid-3-ulose (**1**). This paper describes the complete experimental details of this research and, in addition, reports the conversion of the cyanomethyl glycoside into derivatives which might have utility as intermediates in nucleoside synthesis.

The rational explanation for the introduction of branched-chains at C-3 of sugars has previously been given (2). Of the various procedures which have been developed for the introduction of branched-chains into sugars (3), the nitromethane condensation to 3-ketoses (2, 3) parallels the acetonitrile condensation as each procedure affords a branched-chain glycoside having a tertiary hydroxyl at the branch site. The cyanomethyl glycoside, however, would on reduction yield an homologous aminoalkyl glycoside of those obtained by the reduction of the branched-chain nitromethyl carbohydrates.

Addition of acetonitrile to methyl 4,6-*O*-benzylidene-2-deoxy-α-D-*erythro*-hexopyranosid-3-ulose (**1**) in anhydrous ammonia at −50 to −60° in the presence of lithium amide proceeded stereoselectively to yield only one crystalline branched-chain cyanomethyl glycoside (**2**) in almost quantitative yield. In contrast, the nitromethane condensation to the same ketose (**1**) had afforded both the *ribo* and *arabino* branched-chain nitromethyl glycosides (2). The proof of structure of the branched-chain cyanomethyl glycoside (**2**) makes use of a parallel line of reasoning utilized in the proof of structures of the two 3-*C*-nitromethyl glycosides hitherto described (shown in Scheme 1).

As shown by previous authors (2, 4–7), deductions of probable structure of condensation products obtained from keto sugars based on conformational analysis can be fallacious because of the subsequent elimination of water from the branched-chain sugar followed by recombination of water to give an epimer of the original branched-chain sugar (4).

Debenzylidenation of the cyanomethyl glycoside (**2**) over Dowex 50W-X8 (H^+), under careful monitoring to prevent excessive deglycosidation and anomerization, yielded the crystalline 3-*C*-cyanomethyl glycoside (**3**) in 95% yield. The unblocked glycoside (**3**) readily condensed with

[1]Revision received September 13, 1973.

Can. J. Chem. Downloaded from www.nrcresearchpress.com by 210.87.254.6 on 09/05/12
For personal use only.

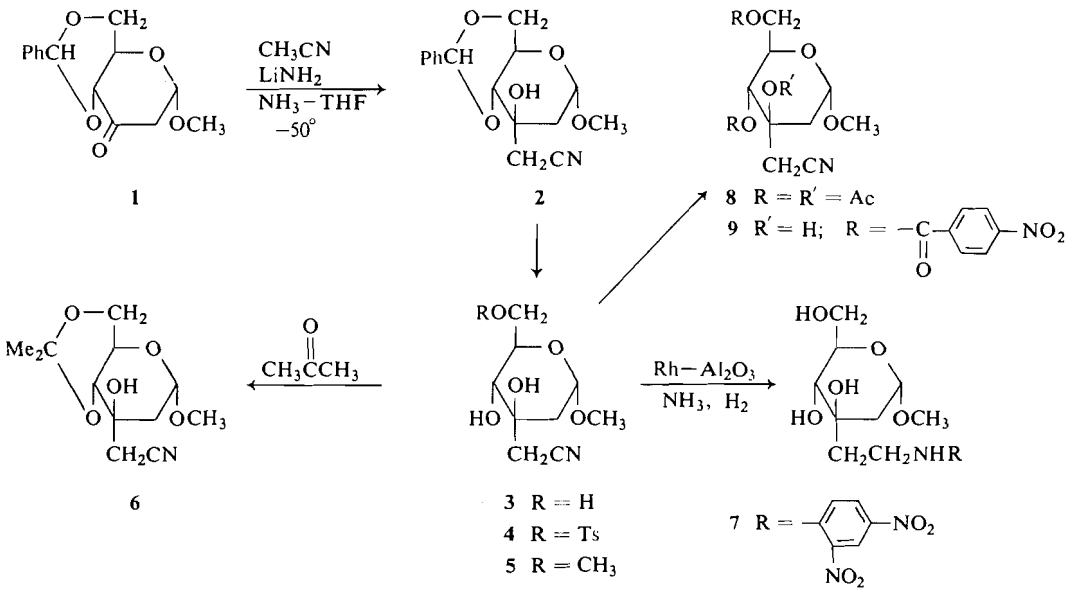

SCHEME 1

acetone to yield only one crystalline monoisopropylidene derivative, namely, the 4,6-*O*-isopropylidene derivative (**6**) in 72% yield. The n.m.r of **6** in DMSO-d_6 showed the presence of a singlet at τ 5.40 which disappeared on addition of D_2O which is attributed to the presence of an unsubstituted tertiary hydroxyl group, and thus, **6** must be methyl 4,6-*O*-isopropylidene-3-*C*-cyanomethyl-2-deoxy-α-D-*arabino*-hexopyranoside. If the cyanomethyl glycoside possessed the *ribo* configuration one might reasonably expect (2) the formation of both the 4,6- and the 3,4-*O*-isopropylidene derivative. The absence of a *cis* glycol at C-3 and C-4 was further confirmed in the following way. The unblocked glycoside **3** was preferentially tosylated to afford the crystalline 6-*O*-tosylate derivative (**4**) (n.m.r. of **4** in DMSO-d_6 showed the presence of a doublet at τ 4.85 and a singlet at τ 5.50 (both disappeared on addition of D_2O) which are attributed to the C-4 and -3 hydroxyl groups, respectively). The monotosylate **4** failed to condense with acetone thus indicating the absence of a *cis* glycol on C-3 and -4. To confirm this supposition an attempt was then made to convert **4** into a 3,6-anhydro compound by treatment with methanolic sodium methoxide. Quite unexpectedly, the only product formed was the 6-*O*-methyl derivative (**5**). This anomalous result might be due to electronic factors (8) which prevented the anhydro formation. Compound **2** showed an hydroxyl absorption (by high resolution infrared spectroscopy in CCl_4 solution (9, 10)) at 3500 cm^{-1} which is similar to that exhibited by the *arabino* 3-*C*-nitromethyl analog (2). Application of the elegant method of Nakanishi and Dillon (11) for determining the chirality of cyclic α-glycols to **5** (negative Cotton effect) confirmed the *arabino* configuration and compound **2** is 4,6-*O*-benzylidene-3-*C*-cyanomethyl-2-deoxy-α-D-*arabino*-hexopyranoside.

Reduction of the cyanomethyl glycoside (**3**) over rhodium on alumina in the presence of ammonia gave, in high yield, a branched-chain aminoethyl glycoside. The latter was characterized as its crystalline *N*-2,4-dinitrophenyl derivative (**7**).

For possible use in nucleoside synthesis, the unblocked cyanomethyl glycoside (**3**) was converted, by treatment with acetic anhydride in the presence of *p*-toluenesulfonic acid, into the crystalline 3,4,6-tri-*O*-acetate derivative (**8**). Compound **3** was also transformed into the 4,6-*O*-di-*p*-nitrobenzoate ester (**9**). Direct fusion of either **8** or **9** with 2,6-dichloropurine gave very low yields of nucleosides which were not characterized.

Experimental

General Considerations

The general considerations have been described previously (2). The ammonia gas was dried over sodium hydroxide. Methyl 4,6-*O*-benzylidene-2-deoxy-α-D-*ery-*

Can. J. Chem. Downloaded from www.nrcresearchpress.com by 210.87.254.6 on 09/05/12
For personal use only.

Can. J. Chem. Downloaded from www.nrcresearchpress.com by 210.87.254.6 on 09/05/12
For personal use only.

thro-hexopyranosid-3-ulose (12), prepared by the dimethyl sulfoxide – acetic anhydride procedure, was freed of mercaptans by treatment with charcoal in dichloromethane, filtration, evaporation and subsequent sublimation under vacuum at 130–135°.

Methyl 4,6-O-Benzylidene-3-C-cyanomethyl-2-deoxy-α-D-arabino-hexopyranoside (2)

To a stirred solution of lithium amide in liquid ammonia (from 0.220 g of lithium in 125 ml of ammonia cooled to −50 to −60° containing a few crystals of ferric nitrate) was added (by injection with a syringe into a three-necked flask fitted with an injector septum) anhydrous acetonitrile (16 ml), and the solution stirred for 20 min. A solution of methyl 4,6-*O*-benzylidene-2-deoxy-α-D-*erythro*-hexopyranosid-3-ulose (1.240 g) in anhydrous tetrahydrofuran (40 ml) was then added by means of the syringe to the rapidly stirred solution kept at −50° for 3 h (or until all starting material was consumed as evidenced by monitoring by t.l.c. (silica gel G, 19:1 chloroform – ethyl acetate). Ammonium chloride (1.6 g) was added to neutralize the lithium amide and the ammonia was allowed to evaporate. The residue was extracted three times with tetrahydrofuran, filtered, and evaporated to yield a solid. This solid was dissolved in dichloromethane (50 ml) and the latter solution washed with water (2 × 10 ml), dried over sodium sulfate, filtered, and evaporated to yield 1.4 g of product which was recrystallized from ethyl acetate – petroleum ether (b.p. 35–60°) to yield **2** (1.1 g, 75%); m.p. 170°; $[\alpha]_D^{22}$ +69° (*c* 1, chloroform); ν (5 m*M*, CCl_4) 3500 (OH), 2200 cm^{-1} (C≡N); τ ($CDCl_3$) 7.85 (m, 2p, H-2), 7.30 (s, 2p, H-1′), 6.60 (s, OCH_3), 5.50–6.60 (m, H-4, H-5, H-6, C-3OH), 5.50 (t, H-1), 4.40 (s, C-7H); τ (DMSO-d_6) 5.20 (s, C-3OH). Addition of D_2O exchanged the hydrogen on C-3OH.

Anal. Calcd. for $C_{16}H_{19}NO_5$: C, 62.95; H, 6.23; N, 4.59. Found: C, 62.85; H, 6.09; N, 4.34.

Methyl 3-C-Cyanomethyl-2-deoxy-α-D-arabino-hexopyranoside (3)

Methyl 4,6-*O*-benzylidene-3-*C*-cyanomethyl-2-deoxy-α-D-*arabino*-hexopyranoside (0.120 g) in methanol (5 ml) was debenzylidenated with Dowex 50W-X8 (H^+ form) (0.260 g) for about 4 h. The reaction was monitored by t.l.c. (silica gel G, 5:5:1 benzene – ethyl acetate – methanol). When a trace of starting material was still present the resin was removed by filtration and the filtrate evaporated to dryness. Silica gel (Grade II) column (15 g) chromatography of this product with the above solvent system as developer afforded 0.067 g (95%) of product **3** which was crystallized from ethyl acetate – petroleum ether (b.p. 30–60°); m.p. 103°; $[\alpha]_D^{22}$ +129° (*c* 1, methanol); τ (DMSO-d_6) 5.20 (q, H-1), 5.15 (d, C-4OH), 5.50 (t, C-6OH), 5.75 (s, C-3OH), 6.40 (d, H-6), 6.70 (s, OCH_3), 6.20–7.0 (m), 7.30 (s, CH_2CN), 8.1 (m, H_{2a} and H_{2e}). The peaks at τ 5.15, 5.55, and 5.75 disappeared on addition of D_2O.

Anal. Calcd. for $C_9H_{15}NO_5$: C, 49.8; H, 7.0; N, 6.5. Found: C, 50.0; H, 7.14; N, 6.3.

Methyl 3-C-Cyanomethyl-2-deoxy-6-O-tosyl-α-D-arabino-hexopyranoside (4)

To a 0° solution of methyl 3-*C*-cyanomethyl-2-deoxy-α-D-*arabino*-hexopyranoside (0.110 g) in anhydrous pyridine (5 ml) was added freshly recrystallized *p*-toluenesulfonyl chloride (0.130 g). The solution, kept at 0° for about 17 h, was monitored by t.l.c. (silica gel G, 90:5:0.5 dichloromethane – ethyl acetate – ethanol). When a trace of starting material remained, the reaction was quenched by the addition of water (30 ml). The reaction mixture was extracted with dichloromethane (5 × 10 ml), dried over sodium sulfate, and evaporated to dryness. Traces of pyridine were removed by distillation of ethanol and toluene from the product. Silica gel column (15 g) chromatography with 90:5:0.5 dichloromethane – ethyl acetate – ethanol as developer afforded 0.168 g (88%) of crystals which were recrystallized from ethyl acetate – *n*-hexane, to give pure **4**; m.p. 107–108°; $[\alpha]_D^{24}$ +65° (*c* 2, dichloromethane); τ (DMSO-d_6) 4.85 (d, C4-OH, disappeared on addition of D_2O), 5.25 (q, H-1), 5.50 (s, C_3-OH), disappeared on addition of D_2O), 5.60–6.90 (m, H-4, H-5, H-6), 6.75 (s, OCH_3), 7.25 (s, CH_2CN), 7.58 (s, CH_3 of tosyl), 8.00 (m, H-2).

Anal. Calcd. for $C_{16}H_{21}NO_7S$: C, 51.8; H, 5.70; N, 3.78. Found: C, 52.0; H, 5.46; N, 3.50.

Methyl 3-C-Cyanomethyl-4,6-O-isopropylidene-α-D-arabino-hexopyranoside (6)

To a solution of methyl 3-*C*-cyanomethyl-2-deoxy-α-D-*arabino*-hexopyranoside (0.049 g) in anhydrous acetone (2 ml) was added 2,2-dimethoxypropane (2 ml) and bis(*p*-nitrophenyl)phosphate (0.010 g). After the mixture was stirred at room temperature for 0.5 h (monitored by t.l.c., 5:5:1 benzene – ethyl acetate – methanol) the reaction was stopped by the addition of sodium hydrogen carbonate, filtered, and evaporated to yield a homogeneous solid (by t.l.c. and n.m.r.) which was crystallized from ether – *n*-hexane to afford pure **5** (0.049 g, 72%); m.p. 89°; $[\alpha]_D^{24}$ +79° (*c* 1, chloroform); τ (DMSO-d_6), 5.20 (d, H-1), 5.40 (s, C3-OH, disappeared on addition of D_2O), 6.00–6.80 (H-5, H-6), 6.70 (s, OCH_3), 7.30 (s, H-3′), 8.55, 8.65 (s, isopropylidene group).

Anal. Calcd. for $C_{12}H_{19}NO_5$: C, 56.20; H, 7.47; N, 5.46. Found: C, 56.13; H, 7.48; N, 5.35.

Attempt to Prepare Methyl 3-C-Cyanomethyl-2-deoxy-3,4-O-isopropylidene-6-O-tosyl-α-D-arabino-hexopyranoside

The monotosylate **4** was treated with a mixture of acetone, 2,2-dimethoxypropane, and bis(*p*-nitrophenyl)-phosphate for 3 days and the product worked up as described for the preparation of compound **5**. The product, analyzed by n.m.r. and t.l.c., showed only unreacted starting material.

Methyl 3-C-Cyanomethyl-2-deoxy-6-O-methyl-α-D-arabino-hexopyranoside (5)

To a solution of the monotosylate **4** (0.046 g) in anhydrous methanol (2 ml) was added a 1 *N* methanolic solution of sodium methoxide (0.75 mmol). The reaction mixture was heated at about 60° for 7 h and monitored by t.l.c. (5:5:1 benzene – ethyl acetate – methanol). After the solvent was removed under reduced pressure, the residue was extracted with dichloromethane and filtered to yield 0.028 g (95%) of crystalline material. This material was dissolved in ethyl acetate, filtered through a bed of Celite, evaporated to dryness, and the residue recrystallized from ethyl acetate – *n*-hexane to yield 0.019 g of pure **5**; m.p. 105–107°; $[\alpha]_D^{23}$ +113° (*c* 1,

dichloromethane); ν (film) 3500 (OH), 2260 cm^{-1} (C≡N); τ (DMSO-d_6) 5.0 (d, $J = 8$ Hz, C4-OH, disappeared on addition of D_2O), 5.2 (m, H-1), 5.7 (s, C3-OH, disappeared on addition of D_2O), 6.0–7.0 (m), 6.7 (two s, OCH_3), 7.3 (d, $J = 1$ Hz, CH_2CN), 8.1 (m, H-2); c.d. of **5** and $Pr(DPM)_3$ is $\Delta\varepsilon_{312} = -0.9$ (in CCl_4).

Anal. Calcd. for $C_{10}H_{17}NO_5$: C, 52.0; H, 7.40; N, 6.10. Found: C, 51.59; H, 7.15; N, 6.09.

Methyl 2-Deoxy-3-C-ethyl-2'-(2,4-dinitroanilino)-α-D-arabino-hexopyranoside (7)

A solution of methyl 3-*C*-cyanomethyl-2-deoxy-α-D-*arabino*-hexopyranoside (0.178 g) in ethanol (10 ml) saturated with ammonia was reduced with hydrogen at room temperature and 60 p.s i. pressure over rhodium on alumina (0.120 g). The reaction was complete in 24 h as evidenced by monitoring by silica gel t.l.c. (5:5:1 benzene – ethyl acetate – methanol). The catalyst was removed by filtration and washed with ethanol. The filtrate was evaporated to dryness to yield 0.180 g of a syrup (ninhydrin positive); τ ($CDCl_3$) 6.8–8.5 (m, $CH_2CH_2NH_2$), 6.6 (OCH_3).

The branched-chain amino sugar (0.146 g) was dissolved in ethanol and allowed to react for 16 h with 2,4-dinitrofluorobenzene (0.200 g) in the presence of sodium hydrogen carbonate (0.160 g) until all starting material was consumed as evidenced by silica gel t.l.c. (5:5:1 benzene – ethyl acetate – methanol). The product, freed from solvent, was purified by preparative silica gel t.l.c. using the above developer. The main fraction (R_f 0.3) (0.078 g, 31%) was crystallized from isopropanol; m.p. 92–95°; $[\alpha]_D^{23}$ +75° (*c* 1, methanol); τ ($CDCl_3$) 1.2, 1.65, 1.80 (d, aromatic H), 3.10 (d, $J = 10$ Hz), 5.10 (m, H-1), 5.80 (s, OH), 5.90–6.70 (m), 6.55 (s, OCH_3), 7.70–8.20 (m, CH_2CH_2N and H-2).

Anal. Calcd. for $C_{15}H_{21}N_3O_9$: C, 46.60; H, 5.48; N, 10.8. Found: C, 46.34; H, 5.29; N, 10.51.

Methyl 3,4,6-Tri-O-acetyl-3-C-cyanomethyl-2-deoxy-α-D-arabino-hexopyranoside (8)

Methyl 3-*C*-cyanomethyl-2-deoxy-α-D-*arabino*-hexopyranoside (0.440 g) was acetylated with acetic anhydride (10 ml) in the presence of *p*-toluenesulfonic acid monohydrate (0.220 g) at room temperature for 1.5 h. After the addition of ice and water, the reaction mixture was neutralized with sodium hydrogen carbonate and then extracted with dichloromethane (5 × 20 ml). The combined dichloromethane extracts were washed with aqueous sodium hydrogen carbonate, water, dried over sodium sulfate, filtered, and evaporated to yield 0.636 g (90%) of a syrup which was crystallized from ether – *n*-hexane; m.p. 93–95°; $[\alpha]_D^{22}$ +105° (*c* 1, ethanol); ν (film) 2260 cm^{-1} (C≡N); τ ($CDCl_3$) 7.80, 7.90, 7.95 (3OAc).

Anal. Calcd. for $C_{15}H_{21}NO_8$: C, 52.5; H, 6.12; N, 4.08. Found: C, 52.6; H, 5.84; N, 3.84.

Methyl 3-C-Cyanomethyl-2-deoxy-4,6-di-O-p-nitrobenzoyl-α-D-arabino-hexopyranoside (9)

To a solution, cooled to 0°, of methyl 3-cyanomethyl-2-deoxy-α-D-*arabino*-hexopyranoside (0.824 g) in anhydrous pyridine (12 ml) was added *p*-nitrobenzoyl chloride (1.458 g). The reaction mixture was kept at 0° for 2 h and then at room temperature for 2 h. The product was worked up as described for the preparation of the acetate **8**. Compound **9** was recrystallized from 1:1 dichloromethane – ethyl acetate to yield 0.99 g (52%) of pure **9**; m.p. 199–200°; $[\alpha]_D^{23}$ +165° (*c* 1, dichloromethane); τ (DMSO-d_6), 4.6 (s, C3-OH, disappeared on addition of D_2O), 4.6–6.4 (m), 6.65 (s, OCH_3), 7.2 (s, CH_2CN), 7.8 (m, H-2).

Anal. Calcd. for $C_{23}H_{21}N_3O_{11}$: C, 53.6; H, 4.10; N, 8.10. Found: C, 53.67; H, 4.20; N, 8.27.

This research was supported by the National Research Council of Canada. The authors wish to thank Dr. Dillon (11) for determining the circular dichroism of a mixture of **5** and $Pr(DPM)_3$ and deducing the configuration of C-3 of compound **2**.

1. A. ROSENTHAL and G. SCHÖLLNHAMMER. Carbohydr. Res. **15**, 421 (1970).
2. A. ROSENTHAL and K. S. ONG. Can. J. Chem. **48**, 3034 (1970).
3. H. GRISEBACH and R. SCHMID. Angew. Chem. Int. Ed. **11**, 159 (1972).
4. H. P. ALBRECHT and J. G. MOFFATT. Tetrahedron Lett. 1063 (1970).
5. A. ROSENTHAL, K. S. ONG, and D. BAKER. Carbohydr. Res. **13**, 113 (1970).
6. G. J. LAURENS. Tetrahedron Lett. 3733 (1969).
7. S. W. GUNNER, R. D. KING, W. GOVEREND, and N. R. WILLIAMS. J. Chem. Soc. C, 1954 (1970).
8. N. R. WILLIAMS. Adv. Carbohydr. Chem. **25**, 109 (1970).
9. H. SPEDDING. Adv. Carbohydr. Chem. **19**, 23 (1964).
10. K. N. SLESSOR and A. S. TRACY. Can. J. Chem. **47**, 3989 (1969).
11. K. NAKANISHI and J. DILLON. J. Am. Chem. Soc. **93**, 4058 (1971).
12. A. ROSENTHAL and P. CATSOULACOS. Can. J. Chem. **46**, 2868 (1968).

Can. J. Chem. Downloaded from www.nrcresearchpress.com by 210.87.254.6 on 09/05/12
For personal use only.

Studies on Enaminoketones

IVO JIRKOVSKY
Ayerst Research Laboratories, Montreal, Quebec
Received July 23, 1973

A series of *N*-substituted 3-amino-2-cyclohexen-1-ones and 3-amino-5,5-dimethyl-2-cyclohexen-1-ones (**1–9**) has been prepared. Halogenation of these compounds with bromine, NBS, cyanogen bromide, and iodine is described. The tendency of enaminoketones to form salts of the corresponding enol–ketimine form was observed and structures of the salts are supported by their p.m.r. and i.r. properties. The reaction of 3-benzylamino-2-bromo-5,5-dimethyl-2-cyclohexen-1-one with concentrated sulfuric acid effected debenzylation. Treatment of 3-benzylamino-2-iodo-5,5-dimethyl-2-cyclohexen-1-one with dibenzoyl peroxide gave 8,8*a*-dihydro-5-iodo-8,8-dimethyl-2,3-diphenyl-4*H*-1,4-benzoxazine-6,7-diol. The above secondary enaminoketones **1–9** were shown to react with phenyl isocyanates, phenyl isothiocyanate, and methyl isothiocyanate under fusion conditions to yield substituted 2-amino-6-oxo-1-cyclohexene-1-carboxamides and corresponding thiocarboxamides. 2-Benzylamino-6-oxo-*N*-phenyl-1-cyclohexene-1-carboxamide and its 5,5-dimethyl analog were found to undergo facile transamination in position 2, when heated with a primary amine. This reaction is of synthetic utility for the preparation of biologically active derivatives with a basically substituted side chain. Addition of 4-methylamino-3-pentene-2-one to phenyl isocyanate afforded 2-acetyl-3-methylaminoisocrotonanilide; the spectroscopic properties of this product are discussed.

Une série d'amino-3 cyclohexen-2 ones-1 et d'amino-3 diméthyl-5,5 cyclohexène-2 ones-1, *N*-substituées a été préparée. L'halogénation de ces composés par le brome, la NBS, le bromure de cyanogène et l'iode est décrite. La tendance des énaminocétones à former les sels de la forme énol–cétimine correspondante a été observée et les structures de ces sels ont été établies à partir de leurs propriétés en r.m.n. et i.r. La réaction du benzylamino-3 bromo-2 diméthyl-5,5 cyclohexène-2 one-1 avec l'acide sulfurique conc. produit une débenzylation. Le triatement du benzylamino-3 iodo-2 diméthyl-5,5 cyclohexène-2 one-1 par le peroxyde dibenzoique conduit au dihydro-8,8*a* iodo-5 diméthyl-8,8 diphényl-2,3 4*H*-benzoxazine-1,4 diol-6,7. On a montré que les énaminocétones **1–9** secondaires ci-dessus réagissent avec les isocyanates de phényle, l'isothiocyanate de phényle et l'isothiocyanate de méthyle, sous des conditions de fusion, pour donner les amino-2 oxo-6 cyclohexène-1 carboxamides-1 substituées et les thiocarboxamides correspondantes. On a trouvé que la benzylamino-2 oxo-6 *N*-phényl-cyclohexène-1 carboxamide-1 et ses analogues diméthyles en 5,5 subissent facilement une transamination en position 2, lorsqu'ils sont chauffés en présence d'une amine primaire. Cette réaction présente un intérêt synthétique pour la préparation de dérivés biologiquement actifs avec une substitution basique. L'addition de méthylamino-4 pentène-3 one-2 à l'isocyanate de phényle conduit à l'acétyl-2 méthylamino-3 isocrotonanilide; les propriétés spectroscopiques de ce composé sont discutées. [Traduit par le journal]

Can. J. Chem., **52**, 55 (1974)

The purpose of the present work was to investigate the versatility of some functionalized enaminoketones as points of departure in drug synthesis and to add to the existing knowledge of the chemistry of enaminoketones (vinylogous amides). The enaminoketone moiety has received little attention in medicinal chemistry. Since this system has a tendency to form dipolar structures, it may play a role in binding, anionic–cationic interactions, or charge-transfer complexes, and it could be an effective carrier in combination with a pharmacologically active group.

Enaminoketones in general are active toward electrophiles. For example, the nucleophilicity of the carbon β to the nitrogen has been well documented in the literature (1–9). Due to our interest in a related problem, we have examined bromination of simple enaminoketones. To avoid stereochemical complications about the double bond, the studies were confined to enaminoketones with the fixed *trans-s-trans* configuration. The requisite compounds of varied structure **1–9** (Table 1) have been prepared by the condensation of dihydroresorcinol or dimedone with corresponding primary amines.

The relevant p.m.r. and i.r. data are recorded in Table 2 for comparative purposes. Structures of the salts **10** and **11** clearly follow from the presence of one-proton peaks due to OH, NH^+, and vinylic proton. All three peaks disappeared upon treatment with D_2O. The structural assignments of **10** and **11** are further supported by their infrared spectra (*cf.* Table 2). The u.v.

Can. J. Chem. Downloaded from www.nrcresearchpress.com by 210.87.254.5 on 09/05/12
For personal use only.

Can. J. Chem. Downloaded from www.nrcresearchpress.com by 210.87.254.5 on 09/05/12
For personal use only.

TABLE 1. *N*-Substituted 3-amino-2-cyclohexen-1-ones

	No.	R	R_1	R_2	Melting point (°C)	Crystallization solvent	% yield	Molecular formula	Analysis (%) Found C	H	N	Calculated C	H	N
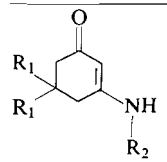 1-9	1	H	H	$-CH_2-C_6H_5$	124–125	AcOEt	90	$C_{13}H_{15}NO$	77.08	7.63	6.97	77.58	7.51	6.96
	2	H	H	$-CH_2-C_4H_3O$	103–104	C_6H_6	95	$C_{11}H_{13}NO_2$	69.00	6.67	7.53	69.09	6.85	7.33
	3[a]	H	H	$-C_6H_4-Cl$	190	AcOEt	82	$C_{12}H_{12}ClNO$	65.05	5.52	6.00	65.01	5.46	6.32
	4	H	H	$-C_6H_4-CF_3$	158	C_6H_6	71	$C_{13}H_{12}F_3NO$	61.19	4.47	5.39	61.30	4.75	5.50
	5	H	H	$-C_6H_4-COOH$	259–260	H_2O–EtOH	60	$C_{13}H_{13}NO_3$	67.47	5.90	5.93	67.52	5.67	6.06
	6[a]	CH_3	CH_3	$-CH_2-C_6H_5$	130–131	C_6H_6	92	$C_{15}H_{19}NO$	78.36	8.13	6.29	78.56	8.35	6.11
	7	CH_3	CH_3	$-C_6H_4-OH$	241–242	MeOH	92	$C_{14}H_{17}NO_2$	72.36	7.46	6.03	72.70	7.41	6.06
	8	CH_3	CH_3	$-C_6H_5$	224–225	AcOEt	77	$C_{20}H_{21}NO$	82.06	7.25	4.70	82.44	7.26	4.81
	9	CH_3	CH_3	$-CH_2-CH(OH)CH_3$	116–117	C_6H_6	95	$C_{11}H_{19}NO_2$	66.85	9.62	6.89	66.97	9.71	7.10
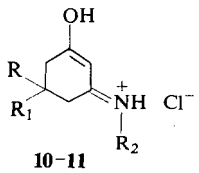 10–11	10	H	H	$-CH_2-C_6H_5$	131–132	CH_3CN	—	$C_{13}H_{16}ClNO$	65.48	6.82	5.77	65.68	6.78	5.89
	11	CH_3	CH_3	$-CH_2-C_6H_5$	168–170	CH_2Cl_2–Et_2O	—	$C_{15}H_{20}ClNO$	67.65	7.52	5.12	67.78	7.58	5.27

[a]5,5-Dimethyl-3-benzylamino-2-cyclohexen-1-one (6) is a known compound which has served as a model in numerous spectroscopic studies (10–13). Ramalingam *et al.* (14) reported recently the preparation of 3-*p*-chloroanilino-2-cyclohexen-1-one (3), m.p. 186–187°. Spectral properties of this compound are in general agreement with our findings, however, there is a considerable discrepancy in the results of elemental analysis. The values C, 64.90% and H, 6.80% as required for the formula $C_{12}H_{12}ClNO$ in the paper (14) are in error.

TABLE 2. Some p.m.r. and i.r. data of *N*-substituted 3-amino-2-cyclohexen-1-ones

No.	Proton magnetic resonance[a] spectra δ_{TMS} ($CDCl_3$) —CH=[b]	N—CH_2[c]	NH[d]	Other	Selected i.r. absorption maxima frequencies (cm^{-1}) (0.2 *M* $CHCl_3$ solutions)[e]
1	5.12	4.20 $d^{5.5}$	6.33		3420, 3250, 1585, 1515
2	5.18	4.23 d^{5}	5.88		3440, 3270, 1595, 1510
3	5.44	—	8.19		3410, 3245, 1605, 1575, 1520[g]
4	5.50	—	8.14		3400, 3250, 1620sh, 1580, 1520
5[f]	5.56	—	9.06		3420, 3405, 3215, 3160, 1650, 1600, 1560, 1520[h]
6	5.10	4.22 $d^{5.5}$	6.35		3420, 3220, 1580, 1515[i]
7[f]	4.90	—	8.19	9.60 b, ex (OH)	3225, 3060, 1595, 1565, 1545[h]
8	5.62	—	7.60		3400, 3250, 1605, 1575, 1515
9	5.09	3.07 m	6.25	4.83 b, ex (OH)	3420, 3310, 1600–1525[j]
10	6.30 ex	4.53 d^{6}	11.32	11.38 s, ex (OH)	3210, 3160, 3100–2600,[j] 2560, 2460, 1605–1520[j]
11	6.28 ex	4.50 d^{6}	11.55	12.65 s, ex (OH)	3200, 3150, 3100–2600,[j] 2510, 2460, 1600–1520[j]

[a]Abbreviations: s, singlet; d, doublet; m, multiplet; ex, D_2O exchangeable; superscripts are *J* values in H_z.
[b]Singlets.
[c]Center of doublet; in deuterated form a singlet.
[d]Broad signals, all D_2O exchangeable.
[e]Relative intensities of bands are dependent on concentration, *cf.* ref. 16.
[f]Recorded in DMSO-d_6.
[g]Compare with ref. 14.
[h]Recorded in Nujol mull.
[i]Compare with ref. 12.
[j]Broad and indefinite, coalescent bands.

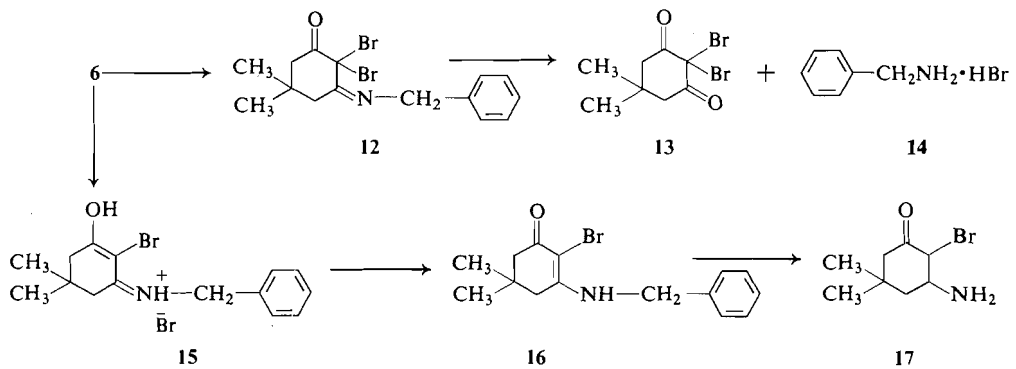

SCHEME 1

spectra of **10** and **11** exhibited strong maxima at 288 (ε = 25 900) and 291 nm (ε = 28 300), respectively. The i.r. spectra of compounds **1**–**11** reveal that a trio of absorption bands (15) consistently appears in the regions 1620–1600 (moderate or very weak), 1595–1560 (very strong), and 1525–1495 cm^{-1} (medium strong). These bands tend to coalesce in diluted solutions and their positions do not vary greatly with substituents on the nitrogen.

Bromination of *trans*-enaminoketones appears to depend upon the nature of the *N*-substituent and reaction conditions (Scheme 1). For example, when **6** was titrated with bromine in aqueous tetrahydrofuran until yellow coloration was persistent, both 5,5-dimethyl-2,2-dibromo-1,3-cyclohexadione (**13**) and benzylamine hydrobromide (**14**) were isolated in a good yield.

Evidently, the intermediate ketimine **12** is readily hydrolyzed (17). Bromination of **6** using 1 equiv. of bromine in dry chloroform gave the bromide–hydrobromide **15** which was converted into α-bromoenaminoketone **16** on treatment with cold sulfuric acid or upon crystallization from ethanol. Heating of **16** with concentrated sulfuric acid at 65° resulted in a facile cleavage of the benzyl group and **17** was obtained. As expected by analogy with **6**, reaction of a chloroform solution of **3** with bromine gave **18**, however, this salt did not suffer dehydrobromination upon recrystallization from methanol or ethanol (Scheme 2).

Can. J. Chem. Downloaded from www.nrcresearchpress.com by 210.87.254.5 on 09/05/12
For personal use only.

TABLE 3. *N*-Substituted 3-amino-2-halogeno-2-cyclohexen-1-ones

No.	X	R = R_1	R_2	Melting point (°C) (solvent)
16	Br	CH_3	CH_2—C$_6$H$_5$	183–184 (ethanol)
17	Br	CH_3	H	204–206 (ethyl acetate)
20	Br	CH_3	CH_2—CH(OH)—CH_3	106–108 (benzene–ether)
21	Br	H	CH_2—(furan)	123–124 (benzene–hexane)
22	Br	H	—C$_6$H$_4$—Cl	143–145 (benzene)
23	Br	H	—C$_6$H$_4$—CF_3	120–121 (benzene-hexane)
24	I	CH_3	CH_2—C$_6$H$_5$	153–154 (methanol–water)

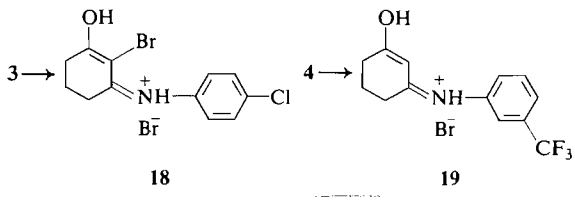

18 **19**

SCHEME 2

Decomposition of **18** with cold concentrated sulfuric acid yielded **22**. The p.m.r. spectrum (DMSO-d_6) of the salt **15** showed two low-field exchangeable signals at δ 8.1 (broad, NH^+) and 8.4 (broad singlet, OH); the spectrum of **18** revealed similar signals at δ 8.8 and 10.3. Bromination of **4** with elemental bromine did not take place, and when the reaction mixture was evaporated and crystallized from ethanol, a nearly quantitative yield of **19** was obtained. This product was identical to that obtained by short treatment of **4** with hydrogen bromide in ethanol. The deactivating effect of the trifluoromethyl group apparently reduces an excess of electron density at —CH=, and thus, bromination under mild conditions does not proceed. The p.m.r. spectrum (DMSO-d_6) of **19**, with an exchangeable singlet at δ 5.75 (—CH=) and two exchangeable signals at δ 11.5 (NH^+) and 12.1 (OH), was consistent with the structure. When discussing p.m.r. spectra of the above salts, it must be pointed out that these tautomers were found to be reasonably stable in cold, dry DMSO. The tendency of enaminoketones to form salts of the corresponding enolic form of ketimines (**10**, **11**, **15**, **18**, **19**) is not surprising and has been already indicated by Leonard and Adamcik (18) and Meyers *et al.* (19). Another argument in favor of the *O*-protonated form (18) of the salts **15**, **18**, **19** is given by their i.r. spectra in Nujol (see Experimental part).

Bromination with *N*-bromosuccinimide in aqueous methanol is suitable for all types of enaminoketones, even in the presence of the furan ring as in **21**. The method is fast, clean, and the yields of **16** and **20–23** (Table 3) were over 70%. It was later found that the reaction of the enaminoketones with cyanogen bromide in ethanol or benzene at 70° affords identical bromo derivatives in high yields. All halogenated secondary enaminoketones showed an i.r. absorption at 3345–3360 cm^{-1}, and a strong and broad band at 1560–1575 cm^{-1} with a shoulder at 1625–1645 cm^{-1} (in chloroform).

Brominated *trans*-enaminoketones are poorly reactive species and the bromine cannot be readily displaced. In contrast, we have observed two interesting reactions of the iodo derivative **24** which was prepared by treatment of **6** with iodine in chloroform. When heated with potassium cyanide in aqueous ethanol, **24** was con-

Can. J. Chem. Downloaded from www.nrcresearchpress.com by 210.87.254.5 on 09/05/12
For personal use only.

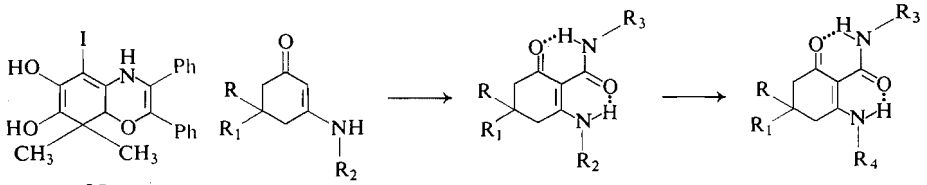

25

SCHEME 3

TABLE 4. Derivatives of 2-amino-6-oxo-1-cyclohexene-1-carboxamide

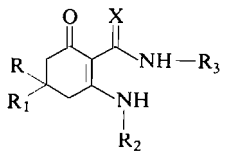

No.	R = R$_1$	R$_2$	R$_3$	X
26	H	Benzyl	Phenyl	O
27	H	*p*-Chlorophenyl	Phenyl	O
28[ab]	H	—CH_2CH_2—NH—CH_3	Phenyl	O
29	CH_3	Benzyl	Phenyl	O
30[ab]	CH_3	—CH_2CH_2—NH_2	Phenyl	O
31[b]	CH_3	—CH_2—CH(OH)—CH_3	Phenyl	O
32[ab]	CH_3	—$CH_2CH_2CH_2$—NH—CH_3	Phenyl	O
33[ab]	CH_3	—$CH_2CH_2CH_2$—$N(CH_3)_2$	Phenyl	O
34	CH_3	Benzyl	*p*-Chlorophenyl	O
35[c]	CH_3	—$CH_2CH_2CH_2$—NH—CH_3	*p*-Chlorophenyl	O
36	CH_3	Benzyl	Methyl	S
37	CH_3	Benzyl	Phenyl	S
38	CH_3	Methyl	Phenyl	S
39	CH_3	Methyl	*p*-Nitrophenyl	S

[a]Isolated and analyzed as hydrochloride.
[b]Prepared from 29.
[c]Prepared from 34.

verted into the parent compound **6**. The reaction of **24** with 1 mol dibenzoyl peroxide afforded an unusual heterocyclic compound **25** in a yield of 72%. Corroboration of the structure was obtained by elemental analysis, i.r., p.m.r., and mass spectra. Under similar conditions, the bromo derivative **16** did not react with dibenzoyl peroxide.

In our earlier experiments, **6** had failed to react with phenyl isocyanates in boiling tetrahydrofuran, benzene, toluene, or xylene. It was soon discovered that this reaction can be carried out without a solvent at 115–145°. Under these conditions, the reaction was rapid, clean, and quantitative. The products were *cis*-vinylogous ureas cross-conjugated with the original *trans*-enaminoketone function (Scheme 3). The assignment of the structures was based on elemental analyses, spectral data, and subsequent transformations. It was immediately obvious that the vinyl proton signal was absent in the p.m.r. spectra of all products. The lack of a distinct NH stretching band in the i.r. spectra (chloroform) can be attributed to strong intramolecular hydrogen bonding. The formation of a hydrogen bond by the oxygen of an amido group increases the hydrogen bond forming power of the hydrogen atom of the same amide group. Thus, one can visualize the existence of two six-membered chelate rings. Remarkably, these compounds (Scheme 3, R_2 = benzyl) undergo a facile transamination when heated with a higher boiling primary amine R_4—NH_2.

Methyl isocyanate and allyl isocyanate failed to react with both enaminoketones **1** and **6**. In one experiment, **29** was prepared in a moderate yield when refluxing a mixture of **6** and phenyl isocyanate in benzene for 4 days. The reaction of secondary enaminoketones with phenyl isothiocyanates has been reported by Goerdeler and Keuser (3); the results (compounds **38** and **39**) are included in Table 4.

Treatment of **6** with hydrazine hydrate in boiling ethanol afforded a yellowish, crystalline compound. Elemental analysis corresponded to the empirical formula $C_{15}H_{19}N_5$. The i.r. spectrum (Nujol) exhibited strong bands at 3360, 3260, and typical ring stretching modes of pyrazole at 1552 and 1497 cm^{-1}. The p.m.r. spectrum (DMSO-d_6) showed a broad resonance centered at δ 5.80 which integrated for two protons (NH_2), and two low-field signals at δ 8.39 and

Can. J. Chem. Downloaded from www.nrcresearchpress.com by 210.87.254.5 on 09/05/12
For personal use only.

Can. J. Chem. Downloaded from www.nrcresearchpress.com by 210.87.254.5 on 09/05/12
For personal use only.

11.50, each equivalent to a single proton (NH). Characteristic singlets for methyl and methylene protons had chemical shifts similar to those observed in the spectrum of the starting material. Considered in conjunction with the fact that hydrazones are more stable than enehydrazines, only structures **40***a* and **40***b* are consistent with the data.

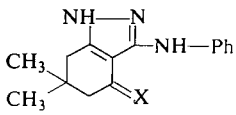

40*a* X = N—NH_2
41 X = O

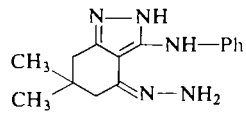

40*b*

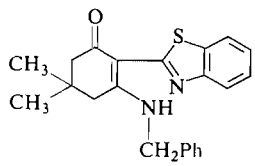

42

The preference for the structure **40***a* with one endocyclic double bond in the six-membered ring is supported by the known strain theory (20). Acidic hydrolysis of **40***a* provided **41**. We next attempted to prepare the hitherto unknown vinylogous guanidine from the readily available vinylogous thiourea **37** via the *S*-methyl isothiuronium salt. However, methylation of **37** with dimethyl sulfate was unsuccessful. The reaction gave the benzothiazol derivative **42** (10%) as the only identifiable product. With sulfuric acid as catalyst, the oxidation product **42** was obtained in a quantitative yield.

Before our work had been completed, Böhme and Willinger published a paper (21) reporting the addition of primary and secondary enaminoketones to phenyl isocyanate to yield ureas R—CO—CH=CH—$N(R_1)$—CONH—Ph. The authors claim that the structures of products are secured by p.m.r. spectroscopy, however, no spectral data are presented in detail. Since our results were not in agreement with their assignment, we have reinvestigated a model experiment as described by Böhme and Willinger (21). Equivalent amounts of phenyl isocyanate and 4-methylamino-3-penten-2-one (**43**) were heated in benzene; the product precipitated shortly after refluxing began. Elemental analysis attested to a 1:1 adduct and the melting point 178–179° coincided with the reported value (21). However, the p.m.r. spectrum in DMSO-d_6 revealed complete absence of the initial vinyl proton (δ 4.98) and displayed two low-field signals, a sharp singlet at δ 10.00 and an obscured quartet at δ 11.50, both integrating for one proton and assignable only to NH protons. Moreover, spin–spin coupling of *N*-methyl protons with that on nitrogen confirmed that the structure **44** was out of question. The resonance absorption due to the *N*-methyl protons was observed as a doublet (J = 5 Hz) at δ 2.97 which collapsed into singlet upon addition of deuterium oxide to the sample. The p.m.r. spectrum showed no minor additional peaks, thus indicating that the product was a pure geometrical isomer **45** or **46**. However, the spectrum of one isomer is not particularly informative in this respect. Dudek and co-workers (11, 22) measured the n.m.r. spectra of **43** in solutions and were able to detect only the chelated *cis* isomer. They have also demonstrated that

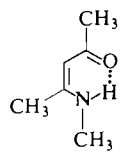

43

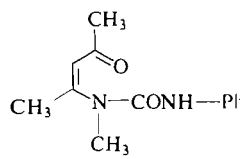

44

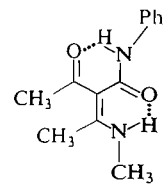

45

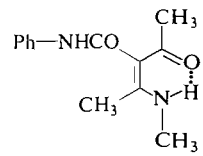

46

stability of this form is increased in very dilute solutions. The reaction of **43** with phenyl isocyanate is fast and takes place under mild conditions in a large amount of solvent. Therefore, it is reasonable to expect formation of **46** where the *cis* stereochemistry of the enaminoketone is retained.

As illustrated, the isomer **45** may be chelated completely, whereas the carbonyl of the Ph—NH—CO grouping in the isomer **46** does not participate in the intramolecular hydrogen bonding. A dilution study of the i.r. spectrum of **29** (a model compound for **45**) in chloroform showed absence of bands corresponding to the stretching of free N—H, and proved that both intensity and frequency (near 3050 cm^{-1}) of a band associated with NH modes were concentration independent. In contrast, the i.r. spectrum

Can. J. Chem. Downloaded from www.nrcresearchpress.com by 210.87.254.5 on 09/05/12
For personal use only.

of the product under discussion was sensitive to the concentration in chloroform, and both intra- and intermolecular hydrogen bonding could be detected. Hydrogen bond absorption at 3290 cm^{-1} gradually diminished in intensity on dilution, with a simultaneous increase in intensity of the 3430 cm^{-1} free NH absorption peak. The i.r. spectra determined in Nujol and KBr were practically identical; as was to be expected, the 3430 cm^{-1} band disappeared and the N—H absorption occurred at 3270 cm^{-1}. The carbonyl frequencies of the undissolved compound appeared at 1655 (weaker) and 1635 cm^{-1}. The first of these behaved like an ordinary amide I band and was found stronger and shifted in dilute solutions to 1660 (chloroform) and 1668 cm^{-1} (dioxane). Different character of the second carbonyl band was manifested with a lowering of the frequency in solutions; the spectra in chloroform and in dioxane showed bands near 1600 cm^{-1}, which can be expected for chelated *cis*-enaminoketones (23, 24). The above spectroscopic data strongly favor structure **46**.

Assignment of a configuration to a substituted enaminoketone cannot be based on the location of u.v. absorption bands. On the other hand, a close correlation of the molar extinction coefficients indicates similarity in structure and stereochemistry (25).

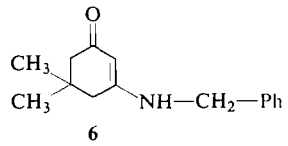

6

λ_{max}^{EtOH} 291 nm, ϵ = 30 900

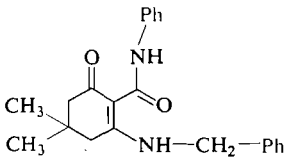

29

λ_{max}^{EtOH} 295 nm, ϵ = 27 900
230 nm, ϵ = 7040

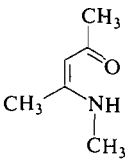

43

λ_{max}^{MeOH} 309 nm, ϵ = 18 100

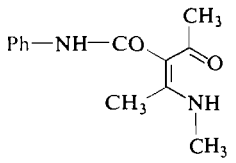

46

λ_{max}^{EtOH} 313 nm, ϵ = 15 200
248 nm, ϵ = 15 200

Hence, compound **46** does not duplicate the skeletal features of **29** because their molar absorptivities are not comparable. In the chelated form, **29** represents a homogeneous chromophore unit, and the location and intensity of the main absorption band would be normal for a *trans*-enaminoketone. In contrast, the u.v. spectrum of **46** contains two maxima of equal intensity, and the molar absorptivity at 313 nm would be adequate for a *cis*-enaminoketone (25).

Most of the described enaminoketones have shown an appreciable antiinflammatory activity. Some results are displayed in Table 5. The antiinflammatory effect was measured by the reduction of pedal inflammation, and expressed as % inhibition from control rats after innoculation of Freund's adjuvant.

Administration of **28** also produced 68% inhibition of carrageenin-induced edema at 100 mg/kg. Both **28** and **35** were effective in the "curative polyarthritis" test and showed an activity intermediate between mefenamic acid and aminopyrin. Several compounds, namely the iodo derivative **25**, exhibited an interesting antimicrobial activity *in vitro*.

Experimental

All melting points (uncorrected) were determined on a Kofler hot-stage apparatus. Infrared results were obtained with a Perkin-Elmer 225 spectrometer. A Zeiss DMR 21 spectrophotometer was used to measure the u.v. spectra. Proton magnetic resonance spectra were recorded on a Varian A-60A instrument using deuteriochloroform as solvent, unless otherwise stated; resonance positions

TABLE 5. Antiinflammatory activity of selected compounds

Compound	Daily dose (mg/kg)	Inhibition (%)	On day
8	75	40	14
28	100	36	3
31	100	38	14
35	100	43	3

Can. J. Chem. Downloaded from www.nrcresearchpress.com by 210.87.254.5 on 09/05/12
For personal use only.

are given on the δ scale (p.p.m.) relative to internal tetramethylsilane.

Preparation of Enaminoketones 1–9

A mixture of 0.01 mol of 1,3-cyclohexanedione or 5,5-dimethyl-1,3-cyclohexanedione, 0.01 mol of the primary amine, and 100 ml of dry benzene was refluxed under a Dean–Stark water trap for 12 h. The mixture was cooled, and if no product separated, benzene was distilled off under reduced pressure, and the residue was recrystallized from a suitable solvent. The conversion of enaminoketones **1** and **6** into the corresponding hydrochlorides **10** and **11** was carried out in a standard manner.

3-Benzylimino-2-bromo-5,5-dimethyl-1-cyclohexen-1-ol Hydrobromide (15)

A solution of bromine (2.7 g, 0.017 mol) in chloroform (30 ml) was added during 10 min to a stirred solution of **6** (3.45 g, 0.015 mol) in chloroform (80 ml). The reaction was slightly exothermic. The resulting mixture was stirred for 3 h, 50 ml of dry ether was added, and 4 g (85%) of the hydrobromide were filtered off, m.p. 159–162°. An analytical sample was obtained by recrystallization from chloroform as white crystals: m.p. 160–162°; i.r. (Nujol) 3250–3150, 2900–2500, 1615, and 1565 cm^{-1}.

Anal. Calcd. for $C_{15}H_{19}Br_2NO$: C, 46.30; H, 4.89; N, 3.61; Br, 41.10. Found: C, 46.12; H, 4.90; N, 3.70; Br, 41.70.

The hydrobromide **18** was prepared similarly from **3**: m.p. 142–143° (methanol); i.r. (Nujol) 3110 (broad), 2450 (broad), 1605 (weak), and 1565 cm^{-1}.

Anal. Calcd. for $C_{12}H_{12}Br_2ClNO$: C, 37.78; H, 3.17; N, 3.67. Found: C, 38.06; H, 3.24; N, 3.82.

3-Benzylamino-2-bromo-5,5-dimethyl-2-cyclohexen-1-one (16)

(*a*) Two recrystallizations of **15** from ethanol yielded a crystalline compound: m.p. 183–184°; i.r. ($CHCl_3$) 3350 and 1565 cm^{-1}; p.m.r. 1.07 (s, 6H, CH_3), 2.42 and 2.46 (2s, 4H, CH_2), 4.57 (d, J = 6.5 Hz, 2H, CH_2—N), 6.31 (b, 1H, NH), 7.32 (m, 5H, aromatic).

Anal. Calcd. for $C_{15}H_{18}BrNO$: C, 58.45; H, 5.85; N, 4.55; Br, 25.95. Found: C, 58.51; H, 5.98; N, 4.73; Br, 26.13.

(*b*) The hydrobromide **15** was dissolved in a small amount of cold concentrated sulfuric acid, the solution was poured onto crushed ice and extracted with chloroform. Customary work-up of the organic layer afforded solid material which crystallized from acetone as colorless crystals, m.p. 183–184°.

In an identical manner, **18** was converted to **22**: m.p. 143–145° (benzene, depressed by 20° on admixture with **18**).

Anal. Calcd. for $C_{12}H_{11}BrClNO$: C, 47.94; H, 3.69; N. 4.66. Found: C, 47.84; H, 3.63; N. 4.37.

3-Amino-2-bromo-5,5-dimethyl-2-cyclohexen-1-one (17)

A solution of **15** (500 mg) in concentrated sulfuric acid (10 ml) was stirred at 65° for 90 min, allowed to cool, then poured into ice and extracted with chloroform. The organic layer was washed consecutively with water, sodium bicarbonate, and saturated brine solution. Removal of the solvent gave a solid which was recrystallized from ethyl acetate to afford **17** as colorless crystals (210 mg, 75%): m.p. 204–206°; i.r. (Nujol) 3360, 3320, 3260, 3160, 1650, and 1530 cm^{-1}; u.v. λ_{max}MeOH 291 nm (21 450); p.m.r. (DMSO-d_6) 0.98 (s, 6H, CH_3), 2.22 (s, 2H, CH_2CO), 2.43 (s, 2H, CH_2), 7.00 (very broad, 2H, NH_2).

Anal. Calcd. for $C_8H_{12}BrNO$: N, 6.42; Br, 36.66. Found: N, 6.70; Br, 36.87.

3-(m-Trifluoromethylphenylimino)-1-cyclohexen-1-ol Hydrobromide (19)

A solution of bromine (340 mg, 2.12 mmol) in chloroform (20 ml) was added to a stirred solution of **4** (510 mg, 2 mmol) in chloroform (30 ml). The mixture was stirred for 2 h and evaporated to dryness. The residue was dissolved in hot ethanol, and the precipitated salt which was separated by addition of ether was removed by filtration and washed with acetone. Recrystallization from acetone–ethanol–ether gave colorless crystalline material: 600 mg (89%); m.p. 204–206°; i.r. (Nujol) 3180, 2580, 2500, 1615 (weak), 1605 (weak), 1555, and 1530 cm^{-1}.

Anal. Calcd. for $C_{13}H_{13}BrF_3NO$: C, 46.45; H, 3.89; N, 4.16; Br, 23.78. Found: C, 46.71; H, 3.86; N, 4.21; Br, 23.54.

Bromination with N-Bromosuccinimide

In a typical experiment, **4** (7.65 g, 0.030 mol) was added in portions into a stirred suspension of *N*-bromosuccinimide (5.7 g, 0.032 mol) in 65 ml of methanol–water (9:1) kept at 0°. The reaction mixture was stirred for 60 min, allowed to stand overnight, then poured into 130 ml of 10% sodium bicarbonate, and extracted with chloroform. The combined extracts were washed with water, dried over magnesium sulfate, filtered, and evaporated. The residue was crystallized from a benzene–hexane mixture to give 7.1 g (71%) of 2-bromo-3-(*m*-trifluoromethylphenylamino)-2-cyclohexen-1-one **23**: m.p. 120–121°; i.r. ($CHCl_3$) 3345, 1645, and 1575 cm^{-1}; p.m.r. 2.03 (m, 2H, 5-CH_2), 2.62 (t, J = 6 Hz, 4H, remaining CH_2).

Anal. Calcd. for $C_{13}H_{11}BrF_3NO$: C, 46.73; H, 3.32; N, 4.19; Br, 23.92. Found: C, 46.73; H, 3.35; N, 4.13; Br, 23.91.

The same procedure was applied to **3** and **6** to produce **22** (75%) and **16** (88%). Compound **20** was prepared in a similar manner in 76% yield: m.p. 106–108° (benzene–ether); p.m.r. 1.08 (s, 6H, 5,5-*gem*-dimethyl), 1.27 (d, J = 6 Hz, 3H, CH_3), 2.36 (s, 2H, CH_2CO), 2.45 (s, 2H, CH_2—C=), 3.3 (m, 2H, CH_2—N), 3.83 (s, 1H, OH), 4.03 (m, 1H, CH—O), 6.22 (b, 1H, NH).

Anal. Calcd. for $C_{11}H_{18}BrNO_2$: C, 47.84; H, 6.57; N, 5.07; Br, 28.95. Found: C, 47.70; H, 6.51; N, 4.89; Br, 28.88.

In a similar way **2** was converted into **21** (71%): m.p. 123–124° (benzene–hexane); p.m.r. 4.48 (d, J = 6.5 Hz, 2H, CH_2—N), 5.85 (b, 1H, NH), 6.30 (m, 2H, β protons of furan), 7.39 (m, 1H, α proton of furan).

Anal. Calcd. for $C_{11}H_{12}BrNO_2$: C, 48.89; H, 4.47; N, 5.19; Br, 29.60. Found: C, 49.00; H, 4.46; N, 5.26; Br, 29.54.

Bromination with Cyanogen Bromide

Representative procedure: to a stirred solution of **6** (230 mg) in 30 ml of benzene was added cyanogen bromide (150 mg) at 70° and the temperature was maintained overnight. The benzene was removed by distillation and the crude product was recrystallized from ethanol to give 280 mg (91%) of **16**, m.p. 184°, identical in every respect with an authentic sample.

Can. J. Chem. Downloaded from www.nrcresearchpress.com by 210.87.254.5 on 09/05/12
For personal use only.

*3-Benzylamino-2-iodo-5,5-dimethyl-2-cyclohexen-1-one (**24**)*

To a solution of **6** (2.29 g, 0.01 mol) in chloroform (60 ml) was added with stirring a solution of iodine (2.54 g, 0.01 mol) in chloroform (100 ml). The mixture was stirred at room temperature for 3 h, then washed successively with 30% aqueous solution of sodium thiosulfate, 10% sodium bicarbonate, and with water. Removal of the chloroform gave a solid which was recrystallized from aqueous methanol: m.p. 153–154°; yield 3 g (85%); i.r. ($CHCl_3$) 3340, 1630, and 1560 cm^{-1}; p.m.r. 1.01 (s, 6H, CH_3), 2.40 (s, 4H, CH_2) 4.55 (d, J = 6 Hz, 2H, CH_2—N) 6.10 (m, 1H, NH), 7.3 (m, 5H, aromatic).

Anal. Calcd. for $C_{15}H_{18}INO$: C, 50.71; H, 5.11; N, 3.94. Found: C, 50.58; H, 5.06; N, 4.13.

*8,8a-Dihydro-5-iodo-8,8-dimethyl-2,3-diphenyl-4H-1,4-benzoxazine-6,7-diol (**25**)*

A mixture of **24** (10 g, 0.028 mol), dibenzoyl peroxide (6.8 g, 0.028 mol), and benzene (270 ml) was refluxed for 15 h. After cooling, the reaction mixture was washed successively with a solution of sodium thiosulfate and sodium bicarbonate. The organic phase was dried over magnesium sulfate, filtered, and evaporated. The solid residue crystallized from a benzene–hexane mixture to yield 9.6 g (72%) of **25**. An analytical sample was obtained by recrystallization from benzene: m.p. 212–215°; i.r. ($CHCl_3$) 3430, 3400, 1655, 1645, and 1620 (weak) cm^{-1}; p.m.r. 0.78 (s, 6H, CH_3), 4.8 (b, exchangeable, 2H, OH), 6.32 (s, 1H, CH), 6.90 (b, 1H, NH), 7.24 (m, 10H, aromatic); mass spectrum *m/e* (relative intensity) 473 (17, M^+), 458 (37, $M - CH_3$), 368 (100, $M - C_6H_5CO$), 241 (55 368 − I).

Anal. Calcd. for $C_{20}H_{20}INO_3$: C, 55.82; H, 4.26; N, 2.96; I, 26.81. Found: C, 55.80; H, 4.44; N, 2.84; I, 27.48.

Reaction of Enaminoketones with Isocyanates and Isothiocyanates

A mixture of **6** (20 g, 0.087 mol) and phenyl isocyanate (11.9 g, 0.1 mol) was heated at 130–135° with stirring for 90 min. The resulting amber-like material was crystallized from ethanol to give 23 g (76%) of **29** as white crystals, m.p. 133–134°. Recrystallization from acetone afforded the analytical sample: m.p. 134°; i.r. ($CHCl_3$) 3050, 1630, 1608, 1590, 1570, 1535, and 1500 cm^{-1}; i.r. (Nujol) 2950, 1630, 1588, 1565, 1520, and 1500 cm^{-1}; u.v. λ_{max}EtOH 295 nm (32 050); p.m.r. 1.01 (s, 6H, CH_3), 2.33 (s, 2H, CH_2CO), 2.42 (s, 2H, CH_2—C═), 4.53 (d, J = 6 Hz, 2H, CH_2—N), 7.30 (m, 10H, aromatic), 12.5 (b, 1H, NH), 12.8 (b, 1H, NH).

Anal. Calcd. for $C_{22}H_{24}N_2O_2$: C, 75.83; H, 6.94; N, 8.04. Found: C, 75.86; H, 7.09; N, 8.05.

This example is representative of the manner in which the following compounds were prepared:

26: m.p. 118° (isopropanol); 88%; p.m.r. 4.52 (d, J = 6 Hz, 2H, CH_2—N), 12.5 (b, 1H, NH), 12.75 (b, 1H, NH).

Anal. Calcd. for $C_{20}H_{20}N_2O_2$: C, 74.97; H, 6.29; N, 8.74. Found: C, 74.94; H, 6.35; N, 8.62.

27: m.p. 177° (ethanol); 70%; i.r. ($CHCl_3$) broad bands at 3090, 2880, and 2800 cm^{-1}, 1630 and 1575 cm^{-1}; p.m.r. 12.45 (b, 1H, NH), 14.1 (b, 1H, NH).

Anal. Calcd. for $C_{19}H_{17}ClN_2O_2$: C, 66.96; H, 5.03; N, 8.21; Cl, 10.40. Found: C, 66.91; H, 5.19; N, 8.16; Cl, 10.23.

34: m.p. 202–204° (benzene); 85%; i.r. and p.m.r. spectra similar to those of **29**; u.v. λ_{max}EtOH 297 nm (39 000).

Anal. Calcd. for $C_{22}H_{23}ClN_2O_2$: C, 69.04; H, 6.06; N, 7.32; Cl, 9.28. Found: C, 69.19; H, 6.36; N, 7.12; Cl, 9.01.

37: m.p. 149–150° (ethanol); 86%; i.r. ($CHCl_3$) 2740 (broad), 1590, 1570, 1515 (broad), and 1470 cm^{-1}; u.v. λ_{max}EtOH 279 and 319 nm (29 700 and 20 350, respectively); p.m.r. 1.00 (s, 6H, CH_3), 2.40 (s, 2H, CH_2CO), 2.51 (s, 2H, CH_2—C═), 4.61 (d, J = 6 Hz, 2H, CH_2—N), 7.36 (m, 10H, aromatic), 14.7 (b, 2H, NH).

Anal. Calcd. for $C_{22}H_{24}N_2OS$: C, 72.49; H, 6.64; N, 7.69; S, 8.78. Found: C, 72.19; H, 6.63; N, 8.00; S, 8.83.

36: m.p. 183–184° (ethanol); 66%; p.m.r. 0.95 (s, 6H, CH_3), 2.33 (s, 2H, CH_2CO), 2.47 (s, 2H, CH_2—C═), 3.15 (d, J = 5 Hz, 3H, CH_3—N), 4.60 (d, J = 6 Hz, 2H, CH_2—N), 13.00 (b, 1H, NH), 14.6 (b, 1H, NH).

Anal. Calcd. for $C_{17}H_{22}N_2OS$: C, 67.51; H, 7.33; N, 9.26; S, 10.61. Found: C, 67.82; H, 7.41; N, 9.04; S, 10.59.

*3-Benzylamino-2-(benzothiazol-2-yl)-5,5-dimethyl-2-cyclohexen-1-one (**42**)*

A vigorously stirred mixture of **37** (3.6 g), tetrahydrofuran (100 ml), water (15 ml), and dimethyl sulfate (1 g) was refluxed for 3 h. Five drops of concentrated sulfuric acid were added and heating was continued for 12 h. The reaction mixture was allowed to cool, the tetrahydrofuran was removed *in vacuo*, and the residue was taken between chloroform and water. The organic layer was separated, washed with water and saturated brine solution, dried over magnesium sulfate, filtered, and evaporated. The crude product was recrystallized from a benzene–hexane mixture to afford 3.5 g (98%) of white crystals: m.p. 203–205°; i.r. ($CHCl_3$) 3050, 2860, 1600, 1585, and 1485 cm^{-1}; p.m.r. 4.65 (d, J = 5.5 Hz, becomes a sharp singlet after deuteration, 2H, CH_2—N), 7.1–8.1 (m, 9H, aromatic), 13.25 (b, 1H, NH).

Anal. Calcd. for $C_{22}H_{22}N_2OS$: C, 72.90; H, 6.12; N, 7.73; S, 8.83. Found: C, 72.98; H, 6.24; N, 7.53; S, 8.86.

*3-Anilino-1,5,6,7-tetrahydro-6,6-dimethyl-4H-indazol-4-one Hydrazone (**40a**)*

A mixture of **29** (15 g), 85% aqueous hydrazine hydrate (130 ml), and ethanol (250 ml) was refluxed for 15 h. After cooling, some 100 ml of ethanol were removed under reduced pressure, and the remaining solution was diluted with 50 ml of water. The crystalline material that had deposited on chilling was collected and dried; yield 10 g (90%); m.p. 217–219°. Recrystallization from aqueous ethanol afforded pure **40*a***: m.p. 219–220°; i.r. (Nujol) 3360, 3260, 3060, 1610, 1595, 1552, 1530, and 1497 cm^{-1}; i.r. (saturated solution in $CHCl_3$) 3470, 3400, 3330, 1628, 1597 (strong) cm^{-1}; u.v. λ_{max}EtOH 252 and 273 nm (20 200 and 17 900 respectively); p.m.r. (DMSO-d_6) 1.01 (s, 6H, CH_3), 2.30 and 2.48 (singlets, 4H, CH_2), 5.80 (b, exchangeable, 2H, NH_2), 6.6–7.6 (m, 5H, aromatic), 8.38 (b, exchangeable, 1H, NH), 11.50 (b, exchangeable, 1H, NH).

Anal. Calcd. for $C_{15}H_{19}N_5$: C, 66.89; H, 7.11; N, 26.00. Found: C, 67.00; H, 6.96; N, 25.98.

*3-Anilino-1,5,6,7-tetrahydro-6,6-dimethyl-4H-indazol-4-one (**41**)*

A mixture of **40*a*** (20 g), concentrated hydrochloric acid (400 ml), and ethanol (800 ml) was refluxed for 24 h.

Can. J. Chem. Downloaded from www.nrcresearchpress.com by 210.87.254.5 on 09/05/12
For personal use only.

Ethanol was removed in a rotavapor, and the remaining solution was basified upon cooling to p*H* 9 with diluted sodium hydroxide. The mixture was extracted with chloroform, the combined extracts were washed with water, dried over magnesium sulfate, and filtered. The filtrate was concentrated and kept overnight in an icebox to deposit 12.3 g (65%) of shiny hexagonal plates, m.p. 268–270°. An analytical sample was obtained by recrystallization from methanol: m.p. 270–271°; i.r. (Nujol) 3400, 3230, 1618, and 1540 cm^{-1}; u.v. λ_{max}EtOH 244, 255, 262, and 312 nm (the corresponding ε values were 19 300, 15 630, 15 200, and 8400); p.m.r. (DMSO-d_6) 1.06 (s, 6H, CH_3), 2.30 and 2.68 (singlets, 4H, CH_2), 6.7–7.7 (m, 5H, aromatic), 7.98 (b, 1H, NH), 9.93 (b, 1H, NH).

Anal. Calcd. for $C_{15}H_{17}N_3O$: C, 70.56; H, 6.71; N, 16.46. Found: C, 70.84; H, 6.72; N, 16.55.

*2-(2-Hydroxypropyl)amino-4,4-dimethyl-6-oxo-N-phenyl-1-cyclohexene-1-carboxamide (**31**)*

A mixture of **29** (10 g) and 1-amino-2-propanol was heated at 110–120° for 15 h, then at 160° for 5 h. The reaction mixture was cooled to 50–60° and partitioned between water and chloroform. The organic layer was washed successively with diluted hydrochloric acid, water, saturated brine solution, then dried over magnesium sulfate, filtered, and evaporated. The residue was applied to a column of silica gel which was eluted with benzene–chloroform (1:1), chloroform, and finally with 1% of methanol in chloroform. The main fraction was collected and recrystallized from benzene to give 5.2 g (57%) of white prismatic crystals: m.p. 160–161°; i.r. ($CHCl_3$) 3450–3300 (broad and weak), 3050, 1625, 1605, 1595, 1570, 1530 (strong), and 1445 cm^{-1}; p.m.r. 1.00 (s, 6H, 4,4-*gem*-dimethyl), 1.25 (d, J = 6 Hz, 3H, CH_3), 2.30 and 2.37 (singlets, 4H, CH_2), 3.28 (obscured triplet, J = 5.5 Hz, 2H, CH_2N), 4.00 (m, 1H, —CH—O), 6.83–7.76 (m, 5H, aromatic), 12.50 (b, 2H, NH).

Anal. Calcd. for $C_{18}H_{24}N_2O_3$: C, 68.33; H, 7.65; N, 8.85. Found: C, 68.03; H, 7.57; N, 8.78.

*Transamination of **29** and **34***

In a typical run, a mixture of **29** (15 g) and 3-(methylamino)propylamine (15 g) was heated at 130° for 18 h. After cooling, the mixture was diluted with ice water and extracted four times with 50 ml of chloroform. The combined extracts were washed with 30 ml of diluted hydrochloric acid (1:1), dried over magnesium sulfate, and filtered. The product was precipitated by diluting the filtrate with 200 ml of dry ether. Crystalline material was collected by filtration and recrystallized from ethanol to yield 11.8 g (75%) of **32**, m.p. 222–225°. The work-up is based on the fact that the salt is soluble in chloroform. An analytical sample was crystallized from ethanol: m.p. 224–225°; p.m.r. (DMSO-d_6) 2.53 (s, 3H, CH_3—N) 2.97 (t, J = 7 Hz, 2H, CH_2—N), 3.58 (q, J = 7 Hz, after exchange collapses to a triplet, 2H, CH_2—N^+) 9.17 (b, 2H, NH_2^+), 12.17 (m, 1H, NH), 12.60 (s, 1H, NHCO).

Anal. Calcd. for $C_{19}H_{27}N_3O_2$·HCl: C, 62.37; H, 7.71; N, 11.48; Cl, 9.69. Found: C, 62.24; H, 7.62; N, 11.32; Cl, 9.44.

Under similar conditions **28** was prepared in 65% yield, m.p. 211—213° (ethanol). However, this salt was hygroscopic and we could not obtain satisfactory analytical values. By the same procedure, compound **30** was prepared from **29** and ethylenediamine in 72% yield. An analytical sample of **30** was crystallized from ethanol: m.p. 243–245°; p.m.r. (DMSO-d_6) 3.05 and 3.75 (obscured triplets, J = 6 Hz, 4H, CH_2—CH_2), 8.50 (b, 2H, NH_2), 9.73 (b, 1H, NH), 10.10 (s, 1H, NHCO).

Anal. Calcd. for $C_{17}H_{23}N_3O_2$·HCl: C, 60.47; H, 7.15; N, 12.50; Cl, 10.45. Found: C, 60.80; H, 7.14; N, 12.80; Cl, 10.24.

The reaction of **29** with 3-(dimethylamino)propylamine afforded **33**: m.p. 192–194°; yield 38%; p.m.r. (DMSO-d_6) 2.76 (s, 6H, CH_3—N), 12.30 (b, 1H, NH), 12.65 (s, 1H, NHCO).

Anal. Calcd. for $C_{20}H_{29}N_3O_2$·HCl: N, 11.06; Cl, 9.33. Found: N, 10.91; Cl, 9.24.

In a similar manner treatment of **34** with 3-(methylamino)propylamine allowed the preparation of **35**: m.p. 246–248° (ethanol–acetonitrile); yield 68%; p.m.r. (DMSO-d_6) 2.55 (s, 3H, CH_3—N), 7.32 and 7.63 (pair of doublets, J = 8.5 Hz, 4H, aromatic), 9.1 (b, 2H, NH_2^+), 12.00 (b, 1H, NH), 12.68 (s, 1H, NHCO).

Anal. Calcd. for $C_{19}H_{26}ClN_3O_2$·HCl: N, 10.50; Cl, 17.71. Found: N, 10.56; Cl, 17.57.

*4-Methylamino-3-pentene-2-one (**43**)*

This compound was prepared by the method of Holtzclaw *et al.* (24): b.p. 85–86°/10 mm Hg; m.p. 39–40°; the i.r. and p.m.r. data were identical with those reported in the literature (24, 11).

*2-Acetyl-3-methylaminoisocrotonanilide (**46**)*

A solution of **43** (3.4 g, 0.03 mol) and phenyl isocyanate (3.6 g 0.03 mol) in benzene (50 ml) was refluxed for 30 min. After cooling, the mixture was evaporated to dryness and the solid residue was crystallized from acetone–ether to yield 5.6 g (80%) of the title compound. An analytical sample was crystallized from acetone – ethyl acetate: m.p. 178–179°; p.m.r. (DMSO-d_6) 2.03 (broad s, 6H, CH_3), 2.97 (d, J = 5 Hz, 3H, CH_3—N), 6.83–7.91 (m, 5H, aromatic), 10.00 (s, 1H, NHCO), 11.50 (b, 1H, NH).

Anal. Calcd. for $C_{13}H_{16}N_2O_2$: C, 67.22; H, 6.94; N, 12.06. Found: C, 67.11; H, 7.03; N, 12.02.

Technical assistance by Mr. S. Toutounji is gratefully acknowledged. The author wishes to thank Dr. G. Schilling, Mr. A. Verwijs, and Mrs. J. Jachner for recording and discussing the p.m.r., i.v., and u.v. spectra.

1. F. Zymalkowski and H. J. Rimek. Arch. Pharm. **294**, 759 (1961).
2. G. H. Alt and A. J. Speziale. J. Org. Chem. **29**, 798 (1964).
3. J. Goerdeler and U. Keuser. Chem. Ber. **97**, 2209 (1964).
4. K. Wiesner, I. Jirkovsky, M. Fishman, and C. A. J. Williams. Tetrahedron Lett. 1523 (1967).
5. J. M. Bobbitt and C. P. Dutta. Chem. Commun. 1429 (1968).
6. Ch. Ruangsiyanand, H. J. Rimek, and F. Zymalowski. Chem. Ber. **103**, 2403 (1970).
7. E. Schmitz and H. Striegler. J. Prakt. Chem. **313**, 1125 (1971).
8. T. Kametani, M. Ihara, and K. Takahashi. Chem. Pharm. Bull. **20**(7), 1588 (1972).
9. P. W. Hickmott and G. Sheppard. J. Chem. Soc. Perkin Trans. I, 1038 (1972).

10. K. KOTERA. J. Pharm. Soc. Jap. **80**, 1275 (1960).
11. G. O. DUDEK and R. H. HOLM. J. Am. Chem. Soc. **84**, 2691 (1962).
12. P. CRABBE, B. HALPERN, and E. SANTOS. Tetrahedron, **24**, 4299 (1968).
13. CH. KASHIMA, M. YAMAMOTO, and N. SUGIYAMA. J. Chem. Soc. (C), 111 (1970).
14. K. RAMALINGAM, M. BALASUBRAMANIAN, and V. BALIAH. Ind. J. Chem. **10**, 62 (1972).
15. K. KOTERA. Yak. Zass. **80**, 1275 (1960).
16. J. DABROWSKI. Spectrochim. Acta, **19**, 475 (1963).
17. B. HALPERN and L. B. JAMES. Aust. J. Chem. **17**, 1282 (1964).
18. N. J. LEONARD and J. A. ADAMCIK. J. Am. Chem. Soc. **81**, 595 (1959).
19. A. I. MEYERS, A. H. REINE, and R. GAULT. J. Org. Chem. **34**, 698 (1969).
20. H. C. BROWN, J. H. BREWSTER, and H. SHECHTER. J. Am. Chem. Soc. **76**, 467 (1954).
21. H. BÖHME and G. WILLINGER. Arch. Pharm. **302**, 974 (1969).
22. G. O. DUDEK and G. P. VOLPP. J. Am Chem. Soc. **85**, 2697 (1963).
23. N. H. CROMWELL *et al*. J. Am. Chem. Soc. **71**, 3337 (1949).
24. H. F. HOLTZCLAW, JR., J. P. COLLMAN, and R. M. ALIRE. J. Am. Chem. Soc. **80**, 1100 (1958).
25. D. L. OSTERCAMP. J. Org. Chem. **35**, 1632 (1970).

Can. J. Chem. Downloaded from www.nrcresearchpress.com by 210.87.254.5 on 09/05/12
For personal use only.

Steric and Electronic Factors in 1,3-Dipolar Cycloadditions. The Stereochemical Course of the Addition of Dimethyl Aryl- and Alkyldiazomethylphosphonates to Norbornadiene

HUGUETTE COHEN AND CLAUDE BENEZRA

Department of Chemistry, University of Ottawa, Ottawa, Canada, K1N 6N5

Received July 16, 1973

The addition of 14 dimethyl aryl- and alkyldiazomethylphosphonates, $RC(N_2)P(O)(OCH_3)_2$, to norbornadiene has been studied and the stereochemistry of the resulting *exo*-Δ^1-pyrazolines determined by n.m.r. The *anti*/*syn* ratio of the cycloadducts is discussed in terms of steric and electronic factors. For alkyldiazomethylphosphonates steric factors are the dominant ones, while with aryldiazomethylphosphonates electronic factors seem to be of importance.

L'addition de 14 aryl- et alkyldiazomethylphosphonates, $RC(N_2)P(O)(OCH_3)_2$ au norbornadiène a été étudiée et la stéréochimie des Δ^1-pyrazolines-*exo* formées a été déterminée par r.m.n. Le rapport *anti*/*syn* des produits d'addition est discuté en termes de facteurs stériques et électroniques. Pour les alkyldiazomethylphosphonates, ce sont les facteurs stériques qui sont prédominants alors que pour les aryldiazomethylphosphonates les facteurs électroniques sont importants.

Can. J. Chem., **52**, 66 (1974)

1,3-dipolar cycloaddition reactions provide a general route to five-membered rings containing several heteroatoms (1). The most generally accepted mechanism is the one proposed by Huisgen (1), namely, that cycloaddition is a concerted "no-mechanism" reaction (2). Recently, Firestone (3) has proposed a two-step diradical mechanism. A clear assignment of the role of steric and electronic factors should give some insight into the mechanism of such reactions: steric factors should be more important in a concerted one-step than in a two-step reaction.

Although 1,3-dipolar cycloadditions with activated double bonds are well documented, there has been no systematic study of the reaction of dipoles with isolated double bonds whose reactivity stems from their strain. With dimethyl diazoalkylphosphonates, $RC(N_2)P(O)(OCH_3)_2$, the addition to an olefin such as norbornadiene results in the formation of two Δ^1-pyrazolines (Fig. 1) and the *anti* to *syn*[1] ratio should give some information about the influence of the R group. For R = CH_3 and C_6H_5 we found recently (4) that the distribution of adducts could not be explained by consideration of steric factors only and we therefore undertook the study of the addition of 14 dimethyl alkyl- and aryldiazomethylphosphonates to norbornadiene. The results are reported here.

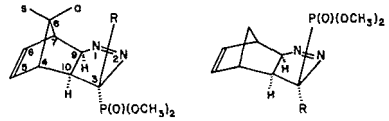

FIG. 1. *Anti* and *syn* pyrazolines.

Results

All the diazomethylphosphonates necessary for this study, except the *p*-nitrophenyl derivative **5**, were prepared by a general route devised by Seyferth and co-worker (5) from α-ketophosphonates whose tosylhydrazone derivatives decomposed in basic medium to yield the desired starting material. Because of the reactivity of trialkyl phosphite toward *p*-nitroaromatics (6), the Regitz "diazo transfer method" (7) was used to make compound **5**.[2] The synthesis and ^{13}C n.m.r. spectra of some of them (**1–5** and **7**) have appeared recently (8).

All cycloadditions were carried out under the same conditions, as described previously (4); a

[1]The words *anti* and *syn* refer to the relative position of the C_8 bridge and of the dimethylphosphono group.

[2]After our manuscript (ref. 8) had been submitted for publication, a paper by Regitz and co-workers (7*b*) described compounds **2** and **5**. The physical constants and the spectral data of their compounds agreed well with those of our compounds.

Can. J. Chem. Downloaded from www.nrcresearchpress.com by 210.87.254.105 on 09/05/12
For personal use only.

Can. J. Chem. Downloaded from www.nrcresearchpress.com by 210.87.254.105 on 09/05/12
For personal use only.

mixture of the diazophosphonate, norbornadiene in more than 40-fold excess, and methylene chloride was heated at 55–60°.[3] The addition reaction was fast (24 h for more than 90% completion) with components **1–6**, **9–11**, and **14**, and much slower for derivatives **7**, **8**, **12**, and **13**. See Experimental section for details.

The configurations of the pyrazolines were determined essentially by proton n.m.r. and the *anti*/*syn* ratio could be estimated directly on the n.m.r. spectrum of the crude by integrations of the signal due to the H_9 protons.[4] The n.m.r. spectra of some of the *aryl* pyrazolines (**14–23**, and **26**) have been described elsewhere (9). Of the four possible diastereomeric pyrazolines only the *exo* adducts were formed, a result quite common in addition to the bicyclo[2.2.1]heptene or -heptadiene systems (10). The *exo* attachment of the pyrazoline ring is proved by the existence of a 2.0 Hz long-range $H_{8s}CCCH_{10}$ coupling (11) and the absence of any H_{10},H_4 vicinal coupling. The configuration at C_3 is based essentially on the existence of a large (19–20 Hz) P,H_{10} coupling in the *anti* epimer and of a small (6–8 Hz) P,H_{10} coupling in the *syn* derivative. This is in accord with the known dihedral angular dependence of P—C—C—H coupling (12) in phosphonates; Dreiding models show that the pyrazoline ring is planar in this system and that the dihedral P,H angles are near 0° in the *anti* epimer (large $^3J_{PH}$ coupling) and near 120° in the *syn* epimer (small $^3J_{PH}$ coupling) (12).

Although this contrasting difference in P,H vicinal coupling allows unambiguous assignments to be made, it is not always sufficient because, in the case of the alkyl derivatives, the H_{10} signal lies under the absorptions of the alkyl protons. In those cases, the stereospecificity of P—C—N=N—C—H *homoallylic* couplings (9), 4–4.8 Hz in the *anti* configuration and 5.5–6.6 Hz in the *syn* configuration, allows unambiguous assignments to be made.

In the case of the *syn* benzyl derivative **39**, the signal for H_9 is shifted upfield (δ 3.40 p.p.m.) as compared with the usual 4.67–4.83 p.p.m. range for this absorption in *syn* derivatives. There is no doubt about the assigned configuration since the P,H_{10} coupling is 6.0 Hz (P,H_{10} = 18.0 Hz in the *anti* epimer). This unusual shielding effect probably corresponds to a preferred conformation of the phenyl ring; additional evidence for preferred conformation is the finding that vicinal *P*—C—CH_2(C_6H_5) couplings are different for the two benzylic hydrogens.

The mixture of epimeric pyrazolines was separated on a silica gel column chromatograph. In one instance, it was not possible to isolate pure *syn* derivative (compound **24**) and the amount of this epimer was estimated by n.m.r. of **24** with the starting diazo compound. The results of cycloaddition are summarized in Table 1.

Discussion

All the pyrazolines isolated possess the *exo* configuration. Radical (13) as well as electrophilic (10) additions to norbornene lead mostly, if not exclusively, to products resulting from *exo* attack. Additions to norbornadiene are more complex. Homolytic additions usually give mixtures of nortricyclene derivatives, as well as *exo*-norbornene derivatives (14). Some *endo* products have been reported for the addition of thiols to polyhalonorbornadienes (15). Addition of carbenes to norbornadiene leads to a fair amount of *endo* attack (16). In contrast to the number of products obtained with norbornadiene in radical, electrophilic, or carbenic

TABLE 1. Results of the cycloaddition reactions

Diazo compound $RC(N_2)P(O)(OCH_3)_2$		Amount of pyrazolines (%)	
No.	R	*anti*[a]	*syn*
1	*p*-$CH_3OC_6H_4$	95	5
2	*p*-$CH_3C_6H_4$	90	10
3	*p*-BrC_6H_4	90	10
4	C_6H_5	95	5
5	*p*-$NO_2C_6H_4$	93	7
6	*p*-$CH_3OCOC_6H_4$	91	9
7	*o*-$CH_3OC_6H_4$	~100[b]	~0
8	α-Naphthyl	~100[b]	~0
9	β-Naphthyl	90	10
10	CH_3	75	25
11	C_2H_5	60	40
12	iso-C_3H_7	50	50
13	*tert*-C_4H_9	0	100[b]
14	$C_6H_5CH_2$	55	45

[a]% *anti* + % *syn* = 100; estimated accuracy ±2%;
[b]Estimated by n.m.r. and confirmed by chromatographic separation: no trace of the other epimer could be detected.

[3]The reaction was followed by n.m.r.: appearance of new P—OCH_3 peaks and of characteristic H_9 absorptions.

[4]The estimate was confirmed within ±2% by chromatographic separation of the mixture.

TABLE 2. Pyrazolines

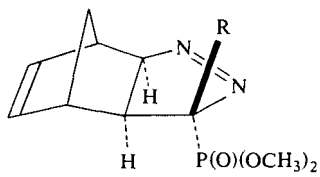

anti

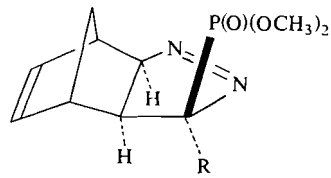

syn

Compound No.	R	Compound No.
15	*p*-$CH_3OC_6H_4$	**16**
17	*p*-$CH_3C_6H_4$	**18**
19	*p*-BrC_6H_4	**20**
21	C_6H_5	**22**
23	*p*-$NO_2C_6H_4$	**24**
25	*p*-$CH_3OCOC_6H_4$	**26**
27	*o*-$CH_3OC_6H_4$	—
28	α-Naphthyl	—
29	β-Naphthyl	**30**
31	CH_3	**32**
33	C_2H_5	**34**
35	iso-C_3H_7	**36**
—	*tert*-C_4H_9	**37**
38	$C_6H_5CH_2$	**39**

additions, only adducts resulting from *exo* attack have been reported in 1,3-dipolar cycloaddition reactions. Thus, although the exclusive formation of *exo*-Δ^1-pyrazolines is certainly striking, it is not unprecedented: additions of nitrilimines (17*a*), azides (17*b*), and diazoalkanes (18) to norbornadiene give mono- and bisadducts resulting from exclusive *exo* attack.

The results shown in Table 1 clearly reveal that steric factors are dominating, except in the case of the aromatic derivatives. This is particularly striking for the alkyldiazophosphonates **10–13**: as the size of the R group increases from methyl to *tert*-butyl, the amount of *syn*-pyrazoline increases from 25 to 100%. This is in accord with a concerted mechanism of addition. Incidentally, this would suggest that the dimethylphosphono group is almost as bulky as an isopropyl group.

It is more difficult to explain the results for the aromatic derivatives (**15–30**). A consideration of most of the 1,3-dipolar cycloadditions studied by Huisgen's group shows that kinetic control of the reaction is important (2). We have evidence that the reactions we are studying are also kinetically controlled: there was no change in the *anti*/*syn* ratio with time and the pyrazolines did not epimerize when submitted to the same conditions. Therefore, the *anti*/*syn* ratio of the products should reflect the differences in energy between the transition states leading to the *anti* and to the *syn* pyrazolines, respectively.

Steric factors alone could not explain the predominance of the *anti* derivatives. From the *A* values of the phenyl group (3.0 kcal/mol) (19) and of the $P(O)(OCH_3)_2$ group (2–3 kcal/mol),[5] there seems to be little difference in size between those two groups and one would expect a 1:1 *anti*/*syn* ratio rather than the ~9:1 ratio observed. Of course, these *A*-values should be considered as indicative only, since they refer to 1,3-diaxial interactions in the cyclohexane system. In fact, depending on its orientation, a phenyl group can be "smaller" than predicted from the *A*-value (20) and, indeed, there are examples in the literature where a phenyl–methyl nonbonded 1,3-diaxial interaction in a cyclohexyl derivative seems to be preferred to a corresponding methyl–methyl interaction (21). A possible explanation is therefore that the phenyl group, at least in the system studied here, is smaller than the dimethylphosphonate. This interpretation does not seem satisfactory to us

[5]J. L. Bravet and C. Benezra, unpublished results.

Can. J. Chem. Downloaded from www.nrcresearchpress.com by 210.87.254.105 on 09/05/12
For personal use only.

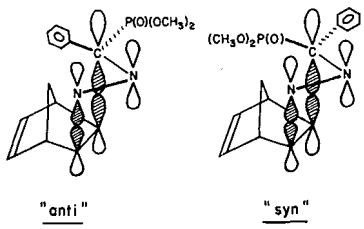

FIG. 2. Transition states leading to the *anti* and to the *syn* Δ^1-pyrazolines respectively.

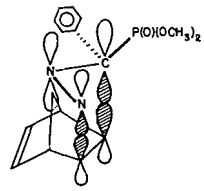

FIG. 3. Transition state leading to the *anti* Δ^1-pyrazoline with an "anti" arrangement of the phenyl *vs.* the nitrogen end of the dipole.

because of the results for the *o*-methoxyphenyl (**7**) and the α-naphthyl (**8**) derivatives: it is evident that the α-naphthyl group, at least, is bulkier than the phosphorus moiety and, still, only the *anti* derivative is obtained.

We rather favor a dominating effect of electronic factors in the aryl derivatives. Since we get mostly the *anti* derivatives, this means that the transition state leading to these products is stabilized, as compared with that for the *syn* ones (Fig. 2). This stabilization can be envisaged in three different ways.

In the transition state of 1,3-dipolar cycloadditions, the dipole is bent (2). Stabilization of the "anti" arrangement depicted in Fig. 2 can occur by favorable coulombic interaction between the phenyl ring and the nitrogen end of the dipole. Such an electrostatic effect can occur only when the phenyl and the nitrogen end of the dipole are *cis* to each other.

Stabilization can also occur from resonance: the steric hindrance of the C_8 bridge could cause the aromatic ring to be *coplanar* with the dipole in the "*anti*" arrangement, while in the "*syn*" alternative, the aromatic ring is a free rotor.

Finally, the dipole in an "*anti*" arrangement (with the aromatic ring *cis* to the nitrogen end of the dipole) could react *faster* than in the other conformation.[6] This difference is not unprecedented in the literature. For instance, the *cis* and *trans* forms of azomethine ylide dicarboxylic esters have a very different reactivity (22). In the particular case of the addition to norbornadiene, it is not possible to draw a clear-cut conclusion concerning this point; the arrangement depicted in Fig. 3 (with the phenyl "*trans*" to the nitrogen end of the dipole), which could also lead to the *anti* pyrazoline, seems to be precluded for steric reasons. It is of interest to note that there is no substituent effect: the difference between the *anti*/*syn* ratio found in the case of the *p*-methoxyphenyl derivative for instance and of the *p*-nitrophenyl is within experimental error (±2%).

Preliminary results for the addition of dimethyl aryldiazomethylphosphonates to 7-oxabenzonorbornadiene indicate that the effect of the —CH_2— bridge is not important: essentially the same *anti*/*syn* ratio is obtained. It seems therefore that polar effects predominate for aryldiazophosphonates. More work along those lines is in progress.

Experimental

Trimethyl phosphite was purchased from Aldrich Company and distilled before use. The benzoyl and naphthyl derivatives were prepared according to a published procedure (5). Silicic acid (Merck (0.05–0.20 mm)) was used for column chromatography. The i.r. spectra were recorded on a Beckman-20 i.r. Spectrometer either in chloroform solutions or as Nujol mulls. The n.m.r. spectra were run on a HA-100 Varian Spectrometer in deuteriochloroform solutions and chemical shifts are given in δ p.p.m. values with TMS as internal reference. Analyses were performed in Organic Microanalyses Laboratories (Dr. C. Daesslé) in Montreal. Norbornadiene was purchased from Aldrich Company and used as such.

Preparation of p-Carbomethoxybenzoyl Chloride

Since the preparation of *p*-carbomethoxybenzoyl chloride has not been described yet and since that of the monomethyl ester of terephthalic acid is described in a patent (23), we give here detailed procedures, starting from the commercially available dimethyl terephthalate (purchased from Baker).

$$p\text{-MeOOC—C}_6\text{H}_4\text{—COOMe} \xrightarrow[(2)\ SOCl_2]{(1)\ HO^-} p\text{-MeOOC—C}_6\text{H}_4\text{—COCl}$$

In a three-necked round-bottom flask equipped with a condenser, a dropping funnel, and a mechanical stirrer, was put dimethyl terephthalate (45 g) in 200 ml anhy-

[6]A referee suggested that determination of the frontier orbital energies and of the coefficients of the terminal atoms in the HOMO of the dipole could perhaps show that the *cis* form of the dipole (Fig. 2, transition state "*anti*") reacts faster than the *trans* form (Fig. 2, "*syn*"). This could indeed lead to conclusive results and those calculations will be undertaken and reported later.

Can. J. Chem. Downloaded from www.nrcresearchpress.com by 210.87.254.105 on 09/05/12
For personal use only.

Can. J. Chem. Downloaded from www.nrcresearchpress.com by 210.87.254.105 on 09/05/12
For personal use only.

TABLE 3. Ketophosphonates $RC(O)P(O)(OCH_3)_2$

R	RCOCl (g)	$P(OCH_3)_3$ (ml)	$RCOP(O)(OCH_3)_2$	Boiling point	Analysis (%) Calcd.	Analysis (%) Found	Infrared	Nuclear magnetic resonance
p-$CH_3OCOC_6H_4$[a]	27.1	19	23.55[b]	165–170° (0.015 Torr)	C 48.54 H 4.81 P 11.38	48.71 4.64 10.92	C=O 1660[c] P=O 1240 POC 1050	3.91 (d, 6H, $POCH_3$, J_{PH} = 11.2), 8.06, 8.15, 8.23, 8.32[d] (4H aromatic)
α-Naphthyl	18.7	12	23.8	Oil	C 58.87 H 4.94 P 11.68	58.78 5.01 11.65	C=O 1670 P=O ~1250 POC 1040	3.93 (d, 6H, $POCH_3$, J_{PH} = 10.8), 7.45–9.05 (m, 7H, H aromatic)
β-Naphthyl	18.8	12	23.8	Oil	C 58.87 H 4.94 P 11.68	59.11 4.97 11.31	C=O 1650[e] P=O 1240 POC 1050	3.94 (d, 6H, $POCH_3$, J_{PH} = 10.9), 7.28–8.20 (m, 7H, H aromatic)
C_2H_5[a]	31	12	29.70[b]	70° (0.05 Torr)	C 36.15 H 6.67 P 18.64	36.49 6.61 18.72	C=O 1700 P=O 1265 POC ~1040	1.11 (d of t, 3H, CH_3CH_2, J_{HH} = 7.25, $^4J_{PH}$ = 1.0), 2.86 (d of 9, 2H, CH_3CH_2—, $^3J_{PH}$ = 1.0), 3.88 (d, 6H, $POCH_3$, J_{PH} = 11.0)
$C_6H_5CH_2$	15.4	15	19.72[b]	125° (0.1 Torr)	C 52.40 H 5.72 P 13.51	52.27[f] 5.63 13.33	C=O 1675 P=O 1210 POC ~1030	3.76 (d, 2H, CH_2(CO), J_{PH} = 11), 3.81 (d, 6H, P—O—CH_3, J_{PH} = 11.2), 2 multiplets at ~7.3 and ~7.8 (5H, H aromatic)

[a]Both ketophosphonates purified by distillation under vacuum.
[b]After distillation.
[c]The $(CO)OCH_3$ absorption appeared at 1720 cm^{-1}.
[d]AA'BB' part of an AA'BB'X (X = P); positions of main absorptions given.
[e]There was another strong absorption at 1625 cm^{-1}.
[f]Analysis performed by Chemalytics Inc., Tempe, Arizona (Dr. A. M. Yates).

TABLE 4. Tosylhydrazones $RC(NNHTS)P(O)(OCH_3)_2$

R	$RCOP(O)(OCH_3)_2$ (g)	Hydrazone[a] (g)	Melting point	Analysis (%) Calcd.	Found
p-$CH_3OCOC_6H_4$	20	25.8	118–120°	C 49.09	49.05
				H 4.78	4.75
				N 6.36	6.08
				P 7.02	6.71
α-Naphthyl	18.5	26.7	127°	C 55.42	55.68
				H 4.88	4.98
				N 6.46	6.60
				P 7.14	7.00
β-Naphthyl	18.5	26.9	193–194°	C 55.42	55.27
				H 4.88	4.89
				N 6.46	6.50
				P 7.14	6.97
C_2H_5	20.7	34	155–160°	C 43.11	42.85
				H 5.72	5.59
				N 8.37	8.51
				P 9.26	9.50
$C_6H_5CH_2$	11.4	16.8	125–126°	C 51.52	51.10[b]
				H 5.33	5.44
				N 7.07	7.44
				P 7.81	7.46

[a]Purified by recrystallization in methanol.
[b]Analysis performed by Chemalytics Inc., Tempe, Arizona (Dr. A. M. Yates).

drous methanol. A solution of KOH (12.9 g) in methanol (250 ml) was added dropwise for 3.30 h while the temperature of the reaction mixture was maintained at 75° (or a little less). After cooling to room temperature, the precipitate was filtered and was further dissolved in water (1500 ml); only the monosalt was soluble and the unreacted diester was filtered off. The filtrate was acidified with a 10% HCl solution (pH 2) and a precipitate formed which was filtered and washed several times with water. The monoacid was dried (at a temperature less than 80°) and 28.5 g were obtained (m.p. 221°, lit. (24) m.p. 230°).

This acid was dissolved in 15 ml anhydrous benzene to which 1 drop of pyridine had been added. Then thionyl chloride (80 ml, from a freshly opened new bottle) was added and the mixture was refluxed for 5 h. Excess $SOCl_2$ and benzene were removed by distillation under vacuum (water pump); 50 ml anhydrous benzene were added and further distillation (water pump) removed the remaining $SOCl_2$. The monochloride (27.10 g) was purified by crystallization from cyclohexane, m.p. 52–53° (b.p. 90°, 0.015 Torr)., i.r. ($CHCl_3$): 1730 ($COOCH_3$), 1785 ($COCl$).

Anal. Calcd. for $C_9H_7ClO_3$ (mol. wt. 198.61): C, 54.43; H, 3.55; Cl, 17.85. Found: C, 54.49; H, 3.68; Cl, 18.02.

Preparation of the Ketophosphonates and of the Diazophosphonates

The ketophosphonates were prepared from the acyl chlorides, according to Seyferth's general procedure (5). It is very important for the preparation of the p-carbomethoxyphenyl and benzyl derivatives that the Arbuzov reaction be conducted in dilute solution to avoid polymerization. In a typical run, to an anhydrous, vigorously stirred benzene (200 ml) solution of phenylacetyl chloride (20 g) was added an anhydrous benzene (100 ml) solution of trimethyl phosphite (10 g) over 4 h with cooling in an ice-bath. After the addition was completed, the mixture was left under nitrogen, for 24 h at room temperature, then the benzene was distilled off and the phosphonate separated by distillation.

The diazophosphonates, except the p-nitrophenyl derivative (8), were prepared from the tosylhydrazone derivatives of the ketophosphonates, as described previously (4).

Tables 3–5 give the details (weight, analysis, etc.) for new compounds, as well as the spectral data.

Kinetic Studies of the Cycloaddition Reaction

All the runs were done at the same time by heating mixtures of 1 mmol of the diazophosphonate, 5 ml norbornadiene, and 0.5 ml of CH_2Cl_2 in the same bath, at a temperature of 55–60 °C. A sample was taken after 2, 5, 10, 24, and 50 h, evaporated to dryness (no more norbornadiene present), and the T-60 n.m.r. spectrum in $CDCl_3$ was taken. It was possible to estimate the amount of cycloadducts formed by integrating the signal due to H_9 which was well isolated from the others and by comparing it with the CH_3O signals. Since the CH_3O signals were quite different in the pyrazolines and in the diazo compounds, it was also possible to estimate the com-

Can. J. Chem. Downloaded from www.nrcresearchpress.com by 210.87.254.105 on 09/05/12
For personal use only.

Can. J. Chem. Downloaded from www.nrcresearchpress.com by 210.87.254.105 on 09/05/12
For personal use only.

TABLE 5. Diazomethylphosphonates $RC(N_2)P(O)(OCH_3)_2$

R	Hydrazone (g)	Diazo compound[a] (g)	Analysis (%) Calcd.	Analysis (%) Found	Infrared	Nuclear magnetic resonance
p-$CH_3OCOC_6H_4$ **6**	15.6	9.56 (orange crystal m.p. 48° dec. 140°)	C 46.48 H 4.61 N 9.86 P 10.90	46.81 4.62 9.71 10.89	C=N_2 2080[b] P=O 1240 POC 1040	3.82 (d, 6H, $POCH_3$, J_{PH} = 12.2), 3.90 (s, 3H, CH_3OCO), 8.05, 7.96, 7.19, 7.15[c] (AA′BB′, 4H, H aromatic)
α-Naphthyl **8**	13	4.4 (yellow oil)	C 56.53 H 4.74 N 10.13 P 11.21	56.30 4.95 10.27 10.93	C=N_2 2080 P=O ~1220 POC 1030	3.81 (d, 6H, $POCH_3$, J_{PH} = 10.5), 7.73 (complex m, fine structure 7H)
β-Naphthyl **9**	12	8.0 (orange crystal m.p. 40° dec. 137°)	C 56.53 H 4.74 N 10.13 P 11.21	56.40 4.85 9.85 10.98	C=N_2 2080 P=O ~1240 POC 1030	3.78 (d, 6H, $POCH_3$, J_{PH} = 12.0), 7.20–7.90 (m, 7H, fine structure)
C_2H_5 **11**	18	6.5 (yellow oil)	C 33.71 H 6.22 N 15.72 P 17.38	33.97 6.44 15.67 17.52	C=N_2 2080 P=O 1265 POC ~1040	1.17 (t, 3H, CH_3CH_2, J_{HH} = 7.5), 2.20 (d of q, 2H, CH_3CH_2, J_{PH} = 9.5), 3.75 (d, 6H, $POCH_3$, J_{PH} = 12.0)
$C_6H_5CH_2$ **14**	11.0	7.3 (yellow oil)	N 9.46 P 10.45	9.45 10.45	C=N_2 2030 P=O ~1290 POC ~1050	3.42 (d, 2H, $CH_2C_6H_5$, J_{PH} = 9.6), 3.67 (d, 6H, $POCH_3$, J_{PH} = 12.0), 7.27 (m, H aromatic)

[a]All the diazo compounds were purified by chromatography on a silica gel column.
[b]CO at 1715 cm^{-1}.
[c]AA′BB′ part of an AA′BB′X (X = P) spectrum, the positions of the 4 main peaks (2 of them are doubled by $^4J_{PH}$ coupling) are given.

TABLE 6. % completion of the cycloaddition reaction

Diazo compound No.	Reaction time (h) 1	2	5	10	24	50
1	n.m.[a]	20	40	55	90	90
2	n.m.	15	30	50	90	90
3	n.m.	25	30	55	90	95
4	n.m.	30	55	70	90	95
5	0	n.m.	50	65	75	95
7	0	0	0	8	11	60
10	—	75	83	100[b]	—	—
11	—	25	50	60	90	—
12	0	0	0	0	10	45

[a]Not measurable.
[b]No more trace of the starting material.

Can. J. Chem. Downloaded from www.nrcresearchpress.com by 210.87.254.105 on 09/05/12
For personal use only.

TABLE 7. Cycloaddition conditions; cycloadducts

$RC(N_2)P(O)(OCH_3)_2$		Products isolated		Pyrazoline				
						Analysis %		
R	Reaction time (h)	Compound	Weight (g)	Compound	Melting point	Calcd.	Found	Infrared[a]
p-$CH_3OC_6H_4$	24	Diazo **1**	0.210	*anti* **15**	129–130°	C 59.48 H 6.16	59.86 6.34	P═O ~1240
		syn **16**	0.180			N 8.16 P 8.89	8.29 8.85	P—OC ~1050
1		*anti* **15**	1.97					
				syn **16**	Oil	C 59.48 H 6.16	59.17 6.50	P═O ~1250
						N 8.16 P 8.89	8.50 9.10	P—OC ~1050
p-$CH_3C_6H_4$	24	Diazo **2**	0.260	*anti* **17**	108–109°	C 61.44 H 6.36	61.57 6.50	P═O ~1230
		syn **18**	0.300			N 8.42 P 9.31	8.64 9.10	P—OC ~1040
2		Mixture	0.210					
				syn **18**	Oil	C 61.44 H 6.36	61.57 6.42	P═O ~1240
		anti **17**	2.98			N 8.42 P 9.31	8.64 9.50	P—OC ~1050
p-BrC_6H_4	24	Diazo **3**	0.100	*anti* **19**	147–148°	C 48.36 H 4.56	48.06 4.86	P═O ~1230
		syn **20**	0.340			N 7.05 P 7.80	7.15 8.05	P—OC ~1040
3		*anti* **19**	3.100					
				syn **20**	Oil	C 48.36 H 4.56	48.26 4.80	P═O ~1220
						N 7.05 P 7.80	6.91 7.50	P—OC ~1050

Can. J. Chem. Downloaded from www.nrcresearchpress.com by 210.87.254.105 on 09/05/12
For personal use only.

TABLE 7 (*Continued*)

$RC(N_2)P(O)(OCH_3)_2$		Products isolated		Pyrazoline				
						Analysis %		
R	Reaction time (h)	Compound	Weight (g)	Compound	Melting point	Calcd.	Found	Infrared[a]
C_6H_5[b]	24	Diazo **4**	0.2	*syn* **22**	Oil	C 60.37 H 6.02	60.56 6.04	P=O ~1240
4		*syn* **22**	0.1			N 8.80 P 9.73	8.72 9.35	P—OC ~1050
		anti **21**	1.9					
p-$NO_2C_6H_4$	24	Diazo **5**	0.280	*anti* **23**	124°	C 52.90 H 4.99	53.19 5.05	P=O ~1240
5		*syn* **24**[c]	0.230			N 11.56 P 8.52	11.81 8.77	P—OC ~1100
		anti **23**	0.980					
p-$CH_3OCOC_6H_4$	24	Diazo **6**	0.150	*anti* **25**	149°	C 57.46 H 5.63	57.74 6.03	P=O ~1240 P—OC ~1050
		syn **26**	0.332			N 7.44 P 8.23	7.61 8.37	CO 1725
6		*anti* **25**	3.290	*syn* **26**	145°	C 57.46 H 5.63	57.20 5.59	P=O ~1240 P—OC ~1050
						N 7.44 P 8.23	7.73 8.31	CO 1725
o-$CH_3OC_6H_4$	54	Diazo **7**	0.780	*anti* **27**	94–95°	C 59.48 H 6.16	59.22 6.20	P=O ~1270
7		*anti* **27**	3.570			N 8.16 P 8.89	8.28 9.09	P—OC ~1050
α-Naphthyl	168	Diazo **8**	0.120	*anti* **28**	136–138°	C 65.21 H 5.74	65.48 5.71	P=O ~1230
8		*anti* **28**	3.130			N 7.60 P 8.40	8.01 8.74	P—OC 1050
β-Naphthyl	24	Diazo **9**	0.110	*anti* **29**	128°	C 65.21 H 5.74	65.31 5.76	N=N 1550 P=O ~1230
		syn **30**	0.250			N 7.60 P 8.40	7.86 8.23	P—OC ~1050
9		*anti* **29**	1.970	*syn* **30**	Oil	C 65.21 H 5.74	65.47 5.53	P=O ~1230
						N 7.60 P 8.40	7.78 8.59	P—OC ~1050

Can. J. Chem. Downloaded from www.nrcresearchpress.com by 210.87.254.105 on 09/05/12
For personal use only.

TABLE 7 (*Concluded*)

$RC(N_2)P(O)(OCH_3)_2$ R	Reaction time (h)	Products isolated Compound	Weight (g)	Pyrazoline Compound	Melting point	Analysis % Calcd.	Found	Infrared[a]
C_2H_5	27	No diazo left		*anti*[e] **33**	Oil	C 53.33 H 7.05	53.25 7.16	P=O ~1230
		Mixture **33** + **34**	1.990			N 10.36 P 11.46	10.18 11.43	P—OC ~1040
11		*syn* **34**	2.79					
				syn[e] **34**	Oil	—		P=O 1230 P—OC 1040
iso-C_3H_7	216	Diazo **12**	0.320	*anti*[e] **35**	Oil	C 54.92 H 7.44	54.57 7.14	P=O ~1230
		Mixture **35**+**36**[d]	1.390			N 9.85 P 10.98	9.64 11.10	P—OC ~1050
12		*syn* **36**	1.360					
				syn[e] **36**	Oil	—		P=O ~1230 P—OC ~1040
tert-C_4H_9	26 days	Diazo **13**	1.900	*syn* **37**	Oil	C 56.36 H 7.77	55.98 8.12	P=O ~1230
		syn **37**	1.040			P 10.38	10.12	P—OC ~1040
13		Unidentified	0.440					
$C_6H_5CH_2$	24	Diazo **14**	0.44	*anti* **38**	82–83°	C 61.47 H 6.37	61.22 6.45	P=O ~1220
		syn **39**	1.00			N 8.43 P 9.32	8.55 9.33	P—OC ~1040
14		*anti* **38**	1.55					
				syn **39**	128–129°	C 61.47 H 6.37	61.10 6.57	P=O ~1230
						N 8.43 P 9.32	8.46 9.54	P—OC ~1040

[a]Cm^{-1}.
[b]The *anti* derivative **20** has been described (4).
[c]The *syn* pyrazoline was identified in a mixture with the diazo compound, by n.m.r.
[d]Pure samples of *anti* **33** and **35** respectively could be obtained by further chromatography.
[e]Analyzed as a 1:1 mixture of *syn* + *anti*.

Can. J. Chem. Downloaded from www.nrcresearchpress.com by 210.87.254.105 on 09/05/12
For personal use only.

TABLE 8. Nuclear magnetic resonance spectra of the pyrazolines (chemical shifts in δ p.p.m.)

R	8	4	10	7	P—OCH_3	9	5,6	Others
p-$CH_3OCOC_6H_4$	C 0.69	2.42	2.80	3.54	3.70	5.19	6.20	3.93
	Δδ 0.64							(CH_3OCO)
anti **25**	δ_s 1.01							7.85, 7.93
	δ_a 0.37							8.09, 8.17[a]
p-$CH_3OCOC_6H_4$	C 1.49	3.36	2.32	3.65	3.83	4.79	6.25[b]	8.04, 7.95
	Δδ 0.26	or		or	3.51			7.59, 7.50
syn **26**	δ_s 1.49	3.65		3.36				(4H aromatic,
	δ_a 1.23							AA′BB′)
α-Naphthyl	C 0.65	2.24	3.16	3.55	3.29	5.25	6.21	7.39–7.61
	Δδ 0.57				3.68			(m, 7H aromatic)
anti **28**	δ_s 0.94							
	δ_a 0.36							
β-Naphthyl	C 0.71	2.46	2.87	3.56	3.73	5.19	6.18	7.37–8.31
	Δδ 0.50				3.47			(m, 7H aromatic)
anti **29**	δ_s 0.96							
	δ_a 0.46							
β-Naphthyl	C 1.38	3.42	2.45	3.66	3.84	4.78	6.25[b]	7.32–7.90
	Δδ 0.20	or		or	3.46			(m, 7H aromatic)
syn **30**	δ_s 1.48	3.66		3.42				
	δ_a 1.28							
C_2H_5	—	2.71	—	3.52	3.78	5.25	6.21	
anti **33**					3.71			
C_2H_5	C 1.28	3.05	~2	3.55	3.90	4.69	6.23[b]	0.69
	Δδ 0.21	or		or	3.87			(t, CH_3)
syn **34**	δ_s 1.39	3.55		3.05				
	δ_a 1.18							
iso-C_3H_7		2.75	2.34	3.50	3.63	4.98	6.16	1.63, 1.29,
anti **35**					3.67			(2d, 6H, nonequivalent
								$CHMe_2$)
iso-C_3H_7		3.09	1.87	3.56	3.87	4.67	6.21[b]	0.56, 1.22
syn **36**		or		or	3.80			(2d, 6H, nonequivalent
		3.56		3.09				$CHMe_2$)
tert-C_4H_9	C 1.23	3.05	1.94	3.55	3.82	4.72	6.24[b]	1.03 (s, $(CH_3)_3C$)
	Δδ 0.17	or		or				
syn **37**	δ_A 1.32	3.55		3.05				
	δ_B 1.15							

Can. J. Chem. Downloaded from www.nrcresearchpress.com by 210.87.254.105 on 09/05/12
For personal use only.

TABLE 8 (*Concluded*)

R		8	4	10	7	P—OCH_3	9	5,6	Others
$C_6H_5CH_2$	C	1.03	2.84	2.47	3.57	3.45	5.05	6.21	3 (m, 2H, CH_2Ph),
	$\Delta\delta$	0.31				3.34			7.20–7.60
anti **38**	δ_A	1.34							(m, H aromatic)
	δ_B	0.72							
$C_6H_5CH_2$	C	1.10	2.99	1.90	3.28	3.94	3.40	6.08[b]	3.29 (ABX m, 2H, CH_2Ph,
	$\Delta\delta$	0.34	or		or	3.92			$\delta_A = 3.58$, $\delta_B = 3.04$,
syn **39**	δ_s	1.27	3.28		2.99				$J_{AB} = 14.0$, $J_{PA} = 6.2$,
	δ_a	1.01							$J_{PB} = 8.1$)

[a]AA′BB′ part of an AA′BB′X spectrum (X = ^{31}P). The main absorptions are given.
[b]Center of an eight-line multiplier.

Can. J. Chem. Downloaded from www.nrcresearchpress.com by 210.87.254.105 on 09/05/12
For personal use only.

TABLE 9. Nuclear magnetic resonance spectra of pyrazolines (coupling constants[a] in Hz)

R	H_{8a},H_{8s}	H_9,H_{10}	H_{8s},H_9	H_{8s},H_{10}	H_5,H_6	P,H_{10}	P,H_9	P—OCH_3	Others[b]
p-$CH_3OCOC_6H_4$ *anti* **25**	10.0	6.5	1.0	1.5	4.8[c]	19.5	4.0	10.0[d]	P,H aromatic = 2.25
p-$CH_3OCOC_6H_4$ *syn* **26**	9.2	6.0	—	—	6.0	6.0	6.0	10.5	P,H aromatic = 2.25 5,4 = 6,7 = 3.2
α-Naphthyl *anti* **28**	10.0	6.4	1.0	1.6	4.5[c]	19.2	4.0	10.8	—
β-Naphthyl *anti* **29**	10.0	6.0[d]	—	—	4.5[c]	20.0	4.4	10.8	—
β-Naphthyl *syn* **30**	9.2	6.0		—	5.6	6.0		10.8	5,4 = 6,7 = 3.2
C_2H_5 *anti* **33**	9.2	6.8	1.0	—	—	—	4.8	11.2	
C_2H_5 *syn* **34**	8.0	6.6	1.0	—	6.0	—	6.6	10.2	CH_3CH_2 = 7.2 5,4 = 6,7 = 3.2
iso-C_3H_7 *anti* **35**	—	6.2	1.2	1.6	—	20.0		11.0[d]	$CH(CH_3)_2$ = 6.4
iso-C_3H_7 *syn* **36**	—	6.5	1.0	1.5	5.7	6.5	6.5	10.8	$CH(CH_3)_2$ = 5.2 5,4 = 6,7 = 3.2
tert-C_4H_9 *syn* **37**	10.0	6.4	1.0	—	—	6.4	6.4	10.0	
$C_6H_5CH_2$ *anti* **38**	9.0	6.0	—	1.5	—	18.0	—	10.2	
$C_6H_5CH_2$ *syn* **39**	10.0	6.0	—	1.5	6.0	6.0	—	10.6	*p*-CCH_2Ph: 6.2 and 8.1 5,4 = 6,7 = 3.0

[a] ± 0.2 Hz.
[b] All the H_9 resonances show, in addition, a small coupling (1.0 Hz) with one of the bridgehead (the upfield one in the *anti* derivatives).
[c] $W_{1/2}$.
[d] ± 0.5 Hz.

Can. J. Chem. Downloaded from www.nrcresearchpress.com by 210.87.254.105 on 09/05/12
For personal use only.

pletion of the reaction in this way. The % completion given here can be estimated to be accurate within ±5%. For the *tert*-butyl derivative **13**, there was no noticeable reaction after 50 h. No kinetic studies were done on **6**, **8**, **9**, and **14** (Table 6).

General Procedures for the Cycloaddition Reactions

A mixture of norbornadiene (40 ml), diazophosphonate (3 g), and CH_2Cl_2 (3 ml) was warmed at a bath temperature never exceeding 55–60°. The proportions were changed slightly for the *p*-methylphenyldiazo derivative **2** (norbornadiene, 50 ml, diazo compound, 3.42 g, and CH_2Cl_2, 5 ml) and for the *p*-nitrophenyldiazo derivative **5** (norbornadiene, 35 ml, diazo compound, 2 g, CH_2Cl_2, 2 ml). The reaction time varied from 24 h to 26 days (see Table 7). The addition with the phenyl **4** and the methyl **10** derivatives have been described (4). The reaction time was 24 h for both reactions.

General Procedure for the Isolation of the Cycloadducts

The reaction mixture was poured as such on a 180 g silica gel column chromatograph. Excess diazo compound was eluted with ether while the pyrazolines came out with MeOH–ether mixtures. In the case of the aryl derivatives, the *syn* epimer was eluted first (5% MeOH in ether) and then the *anti* (10% MeOH in ether). Separation was much more difficult with alkyl derivatives. The addition of the methyl derivative **10** has already been described (4). For all the alkyl derivatives, the excess diazo compound was eluted with pure ether. In the case of the ethyl **11** and the isopropyl **12** derivatives, the *anti* epimer was eluted before the *syn*; the eluent in both cases was a 20% solution of MeOH in ether. As to the *tert*-butyl diazo compound **13**, only one pyrazoline (*syn*) could be detected and was isolated with MeOH–ether (20:80).

Nuclear Magnetic Resonance Spectra of the Pyrazolines (Tables 8 and 9)

Those spectra are typical of a *syn* or an *anti* configuration. For all isomers, H_8 appears as an AB quartet, the center (C) of which is given; H_{8s} (*syn* to the 5,6 double bond) is assigned the low-field signals because of long-range couplings with H_9 and H_{10} protons; otherwise (*e.g.* compound **36**) the assignment (*s* or *a*) is not specified (δ_A and δ_B are given). P—OCH_3 gives two doublets (unequivalent OCH_3's).

In the *anti* isomers, the bridgehead protons (H_4 and H_7) are broad singlets > 1.0 p.p.m. apart; H_{10} gives rise to a d or d of d signal (eight lines in all) by coupling with H_9, H_{8s}, and P; H_9 appears as a d of d (coupling with P, H_{10}; fine resolution shows each signal as a t, due to coupling with H_{8s} and either H_4 or H_7); H_5 and H_6 each give a narrow multiplet; $w_{\frac{1}{2}}$ is given.

In the *syn* isomers the bridgehead protons are broad s 0.3–0.5 p.p.m. apart, and no assignment is made; H_{10} gives rise to a t signal (in fact it is a d of d by coupling with H_9 and P; the fine structure reveals further long-range coupling with H_{8s}); H_9 appears as a t (in fact d of d, by coupling with P and H_{10}; also small couplings with H_{8s} and either H_4 or H_7 are visible); H_5 and H_6 give an eight-line multiplet (AB part of an ABXY spectrum by coupling with H_4 and H_7) the center of which is given in Table 8.

The authors wish to thank the National Research Council of Canada for financial support of this work (operating grant A-5496) and the Rector of the University of Ottawa for a stipend to one of us (H.C.).

1. R. HUISGEN. Angew. Chem. Int. Ed. **2**, 633 (1963).
2. R. HUISGEN. J. Org. Chem. **33**, 2291 (1968).
3. R. A. FIRESTONE. J. Org. Chem. **33**, 2285 (1968); **37**, 2181 (1972).
4. H. J. CALLOT and C. BENEZRA. Can. J. Chem. **50**, 1078 (1972).
5. R. S. MARMOR and D. SEYFERTH. J. Org. Chem. **36**, 128 (1971).
6. J. E. CADOGAN. Q. Rev. **22**, 222 (1968).
7. (*a*) M. REGITZ, W. ANSCHÜTZ, and A. LIEDHEGENER. Chem. Ber. **101**, 3734 (1968); (*b*) H. SHERER, A. HARTMANN, M. REGITZ, B. D. TUNGGAL, and H. GUNTHER. Chem. Ber. **105**, 3357 (1972).
8. N. GURUDATA, C. BENEZRA, and H. COHEN. Can. J. Chem. **51**, 1142 (1973).
9. H. COHEN and C. BENEZRA. Org. Magn. Res. **5**, 205 (1973).
10. C. W. JEFFORD and F. DELAY. J. Am. Chem. Soc. **94**, 4794 (1972) and references therein.
11. L. M. JACKMAN and S. STERNHELL. Applications of nmr spectroscopy in organic chemistry. 2nd Ed., Pergamon Press, Oxford. 1969. p. 334.
12. C. BENEZRA. Tetrahedron Lett. 4471 (1969); J. Am. Chem. Soc. **95**, 6890 (1973).
13. H. C. BROWN and J. H. KAWAKAMI. J. Am. Chem. Soc. **92**, 201 (1970).
14. (*a*) S. J. CRISTOL, G. D. BRINDELL, and J. A. REEDER. J. Am. Chem. Soc. **80**, 635 (1958); (*b*) D. J. TRECKER and J. P. HENRY. J. Am. Chem. Soc. **85**, 3204 (1963); (*c*) H. J. CALLOT and C. BENEZRA. Can. J. Chem. **49**, 500 (1971); (*d*) H. G. KUIVILA and C. R. WARNER. J. Org. Chem. **29**, 2845 (1964).
15. D. I. DAVIES and P. J. ROWLEY. J. Chem. Soc. C, 2245 (1967).
16. R. R. SAUERS and P. E. SONNET. Tetrahedron, **20**, 1029 (1964).
17. R. HUISGEN, R. GRASHEY, and J. SAUER. Cycloaddition reactions of alkenes. *In* The chemistry of alkenes. *Edited by* S. Patai. Interscience Publishers, London. 1964. (*a*) p. 816 (*b*) p. 836.
18. N. FILIPESCU and J. R. DEMEMBER. Tetrahedron, **24**, 5181 (1968).
19. J. A. HIRSCH. Table of conformational energies—1967. *In* Topics in stereochemistry. Vol. 1. *Edited by* N. L. Allinger and E. L. Eliel. Interscience Publishers, New York. 1967. p. 199.
20. N. L. ALLINGER and M. T. TRIBBLE. Tetrahedron Lett. 3259 (1971) and references therein.
21. B. L. SHAPIRO, M. J. GATTUSO, N. F. HEPFINGER, R. S. SHONE, and W. L. WHITE. Tetrahedron Lett. 219 (1971).
22. R. HUISGEN, W. SCHEER, H. MÄDER, and E. BRUNN. Angew Chem. Int. Ed. **8**, 604 (1969).
23. B. W. HOTTEN. U.S. Patent No. 2 808 428; Chem. Abstr. **52**, 2918c (1958).
24. Dictionary of organic compounds. 4th Ed. Eyre and Spottiswoode Publishers Ltd., London. 1965. p. 2949.

Reactions of Keten Acetals. Part I. A Simple Synthesis of Some Naturally Occurring Anthraquinones[1]

JACQUES BANVILLE, JEAN-LOUIS GRANDMAISON, GÉRARD LANG, AND PAUL BRASSARD

Département de Chimie, Université Laval, Québec, Québec G1K 7P4

Received July 16, 1973

A study of the condensation of keten acetals with some halonaphthoquinones has led to the simple and regiospecific synthesis of some naturally occurring anthraquinones: catenarin, helminthosporin, emodin, and chrysophanol. The results show unambiguously that a previously proposed mechanism is erroneous. The reaction of these acetals with chloromaleic anhydride also provided a one-step preparation of some substituted phthalic anhydrides.

L'étude de la condensation d'acétals de cétènes avec des halogénonaphtoquinones a permis la synthèse facile et régiospécifique de quelques anthraquinones naturelles: la caténarine, l'helminthosporine, l'émodine et le chrysophanol. Les résultats obtenus démontrent que le mécanisme déjà proposé pour cette réaction est erronée. La réaction de ces acétals avec l'anhydride chloromaléique donne en une seule étape des anhydrides phtaliques substitués.

Can. J. Chem., **52**, 80 (1974)

Although keten acetals are very reactive and readily accessible (1, 2), their use in the synthesis of naturally occurring compounds has been considered only rarely. McElvain *et al.* (3–5) have studied the reactions of keten diethyl acetal (**1***b*) with enedione systems and have shown in particular that *p*-benzoquinone, halo-*p*-benzoquinones, and 1,4-naphthoquinone yield 2-ethoxy furans. However under essentially similar conditions 2-bromonaphthoquinone gives a 21% yield of 1,3-diethoxyanthraquinone (xanthopurpurin diethyl ether). Moreover they have proposed mechanisms whereby complex series of processes are initiated by the attack of **1***b*, in the first three cases, on an unsubstituted carbon atom and, in the last instance, on the halogen-bearing one.

The existence of two very different reaction paths and, apparently, modes of attack has led us to examine the factors which determine the course of the reaction and the eventual regiospecificity of the process as applied to the synthesis of anthraquinones. This seemed to be particularly promising since the required isomeric naphthazarins and juglones were known. For ease in identifying the reaction products in mixtures that are often complex, keten dimethyl acetal was used in work of a more exploratory nature, whereas the more readily accessible diethyl acetal was chosen for some of the purely synthetic part. No other particular advantage was found for either of these reagents.

Reactions of Keten Acetals with Halonaphthazarins

It was first established that the presence of the two hydroxyl groups in chloronaphthazarin (**3**) did not prevent or affect a reaction similar to that described for bromonaphthoquinone. Moreover since both 6- and 7-chloro-2-methylnaphthazarin had been identified previously (6), these compounds could readily serve in assessing the proposed dual mode of attack and in providing a very simple synthesis of catenarin (**7***b*). According to McElvain's mechanism, 7-chloro-2-methylnaphthazarin (**5**) should have provided the diethyl ether **7***a*. However the properties of the compound obtained from it, after deethylation, were quite different from those ascribed to catenarin and were correlated to the isomeric substance **8***b*. When carried out with 6-chloro-2-methylnaphthazarin (**4**), the reaction effectively led to the formation of catenarin. In each case, only one quinonic product was obtained as ascertained by t.l.c. and n.m.r. thus clearly establishing that the proposed mechanism is wrong, that only one mode of attack occurs and that the reaction is completely regiospecific. These results were also extended by the reaction of **3** with isopropenylketen diethyl acetal (**2**) which produced **9***a* and thence helminthosporin (**9***b*). In this case the reaction is more efficient

[1]During the preparation of this paper, one of the authors (G.L.) obtained unauthorized patents covering part of the material described here in detail (Fr. 2,112,941; Ger. Offen. 2,144,771–2,144,774).

Can. J. Chem. Downloaded from www.nrcresearchpress.com by 210.87.254.6 on 09/05/12
For personal use only.

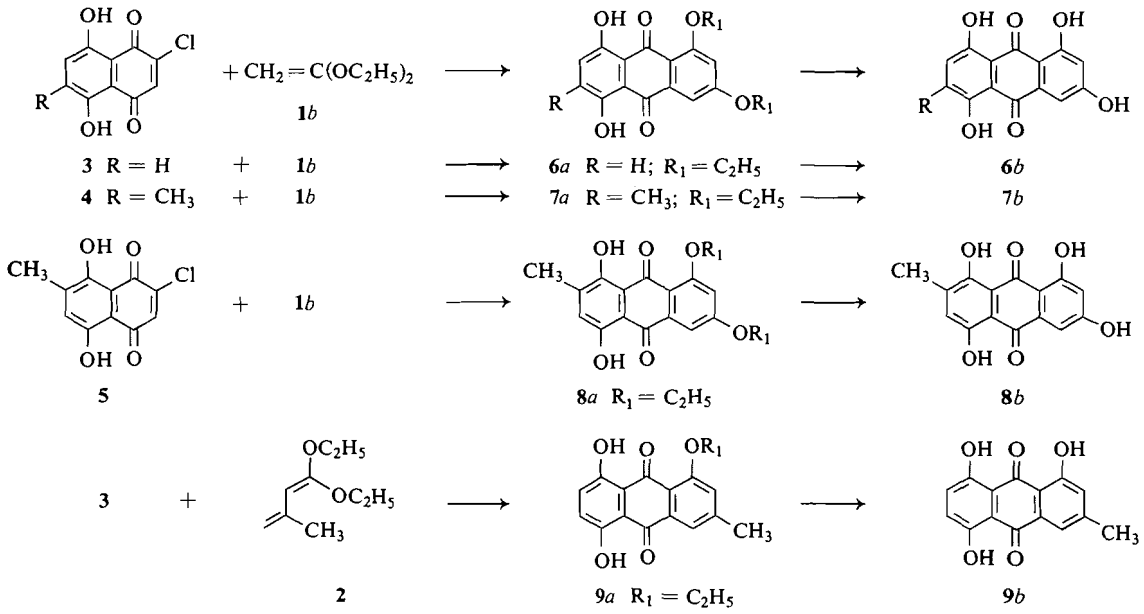

SCHEME I

and produces a much higher yield than with the unconjugated acetals (Scheme 1).

Reactions of Keten Acetals with Bromojuglones

For a more detailed study of the reaction, 2- and 3-bromojuglones were chosen since numerous synthetic applications could be envisaged. Upon adding 3-bromojuglone (**14**) to the theoretical amount (5 equiv.)[2] of keten dimethyl acetal (**1***a*) in the absence of solvent a vigorous reaction ensues and a 60% yield of 1,3-dimethoxy-8-hydroxyanthraquinone (**19***a*) is produced and could be converted into the known 1,3,8-trimethoxyanthraquinone. Under similar conditions 2-bromojuglone (**18**) reacts slowly even at 100° and gives 1,3-dimethoxy-5-hydroxyanthraquinone (53%) and, after methylation, the known 1,3,5-trimethoxyanthraquinone. In both cases t.l.c. revealed no trace of the other isomer. These reactions, therefore, establish that the process is also completely regiospecific in the case of juglones and, though electronic effects modify sharply the reactivity, they do not alter the product-determining step.

The only convenient starting material available for the synthesis of the important natural product emodin (**22***b*) by this method is 8-chloro-7-methyljuglone (**13**). By successive bromination and dehydrobromination of three 8-chlorojuglones the corresponding 3-bromo derivatives were obtained in high yields. The structures were assumed to be those predicted on the basis of the work of Thomson (7) on juglone itself (**10**) and were established unambiguously but indirectly by the substitution patterns in the anthraquinones obtained from them (Scheme 2). By varying the ratios of the reactants, the solvents, the reaction times, and by adding a catalyst ($Hg(OAc)_2$) (8) known to be effective in a reaction of enol ethers, no marked effects were observed. The results are summarized in Table 1. These experiments did establish that an excess of keten acetals should be avoided, that the best results are obtained in the absence of solvent and that free *peri*-hydroxyl groups favor the reaction (Scheme 3). Under these conditions no starting material or other quinonic by-product is isolated or detected. However when only 2 equiv. of **1***a* are used, a small amount (8%) of another substance is formed which probably is methyl (3-bromo-8-chloro-5-hydroxy-7-methylnaphthoquinonyl-2)-acetate. During chromatography (silica gel) the bromine is lost in part and the product could not be adequately purified. The reaction of 3-bromo-8-chlorojuglone (**15**) with isopropenylketen diethyl acetal was also found

[2]During the condensation hydrogen bromide and methanol are eliminated, which react further with the keten acetal.

Can. J. Chem. Downloaded from www.nrcresearchpress.com by 210.87.254.6 on 09/05/12
For personal use only.

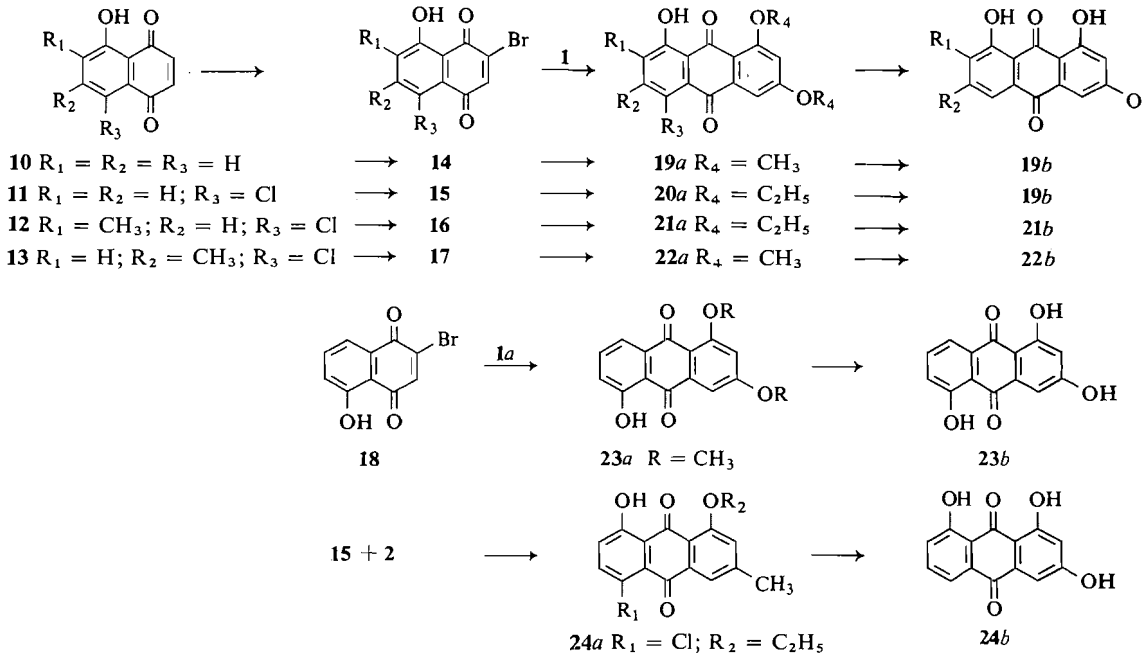

SCHEME 2

TABLE 1. Condensation of 3-bromo-8-chloro-7-methyljuglone (**17**) (600 mg) with keten dimethyl acetal (**1***a*)

Equivalents of acetal	Solvent	Conditions	Yield of **22***a* (%)
2	C_6H_6 (10 ml)	Refluxed 10 min	13
5	C_6H_6 (10 ml)	Refluxed 10 min	25
7	C_6H_6 (10 ml)	Refluxed 10 min	12
3	C_6H_6 (10 ml)	Refluxed 12 h	22
5	C_6H_6 (10 ml)	Refluxed 12 h	30
8	C_6H_6 (10 ml)	Refluxed 12 h	23
5	C_6H_6 (10 ml)	$Hg(OAc)_2$ (32 mg) Refluxed 12 h	19
5	DME (10 ml)	Refluxed 12 h	26
5	C_6H_6 (200 ml)	Refluxed 12 h	19
5	None	100 °C 1 h	57

to be particularly efficient giving a good yield of the corresponding chloroanthraquinone (**24***a*). However a reaction carried out with a chloroketen acetal in the hope of obtaining conveniently substituted chloroanthraquinones was disappointing as the reagent was found to be insufficiently reactive.

The conversion of the chlorinated anthraquinone ethers (**20***a*–**22***a*, **24***a*) to the polyhydroxyanthraquinones (**19***b*, **21***b*, **22***b*, **24***b*) can be carried out efficiently by known methods either (*A*) by reduction with sodium hydrosulfite (9, 10) followed by demethylation with aluminium chloride at 180° (11) or (*B*) by treatment with hydriodic acid and red phosphorus followed by reoxidation with chromic acid (12).

Reactions of Keten Acetals with Chloromaleic Anhydride

Keten dimethyl and diethyl acetals (**1***a*, *b*) as well as isopropenylketen diethyl acetal (**2**) have been found to react vigorously with chloromaleic anhydride and to give directly in moderate yields 3,5-dimethoxy- 3,5-diethoxy- and 3-eth-

Can. J. Chem. Downloaded from www.nrcresearchpress.com by 210.87.254.6 on 09/05/12
For personal use only.

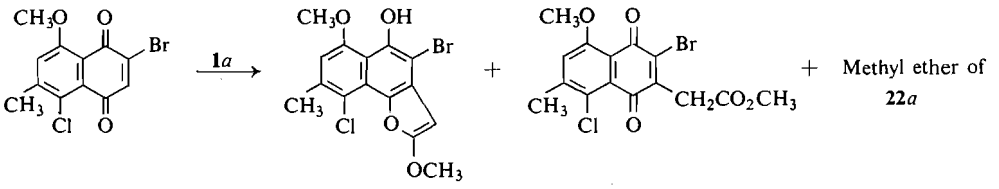

25 26

SCHEME 3

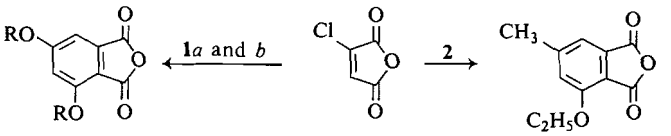

27a R = CH_3
27b R = C_2H_5

28

SCHEME 4

oxy-5-methylphthalic anhydrides. These reactions, therefore, provide very convenient syntheses of these important intermediates (Scheme 4).

Conclusion

In conclusion, this paper illustrates a few very practical syntheses of anthraquinones and numerous other applications of the procedure can be envisaged with minor modifications of the method. The original mechanism proposed by McElvain has been found to be erroneous but no other can be proposed with certainty at present. The intermediate formation of a zwitterion followed by a 1,4-dipolar addition of keten acetal and a triple elimination seems to represent the most plausible series of processes; however, a mechanism involving an oxidative step, as suggested by the reaction with a juglone ether cannot be discounted.

Since all benzoquinones and some naphthoquinones invariably yield 2-alkoxy furans numerous attempts have been made to decrease the ease with which this course is taken. Condensations involving various dibenzoquinones, dihalobenzoquinones (with or without the addition of Lewis acids), and halogenated benzoquinone imines, imides, and chloroimides have not given encouraging results.

Experimental

Reactions of Keten and Isopropenylketen Diethyl Acetal with Chloronaphthazarins

General Procedure a

To a solution of 1.0 g of the chloronaphthazarin (3–5) in 10 ml of anhydrous benzene are added 5 equiv. of keten diethyl acetal (**1***b*) (2). The solution which darkens immediately is allowed to stand for 1 h and then refluxed for 1 h. The crystals that separate on cooling are washed with petroleum ether (b.p. 30–60°) and recrystallized from the appropriate solvent.

1,3-Diethoxy-5,8-dihydroxyanthraquinone (**6***a*) is obtained from chloronaphthazarin (**3**) (13), m.p. 203–204° (toluene) (23%); λ_{max} (EtOH) 230, 277.5, 296, 470, 490 nm (log ε 4.59, 4.32, 4.03, 4.07, 4.04); ν_{max} (KBr) 1610 (sh), 1598 cm^{-1}; δ (90 MHz) ($CDCl_3$) 1.47 t (J = 7.0 Hz) (3-OCH_2CH_3), 1.57 t (J = 7.0 Hz) (1-OCH_2CH_3), 4.20 q (J = 7.0 Hz) (1,3-OCH_2—), 6.72 d (J = 2.5 Hz) (2-CH), 7.19 s (6,7-CH), 7.42 d (J = 2.5 Hz) (4-CH), 12.75 s and 13.44 s (5,8-OH).

Anal. Calcd. for $C_{18}H_{16}O_6$: C, 65.85; H, 4.91. Found: C, 65.46; H, 4.90.

6,8-Diethoxy-1,4-dihydroxy-3-methylanthraquinone (**7***a*) is prepared from 6-chloro-2-methylnaphthazarin (**4**) (6), m.p. 174–175° (benzene) (34%); λ_{max} (EtOH) 231.5, 277, 300 (sh), 480 nm (log ε 4.60, 4.31, 4.04, 4.12); ν_{max} (KBr) 1615 (sh), 1595 (sh), 1580 cm^{-1}; δ (90 MHz) ($CDCl_3$) 1.47 t (J = 7.0 Hz) (6-OCH_2CH_3), 1.57 t (J = 7.0 Hz) (8-OCH_2CH_3), 2.33 s (3-CH_3), 4.22 q (J = 7.0 Hz) (6,8-OCH_2—), 6.72 d (J = 2.2 Hz) (7-CH), 7.04 s (2-CH), 7.42 d (J = 2.2 Hz) (5-CH), 12.83 s and 13.88 s (1,4-OH).

Anal. Calcd. for $C_{19}H_{18}O_6$: C, 66.66; H, 5.29. Found: C, 66.23; H, 5.33.

6,8-Diethoxy-1,4-dihydroxy-2-methylanthraquinone (**8***a*) is obtained from 7-chloro-2-methylnaphthazarin (**5**) (6), m.p. 186–187° (toluene) (47%); λ_{max} (EtOH) 231.5, 275, 301 (sh), 480 nm (log ε 4.56, 4.28, 4.01, 4.06); ν_{max} (KBr) 1618, 1590, 1575 cm^{-1}; δ (90 MHz) ($CDCl_3$) 1.47 t (J = 7.0 Hz) (6-OCH_2 CH_3), 1.56 t (J = 7.0 Hz) (8-OCH_2CH_3), 2.30 s (2-CH_3), 4.18 q (J = 7.0 Hz) (6,8-OCH_2—), 6.68 d (J = 2.5 Hz) (7-CH), 7.08 s (3-CH), 7.39 d (J = 2.5 Hz) (5-CH), 13.16 s and 13.48 s (1,4-OH).

Anal. Calcd. for $C_{19}H_{18}O_6$: C, 66.66; H, 5.29. Found: C, 66.92; H, 5.25.

1-Ethoxy-5,8-dihydroxy-3-methylanthraquinone (**9***a*): Equimolar quantities of chloronaphthazarin (1 g) and isopropenylketen diethyl acetal (**2**) (14) are dissolved in anhydrous benzene (10 ml). The reaction mixture is then refluxed for 1 h, cooled, and diluted with a small amount

Can. J. Chem. Downloaded from www.nrcresearchpress.com by 210.87.254.6 on 09/05/12
For personal use only.

Can. J. Chem. Downloaded from www.nrcresearchpress.com by 210.87.254.6 on 09/05/12
For personal use only.

of petroleum ether. The precipitated solid is recrystallized from petroleum ether, m.p. 186–187° (72%); λ_{max} (EtOH) 230, 255, 287 (sh), 475 nm (log ε 4.59, 4.12, 3.86, 3.98); ν_{max} (KBr) 1622, 1596 cm^{-1}; δ (90 MHz) ($CDCl_3$) 1.58 t (J = 7.0 Hz) (1-OCH_2CH_3), 2.47 s (3-CH_3), 4.34 q (J = 7.0 Hz), 7.07 bs (2-CH), 7.73 bs (4-CH), 7.21 s (6,7-CH), 12.82 s and 13.32 s (5,8-OH).

Anal. Calcd. for $C_{17}H_{14}O_5$: C, 68.45; H, 4.73. Found: C, 68.51; H, 4.62.

Polyhydroxyanthraquinones (from Naphthazarins)

The diethoxy or ethoxy methyl dihydroxyanthraquinone (**7***a*–**9***a*) (500 mg) is added to a solution of 5 g of anhydrous $AlCl_3$ in 20 ml of nitrobenzene. The mixture is stirred for 24 h at 80° and then poured into 500 ml of ice and water. The nitrobenzene is extracted with petroleum ether and the aqueous solution heated to 80°. Upon cooling, crystals of the deethylated compound are recovered and crystallized from the appropriate solvent.

1,4,6,8-Tetrahydroxy-3-methylanthraquinone (catenarin) (**7***b*) from **7***a*, m.p. 244–246° (EtOH) (90%) (lit. (15) m.p. 246°); λ_{max} (EtOH) 231, 255.5, 279, 302, 475, 490, 505 (sh), 515 (sh) nm (log ε 4.46, 4.17, 4.19, 3.99, 4.07, 4.11, 4.02, 3.95); ν_{max} (KBr) 3300, 1610 (sh), 1598 cm^{-1}; δ (90 MHz) ($(CD_3)_2SO$) 2.09 s (3-CH_3), 6.40 d (J = 2.5 Hz) (7-CH), 6.87 d (J = 2.5 Hz) (5-CH), 6.94 s (2-CH), 11.90 s and 12.90 s (1,4,8-OH).

Tetraacetate, m.p. 235° (lit. (15) m.p. 234–235°).

1,4,6,8-Tetrahydroxy-2-methylanthraquinone (**8***b*) from **8***a*, m.p. 273–274° (EtOH) (90%); λ_{max} 231.5, 252.5, 280.5, 300, 485, 505, 515 nm (log ε 4.51, 4.20, 4.26, 4.05, 4.18, 4.08, 4.02); ν_{max} (KBr) 3338, 1602, 1590 (sh) cm^{-1}; δ (90 MHz) ($(CD_3)_2SO$) 2.14 (2-CH_3), 6.45 d (J = 2.0 Hz) (7-CH), 6.95 d (J = 2.0 Hz) (5-CH), 6.98 s (3-CH), 11.89 s, 12.28 s and 12.50 s (1,4,8-OH).

Anal. Calcd. for $C_{15}H_{10}O_6$: C, 62.94; H, 3.52. Found: C, 63.13; H, 3.43.

Tetraacetate, m.p. 221°.

1,5,8-Trihydroxy-3-methylanthraquinone (helminthosporin) (**9***b*) from **9***a*, m.p. 226–227° (pyridine) (almost quantitative) (lit. (16) m.p. 226–227°); λ_{max} (EtOH) 231, 255, 289, 480 (sh), 490, 510 (sh), 520 (sh) nm (log ε 4.67, 4.30, 3.95, 4.11, 4.13, 4.01, 3.91); ν_{max} (KBr) 1598 cm^{-1}; δ (90 MHz) ($CDCl_3$) 2.47 s (3-CH_3), 7.10 bs (2-CH), 7.69 bs (4-CH), 7.28 s (6,7-CH), 12.08 s, 12.27 s and 12.97 s (1,5,8-OH).

Triacetate, m.p. 223° (lit. (16) m.p. 224°).

8-Chlorojuglones

These compounds were prepared according to Cooke *et al.* (17, 18).

8-Chlorojuglone (**11**), m.p. 197–198° (lit. (17) m.p. 201°); λ_{max} (EtOH) 211.5, 254, 430 nm (log ε 4.51, 4.14, 3.66); ν_{max} (KBr) 1665, 1645, 1600 cm^{-1}; δ (60 MHz) ($CDCl_3$) 7.01 s (2,3-CH), 7.50 dd (J = 9.5 Hz; Δν = 24.2 Hz) (6,7-CH), 12.65 s (5-OH).

8-Chloro-6-methyljuglone (**12**) was prepared from 20.0 g of 5-chloro-2-methoxytoluene, 24.0 g of maleic anhydride, 226 g of anhydrous $AlCl_3$ and 50 g of NaCl by heating at 200° for 2 min. The crude material obtained after hydrolysis was extracted (Soxhlet) with petroleum ether (b.p. 30–60°) and chromatographed on silica gel (benzene), m.p. 160.5–161.0° (petroleum ether) (24%); λ_{max} (EtOH) 217, 258, 338, 430 nm (log ε 4.35, 3.93, 4.14, 3.43); ν_{max} (KBr) 1670, 1645, 1597 cm^{-1}; δ (60 MHz) ($CDCl_3$) 2.35 s (6-CH_3), 6.95 s (2,3-CH), 7.53 s (7-CH), 13.10 s (5-OH).

Anal. Calcd. for $C_{11}H_7ClO_3$: C, 59.64; H, 3.17. Found: C, 59.59; H, 3.09.

8-Chloro-7-methyljuglone (**13**), m.p. 158–159° (lit. (18) m.p. 159–161°); λ_{max} (EtOH) 217, 256, 340, 425 nm (log ε 4.54, 4.12, 3.11, 3.69); ν_{max} (KBr) 1670, 1655, 1615 cm^{-1}; δ (60 MHz) ($CDCl_3$) 2.52 s (7-CH_3), 6.99 s (2,3-CH), 7.25 s (6-CH), 12.60 s (5-OH).

3-Bromo-8-chlorojuglones

These quinones are prepared by the methods of Wheeler and Scott (19) and Thomson (7). A suspension of the chlorojuglone (**11**–**13**) (1 to 3 g) and a five-fold excess of Br_2 in CCl_4 (4 to 12 ml) is stirred for 5 h at room temperature and evaporated to dryness under vacuum. The residue dissolved in absolute ethanol (12 to 36 ml) is refluxed for 3 min and a nearly quantitative yield of the 3-bromo-8-chlorojuglone (**16**–**18**) is obtained on cooling.

3-Bromo-8-chlorojuglone (**15**) is obtained from **11**, m.p. 202–203° (dichloroethane); λ_{max} (EtOH) 216, 260, 285, 435 nm (log ε 4.41, 3.86 3.92, 3.62); ν_{max} (KBr) 1655, 1635, 1595 cm^{-1}; δ (90 MHz) ($(CD_3)_2CO$) 7.59 s (2-CH), 7.59 dd (J = 9.5 Hz; Δν = 19.3 Hz) (6,7-CH), 12.30 s (5-OH).

Anal. Calcd. for $C_{10}H_4BrClO_3$: C, 41.77; H, 1.39. Found: C, 41.91; H, 1.40.

3-Bromo-8-chloro-6-methyljuglone (**16**) from **12**, m.p. 144–145° (CCl_4); λ_{max} (EtOH) 221, 265 (sh), 290, 440 nm (log ε 4.43, 3.83, 3.91, 3.62); ν_{max} (KBr) 1650, 1635, 1600 cm^{-1}; δ (60 MHz) ($CDCl_3$) 2.35 s (6-CH_3), 7.46 s (2-CH), 7.52 s (7-CH), 12.65 s (5-OH).

Anal. Calcd. for $C_{11}H_6BrClO_3$: C, 43.82; H, 2.01. Found: C, 44.03; H, 1.91.

3-Bromo-8-chloro-7-methyljuglone (**17**) from **13**, m.p. 187.5–188.0° (EtOH); λ_{max} (EtOH) 221, 259, 289, 435 nm (log ε 4.31, 3.67, 3.79, 3.60); ν_{max} (KBr) 1666, 1640, 1600 cm^{-1}; δ (60 MHz) ($CDCl_3$) 2.52 s (7-CH_3), 7.28 s (2-CH), 7.51 s (6-CH), 12.40 s (5-OH).

Anal. Calcd. for $C_{11}H_6BrClO_3$: C, 43.82; H, 2.01. Found: C, 43.58; H, 2.10.

3-Bromo-8-chloro-5-methoxy-7-methylnaphthoquinone (methyl ether of **17**): The juglone **17** (1.0 g) is dissolved in 20 ml of $CHCl_3$, two portions of iodomethane (1.0 ml) and Ag_2O (0.6 g) are added at 6 h intervals and the mixture stirred at room temperature for 14 h. The methyl ether is obtained in almost quantitative yield, m.p. 205–206° (dichloroethane); λ_{max} (EtOH) 219, 258, 280 (sh), 415 nm (log ε 4.53, 4.10, 4.04, 3.62); ν_{max} (KBr) 1665, 1662, 1583 cm^{-1}; δ (60 MHz) ($CDCl_3$) 2.54 s (7-CH_3), 4.02 s (5-OCH_3), 7.28 s (6-CH), 7.43 s (2-CH).

Anal. Calcd. for $C_{12}H_8BrClO_3$: C, 45.67; H, 2.55. Found: C, 45.79; H, 2.45.

Reactions of Keten and Isopropenylketen Acetals with Bromojuglones

General Procedure b

Keten dimethyl acetal (**1***a*) (20)[3] (1.04 g; 0.0118 mol) is added all at once to the bromojuglone (0.00238 mol). A vigorous reaction ensues and the mixture is kept at 100° for 1 h. The volatile by-products are then evaporated under vacuum and the residue chromatographed on 100 g

[3]In this procedure, ref. 20, benzene is advantageously replaced by xylene.

Can. J. Chem. Downloaded from www.nrcresearchpress.com by 210.87.254.6 on 09/05/12
For personal use only.

of silica gel. A mixture of benzene and ether (19:1) elutes the 8-hydroxy-1,3-dimethoxyanthraquinone.

8-Hydroxy-1,3-dimethoxyanthraquinone (**19***a*) was obtained from **14** (7), m.p. 217.5–218° (EtOH and sublimed) (61%); λ_{max} (EtOH) 222, 242, 270 (sh), 279, 420 nm (log ε 4.54, 4.14, 4.30, 4.33, 4.02); ν_{max} (KBr) 1666, 1625, 1596 cm^{-1}; δ (60 MHz) ($CDCl_3$) 4.03 s (3-OCH_3), 4.08 s (1-OCH_3), 6.87 d (J = 2.5 Hz) (2-CH), 7.45 d (J = 2.5 Hz) (4-CH), 7.5–8.0 m (5,6,7-CH), 13.30 s (8-OH).

Anal. Calcd. for $C_{16}H_{12}O_5$: C, 67.60; H, 4.25. Found: C, 67.80; H, 4.35.

1,3,8-Trimethoxyanthraquinone was prepared by refluxing for 3 h a mixture of **19***a* (0.21 g), dimethyl sulfate (1.8 g), anhydrous K_2CO_3 (2.0 g) and acetone (20 ml), m.p. 194.5–195.0° (EtOH) (85%) (lit. (21) m.p. 195–196°); λ_{max} (EtOH) 219, 275, 395 nm (log ε 4.51, 4.38, 3.89); ν_{max} (KBr) 1660, 1603 cm^{-1}; δ (60 MHz) ($CDCl_3$) 3.99 s, 4.01 s and 4.03 s (1,3,8-OCH_3), 6.84 d (J = 2.5 Hz) (2-CH), 7.3–8.0 m (4,5,6,7-CH).

5-Hydroxy-1,3-dimethoxyanthraquinone (**23***a*) from **18** (22), m.p. 199–199.5° (EtOH and sublimed) (53%); λ_{max} (EtOH) 228, 248, 278, 404 nm (log ε 4.49, 4.12, 4.31, 3.99); ν_{max} (KBr) 1665, 1645, 1605 cm^{-1}; δ (60 MHz) ($CDCl_3$) 4.01 s (3-OCH_3), 4.04 s (1-OCH_3), 6.85 d (J = 2.5 Hz) (2-CH), 7.52 d (J = 2.5 Hz) (4-CH), 7.2–7.9 m (5,7,8-CH), 12.40 s (5-OH).

Anal. Calcd. for $C_{16}H_{12}O_5$: C, 67.60; H, 4.25. Found: C, 67.85; H, 4.05.

1,3,5-Trimethoxyanthraquinone was prepared from **23***a* as above for the 1,3,8-isomer, m.p. 201.5–202° (EtOH) (85%) (lit. (23) m.p. 203°); λ_{max} (EtOH) 226, 276, 283 nm (log ε 4.51, 4.39, 4.01); ν_{max} (KBr) 1660, 1605 cm^{-1}; δ (60 MHz) ($CDCl_3$) 3.98 s, 4.02 s and 4.06 s (1,3,5-OCH_3), 6.80 d (J = 2.5 Hz) (2-CH), 7.48 d (J = 2.5 Hz) (4-CH), 7.2–8.0 m (6,7,8-CH).

4-Chloro-1-hydroxy-6,8-dimethoxy-3-methylanthraquinone (**22***a*) from **17**, m.p. 213–213.5° (EtOH and sublimed) (57%); λ_{max} (EtOH) 227, 271, 282 (sh), 430 nm (log ε 4.57, 4.31, 4.27, 4.02); ν_{max} (KBr) 1677, 1625, 1592 cm^{-1}; δ (60 MHz) ($CDCl_3$) 2.45 s (3-CH_3), 3.97 s (6-OCH_3), 4.00 s (8-OCH_3), 6.75 d (J = 2.5 Hz) (7-CH), 7.20 s (2-CH), 7.43 d (J = 2.5 Hz) (5-CH), 13.60 s (1-OH).

Anal. Calcd. for $C_{17}H_{13}ClO_5$: C, 61.36; H, 3.93; Found: C, 61.31; H, 3.86.

General Procedure a (see first Section)

This method gave products analogous to the foregoing.

5-Chloro-1,3-diethoxy-8-hydroxyanthraquinone (**20***a*) from **15** and **1***b*, m.p. 182–182° (benzene – petroleum ether) (33%); λ_{max} (EtOH) 223, 229 (sh), 271, 422, 430, 437 nm (log ε 4.46, 4.43, 4.27, 4.00, 4.00, 4.00); ν_{max} (KBr) 1670, 1631, 1626, 1598 cm^{-1}; δ (90 MHz) ($CDCl_3$) 1.46 t (J = 7.0 Hz) (3-OCH_2CH_3), 1.59 t (J = 7.0 Hz) (1-OCH_2CH_3), 4.19 q (J = 7.0 Hz) (1,3-OCH_2—), 6.72 d (J = 2.5 Hz) (2-CH), 7.33 d (J = 2.5 Hz) (4-CH), 7.34 dd (J = 8.5 Hz; Δν = 32.9 Hz) (7,6-CH), 13.74 s (8-OH).

Anal. Calcd. for $C_{18}H_{15}ClO_5$: C, 62.34; H, 4.35. Found: C, 62.72; H, 4.26.

4-Chloro-6,8-diethoxy-1-hydroxy-2-methylanthraquinone (**21***a*) from **16**, m.p. 160–161° (petroleum ether) (40%); ν_{max} (KBr) 1671, 1630, 1600 cm^{-1}; δ (60 MHz) ($CDCl_3$) 1.49 t (J = 7.5 Hz) (6-OCH_2CH_3), 1.56 t (J = 7.5 Hz) (8-OCH_2CH_3), 2.34 s (2-CH_3), 4.23 q (J = 7.5 Hz) (6,8-OCH_2—), 6.69 d (J = 2.5 Hz) (7-CH), 7.38 d (J = 2.5 Hz) (5-CH), 7.44 s (3-CH).

Anal. Calcd. for $C_{19}H_{17}ClO_5$: C, 63.23; H, 4.75. Found: C, 63.06; H, 4.92.

4-Chloro-6,8-diethoxy-1-hydroxy-3-methylanthraquinone (**22***a'*, R_4 = C_2H_5) from **17**, m.p. 198–199° (petroleum ether) (40%).

Anal. Calcd. for $C_{19}H_{17}ClO_4$: C, 63.25; H, 4.75. Found: C, 63.35; H, 4.57.

5-Chloro-1-ethoxy-8-hydroxy-3-methylanthraquinone (**24***a*) from **15** and isopropenylketen diethyl acetal (**2**) as for **9***a*, m.p. 212–213° (benzene – petroleum ether) (75%); λ_{max} (EtOH) 226.5, 260, 277 (sh), 420, 432 nm (log ε 4.61, 4.29, 4.04, 3.97, 3.96); ν_{max} (KBr) 1676, 1635 (sh), 1631, 1600 cm^{-1}; δ (90 MHz) ($CDCl_3$) 1.58 t (J = 7.0 Hz) (1-OCH_2CH_3), 2.49 s (3-CH), 4.30 q (J = 7.0 Hz) (1-OCH_2—), 7.08 bs (2-CH), 7.37 dd (J = 9.0 Hz; Δν = 33.40 Hz) (7,6-CH), 7.69 bs (4-CH), 13.58 s (8-OH).

Anal. Calcd. for $C_{17}H_{12}ClO_4$: C, 64.66; H, 3.84. Found: C, 64.32; H, 3.95.

Reaction of Keten Dimethyl Acetal with 3-Bromo-8-chloro-5-methoxy-7-methylnaphthoquinone

A mixture of the methyl ether of **17**, (0.631 g; 0.002 mol) and keten dimethyl acetal (**1***a*) (0.88 g; 0.01 mol) is heated at 120° for 1 h and then at 140° for ½ h. The volatile by-products are then evaporated under vacuum and the residue chromatographed on 100 g of silica gel. Benzene elutes 0.032 g (5%) of 4-bromo-9-chloro-5-hydroxy-2,6-dimethoxy-8-methylnaphtho[1,2-*b*]furan (**25**), a colorless and unstable compound which is slowly converted into **26**; ν_{max} ($CHCl_3$) 3345, 1605 cm^{-1}; δ (60 MHz) ($CDCl_3$) 2.51 s (8-CH_3), 4.10 s (2,6-OCH_3), 5.78 s (3-CH), 6.68 s (7-CH), 10.40 s (5-OH).

A mixture of benzene and ether (19:1) next elutes 0.285 g (38%) of methyl 3-bromo-8-chloro-5-methoxy-7-methylnaphthoquinonylacetate (**26**), m.p. 171.0–171.5° (CCl_4); λ_{max} (EtOH) 219, 259, 381, 415 nm (log ε 4.38, 3.96, 3.88, 3.55); ν_{max} (KBr) 1730, 1678 cm^{-1}; δ (60 MHz) ($CDCl_3$) 2.51 s (7-CH_3), 3.77 s (CO_2CH_3), 3.90 s (—CH_2—), 4.01 s (5-OCH_3), 7.28 s (6-CH).

Anal. Calcd. for $C_{15}H_{12}BrClO_5$: C, 46.47; H, 3.12. Found: C, 46.22; H, 3.08.

Upon flushing the column with ethyl acetate and separating the residue by preparative t.l.c., 0.041 g (6%) of 4-chloro-1,6,8-trimethoxy-3-methylanthraquinone (methyl ether of **22***a*) is obtained, m.p. 219.5–220° (EtOH); λ_{max} (EtOH) 221, 273, 400 nm (log ε 4.28, 4.00, 3.51); ν_{max} (KBr) 1668, 1601 cm^{-1}; δ (60 MHz) ($CDCl_3$) 2.52 s (3-CH_3), 3.99 s, 4.00 s and 4.01 s (1,6,8-OCH_3), 6.78 d (J = 2.5 Hz) (7-CH), 7.25 s (2-CH), 7.29 d (J = 2.5 Hz) (5-CH).

Anal. Calcd. for $C_{18}H_{15}ClO_5$: C, 62.34; H, 4.36. Found: C, 62.44; H, 4.12.

Polyhydroxyanthraquinones (from Juglones)

Method A (Reduction Step)

To a solution of NaOH (1.4 g) in equal volumes of ethanol and water (40 ml each) is added the 5-chloro 8-hydroxy-1,3-dimethoxy anthraquinone (7.16×10^{-4} mol) and $Na_2S_2O_4$ (7.7 g). The mixture is stirred for 18 h under nitrogen and then aerated for 1 h, acidified with dilute HCl and extracted with chloroform.

1-Hydroxy-3-methyl-6,8-dimethoxyanthraquinone from **22***a*, m.p. 211.0° (EtOH) (94%); λ_{max} (EtOH) 225, 269, 280, 298, 430 nm (log ε 4.57, 4.29, 4.31, 4.05, 4,00); ν_{max} (KBr) 1670, 1632, 1595 cm^{-1}; δ (60 MHz) ($CDCl_3$)

Can. J. Chem. Downloaded from www.nrcresearchpress.com by 210.87.254.6 on 09/05/12
For personal use only.

2.44 bs (3-CH_3), 3.99 s (6-OCH_3), 4.03 s (8-OCH_3), 6.79 d (J = 2.5 Hz) (7-CH), 7.11 bs (2-CH), 7.45 d (J = 2.5 Hz) (5-CH), 7.60 bs (4-CH), 13.10 s (8-OH).

Anal. Calcd. for $C_{17}H_{14}O_5$: C, 68.45; H, 4.73. Found: C, 68.70; H, 4.51.

Method A (Demethylation Step)

To a molten mixture of $AlCl_3$ (10.0 g) and NaCl (2.0 g) at 180° is added at once the hydroxy dimethoxy anthraquinone (**19***a*, **23***a*, or the preceding compound) (100 mg). After cooling to 120° the melt is hydrolyzed with ice (300 g) and concentrated HCl (10 ml). The precipitate is extracted with chloroform and the organic solution washed with water, dried and evaporated to dryness.

1,3,5-Trihydroxyanthraquinone (**23***b*) from **18**, m.p. 320–322° dec. (benzene) (84%) (lit. (23) m.p. 314–315°); λ_{max} (EtOH) 227, 246, 280, 322, 415 nm (log ε 4.31, 4.13, 4.19, 3.38, 3.92); ν_{max} (KBr) 1610, 1580 (sh) cm^{-1}; δ (90 MHz) ($(CD_3)_2SO$) 6.52 d (J = 2.0 Hz) (2-CH), 7.06 d (J = 2.0 Hz) (4-CH), 7.17–7.90 m (6,7,8-CH), 12.28 and 12.64 2 s (1,5-OH).

1,3,8-Trihydroxyanthraquinone (**19***b*) from **19***a*, m.p. 287–287.5° dec. (EtOH) (98%) (lit. (21) m.p. 287–288°); λ_{max} (EtOH) 215, 245, 265, 285, 321, 430 nm (log ε 4.44, 4.23, 4.21, 4.25, 3.53, 4.02); ν_{max} (KBr) 1670, 1620, 1575 cm^{-1}; δ (90 MHz) ($(CD_3)_2SO$) 6.55 d (J = 2.0 Hz) (2-CH), 7.09 d (J = 2.0 Hz) (4-CH), 7.20–7.90 m (5,6,7-CH), 11.96 bs (1,8-CH).

1,6,8-Trihydroxy-3-methylanthraquinone (emodin) (**22***b*), from 1-hydroxy-6,8-dimethoxy-3-methylanthraquinone, m.p. 258–259° dec. (MeOH) (96%) (lit. (10) m.p. 259–260° dec.); λ_{max} (EtOH) 221, 253, 266, 289, 438 nm (log ε 4.41, 4.15, 4.12, 4.19, 3.94); ν_{max} (KBr) 1680, 1631, 1598 cm^{-1}; δ (90 MHz) ($(CD_3)_2SO$) 2.37 bs (3-CH_3), 6.52 d (J = 2.5 Hz) (7-CH), 7.03 d (5-CH), 7.04 d (2-CH), 7.36 d (J = 1.5 Hz) (4-CH), 11.93 and 12.02 2 s (1,8-OH).

Method B

To a solution of a 5-chloro-1,3-diethoxy 8-hydroxy anthraquinone or 5-chloro-1-ethoxy 8-hydroxy-3-methyl anthraquinone (1.0 g) in acetic acid (20 ml) are added hydriodic acid (d = 1.57) (1.0 ml) and red phosphorus (1.0 g). The mixture is refluxed for 5 h, poured in ice and water and filtered after several hours. The crystalline product is then extracted with chloroform and the residue, upon evaporation of the solvent, oxidized with an equal weight of chromic oxide in acetic acid (50 ml) at 60° for 0.5 h. The polyhydroxylated anthraquinone is then recovered by dilution with water and extraction by chloroform.

1,3,8-Trihydroxyanthraquinone (**19***b*) from **20***b*, m.p. 287° (ethyl acetate) (85%).

Triacetate, m.p. 194–195° (lit. (21) m.p. 195°).

1,6,8-Trihydroxy-2-methylanthraquinone (**21***b*) from **21***a*, m.p. 287–288° (EtOH) (74%) (lit. (24) m.p. 283–284°); λ_{max} (EtOH) 225, 251, 272, 290, 433 nm (log ε 4.43, 4.14, 4.25, 4.21, 3.98); ν_{max} (KBr) 1665, 1613 cm^{-1}; δ (90 MHz) ($(CD_3)_2SO$) 2.19 s (2-CH_3), 6.49 d (J = 2.0 Hz) (7-CH), 7.00 d (J = 2.0 Hz) (5-CH), 7.46 s (3,4-CH), 11.89 and 12.28 2 s (1,8-OH).

Triacetate, m.p. 205.5–206° (lit. (24) m.p. 204°).

1,6,8-Trihydroxy-3-methylanthraquinone (emodin) (**22***b*) from **22***a*′, m.p. 256° (acetic acid) (80%).

Triacetate, m.p. 193° (lit. (25) m.p. 193–194°).

1,8-Dihydroxy-3-methylanthraquinone (chrysophanol) (**24***b*) from **24***a*, m.p. 192–193° (EtOH) (66%) (lit. (26) m.p. 196°); λ_{max} (EtOH) 226, 256, 277, 287, 425 nm (log ε 4.58, 4.32, 3.98, 4.01, 4.02); ν_{max} (KBr) 1676, 1625, 1604 cm^{-1}; δ (90 MHz) ($CDCl_3$) 2.45 s (3-CH_3), 7.10 bs (2-CH), 7.65 bs (4-CH), 7.2–8.0 m (5,6,7-CH), 11.97 and 12.08 2 s (1,8-OH).

Diacetate, m.p. 206–208° (lit. (27) m.p. 208°).

Reactions of Keten and Isopropenylketen Acetals with Chloromaleic Anhydride

To a solution of chloromaleic anhydride (2.64 g), 0.020 mol) in anhydrous ethyl ether (20 ml) is added rapidly 0.10 mol of the keten acetal (**1***a* or **1***b*) or 0.04 mol of isopropenylketen diethyl acetal (**2**). After the vigorous reaction has subsided, the reaction mixture is allowed to rest for 12 h at room temperature and then filtered.

3,5-Dimethoxyphthalic anhydride (**27***a*), m.p. 148–149° (petroleum ether) (32%) (lit. (28) m.p. 149°); ν_{max} (KBr) 1845, 1790, 1770 cm^{-1}; δ (60 MHz) ($CDCl_3$) 4.03 s (5-OCH_3), 4.08 s (3-OCH_3), 6.86 d (J = 2.0 Hz) (4-CH), 7.11 d (J = 2.0 Hz) (6-CH).

3,5-Diethoxyphthalic anhydride (**27***b*), m.p. 137° (dioxan–cyclohexane) (37%) (lit. (29) m.p. 130°).

3-Ethoxy-5-methylphthalic anhydride (**28**), m.p. 158–159° (acetone) (50%); ν_{max} (KBr) 1837, 1775 cm^{-1}; δ (60 MHz) ($(CD_3)_2CO$) 1.46 t (J = 7.0 Hz) (3-OCH_2CH_3), 2.54 s (5-CH_3), 4.34 q (J = 7.0 Hz) (3-OCH_2—), 7.38 m (2,4-CH).

Anal. Calcd. for $C_{11}H_{10}O_4$: C, 64.07; H, 4.89. Found: C, 64.13; H, 4.66.

1. S. M. McElvain. Chem. Rev. **45**, 453 (1949).
2. S. M. McElvain and D. Kundiger. Organic syntheses. Coll. Vol. III. p. 506.
3. S. M. McElvain and H. Cohen. J. Am. Chem. Soc. **64**, 260 (1942).
4. S. M. McElvain and E. L. Engelhardt. J. Am. Chem. Soc. **66**, 1077 (1944).
5. S. M. McElvain, E. R. Degginger, and J. D. Behun. J. Am. Chem. Soc. **76**, 5736 (1954).
6. P. C. Arora and P. Brassard. Can. J. Chem. **45**, 67 (1967).
7. R. H. Thomson. J. Org. Chem. **13**, 377 (1948).
8. R. I. Hoaglin, D. T. Kubler, and A. E. Montana. J. Am. Chem. Soc. **80**, 5460 (1958).
9. I. Yosioka, H. Yamauchi, K. Morimoto, and I. Kitagawa. Tetrahedron Lett. 1149 (1968).
10. M. V. Sargent, D. O'N. Smith, and J. A. Elix. J. Chem. Soc. (C), 307 (1970).
11. J. Smith and R. H. Thomson. J. Chem. Soc. 1008 (1961).
12. H. Raistrick and J. Ziffer. Biochem. J. **49**, 563 (1951).
13. D. B. Bruce and R. H. Thomson. J. Chem. Soc. 1089 (1955).
14. S. M. McElvain and L. R. Morris. J. Am. Chem. Soc. **74**, 2657 (1952).
15. W. K. Anslow and H. Raistrick. Biochem. J. **35**, 1006 (1941).
16. H. Raistrick, R. Robinson, and A. R. Todd. J. Chem. Soc. 488 (1933).
17. R. G. Cooke, H. Dowd, and W. Segal. Aust. J. Chem. **6**, 38 (1953).

18. R. G. COOKE and H. DOWD. Aust. J. Chem. **6**, 53 (1953).
19. A. S. WHEELER and J. W. SCOTT. J. Am. Chem. Soc. **41**, 833 (1919).
20. S. M. MCELVAIN, H. I. ANTHES, and S. H. SHAPIRO. J. Am. Chem. Soc. **64**, 2525 (1942).
21. W. K. ANSLOW, J. BREEN, and H. RAISTRICK. J. Chem. Soc. 427 (1940).
22. A. H. CARTER, E. RACE, and F. M. ROWE. J. Chem. Soc. 236 (1942).
23. B. S. JOSHI, N. PARKASH, and K. VENKATARAMAN. J. Sci. Ind. Res. **13B**, 246 (1954). Chem. Abstr. **49**, 11611f.
24. N. R. AYYANGAR. Ind. J. Chem. **5**, 530 (1967).
25. O. FISCHER and H. GROSS. J. Prakt. Chem. **84**, 369 (1911).
26. R. EDER and C. WIDMER. Helv. Chim. Acta, **5**, 3 (1922).
27. O. FISCHER, F. FALCO, and H. GROSS. J. Prakt. Chem. **83**, 208 (1911).
28. H. BROCKMANN, F. KLUGE, and H. MUXFELDT. Chem. Ber. **90**, 2302 (1957).
29. P. FRITSCH. Ann. **296**, 358 (1897).

Can. J. Chem. Downloaded from www.nrcresearchpress.com by 210.87.254.6 on 09/05/12
For personal use only.

Synthèse de méthyl-3 furoquinones

RICHARD HUOT ET PAUL BRASSARD
Département de Chimie, Université Laval, Québec, Québec G1K 7P4

Reçu le 17 juillet 1973

Les auteurs proposent deux nouvelles solutions au problème de la synthèse de méthyl-3 furoquinones. Ces méthodes ont l'avantage de requérir des substrats et des réactifs facilement accessibles. Une nouvelle synthèse de la tanchinone I(**26**) illustre l'un des procédés qui devraient en principe s'appliquer également à la synthèse d'isotanchinones. Au cours de cette étude, quelques transformations inédites ont aussi été observées.

The authors propose two new solutions to the problem of the synthesis of 3-methylfuranquinones. The methods have the advantage of requiring readily accessible substrates and reagents. A new synthesis of tanshinone I(**26**) illustrates one of the processes which in principle should also be applicable to the preparation of isotanshinones. Several novel transformations have been observed in the course of this study.

Can. J. Chem., **52**, 88 (1974)

Can. J. Chem. Downloaded from www.nrcresearchpress.com by 210.87.254.6 on 09/05/12
For personal use only.

Synthèses de furonaphtoquinones

Les quinones comportant un hétérocycle oxygéné ont souvent été isolées de sources naturelles (1) et, puisque certaines proviennent probablement des composés hydroxylés correspondants, nous avons recherché des méthodes de synthèse à l'aide de ces intermédiaires. Depuis le début de ces travaux, un certain nombre de synthèses de méthyl-3 furoquinones ont été réalisées (2–4). Nos méthodes constituent toutefois des procédés nouveaux et de plus cette étude nous a permis d'observer des réactions inédites concernant la formation d'alkyl-2 furoquinones.

Le problème principal, celui de la préparation de méthyl-3 furoquinones, a été abordé par l'étude de la synthèse du dihydro-4,5 méthyl-3 dioxo-4,5 naphto[1,2-*b*]furanne (**14***b*). King et Read (5) avaient déjà obtenu cette substance par une méthode qui s'est avérée inapplicable à la synthèse des tanchinones. La façon la plus directe d'envisager la préparation consiste sans doute à introduire dans l'hydroxy-2 naphtoquinone (**1**) une chaîne fonctionnalisée susceptible de se cycliser en méthyl-3 furoquinone. Puisque ce groupement doit contenir trois atomes de carbone, le propanal ou ses dérivés semblaient être des réactifs tout désignés pour opérer cette transformation. Toutefois, des condensations directes entre l'hydroxy-2 ou la chloro-3 méthoxy-2 naphtoquinone et le propanal en présence de NaH ne donnèrent aucun résultat utile.

Une observation inédite sur la réaction de quinones avec certains halogénures d'alkyles semblait offrir quelqu'espoir de succès par la condensation de l'hydroxy-2 naphtoquinone et du bromo-2 propanal. Une première tentative ne conduisit qu'à une faible quantité de dihydro-4,5 méthyl-2 dioxo-4,5 naphto[1,2-*b*]furanne (**2**) obtenu sans doute par la cyclisation de l'hydroxy-3 (bromo-2 propényl)-2 naphtoquinone intermédiaire, une réaction analogue à celle observée par Hooker (6). Il s'agit, à notre connaissance, du premier cas de condensation de ce genre avec des aldéhydes α-halogénés et d'un exemple rare de synthèse directe d'une furoquinone à partir d'une hydroxyquinone. Un second assai, effectué avec le même aldéhyde en présence de HBr, donna un mélange complexe de produits: la bromo-3 hydroxy-2 naphtoquinone (**3**), le dihydro-4,5 méthyl-2 dioxo-4,5 naphto[1,2-*b*]furanne (**2**), le dihydro-4,9 méthyl-2 dioxo-4,9 naphto[2,3-*b*]-furanne (**4**), l'α-formyléthyl-2 hydroxy-3 naphtoquinone (**5***b*) et deux autres substances qui n'ont pas été identifiées. Le produit attendu (**5***b*) a donc été obtenu mais avec un rendement de seulement 9%. Le spectre de r.m.n. de **5***b* surprend par la faiblesse du couplage entre le proton aldéhydique et celui en α du carbonyle, mais sa structure a été confirmée puisqu'il se transforme facilement en dihydro-4,5 méthyl-3 dioxo-4,5 naphto[1,2-*b*]-furanne (**14***b*) (Schéma 1).

Une troisième tentative pour préparer l'aldéhyde **5***b* devait faire intervenir l'époxydation de l'hydroxy-3 propényl-2 naphtoquinone (**6**) suivie d'une transposition catalysée par BF_3. Les essais d'époxydation par le peroxyde d'hydrogène en milieu basique se sont avérés vains mais l'emploi de l'acide perbenzoïque dans le chloroforme

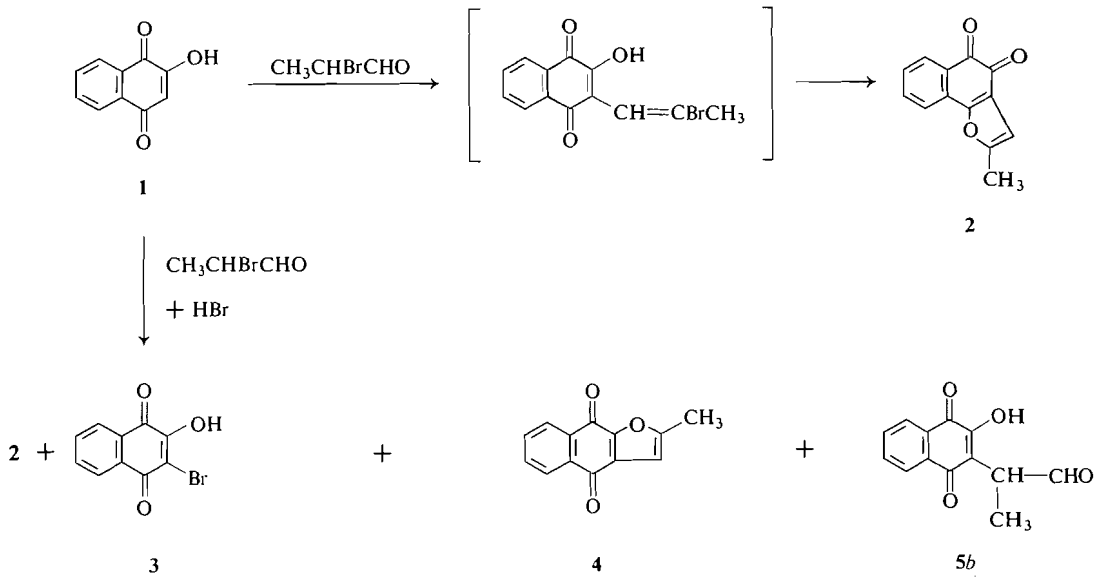

SCHÉMA 1

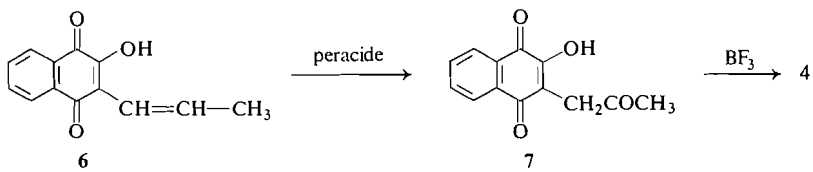

SCHÉMA 2

conduit directement à l'acétonyl-2 hydroxy-3 naphtoquinone (**7**) avec un rendement de 73%. Ce composé s'identifie facilement par son spectre de r.m.n. qui présente deux singulets à δ 2.29 et 3.73 p.p.m. et par le fait qu'il se transforme en furanne **4** sous l'action de BF_3 (Schéma 2).

Nous avons aussi tenté de préparer l'aldéhyde **5***b* par l'oxydation, d'après la méthode de Lemieux et Rudloff (7), de l'hydroxy-3 α-méthylallyl-2 naphtoquinone (**11***b*) qui s'obtient par transposition de Claisen des éthers γ-méthylallyliques des hydroxynaphtoquinones décrits par Fieser (8). L'alkylation du sel d'argent de **1** par le bromure de crotyle donne un mélange des éthers *o*- et *p*-quinoniques et du produit *C*-alkylé. La proportion des éthers par rapport au produit hydroxylé a été porté à 67% du mélange en employant un solvant moins polaire (benzène) que celui (éther éthylique) préconisé par Fieser. Le rendement en substances alkylées est de 64% mais une certaine quantité de **1** peut être récupérée. La pyrolyse des éthers par contre conduit quantitativement au produit transposé.

L'hydroxy-3 α-méthylallyl-2 naphtoquinone (**11***b*), par acétylation réductive et oxydation au moyen de OsO_4 et $NaIO_4$, est transformé en l'aldéhyde **13***b* attendu. La méthanolyse acide de ce dernier et l'oxydation par l'air en milieu basique donnent l'α-formyléthyl-2 hydroxy-3 naphtoquinone (**5***b*). L'α-formylméthyl-2 hydroxy-3 naphtoquinone (**5***a*), préparée de façon analogue, se cyclise en dihydro-4,5 dioxo-4,5 naphto[1,2-*b*]-furanne (**14***a*) par chauffage dans l'acide polyphosphorique. L'aldéhyde **5***b* ne donne pas de réaction semblable, la substance étant trop insoluble dans ce milieu. Toutefois la réduction de **5***b* par le zinc et l'action de HCl suivies d'une oxydation par CrO_3 conduisent à la méthyl-3 furoquinone **14***b* (Schéma 3).

Synthèse de la tanchinone I

Nous avons utilisé comme matière première pour cette synthèse le diméthoxy-3,4 méthyl-8 phénanthrène (**15**) déjà préparé par Pschorr (9). Le clivage des éthers par BBr_3 suivi de l'oxydation par Ag_2O conduit à la méthyl-8 phénan-

Can. J. Chem. Downloaded from www.nrcresearchpress.com by 210.87.254.6 on 09/05/12
For personal use only.

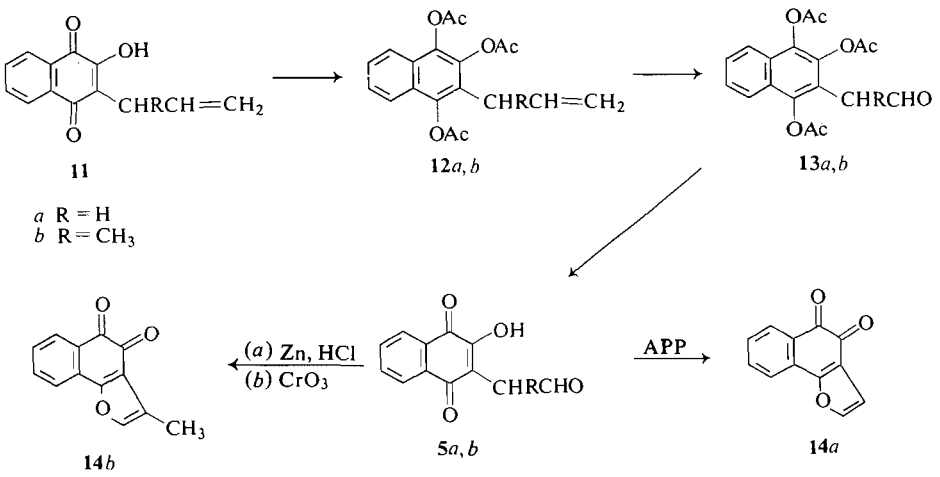

SCHÉMA 3

thrènequinone-3,4 (**16**) avec un rendement global de 62%. Les caractéristiques physiques et spectrales diffèrent toutefois sensiblement de celles déjà publiées (2). Le spectre de masse de la substance révèle un pic moléculaire à *m/e* 222 et les bandes infrarouges ($\nu_{C=O}$ 1662, 1630 cm^{-1}) semblent conformes aux valeurs attendues (10). Par une réaction de Thiele, la quinone **16** donne un triacétate (**17**) qui fut ensuite saponifié par MeONa et oxydé par l'air avec un rendement de 76% pour les trois étapes. Le spectre infrarouge de la substance **18** est comparable à celui déjà publié (2) mais sont point de fusion est toutefois sensiblement plus élevé.

L'alkylation du sel d'argent de l'hydroxyquinone **18** dans le benzène procède assez mal, car la majeure partie de la quinone de départ est récupérée; d'ailleurs la réaction ne donne que deux des trois produits attendus (l'*o*-quinone n'a pas été isolée). Par contre, dans l'hexaméthylphosphotriamide, les éthers s'isolent avec un bon rendement (70%). La façon classique de séparer les produits par extraction des substances acides à l'aide de l'ammoniaque diluée ne s'opère qu'avec difficulté vu la faible solubilité des sels correspondants. (Nous avons toutefois constaté que la méthyl-8 γ-méthylallyloxy-3 phénanthrènequinone-1,4 (**20**), par chromatographie sur gel de silice, donne lieu à une transposition totale. Cette méthode permet donc d'isoler directement le produit **22** sans avoir recours à l'isolement et à la pyrolyse de l'éther. Une partie de ce produit (**20**) cependant se transpose de façon nonconcertée et donne une proportion importante (~40%) d'hydroxy-3 méthyl-8 γ-méthylallyl- phénanthrènequinone-1,4 (**19**), sans doute par u mécanisme ionique).

Après une acétylation réductive de la substanc **22** et une oxydation par la méthode de Lemieu (7), l'aldéhyde **24** s'obtient avec un excellen rendement. La méthanolyse acide de ce dernie donne toutefois un acétal difficile à hydrolyser mais la saponification par l'hydroxyde de sodiur dans le diméthylsulfoxyde suivie d'une cyclisatio par l'acide chlorhydrique et une oxydation pa l'acide chromique permet de compléter la syn thèse (Schéma 4).

Partie expérimentale

I Synthèse de furonaphtoquinones

(A) Réaction avec le bromo-2 propanal

On chauffe à reflux pendant 4 h un mélange de hydroxy 2 naphtoquinone (**1**) (1.8 g), d'acétate de sodium anhydr (2.4 g), de bromo-2 propanal (3.0 ml) (11) et d'acétat d'éthyle (50 ml); puis on ajoute de l'eau (100 ml) et o acidifie avec de l'acide chlorhydrique dilué. On chromat graphie le solide brun obtenu sur gel de silice et on élu successivement avec le benzène, le chloroforme et l'éthe Des premières fractions, on isole le dihydro-4,5 méthyl- dioxo-4,5 naphto[1,2-*b*]furanne (2), p.f. 164–164.5 (EtOH) (5%) (litt. (12) 164–164.5°); ν_{max} (KBr) 1710, 168 cm^{-1}; δ ($CDCl_3$) (60 MHz) 2.33 d (J = 1.0 Hz) (CH_3-2 6.40 q (J = 1.0 Hz) (CH-3). Les spectres sont identiqu à ceux de la substance authentique préparée d'apr Hooker et Steyermark (12).

Les autres fractions contiennent de l'hydroxynapht quinone (**1**) et une huile qui n'a pas cristallisé.

(B) Réaction du bromo-2 propanal en présence d'acide bromhydrique

On ajoute lentement à 0° du brome (4.8 g) à une sol tion de propanal (1.8 g) dans de l'acétate d'éthyle (100 ml

Can. J. Chem. Downloaded from www.nrcresearchpress.com by 210.87.254.6 on 09/05/12
For personal use only.

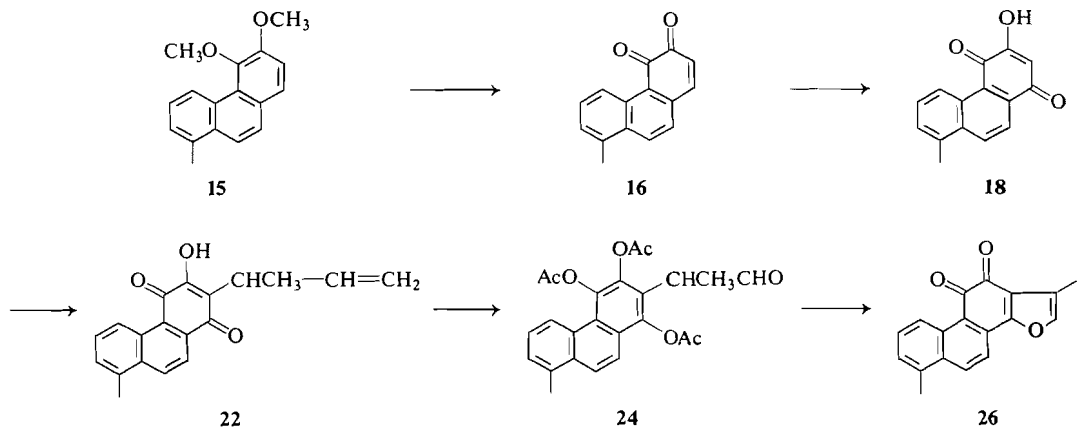

SCHÉMA 4

Lorsque la solution devient incolore, on y ajoute de l'hydroxynaphtoquinone (**1**) (3.5 g) et on porte le mélange à l'ébullition pendant 3 h. Après refroidissement, on ajoute de l'éther (1 l) et on extrait les hydroxyquinones avec une solution de bicarbonate de sodium à 5% (3 × 200 ml). On acidifie la solution aqueuse et on l'extrait avec l'éther. On évapore le solvant organique et on chromatographie le résidu sur gel de silice (benzène, puis chloroforme). On isole ainsi les produits suivants:

La bromo-3 hydroxy-2 naphtoquinone (**3**), p.f. 202–203° (benzène) (4%) (litt. (13) p.f. 202°); ν_{max} (KBr) 3160, 1675, 1640 cm^{-1}. Éther méthylique (CH_2N_2), p.f. 163–164° (litt. (14) p.f. 163–164°).

L'α-formyléthyl-2 hydroxy-3 naphtoquinone (**5***b*) p.f. 119–120° (benzène, éther de pétrole) (9%); ν_{max} (KBr) 3340, 2720, 1720, 1670, 1645 cm^{-1}; δ ($CDCl_3$) (60 MHz) 1.45 d (J = 7.0 Hz) (CH_3), 3.88 qd (J = 7.0, <1 Hz) (CH), 9.80 d (J < 1 Hz) (CHO). Leucotriacetate, p.f. 153–155°.

Anal. Calc. pour $C_{19}H_{18}O_7$: C, 63.68; H, 5.06. Trouvé: C, 63.81; H. 5.06.

Deux produits, en très faible rendement, que l'on n'a pas identifié, un composé jaune, p.f. 177–178° (benzène); ν_{max} (KBr) 3260, 1670, 1650 cm^{-1}; une substance rouge, p.f. 171–172° (benzène); ν_{max} (KBr) 3100, 1650 cm^{-1}.

Le composé **4**, p.f. 247°, s'isole de la phase organique à l'état de traces après extraction au bicarbonate.

Le composé **2**, p.f. 164–165°, s'obtient également à l'état de traces de la solution aqueuse, après avoir laissé reposer celle-ci pendant 2 jours.

(C) Synthèse et cyclisation de l'acétonyl-2 hydroxy-3 naphtoquinone

Acétonyl-2 hydroxy-3 naphtoquinone (7)

On laisse réagir pendant 24 h à la température ambiante la propényl-2 hydroxy-3 naphtoquinone (**6**) (560 mg) (6) dans une solution d'acide perbenzoïque dans le chloroforme (0.23 *N*; 12 ml). Par refroidissement, on obtient la quinone **7**, p.f. 179–179.5° (benzène) (73%) (litt. (15) p.f. 177–177.5°, (12) 176.5–177.5°); ν_{max} (KBr) 3275, 1710, 1685, 1650 cm^{-1}; δ ($CDCl_3$) (60 MHz) 2.29 s (CH_3), 3.73 s (CH_2), 7.48 s (OH).

Dihydro-4,9 méthyl-2 dioxo-4,9 naphto[2,3-b]furanne (4)

On ajoute lentement de l'éthérate de trifluorure de bore (1.0 ml) à une solution de la quinone **7** (410 mg) dans du benzène (15 ml) à 10° et on agite pendant 16 h à la température ambiante. Après avoir versé le mélange réactionnel dans de l'eau glacée (50 ml) et extrait avec de l'éther, on obtient un solide huileux que l'on chromatographie sur gel de silice. Le benzène élue le naphtofuranne **4**, p.f. 245–245.5° (benzène) (46%) (litt. (12) p.f. 246–247°); ν_{max} (KBr) 1680 cm^{-1}; δ (CF_3COOH) (60 MHz) 2.57 s (CH_3-2) 6.76 s (CH-3). Cette substance est identique à celle mentionnée dans la section B.

(D) Synthèse de dihydro-4,5 dioxo-4,5 naphto[1,2-b]-furannes

Alkylation de l'hydroxy-2 naphtoquinone

Méthode A (16). On a repris l'expérience de Fieser (17) (avec le sel d'argent de la quinone **1** (30 g) et le bromure de crotyle (16 g)) mais en substituant le benzène (200 ml) à l'éther comme solvant. On isole de la façon préconisée les produits suivants:

L'hydroxy-3 γ-méthylallyl-2 naphtoquinone (**8**), p.f. 127–128° (EtOH) (21%) (litt. (17) p.f. 132–133°); ν_{max} (KBr) 3390, 1680, 1658 cm^{-1}.

La γ-méthylallyloxy-4 naphtoquinone-1,2 (**9**), p.f. 122–123 (éther de pétrole) (22%) (litt. (17) p.f. 120°); ν_{max} (KBr) 1720, 1665 cm^{-1}.

La γ-méthylallyloxy-2 naphtoquinone-1,4 (**10**), p.f. 138–139° (éther de pétrole) (21%) (litt. (17) p.f. 137°); ν_{max} (KBr) 1690, 1654 cm^{-1}.

Méthode B. On agite pendant 10 min un mélange du sel d'argent de la quinone **1** (3.0 g) et de bromure de crotyle (1.6 g) dans de l'hexaméthylphosphotriamide (25 ml) à la température ambiante. Après avoir versé le mélange dans de l'eau (200 ml) et extrait au benzène, on isole de la façon habituelle les substances suivantes: le produit *C*-alkylé **8** (0.4 g) (16)%, l'éther *o*-quinonique **9** (0.3 g) (12%) et l'éther *p*-quinonique **10** (1.4 g) (58%).

Triacétoxy-1,3,4 allyl-2 naphtalène (12a)

On chauffe pendant 2 min un mélange d'allyl-2 hydroxy-3 naphtoquinone **11***a* (2.5 g), p.f. 114–114.5°

Can. J. Chem. Downloaded from www.nrcresearchpress.com by 210.87.254.6 on 09/05/12
For personal use only.

Can. J. Chem. Downloaded from www.nrcresearchpress.com by 210.87.254.6 on 09/05/12
For personal use only.

(litt. (16) p.f. 116°), de zinc en poudre (8.0 g), d'acétate de sodium fondu (4.0 g) et d'anhydride acétique (20 ml). L'hydrolyse partielle du milieu réactionnel et l'extraction du produit brut par le chloroforme chaud permet d'obtenir le triacétate **12***a*, p.f. 156–157° (benzène – éther de pétrole) (81%) (litt. (16) p.f. 155.5°); ν_{max} (KBr) 1770 cm^{-1}; δ ($CDCl_3$) (60 MHz) 2.29, 2.38 et 2.42 3s (acétates), 3.41 m (—CH_2—), 5.06 m (=CH_2), 5.83 m (—CH=).

Triacétoxy-1,3,4 α-méthylallyl-2 naphtalène (12b)

On obtient ce produit à partir de l'hydroxy-3 α-méthylallyl-2 naphtoquinone-1,4 (**11***b*), p.f. 66–67° (litt. (17) p.f. 69°) d'une façon analogue à la précédente, p.f. 140–142° (benzène – éther de pétrole) (61%); ν_{max} (KBr) 1775 cm^{-1}; δ ($CDCl_3$) (60 MHz) 1.44 d (J = 7.0 Hz) (CH_3), 2.26, 2.36 et 2.40 3s (acétates) 3.79 (—CH—), 5.09 m (=CH_2), 6.05 m (—CH=).

Anal. Calc. pour $C_{20}H_{20}O_6$: C, 67.40; H, 5.65. Trouvé: C, 67.78; H. 5.69.

Triacétoxy-1,3,4 formylméthyl-2 naphtalène (13a)

On agite pendant 1 h une solution du triacétate **12***a* (1.2 g) dans un mélange de dioxanne (20 ml), d'eau (2 ml) et d'une solution aqueuse de tétroxyde d'osmium à 1% (4 ml). Lorsque la solution noircit, on ajoute du périodate de sodium (2.2 g) en trois portions égales à intervalles de 12 h. Au bout de 26 h, on verse le mélange réactionnel dans de l'eau, on extrait au chloroforme et on lave la solution organique successivement avec de l'eau et avec une solution saturée de sulfure d'hydrogène. On obtient l'aldéhyde **13***a* par chromatographie sur gel de silice en éluant avec un mélange de benzène et de chloroforme (1:1), p.f. 158–159° (benzène) (75%); ν_{max} (KBr) 2715, 1775, 1730 cm^{-1}; δ ($CDCl_3$) (60 MHz) 2.31, 2.44 et 2.45 3s (acétates), 3.56 d (J = 2.0 Hz) (CH_2), 9.55 t (J = 2.0 Hz) (CHO).

Anal. Calc. pour $C_{18}H_{16}O_7$: C, 62.78; H, 4.68. Trouvé: C, 62.83; H, 4.71.

Triacétoxy-1,3,4 α-formyléthyl-2 naphtalène (13b)

Le triacétate **12***b* (0.95 g) donne dans les mêmes conditions l'aldéhyde **13***b*, p.f. 153–155° (benzène) (37%); ν_{max} (KBr) 2720, 1780, 1727 cm^{-1}; δ ($CDCl_3$) (60 MHz) 1.36 d (J = 7.0 Hz) (CH_3), 2.26 et 2.39 (3:6) 2s (acétates), 3.73 qd (J = 7.0, <1 Hz) (CH), 9.70 q (J < 1 Hz).

Anal. Calc. pour $C_{19}H_{18}O_7$: C, 63.68; H, 5.06. Trouvé: C, 63.81; H, 5.06.

Formylméthyl-2 hydroxy-3 naphtoquinone (5a)

On dissout du triacétate **13***a* (344 mg) dans du méthanol contenant une goutte d'acide chlorhydrique concentré. A ce mélange refroidi, on ajoute une solution d'hydroxyde de sodium à 30% (10 ml). On laisse reposer 30 min, on acidifie, puis on ajoute une solution de chlorure ferrique (6 ml) (18) et, après 10 min, de l'eau (75 ml). On extrait la quinone avec de l'éther d'où on la récupère par lavage avec une solution de bicarbonate de sodium à 5%. La quinone **5***a* s'obtient alors par acidification de cette solution et extraction à l'éther, p.f. 160–161° déc. (benzène – éther de pétrole) (83%); ν_{max} (KBr) 3110, 2725, 1715, 1685, 1645 cm^{-1}; δ ($CDCl_3$) (60 MHz) 3.76 d (J = 1.0 Hz) (CH_2), 7.36 s (OH), 9.78 t (J = 1.0 Hz) (CHO).

Anal. Calc. pour $C_{12}H_8O_4$: C, 66.66; H, 3.73. Trouvé: C, 66.44; H, 3.68.

α-Formyléthyl-2 hydroxy-3 naphtoquinone (5b)

Cette naphtoquinone se prépare par une méthode analogue à celle du paragraphe précédent (65%) et est identique au produit décrit à la section B.

Dihydro-4,5 dioxo-4,5 naphto[1,2-b]furanne (14a)

On chauffe sur bain-marie pendant 10 min un mélange de l'aldéhyde **5***a* (108 mg) et d'acide polyphosphorique (7.0 g). Après refroidissement, on verse le mélange réactionnel dans de l'eau glacée et on extrait par de l'acétate d'éthyle. On lave ensuite la phase organique avec une solution de bicarbonate de sodium à 5%. On évapore le solvant et chromatographie le résidu sur gel de silice. Le benzène élue le naphtofuranne **14***a*, p.f. 212–212.5° (benzène (10%) (litt. (12) p.f. 209.5–210°); ν_{max} (KBr) 1708, 1685 cm^{-1}; δ ($CDCl_3$) (60 MHz) 6.86 d (J = 2.0 Hz) (CH-3), 7.48 d (J = 2.0 Hz) (CH-2).

Dihydro-4,5 méthyl-3 dioxo-4,5 naphto[1,2-b]furanne (14b)

A de l'acide acétique à 70% (10 ml), on ajoute l'aldéhyde **5***b* (100 mg), du zinc en poudre (100 mg) et de l'acide chlorhydrique (1:3) (2 ml) puis on porte le mélange à reflux pendant 5 min. Après avoir éliminé l'excès de zinc par filtrage, on oxyde l'hydroquinone par addition d'acide chromique (30 mg) dans de l'eau (1 ml). La furoquinone **14***b* cristallise alors dans le milieu réactionnel, p.f. 166–167° (acétone-eau) (58%) (litt. (3) p.f. 168°); ν_{max} (KBr) 1705, 1680, 1650 cm^{-1}; δ ($CDCl_3$) (60 MHz) 2.30 d (J = 1.0 Hz) (CH_3), 7.33 q (J = 1.0 Hz) (CH-2).

11 Synthèse de la tanchinone 1

Méthyl-8 phénanthrènequinone-3,4 (16)

On porte à l'ébullition une solution de diméthoxy-3,4 méthyl-8 phénanthrène (**15**) (5.0 g), p.f. 65–66°, (préparé d'après Pschorr (9)) dans le benzène (150 ml), on ajoute goutte à goutte une solution de tribromure de bore (15 g) dans le même solvant (25 ml) et on continue de chauffer à reflux pendant 3 h. Après avoir refroidi le milieu réactionnel, on le verse dans de l'eau (200 ml), on extrait à l'éther, puis on oxyde l'hydroquinone par addition d'oxyde d'argent (14.0 g) et de sulfate de magnésium anhydre (14.0 g). On agite la suspension pendant 3 h à la température ambiante, filtre et extrait le résidu de façon continue (Soxhlet). Par concentration des extraits, on obtient la quinone **16**, p.f. 192° déc. (éther) (2.85 g), (60%) (litt. (2) p.f. 176–177° déc.); ν_{max} (KBr) 1662, 1630 cm^{-1} δ ($CDCl_3$) (90 MHz) 2.65 s (CH_3-8), 6.46 d (J = 10.0 Hz) (CH-2), 7.48 d (J = 10.0 Hz) (CH-1); *m/e* 222 (M^+).

Anal. Calc. pour $C_{15}H_{10}O_2$: C, 81.51; H, 4.53. Trouvé C, 81.54; H, 4.62.

Triacétoxy-1,3,4 méthyl-8 phénanthrène (17)

On agite pendant 1 h une suspension de méthyl-8 phénanthrènequinone-3,4 (4.4 g) dans de l'anhydride acétique (75 ml) auquel on ajoute quelques gouttes d'acide sulfurique concentré. On isole le triacétate **17** de la façon habituelle, p.f. 174–175° (benzène) (6.2 g, 85%); ν_{max} (KBr) 1770, 1760 cm^{-1}; δ ($CDCl_3$) (90 MHz) 2.34, 2.45 et 2.49 3s (acétates), 2.71 s (CH_3-8).

Hydroxy-3 méthyl-8 phénanthrènequinone-1,4 (18)

On agite à 5° pendant 1 h une suspension du triacétate **17** (6.2 g) et de méthylate de sodium (6.5 g) dans du méthanol absolu (50 ml). On recueille le sel de sodium de la quinone correspondante **18** et le décompose dans l'eau par addition d'acide chlorhydrique dilué, p.f. 238° déc. (benzène) (3.6 g, 82%) (litt. (2) p.f. 203–205° déc.); ν_{max}

Can. J. Chem. Downloaded from www.nrcresearchpress.com by 210.87.254.6 on 09/05/12
For personal use only.

(KBr) 3325, 1654, 1633 cm^{-1}; δ ($(CD_3)_2SO$) (90 MHz) 2.68 s (CH_3-8), 6.14 s (CH-2); *m/e* 238 (M^+).

Réaction du bromure de crotyle avec le sel d'argent de l'hydroxy-3 méthyl-8 phénanthrènequinone-1,4

Méthode A. On agite à la température ambiante une suspension du sel d'argent de la quinone **18** (13.7 g) dans une solution de bromure de crotyle (8.1 g) dans du benzène anhydre (100 ml). Après 90 min on filtre et on lave abondamment le résidu avec le même solvant (l'extraction de ce résidu au soxhlet permet de récupérer 1.9 g de l'hydroxyquinone **18**). Par concentration des extraits jusqu'à un volume de 75 ml et addition d'éther de pétrole (25 ml), on obtient encore 0.4 g de cette quinone. La chromatographie du filtrat sur gel de silice permet par élution avec de l'éther de pétrole et ensuite avec du benzène d'isoler successivement les produits suivants:

Une substance inconnue, p.f. 222–223° (benzène – éther de pétrole) (0.9 g); ν_{max} (KBr) 1800, 1740, 1705 cm^{-1}.

L'hydroxy-3 méthyl-8 α-méthylallyl-2 phénanthrènequinone-1,4 (**22**), p.f. 201–202° (benzène – éther de pétrole) (1.4 g, 12%); ν_{max} (KBr) 3350, 1654, 1634 cm^{-1}; δ ($CDCl_3$) (60 MHz) 1.43 d (J = 7.0 Hz) (CH_3), 2.70 s (CH_3-8), 4.00 m (—CH—), 5.11 m ($=CH_2$), 6.30 m (—CH=), 7.88 s (OH).

Anal. Calc. pour $C_{19}H_{16}O_3$: C, 78.06; H, 5.51. Trouvé: C, 78.00; H, 5.60.

L'hydroxy-3 méthyl-8 γ-méthylallyl-2 phénanthrènequinone-1,4 (**19**), p.f. 186–187° (benzène – éther de petrole) (2.2 g, 18%); ν_{max} (KBr) 3350, 1655, 1632 cm^{-1}; δ ($CDCl_3$) (60 MHz) 1.57 m (CH_3), 2.72 s (CH_3-8), ~3.3 m (CH_2), ~5.65 m (CH=CH), 7.88 s (OH).

Anal. Trouvé: C, 77.59; H, 5.49.

L'hydroxyquinone **18** (0.6 g).

La méthyl-8 γ-méthylallyloxy-3 phénanthrènequinone-1,4 (**20**) s'obtient dans la solution benzénique après extraction du mélange réactionnel avec de l'ammoniaque (1:1) et aussi dans les dernières fractions lorsque l'on chromatographie rapidement, p.f. 148–149° (benzène – éther de pétrole); ν_{max} (KBr) 1675, 1640, 1628, 1622 cm^{-1}; δ ($CDCl_3$) (60 MHz) 1.75 m (CH_3), 2.68 s (CH_3-8), ~4.5 m (CH_2), ~5.8 m (CH=CH), 6.03 s (CH-2).

Anal. Trouvé: C, 78.31; H, 5.47.

On n'isole jamais par cette méthode la méthyl-8 γ-méthylallyloxy-1 phénanthrènequinone-3,4 (**21**).

Méthode B. On agite à la température ambiante pendant 1 h une suspension du sel d'argent de l'hydroxyquinone **18** (344 mg) et de bromure de crotyle (225 mg) dans de l'hexaméthylphosphotriamide (HMPT) (5 ml) puis on verse le mélange dans de l'eau (100 ml) et l'on extrait à l'éther. Les hydroxyquinones s'isolent par extraction avec de l'ammoniaque aqueuse (1:1) et ensuite acidification. On obtient ainsi par chromatographie sur gel de silice (15 g), en éluant avec le benzène puis l'acétate d'éthyle, le produit *C*-alkylé **19** (21 mg, 7%) et l'hydroxyquinone **18** (83 mg). La solution éthérée contient un mélange des éthers **20** et **21** (132 mg, 45%) que l'on peut convertir quantitativement en l'hydroxyquinone **22** par chauffage à 150° pendant 10 min.

Triacétoxy-1,3,4 méthyl-8 α-méthylallyl-2 phénanthrène (23)

Cette substance se prépare à partir de l'hydroxyquinone **22** comme le triacétate **12***a*, p.f. 198–199° (benzène – éther de pétrole) (80%); ν_{max} (KBr) 1781, 1758 cm^{-1}; δ ($CDCl_3$) (60 MHz) 1.45 d (J = 7.0 Hz) (CH_3), 2.32, 2.43 et 2.44 3s (acétates), 2.72 s (CH_3-8), 3.88 m (—CH—), ~5.15 m ($=CH_2$), 6.00 m (—CH=).

Anal. Calc. pour $C_{25}H_{24}O_6$: C, 71.41; H, 5.75. Trouvé: C, 71.10; H, 5.81.

Triacétoxy-1,3,4 α-formyléthyl-2 méthyl-8 phénanthrène (24)

On agite pendant 2.5 h à la température ambiante, un mélange du triacétate (**23**) (420 mg), de dioxanne (10 ml), d'eau (2 ml) et d'une solution aqueuse de tétroxyde d'osmium à 1% (1.5 ml). On ajoute alors du periodate de sodium (550 mg) en trois portions égales à une heure d'intervalle. Après 26 h, on isole l'aldéhyde **24** comme pour **13***a*, p.f. 198–199° (benzène – éther de pétrole) (390 mg, 95%); ν_{max} (KBr) 2725, 1780, 1755, 1730 cm^{-1}; δ ($CDCl_3$) (60 MHz) 1.36 d (J = 7.0 Hz) (CH_3), 2.32, 2.43 et 2.44 3s (acétates), 2.70 s (CH_3-8), 3.76 qd (J = 7.0, <1 Hz) (—CH—), 9.75 d (J < 1 Hz) (CHO)

Anal. Calc. pour $C_{24}H_{22}O_7$: C, 68.23; H, 5.24. Trouvé: C, 68.46; H, 5.25.

α-Formyléthyl-2 hydroxy-3 méthyl-8 phénanthrènequinone-1,4 (25)

On fait barboter de l'air pendant 30 min dans un mélange du triacétate **24** (100 mg), de diméthylsulfoxyde (2 ml) et d'une solution aqueuse d'hydroxyde de sodium à 5% (5 ml). On obtient la quinone **25** par dilution avec de l'eau (100 ml) et acidification, p.f. 199–200° (benzène) (84%); ν_{max} (KBr) 3340, 2725, 1725, 1661, 1638 cm^{-1}; δ ($CDCl_3$) (60 MHz) 1.46 d (J = 7.0 Hz) (CH_3), 2.74 s (CH_3-8), 3.89 qd (J = 7.0, <1 Hz) (CH), 7.59 s (OH), 9.85 d (J < 1 Hz) (CHO).

Anal. Calc. pour $C_{18}H_{14}O_4$: C, 73.45; H, 4.79. Trouvé: C, 73.65; H, 5.11.

Par une méthanolyse acide, suivie d'une oxydation avec un grand excès de chlorure ferrique, le triacétate **24** (212 mg) donne un mélange de la quinone **25** (62 mg, 42%) et de l'acétal méthylique correspondant, p.f. 154–156° (benzène) (60 mg, 35%); ν_{max} (KBr) 3350, 1654, 1630, 1120, 1115, 1090, 1055 cm^{-1}; δ ($CDCl_3$) (60 MHz) 1.32 d (J = 7.0 Hz) (CH_3), 2.72 s (CH_3-8), 3.30 et 3.47 2s (OCH_3), 5.09 d (J = 9.0 Hz) (CH-1′), 7.53 s (OH) (le signal d'un proton CH-2′ est en partie masqué par les bandes dues aux groupes méthoxyle).

Anal. Calc. pour $C_{20}H_{20}O_5$: C, 70.57; H, 5.92. Trouvé: C, 70.50; H, 5.79.

Tanchinone I (26)

On dissout du triacétate **24** (84 mg) dans le diméthylsulfoxyde (2 ml) et, sous atmosphère d'azote, on y verse une solution d'hydroxyde de sodium à 10% (2 ml). Après 3 min on acidifie avec de l'acide chlorhydrique (1:3) et on ajoute quelques cristaux de chlorure stanneux. On dilue alors avec de l'acide acétique à 70% (10 ml) et on ajoute de l'acide chromique (40 mg) dissous dans de l'eau (1 ml). Il se forme un précipité que l'on chromatographie sur gel de silice en éluant avec le chloroforme. On obtient ainsi la tanchinone I dont le spectre infrarouge est identique à celui de la substance authentique;[1] p.f. 234–234.5°

[1]Les auteurs désirent remercier M. le Professeur H. Kakisawa qui a bien voulu leur fournir un échantillon de tanchinone I.

(benzène – éther de pétrole) (15 mg, 33%) (litt. (2) p.f. 233–234°); ν_{max} (KBr) 1676, 1665, 1595 cm^{-1}; λ_{max} (EtOH) 247, 265 (épaulement), 327, 420 nm (log ε 4.51, 4.23, 3.47, 3.74).

On récupère aussi lors de cette opération de la quinone **25** (25 mg, 55%).

1. R. H. THOMSON. Naturally occurring quinones. Academic Press. London. 1971.
2. A. C. BAILLIE et R. H. THOMSON. J. Chem. Soc. (C), 48, 1968.
3. H. KAKISAWA et Y. INOUYE. Bull. Chem. Soc. Jap. **42**, 3318 (1969).
4. H. KAKISAWA et M. TATEISHI. Bull. Chem. Soc. Jap. **43**, 824 (1970).
5. T. J. KING et G. READ. J. Chem. Soc. 5090 (1961).
6. S. C. HOOKER. J. Am. Chem. Soc. **58**, 1163 (1936).
7. R. U. LEMIEUX et E. VON RUDLOFF. Can. J. Chem. **33**, 1701 (1955).
8. L. F. FIESER. J. Am. Chem. Soc. **48**, 3201 (1926); **49**, 857 (1927).
9. R. PSCHORR. Chem. Ber. **39**, 3106 (1906).
10. M. L. JOSIEN, N. FUSON, M. J. LEBAS et T. M. GREGORY. J. Chem. Phys. **21**, 331 (1953).
11. J. U. NEF. Ann. **335**, 247 (1904).
12. S. C. HOOKER et A. STEYERMARK. J. Am. Chem. Soc. **58**, 1202 (1936).
13. K. FRIES et K. SCHIMMELSCHMIDT. Ann. **484**, 245 (1930).
14. L. F. FIESER et R. H. BROWN. J. Am. Chem. Soc. **71**, 3609 (1949).
15. E. F. PRATT et R. G. RICE. J. Am. Chem. Soc. **79**, 5489 (1957).
16. L. F. FIESER. J. Am. Chem. Soc. **48**, 3201 (1926).
17. L. F. FIESER. J. Am. Chem. Soc. **49**, 857 (1926).
18. L. F. FIESER. Organic experiments. 2ième édition. Raytheon Education Co., Lexington, Mass. 1968. p. 275.

Can. J. Chem. Downloaded from www.nrcresearchpress.com by 210.87.254.6 on 09/05/12
For personal use only.

Matrix Infrared and Laser Raman Spectra, Molecular Structures and Normal Coordinate Analyses of Germanium Difluoride, Monomer GeF_2, and Dimer $(GeF_2)_2$

H. HUBER, E. P. KÜNDIG, G. A. OZIN,[1] AND A. VANDER VOET

Lash Miller Chemical Laboratories and Erindale College, University of Toronto, Toronto, Ontario

Received September 5, 1973

Matrix infrared and laser Raman spectra are reported for GeF_2 and $(GeF_2)_2$ in both N_2 and Ar matrices. Raman depolarization measurements for the monomer in N_2 matrices identify ν_1 at 653 cm^{-1}. Warm-up experiments identify infrared and Raman lines at 665, 478 cm^{-1} and 669, 465, and 424 cm^{-1} respectively, with the first stage of the polymerization of GeF_2 monomer and are assigned to GeF stretching modes of the dimer $(GeF_2)_2$, having a centrosymmetric C_{2h} non-planar structure, containing a double fluorine bridge similar to the structure proposed for $(SeO_2)_2$. A normal coordinate analysis is performed on the dimer using a force field transferred from the monomer. The results provide additional evidence for the correctness of the vibrational and stereochemical assignments for the dimer.

Les spectres infrarouges et Raman laser de GeF_2 et $(GeF_2)_2$ dans des matrices d'azote et d'argon sont décrits. Les mesures de dépolarisation Raman pour le monomère dans des matrices d'N_2 permettent d'identifier ν_1 à 653 cm^{-1}. Des expériences de réchauffement permettent de faire correspondre les bandes infrarouge á 665 et 478 cm^{-1} et les bandes Raman à 669, 465 et 424 cm^{-1} avec le premier stade de polymérisation du monomère GeF_2. Ces bandes ont été attribuées aux vibrations d'élongation de GeF du dimère $(GeF_2)_2$ qui, présentant une structure centrosymétrique C_{2h} non plane et un double pont fluor a une structure semblable à celle proposée pour $(SeO_2)_2$. Une analyse par coordonnées normales a été fait pour le dimère en transférant le champ de force du monomère. Les résultats apportent une preuve supplémentaire de l'exactitude des attributions vibrationnelles et stéréochimiques du dimère.

[Traduit par le journal]

Can. J. Chem., **52**, 95 (1974)

Introduction

In the only reported matrix infrared study (1) of monomeric GeF_2 produced by vaporizing solid $(GeF_2)_n$ (a fluorine bridged polymer) (2), the spectra were always found to be complicated by the presence of higher aggregates in the matrix. This was unavoidable and not necessarily the result of poor isolation, as mass spectroscopic data (3) for the vapor above solid GeF_2 had previously shown the presence of $[GeF_2]_x$ where $x =$ 1, 2, 3, and 4.

We were particularly interested in the germanium difluoride dimer $(GeF_2)_2$, as it was conceivable that it might have a similar molecular configuration to that of the recently reported double oxygen bridged dimer $(SeO_2)_2$ (4). It is noteworthy that chemical and spectroscopic properties of the related silicon difluoride dimer $(SiF_2)_2$ are indicative of a radical species containing a silicon–silicon bond (5).

Experimental

Solid germanium difluoride is normally prepared on the gram scale by reacting gaseous GeF_4 with Ge powder in the temperature range 150–300 °C (6). Consequently, it seemed reasonable to try to prepare spectroscopically pure monomeric GeF_2 for matrix infrared and Raman studies, by an analogous reaction employing a high temperature gas flow knudsen cell technique. In this way, gaseous GeF_4 (prepared from $BaGeF_6$ by the standard literature procedure (7) and purified by trap-to-trap distillation) diluted with N_2 or Ar (Matheson 99.99%) matrix gases ($M/A \cong$ 100–1000) was flowed at a rate of approximately 2–4 mmol per h into a stainless steel knudsen cell (orifice size 0.5 mm) containing Ge powder. The knudsen cell was resistively heated to 300–350 °C and the effusing vapors were subsequently condensed onto either a highly polished aluminum tip for matrix Raman experiments, or a caesium iodide plate for matrix infrared experiments, cooled to 4.2 or 10 °K by an Air Products liquid helium transfer system or a Displex closed cycle helium refrigerator system. Typical matrix depositions in the Raman lasted 3–4 h and in the infrared 1–2 h. Matrix Raman spectra were recorded on a Spex 1401 spectrometer using Carson argon ion laser excitation (4880 Å at approximately 100 mW). Raman depolarization measurements on matrix isolated species were recorded whenever possible, by methods described previously (8). Matrix infrared spectra were recorded on a Perkin–Elmer 180 spectrometer. Normal coordinate calculations were performed on an IBM 7094 computer using Schatschneiders GMAT and GVIB.

Results and Discussion

The matrix infrared and Raman spectra of the effusing vapors condensed at 4.2 °K in N_2 and Ar matrices were essentially the same except for

[1]To whom all correspondence should be addressed.

Can. J. Chem. Downloaded from www.nrcresearchpress.com by 210.87.254.40 on 09/05/12
For personal use only.

TABLE 1. Matrix Raman* spectra† of $(GeF_2)_x$ in N_2‡ (where $x = 1, 2, 3.....n$)

Effusing vapors§ condensed at 4.2 °K	Successive warm-up experiments at 30, 35, and 40 °K			
A	B	C	D	Assignment
~702 vvw	~702 vvw	~702 ww	~702 vvw	$\nu_3 GeF_2$?
	669 ms	669 ms	669 ms	$(GeF_2)_2$
653 s(pol)	653 s	653 s	653 s	$\nu_1 GeF_2$
~592 vvw	~592 vw	~592 w	592 m	$(GeF_2)_n$
~533 vvw	~533 vw	533 m	533 m	$(GeF_2)_3$?
~465 ww	465 m	465 m	465 m	$(GeF_2)_2$
	~424 w	~424 w	~424 w	$(GeF_2)_2$

*For matrix infrared data, see text.
†$M/A \cong 200$.
‡The spectra in Ar matrices were of poorer quality than those in N_2. Bands were observed at 659 s, 689 vw, and 705 vw. ν_1 of GeF_2 in Ar is assigned at 659 cm^{-1}.
§Because of the broadness of the weaker lines their frequencies could not be measured to better than ±3 cm^{-1}.

small matrix shifts (Table 1). The Raman spectra in N_2 matrices tended to be of higher quality than those in Ar. A typical matrix Raman recording at $M/A \cong 200$ is shown in Fig. 1*a*. Notable features of these spectra were the complete conversion of GeF_4 to GeF_2 (confirmed by the absence of ν_1 GeF_4 738 cm^{-1}) and the presence of a very strong line at 653 cm^{-1} in N_2 and 649 cm^{-1} in Ar. Owing to the high gain conditions required in these experiments, a steeply rising baseline was experienced at frequencies below 300 cm^{-1} and it was not possible to observe the bending mode of GeF_2 (previously observed in the infrared at 263 cm^{-1} (1)). However, Raman depolarization measurements for GeF_2 in N_2 matrices were successful and identified the strongest line at 653 cm^{-1} ($\rho_p \cong 0.55$) as ν_1. This would indicate that Margrave's infrared assignment (1) for ν_1 of GeF_2 is incorrect and that the asymmetric GeF stretching is *higher* than the symmetric mode. This is not unusual as evidenced by the Raman spectrum of gaseous and matrix isolated SeO_2 (4). For the purposes of our calculations we have accepted the veracity of our assignment for ν_1 and ν_3 on the basis of the fact that (*a*) the band at about 649–653 cm^{-1} of GeF_2 is observed both in the matrix infrared and Raman spectra, (*b*) it is the strongest and sharpest line in the Raman spectrum, and (*c*) it is polarized. It could be argued that this band might coincide with the stretching frequency of monomeric GeF (9), but if this were the case, one would expect to see bands corresponding to GeF_4 (particularly ν_1 at 738 cm^{-1}), which in the matrix Raman experiments were not observed.

By recording the matrix infrared and Raman spectra after successive diffusion controlled warm-up experiments in the temperature ranges 35–40 °K, the progress and results of the polymerization process of GeF_2 monomer in the matrix were observed (Table 1 and Fig. 1*b–d*). The best Raman results were obtained in a N_2 matrix where three lines were observed to grow in at

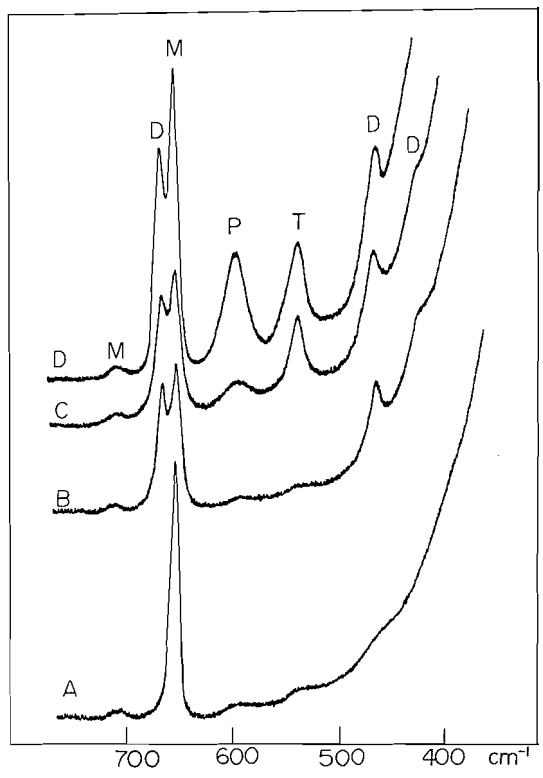

FIG. 1. The matrix Raman spectrum of (*A*) monomeric GeF_2 in N_2 ($M/A \cong 200$) at 4.2 °K, (*B*)–(*D*) and after successive diffusion controlled warm up experiments at 35–40 °K. (M = monomer, D = dimer, T = trimer, P = polymer.)

Can. J. Chem. Downloaded from www.nrcresearchpress.com by 210.87.254.40 on 09/05/12
For personal use only.

TABLE 2. Observed and calculated matrix infrared and Raman frequencies for germanium difluoride dimer, $(GeF_2)_2$

Raman† (N_2 matrix)	Infrared (Ar matrix)	Calculated* frequency	Assignment C_{2h} and approximate description of mode	
669s		663	a_g	νGeF_t
	665s	671	b_u	νGeF_t
	478m	471	b_u	νGeF_b
465ms		473	a_g	νGeF_b
424w		436	b_g	νGeF_b
		282	a_u	νGeF_b
		273	b_u	δGeF_t
		241	a_g	δGeF_t
		204	b_g	δGeF_t
		141	a_u	δGeF_t
		137	a_g	$\nu GeGe$

*Scans covered range 270–1000 cm^{-1} in N_2 matrices.
†Torsional force constants put to zero.

669s, 465ms, and 424w cm^{-1} and could be associated with the *first* stage of the polymerization process to $(GeF_2)_2$. Further prolonged warming at 30–40 °K produced higher aggregate species, yielding lines at 533 cm^{-1} (probably $(GeF_2)_3$ trimer), and finally 592 cm^{-1} (probably polymer, evidenced by the fact that solid $(GeF_2)_n$ has a strong band in this region). The corresponding matrix infrared experiments were also performed where the most useful results were obtained in argon matrices. At $M:A \cong 1:1000$, the infrared spectra showed the presence of only monomeric GeF_2 ($\nu_1 \cong 647$, $\nu_3 \cong 677$ cm^{-1}),[2] which did not appear to diffuse appreciably during matrix warm-up. However, at higher M/A ratios (1:250), monomeric GeF_2 was again observed, but under these higher concentration conditions, aggregation during warm-up was observed. Infrared absorptions at 665 and 478 cm^{-1} could be ascribed to the first stage of the polymerization and are assignable to $(GeF_2)_2$. Absorptions at 531 and 611 cm^{-1} grew in on further warm-up at 30–40 °K and are assignable to higher aggregate species than the dimer (*cf.* Raman lines at 533 and 592 cm^{-1}).

The infrared and Raman lines observed in the regions 669–665 cm^{-1} and 478–424 cm^{-1} are most satisfactorily assigned to terminal and bridge GeF stretching modes respectively, by comparison with other bridged fluorides (10).

[2]Reproducible fine structure was observed on the ν_3 and ν_1 GeF stretching vibrations of the GeF_2 monomer in Ar matrices at 677.0, 675.0, 673.5, 671.7 cm^{-1} and 647.0, 644.5, 643.0, 641.5 cm^{-1} respectively, which corresponds to the normal Ge isotope structure (see Margrave and co-workers (1)).

It is noteworthy that the Raman spectrum of the dimer $(GeF_2)_2$ is quite similar to the Raman spectrum of matrix isolated $(SeO_2)_2$ (4). Qualitatively the results suggest that the three Raman bands associated with $(GeF_2)_2$ could be assigned to $\nu GeF_{terminal}$ (669 cm^{-1}) and νGeF_{bridge} (465 and 424 cm^{-1}) stretching modes analogous to the $\nu SeO_{terminal}$ (1002 cm^{-1}) and νSeO_{bridge} (660 and 543 cm^{-1}) stretching modes for $(SeO_2)_2$. The lone pair of electrons on germanium in $(GeF_2)_2$ is likely to be stereochemically active as it is found to be in the $(GeF_2)_n$ chain polymer and $(SeO_2)_2$, giving an essentially tetrahedral coordination around each germanium atom.

Of the two chemically most likely structures, the C_{2h} chair form and the C_{2v} boat form, the C_{2h} molecule is favored on the basis of the *absence* of infrared and Raman coincidences. (See Table 2 and the section on normal coordinate calculations.)

Normal Coordinate Calculations for $(GeF_2)_2$

To provide additional evidence for our vibrational and stereochemical assignments for the $(GeF_2)_2$ molecule we have computed the vibrational frequencies for the double fluorine bridged dimers in the chair C_{2h} and boat C_{2v} configurations shown below (similar to those proposed for the $(SeO_2)_2$ species) using a force field transferred from GeF_2. Internal and symmetry coordinates are the same as those defined for $(SeO_2)_2$ (4).

Let us formalize the normal coordinate calculations for the germanium difluoride dimer, $(GeF_2)_2$. The molecular dimensions were in part derived from those of the monomer (bond length 1.73 Å, bond angle 97°10′ (11)) and from the poly-

Can. J. Chem. Downloaded from www.nrcresearchpress.com by 210.87.254.40 on 09/05/12
For personal use only.

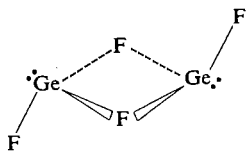

C_{2h}

$\Gamma_{vib} = 4a_g(R) + 2b_g(R) + 2a_u(IR) + 4b_u(IR)$
$\Gamma_{vib}^{GeF_t} = a_g$
$\Gamma_{vib}^{GeF_b} = a_g + b_g$

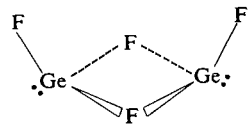

C_{2v}

$\Gamma_{vib} = 5a_1(IR/R) + 2a_2(R) + 3b_1(IR/R) + 2b_2(IR/R)$
$\Gamma_{vib}^{GeF_t} = a_1 + b_2$
$\Gamma_{vib}^{GeF_b} = a_1 + a_2 + b_1 + b_2$

meric solid (terminal bond length 1.79 Å and bridge bond lengths 2.09 and 1.91 Å (2)). The same general shape as the selenium dioxide dimer, was assumed, that is, ∠ F_b—Ge—F_b = 60°, ∠ Ge—F_b—Ge = 120°, ∠ F_t—Ge—plane of the bridged "ring" = 125°, the bond lengths to be Ge—F_t = 1.79 Å, and Ge—F_b = 2.00 Å. The force field of GeF_2 is of some interest in that the spectrum is not yet fully established in the literature (1). If one performs an approximate Wilson GF calculation on the frequencies observed, both with Margrave's assignment and with ours, then the force constants which result are shown below:

	Matrix	
Force constant*	Infrared (ref. 1)	Raman (this work)
f_r	4.18	4.16
f_{rr}	0.37	−0.11
$f_{r\alpha}$	0.46	0.41
f_α	0.39	0.38

*In mdyn/Å, mdyn/rad, or mdyn/rad².

The most noticeable difference between the force constants based on Margrave's assignment and ours is the sign and magnitude of f_{rr}.

For the purpose of calculation of the force field of the dimeric species, we have used our assignment of the monomer, for the reasons described in the text. The final force constants for $(GeF_2)_2$ used in the normal coordinate calculations are listed in Table 3. The calculated and observed spectra for the C_{2h} molecule are shown in Table 2 together with the vibrational assignments and approximate description of the modes.

TABLE 3. Force field* for germanium difluoride dimer† $(GeF_2)_2$

Force constant	Value
f_{r_t}	4.16
f_{r_b}	1.55
$f_{r_tr_t}$	0.31
$f_{r_tr_b}$	0.20
$f_{r_t\alpha}$	0.31
$f_{r_b\alpha}$	0.25
$f_{r_b\beta}$	0.20
f_α	0.29
f_β	0.19
f_γ	0.025
$f_{\alpha\alpha}$	0.029

*Nomenclature the same as ref. 4.
†All force constants not listed above are assumed to be zero; units in mdyn/Å, mdyn/rad or mdyn/rad².

The agreement between the number, frequencies, and intensities of the observed Raman active germanium–fluorine stretching modes together with the calculated frequencies of vibration, provides convincing evidence that $(GeF_2)_2$ has been isolated and that the centrosymmetric chair (C_{2h}) configuration is favored.

It is interesting to note that the value of the ratio k_b/k_t for $(GeF_2)_2$ which gives the best frequency fit for the GeF bridge and terminal stretching modes (*i.e.* 0.38) is also very close to the value found for the only other well defined *dimeric* bridged fluoride Al_2F_6 (12), (k_b/k_t = 0.408) and follows the trend found for other bridged fluorides (10), and lies in the lower range k_b/k_t = 0.25–0.40 rather than the higher range k_b/k_t = 0.5–0.75, commonly found for bridged chlorides (10).

We thank the National Research Council of Canada and the Research Corporation for financial assistance.

1. J. W. HASTIE, R. HAUGE, and J. L. MARGRAVE. J. Phys. Chem. **72**, 4492 (1968).
2. J. TROTTER, A. AKHTAR, and N. BARTLETT. J. Chem. Soc. (A), 30 (1966).
3. K. F. ZYMBOV, J. W. HASTIE, R. HAUGE, and J. L. MARGRAVE. Inorg. Chem. **7**, 608 (1968).
4. G. A. OZIN and A. VANDER VOET. J. Mol. Struct. **10**, 173 (1971).
5. (*a*) G. A. OZIN and A. VANDER VOET. Unpublished results. (*b*) H. P. HOPKINS, J. C. THOMPSON, and J. L.

Can. J. Chem. Downloaded from www.nrcresearchpress.com by 210.87.254.40 on 09/05/12
For personal use only.

MARGRAVE. J. Am. Chem. Soc. **90**, 901 (1968). (*c*) C. S. LIU, J. L. MARGRAVE, J. C. THOMPSON, and P. L. TIMMS. Can. J. Chem. **50**, 459 (1972). (*d*) C. S. LIU, J. L. MARGRAVE, J. C. THOMPSON. Can. J. Chem. **50**, 465 (1972). (*e*) C. S. LIU, J. C. THOMPSON. J. Organomet. Chem. **38**, 249 (1972).
6. N. BARTLETT and K. C. YU. Can. J. Chem. **39**, 80 (1961).
7. G. BRAUER. Handbook of preparative inorganic chemistry. Academic Press, New York. 1963. p. 215.
8. H. HUBER, G. A. OZIN, and A. VANDER VOET. Nature, **236**, 166 (1971); G. A. OZIN and A. VANDER VOET. J. Chem. Phys. **56**, 4768 (1972).
9. G. HERZBERG. Diatomic molecules. D. Van Nostrand Co. Inc., New York.
10. (*a*) I. R. BEATTIE, K. M. S. LIVINGSTON, G. A. OZIN, and D. J. REYNOLDS. J. Chem. Soc. A, 958 (1969). (*b*) I. R. BEATTIE, T. R. GILSON, and G. A. OZIN. J. Chem. Soc. A, 813, 2765 (1968).
11. H. TAKEO, R. F. CURL, and P. W. WILSON. J. Mol. Spectrosc. **38**, 464 (1971).
12. A. SNELSON. J. Phys. Chem. **71**, 3202 (1967).

Can. J. Chem. Downloaded from www.nrcresearchpress.com by 210.87.254.40 on 09/05/12
For personal use only.

The 2980 Å Absorption Spectrum of 1,2,5-Selenadiazole

A. W. RICHARDSON

Chemistry Department, Bishop's University, Lennoxville, Quebec

Received March 30, 1973

The u.v. absorption spectrum of 1,2,5-selenadiazole in the 3050–2600 Å region has been recorded and, by analogy to previous studies of furazan (1,2,5-oxadiazole) and 1,2,5-thiadiazole, an interpretation of the spectrum in terms of an allowed electronic transition involving primarily activity of ν_5, a symmetric ring in-plane bending vibration, and ν_{10}, a ring out-of-plane bending vibration, has been made. This analysis indicates that the excited state is non-planar, and the barrier to planarity has been calculated to be in the order of 115 cm^{-1}.

Le spectre d'absorption u.v. du séléna-1,2,5 diazole dans la région de 3050 à 2600 Å a été enregistré. Par analogie avec des études antérieures sur le furazane (oxa-1,2,5 diazole) et sur le thia-1,2,5 diazole, on a interprété le spectre en fonction d'une transition électronique permise impliquant surtout l'activité de ν_5, une vibration symétrique de déformation du cycle dans le plan, et de ν_{10}, une vibration de déformation du cycle hors du plan. Cette analyse a montré que l'état excité est non-planaire; la barrière à la planéité a été évaluée à environ 115 cm^{-1}. [Traduit par le journal]

Can. J. Chem., **52**, 100 (1974)

Introduction

We have recently reported the results of our investigations of the first u.v. absorption spectra of furazan (1,2,5-oxadiazole) (1) and 1,2,5-thiadiazole (2). In both cases, analysis of the u.v. spectrum shows that the electronic transition is from a planar ground state to a non-planar excited state and that the barrier to planarity in the excited state is relatively small, being in the order of 215 cm^{-1} for furazan and 460 cm^{-1} for 1,2,5-thiadiazole. The investigation of the u.v. absorption spectrum of 1,2,5-selenadiazole was undertaken in order to extend the series of molecules studied.

Experimental

1,2,5-Selenadiazole was prepared by the reaction of ethylenediamine with SeO_2 in dimethylformamide (3). The product was first separated by steam distillation, then extracted into pentane, and concentrated. Final purification was effected by g.l.c. using a 20 ft × ¼ in. column of 30% SE 30 on 45/60 Chrom W with a Varian Aerograph autoprep 700 gas chromatograph. Because of the low yield of the reaction and difficulties of purification, the purity of the compound was not as good as desired, but was, nevertheless, in excess of 95%.

Low resolution spectra of 1,2,5-selenadiazole vapor in a 10 cm cell were recorded on a Cary model 14 spectrometer. Higher resolution spectra were recorded photoelectrically on a Jarrell–Ash 0.5 m spectrometer equipped with a photomultiplier using a 150 W d.c. xenon lamp as a source. For the latter studies, an excess of 1,2,5-selenadiazole was kept in a 1 m fused silica absorption cell with a side arm and the vapor pressure of the sample was controlled by varying the temperature of a slush bath on the side arm. Some spectra were also recorded with the vapor at a fixed pressure but heated to about 75 °C by wrapping the absorption cell with heating tapes.

Observations

The absorption spectrum of 1,2,5-selenadiazole vapor in the 3100–2700 Å region as recorded on a Cary model 14 spectrophotometer is shown in Fig. 1. The diffuseness of the spectrum is apparent from this tracing and was verified by higher resolution spectra recorded on the Jarrell–Ash 0.5 m spectrometer.

The measured wavenumbers of the maxima of the vibronic bands listed in Table 1 were taken

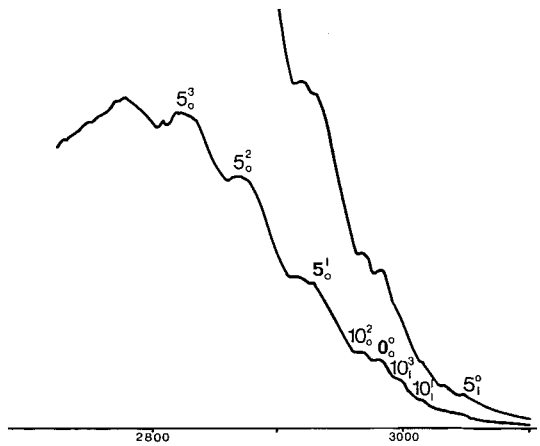

FIG. 1. Ultraviolet absorption spectrum of 1,2,5-selenadiazole vapor at room temperature as recorded on the Cary model 14 spectrophotometer. Only the pressure of sample in the cell was changed between the two traces.

Can. J. Chem. Downloaded from www.nrcresearchpress.com by 210.87.254.6 on 09/05/12
For personal use only.

TABLE 1. Observed bands in the 2980 Å absorption spectrum of 1,2,5-selenadiazole (Jarrell–Ash measurements)

$\bar{\nu}_{obs}$ (cm^{-1})	Assignment*	$\bar{\nu}_{calcd.}$ (cm^{-1})‡
32 566	4_1^0	32 561
32 675	$5_1^0 10_1^3$	32 681
32 832	5_1^0	32 840
33 003	$5_1^0 10_0^2$	33 010
33 170	10_1^1	—
33 407	10_1^3	—
33 566	0_0^0	—
33 736	10_0^2	—
34 171	5_0^1	34 171
34 783	5_0^2	34 776

*A v'–v'' transition in the Kth normal mode is labelled $K_{v''}^{v'}$.

‡Frequencies calculated using $\nu_4'' = 1005\ cm^{-1}$, $\nu_5'' = 726\ cm^{-1}$, $\nu_{10}'' = 438\ cm^{-1}$ (5), $\nu_5' = 605\ cm^{-1}$.

from traces obtained with the Jarrell–Ash spectrometer and are the averages of about 10 measurements, except for the very weak bands for which only 3 measurements were made. Due to the diffuseness of the bands, the uncertainty in the average values listed is about $\pm 8\ cm^{-1}$.

Analysis

Investigation of the microwave spectrum of 1,2,5-selenadiazole has shown that the spectrum is compatible with the molecule being planar with C_{2v} symmetry as expected (4). Similarly, the i.r. and Raman spectra have been interpreted in terms of a planar C_{2v} structure and assignments made for all 15 normal modes of vibration (5).

By analogy to the analyses of the u.v. absorption spectra of furazan (1) and 1,2,5-thiadiazole (2), the bands in the u.v. spectrum of 1,2,5-selenadiazole have been assigned as shown in Table 1. The wavenumbers of the hot bands calculated using the vapor phase i.r. values of $\nu_5'' = 726$ and $\nu_4'' = 1005\ cm^{-1}$ (5) agree with the observed wavenumbers within experimental error.

As was done for furazan (1) and 1,2,5-thiadiazole (2), the $G_0'(v_{10}')$ term values were calculated from the observed u.v. wavenumbers and the i.r. value of $\nu_{10}'' = 438\ cm^{-1}$ and fitted to a double minimum potential function (6). For 1,2,5-selenadiazole, it was not possible to carry out this fitting very accurately since the data are not too accurate and there are only four pieces of data to be used with the potential function which contains three parameters. From a number of calculations which were made, it is possible to conclude that the barrier to planarity in the excited state is in the order of $115\ cm^{-1}$; however, the uncertainty in this value is rather large, being $\pm 30\ cm^{-1}$ at least.

The author thanks the National Research Council of Canada and the Crabtree Fund of Bishop's University for financial support of this work, and Dr. J. C. D. Brand and the Chemistry Department of the University of Western Ontario for use of the Jarrell-Ash and Cary spectrophotometers. Mr. T. England prepared the sample of 1,2,5-selenadiazole and recorded most of the spectra used in the present analysis.

1. B. J. FORREST and A. W. RICHARDSON. Can. J. Chem. **50**, 2088 (1972).
2. E. FIRKINS and A. W. RICHARDSON. Chem. Commun. 1368 (1971).
3. V. BERTINI. Angew. Chem. Int. Ed. **6**, 563 (1967).
4. G. L. BLACKMAN, R. D. BROWN, F. R. BURDEN, and J. E. KENT. Chem. Phys. Lett. **1**, 379 (1967).
5. E. BENEDETTI and V. BERTINI. Spectrochim. Acta, **24**A, 57 (1968).
6. J. B. COON, N. W. NAUGLE, and R. D. MCKENZIE. J. Mol. Spectrosc. **20**, 107 (1966).

Can. J. Chem. Downloaded from www.nrcresearchpress.com by 210.87.254.6 on 09/05/12
For personal use only.

Identification of Intermediates in the Photolysis of Mercaptans in Dilute Glass Matrices. II

ALLEN JOHN ELLIOT AND FRANK CUTHBERT ADAM
Department of Chemistry, University of Calgary, Calgary, Alberta T2N 1N4

Received June 5, 1973

Dilute solutions of aliphatic thiols have been prepared and photolyzed at 253.7 nm in 3-methylpentane glasses at 77 °K. The major products formed initially are thiyl radicals RS· and hydrogen atoms. Both of these are hot and yield solvent radicals by abstraction reactions, and relatively small amounts of RS_2·, RS·, and possibly $R_1R_2C{=}S$. Thermal annealing of the matrices is accompanied by loss of hydrocarbon radicals through cage reactions and concommitant increase in the RS· concentration. An intermediate radical of the type $R_1R_2\dot{C}SH$ may also be produced in the annealing process. The photometric and spin resonance characteristics of RS·, RS_2· and $R_1\dot{C}H{-}SH$ are discussed and related to other systems in which these intermediates are observed. RS· is characterized in the amorphous phase by an absorption at 405 nm and a broad asymmetrical e.p.r. resonance near $g \simeq 2.0$. RS_2· has a non-axial g-tensor with principal values of about 2.06, 2.02, and 2.00 and has no detectable absorptions between 350 and 1200 nm. The photolytic behavior of these metastable radical species is also investigated.

Des solutions de thiols aliphatiques ont été préparées et irradiées à 253.7 nm dans des matrices de méthyl-3 pentane à 77 °K. Les principaux produits formés au début de la photolyse sont des radicaux thiyle RS· et des atomes d'hydrogène. Ces deux produits sont chauds et conduisent à des radicaux du solvant par des réactions d'abstraction. On détecte également de faibles quantités de RS_2·, RS· et peut être de $R_1R_2C{=}S$. Le réchauffement des matrices s'accompagne de la disparition des radicaux hydrocarbure par des réactions de cage et de l'accroissement simultané de la concentration en RS·. Un radical intermédiaire du type $R_1R_2\dot{C}SH$ peut aussi être formé au cours du réchauffement. Les caractéristiques photométriques et de résonnance de spin de RS·, RS_2· et $R_1\dot{C}H{-}SH$ sont discutées et comparées à celles des autres systèmes dans lesquels ces intermédiaires sont observés. RS· est caractérisé dans la phase amorphe par une absorption à 405 nm et une large bande asymétrique en r.p.e. proche de $g \simeq 2.0$. RS_2· présente un tenseur-g non axial dont les principales composantes sont environ 2.06, 2.02 et 2.00. Ce radical ne présente pas d'absorptions détectables entre 350 et 1200 nm.
La conduite photolytique de ces espèces radicalaires métastables a aussi été étudiée.
[Traduit par le journal]

Can. J. Chem., **52**, 102 (1974)

Introduction

The role of sulfur containing substances in the decomposition pathways of biological materials subjected to high energy radiation has been the topic of many investigations since the observation was first made by Gordy *et al.* (1) that, regardless of what the initial process of disruption might be, the damage site eventually ended up on sulfur atoms contained in such amino acid constituents as cysteine or cystine present in the parent organic material. This transfer was inferred by the appearance of terminal radical species characterized by a large variation in the principal g-tensor values, not obtained in biological systems which do not contain sulfur atoms. In fact, irradiation of single crystals of cystine·HCl at room temperature gives oriented radicals with non-axial g-tensor elements (2.052, 2.029, and 2.003) similar (2) to those found in larger biological molecules. These radicals appear to be much the same as thos obtained by 253.7 nm photolysis (3) and b γ-radiolysis (4) of cysteine·HCl·H_2O or L-Penicill amine·HCl (5) at room temperature. Radical with analogous g-tensor elements are also ob tained from the γ-irradiation of pure polycrystal line alkyl disulfides (6) and thiols (7), and b photolysis of neat mercaptans (8) at 77 °K. I most cases the observed resonance has bee attributed to the thiyl radical RS· as wa originally suggested by Kurita and Gordy (2 and that the stability of this species at roor temperature was due to its lack of mobility an extreme unreactivity in the solid state. O melting or dissolving the crystallites, the thi radicals combine to yield disulfide, which, in th case of thiols, is one of the major products (9 In several of the above single crystal studies th initial irradiation was also carried out at lowe temperatures, generally 77 °K. It was shown tha

Can. J. Chem. Downloaded from www.nrcresearchpress.com by 210.87.254.6 on 09/05/12
For personal use only.

Can. J. Chem. Downloaded from www.nrcresearchpress.com by 210.87.254.6 on 09/05/12
For personal use only.

while the room temperature radical was indeed common to both disulfides and thiols, it was never the initial product formed, but results from a sequence of solid state reactions which appear to be peculiar to the individual substances and depend upon the particular mode of radiation damage or upon the precise experimental conditions. By way of example, γ-irradiated single crystals of cysteine·HCl·H_2O at 77 °K produces a radical which also has a strongly anisotropic, but axial, g-tensor with $g \simeq 2.29$ and $g \simeq 1.99$, and a roughly isotropic proton hyperfine structure characteristic of electron coupling to two non-equivalent hydrogen nuclei (10) ($\Delta H \simeq$ 14 G, 38 G). No such resonance is observed in the cystine system even though the final radical at high temperature appears to be much the same for both compounds. This low temperature axially-symmetric radical clearly has the large g-shifts expected for the RS· radical and the hyperfine splitting is what might be expected from the β-coupling of the analogous hydrocarbon fragment $RCH_2—\dot{C}H_2$. Neglecting the small anisotropy, and the B_0 term, in the familiar expression (11)

$$a_H = B_0 + B_2 \cos^2 \theta$$

one obtains a value for B_2 = 33–40 G which is comparable to the value of 45–50 G obtained for hydrocarbon radicals (12). The chief difference between the low and the high temperature form of RS· is that the latter has been assumed to have "relaxed" due to the thermal treatment of the crystal, and to have taken on a more stable non-linear configuration in the fields of the crystalline environment (5). The marked difference in proton hyperfine structure is however a little difficult to rationalize using the same argument. Yet another assignment of e.p.r. signals to thiyl radicals arises in the aqueous phase oxidation of simple thiols where a resonance is obtained with averaged g-values near 2.011 and proton hyperfine structure appropriate to the RS· radical (13, 14). The magnitude of the coupling ($\Delta H \simeq 9.5$ G) seems low, while the rotationally averaged g-value of 2.01 corresponds to neither of the assignments given above for thiyl in the solid state determinations. Radiolysis of thiols in the basic pH range yields nothing at all which may be attributed to RS· radicals (15). Regardless of whether the irradiation or photolysis of thiols is carried out in the solid (9), vapor (16), or liquid phase (using either protic (17) or aprotic (18) media) the major product appears to be the disulfide molecule RSSR, which suggests that somewhere along the line, the thiyl radical has indeed been produced in the system, and that its eventual fate is combination with its own kind.

The non-axial g-tensor elements characteristic of the solid state high temperature form of RS· may also be obtained when dilute glassy solutions of thiols in inert matrices are photolyzed at low temperatures. For instance, 0.1 M ethanethiol in 3-methylpentane at 77 °K has been photolyzed at 253.7 nm to give a radical which is characteristic of the solvent and a second species characterized by g-tensor elements of 2.063, 2.027, and 1.999, and a poorly resolved hyperfine doublet of about 9 G (19). Although one might have expected the "field-free" thiyl radical in this particular matrix, there is obviously a much closer resemblance to the "thermalized" configuration of the single crystal studies. Since the thiol molecules are presumably physically isolated in the glassy solid solution, being present at ~1.2 mol%, then the major products of photolysis (19) (H_2, thioethers, and disulfides) have been explained by the following simple scheme:

$$[1] \quad EtSH \xrightarrow{h\nu} EtS\cdot + H^* \qquad [2a] \quad H^* + MH \rightarrow M\cdot + H_2$$

$$[2b] \quad H^* + MH \rightarrow MH^* + H\cdot \qquad [3a] \quad H\cdot + EtSH \rightarrow EtS\cdot + H_2$$

$$[3b] \quad H\cdot + H\cdot \rightarrow H_2$$

On slight warming of the matrix, cage reactions begin to occur

$$[4] \quad M\cdot + EtS\cdot \rightarrow EtSM$$

Warming to the melting point of the matrix allows diffusion reactions to begin so that

$$[5] \quad 2\,EtS\cdot \rightarrow EtSSEt$$

In these equations, H* is taken to be a "hot" hydrogen atom and MH is, in the reference cited, 3-methylpentane. The primary assumption made is that while initially hot hydrogen atoms are produced, some of these may be thermalized by third body collisions and diffuse out of the cage in which the photolytic absorption took place.

The use of dilute rigid glasses has one distinct

Can. J. Chem. Downloaded from www.nrcresearchpress.com by 210.87.254.6 on 09/05/12
For personal use only.

advantage over the studies employing single crystals, polycrystalline samples, or thin films of thiols (20) in that large concentrations of thiyl radicals may be built up without, at the same time, having to deal with the possible biomolecular reactions between the reaction intermediates and the parent thiol molecules. If such processes are of little importance, then in dilute glassy solutions the scheme outlined above should be reasonably independent of thiol concentration with results similar to those obtained in the solid state. In order to test the relative importance of such reactions and to further determine the physical properties of the thiyl radical, a variety of alkyl thiols at different concentrations have been photolyzed in various hydrocarbon glasses. Solid state reactions may be induced following photolysis by careful thermal annealing of the glasses and may be followed by both e.p.r. and optical spectroscopic techniques. Warming the glasses to the melting point results in solutions which have been subjected to product analysis at room temperature.

Experimental

The 3-methylpentane (3MP) was Aldrich Chemicals "puriss" grade and was dried over lithium aluminum hydride. Before use it was run through an activated silica gel column and then distilled in small amounts (~50 ml). Ethanethiol (EtSH) and isopropylmercaptan (*i*-PrSH) were obtained from the Aldrich Chemical Company, *tert*-butyl mercaptan (*t*-BuSH) from Eastman Organic Chemicals, and *n*-butyl mercaptan (*n*-BuSH) was obtained from the J. D. Baker Chemical Company. The thiols were fractionally distilled before use. H_2S gas was used as supplied from the Matheson Company. Thiol solutions were prepared in either of two ways. In one, the solutions were mixed in volumetric flasks and subsequently transferred to Suprasil e.s.r. tubes (3 mm i.d.), or tubular optical cells (16 mm i.d.) on the vacuum system. The samples were then degassed by repeated freeze-pump-thaw cycling and then sealed off from the line under high vacuum. All glassware was heated to annealing temperature before use. Other samples were prepared using only high vacuum techniques in which the sulfhydryl or 3MP vapors were metered through calibrated bulbs and frozen in the sample cell, sealed off, and mixed after the components had been returned to room temperature. The samples were then refrozen ready for use. Both techniques produced the same spectral effects, so that what follows cannot be related to the presence of oxygen or water in the thiol–hydrocarbon solutions.

Photolyses were carried out at 253.7 nm in a clear quartz Dewar filled with fresh pure liquid nitrogen, with the cell situated 3 cm away from a Hanovia 87A45 low pressure resonance mercury lamp enclosed in a housing with a 1½ in. aperture. A Gates P-109 high pressure 100 W mercury lamp or a 500 W tungsten projection lamp, each with appropriate Corning filters, were used for photobleaching experiments.

Cysteine·HCl·H_2O was recrystallized several times from air-free water. The X-band e.p.r. homodyne spectrometer has been described elsewhere (21). The cavity was cooled using a conventional nitrogen gas flow system with a liquid nitrogen heat exchanger directly below the cavity. Special care was required in this system in order to catch some of the earlier processes occurring in the photolyzed glasses. Only pure liquid nitrogen (containing no oxygen) was used and every advantage was taken of the altitude of Calgary (ambient atmospheric pressure ~660 Torr) to obtain these initial spectra. The entire range of temperatures available for 3MP is less than 15 °C, lying between the temperature of boiling nitrogen and the melting point of the glass near 90 °K.

Low temperature absorption spectra were carried out on a modified Beckman DU2400 spectrophotometer.

Glasses could be photolyzed, melted, and brought to room temperature so that g.l.c. analyses could be carried out on a Varian series 1800 chromatograph. Liquid phase analyses were effected on a 3% Squalane or SE-30 silicon rubber column. The vapors were also investigated using a Poropak Q column. Isothermal analysis at 90 °C was used in each case. Hydrogen analyses were carried out using a palladium thimble technique described elsewhere (22). We will not deal extensively with the results of these analyses at the present time except to note that the main products of photolysis of RSH are H_2, RSSR, and RSM where M represents incorporation of the solvent. Chromatographic peaks corresponding to the last named change when different solvents or different thiols are used. The ratio of peak areas, RSSR to RSM, increase as the concentration of the thiol in the glass increases. There are at least three RSM peaks corresponding to different isomers. Subsidiary peaks are also observed which correspond to fragmentation of the solvent molecule (lower alkanes and alkenes) and of the solute molecules. The latter is indicated by the presence of H_2S peaks detected using a Varian H^3 electron capture detector. In any case, the amount of these subsidiary products represents less than 10% of the total hydrogen yield.

Results

We have repeated the experiments of Wheaton and Ormerod (4) on both single crystals and polycrystalline cysteine·HCl samples, to further determine the characteristics of the axial form of RS·. We find in agreement with these authors that the integrated e.p.r. signal obtained increases as the crystals are warmed from 77 °K to about 180–200 °K and then decreases at higher temperatures. Not noted by Wheaton and Ormerod was the fact that while the crystals at 77 and 300 °K are pale yellow, the color intensifies quite markedly at intermediate temperatures near 180 °K. The results are in agreement with Henriksen (22) who found that while γ-irradiated polycrystalline cysteine·HCl crystals were yellow at low temperatures, those irradiated at room temperature were colorless. Samples irradiated at low temperatures and warmed also

Can. J. Chem. Downloaded from www.nrcresearchpress.com by 210.87.254.6 on 09/05/12
For personal use only.

show the characteristic fading exhibited by single crystals. While the e.p.r. spectrum of single crystals shows the axial g-tensor symmetry and hyperfine structure already referred to, the polycrystalline samples exhibited e.p.r. spectra similar to those obtained by Henriksen; the low field absorption near $g = 2.2$ obtained in single crystals is broadened beyond detection and an unsymmetrical resonance devoid of resolved hyperfine structure remains near $g = 2.0$. From these results one can conclude that the axially symmetric RS· is probably colored and should be difficult to detect by e.p.r. in a homogeneous rigid solution except that perhaps a broad signal with no distinct hyperfine structure may be obtained near $g = 2.00$. The resonance will occur with considerably reduced sensitivity since using differential recording techniques, one normally "sees" only a small fraction of the radicals actually present because of the extreme anisotropic broadening.

We have also repeated the work reported earlier from this laboratory (19) paying much greater attention to the temperature control and details of the thermal annealing processes. In view of the color changes mentioned above, we have also obtained low temperature absorption spectra to follow these processes optically as closely as is possible using different sample sizes.

Generally speaking the 77 °K photolysis of dilute glassy solutions containing alkyl thiols gives results which are similar to those obtained by γ-irradiation of the crystalline cysteine system insofar as the most intense yellow coloration and broad e.p.r. absorption near $g = 2.00$ occur only after thermal annealing, being either absent or substantially reduced in freshly photolyzed samples. As before (19) a resonance A is obtained, characterized by an anisotropic g-tensor with principal values near 2.06, 2.02, and 2.00. The spectrum is similar to that obtained by photolysis of the pure thiol at 77 °K. For reference, the spectrum obtained for neat ethanethiol (EtSH) appears in Fig. 1; it is similar to the spectrum obtained elsewhere (8) and the 9 G hyperfine splitting seen is characteristic of a normal alkyl substituent; iso- and *tertiary*-alkyl thiols do not exhibit any such hyperfine structure. Superimposed on A initially is a six-line proton hyperfine spectrum B characteristic of the solvent and giving a total spectrum such as in Fig. 2 which is that obtained for 0.1 *M* EtSH in 3MP. The six line solvent radical spectrum B is similar to that obtained from γ-radiolysis of 3MP (19) except that there is additional detail in the photolytically produced spectrum which has been attributed to a small amount of ethyl radicals (23). This additional featuring does not depend on the particular substrate, and photolysis of a 0.02 *M* H_2S in 3MP or any of the alkyl thiols glasses gives essentially the same spectrum if the temperature is kept low enough.

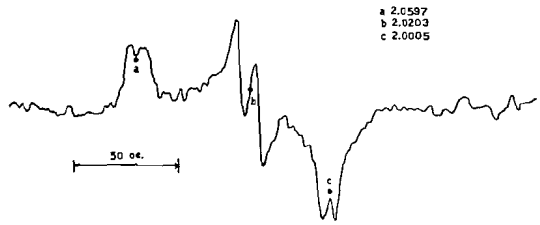

FIG. 1. Radical A; obtained from a 3 h 253.7 nm photolysis of neat ethanethiol at 77 °K.

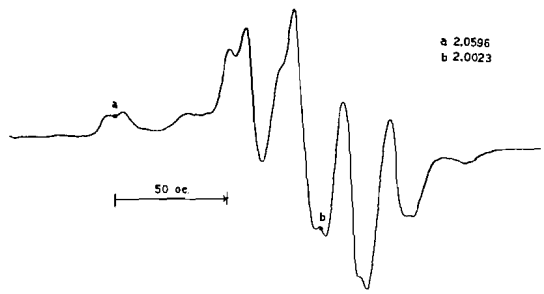

FIG. 2. A 4 h 253.7 nm photolysis of 0.1 *M* ethanethiol, 3-methylpentane glass at 77 °K.

As the matrix is warmed, loss of the hyperfine detail occurs first and the total intensity of B steadily decreases; the glasses become more intensely yellow, and the e.p.r. signal becomes asymmetric relative to the baseline near $g = 2.0$. Other intermediate hyperfine patterns may also grow in, as for example in 0.01 EtSH in 3MP, where the odd line spectrum shown in Fig. 3 is obtained at the expense of B. These intermediate species are characteristic of the solute and will be designated as type C absorptions. As the matrix is further warmed, eventually all proton hyperfine structure is lost and there remains only the unchanged absorption due to A, along with a broad asymmetrical signal near $g = 2.00$, which will be called a type D resonance. A typical terminal spectrum appears in Fig. 4. The signals of both A and D vanish as the melting point of the glass is approached. None of the above transformations is thermally reversible.

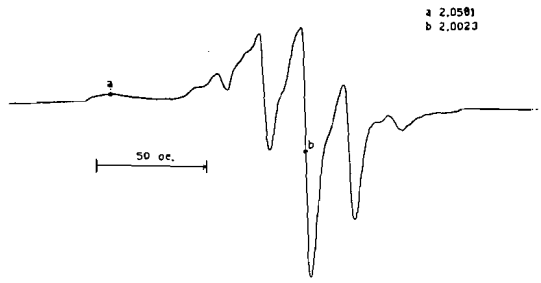

FIG. 3. Sample of Fig. 2 warmed slightly. Solvent radical replaced by species C.

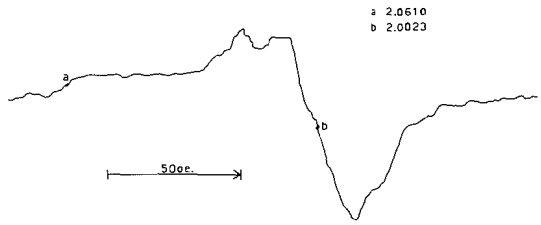

FIG. 4. Sample of Fig. 3 warmed to ~85 °K.

Following the initial photolysis, glasses of increasing concentration show greater optical absorption at 400 nm, and greater intensity in the low-field A absorption relative to B. Regardless of the color initially present, all glasses become more intensely yellow upon warming as can be seen from Fig. 5 which can be considered as representative. Both color and e.p.r. spectrum appear to disappear simultaneously as the matrix is warmed to the melting point.

Glasses containing EtSH were also photolyzed at 77 °K and then warmed until the glass had become an intense yellow. The sample was then returned to 77 °K and photolyzed again. Wavelengths greater than 300 nm produce no change but photolysis at 253.7 nm for an additional period results in a considerable reduction in intensity of the 400 nm peak, loss of the five line spectrum and a substantial increase in the A resonance at $g = 2.06$. The optical results in Fig. 5 and the e.p.r. spectrum in Fig. 6 are typical results. The lines which appear in Fig. 6 resemble the ethyl spectrum (24) rather more than the 3MP radicals seen in Fig. 2. The latter spectrum would have been expected if resumption of the primary photolysis were the only process occurring.

Photolysis of thiols in ethylene glycol – water matrices (80–20) produces no visible coloration.

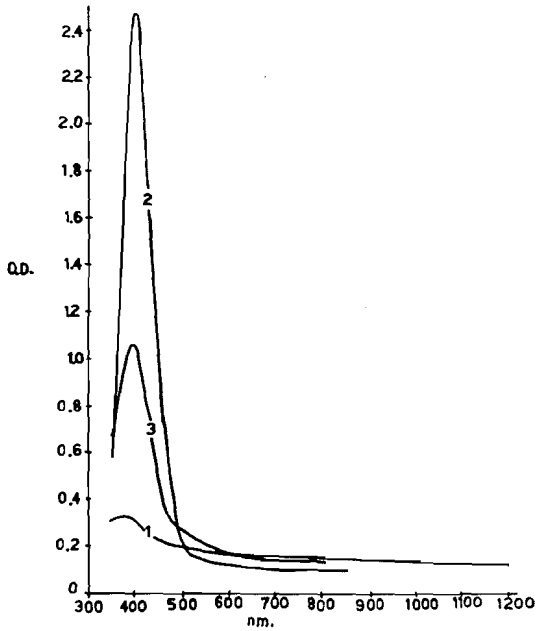

FIG. 5. Optical spectra of 0.01 *M* ethanethiol, 3-methylpentane glass photolyzed at 253.7 nm, for 1 h at 77 °K (*1*). On warming (*2*) is obtained. This is recooled to 77 °K and photolyzed for an additional half hour to obtain (*3*).

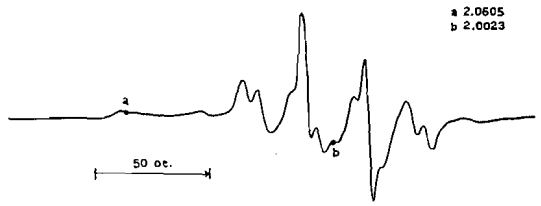

FIG. 6. Electron spin resonance spectrum corresponding to (*3*) of Fig. 5.

Discussion

The Thiyl Species RS· (Radical C)

The results cited for EtSH raise a number of perplexing questions. Regardless of whether one chooses the yellow coloration or the low field resonance A to be indicative of the presence of EtS·, because of the delayed appearance of the former and constant intensity of the latter, neither is consistent with the simple reaction scheme cited in the Introduction which suggests that the maximum EtS· concentration should be present immediately after photolysis. The thiyl concentration should then decrease as the matrix is warmed due to cage reactions with the solvent radicals as recorded by the changes in e.p.r.

Can. J. Chem. Downloaded from www.nrcresearchpress.com by 210.87.254.6 on 09/05/12
For personal use only.

Can. J. Chem. Downloaded from www.nrcresearchpress.com by 210.87.254.6 on 09/05/12
For personal use only.

spectrum. The difficulty can be resolved if it may be assumed that the thiyl radicals formed in the photolytic act are "hot", and can either react or rearrange in such a way as to disguise their presence. Since the product analysis requires that it is the S—H, rather than the C—S bond which breaks, then the energy available to the fragments RS and H is about 1.1 eV, which is the difference in energy between the incident proton (~4.9 eV), and the S—H bond energy (25) (~3.8 eV). Ordinarily the hydrogen atom would carry off over 95% of this energy, because of the fragment mass ratios, and would appear to be "hot", while the thiyl part will remain kinetically "cool". If the excess energy were more equally distributed the following reaction might be expected to occur and should be placed in the scheme presented in the Introduction

$$[1] \qquad \mathrm{EtSH} \xrightarrow{h\nu} \mathrm{EtS^*} + \mathrm{H^*}$$

$$[2c] \qquad \mathrm{EtS^*} + \mathrm{MH} \rightarrow \mathrm{EtSH} + \mathrm{M}\cdot$$

If this process were efficient enough (as appears to be required for certain rate studies carried out at higher temperatures (26), the presence of the thiyl radical would be completely masked but would appear again by relaxation of the matrix through the cage reaction

$$[4b] \qquad \mathrm{M}\cdot + \mathrm{EtSH} \rightarrow \mathrm{MH} + \mathrm{EtS}\cdot$$

As noted above, for this to occur EtS must carry away an unusually large share of the photon energy. That this should indeed be the case can be justified by the following argument based on the magnitude of the $g_\parallel$ tensor element for the RS· radical.

The g-shifts so characteristic of these sulfur containing radicals are given in a molecular fixed frame by the general expression (27)

$$\Delta g_{ij} = -2 \sum_k \sum_n \zeta_k \frac{\langle 0|L_i|n\rangle\langle n|L_j|0\rangle \rho_k}{E_n - E_0}$$

wherein the sums are over the atomic centers k and energy states n, with ρ_k being the spin density, and ζ_k the spin-orbital parameter for the atom k. Since $\zeta_C = -28\ \mathrm{cm}^{-1}$ while $\zeta_S = -382\ \mathrm{cm}^{-1}$, only that spin density on sulfur atoms will be important. In the one electron orbital approximation for which this equation is valid, radicals with z-axis symmetry (*e.g.* $CH_3S\cdot$ or *t*-BuS·, with C_3 symmetry) have isoenergetic p_x and p_y atomic orbitals containing three electrons. Accordingly two degenerate configurations will result and the resonance denominator $E_n - E_0$ tends to zero for these two configurations. Since the numerator will not vanish, $\Delta g_{zz} = \Delta g_\parallel$ will become infinite. One can assume that the Jahn–Teller effect (28) or other non-axial field effects will lift this degeneracy with the result that $\Delta g_\parallel$ will remain finite, but presumably large. On the other hand, $\Delta g_{xx} = \Delta g_{yy} = \Delta g_\perp$ will be determined by configurational mixing of states of sufficiently high energy, so that $g_\perp$ will be relatively unchanged from the free electron value at 2.0023. The observed shift $\Delta g_{zz} = \Delta g_\parallel$ is 0.21 for the low temperature cysteine radical. Using the appropriate parameters with $\rho_S \simeq 1$, one calculates an energy difference of $E_n - E_0 \simeq 3000\ \mathrm{cm}^{-1}$ which means that RS· must have at least one low-lying excited electronic state in the range 0 to 1.1 eV and may well be "hot" in the sense that it can carry off excess electronic energy in this metastable state. Naturally enough the occurrence of hot thiyl will decrease the energy available to the H atom, making it less reactive and so increasing the probability that it will be able to diffuse out of the cage in which it was formed initially. The increasing yellow coloration of successively more concentrated thiol glasses reflects the increased probability that a diffusing hydrogen atom will encounter a thiol molecule before becoming completely thermalized. Accordingly we assign the yellow coloration of the glasses to signify the presence of the RS· radical in agreement with the observations made on the single crystal experiments, and ascribe the tardy appearance of this absorption in thermal annealing experiments to be a result of hot reactions involving the RS· radical, resulting in the reformation of the thiol molecule. The low field resonance A must therefore arise from a different sulfur radical since its concentration does not increase and fall with that of RS·, as would be expected of a "thermalized" isomer.

The thiyl radical may be characterized by an axial **g**-tensor with $g \simeq 2.2$, $g \simeq 2.0$ and hyperfine coupling following the β-coupling relationship $a_H \simeq 36 \cos^2 \theta$. Distinctive hyperfine structure is not observed in randomly oriented RS· and only a broad resonance may be detected at $g = 2.0$ when the radical is present in high concentration. Optically, RS· has a forbidden $n_p \rightarrow \pi_p$ transition near $3000\ \mathrm{cm}^{-1}$, and appears yellow due to a transition near 400 nm. The latter

absorption does not contribute to the g-tensor elements and is accordingly assigned to be a $n_s \rightarrow \pi_p$ transition involving the 3s electrons in sulfur.

The Hydrocarbon Radicals B

The spectrum B is similar to that obtained from photolysis of HI in 3MP containing ethylene (23) and is considered to be the 3MP·radical (ΔH = 24 G) in the presence of some ethyl radical (ΔH = 27 G). In the photolysis of the thiols, ethane and ethylene are among the most plentiful of the subsidiary by-products according to g.l.c. analysis and arise in a large part from fragmentation of the solvent. Although more mobile (23) in glassy 3MP matrices, ethyl will behave in much the same manner as the more abundant 3MP· and react to produce RS· and the other observed intermediates such as C.

The Radical Species C (R'ĊHSH)

The five line spectrum which is obtained for EtSH in Fig. 3 appears to be characteristic of this particular solute. Glasses of the other thiols do not produce the same five-line spectrum but give changing proton hyperfine spectra which suggest formation of analogous intermediate species at the expense of the solvent radical spectrum, which all exhibit initially, and growth of yellow RS· color, which is also common to all of the systems. Since the temperature at which these processes occur is that at which cage reactions are observed, we presume that the reaction which produces thiyl also results in the formation of other radicals. Thus

[4c] $\quad M\cdot + EtSH \rightarrow EtS\cdot + MH$

or

[4d] $\quad \rightarrow \dot{C}H_2CH_2SH + MH$

or

[4e] $\quad \rightarrow CH_3\dot{C}HSH + MH$

Reference to Fig. 3 shows that each hyperfine line is sharper on the high field side, and is slightly asymmetrical relative to the baseline. This general shape is indicative of a small near-axial g-tensor anisotropy which is slightly greater than the line width but smaller than the hyperfine splitting, suggesting a small but finite spin density on the sulfur atom; so our choice for absorption B is the radical $CH_3\dot{C}HSH$. This is in agreement with other work (29) which finds the four protons of the α-isomer to be coupled more or less equally while those of β-isomer are not. The abstraction which has occurred to produce Fig. 3 is not the low energy process (30) (S—H abstraction, $\Delta E_{act} \sim 4$ kcal mol^{-1}) but rather a higher energy, cage-controlled reaction (αC—H abstraction $E_{act} \lesssim 8$ kcal mol^{-1}) which has occurred. The C signal so produced then disappears by thermally induced irreversible isomerization to thiyl

$$CH_3\dot{C}HSH \rightarrow CH_3CH_2S\cdot$$

or perhaps by "repair" reaction due to thermal relaxation of the cage

$$CH_3CH_2SH + CH_3\dot{C}HSH \rightarrow CH_3CH_2S\cdot + CH_3CH_2SH$$

Resonance C is therefore ascribed to radicals of the type R'ĊHSH.

The Radical Species A ($RS_2\cdot$)

So far no mention has been made of the structure appropriate to radical A, except that it is unlikely to be the RS· radical. In dilute thiol glasses it is formed only during the initial photolysis and in spite of the fact that it is paramagnetic, it does not undergo any subsequent cage reactions with other radicals. This suggests that radical A is relatively isolated in the matrix and is formed as a result of attack by diffusing hydrogen atoms which are present in the glass only during the photolysis period. The concentration dependence of A suggests its precursor competes satisfactorily against RSH for the available hydrogen atoms which in turn suggests that it has even a lower energy of activation for reaction than does the thiol molecule itself. Bearing in mind that solid disulfides, as well as thiols, yield this very stable free radical, one must consider the possibility that the radical A contains two skeletal sulfur atoms rather than just one. We believe the most likely structure for the A type radical is $RS_2\cdot$ and that it results from reactions involving dimers of the parent mercaptan (which will explain its concentration dependence) or by cleavage of the C—S bond in the case of disulfides. In the present situation, $RS_2\cdot$ could result by means of two separate pathways involving a thiol–thiyl complex.

$$H + (RSH)_2 \rightarrow [RS\cdot \ldots HSR] + H_2$$

$$[RS\cdot \ldots HSR] \rightarrow RS_2\cdot + HR$$

Can. J. Chem. Downloaded from www.nrcresearchpress.com by 210.87.254.6 on 09/05/12
For personal use only.

Can. J. Chem. Downloaded from www.nrcresearchpress.com by 210.87.254.6 on 09/05/12
For personal use only.

Alternatively

$$(RSH)_2 \xrightarrow{h\nu} RSSR + H_2$$

and subsequently

$$H + RSSR \rightarrow [RS \ldots HSR] \rightarrow RS_2\cdot + HR$$

The effect of the last reaction has been observed in the aqueous phase (31). While association of thiols in non-polar media was once thought to be unlikely (32), recent studies (33) show the association constant may be as high as $K_{eq} = 0.01$ for EtSH in hydrocarbon solutions at room temperature. This constant is presumably larger at lower temperatures.

The general ingredients for the intermediate, a thiyl radical in close proximity to an undamaged thiol molecule, is a general feature of all solid state investigations involving the photolysis and radiolysis of pure thiols. In addition the radiolysis of disulfide systems is known to produce disulfide negative ions (34) and the above intermediate is simply the proton adduct of such a negative ion. In most single crystal studies there is a plentiful source of protons. For instance most cystine studies are performed using the double hydrochloride salt. These factors may account in part for the ubiquitous appearance of this radical in many of the systems subjected to photolytic or ionizing radiation such as those studied by Gordy *et al.* (1).

The observed properties of the radical A are consistent with the structure $RS_2\cdot$ since the molecule is almost surely nonlinear with the spin density most likely distributed over both sulfur atoms in a π^* molecular orbital. This in itself would reduce the proton hyperfine coupling by a half and *g*-shift by at least this amount if any stability at all is gained by π-bond formation. With the introduction of the S—S bond, other low energy excitations ($\pi_{ss}^* \rightarrow \sigma_{ss}^*$) not found in RS· become possible and these will contribute to the non-axial character of the g-tensor. The *g*-value anisotropy should be relatively independent of the particular alkyl group, as is observed, and the stability of $RS_2\cdot$ can be accredited to the relatively low potential for the formation of bonds at this position. For instance (35) the HSS—H bond energy is 72 kcal mol^{-1} compared to HS—H energy of about 90 kcal mol^{-1}, making H-atom abstraction by $RS_2\cdot$ extremely unlikely. This radical also appears to be the stable entity in amine solutions of elemental sulfur (36).

Photochemical Behavior of RS·, $RS_2\cdot$, and R'ĊHSH

As noted in the Results section, when a photolyzed glass containing EtSH was warmed to produce RS· and RĊHSH, cooled, and rephotolyzed at 253.7 nm both of these species disappeared while the spectrum of $RS_2\cdot$ grew rapidly. On this basis one can presume that $CH_3\dot{C}HSH$ and $CH_3CH_2S\cdot$ are photochemically active in the 250 nm region while $RS_2\cdot$ is not.

The following reactions appear feasible at 77 °K:

$$CH_3\dot{C}HSH \xrightarrow{h\nu} CH_3CH_2S\cdot{}^{**}$$

and

$$CH_3CH_2S\cdot \xrightarrow{h\nu} CH_3CH_2S^{**}$$

$$CH_3CH_2S\cdot{}^{**} \rightarrow CH_3CH_2\cdot + \cdot S\cdot$$

followed by

$$\cdot S\cdot + CH_3CH_2S\cdot \rightarrow CH_3CH_2S_2\cdot$$

$$n\cdot S\cdot \rightarrow \cdot S_n\cdot$$

If sulfur atoms are indeed produced, there is enough energy that either ^1D or ground state ^3P atoms can be formed. The fate of ^1D atoms in hydrocarbon solvents is immediate insertion (37) or thermalization to the lower ^3P states. The latter are known to be unreactive toward hydrocarbon matrices (37). The solvent mercaptan MSH has not been detected among the products, which suggests that photolysis of EtS· produces only ^3P atoms, presumably from a lower energy excited quartet state of the radical. Under the conditions of the second photolysis, $S(^3P)$ would most probably react with the excess RS· present in the matrix and this accounts for the increase in the $RS_2\cdot$ signal.

During the primary photolysis, since there are relatively few RS· radicals free in the matrix, but a high concentration of solvent radicals, the most likely product would be MS· with M being the 3MP radical. These molecules would be spectroscopically indistinguishable from RS· and subject to further photolysis with the eventual formation of $(S)_x$. Since this radical has a principle g-value (38) of 2.042, an absorption maximum should be observed in the low temperature glasses (Figs. 2–4) or in frozen neat thiols (Fig. 1). Its absence shows that secondary photolysis of RS· is unimportant during the primary photolysis and supports the idea that "hot" thiyl radicals are indeed formed and that most of

these react by an immediate abstraction from the solvent.

The authors would like to express their gratitude to the Department of National Defence whose financial help initiated this project and to the National Research Council of Canada for continuing support. Thanks are also due to Mr. Glen Smith, Mr. L. Peters, Mr. R. Wickson, and Mrs. R. Sniatycka whose technical help was much appreciated during certain phases of the work.

1. W. GORDY, W. B. ARD, and H. SHIELDS. Proc. Natl. Acad. Sci. **43**, 987 (1957).
2. T. KURITA and W. GORDY. J. Chem. Phys. **34**, 282 (1961).
3. E. L. THOMSEN and S. O. NIELSEN. J. Chem. Phys. **57**, 1095 (1972).
4. R. F. WHEATON and M. G. ORMEROD. Trans. Faraday Soc. 1638 (1968).
5. E. E. BUDZINSKI and H. C. BOX. J. Phys. Chem. **75**, 2564 (1971).
6. F. K. TRUBY, C. MACCALLUM, and J. E. HESSE. J. Chem. Phys. **37**, 2777 (1962).
7. T. HENRIKSEN. J. Chem. Phys. **37**, 2189 (1962).
8. D. H. VOLMAN, J. WOLSTENHOLME, and S. G. HADLEY. J. Phys. Chem. **71**, 1798 (1967).
9. D. B. PETERSON, J. HOLIAN, and W. M. GARRISON. J. Phys. Chem. **73**, 1568 (1969).
10. K. AKASAKA. J. Chem. Phys. **43**, 1182 (1965).
11. C. HELLER and H. M. MCCONNELL. J. Chem. Phys. **34**, 1535 (1960).
12. F. C. ADAM and F. W. KING. J. Chem. Phys. **58**, 2446 (1973).
13. W. WOLF, J. C. KERTESZ, and W. C. LANDGRAF. J. Magn. Res. **1**, 618 (1969).
14. W. A. ARMSTRONG and W. G. HUMPHREYS. Can. J. Chem. **45**, 2589 (1967).
15. P. NETA and R. W. FESSENDEN. J. Phys. Chem. **75**, 2277 (1971).
16. R. P. STEER and A. R. KNIGHT. Can. J. Chem. **47**, 1335 (1969).
17. G. E. ADAMS, G. S. MCNAUGHTON, and B. D. MICHAEL. *In* Chemistry of ionization and excitation. *Edited by* R. R. A. Johnson and G. Scholes. Taylor and Francis, London. 1967. p. 281.
18. J. ESSER and J. A. STONE. Can. J. Chem. **51**, 192 (1973).
19. J. SKELTON and F. C. ADAM. Can. J. Chem. **49**, 3536 (1971).
20. P. S. H. BOLMAN, I. SAFAIEK, D. A. STILES, W. J. R. TYERMAN, and O. P. STRAUSZ. Can. J. Chem. **48**, 3872 (1970).
21. L. J. AARONS and F. C. ADAM. Can. J. Chem. **50**, 1390 (1970).
22. T. HENRIKSEN. J. Chem. Phys. **36**, 1258 (1962).
23. S. ADITYA and J. E. WILLARD. J. Am. Chem. Soc. **83**, 229 (1966).
24. (*a*) P. B. AYSCOUGH and C. THOMSON. Trans. Faraday Soc. **58**, 1477 (1962); (*b*) E. L. COCHRAN, F. J. ADRIAN, and V. A. BOWERS. J. Chem. Phys. **34**, 1161 (1961).
25. J. G. CALVERT and J. N. PITTS. Photochemistry. John Wiley and Sons, New York. 1966.
26. W. A. PRYOR, G. GOJON, and J. P. STANLEY. J. Am. Chem. Soc. **95**, 945 (1973).
27. A. CARRINGTON and A. D. MACLACHLAN. Introduction to magnetic resonance. Harper and Row, New York. 1967.
28. H. A. JAHN and E. TELLER. Proc. R. Soc. London, A**161**, 200 (1937).
29. (*a*) J. Q. ADAMS. J. Am. Chem. Soc. **92**, 4535 (1970). (*b*) P. J. DRUSIC and J. K. KOCHI. J. Am. Chem. Soc. **93**, 846 (1971).
30. G. GREIG and J. C. J. THYNNE. Trans. Faraday Soc. 379 (1966).
31. (*a*) M. SIMIC and M. Z. HOFFMAN. J. Am. Chem. Soc. **92**, 6096 (1970); (*b*) J. W. PURDIE, H. A. GILLIS, and N. V. KLASSEN. To be published.
32. (*a*) T. G. TEATLY, G. HOPKINS, and L. HUNTER. Nature, **149**, 218 (1942). (*b*) A. E. LUTSKII, A. K. KULCHITSKAYA, E. M. OBUKHOVA, S. A. VOLCHENOK, and G. I. SHEREMET'EVA. J. Gen. Chem. U.S.S.R. **36**, 1597 (1966).
33. S. H. MARCUS and S. I. MILLER. J. Am. Chem. Soc. **88**, 3719 (1966).
34. T. SHIDA. J. Phys. Chem. **72**, 2597 (1968).
35. N. J. FRISWELL and B. G. GOWENLOCK. Adv. Free Radical Chem. 226 (1967).
36. W. G. HODGSON, S. A. BUCKLER, and G. PETERS. J. Am. Chem. Soc. **85**, 543 (1963).
37. H. E. GUNNING and O. P. STRAUSZ. Adv. Photochem. **4**, 143 (1966).
38. D. A. STILES, R. KEWLEY, O. P. STRAUSZ, and H. E. GUNNING. Can. J. Chem. **43**, 2442 (1965).

Can. J. Chem. Downloaded from www.nrcresearchpress.com by 210.87.254.6 on 09/05/12
For personal use only.

Reactions of Nitro Sugars. XXXI. Formation of 2,3- and 3,4-Unsaturated Derivatives in the 6-Deoxyhexose Series[1,2]

HANS H. BAER AND CHUNG-WAI CHIU

Department of Chemistry, University of Ottawa, Ottawa, Canada K1N 6N5

Received June 25, 1973

The methyl 3,6-dideoxy-3-nitrohexopyranosides having the α-L-*gluco* (**1**), α-L-*manno* (**2**), α-L-*galacto* (**3**), and α-L-*talo* (**4**) configurations and their 2,4-diacetates (**6**, **11**, **16**, and **18**, respectively) served as starting materials for the preparation of 2,3- and 3,4-unsaturated derivatives. The reactions employed included dehydroacetylation of diacetates and of some monoacetates (**5**, **7**, and **12**) that had been obtained by partial acetylation or partial acid-catalyzed de-*O*-acetylation, and also dehydrations occurring under conditions of acetylation. The following nitroolefins were obtained: methyl 3,4,6-trideoxy-3-nitro-α-L-*erythro*-hex-3-enopyranoside (**8**) and its 2-acetate (**9**), the corresponding α-L-*threo* isomer (**13**) and its 2-acetate (**10**) and 2-*O*-methyl derivative (**20**), and methyl 2,3,6-trideoxy-3-nitro-α-L-*erythro*-hex-2-enopyranoside (**14**) and its 4-acetate (**15**) as well as the 4-acetate (**17**) of the corresponding α-L-*threo* isomer. In addition, 1,4-di-*O*-acetyl-2,3,6-trideoxy-3-nitro-α-L-*threo*-hex-2-enose (**19**) was obtained by acetolysis of **17**. Factors assumed to be responsible for a pronounced regioselectivity in some of the reactions are discussed.

Les didéoxy-3,6 nitro-3 hexopyranosides de méthyle possédant les configurations α-L-*gluco* (**1**), α-L-*manno* (**2**), α-L-*galacto* (**3**) et α-L-*talo* (**4**) ainsi que leurs dérivés diacétates-2,4 (**6**, **11**, **16** et **18**, respectivement) ont servi de composés de départ pour la préparation des dérivés insaturés en position 2,3 et 3,4. Les réactions utilisées comprennent la déhydroacétylation des diacétates et de certains monoacétates (**5**, **7** et **12**) obtenus par acétylation partielle ou par de-*O*-acétylation partielle catalysée par un acide, ainsi que des déshydratations dans les conditions d'acétylation. On a obtenu les nitrooléfines suivantes: tridéoxy-3,4,6 nitro-3 α-L-*erythro* hexèno-3 pyranoside de méthyle (**8**) et son dérivé acétate (**9**), son isomère α-L-*thréo* correspondant (**13**) et son acétate-2 (**10**) et son dérivé *O*-méthyl-2 (**20**) ainsi que le tridéoxy-2,3,6 nitro-3 α-L-*erythro* hexeno-2 pyranoside de méthyle (**14**), son acétate-4 (**15**) et l'acétate-4 (**17**) de son isomère α-L-*thréo* correspondant. En plus, on a obtenu par acétolyse de **17** le di-*O*-acétyl-1,4 tridéoxy-2,3,6 nitro-3 α-L-*thréo* hexène-2 ose (**19**). On discute aussi des facteurs susceptibles d'être responsables de la régiosélectivité prononcée de certaines de ces réactions. [Traduit par le journal]

Can. J. Chem., **52**, 111 (1974)

Introduction

Unsaturated nitro sugars possess great potential as intermediates for synthesis of deoxy, diamino, and branched-chain sugars, disaccharides, and carbohydrate derivatives bearing various kinds of other functionalities (1). In continuing our studies in this field we decided to attempt the preparation of unsaturated compounds derived from the four methyl 3,6-dideoxy-3-nitro-α-L-hexopyranosides (**1**–**4**) which have so far become available (2–4). Possession of such nitroalkenes would be valuable for the design of syntheses of several antibiotics sugars whose common structural feature is a nitrogenous function in position 3 and deoxy functions in positions 6 and 2 or 4 (5). The work to be reported is part of a project of which some other aspects, namely the preparation of saturated and unsaturated methyl ethers derived from **1** and their utilization in the synthesis of amino sugars, are being communicated elsewhere (6).

The most widely used method for making α-nitroalkenes is the base-induced dehydroacetylation of β-nitroalkyl acetates, *i.e.*, the Schmidt–Rutz reaction or modifications thereof (1, 7, 8). No monoacetates of compounds **1**–**4** that could serve the purpose were known, so that it became necessary to devise ways of preparing some of them. Another possible approach to be attempted was dehydroacetylation of the diacetates of **1**–**4** which presumably would be more convenient to prepare than the monoacetates. Although a given diacetate could give rise to positional isomers having 2,3- and 3,4-unsaturation, it was thought that different configurations at C-2 and C-4 might cause preferential elimination of acetate in one direction or the other, and that in any event, mixtures of isomers might be separable

[1]For Part XXX in this series, see ref. 6.

[2]From the Ph. D. Thesis of C. W. Chiu, University of Ottawa, Ottawa, Canada, 1971. Presented before the 8th International Symposium on the Chemistry of Natural Products (IUPAC), New Delhi, India, February, 1972.

Can. J. Chem. Downloaded from www.nrcresearchpress.com by 210.87.254.5 on 09/05/12
For personal use only.

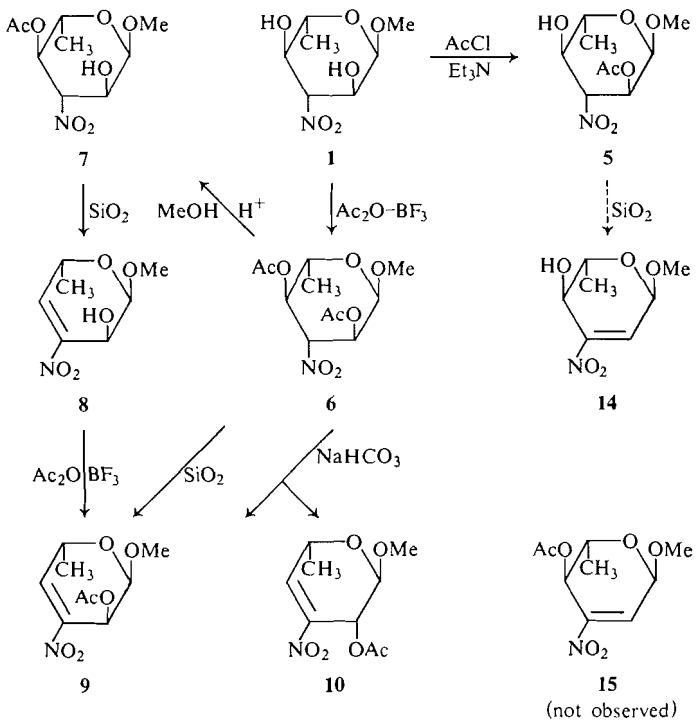

SCHEME 1

without undue labor. Of course this approach was predicated on the actual formation of stable monounsaturated derivatives from the diacetates, which was by no means a trivial point. In fact, chances for success seemed doubtful at the outset as it had to be recalled that Schmidt–Rutz reaction of analogous compounds in the hexose series (as opposed to the 6-deoxyhexose series) had resulted in exclusive double dehydroacetylation giving unstable 3-nitro-2,4-dienes which then underwent spontaneous self addition in the manner of the Diels–Alder reaction (9). Nevertheless, it was reasoned that the electron-donating effect of the methyl group at C-5 (taking the place of an electron-withdrawing acetoxymethyl group in the hexose derivatives) might make the diacetates of **1–4** less susceptible to such a complication.

Results

The reactions that were performed starting with methyl 3,6-dideoxy-3-nitro-α-L-glucopyranoside (**1**) are outlined in Scheme 1. In accordance with the previously observed (6), greater reactivity of its 2-hydroxyl group, compound **1** upon treatment with 1 mol of acetyl chloride and triethylamine (10, 11) gave predominantly the 2-acetate **5** (yield, 51%). Conversely, the greater reactivity at position 2 is also reflected in an enhanced lability of the 2-acetyl group in the diacetate **6** towards acid-catalyzed methanolysis. This procedure effected partial de-*O*-acetylation affording the 4-acetate **7** in 45% yield. On the other hand, positional reactivities appeared inverse in base-catalyzed dehydroacetylation. Thus, action of (basic) silica gel upon **6** effected elimination of acetic acid to give the 3,4-unsaturated monoacetate **9**, but the 2,3-unsaturated isomer **15** was not observed. Similar treatment of the 4-acetate **7** produced methyl 3,4,6-trideoxy-3-nitro-α-L-*erythro*-hex-3-enopyranoside (**8**) from which **9** could be obtained by acetylation. (Partial methanolysis of **6** followed by chromatography of the product mixture on a silica gel column thus constitutes a simple approach to **8** although the yield is low, with much **1** being recovered by competing, total de-*O*-acetylation.) By contrast to the dehydroacetylation of **7**, action of silica gel upon the isomeric monoacetate **5** was rather ineffective. Although some dehydroacetylation seemed to occur, efforts to isolate the expected nitroolefin **14** were not deemed worthwhile since

Can. J. Chem. Downloaded from www.nrcresearchpress.com by 210.87.254.5 on 09/05/12
For personal use only.

Can. J. Chem. Downloaded from www.nrcresearchpress.com by 210.87.254.5 on 09/05/12
For personal use only.

this compound proved more easily accessible by another route (see below).

Performance of the Schmidt–Rutz reaction (7) with **6** under the customary conditions (refluxing in dry benzene in the presence of sodium bicarbonate) indicated that nitroolefins can indeed be obtained in this way in the 6-deoxyhexose series, albeit in moderate yield. However, an unexpected observation was made. While of the two crystalline products isolated the minor one (yield, 4%) was the Δ^3-α-L-*erythro* acetate **9**, the major product (yield, 21%) was not the expected Δ^2-α-L-*erythro* isomer **15** but proved to be the Δ^3-α-L-*threo* isomer **10**. A rationale for the observed 2-epimerization will be offered below.

In Scheme 2 are depicted reaction sequences departing from methyl 3,6-dideoxy-3-nitro-α-L-mannopyranoside (**2**). Its diacetate **11**, smoothly obtained by boron trifluoride-catalyzed acetylation (12), was selectively de-*O*-acetylated in the 2-position by methanolic hydrogen chloride to give the 4-acetate **12** which was dehydroacetylated by silica gel to furnish methyl 3,4,6-trideoxy-3-nitro-α-L-*threo*-hex-3-enopyranoside (**13**). All these steps gave high yields. Direct dehydroacetylation of **11** produced what, according to the n.m.r. spectrum, was an unequal mixture of two nitroolefins. The strongly preponderant product proved identical with the previously obtained, unexpected Schmidt–Rutz product from the α-L-*gluco* diacetate **6**, *i.e.*, it was the acetate (**10**) of **13**. This was confirmed by its methanolysis giving **13**. The minor nitroolefin from **11** could not be isolated but probably was the Δ^2-α-L-*erythro* acetate **15** which, as mentioned above, had been expected but failed to arise from **6**. However, **15** and its parent methyl 2,3,6-trideoxy-3-nitro-α-L-*erythro*-hex-2-enopyranoside (**14**), whose attempted preparation from **5** had also been unfruitful, were obtained in an alternative way. When **2** was subjected to the conditions of partial acetylation with acetyl chloride – triethylamine, more than half was recovered unchanged and a small proportion of diacetate **11** was formed but the main reaction product was **14**. It was isolated in 47% yield (based on consumed **2**) and was subsequently acetylated to **15**.

Methyl 3,6-dideoxy-3-nitro-α-L-galactopyranoside (**3**) was readily acetylated (with boron trifluoride catalysis) to give its diacetate **16** which upon dehydroacetylation by silica gel yielded a separable mixture of methyl 4-*O*-acetyl-2,3,6-trideoxy-3-nitro-α-L-*threo*-hex-2-enopyranoside (**17**) and the previously prepared isomer **9**, the latter being in slight preponderance (Scheme 3).

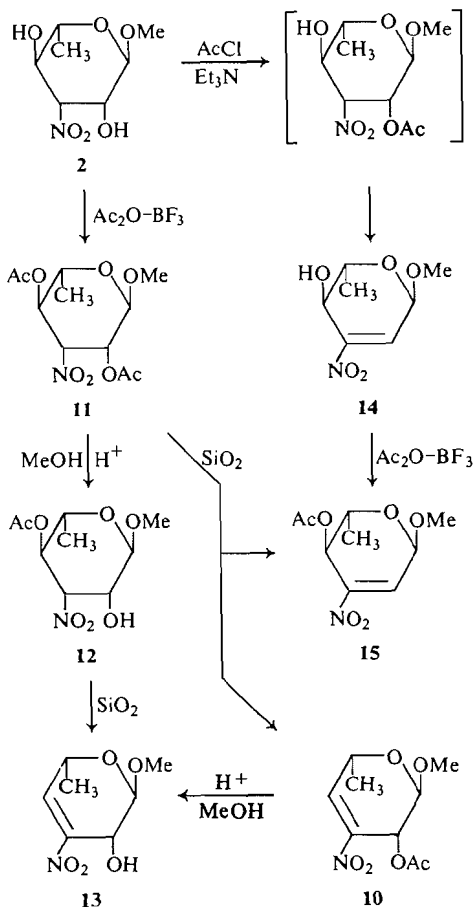

SCHEME 2

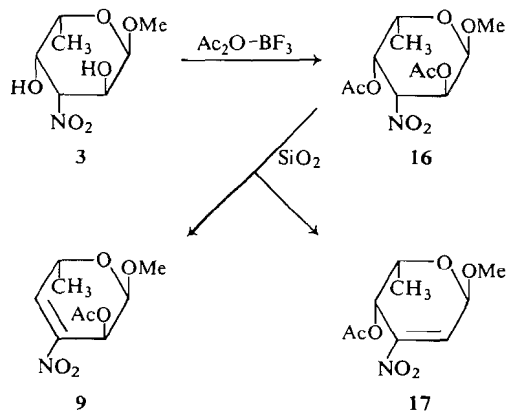

SCHEME 3

Can. J. Chem. Downloaded from www.nrcresearchpress.com by 210.87.254.5 on 09/05/12
For personal use only.

Partial acetylation or deacetylation was not studied in this series.

Scheme 4 depicts the reactions carried out starting from methyl 3,6-dideoxy-3-nitro-α-L-talopyranoside (**4**). The diacetate **18** proved difficult to prepare in entirely pure form because of its tendency to eliminate acetic acid; it was once obtained in crystalline state but failed to crystallize in all subsequent preparations. This instability no doubt is due to crowding of the two *syn*-diaxial acetoxyl groups. Increase in the amount of boron trifluoride catalyst promoted elimination, and quantitative conversion of **4** into an approximately 1:1 mixture of the nitroolefin acetates **10** and **17** took place at 0° under conditions that would normally afford simple acetylation. (A similar mixture of **10** and **17** was produced from **18** by the action of silica gel.) Prolonged treatment with acetic anhydride containing a still larger proportion of catalyst caused acetolysis at C-1, presumably in intermediate **17**, to give 1,4-di-*O*-acetyl-2,3,6-trideoxy-3-nitro-α-L-*threo*-hex-2-enopyranose (**19**). This reaction occurred at −15°, which is quite remarkable.[3] Methanolysis of a mixture of the acetates **10** and **17** by methanol containing 3% hydrogen chloride (2 days at room temperature) gave, in addition to **13** from **10** as expected (*cf.* also Scheme 2), an unexpected product that evidently arose from **17**, namely, methyl 3,4,6-trideoxy-2-*O*-methyl-3-nitro-α-L-*threo*-hex-3-enopyranoside (**20**). It is assumed that **20** was formed by a concerted reaction involving attack of methanol at C-2 and allylic shift of the double bond with elimination of acetic acid. An analogous reaction was observed when 3-acetoxy-2-nitrocyclohexene was refluxed in methanol, the product being 3-methoxy-2-nitrocyclohexene (15). The conversion of **13** into **20** by diazomethane has been reported earlier (6).

Proof of Structure

The structures and configurations of all new products were established by n.m.r. spectroscopy insofar as they did not follow unambiguously from the mode of synthesis. Thus, the 2-acetate **5** and the 4-acetate **7** were distinguished by their lowest field signal, which is attributable to the ring proton at the acetylated position and which is a quartet in **5** ($J_{1,2}$ = 3.5, $J_{2,3}$ = 11 Hz) and a triplet (J = 10 Hz) in **7**. Similarly, the monoacetate **12** revealed the position of its acetyl group by giving at lowest field a signal with large splittings ($J_{3,4}$ = 10.5, $J_{4,5}$ = 10 Hz). The spectra of the nitroolefin acetates **9**, **10**, **15**, and **17** are depicted in Figs. 1 and 2 together with the half-chair conformations assigned to the compounds. Inspection of the figures and Table 1 shows that the multiplets attributable to H-5 incur a downfield shift in the olefins relative to the H-5 signals of the saturated acetyl compounds which fall in the range τ 5.9–6.3. They are shifted to about τ 5.4 in the Δ^3-olefins and τ 5.7–6.0 in the Δ^2-olefins. The observed coupling constants $J_{1,2}$ and $J_{4,5}$ are in accord with the geometrical requirements of the $^1H_0$ conformation of **9** and **10** and the $^5H_0$ conformation of **15** and **17**, which are the conformations that possess an axial (or pseudoaxial) anomeric methoxyl group and an equatorial (or pseudoequatorial) *C*-methyl group and are therefore predicted to be preferred to the alternate half-chair forms. The same applies, *mutatis mutandis*, to the 1,4-diacetate **19**. In all the nitroolefins, H-1, -2, and -4 each have only one neighboring proton so that vicinal coupling should result in doublets. However, the signal multiplicities were more complex due to long-range coupling. Thus, H-2 in **9** gave a narrow septet owing to coupling across four bonds ($J_{2,4}$ = 1 Hz) as well as five bonds ($J_{2,5}$ = 2.5 Hz). Double irradiation of the H-2 signal caused the H-4 quartet to collapse to a doublet, and the complex multiplet of H-5 became an octet as expected ($J_{4,5}$ = 1.5–2 Hz and $J_{5,6}$ = 7 Hz). In **10**, on the other hand, only homoallylic coupling between H-2 and H-5 was observed and no allylic coupling between H-2 and H-4, the H-4 signal being a doublet ($J_{4,5}$ = 2 Hz) and the H-2 signal, a quartet ($J_{1,2}$ = 1, $J_{2,5}$ = 2.5 Hz). This supports the structure allocated to **10**, since, in the $^1H_0$ form shown, the dihedral angle between

[3]Numerous nitro glycosides, including **1**, **2**, and **3** as shown in the present work, have been acetylated with high yields at 0° (some at room temperature) without noticeably incurring acetolysis (12). Acetolysis of **1** has been observed (13) under moderately forcing conditions (3 h at 40°). Methyl pentopyranosides have been stated (13) to suffer cleavage even at low temperatures, but a nitro group at C-3 evidently tends to stabilize the glycosidic bond to some extent towards acidic rupture (10, 14), and we have been able to prepare the 2,4-diacetate from methyl 3-deoxy-3-nitro-β-D-arabinopyranoside at 0° in 90% yield (see Experimental). The only previous instance of high glycoside sensitivity in the nitro sugar series was methyl 3,6-dideoxy-2-*O*-methyl-3-nitro-α-L-glucopyranoside which gave its 4-acetate at −60° but underwent acetolysis at 0° (6).

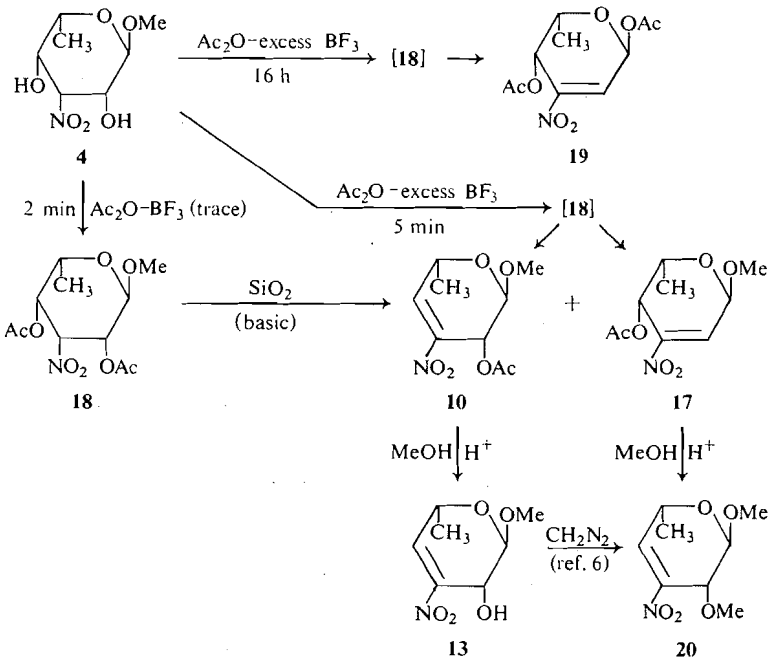

SCHEME 4

H-4 and a quasi-equatorial H-2 is estimated to be about 40° which corresponds (16) to very small allylic coupling (0.3 Hz). Similarly, the Δ^2-olefin **15** showed long-range coupling between H-1 and H-4 as well as between H-2 and H-4, giving rise to quartets for H-1 and H-2 and a doublet of triplets for H-4. By contrast, the stereoisomer **17** which bears a pseudoequatorial H-4 exhibited no significant long-range coupling and the same was true for the stereochemically analogous diacetate **19**.

Discussion

The proportionate formation of different olefinic products in acetylations with subsequent dehydroacetylation of the various nitro glycosides bears comment. In the dehydroacetylation, by silica gel, of the α-L-*manno* diacetate **11** (Scheme 2), a strong preponderance of the Δ^3-olefin **10** was observed even though one might have expected a preferential elimination of the axial C-2 acetoxyl group leading to the Δ^2-olefin **15** as the major product. That such a C-2 acetoxyl is capable of elimination was demonstrated by the attempted monoacetylation of **2** which led, presumably via the 2-acetate, to the hydroxy olefin **14**. However, in the α-L-*gluco* series (Scheme 1) the reactivity of the 4-acetoxyl in the silica-induced elimination was also distinctly higher than that of the 2-acetoxyl (though they are both equatorial); compare the facile reaction of **7** with the sluggish one of **5**, and note the reaction of **6** giving **9** but not **15**. A factor contributing to these differences could be the electron-withdrawing effect of the glycosidic center which should render more difficult the expulsion of an anion from the neighboring carbon[4] just as, conversely, it increases the acidity of a hydroxyl group in this position. The preferential acetylation and de-*O*-acetylation observed in the present work, and similarly the preferential methylation by diazomethane reported previously (6), doubtless are due to this inductive effect. But some of the results obviously cannot be explained in this way and suggest that an alternative or additional factor operates. Thus, dehydroacetylation of the α-L-galactoside **16** gave only slightly less of the Δ^2-olefin **17** than of the Δ^3-olefin **9**, and the α-L-taloside **18** gave olefins **17** and **10** in approximately equal amounts. Furthermore, when the

[4]The same explanation has been considered for the fact that the ring opening (retrograde nitroalkane–aldehyde addition) which **1** undergoes in strongly alkaline medium takes place between C-3 and C-4 rather than between C-3 and C-2: release of C-3 as nitronate ion from its bonding with C-2 is disfavored (4).

Can. J. Chem. Downloaded from www.nrcresearchpress.com by 210.87.254.5 on 09/05/12
For personal use only.

Can. J. Chem. Downloaded from www.nrcresearchpress.com by 210.87.254.5 on 09/05/12
For personal use only.

TABLE 1. Nuclear magnetic resonance data (100 MHz in chloroform-*d*)

	Chemical shifts (τ)*								Coupling constants (Hz)				
Compound	H-1	H-2	H-3	H-4	H-5	OMe	OAc	C—Me	$J_{1,2}$	$J_{2,3}$	$J_{3,4}$	$J_{4,5}$	Long range
5	5.06d	4.80q	5.14q	6.24m	6.31m	6.64	7.98	8.68	3.5	11	9		
6	5.01d	4.74q	5.07t	4.81t	$6.16m_8$	6.62	7.98, 7.98	8.79	3.5	10	10	10	
7	5.22d	5.80q	5.26t	4.86t	$6.20m_8$	6.56	8.00	8.83	4	10	10	10	
8	5.02d	5.22m	—	2.99q	$5.46m_{12}$	6.47	—	8.54	4.5	—	—	1.5–2	1,‡ 2§
9	4.91d	$4.08m_7$	—	2.73q	$5.36m_{12}$	6.54	7.91	8.59	4.3	—	—	1.5–2	1,‡ 2.5§
10	5.12d	4.28q	—	2.56d	$5.46m_{12}$	6.57	7.93	8.55	1	—	—	2	2.5§
11	5.26d	4.49q	5.10q	4.41t	$6.25m_8$	6.62	7.94, 7.97	8.75	1.5	3.5	10.5	10	
12	5.27d	5.54q	5.21q	4.41t	$6.26m_8$	6.61	7.98	8.76	2	3	10.5	10	
13	5.08d	5.46	—	2.74d	$5.51m_{12}$	6.58	—	8.57	0.7	—	—	1.5	2§
14	4.88q	2.97q	—	5.60m	$6.00m_8$	6.55	—	8.62	3.5	—	—	8.5	1,† 1‡
15	4.83q	2.90q	—	$4.18m_6$	$5.93m_8$	6.54	7.97	8.71	3.5	—	—	8.3	1,† 1.3‡
16	4.96d	4.40q	4.96q	4.31q	5.88q	6.63	7.96, 7.98	8.84	3.5	11	3.5	1	
17	4.76d	2.73d	—	4.11d	$5.77m_8$	6.55	7.92	8.75	3.5	—	—	2.5	
18	5.10d	4.41q	5.15t	4.19q	$5.95m_8$	6.61	7.92, 7.94	8.78	1.5	3.5	3.5	1.5	
19	3.33d	2.65d	—	4.13d	$5.72m_8$	—	7.92, 7.92	8.75	3.5	—	—	2.5	
20	5.05d	5.79q	—	2.72d	$5.53m_{12}$	6.51, 6.58	—	8.57	1	—	—	1.8	1.8§

*Where necessary, signal multiplicities were evaluated at 250 Hz sweep width. For ring protons only, multiplicities are indicated as s (singlet), d (doublet), t (triplet), q (quartet), m (multiplet), and m_x (sextet, septet, etc.). The C—Me signal always was a doublet with $J_{5,6}$ = 6–7 Hz. Compounds 5, 7, 8, 12, 13, and 14 showed a (usually broad) OH signal in the τ 6.8–7.3 region which was removed by deuterium exchange.

†$J_{1,4}$.

‡$J_{2,4}$.

§$J_{2,5}$.

Can. J. Chem. Downloaded from www.nrcresearchpress.com by 210.87.254.5 on 09/05/12
For personal use only.

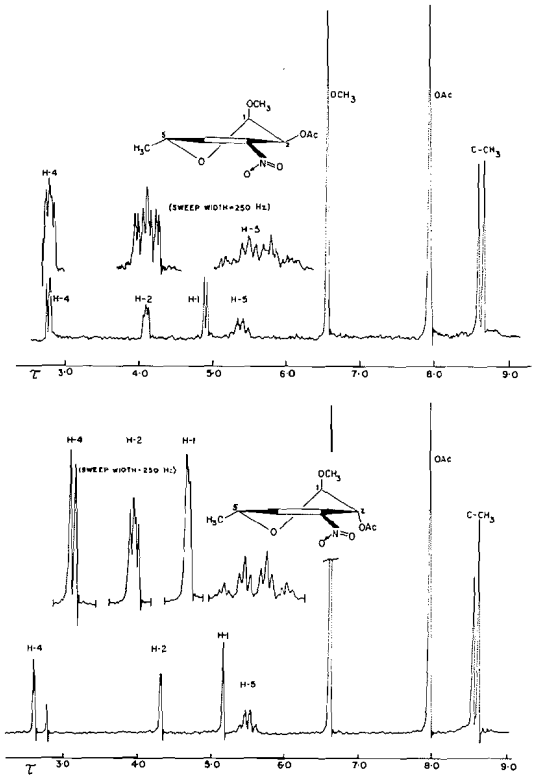

FIG. 1. Nuclear magnetic resonance spectra of **9** (top) and **10** (bottom), in chloroform-*d*.

α-L-glucoside diacetate **6** was subjected to dehydroacetylation by sodium bicarbonate in refluxing benzene (Schmidt–Rutz conditions, as opposed to reaction with silica gel), only a small amount (4%) of **9** was produced and the major product was its 2-epimer **10** while the expected Δ^2-olefin **15** was not encountered under those conditions either. Whether **15** was an intermediate on the route to **10** remains to be investigated; a mechanism could be envisaged. However, it is already apparent that **10** is more stable thermodynamically than both **9** and **15**. We are inclined to regard this as a manifestation of the $A^{(1,2)}$ effect (17), the nonbonded interaction between a group (here NO_2) situated at an endocyclic double bond in a six-membered ring and an adjacent, quasi-equatorial group (here $OCOCH_3$). Inspection of the conformational formulas in Figs. 1 and 2 shows that **9** and **15** are subject to this strain whereas **10** is free from it. Compound **17** also lacks $A^{(1,2)}$ strain, which might compensate for the inductive effect that should counteract formation of **17** in the α-L-*galacto* and α-L-*talo* series.

Experimental

For general preparative and instrumental techniques see earlier articles from this laboratory, *e.g.*, refs. 3, 4, 6, and 9–12. Optical rotations refer to chloroform solutions at about 25°. Infrared data were obtained from Nujol mulls unless otherwise indicated. Column chromatography was performed on Silica Gel 7734 (0.05–0.22 mm, 70–325 mesh ASTM) of E. Merck A. G., Darmstadt; an aqueous slurry showed p*H* 7.5. The following solvents were employed: *A*, 5% methanol in chloroform; *B*, *C*, and *D*, 20, 10, and 2% ethyl acetate in benzene, respectively.

The nitro glycosides **1** (2–4) and **2**–**4** (3, 4) were prepared as reported.

Methyl 2-O-Acetyl-3,6-dideoxy-3-nitro-α-L-glucopyranoside (5)

A mixture of **1** (2.92 g), anhydrous ether (30 ml), and acetyl chloride (1 ml) was cooled to 0° and triethylamine (1.97 ml) was added dropwise with stirring which was continued for 1 h at 0° and 4 h at room temperature. A white precipitate was removed by filtration and t.l.c. (solvent *B*) of the evaporated filtrate showed four spots attributable to unreacted **1**, the 4-acetate **7**, the 2-acetate **5**, and the diacetate **6**, in order of increasing mobility. Separation on a column using the same solvent furnished

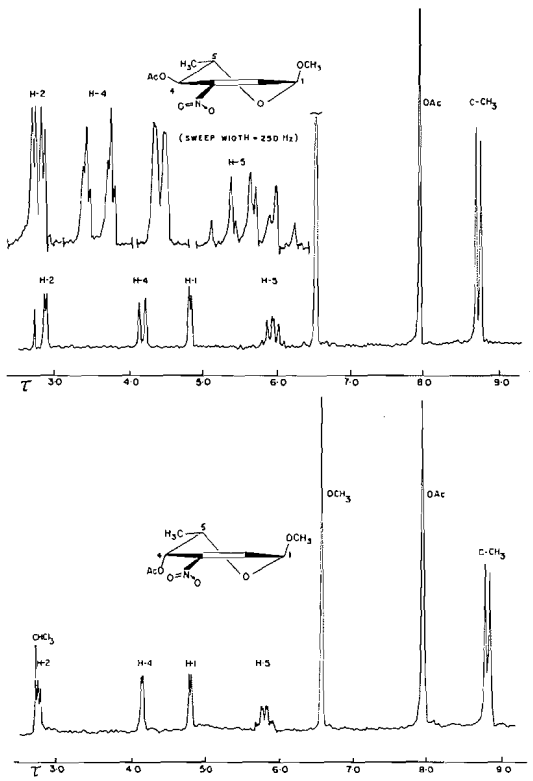

FIG. 2. Nuclear magnetic resonance spectra of **15** (top) and **17** (bottom), in chloroform-*d*.

Can. J. Chem. Downloaded from www.nrcresearchpress.com by 210.87.254.5 on 09/05/12
For personal use only.

crystalline **6** (667 mg, m.p. 111–113°), syrupy but homogeneous **5** (1.222 g), crystalline **7** (200 mg, m.p. 109–111°), and crystalline **1** (937 mg, m.p. 141–143°). Compounds **1**, **6**, and **7** were identified also by their i.r. spectra.

Colorless **5** (yield 35%, or 51% taking recovered **1** into account) exhibited $[\alpha]_D$ −133.5° (*c*, 1); ν_{max}($CHCl_3$) 3600, 3350 (OH), 1742 (ester CO), 1558, and 1364 cm^{-1} (NO_2).

Anal. Calcd. for $C_9H_{15}NO_7$ (249.2): C, 43.37; H, 6.07; N, 5.62. Found: C, 43.38, H, 6.27; N, 5.77.

Methyl 2,4-Di-O-acetyl-3,6-dideoxy-3-nitro-α-L-glucopyranoside (6)

Compound **1** (1 g) was dissolved in acetic anhydride (5 ml), the solution was cooled in an ice-bath, and boron trifluoride etherate (3 drops) was added with stirring. After 15 min the reaction mixture was poured into briskly stirred ice water and the white solid that separated was collected, washed, and dried (1.345 g, 95%). It melted at 109–111° and at 113–113.5° upon recrystallization from methanol; $[\alpha]_D$ −155.3° (*c*, 1.3); ν_{max} 1740 and 1545 cm^{-1} without hydroxyl absorption; lit. (13) m.p. 109–110°, $[\alpha]_D$ −154° (*c*, 1).

Anal. Calcd. for $C_{11}H_{17}NO_8$ (291.2): C, 45.36; H, 5.88; N, 4.81. Found: C, 45.39; H, 5.80; N, 4.83.

Methyl 4-O-Acetyl-3,6-dideoxy-3-nitro-α-L-glucopyranoside (7)

A solution of **6** (500 mg) in a mixture of *N* methanolic hydrogen chloride (9 ml) and acetone (1 ml) was kept at 45–50°. Progress of the reaction was monitored by t.l.c. with solvent *A*. After 2 h, when **6** had completely disappeared, the solution was evaporated to give a yellow syrup which, while still slightly acidic, was chromatographed on a column (20 g of silica gel) by use of solvent *A*. The fractions containing the monoacetate **7** yielded crystals (148 mg, 34.7%) which upon recrystallization from ether – petroleum ether melted at 112–113°; $[\alpha]_D$ −178.5° (*c*, 1); ν_{max} 3460 (OH), 1746 (ester CO), and 1555 cm^{-1} (NO_2). The i.r. spectrum was clearly distinct in the fingerprint region from that of **5**.

Anal. Calcd. for $C_9H_{15}NO_7$ (249.2): C, 43.37; H, 6.07; N, 5.62. Found: C, 43.28; H, 5.96; N, 5.70.

Methyl 3,4,6-Trideoxy-3-nitro-α-L-erythro-hex-3-enopyranoside (8)

A solution of **6** (2.91 g) in a mixture of *N* methanolic hydrogen chloride (40 ml) and acetone (4 ml) was kept at 45–50° for 1 h and then at room temperature for 9 h. Thin-layer chromatography with solvent *A* or *B* indicated the complete consumption of **6** in the process. The solution was then cooled (0°) and, in contrast to the aforedescribed preparation of **7**, *neutralized* with silver carbonate prior to evaporation. The syrup obtained was chromatographed on 120 g of silica gel with solvent *A*, 5-ml fractions being collected. The fractions were inspected by t.l.c. and appropriately pooled so that a fast-moving and a slow-moving material were separated. The latter crystallized (1.0 g) and was identified by its m.p. of 139–141° and by its i.r. spectrum as **1**. The fast-moving material was a colorless syrup (1.275 g) which was revealed by its i.r. spectrum to be a mixture of unsaturated (ν_{max} 1520 cm^{-1}) and saturated (ν_{max} 1560 cm^{-1}) nitro compounds. The n.m.r. spectrum showed olefinic proton and acetyl resonances and suggested that acetylated component(s) preponderated. The mixture was therefore subjected once more to methanolysis at 45–50° for 1 h followed by neutralization with silver carbonate and chromatography on silica gel (50 g) as described before. Another 845 mg of crystalline **1** was thus produced (combined yield, 88.5%), whereas the fast-moving fractions this time gave crystalline **8** (200 mg, 10.6%); m.p. 115–116°; $[\alpha]_D$ −362° (*c*, 0.9); ν_{max} 3380 (OH) and 1515 cm^{-1} (nitroalkene); λ_{max} 247 nm (ε, 4100 in chloroform).

Anal. Calcd. for $C_7H_{11}NO_5$ (189.2): C, 44.44; H, 5.86; N, 7.41. Found: C, 44.58; H, 6.01; N, 7.64.

When pure crystalline monoacetate **7** was slowly passed through a silica gel column with solvent *A*, the effluent contained a considerable proportion of **8**, according to spectra.

Methyl 2-O-Acetyl-3,4,6-trideoxy-3-nitro-α-L-erythro-hex-3-enopyranoside (9) and Methyl 2-O-Acetyl-3,4,6-trideoxy-3-nitro-α-L-threo-hex-3-enopyranoside (10)

Dehydroacetylation of 6

A mixture of the diacetate **6** (950 mg), sodium bicarbonate (4.75 g; dried at 120°), and freshly activated, powdered Drierite (0.5 g) was heated in refluxing benzene (50 ml, dried over sodium), with brisk magnetic stirring. After 40 h the reaction mixture was filtered and the filtrate evaporated to give a yellow syrup (810 mg) the n.m.r. spectrum of which indicated that it was a 3:2 mixture of nitroolefin and starting material. It was therefore subjected to a second treatment as above, with fresh reagents, and dehydroacetylation was monitored by i.r. spectroscopy of samples withdrawn from time to time. Refluxing was stopped when, after 16 h, the nitroalkane peak at 1560 cm^{-1} had been fully replaced by the nitroalkene peak at 1520 cm^{-1}. Work-up then gave a brownish syrup (500 mg) that showed four mobile spots, trailing, and an immobile spot on t.l.c. with solvent *C*. The syrup was chromatographed on a 30-g column with the same solvent. The first few 5-ml fractions gave an unidentified, brownish solid (14 mg). The product corresponding to the second fastest spot emerged as slightly yellow crystals (160 mg, 21%). Recrystallization from ether – petroleum ether furnished pure **10** as small, colorless cubes, m.p. 81–81.5°; $[\alpha]_D$ −165° (*c*, 0.8); ν_{max} ($CHCl_3$) 1735 (ester CO), 1675 (C=C), and 1520 cm^{-1} (nitroalkene); λ_{max} 247 nm (ε 5700, in chloroform).

The product corresponding to the third spot was **9**. It was obtained from the column as a syrup (30 mg, 4%) which crystallized from a small amount of ether upon addition of petroleum ether to incipient turbidity and storing overnight in a refrigerator. The small colorless crystals showed m.p. 98–99°; $[\alpha]_D$ −259° (*c*, 0.8); ν_{max} ($CHCl_3$) 1745 (ester CO), 1680 (C=C), and 1522 cm^{-1} (nitroalkene), with a fingerprint pattern distinctly different from that of the isomer (**10**); λ_{max} 247 nm (ε 5250, in chloroform).

Anal. Calcd. for $C_9H_{13}NO_6$ (231.2): C, 46.75; H, 5.67; N, 6.06. Found for **9**: C, 46.58; H, 5.69; N, 6.21. Found for **10**: C, 46.73; H, 5.84; N, 6.22.

A yellow syrup (30 mg) eluted subsequently from the column could not be identified.

Partial dehydroacetylation to give **9** also occurred when **6** (500 mg) was merely chromatographed slowly on 250 g of silica gel (solvent *C*). The olefin **9** and unchanged **6** (which on t.l.c. moves marginally faster) were collected

Can. J. Chem. Downloaded from www.nrcresearchpress.com by 210.87.254.5 on 09/05/12
For personal use only.

together as a crystalline material (350 mg) consisting of about equal proportions of both (n.m.r. spectrum). The mixture was rechromatographed on a smaller column (30 g). Of 18 5-ml fractions containing carbohydrate, the first 13 gave 262 mg of a similar mixed product as before, and from the last 5 fractions was obtained 32 mg of crystalline **9**, m.p. 97–98°. It was identified by its n.m.r. spectrum.

See also subsequent sections for dehydroacetylations leading to **9** or **10**, together with other isomers.

Acetylation of ***8***

Compound **8** (30 mg) was treated for 5 min at 0° with acetic anhydride (1 ml) and boron trifluoride etherate (1 drop). Excess anhydride was decomposed by ice water, and **9** (33 mg, 90%) was obtained by chloroform extraction, evaporation, and crystallization from ether – petroleum ether; m.p. 97–99°; $[\alpha]_D$ −269° (*c*, 0.9). The n.m.r. spectrum was identical with that of **9** from **6**.

*Methyl 2,4-Di-O-acetyl-3,6-dideoxy-3-nitro-α-L-mannopyranoside (**11**)*

Anhydrous glycoside **2** (400 mg) was acetylated with acetic anhydride (5 ml) and boron trifluoride etherate (3 drops) as described for the preparation of **6**. The crude product (535 mg, 95%) showed m.p. 140–142°, raised to 142–143° by recrystallization from methanol; $[\alpha]_D$ −8.6° (*c*, 1.4); ν_{max} 1750 (ester CO) and 1570, 1552 cm^{-1} (NO_2 giving a doublet in Nujol; only a single band at 1560 cm^{-1} was present in a chloroform solution spectrum).

Anal. Calcd. for $C_{11}H_{17}NO_8$ (291.2): C, 45.36; H, 5.88; N, 4.81. Found: C, 45.37; H, 6.05; N, 4.94.

*Methyl 4-O-Acetyl-3,6-dideoxy-3-nitro-α-L-mannopyranoside (**12**)*

The diacetate **11** (1.0 g) was methanolyzed in 3% methanolic hydrogen chloride (25 ml) at 45–50°. The reaction was monitored by t.l.c. (solvent *B*) and was stopped by solvent removal as soon as **11** had all disappeared (after 90 min). The still slightly acidic residue of evaporation was chromatographed with solvent *B* on 25 g of silica gel. The fast-moving product eluted was **12**. It was isolated as white crystals (652 mg, 76%), m.p. 159–160°; $[\alpha]_D$ −37.5° (*c*, 0.9); ν_{max} 3500 (OH), 1720 (ester CO), and 1550 cm^{-1} (NO_2).

Anal. Calcd. for $C_9H_{15}NO_7$ (249.2): C, 43.37; H, 6.07; N, 6.62. Found: C, 43.34; H, 6.17; N, 5.77.

Subsequent fractions from the column yielded 150 mg (21%) of **2**.

*Methyl 3,4,6-Trideoxy-3-nitro-α-L-threo-hex-3-enopyranoside (**13**)*

From ***12***

The monoacetate **12** (50 mg) was placed on a column of silica gel (10 g) which was slowly eluted with solvent *C*. The eluate was evaporated to give a colorless syrup (33 mg, 87%) of **13**; $[\alpha]_D$ −198° (*c*, 1); ν_{max} ($CHCl_3$) 3600 (OH), 1675 (C=C) and 1522 cm^{-1} (nitroalkene); λ_{max} 251 nm (ε 5000, chloroform).

From ***10***

Compound **10** (40 mg) was treated with 3% methanolic hydrogen chloride for 48 h at room temperature. The pale yellow syrup obtained upon solvent evaporation was purified by passage through a short column using solvent *C*. It was thus obtained in colorless form, showed $[\alpha]_D$ −195° (*c*, 0.8), and its n.m.r. spectrum was identical with that of **13** from **12**. The yield was 21 mg (65%).

*Methyl 2,3,6-Trideoxy-3-nitro-α-L-erythro-hex-2-enopyranoside (**14**)*

The crystalline monohydrate of **2** (1.37 g) was dried for 4 h in an oil-pump vacuum at 80°. The resulting syrup of anhydrous **2** and acetyl chloride (0.44 ml, 1.02 equiv.) were dissolved in dry ether (40 ml) which was cooled to 0°. Triethylamine (0.85 ml, 1.0 equiv.) was added dropwise with stirring, and the reaction was allowed to proceed for 1 h at 0° and 2 h at room temperature. The precipitate of triethylammonium chloride was removed and the solution evaporated to give a syrup which exhibited 4 spots on t.l.c. (solvent *B*). Separation was effected on a 100-g column using the same solvent. The fastest moving component was isolated as crystals (88 mg) that melted at 142–144° and were identified (n.m.r. spectrum) as diacetate **11**. The second fastest component was colorless, crystalline **14** (227 mg). Recrystallization from ether – petroleum ether furnished long prisms, m.p. 124–125°; $[\alpha]_D$ +162.6° (*c*, 1); ν_{max} ($CHCl_3$) 3600 (OH) and 1523 cm^{-1} (nitroalkene); λ_{max} 247 nm (ε 3700, in chloroform).

Anal. Calcd. for $C_7H_{11}NO_5$ (189.2): C, 44.4; H, 5.86; N, 7.41. Found: C, 44.58; H, 6.01; N, 7.64.

A small amount of syrupy material (25 mg) corresponding to the third t.l.c. spot was then eluted from the column and identified by its n.m.r. spectrum as **13**. The most slowly moving component was finally collected and proved to be unchanged **2** (800 mg). Based on the amount of **2** that had actually reacted, the yields of **11**, **13**, and **14** were 14, 6, and 54%, respectively.

*Methyl 4-O-Acetyl-2,3,6-trideoxy-3-nitro-α-L-erythro-hex-2-enopyranoside (**15**)*

A droplet of boron trifluoride etherate was added to an ice-cold solution of **14** (30 mg) in acetic anhydride (0.5 ml). After 2 min the mixture was worked up by adding ice water and extracting the product into chlorofrom. Evaporation of the extract with added portions of toluene gave a syrup which was crystallized from ether – petroleum ether. Crystalline **15** (25 mg, 68%) showed m.p. 81–81.5°; $[\alpha]_D$ +99.3° (*c*, 1.1); λ_{max} 247 nm (ε 3600, in chloroform); ν_{max} ($CHCl_3$) 1750 (ester CO) and 1533 cm^{-1} (nitroalkene).

Anal. Calcd. for $C_9H_{13}NO_6$ (231.2): C, 46.75; H, 5.67; N, 6.06. Found: C, 46.77; H, 5.51; N, 6.25.

Dehydroacetylation of ***11***

The diacetate **11** (100 mg) was passed very slowly through a 10-g column of silica gel by means of solvent *D*. Evaporation of the eluate furnished a crystalline material (70 mg) whose 60-MHz n.m.r. spectrum suggested that it was largely **10** with an admixture of a second nitroolefinic component, probably **15**. Recrystallization from ether – petroleum ether afforded small crystals, m.p. 78–80°, that gave a spectrum identical with that of **10** obtained from **6**.

*Methyl 2,4-Di-O-acetyl-3,6-dideoxy-3-nitro-α-L-galactopyranoside (**16**)*

The glycoside **3** (200 mg) was treated with acetic anhydride (3 ml) and boron trifluoride etherate (3 drops) for 5 min at 0°. Work-up with ice water afforded **16** as a white solid (260 mg, 92.5%) which was recrystallized from ethyl acetate – petroleum ether to give fine needles, m.p.

Can. J. Chem. Downloaded from www.nrcresearchpress.com by 210.87.254.5 on 09/05/12
For personal use only.

122–123°; $[\alpha]_D$ −171° (*c*, 1.2); ν_{max} 1742 (ester CO) and 1558 cm^{-1} (NO_2).

Anal. Calcd. for $C_{11}H_{17}NO_8$ (291.2): C, 45.36; H, 5.88; N, 4.81. Found: C, 45.52; H, 6.00; N, 4.67.

*Methyl 4-O-Acetyl-2,3,6-trideoxy-3-nitro-α-L-threo-hex-2-enopyranoside (**17**)*

*By Dehydroacetylation of **16***

The diacetate **16** (110 mg) was passed through a 10-g silica gel column by means of solvent *D* at a flow rate of about 1 drop per 2 seconds. The entire effluent was evaporated to give a syrup that appeared to be a 1.3:1 mixture of **9** and **17** according to t.l.c. (ethyl acetate – carbon tetrachloride, 1:4) and n.m.r. spectrum. The syrup was passed through a similar column of fresh silica gel (10 g), this time using the solvent just mentioned, whereby fractions corresponding to a faster-moving and a more slowly moving t.l.c. spot could be separated. The former furnished crystals (32 mg) of **17**, m.p. 89–90°; $[\alpha]_D$ +27.5° (*c*, 0.75); ν_{max} ($CHCl_3$) 1750 (ester CO) and 1530 cm^{-1} (nitroalkene); λ_{max} 247 nm (ε 3700, in chloroform).

Anal. Calcd. for $C_9H_{13}NO_6$ (231.2): C, 46.75; H, 5.67; N, 6.06. Found: C, 46.88; H, 5.81; N, 6.18.

The slow-moving fractions gave 37 mg of crystals, m.p. 97–99°, that were identified by i.r. and n.m.r. spectra as **9**.

*By action of acetyl chloride on **4***

To a magnetically stirred, ice-cold solution of glycoside **4** (100 mg) in anhydrous ether (5 ml) was added acetyl chloride (1 ml) followed by triethylamine (1 ml, dropwise). The reaction mixture was kept at 0° for 5 min and then stirred at room temperature for 30 min. More ether (20 ml) was then added and the mixture was extracted twice with water (40 ml). Evaporation of the dried ($MgSO_4$) ether layer gave a colorless syrup from which 10 mg (9%) of **17**, m.p. 89.5–90°, was obtained by crystallization from ether – petroleum ether. The n.m.r. spectrum was identical with that of **17** produced from **16**.

*Reaction of **4** with Acetic Anhydride and Boron Trifluoride*

*Methyl 2,4-Di-O-acetyl-3,6-dideoxy-3-nitro-α-L-talopyranoside (**18**)*

A mixture of **4** (300 mg) and acetic anhydride (10 ml) was cooled in an ice-bath for 15 min. One small drop of boron trifluoride etherate was then introduced, and after 2 min the reaction mixture was poured into ice water which, upon decomposition of the anhydride, was extracted with chloroform (2 × 20 ml). Evaporation of the dried extract gave a colorless syrup which was crystallized from absolute ethanol (5 ml) by adding petroleum ether to incipient turbidity and cooling overnight. The prisms (268 mg, 64%) showed m.p. 78–79°; $[\alpha]_D$ −56.5° (*c*, 1.3); ν_{max} ($CHCl_3$) 1745 (ester CO) and 1555 cm^{-1} (NO_2).

Anal. Calcd. for $C_{11}H_{17}NO_8$ (291.2): C, 45.36; H, 5.88; N, 4.81. Found: C, 45.34; H, 5.70; N, 4.93.

In repeat experiments the syrupy diacetate failed to crystallize, probably because of contamination by nitroolefins. When the product (120 mg) was passed through a 10-g silica gel column by means of solvent *D* (flow rate, 1 drop in 2 s), it suffered complete dehydroacetylation. The colorless syrup that was recovered (91 mg) was clearly revealed by its n.m.r. spectrum to be a 1:1 mixture of **10** and **17**. (Table 1 shows that only the acetyl signals coincide.)

A mixture of **10** and **17** giving an identical n.m.r. spectrum was also obtained directly from **4** (100 mg) when acetylation and subsequent work-up were carried out as described above, except that a higher catalyst concentration (3 drops in 2 ml of acetic anhydride) was employed and a reaction time of 5 min was allowed. The pale yellow syrup obtained weighed 110 mg (99%). A part of **10** (20 mg) crystallized from ether (1 ml) upon addition of petroleum ether (10 ml) and cooling; it showed m.p. 79–80° and $[\alpha]_D$ −166° (*c*, 1).

*1,4-Di-O-acetyl-2,3,6-trideoxy-3-nitro-α-L-threo-hex-2-enose (**19**)*

A mixture of **4** (1.0 g) and acetic anhydride (10 ml) containing boron trifluoride etherate (0.4 ml) was stored for 16 h at 0°. (It was found in another experiment that the reaction proceeded also at −15° but afforded a lower yield). Work-up with ice water, extraction with chloroform (3 × 50 ml), and evaporation of the extract with subsequent coevaporation of several portions of toluene gave a slightly yellow syrup. Crystallization of **19** (341 mg) occurred from a minimum amount of absolute ethanol upon careful addition of petroleum ether and cooling. The product showed m.p. 140–141°; $[\alpha]_D$ +149° (*c*, 0.8); ν_{max} 1760, 1738 (ester CO), and 1540 cm^{-1} (NO_2); λ_{max} 245 nm (ε 5500, in chloroform).

Anal. Calcd. for $C_{10}H_{13}NO_7$ (259.2): C, 46.33; H, 5.06; N, 5.40. Found: C, 46.13; H, 5.10; N, 5.33.

Evaporation of the mother liquor gave a yellow syrup (450 mg) which was chromatographed on silica gel by use of chloroform containing 2% of methanol. The first 30 ml of eluate that contained product yielded 72 mg of crystals, m.p. 80–82° and $[\alpha]_D$ −163°, identified as **10**. The subsequent fractions gave a syrup that appeared to be a mixture of **10**, **17**, and **19**.

*Methyl 3,4,6-Trideoxy-2-O-methyl-3-nitro-α-L-threo-hex-3-enopyranoside (**20**)*

A 1:1 mixture of **10** and **17** (90 mg, obtained by boron trifluoride-catalyzed acetylation of **4**) was dissolved in 3% methanolic hydrogen chloride (15 ml). After standing at room temperature for 2 days the solution was evaporated and the residue chromatographed on a small column with solvent *C*. The 2-*O*-methyl derivative **20** was eluted first. It was a colorless oil (38 mg), $[\alpha]_D$ −113° (*c*, 1.1); ν_{max} ($CHCl_3$) 1670 (C=C) and 1520 cm^{-1} (nitroalkene), without ester or hydroxyl bands; λ_{max} 247 nm (ε 4900, in chloroform). The i.r. and n.m.r. spectra of the product were identical with those of **20** obtained (6) by methylation of **13** with diazomethane.

Further elution of the column furnished 14 mg of **13** that was identified by its n.m.r. spectrum and t.l.c.

Methyl 2,4-Di-O-acetyl-3-deoxy-3-nitro-β-D-arabinopyranoside

Methyl 3-deoxy-3-nitro-β-D-arabinopyranoside (**18**) (50 mg) was allowed to react with acetic anhydride (1 ml) and boron trifluoride etherate (1 drop) for 15 min at 0°. Excess anhydride was decomposed with ice water (20 ml) and the product extracted with ether (2 × 20 ml). Evaporation of the dried extract gave the diacetate as a faintly yellow syrup (65 mg, 91%) that failed to crystallize; $[\alpha]_D$ −195° (*c*, 1.2); ν_{max} ($CHCl_3$) 1750 (ester CO), and 1560, 1370 cm^{-1} (NO_2). Hydroxyl absorption was absent. The n.m.r. data (100 MHz in $CDCl_3$): τ 4.37 (q, $J_{1,2}$ = 3.5 and

$J_{2,3}$ = 11 Hz, H-2), 4.43 (m, H-4), 4.97 (d, $J_{1,2}$ = 3.5 Hz, H-1), 5.02 (q, $J_{2,3}$ = 11 and $J_{3,4}$ = 3.5 Hz, H-3), 6.12 (d, $J_{4,5e}$ = 1.5 Hz, H-5e), 6.14 (d, $J_{4,5a}$ = 2 Hz, H-5a), 6.63 (s, 3H, OCH_3), 7.94 (s, 6H, OAc).

Anal. Calcd. for $C_{10}H_{15}NO_8$ (277.2): C, 43.32; H, 5.45; N, 5.05. Found: C, 43.34; H, 5.58; H, 5.20.

Support of this work by the National Research Council of Canada is gratefully acknowledged. Dr. Karel Čapek, visiting scientist in this laboratory (1967–1968), is thanked for contributing preliminary studies on some acetylation procedures in the course of which he prepared crystalline **11** and **16** for the first time.

1. H. H. Baer. Adv. Carbohydr. Chem. Biochem. **24**, 67 (1969).
2. A. C. Richardson and K. A. McLauchlan. J. Chem. Soc. 2499 (1962); K. Čapek, J. Štefková, and J. Jarý. Coll. Czech. Chem. Commun. **31**, 1854 (1966).
3. H. H. Baer and K. Čapek. Can. J. Chem. **47**, 99 (1969).
4. J. Kovář, K. Čapek, and H. H. Baer. Can. J. Chem. **49**, 3960 (1971).
5. S. Hanessian and T. H. Haskell. *In* The carbohydrates. Vol. IIA. *Edited by* W. Pigman and D. Horton. Academic Press, New York, N.Y. 1970. p. 139.
6. H. H. Baer and C. W. Chiu. Carbohydr. Res. In press.
7. A. Schmidt and G. Rutz. Ber. **61**, 2142 (1928); H. B. Hass, A. G. Susie, and R. L. Heider. J. Org. Chem. **15**, 8 (1950).
8. H. H. Baer and L. Urbas. *In* The chemistry of the nitro and nitroso groups. Pt. 2. *Edited by* H. Feuer. Interscience Publishers, New York, N.Y. 1970. p. 75.
9. H. H. Baer and F. Kienzle. J. Org. Chem. **33**, 1823 (1968).
10. H. H. Baer, W. Rank, and F. Kienzle. Can. J. Chem. **48**, 1302 (1970).
11. W. Rank and H. H. Baer. Can. J. Chem. **49**, 3236 (1971).
12. H. H. Baer, F. Kienzle, and F. Rajabalee. Can. J. Chem. **46**, 80 (1968).
13. F. W. Lichtenthaler, J. Breunig, and W. Fischer. Tetrahedron Lett. 2825 (1971).
14. J. Kovář and H. H. Baer. Can. J. Chem. **49**, 3238 (1971).
15. H. H. Baer, D. C. Shields, and G. G. Dawson. Can. J. Chem. **51**, 2843 (1973).
16. B. Coxon, H. J. Jennings, and K. A. McLauchlan. Tetrahedron, **23**, 2395 (1967).
17. F. Johnson and S. K. Malhotra. J. Am. Chem. Soc. **87**, 5492 (1965).
18. H. H. Baer and A. Ahammad. Can. J. Chem. **41**, 2931 (1963).

Can. J. Chem. Downloaded from www.nrcresearchpress.com by 210.87.254.5 on 09/05/12
For personal use only.

Can. J. Chem. Downloaded from www.nrcresearchpress.com by 210.87.254.105 on 09/05/12
For personal use only.

A Stereospecific Synthesis of L-Desosamine[1]

HANS H. BAER AND CHUNG-WAI CHIU
Department of Chemistry, University of Ottawa, Ottawa, Canada K1N 6N5

Received August 16, 1973

L-Desosamine (3,4,6-trideoxy-3-dimethylamino-L-*xylo*-hexose), the enantiomer of a widely distributed antibiotics component, was synthesized by borohydride reduction of methyl 3,4,6-trideoxy-3-nitro-α-L-*erythro*-hex-3-enopyranoside followed by catalytic hydrogenation of the nitro group, *N,N*-dimethylation of the resulting saturated amino glycoside, and acid hydrolysis of the glycosidic bond.

On a synthétisé la L-désosamine (tridéoxy-3,4,6 diméthylamino-3 L-*xylo*-hexose), qui est l'énantiomère d'un composé très répandu chez les antibiotiques. Cette synthèse fut réalisée en soumettant le tridéoxy-3,4,6 nitro-3 α-L-*érythro*-hexène-3 pyrannoside de méthyle à une réduction avec de l'hydrure de bore, suivie par une hydrogénation catalytique du groupe nitro; l'amino glycoside saturé résultant est soumis à une réaction de *N,N*-diméthylation puis à une hydrolyse acide du lien glycosidique.
[Traduit par le journal]

Can. J. Chem., **52**, 122 (1974)

Several macrolide antibiotics, including the widely used erythromycin, contain the carbohydrate component 3,4,6-trideoxy-3-dimethylamino-D-*xylo*-hexose (desosamine) (1). A stereospecific synthesis of this sugar, departing from a derivative of 3-amino-3-deoxy-D-glucose and employing sulfonylation followed by iodide exchange and reduction in positions 4 and 6, has been accomplished (2). Nonstereospecific syntheses of DL-desosamine starting from noncarbohydrate precursors have also been reported (3, 4). We now describe a stereospecific synthesis of the title compound (**5**), the enantiomer of the natural product.

Methyl 3,4,6-trideoxy-3-nitro-α-L-*erythro*-hex-3-enopyranoside (**1**) recently has become available (5) by way of a simple procedure from methyl 3,6-dideoxy-3-nitro-α-L-glucopyranoside which, in turn, can readily be made (6) from methyl α-L-rhamnopyranoside or any stereoisomeric methyl 6-deoxy-α-L-hexopyranoside. Reduction of **1** with sodium borohydride in ethanol afforded 3,4,6-trideoxy-3-nitro-α-L-*xylo*-hexopyranoside (**2**) in nearly quantitative yield. The highly stereoselective formation of the L-*xylo* configuration in this reaction was in keeping with the results of previous borohydride reductions of unsaturated 3-nitro hexopyranosides (7, 8), and with the generally observed tendency of the nitro group in this position to acquire equatoria orientation (9). Proof of configuration was fur nished by the n.m.r. data of **2** and of its 2-acetat (**3**). Both compounds exhibited 10–12 Hz cou pling constants $J_{2,3}$ and $J_{3,4a}$, which indicated H- to be axial. Platinum-catalyzed hydrogenation o **2** in the presence of dilute hydrochloric acid fol lowed by anion exchange gave methyl 3-amino 3,4,6-trideoxy-α-L-xylo-hexopyranoside (**4**) i 96% yield. Eschweiler–Clarke methylation of **4** le to an oily *N,N*-dimethylamino derivative whic exhibited the expected n.m.r. signals but was no characterized further. Acid hydrolysis of th material furnished 3,4,6-trideoxy-3-dimethyl amino-L-*xylo*-hexose (L-desosamine) in abou 65% yield from **4**. Both the amorphous free bas (**5**) and a crystalline hydrochloride (**6**; the anomer) were prepared, and their spectral an other physical data agreed fully with those re ported for the natural D-enantiomer. Thes reactions are outlined in Scheme 1.

Experimental

Methyl 3,4,6-Trideoxy-3-nitro-α-L-xylo-hexopyranoside (2)

To a magnetically stirred, ice-cold solution of the u saturated glycoside **1** (5) (130 mg) in ethanol (10 ml) w added sodium borohydride (52 mg) in small portions. T reaction was allowed to continue for 15 min. Methan (15 ml) was then added and the solution was deionized b treatment with 4 ml of Amberlite IR-120(H^+). The filtra was evaporated and boric acid was removed by evapor tion of several portions of methanol from the residu The resulting colorless syrup (128 mg) appeared homo enous on t.l.c. (ethyl acetate – carbon tetrachlorid 2:3). Crystallization from ether – petroleum ether gave

[1]Abstracted from the Ph.D. thesis of C. W. Chiu, University of Ottawa, Ottawa, 1971 and presented before the VIIIth International Symposium on the Chemistry of Natural Products (IUPAC), New Delhi, India, February 1972.

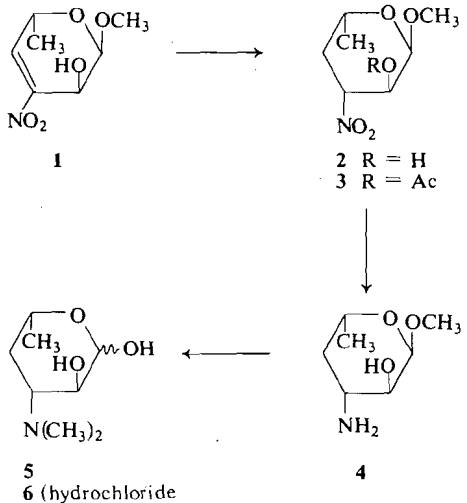

SCHEME 1

showing m.p. 56–57°; $[\alpha]_D$ −198° (*c*, 1 in $CHCl_3$); ν_{max} (Nujol) 3440 (OH) and 1545 cm^{-1} (nitroalkane); n.m.r. (100 MHz in $CDCl_3$): τ 5.20 (1H, d, $J_{1,2}$ = 3.5 Hz, H-1), 5.25 (1H, m, H-3), 5.90 (1H, m, becoming q upon deuterium exchange, $J_{1,2}$ = 3.5 Hz, $J_{2,3}$ = 10 Hz, H-2), 6.07 (1H, m, H-5), 6.59 (3H, s, OCH_3), 7.75 (1H, octet, $J_{3,4e}$ = 4 Hz, $J_{4a,4e}$ = 12 Hz, $J_{4e,5}$ = 2 Hz, H-4e), 8.12 (1H, q, $J_{3,4a} = J_{4a,4e} = J_{4a,5}$ = 12 Hz, H-4a), 8.77 (3H, d, $J_{5,6}$ = 6 Hz, *C*—CH_3).

Anal. Calcd. for $C_7H_{13}NO_5$ (191.2): C, 43.97; H, 6.85; N, 7.33. Found: C, 43.95; H, 6.87; N, 7.50.

Methyl 2-O-Acetyl-3,4,6-trideoxy-3-nitro-α-L-xylo-hexopyranoside (3)

A sample of **2** (20 mg) was acetylated (5 min at 0°) with acetic anhydride (1 ml) and boron trifluoride etherate (1 drop). Work-up by treatment with ice water and chloroform extraction furnished **3** as a slightly yellow oil (24 mg, 95%). After bulb-to-bulb vacuum distillation at 120° and 1 mm Hg, the product showed $[\alpha]_D$ −173° (*c*, 1.3 in $CHCl_3$); ν_{max} (neat) 1745 (ester CO), 1550 and 1370 cm^{-1} (NO_2); n.m.r. (100 MHz in $CDCl_3$): τ 4.74 (1H, q, $J_{1,2}$ = 3.5 Hz, $J_{2,3}$ = 11–11.5 Hz, H-2), 5.01 (2H, superimposed sextet and doublet assigned to H-3 and H-1, respectively, $J_{1,2}$ = 3.5 Hz, $J_{2,3} = J_{3,4a}$ = 11 Hz, $J_{3,4e}$ = 4.5 Hz), 6.03 (1H, m, H-5), 7.64 (1H, octet, $J_{3,4e}$ = 4.5 Hz, $J_{4a,4e}$ = 11–11.5 Hz, $J_{4e,5}$ = 2 Hz, H-4e), 7.99 (3H, s, OAc), 8.09 (1H, q, $J_{3,4a} = J_{4a,4e} = J_{4a,5}$ = 11–11.5 Hz, H-4a), 8.80 (3H, d, $J_{5,6}$ = 6 Hz, *C*—CH_3), 6.65 (3H, s, OCH_3).

Anal. Calcd. for $C_9H_{15}NO_6$ (233.2): C, 46.35; H, 6.48; N, 6.01. Found: C, 46.51; H, 6.55; N, 6.13.

Methyl 3-Amino-3,4,6-trideoxy-α-L-xylo-hexopyranoside (4)

Compound **2** (282 mg) was hydrogenated (4 h at ordinary temperature and pressure) with platinum catalyst (from 200 mg of PtO_2) in a mixture of ethanol (4 ml), water (16 ml), and *N* HCl (1.5 ml). The filtered solution was evaporated to give the hydrochloride of **4** as an amorphous, hygroscopic solid (292 mg). The product was deionized by treatment with 5 ml of Dowex 1X8 (carbonate form) in a mixture of water (10 ml) and methanol (10 ml). Evaporation of the colorless solution then gave crystalline **4** (240 mg, 96%) which was subsequently recrystallized from methanol; m.p. 138–139°; $[\alpha]_D$ −179° (*c*, 0.9 in methanol); ν_{max} (Nujol) 3360, 3290, and 3260–3020 (NH and OH), 1597 cm^{-1} (NH_2); n.m.r. (60 MHz in D_2O, with reference to τ_{DOH} 5.28): τ 5.83–6.33 (1H, m, H-5), 6.73 (3H, s, OCH_3), 6.78 (1H, q, $J_{1,2}$ = 4 Hz, $J_{2,3}$ = 10 Hz, H-2), 7.17 (1H, sextet, $J_{2,3} = J_{3,4a}$ = 10 Hz, $J_{3,4e}$ = 4 Hz, H-3), 8.24 (1H, octet, $J_{3,4e}$ = 4 Hz, $J_{4a,4e}$ = 13 Hz, $J_{4a,5}$ = 10 Hz, H-4e), 8.93 (1H, sextet, $J_{3,4a} = J_{4a,5}$ = 10 Hz, $J_{4a,4e}$ = 13 Hz, H-4a), 8.95 (3H, d, $J_{5,6}$ = 6 Hz, *C*—CH_3). The anomeric proton signal was obscured by the DOH peak but was seen in an acetone-d_6 spectrum to be a 3.5 Hz doublet.

Anal. Calcd. for $C_7H_{15}NO_3$ (161.2): C, 52.15; H, 9.38; N, 8.69. Found: C, 52.31; H, 9.23; N, 8.79.

A sample of **4** was *N*-acetylated, whereupon the following substituent proton resonances were found (in $CDCl_3$): τ 4.60 (broad, NH), 6.59 (s, OCH_3), 8.02 (s, *N*—Ac), and 8.84 (d, *C*—CH_3).

3,4,6-Trideoxy-3-dimethylamino-L-xylo-hexose (5)

The amino glycoside **4** (230 mg) was refluxed for 4 h in a mixture of 98–100% formic acid (2 ml) and 37–41% formaldehyde (1 ml). The reaction mixture was then evaporated with several portions of added *N* hydrochloric acid and ethanol at a bath temperature of 45°, to give a yellow syrup. The syrup was dissolved in methanol (10 ml) and water (10 ml), and the solution was stirred for 2 h with 4 ml of Dowex 1X8 (carbonate form). Removal of the solvent gave a syrup which was passed through a silica gel column with methanol–chloroform (3 : 2) in an unsuccessful attempt at purification. A 60 MHz spectrum in $CDCl_3$ showed an H-1 doublet at τ 5.13 ($J_{1,2}$ = 3–4 Hz), singlets for OCH_3 and $N(CH_3)_2$ at τ 6.53 and 7.70, respectively, and a *C*—CH_3 doublet at τ 8.78, in accordance with the structure of an *N,N*-dimethylated glycoside.

The above product was refluxed for 4 h in 6 *N* HCl (5 ml). The hydrolyzate was evaporated with the addition of several portions of water and ethanol in order to remove most of the acid. The product was then stirred for 3 h with Dowex 1X8 (OH^-) in methanol–water (1:1, 30 ml). Solvent removal followed by chromatography of the remaining syrup on silica gel using methanol–chloroform (2:3) as eluent furnished 165 mg (66%) of **5** as a colorless syrup; $[\alpha]_D$ −42.4°, $[\alpha]_{578}$ −42.9°, $[\alpha]_{546}$ −46.8°, $[\alpha]_{436}$ −76.5° (*c*, 0.85 in water).

A 60 MHz n.m.r. spectrum of **5** in D_2O was identical in every detail with the published (11) spectrum of D-desosamine.

3,4,6-Trideoxy-3-dimethylamino-α-L-xylo-hexose Hydrochloride (6)

A solution of **5** (50 mg) in *N* HCl (2 ml) was evaporated with addition of water and ethanol to give a film that was dried *in vacuo*. The hydrochloride **6** crystallized from a minimum amount of absolute ethanol upon cautious addition of ether and cooling. The colorless crystals (60 mg) melted at 173–175° with decomposition, and at 183–184° after two further recrystallizations. The D-enantiomer showed m.p. 182° (2), 183–184° (12), 189–191° (13), 189–191° (14). The optical rotation of **6** (*c*, 0.75 in water):

Can. J. Chem. Downloaded from www.nrcresearchpress.com by 210.87.254.105 on 09/05/12
For personal use only.

$[\alpha]_D$ −64° (2 min) → −50° (16 h) → −52.5° (24 h) → −52° (48 h); $[\alpha]_{546}$ −73.5° (2 min) → −60° (16 h) → −61.5° (24 h) → −62° (48 h); $[\alpha]_{436}$ −121.5° (2 min) → −100° (16 h) → −101° (24 h) → −106° (48 h). For the D-enantiomer, no mutarotation data are recorded in the literature; only $[\alpha]_D$ values are given which presumably correspond to minimum readings: +48° (2), +49.5° (13), and +50.7° (14). The i.r. spectrum of **6** in KBr agreed very well with the spectrum of the D-enantiomer reproduced in ref. 3.

Support of this work by the National Research Council of Canada is gratefully acknowledged.

1. S. HANESSIAN and T. H. HASKELL. *In* The carbohydrates. Vol. IIA. *Edited by* W. Pigman and D. Horton. Academic Press, New York, N.Y. 1970. p. 139.
2. A. C. RICHARDSON. Proc. Chem. Soc. 131 (1963).
3. F. KORTE, A. BILOW, and R. HEINZ. Tetrahedron, **18**, 657 (1962).
4. H. NEWMAN. J. Org. Chem. **29**, 1461 (1964).
5. H. H. BAER and C. W. CHIU. Can. J. Chem. Can. J. Chem. **52**, 111 (1974).
6. A. C. RICHARDSON and K. A. MCLAUGHLAN. J. Chem. Soc. 2499 (1962); H. H. BAER and K. ČAPEK. Can. J. Chem. **47**, 99 (1969).
7. H. H. BAER and W. RANK. Can. J. Chem. **50**, 1292 (1972).
8. H. H. BAER and C. W. CHIU. Carbohydr. Res. In press.
9. H. H. BAER and J. KOVÁŘ. Can. J. Chem. **49**, 1940 (1971); J. KOVÁŘ, K. ČAPEK, and H. H. BAER. Can. J. Chem. **49**, 3960 (1971).
10. W. ESCHWEILER. Ber. **38**, 880 (1905); H. T. CLARKE, H. B. GILLESPIE, and S. S. WEISSHAUS. J. Am. Chem. Soc. **55**, 4571 (1933); A. C. RICHARDSON. J. Chem. Soc. 2758 (1962).
11. P. W. K. WOO, H. W. DION, L. DURHAM, and H. S. MOSHER. Tetrahedron Lett. 735 (1962).
12. E. H. FLYNN, M. V. SIGAL, JR., P. F. WILEY, and K. GERZON. J. Am. Chem. Soc. **76**, 3121 (1954).
13. H. BROCKMANN, H. B. KÖNIG, and R. OSTER. Chem. Ber. **87**, 856 (1954).
14. C. H. BOLTON, A. B. FOSTER, M. STACEY, and J. M. WEBBER. J. Chem. Soc. 4831 (1961).

Can. J. Chem. Downloaded from www.nrcresearchpress.com by 210.87.254.105 on 09/05/12
For personal use only.

A New Synthesis of 4-(4-Methyl-4-hydroxyamyl)-Δ^3-cyclohexenecarboxaldehyde

KUNIO KOGAMI,[1] OSAMU TAKAHASHI,[1] AND JU KUMANOTANI[2]

The Engineering Research Institute, The University of Tokyo, Tokyo, Japan

Received June 6, 1973

A new synthetic route of 4-(4-methyl-4-hydroxyamyl)-Δ^3-cyclohexenecarboxaldehyde (Lyral) from myrcene (**1**) was investigated. It involves subjecting **1** first to the diene synthesis with acrolein (**2**) followed by hydration of the morpholine enamine of the adduct in 50% sulfuric acid at 0–5° and the subsequent hydrolysis in diluted sulfuric acid at 15–20°.

The present method is superior in simplicity as well as productivity for the preparation of Lyral to any other methods hitherto reported.

On a étudié une nouvelle méthode synthétique pour l'obtention du (méthyl-4 hydroxy-4 amyl)-4 cyclohexène-Δ^3 carboxaldéhyde (Lyral) à partir du myrcène (**1**). Cette méthode implique tout d'abord la réaction de **1** avec l'acroléine (**2**) suivie par l'hydratation de la morpholine énamine du composé d'addition dans l'acide sulfurique 50% à 0–5° puis par une hydrolyse dans l'acide sulfurique dilué à 15–20°.

La méthode que l'on présente, est supérieure à cause de la simplicité ainsi que du rendement obtenu pour la préparation du Lyral, à toutes les méthodes connues jusqu'à cette date.

[Traduit par le journal]

Can. J. Chem., **52**, 125 (1974)

4-(4-Methyl-4-hydroxyamyl)-Δ^3-cyclohexenecarboxaldehyde and its structural isomer (Lyral) have been prepared from myrcene (**1**) by two routes of low yield: (*a*) Diels–Alder condensation of 2-hydroxy-2-methyl-6-methylene-Δ^7-octene (myrcenol) prepared by acetoxylation of **1** and subsequent saponification with acrolein (**2**) (1) and (*b*) that of 2-hydroxy-2-methyl-6-methylene-$\Delta^{3,7}$-octadiene and 3-hydroxy-2,6-dimethylene-Δ^7-octene prepared by the reduction of photooxidized myrcene with **2** and subsequent selective hydrogenation (2). The former gives 15% of the theoretical yield of Lyral from **1** and the latter 20%.

The present paper describes a new, successful synthesis giving as much as 65% of the theoretical yield of hydroxyaldehydes, 4-(4-methyl-4-hydroxyamyl)-Δ^3-cyclohexene-carboxaldehyde (**5**) and 5-(4-methyl-4-hydroxyamyl)-Δ^4-cyclohexene-carboxaldehyde (**6**) by the procedure shown in Scheme 1. **1** was reacted with **2** according to the method described in the literature (**3**). The reaction time, temperature, and yield of cycloadduct, Myrac aldehydes (**3** and **4**, the ratio **3**:**4** of 80:20) are given in Table 1. The morpholine enamines of **3** and **4** were obtained quantitatively by condensation of the aldehydes with morpholine in the molar ratio 1:1.4 in toluene using phosphoric acid as catalyst. The enamine purified by distillation was used in the hydration and hydrolysis (Table 2) (4, 5). The desired hydroxyaldehydes, **5** and **6**, were obtained in the mixture at a good yield (71%) but the estimation of isomers by g.l.c. was found to be very difficult. The dimethyl acetals were prepared and gave an isomer ratio **5**:**6** of 70:30. Comparison of the isomer ratios between the Myrac aldehydes and the Lyral dimethylacetals obtained suggests that **5** is more easily cyclized to a mixture of isomers of 1,1-dimethyl-7-methylal-octaline than **6** (6, 7).

Protection of the aldehyde group in the Myrac aldehydes by conversion into the dimethyl acetal, diacetate, or sodium hydrogen sulfite-adduct instead of enamine, resulted in only a small amount of the hydroxyaldehydes. Without protecting the aldehyde group, however, hardly any hydration took place.

Experimental

Materials

Myrcene (**1**) consisting of a mixture of 76% myrcene, 12% dipentene, 2% β-pinene, and 10% of other terpene hydrocarbons was purchased from the LDRT Co., Ltd.; b.p. 163–178°; d_{20}^{20} 0.8104; n_D^{20} 1.4740. Myrac aldehydes, **3** and **4**, and Lyrals, **5** and **6**, were purchased from the IFF Co., Ltd. Myrac aldehydes: b.p. 136–138°/4 Torr; d_{25}^{25} 0.9326; n_D^{25} 1.4896. Lyrals: b.p. 126–130°/1 Torr; d_{25}^{25} 0.9956; n_D^{25} 1.4893. Acrolein (**2**) and morpholine were of chemically pure grade reagent and used without further purification.

[1]Present address: T. Hasegawa Co., Ltd, 9, 4-Chome, Honcho, Nihonbashi, Chuo-ku, Tokyo 103, Japan.

[2]Institute of Industrial Science, University of Tokyo, 22–1, 7-Chome, Roppongi, Minato-ku, Tokyo 106, Japan.

Can. J. Chem. Downloaded from www.nrcresearchpress.com by 210.87.254.42 on 09/05/12
For personal use only.

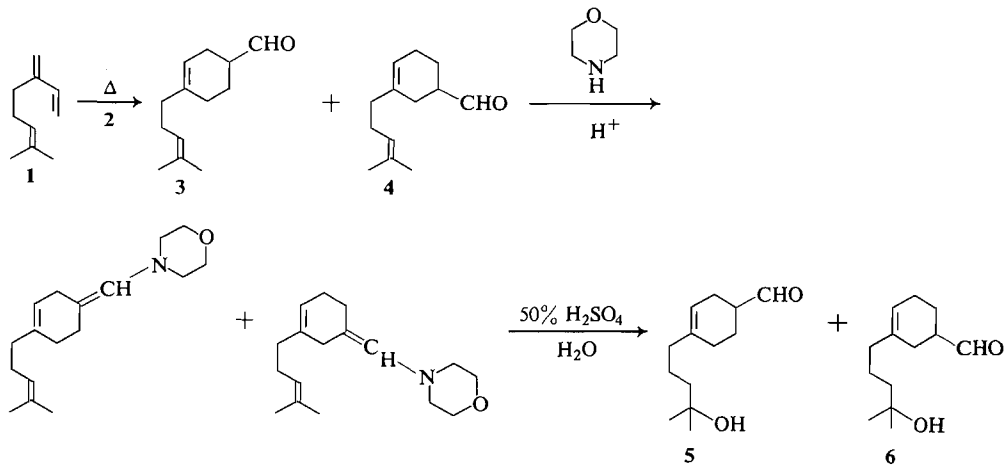

SCHEME 1

TABLE 1. Diels-Alder reaction of myrcene (**1**) with acrolein (**2**)[a]

Run	Hydroquinone (g)	Reaction		Myrac aldehydes yield		Ratio of isomer (%)[b]	
		Temperature (deg)	Time (h)	In g	In %	**3**	**4**
1	3.5	110–120	4.5	510	95.0	81	19
2	3.5	110–120	4.5	506	94.3	80	20
3	3.3	130–140	2.0	516	96.1	78	22
4	3.3	150–160	1.0	504	94.0	77	23

[a]1 (2.8 mol, 500 g) was reacted with 2 (3.59 mol, 201 g in Run 1 and 2.98 mol, 167 g in Runs 2–4).
[b]Based on the Myrac aldehyde dimethyl acetals (3′ + 4′) estimated by g.l.c.

TABLE 2. Hydration of morpholine enamines and other derivatives

Run	Derivative	Amount		$[H_2SO_4]$		Reaction		Yield of Lyral	
		In g	In mol	Wt. %	g	Temperature (dec.)	Time (min)[a]	In g	In %
1	Enamine	100	0.38	40	300	−2 to 10	65	31	40
2	Enamine	100	0.38	50	300	−2 to 10	45	54	70
3	Enamine	100	0.38	60	300	−2 to 10	10	31	40
4	Enamine	100	0.38	40	300	10 to 20	65	50	65
5	Enamine	100	0.38	50	300	10 to 20	20	46	60
6	Enamine	100	0.38	60	300	−15 to −5	5	53	69
7	Enamine	100	0.38	50	300	0 to 5	50	55	71
8	Enamine	100	0.38	50	600	0 to 5	50	53	69
9	Enamine	350	1.33	50	1050	0 to 5	65	260	67.5
10	Enamine	350	1.33	50	1050	−2 to 10	50	270	70
11	Myrac aldehydes	73	0.38	50	300	0 to 5	50	0	0
12	Myrac aldehydes	73	0.38	50	300	−2 to 10	50	0	0
13	Dimethyl acetal	90	0.38	50	300	0 to 5	50	2	2.6
14	Diacetate	112	0.38	50	300	0 to 5	60	3	3.8
15	Sodium hydrogen sulfite adduct	112	0.38	50	300	0 to 5	60	3	3.8

[a]Values indicate the time at which a maximum peak of Lyral was observed on the analysis of hydrated products by g.l.c.

Can. J. Chem. Downloaded from www.nrcresearchpress.com by 210.87.254.42 on 09/05/12
For personal use only.

Can. J. Chem. Downloaded from www.nrcresearchpress.com by 210.87.254.42 on 09/05/12
For personal use only.

Spectral Data

Infrared spectra were obtained with a Nihon Bunko IR-spectrometer, Model IR-S. Nuclear magnetic resonance spectra were determined in carbon tetrachloride with tetramethylsilane as internal standard on a JEOL 4H-100 spectrometer. Mass spectra were measured by means of a Hitachi RMU-6E mass spectrometer under the following conditions: ionization energy 70 eV; ionization current 80 μA; ionization potential 1800 V. The pressure of ion source and ionization chamber was kept at 10^{-4} to 10^{-5} Torr. A column (2 m × 3 mm) containing Carbowax 20 M (10 wt. %) on Celite 545 SK (100–120 mesh) was used for g.l.c.; the column temperature was fixed at 180° and helium was used as a carrier gas.

*Cyclic Adduct of Myrcene (**1**) with Acrolein (**2**)*

Compounds **1** (500 g, 2.8 mol), **2** (167 g, 2.98 mol), and hydroquinone (3.3 g) were placed into a 1-l stainless steel autoclave, the temperature of which was elevated to 110° in 30 min under stirring, kept at 110–120° for 4.5 h, and then lowered. The resulting product was distilled *in vacuo* with a packed column type rectifier to give the following fractions: (*i*) b.p. 30–135°/4 Torr, 94 g; (*ii*) b.p. 136–138°/4 Torr, 506 g; (*iii*) residue, 27 g. Fraction *i* was found to be a mixture of other terpene hydrocarbons except **1**. Fraction *ii* was identified as Myrac aldehydes by comparing the n.m.r., i.r., and mass spectra with those of authentic samples (IFF Co., Ltd.): aldehyde content 99.8% (hydroxylamine method); d_{25}^{25} 0.9323; n_D^{25} 1.4893 (Run 2, Table 1). The Myrac aldehydes are difficult to separate by g.l.c. Therefore, they were converted into dimethylacetal derivatives (**3′** and **4′**) with methanol containing 1% *p*-toluenesulfonic acid; **3′** and **4′** were separated from the mixture by repeated preparative g.l.c. The obtained ratio (**3′**:**4′** of 80:20) was found to agree with that of Canet and Mousseron (3). The analytical conditions and retention times of the isomers were as follows: gas chromatograph, Kotaki GU-21 with a thermal conductivity type detector; column, stainless steel (2 m × 3 mm); packing material, support, Celite 545 SK (60–80 mesh) and liquid phase, Carbowax 20 M (10 wt. %); column temperature, 180°; helium pressure, 14 p.s.i.; flow rate, 40 ml/min; chart speed, 0.5 cm/min; retention times, **3′**, 5 min 40 s, **4′**, 6 min 25 s.

Spectral data were as follows; n.m.r. spectra (δ, p.p.m.): **3′**, 1.72 and 1.82 (singlets, —HC=C(CH_3)$_2$), 1.9–2.8 (superimposed, —CH_2—, =CH—CH_2—, —CH—), 3.58 (singlet, (OCH_3)$_2$), 4.40 (doublet, —CH(OCH_3)$_2$), 5.54 (broad singlet, —CH=C(CH_3)$_2$), 5.58 (broad singlet, —CH=CH—); **4′**, 1.74 (singlet, 1.84 (singlet, —CH=C(CH_3)$_2$), 1.9–2.8 (superimposed, —CH_2—, =CH—CH_2—, —CH—), 3.60 (singlet, (OCH_3)$_2$), 4.08 (doublet, —CH(OCH_3)$_2$), 5.52 (broad singlet, —CH=C(CH_3)$_2$), 5.90 (broad singlet, —CH=CH—). Both the i.r. and mass spectra of **3′** were almost superimposable on those of **4′**. Infrared spectra (neat, cm^{-1}): 2830 (CH(OCH_3)$_2$), 1200–1040 (C—O—C—O—C), 828 (—C=CH—). Mass spectra (*m/e*): 206 M^+; 191 (M − 15, CH_3); 174 (M − CH_3OH), 137 (M − 67, (CH_3)$_2$—C=CH—CH_2—); 123 (M − 83), 105 (M − 69–32), 75 (base peak, CH_3O=C^+H—OCH_3); 41 (CH_3—C=CH_2).

Synthesis of Morpholine Enamines of Myrac Aldehydes

Morpholine (329 g, 3.80 mol) was added to the solution of Myrac aldehydes (450 g, 2.33 mol) in toluene (1600 ml) containing 85% phosphoric acid (4.5 g) at room temperature. After refluxing the mixture at 112–148° for 8 h, the theoretical amount of water was stripped off. The residue obtained by removal of toluene and morpholine from the resultant solution was submitted to distillation *in vacuo*: (*i*) b.p. 70–130°/0.05 Torr, 8 g; (*ii*) b.p. 130–139°/0.05 Torr (morpholine enamine), 426 g; (*iii*) residue, 16 g. Characteristic properties of the morpholine enamine were as follows: b.p. 130–139°/0.05 Torr, d_{25}^{25} 0.9339; n_D^{25} 1.5165; n.m.r. (δ, p.p.m.): 1.62 (6 H, doublet, —CH_3), 1.28–2.8 (10 H, multiplet, —CH_2—), 2.53 (4 H, multiplet, —N—CH_2—), 3.60 (4 H, triplet, —CH_2—CH_2—O—CH_2—CH_2—), 5.05 (1 H, broad singlet, isopropylidene olefine), 5.32 (1 H, broad singlet, cyclohexene olefine), 5.38 (1 H, broad singlet, =CN—N—); i.r. (cm^{-1}): 1665 (=CH—N—), 1120 (C—N); mass spectrum (*m/e*); 261 (M^+), 246 (M − 15), 204 (M − 57), 192 (M − 69, (CH_3)$_2$—C=CH—CH_2—), 178 (M − 83), 105 (192–87), 100 (—CH_2—N(—CH_2—CH_2—)$_2$O), 91, 86 (—N(—CH_2—CH_2—)$_2$O), 79, 69, 41 (base peak, CH_3—C=CH_2).

Hydration of Morpholine Enamine and Other Derivatives

Rectified morpholine enamine (100 g, 0.38 mol) was added immediately to 50% sulfuric acid (300 g) with vigorous stirring at 0–5° (4, 5). Further stirring was continued for 50 min at the same temperature. The reaction mixture was poured into 1 kg of ice water. The mixture was stirred at 15–20° for 5 h and an oily product separated and was extracted with benzene. The benzene solution was washed with an aqueous solution of 5% sodium carbonate until the wash solution was substantially alkaline. After removal of the benzene, the remaining oil was distilled *in vacuo*: (*i*) b.p. 102–105°/1 Torr, 12 g; (*ii*) b.p. 105–126°/1 Torr, 4 g; (*iii*) b.p. 126–130°/1 Torr, 55 g (Lyral, theoretical yield 71%), d_{25}^{25} 0.9958, n_D^{25} 1.4895; (*iv*) b.p. 130–138°/1 Torr, 1.1 g; (*v*) residue, 5.3 g (Run 7, Table 2). Fraction (*i*) with the following properties was estimated by g.l.c. to be a mixture of 1,1-dimethyl-7-methylaloctaline and 1,1-dimethyl-6-methylaloctaline (6), accompanied by a small amount of Myrac aldehydes; d_{25}^{25} 0.9877, n_D^{25} 1.5031, aldehyde content (hydroxylamine method) 100%. The spectral data of the mixture of dimethyl octaline isomers separable by preparative gas chromatography were as follows: n.m.r. (δ, p.p.m.): 1.00 (6 H, singlet, (CH_3)$_2$), 1.5 (complex, —CH_2—), 1.7–2.6 (complex, =CH—CH_2— and —CH—), 5.4 (broad singlet, =CH—), and 9.66 (singlet, aldehyde proton); i.r. (cm^{-1}): 2820, 2720 (ν CH of CHO), 1730 (ν C=O), 1390, 1370 (CH_3—C—CH_3), 1205, 1180 (CH_3—C—CH_3), and 805 (δ, CH=CH—); mass spectrum (*m/e*): 192 (M^+), 177 (M − 15), 163 (M − 29), 159 (M − 15 − 18), 149 (177 − 28), 136, 107 (149 − 42), 105, 93, 91, and 41 (base peak). Fraction (*iii*) was identified to be Lyral and structural isomer by comparing the n.m.r., i.r., and mass spectra with those of an authentic

sample, Lyral of the IFF Co., Ltd. The fraction gave 99.5% aldehyde estimated by oximation, corresponding to 65.3% theoretical yield based on the **1** used, the fragrance of which was very pleasant like that of a fine lilac-lily. The spectral data found: n.m.r. (δ, p.p.m.): 1.12 (6 H, singlet, $-CH_3$), 1.36 (broad singlet, $-CH_2$), 1.7–2.5 (complex, $=C-CH_2-$ and $-CH-$), 3.2 (1 H, singlet, —OH), 5.4 ($=CH-$), and 0 (1 H, CHO); i.r. (neat, cm^{-1}): 3480 (associated —OH), 2860, 2740 (ν CH of CHO), 1730 (ν C=O), 1385, 1370 (CH_3-C-CH_3), 1210, 1160 (CH_3-C-CH_3), 1130 (ν $-C-OH$), 910 (δ CH of CHO), and 805 (δ $-C=C-H$); mass spectrum (*m/e*): 210 (M^+), 192 (M − 18), 136 (192 − ($CH_2=CH-CHO$)), 59 (base peak, $(CH_3)_2-C-OH$) and 29 (CHO).

Direct hydration of unprotected Myrac aldehydes gave very low yields. Therefore a modification of the conversion of aldehydes into the dimethyl acetal, diacetate, and sodium hydrogen sulfite adduct by the usual method (8), was attempted. However, the hydration of these derivatives resulted in only a small percent of Lyral (Table 2). Hence we suggest the use of morpholine enamine.

The authors wish to express their gratitude to Mr. S. Hasegawa, the President of T. Hasegawa, Co., Ltd. for his kind financial support and permission to publish this paper.

1. R. W. TEEGARDEN, F. HAVEN, and L. STEINBACH. U.S. Patent No. 2947780 (1960).
2. T. MOROE, A. KOMATSU, T. MATSUI, and K. UEDA. Jap. Patent No. 6908494 (1969).
3. M. M. CANET and M. MOUSSERON. Bull. Soc. Chim. Fr. 394 (1956).
4. G. H. ALT and A. J. SPEZIEALE. J. Org. Chem. **26**, 3761 (1961).
5. K. KOGAMI, F. TAKAHASHI, M. MONDA, and JU KUMANOTANI. Soap, Perfum. Cosmet. 819 (1969).
6. G. OHLOFF. U.S. Patent No. 2933506 (1960).
7. A. VAN DER GEN, K. WIEDHAUP, J. J. SWOBODA, H. C. DUNATHAN, and W. S. JOHNSON. J. Am. Chem. Soc. **95**, 2656 (1973).
8. P. S. BEDOUKIAN. J. Am. Chem. Soc. **67**, 1430 (1945).

Can. J. Chem. Downloaded from www.nrcresearchpress.com by 210.87.254.42 on 09/05/12
For personal use only.

Aziridine Induced Isomerization of Isomaleimides to Maleimides[1]

P. JOSEPH-NATHAN, V. MENDOZA, AND E. GARCÍA G.[2]

Departamento de Química del Centro de Investigación y de Estudios Avanzados, Instituto Politécnico Nacional, P.O. Box 14-740, México 14, D.F., México

Received May 28, 1973

Treatment of *N*-phenylisomaleimide with aziridine gave 3-(*N'*-aziridinyl)-*N*-phenylsuccinimide identical with the adduct formed between *N*-phenylmaleimide and ethylenimine. The isomerization proceeded through the intermediate **2** whose decomposition in solution to a mixture of **3**, **4**, and **5** is also described.

Le traitement de la *N*-phénylmaleisoimide par l'aziridine fournit la (*N'*aziridinyl)-3 *N*-phényl succinimide identique avec le composé formé dans la réaction entre la *N*-phénylmaleimide et l'éthylenimine. L'isomérisation se produirait par l'intermédiaire de 2 dont la décomposition en solution pour donner **3**, **4** et **5** est aussi discuté. [Traduit par le journal]

Can. J. Chem., **52**, 129 (1974)

The cyclization of *N*-substituted maleamic acids either to the corresponding maleimides (**3**) or isomaleimides (**1**) under various reaction conditions, is well documented (1, 2). The isomerization (3, 4) of **1** into **3** may proceed (5) through nucleophilic attack of an acetate ion on the carbonyl carbon of **1**, followed by ring opening and a recyclization in which the nitrogen of the intermediate reexpels the acetate ion.

In a recent work we described (6) the reaction of substituted *N*-phenylmaleimides (**3**) with aziridine, which lead to adducts (**4**) showing unexpected p.m.r. spectra. Considering the analogy in structure between maleimides and isomaleimides and having also in mind the chemical properties of aziridine (7), it seemed interesting to react ethylenimine with isomaleimides, since either a direct adduct should be formed or an isomerization of the isomaleimide to maleimide could occur.

The latter process took place when room-temperature treatment of an ethereal solution of *N*-phenylisomaleimide (**1**) with aziridine gave in an almost quantitative yield exclusively 3-(*N'*-aziridinyl)-*N*-phenylsuccinimide (**4**), identified by direct comparison with a sample obtained (6) by treatment of aziridine with *N*-phenylmaleimide (**3**).

When aziridine is added dropwise to an ethereal solution of *N*-phenylisomaleimide (**1**) below 0 °C, a compound m.p. 80–81° (dec.) was isolated in almost quantitative yields. It showed i.r. absorption bands at 1715 and 1672 cm^{-1} due to carbonyl groups and u.v. maxima at 223 and 300 nm (ε 10 700 and 650). In the n.m.r. spectrum the presence of five aromatic protons located between 7.1 and 7.8 p.p.m., showing exactly the same pattern as the ring protons of acetanilide, were found. In addition, an AB system ($\delta_A = 6.35$, $\delta_B = 6.50$; $J_{AB} = 12$ Hz) attributable to a *cis* CH=CH moiety and a singlet (4H) at 2.45 p.p.m. corresponding to the aziridinyl ring protons, could be recognized. Therefore structure **2** was assigned to this intermediate, which is very unstable, since it easily undergoes transformation into **4** even when a solid sample is kept at −10 °C during two days.

The transformation of **1** to **4** can be rationalized as an attack of the aziridine electron pair on the carbonyl group of the isomaleimide, followed by cleavage of the carbonyl–oxygen single bond, leading to the anion of the enol of an amide, which, after electron redistribution and protonation, affords **2**; this in turn reacts to yield 3-(*N'*-aziridinyl)-*N*-phenylsuccinimide (**4**) by a stepwise process in which ring closure is accompanied by expulsion of the aziridine residue, followed by a Michael recombination of both species. Evidence for this process was obtained when a chloroform solution of pure **2** after standing at room temperature for several hours, gave a mixture of **3**, **4**, **5**, and some polymeric material which was not studied.

Compounds **3** and **4** were identified by direct comparison with authentic specimens (6), while

[1]Presented at the VIII Congreso Mexicano de Química Pura y Aplicada, Querétaro, Qro. México, March, 1973.

[2]Recipient of a CoNaCyT (México) Scholarship (1970–1973).

Can. J. Chem. Downloaded from www.nrcresearchpress.com by 210.87.254.6 on 09/05/12
For personal use only.

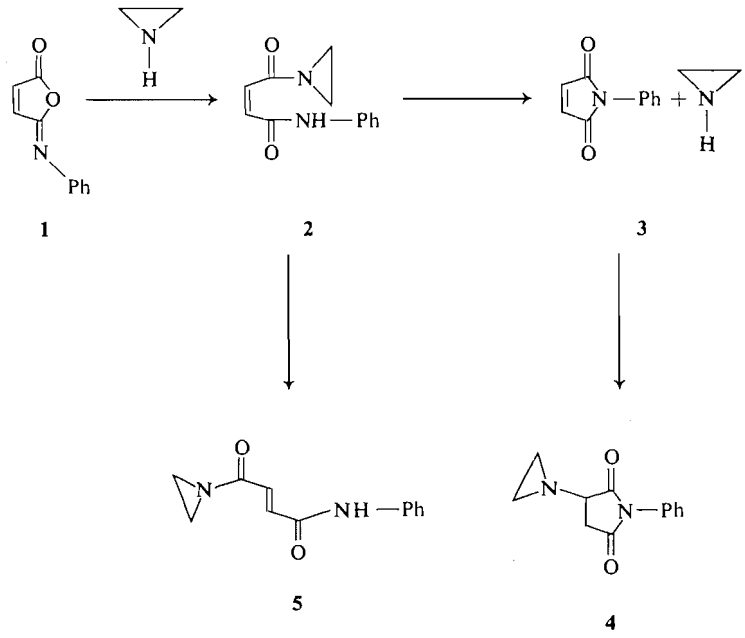

SCHEME 1

the structure of **5** was deduced spectroscopically. It analyzed correctly for $C_{12}H_{12}O_2N_2$, showing i.r. bands at 3425 and 3325 (NH group), 1665 (amide carbonyls), and 1600 cm^{-1} (aromatic double bonds) and u.v. absorption at 228 and 306 nm (ε 10 900 and 6200). The n.m.r. spectrum showed a singlet (2H) at 7.25 p.p.m. due to two vinyllic protons, superimposed on the signals of the five aromatic protons (7.1 to 7.8 p.p.m.), and a singlet (4H) at 2.36 p.p.m. corresponding to the aziridinyl methylene groups. Comparison of the i.r. (8), u.v. (9), and p.m.r. (10) properties of **2** and **5** is also congruent with a *cis–trans* pair of isomers.

Catalytic hydrogenation of **5** afforded *N*-(4-(*N'*-phenyl)succin)aziridine which showed in addition to the aromatic protons, the presence of a broad peak (4H) at 2.80 p.p.m. corresponding to the CH_2—CH_2 protons of the succinic chain and a sharp singlet (4H) at 2.30 p.p.m. attributable to the aziridinyl protons. It is interesting to mention that only a small amount of the three-membered ring was opened to an *N*-ethyl group during this hydrogenation performed in the presence of Adams catalyst, while compound **4** was transformed in high yields into 3-(*N'*-ethyl)-*N*-phenylsuccinimide using 10% Pd on charcoal catalyst (see Experimental). In addition, hydrogenation of **2** with Pd–C catalyst gave *N*-phenylsuccinimide identified with a sample obtained by hydrogenation of *N*-phenylmaleimide (**3**).

A sample of **2** was also treated under the acetate ion conditions in which the transformation of **1** into **3** was described (5). This resulted in the formation of **3** in good yields. Under the reaction conditions, the free aziridine that should be formed very probably reacts further with the acetic anhydride in a similar way as a compound of type **4** was derivatized previously (6), thereby precluding the Michael addition. These reactions are outlined in Scheme 1.

Experimental

3-(N'-Aziridinyl)-N-phenylsuccinimide (4)

A stirred solution of 5 g of *N*-phenylisomaleimide (**1**) in 200 ml of ether was treated dropwise with aziridine until the yellow color disappeared. The stirring was continued awhile and the precipitate filtered, yielding 5 g of **2** m.p. 119–120°. Recrystallization from acetone–hexane gave white needles: m.p. 122–123°; λ_{max} 221 nm; ε 7000; i.r. 1790 and 1722 (imide carbonyls), and 1600 cm^{-1} (aromatic double bonds). The n.m.r. showed the aromatic protons as a broad signal (5H) centered at 7.4 p.p.m. and the characteristic signals due to the succinimide and aziridine ring protons previously found (6) in similar compounds.

Anal. Calcd. for $C_{12}H_{12}N_2O_2$: C, 66.65; H, 5.59; N, 12.95; O, 14.80. Found: C, 66.46; H, 5.42; N, 12.94; O, 14.82.

The substance showed no depression on admixture

Can. J. Chem. Downloaded from www.nrcresearchpress.com by 210.87.254.6 on 09/05/12
For personal use only.

Can. J. Chem. Downloaded from www.nrcresearchpress.com by 210.87.254.6 on 09/05/12
For personal use only.

with a sample obtained by treatment of *N*-phenylmaleimide (**3**) (11) with aziridine (6) and their i.r. spectra were identical.

1-Aziridinyl-4-(N'-phenyl)maleidiamide (2)

A solution of 5 g of **1** in 200 ml of ether was treated as previously with aziridine, but the addition was performed very slowly (45 min) and the solution maintained in an ice bath with NaCl. The precipitate was filtered immediately after decoloration of the solution and washed with cold pentane. This yielded 5 g of solid: m.p. 82–83° (dec.); λ_{max} 223 and 300 nm; ε 10 700 and 650; i.r. 1715 and 1672 (amide carbonyls), 1620, and 1600 cm^{-1} (double bonds). No microanalytical results for the compounds were obtained, since when a sample is kept during 48 h at −10° it transforms quantitatively to 3-(*N'*-aziridinyl)-*N*-phenylsuccinimide (**4**), identified by standard procedures.

Decomposition of 2

A solution containing 1.5 g of freshly prepared **2** in 100 ml of chloroform was stored at room temperature for 6 h. Upon addition of 25 ml of hexane, a pink solid was precipitated and removed by filtration yielding around 100 mg of a polymeric material which was discarded. The filtrate was diluted with 50 ml of ethyl acetate and concentrated under vacuum at room temperature to a small volume (~20 ml). Addition of several drops of hexane caused precipitation of a white solid which was filtered yielding ~300 mg of **5**, m.p. 161–163° (dec.). Recrystallization from ethyl acetate – hexane gave white needles; m.p. 162–163° (dec.); λ_{max} 228 and 306 nm; ε 10 900 and 6180; i.r. 3425 and 3325 (N—H group), 1665 (amide carbonyls), and 1600 cm^{-1} (double bonds).

Anal. Calcd. for $C_{12}H_{12}N_2O_2$: C, 66.65; H, 5.59; N, 12.95; O, 14.80. Found: C, 66.60; H, 5.50; N, 12.98; O, 14.89.

The filtrate was concentrated at room temperature yielding ~200 mg of white needles, m.p. 122–123° which were identified as 3-(*N'*-aziridinyl)-*N*-phenylsuccinimide (**2**) by standard procedures.

Further concentration of the filtrate followed by addition of hexane yielded around 100 mg of yellow needles, m.p. 88–89° identified by direct comparison with an authentic sample (11) of *N*-phenylmaleimide.

Hydrogenation of 5

A solution of 180 mg of **5** was hydrogenated as previously. The residue was treated with hexane yielding 100 mg of *N*-(4-(*N'*-phenyl)succin)aziridine, m.p. 102–104°. The analytical sample from ether–hexane showed m.p. 105–107°; λ_{max} 207 and 243 nm; ε 16 000; i.r. 3430 (N—H group), 1670 (carbonyls), and 1590 cm^{-1} (double bonds).

Anal. Calcd. for $C_{12}H_{14}N_2O$: C; 66.04, H; 6.47; N, 12.89; O, 14.66. Found: C, 65.97; H, 6.40; N, 12.66; O, 14.79.

From the mother liquors, a small amount (20 mg) of *N*-(4-(*N'*-ethyl)succin)aniline, m.p. 165–166° was isolated. The analytical sample obtained from chloroform–hexane showed m.p. 166–167°; λ_{max} 206 and 244 nm; ε 14 200 and 12 000; i.r. 3430 (NH group), 1670 (carbonyls), and 1605 cm^{-1} (double bonds). The p.m.r. spectrum showed the aromatic protons between 7.0 and 7.6 p.p.m., a broad singlet (4H) at 2.65 p.p.m. due to the CH_2—CH_2 moiety and an ethyl group as quartet and triplet (J_t = 7 Hz) at 3.23 and 1.12 p.p.m. respectively.

3-(N'-Ethyl)-N-phenylsuccinimide

An ethyl acetate solution containing 500 mg of **4** was hydrogenated in the presence of 50 mg of 10% Pd on charcoal and worked-up as usual. The residue crystallized from carbon tetrachloride yielding 450 mg of the title compound, m.p. 103–104°. The analytical sample obtained from the same solvent showed m.p. 105–106°; λ_{max} 220 nm; ε 7000; i.r. 1785 and 1718 (imide carbonyls), and 1595 cm^{-1} (double bonds). The n.m.r. spectrum showed the aromatic protons between 7.2 and 7.6 p.p.m., a quartet (J = 7 Hz) at 2.83 (2 H) and a triplet (J = 7 Hz) at 1.20 p.p.m. (3 H) corresponding to the *N*-ethyl group and an ABX system $\delta_A = 2.75$, $\delta_B = 3.12$, $\delta_X = 3.97$ p.p.m.; $J_{AB} = 18$, $J_{AX} = 6$, and $J_{BX} = 8$ Hz corresponding to the succinimide ring protons.

Anal. Calcd. for $C_{12}H_{14}N_2O_2$: C, 66.04; H, 6.47; N, 12.84; O, 14.66. Found: C, 65.89; H, 6.29; N, 12.97; O, 14.77.

Transformation of 2 into 3

A solution containing 1 g of freshly prepared **2** and 2 g of AcONa in 4 ml of Ac_2O was kept at room temperature during 48 h. Addition of ice water and extraction with ether followed by work-up as usual, gave a residue from which 523 mg of **3** could be isolated and identified with an authentic sample by standard methods.

1. T. M. Pyriadi and H. J. Harwood. J. Org. Chem. **36**, 821 (1971).
2. T. M. Pyriadi. J. Org. Chem. **37**, 4184 (1972).
3. D. Y. Curtin and L. L. Miller. Tetrahedron Lett. 1869 (1965).
4. M. L. Ernst and G. L. Schmir. J. Am. Chem. Soc. **88**, 5001 (1966).
5. R. J. Cotter, C. K. Sawer, and J. M. Whelan. J. Org. Chem. **26**, 10 (1961).
6. P. Joseph-Nathan, V. Mendoza, and E. García G. J. Org. Chem. **37**, 3950 (1972).
7. O. C. Dermer and G. E. Man. Ethylenimine and other aziridines. Academic Press, New York. 1969. Chapt. 3.
8. N. B. Colthup, L. H. Daly, and S. E. Wiberley. Introduction to infrared and Raman spectroscopy. Academic Press, New York. 1964. p. 378.
9. A. E. Gillman and E. S. Stern. An introduction to electronic absorption spectroscopy in organic chemistry. E. Arnold Ltd., London. 1962. pp. 267–274.
10. P. Joseph-Nathan and E. Díaz. Introducción a la resonancia magnética nuclear. Limusa-Wiley, Mexico City. 1970. pp. 128–131.
11. V. Mendoza, P. Joseph-Nathan, and C. Pérez. Rev. Soc. Quím. Méx. **15**, 103 (1971).

Photocyclization Reactions of Aryl Polyenes. VII.[1] The Photocyclization of 1-Phenyl-4-thienyl- and 1,4-Dithienyl-1,3-butadienes[2]

CLIFFORD C. LEZNOFF, WOLFGANG LILIE, AND CARL MANNING
Department of Chemistry, York University, Downsview, Ontario

Received June 25, 1973

The photocyclization–oxidation reaction of 1-phenyl-4-(2′-thienyl)-1,3-butadiene gave 4-phenylbenzo[*b*]thiophene. Similarly, irradiation of 1-phenyl-4-(3′-thienyl)-1,3-butadiene gave 7-phenylbenzo[*b*]thiophene. Thus, photocyclization occurs exclusively to the thiophene ring. Irradiation of 1,4-di(2′-thienyl)-1,3-butadiene and 1,4-di(3′-thienyl)-1,3-butadiene yielded 4-(2′-thienyl)benzo[*b*]thiophene and 7-(3′-thienyl)benzo[*b*]thiophene, respectively. Photocyclization of 1-(2′-thienyl)-4-(3′′-thienyl)-1,3-butadiene gave an inseparable mixture of 4-(3′-thienyl)benzo[*b*]thiophene and 7-(2′-thienyl)benzo[*b*]thiophene.

La réaction de photocyclisation–oxydation du phényl-1 (thiènyl-2′)-4 butadiène-1,3 a conduit au phényl-4 benzo[*b*]thiophène. De façon similaire, l'irradiation du phényl-1 (thiènyl-3′)-4 butadiène-1,3 a conduit au phényl-7 benzo[*b*]thiophène. Par suite, la photocyclisation se produit exclusivement à l'anneau du thiophène. L'irradiation du di(thienyl-2′)-1,4 butadiène-1,3 et du di(thienyl-3′)-1,4 butadiène-1,3 a conduit au (thiènyl-2′)-4 benzo[*b*]thiophène et au (thiènyl-3′)-7 benzo[*b*]thiophène, respectivement. La photocyclisation du (thiènyl-2′)-1, (thienyl-3′′)-4 butadiène-1,3 a conduit à un mélange inséparable de (thiènyl-3′)-4 benzo[*b*]thiophène et de (thiènyl-2′)-7 benzo[*b*]thiophène.

[Traduit par le journal]

Can. J. Chem., **52**, 132 (1974)

The photocyclization–oxidation reaction of stilbene-like molecules has received much attention in recent years from both preparative (1) and mechanistic (2) points of view. The photocyclization–oxidation of 1,2-diarylethylenes, where one or both of the aryl groups represents heteronuclear aromatic groups has led to the synthesis of some interesting heterocyclic aromatic compounds (3, 4).

The related photocyclization–oxidation of 1,4-diphenyl-1,3-butadiene gave 1-phenylnaphthalene (5). This photoreaction has been extended to a wide variety of 1,4-diaryl-1,3-butadienes where the aryl groups are phenyl, substituted phenyl (6), and polynuclear aromatic groups (7, 8) and it was shown that photocyclization always occurred to the polynuclear aromatic substituent (7, 8).

It was of some interest to determine the feasibility of using 1,4-diaryl-1,3-butadienes, where the aryl groups are heteronuclear aromatic groups, as a means of synthesizing polynuclear heteroaromatic systems by photocyclization. Although we had shown that the direction of photocyclization in 1,4-diaryl-1,3-butadienes can be predicted by molecular orbital calculations (8), when the aryl groups are aromatic hydrocarbons, Laarhoven *et al.* (9) had previously shown in the stilbene series that simple m.o. calculations were unreliable when applied to five-membered ring heteroaromatic groups such as thiophene. Furthermore, Kellogg *et al.* (4) had shown that although 1,2-di(2′-thienyl)ethene and 1-(2′-thienyl)-2-(3′′-thienyl)ethene photocyclize to give dithiaphenanthrenes, the 1,2-di(3′-thienyl)ethene failed to give a dithiaphenanthrene. Thus the lack of a suitable means of prediction of the photocyclization reaction and the failure of one dithienylethene to give tractable products made a detailed investigation of 1-phenyl,4-thienyl-1,3-butadienes and 1,4-dithienyl-1,3-butadienes very desirable.

Irradiation of 1×10^{-3} *M* solutions of 1-phenyl-4-(2′-thienyl)-1,3-butadiene (**1**) in dry benzene containing 2×10^{-3} *M* iodine gave, after 3 days, 4-phenylbenzo[*b*]thiophene (**2**), in 15% yield, identical to the known compound (10). As shown in Scheme 1, photocyclization of **1** can occur to the thiophene ring to give **2**, as observed, or photocyclization can occur to the phenyl group to give the known 1-(2′-thienyl)naphthalene (**3**) (11).

[1]For Part VI see ref. 8.

[2]Presented in part at the 55th Chemical Conference of The Chemical Institute of Canada, June, 1972.

Can. J. Chem. Downloaded from www.nrcresearchpress.com by 210.87.254.42 on 09/05/12
For personal use only.

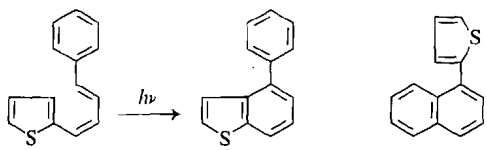

1 2 3

SCHEME 1

The spectral properties of the photoproduct were identical to **2**, synthesized previously (10), and comparison of the n.m.r. spectra of the photoproduct and **3**, previously synthesized (11), showed that less than 5%, if any, of **3** existed in the photoproduct. Vapor phase chromatography was not useful, as a mixture of synthesized **2** and **3** could not be separated on a variety of columns.

Similarly, irradiation of 1-phenyl-4-(3′-thienyl)-1,3-butadiene (**4**) gave exclusive formation of 7-phenylbenzo[*b*]thiophene (**5**), in 39% yield, identical to the known compound (12).

As shown in Scheme 2, photocyclization can occur to the thiophene ring to give **5** or to the phenyl ring to give the known 1-(3′-thienyl)-naphthalene (**6**) (13). Comparison of the n.m.r. spectra of the photoproduct and the known product **6**, however, showed that less than 5%, if any, of **6** was formed.

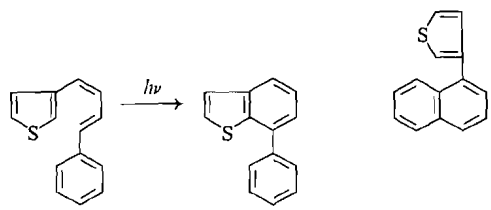

4 5 6

SCHEME 2

It was possible that **3** and **6** were formed in the photocyclization of **1** and **4**, respectively, but that **3** and **6** underwent further photocyclization reactions or suffered decomposition. Irradiation of **3** and **6**, however, led to complete recovery of the starting materials.

It has thus been shown that 1-phenyl-4-thienyl-1,3-butadienes undergo photocyclization exclusively to the thiophene nucleus. This selective mode of cyclization enables the synthesis of 4- and 7-arylbenzo[*b*]thiophenes to be simply accomplished.

The photocyclization of **1** and **4** to give **2** and **5**, respectively, showed that the photocyclization–oxidation reaction to the thiophene ring occurs in high yield to both the 2 and 3 positions of the thiophene nucleus. Due to the unreliability of simple m.o. calculations involving the thiophene nucleus (9), we were unable to predict in advance whether cyclization would occur to the 2 or 3 positions in competitive cyclizations. To elucidate this point a series of 1,4-dithienyl-1,3-butadienes were irradiated.

Thus, photocyclization of 1,4-di(2′-thienyl)-1,3-butadiene (**7**) was irradiated as before to give 4-(2′-thienyl)benzo[*b*]thiophene (**8**) as shown in Scheme 3.

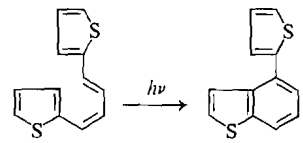

7 8

SCHEME 3

Compound **8** was readily synthesized by a route similar to that described for 1-arylnaphthalenes (**6**).

Similarly, irradiation of 1,4-di(3′-thienyl)-1,3-butadiene (**9**) gave 7-(3′-thienyl)benzothiophene (**10**), as shown in Scheme 4. Compound **10** exhibited a strong parent ion in the mass spectrum. The u.v. spectrum of **10** was very similar to that of 4-(3′-thienyl)benzothiophene (**11**) described below and is consistent with the assigned structure. The n.m.r. spectrum of **10** shows complex absorption between 7 and 8 p.p.m. The spectral data and the mode of synthesis are consistent with structure assigned to **10**.

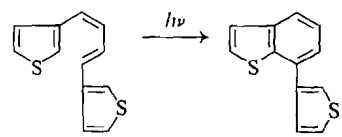

9 10

SCHEME 4

Irradiation of 1-(2′-thienyl)-4-(3′′-thienyl)-1,3-butadiene (**12**) as before gave a mixture of products, inseparable even by vapor phase chromatography. As shown in Scheme 5, photocyclization–oxidation of **12** can occur to the 3′ position of the 1-thienyl group to give **11** and to the 2′′ position of the 4-thienyl group to give 7-(2′-thienyl)benzo[*b*]thiophene (**13**).

Compound **11** was synthesized in the same

Can. J. Chem. Downloaded from www.nrcresearchpress.com by 210.87.254.42 on 09/05/12
For personal use only.

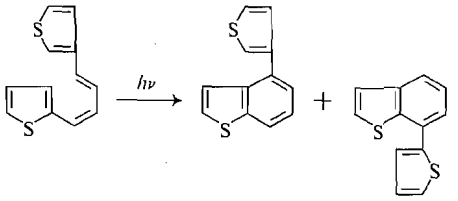

12 11 13

SCHEME 5

way as described above for the synthesis of **8**, except that 3-thienyllithium was used instead of 2-thienylmagnesium bromide. Comparison of the photoproduct from **12**, isolated as a single fraction by t.l.c., indicated the presence of **11**, but also showed that the photoproduct was not solely **11**. Although the mass spectrum of the photoproducts gave a parent ion identical to that of **11**, the cleavage pattern was slightly different. The i.r. and the n.m.r. spectra of the photoproducts were similar but not identical to **11**. The u.v. spectra of **11** and the photoproducts were informative and indicated that the composition of the photoproducts could be explained by a mixture of **11** and **13**.

The u.v. spectra of thienyl compounds are quite informative. Conjugation of the thienyl group with other chromophores is more readily achieved through attachment to the 2 position. This extended conjugation in 2-substituted thiophenes is reflected in a bathochromic shift when compared to 3-substituted thiophenes. For example, 1,2-di(2′-thienyl)ethene, 1-(2′-thienyl)-2-(3′-thienyl)ethene, and 1,2-di(3′-thienyl)ethene exhibit λ_{max} values at 338, 316, and 291 nm, respectively (4); the phenylthienyl butadienes **1** and **4** at 360 and 340 nm, respectively (14); and the dithienylbutadienes **7**, **12**, and **9** at 375, 352, and 332 nm, respectively (14, 15). Thus, it is not surprising that the λ_{max} value for **8** at 300 nm exhibits a bathochromic shift when compared to **11** at 282 nm. Also the λ_{max} value for **10** is 280 nm and hence one should expect a λ_{max} value for **13** of ~300 nm. The u.v. spectrum of the photoproducts from **12** shows λ_{max} at 282 nm corresponding to **11** and a shoulder at ~300 nm corresponding to **13** and is consistent with the u.v. predicted for a mixture of **11** and **13**.

Some time ago Wynberg and van Driel reported the photoisomerization of 2-phenylthiophene to 3-phenylthiophene (16) as well as related photoisomerizations. Thus it is possible that photoproduct **8** could isomerize to **11** and photoproduct **13** could isomerize to **10** under the irradiation conditions. We feel this is highly unlikely as our irradiation conditions (low pressure mercury lamp, room temperature, and Pyrex vessels) are quite different from those of Wynberg and van Driel. Thus the properties of compound **8**, synthesized by both classical and photochemical means, were identical and hence photoisomerization of **8** to **11** had not occurred.

The photocyclization–oxidation reactions of **1**, **4**, **7**, **9**, and **12** described in this paper occur with equal facility to both the 2 and 3 positions of the thienyl moiety. Kellogg *et al.* (4) showed that the 1,2-di(3′-thienyl)ethene failed to cyclize and demonstrated that the failure to isolate a phenanthrene was due to complications in the oxidation of the dihydro intermediate and not in the photocyclization step (4). The facile photocyclizations of **1**, **4**, **7**, **9**, and **12** to both the 2 and 3 positions of the thiophene nucleus support their results.

The fact that photocyclization of **1** and **4** occurs exclusively to the thiophene nucleus is not too surprising as formation of the dihydro intermediates leading to **2** and **5** results in the destruction of the aromaticity of the thiophene nucleus, but photocyclization to **3** and **6** would give dihydro intermediates resulting from destruction of the much more resonance stabilized aromatic phenyl group.

Thus, the photocyclization–oxidation reaction of thienylbutadienes provides a facile route to the synthesis of 4- and 7-arylbenzo[*b*]thiophenes and could be readily adapted to more complex heterocyclic aromatic compounds.

Experimental

All m.p.'s were determined on a Kofler hot stage and are uncorrected. The i.r. spectra were recorded on a Unicam SP1000 spectrometer as neat liquids. The u.v. spectra were measured using a Unicam SP800A spectrometer and cyclohexane as solvent. The n.m.r. spectra were measured on a Varian A60 spectrometer using tetramethylsilane as an internal standard ($\delta = 0$ p.p.m.) and deuteriochloroform as solvent. Mass spectra were recorded on a Hitachi-Perkin-Elmer RMU-6 mass spectrometer. The number in brackets after the mass peak represents the percentage of base peak. Silica gel was used for thin- and thick-layer chromatography. All photochemical reactions were carried out in a Rayonet photochemical reactor using RPR 3500 Å lamps. Microanalyses were performed by Dr. C. Daessle of Montreal.

Irradiation of the Butadienes

The irradiations of **1** (14), **4** (14), **7** (15), **9** (14), and **12** (14) were carried out in a manner previously des

Can. J. Chem. Downloaded from www.nrcresearchpress.com by 210.87.254.42 on 09/05/12
For personal use only.

TABLE 1. Thienylbenzo[*b*]thiophenes

Compound	Substituent	Method of synthesis	Yield (%)	Molecular formula	Analysis (%) Found C	Found H	Calculated C	Calculated H
8	4-(2′-Thienyl)	Photochemical	49	$C_{12}H_8S$	66.55	4.06	66.66	3.74
		Grignard	10					
10	7-(3′-Thienyl)	Photochemical	62	$C_{12}H_8S$	66.41	3.54	66.66	3.74
11	4-(3′-Thienyl)	Photochemical	22*	$C_{12}H_8S$	66.44	3.86	66.66	3.74
		Grignard	15					

*This yield represents a mixture of **11** and 13.

TABLE 2. Spectral characteristics of thienylbenzo[*b*]thiophenes

Compound	Substituent	Ultraviolet spectra λ_{max}(nm) (ε)	Infrared spectra γ(cm^{-1})	Mass spectra* *m/e* M^+, other peaks
8	4-(2′-Thienyl)	300 (10 000)	1575(m), 801(m), 758(s)	216(100), 171(23)
10	7-(3′-Thienyl)	281 (7320)	1460(s), 860(m), 775(s)	216(100), 171(30)
11	4-(3′-Thienyl)	282 (7050)	1580(m), 798(m), 775(s)	216(100), 171(30)

*Number in parentheses represents % of base peak.

cribed. The analytical and spectral data of the unknown photoproducts are given in Tables 1 and 2, respectively. The n.m.r. spectra of the photoproducts, although generally uninformative, showed complex absorption between 7 and 7.7 p.p.m. The lack of absorption at 8.2 p.p.m. in the photoproducts eliminated the possible formation of **3** and **6** in the irradiation of **1** and **4**, respectively.

Synthesis of 4-(2′-Thienyl)benzo[b]thiophene(8) and 4-(3′-Thienyl)benzo[b]thiophene (11)

Compound **8** was synthesized according to the previously described method for the synthesis of 1-arylnaphthalenes (6, 17) except that 4-oxo-4,5,6,7-tetrahydrothionaphthene (purchased from Aldrich Chemical Co.) and 2-thienylmagnesium bromide were used as reactants.

The synthesis of **11** was the same as that described for the known **6** (13), except that 3-thienyllithium was used as a reactant. The analytical and spectral data of **8** and **11** are given in Tables 1 and 2, respectively.

The authors gratefully acknowledge the help of the Atkinson Charitable Foundation for a grant in aid of this research.

1. C. S. WOOD and F. B. MALLORY. J. Org. Chem. **29**, 3373 (1964); E. V. BLACKBURN and C. J. TIMMONS. Q. Rev. **23**, 482 (1969).
2. H. GÜSTEN and L. KLASINC. Tetrahedron, **24**, 5499 (1968); K. A. MUSZKAT and E. FISCHER. J. Chem. Soc. (B) 662 (1967); F. B. MALLORY, C. S. WOOD, and J. T. GORDON. J. Am. Chem. Soc. **86**, 3094 (1964); W. M. MOORE, D. D. MORGAN, and F. R. STEIMETZ. J. Am. Chem. Soc. **85**, 829 (1963); M. V. SARGENT and C. J. TIMMONS. J. Am. Chem. Soc. **85**, 829 (1963); M. V. SARGENT and C. J. TIMMONS. J. Am. Chem. Soc. **85**, 2186 (1963).
3. W. CARRUTHERS and H. N. M. STEWART. J. Chem. Soc. 6221 (1965).
4. R. M. KELLOGG, M. B. GROEN, and H. WYNBERG. J. Org. Chem. **32**, 3093 (1967).
5. G. J. FONKEN. Chem. Ind. 1327 (1962).
6. C. C. LEZNOFF and R. J. HAYWARD. Can. J. Chem. **48**, 1842 (1970).
7. R. J. HAYWARD and C. C. LEZNOFF. Tetrahedron, **27**, 2085 (1971).
8. R. J. HAYWARD, A. C. HOPKINSON, and C. C. LEZNOFF. Tetrahedron, **28**, 439 (1972).
9. W. H. LAARHOVEN, TH. J. H. M. CUPPEN, and R. J. F. NIVARD. Rec. Trav. Chim. **87**, 687 (1968).
10. M. C. KLOETZEL, J. E. LITTLE, JR., and D. M. FRISCH. J. Org. Chem. **18**, 1511 (1953).
11. N. V. STULIN and N. I. PUTOKHIN. Khim. Geterosikl. Soedin. Akad. Nauk. Latv. SSR, 512 (1965).
12. D. W. H. MACDOWELL and THOMAS D. GREENWOOD. J. Heterocycl. Chem. **2**, 44 (1965).
13. D. W. H. MACDOWELL, R. A. JOURDENAIS, R. NAYLOR, and G. E. PAULOVICKS. J. Org. Chem. **36**, 2683 (1971).
14. P. RIBEREAU, G. QUEGUINER, and P. PASTOUR. Bull. Soc. Chim. Fr. 1581 (1972).
15. P. RIBEREAU and P. PASTOUR. Bull. Soc. Chim. Fr. 2076 (1969).
16. H. WYNBERG and H. VAN DRIEL. J. Am. Chem. Soc. **87**, 3998 (1965).
17. F. G. BADDAR, L. S. EL-ASSAL, and M. GINDY. J. Chem. Soc. 1270 (1948); F. G. BADDAR, L. S. EL-ASSAL, and N. A. DOSS. J. Chem. Soc. 1027 (1959).

Can. J. Chem. Downloaded from www.nrcresearchpress.com by 210.87.254.42 on 09/05/12
For personal use only.

Long-range Proton–Proton Coupling Constants in the Vinylpyridines. Conformational Preferences of the Vinyl Group and Molecular Orbital Calculations

J. Brian Rowbotham[1] and Ted Schaefer

Chemistry Department, University of Manitoba, Winnipeg, Manitoba R3T 2N2

Received July 18, 1973

The p.m.r. spectra of 2-vinylpyridine, 2-methyl-5-vinylpyridine, and 4-vinylpyridine are examined for long-range coupling constants between the vinylic and ring protons. Those over six, seven, and eight bonds from the vinyl group to ring or methyl protons in the *para* position are dominated by a π electron mechanism. Those over five bonds between the α proton and a ring proton in the *meta* position indicate that the vinyl group prefers to lie *cis* to the nitrogen in 2-vinylpyridine but *trans* in the 5-vinylpyridine. INDO-MO-FPT calculations of coupling constants between vinyl protons and ring protons, carbon-13, and nitrogen-14 nuclei are presented in graphical form.

Les spectres de résonnance magnétique du proton de la vinyl-2 pyridine, de la méthyl-2 vinyl-5 pyridine et de la vinyl-4 pyridine ont été examinés en vue de l'étude des constantes de couplage à longue distance entre les protons vinyliques et les protons du cycle. Les constantes de couplage à travers six, sept ou huit liaisons entre les protons du groupe vinyle et celui du cycle ou du méthyle en position *para* sont régies principalement par un mécanisme d'électrons π. Celles à travers cinq liaisons entre le proton en α et un proton du cycle en position *méta* montrent que le groupe vinyle préfère, par rapport à l'azote, la conformation cis dans la vinyl-2 pyridine et la conformation *trans* dans la vinyl-5 pyridine. Les calculs INDO-MO-FPT des constantes de couplage entre les protons vinyliques et ceux du cycle, les noyaux de carbone-13 et d'azote-14 sont représéntés sous forme graphique.

[Traduit par le journal]

Can. J. Chem., **52**, 136 (1974)

Introduction

The magnitudes and signs of the spin–spin coupling constants between methyl protons and ring protons or fluorine nuclei in the methyl derivatives of the fluoropyridines are consistent with a model in which the nitrogen atom polarizes the σ electron core primarily at the C-2 and -6 positions, leaving the π electron contributions to the coupling mechanisms relatively unaffected (1). The results imply appreciable σ electron contributions to the couplings over four and five bonds, $^4J_o^{H,CH_3}$ and $^5J_m^{H,CH_3}$.

In ring-substituted styrene derivatives the experimental long-range coupling constants between aromatic and vinylic protons have been compared with those calculated by valence bond and molecular orbital methods (2). The couplings over six and seven bonds between the vinylic protons and the *para* ring proton depend on a π electron mechanism, those over five bonds from *ortho* or *meta* to vinylic protons are dominated by a σ electron mechanism, and the other couplings may evidently have contributions from both mechanisms. The MO-INDO-FPT calculations evidently tend to overestimate the magnitudes of some of these long-range couplings (2), as has been found for benzaldehyde (3) and toluene derivatives (4).

In this paper the long-range proton coupling constants between vinylic and ring or methyl protons are reported for 2-vinyl-, 3-vinyl-6-methyl-, and 4-vinylpyridine. They are discussed in terms of the coupling mechanisms, and conformational preferences of the vinyl group are deduced on the basis of the coupling over five bonds between the α proton on the sidechain and the *meta* ring proton. The contact contributions to the couplings between the vinyl protons and ring protons carbon-13 and nitrogen-14 nuclei, are calculated in the INDO approximation of molecular orbital theory.

The numbering scheme[2] for the protons is given in **1**, **2**, and **3**.

[1]Postdoctoral fellow, 1971–1973.

[2]The scheme is most convenient for our purposes but does not follow the normal pattern.

Can. J. Chem. Downloaded from www.nrcresearchpress.com by 210.87.254.40 on 09/05/12
For personal use only.

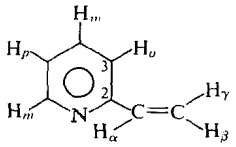

1

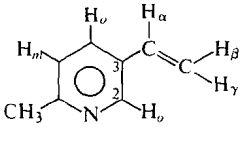

2

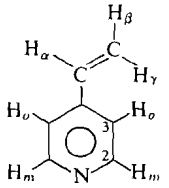

3

Experimental

All p.m.r. spectra were recorded in the sweep frequency mode on an HA100D spectrometer at sweep rates of 0.01 or 0.02 Hz/s and were repeatedly calibrated by reading manual and sweep frequency oscillators.

1. 2-Vinylpyridine

A fresh sample (Baker), inhibited with 0.1% *t*-butylcatechol, formed a precipitate (polymer) in most common solvents after a few hours. In CCl_4 a precipitate formed within a day of degassing the sample. As a compromise, a 15% (w/w) solution in CCl_4 was degassed by a single freeze–pump–thaw cycle. This solution remained clear in the presence of internal tetramethylsilane (TMS) for a period of several weeks.

The linewidths at half-height were scarcely less than 0.2 Hz, the peaks from H_6 being rather broad due to partially relaxed coupling to the quadrupolar ^{14}N nucleus. Fortunately, the spectrum was practically first-order at 100 MHz so that all observable coupling constants caused a well-defined splitting of peaks. The signs of the small couplings were related to those of the large couplings by double resonance experiments under conditions of weak irradiation (5).

2. 3-Vinyl-6-methylpyridine

A gob of the viscous material (Aldrich) was dissolved in CS_2. Addition of TMS caused precipitation of polymer. The supernatant liquid was filtered through a plug of facial tissue into the sample tube. The sample was degassed by a number of freeze–pump–thaw cycles and had a concentration of 10–15% (w/w) in the solvent consisting of about 2:1 v/v CS_2/TMS. Linewidths at half-height were 0.15 Hz for all protons except H_6. The methyl protons were decoupled while calibrating the spectrum of the remaining protons.

3. 4-Vinylpyridine

A 10% (w/w) solution in CCl_4 was degassed by a single freeze–pump–thaw cycle. Polymerization occurred during the spectral calibrations and did not allow time for double resonance experiments.

4. INDO Molecular Orbital Calculations (6,7)

These were performed as described in detail for other molecules (4,8). The geometry of the pyridine ring was taken from microwave data (9). Standard geometry (10) was assumed for the vinyl group and the C—C bond between ring and vinyl carbon atoms was allowed to bisect the concomitant internal ring angle. Convergence to 10^{-3} Hz was demanded in the computed couplings.

Results and Discussion

1. Spectral Analyses

(a) 2-Vinylpyridine

All parameters were allowed to vary in an iteration by the computer program LAME (11), yielding a r.m.s. error of 0.017 Hz. Standard deviations were less than 0.003 Hz for all parameters other than those for H_6, where they were less than 0.01 Hz. Not all transitions were assigned for H_6 (broad peaks) and some correlation coefficients involving this proton were as large as 0.24. Noniterative simulations set upper limits of 0.07 Hz on $^5J_{o,\gamma}$ and 0.03 Hz on $^6J_{m,\beta}$ and $^6J_{m,\gamma}$.

(b) 3-Vinyl-6-methylpyridine

An iteration, holding at 0.0 Hz all couplings less than 0.1 Hz in magnitude, was performed on the spectrum for which the methyl protons were decoupled. The r.m.s. deviation between observed and calculated transitions was 0.0197 Hz; the largest standard deviations occurred for the shift of H_6, 0.021 Hz (broad peaks), and for $^4J_m^{H_4,H_6}$, 0.007 Hz. All correlation coefficients were less than 0.17, except that there was one of 0.63 between the shift of H_4 and $^3J_o^{H_3,H_4}$. The best fit was obtained when $^5J_{o,\gamma}$ equalled ± 0.1 Hz for H_2 and 0.0 Hz for H_4.

For the single resonance spectrum the couplings to the methyl group were varied for a best fit to the whole spectrum. All signs are based on an analogy with those found in styrene derivatives (2), 2-vinylpyridine, and methyl derivatives of pyridine (1). Because of the magnitudes observed for the methyl proton couplings to the vinyl protons over seven and eight bonds (Table 1) they are given the signs expected on the basis of the methyl group replacement technique (12).

(c) 4-Vinylpyridine

The chemical shifts and coupling constants for the ring protons were adjusted by trial and error, followed by an iteration for the sidechain proton spectrum and the long-range coupling constants. The r.m.s. deviation was 0.012 Hz, the standard deviations for all parameters were less than 0.003 Hz, the worst assignment was 0.031 Hz and all correlation coefficients were small except that between $^6J_{m,\beta}$ and $^5J_{o,\beta}$, which was 0.30.

Can. J. Chem. Downloaded from www.nrcresearchpress.com by 210.87.254.40 on 09/05/12
For personal use only.

TABLE 1. Long-range coupling constants in Hz between vinylic and ring protons in vinylpyridines and 3-bromostyrene

Parameter	2-Vinylpyridine, **1***	3-Vinyl-6-methylpyridine, **2**†	4-Vinyl-pyridine, **3**‡	3-Bromo-styrene§
$^4J_{o,\alpha}$	−0.25	(−)0.53[4],(−)0.52	(−)0.52	−0.50
$^5J_{o,\beta}$	0.24	(+)0.12	(+)0.15	0.17,0.19[6]
$^5J_{o,\gamma}$	<0.07	±0.1±0.03[2]0.0[4]	0.0	<0.07
$^5J_{m,\alpha}$	0.25[4],0.24	(+)0.50	(+)0.35	0.33
$^6J_{m,\beta}$	<0.03	0.0	0.0	<0.07
$^6J_{m,\gamma}$	<0.03	0.0	0.0	<0.07
$^6J_{p,\alpha}$	−0.24	(+)0.25±0.03(^7J,CH_3)	—	−0.25
$^7J_{p,\beta}$	0.22	(−)0.25±0.03(^8J,CH_3)	—	0.28
$^7J_{p,\gamma}$	0.22	(−)0.25±0.03(^8J,CH_3)	—	0.25

*In CCl_4, 15% (w/w).
†In 2:1 v/v CS_2, TMS, 10–15% (w/w).
‡In CCl_4, 10% (w/w).
§In CS_2, ref. 2, 5 mol %.

In Table 1 the long-range couplings between the vinylic protons and ring or methyl protons are given. The corresponding parameters for 3-bromostyrene (2) are included for the purposes of comparison. In Table 2 the remaining spectral parameters are displayed.

2. Theoretical Coupling Constants (INDO)

In almost all instances the calculated couplings between the ring protons and the vinylic protons do not differ significantly from those calculated by the same technique by Barfield *et al.* (2) (BMPR). When they do differ significantly they are mentioned in the text. In view of their large number, involving twists about the ring-vinyl C—C bond between 0 and 180° at 30 or 45° intervals, they are not reproduced here[3] in tabular form. However, graphs of their conformational dependence are shown in Fig. 1*a*. In addition, the calculated couplings between the vinylic protons themselves and their couplings to carbon-13 and nitrogen-14 nuclei in the ring are shown in Figs. 1*a* and *b*. These couplings will not be discussed, particularly as there are few experimental values available at present for comparison.

*3. Couplings between Vinylic and Ring or Methyl Protons in the para Position in **1**, **2**, and **3**.*

BMPR give convincing theoretical and experimental evidence for the π electron transmission of these couplings over six and seven bonds in planar and nonplanar conformations of styrene derivatives (2). Replacement of the ring proton by a methyl group should therefore entail (12) $-{}^7J_{CH_3,\alpha} = {}^6J_{p,\alpha}$; $-{}^8J_{CH_3,\beta} = {}^7J_{p,\beta}$; $-{}^8J_{CH_3,\gamma} = {}^7J_{p,\gamma}$. Although the spectral complexity precluded the determination of the signs of the methyl proton couplings in **2**, their magnitudes are indeed equal, to within experimental error, to the corresponding ring-vinylic proton couplings in **1** and in 3-bromostyrene (Table 1); in agreement with our previous model for the methyl derivatives of the fluoropyridine (compound **3** of ref. 1).

Our INDO computations do not differ significantly from those (2) for styrene and agree very well with experiment.

Conformational Preferences of the Vinyl Group

In accordance with the assumptions made about the styrene derivatives (2), **3** is taken as existing in the rapidly interconverting and equally populated conformers **4** and **5**.

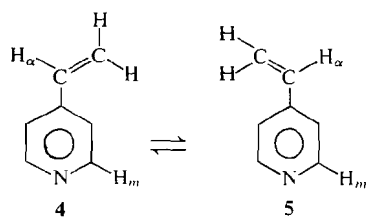

4 **5**

Similar planar conformations are assumed to exist for **1** and **2**.

Now, the coupling corresponding to $^5J_{m,\alpha}$ i

[3]A complete set of tabular data is available, at a nominal charge, from the Depository of Unpublished Data, National Science Library, National Research Council of Canada, Ottawa, Canada K1A OS2.

Can. J. Chem. Downloaded from www.nrcresearchpress.com by 210.87.254.40 on 09/05/12
For personal use only.

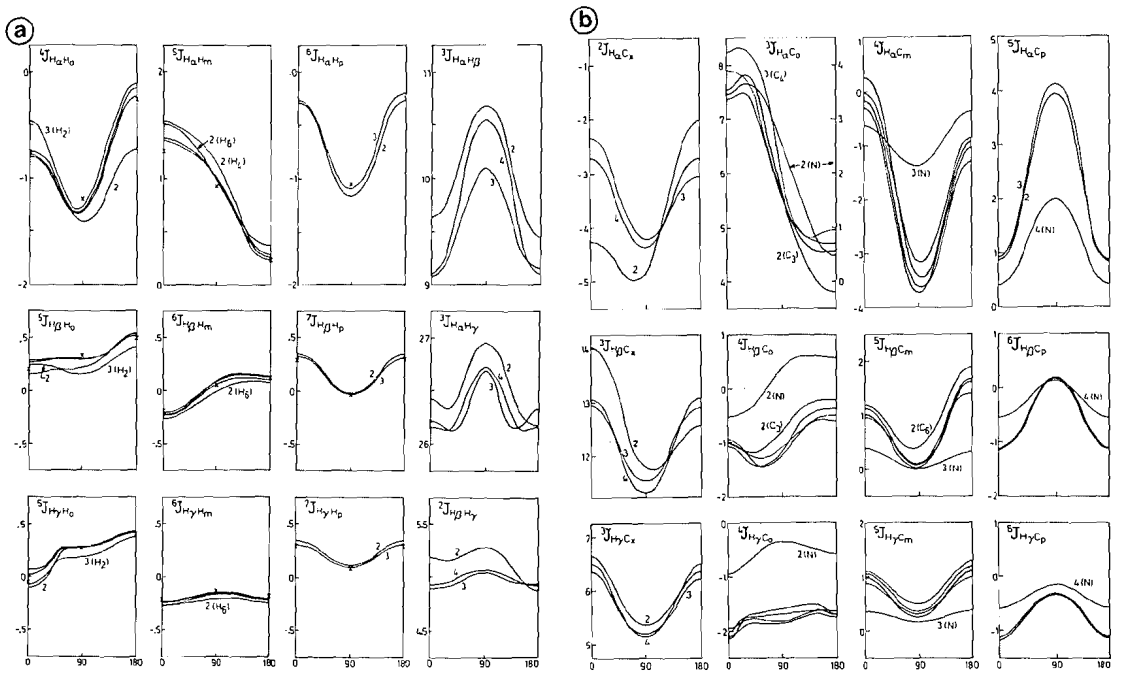

FIG. 1*a* and *b*. Long-range coupling constants in Hz between sidechain protons and ring protons, carbon-13, and nitrogen-14 in 2-, 3-, and 4-vinylpyridines as calculated by MO-INDO-FPT. They were determined every 30 or 45° and smooth curves were then drawn through the values. Calculated points for styrene (ref. 2) are indicated by crosses. The 0° conformation is planar with the vinyl double bond *cis* to either the coupling ring position (columns 1, 2, 6, and 7) or to the ring nitrogen (columns 3, 4, 5, and 8). The plot for $^3J_{H_\alpha,N}$ in 2-vinylpyridine has a unique scale. *Ortho* (*o*), *meta* (*m*), and *para* (*p*) refer to the positions of protons or carbon atoms relative to the point of substitution of the vinyl group. C_x refers to the carbon atom of the ring to which the vinyl group is attached.

TABLE 2. The other spectral parameters for the vinylpyridines

Parameter	1	2*	3
ν_2†	—	838.0	847.0
ν_3	716.46	—	715.0
ν_4	747.65	743.7	—
ν_5	699.57	691.4	715.0
ν_6	847.0	243.0	847.0
ν_α	671.18	656.9	657.39
ν_β	536.83	517.0	537.13
ν_γ	620.48	564.3	587.14
$^3J_o^{H,H}$	7.83[3,4],7.54[4,5],4.79	7.99	5.10
$^4J_m^{H,H}$	1.15[3,5],1.87	2.37	1.92[3,5],0.0
$^5J_p^{H,H}$	1.01	0.86	0.92
$^3J_{\alpha,\beta}^{H,H}$	10.77	10.96	10.86
$^3J_{\alpha,\gamma}^{H,H}$	17.44	17.62	17.57
$^2J_{\beta,\gamma}^{H,H}$	1.66	0.96	0.08

*$^4J_o^{H,CH_3} = -0.48 \pm 0.02$, $^5J_m^{H,CH_3} = 0.30 \pm 0.02$, $^5J_m^{H_6,CH_3} = 0.2 \pm 0.1$.
†In Hz at 100 MHz to low field of internal TMS, coupling constants in Hz.

highly stereospecific in toluene (13), benzaldehyde (3), phenol (14), aniline (15), and styrene (2) derivatives. It is always less than 0.1 Hz in conformations analogous to **5**, but lies between 0.5 and 0.8 Hz in conformations analogous to **4**. In particular, $^5J_{m,\alpha}$ is 0.33 Hz in 3-bromostyrene, 0.36 Hz in 3,4-dichlorostyrene, and 0.07 Hz in 2,5-dichlorostyrene (2). The latter apparently exists predominantly in form **6**, whereas the former two compounds have very nearly equal pop-

Can. J. Chem. Downloaded from www.nrcresearchpress.com by 210.87.254.40 on 09/05/12
For personal use only.

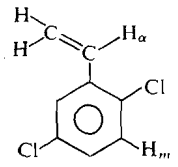

6

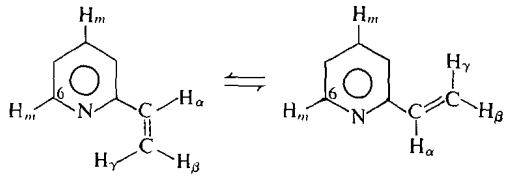

9 10

ulations of the two coplanar forms. In **3** the coupling is 0.35 Hz, implying the absence of a nitrogen substituent effect on $^5J_{m,\alpha}$. We shall assume $^5J_{m,\alpha} = 0.65$ Hz for **4** and $^5J_{m,\alpha} = 0.05$ Hz for **5**. A zero magnitude in **5** would slightly alter the following equilibrium constants.

Turning to **2**, one finds $^5J_{m,\alpha} = 0.50$ Hz, indicating a preference of **7** over **8**. As there exists

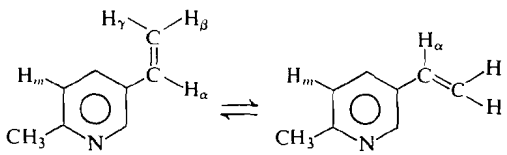

7 8

little or no effect of the nitrogen atom on this coupling in **3**, it appears reasonable that it be absent in **2**. Therefore write $0.50 = 0.05p_8 + 0.65p_7$ where $p_7 + p_8 = 1$, and find $p_7 = 0.75$ or an equilibrium constant of $K = p_7/p_8 = 3.0$ corresponding to a free energy difference of 655 cal/mol at 300 °K. For 3-vinylpyridine INDO computes the form analogous to **7** as more stable than that analogous to **8** by 409 cal/mol. If the entropies of the two conformers are the same, one has $K = 2.0$ at 300 °K. The computed dipole moments of 3-vinylpyridine are 1.95 and 2.08 D for the two forms, so that dipole moment measurements will not shed appreciable light on the conformational preferences of **2**. The observed dipole moment of 3-vinylpyridine in benzene solution is 2.36 D (16), not very different from the 2.21 D in pyridine itself.

An error estimate for K is obtained on the assumption that $^5J_{m,\alpha}$ is 0.05 ± 0.05 Hz in **8** and is 0.70 ± 0.05 Hz in **7**, yielding $K = 3.0 \pm 1$. There is little doubt that **7** is more stable than **8** in CS_2 solution.

$^5J_{m,\alpha}$ is 0.25 Hz to H_4 and 0.24 Hz to H_6 in **1**. Assuming an equilibrium between the conformers **9** and **10**, a comparison of these magnitudes with those in **2** and **3** implies that the nitrogen atom reduces at least one of these couplings. Otherwise their sum would be 0.7 Hz. The coupling is dominated by a σ electron mechanism and hence it is likely that the coupling to H_6, via the N—C bond, is reduced[4] more than the coupling to H_4. An assumption of no substituent effect on the latter leads to $p_9/p_{10} = K = 2.0$. If both couplings in **1** are equally reduced by the nitrogen atom, then $K = 1.0$. INDO calculates **9** more stable than **10** by 2.78 kcal/mol, $K \sim 100$. The calculated dipole moments are 2.05 D for **10** and 2.35 D for **9**. The observed dipole moment (16) in benzene solution is 1.86 D, suggesting **10** as much more stable than **9**, *i.e.*, $K \ll 1$. If this were true, then $^5J_{m,\alpha}$ in **10** would be the first example where an anti zigzig coupling path over five bonds in an aromatic system is larger than 0.1 Hz. In fact, all known couplings across the nitrogen atom, involving a sidechain proton and having a substantial σ electron contribution, are smaller in magnitude than in the corresponding benzene derivatives (1, 17). Therefore it is probably safe to conclude that $K > 1$ in our solution.

In the next section the conclusions about the conformational preferences of **1** and **2** are examined in terms of the couplings between vinylic and *ortho* ring protons.

5. *Couplings over Four and Five Bonds from Vinylic to ortho Ring Protons*

(a) The α Proton Coupling, $^4J_{o,\alpha}$

The INDO calculations on styrene (2) and on 3 agree in finding $^4J_{o,\alpha}$ as given in **11**, with an average value of −0.51 Hz, in line with the observed values in 3-bromostyrene and in **3** (Table 1). The computations for **2** yield a smaller magnitude o

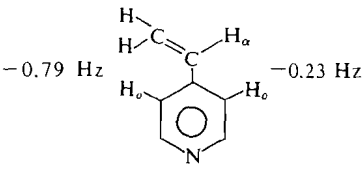

−0.79 Hz −0.23 Hz

11

[4]Our INDO calculations, on the other hand, predict small increase in both couplings over those calculated f $^5J_{m,\alpha}$ in styrene.

Can. J. Chem. Downloaded from www.nrcresearchpress.com by 210.87.254.40 on 09/05/12
For personal use only.

Can. J. Chem. Downloaded from www.nrcresearchpress.com by 210.87.254.40 on 09/05/12
For personal use only.

$^4J_{o,\alpha}$ than in **3** for all orientations of the vinyl group when H_2 is involved, but about the same magnitude as in **3** when H_4 is coupled. In fact, both couplings are observed to have the same magnitude in **2** and are equal to those in **3**. Escape from the conundrum is provided by the suggestion that $^4J_{o,\alpha}$ is not, in fact, stereospecific in **2** and that its values in **2** are not inconsistent with the conformational deductions based on $^5J_{m,\alpha}$.

Support for this suggestion comes from the value of −0.47 Hz in 2,5-dichlorostyrene which exists in form **6** (2). If the INDO predictions were correct its value would not be effectively equal to $^4J_{o,\alpha}$ in 3-bromostyrene and in **3**.

On the other hand, the equality of the two values of $^4J_{o,\alpha}$ in **2** might be taken as indicating $K = p_9/p_{10} = 1.0$. However, it then follows that $^5J_{m,\alpha}$ in **7** is 1.0 Hz, much too large when its values in **3** and in 3-bromostryene are considered. One is forced to conclude that $^4J_{o,\alpha}$ is not stereospecific in **2** or that the nitrogen atom has a large substituent effect on $^4J_{o,\alpha}$ to H_2, in **2**, causing a fortuitous equality of the two values. A nonstereospecificity of $^4J_{o,\alpha}$ implies a preponderant π electron mechanism, operating via the conjugated C—C bond between the sidechain and the aromatic nucleus (2).

The INDO predictions overestimate $^4J_{o,\alpha}$ as −0.75 Hz for **1** in *both* forms **9** and **10**, the average value being 0.25 Hz greater in magnitude than in **3**; instead of 0.25 Hz smaller in magnitude, as observed. There clearly occurs a nitrogen substituent effect on $^4J_{o,\alpha}$ in **1** and conformational deductions cannot be made from this coupling.

A similar substituent effect is found in a butadiene derivative (18). In **12** the chlorine atom plays a role analogous to the nitrogen atom in **13** and reduces $^4J_{1,3}$ by 0.23 Hz in magnitude from its value in butadiene itself (19, 20).

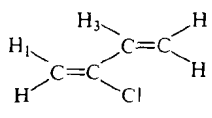

12

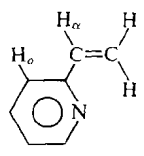

13

(b) The β and γ Couplings, $^5J_{o,\beta}$ and $^5J_{o,\gamma}$

These couplings are evidently dominated by a σ electron mechanism in the styrene derivatives and are stereospecific (2). Thus, $^5J_{o,\beta}$ in form **9** of 2-vinylpyridine should be larger than in **10**. The observed value of 0.24 Hz is somewhat larger than in 4-vinylpyridine and 3-bromostyrene and is thus in agreement with the conformational deductions based on $^5J_{m,\alpha}$. However, in **2** the value of $^5J_{o,\beta}$ is 0.12 Hz to both *ortho* ring protons and is not significantly smaller than in **3**.

The only observable $^5J_{o,\gamma}$ is to H_2 in **2** and if it is positive, then conformer **7** is favored according to our INDO calculations. However, an observable coupling $^5J_{o,\gamma}$ might then also be expected for form **9** of 2-vinylpyridine, the predominant conformer. Yet it is not present.

Conclusions

A π electron mechanism accounts for the couplings over six and seven bonds between the sidechain protons and the ring protons in the *para* position of the vinyl derivatives of pyridine. Conformational deductions can be tentatively made from the observed couplings over five bonds from ring protons in the *meta* position to the α protons of the sidechain. In CCl_4 solution 2-vinylpyridine has a preference for the conformation in which the vinyl group lies *cis* to the nitrogen atom and the opposite holds for a CS_2 solution of 3-vinyl-6-methylpyridine. It is suggested that the coupling over four bonds between a ring proton and the α sidechain proton may not be stereospecific in these compounds and may therefore be transmitted mainly by a π electron mechanism, in agreement with valence bond computations (2). In that event the nitrogen atom in 2-vinylpyridine exerts a substantial substituent effect on a π electron coupling, and the model developed for the methyl derivatives of the fluoropyridines may well be too simple (1).

1. J. B. ROWBOTHAM and T. SCHAEFER. Can. J. Chem. **50**, 2344 (1972).
2. M. BARFIELD, C. J. MACDONALD, I. R. PEAT, and W. F. REYNOLDS. J. Am. Chem. Soc. **93**, 4195 (1971).
3. R. WASYLISHEN and T. SCHAEFER. Can. J. Chem. **49**, 3216 (1971).
4. R. WASYLISHEN and T. SCHAEFER. Can. J. Chem. **50**, 1852 (1972).
5. R. FREEMAN and W. A. ANDERSON. J. Chem. Phys. **37**, 2053 (1962).
6. J. A. POPLE, J. W. MCIVER, JR., and N. S. OSTLUND. J. Chem. Phys. **49**, 2960, 2965 (1968).
7. P. A. DOBOSH. Program Number 141, Quantum Chemistry Program Exchange, University of Indiana, Bloomington, Indiana.
8. R. WASYLISHEN and T. SCHAEFER. Can. J. Chem. **50**, 2989 (1972).

9. B. BAK, L. HANSEN, and J. ROSTRUP-ANDERSON. J. Chem. Phys. **22**, 2013 (1954).
10. J. A. POPLE and M. GORDON. J. Am. Chem. Soc. **89**, 4253 (1967).
11. C. W. HAIGH and J. M. WILLIAMS. J. Mol. Spectrosc. **32**, 398 (1969).
12. R. HOFFMAN and S. GRONOWITZ. Arkiv Kemi, **16**, 471 (1960).
13. H. M. HUTTON, J. B. ROWBOTHAM, B. H. BARBER, and T. SCHAEFER. Can. J. Chem. **49**, 2033 (1971).
14. S. FORSÉN and R. A. HOFFMAN. J. Mol. Spectrosc. **20**, 168 (1966).
15. R. WASYLISHEN, J. B. ROWBOTHAM, L. ERNST, and T. SCHAEFER. Can. J. Chem. **50**, 2575 (1972).
16. G. FAVINI. Gazz. Chim. Ital. **93**, 635 (1963).
17. J. B. ROWBOTHAM, R. WASYLISHEN, and T. SCHAEFER. Can. J. Chem. **49**, 1799 (1971).
18. A. A. BOTHNER-BY and E. MOSER. J. Am. Chem. Soc. **90**, 2347 (1968).
19. R. T. HOBGOOD and J. H. GOLDSTEIN. J. Mol. Spectrosc. **12**, 76 (1964).
20. G. SCHRUMPF, G. BECHER, and W. LÜTTKE. J. Mag. Res. **10**, 90 (1973).

Can. J. Chem. Downloaded from www.nrcresearchpress.com by 210.87.254.40 on 09/05/12
For personal use only.

Influence of Lewis Acids on the Diels–Alder Reaction. VI. Reaction of 2,5-Dimethyl- and 2,5-Diphenylfuran with Ethyl Propiolate[1]

A. W. McCulloch and A. G. McInnes

Atlantic Regional Laboratory, National Research Council of Canada, Halifax, Nova Scotia

Received July 2, 1973

The $AlCl_3$-promoted reactions of 2,5-dimethyl- and of 2,5-diphenylfuran with ethyl propiolate afford as major products ethyl 2,6-dimethyl-3-hydroxybenzoate (**6***a*) and ethyl 3,5-diphenyl-2-hydroxybenzoate (**8***b*), respectively. Also isolated from these reactions were ethyl 2,4-dimethyl-5-hydroxybenzoate (**7***a*), ethyl 3,5-dimethyl-2-hydroxybenzoate (**8***a*), ethyl 2,4-diphenyl-5-hydroxybenzoate (**7***b*), and ethyl 2,6-diphenyl-3-hydroxybenzoate (**6***b*). Minor by-products were *trans* ethyl 3-(2,5-dimethyl-3-furyl)-acrylate (**10**) and ethyl 3-acetyl-2-(2,5-dimethyl-3-furyl)-5-methyl-cyclopenta-2,5-dienecarboxylate (**11**).

Les réactions catalysées par $AlCl_3$ du diméthyl-2,5 et du diphényl-2,5 furanne avec le propiolate d'éthyle ont conduit majoritairement au diméthyl-2,6 hydroxy-3 benzoate d'éthyle (**6***a*) et au diphényl-3,5 hydroxy-2 benzoate d'éthyle (**8***b*) respectivement. On a aussi isolé de ces réactions les produits suivants: le diméthyl-2,4 hydroxy-5 benzoate d'éthyle (**7***a*), le diméthyl-3,5 hydroxy-2 benzoate d'éthyle (**8***a*), le diphényl-2,4 hydroxy-5 benzoate d'éthyle (**7***b*) et le diphényl-2,6 hydroxy-3 benzoate d'éthyle (**6***b*). Les produits secondaires mineurs ont été le *trans* (diméthyl-2,5 furyl-3)-3 acrylate d'éthyle (**10**) et le carboxylate d'acétyl-3 (diméthyl-2,5 furyl-3)-2 méthyl-5 cyclopentadiène-2,5 (**11**). [Traduit par le journal]

Can. J. Chem., **52**, 143 (1974)

Introduction

In a number of previous reports we have described a one-step synthesis of substituted aromatic compounds, involving rearrangement of substituted oxa- or azanorbornadienes formed by $AlCl_3$-promoted Diels–Alder reactions of various substituted furans or pyrroles with acetylenic dienophiles (*1*–*3*). In the most recent example we described the reactions of 2-methyl- and 2-phenylfuran with ethyl propiolate (*3*). Although in theory each of the latter reactions could lead to formation of two 1:1 adducts, **1** and **2**, which on rearrangement would give the phenolic compounds **3** and **4**, in practice the predominant products were **3***a* and **3***b*, with negligible **4***a* and no **4***b* being isolated. The regioselectivity of these reactions is in accord with that predicted for 1-substituted dienes (*4*). The present communication details the results of a study of the corresponding reactions of 2,5-dimethyl- and 2,5-diphenylfuran with ethyl propiolate.

Results and Discussion

In principle, Diels–Alder reaction of a 2,5-disubstituted furan with ethyl propiolate will produce a 1:1 adduct of type **5**. Where the diene is symmetrically substituted only one monoadduct is possible. Rearrangement of such a compound in a manner analogous to that described previously (*1*) can, however, proceed in three ways depending on the shift of the substituent R as shown in Scheme 1, resulting in the formation of phenolic compounds of types **6**, **7**, and **8**. In practice we have observed that under most reaction conditions the intermediate adducts **5***a* and **5***b* cannot be isolated (see below), but rearrange spontaneously in the presence of $AlCl_3$ to the expected aromatic derivatives. The reaction of 2,5-dimethylfuran with ethyl propiolate (60 min at room temperature) gave isolated yields of **6***a* (25.3%), **7***a* (4.9%), and **8***a* (10.2%), while the corresponding reaction of 2,5-diphenylfuran afforded **6***b* (6.4%), **7***b* (0.8%), and **8***b* (46.2%).

A detailed study of the effect of reaction parameters (solvent, temperature, $AlCl_3$ concentration) on the product composition from these reactions was prevented by (*i*) the difficulty in accurately measuring small amounts of isomer **7** formed in each reaction and (*ii*) the competitive diene polymerization observed in the case of 2,5-dimethylfuran. A limited study, however, was conducted in the case of the reaction of 2,5-diphenylfuran. The results obtained (Table 1) allow the following conclusions to be drawn:

[1]Issued as NRCC No. 13495.

Can. J. Chem. Downloaded from www.nrcresearchpress.com by 210.87.254.6 on 09/05/12
For personal use only.

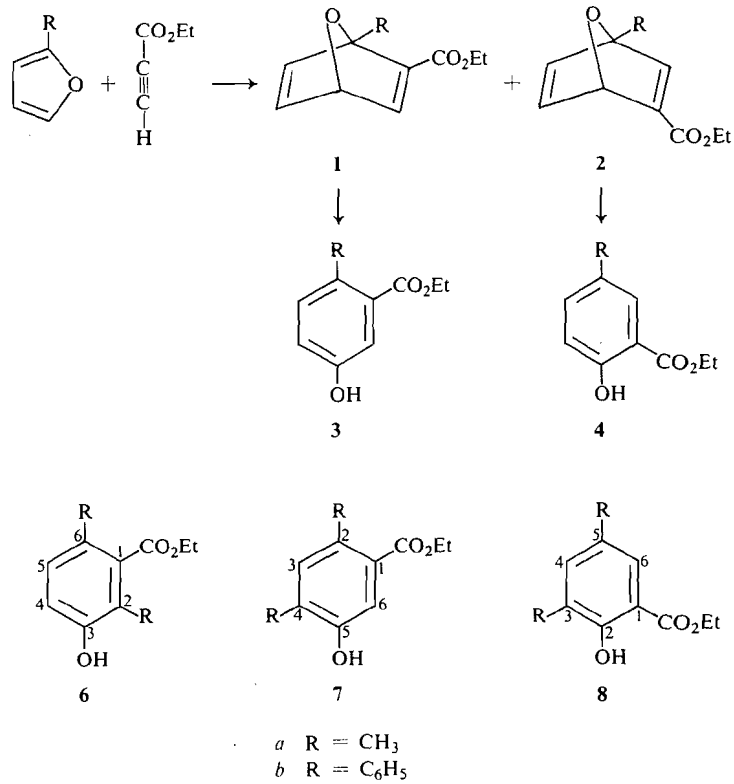

a R = CH_3
b R = C_6H_5

(*a*) at a given temperature the product ratio **8***b*:**6***b* is significantly affected by variation in solvent; (*b*) in the presence of excess amounts of dienophile there is a significant reduction in the ratio **8***b*:**6***b*; (*c*) production of **8***b* is preferred over that of **6***b* to a greater extent when higher concentrations of $AlCl_3$ are employed; and (*d*) use of higher reaction temperatures results in a decrease in the ratio **8***b*:**6***b*.

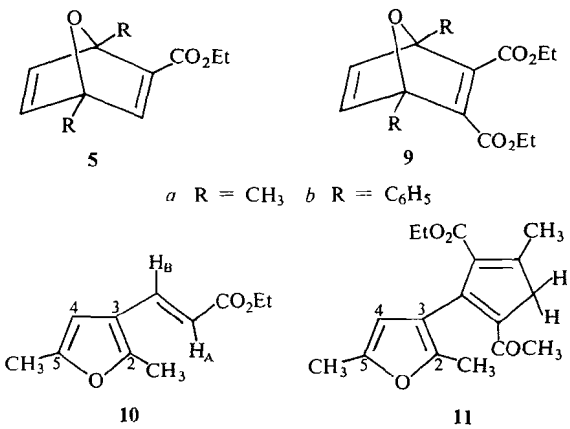

a R = CH_3 *b* R = C_6H_5

It also became evident during this study that overall yields in 1 h at room temperature are moderate (50–60%), whereas at 80° or above conversion to aromatics appears (from p.m.r.) to be essentially complete.

Aromatization of adducts **5** can be envisaged in two ways, both initiated by complexing with the Lewis acid. Before attempting to rationalize our experimental observations it is necessary to first discuss both of these routes.

The first proposed mechanism (Scheme 1) is analogous to that postulated previously (1). Fission of the oxygen bridge, initiated by coordination of the Lewis acid with the bridge oxygen atom, leads to carbonium ions *A* and *B*. These in turn can lead as shown to products **6**, **7**, and **8**. Complexing at the ester carbonyl of **5** can also initiate an aromatization–rearrangement process (Scheme 2), yielding in this case only **6**.

Can. J. Chem. Downloaded from www.nrcresearchpress.com by 210.87.254.6 on 09/05/12
For personal use only.

Can. J. Chem. Downloaded from www.nrcresearchpress.com by 210.87.254.6 on 09/05/12
For personal use only.

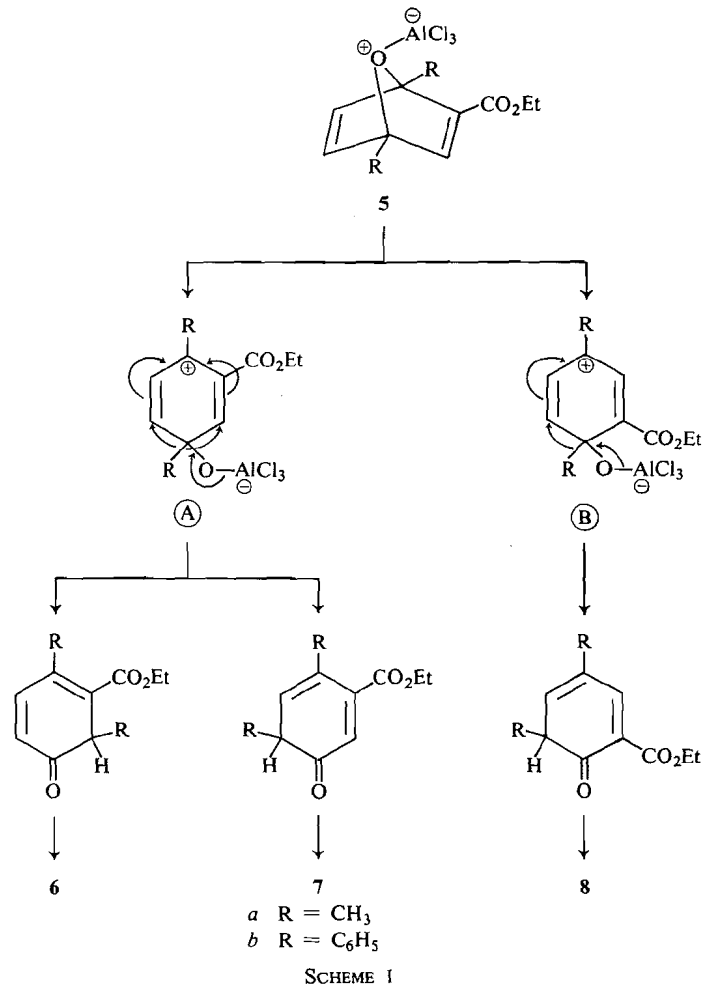

a R = CH_3
b R = C_6H_5

SCHEME I

TABLE 1. Effect of varying reaction parameters on product ratio **8***b*:6*b*

Reactant ratios DPF : EP : $AlCl_3$	Solvent*	Time (h)	Temperature (°C)	Product ratio† **8***b*:6*b*
1 : 1 : 1	CH_2Cl_2	1	25	6.3
1 : 1 : 2	CH_2Cl_2	1	25	8.7
1 : 5 : 1	CH_2Cl_2	1	25	2.9
1 : 1 : 1	C_6H_6	4	25	7.3
1 : 1 : 2	C_6H_6	1	25	8.9
1 : 1 : 1	C_6H_6	4	80	3.6
1 : 1 : 1	$ClCH_2CHCl_2$	1	25	7.5
1 : 3 : 1	$ClCH_2CHCl_2$	16	87	2.8
1 : 1 : 1	$C_6H_5CH_3$	1	25	7.5
1 : 5 : 1	$C_6H_5CH_3$	1	110	2.4

*Solutions were in all cases 0.1 *M* in 2,5-diphenylfuran (DPF).
†Based on peak heights of ester methyl resonances in p.m.r. spectrum of the crude reaction product.

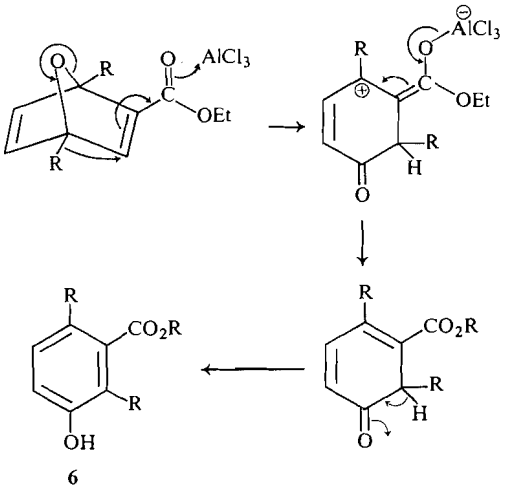

SCHEME 2

Our experimental results show that the isomer distribution in the product is highly dependent on the nature of the substituent R. We have to explain (*i*) the preferred formation of **6** over **7** in both reactions and (*ii*) the predominance of **6***a* and **8***b* in the individual reactions.

On the basis of charge density considerations substituent migration in *B* would be expected to result in production of **8** (Scheme 1). Similarly, in the case of *A* charge density and steric considerations would favor substituent migration leading to **7** rather than **6**. The observed predominance of **6** over **7** can therefore be accounted for only by an alternative mechanism of formation, namely Scheme 2.

Two types of steric interaction in carbonium ions *A* and *B* (Scheme 1) must moreover be considered. These are (*i*) eclipsed interaction at the necessarily planar carbonium ion center in *A*, between the group R and the adjacent carbethoxyl substituent, serving to destabilize *A*, and (*ii*) two skew-type interactions in *B*, between the carbethoxyl and adjacent —R and —$OAlCl_3$ groups, which would tend to destabilize *B*. The relative importance of these steric effects will be significantly dependent on the nature of the group R. It is obvious that when R is phenyl the eclipsed interaction in *A* will be highly unfavorable; for this reason the pathway through *B* leading to **8***b* predominates. When R is methyl, on the other hand, the eclipsed interaction of *A* will be much less severe: in fact the skew interactions present in *B* might in this case play an important role in determining product composition. Increased yields of **6***a* and **7***a* (relative to **8***a*) would therefore be expected.

Production of **8** necessitates coordination of the Lewis acid at the bridge oxygen atom of **5**. If, however, the Lewis acid coordinates more readily at the ester carbonyl oxygen, promoting rearrangement to **6**, we might expect the latter compound to be favored relative to **8** by use of a limited concentration of $AlCl_3$. In fact we observe that in the presence of an excess of dienophile, conditions which would reduce the amount of free $AlCl_3$ (by formation of propiolate–$AlCl_3$ complex), the ratio **8***b*:**6***b* is greatly reduced. Moreover, this ratio, as expected, increases when an excess of $AlCl_3$ is employed.

Isolation of the intermediate adduct was only possible in the case of **5***a*, and then only when the reaction was carried out at $-60°$. This is in accord with our previous work which showed that aromatization of adducts having bridgehead phenyl substituents occurred more readily than that of the corresponding compounds with bridgehead methyl groups (1). It is interesting to note also that aromatization of **5** occurs more readily than that of adducts of type **9**. This may be attributable to the fact that there is less stabilization of the incipient carbonium ion formed by bridge cleavage in **9**, due to the presence of two electron-withdrawing groups on the ring.

A minor by-product isolated from the reaction of 2,5-dimethylfuran with ethyl propiolate was identified as the Michael-type addition product **10** (2–3%). Analogous compounds were previously obtained from the reactions of 2-methyl- and 2-phenylfuran with ethyl propiolate (3). In the present case, where both α positions of the furan ring are substituted, the product obtained is substituted in the β position.

A second, very minor (~1%) by-product isolated from the reaction of 2,5-dimethylfuran, after *basic* work-up (see Experimental) was the cyclopentadiene **11**. This compound probably arises via reaction of **10** with 1,2-diacetylethylene, an autoxidation product of the diene.

Structures

The structures of all reaction products were elucidated on the basis of their p.m.r. (Tables 2 and 3), i.r., and mass spectral data (see Experimental).

Can. J. Chem. Downloaded from www.nrcresearchpress.com by 210.87.254.6 on 09/05/12
For personal use only.

TABLE 2. Proton magnetic resonance data for aromatic products **6**, **7**, and **8**

Compound	Chemical shifts (δ)* —$CO_2CH_2CH_3$	—OH†	Substituents, R	Aromatic hydrogens
7a	4.35 (2H, q) 1.36 (3H, t)	5.50 (b)	2.49 (3H, s), 2.25 (3H, s) Both long-range coupled to H_3	H_3 (6.99, bs, $J_{36}\sim 0.3$ Hz, long-range coupled to both methyls) H_6 (7.43, s, $J_{36}\sim 0.3$ Hz)
6*a*	4.40 (2H, q) 1.37 (3H, t)	6.16 (b)	2.20 (3H, s), 2.15 (3H, s) Both long-range coupled to H_5	H_4 and H_5. 'Quartet' centered at 6.73, $J_{45}=8.5$, $\Delta\nu_{45}=10.1$ Hz, H_5 is at lower field than H_4 and is long-range coupled to both methyls
8*a*	4.37 (2H, q) 1.38 (3H, t)	10.88 (s)	2.22 (6H, bs)	H_4 (7.09, m, $J_{46}=1.8$, $\Delta\nu_{46}=22.7$ Hz; long-range coupled to both methyls) H_6 (7.47, m, $J_{46}=1.8$ Hz; long-range coupled to both methyls)
7b	4.09 (2H, q) 0.97 (3H, t)	6.13 (b)	7.6–7.2 (10H, m)	H_3 and H_6 obscured by multiplet for protons of two phenyl substituents
6*b*	3.77 (2H, q) 0.73 (3H, t)	5.54 (b)	7.5–7.25 (10H, m)	H_4 and H_5. Quartet centered at 7.10, $J_{45}=8.5$, $\Delta\nu_{45}=16.4$ Hz
8*b*	4.45 (2H, q) 1.43 (3H, t)	11.39 (s)	7.7–7.2 (10H, m)	H_4 and H_6. Quartet centered at 7.94, $J_{46}=2.4$, $\Delta\nu_{46}=20.2$ Hz

*b = broad; s = singlet; t = triplet; q = quartet; m = multiplet.
†Replaceable by deuterium.

TABLE 3. Proton magnetic resonance data for **5***a*, **10**, and **11**

Compound	Chemical shifts (δ)* Olefinic and ring —CH=	—CH_3	—$CO_2CH_2CH_3$	—CH_2—
5*a*	H_5 and H_6. Quartet centered at 6.90; $\Delta\nu_{56}=12.7$, $J_{56}=5.2$ Hz H_3 (7.58, s)	1.75 (3H, s), 1.84 (3H, s)	4.22 (2H, q) 1.27 (3H, t)	—
10†	H_4 (6.08, bs, $J_{4,CH_3}\approx 0.8$ Hz). H_A and H_B. Quartet centered at 6.75, $\Delta\nu_{AB}=91.7$, $J_{AB}=15.5$ Hz	2.25 (3H, bs, $J_{4,CH_3}\approx 0.8$ Hz, methyl at C-5) 2.34 (3H, s, methyl at C-2)	4.25 (2H, q) 1.32 (3H, t)	—
11	H_4 (6.68, q, $J_{4,CH_3}\approx 1.0$ Hz	2.51 (3H, s, methyl at C-2) 2.14 (3H, d, $J_{4,CH_3}\approx 1.0$ Hz, methyl at C-5) 2.27 (3H, s, acetyl methyl) 1.78 (3H, s, allylic methyl)	4.28 (2H, q) 1.18 (3H, t)	3.53 (2H, s)

*bs = broad singlet; s = singlet; d = doublet; t = triplet; q = quartet.
†In benzene-d_6.

Can. J. Chem. Downloaded from www.nrcresearchpress.com by 210.87.254.6 on 09/05/12
For personal use only.

Can. J. Chem. Downloaded from www.nrcresearchpress.com by 210.87.254.6 on 09/05/12
For personal use only.

Compound 5a

The structure of this product follows unambiguously from its mode of formation and its spectral properties. The p.m.r. spectrum shows signals for three olefinic hydrogens, two of which comprise an AB system centered at δ 6.90 with a vicinal coupling of 5.2 Hz; the remaining olefinic hydrogen was observed as a singlet at δ 7.58, consistent with its location adjacent to the carbethoxyl group. Signals for two nonequivalent *C*-methyl groups were also observed; the chemical shifts of these were in accord with those of the bridgehead methyl substituents of adducts of type **9** (1).

Compounds 6, 7, and 8

By analogy with previous work in this and other laboratories (1, 2, 5) acid-catalyzed rearrangement of the oxanorbornadiene system **5** would be expected to lead only to the hydroxyaromatics **6**, **7**, and **8**. All compounds were found to have the expected molecular weights (mass spectra). The products were differentiated on the basis of the following evidence.

(*a*) The substitution pattern of the aromatic ring in each case was readily ascertained from the p.m.r. spectrum (Table 2). Typical coupling constants were observed for spin–spin coupling between two *ortho* (**6***a* and *b*), *meta* (**8***a* and *b*), or *para* (**7***a* and *b*) aromatic hydrogens.

(*b*) The presence of nonbonded phenolic hydroxyl groups in **6** and **7** was indicated by their base solubility and by the chemical shifts of their hydroxyl protons (very broad signals, in the range δ 5.50–6.20). In contrast, compounds **8***a* and *b*, which were only sparingly soluble in base, showed sharp signals for bonded hydroxyl at characteristically low-field (δ 10.88 in **8***a*, δ 11.39 in **8***b*).

(*c*) The i.r. spectra of **6***a* and *b* and of **7***a* and *b* showed absorptions for nonbonded ester carbonyl (1725–1730 cm^{-1} for **6**, 1719–1722 cm^{-1} for **7**) and nonbonded phenolic hydroxyl (3570–3615 cm^{-1} for **6**, 3570–3610 cm^{-1} for **7**) under conditions of high dilution (0.005 *M* in CCl_4). At increasing concentrations absorptions for both free and intermolecularly hydrogen-bonded ester and hydroxyl were observed (see Experimental). The spectra of **8***a* and *b*, on the other hand, showed absorptions for intramolecularly hydrogen-bonded ester carbonyl (1662–1678 cm^{-1}) and hydroxyl (3150–3180 cm^{-1}) groups, under the same conditions.

(*d*) Low-field chemical shifts of one aromatic hydrogen in **7***a* and **8***a* suggested that these were deshielded by an *ortho* carbethoxyl substituent. Such deshielding was absent in the spectrum of **6***a*, and could not be ascertained in the phenyl-substituted **7***b* and **8***b*.

(*e*) The chemical shifts of the carbethoxyl methylene and methyl hydrogens of **6***b* and **7***b* suggested an *ortho* phenyl substituent. This shielding effect was noticeably absent in the spectrum of **8***b*. We have observed similar effects previously in the spectra of diethyl 3-hydroxy-6-phenylphthalates (1) and ethyl 5-hydroxy-2-phenylbenzoates (3).

(*f*) The high-field aromatic hydrogen of **7***a* was long-range coupled to the protons of both methyl substituents; the low-field proton was not coupled to either. The low-field aromatic proton of **6***a* was also long-range coupled to the hydrogens of both methyl substituents, while there was no detectable coupling of this type in the case of the high-field proton. In the case of **8***a*, both aromatic hydrogens were long-range coupled, each with the hydrogens of both methyl groups. Such coupling exists in methyl-substituted aromatics when the methyl group is located *ortho* or *para* to a ring hydrogen: it is greatly reduced when the orientation is *meta* (6).

Compound 10

The structure of **10** was readily deduced on the basis of the following spectral properties.

(*a*) The p.m.r. spectrum (Table 3) showed a characteristic AB system for two olefinic hydrogens, and a broad singlet for a single furan ring proton. The latter was coupled to the hydrogens of one of the two ring methyl groups. The value of the coupling between the two olefinic hydrogens suggests that these have a *trans* orientation.

(*b*) The i.r. spectrum (in CCl_4) showed strong absorptions for conjugated ester carbonyl (1717 cm^{-1}) and conjugated double bond (1638 cm^{-1}). The *trans* stereochemistry of the double bond was confirmed by an absorption at 975 cm^{-1}.

Compound 11

(*a*) Mass measurement of the parent molecular ion confirmed the molecular formula $C_{17}H_{20}O_4$.

(*b*) The most characteristic feature of the p.m.r. spectrum was the appearance of signals for four *C*-methyl groups. One of these (δ 2.14) was a doublet and was shown to be coupled ($J \approx 1$ Hz) to the one-proton quartet at δ 6.65. These signals were therefore assigned to the methyl and adjacent hydrogen on the furan ring. The chemical shifts of the remaining methyl

Can. J. Chem. Downloaded from www.nrcresearchpress.com by 210.87.254.6 on 09/05/12
For personal use only.

resonances were consistent with these groups being allylic (δ 1.78), acetyl (δ 2.27), or on a furan ring (δ 2.51). The two-proton singlet at δ 3.50 was in accord with a cyclopentadiene methylene (δ 2.90) deshielded by a β-carbonyl group.

(*c*) The i.r. spectrum was characterized by a strong absorption at 1710 cm^{-1} with a shoulder at 1700 cm^{-1}, consistent with conjugated ketone or ester carbonyl functions.

These $AlCl_3$-promoted rearrangements of **5** are further examples of the one-step preparation of aromatic compounds via Diels–Alder reaction of five-membered heterocycles with acetylenic dienophiles. As we have observed before (1, 3) yields are limited by competitive polymerization when alkyl-substituted furans are used. This is not a problem in the case of 2,5-diphenylfuran.

Experimental

The p.m.r. spectra were recorded with a Varian A-60A spectrometer equipped with a V-6058A spin-decoupler, using $CDCl_3$ as solvent (unless otherwise stated) and tetramethylsilane as internal standard. The chemical shifts and coupling constants reported are judged to have an accuracy of ±0.02 p.p.m. and ±0.2 Hz respectively. Values of small long-range couplings were estimated by comparison of the half-band widths of the appropriate coupled and decoupled signals. The i.r. spectra were obtained on a Perkin-Elmer model 521 spectrometer, and the mass spectra with a Dupont-CEC model 21-491 spectrometer.

Reaction of 2,5-Dimethylfuran with Ethyl Propiolate

(*a*) To a stirred suspension of $AlCl_3$ (6.92 g) in CH_2Cl_2 (75 ml) was added a solution of ethyl propiolate (5.0 g) in CH_2Cl_2 (100 ml). To this was then added 2,5-dimethylfuran (4.90 g) in CH_2Cl_2 (75 ml), with external cooling to maintain the temperature < 30°, to give a mixture 0.2 *M* in all three reagents. After stirring at room temperature for 60 min, the dark red solution was shaken vigorously with cold water (250 ml). The CH_2Cl_2 layer was separated and the aqueous layer washed with CH_2Cl_2. The combined CH_2Cl_2 solutions were dried (Na_2SO_4) and evaporated. The residue (9.04 g) was chromatographed on SiO_2, using petroleum ether (b.p. 60–80°), and then 5, 10, and 25% EtOAc – petroleum ether as successive elutants. From this column, in order of their elution, were obtained:

(*i*) Compound **8***a* (0.99 g, 10.2%) as an almost colorless oil, n_D^{24} = 1.5190. Final purification was achieved by preparative g.l.p.c. (5% Carbowax on Chromosorb G, at 160°). This gave a colorless solid, m.p. 24–26°. Parent molecular ion at *m/e* 194 ($C_{11}H_{14}O_3$ requires 194); ν_{max} (0.01 or 0.005 *M* in CCl_4): 3180 (broad), 1662 cm^{-1}.

(*ii*) Compound **10** (0.208 g, 2.1%) as a yellow oil. Final purification was achieved by preparative g.l.p.c. (5% Carbowax on Chromosorb G, at 160°). Parent molecular ion at *m/e* 194 ($C_{11}H_{14}O_3$ requires 194); ν_{max} (liquid film): 1710, 1634, 1603, 1570, 975 cm^{-1}; ν_{max} (0.007 *M* in CCl_4): 1717, 1638 cm^{-1}.

(*iii*) Compound **7***a* as a pale yellow solid (0.48 g, 4.9%). Final separation from trace amounts of **6***a* was achieved by preparative t.l.c. (25% EtOAc in petroleum ether (b.p. 80–100°)). This gave a pale yellow solid, m.p. 66.5–67.5°. Parent molecular ion at *m/e* 194 ($C_{11}H_{14}O_3$ requires 194); ν_{max} (0.005 *M* in CCl_4): 3610 (s), 3435 (weak and broad), 1719, 1685 (wk) cm^{-1}; ν_{max} (0.01 *M* in CCl_4): 3610 (weak), 3440 (s), 1719, 1685 (s) cm^{-1}.

(*iv*) Compound **6***a* as a pale yellow oil (2.45 g, 25.3%). Final purification was achieved by column or preparative t.l.c. This gave a pale yellow oil, n_D^{24} = 1.5201. Parent molecular ion at *m/e* 194 ($C_{11}H_{14}O_3$ requires 194); ν_{max} (0.005 *M* in CCl_4): 3615, 3445 (very weak), 1725 cm^{-1}; ν_{max} (0.01 *M* in CCl_4): 3615, 3445 (weak), 1723, 1690 (shoulder) cm^{-1}.

(*b*) The reaction was repeated under the same conditions as in *a* above, using $AlCl_3$ (34.6 g), ethyl propiolate (25.0 g), 2,5-dimethylfuran (24.5 g), and CH_2Cl_2 (1250 ml), *i.e.* a mixture 0.2 *M* in all three reagents. In this case the crude reaction product was dissolved in ether and the solution thoroughly extracted with 5% NaOH. The basic extract was then acidified with HCl. The acid solution was extracted with ether; evaporation of solvent from the dried (Na_2SO_4) extract gave a dark red gummy residue (19.51 g).

The base-insoluble material (18.38 g), which was recovered after washing with water, drying, and evaporation, was chromatographed on SiO_2 ($CHCl_3$). The products in order of their elution were:

(*i*) Compound **8***a* (4.75 g, 9.8%), identical to that obtained in *a* above.

(*ii*) Compound **10** (1.44 g, 3.0%), identical to that obtained in *a* above.

(*iii*) Compound **11** as yellow-orange rosettes (0.82 g, 1.14%), m.p. 76–77° (from petroleum ether (b.p. 60–80°)). Ion of highest mass at *m/e* 288.1363 (calculated for $C_{17}H_{20}O_4$, 288.13616); ν_{max} (KBr): 1710, 1700 (sh), 1612, 1602 cm^{-1}; ν_{max} (0.01 *M* in CCl_4): 1715 cm^{-1}.

The base-soluble portion of the product was chromatographed on SiO_2 ($CHCl_3$). This afforded, in order of their elution:

(*i*) Compound **8***a* (0.76 g, 1.6%; total yield of **8***a*, 11.4%).

(*ii*) A mixture of **7***a* and **6***a* (10.97 g, 22.6%; ratio **6***a*:**7***a* = 5:1).

Preparation of 5a

2,5-Dimethylfuran (4.99 g) and ethyl propiolate (5.03 g) were reacted in the presence of $AlCl_3$ (6.65 g) in CH_2Cl_2 (100 ml), *i.e.* a mixture 0.5 *M* in all three reagents. In this case solutions were prepared as before, cooled to −60°, mixed, and the reaction continued at −60° for 15 min. Work-up identical to that used above in the preparation of **6**–**8***a* gave a residue which was chromatographed on SiO_2 ($CHCl_3$). Compound **5***a* was obtained as a pale yellow oil (1.45 g, 14.6%). It could be purified by preparative t.l.c., but proved to be highly unstable.

In its purest state **5***a* was obtained as a pale yellow oil, n_D^{25} = 1.4868 (slow increase with time suggested decomposition, confirmed by p.m.r.). Parent molecular ion at *m/e* 194 ($C_{11}H_{14}O_3$ requires 194), base peak at *m/e* 96 ($C_6H_8O^+$, formed by retrogression); ν_{max} (CCl_4): 1712 cm^{-1}.

Reaction of 2,5-Diphenylfuran with Ethyl Propiolate

(*a*) To a stirred suspension of $AlCl_3$ (6.65 g) in CH_2Cl_2

(75 ml) was added a solution of ethyl propiolate (4.90 g) in CH_2Cl_2 (100 ml). To this was then added 2,5-diphenylfuran (11.0 g) in CH_2Cl_2 (75 ml), with external cooling to maintain the temperature $< 30°$, to give a mixture 0.2 *M* in all three reagents. Stirring was continued at room temperature for 1 h. The dark green mixture was then shaken vigorously with an equal volume of ice water. The CH_2Cl_2 layer was separated and the aqueous layer washed with CH_2Cl_2. The combined CH_2Cl_2 solutions were dried (Na_2SO_4) and evaporated. The residue was taken up in ether and extracted thoroughly with 5% NaOH. The basic extract was acidified with HCl and the solution then extracted with ether. Evaporation of solvent from the dried extract afforded a greenish solid (2.12 g).

The base-insoluble portion of the crude product was a sticky orange solid; trituration of the latter with cold MeOH followed by crystallization from MeOH afforded compound **8***b* as colorless needles (7.12 g, 44.8%), m.p. 102–103°. Parent molecular ion at *m/e* 318 ($C_{21}H_{18}O_3$ requires 318); ν_{max} (0.01 or 0.005 *M* in CCl_4): 3150 (broad), 3100, 3080, 1678 cm^{-1}.

The reddish methanolic mother liquors were evaporated to dryness to give a highly viscous red-brown oil which slowly solidified. This material (4.18 g) proved to be mainly 2,5-diphenylfuran.

The base-soluble fraction of the crude product (2.12 g) was chromatographed on SiO_2 (25% EtOAc in petroleum ether).

A small amount of compound **8***b* (0.21 g, 1.3%, total yield of **8***b* = 46.1%) eluted first. Isomers **6***b* and **7***b* eluted together and were obtained as a colorless solid. Fractionation by preparative t.l.c. (25% EtOAc in petroleum ether) gave the pure isomers as follows:

Compound **7***b* as cream-colored rosettes (0.13 g, 0.8%), m.p. 120–122°. Parent molecular ion at *m/e* 318 ($C_{21}H_{18}O_3$ requires 318); ν_{max} (0.01 *M* in CCl_4): 3570, 3440 (weak and broad), 3070, 1722, 1690 (sh), 1621 cm^{-1}; ν_{max} (0.005 *M* in CCl_4): 3570, 3070, 3040, 1722, 1620 cm^{-1}.

Compound **6***b* as cream-colored needles (1.02 g, 6.4%), m.p. 145.5–147°. Parent molecular ion at *m/e* 318 ($C_{21}H_{18}O_3$ requires 318); ν_{max} (0.005 *M* in CCl_4): 3570, 3075, 1730 cm^{-1}; ν_{max} (0.01 *M* in CCl_4): 3570, 3450(w), 1730, 1695(w) cm^{-1}.

(*b*) A series of separate experiments under a variety of reaction conditions (temperature, solvent, $AlCl_3$ concentration, dienophile concentration) were carried out in a manner similar to *a* above. The product composition was in each case estimated from the p.m.r. spectrum of the crude product. The results are detailed in Table 1.

We gratefully acknowledge the excellent technical assistance of Mrs. M. G. Flack. Thanks are also due to Mr. P. F. Seto for the i.r. spectra and Mr. D. Embree for the mass measurement of compound **10**.

1. A. W. McCulloch, B. Stanovnik, D. G. Smith, and A. G. McInnes. Can. J. Chem. **47**, 4319 (1969).
2. R. C. Bansal, A. W. McCulloch, and A. G. McInnes. Can. J. Chem. **48**, 1472 (1970).
3. A. W. McCulloch and A. G. McInnes. Can. J. Chem. **49**, 3152 (1971).
4. J. Sauer. Angew. Chem. Int. Ed. **6**, 22 (1967).
5. P. Vogel, B. Willhalm, and H. Prinzbach. Helv. Chim. Acta, **52**, 584 (1969); L. Mavoungou Gomes, C. R. **270**, C, 347 (1970).
6. S. Sternhell. Quart. Rev. **23**, 236 (1969); L. M. Jackman and S. Sternhell. Applications of nuclear magnetic resonance spectroscopy in organic chemistry. 2nd ed. Pergamon Press, New York. 1969. p. 330.

Can. J. Chem. Downloaded from www.nrcresearchpress.com by 210.87.254.6 on 09/05/12
For personal use only.

A Proton Magnetic Resonance Study of 1,4-Dichlorobenzene-^{13}C Partially Oriented in Nematic Phases

E. E. BURNELL

Chemistry Department, University of British Columbia, Vancouver, British Columbia V6T IW5

AND

P. DIEHL AND W. NIEDERBERGER

Physics Department, University of Basel, Basel, Switzerland

Received July 5, 1973

The p.m.r. spectra of 1,4-dichlorobenzene-(^{13}C and ^{12}C) partially oriented in nematic phases have been measured and analyzed, and the geometry of the molecule has been determined. The angle $\angle C_1C_2H$ is found to be 119.4° and $\angle C_1C_2C_3$ 120.3°. The J_{CH} are determined using spectra of samples with differing degrees of orientation.

Les spectres r.m.p. du dichloro-1,4 benzène (^{13}C et ^{12}C) partiellement orienté dans une phase nématique ont été mesurés et analysés et la géométrie de la molécule a été déterminée. On a trouvé que l'angle $\angle C_1C_2H$ est de 119.4° et que celui de $\angle C_1C_2C_3$ est de 120.3°. Les constantes J_{CH} ont été déterminées en utilisant les spectres d'échantillons possédant différents degrés d'orientation.

[Traduit par le journal]

Can. J. Chem., **52**, 151 (1974)

Introduction

The n.m.r. spectra of molecules partially oriented in nematic phases have been extensively used to determine relative internuclear distances (1). 1,4-Dichlorobenzene (Fig. 1) has been studied twice by this method (2, 3). In both cases only the proton spectrum was observed, hence only the relative proton geometry was determined.

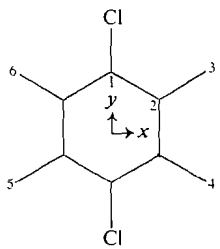

FIG. 1. 1,4-Dichlorobenzene.

With the use of time averaging techniques, proton spectra of molecules containing ^{13}C in natural abundance can be obtained and more complete geometrical information is available. This technique is particularly useful when the proton spectrum is relatively simple, such that the spectra of molecules containing ^{13}C are not obscured by the intense lines of the ^{12}C compound. This is the case with the n.m.r. spectrum of 1,4-dichlorobenzene oriented in a nematic phase (Fig. 2). The spectrum, as in the previous studies, consists of two sets of lines separated by several kHz and symmetrically displaced about the center.

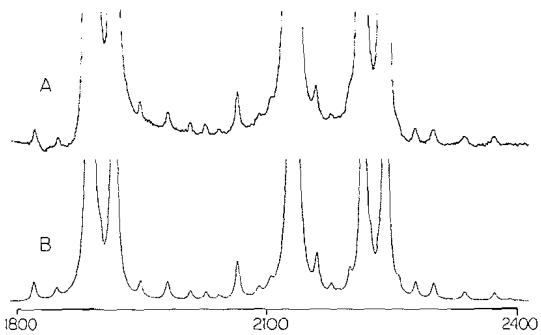

FIG. 2. (*A*) 100 MHz spectrum of partially oriented 1,4-dichlorobenzene obtained after 125 accumulations on a Varian C-1024 time averaging computer in Basel. Concentration 25 mol %; temperature ~30 °C. Only the upfield portion of the spectrum is shown. (*B*) Calculated spectrum with a linewidth of 6 Hz. The center of the spectrum is at 0 Hz.

All six ^{13}C—H dipole–dipole coupling constants have been determined and used to obtain

Can. J. Chem. Downloaded from www.nrcresearchpress.com by 210.87.254.5 on 09/05/12
For personal use only.

the molecular geometry. Some of the problems with the analysis are discussed below.

Experimental

Using one of the lines of the ^{12}C spectrum to provide a lock signal, spectra (see Fig. 2) were obtained from two separate samples with time averaging techniques on HA-100 spectrometers operated in the HA mode. Sample I, run in Basel, was ~25 mol% 1,4-dichlorobenzene dissolved in the nematic phase of *N*-(*p*-ethoxybenzylidene)-*p'*-*n*-butylaniline (EBBA) and 125 scans were accumulated at ~30 °C with a linewidth of ~6 Hz. Sample II, run in Vancouver, was ~20 mol % in EBBA and 77 scans were accumulated at ~30 °C with a linewidth of ~6 Hz.

Only the highfield multiplet of peaks was time averaged and drawn out using a scale of 1000 Hz = 50 cm. The splitting between the low- and highfield multiplets ($=3D_{34}$) was measured before and after time averaging. The program LEQUOR (4) was modified to analyze simultaneously the three spectra (*i*) ^{13}C at position 1, (*ii*) ^{13}C at position 2, and (*iii*) no ^{13}C. The couplings between ^{13}C and H are obtainable as $2D_{CH} + J_{CH}$ only. The parameters obtained, fitting to about 30 lines, are in Table 1.

TABLE 1. Spectral parameters (in Hz) from the p.m.r. spectra of *p*-dichlorobenzene-^{13}C oriented in EBBA

Parameter	Value	
	Sample I	Sample II
$D_{13} + \frac{1}{2}J_{13}$	213.8 ± 1.6	366.1 ± 2.1
$D_{14} + \frac{1}{2}J_{14}$	−54.7 ± 1.6	−93.3 ± 2.1
$D_{23} + \frac{1}{2}J_{23}$	288.3 ± 1.0	475.5 ± 1.4
$D_{24} + \frac{1}{2}J_{24}$	−386.9 ± 0.9	−647.7 ± 1.4
$D_{25} + \frac{1}{2}J_{25}$	−0.9 ± 3.9	9.8 ± 5.6
$D_{26} + \frac{1}{2}J_{26}$	57.8 ± 3.9	89.7 ± 5.7
D_{34}	−1376.4 ± 0.2	−2301.2 ± 0.3
D_{35}	9.2 ± 0.1	17.8 ± 0.2
D_{36}	109.3 ± 0.1	186.6 ± 0.2
J_{34}[a]	8.551	8.551
J_{35}[a]	0.391	0.391
J_{36}[a]	2.579	2.579
R.m.s. error	0.5	0.8

[a]Assumed from ref. 6.

Results and Discussion

Four coordinates are needed to specify the relative carbon and proton geometry of 1,4-dichlorobenzene, assuming D_{2h} symmetry and a C_2—C_3 bond length of 1.3974 Å (5). In addition, two orientation parameters are needed to specify the average orientation of the molecule in the magnetic field. In principle, the nine dipole–dipole coupling constants determined from the spectrum are more than sufficient to determine the geometrical and orientational parameters. However, two problems exist:

(*i*) As pointed out above, because of the large chemical shift between ^{13}C and H, only the sum $2D_{CH} + J_{CH}$ can be determined from an analysis of the spectrum. Previous high-resolution studies of 1,4-dichlorobenzene have determined only J_{23}, J_{25}–J_{24}, and J_{26}–J_{24} (6); J_{13} and J_{14} have not, to the author's knowledge, been reported. Hence, J_{13}, J_{14}, and J_{24} must be treated as unknowns. A solution to this problem is to obtain spectra with different orientations; the D_{ij} are proportional to the orientation and the J_{ij} are constant, and hence both can be determined.

(*ii*) The second problem is that there is a large covariance between D_{13} and D_{14}; D_{23} and D_{24}; and D_{25} and D_{26}, as reflected in the large error reported for these parameters in Table 1. Consequently, only the sums of these couplings can be accurately determined. However, when two spectra with different orientations were used for the analysis, the large covariance no longer proved troublesome. Another possible approach is to treat the sums of the D_{ij} as measurables.

The iterative weighted least squares program SHAPE (7) was modified to fit the two sets of D_{ij} reported in Table 1 in order to obtain the coordinates, J_{13}, J_{14}, J_{24}, and the four orientation parameters. Results are in Table 2, where the weighted r.m.s. error of the fit from SHAPE was 0.17 Hz. We note that the geometrical coordinates are well determined, but that the J_{CH} are not. However, the J_{CH} are of the same order of magnitude as those reported for benzene (8). The accuracy could be increased by measuring yet more spectra at different orientations.

From the coordinates in Table 2, the angle $\angle C_1C_2H_3$ equals 119.4 ± 2.0°, and the angle $\angle C_1C_2C_3$ equals 120.3 ± 2.0°. The value of $\angle C_1C_2H_3$ agrees with that of 119°37′ reported by Bulthuis *et al.* (3). The ratio r_{36} to r_{34} of 1.726 agrees with previous values reported from analyses of n.m.r. spectra of molecules dissolved in nematic phases (2, 3).

Conclusion

The two spectra of 1,4-dichlorobenzene at different orientations in EBBA give accurate geometrical information about the proton and carbon skeleton of the molecule. This information has been obtainable because the proton spectrum of the ^{12}C molecule is simple (six lines each side of center), and most of the proton lines due to coupling to the ^{13}C are observed. The ^{13}C spectra

Can. J. Chem. Downloaded from www.nrcresearchpress.com by 210.87.254.5 on 09/05/12
For personal use only.

Can. J. Chem. Downloaded from www.nrcresearchpress.com by 210.87.254.5 on 09/05/12
For personal use only.

TABLE 2. Geometrical, orientational, and indirect spin–spin coupling parameters of *p*-dichlorobenzene*

Geometrical parameter	Value (Å)	Bond angle	Value (°)	Orientational parameter	Value		Coupling parameter	Value (Hz)
					Sample I	Sample II		
$x(1)$	(0)	$C_1C_2C_3$	120.3 ± 2.0	S_{xx}	-0.0735 ± 0.0005	-0.1258 ± 0.0009	J_{13}	-1 ± 11
$x(2)$	1.212 ± 0.002	$H_3C_2C_3$	120.3 ± 0.1	S_{xx}	-0.1069 ± 0.0007	-0.1758 ± 0.0011	J_{14}	9.9 ± 2.6
$x(3)$	2.162 ± 0.005	$C_1C_2H_3$	119.4 ± 2.0				J_{23}‡	(166.98)
$y(1)$	1.408 ± 0.057						J_{24}	3.0 ± 2.7
$y(2)$†	(0.6987)						J_{25}§	1.3
$y(3)$	1.253 ± 0.003						J_{26}§	8.3

*Weighted r.m.s. error from SHAPE = 0.17 Hz. Values in brackets are assumed. The origin is taken as the center of symmetry of the molecule.
†Assumed from benzene (5).
‡From Read *et al.* (6).
§Set from ref. 6 so that $J_{25} = J_{24} - 1.768$ Hz and $J_{26} = J_{24} + 5.285$ Hz.

of other simple molecules can be measured and interpreted in a similar way. However, lack of information about the J_{CH} may lead to problems, especially for carbon not directly bonded to hydrogen.

Corrections for molecular vibrations (9) have not been applied because the results are not considered of sufficient accuracy. The various effects of other nuclear motions (10) and any anisotropy in the indirect spin–spin coupling constants have also been neglected. Work on $^{13}CH_3F$ yields ambiguous results which point out the possibility of difficulties in the interpretation of D_{13C-H} couplings.[1]

The authors are grateful to the Swiss National Foundation for the Advancement of Science and to the National Research Council of Canada for financial support.

[1]E. E. Burnell and J. R. Council, unpublished results.

1. P. DIEHL and C. L. KHETRAPAL. NMR—Basic principles and progress. Vol. 1. Springer-Verlag. 1969.
2. A. SAUPE. Mol. Cryst. **1**, 527 (1966).
3. J. BULTHUIS, J. GERRITSEN, C. W. HILBERS, and C. MACLEAN. Rec. Trav. Chim. **87**, 417 (1968).
4. P. DIEHL, H. P. KELLERHALS, and W. NIEDERBERGER. J. Magn. Res. **4**, 352 (1971).
5. A. LANGSETH and B. P. STOICHEFF. Can. J. Phys. **34**, 350 (1956).
6. J. M. READ, JR., R. W. GRECELY, and J. H. GOLDSTEIN. J. Mol. Spectrosc. **25**, 107 (1968).
7. P. DIEHL, P. M. HENRICHS, and W. NIEDERBERGER. Mol. Phys. **20**, 139 (1971).
8. G. ENGLERT, P. DIEHL, and W. NIEDERBERGER. Z. für Naturf. **26a**, 1829 (1971).
9. P. DIEHL and W. NIEDERBERGER. J. Magn. Res. **9**, 495 (1973), and references therein.
10. A. D. BUCKINGHAM, E. E. BURNELL, and C. A. DELANGE. Mol. Phys. **16**, 299 (1969).

Can. J. Chem. Downloaded from www.nrcresearchpress.com by 210.87.254.5 on 09/05/12
For personal use only.

Theoretical Studies of some Nonbenzenoid Hydrocarbons. II

ARCHANA DASGUPTA AND NADNA K. DASGUPTA[1]

Department of Chemistry, The University of Alberta, Edmonton, Alberta T6G 2E1

Received July 6, 1973

A semiempirical self-consistent field molecular orbital study has been made on some nonbenzenoid hydrocarbons using a resonance integral value proposed by Lo and Whitehead (2, 4), Chung and Dewar (3), Dewar and Harget (7), and Yamaguchi *et al.* (6) without using configuration interaction. It has been observed that spectral transitions calculated using the β-value proposed by Lo and Whitehead and Chung and Dewar are in good agreement with experiment and comparable to those calculated by the β-value proposed by Yamaguchi *et al.* and Dewar *et al.*

On a effectué une étude semiempirique SCF MO sur plusieurs hydrocarbures du type non-benzénique en utilisant la valeur intégrale de résonnance proposée par Lo et Whitehead (2, 4), Chung et Dewar (3), Dewar et Harget (7) et Yamaguchi *et al.* (6) sans tenir compte des interactions de configuration. Il fut observé que les transitions spectrales calculées en utilisant la valeur-β proposée par Lo et Whitehead et Chung et Dewar, sont en accord avec les données expérimentales et sont comparables à celles calculées à partir de la valeur-β proposée par Yamaguchi *et al.* et Dewar *et al.* [Traduit par le journal]

Can. J. Chem., **52**, 155 (1974)

Introduction

In a previous paper (1), we reported the results of calculations on some nonbenzenoid hydrocarbons with 16π electrons using the self-consistent field molecular orbital (s.c.f. m.o.) method with resonance integral values proposed by Lo and Whitehead (2) and Chung and Dewar (3). It has been shown that properties such as bond length, heat of atomization, and resonance energy for conjugated hydrocarbons (2–4) can be predicted with reasonably good accuracy. It was observed in our previous paper (1), that the theoretically predicted spectral data were also in good agreement with experiment. This inspired us to apply these same methods to other nonbenzenoid hydrocarbons such as azulene, Hafner's hydrocarbons (aceazulylene and aceheptylene), azupyrene, dicyclohepta[*cd*,*gh*]pentalene, cyclohepta[*def*]fluorene, and azuleno[8,8*a*,1-2-*def*]heptalene and in addition to compare the results with those calculated by the method of Dewar and Harget (7) a "β-variable method". The "β-variable method" has been successfully applied by various authors such as Nishimoto and Forster (5), Yamaguchi *et al.* (6), and Dewar *et al.* (7).

Among these molecules, azulene (ref. 8 and references therein) and Hafner's hydrocarbons (9) were studied extensively with different set of parameters. Azupyrene, cyclohepta[*def*]fluorene and dicyclohepta[*cd*,*gh*]pentalene have been studied by Heilbronner and co-workers (10) using a modified Pariser–Parr–Pople (11, 12) method in which many of the two electron repulsion integrals which have been included here were neglected.

Although the hydrocarbon azuleno[8,8*a*,1,2-*def*] heptalene has not been synthesized, its methyl derivative, 11 methyl azuleno[8,8*a*,1,2-*def*]heptalene, has been synthesized by Hafner *et al.* (13). Azupyrene (14) has been synthesized recently. However, no report of the synthesis of dicyclohepta[*dc*,*gh*]pentalene has been found in the literature and the attempts to synthesize cyclohepta[*def*]fluorene (15) have so far been unsuccessful.

In this paper we shall use dicycloheptapentalene, cycloheptafluorene, and azulenoheptalene for dicyclohepta[*cd*,*gh*]pentalene, cyclohepta[*def*] fluorene, and azuleno[8,8*a*,1,2-*def*]heptalene, respectively.

Method and Parameters

The self-consistent field method applied here is similar to that of Pariser–Parr (11) and Pople (12) within the zero-differential-overlap approximation. The orbitals are expressed as eigenvectors of the matrix representation of the closed shell Hartree–Fock operator (16). The diagonal and off-diagonal matrix elements, $F_{\mu\mu}$ and $F_{\mu\nu}$, may be represented as follows:

[1]On leave of absence from the Visva-Bharati University, Santiniketan, West Bengal, India.

Can. J. Chem. Downloaded from www.nrcresearchpress.com by 210.87.254.40 on 09/05/12
For personal use only.

Can. J. Chem. Downloaded from www.nrcresearchpress.com by 210.87.254.40 on 09/05/12
For personal use only.

[1] $$F_{\mu\mu} = \alpha_\mu + \sum_{m=1} q_m\gamma_{\mu m} - \tfrac{1}{2}q_m\gamma_{\mu\mu}$$

with

$$\alpha_\mu = -I - \sum_{\substack{m=1 \\ m\neq\mu}}^{n} \gamma_{\mu m}$$

where I is the ionization energy of the carbon atom in its sp^2 valence state and is equal to 11.16 eV (17).

[2] $$F_{\mu\nu} = \beta_{\mu\nu} - \tfrac{1}{2}p_{\mu\nu}$$

for neighboring μ and ν and for non-neighboring centers $\beta_{\mu\nu}$ is assumed to be zero.

For the calculation of the resonance integral, $\beta_{\mu\nu}$, four methods were utilized:

(*i*) In the first method, designated as s.c.f.(*a*), $\beta_{\mu\nu}$ depending on internuclear distance was calculated by the method of Lo and Whitehead (2).

(*ii*) In the second method, s.c.f.(*b*), a constant value of β, −1.7901 eV (1), determined by the method of Chung and Dewar (3), was used.

(*iii*) The third method, s.c.f.(*c*), is that due to Dewar and Harget (7*c*). At each iteration the bond lengths, $r_{\mu\nu}$ are calculated from the relation,

[3] $$r_{\mu\nu}\,(\text{Å}) = 1.512 - 0.174p_{\mu\nu}$$

where $p_{\mu\nu}$ is the π-bond order of the bond μν. This is then used in a recalculation of the two center core integrals, $\beta_{\mu\nu}$, and two center repulsion integrals, $\gamma_{\mu\nu}$, between neighboring centers, with

[4] $$\beta_{\mu\nu} = -6.927S_{\mu\nu}$$

with $S_{\mu\nu}$ the overlap integral between two π_{2p} orbitals with orbital exponent 1.59.

(*iv*) The β-variable method as proposed by Yamaguchi *et al.* (6) is the s.c.f.(*d*) method. It is similar to the s.c.f.(*c*) method with $r_{\mu\nu}$ and $\beta_{\mu\nu}$ determined from

[5] $$r_{\mu\nu}(\text{Å}) = 1.520 - 0.186p_{\mu\nu}$$

[6] $$\beta_{\mu\nu} = \beta_0 \exp\,[a(r_0 - r_{\mu\nu})]$$

where r_0 is the C—C distance for benzene, a = 1.7 Å^{-1} and β_0 is the resonance integral in benzene. It has been suggested (18) that the value of β_0 depending on a given bond length decreases as the number of rings increases. Hence for azulene we used −2.28 eV (19) for β_0 which gives a good fit for the spectra of naphthalene. For large molecules we used −2.15 eV which also gives a good fit for the spectra of phenanthrene and pyrene.

The bond order and charge density are defined as

$$p_{\mu\nu} = 2\sum_{i=1}^{n} C_{\mu i}C_{\nu i}$$

and

$$q_\mu = 2\sum_{i=1}^{n} C_{\mu i}^2$$

They are obtained from the eigenvector components $C_{\mu i}$. Eigenvectors produced by Hückel calculations were used for the first s.c.f. iteration and the iterative procedure continued until self-consistency was achieved within the desired degree of accuracy of 10^{-5} for the components of vectors of successive iterations.

The one center two electron repulsion integrals $\gamma_{\mu\mu}$ were calculated from the valence state ionization energy, I_μ (17), and electron affinity, A_μ, given by $\gamma_{\mu\mu} = I_\mu - A_\mu = 11.134$ eV.

Two center repulsion integrals $\gamma_{\mu\nu}$ were calculated by Ohno's formula (21) except in the s.c.f.(*d*) method, where the Mataga–Nishimoto (20) formula was used. In all cases, the $\gamma_{\mu\nu}$ between non-neighboring centers were calculated from the initial geometries discussed below and not varied during the course of the iterations. In the s.c.f.(*a*) and (*b*) methods, the same procedure was used for the $\gamma_{\mu\nu}$ and $\beta_{\mu\nu}$ between neighboring atoms while in the s.c.f.(*c*) and (*d*) methods, the $\gamma_{\mu\nu}$ and $\beta_{\mu\nu}$ were recalculated after each iteration on the basis of the bond length – bond order relations discussed above.

Geometry of the Molecules

The structure of azulene (22), and some derivatives of aceazulylene (23) and aceheptylene (24) are known. Azulene and aceheptylene are planar and aceazulylene is almost planar. Two center repulsion integrals, $\gamma_{\mu\nu}$, were calculated from the structure of azulene and aceheptylene; for aceazulylene a planar geometry very close to that reported was used and for other molecules with no reported structure, a reasonable planar geometry was used as shown in Fig. 1. For the "β variable" method only the adjacent $\gamma_{\mu\nu}$ were varied as stated earlier.

Results and Discussion

Table 1 contains the charge density of all the molecules. There is some variation of results among the different methods for all molecules

Can. J. Chem. Downloaded from www.nrcresearchpress.com by 210.87.254.40 on 09/05/12
For personal use only.

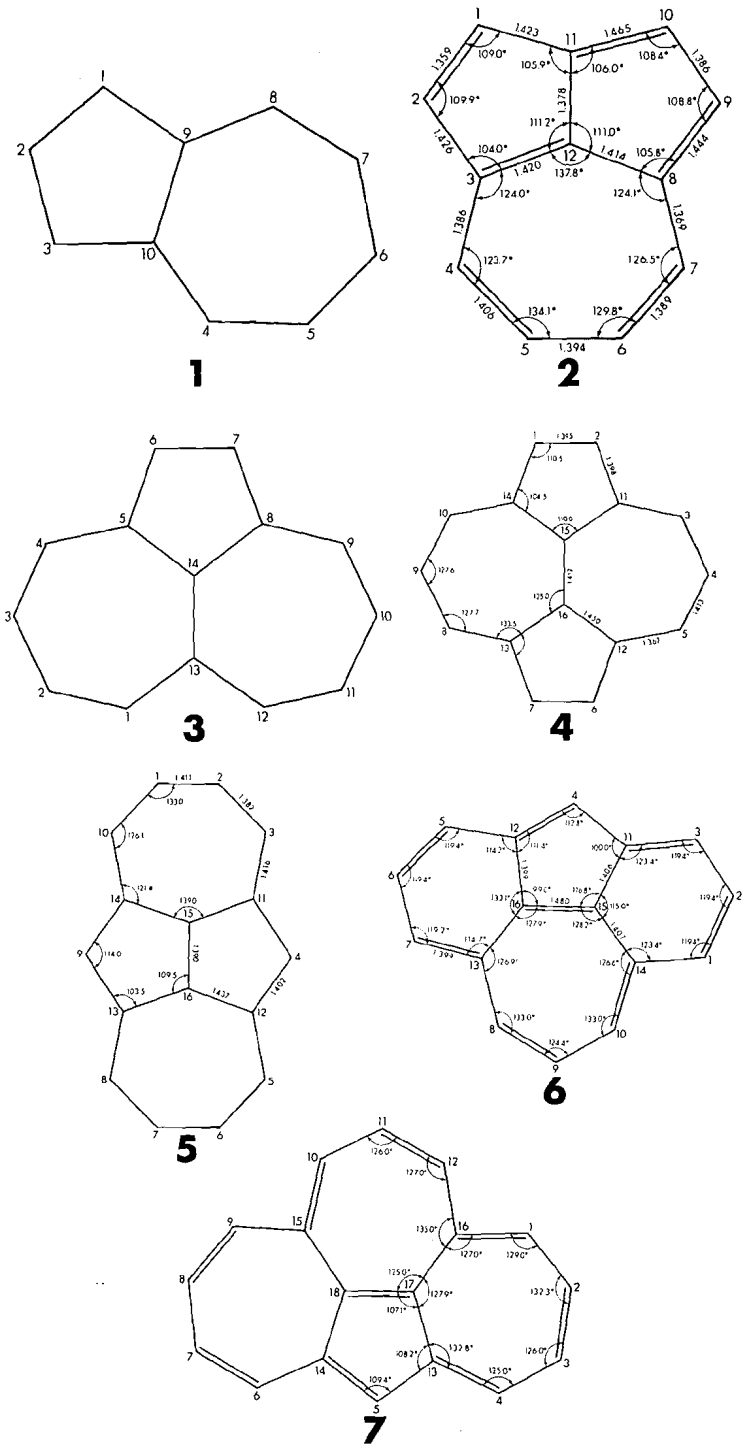

FIG. 1. Planar geometry of molecules **1**, azulene; **2**, aceazulelylene; **3**, aceheptylene; **4**, azupyrene; **5**, dicycloheptpentalene; **6**, cycloheptfluorene (all bonds equal to 1.40 Å except otherwise mentioned); 7, azulenoheptalene (all bonds equal to 1.40 Å).

TABLE 1. Charge density

Molecule	Center	Charge density s.c.f.(*a*)	s.c.f.(*b*)	s.c.f.(*c*)	s.c.f.(*d*)
1	1,3	1.092	1.110	1.090	1.091
	2	0.965	0.961	0.982	1.003
	4,8	0.892	0.864	0.868	0.909
	5,7	1.051	1.067	1.073	1.015
	6	0.931	0.906	0.895	0.939
	9,10	1.017	1.026	1.030	1.013
2	1	0.930	0.880	0.931	0.959
	2	1.116	1.160	1.111	1.091
	3	0.921	0.886	0.921	0.937
	4	0.953	0.960	0.958	0.939
	5	0.985	0.974	0.980	0.962
	6	0.969	0.973	0.978	0.963
	7	0.971	0.961	0.959	0.947
	8	0.908	0.886	0.919	0.935
	9	1.114	1.157	1.115	1.089
	10	0.923	0.883	0.928	0.948
	11	1.129	1.165	1.120	1.112
	12	1.081	1.114	1.081	1.119
3	1	1.073	1.122	1.078	1.038
	2	0.908	0.859	0.901	0.935
	3	1.076	1.125	1.084	1.048
	4	0.902	0.842	0.891	0.925
	5	1.084	1.111	1.086	1.072
	6	1.032	1.046	1.038	1.063
	7	1.036	1.047	1.038	1.060
	8	1.081	1.111	1.086	1.076
	9	0.901	0.841	0.891	0.923
	10	1.076	1.125	1.084	1.049
	11	0.911	0.859	0.901	0.938
	12	1.073	1.121	1.079	1.035
	13	0.861	0.822	0.853	0.893
	14	0.987	0.971	0.990	0.945

and, except for azulene, some variation in order. The most discrepancies in sequence occur between the s.c.f.(*d*) and the other methods. This is due to the fact that the β and γ integrals are determined by quite different methods, directed towards good spectral prediction in the s.c.f.(*d*) whereas in the other methods the integrals are determined by methods directed towards obtaining reasonable heats of atomization. Such differences in order that arise in the first three methods occur among centers which are grouped into distinct and reasonably narrow range of charge density. Hence, for practical purposes there is excellent agreement among the predictions.

According to the s.c.f.(*a*) and s.c.f.(*b*) methods the highest charge density for molecule **7** is found to be at centers 10 and 12. This is also in agreement with chemical properties of the molecule because protonation (13) takes place at this position. However, in case of the s.c.f.(*d*) method there is some ambiguity. An interesting feature is the charge density at center 4 of cycloheptfluorene which is very high.

From Table 1 it is clear that the charge density is very sensitive towards choices of parameters. This is also reflected in the calculation of the π dipole moment shown in Table 2. The only experimental value available is for azulene 1.0 D (25). Bloor (8) has reported a value of 3.19 D from theoretical calculations using configuration interaction. The values obtained by the present methods are all considerably closer to the experimental result. The distinctly lower values obtained by the s.c.f.(*a*), (*b*), and (*c*) methods indicated that the charge

Can. J. Chem. Downloaded from www.nrcresearchpress.com by 210.87.254.40 on 09/05/12
For personal use only.

TABLE 1. (*Concluded*)

Molecule	Center	Charge density s.c.f.(*a*)	s.c.f.(*b*)	s.c.f.(*c*)	s.c.f.(*d*)
4	1,2,6,7	1.032	1.040	1.037	1.042
	3,5,8,10	0.859	0.828	0.830	0.909
	4,9	1.117	1.130	1.131	1.037
	11,12,13,14	1.095	1.112	1.116	1.070
	15,16	0.911	0.910	0.902	0.921
5	1,2,6,7	0.984	0.984	0.983	0.979
	3,5,8,10	0.979	0.973	0.979	0.964
	4,9	1.154	1.170	1.168	1.107
	11,12,13,14	0.895	0.894	0.882	0.948
	15,16	1.131	1.128	1.143	1.110
6	1,7	1.020	1.016	1.009	1.021
	2,6	1.021	1.024	1.026	1.006
	3,5	0.952	0.948	0.949	0.964
	4	1.244	1.224	1.192	1.169
	9	1.132	1.126	1.116	1.022
	8,10	0.767	0.779	0.799	0.856
	11,12	0.974	0.983	0.990	1.026
	13,14	1.054	1.051	1.050	1.013
	15,16	1.024	1.024	1.023	1.019
7	1,9	1.102	1.108	1.079	1.028
	2,8	0.868	0.863	0.894	0.937
	3,7	1.116	1.120	1.095	1.043
	4,6	0.854	0.849	0.890	0.933
	5	1.056	1.057	1.048	1.063
	10,12	1.205	1.204	1.161	1.078
	11	0.810	0.803	0.832	0.913
	13,14	1.095	1.098	1.091	1.085
	15,16	0.799	0.795	0.812	0.898
	17,18	1.030	1.034	1.038	1.010

TABLE 2. Dipole moment (D)

Molecule	Dipole moment s.c.f.(*a*)	s.c.f.(*b*)	s.c.f.(*c*)	s.c.f.(*d*)
1	1.79	2.27	2.20	2.74
2	2.03	2.05	1.98	2.87
3	1.45	1.47	1.55	2.32
4	0	0	0	0
5	0	0	0	0
6	4.28	4.00	3.54	4.25
7	0.43	0.29	0.68	1.32

densities predicted by these methods are more reliable than those obtained from the s.c.f.(*d*) method.

The predicted π dipole moment of cycloheptfluorene (4.28, 4.00, 3.54, and 4.25 D) is rather high and this suggests that in the ground state there is probably charge separation in the molecule. This phenomenon and high charge density at center 4 of this molecule make it very much reactive and unstable.

Bond Order and Bond Length

Table 3 contains the calculated bond orders and bond lengths and the available experimental

Can. J. Chem. Downloaded from www.nrcresearchpress.com by 210.87.254.40 on 09/05/12
For personal use only.

TABLE 3. Bond order and bond length

Molecule	Bond	Bond order				Bond length				
		s.c.f.(*a*)	s.c.f.(*b*)	s.c.f.(*c*)	s.c.f.(*d*)	s.c.f.(*a*)	s.c.f.(*b*)	s.c.f.(*c*)	s.c.f.(*d*)	Exptl.
1	1– 2	0.665	0.662	0.662	0.657	1.394	1.394	1.397	1.398	1.391[a]
	1– 9	0.607	0.610	0.616	0.619	1.403	1.403	1.405	1.405	1.413[a]
	4– 5	0.642	0.653	0.657	0.655	1.398	1.396	1.398	1.398	1.401[a]
	4–10	0.631	0.608	0.608	0.614	1.399	1.403	1.406	1.408	1.383[a]
	5– 6	0.653	0.648	0.646	0.646	1.396	1.397	1.400	1.400	1.385[a]
	9–10	0.231	0.283	0.260	0.270	1.468	1.457	1.467	1.470	1.483[a]
2	1– 2	0.839	0.785	0.848	0.806	1.365	1.374	1.364	1.370	1.359[b]
	2– 3	0.401	0.470	0.386	0.450	1.438	1.426	1.445	1.436	1.426[b]
	3– 4	0.726	0.630	0.743	0.670	1.384	1.399	1.383	1.395	1.386[b]
	4– 5	0.556	0.654	0.532	0.611	1.412	1.396	1.420	1.406	1.406[b]
	5– 6	0.737	0.652	0.761	0.688	1.382	1.396	1.380	1.392	1.394[b]
	1–11	0.420	0.465	0.405	0.444	1.434	1.427	1.442	1.437	1.423[b]
	3–12	0.360	0.416	0.359	0.399	1.444	1.435	1.450	1.446	1.421[b]
	11–12	0.725	0.642	0.727	0.681	1.384	1.398	1.386	1.393	1.378[b]
	9–10	0.862	0.790	0.849	0.808	1.361	1.373	1.364	1.370	1.386[b]
	8– 9	0.372	0.466	0.385	0.450	1.442	1.427	1.445	1.436	1.444[b]
	7– 8	0.728	0.630	0.742	0.671	1.383	1.399	1.383	1.395	1.369[b]
	6– 7	0.559	0.655	0.533	0.612	1.411	1.395	1.419	1.406	1.389[b]
	10–11	0.377	0.459	0.404	0.439	1.441	1.428	1.442	1.438	1.465[b]
	8–12	0.381	0.420	0.360	0.396	1.441	1.434	1.449	1.446	1.417[b]
3	1– 2	0.853	0.778	0.847	0.799	1.362	1.375	1.365	1.371	1.369[c]
	2– 3	0.402	0.500	0.409	0.481	1.437	1.421	1.441	1.431	1.422[c]
	3– 4	0.855	0.776	0.849	0.792	1.362	1.375	1.364	1.373	1.355[c]
	4– 5	0.378	0.469	0.383	0.460	1.441	1.426	1.445	1.435	1.437[c]
	5– 6	0.737	0.627	0.732	0.662	1.382	1.400	1.385	1.397	1.393[c]
	6– 7	0.567	0.675	0.563	0.630	1.410	1.392	1.414	1.403	1.393[c]
	1–13	0.387	0.466	0.395	0.448	1.440	1.427	1.443	1.437	1.441[c]
	5–14	0.354	0.438	0.378	0.410	1.445	1.431	1.446	1.444	1.473[c]
	13–14	0.736	0.612	0.715	0.659	1.382	1.402	1.388	1.397	1.399[c]
	7– 8	0.732	0.626	0.732	0.662	1.382	1.400	1.385	1.397	1.398[c]
	8– 9	0.378	0.468	0.383	0.458	1.441	1.426	1.445	1.435	1.434[c]
	9–10	0.852	0.775	0.848	0.793	1.363	1.375	1.364	1.373	1.360[c]
	10–11	0.405	0.500	0.409	0.480	1.437	1.421	1.441	1.431	1.413[c]
	11–12	0.855	0.779	0.847	0.800	1.362	1.375	1.365	1.371	1.367[c]
	12–13	0.377	0.464	0.396	0.446	1.441	1.427	1.443	1.437	1.450[c]
	8–14	0.369	0.440	0.378	0.410	1.443	1.431	1.446	1.444	1.466[c]

bond lengths. Several relations between bond length and bond order exist in the literature. In the s.c.f.(*a*) and s.c.f.(*b*) methods we used the relation of Dewar and Gleicher (7*a*),

$$r_{\mu\nu} = 1.504 - 0.166p_{\mu\nu}$$

because Lo and Whitehead (2) have shown that the length of a single bond in aromatic compound is best represented by a value of 1.505 Å. In the s.c.f.(*c*) and (*d*) method we used a different relation as discussed earlier (eqs. 3 and 5). The agreement between theoretical and experimental bond lengths is reasonable and in some cases it is good.

The theoretical bond lengths of these non-benzenoid molecules display an interesting feature: a bond between two different types of rings has a tendency to have single bond character and bonds between the same types of ring have a tendency to have aromatic character. Thus the 9–10 bond of azulene, the 3–12 and 8–12 bonds of aceazulylene, the 8–14 and 5–14 bonds of aceheptylene, the 12–16, 13–16, 11–15, and 14–15 bonds of azupyrene, dicycloheptapentalene, and cycloheptfluorene have the tendency to have single bond character with a bond order of the order of 0.46 or less. Again the 11–12 bond of aceazulylene, the 13–14 bond of aceheptylene, the 15–16 bonds of azupyrene and dicycloheptapentalene have the tendency to have aromatic character with a bond order of the order of 0.6 to 0.74. The 15–16 bond of hypo-

Can. J. Chem. Downloaded from www.nrcresearchpress.com by 210.87.254.40 on 09/05/12
For personal use only.

TABLE 3. (*Concluded*)

Molecule	Bond	Bond order				Bond length				
		s.c.f.(*a*)	s.c.f.(*b*)	s.c.f.(*c*)	s.c.f.(*d*)	s.c.f.(*a*)	s.c.f.(*b*)	s.c.f.(*c*)	s.c.f.(*d*)	Exptl.
4	1– 2	0.778	0.784	0.806	0.774	1.375	1.374	1.372	1.376	
	1–14	0.503	0.498	0.474	0.507	1.421	1.421	1.430	1.426	
	3–11	0.629	0.604	0.610	0.608	1.400	1.404	1.406	1.407	
	3– 4	0.642	0.650	0.650	0.653	1.397	1.396	1.399	1.399	
	11–15	0.415	0.453	0.457	0.433	1.435	1.429	1.433	1.439	
	15–16	0.657	0.595	0.594	0.641	1.395	1.405	1.409	1.401	
5	1– 2	0.492	0.519	0.465	0.529	1.422	1.418	1.431	1.422	
	2– 3	0.794	0.775	0.814	0.762	1.372	1.375	1.370	1.378	
	3–11	0.474	0.489	0.451	0.505	1.425	1.423	1.434	1.426	
	4–11	0.628	0.619	0.628	0.624	1.400	1.401	1.403	1.404	
	11–15	0.423	0.436	0.441	0.418	1.434	1.432	1.435	1.442	
	15–16	0.665	0.639	0.635	0.678	1.399	1.398	1.402	1.394	
6	1– 2	0.658	0.657	0.653	0.656	1.395	1.395	1.398	1.398	
	2– 3	0.679	0.677	0.679	0.673	1.391	1.392	1.394	1.395	
	3–11	0.565	0.572	0.576	0.578	1.410	1.409	1.412	1.413	
	4–11	0.596	0.600	0.607	0.609	1.406	1.405	1.407	1.407	
	1–14	0.584	0.589	0.599	0.595	1.407	1.407	1.408	1.410	
	8–13	0.562	0.569	0.575	0.579	1.411	1.410	1.412	1.413	
	8– 9	0.654	0.653	0.654	0.657	1.396	1.396	1.398	1.398	
	11–15	0.445	0.422	0.394	0.394	1.431	1.434	1.443	1.447	
	13–16	0.442	0.419	0.386	0.393	1.431	1.435	1.445	1.447	
	15–16	0.562	0.614	0.668	0.671	1.411	1.402	1.396	1.395	
7	1– 2	0.808	0.807	0.872	0.844	1.370	1.370	1.360	1.364	
	2– 3	0.464	0.463	0.368	0.415	1.427	1.427	1.448	1.443	
	3– 4	0.806	0.806	0.872	0.843	1.370	1.370	1.360	1.364	
	4–13	0.428	0.426	0.349	0.388	1.433	1.433	1.451	1.448	
	5–13	0.634	0.633	0.645	0.636	1.399	1.399	1.400	1.402	
	1–16	0.424	0.425	0.351	0.386	1.434	1.433	1.451	1.448	
	10–15	0.578	0.588	0.607	0.595	1.408	1.406	1.406	1.410	
	10–11	0.649	0.645	0.647	0.652	1.396	1.397	1.399	1.399	
	13–17	0.499	0.505	0.541	0.528	1.421	1.420	1.418	1.422	
	16–17	0.534	0.520	0.555	0.567	1.415	1.418	1.415	1.415	
	17–18	0.479	0.487	0.405	0.398	1.425	1.423	1.442	1.446	

[a]Reference 22.
[b]Reference 23.
[c]Reference 24.

thetical molecule cycloheptfluorene is an exception. Although it belongs to different types of rings it has no tendency to have single bond character. However, the molecule azulenoheptalene shows no such marked tendency.

Another interesting feature of these molecules is that some of the peripheral bond lengths are close to the aromatic value and the differences between them and the rest are pronounced. Thus the predicted peripheral bonds of azulene, the 7-membered ring of aceazulylene, the 5-membered ring of aceheptylene, the 7-membered rings of azupyrene, the 5-membered rings of dicycloheptpentalene, and the 5–13, 5–14, 10–15, 10–11, 11–12, and 12–16 bonds of azulenoheptalene exhibit this phenomenon.

Another interesting feature concerning the structure of molecules **2** and **3** is worthy of comment. The chemistry of these molecules proceeds to generate azulene derivatives. This has led to the possible consideration that in the ground state the two 5-membered rings of **2** or two 7-membered rings of **3** are probably not equivalent. The present calculations indicate that they are, even though the experimental structure for **2** indicates some variation.

Spectra

Table 4 contains the theoretical and experimental singlet $\pi^* \leftarrow \pi$ transition energies and oscillator strength along with other theoretical results from these molecules. The oscillator

Can. J. Chem. Downloaded from www.nrcresearchpress.com by 210.87.254.40 on 09/05/12
For personal use only.

Can. J. Chem. Downloaded from www.nrcresearchpress.com by 210.87.254.40 on 09/05/12
For personal use only.

TABLE 4. Transition energies[a]

		Theoretical											
		s.c.f.(*a*)		s.c.f.(*b*)		s.c.f.(*c*)		s.c.f.(*d*)		Other work		Exptl.	
Molecule	Symmetry	eV	*f*	eV	*f*	eV	*f*	eV	*f*	eV	*f*	eV	log(ε)/*f*[a]
1	$^1B_1$	2.28	0.13	1.97	0.08	2.07	0.10	2.18	0.10	2.05[c]	0.025[c]	1.96[d]	0.009[d]
	$^1A_1$	3.63	0.85	3.60	0.79	2.64	0.80	4.02	0.90	3.53[c]	0.005[c]	3.50, 3.66[d]	0.08[d]
		3.94	0.75	3.72	0.71	3.72	0.73						
	$^1B_1$	4.10	0.47	4.12	0.46	4.06	0.46	4.52	0.48	4.41[c]	0.13[c]	4.48[d]	
	$^1A_1$							4.13	0.86	4.78[c]	1.88[c]	4.52[d]	1.10[d]
	$^1B_1$	5.05	0.28	4.81	0.32	4.82	0.30	5.46	0.37	5.63[c]	0.41[c]	5.24[d]	0.38[d]
	$^1A_1$							6.18	0.06	6.03[c]	0.010[c]		
	$^1B_1$	6.17	0.22	6.03	0.26	6.04	0.24			6.41[c]	0.19[c]	6.42[d]	0.65[d]
	$^1A_1$	6.64	0.01	6.55	0.07	6.55	0.02	6.38	0.09	6.72[c]	0.39[c]		
2[b]	$^1B_2$	2.31	0.09	1.67	0.03	2.28	0.07	1.72	0.02	1.73[e]	0.003[e]	1.84[f]	
	$^1A_1$			2.95	0.18	3.07	0.35	3.01	0.20	2.91[e]	0.001[e]	2.60[f]	2.94[f]
	$^1A_1$	3.25	0.44										
	$^1A_1$			3.80	0.86	3.92	0.42	3.83	0.73	3.64[e]	0.073[e]	3.40[f]	3.21[f]
	$^1B_2$	3.50	0.28	3.59	0.49	3.52	0.29	3.85	0.67	3.86[e]	0.11[e]	3.75[f]	4.80[f]
	$^1A_1$	4.01	0.35										
				4.01	0.52	4.05	0.81						
	$^1A_1$	4.10	0.81										
	$^1A_1$							4.31	0.53				
	$^1B_2$	4.36	0.41	4.17	0.46	4.20	0.41	4.33	0.53	4.79[e]	0.39[e]	4.71[f]	4.65[f]
3[b]	$^1B_2$			1.68	0.07	2.21	0.16	1.62	0.07	1.52[e]	0.014[e]	1.56[f]	2.108[f]
	$^1B_2$	2.31	0.19										
	$^1A_1$			3.29	0.17	3.35	0.37	3.31	0.20	2.89[e]	0.009[e]	2.94[f]	2.81[f]
	$^1B_2$	3.26	0.37	3.28	0.70	3.31	0.41	3.40	0.72	3.47[e]	0.30[e]	3.34[f]	4.09[f]
	$^1A_1$	3.48	0.41	3.62	0.60			3.52	0.62				
	$^1A_1$	4.02	0.54	4.13	0.53	3.93	0.54	4.27	0.56	3.82[e]	0.14[e]	3.97[f]	4.0[f]
	$^1A_1$	4.25	0.39			4.20	0.43						
	$^1B_2$	4.45	0.38	4.25	0.35	4.35	0.31	4.41	0.37	4.48[e]	0.019[e]		
	$^1B_2$			4.35	0.62	4.37	0.42	4.42	0.65				
	$^1A_1$									4.57[e]	0.53[e]	4.77[f]	
	$^1A_1$					5.18	0.31	5.25	0.46				
	$^1B_2$	4.51	0.33	5.20	0.07	5.47	0.15	5.43	0.06	4.95[e]	1.44[e]	4.94[f]	

Can. J. Chem. Downloaded from www.nrcresearchpress.com by 210.87.254.40 on 09/05/12
For personal use only.

TABLE 4. (*Continued*)

		Theoretical											
		s.c.f.(*a*)		s.c.f.(*b*)		s.c.f.(*c*)		s.c.f.(*d*)		Other work		Exptl.	
Molecule	Symmetry	eV	*f*	eV	*f*	eV	*f*	eV	*f*	eV	*f*	eV	log(ε)/*f*[a]
4	$^1B_{1g}$	1.96	0	1.83	0	1.71	0	1.73	0	1.82[g]	0[g]	(1.61)[h]	1–1.65[h]
	$^1B_{2u}$							2.94	0.78	2.54[g]	0.2[g]	2.57[h]	4.11[h]
	^1A_g	3.28	0	3.09	0	3.20	0	3.09	0	3.05[g]	0[g]		
	$^1B_{2u}$	3.31	0.77	3.27	0.74	3.24	0.71					3.03[h]	2.92[h]
	$^1B_{3u}$	3.59	1.03	3.51	0.73	3.66	0.71	3.61	0.82	3.20[g]	0.1[g]	3.61[h]	4.13[h]
	$^1B_{3u}$	3.69	0.83	3.81	0.99	3.65	0.98	3.84	1.03	3.72[g]	1.7[g]		
	$^1B_{2u}$	3.81	0.77	3.98	0.74	3.97	0.71	4.13	0.76	3.91[g]	0.0004[g]		
	$^1B_{2u}$	4.30	0.26	4.07	0.23	4.14	0.23	4.18	0.31	4.18[g]	2.1[g]	4.15[h]	4.32[h]
	$^1B_{1g}$	4.33	0	4.17	0	4.30	0	4.25	0				
	$^1B_{3u}$	4.92	0.55	4.59	0.59	4.50	0.59	4.62	0.60			4.64[h]	5.03[h]
	^1A_g	4.78	0	4.98	0	4.93	0	5.16	0				
5	$^1B_{1g}$	1.74	0	1.72	0	1.54	0	1.72	0	1.84[g]	0[g]		
	$^1B_{3u}$									2.64[g]	0.5[g]		
	^1A_g	3.34	0	3.08	0	3.33	0	3.03	0	2.93[g]	0[g]		
	$^1B_{2u}$	3.29	1.24	3.25	1.27	3.30	1.20	3.02	1.34	3.20[g]	0.2[g]		
	$^1B_{3u}$	3.61	0.59	3.57	0.63	3.60	0.60	3.67	0.67	3.47[g]	0.4[g]		
	$^1B_{2u}$	3.91	0.17	3.62	0.17	3.82	0.15	3.70	0.21				
	$^1B_{1g}$	4.12	0	3.84	0	4.16	0	4.00	0				
	$^1B_{3u}$	3.80	0.63	3.87	0.61	3.91	0.60	3.91	0.62	4.01[g]	2.5[g]		
	$^1B_{2u}$	3.92	0.97	4.00	0.97	3.99	0.90	4.07	1.01				
	^1A_g	4.68	0	4.77	0	4.68	0	4.84	0				
	^1A_g	4.97	0	5.02	0	4.89	0	4.93	0				
	$^1B_{3u}$	5.38	0.19	5.25	0.19	5.25	0.21	5.16	0.19				
6[b]	$^1B_2$	0.64	0.07	0.77	0.09	0.96	0.13	0.71	0.10	0.22[g]	0.01[g]		
	$^1A_1$	2.31	0.22	2.37	0.27	2.47	0.33	2.42	0.29	1.98[g]	0.2[g]		
	$^1A_1$	2.47	0.15	2.49	0.19	2.51	0.24	2.47	0.23	2.22[g]	0.03[g]		
	$^1B_2$	3.23	0.48	3.37	0.48	3.42	0.46	3.42	0.54	3.39[g]	0.004[g]		
	$^1B_2$	3.61	0.56	3.69	0.51	3.75	0.45	3.73	0.50	3.45[g]	0.02[g]		
	$^1B_2$	3.85	0.78	3.77	0.85	3.64	0.91	3.82	0.92	3.90[g]	1.6[g]		
	$^1B_2$	4.02	0.05	4.21	0.09	4.31	0.12	4.17	0.02				
	$^1B_2$	4.13	0.00	4.23	0.00	4.30	0.01	4.38	0.17				
	$^1A_1$	4.24	0.51	4.26	0.47	4.25	0.42	4.25	0.47				
	$^1A_1$	4.42	0.11	4.48	0.09	4.59	0.08	4.49	0.09				

Can. J. Chem. Downloaded from www.nrcresearchpress.com by 210.87.254.40 on 09/05/12
For personal use only.

TABLE 4. (*concluded*)

		Theoretical											
		s.c.f.(*a*)		s.c.f.(*b*)		s.c.f.(*c*)		s.c.f.(*d*)		Other work		Exptl.	
Molecule	Symmetry	eV	*f*	eV	*f*	eV	*f*	eV	*f*	eV	*f*	eV	log(ε)/*f*[a]
7	$^1B_2$	1.43	0.00	1.41	0.01	1.58	0.04	1.18	0.03			1.15[i]	1.74[i]
	$^1A_1$	2.64	0.05	2.57	0.04	2.81	0.01	2.38	0.00			2.13[i]	2.44[i]
	$^1A_1$	3.21	0.03	3.21	0.01	3.52	0.02	3.18	0.28			3.12[i]	3.67[i]
	$^1A_1$							3.23	0.36				
	$^1A_1$	3.46	0.87	3.55	0.89	3.49	0.87	3.44	0.98				
	$^1B_2$	3.45	0.78	3.46	0.77	3.68	0.59						
	$^1B_2$	3.78	0.67	3.76	0.14	3.67	0.63	3.67	0.58			3.68[i]	3.88[i]
	$^1B_2$	3.79	0.09										
	$^1B_2$					4.06	0.07	4.08	0.66				
	$^1B_2$	4.33	0.80	4.26	0.78	4.22	0.54	4.13	0.27			4.15[i]	4.88[i]
	$^1B_2$	4.44	0.38					4.26	0.32				
	$^1A_1$	4.82	0.63	4.37	0.38	4.53	0.47	4.60	0.76				
	$^1A_1$			4.74	0.65	4.80	0.71						
	$^1B_2$							5.19	0.04				
	$^1A_1$	5.13	0.02	5.17	0.01	5.02	0	5.27	0.00			5.32[i]	4.40[i]

[a]For azulene *f* values have been quoted.
[b]Symmetry designation has been given considering C_{2v} symmetry.
[c]Reference 6.
[d]References 25, 31.
[e]Reference 9*e*.
[f]References 32, 9*e*.
[g]Reference 10.
[h]Reference 14.
[i]Reference 13.

TABLE 5. Ionization energy (eV)

	Ionization energy								
	Uncorrected				Corrected				
Molecule	s.c.f.(*a*)	s.c.f.(*b*)	s.c.f.(*c*)	s.c.f.(*d*)	s.c.f.(*a*)[a]	s.c.f.(*b*)[a]	s.c.f.(*c*)[b]	s.c.f.(*a*)[c]	s.c.f.(*b*)[c]
1	9.10	9.06	9.11	8.53	7.78	7.73	7.47	8.93	8.90
2	9.36	9.23	9.38	8.55	8.03	7.90	7.49	9.17	8.89
3	8.86	8.58	8.85	8.00	7.53	7.25	6.94	8.87	8.49
4	8.75	8.82	8.72	8.21	7.42	7.49	7.15	8.63	8.71
5	9.10	8.95	9.19	8.46	7.77	7.62	7.40	8.92	8.76
6	7.82	7.90	8.02	7.44	6.49	6.57	6.38	7.50	7.58
7	8.28	8.31	8.46	7.71	6.95	6.98	6.65	8.07	8.10

[a]Correction made according to Bloor's formula (8).
[b]Correction made according to Kuni and Kuroda's formula (30).
[c]Difference between the total π energy of the molecule and positive ion.

strengths were obtained from the relation (26)

$$f = 1.085 \times 10^{-5}\bar{\nu}\mu^2$$

where $\bar{\nu}$ is the transition energy in cm^{-1} and μ is the dipole length for the corresponding transition in Å.

As far as possible, we have tried to obtain one-to-one correlation between the theoretical and experimental transitions, but since the molecules are not so simple, this is difficult. Hence, in some cases, we have attempted a general correlation over quite a wide spectral region.

For azulene the correlation between the experimental and these methods is good. However, the s.c.f.(*a–c*) methods do not provide any transition and the s.c.f.(*d*) method provides a poor value to correspond to the 4.52 eV transition for which other workers (6) have indicated some correlation. This may be due to not considering configuration interaction. Apart from this the agreement between these methods and other theoretical results is also good.

For aceazulylene, in the s.c.f.(*a*) method, the correlation between theoretical and experimental transition energies is good in the higher region only. For the s.c.f.(*d*) method the overall correlation is good except for the transition energy corresponding to 3.01 eV which can only be correlated to experimental values from 2.60 to 3.40 eV. It is seen that among the four methods the s.c.f.(*b*) method gives the best correlation although the correspondence between the theoretical value of 4.17 eV and the experimental value of 4.71 eV is not good. These methods give good agreement with those results calculated by DasGupta and Ali (9*c*), who used configuration interaction (c.i.), and by Yamaguchi *et al.* (9*e*) using a "β variable method" with c.i. In the case of aceheptylene the same situation is seen, *i.e.*, the s.c.f.(*b*) method gives a better correlation than the other three so far as theoretical and experimental transition energies are concerned, and the agreement between s.c.f.(*b*) and other theoretical results is also better than the other three.

The predicted transitions for azupyrene can be correlated beautifully with experimental ones (14). The same is also true for azulenoheptalene. The agreement among the results calculated by the four methods is also noteworthy.

For the other two molecules, dicycloheptapentalene and cyclopheptfluorene, which have not been synthesized, we compared our results with those of Heilbronner and co-workers (10). The agreement between these methods and that of Heilbronner is good.

Ionization Energy

It is well known (28) that ionization energies calculated by Koopman's (27) theorem are 1 to 2 eV too high. This discrepancy may be due to π-orbital deformation and σ-core contraction in the ionized molecule (29). Bloor (8) has proposed a general correction for hydrocarbons

$$I = -(\varepsilon_h + 1.33)$$

where ε_h is the orbital energy of the highest occupied orbital. For the "β variable" method the ionization energy is given by the following equation proposed by Kuni and Kuroda (30)

$$I = -(\varepsilon_h + 1.06)$$

with ε_h as defined above.

Table 5 contains the values for the uncorrected ionization energy based on Koopman's

Can. J. Chem. Downloaded from www.nrcresearchpress.com by 210.87.254.40 on 09/05/12
For personal use only.

theorem, the corrected ionization energy as proposed by Bloor (8) and Kuni and Kuroda (30). It also contains the ionization energies for these molecules calculated as the difference in total π energy of the neutral molecule and the positive ions. It is expected that since identical basic integrals were used in all cases these values should include the correction due to π-orbital deformation neglecting, however, the σ-core contraction.

Summary

The charge densities, bond lengths, dipole moments, and ionization energies predicted by the methods of Lo and Whitehead, Chung and Dewar, and Dewar and Harget are all consistent with one another even though the latter method differs from the others in that the $\beta_{\mu\nu}$ and some $\gamma_{\mu\nu}$ integrals are recalculated at each iteration. Such consistency is based upon the common fundamental intent of these methods to give reasonable prediction of heats of atomization.

Spectral transitions can also be reasonably correlated with the predictions of all four methods. It is seen, however, that the s.c.f.(*b*) method is better than the other methods in predicting spectral transitions of these non-benzenoid compounds. It is surprising that a method whose parameters are evaluated solely from ground state functions should yield better results than a method (s.c.f.(*d*)) which has been fitted to the spectral transitions of alternants.

The authors would like to express their gratitude to Professor F. W. Birss for many stimulating discussions, helpful comments, and financial support. They are also grateful to Computing Services of the University of Alberta for computational facilities.

1. F. W. Birss and N. K. Das Gupta. Can. J. Chem. **49**, 2840 (1971).
2. D. H. Lo and M. A. Whitehead. Can. J. Chem. **46**, 2027 (1968).
3. A. L. H. Chung and M. J. S. Dewar. J. Chem. Phys. **42**, 756 (1965).
4. D. H. Lo and M. A. Whitehead. Can. J. Chem. **46**, 2041 (1968).
5. K. Nishimoto and L. S. Forster. Theor. Chim. Acta, Berl. **3**, 407 (1965).
6. H. Yamaguchi, T. Nakajima, and T. L. Kuni. Theor. Chim. Acta, Berl. **12**, 349 (1968).
7. (*a*) M. J. S. Dewar and G. J. Gleicher. J. Am. Chem. Soc. **87**, 685 (1965); **87**, 692 (1965); (*b*) M. J. S. Dewar and C. DeLlano. J. Am. Chem. Soc. **91**, 789 (1969); (*c*) M. J. S. Dewar and A. J. Harget. Proc. R. Soc. London, **A315**, 443, 457 (1970).
8. J. E. Bloor. Can. J. Chem. **43**, 3026 (1965).
9. (*a*) M. A. Ali and C. A. Coulson. Mol. Phys. **4**, 65 (1961); (*b*) H. Chatterjee and M. A. Ali. Tetrahedron, **20**, 2829 (1964); (*c*) N. K. Das Gupta and M. A. Ali. Theor. Chim. Acta, Berl. **4**, 101 (1966); (*d*) A. Julg and P. Francois. Theor. Chim. Acta, Berl. **7**, 249 (1967). (*e*) H. Yamaguchi, T. Terasaka, and T. Nakajima. Theor. Chim. Acta, Berl. **18**, 255 (1970).
10. P. Baumgartner, E. Weltin, G. Wagniere, and E. Heilbronner. Helv. Chim. Acta, **48**, 751 (1965).
11. R. Pariser and R. G. Parr. J. Chem. Phys. **21**, 466, 767 (1953).
12. J. A. Pople. Trans. Faraday. Soc. **49**, 1375 (1953).
13. K. Hafner, G. Hafner-Schneider, and F. Baur. Angew. Chem. Int. Ed. **7**, 808 (1968).
14. A. G. Anderson, Jr., A. A. MacDonald, and A. F. Montana. J. Am. Chem. Soc. **90**, 2993 (1968).
15. D. H. Reid, W. H. Stafford, and J. P. Ward. J. Chem. Soc. 1193 (1955); R. Munday and I. O. Sutherland. J. Chem. Soc. C, 1427 (1969).
16. C. C. J. Roothan. Rev. Mod. Phys. **23**, 69 (1951).
17. J. Hinze and H. H. Jaffe. J. Am. Chem. Soc. **84**, 540 (1962).
18. K. Nishimoto and R. Fujishiro. Bull. Chem. Soc. Jap. **37**, 1660 (1964).
19. A. DasGupta and N. K. DasGupta. Unpublished results.
20. N. Mataga and K. Nishimoto. Z. Phys. Chem. **13**, 140 (1957).
21. K. Ohno. Theor. Chim. Acta, **2**, 219 (1964).
22. J. M. Robertson, H. M. M. Shearer, G. A. Sim, and D. G. Watson. Acta Cryst. **15**, 1 (1962).
23. H. J. Lindner. J. Chem. Soc. B, 907 (1970).
24. R. Quasba, F. Brandl, W. Hope, and R. Huber. Acta Cryst. **B25**, 1198 (1969).
25. E. Heilbronner. *In* Nonbenzenoid aromatic compounds. *Edited by* D. Ginsberg. Interscience Publishers, Inc., N.Y. 1959. p. 196.
26. L. Salem. The molecular orbital theory of conjugated systems. W. A. Benjamin, Inc. N.Y. 1966. p. 358.
27. T. Koopman. Physica, **1**, 104 (1934).
28. C. Moser. J. Chim. Phys. **52**, 24 (1955).
29. J. R. Hoyland and L. Goodman. J. Chem. Phys. **33**, 946 (1960).
30. T. L. Kuni and H. Kuroda. Theor. Chim. Acta, Berl. **11**, 97 (1968).
31. R. Pariser. J. Chem. Phys. **25**, 1112 (1956); G. R. Hunt and I. G. Ross. J. Mol. Spectrosc. **9**, 52 (1962).
32. K. Hafner and J. Schneider. Liebigs. Ann. Chem. **624**, 37 (1959).

Can. J. Chem. Downloaded from www.nrcresearchpress.com by 210.87.254.40 on 09/05/12
For personal use only.

Cinétique de la pyrolyse du sous-oxyde de carbone et de sa réaction avec l'oxyde nitreux

MICHEL-M. BONNEAU ET CYRIAS OUELLET
Département de Chimie, Université Laval, Québec, Québec G1K 7P4

Reçu le 27 juin 1973

Dans le domaine de 600–700 °C et 20–100 mm Hg dans des réacteurs en Vycor, la vitesse de pyrolyse de C_3O_2 est proportionnelle au rapport surface/volume et son énergie d'activation globale dépend aussi de la surface. Cette réaction est du premier ordre aux basses pressions et est fortement inhibée par NO. Par contre, la réaction de C_3O_2 avec N_2O n'est pas inhibée par NO; elle est du premier ordre par rapport à chacun des réactifs, a une énergie d'activation globale de 52 kcal mol^{-1} et est partiellement affectée par le rapport surface/volume. L'analyse donne le bilan $4C_3O_2 + N_2O = N_2 + CO_2 + 7CO + 4C(s)$. Nous proposons une initiation bimoléculaire hétérogène suivie d'une chaîne courte du type $C_n + C_3O_2 \rightarrow 2CO + C_{n+1}$. On examine le rôle de C_2O.

In the range 600–700 °C and 20–100 mm Hg in Vycor vessels, the velocity of C_3O_2 pyrolysis is proportional to the surface/volume ratio and its overall activation energy is also surface-sensitive. This reaction is first-order at the lower pressures and is strongly inhibited by NO. On the contrary, the reaction of C_3O_2 with N_2O is not inhibited by NO; it is first-order in each reactant, shows an overall activation energy of 52 kcal mol^{-1}, and is partially surface dependent. Analysis shows the material balance $4C_3O_2 + N_2O = N_2 + CO_2 + 7CO + 4C(s)$. We suggest a bimolecular heterogeneous initiation followed by a short chain of the type $C_n + C_3O_2 \rightarrow 2CO + C_{n+1}$. The part played by C_2O is discussed.

Can. J. Chem., 52, 167 (1974)

Introduction

Nous avons étudié la pyrolyse de C_3O_2 et sa réaction avec N_2O à des pressions et températures moyennes, 20–100 mm Hg et 600–700 °C, où ces réactions s'effectuent à des vitesses commodément mesurables et comparables à celle de la combustion lente de C_3O_2 (1). La pyrolyse a déjà été étudiée à des concentrations de C_3O_2 inférieures à 1% dans un gaz inerte, d'une part en régime dynamique entre 650 et 750 °C par mesure du dépôt de carbone formé (2), d'autre part entre 1200 et 2500 °C dans des ondes de choc (3). Dans ces conditions, la réaction présumément homogène était du premier ordre par rapport à C_3O_2 et affectée d'énergies d'activation de 52 et 61 kcal mol^{-1} respectivement. La combustion lente (1) semble être initiée sur la paroi et est fortement inhibée par NO. C'est ce qui nous a amenés à étudier les réactions de C_3O_2 avec les oxydes d'azote. Après des essais préliminaires avec NO (réaction très lente), nous avons entrepris l'étude de la réaction avec N_2O.

On sait qu'à la température ambiante C_3O_2 réagit avec l'oxygène atomique (4, 6, 7) pour donner soit 3 CO soit $CO_2 + C_2O$. La photolyse à 3000 Å donne naissance à C_2O dans son état fondamental triplet, qui réagit rapidement avec NO (5–7).

Méthode expérimentale

Nous avons étudié ces réactions en système statique dans des cylindres de 22 × 4.5 cm en Vycor et en quartz, dont le rapport surface/volume de 1.1 cm^{-1} pouvait être porté à 3.2 et à 5.0 cm^{-1} par addition de tubes de Vycor de 2 × 1 cm. On enregistrait la pression au moyen d'un capteur électro-magnétique Pace (modèle P 7) et on analysait les échantillons à 25 °C dans un chromatographe à gaz F et M (modèle 700). On préparait le C_3O_2 par déshydratation de l'acide malonique (8) et on le conservait à −196 °C pour prévenir la polymérisation. Pour en contrôler la pureté, on comparait son spectre i.r. à celui qui a été publié (9). Le N_2O était de marque Matheson, L. B. Les mélanges gazeux étaient préparés à la température ambiante et séjournaient 30 min avant d'être introduits dans le réacteur. On dosait C_3O_2 sur brique pilée contenant 23% d'Apiezon M selon (10), CO_2 et N_2O sur charbon activé. Pour N_2, CO, NO et O_2, on utilisait une colonne de Porapak S 180/200 M en série avec une colonne de tamis moléculaire 13 X. A noter que C_3O_2, CO_2 et N_2O sont retenus par la première (11).

Résultats

Pyrolyse de C_3O_2

Quelques expériences préliminaires ont confirmé que la réaction obéit à l'équation $C_3O_2 = C(solide) + 2CO$ et, en particulier, qu'il n'y a pas production de CO_2. Aux basses pressions initiales de C_3O_2, la réaction est du premier ordre, mais aux pressions initiales élevées dans les réacteurs de $S/V = 3.2$ ou 5.0, la réaction est d'ordre zéro

Can. J. Chem. Downloaded from www.nrcresearchpress.com by 210.87.254.42 on 09/05/12
For personal use only.

Can. J. Chem. Downloaded from www.nrcresearchpress.com by 210.87.254.42 on 09/05/12
For personal use only.

au début et ne devient du premier ordre que lorsque la pression de C_3O_2 tombe en-dessous d'une certaine valeur qui se situe vers 30 ou 50 mm Hg selon le réacteur employé.

Pour étudier l'influence des facteurs pression, surfaces, additifs et température, nous avons comparé les valeurs de la vitesse initiale de la pyrolyse exprimées en mm Hg s^{-1}. On voit sur la fig. 1 les effets de la pression initiale du C_3O_2 et du rapport surface/volume du réacteur. La vitesse initiale croît linéairement avec la pression jusqu'à une valeur limite d'autant plus élevée que la surface est plus grande. Incidemment, les vitesses sont les mêmes dans les réacteurs de $S/V = 1.1$ cm^{-1} en Vycor et en quartz. Donc, la réaction n'est pas sensible à de petites différences de nature de la surface. Si l'on compare les vitesses initiales observées dans les mêmes conditions mais dans des réacteurs de S/V différents, on obtient les valeurs de la fig. 2. En extrapolant, on trouve que la vitesse serait nulle à $S/V = 0$, c.-à-d. en l'absence de paroi. Il semble donc que la pyrolyse soit entièrement hétérogène dans les conditions de nos expériences.

NO exerce un effet inhibiteur puissant comme le montre la fig. 3. En revanche, l'argon ne modifie pas la vitesse, même à une pression triple de celle de C_3O_2.

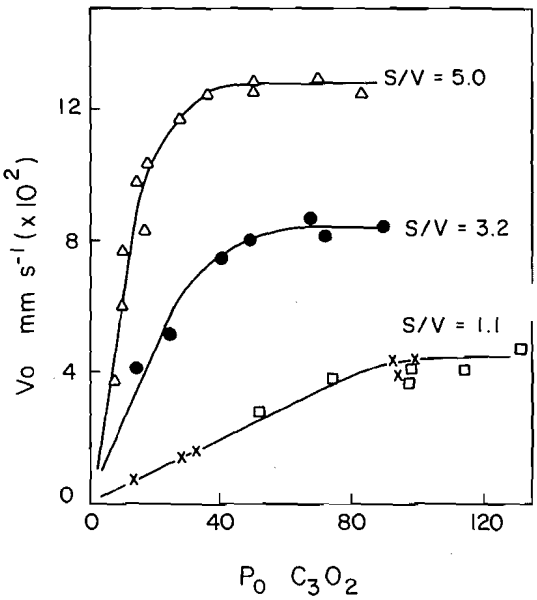

FIG. 1. Influence de la pression de C_3O_2 sur la vitesse initiale de la pyrolyse à 653 °C dans des réacteurs en Vycor (△, ○, □) et en quartz (×) ayant des rapports surface/volume différents.

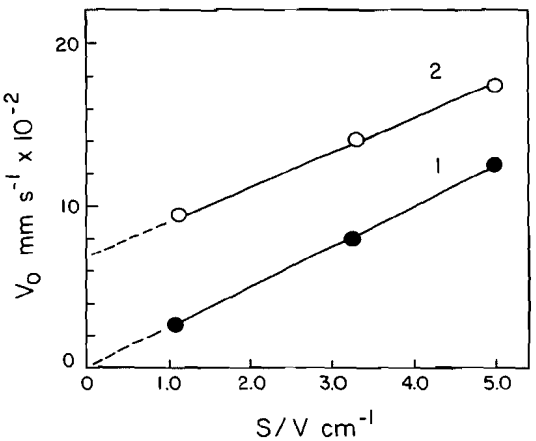

FIG. 2. Influence du rapport surface/volume sur les vitesses initiales (1) et de la pyrolyse de C_3O_2 à $P_0 = 50$ mm et (2) de sa réaction avec N_2O à $P_0 = 50 + 50$ mm à 654 °C.

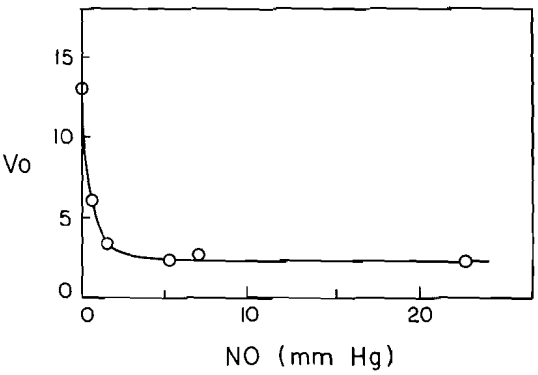

FIG. 3. Influence de NO sur la vitesse initiale de la pyrolyse à 39 mm Hg et 653 °C dans un réacteur de $S/V = 5.0$ cm^{-1} (V_0 mm Hg s^{-1} × 10^2).

Les mesures de l'énergie d'activation apparente nous ont donné des résultats d'une reproductibilité médiocre (fig. 4), mais un fait ressort clairement de plusieurs séries d'expériences: cette énergie est très grande (~100 kcal mol^{-1}) en-dessous de 650 °C et petite (~10 kcal mol^{-1}) au-dessus de 650 °C dans le réacteur à grande surface $S/V = 5$. Par contre, elle n'est que d'environ 40 kcal mol^{-1} dans le réacteur $S/V = 1$.

Réaction de C_3O_2 avec N_2O

Dès l'introduction d'un mélange $1C_3O_2 : 1N_2O$ dans un réacteur neuf, la pression croît et tend vers une valeur finale de 3/2 fois la pression initiale. La vitesse de cette augmentation de pression s'accroît lors des expériences suivantes puis devient reproductible. C'est l'indication d'un

Can. J. Chem. Downloaded from www.nrcresearchpress.com by 210.87.254.42 on 09/05/12
For personal use only.

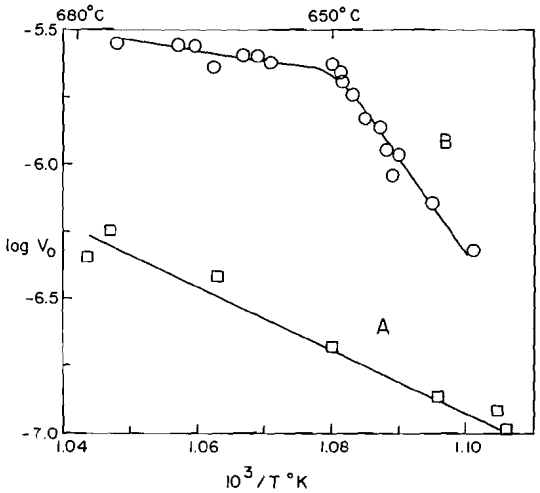

FIG. 4. Influence de la température sur la vitesse initiale de la pyrolyse à 55 mm Hg dans les réacteurs en Vycor S/V = 1.1 cm^{-1} (*A*) et 5.0 cm^{-1} (*B*) (V_0 mol l^{-1} s^{-1}).

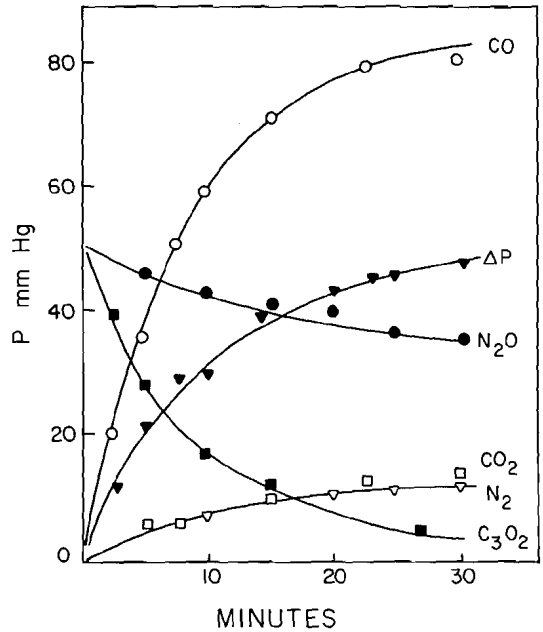

FIG. 5. Evolution des espèces chimiques au cours d'une réaction à 653 °C dans le réacteur S/V = 1.1 cm^{-1}.

effet de surface attribuable à un dépôt de carbone qui devient visible par la suite. La vitesse initiale dépend du rapport surface/volume du réacteur comme le montre la droite supérieure de la fig. 2. A la différence de la pyrolyse de C_3O_2, qui paraissait entièrement hétérogène, sa réaction avec N_2O semble avoir une composante homogène résiduelle à $S/V = 0$.

Dans ce qui suit, il sera d'abord question des résultats obtenus dans le réacteur en Vycor à surface minimum S/V = 1.1, jusqu'à indication du contraire.

La fig. 5 montre les pressions partielles des espèces obtenues à partir d'échantillons prélevés à diverses époques au cours d'une série de réactions de mélanges équimoléculaires de C_3O_2 et de N_2O à 654 °C. On remarque que 4 molécules de C_3O_2 disparaissent pour chaque molécule de N_2O consommée. La quantité de CO formée est environ 7 fois celles de N_2 et de CO_2. Faisant arbitrairement correspondre 50 mm Hg à 1 mole de C_3O_2 ou de N_2O, soit en tout à 68 + 44 = 112 g, on retrouve à la fin de la réaction 100 ± 1 g d'après les pressions partielles des espèces présentes. Le déficit de 12 g est attribué à la perte d'une mole de carbone C(s) par mole de C_3O_2 disparue. En utilisant des coefficients entires, ce bilan s'exprime par l'équation 1*a*

$$[1a]\quad 4C_3O_2 + 4N_2O = N_2 + 3N_2O + CO_2 + 7CO + 4C(s)$$

qui s'accorde aussi avec l'augmentation de 50% de la pression totale. Pour vérifier que ce bilan inusité n'était pas fortuit, nous avons, au cours de réactions à plusieurs températures, analysé des échantillons prélevés à des temps et à des pourcentages de réaction différents. Le tableau 1 montre que l'équation 1*a* s'applique dans un domaine assez étendu.

Il est peu probable que ces valeurs résultent d'une simple superposition de la pyrolyse de C_3O_2 et de celle de N_2O. Pour en être plus sûrs, nous avons mesuré les vitesses de chacune de ces réactions dans les conditions mêmes de nos expériences: 654 °C, pressions initiales de 50 mm, réacteurs S/V = 1.1 et 5.0 cm^{-1}. Remarquons que la comparaison est facilitée par le fait que l'augmentation de pression est de 50% pour $N_2O = N_2 + \frac{1}{2}O_2$ ainsi que pour [1*a*]. Les résultats sont consignés au tableau 2. Les nombreuses données existantes (12) sur la pyrolyse de N_2O sont difficilement transposables à nos conditions expérimentales: nous avons déterminé empiriquement les vitesses, en l'absence (−) et en présence (+) d'une couche de carbone provenant de pyrolyses préalables de C_3O_2. On voit que le réacteur S/V = 1.1 cm^{-1}, la réaction entre C_3O_2 et N_2O est nettement plus rapide que chacune des pyrolyses prise séparément. On note

TABLEAU 1. Pressions partielles en mm Hg des produits de quelques réactions à partir de mélanges 1:1 de $P_0 = 100 \pm 1$ mm Hg; $S/V = 1.1$ cm^{-1}

t (°C)	Temps (min)	ΔP	CO	CO_2	N_2	$(CO + CO_2)/\Delta P$	CO/N_2	CO_2/N_2
614	15	20.7	34.9	5.3	4.8	1.95	7.3	1.1
653	5	22.0	37.2	5.6	5.5	1.95	6.8	1.0
653	15	40.5	72.5	9.8	9.7	2.02	7.4	1.0
684	5	34.4	60.0	8.1	8.1	1.98	7.4	1.0

TABLEAU 2. Vitesses initiales de trois réactions dans des réacteurs de $S/V = 1.1$, 3.2 et 5.0 cm^{-1} avec (+) et sans (−) dépôt de carbone à 654 °C et 50 mm Hg de chaque réactif

Réaction	S/V (cm^{-1})	C	$V_0 \times 10^2$ (mm s^{-1})
$C_3O_2 = 2CO + C$	1.1	+	2
	3.2	+	8
	5.0	+	10
$N_2O = N_2 + \frac{1}{2}O_2$	1.1	−	0.2
	1.1	+	0.6
	5.0	−	0.6
	5.0	+	30.0
$C_3O_2 + N_2O =$ produits	1.1	+	10
	3.2	+	14
	5.0	+	17

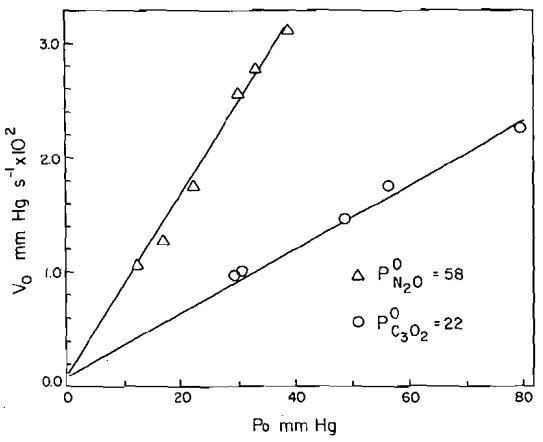

FIG. 6. Ordres relatifs aux pressions initiales de chacun des réactifs à 610 °C dans le réacteur $S/V = 1.1$ cm^{-1}.

que le carbone accélère la décomposition de N_2O. L'accélération considérable observée dans le réacteur $S/V = 5.0$ cm^{-1} est peut-être le résultat d'une oxydation du carbone et d'autoéchauffement, mais la quantité ainsi oxydée ne peut être grande, car le rapport $CO/CO_2 \sim 7$ se retrouve dans ce réacteur lors de notre réaction $C_3O_2 + N_2O$.

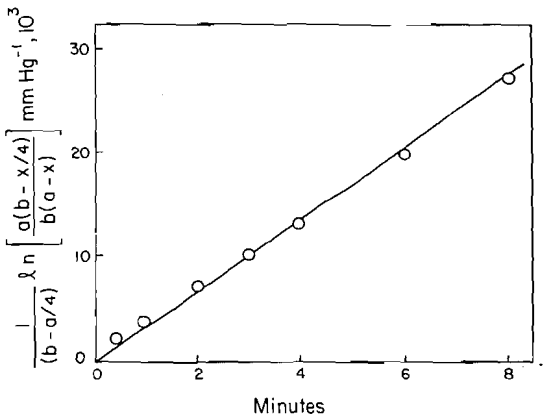

FIG. 7. Ordre global au cours d'une réaction d'un mélange 1 C_3O_2:1 N_2O à $P_0 = 120$ mm et à 665 °C dans le réacteur $S/V = 1.1$ cm^{-1}.

La réaction à 610 °C est du premier ordre (fig. 6) par rapport à chacun des réactifs et le deuxième ordre global (fig. 7) se maintient à 665 °C jusqu'à au moins 80% de conversion suivant l'équation 2.

$$[2] \qquad \frac{1}{(b - a/4)} \ln \frac{a(b - x/4)}{b(a - x)} = kt$$

où $a = P_0$ (C_3O_2), $b = P_0$ (N_2O) et $x = \Delta P$. Nous avons aussi vérifié que l'ordre global est de 2 à 618 °C. Donc l'ordre ne varie pas avec la température.

L'influence de la température sur la vitesse initiale V_0 est illustrée sur la fig. 8, où les cercles blancs proviennent de températures ascendantes et les carrés noirs de températures décroissantes. L'énergie d'activation apparente est de 51 ± 2 kcal mol^{-1}. On ne retrouve pas les anomalies observées lors de la pyrolyse de C_3O_2.

Il est difficile d'établir avec certitude l'importance relative des effets de surface. A 654 °C, nous avons observé la même vitesse et la même stoechiométrie dans les réacteurs $S/V = 1.1$ cm^{-1} en Vycor et en quartz, probablement parce que la surface active est la couche de carbone. La

Can. J. Chem. Downloaded from www.nrcresearchpress.com by 210.87.254.42 on 09/05/12
For personal use only.

Can. J. Chem. Downloaded from www.nrcresearchpress.com by 210.87.254.42 on 09/05/12
For personal use only.

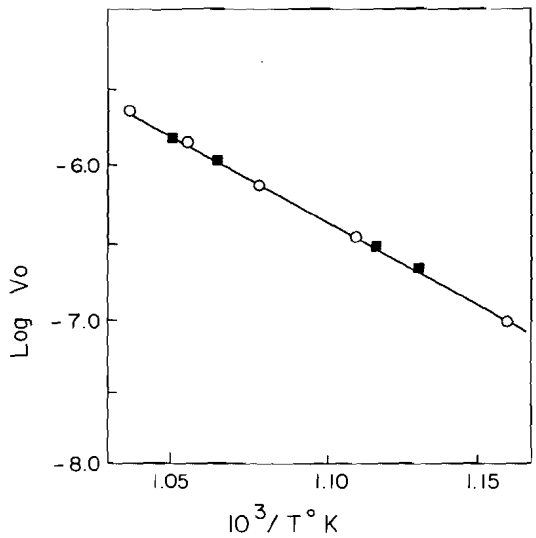

FIG. 8. Influence de températures ascendantes (○) et descendantes (■) sur la vitesse initiale dans le réacteur $S/V = 1.1\ cm^{-1}$. $P_0(C_3O_2) = 22$ mm; $P_0(N_2O) = 30$ mm (V_0 mol l^{-1} s^{-1}).

stoechiométrie reste la même dans le réacteur $S/V = 5.0\ cm^{-1}$ où la vitesse est beaucoup plus grande. Dans une série d'expériences avec des mélanges 1:1 à 654 °C dans le réacteur $S/V = 5.0\ cm^{-1}$, nous avons trouvé (11) que la réaction est encore du deuxième ordre aux basses pressions, comme dans le cas de la fig. 7, mais qu'elle devient du premier ordre au-dessus d'environ 40 mm. Cette discontinuité ne se manifeste que dans le réacteur $S/V = 5.0\ cm^{-1}$, et dans à peu près les mêmes conditions que la discontinuité visible sur les figs. 1 et 4. Il n'est pas possible de dire si cet effet est dû à la saturation de la surface par l'un des réactifs ou à un phénomène de diffusion.

Il est remarquable que l'addition de NO à des concentrations de 10% de celle des réactifs dans des mélanges 1:1 ne modifie ni la vitesse ni le ΔP dans les réacteurs $S/V = 1.1$ et 5.0 à 654 °C. Rappelons que NO inhibe fortement la pyrolyse et la combustion (1) de C_3O_2. L'addition de 110 mm d'argon à un mélange de 53 mm accroît la vitesse initiale de 30%, ce qui suggère la présence de chaînes courtes. L'addition de 53 mm de CO à ce même mélange ne modifie ni la vitesse, ni le ΔP ni la composition des produits. Donc, les réactions possibles $CO + C_2O \rightarrow C_3O_2$ et $CO + N_2O \rightarrow CO_2 + N_2$ ne perturbent pas la cinétique de notre réaction dans les conditions de nos expériences.

Discussion

La pyrolyse de C_3O_2 et la réaction de ce dernier avec N_2O ont des caractères cinétiques très différents.

La cinétique de la pyrolyse semble entièrement déterminée par une réaction hétérogène. Les anomalies visibles sur la fig. 4 ne permettent aucun rapprochement avec les données obtenues dans des conditions totalement différentes (2, 3), c.-à-d. à très faibles concentrations. Notons seulement que l'énergie d'activation apparente que nous observons entre 600 et 650 °C, soit ~100 kcal mol^{-1}, n'est pas impensable vu que l'enthalpie de la réaction 3 est de 86 kcal mol^{-1} (5–7), mais que cela exigerait un facteur pré-exponentiel peu vraisemblable. Il est possible que le bas coefficient de température (fig. 4) observé au-dessus de 654 °C dans le réacteur à grande surface soit dû à la limitation de la vitesse par un processus de diffusion.

Les étapes de la pyrolyse sont probablement [3] et [4]

$$[3] \qquad C_3O_2 \xrightarrow{\text{paroi}} CO + C_2O$$

$$[4] \qquad C_2O \longrightarrow CO + C$$

Nous pensons que la première au moins de ces étapes est hétérogène et qu'elle est la même qui amorce les chaînes de la combustion (1).

L'inhibition par NO pourrait résulter de la capture [5] de C_2O par le radical NO.

$$[5] \qquad C_2O + NO \rightarrow X$$

Cette réaction est déjà rapide à la température ambiante (5–7), mais on ignore encore la nature du produit X. Nous n'avons pas vérifié si, dans nos expériences, on voit apparaître de petites quantités de N_2, CO_2, NO_2 ou N_2O en présence de NO comme c'est le cas à froid (6, 7). Il se peut qu'à haute température le produit X soit instable et agisse simplement comme intermédiaire pour propager la chaîne. Ce qui nous fait penser que la capture de C_2O n'est pas responsable de l'inhibition de la pyrolyse, c'est que NO n'inhibe pas la réaction de C_3O_2 avec N_2O. Ce contraste s'expliquerait facilement si les deux réactions étaient amorcées par des processus différents; par exemple si NO inhibait la pyrolyse en bloquant sur la surface un site actif qui n'intervient pas dans la réaction entre C_3O_2 et N_2O. Le processus ainsi inhibé serait [3] et le C_2O intervenant dans la réaction avec N_2O aurait une origine différente de [3].

Can. J. Chem. Downloaded from www.nrcresearchpress.com by 210.87.254.42 on 09/05/12
For personal use only.

Pour ce qui est de la réaction entre C_3O_2 et N_2O, l'invariabilité des ordres, du coefficient de température et du bilan [1*a*] que nous écrirons [1*b*]

[1*b*] $4C_3O_2 + N_2O = N_2 + CO_2 + 7CO + 4C(s)$

montre que la disparition des deux réactifs ne résulte pas de la simple addition de leurs décompositions respectives. Nous chercherons un mode d'inhibition par NO et un mécanisme de formation du carbone.

L'initiation par décomposition de C_3O_2 selon [3] nous paraît incompatible avec l'absence d'inhibition par NO. La pyrolyse de N_2O dont l'énergie d'activation (12) est de 59 kcal mol^{-1}, pourrait amorcer la chaîne suivante

[6] $M + N_2O \rightarrow N_2 + O + M$

[7] $O + C_3O_2 \rightarrow CO_2 + C_2O$

[8] $O + C_3O_2 \rightarrow 3CO$

[4] $C_2O \rightarrow CO + C$

Pour respecter le rapport $CO_2/N_2 = 1$, il faudrait que [8] devînt négligeable par rapport à [7] à haute température, car [8] est nettement la plus rapide à la température ambiante (4, 6, 7). Il faudrait encore que les vitesses de $O + N_2O = 2NO$ et $O + N_2O = N_2 + O_2$ fussent négligeables par rapport à celle de [7]. De plus, pour obtenir le premier ordre par rapport à chacun des réactifs, il faudrait soit postuler la réversibilité de [6], soit identifier M à C_3O_2, c.-à-d. supposer que le transfert d'énergie à N_2O est beaucoup plus efficace dans les chocs avec C_3O_2 qu'entre les molécules N_2O.

L'initiation par réaction bimoléculaire selon [9]

[9] $C_3O_2 + N_2O \xrightarrow{\text{paroi}} N_2 + C_3O_3$

[10] $C_3O_3 \longrightarrow CO_2 + C_2O$

[4] $C_2O \longrightarrow CO + C$

fait intervenir un intermédiaire instable hypothétique C_3O_3, mais élimine les complications dues à la présence d'atomes O libres et respecte le rapport $CO_2/N_2 = 1$.

Pour rendre compte de la stoechiométrie, nous postulons une chaîne rapide du type [11]–[13] au cours de laquelle C_1, C_2, C_3 ... s'additionnent sur le carbone central de OCCCO.

[11] $C + C_3O_2 \rightarrow 2CO + C_2$

[12] $C_2 + C_3O_2 \rightarrow 2CO + C_3$

[13] $C_3 + C_3O_2 \rightarrow 2CO + C_4$

La suite d'étapes [9]–[13] rend compte de la production, à partir d'une seule molécule de N_2O, de $1N_2$, $1CO_2$, 7CO et 4C. Nous choisissons arbitrairement une terminaison en C_4 parce qu'elle concorde avec nos résultats; mais cette terminaison nous paraît plausible puisque C_4 étant la maille élémentaire du graphite, a des chances d'être moins réactif que C_1, C_2 et C_3. Pour conserver le rapport $CO_2/N_2 = 1$, il faut en plus supposer que les vitesses de réactions telles que $C + N_2O \rightarrow N_2 + CO$ sont négligeables par rapport à celles de [11]–[13] (13).

Nous avons omis de dire si la chaîne se propage en phase gazeuse ou sur la surface, car plusieurs réactions du carbone gazeux sont connues (13, 14). On peut obtenir des valeurs approximatives des enthalpies de réaction à partir des enthalpies de formation (ramenées à 1000 °K) des molécules. Ces dernières sont d'environ -10 kcal mol^{-1} pour C_3O_2 (15, 16), 27 pour N_2O, -86 pour CO_2, -21 pour CO et 5 pour N_2. Celle de C_2O serait d'environ 98 (5, 17) et celles de C_1, C_2, C_3 d'environ 174, 205 et 191 respectivement (16). On trouve ainsi que l'enthalpie de [9] et [10] combinées serait à peu près nulle. Celle de [4] serait de 55 kcal mol^{-1}, alors que celles de [11], [12] et [13] seraient négatives. La réaction globale [1*b*] pourrait donc, à la rigueur, avoir lieu entièrement en phase gazeuse, mais les effets de surface observés et les réactions secondaires possibles de O et de C signalées plus haut nous incitent à penser que la paroi intervient au moins pour la réaction 9.

L'énergie d'activation apparente de 52 kcal mol^{-1} que nous observons pour la réaction de C_3O_2 avec N_2O concorde avec l'énergie D(C—CO) = 52 de dissociation (17) du radical C_2O, de sorte que la vitesse de la réaction est vraisemblablement limitée par celle de l'étape [4]. Cette même valeur a été trouvée pour la pyrolyse de C_3O_2 par nos prédécesseurs (2). Quant aux anomalies (fig. 4) que nous avons remarquées aux fortes concentrations en présence d'un grand rapport S/V (11), leur explication exigerait une exploration expérimentale systématique.

Nous remercions le Conseil national de recherches du Canada qui a subventionné ce travail et accordé une bourse à M.-M.B. Nous remercions aussi MM. Pierre Gagnon et Claude Fouquet pour leur aide technique.

1. J. LEBEL et C. OUELLET. Can. J. Chem. **49**, 447 (1971).
2. H. B. PALMER et T. J. HIRT. J. Am. Chem. Soc. **84**, 113 (1962); H. B. PALMER et W. D. CROSS. Carbon, **3**, 475 (1966).

3. H. KIJEWSKI, J. TROE et H. GG. WAGNER. Z. Phys. Chem. N.F. **68**, 321 (1969).
4. H. VON WEYSSENHOFF, S. DONDES et P. HARTECK. J. Am. Chem. Soc. **84**, 1526 (1962); G. LIUTI, C. KUNZ et S. DONDES. J. Am. Chem. Soc. **89**, 5542 (1967).
5. C. WILLIS et K. D. BAYES. J. Am. Chem. Soc. **88**, 3203 (1966).
6. D. G. WILLIAMSON et K. D. BAYES. J. Am. Chem. Soc. **89**, 3390 (1967); K. H. BECKER et K. D. BAYES. J. Chem. Phys. **48**, 653 (1968).
7. W. L. SHACKLEFORD, F. N. MASTRUP et W. C. KREYE. J. Chem. Phys. **57**, 3933 (1972).
8. D. A. LONG, F. S. MURFIN et R. L. WILLIAMS. Proc. R. Soc. London, A**223**, 251 (1954).
9. A. O. DIALLO et P. BARCHEWITZ. J. Chim. Phys. **61**, 1296 (1964).
10. T. J. HIRT et H. B. PALMER. Anal. Chem. **34**, 164 (1962); Carbon, **1**, 65 (1963).
11. M.-M. BONNEAU. Thèse de maîtrise, Université Laval, Québec, Québec. 1971.
12. H. S. JOHNSTON. J. Chem. Phys. **19**, 663 (1951); E. S. FISHBURNE et R. EDSE. J. Chem. Phys. **41**, 1297 (1964); H. A. OLSCHEWSKI, J. TROE et H. GG. WAGNER. Ber. Bunsenges. Phys. Chem. **70**, 450 (1966); D. GUTMAN, R. L. BELFORD, A. J. HAY et R. PANIROW. J. Phys. Chem. **70**, 1793 (1966); G. DORTHE et M. DESTRIAU. Bull. Soc. Chim. Fr. 2407 (1971).
13. D. HUSAIN et L. U. KIRSH. Trans. Faraday Soc. **67**, 2025 (1971).
14. P. S. SKELL, J. J. HAVEL et M. J. MCGLINCHEY. Acc. Chem. Res. **6**, 97 (1973); P. S. SKELL, J. E. VILLAUME, J. H. PLONKA et F. A. FAGONE. J. Am. Chem. Soc. **93**, 2699 (1971).
15. B. D. KYBETT, G. K. JOHNSON, C. K. BARKER et J. L. MARGRAVE. J. Phys. Chem. **69**, 3603 (1965).
16. S. W. BENSON. Thermochemical kinetics. Wiley, New York. 1968. pp. 195–201.
17. C. WILLIS et C. DEVILLERS. Chem. Phys. Lett. **2**, 51 (1968).

Can. J. Chem. Downloaded from www.nrcresearchpress.com by 210.87.254.42 on 09/05/12
For personal use only.

The Charge Transfer Spectra of d^8 Transition Metal Halide Complexes and the 1849 Å Photolysis of Aqueous $PtCl_4^{2-}$

JOHN L. H. BATISTE AND ROBERT RUMFELDT

Department of Chemistry, University of Windsor, Windsor, Ontario N9B 3P4

Received May 30, 1973

The ultraviolet spectra of the d^8 complexes PtX_4^{2-}, AuX_4^-, and $Pd_2X_6^{2-}$ (X = Cl^- or Br^-) are reported. The assignments are based on a standard ordering of molecular orbital energy levels and on the trends in the band frequencies as related to the different metals and ligands. In addition to the low intensity d–d bands, two distinct high intensity regions are identified, an initial set of charge transfer ligand to metal bands followed by a sequence of essentially d → p bands. The 1849 Å irradiation of aqueous $PtCl_4^{2-}$ results in a redox reaction via photoelectron formation with $\phi e_{aq}^- = 0.25 \pm 0.02$. The primary photolytic act is interpreted as initial excitation of the d → p transition $^1A_{1g} \rightarrow {}^1E_u(3)$ ($e_g\pi^* \rightarrow a_{2u}\pi^*$).

On a étudié les spectres des complexes d^8 PtX_4^{2-}, AuX_4^- et $Pd_2X_6^{2-}$ (X = Cl^- ou Br^-) dans l'ultraviolet. Les différentes attributions se rapportant aux différents métaux et coordinats sont basées sur un classement standard des niveaux énergétiques d'orbitale moléculaire et sur les tendances exhibées par les fréquences des bandes. En plus des bandes d–d de faible intensité, on a pu identifier deux régions distinctes de haute intensité, une série initiale de bandes du type transfert de charges coordinatmétal puis une série composée principalement de bandes du type d → p. L'irradiation à 1849 Å du $PtCl_4^{2-}$ aqueux a conduit à une réaction redox via la formation de photoélectrons avec $\phi e_{aq}^- = 0.25 \pm 0.02$. La première étape photolytique est représentée par l'excitation initiale de la transition d → p $^1A_{1g} \rightarrow {}^1E_u(3)$ ($e_g\pi^* \rightarrow a_{2u}\pi^*$). [Traduit par le journal]

Can. J. Chem., **52**, 174 (1974)

Introduction

Following an earlier study of the γ-radiolysis of aqueous $PtCl_4^{2-}$ (1) some preliminary experiments were carried out to determine the effects of u.v. light on the same system. In addition to photohydrolysis anticipated from the work of Balzani and Carassiti (2), N_2 evolution was observed when aqueous $PtCl_4^{2-}$–N_2O solutions were illuminated with 1849 Å light. The formation of N_2, exclusive of that part emanating from direct photodissociation of N_2O, is suggestive of photoelectron formation.

Although only a limited number of transition metal complexes have been reported as sources for the photolytic production of hydrated electrons it is possible to identify three common features, these being that the ion used (*i*) be relatively inert towards e_{aq}^-, (*ii*) forms a stable complex of the same stoichiometry and one equivalent higher in oxidation state, and (*iii*) that the exciting radiation is in the charge transfer region (3). Since $PtCl_4^{2-}$ is obviously lacking in the first two characteristics it seemed in prospect that a unifying feature might be revealed in the charge transfer spectrum of $PtCl_4^{2-}$. Thus, the present study was prompted both by an inherent interest in the previously uninvestigated spectral region effected by 1849 Å light and by the expectation that the resultant data might provide a reasonable basis for rationalizing the short wavelength photochemistry of $PtCl_4^{2-}$.

While there is considerable spectral data available on the low intensity d–d bands (4), only two charge transfer bands appearing as moderately intense overlapping bands centered at about 45 000 cm^{-1} have been reported for $PtCl_4^{2-}$. The origin of the two bands have been variously interpreted as arising from the transitions $^1A_{1g} \rightarrow {}^1A_{2u}$ ($b_{2u}\pi \rightarrow b_{1g}\sigma^*$) and $^1A_{1g} \rightarrow {}^1E_u(1)$ ($e_u\pi \rightarrow b_{1g}\sigma^*$) (5, 6) to the combination $^1A_{1g} \rightarrow {}^1A_{2u} + {}^1E_u(1)$ for the first band with the high frequency band being due to either $^1A_{1g} \rightarrow {}^1E_u(2)$ ($^1e_u\sigma \rightarrow b_{1g}\sigma^*$) or a 5d → 6p transition (7, 8). Neglecting the high energy $3a_{1g}\sigma^*$ orbital, it can be easily shown, using the molecular orbital energy diagram given in Fig. 1, that there are eight fully allowed transitions anticipated for the u.v. spectrum of $PtCl_4^{2-}$. Since only two bands have thus far been reported, the region beyond 45 000 cm^{-1} promised to be rich in spectral data.

In this study an attempt has been made to examine and interpret the band structure of $PtCl_4^{2-}$ in the spectral region of 1849 Å. How-

Can. J. Chem. Downloaded from www.nrcresearchpress.com by 210.87.254.42 on 09/05/12
For personal use only.

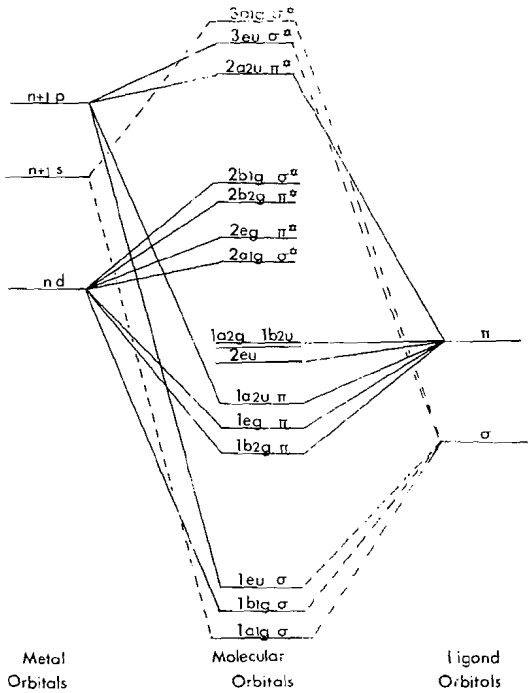

FIG. 1. Molecular orbital scheme for ML_4^{z-} ions of D_{4h} symmetry.

ever, since the interpretation of one complex is but an isolated statement, the study was extended to include an examination of $PtBr_4^{2-}$ as well as the chlorides and bromides of Pd(II) and Au(III) so that spectral frequency trends could substantiate the assignments offered.

Experimental

Materials

The salts, tetra-*n*-butylammonium bromide and chloride (Eastman Organic Chemicals), potassium tetrachloroplatinate(II) (Fisher Scientific), and potassium tetrachloropalladate(II) (Fisher Scientific) were used as received. The gold complexes were prepared from hydrogen tetrachloroaurate(III) (Fisher Scientific). The tetra-*n*-butylammonium salts of the bromide and chloride complexes of platinum(II), palladium(II), and gold(III) were prepared by the methods described by Mason and Gray (5) with the exception that saturated K_2PtCl_4 and K_2PdCl_4 solutions were used.

The solvents used in preparing spectral solutions were acetonitrile (Fisher Scientific), deuterium oxide (99.7 Atom %D, Merck, Sharp and Dohme), and quadruple-distilled water.

Spectra

Spectra were recorded using a Beckman Model DK-1A Far UV recording spectrophotometer. For wavelengths shorter than 200 mμ variable pathlength cells (Research and Industrial Instrument Company) were employed. Pathlengths of 0.01 and 0.0074 cm were achieved by closing the cells onto a Teflon spacer. In addition a matching pair of fixed pathlength cells (0.028 cm) were also used. Calibration of these cells was achieved using solutions of known concentration of K_2PtCl_6 ($\varepsilon_{262\ m\mu}$ = 24 500 M^{-1} cm^{-1}).

In addition, for spectra recorded below 200 mμ, the cell chamber was vigorously purged with high purity nitrogen to minimize light absorption by atmospheric gases The nitrogen purge also served to partially thermostat the cell chamber (22–24 °C).

The observed spectra were resolved into a sum of Gaussian curves by a trial and error method similar to that described by Chatt, Gamlen, and Orgel (9). The additional criterion of seeking the smallest number smooth symmetrical bands was imposed since it is easily shown (10) that a Gaussian curve can always be decomposed into a large number of smaller Gaussian curves. The bands thus resolved were tested with respect to relationships derived from the Gaussian equation $\varepsilon = \varepsilon_{max} \exp[-(w/\theta)^2]$. Based on an average of seven determinations, the precision in the calculated extinction coefficients at high frequencies was ± 5%.

Following the suggestion of Mason and Gray (5) it was found that films of the tetra-*n*-butylammonium salts of both the tetrabromo- and tetrachloroplatinate(II) thin enough for high frequency studies could be deposited on a quartz plate. Low temperature (≃ 140 °K) spectra of these samples were obtained using an Air Products Cryo-Tip Model AC-1-110 equipped with a vacuum shroud Model WMX-17. Although only limited use was made of this technique, the enhanced resolution was an invaluable aid in resolving bands which were highly overlapped in the solution spectra.

A frequency of about 55 000 cm^{-1} constituted the upper limit of reliable measurement since increasing slit widths entailed serious loss of resolution and beyond 57 000 cm^{-1} stray light can produce imaginary bands of significant intensity. Thus, under the conditions employed here bands for which the maximum occurred at or beyond 55 500 cm^{-1} could not be completely observed. In fact bands peaking beyond 55 500 cm^{-1} gave the appearance of being "chopped" thereby giving rise to an artificial maximum of anomalously low intensity and frequency.

Photolyses

The photochemical procedures employed here are essentially the same as previously described (11). Interposing a 2 cm water filter totally suppressed N_2 formation in the N_2O–$PtCl_4^{2-}$ solutions thus ensuring that the effects observed were due to the 1849 Å radiation. Furthermore, the cellholder employed was such that only the solution phase was irradiated, the gas phase being shielded from the incident radiation. Actinometry was by the aqueous N_2O system reported by Dainton and Fowles (12) except that a value of 1.46 cm^{-1} for ε_{H_2O} was used (13).

Results

$PtCl_4^{2-}$ and $PtBr_4^{2-}$

Rapid hydrolysis precluded an acceptable aqueous spectrum of $PtBr_4^{2-}$ but $PtCl_4^{2-}$ was sufficiently stable in H_2O and D_2O to permit a

Can. J. Chem. Downloaded from www.nrcresearchpress.com by 210.87.254.42 on 09/05/12
For personal use only.

Can. J. Chem. Downloaded from www.nrcresearchpress.com by 210.87.254.42 on 09/05/12
For personal use only.

TABLE 1. Electronic spectra of chloride complexes[a]

Transition		$PtCl_4^{2-}$		$[(n\text{-}C_4H_9)_4N]_2PtCl_4$			
		H_2O	D_2O	CH_3CN	Film	$[(n\text{-}C_4H_9)_4N]_2Pd_2Cl_6$	$[(n\text{-}C_4H_9)_4N]AuCl_4$
$^1A_{1g}\rightarrow{}^1A_{2g}$	$(b_{2g}\pi^*\rightarrow b_{1g}\sigma^*)$	25 740(63.3)	25 750(62.0)	24 750(59.6)[b]	—	22 200(350)[b]	21 930(17.3)[b]
$^1A_{1g}\rightarrow{}^1E_g$	$(e_g\pi^*\rightarrow b_{1g}\sigma^*)$	30 650(79.1)	30 650(76.7)	29 500(66.4)[b]	—	24 940(490)[b]	26 520(319)[b]
$^1A_{1g}\rightarrow{}^1B_{1g}$	$(a_{1g}\sigma^*\rightarrow b_{1g}\sigma^*)$	38 000(500)	38 000(514)	37 500(453)	—	—	—
$^1A_{1g}\rightarrow{}^1A_{2u}$	$(b_{2u}\pi\rightarrow b_{1g}\sigma^*)$	43 200(6 170)	43 320(6 420)	41 530(4 100)	42 500	B 30 310(1 935)[c]	31 050(5 750)
$^1A_{1g}\rightarrow{}^1E_u(1)$	$(e_u\pi\rightarrow b_{1g}\sigma^*)$	46 470(10 330)	46 650(10 230)	44 300(10 360)	45 700	T 34 980(2 200)	
$^1A_{1g}\rightarrow{}^1E_u(2)$	$(e_u\sigma\rightarrow b_{1g}\sigma^*)$	52 400(18 840)	52 740(20 960)	51 000(15 100)	52 000	B 41 190(32 000)[c] T 48 440(28 100)	44 150(47 800)
$^1A_{1g}\rightarrow{}^1B_{1u}$	$(b_{2g}\pi^*\rightarrow a_{2u}\pi^*)$	—	—	—	—	52 200(28 400)	—
$^1A_{1g}\rightarrow{}^1E_u(3)$	$(e_g\pi^*\rightarrow a_{2u}\pi^*)$	~56 500(> 40 000)[d]	~56 500(> 40 000)[d]	54 230(50 400)	54 400	56 000(> 30 000)[d]	> 57 000[d]

[a]Frequency in cm^{-1} (extinction coefficient (M^{-1} cm^{-1})).
[b]Reference 5.
[c]Bridging ligand (B), terminal ligand (L).
[d]Estimated from frequency shifts and/or ε_{max} at effective cutoff.

TABLE 2. Electronic spectra of bromide complexes[a]

Transition		Electronic spectra			
		$[(n\text{-}C_4H_9)_4N]_2PtBr_4$			
		CH_3CN	Film	$[(n\text{-}C_4H_9)_4N]Pd_2Br_6$	$[(n\text{-}C_4H_9)_4N]AuBr_4$
$^1A_{1g}\rightarrow{}^1A_{2g}$	$(b_{2g}\pi^*\rightarrow b_{1g}\sigma^*)$	23 150(126)	—	—	
$^1A_{1g}\rightarrow{}^1E_g$	$(e_g\pi^*\rightarrow b_{1g}\sigma^*)$	26 880(187)	—	20 600(848)[b]	21 740(1 560)[b]
$^1A_{1g}\rightarrow{}^1B_{1g}$	$(a_{1g}\sigma^*\rightarrow b_{1g}\sigma^*)$	30 100(2 100)	30 000	—	—
$^1A_{1g}\rightarrow{}^1A_{2u}(1)$	$(b_{2u}\pi\rightarrow b_{1g}\sigma^*)$	33 300(4 790)	33 000	B 24 520(3 010)[c]	25 400(4 775)
$^1A_{1g}\rightarrow{}^1E_u(1)$	$(e_u\pi\rightarrow b_{1g}\sigma^*)$	36 100(8 600)	35 900	T 30 330(3 910)	
$^1A_{1g}\rightarrow{}^1E_u(2)$	$(e_u\sigma\rightarrow b_{1g}\sigma^*)$	43 350(16 800)	43 100	B 36 710(33 100)[c] T 43 590(20 100)	39 150(48 625)
$^1A_{1g}\rightarrow{}^1B_{1u}$	$(b_{2g}\pi^*\rightarrow a_{2u}\pi^*)$	—	—	46 300(10 550)	—
$^1A_{1g}\rightarrow{}^1E_u(3)$	$(e_g\pi^*\rightarrow a_{2u}\pi^*)$	47 200(48 300)	46 900	50 120(42 300)	50 300(14 000)
$^1A_{1g}\rightarrow{}^1A_{2u}(2)$	$(a_{1g}\sigma^*\rightarrow a_{2u}\pi^*)$	50 740(46 600)	51 000	~53 000(24 000)[d]	53 330(17 700)
$^1A_{1g}\rightarrow{}^1E_u(A)$	$(b_{2g}\pi^*\rightarrow e_u\pi^*)$	53 600(27 900)	53 800	> 56 000(25 000)[e]	> 56 000(27 000)[e]
$^1A_{1g}\rightarrow{}^1A_{2u}(3)$	$(e_g\pi^*\rightarrow e_u\pi^*)$	56 600(30 000)[e]	—	—	—

[a]Frequency in cm^{-1} (extinction coefficient (M^{-1} cm^{-1})).
[b]Reference 5.
[c]Bridging ligand (B), terminal ligand (T).
[d]Severe overlap from unresolved high frequency absorption precluded accurate analysis. Frequency approximated from weakly distinguished peak at 52 600 cm^{-1}.
[e]Estimated from frequency shifts and/or ε_{max} at effective cutoff.

spectrum to be recorded. Unfortunately the strong band occurring in the region of 55 000 cm^{-1} (which is of special interest because of the 1849 Å photolyses) was partially obscured by the effective solvent cutoff. On the other hand, acetonitrile proved to be a suitable solvent since it provided a medium in which the tetra-*n*-butylammonium salts of $PtCl_4^{2-}$ and $PtBr_4^{2-}$ were stable and because the accompanying red shift effectively brought the high frequency bands into a more observable region. The spectra thus recorded for $PtCl_4^{2-}$ and $PtBr_4^{2-}$ are illustrated in Figs. 2 and 3.

In addition spectra were also obtained with low temperature thin film samples of $PtCl_4^{2-}$ and $PtBr_4^{2-}$. The improved resolution thus

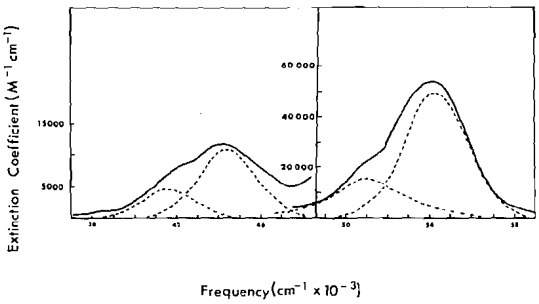

FIG. 2. Electronic spectrum of $[(n\text{-}C_4H_9)_4N]_2PtCl_4$ in CH_3CN with pathlength 0.01 cm: —, observed spectrum; ···, Gaussian components.

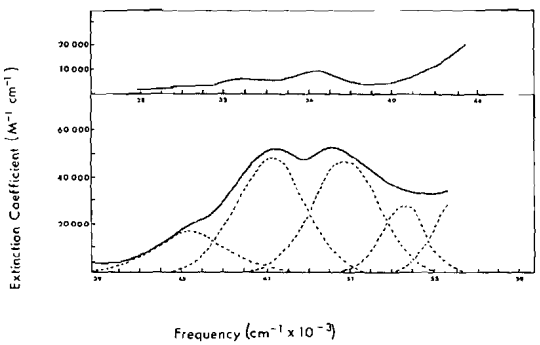

FIG. 3. Electronic spectrum of $[(n\text{-}C_4H_9)_4N]_2PtBr_4$ in CH_3CN with pathlength 0.01 cm: —, observed spectrum; ···, Gaussian components.

achieved tended to reveal well defined peaks for those bands which appeared only as shoulders in solution. For example, whereas the 53 600 cm^{-1} band of $PtBr_4^{2-}$ in CH_3CN was determined principally as a residual after resolving out the lower frequency bands, with the thin film sample the band exhibited a clearly distinguished peak at 53 800 cm^{-1}. The frequencies of the other bands are summarized in Tables 1 and 2.

Although the bands at 50 740 and 53 600 cm^{-1} observed for $PtBr_4^{2-}$ would occur too far into the u.v. to be observed for $PtCl_4^{2-}$, comparison of the intensities and peak separations of the initial four charge transfer bands reveals a

Can. J. Chem. Downloaded from www.nrcresearchpress.com by 210.87.254.42 on 09/05/12
For personal use only.

striking similarity in the spectra of the two compounds.

$Pd_2Cl_6^{2-}$ and $Pd_2Br_6^{2-}$

As it was not practicable to use aqueous solutions due to rapid hydrolysis, the spectra of the Pd(II) halides shown in Figs. 4 and 5 were obtained using solutions of the tetra-*n*-butylammonium salts in CH_3CN. Under these conditions the Pd(II) complexes exist as the dimers $Pd_2Cl_6^{2-}$ and $Pd_2Br_6^{2-}$. As the terminal and bridging ligands are non-equivalent the Pd(II) complexes will belong to a symmetry lower than D_{4h} which applies to the Pt(II) complexes.

A charge transfer spectra of PdX_4^{2-} in aqueous HX solutions (X = Cl or Br) has been reported (7). If allowance is made for the red shift which normally accompanies the change from H_2O to CH_3CN the principal differences observed in the spectra of PdX_4^{2-} and $Pd_2X_6^{2-}$

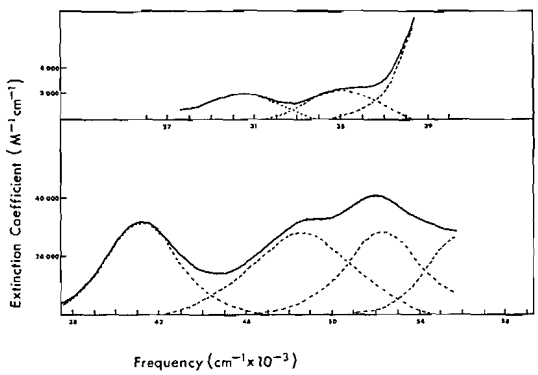

FIG. 4. Electronic spectrum of $[(n\text{-}C_4H_9)N]_2Pd_2Cl_6$ in CH_3CN with pathlength 0.01 cm: —, observed spectrum; ···, Gaussian components.

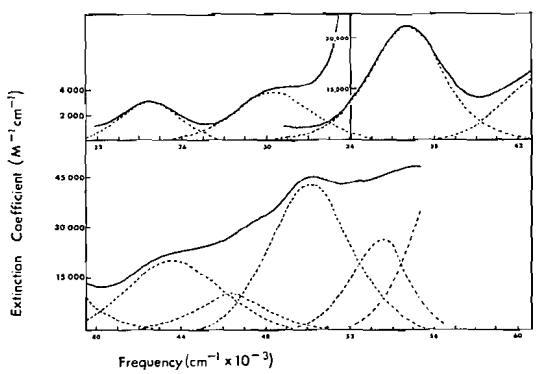

FIG. 5. Electronic spectrum of $[(n\text{-}C_4H_9)N]_2Pd_2Br_6$ in CH_3CN with pathlength 0.01 cm: —, observed spectrum; ···, Gaussian components.

are a decrease in the intensity of the transition $^1A_{1g} \rightarrow {}^1E_u(1) + {}^1A_{2u}$ and a splitting of this band and that due to the transition $^1A_{1g} \rightarrow {}^1E_u(2)$ for the $Pd_2X_6^{2-}$ complexes. The latter effect is seen as a result of the non-equivalence of the terminal and bridging ligands.

Perhaps the most notable feature of the Pd(II) spectra is the remarkable similarity between $PtBr_4^{2-}$ and $Pd_2Br_6^{2-}$. This is most easily seen by comparison of the data given in Table 2.

$AuCl_4^-$ and $AuBr_4^-$

Again to avoid hydrolysis, solutions were prepared using $[(n\text{-}C_4H_9)_4N][AuCl_4]$ and $[(n\text{-}C_4H_9)_4N][AuBr_4]$ in CH_3CN, the spectra of which are illustrated in Figs. 6 and 7. The aqueous spectra have been reported (7) and whilst the frequencies of the first two charge transfer bands seem to exhibit only a slight solvent effect, the intensity of the second band ($^1A_{1g} \rightarrow {}^1E_u(2)$) appears to be quite solvent sensitive (see Tables 1 and 2).

The frequency shift accompanying the change from Cl^- to Br^- is approximately 5000 cm^{-1} which is comparable to that observed with the Pd(II) complexes. Accordingly, it is noteworthy that there was no evidence for a band in the region 55 000–56 000 cm^{-1} for $AuCl_4^-$ to correspond to the 50 300 cm^{-1} band in the $AuBr_4^-$ spectrum. Although this region imposes experimental difficulties the absence of any evidence for even the onset of a band would seem to imply that this band has been shifted by more than 7000 cm^{-1} in the $AuCl_4^-$.

Photolysis of Aqueous $PtCl_4^{2-}$

From several preliminary experiments it was found that N_2O had no measurable effect on

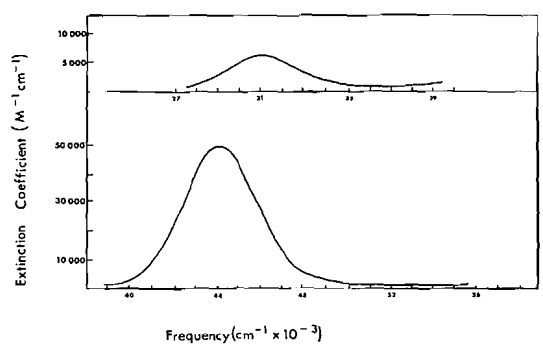

FIG. 6. Electronic spectrum of $[(n\text{-}C_4H_9)_4N]AuCl_4$ in CH_3CN with pathlength 0.007$_4$ cm.

Can. J. Chem. Downloaded from www.nrcresearchpress.com by 210.87.254.42 on 09/05/12
For personal use only.

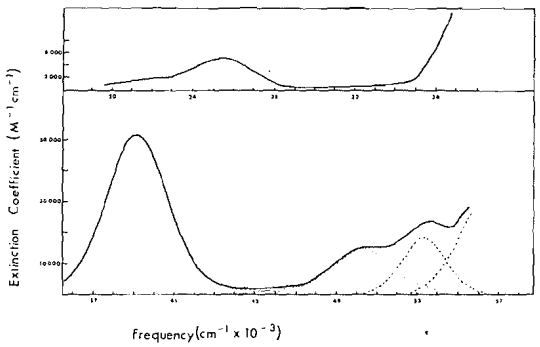

FIG. 7. Electronic spectrum of $[(n\text{-}C_4H_9)_4N]AuBr_4$ in CH_3CN with pathlength 0.007$_4$ cm: —, observed spectrum; ···, Gaussian components.

the photochemistry of aqueous $PtCl_4^{2-}$ when the incident radiation was of wavelength 2537 Å or longer. On the other hand, N_2 was produced when 1849 Å light was used. The N_2 yields from solutions for which $[PtCl_4^{2-}]$ varied from 10^{-4} to 8.6×10^{-3} M and $[N_2O]$ from 2×10^{-2} to 9×10^{-3} M were linear with respect to radiation time; however, the dependence on $[PtCl_4^{2-}]$ and $[N_2O]$ was complex.

It is well known that at 1849 Å N_2O undergoes direct photodissociation with the primary yield ($\gamma_{N_2}^0$) assumed to be unity (12). Due to filtering effects of the solvent and other absorbing solutes the anticipated yield due to photolysis of N_2O ($\gamma(N_2)$) can be calculated from the relationship

$$[1]\quad \gamma(N_2) = \gamma_{N_2}^0 \frac{\varepsilon_{N_2O}[N_2O]}{\varepsilon_{N_2O}[N_2O] + \varepsilon_{PtII}[PtII] + \Sigma_{H_2O}}$$

where $\Sigma_{H_2O} = 1.46\ cm^{-1}$ is the linear extinction coefficient of H_2O (13). For all solutions employed in this study the actual yields measured, $\phi(N_2)$, were significantly greater than $\gamma(N_2)$. For example where $[PtCl_4^{2-}] = 1.0 \times 10^{-3}$ M and $[N_2O] = 2.0 \times 10^{-2}$, $\gamma(N_2) = 0.035$; however, $\phi(N_2) = 0.21 \pm 0.02$. Thus, the 1849 Å photolysis of aqueous $PtCl_4^{2-}$ must generate a species (denoted "x") which reacts with N_2O to produce N_2 and the yield of this species would be $\phi(x) = \phi(N_2) - \gamma(N_2)$.

Whereas $\phi(N_2)$ decreased, $\phi(x)$ increased with increasing $[PtCl_4^{2-}]$ reaching an apparent plateau at $[PtCl_4^{2-}] = 1 \times 10^{-3}$ M, but thereafter $\phi(x)$ decreased. These phenomena were interpreted as the results of both an inner filter effect and competitive scavenging by N_2O of the species "x".

In several experiments it was found that the yield of "x" was reduced by addition of $[SF_6] = 1.4 \times 10^{-4}$ M. Although the yield reduction exceeded the experimental error it was not sufficiently large to provide the basis of a reliable kinetic analysis. Using a F^- specific ion electrode, a yield of F^- was found; however, quantitative interpretation was not practicable since control experiments using $PtCl_4^{2-}$ solutions containing measured amounts of F^- when irradiated revealed a substantial decrease in the detectable F^-. It is known that the three solutes $PtCl_4^{2-}$, N_2O, and SF_6 are all efficient scavengers of e_{aq}^- with SF_6 being highly specific (14, 15) ($k_{e+PtCl_4^{2-}} = 9 \times 10^9\ M^{-1}\ s^{-1}$ (16), $k_{e+N_2O} = 8.7 \times 10^9\ M^{-1}\ s^{-1}$ (17), and $k_{e+SF_6} = 1.65 \times 10^{10}\ M^{-1}\ s^{-1}$ (14)).

Although the identity of "x" is not unambiguously established, the data is consistent with $x = e_{aq}^-$. Accordingly the yields would be represented by modifying eq. 1 to

$$[2]\quad \phi(x) = \phi_{e_{aq}^-} \frac{\varepsilon[PtII]}{\sum_i \varepsilon_i[S_i]} \times \frac{1}{1 + k_{PtII}[PtII]/k_{N_2O}[N_2O]}$$

where $\phi_{e_{aq}^-}$ is the primary yield of e_{aq}^- and the final term represents the competitive scavenging. The values of $\phi_{e_{aq}^-}$ thus calculated are given in Table 3 and are seen to be relatively constant except at very high $[PtCl_4^{2-}]$ where the departure from homogeneous kinetics would be severe due to the exceedingly high optical density of the solution.

Spectrophotometric analysis of the photolyzed solutions revealed the presence of $PtCl_6^{2-}$ and after the solutions were made 1 M in HCl and sufficient time allowed for anation to be com-

TABLE 3. Analysis of yield data from the photolysis of aqueous $PtCl_4^{2-}$ [a]

$[PtCl_4^{2-}]$ ($\times 10^3$)	$\phi(N_2)$ [b]	$\gamma(N_2)$ [c]	$\phi(X)$	$\phi_{e_{aq}^-}$ [d]
0.1	0.33 ±0.02	0.21	0.12	0.23
0.2	0.30 ±0.02	0.17	0.17	0.25
0.5	0.27 ±0.02	0.07	0.20	0.25
1.0	0.21 ±0.02	0.03	0.18	0.21
8.6	0.006±0.001	0.00	0.006	0.09

[a] All data for 1849 Å irradiations.
[b] Actual yield measured.
[c] Calculated from eq. 1.
[d] Calculated from eq. 2.

Can. J. Chem. Downloaded from www.nrcresearchpress.com by 210.87.254.42 on 09/05/12
For personal use only.

Can. J. Chem. Downloaded from www.nrcresearchpress.com by 210.87.254.42 on 09/05/12
For personal use only.

plete the yield relationship was found to be $\phi(N_2) = \phi(PtCl_6^{2-})$. However, as the $PtCl_6^{2-}$ analysis involved more potential errors as well as the necessity of much longer irradiation times this datum merely establishes qualitative confirmation of the redox reaction.

Discussion

On the basis of the molecular orbital energy diagram shown in Fig. 1 two general classes of charge transfer bands are anticipated for the d^8 complexes studied here. The first of these can be designated as ligand to metal (L → M) and involve electron transfer from orbitals localized mainly on the ligands to the essentially metal $b_{1g}(x^2 - y^2)$ orbital. In the second, the molecular orbitals correspond to the metal d- and p-orbitals as the donor and receptor orbitals, respectively (d → p). In the event that in the excited states for these transitions a degree of back bonding occurred by the halide "open" d-orbitals via a_{2u}^* or e_u^* orbitals then these transitions could acquire some metal to ligand (M → L) character. With respect to complexes studied here the L → M bands should be characterized by a shift to lower energy following the series Pt(II), Pd(II), to Au(III) whereas the d → p transitions should exhibit a trend to higher frequencies over the same series. Accordingly, the proposed assignments listed in Tables 1 and 2 are based on the orbital ordering illustrated in Fig. 1 in conjunction with the shifts in band frequencies as related to changes in the central metal and ligands.

In order to include the dimeric Pd complexes in a single scheme of assignments with the square planar Pt and Au complexes an additional assumption was necessary. An effective local symmetry about the Pd atom of C_{2v} was assumed and on this basis an initial choice of assignments was made. These were subsequently listed with the equivalent transitions in the D_{4h} scheme. Apart from the splitting of the L → M bands due to the non-equivalence of the bridging and terminal ligands and the increased intensity of the observed ligands field bands, the most significant ramification of the lower symmetry is that the otherwise orbitally forbidden $^1A_{1g} \rightarrow {}^1B_{1u}$ transition becomes allowed.

The low intensity d → d transitions, a résumé of which is included in Tables 1 and 2, have been the subject of numerous investigations (4), and do not warrant further comment here. Of the intense bands, the assignments for the L → M transitions are in essential agreement with those given by Mason and Gray (5). The alternate assignment (8) for the second charge transfer band in PtX_4^{2-} as $^1A_{1g} \rightarrow {}^1E_u(2)$ was rejected since this would impose the unreasonable conclusion that the same transition in AuX_4^- would occur at or below the same frequency. The separation of the $^1A_{2u}$ and $^1E_u(1)$ states in PtX_4^{2-} has been interpreted (6) as a result of the bonding character of the $e_u\pi$ orbital. This corresponds to an enhanced bond order which in turn provides a partial basis for the relative stability of PtX_4^{2-} and the qualitative conclusion that PtX_4^{2-} is more covalent than AuX_4^-. Since covalency would be contingent upon mixing of predominantly ligand p-orbital combinations with the metal d-orbitals, a reasonable consequence might be the introduction of weak matrix elements into the $^1A_{1g} \rightarrow {}^1E_u(2)$ transition thereby explaining the pronounced increase in intensity on going from PtX_4^{2-} to AuX_4^-.

The additional intense bands must be assigned to transitions involving orbitals other than the metal $b_{1g}(x^2 - y^2)$ and based on the orbital scheme shown in Fig. 1 it can be seen that these transitions will involve excitation from the predominantly metal d-orbitals ($b_{2g}(xy)$, $e_g(xz,yz)$, and $a_{1g}(z^2)$) to either the a_{2u}^* or e_u^* orbitals. The first fully allowed transition of this nominal d → p sequence is $^1A_{1g} \rightarrow {}^1E_u(3)$ ($e_g^* \rightarrow a_{2u}^*$) and whilst this transition is fully observed only in $PtCl_4^{2-}$ amongst the chlorides, it is observed in all three bromide spectra and the pronounced shift to higher energy on going from $PtBr_4^{2-}$ to $AuBr_4^-$ is consistent with d → p transitions. For the remaining observed bands the assignments proposed have been based on a natural energy sequence derived from the ordering of $b_{2g}^* > e_g^* > a_{1g}^*$ for the metal d-orbitals and $e_u^* > a_{2u}^*$.

The spectra of these complexes can conveniently be divided into three regions in the order of increasing energy, ligand fields bands, CTTM, and d → p. In parallel fashion irradiation of aqueous $PtCl_4^{2-}$ leads to a different photochemistry in each of these regions. Balzani and Carasiti (2) have shown that within the ligand field region wavelength independent photohydrolysis occurs with $\phi(Cl^-) \simeq 0.2$. Using 2537 Å light the result is again only photohydrolysis but with $\phi(\text{—Cl}) = 0.90$ suggesting a different active precursor state. Although not precisely defined, the precursor states must correlate with a configuration involving popula-

Can. J. Chem. Downloaded from www.nrcresearchpress.com by 210.87.254.42 on 09/05/12
For personal use only.

tion of the $b_{1g}\sigma^*$ $(x^2 - y^2)$ orbital. Since this will produce increased metal–ligand repulsion, the natural consequence is seen as hydrolysis.

The 1849 Å irradiations reported here demonstrate that excitation in this region results in a photochemistry quite distinct from that observed at longer wavelengths. Following the proposed assignments, the $^1E_u(3)$ state will be formed initially; however, if the pattern of internal conversion and intersystem crossing which characterize the ligand field (2, 18) excitation is also operative in this region, then the immediate precursor to photoelectron formation should be identified with a state lying lower in energy. The $^1E_u(2)$ and $^1E_u(1)$, although below the $^1E_u(3)$, are not configurationally compatible with $^1E_u(3)$ and such a conversion should either be prohibited or at least very slow. Furthermore, since the $^1E_u(2)$ or $^1E_u(1)$ states involve population of the $b_{1g}\sigma^*(x^2 - y^2)$ orbital it is expected that their participation would ultimately lead to hydrolysis not the formation of e_{aq}^-. It is interesting to note that whereas $^1B_{1u}$ and $^3B_{1u}$ states are not observed due to orbital and spin selection rules, they are configurationally similar to the $^1E_u(3)$ state and could contribute to the primary photophysical processes. In any event the immediate precursor state should be one in which electron density has been transferred to the a_{2u}^* orbital. With $PtCl_4^{2-}$, because of the square planar geometry, the C_4-axis should be a region of high solvent sensitivity thus charge transfer to the a_{2u}^* orbital which is colinear with the C_4-axis should provide a natural path for the ultimate electron transfer to the solvent.

Photoelectron formation has been mainly associated with the photolysis of simple anions (*e.g.* halides, pseudohalide, and some main group oxyanions) or cyanometal complexes. In the former cases the initiating excitation is generally assigned to a CTTS band (19) whilst for the latter the proposed bands are CTTL or CTTS (3). In both cases excitation is readily seen to result in a transfer of electron density to solvent sensitive orbitals. Thus, a similarity can be established between these systems and $PtCl_4^{2-}$. In comparison then it is a significant feature that different spectroscopic transitions can ultimately result in the same photochemistry. Consequently the photochemical activity alone should not be regarded as a substantive basis for postulating the presence of a specific spectroscopic assignment.

Finally, while we do not dispute the utility of the criteria proposed by Waltz and Adamson (3) for selecting probable photoelectron sources, the $PtCl_4^{2-}$ system which so clearly fails these criteria demonstrates that photoelectron formation is not limited to a restricted group of transition metal complexes but at sufficiently short wavelengths could be a general phenomenon.

The authors wish to acknowledge the financial assistance of the National Research Council of Canada and for the award of a studentship to J.H.B. We also thank Mr. D. V. Jindal who performed some preliminary photolyses.

1. F. S. Dainton and R. Rumfeldt. Proc. R. Soc. A, **298**, 239 (1967).
2. (*a*) V. Balzani and V. Carassiti. J. Phys. Chem. **72**, 383 (1968); (*b*) F. Scandola, O. Traverso, and V. Carasiti. Mol. Photochem. **1**, 11 (1969).
3. W. L. Waltz and A. W. Adamson. J. Phys. Chem. **73**, 4250 (1969).
4. (*a*) R. F. Fenske, D. A. Martin, and K. R. Ruedenberg. Inorg. Chem. **1**, 441 (1962); (*b*) D. S. Martin and C. A. Lenhardt. Inorg. Chem. **3**, 1368 (1964); (*c*) D. S. Martin, M. A. Tucker, and A. J. Kassman. Inorg. Chem. **4**, 1682 (1965); **5**, 1298 (1966); (*d*) D. S. Martin, J. G. Foss, M. E. McCarville, M. A. Tucker, and A. J. Kassman. Inorg. Chem. **5**, 491 (1966).
5. W. R. Mason and H. B. Gray. J. Am. Chem. Soc. **90**, 5721 (1968).
6. H. B. Gray and C. J. Ballhausen. J. Am. Chem. Soc. **85**, 260 (1963).
7. A. J. McCaffery, P. N. Schatz, and P. J. Stephens. J. Am. Chem. Soc. **90**, 5730 (1968).
8. C. K. Jorgensen. Adv. Chem. Phys. **5**, 119 (1963).
9. J. Chatt, G. A. Gamlen, and L. E. Orgel. J. Chem. Soc. 486 (1958).
10. J. W. Perram. J. Chem. Phys. **49**, 4245 (1968).
11. R. Rumfeldt. Can. J. Chem. **49**, 1262 (1971).
12. F. S. Dainton and P. Fowles. Proc. R. Soc. A, **287**, 295 (1965).
13. M. F. Fox and E. Hayon. J. Phys. Chem. **76**, 2703 (1972).
14. K.-D Asmus and J. H. Fendler. J. Phys. Chem. **72**, 4285 (1968).
15. M. Crawford and R. Rumfeldt. Can. J. Chem. **49**, 3336 (1971).
16. J. H. Baxendale, E. M. Fielden, C. Capellos, J. M. Francis, J. V. Davies, M. Ebert, C. W. Gilbert, J. P. Keene, E. J. Land, A. J. Swallow, and J. M. Nosworthy. Nature, London. **201**, 468 (1964).
17. S. Gordon, E. J. Hart, M. S. Matheson, J. Rabani, and J. K. Thomas. Discuss. Faraday Soc. **36**, 193 (1963).
18. V. S. Sastri and C. H. Langford. J. Am. Chem. Soc. **91**, 7534 (1969).
19. (*a*) M. S. Matheson, W. A. Mulac, and J. Rabani. J. Phys. Chem. **67**, 2613 (1963); (*b*) G. Stein. Solvated electron. Adv. Chem. Ser. No. 50. American Chemical Society, Washington, D.C. 1965. p. 230.

Erratum: Conformation of Bridged Diphenyls. III. Crystal Structure of 2-(2′-Carbomethoxy-4′-nitrophenoxy)-1,3,5-trichlorobenzene

E. A. H. GRIFFITH,[1] W. D. CHANDLER, AND B. E. ROBERTSON

Division of Natural Sciences and Mathematics, University of Saskatchewan, Regina, Saskatchewan S4S 0A2

(Ref.: Can. J. Chem. **50**, 2979 (1972))

Received October 12, 1973

Can. J. Chem., **52**, 182 (1974)

Dr. George Ferguson has drawn our attention to the possibility that a computational error led to the unusual shapes of the thermal ellipsoids in Figs. 5 and 6 of this paper. A recalculation supports this suggestion; corrected versions of these figures are shown below. The section beginning on line 13, column 2, p. 2984 to the end of the same paragraph should be deleted.

In Table 1(*b*) the number for the *z* fractional coordinate of atom H(14,1) should read −261(9).

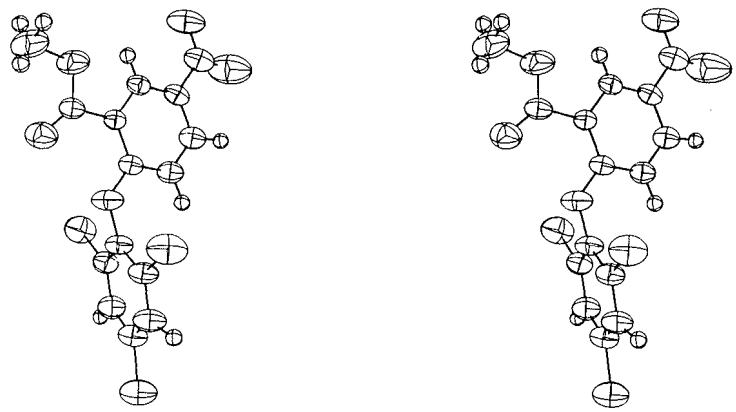

FIG. 5. Stereoscopic view of molecule 1. The thermal ellipsoids have been scaled to include 50% probability.

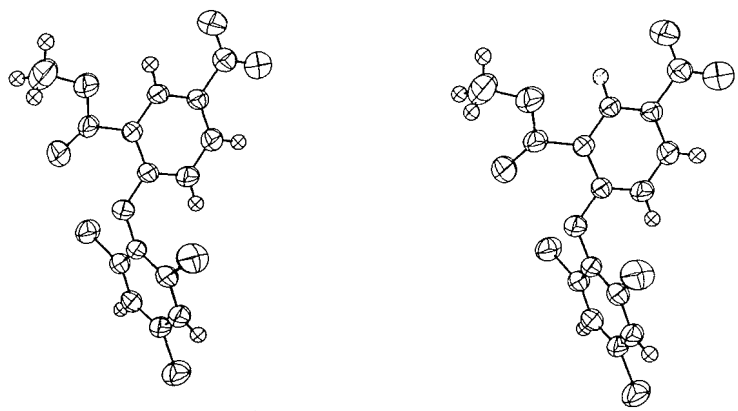

FIG. 6. Stereoscopic view of molecule 2. The thermal ellipsoids have been scaled to include 50% probability.

[1]Present address: Department of Chemistry, University of South Carolina, Columbia, South Carolina 29208.

Can. J. Chem. Downloaded from www.nrcresearchpress.com by 210.87.254.42 on 09/05/12
For personal use only.

Can. J. Chem. Downloaded from www.nrcresearchpress.com by 210.87.254.5 on 09/05/12
For personal use only.

Photochemistry of Glycosyl Azides

JAN PLENKIEWICZ,[1] GEORGE W. HAY, AND WALTER A. SZAREK[2]

Department of Chemistry, Queen's University, Kingston, Ontario

Received August 16, 1973

Irradiation with u.v. light of a methanolic solution of β-D-glucopyranosyl (**1**), α-D-mannopyranosyl (**3**), or β-D-galactopyranosyl (**4**) azide affords in good yield the corresponding next-lower aldose. In the case of β-maltosyl (**6**), β-D-ribofuranosyl (**7**), or α-L-arabinopyranosyl (**8**) azide, there was observed the formation of an intermediate which, on standing in the dark, reverts back to starting material.

L'irradiation avec de la lumière ultra-violette d'une solution méthanolique d'azothydrure de β-D-glucopyrannosyle (**1**), d'α-D-mannopyrannosyle (**3**) ou de β-D-galactopyrannosyle (**4**), a conduit avec des bons rendements aux aldoses immédiatement inférieurs correspondants. Dans le cas des azothydrures de ß-maltosyle (**6**), de β-D-ribofurannosyle (**7**) ou d'α-L-arabinopyrannosyle, on a observé la formation d'un intermédiaire qui redonne le produit initial lorsqu'on le laisse à la noirceur.

[Traduit par le journal]

Can. J. Chem., 52, 183 (1974)

The photochemistry of various types of organic azides has been extensively studied (1). Generally, photolysis of azides results in elimination of molecular nitrogen and formation of products which can be rationalized by the intermediacy of a nitrene (for reviews on nitrenes see ref. 2), although the existence of such an intermediate has not been proven in all cases. A variety of reactions is available to photochemically-generated nitrenes, namely, abstraction of hydrogen by the nitrene, rearrangement of a hydrogen or carbon function to the electron-deficient nitrogen, and insertion of the nitrene into a saturated bond or addition to multiple bonds. In the field of carbohydrate chemistry, it has been found that photolysis of primary azides in sugar systems, followed by mild hydrolysis of the resultant imino derivatives, is an excellent method for the preparation of ω-aldehydo derivatives of glycosides (3), 6-aldehydo analogs of such polysaccharides as amylose (4, 5), starch (4), and cellulose (6, 7), and 5′-aldehyde analogs of nucleosides (8); the photolysis presumably occurs by way of an intermediate nitrene ($R—CH_2N:$) which rearranges by a 1,2-hydrogen migration. Photolysis of secondary azides of sugars also leads to carbonyl derivatives, but the yields of the keto sugars are low (9). In this Communication we report some results of an investigation of the photochemistry of glycosyl azides. Two salient features of this work are the facile degradation by u.v. light of some of the azides to the corresponding next-lower aldose, and the observation, in some cases, of the formation of an intermediate which, on standing in the dark, reverts back to starting material.

The first type of behavior was exhibited by aldohexopyranosyl azides. The experiments involved irradiation[3] of a solution of the glycosyl azide[4] (1.5 g) in methanol (65 ml) for 4 h, at the end of which time t.l.c. on silica gel (1:2:3, v/v, methanol – ethyl acetate – benzene or 3:1 ethanol–benzene) indicated that all of the starting material had been consumed, and showed the presence of a slower-moving component and a nonmigrating component; the reaction mixture was concentrated, and the former component

[1]On leave from the Department of Chemistry, Technical University of Warsaw (Politechnika), Warsaw 10, Poland.

[2]To whom correspondence should be addressed.

[3]Irradiations were performed with a 450-W Hanovia medium-pressure mercury-arc lamp (Cat. No. 679A-36) contained in a water-cooled, quartz immersion-well; a Vycor 7010 filter-sleeve was employed. The whole assembly was mounted in a borosilicate glass reaction-vessel.

[4]Details of the preparation of the glycosyl azides employed in the study described in this Communication, together with their physical constants, will be reported later. As a typical example, β-D-galactopyranosyl azide (**4**) exhibits weak absorption in its u.v. spectrum (methanol) at 275 nm (ε 38.4).

was isolated by column chromatography. Thus, β-D-glucopyranosyl azide (**1**) and α-D-mannopyranosyl azide (**3**) afforded D-arabinose (**2**) in 47 and 60% yields, respectively, whereas β-D-galactopyranosyl azide (**4**) gave D-lyxose (**5**) in 65% yield.

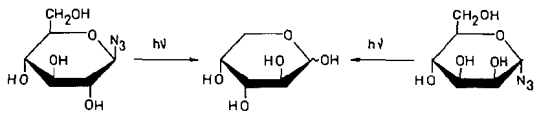

1 **2** **3**

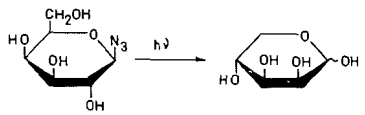

4 **5**

When 4-*O*-α-D-glucopyranosyl-β-D-glucopyranosyl azide (**6**, β-maltosyl azide) was irradiated under the conditions described above, t.l.c. (2:3, v/v, benzene–ethanol) again indicated after 4 h that all of the starting compound had been converted into a slower-moving material, which was revealed as an elongated spot suggestive of the presence of more than one compound, and a nonmigrating component. The i.r. spectrum of the reaction mixture (determined with a smear obtained by rapidly evaporating a small aliquot) did not show any absorption at $\sim 2130\ cm^{-1}$ attributable to an azido group, but showed a broad band centered at $\sim 1670\ cm^{-1}$. However, after the reaction mixture had been kept for 2 h in the dark, the i.r. spectrum showed a weak absorption at $2125\ cm^{-1}$. After 50 h, a very strong absorption attributable to an azido group was observed in the spectrum; moreover, t.l.c. indicated the presence of a considerable amount of starting material.[5] Column chromatography afforded 0.91 g of the starting azide (**6**) and 0.40 g of slower-moving material. The i.r. spectrum of the latter showed a broad band at $\sim 1670\ cm^{-1}$; acid-catalyzed hydrolysis of this material afforded glucose and arabinose, a result which suggests the presence of some 3-*O*-α-D-glucopyranosyl-D-arabinose, the disaccharide expected to be formed by photochemical degradation of β-maltosyl azide (**6**). The identity of the substance giving rise to the absorption at $\sim 1670\ cm^{-1}$ has not been established. It is noteworthy that, whereas during the irradiation of the aldohexopyranosyl azides **1**, **3**, and **4** there was an immediate and steady evolution of gas, in the case of β-maltosyl azide (**6**) very little gas appeared to be liberated.

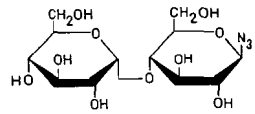

6

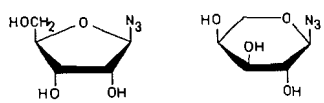

7 **8**

The unusual behavior exhibited by β-maltosyl azide, namely, the formation upon irradiation of an intermediate which, on standing in the dark, reverts back to starting material, was also observed with β-D-ribofuranosyl azide (**7**) and α-L-arabinopyranosyl azide (**8**). In the latter two cases the presence of starting material could not be detected by t.l.c. after 2 h of irradiation; longer periods of irradiation resulted in severe streaking of the chromatograms.

The results described in this Communication indicate that the irradiation with u.v. light of appropriate glycosyl azides should be a convenient one-carbon, chain-shortening procedure (for other photochemical degradations of carbohydrate derivatives see ref. 10) in synthetic carbohydrate chemistry. An investigation of the second type of behavior is in progress.

The authors are grateful to the National Research Council of Canada for its generous financial support of this work, and to Professor J. K. N. Jones for his interest and counsel.

[5]The same observations were recorded on irradiating β-maltosyl azide (**6**) for 11 h and then keeping the reaction mixture in the dark for 48 h.

1. A. REISER and H. M. WAGNER. *In* The chemistry of the azido group. *Edited by* S. Patai. Interscience Publishers, London. 1971. Chapt. 8.
2. (*a*) L. HORNER and A. CHRISTMANN. Angew. Chem. Int. Ed. Engl. **2**, 599 (1963); (*b*) R. A. ABRAMOVITCH and B. A. DAVIS. Chem. Rev. **64**, 149 (1964); (*c*) W. LWOWSKI. Angew. Chem. Int. Ed. Engl. **6**, 897 (1967); (*d*) W. LWOWSKI (*Editor*). Nitrenes. Interscience Publishers, New York. 1970.
3. D. HORTON, A. E. LUETZOW, and J. C. WEASE. Carbohydr. Res. **8**, 366 (1968).

Can. J. Chem. Downloaded from www.nrcresearchpress.com by 210.87.254.5 on 09/05/12
For personal use only.

4. D. M. CLODE and D. HORTON. Carbohydr. Res. **17**, 365 (1971).
5. D. HORTON, A. E. LUETZOW, and O. THEANDER. Carbohydr. Res. **27**, 268 (1973).
6. D. M. CLODE and D. HORTON. Carbohydr. Res. **12**, 477 (1970); **19**, 329 (1971).
7. D. HORTON, A. E. LUETZOW, and O. THEANDER. Carbohydr. Res. **26**, 1 (1973).
8. D. C. BAKER and D. HORTON. Carbohydr. Res. **21**, 393 (1972).
9. D. M. CLODE and D. HORTON. Carbohydr. Res. **14**, 405 (1970); R. L. WHISTLER and L. W. DONER. J. Org. Chem. **35**, 3562 (1970).
10. A. E. EL ASHMAWY, D. HORTON, and K. D. PHILIPS. Carbohydr. Res. **9**, 350 (1969); R. W. BINKLEY and W. W. BINKLEY. Carbohydr. Res. **23**, 283 (1972).

Can. J. Chem. Downloaded from www.nrcresearchpress.com by 210.87.254.5 on 09/05/12
For personal use only.

Direct Formation of the Carbonyl Anion of Diisopropyl Formamide[1]

ROBERT R. FRASER AND PATRICK R. HUBERT
Department of Chemistry, University of Ottawa, Ottawa, Canada K1N 6N5

Received August 3, 1973

The reaction of diisopropyl formamide with lithium diisopropylamide produces, by abstraction of the formyl proton, the carbonyl anion, $LiCON[CH(CH_3)_2]_2$. Reactions of this anion with benzaldehyde, benzophenone, ethyl benzoate, acetone, and propionaldehyde occur in yields ranging from 30–92%. Thus, this anion provides a useful method for the synthesis of α-hydroxy and α-keto acids, particularly in cases where cyanohydrin formation is difficult.

La réaction de la diisopropyl formamide avec la diisopropylamide de lithium a produit, par enlèvement du proton formyle, l'anion carbonyle $LiCON[CH(CH_3)_2]_2$. Les réactions de cet anion avec de la benzaldéhyde, de la benzophénone, du benzoate d'éthyle, de l'acétone et de la propionaldéhyde se font avec des rendements variant de 30–92%. Par suite grâce à cet anion on obtient une méthode utile pour la synthèse de α-hydroxy et α-cétoacides, particulièrement dans les cas où la formation de cyanohydrines est difficile. [Traduit par le journal]

Can. J. Chem., **52**, 185 (1974)

Recently much work (1) has been devoted to the formation of carbanions whose utility in synthesis derive from their being "carbonyl anion equivalents" (2). Naturally it would be much easier and more valuable if carbonyl anions could be directly formed and reacted. There is evidence in the literature that this should be possible. Both alkoxide (3*a*) and amide (3*b*) anions undergo reversible addition to carbon monoxide at high pressure. Alkyllithiums have also been shown to add to carbon monoxide (3*c*). Furthermore, Schöllkopf and Gerhart (4) have postulated the carbanion of diethylformamide $\overset{\overset{\displaystyle O}{\|}}{\ominus CN(Et)_2}$ as the probable intermediate[2] in the conversion of the mercuriamide, $Hg[CON(Et)_2]_2$ by reaction with butyllithium and benzophenone into the hydroxyamide $(C_6H_5)_2C(OH)CON(C_2H_5)_2$. We wish to report a new method of formation of an acyl carbanion, specifically, by direct abstraction of the formyl proton of diiso-

[1]Support for this work by the National Research Council of Canada is gratefully acknowledged.

[2]Alternatively, the intermediate involving coordination of mercury to the carbene form of the anion, *i.e.*, $\left(\begin{array}{c} LiO \\ \diagdown \\ C \\ \diagup \\ (Et)_2N \end{array}\right)_2 \leftarrow Hg—(n\text{-}Bu)_2$ was suggested (4).

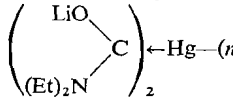

4. D. M. CLODE and D. HORTON. Carbohydr. Res. **17**, 365 (1971).
5. D. HORTON, A. E. LUETZOW, and O. THEANDER. Carbohydr. Res. **27**, 268 (1973).
6. D. M. CLODE and D. HORTON. Carbohydr. Res. **12**, 477 (1970); **19**, 329 (1971).
7. D. HORTON, A. E. LUETZOW, and O. THEANDER. Carbohydr. Res. **26**, 1 (1973).
8. D. C. BAKER and D. HORTON. Carbohydr. Res. **21**, 393 (1972).
9. D. M. CLODE and D. HORTON. Carbohydr. Res. **14**, 405 (1970); R. L. WHISTLER and L. W. DONER. J. Org. Chem. **35**, 3562 (1970).
10. A. E. EL ASHMAWY, D. HORTON, and K. D. PHILIPS. Carbohydr. Res. **9**, 350 (1969); R. W. BINKLEY and W. W. BINKLEY. Carbohydr. Res. **23**, 283 (1972).

Can. J. Chem. Downloaded from www.nrcresearchpress.com by 210.87.254.5 on 09/05/12
For personal use only.

Direct Formation of the Carbonyl Anion of Diisopropyl Formamide[1]

ROBERT R. FRASER AND PATRICK R. HUBERT
Department of Chemistry, University of Ottawa, Ottawa, Canada K1N 6N5

Received August 3, 1973

The reaction of diisopropyl formamide with lithium diisopropylamide produces, by abstraction of the formyl proton, the carbonyl anion, $LiCON[CH(CH_3)_2]_2$. Reactions of this anion with benzaldehyde, benzophenone, ethyl benzoate, acetone, and propionaldehyde occur in yields ranging from 30–92%. Thus, this anion provides a useful method for the synthesis of α-hydroxy and α-keto acids, particularly in cases where cyanohydrin formation is difficult.

La réaction de la diisopropyl formamide avec la diisopropylamide de lithium a produit, par enlèvement du proton formyle, l'anion carbonyle $LiCON[CH(CH_3)_2]_2$. Les réactions de cet anion avec de la benzaldéhyde, de la benzophénone, du benzoate d'éthyle, de l'acétone et de la propionaldéhyde se font avec des rendements variant de 30–92%. Par suite grâce à cet anion on obtient une méthode utile pour la synthèse de α-hydroxy et α-cétoacides, particulièrement dans les cas où la formation de cyanohydrines est difficile. [Traduit par le journal]

Can. J. Chem., **52**, 185 (1974)

Recently much work (1) has been devoted to the formation of carbanions whose utility in synthesis derive from their being "carbonyl anion equivalents" (2). Naturally it would be much easier and more valuable if carbonyl anions could be directly formed and reacted. There is evidence in the literature that this should be possible. Both alkoxide (3*a*) and amide (3*b*) anions undergo reversible addition to carbon monoxide at high pressure. Alkyllithiums have also been shown to add to carbon monoxide (3*c*). Furthermore, Schöllkopf and Gerhart (4) have postulated the carbanion of diethylformamide $\overset{\overset{\displaystyle O}{\|}}{\ominus CN(Et)_2}$ as the probable intermediate[2] in the conversion of the mercuriamide, $Hg[CON(Et)_2]_2$ by reaction with butyllithium and benzophenone into the hydroxyamide $(C_6H_5)_2C(OH)CON(C_2H_5)_2$. We wish to report a new method of formation of an acyl carbanion, specifically, by direct abstraction of the formyl proton of diiso-

[1]Support for this work by the National Research Council of Canada is gratefully acknowledged.

[2]Alternatively, the intermediate involving coordination of mercury to the carbene form of the anion, *i.e.*, $\left(\begin{array}{c} LiO \\ \diagdown \\ C \\ \diagup \\ (Et)_2N \end{array}\right)_2 \leftarrow Hg—(n\text{-}Bu)_2$ was suggested (4).

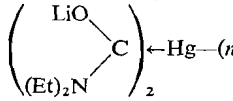

Can. J. Chem. Downloaded from www.nrcresearchpress.com by 210.87.254.5 on 09/05/12
For personal use only.

TABLE 1. Reactions of $LiC(=O)-N[CH(CH_3)_2](LiA)$ with electrophiles

Electrophile	Product[a]	Yield(%)[b]
Acetone	$(CH_3)_2C(OH)A$	30
Benzaldehyde	C_6H_5CHOHA	51
Benzophenone	$(C_6H_5)_2C(OH)A$	92
Ethyl benzoate (1 equiv.)	$C_6H_5C(=O)A$	45
Ethyl benzoate (0.5 equiv.)	$(C_6H_5)C(OH)A_2$	42
Methyl iodide	CH_3A	20[c]
Propionaldehyde	CH_3CH_2CHOHA	41
Propyl iodide	—	0[c]
D_2O	DA	70[c]

[a]All products possess n.m.r. spectra and combustion analyses in accord with their assigned structures.
[b]Yields are of pure products isolated and purified by column chromatography unless stated otherwise.
[c]Analysis by n.m.r. integration measurements.

propyl formamide, and to describe the reactivity of this anion toward a number of electrophiles.

When diisopropyl formamide is added to a solution of lithium diisopropylamide in tetrahydrofuran (THF) at -78 °C, abstraction of the formyl proton by the nitrogen base takes place as indicated by the following observations. Addition, after 4 min, of an equivalent of D_2O gives back amide in which 70% of the formyl proton has been replaced by deuterium (n.m.r. integration). Similarly, addition of benzophenone gives a 92% yield of the hydroxyamide $(C_6H_5)_2C(OH)$-$CONR_2$ (throughout this paper R = $CH(CH_3)_2$). Addition of other electrophiles results in the formation of a variety of products whose structures and yields (isolated) are given in Table 1. These results clearly demonstrate that the carbonyl anion[3] has been successfully formed. They also provide a convenient method for the synthesis of a variety of structures for which existing methods are often tedious; i.e., α-hydroxy acids, α-keto acids, and hydroxymalonic acids. Use of this anion in place of cyanide for the purpose of making α-hydroxy acids provides obvious advantages of safety in handling and better reactivity towards ketones which form cyanohydrins with difficulty or not at all (*e.g.*, benzophenone (5)).

The widely differing yields for reactions of this carbonyl anion most probably result from the presence of a mobile equilibrium ($K_{eq} \cong 2$)

$$HCONR_2 + LiNR_2 \rightleftharpoons Li{-}CONR_2 + HNR_2$$

Thus, the formation of 70% deuterated amide probably indicates the position of this equilibrium, since quenching of the carbanion with D_2O ought to be rapid. On the other hand, addition of less reactive electrophiles gives rise to yields which likely reflect the reactivity of the carbanion towards the electrophile, relative to that of the nitrogen anion.

It is interesting to note that dimethyl formamide (DMF) under the same reaction conditions fails to give an adduct with benzophenone. Instead, the only isolable product was diphenylcarbinol (17% yield). Reduction in this instance is attributed to a hydride transfer by the intermediate $HC(O^-)NR_2N(CH_3)_2$. Increasing the bulk of the substituents on the amide nitrogen likely prevents formation and subsequent reaction of this type of intermediate. An alternative explanation based on differing acidities of the formyl protons of DMF and diisopropyl formamide seems unlikely in view of our observation that these two "acids" show comparable rates of H–D exchange in DMSO-d_6 (0.5 *M* in potassium *t*-butoxide).

[3]Abstraction of the formyl proton by lithium diisopropyl amide is also of theoretical interest. Over ten years ago Breslow (6) proposed that the first step in the polymerization of formaldehyde to "formose" was the generation of the $H{-}C(=O)^{\ominus}$ anion. Though the base used herein is far stronger than that used in "formose" production it demonstrates that carbonyl carbanions can be formed by proton abstraction.

Work on extension of the utility of the anion of diisopropyl formamide to include its reaction with other electrophiles is currently in progress.

Experimental

Standard Procedure

To a solution of diisopropyl amine (2.6 mmol) in 50 ml THF at −78° is added 2.6 mmol of methyllithium followed after 2 min by 2.6 mmol of diisopropyl formamide. After 5 min benzophenone (2 mmol) is added and the solution stirred for 45 min. Warming to room temperature, then removing solvent, dissolving in methylene chloride, washing with water, drying, and evaporating solvent gave a solid which was subjected to column chromatography. Elution from silica with chloroform gave 570 mg (92% of theory) of solid, m.p. 150.5–151°.

1. K. OSHIMA, K. SHIMOJI, H. TAKAHASHI, H. YAMAMOTO, and H. NOZAKI. J. Am. Chem. Soc. **95**, 2694 (1973); J. E. RICHMAN, J. L. HERRMANN, and R. H. SCHLESSINGER. Tetrahedron Lett. 3267 (1973) and references therein.
2. D. SEEBACH. Angew. Chem. Int. Ed. **8**, 639 (1969).
3. (*a*) J. A. CHRISTIANSEN and J. C. GJALDBACK. Chem. Abstr. **38**, 3898 (1944), F. ADICKES and G. SCHAFER. Ber. **65B**, 950 (1932). (*b*) H. WINTELER, A. BIELER, and A. GUYER. Helv. Chem. Acta. **37**, 2370 (1954). (*c*) P. JUTZI and F. W. SCHRÖDER. J. Organometallic. Chem. **24**, 1 (1970).
4. U. SCHÖLLKOPF and F. GERHART. Angew. Chem. **79**, 819, 990 (1967).
5. Houben-Weyl Methoden der Organische Chemie. Vol. 8. Georg Thieme Verlag, Stuttgart. 1952. p. 274.
6. R. BRESLOW. Tetrahedron Lett. No. 21, 22 (1959).

Can. J. Chem. Downloaded from www.nrcresearchpress.com by 210.87.254.5 on 09/05/12
For personal use only.

o-Nitrophenylethylene Glycol: a Photosensitive Protecting Group for Aldehydes and Ketones

JACQUES HÉBERT[1] AND DENIS GRAVEL

Department of Chemistry, University of Montreal, P.O. Box 6128, Montreal, Quebec

Received August 10, 1973

o-Nitrophenylethylene glycol (**1**) was synthesized and found to be useful as a photochemically labile blocking group for aldehydes and ketones. The acetals obtained are cleaved smoothly upon irradiation at 3500 Å, regenerating the parent carbonyl compound in very good yield.

L'*o*-nitrophényléthylène glycol (**1**) a été synthétisé et développé comme groupement protecteur photochimiquement labile pour les aldéhydes et les cétones. Les acétals ainsi formés se scindent très facilement par irradiation à 3500 Å pour régénérer les composés carbonylés parents avec de très bons rendements.

Can. J. Chem., **52**, 187 (1974)

The photochemical isomerization of *o*-nitrobenzaldehyde (1) and of various *o*-nitrobenzyl derivatives (2) has been investigated actively since the beginning of this century. The greatest portion of the work done in this field has been reported by Tanasescu (ref. 3*a* and later papers, in particular ref. 3*b*) and dealt mainly with the photochemical cleavage of *o*-nitrobenzylidene acetals. The key step in this general reaction involves the transfer of an oxygen atom from the nitro group to the benzylic position.

In 1966, Barltrop *et al.* (4) reported new photosensitive blocking groups for the amino and carboxyl functions of amino acids based on the above concept. Since then, the use of *o*-nitrobenzyl derivatives as photosensitive protecting groups in peptide (5) and carbohydrate chemistry (6) has attained a high degree of sophistication due to the efforts of Patchornik and co-workers (5, 6).

We wish to report here the synthesis of *o*-nitrophenylethylene glycol (**1**) and its application as a photosensitive protecting group for the carbonyl function (Scheme 1).

The title compound (**1**) (m.p. 95–96°) was obtained in 78% yield by alkaline hydrolysis of

[1]NRCC Postgraduate Scholarship Holder 1969–1973.

Work on extension of the utility of the anion of diisopropyl formamide to include its reaction with other electrophiles is currently in progress.

Experimental

Standard Procedure

To a solution of diisopropyl amine (2.6 mmol) in 50 ml THF at −78° is added 2.6 mmol of methyllithium followed after 2 min by 2.6 mmol of diisopropyl formamide. After 5 min benzophenone (2 mmol) is added and the solution stirred for 45 min. Warming to room temperature, then removing solvent, dissolving in methylene chloride, washing with water, drying, and evaporating solvent gave a solid which was subjected to column chromatography. Elution from silica with chloroform gave 570 mg (92% of theory) of solid, m.p. 150.5–151°.

1. K. OSHIMA, K. SHIMOJI, H. TAKAHASHI, H. YAMAMOTO, and H. NOZAKI. J. Am. Chem. Soc. **95**, 2694 (1973); J. E. RICHMAN, J. L. HERRMANN, and R. H. SCHLESSINGER. Tetrahedron Lett. 3267 (1973) and references therein.
2. D. SEEBACH. Angew. Chem. Int. Ed. **8**, 639 (1969).
3. (*a*) J. A. CHRISTIANSEN and J. C. GJALDBACK. Chem. Abstr. **38**, 3898 (1944), F. ADICKES and G. SCHAFER. Ber. **65B**, 950 (1932). (*b*) H. WINTELER, A. BIELER, and A. GUYER. Helv. Chem. Acta. **37**, 2370 (1954). (*c*) P. JUTZI and F. W. SCHRÖDER. J. Organometallic. Chem. **24**, 1 (1970).
4. U. SCHÖLLKOPF and F. GERHART. Angew. Chem. **79**, 819, 990 (1967).
5. Houben-Weyl Methoden der Organische Chemie. Vol. 8. Georg Thieme Verlag, Stuttgart. 1952. p. 274.
6. R. BRESLOW. Tetrahedron Lett. No. 21, 22 (1959).

o-Nitrophenylethylene Glycol: a Photosensitive Protecting Group for Aldehydes and Ketones

JACQUES HÉBERT[1] AND DENIS GRAVEL

Department of Chemistry, University of Montreal, P.O. Box 6128, Montreal, Quebec

Received August 10, 1973

o-Nitrophenylethylene glycol (**1**) was synthesized and found to be useful as a photochemically labile blocking group for aldehydes and ketones. The acetals obtained are cleaved smoothly upon irradiation at 3500 Å, regenerating the parent carbonyl compound in very good yield.

L'*o*-nitrophényléthylène glycol (**1**) a été synthétisé et développé comme groupement protecteur photochimiquement labile pour les aldéhydes et les cétones. Les acétals ainsi formés se scindent très facilement par irradiation à 3500 Å pour régénérer les composés carbonylés parents avec de très bons rendements.

Can. J. Chem., **52**, 187 (1974)

The photochemical isomerization of *o*-nitrobenzaldehyde (1) and of various *o*-nitrobenzyl derivatives (2) has been investigated actively since the beginning of this century. The greatest portion of the work done in this field has been reported by Tanasescu (ref. 3*a* and later papers, in particular ref. 3*b*) and dealt mainly with the photochemical cleavage of *o*-nitrobenzylidene acetals. The key step in this general reaction involves the transfer of an oxygen atom from the nitro group to the benzylic position.

In 1966, Barltrop *et al.* (4) reported new photosensitive blocking groups for the amino and carboxyl functions of amino acids based on the above concept. Since then, the use of *o*-nitrobenzyl derivatives as photosensitive protecting groups in peptide (5) and carbohydrate chemistry (6) has attained a high degree of sophistication due to the efforts of Patchornik and co-workers (5, 6).

We wish to report here the synthesis of *o*-nitrophenylethylene glycol (**1**) and its application as a photosensitive protecting group for the carbonyl function (Scheme 1).

The title compound (**1**) (m.p. 95–96°) was obtained in 78% yield by alkaline hydrolysis of

[1]NRCC Postgraduate Scholarship Holder 1969–1973.

Can. J. Chem. Downloaded from www.nrcresearchpress.com by 84.22.46.98 on 09/08/12
For personal use only.

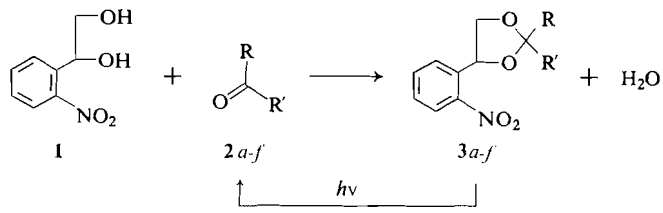

SCHEME 1

o-nitrostyrene oxide (7) using potassium carbonate in aqueous dioxane. The acetals (**3***a–f*) of cyclohexanone (**3***a*), *p*-nitrobenzaldehyde (**3***b*), benzophenone (**3***c*), 5-pregnen-3β-ol-20-one acetate (**3***d*), 5-androsten-3β-ol-17-one acetate (**3***e*), and testosterone (**3***f*) were prepared and characterized by n.m.r., i.r., u.v., and mass spectrometry. In the standard experimental procedure, a solution of 10 mmol of carbonyl compound (**2**), 30 mmol of **1** and 100 mg of *p*-toluenesulfonic acid in 125 ml of benzene is heated to reflux in the flask of a Soxhlet apparatus, the extraction thimble of which is filled with anhydrous magnesium sulfate to ensure adequate water removal. After the usual work-up, the residue is passed through a silica gel column in order to obtain the pure acetal (**3**). Melting points, yields and reaction times are reported in Table 1.

The protecting group is removed by irradiation of a 2.5×10^{-3} *M* solution of the acetal in benzene (0.5 mmol in 200 ml benzene) at room temperature for 6 h. A pyrex vessel and light of wavelength longer than 3200 Å are used (Rayonet, 3500 Å lamps). The red-brown residue is chromatographed on silica gel. Yields of regenerated carbonyl compounds (**2***a–f*) reported in Table 2 are generally good, except in the case of testosterone (**2***f*). For the latter, irradiation of the $\Delta^{5,6}$ acetal yields the deconjugated parent ketone which has a low degree of stability under the reaction conditions and either reconjugates, oxidizes, or cleaves in a Norrish type I manner (8).

The mechanism of this photochemical reaction (Scheme 2) is most probably analogous to that postulated for the rearrangement of *o*-nitrobenzaldehyde (9). The key steps would involve intramolecular abstraction of the benzylic hydrogen giving either **5***a* or **5***b*, rearrangement to hemiacetal **6** and collapse of the latter to the free carbonyl compound **2** and α-hydroxy-*o*-nitrosoacetophenone (**4**). The sensitivity to u.v. light of compound **4** prevented its isolation.

o-Nitrophenylethylene glycol is, to our knowledge, the first photochemically labile protecting group for aldehydes and ketones. Although the method has some obvious limitations it should nevertheless prove useful in organic synthesis since it allows the selective removal of an acetal under anhydrous and chemically inert conditions.

TABLE 1. Preparation of acetals (**3***a–f*)

Acetals	Melting point[a] (°C)	Reaction time (h)	% yield of acetals
3*a*	[b]	1	96
3*b*	118–119[c]		
	111–112[d]	2	97
3*c*	115–116	12	94
3*d*	[e]	7	58
3*e*	[e]	2	89
3*f*	[e]	20	70

[a]All melting points are uncorrected.
[b]Boiling point 142 °C/0.25 mm Hg.
[c]*Cis* isomer.
[d]*Trans* isomer.
[e]Mixture of diastereoisomers.

TABLE 2. Irradiation of acetals (**3***a–f*)

Acetals	% yield carbonyl compound	% unreacted acetal
3*a*	85[a]	—
3*b*	86	11
3*c*	90	7
3*d*	83	13
3*e*	74[b]	15
3*f*	31	14

[a]Characterized as its 2,4-dinitrophenylhydrazone.
[b]Comprising 2/3 androstenone acetate and 1/3 13-α-androstenone acetate.

Can. J. Chem. Downloaded from www.nrcresearchpress.com by 84.22.46.98 on 09/08/12
For personal use only.

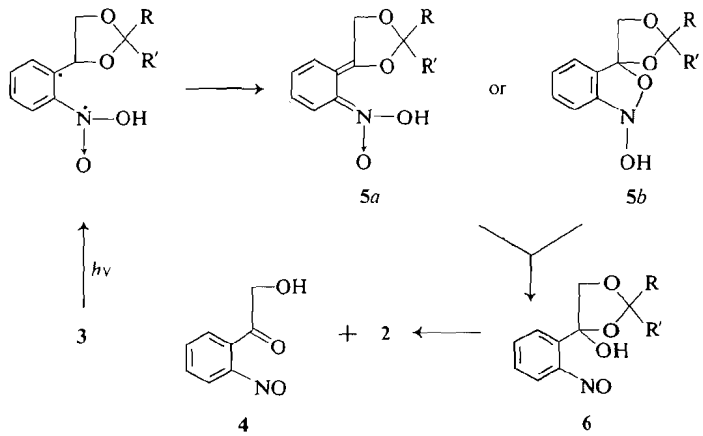

SCHEME 2

Support of this research by the National Research Council of Canada is gratefully acknowledged.

1. G. CIAMICIAN and P. SILBER. Chem. Ber. **35**, 1992 (1902).
2. (*a*) F. SACHS and S. HILPERT. Chem. Ber. **37**, 3425 (1904); (*b*) E. BAMBERGER and F. ELGER. Ann. **371**, 319 (1909); (*c*) G. SCHULTZ and K. L. GANGULY. Chem. Ber. **58**, 702 (1925); (*d*) I. TANASESCU. Bull. Soc. Chim. Fr. 1443 (1926); (*e*) J. A. BERSON and E. BROWN. J. Am. Chem. Soc. **77**, 447 (1955).
3. (*a*) I. TANASESCU. Bull. Soc. Stiinte Cluj, **2**, 111 (1924); (*b*) I. TANASESCU. Rev. Roum. Chem. **5**, 35 (1960).
4. J. A. BARLTROP, P. J. PLANT, and P. SCHOFIELD. Chem. Commun. 822 (1966).
5. A. PATCHORNIK, B. AMIT, and R. B. WOODWARD. J. Am. Chem. Soc. **92**, 6333 (1970).
6. (*a*) U. ZEHAVI, B. AMIT, and A. PATCHORNIK. J. Org. Chem. **37**, 2281, 2285 (1972); (*b*) P. M. COLLINS and N. N. OPARAECHE. Chem. Commun. 532 (1972); (*c*) B. AMIT, U. ZEHAVI, and A. PATCHORNIK. Proceedings, 42nd Meeting of the Israel Chemical Society, Dec. 1972. p. 60; (*d*) U. ZEHAVI and A. PATCHORNIK. Proceedings, 42nd Meeting of the Israel Chemical Society, Dec. 1972. p. 61.
7. C. O. GUSS. J. Org. Chem. **17**, 678 (1952).
8. (*a*) H. J. RINGOLD and S. K. MALHOTRA. Tetrahedron Lett. **15**, 669 (1962); (*b*) L. A. PAQUETTE and G. V. MEEHAN. J. Org. Chem. **34**, 450 (1969) and references cited therein.
9. (*a*) P. DE MAYO and S. T. REID. Quart. Rev. **15**, 414 (1961); (*b*) D. C. NECKERS. Mechanistic organic photochemistry. Reinhold Publishing Corp., N.Y. 1967. p. 207; (*c*) R. O. KAN. Organic photochemistry. McGraw-Hill Co., New York. 1966. p. 218.

Can. J. Chem. Downloaded from www.nrcresearchpress.com by 84.22.46.98 on 09/08/12
For personal use only.

Can. J. Chem. Downloaded from www.nrcresearchpress.com by 210.87.254.6 on 09/05/12
For personal use only.

Canadian Journal of Chemistry

Published by
THE NATIONAL RESEARCH COUNCIL OF CANADA

Journal canadien de chimie

Publié par
LE CONSEIL NATIONAL DE RECHERCHES DU CANADA

Volume 52 Number 2 January 15, 1974 Volume 52 numéro 2 15 janvier 1974

Application of Adiabatic Rapid Passage Nuclear Magnetic Resonance Techniques to the Study of Molecular Motions in Solids

J. A. RIPMEESTER[1,2] AND B. A. DUNELL

Department of Chemistry, University of British Columbia, Vancouver 8, British Columbia

Received July 11, 1973

The adiabatic rapid passage (ARP) technique was applied to the study of molecular motion in solids. Second moments and spin–lattice relaxation times for solid furan and benzene were derived using ARP methods from 77 °K to the respective melting points. Unusual variations of the ARP signal height and shape with temperature were observed for these solids. These effects were interpreted as being due to the presence of short rotating frame relaxation times. New information regarding molecular motion in solid furan, as well as acetic acid-d_1, was obtained. Also some quantitative statements have been made regarding the conditions required to observe an ARP signal in the solid state.

La technique du passage rapide adiabatique (PRA) a été appliquée pour étudier les mouvements moléculaires dans les solides. Les moments seconds et les temps de relaxation spin–réseau ont été obtenus pour le furanne et le benzène solides en utilisant des méthodes PRA de 77 °K jusqu'à leurs points de fusion respectifs. Des variations inhabituelles de la hauteur et de la forme du signal PRA, en fonction de la température, ont été observées pour ces solides. L'origine de ces effets a été attribuée à la présence de temps de relaxation dans le referentiel tournant courts. De nouvelles informations ont été recueillies sur les mouvements moléculaires dans le furanne solide aussi bien que dans l'acide acétique-d_1. Quelques conclusions sont aussi émises sur les conditions requises pour l'observation d'un signal PRA à l'état solide. [Traduit par le journal]

Can. J. Chem., **52**, 191 (1974)

Introduction

Previous publications (1, 2*a*) from this laboratory have reported the experimental conditions under which such useful n.m.r. parameters as second moments and spin–lattice relaxation times may be obtained using the adiabatic rapid passage (ARP) technique in the study of solids. We have extended ARP measurements to conditions under which molecular motion occurs in solid systems in order to establish the applicability of the ARP technique in this area of interest. During the course of these investigations, unusual effects were noted. In some solids where motional narrowing of the resonance line took place, it was observed that the ARP signal appeared distorted, and the signal intensity was anomalously low (3).

We have observed this phenomenon in various solids and have related this to the presence of short rotating frame relaxation times due to slow molecular motions. We have also attempted to measure second moments and spin–lattice relaxation times for these solids.

Janzen (2*b*) has discussed the necessary conditions for adiabatic rapid passage in solids. The stringency of the adiabatic condition (1, 2*b*, 4, 5)

$$[1] \qquad dH_0/dt \ll \gamma H_1^2$$

depends on the purpose of the experiment and the

[1]Present address: Division of Chemistry, National Research Council of Canada, Ottawa.

[2]NRCC Scholarship holder, 1967–1970.

Can. J. Chem. Downloaded from www.nrcresearchpress.com by 210.87.254.6 on 09/05/12
For personal use only.

accuracy expected. Measurement of T_1, in which the shape of the ARP signal is not critical, requires that γH_1^2 be only about 5 times greater (1) than dH_0/dt. Here dH_0/dt is the rate at which the main magnetic field is swept in the ARP experiment, γ is the magnetogyric ratio of the nucleus in question, and H_1 is the radio frequency field amplitude. The rapid passage condition requires that the time of passage through the region of resonance, or through the ARP line, be short compared with T_1. It may be written

$$[2] \qquad t_p \simeq \delta H/(dH_0/dt) \ll T_1$$

where δH is the width at half-height of the ARP signal.

The ARP signal is proportional to the component of the magnetization in the rotating frame in phase with the r.f. field, namely,

$$[3] \quad M_{xr} = M_0 H_1 [H_1^2 + h^2 + H_L^2]^{-1/2}$$

where h is the distance from resonance in G. H_L is the local field and is related to the second moment of the unsaturated absorption line ΔH_2^2 by

$$[4] \qquad H_L = (\Delta H_2^2/3)^{1/2}$$

The signal width at half height δH is given by

$$[5] \qquad \delta H = [12(H_1^2 + H_L^2)]^{1/2}$$

so the second moment can be obtained from the ARP line if H_1 is known.

It is convenient to mention here three ways of obtaining T_1 by ARP methods. In the two-pass "$\pi - \pi/2$" ARP experiment the first passage is used to invert the magnetization, which had been allowed to attain equilibrium in a field above resonance (*i.e.*, in $H_0 > \omega_0/\gamma$). After a time t, the second passage is used to sample the partially recovered magnetization. The relation between the magnetization M_t at time t and the initial equilibrium magnetization M_0 is

$$[6] \qquad M_t = M_0(1 - 2\exp(-t/T_1))$$

In the null method, t is adjusted so that $M_t = 0$, and

$$[7] \qquad T_1 = t_{null}/\ln 2$$

When T_1 is long, the two-pass experiment is inconvenient because of the very long waiting required to allow the elapse of several times T_1 so that the equilibrium magnetization will be re-established before a new value of t is chosen. Under these circumstances it is convenient to reduce the magnetization to zero by successive passages through resonance and then sample the partially recovered magnetization at a time t later. Again the experiment is repeated for various times t, but without the necessity of waiting between successive experiments. The recovery of magnetization is given by

$$[8] \qquad M_t = M_0(1 - \exp(-t/T_1))$$

T_1 is obtained from either eq. 6 or 8 by a semi-logarithmic plot of M_t against t.

Experimental

Acetone, benzene, and furan were spectroscopic grade chemicals. Acetic acid-d_1 was purchased from Stohler Isotope Chemicals. Samples of each were sealed in Pyrex tubes after degassing by successive freeze–pump–thaw cycles.

The magnetic field was supplied by a Varian 6 in. electromagnet. The field was swept by directing the square wave, or single square step, output of a Servomex LF-51 Mk II waveform generator directly into the sweep input of the electromagnet power supply. Sweep rates used range from 200 to 300 G/s.

The 8 MHz radio frequency field of 0.69 G amplitude was obtained from a Varian V-4210A r.f. unit. The ARP signal was taken directly from the output of the diode stage in the receiver and displayed on an oscilloscope screen. Measurements were made directly from the oscilloscope display, or photographs made thereof.

Results and Discussion

ARP Experiments on Furan

(a) Background Information

Solid furan is known to have two distinct solid phases (6, 7). The structure stable below 150 °K is tetragonal (7) and the structure is ordered in the sense that each molecule has only a single allowed orientation. The phase stable between 150 °K and the melting point is orthorhombic, space group *Cmca*. This high temperature phase is disordered; there are four allowed orientations of the furan molecule such that the disorder is about an axis at right angles to the molecular plane. Dielectric (8) and broadline n.m.r. (9) studies have shown that the disorder in the high temperature phase is dynamic. The dielectric (8) and n.m.r. (9) results are consistent with essentially stationary molecules in the low temperature phase and with a high temperature phase model in which the molecules reorient rapidly about the out-of-plane axis with an activation energy of about 2 kcal/mol.

Can. J. Chem. Downloaded from www.nrcresearchpress.com by 210.87.254.6 on 09/05/12
For personal use only.

(b) Calculations

Since the molecular structure (10) as well as the crystal structure (7) of both phases of solid furan is well defined, second moments may be calculated for both these phases using the proton coordinates given in the X-ray structure.

For the low temperature phase we assume that the lattice is rigid and we use Van Vleck's formula (11). Contributions from interactions with nuclei within a sphere of radius 5 Å were taken into account. Contributions from outside this sphere were estimated by an integral.

For the high temperature phase we use the expressions tabulated by Rigny and co-workers (12), and we assume that the furan molecules reorient by jumping randomly between their four allowed sites. Contributions from a block of 27 unit cells were taken into account in this case.

The second moments calculated in this manner were 5.12 G^2 for the rigid lattice case and 1.45 G^2 for the rotator phase.

(c) ARP Experiments

The ARP signals obtained for furan between 77 °K and ~170 °K appeared to be true ARP signals, with no obvious evidence of distortion (see Fig. 1). Second moments were derived from the ARP signal at temperatures above and below the phase transition using eqs. 4 and 5. Values obtained were 4.95 and 1.42 G^2 at 137 and 164 °K respectively, and are in excellent agreement with values calculated for the motional models considered.

Spin–lattice relaxation times (T_1) were measured in the solid between 77 °K and the melting point, and also over a limited temperature range in the liquid (Fig. 2). For measurements in the

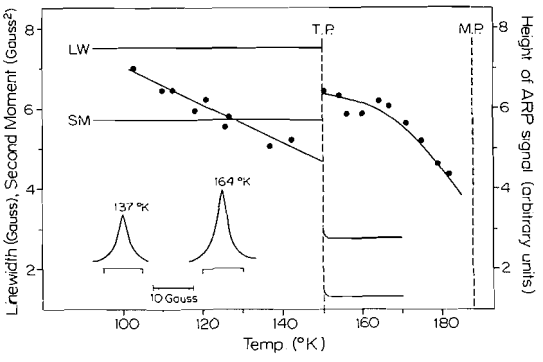

FIG. 1. Linewidth and second moment (from C.W. measurements, ref. 9) and height of the ARP signal as a function of temperature for furan. Also shown are some representative ARP signal shapes.

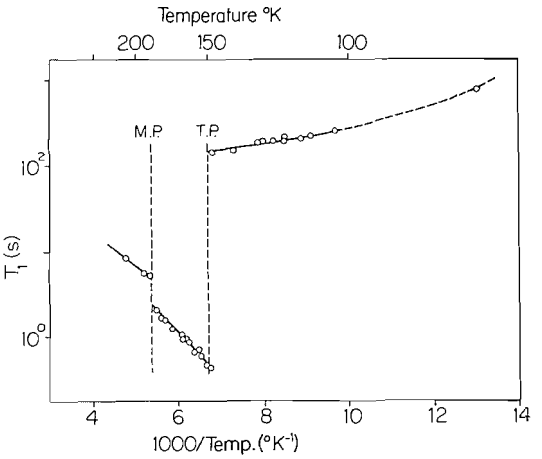

FIG. 2. Spin–lattice relaxation times (T_1) for furan as a function of inverse temperature.

low temperature phase we used the technique which required eq. 8 to extract the T_1 values. The other datum points were measured using the two-pass "$\pi - \pi/2$" experiment and eq. 6. In the low temperature phase T_1 varies only slightly with temperature and is quite long. In agreement with conclusions reached from second moment considerations, the long T_1's suggest that nuclear dipolar relaxation due to molecular reorientation is essentially absent in this phase.

In the high temperature phase, T_1 is much shorter and increases with temperature. From the second moment data and the sense of the T_1 slope above the transition temperature we may conclude that motions are fast ($\omega_0\tau_c \ll 1$, where τ_c is the correlation time for motion). If we assume that the molecular reorientation is an activated process so that we can write

$$[9] \qquad \tau_c = \tau_0 \exp(E_a/RT)$$

where τ_0 is an inverse frequency factor and E_a an activation energy, we derive a value of 2.35 ± 0.1 kcal/mol for E_a from the slope of the semi log plot of T_1 *vs.* inverse temperature. In the extreme narrowing region, where $\omega_0\tau_c \ll 1$ for the motion, T_1 is related to τ_c by (13)

$$[10] \qquad T_1^{-1} = (2/3)\gamma^2\Delta H_2^2(\text{MOD})(5\tau_c)$$

where ΔH_2^2(MOD) is the part of the second moment modulated by the motion. Using the calculated second moments to find ΔH_2^2(MOD), we find that immediately above the transition point $\tau_c = 2.5 \times 10^{-10}$ s, and from eq. 9 we find $\tau_0 \sim 1 \times 10^{-13}$ s. Apparently the molecular

Can. J. Chem. Downloaded from www.nrcresearchpress.com by 210.87.254.6 on 09/05/12
For personal use only.

reorientation is extremely fast in the high temperature phase of furan, a conclusion also reached in the dielectric study (8).

The variation of the ARP signal amplitude with temperature is not unusual in the low temperature phase, and probably reflects only the change in energy level populations according to the Boltzman factor. However, in the high temperature phase between ~170 °K and the melting point the ARP signal height decreased more rapidly with temperature. Since the ARP conditions as they are written in eqs. 1 and 2 are apparently satisfied, this anomalous signal intensity loss is probably due to the presence of a rotating frame spin–lattice relaxation time ($T_{1\rho}$) comparable in magnitude to the time of passage $t_p = \delta H/(dH_0/dt) \sim 10^{-2}$ to 10^{-3} s. Such a short $T_{1\rho}$ suggests that slow molecular motions are taking place in the solid with correlation times τ_c such that $\gamma H_L \tau_c \geqslant 1$. This loss of intensity of the ARP signal was checked further for benzene (see next section) where such slow motions are known to exist.

ARP Experiments on Benzene

(a) Background Information

Solid benzene has been the subject of a number of n.m.r. studies (14–17). These include measurements of second moments (14), line widths (14), and spin–lattice relaxation times (14–17) as a function of temperature. From these studies it has been concluded that reorientation of the benzene molecules about their hexad axes takes place with frequencies greater than $\sim 10^5$ s^{-1} above ~100 °K. The correlation times in s as a function of temperature are given by (16) $\tau_c = 9.2 \times 10^{-15} \exp(4200/RT)$ or (15) $\tau_c = 1.82 \times 10^{-14} \exp(3950/RT)$ depending on the detailed model chosen for the motion.

Measurement of the dipolar relaxation rate for benzene (17) also has revealed the presence of a slow motion immediately below the melting point. This motion does not occur rapidly enough to narrow the resonance line; the activation energy for this process was 16 kcal/mol. Van Steenwinkel (17) proposed that the motion in question is a rotation of the molecule about a C_2 axis, although recently O'Reilly and Peterson (18) suggested that it is a molecular diffusion.

(b) ARP Experiments

Between ~80 and 170 °K the ARP signal was distorted (Fig. 3), so that second moment data could not be obtained from the ARP signal width

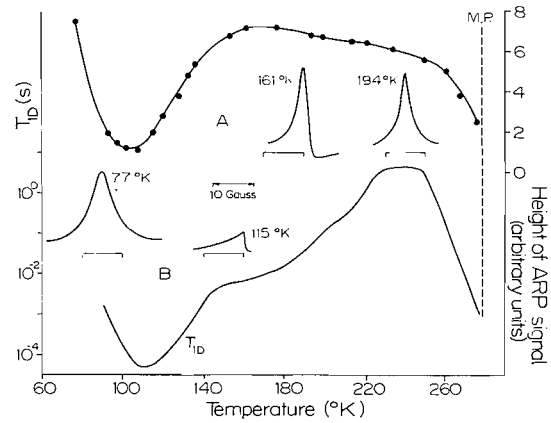

FIG. 3. Height of the ARP signal, and the time constant (T_{1D}) characterizing the dipolar energy relaxation rate (ref. 17) as a function of temperature for benzene. ARP signal shapes are shown as well for various temperatures.

at half height. At 77 and ~190 °K, the ARP signals appeared to be free of distortion, and linewidth measurements yielded second moments of 10.0 and 1.55 G^2. These values are in good agreement with those obtained by Andrew and Eades (14) using C. W. methods, namely 9.80 and 1.60 G^2.

Between ~80 and 150 °K, and just below the benzene melting point, the ARP signal height was anomalously low. At 105 °K, the signal amplitude was about 15% of its expected value.

Spin–lattice relaxation times were measured for benzene between ~90 °K and the melting point using the two-pass "$\pi - \pi/2$" experiment and eq. 6. Between ~125 and 150 °K, T_1 was too short for our particular instrumentation (the sweep rate was the limiting factor); the shortest T_1's measured were ~0.02 s. Although the anomalous signal amplitude loss made the measurements more difficult, the validity of the T_1 measurement seems to be unaffected. The temperature dependence of the correlation times (in s) derived from the relaxation time data can be expressed as

$$\tau_c = 8.0 \times 10^{-15} \exp(4100/RT)$$

in reasonable agreement with the previously quoted correlation time parameters.

It can be seen from Fig. 3 that the temperature regions where the anomalous signal loss was observed for benzene coincide approximately with the temperature regions where the relaxation times for the dipolar energy (T_{1D}) were observed

Can. J. Chem. Downloaded from www.nrcresearchpress.com by 210.87.254.6 on 09/05/12
For personal use only.

to be short. Since both T_{1D} and $T_{1\rho}$ in systems with classical motions (such as benzene) are governed by slow motional processes, the observation of short T_{1D} values also implies that $T_{1\rho}$ (measured with weak H_1 fields of ~ 1 G) will be short. It is then quite obvious that when, during a sweep through resonance, the magnetization is aligned along the H_1 field, relaxation will take place if the rotating frame relaxation time is of the order of or shorter than, the time of passage $\delta H/(dH_0/dt)$. This then would cause a loss of amplitude and signal distortion, the degree of which would depend on the exact values for the sweep rate and rotating frame relaxation time. Rotating frame relaxation in the strong collision limit ($H_1 \sim H_L$), which can take place in benzene near ~ 100 °K, has been treated theoretically by Slichter and Ailion (19). A calculation of the dipolar relaxation rate in benzene has been presented by Haeberlen (20).

The inequalities [1] and [2] may be reconsidered here. In this work $\gamma H_1^2/(dH_0/dt)$ ranges from 40 to 65. If other criteria are satisfied, second moments which agree with the C.W. values to within 4% under these conditions can be calculated from the ARP line. With respect to inequality (2), we find that on the high temperature side of the T_1 minimum, signal distortions disappear as the temperature increases above about 180 °K. At this temperature, T_1 and $T_{1\rho}$ are equal to ~ 0.05 s. (T_1 and $T_{1\rho}$ should be equal in the extreme narrowing limit.) Our sweep rate was such that we find

$$(T_{1\rho}/\delta H)(dH_0/dt), (T_1/\delta H)(dH_0/dt) > 3.6$$

represents the condition required to give an ARP signal of satisfactory shape for the other existing experimental conditions.

As far as the measurement of T_1 in the presence of a very short $T_{1\rho}$ is concerned, it is evident that meaningful data may be obtained as long as an ARP signal can be observed, and a constant sweep rate is employed in any single T_1 determination. It should be noted that when $T_{1\rho}$ is very short the use of eq. 8 is probably preferable to the use of eq. 6 for the two-pass "$\pi - \pi/2$" experiment, as, instead of the magnetization being inverted during the first pass, it is actually reduced essentially to zero by the rapid rotating frame relaxation. This is illustrated in Fig. 4, where some magnetization recovery curves are shown. The magnetization recovery curve normalized according to eq. 6 at 234 °K passes through unity

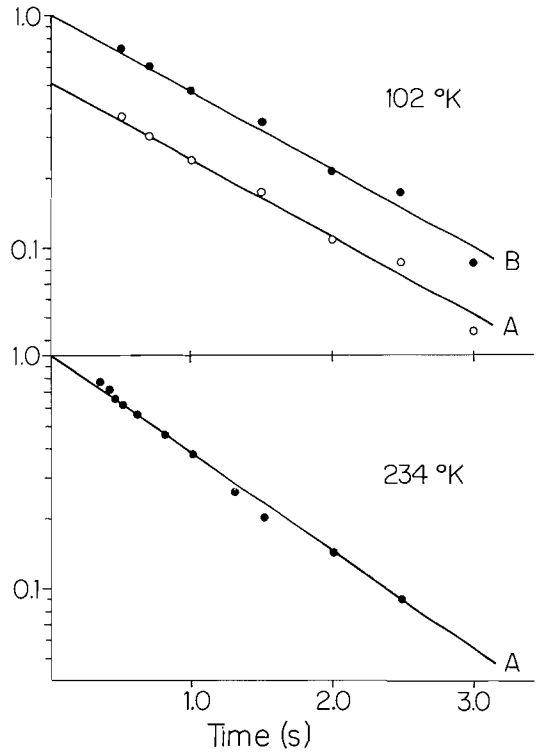

FIG. 4. Magnetization recovery curves for benzene at 102 °K and 234 °K. The ordinate is $(M_t - M_0)/M_0$ for B and $(M_t - M_0)/2M_0$ for A.

when extrapolated to $t = 0$. When $T_{1\rho}$ is very short, as it is at 120 °K, the normalized recovery curve extrapolated to a value of ~ 0.5 at $t = 0$. If this second curve is normalized according to eq. 8, however, extrapolation to zero time again results in a value of unity (see Fig. 4).

The Null Method for Determining T_1

Two systems were investigated in order to determine whether the ARP null method described earlier is at all a useful technique to measure T_1. The solids investigated were acetone and acetic acid-d_1. Only methyl group rotation takes place in these solids (21, 22), and the extreme narrowing limit for this motion exists in the entire region of study. With the H_1 and sweep rates used, the ARP conditions were all satisfied. Some initial determinations of M_t as a function of time at specific temperatures showed that the magnetization recoveries were non-exponential. In cases like this, null determinations of T_1 are especially suitable, although any single, exact T_1 is not really defined.

Semilog plots of t_{null} as a function of inverse

Can. J. Chem. Downloaded from www.nrcresearchpress.com by 210.87.254.6 on 09/05/12
For personal use only.

temperature are shown in Fig. 5 for both substances. The T_1's increase with temperature as is expected for motions in the extreme narrowing limit. Activation energies indicated are 1.36 kcal/mol for acetone, and 0.77 kcal/mol for acetic acid-d_1. The results obtained for acetone compare well with these obtained in a recent study (23) using pulsed n.m.r.

These results indicate that if the ARP conditions are satisfied, the null method gives reasonable results for T_1 determinations.

Conclusions

In summary, in a solid an ARP signal which is satisfactory for many purposes may be observed under the condition that

$$[11] \qquad \frac{\delta H}{T_1}, \frac{\delta H}{T_{1\rho}} \ll \frac{dH_0}{dt} \ll \gamma H_1^2$$

where the first inequality implies a factor of ~ 4, the second 5–30 (see ref. 2, 2*a*).

The conditions that must be observed in order to extract second moment information from the ARP signal are the more demanding ones, and in the following order of magnitude calculations we assume a factor of 25 or 30 for the second inequality. The maximum H_1 field available in the Varian V-4210 r.f. unit is of the order of ~ 1 G. This implies that when using a H_1 field of this magnitude to observe a proton or fluorine resonance with a local field H_L of 1.8 G (this corresponds to an absorption line with a second moment of ~ 10 G^2) the maximum allowable sweep rate will be ~ 1000 G/s, and an undistorted ARP signal should be observed with T_1's and $T_{1\rho}$'s as short as 30 ms. However, in the study of molecular motion in solids containing protons or fluorine, $T_{1\rho}$ very often is shorter than 30 ms. This then limits the extraction of second moment data to ARP signals obtained either in the rigid lattice or extreme narrowing region for the motion. The advantages of the ARP method for determining second moments have been pointed out previously: simplicity of equipment required, ease and rapidity of measurement, and independence of saturation and modulation effects normally encountered in C.W. n.m.r.

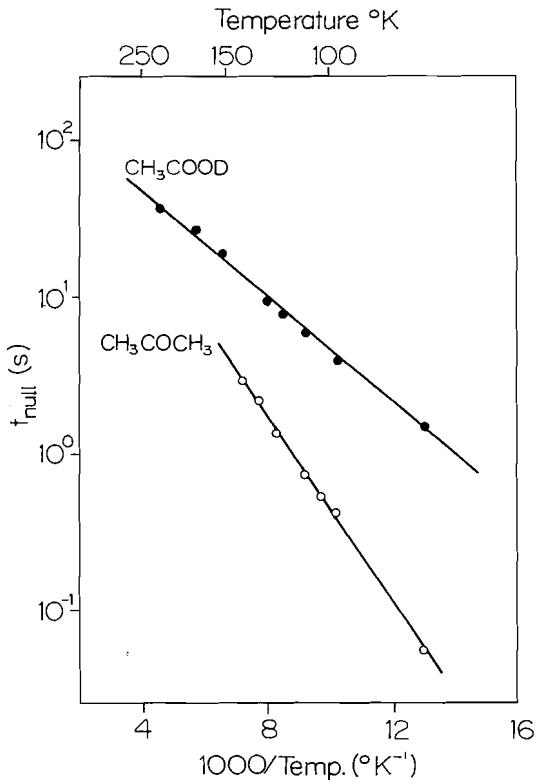

FIG. 5. Spin–lattice relaxation times (t_{null}) for solid acetone and acetic acid-d_1 as a function of inverse temperature.

It is of interest to point out that in the ARP experiments reported here the condition on the right side of eq. 11 was always satisfied ($\gamma H_1^2/(dH_0/dt) \sim 50$). The distortions of the ARP signal observed were due to the condition on the left side of eq. 11 not being fulfilled. However, short T_1 values cause a distortion of the ARP signal different from that caused by short $T_{1\rho}$ values. This difference is illustrated in Fig. 3 where A denotes an ARP signal distorted due to a short T_1, and B denotes a signal distorted due to a short $T_{1\rho}$.

For the measurement of T_1, only the amplitude of the ARP signal is required so that the conditions as given in eq. 11 do not need to be strictly adhered to. For reliable measurements one of the methods where M_t is determined as a function of time should be used. The null method, as well as the symmetric sweep method, can lead to relatively large errors if the ARP conditions are not satisfied. A drawback in determining T_1's using ARP of course exists when $T_{1\rho}$ is very short, and a loss in signal intensity decreases the accuracy of measurement.

We have also used the amplitude of the ARP signal to detect temperature regions where $T_{1\rho}$ is short ($\leq \sim 0.01$ s). Of course, previously (24) $T_{1\rho}$ measurements have been made which em-

ployed an ARP to obtain alignment of the magnetization with the H_1 field. $T_{1\rho}$ measurements on solids using ARP methods and C.W. equipment have not as yet been reported, but if accurate control of the magnetic field sweep is obtained, such measurements should be possible using an adiabatic half passage into the center of the resonance.

The authors are most grateful to the National Research Council of Canada for financial assistance in the form of a Scholarship to J.A.R. and a grant-in-aid to B.A.D. Discussions with Dr. W. R. Janzen have been most useful.

1. W. R. JANZEN, T. J. R. CYR, and B. A. DUNELL. J. Chem. Phys. **48**, 1246 (1968).
2. (*a*) W. R. JANZEN. Chem. Phys. Lett. **12**, 35 (1971). (*b*) W. R. JANZEN. To be published.
3. C. A. FYFE, B. A. DUNELL, and J. A. RIPMEESTER. Can. J. Chem. **49**, 3332 (1971).
4. A. G. REDFIELD. Phys. Rev. **101**, 67 (1956).
5. A. ABRAGAM. The principles of nuclear magnetism. Oxford University Press. 1961. pp. 65–68, 539–554.
6. G. B. GUTHRIE, D. W. SCOTT, W. N. HUBBARD, C. KATZ, J. P. MCCULLOUGH, M. E. GROSS, K. D. WILLIAMSON, and G. WADDINGTON. J. Am. Chem. Soc. **74**, 4662 (1952).
7. R. FOURME. Acta Cryst. **B28**, 2984 (1972).
8. F. FRIED and B. J. LASSIER. J. Chim. Phys. **63**, 1 (1966).
9. F. FRIED. C. R. Acad. Sci. Paris, **262**, 1497 (1966).
10. B. BAK, L. HANSEN, and J. RASTRUP-ANDERSON. Disc. Faraday Soc. **19**, 30 (1955).
11. J. H. VAN VLECK. Phys. Rev. **74**, 1168 (1948).
12. J. MICHEL, M. DRIFFORD, and P. RIGNY. J. Chim. Phys. **67**, 31 (1970).
13. S. ALBERT, H. S. GUTOWSKY, and J. A. RIPMEESTER. J. Chem. Phys. **56**, 2844 (1972).
14. E. R. ANDREW and R. G. EADES. Proc. R. Soc. **A218**, 537 (1953).
15. J. E. ANDERSON. J. Chem. Phys. **43**, 3575 (1965).
16. U. HAEBERLEN and G. MAIER. Z. Naturforsch. **22a**, 1236 (1967).
17. R. VAN STEENWINKEL. Z. Naturforsch. **24a**, 1526 (1969).
18. D. E. O'REILLY and E. M. PETERSON. J. Chem. Phys. **56**, 5536 (1972).
19. C. P. SLICHTER and D. C. AILION. Phys. Rev. **135A**, 1099 (1964).
20. U. HAEBERLEN. Z. Naturforsch. **25a**, 1459 (1970).
21. H. S. GUTOWSKY and G. E. PAKE. J. Chem. Phys. **18**, 162 (1950).
22. B. A. DUNELL, L. W. REEVES, and K. O. STRØMME. Trans. Faraday Soc. **57**, 373 (1961).
23. P. S. ALLEN, A. W. K. KHANZADA, and C. A. MCDOWELL. J. Mol. Struct. **14**, 9 (1972).
24. D. C. AILION and C. P. SLICHTER. Phys. Rev. **137A**, 235 (1965).

Can. J. Chem. Downloaded from www.nrcresearchpress.com by 210.87.254.6 on 09/05/12
For personal use only.

The Crystal and Molecular Structure of Dinitrato(triphenylphosphine)mercury(II)

SIMON H. WHITLOW

Inland Waters Directorate, Department of the Environment, Ottawa, Canada

Received July 18, 1973

The structure of dinitrato(triphenylphosphine)mercury(II), $Hg(NO_3)_2.P(C_6H_5)_3$, has been determined from single-crystal X-ray data measured on a computer-controlled diffractometer. The crystals are monoclinic, have a unit cell of dimensions $a = 10.39(1)$, $b = 9.56(1)$, $c = 19.44(2)$ Å, $\beta = 94.3(1)°$, which contains 4 molecules, and they belong to the space group, $P2_1/c$. The structure has been refined by least-squares methods from 2470 independent observed reflections to a conventional R-factor of 0.061. The Hg atom has a distorted tetrahedral coordination with Hg—O bond lengths of 2.190(8), 2.428(8), and 2.560(9) Å and an Hg—P bond distance of 2.359(3) Å. There are 2 distinct types of NO_3 groups bonded to Hg. One is an unshared, unidentate ligand and the other acts as a bridging group joining 2 Hg atoms. Chains of —Hg—NO_3—Hg— atoms are formed which follow crystallographic two-fold screw axes in the b-direction.

La structure du dinitrato(triphénylphosphine) de mercure(II), $Hg(NO_3)_2.P(C_6H_5)_3$ a été déterminée à partir des mesures de diffraction des rayons-X par un monocristal effectuées sur un diffractomètre automatique. Ces cristaux sont monocliniques; les dimensions de la maile sont $a = 10.39(1)$, $b = 9.56(1)$, $c = 19.44(2)$ Å, $\beta = 94.3(1)°$. Elle contient 4 molécules et le groupe spatial est $P2_1/c$. L'affinement de la structure par moindres carrés à porté sur 2470 réflections observées indépendantes et a été poursuivi jusqu'au facteur R conventionnel de 0.061. L'atome de Hg présente une coordination tétraédrique déformée, les longueurs des liaisons Hg—O étant 2.190(8), 2.428(8) et 2.560(9) Å, celle de la liaison Hg—P valant 2.359(3) Å. On peut distinguer 2 types de groupements NO_3 liés au Hg. L'un est un ligand non partagé, monodentate, l'autre constitue un pont reliant 2 atomes de Hg. Il y a des chaines d'atomes —Hg—NO_3—Hg— qui suivent les axes cristallographiques hélicoidaux d'ordre 2 de la direction-b. [Traduit par le journal]

Can. J. Chem., **52**, 198 (1974)

Recent awareness of high mercury concentrations in the environment has led to increased research activity in the field of organo-mercury compounds. The nature of the bonding between Hg and lighter atoms is of interest, interactions between Hg and nutrients being of special concern in view of the enrichment processes known to occur in the food chain. Spectroscopic methods have been used to demonstrate the association of mercuric and nitrate ions in aqueous solution (1) and also to predict structural features in the solid state. From the infrared spectral assignments for a series of triphenylphosphine–Hg compounds, Davis *et al.* (2) proposed a dimeric structure for solid $Hg(NO_3)_2.P(C_6H_5)_3$ containing both bridging and unshared NO_3 groups. The present investigation was undertaken to determine the crystal structure of this compound and to verify and extend the structural conclusions inferred by the infrared analysis.

Experimental

Dinitrato(triphenylphosphine)mercury(II), $Hg(NO_3)_2.P(C_6H_5)_3$, which was prepared by reacting triphenylphosphine and $Hg(NO_3)_2$ in acetone, crystallizes as irregular white prisms elongated along either a or b. The crystal selected for X-ray intensity measurements was approximately equidimensional measuring ~0.25 mm in diameter. This was mounted in a random orientation on a four-circle computer-controlled diffractometer. The orientation matrix and lattice parameters were determined by a least-squares refinement of the angular settings of 12 strong reflections aligned under computer control. For these measurements a small counting aperture was used with a take-off angle of 2° and a graphite monochromator (Mo $K\alpha_1 = 0.70926$ Å). The conditions for systematically absent reflections were determined from Weissenberg and precession photographs: $h0l$, $l = 2n + 1$ and $0k0$, $k = 2n + 1$. These uniquely specify the space group $P2_1/c$ (C_{2h}^5). The unit cell constants determined at 20 °C and crystal data are summarized as follows:

$Hg(NO_3)_2.P(C_6H_5)_3$ mol. wt. = 586.89

Monoclinic, $P2_1/c$, $a = 10.39(1)$, $b = 9.56(1)$, $c = 19.44(2)$ Å, $\beta = 94.3(1)°$, $V = 1924.2$ Å^3. $F(000) = 1120$e, $D_m = 2.00$, $D_c = 2.02$ g cm^{-3}, $Z = 4$.

Intensity data for 3413 independent reflections with $2\theta \leqslant 50°$ were collected using the θ–2θ scan technique. Background readings were taken for 15s either side of each scan and 3 standard reflections (400, 0010, and 060) were recorded every 25 measurements for checking and scaling purposes. The take-off angle was optimized at 4.5° for the data collection and individual scan widths

Can. J. Chem. Downloaded from www.nrcresearchpress.com by 210.87.254.42 on 09/05/12
For personal use only.

Can. J. Chem. Downloaded from www.nrcresearchpress.com by 210.87.254.42 on 09/05/12
For personal use only.

were taken as $(2.1 + 0.5 \tan \theta)°$ to allow for the wavelength dispersion and crystal mosaicity. Attenuators were used to prevent overloading the scintillation counter and a pulse height analyzer was employed, in addition to the monochromator, for energy discrimination. Although the crystal became brown during the course of the data collection, the standard reflection intensities, which fluctuated $< 5\%$, showed no systematic decomposition with time. Lorentz and polarization corrections were applied to the intensities and weights based on counting statistics and instrument stability (3) were assigned. Where the net intensity for a reflection was $< 1.65\ \sigma(I)$, where $\sigma(I)$ is the associated standard deviation, the reflection was classified unobserved. At this significance level 943 reflections (28%) were considered to be unobserved and were assigned threshold values equal to $1.65\ \sigma(I)$.[1]

The crystal was measured for absorption corrections by means of a micrometer eyepiece mounted on the diffractometer telescope. Although the crystal was an irregular shape, it was approximately equidimensional; the 12 enveloping faces were between 0.14 and 0.10 mm from the center of the crystal and enclosed a volume of 0.009 mm^3. Absorption corrections ($\mu = 82.92\ cm^{-1}$) were calculated by the Gaussian quadrature method using a 512 point grid. The calculated transmission factors varied between 0.268 and 0.209.

Solution and Refinement of the Structure

Most of the calculations required in the analysis were done using the X-RAY system of crystallographic programs (4). The Hg and P atom positions were established from the sharpened Patterson function and the other non-hydrogen atoms were located from subsequent Fourier or difference-Fourier summations, Neutral atomic scattering factors were used to represent all atoms (5) and for Hg the real and imaginary components of anomalous dispersion ($\Delta f' = -2.7$, $\Delta f'' = 10.3$) (6) were included. The atomic parameters were refined by a blocked, full-matrix least-squares treatment, the C atoms of the 3 phenyl groups being refined in separate matrices. The quantity minimized was $\Sigma w(|F_o| - |F_c|)^2$ where the weight, w, is equal to $1/\sigma^2(F_o)$ (3); $|F_o|$ and $|F_c|$ are the amplitudes of the observed and calculated structure factors. Reflections considered to be unobserved were excluded from the refinement. The initial R index, $R = \Sigma||F_o| - |F_c||/\Sigma|F_o|$ was 0.40 with only the Hg and P atoms included. The C atoms of the phenyl rings were readily located from a difference-Fourier summation but the NO_3 groups were less well resolved. It was only after refining anisotropic temperature parameters for the Hg atom that the positions of the N and O atoms became unambiguous. Refinement of the coordinates of all the non-hydrogen atoms, anisotropic temperature parameters for Hg and isotropic factors for remainder, gave an R value of 0.063 and a weighted residual, $R_w = [\Sigma w(|F_o| - |F_c|)^2/\Sigma w F_o^2]^{1/2}$, of 0.041. A difference-Fourier map at this stage suggested the locations of some of the phenyl H atoms and the 15 H atoms were included at calculated positions 1.08 Å from the respective C atom with isotropic temperature factors of 4.0 $eÅ^{-2}$, but these were not refined.[2] An extinction parameter was determined ($g = 5.5 \times 10^{-3}$) and applied since for many of the strong reflections F_o was less than F_c. Attempts to determine and refine anisotropic thermal parameters for the P, N, O, and C atoms, while adding many more parameters to the refinement, did not significantly improve the model and are not reported. The final R value is 0.061 and R_w is 0.039 for the 2470 observed reflections.[2] There are 20.7 observations for each parameter refined and in the last least-squares cycle (unblocked, full-matrix) the average shift to error ratio was 0.07. The largest residual electron density on the final difference-Fourier map (1.4 $eÅ^{-3}$), which is ~0.05 of a C atom peak, occurred near the Hg position; residual background fluctuations were $\sim \pm 0.7\ eÅ^{-3}$. The refined positional and thermal parameters of the atoms are given in Table 1.

TABLE 1. Fractional atomic coordinates $\times 10^4$ and thermal parameters $\times 10^3$ with standard deviations in parentheses

Atom	x	y	z	$U(Å^2)$
Hg	1338(1)	169(1)	2591(1)	*
P	2768(3)	−57(4)	3586(1)	37(1)
N(1)	1750(11)	86(13)	1166(6)	73(3)
O(1)	739(8)	−210(10)	1502(4)	71(3)
O(2)	2688(10)	568(11)	1482(6)	99(4)
O(3)	1643(9)	−170(12)	547(5)	96(3)
N(2)	1193(12)	3433(11)	2461(6)	63(3)
O(4)	945(7)	4719(9)	2322(4)	61(2)
O(5)	289(8)	2584(9)	2441(5)	59(3)
O(6)	2291(10)	3062(10)	2612(5)	84(3)
C(A1)	2072(11)	646(12)	4326(6)	43(3)
C(A2)	1136(12)	1695(14)	4241(7)	57(4)
C(A3)	624(13)	2253(14)	4834(7)	67(4)
C(A4)	1044(13)	1775(14)	5460(7)	67(4)
C(A5)	1953(13)	744(14)	5552(7)	64(4)
C(A6)	2484(11)	195(14)	4976(6)	59(4)
C(B1)	4257(11)	811(12)	3461(6)	44(3)
C(B2)	4774(12)	1728(13)	3935(6)	48(4)
C(B3)	5989(14)	2323(14)	3836(7)	64(4)
C(B4)	6605(13)	1980(14)	3262(7)	62(4)
C(B5)	6082(12)	1078(13)	2782(7)	56(4)
C(B6)	4914(11)	460(12)	2884(6)	53(4)
C(C1)	3143(11)	−1862(12)	3795(6)	39(3)
C(C2)	2135(11)	−2809(13)	3783(6)	46(3)
C(C3)	2364(12)	−4171(13)	3987(6)	54(4)
C(C4)	3593(13)	−4583(14)	4189(6)	63(4)
C(C5)	4610(13)	−3668(14)	4187(7)	60(4)
C(C6)	4382(12)	−2281(13)	3985(6)	48(4)

*Anisotropic thermal parameters for Hg: U_{11} 0.0486(3), U_{12} 0.0502(4), U_{33} 0.0437(3), U_{12} 0.0057(4), U_{13} −0.0052(2), U_{23} 0.0003(4) where the temperature factor is of the form $\exp[-2\pi^2(U_{11}h^2a^{*2} + \ldots + 2U_{23}klb^*c^* \cos \alpha^*)]$.

[1]In the data set reflections with $k + l = 2n + 1$ tend to have weak intensities, many of these being classified unobserved. This is a consequence of the y-coordinates of the Hg and P atoms being approximately zero and not contributing strongly to this class of reflections.

[2]The hydrogen atom coordinates and the final structure factor list have been deposited and are available from the Depository of Unpublished Data, National Science Library, National Research Council of Canada, Ottawa, Canada K1A 0S2.

Can. J. Chem. Downloaded from www.nrcresearchpress.com by 210.87.254.42 on 09/05/12
For personal use only.

Discussion

The proposal of Davis *et al.* (1) that there are 2 different types of NO_3 groups in the compound has been confirmed by the X-ray analysis. Although the compound forms infinite chains rather than the simple dimers suggested, the predictions of an unshared, monodentate NO_3 ligand and a bridging, bidentate NO_3 group have been verified.

A view (7) of the molecule giving the atom labelling is shown in Fig. 1 and the crystal packing is illustrated in Fig. 2. In both figures the H atoms have been omitted for clarity. It is apparent from these diagrams and the bond distances (uncorrected for thermal vibration) in Table 2, that there are 2 distinct types of NO_3 ligand present: one associated with a single Hg atom, and the other bridging between 2 Hg atoms. The unshared group, N(1)O(1)O(2)O(3), is strongly bonded to Hg with an Hg—O(1) distance of 2.19(1) Å. This distance is shorter than those usually found in tetrahedrally-coordinated Hg complexes (*e.g.* 2.32 and 2.37 Å in $HgCl_2((C_6H_5)_3AsO)_2$ (8)) but longer than in the linearly-coordinated mercuric oxide where the Hg—O bond lengths are 2.03 Å (9). There is a possibility of an unsymmetric bidentate interaction between this nitrate group and the Hg atom since the Hg—O(2) distance of 2.69(1) Å is shorter than the sum of the van der Waals radii of Hg, 1.5 Å (10), and O, 1.4 Å (11). However, the geometry of the NO_3 group itself produces a second close metal–oxygen interaction and this contact is probably best explained on a steric basis. The second nitrate group, N(2)O(4)O(5)O(6), links Hg atoms into infinite —Hg—NO_3—Hg— chains along the *b*-direction (Fig. 2). The Hg atoms are separated by 5.526 Å and are connected to the nitrate group in a *syn–anti* (12) arrangement through Hg—O bonds of 2.43(1) and 2.56(1) Å.

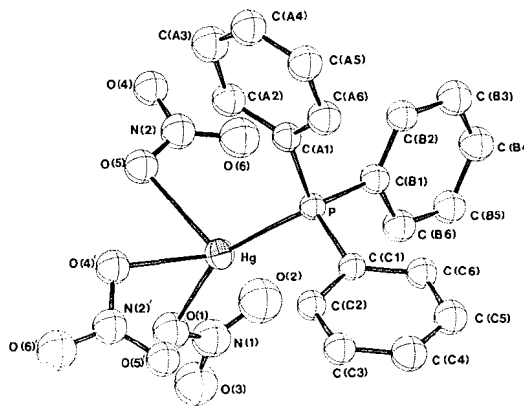

FIG. 1. The molecular configuration of $Hg(NO_3)_2.P(C_6H_5)_3$ with 40% probability thermal ellipsoids. The nitrate group designated by primes is related to its counterpart by symmetry.

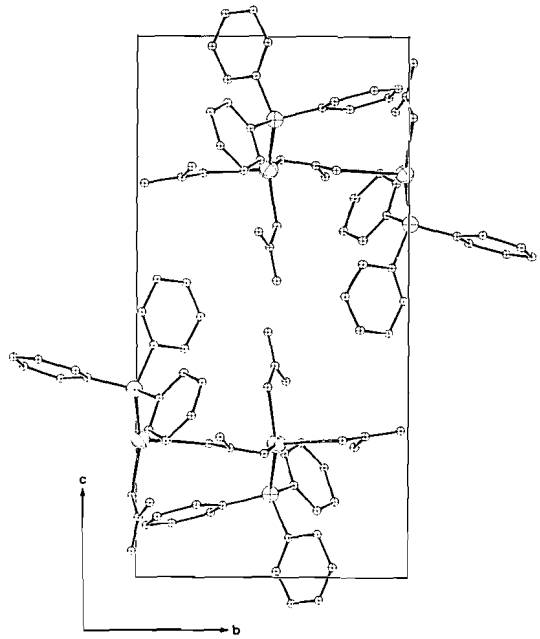

FIG. 2. The molecular packing viewed perpendicular to the *bc*-plane.

The coordination about Hg is best described as a very distorted tetrahedral arrangement considering only the 3 closest O atoms and the P atom. A measure of the distortion from tetrahedral symmetry is given by the angles at Hg between the 4 contacts which range between 76.0 and 153.0°. A somewhat similar distorted tetrahedral environment is found in $Hg(C_{13}H_{11}N_4S)_2.2C_5H_5N$ where the valency angles at Hg (considering the weak Hg—N bonds) vary between 70 and 155° (13). If the additional weak Hg—O(2) bond (*i.e.* the bidentate interaction) is included, the geometry becomes a distorted square pyramidal arrangement with O(5) at the apex. In this description, the Hg atom is only 0.2 Å from the plane defined by the four basal atoms O(1), O(2), O(4), and P. A still different coordination has recently been reported for the related compound, $Hg(SCN)_2.As(C_6H_5)_3$ (14). In this struc-

Can. J. Chem. Downloaded from www.nrcresearchpress.com by 210.87.254.42 on 09/05/12
For personal use only.

TABLE 2. Selected interatomic distances and angles

Bond	Distance† (Å)	Bonds	Angle† (deg)
Hg—P	2.359(3)	P—Hg—O(1)	153.2(2)
—O(1)	2.190(8)	—O(2)	109.6(2)
—O(4)*	2.428(8)	—O(5)	114.3(2)
—O(5)	2.560(9)	—O(4)*	118.9(2)
		O(1)—Hg—O(2)	51.4(3)
—O(2)	2.686(11)	—O(5)	87.2(3)
—O(6)	2.936(10)	—O(4)*	80.3(3)
—O(5)*	2.991(9)	O(2)—Hg—O(5)	91.4(3)
		—O(4)*	130.8(3)
P—C(A1)	1.788(12)	O(5)—Hg—O(4)*	76.0(3)
—C(B1)	1.788(12)		
—C(C1)	1.808(11)	O(1)—N(1)—O(2)	118(1)
		—O(3)	115(1)
N(1)—O(1)	1.31(1)	O(2)—N(1)—O(3)	126(1)
—O(2)	1.20(2)	O(4)—N(2)—O(6)	120(1)
—O(3)	1.22(2)	—O(5)	119(1)
N(2)—O(4)	1.28(1)	O(5)—N(2)—O(6)	121(1)
—O(5)	1.24(1)		
—O(6)	1.21(2)		
mean C—C	1.387	mean C—C—C	120.0

*Atom at $-x, y - 1/2, -z + 1/2$.
†Standard deviations in parentheses.

ture the Hg coordination is apparently trigonal with 2 additional contacts at larger distances.

The nitrate groups have bond lengths between 1.20 and 1.31 Å and O—N—O angles between 115 and 126°. The N(1)O(1)O(2)O(3) group is clearly monodentate: the long N(1)—O(1) distance, 1.31 Å (compared to 1.20 and 1.22 Å for O(2) and O(3)) and the large O(2)—N(1)—O(3) angle of 126° indicate coordination through O(1). The nature of the interactions between the N(2)O(4)O(5)O(6) group and Hg is less apparent from the structure of the group. While O(6) with an N—O bond distance of 1.21 Å is uncoordinated, some coordination to Hg via O(4), and to a lesser extent O(5), is likely. Considering both NO_3 groups there exists an inverse correlation between the N—O bond distances and the respective Hg—O bond lengths. Thus the N—O bonds involving oxygen atoms O(1), O(4), and O(5) shorten as the corresponding Hg—O bond lengths increase. This relationship involving 3 of the N—O bond lengths supports the tetrahedral description of the Hg coordination.

The coordination about P is much more nearly tetrahedral than is the case for Hg: the Hg—P—C angles average 110.9°, the C—P—C angles, 107.7°. The Hg—P bond length of 2.359(3) Å is in good agreement with other reported values, *e.g.* 2.36 in $HgCl(CH_3CH_2O)_2PO$ (15), and the average P—C distance of 1.80 Å is within the range 1.72 to 1.80 Å commonly observed for four-coordinated phosphorus (16). The torsion angles, HgPC(1)/C(1)C(2)C(6), for the 3 phenyl rings are 25, 52, and 45°, respectively, with the rings being displaced away from each other; apart from the C atoms actually bonded to P there are no C...C inter-ring contacts <3 Å. Within each phenyl ring the geometry is normal: the C—C bond lengths determined range between 1.34(2) and 1.41(2) Å; the C—C—C angles between 119(1) and 123(1)°. The average C—C bond distance of 1.378 Å and the mean C—C—C angle of 120.0° are in agreement with reported values (16).

The —Hg—NO_3—Hg— chains along *b* (Fig. 2) are the most important feature of the unit cell packing. These chains follow two-fold crystallographic screw axes so that successive $-P(C_6H_5)_3$ groups are translated and rotated to opposite sides of the chain with the result that there are no C...C interactions between different molecules <3.5 Å. A rather similar helical chain is found in $Hg[(i\text{-}C_3H_7O)_2PS_2]_2$ (17) where one of the isopropyl-phosphorodithioate groups acts as a bridging unit between 2 Hg atoms. In $Hg(NO_3)_2.P(C_6H_5)_3$ the closest non-bonded contacts between molecules occur along the chain, the four shortest distances (2.98 to 3.22 Å) being between non-equivalent NO_3 groups. Disregarding the H atoms, the shortest contact distances between chains involve the oxygen atom O(6) with C(A3) at $x, -y + 1/2, z + 1/2$ of 3.25 Å and with C(C3) at $x, -y - 1/2, z + 1/2$ of 3.24 Å.

The author is grateful to Dr. A. R. Davis for suggesting the problem and supplying the crystals and to Dr. S. R. Hall of the Mines Branch, Department of Energy, Mines and Resources for assistance with the data collection.

1. A. R. DAVIS and D. E. IRISH. Inorg. Chem. 7, 1699 (1968).
2. A. R. DAVIS, C. J. MURPHY, and R. A. PLANE. Inorg. Chem. 9, 423 (1970).
3. E. J. GABE, J. P. GLUSKER, J. A. MINKIN, and A. L. PATTERSON. Acta Cryst. 22, 366 (1967).
4. J. M. STEWART, F. A. KUNDELL, and J. C. BALDWIN. Comp. Sci. Center Rept. Univ. of Maryland. 1970.
5. P. A. DOYLE and P. S. TURNER. Acta Cryst. A24, 390 (1968).
6. International tables for X-ray crystallography. Vol. III. Kynoch Press, Birmingham. 1968. p. 215.

7. C. K. JOHNSON. ORTEP, Report ORNL-3794, Oak Ridge Nat. Lab., Oak Ridge, Tennessee, 1965.
8. C. I. BRÄNDÉN. Acta Chem. Scand. **17**, 1363 (1963).
9. K. AURIVILLIUS. Acta Chem. Scand. **10**, 852 (1956).
10. D. GRDENIĆ. Q. Rev. **19**, 303 (1965).
11. L. PAULING. The nature of the chemical bond. 3rd ed. Cornell Univ. Press, Ithaca, N.Y. 1967. p. 260.
12. C. C. ADDISON, N. LOGAN, and S. C. WALLWORK. Q. Rev. **25**, 289 (1971).
13. M. M. HARDING. J. Chem. Soc. 4136 (1958).
14. R. C. MAKHIJA, A. L. BEAUCHAMP, and R. RIVEST. Chem. Commun. 1043 (1972).
15. J. BENNETT, A. PIDCOCK, C. R. WATERHOUSE, P. COGGON, and A. T. MCPHAIL. J. Chem. Soc. (A), 2094 (1970).
16. F. K. ROSS, L. MANOJLOVIC-MUIR, W. C. HAMILTON, F. RAMIREZ, and J. E. PILOT. J. Am. Chem. Soc. **94**, 8738 (1972).
17. S. L. LAWTON. Inorg. Chem. **10**, 328 (1971).

Can. J. Chem. Downloaded from www.nrcresearchpress.com by 210.87.254.42 on 09/05/12
For personal use only.

Solvation Enthalpies of Some Alkali Metal and Tetraalkylammonium Salts in Dioxane–Water Mixtures

OM N. BHATNAGER AND A. N. CAMPBELL
Department of Chemistry, University of Manitoba, Winnipeg, Manitoba R3T 2N2
Received February 20, 1973

Enthalpies of solution of LiCl, NaCl, $(CH_3)_4NBr$, $(C_2H_5)_4NBr$, $(C_3H_7)_4NBr$, and $(C_4H_9)_4NBr$ in dioxane–water mixtures varying in composition from 20 to 64.5% dioxane have been determined. Values of standard enthalpy of solution, ΔH_s^0, were obtained using the extended Debye–Hückel equation.

Using these ΔH_s^0 and the lattice energies (U) of these salts, solvation enthalpies have been evaluated.

Les enthalpies des solutions de LiCl, NaCl, $(CH_3)_4NBr$, $(C_2H_5)_4NBr$, $(C_3H_7)_4NBr$, et $(C_4H_9)_4NBr$ dans des mélanges dioxanne–eau dont la composition varie entre 20 et 64.5% de dioxanne ont été déterminées. Les valeurs des enthalpies standard de solution ΔH_s^0, ont été obtenues par l'équation étendue de Debye–Huckel.

L'utilisation de ces ΔH_s^0 et des énergies de réseau (U) de ces sels a permis d'évaluer les enthalpies de solvatation. [Traduit par le journal]

Can. J. Chem., **52**, 203 (1974)

Introduction

The problem of the nature of electrolyte solutions has been attacked, as indeed it can only be attacked, by a study of the physical properties of such solutions. The results have been interpreted in the light of solute–solvent, solute–solute, and solvent–solvent interactions, hydrogen bonding, etc. Among the methods used, one which has recently come into prominence is the study of ion–solvent interactions from the enthalpies of solution and of solvation. In order to elucidate the effects of hydrogen bonding and of dielectric constant, such studies have been made on substituted amide solvents (1–5), alcohols (6, 7), propylene carbonate, (8), dimethyl sulfoxide (8), and dioxane–water mixtures (9). We have been interested in dioxane–water mixtures for some time and have reported the thermodynamic properties of sodium chlorate and lithium chlorate (10, 11) in these mixed solvents. In this paper, we report the enthalpies of solution and of solvation of NaCl and LiCl in 44.5 and 64.5% and of $(CH_3)_4NBr$, $(C_2H_5)_4NBr$, $(C_3H_7)_4NBr$, and $(C_4H_9)_4NBr$ in 20, 44.5 and 64.5% dioxane–water mixtures at 25 $\pm$ 0.002 °C. The unique behavior of tetraalkylammonium salts in water is attributed to water – hydrophobic group interactions. It is of interest to see how this behavior changes in passing from water to 64.5% dioxane–water mixtures.

Experimental

Purification of Salts

NaCl

Analytical reagent grade NaCl was twice recrystallized from conductivity water and dried at 180 °C for 3 days.

LiCl

Anhydrous reagent grade LiCl was further dried in a vacuum oven whose temperature was gradually and slowly raised to 200 °C. The salt was dried for 4 d.

$(CH_3)_4NBr$

Tetramethylammonium bromide (Me_4NBr) was recrystallized from methanol–water mixtures and dried at 95 °C in a vacuum oven for one week.

$(C_2H_5)_4NBr$

Tetraethylammonium bromide (Et_4NBr) was recrystallized twice from acetone–ether mixture and dried in a vacuum oven for 3 days at 95 °C.

$(C_3H_7)_4NBr$

Tetrapropylammonium bromide (Pr_4NBr) was recrystallized from ethylacetate–ethanol mixture and dried at 75 °C in a vacuum oven for 2 days.

$(C_4H_9)_4NBr$

Tetrabutylammonium bromide (Bu_4NBr) was recrystallized from acetone–ether mixture and dried at 60 °C in a vacuum oven for 2 days.

Gravimetric analysis on each salt (by precipitating the bromide with silver nitrate) indicated the purity to better than 99.7 mol% for all the salts.

All compounds were stored in ground glass joint bottles in a vacuum dry box. The tetraalkylammonium salts were stored in brown colored bottles. The samples were also made up in the dry box. Before proceeding with the actual experimental work in dioxane–water mixtures, a few samples of each salt were run in water. The values of

Can. J. Chem. Downloaded from www.nrcresearchpress.com by 210.87.254.40 on 09/05/12
For personal use only.

Can. J. Chem. Downloaded from www.nrcresearchpress.com by 210.87.254.40 on 09/05/12
For personal use only.

enthalpies of solution, ΔH_s, were in good agreement with the literature values.

Our purification of dioxane has been given elsewhere (10). The mixtures of dioxane with water were made by weighing.

Apparatus and Procedure

A new submarine type calorimeter (OB-1) has been designed which is capable of working with solid as well as gaseous compounds. Our design is based on the designs given by Held and Criss (1), Nutter (12), and Vanderzee and Rodenburg (13). The double walled silvered Dewar flask had a capacity of about 300 ml and the design was such that it had a very small vapor space and short equilibrium time, (< 5 min). The precise details of the calorimeter design, temperature measuring systems, and procedure are given elsewhere (14). The bath was controlled to better than $\pm 0.002°$ and all the measurements were made at 25 °C.

Results and Discussion

The enthalpies of solution (ΔH_s) for various electrolytes as a function of concentration in 20, 44.5, and 64.5% mixtures are given in Tables 1, 2, and 3, respectively. All data are extrapolated to infinite dilution using the extended Debye–Hückel equation

$$[1] \quad \rho = \Delta H_s^0 - 2.303RT^2 \left(\frac{dB}{dT}\right) (\nu_+ \cdot \nu_- \cdot m)$$

where

$$[2] \quad \rho = \Delta H_s - \frac{\nu}{2} |Z_+ \cdot Z_-| \delta_H I^{1/2} \alpha$$

$$[3] \quad \alpha = \left[(1 + I^{1/2})^{-1} - \frac{\sigma(I^{1/2})}{3} \right]$$

and

$$[4] \quad \sigma(I^{1/2}) = \frac{3}{I^{3/2}} [1 + I^{1/2} - (1 + I^{1/2})^{-1} - 2 \ln (1 + I^{1/2})]$$

In this equation δ_H is the Debye–Hückel constant, the values of this in dioxane–water mixtures are given by Harned and Owen (15). B is a constant at a given temperature, $\sigma(I^{1/2})$ is a function of ionic strength, I; the values of this are tabulated by Brinkley and Brinkley (see ref. 15, p. 176). The rest of the terms have their usual meaning. At infinite dilution *i.e.* $m = 0$, $\rho^0 = \Delta H_s^0$. The advantages of using ρ *vs.* m plots are discussed by Criss and Cobble (16). Values of m, $m^{1/2}$, ΔH_s, $\delta_H I^{1/2} \alpha$, and ρ are also given in Tables 1–3. The extrapolated enthalpies of solution are given just below the data for each salt.

The most unusual feature in the application of the extended Debye–Hückel equation is the large correction factor in the case of NaCl; in some cases the corrections are far greater than the ΔH_s value. Since the enthalpies of solution of NaCl in 44.5 and 64.5% dioxane–water mixtures are quite small, we were obliged to confine our work to higher concentrations to minimize the experimental errors and this causes the large correction factor. The plots of ρ *vs.* m for NaCl in 20 (ref. 9), 44.5, and 64.5% dioxane–water mixtures were in good agreement with the Debye–Hückel slopes except in the case of 64.5% dioxane–water mixture where there were small deviations at higher concentrations indicating some ion association.

For all the electrolytes we have studied so far, with the exception of the tetraalkylammonium salts, the standard enthalpies of solution, ΔH_s^0, become more exothermic (*i.e.* less endothermic) in passing from pure water to 64.5% dioxane–water mixtures, indicating a structure breaking effect of the ions. The ΔH_s^0 values of the tetraalkylammonium salts in water and in dioxane–water mixtures are given in Table 4. The ΔH_s^0 values of these salts in water become more exothermic in going from Me_4NBr to Bu_4NBr but in passing from Bu_4NBr to Am_4NBr there is a sharp change in the value of ΔH_s^0, it actually changes sign, *i.e.* it becomes endothermic. In 20% dioxane the general trend is the same except that the change occurs between Pr_4NBr and Bu_4NBr. In 44.5 and 64.5% dioxane–water mixtures, however, this change occurs between Me_4NBr and Et_4NBr, *i.e.* the ΔH_s^0 values become more endothermic with the increase in the cation size, with the exception of Me_4NBr.

Another interesting feature is exhibited if we look at the ΔH_s^0 values in various dioxane–water mixtures. Me_4NBr shows a very slight increase in the ΔH_s^0 value in passing from pure water to 44.5% dioxane–water mixture and a sharp decrease in passing from 44.5 to 64.5% dioxane–water mixture, while Et_4NBr, Pr_4NBr, and Bu_4NBr all show a steady increase in the ΔH_s^0 values in going from pure water to 64.5% dioxane–water mixture. The increase has a definite trend and the amount of increase in ΔH_s^0 values increases with the ionic size of the cation. From the data it is clear that all the tetraalkyl salts except Me_4NBr are net structure makers in these mixtures. In recent years the standard heat capacities of solution, ΔC_p^0, of Me_4NBr, Et_4NBr, Pr_4NBr, Bu_4NBr, and Am_4NBr in water have been determined by Ahluwalia

TABLE 1. Enthalpy of solution and ρ values of some uni-univalent electrolytes in 20% dioxane–water mixtures

$m \times 10^3$	$m^{1/2} \times 10^2$	ΔH_s (cal/mol)	$\delta_H I^{1/2}\alpha$	ρ (cal/mol)
Tetramethylammonium bromide				
2.0125	4.4861	5 860	43	5 817
4.3027	6.5595	5 823	62	5 761
4.6232	6.7994	5 779	64	5 715
7.3047	8.5467	5 751	79	5 672
10.2541	10.1262	5 723	93	5 630
14.4807	12.0336	5 600	109	5 491
$\rho^0 = \Delta H_s^0 = 5\ 860 \pm 10$ cal/mol				
Tetraethylammonium bromide				
1.3252	3.6403	1 910	35	1 875
1.9021	4.3613	1 915	42	1 873
3.7298	6.1072	1 955	58	1 897
4.6498	6.8189	1 965	64	1 901
5.5377	7.4415	1 984	70	1 913
6.9864	8.3584	2 005	78	1 927
$\rho^0 = \Delta H_s^0 = 1\ 870 \pm 8$ cal/mol				
Tetrapropylammonium bromide				
1.7502	4.1835	944	40	904
3.7501	6.1238	964	58	906
4.5046	6.7116	970	63	907
6.2511	7.9064	983	74	909
7.5757	8.7038	992	81	911
$\rho^0 = \Delta H_s^0 = 902 \pm 6$ cal/mol				
Tetrabutylammonium bromide				
2.3987	4.8976	1 650	46	1 604
2.8265	5.3165	1 719	51	1 658
3.6275	6.0228	1 947	57	1 890
4.6464	6.8165	2 154	64	2 090
5.1021	7.1429	2 265	67	2 198
$\rho^0 = \Delta H_s^0 = 1\ 075 \pm 4$ cal/mol				

and co-workers (23, 24). More recently Mastroianni and Criss (7) have reported the ΔC_p^0 values of Me_4NBr and Bu_4NBr solutions in water at various temperatures. Me_4NBr exhibits a negative ΔC_p^0 value like the simple ions while all other salts of the tetraalkyl series exhibit positive values. The negative ΔC_p^0 value for Me_4NBr in water supports the view of various other workers (8, 17–21) that it behaves like a normal electrolyte, *i.e.* it breaks the water structure. This behavior is clear from the trend in passing from 44.5 to 64.5% dioxane–water. The increase in the ΔH_s^0 value of Me_4NBr in passing from pure water to 44.5% cannot be explained on the basis of normal behavior. The positive ΔC_p^0 values for the rest of the tetraalkyl ammonium bromide salts in water indicate that these salts increase the structure of water (7, 22, 23). Since the ΔH_s^0 values become more endothermic in passing from pure water to 64.5% dioxane–water mixtures, a similar conclusion can be drawn for these salts in dioxane–water mixtures.

Mastroianni and Criss (7) have measured the ΔH_s^0 values of Me_4NBr and Bu_4NBr in water over a wide range of temperature. By increasing the temperature, the hydrogen bonding and dielectric constant decrease; the introduction of dioxane into water has an effect similar to that of raising the temperature. In this way the behavior of Bu_4NBr in water at different temperatures and of Et_4NBr, Pr_4NBr, and Bu_4NBr in dioxane–water mixture appears similar.

Can. J. Chem. Downloaded from www.nrcresearchpress.com by 210.87.254.40 on 09/05/12
For personal use only.

Can. J. Chem. Downloaded from www.nrcresearchpress.com by 210.87.254.40 on 09/05/12
For personal use only.

TABLE 2. Enthalpy of solution and ρ values of some uni-univalent electrolytes in 44.5% dioxane–water mixture

$m \times 10^3$	$m^{1/2} \times 10^2$	ΔH_s (cal/mol)	$\delta_H I^{1/2}\alpha$ (cal/mol)	ρ (cal/mol)
Sodium chloride				
28.880	16.990	439	376	63
42.280	20.560	448	444	4
49.671	22.280	450	476	− 26
67.892	26.050	463	544	− 81
153.123	39.130	507	757	−250
165.412	40.670	519	780	−261
	$\rho^0 = \Delta H_s^0 = +170 \pm 2$ cal/mol			
Lithium chloride				
1.7919	4.2331	−10 049	102	−10 151
3.2192	5.6737	−10 010	135	−10 145
5.6219	7.4979	− 9 945	177	−10 122
8.0388	8.9659	− 9 920	209	−10 129
8.8933	9.4304	− 9 901	219	−10 120
13.2170	11.4960	− 9 831	264	−10 095
17.2052	13.1160	− 9 815	298	−10 113
21.4123	14.6320	− 9 772	329	−10 101
	$\rho^0 = \Delta H_s^0 = -10\,160 \pm 34$ cal/mol			
Tetramethylammonium bromide				
1.2085	3.4763	5 948	84	5 864
2.5127	5.0126	5 794	96	5 698
3.0195	5.4949	5 779	131	5 648
5.5013	7.4100	5 393	175	5 218
7.6105	8.7238	5 122	204	4 918
	$\rho^0 = \Delta H_s^0 = 6070 \pm 12$ cal/mol			
Tetraethylammonium bromide				
1.4416	3.7968	2 122	92	2 030
2.4080	4.9071	2 121	118	2 003
3.3653	6.0440	2 115	144	1 971
3.9488	6.2839	2 128	149	1 978
5.8013	7.6166	2 097	179	1 918
	$\rho^0 = \Delta H_s^0 = 2\,065 \pm 6$ cal/mol			
Tetrapropylammonium bromide				
2.1394	4.6253	2 695	111	2 584
3.6139	6.0115	2 700	144	2 556
3.9647	6.2965	2 705	150	2 555
4.8100	6.9354	2 695	164	2 531
5.2679	7.2580	2 702	172	2 530
7.5786	8.7055	2 703	204	2 499
	$\rho^0 = \Delta H_s^0 = 2\,610 \pm 9$ cal/mol			
Tetrabutylammonium bromide				
1.9498	4.4156	4 907	100	4 807
3.9327	6.2711	5 053	145	4 908
4.7213	6.8711	5 170	163	5 007
6.1482	7.8410	5 263	184	5 079
7.0025	8.3680	5 335	196	5 139
	$\rho^0 = \Delta H_s^0 = 4\,680 \pm 9$ cal/mol			

TABLE 3. Enthalpy of solution and ρ values of some uni-univalent electrolytes in 64.5% dioxane–water mixture

$m \times 10^3$	$m^{1/2} \times 10^2$	ΔH_s (cal/mol)	$\delta_H I^{1/2}\alpha$ (cal/mol)	ρ (cal/mol)
Sodium chloride				
11.095	10.530	110	585	− 475
13.391	11.570	140	639	− 499
27.584	16.610	135	887	− 752
40.602	20.150	130	1051	− 921
53.989	23.250	120	1189	−1 069
68.373	26.150	132	1314	−1 182
	$\rho^0 = \Delta H_s^0 = -280 \pm 5$ cal/mol			
Lithium chloride				
1.5013	3.8746	−10 879	226	−11 105
3.5214	5.9341	−10 731	344	−11 075
5.1316	7.1630	−10 666	408	−11 072
7.1117	8.4330	−10 581	476	−11 057
8.8437	9.4041	−10 493	527	−11 020
11.1693	10.5680	−10 411	587	−10 999
11.8910	10.9045	−10 403	605	−11 008
16.7860	12.9560	−10 243	708	−10 951
24.8900	15.7765	−10 006	847	−10 853
	$\rho^0 = \Delta H_s^0 = -11\,115 \pm 32$ cal/mol			
Tetramethylammonium bromide				
1.6050	4.0062	5 160	233	4 927
1.7790	4.2178	5 143	245	4 898
2.0436	4.5206	5 140	262	4 878
4.9016	7.0011	4 962	399	4 563
5.4610	7.3898	4 893	420	4 473
9.3170	9.6524	4 561	472	4 089
	$\rho^0 = \Delta H_s^0 = 5\,100 \pm 10$ cal/mol			
Tetraethylammonium bromide				
1.4963	3.8678	2 492	225	2 267
2.0709	4.5597	2 469	264	2 205
3.3672	5.8025	2 420	333	2 087
3.6283	6.0232	2 311	346	1 965
5.1697	7.1895	2 367	409	1 958
5.3595	7.3205	2 321	416	1 905
7.7485	8.8022	2 227	495	1 728
	$\rho^0 = \Delta H_s^0 = 2\,395 \pm 8$ cal/mol			
Tetrapropylammonium bromide				
1.5011	3.8744	3 380	226	3 154
2.7438	5.2381	3 341	300	3 041
3.1035	5.5709	3 330	321	3 009
3.9035	6.2478	3 310	358	2 952
6.0021	7.7473	3 245	439	2 806
9.2520	9.6187	3 151	539	2 612
	$\rho^0 = \Delta H_s^0 = 3\,295 \pm 5$ cal/mol			
Tetrabutylammonium bromide				
1.5218	3.9010	5 658	226	5 432
2.1386	4.6245	5 642	268	5 374
3.3012	5.7456	5 605	330	5 275
4.6590	6.8256	5 595	390	5 205
4.8118	6.9367	5 581	396	5 185
5.5642	7.4593	5 545	424	5 121
	$\rho^0 = \Delta H_s^0 = 5\,540 \pm 11$ cal/mol			

Can. J. Chem. Downloaded from www.nrcresearchpress.com by 210.87.254.40 on 09/05/12
For personal use only.

TABLE 4. Standard enthalpy of solution, ΔH_s^0 (cal/mol), of tetraalkylammonium bromides in water and dioxane–water mixtures

Salts	ΔH_s^0 (cal/mol)			
	Water	20% Dioxane	44.5% Dioxane	64.5% Dioxane
Me_4NBr	5 745*	5 860	6 070	5 100
Et_4NBr	1 430*	1 870	2 065	2 395
Pr_4NBr	−1 055*	902	2 610	3 295
Bu_4NBr	−2 050*	1 075	4 680	5 540
Am_4NBr	+796†	—	—	—

*Data from ref. 23.
†Datum from ref. 24.

TABLE 5. Enthalpies of solvation ($-\Delta H_{solv}^0$, kcal/mol) of some uni-univalent electrolytes in dioxane–water mixtures and amide solvents

Dioxane-water mixtures

Salt	Lattice energy ($-U$, kcal/mol)	$-\Delta H_{solv}^0$ (kcal/mol)		
		20% Dioxane	44.5% Dioxane	64.5% Dioxane
LiCl	200.20*	209.66‖	210.41	211.31
NaCl	183.50*	182.90‖	183.33	183.78
$LiClO_3$	202.43†		206.23	207.66
$NaClO_3$	183.80†		178.88	180.80
$(CH_3)_4NBr$	131.09‡	125.23	125.02	125.99
$(C_2H_5)_4NBr$	122.84‡	120.97	120.78	120.45
$(C_3H_7)_4NBr$	119.09‡	118.19	116.48	115.80
$(C_4H_9)_4NBr$	118.07‡	117.00	113.39	112.53

Amide solvents¶

Salt	Lattice energy ($-U$, kcal/mol)		$-\Delta H_{solv}^0$ (kcal/mol)		
			Dimethylformamide	Formamide	*n*-Methylformamide
$LiClO_4$	169.40§	191.80†	213.80	202.60	205.60
$NaClO_4$	153.80§	174.90†	182.75	176.60	178.25
$KClO_4$	139.70§	165.10†	167.40	161.60	163.60
$RbClO_4$	134.90§	159.50†	161.45	155.45	156.80
$CsClO_4$	128.60§	152.20†	153.97	147.60	149.10
NH_4ClO_3	136.10§	157.00†	165.50	156.20	158.55

*Values taken from ref. 24.
†Values taken from ref. 28.
‡Values taken from ref. 5.
§Values taken from ref. 26.
‖ΔH_s^0 data taken from ref. 9.
¶ΔH_s^0 data for calculating $-\Delta H_{solv}^0$ taken from ref. 26.

Enthalpies of Solvation

The enthalpy of solvation (ΔH_{solv}^0) of an electrolyte can be calculated using lattice energy (U) and the standard enthalpy of solution (ΔH_s^0) of the electrolyte.

$$[5] \qquad \Delta H_{solv}^0 = \Delta H_s^0 + U$$

The lattice energies of most uni-univalent alkali metal halides are given in the literature (25). These values can also be calculated for the simple planar molecules from Kapustinskii's equation (26).

$$[6] \quad U = 287.2\left[\frac{\nu Z_1 Z_2}{\gamma_1 + \gamma_2}\left(\frac{1 - 0.345}{\gamma_1 + \gamma_2}\right)\right] \text{kcal}$$

where ν is the total number of ions, Z_1 and Z_2 are the electric charges, and γ_1 and γ_2 the ionic radii of anions and cations in Å.

Can. J. Chem. Downloaded from www.nrcresearchpress.com by 210.87.254.40 on 09/05/12
For personal use only.

This seems to work well with the simple alkali halides but when the anions are of the XO_2^-, XO_3^-, or XO_4^- type, the values of lattice energies calculated from this formula are in serious error. Recently Paul and co-workers (27) calculated the lattice energies of some alkali metal perchlorates using eq. 6 and the effective thermochemical radii of Kapustinskii. Arvindakshan (28) has shown from crystallographic studies that the Cl—O distance in the ClO_3^- ion of $NaClO_3$ is 1.49 Å; the three oxygens form an equilateral triangle with each side being 2.37 Å while the chlorine atom is situated above the plane of oxygen at 0.50 Å.

The structure of $NaClO_4$ is somewhat similar to that of $NaClO_3$. In such a case what should be the effective thermochemical radii of ClO_3^- or ClO_4^- ions? The same argument applies to all kinds of anions having a structure of the type XO_2^-, XO_3^-, and XO_4^-. Morris (29) suggested an alternative approach for calculating the lattice energies of salts involving such ions. Using the lyotropic numbers and enthalpies of hydration he has tabulated the lattice energies of alkali metal nitrites, nitrates, chlorates, perchlorates, and thiocyanates. Though the lattice energy of $LiClO_3$ is not given in this table it is easy to calculate and was found to be -202.43 kcal. The lattice energies and enthalpies of solvation of all the electrolytes we have studied are given in Table 5 along with the corrected values of the enthalpies of solvation of alkali metal perchlorates in various amide solvents, using the data for ΔH_s^0 of Paul and co-workers (27). At present not enough data are available to obtain the ionic enthalpies of solvation but in future studies we intend to include those calculations.

1. R. P. Held and C. M. Criss. J. Phys. Chem. **69**, 2611 (1965).
2. R. P. Held and C. M. Criss. J. Phys. Chem. **71**, 2487 (1967).
3. Om N. Bhatnagar and C. M. Criss. J. Phys. Chem. **73**, 174 (1969).
4. C. De Visser and G. Somsen. Recueil, **90**, 81, 1129 (1971); **91**, 943 (1972).
5. C. De Visser and G. Somsen. J. Chem. Thermodyn. **4**, 313 (1972).
6. M. J. Mastroianni and C. M. Criss. J. Chem. Eng. Data, **17**, 222 (1972).
7. M. J. Mastroianni and C. M. Criss. J. Chem. Thermodyn. **4**, 321 (1972).
8. C. V. Krishnan and H. L. Friedman. J. Phys. Chem. **73**, 3934 (1969).
9. D. Feakins, B. C. Smith, and L. Thakur. J. Chem. Soc. 714 (1966).
10. A. N. Campbell and O. N. Bhatnagar. Can. J. Chem. **49**, 217 (1971).
11. A. N. Campbell and O. N. Bhatnagar. Can. J. Chem. **50**, 1627 (1972).
12. J. D. Nutter. Ph.D. Thesis, University of Nebraska, Lincoln, Nebraska. 1964.
13. C. E. Vanderzee and W. W. Rodenburg. J. Chem. Thermodyn. **3**, 267 (1971).
14. O. N. Bhatnagar and A. N. Campbell. Chem. Instrum. **4**, 179 (1973).
15. H. S. Harned and B. B. Owen. The physical chemistry of electrolyte solutions. 3rd Ed. Reinhold Publishing Corporation. 1958. p. 720.
16. C. M. Criss and J. W. Cobble. J. Am. Chem. Soc. **83**, 3223 (1961).
17. W. R. Wen and S. Saito. J. Phys. Chem. **68**, 2639 (1964).
18. R. L. Kay and D. F. Evans. J. Phys. Chem. **69**, 4216 (1965); **70**, 366, 2325, 2336 (1966).
19. R. L. Kay, T. Vituccio, C. Zawoyski, and D. F. Evans. J. Phys. Chem. **70**, 2336 (1966).
20. K. W. Bunzel. J. Phys. Chem. **71**, 1358 (1967).
21. R. H. Wood and H. L. Anderson. J. Phys. Chem. **71**, 1871 (1967).
22. H. S. Frank and W. Y. Wen. Discuss. Faraday Soc. **24**, 133 (1957).
23. T. S. Sarma, R. K. Mohanty, and J. C. Ahluwalia. Trans. Faraday Soc. **65**, 2333 (1969).
24. R. K. Mohanty and J. C. Ahluwalia. J. Chem. Thermodyn. **4**, 53 (1972).
25. M. L. Huggins. J. Chem. Phys. **5**, 143 (1937).
26. A. F. Kapustinskii. Q. Rev. **10**, 283 (1956).
27. R. C. Paul, D. P. Gill, J. P. Singla, and S. P. Narula. J. Chem. Soc. Dalton, 622 (1971).
28. C. Arvindakshan. Z. Kristallogr. **111**, 241 (1959).
29. D. F. C. Morris. J. Inorg. Nucl. Chem. **6**, 295 (1958).

Can. J. Chem. Downloaded from www.nrcresearchpress.com by 210.87.254.40 on 09/05/12
For personal use only.

Synthèse d'α-L-Fucopyrannosides

MARIE-EDITH RAFESTIN, DIDIER DELAY ET MICHEL MONSIGNY

Laboratoire de Chimie Biologique et Centre de Biophysique Moléculaire, 45045 Orléans, Cedex, France

Reçu le 12 juin 1973

Le chloro-1 trichlorosulfate-2,3,4 β-L-fucopyrannose (**1**) est préparé par réaction du chlorure de sulfuryle sur le L-fucose, à basse température (rendement, 47%). Le chloro dérivé (**1**) réagit sur les alcools en conduisant principalement à l'α-L-fucoside correspondant. Le *p*-nitrobenzyl α-L-fucoside est obtenu avec un rendement de 35%, à partir de (**1**). A partir du L-fucose, l'α-L-fucoside est obtenu en trois étapes seulement.

The β-L-fucopyranosyl chloride 2,3,4-tri(chlorosulfate) (**1**) has been prepared by reaction of sulfuryl chloride with L-fucose at low temperature (yield, 47%). This β-L-fucopyranosyl chloride (**1**) gave high yields of the α-L-fucoside by reaction with alcohols. The *p*-nitrobenzyl α-L-fucoside has been prepared (yield, 35%). From L-fucose, the α-L-fucoside is obtained in three steps.

Can. J. Chem., **52**, 210 (1974)

Introduction

La réaction du chlorure de sulfuryle sur les sucres réducteurs, à basse température, conduit dans les conditions d'isolement décrites par Jennings et Jones (1, 2) à des trichloro-1,4,6 tridésoxy-1,4,6 dichlorosulfate-2,3 hexopyrannose pour les hexopyrannoses et à des dichloro-1,4 dichlorosulfate-2,3 pentopyrannose pour les pentoses. Par modification des conditions d'isolement, Jennings décrit ultérieurement (3–5) la préparation de chloro-1 trichlorosulfate-2,3,4 pentopyrannose. Ces composés permettent, grâce à la non participation des groupes chlorosulfates (6), de préparer des α-pentopyrannosides à partir de chloro-1 β-pentopyrannose et des β-pentopyrannosides à partir de chloro-1 α-pentopyrannose.

En utilisant le D-xylose, Jennings (4) a obtenu l'anomère β du chloro-1 trichlorosulfate-2,3,4 D-xylopyrannose qui, par condensation avec le méthanol ou le tétra-*O*-acétyl-1,2,3,4 β-D-mannopyrannoside, conduit aux α-D-xylopyrannosides correspondants.

Nous décrivons dans ce mémoire la préparation du chloro-1 trichlorosulfate-2,3,4 β-L-fucopyrannose et la préparation des méthyl et *p*-nitrobenzyl α-L-fucopyrannosides. Le *p*-nitrobenzyl α-L-fucopyrannoside est un intermédiaire intéressant pour préparer des supports utilisables en chromatographie d'affinité (7).

Résultats et discussion

Dans les conditions analogues à celles décrites par Jennings (4) pour les pentoses, le L-fucose est substitué par le chlorure de sulfuryle pour donner le chloro-1 trichlorosulfate-2,3,4 β-L-fucopyrannose cristallisé. Les résultats de l'analyse élémentaire, la valeur de la masse moléculaire et les données de spectroscopie r.m.n. permettent de conclure que le groupement $—C_5—CH_3$ n'est pas modifié et que trois des groupements hydroxylés sont substitués par un groupement SO_2Cl. Le spectre r.m.n. est complexe et en première analyse, seuls les protons du CH_3 et celui du carbone 5 sont individualisés.

La condensation du chloro-1 trichlorosulfate-2,3,4 β-L-fucopyrannose avec le méthanol, en présence de carbonate d'argent et de perchlorate d'argent conduit au méthyl trichlorosulfate-2,3,4 L-fucopyrannoside qui cristallise. Ce composé après élimination des groupements chlorosulfates et *O*-acétylation conduit au méthyl tri-*O*-acétyl-2,3,4 L-fucopyrannoside (**4**). L'analyse chromatographique de ce composé montre la présence des deux anomères α et β. Les surfaces de pics obtenus sont dans les rapports 89 et 11. Le pouvoir optique rotatoire du mélange correspond à 87% d'anomère α. Ce résultat permet de conclure que le composé (**1**) est effectivement l'anomère β du chloro-1 trichlorosulfate-2,3,4 L-fucopyrannose qui, par inversion de Walden, conduit essentiellement à l'α-fucopyrannoside avec une grande spécificité (88%). Le spectre r.m.n. permet d'arriver aux mêmes conclusions et les valeurs de déplacements chimiques et de constantes de couplage sont en parfait accord avec celles obtenues par Leaback *et al.* (8).

La condensation de (**1**) et de l'alcool *p*-nitro-

Can. J. Chem. Downloaded from www.nrcresearchpress.com by 210.87.254.105 on 09/05/12
For personal use only.

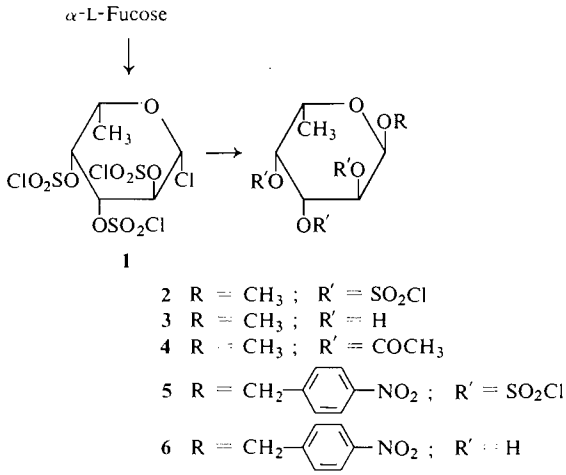

SCHÉMA 1

benzylique en présence de carbonate d'argent permet d'obtenir le composé (**5**) qui après déchlorosulfatation conduit au *p*-nitrobenzyl α-L-fucopyrannoside (**6**) cristallisé avec un rendement de 35% (schéma I). A titre de comparaison, Flowers *et al.* (9) ont préparé l'anomère β du benzyl L-fucopyrannoside à partir du bromo-1 tri-*O*-acétyl-2,3,4 α-L-fucopyrannose avec un rendement du même ordre de grandeur (37%).

D'une façon générale le bromo-1 tri-*O*-acétyl-2,3,4 α-L-fucopyrannose conduit au β-L-fucopyrannoside; c'est ainsi que Zehavi et Patchornik (10) en utilisant les conditions de synthèse de Koenigs et Knorr précisées par Zemplen (11) ont obtenu l'orthonitrobenzyl β-L-fucopyrannoside. Rachaman et Jeanloz (12, 13) avec le nitrométhane comme solvant et le cyanure mercurique comme catalyseur ont obtenu des β-L-fucopyrannosyl *N*-acétylglucosamine. Par contre, Flowers *et al.* (9), Levy *et al.* (14) et Shaban et Jeanloz (15) ont obtenu dans des conditions analogues, mais sur des partenaires hydroxylés différents, des α-L-fucopyrannosides.

Récemment, Dejter-Juszynski et Flowers (16) ont proposé une synthèse stéréospécifique d'α-L-fucopyrannosides par condensation d'aglycone sur un bromo-1 α-L-fucopyrannose portant un groupement non participant sur le carbone 2, et des groupements participants sur les carbones 3 et 4. La condensation s'effectue en présence de nitrométhane. Cette méthode conduit à l'α-L-fucoside en une dizaine d'étapes. La méthode que nous décrivons dans ce papier conduit au même résultat en trois étapes.

Ainsi donc, le chloro-1 trichlorosulfate-2,3,4 β-L-fucopyrannose (**1**) apparaît comme un excellent intermédiaire pour la préparation d'α-L-fucosides. En effet, grâce à l'élimination aisée des groupements chlorosulfates (Jennings et Jones (17)) et grâce à la non participation de ces groupements, la condensation de (**1**) sur un alcool conduit à un α-L-fucopyrannoside avec un rendement comparable à l'obtention de l'anomère β à partir de l'acéto-bromo-α-L-fucose.

Partie expérimentale

L'α-L-fucose (Sigma) est séché avant utilisation sur P_2O_5 pendant une nuit. La pyridine (RP Prolabo) est séchée sur pastilles de potasse puis redistillée. Le chlorure de sulfuryle est redistillé. Le chloroforme sans éthanol est préparé selon le procédé suivant: le chloroforme est agité avec un petit volume d'acide sulfurique (environ 5% du volume de $CHCl_3$) puis lavé à l'eau, séché sur $CaCl_2$ et redistillé. Le méthanol anhydre est préparé par distillation à reflux sur tournure de magnésium. Le carbonate d'argent est préparé extemporanément, à l'obscurité, suivant le procédé de Wolfrom et Lineback (18).

Les points de fusion ont été déterminés à l'aide du microscope à platine chauffante (Leitz) et ne sont pas corrigés. Les pouvoirs optiques rotatoires ont été mesurés sur le polarimètre Perkin-Elmer modèle 141. Les spectres infra-rouge ont été enregistrés, en utilisant des pastilles de bromure de potassium, sur un spectromètre Perkin-Elmer modèle 257. Les spectres de résonance magnétique nucléaire ont été réalisés, à température ambiante, sur le spectromètre Bruker à 90 MHz en utilisant le chloroforme ou l'acétone deutériés. Les signaux du tétraméthylsilane ont été pris comme référence pour la mesure des déplacements chimiques. La détermination de masse moléculaire a été réalisée sur l'osmomètre à tension de vapeur Mechrolab 302 B. Les expériences ont été faites à 37° avec le toluène comme solvant et le benzyle comme étalon.

La chromatographie en phase gazeuse a été réalisée sur un appareil Varian Aerograph 1520; colonne de verre (150 × 0.2 cm) remplie de chromosorb W 100–120 mesh imprégné de ECNSS-M (A.S.L.) (3% p/p); gaz porteur N_2, débit 30 ml/mn; température 150°; détecteur à ionisation de flamme. Les chromatographies sur couche mince ont été réalisées sur silica gel G (Merck), la détection étant obtenue par chauffage des plaques après pulvérisation d'acide sulfurique à 5% (pour les chlorosulfates pulvérisation du mélange aniline–pyridine–*n*-butanol 1:2:7, Crank (19)). Les chromatographies sur colonne ont été réalisées sur silice Merck (70–325 mesh ASTM). La composition du solvant, qui dépend de la nature des composés à isoler, est prédéterminée par la chromatographie sur couche mince.

Chloro-1 trichlorosulfate-2,3,4 β-L-fucopyrannose (1)

De l'α-L-fucose (5 g) dans de la pyridine (20 ml) et du chloroforme (50 ml) est porté à −70° par un mélange réfrigérant acétone–carboglace. Du chlorure de sulfuryle (12 ml) est ajouté goutte à goutte. Le mélange est maintenu sous agitation constante à −70° pendant 2 h, puis la température est portée entre −10 et 0° et une nouvelle addition de chloroforme (50 ml) est effectuée. La tempéra-

Can. J. Chem. Downloaded from www.nrcresearchpress.com by 210.87.254.105 on 09/05/12
For personal use only.

Can. J. Chem. Downloaded from www.nrcresearchpress.com by 210.87.254.105 on 09/05/12
For personal use only.

ture est maintenue entre -10 et 0° pendant 30 min, avant d'isoler le produit de condensation. La phase chloroformique est lavée avec une solution d'acide sulfurique à 10% puis avec une solution saturée de bicarbonate de sodium et enfin avec de l'eau. La solution est séchée sur sulfate de sodium anhydre puis concentrée. Le sirop obtenu est repris par le chloroforme (50 ml) et le chlorosulfate est recristallisé par addition d'éther de pétrole (6.6 g; rendement, 47%): p.f. 128°; $[\alpha]_{589}^{25}$ $-30°$, $[\alpha]_{546}^{25}$ $-34°6$ (*c*, 1 dans le chloroforme).

Anal. calc. pour $C_6H_8O_{10}S_3Cl_4$: C, 15.06; S, 20.08; Cl, 29.70. Trouvé: C, 15.01; S, 20.17; C, 29.71.

Masse moléculaire calc. 478; Trouvée: 462 ± 20; ν_{max} (KBr): 2990 (C—CH_3), 1420 (OSO_2Cl, C—CH_3), 1190 (OSO_2Cl), 675 cm^{-1} (C—Cl); r.m.n. ($CDCl_3$) τ: 4.55–4.89 (H-1, H-2, H-3, H-4), 5.92 (q, J = 6.5 Hz, H-5), 8.46 (d, J = 6.5 Hz, C—CH_3); r.m.n. (acétone deutériée) τ: 3.55–4, 4.54 (d, J = 9 Hz) (H-1, H-2, H-3, H-4), 5.28 (q, J = 6.5 Hz, H-5), 8.48 (d, J = 6 Hz, C—CH_3).

Méthyl trichlorosulfate-2,3,4 L-*fucopyrannoside (2)*

Des cristaux de chloro-1 trichlorosulfate-2,3,4 β-L-fucopyrannose (**1**) (2 g) sont dissous dans du chloroforme et du méthanol anhydre (20 ml) est additionné. La solution est agitée à l'abri de la lumière en présence de carbonate d'argent (6 g), de perchlorate d'argent (80 mg) et de drierite (2 g) pendant une dizaine d'heures. La solution est concentrée en un sirop qui cristallise. Après redissolution dans le méthanol (50 ml) le composé **2** est recristallisé par addition d'eau distillée (1.13 g; rendement, 57%): $[\alpha]_{546}^{25}$ $-139°$, $[\alpha]_{589}^{25}$ $-119°5$ (*c*, 1 dans le chloroforme); ν_{max} (KBr): 2985 (C—CH_3), 2930, 2840 (O—CH_3), 1420 (C—CH_3, OSO_2Cl), 1190 cm^{-1} (OSO_2Cl); r.m.n. ($CDCl_3$) τ: 4.55–4.9 (H-2, H-3, H-4), 5.02 (d, J = 3.5 Hz, H-1), 5.75 (q, J = 6.5, H-5), 6.46 (s, OMe), 8.56 (d, J = 6 Hz, C—CH_3).

Méthyl tri-O-acétyl-2,3,4 L-*fucopyrannoside (4)*

A une solution de méthyl trichlorosulfate-2,3,4 L-fucopyrannoside (**2**) (2 g) dans le méthanol sont ajoutés du carbonate de baryum (200 mg environ) puis de faibles quantités d'une solution d'iodure de sodium (8 g d'iodure de sodium dans 20 ml d'une solution méthanol–eau v:v (17)). L'addition d'iodure de sodium est arrêtée lorsqu'une nouvelle addition ne libère plus d'iode. La solution est ensuite évaporée à siccité (**3**). Le mélange, repris dans la pyridine (4 ml) et l'anhydride acétique (2 ml), est porté à 100° pendant une demi-heure. Après refroidissement à 20° l'anhydride acétique en excès est détruite par addition d'eau distillée (50 ml). Le composé (**4**) est extrait par le chloroforme (3 × 25 ml). Les phases chloroformiques sont lavées successivement avec une solution d'acide sulfurique à 10%, une solution saturée de bicarbonate de sodium et avec de l'eau. La solution chloroformique évaporée donne un sirop: $[\alpha]_{546}^{25}$ $-153°$, $[\alpha]_{589}^{25}$ $-131°$ (*c*, 1 dans le chloroforme) (litt. (17) $[\alpha]_{589}^{25}$ $-152°$); ν_{max} (KBr): 2985 (C—CH_3), 2940, 2840 (O—CH_3), 1750 (C=O), 1440 (C—CH_3), 1375, 1230 cm^{-1} (C—O); r.m.n. ($CDCl_3$) τ: 4.6–4.85 (H-2, H-3, H-4), 5.08 (d, J = 3.5 Hz, H-1), 5.88 (J = 6.5 Hz, H-5), 6.6 (s, O—CH_3), 8.86 (d, J = 6.5 Hz, C—CH_3) (litt. (17) ($CDCl_3$) τ: 4.55–4.9 (H-2, H-3, H-4), 5.08 (d, J = 3.5 Hz, H-1), 5.78 (J = 6.5 Hz, H-5), 6.6 (s, OCH_3), 8.86 (d, J = 6.5 Hz, C—CH_3)).

p-Nitrobenzyl α-L-*fucopyrannoside (6)*

Des cristaux de chloro-1 trichlorosulfate-2,3,4 β-L-fucopyrannoside (**1**) (2.4 g) sont dissous dans du chloroforme (20 ml) et de l'alcool *p*-nitrobenzylique est ajouté en excès (1.53 g). Le mélange est maintenu sous agitation constante à l'abri de la lumière pendant six jours en présence de carbonate d'argent (10 g) et de drierite (3 g). La solution chloroformique (**5**) est évaporée puis reprise par le méthanol (10 ml). Du carbonate de baryum (500 mg environ) et des quantités suffisantes d'une solution méthanolique d'iodure de sodium (17) sont additionnées à la solution. Le mélange est purifié par passage sur colonne de silice (3 × 80 cm) avec le système solvant: acétate d'éthyle–méthanol (5:1). La fraction de tête correspond à l'alcool *p*-nitrobenzylique, la seconde fraction contient le *p*-nitrobenzyl α-L-fucopyrannoside (**6**) (370 mg, rendement, 31%). Après dissolution dans l'acétone (5 ml), le composé (**6**) cristallise par addition d'éthoxyéthane: p.f. 149–151°; $[\alpha]_{546}^{25}$ $-167°$, $[\alpha]_{589}^{25}$ $-142°$ (*c*, 1 dans l'éthanol); ν_{max} (KBr): 3300 (OH), 3000 (C—CH_3), 2930–2910 (CH_2), 1520 (NO_2), 1455 (C—CH_3), 1355 (NO_2), 855 (NO_2), 810 (C—H noyau phényle); r.m.n. (acétone deutériée) τ: 1.77 et 2.25 (2d, J = 8 Hz, 4 H aromatiques), 8.6 (d, J = 7 Hz, C—CH_3).

Les auteurs remercient Monsieur le Professeur J. K. N. Jones (Chown Research Laboratory, Queen's University, Kingston, Ontario) pour les conseils et les suggestions qu'il leur a apportés, et Monsieur le Professeur Ch. Sadron, Directeur du Centre de Biophysique Moléculaire pour l'intéret qu'il a porté à ce travail.

1. H. J. Jennings et J. K. N. Jones. Can. J. Chem. **40**, 1408 (1962).
2. H. J. Jennings et J. K. N. Jones. Can. J. Chem. **43**, 2372 (1965).
3. H. J. Jennings. Chem. Commun. 722 (1967).
4. H. J. Jennings. Can. J. Chem. **46**, 2799 (1968).
5. H. J. Jennings. Can. J. Chem. **47**, 1157 (1969).
6. B. Coxon, H. J. Jennings et K. A. McLaughlan. Tetrahedron, **23**, 2395 (1967).
7. M. Monsigny et M. E. Rafestin. En préparation.
8. D. H. Leaback, E. L. Heath et S. Roseman. Biochem. **8**, 1351 (1969).
9. H. M. Flowers, A. Levy et N. Sharon. Carbohydr. Res. **4**, 189 (1967).
10. U. Zehavi et A. Patchornik. J. Org. Chem. **37**, 2285 (1972).
11. G. Zemplen. Ber. **62**, 990 (1929).
12. E. S. Rachaman et R. W. Jeanloz. Carbohydr. Res. **10**, 429 (1969).
13. E. S. Rachaman et R. W. Jeanloz. Carbohydr. Res. **10**, 435 (1969).
14. A. Levy, H. M. Flowers et N. Sharon. Carbohydr. Res. **4**, 307 (1967).
15. M. A. E. Shaban et R. W. Jeanloz. Carbohydr. Res. **20**, 399 (1971).
16. M. Dejter-Juszynski et H. M. Flowers. Carbohydr. Res. **23**, 41 (1972).
17. H. J. Jennings et J. K. N. Jones. Can. J. Chem. **41**, 1151 (1963).
18. M. L. Wolfrom et D. R. Lineback. Meth. Carb. Chem. **2**, 342 (1962).
19. G. Crank. M.Sc. Thesis. Queen's University, Kingston, Ontario, 1960.

Vibrational Spectra of the Hexacarbonyl Manganese(I) Cation

R. A. N. McLEAN

Department of Chemistry, University of Ife, Ile-Ife, Nigeria

Received July 16, 1973

The infrared and Raman spectra of the hexacarbonylmanganese cation as $Mn(CO)_6^+PF_6^-$ were assigned by comparison with other hexacarbonyl species. The CO stretching force constants for $Mn(CO)_6^+$ and $Re(CO)_6^+$ as indicated by the CO stretching vibrational frequencies are not significantly different. However, the Mn—C force constant in $Mn(CO)_6^+$ is likely to be considerably less than the Cr—C force constant in $Cr(CO)_6$, whereas $Re(CO)_6^+$ and $W(CO)_6$ have similar values. It is postulated that, although $Mn(CO)_6^+$ has equal metal–carbon π bonding to $Re(CO)_6^+$, the metal–carbon σ bonding is less for $Mn(CO)_6^+$.

Les spectres infrarouge et Raman du cation de l'hexacarbonylmanganèse $Mn(CO)_6^+PF_6^-$, ont été analysés par comparaison avec d'autres espèces hexacarbonyles. Les constantes de force d'élongation du lien CO pour $Mn(CO)_6^+$ et $Re(CO)_6^+$ ne diffèrent pas de façon importante comme le montrent les fréquences de vibration attribuables à l'élongation du lien CO. Cependant, la constante de force de Mn—C dans $Mn(CO)_6^+$ sera vraisemblablement beaucoup plus petite que la constante de force Cr—C dans $Cr(CO)_6$, alors que celles de $Re(CO)_6^+$ et $W(CO)_6$ ont des valeurs semblables. On en conclut alors que, bien que $Mn(CO)_6^+$ possède une liaison π métal–carbone équivalente à celle dans $Re(CO)_6^+$, la liaisons métal–carbone est plus faible pour $Mn(CO)_6^+$. [Traduit par le journal]

Can. J. Chem., **52**, 213 (1974)

Introduction

Full details of the vibrational spectra of the neutral hexacarbonyls of Group VIA (ref. 1 and references therein), and two ionic hexacarbonyls have been published (2). Bonding in these and related species continues to attract considerable attention (3–8) and further spectroscopic data is useful for comparison with these studies.

We have shown earlier that although there is a considerable increase in the CO force constant (and bond order) from $W(CO)_6$ to $Re(CO)_6^+$ the metal–carbon stretching force constants are almost equal (9). (*Note*: the constraints placed on the force field in that work, because of the limited data available, produced rather different values for the force constants and interaction constants in the neutral hexacarbonyls than those obtained from using a complete quadratic valence force field (1), though with the same trends in primary valence force constants. As these trends are also indicated by weighted average frequencies we now prefer to discuss these rather than the force constants produced by a rather artificial force field.) We now present i.r. and Raman spectral data on the first row metal hexacarbonyl cation, $Mn(CO)_6^+$, and comment on the bonding trends implied by these results in comparison with the previously reported spectra of $V(CO)_6^-$, $Re(CO)_6^+$, and $Cr(CO)_6$.

Experimental and Results

The salt used for the investigation was $Mn(CO)_6^+PF_6^-$ prepared by the high pressure carbonylation of $Mn(CO)_5Cl$ with $AlCl_3$ as Lewis acid (10) and precipitating with NH_4PF_6 in degassed tetrahydrofuran. The spectra were recorded as in the earlier study (2) and the results are given in Tables 1 and 2. As $Mn(CO)_6^+PF_6^-$ decomposes to $Mn(CO)_5H$ immediately on exposure to wet solvents, the acetonitrile used was distilled from phosphorus pentoxide. Surprisingly for a white compound it was extremely difficult to obtain a Raman spectrum either in solution or in the solid state due to the presence of a fluorescing impurity. A sample of analytical purity was used but it was only after a third recrystallization from acetonitrile that a very poor Raman spectrum in the solid state was obtained. No Raman spectrum could be obtained of solutions. The combination bands in the i.r. spectra were used to confirm the Raman assignments. The spectral assignments, both of fundamentals and combinations, are fairly straightforward by comparison with the position and intensity of corresponding bands of the other hexacarbonyl species (1, 2). The fundamental frequencies in Table 2 are for the solid state. The only significant differences between the solid state and solution spectra are in ν_1 and ν_3.

Can. J. Chem. Downloaded from www.nrcresearchpress.com by 210.87.254.40 on 09/05/12
For personal use only.

TABLE 1. Vibrational frequencies* in cm^{-1} for $Mn(CO)_6^+PF_6^-$

(*A*) Infrared spectrum

Assignment	Frequency (cm^{-1}) Solution (in acetonitrile and nitromethane)	Solid†
ν_9	—	101 (vw)
ν_5(?)	—	349 (vw)
ν_2(?)	—	376 (vw)
ν_8	412 (500)	414 (s)
ν_{12} ($\nu_8 + \nu_{11}$?)	—	500 (m)
ν_4 (PF_6^-)	559 (600)	557 (s)
ν_7	636 (800)	636 (vw)
—	—	780 (vw)
$\nu_2 + \nu_8$ ($\nu_4 + \nu_8$?)	—	796 (sh)
ν_3 (PF_6^-), ($\nu_5 + \nu_{12}$?)	840 (3000)	840 (vs)
$\nu_4 + \nu_{12}$?	—	880 (sh)
$\nu_8 + \nu_{10}$	—	932 (vw)
$\nu_5 + \nu_7$	—	983 (m)
$\nu_4 + \nu_7$, ($\nu_2 + \nu_7$?)	—	1018 (m)
$\nu_7 + \nu_{10}$	—	1152 (m)
ν_6 (^{13}CO)	2060 (sh)	2065 (sh)
ν_6	2095 (2000)	2095 (vs)
$\nu_1 + \nu_9$	—	2285 (vw)
$\nu_2 + \nu_6$	2479 (sh)	2479 (sh)
$\nu_4 + \nu_6$	2483 (8)	2487 (m)
$\nu_3 + \nu_8$	2541 (10)	2540 (m)
$\nu_1 + \nu_8$	2599 (2)	2596 (w)
$\nu_3 + \nu_7$	2760 (3)	—
$\nu_3 + \nu_6$	4201 (2)	4198 (vw)
$\nu_1 + \nu_6$	4283 (10)	4278 (w)

(*B*) Raman spectrum (solid)

Assignment	Frequency (cm^{-1})
ν_{11} ?	90 (vs)
	110 (vs)
ν_2	384 (s)
ν_4	390 (sh)
ν_5(PF_6^-)	472 (ms)
ν_{10}	520 (vw)
ν_2 (PF_6^-)	573 (m)
ν_1 (PF_6^-)	749 (s)
ν_3	2125 (m)
ν_1	2192 (w)

*Errors ±1 cm^{-1} for i.r., ±5 cm^{-1} for Raman.
†Relative intensities given in parentheses: vw = very weak, w = weak, m = medium, s = strong, vs = very strong.

The observed combination bands below 3000 cm^{-1} are very close to the sum of the corresponding fundamentals and the intensity patterns are mostly the same as in the related hexacarbonyls (1, 2). The CO combination bands, $\nu_1 + \nu_6$ and $\nu_3 + \nu_6$ have anharmonic corrections of the order of those for the other hexacarbonyls (11) ($X_{16} = -9\,cm^{-1}$, $X_{36} = -22\,cm^{-1}$, *cf.* $Cr(CO)_6$, $X_{16} = -8\ cm^{-1}$, $X_{36} = -21\ cm^{-1}$).

TABLE 2. Fundamental vibrations* of $Mn(CO)_6^+$

Assignment	Representation	Normal mode	ν(cm^{-1})
ν_1	A_{1g}	ν(CO)	2192
ν_2	A_{1g}	ν(MC)	384
ν_3	E_g	ν(CO)	2125
ν_4	E_g	ν(MC)	390
ν_5	T_{1g}	δ(MCO)	347
ν_6	T_{1u}	ν(CO)	2095
ν_7	T_{1u}	δ(MCO)	636
ν_8	T_{1u}	ν(MC)	412
ν_9	T_{1u}	δ(CMC)	101
ν_{10}	T_{2g}	δ(MCO)	500
ν_{11}	T_{2g}	δ(CMC)	110 ?
ν_{12}	T_{2u}	δ(MCO)	500
ν_{13}	T_{2u}	δ(CMC)	—

*Solid state values.

Considering the anharmonic defects to be equal to those of $Cr(CO)_6$ ($\omega_1 - \nu_1$, 21 cm^{-1}; $\omega_3 - \nu_3$, 19 cm^{-1}; $\omega_6 - \nu_6$, 43 cm^{-1} (11)) the following harmonic values (±5 cm^{-1}) for the CO vibrations of $Mn(CO)_6^+$ are obtained: $\omega_1 = 2213$ cm^{-1}, $\omega_3 = 2144$ cm^{-1}, $\omega_6 = 2138$ cm^{-1} (average, $\bar{\omega} = 2153 \pm 5$ cm^{-1}). The corresponding values for $Re(CO)_6^+$ (2) are 2224, 2139, and 2131 cm^{-1}, respectively ($\bar{\omega} = 2149 \pm 5$ cm), for $Cr(CO)_6$ (1) 2133, 2037, 2027 cm^{-1}, respectively ($\bar{\omega} = 2048$ cm^{-1}), and for $V(CO)_6^-$ (2) 2036, 1908, 1895 cm^{-1}, respectively ($\bar{\omega} = 1923$ cm^{-1}) (6).

Discussion

The order of the average harmonic CO stretching frequency through the series of metal hexacarbonyls now studied (1, 2) is $Mn(CO)_6^+ > Re(CO)_6^+$ ($\approx$2150 cm^{-1}) > $Mo(CO)_6 > Cr(CO)_6$ and $W(CO)_6$ ($\approx$2050 cm^{-1}) > $V(CO)_6^-$ ($\approx$1920 cm^{-1}).

The effect of the metal (and particularly its charge) on "back-donation" from the metal d orbitals to the π^* orbitals of the CO ligand and on the σ donation to the metal and the resultant effect on the CO stretching force constant has been well discussed (1, 2, 4, ref. 7 and references therein).

The CO force constant for $Mn(CO)_6^+$ will not be significantly different from that of $Re(CO)_6^+$. This is the same result as that obtained with $Cr(CO)_6$ and $W(CO)_6$, but contrasts with the re-

Can. J. Chem. Downloaded from www.nrcresearchpress.com by 210.87.254.40 on 09/05/12
For personal use only.

Can. J. Chem. Downloaded from www.nrcresearchpress.com by 210.87.254.40 on 09/05/12
For personal use only.

sults of molecular orbital calculations (3) on $Mn(CO)_6^+$ and $Re(CO)_6^+$, in which $Mn(CO)_6^+$ was found to have twice the amount of $d \rightarrow \pi^*$ backbonding of $Re(CO)_6^+$. However the CO force constants indicate that $Mn(CO)_6^+$ has about the same amount of $d \rightarrow \pi^*$ backbonding as $Re(CO)_6^+$.

The change in the T_{1u} metal–carbon (M—CO) stretching vibration through the series $V(CO)_6^-$ (460 cm^{-1}), $Cr(CO)_6$ (440 cm^{-1}), $Mn(CO)_6^+$ (410 cm^{-1}), which is the opposite of the order of the CO stretching vibrations, has been cited as evidence for the decreased M—C bond strength in that order (4, 13). This was explained by the decreased M—C π bonding through the series with the σ bonding being constant or indeed decreasing slightly with the π bonding. An examination of all the M—C stretching vibrations for $V(CO)_6^-$, $Cr(CO)_6$, and $Mn(CO)_6^+$ (Table 3) shows that the differences between the average M—C stretching frequencies are not as great as for the T_{1u}. The difference between $Cr(CO)_6$ and $Mn(CO)_6^+$ is more significant than that between $V(CO)_6^-$ and $Cr(CO)_6$. Since in the heavier metal species σ bonding in the M—C bond increases with the nuclear charge (see below) we believe this also holds for the first row series and that the decreased π bonding in $Mn(CO)_6^+$ outweighs the increase in σ bonding in the M—C bond compared to $Cr(CO)_6$. Comparison of $Re(CO)_6^+$ and $W(CO)_6$ shows no significant difference between the average M—C stretching vibration (393 and 397 cm^{-1}, respectively) and the M—C force constants, as discussed earlier (2, 9). There seems no doubt that the other properties of $Re(CO)_6^+$ (12, 14) support this relative strengthening of the metal–carbon bond compared to $Mn(CO)_6^+$.

We have suggested earlier that the Re—C σ bonding is stronger than the W—C σ bonding (already considerably greater than Cr—C and Mo—C σ bonding) and it is pertinent to speculate on the reasons for the relatively weaker σ bonding of $Mn(CO)_6^+$. It seems likely that the less diffuse orbitals of the first row metals are more affected by the nuclear charge and are less available for effective overlap with carbon when there is a high nuclear charge. A corollary to this argument is the prediction that if it is possible to make hexacarbonyl dications then $Os(CO)_6^{2+}$ will be more stable than $Fe(CO)_6^{2+}$.

TABLE 3. M—C stretching vibrations

Mode	Frequency (cm^{-1})		
	$Mn(CO)_6^+$	$Cr(CO)_6$	$V(CO)_6^-$
A_{1g}	384	381	374
E_g	390	394	393
T_{1u}	412	440	460
Weighted average	400	415	423

I thank Professor E. W. Abel for his encouragement and the Salters' Company and the Research Committee of the University of Ife for financial support.

1. L. H. JONES, R. S. McDOWELL, and M. GOLDBLATT. Inorg. Chem. **8**, 2349 (1969).
2. E. W. ABEL, R. A. N. McLEAN, S. P. TYFIELD, P. S. BRATERMAN, A. P. WALKER, and P. J. HENDRA. J. Mol. Spectrosc. **30**, 29 (1969).
3. N. A. BEACH and H. B. GRAY. J. Am. Chem. Soc. **90**, 5114 (1968).
4. K. G. CAULTON and R. F. FENSKE. Inorg. Chem. **7**, 1273 (1968).
5. D. A. BROWN and R. M. RAWLINSON. J. Chem. Soc. A, 1530 (1969).
6. R. L. DEKOCK, A. C. SARAPU, and R. F. FENSKE. Inorg. Chem. **10**, 38 (1971).
7. M. B. HALL and R. F. FENSKE. Inorg. Chem. **11**, 1619 (1972).
8. I. H. HILLIER and V. R. SAUNDERS. Mol. Phys. **22**, 1025 (1971).
9. E. W. ABEL, R. A. N. McLEAN, M. G. NORTON, and S. P. TYFIELD. Chem. Commun. 900 (1968).
10. T. KRUCK and M. NOACK. Chem. Ber. **96**, 3028 (1963).
11. J. M. SMITH and L. H. JONES. J. Mol. Spectrosc. **20**, 248 (1966).
12. E. W. ABEL and S. P. TYFIELD. Adv. Organomet. Chem. **8**, 117 (1970).
13. R. W. CATTRALL and R. J. H. CLARK. J. Organomet. Chem. **6**, 157 (1966).
14. E. W. ABEL and S. P. TYFIELD. Can. J. Chem. **47**, 4627 (1969).

Homogeneous Gas-phase Pyrolyses using a Wall-less Reactor. IV. Comparative Surface–Nonsurface Effects with Cyclopropane

DONALD M. KULICH, JAY E. TAYLOR, AND DAVID A. HUTCHINGS[1]

Department of Chemistry, Kent State University, Kent, Ohio 44242

Received December 11, 1972[2]

The rates of pyrolysis of cyclopropane in nitrogen have been determined using a wall-less reactor at temperatures of 600–740 °C and a total pressure of 1 atm. In the presence of oxidized stainless steel, quartz, or carbon coated steel rods the rate of conversion to propylene is 1.9 times the rate under homogeneous conditions. A maximum in surface effect was observed at $S/V = 0.6$ cm^{-1}. A small but increased amount of methane and ethene are formed under surface conditions as compared to homogeneous conditions. Several possible mechanisms for the rate enhancement by surface are discussed. The most likely possibility is surface interaction with the cyclopropane molecule to form the diradical followed by its surface promoted conversion to propene. The importance of determining surface effects by comparing surface rates with *totally* homogeneous rates is emphasized.

On a évalué les différentes vitesses de pyrolyse dans l'azote du cyclopropane en utilisant un réacteur sans paroi à des températures de 600 à 740 °C et à une pression totale d'un atmosphère. En présence de tiges d'acier recouvertes de quartz, de carbone ou d'acier inoxydable oxydé, la vitesse de transformation en propylène est supérieure par un facteur de 1.9 à celle enregistrée dans des conditions homogènes. On a observé à $S/V = 0.6$ cm^{-1} un effet de surface maximum. De même, une légère augmentation de la quantité produite de méthane et d'éthane a été enregistrée dans les conditions impliquant une surface par rapport aux conditions homogènes. On discute de plusieurs mécanismes probables tenant compte de l'augmentation de vitesse due à une interaction surface-cyclopropane conduisant à un biradical puis à sa transformation, favorisée par la surface, en propène. On discute aussi de l'importance d'évaluer les effets de surface par comparaison entre les vitesses observées lors de la présence d'une surface et celles obtenues dans des conditions *parfaitement* homogènes. [Traduit par le journal]

Can. J. Chem., 52, 216 (1974)

Introduction

In the first determinations of the absolute effects of surfaces on various gas-phase pyrolyses using the wall-less reactor, results ranging from activation to inhibition have been noted. The compounds reported to date include neopentane (1, 2) and ethane under both oxidative and nonoxidative conditions (3) and now cyclopropane. Neopentane exhibits a strong positive surface effect with alteration of both products and activation energy. Ethane has a negligible surface effect at low surface to volume ratios; ethane with oxygen is positively affected by surface at very low conversions and is inhibited at higher conversions.

Previous investigations of the thermal isomerization of cyclopropane have been carried out in reactors having walls of glass (4–6), seasoned glass or silica (7–9), and recently gold-lined steel (10). It has been generally assumed that the reaction proceeds without notable surface effect. The isomerization may be considered to proceed as follows

[1] 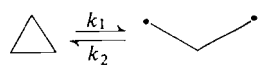

[2] 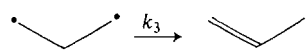

Studies on the geometric isomerization of dideuterocyclopropanes by Rabinovitch and co-workers (8, 9) and the discussion of O'Neal and Benson (11) present convincing arguments favoring a biradical mechanism.

Experimental support for an entirely homogeneous process has been given by Davis and Scott (4) and Chambers and Kistiakowsky (5), who compared packed with unpacked clean glass reactors and detected no significant deviation in the observed rate values. Using a silica vessel, Rabinovitch *et al.* (8) observed that seasoning of the reactor was necessary to establish reproducible rates. Pritchard, Sowden, and Trotman-Dickenson (7) also noted differences between runs carried out in an aged

[1]Present address: Research Division, The Goodyear Tire and Rubber Co., Akron, Ohio 44316.

[2]Revision received September 24, 1973.

Can. J. Chem. Downloaded from www.nrcresearchpress.com by 210.87.254.5 on 09/05/12
For personal use only.

Can. J. Chem. Downloaded from www.nrcresearchpress.com by 210.87.254.5 on 09/05/12
For personal use only.

Pyrex vessel and runs following exposure of the reactor vessel to air.

Catalytic isomerization of cyclopropane to propene by platinum black, alumina, and zeolite has been clearly demonstrated (12, 13).

Wall effects at very low pressures (0.1 Torr or less) have been reported by Kennedy and Pritchard (6) and Rabinovitch, Gilderson, and Blades (14). However, at very low pressures the mean free path exceeds the size of the reaction vessel and the molecules become predominantly energized by collisions with the walls. Theoretical treatments of this low pressure effect have been advanced (15–17).

The purpose of this paper is to present evidence concerning the existence of surface effects in the pyrolysis of cyclopropane at 1 atm total pressure. A comparison is made of the homogeneous rate with the rate in the presence of surface at low surface to volume ratios. These homogeneous data are in contrast with the prior concept of a "homogeneous" reaction in that there is a total absence of any contact of the reactant with surface from the time it attains reaction temperature to the time the reaction is quenched.

Experimental

The use of the wall-less reactor for comparative homogeneous–heterogeneous studies has been described (1, 3); however, one additional change was incorporated for this work. An opaque quartz tube has been substituted for the previously used stainless steel reactor.

Both the center-point sampling and cross-sectional analysis techniques as previously described (1) were used in the determination of rate data. The latter procedure is the more accurate for the determination of comparative rates either with or without surface. Center-point sampling is excellent for the determination of activation energies where a series of runs can be made without changing the position of the sampling tube. If the sampling tube position is altered (as with comparative surface–nonsurface runs), the technique is less accurate.

All reactions are done at a total pressure of 1 atm. The concentration of cyclopropane varies due to diffusion of the injected center stream into the "blanket" nitrogen stream. The overall average concentration of cyclopropane is ~1% (see Fig. 1).

The cyclopropane was purified by removal of oxygen using the procedure previously described (3).

Results

A distinct and significant rate enhancement of the isomerization of cyclopropane occurs in the presence of surfaces as compared to the homogeneous rate (see Figs. 2 and 3). It is further noted that the rate increases with in-

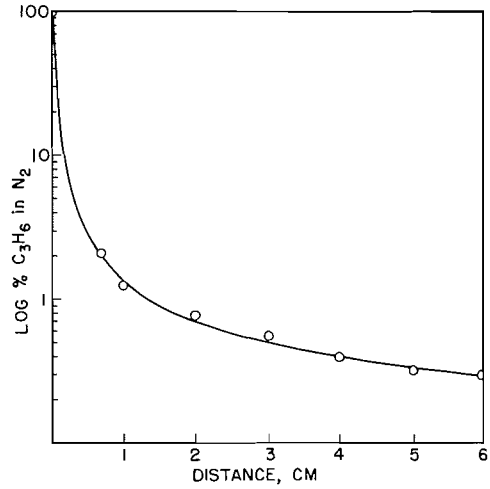

FIG. 1. Plot of the variation of log of cyclopropane concentration with distance traversed in the wall-less reactor. Each point on the curve is a weighted average of the total cyclopropane concentrations at that distance from the inlet tube. The experimental conditions are identical (except temperature) for all experiments described in this paper. Pressure, ~740 Torr (atmospheric); temperature, 660 °C; total averaged concentration of cyclopropane, 1.8% between 0 and 6 cm downstream. In view of the warm-up period required, the averaged concentration at reaction temperature is about 1%. Due to the design of the surface insert with rods parallel to the gas flow, no significant alteration of the flow pattern was noted upon placing the surface insert in the reactor. Inlet tube ~360 °C, sampling tube ~400 °C. 1 cm = 0.0360 s.

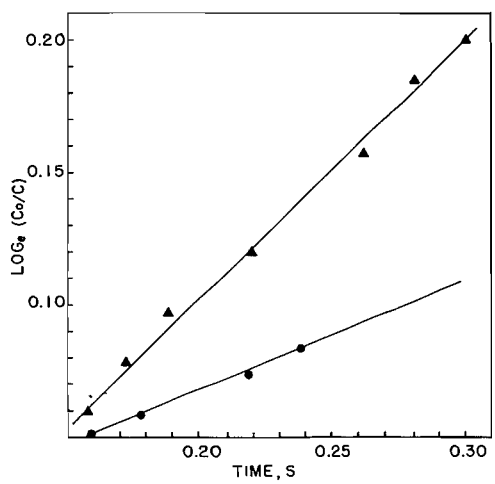

FIG. 2. Comparative rates of pyrolysis of cyclopropane at 672 °C. ●, Homogeneous, ▲, $S/V = 1.2\ cm^{-1}$ with an oxidized stainless steel surface. The data are taken with center-point sampling and are uncorrected. They are presented to show the consistency within each curve and the semiquantitative difference in rates.

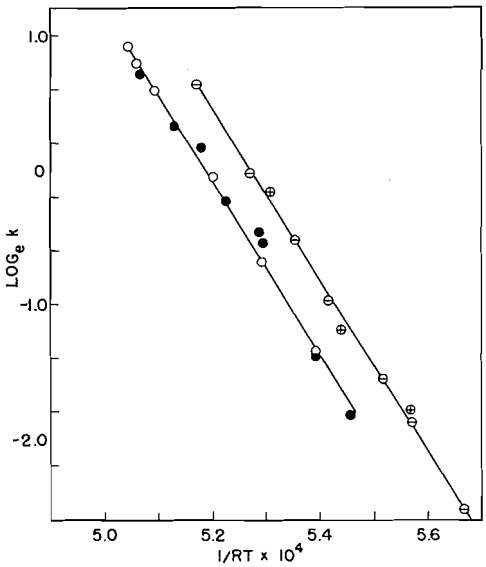

FIG. 3. Arrhenius plot of rate constants for cyclopropane pyrolysis. The data are taken in part by center-point sampling (P) which gives more consistent data for activation energies and the remainder by cross-sectional analysis (S) which permits a better absolute determination of comparative rates. The (P) data are corrected by adding a constant factor to $\log k$ to give consistency with the (S) data. ○, (P) corr., homogeneous; ●, (S) homogeneous; ⊖, (P) corr., oxidized stainless steel; ⊕, (S) oxidized stainless steel.

creasing surface up to an optimum at surface to volume (S/V) ratios of about 0.6 cm^{-1} (see Table 1).

The variation in activation energy upon adding a surface is within experimental error since the values are 64.0 ± 2 kcal/mol homogeneous, and 64.5 ± 2 kcal/mol with oxidized stainless steel.

The design of the surface insert is such that the reactant gas encounters only rods set parallel to the stream flow thereby minimizing turbulence. It has been observed (3) that pure ethane exhibits a negligible surface effect at $S/V = 1.2$ with stainless steel. Laidler and Wojciechowski (18) noted only a small surface effect at $S/V = 25$ with quartz. Using identical experimental conditions to the cyclopropane studies (except temperature) ethane decomposes at the same rate in either the presence or absence of surface thereby supporting the reality of the cyclopropane data.

Although the products methane and ethene are formed in minute quantities under homogeneous conditions, there is a significant increase in their formation in the presence of a stainless steel surface (see Table 2). Deposition of carbon was noted on the stainless steel surface.

Other surfaces including quartz and carbon coated steel are similar to stainless steel in their relative effects upon the rate of reaction (see Table 3). Although there do appear to be slight differences among the surfaces examined, the primary importance of Table 3 is to establish that all three surfaces increase the rate of pyrolysis to a roughly equivalent degree.

Oxygen has a negligible effect upon the rate of reaction (Table 3). This is in sharp contrast to ethane (3) and propane (19) whose rates of pyrolysis are greatly increased by oxygen. This lack of

TABLE 1. Variation of rate constant with increased surface. Oxidized stainless steel rods, equally spaced throughout a 5.2 cm i.d. quartz reactor tube, provide the surface. Because of the outward diffusion of the cyclopropane stream as it flows downward, an increasing number of rods are contacted with time of flow. The data are taken at 676–680 °C using the cross-sectional technique and the rate constants are corrected to 678 °C*

t (s)	Number of rods	S/V	Conversion (%)	k (s^{-1})
0.210	40	0.79	17.7	0.95
0.212	35	0.69	17.9	0.97
0.212	30	0.60	24.2	1.22
0.213	20	0.42	23.7	1.18
0.215	15	0.32	17.5	0.89
0.215	10	0.23	16.3	0.78
0.215	10	0.23	15.8	0.75
0.220	0	0	13.9	0.65
0.220	0	0	12.9	0.64

*The temperatures of the heterogeneous data do not exceed in average 3° greater than the listed temperatures. The actual value error is generally less.

TABLE 2. Analysis of minor products under surface and nonsurface conditions. Temperature, 678 °C; reaction times, 0.237 s homogeneous, and 0.229 s with 40 stainless steel rods ($S/V = 0.79$)

Reaction products	Yield (%)	
	Homogeneous	$S/V = 0.79$
C_3H_6	13.1	17.7
C_2H_4	0.00001*	0.0162
CH_4	0.0001*	0.0016

*Because of the very low concentrations the data are difficult to reproduce. The comparison between the homogeneous and heterogeneous systems is valid qualitatively, however.

Can. J. Chem. Downloaded from www.nrcresearchpress.com by 210.87.254.5 on 09/05/12
For personal use only.

TABLE 3. Effects of three surfaces and oxygen on cyclopropane pyrolysis*

Surface	O_2 added	Time (s)	Conversion (%)
None	No	0.246	1.9
None	Yes	0.246	1.9
Carbon	No	0.155	4.0
Carbon	Yes	0.155	3.6
Quartz	No	0.155	3.8
Quartz	Yes	0.155	3.8
Oxidized stainless steel	No	0.155	3.3
Oxidized stainless steel	Yes	0.155	3.0

*Conditions: point sampling technique, 0.4% O_2 added to the N_2 when indicated, 643 °C reaction temperature, $S/V = 1.2\ cm^{-1}$.

sensitivity of cyclopropane to oxygen has been recorded earlier (20).

Discussion

From a consideration of the assigned mechanism for cyclopropane isomerization and the observed surface effect, several alternate possibilities for this surface interaction can be envisaged.

It is unlikely that the observed surface effect is due to collisional activation. An investigation at very low pressures by Pritchard and coworkers (6, 7) suggests that a collision of a cyclopropane molecule with the reactor wall is ~60 times as efficient as a collision with a nitrogen molecule. However, at 1 atm pressure the ratio of heterogeneous to homogeneous contacts by cyclopropane is very small ($\sim 1:10^6$ at $S/V = 1$), and the increased efficiency of energy transfer by the surface will not be significant. It should be noted that the energy transfer studies were carried out in a conditioned reaction vessel ($S/V = 0.4\ cm^{-1}$); the data of this paper indicate a surface effect at this value of S/V (Table 1), although differences in temperature, reaction times, and the types of reactors (flow *vs.* static) prevent a quantitative comparison. Energy transfer studies of various gases in cyclopropane using a sound absorption technique do support the chemically oriented observations of the relative efficiencies of various gases (21, 22).

It is also unlikely that surface influences only the final step, k_3 (reaction 2). Using the data of O'Neal and Benson (11), the half-life t of the biradical is estimated to be $<10^{-11}$ s. From the Einstein relation

$$[3] \qquad \bar{x}^2 = 2Dt$$

and an estimated diffusion constant of $D = 1\ cm^2/s$, the biradical will only travel an average distance ($\bar{x}$) of $<10^{-4}$ mm at 700 °C and 1 atm pressure within its half-life. Since the average distance to each rod is 3 mm, the number of contacts of the biradical with the surface will be very small.

However, the time (<0.04 s) required for a cyclopropane molecule to diffuse to the surface is short relative to its half-life (~0.6 s at 700 °C) and the reaction time (~0.2 s). If the surface interaction is limited to the equilibrium step and the biradical diffuses from its adsorbed site, there will then be no overall change in rate since the reverse reaction must necessarily be proportionally increased. The surface effect is therefore nullified since $k_1/k_2 = K$.

However, k_3 can be independently altered by surface. It therefore appears that the combination of surface effects in both the equilibrium and final steps of reactions 1 and 2 provides the best explanation.

[4]

With the enhanced rate of biradical formation as above, the probability of formation of the biradical upon contact of a cyclopropane molecule with the surface is greatly increased. If the rate of migration of hydrogen within the biradical is correspondingly increased such that it is competitive with the reverse reaction, then an overall rate enhancement will be noted.

The variation of activation energy upon adding a surface is within experimental error. However, the change of activation energy calculated from the alteration in rate is also roughly within experimental error. At $S/V = 0.6\ cm^{-1}$ the rate increases by a factor of 1.9 over the homogeneous rate. Assuming the entire effect is due to a variation of activation energy, the change in the latter would be only 1.2 kcal/mol.

A maximization in surface effect at $S/V = 0.6\ cm^{-1}$ is seen in Table 1. Because of the difficulty of reproducibility of surface data the shape of the curve is subject to question. The fall-off in rate may be attributed to polymerization of propene on the surface. Surface promoted secondary decomposition does occur (Table 2) and is responsible for the formation of methane and ethene. Although the surface insert was not preconditioned, it should become conditioned with the

Can. J. Chem. Downloaded from www.nrcresearchpress.com by 210.87.254.5 on 09/05/12
For personal use only.

flowing reactant. It was noted that the oxidized steel surface especially promoted carbon deposition. Deposition on the surface may be of greater importance than the chemical nature of the surface since quartz, stainless steel, and carbon influence the rate to about the same degree (Table 3).

In summary, in the absence of a surface, $\log_{10} A = 14.52$ and $E_{act} = 64.0 \pm 2$ kcal/mol for the pyrolysis of cyclopropane. In the presence of a surface with $S/V = 0.6\ cm^{-1}$ for oxidized stainless steel, $\log_{10} A = 14.70$ and $E_{act} = 64.5 \pm 2$ kcal/mol.

In view of the data presented, conditioning and the use of packed and unpacked reactors can be unsatisfactory as definitive evidence for or against surface effects. Conditioning may simply achieve reproducible heterogeneous behavior. Only a detailed evaluation of the influence of surface beginning with a totally homogeneous system can insure reliable observations.

Acknowledgment is made to the donors of The Petroleum Research Fund, administered by the American Chemical Society, for partial support of this research.

1. J. E. TAYLOR, D. A. HUTCHINGS, and K. J. FRECH. J. Am. Chem. Soc. **91**, 2215 (1969).
2. D. A. HUTCHINGS, J. E. TAYLOR, and K. J. FRECH. J. Phys. Chem. **73**, 3167 (1969).
3. J. E. TAYLOR and D. M. KULICH. Int. J. Chem. Kinet. **5**, 455 (1973).
4. B. R. DAVIS and D. S. SCOTT. Ind. Eng. Chem. Fundam. **3**, 20 (1964).
5. T. S. CHAMBERS and G. B. KISTIAKOWSKY. J. Am. Chem. Soc. **56**, 399 (1934).
6. A. D. KENNEDY and H. O. PRITCHARD. J. Phys. Chem. **67**, 161 (1963).
7. H. O. PRITCHARD, R. G. SOWDEN, and A. F. TROTMAN-DICKENSON. Proc. R. Soc. A, **217**, 563 (1953).
8. B. S. RABINOVITCH, E. W. SCHLAG, and K. B. WIBERG. J. Chem. Phys. **28**, 504 (1958).
9. E. W. SCHLAG and B. S. RABINOVITCH. J. Am. Chem. Soc. **82**, 5996 (1960).
10. D. W. JOHNSON, O. A. PIPKIN, and C. M. SLIEPCEVICH. Ind. Eng. Chem. Fundam. **11**, 244 (1972).
11. H. E. O'NEAL and S. W. BENSON. J. Phys. Chem. **72**, 1866 (1968).
12. V. N. IPATIEFF. Catalytic reactions at high pressures and temperatures. The Macmillan Co., New York, New York. 1968. p. 155.
13. B. D. FLOCKHART, L. MCLOUGHLIN, and R. C. PINK. Chem. Commun. 818 (1970).
14. B. S. RABINOVITCH, P. W. GILDERSON, and A. T. BLADES. J. Am. Chem. Soc. **86**, 2994 (1964).
15. M. C. LIN and K. J. LAIDLER. Trans. Faraday Soc. **64**, 94 (1968).
16. K. J. LAIDLER. Theories of chemical reaction rates. McGraw-Hill Book Co., New York, New York. 1969. pp. 145–148.
17. G. L. PRATT. J. Chem. Soc. 6050 (1963).
18. K. J. LAIDLER and B. W. WOJCIECHOWSKI. Proc. R. Soc. A, **260**, 91 (1961).
19. M. NICLAUSE, R. MARTIN, A. COMBES, and M. DZIERZYNSKI. Can. J. Chem. **43**, 1120 (1965).
20. R. A. DAY, JR. and R. N. PEASE. J. Am. Chem. Soc. **63**, 912 (1941).
21. A. G. WELSH and J. E. TAYLOR. J. Acoust. Soc. Am. **47**, 1274 (1970).
22. A. G. WELSH and J. E. TAYLOR. J. Chem. Phys. **53**, 2529 (1970).

Can. J. Chem. Downloaded from www.nrcresearchpress.com by 210.87.254.5 on 09/05/12
For personal use only.

The γ-Radiolysis of Ethane. III. The Effect of Density on Ion Scavenging Reactions above the Critical Temperature

PATRICK T. HOLLAND AND JOHN A. STONE
Chemistry Department, Queen's University, Kingston, Ontario

Received August 20, 1973

The radiolysis of ethane has been studied over the density range 0.0018–0.5 g cc^{-1} at a temperature just above the critical point. The variations of product yields with increasing density are consistent with increasing collisional stabilization of excited species. Electron scavenging by sulfurhexafluoride in ethane at 0.275 g cc^{-1} is accurately described by an expression used for liquid phase scavenging with $G_{\text{free ions}} = 0.65$. At 0.052 g cc^{-1} a much higher yield of free ions is observed and at high sulfurhexafluoride concentrations there is a sensitized decomposition of ethane.

Ammonia-d_3 scavenges ions at all densities but in the region around 0.07 g cc^{-1} a mechanism operates which produces more than one hydrogen molecule per ion scavenged. The freely diffusing ions do not appear to be readily scavenged by ammonia-d_3.

La radiolyse de l'éthane a été étudiée dans l'intervalle de densité 0.0018–0.5 g cc^{-1}, à une température juste au dessus celle du point critique. Les variations des rendements en produit lorsque la densité augmente sont cohérentes avec l'accroissement de la stabilisation par choc des espèces excitées. Le piégeage des électrons par l'hexafluorure de soufre dans l'éthane à la densité 0.275 g cc^{-1} est décrit avec précision par une expression utilisée pour le piégeage en phase liquide avec $G_{\text{ions libres}} = 0.65$. Pour une densité de 0.52 g cc^{-1} on observe un plus grand rendement en ions libres et pour des concentrations élevées en hexafluorure de soufre on note une décomposition sensible de l'éthane.

L'ammoniac-d_3 piège les ions à toutes les densités mais aux environs de 0.07 g cc^{-1} apparait un mécanisme qui produit plus d'une molécule d'hydrogène par ion piégé. Les ions pouvant diffusés aisément ne semblent pas être facilement piégés par l'ammoniac-d_3. [Traduit par le journal]

Can. J. Chem., **52**, 221 (1974)

Introduction

The important role played by ionic intermediates in the radiolysis of saturated hydrocarbons is well recognized as is the effect of phase density on their behavior. In the liquid phase few electrons escape from their geminate ions leading to a short ($<10^{-9}$ s (1)) lifetime for the majority of ion–electron pairs. Information on these lifetimes is obtained mainly from the concentration dependence of scavenging reactions (2–4). In the gas phase essentially all electrons excape the coulombic fields of the geminate ions and homogeneous charge combination occurs with a rate constant of $10^{-7} - 10^{-5}$ cc ions $^{-1}$ s^{-1} (5, 6). At normal dose rates ($<10^{19}$ eV g^{-1} s^{-1}) scavenging of both positive ions and electrons may be accomplished with a very low concentration of an efficient scavenger ($k \sim 10^{-9}$ cc molecule^{-1} s^{-1}).

In spite of all the work devoted to the study of hydrocarbon radiolysis little effort has been made to study the effect of density on product yields and on the behavior of ionic intermediates.

Increasing density is expected to lead to collisional stabilization of excited species, both ionic and non-ionic, and hence to a decrease in the yields of products formed via molecular fragmentation. Carmichael, Gordon, and Ausloos (7) found that many of the changes in the relative yields of isotopic products in the system ethane – ethane-d_6 – nitric oxide over the density range 0.001–0.107 g cc^{-1} are consistent with decreasing fragmentation as the density increases. Wodetzki, McCusker, and Peterson (8, 9) measured the yields of the three major products of ethane radiolysis (hydrogen, ethylene, and butane) over the range 0.001–0.293 g cc^{-1} in the presence and absence of ethylene and nitric oxide which were presumed to be simple free radical scavengers. Again collisional stabilization was noted but the quantitative aspects of the arguments presented must be treated with caution since both solutes are now known to scavenge ions as well as free radicals (10). An important feature of this work is the use of experimentally measured dosimetry for the region 0.001–0.075 g cc^{-1} where there is a decrease in the importance of energy deposition by the γ-field in the vessel walls relative to that in the sample itself. We have made use of these results in our dosimetry.

Miyazaki (11) studied the effect of density

(0.0032–0.15 g cc^{-1}) on the radiolysis of isobutane at 150 °C and found increasing stabilization of the molecular ion with increasing density as judged by a decreased yield of the fragment ion $C_3H_7^+$. A similar stabilization of the *n*-butane molecular ion was previously observed (12).

Ethane is the only paraffin that can be studied over a wide range of density as a single phase at a convenient temperature (critical temperature = 305 °K). We have made a detailed study of product yields from ethane over the density range 0.0018–0.5 g cc^{-1} in the presence and absence of the charge scavengers sulfurhexafluoride (for electrons) and ammonia-d_3 (for positive ions). These scavengers were chosen for their high efficiency (13) and for their apparent lack of complicating secondary reactions. However in spite of these advantages the overall chemistry of their behavior is not known.

Experimental

The purification of the ethane and the product analysis have been described (14). The isotopic composition of the hydrogen from the ethane/ammonia-d_3 system was determined with a calibrated AEI-MS 10 Mass spectrometer.

The high density samples were irradiated in stainless steel vessels fitted with stainless steel valves. The volumes ranged from 3.05 to 81 cc. A 526 cc Pyrex flask with greased stopcock was used for the lowest density samples (0.00183 g cc^{-1}).

Energy deposition in the smallest vessels used for densities above 0.05 g cc^{-1} was determined by radiolysis of liquid cyclohexane for which $G(H_2)$ extrapolated to zero dose is 5.55 (15). Dosimetry for the glass bulb was obtained by radiolysis of gaseous ethylene ($G(H_2) = 1.20$ (16)). No dose rates were experimentally determined for samples in the density range 0.002–0.05 g cc^{-1}. Here dose rates were chosen to give a smooth transition for $G(H_2)$ for pure ethane between the low and high density experimental points (Fig. 2). This is in agreement with the hydrogen yield curve of ref. 8 for which internal dosimetry with tritium was obtained. As an example of the corrections required, the 81 cc cylindrical vessel with diameter 3.5 cm had an energy deposition rate of 9.05×10^{19}eV g^{-1} h^{-1} at an ethane density of 0.00183 g cc^{-1}, this dose rate dropped to 6.07×10^{19}eV g^{-1} h^{-1} at 0.0118 g cc^{-1}. This decrease can be characterized and qualitatively explained by the relationship between the range of wall generated electrons and the cell diameter (17). These dose rates should be accurate to better than ±10% as opposed to ±2% at the lower and higher densities.

All irradiations were performed in a ^{60}Co γ-source at 313±2 °K. A 10 °K increase in temperature did not measurably affect the product yields for pure ethane.

Results

The major products of the radiolysis of ethane alone are the same as those found for the liquid phase radiolysis at 196 °K (14). The dose dependences of the yields were determined at 0.102, 0.203, and 0.327 g cc^{-1}. There was no noticeable effect of density on the shapes of the yield curves; the ones for 0.203 g cc^{-1} are shown in Fig. 1. Figure 2 shows the effect of density on product yields at 1.0×10^{19} eV g^{-1} at which dose the yield curves of all products except ethylene show little departure from linearity.

The addition of sulfurhexafluoride results in the reduction of product yields but the dose dependences of these yields at 0.052 (Fig. 3) and 0.275 g cc^{-1} in the presence of 3 mol% sulfurhexafluoride are closely similar to those in the absence of electron scavenger. The effects of increasing concentrations of sulfurhexafluoride on product yields at 0.052 and 0.275 g cc^{-1} are shown in Figs. 4 and 5 respectively. Figure 6 shows the effect of 3 mol% of sulfurhexafluoride on product yields at different densities. This concentration was chosen since here, as seen in Figs. 4 and 5, the variations of product yields with concentration are minimal.

The only new product observed when ammonia-d_3 is present is HD. Its yield at 5 mol% was linear with dose at 0.051 g cc^{-1} (Fig. 7) and at 0.25 g cc^{-1}. Figures 8 and 9 show the effect

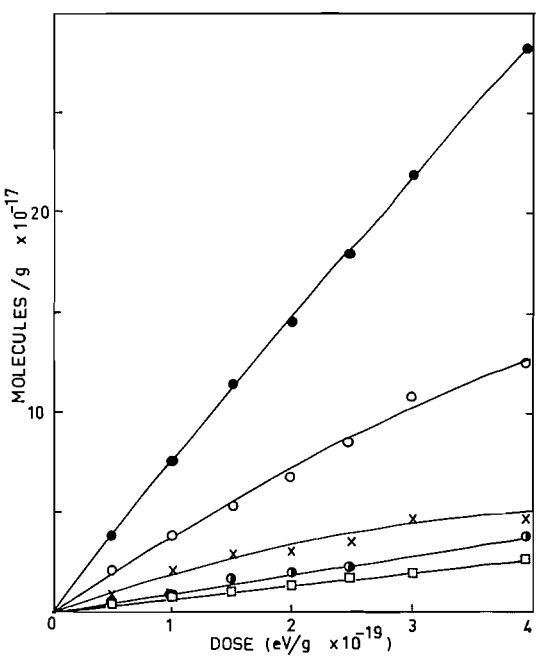

FIG. 1. The dose dependence of product yields in ethane at 0.203 gm cc^{-1}: (●), hydrogen; (○), *n*-butane; (×), ethylene; (□), propane; (◑), methane.

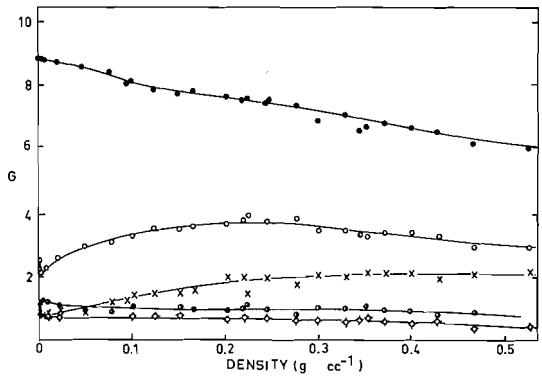

FIG. 2. The effect of density on product yields in ethane: (●), hydrogen; (○), *n*-butane; (×), ethylene; (◇), propane; (◑), methane; dose = 1 × 10^{19} eV g^{-1}.

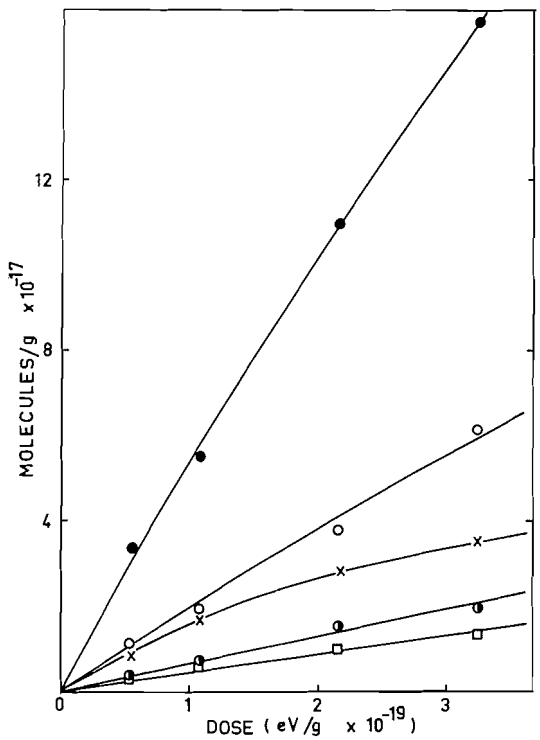

FIG. 3. The dose dependence of the product yields in the system ethane/3 mol% sulfurhexafluoride: (●), hydrogen; (○), *n*-butane; (×), ethylene; (□), propane; (◑), methane. (0.052 g cc^{-1} ethane).

of increasing ammonia-d_3 concentration on product yields at 0.051 and 0.25 g cc^{-1}, respectively. The effect of ammonia-d_3 over the whole density range was studied at an arbitrary concentration of 5 mol% (Fig. 10).

Table 1 shows the yields of products in the

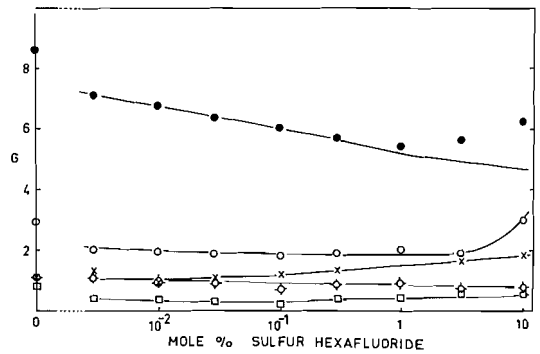

FIG. 4. The effect of sulfurhexafluoride on the yields of products from ethane at 0.052 g cc^{-1}: (●), hydrogen; (○), *n*-butane; (×), ethylene; (□), propane; (◇), methane; the curve drawn through the hydrogen points is calculated as described in the text; dose = 1 × 10^{19}eV g^{-1}.

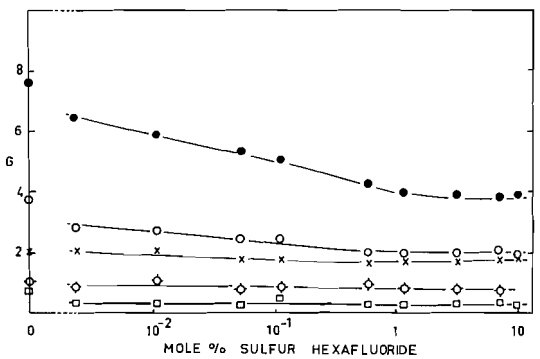

FIG. 5. The effect of sulfurhexafluoride on the yields of products from ethane at 0.275 g cc^{-1}: (●), hydrogen; (○), *n*-butane; (×), ethylene; (□), propane; (◇), methane; the curve drawn through the hydrogen points is calculated as described in the test; dose = 1 × 10^{19}eV g^{-1}.

presence of both electron and positive ion scavengers.

Discussion

4·2 ion–electron pairs are produced for every 100 eV of energy absorbed in gaseous ethane (18). We assume that this value holds with increasing density. At the lowest density we employ (0.0018 g cc^{-1} *i.e.* 1100 Torr) there will be gas phase behavior *i.e.* essentially no geminate ions and charge neutralization occurring with a rate constant of 10^{-5} – 10^{-7} cc ions^{-1} s^{-1} (5, 6). Equating the rate of formation of ions to their rate of disappearance at our dose rate of 2.8 × 10^{16} eV g^{-1} s^{-1} yields a half life for an ion of about

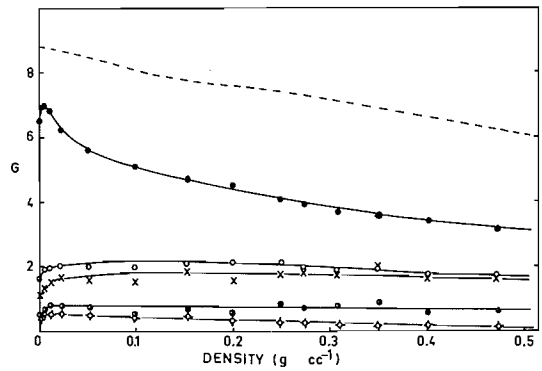

FIG. 6. The effect of density on product yields in the system ethane/3 mol% sulfurhexafluoride: (●), hydrogen; (○), *n*-butane; (×), ethylene; (◇), propane; (◑), methane; the broken line represents the hydrogen yield in the absence of scavenger; dose = 1×10^{19}eV g^{-1}.

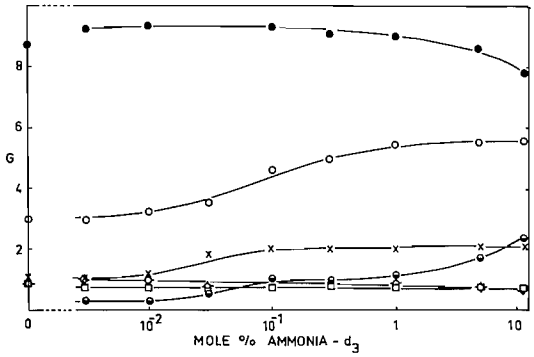

FIG. 8. The effect of ammonia-d_3 on the yields of products from ethane at 0.051 gm cc^{-1}: (●), H_2 (◒), HD; (○), *n*-butane; (×), ethylene; (□), propane; (◇), methane; dose = 1.4×10^{19}eV g^{-1}.

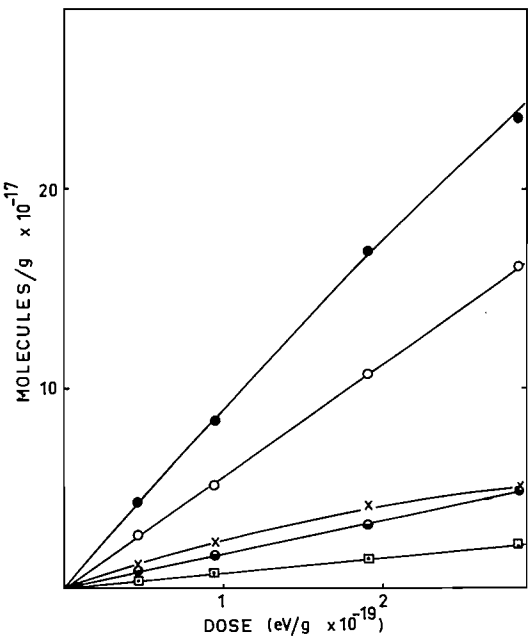

FIG. 7. The dose dependence of the product yields in the system ethane/5 mol% ammonia-d_3: (●), H_2; (◒), HD; (○), *n*-butane; (×), ethylene; (□), propane; (·), methane. (0.051 g cc^{-1} ethane).

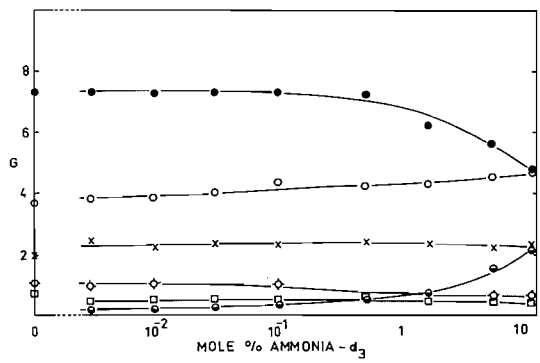

FIG. 9. The effect of ammonia-d_3 on the yields of products from ethane at 0.25 g cc^{-1}: (●), H_2; (◒), HD; (○), *n*-butane; (×), ethylene; (□), propane; (◇), methane; dose = 0.93×10^{19}eV g^{-1}.

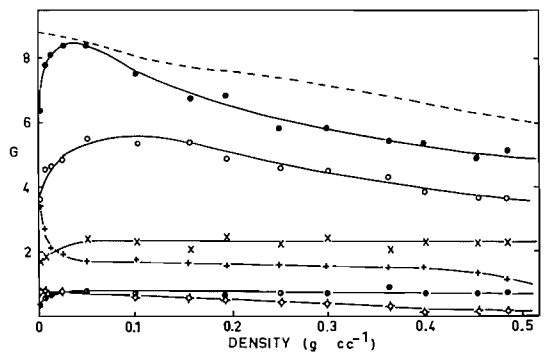

FIG. 10. The effect of density on product yields in the system ethane/5 mol% ammonia-d_3: (●), H_2; (+), HD; (○), *n*-butane; (×), ethylene; (◇), propane; (◑), methane; the broken line represents the hydrogen yield in the absence of scavenger; dose = 0.93×10^{19} eV g^{-1}.

10^{-4} s. This half life for homogeneous combination decreases by 1/density for the same dose rate with increasing density if the rate constant is independent of density. With increasing density geminate combination will become significant and the much decreased half life of geminate ion pairs will increase the probability of neutralization before secondary reactions can occur.

TABLE 1. Ethane radiolysis in the presence of 5 mol% ND_3 and 3 mol% SF_6 (1×10^{19}eV g^{-1})

Density (g cc^{-1})	$G(H_2)$	$G(HD)$	$G(CH_4)$	$G(C_2H_4)$	$G(C_3H_8)$	$G(nC_4H_{10})$
0.05	4.85	0.15	0.43	1.92	0.54	3.07
0.25	3.79	0.15	1.00	2.05	0.33	3.26
0.49	2.67	0.11	0.76	1.92	0.28	3.95

TABLE 2. G values for products from the radiolysis of ethane at low density

	G value	
Product	This work (1.8×10^{-3}g cc^{-1}, 313 °K)	Reference 16 (9.6×10^{-4}g cc^{-1}, 298 °K)
Hydrogen	8.7	8.8
Butane	2.5	2.5
Ethylene	1.2	2.0*
Propane	0.75	~0.8
Methane	0.75	0.39

*Contains nitric oxide.

Ausloos and co-workers (10, 19) and Bennet, Lias, and Field (20) have shown that the predominant reaction of the major ions produced in ethane at pressures up to 5 Torr is condensation with the parent molecule.

[1] $C_2H_6^+ + C_2H_6 \rightarrow (C_2H_6)_2^+$ $k \sim 10^{-10}$ cc molecule^{-1} s^{-1}

[2] $C_2H_5^+ + C_2H_6 \rightarrow C_4H_{11}^+$ $k \sim 10^{-10}$ cc molecule^{-1} s^{-1}

[3] $C_2H_4^+ + C_2H_6 \rightarrow C_4H_{10}^+$ $k \sim 10^{-11}$ cc molecule^{-1} s^{-1}

The half-life of an ion with respect to such a reaction is $1/k[C_2H_6]$ *i.e.* $\sim 3 \times 10^{-10}$ s for the $C_2H_6^+$ and $C_2H_5^+$ ions and $\sim 3 \times 10^{-11}$ s for the $C_2H_6^+$ ions at 0.0018 g cc^{-1}. These values will decrease with increasing density. Therefore all free ions will take part in condensation reactions prior to neutralization and the products should be amenable to scavenging by low concentrations ($< 10^{-4}$ M) of efficient scavengers. Higher concentrations will be required to compete with geminate charge combination.

Pure Ethane

The overall trends in the yields of hydrogen, butane, and ethylene with increasing density are in agreement with those of Wodetzki, McCusker, and Peterson (9). The yields at 0.0018 g cc^{-1} (1100 Torr) are in good agreement with those of Yang and Gant (16) obtained at 600 Torr (Table 2) which shows that there is little effect of pressure on overall yields over this pressure range. Their high ethylene yield was obtained in the presence of 6 mol% nitric oxide; as discussed previously complications can occur with this additive.

As is usual in gas phase radiolysis of hydrocarbons the mass balance of the products is poor. It does improve with increasing density *e.g.* at 1×10^{19} eV g^{-1} the values are $C_2H_{6.9}$, $C_2H_{6.7}$, and $C_2H_{6.24}$ at 0.0018, 0.10, and 0.52 g cc^{-1} respectively. The missing carbon rich products were not identified. Acetylene and a product with a chromatographic retention time equal to that of butene-1 were found in such small yields ($G \sim 0.1$) that their dose dependences could not be determined. The ethylene yield shows the greatest departure from linearity with dose and the poor mass balance will be in part related to this behavior. The better mass balance with increasing density may be related to decreasing primary fragmentation of the ethane ion, leading to increased ethyl radical and ethylene yields via neutralization of ethane ions ($C_2H_6^+$ or $(C_2H_6)_2^+$). This collisional stabilization is indicated by the increase in *n*-butane yields with increasing density which is accompanied by decreases in the hydrogen, methane, and propane yields. At 0.529 g cc^{-1} the product yields are almost identical to

those estimated for liquid ethane at 195 °K (14) leading to the conclusion that phase density is more important than temperature in defining the radiolytic reaction path.

Ethane Plus Sulfurhexafluoride

Sulfurhexafluoride scavenges electrons with high efficiency in the gas phase ($k_{e+SF_6} = 10^9 - 10^{10}$ Torr^{-1} s^{-1}) (21) and charge scavenging in liquid hydrocarbons is at or near the diffusion controlled rate (22). The products of reaction of the sulfurhexafluoride anion with hydrocarbon cations are not known but they apparently do not include hydrogen. $\Delta G(H_2)$ may therefore be equated to the number of electrons scavenged if the efficiency of hydrogen production per neutralization event in the absence of scavenger is known.

At 0.275 g cc^{-1} with high sulfurhexafluoride concentration $\Delta G(H_2) = 3.9$ and we may therefore assume unit efficiency of H_2 formation for ion–electron combination. An empirical expression which accurately fits scavenging curves for irradiated liquid hydrocarbons is (13)

$$[I] \qquad \Delta G(H_2) = G_{fi} + \frac{G_{gi}\sqrt{\alpha c}}{1 + \sqrt{\alpha c}}$$

where G_{fi} and G_{gi} are the yields of free and geminate ion pairs respectively, c is the molar concentration of scavenger and α is a constant for a given hydrocarbon/scavenger system which describes the competition between ion scavenging and geminate ion recombination. For ethane $G_{fi} + G_{gi} = 4.2$. The experimental $G(H_2)$ values shown in Fig. 5 for 0.275 g cc^{-1} and the $\Delta G(H_2)$ values for the same results in Fig. 11 are fitted well by expression I when $G_{fi} = 0.65$ and $\alpha =$ 130 M^{-1}. There are no comparable results reported for low density hydrocarbons but the free ion yield may be compared with values obtained for ethane at much lower temperatures and higher densities.

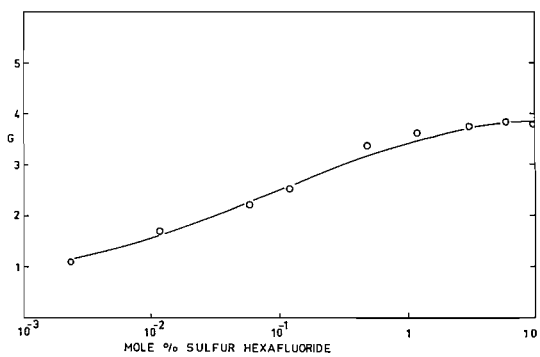

FIG. 11. The decrease in $G(H_2)$ upon the addition of sulfurhexafluoride to ethane at 0.275 g cc^{-1}; dose = 1×10^{19} eV g^{-1}.

Schmidt and Allen (23) find that the probability P that an electron ion pair will escape geminate combination is given by

$$[II] \quad P = \frac{G_{fi}}{G_{fi} + G_{gi}} = \left(\frac{4}{\pi^{1/2}}\right) \times \int_0^\infty \left(\frac{r}{b}\right)^2 \exp\left(-\left(\frac{r}{b}\right)^2 - \left(\frac{r_c}{r}\right)\right) dr$$

Where r_c is the critical distance at which the potential energy of the ion–electron pair is equal to the thermal energy kT and b is the most probable value of the ion–electron distance r at thermalization. From the plot of P *vs.* (b/r_c) given in ref. 24, for $G_{fi} = 0.65$ *i.e.* $P = 0.155$, $(b/r_c) = 0.48$. Using the Debye equation (24) the calculated dielectric constant ε for ethane at 0.275 g cc^{-1} is 1.33 and hence $r_c = e^2/\varepsilon kT = 4.0 \times 10^{-6}$ cm at 313 °K; hence $b = 1.93 \times 10^{-6}$ cm. Schmidt and Allen (23) suggest that bd, where d is the density, remains constant for a given liquid hydrocarbon but Robinson, Fuochi, and Freeman (25) have shown that for the lower hydrocarbons and olefins bd decreases with increasing temperature. From conductance experiments they obtain bd values of 81, 69, and 65 $\times 10^{-8}$ g cm^{-2} for liquid ethane (density 0.63–0.55 g cc^{-1}) at temperatures of 120, 148, and 183 °K respectively. Extrapolation of these bd values to 313 °K cannot be made with confidence but we may conclude that a value of 53 $\times 10^{-8}$ g cm^{-2} at 313 °K is reasonable. Decreasing density therefore leads, as expected, to an increased yield of free ions and a larger average distance at which thermalization occurs.

At 0.052 g cc^{-1} sulfurhexafluoride causes a considerable reduction in $G(H_2)$ but a quantitative interpretation of its dependence on solute concentration is not possible. The maximum decrease in $G(H_2)$ is 3.3 which occurs at 1 mol% solute. Above this concentration $G(H_2)$ increases again, a behavior not observed at 0.275 g cc^{-1}. At these high concentrations the electron fraction of sulfurhexafluoride is very high (*e.g.* 10 mol% is 30 electron%) so that considerable primary ionization of the solute will occur. The ionization potential of sulfurhexafluoride (~15.4 eV (26)) is much higher than that of ethane (~11.5 eV) so

that charge transfer to form an electronically excited ethane ion which subsequently decomposes is energetically possible. The concurrent increase in G(butane) would suggest decomposition to either an ethyl radical ion and H atom or to hydrogen and an ethylene ion which subsequently gives $C_4H_{10}^+$ via reaction 3. The absence of an increase in $G(H_2)$ at high sulfurhexafluoride concentrations at 0.275 g cc^{-1} must be ascribed to collisional deactivation of the excited $C_2H_6^+$ followed by neutralization by SF_6^-.

If unit efficiency is assumed for hydrogen formation from ion–electron combination at 0.052 g cc^{-1} the experimental $G(H_2)$ points below 1 mol% sulfurhexafluoride are reasonably well fitted by expression I with $G_{fi} = 1.1$ and $G_{gi} = 3.1$ (Fig. 4). P is therefore 0.26 and $b/r_c = 0.7$. The calculated dielectric constant is 1.06 leading to $r_c = 5.04 \times 10^{-6}$ cm, $b = 350$ Å and $bd = 18 \times 10^{-8}$ g cm^{-2} *c.f.* 53×10^{-8} g cm^{-2} at 0.275 cc^{-1}. If however it is assumed that the latter value of bd applies at the lower density then $b = 10.2 \times 10^{-6}$ cm, $b/r_c = 2.02$ and from expression 5 $P = 0.60$ *i.e.* $G_{fi} = 2.5$ and $G_{gi} = 1.7$. This is a minimum value for G_{gi} since it is exactly equal to the maximum value of $\Delta G(H_2)$ and some geminate ions will be scavenged at 3×10^{-3} mol% sulfurhexafluoride. G_{fi} therefore lies in the range 1.1 to 2.5 at 0.052 g cc^{-1} and the distribution of ion–electron distances at thermalization appears to maximize at a lower value than is predicted by the simple gaussion expression II.

At 0.275 g cc^{-1} and the lowest concentration of sulfurhexafluoride employed $\Delta G(H_2) = 1.12$ which is attributable to free ions and the longest lived geminate ions. At the same time ΔG(butane) = 1.0 and ΔG(propane) = 0.3 while there is no change in the measured ethylene yield. Similar considerations apply at 0.052 g cc^{-1}. The long lived ions therefore yield mainly butane and propane subsequent to neutralization. This is consistent with the formation of dimer ions via reactions 1–3 but is not conclusive evidence for their presence. Indeed it appears that the butane is formed mainly by the dimerization of ethyl radicals since the addition of a small amount of deuterium sulfide (0.1 mol%) as radical scavenger almost completely eliminates the formation of butane ($G = 0.4$). Neutralization of the long lived ions may therefore yield ethyl radicals. An alternate explanation of the above result would involve charge exchange with D_2S

[4] $$(C_2H_6)_2^+ + D_2S \rightarrow 2C_2H_6 + D_2S^+$$

We do not favor this mechanism since the yield of D_2 is negligibly small ($\sim$0.05). The short lived ions would produce D_2 via the suggested neutralization (27).

[5] $$D_2S^+ + e \rightarrow D_2 + S$$

while the longer lived ones would react with D_2S to form D_3S^+ or $D_5S_2^+$ which would still produce D_2 or a D atom which would be scavenged by D_2S to yield D_2.

At least 50% of the propane yield has long lived ionic precursors, the remainder being little affected by increasing scavenger concentration. The butane yield also decreases to a small extent after the first addition of sulfurhexafluoride. This illustrates the present lack of knowledge of the secondary reactions which occur after neutralization by SF_6^-. For example Bansal and Schuler (28) find that electron scavenging by sulfurhexafluoride in liquid cyclohexane does not affect the yield of cyclohexyl radicals whereas Sagert and Blair (29) find that the normal products of radical combination and disproportionation are reduced in yield. In the present work formation of butane and propane subsequent to neutralization of hydrocarbon cations by SF_6^- cannot be ruled out.

$G(H_2)$ attains a minimum value at $\sim$3 mol% sulfurhexafluoride and Fig. 6 shows that at this concentration the maximum $\Delta G(H_2)$ occurs around 0.3 g cc^{-1}. Electron scavenging must be most efficient at the lowest densities and hence some ion–electron combinations do not lead to hydrogen production. At 0.0018 g cc^{-1} $\Delta G(H_2) = 2.4$ implying that only $\sim$60% of the ions yield H_2 upon neutralization. This is confirmed by ammonia-d_3 scavenging (see later). The ions that do not lead to hydrogen production are probably acetylenic or olefinic ones which take part in "polymer" formation as suggested by the poor carbon/hydrogen balance. With increasing density G(butane) and G(ethylene) increase as collisional stabilization occurs. The increase in $\Delta G(H_2)$ is due to the presence of more molecular ions. There is no readily available explanation for the maximum in the $G(H_2)$ curve at very low density.

$\Delta G(H_2)$ decreases at the highest densities probably due to a combination of events including less efficient scavenging of very short-lived geminate electrons and collisional stabilization of molecular excited states formed either directly or by ion–electron combination.

The almost complete elimination of propane formation at the highest densities rules out a major contribution to its formation from the insertion of methylene radicals formed from nonionic states as has been suggested to occur at lower densities (7). The carbon/hydrogen balance is, as usual, much better at the higher densities although an improvement is noted at low densities over the results obtained in the absence of scavenger. No new products were observed in this system.

Ethane plus Ammonia-d_3

The HD formed when ammonia-d_3 is used as an ion scavenger is believed to arise by exothermic proton transfer (2)

[6] $$MH^+ + ND_3 \rightarrow M\cdot + NHD_3^+$$

[7a] $$NHD_3^+ + e \rightarrow NHD_2 + D\cdot$$

[7b] $$\rightarrow ND_3 + H\cdot$$

[8] $$D\cdot(H\cdot) + MH \rightarrow HD(H_2) + M\cdot$$

G(ions scavenged) is given by 4/3 G(HD) if there is no isotope effect in reaction 7 as appears to be true in liquid cyclohexane (30). With the proton affinity of ammonia taken as 205 kcal mol^{-1} (31) proton transfer is exothermic in the gas phase for $C_4H_{10}^+$, $C_4H_9^+$, $C_3H_8^+$, $C_3H_7^+$, $C_2H_6^+$, $C_2H_5^+$, $C_2H_4^+$, $C_2H_3^+$, and $C_2H_2^+$. Since $(C_2H_6)_2^+$ is thermally unstable with respect to dissociation to $C_2H_6^+$ and C_2H_6 (20) the recombination energy of $(C_2H_6)_2^+$ can be only slightly smaller than that of $C_2H_6^+$ and it too should react with ammonia.

The changes in yields with density observed in the presence of 5 mol% ammonia-d_3 (Fig. 10) are difficult to explain on the basis of the above reaction scheme. If G(ions scavenged) is taken as 4/3 G(HD) then G(HD) = 3.4 at 0.0018 g cc^{-1} represents more ions scavenged than the total ion yield. (A similar observation was made for the gaseous system methylcyclohexane/ammonia-d_3 (32)). Also in the intermediate density region (0.01–0.2 g cc^{-1}) the n-butane yields are much higher than expected. The maximum increase of 2.5 occurs at 0.07 g cc^{-1}. The maximum increase expected on the basis of the above mechanism would be 4/3 G(HD) = 2.4 which assumes that each ion scavenged gives one C_2H_5 radical and the resulting D· or H· another and that none of the ions scavenged normally leads to butane formation. However the SF_6 results (Figs. 4 and 5) show that at least 1 G of scavengeable ions lead to butane formation. The excess butane at 0.07 g cc^{-1} is therefore at least 1 G.

The following mechanism can qualitatively explain the observed yields and is consistent with the known radiolytic behaviour of ammonia.

(i) At low density (~0.002 g cc^{-1})

[9] $$ND_3H^+ + ND_3 \rightarrow ND_4^+ + ND_2H$$

[10] $$ND_4^+ + nND_3 \rightarrow ND_4(ND_3)_n^+$$

[11] $$ND_4(ND_3)_n^+ + e \rightarrow (n+1)ND_3 + D\cdot$$

(ii) At higher densities

[12a] $$ND_3H^+ + e \rightarrow ND_2H^* + D\cdot$$

[12b] $$\rightarrow ND_3^* + H\cdot$$

[13a] $$ND_2H^* \rightarrow \cdot ND_2(NDH) + H\cdot(D\cdot)$$

[13b] $$\xrightarrow{M} ND_2H$$

[14a] $$ND_3^* \rightarrow \cdot ND_2 + D\cdot$$

[14b] $$\xrightarrow{M} ND$$

The exchange reaction (9) has been observed mass spectrometrically (33) and has been suggested to occur in the gas phase radiolysis (32) with an estimated rate constant of $\sim 10^{12}$ l mol^{-1} s^{-1} (33). At 0.0018 g cc^{-1} and 5 mol% ammonia-d_3 this reaction will be essentially complete before neutralization occurs. The clustering reaction (10) has been observed in pure ammonia (34). We propose that this reaction can occur at low density in the ethane/5 mol% ammonia-d_3 system and thereby dissipate some of the neutralization energy so that only one D·(H·) is produced per ion scavenged. This mechanism appears to operate in the radiolysis of pure gaseous ammonia (35). Thus at 0.0018 g cc^{-1} we postulate that G(HD) is a direct measure of proton transfer to ammonia-d_3. $\Delta G(H_2)$ at this density is 2.4, the same value obtained with 3 mol% sulfurhexafluoride, indicating that scavenging is complete. Thus there must remain 4.2 − 3.4 = 0.8 G units of charge which cannot be scavenged by ammonia-d_3 in a reaction sequence leading to HD formation. A possibility is a condensation type reaction such as has been observed for CH_3^+ (36).

At increased density geminate recombination will compete with the exchange and clustering reactions and the neutralization reaction (12) will assume importance. The increased n-butane yields can now be explained by further decompo-

sition of excited ammonia to yield $\cdot ND_2$ and D·(H·) radicals which can both form ethyl radicals by abstraction (37). G(proton transfer) will be approximated by G(HD) as the probability of an H· from the double elimination is 0.5 in the absence of an isotope effect. These reactions producing two hydrogen atoms have been proposed in the radiolysis of gaseous ammonia (38) but have been discarded in favor of the cluster mechanism. At high density the excited ammonia will be collisionally stabilized, only one hydrogen atom will be produced and the liquid phase situation of G(proton transfer) = 4/3 G(HD) will pertain.

G(HD) is constant for 5 mol% ammonia-d_3 from 0.05 to 0.4 g cc^{-1} which superficially would indicate a constant scavenging efficiency over this density range. The situation however is much more complex. As the density increases the number of geminate ion pairs will increase and hence the efficiency of scavenging will decrease. However, a constant 5 mol% of ammonia-d_3 means an increasing molar concentration which at constant density would imply increased scavenging efficiency. With increasing density the mobility of scavenger and scavengeable ions will decrease leading to reduced scavenging efficiency. The net result of all these effects is the constancy of G(HD).

The rapid rise in $G(H_2)$ to a value equal to that in the absence of ammonia-d_3 at 0.05 g cc^{-1} is accommodated by the above mechanism if, in this density region, clustering has become minimal and collisional deactivation of excited ammonia is still ineffective in preventing the formation of two hydrogen atoms (H· or D·) per ion scavenged. Comparison of the $G(H_2)$ curve with that for pure ethane suggests that collisional deactivation has become significant at 0.1 to 0.15 g cc^{-1}.

The presence of 3 mol% sulfurhexafluoride almost completely eliminates the production of HD while $G(H_2)$ is decreased to values close to those obtained with the electron scavenger alone (Table 1 and Fig. 6). The yield of butane is larger than in the presence of sulfurhexafluoride alone but at 0.05 and 0.25 g cc^{-1} is less than that for the 5% ammonia-d_3/ethane system. This is as expected since proton transfer from the molecular ion to yield an ethyl radical still occurs.

From Figs. 8 and 9 it is obvious that extrapolation of G(HD) to low concentrations of ammonia-d_3 does not give the expected yield of free ions. Certainly the yield is higher at the lower density as expected but at both densities the magnitude is about four times less than that estimated from the sulfurhexafluoride results. Either the free ions are not scavenged by ammonia-d_3 or, if they are, the expected products do not appear. At 0.25 g cc^{-1} the propane yield is reduced considerably by the very lowest concentration of ammonia-d_3 but at 0.05 g cc^{-1} it is little affected. There is no change in the butane yield at this point at either density which is not significant since, as the sulfurhexafluoride results showed, the easily scavenged ions are precursors mainly of butane.

The HD yields cannot be fitted by expression I, an observation that was also made for ion scavenging by neopentane-d_{12} in ethane at 0.25 g cc^{-1} (39). Exchange of the ammonia-d_3 with adventitious water cannot be ruled out although every precaution was taken against this possibility. The ethane was purified by distillation off molecular sieve at 198 °K and stored under pressure. The gas handling line was saturated with D_2O and then flamed under vacuum. Samples were prepared in random order of concentration and reasonably smooth curves of G(HD) against concentration were obtained (Figs. 8 and 9). The step in the curve in Fig. 9 does not appear to be an experimental artefact since it also appears in the curves for butane and ethylene but not in those of the other products. Experiments with other positive ion scavengers are obviously required to help elucidate the nature of the free ions in this system.

Conclusion

Sulfurhexafluoride and ammonia-d_3 scavenge electrons and positive ions respectively in ethane over a range of densities. The interpretation of the results of this scavenging at low ($\sim$0.002 g cc^{-1}) and high ($\sim$0.5 g cc^{-1}) density is consistent with our knowledge of gas phase and liquid phase hydrocarbon radiolysis. At intermediate densities the interpretation is not straightforward and work with more specific ion scavengers is required. The concept of decreased molecular fragmentation with increasing density is consistent with the results of this study.

The authors thank the National Research Council of Canada for financial assistance.

1. Robert H. Schuler, and Pierre P. Infelta. J. Phys. Chem. **76**, 3812 (1972).
2. F. Williams. J. Am. Chem. Soc. **86**, 3954 (1964).
3. G. R. Freeman. J. Chem. Phys. **46**, 2822 (1967).

4. A. HUMMEL. J. Chem. Phys. **49**, 4840 (1968).
5. R. C. GUNTON and T. M. SHAW. Phys. Rev. **140**, A759 (1965).
6. D. E. WILSON and D. A. ARMSTRONG. J. Phys. Chem. **75**, 444 (1971).
7. H. H. CARMICHAEL, R. GORDON, JR., and P. AUSLOOS. J. Chem. Phys. **42**, 343 (1965).
8. C. M. WODETZKI, P. A. MCCUSKER, and D. B. PETERSON. J. Phys. Chem. **69**, 1045 (1965).
9. C. M. WODETZKI, P. A. MCCUSKER, and D. B. PETERSON. J. Phys. Chem. **69**, 1056 (1965).
10. P. AUSLOOS, R. E. REBBERT, and L. WAYNE SIECK. J. Chem. Phys. **54**, 2612 (1971).
11. T. MIYAZAKI. J. Phys. Chem. **71**, 4282 (1967).
12. T. MIYAZAKI and S. SHIDA. Bull. Chem. Soc. Jap. **37**, 1352 (1964).
13. K.-D. ASMUS, J. M. WARMAN, and R. H. SCHULER. J. Phys. Chem. **74**, 246 (1970).
14. P. T. HOLLAND and J. A. STONE. Can. J. Chem. **48**, 1078 (1970).
15. P. J. DYNE and J. A. STONE. Can. J. Chem. **39**, 2381 (1961).
16. K. YANG and P. L. GANT. J. Phys. Chem. **65**, 1561 (1961).
17. P. T. HOLLAND. Ph.D. Thesis. Queen's University, 1970.
18. G. G. MEISELS. J. Chem. Phys. **41**, 51 (1964).
19. S. K. SEARLES, L. WAYNE SIECK, and P. AUSLOOS. J. Chem. Phys. **53**, 849 (1970).
20. S. L. BENNET, S. G. LIAS, and F. H. FIELD. J. Phys. Chem. **76**, 3919 (1972).
21. L. G. CHRISTOPHOROU. J. Phys. Chem. **76**, 3730 (1972).
22. GEORGE W. KLEIN and ROBERT H. SCHULER. J. Phys. Chem. **77**, 978 (1973).
23. W. F. SCHMIDT and A. O. ALLEN. J. Phys. Chem. **72**, 3730 (1968).
24. G. M. BARROW. Physical chemistry. 2nd ed. McGraw–Hill. 1966. p. 432.
25. M. G. ROBINSON, P. G. FUOCHI, and G. R. FREEMAN. Can. J. Chem. **49**, 3657 (1971).
26. D. C. FROST, C. A. MCDOWELL, J. S. SANDHU, and D. A. BROOM. Adv. Mass Spectrom. **4**, 781 (1968).
27. G. MEISSNER and A. HENGLEIN. Ber. Bunsenges Phys. Chem. **69**, 264 (1965).
28. K. M. BANSAL and R. H. SCHULER. J. Phys. Chem. **74**, 3924 (1970).
29. N. H. SAGERT and A. S. BLAIR. Can. J. Chem. **45**, 1351 (1967).
30. K.-D. ASMUS. Int. J. Radiat. Phys. Chem. **3**, 419 (1971).
31. J. W. D. CONNOLLY and K. H. JOHNSON. Chem. Phys. Lett. **10**, 616 (1971).
32. W. J. HOLTSLANDER and G. R. FREEMAN. Can. J. Chem. **45**, 1649 (1967).
33. M. S. B. MUNSON and F. H. FIELD. J. Am. Chem. Soc. **87**, 4242 (1965).
34. A. HOGG and P. KEBARLE. J. Chem. Phys. **43**, 449 (1965).
35. C. WILLIS, A. W. BOYD, and O. J. MILLER. Can. J. Chem. **47**, 3007 (1969).
36. W. T. HUNTRESS and D. D. ELLMAN. J. Am. Chem. Soc. **92**, 3565 (1970).
37. M. NISHIKAWA, K. KUROTA, and N. MATSURA. Bull. Chem. Soc. Jap. **42**, 116 (1962).
38. A. ANDERSON and J. WINTER. *In* The chemistry of ionization and excitation. *Edited by* G. R. A. Johnson and G. Scholes. Taylor and Francis, London. 1967. p. 197.
39. G. MATSUSHITA and J. A. STONE. Can. J. Chem. **49**, 3287 (1971).

Titanium(IV) Chloro- Derivatives of Strong Monobasic Acids

J. R. DALZIEL, R. D. KLETT, P. A. YEATS, AND F. AUBKE[1]

Department of Chemistry, The University of British Columbia, Vancouver 8, British Columbia

Received June 6, 1973

The interaction of the monobasic protonic acids HSO_3F, HSO_3CH_3, HPO_2F_2, and HCO_2CF_3 with titanium(IV) chloride at room temperature is studied with either the acid or the metal halide in excess. Whereas with the acid in excess products of the type $TiCl_2Y_2$, with Y = oxyacid group, are formed, the excess of $TiCl_4$ results in the formation of $TiCl_{3.33}(SO_3F)_{0.66}$, $TiCl_3SO_3CH_3$, and again $TiCl_2(PO_2F_2)_2$ and $TiCl_2(CO_2CF_3)_2$.

The first two compounds are also obtained by ligand redistribution reactions with $TiCl_4$ in excess, *e.g.*

$$TiCl_2(SO_3CH_3)_2 + TiCl_4 \xrightarrow{25\,^\circ C} 2TiCl_3SO_3CH_3$$

in quantitative yield.

Vibrational spectra for the PO_2F_2, SO_3F and the previously reported SO_3CF_3 derivatives are interpreted in terms of hexacoordinated titanium and generally bi- or tridentate oxyacid groups. In $TiCl_{3.33}(SO_3F)_{0.66}$ evidence for a highly unusual tetradentate SO_3F group is presented, where coordination to titanium involves all three oxygens as well as fluorine.

L'interaction des acides protoniques monobasiques, HSO_3F, HSO_3CH_3, HPO_2F_2 et HCO_2CF_3 avec le chlorure de titane(IV) a été étudiée à température ambiante en employant soit l'acide, soit l'halogénure métallique en excès.

Lorsque l'acide est en excès, on note la formation de produits du type $TiCl_2Y_2$ où Y = groupe oxyacide; par contre, l'excès de $TiCl_4$ conduit à la formation de $TiCl_{3.33}(SO_3F)_{0.66}$, de $TiCl_3SO_3CH_3$, de $TiCl_2(PO_2F_2)_2$ et de $TiCl_2(CO_2CF_3)_2$.

Les deux premiers composés sont aussi obtenus quantitativement à l'aide de réactions de redistribution du coordinat en présence d'un excès de $TiCl_4$, *e.g.*

$$TiCl_2(SO_3CH_3)_2 + TiCl_4 \xrightarrow{25\,^\circ C} 2TiCl_3SO_3CH_3$$

Les spectres de vibration des dérivés PO_2F_2-, SO_3F- et SO_3CF_3-, lequel a déjà été rapporté, sont interprétés en fonction de titanium hexacoordonné et de groupes oxyacides généralement bi ou tricoordonnés. Dans le $TiCl_{3.33}(SO_3F)_{0.66}$, on met en évidence la présence d'un groupe SO_3F tétracoordonné assez inhabituel où la coordination du titanium implique les trois oxygènes ainsi que le fluor.

[Traduit par le journal]

Can. J. Chem., **52**, 231 (1974)

Introduction

There are a number of reports (1–6) on the interaction of titanium(IV) chloride with strong monobasic protonic acids, indicating substitution of Cl by the acid group Y according to

[1] $$TiCl_4 + nHY \rightarrow TiCl_{(4-n)}Y_n + nHCl$$

It appears that the degree of substitution depends on the mole ratio of reactants as well as on the reaction temperature. Complete substitution seems to occur only in the reaction of $TiCl_4$ with anhydrous HF (1, 2). Generally incomplete substitution and the formation of well defined mixed titanium(IV) chloride derivatives occurs as *e.g.* in the system $TiCl_4$–HSO_3CF_3, first investigated by Noftle and Cady (3). At room temperature a slight excess of trifluoromethane sulfonic acid will result in the formation of $TiCl_2(SO_3CF_3)_2$, while with $TiCl_4$ in excess only $TiCl_3SO_3CF_3$ is formed together with HCl. Trisubstituted $TiCl(SO_3CF_3)_3$ was formed (4) when an excess of acid was allowed to react for 16 h with $TiCl_4$ at 100 °C.

We have been interested for some time in tin(IV) chloro-derivatives of oxyacids (7–9), in particular fluorosulfates, and became interested in the related titanium(IV) compounds in the search for structural similarities. The ability of monobasic oxyacid groups to function as bidentate ligands with bonding through oxygen has been demonstrated for the tin(IV) compounds, and the tendency of titanium(IV) compounds to expand their coordination number, most frequently to six, is well documented (10). However all previous reports on titanium chloride sulfonates (3–6) did not include structural studies such as vibrational spectra.

[1]To whom correspondence should be addressed.

Can. J. Chem. Downloaded from www.nrcresearchpress.com by 210.87.254.6 on 09/05/12
For personal use only.

Can. J. Chem. Downloaded from www.nrcresearchpress.com by 210.87.254.6 on 09/05/12
For personal use only.

Because of the thermal instability of higher substituted titanium(IV) fluorosulfates (1), we restricted the study to mono- and disubstituted compounds of the general type $TiCl_3Y$ and $TiCl_2Y_2$, where Y is the monobasic acid group, which can all be synthesized without raising the temperature above 25 °C.

Again in analogy to observations on tin(IV) compounds (7, 9) we became interested in possible ligand exchange reactions of the type

$$[2] \qquad TiCl_2Y_2 + TiCl_4 \rightarrow 2TiCl_3Y$$

as additional synthetic routes. In the SO_3F system additional fluorosulfonating agents were found in $S_2O_6F_2$ (12*a*), $BrOSO_2F$ (12*b*), and $Sn(SO_3F)_4$ (1).

Experimental

Chemicals

Titanium(IV) chloride (Matheson, Coleman and Bell), sulfurylchloride (British Drug House), methanesulfonic acid (Aldrich Chemicals), trifluoromethanesulfonic acid (Minnesota Mining and Manufacturing Company), and trifluoroacetic acid (Eastman Kodak) were purified by repeated distillation at reduced pressures before use.

Technical grade fluorosulfuric acid (Baker and Adamson) was doubly distilled under atmospheric pressure as described before (13). Technical grade difluorophosphoric acid (Ozark–Mahoning Chemical Company) was purified after storing over P_2O_5 by repeated distillation at 100 mm Hg pressure in a Pyrex system (14). Peroxydisulfuryl difluoride (15), bromine(I) fluorosulfate (16), tin(IV) tetrakisfluorosulfate (7), and trimethyltin(IV) trifluoromethane sulfonate (4) all were prepared according to published methods. Both $TiCl_2(SO_3CF_3)_2$ and $TiCl_3SO_3CF_3$ were synthesized according to Noftle and Cady (3).

Instrumentation

Infrared spectra were recorded on a Perkin–Elmer 457 grating spectrophotometer. Silver chloride, cesium iodide, silver bromide, and KRS-5 windows (all from Harshaw Chemicals) were used either with Nujol or without any mulling agent.

Raman spectra on the solid samples were obtained with a Cary 81 spectrometer, equipped with a model 125 He–Ne gas laser (Spectra Physics Corp.). The 6328 Å wavelength line was used as exciting light. The samples were contained in 5 mm o.d. Pyrex tubes with flat bottoms.

All manipulations of solid materials were carried out in a Vacuum Atmosphere Corp. Dri-Lab model no. He-43-2 filled with purified dry nitrogen and equipped with Dri-Train model no. HE-93B. Volatile materials were handled in Pyrex vacuum lines fitted with Teflon stem stopcocks (Kontes glassware).

Reactions

All chloride substitution reactions were carried out in about 100 ml two part reaction flasks, fitted with Teflon coated stirring bars, Teflon stem stopcocks (Kontes glassware), and P_2O_5 guard tubes. Either the acid or titanium(IV) chloride was kept in excess. Reactions with HSO_3CH_3 and HSO_3F in a slight excess were performed in SO_2Cl_2 solution. The solid reaction-products were filtered in a dry atmosphere, using an apparatus described by Shriver (17), and washed with sulfuryl chloride.

The ligand redistribution reactions were carried out in reactors similar to those described above. An approximately 10–15 fold excess of $TiCl_4$ was added to the finely powdered substrate and stirred magnetically for about 1 h at room temperature. The excess $TiCl_4$ was removed by vacuum distillation and the course of the reaction was followed by weighing the reaction vessel before and after completing the reaction.

Reactions with either $S_2O_6F_2$ or $BrOSO_2F$ as reactants were carried out in one part reactors, fitted with Teflon coated magnetic stirring bars and Teflon stem stopcocks.

Analysis

All compounds are found to be yellow and extremely moisture sensitive. On heating at atmospheric pressure, decomposition often preceded by shrinking of the solid is observed.

Chloride was determined by volumetric titration with silver nitrate solution, using potentiometric endpoint detection. The quantitative determinations of titanium, sulfur, phosphorus, and fluorine were carried out by Alfred Bernhardt Microanalytical Laboratories, 5251 Elbach, West Germany. The results are listed below.

Anal. Calcd. for $TiCl_{3.3}(SO_3F)_{0.66}$: Ti, 20.60; S, 9.21; F, 5.46; Cl, 50.90. Found: Ti, 20.86; S, 9.48; F, 5.51; Cl, 50.77.

Anal. Calcd. for $TiCl_2(SO_3F)_2$ (dec. pt. = 108 °C): Ti, 15.11; S, 20.23; Cl, 22.37. Found: Ti, 15.38; S, 20.32; Cl, 22.40.

Anal. Calcd. for $TiCl_3SO_3CH_3$ (dec. pt. = 215 °C): Ti, 19.21; S, 12.86; Cl, 42.65. Found: Ti, 19.52; S, 12.75; Cl, 42.35.

Anal. Calcd. for $TiCl_2(SO_3CH_3)_2$ (dec. pt. = 205 °C): Ti, 15.50; S, 20.75; Cl, 22.95. Found: Ti, 15.64; S, 21.05; Cl, 23.05.

Anal. Calcd. for $TiCl_2(PO_2F)_2$ (dec. pt. = 195 °C): Ti, 14.93; P, 19.31; Cl, 22.11. Found: Ti, 15.16; P, 19.09; Cl, 21.90.

Anal. Calcd. for $TiCl_2(CO_2CF_3)_2$ (dec. pt. = 180 °C): Ti, 13.89; F, 33.06; Cl, 20.56. Found: Ti, 14.26; F, 32.91; Cl, 20.35.

Both $TiCl_3SO_3CF_3$ and $TiCl_2(SO_3CF_3)_2$ have been analyzed previously (3, 4). Their purity was checked by a chloride determination.

Listing of Vibration Frequencies

$TiCl_2(CO_2CF_3)_2$: i.r.; 1655 ms, sh, 1585 vs, b, 1480 vs, b, 1340 w, sh, 1235 m, sh, 1190 vs, b, 965 vw, sh, 870 ms, 835 m, sh, 790 ms, 745 ms, 720 s, 620 s, 555 vw, 520 ms, 470 ms, sh, 440 vs, b, 400 vs, 320 ms. Raman; 1650 m, sh, 1593 vs, 1497 m, 1350 w, 1230 w, sh, 1199 ms, 879 m, 835 ms, 791 m, 737 ms, 622 s, 558 s, 530 w, sh, 461 s, 443 s, 391 s, 350 vw, sh.

$TiCl_2(SO_3CH_3)_2$ (from 1500 cm^{-1} down): Raman; 1416 m, 1308 s, 1175 w, 1060 m, sh, 1016 w, sh, 1007 s, 968 s, 860 vw, 789 s, 566 w, 537 w, 500 m, 410 vs, 395 sh, 260 w.

$TiCl_3SO_3CH_3$ (from 1500 cm^{-1} down): Raman; 1406 m, 1337 w, 1215 m, 1145 s, sh, 1133 s, 1094 s, 977 m, 803 s, 576 mw, 566 w, 544 vw, 523 w, 500 w, 424 s, 410 s, 395 ms, 274 w.

TABLE 1. Ligand substitution reactions

No.	$TiCl_4$ (mmol)	Acid	Amount (mmol)	Solvent	T (°C)	Reaction product*
1	~45.0	HSO_3CH_3	15.4	None	0–25	$TiCl_3SO_3CH_3$
2	8.49	HSO_3CH_3	18.65	SO_2Cl_2	25	$TiCl_2(SO_3CH_3)_2$
3	~50.0	HSO_3F	10.5	None	0–25	$TiCl_{3.33}(SO_3F)_{0.66}$
4	15.47	HSO_3F	34.10	SO_2Cl_2	25	$TiCl_2(SO_3F)_2$
5	~50.0	HPO_2F_2	26.5	None	0–25	$TiCl_2(PO_2F_2)_2$
6	9.45	HPO_2F_2	20.8	SO_2Cl_2	0–25	$TiCl_2(PO_2F_2)_2$
7	~50.0	HCO_2CF_3	12.06	None	0–25	$TiCl_2(CO_2CF_3)_2$
8	8.03	HCO_2CF_3	20.2	SO_2Cl_2	25	$TiCl_2(CO_2CF_3)_2$

*Isolated by filtration. In all instances HCl was evolved.

Results and Discussion

Synthesis

The solvolysis of titanium(IV) chloride at room temperature or lower by monobasic protonic acids has been studied under two different conditions: (*a*) $TiCl_4$ was present in a large excess, acting as a reactant and diluting agent; (*b*) the acid was present in a slight excess over the amount required for disubstitution and SO_2Cl_2 was used as solvent. In all instances the reactions occurred very readily with evolution of gas and heat. Initial cooling to about −50 °C was required. Yellow precipitates were formed instantaneously, allowing separation either by removal of the excess $TiCl_4$ or by filtration. In all cases well defined products were obtained rather than mixtures, however, distinct differences became apparent depending on the type of acid. Details of these reactions are summarized in Table 1.

Substitution of HSO_3F by $BrOSO_2F$ or $S_2O_6F_2$ again yielded Cl_2 gas as well as $TiCl_{3.3}(SO_3F)_{0.66}$ when an excess of $TiCl_4$ was present. With a slight excess of $S_2O_6F_2$ at −20 °C only $TiCl_2(SO_3F)_2$ was formed. At higher temperatures $S_2O_6F_2$ is capable of further substitution, however, in contrast to the reaction of $SnCl_4$ with $S_2O_6F_2$ where at about 120 °C $Sn(SO_3F)_4$ is obtained (7), no well defined products could be isolated. Apparently thermal decomposition occurs.

Another route to $TiCl_{3.33}(SO_3F)_{0.66}$ was discovered when the above mentioned $Sn(SO_3F)_4$ was reacted with an excess of $TiCl_4$ at room temperature. Complete SO_3F group transfer according to

$$[3]\quad Sn(SO_3F)_4 + 6TiCl_4 \xrightarrow[1\ h/TiCl_4]{25\ °C} 6TiCl_{3.33}(SO_3F)_{0.66} + SnCl_4$$

was observed. The reaction appears to be a ligand redistribution reaction, very similar in respect to the reaction conditions to the reaction of $Sn(SO_3F)_4$ with $SnCl_4$ to give $SnCl_2(SO_3F)_2$ (7).

Further examples of such ligand redistribution reactions were subsequently observed. The transfer of a SO_3CF_3 group from tin to titanium is found in the reaction of $(CH_3)_3SnSO_3CF_3$ with $TiCl_4$

$$[4]\quad (CH_3)_3SnSO_3CF_3 + TiCl_4 \xrightarrow[1\ h/TiCl_4]{25\ °C} (CH_3)_3SnCl + TiCl_3SO_3CF_3$$

where trimethyltin(IV) chloride can be removed from the reaction mixture by vacuum sublimation. Also the exchange reactions between different titanium compounds were observed (6, 7).

$$[5]\quad TiCl_2(SO_3F)_2 + 2TiCl_4 \xrightarrow[1\ h/TiCl_4]{25\ °C} 3TiCl_{3.33}(SO_3F)_{0.66}$$

and

$$[6]\quad TiCl_2(SO_3CX_3)_2 + TiCl_4 \xrightarrow[1\ h/TiCl_4]{25\ °C} 2TiCl_3SO_3CX_3 \text{ with } X = F \text{ or } H.$$

Both $TiCl_2(CO_2CF_3)_2$ and $TiCl_2(PO_2F_2)_2$ did not undergo ligand scrambling under the conditions mentioned above. The starting materials could be recovered completely from the mixture. The reaction conditions for all ligand exchange reactions are summarized in Table 2. All compounds formed via ligand redistribution were found to be identical to those obtained by solvolysis or the interaction of $BrOSO_2F$ or $S_2O_6F_2$ with $TiCl_4$. Whereas both reactions 3 and 4 are undoubtedly ligand redistribution reactions between SO_3F or SO_3CF_3 on the one hand and Cl on the other as the migrating ligands, the remaining reactions 5 and 6 can also be regarded as

Can. J. Chem. Downloaded from www.nrcresearchpress.com by 210.87.254.6 on 09/05/12
For personal use only.

TABLE 2. Ligand redistribution reactions with titanium(IV) chloride at 25 °C

No.	Substrate	Amount (mmol)	Time (h)	Reaction products
1	$Sn(SO_3F)_4$	1.69	1.0	$TiCl_{3.33}(SO_3F)_{0.66}$, $SnCl_4$
2	$(CH_3)_3SnSO_3CF_3$	1.83	1.0	$TiCl_{3.33}(SO_3F)_{0.66}$, $(CH_3)_3SnCl$
3	$TiCl_2(SO_3CF_3)_2$	4.31	1.0	$TiCl_3SO_3CF_3$
4	$TiCl_2(SO_3CH_3)_2$	16.5	1.0	$TiCl_3SO_3CH_3$
5	$TiCl_2(SO_3F)_2$	29.9	20.0	$TiCl_{3.33}(SO_3F)_{0.66}$
6	$TiCl_2(PO_2F_2)_2$	15.3	24.0	No reaction
7	$TiCl_2(CO_2CF_3)_2$	18.2	24.0	No reaction

complex formation reactions with *e.g.* $TiCl_4$ as acceptor and $TiCl_2(SO_3CF_3)_2$ as oxygen donor ligand resulting in a complex of the type $TiCl_2(SO_3CF_3)_2 \cdot TiCl_4$. Such a formulation would imply two distinctively different environments for titanium.

Although a large number of $TiCl_4$ – oxygen donor complexes are reported (10, 18, 19), the closest analog $TiCl_4 \cdot 2SO_2Cl_2$ (20, 21) is thermally stable only below the melting point of −43.7 °C, quite different from our observations in this respect. Also, all redistribution reactions have precedents among tin(IV) and organotin(IV) compounds (7–9), where ^{119}Sn Mössbauer spectroscopy provides unambiguous evidence for true ligand redistribution. Additional evidence in favor of ligand scrambling will come from the vibrational spectra.

When comparing Tables 1 and 2, it becomes apparent that the conditions for both reaction types are very similar and that the reaction products have identical composition whenever $TiCl_4$ is present in a large excess. It can be concluded, that the observed diversity of the solvolysis reactions may arise from a combination of solvolysis and ligand redistribution reactions. So, for example, in the $TiCl_4$–HSO_3CF_3 system, initial solvolysis, producing possibly mono and disubstituted products, may be followed by a ligand redistribution, producing *only* $TiCl_3SO_3CF_3$. Alternative explanations for the observed differences in the solvolysis of $TiCl_4$ such as assuming subtle differences in the solvolyzing ability of the five acids employed are not very convincing.

A final comment remains to be made: the thermal decomposition of $TiCl_3SO_3CF_3$ to $TiCl_4$ and $TiCl_2(SO_3CF_3)_2$ described by Noftle and Cady (3) presents a reversal of the ligand redistribution reaction 6. Likewise $TiCl_3SO_3CH_3$ can be converted back into $TiCl_2(SO_3CH_3)_2$ with loss of $TiCl_4$ at 145 °C *in vacuo*. $TiCl_{3.33}(SO_3F)_{0.66}$ was found to be thermally stable up to +70 °C *in vacuo*, however the decomposition appears to be rather complex. No well defined products could be isolated as residues.

Vibrational Spectra

To simplify matters, the discussion will be restricted to the following compounds: (*a*) $TiCl_2(PO_2F_2)_2$, (*b*) $TiCl_2(SO_3CF_3)_2$ and $TiCl_3SO_3CF_3$, and (*c*) $TiCl_2(SO_3F)_2$ and $TiCl_{3.33}(SO_3F)_{0.66}$.

The observed Raman and i.r. frequencies for the remaining compounds are listed in the Experimental section.

Emphasis will be placed on the interpretation of absorption bands due to the monobasic acid groups, in particular the stretching modes, which should be indicative of the presence of ionic, mono- or polyfunctional groups. Additional interest centers around the occurrence of Ti—Cl stretching modes.

(a) $TiCl_2(PO_2F_2)_2$

The observed i.r. frequencies in the region of 2000–250 cm^{-1} and the Raman shifts are listed in Table 3 together with the estimated intensities. Also listed are frequencies reported for KPO_2F_2 (14, 21) and $(CH_3)_2Sn(PO_2F_2)_2$ (22) where bidentate bridging PO_2F_2-groups were postulated on the basis of vibrational and ^{119}Sn Mössbauer spectra. This is analogous to dimethyl tin(IV) derivatives of other monobasic oxyacids (7, 22). A similar structure for this group, with bridging via oxygen rather than fluorine has also been postulated for $Fe(PO_2F_2)_3$ (23, 24), $In(PO_2F_2)_3$ (23), and $(CH_3)_2GaPO_2F_2$ (25) based on evidence from vibrational and ^{57}Fe Mössbauer spectra. A force field calculation for the $PO_2F_2^-$ ion was reported very recently (26).

The observed frequencies listed in Table 3, indicate the presence of only one type of PO_2F_2 group in $TiCl_2(PO_2F_2)_2$, and the positions of the PO_2 and PF_2 stretching modes in particular are

Can. J. Chem. Downloaded from www.nrcresearchpress.com by 210.87.254.6 on 09/05/12
For personal use only.

TABLE 3. Vibrational spectra (cm^{-1}) of $TiCl_2(PO_2F_2)_2$ and related compounds

$TiCl_2(PO_2F_2)_2$		Infrared (cm^{-1})		Approximate description
Infrared	Raman	$(CH_3)_2Sn(PO_2F)_2$	KPO_2F_2	
~1265 br, sh				
1215 vs, br	1210 s	1258	1310	vas PO_2
1155 s, br	1162 s, sh 1155 s	1168	1148	vsym PO_2
972 s	965 w, sh	928	850	vas PO_2
922 ms	930 s	888	832	vsym PF_2
576 ms, br	572	540	518§	δPO_2
521 w, sh	530 m	506	503	δPF_2
492 s	495 m	485	495	δPO_2
435 s	447 s, sh			vTiO?
415 vs, br	431 vs, br 424 s, sh			vTiCl
374 w, sh		350	356§	ρPF_2

*Abbreviations: vs = very strong, s = strong, m = medium, w = weak, vw = very weak, sh = shoulder, br = broad, v = stretch, δ = bend, ρ = rock, as = asymmetric, s = symmetric.
†Reference 22.
‡Reference 14.
§Denotes obtained from Raman spectrum.

consistent with previous findings (22–25) for a bidentate bridging group. The symmetrical PO_2 stretching mode is found slightly higher than for the $PO_2F_2^-$ ion but the asymmetrical PO_2 stretching is lowered by about 100 cm^{-1}. This and the concommittant increase for both PF_2 stretching modes again by approximately 100 cm^{-1}, as well as the positions of the remaining deformation modes is very consistent with previous findings (22–25).

A clear distinction whether a bidentate PO_2F_2 group acts bridging or chelating cannot be made with the aid of vibrational spectra only. A polymeric structure however, and thus the presence of bridging PO_2F_2 groups, is more in accord with earlier stated observations on the solubilities and physical properties of all titanium(IV) chloro derivatives discussed here. Bonding to titanium in $TiCl_2(PO_2F_2)_2$ seems to involve oxygen only, whereas the position of the PF_2 stretches, νPF_2 average in $TiCl_2(PO_2F_2)_2$ and OPF_3 (27, 28) are identical, when Lehmann's (29) rule is applied. This rules out any appreciable interaction via fluorine bridges.

It is implied but not discussed here that a similar bridging group is found for $TiCl_2(O_2CCF_3)_2$.

(b) $TiCl_2(SO_3CF_3)_2$ and $TiCl_3SO_3CF_3$

The observed vibrational frequencies for these two compounds are listed in Table 4.

An unambiguous assignment of vibrational modes, even in the stretching region only, is difficult and problematic for SO_3CF_3-compounds. This is best illustrated by two independent vibrational studies (30, 31) of ions of the general type $SO_3CX_3^-$, involving normal coordinate analysis and force field calculations. Due to mixing of CF_3 and SO_3 vibrational modes and the accidental coincidence of these modes in particular in the stretching region, the proposed assignments for the observed bands differ widely.

As discussed earlier (32), where the SO_3CF_3 group acts as a mono- or bifunctional group, the degeneracy of the *E* modes in $SO_3CF_3^-$ will be removed. This should be most obvious for the SO_3 modes but the CF_3 modes should also be affected. As a result splittings or band broadening effects are expected and best detected in the stretching range. Besides the increase in the number of vibrations, differences in band positions should allow a distinction between a mono and a bidentate group in analogy to SO_3F compounds.

From the findings for $TiCl_2(PO_2F_2)_2$ it is reasonable to expect for $TiCl_2(SO_3CF_3)_2$ structural similarity and hence a bidentate SO_3CF_3 group. This is indeed the case as can be seen from Table 4 and the previously (32) reported vibrational frequencies for a bidentate bridging SO_3CF_3 group in $(CH_3)_3SnSO_3CF_3$.

Thus again a bidentate SO_3CF_3 group and a polymeric structure appear most reasonable for $TiCl_2(SO_3CF_3)_2$. The compound $TiCl_3SO_3CF_3$ appears to have far fewer absorption bands in the region of 1500–500 cm^{-1} where the majority of SO_3CF_3 stretching and bending modes occur.

Can. J. Chem. Downloaded from www.nrcresearchpress.com by 210.87.254.6 on 09/05/12
For personal use only.

Can. J. Chem. Downloaded from www.nrcresearchpress.com by 210.87.254.6 on 09/05/12
For personal use only.

TABLE 4. Vibrational spectra of $TiCl_3SO_3CF_3$, $TiCl_2(SO_3CF_3)_2$, $TiCl_{3.33}(SO_3F)_{0.66}$, and $TiCl_2(SO_3F)_2$*

$TiCl_3SO_3CF_3$		$TiCl_2(SO_3CF_3)_2$		$TiCl_{3.33}(SO_3F)_{0.66}$			
Infrared (cm^{-1})	Raman (cm^{-1})	Infrared (cm^{-1})	Raman (cm^{-1})	Infrared (cm^{-1})	Raman (cm^{-1})	$TiCl_2(SO_3F)_2$ i.r. (cm^{-1})	Comments
			1364 m				
1272 m, vs	1275 ms	1358 s	1353 w	1248 vs, br	1260 ms 1248 m	1380 m, sh 1342 s	
1225 s, b	1233 ms 1213 ms	1235 vs, sh	1228 ms, br	1205 vw 1188 vw		1195 m, sh	SO_3 and CF_3 stretching modes
1205 m	1202 m	1215 vs, b 1145 vw	1210 m, sh				
1120 m	1110 mw	1105 s	1103 vs	1082 m, sh 1070 s	1082 s	1080 ms, sh 1020 s, b	
1050 m, sh 1031 s	1063 s 1036 ms	1040 m, sh 1006 ms	1042 996 m	870 vw			
		780 w	784 vs				νSF and νSC
780 mw	785 s					846 ms	
				650 s 643 s, sh	676 ms	732 vs	
630 s	662 m	635 s	644 m				SO_3 and CF_3 bending modes
		605 ms	601 ms	592 m	590 ms	630 s	
595 m, sh	591 s	582 m	580 m, sh				
525 ms	533 ms	536 m	540 w, sh	579 m	570 ms	616 m, sh	
490 m	514 w	520 ms	524 s				
452 vs	455 vs	462 vs	468 vs	495 ms		578 m, sh	TiO and TiCl stretching range
428 vs	433 vs	458 vs	445 s	464 s	461 m, sh	555 ms	
		438 vs	435 s, sh	430 vs	444 vs		
391 m,sh	391 m	384 m	384 m	415 vs		445 s (448)†	
	361 ms		371 s				
	320 m	330 m	335 m	390 ms	390	418 sh 390 m† 363 ms†	Torsion modes

*For abbreviations see footnotes to Table 3.
†From Raman spectrum.

Can. J. Chem. Downloaded from www.nrcresearchpress.com by 210.87.254.6 on 09/05/12
For personal use only.

Indeed good correspondence generally between the observed bands and the ones reported for a $SO_3CF_3^-$ (30, 31) ion are found indicating that the E modes may not be split to any large degree. Observed splittings in the 1230–1200 cm^{-1} and in the 1050 cm^{-1} range appear to affect modes originally assigned as A_1 modes with the highest frequency being assigned as CF_3 stretching mode (30). The other CF_3 stretch found at 1167 cm^{-1} in $AgSO_3CF_3$ (30) is noticeably lowered by about 40–50 cm^{-1}. A further departure is found in the range of 760–780 cm^{-1}, where the intense Raman band may be regarded as an S—C stretch. This band is found at 785 cm^{-1} for $TiCl_3SO_3CF_3$, and thus about 25 cm^{-1} higher than for ionic $SO_3CF_3^-$ (30).

The two most likely models to fit the observations are a tridentate SO_3CF_3 group with all three oxygens equally involved in bonding to titanium, and the $SO_3CF_3^-$ ion. There appear to be no published precedents for the former.

Our preference for the tridentate SO_3CF_3 group in $TiCl_3SO_3CF_3$ and thus a polymeric structure is based on the following arguments: (*i*) There are, as pointed out, some deviations, positional changes or band broadening, in the vibrational spectra. (*ii*) The coordination number 3 for tetravalent titanium in $TiCl_3{}^+SO_3F^-$ is unprecedented, whereas coordination number 6 appears to be the rule (10). (*iii*) As will be seen later, a tridentate group fits very well into the structural pattern of this group of compounds and explains the observed reactions rather well.

(c) $TiCl_2(SO_3F)_2$ and $TiCl_{3.33}(SO_3F)_{0.66}$

Of these two compounds $TiCl_{3.33}(SO_3F)_{0.66}$ is found to give rise to a very simple uncomplicated spectrum. The vibrational frequencies are listed in Table 4. As can be seen, only the six fundamentals are observed in the i.r. region and any splitting of E modes in the Raman spectrum is either very small as is the case for the band at $\sim$1250 cm^{-1} or not observed as found in the range of the deformation modes. This indicates C_{3v} symmetry. Besides a small positional change observed for ν_4, the asymmetric SO_3 stretch, which is found lower by about 30 cm^{-1} than for KSO_3F, good correspondance is observed with one exception, the SF stretching mode occurs at $\sim$650 cm^{-1}. There are no precedents for such drastic lowering. In previous reports (7, 8, 32 and references therein), where mono-, bi-, or tridentate SO_3F groups are postulated, νSF is generally found in the range of 820–870 cm^{-1} and even for $TiCl_2(PO_2F_2)_2$ the PF_2 stretching modes are found $\sim$100 cm^{-1} higher than the corresponding bands in KPO_2F_2.

The most logical explanation for the observed frequency lowering in $TiCl_{3.33}(SO_3F)_{0.66}$ is the assumption that here the SO_3F is bonded to titanium not only over all three oxygens but also over fluorine, that is, SO_3F functions as a tetradentate ligand. Even though there are no precedents for such a configuration, the unusual stoichiometry of the compound is easily explained by assuming, in good agreement with our observations in the TiCl stretching range, that Cl is monodentate. For tetradentate fluorosulfate, the stoichiometry $TiCl_{3.33}(SO_3F)_{0.66}$ (or $Ti_3Cl_{10}(SO_3F)_2$) would allow hexacoordination for titanium, which is fairly common indeed for tetravalent titanium. Support is derived from the $TiCl_4$–HSO_3CF_3 system and possibly also from $TiCl_4$–HSO_3CH_3, where only three potential coordination sites are available for each anionic group and where under similar experimental conditions $TiCl_3SO_3CF_3$ and $TiCl_3SO_3CH_3$ are formed, as discussed earlier, with possible hexacoordination around titanium.

For $TiCl_2(SO_3F)_2$, the presence of bidentate SO_3F groups would be expected and structural similarities to the previously discussed compounds $TiCl_2(PO_2F_2)_2$ and $TiCl_2(SO_3CF_3)_2$ or to the previously reported $SnCl_2(SO_3F)_2$ (6) should be reflected in the vibrational spectra. However a number of disturbing features are noted in the i.r. spectrum, listed in Table 4. The strong band at 1020 cm^{-1} is decidedly too low to fit the pattern of such a bidentate SO_3F group in $SnCl_2(SO_3F)_2$ (7), as well as in other organo tin(IV) fluorosulfates (7) where this band is found in the rather narrow range of 1068–1087 cm^{-1}. Furthermore a strong band at $\sim$750 cm^{-1} assignable only as SF stretch is decidedly too low when compared to previous findings (7, 8). A second band in this region at 850 cm^{-1} and the unusual broadness in particular in the SO stretching range suggest the presence of two distinctively different fluorosulfate groups. It is interesting to note, that bands at 1380, 1195, and 1080 cm^{-1} in the SO stretching range, at 846 cm^{-1} in the SF stretching range, and deformation modes at 630, 578, 555, and 418 cm^{-1} agree well with previous findings for a bidentate SO_3F group (7, 8). However the occurrence of additional bands in all areas is rather disturbing and prevents a reasonable structural assignment for $TiCl_2(SO_3F)_2$.

Can. J. Chem. Downloaded from www.nrcresearchpress.com by 210.87.254.6 on 09/05/12
For personal use only.

All compounds discussed here have strong absorption bands in the range of 400–500 cm^{-1}, where none of the acid groups have any bands. Previous reports on TiCl stretching frequencies (33) suggest a range of 370–450 cm^{-1} with a strong dependence on the coordination number of Ti for terminally bonded chlorine and a range of 250–290 cm^{-1} for bridging chlorine (35). However these reports are concerned with compounds containing the $TiCl_6^{2-}$ anion or with donor–acceptor complexes of the type $TiCl_4L_2$ with L being a strong Lewis base where hexacoordination is postulated. The frequencies are therefore considerably lower (360–390 cm^{-1}). Some examples however have $TiCl_2$ stretching modes in the same range (35) *e.g.* $TiOCl_2$ at 407 and 430 cm^{-1}. It is therefore reasonable to expect TiCl stretching modes for the oxyacid derivatives in this area.

Titanium–oxygen stretching modes are commonly found at higher frequencies (a summary is found in ref. 23) but again the compounds are not strictly comparable and both the coordination number and the donor properties of the oxyacid are quite different as *e.g.* in $OTi(PO_2Cl_2)_2$ (23) where bands between 970 and 728 cm^{-1} are cited as Ti—O stretching modes. For $Ti(OCH_3)_4$ νTiO are found at 588 and 533 cm^{-1} (36). A lowering for the oxyacid derivatives seems likely in this case considering the poor donor abilities of the oxyacid groups.

The great complexity of the spectra, *e.g.* for $TiCl_2(SO_3CF_3)_2$ suggests that both TiCl and TiO stretches fall in the same area and may in fact overlap, accounting for some of the rather broad bands. A distinction and subsequently a conclusion in regard to the linearity or nonlinearity of $TiCl_2$ groups or the planarity of $TiCl_3$ groups does not appear possible. It seems however, that the $TiCl_n$ groups do not involve chlorine bridging and also, comparing this region for $TiCl_2(SO_3CF_3)_2$ and $TiCl_3SO_3CF_3$, that the latter is probably not just an adduct of the type $TiCl_2(SO_3CF_3)_2 \cdot TiCl_4$.

While a fairly good picture regarding the oxyacid group can be obtained from vibrational spectra, definite structural views will have to await X-ray diffraction studies. For $TiCl_{3.33}(SO_3F)_{0.66}$ a fluorosulfate bridged cluster with perhaps two or even three different environments for titanium may be expected and a formulation like $Ti_3Cl_{10}(SO_3F)_2$ may be more adequate.

Conclusion

The proposed structures with hexacoordination as the rule and the tendency towards hexacoordination as the driving force in the observed ligand substitution reactions do involve either two or three oxygen atoms and in the case of the SO_3F group even fluorine coordinated to titanium.

The failure of $TiCl_2(CO_2CF_3)_2$ and $TiCl_2(PO_2F_2)_2$ to undergo ligand redistribution must be attributed to the absence of suitable non-coordinated oxygen in the oxyacid group. The observed differences in the stoichiometries of the products of the ligand redistribution is attributed to the different functionalities of the oxyacid group.

Financial support by the National Research Council of Canada is gratefully acknowledged. P.A.Y. gratefully acknowledges financial support of a MacMillan Family Foundation fellowship.

1. O. RUFF and W. IPSEN. Chem. Ber. **36**, 1777 (1903).
2. O. RUFF and W. PLATO. Chem. Ber. **37**, 673 (1904).
3. R. E. NOFTLE and G. H. CADY. Inorg. Chem. **5**, 2182 (1966).
4. M. SCHMEISSER, P. SARTORI, and B. LIPPSMEIER. Chem. Ber. **103**, 868 (1970).
5. (*a*) E. HAYEK, J. PUSCHMANN, and S. CZALOUN. Monatsh. **85**, 359 (1954); (*b*) M. J. FRAZER, W. GERRARD, and F. W. PARRETT. J. Chem. Soc. 342 (1965).
6. R. FELD. J. Chem. Soc. 3963 (1964).
7. P. A. YEATS, B. L. POH, B. F. E. FORD, J. R. SAMS, and F. AUBKE. J. Chem. Soc. A, 2188 (1970).
8. P. A. YEATS, J. R. SAMS, and F. AUBKE. Inorg. Chem. **11**, 2634 (1972).
9. P. A. YEATS, D. R. KLETT, and F. AUBKE. To be published.
10. R. J. H. CLARK. The chemistry of titanium and vanadium. Elsevier Publishing Company, Amsterdam. 1968.
11. P. A. YEATS. Unpublished observation; A. A. WOOLF. *In* New pathways in inorganic chemistry. *Edited by* E. A. V. EBSWORTH, A. G. MADDOCK, and A. G. SHARPE. Cambridge University Press, London. 1968. p. 356.
12. (*a*) F. B. DUDLEY and G. H. CADY. J. Am. Chem. Soc. **79**, 513 (1957); (*b*) J. E. ROBERTS and G. H. CADY. J. Am. Chem. Soc. **82**, 352 (1960).
13. J. BARR, R. J. GILLESPIE, and R. C. THOMPSON. Inorg. Chem. **3**, 1149 (1964).
14. R. C. THOMPSON and W. REED. Inorg. Nucl. Chem. Lett. **5**, 581 (1969).
15. G. H. CADY and J. M. SHREEVE. Inorg. Synth. **7**, 124 (1963).
16. F. AUBKE and R. J. GILLESPIE. Inorg. Chem. **7**, 599 (1968).
17. D. F. SHRIVER. The manipulation of air sensitive compounds. McGraw–Hill Book Company, New York. 1969. p. 147.
18. I. LINDQUIST. Inorganic adduct molecules of oxo-compounds. Springer Verlag, Berlin. 1963.
19. R. FELD and P. L. COWE. The organic chemistry of titanium. Butterworths, London. 1965.

20. G. P. LUSCHINSKII. J. Gen. Chem. U.S.S.R. **7**, 207 (1937); G. P. LUSCHINSKII. Chem. Abstr. **31**, 4613 (1937).
21. K. BUEHLER and W. BUES. Z. Anorg. Allg. Chem. **308**, 62 (1961).
22. T. H. TAN, J. R. DALZIEL, P. A. YEATS, J. R. SAMS, R. C. THOMPSON, and F. AUBKE. Can. J. Chem. **50**, 1843 (1972).
23. J. WEIDLEIN. Z. Anorg. Allg. Chem. **358**, 13 (1968).
24. I. PEBLER and K. DEHNICKE. Z. Naturforsch. B. **26**, 747 (1971).
25. B. SCHAIBLE and J. WEIDLEIN. J. Organomet. Chem. **35**, C7 (1972).
26. H. W. ROESKY, R. PANZER, and J. GOUBEAU. Z. Anorg. Allg. Chem. **392**, 42 (1972).
27. M. L. DELWAULLE and F. FRANCOIS. J. Chem. Phys. **45**, 50 (1948); J. Chem. Phys. **26**, 87 (1949).
28. H. S. GUTOWSKY and A. D. LIEHR. J. Chem. Phys. **20**, 1652 (1952).
29. W. J. LEHMANN. J. Mol. Spectrosc. **7**, 261 (1961).
30. H. BURGER, K. BURCYZYK, and A. BLASCHETTE. Monatsh. Chem. **101**, 102 (1970).
31. M. G. MILES, G. DOYLE, R. P. COONEY, and R. S. TOBIAS. Spectrochim. Acta, A, **25**, 1515 (1969).
32. P. A. YEATS, J. R. SAMS, and F. AUBKE. Inorg. Chem. **10**, 1877 (1971).
33. G. S. KYKER and E. P. SCHRAM. Inorg. Chem. **8**, 2313 (1969).
34. N. SERPONE, P. H. BIRD, D. G. BICKLEY, and D. W. THOMPSON. Chem. Commun. 217 (1972).
35. K. DEHNICKE. Bericht, **98**, 290 (1965).
36. H. KRIEGSMANN and E. LICHT. Z. Elektrochem. **62**, 1163 (1958).

Can. J. Chem. Downloaded from www.nrcresearchpress.com by 210.87.254.6 on 09/05/12
For personal use only.

The Quenching of $O_2(^1\Sigma_g^+)$ by Aliphatic Hydrocarbons

J. A. DAVIDSON AND E. A. OGRYZLO

Department of Chemistry, University of British Columbia, Vancouver, British Columbia

Rate constants for the quenching of $O_2(^1\Sigma_g^+)$ in the gas phase have been determined for 12 aliphatic hydrocarbons. The values are discussed in terms of a mechanism in which the magnitudes of the rate constants are determined by the abilities of the quenchers to become vibrationally excited when $O_2(^1\Sigma_g^+)$ is relaxed to $O_2(^1\Delta_g)$. The resulting equations are tested quantitatively by relating the rate constants to the absorption spectra of the quenchers at the frequencies of the $O_2(^1\Sigma_g^+ - {}^1\Delta_g)$ transition.

Les constantes de vitesse de désactivation de l'O_2 $(^1\Sigma_g^+)$ en phase gazeuse, ont été déterminées pour 12 hydrocarbures aliphatiques. La discussion des valeurs trouvées est faite dans le cadre d'un mécanisme où la grandeur des constantes de vitesse est fonction des possibilités des désensibilisateurs à passer dans des états excités de vibration lorsque l'O_2 est relaxé de l'état 1 Σ_g^+ à l'état $^1\Delta_g$. Les équations résultantes sont controlées quantitativement en reliant les constantes de vitesse aux spectres d'absorption des désensibilisateurs aux fréquences de la transition de l'O_2 $(^1\Sigma_g^+ - {}^1\Delta_g)$.

[Traduit par le journal]

Can. J. Chem., **52**, 240 (1974)

In the last five years a number of laboratories have reported rate constants for the quenching of $O_2(^1\Sigma_g^+)$ in the gas phase (1–6). It would appear that in all cases the quenching did not involve chemical reaction, and $O_2(^1\Sigma_g^+)$ was relaxed to $O_2(^1\Delta_g)$ which lies only 15 kcal below it (7, 8). However, it proved more difficult to understand the rather large variation in quenching efficiencies reported. Recently a correlation of these rate constants with the vibrational frequencies of the quencher has been noted (6). Consequently it has been proposed that the relaxation rate is dominated by the ability of the quencher to become vibrationally excited in the process (9). A theoretical basis for such a mechanism has been presented by Merkel and Kearns (10), chiefly to explain similar trends observed in the solvent quenching of $O_2(^1\Delta_g)$. Starting with the Fermi golden rule for radiationless relaxation, their equations indicate that the quenching ability of a solvent should be related to its extinction coefficient at 5200 cm^{-1} (the $^1\Sigma_g^+ - {}^1\Delta_g$ energy gap). The very fact that molecules such as H_2 are very good quenchers of $O_2(^1\Sigma_g^+)$ (11) and yet show no intrinsic absorption in the infrared, suggests that this simple description will, at the very least, require some modification. In the present study we have investigated a series of structurally similar molecules which do show an infrared absorption to determine whether this property can be related to the quenching efficiencies.

Experimental

$O_2(^1\Sigma_g^+)$ was generated in a conventional flow discharge system utilizing microwave excitation (1). The flow tube itself was a jacketed 25 mm i.d. Pyrex vessel 100 cm in length. The pressure of O_2 within the tube was maintained at 3.0 Torr which yielded a linear flow rate of 550 cm/s. The quencher generally comprised less than 1% of the total gas mixture. Oxygen atoms were removed with the addition of mercury vapor to the stream (1), and a trace of NO_2 was added after the discharge to guarantee that no atoms escaped into the observation tube. The $O_2(^1\Sigma_g^+)$ is formed in an energy pooling process between pairs of $O_2(^1\Delta_g)$ molecules. The quencher concentration was determined by following the decrease in pressure in a calibrated volume using a Texas Instruments (Model 145) quartz spiral gauge. Pressure drops were kept sufficiently small that the total pressure remained essentially constant during the course of a measurement. The quencher was introduced into the center of the main gas flow so as to facilitate mixing. All measurements were made 30 cm downstream from the point of introduction to insure that thorough mixing had been achieved and that steady state conditions had been reached in the energy pooling reactions (12).

The emission of $O_2(^1\Sigma_g^+)$ at 7619 Å and the $(O_2(^1\Delta_g))^2$ dimol emission at 6340 Å were simultaneously monitored using a Hamamatsu TV R-213 photomultiplier tube and a Zeiss variable wavelength interference filter. With this arrangement, the observed decrease in the intensity of $O_2(^1\Sigma_g^+)$ emission could be corrected for changes in $(O_2(^1\Delta_g))^2$ concentration due to quenching or simple dilution of the flowing gas mixture. Rate constants were calculated from Stern–Volmer plots of log (I_0/I) against quencher concentration [Q], where I_0 is the 7619 Å emission intensity in the absence of quencher and I is the intensity at quencher concentration [Q], corrected for any changes in $(O_2(^1\Delta_g))^2$. For convenience and better reproducibility all rate constants were determined

TABLE 1. Rate constants for the process: $O_2(^1\Sigma_g^+) + Q \rightarrow O_2(^1\Delta_g) + Q$

Quencher	k_q (1 mol^{-1} s^{-1}) Other determinations	This work
Methane	5.0×10^7 (14) 4.5×10^7 (5) 6.6×10^7 (4) 8.0×10^6 (1, 3)	4.4×10^7
Ethane	2.8×10^8 (14) 2.2×10^8 (4)	1.9×10^8
Propane	2.2×10^8 (5)	2.7×10^8
2-Methylpropane		2.9×10^8
Cyclopropane		3.7×10^8
Butane		3.8×10^8
Pentane		4.5×10^8
Methylcyclopentane		5.2×10^8
Hexane		5.5×10^8
Cyclohexane		5.8×10^8
Methylcyclohexane		5.8×10^8
Heptane		6.0×10^8

relative to the quenching constant for CO_2 (2.0×10^8 l mol^{-1} s^{-1}) because of the excellent agreement between several determinations (9). This eliminated problems associated with changing wall conditions since it provided a constant check with the wall-decay rate constant.

The hydrocarbons were obtained from Matheson and MCB, dried with P_2O_5 and separated from less condensible gases. Matheson "extra dry" oxygen was used without further purification. Flow rates of all quenchers were determined by following the pressure drop in a calibrated volume.

The infrared absorption spectra of the hydrocarbons were obtained with a Cary-14 spectrometer (10 000 – 4 000 cm^{-1}) and a Perkin–Elmer model 457 spectrometer (4000–250 cm^{-1}). Where possible, spectra were taken of the gas phase species. However, because of the limited path lengths available, liquid spectra had to be taken with the less volatile hydrocarbons. Although some broadening and a slight wavelength shift does occur on condensation, it is not great with this series of hydrocarbons.

Results and Calculations

Rate constants determined in this study are listed in Table 1, together with values obtained by other laboratories. The precision in several determinations of the same rate constant was generally quite high ($\pm 5\%$ standard deviation). However, since systematic errors have always proven difficult to assess in discharge flow systems (13), we can only hope that in this case the standard deviation is also a good measure of the accuracy of the determinations. There is, in fact, good agreement with the most reliable values reported previously.

The quenching constants appear roughly related to the size of the hydrocarbon, increasing by more than an order of magnitude between CH_4 and C_7H_{16}. This suggests a possible correlation with the strength of infrared absorption of the quencher since this is known to increase with molecular size.

The quenching process can be considered to occur through the following sequence of elementary processes:

$$^1\Sigma + Q \underset{k_{-1}}{\overset{k_1}{\rightleftharpoons}} [^1\Sigma\cdot Q] \overset{k_2}{\rightarrow} [^1\Delta\cdot Q] \overset{k_3}{\rightarrow} {}^1\Delta + Q$$

Assuming that $[^1\Sigma\cdot Q]$ is just a collision complex and that the rate controlling process is the step characterized by k_2 then the experimental quenching constant k_q is equal to k_1k_2/k_{-1}. The rate constant k_2 describes a radiationless relaxation in a polynuclear complex, and can be calculated with the well known Fermi golden rule $k_2 = 2\pi\rho|\beta|^2/\hbar^2$ where ρ is the density of states in the product and $|\beta|$ is the matrix element of H′, the perturbation Hamiltonian between the initial and final states: $\langle ^1\Delta\cdot Q|H'|^1\Sigma\cdot Q\rangle$. Assuming that the interaction between the quencher and oxygen is "dipolar" one obtains in the Born–Oppenheimer approxi-

mation (10)

$$[1]\quad k_2 \approx \frac{2\pi\rho}{\hbar^2}\left(\beta_{el}\sum_{mn}\langle {}^1\Delta_m|{}^1\Sigma_0\rangle\langle Q_n\left|\frac{\delta\mu}{\delta r}\right|Q_0\rangle\right)^2$$

where β_{el} is the purely electronic wave function which would not be expected to change much between quenchers. ${}^1\Sigma_0$ and ${}^1\Delta_m$ are the initial and final vibrational wave functions of oxygen and Q_0 and Q_n those of the quencher. $\langle {}^1\Delta_m|{}^1\Sigma_0\rangle$ will be recognized as the Franck–Condon factor for the radiative transition of $O_2({}^1\Sigma_g{}^+)$ to the mth vibrational level of $O_2({}^1\Delta_g)$ and $\langle Q_n|\delta\mu/\delta r|Q_0\rangle$ is related to the probability of optical excitation of the quencher to the nth vibrational level. This theoretical model therefore predicts that the rate constant is determined by the overlap of the absorption spectrum of the quencher with the emission spectrum of $O_2({}^1\Sigma_g{}^+)$ in its transition to $O_2({}^1\Delta_g)$, *i.e.*,

$$[2]\qquad k_q = C\int_0^\infty \varepsilon_q(\nu) f_{O_2}(\nu)d\nu$$

This assumes that k_1, k_{-1} and ρ do not change appreciably for any series of quenchers. The integral in eq. 2 can be approximated in a number of different ways. Merkel and Kearns (10) found it useful to write this equation in terms of the extinction coefficients of the quencher at the transition frequencies in O_2.

Only theoretical values have been determined for the Franck–Condon factors of the $O_2({}^1\Sigma_g{}^+ \rightarrow {}^1\Delta_g)$ transition (15). These are

Franck-Condon factor	Transition	Frequency (cm^{-1})
0.98	(0,0)	5238
2.3×10^{-2}	(0,1)	3755
3.7×10^{-4}	(0,2)	2297
5.1×10^{-6}	(0,3)	865

Using these Franck–Condon factors, eq. 2 can then be written in the form:

$$k_q = C[0.98 \times \varepsilon_q \text{ at } 5238\ cm^{-1} + 2.3\times10^{-2}\times\varepsilon_q \text{ at } 3755\ cm^{-1} + 3.7\times10^{-4}\times\varepsilon_q \text{ at } 2297\ cm^{-1} + 5.1\times10^{-6}\times\varepsilon_q \text{ at } 865\ cm^{-1}]$$

Values of ε_q at the first three frequencies are listed in Table 2. A very low Franck–Condon factor makes absorption at 865 cm^{-1} insignificant. The proportionality constant C was fixed to make k_q for C_7H_{16} equal to 6×10^8. The calculated quenching constants are listed in Table 2 and plotted against the experimental values in Fig. 1 as open rectangles.

The correlation clearly leaves something to be desired. The most obvious source of error is the use of extinction coefficients rather than overlap integrals. It is possible that this approximation is more valid in the condensed phase studies of Merkel and Kearns (10) where absorption bands are broad. In the gas phase these bands are often quite sharp and considerable error could be introduced. Since the only experimental observation of the $O_2({}^1\Sigma_g{}^+ - {}^1\Delta_g)$ emission reports only a rather diffuse O—O band (16) we have had to compute the structures of these bands. Assuming that the selection rules for changes in rotational quantum number are those characteristic of induced transitions ($\Delta J = 0, \pm1, \pm2$) the synthetic bands shown in Fig. 2 were generated. Since the process with which we are concerned is non-photonic, we have not included the ν^4 dependence normally implicit in emission spectra. Using the above Franck–Condon factors, eq. 3 can be written in the more exact form:

$$k_q = C[0.98 \times \text{overlap at } 5238\ cm^{-1} + 2.3\times10^{-2}\times\text{overlap at } 3755\ cm^{-1} + 3.7\times10^{-4}\times\text{overlap at } 2297\ cm^{-1} + 5.1\times10^{-6}\times\text{overlap at } 865\ cm^{-1}]$$

The absorption spectra of the quenchers in these four spectral regions were determined and the overlap integrals were calculated with the aid of a computer. The results are listed in Table 3 under the headings (0,0), (0,1), (0,2), and (0,3). Choosing a value of C to make $k_q = 6\times10^8$ for C_7H_{16}, the other quenching constants were calculated and are listed in the last column of Table 3. In Fig. 1 these are plotted against the experimentally determined values (as open circles). There is a somewhat improved correlation with these rate constants calculated from the spectral overlap. However, two points may be noteworthy. CH_4 is more than ten times as effective as its absorption spectrum would predict. This appears well beyond the combined experimental uncertainties. Secondly, the cyclic hydrocarbons do not possess the larger rate constants which their absorption at the O_2 frequencies would predict.

Before considering the possibility that other

TABLE 2. Extinction coefficients and calculated quenching constants

Quencher	Extinction coefficient at 5240 cm^{-1}	3755 cm^{-1}	2300 cm^{-1}	k_q(calcd)
Methane	0.0003	0.0246	0.00755	3.25×10^6
Ethane	0.0234	0.237	0.145	1.08×10^8
Propane	0.0391	0.122	0.177	1.52×10^8
2-Methylpropane	0.0564	0.187	0.206	2.2×10^8
Cyclopropane	0.123	0.102	0.206	6.05×10^8
Butane	0.0437	0.221	0.366	1.78×10^8
Pentane	0.107	0.376	0.396	4.2×10^8
Methylcyclopentane	0.134	0.605	0.611	5.38×10^8
Hexane	0.135	0.505	0.528	5.33×10^8
Cyclohexane	0.130	0.708	0.235	5.33×10^8
Methylcyclohexane	0.166	0.638	0.597	6.57×10^8
Heptane	0.153	0.557	0.618	6.0×10^8

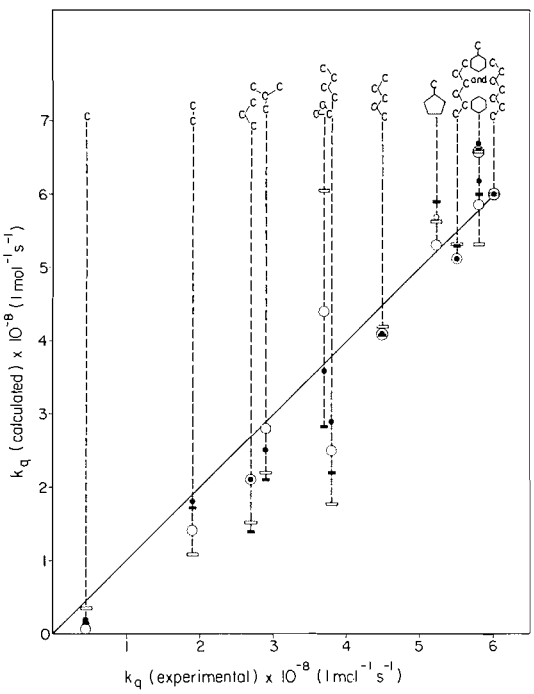

FIG. 1. Correlation between the experimental $O_2(^1\Sigma_g^+)$ quenching constants and those calculated from the i.r. absorption spectra of the quenchers: □ = values from extinction coefficients at three wavelengths and normal Franck–Condon factors. ■ = values from extinction coefficients at three wavelengths and "best-fit" Franck–Condon factors. ○ = values from overlap integrals and normal Franck–Condon factors. ● = values from overlap integrals and "best-fit" Franck–Condon factors.

factors determine the efficiency of a quencher, there is reason to question the free-molecule Franck–Condon factors which we have used. For example, studies of the infrared absorption of O_2 have shown (17) that quite different Franck–Condon factors can occur when the transitions are collision induced. Since collision induced values will be almost impossible to obtain for the $^1\Sigma_g^+ - {}^1\Delta_g$ transition in oxygen we have simply varied the Franck–Condon factors to see whether a better fit could be obtained with any particular set. The black circles in Fig. 1 represent the best fit we could obtain. In this case the Franck–Condon factors used were 0.72, 0.205, 0.039, and 0.0039 for the (0,0), (0,1), (0,2), and (0,3) transitions, respectively. Though these values are not unreasonable for an induced transition, and some improvement can be seen for CH_4, C_2H_5, cyclopropane, and C_4H_{10}, the remaining constants do not show an improvement or become worse. We have also applied these "best-fit" Franck–Condon factors to the extinction coefficient data in Table 1 and then recalculated k_q. These values are plotted as solid rectangles in Fig. 1. No significant improvement can be said to occur.

Conclusions

The quenching of $O_2(^1\Sigma_g^+)$ by saturated hydrocarbons does seem to be dominated by the ability of the hydrocarbon to become vibrationally excited by the $^1\Sigma_g^+ - {}^1\Delta_g$ transition in oxygen. However, the fact that varying the Franck–Condon factors does not produce a significantly improved correlation between the calculated and experimental rate constants suggests that the model assumed has some shortcomings. Most disconcerting is the exceptionally low quenching constant calculated for

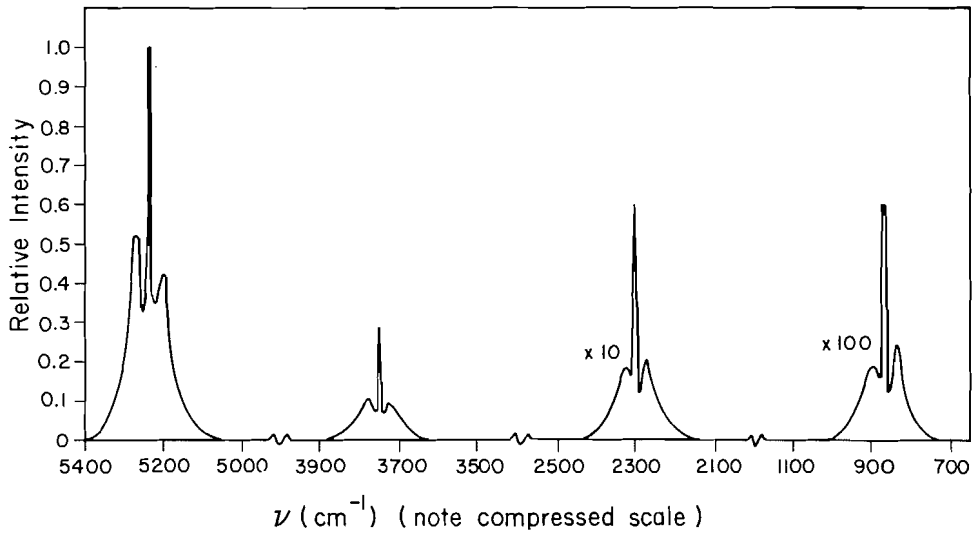

FIG. 2. Computed "induced" emission bands for the $O_2(^1\Sigma_g^+ - {}^1\Delta_g)$ transition.

TABLE 3. Overlap integrals and calculated quenching constants

Quencher	Overlap integral 0,0 overlap $\times 10^{-2}$	0,1 overlap $\times 10^{-3}$	0,2 overlap $\times 10^{-3}$	0,3 overlap $\times 10^{-4}$	k_q(calcd)
Methane	0.022	0.226	0.0068	0.0000	5.3×10^6
Ethane	1.72	1.32	1.16	0.79	1.4×10^8
Propane	2.74	1.44	1.28	0.455	2.1×10^8
2-Methylpropane	3.71	1.64	1.53	0.272	2.8×10^8
Cyclopropane	6.09	0.951	1.13	6.91	4.4×10^8
Butane	3.71	1.64	1.53	0.222	2.8×10^8
Pentane	5.31	2.63	2.8	1.19	4.1×10^8
Methylcyclopentane	6.72	4.05	3.96	1.27	5.3×10^8
Hexane	6.56	3.41	3.63	1.15	5.1×10^8
Cyclohexane	7.62	4.36	3.35	1.60	6.0×10^8
Methylcyclohexane	8.43	4.54	4.20	2.04	6.6×10^8
Heptane	7.77	4.03	4.28	1.09	6.0×10^8

methane. This, no doubt, is a result of the method employed in evaluating the overlap integrals. The use of the infrared absorption spectrum precludes any contribution from transitions which are not observed in the normal infrared spectrum. The calculated $O_2(^1\Sigma_g^+) \rightarrow O_2(^1\Delta_g)$ emission spectrum ($\Delta J = 0, \pm 1, \pm 2$) restricts contributions to the overlap integral to relatively narrow spectral regions. These effects would be expected to have the greatest effect on relatively simple molecules and points up the approximate nature of applying photonic selection rules to processes which are non-photonic.

1. S. J. ARNOLD, M. KUBO, and E. A. OGRYZLO. Adv. Chem. Ser. **77#3**, 133 (1968).
2. T. D. CLARK and R. P. WAYNE. Proc. R. Soc. (Lond.), **A314**, 111 (1969).
3. F. STUHL and K. H. WELGE. Can. J. Chem. **47**, 1870 (1969).
4. S. V. FILSETH, A. ZIA, and K. H. WELGE. J. Chem. Phys. **52**, 5502 (1970).
5. K. H. BECKER, W. GROTH, and U. SCHWATH. Chem. Phys. Lett. **8**, 259 (1971).

6. J. A. DAVIDSON. Ph.D. Thesis. Case Western Reserve University, Cleveland, Ohio. 1971.
7. D. F. EVANS. Chem. Commun. 367 (1969).
8. H. LAKUSTA, J. A. DAVIDSON, and E. A. OGRYZLO. Unpublished results.
9. J. A. DAVIDSON and E. A. OGRYZLO. Chemiluminescence and bioluminescence. Plenum Press, New York. 1973. p. 111.
10. P. B. MERKEL and D. R. KEARNS. J. Am. Chem. Soc. **94**, 7244 (1972).
11. F. STUHL and H. NIKI. Chem. Phys. Lett. **7**, 473 (1971).
12. S. J. ARNOLD and E. A. OGRYZLO. Can. J. Phys. **45**, 2053 (1967).
13. K. FURUKAWA and E. A. OGRYZLO. Chem. Phys. Lett. **12**, 370 (1971).
14. J. A. DAVIDSON, K. E. KEAR, and E. W. ABRAHAMSON. J. Photochem. **1**, 307 (1973).
15. R. W. NICHOLLS. J. Res. Natl. Bur. Stand., **69A**, 369 (1965).
16. J. F. NOXON. Can. J. Phys. **39**, 1110 (1961).
17. V. I. DIANOV-KLOKOV. Opt. Spectrosc. **17**, 76 (1964).

Effects of Solvent on the 1,2-Hydrogen Shift to a Divalent Carbon

MICHAEL T. H. LIU[1] AND DAVID H. T. CHIEN

Department of Chemistry, University of Prince Edward Island, Charlottetown, Prince Edward Island

Received June 26, 1973

The thermal decomposition of 3-chloro and 3-bromo-3-ethyldiazirine in various solvents has been investigated. A comparison was made between the decomposition in gas phase and in solution. The nature of the solvent does not affect the rate of diazirine decomposition, but does alter the subsequent reactions of the carbene. The results show that the *cis* olefin is predominant in a non-polar solvent but less so in polar solvent. These results were successfully explained by considering the electrostatic interaction of the $CH_3^{\delta+}$ and $Cl^{\delta-}$ groups.

On a étudié la décomposition thermique du chloro-3 et du bromo-3 éthyl-3 diazirine dans plusieurs solvants. On a effectué une comparaison entre le décomposition en phase gazeuse et en solution. La nature du solvant ne change pas la vitesse de décomposition de la diazirine mais, par contre, affecte les réactions subséquentes du carbène. Les résultats montrent que l'oléfine *cis* est le produit principal obtenu dans un solvant non-polaire alors qu'on en obtient moins dans un solvant polaire. On explique, avec succès, ces résultats en considérant l'interaction électrostatique des groupes $CH_3^{\delta+}$ et $Cl^{\delta-}$.

[Traduit par le journal]

Can. J. Chem., **52**, 246 (1974)

Introduction

The thermal decomposition of a number of substituted diazirines has been investigated (1, 2). The results indicate that the decomposition is a unimolecular reaction and is consistent with a mechanism in which the breaking of the two C—N bonds occur in a step-wise manner (2–4). In the gas phase pyrolysis of 3-chloro-3-ethyldiazirine (1), it was suggested that the decomposition involves the intermediate formation of a carbene which, in turn, gives rise to a mixture of *cis* and *trans* 1-chloropropene. Since few unimolecular reactions have been studied in more than one phase, the present work was undertaken to provide a comparison between unimolecular reactions in gas phase and in solution. In addition, we have examined the effects of solvents on the rearrangement of a carbene, a problem on which little information can be found in the literature.

Experimental

Infrared and nuclear magnetic resonance spectra were obtained with Perkin–Elmer Model 137 and Varian Associates T60 instruments. The ultraviolet spectra were measured with a Unicam SP 800 spectrophotometer.

Materials

Cyclohexene was passed through a silica gel column and fractionally distilled. Anisole, *t*-butanol, and dimethylsulfoxide (DMSO) were distilled before use. Hexamethylphosphoramide (HMPA) was used without further purification. All solvents used were research grade. 3-Chloro-3-ethyldiazirine was prepared from the corresponding amidine hydrochloride by oxidation with sodium hypochlorite in the presence of LiCl in DMSO solution; 3-bromo-3-ethyldiazirine was synthesized by a similar procedure with the use of freshly prepared NaOBr. The n.m.r. and i.r. spectra of the diazirines were in agreement with the data reported by Graham (5) and Ettinger (6). The physical constants of the diazirines are listed in Table 1.

Kinetic Procedure

The rates of reaction were measured by following the disappearance of diazirine. The concentration of the diazirine is approximately 2.0×10^{-2} *M*. The procedure employed is similar to the one which was described in a previous paper (2).

Reaction Products

In the decomposition of 3-chloro-3-ethyldiazirine and 3-bromo-3-ethyldiazirine in various solvents, the only products found were nitrogen, 1-chloropropene (*cis* and *trans*), and 1-bromopropene (*cis* and *trans*), respectively. The ratio of the *cis* and *trans* olefins was determined by g.l.p.c. using a 12 ft column packed with 60–80 mesh Chromosorb P containing 20% dinonyl phthalate. The agreement between the rate constants obtained by following the disappearance of reactant or by following the appearance of products was ±3%.

Results and Discussion

The gas phase decomposition of 3-chloro-3-ethyldiazirine (1) over the 100–145 °C temperature range gave *cis* and *trans* 1-chloropropene and nitrogen as the only products. The olefin mixtures consisted of 78% of the *cis* and 22% of the *trans* isomer. The results yield

[1]To whom correspondence should be addressed.

Can. J. Chem. Downloaded from www.nrcresearchpress.com by 210.87.254.105 on 09/05/12
For personal use only.

TABLE 1. Physical data of 3-halo-3-ethyldiazirine

Compound	I.r. (N=N) (cm^{-1})*	λ_{max} (nm) (ε_{max} l m^{-1} cm^{-1})	N.m.r. δ*
3-Chloro-3-ethyldiazirine	1570	360 (71.5)†	2.0 (quartet, 2H) 1.0 (triplet, 3H)
3-Bromo-3-ethyldiazirine	1567	362 (105.4)‡	2.0 (quartet, 2H) 1.0 (triplet, 3H)

*In CCl_4 solution.
†In cyclohexene solution.
‡In 1-dodecene solution.

$$k_{gas} = 10^{13.99\pm0.05} \times \exp(-30.45 \pm 0.09/RT)\ s^{-1}$$

in which $R = 0.00198$ kcal mol^{-1} deg^{-1}; the standard deviation is cited in each case.

In our present work, the decomposition of 3-chloro-3-ethyldiazirine and 3-bromo-3-ethyldiazirine were examined in various solvents: cyclohexene, anisole, *t*-butanol, DMSO, and HMPA. The absence of any product resulting from addition or insertion of the carbenes to solvent molecules suggests that the rearrangements are fast. The decompositions were strictly first order under the conditions employed in the experiments. Rate constants were determined at 8 temperatures (Table 2). At each temperature, a series of runs of various duration was carried out and the first order rate constants were obtained from the usual plots. The Arrhenius expressions calculated from the data by the method of least squares are as follows:

3-Chloro-3-ethyldiazirine

$$k_{cyclohexene} = 10^{13.81\pm0.24} \times \exp(-29.60 \pm 0.04/RT)\ s^{-1}$$

$$k_{anisole} = 10^{12.96\pm0.16} \times \exp(-28.05 \pm 0.27/RT)\ s^{-1}$$

$$k_{t\text{-butanol}} = 10^{12.53\pm0.11} \times \exp(-27.48 \pm 0.18/RT)\ s^{-1}$$

$$k_{DMSO} = 10^{12.97\pm0.10} \times \exp(-28.10 \pm 0.17/RT)\ s^{-1}$$

$$k_{HMPA} = 10^{13.31\pm0.19} \times \exp(-28.64 \pm 0.31/RT)\ s^{-1}$$

3-Bromo-3-ethyldiazirine

$$k_{anisole} = 10^{13.20\pm0.14} \times \exp(-28.09 \pm 0.23/RT)\ s^{-1}$$

In solution the bromo compound decomposes twice as fast as the chloro compound over the entire temperature range. A similar result has been noted in the thermal decomposition of 3-chloro-3-phenyldiazirine and 3-bromo-3-phenyldiazirine (7) and was rationalized in terms of the highly polarizable bromine atom. For the 3-chloro-3-ethyldiazirine, the rates in solution were increased by a factor of approximately 2 as compared with rates in gas phase.

Perhaps the really striking feature of the present results is the similarity of the rate constants as shown in Table 2. While there is good evidence that the thermal decomposition of diazirines proceed via a step-wise mechanism (3), it is not certain if the carbene precursor is a diradical or a diazomethane intermediate. The data obtained thus far could be interpreted in terms of either one of the above or a combination of both. We will not discuss the mechanism of diazirine decomposition here but note that work on other substituted chlorodiazirines, which will be reported later, supports a polarized radical-like transition state for the decomposition of diazirines.

While the nature of the solvent does not affect the rate of diazirine decomposition, it does alter the subsequent reactions of the carbene. The results, Table 3, show that the relative yields of the olefin were independent of percentage conversion and temperature in the range studied, but that the percentage *trans* isomer increased with increasing solvent polarities. The relative yields of *cis* and *trans* 1-bromopropene in the decomposition of 3-bromo-3-ethyldiazirine were similar to those of the chloro compound. The similarity between these two sets of compounds is not surprising since the equilibrium values of *cis*/*trans* at 150 °C for 1-chloropropene and 1-bromopropene were 2.52 and 2.60, respectively (12). Furthermore, it was found that the *cis*/*trans* ratios of the 1-halo-1-propenes was independent of the halogen in the halopropene. A number of related cases have been discussed in the literature. (13). It is noteworthy to mention that in the gas phase

Can. J. Chem. Downloaded from www.nrcresearchpress.com by 210.87.254.105 on 09/05/12
For personal use only.

TABLE 2. Rate constants for the decomposition of 3-halo-3-ethyldiazirines in various solvents

Solvent	3-Chloro-3-ethyldiazirine Temperature (°C)	3-Chloro-3-ethyldiazirine $k \times 10^4$ (s^{-1})	3-Bromo-3-ethyldiazirine Temperature (°C)	3-Bromo-3-ethyldiazirine $k \times 10^4$ (s^{-1})
Cyclohexene	80.6	0.35	100	4.74
	84.8	0.51		
	89.6	0.94		
	94.6	1.70		
	100.4	3.29		
	105.6	5.36		
	109.0	7.73		
	114.6	13.09		
Anisole	80.0	0.39	74.9	0.35
	85.2	0.72	80.1	0.66
	89.8	1.07	85.1	1.17
	95.0	1.90	90.2	2.11
	99.9	3.21	95.2	3.41
	104.9	5.36	100.1	5.48
	110.0	8.69	105.1	9.25
	114.8	14.20	110.2	15.35
t-Butanol	80.0	0.34		
	85.4	0.61		
	90.0	1.01		
	95.0	1.64		
	99.7	2.70		
	105.0	4.32		
	110.0	7.26		
	115.2	11.98		
DMSO	80.1	0.39	100	6.01
	84.9	0.65		
	89.7	1.16		
	94.8	1.93		
	100.2	3.31		
	104.0	4.91		
	109.9	8.87		
	114.9	14.20		
HMPA	80.0	0.37	100	6.09
	85.0	0.70		
	90.0	1.23		
	95.0	1.97		
	100.0	3.53		
	105.0	5.86		
	110.0	9.48		
	115.0	14.66		
1-Dodecane			100	5.18

pyrolysis of 1,1-dichloropropane (14), the observed *cis*/*trans* ratio of the 1-chloropropene produced was 1.20.

The increased stability of *cis* over *trans* 1-chloropropene has been attributed to electrostatic attraction between the $CH_3^{\delta+}$ and $Cl^{\delta-}$ groups (15). The carbene generated from the thermal decomposition of 3-chloro-3-ethyldiazirine is probably in its singlet state, since the ground state of chloromethylcarbene was shown to be a singlet (16). The 1,2-hydrogen shift in chloroethylcarbene (singlet state) is shown **1**

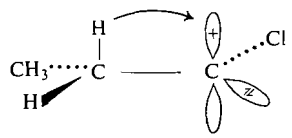

1

Can. J. Chem. Downloaded from www.nrcresearchpress.com by 210.87.254.105 on 09/05/12
For personal use only.

TABLE 3. Relative distribution of *cis–trans* olefin as a function of temperature, reaction time, and polarity of solvents

Solvent	Reaction temperature (°C)	Reaction times (min)	Olefin		Dipole moment (Debye)
			% *cis*	% *trans*	
3-Chloro-3-ethyldiazirine					
Cyclohexene	114.6	96	81.7	18.3	0.76*
Anisole	85.2	145	81.1	18.9	1.38†
	95.0	85	80.6	19.4	
	95.0	120	81.2	18.8	
	85.2	100	80.3	19.7	
t-Butanol	85.4	160	76.5	23.5	1.88*
	95.0	85	76.7	23.3	
DMSO	80.1	1110	74.2	25.8	3.96†
	100.2	110	73.7	26.3	
	100.2	300	74.3	25.7	
	109.9	30	73.5	26.5	
HMPA	80.0	161	65.7	34.3	5.3‡
	90.0	120	66.3	33.7	
	90.0	100	66.2	33.8	
	100.0	80	65.5	34.5	
	100.0	58	66.7	33.3	
1-Dodecene	100.1	35	80.1	19.9	0.52§
	100.1	60	79.3	20.7	
Anisole	85.1	160	78.4	21.6	1.38
	90.2	90	78.5	21.5	
	90.2	130	79.3	20.7	
	100.1	40	78.4	21.6	
DMSO	100.1	30	73.5	26.5	3.96
	100.1	51	72.6	27.4	
HMPA	100.1	30	64.1	35.9	5.3
	100.1	50	65.6	34.4	

*Reference 8.
†Reference 9.
‡Reference 10.
§Reference 11.

in which the hydrogen bonded to the α-carbon migrates to the vacant p-orbital of the sp^2-hybridized divalent carbon giving rise to a mixture of isomeric olefins. From our experiments, it was concluded that the *cis* olefin is predominant in a non-polar solvent but less so in polar solvent. Thus, the interaction between $CH_3^{\delta+}$ and $Cl^{\delta-}$ must be more effective than that of $CH_3^{\delta+}$ and the lone pair although the evaluation of electronegativity for the lone pair and $Cl^{\delta-}$ is not available. If $Cl^{\delta-}$ were more effective and more electronegative than the lone pair, the solvent interaction in the polar medium must be much more stronger at the $Cl^{\delta-}$ than at the lone pair. Consequently, electronic and steric effects would favor the *trans* isomer as illustrated below.

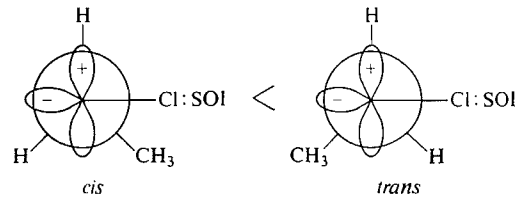

There could be other factors which determine the stereochemistry. For example, *t*-butanol may protonate the intermediate to produce the corresponding carbonium ion. However, this is rather unlikely since the percentage *trans* isomer varies linearly with the increase in dipole moment of the solvent.

These results can be summarized by stating that the thermodynamically unstable *trans* olefin

Can. J. Chem. Downloaded from www.nrcresearchpress.com by 210.87.254.105 on 09/05/12
For personal use only.

is preferentially formed in a polar medium. This statement is substantiated by the results obtained for the bromo compound. In the decomposition of diethyl diazosuccinate (17), a similar solvent effect was observed in which the thermodynamically unfavorable *cis* diethylmaleate was predominant in the polar solvents. These stereochemical results were successfully explained by considering the conformations of the singlet carbene. This similar behavior in the stereochemistry in the 1,2-hydrogen shift to a carbene is very interesting.

Grateful acknowledgment is made by one of us, M.T.H.L. for a grants-in-aid of research from National Research Council of Canada and from the Senate Research Committee of U.P.E.I. The authors wish to thank Professor I. Moritani for valuable suggestions and Mrs. S. MacQuarrie for secretarial help. The authors also wish to thank Drs. J. R. Duffy and M. P. Madan and J. A. Rigney for expressing an interest in their work.

1. H. M. FREY and M. T. H. LIU. J. Chem. Soc. A, 1916 (1970).
2. M. T. H. LIU and K. TORIYAMA. Can. J. Chem. **50**, 3009 (1972).
3. M. T. H. LIU and K. TORIYAMA. Can. J. Chem. **51**, 2393 (1973).
4. E. SCHMITZ. 23rd International congress of pure and applied chemistry. Vol. II. Butterworths, London. 1971. p. 283.
5. W. H. GRAHAM J. Am. Chem. Soc. **87**, 4396 (1965).
6. R. ETTINGER. J. Chem. Phys. **40**, 1693 (1964).
7. M. T. H. LIU and K. TORIYAMA. J. Phys. Chem. **76**, 797 (1972).
8. A. L. MCCLELLAN. Tables of experimental dipole moments. W. H. Freeman and Co., San Francisco. 1963.
9. Handbook of Chemistry and Physics. The Chemical Rubber Company. 1969.
10. J. E. DUBOIS and H. VIELLARD. J. Chem. Phys. **62**, 699 (1965).
11. G. CEISELER and E. PILZ. Chem. Ber. **95**, 92 (1962).
12. P. I. ABELL and P. K. ADOLF. J. Chem. Thermodyn. **1**, 333 (1969).
13. E. L. ELIEL. Stereochemistry of carbon compounds. McGraw–Hill, New York. 1962. p. 341.
14. K. A. HOLBROOK and K. A. W. PARRY. J. Chem. Soc. B, 1762 (1971).
15. J. W. CRUMP. J. Org. Chem. **28**, 953 (1963).
16. R. A. Moss and A. MAMANTOV. J. Am. Chem. Soc. **92**, 6951 (1970).
17. Y. YAMAMOTO and I. MORITANI. Tetrahedron **26**, 1235, (1970).

Can. J. Chem. Downloaded from www.nrcresearchpress.com by 210.87.254.105 on 09/05/12
For personal use only.

Chemically Induced Dynamic Electron Polarization. IV. The Photolysis of 1,4-Naphthoquinone

SAU-KING WONG, DOUGLAS A. HUTCHINSON, AND JEFFREY K. S. WAN
Department of Chemistry, Queen's University, Kingston, Ontario

Received May 4, 1973

Electron spin resonance emission was studied from the photochemically produced 1,4-naphthosemiquinone radical in liquid methanol, ethanol, isopropanol, ethylene glycol, and in acetic acid in the presence of 2,6-di-*tert*-butylphenol. This chemically induced dynamic electron polarization is due to the optically spin polarized triplets of the parent quinone and their subsequent hydrogen abstraction reaction with retention of the polarization in the resultant semiquinone radicals. In the acetic acid – 2,6-di-*tert*-butylphenol system, emission was observed also from the phenoxy counter radical. The magnitude of the polarization at constant microwave power was found to be temperature dependent. The comparison of the photochemical theory and the radical-pair theory is examined in the light of some of the results obtained.

On a étudié l'émission de résonance électronique de spin du radical de la naphtosemiquinone-1,4, préparée photochimiquement dans le méthanol, l'éthanol, l'isopropanol, l'éthylène glycol et l'acide acétique en présence de diterbutyl-2,6 phénol liquides. Cette polarisation électronique dynamique, chimiquement produite, est dûe aux états triplets, dont les spins sont optiquement polarisés de la quinone parente, qui subit par la suite une réaction d'abstraction d'un atome d'hydrogène accompagnée de la rétention de la polarisation dans le radical semiquinonique résultant. Dans le système acide acétique – diterbutyl-2,6 phénol on observe aussi une émission dûe au radical complémentaire phénoxy. On a trouvé que l'importance de la polarisation dépend de la température lorsque la puissance de la microonde reste constante. La théorie photochimique et la théorie des "paires de radicaux" sont comparées à la lumière de quelques-uns des résultats obtenus. [Traduit par le journal]

Can. J. Chem., **52**, 251 (1974)

Introduction

Recently we have reported the observation of the totally emissive e.s.r. of 1,4-naphthosemiquinone radicals produced in the pulsed photolysis of 1,4-naphthoquinone in isopropanol (1). It was concluded that a spin polarization arising from intersystem crossing to the triplet quinone may result in a spin polarization for the doublet radical, when the chemical hydrogen abstraction rate is comparable to the spin–lattice relaxation rate of the triplet molecule. A formal theoretical development of this model has been given (2). The model also predicts that the counter radical from the hydrogen donor must have the same sign of electron polarization. Thus, in a recent communication (3) on the observation of a photo-radical pair of durosemiquinone radical and the 2,6-di-*tert*-butylphenoxy radical, the results that both radicals are totally emissive support strongly the photochemical theory. In the present paper, we describe the detailed study of the photolysis of 1,4-naphthoquinone in a variety of solvents. The chemically induced dynamic electron polarization (c.i.d.e.p.) results of this system are discussed in the light of the radical-pair theory (4) and our photochemical theory.

Experimental

1,4-Naphthoquinone (Aldrich) after purification with petroleum ether in a Soxhlet extractor was recrystallized from methanol. The sample could be further purified by sublimation but the experimental results in control experiments indicated no significant difference. 1,4-Dihydroxynaphthalene (Aldrich) was recrystallized successively from 95% ethanol, hot water, and benzene with a small amount of water. 2,6-Di-*tert*-butylphenol was recrystallized from benzene.

Most of the sample solutions were first made saturated at room temperature and were diluted to twice the volume with the same solvent. The sample solutions contained in 4 mm o.d. Pyrex tubings were degassed and sealed off under 10^{-5} Torr vacuum. All runs were at room temperature unless otherwise specified.

A Varian 4502 x-band spectrometer using 100 kHz modulation was employed for the e.s.r. study. The sample temperature was controlled by the Varian variable temperature accessory. An optical transmission cavity was used and the light source was a 200 W super-pressure mercury d.c. lamp. The reproducible light pulses were obtained by using a rotating disk capable of varying the dark-to-light ratio between 20 and 200 with the light period being as short as 200 μs. The characteristics of the light pulse was monitored by a phototube and is shown in Fig. 1. The rotating sector in our experiments served

Can. J. Chem. Downloaded from www.nrcresearchpress.com by 210.87.254.5 on 09/05/12
For personal use only.

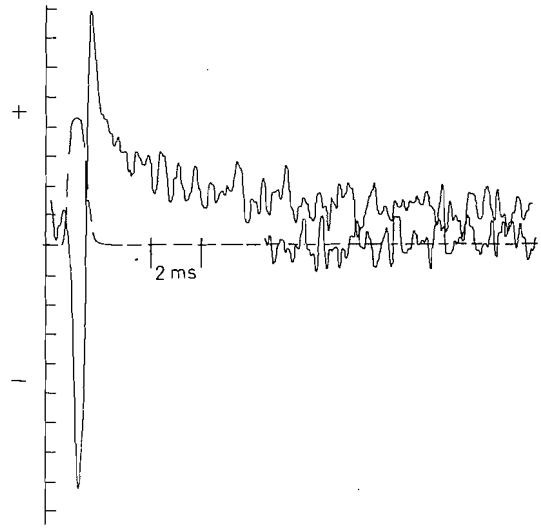

FIG. 1. Time dependence of the e.s.r. signal intensity at constant magnetic field of the photo-produced 1,4-naphthosemiquinone radical: absorption (+); emission (−). Also shown in dotted line is the shape of the light pulse.

only as a means to give reproducible and reasonably fast recurrent light pulses. The sector used here, however, is different from the conventional ones used in photochemical experiments, since our sector was designed to have a light-to-dark ratio of at least 1:20. The light pulse provided by the sector is still relatively long for quantitative study of the initial polarization, but we believe that we were looking at the intermediate stage between a truly time-resolved and a truly steady-state condition. This is supported by the experimental decay curves showing the actual conversion of the signal from emission to absorption.

The zero-line (base-line) shown in Fig. 1 represents only an example of the noise level. The base-lines for all other decay curves were represented simply by a straight line to show more clearly the feature of the emission. The emission is represented in the decay curves by the (−) signal, following which the signal converts rapidly to the absorption mode (+) and then decays chemically. All the decay curves were measured at the maximum position of the first derivative e.s.r. lines. A Fabri-tek 1074 instrument computer was used to measure and time-average the changes in e.s.r. signal amplitude at some predetermined constant magnetic field and during the intermittent irradiation. Pre-triggering was accomplished by means of a miniature photocell. Normally 10^3 to 10^4 sweeps were required for each observation. Further time-averaging beyond 10^4 sweeps offered little improvement under the present experimental condition.

The time response of the present detection system was limited mainly by the Varian 100 kHz modulation unit and was probably not better than about 150 μs. Future experiments, however, will be improved by using a 2 MHz modulation unit.

Results and Discussion

The following experiments involve studies of the photolyses of 1,4-naphthoquinone in various solvents. Some of the results are difficult, if not impossible, to interpret by the radical-pair theory (4). On the other hand the photochemical theory (2) provides a ready interpretation for the experiments. The preference for the photochemical theory over the radical-pair theory emerges in five stages. Accordingly, the results of the experiments are grouped into five sections. The first section indicates the S—T_0 mixing mechanism of the radical-pair theory is unlikely; the second section rules it out. However, the S–$T_{\pm 1}$ mixing mechanism is still a possibility at this stage. The third section, which describes concentration effects, eliminates the S–$T_{\pm 1}$ mixing mechanism of the radical-pair theory and the fourth and fifth sections provide further tests for the validity of the photochemical theory.

For the sake of convenience, the subsequent discussion employs the following abbreviations: NQ for 1,4-naphthoquinone, $\dot{N}QH$ for 1,4-naphthosemiquinone radical, and NQH_2 for 1,4-dihydroxynaphthalene.

Photolysis of 1,4-Naphthoquinone in Isopropanol

The 1,4-naphthosemiquinone radical has been postulated as an intermediate in the photolysis of the parent quinone (5); similar mechanisms of other simple quinones have been established (6, 7). In the photoreduction system the precursors of the semiquinone radicals are usually triplet states of the parent quinones. For 1,4-benzoquinone, NQ, and anthraquinone, the lowest triplet states are probably n–π^* in character (8). Thus, a simplified mechanism of the photoreduction of NQ in isopropanol is

$$[1] \qquad NQ + h\nu \rightarrow {}^1NQ \rightsquigarrow {}^3NQ$$

$$[2] \qquad {}^3NQ + (CH_3)_2CHOH \rightarrow \dot{N}QH + (CH_3)_2\dot{C}OH$$

$$[3] \qquad 2\,\dot{N}QH \rightarrow NQ + NQH_2$$

The major product of the photoreduction is the NQH_2; no cross product between $\dot{N}QH$ and $(CH_3)_2\dot{C}OH$ was found (5).

The e.s.r. spectrum of the $\dot{N}QH$ radical in the photolysis system has been observed (9). The semiquinone radicals give a totally emissive spectrum for all hyperfine components during and immediately after the light pulse. Although this result has been reported previously in a

Can. J. Chem. Downloaded from www.nrcresearchpress.com by 210.87.254.5 on 09/05/12
For personal use only.

Can. J. Chem. Downloaded from www.nrcresearchpress.com by 210.87.254.5 on 09/05/12
For personal use only.

preliminary communication (1), it is now instructive to attempt to interpret it by the radical-pair theory.

Since the results of product analysis show no cross products, it appears that the semiquinone radicals escape from the initial cage combination with the isopropanol radicals. Thus one would expect that $\dot{N}QH$–$(CH_3)_2\dot{C}OH$ encounters play a minor role in inducing electron spin polarization on the semiquinone radical. Eventually another semiquinone radical is encountered; this leads to self-disproportionation. These $\dot{N}QH$–$\dot{N}QH$ encounters should be the major source of electron spin polarization in the radical-pair theory.

If one examines $\dot{N}QH$–$\dot{N}QH$ encounters, a number of difficulties arise in a radical-pair theory interpretation. In an $\dot{N}QH$–$\dot{N}QH$ encounter, S–T_0 mixing cannot produce electron spin polarization. Thus one must consider S–$T_{\pm 1}$ mixing (4*d*, *f*), but this produces two difficulties. Firstly, the hyperfine interaction is not sufficient to account for the observed polarization. Secondly, the electron spin – rotation interaction, which can be quite large, is associated with broad lines. The observed e.s.r. spectrum consists of narrow lines.

Thus, it is only with difficulty that one can interpret the semiquinone radical spectrum by the radical-pair theory. This is not the case with the photochemical theory; it predicts the same polarization for all hyperfine components of $\dot{N}QH$. In addition, the photochemical theory predicts both $\dot{N}QH$ and the solvent radicals to have the same polarization. The results of the next section allow one to make a further comparison of these two theories.

The Photolysis of NQ in Acetic Acid in the Presence of 2,6-Di-tert-butylphenol (Ph'OH)

In the photochemical system of NQ in isopropanol, the shortlived isopropanol radical has eluded experimental detection; one reason is that $(CH_3)_2\dot{C}OH$ readily reacts with a quinone to form a semiquinone (10). Thus it may be possible to stabilize the "counter" radical by using a hydrogen donor which would react rapidly with the spin-polarized triplet quinone

[4] $$^3NQ + Ph'OH \rightarrow \dot{N}QH + Ph'\dot{O}$$

2,6-Di-*tert*-butylphenol was chosen as the hydrogen donor.

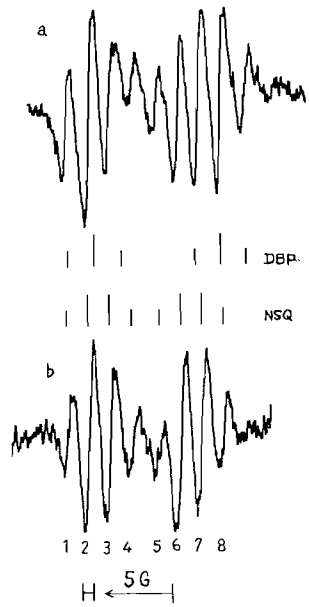

FIG. 2. (*a*) Electron spin resonance spectra of the 1,4-naphthosemiquinone radical and the 2,6-di-*tert*-butylphenoxy radical in acetic acid; (*b*) e.s.r. spectra of the semiquinone radical produced in acetic acid containing the parent quinone and 1,4-dihydroxynaphthalene. The hyperfine lines are numbered for subsequent reference.

The e.s.r. spectra of both the $\dot{N}QH$ and $Ph'\dot{O}$ radicals were observed. The overlapping spectra are shown in Fig. 2. All the hyperfine lines, including those of $\dot{N}QH$ and the nonoverlapping lines belonging to $Ph'\dot{O}$, exhibit emission during and immediately after the light pulse. Thus, both radicals have the same polarization in the totally emissive mode.

The NQ–isopropanol results of the previous section indicated that the S–T_0 mixing mechanism of the radical-pair theory was an unlikely explanation. The results of this section show it to be impossible for two reasons. Firstly, a large *g* value difference is required for all hyperfine components of a radical to be polarized in the same mode. The *g* value difference between $\dot{N}QH$ and $Ph'\dot{O}$ is only 0.0003. Secondly, the S–T_0 mixing predicts *opposite* polarization between a radical and its counter radical.

The experimental observation of this section can only be explained by S–$T_{\pm 1}$ mixing in the radical-pair theory or by the photochemical theory. With the S–$T_{\pm 1}$ mixing mechanism, one encounters the difficulties already mentioned in the previous section. The results of the following

Can. J. Chem. Downloaded from www.nrcresearchpress.com by 210.87.254.5 on 09/05/12
For personal use only.

sections present a radical-pair theory interpretation with further difficulties.

The Photolysis of NQ in Acetic Acid in the Presence of NQH_2

If the phenol is replaced with NQH_2 as the hydrogen donor only semiquinone radicals are

[5] $$^3NQ + NQH_2 \rightarrow \dot{N}QH + \dot{N}QH$$

produced. This removes the complication of overlapping spectra for two different radicals. E.s.r. spectra were recorded for this system for various concentrations of NQ and NQH_2. The results are shown in Fig. 3; as in the previous system all hyperfine lines of ṄQH are emissive. Of greater importance is the concentration dependence of the polarization.

From the maxima of the absorption parts of the experimental decay curves, the initial ṄQH concentrations immediately after the light pulse are approximately equal for the four solutions studied. But the magnitude of the emission parts of the curves is very sensitive to NQH_2 concentration (see Fig. 3). The interpretation of this result provides a test for the $S-T_{\pm 1}$ mixing mechanism of the radical-pair theory and the photochemical theory.

The $S-T_{\pm 1}$ mixing mechanism does not consider the initial polarization of ṄQH; it only deals with the polarization resulting from the formation of a radical pair ṄQH–ṄQH.

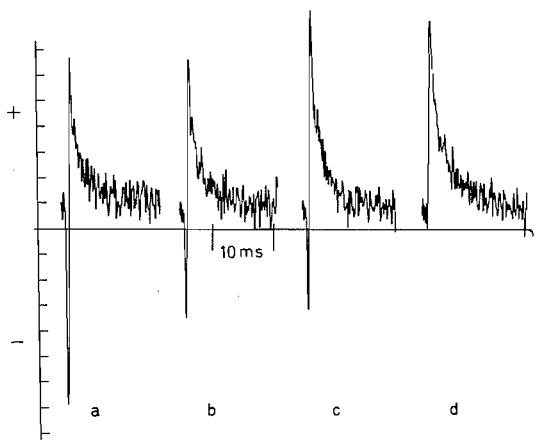

FIG. 3. Electron polarization of 1,4-naphthosemiquinone radical produced in the photolysis of the parent quinone in acetic acid containing various concentrations of 1,4-dihydroxynaphthalene: the concentrations are (*a*) 0.167 *M*; (*b*) 0.084 *M*; (*c*) 0.056 *M*; (*d*) 0.028 *M*. The concentrations of quinone are 0.024 *M* for solutions (*a*) and (*c*), and 0.012 *M* for solutions (*b*) and (*d*).

Thus it can explain a concentration dependence of the total intensity curve but not of the initial emission intensity relative to the subsequent absorption intensity.

On the other hand the photochemical theory fixes its attention on the initial polarization of ṄQH. The initial polarization is responsible for the emission part of the intensity curves of Fig. 3. This polarization depends on the hydrogen abstraction rate relative to the spin–lattice relaxation rate of the polarized triplet quinones (1–3). If the spin–lattice relaxation rate remains approximately constant in the same solvent and at the same temperature, an increase in the hydrogen abstraction rate yields an increase in the magnitude of the initial polarization. Thus, the photochemical theory provides a relatively straightforward explanation for the results shown in Fig. 3; the radical-pair theory is unable to do so.

Photolysis of NQ in Methanol, Ethanol, Isopropanol, and Ethylene Glycol

The experimental results of the previous section provide evidence in favor of the photochemical theory over the radical-pair theory. This section provides additional tests for the photochemical theory. The photolysis of NQ was carried out in methanol, ethanol, isopropanol, and ethylene glycol. Two factors are varied in this study: the chemical reactivity of the solvent with the triplet quinone and the spin–lattice relaxation rate. The spin–lattice relaxation rate decreases with an increase in solvent viscosity. Both factors affect the resultant observed magnitude of the polarization of ṄQH.

Strong emission was observed in isopropanol, very weak emission in ethanol, and no emission in methanol. The e.s.r. spectrum of ṄQH in ethylene glycol was totally emissive, and the relative polarization magnitude, as determined from the values of the maximum emission to the maximum absorption in the decay curves, is several times larger than that observed in isopropanol.

These results are in accord with what the photochemical theory predicts. The rate of hydrogen abstraction should increase from methanol to ethanol to isopropanol. This provides an explanation for the increasing emission for this sequence of alcohols as solvents. The hydrogen abstraction rate for ethylene glycol is not known; it would be reasonable to

Can. J. Chem. Downloaded from www.nrcresearchpress.com by 210.87.254.5 on 09/05/12
For personal use only.

assume that it lies somewhere between that for ethanol and isopropanol. However, ethylene glycol has a large viscosity (19.0 cP at 20 °C) compared to the other alcohols (*e.g.* 2.86 cP at 15 °C for isopropanol). This large increase in viscosity, which greatly reduces the spin–lattice relaxation rate, explains the large initial emission in ethylene glycol.

At the present time it is not possible to distinguish NQ triplet depolarization from $\dot{N}SQ$ spin–lattice relaxation. The reduction of either or both would favor a stronger observed emission. Recently, Atkins and co-workers (11) developed a method for the determination of electron spin–lattice relaxation rates of radicals from the decay curves of their e.s.r. emission.

The Effects of Temperature

Since temperature affects both the hydrogen abstraction rate and the spin–lattice relaxation rate, temperature dependent studies should provide additional tests for the photochemical theory. Accordingly, the photolysis of NQ in methanol was carried out at temperatures between −50 and 25 °C. The results are shown in Fig. 4. This experiment clearly indicates the increase in emission with a decrease in temperature, from undetectable at room temperature to strong at −50 °C. Similar temperature dependent results were observed using ethanol and isopropanol as solvents.

One would expect the temperature to decrease both the hydrogen abstraction rate and the spin–lattice relaxation rate. According to the photochemical theory, a decrease in the hydrogen abstraction rate would decrease the emission character of the $\dot{N}QH$ radical, whereas a decrease in the spin–lattice relaxation rate would enhance the emission. The experimental results indicate that the temperature effect on the spin–lattice relaxation is more pronounced than on the hydrogen abstraction rate. This is reasonable since the hydrogen abstraction is a photochemical reaction involving an excited triplet quinone molecule, and primary photochemical reactions are less temperature dependent.

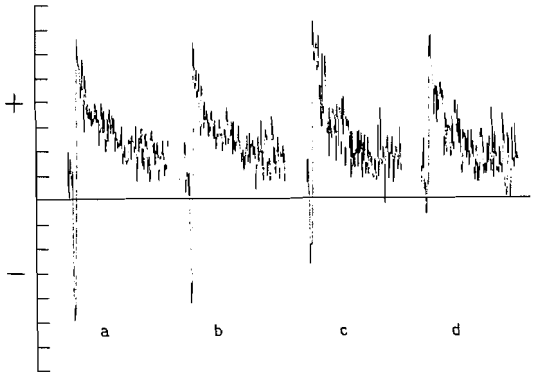

FIG. 4. Temperature dependence of polarization of 1,4-naphthosemiquinone radical in methanol: (*a*) −50 °C; (*b*) −25 °C; (*c*) 0 °C; (*d*) 25 °C. The hyperfine line studied is number 7.

Summary

The c.i.d.e.p. results obtained in the photolysis of NQ are readily interpreted by the photochemical theory. While the $S–T_{\pm 1}$ mixing mechanism of the radical-pair theory explains the total emissive nature and the same sign of the polarization for both radicals, it fails to account for the major influence of the concentration of the hydrogen donor. Thus, although there are other systems which can be interpreted by the radical-pair theory, the results of this work show up some deficiencies of the radical-pair theory.

The photochemical theory, which gives a satisfactory explanation of the present results, also has its deficiencies. The principal deficiency is that it cannot give quantitative predictions of the electron polarization in general photochemical systems. In order to do so, the following difficulties must be overcome: prior information is required on the population and depopulation of triplet sublevels and on the zero field splittings of the triplet sublevels. The chemical reaction rate, spin–lattice relaxation rates of the depolarization, and overall decay rates of the radical are required. The spin–lattice relaxation times of triplet organic molecules in liquid solutions are virtually impossible to determine experimentally at the present time. The measurement of chemical hydrogen abstraction rates is not easy because the rates must be very large before polarization can be induced. However, some recent work offers hope that some of these difficulties may be overcome. Ayscough and Sealy (12) have recently proposed a kinetic e.s.r. method to measure the rates of hydrogen abstraction by photoexcited triplet carbonyl compounds. Also, it is possible that the analysis of Atkins and co-workers (11) can be extended to estimate the spin–lattice relaxation times of

the semiquinone radical and perhaps set limits for the triplet quinones.

In spite of its present difficulties, the photochemical theory has some possible future applications (13). The importance of organic triplet states in photochemistry has been well recognized in the past decade. The fact that the repopulation of the lowest excited singlets can result from thermal equilibrium existing in the triplet states has led many authors (ref. 14 and references therein) to question whether the photochemical reactivity in some organic systems originates directly from the triplet states. It is possible with further development of the photochemical c.i.d.e.p. theory that this question can be answered partially by the direct observation of e.s.r. of the resulting radicals.

Finally, it is not difficult to recognize that both the radical-pair theory and the photochemical theory are *simplified models* constructed for the purpose of describing complicated phenomena. Perhaps a more comprehensive description of c.i.d.e.p. phenomena will emerge from either the incorporation of some of the ideas of the photochemical theory into the radical-pair theory or the incorporation of some of the ideas of the radical-pair theory into the photochemical theory. It is hoped that the experimental results of this work may stimulate such effects.

This research is supported by the National Research Council of Canada and by the School of Graduate Studies and Research at Queen's University. We wish to thank the referees for their valuable comments.

1. S. K. WONG and J. K. S. WAN. J. Am. Chem. Soc. **94**, 7197 (1972).
2. S. K. WONG, D. A. HUTCHINSON, and J. K. S. WAN. J. Chem. Phys. **58**, 985 (1973).
3. S. K. WONG, D. A. HUTCHINSON, and J. K. S. WAN. J. Am. Chem. Soc. **95**, 622 (1973).
4. (*a*) R. KAPTEIN and J. L. OOSTERHOFF. Chem. Phys. Lett. **4**, 195 (1969). (*b*) H. FISCHER. Chem. Phys. Lett. **4**, 611 (1969). (*c*) F. J. ADRIAN. J. Chem. Phys. **54**, 3918 (1971). (*d*) F. J. ADRIAN. Chem. Phys. Lett. **10**, 70 (1971). (*e*) F. J. ADRIAN. J. Chem. Phys. **57**, 5107 (1972). (*f*) P. W. ATKINS, R. C. GURD, K. A. MCLAUCHLAN, and A. F. SIMPSON. Chem. Phys. Lett. **8**, 55 (1971). (*g*) P. W. ATKINS. Chem. Phys. Lett. **18**, 290 (1973). (*h*) G. T. EVANS, P. D. FLEMING, and R. G. LAWLER. J. Chem. Phys. **58**, 2071 (1973).
5. J. RENNERT, S. JAPER, and M. GUTTMAN. Photochem. Photobiol. **6**, 485 (1967).
6. N. K. BRIDGE and G. PORTER. Proc. R. Soc. Lond. A, **244**, 259, 275 (1958).
7. F. WILKINSON, G. M. SEDDON, and K. TICKLE. Ber. Bunsenges. Phys. Chem. **72**, 315 (1968).
8. F. WILKINSON. J. Phys. Chem. **66**, 2569 (1962); H. H. DEARMAN and A. CHAN. J. Chem. Phys. **44**, 416 (1966); N. A. SHCHEGLAVA, D. N. SHIGORIN, G. G. YAKOBSON, and L. SH. TUSHISHVILI. RUSS. J. Phys. Chem. **43**, 1112 (1969).
9. S. K. WONG, W. SYTNYK, and J. K. S. WAN. Can. J. Chem. **50**, 3052 (1972).
10. F. WILKINSON. J. Phys. Chem. **66**, 2569 (1962).
11. P. W. ATKINS, K. A. MCLAUCHLAN, and P. W. PERCIVAL. Mol. Phys. **25**, 281 (1973).
12. P. B. AYSCOUGH and R. C. SEALY. J. Photochem. **1**, 83 (1972).
13. S. K. WONG and J. K. S. WAN. J. Chem. Phys. In press.
14. C. M. O'DONNELL and T. S. SPENCER. J. Chem. Educ. **49**, 822 (1972).

Can. J. Chem. Downloaded from www.nrcresearchpress.com by 210.87.254.5 on 09/05/12
For personal use only.

The Ultraviolet Flash Photolysis of Ozone and the Reactions of $O(^1D)$ and $O_2(^1\Sigma_g^+)$

D. R. SNELLING

Defence Research Establishment Valcartier, and, *Centre de Recherches sur les Atomes et les Molecules, P.O. Box 880, Courcelette, Quebec*

Received May 30, 1973

The decomposition of ozone has been studied following a short duration u.v. light pulse. From an analysis of the O_3 decomposition curves for $O_3:N_2$, $O_3:N_2:O_2$ and $O_3:O_2$ mixtures it is shown that the relative rate constant for $O(^1D)$ deactivation by N_2 and O_2 is given by $k_{N_2}/k_{O_2} = 0.7 \pm 0.25$. It is also shown that $O_2(^1\Sigma_g^+)$ is formed in at least 75% of the collisions in which $O(^1D)$ is deactivated by O_2. The rate constants of the reactions $O_2(^1\Sigma_g^+) + O_3 \rightarrow 2O_2 + O$ and $O + O_2 + O_2 \rightarrow O_3 + O_2$ are found to be $(2.3 \pm 0.5) \times 10^{-11}$ cm^3 molecule^{-1} s^{-1} and $(5.0 \pm 0.5) \times 10^{-34}$ cm^6 molecule^{-2} s^{-1}, respectively, at (295 ± 1) °K.

La décomposition de l'ozone a été étudiée après une brève exposition à la lumière ultraviolette. Une analyse des courbes de décomposition de O_3 pour des mélanges $O_3:N_2$, $O_3:N_2:O_2$ et $O_3:O_2$ a montré que la constante de vitesse relative est égale à $k_{N_2}/k_{O_2} = 0.7 \pm 0.25$ pour la désactivation de $O(^1D)$ par N_2 et O_2. De même on a montré que $O_2(^1\Sigma_g^+)$ est formé lors, d'au moins, 75% des collisions impliquant la désactivation de $O(^1D)$ par O_2. Les constantes de vitesses des réactions $O_2(^1\Sigma_g^+) + O_3 \rightarrow 2O_2 + O$ et $O + O_2 + O_2 \rightarrow O_3 + O_2$ sont égales expérimentalement à $(2.3 \pm 0.5) \times 10^{-11}$ cm^3 molécule^{-1} s^{-1} et à $(5.0 \pm 0.5) \times 10^{-34}$ cm^6 molécule^{-2} s^{-1} respectivement à (295 ± 1) °K.

[Traduit par le journal]

Can. J. Chem., **52**, 257 (1974)

Introduction

An understanding of the processes occurring in the u.v. photolysis of ozone in the Hartley continuum is of fundamental importance to chemical aeronomy. O_3 photolysis at wavelengths less then approximately 3100 Å produces $O(^1D)$ atoms (1), and the deactivation of these atoms by O_2 leads to production of $O_2(^1\Sigma_g^+)$ by the energy exchange process

[1] $$O(^1D) + O_2(^3\Sigma_g^-) \rightarrow O(^3P) + O_2(^1\Sigma_g^+)$$

The efficiency (Φ) of this process (*i.e.* the fraction of $O(^1D) + O_2$ quenching collisions which lead to $O_2(^1\Sigma_g^+)$ production) is in question (see ref. 2 for a review of available information) with values of Φ reported ranging from less than 10^{-2} to unity. This process is a major source of $O_2(^1\Sigma_g^+)$ in the atmosphere.

Previous work in this laboratory has shown that $O_2(^1\Sigma_g^+)$ is not formed directly by O_3 photolysis at 2537 Å (3) nor by flash photolysis in the wavelength range 2400–3000 Å (4). The O_2 produced by O_3 photolysis at 2537 Å is in the $^1\Delta_g$ state (3) and is formed with a quantum yield of close to unity (5).

The $O(^1D)$ reactions are also of aeronomic interest since the reaction of $O(^1D)$ with H_2O is thought to be one of the principal mechanisms for producing OH and thus initiating the water catalyzed decomposition of O_3 in the stratosphere. Since the reactions of $O(^1D)$ with O_2 and N_2 are almost collision limited the $O(^1D)$ is in photochemical equilibrium in the stratosphere. Thus, relative rates of the $O(^1D)$ reactions with H_2O, N_2, and O_2 are sufficient to estimate the stratospheric OH production which results from $O(^1D)$ formation by the solar u.v. photodissociation of O_3.

In an earlier publication (4) we have described the apparatus used in this work and reported a measurement of the relative rate of $O(^1D)$ reaction with H_2O and N_2. The technique employed involved fitting experimental ozone decay curves to a proposed mechanism by numerically integrating the appropriate rate equations. The use of very low O_3 pressures (0.015 Torr) allowed the fast reactions of $O(^1D)$ and $O_2(^1\Sigma_g^+)$ to be readily separated from the slower reactions of $O(^3P)$ and $O_2(\Delta)$.

In this paper we report on determination of the relative rates of $O(^1D)$ with N_2 and O_2 and the efficiency of $O_2(^1\Sigma_g^+)$ formation (Φ) in the reaction of $O(^1D)$ with O_2. The rate of reaction of $O_2(^1\Sigma_g^+)$ with O_3 and the three body recombination rate $O + O_2 + O_2 \rightarrow O_3 + O_2$ have also been measured. The results obtained in this

Can. J. Chem. Downloaded from www.nrcresearchpress.com by 210.87.254.40 on 09/05/12
For personal use only.

work are critically compared with literature values.

Experimental

A detailed description of the apparatus and the experimental procedure has been given previously (4), hence only a brief summary will be given here.

The cylindrical photolysis cell (53 cm long, 18 cm in diameter) contained a set of 3 multiple reflection mirrors and two quartz flash lamps which were supported by metal end plates. One end plate contained two quartz windows to provide for entrance and exit of the 2537 Å low pressure mercury resonance radiation. Absorption of this radiation was used to monitor the O_3 concentration. For these experiments the multiple reflection mirrors were set to provide 12 traversals of the cell for a total path length of ≈ 5 m. With this optical arrangement ozone absorption measurements were confined to the center of the photolysis cell, and the long path length allowed very low ozone pressures (≈ 0.015 Torr) to be used. The 2537 Å radiation was isolated and detected by a Medium Quartz Hilger spectrometer fitted with a 1P28 photomultiplier. The spectrometer was used with a band pass of 2 Å in order to reduce the effect of scattered light from the flash lamps.

The photomultiplier signal was displayed on an oscilloscope and the trace photographed on Polaroid film. The signals recorded on the Polaroid prints were measured and processed automatically. Measurements were taken every 0.25 mm across the 80 mm oscilloscope trace and for each measurement the fraction of ozone decomposed was calculated; all the values falling in selected time intervals were then averaged. Finally the results of several (5–10) experiments were averaged to provide graphs of fractional ozone decomposition *vs.* time.

The flash photolysis driver circuit and the methods of ozone production and mixture preparation have all been described previously (4).

Results

The following photomultiplier signals were recorded for each experiment: V_0 the voltage with the cell empty, V_i the voltage with the ozone mixture in the cell before photolysis, and V_t the voltages observed as a function of time following the photolysis flash.

Using Beer's law, the initial O_3 pressure (P) in Torr can be calculated from the relationship

$$V_0/V_i = \exp(306 \times P/760 \times 273/T \times L)$$

where T is the absolute temperature (295 ± 1 °K for these experiments), L is the path length in cm, and the absorption coefficient of O_3 at 2537 Å is 306 cm^{-1} (6). For all the experiments, gas mixtures were added until a transmission of 5% was attained, *i.e.* ≈ 0.014 Torr of O_3.

The fractional ozone decomposition at time t (f_t) is given by

$$f_t = \log(V_t/V_i)/\log(V_0/V_i)$$

Ozone decomposition as a function of time has been measured for various ozone added gas mixtures, and the results are shown in Figs. 1 to 7. The experimental data has been fitted by theoretical curves which were obtained by numerically integrating the appropriate rate equations. These theoretical curves are discussed in a following section.

The precision of these results, as judged from the standard deviations of a set of 5 to 10 separate experiments, depended somewhat on the fraction of O_3 decomposed (f_t). Typically the standard deviation was $\approx 1\%$ of f_t. Thus the plotting symbols in Figs. 1 to 7 represent approximately 2 to 3 standard deviations in the ordinate. From the calibrations of the oscilloscope time base it was determined that the plotting symbols represent approximately 3 to 5 standard deviations in the abscissa.

For experiments at higher O_2 pressures it was found that a small amount of O atoms was produced by photolysis of O_2, presumably in the Herzberg continuum. The amount of O atoms formed was determined by flashing pure O_2 and determining the production of O_3 by the reaction sequence

$$O_2 + h\nu \rightarrow 2O$$

$$O + O_2 + O_2 \rightarrow O_3 + O_2$$

The O atom production was always much less than the O_3 initially present (≈ 0.014 Torr), and reached a maximum of 3.7×10^{-4} Torr for an O_2 pressure of 37 Torr. This O atom production was taken into account by plotting the fraction of O_3 decomposed relative to the sum of the O_3 initially present $[O_3]_i$ and the O formed, $[O]_i$, *i.e.*

$$f_t = \frac{[O_3]_i + [O]_i - [O_3]_t}{[O_3]_i + [O]_i}$$

The O atom production was included in the model calculations, and the values of f_t were calculated as defined above.

The time and wavelength distribution of the photolysis flash have been described in detail previously (4).

Discussion

Reaction Scheme and Integration of Rate Equations

The relevant reactions and their rate constants are listed in Tables 1 and 2, respectively. All rate constants are given in molecular units (cm^3, molecule, and s). The reactions have been

Can. J. Chem. Downloaded from www.nrcresearchpress.com by 210.87.254.40 on 09/05/12
For personal use only.

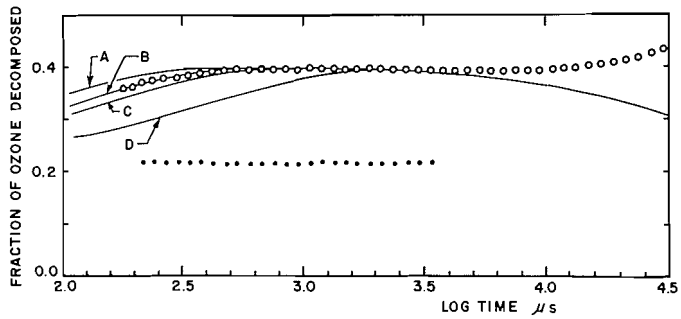

FIG. 1. Experimental conditions: open circles, O_3 pressure 0.0146 Torr, O_2 pressure 5.40 Torr; solid circles, O_3 pressure 0.0145 Torr, N_2 pressure 31.9 Torr. Flash energy 976 J. For details of computed O_3 decay curves see Table 3 and text.

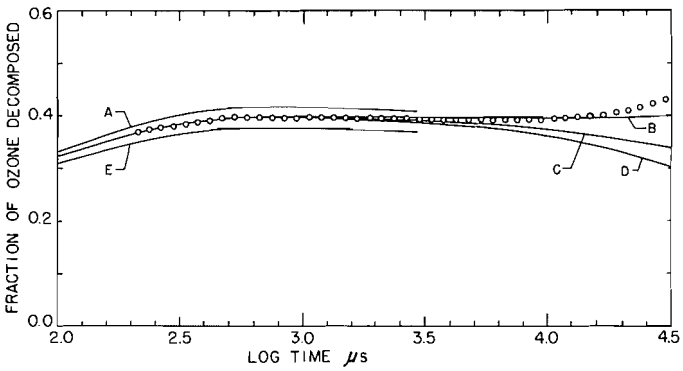

FIG. 2. Experimental conditions: open circles same as for Fig. 1 *i.e.* O_3 pressure 0.0146 Torr, O_2 pressure 5.40 Torr. For details of computed O_3 decay curves see Table 3 and text.

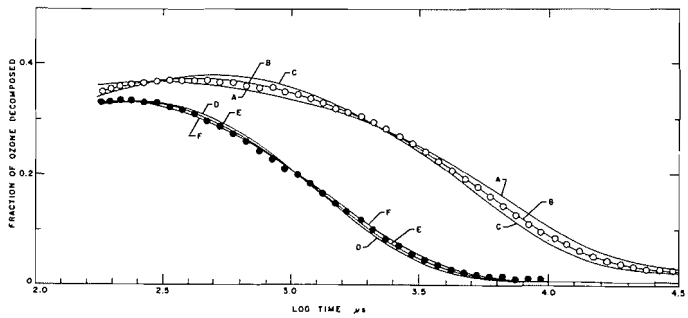

FIG. 3. Experimental conditions: open circles, O_3 pressure 0.0146 Torr, O_2 pressure 17.60 Torr; solid circles, O_3 pressure 0.0146 Torr, O_2 pressure 36.90 Torr. Flash energy 976 J. For details of computed curves see Table 3 and text.

arbitrarily divided into two groups: principal reactions and reactions of secondary importance because of their slow rates or because of the presence of more important competing reaction.

The rate of O_3 photolysis has been shown (4) to be proportional to O_3 concentration and can be represented by $k_1 I_t[O_3]$ where I_t is the time dependent relative flash intensity and k_1 is an empirically determined constant which depends on flash lamp intensity, cell geometry, etc.

The calculated O_3 decay curves were obtained by a numerical integration of the appropriate rate expressions using a Runge–Kutta integration routine. It proved difficult to integrate the rate expressions directly, because the very large O(D) reaction rates necessitated too small a time

Can. J. Chem. Downloaded from www.nrcresearchpress.com by 210.87.254.40 on 09/05/12
For personal use only.

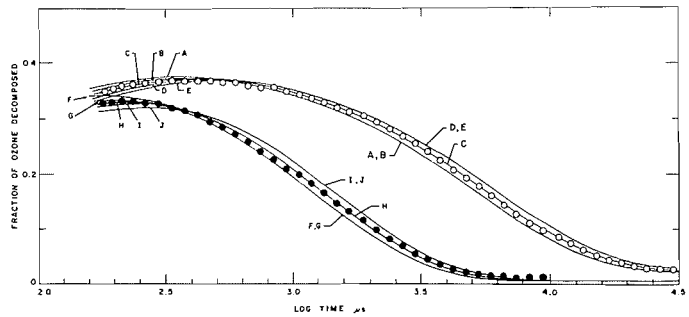

FIG. 4. Experimental conditions: same as for Fig. 3, *i.e.*, open circles, pressure 0.0146 Torr, O_2 pressure 17.60 Torr; solid circles, O_3 pressure 0.0146 Torr, O_2 pressure 36.90 Torr. Flash energy 976 J. For details of computed curves see Table 3 and text.

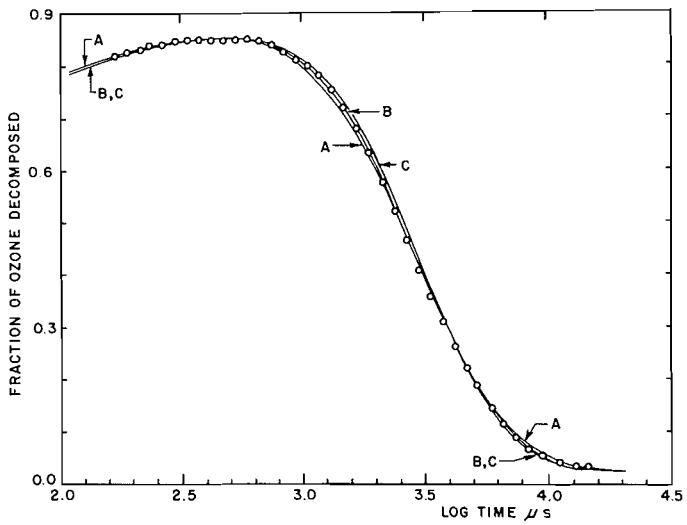

FIG. 5. Experimental conditions: O_3 pressure 0.0148 Torr, O_2 pressure 28.29 Torr. Flash energy 2840 J. For details of computed curves see Table 3 and text.

step for the integration to be practical. Since $k_2 \geqslant 2 \times 10^{-11}$ (12), and the minimum O_2 pressure used in our experiments was 5 Torr, the time constant for O(D) disappearance was always less than 0.3 μs. Since this time constant was short, compared to the flash duration (≈ 10 μs), the O(D) was taken to be in photochemical equilibrium. The steady state O(D) concentration is then given by $[O(D)] = k_1 I_t [O_3]/(k_2[O_2] + k_3[N_2] + k_8[O_3])$. The rate of an individual O(D) reaction, *e.g.* deactivation by O_2, is then given by $k_2[O_2][O(D)]$ and, hence, only relative O(D) reaction rates are required to compute the fraction of O(D) participating in the various reactions.

The constant k_1 in the expression for the rate of photolysis of ozone was empirically determined as described previously (4) by computer fitting data for O_3/N_2 or $O_3/N_2/SF_6$ mixtures in the period 200 to 800 μs following the flash. (SF_6, a gas which does not deactivate O(D) (12), was sometimes added as an inert diluent.) Typical O_3/N_2 data are shown in Fig. 1 where it can be seen that no further O_3 decomposition occurs in the period 200 to 800 μs following the flash. Thus the O_3 decomposition in the time period 0 to 800 μs results from O_3 photolysis with a very small contribution from reaction 8. (The slow reactions of O and $O_2(\Delta)$ with O_3, reactions 7 and 5, respectively, do not occur at these short times. See ref. 4 for a detailed description of the processes occurring at longer times in O_3/N_2 and $O_3/N_2/SF_6$ mixtures.) k_1 was determined by integrating the rate equations

Can. J. Chem. Downloaded from www.nrcresearchpress.com by 210.87.254.40 on 09/05/12
For personal use only.

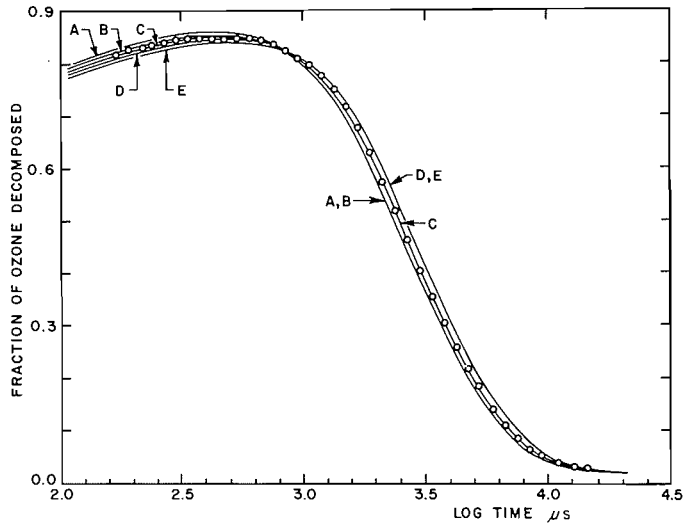

FIG. 6. Experimental conditions: same as Fig. 5; *i.e.* O_3 pressure 0.0148 Torr, O_2 pressure 28.29 Torr. Flash energy 2840 J. For details of computed curves see Table 3 and text.

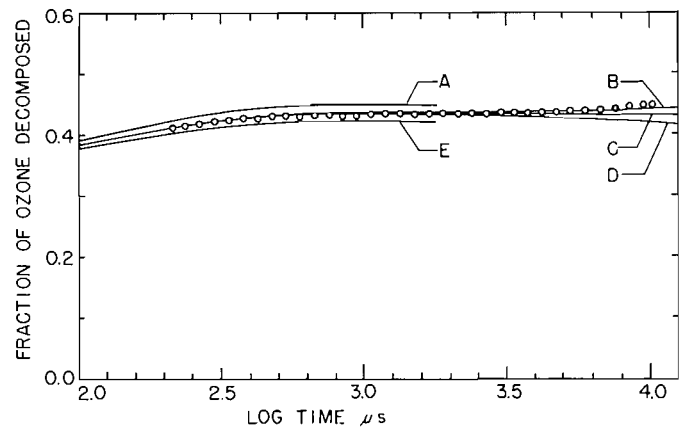

FIG. 7. Experimental conditions: O_3 pressure 0.0144 Torr, O_2 pressure 1.86 Torr, N_2 pressure 3.73 Torr, Ar pressure 5.56 Torr. Flash energy 976 J. For details of computed curves see text.

with photolysis and the O(D) reactions 2, 3, and 8 included and varying k_1 in order to obtain the observed amount of O_3 decomposition in these mixtures. It should be pointed out that there is some uncertainty in the relative rates of O(D) reaction with O_3 and N_2 and also in the products of reaction 8. (This point has been discussed in some detail in our earlier publication (4).) However, all our experiments have been performed with a large excess of O_2 and/or N_2 so that reaction 8 is of only very minor significance. All the O_3/N_2 experiments were performed with at least a thousandfold excess of N_2 over O_3, so that for the relative rates assumed in Table 1, less than 2% of the O(D) formed reacts with O_3. We have arbitrarily assumed that the products of this reaction are $2O_2$ although at least part of the reaction may proceed to give $2O + O_2$ (2). The O_3/N_2 experiments were repeated at frequent intervals throughout this work since a slow decrease in flash lamp intensity (typically 1% loss of intensity/100 flashes) and hence O_3 photolysis occurred. This loss of intensity could be recovered by cleaning the flash lamps with HF and was probably caused by deposits forming on the flash tubes.

Can. J. Chem. Downloaded from www.nrcresearchpress.com by 210.87.254.40 on 09/05/12
For personal use only.

TABLE 1. Reaction scheme*

Principal Reactions	
[1]	$O_3 + h\nu \rightarrow O_2(\Delta) + O(D)$
[2]	$O(D) + O_2 \rightarrow O_2(\Sigma) + O$
	$\rightarrow O_2 + O$
[3]	$O(D) + N_2 \rightarrow N_2 + O$
[4]	$O_2(\Sigma) + O_3 \rightarrow 2O_2 + O$
[5]	$O_2(\Delta) + O_3 \rightarrow 2O_2 + O$
[6]	$O + O_2 + O_2 \rightarrow O_3 + O_2$
[7]	$O + O_3 \rightarrow 2O_2$
Secondary Reactions	
[8]	$O(D) + O_3 \rightarrow 2O_2$
	$\rightarrow 2O + O_2$
[9]	$O_2(\Sigma) + M \rightarrow O_2 + M$
[10]	$O_2(\Delta) + M \rightarrow O_2 + M$

*The excited states of atomic and molecular oxygen $O(^1D)$, $O_2(^1\Delta_g)$ and $O_2(^1\Sigma_u^+)$ are abbreviated by $O(D)$, $O_2(\Delta)$ and $O_2(\Sigma)$, respectively.

Gas heating was included in all the model calculations as described below. It was assumed that both the excess energy available in the photolysis reaction and the heat liberated by O_3 decomposition were rapidly equilibrated. The consequent temperature rise was then calculated from the known heat capacity of the mixture. Since the mixtures used were very dilute in O_3 this heating term was small (usually less than 5 °C) and had only a small effect on reactions 5, 6, and 7, all of which have an energy of activation. The rate constants used in the model calculations for each of the curves in Figs. 1 to 7 are listed in Table 3.

Experiments with O_3/O_2 Mixtures

Four O_3/O_2 mixtures were studied and the results are given in Figs. 1 to 6. From these results and model calculations a consistent set of values for Φ, k_4, and k_6 was determined by trial and error. The calculated curves in Figs. 1 to 6 are presented to show the best fit obtainable and the sensitivity of this best fit to changes in Φ, k_4, and k_6.

Figure 1

From Table 2 it can be seen that there are two literature values of k_4 which differ by a factor of almost 4. For all our results we have found that our data are consistent with the higher of the two values. In Fig. 1, four calculated curves are shown for fixed Φ and k_6 and variable k_4. The data are clearly inconsistent with a value of k_4 of 7×10^{-12} (13) but are in good agreement with the higher value of k_4 of 2.5×10^{-11} (14). We conclude from the calculated curves in Fig. 1 that the best fit value of k_4 is 2.4×10^{-11} with upper and lower error limits of 3.7×10^{-11} and 1.84×10^{-11}, respectively. The degree of fit is more sensitive to a reduction in k_4 than an increase.

Figure 2

For the calculated curves A, D, and E in Fig. 2, k_4 and k_6 were held constant and Φ was varied. It can be seen from these curves that $\Phi = 0.85$ provides the best fit and that $\Phi = 0.75$ or 0.95 are clearly inconsistent with the data. Because of the controversy involving the value of Φ we have deliberately been somewhat conservative in our estimate of the error limits for this quantity. It will be shown in later discussion that for the data at the highest O_2 pressure it is often possible to obtain a satisfactory fit to the data for $\Phi = 0.75$ or 0.95 by varying both k_4 and k_6. However, for the data at the lowest O_2 pressure (Figs. 1 and 2) variations in k_6 have a much reduced effect and it is no longer possible to fit the data by this means.

It is apparent from an examination of Fig. 2 that curve D underestimates the O_3 decomposition at longer times. Therefore, taking account of the uncertainty in k_7, we have tried doubling k_7 to improve the fit (curve C). Even with this large increase in k_7 the fit to the data is very little improved. Because of the effects of small quantities of H_2O on the rate of O_3 decomposition observed previously (4), we have calculated the O_3 decomposition that would result from the presence of 0.015 Torr of H_2O in the mixture. For this calculation (curve B) the rate constants given in ref. 4 were used with a relative rate for the $O(D) + H_2O$ reaction of 3.5. For these calculations the significant reactions (additional to those shown in Table 1) for the time period shown in Fig. 2 are

$$O(D) + H_2O \rightarrow 2OH$$
$$O + OH \rightarrow O_2 + H$$
$$H + O_3 \rightarrow OH + O_2$$
$$2OH \rightarrow H_2O + O$$

The first reaction results in OH production which leads to a catalyzed $O + O_3$ reaction by the second two reactions while the OH decays slowly by the fourth reaction. Although this curve (B) is a much better fit to the data, it is not

Can. J. Chem. Downloaded from www.nrcresearchpress.com by 210.87.254.40 on 09/05/12
For personal use only.

TABLE 2. Rate constants for reactions listed in Table 1

Reaction	Rate constants*	Comments†	Reference
[1]	$K_1 I_t$	See text	
[2]	$1.0(\Phi)$	See text‡§	
[3]	0.7	‡§	3
[4]	7×10^{-12}	§	13
	2.5×10^{-11}		14
[5]	3.5×10^{-15}(295 °K)	$E = 5600$	11, 15
[6]	$(3.5 \text{ to } 9) \times 10^{-34}$(295 °K)	$E = -2000$§	7–9
[7]	1×10^{-14}(295 °K)	$E = 4000$	7–9
[8]	9.7	‡	3
[9]	$1 \times 10^{-16}(M = O_2)$		10
	$2.2 \times 10^{-15}(M = N_2)$		
[10]	$2.2 \times 10^{-18}(M = O_2)$		10
	$\leqslant 3 \times 10^{-21}(M = N_2)$		

*Wherever possible rate constants have been taken from recent review articles (7–10). When this was not possible a publication which summarizes the information available has been chosen.
†Where applicable energy of activation is given in cal/mol.
‡Relative rates with $k_2 = 1.0$; see text for discussion. Φ is the efficiency of $O_2(\Sigma)$ formation in reaction 2, and k_2 represents the total rate of deactivation of O(D) by O_2.
§These rate constants were determined in this work by fitting the experimental data, and the values given in the table represent literature values for comparison.

TABLE 3. Rate constants used to obtain calculated curves shown in Figs. 1–6*

Rate constants	Curve A	B	C	D	E	F	Figure number	Comments
$k_4 \times 10^{11}$	3.7	2.45	1.84	0.7			1	$k_6 = 5 \times 10^{-34}$, $\Phi = 0.85$, for all curves
Φ	0.95	0.85	0.85	0.85	0.75		2	$k_6 = 5 \times 10^{-34}$, $k_4 = 2.4 \times 10^{-11}$, for all curves†
$k_4 \times 10^{11}$	4.3	2.3	1.7	1.8	2.3	3.1	3	
$k_6 \times 10^{34}$	4.44	5.22	6.00	5.58	5.15	4.65		
Φ	0.75	0.85	0.95	0.95	0.85	0.75		
$k_4 \times 10^{11}$	3.3	2.8	2.3	2.0	1.7		4	For all curves $\Phi = 8.85$
$k_6 \times 10^{34}$	5.65	5.65	5.15	4.71	4.71			
$k_4 \times 10^{11}$	2.9	2.7	2.3	2.0	1.8		4	For all curves $\Phi = 0.85$ Data are for curves F, G, H, I, J, respectively.
$k_6 \times 10^{34}$	5.72	5.72	5.21	4.80	4.80			
$k_4 \times 10^{11}$	2.48	2.10	1.84				5	
$k_6 \times 10^{34}$	4.50	4.83	5.00					
Φ	0.75	0.85	0.95					
$k_4 \times 10^{11}$	2.45	2.27	2.10	1.90	1.78		6	For all curves $\Phi = 0.85$
$k_6 \times 10^{34}$	5.08	5.08	4.83	4.44	4.44			

*For the reactions not listed in this table the rate constants given in Table 2 were used unless otherwise stated. For rate constants used for calculated curves in Fig. 7 see text.
†For curve C, $k_7 = 2.0 \times 10^{-14}$, twice the rate given in Table 2, was assumed. For curve B see text.

entirely satisfactory. Furthermore, we consider it unlikely that so much water could have been present in the gas mixtures used. The high purity O_2 used was passed through a liquid-nitrogen-cooled trap and the apparatus was always pumped to better than 10^{-5} Torr between experiments and the subsequent pressure increase was slow (typically 10 min to attain 10^{-3} Torr).

Similar observations of an enhanced rate of O_3 decomposition were encountered in our earlier works (4) with O_3/N_2 and $O_3/N_2/SF_6$ mixtures. As discussed previously (4) a possible explanation of this effect lies in the vibrationally

Can. J. Chem. Downloaded from www.nrcresearchpress.com by 210.87.254.40 on 09/05/12
For personal use only.

Can. J. Chem. Downloaded from www.nrcresearchpress.com by 210.87.254.40 on 09/05/12
For personal use only.

excited O_2 formed in reaction 7. It is known (15) that vibrational energy released in this reaction readily transfers to O_3 and leads to enhanced rates for reactions 5 and 7. The vibrational energy of the O_2 produced in reaction 7 will probably be rapidly equilibrated by V–V energy transfer to ground state O_2. If the predominant loss of O_2 vibrational quanta occurs by V–V transfer to O_3 and the excited O_3 decays sufficiently slowly by V–T processes, significant vibrational excitation of the O_3 will result.

As has been pointed out previously (4) it is difficult to model this mechanism because the energy transfer mechanism is not well defined and the effect of O_3 vibrational energy in overcoming the barrier to reaction in reactions 5 and 7 is not known. However, qualitatively it will lead to enhanced reaction rates for reactions 5 and 7 and thus an enhanced rate of O_3 destruction.

Similar effects were not observed at higher O_2 pressures. This is demonstrated by the data in Figs. 3 to 6 where the ultimate O_3 concentration is entirely consistent with model calculations using the rates for reactions 5, 6, and 7 given in Table 2. (If enhanced reactivity of O with O_3 occurred directly, or was catalyzed by H_2O, then this would reduce the ultimate O_3 concentration.) This is entirely consistent with the mechanism discussed above, since at higher O_2 pressures the predominant decay process for O atoms is reaction 6 rather than 7 and a larger fraction of any vibrational energy liberated in reaction 7 will, after equilibration, be in the O_2 rather than the O_3.

Figure 3

For the two sets of data in Fig. 3, calculated curves are shown for $\Phi = 0.75$, 0.85, and 0.95. For each value of Φ, k_4 and k_6 were varied in order to obtain the best fit to the data.

For the top curves ($P_{O_2} = 17.6$ Torr) it can be seen that no satisfactory fit to the data can be obtained for $\Phi = 0.75$ or 0.95, thus supporting the limits obtained for this quantity from the data in Fig. 2. For $\Phi = 0.85$ the best fit (curve B) values of k_6 and k_4 were 5.22×10^{-34} and 2.3×10^{-11}, respectively. The latter value is consistent with the value obtained from Fig. 1.

For the lower set of curves ($P_{O_2} = 36.9$ Torr) a satisfactory fit could be obtained for all the values of Φ (0.75, 0.85, and 0.95), although the best fit is obtained for $\Phi = 0.85$. For $\Phi = 0.85$ (curve E) the best fit values of k_4 and k_6 were almost identical to those obtained for the upper curves. From curve D it can be seen that the higher value of Φ (0.95) can be accommodated by decreasing k_4 and increasing k_6. The reverse is true for the lower value of Φ (0.75). A comparison of the curves for $\Phi = 0.75$ and 0.95 (F and D) with that for 0.85 (curve E) indicates the effect on the best fit values of k_4 and k_6 produced by the uncertainty in Φ. From a comparison of the rate constants used for D, E, and F, it is apparent that increasing Φ from 0.85 to 0.95 is compensated for by changes in k_4 and k_6 of -0.5×10^{-11} and $+0.43 \times 10^{-34}$, respectively. The corresponding changes in k_4 and k_6 for $\Phi = 0.75$ are $+0.8 \times 10^{-11}$ and -0.5×10^{-34}, respectively. Thus the average variations in k_4 and k_6 are 0.65×10^{-11} and 0.5×10^{-34} and they reflect the uncertainties in k_4 and k_6 produced by the uncertainty in Φ of ± 0.1. These quantities will be used in the following section.

Figure 4

In Fig. 4 the effect of varying k_4 and k_6 with a fixed value of Φ (0.85) is shown for the same data as in Fig. 3. For both sets of curves it is apparent that with a fixed value of k_6 and varying k_4 the calculated curves coincide at longer times. Thus the best fit k_6 is independent of k_4 and will only be affected by errors in the assumption that $\Phi = 0.85$. For both sets of data it can be seen that the best fit values of k_4 and k_6 obtained (curves C and H) are almost identical. It is also concluded that curves A and E (upper data) and curves F and J (lower data) are an unacceptable fit to the data and thus represent the error limits obtained for k_4 and k_6. These limits are somewhat smaller for curves F and J and will thus be used in the following discussion. From a comparison of the rate constants used for curves F and J we conclude that the limits for k_4 are (1.8 to 2.9) $\times 10^{-11}$ and for k_6 (4.80 to 5.72) $\times 10^{-34}$. We must also consider the additional uncertainty in these rate constants due to the uncertainty in Φ discussed in Fig. 3. We have arbitrarily added half the uncertainty in k_4 and k_6 due to errors in Φ, since we consider that the error limits on Φ are conservative. Thus the final error limits on k_4 and k_6 are (1.5 to 3.2) $\times 10^{-11}$ and (4.6 to 6.0) $\times 10^{-34}$, respectively.

Figure 5

Figure 5 shows the computed curves for a best

Can. J. Chem. Downloaded from www.nrcresearchpress.com by 210.87.254.40 on 09/05/12
For personal use only.

fit to the fourth set of O_3/O_2 data for $\Phi = 0.75$, 0.85, and 0.95. Again a satisfactory fit to the data can be obtained for all values of Φ (although $\Phi = 0.85$ provides the best fit) as was observed for the higher O_2 pressure data in Fig. 3. However, for the data in Fig. 5, the changes in k_4 and k_6 required to accommodate the extreme values of Φ are smaller than for the data in Fig. 3. The best fit values of k_4 (2.06×10^{-11}) and k_6 (4.80×10^{-34}) are consistent within experimental error with those obtained for the data in Fig. 4 (curves C and H).

Figure 6

Figure 6 is similar to Fig. 4 in that the effect of varying k_4 and k_6 with a fixed value of Φ is shown. We conclude that curves A and E represent an unacceptable fit to the data while curve C (almost identical to curve B, Fig. 5) provides the best fit. Using the same procedure as for Fig. 4 (*i.e.* adding half the uncertainty due to possible errors in Φ obtained in Fig. 5) we conclude that the best fit values of k_4 and k_6 are 2.1×10^{-11} and 4.83×10^{-34}, respectively, and the error limits for k_4 and k_6 are (1.67 to 2.67) $\times 10^{-11}$ and (4.30 to 5.18) $\times 10^{-34}$.

Summary of Conclusions from O_3/O_2 Results

For convenience we summarize the conclusions drawn from the data in Figs. 1 to 6. In each case the best estimate and upper and lower limits are given in that order. Fig. 1: $k_4 \times 10^{11}$ (2.40, 3.7, 1.84). Fig. 2: Φ (0.85, 0.95, 0.75). Fig. 3: Φ (0.85, 0.95, 0.75). Fig. 4: $k_4 \times 10^{11}$ (2.3, 3.2, 1.5); $k_6 \times 10^{34}$ (5.18, 6.0, 4.6). Figs. 5 and 6: $k_4 \times 10^{11}$ (2.1, 2.87, 1.67); $k_6 \times 10^{34}$ (4.83, 5.18, 4.30). We conclude finally from a comparison of all of these results that $\Phi = 0.75 \pm 0.10$, $k_4 = (2.3 \pm 0.5) \times 10^{-11}$, and $k_6 = (5.0 \pm 0.5) \times 10^{-34}$.

There are two possible effects which must be considered and which would result in the values of Φ obtained being a lower limit. Firstly, there is the possibility that part of the photolysis results in production of $O(^3P)$ rather than $O(^1D)$. If a certain fraction, f, of the O_3 photolysis resulted in $O(^3P)$ production then all the calculated curves would be identical provided that Φ is decreased by an amount f. Figure 2 of ref. 4 shows the wavelength distribution of the flash lamp output and the wavelength distribution of the flash energy absorbed by O_3. These data show that almost all the O_3 absorption occurs at $\lambda \leqslant 2950$ Å, well below the threshold for $O(^1D)$ production of 3100 Å. This occurs since the O_3 absorption coefficient is very small at 2950 Å and drops rapidly towards longer wavelengths. Thus we consider it unlikely, but cannot rule out completely, that any significant fraction of the O_3 photolysis results in $O(^3P)$ production. A second possibility is that part of the $O_2(\Sigma) + O_3$ reaction occurs by physical deactivation of $O_2(\Sigma)$ rather than destruction of O_3. This possibility which cannot be discounted but seems somewhat unlikely would similarly result in an increase in Φ. Since these two effects cannot be ruled out we conclude finally that $\Phi \geqslant 0.75$.

$O_3/O_2/N_2$ Experiments

After establishing the mechanism for the O_3/O_2 mixtures several experiments were performed with $O_3/O_2/N_2$ mixtures to obtain the relative rates of O(D) deactivation by N_2 and O_2. One of these experiments is shown in Fig. 7. (The argon was added as an inert diluent which does not deactivate O(D) (12).) For the model calculations the values of Φ, k_4, and k_6 deduced above were used and k_3 was varied to obtain the best fit to the data. In Fig. 7, for curves B, C, and D, $k_3 = 0.7$ and for curves A and E, k_3 is 0.55 and 0.85, respectively. At longer times curve C shows the effect of increasing k_7 ($k_7 = 2.0 \times 10^{-14}$) and curve B shows the effect of including 0.005 Torr of H_2O (see discussion of Fig. 2). At longer times, curve B is a satisfactory fit to the data but, as discussed above, we feel that the enhanced O_3 decomposition is caused by vibrational excitation of the O_3.

Returning to the fit at shorter times we conclude from Fig. 7 that $k_3 = 0.7$ provides a satisfactory fit to the data while the curves for $k_3 = 0.55$ or 0.85 are unacceptable. If $\Phi = 0.75$ or 0.95 is used then different best fit values of k_3 are found. Because of this additional uncertainty we have adopted 0.7 ± 0.25 as our best estimate of k_3/k_2.

Comparison Of Various Determinations of Φ, k_3, k_4, and k_6

Comparison of Φ Values

Determinations of Φ may be conveniently divided into two groups: those in which the $O_2(\Sigma)$ was detected by its emission at 7619 Å and those in which the presence of $O_2(\Sigma)$ was inferred, less directly, by its subsequent reactions.

The former group, while providing very

Can. J. Chem. Downloaded from www.nrcresearchpress.com by 210.87.254.40 on 09/05/12
For personal use only.

specific identification of $O_2(\Sigma)$, is subject to the difficulties of making absolute $O_2(\Sigma)$ emission measurements (16, 17) or measuring $O_2(\Sigma)$ emission relative to some internal standard such as the NO_2 continuum (18) or the $O_2(\Delta)$ emission (20). Because of the inherent difficulty of these measurements, and their frequent dependence on other quantities such as Einstein *A* factors or rates of specific reactions, the results are necessarily less reliable. In this group we may include the measurements of Noxon (16), Young and Black (17), Gilpin *et al.* (14), Snelling and Gauthier (20), and Izod and Wayne (18). All of these measurements, with the exception of those in ref. 18, are consistent with a Φ of unity. The results of Izod and Wayne (18) have been criticized by Clark (19) who showed that vortex formation around the photolysis window could have led to large errors in Φ. However, this question has not been completely resolved (see ref. 29 and references contained therein) and the low values of Φ (≈ 0.01) remains very uncertain.

Probably the most reliable measurements of those listed above are refs. 16 and 20. Noxon (16) deduced that Φ was probably near unity and certainly $\geqslant 0.3$. Snelling and Gauthier (20) measured the relative intensities of $O_2(\Sigma)$ and $O_2(\Delta)$ from photolysis of O_3/O_2 mixtures and concluded that $\Phi = 0.85$. This result was very dependent on the value k_4 used in the derivation of Φ (*i.e.* 2.5×10^{-11} or 7×10^{-12}, see Table 2). The higher of these two values was chosen at the time and our own measurement of 2.3×10^{-11} for k_4 now supports this earlier choice. However, the result is still dependent on the Einstein *A* factors for the $O_2(\Sigma)$ and $O_2(\Delta)$ emissions as well as the rate of reaction 4. Taking account of these uncertainties, and the experimental error, a value of $\Phi \geqslant 0.5$ seems reasonable.

We now turn to the second group of Φ determinations. From flash photolysis experiments, Biedenkapp and Bair (21) concluded that $\Phi = 0.6$ to 1.0. Jones *et al.* (22) interpreted O_3 quantum yield measurements to indicate that $\Phi \leqslant 0.2$, but similar experiments (23) were consistent with $\Phi = 0.6$. There was rather a large scatter in the former experimental results and the latter work seems more reliable.

We may summarize the above discussion by noting that experiments favoring a Φ value of unity are both more numerous and more reliable. Taking account of experimental errors in the various determinations a value of $\Phi \geqslant 0.5$ is indicated. In the following discussion we consider in some detail three further experiments which indicate a lower value for Φ (24, 25, 29).

McGrath and co-workers, using flash photolysis techniques, concluded that $\Phi = 0.4 \pm 0.1$ (24) and that vibrationally excited $O_2(^3\Sigma_g^-)$ was formed with a yield of $\geqslant 0.3$ (25). The conclusion that $\Phi = 0.4$ was based on experiments similar to our own, hence, the different conclusions are somewhat surprising and the two experiments will be compared in some detail.

The principal experimental differences are that Langley and McGrath used an O_3 pressure of 1.0 Torr and their measurements of O_3 decomposition were confined to the period 1 to 2 ms following the flash, using monitoring radiation at 2900 Å. The mixtures were diluted with 100 Torr of Ar. These mixtures were 4 to 25 times less dilute than those used in our work and hence considerable temperature increases are to be anticipated. The O_3 decay curves were stated to be linear in the 1 to 2 ms time region and were extrapolated to obtain the O_3 decomposition immediately following the flash. Detailed experimental conditions were not given but the fractions of O_3 decomposed after the flash were stated to be 0.16 for $O_3/N_2/Ar$ mixtures, 0.32 for O_3/Ar mixtures, and 0.22 for $O_3/O_2/Ar$ mixtures. The simple 2:1 ratio for O_3/Ar compared to $O_3/N_2/Ar$ was explained as photolysis followed by reaction 8 for O_3/Ar mixtures and photolysis alone for $O_3/N_2/Ar$ mixtures, where O(D) is deactivated by N_2 rather than reacting with O_3. The O_3 decomposition for $O_3/Ar/O_2$ mixtures was then attributed to photolysis followed by reactions 2 and 4 and Φ was thus deduced to be $(1 - (0.32 - 0.22)/0.16) = 0.37$. In the absence of O_3 decay curves and detailed experimental conditions for ref. 24 it is difficult to compare the two experiments. However, we feel our experiments are more reliable for the following reasons.

Firstly, the simple 2:1 relationship noted above is only expected if O_3 is optically thick to photolysis radiation. For the optically thin limit (*i.e.* absorption of photolysis radiation proportional to O_3 concentration) the $O(D) + O_3$ reaction depletes the O_3 during the flash (the lifetime of O(D) will be $\lesssim 0.1$ μs) and hence reduces the amount of O_3 photolysis in the O_3/Ar experiments below that found in the $O_3/N_2/Ar$ experiments. If we assume that the

Can. J. Chem. Downloaded from www.nrcresearchpress.com by 210.87.254.40 on 09/05/12
For personal use only.

observed fractional O_3 decomposition for $O_3/N_2/Ar$ mixtures (0.16) to represent the fraction of O_3 photolyzed, then the calculated fraction of O_3 photolyzed for O_3/Ar mixtures is 0.15. This calculated value which was obtained using our Runge–Kutta integration routine is independent of the time dependence of the flash provided, as in this case, the O(D) lifetime is short compared to the flash duration. Thus the fractional O_3 decomposition, immediately after the flash, for these mixtures is expected to be 2×0.15 or 0.30 rather than 0.32. (Although a detailed description of the apparatus is not given the conditions appear to correspond more closely to the optically thin than the optically thick regime. The reaction vessel was a 20 mm o.d. quartz tube, and even for the peak of the O_3 absorption at 2550 Å, the transmission of photolysis radiation for a single pass through the reaction vessel $\geqslant 50\%$.) Thus the 2:1 ratio observed is somewhat surprising since for the optically thin regime the O_3 decomposition for O_3/Ar mixtures is expected to be $\approx 2 \times 0.15$ or 0.30 rather than 0.32. Furthermore, with the large value of k_8/k_3 (see Table 2) it is not clear that enough N_2 was added to completely deactivate O(D).

Secondly, in the absence of detailed modeling the extrapolation procedure is somewhat uncertain. In this context the products of reaction are uncertain and may involve excited states of O_2 (23) which are capable of decomposing O_3. Furthermore the high O_3 pressure used and large temperature increases which can be expected (≈ 50–$100°$) make reactions 5 and 7 much more important than in our work. It should be noted that even a 5% uncertainty in the observed (24) fractional O_3 decompositions of 0.32 and 0.22 leads to an uncertainty in Φ of 0.37 ± 0.20.

Thirdly, the experimental results and the value of Φ of 0.37 were used to deduce a value of k_2/k_8 of 0.79 whereas the available information (2, 3, 14, 23, 30) indicates that k_2/k_8 is 0.10 to 0.20. An examination of eq. 6, ref. 24 indicates that a higher value of Φ would result in a lower value of k_2/k_8 and better agreement with other values of this quantity.

In summary because of the uncertainties discussed above and because we have used a much lower O_3 pressure (0.014 Torr) and taken O_3 decay measurements as early as 200 μs following the flash we consider that our results are more reliable. The precision of our results has been established by averaging up to 10 separate experiments.

From other flash photolysis experiments McCullough and co-worker (25) have deduced that $O_2(^3\Sigma_g^-)\, v > 0$ is formed in reaction 2 with an efficiency $\geqslant 0.30$; this result is again in conflict with our results that $\Phi \geqslant 0.75$. It was observed (25) that at $t = 20$ μs, O_2 $v = 13$ and 14 increased with addition of up to 20 Torr of O_2 to mixtures containing O_3 (20 Torr) and He (215 Torr). It was also observed that no increase in O_2 $v = 15$ occurred. The results were analyzed by a simple mechanism involving production of vibrationally excited O_2 in reactions 2 and 8. (It should be noted that reaction 8 is 139 kcal/mol exothermic and population of vibrational levels of O_2 up to the dissociation limit is possible.) The ratio of vibrationally excited O_2 with ($[O_2]_v$) and without ($[O_2]_v^1$) addition of O_2 was deduced to be

$$[O_2]_v/[O_2]_v^1 = 1 + (k_2(v)/k_8(v))[O_2]/[O_3]$$

where $k_2(v)$ and $k_8(v)$ are the specific rates of reactions 2 and 8 to produce O_2 in vibrational level v. From the observed increase of O_2 $v = 13$ and 14 with added O_2, and using $k_8 = 6 \times 10^{-11}$ in the equation above, $k_2(13)$ and $k_2(14)$ were found to be 1.4×10^{-11} and 0.4×10^{-11}, respectively (25). Finally, assuming $k_2 = 6 \times 10^{-11}$, it was concluded that $(k_2(13) + k_2(14)/k_2 \geqslant 0.3$ (where k_2 is the total rate constant for reaction 2, *i.e.* the rate of deactivation of O(D) by O_2). In the analysis (25) it appears that the rate of production of O_2 $v = 13$ and 14 in reaction 8 has been incorrectly set equal to the total rate of reaction 8. The value of k_8 used (6×10^{-11}) (21) is somewhat slower than indicated by more recent work, $(2.5 \pm 1.0) \times 10^{-10}$ (14), and $(3.5 \pm 0.3) \times 10^{-10}$ (26). If $k_8 = 3.5 \times 10^{-10}$ had been used in the analysis of McCullough and co-worker then $k_2(v)$ values of 8.2×10^{-11} ($v = 13$) and 2.3×10^{-11} ($v = 14$) would have been obtained. The combined rate into $v = 13$ and 14 is then higher than the total rate of quenching of O(D) by O_2(12). However, as noted above, it is the specific rate of reaction 8 to produce vibrationally excited O_2 which should have been used in the analysis. Since vibrationally excited O_2 is not the only product of reaction 8 (27, 29, 32) and since the complete initial distribution of vibrators is not known, the specific rates $k_8(v)$ cannot be readily calculated.

However, in a recent series of papers, Webster

Can. J. Chem. Downloaded from www.nrcresearchpress.com by 210.87.254.40 on 09/05/12
For personal use only.

and Bair (27, 28) have determined the initial distribution of O_2 in levels $v = 14$ to 21 from the reaction of O(D) with O_3. This initial distribution was consistent with a vibrational temperature of 23 400 °K and it was further shown that $\approx 6\%$ of the O(D) + O_3 reaction produced vibrationally excited O_2. This latter conclusion is in satisfactory agreement with an earlier estimate that $\geqslant 90\%$ of the O(D) + O_3 reactive collisions produced 2O + O_2 (32). Thus, from these findings we can estimate that $k_8(13)/k_8 \approx k_8(14)/k_8 \approx 3 \times 10^{-3}$ where $k_8(13)$ and $k_8(14)$ are the rate constants for formation of O_2 $v = 13$ and 14 and k_8 is the total rate constant for reaction 8. Thus, for $k_8 = 3.5 \times 10^{-10}$, $k_8(13) \approx k_8(14) \approx 10^{-12}$. Substituting these values into the equation of McCullough and co-worker above gives $k_2(13) = 2.3 \times 10^{-13}$ and $k_2(14) = 7 \times 10^{-14}$. The rate of production of vibrationally excited O_2 is then a minor process since the total rate of reaction 2 is 6×10^{-11} (12).

However, this conclusion should be adopted with some caution since this rather simple analysis neglects several important processes. Firstly, excitation of $O_2(v = 14)$ in reaction 2 is approximately 10 kcal endothermic. As noted by McCullough and co-worker the O(D) may be translationally hot since reaction 1 is $\approx$ 19 kcal exothermic (for $\lambda = 2550$ Å, the peak wavelength of O_3 absorption). Classically, the O(D) atom would have 2/3 of the available translational energy. Thus, if no energy is lost in vibrational or rotational excitation of O_2 then the O(D) atom would have $\approx$12 kcal of translational energy. However, it seems unlikely that sufficient translational energy will survive for the experimental conditions of McCullough and co-worker (25) (O_2, 20 Torr; He, 200 Torr) to account for substantial excitation of $O_2(v = 14)$ by [2]. Secondly, the effect of V–V energy transfer was not considered explicitly and it was assumed that no appreciable relaxation of vibrationally excited O_2 occurred in the 20 μs following the flash. This latter assumption is in direct conflict with the deductions of Fitzsimmons and Bair (31) that V–V energy transfer from $O_2(v = 1)$ to O_3 occurred with a probability of 4.3×10^{-3} and that this probability increased linearly with v. For the experimental conditions of McCullough and co-worker there would be $\approx$4000 collisions of vibrationally excited O_2 with O_3 in the first 20 μs and about the same number with O_2 at the highest O_2 pressure used. Thus, it seems very unlikely that V–V transfer can be neglected and, in fact, the observed increase of O_2 in levels $v = 13$ and 14 may be the result of vibrational deactivation of $O_2(v \geqslant 15)$ by O_2. Substantial population of levels $v \geqslant 15$ has been demonstrated by Webster and Bair (28).

During the preparation of this manuscript further analyses of these results were published (37) and the distribution of products in reaction 8 was accounted for by including a factor γ which is the fraction of reactive collisions leading O_2 productions in vibrational levels 13 and 14. The modified expression for $[O_2]_v^1/[O_2]_v^1$ was deduced to be

$$[O_2]_v/[O_2]_v^1 = (\gamma k_8 + \alpha_v k_2[M])/(\gamma k_8 + \gamma k_2[M])$$

where α_v is the fraction of reaction 2 leading to production of O_2 in levels $v = 13$ and 14, *i.e.* $\alpha = (k_2(13) + k_2(14)/k_2$. By fitting this expression to the experimental data for various values of γ corresponding values of α_v were deduced and a graph of α_v *vs.* γ constructed. Using an upper limit for γ of 0.1 from ref. 32 it was considered that $\alpha_v \leqslant 0.5$ and this result was coupled with the conclusion from the earlier work (25) that $\alpha_v \geqslant 0.3$ to give $0.3 \leqslant \alpha_v \leqslant 0.5$ and hence $0.06 \leqslant \gamma \leqslant 0.1$. However, as has been suggested above this lower limit to α_v is probably incorrect because the rate of production of O_2 $v = 13$ and 14 was incorrectly set equal to the total rate of reaction 8. In fact it has been estimated above, from the work of Bair and co-workers, that $\gamma \simeq 6 \times 10^{-3}$ for which $\alpha_v = 0.03$. Therefore we feel that this new analysis does not substantiate the higher values of α_v claimed and that a more detailed analysis of the results, including the possible effects of vibrational–vibrational energy transfer from O_2 to O_2 and O_3, is required.

We should note at this point that the possibility of vibrationally excited O_2 participating in the decomposition of O_3 in our experiments has not been considered. However, even if O_2 were formed with sufficient vibrational excitation to decompose O_3 we consider it unlikely that this would occur in a one step process. In fact the evidence indicates that O_2 vibrational energy is lost in single quantum steps (31) and that considerable vibrational excitation of the O_3 occurs by V–V processes (15). Even if the one step O_3 dissociation process were to occur with collisionally limited rate the vibrationally ex-

Can. J. Chem. Downloaded from www.nrcresearchpress.com by 210.87.254.40 on 09/05/12
For personal use only.

cited O_2 would have to survive more than 2500 collisions with O_2 for our experimental conditions. Thus we consider that this process is extremely unlikely under our experimental conditions.

Very recently (29) Giachardi and Wayne have studied O_3 decomposition in a flow system by monitoring both the O_3 decomposition and the O atom production. These quantities were measured for O_3/N_2 mixtures in order to establish the amount of photolysis. (This is equivalent to our procedure for obtaining k_1.) The increased O_3 decomposition and O atom production for O_3/O_2 mixtures were then interpreted to show that $\Phi = 0.5$ to 0.6. However, in establishing the amount of photolysis from graphs of $\Delta[O_3]$ *vs.* $[O_3]$ or $[O]$ *vs.* $[O_3]$ for O_3/N_2 mixtures, reaction 8 appears to have been neglected, although insufficient N_2 was present to completely suppress this reaction. If a correction for this reaction is applied to their data then the experimental values of $\Delta[O_3]$ must be reduced to account for the O_3 destroyed in reaction 8. We can readily apply a correction to their data by noting that the $\Delta[O_3]$ data in Fig. 3, ref. 29 should be divided by $1 + k_8[O_3]/(k_8[O_3] + k_3[N_2])$ to correct for the additional O_3 destruction in reaction 8. A similar correction to the O_3/O_2 data from Fig. 5 of ref. 29 is obtained by setting their $\Phi(O_2)$ equal to $1 + \alpha k_2[O_2]/(k_2[O_2] + k_8[O_3]) + k_8[O_3]/(k_8[O_3] + k_2[O_2])$ rather than $1 + \alpha$. α, which is equivalent to our Φ, is the fraction of reaction 2 producing $O_2(^1\Sigma_g^+)$. Relative O(D) reaction rates are sufficient to make this correction. As discussed previously k_8/k_2 is 5 to 10 (2, 3, 14, 23) and the measurements of k_3/k_2 to be discussed later indicate that $k_3/k_2 = 0.8 \pm 0.2$. From these results we conclude that k_8/k_3 is between 5 and 15. We have applied the corrections outlined above assuming values of k_8/k_3 of 5, 10, and 15 and corresponding values of k_8/k_2 of 4, 8, and 12. With these corrections the parameter β of ref. 29 (equivalent to our k_1) was 3.03, 2.85, and 2.72 (units s^{-1}) for the three assumed values of the relative $O(^1D)$ rates and the corresponding values of α (our Φ) were 0.71, 0.81, and 0.91. The uncorrected values were $\beta = 3.26\ s^{-1}$ and $\alpha = 0.61$. The intermediate quantum yield for O_3/He mixtures (see ref. 29) is increased from 1.89 to 2.04, 2.16, and 2.27 for β equal to 3.03, 2.85, and 2.72. Several points should be noted concerning these results.

For the largest value of k_8/k_3 the fit to the O_3/N_2 data is somewhat poor, being too high for the higher O_3 concentrations and too low for the lower O_3 concentrations. A further indication that the highest value of k_8/k_3 is not consistent with the data is the value of 2.27 for the intermediate quantum yield in O_3/He mixtures which should be 2.0 for a mechanism involving photolysis followed by reaction 8. However, the lowest value of k_8/k_3 increases the intermediate quantum yield from 1.84 to 2.04 yielding better agreement with the prepared mechanism. For the two lowest values of k_8/k_3 the calculated curves appear to be in satisfactory agreement with data shown in Figs. 3 and 5 of ref. 29.

We have also applied the correction using values of $k_8:k_3:k_2$ of 5:1.7:1 listed in ref. 29, the values of β and α obtained were 3.11 s^{-1} and 0.65, respectively. However the values of k_3 and k_2 were based on earlier work of Noxon (16) and more recent results from this group (36) indicate that $k_3/k_2 = 0.7$–0.8 which would lead to a set of relative rates $k_8:k_3:k_2$ of 5:0.7–0.8:1.0 *i.e.* $k_8/k_3 = 6.7$ and $k_8/k_2 = 5$. These relative rates would produce a correction intermediate between the two lowest values of k_8/k_3 and k_8/k_2 used above.

From the above discussion we conclude that the results of Giachardi and Wayne are probably consistent with $\alpha = 0.75$. However, we have only applied the corrections to the typical examples of the data given in ref. 29 and correcting all the data may change the quantitative results. Thus the values of β and α deduced above should be regarded as first approximations.

We have not attempted to apply a similar correction to the O atom data of Giachardi and Wayne since this correction is more complicated and will be dependent on the fraction $O(D) + O_3$ reactive collisions which produce $2O + O_2$. There is no general agreement on this latter quantity (23, 27, 29, 32, 33).

From the above discussion we conclude that the experiments indicating a value of Φ less than 0.75 can be reinterpreted and it appears very likely that $\Phi \geqslant 0.75$.

Comparison of k_3 Values

Since our primary concern here is with relative O(D) rates and the fate of O(D) in the atmosphere this discussion will be concerned with the available information on k_3/k_2. There now appears to be rather good agreement on k_3/k_2 since

recent results have provided values of 0.7 to 0.8 (36), 0.64 (34), 1.0 (35), 0.72 ± 0.08 (3), which are in good agreement with our own value of 0.7 ± 0.25. All these measurements are in agreement with $k_3/k_2 = 0.8 \pm 0.2$.

Comparison of k_4 Values

As discussed above and shown in Table 2 there are two reported values of k_4. Our own measurement $k_4 = (2.3 \pm 0.5) \times 10^{-11}$ is in excellent agreement with the higher of these two values obtained by Gilpin *et al.* (14) who found $k_4 = 2.5 \times 10^{-11}$.

Comparison of k_6 Values

This is the principal reaction responsible for formation of O_3 in the atmosphere below 100 km and has been the object of many studies. Most of the available information, which has been discussed in recent review articles (2, 7, 9), indicates that k_6 is between 4×10^{-34} and 9×10^{-34}. Our own value of 4.9×10^{-34} is in the lower range of these reported values.

The author is greatly indebted to A. Tardif who designed the flash photolysis cell and performed many of the experiments. The author is also indebted to J. Oman for his painstaking help in performing these experiments.

1. W. B. DeMore and O. F. Raper. J. Chem. Phys. **44**, 1780 (1966).
2. H. I. Schiff. Ann. Géophys. **28**, 67 (1972).
3. M. Gauthier and D. R. Snelling. J. Chem. Phys. **54**, 4317 (1971).
4. C. J. Fortin, D. R. Snelling, and A. Tardif. Can. J. Chem. **50**, 2747 (1972).
5. I. T. N. Jones and R. P. Wayne. Proc. R. Soc. London, A**321**, 409 (1971).
6. E. C. Y. Inn and Y. Tanaka. J. Opt. Soc. Am. **43**, 870 (1954).
7. H. I. Schiff. Can. J. Chem. **47**, 1903 (1969).
8. K. Schofield. Planet. Space Sci. **15**, 643 (1967).
9. H. S. Johnston. Gas phase reaction kinetics of neutral oxygen species. U.S. Dept. of Commerce NSRDS-NBS20. 1968.
10. K. H. Becker, W. Groth, and U. Schurath. Chem. Phys. Lett. **8**, 259 (1971).
11. F. D. Findlay and D. R. Snelling. J. Chem. Phys. **54**, 2750 (1971).
12. R. J. Donovan and D. Husain. Chem. Rev. **70**, 489 (1970).
13. T. P. J. Izod and R. P. Wayne. Proc. R. Soc. London, A**308**, 81 (1968).
14. R. Gilpin, H. I. Schiff, and K. H. Welge. J. Chem. Phys. **55**, 1087 (1971).
15. V. D. Baiamonte, D. R. Snelling, and E. J. Bair. J. Chem. Phys. **44**, 673 (1966).
16. J. F. Noxon. J. Chem. Phys. **52**, 1852 (1970).
17. R. A. Young and G. Black. J. Chem. Phys. **47**, 2311 (1967).
18. T. P. J. Izod and R. P. Wayne. Chem. Phys. Lett. **4**, 208 (1969).
19. I. D. Clark. Chem. Phys. Lett. **5**, 317 (1970).
20. D. R. Snelling and M. Gauthier. Chem. Phys. Lett. **9**, 254 (1971).
21. D. Biedenkapp and E. J. Bair. J. Chem. Phys. **52**, 6119 (1970).
22. I. T. N. Jones, U. B. Kaczmar, and R. P. Wayne. Proc. R. Soc. London, A**316**, 431 (1970).
23. G. von Ellenrieder, E. Castellano, and H. J. Schumacher. Chem. Phys. Lett. **9**, 152 (1971).
24. K. F. Langley and W. D. McGrath. Planet. Space Sci. **19**, 416 (1971).
25. D. W. McCullough and W. D. McGrath. Chem. Phys. Lett. **12**, 98 (1971).
26. R. F. Heidner III, D. Husain, and J. R. Wiesenfeld. Chem. Phys. Lett. **16**, 530 (1972).
27. H. Webster III and E. J. Bair. J. Chem. Phys. **56**, 6104 (1972).
28. H. Webster III and E. J. Bair. J. Chem. Phys. **57**, 3802 (1972).
29. D. J. Giachardi and R. P. Wayne. Proc. R. Soc. London, A**330**, 131 (1972).
30. D. R. Snelling and E. J. Bair. J. Chem. Phys. **47**, 228 (1967).
31. R. V. Fitzsimmons and E. J. Bair. J. Chem. Phys. **40**, 451 (1964).
32. V. D. Baiamonte, L. G. Hartshorn, and E. J. Bair. J. Chem. Phys. **55**, 3617 (1971).
33. H. Webster III and E. J. Bair. J. Chem. Phys. **53**, 4532 (1970).
34. M. Loewenstein. J. Chem. Phys. **54**, 2282 (1971).
35. W. B. DeMore. J. Chem. Phys. **52**, 4309 (1970).
36. I. D. Clark and J. F. Noxon. J. Chem. Phys. **57**, 1033 (1972).
37. D. W. McCullough and W. D. McGrath. J. Photochem. **1**, 241 (1972).

Can. J. Chem. Downloaded from www.nrcresearchpress.com by 210.87.254.40 on 09/05/12
For personal use only.

Infrared Chemiluminescence from the Reactions of Oxygen Atoms with Halomethanes

S. J. ARNOLD, G. H. KIMBELL, AND D. R. SNELLING

Centre de Recherches pour la Defense, Defence Research Establishment, Valcartier, Québec

Received July 6, 1973

Infrared chemiluminescence from vibrationally excited CO was observed when CH_3Cl, CH_2Cl_2, $CHCl_3$, or CH_2Br_2 was introduced into a stream of oxygen atoms. Emission from vibrationally excited HCl was also observed from CH_2Cl_2 and $CHCl_3$. The mechanisms describing the reactions of oxygen atoms with these molecules are discussed in detail. The reaction step responsible for the formation of CO† is postulated to be

$$O + CX_1X_2 \rightarrow CO\dagger + X_1 + X_2 \ (X_1, X_2 = \text{H or halogen})$$

and for HCl†

$$H + Cl_2 \rightarrow HCl\dagger + Cl$$

La chimiluminescence infrarouge de CO vibrationnellement excité est observée lorsque CH_3Cl, CH_2Cl_2, $CHCl_3$ ou CH_2Br_2 est introduit dans un courant d'atomes d'oxygène. L'émission de HCl vibrationnellement excité est aussi observée avec CH_2Cl_2 et $CHCl_3$. Les mécanismes qui décrivent les réactions des atomes d'oxygène avec ces molécules sont discutés en détail. On suppose que l'étape de la réaction responsable de la formation de CO† est

$$O + CX_1X_2 \rightarrow CO\dagger + X_1 + X_2 \ (X_1, X_2 = \text{H ou halogène})$$

pour la formation de HCl† ce serait.

$$H + Cl_2 \rightarrow HCl\dagger + Cl$$

[Traduit par le journal]

Can. J. Chem., **52**, 271 (1974)

Introduction

The recent discoveries of hydrogen halide and carbon monoxide chemical lasers have prompted numerous studies of chemical systems capable of producing i.r. chemiluminescence. Among these are studies of the reactions of oxygen atoms with CS_2, C_2H_2, and CH_3C_2H (1–3). In these reactions carbon monoxide is produced with very high vibrational excitation. No reports of similar chemiluminescence studies, or in fact, of any systematic investigations of the reactions of oxygen atoms with halogenated methanes have appeared in the literature. Harteck and Kopsch (4) in 1930 tabulated the reaction products and reported visible chemiluminescence from the reactions of oxygen atoms with chloromethanes. Recently, the rates of oxygen atom reactions with CH_3Cl, CH_3Br, CH_3F (5), and $CHCl_3$ (6) have been measured.

Lin (7) has observed, in chemical laser studies, that $O(^1D)$ atoms, obtained from the u.v. photolysis of ozone, readily insert into the C—H bonds of molecules such as CH_nX_{4-n} (X = F, Cl) and that the resulting unstable alcohol eliminates HX (X = F, Cl) producing vibrationally excited HF or HCl. In recent experiments on the reactions of $O(^3P)$ atoms with $CHBr_3$, however, Lin (8) has observed that CO was the lasing molecule and that the reaction mechanism was considerably more complex.

The present experiments show that intense i.r. chemiluminescence is produced when oxygen atoms react with CH_3Cl, CH_2Cl_2, $CHCl_3$, and CH_2Br_2. The chemiluminescence arises from vibrationally excited CO and, also, in the case of chloromethanes from vibrationally excited HCl.

Experimental

The apparatus used in these experiments is identical to that shown in Fig. 1 of ref. 3*b*. The reaction cell consisted of a 1.5 in. glass "tee" equipped with an NaCl window, which was pumped by an Edwards 660 l/min two stage pump. Oxygen atoms produced by the passage of an oxygen–helium mixture through a 2450 MHz microwave discharge entered the cell through the center tube of the concentric mixer. The halogenated methane in a helium buffer entered through five holes in the outer tube of the concentric mixer. Carbon monoxide, when introduced, was premixed with the halogenated methane – helium mixture.

The spectra were recorded using a McPherson Model 218 0.3 m monochromator equipped with a 300 line/mm grating, a Dry Ice – acetone cooled PbS detector, a phase sensitive PAR Model HR-8 amplifier, and a Hewlett–Packard Model 7100 B strip chart recorder. This assembly

Can. J. Chem. Downloaded from www.nrcresearchpress.com by 210.87.254.40 on 09/05/12
For personal use only.

TABLE 1. Reaction products observed in CH_nX_{4-n}–O_2 atomic flames

Chloromethane	Products
CH_3Cl	CO*, CO_2*, HCl*, CH_2Cl_2, $CHCl_3$
CH_2Cl_2	CO, CO_2, HCl, Cl_2*, CCl_2O*, $C_2H_2Cl_2$, $C_2H_2Cl_2O$, C_2H_2, CH_4,
$CHCl_3$	CO, CO_2, HCl*, Cl_2*, CCl_2O*, CCl_4

*Also observed in a mass spectrometric study by Harteck and Kopsch (*4a* and *b*).

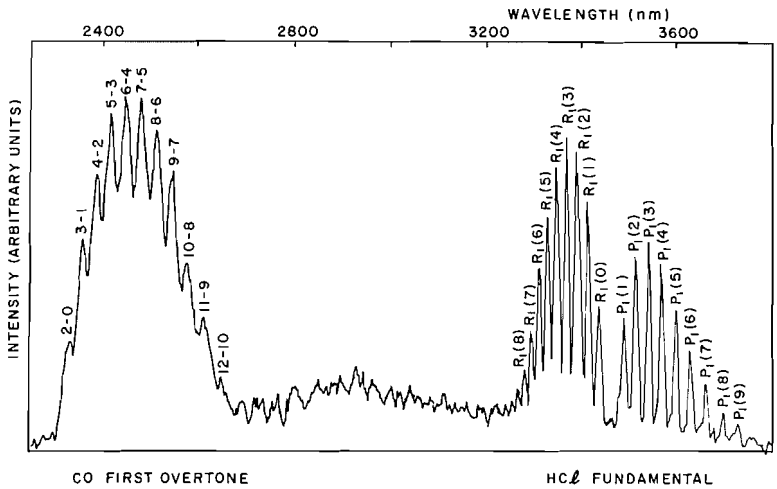

FIG. 1. The CO first overtone emission and the HCl fundamental emission from the CH_2Cl_2/O_2 atomic flame. Flow rates $CH_2Cl_2:O_2:He$, 200:54:4800 μmol/s, total pressure, 8.4 Torr, temperature 373 °K.

permitted spectral studies in the region 1500–4000 nm. The entire optical path was flushed with dry nitrogen to minimize absorption by atmospheric water vapor. A 500 °C black body source was used to provide a relative measurement of the sensitivity of the detection system as a function of wavelength.

Temperatures in the reaction zone were measured with a glass coated chromel–alumel thermocouple.

Reaction products, trapped at liquid nitrogen temperatures, were analyzed by means of a CEC Model 72-104 mass spectrometer and a Perkin–Elmer Model 900 vapor phase chromatograph.

All gases used were of the highest purity available from Matheson and were used without further purification. The CH_2Cl_2 and CH_2Br_2 were supplied by J. T. Baker Chemical Company and the $CHCl_3$ and CCl_4 by the Fisher Scientific Company. Gas flows were measured using Matheson rotameters.

Results

Infrared chemiluminescence was observed from the reaction of oxygen atoms with CH_3Cl, CH_2Cl_2, $CHCl_3$, and CH_2Br_2. No i.r. chemiluminescence in the region 1500–4000 nm could be detected from the reaction of oxygen atoms with CCl_4. In the case of the chlorinated methanes mass spectrometric and vapor phase chromatographic analysis of the reaction products yielded the results shown in Table 1.

The pressure for all experiments was (8.4 ± 0.2) Torr. The flow rates of the inert buffer, He, and of O_2 were 4.8 and 5.4 × 10^{-2} mmol/s, respectively.

Methylene Chloride

Strong i.r. chemiluminescence was observed from the reaction of oxygen atoms with CH_2Cl_2. As is shown in Fig. 1, two emitting species were present. First overtone emission from CO† was observed in the region 2300–2800 nm, fundamental emission from HCl† in the region 3250–3800 nm, and first overtone emission from HCl† in the region 1700–2100 nm (see Fig. 2).

It was suggested[1] that vibrationally excited CO might arise from an electronic to vibration energy transfer process between electronically excited He formed in the discharge and CO ($v = 0$) formed as a result of the chemical reaction. This process although feasible, does not take place under the present experimental conditions. When the CH_2Cl_2 was replaced by CO no emission from vibrationally excited CO was

[1]Suggested by the referee.

Can. J. Chem. Downloaded from www.nrcresearchpress.com by 210.87.254.40 on 09/05/12
For personal use only.

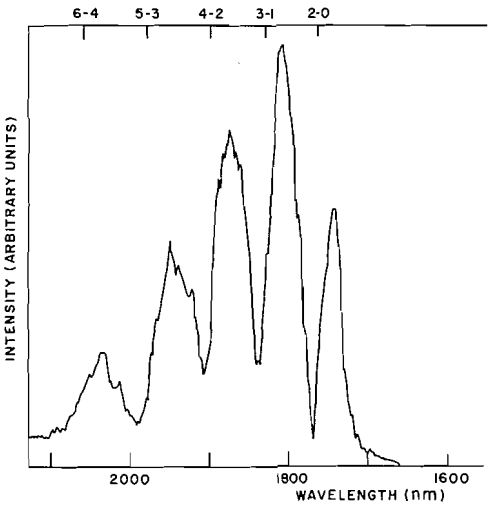

FIG. 2. The HCl overtone emission from the CH_2Cl_2/O_2 atomic flame for the experimental conditions of Fig. 1.

detectable. (The CO flow was varied between 5.4×10^{-4} and 5.4×10^{-2} mmol/s.)

Only the first 12 vibrational levels of CO† were appreciably populated. Figure 3 shows a plot of the relative vibrational level population, Nv, calculated according to the method of Hancock and Smith (1*a*), against vibrational number, v, for conditions of maximum total emission intensity (CH_2Cl_2:O_2 ratio of 3.7:1.0). Under these conditions the system did not exhibit a complete population inversion. As in the case of the oxygen atom – C_2H_2 system (3*b*), when vibrationally "cold" CO was premixed with the C_2H_2–He mixture, a vibrational population inversion was marginally sustained at the 7–6 and 6–5 transitions.

The relative vibrational level distribution appeared to be independent of the amount of fuel added. When the CH_2Cl_2 concentration was varied by a factor of 10 no apparent change in the distribution was observed. In addition, when the microwave power into the oxygen line was varied from 50 to 150 W no change in the distribution was observed, although the total emission intensity increased by a factor of 2. Thus it seems unlikely that vibrational deactivation by fuel molecules or by combustion products plays an important part in altering the vibrational energy distribution of the product CO. Similar results were observed when $CHCl_3$ was used as a fuel. However, the residence time in the viewed region of ~8 ms is of the same order of magnitude as the radiative lifetime of the vibrational levels of CO (5 ms for $v = 8$, 10.7 ms for $v = 3$). Hence, although the relative vibrational level distributions for various fuels can be compared one with another, they represent partially relaxed distributions with the populations in the higher vibrational levels reduced with respect to those in the lower vibrational levels.

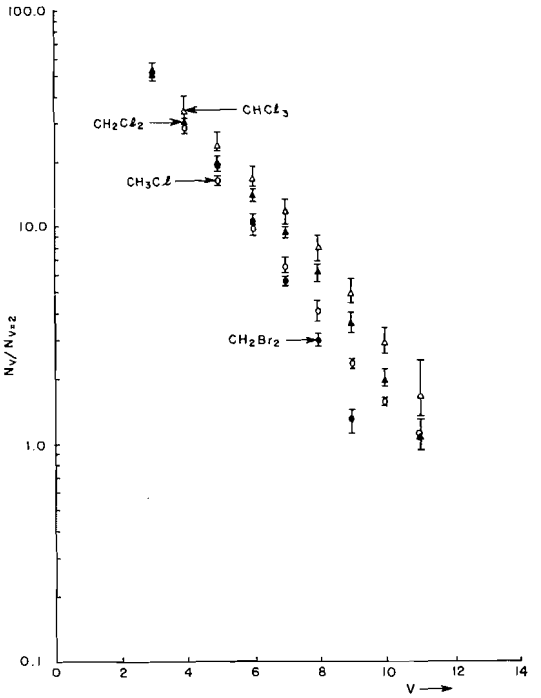

FIG. 3. Relative vibrational level population of CO† produced in CH_nX_{4-n}/O_2 (X = Cl, Br) atomic flames. The error bars represent the spread in data for the following number of separate experimental determinations: $CHCl_3 = 10$, $CH_2Cl_2 = 10$, $CH_3Cl = 5$, $CH_2Br_2 = 8$.

A rotational analysis of the emission in the region 3250–3800 nm indicated that both the first and second vibrational levels of HCl† were appreciably populated. Observations of the first overtone of HCl† indicated that the 3rd, 4th, 5th, and 6th vibrational levels were also weakly populated (Fig. 2). Detailed analysis of the emission from the fundamental in the upper vibrational levels was not attempted since the sensitivity of the cooled PbS detector fell rapidly in this region.

Chloroform

Infrared chemiluminescence from CO† and HCl† was observed from the reactions of oxygen atoms with $CHCl_3$. As in the case of CH_2Cl_2 only the first 12 vibrational levels of CO† were

Can. J. Chem. Downloaded from www.nrcresearchpress.com by 210.87.254.40 on 09/05/12
For personal use only.

TABLE 2. Summary of elementary reactions and their rate constants of importance in the reactions of oxygen atoms with chlorinated methanes. Units are in cm^3 $molecule^{-1}$ s^{-1}

Reaction	Rate constant	Temperature (°K)	Reference
$OH + CH_4 \rightarrow H_2O + CH_3$	$1.2 \times 10^{-10} \exp\{-5910/RT\}$	300–1850	15
$O + OH \rightarrow O_2 + H$	$(5 \pm 2) \times 10^{-11}$	300	10
$O + CH_3Cl \rightarrow OH + CH_2Cl$	$3.0 \times 10^{-11} \exp\{-7930/RT\}$	350–950	5*a*
	$4.2 \times 10^{-11} \exp\{-(3880 \pm 220)/RT\}$	336–662	5*b*
$O + CH_2Cl_2 \rightarrow OH + CHCl_2$	No known value		
$O + CHCl_3 \rightarrow OH + CCl_3$	2.5×10^{-15}	300	6
$H + CH_3Cl \rightarrow HCl + CH_3$	No known value		
$H + CH_2Cl_2 \rightarrow HCl + CH_2Cl$	$1.8 \times 10^{-11} \exp\{-6100/RT\}$	298–460	14
$H + CHCl_3 \rightarrow HCl + CHCl_2$	No known value		
$H + CCl_4 \rightarrow HCl + CCl_3$	2×10^{-14}	300	13
$H + HCl \rightarrow H_2 + Cl$	$3.8 \times 10^{-11} \exp\{-3500/RT\}$	195–497	21
$H + Cl_2 \rightarrow HCl + Cl$	1.0×10^{-11}	300	22
$Cl + H_2 \rightarrow HCl + H$	$6.0 \times 10^{-11} \exp\{-4300/RT\}$	195–497	21
$Cl + CH_3Cl \rightarrow HCl + CH_2Cl$	$5.66 \times 10^{-11} \exp\{-3300/RT\}$	273–573	24
$Cl + CH_2Cl_2 \rightarrow HCl + CHCl_2$	$4.5 \times 10^{-11} \exp\{-3000/RT\}$	273–573	24
	$(5.5 \pm 0.5) \times 10^{-13}$	298	25
$Cl + CHCl_3 \rightarrow HCl + CCl_3$	$1.2 \times 10^{-11} \exp\{-3350/RT\}$	273–573	24

appreciably populated. The relative vibrational level distribution was similar to that found in the CH_2Cl_2 case as shown in Fig. 3, although the maximum total emission intensity ($CHCl_3$:O_2 ratio of 4.9:1.0) was only 0.45 of that observed in the CH_2Cl_2 case.

The emission from HCl† was also considerably weaker than that observed in the CH_2Cl_2 case. Observations of the first overtone emission of HCl† indicated weak population of $v \leqslant 5$.

Methyl Chloride

Very weak i.r. chemiluminescence attributable to the first overtone of CO† was observed when oxygen atoms reacted with CH_3Cl. No emission attributable to HCl† could be detected. The first 12 vibrational levels of CO† were populated with the relative vibrational level distribution indicated on Fig. 3. The maximum total emission intensity of CO† (CH_3Cl:O_2 ratio of 2:1) was about 0.1 of that observed in the CH_2Cl_2 case.

Methylene Bromide

Very weak i.r. chemiluminescence attributable to the first overtone of CO† was observed when oxygen atoms reacted with CH_2Br_2. The relative vibrational level distribution is also shown in Fig. 3. The spectroscopic assembly did not permit observation of the wavelength region where the fundamental of HBr is found. No emission attributable to the overtone of HBr could be detected. Emission attributable to the excited bromine atom $^2P_{1/2}$ was observed at 2713.7 nm.

Discussion

Thermochemical data required in the following discussion have been taken from the JANAF thermochemical tables (*9a*) unless otherwise specified. (Thermochemical data for $CHCl_2$ and CH_2Cl are from ref. *9b*.) Relevant rate constants in units of cm^3 $molecule^{-1}$ s^{-1} are given in Table 2.

It seems likely that the initial reaction steps are the abstraction of a hydrogen atom from the halomethane

[1] $O + CH_{4-n}X_n \rightarrow OH + CH_{3-n}X_n$ (X = Cl or Br)

followed rapidly by

[2] $O + OH = H + O_2 + 16.8$ kcal/mol

where $k_2 = (5 \pm 2) \times 10^{-11}$ at 300 °K (10).

Chloroform

The initial reaction steps for chloroform are, therefore,

[3*a*] $O + CHCl_3 = OH + CCl_3 + 6.6$ kcal/mol

[3*b*] $= OCl + CHCl_2 - 12.2$ kcal/mol

followed by reaction 2. Froben (6), who measured $k_{3a} + k_{3b} = 2.5 \times 10^{-15}$ at 300 °K in an e.p.r. study of the reactions of oxygen atoms with $CHCl_3$, observed no hydrogen atoms present in the system and suggested that either the hydrogen atoms produced by reaction 2 were rapidly consumed or that oxygen atom attack of $CHCl_3$ proceeded by reaction 3*b*. This latter possibility

Can. J. Chem. Downloaded from www.nrcresearchpress.com by 210.87.254.40 on 09/05/12
For personal use only.

Can. J. Chem. Downloaded from www.nrcresearchpress.com by 210.87.254.40 on 09/05/12
For personal use only.

is considered unlikely as reaction 3*b* is 12.2 kcal/mol endothermic.

Mechanism of Loss of Hydrogen Atoms

Clark and Tedder (11) have considered in detail the reactions of hydrogen atoms with $CHCl_3$. They considered the initial steps to be

[4*a*] $H + CHCl_3 = HCl + CHCl_2 + 26.6$ kcal/mol

[4*b*] $= H_2 + CCl_3 + 8.4$ kcal/mol

and concluded that hydrogen atom abstraction was faster than halogen atom abstraction with the relative rates, k_{4b}/k_{4a}, being 3.3–3.4. They then proposed that reactions 4 were followed by the formation of an excited molecule intermediate, CH_nX_{4-n}*.

If route 4*a* is followed

[5*a*] $H + CHCl_2 \rightarrow CH_2Cl_2^* \rightarrow CH_2Cl_2$ (stabilization)

[5*b*] $= HCl + CHCl + 15$ kcal/mol (decomposition)

and

[6*a*] $CHCl + H_2 = CH_3Cl + 100.7$ kcal/mol

Similarly if route 4*b* is followed

[5*c*] $H + CCl_3 \rightarrow CHCl_3^* \rightarrow CHCl_3$ (stabilization)

[5*d*] $= HCl + CCl_2 + 36.2$ kcal/mol (decomposition)

and

[6*b*] $CCl_2 + H_2 = CH_2Cl_2 + 79.8$ kcal/mol

From the ratio of the observed products, $CHCl_3:CH_2Cl_2:CH_3Cl$ of $\sim 20:1:0.08$, Clark and Tedder have inferred stabilization to decomposition ratios of the excited molecule intermediates in reactions 5*a* and 5*c*.

In the present experiments it is important to consider whether hydrogen atom attack on the parent compound, $CHCl_3$, can be competitive in the time scale, *i.e.* residence time of 8 ms. The rate constant for reaction 4 is not known, although Cremer, Curry, and Polanyi (12), in a 1933 study, concluded that the activation energy was less than 4.3 kcal/mol. However, the rate constants for the reactions of hydrogen atoms with CCl_4 and CH_2Cl_2 have been measured. Vance and Bauman (13), in 1938, obtained a value of 2×10^{-14} at 300 °K for the rate constant for the $H + CCl_4$ reaction and Combourieu, LeBras, and Paty (14), in 1972, a value of 7.1×10^{-16} at 300 °K for the rate constant for the $H + CH_2Cl_2$ reaction. Limits on the half-life of the decay of hydrogen atoms can be calculated using these two values. Thus

$$\tau_H = 1/(k[CHCl_3])$$

lies between 3 and 93 ms. Consequently, it is very difficult on the basis of these calculations to say whether reactions 4 are important loss mechanisms for hydrogen atoms. We considered that the recently obtained value for the rate constant for the $H + CH_2Cl_2$ reaction is more reliable than that for the $H + CCl_4$ reaction. Therefore, it is concluded that the value of the rate constant for the $H + CHCl_3$ reaction is probably closer to the value for the $H + CH_2Cl_2$ reaction than to the value for the $H + CCl_4$ reaction; thus τ lies closer to the calculated upper limit. For the purpose of the present discussion, therefore, reactions 4 are neglected. Furthermore, since reactions 5*a* and 5*c* are likely to be collision limited, *i.e.* $\sim 4 \times 10^{-10}$, a steady state concentration of CCl_3 or $CHCl_2$ radicals of 10^{12} molecule cm^{-3} or greater will ensure that the lifetime of H atoms for reactions 5*a* and 5*c* will be less than 2.5 ms.

Other possible loss mechanisms for hydrogen atoms such as

[7*a*] $O_2 + H + M \rightarrow HO_2 + M$

[7*b*] $H + O_2 = OH + O - 16.8$ kcal/mol

are unlikely. The first is a three body process and the second is endothermic.

The possibility that OH radicals are lost by attack on the parent compound, $CHCl_3$,

[8] $OH + CHCl_3 \rightarrow H_2O + CCl_3$

rather than producing hydrogen atoms by reaction 2 has also been considered. If the rate of attack of OH on $CHCl_3$ is of the same order of magnitude as its rate of attack on CH_4 ($1.2 \times 10^{-10} \exp\{-5910/RT\}$) (15), then the first order decay of OH via reaction 2 is more than 100 times faster than via reaction 8. Consequently, reaction 8 can be neglected under the present experimental conditions. (For this calculation we have assumed that initially 5% of the O_2 dissociated and we have calculated the OH lifetime for reaction 2 when 1/2 the O atoms are consumed, *i.e.* $[O] = 0.05[O_2]$.)

The question of whether reactions 5 proceed predominantly by stabilization or decomposition does not appear to be entirely clear. The mech-

Can. J. Chem. Downloaded from www.nrcresearchpress.com by 210.87.254.40 on 09/05/12
For personal use only.

anism of the thermal decomposition of chloroform, itself, is also not certain. The most recent work of Shilov and Sabirova (16) favors decomposition of $CHCl_3$* via reaction 5*d* while earlier work by Semeluk and Bernstein (17) indicates that decomposition proceeds by the splitting off of a chlorine atom. Clark and Tedder (11) state that stabilization of the excited molecule intermediates (reactions 5*a* and 5*c*) predominates in their system. Combourieu *et al.* (14), however, in studying the reactions of hydrogen atoms with CH_2Cl_2 indicate that no stabilization of the intermediate $CDHCl_2$* was observed when deuterium atoms replaced hydrogen atoms.

The stabilization to decomposition ratios (S/D) obtained by Clark and Tedder at a pressure of 0.23 Torr for halomethanes formed from the H + CCl_2X (X = F, Cl, Br, or D) reaction varied from 1.8 for $CHFCl_2$ to 10.9 for CCl_2DH. Assuming that 10 collisions (18) will remove the excess energy of the activated molecule and assuming a collision rate of 10^7 collision $Torr^{-1}$ s^{-1} then at 0.23 Torr the time for 10 collisions is 5 μs. Since in this time only 10–25% of the molecules decompose, it must be concluded that the first order decay rate is of the order of 3×10^4 s^{-1}. This rate is many orders of magnitude lower than that calculated by Chang (19) for $CHCl_3$* formed from the H + CCl_3 reaction. He estimated a threshold energy of 64 kcal/mol for decomposition of $CHCl_3$* via reaction 5*d* and calculated first order decomposition rates of 7×10^9, 6×10^{10}, and 2.5×10^{11} s^{-1} for $CHCl_3$* with 16, 26, and 36 kcal/mol of excess energy above the threshold energy required for decomposition. The $CHCl_3$* intermediate formed in reaction 5*d* would have ~32 kcal/mol excess energy above the threshold required for decomposition. While these calculations are very dependent on the assumed threshold energy (which is somewhat uncertain because of possible error (±5 kcal/mol) in the heat of formation of CCl_3 and the lack of information on the energy of activation of the reverse of reaction 5*d*), it seems most unlikely that these calculations are sufficiently in error to be consistent with the results of Clark and Tedder.

The conclusions of Clark and Tedder on the fate of $CHFCl_2$* formed by the reaction H + $CFCl_2$ have also been criticized (20). Clark and Tedder obtained an S/D ratio of 1.8 at 0.23 Torr which should be compared with an S/D ratio of 0.06 at 60 Torr observed by Medvedev *et al.* (20). (This latter observation was found to be consistent with theoretical calculations of the first order decomposition rate of $CHFCl_2$* using reasonable thermodynamic parameters (20).) It should be noted that Clark and Tedder find experimental decomposition to stabilization ratios rates approximately 10^4 times less than Medvedev *et al.* (20) when allowance is made for the different pressures used.

The experimental and theoretical work discussed above indicates that the conclusions of Clark and Tedder are in error. It seems possible that the products they observed may have resulted from surface reactions since they used very low pressures and long contact times. It should be noted that their conclusions were not verified by varying the pressure in their reaction vessel or by varying the surface to volume ratio.

The products of the reaction of oxygen atoms with $CHCl_3$ are shown in Table 1. The fact that no CH_2Cl_2 or CH_3Cl was observed reinforces the above argument that stabilization does not occur. It also indicates that the CHCl and CCl_2 radicals formed in reactions 5*b* and 5*d* react predominately by some reaction other than [6], which is to be expected, as molecular hydrogen is not likely to be formed in large amounts in this system.

Formation of Vibrationally Excited CO

In their study of the reactions of oxygen atoms with C_2H_2, Thrush and co-workers (3*a*) have suggested that the elementary reaction steps responsible for the formation of vibrationally excited CO were

[9] $O + C_2H_2 = CO\dagger + CH_2 + 48.2$ kcal/mol

[10] $O + CH_2 = CO\dagger + 2H + 73.8$ kcal/mol

Lin (8) has suggested that reactions 9 and 10 are responsible for the pumping of the CO chemical laser formed when C_2H_2 is flash photolyzed in the presence of SO_2 (a source of $O(^3P)$ atoms).

Thus it seems reasonable to suppose that the CHCl and CCl_2 radicals, formed in reactions 5*b* and 5*d*, react with oxygen atoms in a manner analogous to reaction 10.

[11] $O + CHCl = CO\dagger + H + Cl + 85$ kcal/mol

[12] $O + CCl_2 = CO\dagger + 2Cl + 85$ kcal/mol

If during the collision the fragments combine in such a way as to produce HCl or Cl_2 the heat of reaction will increase accordingly to 188 and 143 kcal/mol respectively. Reaction 11 could

Can. J. Chem. Downloaded from www.nrcresearchpress.com by 210.87.254.40 on 09/05/12
For personal use only.

then contribute to the vibrationally excited HCl observed and reaction 12 to the production of molecular chlorine. The exothermicities of reactions 11 and 12 are sufficient to populate CO up to and including $v = 15$. Experimentally, it was difficult to observe levels above $v = 12$; nevertheless this is in reasonable accord with the exothermicities of some combination of reactions 11 and 12. It is therefore suggested that these reactions are responsible for the observation of vibrationally excited CO.

Formation of Vibrationally Excited HCl

Vibrationally excited HCl can be formed via a number of reactions, *i.e.* 4*a*, 5*b*, 5*d*, although none of these reactions is sufficiently exothermic to produce HCl in $v = 6$ as observed. A major product of the reaction of oxygen atoms with $CHCl_3$ is molecular chlorine. This can be produced by recombination of Cl atoms following either reaction 12 or the reaction

[13] $H + HCl = H_2 + Cl + 1.1$ kcal/mol

Thus, the reaction of hydrogen atoms with Cl_2 becomes possible via

[14] $H + Cl_2 = HCl\dagger + Cl + 45.2$ kcal/mol

which can produce HCl† in levels up to $v = 6$.

Both reactions 13 and 14 are very fast with $k_{13} = 3.8 \times 10^{-11} \exp\{-3500/RT\}$ (21) and $k_{14} = 1.0 \times 10^{-11}$ (22). Clark and Tedder, however, neglected reaction 13 in their study of the reactions of hydrogen atoms with $CHCl_3$. The value of k_{13} which they used to eliminate reaction 13 from consideration was extrapolated from high temperature measurements (23) and was low by a factor of ~ 20. They also assumed the rate of reaction 14 to be equal to the rate of reaction 13 whereas it is a factor of 10 lower (21). Thus the reactions of chlorine atoms become important in their system, especially when HCl is added. The reaction

[15] $Cl + CHCl_3 = HCl + CCl_3 + 7.3$ kcal/mol

which has a value of $k_{15} = 1.15 \times 10^{-11} \exp\{-3350/RT\}$ (24) is thus likely faster than reaction 4 and consequently contributes significantly to the production of CCl_3 radicals used in reactions 5*c* and 5*d*.

The other two main products observed using mass spectrometry and vapor phase chromatography were phosgene ($COCl_2$) and CCl_4. It is possible to form $COCl_2$ via

[16] $O_2 + CCl_3 = COCl_2 + OCl + 47.4$ kcal/mol

and CCl_4 via

[17] $CCl_3 + Cl = CCl_4$

or

[18] $CCl_2 + Cl_2 = CCl_4$

Thus the main reaction scheme proposed to account for the present results is

$$O + CHCl_3 = OH + CCl_3$$
$$O + OH = O_2 + H$$
$$H + CCl_3 \rightarrow CHCl_3^* \rightarrow CCl_2 + HCl$$
$$O + CCl_2 = CO\dagger + 2Cl$$
$$Cl = \tfrac{1}{2}Cl_2$$
$$H + HCl = H_2 + Cl$$
$$H + Cl_2 = HCl\dagger + Cl$$
$$CCl_3 + O_2 = COCl_2 + OCl$$
$$CCl_3 + Cl = CCl_4$$

Methylene Chloride

The initial reaction steps, in direct analogy with the $CHCl_3$ case, are

[19] $O + CH_2Cl_2 = OH + CHCl_2 + 4.4$ kcal/mol

[2] $O + OH = H + O_2 + 16.8$ kcal/mol

The hydrogen atoms produced in reaction 2 may then attack either the parent compound, CH_2Cl_2, via

[20] $H + CH_2Cl_2 = HCl + CH_2Cl + 22.5$ kcal/mol

or the $CHCl_2$ radical formed in reaction 19.

[5*b*] $H + CHCl_2 = HCl + CHCl + 15.0$ kcal/mol

As previously mentioned, the only systematic study of the reactions of hydrogen atoms with CH_2Cl_2 was undertaken by Combourieu *et al.* (14). They proposed reaction 20 as the initial step followed by reaction 13 and

[21] $Cl + CH_2Cl_2 = HCl + CHCl_2 + 5.3$ kcal/mol

which has a rate constant, k_{21} of $(5.5 \pm 0.5) \times 10^{-13}$ at 298 °K (25). Reaction 21 which is analogous to reaction 15 in the $O + CHCl_3$ study was proposed to account for the apparent increase in the rate of consumption of CH_2Cl_2 when HCl was added to the system. The absence of the reaction product $CHDCl_2$ when deuterium atoms replaced hydrogen atoms led them to suggest that the reaction

Can. J. Chem. Downloaded from www.nrcresearchpress.com by 210.87.254.40 on 09/05/12
For personal use only.

[22] $D + CHCl_2 \rightarrow CHDCl_2^* \rightarrow CHDCl_2$

(and also its hydrogen analog) did not occur; the excited molecule intermediate, $CHDCl_2^*$, decomposed rather than stabilized. The additional reaction steps

[23] $H + CH_2Cl = HCl + CH_2 + 11.0$ kcal/mol

[5*b*] $H + CHCl_2 = HCl + CHCl + 15.0$ kcal/mol

[24] $H + CHCl = HCl + CH + 12.2$ kcal/mol

completed their reaction mechanism. Reaction 24 is not very probable because both reactants are likely present in low concentrations. It should be pointed out that Combourieu *et al.* did not find it necessary to postulate a hydrogen atom abstraction reaction analogous to Clark and Tedder's reaction 4*b* in order to explain their results.

In the present experiments, reaction 20 which has a rate constant $k_{20} = 1.8 \times 10^{-11}$ exp $\{-6100/RT\}$ (14) can be neglected because $\tau_{20} = 1/(k_{20}[CH_2Cl_2]) \sim 150$ ms. Vibrationally excited CO is formed by oxygen atom attack on the CHCl radical

[11] $O + CHCl = CO\dagger + H + Cl + 85$ kcal/mol

or on the CCl_2 radical formed in reaction 25

[25] $O + CHCl_2 = OH + CCl_2 + 16$ kcal/mol

Molecular chlorine, an important reaction product, can be formed by recombination of Cl atoms following either reaction 11 or reaction 13. Vibrationally excited HCl is formed via reaction 14, as in the CH_2Cl_2 case.

Phosgene which is also observed as a reaction product in this system may be formed by a reaction analogous to reaction 16

[26] $O_2 + CHCl_2 = CCl_2O + OH + 66.0$ kcal/mol

The other observed reaction products $C_2H_2Cl_2$ and $C_2H_2Cl_2O$ can be formed by dimerization of CHCl radicals followed by addition of oxygen atoms to give $C_2H_2Cl_2O$. The trace amounts of C_2H_2 and CH_4 observed in the present system, as well as in the system of Combourieu *et al.*, may be formed by

[27] $CH + CH = C_2H_2 + 229.8$ kcal/mol

and

[28] $CH + H + (M) \rightarrow CH_2 + (M)$

[29] $CH_2 + H + (M) \rightarrow CH_3 + (M)$

[30] $CH_3 + H + (wall) \rightarrow CH_4 + (wall)$

The presence of trace amounts of C_2H_2 indicates that reaction 24 can occur to a small extent in the present system.

Methyl Chloride

The initial step is again suggested to be hydrogen atom abstraction followed by reaction 2

[31] $O + CH_3Cl = OH + CH_2Cl + 0.6$ kcal/mol

The fact that reaction 31 is very slow, $k_{31} = 4.2 \times 10^{-11}$ exp $\{-(3880 \pm 220)/RT\}$ (5*a*) may account for the greatly reduced intensity of the CO emission observed. Hydrogen atom attack on the parent molecule may again be neglected.

CH_2 radicals are formed via reaction 23 and vibrationally excited CO by reaction 10.

The presence of small amounts of methylene chloride and chloroform in the products suggests that reactions such as

[32] $CH_2Cl + Cl \rightarrow CH_2Cl_2$

and the thermoneutral reaction

[33] $O + CH_2Cl \rightarrow OH + CHCl$

followed by

$CHCl + Cl_2 \rightarrow CHCl_3$

may occur.

Molecular chlorine is not observed as a reaction product. Only small amounts of HCl are observed, presumably formed from reaction 23. Consequently, the reaction sequence responsible for the formation of HCl† in the $CHCl_3$ and CH_2Cl_2 cases (reaction 13, chlorine atom recombination, reaction 14) probably does not occur to any great extent in this system, thus explaining why emission from vibrationally excited HCl could not be detected.

The vibrational level distribution for CO† shown in Fig. 3[2] reflects the differing contribu-

[2]One of the referees has suggested that reactions between oxygen atoms and halogenated methyl radicals may be important. While these reactions could well contribute to the formation of carbon monoxide we consider it unlikely that reactions such as

$O + CCl_3 \rightarrow CO\dagger + Cl_2 + Cl \quad \Delta H = -76$ kcal/mol

$O + CHCl_2 \rightarrow CO\dagger + HCl + Cl \quad \Delta H = -130$ kcal/mol

$O + CH_2Cl \rightarrow CO\dagger + HCl + H \quad \Delta H = -89$ kcal/mol

could account for the CO† observed. With the widely differing exothermicities of the halogenated methyl – oxygen atom reaction one would expect to see widely differing CO distributions for the three parent compounds ($CHCl_3$, CH_2Cl_2, and CH_3Cl) which is not observed. However, the first of the reactions giving $COCl_2 + Cl$ as products may well account for some of the $COCl_2$ observed.

Can. J. Chem. Downloaded from www.nrcresearchpress.com by 210.87.254.40 on 09/05/12
For personal use only.

tions of the three pumping reactions forming CO†

[10] $O + CH_2 = CO\dagger + 2H + 73.8$ kcal/mol

[11] $O + CHCl = CO\dagger + H + Cl + 85$ kcal/mol

[12] $O + CCl_2 = CO\dagger + 2Cl + 85$ kcal/mol

For $CHCl_3$ the dominant pumping reaction is [12], for CH_2Cl_2 reaction 11 and also reaction 12, and for CH_3Cl reaction 10. In the CH_3Cl case, the distribution bends slightly lower with increasing vibrational quantum number whereas in the $CHCl_3$ case the higher vibrational levels are slightly more populated. This is as would be expected because of the greater exothermicity of reaction 12.

It should be added, however, that the actual magnitude of the differences in the vibrational level distribution as the nature of the CX_1X_2 (X_1 and X_2 = H or Cl) changes, although statistically real, is relatively small.

A comparison between the vibrational level distribution for CO† obtained from the halomethanes and from C_2H_2 is shown in Fig. 4. Average values for the data shown in Fig. 3 are given for the halomethanes; the C_2H_2 data is from ref. 3*b*. (These experiments were conducted under the same experimental conditions as the present experiments.) For C_2H_2 the dominant pumping step has been postulated to be reaction 10 (3*a*), the same pumping step as for CH_3Cl. However, for C_2H_2, reaction 9 can also contribute to the population of CO† in levels up to and including the 8th, thus accounting for the slightly greater population in these levels. Thrush and co-workers (3*a*) have also postulated that the reaction

[35] $O + CH \rightarrow CO + H + 175.0$ kcal/mol

occurs for C_2H_2 and is responsible for the population of higher vibrational levels ($v \leqslant 33$). Small contributions from this reaction could explain why the higher levels have a slightly greater population than for CH_3Cl where reaction 10 is the only important pumping step.

The vibrationally excited HCl observed when oxygen atoms react with chloromethanes is formed primarily by the reaction of hydrogen atoms with molecular chlorine (reaction 14). (The molecular chlorine is formed by atom recombination.) This reaction is sufficiently exothermic to populate up to the 6th vibrational level and can thus explain the vibrational level distribution of HCl† shown in Fig. 2. Some contribution to $v = 1$ may arise from reactions 5*d* in the chloroform case and 5*b* in the methylene chloride case.

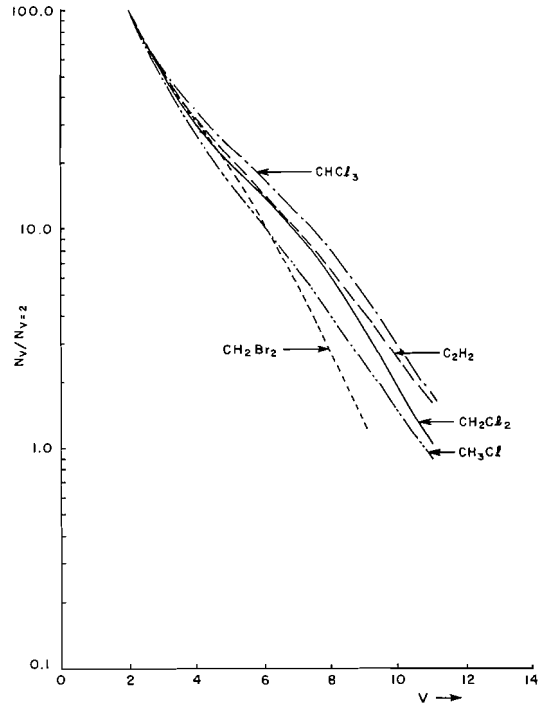

FIG. 4. Comparison of the relative vibrational level population of CO† produced in CH_nX_{4-n}/O_2 (X = Cl, Br) atomic flames with that produced in the C_2H_2/O_2 atomic flame.

Methylene Bromide

The mechanism describing the reactions of oxygen atoms with CH_2Br_2 can be expected to be in direct analogy with that of CH_2Cl_2. The relative vibrational level distribution of CO† shown in Fig. 3 indicates that the levels above $v = 5$ are less populated than for the CH_2Cl_2. As the exothermicities of the pumping steps analogous to reactions 11 and 12 are not known, it is not possible to speculate whether or not this is simply due to a less exothermic pumping step.

The excited $Br(^2P_{1/2})$ atom, responsible for the strong emission line at 2713.7 nm, can easily arise in the energy partitioning in the reaction

[36] $O + CHBr \rightarrow CO\dagger + H + Br$

which should be approximately 80 kcal/mol exothermic in analogy with reaction 11. If this heat of reaction is correct the lowered distribution can in part be accounted for by the 10.5 kcal carried off by the Br atom.

Can. J. Chem. Downloaded from www.nrcresearchpress.com by 210.87.254.40 on 09/05/12
For personal use only.

Conclusions and Summary

The addition of either CH_3Cl, CH_2Cl_2, $CHCl_3$, or CH_2Br_2 to a stream of oxygen atoms results in the observation of i.r. chemiluminescence from vibrationally excited CO†. In the cases of CH_2Cl_2 and $CHCl_3$ i.r. chemiluminescence from vibrationally excited HCl† is also observed.

The addition of vibrationally cold CO results in a marginally sustained vibrational population inversion in the chemically formed CO. This suggests that it should be possible to achieve gain on these transitions in a laser cavity provided the concentration of CO† is sufficient. The CH_2Cl_2 system is the most promising of the three chloromethane oxygen systems studied.

The CO† appears to result from reactions such as $O + CX_1X_2$ where X_1 and X_2 can be either halogen or hydrogen. This reaction is possible following successive stripping of halogen or hydrogen atoms from the parent halomethane by O or H atoms.

Vibrationally excited HCl is likely formed from the reaction $H + Cl_2 \rightarrow HCl + Cl$.

1. (*a*) G. Hancock and I. W. M. Smith. Chem. Phys. Lett. **3**, 573 (1969); (*b*) G. Hancock and I. W. M. Smith. Trans. Faraday Soc. **67**, 2586 (1971); (*c*) G. Hancock and I. W. M. Smith. Chem. Phys. Lett. **8**, 41 (1971); (*d*) G. Hancock, C. Morley, and I. W. M. Smith. Chem. Phys. Lett. **12**, 193 (1971).
2. D. M. Creek, C. M. Melliar-Smith, and N. Jonathan. J. Chem. Soc. A, 646 (1970).
3. (*a*) P. N. Clough, S. E. Schwartz, and B. A. Thrush. Proc. R. Soc. Lond. A, **317**, 575 (1970); (*b*) S. J. Arnold and G. H. Kimbell. Can. J. Chem. **51**, 451 (1973).
4. (*a*) P. Harteck and U. Kopsch. Z. Elektrochem. **36**, 714 (1930); (*b*) P. Harteck and U. Kopsch. Z. Phys. Chem. B, **12**, 327 (1931).
5. (*a*) J. T. Herron and R. E. Huie. J. Phys. Chem. **73**, 1326 (1969); (*b*) W. E. Wilson and J. T. O'Donovan. J. Chem. Phys. **48**, 2829 (1968).
6. F. W. Froben. Ber. Bunsenges. Phys. Chem. **72**, 996 (1968).
7. (*a*) M. C. Lin. J. Phys. Chem. **75**, 3642 (1971); (*b*) M. C. Lin. J. Phys. Chem. **76**, 811 (1972).
8. M. C. Lin. Int. J. Chem. Kinet. **5**, 173 (1973).
9. (*a*) JANAF thermochemical tables, 2nd Ed. National Bureau of Standards, NSRDS–NBS 37, 1971; (*b*) J. A. Franklin and G. Huybrechts. Int. J. Chem. Kinet. **1**, 3 (1969).
10. F. Kaufman. Can. J. Chem. **47**, 1917 (1969).
11. D. T. Clark and J. M. Tedder. Trans. Faraday Soc. **62**, 405 (1966).
12. E. Cremer, J. Curry, and M. Polanyi. Z. Phys. Chem. B, **23**, 445 (1933).
13. J. E. Vance and W. G. Bauman. J. Chem. Phys. **6**, 811 (1938).
14. J. Combourieu, G. LeBras and C. Paty. 14th Symposium (International) on Combustion. August, 1972. University Park, Pa., U.S.A.
15. K. Schofield. Planet. Space Sci. **15**, 643 (1967).
16. A. E. Shilov and R. D. Sabirova. Russ. J. Phys. Chem. **34**, 408 (1960).
17. (*a*) G. P. Semeluk and R. B. Bernstein. J. Am. Chem. Soc. **76**, 3793 (1954); (*b*) G. P. Semeluk and R. B. Bernstein. J. Am. Chem. Soc. **79**, 46 (1957).
18. B. S. Rabinovitch and D. W. Setser. Advances in photochemistry. Vol. 3. Interscience, New York, 1964. p. 1.
19. H. W. Chang. Ph.D. Thesis. Kansas State University, Manhattan, Kansas. 1971.
20. (*a*) B. A. Medvedev. M. A. Teitel'boim and A. E. Shilov. Kinet. Katal. **12**, 269 (1971); (*b*) B. A. Medvedev, M. A. Teitel'boim, and A. E. Shilov. Kinet. Katal. **12**, 749 (1971).
21. A. A. Westenberg and N. de Haas. J. Chem. Phys. **48**, 4405 (1968).
22. F. S. Klein and M. Wolfsberg. J. Chem. Phys. **34**, 1494 (1961).
23. H. Steiner and E. K. Rideal. Proc. R. Soc. Lond. A**173**, 503 (1939).
24. J. H. Knox. Trans. Faraday Soc. **58**, 275 (1962).
25. D. D. Davis, W. Braun, and A. M. Bass. Int. J. Chem. Kinet. **2**, 101 (1970).

The Molecular Structure of 2,5-Dihydrofuran from the Analysis of the Nematic Liquid Crystal Nuclear Magnetic Resonance Spectrum

K. C. COLE AND D. F. R. GILSON

Department of Chemistry, McGill University, P.O. Box 6070, Montreal 101, Quebec

Received August 7, 1973

The nematic phase n.m.r. spectrum of partially oriented 2,5-dihydrofuran has been analyzed. Corrections to the structure for ring puckering and methylene rocking motions, according to the model due to Malloy, give improved agreement between experimental and calculated direct dipole–dipole coupling constants.

Le spectre r.m.n. en phase nématique du dihydro-2,5 furanne partiellement orienté a été étudié. Des modifications de structure tenant compte des mouvements de gauchissement du cycle et de balancement des méthylènes, selon le modèle proposé par Malloy, ont permis d'obtenir un meilleur accord entre les constantes de couplage expérimentales et calculées provenant d'interactions directes dipole–dipole.

[Traduit par le journal]

Can. J. Chem., **52**, 281 (1974)

Introduction

In four-membered ring compounds the out-of-plane vibrational motion leads to a puckering of the ring. The potential function for this vibration usually has a double minimum, and if the lowest vibrational state lies below the hump the molecule is nonplanar in the ground state. Five-membered rings have two out-of-plane vibrations which can interact to give pseudo-rotation unless there is a double bond in the ring in which case the torsional motion about this bond is at much higher energy and the remaining low frequency out-of-plane motion reduces to a one dimensional puckering. Information about ring puckering motions can be obtained from microwave spectroscopy from the dependence of the moments of inertia on the vibrational quantum number and/or from the actual vibrational absorption spectrum in the far i.r. region. The potential function arises from two contributions: a quartic term, originally predicted by Bell (1), due to ring strain which tends to keep the ring in a planar conformation, and a quadratic term due to torsion about bonds tending to force a nonplanar conformation to avoid eclipsing between adjacent methylene groups. The expression used for the potential function is of the form $V(x) = Ax^2 + Bx^4$, where x is a ring puckering coordinate which may be an out-of-plane displacement, a mass weighted normal coordinate, or a dimensionless coordinate. Some confusion has existed over the indiscriminate comparison of potential functions for different molecules and it is necessary to use an appropriate transformation (2) between different coordinate systems. For some molecules the simple quadratic–quartic function does not provide an adequate description of the potential, and exponential functions have been included (3–5) and an extension of the power series to include the hexic term has been suggested (6, 7).

The far i.r. spectrum of 2,5-dihydrofuran and its analysis have received attention from several authors (4, 8–11). The quadratic term has a positive coefficient, and no hump occurs in the potential function, as expected for the case where adjacent methylene groups are absent. Malloy (11) has extended the Ueda–Shimanouchi model (8) by including a methylene rocking motion mixed with the puckering mode and has obtained some improvement in the overall agreement between the observed and calculated i.r. absorption frequencies. In spite of the current interest in molecules of this type there is only limited molecular structural information and the only study of 2,5-dihydrofuran is an early electron diffraction investigation by Beach (12). The present study reports the results of a determination of the structure using the nematic liquid crystal n.m.r. method (13).

The n.m.r. spectrum of a molecule partially oriented in a nematic liquid crystal can be analyzed to give the direct dipole–dipole coupling constants, D_{ij}, which are functions of the inverse cube of internuclear distance and the constants required to describe the average orientation.

Can. J. Chem. Downloaded from www.nrcresearchpress.com by 210.87.254.5 on 09/05/12
For personal use only.

Can. J. Chem. Downloaded from www.nrcresearchpress.com by 210.87.254.5 on 09/05/12
For personal use only.

Using Snyder's notation (14)

$$[1]\quad D_{ij} = \frac{-h\gamma_i\gamma_j}{2\pi^2\sqrt{5}}\left\{C_{3z^2-r^2}\left[\left\langle\frac{(\Delta z_{ij})^2}{r_{ij}^5}\right\rangle - \frac{1}{2}\left\langle\frac{(\Delta x_{ij})^2}{r_{ij}^5}\right\rangle - \frac{1}{2}\left\langle\frac{(\Delta y_{ij})^2}{r_{ij}^5}\right\rangle\right] + C_{x^2-y^2}\frac{\sqrt{3}}{2}\left[\left\langle\frac{(\Delta x_{ij})^2}{r_{ij}^5}\right\rangle - \left\langle\frac{(\Delta y_{ij})^2}{r_{ij}^5}\right\rangle\right] + C_{xz}\sqrt{3}\left[\left\langle\frac{(\Delta x_{ij})(\Delta z_{ij})}{r_{ij}^5}\right\rangle\right] + C_{yz}\sqrt{3}\left[\left\langle\frac{(\Delta y_{ij})(\Delta z_{ij})}{r_{ij}^5}\right\rangle\right] + C_{xy}\sqrt{3}\left[\left\langle\frac{(\Delta x_{ij})(\Delta y_{ij})}{r_{ij}^5}\right\rangle\right]\right\}$$

where the C's are the motional constants and the angular brackets indicate that the distances are averaged over the molecular vibrations. Comparisons between internuclear distances measured by different experimental methods should take account of the vibrational averaging but attempts to correct for these effects have not been very successful (15–18), although Lucas (19, 20) has reconciled the structure of cyclopropane. Molecules with large amplitude anharmonic vibrations, for which the potential functions are known, provide examples where the vibrational corrections of direct dipole–dipole coupling constants can be tested.

Experimental

The n.m.r. spectrum of a solution of 2,5-dihydrofuran (19.5 mol %) in *N*-(*p*-ethoxybenzylidene)-*p*-*n*-butylaniline (EBBA) was obtained at 220 MHz at the Canadian 220 MHz NMR Centre, Sheridan Park, Ontario. The sample temperature was 18 °C. The following computer programs were used: SPECFIT, an iterative procedure for spectrum analysis; GEOFIT, calculates a proton geometry for the molecule as the best fit to the experimental D_{ij} values obtained from SPECFIT; DOUMIN, uses the reduced mass and the potential function as input and calculates the vibrational energy levels, expectation values of the even powers of the puckering coordinate, the Boltzmann population of each level, and the thermal averages of z^2 and z^4 at a selected temperature; PUCKER, transforms input coordinates in any arbitrary axis system to a zero angular momentum axis system and calculates the reduced mass, principal moments of inertia, and D_{ij} values as power series in the puckering coordinate up to the z^4 term. All computations were performed on an IBM 360/75.

Results and Discussion

Rigid Planar Model

The spectrum of 2,5-dihydrofuran in the nematic phase of EBBA consists of three distinct regions (Fig. 1); the resonance due to the olefinic protons, which is symmetrical about its center, and the methylene proton resonances which are split into two regions, symmetrical with respect to each other, by the large coupling constant given by $|\frac{3}{2}D_{13}|$ (or D_{24}). The width of the olefinic resonance gives an estimate of D_{56}. This approximate first order character provided a convenient starting point for the analysis of the spectrum as initial values for the motional constants $C_{3z^2-r^2}$ and $C_{x^2-y^2}$ could be obtained using D_{13} and D_{56} with a molecular geometry based on standard bond lengths and angles. Initially, all J_{ij} values were set at zero. Good agreement with the experimental spectrum was obtained and final refinement, using SPECFIT, gave the coupling constants listed in column I of Table 1. The r.m.s. deviation between experimental and calculated line positions for 77 lines used in the analysis was 0.44 Hz. The spectrum, because of the first order nature, is much more sensitive to the diagonal elements ($D_{ij} + J_{ij}$) for the H_1–H_5 and H_1–H_6 interactions than it is to the off-diagonal elements. This gives rise to a large covariance between D_{ij} and J_{ij} for these interactions, so that the sums $D_{ij} + J_{ij}$ are accurately determined from the anisotropic spectrum, whereas precise values for $^3J_{15}$ and $^4J_{16}$ are not. The isotropic spectrum of 2,5-dihydrofuran consists of only two lines (21), although the liquid crystal spectrum indicates that all the J_{ij} have appreciable magnitudes, including the long range couplings $^4J_{12}$ (+4.19 Hz) and $^4J_{14}$ (+6.66 Hz).[1] The deceptively simple isotropic spectrum results because $|J_{15} + J_{16}| \simeq 0$. In 2,3-dihydrofuran the related coupling constants were found to be $^3J = +2.46$ Hz and $^4J = -2.36$ Hz (21). We have, therefore, adopted values for 2,5-dihydrofuran of $^3J_{15} = +2.4$ Hz and $^4J_{16} = -2.4$ Hz, and adjusted D_{15} and D_{16} accordingly. The resulting improved set of experimental dipole–dipole coupling constants is given in column II of Table 1.

[1]These values of $^4J_{12}$ and $^4J_{14}$ agree reasonably well with those calculated by Barfield *et al.* (22) of +2.52 and +7.51 Hz, respectively.

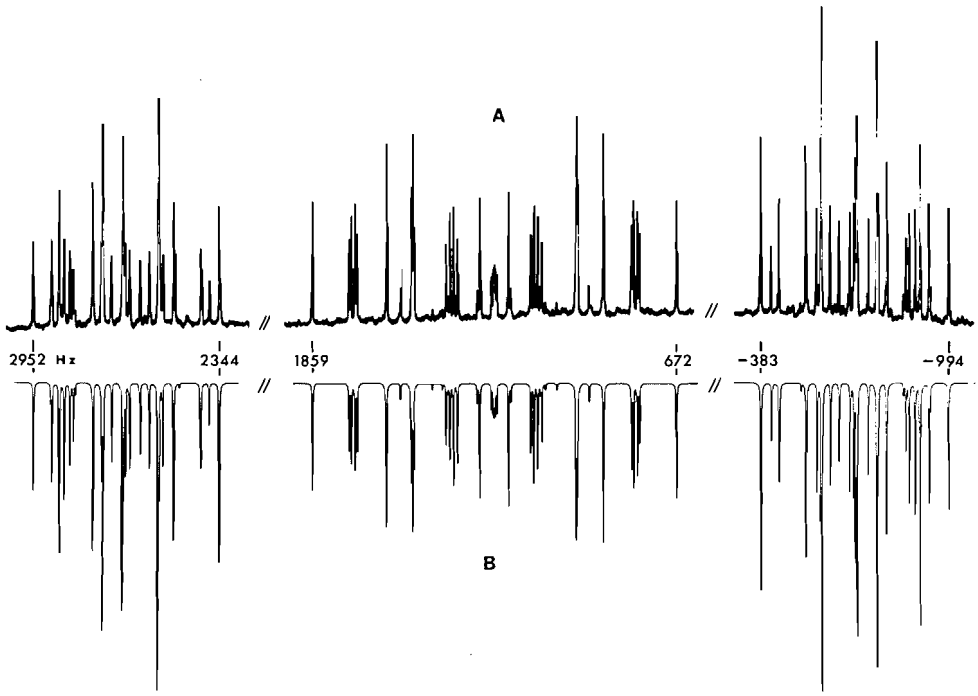

FIG. 1. The 220 MHz n.m.r. spectrum of 2,5-dihydrofuran in EBBA. (*a*) Experimental, (*b*) computer simulated, with linewidth of 2 Hz. The numbers indicate Hz from TMS.

TABLE 1. Experimental and calculated coupling constants (Hz)

	(I) Experimental	(II) Calculated experimental[a]	(III) Calculated rigid planar	ΔD_{ij}	(IV) Calculated pucker plus rocking	ΔD_{ij}	(V) Calculated pucker only	ΔD_{ij}
D_{12}	-154.11 ± 0.10	-154.11	-153.69	-0.42	-154.00	-0.11	-154.09	-0.02
D_{13}	$+2215.33\pm0.44$	$+2215.33$	$+2215.37$	-0.04	$+2215.33$	0.00	$+2215.33$	0.00
D_{14}	-41.44 ± 0.09	-41.44	-39.99	-1.45	-41.12	-0.32	-41.39	-0.05
D_{15}	-230.79 ± 2.24	-232.53	-231.92	-0.61	-232.38	-0.15	-232.50	-0.03
D_{16}	-83.23 ± 0.92	-83.51	-86.24	$+2.73$	-84.22	$+0.71$	-83.64	$+0.13$
D_{56}	-362.19 ± 0.12	-362.19	-362.03	-0.16	-362.15	-0.04	-362.18	-0.01
J_{12}	$+4.19\pm0.10$							
J_{13}[b]	—							
J_{14}	$+6.66\pm0.09$							
J_{15}	$+0.66\pm2.49$	$+2.4$						
J_{16}	-2.68 ± 0.93	-2.4						
J_{56}	$+5.95\pm0.12$							
ν_1[c]	978.95 ± 0.06							
ν_5[c]	1266.72 ± 0.06							
$D_{15}+J_{15}$	-230.13 ± 0.26							
$D_{16}+J_{16}$	-85.91 ± 0.08							
R.m.s. dev.[d]				1.30		0.33		0.06

[a] With assumed values for J_{15} and J_{16}.
[b] J_{13} does not affect the spectrum.
[c] Chemical shifts in Hz from internal TMS.
[d] R.m.s. deviation between experimental and calculated D_{ij}.

Can. J. Chem. Downloaded from www.nrcresearchpress.com by 210.87.254.5 on 09/05/12
For personal use only.

TABLE 2. Geometric parameters and motional constants

	(I)[a] Starting model	(II) Rigid planar	(III) Puckering and rocking	(IV) Puckering alone
d_1	2.5132	2.4521	2.4577	2.4729
d_2[b]	1.7728	1.7728	1.7728	1.7728
d_3	1.3044	1.3324	1.3186	1.3127
d_4	0.8941	0.9157	0.9027	0.8972
$C_{3z^2-r^2}$		−0.12668	−0.12415	−0.12361
$C_{x^2-y^2}$		−0.00049	+0.00028	−0.00092

[a]The starting model was the structure used by Malloy (11). Distances in Å.
[b]Assumed.

Using the program GEOFIT a best fit geometry to the experimental dipolar coupling constants was calculated for a planar rigid molecule. Four distances (Fig. 2) and two motional constants are required to describe the system, and since only relative distances are obtained, one distance can be (arbitrarily) fixed. There are six independent D_{ij} and the system is therefore overdetermined. The parameters obtained are given in column II of Table 2 and the calculated D_{ij} in column III of Table 1. The deviations between experimental and calculated coupling constants are rather large.

Ring Puckering Model with Methylene Rocking

In this model it is assumed that bending occurs only about the C_2—C_5 direction (y axis in Fig. 2), even though this mode is coupled to a ring twisting vibration (10). It is necessary to obtain expressions for the coordinates of each proton as a function of the amount of puckering, with the additional complication of the methylene rocking motion. Furthermore the puckered molecule no longer possesses two perpendicular planes of symmetry and allowance for a third motional constant must be made. The coordinate system used is that employed by Chan *et al.* (23); the out-of-plane displacement of each of the ring atoms at any instant is given by $\pm z$, with the restrictions (8) that neither the center of mass nor the angular momentum shall change during the vibration. The principal moments of inertia of the puckered molecule are independent of the choice of coordinate system but the reduced mass and the motional constants do depend on the choice. It is advisable, therefore, to transform to a system in which the angular momentum is invariant. The coordinates of each atom in the puckered molecule were obtained by expressing each atomic position as the sum of vectors with respect to the origin, Fig. 2, and containing elements given by the fixed planar geometry plus the changes due to puckering and methylene rocking motions. The angle of the methylene rocking motion was taken to be proportional to the puckering angle, as given by Malloy (11). After substitution of the numerical values derived from the planar structure the atomic coordinates were obtained as polynomials in z up to the fourth power.

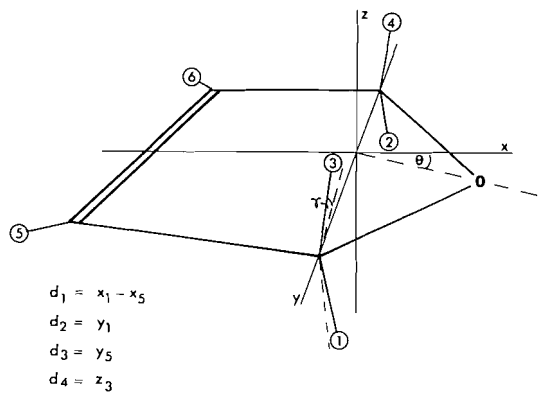

FIG. 2. 2,5-Dihydrofuran. Numbering of proton positions and the geometric parameters used to describe the system. θ is the puckering angle and γ the methylene rocking angle.

These coordinates were used as input for the program PUCKER and the direct dipole–dipole coupling constants were computed as functions of z in the center-of-mass, zero-angular-momentum axis system. In order to calculate the contributions of puckering and rocking motions to these D_{ij} values it is necessary to compute the average values of z^2 and z^4. These were computed using DOUMIN with the reduced mass calculated using PUCKER and the potential function given by Malloy (11) for the semirigid model

Can. J. Chem. Downloaded from www.nrcresearchpress.com by 210.87.254.5 on 09/05/12
For personal use only.

Can. J. Chem. Downloaded from www.nrcresearchpress.com by 210.87.254.5 on 09/05/12
For personal use only.

[2] $V(\text{cm}^{-1}) = 26.38\{2.24Z^2 + Z^4\}$

In this expression Z is a reduced coordinate which requires transformation to a different dimensionless coordinate, X, for use in program DOUMIN:

[3] $V(\text{cm}^{-1}) = 13.19\{2.24X^2 + 0.50X^4\}$

The transition frequencies are also produced by DOUMIN and serve as a check on the calculations. The values agree with the experimental frequencies (8). The values of $\langle z^2 \rangle$ and $\langle z^4 \rangle$, thermally averaged over the occupied levels at 300 °K, are

$$\langle z^2 \rangle = 5.387 \times 10^{-3} \text{ Å}^2$$
$$\langle z^4 \rangle = 7.039 \times 10^{-5} \text{ Å}^4$$

The expressions for the direct dipole–dipole coupling constants are

$$D_{12}^{\text{p}} = D_{12} + 40.2024C_{3z^2-r^2} + 69.6327C_{x^2-y^2}$$
$$D_{13}^{\text{p}} = D_{13} + 412.7024C_{3z^2-r^2} + 238.1117C_{x^2-y^2} + 5.2457\eta$$
$$D_{14}^{\text{p}} = D_{14} + 7.8124C_{3z^2-r^2} + 16.5451C_{x^2-y^2} + 0.1028\eta$$
$$D_{15}^{\text{p}} = D_{15} - 8.8522C_{3z^2-r^2} + 37.8421C_{x^2-y^2} - 33.2369\eta$$
$$D_{16}^{\text{p}} = D_{16} - 8.4720C_{3z^2-r^2} + 3.0494C_{x^2-y^2} - 8.1130\eta$$
$$D_{56}^{\text{p}} = D_{56}$$

The superscript p indicates the D_{ij} value corrected for the average over the puckering motion. The parameter η allows for the third motional constant as $C_{xz} = \eta z$, *i.e.* the motional constant is assumed to be proportional to the out-of-plane displacement. The D_{ij}^{p} values were used with the program GEOFIT to calculate a "planar" geometry, thus accounting for the averaging over the puckering vibration in eq. 1. The parameter η was set at zero. The structural parameters are given in column III of Table 2 and the calculated D_{ij} in column IV of Table 1. The r.m.s. deviation between experimental and calculated D_{ij} has been substantially reduced and the dipole–dipole coupling constants now fit within experimental error. There seemed no point, therefore, in pursuing calculations in which the additional variable η is included. The neglect of C_{xz} is equivalent to assuming that the principal orientation axes coincide with the zero-angular-momentum axes.

Ring Puckering without Methylene Rocking

Calculations were also made for a model in which ring puckering was the only vibration and the Malloy methylene rocking motion was neglected. The reduced mass calculated by PUCKER is changed substantially and thus the values of $\langle z^2 \rangle$ and $\langle z^4 \rangle$ become

$$\langle z^2 \rangle = 4.795 \times 10^{-3} \text{ Å}^2$$
$$\langle z^4 \rangle = 5.576 \times 10^{-5} \text{ Å}^4$$

Following the same computations as before the D_{ij} values and geometric parameters are listed in column V of Table 1 and column IV of Table 2 respectively. There is a further improvement in the fit but the significance is doubtful and does not provide a test of the Malloy model.

In using the r.m.s. deviation between calculated and experimental direct dipole–dipole coupling constants as the criterion for an improved structure, it is appropriate to question the sensitivity of the geometrical parameters and motional constants, designated here by p_j, to changes in the experimental D_{ij} values, ΔD_i. The expressions, eq. 1, are complicated functions of p_j and, for ease of computation, we consider the change in a direct dipole–dipole coupling produced by a change in one of the parameters p_j.

[4] $$\Delta D_i = \sum_j \frac{\partial D_i}{\partial p_j} \cdot \Delta p_j$$

This can be cast in matrix form, the elements of which are obtained from eq. 1 for each D_{ij}, and, after some manipulation, inverted to give Δp_j.

The ΔD_i values used were the experimental errors given in column I of Table 1 with the exceptions of ΔD_{15} and ΔD_{16} which are not well defined because of the uncertainty in J_{15} and J_{16} and were arbitrarily set at 0.50 Hz. The signs of ΔD_i were chosen so as to maximize Δp_j, with the following results,

$$\Delta d_1 = 0.0115 \text{ Å}$$
$$\Delta d_3 = 0.0006 \text{ Å}$$
$$\Delta d_4 = 0.0012 \text{ Å}$$
$$\Delta C_{3z^2-r^2} = 0.0005$$
$$\Delta C_{x^2-y^2} = 0.0003$$

Can. J. Chem. Downloaded from www.nrcresearchpress.com by 210.87.254.5 on 09/05/12
For personal use only.

Thus d_1 is quite sensitive to the errors in the direct dipole–dipole coupling constants and the difference in d_1 for the rigid planar model and the puckering–rocking model is probably not significant, whereas the differences in d_3 and d_4 are significant.

The analysis of the nematic phase n.m.r. spectrum provides only relative positions of the protons but these can be scaled in order to fit the proton geometry to the ring framework. The ring bond lengths and angles given by Beach (12) are insufficient for the present purpose since they are incomplete and were scaled to a C=C distance of 1.34 Å. It is necessary therefore to assume some of the bond lengths for the ring structure. Obviously a wide choice of parameters exists, but some choices are less arbitrary than others. The carbon–carbon single bond length adjacent to a double bond is not well defined and therefore bond lengths of r(C=C) = 1.350 Å and R(C—O) = 1.430 Å were adopted and it was assumed that the C—C—O angle is bisected by the methylene C—H bond directions. The parameters which remain to be determined are the carbon–carbon single bond length, the carbon–proton bond lengths, all bond angles, and a scaling factor required to fit the relative proton positions to the ring atom positions. This last parameter was fixed by varying the scale to achieve reasonable C—H bond lengths. The proposed structure of 2,5-dihydrofuran is given in Fig. 3. The carbon–carbon single bond length is 1.500 Å compared with 1.54 Å obtained by Beach (12) and 1.519 Å obtained for cyclopentene by electron diffraction (24). A shorter than normal single bond is expected for a single bond adjacent to a double bond. If the C_2—C_3 bond is increased to 1.519 Å then either unacceptable values for the proton bond lengths were obtained or the angle COC must be increased to 114°.

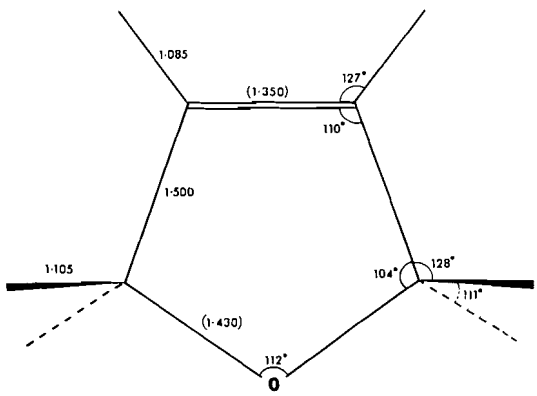

FIG. 3. Structure of 2,5-dihydrofuran. Distances in parentheses are assumed. This structure is scaled to reasonable values for the C—H bond lengths and a different scaling would produce alternative structures.

The puckering angle in 2,5-dihydrofuran calculated for the structure in Fig. 3 with the r.m.s. out-of-plane displacement given by DOUMIN is 16°, compared with the angles of 22 and 29° quoted for cyclopentene from microwave spectroscopic (25) and electron diffraction (24) studies.

The financial support of the National Research Council of Canada is gratefully acknowledged. K.C.C. acknowledges the award of a 1967 Science Scholarship.

1. R. P. BELL. Proc. R. Soc. Lond. A, **183**, 328 (1945).
2. J. S. GIBSON and D. O. HARRIS. J. Chem. Phys. **57**, 238 (1972).
3. L. H. SHARPEN and V. W. LAURIE. J. Chem. Phys. **49**, 221 (1968).
4. T. UEDA and T. SHIMANOUCHI. J. Chem. Phys. **47**, 5018 (1967).
5. W. C. PRINGLE J. Chem. Phys. **54**, 4979 (1971).
6. P. D. ROBINSON and C. H. KIM. J. Chem. Phys. **49**, 2874 (1968).
7. J. LAANE. Appl. Spectrosc. **24**, 73 (1970).
8. T. UEDA and T. SHIMANOUCHI J. Chem. Phys. **47**, 4042 (1967).
9. L. A. CARREIRA and R. C. LORD. J. Chem. Phys. **51**, 3225 (1969).
10. L. A. CARREIRA, I. M. MILLS, and W. B. PERSON. J. Chem. Phys. **56**, 1444 (1972).
11. T. B. MALLOY. J. Mol. Spectrosc. **44**, 504 (1972).
12. J. Y. BEACH. J. Chem. Phys. **9**, 54 (1941).
13. P. DIEHL and C. L. KHETRAPAL. NMR, basic principles and progress. Springer-Verlag. Vol 1. 1969.
14. L. C. SNYDER. J. Chem. Phys. **43**, 4041 (1965).
15. W. BOVÉE, C. W. HILBERS, and C. MACLEAN. Mol. Phys. **17**, 75 (1969).
16. J. BULTHUIS and C. MACLEAN. Chem. Phys. Lett. **7**, 242 (1970).
17. J. BULTHUIS and C. MACLEAN. J. Magn. Resonance, **4**, 148 (1971).
18. N. J. D. LUCAS. Mol. Phys. **22**, 147 (1971).
19. N. J. D. LUCAS. Mol. Phys. **22**, 233 (1971).
20. N. J. D. LUCAS. Mol. Phys. **23**, 825 (1972).
21. P. K. KORVER, P. J. VAN DER HAAK, H. STEINBERG, and TH. J. DEBOER. Rec. Trav. Chim. **84**, 129 (1965).
22. M. BARFIELD, R. J. SPEAR, and S. STERNHELL. J. Am. Chem. Soc. **93**, 5322 (1971).
23. S. I. CHAN, J. ZINN, and W. D. GWINN. J. Chem. Phys. **34**, 1319 (1961).
24. M. I. DAVIS and T. W. MUECKE. J. Phys. Chem. **74**, 1104 (1970).
25. G. W. RATHJENS. J. Chem. Phys. **36**, 2401 (1962).

A CNDO/2 Calculation on the Reaction of Ground State Oxygen Atoms with Olefins

SEIICHIRO KODA[1]

Department of Reaction Chemistry, Faculty of Engineering, the University of Tokyo, Bunkyo-ku, Tokyo, Japan

Received December 5, 1972[2]

A molecular orbital study within the framework of the CNDO/2 method has been made of the reactions of ground state oxygen atoms with olefins. Calculated excitation energies confirm the existence of a certain correlation between those and the logarithm of the reaction rate constants. The location of minima in the simplified potential energy surfaces computed appear to correspond to the reaction intermediates suggested previously.

On a effectué une étude des orbitales moléculaires, à l'intérieur des cadres de la méthode CNDO/2, sur les réactions d'atomes d'oxygène à l'état fondamental avec des oléfines. Les énergies d'excitation calculées ont confirmé l'existence d'une certaine relation entre celles-ci et le logarithme des constantes de vitesse de la réaction. La position des minima dans les surfaces calculées et simplifiées d'énergie potentielle semble correspondre aux intermédiaires de réaction suggérés antérieurement.

[Traduit par le journal]

Can. J. Chem., **52**, 287 (1974)

Introduction

Many investigations on the mechanism of the atomic oxygen ($O(^3P)$) reaction with olefins have been pursued, taking the rate constants (especially, relative ones) and the stereo-specificities of the reactions into account. Some possible intermediates have been suggested by Cvetanović (1) and by Scheer and co-worker (2), but no satisfactory results are obtained by molecular orbital calculations except for the classical work of Sato and co-worker (3) and the several trials of the sulfur atom reactions (4). Our investigation of oxygen atom reactions with metallocenes (5) led us into trying to obtain some information in this reaction system by using a CNDO/2 program. Though the CNDO/2 computer program could not give quantitatively reliable results, it was expected to give some meaningful suggestions of the mechanism involved as demonstrated by the recent success of Pople and Beveridge (6).

At first, we compared some excitation energies of several olefins with the rate constants and then we tried to construct some possible energy surfaces in the reaction system of atomic oxygen with ethylene, though with great simplification.

Calculation

The CNDO/2 programmed by Segal (7) was used. The results obtained were also checked by the CNINDO program by Pople and co-worker (6). The computations were done on the computer Hitac 5020 of Tokyo University Computer Center (3001GQ0212). The structures of all olefins for which calculations were attempted were as follows: the angle of the sp^3 bond was fixed at 109°28′, and that of the sp^2 at 120°; appropriate bond lengths were selected from the literature (8).

Results and Discussion

In order to determine a possible relationship between the rate constant and an excitation energy suggested by Sato and co-worker (LCAO MO calculation) (3), some excitation energies (α, β, γ) were calculated for each olefin as shown in Table 1.

α is the difference between the energy of the ground singlet state and that of the triplet state, the structure of which was taken as that of the ground singlet state. β is the difference between the energy of the ground state and that of the triplet, the structure of which was taken as that of the ground state except that a 90° internal rotation around the olefinic bond was applied. The CNDO/2 calculation where the electronic state is designated to be triplet is considered to give the lowest triplet energy for the corresponding structure. α may be considered as a measure of a vertical excitation to the triplet state. On the other hand, β is considered to be the approximate minimum triplet excitation energy because this state is known to have a perpendicular equilibrium conformation.

[1]Present address: Division of Chemistry, National Research Council of Canada, Ottawa, Canada K1A 0R6.

[2]Revision received October 4, 1973.

Can. J. Chem. Downloaded from www.nrcresearchpress.com by 210.87.254.40 on 09/05/12
For personal use only.

Can. J. Chem. Downloaded from www.nrcresearchpress.com by 210.87.254.40 on 09/05/12
For personal use only.

TABLE 1. The excitation energies

Olefin	Excitation energies* (Hartree units) α	β	γ
Ethylene	0.3775	0.1783	0.7803
Propylene	0.2770	0.1678	0.7034
cis-2-Butene	0.2332	0.1482	0.6365
trans-2-Butene	0.2193	0.1403	0.6222
1-Butene	0.2759	0.1674	0.6927
Isobutene	0.2585	0.1614	0.6616

*For definition of α, β, and γ, see text.

γ is the difference in energy between the highest occupied and the lowest unoccupied molecular orbital in the ground state, and is considered to represent the average singlet–triplet excitation energy. This corresponds to the excitation energy, δ, calculated by Sato and co-worker using a LCAO MO method (3). However, γ and δ do not contain the right amounts of electron interaction expected for the average excitation energy of the singlet and triplet. Therefore, these values have no precise physical meaning and should rather be considered as a kind of quantum-chemical parameter. It is difficult to calculate the energy of upper singlet states by the CNDO/2.

It is more reasonable to compare these excitation energies with activation energies instead of with rate constants. Activation energies have been obtained for some olefins, and it is well recognized that the differences in the rate constants of these reactions are mainly due to the differences in activation energies (9, 10). Plots of log (relative rate constants) *vs.* excitation energy for the reaction of five olefins are presented in Fig. 1. The excitation energies by Sato (δ) are also shown. Though there is a certain relationship, there seems to be no improvement in linearity by applying the CNDO/2 instead of the LCAO MO. Therefore, these rough relationships do not allow one to conclude what kind of excitation in the olefinic part is important in the reactions; they may not be incompatible with a reaction path in which some excitation to a triplet state is induced in the olefinic part by approach of the triplet oxygen atom.[3]

In order to obtain a clearer understanding of

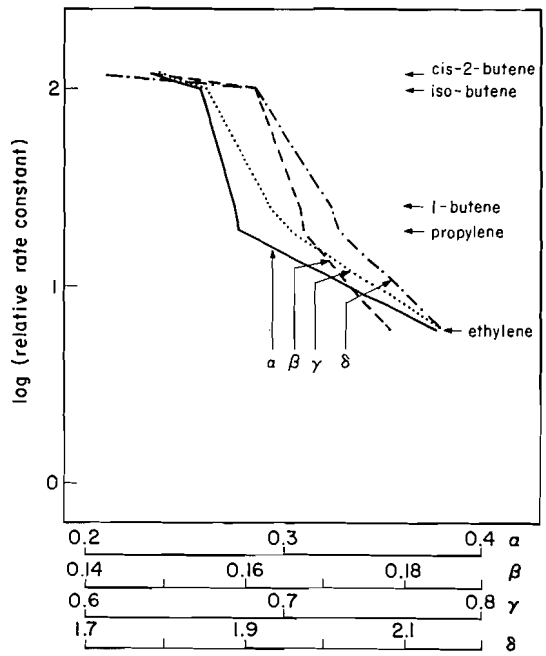

FIG. 1. Plots of log *k* at room temperature *vs.* computed excitation energy of the olefin. The rate data are from ref. 9; α, β, and γ (Hartree units) are from Table 1; δ ($-\beta_0$ unit) is from ref. 3.

the reaction paths, simplified potential energy surfaces were calculated in the neighborhood of the expected positions of minima.[4] Thus, the positions of the atoms in the system were selected as follows. The structure of ethylene (that is, ground state ethylene, C—C = 1.338 Å, ∠HCH = 120°) was kept constant, regardless of the position of O atom. As model I (which may be considered to correspond to an in-front attack by O atom), the atomic oxygen was moved in a plane which was perpendicular to the molecular plane and contained the ethylene molecular axis. As model II (which may be considered to correspond to an in-plane attack), the oxygen was moved in the ethylene molecular plane. The electronic state of the whole system was constrained to be triplet in these calculations. The total energies thus obtained as a function of the position of the O atom are shown as contour lines near the energy mini-

[3]It is not clear when the spin-relaxation occurs but, from a consideration of the available experimental data, it seems to take place only at some later stages of the reaction.

[4]These simplifications were necessary, because of the great number of degrees of freedom in these multi-atom systems. Even if calculations were done without simplifications by the CNDO/2 method, no quantitatively reliable results could be expected, especially for the triplet state, because of the approximate nature of the programs used.

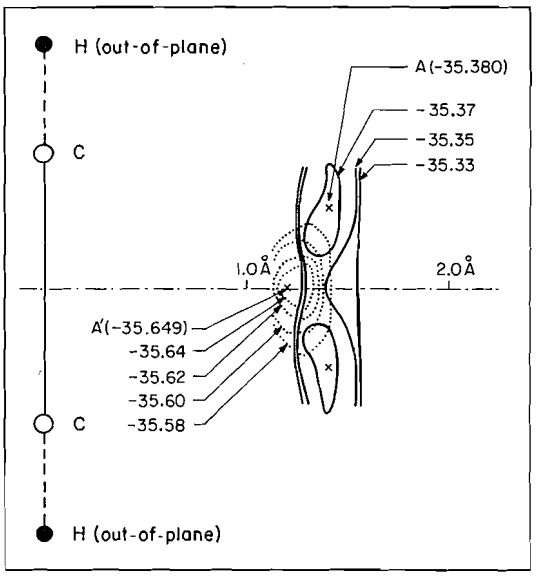

FIG. 2. The contour lines of total energy for model I. The solid lines for the triplet, the dotted lines for the singlet; Hartree units are used.

ma points (A, B) in Figs. 2 and 3. As comparisons, the results when the whole system was constrained to be singlet are also presented in these figures.

It is worthy of note that the energy of A (the structure of the energy minimum point in model I) is a little lower than that of B (that in model II) and also that the oxygen atom is not on the bisector of the C—C bond in the structure A.[5] If the intermediate in oxygen atom reactions is in fact a triplet which has a moderate life-time, it might be approximately illustrated by A or B.[6]

[5]The absolute values of the energy might not be very meaningful. The relative values should be better, though allowance should be made for the possibility that the relative values might be also considerably affected by some other choices of the atomic positions in the ethylene part of the system. Of course, in a higher approximation, the angles and also the bond lengths of the ethylenic part should be changed, but it seems probable that, even in the higher approximation, there are some energy minimum structures corresponding to A and B. This may be exemplified by the fact that a structure of minimum energy was found to be also the one with its oxygen apart from the bisector of the C—C bond, in the calculation of an in-front attack (like model I) where the C—C bond was elongated to 1.438 from 1.338 Å.

[6]The triplet of a moderate life-time is usually the lowest triplet, and the CNDO/2 calculation with a triplet designation is considered to give the lowest triplet, as already stated.

The structure A might be identified as the biradical model suggested by Cvetanović (1) and the structure B might be the model by Scheer and co-worker (2). When an internal 90° rotation around the C—C bond was attempted with these models, the structure of minimum energy (C in Fig. 4) was found to be the one with its oxygen

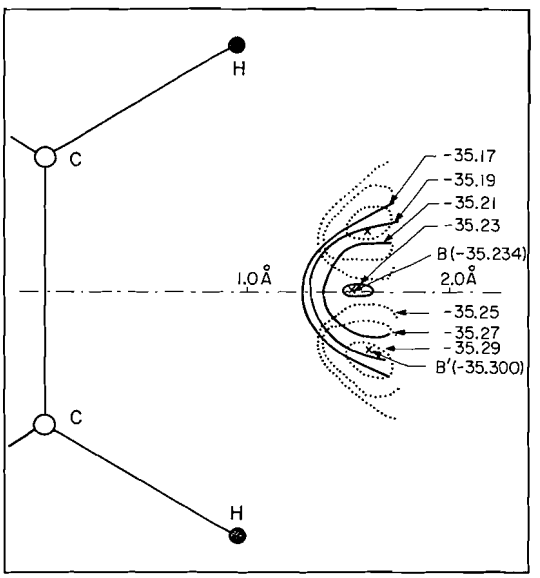

FIG. 3. The contour lines of total energy for model II. The solid lines for the triplet, the dotted lines for the singlet; Hartree units are used.

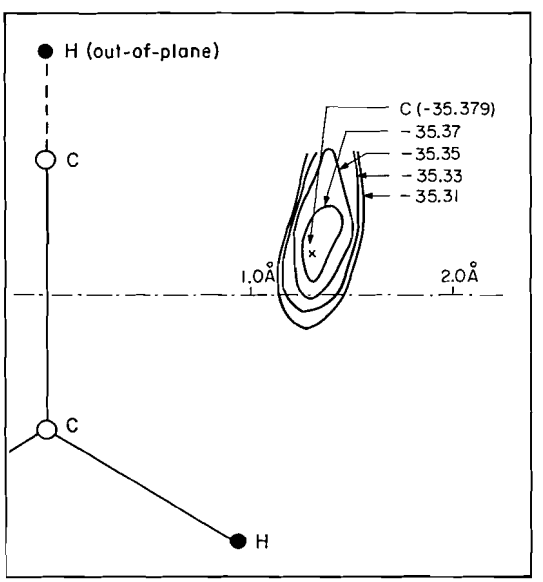

FIG. 4. The contour lines of total energy in 90° rotational structures; Hartree units are used.

Can. J. Chem. Downloaded from www.nrcresearchpress.com by 210.87.254.40 on 09/05/12
For personal use only.

atom nearer to one carbon atom. The total energy is about the same as that of A. Thus a relatively free rotation around the C—C bond seems to exist in the A structure. Thus these considerations support the suggestion of a biradical intermediate, the rotation of which is important in deciding the stereo-specificity, as a possible important intermediate of oxygen atom adding to olefins, though allowance should be made for the fact that the calculations were very limited and not definitive. The energies of singlet states were found to be below those of triplet states, as expected. The change from A to A′ may correspond to the formation of the epoxide.

The author is grateful to Dr. H. Arai, Associate Professor T. Yoshida for their instructions in computation; to Associate Professor S. Tsuchiya and Professor T. Hikita for discussions and encouragement.

1. R. J. Cvetanović. J. Phys. Chem. **74**, 2730 (1970).
2. M. D. Scheer and R. Klein. J. Phys. Chem. **74**, 2732 (1970).
3. S. Sato and R. J. Cvetanović. J. Am. Chem. Soc. **81**, 3223 (1959).
4. O. P. Strauz, R. K. Gosavi, A. S. Denes, and I. G. Csizmadia. Theor. Chim. Acta, **26**, 367 (1972).
5. S. Koda and T. Hikita. Chem. Lett. 353 (1972).
6. J. A. Pople and D. L. Beveridge. Approximate molecular orbital theory. McGraw–Hill, New York. 1970.
7. G. A. Segal. Quantum chemistry program exchange. No. 91. Department of Chemistry, Indiana University, Bloomington, Ind. 47401. 1966.
8. L. E. Sutton. Tables of interatomic distances and configulations in molecules and ions. Chemical Society Special Publications, No. 11 and No. 18. The Chemical Society, London. 1958, 1965.
9. R. Atkinson and R. J. Cvetanović. J. Chem. Phys. **55**, 659 (1971).
10. R. Atkinson and R. J. Cvetanović. J. Chem. Phys. **56**, 432 (1972).

Can. J. Chem. Downloaded from www.nrcresearchpress.com by 210.87.254.40 on 09/05/12
For personal use only.

Synthesis of 3,4,6-Tri-*O*-methyl-D-glucose, -D-galactose, and -D-mannose

JOFFRE M. BERRY, YUEN-MIN CHOY, AND GUY G. S. DUTTON

Department of Chemistry, University of British Columbia, Vancouver, British Columbia V6T 1W5

Received June 14, 1973

Reaction of 1,3,4,6-tetra-*O*-acetyl-D-glucose, -D-mannose, and -D-galactose with dihydropyran and *p*-toluenesulfonic acid in dichloromethane gave the corresponding 2-tetrahydropyranyl ethers. Deacetylation, methylation, and hydrolysis gave 3,4,6-tri-*O*-methyl-D-glucose, 3,4,6-tri-*O*-methyl-D-mannose, and 3,4,6-tri-*O*-methyl-D-galactose in 60, 28, and 25% overall yields, respectively. A small amount of 3,5,6-tri-*O*-methyl-D-galactose was also obtained.

La réaction des tétra-*O*-acétyl-1,3,4,6-D-glucose, -D-mannose et -D-galactose avec le dihydropyranne et l'acide *p*-toluènesulfonique dans le dichlorométhane a conduit aux éthers tétrahydropyrannyl-2 correspondants. La déacétylation, la méthylation puis l'hydrolyse ont conduit au tri-*O*-méthyl-3,4,6-D-glucose, au tri-*O*-méthyl-3,4,6-D-mannose et au tri-*O*-méthyl-3,4,6-D-galactose avec des rendements de 60, 28 et 25%, respectivement. On a aussi obtenu une petite quantité de tri-*O*-méthyl-3,5,6-D-galactose.

[Traduit par le journal]

Can. J. Chem., **52**, 291 (1974)

Studies on the structure of bacterial polysaccharides, many of which contain 1 → 2 linkages, emphasize the need for 3,4,6-tri-*O*-methyl hexoses as reference compounds. Preparation of 1,3,4,6-tetra-*O*-acetyl hexoses is readily accomplished (1, 2); these intermediates may be used for the synthesis of 1 → 2 linked disaccharides and, by suitable blocking, 3,4,6-tri-*O*-methyl sugars.

The route selected involved the preparation of the tetrahydropyranyl ether (3); methyl vinyl ether, isobutene, and tosyl chloride were found less satisfactory reagents. The deacetylated ethers were methylated by the method of Hakomori (4) at a low temperature to minimize degradation and the products obtained by hydrolysis were purified by chromatography (5) to give 3,4,6-tri-*O*-methyl-D-glucose (60%), -D-mannose (28%), and -D-galactose (25%). In addition 3,5,6-tri-*O*-methyl-D-galactose (8%) was also isolated making the total yield of galactose isomers 33%. The pyranose compounds crystallized on seeding and the structures assigned were consistent with the p.m.r. spectra (6) of the sugars and with the mass spectra of the tri-*O*-methyl hexitol acetates (7, 8).

The D-glucose (9, 10), D-galactose (11), and D-mannose (12) compounds have been synthesized previously but each by a different route. The merits of the method presently described are that the same type of intermediate is used in each case; the required 1,3,4,6-tetraacetates may be obtained in 5 h and the syntheses can be completed in three further steps (four, if deacetylation is effected separately).

Experimental

Practical grade dihydropyran was partially dried with Na_2CO_3, then fractionally distilled. The fraction b.p. 83.5–85° was refluxed with sodium and distilled. Reagent grade dichloromethane was distilled from calcium hydride. Anhydrous *p*-toluenesulfonic acid was obtained by heating the hydrate at 95° for 2 h at 10 mm. Solvent systems *A* (ethyl ether – toluene (2:1)) and *B* (butanone–water azeotrope) were used for chromatography. Gas–liquid chromatography (g.l.c.) was carried out on an F and M 720 instrument using a column (5 ft × ¼ in.) of 5% butanediol succinate on 80–120 mesh Diatoport S at 185° and a helium flow of 60 ml/min. Proton magnetic resonance spectra were recorded with a Varian XL-100 instrument, using tetramethylsilane or sodium 4,4-dimethyl-4-silapentanesulfonate as internal standard. Spectra were consistent with the structures assigned; signals from the tetrahydropyranyl ether occurred at τ 8.1–8.7. Optical rotations were measured at 23 ± 1° on a Perkin-Elmer model 141 polarimeter. Melting points are uncorrected.

*1,3,4,6-Tetra-O-acetyl-2-O-(2-tetrahydropyranyl)-α-D-glucopyranose (**1**)*

1,3,4,6-Tetra-*O*-acetyl-α-D-glucopyranose (1) (2 g) was dissolved in absolute dichloromethane (45 ml). Dihydropyran (0.65 ml) and anhydrous *p*-toluenesulfonic acid (10 mg) were added and the mixture was stirred at 0°. Inspection by t.l.c. (silica gel G, solvent *A*) after 1 h showed a small amount of unreacted starting material (R_f 0.19), a major component (R_f 0.50) corresponding to **1**, and faster moving components (dihydropyran condensation products). The reaction mixture was neutralized with pyridine or with anhydrous potassium carbonate and evaporation

Can. J. Chem. Downloaded from www.nrcresearchpress.com by 210.87.254.42 on 09/05/12
For personal use only.

Can. J. Chem. Downloaded from www.nrcresearchpress.com by 210.87.254.42 on 09/05/12
For personal use only.

of the solvent at 30° gave **1** as a syrup (2.5 g). When purified by t.l.c. using solvent *A*, **1** had $[\alpha]_D$ +76° (*c* 1.7, chloroform).

1,3,4,6-Tetra-O-acetyl-2-O-(2-tetrahydropyranyl)-β-D-mannopyranose (2)

This compound was obtained similarly as a syrup from 1,3,4,6-tetra-*O*-acetyl-β-D-mannopyranose (3) (1 g), yield 1.2 g, R_f 0.37 (solvent *A*); $[\alpha]_D$ −41° (*c* 3.8, chloroform).

1,3,4,6-Tetra-O-acetyl-2-O-(2-tetrahydropyranyl)-α-D-galactopyranose (3)

This compound was obtained as a syrup from 1,3,4,6-tetra-*O*-acetyl-α-D-galactopyranose (1) (1 g), yield 1.2 g, R_f 0.50 (solvent *A*); $[\alpha]_D$ +72° (*c* 2.7, chloroform).

3,4,6-Tri-O-methyl-D-glucose (4)

The syrup **1** (2.5 g) in dry methanol (25 ml) was treated with 0.2 *M* sodium methoxide in anhydrous methanol (10 ml) for 30 min at room temperature giving a product with R_f 0.34 (solvent *B*) on t.l.c. Alternatively, the dichloromethane solution of **1** was treated directly with sodium methoxide. The syrup obtained was dried for 45 min on a vacuum pump and then dissolved in dry methyl sulfoxide (5 ml). Methyl sulfinyl anion (2 *M*, 25 ml) was added under anhydrous conditions (13) while keeping the temperature below 25°. The mixture was shaken for 1 h at room temperature, frozen in a Dry Ice – acetone bath and excess methyl iodide (15 ml) was added dropwise with shaking (if warming was detected the mixture was frozen again). The reaction mixture was shaken at room temperature overnight and extracted with petroleum ether (b.p. 65–70°, 100 ml × 10). Evaporation of the solvent and hydrolysis (2 *M* trifluoroacetic acid, 75 ml, reflux, overnight) gave a syrup which was shown by paper chromatography (solvent *B*) to contain **4** (R_f 0.58) and a small amount of tetramethyl sugar. The syrup was dissolved in water (100 ml) which was extracted with chloroform (40 ml × 3) and the water was evaporated. The syrup obtained was purified using solvent *B* on either a cellulose column or on a short column of silica gel (5). 3,4,6-Tri-*O*-methyl-D-glucose (**4**) was obtained as a syrup (775 mg, 60% overall) which crystallized on seeding with the β-anomer. Recrystallization from ether – petroleum ether (1 : 1, 100 ml/g) gave pure 3,4,6-tri-*O*-methyl-β-D-glucose, m.p. 104–106°, mixture m.p. 104–106°; $[\alpha]_D$ +41° → +77° (2½ h, *c* 1.5, water) (lit. (10) m.p. 97–98°; $[\alpha]_D$ +41° → 77.5° (*c* 1.6, water)); p.m.r. (D_2O) τ 4.85 (doublet, $J_{1,2}$ = 3.4 Hz, H-1 of α-D-form), 5.42 (doublet, $J_{1,2}$ = 7.3 Hz, H-1 of β-D-form), 6.61, 6.47, 6.38 (OMe's).

Anal. Calcd. for $C_9H_{18}O_6$: C, 48.64; H, 8.16. Found: C, 48.58; H, 8.21.

3,4,6-Tri-O-methyl-D-mannose (5)

1,3,4,6-Tetra-*O*-acetyl-2-*O*-(2-tetrahydropyranyl)-β-D-mannopyranose (**2**) (1.2 g) was deacetylated to give a product having R_f 0.35 (t.l.c., solvent *B*) which on methylation and hydrolysis afforded **5** as a syrup with R_f 0.60 (paper, solvent *B*), yield 180 mg (28%). Crystalline 3,4,6-tri-*O*-methyl-α-D-mannose was obtained on seeding and was recrystallized from ether – petroleum ether (1 : 1, 100 ml/g), m.p. 104–106°, mixture m.p. 104–106°; $[\alpha]_D$ +20° → +8° (1 h, *c* 0.9, water) (lit. (12) m.p. 104°; $[\alpha]_D$ +21° → 8° (*c* 1.0, water)); p.m.r. (D_2O) τ 4.85 (doublet, $J_{1,2}$ = 4.0 Hz, H-1 of α-D-form), 5.17 (doublet, $J_{1,2}$ = 2.2 Hz, H-1 of β-D-form), 6.51, 6.55, 6.60 (OMe's).

Anal. Calcd. for $C_9H_{18}O_6$: C, 48.64; H, 8.16. Found: C, 48.35; H, 8.14.

3,4,6-Tri-O-methyl-D-galactose (6)

1,3,4,6-Tetra-*O*-acetyl-2-*O*-(2-tetrahydropyranyl)-α-D-galactopyranose (**3**) (1.2 g) was deacetylated to give 2-*O*-(2-tetrahydropyranyl)-D-galactose, R_f 0.29 (t.l.c., solvent *B*). Methylation and hydrolysis gave two components on paper chromatography (solvent *B*); R_f 0.37 corresponding to **6** and a faster moving component (7) with R_f 0.69. Purification by column chromatography gave 3,4,6-tri-*O*-methyl-D-galactose (**6**) (160 mg, 25% overall) which crystallized on seeding, m.p. and mixture m.p. 88–89°; $[\alpha]_D$ +152° → +110° (*c* 1.2, water) (lit. (11) m.p. 88–89°; $[\alpha]_D$ +154° → +110° (*c* 1.0, water)); p.m.r. (D_2O) τ 4.79 (doublet, $J_{1,2}$ = 3.7 Hz, H-1 of α-D-form), 5.46 (doublet, $J_{1,2}$ = 7.2 Hz, H-1 of β-D-form), 6.51, 6.51, 6.61 (OMe's).

Anal. Calcd. for $C_9H_{18}O_6$: C, 48.64; H, 8.16. Found: C, 48.44; H, 8.00.

The column separation also gave **7** (54 mg), $[\alpha]_D$ −15° (*c* 2.0, water), a portion of which was converted to the alditol acetate. This had a retention time of 13.0 min and gave a mass spectrum consistent with the assignment of **7** as 3,5,6-tri-*O*-methyl-D-galactose (7, 8). The alditol acetates of **4**, **5**, and **6** had retention times of 13.2, 13.2, and 14.2 min, respectively.

We are grateful to Drs. D. H. Ball, C. T. Bishop, A. Gauhe, and G. Keilich for gifts of seed crystals and to the National Research Council of Canada for continued financial support.

1. B. Helferich and J. Zirner. Chem. Ber. **95**, 2604 (1962).
2. J. O. Deferrari, E. S. Gros, and I. O. Mastronardi. Carbohydr. Res. **4**, 435 (1967).
3. S. J. Angyal and S. D. Gero. J. Chem. Soc. 5255 (1965).
4. S. Hakomori. J. Biochem. (Tokyo), **55**, 205 (1964).
5. B. J. Hunt and W. Rigby. Chem. Ind. (London), 1868 (1967).
6. E. B. Rathbone and A. M. Stephen. Carbohydr. Res. **21**, 83 (1972).
7. H. Björndal, C. E. Hellerqvist, B. Lindberg, and S. Svensson. Angew. Chem. Int. Ed. **9**, 610 (1970).
8. H. Björndal, B. Lindberg, and S. Svensson. Carbohydr. Res. **5**, 433 (1967).
9. A. K. Mitra, D. H. Ball, and L. Long, Jr. J. Org. Chem. **27**, 160 (1962).
10. R. L. Sundberg, C. M. McCloskey, D. E. Rees, and G. H. Coleman. J. Am. Chem. Soc. **67**, 1080 (1945); Methods Carbohydr. Chem. **5**, 298 (1965).
11. R. Kuhn and H. H. Baer. Chem. Ber. **88**, 1537 (1955); Methods Carbohydr. Chem. **5**, 298 (1965).
12. H. G. Bott, W. H. Haworth, and E. L. Hirst. J. Chem. Soc. 1395 (1930); Methods Carbohydr. Chem. **5**, 298 (1965).
13. P. A. Sandford and H. E. Conrad. Biochemistry, **5**, 1508 (1966).

Molecular Rearrangements. Part IV. Aryl (Alkyl) Amines (1), Thermal Rearrangement of *N*-Benzyl-*N*-Methylaniline

M. Zarif A. Badr[1] and M. M. Aly

Chemistry Department, Faculty of Science, Assiut University, Assiut, Egypt, E.A.R.

Received July 11, 1973

Heating *N*-benzyl-*N*-methylaniline under reflux or heating at ~315° in sealed tubes, in the absence of any promotor for 100 h, resulted in its rearrangement, producing methylamine, diphenylmethane, and dibenzyl together with *o*-toluidine and 4-methylacridine. Heating *N*-methylaniline in a sealed tube under the same conditions, in absence of any promotor, resulted in its rearrangement, producing methylamine and *o*-toluidine together with unidentified neutral products.

When pyrolysis of the tertiary amine was carried out with quinoline as a solvent, the normal products of rearrangement were obtained together with 2- and 4-benzylquinolines and 2,2′-biquinolyl.

The reaction mechanism is discussed on the basis of the products separated, from which it is concluded that the tertiary amine undergoes homolytic fission to benzyl and *N*-methylphenylamino free radicals, followed by a series of homolytic fissions of initially separated intermediate products, during the rearrangement process. Throughout the whole mechanism, the C—N bonds are the only ones to suffer homolytic fission.

Lorsque l'on chauffe la *N*-benzyl *N*-méthylaniline à reflux ou à 315° dans des tubes scellés durant 100 h en absence de promoteur, il se produit un réarrangement qui conduit à la formation de la méthylamine, du dibenzyl et diphénylméthane ainsi que de l'*o*-toluidine et de la méthyl-4 acridine. Lorsque l'on chauffe la *N*-méthylaniline dans un tube scellé dans les mêmes conditions en absence de promoteur, il se produit aussi un réarrangement conduisant à la formation de la méthylamine, de l'*o*-toluidine ainsi que de plusieurs produits neutres non-identifiés.

Lorsque la pyrolyse de l'amine tertiaire est effectuée en utilisant comme solvant, la quinoline, on obtient les produits normaux issus du réarrangement ainsi que les benzyl-2 et -4 quinolines et la biquinolyl-2,2′.

On discute du mécanisme réactionnel en se basant sur les produits séparés à partir desquels il est possible de conclure que l'amine tertiaire subit une fission homolytique entraînant la formation de radicaux libres benzyl et *N*-méthylphénylamine, suivie d'une série de fissions homolytiques des produits séparés à l'origine, comme intermédiaires, durant le processus de réarrangement. Selon le mécanisme complet, les liens C—N sont les seuls à subit une homolytique. [Traduit par le journal]

Can. J. Chem., **52**, 293 (1974)

Aryl alkyl amines were reported (1–3) to rearrange under the influence of acids or Lewis acid catalysts, or by thermal rearrangement of their hydrochlorides in sealed tubes to give ring-alkylated secondary or primary aryl amine derivatives. The alkyl groups mainly enter *para* positions but if such are not free, *ortho* migration will occur. Thus *N*-methylaniline, when rearranged by heating its hydrochloride, gives *p*-toluidine and little *o*-toluidine. Polyalkylation may occur, not only in the successive conversions of a tertiary, through secondary, to primary amine (2*a*); alkyl halide and olefin formation was also established together with isomerization of the alkyl groups during their migrations in such type of aryl amine rearrangement (2*b*–*d*).

Although this rearrangement was regarded at one time as intramolecular (4), it now is concluded that the reaction is intermolecular (5) and occurs through the formation of a carbonium ion intermediate (2*d*).

The photochemical rearrangement process of aromatic amines has also been observed. Although *N*,*N*-dimethylaniline is quite stable under u.v. light, the amine hydrochloride salt can be photolyzed (6).

As far as our observation goes, the aryl amines are not recorded to undergo molecular rearrangement under thermal conditions in absence of any promotor.

The present paper describes a novel rearrangement, involving a C—N bond fission, when *N*-benzyl-*N*-methylaniline is heated at elevated temperature, either alone or in presence of solvent where its nuclear alkylation was observed. Thus, *N*-benzyl-*N*-methylaniline changed on heating in

[1]To whom correspondence should be addressed; Present address: Chemistry Department, University of Libya, P.O. Box 2558, Tripoli, Libya.

Can. J. Chem. Downloaded from www.nrcresearchpress.com by 210.87.254.6 on 09/05/12
For personal use only.

Can. J. Chem. Downloaded from www.nrcresearchpress.com by 210.87.254.6 on 09/05/12
For personal use only.

TABLE 1. Products of pyrolysis of *N*-benzyl-*N*-methylaniline

Exp. No.	Conditions (solvent (g); temperature; time)	Amine in g (%)		Products in g (%)					
		Used	Consumed	Methylamine	Diphenylmethane	Dibenzyl	*o*-Toluidine	4-Methylacridine	Benzylquinoline
1	—; reflux; 100 h[b]	30	15 (50)	Exists	0.75 (5)	0.35 (2.3)	2.25 (15)	4.3 (28.7)	—
2[a]	—; 315°; 100 h	30	14 (46.7)	Exists	0.5 (3.6)	0.52 (3.7)	2.3 (16.4)	3.56 (25.4)	—
3[a]	Quinoline (30); 315°; 100 h	30	15 (43.3)	Exists	0.32 (2.5)	0.35 (2.7)	4.3 (33.1)	3.2 (24.6)	5.6 (32.5)[c]

[a]In nitrogen atmosphere.
[b]Benzaldehyde (0.4 g) separated and identified.
[c]2.2′-Biquinolyl (0.75 g) separated and the benzylquinolines are 41% 2-isomer and 59% 4-isomer.

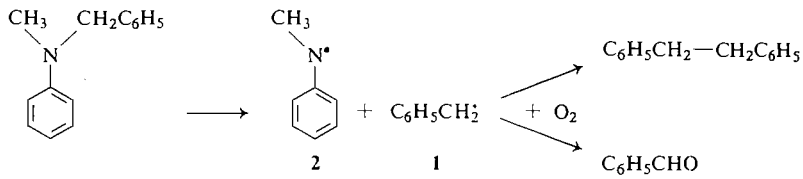

SCHEME 1

a sealed tube in nitrogen atmosphere at ~315°. Methylamine was formed together with *o*-toluidine, diphenylmethane, dibenzyl, and 4-methylacridine in a relatively high yield, and higher boiling products not yet resolved. When heated at its boiling point under reflux for 100 h, the amine gave the same products with the difference that some benzaldehyde was isolated and the yield of dibenzyl was decreased.

The products of these thermal rearrangements differ markedly from those of the proton-catalyzed rearrangement, from which neither dibenzyl nor methylamine, nor diphenylmethane could be expected, and only alkyl halides, and olefins, together with ring-alkylated products, were separated (2).

The presence of dibenzyl, diphenylmethane, and methylamine in the product strongly suggests that the change depends on a free radical mechanism. In order to study this suggestion further, the thermal rearrangement in a higher boiling solvent, such as quinoline, was examined. The normal products of rearrangement were obtained together with 2- and 4-benzylquinoline and 2,2′-biquinolyl, as summarized in Table 1.

These results are consistent with the simplest possible interpretation of the reaction, namely that *N*-benzyl-*N*-methylaniline undergoes homolysis to benzyl free radical (**1**) and *N*-methylphenylamino free radical (**2**). The former then dimerizing to dibenzyl. Separation of benzaldehyde from the amine pyrolysis under reflux in presence of atmospheric oxygen, which acts as scavenger for free radicals having an α-hydrogen (7), is further proof of the separation of benzyl free radical, which gives benzaldehyde (8), as in Scheme 1.

The normal expectation for the behavior of the methylanilino free radical in the reaction mechanism is to abstract hydrogen, resulting in *N*-methylaniline, and to couple with benzyl free radical to give *o*- and *p*-*N*-methylaminodiphenylmethane. Since none of these products was detected under the conditions used, they could be considered as precursors for other products, some of which were separated. The methyl group in *N*-methylaniline is reasonably shifted intramolecularly from the nitrogen atom to the *o*-position of the same nucleus giving rise to *o*-toluidine in relatively high yield, according to Scheme 2 (route *a*). However, methylamine can be considered to be formed from the fission of the CH_3NH—Ar bond in *N*-methylaniline (route *b*). The possibility that isomeric *o*- and *p*-*N*-methylaminodiphenylmethane undergo homolytic fission leading to separation of methylamine and diphenylmethane (route *d*) is not easily accepted, because when the pure isomers are heated under the same conditions of pyrolysis, they were recovered unchanged.

N-Methylaniline is proved to rearrange intramolecularly when heated alone in a sealed tube under the same conditions as the tertiary amine rearrangement producing only *o*-toluidine, together with methylamine, resulting from homolytic fission process (route *b*). Consequently, diphenylmethane can be considered to have resulted from coupling of benzyl and phenyl radicals (see route *c*).

It was reported (9) that acridine was obtained by distillation of 2-aminodiphenylmethane through a red hot tube; it is likely that 2-aminodiphenylmethane is dehydrogenated to a radical followed by cyclization and further dehydrogenation to produce acridine.

Consequently, 2-amino-3-methyldiphenylmethane, plausibly formed as an intermediate product from an intramolecular shift of the methyl group in *N*-methyldiphenylmethane to the *ortho* position of the benzene nucleus (route *e*), could be considered to undergo a dehydrogenation and cyclization process under the homolytic conditions of the reaction, producing 4-methylacridine, which was separated in relatively high yield (29%), as in Scheme 3.

Separation of methylamine, and not benzylamine, during the rearrangement of the amine insures that the migration of the benzyl group precedes that of the methyl group, *i.e.* the reverse

Can. J. Chem. Downloaded from www.nrcresearchpress.com by 210.87.254.6 on 09/05/12
For personal use only.

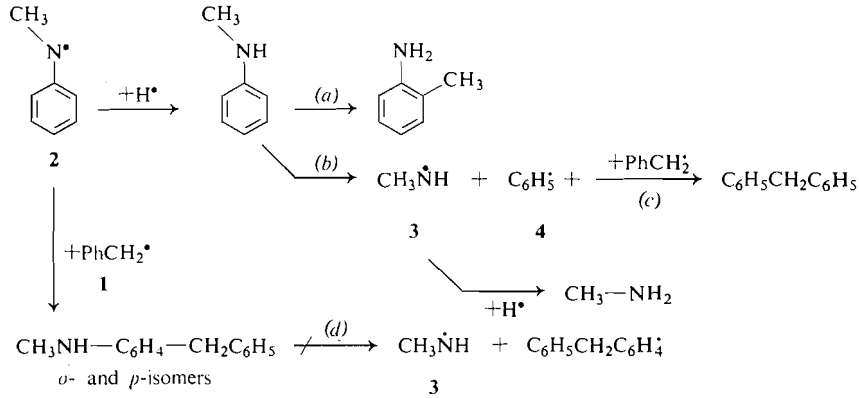

SCHEME 2

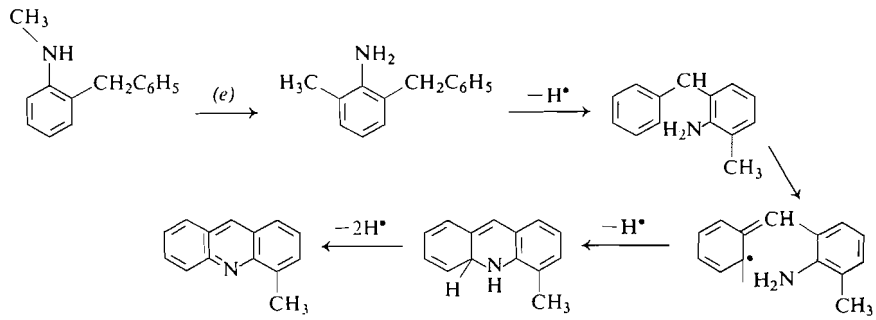

SCHEME 3

order to that observed in case of proton-catalyzed rearrangement (3*a*), and this was further confirmed in general by the nature of other isolated products.

The thermal rearrangement of *N*-benzyl-*N*-methylaniline in quinoline gave the normal rearrangement products together with 2- and 4-benzylquinolines in a ratio similar to that obtained in the pyrolysis of benzyl naphthyl ethers (10) with quinoline as solvent, justifying the similarity in nature of both rearrangements, *i.e.* benzylation of quinoline occurred by intermolecular mechanism involving the attack of benzyl free radical on the quinoline nucleus. However, the absence of methylquinolines among the products of the amine rearrangement and the absence of *p*-toluidine in rearrangements of either tertiary or secondary amines indicates that the methyl group of *N*-methylaniline does not migrate as a free radical in the course of the thermal rearrangement, but possibly through an intramolecular shift.

The formation of 2,2′-biquinolyl strongly suggests the formation of quinolyl free radical from quinoline followed by reaction with other free radicals in the reaction medium; combination with another quinolyl free radical gives 2,2′-biquinolyl, while with a benzyl radical, 2- and 4-benzylquinolines are formed. Further studies on the behavior of such types of compounds under thermal and other comparable conditions are in progress, the results of which will be published on their completion.

Experimental

Analysis

The i.r. spectroscopic analysis was carried out by Pye-Unicam i.r. spectrophotometer, Model SP200G. The u.v. absorptions were carried out by Pye-Unicam u.v. spectrophotometer, Model SP8000. Gas–Liquid chromatographic analysis was carried out by Pye-Unicam gas chromatograph, "Series 104", Dual flame ionization detector, temperature programmed, Model 24. The column used was 20% SE30 on Chromosorb W (35–80) mesh.

N-Benzyl-N-methylaniline (11)

Benzyl chloride (1 mol) and redistilled *N*-methylaniline (1 mol) were warmed for 4 h. The cooled reaction prod-

Can. J. Chem. Downloaded from www.nrcresearchpress.com by 210.87.254.6 on 09/05/12
For personal use only.

Can. J. Chem. Downloaded from www.nrcresearchpress.com by 210.87.254.6 on 09/05/12
For personal use only.

ucts were decomposed with 30% NaOH and extracted with ether. The ethereal extract was dried, evaporated, and the residue fractionated. The amine was collected at b.p. 304–306° (80% yield). It was further purified by redistillation over fused KOH and collected at b.p. 187–188°/26 mm Hg; n_D^{20} 1.6021; picrate from ethanol, m.p. 127° (lit. (11*b*) gives b.p. 161–162/8 mm, $n_D^{29.5}$ 1.6008; picrate m.p. 128–128.5). The purity of the amine has been ascertained by its i.r. spectrum and by t.l.c. using butanol saturated with water as a solvent and the spot was developed by iodine vapor, R_f = 0.56. All the rearrangements of the amine were carried out in duplicate. Details of the conditions and the mean yields of products separated are summarized in Table 1.

Pyrolysis of N-Benzyl-N-methylaniline

(*a*) *N*-Benzyl-*N*-methylaniline (30 g) was heated under reflux for 100 h. The reflux condenser was connected to a gas trap containing glass wool moistened with concentrated hydrochloric acid, adequate precautions being taken to prevent the diffusion of acid vapor to the reaction vessel. The temperature of the boiling liquid dropped progressively during the first 10 h from 306 to 252°, and the contents of the flask acquired a dark brown color. The products were dissolved in ether and shaken several times with concentrated hydrochloric acid to dissolve the amines.

The ethereal layer containing the neutral products (*A*) was dried and evaporated to dryness leaving an oily residue (2.5 g).

The amine hydrochloride solution was made alkaline with NaOH solution in order to liberate the amines which were extracted with ether. The ether layer was removed, dried (Na_2SO_4), and evaporated, leaving the free amines (*B*) (26.6 g).

The contents of the trap were washed with water and left for crystallization whereupon hairy colorless crystals were deposited as methylaminehydrochloride, m.p. and mixture m.p. 223–225° (benzyl derivative, m.p. and mixture m.p. 79–80°; picrate from ethanol, m.p. and mixture m.p. 214–215°).

The neutral products (*A*) were distilled to give benzaldehyde (0.4 g), b.p. 52–54°/10 mm Hg, n_D^{20} 1.5450 (2,4-dinitrophenylhydrazone derivative, m.p. and mixture m.p. 235–236°). Its i.r. spectrum showed a carbonyl stretching vibration at 1698 cm^{-1} and was superimposable upon that of a reference sample. The neutral fraction, b.p. 130–135°/10 mm Hg, solidified and was identified as diphenylmethane (0.75 g), m.p. 25–26°, $n_D^{26.5}$ 1.5805 (2,2′, 4,4′-tetranitro derivative, m.p. and mixture m.p. 170°). On oxidation with potassium dichromate – sulfuric acid mixture, it gave benzophenone (2,4-dinitrophenylhydrazone derivative, m.p. and mixture m.p. 238–239°). The fraction, b.p. 145–155°/10 mm Hg, solidified and was identified as dibenzyl (0.35 g), m.p. and mixture m.p. 51–52° (4,4′-dinitro derivative, m.p. and mixture m.p. 180°). The neutral products were further confirmed by their retention times in g.l.c. analysis.

The amines (*B*) were fractionated into *o*-toluidine (2.25 g) as pale yellow oil, b.p. 94–98°/15 mm Hg, n_D^{15} 1.5680 (picrate from ethanol, yellow crystals, m.p. and mixture m.p. 214–215°; benzoyl derivative, m.p. and mixture m.p. 144–145°). Its i.r. spectrum showed N—H stretching frequency as a doublet at 3363 and 3444 cm^{-1}, due to asymmetric and symmetric stretching of the free NH_2, and was coincident with that of the reference sample. Unchanged *N*-benzyl-*N*-methylaniline (15 g) was recovered as pale yellow oil, b.p. 171–182°/15 mm Hg, n_D^{20} 1.6025 (picrate, m.p. and mixture m.p. 126–127°).

The amine fraction, b.p. 265–272°/15 mm Hg, which solidified on cooling to brownish crystals, m.p. 84°, was identified as 4-methylacridine (4.3 g) crystallized from ethanol as yellow needles, m.p. and mixture m.p. 86-88°. Its i.r. spectrum is superimposable on that of a reference sample.

Anal. Calcd. for $C_{14}H_{11}N$: C, 87.1; H, 5.7; N, 7.3. Found: C, 87.2; H, 5.7; N, 7.3.

(*b*) The amine (30 g) was heated in a sealed tube filled with nitrogen atmosphere, at about 315° for 100 h and the contents of the tube changed similarly to dark brown oil. The tube was chilled in ice and opened whereupon methylamine evolved violently with its characteristic fishy ammoniacal odor. The products were taken up in ether and separated as before, into neutral (*A*) (2.4 g) and amino products (*B*) (27 g).

The neutral products (*A*) were separated by fractional distillation into diphenylmethane (0.5 g), b.p. 128–135°/10 mm Hg, n_D^{30} 1.5680, m.p. and mixture m.p. 25–26°, which is oxidized to benzophenone (2,4-dinitrophenylhydrazone derivative, m.p. and mixture m.p. 237–238°). Dibenzyl (0.52 g) also separated, b.p. 145–150°/10 mm Hg, m.p. and mixture m.p. 178–180°. They were further confirmed by g.l.c.

Fractionation of the amine products (*B*) gave *o*-toluidine (2.3 g) as pale yellow oil, b.p. 90–95°/10 mm Hg, n_D^{15} 1.5683 (picrate from ethanol, m.p. and mixture m.p. 214–215°; acetyl derivative, m.p. and mixture m.p. 110°). Unchanged amine (16 g) was recovered as pale yellow oil, b.p. 165–170°/10 mm Hg, n_D^{15} 1.6023. The amine fraction, b.p. 260–265°/15 mm Hg, was identified as 4-methylacridine, m.p. and mixture m.p. 87–88°.

Thermal Rearrangement in Quinoline as Aromatic Solvent

The amine (30 g) and redistilled quinoline (20 g) were heated together in a sealed tube under nitrogen at about 315° for 100 h. The same changes in color and viscosity of contents were observed and the tube was then chilled in ice and opened.

The products were separated as usual into neutral products (*A*) (2.25 g) and amines (*B*) (42 g).

The neutral products were fractionated into diphenylmethane (0.32 g), b.p. 90–95°/2 mm Hg, n_D^{30} 1.5681, m.p. and mixture m.p. 25–26°; benzophenone was separated on oxidation (2,4-dinitrophenylhydrazone derivative, m.p. and mixture m.p. 237–238°); and dibenzyl (0.35 g), b.p. 115–125°/2 mm Hg, m.p. and mixture m.p. 51–52° (4,4′-dinitro derivative, m.p. and mixture m.p. 179–180°).

The amine products (*B*) were fractionated into *o*-toluidine (4.3 g), b.p. 72–80°/2 mm Hg, n_D^{20} 1.5686 (picrate from ethanol, m.p. and mixture m.p. 213–214°; benzoyl derivative, m.p. and mixture m.p. 144–145°); recovered quinoline (11.2 g) collected at 100–105°/2 mm Hg, n_D^{20} 1.6251; and unchanged *N*-benzyl-*N*-methylaniline (17 g) collected at b.p. 135–142°/2 mm Hg.

The reddish oily amine fraction, b.p. 152–165°/2 mm Hg, was identified as a mixture of 2- and 4-benzylquinolines (6.5 g) by their retention time in g.l.c. analysis, with 41% 2-isomer and 59% 4-isomer. They were further separated by ascending paper chromatography, the benzylquinolines mixture being used as its picrate solution on C.

Can. J. Chem. Downloaded from www.nrcresearchpress.com by 210.87.254.6 on 09/05/12
For personal use only.

Schleicher and Schull paper No. 2316, using butanol saturated with water as solvent; 2-benzylquinoline picrate had R_f 0.71 and 4-benzylquinoline picrate had R_f 0.83. The two isomers were separated by fractional crystallization of their picrates from ethanol; 4-benzylquinoline picrate (9.25 g) separated first as golden yellow crystals, m.p. and mixture m.p. 178–179°. On dilution of the mother liquor with water, 2-benzylquinoline picrate (6.5 g) crystallized out, m.p. and mixture m.p. 155–156°. From the fraction, b.p. 200–210°/2 mm Hg, 4-methylacridine separated (3.2 g), m.p. and mixture m.p. 86–87.5°. Its i.r. spectrum was the same as that of the reference sample. The solid residue in the flask, when triturated with petroleum ether (40–60°), gave crystals, m.p. 192°, identified as 2,2′-biquinolyl (0.75 g); these were recrystallized from ethanol as colorless short needles, m.p. and mixture m.p. 194–195° (picrate, m.p. and mixture m.p. 214–215°). Its i.r. spectrum was superimposable upon that of the reference sample.

Thermal Rearrangement of N-Methylaniline

N-Methylaniline (20 g) was heated in a sealed tube at 310–315° for 100 h. The contents changed to a dark brown oil, and the tube was chilled in ice and opened whereupon methylamine evolved violently with its characteristic fishy ammoniacal odor. Some of the methylamine vapor was collected in a HCl trap and separated as hairy colorless crystals of methylamine hydrochloride, m.p. and mixture m.p. 223–225° (benzoyl derivative m.p. and mixture m.p. 78–80°; picrate from ethanol, m.p. and mixture m.p. 214–215°).

The contents of the tube were separated as usual into neutral (*A*) and amine products (*B*).

The neutral product (0.5 g) was an unidentified dark brown resinous material.

The amine products (*B*) (18.5 g) were treated with an alcoholic solution of oxalic acid whereupon a colorless crystalline solid was precipitated and identified as *o*-toluidine oxalate, m.p. and mixture m.p. 170–171°. The free base was separated by hydrolysis with hot KOH solution and extracted with ether; *o*-toluidine (7 g) was collected as a colorless oil, b.p. 198–200°, n_D^{20} 1.5689 (acetyl derivative m.p. and mixture m.p. 110–112°). On concentration of the remaining mother liquor, crystals of *N*-methylaniline oxalate were separated, m.p. and mixture m.p. 111–113°, from which the free base was separated by the action of hot KOH solution and extraction with ether (10 g), b.p. 193–195°, n_D^{20} 1.5721 (acetyl derivative, m.p. and mixture m.p. 102°).

Preparation of Reference Compounds

N-Methylaniline: prepared by heating acetanilide and sodium in dry xylene, then after, with methyl iodide. Xylene was evaporated and the residue refluxed with 30% alcoholic KOH solution. The alcohol was evaporated and the residue steam distilled. The ethereal extract of the distillate was dried and evaporated. The residual oil of *N*-methylaniline was distilled at 190–192° (lit. (12) b.p. 190–192°), n_D^{20} 1.5720 (picrate from ethanol, m.p. 145°).

Diphenylmethane: prepared by alkylation of benzene with benzylchloride and $AlCl_3$. It was collected at b.p. 261–262°, n_D^{27} 1.5788, m.p. 26° (lit. (13) m.p. 26°, b.p. 261–262°, n_D^{17} 1.5788).

Anal. Calcd. for $C_{13}H_{12}$: C, 92.9; H, 7.1. Found: C, 93.0; H, 7.1.

Dibenzyl: prepared by reduction of benzoin with zinc amalgam and concentrated HCl. It was crystallized from ethanol as white crystals, m.p. 52° (lit. (15) m.p. 52°) (4,4′-dinitro derivative, m.p. 180°).

4-Methylacridine: prepared by heating a mixture of *o*-aminobenzaldehyde, *o*-bromotoluene, and copper powder with anhydrous Na_2CO_3 in nitrobenzene. 4-Methylacridine was extracted and crystallized from petroleum ether (60–80°) or ethanol, m.p. 88° (lit. (14) m.p. 88°).

Anal. Calcd. for $C_{14}H_{11}N$: C, 87.1; H, 5.7; N, 7.3. Found: C, 87.2; H, 5.6; N, 7.3.

2-Benzylquinoline: pale yellow oil, b.p. 235°/14 mm (picrate, m.p. 157°; methiodide, m.p. 219° (dec.); lit. (16), gives picrate m.p. 156–157°).

4-Benzylquinoline: brownish crystals, b.p. 230°/14 mm; m.p. 53° (picrate, m.p. 178–179°; lit. (17) gives b.p. 222–223°/19 mm; picrate, m.p. 178°).

2,2′-Biquinolyl: white crystals from ethanol, m.p. 192° (picrate, m.p. 210° lit. (18), gives m.p. 192°; picrate, m.p. 210°).

1. A. W. HOFMANN and C. A. MARTIUS. Ber. **4**, 742 (1871). A. W. HOFMANN. Ber. **5**, 704 (1872); 7, 526 (1874).
2. (*a*) J. REILLY and W. J. HICKINBOTTOM. J. Chem. Soc. **117**, 103 (1920). (*b*) W. J. HICKINBOTTOM and S. E. A. RYDER. J. Chem. Soc. 1281 (1931). (*c*) W. J. HICKINBOTTOM and G. H. PRESTON. J. Chem. Soc. 1566 (1930). (*d*) W. J. HICKINBOTTOM. J. Chem. Soc. 1700 (1932); 1279 (1935); 404 (1937).
3. (*a*) H. HART and J. R. KASAK. J. Org. Chem. **27**, 116 (1962); (*b*) Y. OGATA, H. TABUCHI, and K. KOSHIDA. Tetrahedron, **20**, 2717 (1964).
4. M. J. S. DEWAR. Nature, **156**, 784 (1946); J. Chem. Soc. 406 (1964); Disc. Faraday Soc. **2**, 50 (1947); Electronic theory of organic chemistry. Clarendon Press, Oxford. 1949. p. 233; Bull. Soc. Chim. Fr. 71c (1951).
5. A. MICHAEL. Ber. **14**, 2105 (1881); J. Am. Chem. Soc. **42**, 787 (1920). E. BECKMANN and E. CORRONS. Ber. **55**, 852 (1922).
6. C. PAC and H. SAKURAI. Tetrahedron Lett. 1865 (1968); Kagaka Zasshi, **72**, 230 (1969).
7. C. WALLING. Free radicals in solution. J. Wiley, London. 1957. p. 398.
8. A. F. WOODWARD and R. B. MESROBIAN. J. Am. Chem. Soc. **75**, 6189 (1953).
9. A. ALBERT. The acridines. Arnold, London. 1951. p. 60. R. M. ACHESON. Acridines. Interscience Publications Inc., N.Y. 1956. FISCHER and SCHUTTE. Ber. **26**, 3085 (1893).
10. M. Z. A. BADR and M. M. ALY. Tetrahedron, **28**, 3401 (1972). M. Z. A. BADR and H. A. H. EL-SHERIEF. Can. J. Chem. **50**, 259 (1972).
11. (*a*) M. GOMBERG and G. G. BUCHLER. J. Am. Chem. Soc. **42**, 2059 (1920). E. WEDENKIND. Ber. **32**, 519 (1899). (*b*) DESAI. J. Indian Inst. Sci. **7**, 250 (1925).
12. P. HEPP. Ber. **10**, 328 (1877).
13. W. W. HARTMAN and R. PHILLIPS. Org. Synth. Col. Vol. II, 232 (1943).
14. H. JONSON and M. FRIEDRICH. J. Am. Chem. Soc. **49**, 1049 (1927).
15. CANNIZARO and ROSSI. Ann. **251**, 121 (1862).
16. H. DECKER and R. POSCHORR. Ber. **37**, 3400 (1904).
17. I. P. RABE and R. PASTENACK. Ber. **46**, 1026 (1913).
18. J. P. WIBAUT and H. D. T. WILLINK. Rec. Trav. Chim. **54**, 804 (1935).

Some Derivatives of 2,5-Xylidine and their Cyclization to Indoles

LARRY J. KRICKA[1] AND JOHN M. VERNON[2]

Department of Chemistry, University of York, Heslington, York Y01 5DD, U.K.

Received July 23, 1973

N-Methyl and *N*-phenyl derivatives of 2,5-xylidine have been characterized, and polysubstituted indoles obtained via cyclization of appropriate derivatives of 2,5-xylidine and 2,5-xylylhydrazine.

On a caractérisé les dérivés *N*-méthylé et *N*-phénylé de la xylidine-2,5. Des indoles polysubstitués ont aussi été obtenus par cyclisation des dérivés appropriés de la xylidine-2,5 et de la xylylhydrazine-2,5.
[Traduit par le journal]

Can. J. Chem., **52**, 299 (1974)

Can. J. Chem. Downloaded from www.nrcresearchpress.com by 210.87.254.40 on 09/05/12
For personal use only.

For an exploration of the possibility of photochemical interconversion of indole and isoindole ring systems (*cf.* 1,2- and 1,3-benzoxazoles (1) and -benzodiazoles (2)), we required new indoles with a substitution pattern the same as that of some isoindoles already available through earlier work (3). We describe some previously ill-characterized *N*-substituted derivatives of 2,5-xylidine and the synthesis of some 1,2,3,4,7-pentasubstituted indoles therefrom. The photochemical isomerization which we sought has not yet been achieved.

Reduction of the nitrosamine obtained from *N*-methyl-2,5-xylidine (**1**)[3] gave 1-methyl-1-(2,5-xylyl)hydrazine (**2**) more simply than its single previously recorded (4) preparation. The hydrazine **2** with ethyl methyl ketone and polyphosphoric acid afforded 1,2,3,4,7-pentamethylindole (**5**) rather than the isomeric 2-ethyl-1,4,7-trimethylindole, in accordance with the usually preferred orientation in Fischer cyclization reactions (see ref. 5 for a comprehensive and recent review). The mass spectrum of the product **5** agreed with that recorded by Russian workers (6), although their work gave no account of the preparation of **5** nor of its further characterization, which have not been reported hitherto. The position of the longest wavelength electronic absorption band (λ_{max} 281 nm) and its subsidiary absorption maxima are like those of 1,2,3-trimethylindole (7).

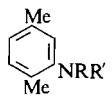

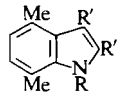

1 R = Me; R′ = H
2 R = Me; R′ = NH_2
3 R = H; R′ = CHPh·COPh
4 R = Ph; R′ = H

5 R = R′ = Me
6 R = H; R′ = Ph
7 R = Me; R′ = Ph
8 R = CH_2Ph; R′ = Ph

A similar Fischer synthesis with the hydrazine **2** and deoxybenzoin gave the indole **7**, but in such poor yield that an alternative route was sought. The acid-catalyzed condensation of 2,5-xylidine and benzoin has been reported (8) to give 4,7-dimethyl-2,3-diphenylindole (**6**), but we obtained instead the α-arylaminoketone **3**, which failed to cyclize on further treatment with acid. Infrared absorptions characteristic of N—H and C=O bonds, mass spectral fragmentation involving loss of a benzoyl group, and analytical figures in support of structure **3** are presented in the Experimental section. Similar intermediates have been isolated in some previous instances of the Bischler synthesis of indoles (5). However, the indole **6** was obtained satisfactorily from **3** in the presence of 2,5-xylidine hydrochloride at 200°. The potassium derivative of **6** was alkylated with methyl iodide or with benzyl chloride to give the pentasubstituted indoles **7** and **8**, respectively.

N-Phenyl-2,5-xylidine (**4**) was prepared via 2′,5′-acetoxylidide by a general method for *N*-phenylation of aromatic amines using bromobenzene and copper powder in presence of potassium carbonate. This method had been employed previously for both 2,3- and 3,5-xylyl

[1]Present address: Department of Clinical Chemistry, The Medical School, University of Birmingham, Birmingham, U.K.

[2]Author to whom correspondence should be addressed; on study leave 1973 at Department of Chemistry, University of British Columbia, Vancouver 8, British Columbia.

[3]Remarkably, the first simple crystalline derivatives of this amine **1** are those described in the Experimental section, although the n.m.r. spectrum of the *N*-acetyl derivative has been reported (19).

Can. J. Chem. Downloaded from www.nrcresearchpress.com by 210.87.254.40 on 09/05/12
For personal use only.

isomers of structure **4** (9, 10), and it was neither known nor expected to cause rearrangement. Surprisingly, our product **4** had the same m.p. (54°) as that reported for either the 3,5- or the 2,6-xylyl isomer (10, 11), but significantly different from the value (29°) given for *N*-phenyl-2,5-xylidine (**4**), which had been obtained via a different route (12).

It was conceivable that migration of a methyl group had occurred in the strongly acidic conditions used by the Czech workers (10) to prepare their 3,5-xylidine via a modified Lossen reaction from 3,5-dimethylbenzoic acid, but repetition of this reaction gave 3,5-xylidine identical (g.l.c. retention time, i.r., n.m.r.) with an authentic sample. Rearrangement during the *N*-phenylation procedure appeared less likely in view of the basic conditions employed, but the high temperature required might have favored the formation of the less crowded 3,5-xylyl structure in our reaction starting from 2,5-xylidine. We therefore repeated the preparation of *N*-phenyl-3,5-xylidine to compare the product, m.p. 52°, with our 2,5-xylyl isomer **4**. Not only was the melting point considerably depressed on admixture, but the two isomers afforded different *N*-acetyl derivatives and they showed characteristically different n.m.r. and i.r. absorptions in accord with the 1,2,5- and 1,3,5-aromatic substitution patterns (see Experimental section); in particular, the equivalence of the ring methyl groups in the n.m.r. spectra was distinctive for all the 3,5-xylidine derivatives.

Probably on account of their low nucleophilicity, diarylamines require vigorous conditions of high temperature and acid catalysis for their condensation with acyloins to give *N*-arylindoles (13), and few such syntheses have been reported. However, we were unable to obtain any indolic product from an attempted reaction of *N*-phenyl-2,5-xylidine (**4**) with benzoin.

Experimental

Infrared spectra were recorded for Nujol mulls and calibrated with polystyrene. Proton n.m.r. spectra were measured at 60 MHz for solutions in deuteriochloroform with tetramethylsilane as internal standard; chemical shifts are given on the τ scale (10 − δ). Mass spectra were recorded with an A.E.I. MS 12 instrument operating at 70 eV. Alumina for chromatography was Laporte type H. Light petroleum was the fraction of b.p. 60–80°, unless otherwise stated.

2,5-Xylidine Derivatives

N-Methyl-2,5-xylidine (**1**) was prepared (14) from *N*-benzylidene-2,5-xylidine (15) and dimethyl sulfate; it was an oil, b.p. 95–96°/10 mm (lit. b.p. 225–227°/735 mm (15)), which with *p*-toluenesulfonyl chloride and alkali afforded *N-methyl-p-toluenesulfon-2,5-xylidide*, m.p. 109–110°(from ethanol); n.m.r. 2.2–3.6 (7H, m, ArH), 6.90 (3H, s, NCH_3), 7.56, 7.69, and 7.83 (each 3H, s, $ArCH_3$).

Anal. Calcd. for $C_{16}H_{19}NO_2S$: C, 66.4; H, 6.6; N, 4.8. Found: C, 66.3; H, 6.6; N, 4.9.

The amine **1** and acetic anhydride in refluxing xylene afforded *N-methyl-2′,5′-acetoxylidide*, m.p. 44° (from light petroleum); i.r. (film) N—H absent, 1660s cm^{-1} (C=O); n.m.r. 2.8–3.0 (3H, m, ArH), 6.81 (3H, s, NCH_3), 7.65 and 7.80 (each 3H, s, $ArCH_3$), and 8.22 (3H, s, $COCH_3$).

Anal. Calcd. for $C_{11}H_{15}NO$: C, 74.5; H, 8.5; N, 7.9. Found: C, 74.1; H, 8.6; N, 7.8.

N-Methyl-*N*-nitroso-2,5-xylidine (i.r. (film) N—H absent, 1519s cm^{-1} (N=O)), obtained (15) as a yellow oil from the amine **1** and cold nitrous acid, was reduced with zinc and acetic acid (*cf.* the procedure for 1-methyl-1-(2,4-xylyl)hydrazine (16)) to 1-methyl-1-(2,5-xylyl)-hydrazine (**2**) (53%), b.p. 64–66°/1.4 mm, which with acetic anhydride gave the acetyl derivative, m.p. 101–102° (lit. m.p. 102–103.5° (4)). The hydrazine **2** and *p*-nitrobenzaldehyde afforded the corresponding *N-methyl-N-(2,5-xylyl)hydrazone* as orange needles, m.p. 85–86° (from methanol); n.m.r. 1.84 and 2.34 (each 2H, d, $p\text{-}O_2NC_6H_4$), 2.75–3.10 (3H, m, ArH), 6.59 (3H, s, NCH_3), 7.68 and 7.78 (each 3H, s, $ArCH_3$).

Anal. Calcd. for $C_{16}H_{17}N_3O_2$: C, 67.8; H, 6.1; N, 14.8. Found: C, 68.0; H, 6.2; N, 15.3.

N-Phenylation of 2′,5′-acetoxylidide (17) with bromobenzene in presence of copper powder and potassium carbonate (*cf.* ref. 10) followed by alkaline hydrolysis gave *N*-phenyl-2,5-xylidine (**4**); the yield of **4** eluted with benzene – light petroleum (1:1 v/v) from a column of alumina was 16%, m.p. 54° (from methanol) (lit. m.p. 29° (12)); i.r. 3350 (N—H), 880, 815s, 750s, 725, 705, and 695s cm^{-1}; n.m.r. 2.6–3.2 (8H, m, ArH), 4.85br (1H, s, NH), 7.82 and 7.92 (each 3H, s, $ArCH_3$).

Anal. Calcd. for $C_{14}H_{15}N$: C, 85.2; H, 7.7; N, 7.1. Found: C, 85.3; H, 7.8; N, 7.0.

With acetic anhydride in refluxing xylene the amine **4** afforded *N-phenyl-2′,5′-acetoxylidide*, m.p. 89.5–91° (from methanol); i.r. N—H absent, 1655 (C=O), 820, 770s, 730 and 695s cm^{-1}; n.m.r. 2.6–3.0 (8H, m, ArH), 7.70 and 7.81 (each 3H, s, $ArCH_3$), and 8.01 (3H, s, $COCH_3$).

Anal. Calcd. for $C_{16}H_{17}NO$: C, 80.3; H, 7.2; N, 5.9. Found: C, 80.2; H, 7.2; N, 5.7.

3,5-Xylidine Derivatives

N-Phenyl-3,5-xylidine, obtained from 3′,5′-acetoxylidide by the same method (10), had m.p. 51–52° (after sublimation at 130°/0.2 mm and recrystallization from methanol) (lit. m.p. 54° (10)); mixture m.p. with the 2,5-isomer **4** 30–35°; i.r. 3370 (N—H), 885, 850s, 755s, 710, and 695s cm^{-1}; n.m.r. 2.6–3.5 (8H, m, ArH), 4.50 br (1H, s, NH), and 7.77 (6H, s, $ArCH_3$). Its *N-acetyl derivative* was prepared as above, m.p. 93.5–95° (from methanol), mixture m.p. with the 2,5-isomer considerably depressed; i.r. N—H absent, 1665 (C=O), 885, 860s, 760s, 705s, and 695s cm^{-1}; n.m.r. 2.6–2.8 (5H, m, ArH),

Can. J. Chem. Downloaded from www.nrcresearchpress.com by 210.87.254.40 on 09/05/12
For personal use only.

3.08 (3H, s, ArH), 7.74 (6H, s, $ArCH_3$), and 7.98 (3H, s, $COCH_3$).

Anal. Calcd. for $C_{16}H_{17}NO$: C, 80.3; H, 7.2; N, 5.9. Found: C, 80.4; H, 7.2; N, 5.8.

1,2,3,4,7-Pentamethylindole (5)

Ethyl methyl ketone (3.0 g), polyphosphoric acid (20 g), and the hydrazine **2** (4.5 g) were heated together for 1 h at 100°, then for 15 min at 200° (*cf.* ref. 18). The reaction mixture was cooled, stirred with water (200 ml), and extracted repeatedly with ether. The combined ether extracts were washed with water, dried ($MgSO_4$), and evaporated to give the *indole* **5** (0.6 g, 10%) as pale buff crystals, m.p. 138–139° (from methanol); u.v. (ethanol) 236 nm (log ε 4.5), 281 (3.8), 290 sh (3.8), and 301 (3.7); i.r. 1603, 1515s, 1403, 1318s, and 802 cm^{-1}; n.m.r. 3.39 (2H, s, ArH), 6.20 (3H, s, NCH_3), 7.55 (6H), and 7.60, 7.76 (each 3H, s, CH_3); mass spectrum *m/e* 188 (15%), 187 (M^+, 100), 186 (42), 173 (20), and 172 (M − CH_3, 65), m* 159.5 (187 → 172).

Anal. Calcd. for $C_{13}H_{17}N$: C, 83.4; H, 9.2; N, 7.5. Found: C, 83.5; H, 9.0; N, 7.7.

N-(α-Phenylphenacyl)-2,5-xylidine (3)

A mixture of benzoin (20 g), 2,5-xylidine (30 ml), and concentrated hydrochloric acid (5 ml) was heated under reflux for 2.5 h; it was then cooled, poured into water, and extracted with ether. The ether extract was washed, dried ($MgSO_4$), and evaporated to yield a yellow oil, from which *N-(α-phenylphenacyl)-2,5-xylidine* (**3**) (14.8 g, 50%) was obtained as yellow crystals, m.p. 73.5–74.5° (from methanol); i.r. 3450br (N—H), 1680s (C=O), 1618, 1600s, 1585, 1530br, 1325, 1250br, 1010, 998, 805, and 700 cm^{-1}; n.m.r. 1.9–2.9 (11H, m, ArH), 3.05 and 3.53 (each 1H, d, $J_{3,4}$ 7 Hz, ArH), 3.9br (1H, CH), 4.65br (1H, NH), 7.78 and 7.83 (each 3H, s, $ArCH_3$); mass spectrum *m/e* 315 (M^+, 5%), 211 (17), and 210 (M − PhCO, 100), m* 140 (315 → 210).

Anal. Calcd. for $C_{22}H_{21}NO$: C, 83.8; H, 6.7; N, 4.4. Found: C, 83.8; H, 6.8; N, 4.6.

4,7-Dimethyl-2,3-diphenylindole (6)

2,5-Xylidine hydrochloride (3.7 g) and compound **3** (7.5 g) were heated for 1 h at 190–200°. The resulting gum was dissolved in benzene and this solution was washed with dilute hydrochloric acid, then with water, dried ($MgSO_4$), and evaporated. The residue afforded the indole **6** (4.0 g, 43%), m.p. 128–129° (from aqueous ethanol) (lit. m.p. 130° (8)).

N-(α-Phenylphenacyl)-2,5-xylidine (**3**) could not be cyclized to the indole **6** by treatment with either cold concentrated sulfuric acid or hot concentrated hydrochloric acid.

1,4,7-Trimethyl-2,3-diphenylindole (7)

Potassium (0.35 g) was added in small pieces to a stirred solution of the indole **6** (2.2 g) in hot xylene (15 ml) under nitrogen. The mixture was heated under reflux and stirred until after 1 h all the potassium had reacted. The apparatus was then fitted with a Friedrichsen condenser (cold finger) containing acetone and solid carbon dioxide, and the mixture was refluxed for a further 5 h with addition of methyl iodide (10 g). The mixture was cooled, poured into water, and extracted with ether. The ether extract was washed, dried ($MgSO_4$), and evaporated to afford the *indole* 7 (1.0 g, 43%) as prisms, m.p. 154–155° (from benzene – light petroleum); i.r. N—H absent, 1600w, 1394s, 1037, 814s, 753, and 713 cm^{-1}; n.m.r. 2.6–2.9 (10H, m, ArH), 3.07 and 3.27 (each 1H, d, $J_{5,6}$ 7 Hz, ArH), 6.14 (3H, s, NCH_3), 7.20 and 7.93 (each 3H, s, $ArCH_3$); *m/e* 311 (M^+, 100%).

Anal. Calcd. for $C_{23}H_{21}N$: C, 88.7; H, 6.8; N, 4.5. Found: C, 88.6; H, 6.9; N, 4.3.

An attempted preparation of the same indole 7 from the hydrazine **2**, which was heated with deoxybenzoin and zinc chloride, gave less pure material (2%) with the same i.r. spectrum.

1-Benzyl-4,7-dimethyl-2,3-diphenylindole (8)

The indole **6** in hot xylene was converted to its potassium derivative as described above. After dropwise addition of benzyl chloride (3 ml) the mixture was refluxed for a further 10 h, after which it was cooled, poured into water, and extracted with ether. Evaporation of the ether extract left a yellow oil which was chromatographed on alumina (200 g), from which light petroleum eluted xylene. Further elution with light petroleum – benzene afforded the *indole* **8** (1.5 g, 26%) as prisms, m.p. 192–193° (from benzene); i.r. N—H absent, 1603w, 1503, 825, 773, and 715 cm^{-1}; n.m.r. 2.5–3.2 (17H, m, ArH), 6.0br (2H, NCH_2Ph), 7.60 and 7.90 (each 3H, s, $ArCH_3$).

Anal. Calcd. for $C_{29}H_{25}N$: C, 89.9; H, 6.5; N, 3.6. Found: C, 89.9; H, 6.6; N, 3.6.

We thank the Science Research Council for a studentship (to L.J.K.) and Mrs. J. E. Humpherson for some experimental assistance.

1. H. GÖTH and H. SCHMID. Chim. (Switz.), **20**, 148 (1966); *cf.* M. OGATA, H. MATSUMATO, and H. KANO. Tetrahedron, **25**, 5205 (1969).
2. H. TIEFENTHALER, W. DÖRSCHELN, H. GÖTH, and H. SCHMID. Tetrahedron Lett. 2999 (1964); Helv. Chim. Acta, **50**, 2244 (1967). H. LABHARDT, W. HEINZELMANN, and J. P. DUBOIS. Pure Appl. Chem. **24**, 495 (1970).
3. C. O. BENDER and R. BONNETT. J. Chem. Soc. C, 3036 (1968). L. J. KRICKA and J. M. VERNON. J. Chem. Soc. (Perkin I), 904 (1972).
4. R. HUISGEN, F. JAKOB, W. SIEGEL, and A. CADUS. Justus Liebigs Ann. Chem. **590**, 1 (1954).
5. R. K. BROWN. Synthesis of the indole nucleus. *In* Indoles Part 1. *Edited by* W. J. Houlihan. Wiley-Interscience, New York. 1972. p. 227 and refs. therein.
6. V. I. VYSOTSKIĬ, R. A. KHMEL'NITSKIĬ, I. I. GRANDBERG, and V. A. BUDYLIN. Izv. Timiryazev. Sel'skokhoz. Akad. 221 (1970); Chem. Abstr. **73**, 124826a (1970).
7. R. L. HINMAN and E. B. WHIPPLE. J. Am. Chem. Soc. **84**, 2534 (1962).
8. E. RITCHIE. J. Proc. Roy. Soc. N.S.W. **80**, 33 (1946); Chem. Abstr. **41**, 3094c (1947).
9. H. BRÄUNIGER and K. F. AHREND. Arch. Pharm. **298**, 627 (1965).

10. J. HEBKÝ, O. ŘÁDEK, and J. KEJHA. Collect. Czech. Chem. Commun. **24**, 3988 (1959).
11. Monsanto Co. Brit. Pat. No. 989 247 (1965); Chem. Abstr. **63**, 14755h (1965).
12. R. J. SUNDBERG and R. H. SMITH, JR. Tetrahedron Lett. 267 (1971).
13. M. B. RICHARDS. J. Chem. Soc. **97**, 977 (1910).
14. Farbwerke Hoechst A.G. Germ. Pat. No. 953 169 (1956); Chem. Abstr. **53**, 8072d (1959).
15. L. PFLUG. Justus Liebigs Ann. Chem. **255**, 168 (1889).
16. H.-H. STROH and E. ROPTA. Chem. Ber. **93**, 1148 (1960).
17. E. BAMBERGER. Ber. **59**, 418 (1926). TH. CURTIUS and A. BERTHO. Ber. **59**, 565 (1926).
18. H. M. KISSMAN, D. W. FARNSWORTH, and B. WITKOP. J. Am. Chem. Soc. **74**, 3948 (1952).
19. R. F. C. BROWN, L. RADOM, S. STERNHELL, and I. D. RAE. Can. J. Chem. **46**, 2577 (1968).

Can. J. Chem. Downloaded from www.nrcresearchpress.com by 210.87.254.40 on 09/05/12
For personal use only.

Quaternary Nitrogen Heterocycles. III.[1] Kinetic and Thermodynamic Control of Pseudobase Formation from the 1-Methyl-3-nitroquinolinium Cation

JOHN W. BUNTING AND WILLIAM G. MEATHREL

Department of Chemistry, University of Toronto, Toronto, Ontario M5S 1A1

Received August 14, 1973

A kinetic study of the formation and decomposition of the pseudobase of the 1-methyl-3-nitroquinolinium cation has revealed that although 1,4-dihydro-4-hydroxy-1-methyl-3-nitroquinoline is the predominant product at equilibrium, the kinetically controlled product is the isomeric pseudobase, 1,2-dihydro-2-hydroxy-1-methyl-3-nitroquinoline. This less stable isomer has been identified from its u.v.–visible spectrum, and the pK_{ROH} value for its formation (9.16) has been measured by the stopped-flow technique.

Une étude cinétique de la formation et de la décomposition de la pseudobase du cation méthyl-1 nitro-3 quinolinium a montré que la pseudobase isomérique, dihydro-1,2 hydroxy-2 méthyl-1 nitro-3 quinoline, est majoritairement formée sous contrôle cinétique bien qu'à l'équilibre la dihydro-1,4 hydroxy-4 méthyl-1 nitro-3 quinoline soit le produit majeur. L'isomère le moins stable, issu du contrôle cinétique, a été identifié à partir de son spectre u.v.–visible; de même la valeur du pK_{ROH} pour sa formation (9.16) a été mesurée à l'aide de la technique à débit interrompu. [Traduit par le journal]

Can. J. Chem., **52**, 303 (1974)

We have previously reported (1) that the pK_{ROH} value for the reversible formation of the pseudobase **2** from the 1-methyl-3-nitroquinolinium cation (**1**) in aqueous solution is 6.74 at 25°. In more basic solution a further ionization constant was measured, $pK_{RO^-} = 13.0$ which was ascribed to the ionization of **2** to the alkoxide ion **3**.

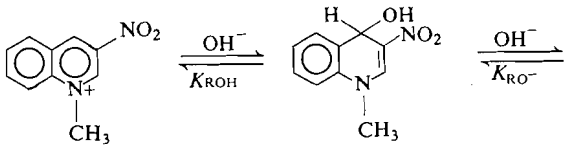

1 **2**

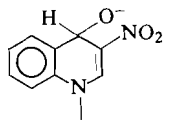

3

Severin and co-workers (2) have definitely established, on the basis of u.v. and p.m.r. spectra, that the predominant pseudobase formed from **1** is the 1,4-dihydroquinoline **2** rather than the corresponding 1,2-dihydroquinoline derivative **4**. In particular, these workers noted that 1,2-dihydro-3-nitroquinolines have absorption maxima at considerably longer wavelengths than the corresponding 1,4-dihydro isomers, *e.g.* λ_{max} for 1,2-dihydro-1-methyl-3-nitroquinoline: 266, 330,

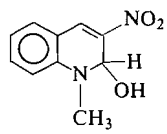

4

510 nm and for 1,4-dihydro-1-methyl-3-nitroquinoline: 240, 420 nm. The long wavelength maxima of 401 and 410 nm, respectively, for the pseudobase and pseudobase anion of the 1-methyl-3-nitroquinolinium cation (1), confirm that these species are predominantly **2** and **3** rather than **4** and/or its alkoxide ion, respectively. The spectral evidence does not, of course, rule out the possibility that small amounts of **4** and its anion are present in equilibrium with **2** and **3**, and such is almost certain to be the case.

We have also recently reported a study on the kinetics of pseudobase formation and decomposition for a number of quaternary heteroaromatic cations (3). In extending this study to the 1-methyl-3-nitroquinolinium cation, we have observed that the p*H* dependence of pseudobase formation from this cation is different from that previously observed for other heterocyclic cations. Further investigation has then established that although **2** is the thermodynamically preferred pseudobase, the kinetically preferred product is **4**.

Results and Discussion

Rapid u.v. spectral changes are observed when aqueous solutions of the 1-methyl-3-nitroquino-

[1]For Part II, see ref. 3.

Can. J. Chem. Downloaded from www.nrcresearchpress.com by 210.87.254.40 on 09/05/12
For personal use only.

Can. J. Chem. Downloaded from www.nrcresearchpress.com by 210.87.254.40 on 09/05/12
For personal use only.

linium cation are mixed in the stopped-flow apparatus with buffers in the range pH 6–12. In all cases, these changes are first-order in the heterocyclic cation over at least 90% of the reaction. Spectral changes, first-order in heterocycle, are also observed when solutions of the pseudobase, **2**, (in 0.01 N KOH) are mixed with buffers (containing 0.01 N HCl) in the range pH 4–7. The pH dependence of the observed pseudo first-order rate constants, k_{obs}, for these reactions is indicated in Fig. 1. A striking feature of this figure is the pH independence of k_{obs} in the range pH 9–12; for similar reactions of other cations, k_{obs} is directly proportional to hydroxide ion concentration in basic solutions (3).

The rate constant, k_{obs}, reflects the rate of approach to equilibrium between the cation and its pseudobase, and is the sum of the individual rate constants, k_f and k_d, for the formation and decomposition of the pseudobase. We have shown previously (3), that in such systems k_f and k_d may be calculated from the equations

$$k_f = \frac{k_{obs}}{1 + [H^+]/K_{ROH}}$$

and

$$k_d = \frac{k_{obs}}{1 + K_{ROH}/[H^+]}$$

Values of k_f and k_d calculated in this way from the data in Fig. 1 are plotted in Fig. 2. The pH profiles for these two pseudo first-order rate constants are quite different from those previously observed for other cations (3); thus eqs. 1 and 2 which were used previously,

$$[1] \qquad k_d = k_1[H^+] + k_2$$

$$[2] \qquad k_f = k_3[OH^-] + k_4$$

are clearly not sufficient in the present case to express the observed pH dependence of k_f and k_d.

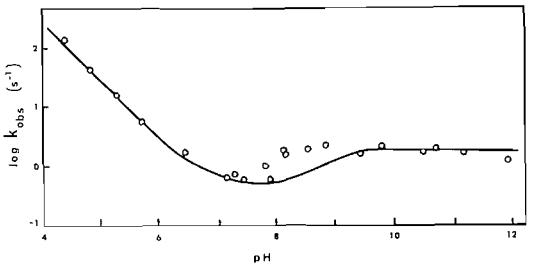

FIG. 1. The pH dependence of k_{obs} (s^{-1}) for reversible pseudobase formation from the 1-methyl-3-nitroquinolinium cation: 25°, ionic strength 0.1.

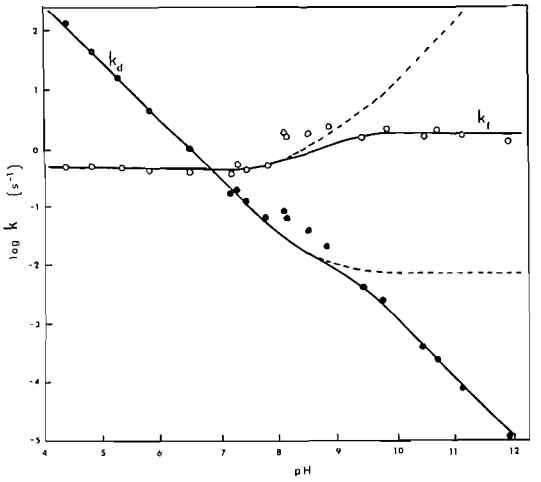

FIG. 2. The pH dependence of k_f and k_d (s^{-1}) for the formation and decomposition of the pseudobase from the 1-methyl-3-nitroquinolinium cation: 25°, ionic strength 0.1.

We have found that a mechanism such as that illustrated in Scheme 1 can be reconciled with the observed pH profiles in Fig. 2. This scheme assumes a species "X" that is in acid–base equilibrium with the cation, **1**; this equilibrium is attained rapidly relative to the establishment of the equilibrium between **1** and the pseudobase, **2**. It is further assumed that the pseudobase may arise by attack of either hydroxide ion (k_3) or a water molecule (k_4) on the heterocyclic cation, in accord with previous observations (3). Similarly, the pseudobase may decompose to the cation either directly by elimination of hydroxide ion (k_2) or via loss of water from its conjugate acid (k_1^1). The use of the rate constants k_2, k_3, and k_4 in this scheme is consistent with eqs. 1 and 2. The constant k_1^1 is related to k_1 of eq. 1 by $k_1^1 = k_1 \cdot K_a$

Since we have separated k_{obs} into k_f and k_d above, we may consider separately the formation of **2** from **1** and of **1** from **2** in Scheme 1. Thus,

$$\frac{d[\mathbf{2}]}{dt} = (k_3[OH^-] + k_4)[\mathbf{1}]$$

$$= k_f([\mathbf{1}] + [X])$$

$$= k_f\left(1 + \frac{K_X}{[H^+]}\right)[X]$$

Hence,

$$k_f = \frac{k_3[OH^-] + k_4}{1 + K_X/[H^+]} = \frac{k_3K_w + k_4[H^+]}{[H^+] + K_X}$$

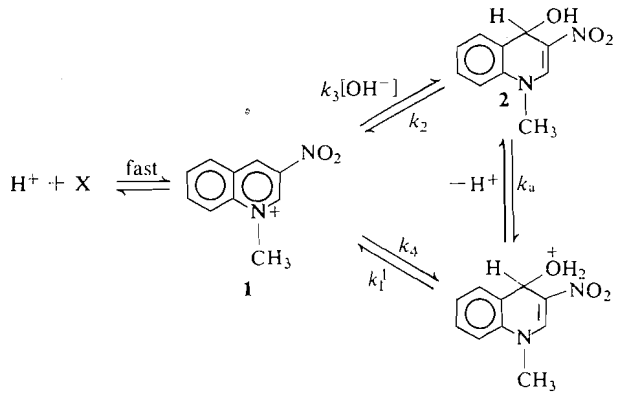

SCHEME I

where K_w is the ionic product of water and K_X is the acid dissociation constant of **1**. This relationship predicts that for $[H^+] \ll K_X$ (high pH),

$$k_f = \frac{k_3K_w + k_4[H^+]}{K_X} \approx \frac{k_3K_w}{K_X}$$

provided that $k_4[H^+] \ll k_3 K_w$. Also, for $[H^+] \gg K_X$ (low pH),

$$k_f = \frac{k_3K_w + k_4[H^+]}{[H^+]} \approx k_4$$

for

$$k_4[H^+] \gg k_3K_w$$

Thus, provided the indicated inequalities hold, k_f is predicted to be pH-independent at both low and high pH which is in agreement with the experimental observation (Fig. 2).

Furthermore, since $k_d/k_f = [H^+]/K_{ROH}$, whenever k_f is independent of pH, k_d will be directly proportional to $[H^+]$ (lines of slope -1 in Fig. 2). Thus at high pH,

$$k_d = \frac{[H^+]}{K_{ROH}} \cdot k_f = \frac{[H^+]}{K_{ROH}} \cdot \frac{k_3K_w}{K_X}$$

and since

$$k_3 = k_2 \cdot K_{ROH}/K_w$$

$$k_d = [H^+] \cdot k_2/K_X$$

At low pH,

$$k_d = \frac{[H^+]}{K_{ROH}} \cdot k_4 = \frac{[H^+]}{K_a} \cdot k_1^1$$

since

$$k_4 = k_1^1 \cdot \frac{K_{ROH}}{K_a}$$

Thus, from the two linear portions of each of k_f and k_d (high and low pH regions of each, respectively), one can obtain values for $k_3K_w/K_X = 1.8\ M^{-1}\ s^{-1}$, $k_4 = 0.43\ s^{-1}$, $k_2/K_X = 1.0 \times 10^7\ M^{-1}\ s^{-1}$ and $k_1^1/K_a = k_1 = 2.8 \times 10^6\ M^{-1}\ s^{-1}$ at 25° and ionic strength 0.1. The curves in Figs. 1 and 2, which are drawn using these values and the above equations, give an acceptable fit to the experimental data.[2]

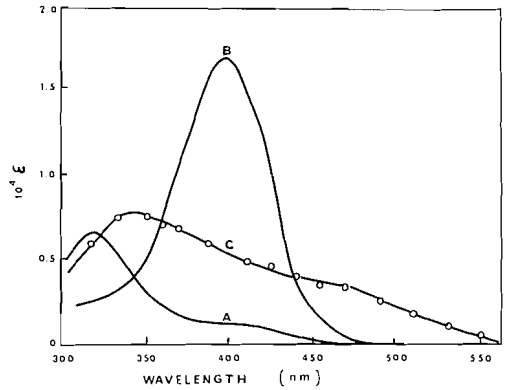

FIG. 3. The absorption spectra of (*A*) the 1-methyl-3-nitroquinolinium cation; (*B*) 1,4-dihydro-4-hydroxy-1-methyl-3-nitroquinoline; (*C*) "X" at pH 10.3 (1,2-dihydro-2-hydroxy-1-methyl-3-nitroquinoline).

In an effort to establish the nature of the species "X" we have studied the u.v.–visible spectrum of the species that is present immediately after mixing a solution of the cation **1** with buffer, pH 10.3, in the stopped-flow apparatus. This spectrum was obtained by repetitive runs at different wavelengths and is plotted in Fig. 3 along with the spectrum of the cation, **1**, and the

[2]The positive deviations from the calculated curve in the vicinity of pH 8 have also been observed for other cations (3). Such deviations appear to arise from an unidentified buffer effect.

Can. J. Chem. Downloaded from www.nrcresearchpress.com by 210.87.254.40 on 09/05/12
For personal use only.

Can. J. Chem. Downloaded from www.nrcresearchpress.com by 210.87.254.40 on 09/05/12
For personal use only.

pseudobase, **2**. The spectrum of "X" indicates a maximum in the vicinity of 340 nm and also absorption in the region 470–550 nm, where neither **1** nor **2** shows any significant absorption. Although no clearly defined maximum is discernible in this long-wavelength region, it is probable that a broad peak does exist but that it is obscured by the relatively intense absorption in the region 370–430 nm by small amounts of **2** which are already present. The spectrum of this unstable species which is rapidly converted to **2** is suggestive of a 1,2-dihydro-3-nitroquinoline system, since such species do have broad maxima in the region 470–510 nm and also a maximum at 320–330 nm (2). Since the kinetic analysis above suggests that this species is in acid–base equilibrium (pK_X) with the cation, **1**, we suggest that this species is the pseudobase **4**, formed by hydroxide attack at C-2 of **1**, and that this equilibrium is established too rapidly to allow observation by the stopped-flow technique. Numerous examples of such very rapid pseudobase formation have been cited previously (3).

We have found that it is possible to measure pK_X by studying the initial optical density at 490 nm as a function of p*H* by mixing a solution of cation, **1**, with various buffer solutions. These data are given in Table 1 and allow the calculation of a consistent $pK_X = 9.16 \pm 0.03$. This pK_X value is, of course, the pK_{ROH} value for formation of the unstable pseudobase, **4**, in the above interpretation of "X" as being **4**. By making use of the equilibrium pK_{ROH} value (6.82 ± 0.02 at 25° and ionic strength 0.1), it can now be calculated that the equilibrium mixture of pseudobases contains only 0.5% **4** and 99.5% **2**.

TABLE 1. Absorbance (490 nm) immediately after mixing solutions of **1** (4.47×10^{-4} *M*) with buffer solutions

p*H*	Optical density (*D*)	pK_X*
8.03	0.082	9.15
8.08	0.093	9.14
8.32	0.147	9.16
8.48	0.205	9.15
8.67	0.290	9.15
8.78	0.350	9.14
8.88	0.420	9.13
9.04	0.480	9.19
9.46	0.780	9.16
9.55	0.820	9.17
9.80	0.920	9.23
9.98	1.000	9.18
10.30	1.160	

*Calculated from $pK_X = pH - \log D/(1.160 - D)$. The cation does not significantly absorb at 490 nm.

With the value of pK_X available, the individual rate constants k_2 and k_3 can now be evaluated from the above kinetic data: $k_3 = 1.8 \times K_X/K_w = 1.3 \times 10^5\ M^{-1}\ s^{-1}$ and $k_2 = 1.0 \times 10^7 \times K_X = 7.1 \times 10^{-3}\ s^{-1}$. Thus values of k_1, k_2, k_3, and k_4 have been obtained for the 1-methyl-3-nitroquinolinium cation, and theoretical curves based on eqs. 1 and 2 for this cation are indicated by dashed lines in Fig. 2. The differences between the experimental and calculated curves in this figure clearly indicate the influence that a kinetically controlled product other than the thermodynamically most stable product has upon the rates of pseudobase formation and decomposition.

In Table 2, values for the parameters k_1, k_2, k_3, and k_4 are compared for the cation, **1**, and the 2-methyl-4-nitroisoquinolinium cation (3). These two cations have somewhat similar pK_{ROH} values, and the similarity of the values of the kinetic parameters for the two cations gives us further confidence that the analysis in terms of the reactions in Scheme 1 is correct.

Support for the assignment of **4** as the kinetically preferred pseudobase and **2** as the thermodynamically more stable product is found in the studies of Severin and co-workers (2) on the reduction of the 1-methyl-3-nitroquinolinium cation, **1**, with sodium borohydride. Thus, although 1,2-dihydro-1-methyl-3-nitroquinoline (red) is produced in this reduction, it subsequently rearranges to the 1,4-dihydro isomer (yellow). These workers have also observed transient red species in reaction solutions (presumably 1,2-dihydroquinolines) during the addition of carbanions to cation **1**, although in all cases only the yellow C-4 adducts could be isolated as reaction products.

Other examples of differences between the kinetically and thermodynamically controlled products from nucleophilic addition reactions to heteroaromatic systems are available in the literature. Thus, although cyanide anion initially attacks pyridinium cations at C-2 and C-6, these adducts rearrange to give the thermodynamically more stable 4-cyano-1,4-dihydropyridine isomers (4). Recent work has also shown that in solutions of sodium amide in liquid ammonia, the anion **5** is initially formed by attack of amide ion on

TABLE 2. Comparison of kinetic parameters* for pseudobase formation

Cation	pK_{ROH}	k_1 (M^{-1} s^{-1})	k_2 (s^{-1})	k_3 (M^{-1} s^{-1})	k_4 (s^{-1})
1-Methyl-3-nitroquinolinium	6.82	2.8×10^{6}	7.1×10^{-3}	1.3×10^{5}	0.43
2-Methyl-4-nitroisoquinolinium†	5.11	1.3×10^{5}	1.1×10^{-2}	8.8×10^{6}	1.04

*At 25°, ionic strength 0.1.
†From ref. 3.

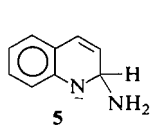

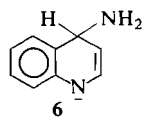

quinoline, but this anion subsequently rearranges to the more stable C-4 adduct, **6** (5).

Experimental

Materials

1-Methyl-3-nitroquinolinium iodide was prepared as previously described (1). Buffers used were those indicated previously (3).

Methods

General experimental methods were as previously described (3). Rate measurements were made on a Durrum-Gibson stopped-flow spectrophotometer at 25°, using buffers of ionic strength 0.1 after mixing. Reactions were followed at 400 nm, using solutions that were 3.59×10^{-5} *M* in the heterocyclic species. The spectrum of the unstable species, **4**, was obtained by mixing a solution (8.87×10^{-5} *M*) of the cation, **1**, with borax buffer, p*H* 10.3. Buffers used for kinetic studies were: succinate (p*H* 4–6); phosphate (p*H* 6–8); borate (p*H* 8–9.5); carbonate (p*H* 9.5–11); phosphate (p*H* 11–12).

This research was supported by an operating grant from the National Research Council of Canada, and the award of a Province of Ontario Graduate Fellowship to W.G.M.

1. J. W. BUNTING and W. G. MEATHREL. Can. J. Chem. **50**, 917 (1972).
2. T. SEVERIN, D. BATZ, and H. LERCHE. Chem. Ber. **101**, 2731 (1968).
3. J. W. BUNTING and W. G. MEATHREL. Can. J. Chem. **51**, 1965 (1973).
4. R. E. LYLE and G. J. GAUTHIER. Tetrahedron Lett. 4615 (1965).
5. J. A. ZOLTEWICZ, L. S. HELMICK, T. M. OESTREICH, R. W. KING, and P. E. KANDETZKI. J. Org. Chem. **38**, 1947 (1973).

Can. J. Chem. Downloaded from www.nrcresearchpress.com by 210.87.254.40 on 09/05/12
For personal use only.

^{13}C Nuclear Magnetic Resonance Studies. 34. The ^{13}C Spectra of Several Methylcyclopentanones and -cyclohexanones[1]

J. B. STOTHERS AND C. T. TAN

Department of Chemistry, University of Western Ontario, London, Ontario N6A 3K7

Received July 13, 1973

The ^{13}C spectra of 16 methyl substituted cyclohexanones and 15 methylcyclopentanones have been determined. These series were chosen as model systems for the study of steric and conformation effects on ^{13}C shieldings. Complete assignments of the individual signals were accomplished by intercomparison of the shielding data within each series and the trends observed are readily interpreted in conformational terms. Each of the cyclohexanones exists preferentially in chair conformations although there is evidence of ring distortion in the tetramethyl derivatives. The cyclopentanones apparently strongly favor half-chair forms with maximum puckering at C-3 and C-4. In general, shielding differences between *cis* and *trans* isomers are pronounced and the assignment of stereochemistry for some *cis–trans* dimethyl derivatives is illustrated.

Further examples of marked *deshielding* trends associated with sterically crowded δ nuclei in *syn*-axial arrangements are described.

Les spectres de ^{13}C de 16 méthylcyclohexanones et de 15 méthylcyclopentanones ont été enregistrés. Ces séries ont été choisies comme références pour l'étude des effets stériques et conformationnels sur les blindages en ^{13}C. L'assignement complet des signaux a été effectué par intercomparaison des effets d'écran à l'intérieur de chaque série et les tendances observées ont été aisément interprétées en termes conformationnels. Toutes les cyclohexanones présentent préférentiellement des conformations chaises bien qu'apparaisse une déformation évidente du cycle dans les dérivés tétraméthylés. Apparemment les cyclopentanones préfèrent nettement les formes demi-chaises avec un "effet gauche" maximum aux carbones 3 et 4. En général les différences d'écran entre les isomères *cis* et *trans* sont prononcées et l'assignement de la stéréochimie de quelques dérivés *cis–trans* diméthylés est décrit.

D'autres exemples de tendances marquées au déblindage liées à l'encombrement stérique de noyaux δ dans des arrangements *syn*-axiaux sont décrits. [Traduit par le journal]

Can. J. Chem., **52**, 308 (1974)

Introduction

The results of carbon-13 n.m.r. studies of a variety of cyclic systems have established that ^{13}C spectroscopy is a powerful method for stereochemical assignments and conformational analysis (1). Several six-membered ring systems, both mono- and polycyclic, have been examined in detail and in general it is found that axial substituents tend to shield the neighboring carbons (C-1, -2, -3, -5, and -6 in a monosubstituted cyclohexane) relative to their positions in the spectrum of the equatorial analogs. The variation of carbon shieldings with substitution in simple five-membered ring derivatives has received much less attention. Apart from studies of a variety of norbornyl derivatives (2) the only detailed examinations of cyclopentane derivatives is that of Christl *et al.* (3) in which several methylcyclopentanes, cyclopentanols, and cyclopentyl acetates were studied. We wish to report the results of a ^{13}C n.m.r. investigation of a series of 16 methylcyclohexanones and 15 methylcyclopentanones to compare the effects of methyl substitution in rings containing a trigonal carbon and to compare the trends observed for the two ring sizes. In addition, some pairs of *cis–trans* dimethyl derivatives were included to illustrate the shielding differences arising from geometrical isomerism demonstrating the utility of ^{13}C n.m.r. for stereochemical assignments.

[1]For Part 33, see ref. 12*b*.

Results and Discussion

The ^{13}C shieldings for the methylcyclohexanones examined in this study are listed in Table 1 and the data for the methylcyclopentanones are given in Table 2. While the results for cyclohexanone, its monomethyl derivatives and cyclopentanone and 3,5-dimethyl have been reported previously (4), these were re-examined to obtain a set of data for the entire series in a common solvent at comparable concentrations.

Methylcyclohexanones: sp^3-Carbon Shieldings

For the parent ketone and its monosubstituted

Can. J. Chem. Downloaded from www.nrcresearchpress.com by 210.87.254.105 on 09/05/12
For personal use only.

TABLE 1. ^{13}C shieldings[a] of some cyclohexanones

Substitution	C-1	C-2	C-3	C-4	C-5	C-6	Me
Nil	211.5	41.9	27.1	25.0	27.1	41.9	
4-Me	211.4	40.6	34.7	31.1	34.7	40.6	20.9
4-*t*-Bu	211.5	41.2	27.6	46.7	27.6	41.2	27.6[b]
3-Me	211.0	49.9	34.1	33.3	25.3	41.0	22.0
cis-3,5-Me_2	210.4	49.3	33.2	42.7	33.2	49.3	22.3
trans-3,5-Me_2	211.0	48.7	29.6	39.6	29.6	48.7	20.8
3,3,5-Me_3	210.5	53.9	35.1	47.2	29.5	49.0	22.4(5-Me); 25.7(*a*-3-Me); 32.0(*e*-3-Me)
3,3,5,5-Me_4	212.0	53.8	36.0	51.5	36.0	53.8	31.3
2-Me	212.9	45.3	36.2	25.2	28.0	41.8	14.7
cis-2,5-Me_2	213.0	44.5	31.3	30.1	32.8	47.5	15.3(2-Me); 19.8(5-Me)
trans-2,5-Me_2	211.8	44.3	35.2	34.2	35.6	50.2	14.4(2-Me); 22.4(5-Me)
cis-2,6-Me_2	213.6	45.3	37.3	25.6	37.3	45.3	14.6
trans-2,6-Me_2	216.2	42.7	34.8	20.3	34.8	42.7	16.0
2,2-Me_2	215.0	45.1	41.1	21.5	27.6	38.2	25.2
2,2,6-Me_3	216.4	45.0	41.8	21.6	36.7	40.6	15.0(6-Me); 25.2, 25.6
2,2,6-Me_3-4-*t*-Bu	216.8	44.3	43.0	42.4	37.8	40.0	15.0(6-Me); 26.0(*a*-2-Me); 27.5(*e*-2-Me); 27.5(Me_3)[c]
2,2,6,6-Me_4	220.0	44.4	40.2	18.1	40.2	44.4	27.6
2,2,6,6-Me_4-4-*t*-Bu	220.1	44.1	41.6	38.8	41.6	44.1	27.4(Me_3)[d]; 27.9(*e*-2,6-Me_2); 28.4(*a*-2,6-Me_2)

[a]In p.p.m. from internal TMS in $CDCl_3$ solutions.
[b]Quaternary carbon, 32.4 p.p.m.
[c]Quaternary carbon, 32.0 p.p.m.
[d]Quaternary carbon, 31.8 p.p.m.

TABLE 2. ^{13}C shieldings[a] of some cyclopentanones

Substitution	C-1	C-2	C-3	C-4	C-5	Me
Nil	219.4	38.1	23.2	23.2	38.1	
3-Me	218.7	46.7	31.8	31.4	38.5	20.3
cis-3,4-Me_2	218.6	45.5	34.1	34.1	45.5	15.0
trans-3,4-Me_2	217.3	47.3	39.2	39.2	47.3	18.1
2-Me	220.9	43.9	31.9	20.7	37.5	14.2
cis-2,3-Me_2	220.9	48.0	34.4	28.1	35.2	9.5 (2-Me); 14.8 (3-Me)
trans-2,3-Me_2	220.3	51.8	39.8	29.6	37.5	12.0 (2-Me); 19.1 (3-Me)
cis-2,4-Me_2	220.0	45.6	40.9	29.6	46.1	14.0 (2-Me); 20.3 (4-Me)
trans-2,4-Me_2	221.0	41.5	39.1	28.0	45.9	15.3 (2-Me); 20.8 (4-Me)
2,4,4-Me_3	220.2	42.7	46.1	33.8	52.5	14.9 (2-Me); 27.9, 29.8
cis-2,5-Me_2	222.7	42.5	28.9	28.9	42.5	15.3
trans-2,5-Me_2	222.3	43.6	30.1	30.1	43.6	14.7
2,2,4-Me_3	222.0	46.5	47.5	27.5	45.8	20.5 (4-Me); 24.3, 24.4
2,2,4,4-Me_4	222.5	45.2	52.3	33.1	52.6	27.4 (2-Me); 30.1 (4-Me)
2,2,5-Me_3	224.1	44.7	36.6	28.0	43.1	15.2 (5-Me); 24.8, 24.1
2,2,5,5-Me_4	226.4	45.2	34.9	34.9	45.2	24.9

[a]In p.p.m. from internal TMS in $CDCl_3$ solutions.

derivatives the assignments were straightforward (4). Since the methylcyclohexanones can be assumed to exist predominantly in chair conformations having equatorial methyl groups, a comparison of the individual shieldings for specific carbons with those for the corresponding carbons in cyclohexanone furnished a set of substituent effects for equatorial methyl groups in this system. These values may be compared with those for methyl substitutions in cyclohexane (5) as shown in Table 3. From the values for equatorial 2- and 3-methyl groups, the shieldings for *cis*-2,6-, *cis*-3,5-, and *trans*-2,5-dimethylcyclohexanone were estimated and compared with those observed as a test of the additivity of these substituent effects. For the 11 possible comparisons the average deviation between the predicted and observed values is 0.5 p.p.m. with a maximum deviation of 1.1 p.p.m. To obtain an estimate of the substituent effects

Can. J. Chem. Downloaded from www.nrcresearchpress.com by 210.87.254.105 on 09/05/12
For personal use only.

TABLE 3. Methyl substituent effects on sp^3 carbons in cyclohexane and cyclohexanone[a]

Parent	Substitution	α	β	γ	δ
Cyclohexane[b]	*e*-Me	6.0	9.0	0.1	−0.2
	a-Me	1.4	5.4	−6.4	−0.1
	gem-Me_2	−3.8	−1.3	2.0	
Cyclohexanone	*e*-2-Me	3.4	9.1	0.2(C-4) −0.1(C-6)	0.9
	a-2-Me	3.6	6.0	−5.9(C-4) −6.2(C-6)	−0.5
	e-3-Me	7.0	8.0(C-2) 8.3(C-4)	−1.8	−0.9
	a-3-Me	5.7	5.9	−5.7	−0.3
	e-4-Me	6.1	7.6	−1.3	

[a]In p.p.m.
[b]Results from ref. 5.

of an axial 3-methyl group, the shieldings of the *cis*-3,5-dimethyl and 3,3,5-trimethyl derivatives were compared and the differences adjusted for the known attenuation of the α, β, and γ effects caused by geminal methyl substitution (5*b*). These results are listed in Table 3. With these effects and the observed shieldings for 3-methylcyclohexanone the shieldings for *trans*-3,5-dimethylcyclohexanone were estimated and found to be in good agreement with experiment; the predicted and observed values, in parentheses, are C-2,6, 48.3 (48.7); C-3,5, 29.7 (29.6); and C-4, 39.2 (39.6) p.p.m. In a similar manner, substituent effects were found for an axial 2-methyl group by comparing the data for 2-methylcyclohexanone and 2,2-dimethylcyclohexanone and for the *cis*-2,6-dimethyl and 2,2,6-trimethyl derivatives; these results are included in Table 3. As a test of the utility of these effects, the estimated shieldings for *trans*-2,6-dimethylcyclohexanone may be compared with those observed: C-2,6, 42.3 (42.7); C-3,5, 34.9 (34.8); and C-4, 19.3 (20.3) p.p.m. As a further test of these axial methyl effects, the individual shieldings for the two conformers of *cis*-2,5-dimethylcyclohexanone were predicted from the results for 2-methylcyclohexanone with the axial 3-methyl effects operative at C-5 and for 3-methylcyclohexanone with the axial 2-methyl effects operative at C-6 as illustrated in Scheme 1. Assuming a 1:1 mixture of the two conformers at equilibrium, the predicted shieldings for *cis*-2,5-dimethylcyclohexanone were obtained from the averaged values for each carbon in the two conformers: C-2, 44.8 (44.5); C-3, 30.9 (31.3); C-4, 29.3 (30.1); C-5, 33.7 (32.8); and C-6, 45.7 (47.5) p.p.m., the observed shieldings are given in parentheses. Since an axial methyl at C-5 has only one *syn*-axial interaction, it is reasonable that conformer A (Scheme 1) will predominate. For a 4:1 mixture of A:B the predicted shieldings become: C-2, 44.9; C-3, 30.7; C-4, 30.4; C-5, 33.7; and C-6, 46.9 p.p.m. which fit somewhat better with those observed. Thus, this sort of analysis provides a crude indication of the equilibrium mixture but, as shown below, the methyl shieldings seem to give a better indication of the relative proportions of conformers.

From Table 3 it is apparent that the differences in substituent effects for axial and equatorial methyl groups are similar for both cyclohexane and cyclohexanone. The attenuation of the α effects of 2-methyl groups in the latter system may be due to the concomitant γ interaction between the methyl group and the carbonyl oxygen. A comparison of the individual effects for the axial methyls with those for the corresponding equatorial methyl groups reveals the consistent shielding trends associated with γ interactions between the methyl groups and *syn*-axial ring protons, *i.e.* those at C-4 and C-6 in the case of an axial 2-methyl group. Although the number of model compounds from which these individual methyl substituent effects were derived is very restricted, the results of the tests for additivity described above indicate that the data in Table 3 may be useful for estimations of shieldings in related systems.

An additional examination of substituent effects is interesting, namely, the perturbations produced by the 4-*t*-butyl group in the three examples included in this study. Comparison of their shieldings with those for the corre-

Can. J. Chem. Downloaded from www.nrcresearchpress.com by 210.87.254.105 on 09/05/12
For personal use only.

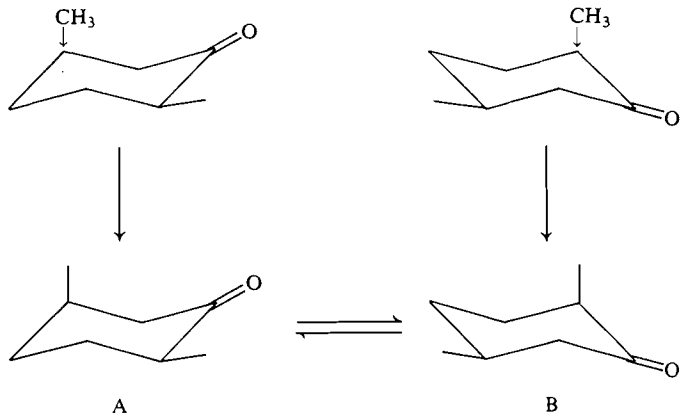

SCHEME 1

sponding ketones lacking the 4-*t*-butyl group shows the following effects: α, 21.1 ± 0.5; β, 1.0 ± 0.5; γ, −0.5 ± 0.2 p.p.m. These are closely similar to the effects found for *t*-butylcyclohexane and *trans*-1,4-di-*t*-butylcyclohexane (6), namely, 21.3, 0.5, and 0.1 p.p.m., respectively. The close agreement indicates that each of the 4-*t*-butyl substituted cyclohexanones exists preferentially in a chair conformation rather than a twist form for which one would expect somewhat different substituent effects. This is certainly not unexpected for 4-*t*-butylcyclohexanone and its 2,2,6-trimethyl derivative but is particularly interesting for the 2,2,6,6-tetramethyl isomer for which the *syn*-axial interaction of the axial methyl groups tends to increase the energy of the chair conformer. It may be noted that a variety of similarly substituted heterocyclic systems (1*c*, 7, 8) have been shown to favor twist conformations and the ring carbon shieldings exhibit substantial deviations from those predicted by assuming additivity of substituent effects.

The results for the ring carbon shieldings in the tetramethylcyclohexanones can also be compared with those predicted from the data for less highly substituted derivatives and the substituent effects listed in Table 3. For example, the shieldings of the 2,2,6,6-tetramethyl derivative may be estimated from the results for *cis*-2,6-dimethyl- and 2,2,6-trimethylcyclohexanone. These estimates together with the corresponding predictions for the 3,3,5,5-tetramethyl isomer are given in Table 4. There is good agreement between the estimated and predicted values for all but the carbons bearing the methyl groups suggesting that a major conformational change does not occur for either tetramethyl system. Evidence confirming the chair conformation for the 3,3,5,5-tetramethyl ketone has been presented by St.-Jacques *et al.* (9). The marked upfield shift found for the methyl-bearing carbons may be indicative of distortion in these systems from perfect chairs as a result of the *syn*-axial interactions of two of the methyl groups. Additional indications of this are discussed below.

TABLE 4. Observed and estimated ring carbon shieldings of tetramethylcyclohexanones[a]

	2,2,6,6-Me_4		3,3,5,5-Me_4	
Carbon	Obs.	Calcd.	Obs.	Calcd.
C-2,6	44.3	39.8	53.8	53.6
C-3,5	40.1	41.4	36.0	31.4
C-4	18.1	17.8	51.5	51.9

[a]In p.p.m. from TMS.

The variations in the methyl carbon shieldings also appear to provide conformational information. Equatorial 3-methyl carbons absorb near 22.3 p.p.m. from the results for *cis*-3,5-dimethylcyclohexanone and the 5-methyl in the 3,3,5-trimethyl derivative. These are selected as models in preference to the 3-methyl derivative since the latter exists to a small extent in a conformation having an axial methyl group. The slightly greater methyl shielding of 3-methylcyclohexanone may be ascribed to this feature. Equatorial 2-methyl carbons are significantly shielded relative to the 3-methyl nuclei, appearing near 14.6 p.p.m. The 7.7 p.p.m. upfield shift presumably arises from the γ interactions of the α-methyl group with the carbonyl oxygen.

Can. J. Chem. Downloaded from www.nrcresearchpress.com by 210.87.254.105 on 09/05/12
For personal use only.

Can. J. Chem. Downloaded from www.nrcresearchpress.com by 210.87.254.105 on 09/05/12
For personal use only.

From the results for the *trans*-3,5- and *trans*-2,6-dimethyl isomers shieldings for axial 3- and 2-methyl carbons can be estimated as 19.3 and 17.4 p.p.m., respectively, since the observed shieldings represent averaged values for axial and equatorial environment. The axial 3-methyl carbon is shielded relative to its equatorial counterpart as expected because of the *syn*-axial interaction with the axial 5-proton. The observed 3 p.p.m. upfield shift is approximately half that exhibited by an axial methyl on a cyclohexane ring (10) which is entirely consistent with the difference in *syn*-axial interactions between the two systems, since in the hydrocarbon an axial methyl is *syn*-axial with respect to two protons. It may be noted that the methyl shielding for 3-methylcyclohexanone, therefore, indicates the presence of about 10% of the axial methyl conformer which agrees very nicely with an expected $-\Delta G^\circ$ of $\sim$1.3 kcal/mol (11*a*). In contrast to the behavior of the 3-methyl group, an axial 2-methyl carbon is apparently deshielded relative to its equatorial counterpart, indicating that the γ interaction of an equatorial methyl with the carbonyl group has a greater shielding effect than the two *syn*-axial interactions of an axial 2-methyl group.

The methyl shieldings for *trans*-2,5-dimethylcyclohexanone are essentially the same as the characteristic values for equatorial 2- and 3-methyl groups as noted above as is expected for the diequatorial conformer which this molecule must adopt almost exclusively. For the *cis*-2,5-dimethyl isomer, however, two conformers are in equilibrium but the observed methyl shieldings of 15.3 and 19.8 p.p.m. differ substantially from the values predicted for a 1:1 mixture, 16.0 and 20.8 p.p.m. In fact, the observed values are close to those predicted for a 4:1 mixture of A:B (Scheme 1) favoring the conformer having an axial 5-methyl, namely, 15.2 and 19.9 p.p.m. Clearly, however, these ^{13}C data do not permit a precise quantitative assessment of the equilibrium populations but do indicate the bias of the system.

In those ketones having *gem*-dimethyl substitution, the *gem*-methyl carbons are deshielded by the mutual β effects of each other (1). In methylcyclohexanes, this shift is 10.4 p.p.m. (5*b*). Thus, the equatorial 3-methyl carbon in the 3,3,5-trimethyl derivative is readily assigned to the 32.0 p.p.m. signal while the remaining methyl signal at 25.7 p.p.m. must arise from the axial 3-methyl group. For the 2,2,6-trimethyl derivative it is not possible to specifically assign the *gem*-methyl signals at 25.2 and 25.6 p.p.m. In both of the tetramethyl isomers which undergo rapid interconversion between equivalent conformers only a single methyl signal is observed which must represent the averaged shieldings for axial and equatorial environments. In each case the observed signal is at lower field than that calculated by simply averaging the *gem*-dimethyl shieldings of the trimethyl derivatives. For example, if there were no additional perturbation on the *gem*-dimethyl shieldings the values for the 3,3,5-trimethyl derivative lead to a prediction of 28.9 p.p.m. for the averaged methyl shieldings in the 3,3,5,5-tetramethyl derivative but the observed value is 31.3 p.p.m. For the 2,2,6-trimethyl and 2,2,6,6-tetramethyl cases, the corresponding values are 25.4 and 27.6 p.p.m. In each case there is a difference of *ca.* 2.3 p.p.m. Initially this finding seemed particularly surprising in view of the general tendency for sterically crowded carbons to exhibit upfield shifts. This generalization, however, refers specifically to γ nuclei separated by three bonds whereas these *syn*-axial interactions are δ effects involving nuclei separated by four bonds. At the time of our first observations of these shifts, we were also examining a variety of other systems which contained similar spatial arrangements of methyl groups relative to hydroxyl and to other methyl groups. The general finding for *syn*-axial orientations, either Me···OH or Me···Me, is a *downfield* shift (12) in striking contrast to the trends for eclipsed or gauche γ interactions. For the tetramethylcyclohexanones it is not possible to estimate the magnitude of the *syn*-axial δ effects since it is known that *both* geminal methyl carbons are deshielded by the *syn*-axial interaction of one (12). It is interesting that the α-methyl shieldings of the 4-*t*-butyl-2,2,6,6-tetramethyl derivative, which is essentially a single conformer, give an averaged shielding of 28.2 p.p.m. which is slightly lower than that observed for 2,2,6,6-tetramethylcyclohexanone, 27.6 p.p.m. This may arise from slightly different distortions of the ring in the two cases but, as noted above, seems too small to indicate a departure from a chair conformation. The fact that the deshieldings of the *syn*-axial methyl carbons appear to be smaller than those found for more

Can. J. Chem. Downloaded from www.nrcresearchpress.com by 210.87.254.105 on 09/05/12
For personal use only.

rigid systems (12) suggests the presence of appreciable ring distortion to decrease the *syn*-axial interactions.

Carbonyl Carbons

The carbonyl carbon shieldings are most affected by axial α-methyl substitution while equatorial α-methyl groups produce smaller downfield shifts. Presumably this difference arises from the differences in steric interactions of the α-methyl groups with the carbonyl oxygen for the two orientations. More remote methyl substitution on the cyclohexanone ring has little affect on the carbonyl absorption. Thus, cyclohexanone carbonyl absorptions are readily distinguished from those of cyclopentanones with the exception of the α-tetramethyl cases in the former systems. With increasing methyl substitution at the α positions, the cyclopentanone carbonyls also exhibit a pronounced downfield shift such that the 226.4 p.p.m. shielding of 2,2,5,5-tetramethylcyclopentanone is the most deshielded carbonyl carbon yet reported (1).

Methylcyclopentanones: *sp*^{3}*-Carbon Shieldings*

The cyclopentanone ring exists in the half-chair form **1** with maximum puckering at C-3

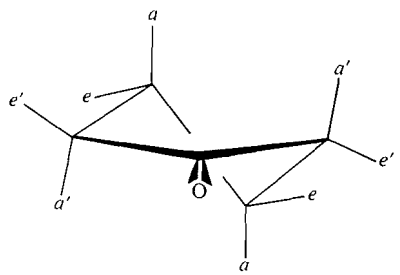

1

and C-4 (11*b*) and consequently there are two orientations for methyl groups at either of the α and β positions, which, for convenience, are denoted axial (*a*) and equatorial (*e*) although these orientations are not strictly comparable to those in cyclohexane systems. Although little is known about the relative energies of the conformations available to the methylcyclopentanones, the ^{13}C results give some qualitative indications of the preferred conformers in a variety of cases. The methyl shieldings appear to be the more informative in this regard. With the assumption that conformations having axial methyls are less stable than their equatorial counterparts, some consistent trends emerge. The shielding for the β-methyl carbon in the 3-methyl, *cis*-2,4-dimethyl, and 2,2,4-trimethyl derivatives is 20.4 ± 0.1 p.p.m., while the α-methyl shielding in the 2-methyl, *trans*-2,5-, and *cis*-2,4-dimethyl derivatives averages 14.3 p.p.m. With these values representative of equatorial and pseudo-equatorial groups, respectively, it is apparent that the shielding influence of the carbonyl group at the α-methyl carbon is less than that found for the cyclohexanones. This is consistent with the larger dihedral angle between the carbonyl and the α-C—CH_3 bonds in cyclopentanones relative to that in cyclohexanones in which these bonds are nearly eclipsed. The similarity of methyl shieldings for *cis*-2,4-dimethylcyclopentanone with respect to the two monomethyl derivatives indicates that this dimethyl derivative is essentially diequatorial. The same conclusion results from a comparison of the ring shieldings with those predicted by additivity of the substituent effects for each of the methyl groups; the latter were obtained by comparison of the shieldings of the monomethyl derivatives with those of cyclopentanone itself. For *cis*-2,4-dimethylcyclopentanone the predicted (and observed) shieldings are: C-2, 44.3 (45.6); C-3, 40.1 (40.9); C-4, 29.3 (29.6); and C-5, 46.1 (46.1) p.p.m. The general trend toward higher field for all ring carbons in the *trans*-2,4-dimethyl derivative is consistent with the presence of axial methyl groups. Similar results obtained from the corresponding comparisons for the 2,5-dimethyl isomers indicated that the *trans* isomer is essentially diequatorial. It is interesting that the α-methyl shieldings for *cis*-2,5- and *trans*-2,4-dimethylcyclopentanones are the same, 15.3 p.p.m., deshielded by 1 p.p.m. relative to their pseudo-equatorial counterparts. This trend toward lower field for axial α-methyl carbons is consistent with the cyclohexanone series.

A comparison of the geminal methyl shieldings in the tri- and tetramethylcyclopentanones reveals the same trend noted earlier for the cyclohexanones, namely, the downfield shift exhibited by *syn*-axial methyl carbons. The 2,2- and 4,4-dimethyl carbons have averaged shieldings of 27.4 and 30.1 p.p.m. in 2,2,4,4-tetramethylcyclopentanone, both of which are significantly downfield from the geminal methyl absorptions in the 2,2,4- and 2,4,5-trimethyl derivatives, respectively. It may be noted that the remaining methyl

shielding in each of the latter compounds is similar to that for an equatorial methyl group indicating that each favors a specific conformation. For 2,2,5,5-tetramethylcyclopentanone the averaged methyl shielding, 24.9 p.p.m., is very close to the α-methyl shieldings in the 2,2,4- and 2,2,5-trimethyl derivatives, in sharp contrast with the situation for the cyclohexanone system but as expected for systems lacking *syn*-axial arrangements of methyls separated by four bonds.

An additional feature illustrated by the results for the cyclopentanone series concerns the trends exhibited by the vicinal methyl substituents in the 2,3- and 3,4-dimethyl derivatives. It is well-established that closely neighboring vicinal methyl groups exhibit upfield shifts which increase with decreasing separation (1, 5). A convenient, albeit approximate, indicator of the magnitude of the shift is provided by the dihedral angle relating the two methyl carbons (2*c*). As a consequence of the puckered nature of the half-chair conformation of cyclopentanone, the dihedral angles relating vicinal substituents differ markedly for equatorial–equatorial and axial–equatorial arrangements. The dihedral angle is significantly smaller for the latter. This difference accounts nicely for the more shielded methyl carbons in the *cis*-2,3- and *cis*-3,4-dimethyl isomers relative to their *trans* counterparts. The ring carbons of the *cis* isomers are shielded relative to those in the *trans* isomers, reflecting the greater steric crowding of the vicinal methyls as well as the shielding effects associated with axial methyl groups. The results, therefore, are readily interpreted in terms of the half-chair conformation of the cyclopentanone ring such that the *trans*-2,3- and -3,4-dimethyl isomers are diequatorial and the *cis* isomers are equilibrium mixtures of axial–equatorial conformers.

Experimental

Materials

Most of the ketones examined in this study were commercially available (Aldrich Chemical Company and Chem Sample Company) and were used without further purification after checking by gas chromatography. Methylation (13) of cyclohexanone and 4-*t*-butylcyclohexanone provided samples of the 2,2,6-trimethyl and 2,2,6,6-tetramethyl derivatives; separation of the isomers in each case was accomplished by gas chromatography on a 20% SE30 column. The 2,2,5-trimethyl- and 2,2,5,5-tetramethylcyclopentanones were similarly obtained from the mixture of 2,5-dimethylcyclopentanone isomers. Oxidation (14) of commercial 3,3,5-trimethylcyclohexanol afforded a sample of the corresponding trimethyl ketone.

^{13}C Spectra

Solutions in deuteriochloroform (10–15% w/v) containing a few drops of TMS were examined in 5-mm tubes using a Varian XL-100-15 system operating at 25.2 MHz in the Fourier transform mode. With 2000 Hz "sweep widths" and the available memory core, the peak positions were determined to ±1 Hz. Off-resonance decoupling was employed to confirm assignments for methyl, methylene, methine, and quaternary carbons.

We wish to thank the National Research Council of Canada for financial support of this study. We are grateful for the technical assistance of Mrs. C. Ferriera.

1. (*a*) G. C. Levy and G. L. Nelson. ^{13}C nuclear magnetic resonance for organic chemists. Wiley-Interscience, New York. 1972; (*b*) J. B. Stothers. Carbon-13 NMR spectroscopy. Academic Press, New York. 1972; (*c*) N. K. Wilson and J. B. Stothers. *In* Topics in stereochemistry. Vol. 8. *Edited by* E. L. Eliel and N. L. Allinger. Wiley-Interscience, New York. 1973. Chapt. 1.
2. (*a*) J. B. Grutzner, M. Jautelat, J. B. Dence, R. A. Smith, and J. D. Roberts. J. Am. Chem. Soc. **92**, 7107 (1970); (*b*) E. Lippmaa, T. Pehk, J. Paasivirta, N. Belikova, and A. Plate. Org. Mag. Res. **2**, 581 (1970); (*c*) J. B. Stothers, C. T. Tan, and K. C. Teo. Can. J. Chem. **51**, 2893 (1973).
3. M. Christl, H. J. Reich, and J. D. Roberts. J. Am. Chem. Soc. **93**, 3465 (1971).
4. F. J. Weigert and J. D. Roberts. J. Am. Chem. Soc. **92**, 1347 (1970).
5. (*a*) D. K. Dalling and D. M. Grant. J. Am. Chem. Soc. **89**, 6612 (1967); (*b*) **94**, 5318 (1972).
6. J. D. Roberts, F. J. Weigert, J. I. Kroschwitz, and H. J. Reich. J. Am. Chem. Soc. **92**, 1338 (1970).
7. G. M. Kellie and F. G. Riddell. J. Chem. Soc. (B), 1030 (1971); K. Pihlaja, G. M. Kellie and F. G. Riddell. J. Chem. Soc. Perkin II, 252 (1972).
8. G. Ellis and R. G. Jones. J. Chem. Soc. Perkin II, 437 (1972).
9. M. St.-Jacques, M. Bernard, and C. Vaziri. Can. J. Chem. **48**, 2386 (1970).
10. F. A. L. Anet, C. H. Bradley, and G. W. Buchanan. J. Am. Chem. Soc. **93**, 258 (1971).
11. E. L. Eliel, N. L. Allinger, S. J. Angyel and G. A. Morrison. Conformational analysis. Interscience, New York. 1965 (*a*) p. 114, (*b*) p. 202.
12. (*a*) S. H. Grover, J. P. Guthrie, J. B. Stothers, and C. T. Tan. J. Mag. Res. **10**, 227 (1973); (*b*) K. R. Stephens, J. B. Stothers, and C. T. Tan. *In* Mass spectrometry and NMR in pesticide chemistry. Plenum Press, New York. 1974.
13. E. J. Corey, R. Hartmann, and R. A. Vatakencherry. J. Am. Chem. Soc. **84**, 2611 (1962).
14. R. Ratcliffe and R. Rodehurst. J. Org. Chem. **35**, 4000 (1970).

Can. J. Chem. Downloaded from www.nrcresearchpress.com by 210.87.254.105 on 09/05/12
For personal use only.

Association of a Europium Shift Reagent with Dialkylnitrosamines

RICHARD A. PERRY AND YUAN L. CHOW

Department of Chemistry, Simon Fraser University, Burnaby 2, British Columbia

Received February 19, 1973[1]

The $Eu(fod)_3$ induced shifts of the n.m.r. signals of various nitrosamines were studied at a constant lanthanide concentration and also at constant nitrosamine concentration. The bound chemical shifts (Δ_B) and binding equilibrium constants (K) were determined. The stoichiometry of the complexes appears to be 1:1 in $CDCl_3$ in agreement with the criteria of two types of existing tests designed to determine Eu–substrate ratio. On the basis of the experimental Δ_B values, the molecular geometry of Eu–nitrosamine complexes were computed according to the principle of pseudo-contact shift. It was concluded that the Eu atom complexed at the oxygen of the nitroso group and that the conformations of nitrosamines in the complexes were basically the same as those of uncomplexed nitrosamines.

Les déplacements chimiques induits par l'$Eu(fod)_3$ des signaux r.m.n. de diverses nitrosamines ont été étudiés pour une concentration constante en lanthanide et aussi pour des concentrations constantes en nitrosamines. Les déplacements chimiques dans le complexe (Δ_B) et la constante de complexation (K) ont été déterminés. La stoechiométrie des complexes se révèle être 1:1 dans le $CDCl_3$ selon les critères des deux types de tests existants pour déterminer le rapport Eu–substrat. Sur la base des valeurs expérimentales Δ_B, la géométrie moléculaire des complexes Eu–nitrosamine a été calculée selon le principe du déplacement chimique de pseudo-contact. On a conclu que l'atome d'Eu complexe l'oxygène du groupe nitroso et que les conformations des nitrosamines dans les complexes sont dans l'ensemble les mêmes que celles des nitrosamines non-complexées. [Traduit par le journal]

Can. J. Chem., **52**, 315 (1974)

Introduction

In recent years, the n.m.r. chemical shifts induced by paramagnetic lanthanide complexes have attracted widespread interest in assignments of the signals of complex organic molecules (1–4). Indeed, scattered in the recent literature, there are numerous cases of empirical applications of lanthanide shift reagents to gain first-order spectrum; the number is increasing exponentially. However, the application of this phenomenon has been recognized to be far reaching in that the magnitudes of the induced shifts should be related to the spatial disposition of each proton with respect to the metal ion (1). Such information, in turn, enables chemists to examine the stereochemistry of an organic molecule.

Because certain nitrosamines are potent producers of cancer in a variety of experimental animals (5), they are candidates for serious consideration as human carcinogens. A sudden upsurge of interest in nitrosamines has arisen recently as a number of these compounds and their precursors have been found in foodstuffs (6). There is certainly a pressing need to know more about the chemistry of nitrosamines so that highly sensitive analytical methods can be developed to describe the distribution of these compounds in the human environment.

In connection with our photochemical studies of nitrosamines (ref. 7 and previous publications), we have been actively studying the stereochemistry of ground state nitrosamines (8, 9). The n.m.r. studies (8–10) have revealed that a nitrosamine molecule has a large charge separation, such as in structure **1**, with the negative pole residing at the oxygen atom. The chemical shifts of nitrosamines have been interpreted satisfactorily by an approximation of the anisotropic effects of the NNO group (8). This structure (**1**) has been supported by various physical measurements (11, 12). Among three

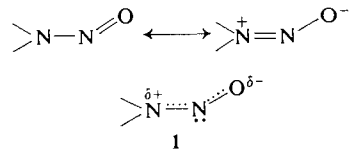

1

possible heteroatoms for coordination, it has been shown that a proton complexes with the oxygen atom of the NNO group exclusively in solution (12, 14) and that Cu(II) ion complexes with the oxygen as well as the nitroso nitrogen atom in the solid state (13).

[1]Revision received October 1, 1973.

Can. J. Chem. Downloaded from www.nrcresearchpress.com by 210.87.254.40 on 09/05/12
For personal use only.

Can. J. Chem. Downloaded from www.nrcresearchpress.com by 210.87.254.40 on 09/05/12
For personal use only.

Trisdipivaloyleuropium, $Eu(dpm)_3$, has been shown to induce shifts of the n.m.r. signals of the structurally related oximes. On the basis of the qualitative studies, whereas Wolkowski (15) has concluded that lanthanide coordinates with the oxygen atom rather than the electron lone pair of the nitrogen, Berlin and Rengaraju (16) have reached the opposite conclusion. It has been shown that an amine generally forms a tighter complex with the Eu shift reagent than an alcohol of comparable structure does (2, 17). In order to clarify the assignments of the n.m.r. signals, applications of $Eu(dpm)_3$ shift reagent on rigid nitrosamine molecules have been reported by two groups recently (18, 19).

The combination of these reports prompts us to undertake a quantitative study on lanthanide induced chemical shifts of dialkylnitrosamines. For this study, tris(2,2-dimethyl-6,6,7,7,8,8,8-heptafluoro-3,5-octanediote)europium, abbreviated as $Eu(fod)_3$, is utilized as the shift reagent.

Experimental

A commercially available $Eu(fod)_3$ (Norell Chemical Co., Landing, N.J.) was stored over P_2O_5 and was used without further purification. Commercial $CDCl_3$ was used as supplied. Some nitrosamines were available from Eastman Kodak Co., Rochester, New York and others were prepared according to the procedure published previously (14). All nitrosamines were distilled twice or recrystallized repeatedly. The n.m.r. spectra were recorded with a Varian XL-100 spectrophotometer at a cavity temperature of 37.5 °C. The least-square calculation and plots were done with a Monroe 1670 Calculator and computer iteration calculations with an IBM 370.

Method A: Nuclear Magnetic Resonance Studies with Constant Nitrosamine Concentration [S]

Approximately 50 mg of a nitrosamine was accurately weighed and was dissolved in 1 ml of $CDCl_3$ (concentration [S] is 0.2–0.7 *M*). To this solution measured portions (20–60 mg each portion) of $Eu(fod)_3$ were added successively and the n.m.r. spectra recorded. The downfield shifts (δ) of each proton were summarized in Table 1.

Method B: Nuclear Magnetic Resonance Studies with Constant Lanthanide Concentration [L]

The stock solutions of $Eu(fod)_3$ in $CDCl_3$ ($\sim 4 \times 10^{-3}$ *M*) and a nitrosamine in $CDCl_3$ (4–5 *M*) were prepared. The $Eu(fod)_3$ solution (0.5 ml) and appropriate amount of nitrosamine solution were placed in a volumetric flask and were diluted with $CDCl_3$ to 2 ml. The results were summarized in Table 2. Control experiments were run with various concentrations of *N*-nitroso-*N*-methylisopropylamine in the absence of $Eu(fod)_3$; within experimental and reading errors, the chemical shifts of protons were shown to be independent of concentration.

Results

Graphic Calculation

The induced shifts of various protons (δ in p.p.m.) of a nitrosamine in method A were plotted against the mol ratio of $Eu(fod)_3$ to nitrosamine ([L]/[S]) according to the equation $\delta = \Delta_B[L]/[S]$ derived by Armitage *et al.* (2, 3). As this equation is operative only when $[S] \gg [L]$, the measurements obtained with $[L]/[S] > 0.7$ (2) have been used to draw straight lines by a least-square computation. Most of the plots show reasonably good straight lines with correlation coefficients of better than 0.99 and converge at the original point (within the range of ± 0.03 unit in the *y*-intercept) as predicted by the equation. In the case of the *syn*-α-CH of *N*-nitroso-*N*-methylisopropylamine, the computed straight line deviates from the zero point by -0.045 unit. The chemical shifts of this proton were difficult to read accurately owing to the spread and the low intensity. The reciprocals of the slopes from these plots were taken as Δ_B, the "bound" chemical shift of each proton. These Δ_B values were appended at the end of each column in Table 1.

The plots of the induced shifts of *N*-nitrosodibenzylamine were found to be, among the cases investigated, the only exceptions in which the points exhibited definite curvature and the straight lines (computed using only $[L]/[S] < 0.9$) deviated considerably from the zero point. We shall return to this case later.

In method B, concentrations of nitrosamine [S] were plotted against the reciprocals of the induced shifts ($1/\delta$), according to eq. 1 (2),

$$[1] \qquad [S] = [L]\Delta_B(1/\delta) - ((1/K) + [L])$$

where Δ_B is the induced shift of the bound complex and K is the binding equilibrium constant. In these experiments the mol ratios of $Eu(fod)_3$ to nitrosamine, [L]/[S], were in the vicinity of 1/100 in order to ensure the applicability of the one-step binding model (2, 3). From these plots, Δ_B and K were calculated from the slopes and *y*-intercepts, respectively. In Table 3, these data were assembled together with the corresponding Δ_B values obtained by method A for comparison.

In the interactions of lanthanide shift reagents with a substrate, the stoichiometry of the complex is undoubtedly one of the vital questions for which 1:1 complexation has been assumed

TABLE 1. Downfield shifts of n.m.r. signals in nitrosamine–Eu complexes by method A*

(*a*) *N*-Nitrosodimethylamine; [S] = 0.762 *M*

Mol ratio [L]/[S]	δ S-CH_3 (7.00)	δ A-CH_3 (6.31)
0.038	0.24	0.16
0.062	0.31	0.20
0.12	0.64	0.40
0.16	0.86	0.56
0.19	1.11	0.65
0.24	1.35	0.83
Δ_B	5.66	3.42

(*b*) *N*-Nitrosodiethylamine; [S] = 0.529 *M*

Mol ratio [L]/[S]	δ S-CH_2 (6.46)	δ S-CH_3 (8.91)	δ A-CH_2 (5.93)	δ A-CH_3 (8.64)
0.052	0.24	0.13	0.16	0.11
0.11	0.66	0.39	0.34	0.24
0.18	0.97	0.53	0.54	0.34
0.25	1.31	0.78	0.78	0.43
0.30	1.65	0.99	0.87	0.53
Δ_B	5.52	3.31	3.01	1.74

(*c*) *N*-Nitrosodibenzylamine; [S] = 0.234 *M*

Mol ratio [L]/[S]	δ S-CH_2 (5.43)	δ S-*o*-H (2.75)	δ A-CH_2 (4.90)	δ A-*o*-H (2.75)
0.25	1.75	0.59	0.91	0.35
0.44	3.00	1.22	1.60	0.69
0.62	3.90	1.70	2.10	0.98
0.86	4.92	2.25	2.61	1.25
1.08	5.66	2.62	2.92	1.46
Δ_B	5.84	2.70	3.12	1.51

(*d*) *N*-Nitrosodiisopropylamine; [S] = 0.425 *M*

Mol ratio [L]/[S]	δ S-CH (5.08)	δ S-CH_3 (8.82)	δ A-CH (5.83)	δ A-CH_3 (8.51)
0.078	0.54	0.24	0.25	0.19
0.15	1.03	0.51	0.49	0.29
0.22	1.52	0.75	0.65	0.39
0.30	2.12	1.02	0.95	0.65
0.39	2.79	1.31	1.21	0.83
Δ_B	5.13	3.43	3.13	2.15

(*e*) *N*-Nitrosodicyclohexylamine; [S] = 0.224 *M*

Mol ratio [L]/[S]	δ S-CH (5.21)	δ S-2-CH_2‡ (8.1)	δ A-CH (6.28)	δ A-2-CH_2 (8.1)
0.23	1.78	0.6	0.65	0.6
0.43	3.19	1.25e; 1.1a	1.23	1.1
0.65	4.55	1.95e; 1.5a	1.75	1.5
0.85	5.94	2.6 e; 2.15a	2.31	1.9
1.11	7.26	3.3 e; 2.65a	2.81	2.3
Δ_B	6.93	3.09e; 2.47a	2.70	2.23

Can. J. Chem. Downloaded from www.nrcresearchpress.com by 210.87.254.40 on 09/05/12
For personal use only.

TABLE 1. (*Continued*)

(*f*) *N*-Nitrosomethylethylamine; [S] = 0.645 *M*

Mol ratio [L]/[S]	*E* isomer δ S-α-CH_3 (6.99)	*E* isomer δ A-α-CH_2 (5.81)	*E* isomer δ A-β-CH_3 (8.64)	*Z* isomer δ A-α-CH_3 (6.30)	*Z* isomer δ S-α-CH_2 (6.40)	*Z* isomer δ S-β-CH_3 (8.93)
0.06	0.42	0.16	0.14	0.24	0.41	0.27
0.11	0.71	0.32	0.23	0.43	0.76	0.47
0.17	1.13	0.54	0.38	0.68	1.18	0.71
0.23	1.86	0.98	0.64	1.17	1.97	1.18
0.30	2.34	1.17	0.80	1.37	2.44	1.40
Δ_B	8.07	4.24	2.78	4.85	8.48	4.88

(*g*) *N*-Nitrosomethylbenzylamine; [S] = 0.354 *M*

Mol ratio [L]/[S]	*E* isomer δ S-CH_3 (7.08)	*E* isomer δ A-CH_2 (4.74)	*E* isomer δ A-*o*-H (2.72)	*Z* isomer δ A-CH_3 (6.32)	*Z* isomer δ S-CH_2 (5.25)	*Z* isomer δ S-*o*-H (2.72)
0.11	0.78	0.38	0.12	0.38	0.79	0.22
0.24	1.50	0.75	0.35	0.64	1.57	0.59
0.49	3.21	1.70	0.93	1.71	3.44	1.55
0.69	4.28	2.27	1.24	2.31	4.58	2.07
0.86	5.03	2.69	1.48	2.72	5.46	2.49
Δ_B	5.95	3.20	1.82	3.29	6.45	3.04

(*h*) *N*-Nitrosomethylphenethylamine; [S] = 0.327 *M*

Mol ratio [L]/[S]	*E* isomer δ S-CH_3 (7.10)	*E* isomer δ A-α-CH_2 (5.72)	*E* isomer δ A-β-CH_2 (7.03)	*E* isomer δ A-*o*-H (2.85)	*Z* isomer δ A-CH_3 (6.52)	*Z* isomer δ S-α-CH_2 (6.28)	*Z* isomer δ S-β-CH_2 (7.30)	*Z* isomer δ S-*o*-H (2.85)
0.07	0.40	0.20	0.16	0.07	0.25	0.51	0.40	0.12
0.17	0.95	0.49	0.33	0.15	0.64	1.13	0.86	0.25
0.26	1.36	0.70	0.50	0.22	0.86	1.60	1.16	0.42
0.37	1.86	0.99	0.70	0.30	1.19	2.13	1.57	0.61
0.47	2.29	1.18	0.83	0.40	1.42	2.61	1.93	0.74
0.61	2.78	1.45	1.02	0.51	1.74	3.15	2.29	0.91
Δ_B	4.61	2.41	1.69	0.83	2.88	5.19	3.77	1.53

(*i*) *N*-Nitrosomethylisopropylamine; [S] = 0.540 *M*

Mol ratio [L]/[S]	*E* isomer δ S-α-CH_3 (7.09)	*E* isomer δ A-CH (5.24)	*E* isomer δ A-β-CH_3 (8.63)	*Z* isomer δ A-α-CH_3 (6.40)	*Z* isomer δ S-CH† (5.0)	*Z* isomer δ S-β-CH_3 (8.89)
0.075	0.60	0.29	0.20	0.27	0.4	0.24
0.14	1.04	0.46	0.35	0.53	1.3	0.49
0.21	1.57	0.85	0.52	0.84	2.2	0.75
0.31	2.23	1.19	0.76	1.19	2.65	1.07
0.39	2.56	1.42	0.82	1.40	4.6	1.20
Δ_B	6.80	3.81	2.24	3.75	12.7	3.27

Can. J. Chem. Downloaded from www.nrcresearchpress.com by 210.87.254.40 on 09/05/12
For personal use only.

TABLE 1. (*Concluded*)

(*j*) *N*-Nitrosomethylcyclohexylamine; [S] = 0.385 *M*

	E isomer			*Z* isomer		
Mol ratio [L]/[S]	δ S-CH_3 (7.04)	δ A-CH (5.70)	δ A-2-CH_2 (8.0)	δ A-CH_3 (6.38)	δ S-CH (5.3)	δ S-2-CH_2 (8.0)‡
0.10	0.86	0.48	0.3	0.46	1.2	0.3
0.21	1.78	0.90	0.6	0.89	2.25	0.6
0.31	2.32	1.20	0.8	1.25	3.1	1.1e; 0.95a
0.43	3.23	1.70	0.9	1.71	4.2	1.6e; 1.2a
0.54	3.95	2.04	1.1	2.18	5.3	2.05e; 1.5a
Δ_B	7.24	3.74	2.05	3.95	9.59	3.89e; 2.79a

*The figures in parentheses represent the chemical shift of the corresponding protons of uncomplexed nitrosamine. The symbols S and A stand for *syn* and *anti*. The S-*o*-H and A-*o*-H are *syn* and *anti ortho*-protons.
†In several cases, the chemical shifts were estimated from the integration curves due to the weak signals.
‡The corresponding 2-methylene signal is separated into the equatorial and the axial signals.

TABLE 2. Downfield shifts of the n.m.r. signals in nitrosamine–Eu complexes by method B

(*a*) *N*-Nitrosomethylethylamine; [L] = 1.025×10^{-3} *M*

	E isomer			*Z* isomer		
[S] (*M*)	S-α-CH_3 δ (1/δ)	A-CH_2 δ (1/δ)	A-β-CH_3 δ (1/δ)	A-α-CH_3 δ (1/δ)	S-CH_2 δ (1/δ)	S-β-CH_3 δ (1/δ)
0.65	0.05(20)	0.03(33)	0.02(50)	0.03(33)	0.055(18)	0.03(33)
0.22	0.15(6.7)	0.085(12)	0.04(25)	0.95(10.5)	0.16(6.3)	0.095(10.5)
0.15	0.185(5.2)	0.10(10)	0.06(17)	0.105(9.5)	0.20(5)	0.115(8.7)

(*b*) *N*-Nitrosomethylisopropylamine; [L] = 1.025×10^{-3} *M*

	E isomer			*Z* isomer	
[S] (*M*)	S-α-CH_3 δ (1/δ)	A-CH δ (1/δ)	A-β-CH_3 δ (1/δ)	A-α-CH_3 δ (1/δ)	S-β-CH_3 δ (1/δ)
0.83	0.05(20)	0.01(100)	0.03(33)	0.025(40)	0.02(50)
0.50	0.06(16.7)	0.025(40)	0.025(40)	0.03(33)	0.025(40)
0.17	0.15(6.7)	0.075(13.3)	0.05(20)	0.07(14.2)	0.06(16.7)
0.10	0.25(4.0)	0.13(7.7)	0.075(13.3)	0.12(8.3)	0.105(9.5)
0.05	0.34(2.9)	0.20(5.0)	0.10(10)	0.175(5.7)	0.15(6.7)

in most of the previous investigations. During the preparation of this manuscript, several reports (3, 20–24) dealing with higher stoichiometry have attracted our attention. Armitage and co-workers (20), by examining the linearity of a plot of [S] *vs.* 1/δ for the 1:1 complex or that of $[S]^2$ *vs.* [S] 1/δ for the 1:2 complex, have established that the stoichiometry of Eu(fod)$_3$–norcamphor complex changes from 1:1 to 1:2 upon changing the solvent from CCl_4 to $CDCl_3$. When this method was applied to *N*-nitrosomethylethylamine, both types of plots were reasonably linear and did not allow differentiation of the stoichiometry. In the case of *N*-nitrosomethylisopropylamine, the former type of plots ([S] *vs.* 1/δ) were definitely linear in contrast to curved graphs of the latter type of plots ($[S]^2$ *vs.* [S] 1/δ).

When the stoichiometric test proposed by ApSimon *et al.* (24) was applied,[2] *N*-nitrosodicyclohexylamine exhibited the experimental point

[2]It must be mentioned that application of this method to the plots of a well established 2:1 complex between 3-(*p*-chlorophenyl)-3,5,5-trimethylcyclohexanone and Eu(fod)$_3$, reported by Shapiro and Johnson Jr. (Figs. 2 and 3 in ref. 3), gives results in which the experimental points are either on the constructed line or below in *disagreement* with the proposal of ApSimon *et al.* (24).

Can. J. Chem. Downloaded from www.nrcresearchpress.com by 210.87.254.40 on 09/05/12
For personal use only.

TABLE 3. Summary of "bound" chemical shifts and binding equilibrium constant

(*a*) *N*-Nitrosomethylethylamine

	E isomer			*Z* isomer		
	S=α-CH_3	A-CH_2	A-β-CH_3	A-α-CH_3	S-CH_2	S-β-CH_3
Δ_B (method A)	8.07	4.24	2.78	4.85	8.48	4.88
Δ_B (method B)	7.94	5.05	3.70	4.85	8.87	4.77
K	55	20	70	43	34	82

(*b*) *N*-Nitrosomethylisopropylamine

	E isomer			*Z* isomer		
	S-α-CH_3	A-CH	A-β-CH_3	A-α-CH_3	S-CH	S-β-CH_3
Δ_B (method A)	6.80	3.81	2.24	3.75	12.7	3.27
Δ_B (method B)	7.81	3.30	2.75	3.98	—	3.24
K	22	58	16	19	—	22

lying below the lines constructed with slopes equal to the induced shifts observed for a high [L]/[S] ratio. In the case of *N*-nitrosodibenzylamine, those experimental points were found to lie above the constructed line. Since a high lanthanide concentration posed difficulties in the experiment, other nitrosamines could not be checked by an ApSimon-type experiment. In view of the fact that the plots of other nitrosamines by method A are rather similar to that of *N*-nitrosodicyclohexylamine, it is suggested that other nitrosamines also have 1:1 stoichiometry. Attempts to investigate stoichiometry in CCl_4 with these methods gave more scatter of the experimental points and ambiguous results.

Computation of the Complex Geometry

Several computer calculations on the determination of the lanthanide position in a complex have been reported (25, 26). According to the proposal of McConnell and Robertson (27) pseudo-contact shift is proportional to the geometric factor given in eq. 2, in which the organic moiety has a fixed geometry.

$$[2] \qquad \Delta_B = \text{constant } (3\cos^2\theta - 1)/\gamma^3$$

where θ is the O—Eu....H angle and γ is the distance in Å between Eu and H atoms. Our aim was to use the experimentally obtained bound chemical shifts (Δ_B) as monitors and to calculate the Eu—O bond length and the Eu—O—N bond angle by varying the conformer population of the nitrosamine in a 1:1 complex. In practice, ratios[3] of Δ_B^1/Δ_B^2 of various protons in the same nitrosamine, rather than bound chemical shift (Δ_B) itself, were used to obtain the best computer fit for the geometrical terms. This design cancelled the constant term in eq. 2 and also eliminated various possible effects, such as a change in the bulk magnetic susceptibility of the solution from variation in [L] and dependence of [S] on individual values of Δ_B.

In this computation, the geometric parameters of a nitrosamine were adapted from those data obtained from X-ray crystallography of nitrosamine–Cu(II) complexes as well as those from electron diffraction measurement of uncomplexed nitrosamines (13). The N—N bond length of *N*-nitrosodimethylamine determined by the latter method is 1.34 Å and that determined by the former method is 1.26 Å. As shown in Table 4, using either N—N bond length did not alter the result significantly. Assumptions were made that the Eu atom was coplanar with the N—N—O plane (8), and, as an approximation, that the nitrosamine had the most stable conformation in the orientation of the C—H bonds eclipsing with the NNO group as shown in **2** and **4** (10). An arbitrary set of the Eu—O bond length and the Eu—O—N bond angle was chosen and θ and γ were calculated. The data of γ and θ together with ratios of Δ_B^1/Δ_B^2 (obtained from method A) were fed into the computer to calculate the errors between the computed Δ_B^1/Δ_B^2 values and the experimental ones.

[3] Δ_B^1, Δ_B^2 etc. are the bound chemical shifts of protons 1, 2, etc. in the same nitrosamine molecule.

Can. J. Chem. Downloaded from www.nrcresearchpress.com by 210.87.254.40 on 09/05/12
For personal use only.

TABLE 4. Parameters of the optimum geometry of the Eu–nitrosamine complexes

Nitrosodialkylamine	Isomer	O—Eu bond length (Å)	N—O—Eu bond angle (°)	Conformer population (%)* 4	2
Dimethyl		3.7	131	33	33
Diethyl		3.8†	129	50	38
		3.7‡	128	50	38
Dibenzyl		3.6	129	45	33
Dicyclohexyl		3.6	128	85	55
Diisopropyl		3.7	131	90	50
Methylethyl	*E*	3.2	130	33	50
		(3.9)§	(130)	(33)	(38)
	Z	3.9	130	48	33
		(3.2)	(130)	(50)	(33)
Methylbenzyl	*E*	3.6	130	33	35
	Z	3.7	128	45	33
Methylphenethyl	*E*	3.4	130	33	43
		(4.2)	(129)	(33)	(43)
	Z	4.2	129	50	33
Methylisopropyl	*E*	3.7	131	33	40
	Z	3.9	122	70	33
Methylcyclohexyl	*E*	3.5	130	33	40
	Z	3.6	126	70	33

*The conformer population is defined as the % time the particular C—H bond spends at the eclipsed position.
†Nitrosamine parameters derived from X-ray data.
‡Nitrosamine parameters derived from electron diffraction data.
§The figures in brackets are the alternative set of optimum parameters.

In the next step, the effect on the errors of changing the conformation at the *syn* and *anti* side was computed. First, the proportion of the *C*-alkyl eclipsed conformation on the *syn* side (**5**) was successively increased by 5%, holding the conformation on the *anti* side (**2**) unaltered;

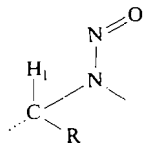

2
anti-CH eclipsed

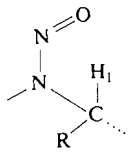

4
syn-CH eclipsed

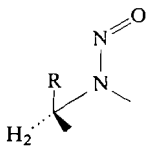

3
anti-CR eclipsed

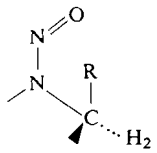

5
syn-CR eclipsed

then the *C*-alkyl eclipsed conformation on the *anti* side (**3**) was increased, similarly holding the conformation on the *syn* side (**4**) unaltered. This process was repeated to obtain the lowest % error by varying the Eu—O bond length and the Eu—O—N bond angles. From this series of computations, we obtained the minimum value of combined individual errors between calculated and experimental ratios of $\Delta_B{}^1/\Delta_B{}^2$. With the optimum geometric parameters, the individual errors were generally less than 4%. At the optimum conditions, there are only three cases where the individual errors were about 10%; for these cases the individual errors were found to be relatively insensitive to variations in the geometric parameters, *e.g.*, change in the bond angle of $\pm 1°$, in the bond length of ± 0.3 Å, and in the conformer population of $\pm 5\%$. For these cases, an alternate set of optimum geometric parameters was also presented in Table 4. These computations yield the % time in which a C—H bond (conformation **2** or **4**) spends at the eclipsed position and is designated as conformer population in Table 4.

Discussion

Previous[4] workers (8–10) have shown the presence of *E* and *Z* isomers for an unsym-

[4]The *Z*–*E* nomenclature (20) is adapted to describe the geometric isomers and *syn*–*anti* nomenclature is exclusively reserved to describe the locations of proton with respect to NNO orientation.

Can. J. Chem. Downloaded from www.nrcresearchpress.com by 210.87.254.40 on 09/05/12
For personal use only.

Can. J. Chem. Downloaded from www.nrcresearchpress.com by 210.87.254.40 on 09/05/12
For personal use only.

metrical nitrosamine and observed the signals due to *syn*- and *anti*-protons when nitrosamines are examined by n.m.r. spectroscopy owing to the restricted rotation of the N—N bond. The n.m.r. spectra are generally complex although they can be interpreted with a certain degree of accuracy if the alkyl groups in the nitrosamine are simple. It has been confirmed by intramolecular comparisons of symmetrical nitrosamines and intermolecular comparisons of unsymmetrical ones that, for acyclic nitrosamines, the n.m.r. signals of the *syn*-methyl and *syn*-methylene protons resonate at a higher field than those of the corresponding *anti*-protons, but the relation is reversed for the methine protons. As shown in Tables 1 and 2, the bound chemical shifts (Δ_B) resulting from Eu complexation invariably produce greater downfield shifts for the *syn*-protons than for the corresponding *anti*-protons. As a consequence, for each nitrosamine, crossover of the chemical shifts occurs at a certain $Eu(fod)_3$ concentration at which the *syn*-protons resonate at a lower field than the *anti*-protons. On the basis of the principle incorporated in the geometric factor of eq. 2, this general trend of Δ_B values suggests that the Eu atom is coordinated with the nitroso oxygen and not with the lone pair electrons of either nitrogen atom. In this connection, aromatic solvent shifts on nitrosamines have been proven to be just the opposite in every respect; the *anti*-protons are shielded more than the corresponding *syn*-protons (8–10).

For the Δ_B values obtained by method A, it has been pointed out by the previous workers (2, 3) that the bound chemical shift (Δ_B) is dependent on nitrosamine concentration [S]. In the present experiments, [S] is purposely set high in order to fulfill the necessary conditions of $[S] \gg [L]$ and $K[S] \gg 1$ that are required in the simplification of the graphic operation (2). Indeed, at the range of $[S] = 0.3$–0.7 *M* in nitrosamine, we have found Δ_B varies only slightly in a few cases. In theory, method B is more amenable for calculation of Δ_B and *K*. In practice, however, since the necessary approximations of $1/K > [S]$ and $\delta \ll \Delta_B$ must be met for operation of eq. 1 (2), the valid nitrosamine concentration [S] is fairly low which leads to feeble n.m.r. signals for accurate reading of the chemical shifts. With the concentration range used in the present experiments and in those published (2), the graphic calculation of Δ_B and *K* by method B is at best a good approximation. From these reasons, we feel that the Δ_B value obtained from method A is more reliable than that obtained from method B; the former set of Δ_B values has been used for computation of the geometry of the nitrosamine complex.

As can be seen in Table 3, the Δ_B values obtained by methods A and B are generally in good agreement. The binding equilibrium constants (*K*) calculated with respect to various protons in the same molecule are, however, not as self-consistent as they should be. It can be seen that whenever Δ_B calculated by method B is smaller than that calculated by method A, the corresponding *K* is at the high extremity. Since the previous workers (2) have shown that Δ_B obtained by method A is generally lower by 5–10% than Δ_B from method B, these high *K* values may not be accurate figures. If we discard these high *K* values, the average binding constant (*K*) can be estimated to be *ca.* 40 for *N*-nitrosomethylethylamine and *ca.* 20 for *N*-nitrosomethylisopropylamine. In spite of the heavy concentration of electron density at the nitroso oxygen atom in a nitrosamine, it is surprising that these *K* values are smaller than those of *n*-propylamine and neopentanol ($K \geqslant 100$) (2).

In Tables 5, 6, and 7, in order to correlate the geometric factors (Eu—O—N bond angle and Eu—O bond length), bound chemical shifts, conformer populations, and other parameters of the relevant nitrosamines are collected together according to the types of α-protons. The bound chemical shifts (Δ_B) of the *syn*-α-methyl protons of various (*E*)-methylnitrosamines correlate inversely with the corresponding Eu—O bond length qualitatively but fail to correlate with Taft σ* constants (29). The picture is pretty much the same with Δ_B of the *syn*-α-methylene protons. In Table 6 the Δ_B of the corresponding *anti*-protons of the same nitrosamines are also listed in the third column to show that the same trend of decrease on Δ_B with those of the *syn*-protons can be observed although not the same type of protons are compared. The optimum Eu—O—N angles remain relatively constant in the vicinity of $130 \pm 1°$ as would be expected in coordination with an analogous series of nitrosamines unless steric hindrance limits the availability of the space. In the computation, a change in the Eu—O—N bond angle from 130 to 128° increases Δ_B by approximately 25%.

TABLE 5. Correlation of *syn*-methyl chemical shifts

(*E*)-Nitrosomethyl-alkylamine	Δ_B	O—Eu bond* length (Å)	N—O—Eu bond angle (°)	Taft† σ*
Ethyl	8.1	3.2	130	−0.10
Cyclohexyl	7.2	3.5	130	−0.15
Isopropyl	6.8	3.7	131	−0.19
Benzyl	6.0	3.6	130	+0.22
Methyl	5.7	3.7	131	0.0
Phenethyl	4.6	4.2	129	+0.08

*The optimum bond length obtained from the computation (Table 4) are adapted.
†Reference 21 (positive values are electron withdrawing substituents).

TABLE 6. Correlation of *syn*-methylene chemical shifts

Nitrosodialkylamine	Δ_B *syn*	Δ_B *anti**	O—Eu bond length (Å)	N—O—Eu bond angle (°)	Conformer population (%)
(*Z*)-Methylethyl	8.5	4.9	3.2	130	100
(*Z*)-Methylbenzyl	6.4	3.3	3.7	128	90
Dibenzyl	5.8	3.1	3.6	129	90
Diethyl	5.5	3.0	3.8	129	100
(*Z*)-Methylphenethyl	5.2	2.9	4.2	129	100

*Δ_B of the corresponding *anti*-α-proton in the same nitrosamine isomer.

TABLE 7. Correlation of *syn*-methine chemical shifts

Nitrosodialkylamine	Δ_B	O—Eu bond length (Å)	N—O—Eu bond angle (°)	Conformer population (%)
(*Z*)-Methylisopropyl	12.7	3.9	122	70
(*Z*)-Methylcyclohexyl	9.6	3.6	126	70
Dicyclohexyl	6.9	3.6	128	85
Diisopropyl	5.1	3.7	131	90

However, in this bond angle range, it has been noted that the calculated individual pseudo-contact shift for the eclipsed proton (H_1) is smaller than that for the noneclipsed proton (H_2), although the latter is located farther from the Eu atom than the former. This indicates the control of the angular factor θ in eq. 2.

In Table 7, it is shown that Δ_B values of *syn*-α-methine protons correlate well with both the Eu—O bond length and the Eu—O—N bond angle. In terms of stereochemistry, the compression from the bulky secondary alkyl groups (isopropyl and cyclohexyl) displaces the Eu position toward the less hindered *anti* side and the angular factor varies more drastically than the distance factor. In the last column of Tables 6 and 7, the percentage of time the *syn*-methylene and *syn*-methine protons spend in the eclipsed position is tabulated. At the present stage there is no way to ascertain whether the computed conformation of the complexes represents the actual shape. However it is noteworthy that the computed "conformer populations" of *N*-nitrosodiisopropylamine in the Eu complex are generally in good agreement with those of the uncomplexed parent nitrosamine (10). The latter figures are obtained by correlating the pertinent chemical shift data with stability of various conformations (10). This shows that the conformation of a nitrosamine is not altered significantly in the Eu complex. Finally it should be mentioned that the population ratios of the *E* and *Z* configurational isomers of the unsymmetrical nitrosamines examined are virtually unaltered, whether free or complexed with $Eu(fod)_3$, as shown by the n.m.r. integrations.

The authors wish to thank the National Research Council of Canada for financial support and Mr. J. M. Pastucha for recording n.m.r. spectra.

Can. J. Chem. Downloaded from www.nrcresearchpress.com by 210.87.254.40 on 09/05/12
For personal use only.

1. C. C. HINKLEY. J. Am. Chem. Soc. **93**, 5258 (1971).
2. (*a*) I. ARMITAGE and L. D. HALL. Can. J. Chem. **49**, (1971); (*b*) I. ARMITAGE, G. DUNSMORE, L. D. HALL, and A. G. MARSHALL. Can. J. Chem. **50**, 2119 (1972).
3. B. L. SHAPIRO and M. D. JOHNSTON, JR. J. Am. Chem. Soc. **94**, 8185 (1972).
4. (*a*) R. VON AMMON and R. D. FISCHER. Angew. Chem. Int. **11**, 675 (1972); (*b*) J. P. BEGUE. Bull. Soc. Chim. Fr. 351 (1972); (*c*) M. R. PETERSON, JR. and G. H. WAHL, JR. J. Chem. Educ. **49**, 790 (1972).
5. W. LIJNSKY and S. S. EPSTEIN. Nature, **225**, 21 (1970); E. C. MILLER and J. A. MILLER. Pharm. Rev. **18**, 805 (1966).
6. S. S. MIRVISH. J. Nat. Cancer Inst. **46**, 1183 (1971).
7. Y. L. CHOW, C. J. COLÓN, H. H. QUON, and T. MOJELSKY. Can. J. Chem. **50**, 1065 (1972).
8. Y. L. CHOW and C. J. COLÓN. Can. J. Chem. **46**, 2827 (1968); Y. L. CHOW, C. J. COLÓN, and J. N. S. TAM. Can. J. Chem. **46**, 2821 (1968).
9. Y. L. CHOW and M. M. FESER. Chem. Commun. 239 (1967).
10. G. J. KARABATSOS and R. A. TALLER. J. Am. Chem. Soc. **86**, 4373 (1964).
11. S. J. KUHN and J. S. MCINTYRE. Can. J. Chem. **44**, 105 (1966).
12. W. S. LAYNE, H. H. JAFFE, and H. ZIMMER. J. Am. Chem. Soc. **85**, 435 (1963).
13. U. KLEMENT and A. SCHMIDPETER. Angew. Chem. **80**, 444 (1968); P. RADEMACHER, R. STØLEVIK, and W. LÜTTKE. Angew. Chem. **80**, 842 (1968).
14. Y. L. CHOW. Can. J. Chem. **45**, 53 (1967).
15. Z. W. WOLKOWSKI. Tetrahedron Lett. 825 (1971).
16. K. D. BERLIN and S. RENGARAJU. J. Org. Chem. **36**, 2912 (1971).
17. J. K. M. SANDERS and D. H. WILLIAMS. J. Am. Chem. Soc. **93**, 641 (1971).
18. R. R. FRASER and Y. Y. WIGFIELD. Tetrahedron Lett. 2215 (1971).
19. J. W. APSIMON and J. D. COONEY. Can. J. Chem. **49**, 2377 (1971).
20. V. G. GIFF, I. M. ARMITAGE, L. D. HALL, and A. G. MARSHALL. J. Am. Chem. Soc. **94**, 8919 (1972).
21. J. K. M. SANDERS, S. W. HANSON, and D. H. WILLIAMS. J. Am. Chem. Soc. **94**, 5325 (1972).
22. K. ROTH, M. GIROSSE, and D. REWICKI. Tetrahedron Lett. 435 (1972).
23. D. F. EVANS and M. WYATT. J. Chem. Soc. Chem. Commun. 312 (1972).
24. J. W. APSIMON, H. BEIERBECK, and A. FRUCHIER. J. Am. Chem. Soc. **95**, 939 (1973).
25. S. FARID, A. ATEYA, and M. MAGGIO. Chem. Commun. 1285 (1971).
26. M. R. WILLCOTT, III, R. E. LENKINSKI, and R. E. DAVIS. J. Am. Chem. Soc. **94**, 1742 (1972).
27. H. M. MCCONNELL and R. E. ROBERTSON. J. Chem. Phys. **29**, 1361 (1958).
28. E. L. ELIEL. J. Chem. Educ. **48**, 163 (1971).
29. J. HINE. Physical organic chemistry. 2nd ed. McGraw-Hill, New York. 1962. p. 97.

Can. J. Chem. Downloaded from www.nrcresearchpress.com by 210.87.254.40 on 09/05/12
For personal use only.

Metabolites of *Hyalodendron* sp.: Bisdethiodi(methylthio)hyalodendrin

GEORGE M. STRUNZ, CHRISTOPHER J. HEISSNER, MASATOSHI KAKUSHIMA, AND MERLYN A. STILLWELL

Canadian Forestry Service, P.O. Box 4000, Fredericton, New Brunswick

Received September 7, 1973

Spectroscopic studies and chemical correlation with hyalodendrin show that a new metabolite of *Hyalodendron* sp. is bisdethiodi(methylthio)hyalodendrin (3-benzyl-6 hydroxymethyl-1,4-dimethyl-2,5-dioxo-3,6-di(methylthio)piperazine).

Les études spectroscopiques et une correlation chimique avec l'hyalodendrine démontrent qu'un métabolite nouveau d'une espèce d'*Hyalodendron* est la bisdethiodi(méthylthio)hyalodendrine (3-benzyl-6-hydroxyméthyl-1,4-diméthyl-2,5-dioxo-3,6-di(méthylthio) piperazine).

Can. J. Chem., **52**, 325 (1974)

A recent addition to the group of biologically active epidithiodiketopiperazine fungal metabolites (1) is hyalodendrin (**1**),[1] produced by a *Hyalodendron* sp. (2, 3). We report here the isolation and identification of a new, related metabolite, bisdethiodi(methylthio)hyalodendrin (**2**), produced in culture by this organism.

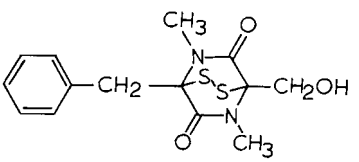

1

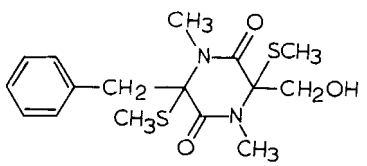

2

Comparison of the spectroscopic characteristics of the new metabolite, $C_{16}H_{22}N_2O_3S_2$, with those of hyalodendrin (**1**), indicated that the former compound is also an *N*-methylserine-*N*-methylphenylalanine diketopiperazine, bearing substitution at the 3 and 6 positions. Thus, **2** displayed i.r. absorption indicative of amide and hydroxyl functionality, as well as peaks attributable to a monosubstituted phenyl group (see Experimental section) (2, 4). In the n.m.r. spectrum (220 MHz, $CDCl_3$), the phenyl hydrogens give rise to multiplets at δ 7.12 (2H) and 7.26 p.p.m. (3H). An AB quartet centered at δ 3.44 (2H, J = 14 Hz) represents the benzylic protons, and demonstrates the tetrasubstituted character of the neighboring carbon atom. Coupling with the hydroxyl proton (J = 6 and 7 Hz), as well as geminal coupling (J = 12 Hz) is observed for the two hydrogens attached to the primary carbinol center, and they appear as doublets of doublets at δ 3.14 and 3.85 p.p.m. The hydroxyl proton is manifested as a broadened unsymmetrical "triplet" at δ 1.43; as expected, irradiation at 314 Hz collapsed the signal for the carbinol protons to an AB quartet (J = 12 Hz). Singlets (3H each) at δ 3.03 and 3.29 p.p.m. represent the methyl groups on the amide nitrogens, and singlets (3H each) at δ 2.13 and 2.30 p.p.m. are assigned to two methylthio groups (5–7), which can only be located at the 3 and 6 positions of the diketopiperazine system, as in structure **2**. The presence of benzyl and —CH_2OH functionality, as well as the two methylthio groups was confirmed by the mass spectral fragmentation pattern (see Experimental section). Ions at *m/e* 132 and 72 can be rationalized in terms of the cleavages indicated in Scheme 1 (*c.f.* ref. 8).

Correlation with hyalodendrin corroborated the formulation **2**. Thus, treatment of the former with sodium borohydride in the presence of methyl iodide and pyridine (5) at 0° gave a di(methylthio) ether, identical in all respects with the metabolite **2**. Sodium borohydride reduction of epidithiodiketopiperazines proceeds with retention of configuration (1, 5).

Isolation of bisdethiodi(methylthio) modifications of epidithiodiketopiperazine metabolites

[1]The absolute configuration of the bridged diketopiperazine system of hyalodendrin is antipodal to that of gliotoxin (2).

Can. J. Chem. Downloaded from www.nrcresearchpress.com by 210.87.254.5 on 09/05/12
For personal use only.

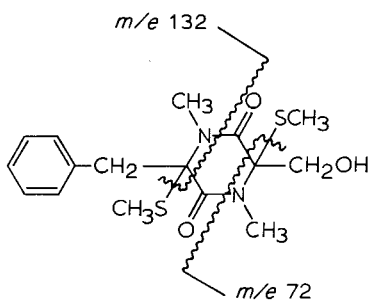

SCHEME 1

has precedents in similar derivatives of sporidesmin (5), acetylaranotin (6), and acetylapoaranotin (7). Since these metabolites lack the striking biological activity of their bridged counterparts (1, 9), it is not surprising that **2** was devoid of antifungal activity in a series of bioassays (3).

Experimental

See ref. 1 for description of instrumentation, etc. The 220 MHz n.m.r. spectrum of **2** was recorded for a solution in deuteriochloroform on a Varian HR-220 instrument at the Canadian 220 MHz N.M.R. Center, Ontario Research Foundation.

Isolation of Metabolites

The production and isolation of hyalodendrin have been detailed elsewhere (2, 3). Material extracted with chloroform from filtered culture medium which had supported growth of *Hyalodendron* sp. for 10 to 12 days was chromatographed on a column of silica gel (Kieselgel: 100–200 mesh, Gebr. Herrmann, Köln). Elution with benzene–chloroform (7:3) afforded hyalodendrin (after crystallization, *ca.* 100 mg/l of culture medium) as described previously (2, 3). Bisdethiodi(methylthio)hyalodendrin (**2**) was subsequently eluted with benzene–chloroform (1:1) and further purified by recrystallization from methylene chloride – cyclohexane to give colorless needles, m.p. 140–140.5°; $[\alpha]_D^{23}$ +64° (*c*, 1.071 in $CHCl_3$); ν_{max} (KBr) *inter alia*, 3375, 1660, 1644, 1636, 1499, 1375, 735, and 700 cm^{-1}; ν_{max} (CCl_4) 3570, 1657, and 1380 cm^{-1}; λ_{max} (EtOH) <220, *ca.* 260 nm (inflection, $\varepsilon \sim 900$). The n.m.r. data are given in the text. Mass spectrum *inter alia*, *m/e* 354 (low intensity, M^+), 323 $(M - CH_2OH)^+$, 307 (base peak) $(M - SCH_3)^+$, 277 $(M - SCH_3 - CH_2O)^+$, 276 $(M - SCH_3 - CH_2OH)^+$, 263 $(M - C_7H_7)^+$, 260 $(M - SCH_3 - SCH_3)^+$, 132 $(C_9H_{10}N)^+$, 91 $(C_7H_7)^+$, and 72 $(C_3H_6NO)^+$. Accurate mass measurements: 307.1107 ($C_{15}H_{19}N_2O_3S$ requires 307.1116), 132.0809 ($C_9H_{10}N$ requires 132.0813).

Anal. Calcd. for $C_{16}H_{22}N_2O_3S_2$: C, 54.21; H, 6.26; O, 13.54; N, 7.90; S, 18.10. Found: C, 54.18; H, 6.30; O, 13.41; N, 7.95; S, 18.02.

While growth of *Hyalodendron* sp. in liquid culture as described above (3) leads to isolation of **1** as the major metabolite, longer fermentation periods appear to favor the formation of **2**.

Conversion of Hyalodendrin into 2

A solution of hyalodendrin (200 mg) in pyridine (1 ml) was treated with methyl iodide (5 ml) at 0° in a nitrogen atmosphere. An ice-cold solution of sodium borohydride (100 mg) in methanol (7 ml) was added dropwise to the stirred suspension and the resulting pale yellow solution was stirred for 30 min at 0°, during which the color faded. Additional methyl iodide (1 ml) was added and the solution was allowed to attain room temperature during 3 h. The resulting pale yellow solution was evaporated *in vacuo* at 30 to 40° and the residue was taken up into methylene chloride and water. The aqueous phase was adjusted to p*H* 6 by addition of 1 *N* HCl and the organic layer was then washed with water, dried ($MgSO_4$), and evaporated. Preparative layer chromatography of the residue on a silica gel plate using the solvent system benzene–hexane–acetone (5:4:1) afforded 215 mg of crude crystalline bisdethiodi(methylthio)hyalodendrin, which was recrystallized from methylene chloride – cyclohexane to give 188 mg (86%) colorless needles, m.p. 138–140°. Crystals melting at 139.5–140° were obtained on further recrystallization from methylene chloride – cyclohexane. Comparison of chromatographic behavior and spectra, and mixture melting point determination established the identity of the product with the natural metabolite **2**.

We thank Mr. A. I. Budd, University of Alberta, Edmonton, for the accurate mass measurements.

1. A. TAYLOR. The toxicology of sporidesmins and other epipolythiadioxopiperazines. *In* Microbial toxins. Vol. 7. Academic Press, Inc., New York. 1971. Chapt. 10. pp. 337–375.
2. G. M. STRUNZ, M. KAKUSHIMA, M. A. STILLWELL, and C. J. HEISSNER. J. Chem. Soc. Perkin I (1973). In press.
3. M. A. STILLWELL, L. P. MAGASI, and G. M. STRUNZ. Can. J. Microbiol. In press.
4. L. J. BELLAMY. The infrared spectra of complex molecules. 2nd ed. John Wiley and Sons, Inc., New York. 1958.
5. R. RAHMAN and A. TAYLOR. Chem. Commun. 1032 (1967); W. D. JAMIESON, R. RAHMAN, and A. TAYLOR. J. Chem. Soc. C, 1564 (1969).
6. R. NAGARAJAN, L. L. HUCKSTEP, D. H. LIVELY, D. C. DELONG, M. M. MARSH, and N. NEUSS. J. Am. Chem. Soc. **90**, 2980 (1968); J. W. MONCRIEF. J. Am. Chem. Soc. **90**, 6517 (1968).
7. N. NEUSS, R. NAGARAJAN, B. B. MOLLOY, and L. L. HUCKSTEP. Tetrahedron Lett. 4467 (1968).
8. R. NAGARAJAN, J. L. OCCOLOWITZ, N. NEUSS, and S. M. NASH. Chem. Commun. 359 (1969).
9. H. C. J. OTTENHEYM, T. F. SPANDE, and B. WITKOP. J. Am. Chem. Soc. **95**, 1989 (1973).

Can. J. Chem. Downloaded from www.nrcresearchpress.com by 210.87.254.5 on 09/05/12
For personal use only.

Vibrational Spectra and Structures of the Solid Phases of Germane

NGUYEN DINH THE, J.-M. GAGNON, R. BELZILE, AND A. CABANA
Département de Chimie, Université de Sherbrooke, Sherbrooke, Québec

Received July 27, 1973

This paper reports the i.r. and Raman spectra of the four solid phases of GeH_4. Pure and mixed isotopic crystals have been examined. Marked spectral changes are observed at every transition. The interpretation of the spectra, based upon the Halford–Hornig approach, provides information on the crystal structure of each form. Phase I is plastic and molecules probably lie at sites of symmetry T or T_d. The spectra of the two intermediate phases are consistent with site symmetries of either D_{2d}, S_4, C_{3v}, or C_3 but the two former are favored. The stable phase below 63 °K is of lower symmetry, the molecules lying at sites of either D_2, C_{2v}, C_2, C_s, or C_1 symmetry. Possible factor groups are proposed for phases II, III, and IV. The molecules are found to occupy only one set of equivalent sites in each of the phases.

On a enregistré les spectres i.r. et Raman des quatre phases solides de la molécule GeH_4 et ceux de la molécule GeD_4 présente à basse concentration dans le GeH_4. Chacune des transitions conduit à des modifications marquées des spectres. L'interprétation de ceux-ci, basée sur l'approche Halford–Hornig, procure des renseignements sur les structures cristallines de toutes les phases. La phase I est une phase plastique où les molécules occupent probablement des sites de symétrie T ou T_d. Les spectres des deux phases intermédiaires sont compatibles avec des symétries de site D_{2d}, S_4, C_{3v}, ou C_3 bien que les deux premiers groupes soient considérés plus probables. La symétrie de la phase stable en dessous de 63 °K est plus basse; les molécules sont situées sur des sites de symétrie D_2, C_{2v}, C_2, C_s ou C_1. On propose certains groupes facteurs pour les trois phases de plus basses températures. On a trouvé que les molécules occupent un seul ensemble de sites équivalents dans chacune des phases solides.

Can. J. Chem., **52**, 327 (1974)

Introduction

Infrared and Raman spectroscopy often yields valuable information on the structure of molecular crystals (1). The information provided by these techniques is particularly useful when the more direct methods of investigation of the structures are not easily applicable. This is the case for all the hydrides of Group IV. We have, for this reason, undertaken a vibrational study of this group of molecules and have already reported some progress on methane (2) and silane (3). In this paper, the infrared and Raman spectra of the various solid modifications of germane will be reported and analyzed with the aim of obtaining information on the structures of the various solid phases.

A calorimetric investigation (4) has shown that germane exhibits three solid–solid phase transformations around 76, 73, and 63 °K. Therefore GeH_4 exists under four crystalline modifications labelled, in order of decreasing temperature, I to IV. Clusius and Faber (4) have observed that except for phase I, all phases are strongly birefringent.

The gas-phase i.r. spectrum has been obtained (5) with a resolution sufficient to resolve the lines due to each isotopic modification of the natural mixture. The isotopic shifts are smaller than the usual bandwidth found in solids and hence it is expected that no isotopic structure will be observed in the solid state spectra.

The i.r. spectra of some of the condensed phases were also previously recorded (6, 7) but the work was not carried out under the best experimental conditions and the spectra were not analyzed in terms of the symmetry of the crystal lattice. The work presented in ref. 7 is very extensive and contains an interesting discussion of frequency shifts which occur upon condensation from the gas.

Experimental

The GeH_4 used in our experiments was obtained from the Matheson Co; the stated purity was 99.99% and has been used without any purification. The GeD_4, from Merck, Sharp, and Dohme of Canada, Ltd., was analyzed by mass spectrometry and found to contain about 10% of the mixed hydrogenated species. Therefore the vibrational spectra of the neat crystals of GeD_4 were not recorded. Mixed crystals containing 0.3% GeD_4 in GeH_4 were used for the i.r. experiments whereas for the Raman experiments the concentration of GeD_4 was increased to 1.8%.

The i.r. spectra were obtained with a Perkin–Elmer (Model 125) prism-grating spectrometer calibrated with reference to the I.U.P.A.C. tables (8). The spectral slit

Can. J. Chem. Downloaded from www.nrcresearchpress.com by 210.87.254.105 on 09/05/12
For personal use only.

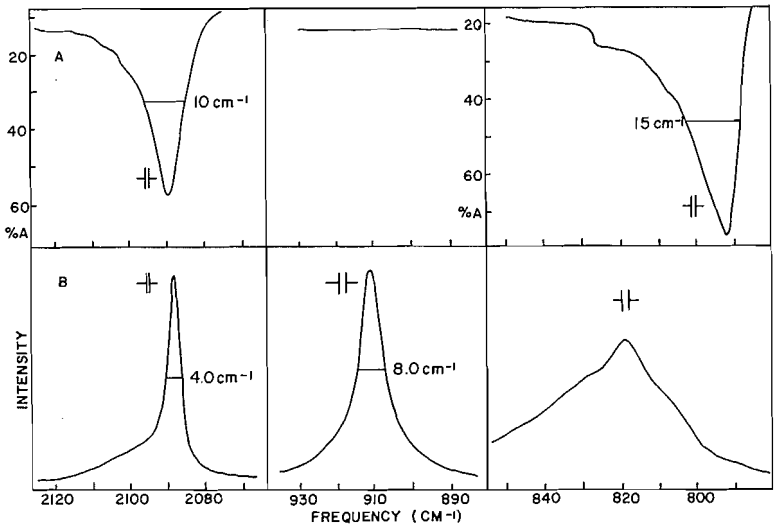

FIG. 1. Pure GeH_4 in phase I. (A) Infrared spectrum of a 1 μ thick sample at 92 °K. (B) Raman spectrum at 95 °K.

width varied in the range 0.5–0.9 cm^{-1} and the frequency accuracy was 0.5 cm^{-1} for sharp peaks.

The Raman spectra were recorded using a Jarrell–Ash (Model 25–100) double monochromator, a Coherent Radiation Laboratory (Model 52A) argon ion laser, an ITT (FW-130) phototube cooled to −60 °C, and a photon counting detection system. The spectra were calibrated with reference to plasma lines from the laser and emission lines from neon (9). The frequencies for sharp peaks are accurate to within 1 cm^{-1} or better and the resolution varied from 0.5 to 2.5 cm^{-1} depending upon the intensity of the various bands.

The cryostats and cells used have been previously described (2, 3). The crystals grown from the liquid phase were perfectly transparent in phase I but invariably shattered at the phase transition.

Results and Discussion

In the gas phase, the symmetry of the molecule is T_d; therefore it has four normal modes of vibrations. These are labelled: ν_1 (A_1), ν_2 (E), ν_3 (F_2), and ν_4 (F_2). All four are Raman active while only the two F_2 modes are allowed in i.r. Forbidden modes often become active in the solid through crystalline perturbations but the intensity of such modes was always found to be very low. In the present study we have failed to detect any i.r. absorption in the region of the forbidden transitions even when samples 50 times thicker than those necessary to record ν_3 and ν_4 were used. Accidental frequency coincidence between ν_1 and ν_3 makes it impossible to check for possible i.r. absorption due to the ν_1 vibration.

Natural germanium is a mixture of five isotopes: ^{70}Ge (20.5%), ^{72}Ge (27.4%), ^{73}Ge (7.8%), ^{74}Ge (36.5%), and ^{76}Ge (7.8%). The gas-phase frequencies of the ν_3 vibrations for the lightest and heaviest germane molecules differ only by 1.2 cm^{-1} and smaller isotopic shifts are expected for ν_1, ν_2, and ν_4 and since the spectral slit widths of the instruments used in the present investigation are at least 0.5 cm^{-1} it cannot be expected that isotopic splitting will be resolved. The five unresolved components will produce rather wide lines particularly in the ν_3 region where the isotopic shifts are largest.

Vibrational Spectra and Structure of Phase I

The i.r. and Raman spectra of neat crystalline GeH_4 in Phase I are reproduced in Fig. 1, and measured frequencies are listed in Table 1. The spectra of the liquid are not reproduced here but it is interesting to note that no noticeable spectral changes were observed upon solidification. The bands were found to be wide both in the liquid phase and in the solid phase I. The widths of the bands observed for the pure solid were characteristic of the plastic phases for related molecules (2, 3, 10). Although all the bands observed for the phase I solid, with the possible exception of ν_2, appeared to result from the overlapping of two or more components, it was impossible to determine the exact number of components responsible for the wide bands

Can. J. Chem. Downloaded from www.nrcresearchpress.com by 210.87.254.105 on 09/05/12
For personal use only.

TABLE 1. Vibrational frequencies of neat GeH_4 crystals (cm^{-1})

Crystal I		Crystal II		Crystal III		Crystal IV		
Infrared	Raman	Infrared	Raman	Infrared	Raman	Infrared	Raman	Assignment
							2110.5	
				2104	2104.1	2108.8	2102.6	
				—	2099.1	2101.4	2099.5	
		2090.2	2106.8	—	2096.4	2094.9	2096.2	
2089.6	~2100	2085.9	2096.1	—	2090.5	2092.9	2092.7	ν_1, ν_3
				2092.3	—	2089.1	2089.6	
				2087.1	—	2086.4	2087.9	
						2084.4		
						2081.4		
—	2088	—	2088.3	—	2085.4	—	2082.8	
—	918.5	—	919.0	—	918.0	—	916.0	ν_2
							827.5	
—	—	856.0	826.5	824.0	822.2	826.6	825.8	
825	820	824.4	803.6	795.4	810.0	821.2	821.2	
791.4	—	796.0	797.2	788.6	797.9	816	817	ν_4
		788				−792.0	808.7	
						−787.2	803.8	
							796.0	

found in any of the vibration regions. Therefore it was impossible to carry out an analysis of the spectra of the neat crystal that would lead to a characterization of the site or factor groups. One should note the different band shapes, widths, and frequencies of the i.r. and Raman ν_4 spectra. It is clear that the i.r. absorption in the ν_4 region is complicated by reflection losses. The complex Raman spectrum in the ν_4 region results from a superposition of quasi-longitudinal and transverse frequencies. A similar phenomenon was observed in the ν_3 region of the Raman spectrum of the high temperature phase of CF_4 (10).

The spectra of mixed isotopic solutions in phase I are interesting if one compares the band widths of the guest and host species. The infrared and Raman spectra of GeD_4 at low concentration in GeH_4 are reproduced in Fig. 2, and measured frequencies are listed in Table 2. Although the band widths of ν_1, ν_2, and ν_3 of the uncoupled GeD_4 molecules are comparable to what they were in the spectrum of the pure crystal of GeH_4, the ν_4 i.r. band of the uncoupled molecule is much sharper than that for the pure crystal (3 cm^{-1} as opposed to 15 cm^{-1}). This relatively narrow and symmetrical band of ν_4 for isolated GeD_4 may be a true singlet. This would indicate a high site symmetry. Since the site group ought to be a sub-group of the point group symmetry of the free molecule, hence only T and T_d site symmetries are acceptable.

Vibrational Spectra and Structures of Phases II and III

The i.r. and Raman spectra of GeD_4 at low concentration in phase II GeH_4 are reproduced in Fig. 3 and Fig. 4 shows the corresponding spectrum for phase III. Upon transition from phase I to phase II all bands become sharper. This reflects increased ordering of the molecules in phase II. The transition from phase II to phase III is not accompanied by a change in the number of observed spectral features but only by a sharpening of the lines. Therefore the same site symmetries will be found compatible with the spectra of both phases II and III. The triply degenerate modes yield i.r. and Raman doublets, while ν_2 and ν_1 are respectively wide and narrow Raman singlets. However, in view of the width of the ν_2 band it is believed to be an unresolved doublet. If this is the case, the site symmetry is either S_4 or D_{2d} but if, on the contrary, the E mode remains degenerate the site symmetry is either C_3 or C_{3v}. The sharp single ν_1 component indicates that only one set of equivalent sites is occupied by the molecules in each of the two phases.

The i.r. and Raman spectra of pure crystalline

Can. J. Chem. Downloaded from www.nrcresearchpress.com by 210.87.254.105 on 09/05/12
For personal use only.

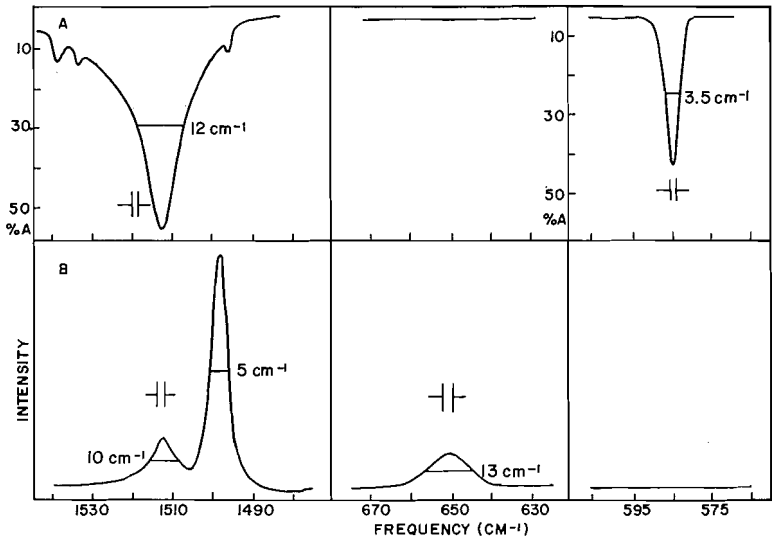

FIG. 2. Mixed crystal in phase I. (A) Infrared spectrum of GeD_4 (0.3%) in GeH_4 at 92 °K. (B) Raman spectrum of GeD_4 (1.8%) in GeH_4 at 95 °K.

TABLE 2. Vibrational frequencies (cm^{-1}) of GeD_4 isolated in crystalline GeH_4*

Crystal I		Crystal II		Crystal III		Crystal IV		
Infrared	Raman	Infrared	Raman	Infrared	Raman	Infrared	Raman	Assignment
		1512	1512.8	—	1513.6	1514.9	1513.0	
1512.3	1512.5	1509.9	1511.0	—	1511.0	1510.9	1509.2	ν_3
						1508.3	1507.0	
—	1497.5	—	1497.0	—	1496.8	—	1494.1	ν_1
—	652.0	—	652.0	—	651.8	—	651.0	ν_2†
				—	—	586.1	—	
584.5	—	585.3	—	—	—	583.9	—	ν_4
		582.9	—			582.1	—	

*Concentration of GeD_4: 0.3% for the i.r. and 1.8% for the Raman.
†ν_2 is a weak Raman band. A spectral slit width of 2.5 cm^{-1} had to be used in order to be able to record this band.

GeH_4 in phases II and III are reproduced in Figs. 5 and 6 respectively. The vibrational frequencies are listed in Table 1. When compared to the spectra of phase I those of phases II and III are found to exhibit several changes. The ν_2 region may seem the less affected but one should note the increased width of this band in phase II relative to phase I; in phase III the width decreases to what it was in phase I. The most striking modifications appear in the ν_4 Raman band where there are three well separated peaks instead of the broad feature found in phase I. It is believed that the two lower frequency peaks are transverse components associated with ν_4 while the peaks at 826.5 cm^{-1} and 822.2 cm^{-1} in phases II and III respectively are longitudinal components. Evidently the same type of complication should be observed in the ν_3 region and indeed it is believed that the 2106.8 cm^{-1} peak in the spectrum of phase II is a longitudinal component associated with ν_3. Similarly, in the Raman spectrum of phase III, it is believed that the two sharp features at 2104 and 2099 cm^{-1} are also longitudinal components. If the crystal density, the index of refraction, and the $\partial\mu/\partial Q$ were known one could check the validity of this proposed assignment by using the Hass–Hornig relation (11) which relates these quantities to the transverse and longitudinal frequencies. Unfortunately the data is not available and the calculation cannot be carried out. Since it is likely that some of the modes are longitudinal components

Can. J. Chem. Downloaded from www.nrcresearchpress.com by 210.87.254.105 on 09/05/12
For personal use only.

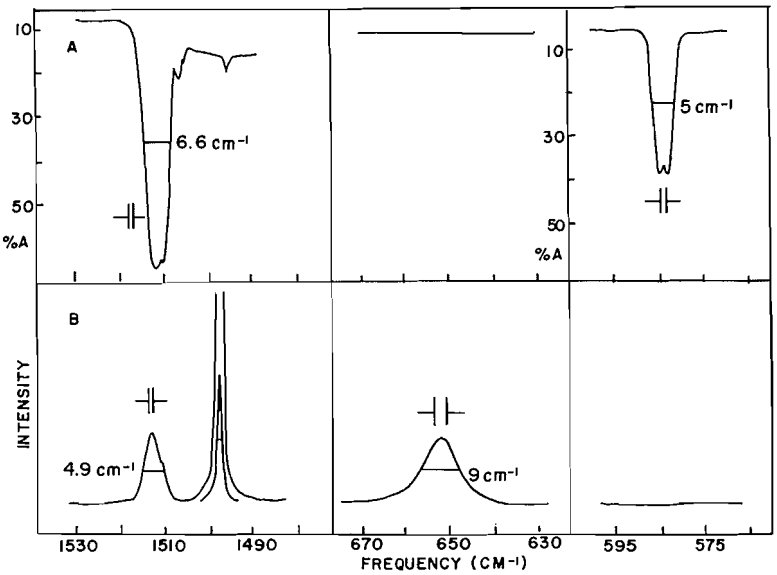

FIG. 3. Mixed crystal in phase II at 75 °K. (A) Infrared spectrum of GeD_4 (0.3%) in GeH_4. (B) Raman spectrum of GeD_4 (1.8%) in GeH_4.

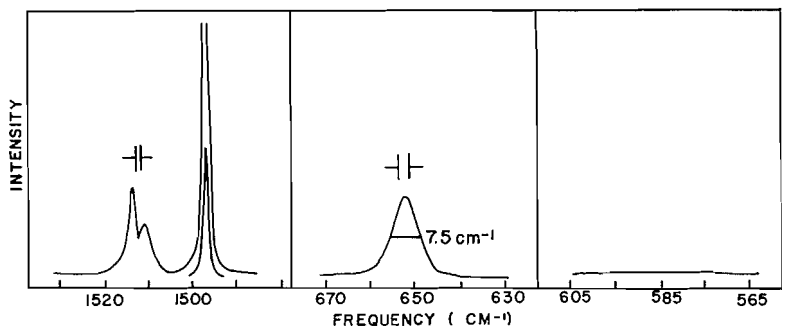

FIG. 4. Raman spectrum of GeD_4 (1.8%) in GeH_4 phase III at 64 °K.

there is some uncertainty in the number of active components in the Raman spectra. Although these longitudinal frequencies are not i.r. active, weak features are, under certain conditions, observed in the i.r. spectrum around the longitudinal frequencies (12, 13); this appears to be the case in these spectra. As a consequence of the ambiguity in the assignment of the observed features the factor group analysis will be more speculative than it usually is in this type of study. Nevertheless the analysis has been carried out based on the number of modes remaining after the exclusion of the bands believed to result from the longitudinal frequencies. This leaves us with the same number of bands in both phases II and III: two for each of the two i.r. and Raman F_2 modes and one for the sharp Raman A_1 mode. The band observed in the ν_2 Raman region is so wide that it most likely contains several unresolved components. Therefore it seems preferable not to use this band in the selection of acceptable factor groups. Table 3 lists pairs of site and factor groups compatible with the spectra. Centrosymmetric structures are excluded since they can never yield separate longitudinal and transverse Raman frequencies (14). Furthermore the elimination of the cubic groups is dictated by the observed birefringence for the crystal in phases II and III (4).

Vibrational Spectra and Structure of GeH_4 below the λ Point at 62.9 °K

The i.r. and Raman spectra of uncoupled GeD_4 molecules in a crystal of GeH_4 below the

Can. J. Chem. Downloaded from www.nrcresearchpress.com by 210.87.254.105 on 09/05/12
For personal use only.

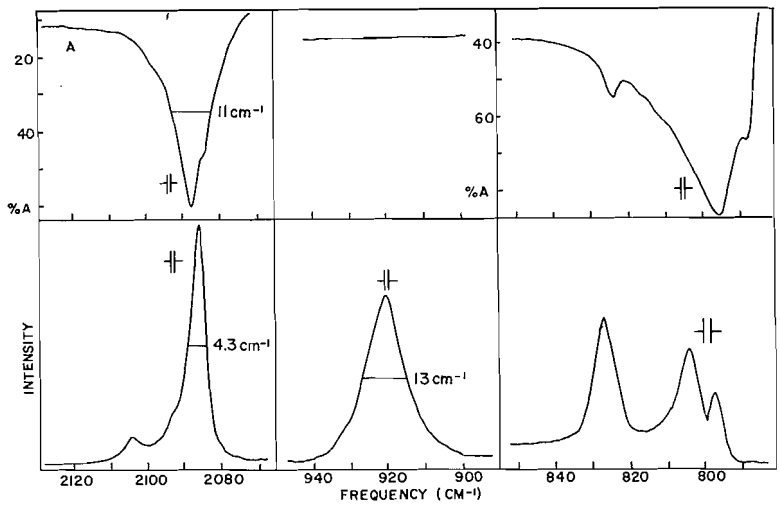

FIG. 5. Pure GeH_4 in phase II at 75 °K. (A) Infrared spectrum of a 1 μ thick sample. (B) Raman spectrum.

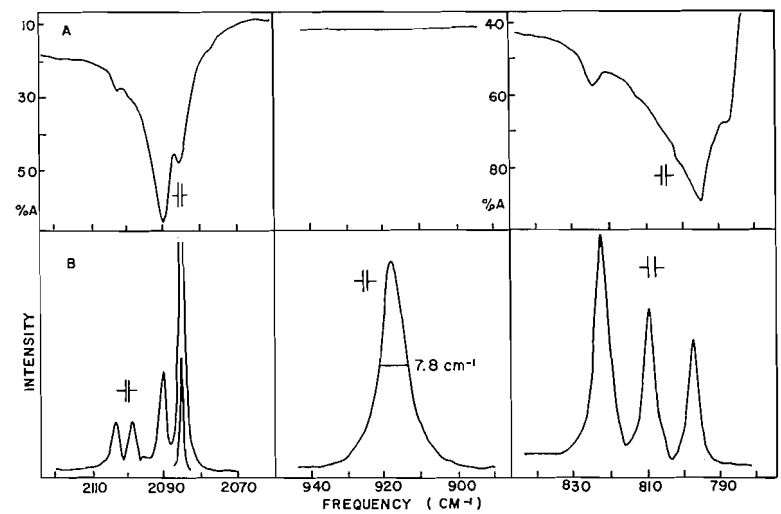

FIG. 6. Pure GeH_4 in phase III. (A) Infrared spectrum of a 1 μ thick sample at 72 °K. (B) Raman spectrum at 65 °K.

λ point at 62.9 °K are reproduced in Fig. 7. The components observed in the spectra of the isolated molecules in phase IV are sharper than those in any of the higher temperature phases. The degeneracy of the gas phase F_2 modes has been completely removed and both the i.r. and Raman spectra display three components in any of the appropriate regions. (Weaker lives observed in the ν_3 region of the i.r. spectrum result from imperfect compensation of atmospheric water vapor and should be ignored.) The ν_2 region reveals a single band, although any site group compatible with the splitting of the F_2 modes into three components (D_2, C_{2v}, C_2, C_s, and C_1) necessarily removes the degeneracy of the $\nu_2(E)$ mode; thus the observed wide band (5.8 cm^{-1}) consists of an unresolved doublet.

The i.r. and Raman spectra of a pure crystal of GeH_4 in phase IV are shown in Fig. 8. The peak at 821.2 cm^{-1} in the ν_4 Raman region is thought to be due to a longitudinal component. A weak band is also observed in the infrared region at the same frequency. Similarly the higher frequency peaks in the ν_3 region of the

Can. J. Chem. Downloaded from www.nrcresearchpress.com by 210.87.254.105 on 09/05/12
For personal use only.

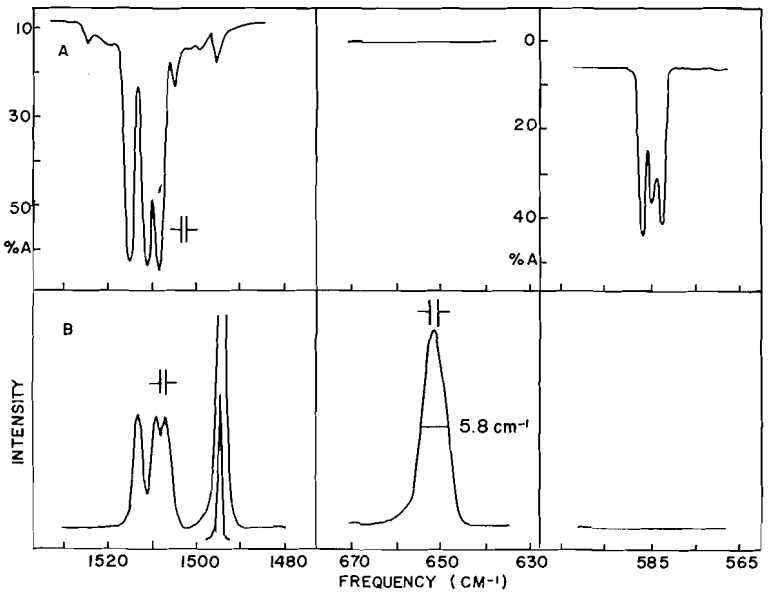

FIG. 7. Mixed crystal in phase IV. (A) Infrared spectrum of GeD_4 (0.3%) in GeH_4 at 10 °K. (B) Raman spectrum of GeD_4 (1.8%) in GeH_4 at 20 °K.

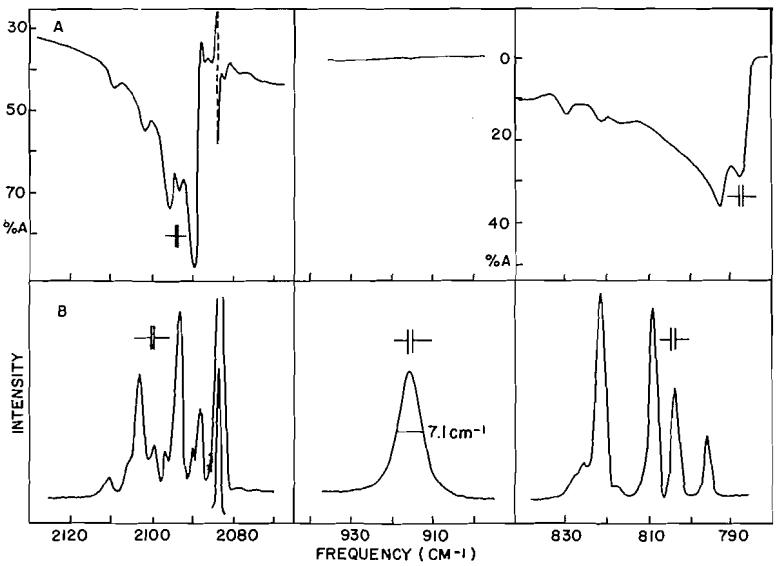

FIG. 8. Pure GeH_4 in phase IV. (A) Infrared spectrum of a 1 μ thick sample at 15 °K. (B) Raman spectrum at 30 °K.

Raman spectrum are probably also longitudinal components. The ν_3–ν_1 region of the Raman spectrum is very complicated and is not useful for a factor group analysis. The infrared spectrum is also not helpful since it is complicated by strong reflection. Therefore we are left, for a factor group analysis, with only the ν_2 and ν_4 portions of the Raman spectrum. Although the ν_2 band is not split, it is wide and likely to result from two or more unresolved components. In the ν_4 region it is likely that the three low frequency components are transverse modes associated with the high frequency longitudinal mode but it cannot be excluded that both lines at

Can. J. Chem. Downloaded from www.nrcresearchpress.com by 210.87.254.105 on 09/05/12
For personal use only.

TABLE 3. Site and factor groups compatible with the number of i.r. and Raman bands of GeH_4 in phases II and III

		Infrared			Raman			
Site	Factor	A_1	E	F_2	A_1	E	F_2	Crystal system*
D_{2d}	D_{2d}	0	0	2	1	2	2	Tetragonal (7)
S_4	S_4	0	1	2	1	2	2	Tetragonal (2)
C_{3v}	C_{3v}	1	1	2	1	1	2	Trigonal (3)
C_3	C_3	1	1	2	1	1	2	Trigonal (2)

*The number in parenthesis is the number of space groups compatible with each set of site and factor groups.

TABLE 4. Site and factor groups compatible with the number of i.r. and Raman bands of GeH_4 in phase IV

		Infrared			Raman			
Site	Factor	A_1	E	F_2	A_1	E	F_2	Crystal system*
C_1	C_1	1	2	3	1	2	3	Triclinic (1)
C_s	C_s	1	2	3	1	2	3	Monoclinic (2)
C_2	C_2	1	2	3	1	2	3	Monoclinic (2)
C_{2v}	C_{2v}	1	1	3	1	2	3	Orthorhombic (5)
D_2	D_2	0	0	3	1	2	3	Orthorhombic (4)

*The number in parenthesis is the number of space groups compatible with each set of site and factor groups.

higher frequencies are longitudinal components. We therefore suggest that the factor group analysis be carried out with these three components being considered. (Any of the site groups found compatible with the splitting observed in the spectra of GeD_4 isolated in GeH_4 requires that a minimum of three components be found in both the ν_3 and ν_4 regions of the i.r. and Raman spectra.) The reported birefringence excludes the cubic groups and the existence of separate longitudinal and transverse frequencies is incompatible with centrosymmetric crystals. With these assumptions one arrives at the possible symmetries listed in Table 4 but the factor group analysis ought to be regarded as very tentative; it is correct as long as our assumptions are valid.

Final Remarks and Conclusions

The analysis of the vibrational spectra of GeH_4 as a pure crystal and of GeD_4 at low concentration in a matrix of GeH_4 has proven to be more difficult than expected. The difficulties arise partly because the intense i.r. absorption of the neat crystals is accompanied by reflection which distorts the bands. The lines at the higher frequencies in the ν_3 and ν_4 regions of the Raman spectra are believed to be longitudinal components associated with the lower frequency transverse components; their presence makes the factor group analysis less certain.

The spectra of the isotopic impurity in the mixed crystals are free from these problems; therefore the results extracted from their analysis may be considered well established. In particular, the sharpness of the ν_1 singlet in all phases (except phase I) suggests that only one type of site is occupied in the solid phases. The spectra do not permit a unique choice of site group in any phase but lead to a limited number of acceptable site symmetries. These are: T or T_d for phase I, S_4 or D_{2d}, or less likely C_3 or C_{3v} for phases II and III. For the phase stable below the 63.9 °K λ point, five possible site groups were found compatible with both the i.r. and Raman spectra; these are C_1, C_s, C_2, C_{2v}, and D_2. An analysis of the orientational effects on the spectra of isolated partially deuterated germane molecules in a matrix of GeH_4 could lead to a unique choice of site symmetries (2, 15) in the three phases stable at the lower temperatures but these compounds are not available to us at present.

Although the work described in this paper is quite extensive it should not be considered more than a preliminary survey of the structures of the four solid phases of germane. Much more experimental data is necessary. In particular it is believed that X-ray diffraction from the heavy

Can. J. Chem. Downloaded from www.nrcresearchpress.com by 210.87.254.105 on 09/05/12
For personal use only.

atoms should yield rather readily the Bravais lattices of the phases stable at the lower temperatures and possibly also of phase I. Such an experiment and a test for piezoelectricity would constitute useful checks of some of the conclusions derived in this study. Although the optical birefringence has already been measured, perhaps it would be worthwhile repeating this experiment using modern techniques.

Financial support was provided by the Ministère de l'Education de la Province de Québec and by the National Research Council of Canada. Thanks are due to Mr. Nguyen Cong Thanh for rerunning several i.r. spectra just prior to this publication.

1. W. VEDDER and D. F. HORNIG. Adv. Spectrosc. **2**, 189 (1961); D. A. Dows. Physics and chemistry of the organic solid state. Vol. 1. Inter-science Publishers, Inc., New York. 1963. p. 657.
2. C. CHAPADOS and A. CABANA. Can. J. Chem. **50**, 3521 (1972); Chem. Phys. Lett. 7, 191 (1970).
3. R. P. FOURNIER, R. SAVOIE, NGUYEN DINH THE, R. BELZILE, and A. CABANA. Can. J. Chem. **50**, 35 (1972).
4. K. CLUSIUS and G. FABER. Z. Phys. Chem. **51B**, 352 (1942).
5. G. R. WILKINSON and M. K. WILSON. J. Chem. Phys. **44**, 3867 (1966).
6. R. M. HEXTER and D. E. MILLIGAN. Proceedings of the Fourth International Symposium on Free Radical Stabilization. 1959.
7. D. C. MCKEAN and A. A. CHALMERS. Spectrochim. Acta, **23A**, 777 (1967).
8. Tables of wavenumbers for the calibration of infrared spectrometers. Butterworths Inc., Washington, D.C. 1961.
9. Handbook of chemistry and physics. The Chemical Rubber Co., Cleveland, Ohio. 1968.
10. R. P. FOURNIER, R. SAVOIE, F. BESSETTE, and A. CABANA. J. Chem. Phys. **49**, 1159 (1968).
11. C. HAAS and D. F. HORNIG. J. Chem. Phys. **26**, 707 (1957).
12. D. W. BERREMAN. Phys. Rev. **130**, 2193 (1963).
13. F. BESSETTE and A. CABANA. Spectrochim. Acta, **25A**, 157 (1969).
14. J. A. KETELAAR, C. HAAS, and J. FAHRENFORT. Physica, **20**, 1259 (1954).
15. R. KOPELMAN. J. Chem. Phys. **47**, 2631 (1967).

Can. J. Chem. Downloaded from www.nrcresearchpress.com by 210.87.254.105 on 09/05/12
For personal use only.

Infrared Spectra of Metal Bisfluorosulfates

CARL STANLEY ALLEYNE, KATHLEEN O'SULLIVAN MAILER, AND ROBERT CLAYTON THOMPSON

Department of Chemistry, The University of British Columbia, Vancouver 8, British Columbia

Received August 17, 1973

The infrared spectra, over the frequency range 250 to 1400 cm^{-1}, of fourteen metal bisfluorosulfates are tabulated and discussed. The fluorosulfates of Fe(II), Co(II), Ni(II), Zn(II), Cd(II), Hg(II), Mg(II), and Ca(II) give simple spectra which are assigned to the fundamental modes of vibration of fluorosulfate groups of C_{3v} symmetry. The spectra of the Mn(II), Cu(II), Ba(II), Pb(II), and Sn(II) compounds are assigned to fluorosulfate groups of reduced symmetry. The spectrum of Sr(II) fluorosulfate suggests the presence of at least two non-equivalent fluorosulfate environments in this compound. The general features of the infrared spectra of compounds containing tridentate coordinated fluorosulfate groups are summarized.

Les spectres infrarouges de quatorze bisfluorosulfates métalliques ont été enregistrés et discutés dans le domaine de fréquence 250 à 1400 cm^{-1}. Les fluorosulfates de Fe(II), Co(II), Ni(II), Zn(II), Cd(II), Hg(II), Mg(II) et Ca(II) donnent des spectres simples qui ont été assignés aux modes fondamentaux de vibration de groupes fluorosulfates présentant la symétrie C_{3v}. Les spectres des composés avec Mn(II), Cu(II), Br(II), Pb(II) et Sn(II) ont été assignés en fonction de groupes fluorosulfates de symétrie réduite. Le spectre du fluorosulfate de Sr(II) suggère la présence d'au moins deux environnements fluorosulfates différents dans ce composé. Les traits généraux des spectres des composés présentant des groupes fluorosulfates tridentates sont résumés. [Traduit par le journal]

Can. J. Chem., **52**, 336 (1974)

Introduction

There have been a number of reports recently on the preparation and characterization of metal fluorosulfate compounds, including binary metal mono- (1, 2), bis- (3–8), tris- (3, 9, 10), and tetrakis- (10, 11) fluorosulfates, chloro- and organotin-fluorosulfates (11–14), oxyfluorosulfates (15–17) and methylcyanide complexes of metal fluorosulfates (18). In most instances infrared spectra have been recorded and evidence regarding structure and bonding has been deduced from the number and energies of observed anion vibrations. The usefulness of infrared spectroscopy in such applications is enhanced by comparisons of the spectra of closely related compounds, as has been done with the alkali metal fluorosulfates (2).

The infrared spectra of calcium, zinc, copper, tin, and cobalt bisfluorosulfates (3, 7, 8) have been reported in some detail previously and incomplete vibrational data are available on the manganese(II), barium(II), cadmium(II), and some transition metal salts (5, 6). Some discrepancies appear where the same compounds were studied by different workers. For example, Bernard, Parent, and Vast (6) observed three absorptions for calcium fluorosulfate in the SO_3 stretching region, 1000–1400 cm^{-1}, while Goubeau and Milne (3) report only two bands. In an attempt to resolve such discrepancies in the literature and to extend the range of metal bisfluorosulfates studied, we have reexamined the spectra of a number of compounds and report for the first time the complete spectra (over the frequency range 250 to 1400 cm^{-1}) of the fluorosulfates of divalent magnesium, strontium, barium, cadmium, mercury, manganese, iron, nickel, and lead.

Experimental

During all preparative manipulations care was taken to avoid exposing solutions and products to atmospheric moisture. Transferring of metal fluorosulfates from reaction vessels to storage ampoules and subsequent handling were done in a nitrogen atmosphere dry box. Vacuum filtrations and washings were done in a manner analogous to that described previously for the preparation of anhydrous chlorosulfates (19).

Calcium, Strontium, Barium, Tin, and Lead Bisfluorosulfates

The calcium, strontium, and barium compounds were obtained as described previously (20) by distilling fluorosulfuric acid onto the anhydrous chlorides until a clear solution was obtained, followed by removal of excess acid under vacuum. This method was also used to prepare the tin and lead compounds and in the case of the former would seem to provide an easier route to $Sn(SO_3F)_2$ than the preparation described in the literature (8).

Can. J. Chem. Downloaded from www.nrcresearchpress.com by 210.87.254.6 on 09/05/12
For personal use only.

TABLE 1. Analytical data

Compound	Calculated (%)			Found (%)		
	Metal	S	F	Metal	S	F
$Mg(SO_3F)_2$	—	28.8	17.1	—	28.9	17.2
$Ca(SO_3F)_2$	16.8	26.9	16.0	16.6	26.7	15.6
$Sr(SO_3F)_2$	30.7	22.4	13.3	30.6	22.5	13.4
$Ba(SO_3F)_2$	40.9	19.1	11.3	40.6	18.8	11.2
$Cd(SO_3F)_2$	36.2	20.6	12.2	35.9	20.6	12.4
$Hg(SO_3F)_2$	—	16.1	9.5	—	16.1	9.4
$Sn(SO_3F)_2$	—	20.2	12.0	—	20.4	11.9
$Pb(SO_3F)_2$	51.1	15.8	9.4	50.8	16.1	9.6
$Mn(SO_3F)_2$	—	25.3	15.0	—	25.1	15.2
$Fe(SO_3F)_2$	22.0	25.2	15.0	22.0	25.1	15.0
$Ni(SO_3F)_2$	—	25.0	14.8	—	25.0	14.9
$Cu(SO_3F)_2$	24.3	24.5	14.5	24.3	24.6	14.3
$Zn(SO_3F)_2$	24.8	24.3	14.4	25.0	24.2	14.4

Magnesium, Nickel, and Iron Bisfluorosulfates

These compounds were prepared by the reaction of an equimolar mixture of the appropriate anhydrous metal chloride and potassium chloride with excess fluorosulfuric acid according to Goubeau and Milne (3). In the preparation of magnesium fluorosulfate the mixture was allowed to react, with constant stirring, at room temperature and required about 2 weeks before a negative test for chloride in the filtered product indicated complete reaction. In the preparation of the nickel and iron compounds the reaction was done under reflux conditions in an atmosphere of nitrogen and in both instances reached completion within 24 h. The metal fluorosulfates were vacuum filtered, washed several times with fluorosulfuric acid and dried under vacuum at temperatures of 50 to 100 °C.

Manganese, Cobalt, Zinc, Copper, and Cadmium Bisfluorosulfates

Cobalt(II) fluorosulfate was prepared as described previously (7) and the other compounds were prepared in an analogous manner by the reaction of the appropriate metal benzoate with excess fluorosulfuric acid. In all cases rapid reaction occurred and the insoluble metal fluorosulfates were filtered, washed several times with fluorosulfuric acid, and dried under vacuum at temperatures of 50 to 100 °C. Anhydrous copper(II) benzoate was prepared as described previously (21) and the other benzoates were prepared by the reaction of the metal chloride and sodium benzoate in aqueous solution, the filtered products being dried under vacuum at room temperature. No attempt was made to characterize these benzoate compounds but it should be noted that the infrared spectra of the cadmium and manganese benzoates showed the presence of water of crystallization. In spite of the presence of water, no difficulties, such as the formation of sulfate impurities, were experienced in the preparation of the fluorosulfate derivatives. Woolf found previously (4) that incompletely dehydrated salts yield good sulfate-free products on reaction with fluorosulfuric acid. Clearly the presence of water may be tolerated when the desired metal fluorosulfate is insoluble in fluorosulfuric acid and can be washed free of the sulfuric acid formed by the reaction of water with fluorosulfuric acid.

Mercury(II) Fluorosulfate

This compound was prepared by the reaction of reagent grade mercury with excess peroxydisulfuryl difluoride according to the method of Roberts and Cady (22).

Analytical data for metal fluorosulfates prepared in this work are given in Table 1. Iron was determined by titration with potassium dichromate. All other analyses were obtained in the A. Bernhardt microanalytical laboratories. The cobalt salt was not analyzed as its infrared spectrum was found to be in satisfactory agreement with samples previously prepared and analyzed in this laboratory (7).

Infrared spectra were obtained on freshly prepared samples mulled in Nujol and hexachlorobutadiene and contained between KRS-5 (Harshaw Chemical Co.) plates which were sealed around the edges with plastic tape. Manipulations were carried out in a dry box and samples were run immediately on a Perkin–Elmer model 457 spectrophotometer. Spectra were calibrated using polystyrene film and frequencies are considered accurate to within ± 4 cm^{-1}. Although all spectra were recorded over the frequency range 250 to 4000 cm^{-1} only the region of the fundamental modes, below 1400 cm^{-1}, is considered here. Attack on cell windows by the samples was not observed except for lead(II) fluorosulfate. This compound attacks potassium bromide plates very rapidly and KRS-5 and silver chloride plates more slowly. Good spectra were obtained for this compound by shielding the plates from the mull using thin polyethylene sheets.

Results

Infrared data on all compounds studied in this work are recorded in Tables 2, 3, and 4. For assignment purposes C_{3v} nomenclature is used (3); where the symmetry of the fluorosulfate group is reduced below C_{3v}, this is usually seen as a splitting of the doubly degenerate E modes.

Can. J. Chem. Downloaded from www.nrcresearchpress.com by 210.87.254.6 on 09/05/12
For personal use only.

Can. J. Chem. Downloaded from www.nrcresearchpress.com by 210.87.254.6 on 09/05/12
For personal use only.

TABLE 2. Infrared spectra of group IIA and IIB bisfluorosulfates*

Infrared frequency (cm^{-1})							
$Mg(SO_3F)_2$	$Ca(SO_3F)_2$	$Sr(SO_3F)_2$	$Ba(SO_3F)_2$	$Zn(SO_3F)_2$	$Cd(SO_3F)_2$	$Hg(SO_3F)_2$	C_{3v} assignment
		1350 sh					
1302 vs	1270 vs	1305 vs	1313 vs	1266 vs	1255 vs	1221 vs	$\nu_4(E)SO_3$ as. stretch
		1238 vs	1250 vs				
1142 s	1119 s	1113 s	1085 s	1118 s	1107 s	1089 s	$\nu_1(A_1)SO_3$ sym. stretch
		1092 s					
862 s	860 s	835 s	815 s	859 s	855 s	856 s	$\nu_2(A_1)$SF stretch
		785 s	806 s				
619 m	613 s	623 m	607 m	613 s	606 s	598 s	$\nu_5(E)SO_3$ as. defn.
		602 m	584 m			581 w	
						574 w	
571 m	568 m	586 s	567 m	567 m	567 m	559 m	$\nu_3(A_1)SO_3$ sym. defn.
		565 s					
424 m	419 m	422 sh	415 sh	419 m	415 m	417 m	$\nu_6(E)$SF defn.
		417 w	410 w				
		401 vw	399 w				
300 m							Lattice mode

*v = very, s = strong, m = medium, w = weak, sh = shoulder, as. = asymmetric, sym. = symmetric, defn. = deformation.

TABLE 3. Infrared spectra of transition metal bisfluorosulfates*

Infrared freqeuncy (cm^{-1})					C_{3v} assignment
$Mn(SO_3F)_2$	$Fe(SO_3F)_2$	$Co(SO_3F)_2$	$Ni(SO_3F)_2$	$Cu(SO_3F)_2$	
1359 m 1297 vs	1261 vs	1266 vs	1262 vs	1306 vs 1223 vs	$\nu_4(E)$
1118 s	1118 s	1114 s	1120 s	1115 s	$\nu_1(A_1)$
836 s	862 s	858 s	859 s	861 s	$\nu_2(A_1)$
604 m 590 m	610 s	614 s	619 s	630 m 604 m	$\nu_5(E)$
573 m 568 sh	568 m	568 m	568 m	564 m	$\nu_3(A_1)$
418 w 412 sh	419 m	422 m	422 m	428 m 416 m	$\nu_6(E)$
			290 m	300 m	Lattice mode

*Abbreviations and approximate description of vibrations as in Table 2.

Group IIA and IIB Bisfluorosulfates

The infrared spectra of magnesium, calcium, zinc, cadmium, and mercury bisfluorosulfates all show six medium to strong intensity bands which may be readily assigned to the six normal modes of vibration of C_{3v} fluorosulfate groups. The spectra of $Ca(SO_3F)_2$ and $Zn(SO_3F)_2$ agree quite well with those reported earlier by Goubeau and Milne (3) with the exception that the ν_2 band frequencies observed here appear to be significantly higher than the previously reported values.

TABLE 4. Infrared spectra of tin and lead bisfluorosulfates*

Infrared frequency (cm^{-1})		
$Sn(SO_3F)_2$	$Pb(SO_3F)_2$	C_{3v} assignment
1290 sh 1240 vs 1180 sh	1265 vs 1219 sh	$\nu_4(E)$
1062 s	1074 s	$\nu_1(A)$
	970 w	Combination band
833 s 772 s	826 m 760 m	$\nu_2(A_1)(+2\nu_6?)$
606 m 592 m 573 s 554 s	599 m 577 m 559 s	$\nu_5(E)$, $\nu_3(A_1)$ (+ combination bands)
403 m 395 sh	408 w 399 w	$\nu_6(E)$

*Abbreviations and approximate description of vibrations as in Table 2.

In contrast to this, the spectra we obtained for $Mg(SO_3F)_2$ and $Ca(SO_3F)_2$ differ significantly from those reported by Bernard, Parent, and Vast (6). These authors do not tabulate frequencies but give spectra in diagram form over the frequency ranges 500–600 cm^{-1} and 1000–1400 cm^{-1}. There is qualitative agreement over the lower frequency range; however, the bands we observe in the 1000–1400 cm^{-1} range are relatively sharper than those reported earlier and, in particular, we observe only one band near 1100 cm^{-1} as opposed to the two bands observed in the earlier work. Since sulfates are known to show strong absorptions in the 1000–1200 cm^{-1} region (23), it is possible that the samples studied previously were significantly contaminated with sulfate impurities. Goubeau and Milne report bands at 250 and 261 cm^{-1} in the spectra of $Ca(SO_3F)_2$ and $Zn(SO_3F)_2$ respectively which they assign to lattice, cation–anion stretching, vibrations. We did not observe these bands, no doubt because they occur too near the frequency limit of our equipment (250 cm^{-1}); however, we do observe a band, presumably of similar origin, at 300 cm^{-1} in the spectrum of $Mg(SO_3F)_2$. The two weak bands at 581 and 574 cm^{-1} in the spectrum of $Hg(SO_3F)_2$ may be combination bands arising from coupling of fundamental modes with lattice vibrations. Such bands have been reported before in the spectra of $Cs(SO_3F)$ (2) and the methyl cyanide complex of zinc(II) fluorosulfate (18).

The spectrum of $Sr(SO_3F)_2$ which, to our

Can. J. Chem. Downloaded from www.nrcresearchpress.com by 210.87.254.6 on 09/05/12
For personal use only.

Can. J. Chem. Downloaded from www.nrcresearchpress.com by 210.87.254.6 on 09/05/12
For personal use only.

knowledge, has not been examined previously, shows a doubling of the bands expected for C_{3v} fluorosulfate. The apparent splitting of all bands including the non-degenerate ν_1, ν_2, and ν_3 vibrations suggests the presence of two non-equivalent fluorosulfate sites of approximate C_{3v} symmetry in the crystal lattice of this compound. The shoulder appearing at 1350 cm^{-1} is probably the $\nu_2 + \nu_6$ combination band.

The infrared spectrum of barium fluorosulfate may be assigned to fluorosulfate anions of reduced, C_s, symmetry. All modes, assigned in C_{3v} symmetry to doubly degenerate vibrations are split while no indication of band splitting is seen in the non-degenerate ν_1 and ν_3 vibrations. The small splitting of 9 cm^{-1} observed in the ν_2 (A_1) band may be the result of the presence of two non-equivalent fluorosulfate sites as proposed for $Sr(SO_3F)_2$; however, it is also possible that it arises from a coupling between equivalent anions in the crystal lattice as has been observed, for example, in potassium nitrate (24). Again, our spectrum of $Ba(SO_3F)_2$ differs significantly from that reported by Bernard *et al.* (6). These authors report a single, rather broad, ν_4 and a split ν_1 band.

Transition Metal Bisfluorosulfates

The infrared spectra of $Cu(SO_3F)_2$ and $Co(SO_3F)_2$ have been reported before and, except for the fact that we observe significantly higher values for the ν_1 and ν_2 vibrations of the copper salt, there is good agreement with the earlier work (3, 7). A band at 262 cm^{-1}, reported previously for $Cu(SO_3F)_2$, was not observed here, possibly due to the fact that it occurs too near the lower frequency limit of our spectrometer.

The spectra of $Fe(SO_3F)_2$, $Co(SO_3F)_2$, $Ni(SO_3F)_2$, and $Cu(SO_3F)_2$ are readily assigned, the first three to fluorosulfate ions of C_{3v} symmetry and that of the copper salt to anions of reduced, C_s, symmetry. Evidence for reduction in fluorosulfate ion symmetry below C_{3v} is also seen in the spectrum of $Mn(SO_3F)_2$ where small splittings are apparent in both ν_5 and ν_6 and a medium intensity band at 1359 cm^{-1}, appearing as a shoulder on a strong and relatively broad band at 1297 cm^{-1}, suggests a splitting of the ν_4 mode.

Tin and Lead Bisfluorosulfates

The infrared spectrum of tin(II) fluorosulfate was reported recently by Birchall, Dean, and Gillespie (8). The spectrum we have obtained for this compound shows better resolution of bands in the region above 1000 cm^{-1}; otherwise, it agrees well with the published one. The spectrum of lead(II) fluorosulfate is very similar to that of the tin compound and both may be assigned to the fundamental modes of C_s fluorosulfate ions plus combination and overtone bands as described previously for $Sn(SO_3F)_2$. The two bands in the ν_2 (SF stretch) region may be accounted for by assigning one to $2 \times \nu_6$ (Birchall *et al.* assigned the higher frequency band in $Sn(SO_3F)_2$ to this overtone) and the other to ν_2.

Discussion

Of the fourteen metal bisfluorosulfates studied here, eight (M = Fe, Co, Ni, Zn, Cd, Hg, Mg, Ca) have infrared spectra which can be unambiguously assigned on the basis of C_{3v} anion symmetry. In none of these spectra is there any indication of symmetry lowering below C_{3v} at the resolution of the instrument used ($\sim$3 cm^{-1}) or of the presence of anions in non-equivalent sites in the crystal lattice. For the anion to maintain C_{3v} symmetry any metal–anion coordination in these compounds must involve tridentate fluorosulfate groups in which all three oxygen atoms are involved in coordination to metal ions in an equivalent manner. One possible structure of this type is the tridentate bridging structure proposed recently for cobalt(II) fluorosulfate (7).

A comparison of the spectrum of the ionic C_{3v} fluorosulfate, $CsSO_3F$ (2), with the spectra of these divalent metal fluorosulfates permits an assessment of spectral changes accompanying increased metal–anion interactions, in the absence of symmetry lowering, and should provide criteria useful in identifying the tridentate form of fluorosulfate coordination. The SF stretching vibration, ν_2, shows the most pronounced shift, going from 715 cm^{-1} in the cesium salt to 855–862 cm^{-1} in the divalent metal salts. Making similar comparisons involving ν_1, ν_3, and ν_5 we note consistent, though much smaller, increases in frequency: from 1078 to 1089–1142 cm^{-1} for ν_1, from 558 to 559–571 cm^{-1} for ν_3 and from 585 to 598–619 cm^{-1} for ν_5. The frequency of the ν_6 vibration does not change significantly and ν_4, which is at $\sim$1295 cm^{-1} in $CsSO_3F$ occurs at about the same frequency in $Mg(SO_3F)_2$ but shifts to lower frequencies (1221–1270 cm^{-1}) in

Can. J. Chem. Downloaded from www.nrcresearchpress.com by 210.87.254.6 on 09/05/12
For personal use only.

the other seven divalent metal compounds. The general criteria for identifying tridentate fluorosulfate groups would seem to be a C_{3v} spectrum with a shift in ν_2, compared to $CsSO_3F$, of ~ 100 cm^{-1} or more to higher frequencies accompanied by smaller increases in ν_1, ν_3, and ν_5 and a decrease in ν_4. Other workers have recently summarized the spectral changes observed on going from ionic SO_3F groups to lower symmetry monodentate or bridging bidentate SO_3F groups (9).

We turn now to a brief discussion of the six metal bisfluorosulfates (M = Cu, Ba, Mn, Sr, Sn, Pb) which do not show simple C_{3v} anion spectra. The spectra of $Cu(SO_3F)_2$ and $Ba(SO_3F)_2$ are readily assignable on the basis of C_s fluorosulfate. Whether the lowering in symmetry in $Ba(SO_3F)_2$ is due to a reduction in the site symmetry of the anion below C_{3v} or to coordination with the cation is uncertain. In the case of $Cu(SO_3F)_2$, on the other hand, it has been pointed out previously (3, 7) that the symmetry lowering is probably due to a form of fluorosulfate coordination in which two oxygen atoms of each fluorosulfate group are more strongly bonded to the metal ion than the third. A similar form of coordination could account for the apparent reduction in symmetry of the SO_3F ions in $Mn(SO_3F)_2$.

The spectra of $Sn(SO_3F)_2$ and $Pb(SO_3F)_2$ also indicate the presence of fluorosulfate ions of reduced symmetry; however, these spectra are further complicated by additional bands which in the case of the tin compound, were previously assigned to combination and overtone bands (8). Such assignments are not entirely satisfactory since it is difficult to understand why the $2 \times \nu_6$ overtone, in particular, should appear so intense in the tin and lead compounds yet not appear in the spectra of the other divalent metal fluorosulfates. The possibility that the two bands near 800 cm^{-1} in each of these compounds are the ν_2 vibrations of two non-equivalent fluorosulfates cannot be ruled out; although, this suggestion is not supported by an observed splitting of the ν_1 vibrations. The evidence for the presence of two types of fluorosulfate groups is much clearer in the case of $Sr(SO_3F)_2$ where there is an apparent splitting of all fundamental modes giving the spectrum the appearance of two superimposed C_{3v} spectra. The postulate of non-equivalent anions in metal fluorosulfates is not without precedence. Yeats *et al.* (11) observed eight bands in the SO and SF stretching region of the spectrum of tin(IV) fluorosulfate which they assigned to the presence of two non-equivalent C_s fluorosulfate groups.

Previous studies on the vibrational spectra of metal fluorosulfates have indicated that the position of the SF stretching vibration, ν_2, is related to the polarizing power of the cation (3) and may therefore be used as a measure of cation–anion interactions in fluorosulfate compounds. It has been suggested that, as the polarizing power of the cation increases, withdrawal of charge through the oxygens of the anion by the cation increases, resulting in increased $p\pi$–$d\pi$ bonding between sulfur and fluorine. Support for this explanation should come from bond length data; however, it appears that crystal structure studies of fluorosulfate compounds (25–29) are neither sufficiently extensive nor sufficiently accurate (the anions in the ammonium and potassium salts are disordered) to permit a meaningful analysis of SF bond length data.

In the alkali metal series (2), the frequency of ν_2 increases regularly with increasing polarizing power of the alkali metal cation. On examining the spectral data obtained in the present work on divalent metal fluorosulfates the only evidence for a similar trend is within the alkaline earth series where ν_2 for the barium salt is significantly less than ν_2 for the calcium and magnesium salts (Table 2). Otherwise, considering all of the divalent metal salts studied here, there is no correlation between ν_2 and cation radius, nor is there a correlation with ionization energy, a property which has been used as a measure of polarizing power by other authors (6). Another indication that, in fluorosulfates of multivalent metals, higher cation polarizing power does not necessarily result in a higher ν_2 frequency, is the observation that on going from iron(II) fluorosulfate to iron(III) fluorosulfate the frequency of ν_2 actually decreases from 865 cm^{-1} to 850 cm^{-1} (3). We conclude from this that the observation of a ν_2 frequency above 800 cm^{-1} is evidence only that cation–anion interactions are stronger than those present in ionic fluorosulfates. One should not take a group of compounds which have high ν_2 frequencies and infer, from the relative values of ν_2, relative degrees of cation–anion interaction, or covalent character, as has been suggested recently (17).

We thank Dr. F. Aubke for supplying us with some peroxydisulfuryl difluoride and the National Research Council of Canada for financial support.

1. D. W. A. SHARP. J. Chem. Soc. 3761 (1957).
2. A. RUOFF, J. B. MILNE, G. KAUFMANN, and M. LEROY. Z. Anorg. Allg. Chem. **372**, 119 (1970).
3. J. GOUBEAU and J. B. MILNE. Can. J. Chem. **45**, 2321 (1967).
4. A. A. WOOLF. J. Chem. Soc. (A), 355 (1967).
5. D. A. EDWARDS, M. J. STIFF, and A. A. WOOLF. Inorg. Nucl. Chem. Lett. **3**, 427 (1967).
6. PIERRE BERNARD, YVES PARENT, and PIERRE VAST. C. R. **267**, Ser. C, 236 (1969).
7. J. M. TAYLOR and R. C. THOMPSON. Can. J. Chem. **49**, 511 (1971).
8. T. BIRCHALL, P. A. W. DEAN, and R. J. GILLESPIE. J. Chem. Soc. (A), 1777 (1971).
9. A. STORR, P. A. YEATS, and F. AUBKE. Can. J. Chem. **50**, 452 (1972).
10. WESLEY M. JOHNSON, RAJENDAR DEV, and GEORGE H. CADY. Inorg. Chem. **11**, 2260 (1972).
11. P. A. YEATS, B. L. POH, B. F. E. FORD, J. R. SAMS, and F. AUBKE. J. Chem. Soc. (A), 2188 (1970).
12. P. A. YEATS, F. B. E. FORD, J. R. SAMS, and F. AUBKE. Chem. Commun. 791 (1969).
13. P. A. YEATS, J. R. SAMS, and F. AUBKE. Inorg. Chem. **10**, 1877 (1971).
14. T. H. TAN, J. R. DALZIEL, P. A. YEATS, J. R. SAMS, R. C. THOMPSON, and F. AUBKE. Can. J. Chem. **50**, 1842 (1972).
15. RAJENDAR DEV and GEORGE H. CADY. Inorg. Chem. **10**, 2354 (1971).
16. W. V. ROCHAT and G. L. GARD. Inorg. Chem. **8**, 158 (1969).
17. RAJENDAR DEV, WESLEY M. JOHNSON, and GEORGE H. CADY. Inorg. Chem. **11**, 2259 (1972).
18. J. B. MILNE. Can. J. Chem. **48**, 75 (1970).
19. J. A. CIRUNA and E. A. ROBINSON. Can. J. Chem. **46**, 1715 (1968).
20. J. BARR, R. J. GILLESPIE, and R. C. THOMPSON. Inorg. Chem. **3**, 1149 (1964).
21. J. LEWIS, Y. C. LIN, L. K. ROYSTON, and R. C. THOMPSON. J. Chem. Soc. 6464 (1965).
22. J. E. ROBERTS and G. H. CADY. J. Am. Chem. Soc. **82**, 353 (1960).
23. KAZUO NAKAMOTO. Infrared spectra of inorganic and coordination compounds. Wiley–Interscience, New York. 1970.
24. J. C. DECIUS. J. Chem. Phys. **23**, 1290 (1955).
25. K. O'SULLIVAN, R. C. THOMPSON, and J. TROTTER. J. Chem. Soc. (A), 2026 (1967).
26. K. O'SULLIVAN, R. C. THOMPSON, and J. TROTTER. J. Chem. Soc. (A), 1814 (1970).
27. A. KVICK, P.-G. JÖNSSON, and I. OLOVSSON. Inorg. Chem. **8**, 2775 (1969).
28. F. H. ALLEN, J. A. LERBSCHER, and J. TROTTER. J. Chem. Soc. (A), 2507 (1971).
29. N. BARTLETT, M. WECHSBERG, G. R. JONES, and R. D. BURBANK. Inorg. Chem. **11**, 1124 (1972).

Can. J. Chem. Downloaded from www.nrcresearchpress.com by 210.87.254.6 on 09/05/12
For personal use only.

Hydrated Electrons Produced by the Flash Photolysis of Co^+, Ni^+, Zn^+, and Cd^+ Ions

NORMAN BASCO, SUNIL K. VIDYARTHI, AND DAVID C. WALKER
Chemistry Department, University of British Columbia, Vancouver, British Columbia

Received August 13, 1973

Hydrated electrons are produced with a quantum yield of about unity when the low valence state ions Co^+, Ni^+, Zn^+, and Cd^+ are photolyzed by light within their absorption bands centered at ~300 nm. The observations seem to offer direct evidence that these absorption bands may be assigned as charge-transfer bands, and specifically as charge-transfer-to-solvent (c.t.t.s.). The ions are probably present as simple aquo complexes, since they were formed initially in very dilute aqueous solution from the divalent sulfate salts; but they may be solvated ion–electron pairs. Cu^+ ions do not show a similar strong charge-transfer band at any wavelengths > 230 nm and the second maximum in the case of Co^+ at 360 nm is not of the c.t.t.s. type.

The experiments used a double flash photolysis method whereby the first flash photolyzed SO_4^{2-} with light at $\lambda < 220$ nm to produce hydrated electrons which then reacted with Co^{2+}, Ni^{2+}, Zn^{2+}, or Cd^{2+} ions present at 10^{-5} to 10^{-6} *M*. The short-lived monovalent ions so formed were photolyzed 10–300 μs later by the second flash of restricted wavelengths.

Des électrons hydratés sont produits, avec un rendement quantique presque unitaire, lorsque des ions à un état de valence vibrationnellement bas, Co^+, Ni^+, Zn^+ et Cd^+ sont photolysés dans les limites de leurs bandes d'absorption centrées à ~300 nm. Les observations effectuées tendent à prouver que ces bandes d'absorption peuvent être attribuées à des bandes de transfert de charges et plus spécialement de transfert de charges au solvant (c.t.t.s.). Les ions sont probablement présents sous forme de complexes aquo simples, puisqu'ils ont été préalablement formés dans des solutions aqueuses très diluées à partir des sels de sulfate divalent: cependant ils peuvent aussi être des paires ion-électron solvatées. Les ions Cu^+ ne possèdent pas une bande de transfert de charges similaire à une longueur d'onde supérieure à 230 nm et, dans le cas de Co^+, le second maximum à 360 nm n'est pas du type c.t.t.s.

On a réalisé les expériences de photolyse en utilisant la méthode de photolyse à double décharge selon laquelle la première décharge sert à photolyser SO_4^{2-} (avec une lumière dont $\lambda < 220$ nm) pour produire des électrons hydratés qui réagissent avec les ions Co^{2+}, Ni^{2+}, Zn^{2+} ou Cd^{2+} présents à des concentrations de 10^{-5} à 10^{-6} *M*. Les ions monovalents de courte durée, ainsi formés ont ensuite été photolysés 10 à 300 μs. plus tard à l'aide de la seconde décharge (avec une lumière dont les longueurs d'onde étaient limitées). [Traduit par le journal]

Can. J. Chem., **52**, 343 (1974)

Introduction

Hydrated electron studies have led to the discovery of many new chemical entities, of which the "hyper-reduced" transition metal ions form an interesting class. Pulse radiolysis studies have shown that several divalent metal ions (as aquo complexes) in water solution have very high reactivities towards e_{aq}^- and thereby form short-lived species having strong absorption bands centered at about 300 nm (1–3). These bands have been identified with the ground state of the unusual monovalent ionic states of the metals (3). At the present time the spectra for Co^+, Ni^+, Zn^+, Cd^+, Ag^0, and others are well documented through liquid phase pulse radiolysis. Some of these have also been observed trapped in acid glasses at 77 °K (4), in metaphosphate glasses at room temperature (5), and by e.s.r. studies in various types of glasses (5–7). Furthermore, the chemical reactivity of these low valence state ions has been studied extensively (8–11).

Their near u.v. absorption bands have already been tentatively attributed to charge-transfer processes (1, 3, 5), largely on the basis of their high extinction coefficient and the spectral position of the band. Ag^0 has a particularly large extinction coefficient and it was possible in that case to observe the band at 315 nm spectrographically (12). Flash photolysis of Ag^0 in this band, and of Tl^0 at ~300 nm, yielded e_{aq}^- (12) thereby providing evidence for the charge-transfer-to-solvent (c.t.t.s.) nature of these bands. This paper describes analogous experiments on the flash photolysis of Co^+, Ni^+, Cu^+, Zn^+, and Cd^+.

Can. J. Chem. Downloaded from www.nrcresearchpress.com by 210.87.254.40 on 09/05/12
For personal use only.

TABLE 1. Transmission characteristics (relative to maximum) of Corning glass filters used between auxiliary lamp and reaction vessel

Filter No.	Wavelength* (nm) of transmission				
	3%	10%	50%	90%	97%
9-54	216	223	240	288	300
7-54†	231(411)	236(401)	253(390)	283(367)	298(353)
0-53	279	290	303	334	344
0-52	339	342	350	380	389
3-74	385	390	415	461	497
3-70	486	493	507	548	573

*Error limit = ± 3 nm.
† 7-54 has a transmission band in the relevant region of the spectrum. The wavelengths in brackets indicate the long wavelength limits of this band. The maximum transmission at ~320 nm is an absolute transmission of 89%.

Experimental Method

A double flash photolysis method was used for these experiments and has been described in detail previously (13). Hydrated electrons were produced in the first flash (called main flash) by u.v. photolysis of SO_4^{2-} ions. They reacted exclusively with the divalent transition metal ions present and then the product of that reaction was subjected to a second photolysis flash (called auxiliary flash). The auxiliary flash lamp was separated from the reaction vessel by a space in which light filters could be placed to restrict the range of wavelengths incident upon the reaction vessel from the auxiliary lamp. Transmission characteristics of the filters used are given in Table 1. The time interval between the firing of the two flash lamps could be varied at will from 1 μs on. A 2 mW He/Ne continuous-wave laser was used (with photomultiplier and oscilloscope) to monitor the concentration of e_{aq}^- in the reaction vessel during and after both photoflashes. In all the systems discussed here e_{aq}^- was the only transient species which absorbed the 633 nm laser light.

Solutions were made from water which had been doubly distilled, pre-irradiated, and subsequently refluxed continuously until used for an experiment (13). Analytical grade Na_2SO_4, $NiSO_4$, $CdSO_4$, $ZnSO_4$, $CuSO_4$, $CoSO_4$ hydrated salts were used to make up the solutions. Matheson prepurified H_2 or Analar 2-propanol were used in some experiments as scavengers for oxidizing radicals and showed that none of the effects reported arose from these species. The solutions were deoxygenated by bubbling with pure He or H_2.

Results are reported for solutions consisting of $\sim 10^{-3}$ *M* Na_2SO_4 plus 10^{-5} to 10^{-6} *M* MSO_4, where M is Co, Ni, Cu, Zn, and Cd. These concentrations were selected for the following reasons. The main flash produced $\sim 10^{-6}$ Me_{aq}^- from 10^{-3} *M* SO_4^{2-} so that an absorbance in the range 0.3 to 0.8 at 633 nm was created in the 42.5 cm cell ($\varepsilon_{(e_{aq}^-)}^{633} = 1.2 \times 10^4\ M^{-1}\ cm^{-1}$ (14)) due to reaction 1.

$$[1] \qquad SO_4^{2-} \xrightarrow[\lambda < 220\ nm]{h\nu} SO_4^- + e_{aq}^-$$

The rate constants for the reaction of Co^{2+}, Ni^{2+}, Cu^{2+}, Zn^{2+}, and Cd^{2+} ions with e_{aq}^- are known to be 1.2, 2.2, 3.0, 0.12, and 5.0 times $10^{10}\ M^{-1}\ s^{-1}$ respectively (3, 14). With these ions present at 10^{-5} to 10^{-6} *M* the mean lifetime of e_{aq}^- was of the order of $1\text{–}5 \times 10^{-5}$ s and reaction 2 was the only significant decay process for e_{aq}^-. (In the absence of M^{2+} e_{aq}^- had a mean lifetime > 100 μs.)

$$[2] \qquad M_{aq}^{2+} + e_{aq}^- \rightarrow M_{aq}^+$$

The auxiliary flash was fired at times between 10^{-5} and 3×10^{-4} s after the main flash. One of the filters listed in Table 1 was always in place to restrict the light from the auxiliary lamp so that hydrated electrons could not be produced by reaction 1 during the auxiliary flash. Consequently the production of absorbance at 633 nm by the auxiliary flash indicated that the product of reaction 2 gave hydrated electrons when illuminated by the light transmitted by the filters used. Since both photolysis flashes were ~20 μs width-at-half-maximum and the hydrated electron lifetime was 10–50 μs, all data are presented as the ratio of the observed absorbance during the peak of the auxiliary flash relative to that during the peak of the main flash. This ratio should be proportional to the fraction of the original e_{aq}^- regenerated during the auxiliary flash.

Results

Figure 1 shows typical transmission curves at 633 nm for solutions of Co^{2+}, Zn^{2+}, and Cd^{2+} at various time delays between flashes and oscilloscope sweep speeds, using filter No. 9-54. The formation of hydrated electrons during the auxiliary flash is interpreted to mean that reaction 3 represents the process which occurs.

$$[3] \qquad M_{aq}^+ \xrightarrow[\lambda > 260\ nm]{h\nu} M_{aq}^{2+} + e_{aq}^-$$

For Co^{2+}, Ni^{2+}, Zn^{2+}, and Cd^{2+} solutions hydrated electrons were produced in reaction 3. For Cu^{2+} solutions no detectable absorption at 633 nm was produced by the auxiliary flash even using filter No. 9-54 which has the shortest wavelength cut off used. Figure 1 shows the type of variation in (*i*) the lifetime of e_{aq}^- following a flash for the different ions, and (*ii*) the lifetime

Can. J. Chem. Downloaded from www.nrcresearchpress.com by 210.87.254.40 on 09/05/12
For personal use only.

TABLE 2. Data showing the effect of various light filters on the yield of e_{aq}^- during the auxiliary flash. For each ion the delay time was constant and the ratio of flash energies (main/auxiliary) was fixed

Metal ion	Delay time	$A_{(aux)}/A_{(main)}$ with Corning filters 9-54	7-54	0-53	0-52	3.74	Uncertainty
Co^{2+} (5×10^{-6} *M*)	30	0.19	0.21	0.15	<0.05	<0.03	±0.04
Ni^{2+} (1.1×10^{-5} *M*)	40	0.24	0.23	0.19	0.07	<0.04	±0.04
Cu^{2+} (6×10^{-6} *M*)	35	<0.04	<0.04	<0.04	<0.04	<0.04	±0.04
Zn^{2+} (2×10^{-5} *M*)	52	0.18	0.15	0.05	<0.02	<0.02	±0.02
Cd^{2+} (1.1×10^{-6} *M*)	50	0.18	0.16	0.045	<0.02	<0.02	±0.02

of M^+ (which can be inferred from the relative auxiliary absorbance as a function of time). By using different filters at a constant time delay it was possible to establish the approximate wavelength range in which the photoionization of M^+ occurred. Representative data are given in Table 2. It is clear that Co^+, Ni^+, Zn^+, and Cd^+ have absorption bands mainly centered around 300 nm which are responsible for electron detachment by reaction 3. For the case of Ni^+ the band apparently also extends slightly further into the visible than for the other three.

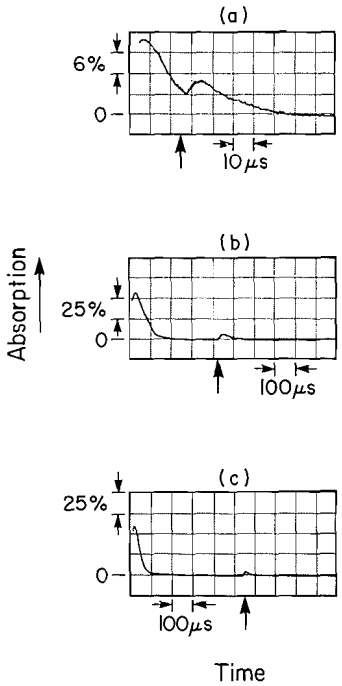

FIG. 1. Oscilloscope traces showing the transmission at 633 nm during the double flash photolysis of 10^{-3} *M* $NaSO_4$ solutions, containing (*a*) 5×10^{-6} *M* Co^{2+}, (*b*) 2×10^{-5} *M* Zn^{2+} and (*c*) 1×10^{-6} *M* Cd^{2+}. The arrows indicate the time at which the auxiliary lamp was fired.

Some time-dependence data are given in Table 3 which show that Co^+ and Ni^+ ions have lifetimes significantly shorter than Cd^+ and Zn^+. These findings are in general accord with pulse radiolysis studies in which, for instance, Zn^+ was shown to decay only via the bimolecular dismutation reaction whereas Ni^+ also had a first order component possibly due to an additional reaction with Ni^{2+} (3).

The absorption spectra of the M^+ ions formed in reaction 2 are well known and coincide with our photoionization region. Both their formation rate and decay rate are in accordance with published data and so we are convinced that these are the species involved in the production e_{aq}^- by photolysis during the auxiliary flash. This is further corroborated by analogy with the data for Ag^0 where the band at 315 nm was observed to be destroyed by the auxiliary flash concurrent with e_{aq}^- formation (12).

Tables 2 and 3 and Fig. 1 show that it is possible to regenerate a substantial fraction of e_{aq}^-; but it was impossible to see them all re-

TABLE 3. Variation of yield of e_{aq}^- during auxiliary flash as a function of delay time. All data were obtained with a 9-54 filter and fixed main/auxiliary flash energies (uncertainty ~±0.04)

Metal ion	Delay time (μs)	$A_{(aux)}/A_{(main)}$
Co^{2+} (5×10^{-6} *M*)	25	0.24
	100	0.05
Ni^{2+} (1.1×10^{-5} *M*)	42	0.25
	112	0.05
Zn^{2+} (2×10^{-5} *M*)	30	0.24
	52	0.18
	650	0.06
Cd^{2+} (1.1×10^{-6} *M*)	50	0.18
	90	0.16
	208	0.08
	800	0.05

Can. J. Chem. Downloaded from www.nrcresearchpress.com by 210.87.254.40 on 09/05/12
For personal use only.

Can. J. Chem. Downloaded from www.nrcresearchpress.com by 210.87.254.40 on 09/05/12
For personal use only.

generated because M^+ was being formed and decaying over comparable time-scales. In order to separate the e_{aq}^- absorption peaks to get reasonably accurate data, minimum delay times of 20 to 50 μs were necessary and at these times only about 25% regeneration of the original e_{aq}^- was observed. However, it is clear that a large fraction was regenerated and for the case of Ag^0 it was shown directly that at least ~80% of the Ag^0 had been destroyed during the auxiliary flash (see Fig. 3, ref. 12).

It is important to show that the production of e_{aq}^- due to photolysis of M^+ at ~300 nm by the auxiliary flash was not merely a trivial side effect of multiple intramolecular excitation of solvated M^+ ions. Consequently we will make an approximate estimate of the quantum yield for hydrated electron production (ϕ).

We define the fraction of M^+ ions which are photolyzed by the auxiliary flash to give hydrated electrons as β, thus $\beta = (c_0 - c')/c_0$ where c_0 and c' are respectively the concentrations of M^+ at the beginning and end of the auxiliary flash. We are assuming here that reaction 3 is the only significant photoinduced *decomposition* step of M^+, though M^+ could be photoexcited and deexcited without dissociation many times during the flash. The concentration (c) of M^+ is quite small, only $\sim 10^{-6}$ M initially, and the mean absorption path length (l) for photolysis by an adjacent flash lamp is only a few centimeters, therefore the absorption by M^+ of light from the flash must be low. Thus to a good approximation the rate of loss of M^+ during the flash is proportional to the instantaneous concentration c, so that upon integration over the flash (and regardless of the shape of the flash) one gets c' given by eq. 4.

$$[4] \qquad c' = c_0 e^{-\phi k}$$

k is related to the total light from the flash and the oscillator strength of the absorber and in fact is equal to $2.3Il\int \varepsilon\, d\lambda$, which approximates to $2.3Il\varepsilon_{max}\Delta\lambda$ for Gaussian or triangular shaped bands (ε_{max} is the extinction coefficient at the band maximum and $\Delta\lambda$ the band width-at-half-height). $2.3Il$ is estimated as before (13) to be $\sim 6 \times 6^{-6}$ einstein nm^{-1} l^{-1} cm^{-1}. It follows then that

$$\beta = (c_0 - c')/c_0 = 1 - e^{-\phi k}$$

and hence that ϕ is given by eq. 5

$$[5] \qquad \phi = k^{-1} \ln(1 - \beta)^{-1}$$

TABLE 4. Estimations of ϕ

M^+	ε_{max}*	$\Delta\lambda$*	k	β	ϕ
Co^+	2 110	~50	0.63	0.5†	1.1
Ni^+	4 800	50	1.44	0.5†	0.48
Zn^+	4 700	75	2.1	0.5‡	0.33
Cd^+	8 080	80	3.9	(0.5)§	(0.18)§
Ag^0	24 000	55	7.9	≥0.9	≥0.29

*Data from ref. 16, except for Ag^0 data which is from ref. 12.
†Probably lower than the true value because of rapid decay of Co^+ and Ni^+.
‡Probably on the high side because of the slow decay of Zn^+.
§The value of ϕ for Cd^+ is almost certainly low because at 1.1×10^{-6} M Cd^{2+} there was barely enough Cd^{2+} to scavenge all e_{aq}^- produced by the main flash.

Values of k for each ion can be calculated from the available data for ε_{max} and $\Delta\lambda$(1–3, 15, 16). The most recent values (16) are presented in Table 4 and have been used in the calculations of k. The β values required correspond to the magnitude of $A_{(aux)}/A_{(main)}$ extrapolated to the time of the main flash. In fact the observed ratio of absorbances decreases with increasing delay time because of loss of M^+ by reaction after the main flash. Typically 20–50 μs delays occur before the ratio can be measured with any accuracy, by which time it had dropped to 0.25 and lower, as seen in Table 3. However, we can take β to be 0.5 knowing that this cannot be in error by more than a factor of two.

Table 4 contains the estimates of ϕ obtained by the use of eq. 5 based on the data presented. For completeness the Ag^0 data (12) is also given and for that species β is taken to be ≥0.9 because the concentration of Ag^0 *during* the auxiliary flash was directly observed to be $<0.2c_0$ (12).

Despite the approximations involved in these estimations it is clear that ϕ is quite close to unity. This then indicates that reaction 3 represents an important, and probably the predominant, effect of light absorption in the bands centered around 300 nm.

Discussion

It is evident that the low valence state ions Cd^+, Zn^+, Co^+, and Ni^+, coordinated only by H_2O (or occasionally SO_4^{2-}), produce hydrated electrons with high efficiency when photolyzed within their near u.v. absorption bands. This seems to be direct evidence that these bands should be assigned as charge-transfer-(to-solvent) bands. It is clear that photoexcitation of the central ion results in electron detachment from the aquo complex; but one cannot decide if electron ejection occurred as a one-step adiabatic photol-

Can. J. Chem. Downloaded from www.nrcresearchpress.com by 210.87.254.40 on 09/05/12
For personal use only.

ysis process or results from subsequent relaxation within a microsecond following an intramolecular excitation.

In fact, Baxendale *et al.* (3) proposed charge transfer as the nature of these bands some years ago and suggested the process as in [6].

$$[6]\quad M^+ H_2O \xrightarrow{h\nu} M^{2+} H_2O^- \text{ (or } M^{2+} + H + OH^-)$$

Our conclusion differs from this only by virtue of the detachment of an electron into the solvent rather than the formation of $H + OH^-$.

It is not obvious why all these low valence state ions, and Ag^0 and Tl^0, should have such bands in the same spectral region. The electronic structures are the following $Co^+(d^8)$, $Ni^+(d^9)$, $Cu^+(d^{10})$, $Zn^+(d^{10}s^1)$, $Cd^+(d^{10}s^1)$, $Ag^0(d^{10}s^1)$, $Tl^0(d^{10}s^2p^1)$. Furthermore, the sizes of the metal ions (and atoms) differ considerably and so could their coordination numbers. It might be argued that Cu^+, with a stable d^{10} structure, could have a charge-transfer band much further into the u.v. than the others, and hence not detectable in the present experiments; but on the same basis one would have expected substantial differences in λ_{max} among the others due to differing ionization potentials. It may be that Cu^+ has a band in the same region but of very low oscillator strength. Indeed, if any correlation can be made, it suggests that it is the oscillator strengths which change in accordance with the expected ionization potentials based on size and outer electronic structure, not the photon energy of the band maximum. The oscillator strengths are Cd^+ (0.31), Zn^+ (0.22), Ni^+ (0.12), Co^+ (0.06), and Ag^0 (0.63). Large oscillator strengths, such as these, are common for c.t.t.s. bands (17–19).

An alternative explanation for the coincidence of the bands at ~300 nm is that they are not due to M^+ species *per se* (lowest electronic states), but rather arise from the occurrence of solvated ion–electron pairs. Perhaps these could be described by $(M^{2+}{}_{aq}.e^-)$ where the electron charge density is mainly associated with the protons of the metal ion's solvation shell. If this is so the photon energy for the charge-transfer-to-solvent transition may be very much less dependent on the nature of the metal ion, so that they can all more or less coincide. Monomeric ion aggregate species are postulated to occur in alkali metal / ammonia solutions as a result of solvated electron attachment to solvated metal ions (20).

The case of Co^+ is interesting in the following respect. This ion gives a double-humped absorption band with maxima at ~300 nm and ~360 nm (1, 16). Our filter data shows that only the 300 nm band can correspond to a charge-transfer-to-solvent process, because hydrated electrons are not produced by wavelengths of ~360 nm. The long wavelength part of the Co^+ band must consequently have a different origin. Perhaps the long wavelength side of the band for the cases of Zn^+ and Cd^+ also does not contain much c.t.t.s. character which would then account for the somewhat smaller quantum yields recorded in Table 4 and the wavelength data in Table 2.

We are most grateful to Dr. G. V. Buxton for providing us with the unpublished data which we have used and for very helpful suggestions regarding the evaluation of the quantum yield. Financial support of this research by the National Research Council of Canada and Defence Research Board of Canada is gratefully acknowledged.

1. G. E. Adams, J. H. Baxendale, and J. W. Boag. Proc. Chem. Soc. 241 (1963).
2. J. H. Baxendale, E. M. Fielden, and J. P. Keene. Proc. Chem. Soc. 242 (1963).
3. J. H. Baxendale, E. M. Fielden, and J. P. Keene. Proc. Roy. Soc. A, **286**, 320 (1965).
4. D. M. Brown and F. S. Dainton. Trans. Faraday Soc. **62**, 1139 (1966).
5. T. Feldmann, A. Treinin, and V. Volterra. J. Chem. Phys. **42**, 3366 (1965).
6. P. N. Moorthy and J. J. Weiss. Am. Chem. Soc. Adv. Chem. **50**, 180 (1965).
7. W. Low and J. L. Suss. Phys. Lett. **7**, 310 (1963).
8. J. H. Baxendale, J. P. Keene, and D. A. Stott. Chem. Commun. 715 (1966).
9. G. V. Buxton, F. S. Dainton, and G. Thielens. Chem. Commun. 201 (1967).
10. D. Meyerstein and W. A. Mulac. J. Phys. Chem. **72**, 784 (1968).
11. G. V. Buxton, F. Dainton, and D. R. McCracken. J. Chem. Soc. Faraday Trans. I, **69**, 243 (1973).
12. N. Basco, S. K. Vidyarthi, and D. C. Walker. Can. J. Chem. **51**, 2497 (1973).
13. N. Basco, G. A. Kenney-Wallace, S. K. Vidyarthi, and D. C. Walker. Can. J. Chem. **50**, 2059 (1972).
14. E. J. Hart and M. Anbar. The hydrated electron. Wiley, N.Y. 1970.
15. J. H. Baxendale, E. M. Fielden, and J. P. Keene. *In* Pulse radiolysis. *Edited by* M. Ebert *et al.* Academic Press, London. 1965. p. 207.
16. G. V. Buxton and R. M. Sellers. To be published.
17. J. Frank and R. L. Platzman. Z. Phys. **138**, 411 (1954).
18. G. Stein and A. Treinin. Trans. Faraday Soc. **55**, 1086 (1959).
19. T. R. Griffiths and M. C. R. Symons. Trans. Faraday Soc. **56**, 1125 (1960).
20. M. Gold, W. L. Jolly, and K. S. Pitzer. J. Am. Chem. Soc. **84**, 2264 (1962).

Catalytic Activation of Molecular Hydrogen by Ruthenium Chloride Complexes in *N,N*-Dimethylacetamide Solution[1]

BENJAMIN C. HUI[2] AND BRIAN R. JAMES

Department of Chemistry, University of British Columbia, Vancouver 8, British Columbia

Received July 30, 1973

N,N-Dimethylacetamide solutions of "$RuCl_3 \cdot 3H_2O$", which is a mixture of Ru(IV) and Ru(III), react with hydrogen under mild conditions in stepwise stoichiometric processes to give finally univalent species ($Ru^{IV} \xrightarrow{1} Ru^{III} \xrightarrow{2} Ru^{II} \xrightarrow{3} Ru^{I}$). Reactions 1 and 2 involve heterolytic activation of H_2 by a Ru^{III} catalyst and likely proceed via a $Ru^{III}H$ intermediate; the same catalyst catalyzes the hydrogenolysis of oxygen to water. Reaction 3 involves a $Ru^{II}H$ intermediate. Kinetic parameters are presented for processes 1–3 and the catalytic water production, and are compared with data for some systems that have been studied previously in aqueous acid chloride solutions. Reactions 1 and 2 occur much more readily in the non-aqueous solvent due to a lower activation energy, while reaction 3 occurs only in the non-aqueous system. A detailed interpretation of the data is limited by the uncertain nature of species present in the amide solvent.

Le "$RuCl_3 \cdot 3H_2O$", qui est un mélange de Ru(IV) et de Ru(III), en solution dans la *N,N*-diméthylacétamide, réagit avec de l'hydrogène dans des conditions douces selon un processus stoechiométrique par étapes pour conduire à l'espèce univalente ($Ru^{IV} \xrightarrow{1} Ru^{III} \xrightarrow{2} Ru^{II} \xrightarrow{3} Ru^{I}$). Les réactions 1 et 2 impliquent une activation hétérolytique de H_2 par le Ru^{III} servant de catalyseur et fort probablement passent par un intermédiaire $Ru^{III}H$; le même catalyseur catalyse l'hydrogénolyse de l'oxygène en eau. La réaction 3 implique un intermédiaire $Ru^{II}H$. On présente les paramètres cinétiques des processus 1–3 ainsi que ceux de la production par catalyse de l'eau et on les compare avec les données de quelques systèmes que l'on a déjà étudié dans des solutions aqueuses de chlorure d'acide. Les réactions 1 et 2 se font beaucoup plus facilement dans des solvants non-aqueux à cause d'une énergie d'activation plus faible alors que la réaction 3 se fait uniquement dans un système non-aqueux. Une interprétation détaillée des résultats est difficile à réaliser à cause de la nature incertaine des produits dans le solvant amide.

[Traduit par le journal]

Can. J. Chem., **52**, 348 (1974)

Introduction

Many transition metal ions and complexes are known to activate molecular hydrogen in both aqueous and non-aqueous solvents (1). Harrod and co-workers (2) first reported on hydrogen activation by ruthenium complexes when they used aqueous hydrochloric acid solutions of ruthenium(III) chloride to catalyze the hydrogen reduction of iron(III) and ruthenium(IV). The mechanism was written as a rate-determining step that involved an overall heterolytic splitting of H_2 to produce an intermediate hydride (reaction 1) which subsequently reacted with the substrates in a faster step (reactions 2, 3):

$$[1] \qquad Ru^{III} + H_2 \underset{k_{-1}}{\overset{k_1}{\rightleftharpoons}} Ru^{III}H + H^+$$

$$[2] \qquad Ru^{III}H + 2Fe^{III} \overset{k_2}{\rightleftharpoons} Ru^{III} + 2Fe^{II} + H^+$$

$$[3] \qquad Ru^{III}H + 2Ru^{IV} \overset{k_3}{\rightleftharpoons} 3Ru^{III} + H^+$$

The postulated reversible reaction 1 was confirmed later by deuterium exchange studies (3, 4).

The ruthenium(III) solutions alone were essentially unreactive toward hydrogen over the reaction times required for substrate reduction (*i.e.*, k_2 (or k_3) $> k_{-1} > k_1$), although over very long reaction times, slow reduction to chlororuthenate(II) species occurred (3, 5). No kinetic data were reported for this slow reaction but it likely proceeded (2) by reaction 1 followed by reaction 4:

$$[4] \qquad Ru^{III}H + Ru^{III} \overset{k_4}{\rightleftharpoons} 2Ru^{II} + H^+$$

where $k_{-1} > k_4$.

The aqueous acid solutions containing blue chlororuthenate(II) were found later to be effective catalysts for the hydrogenation of a number of activated olefins (5). The rate-determining step

[1]Taken from the Ph.D. thesis in Chemistry of B. C. Hui, University of British Columbia, Vancouver, British Columbia, 1969.

[2]Present address: Department of Chemistry, Lakehead University, Thunder Bay, Ontario.

Can. J. Chem. Downloaded from www.nrcresearchpress.com by 210.87.254.5 on 09/05/12
For personal use only.

Can. J. Chem. Downloaded from www.nrcresearchpress.com by 210.87.254.5 on 09/05/12
For personal use only.

in this process was thought to involve hydrogen activation (again heterolytically) according to reaction 5 (*cf.* reaction 1):

[5] $Ru^{II}(olefin) + H_2 \rightleftarrows HRu^{II}(olefin) + H^+$

These studies concluded that less reactive olefins such as ethylene might be hydrogenated if the rate of the back reaction of [5] could be lowered, *e.g.*, by reducing the acidity of the medium. This possibility could not be explored in aqueous solution since ruthenium(II) is unstable in this medium at low acidities (6), and hence studies in the aprotic coordinating solvent *N,N*-dimethylacetamide (DMA) were initiated.

DMA solutions of ruthenium chloride were indeed found to catalyze ethylene hydrogenation (5), but the systems appeared extremely complicated. It eventually became clear that the reactivity of DMA solutions of ruthenium chlorides toward hydrogen was quite different to that observed in aqueous acid solutions (see above), and this paper reports on the investigation of the non-aqueous system in the absence of reducible organic substrates. Reactions such as [1] are found to be very much enhanced in the non-acidic media, and, of more significance, further reduction to univalent ruthenium occurs.

Some of the work presented here has been reported on briefly elsewhere (1, 7, 8).

Experimental

Ruthenium(III) trichloride trihydrate was obtained as $RuCl_3 \cdot 3H_2O$ (40.59% Ru) from Johnson Matthey Limited. The commercially available hydrate, however, is known (2) to be a mixture of Ru^{III} and Ru^{IV} (probably present as $RuCl_3(OH) \cdot 2H_2O$). The compounds $K_2RuCl_5(H_2O)$ and $(NH_4)_2[RuCl_5(OH)]$, available as pure Ru^{III} and Ru^{IV} compounds respectively, were essentially insoluble in DMA, and hence the soluble $RuCl_3 \cdot 3H_2O$ compound was used for the preparation of the stock ruthenium solutions. This has some merit, however, in that the readily available $RuCl_3 \cdot 3H_2O$ compound has been used as such in non-aqueous solvents for a variety of catalytic reactions including hydrogenation, isomerization, oxidation, alkylation, carbonylation and polymerization of olefins (8). The visible absorption spectra of a 3 *M* HCl solution of $RuCl_3 \cdot 3H_2O$, and a measured hydrogen uptake in the same media for reduction to Ru^{III}(2), showed that the material contained 70 ± 3% Ru^{IV}.

Other materials used and the procedure used for following H_2-uptake at constant pressure have been described earlier (9). The solubility of H_2 in DMA has been determined previously in this laboratory (9, 10).

Results

Activation of Hydrogen by Ru^{III}

Equilibrated red-brown solutions of $RuCl_3 \cdot 3H_2O$ (~70% Ru^{IV}) in DMA were found to absorb H_2, initially in an autocatalytic manner (Fig. 1), at measurable rates in the temperature range 30–55°. The stoichiometry of the total uptake at the levelling-off region corresponds to about 0.5 mol H_2 per mol of Ru^{IV}, and presumably involves reduction of Ru^{IV} to Ru^{III}, as in the aqueous 3 *M* HCl solutions according to reaction 6 (the sum of reactions 1 and 3):

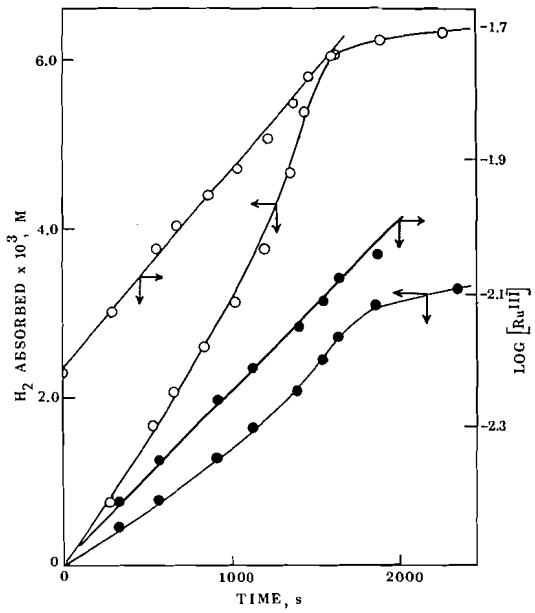

FIG. 1. Autocatalytic reduction of Ru^{IV} to Ru^{III} by H_2 in DMA at 35°. 380 mm H_2; [$RuCl_3 \cdot 3H_2O$]: ○, 0.02 *M*; ●, 0.01 *M*. Uptake and log plots.

[6] $2Ru^{IV} + H_2 \rightarrow 2Ru^{III} + 2H^+$

The color of the solution at this stage was yellowish, and an absorption peak was observed at 450 nm (ε = 1750); aqueous acid solutions containing Ru^{III} chlorides are known to be yellow (2).

It is noted in Fig. 1 that the H_2 uptake does not cease completely at the levelling-off stage and, in fact, at 35° a subsequent much slower reaction of the Ru^{III} with H_2 occurs. This slow reaction ceases after about 15 h, and the uptake again corresponds to 0.5 mol of H_2 per mol of Ru^{III}; this stoichiometry, together with the production of a blue color (see later), are consistent with production of Ru^{II}:

[7] $2Ru^{III} + H_2 \rightarrow 2Ru^{II} + 2H^+$

The blue solution showed an absorption maximum at 650 nm (ε = 1200). Reaction 7 was more

Can. J. Chem. Downloaded from www.nrcresearchpress.com by 210.87.254.5 on 09/05/12
For personal use only.

conveniently studied at higher temperatures (65–80°), where the stoichiometry was again established, although at the highest temperatures the reaction was complicated by yet a further slow reduction to Ru^{I} (see later).

The autocatalytic behavior of reaction 6 (as in the aqueous acid system) may be explained in terms of catalysis of the reaction by Ru^{III}, and fitted by the rate-law shown in eq. 8:

$$[8] \quad -d[H_2]/dt = \tfrac{1}{2}d[Ru^{III}]/dt = k_1[H_2][Ru^{III}]$$

With $[H_2]$ constant during the course of each experiment, the rate-law yields on integration,

$$[9] \quad \log [Ru^{III}] = \log [Ru^{III}]_{t=0} + 2k_1[H_2]t/2.3$$

Plots of log $[Ru^{III}]$ *vs.* time are given in Fig. 1 for the two uptake plots shown; the log plots are linear over the major portion of each experiment and the slopes yield consistent values of k_1. The non-zero initial rates in these systems are due to the presence of ~30% of the ruthenium being present as Ru^{III}. The successful linear analysis using this 30% Ru^{III} figure further substantiates the composition of the $RuCl_3 \cdot 3H_2O$ starting material. k_1 was essentially independent of the $[Ru^{III}]$ from (0.5–2.0) $\times 10^{-2}$ M, and of the $[H_2]$ from (0.4–1.8) $\times 10^{-3}$ M, thus substantiating rate-law [8], and had the value 0.73 ± 0.06 $M^{-1}s^{-1}$ at 35°. It should be noted that this group of experiments were carried out using the DMA as purchased from Eastman Kodak (highest purity). All subsequent studies used the purified solvent, and rates about three times lower were measured, although the general kinetics and observations were identical. Traces of water were the cause of this discrepancy.

Table 1 shows the variation of k_1 with temperature (using purified DMA); the data give a good Arrhenius plot and the activation parameters $\Delta H^{\ddagger} = 19.9 \pm 1.0$ kcal mol^{-1} and $\Delta S^{\ddagger} = +3.2 \pm 2.0$ e.u.

TABLE 1. Temperature dependence data* for Ru^{III}-catalyzed hydrogen reduction of Ru^{IV}

T (°C)	k_1 ($M^{-1}s^{-1}$)
30	0.16
35	0.23
40	0.42
45	0.65
50	1.20
55	1.64

*$[RuCl_3.3H_2O] = 0.02$ M, 1 atm.

Reaction 6 is thus seen to be a Ru^{III}-catalyzed hydrogen reduction of Ru^{IV} in which the reduction product is also the catalyst, and as in the aqueous system, the mechanism outlined by reactions 1 and 3, with 3 being fast, accounts for the kinetics. More evidence to support the mechanism could clearly be sought from systems using other reducible substrates. Some very simple kinetics were observed using molecular oxygen as the substrate, and these results will now be described.

Solutions of $RuCl_3 \cdot 3H_2O$ in DMA reacted with gas mixtures of H_2 and O_2 (H_2:O_2 = 0.1 to 0.5) and the resulting uptake plots were linear for at least 1 h (Fig. 2). The u.v.–visible spectrum of the solution remained unchanged throughout the reaction showing that no reduction of Ru^{IV} takes place and thus the concentration of Ru^{III} remains constant. During a reaction time of 1 h, the partial pressures (and hence their concentrations in solution) remain effectively constant. Thus the reaction is one of pseudo-zero-order. The kinetic results (Table 2) show a good first-order dependence on $RuCl_3 \cdot 3H_2O$ up to 0.02 M, and a first-order dependence on H_2 up to 0.8 $\times 10^{-3}$ M, the reaction being independent of O_2 pressure from 450–700 mm. No deuterium kinetic isotope effect was observed. Ru^{III} is again the active catalyst, and this was further confirmed by using solutions containing purely Ru^{III} (formed via the autocatalytic H_2-

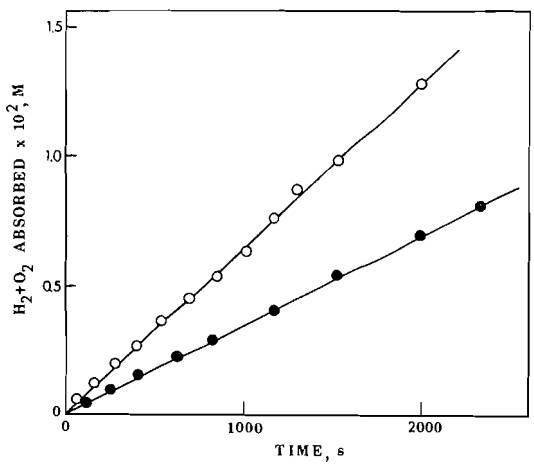

FIG. 2. Rate plots for Ru^{III}-catalyzed hydrogenolysis of O_2 in DMA at 50°. 0.02 M $RuCl_3 \cdot 3H_2O$; ○, 158 mm H_2, 594 mm O_2; ●, 93 mm H_2, 659 mm O_2.

TABLE 2. Ru^{III}-catalyzed hydrogenolysis of oxygen; at 50° unless stated otherwise

$[RuCl_3 \cdot 3H_2O]$ $\times 10^2$ (M)	H_2 (mm)	$[H_2]$ $\times 10^4$ (M)	O_2 (mm)	Rate $\times 10^6$ (M s^{-1})	k_1[a] (M^{-1} s^{-1})
2.00	295	7.7	457	8.00	1.73
1.50	295	7.7	457	5.83	1.68
1.00	295	7.7	457	3.95	1.71
0.50	295	7.7	457	2.06	1.79
2.00	192	5.0	560	5.40	1.80
2.00	158	4.1	594	4.00	1.62
2.00	118	3.1	637	3.04	1.64
2.00	93	2.4	659	2.37	1.64
2.00	54	1.4	698	1.50	1.77
1.50	192	5.0	560	4.12	1.82
1.00	192	5.0	560	2.80	1.86
0.50	192	5.0	560	1.51	1.98
1.10	366	9.7	386	1.93	1.37[b]
1.10	382	1.0	370	2.09	1.43[b,c]
2.00	300	6.9	457	0.77	0.18[d]
2.00	300	7.1	457	1.64	0.39[e]
2.00	298	7.4	457	2.49	0.56[f]
2.00	295	7.6	457	4.23	0.93[g]
2.00	292	8.0	457	11.0	2.29[h]
2.00	288	8.1	457	23.2	4.77[i]
2.00	281	8.3	457	51.2	10.3[j]

[a]Assuming 30% Ru present initially as Ru^{II}.
[b]Using a different batch of $RuCl_3 \cdot 3H_2O$ (found to contain 13% Ru^{III}).
[c]D_2 in place of H_2.
[d]30°.
[e]35°.
[f]40°.
[g]45°.
[h]55°.
[i]60°.
[j]70°.

reduction of Ru^{IV}). The only product detected was water, and the reaction occurring is

$$[10] \qquad 2H_2 + O_2 \rightarrow 2H_2O$$

The rate-law for the oxygen hydrogenolysis is that shown in eq. 8. To determine k_1, the rate of H_2-uptake is required; this is the rate listed in Table 2 and is 2/3 the total measured rate which includes O_2 consumption. The average bimolecular rate constant at 50° is 1.73 M^{-1} s^{-1}. The temperature variation data give a good Arrhenius plot and the activation parameters $\Delta H^{\ddagger} = 19.3 \pm 1.0$ kcal mol^{-1} and $\Delta S^{\ddagger} = +2.3 \pm 2.0$ e.u.

As mentioned earlier, the slower reaction [7] was observed following the autocatalytic Ru^{IV} reduction. This system again seemed likely to involve Ru^{III} as the hydrogen activator, particularly since the formation of the Ru^{II} was not an autocatalytic process. The reaction thus involves Ru^{III} as the substrate as well as the catalyst, and the kinetics were investigated.

An uptake plot for the reaction of $RuCl_3 \cdot 3H_2O$ with H_2 at 80° is shown in Fig. 3. The H_2

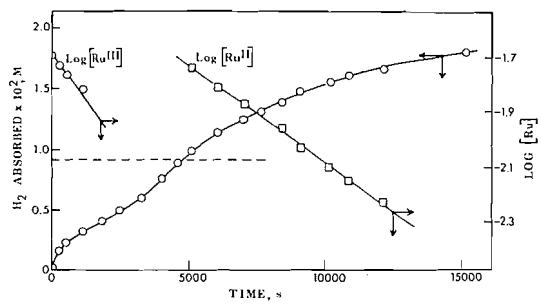

FIG. 3. H_2 reduction of Ru^{III} to Ru^{I} via Ru^{II} in DMA at 80°. 0.02 M Ru^{III}, 187 mm H_2. Uptake and log plots; the dotted line indicates the stoichiometry break used for the $Ru^{III} \rightarrow Ru^{II}$, and $Ru^{II} \rightarrow Ru^{I}$ analyses.

required for the reduction to Ru^{III} could be observed as an "instantaneous" uptake in under 100 s, but at this temperature a quantitative reproducible measurement for this reaction (eq. 6) was impractical and is thus not shown in the figure (spectral data however readily confirm the rapid formation of Ru^{III}). The overall stoichiometry shown in Fig. 3 is thus about 1.0 mol of H_2 per mol of Ru^{III}, the final solution

Can. J. Chem. Downloaded from www.nrcresearchpress.com by 210.87.254.5 on 09/05/12
For personal use only.

TABLE 3. Ru^{III}-catalyzed hydrogen reduction of Ru^{III}; at 80° unless stated otherwise

$[Ru^{III}]$ $\times 10^2$ (M)	H_2 (mm)	$[H_2]$ $\times 10^3$ (M)	k_1 (M^{-1} s^{-1})
2.00	725	2.3	0.24
2.00	546	1.7	0.20
2.00	366	1.2	0.23
2.00	187	0.6	0.23
1.00	725	2.3	0.24
1.00	546	1.7	0.22
1.30[a]	366	1.2	0.33
1.30[a]	366	1.2	0.28[b]
1.30[a]	366	1.2	0.21[c]
2.00	730	2.2	0.16[d]
2.00	735	2.2	0.12[e]
2.00	740	2.1	0.08[f]

[a]Using a different batch of $RuCl_3 \cdot 3H_2O$ and DMA.
[b]0.09 M *p*-toluenesulfonic acid.
[c]0.9 M *p*-toluenesulfonic acid.
[d]75°.
[e]70°.
[f]65°.

being dark brown. The stoichiometry is consistent with reaction 7 followed by a further reaction to give ruthenium(I):

$$[11] \qquad \underset{\text{blue}}{2Ru^{II}} + H_2 \rightarrow \underset{\text{brown}}{2Ru^{I}} + 2H^+$$

There is a distinct inflection region in the uptake plot which results from the two stages of the $Ru^{III} \rightarrow Ru^{II} \rightarrow Ru^{I}$ processes. A considerable part of the first portion of the uptake curve does fit a pseudo-first-order log plot (given in Fig. 3), and the data are consistent with a rate-law of the form:

$$[12] \qquad \frac{-d[H_2]}{dt} = -\frac{1}{2}\frac{d[Ru^{III}]}{dt} = k_1[Ru^{III}]\,[H_2]$$

The log plots were obtained by assuming the decrease in Ru^{III} is proportional to the H_2 uptake. From the slopes, the bimolecular rate constant k_1 was calculated, and the results are summarized in Table 3. An Arrhenius plot gave the following activation parameters: $\Delta H^{\ddagger} = 15.5 \pm 1.5$ kcal mol^{-1}, $\Delta S^{\ddagger} = -16.4 \pm 3.0$ e.u.

The second half of uptake plots such as those shown in Fig. 3, when essentially no Ru^{III} remains, also analyzed well for a standard first-order log plot (included in Fig. 3). This refers to reaction 11 which is found to be first-order in both Ru^{II} and H_2 with a second-order rate-constant of about 0.1 M^{-1} s^{-1} at 80°. This system has been studied separately in more detail using prepared solutions of Ru^{II}, and the data are given in the following section.

Activation of Hydrogen by Ru^{II}; Production of Ru^{I}

Reaction 11 was studied by using as reactant the deep blue Ru^{II} solutions, prepared by subjecting DMA solutions of $RuCl_3 \cdot 3H_2O$ to 1 atm H_2 at room temperature for 15–20 h. Treatment of the Ru^{II} solution with H_2 at 80° results in uptake plots of the type shown in Fig. 4; 0.5 mol H_2 per mol of Ru^{II} are absorbed in a pseudo-first-order manner.

The final brown solutions could also be produced by titanous chloride reduction of the $RuCl_3 \cdot 3H_2O$ solutions in DMA. Nuclear magnetic resonance and infrared spectra gave no evidence for the presence of metal hydride species. The solutions were sensitive to air, and a room temperature stoichiometric oxidation with oxygen (O_2 : Ru = 0.5) yielded Ru^{III} (identi-

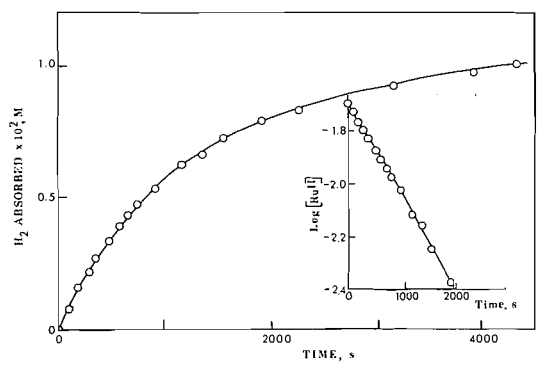

FIG. 4. Rate plot for H_2 reduction of Ru^{II} to Ru^{I} in DMA at 80°. 0.02 M Ru^{II}, 725 mm H_2. Inset: plot of log $[Ru^{II}]$ *vs.* time.

Can. J. Chem. Downloaded from www.nrcresearchpress.com by 210.87.254.5 on 09/05/12
For personal use only.

TABLE 4. Hydrogen reduction of Ru^{II} to Ru^{I}; at 80° unless stated otherwise

$[Ru^{II}]$ $\times 10^2$ (M)	H_2 (mm)	$[H_2]$ $\times 10^3$ (M)	k (M^{-1} s^{-1})
2.00	309	1.0	0.17
2.05	408	1.3	0.17
2.05	551	1.8	0.15
2.05	651	2.1	0.17
2.05	725	2.3	0.18
2.10	725	2.3	0.06[a]
2.10	725	2.3	0.17[b]
1.50	408	1.3	0.18
1.00	408	1.3	0.17
0.50	408	1.3	0.17
2.05	410	1.3	0.12[c]
2.05	410	1.2	0.09[d]
2.05	410	1.2	0.06[e]
2.05	410	1.2	0.04[f]

[a] D_2 in place of H_2.
[b] 0.07 M *p*-toluenesulfonic acid.
[c] 75°.
[d] 70°.
[e] 65°.
[f] 60°.

fied by visible spectroscopy). Reaction with carbon monoxide (1 atm, 60°) yields $Ru^{I}(CO)$ and $Ru^{I}(CO)_2$ successively in solution (12), and the latter is oxidized stoichiometrically to $Ru^{II}(CO)_2$ which can also be formed from reaction of Ru^{II} with 2 moles of carbon monoxide (13). Isolation of a ruthenium(I)–DMA–chloride complex (11) has confirmed further the existence of Ru^{I} in the brown solutions.

The H_2-uptakes, illustrated in Fig. 4, were found to obey the second-order rate-law:

$$[13] \quad -d[H_2]/dt = -\tfrac{1}{2}d[Ru^{II}]/dt = k[Ru^{II}][H_2]$$

Values of k were determined from the slopes of the first-order log plots (Fig. 4) and are summarized in Table 4. A significant kinetic isotope effect was observed, $k_H/k_D \sim 3$; the rate was independent of added acid. The temperature dependence data yielded a good Arrhenius plot and the activation parameters $\Delta H^{\ddagger} = 16.6 \pm 1.0$ kcal mol^{-1}, $\Delta S^{\ddagger} = -13.2 \pm 2.0$ e.u.

Figure 5 shows how the measured rate constant varied with added chloride concentration. k shows a sharp decrease in added Cl^- up to ~ 0.05 M, and then increases and passes through a maximum at ~ 1.0 M. Unfortunately the ionic strength of the solution could not be maintained constant in these chloride variation experiments (14, 15).

Of interest is that in the presence of three-fold excess of triphenylphosphine, the blue Ru^{II} solutions absorb 1 mol of H_2 per mol of Ru^{II} to give purple-red solutions containing the hydridochloro species $HRuCl(PPh_3)_3$ (16, 17). The uptake plots are of a pseudo-first-order type and in accordance with eq. 13 a k value of 0.057 M^{-1} s^{-1} was estimated at 60° (12). The phosphine did not react with the Ru^{II} solutions over the 2 h period of the hydrogenation reaction at this temperature, and the hydride must be formed via reactions 14 and 15:

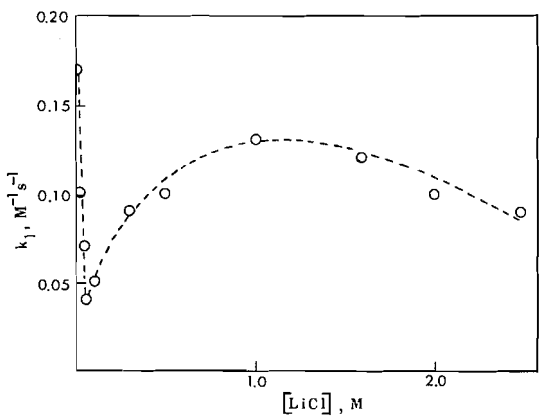

FIG. 5. Effect of added chloride on the rate of Ru^{II} reduction by H_2 in DMA at 80°; 0.02 M Ru^{II}.

$$[14] \quad Ru^{II} + H_2 \xrightarrow{k} HRu^{II} + H^+$$

$$[15] \quad HRu^{II} + PPh_3 \rightarrow HRuCl(PPh_3)_3$$

Can. J. Chem. Downloaded from www.nrcresearchpress.com by 210.87.254.5 on 09/05/12
For personal use only.

TABLE 5. Summary of data for Ru^{III}-catalyzed reductions

Substrate	$k_1(55°)$ (M^{-1} s^{-1})	$\Delta H^{\ddagger}$ (kcal mol^{-1})	$\Delta S^{\ddagger}$ (e.u.)
Ru^{IV}	1.64	19.9	+3.3
O_2	2.29	19.3	+2.3
Ru^{III}	0.04[a]	15.5	−16.4

[a]Extrapolated from data given in Table 3.

Blue solutions of Ru^{II} in 3 *M* HCl (4, 5), when subjected to 1 atm H_2 at 80°, very slowly precipitate metal; a similar observation was noted, however, under inert atmospheres in the absence of H_2.

Discussion

Ruthenium(III) Catalyst

The kinetic data for the Ru^{III}-catalyzed reduction of Ru^{IV}, O_2, and Ru^{III} (eqs. 6, 10, and 7, respectively) all give a hydrogen-uptake rate given by $k_1[Ru^{III}][H_2]$. The reactions must proceed through some intermediate which involves activation of H_2 by Ru^{III}, and it seems likely that in DMA, a moderately high polar solvent, the initial step in these catalytic reductions involves an overall heterolytic splitting of hydrogen according to reaction 1, as demonstrated for some similar systems in aqueous acid solution (2–4). This mechanism has been viewed as involving a four-center transition state in which the released proton is stabilized by the concomitant release of a coordinated basic ligand (18), which in this case could be chloride or solvent. A heterolytic splitting via a ruthenium(V) dihydride intermediate, reaction 16,

$$[16] \quad Ru^{III} + H_2 \rightleftarrows [Ru^{V}H_2] \rightleftarrows Ru^{III}H + H^+$$

seems unlikely, but cannot be completely ruled out; the monohydride could result from reductive elimination of, for example, HCl from the dihydride. Deuterium isotope effects have been found to be small for hydrogen activation processes that are known to involve dihydride formation, and those that overall involve heterolytic splitting of H_2 (ref. 1, p. 407). The observed $k_H/k_D \sim 1$ for the O_2-reduction is thus not diagnostic of mechanism.

A mechanism with reaction 1 rate-determining, followed by faster steps with the substrates (reactions 3, 4, and 17), accounts for the rate-law.

$$[17] \quad 2Ru^{III}H + O_2 \xrightarrow{k} 2Ru^{III} + 2OH^-$$

However, the measured k_1 value at 55° for the Ru^{III} reduction is about 50 times lower than those for the comparable Ru^{IV} and O_2 systems (Table 5); quite different activation parameters are also evident for the Ru^{III} reduction.

A more complete rate-law for a mechanism involving reaction 1 followed by reaction 3 (or [4], or [17]) is readily shown, by assuming a steady state concentration of the hydride, to be of the form:

$$[18] \quad -d[H_2]/dt = k_1[H_2][Ru^{III}] \times \left\{1 - \frac{k_{-1}[H^+]}{k_{-1}[H^+] + k_n[\text{substrate}]}\right\}$$

(where n = 3, 4, 5 for the three systems).

The second term in the bracket represents the competition of the hydride to react with the reducible substrate or regenerate H_2 from the back reaction of [1]. The Ru^{IV} and O_2 systems give essentially the same rate-constants and activation parameters, suggesting that these substrates oxidize $Ru^{III}H$ rapidly, *i.e.* k_3 and k_5 are large ($\gg k_{-1}$), the back reaction is negligible, and the rate-law reduces to its simple form, $k_1[H_2][Ru^{III}]$. The k_1 values for these systems then refer genuinely to the forward reaction of [1]. The much lower k_1 value for the Ru^{III} substrate system could result from the k_{-1} back reaction competing effectively with reaction 4; compared with Ru^{IV} and O_2, Ru^{III} chloride complexes are not as efficient an oxidizing system and in fact chlororuthenate(II) is a strong reducing agent (19). The data suggest that the term $k_{-1}[H^+]/\{k_{-1}[H^+] + k_4[Ru^{III}]\}$ is close to unity, in fact about 49/50 at 55°; the $k_4[Ru^{III}]$ term will be small compared to the $k_{-1}[H^+]$ term, and the rate will still therefore show a first-order dependence on Ru^{III} as observed (Table 3). If this reasoning is correct, then this system should show an inverse acid dependence according to eq. 18 and the fact that the above term must be close to unity gives a dependence inversely proportional to $[H^+]$. There is of course some acid present initially in these Ru^{III}

Can. J. Chem. Downloaded from www.nrcresearchpress.com by 210.87.254.5 on 09/05/12
For personal use only.

Can. J. Chem. Downloaded from www.nrcresearchpress.com by 210.87.254.5 on 09/05/12
For personal use only.

reductions produced according to reaction 6 and possibly from the water of hydration of the $RuCl_3 \cdot 3H_2O$ starting material, although the fate of this water is uncertain. However, the inverse acid dependence noted (Table 3) is much less than anticipated from the above discussion. A possible complication is that addition of acid could affect the distribution of the starting Ru^{III} complexes (particularly hydroxy species) with resulting different activity, especially for the k_{-1} back reaction. A further complication is that in the experiments involving addition of acid, a constant ionic strength is not maintained because of the difficulty of finding a suitable inert anion for Ru^{II} systems (14, 15). Some quite strong support for the contribution of the k_{-1} back reaction in the Ru^{III} system here is the fact that in aqueous 3 *M* HCl solution at 80°, no reduction of Ru^{III} to Ru^{II} is observed at all over several hours (2); this reduction is promoted under the less acid conditions in DMA, presumably by decreasing the rate of the k_{-1} reaction to such an extent that the k_4 rate successfully competes.

For the autocatalytic reduction of Ru^{IV} by H_2 in 3 *M* HCl(2) the values of $\Delta H^{\ddagger}$ and $\Delta S^{\ddagger}$ were 23.1 kcal mol^{-1} and +6 e.u. with $k_1^{65°} = 0.22$ M^{-1} s^{-1} (*cf.* Table 5). The rate of a reaction such as [1] producing ions in solution generally increases with solvent polarity (20); however the dielectric constants for DMA and 3 *M* HCl are both about 30–40 (9), and a more important factor is likely to be the greater basic strength (coordinating ability) of the DMA molecule compared to water (21). The higher k_1 value in DMA is due to a lower activation energy which could result from solvent stabilization of the released proton in the transition state, and/or from a solvent-assisted ligand dissociation from an octahedral Ru^{III} complex (22).

Ruthenium(II) Catalyst

The kinetics of the H_2-reduction of Ru^{II} to Ru^{I} are similar to those observed in the reactions involving activation of H_2 by Ru^{III}, and there is good evidence for formation of an intermediate hydride according to reaction 14. As well as the similarity to the Ru^{III}-catalyzed systems, a Ru^{II}(olefin) system is thought (5) to involve heterolytic splitting of H_2 according to reaction 5. Further, the stabilization of the intermediate hydride as the $HRuCl(PPh_3)_3$ complex by reactions 14 and 15, and the fact that the *k* value of 0.057 M^{-1} s^{-1} determined at 60° for this process is in reasonable agreement with that determined at 60° for H_2-reduction of Ru^{II} to Ru^{I} ($k = 0.04$ M^{-1} s^{-1}), strongly suggest a common mechanism for the two processes via the rate-determining step shown in reaction 14.

Ru^{I} production presumably occurs via reaction 19 (*cf.* reactions 2–4):

$$[19] \qquad Ru^{II}H + Ru^{II} \rightarrow 2Ru^{I} + H^{+}$$

The absence of an acid dependence indicates that reaction 19 is fast compared to the reverse reaction of [14].

The possibility exists that reaction 14 proceeds via oxidative addition and a Ru^{IV} dihydride intermediate (*cf.* reaction 16), particularly since such reactions for Ru^{II} systems are known (23), and also appear likely in some Ru^{II}-catalyzed olefin hydrogenations (8, 16). Of particular interest is the kinetic isotope effect of about 3 observed for reaction 14. This appears to be the largest yet reported for H_2 activation by a metal complex in solution (ref. 1, p. 407), although Hui *et al.* (24) have recently reported a deuterium isotope effect (k_H/k_D) of ~2.6 for reaction of rhodium(II) acetate with H_2, written as reaction 20.

$$[20] \qquad Rh_2(OCOCH_3)_4 + H_2 \rightarrow H_2Rh_2(OCOCH_3)_4$$

The small isotope effects (about unity) invariably measured for systems that *definitely* involve dihydride formation have always involved oxidative addition to square planar d^8 systems. The possibility that larger isotope effects might result with dihydride formation from other geometries and configurations, *e.g.*, octahedral d^6 systems as in Ru^{II}, is currently being investigated further. The small isotope effects observed in systems involving a direct heterolytic H_2 splitting may be rationalized in terms of metal–hydride bond formation and hydrogen–hydrogen bond breaking occurring in a concerted process, and the larger isotope effect of 3 could be consistent with somewhat greater dissociation of the H—H bond prior to formation of the activated complex; this could reflect a weaker metal–hydrogen bond in a Ru^{II} system compared to the Ru^{III} system.

We have no quantitative interpretation for the effect of chloride variation (Fig. 5). Henry (25) has found a remarkably similar chloride dependence for the rate of reaction of ethylene with aqueous palladium(II) chloride solutions;

Can. J. Chem. Downloaded from www.nrcresearchpress.com by 210.87.254.5 on 09/05/12
For personal use only.

he attributed the initial decrease in rate to the presence of different chloro complexes, and the remaining variation to salt effects. Addition of chloride to the blue Ru^{II} solutions does result in some variation of the visible absorption spectra (26), and the two factors noted by Henry could well explain the data of the present system.

The present studies are the first to give direct evidence for the existence of thermodynamically stable Ru^{I} salts in solution, although a number of dimeric and polymeric Ru^{I} carbonyls containing bridging carboxylate ligands have been described (27). The existence of Ru^{I} has sometimes been postulated in aqueous systems. Grube and Nann (28) have attributed the instability of blue Ru^{II} solutions in dilute HCl to disproportionation reactions such as:

$$[21] \qquad 3Ru^{II} \rightarrow Ru^{0}(\text{metal}) + 2Ru^{III}$$

$$[22] \qquad 2Ru^{I} \rightleftarrows Ru^{II} + Ru^{0}(\text{metal})$$

Later studies by Backhouse and Dwyer (29) recognized the disproportionation of Ru^{II} to metal, but they disputed the existence of Ru^{I} in such solutions. Other workers (6) have demonstrated the decomposition of such solutions also arises by reduction of the water, with no metal production:

$$[23] \qquad Ru^{II} + H_2O \rightarrow OH^- + Ru^{III} + \tfrac{1}{2}H_2$$

The nature of the chloro species present in these Ru^{II} solutions at different HCl concentrations remains to be more fully established (see the following section) prior to more meaningful discussion on reactions 21–23. Adamson (30) has suggested that highly labile Ru^{I} may be extremely active in catalyzing chloride exchange in chlororuthenate(III) complexes in aqueous acid, but no evidence for such an intermediate was found.

The nonaqueous solvent plays an important role in producing and hence stabilizing the Ru^{I} species. As for the Ru^{III} systems, the reverse of reaction 14 in aqueous acid solution will hinder any possible H_2-reduction of Ru^{II}, while the more basic DMA will promote the forward reaction. The activation energy for the forward reaction of [14] is about 3 kcal mol^{-1} lower than that for the corresponding Ru^{III} reaction in DMA; the slower rate of the Ru^{II} reduction is seen to result from a less favorable $\Delta S^{\ddagger}$ value (-13 e.u. *vs.* $+3$ e.u.). Differences in $\Delta S^{\ddagger}$ will result mainly from differences in ionic charges of the species involved, but information on this point is lacking.

No quantitative redox potential data are available for the estimation of an equilibrium such as [22]. In aqueous systems such a disproportionation could occur through a hydrogen atom transfer mechanism, as has been suggested for a number of electron transfer reactions between metal aquo ions (ref. 23, p. 469); such a mechanism would be ruled out in a solvent such as DMA, which is undoubtedly coordinated to all the ruthenium species.

Nature of the Species in the DMA Solutions

A more detailed interpretation of the kinetics and mechanisms of the H_2 reductions in DMA is clearly hindered by the lack of information on the nature of the ruthenium complexes in solution, especially the catalytically active Ru^{III} and Ru^{II} species.

The visible absorption spectrum of $RuCl_3 \cdot 3H_2O$ in DMA has been found to vary with concentration, and a limiting spectrum (λ_{max} 415 nm; $\varepsilon \sim 8000$) is reached on successive dilution. Polymer $\rightleftarrows$ dimer $\rightleftarrows$ monomer equilibria seem likely, since they exist for solutions of Ru^{IV} chlorides in aqueous HCl solutions (31). The observed first-order dependence on Ru^{III} suggests a single species of this valency state exists over the concentration range used (or less likely a number of species with equal reactivity); it is also consistent with steps involving Ru^{IV} in the Ru^{IV} reduction process (reaction 3) being relatively fast.

More detailed u.v.–visible spectroscopic measurements on the solutions are in progress (26). If the complexes activating hydrogen are polymeric Ru_n species, then the forward rate-constants determined for reactions 1 and 14 should be multiplied by n. Rose and Wilkinson (32) have reported that the blue Ru^{II} chloride solutions in aqueous HCl or dimethylformamide contain the $Ru_5Cl_{12}^{2-}$ cluster, although there is some difficulty in interpreting the magnetic behavior of the system.

It should be noted that Mercer and Dumas (33) have isolated the Ru^{II}–Ru^{III} mixed-valence cations $Ru_2Cl_{3+n}^{(2-n)+}$ ($n = 0, 1, 2$) from the blue solutions in dilute HCl, and the species are considered to exist in solution. A mixed-valence blue ammine complex $[Ru_2(NH_3)_6Cl_4H_2O]Cl$ has also been isolated by Bottomley and Tong (34). We have subsequently studied further the

Can. J. Chem. Downloaded from www.nrcresearchpress.com by 210.87.254.5 on 09/05/12
For personal use only.

blue solutions in 3 *M* HCl and find no evidence for the presence of any Ru^{III} species (35). Considerable stoichiometric data are presented in this paper on the DMA systems, and are all consistent with reduction steps involving the univalent changes $Ru^{IV} \rightarrow Ru^{III} \rightarrow Ru^{II} \rightarrow Ru^{I}$. The data are not consistent with the presence of Ru^{II}–Ru^{III} species in the blue solutions. A Ru^{II} chloride and a Ru^{I} chloride complex, both containing DMA, have been isolated from the hydrogenation reactions (11).

The homogeneous catalytic combination of hydrogen and oxygen to form water is of interest and was first reported by McDuffie *et al.* (36), who used aqueous acid cupric solutions under severe conditions of temperature and pressure. The ruthenium-catalyzed system reported here is one of the first (12) to be found effective under mild conditions. A number of other systems involving platinum metal complexes have recently been found to be similarly effective (37–39); the mechanisms of these reactions have not been studied in any great detail but hydroxy intermediates seem likely (39).

We thank the National Research Council of Canada for financial support and Johnson Matthey Limited for loan of ruthenium.

1. B. R. JAMES. Homogeneous hydrogenation. Wiley–Interscience, New York. 1973.
2. J. F. HARROD, S. CICCONE, and J. HALPERN. Can. J. Chem. **39**, 1372 (1961).
3. U. SCHINDEWOLF. J. Chim. Phys. **60**, 124 (1963).
4. J. HALPERN and B. R. JAMES. Can. J. Chem. **44**, 671 (1966).
5. J. HALPERN, J. F. HARROD, and B. R. JAMES. J. Am. Chem. Soc. **88**, 5150 (1966).
6. G. A. RECHNITZ and H. A. CATHERINO. Inorg. Chem. **4**, 112 (1965).
7. B. C. HUI and B. R. JAMES. Chem. Commun. 198 (1969).
8. B. R. JAMES. Inorg. Chim. Acta Rev. **4**, 73 (1970).
9. B. R. JAMES and G. L. REMPEL. Discuss. Faraday Soc. **46**, 48 (1968).
10. G. L. REMPEL. Ph.D. Thesis. University of British Columbia, Vancouver, British Columbia. 1968.
11. B. R. JAMES, R. S. MCMILLAN, and E. OCHIAI. Inorg. Nucl. Chem. Letters **8**, 239 (1972).
12. B. C. HUI. Ph.D. Thesis. University of British Columbia. Vancouver, British Columbia. 1969.
13. B. C. HUI and B. R. JAMES. Can. J. Chem. **48**, 3613 (1970).
14. H. H. CADY. Ph.D. Thesis. University of California, Berkeley, California. 1957.
15. J. HALPERN and B. R. JAMES. Can. J. Chem. **44**, 495 (1966).
16. P. S. HALLMAN, B. R. MCGARVEY, and G. WILKINSON. J. Chem. Soc. A, 3143 (1968).
17. B. R. JAMES and L. D. MARKHAM. J. Catal. **27**, 442 (1972).
18. J. HALPERN. J. Phys. Chem. **63**, 398 (1959).
19. G. CHARLOT. Selected constants, oxidation reduction potentials. Pergamon, Paris. 1958.
20. A. A. FROST and R. G. PEARSON. Kinetics and mechanism. 2nd ed. Wiley, New York. 1961. p. 136.
21. V. GUTMANN. Coord. Chem. Rev. **2**, 239 (1967).
22. F. BASOLO and R. G. PEARSON. Mechanisms of inorganic reactions. 2nd ed. Wiley, New York. 1967. pp. 134, 239, 585.
23. W. H. KNOTH. J. Am. Chem. Soc. **94**, 104 (1972).
24. B. C. HUI, W. K. TEO, and G. L. REMPEL. Inorg. Chem. **12**, 757 (1973).
25. P. HENRY. J. Am. Chem. Soc. **86**, 3246 (1964).
26. R. S. MCMILLAN. Work in progress.
27. G. R. CROOKS, B. F. G. JOHNSON, J. LEWIS, I. G. WILLIAMS, and G. GAMLEN. J. Chem. Soc. A, 2761 (1969).
28. G. GRUBE and H. NANN. Z. Elektrochem. **45**, 874 (1939); **46**, 661 (1939).
29. J. R. BACKHOUSE and F. P. DWYER. J. Proc. Roy. Soc. N. S. Wales, **83**, 146 (1949).
30. M. G. ADAMSON. J. Chem. Soc. A, 1370 (1968).
31. J. L. WOODHEAD and J. M. FLETCHER. United Kingdom Atomic Energy Authority, Report AERE R4123. 1962.
32. D. ROSE and G. WILKINSON. J. Chem. Soc. A, 1791 (1970).
33. E. E. MERCER and P. E. DUMAS. Inorg. Chem. **10**, 2755 (1971).
34. F. BOTTOMLEY and S. B. TONG. Can. J. Chem. **49**, 3739 (1971).
35. R. J. KING. M.Sc. Thesis. University of British Columbia, Vancouver, British Columbia. 1973.
36. H. F. MCDUFFIE, E. L. COMPERE, H. H. STONE, L. F. WOO, and C. H. SECOY. J. Phys. Chem. **62**, 1030 (1958).
37. B. C. HUI and G. L. REMPEL. Chem. Commun. 1195 (1970).
38. L. VASKA and M. E. TADROS. J. Am. Chem. Soc. **93**, 7099 (1971).
39. C. A. REED and W. R. ROPER. J. Chem. Soc. Dalton, 1014 (1973).

Can. J. Chem. Downloaded from www.nrcresearchpress.com by 210.87.254.5 on 09/05/12
For personal use only.

Canadian Journal of Chemistry

Published by
THE NATIONAL RESEARCH COUNCIL OF CANADA

Journal canadien de chimie

Publié par
LE CONSEIL NATIONAL DE RECHERCHES DU CANADA

Volume 52 Number 3 February 1, 1974

Volume 52 numéro 3 1 février 1974

Ion Yields and Fragmentation Processes in the Radiolysis of HCl and DCl

PETER F. CARR,[1] PATRICIA CHRISTENSEN,[2] DEREK E. WILSON, AND DAVID A. ARMSTRONG

Department of Chemistry, The University of Calgary, Calgary, Alberta T2N 1N4

Received January 2, 1973[3]

The ionization yield from fast electron impact on DCl under radiolysis conditions at 200 to 650 Torr was found to be 1.006 ± 0.023 times that from HCl. Also primary ionization processes were investigated by mass spectrometry. The relative abundance of Cl^+ from HCl near threshold at 17.4 eV was about twice that from DCl, but processes with onset at and above 21.0 eV did not exhibit an isotope effect. The interpretation of the results and their implications concerning the mechanism of radiolysis of HCl were discussed.

On a trouvé que, dans les conditions de radiolyse de 200 à 650 torr, le rendement d'ionisation du DCl provenant de l'impact d'électrons rapides, est égal à 1.006 ± 0.023 fois celui du HCl. De même, on a étudié à l'aide de la spectrométrie de masse les processus primaires d'ionisation. L'abondance relative de Cl^+ à partir de HCl près de la limite à 17.4 eV est d'environ le double de celle à partir du DCl, alors que les processus, dont le commencement se situe à 21.0 eV et au-dessus, n'ont pas montré d'effet isotopique. On discute de l'interprétation des résultats et de leurs conséquences vis-à-vis du mécanisme de radiolyse du HCl. [Traduit par le journal]

Can. J. Chem., **52**, 359 (1974)

Introduction

Previous publications (1–3) have reported decomposition yields for the radiolysis of gaseous HCl and DCl at normal pressures, and have discussed their mechanisms of radiolysis in the light of experiments with different types of scavenger. The total hydrogen yields, which include the contributions from reactions of scavengable hydrogen atoms (H or D), hot hydrogen atoms (*H* or *D*), electrons, and possibly other primary reactive species, were found to be 8.0 ± 0.3 and 7.4 ± 0.3 molecules per 100 eV for HCl and DCl respectively. Experiments with chlorine as a hydrogen atom scavenger showed that there was an essentially identical yield of "unscavengable" hydrogen in the two systems ($G_{H''} = G_{D''} =$ 2.2 ± 0.2 molecules per 100 eV) and from the effects of the specific electron scavenger SF_6 it was concluded that the primary electron yields were, within experimental error, the same (4.0 ± 0.2 for HCl and 4.1 ± 0.2 for DCl). The only difference between the two isotopic systems was in the yields of scavengable hydrogen atoms[4] ($G_H = 1.8 \pm 0.2$ and $G_D = 1.2 \pm 0.2$ per 100 eV for HCl and DCl respectively). In fact it appeared that the lower total yield of hydrogen from DCl was entirely due to the 0.6 molecule per 100 eV reduction in the contribution of reaction 1 below that of [2]:

[1] $D + DCl \rightarrow D_2 + Cl$

[2] $H + HCl \rightarrow H_2 + Cl$

[1]Present address: St. Patrick's College, Maynooth, Ireland.

[2]Present address: Department of Chemistry, University of Windsor, Windsor, Ontario.

[3]Revision received August 17, 1973.

[4]For practical purposes these may be defined as H atoms having k_{H+HCl}/k_{H+Cl_2} equal to the ratio of 10^{-2} for thermally equilibrated atoms at 298 °K (1) (or the equivalent for D atoms in DCl (3)). Atoms with excess kinetic energy have higher values of k_{H+HCl}/k_{H+Cl_2} and are appropriately referred to as "hot" (2). They contribute to the unscavengable yield.

Can. J. Chem. Downloaded from www.nrcresearchpress.com by 210.87.254.5 on 09/05/12
For personal use only.

The presence of H or D(^{2}S) atoms in irradiated hydrogen halides may result from a number of processes (2). Among these is the formation of superexcited molecules and their dissociation to H or D(^{2}S) and electronically excited Cl atoms. Here, as in the rest of this paper, only equations for the hydrogen isotope reactions are written

$$[3] \qquad HCl \rightarrow HCl^{**}$$

$$[4] \qquad HCl^{**} \rightarrow H + Cl^{*}$$

the analogous ones for deuterium being taken as obvious. If reaction 4 is in competition with preionization:

$$[5] \qquad HCl^{**} \rightarrow HCl^{+} + e$$

larger ion yields and lower atom yields may be observed (4) in the deuterated system. This results from the fact that the dissociation of molecules containing the lighter isotope may be faster than for their deuterated analogs, while the rates of preionization should be similar. For these reasons a direct comparison of the total ion yields in HCl and DCl by a method independent of chemical electron scavenging was desirable. In this study saturation ionization currents were therefore obtained for HCl and DCl under identical conditions or irradiation in an ionization chamber.

The dissociation of electronically excited ions

$$[6] \qquad HCl \rightarrow HCl^{+*} + e \rightarrow H + Cl^{+} + e$$

is also a source of hydrogen atoms (2) and processes of this type were investigated by mass spectrometry. The results provide information concerning primary processes occurring in the extreme low pressure regime. They are discussed in the light of information in the literature and used to gain a further insight into reactions which may produce different yields of scavengable atoms in HCl and DCl under radiolysis conditions.

Experimental

Materials

Matheson HCl of highest purity available was purified further as previously described (1). Similar procedures were used for the DCl, which was guaranteed 99% minimum isotopic purity as supplied by Merck, Sharp, and Dohme of Montreal. Before experiments were done with DCl, the storage bulbs and vacuum lines which would come in contact with it were exposed to it for several hours and then thoroughly evacuated. This procedure was repeated two to three times.

Apparatus and Procedure

Total ionization yields were obtained by measuring saturation ionization currents in a pyrex ionization chamber with coaxial graphite-coated electrodes. The chamber, which was of a type already described (5), was irradiated in an A.E.C.L. gamma cell 220 at room temperature—first with various pressures of HCl and then with DCl. At each pressure ionization currents were measured with a Victoreen model 475A vibrating reed electrometer at collecting voltages in the range 0 to 3000. Saturation currents were determined graphically.

Ionization efficiency curves for HCl^{+}, HCl^{2+}, Cl^{2+} and a few other ions of less importance were studied at electron energies between 5 and 30 eV and at 70 eV with an Atlas-Varian CH5 Series mass spectrometer fitted with a peak matching unit. Measurements at electron energies between 30 and 100 eV were made with an A.E.I. MS10 mass spectrometer. Similar measurements were made for the corresponding ions from DCl. Prior to this the instruments were baked overnight. The DCl was then introduced and time allowed for stabilization of the H:D isotope ratio. Even under the best circumstances a substantial HCl background remained. This precluded determination of ionization cross sections for the ions from DCl and the results are therefore presented in terms of fractional ion abundances. Taking the Cl^{+} ion from DCl as an example the fractional abundance is defined here as (ion current of Cl^{+}) × (Σ ion current of DCl^{+} and all fragment ions at the same electron energy)$^{-1}$. Allowance for contributions to the DCl fragment peaks from the HCl background was made using the previously measured abundances for HCl and the HCl^{+} 36 peak height.

Results

Ionization Yields

Figure 1*a* shows a plot of ionization current *vs.* collecting voltage for 200.0 Torr of both HCl and DCl in the ionization chamber. The points are seen to be accommodated on a single saturation current plateau. Similar plateaus were obtained for the other HCl pressures and for the DCl pressures shown in Fig. 1*b*. It should be noted that the chamber was baked and evacuated several times prior to use with DCl to ensure complete removal of HCl. Further cycles of

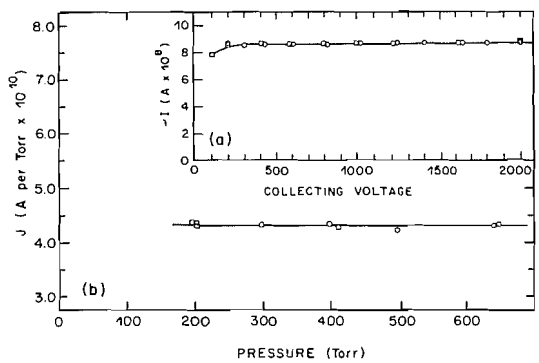

FIG. 1. Circles, HCl; squares, DCl. (*a*) Ionization current plotted as a function of voltage for 200.0 Torr of HCl and DCl; (*b*) saturation ionization current per unit pressure of HCl and DCl plotted as a function of pressure.

Can. J. Chem. Downloaded from www.nrcresearchpress.com by 210.87.254.5 on 09/05/12
For personal use only.

baking and evacuation between successive measurements with DCl produced no change.

The values of the saturation ionization currents divided by the corresponding hydrogen halide pressure are denoted as J and plotted against pressure in Fig. 1*b*.

The mean values of J over all pressures are 4.33 ± 0.04 for DCl and 4.31 ± 0.06 for HCl—both in units of amperes per Torr. The ratio of these two numbers, $1.00_6 \pm 0.02_3$, is related to the W and $G_{\text{ionization}}$ values of the two gases (6) by expression 7:

$$[7] \quad \frac{G_{\text{ionization}}^{\text{HCl}}}{G_{\text{ionization}}^{\text{DCl}}} \frac{J_{\text{DCl}}}{J_{\text{HCl}}} = \frac{W_{\text{DCl}} J_{\text{DCl}}}{W_{\text{HCl}} J_{\text{HCl}}} = \rho_{\text{HCl}}^{\text{DCl}}$$

For HCl and DCl the ratio of stopping powers, $\rho_{\text{HCl}}^{\text{DCl}}$, is unity. Taking $W_{\text{HCl}} = 25.0 \pm 0.04$ (2), $G_{\text{ionization}} (= 100/W) = 4.00 \pm 0.06$ for HCl and, using the above ratio of J values, 4.02 ± 0.08 for DCl.

Ion Abundances

The coincident circles and squares in Fig. 2*b* are plots of HCl^+ ion currents in the 12 to 16 eV region relative to the HCl^+ ion current at 70 eV. These were used to calibrate the energy scale for the corresponding Cl^+ fractional abundances shown in Fig. 2*a*, taking the ionization potential of HCl to be 12.75 eV (7–11). Similar calibrations were made in all other experiments reported here. Figure 3 shows fractional ion abundances for the parent and several other ions of HCl and DCl at higher energies. The early results of Nier and Hanson for HCl (12) extended to energies above 200 eV and are included for comparison. The agreement with the present results in the 40 to 100 eV range is within $\pm 1.5\%$.

As in the case of the Cl^+ ion in Figs. 2*b* and 3 the fractional abundances of Cl^{2+} showed an isotope effect, being about 0.005 less from DCl than from HCl in the 70–100 eV range. The intensities of the HCl^{2+} and DCl^{2+} ions were both much less than those of the Cl^{2+} ions and were not investigated in great detail. However, the fractional abundance of HCl^{2+} became constant at 0.0045 above 80 eV and this agrees with Nier and Hanson's observations (12).

The identity of the HCl_2^+ peak was established by "mass matching" with Cl_2^+ from chlorine which was introduced in some of the HCl samples. Its appearance potential lies in the region of 17 to 18 eV but an accurate determination was precluded by the very low intensity in the thres-

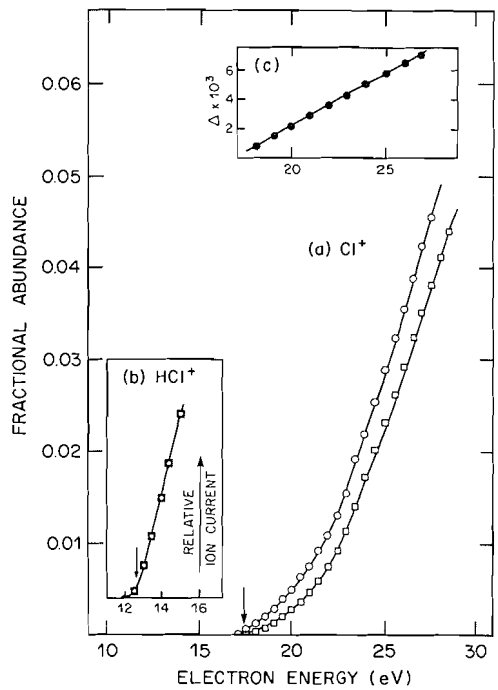

FIG. 2. (*a*) Fractional abundance of Cl^+ from HCl (○) and DCl (□) plotted against electron beam energy; (*b*) HCl^+ ion currents in the threshold region relative to the HCl^+ ion current at 70 eV; (*c*) Plot of Δ, the difference in the fractional abundance of Cl^+ from HCl and DCl, against energy (all data obtained with the Atlas-Varian CH5 mass spectrometer).

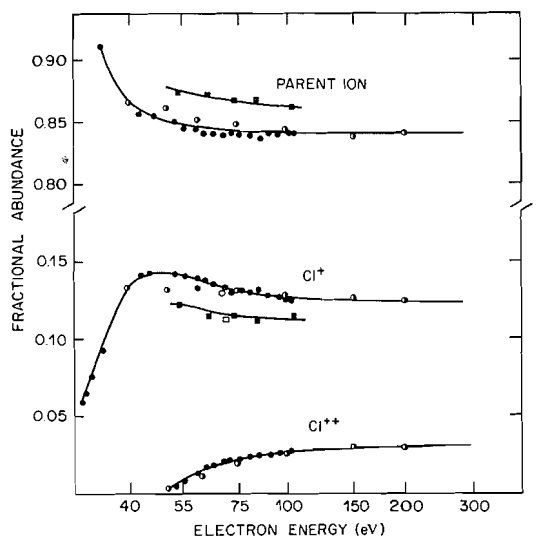

FIG. 3. Fractional abundances: ◑, data of ref. 12; ○, □, this study, Atlas-Varian CH5 mass spectrometer; ●, ■, this study, M.S.10 mass spectrometer; square points are for DCl and round ones for HCl.

hold region (typically $\leqslant 10^{-3}\%$ of HCl^+). At 70 eV the HCl_2^+ ion current increased with the square of the HCl^+ ion current and this behavior resembles that of the H_2Cl^+ ion which is formed (13) in the ion molecule reaction

[8] $$HCl^+ + HCl \rightarrow H_2Cl^+ + Cl$$

showing that HCl_2^+ is probably also produced from a secondary reaction.

Discussion

Total Ionization Yields at High Pressure

The results of the ionization chamber study show that over the pressure range 200 to 600 Torr $G_{ionization}$ is the same in HCl and DCl within an experimental uncertainty of $\pm 2\%$. Hence unless all Cl* atoms produced in reaction 4 undergo chemi-ionization reactions, *viz.*

[9] $$Cl^* + HCl \rightarrow HCl_2^+ + e$$

the competition between reactions 4 and 5 cannot explain the 30% larger yield of H atoms from HCl (*cf.* G_H and G_D in the Introduction). Assuming Cl* is in the $(4s)^2P_{3/2}$ state (14) the appearance potential of HCl_2^+ from the reaction sequence [4]–[9] would be 13.5 eV. As stated in the Results section the observed appearance potential of this ion was in excess of 17 eV and it may be due to reactions between vibrationally excited HCl^+ $(A^2\Sigma^+)$ and HCl.[5] At the present time there is therefore no evidence to support the reaction sequence [4]–[5] as an explanation of the isotope effect on the yields of scavengable H and D atoms.

Ion Fragmentation

The arrows in Figs. 2*a* and 2*b* show respectively the ionization potential of HCl (= 12.75 eV (7 to 11)) and the threshold energy of reaction 6 calculated from D_{HCl} + I.P. of Cl.[6] The present data are consistent with previous mass spectrometric (12, 17) and photoionization (8)[7] studies in that the appearance potential of Cl^+ is within our experimental uncertainty of ± 0.2 eV equal to the calculated threshold energy.

From the data in Fig. 2*a* the ratio of the fractional abundance of Cl^+ from HCl to that from DCl exceeds 2 in the region near threshold and decreases as the electron beam energy rises, becoming constant at 1.14 ± 0.02 above 50 eV. Dissociations from repulsive ionic states probably occur at the higher energies (see below) and would produce Cl^+ ions carrying 2.7 and 5.3% of the total excess kinetic energy available for HCl and DCl respectively. This would result in a 40% greater velocity of the Cl^+ ions from DCl and more of them may therefore be lost from the collection region of the mass spectrometer. If this effect were important it would be greatest at the higher energies and least in the threshold region where the Cl^+ energies are comparable to thermal. As stated above, the ratio of the isotopic abundances shows the opposite behavior. This feature and the correspondence in Fig. 3 of the Cl^+ abundances from HCl observed on three instruments with different source geometries implies that velocity discrimination is not contributing significantly to the observed isotope effect.

The statement in ref. 9 that predissociation of HBr^+ $(A^2\Sigma^+)$ could occur above $v = 4$ through interaction with a nonbonded ionic state (probably the $^4\pi$) led to the suggestion (2) that Cl^+ might be formed from HCl by a similar process in the region near threshold. However, as shown in Fig. 4 even in HCl the Frank–Condon factors calculated (18) for transitions to the vibrational levels of $A^2\Sigma^+$ indicate only a small intensity above the energy for dissociation to $H + Cl^+$ (^3P). This is confirmed by recent photoelectron spectra (10, 11) and it is clear that the predissociation cannot be important. Furthermore, in the energy range 17.4 to 20.6 eV the photoionization yield curves of HCl^+ and Cl^+ exhibit corresponding peaks that do not match known ionic levels (8). The structure has been attributed to superexcited states which preionize either to bound states such as HCl^+ $(A^2\Sigma^+)$ or to

[5]As a check on the ability of our instrument to detect chemi-ionization the spectrum of argon was run under comparable conditions to those used for HCl and Ar_2^+ from $Ar^* + Ar \rightarrow Ar_2^+ + e$ was observed near threshold. The rate constant for this process is 1.7×10^{-9} cm^3 molecule^{-1} s^{-1}, $\sigma_{Ar}^*/\sigma_{Ar^+} = 0.03$ and the lifetime of Ar* is 0.77 μs (ref. 20). Our failure to detect HCl_2^+ at the calculated threshold therefore implies that conditions for reaction 9 are much less favorable than these. The HCl_2^+ ion has previously also been attributed to sticky collisions between Cl^+ and HCl (ref. 21).

[6]$D_{HCl} = 4.43$ and $D_{DCl} = 4.48$ eV from ref. 15, and I.P. of Cl = 12.967 eV from ref. 16.

[7]It may be noted that the difference between the ionization energy to $X^2\Pi_{3/2}$ and $A^2\Sigma^+$ determined in ref. 8 is 4.64 eV, in excellent agreement with 4.65 eV calculated from other spectroscopic data (15 and 7–11). The fact that both ionization energies are low may be due to causes discussed by Berkowitz *et al.* (22).

Can. J. Chem. Downloaded from www.nrcresearchpress.com by 210.87.254.5 on 09/05/12
For personal use only.

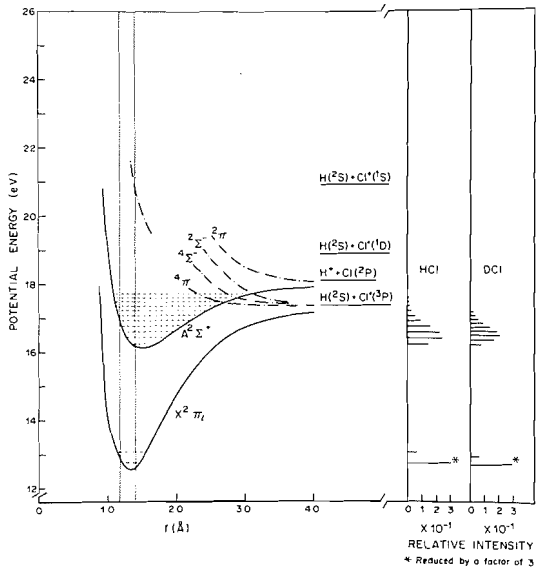

FIG. 4. Potential energy diagram of ionic states of HCl in the 12 to 22 eV region. The relative positions of the repulsive states are taken from ref. 9. The others are based on data in refs. 11, 15, and 18.

nonbonded states correlating with $H(^2S)$ and $Cl^+(^3P)$ at infinite separation (see Fig. 4). This is the energy region in which the difference in the fractional abundances of Cl^+ from HCl and DCl is greatest and the origin of the isotope effect must lie in different rates of crossing of the isotopic species into the bound and unbound ionic levels.

The fractional abundance curves for Cl^+ in Fig. 2*a* show a marked upward rise in the region between 20 and 23 eV and, in agreement with previous mass spectrometric studies (12, 17), the ionization efficiency curve of Cl^+ showed a break at 21.0 ± 0.3 eV. There are also indications of a second break at 22.6 eV (17). From Fig. 2*a* the isotope effect on the processes with onset at and above 21 eV is clearly less than on the lower energy process. To check this further the difference, Δ, between the fractional abundance of Cl^+ from HCl and DCl was plotted against the electron beam energy in Fig. 1*c*. Since the cross sections for the electronic transitions responsible for the low energy process should increase proportionately with electron energy in both HCl and DCl, one anticipates a rise in Δ. The absence of any break supports the view that the processes with appearance potential at and above 21 eV have no detectable isotope effect. It would appear that this can be reconciled most easily with direct transitions between HCl ($X^1\Sigma^+$) and repulsive states of HCl^+ (cf. ref. 19) which cross the Frank–Condon region near 21 eV. The potential energy curves of such states are not known exactly, but the relative levels of some of the ones which correlate with $H(^2S)$ and $Cl^+(^3P)$ are shown in Fig. 4. For the purpose of correlation with radiation chemical data it should be noted that $H(^2S)$ atoms formed from these states would possess excess kinetic energy (*i.e.*, be hot):

$$[10] \qquad HCl \rightarrow HCl^{+**} + e \rightarrow H + Cl^+ + e$$

Thus only the process(es) occurring below 21 eV can be expected to contribute significantly to the yields of scavengable H and D atoms through reaction 6. However, from the relative slopes of the ionization efficiency curves above and below 21 eV it can be estimated that the cross section for these processes constitutes only about 25% of the total cross section for Cl^+ production from HCl. The corresponding fraction from DCl would be ~15%, and the yields of H and D atoms from reaction 6 in the low pressure regime are therefore small.

As seen from Fig. 3 and pointed out in the Results section the fractional abundances of Cl^{2+} from HCl and DCl are 0.030 and 0.025 in the "optical" energy range. This ion is not therefore of great importance. However, it is worth noting that Cl^{2+} probably decays by charge exchange with HCl and, since the recombination energy to Cl^+ is 23.8 eV (2), the conclusions of the preceding paragraph indicate that reaction 11 should have a small or negligible isotope effect:

$$[11] \qquad Cl^{2+} + HCl \rightarrow Cl^+ + H + Cl^+$$

Similar considerations apply to the charge transfer reactions of HCl^{2+} and DCl^{2+}

$$[12] \qquad HCl^{2+} + HCl \rightarrow HCl^+ + H + Cl^+$$

which have a recombination energy of ~23 eV (2). These ions are even less important than Cl^{2+} (see Results).

Conclusions

Total ionization yields in HCl and DCl in the high pressure regime under radiolysis conditions are the same within an experimental uncertainty of ±2%. Ion pair yields of scavengable hydrogen atoms calculated from ($G_{H\text{ or }D}/G_{ionization}$) are 0.45 and 0.30 for H atoms in HCl and D atoms in DCl respectively.

Can. J. Chem. Downloaded from www.nrcresearchpress.com by 210.87.254.5 on 09/05/12
For personal use only.

Assuming maximum efficiency for reactions 11 and 12, combined ion pair yields for scavengable and hot atoms of 0.16 in HCl and 0.14 in DCl can be calculated from the fractional ion abundances for Cl^+, Cl^{2+}, HCl^{2+}, and DCl^{2+} in the optical energy range above 70 eV in Fig. 3. The isotope effect occurs primarily for the low energy processes which are likely to form scavengable atoms. However, the ionization efficiency and fractional abundance curves indicate that these processes can make only small contributions ($\sim$0.04 for HCl and $\sim$0.02 for DCl) to the combined atom yields of 0.16 and 0.14 respectively. Even these are smaller than the radiolytic yields. In fact if reactions 6, 10, 11, and 12 were the only sources of atoms their ion pair yields would have to increase by a factor of 3 in the case of HCl and 2 for DCl in going from mass spectrometric conditions to radiolysis conditions at 600 Torr. Furthermore the dissociations would have to be perturbed to produce exclusively scavengable atoms and processes with large isotope effect would have to become dominant. In the light of the preceding discussion and recognizing that ionic dissociations such as [10] should occur in 10^{-12} s with diatomic molecules, it is evident that there must be other sources of H and D atoms in the irradiated systems. Further work is required to establish what these are.

The authors are indebted to the National Research Council of Canada for financial support and to The University of Calgary for the use of laboratory facilities. Acknowledgment is made to Mr. P. Dale for technical assistance. Also appreciation is expressed to Dr. T. Terwilliger for helpful information and discussion.

1. R. A. Lee, R. S. Davidow, and D. A. Armstrong. J. Chem. Phys. **42**, 1906 (1964).
2. D. E. Wilson and D. A. Armstrong. Rad. Res. Rev. **2**, 297 (1970).
3. D. K. Jardine, D. A. Armstrong, A. W. Boyd, and C. Willis. Can. J. Chem. **49**, 187 (1971).
4. R. L. Platzman. Rad. Res. **17**, 419 (1962).
5. D. E. Wilson and D. A. Armstrong. Can. J. Chem. **40**, 598 (1970).
6. R. S. Davidow and D. A. Armstrong. Rad. Res. **28**, 143 (1966).
7. K. Watanabe. J. Chem. Phys. **26**, 542 (1957).
8. M. Krauss, J. A. Walker, and V. H. Dibeler. J. Res. Natl. Bur. Stand. **72A**, 281 (1968).
9. H. J. Lemka, T. R. Passmore, and W. C. Price. Proc. R. Soc. A, **304**, 53 (1968).
10. D. C. Frost, C. A. McDowell, and D. A. Vroom. J. Chem. Phys. **46**, 4255 (1967); and private communication.
11. M. J. Weiss, G. M. Lawrence, and R. A. Young. J. Chem. Phys. **52**, 2867 (1970).
12. A. O. Nier and E. O. Hanson. Phys. Rev. **50**, 722 (1936).
13. D. P. Stevenson and D. O. Schissler. J. Chem. Phys. **29**, 282 (1958).
14. C. E. Moore. Atomic energy levels. Natl. Bur. Stand. Circ. 467 (1949).
15. G. Herzberg. Spectra of diatomic molecules. Van Nostrand, New York. 1965.
16. R. E. Huffman, J. C. Larabee, and Y. Tanaka. J. Chem. Phys. **47**, 856 (1967).
17. R. Thornburn. Proc. Phys. Soc. **73**, 122 (1959).
18. H. Halmann and I. Laulicht. J. Chem. Phys. **43**, 1503 (1965).
19. F. Fiquet-Fayard. Bull. Soc. Chim. Belg. **73**, 373 (1964).
20. J. L. Franklin. Adv. Chem. Ser. **72**, 1 (1968).
21. A. Henglein. Molecular beams and reaction kinetics. *Edited by* C. Shier. Academic Press, New York. 1970. p. 147.
22. J. Berkowitz, W. A. Chupka, P. M. Guyon, J. H. Holloway, and R. Spohr. J. Chem. Phys. **54**, 5165 (1971).

Can. J. Chem. Downloaded from www.nrcresearchpress.com by 210.87.254.5 on 09/05/12
For personal use only.

Can. J. Chem. Downloaded from www.nrcresearchpress.com by 210.87.254.40 on 09/05/12
For personal use only.

A Mass Spectrometric Study of the Influence of Electronic and Stereochemical Factors on the Hofmann Elimination Process in Quaternary Ammonium Salts

PETER JAMES SMITH

Department of Chemistry and Chemical Engineering, University of Saskatchewan, Saskatoon, Saskatchewan

Received June 6, 1973

The mass spectra of the thermal decomposition products derived from the geometrical isomers of 2-phenylcyclohexyl- and 2-phenylcyclopentyltrimethylammonium salts together with their 2-d_1 analogs have been determined together with the rigid substrate, 3-*endo*-2-*exo*-norbornyltrimethylammonium bromide. It is found that the Hofmann elimination reaction is most favored when the departing groups or atoms have the *anti* coplanar relationship and that the abstracted hydrogen is exclusively the benzylic hydrogen. A series of 1-arylethyltrimethylammonium salts were also examined together with their 1-d_1 and 2-d_3 analogs. It was found that electron-donating substituents on the phenyl ring favor the Hofmann elimination process while electron withdrawers lead to the pyrolytic reaction of halide substitution at carbon.

Les spectres de masse des produits de décomposition thermique des isomères géométriques des sels de phényl-2 cyclohexyl et phényl-2 cyclopentyl triméthylammonium ainsi que de leurs homologues d_1-2 ont été déterminés conjointement à ceux d'un substrat rigide le bromure de *endo*-3 *exo*-2 norbornyltriméthylammonium. On a trouvé que la réaction d'élimination de Hofmann est favorisée lorsque les groupes ou atomes partants sont en positions *anti*-coplanaires et lorsque les hydrogènes éliminés sont exclusivement benzyliques. Une série de sels d'aryl-1 éthyl triméthylammonium ont aussi été examinés ainsi que leurs homologues d_1-1 et d_3-2. On a trouvé que, sur le cycle phényle, des substituants donneurs d'électrons favorisent le processus d'élimination de Hofmann alors que des substituants attracteurs d'électrons conduisent à la réaction pyrolytique de substitution d'un halogène au niveau du carbone.

[Traduit par le journal]

Can. J. Chem., 52, 365 (1974)

Introduction

A mass spectral study of quaternary ammonium ions has received little attention. Due to the nonvolatility of these salts it is necessary for pyrolytic reactions to occur in the source of the mass spectrometer to generate neutral particles which can be vaporized and subsequently ionized.

Competing thermal reactions in the source can generate a variety of neutral molecules which, after subsequent ionization and fragmentation, can lead to a complicated mass spectrum arising from the superimposition of several mass spectra. The most common thermal reaction (1) observed is substitution leading to the nor base and the alkyl halide, eqs. 1 and 2.

[1]
$$\underset{\substack{|\\ X^-\ {}^+N(CH_3)_3}}{RCHR'} \xrightarrow{\Delta} \underset{\substack{|\\ N(CH_3)_2}}{RCHR'} + CH_3X$$
X = halide ion

[2]
$$\underset{\substack{|\\ X^-\ {}^+N(CH_3)_3}}{RCHR'} \xrightarrow{\Delta} \underset{\substack{|\\ X}}{RCHR'} + N(CH_3)_3$$

The other frequently observed pyrolytic process (2) is the Hofmann elimination leading to the formation of an olefin and the hydrogen halide, eq. 3. It is possible for this decomposition

[3]
$$\underset{\substack{|\\ X^-\ {}^+N(CH_3)_3}}{RCHCH_2R'} \xrightarrow{\Delta} RCH = CHR' + N(CH_3)_3 + HX$$

pathway to lead to a variety of olefinic products depending upon the number of different β-hydrogens, eq. 4. The ease of the Hofmann

[4]
$$\underset{\substack{|\\ X^-\ {}^+N(CH_3)_3}}{CH_3\overset{\beta'}{C}H_2\overset{\alpha}{C}H\overset{\beta}{C}H_3} \rightarrow CH_3CH = CHCH_3 + CH_3CH_2CH = CH_2 + N(CH_3)_3 + HX$$

reaction is related to the nature of the anion, X, (2). For example, it has been shown that iodide ion is less able to promote the Hofmann reaction than fluoride and conversely more likely to favor substitution than the more electronegative anion.

The reaction of quaternary ammonium ions with base has been extensively studied in solution (3). Elimination generally proceeds to give the least hindered olefin by the concerted one-step pathway. A study of substituent and kinetic isotope effects (4, 5) has established that

Can. J. Chem. Downloaded from www.nrcresearchpress.com by 210.87.254.40 on 09/05/12
For personal use only.

the reaction is facilitated when the β-hydrogen is made more acidic or the strength of the abstracting base is increased. Indeed, considerable studies have been made with respect to the nature of the transition state for the E2 process, *i.e.*, whether an increase in C—H bond rupture is accompanied by an increase or decrease in C—$\overset{+}{N}$ bond weakening.

The effect of dihedral angle on the ease and stereochemistry of elimination has recently received considerable attention (6). It has long been considered that concerted elimination reactions proceed most readily when the carbon–hydrogen and carbon – leaving group bonds have a *trans-anti* relationship to one another; *cis-syn* eliminations are known, however, and have been most frequently encountered when the geometry of the reacting molecule is such that the reacting bonds are unable to assume the *anti* relationship. DePuy *et al.* (7) have suggested that the essential feature of an E2 reaction is not the *trans* relationship of the departing atoms but coplanarity of the four-atom system H—C—C—Z. This can arise when the C—H and C—Z bonds are directed 180° with respect to one another. It also can arise when the dihedral angle is 0°, in which case the departing atoms have a *cis-syn* relationship. DePuy predicts that E2 processes should proceed most readily when the dihedral angle is 180 or 0° and should be most difficult when the geometry of the molecule is constrained in such a way as to cause the maximum deviation from the coplanar situation.

Accordingly, we have examined, by mass spectrometry, the pyrolysis of five *para*-substituted 1-arylethyltrimethylammonium salts in order to gain an insight into possible electronic factors involved in the pyrolytic processes. The *cis* and *trans* isomers of 2-phenylcyclohexyl- and 2-phenylcyclopentyltrimethylammonium salts were examined together with the rigid substrate, 3-*endo*-phenyl-2-*exo*-norbornyltrimethylammonium bromide in an attempt to examine the stereochemical factors associated with the Hofmann elimination process.

Results and Discussion

The Effect of Geometry on the Hofmann Elimination Process

The compounds which have been investigated include those shown in Series 1 together with their 2-d_1 analogs. As well, 3-*endo*-phenyl-2-*exo*-norbornyltrimethylammonium bromide (**5**) and

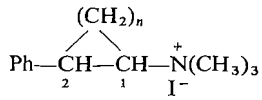

1 $n = 4$, *trans* compound
2 $n = 4$, *cis* compound
3 $n = 3$, *trans* compound
4 $n = 3$, *cis* compound

SERIES 1

its 3-d_1, analog were examined. The mass spectral data for the major ions of the pyrolysis products from **1** to **5** are recorded in Table 1. Figures 1 and 2 are bar graphs of the spectra of the products from **1** and **2**.

It can be seen from the data in Table 1 that the principal ions formed in the source of the mass spectrometer when the *trans* (**1**) and *cis* (**2**) cyclohexyl salts are pyrolyzed (Figs. 1 and 2,

TABLE 1. Percentage total intensity and *m/e* values of the principal ions in the 70 eV spectra of the pyrolysis products from compounds in Series 1 as well as of 3-*endo*-phenyl-2-*exo*-norbornyltrimethylammonium bromide

Compound	*m/e*	% Σ_{40}
1	203(204)*	9
	158	2
	142	14
	84	36
	58	5
2	203(204)*	4
	158	10
	142	6
	84	14
	58	6
3	189(190)*	7
	144	—
	142	15
	84	35
	58	6
4	189(190)*	6
	144	5
	142	10
	84	29
	58	4
5	215(216)*	10
	98	16
	96	5
	94	5
	58	8

*m/e value observed in the spectrum of the pyrolysis products from the deuterated analog (2-d_1 for 1–4 and 3-d_1 for 5).

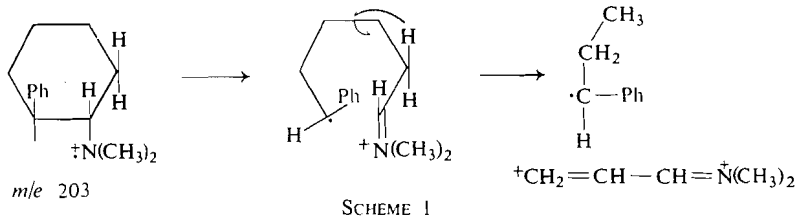

SCHEME 1

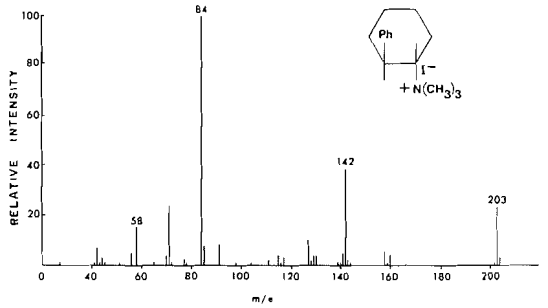

FIG. 1. Mass spectrum (70 eV) of pyrolysis products from **1**.

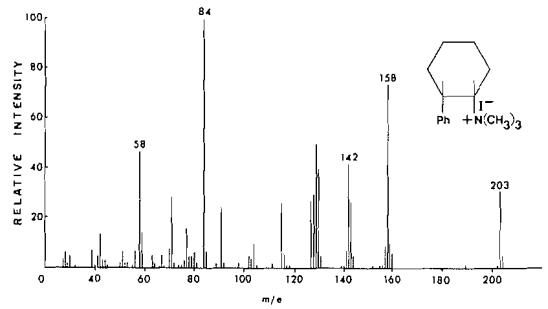

FIG. 2. Mass spectrum (70 eV) of pyrolysis products from **2**.

respectively) correspond to the *trans*- and *cis*-*N*,*N*-dimethyl-2-phenylcyclohexylamine (*m*/*e* 203), 1-phenylcyclohexene (*m*/*e* 158), methyl iodide (*m*/*e* 142), and the M − 1 fragment ion from trimethylamine (*m*/*e* 58). The ions formed from the corresponding *trans* (**3**) and *cis* (**4**) cyclopentyl quaternary ammonium iodides represent the *trans*- and *cis*-*N*,*N*-dimethyl-2-phenylcyclopentylamines (*m*/*e* 189), 1-phenylcyclopentene (*m*/*e* 144) together with the ions at *m*/*e* 142, 84, and 58.

The base peak in the spectra of the pyrolysis products of each of **1**–**4**, as well as their 2-d_1 analogs, is at *m*/*e* 84. This ion could be formed from the *N*,*N*-dimethylamines by the pathway shown in Scheme 1.

The data of particular interest in Table 1 are the percentages of total ion current for the Hofmann products, *i.e.*, 1-phenylcyclohexene (*m*/*e* 158) and 1-phenylcyclopentene (*m*/*e* 144) from the 2-phenylcyclohexyl- and 2-phenylcyclopentyltrimethylammonium iodides, respectively. It is seen that for the *trans* cyclohexyl salt, the olefin represents 2% of the total ion current whereas the *cis* cyclohexyl salt on pyrolysis gives the Hofmann product which carries 10% of the ion current. Consequently, it must be concluded that elimination is more favored from the *cis* isomer than from the *trans*. Similarly, the same conclusion is reached when one examines the *trans* and *cis* cyclopentyl compounds, **3** and **4**, *i.e.*, the olefin represents 0 and 5% of the total ion current, respectively. It is to be noted that the substitution products, *N*,*N*-dimethylamines and methyl iodide, carry a greater percentage of the total ion current for the *trans* substrates (**1** and **3**) where elimination is not as favored.

It is extremely difficult to determine the exact conformation of each of compounds **1**–**4** in the sample probe of the mass spectrometer at approximately 230 °C. In the case of the *cis* cyclohexyl salt more than one conformation provides coplanarity with a dihedral angle of 180° or close to it. The reacting conformer could be the twist-boat since it provides the least crowded situation. The slightly puckered cyclopentane ring provides approximate coplanarity of the C—H and C—$\overset{+}{N}$ bonds with both isomers. For the *cis* isomer undergoing *trans* elimination, the dihedral angle is not far from 180°, while in the *cis* elimination of the *trans* compound the angle is close to 0°. For the *trans* cyclohexyl salt, which undergoes *cis* elimination, the favored conformation, which places the bulky groups in the less crowded equatorial positions, provides a dihedral angle of 60°, far from that required for coplanarity.

The results of this study generally agree with conclusions reached from studies of the E2 reaction in solution where elimination is favored when the departing groups, H and

Can. J. Chem. Downloaded from www.nrcresearchpress.com by 210.87.254.40 on 09/05/12
For personal use only.

$N(CH_3)_3$, have the *anti* coplanar relationship. When the dihedral angle is 60 or 0° elimination is less favored and substitution predominates. Indeed, the mass spectrum of the pyrolysis products from the *trans* cyclopentyl salt, dihedral angle approximately 0°, does not indicate any olefin.

The small amount of elimination product from the pyrolysis of the *trans* cyclohexyl salt (**1**), where the departing groups cannot easily acquire a coplanar relationship, is probably due to the flexibility of the ring. That this is so is suggested by the data in Table 1 for 3-*endo*-phenyl-2-*exo*-norbornyltrimethylammonium bromide (**5**), a rigid system where coplanarity cannot be obtained, the major ions are the *N*,*N*-dimethylamine (*m*/*e* 215), methyl bromide (*m*/*e* 94 and 96), and the usual *m*/*e* 58 ion. An ion, corresponding to the Hofmann product, at *m*/*e* 170 was not observed in the spectrum. The 3-d_1 analog of **5** gave an identical mass spectrum to that obtained for **5** except that the ion corresponding to the *N*,*N*-dimethylamine appeared one mass unit higher (*m*/*e* 216).

The spectra of the 2-d_1 analogs of compounds **1**–**4** were also identical to those of the undeuterated substrates except for the substitution product, the *N*,*N*-dimethylamine. Of particular interest is the observation that the Hofmann elimination product did not contain deuterium and hence must be 1-phenylcyclohexene and 1-phenylcyclopentene rather than the other possible product of β-elimination, *i.e.*, 3-phenylcyclohexene and 3-phenylcyclopentene. Presumably, as has been observed for reactions in solution (8), the acidity of the β-hydrogen and the stability of the product is a predominant driving force for the pyrolytic Hofmann reaction.

The Effect of Electronic Factors on the Pyrolytic Processes

The compounds which have been examined are those shown in Series 2 together with their 1-d_1 and 2-d_3 analogs.

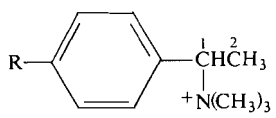

6 R = CF_3
7 R = Cl
8 R = H
9 R = CH_3
10 R = OCH_3

SERIES 2

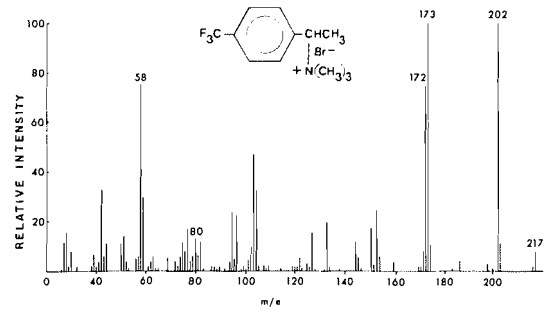

FIG. 3. Mass spectrum (70 eV) of pyrolysis products from **6**.

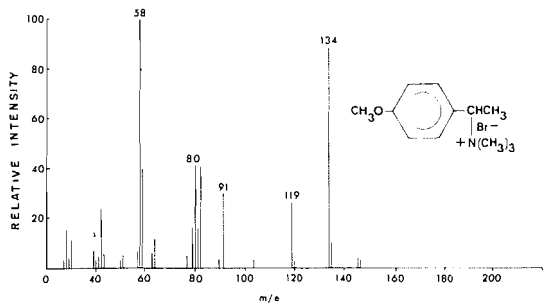

FIG. 4. Mass spectrum (70 eV) of pyrolysis products from **10**.

Figures 3 and 4 are bar graphs of the spectra of pyrolysis products from **6** and **10**. The major ions observed for the substitution reaction, $R—C_6H_4—CH=\overset{+}{N}(CH_3)_2$, and the elimination reaction, $H\overset{+}{B}r$, are shown in Table 2 together with their percentage of the total ion current.

The ion of greatest relative abundance related to the substitution reaction is $R—C_6H_4—CH=\overset{+}{N}(CH_3)_2$. This fragment ion (*m*/*e* 202 in Fig. 3) is formed from the substitution product, *N*,*N*-dimethylamine (*m*/*e* 217 in Fig. 3), by the facile loss of CH_3. (Scheme 2). Confirmation is given by an examination of the spectra of the 1-d_1 and 2-d_3 analogs of the quaternary salts, *i.e.*, for the β-d_3 substrate.

The percentage of the total intensity, % Σ_{40}, for hydrogen bromide was used as a measure of the extent of the pyrolytic elimination reaction in the source. This was necessary since an ion which could be used to measure the substituted styrene product formed could arise, depending upon R, by two pathways. The first pathway, which was predominant for the substrates with electron-withdrawing substituents in the *para* position, involved loss of Br from the alkyl

Can. J. Chem. Downloaded from www.nrcresearchpress.com by 210.87.254.40 on 09/05/12
For personal use only.

Can. J. Chem. Downloaded from www.nrcresearchpress.com by 210.87.254.40 on 09/05/12
For personal use only.

TABLE 2. Percentage total intensity and m/e values of the ions, $R—C_6H_4—CH{=}\overset{+}{N}(CH_3)_2$ and $HBr^{\overset{+}{\cdot}}$, in the 70 eV spectra of pyrolysis products from compounds in Series 2

		$R—C_6H_4—CH{=}\overset{+}{N}(CH_3)_2$		$HBr^{\overset{+}{\cdot}}$	
R	Compound	% Σ_{40}	m/e	% Σ_{40}*	m/e
CF_3	**6**	11.0	202(203)‡	2.7	80(81)†
Cl	**7**	5.1	168(169)	5.1	80(81)
H	**8**	3.9	134(135)	6.1	80(81)
CH_3	**9**	2.1	148(149)	9.0	80(81)
OCH_3	**10**	0	—	16.	80(81)

*Only ^{79}Br is considered.
†m/e value of corresponding ion formed in 70 eV spectra of pyrolysis products from the 2-d_3 analogs of the compounds in Series 2.
‡m/e value of corresponding ion formed in 70 eV spectra of pyrolysis products from the 1-d_1 analogs of the compounds in Series 2.

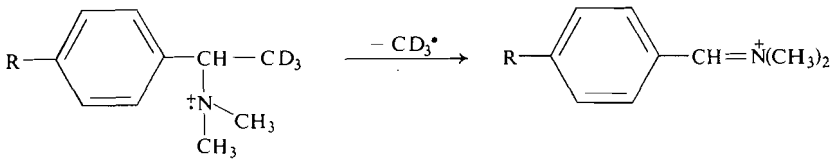

SCHEME 2

bromide[1] formed by the substitution reaction on the benzylic carbon (m/e 173 in Fig. 3) followed by loss of a hydrogen atom from the 2-carbon (m/e 172 in Fig. 3), eq. 5.

[5] $$\left[R—C_6H_4\underset{\displaystyle Br}{\underset{|}{C}}HCH_3\right]^{\overset{+}{\cdot}} \xrightarrow{-Br^{\cdot}} [R—C_6H_4CHCH_3]^+ \xrightarrow{-H^{\cdot}} [R—C_6H_4CH{=}CH_2]^{\overset{+}{\cdot}}$$

The other route for the formation of this ion was by the ionization of the olefin formed in the one-step pyrolytic elimination reaction with halide acting as the abstracting base, eq. 6. This pathway was favored when R was electron donating and, in fact, was followed exclusively for the p-OCH_3 substrate (m/e 134 in Fig. 4).

[6] $$R—C_6H_4\underset{\displaystyle Br^- \quad {}^+N(CH_3)_3}{\underset{|}{C}}HCH_3 \xrightarrow{\Delta} R—C_6H_4CH{=}CH_2 + HBr + N(CH_3)_3$$

It can be seen from the data in Table 2 that the extent of Hofmann elimination increases as the *para* substituent is made more electron donating, *i.e.*, % Σ_{40} for HBr increases from 2.7 to 16 for the p-CF_3 and p-OCH_3 substrates, respectively. Alternatively, the substitution reaction of halide on the N—CH_3 to give methyl bromide and the *N,N*-dimethylamine[2] decreases as the *para* substituent is made more electron donating. These trends are in accord with the competing halide promoted substitution and elimination reactions.

A possible explanation for the enhancement of elimination over that of substitution when R=OCH_3 is that the halide ion, in the crystal or the melt during pyrolysis in the probe, is not as close to the positive onium ion and hence can more readily promote elimination by removal of the 2-hydrogen. On the other hand, for the p-CF_3 substrate, the halide ion is probably in very close proximity to the positive nitrogen and hence not as "available" to effect elimination and consequently substitution predominates. If the halide ion is made more "tightly-bonded" to nitrogen in the crystal it is expected that the melting point of the compound would increase. This is observed as the melting points for compounds **6–10** are 224, 199, 193, 179, and 165°, respectively.

It is possible to invoke some stabilization of the positive nitrogen by electron donation from the ring, which would allow some freeing of the

[1]The relative intensity of the 1-arylethyl bromides in all cases was less than one. The bromide was observed in the spectra of each salt except for the p-OCH_3 substrate.

[2]As measured by % Σ_{40} of $R—C_6H_4CH{=}\overset{+}{N}(CH_3)_2$.

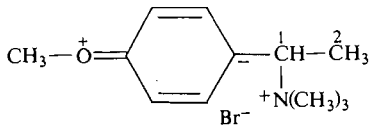

halide anion. This, however, is highly speculative and further work is planned to investigate the electronic and stereochemical factors which effect the pyrolytic reactions.

Experimental

The compounds in Series 1 as well as 3-*endo*-phenyl-2-*exo*-norbornyltrimethylammonium bromide together with their deuterated analogs were graciously supplied by Dr. A. N. Bourns. The substrates shown in Series 2 and their deuterated analogs were donated by Mr. David Tsui. In all cases the deuterated substrates were shown to be better than 99% deuterated.

The mass spectra were determined with an MS-12 mass spectrometer operating at 70 eV and an ion source temperature of 220°. The samples were introduced via the direct probe technique. In all cases the spectra were reproducible when the source temperature was changed by as much as 30°.

Financial assistance by the National Research Council of Canada is gratefully acknowledged.

1. M. HESSE, W. VETTER, and H. SCHMID. Helv. Chim. Acta, **48**, 674 (1965).
2. M. HESSE and H. SCHMID. Liebigs Ann. Chem. **696**, 85 (1966).
3. J. K. BORCHARDT and W. H. SAUNDERS JR. Tetrahedron Lett. 3439 (1972) and earlier papers; P. J. SMITH and A. N. BOURNS. Can. J. Chem. **48**, 125 (1970) and earlier papers; D. V. BANTHORPE. Elimination reactions. Elsevier, Amsterdam 1963.
4. A. FRY. Chem. Soc. Rev. **1**, 163 (1972).
5. D. J. MCLENNAN. Quart. Rev. **21**, 490 (1967).
6. M. PÁNKOVÁ, M. SVOBODA, and J. ZÁVADA. Tetrahedron Lett. 2465 (1972) and earlier papers.
7. C. H. DEPUY, R. D. THURN, and G. F. MORRIS. J. Am. Chem. Soc. **84**, 1314 (1962).
8. G. AYREY, E. BUNCEL, and A. N. BOURNS. Proc. Chem. Soc. 485 (1961) and references therein.

Can. J. Chem. Downloaded from www.nrcresearchpress.com by 210.87.254.40 on 09/05/12
For personal use only.

The Conformation of β-Pseudouridine about the Glycosidic Bond as Studied by ^{1}H Homonuclear Overhauser Measurements and Molecular Orbital Calculations[1]

R. K. NANDA, R. TEWARI, AND G. GOVIL[2]

Tata Institute of Fundamental Research, Homi Bhabha Road, Bombay 400005, India

AND

IAN C. P. SMITH

Division of Biological Sciences, National Research Council of Canada, Ottawa, Canada KIA 0R6

Received July 17, 1973

The conformation of β-pseudouridine about the glycosidic bond has been studied by both the internal nuclear Overhauser effect and CNDO molecular orbital calculations. Both *syn* and *anti* conformations are found to exist in rapid equilibrium, with roughly equal populations of each. The proportion of *syn* to *anti* conformations does not change significantly with p*D* over the range 7.1 to 11.6. The CNDO calculations suggest that the *syn* conformation is stabilized by formation of a hydrogen bond, $C_4{=}O\ldots O{-}H_{5'}$, but the n.m.r. data indicate that if such a bond exists its probability is the same at p*D* 7.1 and 11.6. Major contributions to n.O.e. may occur through conformations other than those which are most stable.

L'effet Overhauser intramoléculaire et des calculs théoriques par la méthode CNDO ont permis d'étudier la conformation de la β-pseudouridine autour de la liaison glycosidique. On a trouvé que les deux conformations, *syn* et *anti*, sont en équilibre rapide, avec des populations sensiblement égales. Les proportions des conformations *syn* et *anti* ne changent pas de manière significative dans l'intervalle de p*D* de 7.1 à 11.6. Les calculs CNDO suggèrent que la conformation *syn* est stabilisée par la formation d'une liaison hydrogène $C_4{=}O\ldots O{-}H_{5'}$, mais les données de la r.m.n. montrent que la probabilité d'existence d'une telle liaison est la même aux p*D* 7.1 et 11.6. Des conformations autres que les conformations les plus stables peuvent avoir des contributions importantes dans le n.O.e. [Traduit par le journal]

Can. J. Chem., **52**, 371 (1974)

Introduction

Nuclear magnetic resonance spectroscopy (n.m.r.) has been used recently (1–4) to derive information about the conformation of β-pseudouridine (β–ψ), which occurs as a minor constituent of transfer RNA. Information about the ribose geometry and the conformation about the exocyclic $C_{4'}{-}C_{5'}$ bond, has been obtained from ^{1}H n.m.r. data. However, direct evidence on the sugar–base torsion angle (χ) could not be obtained by such studies. Indirect evidence has been interpreted both in terms of an appreciable population of *anti* conformer of β–ψ (1–6) as well as that of *syn* conformation stabilized by an O—H...O bond between the 5′-hydroxyl proton and the oxygen on C_4 of the base at high p*H* (7).

Recently, the internal nuclear Overhauser effect (n.O.e.) has been used (8–11) in studies of nucleoside conformations. In particular the technique has been applied to determine the glycosidic bond conformation. In this double resonance experiment enhancement in the intensity of the resonance line of a magnetic nucleus (*i*) is observed when another nucleus (*j*) in its proximity is saturated. The n.O.e. depends on the ^{1}H relaxation mechanisms and a general treatment of this phenomenon has been given recently (12). If the sample is sufficiently dilute, paramagnetic impurities are absent and one is dealing with spin $\frac{1}{2}$ nuclei, then intramolecular dipole–dipole interaction is the dominant factor contributing to n.O.e. Since this interaction depends on the inverse sixth power of internuclear distance r_{ij}, the relative values of n.O.e. yield a rough estimate of various internuclear distances in a rigid molecule. We have chosen β-pseudouridine for this study because of the lack of competing relaxation mechanisms from other base protons (H_5 in uridine), and because of the suggestion that at p*D* 11.6 the *syn* conformation can be stabilized by hydrogen-bond formation (7).

[1]Issued as NRCC Publication Number 13555.
[2]NRCC Visiting Scientist, 1972.

Can. J. Chem. Downloaded from www.nrcresearchpress.com by 210.87.254.6 on 09/05/12
For personal use only.

Can. J. Chem. Downloaded from www.nrcresearchpress.com by 210.87.254.6 on 09/05/12
For personal use only.

Theoretical calculations using molecular orbital theory have also been applied with success in investigations of the conformations of nucleosides and nucleotides (13–17). Studies on glycosidic bond rotation in common nucleosides have been reported by Berthod and Pullman (17) who have used the PCILO method. Such calculations can be used to determine the relative stabilities of individual points in conformational space whereas the n.m.r. investigations give a "time-average" picture.

In this paper we report the n.O.e. experiments on β–ψ which indicate the presence of an equilibrium involving detectable proportions of *syn* and *anti* conformations. Calculations based on complete neglect of differential overlap (CNDO) have enabled a deeper insight into the factors stabilizing the molecule in the two states and into the mechanism of nuclear Overhauser enhancements.

Materials and Techniques

Nuclear Magnetic Resonance Measurements

β–ψ was purchased from Calbiochem. The purity of the sample was better than 95% as indicated by the absence of any unexplained features in the n.m.r. spectra. A solution containing 0.10 *M* β–ψ and 0.10 *M* 3-(trimethylsilyl)propanesulfonic acid sodium salt (DSS, Merck, Sharpe, and Dohme, Canada) in deuterium oxide (D_2O) was prepared. Sample p*D*'s were adjusted using dilute solutions of NaOD (p*D* = meter reading + 0.4) and were then triply lyophilized from D_2O to remove residual HDO. The samples were carefully degassed to remove traces of oxygen. The ^1H n.m.r. measurements were made on a VARIAN XL-100 spectrometer; the radio-frequency field used for the double resonance experiments was calibrated in a separate experiment based on measurements of Bloch–Siegert shifts (18) of the chloroform ^1H resonance in a chloroform–tetramethylsilane mixture. The n.O.e. enhancements were generally measured using changes in the peak height of the H_6 resonance when the ribofuranose protons were irradiated. However, this method could not be used when $H_{1'}$ was irradiated, since $H_{1'}$ and H_6 show a small scalar coupling (1–3). In this case, the integrated area of the H_6 resonance was used. The n.O.e. has been expressed as the percentage difference in the peak height (intensity) when the sugar protons were saturated and when the double resonance field was applied off-resonance. In the latter case the double resonance field was set in a region free from any n.m.r. signal. In this way base line changes and effects arising from the loading of the master oscillator were avoided. About twenty measurements were made in each case. No attempts have been made to interpret n.O.e. results of less than 4% in view of the basic difficulties in such measurements. Double resonance field strengths corresponding to 3–15 Hz were used in the experiments.

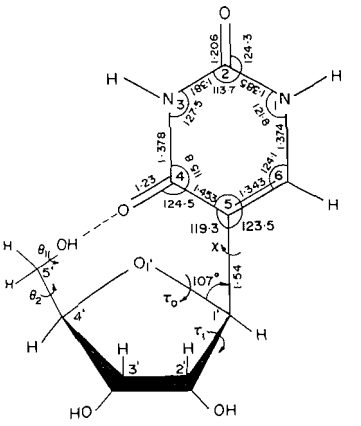

FIG. 1. The primary structure of β–ψ. The H-bonded structure shown here is one of the many conformers which may be present in aqueous solutions.

Theoretical Calculations

The CNDO calculations were performed on a CDC-3600 computer using a slightly modified version (13, 14) of QCPE 142 (19). The input to the program consists of the Cartesian coordinates of the various atoms. The coordinates are calculated using the bond lengths, bond angles and the torsional angles τ_0, τ_1, χ, θ_1, and θ_2 (Fig. 2) which define the conformation of the molecule. The sugar geometry used has been taken from an earlier publication (14), while the base geometry is shown in Fig. 1. The computer time was reduced considerably by replacing the 2′ and 3′ hydroxyl groups by hydrogen atoms. These groups do not come in proximity to either the base or the 5′-CH_2OH group and therefore such a replacement does not affect the basic conclusions drawn in the next section. Their inclusion would affect the relative energies of the various forms of the ribofuranose ring.

Discussion

(a) CNDO Calculations

The calculation of the conformation of β–ψ is a problem in multidimensional conformation space. Specifically, in addition to the conformation of the sugar ring (angles τ_0 and τ_1 as defined in ref. 14) and the rotation χ about the glycosidic bond one has to consider the angles θ_1 and θ_2 which denote rotations about the $C_{5'}$—$O_{5'}$ and $C_{4'}$—$C_{5'}$ bonds, respectively (see Fig. 2 for definitions). Further, these rotations are coupled to one another. In other words, the value of χ which leads to a minimum energy conformation is expected to depend on the sugar ring geometry as well as on θ_1 and θ_2. A further complication is the flexibility of β–ψ both in the ribofuranose ring and in the exocyclic —CH_2OH group (1–4). The H-bonded structure of the type shown in

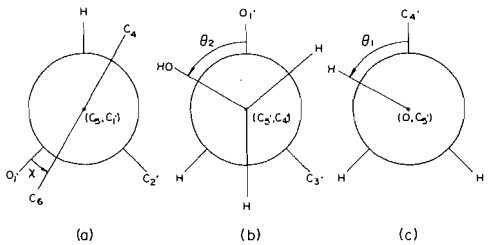

FIG. 2. Notation of the torsional angles χ, θ_2, and θ_1 which determine the overall conformation of β–ψ.

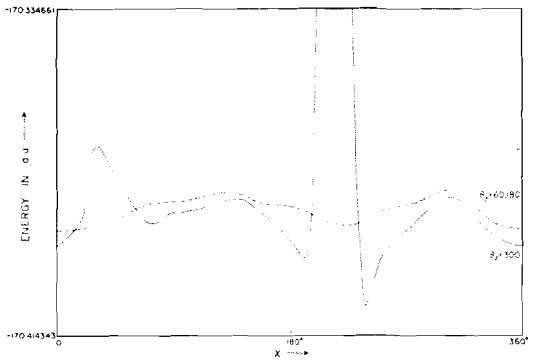

FIG. 3. Potential energy curves of β–ψ (by CNDO) as a function of angle χ for the $C_{3'}$-*endo* ribofuranose ring conformation. The behavior for θ_2 = 60 and 180° is very similar and is shown by the dotted line. The solid line denotes the curve for θ_2 = 300°. The value of θ_1 is 0° in all cases.

Fig. 1 can occur only if $\theta_2 \sim 300°$ and $\theta_1 \sim 0°$. The n.m.r. evidence indicates that the population of the *gauche–gauche* rotamer (θ_2 = 300°) is ~60% in water (1–3) and ~70% in dimethylsulfoxide (4). However, the populations of other conformers (θ_2 = 60 or 180°) are not negligible. The three-bond ^1H–^1H coupling constants of the ribofuranose ring indicate that rapid conformational interconversion is taking place with very little preference for any of the conventional puckered conformations (1–4).

The potential energy of β–ψ has been calculated for all the three possible values of θ_2 namely 60, 180, and 300°. A value of 0° has been assigned to θ_1 so that the effect of intramolecular H-bonding could be studied. The ^1H n.m.r. data has indicated that β–ψ shows some preference in dimethylsulfoxide for small values of θ_1(4). Initially, the calculations were performed using a $C_{3'}$-*endo* ribose conformation. The low energy regions in the χ space were then repeated with $C_{2'}$-*endo*, $C_{3'}$-*exo* and $C_{2'}$-*exo* geometry to check if the puckering of the sugar ring affects the behavior of potential energy curves.

The results for the $C_{3'}$-*endo* conformation are shown in Fig. 3. The profiles for θ_2 = 60 and 180° are remarkably similar, while that for θ_2 = 300° is significantly different. For θ_2 = 60 or 180°, the potential energy curves show two minima, which correspond to $\chi \sim 0°$ (*anti*) and $\chi \sim 220°$ (*syn*). The *anti* conformation is slightly favored over the *syn* conformation, the difference in energies being ~0.6 kcal mol^{-1}. The two minima are connected by a low energy barrier (~5 kcal mol^{-1}). The general nature of the curves does not change very much with a change in the ribose geometry. These results indicate that when θ_2 = 60 or 180°, β–ψ will occur with a distribution of χ angles centered around 0 and 220°. The interconversion between the various configurations should be fast (on the n.m.r. time scale) because the energy barrier is low; this is in accord with a single H_6 n.m.r. resonance (1–4).

With $C_{3'}$-*endo* geometry and θ_2 = 300°, the *syn* conformation (χ = 240°) is stabilized by almost 9 kcal mol^{-1} over the *anti* (χ = 0°) conformation. Such a configuration could be stabilized by a hydrogen bond of the type $C_4{=}O_4 \ldots H{-}O_{5'}$. The O—H . . . O angle is 153° and O—O distance is 2.4 Å. When χ is around 210°, O_4 and the 5′-hydroxyl proton come within 1 Å of each other, leading to the large repulsive energies in this region. Another high energy barrier occurs around $\chi \sim 35°$, which is due to close contact between H_6 and the hydroxyl proton.

The $C_{2'}$-*exo* geometry gives a potential energy curve which closely resembles that for $C_{3'}$-*endo*. However, a very pronounced difference is observed for $C_{2'}$-*endo* and $C_{3'}$-*exo* geometries. For the $C_{2'}$-*endo* conformation, the entire χ region shows very high energy. This behavior can be easily understood since in this case, $C_{2'}$ and $H_{2'}$ are fairly close to the 5′-OH group. For the $C_{3'}$-*exo* conformation, the 5′-OH group is pulled away from sugar base and in the absence of a possible hydrogen bond the *syn* structure is predicted to be less stable than the *anti*.

The CNDO calculations indicate, therefore, that different sugar conformations stabilize the *syn* or *anti* regions to different extents. However,

Can. J. Chem. Downloaded from www.nrcresearchpress.com by 210.87.254.6 on 09/05/12
For personal use only.

Can. J. Chem. Downloaded from www.nrcresearchpress.com by 210.87.254.6 on 09/05/12
For personal use only.

in absence of any quantitative data on the distribution of ribose conformations for β–ψ in solution it is not possible to make predictions on the relative populations of *syn* and *anti* conformers from the CNDO calculations alone.

(b) Nuclear Overhauser Measurements

The results of n.O.e. experiments are given in Table 1. It is seen that the H_6 resonance shows significant enhancements when $H_{1'}$, $H_{2'}$, and $H_{3'}$ are saturated. Since for a rigid structure the n.O.e. depends on r_k, the distance between H_6 and the ribofuranose proton (k) under consideration, the observation of substantial n.O.e. from both $H_{1'}$ and $H_{2'}$ is an indication that significant proportions of both *syn* and *anti* forms are present. At higher pD (11.6) the overall enhancement decreases but the relative values remain the same. This indicates that the population distribution does not change significantly with a change in pD, as has already been suggested by other ^1H n.m.r. data (3). The presence of a single resonance for H_6 indicates that rapid interconversion between conformers about the glycosidic bond must be taking place. Thus, although a hydrogen bond may exist between $C_4{=}O$ and $H{-}O_{5'}$, the n.m.r. data indicate no change in its probability from pD 7.1 to 11.6, and therefore it cannot be responsible for the anomalous ultraviolet absorption spectrum found at basic pH values (7).

A more quantitative discussion of the n.O.e. results is possible only if the distances of H_6 from the various ribofuranose protons are known; these in turn depend primarily on the value of χ and, to some extent, on the ribofuranose ring geometry. For the $C_{3'}$-*endo* conformation the relevant interproton distances are given in Fig. 4. Over the entire χ range the distances of protons $H_{4'}$, $H_{5'}$, and $H_{5''}$ from H_6 are

TABLE 1. Internal nuclear Overhauser effect on the H_6 proton in β–ψ caused by the saturation of the ribofuranose ring proton resonances

Proton irradiated	Nuclear Overhauser effect	
	pD = 7.1	pD = 11.6
$H_{1'}$	22	16
$H_{2'}$	19	11
$H_{3'}$	12	8
$H_{4'}$	2	4
$H_{5'}$ + $H_{5''}$	1	0

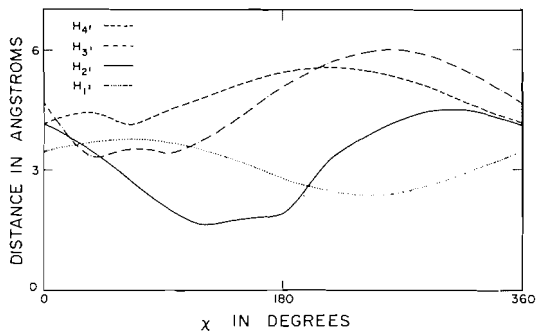

FIG. 4. The distance of the ribofuranose ring protons ($H_{1'}$, $H_{2'}$, $H_{3'}$, and $H_{4'}$) from the base proton H_6. The ring conformation is taken as $C_{3'}$-*endo*. For other ring conformations, the distances for $H_{2'}$ and $H_{3'}$ are slightly different.

greater than 4 Å and these protons do not make any significant contributions to the n.O.e. of H_6. The H-bonded *syn* conformation (χ = 240°) corresponds to an $H_{1'}{-}H_6$ distance of 2.4 Å and clearly, such a conformation would give rise to a large n.O.e., when $H_{1'}$ is irradiated. However, neither the χ = 0° nor the χ = 240° configuration can explain the n.O.e. observed for the $H_{2'}$ and $H_{3'}$ protons, since the relevant distances for both the protons are more than 4 Å. It is evident that these protons relax due to a finite probability of the molecule lying in regions of χ where the relevant interproton distances are lower (*i.e.* χ ~20–40°).

These results can be interpreted semiquantitatively in terms of the energy calculations. The statistical probability (p_i) of finding the molecule in the configuration i, is related to its potential energy E_i by the expression

$$p_i = \frac{\exp(-E_i/RT)}{\sum_i \exp(-E_i/RT)}$$

The n.O.e. (ζ_k) obtained by irradiating one of the ribofuranose protons k can therefore be related to the relevant distances r_k by the expression

$$\zeta_k \propto \sum_i p_i (r_k)_i^{-6}$$

Figure 5 shows the value of $p_i(r_k)_i^{-6}$ as a function of χ, where the p_i values are derived from the potential energy curve for the $C_{3'}$-*endo*, θ_2 = 60° (or 180°) curve. It is evident from Fig. 5, that the points which lead to maximum n.O.e. need not correspond exactly to the most probable values of χ. For example, $H_{2'}$ derives most

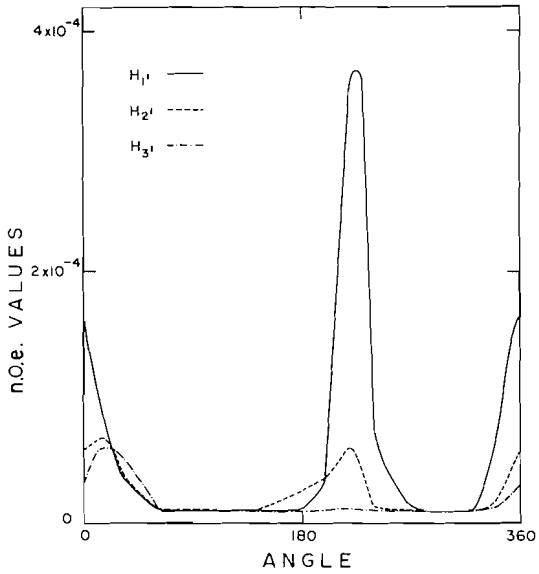

FIG. 5. The value of pr_k^{-6} as a function of χ, for the protons $H_{1'}$, $H_{2'}$, and $H_{3'}$.

of its n.O.e. from the region $\chi = 20$ and 220°, while the maximum dipole–dipole interaction for $H_{3'}$ occurs at $\chi = 20°$. The total n.O.e. for each proton is proportional to the integrated area of the curve. The theoretical values of $\zeta_{1'}$, $\zeta_{2'}$, and $\zeta_{3'}$ (from Fig. 5) when compared with the results in Table 1 indicate that the population of the *anti* conformation is much larger than predicted theoretically from the $C_{3'}$-*endo* geometry. Further, because of the critical r^{-6} dependence of the dipole–dipole contribution to the n.O.e., and the possible contributions of other relaxation, it is not possible to interpret the n.m.r. results in terms of a two-state model in which only the most probable *syn* and *anti* conformations are assumed to provide the dominant relaxation mechanism. If quantitative information on the sugar geometry and the exocyclic hydroxymethyl group conformation is available, then theoretical calculations can be used to interpret n.O.e. results quantitatively. We are currently studying some cyclic nucleotides, where the sugar geometry is rigid and the conformational freedom is restricted to the glycosidic bond. However, in the case of β–ψ the flexibility of both the sugar ring and the exocyclic —CH_2OH group restricts one to qualitative conclusions.

1. F. E. HRUSKA, A. A. GREY, and I. C. P. SMITH. J. Am. Chem. Soc. **92**, 214 (1970).
2. A. A. GREY, F. E. HRUSKA, and I. C. P. SMITH. J. Am. Chem. Soc. **92**, 4088 (1970).
3. R. DESLAURIERS and I. C. P. SMITH. Can. J. Biochem. **50**, 766 (1972).
4. R. DESLAURIERS and I. C. P. SMITH. Can. J. Chem. **51**, 833 (1973).
5. J. D. FISSEKIS and B. M. CREEGAN. J. Org. Chem. **32**, 3595 (1967).
6. A. DUGAICZYK. Biochem. **9**, 1557 (1970).
7. R. W. CHAMBERS. Prog. Nucl. Acid. Res. Mol. Biol. **5**, 349 (1966).
8. R. E. SCHIRMER, J. P. DAVIS, J. H. NOGGLE, and P. A. HART. J. Am. Chem. Soc. **94**, 2561 (1972).
9. J. P. DAVIS and P. A. HART. Tetrahedron, **28**, 2883 (1972).
10. R. J. CUSHLEY, B. L. BLITZER, and S. R. LIPSKY. Biochem. Biophys. Res. Commun. **48**, 1482 (1972).
11. TRAN-DINH SON, W. GUSCHLBAUER, and M. GUERON. J. Am. Chem. Soc. **94**, 7903 (1972).
12. J. H. NOGGLE and R. E. SCHIRMER. The nuclear Overhauser effect: chemical applications. Academic Press, New York. 1971.
13. G. GOVIL and A. SARAN. J. Theor. Biol. **30**, 621 (1971).
14. G. GOVIL and A. SARAN. J. Theor. Biol. **33**, 399 (1971).
15. A. SARAN and G. GOVIL. J. Theor. Biol. **33**, 407 (1971).
16. F. JORDAN and B. PULLMAN. Theor. Chim. Acta, **9**, 242 (1968).
17. H. BERTHOD and B. PULLMAN. Biochim. Biophys. Acta, **232**, 595 (1971).
18. F. BLOCH and A. SIEGERT. Phys. Rev. **57**, 522 (1940).
19. P. A. DOBOSH. Quantum Chemistry Program Exchange (QCPE 142). Indiana University, Bloomington, Indiana, U.S.A.

Can. J. Chem. Downloaded from www.nrcresearchpress.com by 210.87.254.6 on 09/05/12
For personal use only.

Electrochemical Synthesis of Deuterio Organic Compounds. I. Electrochemical Reduction of 1-Halonaphthalenes and Synthesis of 1-Chloro-4-methylnaphthalene[1]

ROGER N. RENAUD

Division of Chemistry, National Research Council of Canada, Ottawa, Canada K1A 0R6

Received July 18, 1973

Electrochemical reduction of 1-chloro-, 1-bromo-, 1-iodo-, 1-chloro-4-methyl-, and 1-bromo-4-methylnaphthalene was done in presence of deuterated water. The deuterium content of the naphthalene obtained reveals that the mechanism for the bromo and the iodo derivatives might involve either a simultaneous transfer of two electrons or an organometallic intermediate, while reduction of the chloro derivative might proceed at least partially via a radical intermediate.

The synthesis of 1-chloro-4-methylnaphthalene from 1-chloro-4-chloromethylnaphthalene was achieved either by selective sodium borohydride reduction or by selective electrochemical reduction.

La réduction électrochimique de naphtalènes et de méthyl-4 naphtalènes halogénés a été faite en présence d'eau deutériée. La teneur en deutérium du naphtalène et du méthyl-4 naphtalène ainsi formés a démontré que les dérivés bromés et iodés semblent préférer un mécanisme de type impliquant soit le transfert simultané de deux électrons ou la formation d'un organométallique intermédiaire. Par contre, les dérivés chlorés semblent préférer un mécanisme radicalaire.

Le chloro-1 méthyl-4 naphtalène a été synthétisé par réduction sélective du chloro-1 chlorométhyl-4 naphtalène soit sur le borohydrure de sodium ou soit électrolytiquement.

Can. J. Chem., **52**, 376 (1974)

Introduction

The electrochemical reduction of halogenated organic compounds to hydrocarbons is well known (1). Furthermore, this reduction is shown to be, in many cases, very selective in the presence of functional groups easily reducible by conventional reducing methods (2–4). The hydrogen donor can be the solvent, the supporting electrolyte, and/or an acidic additive. This method has recently been used for the synthesis of deuterium (and tritium) labelled organic compounds where the isotopic hydrogen source was labelled water. High isotopic purities were obtained by Cockrell and Murray (5) in the synthesis of deuterated anisoles and toluenes from the electrochemical reduction of iodoanisoles and iodotoluenes. Semmelhack and coworkers (6) selectively introduced a deuterium at C-6 in 1,1-dimethyl-4,5,6-trichlorospiro[2.3]-hex-4-ene by this method. The same result was obtained by Bratu (7) in the synthesis of tritiated uracil using tritiated water as the electrophile. Therefore, the electrochemical reduction of halogenated organic compounds seems to offer a relatively good method for the regiospecific introduction of labelled hydrogen in highly substituted aliphatic, aromatic, and heterocyclic compounds. Since the synthesis of labelled compounds is one of the major problems in our laboratory, the electrochemical method was further explored.

It is known that the relative rate of halide ion loss for alkyl halides (8) and aryl halides (9) increases in the following order

$$Cl < Br < I$$

Although iodo and bromo derivatives are reduced more easily than the corresponding chloro homologs, the chloro compounds are generally more readily accessible and less expensive. Since very little is reported in the literature regarding the use of chloro compounds as potential precursors for the synthesis of deuterated derivatives via electrochemical reduction in the presence of D_2O, some preliminary studies were done on 1-chloronaphthalene and 1-chloro-4-methylnaphthalene. The results were compared with the reduction of their bromo and iodo homologs.

The synthesis of 1-chloro-4-methylnaphthalene reported in the literature involved the chlorination of 1-methylnaphthalene to give a mixture of isomeric compounds (10), or the nitration of 1-chloronaphthalene followed by a

[1]NRCC No. 13561.

Can. J. Chem. Downloaded from www.nrcresearchpress.com by 210.87.254.42 on 09/05/12
For personal use only.

Can. J. Chem. Downloaded from www.nrcresearchpress.com by 210.87.254.42 on 09/05/12
For personal use only.

long synthetic procedure (10), or the chlorination of 1-naphthalene acetic acid in a very low yield followed by a thermal decarboxylation of the 1-chloro-4-naphthalene acetic acid (11). The method we have used consists of a chloromethylation of 1-choronaphthalene followed by a selective reductive dechlorination of 1-chloro-4-chloromethylnaphthalene with either sodium borohydride (method A) in 72% yield or electrolytically (method B) in 66% yield.

Experimental

The halogenated naphthalenes were commercially available and analyzed spectroscopically to be highly pure (>98%). Solvents were purified as reported in the literature (23). Melting points are uncorrected. Silica gel was Fisher Scientific 28–200 Mesh Grade 12 and the eluant was petroleum ether. Nuclear magnetic resonance spectra were determined on a Varian A-60 spectrometer using TMS as internal standard. Microanalyses were determined by Mr. H. Séguin, National Research Council of Canada, Ottawa. Mass spectra were determined on a Hitachi Perkin-Elmer RMU-6D instrument and corrected for natural ^{13}C abundance.

1-Chloro-4-chloromethylnaphthalene

1-Chloro-4-chloromethylnaphthalene was prepared according to the method described by Horn and Warren (12), m.p. 76.5–77.5° (lit. (12) 78–79°); n.m.r. ($CDCl_3$): τ 1.7–2.3 (6H, multiplet, aromatic), 4.97 (2H, singlet, methylene).

1-Chloro-4-methylnaphthalene

Method A. $NaBH_4$ Reduction

A mixture of 1-chloro-4-chloromethylnaphthalene (1 g) and sodium borohydride (0.36 g) in DMSO (45 ml) (dried over calcium hydride and distilled under reduced pressure), was stirred at room temperature for 2 h. Then, the excess sodium borohydride was destroyed with methyl iodide (1.4 g) and the mixture was extracted continuously for 4 h with pentane. The pentane solution was concentrated and the residue was distilled in a Späth bulb under reduced pressure to give 0.6 g (72%) of an oil boiling at 70° (0.001 mm pressure). The distillate analyzed to be ~98% pure by v.p.c. (picrate: m.p. 125–126° (lit. (11) 119–121°)); n.m.r. ($CDCl_3$): τ 1.5–3.0 (6H, multiplet, aromatic), 7.43 (3H, singlet, methyl).

Anal. Calcd. for $C_{11}H_9Cl$: C, 74.79; H, 5.14; Cl, 20.12. Found: C, 75.06; H, 5.29; Cl, 19.77.

Method B. Electrochemical Reduction

A solution of freshly distilled dioxane (40 ml), water (15 ml), and lithium perchlorate (2.7 g) was placed in a three-compartment cell separated by coarse fritted glasses and maintained at 20 °C under an atmosphere of nitrogen. The cell was equipped with a reflux condenser, a thermometer, a gas inlet, a mercury reference electrode, a platinum screen anode, and a mercury pool cathode. The cathodic current was supplied from a PAR potentiostat model 173 combined with a PAR coulometer model 179. A potential of 2.0 V *vs.* Hg was applied to the cell until the current stabilized at 8.5 mA. Then, 1-chloro-4-chloromethylnaphthalene (1 g) was added to the cell. The current went up to 110 mA. The electrolysis was continued until the current was down to 40 mA (3.7 equivalent number of coulombs). The solution was filtered, evaporated nearly to dryness under reduced pressure, and then excess water was added. The supernatant oil so obtained was extracted with ether. The ethereal solution was dried over sodium sulfate, filtered, and concentrated *in vacuo*. The crude residue was distilled in a Späth bulb to afford 0.55 g (66%) of a colorless oil analyzing nearly pure 1-chloro-4-methylnaphthalene (picrate: m.p. 125–126° (lit. (11) 119–121°)).

Anal. Calcd. for $C_{11}H_9Cl$: C, 74.79; H, 5.14; Cl, 20.12. Found: C, 74.90; H, 5.19; Cl, 19.88.

Electrochemical Reduction of 1-Halonaphthalene

A solution of dry solvent (dioxane, dimethylformamide, ethanol-*d* or dimethoxyethane) (38 ml), D_2O (13 ml), and supporting electrolyte ($LiClO_4$, LiCl, TBAI) (0.3–0.5 *M*) was placed in the cell described above. The cell was maintained at 20 °C under an atmosphere of nitrogen and carefully protected from moisture in both the anodic and cathodic compartments by Drierite tubes.

A constant potential of 2–3 V *vs.* Hg (calibrated to be +0.18 V *vs.* SCE) was maintained before each run until the current stabilized. Such potentials elicited a steady evolution of hydrogen. However, as soon as the halogenated naphthalene was added (0.006 mol), the evolution of hydrogen ceased completely. A fixed potential of 2–3 V was maintained until 3 to 6 equivalent number of coulombs had been passed. Then, the solution was either diluted with a large excess of water (500 ml) and filtered (in the case of naphthalene) or concentrated under vacuum before the addition of the water (in the case of methylnaphthalene). The supernatant solid or oil was chromatographed on a silica gel column using pentane as the eluant. The compounds thus obtained were analyzed by mass spectrometry for deuterium content. The results are shown in Tables 1, 2, and 3.

Results and Discussion

The deuterium content of the naphthalenes obtained from the electrolysis of the 1-halonaphthalenes (Table 1, runs 1, 2, and 3) indicates that the nature of the halogen is a critical parameter. 1-Chloronaphthalene reduces to naphthalene of significantly lower deuterium content than that obtained from its bromo and iodo homologs under the same experimental conditions. Substitution of a methyl group for a hydrogen in position-4 for the chloro and the bromo derivatives has no substantial effect on the deuterium incorporation in the products (Table 1, runs 4 and 5). A negative increase in potential from −2.5 to −3.0 V (Table 2) causes a slight increase in deuterium introduction in the naphthalene obtained from 1-chloronaphthalene, but an important drop is noticed at −2.4 V. On the contrary, the deuterium content in the naphthalene decreases with a negative increase

TABLE 1. Effect of the nature of the halide and the substituent on deuterium content of products obtained from the electrochemical reduction of 1-substituted-4-halonaphthalene*

Run	X	R	% d_1	% yield
1	Cl	H	50.5	90 (27)†
2	Br	H	92.6	89 (42)
3	I	H	95.7	86 (92)
4	Cl	CH_3	54.0	74 (13)
5	Br	CH_3	90.3	82 (22)

*The electrolysis was done in a dioxane/D_2O solution containing lithium perchlorate as the supporting electrolyte.

†The number in parentheses is the current yield for $RX \xrightarrow{2e/H^+} RH$.

TABLE 2. Effect of potential on deuterium content of naphthalene obtained from the electrochemical reduction of 1-halonaphthalene

Run	X	E (V)	% d_1	% yield
6	Cl	2.4	38	67
7	Cl	2.5	49	78
1	Cl	2.7	50.5	90
8	Cl	3.0	53.1	81
9	Br	2.4	92.6	89
2	Br	2.6	88.7	92
3	I	2.1	95.7	86
10	I	2.6	88.6	85

TABLE 3. Effect of solvent-supporting electrolyte and nature of the electrodes on deuterium content of naphthalene obtained from the electrochemical reduction of 1-chloronaphthalene

Run	Solvent	Electrolyte	Cathode	% d_1	% yield
1	Dioxane	$LiClO_4$	Hg	50.5	90
11	Dioxane	LiCl	Hg	50	78
12	DME	$LiClO_4$	Hg	53	85
13	DMF/EtOD	LiCl	Hg	27*	63
14	EtOD	LiCl	Hg	66	78
15	DMF	TBAI	Pb	50	63
16	EtOD	$NaClO_4$	Al	—	0
17	EtOD	LiCl	C	—	0
18	EtOD	LiCl	Pt	—	0

*The lower deuterium content of naphthalene in run 13 may be due to the presence of some protonated ethanol in the solvent.

in potential when the bromo- or the iodonaphthalene is reduced.

The nature of the solvent and the supporting electrolyte (Table 3, runs 1, and 11–14) does not seem to have a large influence on the deuteration of naphthalene. A lead cathode (run 15) gives a result identical with that obtained with a mercury cathode. However, an aluminum, a carbon, or a platinum electrode (runs 16–18) does not reduce chloronaphthalene under similar conditions (run 14).

It is evident from the results obtained that the chloro derivative cannot always be used for the electrochemical preparation of deuterated compounds unless proton-free or perdeuterio solvents are used. Such conditions are not always practical especially on large-scale syntheses.

The results of the electrochemical reduction of 1-halonaphthalene cannot always be explained by mechanisms proposed for alkyl and aryl halides. A common radical (13) or organometallic radical (14, 15) intermediate for the three halides studied does not explain our results because the deuterium content of the naphtha-

Can. J. Chem. Downloaded from www.nrcresearchpress.com by 210.87.254.42 on 09/05/12
For personal use only.

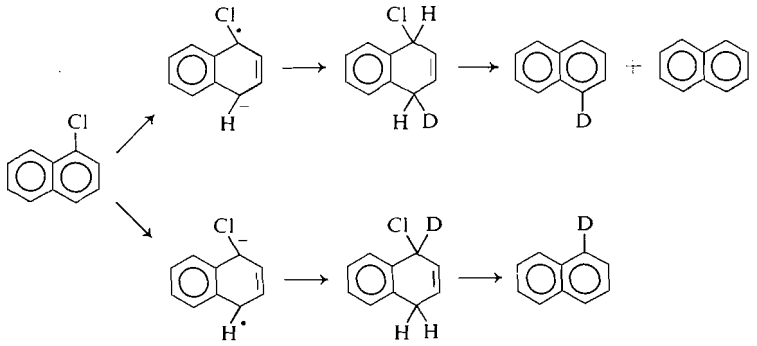

SCHEME 1

lene produced was not the same in each case. Also, the results seem to contradict the postulate that the radical contribution increases through the chloro, bromo, and iodo derivatives (16). The reported relative increase in radical products resulting from an increase in potential (17) for the bromo and the iodo compounds (Table 2, runs 2, 9, 3, and 10) does not apply to the chloro derivative (Table 2, runs 1, 6, 7, and 8). Moreover, the polarographic observation of a two-electron reduction peak to give a carbanion and a chloride anion (17) in 1-chloro-4-nitrobenzene also does not fit the results obtained for 1-chloronaphthalene because of the formation of products resulting from radical intermediates.

The possibility of 1,4-addition in 1-chloronaphthalene followed by aromatization (Scheme 1) is rejected on the basis of a deuterium isotopic effect and by the observation that the deuterium content of the starting material and the product in the electrochemical reduction of 1-chloroperdeuterionaphthalene is identical. Therefore, the electrochemical reduction of 1-chloronaphthalene must occur directly on the C—Cl bond.

Any proposed mechanisms to rationalize the data observed are surely premature and undesirable. However, there are few points worth mentioning. It seems likely that the reduction of the bromo- and the iodonaphthalene prefers, to the extent of over 90% (based on the deuterium content of the product), an ionic pathway via an organometallic radical intermediate (18, 19) and/or a simultaneous transfer of two electrons (Scheme 2, pathways *a* and *b*) to give a carbanion. The existence of the intermediate RHg. (15, 19) is not in contradiction with our result, but the process by which it is formed is still unexplained. On the other hand, the deuterium content of

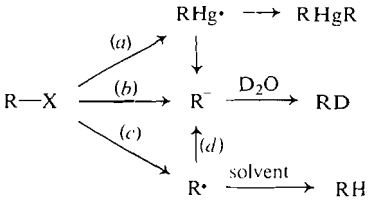

SCHEME 2

naphthalene isolated from the electroreduction of chloronaphthalene seems to indicate simultaneous ionic and radical pathways or a discrete radical pathway followed by a partial transfer of one electron (Scheme 2, pathways *b*, *c*, and *d*).

Work is presently in progress with other substituted halonaphthalenes as well as with related systems in an attempt to elucidate the mechanism of this reaction and thus develop it into a synthetically viable method for the preparation of deuterated compounds.

The author is grateful to J. C. Stephens of the National Research Council of Canada for his technical assistance.

1. C. L. PERRIN. Progress in physical organic chemistry. Vol. 3. John Wiley and Sons, Inc., New York, N.Y. 1965. pp. 256–270.
2. A. J. FRY. Synthetic organic electrochemistry. Harper and Row, Publishers, Inc., New York. 1972. p. 180.
3. A. J. FRY, M. A. MITNICK, and R. G. REED. J. Org. Chem. **35**, 1232 (1970).
4. P. W. BOARD, D. BRITZ, and R. V. HOLLAND. Electrochim. Acta, **13**, 1575, 1633 (1968).
5. J. R. COCKRELL and R. W. MURRAY. J. Electrochem. Soc. **119**, 849 (1972).
6. M. F. SEMMELHACK, R. J. DEFRANCO, and J. STOCK. Tetrahedron Lett. 1371 (1972).
7. C. BRATU. J. Labelled Compds. **7**, 161 (1971).
8. M. V. STACKELBERG and W. STRACKE. Z. Elektrochem. **53**, 118 (1949).
9. D. E. BARTAK, K. J. HAUSER, B. C. RUDY, and M. D. HAWLEY. J. Am. Chem. Soc. **94**, 7526 (1972).

Can. J. Chem. Downloaded from www.nrcresearchpress.com by 210.87.254.42 on 09/05/12
For personal use only.

10. G. CUM and P. B. D. DE LA MARE. J. Chem. Soc. C, 1590 (1967).
11. Y. OGATO, M. OKANO, and Y. KITAMURA. J. Org. Chem. **16**, 1588 (1951).
12. D. H. S. HORN and F. W. WARREN. J. Chem. Soc. 144 (1946).
13. L. EBERSON and H. SCHÄFER. Topics in current chemistry. Vol. 21. Springer-Verlag Berlin, Heidelberg, New York. 1971. p. 133.
14. N. S. HUSH and K. B. OLDHAM. J. Electroanal. Chem. **6**, 34 (1963).
15. J. L. WEBB, C. MANN, and H. M. WALBORSKY. J. Am. Chem. Soc. **92**, 2042 (1970).
16. O. R. BROWN and J. A. ARRISON. J. Electroanal. Chem. **21**, 387 (1969).
17. J. G. LAWLESS and M. D. HAWLEY. J. Electroanal. Chem. **21**, 365 (1969).
18. R. ANNINO, R. E. ERICKSON, J. MICHALOVEC, and B. MCKAY. J. Am. Chem. Soc. **88**, 4424 (1966).
19. H. DOUPEUX, P. M. MARTINET, and J. SIMONET. Bull. Soc. Chim. 2299 (1971).

Can. J. Chem. Downloaded from www.nrcresearchpress.com by 210.87.254.42 on 09/05/12
For personal use only.

Can. J. Chem. Downloaded from www.nrcresearchpress.com by 210.87.254.42 on 09/05/12
For personal use only.

The Synthesis of Analogs of the Hallucinogen 1-(2,5-Dimethoxy-4-methylphenyl)-2-aminopropane (DOM). II.[1] Some Ring-methoxylated 1-Amino- and 2-Aminoindanes

RONALD T. COUTTS AND JERRY L. MALICKY

Faculty of Pharmacy and Pharmaceutical Sciences, University of Alberta, Edmonton, Alberta

Received March 15, 1973[2]

The synthesis of 2-amino-4,7-dimethoxy-5-methylindane (**12***a*), the cyclic analog of the known hallucinogen 1-(2,5-dimethoxy-4-methylphenyl)-2-aminopropane (DOM), is described. The key intermediate was *trans*-2-amino-4,7-dimethoxy-6-methyl-1-indanol (*trans*-**10***a*) which was converted to **12***a* in two ways. The prolonged action of hydrochloric acid on *trans*-**10***a* gave 4,7-dimethoxy-5-methyl-2-indanone (**11***d*), the oxime of which, on catalytic reduction, was converted to **12***a* in low yield. A direct catalytic reduction of *trans*-**10***a* in the presence of hydrochloric acid also gave **12***a*, together with *cis*-2-amino-4,7-dimethoxy-6-methyl-1-indanol (*cis*-**10***a*).

The synthesis and properties of other derivatives of 2-aminoindane, and some derivatives of 1-aminoindane are also described.

On décrit la synthèse de l'amino-2 diméthoxy-4,7 méthyl-5 indane (**12***a*), un analogue cyclique de l'hallucinogène connu (diméthoxy-2,5 méthyl-4 phényl)-1 amino-2 propane (DOM). L'intermédiaire-clef de la synthèse est la *trans*-amino-2 diméthoxy-4,7 méthyl-6 indanol-1 (*trans*-**10***a*) qui peut être transformé en **12***a* selon deux procédés. L'action prolongée de l'acide chlorhydrique sur le *trans*-**10***a* conduit au diméthoxy-4,7 méthyl-5 indanone-2 (**11***d*) dont l'oxime, par réduction catalytique, conduit au produit **12***a* avec des rendements faibles. La réduction catalytique directe du *trans*-**10***a* en présence d'acide chlorhydrique conduit également au produit **12***a* mais aussi au *cis*-amino-2 diméthoxy-4,7 méthyl-6 indanol-1 (*cis*-**10***a*).

On décrit aussi la synthèse et les propriétés de certains autres dérivés de l'amino-2 indane ainsi que de l'amino-1 indane. [Traduit par le journal]

Can. J. Chem., **52**, 381 (1974)

Many ring-methoxylated phenethylamines (**1**) have been shown to possess psychotomimetic activity (1,2) and two conflicting theories have been propounded by Snyder *et al.* (3, 4) and Kang and Green (5) in an attempt to explain why these compounds are active. Both theories related the phenethylamine structures to that of lysergic acid diethylamine (LSD; **2**). In each case, the aromatic ring of the phenethylamines is equated with ring A of LSD but, whereas Snyder *et al.* consider the nitrogen atom of structure **1** to correspond to the N-1 of LSD, or to contribute to the formation of a pseudo-ring C, Kang and Green are of the opinion that the nitrogen atom of the phenethylamines is equivalent to N-6 of LSD at the receptor site in the brain.

In view of this conflict, it seemed desirable to synthesize and evaluate pharmacologically rigid molecules which were structurally related to known psychotomimetic compounds. The initial compounds selected (**12***a* and *b*) possessed an aromatic ring which corresponded to ring A of LSD, and a nitrogen atom in a rigid position comparable to that of N-6 in LSD; the former compound (**12***a*) is the cyclic analog of 1-(2,5-dimethoxy-4-methylphenyl)-2-aminopropane (**3**; DOM), a known potent hallucinogen (6). The synthesis of these two aminoindanes (**12***a* and *b*) and some related compounds is now described. While this work was in progress, Horn and Snyder (7) reported their studies on the steric requirements for catecholamine uptake by rat brain, in which they compared the preferred conformation of amphetamine with 1- and 2-aminoindane.

The starting material for the synthesis of 2-amino-4,7-dimethoxy-5-methylindane (**12***a*) was 2,5-dimethoxy-4-methylbenzaldehyde (**4***a*). This was reacted with malonic acid to give a cinnamic acid derivative (**5***a*) which on catalytic reduction gave 3-(2,5-dimethoxy-4-methyl)propionic acid (**6***a*). Attempts to cyclize the latter to the 1-indanone (**7***a*) using phosphorous oxychloride as the dehydrating agent (8) gave a low yield of an

[1]Reference 18 is considered Part I.

[2]Revision received October 1, 1973.

Can. J. Chem. Downloaded from www.nrcresearchpress.com by 210.87.254.42 on 09/05/12
For personal use only.

impure product. Polyphosphoric acid (*cf.* ref. 9) proved to be a much superior reagent for this purpose.

4,7-Dimethoxy-2-isonitroso-6-methyl-1-indanone (**8***a*) was formed when a solution of the indanone (**7***a*) in ethanolic HCl was treated with freshly prepared ethyl nitrite. Because of its low solubility in ethanol, the pure product crystallized from the solution as it was formed. Numerous attempts, in different solvents and employing different catalysts, were made to reduce the oxime (**8***a*) directly to the amine (**12***a*), but generally a dark red oil, which could not be purified, was obtained. Eventually, catalytic reduction of a suspension of **8***a* in ethanolic HCl containing palladium–charcoal was attempted and a white water-soluble solid was recovered. When an aqueous solution of this solid was basified, the solution turned dark red in color. An ethanolic solution of the same material slowly turned red during a recrystallization process but this color formation could be prevented by the addition of HCl to the ethanol. This behavior was consistent (10) with the product being 2-amino-4,7-dimethoxy-6-methyl-1-indanone (**9***a*) hydrochloride and its i.r. spectrum (ν_{max} 1720 cm^{-1}) and n.m.r. spectrum supported this conclusion, although the compound analyzed indifferently for $C_{12}H_{16}ClNO_3$.

The reduction of 2-amino-1-indanone with sodium borohydride is reported (11) to yield *trans*-2-amino-1-indanol. When the impure **9***a* was so reduced, an amino alcohol, $C_{12}H_{18}ClNO_3$, was isolated (ν_{max} 3350 cm^{-1}; m.p. 193–195°) and concluded to be *trans*-2-amino-4,7-dimethoxy-6-methyl-1-indanol (**10***a*) hydrochloride. The stereochemistry of this product is discussed below.

In view of the doubtful purity of the indanone (**9***a*), an alternative method of preparing the indanol (**10***a*) was sought. Hydrogenation of 2-isonitroso-1-indanones in ethanolic NaOH containing Raney nickel is known to produce 2-amino-1-indanols (12). 4,7-Dimethoxy-2-isonitroso-6-methyl-1-indanone (**8***a*) was reduced under conditions similar to those reported, except that palladium–charcoal was the catalyst employed, and the product isolated was the *trans*-indanol (**10***a*). Prolonged heating of this alcohol in concentrated HCl (11) caused dehydration and deamination, and the product isolated was deduced to be 4,7-dimethoxy-5-methyl-2-indanone (**11***d*); the i.r., n.m.r., and mass spectra were all consistent with this conclusion. The oxime (**11***e*) was readily prepared from compound **11***d* but its reduction to the required 2-aminoindane (**12***a*) proved more difficult than anticipated. Attempted catalytic hydrogenations (10% Pd–C or Pt_2O) in ethanol were unsuccessful and a lithium aluminum hydride reduction gave a very poor yield of the amine, largely because of the insolubility of the oxime in ether or tetrahydrofuran. Catalytic (10% Pd–C) reduction of the oxime in ethanolic HCl, however, gave a 35% yield of 2-amino-4,7-dimethoxy-5-methylindane; a better yield resulted when acetic acid – sulfuric acid was the solvent (10).

The possibility of reducing the amino alcohol (**10***a*) directly to the required amine (**12***a*) was then investigated. As indicated previously, the action of HCl on **10***a* yielded the ketone (**11***d*). It was reasoned that if this **10***a* → **11***d* transition proceeded via the chloro amine (**13**) and possibly the enamine (**14**), these intermediates might be expected to reduce catalytically and give the 2-aminoindane (**12***a*). This, in fact, did occur. When the amino alcohol (*trans*-**10***a*, m.p. 193–195°), dissolved in a dioxane – concentrated HCl solvent, was catalytically reduced (10% Pd–C), two compounds were isolated. The acetone-insoluble product was 2-amino-4,7-dimethoxy-5-methylindane (**12***a*) hydrochloride. The acetone-soluble compound, $C_{12}H_{18}ClNO_3$, was isomeric with the amino alcohol employed in the reduction but differed in melting point (206–208°) and in position of the O—H stretching frequency (ν_{max} 3150 cm^{-1}). This product is concluded to be *cis*-2-amino-4,7-dimethoxy-6-methyl-1-indanol (*cis*-**10***a*) hydrochloride since it can hydrogen bond intramolecularly (**15**) which explains the lower O—H stretching frequency.

To verify that the second product was *cis*-**10***a*, a stereospecific reduction (13, 14) of 2-amino-4,7-dimethoxy-6-methyl-1-indanone (**9***a*) was performed which involved hydrogenation in the presence of Pd–C and $PdCl_2$. The product isolated was identical to *cis*-**10***a*. Further support for the stereochemical assignments given to compounds *cis*-**10***a* and *trans*-**10***a* was obtained from an n.m.r. study of their hydrochlorides in D_2O. Proton H_a in the spectrum of *cis*-**10***a* was a doublet, δ 5.47, $J_{H_aH_b}$ = 5.7 Hz. Proton H_a in the spectrum of *trans*-10*a* was also a doublet, δ 5.52, $J_{H_aH_b}$ = 3.2 Hz. Assuming that the five-

membered ring in *cis*- and *trans*-**10***a* is little distorted from the Dreiding model representation which indicated virtual planarity, it can be predicted from the Karplus equation (15) that the *cis* isomer should have the larger coupling constant.

To confirm that *trans*-**10***a* → *cis*-**10***a* isomerism occurred in concentrated HCl, a solution of the former was heated at 80° and aliquots were removed at various time intervals and evaporated to give white solids whose i.r. spectra were examined. The ν_{max} 3150 cm^{-1} band (*cis* isomer) increased in size at the expense of the ν_{max} 3350 cm^{-1} band (*trans* isomer) with increasing solution time. Prolonged heating gave the ketone (**11***d*).

The experience gained during the preparation of compound **12***a* permitted a more rapid synthesis of 2-amino-4,7-dimethoxyindane (**12***b*). 4,7-Dimethoxy-2-isonitroso-1-indanone (**8***b*) was synthesized from 2,5-dimethoxybenzaldehyde (**4***b*) via the same sequence of reactions described above for the homolog (**8***a*). Catalytic reduction

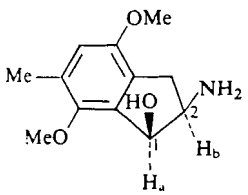

cis-**10***a*

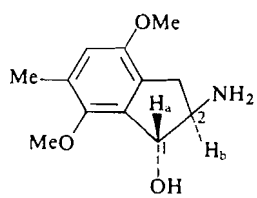

trans-**10***a*

of **8***b* in ethanolic hydrochloric acid gave an excellent yield of 2-amino-4,7-dimethoxy-1-indanone (**9***b*) hydrochloride, whereas the same reduction in ethanolic sodium hydroxide produced 2-amino-4,7-dimethoxy-1-indanol (**10***b*; ν_{max} 3350 cm^{-1}), assumed to be the *trans* isomer. Its reduction in dioxane – concentrated HCl proceeded smoothly and an excellent yield of 2-amino-4,7-dimethoxyindane (**12***b*) hydrochloride resulted.

An attempt to prepare 2-amino-5-bromo-4,7-dimethoxyindane (**12***c*) was unsuccessful. Treatment of 3-(2,5-dimethoxyphenyl)propionic acid (**6***b*) with bromine water gave a monobromo derivative. Since the aromatic protons appeared as singlets (δ 6.80, 7.03) in a 60 MHz n.m.r. spectrum and were therefore *para* to each other, the product was identified as 3-(4-bromo-2,5-dimethoxyphenyl)propionic acid (**6***c*). When this acid was heated in polyphosphoric acid, a low yield of 6-bromo-4,7-dimethoxy-1-indanone (**7***c*) was produced which was converted to the required 6-bromo-4,7-dimethoxy-2-isonitroso-1-indanone (**8***c*) by the action of ethyl nitrite. Catalytic reduction of this product, however, resulted in the removal of the bromine atom. Thus, catalytic reduction of **8***c* in ethanolic HCl yielded 2-amino-4,7-dimethoxy-1-indanone (**9***b*) hydrochloride, and a similar reduction in ethanol and sodium hydroxide gave the corresponding indanol (**10***b*) hydrochloride.

Some tertiary amines were also prepared in this study. When an aqueous solution of 2-amino-4,7-dimethoxy-5-methylindane (**12***a*) containing a slight excess of formaldehyde was hydrogenated catalytically, the product isolated was 4,7-dimethoxy-2-dimethylamino-5-methylindane (**16***f*) hydrochloride. In a similar manner, *cis*- and *trans*-2-dimethylamino-4,7-dimethoxy-6-methyl-1-indanol (**17***f*) hydrochlorides were prepared from *cis*- and *trans*-2-amino-4,7-dimethoxy-6-methyl-1-indanol (**10***a*) hydrochlorides, respectively. The *cis*- (ν_{max} OH, 3190 cm^{-1}) and *trans*-**17***f* hydrochlorides (ν_{max} OH, 3270 cm^{-1}) had similar melting points but a mixture melting point was depressed.

When 4,7-dimethoxy-6-methyl-1-indanone (**7***a*) was reacted with dimethylamine and paraformaldehyde in ethanolic HCl, a good yield of 4,7-dimethoxy-2-(dimethylamino)methyl-6-methyl-1-indanone (**18**) hydrochloride resulted. Reduction of this ketone with sodium borohydride gave the corresponding indanol (**17***g*) hydrochloride (ν_{max} OH, 3310 cm^{-1}), presumably the *trans* isomer, which was catalytically reduced in dioxane – concentrated HCl to 4,7-dimethoxy-2-(dimethylamino)methyl-5-methylindane (**16***g*) hydrochloride.

Various substituted 1-aminoindanes have been found to possess central nervous system activity (16, 17) and since the 1-indanones described above are also precursors of 1-aminoindanes, it was convenient to prepare selected examples of ring-methoxylated 1-aminoindanes to compare their pharmacological properties with their 2-amino counterparts.

The oximes (**19***a* and *b*) were readily obtained by the action of hydroxylamine on the appropriate ketone (**7**). Catalytic reduction of 4,7-dimethoxy-6-methyl-1-indanone oxime (**19***a*) in ethanol or reduction with lithium aluminum hydride gave a good yield of 1-amino-4,7-dimethoxy-6-methylindane (**20***a*). In contrast, a solvent system of acetic acid, ethanol, and sul-

Can. J. Chem. Downloaded from www.nrcresearchpress.com by 210.87.254.42 on 09/05/12
For personal use only.

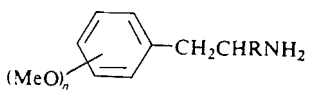

1

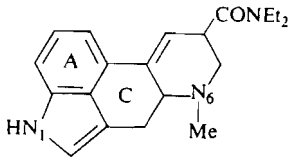

2

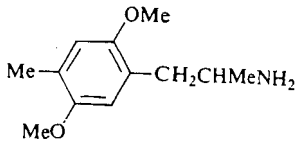

3

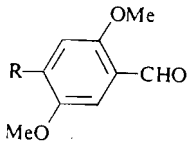

4

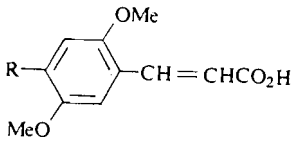

5

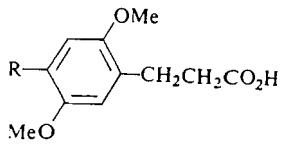

6

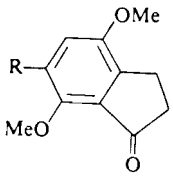

7

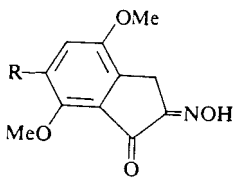

8

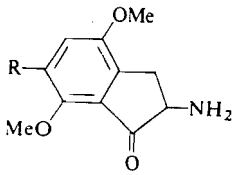

9

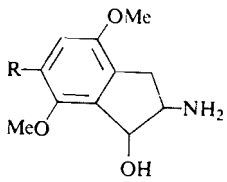

10

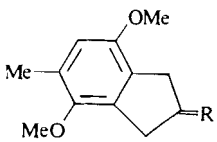

11

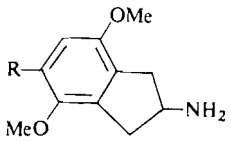

12

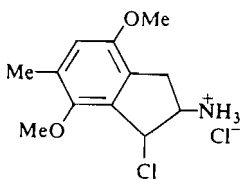

13

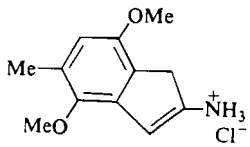

14

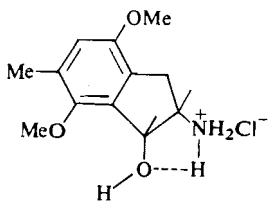

15

Can. J. Chem. Downloaded from www.nrcresearchpress.com by 210.87.254.42 on 09/05/12
For personal use only.

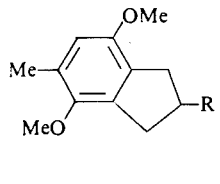

16

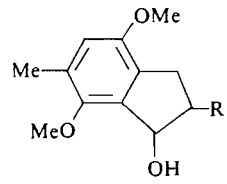

17

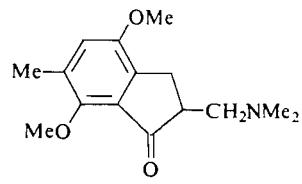

18

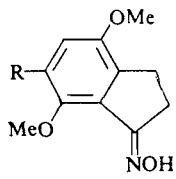

19

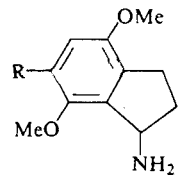

20

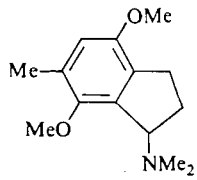

21

a R = Me
b R = H
c R = Br
d R = O
e R = NOH
f R = NMe_2
g R = CH_2NMe_2

furic acid proved necessary in the catalytic reduction of the oxime (**19***b*) to 1-amino-4,7-dimethoxyindane (**20***b*).

Two derivatives of **20***a* and *b* were also prepared. Treatment of **20***b* with a slight excess of bromine water gave a monobromo derivative, $C_{11}H_{16}BrNO_2$, assumed to be 1-amino-6-bromo-4,7-dimethoxyindane (**20***c*). The tertiary amine, 4,7-dimethoxy-1-dimethylamino-6-methylindane (**21**), was the product recovered when a solution of the indane **20***a* and formaldehyde was reduced catalytically.

Some of the aminoindanes just described were subjected to a simple preliminary pharmacological screening in which the effects of an oral or intraperitoneal dose in male rats (150–500 g) were compared with those caused by an oral dose of DOM (10 mg/kg) which reliably caused hypersalivation, pupillary dilation, retraction of scrotum, loss of orientation reflexes, hypomotility, and walking with a slinking gait. This revealed that compounds **12***a* (10 mg/kg oral dose) and **12***c* (30 mg/kg intraperitoneal dose) showed similar pharmacological responses as DOM, but were somewhat less active than DOM. The remaining compounds evaluated, *cis*-**10***a*, *trans*-**10***a*, **12***b*, **16***f*, **16***g*, **20***a*, and **21** were much less active.

Experimental

The conditions employed in the determination of melting points and elemental analyses, and in the recording of i.r. as Nujol mulls, n.m.r., and mass spectra are described in a previous publication (18). Compounds with structures **9**, **10**, **12**, **13**, **16**, **17**, **18**, **20**, and **21**, described below, are racemates. No attempts were made to isolate optically pure compounds.

trans-2,5-Dimethoxy-4-methylcinnamic Acid (5a)

A solution of 2,5-dimethoxy-4-methylbenzaldehyde (19), (9.2 g), malonic acid (12.0 g), dry pyridine (24 ml), and piperidine (0.6 ml) was heated on a steam bath for 3 h, then added to a mixture of concentrated HCl (35 ml) and ice (60 g). Crystallization of the product from ethanol gave the title compound as a yellow solid (11.4 g), m.p. 158–161°; i.r. ν_{max} 1618 (C=C), 1690 (C=O), 2500–2700 (OH) cm^{-1}; n.m.r. ($CDCl_3$) δ 2.25 (s, 3H, CH_3), 3.84 and 3.85 (overlapping singlets, 6H, $(OCH_3)_2$), 6.46 (d, 1H, J = 16.5) and 8.14 (d, 1H, J = 16.5) (*trans* (20, 21) CH=CH), 6.76 (s, 1H) and 6.99 (s, 1H) (aromatic protons), 10.78 (s, br, 1H, exchanges with D_2O, COOH).

Anal. Calcd. for $C_{12}H_{14}O_4$: C, 64.85; H, 6.35. Found: C, 64.95; H, 6.46.

3-(2,5-Dimethoxy-4-methylphenyl)propionic Acid (6a)

A solution of 2,5-dimethoxy-4-methylcinnamic acid (10.0 g) in ethanol was hydrogenated at room temperature and normal pressure under 10% palladium–charcoal (Pd-C) (0.5 g) until the theoretical amount of hydrogen was absorbed. The filtrate on evaporation gave the title compound, m.p. 108–110° (from ethanol); i.r. ν_{max} 1700 (C=O), 2500–2700 (OH) cm^{-1}.

Anal. Calcd. for $C_{12}H_{16}O_4$: C, 64.27; H, 7.19. Found: C, 64.02; H, 7.19.

4,7-Dimethoxy-6-methyl-1-indanone (7a)

The acid (**6***a*, 10.0 g) was stirred in polyphosphoric acid (100 g) at 80° for 1.5 h. The dark yellow mixture was poured into ice water (300 ml), basified with excess $NaHCO_3$, and extracted with chloroform (3 × 200 ml). The washed (H_2O) organic solution was evaporated to

Can. J. Chem. Downloaded from www.nrcresearchpress.com by 210.87.254.42 on 09/05/12
For personal use only.

Can. J. Chem. Downloaded from www.nrcresearchpress.com by 210.87.254.42 on 09/05/12
For personal use only.

give the title indanone (6.8 g), m.p. 104–105.5° (from ethanol); i.r. ν_{max} 1710 (C=O) cm^{-1}; n.m.r. (DMSO-d_6) δ 2.21 (s, 3H, CH_3), 2.35–3.07 (m, 4H, CH_2 groups), 3.73 (s, 3H) and 3.80 (s, 3H) (OCH_3 groups), 7.07 (s, 1H, aromatic proton).

Anal. Calcd. for $C_{12}H_{14}O_3$: C, 69.88; H, 6.84. Found: C, 69.78; H, 6.94.

4,7-Dimethoxy-1-indanone (7b)

This compound was prepared in a similar manner in 58% yield from 3-(2,5-dimethoxyphenyl)propionic acid. The product had m.p. 124–125° (from ethanol) (lit. (22) m.p. 124–125°); i.r. ν_{max} 1701 (C=O) cm^{-1}.

Anal. Calcd. for $C_{11}H_{12}O_3$: C, 68.73; H, 6.30. Found: C, 68.51; H, 6.19.

6-Bromo-4,7-dimethoxy-1-indanone (7c)

This compound (2.6 g), m.p. 109–110° (from ethanol) was prepared in a similar way from 3-(4-bromo-2,5-dimethoxyphenyl)propionic acid (10.0 g); i.r. ν_{max} 1700 (C=O) cm^{-1}.

Anal. Calcd. for $C_{11}H_{11}BrO_3$: C, 48.73; H, 4.09. Found: C, 48.56; H, 4.08.

4,7-Dimethoxy-2-isonitroso-6-methyl-1-indanone (8a)

Freshly prepared ethyl nitrite was bubbled through a solution of 4,7-dimethoxy-6-methyl-1-indanone (11.0 g) in ethanol (100 ml) saturated with HCl gas, for 2 h at 35° then the reaction mixture was left at room temperature for 12 h. The crystalline solid which formed (6.8 g) had m.p. 219–220° (from ethanol); i.r. ν_{max} 1645 (C=N), 1730 (C=O), 3280 br (OH) cm^{-1}.

Anal. Calcd. for $C_{12}H_{13}NO_4$: C, 61.27; H, 5.57; N, 5.96. Found: C, 61.07; H, 5.46; N, 5.72.

4,7-Dimethoxy-2-isonitroso-1-indanone (8b)

This was prepared in 72% yield in a similar manner from 4,7-dimethoxy-1-indanone. The product was purified by dissolving it in 10% NaOH, filtering and acidifying with concentrated HCl. Compound **8***b* had m.p. 233–234.5° (from ethanol); i.r. ν_{max} 1650 (C=N), 1732 (C=O), 3300 br (OH) cm^{-1}.

Anal. Calcd. for $C_{11}H_{11}NO_4$: C, 59.72; H, 5.01. Found: C, 59.50; H, 4.97.

6-Bromo-4,7-dimethoxy-2-isonitroso-1-indanone (8c)

This compound (1.25 g), m.p. 248–250° (from ethanol), was prepared in a similar way from 6-bromo-4,7-dimethoxy-1-indanone (3.0 g); i.r. ν_{max} 1648 (C=N), 1730 (C=O), 3300 br (OH) cm^{-1}.

Anal. Calcd. for $C_{11}H_{10}BrNO_4$: C, 44.02; H, 3.36. Found: C, 43.88; H, 3.28.

2-Amino-4,7-dimethoxy-6-methyl-1-indanone (9a) Hydrochloride

A suspension of 4,7-dimethoxy-2-isonitroso-6-methyl-1-indanone (2.0 g) in ethanol (200 ml) was hydrogenated at room temperature and normal pressure in the presence of 10% Pd–C (0.2 g) until incorporation of hydrogen was complete. The filtrate, initially colorless, slowly turned red on standing. Addition of concentrated HCl decolorized the solution and removal of the solvent gave the title compound as a white solid (1.81 g), m.p. 248–252° (from ethanol–ether); i.r. ν_{max} 1602, 1980, 2450–2630 ($\overset{+}{N}$—H), 1720 (C=O) cm^{-1}; n.m.r. (D_2O) δ 2.33 (s, 3H, CH_3), 2.49–3.71 (m, 2H, CH_2), 3.87 (s, 3H) and 3.95 (s, 3H) (OCH_3 groups), 4.15–4.57 (m, 1H, aliphatic CH), 7.31 (s, 1H, aromatic proton).

Anal. Calcd. for $C_{12}H_{16}ClNO_3$: C, 55.92; H, 6.26; N, 5.44. Found: C, 55.09; H, 6.40; N, 6.60.

2-Amino-4,7-dimethoxy-1-indanone (9b) Hydrochloride

This compound (4.5 g), m.p. 260–262°, was prepared in a similar manner from the isonitroso compound (**8***b*, 5.0 g), using ethanol (200 ml) and concentrated HCl (5 ml) as solvent; i.r. ν_{max} 1592, 1980, 2610–2700 ($\overset{+}{N}$—H), 1712 (C=O) cm^{-1}.

Anal. Calcd. for $C_{11}H_{14}ClNO_3$: C, 54.21; H, 5.79; N, 5.75. Found: C, 53.98; H, 5.98; N, 6.00.

trans-2-Amino-4,7-dimethoxy-6-methyl-1-indanol (10a) Hydrochloride

(*i*) A solution of 2-amino-4,7-dimethoxy-6-methyl-1-indanone hydrochloride (5.0 g) in 50% aqueous methanol (100 ml) was added dropwise to a stirred solution of sodium borohydride (5.0 g) in the same solvent (100 ml). Stirring was continued for a further 3 h, then the solution was acidified with concentrated HCl. The solution was concentrated (60 ml), basified ($NaHCO_3$), and extracted with chloroform (3 × 50 ml). Evaporation of the combined chloroform extracts yielded the indanol (**10***a*, 2.41 g), which was converted to its hydrochloride, m.p. 193–195° (from ethanol–ether); i.r. ν_{max} 1610, 1998, 2420–2650 ($\overset{+}{N}$—H), 3350 (OH) cm^{-1}; mass spectrum *m/e* (% relative abundance) 194 (100), 223 (95) ($C_{12}H_{17}NO_3$); n.m.r. (D_2O) δ 2.33 (s, 3H, CH_3), 2.50–4.23 (m, 3H, C_2—H and CH_2) overlapping 3.87 (s, 6H, $(OCH_3)_2$), 4.82 (s, 4H, DOH from $\overset{+}{N}H_3$, OH), 5.52 (d, 1H, J = 3.2 Hz, C_1—H), 6.98 (s, 1H, aromatic H).

Anal. Calcd. for $C_{12}H_{18}ClNO_3$: C, 55.49; H, 6.98; N, 5.39. Found: C, 55.23; H, 7.16; N, 5.50.

(*ii*) A solution of 4,7-dimethoxy-2-isonitroso-6-methyl-1-indanone (10.0 g) in ethanol (100 ml) and sufficient 10% NaOH to effect solution was hydrogenated at room temperature and normal pressure in the presence of 10% Pd–C (1.0 g) until hydrogen uptake ceased. The filtrate was evaporated and the residue suspended in water (60 ml), then extracted with chloroform and further treated as described in preparation *i* immediately above. This produced **10***a* hydrochloride (6.92 g), m.p. 193–195°, with i.r. and mass spectra identical to the product of preparation *i*.

trans-2-Amino-4,7-dimethoxy-1-indanol (10b) Hydrochloride

This compound (1.98 g), m.p. 182–184° (from ethanol) was the product of the reduction of 4,7-dimethoxy-2-isonitroso-1-indanone (3.0 g) using method *ii* above; i.r. ν_{max} 1602, 2080, 2580–2660 ($\overset{+}{N}$—H), 3350 (OH) cm^{-1}.

Anal. Calcd. for $C_{11}H_{16}ClNO_3$: C, 53.77; H, 6.56; N, 5.70. Found: C, 53.68; H, 7.11; N, 6.02.

4,7-Dimethoxy-5-methyl-2-indanone (11d)

A solution of 2-amino-4,7-dimethoxy-6-methyl-1-indanol hydrochloride (1.0 g) in concentrated HCl (20 ml) and water (10 ml) was heated under reflux. After 15 min a yellow oil separated from the solution. The reaction mixture was cooled, then extracted with chloroform (30 ml), and the latter extract reserved. The procedure was

Can. J. Chem. Downloaded from www.nrcresearchpress.com by 210.87.254.42 on 09/05/12
For personal use only.

repeated on the aqueous layer until evaporation of the chloroform extract gave no residue. The previous chloroform extracts were combined and evaporated to yield a pale yellow oil (0.56 g) which solidified on standing. Crystallization from ethanol yielded the title compound, m.p. 100–102°; i.r. ν_{max} 1750 (C=O) cm^{-1}; n.m.r. ($CDCl_3$) δ 2.32 (s, 3H, CH_3), 3.40 (s, 2H) and 3.51 (s, 2H) (CH_2 groups), 3.71 (s, 3H) and 3.81 (s, 3H) (OCH_3 groups), 6.59 (s, 1H, aromatic proton); mass spectrum *m/e* (% relative abundance) 163 (100), 206 (90) ($C_{12}H_{14}O_3$). This compound was used, without further characterization, in the preparation of the oxime (**11***e*).

*4,7-Dimethoxy-5-methyl-2-indanone Oxime (**11***e*)*

A solution of the indanone (**11***d*, 1.0 g) and hydroxylamine hydrochloride (2.0 g) in ethanol (10 ml) and pyridine (5 ml) was heated at 80° for 5 h then evaporated. The residue was suspended in water and the insoluble portion (0.98 g) was crystallized from ethanol and gave the title compound, m.p. 164–166°; i.r. ν_{max} 3250 br (OH) cm^{-1}; n.m.r. (DMSO-d_6) δ 10.66 (s, 1H, OH).

Anal. Calcd. for $C_{12}H_{15}NO_3$: C, 65.14; H, 6.83; N, 6.33. Found: C, 64.69; H, 6.92; N, 5.99.

*2-Amino-4,7-dimethoxy-5-methylindane (**12***a*) Hydrochloride*

(*i*) A solution of 4,7-dimethoxy-5-methyl-2-indanone oxime (0.5 g) in ethanol (200 ml) and concentrated HCl (5 ml) containing PtO_2 (0.1 g) was hydrogenated at room temperature and normal pressure until the theoretical amount of hydrogen was absorbed. The filtrate was evaporated and the residue was triturated with water (25 ml) and filtered. The aqueous solution was evaporated under reduced pressure and the product obtained (0.18 g) was crystallized from ethanol–ether to give the title compound, m.p. 253–255°; i.r. ν_{max} 1610, 2220–2680 ($\overset{+}{N}$—H) cm^{-1}; n.m.r. (D_2O) δ 2.30 (s, 3H, CH_3), 2.90–3.55 (m, 4H, CH_2 protons), 3.83 (s, 3H) and 3.88 (s, 3H) (OCH_3 protons), 4.10–4.60 (m, 1H, CH), 6.83 (s, 1H, aromatic proton).

Anal. Calcd. for $C_{12}H_{18}ClNO_2$: C, 59.12; H, 7.45; N, 5.75. Found: C, 58.70; H, 7.64; N, 5.85.

(*ii*) A solution of the oxime (**11***e*, 0.5 g) in glacial acetic acid (50 ml) and concentrated H_2SO_4 (0.5 g) containing 10% Pd–C (0.13 g), was hydrogenated to completion at room temperature and normal pressure. To the filtrate was added a solution of NaOH (0.25 g) in water (2 ml), prior to evaporation. The residue was dissolved in water (50 ml), basified with 5% NaOH (3 ml) and extracted with chloroform (3 × 50 ml). The combined chloroform extract was saturated with HCl gas and evaporated to give the title compound (0.32 g), m.p. 253–255° (from ethanol–ether).

(*iii*) A solution of 2-amino-4,7-dimethoxy-6-methylindanol hydrochloride (0.5 g) in dioxane (20 ml) and concentrated HCl (20 ml) containing 10% Pd–C (0.1 g) was hydrogenated at room temperature and normal pressure. Hydrogen was slowly absorbed over 20 h. The filtrate was evaporated under reduced pressure and the residue obtained was suspended in cold acetone (10 ml) and filtered. The insoluble material (0.23 g) was the title compound, m.p. 252–255° (from ethanol–ether).

Products from reactions *ii* and *iii* had i.r. spectra superimposable on that of the product from reaction *i*.

*2-Amino-4,7-dimethoxyindane (**12***b*) Hydrochloride*

This compound (0.91 g), m.p. 245–247° (from ethanol–ether) was the acetone-insoluble product obtained when 2-amino-4,7-dimethoxy-1-indanol (1.0 g) was treated in the manner described in reaction *iii* above; i.r. ν_{max} 1615, 2030, 2380–2700 ($\overset{+}{N}$—H) cm^{-1}; mass spectrum *m/e* (% relative abundance) 162 (100), 193 (86) ($C_{11}H_{15}NO_2$).

Anal. Calcd. for $C_{11}H_{16}ClNO_2$: C, 57.51; H, 7.02; N, 6.10. Found: C, 57.43; H, 7.16; N, 6.23.

*cis-2-Amino-4,7-dimethoxy-6-methyl-1-indanol (**10***a*) Hydrochloride*

(*i*) The acetone solution remaining in the preparation of **12***a* hydrochloride by method *iii* was evaporated and the residue dissolved in water (25 ml), then filtered. The filtrate was basified (5% NaOH) and extracted with chloroform (3 × 25 ml). The combined chloroform extract was saturated with HCl gas and evaporated to yield the title compound (0.25 g), m.p. 206–208° (from ethanol–ether); i.r. ν_{max} 1602, 2480–2700 ($\overset{+}{N}$—H), 3150 br (OH) cm^{-1}; mass spectrum *m/e* (% relative abundance) 194 (100); 223 (75) ($C_{12}H_{17}NO_3$); n.m.r. (D_2O) δ 2.33 (s, 3H, CH_3), 2.60–4.20 (m, 3H, C_2—H and CH_2) overlapping 3.88 and 3.91 (singlets, 6H, $(OCH_3)_2$), 4.80 (s, 4H, DOH from $\overset{+}{N}H_3$, OH), 5.47 (d, 1H, J = 5.7 Hz, C_1—H), 6.95 (s, 1H, aromatic H).

Anal. Calcd. for $C_{12}H_{18}ClNO_3$: C, 55.49; H, 6.98; N, 5.39. Found: C, 55.26; H, 7.24; N, 5.68.

(*ii*) A solution of 2-amino-4,7-dimethoxy-6-methyl-1-indanone hydrochloride (0.5 g) in ethanol (50 ml) was hydrogenated at 50 p.s.i. and room temperature for 15 h (arbitrary) in the presence of 10% Pd–C (0.1 g) and $PdCl_2$ (0.1 g). The filtrate was evaporated and the residue was crystallized from ethanol–ether to give the title compound (0.31 g), m.p. 205–208°, whose i.r. spectrum was identical to that of the product obtained in reaction *i*.

*3-(4-Bromo-2,5-dimethoxyphenyl)propionic Acid (**6***c*)*

A slight excess of bromine water was added dropwise over 4 h to a stirred solution of 3-(2,5-dimethoxyphenyl)-propionic acid (25 g) in dioxane (100 ml) and water (25 ml). The product precipitated from solution during the addition. The solid was collected by filtration and when the filtrate was diluted with water, more product precipitated. The combined solids when crystallized from ethanol yielded the title compound (22.2 g), m.p. 136–137°; i.r. ν_{max} 1702 (C=O), 2500–2700 (OH) cm^{-1}; n.m.r. ($CDCl_3$) δ 2.52–3.12 (m, 4H, CH_2 groups), 3.76 (s, 3H) and 3.81 (s, 3H) (OCH_3 groups), 6.80 (s, 1H) and 7.03 (s, 1H) (aromatic protons), 11.36 (s, br, 1H, exchanges with D_2O, OH).

Anal. Calcd. for $C_{11}H_{13}BrO_4$: C, 45.69; H, 4.53. Found: C, 45.63; H, 4.54.

*Catalytic Hydrogenation of 6-Bromo-4,7-dimethoxy-2-isonitroso-1-indanone (**8***c*)*

(*i*) A solution of the title compound (0.60 g) in ethanol (50 ml) and concentrated HCl (3 ml) was hydrogenated at room temperature and normal pressure for 12 h (arbitrary) in the presence of 10% Pd–C (0.2 g). Evaporation of the filtrate gave 2-amino-4,7-dimethoxy-1-indanone (**9***b*) hydrochloride (0.48 g), m.p. 259–262° (from ethanol–ether). The i.r. was identical to that of **9***b*

Can. J. Chem. Downloaded from www.nrcresearchpress.com by 210.87.254.42 on 09/05/12
For personal use only.

hydrochloride described earlier, and a mixture m.p. was undepressed.

(*ii*) A solution of the title compound (1.0 g) in ethanol (100 ml) and 5% NaOH (5 ml) was hydrogenated as described in *i* immediately above. The filtrate was evaporated and the residue dissolved in chloroform (100 ml). The chloroform solution was washed with water (4 × 50 ml), then saturated with HCl gas and evaporated. The residue (0.64 g), m.p. 180–182° (from ethanol) was *trans*-2-amino-4,7-dimethoxy-1-indanol (**10***b*) hydrochloride. Its i.r. spectrum was superimposable on that of authentic **10***b* hydrochloride and a mixture m.p. was undepressed.

*4,7-Dimethoxy-2-dimethylamino-5-methylindane (**16***f*) Hydrochloride*

A solution of 2-amino-4,7-dimethoxy-5-methylindane hydrochloride (0.50 g) in water (30 ml) and 40% formaldehyde (0.6 g) was hydrogenated at room temperature and normal pressure for 12 h (arbitrary) over 10% Pd–C (0.5 g). The filtrate was basified (NH_4OH) and extracted with chloroform (3 × 30 ml). The washed (H_2O) chloroform extract was saturated with HCl gas and evaporated to give a pale yellow solid (0.21 g), m.p. 194–196° (from ethanol); i.r. ν_{max} 1599, 2440–2700 ($\overset{+}{N}$—H) cm^{-1}; mass spectrum *m/e* (% relative abundance) 71 (100), 235 (57) ($C_{14}H_{21}NO_2$).

Anal. Calcd. for $C_{14}H_{22}ClNO_2$: C, 61.86; H, 8.16; N, 5.15. Found: C, 61.87; H, 8.34; N, 5.42.

*cis-2-Dimethylamino-4,7-dimethoxy-6-methyl-1-indanol (**17***f*) Hydrochloride*

This compound (0.55 g), m.p. 234–236° (from ethanol–ether) was prepared in a similar manner from *cis*-2-amino-4,7-dimethoxy-6-methyl-1-indanol hydrochloride (1.0 g); i.r. ν_{max} 1610, 2480–2700 br ($\overset{+}{N}$—H), 3190 br (OH) cm^{-1}; n.m.r. (DMSO-d_6) δ 2.22 (s, 3H, CH_3), 2.80–3.65 (m, 3H, C_2—H and CH_2) overlapping 2.96 (s, 6H, $N(CH_3)_2$), 3.78 and 3.80 (overlapping s, 6H, $(OCH_3)_2$), 5.31 (d, 1H, J = 5.50 Hz, C_1—H), 6.00–6.50 (br s, 1H, exchanges in D_2O, OH), 6.90 (s, 1H, aromatic H), 9.41–10.83 (br s, 1H, exchanges in D_2O, $\overset{+}{N}H$).

Anal. Calcd. for $C_{14}H_{22}ClNO_3$: C, 58.42; H, 7.71; N, 4.87. Found: C, 58.67; H, 7.97; N, 4.96.

*trans-2-Dimethylamino-4,7-dimethoxy-6-methyl-1-indanol (**17***f*) Hydrochloride*

This compound (0.38 g), m.p. 244–246° (from ethanol) was prepared in a similar manner from *trans*-2-amino-4,7-dimethoxy-6-methyl-1-indanol hydrochloride (0.8 g) except that in this instance the title compound base precipitated on the addition of NH_4OH and was removed, then dissolved in dry ether for conversion to the hydrochloride; i.r. ν_{max} 1610, 2460–2560 ($\overset{+}{N}$—H), 3270 br (OH) cm^{-1}; n.m.r. (DMSO-d_6) δ 2.22 (s, 3H, CH_3), 2.87 (s, 6H, $N(CH_3)_2$), 2.92–3.65 (m, 3H, C_2—H and CH_2), 3.75 and 3.78 (overlapping s, 6H, $(OCH_3)_2$), 5.69 (d, 1H, J = 5.50 Hz, C_1—H), 5.86–6.53 (br s, 1H, exchanges in D_2O, OH), 6.83 (s, 1H, aromatic H), 11.50–12.10 (br s, 1H, exchanges in D_2O, $\overset{+}{N}H$).

Anal. Calcd. for $C_{14}H_{22}ClNO_3$: C, 58.42; H, 7.71; N, 4.87. Found: C, 58.72; H, 8.08; N, 4.80.

A mixture m.p. of *cis*-**17***f* hydrochloride and *trans*-**17***f* hydrochloride was depressed to 228°.

*4,7-Dimethoxy-2-(dimethylamino)methyl-6-methyl-1-indanone (**18**) Hydrochloride*

A solution of 4,7-dimethoxy-6-methyl-1-indanone (10.0 g), dimethylamine hydrochloride (4.05 g) and paraformaldehyde (3.0 g) in ethanol (150 ml) and concentrated HCl (0.2 ml) was heated under reflux for 3 h, concentrated and cooled. The title compound (7.2 g), m.p. 179–180° (from ethanol–acetone), crystallized from solution; i.r. ν_{max} 1710 (C=O), 2450–2550 br ($\overset{+}{N}$—H) cm^{-1}; n.m.r. (DMSO-d_6) δ 2.22 (s, 3H, CH_3), 2.83 (s, 6H, $N(CH_3)_3$), 3.00–3.65 (m, 5H, CH and CH_2 groups), 3.75 (s, 3H) and 3.84 (s, 3H) (OCH_3 groups), 7.18 (s, 1H, aromatic proton).

Anal. Calcd. for $C_{15}H_{22}ClNO_3$: C, 60.09; H, 7.40. Found: C, 59.87; H, 7.67.

*4,7-Dimethoxy-2-(dimethylamino)methyl-6-methyl-1-indanol (**17***g*) Hydrochloride*

A solution of 4,7-dimethoxy-2-(dimethylamino)methyl-6-methyl-1-indanone hydrochloride (2.0 g) in methanol (25 ml) was reduced to the indanol (**17***g*) with sodium borohydride (1.0 g) using essentially the same method as described above for the preparation of **10***a*, method *i*. The chloroform extract of the indanol (**17***g*) was saturated with HCl gas and evaporated to yield the title compound (1.1 g), m.p. 193–194° (from ethanol); i.r. ν_{max} 2450, 2610 br ($\overset{+}{N}$—H), 3310 br (OH) cm^{-1}.

Anal. Calcd. for $C_{15}H_{24}ClNO_3$: C, 59.69; H, 8.01; N, 4.64. Found: C, 59.69; H, 7.83; N, 4.65.

*4,7-Dimethoxy-2-(dimethylamino)methyl-5-methylindane (**16***g*) Hydrochloride*

A solution of 4,7-dimethoxy-2-(dimethylamino)methyl-6-methyl-1-indanol hydrochloride (1.0 g) in dioxane (20 ml) and concentrated HCl (20 ml) containing 10% Pd-C (0.5 g) was hydrogenated at 40 p.s.i. and room temperature for 12 h (arbitrary). The filtrate was evaporated and the residue obtained was shaken with dry acetone and filtered. The insoluble material (0.67 g) was crystallized from ethanol–ether to yield the title compound, m.p. 204–205°; i.r. ν_{max} 2560 br, 2610 br ($\overset{+}{N}$—H) cm^{-1}.

Anal. Calcd. for $C_{15}H_{24}ClNO_2$: C, 63.00; H, 8.46; N, 4.90. Found: C, 62.52; H, 8.72; N, 4.54.

*4,7-Dimethoxy-6-methyl-1-indanone Oxime (**19***a*)*

A solution of 4,7-dimethoxy-6-methyl-1-indanone (7.0 g), hydroxylamine hydrochloride (7.0 g), and pyridine (8 ml) in ethanol (100 ml) was heated at 80° with stirring for 20 min and cooled. A solid precipitated and was washed repeatedly with 5% HCl then crystallized from methanol to yield the title compound (5.7 g), m.p. 228–231°; i.r. ν_{max} 3250 (OH) cm^{-1}.

Anal. Calcd. for $C_{12}H_{15}NO_3$: C, 65.14; H, 6.83. Found: C, 65.10; H, 6.79.

*4,7-Dimethoxy-1-indanone Oxime (**19***b*)*

This compound (2.1 g), m.p. 230–232° (from ethanol) was obtained in the same manner from 4,7-dimethoxy-1-indanone (2.5 g); i.r. ν_{max} 3210 (OH) cm^{-1}.

Anal. Calcd. for $C_{11}H_{13}NO_3$: C, 63.75; H, 6.32; N, 6.76. Found: C, 64.06; H, 6.56; N, 6.67.

*1-Amino-4,7-dimethoxy-6-methylindane (**20a**)*

(*i*) A suspension of finely powdered 4,7-dimethoxy-6-methyl-1-indanone (4.5 g) in sodium-dried ether (200 ml) was added slowly to a stirred suspension of lithium aluminum hydride (1.0 g) in the same solvent (100 ml). The mixture was heated under reflux for 30 h, cooled, and the excess hydride decomposed by the careful addition of cold water. The suspension was filtered and the insoluble material washed well with ether. The combined ether extract was dried ($MgSO_4$) and saturated with HBr gas. The title compound (4.8 g) precipitated, m.p. 214–215° (from ethanol); i.r. ν_{max} 1590, 1998, 2580–2680 ($\overset{+}{N}$—H) cm^{-1}.

Anal. Calcd. for $C_{12}H_{18}BrNO_2$: C, 50.01; H, 6.29; N, 4.86. Found: C, 50.04; H, 6.42; N, 4.86.

(*ii*) A solution of 4,7-dimethoxy-6-methyl-1-indanone oxime (2.0 g) in ethanol (50 ml) containing PtO_2 (0.1 g) was hydrogenated at room temperature and normal pressure for 12 h. The filtrate was evaporated and the residue dissolved in ether. This solution was saturated with HBr gas to yield the title compound (1.84 g), m.p. 214–215°.

*1-Amino-4,7-dimethoxyindane (**20b**) Hydrochloride*

A solution of 4,7-dimethoxy-1-indanone oxime (1.2 g) in glacial acetic acid (25 ml) and concentrated H_2SO_4 (1 ml) was hydrogenated over 10% Pd–C (0.3 g) until the theoretical volume of hydrogen was absorbed (6 h). The filtrate was neutralized ($NaHCO_3$) and evaporated. The residue was suspended in 5% $NaHCO_3$ solution (25 ml) and extracted with chloroform (3 × 25 ml). The chloroform extract was washed (H_2O), dried ($MgSO_4$), saturated with gaseous HBr and evaporated to yield the title compound (1.1 g), m.p. 225–226° (from ethanol); i.r. ν_{max} 1590, 1982, 2600–2700 ($\overset{+}{N}$—H) cm^{-1}.

Anal. Calcd. for $C_{11}H_{16}BrNO_2$: C, 48.19; H, 5.88; N, 5.11. Found: C, 48.06; H, 5.79; N, 4.82.

*1-Amino-6-bromo-4,7-dimethoxyindane (**20c**) Hydrochloride*

A slight excess of bromine water was added dropwise to a stirred solution of 1-amino-4,7-dimethoxyindane hydrochloride (0.5 g) in water (20 ml). The pale red solution was stirred for a further 2 h, basified (10% NaOH) and extracted with ether (2 × 50 ml). The ether solution was dried ($MgSO_4$), saturated with gaseous HCl and evaporated to give an oil which solidified on standing. This was assumed to be the title compound (0.21 g), m.p. 217–219°, (from ethanol–acetone); i.r. ν_{max} 1602, 2010, 2580–2680 ($\overset{+}{N}$—H) cm^{-1}; mass spectrum *m/e* (% relative abundance) 162 (100), 273 (58) ($C_{11}H_{14}{}^{81}BrNO_2$), 271 (60) ($C_{11}H_{14}{}^{79}BrNO_2$).

Anal. Calcd. for $C_{11}H_{15}BrClNO_2$: C, 42.81; H, 4.90; N, 4.54. Found: C, 42.70; H, 4.70; N, 4.79.

*1-Dimethylamino-4,7-dimethoxy-6-methylindane (**21**) Hydrochloride*

This compound (0.42 g), m.p. 209–211° (from ethanol) was prepared from 1-amino-4,7-dimethoxy-6-methylindane hydrochloride (1.5 g) using the method described for the synthesis of **16***f*-hydrochloride; i.r. ν_{max} 1602, 2300–2600 ($\overset{+}{N}$—H) cm^{-1}.

Anal. Calcd. for $C_{14}H_{22}ClNO_2$: C, 61.86; H, 8.16; N, 5.15. Found: C, 62.00; H, 8.17; N, 5.58.

The authors wish to thank the Medical Research Council of Canada for the award of a studentship (to J.L.M.) and an operating grant No. MA-2993 (to R.T.C.). The preliminary pharmacological testing was organized by Dr. D. F. Biggs, of our Faculty.

1. J. R. SMYTHIES, R. J. BRADLEY, V. S. JOHNSTON, F. BENINGTON, R. D. MORIN, and L. C. CLARK. Psychopharmacologia, **10**, 379 (1967).
2. J. R. SMYTHIES, V. S. JOHNSTON, R. J. BRADLEY, F. BENINGTON, R. D. MORIN, and L. C. CLARK. Nature, **216**, 128 (1967).
3. S. H. SNYDER and C. R. MERRIL. Proc. Natl. Acad. Sci. U.S. **54**, 258 (1965).
4. S. H. SNYDER and E. RICHELSON. Proc. Natl. Acad. Sci. U.S. **60**, 206 (1968).
5. S. KANG and J. P. GREEN. Proc. Natl. Acad. Sci. U.S. **67**, 62 (1970).
6. A. T. SHULGIN, T. SARGENT, and C. NARANJO. Nature, **221**, 537 (1969).
7. A. S. HORN and S. H. SNYDER. J. Pharmacol. Exptl. Therap. **180**, 523 (1972).
8. J. LOCKETT and W. F. SHORT. J. Chem. Soc. 787 (1939).
9. J. KOO. J. Am. Chem. Soc. **75**, 1891 (1953).
10. W. E. ROSEN and M. J. GREEN. J. Org. Chem. **28**, 2797 (1963).
11. R. I. THRIFT. J. Chem. Soc. (C), 288 (1967).
12. H. RICHTER and M. SCHENCK. German Patent 937, 953 (1956); Chem. Abstr. **53**, 2191c (1959).
13. British Patent 752,949 (1956) (to Schering A-G); Chem. Abstr. **51**, 8791h (1957).
14. H. RICHTER and M. SCHENCK. German Patent 936, 507 (1955); Chem. Abstr. **53**, 2190d (1959).
15. M. KARPLUS. J. Chem. Phys. **30**, 11 (1959); J. Am. Chem. Soc. **85**, 2870 (1963).
16. Netherland Patent 6, 408,887 (1965) (to Aspro-Nicholas); Chem. Abstr. **62**, 16161c (1965).
17. S. REINHARD. German Patent 2,018,135 (1970); Chem. Abstr. **74**, 22601b (1971).
18. R. T. COUTTS and J. L. MALICKY. Can. J. Chem. **51**, 1402 (1973).
19. A. A. R. SAYIGH, H. ULRICH, and M. GREEN. J. Chem. Soc. 3482 (1964).
20. A. A. BOTHNER-BY and C. NAAR-COLIN. J. Am. Chem. Soc. **83**, 231 (1961).
21. A. A. BOTHNER-BY, C. NAAR-COLIN, and H. GUNTHER. J. Am. Chem. Soc. **84**, 2748 (1962).
22. R. T. ARNOLD and H. E. ZAUGG. J. Am. Chem. Soc. **63**, 1317 (1941).

Can. J. Chem. Downloaded from www.nrcresearchpress.com by 210.87.254.42 on 09/05/12
For personal use only.

The Synthesis of Some Analogs of the Hallucinogen 1-(2,5-Dimethoxy-4-methylphenyl)-2-aminopropane (DOM). III.[1] Some Derivatives of 3-phenylalanine

RONALD T. COUTTS AND JERRY L. MALICKY

Faculty of Pharmacy and Pharmaceutical Sciences, University of Alberta, Edmonton, Alberta

Received June 18, 1973

Syntheses of the hydrochlorides of 3-(2,5-dimethoxyphenyl)alanine, 3-(2,5-dimethoxy-4-methylphenyl) alanine, and 3-(4-bromo-2,5-dimethoxyphenyl)alanine are described. A phenol, $C_{10}H_{14}ClNO_4$, related to the second of these three compounds was also prepared and is concluded to be a monohydrate of the lactone, 3-amino-6-hydroxy-7-methylhydrocoumarin hydrochloride.

On décrit les synthèses des chlorhydrates de (diméthoxy-2,5 phényl)-3 alanine, de (diméthoxy-2,5 méthyl-4 phényl)-3 alanine et de (bromo-4 diméthoxy-2,5 phényl)-3 alanine. On a aussi préparé un dérivé du type phénol, $C_{10}H_{14}ClNO_4$, relié au second de ces trois composés, qui s'est révélé être un monohydrate de la lactone, chlorhydrate d'amino-3 hydroxy-6 méthyl-7 hydrocoumarin.

[Traduit par le journal]

Can. J. Chem., 52, 390 (1974)

When mescaline is administered to animals, the amount which reaches the brain is very low (1, 2). In an attempt to obtain higher brain levels, the amino acid analog, 3-(3,4,5-trimethoxyphenyl)alanine (**1**), was prepared, it being rationalized that this compound would be actively transported across the blood–brain barrier and might be decarboxylated in the brain to yield mescaline (3, 4). When evaluated pharmacologically, however, the amino acid **1** failed to demonstrate any psychotomimetic activity. Mescaline, itself, is a weak psychotomimetic drug and so we decided to prepare for pharmacological evaluation, amino acid analogs of the more potent psychotomimetic drugs, 1-(2,5-dimethoxyphenyl) 2-aminopropane (5), 1-(2,5-dimethoxy-4-methylphenyl)-2-aminopropane (5) (DOM), and 1-(4-bromo-2,5-dimethoxyphenyl)-2-aminopropane (6, 7). The envisaged compounds were not expected to act as substrates for brain decarboxylase enzymes (*cf.* 8); activity *per se* was being investigated. The compounds were interesting for other reasons. Since they were amino acids, they would be expected to be capable of entering the CNS system and might possibly evoke pharmacological effects other than psychotomimetic ones.

For the reasons given, syntheses of 3-(2,5-dimethoxy-4-methylphenyl)alanine (**2***a*), 3-(2,5-dimethoxyphenyl)alanine (**2***b*), and 3-(4-bromo-2,5-dimethoxyphenyl)alanine (**2***c*) were undertaken.

Phenylalanines have been prepared by a variety of methods including one which employed an azlactone as a suitable intermediate (9). This was the method employed in the present investigation and is summarized in Scheme 1. Thus, when 2,5-dimethoxy-4-methylbenzaldehyde was reacted with acetylglycine in the presence of acetic anhydride and sodium acetate, the bright orange azlactone, 4-(2,5-dimethoxy-4-methylbenzylidene)-2-methyl-2-oxazolin-5-one (**3***a*), was formed. Hydrolysis of **3***a* in aqueous acetone gave α-acetamido-2,5-dimethoxy-4-methylcinnamic acid (**4***a*), which was reduced catalytically to *N*-acetyl-3-(2,5-dimethoxy-4-methylphenyl)alanine (**5***a*). Treatment of the latter with hydrochloric acid caused hydrolysis of the amide group and gave the required 3-(2,5-dimethoxy-4-methylphenyl)alanine hydrochloride (**2***a*). In the

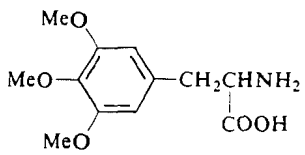

1

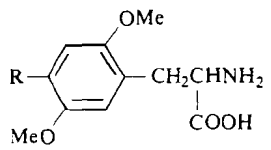

2

a R = Me
b R = H
c R = Br

[1]Part II see ref. 15.

Can. J. Chem. Downloaded from www.nrcresearchpress.com by 210.87.254.42 on 09/05/12
For personal use only.

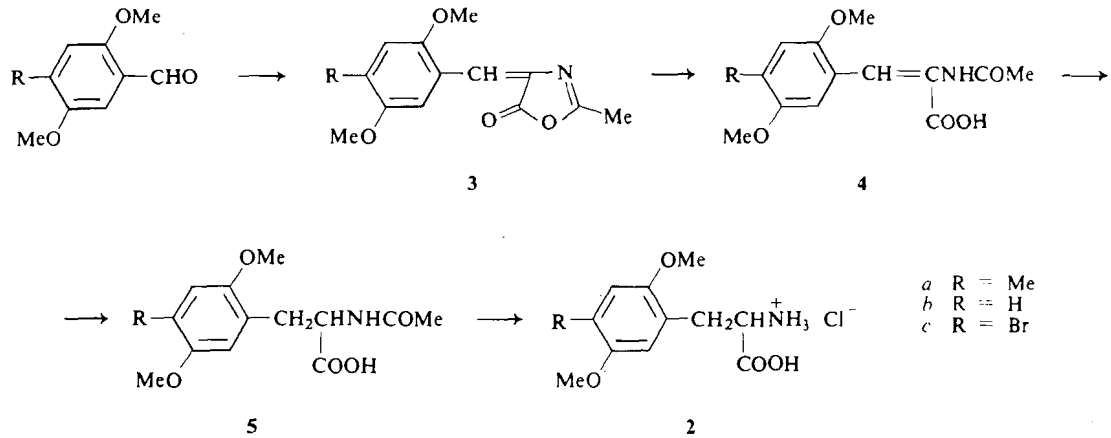

3 4 5 2

SCHEME I

same way, 2,5-dimethoxybenzaldehyde was converted to 3-(2,5-dimethoxyphenyl)alanine hydrochloride (**2***b*) via intermediates **3***b*, **4***b*, and **5***b*.

The action of bromine water on *N*-acetyl-3-(2,5-dimethoxyphenyl)alanine (**5***b*) gave a monobromo derivative. A 60 MHz n.m.r. spectrum of this product showed two one-proton singlet signals (δ 7.03 and 7.18) which indicated that these aromatic protons were *para* to each other, and enabled identification of the bromo compound as *N*-acetyl-3-(4-bromo-2,5-dimethoxyphenyl)alanine (**5***c*). This amide was then hydrolyzed with hydrochloric acid to 3-(4-bromo-2,5-dimethoxyphenyl)alanine hydrochloride (**2***c*).

In view of the study by Ferrini and Glässer (8), it is possible that, in contrast with the dimethyl ether (**2***a*), 3-(2,5-dihydroxy-4-methylphenyl)alanine (**6**) might be a substrate for a brain decarboxylase system and, if so, would produce *in vivo* 2-(2,5-dihydroxy-4-methylphenyl) ethylamine (**7**), a compound with possible psychotomimetic activity. The feasibility of preparing **6** was considered remote since spontaneous lactonization would be expected to occur in an acidic medium and yield the lactone **8**. However, a synthesis of **6** was attempted with the thought in mind that if the lactone **8** did form, it might itself possess pharmacological activity, or alternatively might hydrolyze *in vivo* to the more interesting amino acid **6**.

When 3-(2,5-dimethoxy-4-methylphenyl)alanine (**2***a*) was reacted with phosphorus and hydriodic acid, a small quantity of a product was isolated but could not be purified. 4-(2,5-Dimethoxy-4-methylbenzylidene)-2-phenyl-2-oxazolin-5-one (**9**), prepared for another study (10), was then heated under reflux with phosphorus and hydriodic acid and was converted in low yield to a colorless product, $C_{17}H_{15}NO_4$. The i.r. spectrum of this material displayed bands at 1765 (lactone), 1642 (C=N), and 3440 and 3300 cm^{-1} (free and bonded OH), enabling identification as 4-(2,5-dihydroxy-4-methylbenzyl)-2-

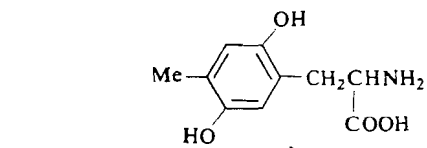

6

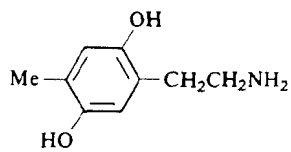

7

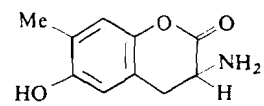

8

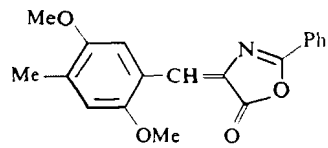

9

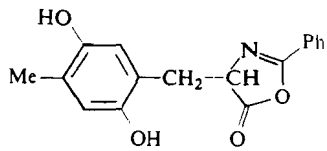

10

Can. J. Chem. Downloaded from www.nrcresearchpress.com by 210.87.254.42 on 09/05/12
For personal use only.

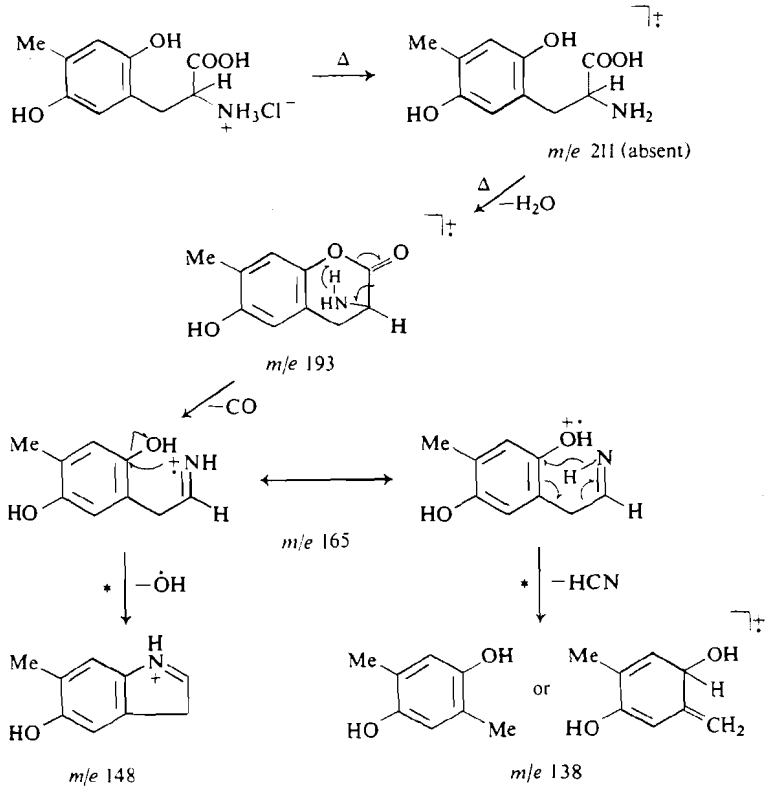

SCHEME 2

phenyl-2-oxazolin-5-one (**10**). The mother liquor remaining after removal of **10** gave a blue color when treated with ninhydrin reagent, suggesting the presence of an α-amino acid (11), but attempts to find the isoelectric point and isolate this product proved unsuccessful.

Treatment of the azlactone **9** with phosphorus and hydriodic acid was repeated but for a longer time. When the p*H* of the reaction mixture was adjusted to 4.5 a solid, which gave a positive ninhydrin reaction, precipitated from solution in modest yield. The compound was amphoteric; it formed a hydrochloride, and an aqueous solution when treated with ferric chloride turned blue, indicative of a phenol. A correct analysis for $C_{10}H_{14}ClNO_4$ was consistent with the product being a monohydrate of the expected lactone **8** hydrochloride, or alternatively, the hydrochloride of amino acid **6**. The carbonyl stretching band in the i.r. spectrum was located at 1765 cm^{-1} which was more indicative (12) of the lactone. However, this stretching frequency is not far removed from the range quoted (13) for α-amino acid hydrochlorides (1730–1755 cm^{-1}) and is reasonably close to the carbonyl stretching frequencies of amino acids **2***a* and *b*. The mass spectrum displayed diagnostic ions of *m/e* 193, 165, 148, and 138 but no ions of greater mass. This, also, suggested the lactone (mass of anhydrous base, 193), but the mass spectrum may be explained in terms of the phenylalanine (**6**) structure if thermal decomposition of the hydrochloride of **6** to the base is followed by dehydration to the lactone **8** prior to fragmentation. The fragment ions of *m/e* 165, 148, and 138 were identified as $C_9H_{11}NO_2$, $C_9H_{10}NO$, and $C_8H_{10}O$, respectively, by accurate mass measurements, and their formation from the lactone molecular ion can be rationalized as illustrated in Scheme 2; the *ortho* effect involved in the *m/e* 165 → *m/e* 148 fragmentation is reminiscent of the expulsion of $\cdot OCH_3$ from *o*-methoxybenzylketoximes (14).

To help distinguish between the two possibilities **6** and **8**, an n.m.r. spectrum of the compound was recorded in DMSO. Since the methylene and methine signals of both structures **6** and **8** would

Can. J. Chem. Downloaded from www.nrcresearchpress.com by 210.87.254.42 on 09/05/12
For personal use only.

Can. J. Chem. Downloaded from www.nrcresearchpress.com by 210.87.254.42 on 09/05/12
For personal use only.

be expected to display ABX coupling patterns, an interpretation of these signals would not permit a choice between the two possibilities. However, when the downfield deuterium-exchangeable signals were examined, it was revealed that signals ascribable to only four protons (*i.e.* $\overset{+}{N}H_3$ and O*H*) were present. This evidence is consistent with the product of the action of phosphorus and hydriodic acid on the azlactone **9** being the hydrochloride of lactone **8** and not of the amino acid **6**, which would give signals for six downfield deuterium-exchangeable protons.

Compounds **2***a* and **8** were subjected to a preliminary pharmacology screening in the rat. Both lacked symptoms characteristic of DOM intoxication. Compound **8** appeared to possess some stimulant properties. Compounds **2***b* and **2***c* await pharmacological evaluation.

Experimental

Melting points (capillary tube) are uncorrected. Infrared spectra were recorded on a Beckman IR-10 spectrophotometer as Nujol mulls, and n.m.r. spectra were taken on a varian A-60D spectrometer with tetramethylsilane as internal standard. Dr. A. M. Hogg and his associates, Department of Chemistry, University of Alberta, recorded the mass spectra on an A.E.I. MS-9 or MS-12 mass spectrometer at an ionizing potential of 70 eV using the direct probe technique. Elemental analysis were determined at the Faculty of Pharmacy and Pharmaceutical Sciences by Mr. W. Dylke.

4-(2,5-Dimethoxy-4-methylbenzylidene)-2-methyl-2-oxazolin-5-one (3a)

A mixture of 2,5-dimethoxy-4-methylbenzaldehyde (22.0 g), acetylglycine (11.0 g), sodium acetate (6.0 g), and acetic anhydride (24 ml) was heated under reflux for 2 h, then cooled to 5°. The orange precipitate was thoroughly washed with water in which the title compound (17.9 g) was insoluble. Recrystallization from benzene gave m.p. 128–130°; i.r. ν_{max} 1650 (C=N), 1795 (C=O) cm^{-1}.

Anal. Calcd. for $C_{14}H_{15}NO$: C, 64.35; H, 5.79; N, 5.36. Found: C, 64.46; H, 5.78; N, 5.29.

4-(2,5-Dimethoxybenzylidene)-2-methyl-2-oxazolin-5-one (3b)

This product (18.2 g), m.p. 129–131° (from benzene), was prepared in the same manner from 2,5-dimethoxybenzaldehyde (22.0 g).

Anal. Calcd. for $C_{13}H_{13}NO$: C, 62.89; H, 5.68; N, 5.64. Found: C, 63.16; H, 5.68; N, 5.40.

α-Acetamido-2,5-dimethoxy-4-methylcinnamic Acid (4a)

A solution of the azlactone **3***a* (15 g) in water (80 ml) and acetone (200 ml) was heated under reflux for 4 h. The acetone was distilled off and insoluble starting material removed by filtration. The title compound (3.2 g) crystallized from the filtrate on cooling. Repeating the procedure with the recovered starting material gave a further 2.1 g of **4***a*. Crystallization from ethanol–water gave m.p. 206–208°; i.r. ν_{max} 1648, 1690 (C=O), 2500–2750 (OH), 3230 (NH) cm^{-1}; n.m.r. (DMSO-d_6) δ 2.00 (s, 3H, $COCH_3$), 2.21 (s, 3H, CH_3), 3.73 (s, 3H) and 3.80 (s, 3H) (OCH_3 groups), 6.81 (s, 1H), 7.26 (s, 1H), and 7.60 (s, 1H) (aromatic protons and CH), 9.17 (s, br, 1H, exchanges with D_2O, OH).

Anal. Calcd. for $C_{14}H_{17}NO_5$: C, 60.20; H, 6.14; N, 5.02. Found: C, 60.45; H, 6.60; N, 5.36.

α-Acetamido-2,5-dimethoxycinnamic Acid (4b)

This product (9.5 g), m.p. 208–209° (from ethanol) was prepared in the same manner from azlactone **3***b* (15.0 g); i.r. ν_{max} 1655, 1695 (C=O), 2400–2600 (OH), 3250 (NH) cm^{-1}.

Anal. Calcd. for $C_{13}H_{15}NO_5$: C, 58.86; H, 5.70; N, 5.28. Found: C, 59.14; H, 6.20; N, 4.91.

N-Acetyl-3-(2,5-dimethoxy-4-methylphenyl)alanine (5a)

A solution of α-acetamido-2,5-dimethoxy-4-methylcinnamic acid (5.0 g) in ethanol (100 ml) containing 10% palladium–charcoal (0.5 g) was hydrogenated at room temperature and 50 p.s.i. until uptake of hydrogen ceased. Evaporation of the filtrate gave a quantitative yield of the title compound, m.p. 159–160° (from ethanol); i.r. ν_{max} 1655 (amide C=O), 1720 (acid C=O), 3310 (NH) cm^{-1}.

Anal. Calcd. for $C_{14}H_{19}NO_5$: C, 59.77; H, 6.81; N, 4.98. Found: C, 59.54; H, 6.73; N, 4.89.

N-Acetyl-3-(2,5-dimethoxyphenyl)alanine (5b)

This product m.p. 160–162° (from ethanol) was similarly prepared in quantitative yield from α-acetamido-2,5-dimethoxycinnamic acid (7.0 g); i.r. ν_{max} 1630 br, 1730 (C=O), 3310 (NH) cm^{-1}.

Anal. Calcd. for $C_{13}H_{17}NO_5$: C, 58.41; H, 6.41; N, 5.24. Found: C, 58.38; H, 6.60; N, 5.21.

N-Acetyl-3-(4-bromo-2,5-dimethoxyphenyl)alanine (5c)

Bromine water was added dropwise to a stirred solution of *N*-acetyl-3-(2,5-dimethoxyphenyl)alanine (1.0 g) in ethanol (100 ml) until a pale orange color persisted. Stirring was continued for a further 0.5 h, then the solution was basified (5% $NaHCO_3$) and evaporated. The mixture was suspended in 5% HCl solution (50 ml) and extracted with chloroform (2 × 30 ml). Evaporation of the chloroform gave an oil which was dissolved in 5% $NaHCO_3$ solution and the solution filtered. Acidification of the filtrate (dilute HCl) gave the title compound (0.62 g), m.p. 178–180° (from ethanol); i.r. ν_{max} 1650, 1730 (C=O), 3310 (NH) cm^{-1}; n.m.r. (DMSO-d_6) δ 1.79 (s, 3H, $COCH_3$) 3.06 (m, 2H, CH_2), 3.78 (s, 6H, OCH_3 groups), 4.15–4.80 (m, 1H, CH), 7.03 (s, 1H), and 7.18 (s, 1H) (aromatic protons), 8.20 (d, 1H, J = 8 Hz, NH).

Anal. Calcd. for $C_{13}H_{16}BrNO_5$: C, 45.10; H, 4.66; N, 4.05. Found: C, 45.04; H, 4.73; N, 3.81.

3-(2,5-Dimethoxy-4-methylphenyl)alanine Hydrochloride (2a)

A suspension of *N*-acetyl-3-(2,5-dimethoxy-4-methylphenyl)alanine (4.0 g) in concentrated HCl (60 ml) was heated under reflux for 4 h, then evaporated to dryness. The residue was suspended in acetone in which the title compound (2.8 g) was insoluble. Crystallization from ethanol gave m.p. 241–242°; i.r. ν_{max} 1580, 1950, 2410–2670 ($\overset{+}{N}$—H), 1745 (C=O) cm^{-1}; n.m.r. (DMSO-d_6)

δ 2.18 (s, 3H, CH_3), 3.18 (d, 2H, J = 6 Hz, CH_2), 3.65–4.23 (m, 7H, overlapping CH and OCH_3 signals), 6.84 (s, 1H) and 7.00 (s, 1H) (aromatic protons), 8.66 (s, br, 4H, exchange with D_2O, $\overset{+}{N}H_3$ and OH).

Anal. Calcd. for $C_{12}H_{17}ClNO_4$: C, 52.46; H, 6.24; N, 5.10. Found: C, 52.40; H, 6.55; N, 4.86.

3-(2,5-Dimethoxyphenyl)alanine Hydrochloride (2b)

This product (1.52 g), m.p. 225° (from ethanol–ether (lit. (8) no m.p. reported)) was obtained similarly by hydrolysis of *N*-acetyl-3-(2,5-dimethoxyphenyl)alanine (2.0 g); i.r. ν_{max} 1585, 2420–2680 ($\overset{+}{N}$—H), 1750 (C=O) cm^{-1}.

Anal. Calcd. for $C_{11}H_{16}ClNO_4$: C, 50.48; H, 6.16; N, 5.35. Found: C, 50.12; H, 6.29; N, 5.35.

3-(4-Bromo-2,5-dimethoxyphenyl)alanine Hydrochloride (2c)

This product (0.41 g), m.p. 252–253° (from ethanol–acetone) was prepared in a similar manner from *N*-acetyl-3-(4-bromo-2,5-dimethoxyphenyl)alanine (0.5 g); i.r. ν_{max} 1590, 2420–2680 ($\overset{+}{N}$—H), 1735 (C=O) cm^{-1}.

Anal. Calcd. for $C_{11}H_{15}BrClNO_4$: C, 38.79; H, 4.44; N, 4.11. Found: C, 39.07; H, 4.62; N, 4.11.

Treatment of 4-(2,5-Dimethoxy-4-methylbenzylidene)-2-phenyl-2-oxazolin-5-one (9) with Phosphorus and Hydriodic Acid

(*i*) To a solution of the title compound (10) (21.0 g) in acetic anhydride (60 ml) containing red phosphorus (18.0 g) was added 50% HI (60 ml) over 1 h. The red reaction mixture was heated under reflux for 3 h, cooled, filtered, and evaporated to a semisolid residue. Water (100 ml) was added and the resulting suspension was shaken several times with ether. This treatment caused the separation of a solid at the interface. The ether extracts were discarded. The aqueous solution remaining gave a positive ninhydrin reaction but attempts to cause precipitation of any product by slowly altering the p*H* of the cooled solution with dilute NH_4OH and dilute HCl were unsuccessful.

The interfacial material (3.1 g), m.p. 262–264° (from ethanol) was 4-(2,5-dihydroxy-4-methylbenzyl)-3-phenyl-2-oxazolin-5-one (**10**); i.r. ν_{max} 1642 (C=N), 1765 (C=O), 3300 br, 3440 (OH) cm^{-1}; mass spectrum *m/e* (% relative abundance) 297 (8) ($C_{17}H_{15}NO_4$).

Anal. Calcd. for $C_{17}H_{15}NO_4$: C, 68.67; H, 5.09; N, 4.71. Found: C, 68.41; H, 5.51; N, 4.48.

(*ii*) The reaction described immediately above was repeated on the title compound (13.0 g) except that heating under reflux was continued for 5 h. The filtrate this time was extracted with ether prior to being evaporated to give a brown oil. To a filtered solution of this oil in water (100 ml), dilute NH_4OH solution was added slowly. At p*H* 4.5, a solid (3.2 g) precipitated, m.p. 250–300° (dec.). An aqueous solution of this material turned blue when treated with ninhydrin reagent. A portion of the solid (1.5 g) was dissolved in concentrated HCl and evaporated. The product (1.1 g, m.p. 245–250°) when crystallized from ethanol–ether, gave 3-amino-6-hydroxy-7-methylhydrocoumarin hydrochloride monohydrate (**8**, 0.44 g), m.p. 255–257°; i.r. ν_{max} 1765 (C=O), 2450–2650 ($\overset{+}{N}$—H), 3120 br, 3300 (OH) cm^{-1}; n.m.r. (DMSO-d_6) δ 2.13 (s, 3H, CH_3), 3.27 (d, 2H, J = 10 Hz, CH_2), 4.57 (t, 1H, J = 10 Hz, CH), 6.85 (s, 1H) and 6.93 (s, 1H) (aromatic protons), 8.10–10.10 (m, br, ~4H, exchanges with D_2O, $\overset{+}{N}$—H and OH protons); mass spectrum *m/e* (% relative abundance) 193 (11) ($C_{10}H_{11}NO_3$), 165 (80) ($C_9H_{11}NO_2$), 148 (18) ($C_9H_{10}NO$), 138 (22) ($C_8H_{10}O_2$) (formula confirmed by accurate mass measurements).

Anal. Calcd. for $C_{10}H_{14}ClNO_4$: C, 48.49; H, 5.70; N, 5.66. Found: C, 48.81; H, 5.96; N, 5.44.

The authors wish to thank the Medical Research Council of Canada for operating grant MA-2993 (to R.T.C.) and a studentship (to J.L.M.), and Dr. D. F. Biggs for assistance in pharmacological evaluations.

1. E. S. Boyd. Arch. Int. Pharmacodyn. **120**, 292 (1959).
2. H. C. B. Debner and D. N. Teller. Arzneim. Forsh. **20**, 903 (1970).
3. R. M. Acheson, D. P. Dearnley, A. O. Plunkett, and V. C. Porter. J. Chem. Soc. 2085 (1963).
4. J. R. Smythies and E. A. Sykes. *In* Amine schizophrenia. Symposium, Atlantic City. 1965. pp. 5–18; Chem. Abstr. **68**, 37785q (1968).
5. A. T. Shulgin, T. Sargent, and C. Naranjo. Nature, **221**, 537 (1969).
6. A. T. Shulgin, T. Sargent, and C. Naranjo. Pharmacology, **5**, 103 (1971).
7. C. F. Barfknecht and D. E. Nichols. J. Med. Chem. **14**, 370 (1971).
8. R. Ferrini and A. Glässer. Biochem. Pharmocol. **13**, 798 (1964).
9. E. Erlenmeyer. Ann. **271**, 164 (1892).
10. R. T. Coutts and J. L. Malicky. Unpublished material.
11. R. L. Shriner, R. C. Fuson, and D. Y. Curtin. The systematic identification of organic compounds. 5th ed. Wiley, New York. 1964. p. 264.
12. L. J. Bellamy. Advances in infrared group frequencies. Methuen. London. 1968. pp. 163–165.
13. A. D. Cross. Introduction to practical infrared spectroscopy. Butterworths, London. 1960. p. 67.
14. R. T. Coutts and J. L. Malicky. Org. Mass Spectrom. **7**, 985 (1973).
15. R. T. Coutts and J. L. Malicky. Can. J. Chem. This issue.

Can. J. Chem. Downloaded from www.nrcresearchpress.com by 210.87.254.42 on 09/05/12
For personal use only.

Can. J. Chem. Downloaded from www.nrcresearchpress.com by 210.87.254.6 on 09/05/12
For personal use only.

The Synthesis of Four Possible *in vitro* Metabolites of the Hallucinogen 1-(2,5-Dimethoxy-4-methylphenyl)-2-aminopropane (DOM)

RONALD T. COUTTS AND JERRY L. MALICKY

Faculty of Pharmacy and Pharmaceutical Sciences, University of Alberta, Edmonton, Alberta

Received June 18, 1973

The synthesis of four possible *in vitro* metabolites of the hallucinogen 1-(2,5-dimethoxy-4-methylphenyl)-2-aminopropane (DOM) is described. These compounds, 1-(2,5-dimethoxy-4-methylphenyl(-2-propanone, the corresponding oxime, 1-(2,5-dimethoxy-4-methylphenyl)-2-propanol, and 1-(2,5-dimethoxy)-4-methylphenyl-2-(hydroxylamino)propane, could be products of side chain metabolic oxidation of DOM.

On décrit la synthèse *in vitro* de quatres métabolites possibles de l'hallucinogène (diméthoxy-2,5 méthyl-4 phényl)-1 amino-2 propane sont décrites. Ces composés, la (diméthoxy-2,5 méthyl-4 phényl)-1 propanone-2, l'oxime correspondante, le (diméthoxy-2,5 méthyl-4 phényl)-1 propanol-2 et le (diméthoxy-2,5 méthyl-4 phényl)-1 hydroxylamino-2 propane, peuvent être des produits de l'oxydation métabolique de la chaîne latérale du DOM. [Traduit par le journal]

Can. J Chem., **52**, 395 (1974)

In 1955, Axelrod (1) reported that amphetamine (**1***a*) was metabolically oxidized by rat liver microsomes to phenylacetone (**2***a*). In view of this observation, it was of interest to us to determine whether the potent hallucinogen, 1-(2,5-dimethoxy-4-methylphenyl)-2-aminopropane(**1***b*, DOM), a ring-substituted amphetamine, was similarly metabolized to the related ketone (**2***b*). A preliminary *in vitro* metabolism of DOM by means of a rabbit microsomal preparation (10 000 *g* supernatant) indicated that, compared to amphetamine, very little metabolism took place although a g.l.c. examination of the products showed that very small quantities of some metabolites had formed. To confirm whether one of these products was the ketone (**2***b*), a synthesis of this compound was undertaken.

While this study was in progress, Ho and co-workers (2, 3) published their findings on the *in vivo* metabolism of DOM in rat and showed that the ketone **2***b* was not formed in that species. In the meantime, Hucker *et al.* (4) claimed that phenylacetone ketoxime (**3***a*) was the major *in vitro* metabolite of amphetamine using rabbit liver, and this ketoxime then hydrolyzed to yield the ketone (**2***a*). Subsequently, Beckett and Al-Sarraj (5) found that 2-hydroxylamino-1-phenylpropane (**4***a*) was, in fact, the primary *in vitro* metabolic product of amphetamine using microsomes from various species and these authors showed that the ketone **2***a*, the oxime **3***a*, and the alcohol **5***a* were chemical or metabolic breakdown products of the hydroxylamine **4***a*.

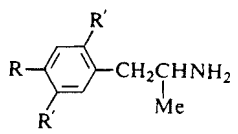

1

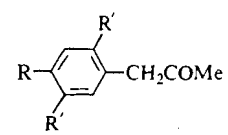

2

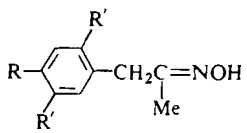

3

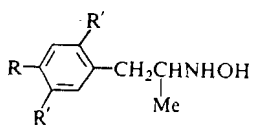

4

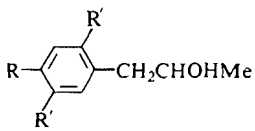

5

a R = R' = H
b R = Me; R' = OMe

These current findings prompted us to extend our studies to the synthesis of the ketone **2***b*, the oxime **3***b*, the hydroxylamine **4***b*, and the alcohol **5***b*, compounds which could be of assistance in the identification of rabbit *in vitro* metabolites and perhaps help identify the unknown minor *in vivo* metabolites of DOM, described by Ho and co-workers (2, 3).

The method selected for the preparation of 1-(2,5-dimethoxy-4-methylphenyl)-2-propanone (**2***b*) required 2,5-dimethoxy-4-methylphenylacetic acid (**9**) as an intermediate. This acid

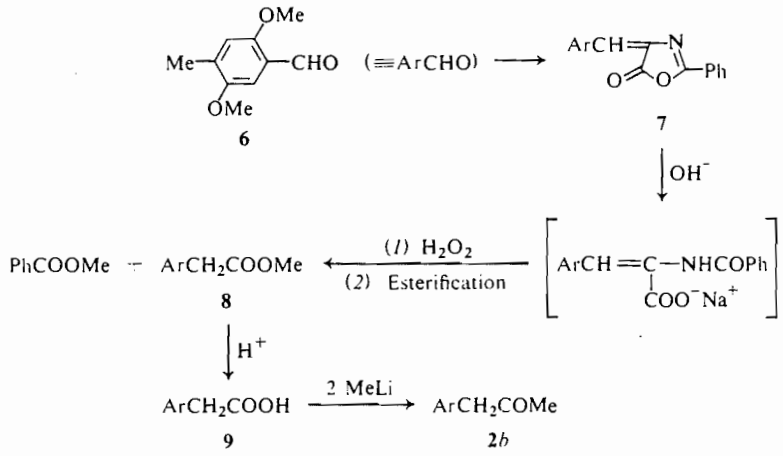

SCHEME 1

was prepared from 2,5-dimethoxy-4-methylbenzaldehyde (**6**) as outlined in Scheme 1. The azlactone, 4-(2,5-dimethoxy-4-methylbenzylidene)-2-phenyl-2-oxazolin-5-one (**7**), was obtained by reacting the aldehyde (**6**) with hippuric acid in the presence of a dehydrating agent (acetic anhydride). The azlactone was hydrolyzed in sodium hydroxide solution and oxidized with hydrogen peroxide (6) to yield a mixture of 2,5-dimethoxy-4-methylphenylacetic acid and benzoic acid. To separate this mixture, the acids were esterified and when a concentrated solution of the mixture of methyl esters was cooled, the less soluble component, methyl 2,5-dimethoxy-4-methylphenylacetate (**8**) precipitated. The acid **9** was regenerated from **8** and reacted with methyllithium to give the required 1-(2,5-dimethoxy-4-methylphenyl)-2-propanone (**2***b*). Ho and Tansey (2) also prepared this ketone in modest yield by the action of iron and ferric chloride on 1-(2,5-dimethoxy-4-methylphenyl)-2-nitropropene (**10**).

1-(2,5-Dimethoxy-4-methylphenyl)-2-propanone oxime (**3***b*) was obtained as an oil when the ketone **2***b* was reacted with hydroxylamine but was conveniently purified and characterized as its hydrochloride. When a synthesis of 1-(2,5-dimethoxy-4-methylphenyl)-2-propanol (**5***b*) was attempted by hydrogenating a solution of the ketone in the presence of palladium–charcoal, the compound failed to incorporate hydrogen. Reduction of the ketone **2***b* with sodium borohydride, however, proved successful.

For the preparation of 1-(2,5-dimethoxy-4-methylphenyl)-2-(hydroxylamino)propane (**4***b*), the feasibility of reducing 1-(2,5-dimethoxy-4-methylphenyl)-2-nitropropene (**10**) was investi-

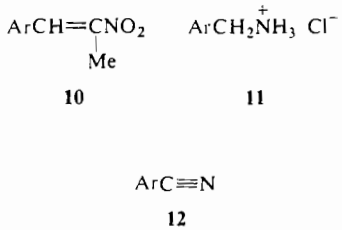

gated. This proved to be a complex reaction. When an ethanolic solution of **10** was hydrogenated catalytically, initial hydrogen incorporation was rapid, then the rate of uptake slowly decreased. When hydrogenation appeared to be complete, the reaction flask was removed from the hydrogenation apparatus and a strong odor of ammonia was discerned. The mixture was stirred at room temperature until the evolution of ammonia ceased and then hydrogenated further. More hydrogen was incorporated. The reaction mixture was separated into basic and neutral products. Fractional crystallization of the bases (as hydrochlorides) gave 1-(2,5-dimethoxy-4-methylphenyl)-2-aminopropane (**1***b*) as the first and minor product. The second compound, $C_{12}H_{19}NO_3.HCl$, was a reducing agent (ammoniacal silver nitrate test); a diagnostic ion, *m/e* 60, shown to be C_2H_6NO by accurate mass measurement, was present in its mass spectrum and is identified as $CH_3CH{=}\overset{+}{N}HOH$. This fragment is observed in the mass spectra of other *N*-hydroxyamphetamine derivatives (7). This basic reduction product, therefore, was concluded to be 1-(2,5-dimethoxy-4-methylphenyl)-2-(hydroxylamino)propane (**4***b*). The neutral products of the reduction of **10** were shown by comparison

Can. J. Chem. Downloaded from www.nrcresearchpress.com by 210.87.254.6 on 09/05/12
For personal use only.

Can. J. Chem. Downloaded from www.nrcresearchpress.com by 210.87.254.6 on 09/05/12
For personal use only.

with authentic samples to be 1-(2,5-dimethoxy-4-methylphenyl)-2-propanone (**2***b*) and the corresponding oxime **3***b*.

The catalytic reduction of 1-(2,5-dimethoxy-4-methylphenyl)-2-nitropropene was repeated using ethanolic HCl as the solvent. This time, hydrogen uptake was rapid and the major product was the oxime (**3***b*); no hydroxylamine (**4***b*) was formed.

The 1-(2,5-dimethoxy-4-methylphenyl)-2-nitro–propene (**10**) employed in these reductions was prepared by reacting 2,5-dimethoxy-4-methyl-benzaldehyde with nitroethane in the presence of ammonium acetate and acetic acid (8). On one occasion, the crude reaction product (**10**) was hydrogenated as just described and an additional reduction product, $C_{10}H_{15}NO_2$.HCl, was isolated and identified by means of its i.r., n.m.r., and mass spectra as 2,5-dimethoxy-4-methylbenzylamine hydrochloride (**11**). It appeared likely that the crude sample of **10** was contaminated with 2,5-dimethoxy-4-methylbenzonitrile (**12**), which catalytically reduced to **11**. This assumption was confirmed when a pure sample of nitrile **12** was isolated from the crude nitropropene (**10**) by fractional crystallization. Other investigators have observed the formation of nitriles in this type of reaction (9, 10).

Nitrile by-product formation could have some significance in the preparation of illicit samples of DOM. If the intermediate (**10**) was not purified prior to reduction, the sample of DOM could contain 2,5-dimethoxy-4-methylbenzylamine as an impurity and this could alter the pharmacological properties of the product in view of the fact that 2,5-dimethoxybenzylamine and related compounds have been reported (11) to possess uterine-contracting properties.

Experimental

Melting points (capillary tube) are uncorrected. Nuclear magnetic resonance spectra were recorded on a Varian A-60D spectrometer, using tetramethylsilane as internal standard. Infrared spectra were recorded on a Beckman IR-10 spectrophotometer as Nujol mulls. Dr. A. M. Hogg and his associates, Department of Chemistry, University of Alberta recorded the mass spectra on an A.E.I. MS-9 or MS-12 mass spectrometer at an ionizing potential of 70 eV using the direct probe technique. Elemental analyses were determined at the Faculty of Pharmacy and Pharmaceutical Sciences by Mr. W. Dylke.

4-(2,5-Dimethoxy-4-methylbenzylidene)-2-phenyl-2-oxazolin-5-one (7)

A mixture of 2,5-dimethoxy-4-methylbenzaldehyde (15.0 g), hippuric acid (15.0 g), acetic anhydride (26.0 g), and anhydrous sodium acetate (7.0 g) was heated at 100° with stirring for 2 h, cooled, and diluted with ethanol (100 ml). An orange-red precipitate of the title compound formed (23.6 g), m.p. 208–210° (from benzene); i.r. ν_{max} 1645 (C=N), 1785 (C=O) cm^{-1}.

Anal. Calcd. for $C_{19}H_{17}NO_4$: C, 70.57; H, 5.30; N, 4.33. Found: C, 70.30; H, 5.52; N, 4.22.

Methyl 2,5-Dimethoxy-4-methylphenylacetate (8) and 2,5-Dimethoxy-4-methylphenylacetic Acid (9)

A solution of 4-(2,5-dimethoxy-4-methylbenzylidene)-2-phenyl-2-oxazolin-5-one (15.0 g) in 10% NaOH solution (100 ml) was heated under reflux for 12 h. The reaction mixture was cooled to 0° and diluted with ice-cold 40% NaOH solution (10 ml). To this solution was added with stirring, a 15% aqueous solution of H_2O_2 at such a rate as to maintain the temperature below 15°. After this addition was complete, the solution was left for 12 h at 25°, then acidified with concentrated HCl (50 ml) and extracted thoroughly with benzene (200 ml). The dried ($MgSO_4$) benzene extract was evaporated to give a solid (15.5 g) which was dissolved in methanol (100 ml) containing concentrated H_2SO_4 (2 ml). This solution was heated under reflux for 5 h, concentrated and cooled. The title ester (**8**, 9.2 g) precipitated, m.p. 66–67° (from ethanol); i.r. ν_{max} 1730 (C=O) cm^{-1}.

Anal. Calcd. for $C_{12}H_{16}O_4$: C, 64.27; H, 7.19. Found: C, 63.96; H, 7.29.

A suspension of this ester (8.0 g) in 10% NaOH solution (50 ml) was heated under reflux for 1 h, cooled and acidified with concentrated HCl. This gave a precipitate of 2,5-dimethoxy-4-methylphenylacetic acid (7.6 g), m.p. 128–129° (from ethanol); i.r. ν_{max} 1700 br (C=O), 2500–2700 (OH) cm^{-1}; n.m.r. ($CDCl_3$) δ 2.20 (s, 3H, CH_3), 3.61 (s, 2H, CH_2), 3.73 (s, 6H, OCH_3 groups), 6.72 (s, 2H, aromatic protons), 10.80 (s, 1H, exchanges with D_2O, OH).

Anal. Calcd. for $C_{11}H_{14}O_4$: C, 62.84; H, 6.71. Found: C, 62.60; H, 6.83.

1-(2,5-Dimethoxy-4-methylphenyl)-2-propanone (2b)

A solution of 2,5-dimethoxy-4-methylphenylacetic acid (9.0 g) in ether (100 ml) was added slowly to a solution of 2.1 *M* methyllithium (Alfa Inorganic, Inc.) (60 ml). The mixture was heated under reflux for 1 h then added to ice water (200 ml) saturated with ammonium chloride. The organic layer was collected and the aqueous portion was extracted with more ether (200 ml). Evaporation of the combined ether solution yielded the ketone (**2***b*, 4.7 g), m.p. 56–58° (from ethanol) (lit. (2) m.p. 49–51°); i.r. ν_{max} 1710 (C=O) cm^{-1}; n.m.r. ($CDCl_3$) δ 2.13 (s, 3H, $COCH_3$), 2.23 (s, 3H, ring CH_3), 3.65 (s, 2H, CH_2), 3.78 (s, 6H, OCH_3 groups), 6.63 (s, 1H) and 6.72 (s, 1H, aromatic protons); mass spectrum *m/e* (% relative abundance) 208 (41) ($C_{12}H_{16}O_3$); 165 (100) ($C_{10}H_{13}O_2$).

Anal. Calcd. for $C_{12}H_{16}O_3$: C, 69.21; H, 7.75. Found: 69.53; H, 7.57.

Acidification of the aqueous solution remaining after the ether extraction caused the precipitation of starting material (**9**, 2.1 g).

1-(2,5-Dimethoxy-4-methylphenyl)-2-propanone Oxime (3b) Hydrochloride

A solution of the propanone (**2***b*, 1.0 g), hydroxylamine hydrochloride (1.0 g), and pyridine (5 ml) in ethanol (10 ml) was heated under reflux for 1 h, then evaporated. The

residue was suspended in 5% HCl solution (25 ml) and extracted with chloroform (2 × 25 ml). Evaporation of the chloroform gave a pale yellow oil (1.1 g), i.r. ν_{max} 3300 (OH) cm^{-1}. A solution of this oil in ether (50 ml) was saturated with gaseous HCl. A crystalline solid (0.64 g) slowly formed, m.p. 114–116°; i.r. ν_{max} 2500 ($\overset{+}{N}$—H) cm^{-1}; n.m.r. ($CDCl_3$) δ 2.04 (s, 3H, aliphatic CH_3), 2.24 (s, 3H, aromatic CH_3), 3.66–3.95 (m, 8H, CH_2 and OCH_3 groups), 6.73 (s, 1H) and 6.80 (s, 1H, aromatic protons), 13.08 (s, br, 2H, $\overset{+}{N}HOH$); mass spectrum *m/e* (% relative abundance) 223 (100) ($C_{12}H_{17}NO_3$).

Anal. Calcd. for $C_{12}H_{18}ClNO_3$: C, 55.49; H, 6.98; N, 5.39. Found: C, 55.46; H, 6.91; N, 5.59.

1-(2,5-Dimethoxy-4-methylphenyl)-2-propanol (5)

A solution of 1-(2,5-dimethoxy-4-methylphenyl)-2-propanone (2.0 g) in methanol (30 ml) was slowly added to a stirred solution of sodium borohydride (2.0 g) in methanol (200 ml) and water (100 ml). Stirring was continued at room temperature for 1 h after the addition, then a slight excess of concentrated HCl was added to decompose the excess hydride. The solvent was removed under reduced pressure and the residue was suspended in water (100 ml) and extracted with chloroform (200 ml). Evaporation of the latter solution gave the title compound (1.2 g), m.p. 80.5–81.5° (from ethanol); n.m.r. (DMSO-d_6) δ 1.01 (d, 3H, J = 6, α-CH_3), 2.12 (s, 3H, ring CH_3), 2.65 (m, 1H (overlaps with DMSO), CH), 3.60–4.27 (m, 8H, overlapping CH_2 and OCH_3 signals), 4.27 (s, br, 1H, exchanges with D_2O, OH), 6.72 (s, 2H, aromatic protons).

Anal. Calcd. for $C_{12}H_{18}O_3$: C, 68.54; H, 8.63. Found: C, 68.62; H, 8.73.

1-(2,5-Dimethoxy-4-methylphenyl)-2-nitropropene (10)

A solution of 2,5-dimethoxy-4-methylbenzaldehyde (15.0 g) and ammonium acetate (6.3 g) in acetic acid (75 ml) and nitroethane (9.9 g) was heated under gentle reflux for 3 h. The dark red solution was evaporated, leaving a red oil which was suspended in water (100 ml) and extracted with chloroform (100 ml). Evaporation of the latter gave an oil which solidified on standing. This crude product (14.4 g, m.p. 79–86°) crystallized from ethanol to give the yellow title compound, m.p. 85–87° (lit. (12) m.p. 85.5–87.5°); i.r. ν_{max} 1320, 1500 (NO_2), 1645 (C=C) cm^{-1}.

Anal. Calcd. for $C_{12}H_{15}NO_4$: C, 60.75; H, 6.37. Found: C, 61.04; H, 6.36.

Catalytic Hydrogenation of 1-(2,5-Dimethoxy-4-methylphenyl)-2-nitropropene

(*i*) A solution of the title compound (7.5 g) in ethanol (300 ml) containing 10% palladium–charcoal (1.0 g) was hydrogenated at room temperature and normal pressure until uptake of hydrogen apparently ceased. When the reaction flask was removed from the hydrogenation apparatus, a pungent ammonia-like odor was evident. The solution was stirred at room temperature for 3 h after which time the basic odor was no longer apparent, then hydrogenation was continued until uptake again ceased. Evaporation of the filtrate gave an oil which was dissolved in chloroform (100 ml) and extracted with 5% HCl solution (2 × 100 ml). The aqueous solution was basified (10% NaOH) and reextracted with chloroform (3 × 100 ml). The combined chloroform extract was dried ($MgSO_4$), saturated with gaseous HCl and evaporated to give a solid which was fractionally crystallized from ethanol–ether. The first product (0.24 g), m.p. 176–178° was 1-(2,5-dimethoxy-4-methylphenyl)-2-aminopropane hydrochloride, confirmed by i.r. spectral comparison and mixture m.p. with authentic DOM. A second product (0.81 g), m.p. 121–123°, was 1-(2,5-dimethoxy-4-methylphenyl)-2-(hydroxylamino)propane hydrochloride; i.r. ν_{max} 2480–2750 ($\overset{+}{N}$—H, $\overset{+}{N}$—OH) cm^{-1}; mass spectrum *m/e* (% relative abundance) 225 (9) ($C_{12}H_{19}NO_3$); 193 (5) ($C_{12}H_{17}O_2$); 166 (100) ($C_{10}H_{14}O_2$); 60 (45) (C_2H_6NO); 44 (18) (C_2H_6N) (Formulae identified by accurate mass measurements).

Anal. Calcd. for $C_{12}H_{20}ClNO_3$: C, 55.06; H, 7.70; N, 5.35. Found; C, 55.06; H, 7.81; N, 5.51.

The chloroform solution remaining after extraction with 5% HCl (see above) was evaporated and the oil which resulted was dissolved in ether and saturated with gaseous HCl. A product separated as an oil from which the ether layer was decanted and treated as described later. Treatment of the oil with ethanol–ether gave a solid (1.1 g), m.p. 112–115°, which was identified by i.r. spectrum and mixture m.p. as the oxime (**3***b*) hydrochloride.

The ether solution referred to above was evaporated and the product obtained was distilled under reduced pressure. An oil, b.p. 130–160° (0.5–1.5 mm) was collected and triturated with ethanol. This gave 1-(2,5-dimethoxy-4-methylphenyl)-2-propanone (**2***b*, 1.7 g), m.p. 55–57°, the i.r. spectrum of which was superimposable on that of the authentic ketone (**2***b*).

(*ii*) A solution of 1-(2,5-dimethoxy-4-methylphenyl)-2-nitropropene (7.0 g) in ethanol (100 ml) and concentrated HCl (7 ml) was hydrogenated at room temperature and normal pressure in the presence of 10% palladium–charcoal (1.0 g). Hydrogen was rapidly incorporated, and when uptake ceased, the filtrate was evaporated to give an oil. This was dissolved in chloroform and separated into basic and neutral fractions as described in (*i*) above. Evaporation of the chloroform solution containing the basic material gave a solid (0.46 g) which was dissolved in ether, and the solution was saturated with gaseous HCl. This gave 1-(2,5-dimethoxy-4-methylphenyl)-2-aminopropane hydrochloride (DOM), m.p. 176–178°, identified (i.r.; mixture m.p.) by comparison with an authentic sample.

The chloroform solution which remained after extracting basic material was evaporated to give a red oil (5.4 g) which was dissolved in ether and saturated with gaseous HCl. 1-(2,5-Dimethoxy-4-methylphenyl)-2-propanone oxime hydrochloride (3.3 g) slowly precipitated. It had an i.r. spectrum and m.p. identical to that of authentic **3***b* hydrochloride, and a mixture m.p. was undepressed.

(*iii*) Crude 1-(2,5-dimethoxy-4-methylphenyl)-2-nitropropene (m.p. 79–86°; i.r. ν_{max} 1320, 1500 (NO_2), 2210 (C≡N) cm^{-1}; see preparation of **10**) (7.0 g) dissolved in ethanol (100 ml) and concentrated HCl (10 ml) was hydrogenated at room temperature and normal pressure with 10% palladium–charcoal (0.7 g) as catalyst. Hydrogen was incorporated rapidly for 2 h then more slowly for 12 h. The filtrate was evaporated to an oil which was dissolved in ethanol (10 ml), cooled, and diluted with

Can. J. Chem. Downloaded from www.nrcresearchpress.com by 210.87.254.6 on 09/05/12
For personal use only.

ether until cloudy. A solid precipitated (0.81 g), which was crystallized from ethanol–ether and gave 2,5-dimethoxy-4-methylbenzylamine hydrochloride (**11**), m.p. 244–246°; i.r. ν_{max} 1598, 2010, 2580–2720 ($\overset{+}{N}$—H) cm^{-1}; n.m.r. (DMSO-d_6) δ 2.16 (s, 3H, CH_3), 3.78 (s, 6H, OCH_3 groups), 3.96 (s, 2H, CH_2), 6.90 (s, 1H) and 7.23 (s, 1H, aromatic protons), 8.00–8.83 (s, br, 3H, exchanges with D_2O, $\overset{+}{N}H_3$).

Anal. Calcd. for $C_{10}H_{16}ClNO_2$: C, 55.17; H, 7.41; N, 6.44. Found; C, 55.41; H, 7.21; N, 6.60.

The filtrate was treated as described in method (*ii*) and 1-(2,5-dimethoxy-4-methylphenyl)-2-propanone oxime hydrochloride (2.8 g) was obtained.

*2,5-Dimethoxy-4-methylbenzonitrile (**12**)*

Crude 1-(2,5-dimethoxy-4-methylphenyl)-2-nitropropene, m.p. 79–86° (see preparation of **10**), (5 g) was fractionally crystallized from ethanol. The initial precipitate was pure **10**; concentration of the mother liquors and repeated crystallization of the resulting precipitate from ethanol gave the title compound (0.6 g), m.p. 127–129°; i.r. ν_{max} 2210 (C≡N) cm^{-1}; n.m.r. ($CDCl_3$) δ 2.33 (s, 3H, CH_3), 3.86 (s, 3H) and 3.93 (s, 3H, OCH_3 groups), 6.87 (s, 1H) and 6.96 (s, 1H, aromatic protons).

Anal. Calcd. for $C_{10}H_{11}NO$: C, 67.77; H, 6.26; N, 7.91. Found: C, 67.82; H, 6.36; N, 7.48.

The authors thank the Medical Research Council of Canada for operating grant MA-2993 (to R.T.C.) and a research studentship (to J.L.M.).

1. J. Axelrod. J. Biol. Chem. **214**, 753 (1955).
2. B. T. Ho and L. W. Tansey. J. Med. Chem. **14**, 156 (1971).
3. B. T. Ho, V. Estevex, L. W. Tansey, L. F. Englert, P. J. Creaven, and W. M. McIsaac. J. Med. Chem. **14**, 158 (1971).
4. H. B. Hucker, B. M. Michniewicz, and R. E. Rhodes. Biochem. Pharmacol. **20**, 2123 (1971).
5. A. H. Beckett and S. Al-Sarraj. J. Pharm. Pharmacol. **24**, 174 (1972).
6. H. R. Snyder, J. S. Buck, and W. S. Ide. *In* Organic synthesis. Vol. 15. Wiley, New York. 1935. p. 31.
7. A. H. Beckett, R. T. Coutts, and F. A. Ogunbona. J. Pharm. Pharmacol. **25**, 190 (1973) and further unpublished findings.
8. A. T. Shulgin. J. Med. Chem. **11**, 186 (1968).
9. A. T. Shulgin. Experientia, **19**, 127 (1963).
10. H. M. Blatter, H. Lukaszewski, and G. deStevens. J. Am. Chem. Soc. **83**, 2203 (1961).
11. A. N. Kudrin and G. S. Koroza. Farmakol. Toksicol. **30**, 718 (1967); Chem. Abstr. **68**, 37794s (1968).
12. A. T. Shulgin. U.S. Patent 3 541 158 (1970); Chem. Abstr. **74**, 53273a (1971).

Can. J. Chem. Downloaded from www.nrcresearchpress.com by 210.87.254.6 on 09/05/12
For personal use only.

Détermination de la vitesse du son dans les sels fondus. Technique et applications

LUCIEN DENIELOU, JEAN-PIERRE PETITET ET CHRISTOPHE TEQUI

Laboratoire de Thermodynamique du liquide salin, (T 16, 4e étage) Université Paris VI, 11 Quai St-Bernard, Paris Ve, France

Reçu le 12 juin 1973

Description d'une technique de mesure de la vitesse du son dans les sels fondus utilisant une méthode impulsionnelle. Le signal provenant du montage est mis en coïncidence avec celui issu d'une ligne à retard formée d'une longueur variable d'eau. Les éléments intermédiaires entre les cristaux émetteurs et récepteurs sont en alumine frittée. Le calcul des corrections dues aux intermédiaires et le calcul d'erreur ont été détaillés. La technique a été appliquée à la mesure de la vitesse du son dans le bromure de potassium, les sulfates alcalins et les chromate, molybdate et tungstate de sodium.

This paper describes a technique for measuring the speed of sound in molten salts employing a pulse method. The signal coming from the sample is made to coincide with that coming from a delay line of a variable length of water. The intervening parts between the emitting and receiving crystals are made of sintered alumina. The calculation of corrections due to the intervening parts and the calculation of error are given in detail. The technique is applied to measure the speed of sound in potassium bromide, alkali sulphates and the chromate, molybdate and tungsten of sodium. [Journal translation]

Can. J. Chem., **52**, 400 (1974)

Introduction

On sait que la détermination simultanée des trois valeurs de la chaleur spécifique à pression constante, de la vitesse du son et du coefficient de dilatation d'un liquide mène à la connaissance d'une série de constantes physiques macroscopiques permettant l'approche de la structure du liquide étudié (1). Dans ce travail, nous nous sommes attachés à décrire une méthode et son application à la détermination de la vitesse du son dans des sels fondus. Il s'avère, en effet, que la vitesse du son, généralement déterminée avec une bonne précision, reste le moyen le plus simple, connaissant la densité, d'obtenir la compressibilité d'un liquide; donnée essentielle pour l'évaluation du volume libre, l'établissement d'une équation d'état et le calcul de certaines fonctions de partition.

Si la littérature contient une quantité importante de résultats concernant les liquides à température ordinaire, en revanche assez peu d'auteurs se sont intéressés aux sels fondus.

C'est dans la perspective particulière d'une étude structurale d'ions complexes MO_4^{2-} (M = S, Cr, Mo, W) associés aux métaux alcalins que nous avons entrepris cette étude, dont nous donnons ici la technique et la méthode.

Méthode

Les sels fondus sont des liquides généralement peu visqueux, ce qui fait que le module de cisaillement est pratiquement nul et qu'il y a peu d'absorption du son dans la gamme de fréquence utilisée. Cependant les fortes températures nécessaires aux expériences réduisent sensiblement l'éventail des méthodes possibles. En effet, les méthodes optiques sont à exclure à cause du rayonnement. Sont à éviter également les méthodes interférométriques à cause des températures élevées qui exigent, par mesure de protection, des intermédiaires entre le liquide et le cristal émetteur. Ces intermédiaires, en provoquant des ondes de réflexions parasites sur les interfaces, risquent de créer des interférences perturbant le phénomène intéressant.

Les techniques utilisant des impulsions de haute fréquence semblent le mieux adaptées au problème.

Le méthode décrite ici est une méthode impulsionnelle. Elle est à rapprocher de celle mise au point par T. A. Litowitz et ses collaborateurs (2) d'une part et G. Petit et M. Blanc (3) d'autre part.

Chaque impulsion issue du circuit électronique est envoyée d'une part dans l'échantillon étudié de longueur fixe et d'autre part, dans une ligne à retard acoustique constituée d'une longueur variable d'eau. L'impulsion issue de la ligne à retard est mise en coïncidence avec le signal provenant de l'échantillon par ajustage de la longueur d'eau. Pour éviter toute ambiguïté, les mesures sont faites sur le premier signal transmis par le sel et la ligne à retard.

Appareillage

Le générateur

Le générateur d'ultrason délivre des impulsions sous forme de pics toutes les millisecondes sur une gamme de fréquence de 0.25 à 6 MHz. Nous avons choisi de faire les mesures sur 4 MHz: ce qui donne une longueur d'onde assez petite compte-tenu des dimensions du matériel, sans pour autant créer des phénomènes d'absorption importants.

Les cristaux émetteurs et récepteurs sont en titanate de

Can. J. Chem. Downloaded from www.nrcresearchpress.com by 210.87.254.42 on 09/05/12
For personal use only.

Can. J. Chem. Downloaded from www.nrcresearchpress.com by 210.87.254.42 on 09/05/12
For personal use only.

barium: le quartz, malgré un plus grand facteur de qualité présente une plus faible sensibilité que le titanate de barium.

Les barres

Notre choix s'est porté sur l'alumine frittée de haute densité: les sels étudiés ne l'attaquant pas, il n'est pas nécessaire d'avoir une atmosphère protectrice. Par ailleurs, sa faible conductivité thermique évite les pertes par conduction et l'installation de forts gradients thermiques dans les sels tout en autorisant des températures d'expérience plus élevées. Enfin, les techniques actuelles d'usinage de l'alumine nous ont permis la réalisation d'un montage commode.

La barre inférieure de 50 mm de diamètre et 400 de longueur est fixe et sert à la fois de liaison avec le récepteur et de creuset. Celui-ci a 40 mm de profondeur sur 28 de diamètre. Il est surmonté d'une partie plus large de 40 mm de hauteur sur 40 de diamètre pour éviter un débordement du sel au cours des manoeuvres de la barre supérieure. Enfin, un logement de 6 mm de diamètre a été aménagé le long d'une génératrice du creuset pour permettre l'installation du thermocouple qui présente ainsi l'avantage d'être immergé dans le sel. Ce système permet d'avoir le fond du creuset et la surface du récepteur parallèles par construction et d'utiliser une petite quantité de sel.

La barre supérieure qui reçoit l'émetteur a 24 mm de diamètre et 400 de longueur. Elle est adaptée à un support mobile métallique monté sur vis calantes qui permet un déplacement horizontal et vertical.

Les faces des barres ont été rectifiées, ce qui assure des couplages meilleurs et la garantie d'un bon parallélisme. Leurs diamètres et celui des cristaux qui leur sont adaptés ont été choisis pour avoir des échos nets tout en évitant, dans la mesure du possible, les réflexions parasites. Bien que la vitesse du son dans l'alumine soit voisine de 10 500 ms^{-1} (4), la fréquence de travail de 4 MHz donne une longueur d'onde de 2 mm: nous pouvons donc avoir ainsi des barres d'un encombrement raisonnable. De plus, dans le même but d'éliminer les réflexions parasites, la barre supérieure est filetée au pas de 100 sur toute sa longueur et la barre inférieure sur 160 mm à partir de sa base.

Le cristal émetteur a été ainsi choisi de 10 mm de diamètre et le récepteur de 24 mm. Ils sont fixés aux extrémités des barres à l'aide de brides métalliques. Pour éviter l'échauffement des transducteurs, on refroidit les barres à leurs extrémités par des circulations d'eau adaptées au filetage de la barre. La température des transducteurs n'excède jamais de 10 °C la température de la salle.

La verticalité de l'ensemble est assurée par un réglage mécanique et le parallélisme des faces est obtenu en réalisant sur l'écran l'écho maximum, un liquide quelconque assurant la transmission. Les barres sont alors fixées une fois pour toute dans leur logement. En cours d'expérience, un palpeur électronique placé sur les cales de mesure au niveau de la barre supérieure contrôle l'immobilité de celle-ci.

L'ensemble du montage est représenté sur la fig. 1.

Chauffage

Le chauffage de l'échantillon est fait par un four de type Chevenard à enceinte refroidie par eau. Il atteint des températures de 1250 °C en fonctionnement continu. Le cycle de montée en température est réglé sur 48 h, précaution nécessaire pour le matériel qui ne souffre pas les chocs thermiques; d'autre part ceci facilite l'établissement d'un équilibre thermique stable et reproductible. Le creuset étant centré au milieu du four et sa taille représentant le 1/10e de la partie chauffante, la température à l'intérieur est bien homogène (5).

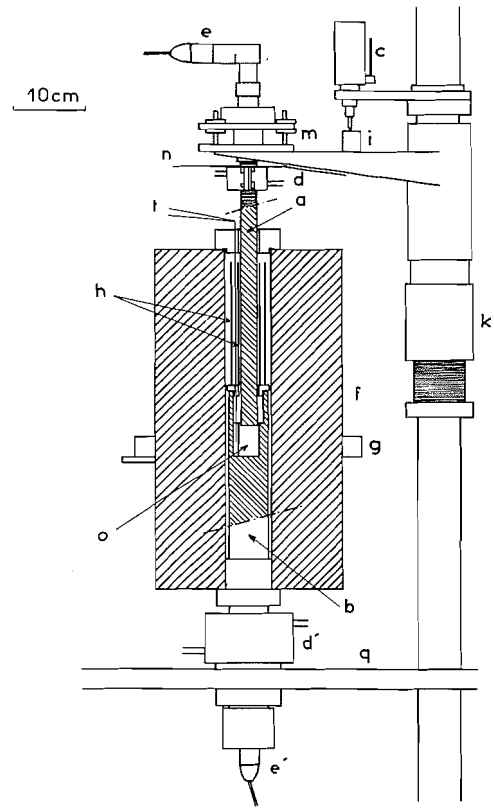

FIG. 1. Vue générale du montage: *e*,*e'*, émetteur et récepteur; *a*,*b*, barres d'alumine; *d*,*d'*, circulations d'eau; *f*, four; *t*, thermocouple; *h*, éléments de céramique; *g*, support du four; *n*, écran protecteur; *m*, système de réglage; *o*, creuset; *k*, vis micrométrique; *c*, controleur électronique; *i*, cale de mesure.

Le calorifugeage est assuré par des éléments concentriques de céramiques, le haut du creuset étant lui-même protégé par un couvercle d'alumine qui ne laisse passer que la barre supérieure et la gaine du thermocouple.

Les performances du montage ne sont pas tant limitées par le four que par le fait qu'au-delà de 1170 °C environ, les signaux s'atténuent. Ce phénomène est produit vraisemblablement par l'établissement de gradients de vitesse engendrés par les gradients de température dans les barres.

Ligne à retard acoustique

La ligne à retard acoustique est constituée d'une longueur variable d'eau. L'émetteur (E) fixe et le récepteur (R) mobile sont immergés dans une cuve remplie d'eau. Ils ont un diamètre de 24 mm et sont étanches. La qualité de l'eau est contrôlée constamment par conductimétrie ($\simeq 4 M\Omega$) et la température mesurée au 1/10e de degré avec un thermomètre à mercure. La tête mobile est adaptée à une vis micrométrique. Les mesures sont faites avec des

cales au micron et complétées par un comparateur au micron dont la course est de 3 mm. La reproductibilité de la ligne à retard est vérifiée avant chaque série de mesures sur un étalon d'acier fixe.

Produits chimiques

Les sels utilisés sont des produits du commerce dont la pureté est garantie par les fabriquants. Chaque sel est chauffé pendant une longue période au-dessus de son point de fusion et conservé à l'étuve à 160 °C jusqu'à utilisation. Le cycle de chauffage au cours d'une expérience étant lui-même très lent, les traces d'eau qui pourraient se trouver dans le réseau du sel sont pratiquement éliminées. Rappelons qu'à cet égard, d'après Bockris (6), l'eau à l'état de trace entraîne une modification de la vitesse du son dans le liquide de l'ordre de grandeur de l'erreur expérimentale.

Discussion

Nous avons vu qu'à température ambiante une très bonne précision peut être obtenue sur la vitesse du son dans un liquide. Par contre, à haute température, la présence d'intermédiaires entre l'échantillon et les transducteurs rend cette précision plus difficile à obtenir.

Au temps de passage d'émetteur à récepteur, il faut déduire le retard dû à ces intermédiaires. Une méthode consiste à mesurer le retard de la première réflexion dans le sel par rapport à l'écho transmis directement. Ce retard est dû à deux fois le parcours de l'échantillon de sel. Mais cette méthode est délicate, vue la faiblesse de la deuxième impulsion reçue et la difficulté de la discerner des parasites. C'est pourquoi la méthode que nous avons utilisée consiste à faire deux séries de mesures, pour des hauteurs de sels différentes. En pratique on trace par point, les courbes de temps de passage relatives aux deux hauteurs de sel en fonction de la température. La différence entre ces deux courbes, à chaque température, donne le temps de passage dans les 30 mm de sel. Cette méthode par différence présente en outre l'avantage d'éliminer un certain nombre d'erreurs systématiques comme, par exemple, les retards dus aux interfaces ou aux défauts d'adaptation des transducteurs.

Le problème de la déformation du groupe d'ondes se trouve aussi résolu, puisque l'erreur qu'elle peut produire (essentiellement le déplacement de la phase au maximum d'amplitude du groupe) est la même pour les deux trajets, les 30 mm de sel n'étant pas la cause d'une déformation supplémentaire appréciable.

Par contre, l'évolution des gradients de température dans les barres d'alumine, pour une même température prise dans le sel, introduit des erreurs participant à la dispersion des points. Ces erreurs[1] sont essentiellement de deux types:

1. Les erreurs sur le temps de passage dans les barres

Celles-ci sont dues à la variation de la vitesse du son dans l'alumine, en fonction de la température. Pour évaluer l'importance de cette erreur, on considère que le temps de passage dans le sel est déduit de la différence entre le temps global (barres + sel) en grande et petite quantités.

En admettant que la vitesse du son dans l'alumine dépende de la température suivant un terme du premier degré:

$$[1] \qquad v = v_0(1 - \beta t)$$

v_0, vitesse du son dans l'alumine à la température ambiante; t, température en d° Celsius; β est supposé constant en première approximation.

Nous pouvons avoir l'ordre de grandeur de cette erreur en calculant la différence de temps de passage du son qu'entraînent deux répartitions différentes des températures le long d'une barre. Une série de mesures a montré qu'il pouvait y avoir des écarts de température de 10 à 25 °C entraînant en conséquence une erreur maximum de 50 ns pour le temps de passage. C'est pourquoi, pour éliminer cette incertitude, on mesure, en plus du temps de passage d'émetteur à récepteur, le temps d'aller et retour d'une impulsion dans chacune des barres. Le temps de passage dans le sel seul est alors égal, pour chaque température, à la différence entre les temps pour le parcours total et le parcours dans les barres seules. La différence qu'il peut y avoir entre la moitié d'un aller et retour et un aller simple (réflexion) disparait naturellement lors de la différence entre les deux séries de mesures pour grande et petite quantités de sel.

Tous ces temps sont exprimés en longueur d'eau parcourue dans la ligne à retard. Un autre avantage de cette façon de procéder est de permettre la mesure des distances d'eau à partir d'une origine arbitraire, la longueur d'eau correspondant à cette origine disparaissant par différence.

[1]Une discussion mathématique plus detaillée de ces erreurs se trouve au Dépôt des documents non publiés. Les photocopies des documents archivés peuvent être obtenues du Dépôt des documents non publiés, Bibliothèque scientifique nationale, Conseil national de recherches du Canada, Ottawa, Canada K1A 0S2.

Can. J. Chem. Downloaded from www.nrcresearchpress.com by 210.87.254.42 on 09/05/12
For personal use only.

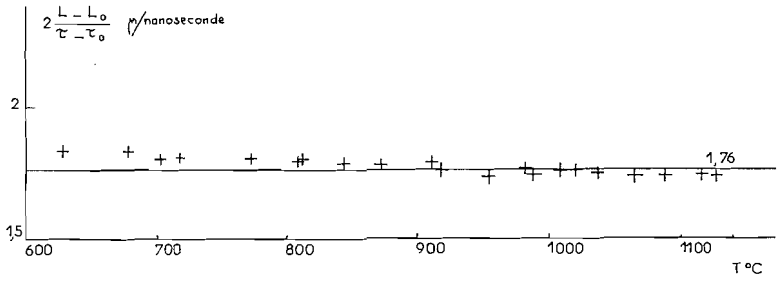

FIG. 2. Représentation de v_0K en fonction de la température.

2. Erreur sur la hauteur de sel traversé

Ayant choisi de faire les mesures sur des hauteurs de sel différant entre elles de 30 mm, la seule chose que l'on puisse dire est qu'entre les deux séries de mesures la barre supérieure est descendue de 30 mm et que la hauteur de sel a diminué d'autant, corrigée de la dilatation des barres.

On montre que la connaissance du temps d'aller et retour d'une impulsion dans une barre d'alumine permet d'en évaluer la longueur.

Sachant que:

$$[2] \qquad l = \int_0^{l_0} (1 + \alpha t(x))\, dx_0$$

avec

$$l_0 = \int_0^{l_0} dx_0$$

où l désigne la longueur d'une barre d'alumine on montre que:

$$[3] \qquad l - l_0 = \frac{v_0 K}{2}(\tau - \tau_0)$$

avec

$$K = \frac{\alpha}{\alpha + \beta}$$

τ désignant le temps de passage du son dans une barre d'alumine. En fait, α et β ne sont pas vraiment constants et nous montrerons plus loin qu'elle en est l'importance.

Enfin, on remarque que dans cette méthode l'erreur est visible sur la dispersion des points et c'est pourquoi nous l'avons adoptée comme mode de correction. Cependant, il reste à lever l'incertitude sur K; pour cela nous l'avons mesuré directement en posant sur le fond du creuset un barreau de silice ($\alpha' = 0.54 \times 10^{-6}$) dont le déplacement avec la température est suivi à l'aide d'un comparateur. D'autre part, à l'aide de la ligne à retard, on suit l'évolution du temps de passage dans la barre d'alumine.

La fig. 2 donne la représentation de:

$$[4] \qquad v_0 K = 2\frac{l - l_0}{\tau - \tau_0}$$

On constate sur cette courbe que, dans le domaine de température 650–1200 °C, v_0K décroît faiblement. Nous avons choisi une valeur moyenne: 1.76 µ ns^{-1}.

Calcul d'erreur

Si u désigne la vitesse du son dans le sel, u_E la vitesse du son dans l'eau, h la hauteur de sel liquide corrigée de la dilatation de l'alumine et h_E la longueur d'eau correspondante, nous aurons la relation:

$$[5] \qquad u = u_E \frac{h}{h_E}$$

ce qui conduit à l'erreur suivante:

$$[6] \qquad \frac{\Delta u}{u} = \frac{\Delta h}{h} + \frac{\Delta u_E}{u_E} + \frac{\Delta h_E}{h_E}$$

Les valeurs de u_E ont été prises par interpolation linéaire sur les valeurs déterminées par Hubbard et Loomis (7). L'erreur sur la vitesse dans l'eau de la ligne à retard est négligeable (moins de 0.0005). De même l'erreur sur la hauteur dont la barre est descendue: la cale de 30 mm est rectifiée au micron, le comparateur donne une précision du micron et le contrôleur-électronique ne bouge pratiquement pas au cours des expériences.

L'erreur provient essentiellement de l'appréciation du temps de parcours corrigé de façon à être ramené à un parcours de 30 mm. Le temps de passage τ_S dans le sel s'écrit:

$$[7] \quad u_E\tau_S = D - d - \left(\frac{B_1 + B_2}{2} - \frac{b_1 + b_2}{2}\right) + \frac{2Kv_0}{u}\left(\frac{B_1 + B_2}{2} - \frac{b_1 + b_2}{2}\right)$$

Can. J. Chem. Downloaded from www.nrcresearchpress.com by 210.87.254.42 on 09/05/12
For personal use only.

Can. J. Chem. Downloaded from www.nrcresearchpress.com by 210.87.254.42 on 09/05/12
For personal use only.

D,d sont les distances dans la ligne à retard correspondant à la transmission émetteur–récepteur respectivement pour la grande et la petite quantité; B,b sont les analogues pour les aller et retour dans chacune des barres respectivement pour la grande (1) et la petite (2); Kv_0 est le coefficient précédemment mesuré; u est une première approximation de la vitesse du son dans le sel. Le dernier terme du second membre est la correction due à la dilatation de l'alumine. Or cette expression [7] correspond exactement au temps de passage dans 30 mm de sel, toute correction faite, soit:

$$[8] \qquad \tau_S = \frac{3 \times 10^{-2}}{u}$$

les erreurs sur les longueurs sont évaluées à 5 μ.

Une évaluation de l'erreur relative sur K due à l'influence de la non-reproductibilité des gradients de température est proche de 0.001; valeur négligeable devant l'erreur due à la détermination de $\Delta(Kv_0)/Kv_0 \simeq 0.02$ sur la courbe fig. 2.

En définitive, l'erreur relative sur la vitesse du son est donnée, dans notre méthode, par l'expression suivante:

$$[9] \quad \frac{\Delta u}{u} = 66.6\frac{u}{u_E}\left\{5 \times 10^{-6} + \left|\frac{1.76}{u}10^{-3} - 1\right| 5 \times 10^{-6} + \frac{0.53}{u}\left(\frac{2}{100} + \frac{\Delta u}{u}\right)\right\}$$

où B a été pris égal à 0.3 mm qui est sa valeur moyenne sur les expériences faites et $\Delta u/u = 0.01$: erreur sur une première évaluation de u en vue des corrections. Nous avons ainsi déterminé des erreurs de 1 à 4 ms^{-1} pour des valeurs de la vitesse du son comprise entre 1000 et 2000 ms^{-1}.

Résultats

Les caractéristiques de la relation entre la vitesse du son et la température sont telles que nous sommes amenés naturellement à rechercher une représentation sous la forme

$$[10] \qquad F(T) = A_0 + A_1T + A_2T^2 + \ldots$$

Ne connaissant pas la température critique, nous n'avons pas cherché une expression en fonction de coordonnées réduites T/T_c ou $(T - T_F)/(T_c - T_F)$, mais nous avons choisi de ramener l'origine des coordonnées à la température de fusion du sel considéré, ce qui donne une signification plus physique aux coefficients

$$[11] \quad F(T) = F'(T - T_F) = F_F(1 + A_1'(T - T_F) + A_2'(T - T_F)^2 + \ldots)$$

La recherche des coefficients a été effectuée par la méthode des moindres carrés, qui est la méthode la plus justifiée dans le cas d'approximants linéaires, tels ceux que nous avons utilisés (8).

Nous avons choisi de considérer le temps de passage en petite quantité comme une correction (ce qui est justifié par sa faible variation en fonction de la température) et lui avons attribué une forme

$$[12] \qquad A + B\theta + C\theta^2 \text{ avec } \theta = T - T_F$$

A chaque valeur expérimentale du temps de passage en grande quantité est soustraite la valeur correspondante interpolée à l'aide du polynôme précédent. Ces dernières valeurs correspondant au temps de passage dans 30 mm de sel, on en déduit autant de valeurs expérimentales de la vitesse.

On peut directement faire le lissage sur les vitesses expérimentales, mais une variante de la méthode utilise une forme mathématique de la vitesse théoriquement plus justifiée: on considère que C_v (la chaleur spécifique à volume constant) varie très peu dans la gamme de température étudiée; sa valeur est essentiellement le résultat de la contribution constante d'un assez grand nombre de degrés de liberté internes des molécules. D'autre part, C_p étant constant dans le liquide, $\gamma = C_p/C_v$ l'est aussi. Or, il existe une relation simple entre γ et la vitesse du son:

$$[13] \qquad \gamma = 1 + \frac{M\alpha_S^2}{C_p}Tu^2$$

où α_s et M, respectivement le coefficient de dilatation du sel et la masse moléculaire, sont également constants. Il est donc intéressant de calculer le produit $A(T) = Tu^2$.

Cette grandeur s'est effectivement révélée pratiquement constante, rendant très précise son approche par un polynôme.

Application

Au préalable et à titre de vérification, nous avons choisi d'expérimenter le montage et la méthode avec une étude de la vitesse du son dans le bromure de potassium. Il n'attaque pas l'alu-

TABLEAU 1. $(TU^2)_T = (TU^2)_F (1 + A(T - T_F) + B(T - T_F)^2)$

Sel	T_F (K)	$(Tu^2)_F$ 10^{-10}	A 10^3	B 10^6	u_F (ms^{-1})	Δu_F (ms^{-1})	Gamme de températ. (K)
KBr	1005	0.164	0.090	0.530	1276	2	1133–1413
Li_2SO_4	1130	0.635	0.148	−0.039	2371*	4	1183–1423
Na_2SO_4	1155	0.487	0.164	−0.130	2053*	4	1213–1448
K_2SO_4	1341	0.408	0.980	−4.04	1743*	2	1373–1463
Rb_2SO_4	1339	0.249	0.040	−0.897	1363*	2	1383–1463
Cs_2SO_4	1274	0.183	−0.122	−0.237	1200*	1.5	1313–1447
Na_2CrO_4	1070	0.397	0.119	−0.074	1926	4	1093–1433
Na_2MoO_4	962	0.311	0.421	−0.396	1798	3	1033–1468
Na_2WO_4	967	0.214	0.441	−0.385	1487	2	1053–1448

*Des valeurs antérieurement publiées ne tiennent pas compte de la méthode de correction décrite ici (11).

TABLEAU 2. Dispersion des mesures

Sel	Nombre de degrés de liberté	σ_1 (ms^{-1})	σ_2 (ms^{-1})	Seuil 0.95 (ms^{-1})
KBr	3	1.8	1	3
Li_2SO_4	10	1.2	0.4	0.9
Na_2SO_4	8	2	0.7	1.6
K_2SO_4	2	2	1.4	6
Rb_2SO_4	6	0.5	0.2	0.5
Cs_2SO_4	10	0.5	0.2	0.4
Na_2CrO_4	9	1.6	0.5	1.2
Na_2MoO_4	12	0.7	0.2	0.5
Na_2WO_4	20	1.6	0.4	0.7

mine et a déjà fait l'objet d'un certain nombre de travaux dont les résultats s'accordent de manière satisfaisante avec les nôtres (9, 6).

Nous présentons ensuite les résultats obtenus dans le cas des sulfates alcalins d'une part, et les chromate, molybdate et tungstate de sodium, d'autre part. Ces résultats sont donnés sous forme de tableaux récapitulatifs (tableaux 1 et 2). Nous avons fait figurer les deux coefficients σ_1 et σ_2 et la valeur de l'intervalle de confiance pour le seuil 0.95, correspondant au nombre de degrés de liberté utilisés. σ_1 et σ_2 sont définis de la façon suivante:

[14] $$\sigma_1 = \sqrt{\frac{1}{n}\sum_{i=1}^{n}[F_i - (A_1' + A_2'\theta_i + A_3'\theta_i^2 + \ldots)]^2}$$

$$\sigma_2 = \frac{\sigma_1}{\sqrt{n - m}}$$

σ_1 désignant l'écart type empirique des valeurs expérimentales, et σ_2 un assez bon estimateur de l'écart type des valeurs lissées, n est le nombre d'expériences; m le nombre de paramètres déterminés. Tous les calculs ont été menés sur un ordinateur C.I.I. 10070.

La comparaison de ces deux tableaux fait ressortir que l'erreur déterminée expérimentalement est pessimiste en regard de l'intervalle de confiance pour le seuil 0.95, ce qui montre que la méthode est satisfaisante. Cependant, on notera une exception pour K_2SO_4 qui donne un intervalle de confiance de 6 ms^{-1} par le calcul; cela provient du fait que le nombre de points expérimentaux en grande quantité est faible, ce qui n'exclut nullement la validité du résultat donné, mais réduit la confiance que l'on peut avoir dans l'estimateur σ_2.

Conclusion

Le travail présenté ici expose une méthode détaillée de la détermination de la vitesse du son dans un sel liquide et la précision que l'on peut en attendre.

Ainsi à l'aide des résultats déjà publiés de calorimétrie (10) et de ceux de densimétrie–dilatométrie à paraître, il est possible d'avoir accès à toute une gamme de grandeurs thermo-

Can. J. Chem. Downloaded from www.nrcresearchpress.com by 210.87.254.42 on 09/05/12
For personal use only.

dynamiques macroscopiques définissant l'état du sel liquide étudié. Ce sera l'objet d'un prochain travail.

1. R. H. Fowler et E. A. Guggenheim. Statistical thermodynamics. Cambridge University Press, London. 1965.
2. T. A. Litovitz, T. Lyon, et L. Peselnick. J. Acoust. Soc. Am. **26**, 273 (1956).
3. G. Petit et M. Blanc. Rev. Int. Hautes Tempér. et Refract. **4** n°3, 18 (1967).
4. L. R. Rossi et W. G. Lawrence. J. Am. Ceram. Soc. **53**, II, 604 (1970).
5. P. Chevenard. Les hautes températures. Lebeau Masson T. I. Paris. 1950. p. 226.
6. N. E. Richard, E. J. Brauner, et J. O'M.Bockris. Brit. J. Appl. Phys. **6**, 387 (1956).
7. J. C. Hubbard et A. L. Loomis. Phil. Mag. n°33, **5**, S.7, 1177 (1928).
8. J. R. Rice. Approximation des fonctions. Dunod. Paris. 1969.
9. J. Marchisio, G. Finiels, and Y. Doucet. C. R. **273** B, 845 (1971).
10. L. Denielou, Y. Fournier, J. P. Petitet, et C. Tequi. Rev. Int. Hautes Tempér. et Réfract. **8**, 119 (1971).
11. L. Denielou, J. P. Petitet, et C. Tequi; C. R. **275** C, 61 (1972); C. R. **274** C, 1865 (1972).

Can. J. Chem. Downloaded from www.nrcresearchpress.com by 210.87.254.42 on 09/05/12
For personal use only.

Isothermal and Photostimulated Emissions of Indole and Tryptophan in Two Polar Matrices at 77 °K

D. MULLER,[1] M. EWALD,[2] AND G. DUROCHER

Département de Chimie, Université de Montréal, C.P. 6128, Montréal 101, Québec

Received June 29, 1973

The isothermal delayed fluorescence along with the visible photostimulated fluorescence and phosphorescence emissions have been recorded and studied for the following systems: a 10^{-3} *M* solution of indole in an ether glassy matrix, a 10^{-3} *M* solution of indole in an ethylene glycol – water glassy matrix (EG–W) (70–30 by volume), a 10^{-3} *M* solution of tryptophan in an EG–W glassy matrix (70–30 by volume). All these experiments have been performed at the temperature of liquid nitrogen. It has also become possible to record the action spectra of the photostimulated emissions which give us information about the entities playing an active part in the recombination processes. The electron–cation recombination after visible light stimulation has been analyzed in terms of a kinetic model based on the assumption that upon neutralization an intermediate state is formed from which the molecule decides what its spin multiplicity will be. It was found that in an EG–W glass at 77 °K about 80% of the recombination events lack the energy necessary to reach the first excited singlet state of the amines studied. In an ether glass this percentage decreases to about 28%. This result is qualitatively in accord with the fact that the photostimulated electrons are more stabilized in an EG–W glass by an amount of energy equal to 1.5 eV.

La fluorescence différée ainsi que la fluorescence et la phosphorescence photostimulées par la lumière visible dans les systèmes suivants ont été enregistrées à la température de l'azote liquide: une solution 10^{-3} *M* en indole dans un verre rigide d'éther, une solution 10^{-3} *M* en indole dans un verre rigide formé de 70% d'éthylène glycol et de 30% d'eau par volume (EG–W), une solution 10^{-3} *M* en tryptophane dans un verre rigide de EG–W (70–30 en volume). En intercalant un monochromateur entre la lampe à xenon servant à la stimulation et l'échantillon, les spectres d'action des émissions photostimulées ont pu aussi être enregistrés nous fournissant ainsi des renseignements quant aux espèces jouant un rôle actif lors du processus de recombinaison conduisant aux luminescences photostimulées. L'analyse de la recombinaison électron–cation, après stimulation dans le visible, a été élaborée en utilisant un modèle cinétique basée sur l'hypothèse qu'au moment de la neutralisation des charges un état intermédiaire est formé à partir duquel la molécule décide de sa multiplicité de spin. Dans un verre de EG–W à 77 °K, il est proposé qu'environ 80% des processus de recombinaison ne possèdent pas suffisamment d'énergie pour que l'amine considéré puisse atteindre l'état premier singulet excité. Ce pourcentage est réduit à 28% dans un verre d'éther. Cette stabilisation supplémentaire dans EG–W est de l'ordre de 1.5 eV pour les électrons photostimulables.

Can. J. Chem., **52**, 407 (1974)

Introduction

It is well known that aromatic amino derivatives give rise photochemically to many interesting reactions such as photoionization, photocyclization, rearrangement, photooxidation, and decomposition.

The photoionizations of aromatic amines can be classified as follows: (*1*) Photoionization in polar fluid solvent via singlet exciplexes formed by the interaction between the lowest excited singlet state of the amines (electron donor) and the ground state of electron acceptor (1–4). (*2*) Photoionization in fluid media by two step excitation via the lowest triplet state (5) or triplet charge transfer state (6) of the amine considered. (*3*) Photoionization in a rigid matrix at 77 °K via a one step excitation producing the co-called "one photon recombination delayed fluorescence" (7–10). (*4*) Photoionization in a rigid matrix by a two step excitation via the lowest triplet state of the amines considered (11–24, 50). (*5*) Photoionization in fluid media by triplet–triplet annihilation during the time of molecular collisions (25, 26).

The fourth phenomenon has been characterized by the following experimental observations: (*1*) Thermoluminescence (13, 19, 27). (*2*) Recombination delayed luminescence (10, 19–30).[3] (*3*) Spectral evidence in the near-infrared and visible for

[1]Present address: Centre Universitaire, Place du 8 mai 1945, 93-St-Denis, France.

[2]Present address: Département de chimie physique, Université de Bordeaux I, 33-Talence, France.

[3]Literature reference 29 was presented at the International Conference in Luminescence, Leningrad, August, 1972.

Can. J. Chem. Downloaded from www.nrcresearchpress.com by 210.87.254.105 on 09/05/12
For personal use only.

Can. J. Chem. Downloaded from www.nrcresearchpress.com by 210.87.254.105 on 09/05/12
For personal use only.

trapped electrons and ions (13, 17, 31, 32). (*4*) Electron spin resonance signals in rigid oxygen free glasses at 77 °K (17, 31–33). (*5*) Near-infrared and visible stimulated luminescence (18, 34–36, 50).

The following series of events have been proposed to explain all the above experimental results: (*1*) Under the action of primary u.v. excitation an electron is ejected from the amine molecule resulting in the appearance of a typical purple color. (*2*) The electron migrates through the rigid matrix and eventually becomes trapped; in the trapped state, it can absorb low-energy radiation (visible or i.r. depending on the nature of the traps). (*3*) The trapped electrons live a long period of time after the exciting radiation is removed and the normal phosphorescence has decayed. When the electron escapes from its trap by thermal or light stimulation it becomes temporarily free to move. (*4*) The electron can either fall into another trap or can recombine with a cation. A part of the energy released in the recombination process is emitted as light and is called thermostimulated emission or photostimulated emission depending on the way the trapped electron is released.

We wish to report in the present study the photostimulated fluorescence and phosphorescence spectra of indole and tryptophan molecules embedded in some polar glassy matrices at 77 °K. The isothermal delayed fluorescence will also be discussed. The purpose of this paper is to show how electrostatic interactions between electrons and rigid matrices can influence the energetics of electron–cation recombination events.

Experimental

(1) Products

Indole from Eastman Kodak was recrystallized from petroleum ether and kept in the dark. Tryptophan from Fisher Scientific Co. was used without further purification. Diethyl ether (Et_2O) was Mallinckrodt "ether anhydrous"; it was dried over sodium, distilled, and kept in the dark. Ethylene glycol (EG) solvent was Matheson, Coleman, and Bell "chromato quality" reagent and water (W) was triply distilled before use. A volume ratio EG/W of 70:30 was used throughout the experiments. Both solvents (EG–W and ether) were checked for any possible interfering emissions when excited at 290 nm either at room temperature or at 77 °K.

(2) Sample Preparation

Concentrations varying between 1×10^{-3} *M* and 5×10^{-3} *M* of amines were prepared at room temperature in the dark. About 3 ml of these solutions were put into a quartz tube (2 mm i.d.) which was immersed in a quartz Dewar containing liquid nitrogen and then subjected to excitation. The freezing of the sample was complete after 15 s. The temperature in the bulk of the sample measured through the use of a thermocouple was constant at 77.8 ± 0.2 °K.

(3) Detection of the Natural Luminescence

All absorption spectra were recorded on a Cary 14 spectrophotometer. Emission spectra were recorded on an Aminco–Bowman spectrofluorophosphorimeter provided with an ellipsoidal condensing mirror at the entrance of the excitation monochromator. Radiation from an Hanovia 150 W xenon arc was passed through a 250 mm grating monochromator (*f*/4.5) blazed at 300 nm (600 l/mm) and focussed onto the cell through the following slit arrangement: $f_1 = 2$ mm, $f_2 = 4$ mm, and $f_3 = 2$ mm. An excitation wavelength of 290 nm (bandwidth = 12 nm) was used in nearly all experiments; and the dose rate was 4×10^{-9} einstein $cm^{-2}\,s^{-1}$. The method of Parker (37) was used to calibrate the excitation light intensity output (38). The luminescence emission was observed perpendicular to the exciting beam using a 250 mm grating monochromator (*f*/4.5) blazed at 500 nm and an 1P28 photomultiplier tube. The XY-recorder has a time response of 0.25 s. The relative response in quanta $s^{-1}\,nm^{-1}$ of the emission monochromator–photomultiplier detector assembly was obtained through the use of a 1000 W tungsten filament quartz–iodine lamp calibrated by the National Bureau of Standards (39).

The natural fluorescence was eliminated by a cylindrical can-type chopper (phosphoroscope) provided with two 60° openings in front of each other. The maximum practical speed was 7000 rev/min, thus giving a 4 ms time resolution. In this work, the rise and decay curves of the delayed fluorescence and the phosphorescence were recorded on the XY-recorder. It was sometimes necessary to use a corning 7-60 filter at the exit of the emission monochromator in order to eliminate the phosphorescence interference in the wavelength region of the delayed fluorescence. In order to reduce the exciting light intensity, neutral density filters (Oriel Optics Corporation) with transmission percentages of 33, 51, and 63 at 290 nm were used at the excitation monochromator output.

(4) Detection of the Stimulated Luminescence

We used the same apparatus as described above but without the phosphoroscope attachment. (The results were the same when the phosphoroscope attachment was used but the sensitivity was reduced.) The excitation and stimulation followed the cycle: (*a*) 0–120 s: excitation at 290 nm with a beam of light containing 4×10^{-9} einstein $cm^{-2}\,s^{-1}$. (*b*) 120–240 s: dark period to allow the natural fluorescence and phosphorescence to decay. (*c*) 240–360 s stimulation with visible light produced by the excitation monochromator through the use of a Wratten filter No. 2B or 16 depending upon the stimulating wavelength (500–700 nm). These filters removed the light of $\lambda < 500$ nm. Corning filters numbers 7-54 or 7-59 were used in front of the PM tube in order to avoid any scattered or stray light from the excitation device. It was confirmed that the stimulation of a fresh sample (unirradiated by step 1) gives no background between 300 and 500 nm. The stimulation period showed pulses as displayed in Figs. 6 and 9; such pulses were recorded at various emission wavelengths. (*d*) 360–420 s: dark period

Can. J. Chem. Downloaded from www.nrcresearchpress.com by 210.87.254.105 on 09/05/12
For personal use only.

until the cycle was started again at some different wavelength of observation.

After having performed a series of 4 cycles at the same wavelength of observation, a decrease in the integrated stimulated luminescence intensity pulses was detected. To avoid this, a new area of the sample was investigated at every 4 cycles. The exciting light intensity was checked after each cycle by measuring the intensity of the natural fluorescence excited at 290 nm and observed at 320 nm. Successive pulses of stimulated emission were recorded at every 10 nm from 290 nm to 550 nm. The integrated area (between 0 and 60 s after the stimulation has started) under each pulse (Fig. 6) gives us the uncorrected intensity of stimulated emission at the particular wavelength of interest. The stimulated fluorescence and phosphorescence spectra must then be corrected for the nonlinear response with wavelength of the emission monochromator–PM system including the filters used and then plotted as shown in Figs. 7 and 10.

By varying the stimulating wavelength and holding the emission wavelength fixed, it appeared possible to record the action spectrum of the stimulated fluorescence spectrum (Figs. 8 and 11).

Photostimulated Luminescence: Kinetic Model

The stimulated emissions of the amines studied in polar solvent matrices have the following kinetic properties: rapid rise of fluorescence and slow fluorescence and phosphorescence exponential decay during the time in which the stimulation is operative (Fig. 6). Therefore, we use the kinetic model proposed by McClain and Albrecht (18) in which an intermediate state A is considered to be formed during the recombination process so that the rate of singlet and triplet production is proportional to A with proportionality constants k_{AS} and k_{AT} respectively as shown schematically in Fig. 1.

The rate equations governing the stimulated emissions are:

$$[1]\quad \frac{d[^1A_1]}{dt} = k_{AS}[A(t)] - (k_F + k_c + k_i)[^1A_1(t)]$$

$$[2]\quad \frac{d[^3A_1]}{dt} = k_i[^1A_1(t)] + k_{AT}[A(t)] - (k_p + k_{ip})[^3A_1(t)]$$

The steady-state condition can only be applied to the singlet state due to its short natural lifetime and we have

$$[3]\quad [A(t)] = \frac{1}{\tau_F k_{AS}}[^1A_1(t)]$$

where τ_F is the observed fluorescence lifetime. Then

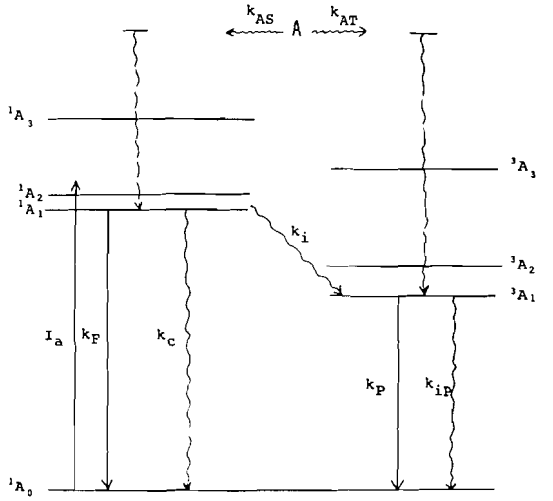

FIG. 1. Schematic diagram of the different processes by which the natural and the stimulated luminescences originate. The intermediate state A chooses between the singlet and the triplet manifold and after the choice has been made, no crossing is allowed between the singlets and the triplets except for the two lower excited states. ⇝ indicates non-radiative and → indicates radiative transitions.

$$[4]\quad \frac{d[^3A_1(t)]}{dt} = \left(k_i + \frac{k_{AT}}{k_{AS}\tau_F}\right)[^1A_1(t)] - \left(\frac{1}{\tau_p}\right)[^3A_1(t)]$$

where τ_p is the observed phosphorescence lifetime. Let us call $F(\bar{\nu},t)$ the stimulated fluorescence quantum rate of production at a particular wave number ($\bar{\nu}$) as a function of time and $P(\bar{\nu},t)$ the stimulated phosphorescence quantum rate at a particular wavenumber $\bar{\nu}$ as a function of time.

$$[5]\quad F(\bar{\nu},t) = s_F k_F\,[^1A_1(t)]$$

$$[6]\quad P(\bar{\nu},t) = s_p k_p\,[^3A_1(t)]$$

s_F and s_p stand for the instrumental sensitivity proportionality constants (response of the emission monochromator–PM system in the P and F region of wavelength). Equation 4 then becomes

$$[7]\quad \frac{dP(\bar{\nu},t)}{dt} = \left(\frac{s_p k_p}{s_F k_F}\right)\left[k_i + \frac{1}{\tau_F}\left(\frac{k_{AT}}{k_{AS}}\right)\right]F(\bar{\nu},t) - \left(\frac{1}{\tau_p}\right)P(\bar{\nu},t)$$

Integration of this equation from time 0.2 to 60 s has been performed graphically using the curves plotted in Figs. 6 and 9. Mathematically,

integration from 0 to infinity gives:

$$[8] \quad \frac{P(\bar{\nu})}{F(\bar{\nu})} = \tau_p\left(\frac{s_p k_p}{s_F k_F}\right)\left[k_i + \frac{1}{\tau_F}\left(\frac{k_{AT}}{k_{AS}}\right)\right]$$

since $P(\bar{\nu},0)$ and $P(\bar{\nu},\infty)$ are zero experimentally. (where $P(\bar{\nu}) = \int_0^\infty P(\bar{\nu},t)dt$ and $F(\bar{\nu}) = \int_0^\infty F(\bar{\nu},t)dt$).

The intensity of the whole stimulated spectrum being defined as

$$[9] \quad I_p = \int_0^\infty P(\bar{\nu})d\nu \quad I_F = \int_0^\infty F(\bar{\nu})d\nu$$

we have for the stimulated phosphorescence to fluorescence ratio

$$[10] \quad \left(\frac{I_p}{I_F}\right)_{st} = \frac{s_p k_p}{s_F k_F}\left(k_i + \frac{\beta(\lambda)}{\tau_F}\right)\tau_p$$

where $\beta(\lambda) = k_{AT}/k_{AS}$; λ is the wavelength of stimulation.

Note that the fact that graphically the integration starts at 0.2 s introduces a negligible error into $F(\bar{\nu})$ due to the nearly exponential form of the decay. A larger error in $F(\bar{\nu})$ and $P(\bar{\nu})$ results from the fact that we stopped the integration at 60 s but, as can be calculated from Figs. 6 and 9, the error on the ratio $P(\bar{\nu})/F(\bar{\nu})$ is about 1%.

We are now concerned with the comparison of this ratio with the one obtained in natural luminescence.

In steady state natural luminescence, the rate equations are

$$[11] \quad \frac{d[^1A_1]}{dt} = I_a - (1/\tau_F)[^1A_1]$$

$$[12] \quad \frac{d[^3A_1]}{dt} = k_i[^1A_1] - (1/\tau_p)[^3A_1]$$

According to the steady state condition applied to both states and using the following definitions: $I_p = s_p k_p[^3A_1]$ and $I_F = s_F k_F[^1A_1]$, we have:

$$[13] \quad \left(\frac{I_p}{I_F}\right)_N = \frac{s_p k_p}{s_F k_F}(k_i\tau_p)$$

Combining eqs. 10 and 13 we have

$$[14] \quad \frac{(I_p/I_F)_{st}}{(I_p/I_F)_N} = 1 + \frac{\beta(\lambda)}{\phi_T}$$

where $\phi_T = k_i\tau_F$ is the quantum yield of production of triplet molecules under steady state excitation.

Results and Discussion

(1) Natural and Delayed Luminescence

(A) Indole

The delayed fluorescence (DF) spectrum of a 10^{-3} *M* solution of indole in ether at 77 °K is apparently identical in shape to the natural fluorescence (F) spectrum as shown in Fig. 2. The intensity ratios I_{DF}/I_F and I_{DF}/I_p are approximately 10^{-4} and 10^{-3} respectively. The phosphorescence spectrum shows a well-defined vibrational structure characterized by the 1350 cm^{-1} (strongly active in Raman (40)) progression and appears to be the $^3L_a \rightarrow {}^1A$ emission (τ_p = 7.2 s Fig. 3). The relative yield ϕ_F/ϕ_P is equal to 4.0 as shown in Fig. 7*a*. The natural fluorescence and the delayed fluorescence spectra both show a mirror image relationship to the lowest energy absorption spectrum and could be attributed to the $^1L_b \rightarrow {}^1A$ emission of the monomer indole (37).

The DF and P intensities have been found to obey the following relationships

$$I_{DF} \propto I_0^{1.8 \pm 0.1}$$

$$I_p \propto I_0^{1.0 \pm 0.1}$$

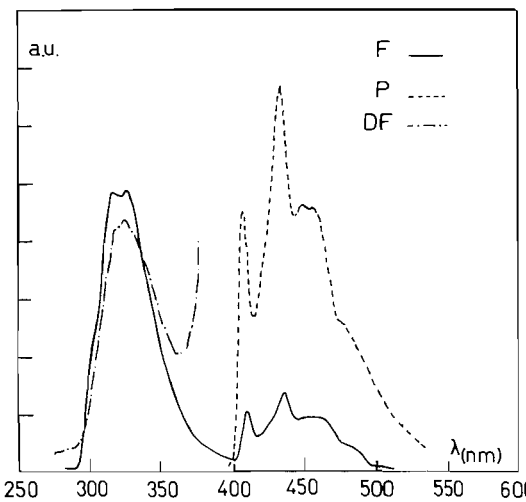

FIG. 2. Indole 10^{-3} *M* in ether at 77 °K: (—), natural fluorescence and phosphorescence uncorrected for the emission monochromator–PM system and without the use of the phosphoroscope assembly; (---), uncorrected phosphorescence spectrum observed through the chopper assembly showing the overlap with the phosphorescence spectrum, the intensity ratio being $I_{DF}/I_P = 10^{-3}$. All these emissions were excited at 290 nm. The ordinate is in arbitrary units.

Can. J. Chem. Downloaded from www.nrcresearchpress.com by 210.87.254.105 on 09/05/12
For personal use only.

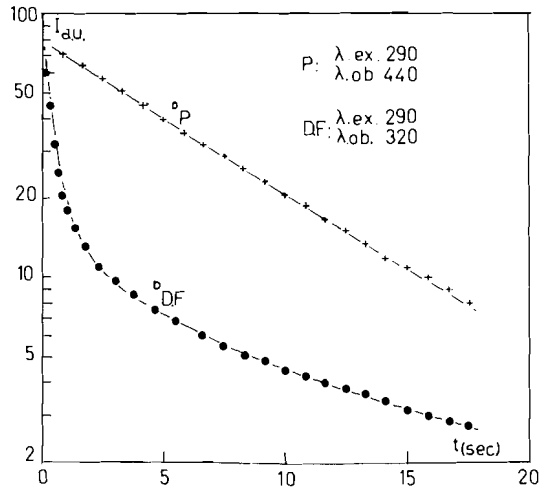

FIG. 3. Indole 10^{-3} M in ether at 77 °K: decay of the DF and P emissions observed through the phosphoroscope assembly. The Corning filter number 7–60 was used in front of the PM tube when recording the DF decay in order to avoid the strong overlapping of the DF and the P spectra.

where I_0 is the exciting light intensity. The decay kinetics of the DF and the P emissions is presented in Fig. 3. The phosphorescence is clearly exponential with a lifetime of 7.2 s while the DF follows a complex law of decay during the first 20 s. Only about 9% of the total DF (the last part of the decay) can be assigned with certainty to isothermal recombination fluorescence. There exists some evidence, based on the rise and decay kinetics of the DF and P emissions, that amine molecules trapped in low temperature rigid matrices might be involved in triplet–triplet annihilation producing a DF emission of short time decay (28, 29). It has also been proposed that the fast component be assigned to isothermal recombination fluorescence (41). The last part (8–20 s) of the DF decay can fit the rate diffusion law $I_{DF} = At^{-m}$ with $m = 0.8$ and A an instrumental sensitivity constant. This law has been derived on the basis of a diffusion controlled recombination of photoejected electrons with their parent cations (43). This result shows that isothermal delayed fluorescence must be involved in the whole DF emission of indole in an ether matrix at 77 °K.

Indole has also been studied in an EG–W rigid glass matrix at 77 °K. The F, DF, and P emissions have the same spectral and kinetic characteristics as those observed in an ether glass except that the DF decay possesses a greater portion of the long decay component (see Fig. 5).

(B) Tryptophan

Indole and tryptophan are well known to have the same spectral and kinetic properties upon u.v. irradiation (46). A 10^{-3} M solution of tryptophan in an EG–W glass at 77 °K has been studied and the results are plotted in Figs. 4 and 5. The spectral properties are the same as those of indole in an ether glass. The relative yield ϕ_F/ϕ_P is also equal to 4.0 as shown in Fig. 10. Again, the phosphorescence decay is exponential with a lifetime of 6.8 s, but the DF decay strongly differs from that observed in the indole–ether system (see Fig. 5). A larger fraction (about 23%) of the total DF can be attributed with certainty to isothermal recombination fluorescence. The last part of the decay (7–20 s) can be fitted to the rate diffusion equation ($I_{DF} = At^{-m}$) with $m = 0.9$. This difference in behavior can only be attributed to the solvent matrix since indole in EG–W gives the same DF decay. This means that on the average, the electron takes a longer time to recombine with their parent cation in EG–W than in ether.

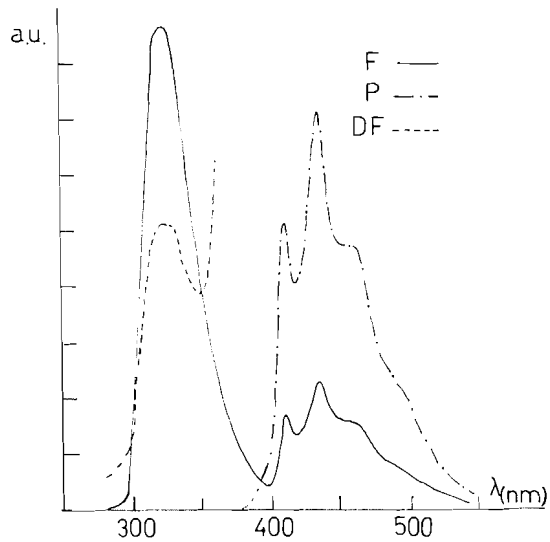

FIG. 4. Tryptophan 10^{-3} M in EG–W (70–30) at 77 °K: (—), uncorrected natural fluorescence and phosphorescence observed without the chopper assembly; (-·-·), uncorrected phosphorescence spectrum observed through the chopper assembly; (---), uncorrected delayed fluorescence spectrum observed through the chopper assembly showing strong overlapping with the phosphorescence spectrum, the DF/P intensity ratio is 3×10^{-5}. The ordinate is in arbitrary units.

Can. J. Chem. Downloaded from www.nrcresearchpress.com by 210.87.254.105 on 09/05/12
For personal use only.

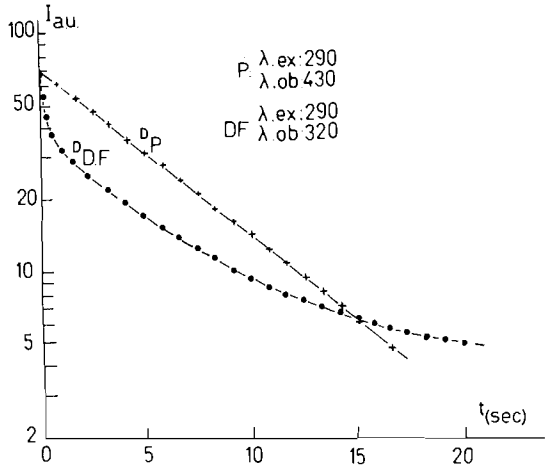

FIG. 5. Tryptophan 10^{-3} M in EG–W (70–30) at 77 °K: decay of the DF and the P emissions observed through the phosphoroscope assembly. The Corning filter 7-60 was used as explained in the caption of Fig. 3.

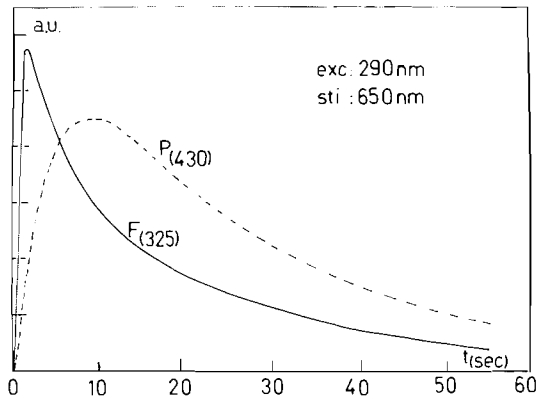

FIG. 6. Indole 10^{-3} M in ether at 77 °K: time dependence of the F and P stimulated emissions respectively at 325 nm and 430 nm when the visible stimulating illumination (650 nm) began at $t = 0$. The sample was pre-irradiated for 2 min at 290 nm.

In fact greater interactions are predicted in an EG–W glass. This could easily be explained on the basis of the dielectric field theory. The coulombic interaction between the ejected electron and the parent cation is inversely proportional to the dielectric constant of the medium. The kinetic energy of the thermal electron is $kT = e^2/\varepsilon r_c$ where r_c is the distance between the electron and the cation in the medium of dielectric constant ε (51). This relation predicts that the average distance between the electron and the amine cation is shorter in EG–W than in ether. This is confirmed when one compares the m values obtained from the relation $I_{DF} = At^{-m}$ in both solvents: 0.9 in EG–W and 0.8 in ether which means that the electron distribution maximum is closer to the amine cation in the EG–W glassy matrix (43).

(2) Stimulated Luminescence

(A) Indole

Two 10^{-3} M solutions of indole in ether and in a EG–W glass at 77 °K have been subjected to the periodic cycle described in detail in the Experimental section. The dependence of stimulated emission intensity over the time of visible stimulation at 650 nm is shown in Fig. 6 for the ether solution. The photoionization of the solute has been performed at 290 nm in the first S_0–S_1 absorption of the solute indole molecule. Immediately after the visible stimulation is applied, the emission centered at 325 nm (fluorescence) rises instantaneously (with the time constant of the

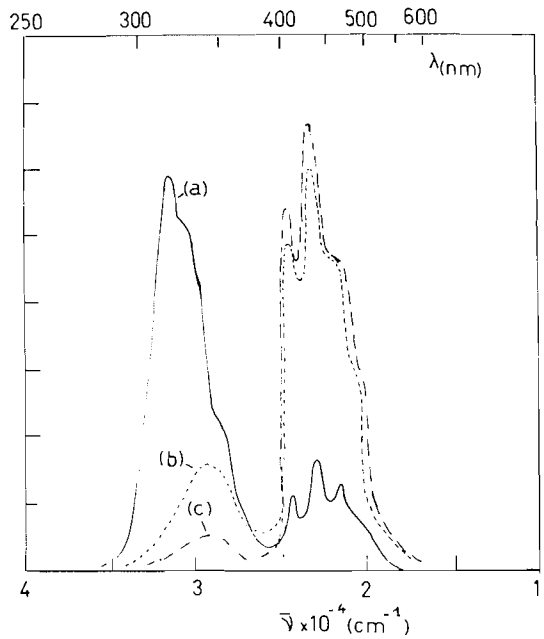

FIG. 7. (*a*) Corrected natural F and P spectra (obtained without the chopper assembly) for a 10^{-3} M solution of indole in ether at 77 °K. (*b*) Stimulated luminescence obtained by plotting point by point the graphical integration of curves like those in Fig. 6 after correcting for the non-linear response of the emission monochromator–PM system and the optical filters used. This is for a 10^{-3} M solution of indole in an ether matrix at 77 °K. (λ_{sti} = 650 nm). (*c*) The same as in (*b*) except that spectra are obtained for a 10^{-3} M solution of indole in an EG–W glass at 77 °K. All these emission spectra are in relative units of quanta $cm^{-2}\,s^{-1}$ per unit wavelength interval.

Can. J. Chem. Downloaded from www.nrcresearchpress.com by 210.87.254.105 on 09/05/12
For personal use only.

Can. J. Chem. Downloaded from www.nrcresearchpress.com by 210.87.254.105 on 09/05/12
For personal use only.

recorder used), reaches a maximum and then decreases nearly exponentially with time during the visible irradiation, at least during the first minute of this stimulation. On the other hand, the emission centered at 430 nm can be kinetically ascribed to the phosphorescence of the indole molecule for the rise of this emission follows the rise of the natural phosphorescence of the solute in the same matrix. The decay of the stimulated phosphorescence with the time of stimulation also follows a first order rate law with the same time constant (23.5 s) as that for the stimulated fluorescence. This kinetic result gives support to the assumption made in the kinetic section above that both the singlet and triplet states are populated by the same recombination mechanism. On the other hand, in an EG–W glass matrix, although

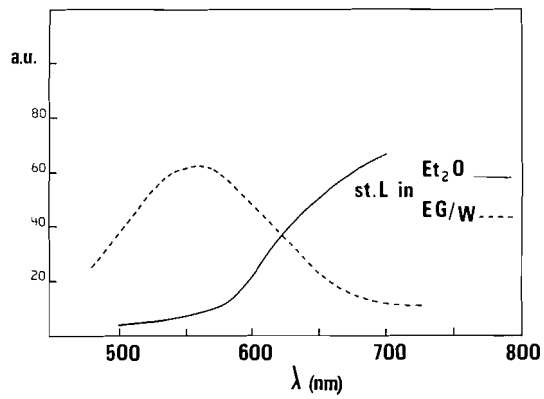

FIG. 8. Corrected action spectra of the stimulated luminescence of indole observed at 325 nm in ether and EG–W rigid glasses at 77 °K.

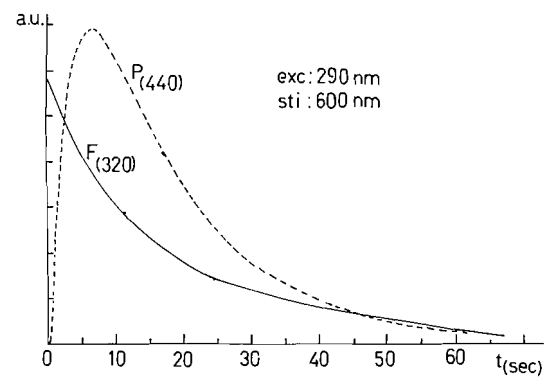

FIG. 9. Tryptophan 10^{-3} *M* in EG–W at 77 °K: time dependence of the F and P stimulated emissions respectively at 320 nm and 440 nm when the visible stimulating illumination (600 nm) began at $t = 0$. The sample was pre-irradiated 2 min at 290 nm.

the stimulated pulses, for both the fluorescence and the phosphorescence, obey first order kinetics, the P decay (time constant 15.7 s) is faster than the F decay (23.5 s). In Fig. 9 are shown the stimulated pulses for tryptophan in EG–W which are analytically similar to those of indole in EG–W.

The integrated area under each emission curve allows us to calculate the following intensity ratios

$$(I_p/I_F)_N = 0.25$$

$$(I_p/I_F)_{st\ (E)} = 3.3$$

$$(I_p/I_F)_{st\ (EG)} = 14$$

where st(E) stands for stimulated emission in an ether glass and st(EG) for stimulated emissions in an EG–W glass matrix.

The fact that the stimulated fluorescence spectrum does not coincide with any of the natural fluorescence or the delayed fluorescence spectra is rather puzzling. This has been observed for indole in both solvents and also for diphenylamine in ether (44). Tryptophan (Fig. 10) and carbazole (44) did not show this effect in either solvent used. The red shift might arise from changes in the interaction of the excited molecule with the surrounding solvent molecules during the dead time allowed before the stimulation or might de due to the recombination of the electron with an entity other than the monomer cation, a cation trapped in an aggregate of solute molecules for example. The DF emission band has a maximum at 340 nm identical with the one attributed to the aggregated tryptophan molecules by Aksentsev *et al.* (45). On the other hand, changes in the interaction of the excited molecule with the surrounding solvent molecules resulting either in the formation of exciplexes (42) or in a lowering of the excited singlet state energy as a result of reorientation of surrounding solvent molecules (46) are much less probable in rigid matrices at 77 °K. More experiments on concentration effects will be necessary in order to elucidate the nature of the apparent red shift observed in the stimulated fluorescence spectra of indole in both solvents.

By holding the wavelength of the stimulated emission fixed at 325 nm for example (Fig. 8) and by varying the wavelength of the visible light of stimulation one might be able to reproduce the absorption spectra of the species responsible for the recombination event if the quantum yield of emission is independent of the excitation wavelength. (See Fig. 11 and part B on tryptophan for

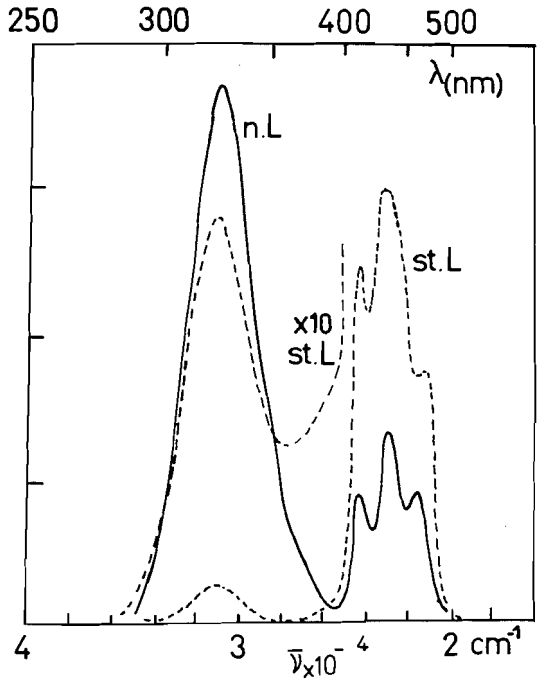

FIG. 10. Tryptophan 10^{-3} *M* in EG–W at 77 °K: (—), corrected natural F and P spectra (obtained without the chopper assembly); (---), stimulated luminescence obtained by plotting point by point the graphical integration of curves displayed in Fig. 9 after correcting for the non-linear response of the emission monochromator–PM system and the optical filters used. All these emission spectra are in relative units of quanta $cm^{-2}\ s^{-1}$ per unit wavelength interval (λ_{stl} = 600 nm).

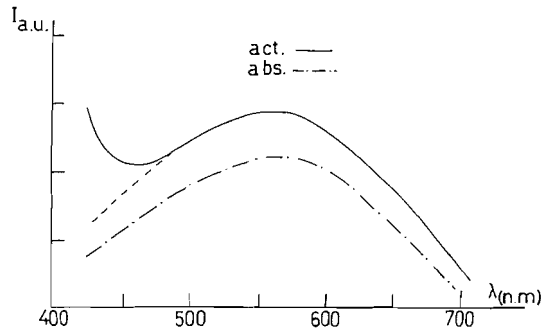

FIG. 11. Tryptophan 10^{-3} *M* in EG–W at 77 °K: (-·-·), absorption spectrum of a pre-irradiated sample in the visible region. An optical density of 0.18 has been obtained for the sample contained in a 1 mm optical path cell. (—), corrected action spectra of the stimulated luminescence observed at 325 nm.

comparison with the absorption spectra of the trapped electrons in the EG–W glass.) Figure 8 shows that the majority of photostimulated electrons are more stabilized in the EG–W glass than in the ether glass. Shida, Iwata, and Watanabe (52) have recently published the absorption spectrum of the electrons trapped in an ether glass matrix and showed that the maximum lies at 1 eV in the near infrared region. Our results could then probably be interpreted in terms of electron stimulation between 500 and 700 nm in the high energy absorption tail of the trapped electrons in ether.

(B) Tryptophan

The behavior of a 10^{-3} *M* solution of tryptophan in both glasses is generally similar to that of indole and for this reason, Figs. 9, 10, and 11 only show the results in the EG–W glassy matrix. The decay of both the stimulated fluorescence and phosphorescence with time during stimulation follows a first order mechanism (Fig. 9) but with different time constants of 23.5 s for the fluorescence and 15.7 s for the phosphorescence. This has been found to be a matrix effect and is unrelated to the solute molecule (44).

In Fig. 10, are plotted, at different wavelengths, the area under the curves found in Fig. 9 in order to obtain the spectra of stimulated fluorescence and phosphorescence. The corrected natural emission spectra are also reproduced and the following intensity ratios obtained:

$$(I_p/I_F)_N = 0.25$$

$$(I_p/I_F)_{st(EG)} = 11$$

The corrected action spectrum of the stimulated emission observed at 325 nm, has been plotted in Fig. 11 along with the absorption spectrum of the same solution in a cell of 1 mm optical path length. The absorption band shows a maximum at 560 nm, with an optical density of 0.18. Hase (31) obtained the same spectra for a u.v. irradiated tryptophan solution in an EG–W (70–30) at 77 °K. This is a strong indication that one may use corrected action spectra of stimulated emissions when discussing the entities responsible for the appearance of stimulated emission. We stress here that the trapped electrons (at least a part of them), when released from their potential wells upon visible stimulation, recombine with amine cations to produce the F and P spectra observed. Not all the released electrons will recombine with the cations; some of these will react with the solvent molecules to induce

Can. J. Chem. Downloaded from www.nrcresearchpress.com by 210.87.254.105 on 09/05/12
For personal use only.

Can. J. Chem. Downloaded from www.nrcresearchpress.com by 210.87.254.105 on 09/05/12
For personal use only.

the solvent decomposition (31). The polar solvent plays the role of positive point charges in competition with the positive cation in the electrostatic coulomb attraction of the released electron. This competition will definitely reduce the velocity and the kinetic energy of the released electrons, the question is: Do all the released electrons have sufficient energy to recombine at the singlet level when they collide with the positive cation?

(3) Discussion based upon the Kinetics of the F and P Photostimulated Emissions

In eq. 14, $\beta(\lambda)$ $(= k_{AT}/k_{AS})$ is defined as the frequency of direct population of the triplet state after the recombination event has taken place; this means the number of molecules in the triplet manifold compared to the number in the singlet manifold. If the electrons have sufficient energy to recombine at the excited singlet and triplet levels (as is the case in hydrocarbon rigid matrices (35, 48)) it has been proposed that $\beta(\lambda) = 3$ in view of the triplet spin degeneracy (48). Applying this value of $\beta(\lambda)$ in eq. 14 along with the intensity ratios obtained for indole in ether, one gets a value of 0.25 for the triplet quantum yield ϕ_T. The triplet quantum yield of indole and tryptophan is not likely to vary much in the different glassy solvents used at 77 °K since the natural P/F ratios are the same and the phosphorescence lifetimes are also approximately the same. So this ϕ_T value along with the value of $\beta(\lambda) = 3$ will certainly not explain the large increase in the ratio $[(I_P/I_F)_{st}]/[(I_P/I_F)_N]$ (13.2 to 56.0) in going from the ether matrix to the EG–W matrix.

The triplet yield is defined as

$$[15] \qquad \phi_T = \frac{k_i}{k_F + k_c + k_i}$$

We have found experimentally that the ratio $\phi_P/\phi_F = 0.25$ and moreover ϕ_F is known to be 0.6 for indole and tryptophan in an EG–W glass (46). The phosphorescence quantum yield (calculated as $\phi_P = 0.15$) is related to the triplet quantum yield by the relation

$$[16] \qquad \phi_P = \phi_T q_P = \frac{k_i}{k_F + k_c + k_i} \cdot \frac{k_P}{k_P + k_{iP}}$$

where q_P is the phosphorescence quantum efficiency. The phosphorescence lifetime is defined as

$$[17] \qquad \tau_P = \frac{1}{k_P + k_{iP}} = 7.2 \text{ s}$$

If the indole ring is considered as an aromatic hydrocarbon and the theory of Siebrand (49) is applied to calculate the non-radiative rate parameter k_{ip} using the following values, triplet energy $E_T = 24700\ \text{cm}^{-1}$ and $\eta = 0.44$, a value of $0.080\ \text{s}^{-1}$ is obtained for k_{ip}. From [16] and [17] the triplet quantum yield is evaluated to be $\phi_T = 0.36$. Assuming that the approximation made is valid and taking into account the inherent experimental error in the measurement of ϕ_F (46), it can be concluded that internal conversion $(S_1–S_0)$ is not operative in these systems.

Now looking back on eq. 14 we find that the only varying parameter is $\beta(\lambda)$. For indole in an ether glass $\beta(650\text{ nm}) = 4.4$; for indole in EG–W glass $\beta(650) = 20$ and for tryptophan in an EG–W glass $\beta(600) = 16$. We interpret this result to mean that in an ether glass about 18% of the indole cations interacting with electrons recombine at the singlet level compared to the statistical ratio $(\beta = k_{AT}/k_{AS} = 3)$ of 25% and that in an EG–W glass, only about 5% of the indole cations recombine at the singlet level. If we can assume that all recombination events producing an energy equal to or higher than the first singlet energy level give rise to an observed $\beta \approx 3$ (47) then we can conclude that in ether for the 18% of the cations recombining at the singlet level there will be 54% of the cations recombining at the triplet level and then 28% of the overall recombination events are deficient in energy to populate the first excited singlet level of the indole solute molecule. This percentage is increased to 80% in an EG–W glassy matrix. Moreover these results seem to indicate a dependence of β on the wavelength of stimulation which is understandable in terms of the excess of kinetic energy of the recombining species after the detrapping has occurred.

More quantitative experiments are needed to obtain a better value for ϕ_T before taking the above figures as absolute; nevertheless, we feel that these figures are indicative of the physical interaction the electron experiences in both glassy matrices. Similar results have been obtained for the diphenylamine and carbazole molecules trapped in rigid polar matrices. This will be the subject of another publication (44).

Can. J. Chem. Downloaded from www.nrcresearchpress.com by 210.87.254.105 on 09/05/12
For personal use only.

Conclusion

The results of the experiments discussed in this paper show that the nature of the solid polar matrix affects first the kinetics of the isothermal delayed fluorescence and second the energetics of charge recombination in the bulk of the rigid glass.

On the basis of theoretical and experimental facts, it was proposed that when ejected from the parent molecule, the electron should be trapped at a shorter distance of the cation in an EG–W glass than in an ether glass. This has been confirmed by the study of the delayed fluorescence decay in both solvents.

In discussing the kinetics of the photostimulated emissions, the model proposed by McClain and Albrecht (18) has been used in which it was assumed that the rate-determining step of the recombination process precedes the formation of an intermediate state A (charge transfer character) from which the singlet $[^1A_1]$ or the triplet $[^3A_1]$ state can be formed. The fact that both the stimulated fluorescence and phosphorescence decayed exponentially and with approximately the same time constant upon visible stimulation is an indication that the singlet and triplet states are populated from the same origin. Moreover the exponentiality might indicate that a single trapping site is responsible in the detrapping of the electrons when the stimulation is applied at 650 nm. Hase (31) has shown that in EG–W glasses two kinds of traps exist with absorption maxima centered at 550 nm and 615 nm. When photobleaching is applied the maximum at 615 nm corresponds to the fast component in the disappearance of the trapped electrons. It is then likely that stimulation at 650 nm will first act only on this second kind of trap.

Based upon the kinetic parameters obtained and the experimental intensity ratios (I_p/I_F) it was concluded that about 28% of the amine molecules do not have sufficient energy to reach the first singlet level after the recombination event in an ether matrix (when stimulated at 650 nm) while this percentage is increased to about 80% in an EG–W (70–30) rigid glass (when stimulated at 650 nm).

The corrected action spectra of the stimulated emissions seem to confirm that the electron is involved in the recombination event and that more energy is needed to release an electron in an EG–W glass than in an ether glass. This means that the electrostatic interactions are playing a more important role in an EG–W glass; they tend to stabilize the electron in potential wells of the matrix much more efficiently than does the ether matrix. All our experimental results are in line with this.

Many more experimental and theoretical studies will be needed in order to bring clarification on the nature of the trapping sites in molecular misoriented glassy solids.

We wish to thank the National Research Council of Canada for financial support. Mr. Aurèle Blanchette has provided valuable technical assistance to a part of this work.

1. H. LEONHARDT and A. WELLER. Z. Phys. Chem. **29**, 277 (1961); Ber. Bunsenges. Phys. Chem. **67**, 791 (1963).
2. Y. NAKATO, N. YAMAMOTO, and H. TSUBOMURA. Bull. Chem. Soc. Jap. **40**, 2481 (1967).
3. N. MATAGA and O. TANIMOTO. Theor. Chim. Acta, **15**, 111 (1969).
4. T. R. HOPKINS and R. LUMRY. Photochem. Photobiol. **15**, 555 (1972).
5. K. KAWAI, N. YAMAMOTO, and H. TSUBOMURA. Bull. Chem. Soc. Jap. **43**, 2266 (1970).
6. R. POTASHNIK, M. OTTOLENGHI, and R. BENSASSON. J. Phys. Chem. **73**, 1912 (1969); A. ALCHALAL and M. OTTOLENGHI. Chem. Phys. Lett. **17**, 117 (1972).
7. E. C. LIM, C. P. LAZZARA, M. Y. YANG, and G. W. SWENSON. J. Chem. Phys. **43**, 970 (1965).
8. M. EWALD and G. DUROCHER. Chem. Phys. Lett. **8**, 479 (1971).
9. M. EWALD and G. DUROCHER. Chem. Phys. Lett. **12**, 385 (1971).
10. M. EWALD. Thèse de doctorat d'état. Université de Paris Sud, Centre d'Orsay, 1972.
11. G. N. LEWIS and D. LIPKIN. J. Am. Chem. Soc. **64**, 2801 (1942).
12. G. N. LEWIS and J. BIGELEISEN. J. Am. Chem. Soc. **65**, 2424 (1943).
13. H. LINSCHITZ, M. G. BERRY, and D. SCHWEITZER. J. Am. Chem. Soc. **76**, 5833 (1954).
14. J. JOUSSOT-DUBIEN and R. LESCLAUX. C. R. Ac. Sci. **258**, 4260 (1964).
15. K. D. CADOGAN and A. C. ALBRECHT. J. Chem. Phys. **43**, 2550 (1965); J. Phys. Chem. **72**, 929 (1968).
16. M. EWALD and B. MUEL. C. R. Ac. Sci. **268B**, 973 (1969).
17. A. BERNAS, M. GAUTHIER-BODARD, D. GRAND, and D. LEONARDI. Int. J. Radiat. Phys. Chem. **1**, 229 (1969).
18. W. M. MCCLAIN and A. C. ALBRECHT. J. Chem. Phys. **43**, 465 (1965).
19. J. MOAN and H. B. STEEN. J. Phys. Chem. **75**, 2887 (1971).
20. F. KIEFFER and M. MAGAT. Actions chimiques et biologiques des radiations. No. 14. Masson, Paris. (1971). p. 135.

21. R. GUERMONPREZ, C. HELENE, and M. PTAK. J. Chim. Phys. **64**, 1376 (1967).
22. M. AUBAILLY, M. BAZIN, and R. SANTUS. Chem. Phys. Lett. **12**, 70 (1971).
23. J. JOUSSOT-DUBIEN and R. LESCLAUX. Isr. J. Chem. **8**, 181 (1970).
24. R. LESCLAUX and J. JOUSSOT-DUBIEN. Organic molecular photophysics, *Edited by* J. B. Birks. J. Wiley and Sons. 1973. p. 457.
25. R. C. JARNAGIN. Acc. Chem. Res. **4**, 420 (1971).
26. M. OTTOLENGHI. Chem. Phys. Lett. **12**, 339 (1971).
27. J. MOAN. Ber. Bunsenges. für Phys. Chem. **75**, 668 (1971).
28. M. EWALD, D. MULLER, and G. DUROCHER. Spectrochim. Acta, **29A**, 1051 (1973).
29. M. EWALD, D. MULLER, and G. DUROCHER. Izvestiza Akad. Nauk. SSSR, **37**, N3, 470 (1973).
30. J. MOAN and H. B. STEEN. J. Phys. Chem. **75**, 2893 (1971).
31. H. HASE. J. Phys. Soc. Jap. **24**, 589 (1968).
32. H. HASE, M. NODA, and T. HIGASHIMURA. J. Chem. Phys. **55**, 5411 (1971).
33. M. T. PAILTHORPE and C. H. NICHOLLS. Photochem. Photobiol. **14**, 135 (1971).
34. E. DOLAN and A. C. ALBRECHT. J. Chem. Phys. **37**, 1149 (1962).
35. W. M. MCCLAIN and A. C. ALBRECHT. J. Chem. Phys. **44**, 1594 (1966).
36. R. SANTUS, M. AUBAILLY, and C. HELENE. C. R. Ac. Sci. **272**, 2008 (1971).
37. C. A. PARKER. Photoluminescence of solutions. Elsevier, Amsterdam. 1968.
38. Y. BEAUCHAMP, L. FOISY, and G. DUROCHER. Unpublished results.
39. R. STAIR, W. E. SCHNEIDER, and J. K. JACKSON. Appl. Opt. **2**, 1151 (1963).
40. K. W. F. KOHLRAUSCH and R. SEKA. Chem. Ber. **71B**, 1563 (1938).
41. M. AUBAILLY, M. BAZIN, and R. SANTUS. Chem. Phys. Lett. **14**, 422 (1972).
42. M. S. WALKER, T. W. BEDNAR, and R. LUMRY. J. Chem. Phys. **47**, 1020 (1967).
43. P. DEBYE and J. O. EDWARDS. J. Chem. Phys. **20**, 236 (1952).
44. D. MULLER, M. EWALD, and G. DUROCHER. Can. J. Spectrosc. To be published.
45. S. L. AKSENTSEV, V. I. OLENEV, and Y. A. VLADIMIROV, Biofiz. **10**, 877 (1965).
46. J. EISENGER and G. NAVON. J. Chem. Phys. **50**, 2069 (1969).
47. A. DEROULEDE. J. Lumin. **3**, 302 (1971); C. DENIAU, A. DEROULEDE, F. KIEFFER, and J. RIGAUT. J. Lumin. **3**, 325 (1971).
48. B. BROCKLEHURST, G. PORTER, and J. M. YATES. J. Phys. Chem. **68**, 203 (1964).
49. W. SIEBRAND. The triplet state. Cambridge University Press. 1967.
50. YU. A. VLADIMIROV, D. I. ROSHCHUPKIN, and E. E. FESENKO. Photochem. Photobiol. **11**, 227 (1970).
51. L. ONSAGER. Phys. Rev. **54**, 554 (1938).
52. T. SHIDA, S. IWATA, and T. WATANABE. J. Phys. Chem. **76**, 3683 (1972).

Can. J. Chem. Downloaded from www.nrcresearchpress.com by 210.87.254.105 on 09/05/12
For personal use only.

Etude de l'effet des cations alcalins sur la structure du succinate de cuivre[1]

P. SHARROCK ET T. THEOPHANIDES

Département de Chimie, Université de Montréal, Montréal 101, Québec

Received April 12, 1973

De nouveaux sels complexes du cuivre du genre $M_2Cu(succinate)_2 . xH_2O$, où M = Li, Na, K et NH_4; $0 \leqslant x \leqslant 5\frac{1}{2}$ ont été synthétisés. Ces complexes ont été étudiés par leurs spectres infrarouges et visibles, diagrammes thermogravimétriques, diagrammes de rayons X, et susceptibilités magnétiques.

New complex-salts of copper of the general formula $M_2Cu(succinate)_2 . xH_2O$, where M = Li, Na, K, and NH_4; $0 \leqslant x \leqslant 5\frac{1}{2}$ were synthesized. The complexes were studied by infrared and visible spectroscopy, thermogravimetry, X-ray powder patterns, and magnetic susceptibility measurements.

Can. J. Chem., **52**, 418 (1974)

Introduction

Les acides carboxyliques donnent de nombreux sels métalliques avec des structures complexes (1). Les déterminations de structures cristallines par diffraction de rayons X se multiplient et de nombreuses isoméries de liaison COO—M ont été trouvées.

Les carboxylates dinucléaires à structure cage ont été les plus remarqués et font maintenant le sujet de recherches théoriques avancées (2). Certains auteurs recherchent l'importance du choix du métal dans la nature du lien métal–métal de la structure cage (3), d'autres examinent les influences qui s'exercent sur les groupes COO et qui ont pour conséquence l'adoption de la structure cage (4). Plusieurs sels doubles de l'acétate de cuivre avec les acétates des métaux alcalins (5, 6) et alcaline-terreux (7, 8) sont connus. L'acide oxalique donne des complexes du genre $K_2[Cu(C_2O_4)]_2 . 2H_2O$ (9) et les acides tartrique, trihydroxyglutarique et l-glutamique donnent aussi des "sels mixtes" (10–12). Tous ces sels ont en commun une structure polymère où les groupes carboxyliques sont à pont et hétéronucléaires. L'étude des susceptibilités magnétiques en fonction de la température (9, 10) révèle que les systèmes sont très sensibles à l'environnement du cuivre.

Une étude par hétérométrie (13) indique l'existence d'un sel complexe du cuivre et des métaux alcalins avec l'acide succinique. La série des complexes insolubles que forme le cuivre avec les acides α,ω-dicarboxyliques est connue depuis longtemps (14). Le succinate de cuivre est un exemple typique de carboxylate de cuivre à structure cage. Nous avons cherché à isoler les sels complexes que forment l'acide succinique avec le cuivre et les métaux alcalins dans le but d'étudier, par susceptibilité magnétique et par spectroscopie infra-rouge et visible, l'effet des métaux alcalins sur la structure cage polymérique trouvée dans le succinate de cuivre.

Résultats et discussion

La formation des sels complexes peut s'expliquer comme suit:

$$[1] \quad 2(M_2succinate) + Cu^{2+} \rightarrow M_2Cu(succinate)_2 + 2M^+$$

où M = Li, Na, K, NH_4 et Cu (voir les analyses élémentaires dans le tableau 1). Les couleurs observées lors de la préparation des sels complexes (voir partie expérimentale) montrent que le succinate de cuivre se forme d'abord et réagit ensuite avec le succinate d'alcali pour donner le sel complexe. L'eau décompose les sels complexes pour donner le succinate de cuivre mélangé à une solution aqueuse de succinate d'alcali. Le succinate de cuivre peut donc être considéré comme un intermédiaire dans la réaction de formation des sels complexes. Les sels complexes isolés sont insolubles dans les solvants organiques et sont très probablement de nature polymère. Le succinate de cuivre est insoluble (0.3g/l) car il est formé de chaines linéaires infinies d'unités dinucléaires reliées entre elles par deux acides succiniques (15). Les sels complexes contiennent des quantités variables d'eau, allant de 1 pour le sel de potassium jusqu'à 5½ pour les sels de sodium et de lithium. Cette quantité d'eau n'est pas surpre-

[1]Extrait d'une partie de la thèse de maîtrise de M. Sharrock déposée en novembre 1972, à l'Université de Montréal.

Can. J. Chem. Downloaded from www.nrcresearchpress.com by 210.87.254.6 on 09/05/12
For personal use only.

TABLEAU 1. Analyses élémentaires

Complexe	%C		%H		%Cu	
	calc.	trouvé	calc.	trouvé	calc.	trouvé
$Na_2Cu(Succ)_2.5½H_2O$	21.85	21.54	4.31	4.27	14.45	14.80
$Na_2Cu(Succ)_2.2H_2O$	25.42	25.71	3.18	3.02	16.85	17.15
$Na_2Cu(Succ)_2.H_2O$	26.70	26.41	2.78	2.67	17.80	17.85
$Na_2Cu(Succ)_2$	28.13	28.35	2.34	2.44	18.60	18.90
$K_2Cu(Succ)_2.H_2O$	24.55	24.81	2.56	2.32	16.22	15.75
	24.55	24.34	2.56	2.32	16.22	16.22
$Li_2Cu(Succ)_2.5½H_2O$	23.48	23.54	4.64	4.74	24.20	24.34
	23.48	23.82	4.64	4.53	24.20	—

nante pour un complexe de cuivre, puisque le tartrate et le sulfate de cuivre cristallisent précisément avec 5 molécules d'eau (10).

Le diagramme thermogravimétrique du sel complexe de sodium (Fig. 1) comprend deux plateaux qui correspondent à la perte successive de 3½ et de 2 molécules d'eau. Dans les 5½ molécules d'eau présentes dans le complexe, il y a donc $2H_2O$ de coordination et $3½H_2O$ de cristallisation. Les analyses thermogravimétriques ont permis d'établir que l'eau de cristallisation peut être enlevée simplement en tirant sous vide alors que l'eau coordonnée ne se perd qu'au dessus de 100 °C. Le sel complexe de lithium est différent, car il se dismute à une température inférieure à 100 °C sous l'action des molécules d'eau libérées. Les sels complexes se décomposent à 250 °C sous vide pour donner le succinate d'alcali et du cuivre mélangé à une faible quantité d'oxyde de cuivre (les produits à ce stade sont de couleur marron-noir et ont été identifiés par rayons X et spectroscopie infrarouge). Nous avons identifié par son spectre infrarouge le produit sublimé comme étant de

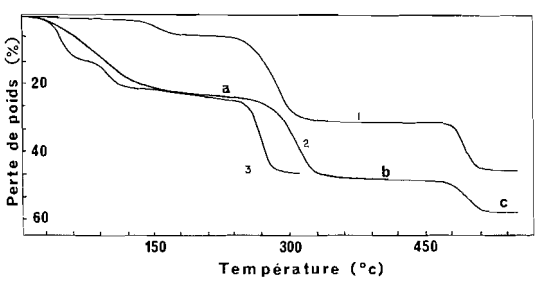

FIG. 1. Diagrammes thermogravimétriques: *1*: $K_2Cu(C_4H_4O_4)_2.H_2O$, chauffage: 4 °C/min. *2*: $Na_2Cu(C_4H_4O_4)_2.5½H_2O$, chauffage: 4 °C/min, sous vide. *3*: $Na_2Cu(C_4H_4O_4)_2.5½H_2O$, chauffage: 2 °C/min, *a* = sels complexes anhydres, *b* = succinates d'alcali + Cu, *c* = carbonates d'alcali + Cu.

l'anhydride succinique. La décomposition thermique suit la réaction 2:

[2] $M_2Cu(\text{succinate})_2 \rightarrow M_2(\text{succinate}) + Cu + \text{anhydride succinique}$

Aux températures plus élevées, nous assistons à la transformation des succinates d'alcali en carbonates d'alcali. Ces résultats concordent avec les observations antérieures (16, 17). Les carbonates ont été identifiés par leur spectres infra-rouges (18). Nous remarquons cependant que vers 230 °C le succinate de cuivre pur se décompose pour donner de l'oxyde de cuivre. La perte de poids observée est de 62.3% (théor: 63.1%). Une structure cage est toujours accompagnée par un moment magnétique plus petit que la moyenne de 1.7 M.B. observée pour les sels de cuivre(II). Ainsi, les benzoates de cuivre, où une interaction par délocalisation des spins via les carboxylates à pont est un mécanisme invoqué pour interpréter les résultats des mesures de susceptibilité (19). Le succinate de cuivre dihydraté est un autre exemple de carboxylate de cuivre à structure cage et son moment magnétique est de 1.34 M.B. à température ambiante (20). Les moments magnétiques observés pour les sels complexes sont assez élevés pour pouvoir affirmer que la structure cage n'est pas présente. En effet à température ambiante elles s'échelonnent entre 1.76 et 1.94 M.B. pour les sels sous leurs différentes formes.

Les sels complexes de lithium et de sodium ont la même couleur bleu-foncé et leurs spectres visibles sont identiques et sont représentés sur la fig. 2. Le sel de potassium, par contre, est bleu-vert. Il est normal que le sel complexe de potassium ait un spectre visible différent car il cristallise avec moins d'eau. Le spectre du succinate de cuivre dihydraté de couleur verte est représenté

Can. J. Chem. Downloaded from www.nrcresearchpress.com by 210.87.254.6 on 09/05/12
For personal use only.

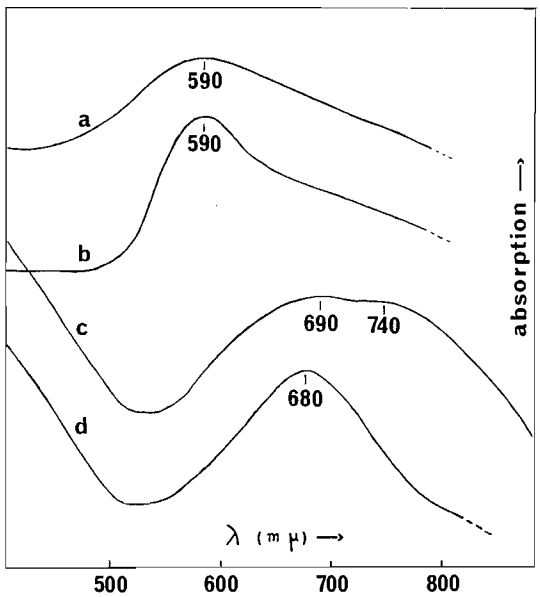

FIG. 2. Spectres visibles; a = $Na_2Cu(C_4H_4O_4)_2.5\frac{1}{2}H_2O$, b = $Li_2Cu(C_4H_4O_4)_2.5\frac{1}{2}H_2O$, c = $K_2Cu(C_4H_4O_4)_2.H_2O$, d = $Cu(C_4H_4O_4).2H_2O$.

par la fig. 2*d* et a déjà été discuté (20, 21). La couleur bleue des sels complexes indique une coordination octaédrique. Les diagrammes de poudre des succinates de Cu(II) avec le Li et le Na se ressemblent (tableau 2). Les six premières raies importantes ont des intensités semblables et correspondent à des valeurs de d qui coincide, compte tenu d'une précision de 0.3 lorsque $d \leqslant 3$ Å et de 0.7 lorsque $d \geqslant 3$ Å. Il semble donc que ces deux sels complexes soient isostructuraux. Le sel complexe de potassium présente un diagramme de poudre bien différent.

Spectres infrarouges

L'utilité des spectres infrarouges dans la détermination de la structure des carboxylates a été mise en doute par de nombreux auteurs (22). Dans le cas des sels de sodium des acides dicarboxyliques, y compris l'acide succinique, quatre fréquences C=O résultent de l'interaction des deux groupes carboxyliques (23). L'attribution des bandes du succinate de cuivre a déjà été faite et correspond à une forme *cis* ou éclipsée de la chaine organique (24). Les spectres infrarouges observés des succinates de Cu(II) avec les cations lithium et sodium présentent des caractères identiques (voir fig. 3*a*, *b*, *c*). Le spectre du sel complexe de sodium hydraté ($5\frac{1}{2}H_2O$) ressemble beaucoup au spectre du succinate de cuivre dihydraté. On a constaté qu'une simple deshydratation conduit à un éclatement des bandes pour aboutir à un spectre beaucoup plus complexe. Ceci est à l'encontre des résultats observés sur les succinates des terres rares (25). Les sels complexes de sodium et de lithium ont une absorption très forte vers 650 cm^{-1} attribuée à l'eau et dont la structure fine provient des modes de déformation des carboxyles. Le spectre du sel complexe de potassium dans cette région ressemble au succinate de sodium anhydre. Le spectre infrarouge du sel complexe de lithium possède trois petites bandes autour de 2950 cm^{-1} qui correspondent aux fréquences d'élongation C—H alors que les autres n'en ont que deux. Les fréquences observées et leurs attributions figurent dans le tableau 3.

Conclusion

Il a été établi que l'acide succinique forme des sels complexes avec le cuivre et les alcalis. Ces composés répondent à la formule, $M_2Cu(succinate)_2.xH_2O$. Nous proposons pour ces sels complexes la structure présentée dans la fig. 4. Cette structure ne comprend pas d'unités

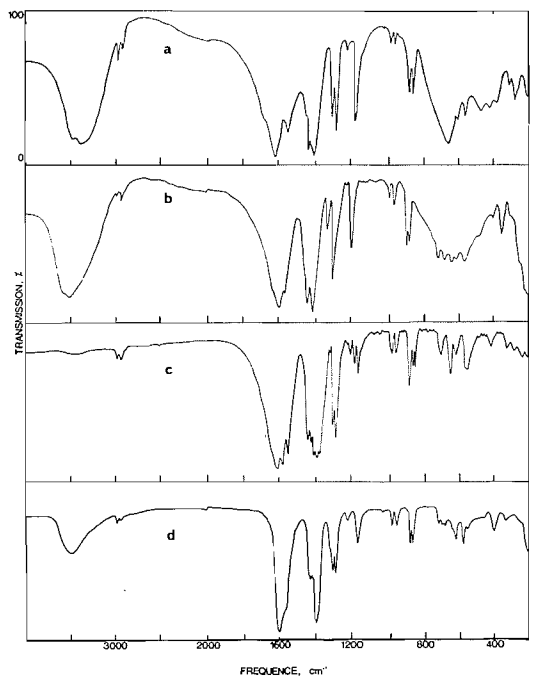

FIG. 3. Spectres infrarouges; a = sel de lithium, b = sel de sodium hydraté (avec $5\frac{1}{2}H_2O$), c = sel de sodium anhydre, d = sel de potassium.

Can. J. Chem. Downloaded from www.nrcresearchpress.com by 210.87.254.6 on 09/05/12
For personal use only.

TABLEAU 2. Diagrammes de poudres (Å)

$Li_2Cu(Succ)_2.5½H_2O$		$Na_2Cu(Succ)_2.5½H_2O$		$K_2Cu(Succ)_2.H_2O$	
Intensité	*d*	Intensité	*d*	Intensité	*d*
90	8.09	90	8.69	100	10.28
100	7.26	100	7.18	50	7.79
15	6.48	25	6.39	75	6.34
10	5.88	10	5.43	2	5.75
5	5.44	8	5.14	5	4.75
5	5.10	10	4.874	5	4.240
15	4.745	8	4.552	5	3.900
20	4.255	20	4.133	10	3.496
20	4.058	5	3.917	3	3.357
25	3.821	50	3.677	10	3.148
10	3.711	10	3.372	3	3.012
10	3.640	30	3.153	2	2.801
20	3.443	10	2.998	2	2.706
10	3.293	8	2.881	7	2.581
15	3.153	5	2.648	7	2.458
25	3.038	15	2.453	16	2.298
15	2.829	15	2.393	2	2.139
5	2.698	5	2.282		
8	2.605	8	2.127		
5	2.546	10	2.054		
10	2.439				
10	2.364				
8	2.278				
7	1.686				

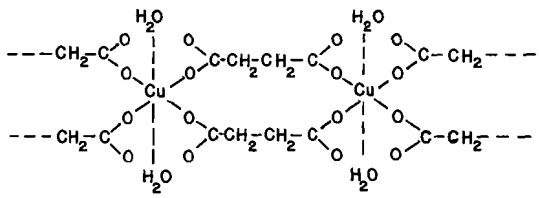

FIG. 4. Structure proposée pour les nouveaux sels complexes.

dimères comme dans le succinate de cuivre dihydraté. Il est logique de penser que les sels complexes contiennent aussi des chaines d'acide succinique. Les molécules d'eau de cristallisation seraient dans des interstices vraisemblablement reliées entre elles par un réseau de liens-H. Dans la fig. 4, les atomes d'alcali, qui ont été omis, sont liés aux oxygènes "libres" des carboxylates. Le cuivre complète sa coordination octaèdrique avec les deux molécules d'eau coordonnées. Si ces deux molécules sont enlevées, il en résulte une coordination de géométrie plan carré, assez commune pour le cuivre(II).

Nos résultats sont en accord avec les travaux antérieurs sur les sels complexes de l'acétate de cuivre et de lithium (6). Il a été trouvé que la population de "monomères" est plus grande que celle de "dimères" (comportant deux cuivres). Le rôle de la structure cage est tout de même important, puisque nous observons la formation préalable d'unités dimères avant l'obtention des sels complexes. La structure cage est stabilisée par les ligands donneurs en position axiale, mais si ces donneurs d'électrons sont trop forts, ils entrent directement en compétition avec les carboxylates et la structure cage est alors détruite, par exemple $Cu(NH_3)_2(CH_3COO)_2$ (26) et $Cu(CH_3COO)_2.3py$ (27). Inversement, les substituants électronégatifs sur le groupement carboxylate laissent une charge résiduelle plus grande sur les atomes de cuivre. Ainsi, le trifluoroacétate de cuivre n'est pas un dimère (28). Les chloroacétates de cuivre illustrent bien ces tendances. En effet, l'α-picoline comme ligand donneur axial stabilise la structure cage en compensant l'effet des chlores (29).

Dans notre cas, la première étape est la formation d'une structure cage, où les positions axiales sont occupées par des carboxylates d'alcali comme cela a déjà été suggéré (6). Les propriétés donneurs du succinate d'alcali et sa haute concentration font qu'en une deuxième étape la structure cage s'ouvre pour donner le

Can. J. Chem. Downloaded from www.nrcresearchpress.com by 210.87.254.6 on 09/05/12
For personal use only.

TABLEAU 3. Spectres infrarouge des complexes (cm^{-1})

Infrarouge				
Na*	Na.$5\frac{1}{2}H_2O$	K	Li	Attribution†
245 F		340 F	309 m	?
290 m			331 f	
326 m	360 m			
410 m	396 m	397 m	385 f	
			420 m	ν CO_2
	480 f	548 f	475 m	
560 mL	563 m	573 m	500 e	
570 m	603 m		560 m	
610 m	632 m	617 m	600 f	b CO_2
642 m	675 m	640 e		
		678 f	685 FL	
693 m	722 m	690 f		
		710 f		
855 m				
868 m	881 F	878 m	875 m	r CH_2
880 m	891 F	890 m	892 m	
963 m	970 m	960 m	970 m	
988 m		990 m	996 m	ν C—C
	1000 m	1046 f		
	1064 f			
1159 m	1110 f			
1179 m	1134 f	1170 m	1172 F	t CH_2
1200 m	1188 F	1216 f	1207 f	
1218 f	1223 f			
1288 F	1290 F	1290 m	1284 F	
1300 m		1301 m	1308 F	w CH_2
	1330 m	1315 e		
1375 F			1397 F	
1340 F				s CH_2
1403 F	1402 F	1400 F		
1420 F	1428 F	1430 F	1425 e	ν_s CO
1438 F				
1544 F	1557 F		1550 F	
1574 F	1588 FL		1615 FL	ν_{as} CO
1610 FL	1630 e	1600 FL		
			1690 e	b H_2O
2918 m	2912 m	2925 f	2910 f	ν_s CH
			2928 f	
2965 m	2972 f	2965 f	2980 m	ν_{as} CH
	3385 FL	3450 FL	3300 FL	ν OH
	3500 e		3450 e	

*Désigne le sel complexe du Na (anhydre).
†r = rocking (balancement); b = bending (déformation); ν = stretching (vibration de valence); t = twisting (torsion de CH_2); w = wagging (balancement hors du plan); s = scissoring (déformation hors du plan); indice s = symmetrical (symétrique) et as = asymmetrical (asymétrique). f = faible; m = medium; F = fort; L = large; e = épaulement.

sel complexe. Les carboxyles, en devenant monodentates pour le cuivre, libèrent les sites de coordination où viennent se placer les molécules d'eau. La plus grande facilité de formation du sel complexe de sodium est sans doute relié à sa taille favorable. Les résultats montrent que la structure cage découle d'un équilibre instable dans les carboxylates de cuivre. Ceci confirme l'hypothèse que la force de la liaison Cu—Cu est très faible.

Partie expérimentale

Synthèses

$K_2Cu(succinate)_2.H_2O$

On prépare une solution saturée de succinate de potassium dans l'alcool dénaturé à 90%. On filtre la solution et on y ajoute petit à petit une solution (verte) de $CuCl_2$ dans de l'alcool à 90%. On obtient un précipité bleu. Après chaque addition de Cu^{2+} on filtre un échantillon, on vérifie que l'addition de Cu donne toujours un précipité bleu et on continue. Si on ajoute trop de Cu le précipité devient vert (et la solution devient trans-

Can. J. Chem. Downloaded from www.nrcresearchpress.com by 210.87.254.6 on 09/05/12
For personal use only.

TABLEAU 4. Décomposition et perte de poids en chauffant les complexes

$Na_2Cu(C_4H_4O_4)_2.5\frac{1}{2}H_2O$		$Li_2Cu(C_4H_4O_4)_2.5\frac{1}{2}H_2O$
↓	Calc. 14.3% Expér. 14.0%	↓ Calc. 24.2% Expér. 23.2%
$Na_2Cu(C_4H_4O_4)_2.2H_2O$		$Li_2Cu(C_4H_4O_4)_2$
↓	Calc. 22.5% Expér. 22.0% 22.8% (vide)	↓ Calc. 48.7% Expér. 48.0%
$Na_2Cu(C_4H_4O_4)_2$		
↓	Calc. 45.4% Expér. 46.3%	
$Na_2C_4H_4O_4 + CuO$		$Li_2C_4H_4O_4 + CuO$
↓	Calc. 48.8% Expér. 48.2%	
$Na_2C_4H_4O_4 + Cu$ (sous vide)		
↓	Calc. 57.9% Expér. 57.8%	
$Na_2CO_3 + CuO$		
↓	Calc. 61.4% Expér. 60.6%	
$Na_2CO_3 + Cu$ (sous vide		
$K_2Cu(C_4H_4O_4)_2.H_2O$		
↓	Calc. 4.6% Expér. 5.2%	
$K_2Cu(C_4H_4O_4)_2$		
↓	Calc. 30.1% Expér. 31.6%	
$K_2C_4H_4O_4 + CuO$		
↓	Calc. 34.2% Expér. 33.9%	
$K_2C_4H_4O_4 + Cu$ (sous vide)		
↓	Calc. 48.5% Expér. 48.0%	
$K_2CO_2 + Cu$ (sous vide)		
↓	Calc. 44.4% Expér. 45.5%	
$K_2CO_3 + CuO$		

parente). Vers la fin de la réaction, on filtre et on lave avec 100 ml d'éther. Etant donné que $K_2Cu(succinate)_2$ ne commence à "s'hydrolyser" visiblement qu'avec du méthanol contenant 40% d'eau et que la décomposition est très lente et partielle dans le méthanol avec 30% d'eau, on lave le produit bleu avec du méthanol contenant 10% d'eau. On lave avec 300 ml de solvant, au total, en portions de 50 à 75 ml; puis, on rince avec du méthanol pur et on laisse sécher.

$Na_2Cu(succinate)_2.2H_2O$

Etant donné que le succinate de sodium dissout dans l'eau est précipité par l'addition d'éthanol, on prend 15 ml de solution saturée dans l'eau et on verse lentement par dessus 100 ml de *n*-propanol. Aussitôt, on ajoute une petite quantité de solution verte de $CuCl_2$ dans l'éthanol. On obtient un précipité bleu. Ensuite, on procède comme avec le sel de potassium et on lave avec deux fois 200 ml de méthanol à 10% d'eau puis avec 50 ml du même solvant, suivi d'un rinçage au méthanol pur.

$(NH_4)_2Cu(succinate)_2.2H_2O$

On dissout 4.2 g de succinate d'ammonium dans 4.2 ml d'eau et on prépare une solution de 1.85 g de $CuCl_2$ dans

Can. J. Chem. Downloaded from www.nrcresearchpress.com by 210.87.254.6 on 09/05/12
For personal use only.

Can. J. Chem. Downloaded from www.nrcresearchpress.com by 210.87.254.6 on 09/05/12
For personal use only.

20 ml de méthanol avec 10% d'eau. On ajoute 2 ml de cette solution de Cu^{2+} à la solution de ligand, ce qui donne une solution bleu-foncé à laquelle on ajoute 20 ml de *n*-propanol, ce qui donne deux phases. La phase inférieure pâteuse est de couleur bleue. On ajoute en tout, 10 ml de la solution Cu^{2+} par petites portions et on observe un début de coagulation dans la phase bleue; alors on ajoute 10 ml de méthanol à 10% d'eau, puis une autre portion de 50 ml du même mélange. Le produit récolté est bleu-royal. L'addition à la solution mère de plus de cuivre donne une solution gris-vert qui se transforme lentement en produit bleu.

Autres méthodes

On fait réagir le succinate de cuivre vert, solide, avec une solution presque saturée de succinate d'alcali en proportion stochiométrique, pour former un mélange visqueux. Il ne se forme rien au début, mais après une attente plus ou moins longue (deux jours pour le sodium, un mois pour le lithium) des cristaux apparraissent et grandissent lentement. Cette méthode donne un sel complexe contenant plus d'eau de cristallisation que dans les préparations précédentes et il est assez difficile d'extraire les cristaux bleus du succinate vert qui n'a pas réagi, ainsi que des cristaux blancs de succinate d'alcali. Cependant, quelques gros cristaux peuvent être isolés et leurs analyses sont satisfaisantes.

Données analytiques (tableau 4)

Le carbone, l'hydrogène et l'azote ont été déterminés par leurs microanalyses chez Chemalytics Inc., Tempe, Arizona et par le Dr. Daesslé à Montréal. Le cuivre a été dosé par absorption atomique sur un Perkin–Elmer 403, à la longueur d'onde 3247.5 Å.

Spectres infrarouges

Les spectres ont été enregistrés en suspension dans le Nujol et aussi dans les pastilles de KBr et de KCl. Un spectrophotomètre infrarouge Perkin–Elmer 621 a été utilisé pour enregistrer les spectres entre 4000 cm^{-1} et 200 cm^{-1}. Les fréquences ont été calibrées avec un film de polystyrène et la précision des maxima d'absorption est de ± 5 cm^{-1} entre 4000 et de 2000 cm^{-1}, et de ± 2 cm^{-1} pour le reste du spectre.

Susceptibilité magnétique

La susceptibilité magnétique des composés a été mesurée sur une électrobalance de Cahn avec un électro-aimant Alpha par la méthode de Faraday. Les mesures ont été effectuées à la température ambiante (22 °C).

Spectres visibles

Les spectres visibles des composés ont été pris sur un Cary 14. Les échantillons étaient broyés dans le Nujol et les spectres d'absorption de ces suspensions étaient enregistrés. Généralement, un grillage fin était introduit dans le faisceau de référence pour compenser l'opacité des échantillons.

Diagrammes de poudres

Tous les films de poudre ont été pris dans une caméra Debye–Scherrer (114.54 mm de diamètre) en utilisant la radiation filtrée du cuivre $\lambda CuK\bar{\alpha} = 1.5418$ Å. Les échantillons finement broyés ont été introduits dans des capillaires de quartz de 0.3 mm.

Analyses thermogravimétriques

Les analyses thermogravimétriques ont été effectuées sur des échantillons d'environ 50 mg dans un panier en aluminium. La température était controlée par un programmeur linéaire et suivie sur papier graphique par l'intermédiaire d'un thermocouple chromel–alumel avec jonction froide (0 °C) branché sur un suiveur de spot. Le poids mesuré par l'électrobalance était aussi enregistré sur le même graphique en utilisant la deuxième plume d'un "Graphispot". Le panier était enfermé dans un long tube en verre, ce qui permettait de faire des mesures sous vide. Les résultats sont représentés dans le tableau 3.

Nous remercions le Conseil National de Recherches du Canada pour l'aide financière accordée à ce travail.

1. J. C. Speckman and H. H. Mills. J. Chem. Soc. 1164 (1961).
2. R. W. Jotham, S. F. A. Kettle, and J. A. Marks. J. Chem. Soc. Dalton, 428 (1972). R. W. Jotham and S. F. A. Kettle. Inorg. Chem. **9**, 1390 (1970).
3. F. A. Cotton and J. G. Norman. J. Am. Chem. Soc. **94**, 5697 (1972); M. A. Porai-Koshits, A. S. Antsyshkina, G. G. Sadikov, and G. A. Kukina. Sov. Phys.-Cristallogr. **16**, 1047 (1972).
4. J. Lewis, F. E. Mabbs, L. K. Royston, and W. R. Smail. J. Chem. Soc. (A), 291 (1969).
5. H. D. Hardt and G. Streit. Z. Anorg. Allgem. Chem. **350**, 84 (1967).
6. K. Sawada, K. Otaki, and M. Tanaka. J. Inorg. Nucl. Chem. **34**, 625 (1972).
7. D. E. Billing, B. J. Hathaway, and P. Nicholls. J. Chem. Soc. (A), 1877 (1970).
8. D. A. Langs and C. R. Hare. Chem. Commun. 890 (1967).
9. D. Y. Jeter and W. E. Hatfield. Inorg. Chim. Acta, **6**, 523 (1972).
10. R. L. Belford, R. J. Missavage, I. C. Paul, N. D. Chasteen, W. E. Hatfield and J. F. Villa. J. Chem. Soc. (D), 508 (1971).
11. E. G. Chikryzova and E. E. Topaly. Russ. J. Inorg. Chem. **16**, 708 (1971).
12. Z. B. Bakasova, L. I. Potemko, and I. G. Druzhinin. Russ. J. Inorg. Chem. **17**, 262 (1972).
13. M. Bobtelsky and I. Bar-Gadda. Bull. Soc. Chim. Fr., 276 (1953).
14. J. Amiel. Bull. Soc. Chim. Fr. **6**, 251 (1939); J. Ploquin. Bull. Soc. Chim. Fr. 757 (1951); O. Osai, M. Kishita, and M. Kubo. J. Phys. Chem. **63**, 96 (1959).
15. B. H. O'Connor and E. N. Maslen. Acta Cryst. **20**, 824 (1966).
16. S. Gal, T. Meisel, and L. Erdey. J. Therm. Anal. **1** (2), 159 (1969).
17. K. C. Paul, G. V. Chandrashekhar, M. V. George, and C. N. R. Rao. Can. J. Chem. 257 (1968).
18. C. J. H. Schutte and K. Buijs. Spectrochim. Acta, **17**, 921, 927 (1961).
19. R. A. Zelonka and M. C. Baird. Inorg. Chem. **11**, 134 (1972).
20. L. Dubiki, C. M. Harris, E. Kokot, and R. L. Martin. Inorg. Chem. **5**, 93 (1966).

21. L. DUBIKI and R. L. MARTIN. Inorg. Chem. **5**, 2203 (1966).
22. C. OLDHAM. Prog. Inorg. Chem. **10**, 223 (1968).
23. C. G. BADIEL, C. D. CAVENDISH, and W. O. GEORGE. J. Mol. Struct. **5**, 263 (1970).
24. Y. KURODA and M. KUBO. J. Phys. Chem. **64**, 759 (1960).
25. B. S. AZIKOV, S. E. KHARZEEVA, Z. A. GRANKINA, and V. V. SEREBRENNIKOV. Chem. Abstr. **67**, 68930s.
26. YU. A. SIMONOV, A. V. ABLOV, and T. I. MALINOVSKII. Sov. Phys.-Cristallogr. **8**, 205 (1963).
27. K. ANZENHOFER and L. N. A. TEN ROUWELAAR. Rec. Trav. Chim. Pays-Bas, **86**, 801 (1967).
28. R. C. THOMPSON and D. B. W. YAWNEY. Can. J. Chem. 1240 (1965).
29. G. DAVEY and F. S. STEPHENS. J. Chem. Soc. (A), 2803 (1970); 1917 (1971).

Can. J. Chem. Downloaded from www.nrcresearchpress.com by 210.87.254.6 on 09/05/12
For personal use only.

Revised Rate Constants for Quenching Reactions of Excited CO_2^+, N_2O^+, and N_2^+

C. G. FREEMAN AND L. F. PHILLIPS

Chemistry Department, University of Canterbury, Christchurch, New Zealand

Received June 19, 1973

Data for the quenching of fluorescence excited by 58.4 nm irradiation of CO_2, N_2O, and N_2 have been recalculated in the light of improved absorption coefficients for 58.4 nm radiation. The new rate constants for quenching of CO_2^+ are in better agreement with results obtained from experiments with electron beam excitation; for N_2^+ the disagreement is greater than before.

Les données pour l'extinction de la fluorescence, induite par l'irradiation à 58.4 nm, de CO_2, N_2O et N_2 ont été recalculées en utilisant des coefficients d'absorption perfectionnés pour la radiation à 58.4 nm. Les nouvelles constantes de vitesse pour l'extinction de CO_2^+ sont en meilleur accord avec celles obtenues lors d'expériences où l'excitation est provoquée par un faisceau d'électrons. Par contre pour N_2^+ le désaccord est plus grand qu'avant. [Traduit par le journal]

Can. J. Chem., **52**, 426 (1974)

Introduction

We previously reported rate constants for quenching reactions of electronically excited ions derived from experiments in which the excitation was produced by absorption of the 58.4 nm radiation in a mixture of the parent and quencher gases (1, 2). The main problem in interpreting these results was that of properly correcting for the absorption of exciting radiation by the quencher molecules. The results were quite critically dependent upon the values assumed for absorption coefficients of parent and quencher gases at 58.4 nm, and for consistency we chose to use absorption coefficient values which had all been measured by a simple method in our own laboratory (3). The recent measurements by Starr and Loewenstein (4) indicate that our absorption coefficient data was subject to a systematic error, possibly as a result of incomplete collimation of the exciting beam. The difference between our absorption coefficients and theirs amounts to almost a constant factor, with the notable exception of the results for hydrogen. Unfortunately the results for hydrogen were deeply involved in the initial experiments by which a curve of growth was obtained for CO_2^+ emission as a function of CO_2 pressure in the cell (1). Therefore we have considered it necessary to recalculate the previous quenching results.

Results

The absorption coefficient results from refs. 3 and 4 are compared in Table 1. In the present calculations we have used the values from ref. 4. For ethane we revised the value given in ref. 3 upwards to 1720 cm^{-1}, *i.e.* by a factor which is the average of those for the other gases in the table. The recalculated quenching coefficients (calculated as described in refs. 1 and 2) are given together with those of Mackay and March (5) in Table 2.

TABLE 1. Absorption coefficients (cm^{-1} at standard temperature and pressure) for various gases at 58.4 nm

	Absorption coefficient		
Absorber	Starr and Loewenstein (4)	Bennett *et al.* (3)	Difference (%)
N_2	589 ± 30	510	+15.5
O_2	611 ± 35	520	+17.5
Ar	928 ± 48	785	+18.2
CO_2	979 ± 62	790	+23.9
CO	578 ± 51	490	+18.0
NO	691 ± 43	570	+21.2
N_2O	985 ± 62	820	+20.1
NH_3	756 ± 46	650	+16.3
CH_4	834 ± 54	660	+26.4
H_2	167 ± 8	175	−4.6
H_2S	785 ± 73	—	—
C_2H_6	—	1420	—

For N_2O^+ $A(000)$ the recalculation gives slightly lower quenching rates for all quencher gases except O_2 and Ar. (The previous values for O_2 and Ar contained numerical errors which were discovered during the present recalculations.) The lifetime of N_2O^+ $A(000)$ was taken to be 2.6×10^{-7} s (6). The estimated uncertainty of the rate constants due to errors in our

TABLE 2. Recalculated quenching rate constants in units of 10^{-9} cm^3 molecule^{-1} s^{-1}. Results of Mackay and March (5) in parentheses

Quencher	N_2^+ $B(0)$	N_2O^+ $A(000)$	CO_2^+ $B(000)$	CO_2^+ $A(300)$	CO_2^+ $A(000)$
N_2	1.1(0.58)	0.45	1.7(0.55)	1.7(0.25)	1.9
CO_2	2.2(1.0)	>0.24	1.9(1.1)	1.5(2.0)	0.42
H_2	0.56(1.16)	3.3	2.2(1.0)	2.5	3.3
O_2	1.6(0.73)	1.4	2.0(2.2)	1.8(1.4)	2.3
NO	1.6(0.76)	1.8	1.9(0.55)	1.4(0.43)	1.3_5
C_2H_6	2.6	2.3	1.8	2.1	3.7
N_2O	2.9	1.5	2.3	2.0	1.2
CO	0.43	0.86	1.9	2.1	2.6
Ar	0.46	0.80	1.6	1.6	1.7
He	<0.03	<0.03	0.5	0.16	0.1
Ne	—	—	1.0	0.22	0.06

intensity measurements is ±15% except for CO_2, for which only a lower limit is specified. To this uncertainty must be added a further ±25% which corresponds to the effect of Starr and Loewenstein's stated limits of error in the absorption coefficients at 58.4 nm. The sensitivity of the results to the values of the absorption coefficients is an unfortunate feature of our method.

For N_2^+ all of the rate constants are higher than before and in worse agreement with the results of Mackay and March (5) and of a number of other workers (7). The reason for this discrepancy remains obscure at present; possibly N_2 is more sensitive than other gases to the presence of radiation other than the 58.4 nm line in the output of our lamp and filter combination. The estimated uncertainty of the rate constants due to the intensity measurements is ±15%, except for He where it amounts to a factor of 2 in the upper limit. The rate constant for quenching by parent gas is critically dependent on the ratio of absorption coefficients of N_2 and CO_2. The lifetime value used here for N_2^+ $B(0)$ is 6.6×10^{-8}s (8, 9). (Mackay and March used 5.86×10^{-8}s.)

For CO_2^+ $B(000)$ the revised rate constants are all about 30% lower than before. The agreement with Mackay and March is thereby improved, but marked differences remain for quenching by NO, N_2, and H_2. The estimated uncertainty of the rate constant values due to the intensity measurements alone is ±25% for He, and ±15% for other quenchers. For the lifetime of the B-state of CO_2^+ we use 1.4×10^{-7}s (9–11). (Mackay and March, 1.18×10^{-7}s.)

For CO_2^+ $A(300)$ observed at 314 nm the previous values contained a numerical error; this combined with the new absorption coefficient data causes the new values to be lower by approximately a factor of 2. The values are now closer to those of Mackay and March, but there is still considerable disagreement with their results for NO and N_2. Estimated uncertainties in the rate constants are as for CO_2^+ $B(000)$. For the lifetime of the A-state of CO_2^+ we use 1.5×10^{-7}s (9–11). (Mackay and March, 1.13×10^{-7}s.)

For CO_2^+ $A(000)$ observed at 351 nm the new results are all somewhat lower than before but the difference is only about 10%. Because of the low emission intensity this upper state gives the least satisfactory Stern–Volmer plots. The estimated uncertainty of the rate constants due to our intensity measurements is a factor of 2 for He, and ±20% for the other quenchers. Our rate constants for CO_2^+ quenching are in general larger than the maximum values predicted from the Langevin formula (2). In this respect the recalculation has reduced the gap between our experiments and the theory but has not entirely eliminated it.

This work was supported by the New Zealand Universities Research Committee and by Grant AF-AFOSR-71-2134 from the United States Air Force Office of Scientific Research.

1. C. A. WINKLER, J. B. TELLINGHUISEN, and L. F. PHILLIPS. J. Chem. Soc. Faraday II. **68**, 121 (1972).
2. J. B. TELLINGHUISEN, C. A. WINKLER, C. G. FREEMAN, M. J. MCEWAN, and L. F. PHILLIPS. J. Chem. Soc. Faraday II. **68**, 833 (1972).
3. S. W. BENNETT, J. B. TELLINGHUISEN, and L. F. PHILLIPS. J. Phys. Chem. **75**, 719 (1971).
4. W. L. STARR and M. LOEWENSTEIN. J. Geophys. Res. **77**, 4790 (1972).

5. G. I. MACKAY and R. E. MARCH. Can. J. Chem. **50**, 1 (1972).
6. I. E. DAYTON, F. W. DALBY, and R. G. BENNETT. J. Chem. Phys. **33**, 179 (1960).
7. B. BROCKLEHURST and F. A. DOWNING. J. Chem. Phys. **46**, 1976 (1967); K. B. MITCHELL. J. Chem. Phys. **53**, 1795 (1970); E. J. COMES and F. SPEIER. Chem. Phys. Lett. **4**, 13 (1969).
8. R. G. BENNETT and F. W. DALBY. J. Chem. Phys. **31**, 434 (1959).
9. A. CORNEY. Adv. Electron. Electron Phys. **29**, 116 (1970).
10. J. DESESQUELLES, M. DUFAY, and M. C. POULIZAC. Phys. Lett. A, **27**, 96 (1968).
11. M. C. POULIZAC and M. DRUETTA. C. R. B, **269**, 114 (1969).

Chemical Relaxations in Aqueous Micellar Solutions by Ultrasonic Spectroscopy. I. Alkali Metal Hexyl and Octyl Sulfates

DOUGLAS A. W. ADAIR AND VINCENT C. REINSBOROUGH
Chemistry Department, Mount Allison University, Sackville, New Brunswick E0A 3C0
AND
NICK PLAVAC AND JOHN P. VALLEAU
Lash Miller Chemical Laboratories, University of Toronto, Toronto, Ontario M5S 1A1

Received June 22, 1973

Ultrasonic absorption studies have been performed in dilute micellar solutions of Li, Na, and K octylsulfates, Na methylhexylsulfate, and Na hexylsulfate at 40° by the pulse technique in the range 13–143 MHz. Chemical relaxations associated with micelle formation were found in each system. The single-valued relaxation frequencies were concentration independent in solutions as concentrated as twice the critical micelle concentration. The relaxation data can be accounted for in terms of monomer–micelle association–dissociation.

Des études d'absorption ultrasonique ont été effectuées sur des solutions micellaires diluées d'octylsulfates de Li, Na et K, de méthylhexylsulfate de Na et d'hexylsulfate de Na, à 40° par la méthode des pulsations, entre 13 et 143 MHz. Des relaxations chimiques associées à la formation de micelles ont été trouvées dans chaque système. Les fréquences de relaxation de valeur unique sont indépendantes de la concentration dans des solutions aussi concentrées que deux fois la concentration critique en micelles. Les données de relaxation peuvent être interprétées en termes d'association–dissociation monomère–micelle. [Traduit par le journal]

Can. J. Chem., **52**, 429 (1974)

Introduction

In recent years, ultrasonic absorption studies in surfactant solutions have revealed chemical relaxations associated with micelle formation (1–8). Investigators are not agreed upon the mechanism giving rise to these relaxations. The relaxation frequencies generally are less than 1 MHz and thus well below the lower limit of the pulse technique, the most accurate of the ultrasonic methods. In this study, the pulse technique was applied to micellar solutions of alkali metal octyl and hexyl sulfates which showed chemical relaxations in the appropriate range.

Experimental

Ultrasonic absorption measurements were made with the solutions thermostatted in a double-walled cell at 40.0 ± 0.2 °C using the pulse technique described previously at 13, 39, 65, 91, and 143 MHz (9, 10). This particular temperature was chosen so that comparison could be made with the critical micelle concentrations reported in the literature. The estimated error in the sound absorption measurements was less than 2% and the precision was ±1%.

Sodium hexyl and octyl sulfates were Mann Research reagents (> 99%) and were used without further purification. Sodium methylheptylsulfate, potassium and lithium octylsulfate were prepared according to Dreger and coworkers (11). After three re-crystallizations (one from butanol and two from water) the purities of the three salts were found by analysis (12) to be > 99%.

Results

Excess ultrasonic absorption could not be detected in any of the soap solutions below the critical micelle concentration (c.m.c.). However, all showed excess absorption above the c.m.c. This absorption increased linearly with the differences between the total concentration of the solutions and the c.m.c. The absorption data were fitted by a least squares method to the equation for a single relaxation where f_c is the

$$[1] \qquad \frac{\alpha}{f^2} = \frac{A}{1 + \left(\frac{f}{f_c}\right)^2} + B$$

relaxation frequency. A is related to the relaxation process while B is the absorption contribution from the background, *i.e.*, the viscous "classical absorption" and absorption due to processes with much higher relaxation frequencies.

Table 1 lists the values of f_c, A, B, the standard deviation, and the c.m.c. obtained for the surfactants, Li, Na, and K octylsulfates, Na methylheptylsulfate, and Na hexylsulfate at 40 °C. The c.m.c. values were determined from graphs such as Fig. 1 which graphically represents the concentration dependence of A and B

Can. J. Chem. Downloaded from www.nrcresearchpress.com by 210.87.254.5 on 09/05/12
For personal use only.

TABLE 1. Relaxation parameters obtained by assuming f_c to be independent of concentration

Solute	Concentration (m)	$10^{17}A$ (cm^{-1} Hz^{-2})	$10^{17}B$ (cm^{-1} Hz^{-2})	f_c (MHz)	Standard deviation $\times 10^{17}$	c.m.c. (m)
Li octylsulfate	0.1199	17.2	14.2			
	0.1350	26.0	14.7			
	0.1499	59.7	14.7	9.35	0.27	0.124
	0.2000	181	14.6			
	0.2500	273	15.3			
Na octylsulfate	0.1200	27.8	14.7			
	0.1350	90.6	14.9_5			
	0.1500	152.6	15.0	7.7	0.27	0.115
	0.2000	371	15.4			(0.13)*
	0.2500	537	16.3			
K octylsulfate	0.1200	94.0	14.3			
	0.1349	151	14.8			
	0.1500	264	14.8	6.8	0.23	0.101
	0.2000	497	15.2			
	0.2499	692	16.2			
Na methylheptylsulfate	0.1727	46.9	14.9			
	0.1803	65.8	14.9	12.7	0.22	0.157
	0.1926	87.1	15.6			(0.17)*
	0.2027	115	15.6			
Na hexylsulfate	0.4499	44.4	18.0			
	0.5000	99.4	18.5			
	0.6433	313	19.9	27.1	0.90	0.428
	0.6983	371	23.4			(0.29–0.52)†
	0.7998	483	24.5			

*Reference 13.
†Reference 14.

for the Na octylsulfate solutions. The c.m.c. was assumed to be the concentration for which A was zero. This method of defining the c.m.c. may well be the most precise method available, since the linear dependence of A in its sharp rise gives a clearly delineated origin.

The relaxation frequencies listed in Table 1 were obtained by minimizing the overall variance of the absorption data for all the micellar concentrations of a particular solute. In other words, f_c was assumed to be independent of concentration and single-valued. When the "best values" of A, B, f_c, and the standard deviations were obtained treating each concentration independently of the others, the f_c values appear somewhat scattered and A and B show a rather ragged linear concentration dependence. As an example, Table 2 notes the values obtained for Na octylsulfate solutions. Comparing these numbers with the corresponding values in Table 1 where f_c was assumed independent of concentration indicates that this assumption leads to more smoothly changing curves for A and B and to no significant increase in the overall standard deviation.

The curves that have been fitted according to the "best values" given in Table 1 for Na hexylsulfate solutions are shown in Fig. 2 along with the experimentally determined ultrasonic absorptions for each concentration. The fit is seen to be satisfactory despite the fact that most of the relaxation frequencies in Table 1 are slightly lower than the lowest observed ultrasonic frequency for 13 MHz. In other words, in these instances only the upper portion of the ultrasonic absorption curve has been observed and it is being assumed that the lower portion of the curve is given by eq. 1 with the same parameters.

Discussion

Our observations substantiate the following findings of Zana and co-workers (4–7) from ultrasonic absorption studies in other surfactant solutions:

(*a*) that the observed chemical relaxations are

Can. J. Chem. Downloaded from www.nrcresearchpress.com by 210.87.254.5 on 09/05/12
For personal use only.

TABLE 2. Values of A, B, f_c, and the standard error at 40 °C in sodium octylsulfate solutions

Concentration (m)	$10^{17}A$ (cm^{-1} Hz^{-2})	$10^{17}B$ (cm^{-1} Hz^{-2})	f_c (MHz)	Standard deviation $\times 10^{17}$
0.1350	81	14.9	8.2	0.10
0.1500	105	14.8	10.0	0.06
0.2000	289	14.9	9.1	0.40
0.2500	770	16.7	6.0	0.28

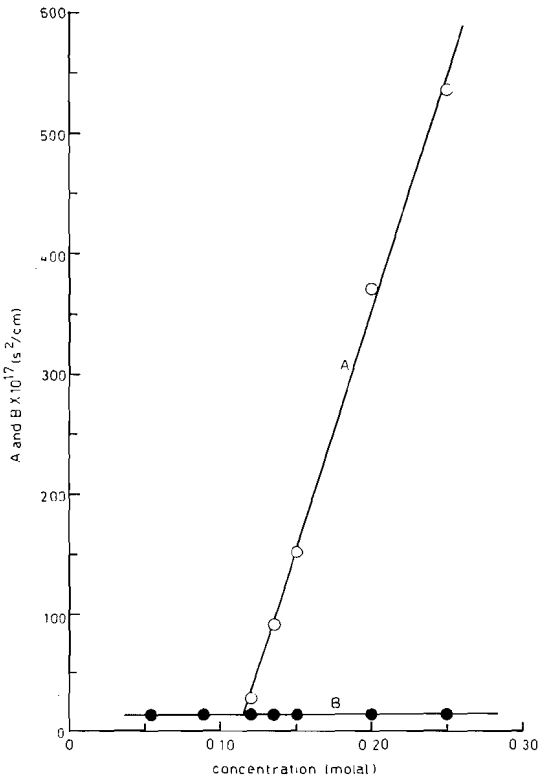

FIG. 1. A and B values for sodium octylsulfate solutions at 40 °C. Open circles are A values; closed circles, B.

associated with micellization, because only at concentrations greater than the c.m.c. were relaxations noted. Moreover, the excess absorption appeared as soon as the solute concentration exceeded the c.m.c.;

(*b*) that the counterion is likely not involved in the relaxation process in anionic surfactants (Zana and co-workers were in disagreement with Yasunaga and co-workers (1, 2) on this point). Changing the counterion from Li to Na to K in the octylsulfate series had little effect upon the relaxation frequency. In fact, the overall standard deviation was not markedly increased if a common f_c of 7.7 MHz was assigned to these three micellar systems. Doing so increased the overall standard deviation for the lithium salt by only 13%, the potassium salt by 8%, and the sodium salt by 1%;

(*c*) that the relaxation frequency is very much dependent upon the hydrocarbon chain length of the surfactant ion. Shortening the hydrocarbon chain by two methyl groups shifted the f_c from 27.1 MHz for Na hexylsulfate to 7.7 MHz for Na octylsulfate. For solutions of Na decylsulfate, no excess absorption could be detected which is an indication that any relaxation associated with micelle formation in this system must have a characteristic frequency of less than 1 MHz. Even slight branching of the hydrocarbon chain as in the Na methylheptylsulfate case had more effect than altering the counterion.

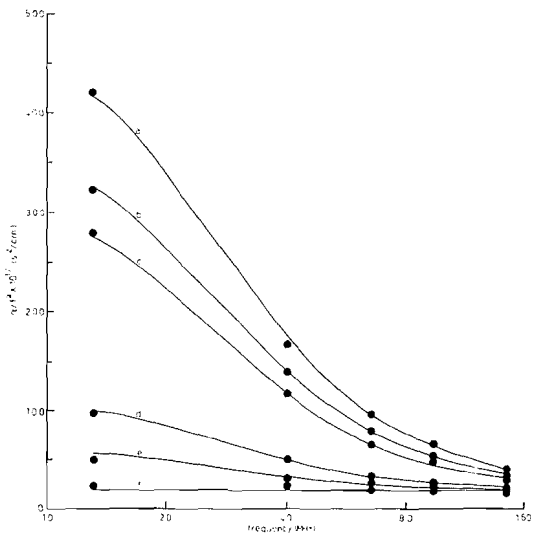

FIG. 2. Ultrasonic absorption in the 10–150 MHz range for sodium hexylsulfate solutions at 40 °C. Concentrations: *a*, 0.800 *m*; *b*, 0.698 *m*; *c*, 0.643 *m*; *d*, 0.500 *m*; *e*, 0.450 *m*; *f*, 0.396 *m*. The circles represent the experimental points while the curves have been fitted according to the single relaxation equation.

Can. J. Chem. Downloaded from www.nrcresearchpress.com by 210.87.254.5 on 09/05/12
For personal use only.

Can. J. Chem. Downloaded from www.nrcresearchpress.com by 210.87.254.5 on 09/05/12
For personal use only.

Our results depart significantly from those of previous investigators in similar systems in that the relaxation frequency in all cases was found to be independent of concentration in the dilute micellar ranges, *i.e.* from the c.m.c. to roughly twice the c.m.c. Over the same concentration range, Graber, Lang, and Zana (6) reported a three-fold linear increase in the relaxation frequency with micellar solutions of alkali metal decanoates. This is typical of the few investigations in micellar solutions reported to date. Exploratory studies in this laboratory with alkylsulfates into the higher concentration range do, however, reveal some increase in f_c with a maximum in A in solutions more concentrated than twice the c.m.c. This will be examined more closely in a later paper, but there is a distinct possibility that we are examining a different type of chemical relaxation from that encountered previously in micellar solutions.

A referee has brought to our attention a recent paper by Rassing, Sams, and Wyn-Jones (15) who employed a resonance technique to measure ultrasonic absorption in concentrated sodium octylsulfate solutions over the range 1–20 MHz. At 0.40 M, the relaxation frequency was found to be 2.1 MHz at 40 °C. The pulse apparatus in our laboratory for the same solution gave the following relaxation parameters for our absorption data: $f_c = 11.0$ MHz, $A = 524 \times 10^{-17}$, $B = 18.1 \times 10^{-17}$, and s.d. $= 0.22 \times 10^{-17}$ (α/f^2 at 13.55 MHz was 227×10^{-17}). When the absorption data were fitted to the relaxation equation with $f_c = 2.1$ MHz, unrealistic $10^{17}A$ and $10^{17}B$ values of 9 100 and 24.8 were obtained. Moreover, the standard deviation was increased 22-fold. There is no reason to suspect experimental error; the most plausible explanation is that there are in fact two relaxations corresponding to two different mechanisms. Each technique is limited by its operating frequency range in bringing both relaxations under full display.

The model giving rise to the relaxation observed in the present study must predict a single, concentration-invariant relaxation frequency. Suppose that the chemical relaxation was associated with one of the stepwise equilibria involved in micelle formation

$$[2] \qquad \mathrm{m} + \mathrm{M}_n \underset{k_d}{\overset{k_a}{\rightleftharpoons}} \mathrm{M}_{n+1}$$

where m represents the monomeric surfactant ion, and M_n and M_{n+1} represent the micelles formed from n and $(n + 1)$ monomers respectively. For a single such reaction, it can be shown (16) that

$$[3] \qquad 2\pi f_c = k_d + k_a([\mathrm{m}] + [\mathrm{M}_n])$$

In dilute micellar solutions with n large and the c.m.c. approximating the monomer concentration, this equation simplifies to

$$[4] \qquad 2\pi f_c \cong k_d + k_a \text{ c.m.c.}$$

which predicts the concentration independent f_c found experimentally.

It is, of course, possible that several different micelle formation steps, corresponding to differing values of n, may take part in the absorption. However, it will be dominated by processes for which there are high concentrations of micelles and $[\mathrm{M}_n] \simeq [\mathrm{M}_{n+1}]$. The separate rate constants can be estimated on this assumption for which the association constant $Q \simeq \text{c.m.c.}^{-1}$ (3). Equation 4 then reduces to $k_a \simeq \pi f_c/\text{c.m.c.}$ The resulting approximate values of k_a, k_d, and Q are given in Table 3 for the five micellar systems.

The forward reaction rate is remarkably constant over the five systems. This suggests, at first hand, that the monomer–micelle association process is largely diffusion controlled. Diffusion coefficients calculated from these rate constants using Smoluchowski's expression are approximately 10^{-4} cm^2 s^{-1}. Lindman and Brun (17) obtained the self diffusion coefficient for the closely related octanoate ion in sodium octanoate solutions as 0.7×10^{-5} cm^2 s^{-1} at 25°. The assumption is then reasonable when the higher temperature of the present work and the approximate nature of Smoluchowski's expression are taken into account.

The formation constants are a relative measure of the stability of the micelles in each system. Sodium hexylsulfate micelles are seen to be the least stable. The C_6 member is generally considered the shortest chained surfactant to show clearly discernible micellization. The lower overall standard deviation obtained with this system when the data were fitted to the curve for a single relaxation indicates that the approximations are beginning to fail slightly.

An alternative treatment of ultrasonic relaxation in micelle systems was proposed by Sams, Wyn-Jones, and Rassing (8); it leads to quite

TABLE 3. Approximate rate constants and equilibrium constants for micelle formation in some alkali metal alkylsulfate solutions at 40°

Solute	$10^{-7}k_a$ (kg mol^{-1} s^{-1})	$10^{-7}k_d$ (s^{-1})	Q (kg mol^{-1})
K octylsulfate	21	2.2	10
Na octylsulfate	21	2.4	9
Li octylsulfate	23	2.9	8
Na methylheptylsulfate	21	3.1	7
Na hexylsulfate	20	8.5	2

different predictions. Both treatments assume a hierarchy of micelle growth steps, like [2], are responsible for the sound absorption. However, it is not possible to cope with the analysis of several interacting steps having arbitrary kinetic parameters, nor could we hope to extract detailed information on them from the rather straightforward, uncomplicated experimental results. The two treatments attempt to approximate the situation using a restricted set of parameters, but they do this in quite different ways. The treatment outlined above notes that the ultrasonic absorption is likely to be dominated by a small number of steps near the mean micelle size, and to approximate the absorption as being by a single such step. The theory of Sams, Wyn-Jones, and Rassing, on the contrary, includes an infinite hierarchy of such steps but makes arbitrary assumptions concerning the rate constants, to enable a simple summation of the many steps. It leads to a relaxation frequency that is a linear function of the total concentration, a result actually observed for certain systems (1, 2, 4, 6), but the assumptions are open to question. It is difficult to reconcile micelle formation with a kinetic scheme in which the association constants for successive steps become asymptotically constant with increasing n. There is then no monomer concentration which gives rise to a micelle of finite size. Further studies on more concentrated micellar solutions are now being pursued in this laboratory to obtain a suitable model.

Financial support of this work came from the National Research Council of Canada.

1. T. YASUNAGA, H. OGURI, and M. MIURA. J. Colloid Interface Sci. **23**, 352 (1967).
2. T. YASUNAGA, S. FUJII, and M. MIURA. J. Colloid Interface Sci. **30**, 399 (1969).
3. V. C. REINSBOROUGH and J. P. VALLEAU. Aust. J. Chem. **21**, 2905 (1968).
4. R. ZANA and J. LANG. C. R. Acad. Sc. Paris, Ser. C. **266**, 893 (1968).
5. R. ZANA and J. LANG. C. R. Acad. Sc. Paris, Ser. C. **266**, 1347 (1968).
6. E. GRABER, J. LANG, and R. ZANA. Kolloid Z. Z. Polym. **238**, 470 (1970).
7. E. GRABER and R. ZANA. Kolloid Z. Z. Polym. **238**, 479 (1970).
8. P. J. SAMS, E. WYN-JONES, and J. RASSING. Chem. Phys. Lett. **13**, 233 (1972).
9. J. P. VALLEAU and S. J. TURNER. Can. J. Chem. **42**, 1186 (1964).
10. S. C. CHAN and J. P. VALLEAU. Can. J. Chem. **46**, 853 (1968).
11. E. E. DREGER, G. I. KEIM, G. D. MILES, L. SHEDLOVSKY, and J. ROSS. Ind. Eng. Chem. **36**, 610 (1944).
12. S. R. EPTON. Trans. Faraday Soc. **44**, 226 (1948).
13. K. SHINODA, T. NAKAGAWA, B. TAMAMUSHI, and T. ISEMURA. Colloidal surfactants. Academic Press, New York. 1963. p. 48.
14. M. RAISON. Mem. Serv. Chim. Etat (Paris), **39**, 291 (1954).
15. J. RASSING, P. J. SAMS, and E. WYN-JONES. J. Chem. Soc. Faraday II, **69**, 180 (1973).
16. M. EIGEN and L. DE MAEYER. Technique of organic chemistry. *Edited by* S. L. Friess, E. S. Lewis, and A. Weissberger. Vol. 8, Part 2. Interscience, New York. 1963. p. 901.
17. B. LINDMAN and B. BRUN. J. Colloid and Interface Sci. **42**, 388 (1973).

Can. J. Chem. Downloaded from www.nrcresearchpress.com by 210.87.254.5 on 09/05/12
For personal use only.

Microwave Spectrum of *N*-Methyl Morpholine

S. C. Dass and R. Kewley

Department of Chemistry, Queen's University, Kingston, Ontario

Received September 6, 1973

The microwave spectrum of *N*-methyl morpholine has been investigated within the 8 to 40 GHz region. The observed rotational constants for the ground vibrational state are (in MHz), $A = 4821.235(0.077)$, $B = 2342.579(0.004)$, and $C = 1719.452(0.003)$. The dipole moment components have been determined as (in D), $\mu_a = 1.21(0.02)$, $\mu_c = 0.10(0.03)$, and $\mu = 1.21(0.02)$. The values of these parameters show that the observed spectrum is due to the chair form with an equatorial methyl group. The ^{14}N nuclear quadrupole coupling constants have the values (in MHz), $\chi_{aa} = 2.4(0.1)$, $\chi_{bb} = 2.6(0.3)$ and $\chi_{cc} = -5.0(0.2)$. Sets of rotational transitions due to six excited vibrational states have also been assigned.

Le spectre microonde de la *N*-méthylmorpholine a été étudié dans la région allant de 8 à 40 GHz. Les constantes de rotation observées pour l'état de vibration fondamental sont (en MHz). $A = 4821.235(0.077)$, $B = 2342.579(0.004)$ et $C = 1719.452(0.003)$. Les composantes du moment dipolaire correspondent à (en D), $\mu_a = 1.21(0.02)$, $\mu_c = 0.10(0.03)$ et $\mu = 1.21(0.02)$. Les valeurs de ces paramètres montrent que le spectre observé correspond à celui de la forme chaise avec le groupe méthyle en position équatoriale. Les constantes de couplage du quadrupole nucléaire ^{14}N correspondent (en MHz) à $\chi_{aa} = 2.4(0.1)$, $\chi_{bb} = 2.6(0.3)$, et $\chi_{cc} = -5.0(0.2)$. On a aussi attribué à six états excités de vibration des séries de transitions de rotation. [Traduit par le journal]

Can. J. Chem., **52**, 434 (1974)

Introduction

The microwave spectra of a number of unsubstituted six-membered ring compounds have been studied recently. For example tetrahydropyran (1), morpholine (2), and 1,3-dioxane (3) were investigated in this laboratory. In each case the observed spectrum was assigned to the chair conformer. For a substituted chair form different isomeric forms are possible due to the axial and equatorial substituent positions. This has been observed by microwave spectroscopy for the F substituent of cyclohexyl fluoride (4) and the NH hydrogen of piperidine (5). Intensity measurements have shown the equatorial form to be more stable, by 259 ± 25 cal mol^{-1} and 248 ± 150 cal mol^{-1} in cyclohexyl fluoride (6) and piperidine (5), respectively. For morpholine only the spectrum of the equatorial form was detected, probably due to the difficulty encountered in assigning the axial NH spectrum.

From a theoretical study and from dipole moment measurements Allinger and co-workers (7, 8) concluded that the methyl group in *N*-methyl piperidine should strongly prefer the equatorial position and also that the NH hydrogen of piperidine might prefer to be either axial or equatorial, since the energy difference between the two arrangements should not be very large. The observed infrared and Raman spectra and vibrational frequencies calculated by Anisimova and Pentin (9) showed that the spectra of gaseous, liquid, and solid *N*-methyl piperidine can be correctly interpreted on the basis of the presence of only the equatorial conformer.

No structural data were found in the literature for *N*-methyl morpholine. Three n.m.r. studies by Harris and Spragg (10) gave no conclusive evidence for the conformation. The present investigations on *N*-methyl morpholine were therefore undertaken to confirm the orientation of the methyl group with respect to the ring. An additional feature of interest in the molecule is the possibility of studying the rotation of the methyl group, which has not been done in previous microwave studies of six-membered ring compounds.

Experimental

The sample of *N*-methyl morpholine was purchased from the Aldrich Chemical Company and was used without further purification. Initially the region 26.5–40 GHz was recorded with a Hewlett–Packard Model 8460A MRR Spectrometer at Rice University. Further work, in the 8–30 GHz region, was done with a conventional 100 kHz Stark modulation spectrometer with oscilloscope display (1, 3). The spectrum was observed at room temperature and with sample pressures in the range about 10–100 Torr. The accuracy of measurement for the Hewlett–Packard spectrometer is better than 0.05 MHz whereas for the 100 kHz Stark modulation instrument the accuracy is about ± 0.2 MHz.

A Perkin–Elmer model 180 spectrometer was used to record the gas phase infrared spectrum. A 10 cm metal

Can. J. Chem. Downloaded from www.nrcresearchpress.com by 210.87.254.40 on 09/05/12
For personal use only.

TABLE 1. Rotational constants of *N*-methyl morpholine in the ground vibrational state

	A (MHz)	*B* (MHz)	*C* (MHz)	κ (asymmetry parameter)
Observed*	4 821.235±0.077	2 342.579±0.004	1 719.452±0.003	−0.598212
Calculated†				
Equatorial Me	4 874.70	2 352.37	1 736.18	−0.607332
Axial Me	3 903.15	2 862.93	2 226.64	−0.240942

*Uncertainties quoted are one standard error in quantity.
†Assumed structure for calculated values: C—O = 1.410 Å, C—C = 1.533 Å, C—N = 1.470 Å, C—H = 1.108 Å. ∠COC = 111.7°, ∠CNC = 110.0°, all C tetrahedral, chair form.

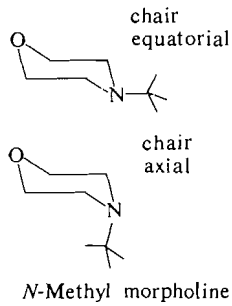

FIG. 1. Chair equatorial and chair axial conformers of *N*-methyl morpholine.

cell with polyethylene windows was used to record the spectrum below 650 cm^{-1}.

Microwave Spectrum

Ground Vibrational State

Figure 1 shows the chair equatorial and chair axial forms of *N*-methyl morpholine. For both conformers the *a*-axis is calculated to pass close to the N and O atoms, the *b*-axis being perpendicular to the symmetry plane so that no *b*-type transitions are expected. In the equatorial form the *a*-component of the dipole moment should be appreciably larger than the *c*-component, while in the axial form the *c*-component is expected to be rather larger than the *a*-component.

N-Methyl morpholine was found to have a fairly rich spectrum. It was quite easy to pick out the pairs of strong transitions of the type $J_{0,J} \rightarrow J + 1_{0,J+1}$ and $J_{1,J} \rightarrow J + 1_{1,J+1}$ for $J = 7$, 8, 9, and 10 on a 26.5 to 40 GHz scan, at a Stark field of 1100 V cm^{-1}. The assignment of other *a*-type R-branch lines was then accomplished giving a total of 65 rotational transitions assigned in the 11 to 40 GHz region.[1] The rotational constants derived from a least squares fit are given in Table 1. Also given in Table 1 are rotational constants calculated from assumed structures. It is quite clear that the assigned lines are due to the equatorial form. Although a number of *c*-type lines were searched for at their predicted frequencies none were found, indicating a small μ_c dipole component.

Attempts were made to locate lines which might be due to the axial methyl conformer. However there appeared to be too few additional lines beyond those of the equatorial form for an axial assignment to be made. This indicates that the proportion of axial conformer must be small. No serious attempts were made to find lines of boat conformers in view of their absence in all previous similar molecules studied by microwave spectroscopy.

^{14}N Quadrupole Coupling

The effect of ^{14}N quadrupole splitting in *N*-methyl morpholine was found to be very small for the observed R-branch lines, completely unresolved in most cases. Two hyperfine peaks were seen for each of fourteen transitions. One of the peaks is due to the $F = J \rightarrow J + 1$ hyperfine component and the other to the two unresolved components $F = J - 1 \rightarrow J$ and $F = J + 1 \rightarrow J + 2$. The observed splittings and the derived quadrupole coupling constants are given in Table 2. The diagonal elements of the ^{14}N quadrupole tensor, referred to the principal inertial axes of the molecule, were calculated by the procedure described in ref. 2.

The nuclear quadrupole coupling constants are similar in value to those measured for morpholine (2): $\chi_{aa} = 2.22$ MHz, $\chi_{bb} = 2.51$ MHz, and $\chi_{cc} = -4.73$ MHz. A direct comparison between the two sets of constants may be made because the angle between the bond axis, N—H or N—CH_3, and the principal *a*-axis changes only by about 2° between the two

[1]Photocopies of the tables of observed transition frequencies for the ground and excited states of *N*-methyl morpholine may be obtained from the Depository of Unpublished Data, National Science Library, National Research Council of Canada, Ottawa, Canada K1A 0S2.

Can. J. Chem. Downloaded from www.nrcresearchpress.com by 210.87.254.40 on 09/05/12
For personal use only.

TABLE 2. ^{14}N nuclear quadrupole hyperfine doublet splittings and coupling constants for *N*-methyl morpholine

	ν_{obsd} (MHz)			
$J_{K_{-1}K_1} \rightarrow J+1_{K'_{-1}K_1'}$	$F = J-1 \rightarrow J$ and $F = J+1 \rightarrow J+2$	$F = J \rightarrow J+1$	$\Delta\nu_{obsd}$ (MHz)	$\Delta\nu_{obsd} - \Delta\nu_{calcd}$ (MHz)
$6_{15} \rightarrow 7_{16}$	28 724.62	28 724.99	0.37	−0.02
$6_{34} \rightarrow 7_{35}$	28 771.87	28 772.05	0.18	0.02
$6_{51} \rightarrow 7_{52}$	28 808.61	28 808.93	0.32	0.00
$6_{52} \rightarrow 7_{53}$	28 804.75	28 805.06	0.31	0.01
$6_{60} \rightarrow 7_{61}$	28 727.43	28 727.88	0.45	−0.05
$6_{61} \rightarrow 7_{62}$	28 727.43	28 727.88	0.45	−0.05
$7_{16} \rightarrow 8_{17}$	32 132.48	32 132.84	0.36	−0.01
$7_{53} \rightarrow 8_{54}$	33 003.52	33 003.69	0.17	−0.03
$7_{70} \rightarrow 8_{71}$	32 821.80	32 822.33	0.53	0.07
$7_{71} \rightarrow 8_{72}$	32 821.80	32 822.33	0.53	0.07
$8_{17} \rightarrow 9_{18}$	35 456.14	35 456.51	0.37	0.06
$8_{26} \rightarrow 9_{27}$	38 523.08	38 523.34	0.26	0.01
$8_{27} \rightarrow 9_{28}$	34 927.27	34 927.42	0.16	−0.02
$9_{18} \rightarrow 10_{19}$	38 779.17	38 779.38	0.21	−0.04

Coupling constants (MHz)	
χ_{aa} =	2.4±0.1
χ_{bb} =	2.6±0.3
χ_{cc} =	−5.0±0.2

TABLE 3. Stark effect coefficients and dipole moment components of *N*-methyl morpholine

		$10^6 \times \Delta\nu/E^2$ (MHz cm^2 V^{-2})	
Transition	*M*	Observed	Calculated
$2_{11} \rightarrow 3_{12}$	1	−4.60	−4.41
$2_{11} \rightarrow 3_{12}$	2	−16.3	−15.8
$3_{13} \rightarrow 4_{14}$	1	0.238	0.284
$3_{13} \rightarrow 4_{14}$	2	2.40	2.81
$3_{03} \rightarrow 4_{04}$	3	2.05	2.18
$4_{14} \rightarrow 5_{15}$	2	0.739	0.619
$4_{14} \rightarrow 5_{15}$	3	1.71	1.80

Dipole component	Value (D)
μ_a	1.21±0.02
μ_c	0.10±0.03
μ	1.21±0.02

molecules. The coupling constants are slightly larger in *N*-methyl morpholine, which parallels the increase from NH_3, $eqQ = -4.08$ MHz (11), to $N(CH_3)_3$, $eqQ = -5.47$ MHz (12).

Dipole Moment

A confirmatory piece of evidence for the equatorial conformer comes from the dipole moment components of the molecule. The Stark coefficients were determined from the linear plots of Stark shift against the square of the applied field, using fields up to 3800 V cm^{-1}. The dipole components were found from a least squares fitting procedure to the coefficients, giving each coefficient equal weight. The results are summarized in Table 3. The μ_c was less well determined since most of the Stark coefficients are fairly insensitive to this component. μ_b was assumed to be zero. As expected μ_a was found to be considerably larger than μ_c, confirming the equatorial form. The value of the total dipole moment is close to the solution values, see below, which were considered to be consistent with 98% abundance of the equatorial form (13). The Stark cell was calibrated on the basis of μ_{OCS} = 0.71512 ± 0.00003 D (14).

It is interesting to compare the dipole moments of the following molecules (references in parentheses):

	Dipole moment (D)	
Molecule	Microwave	Solution
1 Morpholine	1.55 (2)	1.54–1.56 (13)
2 *N*-Methyl morpholine	1.21 (This work)	1.29–1.36 (13)
3 Piperidine	0.80 (5)	1.16 (8), 1.19 (15)
4 *N*-Methyl piperidine	—	0.95 (8)

The microwave values for **1** and **2** solution

Can. J. Chem. Downloaded from www.nrcresearchpress.com by 210.87.254.40 on 09/05/12
For personal use only.

TABLE 4. Ground and excited states of *N*-methyl morpholine

State	*A* (MHz)	*B* (MHz)	*C* (MHz)	Δ_c(a.m.u. Å^2)	ν (cm^{-1}) Microwave	ν (cm^{-1}) Infrared*
Ground	4 821.235	2 342.579	1 719.452	−26.642†	—	—
e.s. 1	4 804.77	2 343.38	1 720.15	−27.046	180 ± 10	176 m
2	4 820.30	2 340.21	1 718.56	−26.728	226 ± 10	225 vvw
3	4 820.96	2 340.90	1 718.06	−26.564	267 ± 10	252 vw
4	4 792.75	2 343.91	1 720.33	−27.291	270 ± 15	274 w, br
5	4 806.66	2 341.10	1 719.12	−27.038	357 ± 25	332 s
6	4 804.60	2 341.66	1 718.68	−26.956	361 ± 25	332 s

Additional infrared frequencies (cm^{-1}): 418 w, 435 w, 496 w, 550 w, br, 620 s.

*w = weak, m = medium, s = strong, br = broad, v = very.
†$\Delta_c = I_c - I_a - I_b$; conversion factor 505377 a.m.u. Å^2.

values for **3** and **4** indicate that the dipole moment decreases by about 0.3 D when the H at N is replaced by a CH_3 group. But the microwave value for **3** compared with solution value of **4** indicates an increase. However the value reported by Buckley, Costain, and Parkin (5) for **3** was not obtained by direct measurements, and is considerably smaller than the value in solution. The above comparison shows that the solution values for piperidine are more likely correct than the value reported by Buckley, Costain, and Parkin.

Excited Vibrational States

In addition to the ground state lines, a number of satellite lines were found on both the high and low frequency sides. A total of six vibrational states were identified. The rotational constants given in Table 4 were derived from the frequencies of assigned *R*-branch lines.[2] The corresponding vibrational frequencies were estimated on the basis of relative intensities of several lines for each state. The frequencies are between 180 and 361 cm^{-1}, see Table 4. The methyl torsion and six ring deformation frequencies are expected to fall below 700 cm^{-1}.

The ground state lines are not split by the internal rotation of the methyl group, indicating a high barrier to rotation. For the pair of ground state transitions $10_{1,10} \rightarrow 11_{1,11}$ and $10_{0,10} \rightarrow 11_{0,11}$, there were four satellite lines on the higher frequency side, see Fig. 2. Their spacing are such that for some time it was thought that these doublet lines were the *A* and *E* components of the first excited state of methyl torsion. A considerable amount of time was spent trying to calculate the barrier height from these split-

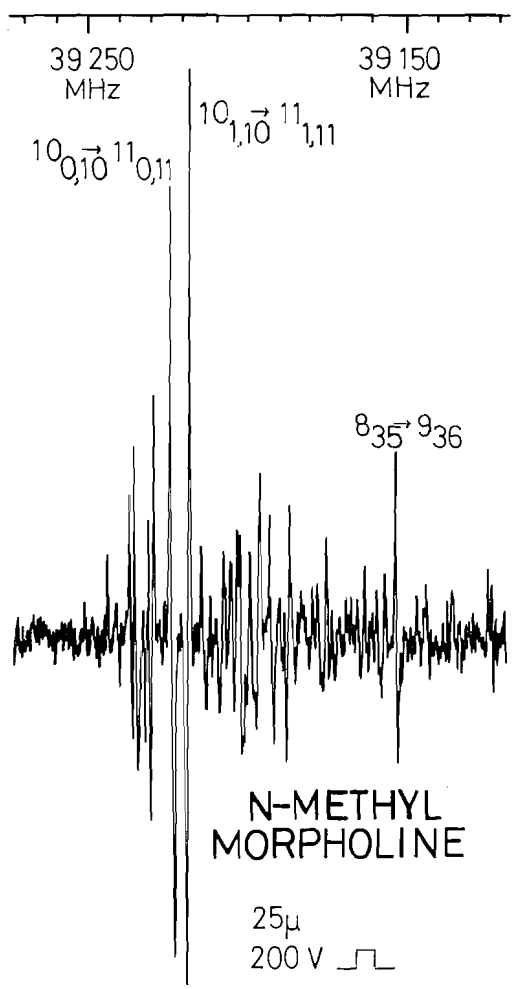

FIG. 2. Vibrational satellite pattern associated with the $10_{0,10} \rightarrow 11_{0,11}$ and $10_{1,10} \rightarrow 11_{1,11}$ transitions of *N*-methyl morpholine. The doublet lines on the high frequency side are accidental, being due to two ring deformation modes. The methyl torsion satellites are amongst the group of lines on the low frequency side.

[2]Frequencies available on request. See footnote 1 for details.

Can. J. Chem. Downloaded from www.nrcresearchpress.com by 210.87.254.40 on 09/05/12
For personal use only.

Can. J. Chem. Downloaded from www.nrcresearchpress.com by 210.87.254.40 on 09/05/12
For personal use only.

tings. However the observed pattern could not be made to fit with calculation, even after taking into account first order perturbation coefficients, which are important in the case of asymmetry near degeneracy. Theory described in refs. 16 and 17 was used in the calculations. In addition the A and E lines should have the same intensity for a CH_3 group while Fig. 2 shows that there is some difference in intensity between the "doublet" members. Therefore we conclude that these lines belong to two ring deformation modes rather than methyl torsion.

The infrared and Raman spectra of N-methyl morpholine were not found in the literature for frequencies below 700 cm^{-1}. The gas phase infrared spectrum was therefore recorded between 150 cm^{-1} and 700 cm^{-1}. The observed band frequencies are given in Table 4 for comparison with the frequencies obtained from relative intensity measurements on the microwave lines. Fairly good agreement was found between the two sets of data. It may be noted that the lowest frequency ring deformation mode was assigned to be 200 $\pm$ 50 cm^{-1} (2) and 171 cm^{-1} (18) in morpholine, 178 cm^{-1} in N-methyl piperidine (9) and 165 cm^{-1} in methyl cyclohexane (19, 20). The next higher band, 245 cm^{-1} in N-methyl piperidine (9) and 237 cm^{-1} in methyl cyclohexane (19, 20), was assigned to methyl torsion. Therefore it seems appropriate, for N-methyl morpholine, to assign the lowest band, at 176 cm^{-1}, to a ring deformation mode.

In view of the methyl torsion assignment, 245 cm^{-1}, in N-methyl piperidine (9) the likely possibilities for assignment to this mode in N-methyl morpholine are the frequencies 226, 267, and 270 cm^{-1}, see Table 4. If Δ is the moment of inertia difference, it is expected that the quantity $\Delta_c = I_c - I_a - I_b$ should undergo only a slight change when methyl torsion is excited, with larger changes usually occurring for excitation of ring deformation modes. Examination of the moments of inertia of a number of other molecules in which the methyl carbon lies in a molecular symmetry plane leads to the conclusion that the change in Δ_c is in fact small, and usually negative. For example the first excited torsional state of N-methyl ethyleneimine (21) has $\delta(\Delta_c) = -0.224$ a.m.u. Å^2 relative to the ground state (where $\varepsilon(\Delta)$ = change in Δ_c). On this basis the 270 cm^{-1} vibration, with $(\Delta_c) = -0.649$ a.m.u.Å^2 can probably be ruled out as the torsional mode. We shall therefore just consider the 226 cm^{-1} and 267 cm^{-1} frequencies. For each of these frequencies the corresponding s value has been calculated, with the aid of tabulated Mathieu eigenvalues (22), and the threefold barrier evaluated from the expression $V_3 = s \times F/4.6602$. F was calculated from the assumed structure as 163.616 GHz, with I_{CH_3} assumed as 3.200 a.m.u. Å^2. The results of these calculations are:

$\nu(cm^{-1})$	$\delta(\Delta_c)$ a.m.u. Å^2	s	V_3 (cal mol^{-1})
226	−0.086	98	3440 ± 150
267	+0.078	130	4560 ± 250

The first V_3 value is close to the values 3462 $\pm$ 35 cal mol^{-1} for N-methyl ethyleneimine (21) and 3434 $\pm$ 40 cal mol^{-1} for dimethylamine (23). On the other hand the second value is close to that for trimethylamine, which is 4400 cal mol^{-1} (12). The latter molecule appears to be structurally the most similar to N-methyl morpholine so perhaps the higher V_3 value should be preferred. A definite decision between the two values cannot be made with certainty from the present data. To decide the issue a microwave study of CD_3 N-methyl morpholine would be valuable.

The authors would like to express their thanks to Dr. R. F. Curl of Rice University, Houston, Texas for the use of the Hewlett-Packard spectrometer in the initial stages of this investigation. They would also like to thank Dr. H. Dreizler for a valuable discussion of internal rotation. Support for the initial part of the work was provided by grant number GP 29374 from the National Science Foundation, U.S.A. The later stages of the study were supported by grant A-2046 from the National Research Council of Canada.

1. V. M. Rao and R. Kewley. Can. J. Chem. **47**, 1289 (1969).
2. J. J. Sloan and R. Kewley. Can. J. Chem. **47**, 3453 (1969).
3. R. Kewley. Can. J. Chem. **50**, 1690 (1972).
4. L. Pierce and R. Nelson. J. Am. Chem. Soc. **88**, 216 (1966); L. Pierce and J. F. Beecher. J. Am. Chem. Soc. **88**, 5406 (1966).
5. P. J. Buckley, C. C. Costain, and J. E. Parkin. Chem. Commun. 668 (1968).
6. L. H. Scharpen. Symposium on molecular structure and spectroscopy. Columbus, Ohio. 1968. Paper N2.
7. N. L. Allinger and J. C. Tai. J. Am. Chem. Soc. **87**, 1227 (1965).
8. N. L. Allinger, J. G. D. Carpenter, and F. M. Karkowski. J. Am. Chem. Soc. **87**, 1232 (1965).
9. O. S. Anisimova and Yu. A. Pentin. Vestrik Moskovskago Universiteta. Kihimiya, **24**, 7 (1969).
10. R. K. Harris and R. A. Spragg. Chem. Commun. 314 (1966); J. Chem. Soc. B, 684 (1968); 1128 (1968).

11. G. R. GUNTHER-MOHR, R. L. WHITE, A. L. SCHAWLOW, W. E. GOOD, and D. K. COLES. Phys. Rev. **94**, 1184 (1954).
12. D. R. LIDE and D. E. MANN. J. Chem. Phys. **28**, 572 (1958).
13. M. J. ARONEY, C. Y. CHEN, R. J. W. LEFÈVRE, and J. D. SAXBY. J. Chem. Soc. 4269 (1964).
14. F. H. DE LEEUW and A. DYMANUS. Chem. Phys. Lett. **7**, 288 (1970).
15. M. J. ARONEY and R. J. W. LEFÈVRE. J. Chem. Soc. 3002 (1958).
16. D. R. HERSCHBACH. J. Chem. Phys. **31**, 91 (1959).
17. V. DOBYNS. J. Chem. Phys. **43**, 4534 (1965).
18. L. MÉDARD. J. Chim. Phys. **33**, 626 (1936); R. A. FRIEDEL and D. S. MCKINNEY. J. Am. Chem. Soc. **69**, 604 (1947).
19. U. A. ZIRNIT and M. M. SUSHCHINSKII. Opt. i spektr. **15**, (2), 180 (1963).
20. G. N. ZHIZHIN and KH.E. STERIN. Zhurnal Prikladnoi Spektroskopii (J. Appl. Spect., Engl. transl.). **5**, (4), 506 (1966).
21. M. D. HARMONY and M. SANCHO. J. Chem. Phys. **47**, 1911 (1967).
22. E. O. STEJSKAL and H. S. GUTOWSKY. J. Chem. Phys. **28**, 388 (1958); D. R. HERSCHBACH. Tables for the internal rotation problem. Department of Chemistry, Harvard University. 1957.
23. J. E. WOLLRAB. Ph.D. Thesis. Stanford University, 1965.

Can. J. Chem. Downloaded from www.nrcresearchpress.com by 210.87.254.40 on 09/05/12
For personal use only.

Electron Mobilities and Ranges in Liquid C_1–C_3 Hydrocarbons and in Xenon: Effects of Temperature and Field Strength[1]

MAURICE G. ROBINSON AND GORDON R. FREEMAN

Chemistry Department, University of Alberta, Edmonton, Alberta, T6G 2G2

Received August 10, 1973

Electron mobilities were measured in ethane, ethylene, propane, cyclopropane, and propylene to complete the studies of the lower hydrocarbons. The effect of temperature on the mobilities in these liquids and in methane, *n*-butane, and xenon were also measured. Examples of the data are given in the order mobility (cm^2/Vs), temperature (K), Arrhenius temperature coefficient (kcal/mol): methane, 430, 140, −0.16; ethane, 0.97, 200, ~3; ethylene, 0.0030, 170, —; propane, 0.55, 238, ~3; *n*-butane, 0.073, 250, ~4; cyclopropane, 0.0043, 234, ~4; propylene, 0.008, 234, ~4; xenon, ~1200 at 40 V/cm, 198, 0. The mobilities in the C_2–C_4 hydrocarbons are independent of applied electric field strength E up to 20 kV/cm; that in methane is independent of E up to 2 kV/cm; that in xenon decreases as $E^{-1/2}$ between 33 and 300 V/cm and decreases slightly more rapidly at higher field strengths. The density-normalized ranges of the secondary electrons in each of the liquids is independent of temperature. The correlation between the ranges of the secondary electrons and the mobilities of thermal electrons observed in other liquids (ref. 2) persists for the simple hydrocarbons.

Les mobilités électroniques, u_e, dans les hydrocarbures liquides ont été mesurées pour l'éthane, l'éthylène, le propane, le cyclopropane, et le propylène. L'effet de la température sur les mobilités dans le méthane, le *n*-butane, et le xénon a également été mesuré. La mobilité (cm^2/Vs) à une certaine température (K), et le coefficient d'Arrhenius (kcal/mol) sont respectivement pour le méthane, 430, 140, −0.16; l'éthane, 0.97, 200, ~3; l'éthylène, 0.0030, 170, —; le propane, 0.55, 238, ~3; le cyclopropane, 0.0043, 234, ~4; le *n*-butane, 0.073, 250, ~4; et le xénon, ~1200 à 40 V/cm, 198, 0. Dans les hydrocarbures C_2–C_4, la valeur de u_e est indépendante de la valeur du champ électrique E jusqu'à 20 kV/cm; dans le méthane u_e est indépendante de E jusqu'à 2 kV/cm; dans le xénon $u_e \propto E^{-1/2}$ pour $33 \leqslant E \leqslant 300$ V/cm. Le parcours des électrons secondaires produits lors de l'irradiation d'un liquide donné, normalisé pour sa densité, est indépendant de la température. La corrélation qui existe pour plusieurs liquides entre le parcours des électrons secondaires et la mobilité des électrons thermiques (ref. 2) est également valable pour les hydrocarbures C_1–C_4.

Can. J. Chem., **52**, 440 (1974)

Introduction

The penetration ranges of low energy (~10 eV) electrons into the simplest liquid hydrocarbons, C_1 to C_3, have recently been estimated (1). The density-normalized range *bd* was related to the degree of sphericity and isotropy of polarizability of the molecules. It has since been shown that there is also a correlation between the mobility of thermal electrons and the penetration range of low energy electrons in a given liquid (2); electron ranges are large in liquids in which the mobilities are high, and vice versa. As the electron mobilities in the C_2 and C_3 hydrocarbons have not yet been reported, it was of interest to make these measurements and test the correlation. Of particular interest with regard to the correlation is the large difference between the electron ranges in methane and ethane (1).

The Arrhenius temperature coefficient E_u for electron mobility in liquid hydrocarbons is inversely related to the magnitude of the mobility, being near zero for high mobilities and near 4 kcal/mol for low mobilities (2–4). Electrons in methane (5, 6), argon (7–9), krypton (7, 8), and xenon (8, 10) have very high mobilities, and since unusual temperature effects had been noted in argon (7, 9) and krypton (7), it was of interest to measure the effect of temperature on electron mobilities in methane and xenon. Measurements were made in the other hydrocarbons to complete the series of C_1 to C_3 molecules.

Experimental

Materials and Purification

Ethane, propane, butane, and propylene were obtained from Phillips Petroleum, while methane, xenon, and cyclopropane were from Matheson, Linde, and Ohio Chemical respectively. The gases were Research Grade with the exception of cyclopropane.

The C_2, C_3, and C_4 hydrocarbons were introduced

[1]Supported by the National Research Council of Canada.

Can. J. Chem. Downloaded from www.nrcresearchpress.com by 210.87.254.6 on 09/05/12
For personal use only.

Can. J. Chem. Downloaded from www.nrcresearchpress.com by 210.87.254.6 on 09/05/12
For personal use only.

into a high vacuum system, previously evacuated to $< 10^{-6}$ Torr, through a column of sodium hydroxide pellets. After a rigorous deaeration treatment of trap-to-trap distillations, retaining the middle fraction, and freeze–pump–thaw cycles, the liquified hydrocarbons were treated with either a potassium metal film or sodium potassium alloy. Ethane and propylene were held over a potassium mirror for 48 h at 200 K and 233 K respectively. Ethylene was held over a potassium mirror for 4 days at 198 K. In each case the mirror was regenerated several times during the treatment. Cyclopropane, propane, and butane were stirred with a low melting sodium/potassium alloy (20/80) for 2 h, the first two compounds at 263 K and the third at 298 K.

Methane was introduced directly into the vacuum system and deaerated by trap-to-trap distillations, pumping away at least half of the sample. It was then electrolyzed at 1 kV/cm and 113 K for 1 h.

Xenon was purified by passing the gas slowly through a 60 cm long glass tube (approximately 0.8 cm diameter) coated with a film of sodium metal. The gas was passed through the tube eight times and the mirror regenerated twice during this procedure.

Equipment and Technique

(a) Conductance Cells

The large cell (25 cm^3) used for the hydrocarbons had stainless steel electrodes. An inner 30 mm diameter collecting electrode was surrounded by a guard electrode and was 3 mm from a parallel, 38 mm diameter, high voltage electrode. The electrodes were sealed in a glass envelope which had an inlet for entry of the hydrocarbon, and a side arm with storage bulb and break seals to facilitate transfer and storage of the material.

A small (5 cm^3) parallel plate cell with a guard electrode was used for the xenon. This has been described in ref. 10.

The electrical connections to both types of cells were kept as short as possible and shielded up to the cell wall with copper braid.

(b) Temperature Control

This was effected by placing the cell in an insulated styrofoam box which was cooled by a regulated stream of cold nitrogen gas. Stabilization to $\pm 0.5°$ was achieved with this system.

(c) Determination of Free Ion Yields

The free ion yields were measured by the charge clearing technique (1, 2, 11) with the field applied across the electrodes throughout the experiment. A description of the method and circuits used is given in ref. 10.

(d) Electron Conductance Transient (ECT)

This was measured in the hydrocarbon liquids using the circuit shown in Fig. 1. The amplifier had a gain of 10^5 and a response decay halflife of 60 ns. A 1 μs X-ray beam pulse from a Van de Graaff generator was used, except for methane and xenon when the pulse length was 100 ns. The amplifier circuit used for measuring the ECT in xenon is given in ref. 10, Fig. 3*b*.

(e) Dosimetry

Thermoluminescence dosimetry using lithium fluoride crystals was used throughout. This has been described for the hydrocarbons in ref. 1. A thorough treatment of the dosimetry for xenon, in which photoelectric absorption is important, is given in ref. 10.

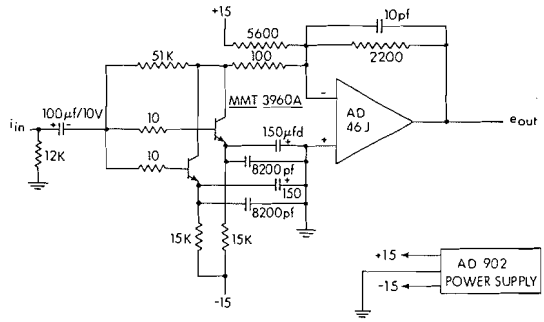

FIG. 1. Circuit for measuring the electron conductance transient (model 4). Gain = 10^5, noise ≃ 15 nA peak, signal decay halflife = 60 ns.

(f) Physical Properties of the Liquids

The densities and dielectric constants of the liquids are listed in Table 1 and were taken from or calculated from data in the references indicated.

Results and Discussion

The free ion yields and electron mobilities were measured as functions of field strength and temperature in the liquids at their vapor pressures, up to a maximum of about 5 atm.

Free Ion Yields and Electron Ranges

The experimental values of the free ion yields were analyzed with the aid of a model that treats the effects of applied electric field strength and temperature (12). The model is based upon the single ion-pair spur approximation and has been examined under a variety of conditions (12–17). Only the relevant equations are given here.

The free ion yield G_{fi}^{E} in the presence of an applied field E is given by [1].

$$[1] \qquad G_{fi}^{E} = G_{tot} \int_0^\infty F(y)\phi(y,E)dy$$

where G_{tot} is the total ionization yield, $F(y)dy$ is the fraction of thermalized electron–ion pairs that have initial intrapair separation distances between y and $y + dy$, and $\phi(y,E)$ is the probability that a pair with initial separation distance y will escape geminate neutralization in the presence of an applied field E.

The probability function $\phi(y,E)$ is given by [2] (17–19).

$$[2] \quad \phi(y,E) = e^{-r/y}\left\{1 + e^{-2\beta y}\sum_{n=1}^{\infty}\frac{(2\beta y)^n}{(n+1)!} \times \sum_{j=0}^{n-1}(n-j)\frac{(r/y)^{j+1}}{(j+1)!}\right\}$$

TABLE 1. Physical properties, ion yields, electron ranges and mobilities

Liquid	Temp. (°K)	ε^a	d^b (g/cm³)	G_{tot}	$G_{fi}{}^0$	b_{GP} (Å)	$b_{GP}d$ (10^{-8}g/cm²)	α^{ac} (Å³)	u_e (cm²/Vs)
Methane	140	1.55	0.379	3.7	1.13	592	224	0.0	430
	118	1.63	0.417		0.92	558	233		510
	98	1.68	0.448		0.74	553	248		560
Ethane	200	1.77	0.533	4.0	0.158	106	57	0.7	0.97
	168	1.83	0.567		0.094	101	57		0.27
	146	1.88	0.590		0.068	99	58		0.057
	127	1.92	0.614		0.045	98	60		0.008
Propane	238	1.76	0.572	4.1	0.166	91	52	0.9	0.55
	205	1.85	0.612		0.102	84	52		0.14
	175	1.92	0.646		0.070	82	53		0.05
n-Butane	293	1.78	0.583	4.1	0.225	93	54	~1	0.27
	271	1.81	0.604		0.182	81	49		0.15
	250	1.85	0.623		0.130	75	46		0.073
	219	1.90	0.652		0.084	71	46		0.013
Cyclopropane	260	1.83	0.650	4.1	0.078	60	39	1.45[f]	0.011[g]
	234	1.89	0.683		0.049	54	37		0.0043[g]
Ethylene	170	1.81	0.570	3.9	0.010	41	23	2.1	0.0030[g]
Propylene	234	1.96	0.602	4.0	0.042	49	30	2.1	0.008[g]
	214	2.07	0.625		0.031	45	28		0.003[g]
Xenon	198	1.83[d]	2.82[e]	16	9.37	840	2370[h]	0.0	[i]
	186	1.87	2.91		8.98	810	2370[h]		
	169	1.92	3.05		8.72	780	2370[h]		

[a]Calculated from the data and references given in ref. 1.
[b]Reference 31.
[c]Reference 2.
[d]Calculated from the Clausius–Mosotti equation, using $\alpha = 4.01$ Å³ (*e*).
[e]Reference 32.
[f]Reference 33.
[g]The initial conductance transient was corrected for the contribution of the heavy positive ions.
[h]Assumed to be independent of temperature.
[i]See Fig. 7.

where $r = \xi^2/\varepsilon kT$, $\xi = 4.80 \times 10^{-10}$ e.s.u., ε is the dielectric constant of the medium, k is Boltzmann's constant, T is the absolute temperature and $\beta = \xi E/600kT$.

At zero field strength eq. 1 reduces to [3].

$$[3] \qquad G_{fi}{}^0 = G_{tot} \int_0^\infty F(y)\, e^{-r/y} dy$$

It has recently been shown that a distribution function $F(y)$ having a Gaussian core and a power function tail, designated *YGP*, satisfies the whole range of free ion yields obtained in all of the liquids at all values of E and T studied so far (17). The distribution *YGP* is represented by [4].

$$[4] \begin{cases} F(y) = 0.96[(4y^2/\pi^{1/2}b_{GP}{}^3) \exp(-y^2/b_{GP}{}^2)] & y < 2.4b_{GP} \\ F(y) = 0.96\,[(4y^2/\pi^{1/2}b_{GP}{}^3) \exp(-y^2/b_{GP}{}^2) + 0.5(b_{GP}{}^2/y^3)] & y > 2.4b_{GP} \end{cases}$$

where 0.96 is a normalization factor (inadvertently omitted from the distribution function *YGP* in ref. 17) and b_{GP} is the dispersion parameter and is also the most probable value of y.

Typical results for the effects of field strength and temperature on the free ion yields in ethane are shown in Fig. 2. The free ion yields increased with increase in either field strength or temperature. The solid curves in Fig. 2 were calculated using eqs. 1, 2, and 4. The value of G_{tot} was assumed to be equal to the ionization yield in the gas phase (20–24). The electron range dispersion b_{GP} was used as an adjustable parameter and at each temperature the value was chosen that gave the minimum average difference between the calculated and experimental points. The best values of b_{GP} are listed in Table 1.

Propane, *n*-butane, cyclopropane, ethylene, and propylene showed similar behavior and the results are summarized in Table 1. The yields obtained in the alkanes are in general agreement with those reported earlier (1, 25), but those in

Can. J. Chem. Downloaded from www.nrcresearchpress.com by 210.87.254.6 on 09/05/12
For personal use only.

Can. J. Chem. Downloaded from www.nrcresearchpress.com by 210.87.254.6 on 09/05/12
For personal use only.

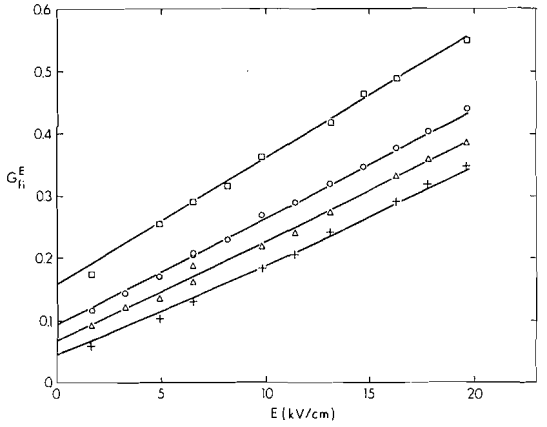

FIG. 2. Free ion yields in ethane as functions of applied electric field strength E and temperature. The curves were calculated from eq. 1 and data in Table 1. □, 200 K; ○, 168 K; △, 146 K; +, 124 K.

cyclopropane and the olefins are ~35% lower than the earlier values (1). However, the yields in the latter compounds are small, and the measurements had been done near the lower limits of the equipment. The present results are considered to be more reliable because larger conductance cells were used.

In methane the free ion yield increased greatly with applied field strength but only slightly with temperature (Fig. 3). The curves were calculated in the same way as those for the other hydrocarbons. The best value of b_{GP} at each temperature is listed in Table 1.

In each of the hydrocarbons the density-normalized range, $b_{GP}d$, of the secondary electrons is independent of temperature, within experimental error. This substantiates the usefulness of the distribution function *YGP* (eq. 4) in the single-ion-pair-per-spur model (17).

The earlier suggested inverse correlation between $b_{GP}d$ and the anisotropy of polarizability α^a of the molecules (2) is roughly supported by the results in Table 1. However, it is becoming increasingly clear that some other factor is very important in determining epithermal electron ranges in liquids.

The free ion yield in xenon increased with applied field strength, but the effect of temperature over the range 172 to 200 °K was smaller than the scatter in the measurements (Fig. 4). The yields were too large to be explained by putting G_{tot} in eq. 1 equal to the gas phase ionization yield. Both G_{tot} and b_{GP} were therefore used as adjustable parameters in the calculations. The best fit to the experimental results was obtained with $G_{tot} = 16$. The final curves were calculated by keeping $b_{GP}d$ constant, independent of temperature, and the best value was 2.37×10^{-5} g/cm^2. Calculated curves that were needed for the mobility determinations at three temperatures are shown in Fig. 4 to illustrate the behavior.

The present yields in methane and xenon are ~20% larger than those reported earlier (1, 10). This is outside the usually obtained reproducibility of ~10% and might be related to the fact that these yields are much larger than those normally measured with the equipment.

Electron Mobilities

In most of these systems the mobilities u_+ of the positive ions were several orders of magnitude smaller than those of the electrons. Under these

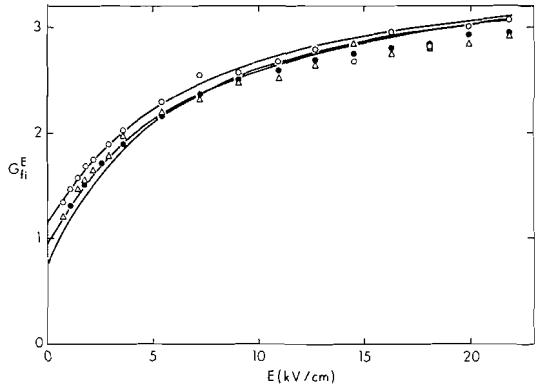

FIG. 3. Free ion yields in methane as functions of applied electric field strength and temperature. The curves were calculated from eq. 1 and data in Table 1. ○, 140 K; △, 118 K; ●, 98 K.

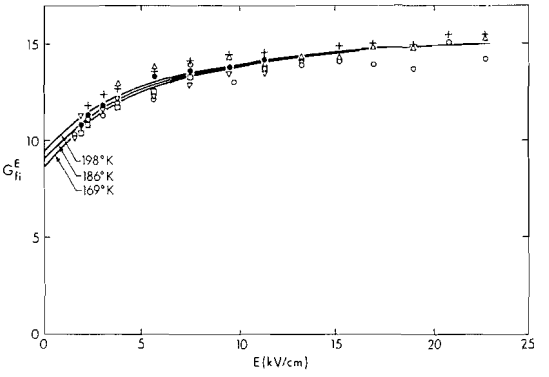

FIG. 4. Free ion yields in xenon as functions of applied electric field strength and temperature. The curves were calculated from eq. 1 and data in Table 1. □, 200 K; +, 195 K; △, 189 K; ○, 183 K; ▽, 178 K; ●, 172 K.

Can. J. Chem. Downloaded from www.nrcresearchpress.com by 210.87.254.6 on 09/05/12
For personal use only.

circumstances the electron mobility u_e was obtained from the peak current i_0 of the electron conductance transient (ECT) that occurred after a short pulse of X-rays irradiated the liquid:

$$[5] \quad u_e \approx (u_+ + u_e) = 6.24 \times 10^{20}\, i_0/\text{dose}.A.E.G_{fi}{}^E$$

where i_0 is in amps, the pulse dose in eV/cm^3, A the area of the collecting electrode in cm^2, and E is the applied field strength in V/cm. When necessary the value of the peak current was corrected for decay during the 0.1 or 1 μs pulse to obtain i_0. The corrections were made empirically, using a separate calibration curve for each amplifier. The calibrations were made by comparing the input and output of a given amplifier, when fed a known input current pulse with a series of known first order decay rates.

Electron mobilities in ethane, propane, *n*-butane, cyclopropane, ethylene, and propylene were independent of field strength up to 20 kV/cm. The values are listed in Table 1. The mobilities increased with increasing temperature; Arrhenius plots are shown in Fig. 5. The plots are not strictly linear, the slope decreasing slightly at the higher mobilities and temperatures. The Arrhenius temperature coefficients E_u are approximately 3 kcal/mol for liquids with mobilities of about 0.2 cm^2/Vs and 4 kcal/mol at the lower mobilities, <0.1 cm^2/Vs.

The mobility of electrons in methane was independent of field strength up to 2 kV/cm and decreased slightly with increasing temperature (Fig. 6 and Table 1). The variation with temperature corresponds to an Arrhenius coefficient of -0.16 kcal/mol or to $T^{-0.7}$.

In xenon the mobility decreased approximately as $E^{-1/2}$ at field strengths between 33 and 300 V/cm, and decreased slightly more rapidly at higher field strengths (Fig. 7). The mobility appeared to be independent of temperature in the range from 169 to 202 K, although a $T^{\pm 1}$ dependence could exist within the scatter of the results. The values are about 50% lower than those reported by Miller, Howe, and Spear for 163 K (8),

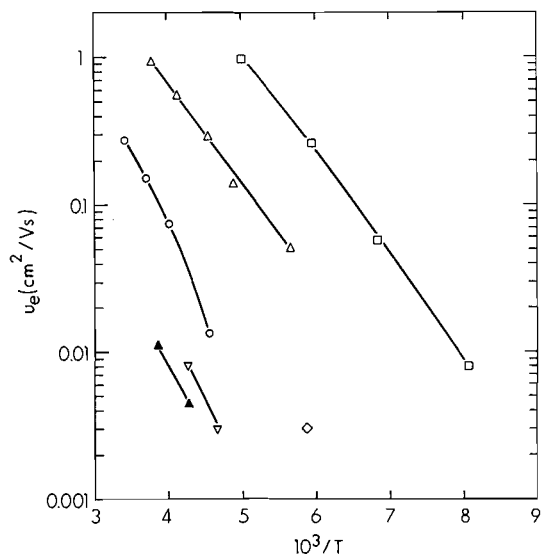

FIG. 5. Arrhenius plots of electron mobilities in hydrocarbon liquids. □, ethane; △, propane; ○, *n*-butane; ▲, cyclopropane; ◇, ethylene; ▽, propylene.

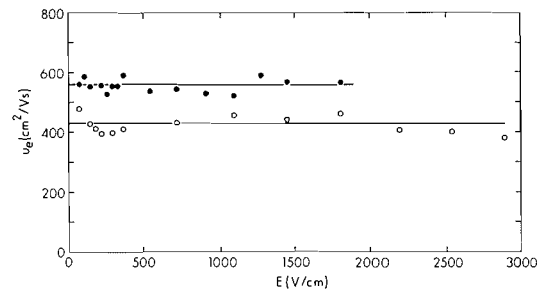

FIG. 6. Electron mobilities in methane at 98 K (●) and 140 K (○) as functions of applied electric field strength.

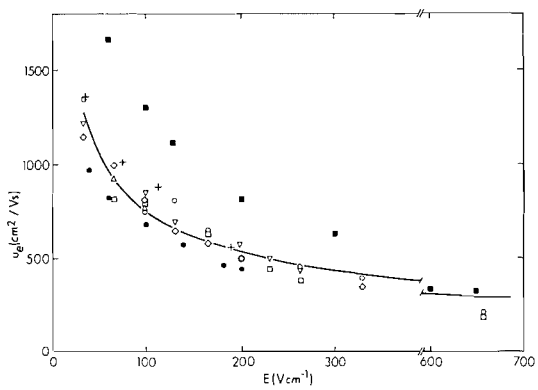

FIG. 7. Electron mobilities in xenon as functions of applied electric field strength at 202 K (△), 198 K (▽), 186 K (□), 182 K (+), 180 K (○), and 169 K (◇). ■, 163 K, ref. 8; ●, 183 K, ref. 10. The solid curve corresponds to 7500 $E^{-1/2}$.

Can. J. Chem. Downloaded from www.nrcresearchpress.com by 210.87.254.6 on 09/05/12
For personal use only.

but are in satisfactory agreement with those reported from this laboratory for 183 K (10).

The anomalous temperature dependence of electron mobilities in argon (7, 9) and krypton (7) was not observed in xenon over the temperature range that could be used with the present apparatus. A conductance cell that will withstand higher pressures is being constructed to allow measurements to be made at temperatures approaching the critical temperature. Similar measurements will also be made on methane.

The general correlation between the ranges of epithermal electrons and the mobilities of thermal electrons observed in other liquids (2, 26) persists for the simple hydrocarbons (Table 1). However, there is an apparent inversion of the correlation for cyclopropane and propylene which is not readily explained.

Ion Mobilities

Electron mobilities in the olefins and cyclopropane were so low that it was of interest to measure the ion mobilities for comparison. The sum of the anion and cation mobilities $(u_+ + u_-)$ was determined using an equation analogous to [5].

Nitrous oxide was added to scavenge the electrons in ethylene at 170 K. The ECT was destroyed and an ion conductance transient (ICT) was observed. The decay half life of the ICT was $\sim$10 ms at 10 kV/cm, compared to $\sim$0.2 ms for the ECT. The value $(u_+ + u_-) = 0.0023$ cm^2/Vs was obtained at field strengths 10–20 kV/cm, not much smaller than the electron mobility 0.0030 cm^2/Vs. By assuming that the ion–electron and ion–ion neutralization reactions would be diffusion controlled, and knowing the pulse dose (2×10^{11} eV/cm^3) and the free ion yield, it was demonstrated that the neutralization half life of the ECT would have been two orders of magnitude greater than the decay halflife observed, and that of the ICT would have been one order of magnitude greater than the observed value. The ECT apparently decayed through electron capture by trace impurities in the "purified" ethylene, whereas the ICT decayed mainly by the ions being drawn to the electrodes.

Since the ECT decayed by negative ion formation, the ion mobilities could be measured without adding nitrous oxide, simply by using a slower sweep time on the measuring oscilloscope. This procedure gave $(u_+ + u_-) = 0.0024$ cm^2/Vs in ethylene at 170 K, in agreement with the value from the nitrous oxide technique. The identities of the ions are not known in either case, but their mobilities are similar.

It has been found in many hydrocarbons (27–30) that $u_-/u_+ \approx 2$. The values of u_e recorded in Table 1 and Fig. 5 were obtained by subtracting $u_+ = (u_+ + u_-)/3$ from the total $(u_+ + u_e^-)$ derived from eq. 5.

Similar treatment of data from propylene gave $(u_+ + u_e) = 0.005$ at 243 K and 0.002 at 214 K, while in cyclopropane the values were 0.003 at 260 K and 0.002 cm^2/Vs at 234 K.

We are grateful to the staff of the Radiation Research Center for help with the electronics.

1. M. G. Robinson, P. G. Fuochi, and G. R. Freeman. Can. J. Chem. **49**, 3657 (1971).
2. J.-P. Dodelet and G. R. Freeman. Can. J. Chem. **50**, 2667 (1972).
3. W. F. Schmidt and A. O. Allen. J. Chem. Phys. **52**, 4788 (1970).
4. R. M. Minday, L. D. Schmidt, and H. T. Davis. J. Chem. Phys. **54**, 3112 (1971).
5. P. G. Fuochi and G. R. Freeman. J. Chem. Phys. **56**, 2333 (1972).
6. W. F. Schmidt and G. Bakale. Chem. Phys. Lett. **17**, 617 (1972).
7. H. Schnyders, S. A. Rice, and L. Meyer. Phys. Rev. **150**, 127 (1966).
8. L. S. Miller, S. Howe, and W. E. Spear. Phys. Rev. **166**, 871 (1968).
9. J. A. Jahnke, L. Meyer, and S. A. Rice. Phys. Rev. A, **3**, 734 (1971).
10. M. G. Robinson and G. R. Freeman. Can. J. Chem. **51**, 641 (1973).
11. W. F. Schmidt and A. O. Allen. (*a*) Science, **160**, 301 (1968); (*b*) J. Phys. Chem. **72**, 3730 (1968).
12. L. Onsager. Phys. Rev. **54**, 554 (1938).
13. G. R. Freeman. J. Chem. Phys. **39**, 1580 (1963).
14. A. Jahns and W. Jacobi. Z. Naturforsch. **21a**, 1400 (1966).
15. A. Hummel and A. O. Allen. J. Chem. Phys. **46**, 1602 (1967).
16. J.-P. Dodelet, P. G. Fuochi, and G. R. Freeman. Can. J. Chem. **50**, 1617 (1972).
17. J.-P. Dodelet, K. Shinsaka, U. Kortsch, and G. R. Freeman. J. Chem. Phys. **59**, 2376 (1973).
18. J. Terlecki and J. Fintak. Int. J. Radiat. Phys. Chem. **4**, 469 (1972).
19. G. R. Freeman and J.-P. Dodelet. Int. J. Radiat. Phys. Chem. **5**, 371 (1973).
20. G. G. Meisels. J. Chem. Phys. **41**, 51 (1964).
21. P. Alder and H. K. Bothe. Z. Naturforsch. **20a**, 1700 (1965).
22. R. M. Leblanc and J. A. Herman. J. Chim. Phys. **63**, 1055 (1966).
23. R. Cooper and R. M. Mooring. Aust. J. Chem. **21**, 2417 (1968).
24. T. A. Stoneham, D. R. Ethridge, and G. G. Meisels. J. Chem. Phys. **54**, 4054 (1971).

25. W. F. SCHMIDT and A. O. ALLEN. J. Chem. Phys. **52**, 2345 (1970).
26. J.-P. DODELET, K. SHINSAKA, and G. R. FREEMAN. J. Chem. Phys. **59**, 1293 (1973).
27. I. ADAMCZEWSKI. Brit. J. Appl. Phys. **16**, 759
28. A. HUMMEL and A. O. ALLEN. J. Chem. Phys. **44**, 3426 (1966).
29. W. F. SCHMIDT. Z. Naturforsch. **23b**, 126 (1968).
30. P. H. TEWARI and G. R. FREEMAN. J. Chem. Phys. **49**, 4394 (1968).
31. R. W. GALLANT. Physical properties of hydrocarbons. Vol. 1 and 2. Gulf Publishing Co., Houston, Texas. 1968 and 1970.
32. G. A. COOK. Argon, helium and the rare gases. Vol. 1. Interscience, New York. 1961.
33. N. J. AVERY, R. J. W. LEFEVRE, W. LUETTKE, G. L. D. RITCHIE, and P. J. STILLS. Aust. J. Chem. **21**, 2551 (1968).

Can. J. Chem. Downloaded from www.nrcresearchpress.com by 210.87.254.6 on 09/05/12
For personal use only.

Chemistry of Proximal π-Bond Systems. Part II.[1] Synthesis of 2,3-Dimethylenebicyclo[2.2.2]octa-5,7-diene

D. N. BUTLER AND R. A. SNOW

Chemistry Department, York University, Toronto, Ontario M3J 1P3

Received September 27, 1973

The new $C_{10}H_{10}$ hydrocarbon, 2,3-dimethylenebicyclo[2.2.2]octa-5,7-diene (**7**), has been synthesized. Diels–Alder additions to **7** afford a useful route to annelated barrelenes.

On a synthétisé le diméthylène-2,3 bicyclo[2.2.2]octadiène-5,7,7 (**7**) un nouvel hydrocarbure de formule $C_{10}H_{10}$. Les réactions d'addition de Diels–Alder sur le composé **7** fournissent une manière utile d'arriver aux barrelènes. [Traduit par le journal]

Can. J. Chem., **52**, 447 (1974)

The widespread interest in the chemistry of the C_nH_n hydrocarbons has for the most part focused upon those isomers composed entirely of methine units *i.e.* $(CH)_n$ (1). The simple conception of replacing any vinylene (—CH=CH—) bridge or ring fragment in the $(CH)_n$ isomers by vinylidene ($\diagdown C{=}CH_2$) leads to a fertile, yet largely unexplored area of hydrocarbon chemistry best represented by the C_6H_6 isomers (fulvene (2), dimethylenecyclobutene (3), and radialene (4)), but sparsely investigated for C_8H_8 and $C_{10}H_{10}$ (5). A casual inspection of these systems reveals their chemical potential for the discovery of new compounds and reactions attending the symmetries and proximities of the various orbitals involved in their construction. As a logical consequence to our interest in bridged, vicinal dienes (6), we have synthesized the $C_{10}H_{10}$ hydrocarbon, 2,3-dimethylenebicyclo[2.2.2]octa-5,7-diene (**7**) as shown in Scheme 1.

The cyclooctatetraene – fumaryl chloride adduct was treated with methanol to provide the starting material **1** (7). This dienophile reacted with the dienone **2** (8) to form a mixture of adducts from which pure **3** (presumably the *exo* isomer (9)) could be fractionally crystallized. Application of the useful photoaromatization route developed by Warrener and co-workers (10) led to the key intermediate **4** of the synthesis along with hydrocarbon **5**. The corresponding *cis*-dimethyl bicyclo[2.2.2]octa-5,7-diene-2,3-dicarboxylate (**8**) has been secured by Warrener and co-workers (11) via the *o*-chloranil adduct – photoaromatization variation of this synthesis. Unlike compound **8** which was crystalline, repeated attempts to isolate the *trans* isomer **4** led to the formation of benzene and dimethyl fumarate. This facile fragmentation required that the irradiation (and subsequent operations) of **3** be conducted at ice temperature. The remaining steps of the synthesis followed the base-catalyzed bis-*p*-toluenesulfonate elimination route to bridged, vicinal dienes (6) we had developed earlier, modified to respect the thermal lability of the dihydrobarrelene intermediates **4** and **6***a*, and *b*.

The structure of the tetraene **7** followed from its mode of formation and spectral data (see Fig. 1). The u.v. spectrum is unremarkable, being very similar to the related triene **9** (6). The hydrocarbon **7**, m.p. 40°, is a colorless, highly volatile

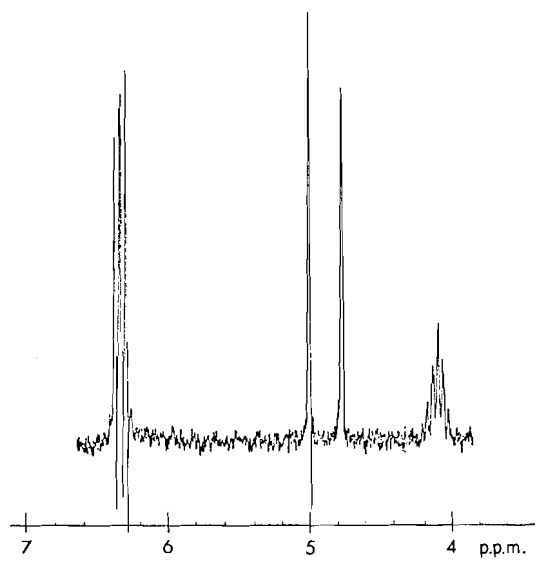

FIG. 1. Proton magnetic resonance spectum of **7** in 10% CCl_4 solution.

[1]For Part I see ref. 6.

Can. J. Chem. Downloaded from www.nrcresearchpress.com by 210.87.254.105 on 09/05/12
For personal use only.

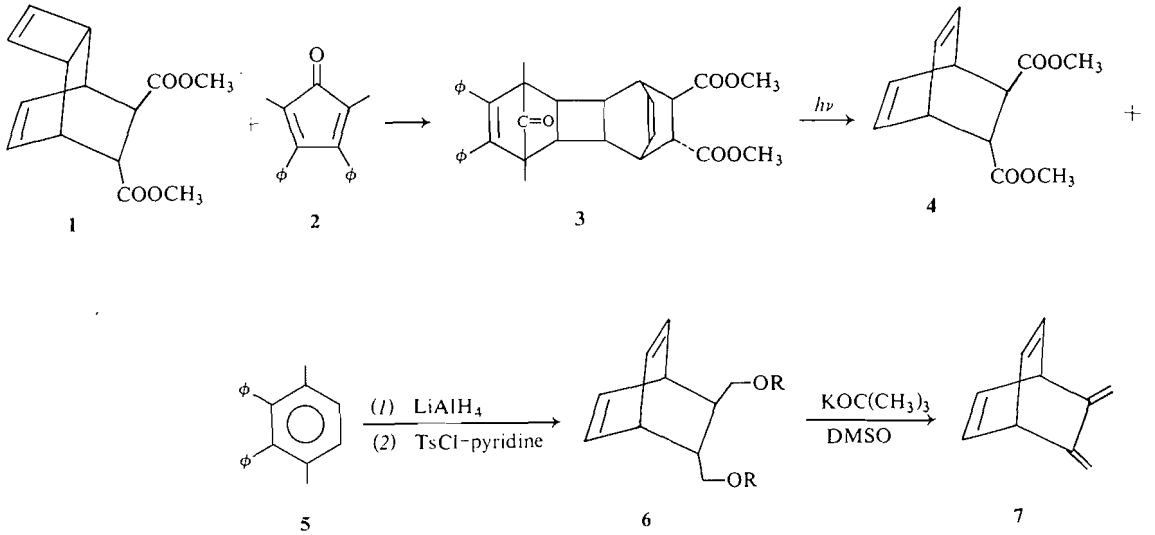

1 2 3 4

5 6 7

a R = H
b R = Ts = *p*-Toluenesulfonyl

SCHEME 1

solid, readily subliming at 30°/15 mm. It is stable at room temperature, partially polymerizing to an amorphous solid over several months. Although the mass spectrum revealed benzene as a prominent peak, in thermolysis experiments up to 350° we have not been able to detect any retro $4\pi + 2\pi$ cycloaddition. This observation precludes **7** as a likely source for butatriene, in common with similar results for the two benzo analogs, **10** and **11** (6). The molecule is similarly

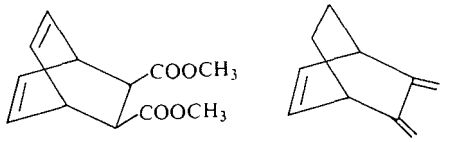

8 9

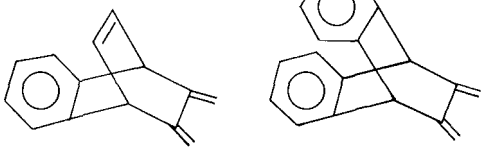

10 11

inert to photochemical excitation. Disappointingly, in all experiments so far tried we have not observed anything other than starting material or polymer upon irradiation under a variety of conditions.

The Diels–Alder chemistry of **7** was easily observed. The tetracyanoethylene, maleic anhydride, and dimethyl acetylenedicarboxylate adducts all formed quantitatively, and provide a facile route to the annelated barrelenes **11**, **12**, and **13**, respectively. These are related to current interest in C_8H_8 chemistry (12). Dehydrogenation (DDQ) of **13** provided the benzobarrelene diester **14**.

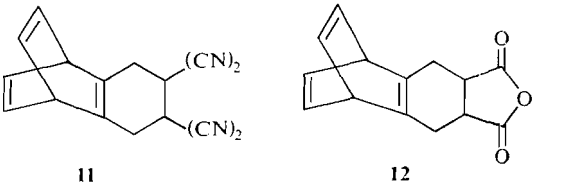

11 12

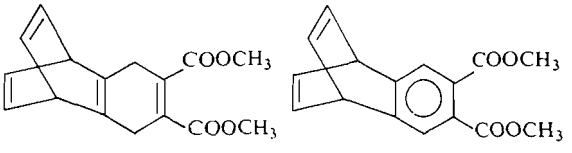

13 14

Experimental

All melting points are uncorrected. The i.r. spectra were taken on a Unicam SP1000 spectrophotometer as liquid films or KBr discs. The p.m.r. spectra were recorded on a Varian HA 100 instrument in carbon tetrachloride or deuteriochloroform using tetramethylsilane as the internal standard. Mass spectra were taken at 70 eV using a Hitachi-Perkin Elmer RMU-6E instrument.

Can. J. Chem. Downloaded from www.nrcresearchpress.com by 210.87.254.105 on 09/05/12
For personal use only.

Can. J. Chem. Downloaded from www.nrcresearchpress.com by 210.87.254.105 on 09/05/12
For personal use only.

The u.v. spectra were run on a Unicam SP800A spectrophotometer. Gas–liquid partition chromatographic analyses were obtained on a Varian Model 1700 instrument fitted with a 7 ft × ¼ in. glass column packed with 6% SE30 – 4% QF 1 on Chromosorb W. Microanalyses were obtained from A. B. Gygli, Toronto.

Preparation of Adduct **3**

A mixture of dimethyl (*anti*)-tricyclo[4.2.2.0^{2,5}]deca-3,9-diene-(*trans*)-7,8-dicarboxylate (50.7 g) (7) and 2,5-dimethyl-3,4-diphenylcyclopenta-2,4-dieneone dimer (53.6 g) (8) in chloroform (300 ml) was heated under reflux for 48 h. The resulting red solution was cooled, filtered from a little polymer, and evaporated under vacuum to a red-brown glass which after three recrystallizations from ethyl acetate afforded the adduct **3** as white crystals (78.3 g), m.p. 188° (dec.); $\nu_{C=O}$ 1765, 1727 cm^{-1} (KBr); δ ($CDCl_3$) 1.18 (s, 3H) and 1.22 (s, 3H) (bridgehead methyls), 2.03 (broad s, 4H, cyclobutane), 2.94–3.28 (m, 4H, bridgehead and C*H*—$COOCH_3$), 3.71 (s, 3H) and 3.76 (s, 3H) (ester methyls), 6.27–6.68 (m, 2H, vinyl), 6.90–7.32 (m, 10H, aromatic) p.p.m.; no parent ion, *m/e* 258, **5** (base peak).

Anal. Calcd. for $C_{33}H_{32}O_5$: C, 77.93; H, 6.34. Found: C, 77.86; H, 6.27.

Dimethyl Bicyclo[2.2.2]octa-5,7-diene-2,3-(trans)-dicarboxylate (4)

The adduct **3** (2.03 g) in acetone (40 ml) was irradiated (450 W Hanovia medium pressure Hg lamp) at 0° for 3.5 h. The solvent was removed under vacuum keeping the temperature at < 10°. The resulting yellow oil was subjected to chromatography in a cold room on silica gel (Woelm: activity grade 1) (40 × 2.5 cm) using petroleum ether (30–60°) until 1,4-dimethyl-2,3-diphenylbenzene (**5**) (0.97 g, 94%) was eluted. Development with 5% ether – petroleum ether and evaporation at 5° under vacuum afforded the colorless oil **4** (0.55 g, 62%) which could not be induced to crystallize and because of its thermal instability was not analyzed. The following spectral properties are consistent with the proposed structure: i.r. ν_{max} 1603 (C=C, weak), 1734 (C=O ester, strong), 2960, 3010, 3075 (C—H stretch, medium) cm^{-1} (liquid film); p.m.r. δ (CCl_4) 2.89 (d, J = 1.0 Hz, 2H, C*H*—$COOCH_3$), 3.60 (s, 6H, ester methyls), 3.95 (m, 2H, bridgehead), 6.11–6.51 (m, 4H, vinyl) p.p.m.

Thermal Decomposition of **4**

A 10% solution of the diester **4** in CCl_4 contained in a p.m.r. tube was warmed to 30° in the spectrometer and the changes in the spectrum observed with time. Signals due to **4** diminished with the simultaneous appearance of absorptions corresponding to benzene and dimethyl fumarate ($T_{\frac{1}{2}}$ = 20 min).

(trans)-2,3-Bis(hydroxymethyl)bicyclo[2.2.2]octa-5,7-diene Di-p-toluenesulfonate (6b)

The adduct **3** (10.53 g) in acetone (250 ml) was irradiated for 5.5 h under the conditions set out above. The solvent was removed at 5° and the resulting oil subjected to vacuum (0.001 mm) at 5° for 1 h to remove all residual solvent. The viscous product was dissolved in dry ether (100 ml) at ice temperature and added dropwise over 0.5 h to a stirred suspension of $LiAlH_4$ (1.5 g) in dry ether (150 ml) also cooled in ice. The mixture was stirred for 1 h at 0°, then 4 h at room temperature. Excess hydride was decomposed at 0° by the careful addition of 30% aqueous KOH (2 ml) followed by water (2 ml). The resulting suspension was filtered and the filter cake washed thoroughly with ether. The combined filtrates were dried ($MgSO_4$) and evaporated under vacuum at 10° to afford the crude diol **4***a* mixed with 1,4-dimethyl-2,3-diphenylbenzene (**5**) (as observed in the p.m.r. spectrum of the mixture). This mixture was dissolved in pyridine (40 ml) and cooled at 0°. Then *p*-toluenesulfonyl chloride (10.0 g) was added with vigorous stirring and the reaction mixture allowed to stand for 2 h at 0° and overnight at 5°. It was then poured over crushed ice (100 g) and the mixture acidified with cold 2 *N* HCl. The gummy precipitate was extracted into chloroform (3 × 50 ml) and the extract washed with water (4 × 75 ml), dried ($MgSO_4$), and evaporated under vacuum to leave a red oil. This was rubbed with ether at 0° to afford crystalline di-*p*-toluenesulfonate **6***b* (3.4 g, 36%) collected in the usual way. Recrystallization from ether–methanol provided pure **6***b*, m.p. 105.5° (dec.); p.m.r. δ ($CDCl_3$) 1.18–1.45 (m, 2H), 2.45 (s, 6H), 3.43–3.88 (m, 6H), 5.93–6.50 (m, 4H), 7.35 (d, J = 9 Hz, 4H), 7.66 (d, J = 9 Hz, 4H) p.p.m.

Anal. Calcd. for $C_{24}H_{26}S_2O_6$: C, 60.72; H, 5.52. Found: C, 60.87; H, 5.47.

2,3-Dimethylenebicyclo[2.2.2]octa-5,7-diene (7)

To a stirred solution of the di-*p*-toluenesulfonate **6***b* (1.49 g) in dimethylsulfoxide (10 ml) at 20° was added potassium *t*-butoxide (0.9 g). The dark green reaction mixture was stirred for 1.5 h. Then petroleum ether (30–60°, 10 ml) was added and the mixture poured over crushed ice (100 g). The organic layer was separated, the aqueous phase extracted with petroleum ether (2 × 40 ml) and the combined organic phase washed with water (4 × 100 ml), dried ($MgSO_4$), evaporated to a low volume under vacuum, and washed through a column of alumina (Woelm: activity grade 1) (5 × 2 cm) with petroleum ether (50 ml). Evaporation (bath temperature 5°) under vacuum left a waxy solid which was sublimed (25°/0.01 mm) onto a Dry Ice cooled cold finger to afford long white needles of the tetraene **7** (0.31 g, 75%), m.p. 40°; i.r. ν_{max} 888 (strong), 1584 (weak), 1618 (medium), 2990 (medium), 3060 (weak, shoulder) cm^{-1} (liquid film); p.m.r. δ (CCl_4) 4.08 (m, 2H, bridgehead), 4.75 (s, 2H, outside methylene), 4.98 (narrow d, J = 0.3 Hz, inside methylene), 6.32 (m, 4H, vinyl) p.p.m.; λ_{max} (log ε) (cyclohexane) 242 (3.96), 221 (3.79) nm; *m/e* M^+ 130.

Anal. Calcd. for $C_{10}H_{10}$: C, 92.26; H, 7.74. Found: C, 92.23; H, 7.81.

Tetracyanoethylene Adduct **11**

The tetraene **7** (0.021 g) and freshly sublimed tetracyanoethylene (TCNE) (0.021 g) were stirred for 1 h in tetrahydrofuran (0.4 ml) at 20°. Evaporation and recrystallization (ether–tetrahydrofuran) provided the adduct **11**, m.p. 223–224°; p.m.r. δ ($CDCl_3$) 3.22 (s, 4H), 4.53 (m, 2H), 6.80 (m, 4H) p.p.m.; *m/e* M^+ 258.

Anal. Calcd. for $C_{16}H_{10}N_4$: C, 74.41; H, 3.90. Found: C, 74.64; H, 3.78.

Maleic Anhydride Adduct **12**

A solution of the tetraene **7** (0.032 g) and maleic anhydride (0.025 g) in dry chloroform (3 ml) was subjected to reflux for 4 h. Evaporation and recrystallization from ether provided the adduct **12**, m.p. 158–159° (dec.); p.m.r.

δ ($CDCl_3$) 2.32–2.93 (m, 4H), 3.27 (m, 2H), 4.47 (m, 2H), 6.70 (m, 4H) p.p.m.; *m/e* M^+ 228.

Anal. Calc. for $C_{14}H_{12}O_3$: C, 73.67, H, 5.30. Found: C, 73.51; H, 5.34.

Dimethyl Acetylenedicarboxylate Adduct ***13***

A solution of tetraene **7** (0.115 g) and dimethyl acetylenedicarboxylate (0.130 g) in carbon tetrachloride (2.5 ml) was heated to reflux for 10 h. Evaporation and recrystallization from methanol provided the pure adduct **13**, m.p. 60.5–61°; p.m.r. δ (CCl_4) 3.10 (s, 4H), 3.66 (s, 6H), 4.38 (m, 2H), 6.64 (m, 4H) p.p.m.; *m/e* M^+ 272.

Anal. Calcd. for $C_{16}H_{16}O_4$: C, 70.58; H, 5.92. Found: C, 70.74; H, 6.05.

*Dimethyl Benzobarrelenedicarboxylate (**14**)*

A solution of the adduct **13** (0.100 g) in benzene (2 ml) was stirred with 2,3-dichloro-5,6-dicyano-*p*-benzoquinone (DDQ) (0.095 g) for 8 h. The whole reaction mixture was then put onto a column of alumina (Woelm: activity grade 1) (8 × 1 cm) and eluted with benzene (50 ml). The total eluate was evaporated and the product recrystallized from methanol to give **14** (0.095 g), m.p. 103–104°; p.m.r. δ (CCl_4) 3.78 (s, 6H), 4.92, (m, 2H), 6.81 (m, 4H), 7.40 (s, 2H) p.p.m.; *m/e* M^+ 270.

Anal. Calcd. for $C_{16}H_{14}O_4$: C, 71.10; H, 5.22. Found: C, 71.30; H, 5.18.

Thermal Behavior of Tetraene ***7***

(*a*) The tetraene **7** (0.08 g) was heated for 20 h at 80° in carbon tetrachloride (0.6 ml) under N_2. Some polymeric material precipitated, but the p.m.r. spectrum revealed only starting material. In particular no resonance for benzene was found.

(*b*) A sample of **7** (0.08 g) was sealed in glass under N_2 and kept at 40° for 4 months. Upon opening there was recovered starting material (0.024 g) and an amorphous polymer (0.048 g).

(*c*) Injection of an ethereal solution of **7** through the injection port of the g.l.p.c. instrument over the temperature range 200–350° revealed no sign of decomposition products.

Irradiation of Tetraene ***7***

A 2% solution of the tetraene **7** in pentane was deoxygenated, sealed under N_2 and irradiated for 10 h (Hanovia 450 W medium pressure Hg lamp) at 0°. The solution became yellow and deposited a sticky yellow polymer. Analysis (g.l.p.c. and p.m.r.) of the supernatant solution revealed only starting material.

1. L. T. Scott and M. Jones. Chem. Rev. **72**, 181 (1972).
2. D. Meuche, N. Nevenschwander, H. Schaltegger, H. V. Schlunegger. Helv. Chim. Acta, **47**, 1211 (1964).
3. W. D. Huntsman and H. J. Wristers. J. Am. Chem. Soc. **89**, 342 (1967).
4. P. A. Waitkus, E. B. Sanders, L. I. Peterson, and G. W. Griffin. J. Am. Chem. Soc. **89**, 6318 (1967).
5. (*a*) L. A. Carpino. J. Am. Chem. Soc. **85**, 2144 (1963); (*b*) F. R. Farr and N. L. Bauld. J. Am. Chem. Soc. **92**, 6695 (1970); (*c*) J. A. Elix, M. V. Sargent, and F. Sondheimer. J. Am. Chem. Soc. **92**, 962 (1970); (*d*) L. A. Paquette and M. J. Broadhurst. J. Org. Chem. **38**, 1893 (1973).
6. D. N. Butler and R. A. Snow. Can. J. Chem. **50**, 795 (1972).
7. v. M. Avram, G. Mateescu, and C. D. Nenitzescu. Ann. **636**, 174 (1960).
8. C. F. H. Allen and J. A. Van Allen. J. Am. Chem. Soc. **72**, 5165 (1950).
9. C. M. Anderson, I. W. McCay, and R. N. Warrener. Tetrahedron Lett. 2735, (1970).
10. C. M. Anderson, J. B. Bremner, H. H. Westberg, and R. N. Warrener. Tetrahedron Lett. 1585, (1969).
11. E. E. Ninn, W. S. Wilson, and R. N. Warrener. Tetrahedron Lett. 175, (1972).
12. R. K. Russell and L. A. Paquette. Tetrahedron Lett. 2855, (1973).

Can. J. Chem. Downloaded from www.nrcresearchpress.com by 210.87.254.105 on 09/05/12
For personal use only.

The Mechanism of Bromination of 2(1*H*)-Pyrimidinone, its *N*-Methyl and *N,N'*-Dimethyl Derivatives in Aqueous Acidic Solution

OSWALD S. TEE[1] AND SUJIT BANERJEE

Department of Chemistry, Sir George Williams University, Montreal 107, Quebec

Received August 20, 1973

Rates of bromination at the 5-positions of the title compounds have been measured in aqueous sulfuric acid solutions. The reaction involves a rapid irreversible formation of a 5-bromo-4,6-dihydroxyhexahydro-2-oxopyrimidine which undergoes slow acid-catalyzed conversion to the corresponding 5-bromopyrimidinone. If excess bromine is present the latter product reacts further to produce a 5,5-dibromo-4,6-dihydroxyhexahydropyrimidine.

Les vitesses de bromation des positions-5 dans les composés du titre ont été mesurées dans des solutions aqueuses d'acide sulfurique. La réaction implique la formation rapide irréversible de la bromo-5 dihydroxy-4,6 hexahydro oxo-2 pyrimidine qui se transforme lentement, sous une catalyse acide, en bromo-5 pyrimidinone correspondante. Ce dernier produit continue de réagir en présence d'un excès de brome, pour donner la dibromo-5,5 dihydroxy-4,6 hexahydro pyrimidine.

[Traduit par le journal]

Can. J. Chem., **52**, 451 (1974)

Can. J. Chem. Downloaded from www.nrcresearchpress.com by 210.87.254.42 on 09/05/12
For personal use only.

Due to their biological and pharmacological importance, pyrimidines have been extensively studied from a synthetic standpoint (1) but only recently have mechanistic studies been forthcoming (2). As part of a study of the electrophilic substitution of heteroaromatic compounds Katritzky and co-workers (3, 4) studied deuteration at the 5-position of 2(1*H*)-pyrimidinone **1**(R^1 = H), 1-methyl-2(1*H*)-pyrimidinone **1** (R^1 = Me), and the 1,2-dihydro-1,3-dimethyl-2-oxopyrimidinium ion **2** ($R^1 = R^2$ = Me). They concluded that these exchanges occur via the covalent hydrates **3** ($R^1 = R^2$ = H) and **3**(R^1 = Me; R^2 = H), and the pseudo-base **3** ($R^1 = R^2$ = Me), respectively. A subsequent study of the nitration of these same derivatives (5) showed that **1**(R^1 = H) and **1**(R^1 = Me) react as their free bases but that the cation **2**($R^1 = R^2$ = Me) is unreactive.

Following an earlier communication (6), we now present more complete results of a study of the bromination of these pyrimidines in aqueous sulfuric acid solutions. Initially it was found that **1**(R^1 = H), **1**(R^1 = Me), and the cation **2**($R^1 = R^2$ = Me; anion = Cl^- or HSO_4^-) react rapidly with bromine in aqueous solution at room temperature. Removal of the water under reduced pressure followed by recrystallization of the solid residue gave the 5-bromo derivatives: **6**(R^1 = H), **6**(R^1 = Me), **5**($R^1 = R^2$ = Me; anion = Br^-). The facility with which the quaternary salts reacted also suggested the intermediacy of the pseudo-base **3**($R^1 = R^2$ = Me) and thus, by analogy, that the parent compound **1**(R = H) reacts via its covalent hydrate **3**($R^1 = R^2$ = H). The changes occurring during bromination were then monitored spectrophotometrically. Upon addition of aqueous bromine to an acidic solution of the cation **2**($R^1 = R^2$ = Me), the u.v. absorption of the latter disappeared immediately but only slowly was it replaced by absorptions appropriate to the 5-bromo cation **5**($R^1 = R^2$ = Me). Similar behavior is exhibited by the other substrates **1**(R^1 = H or Me), namely, that the solution obtained from mixing equimolar quantities of solutions of these substrates and bromine had no significant absorption above 220 nm. These observations suggested the initial formation of nonaromatic adducts of the type **4** (see Scheme 1) for which there are precedents.

Barbieri *et al.* have isolated derivatives of the type **11** formed during the bromination of some 2-sulfonamidopyrimidines (7). Likewise the bromination of 1,3-dimethyluracil has been postulated (8) to occur via the intermediate **12**(R^1 = Me; R^2 = H) and thymine reacts with bromine to form the 5-bromo-5-methylhexahydropyrimidine **12**(R^1 = H; R^2 = Me) (9). Furthermore, with excess bromine uracils give 5,5-dibromo derivatives **12**(R^2 = Br) (1, 2).

Attempts to isolate and characterize the adducts **4** failed, giving white labile materials

[1]Author to whom correspondence should be addressed.

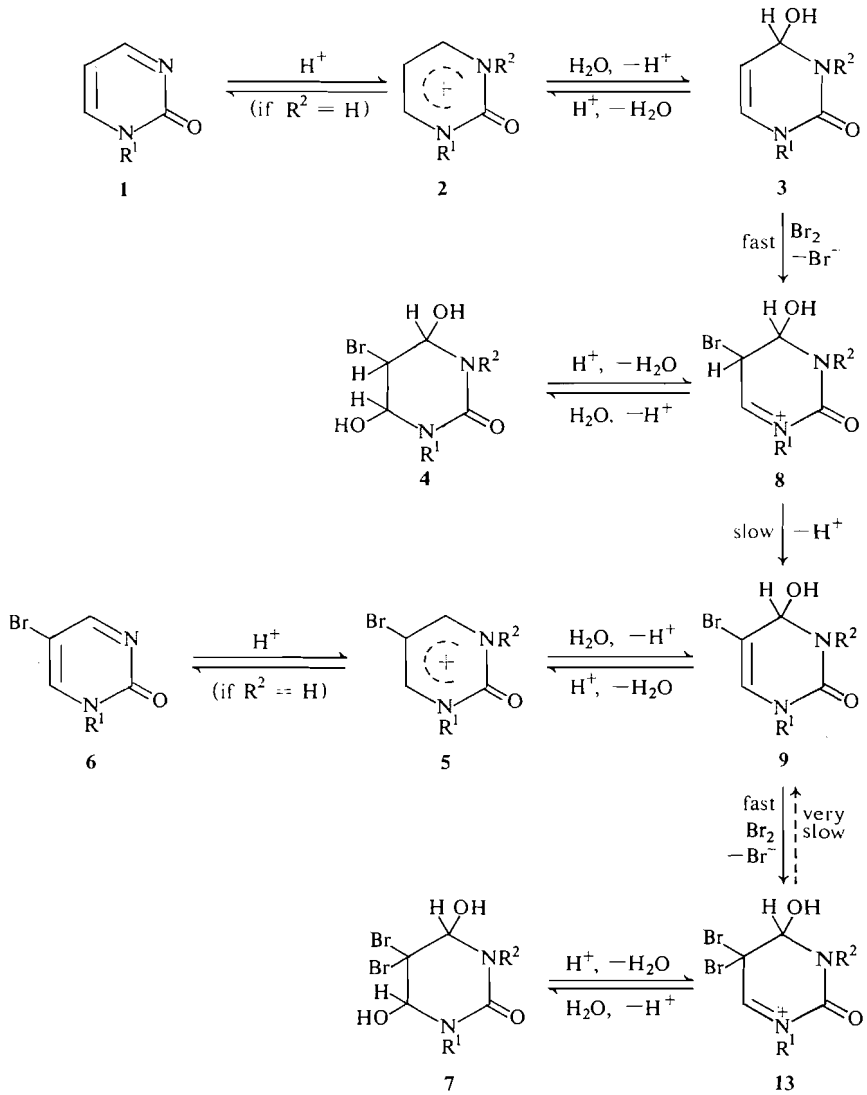

SCHEME 1

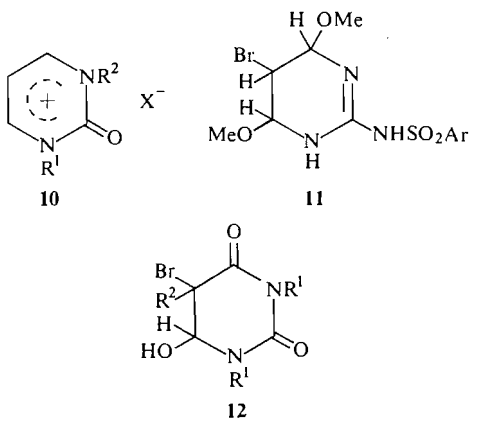

which readily transform to the 5-bromo products **5** or **6**. However they may be observed using n.m.r. spectroscopy. Upon addition of bromine to D_2O solutions of **1**(R^1 = H or Me), and **2**(R^1 = R^2 = Me) signals appropriate to **4** are observed. The 5-proton appears as a complex multiplet centered at δ 4.4 and the 4,6-protons as a multiplet at δ 5.0 with relative integrated intensities of approximately 1:2. The *N*-methyl protons, if present, appear at δ 2.88. Repeat experiments using substrates having deuterium at the 5-position give spectra lacking the absorptions at δ 4.4 and showing much simplification of the multiplet at δ 5.0. The complexity of the

Can. J. Chem. Downloaded from www.nrcresearchpress.com by 210.87.254.42 on 09/05/12
For personal use only.

TABLE 1. Variation of the rate of appearance of the brominated product **5** with acidity for the substrates **10** at 30 °C

R^1	R^2	X^-	$[H_2SO_4]$ (M)	$[H_3O^+]$* (M)	$k_{obs} \times 10^4$† (min^{-1})
H	H	Cl^-	0.250	0.261	1.88
			0.300	0.311	2.19
			0.400	0.411	3.19
			0.500	0.511	4.12
Me	H	Cl^-	0.250	0.261	6.10
			0.350	0.361	7.95
			0.400	0.411	9.5
			0.500	0.511	12.0
Me	Me	HSO_4^-‡	0.050	0.059	5.91
			0.100	0.110	10.8
			0.250	0.261	28.3
			0.300	0.311	34.1
			0.430	0.441	53.3
			0.500	0.511	63.3
			0.665	0.677	80.6
			0.690	0.702	84.0§
			0.500	0.511	34.5‖
			0.75	—	72.6‖
			1.00	—	97.1‖

*Calculated from the molarity of H_2SO_4 assuming the second dissociation constant of H_2SO_4 is $K_2 = 1.2 \times 10^{-2}$ (12).
†Average from two or more determinations. Estimated errors are less than 5%.
‡Data for this compound are shown in Fig. 1.
§Single run.
‖At 25 °C.

multiplets and the *N*-methyl absorptions suggest that the species **4** may be present in more than one diastereomeric form.

With time the n.m.r. absorptions we assign to **4** decrease, and are replaced by those appropriate to the 5-bromo derivatives **5** and **6**. These also react with bromine to give materials with no significant u.v. absorptions and which are presumably the 5,5-dibromo-4,6-dihydroxyhexahydropyrimidines **7**. Indeed for **7**($R^1 = R^2$ = Me) a white crystalline material was isolated whose elemental analysis, n.m.r., and mass spectra are consistent with the proposed structure. The n.m.r. (in DMSO-d_6) shows two singlets: δ 2.87, area 3 (*N*—Me); δ 5.00, area 1 ($C_{4,6}$—H). The mass spectrum has three peaks at *m/e* 316, 318, 320 (approximate ratio 1:2:1) as expected for **7**($R^1 = R^2$ = Me) having two bromines.

The bromination of the title compounds seems, then, to involve a rapid reaction with bromine to give adducts **4** which slowly undergo elimination to yield the 5-bromo derivatives **5** and **6**. The kinetics of this latter process were measured spectrophotometrically by monitoring the u.v. absorption of the products as a function of time. At fixed acid concentrations, first-order kinetics were observed for all three substrates and the rate constants presented in Table 1 were obtained. Part of these data are shown in Fig. 1. Clearly the process being followed is acid catalyzed, as would be expected for the dehydration **4** ⇄ **8** → **9** ⇄ **5** (see Appendix). The presence of *N*-methyl groups facilitates the reaction, presumably by increasing the proportion of **8** relative to **4**.

Kinetics were also measured in stronger acid (1.0–2.19 M H_2SO_4) for **2**($R^1 = R^2$ = Me, HSO_4^-) but a minor complication arises in this region in that first-order plots for the increase of product absorbance are significantly curved (10). This we believe to be due to the formation of some **7**($R^1 = R^2$ = Me) which in a very slow process reverts to **5**($R^1 = R^2$ = Me) and so precludes accurate measurement of A_∞.

As the acidity of the medium increases, the proportion of the pseudo-base **3** relative to the cation **2** is decreased (3, 4). Consequently at the higher acid concentrations it is observed that the time for the initial rapid disappearance of bromine is perceptibly longer, since the conversion **2** → **4** is retarded. At the same time, however, the increased acidity facilitates the process **4** → **5**, and at higher acidities it is quite possible

Can. J. Chem. Downloaded from www.nrcresearchpress.com by 210.87.254.42 on 09/05/12
For personal use only.

TABLE 2. Variation of rate of appearance of the brominated product **5**($R^1 = R^2 = Me$) with the acidity function H_0 for the substrate **10**($R^1 = R^2 = Me$; $X = HSO_4$) at 30 °C

$[H_2SO_4]$ (M)	H_0	$k_{obs} \times 10^2$* (min^{-1})	$\log k_{obs}$†
1.00	−0.30	1.75	−1.7570
1.28	−0.48	2.66	−1.5751
1.50	−0.61	3.68	−1.4342
2.00	−0.89	5.96	−1.2248
2.19	−0.99	8.47	−1.0721

*Average of two or more determinations. Estimated errors less than 5%.
†These values are plotted against H_0 in Fig. 2.

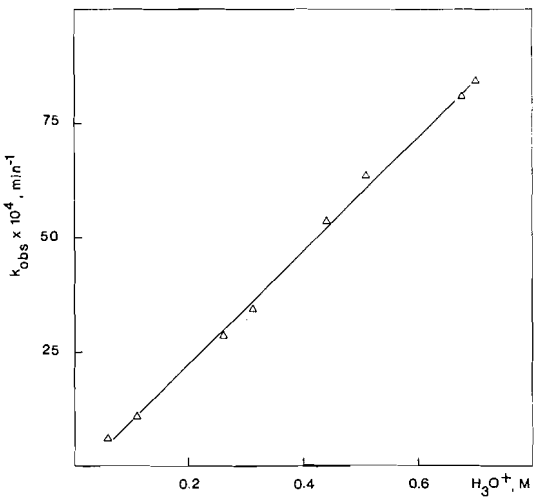

FIG. 1. Variation of the rate of appearance of the product **5**($R^1 = R^2 = Me$) with acidity (30 °C).

that **2** (through **3**) and **5** (through **9**) may compete for bromine and that some of **5** be converted to the dibromo product **7**. This would explain why the A_∞ measured is less than anticipated but does not explain the curvature we have observed. The absorbance measured after 10 half-lives (A_∞) did not remain constant but gradually increased well after the reaction should have theoretically gone to completion if it was strictly limited to the conversion **4** → **5**. This observation suggests a further slow formation of the 5-bromo product **5**. In a separate experiment it was noted that when the 5,5-dibromo adduct **7** was dissolved in 2 M H_2SO_4 solution absorption appropriate to **5** appeared very gradually over an extended period of time.

It seems likely, therefore, that the inaccurate value of A_∞, which leads to the curvature of the first-order plots, is due to a slow conversion of **7** to **5**. Although this reaction does not occur significantly during the normal time of measurement of absorbance values, it influences the final absorbance value to a small extent. Hence on lowering A_∞ slightly to correct for this reaction, good straight first-order plots were obtained for the rate of appearance of **5**. Values of A_∞ were chosen to give the best least squares fit of the absorbance data to a first-order plot. Rate constants derived from such plots are shown in Table 2, and they exhibit a linear dependence upon acidity as anticipated (see Fig. 2).

Experiments were also carried out in which the initial bromine concentration was more than twice that of the pyrimidine substrate. Under these conditions one cannot directly observe the appearance of **5** since it reacts rapidly with bromine to give **7** (via **9**). However, following the rapid consumption of 1 mol equiv. of bromine during the formation of **4**, one can

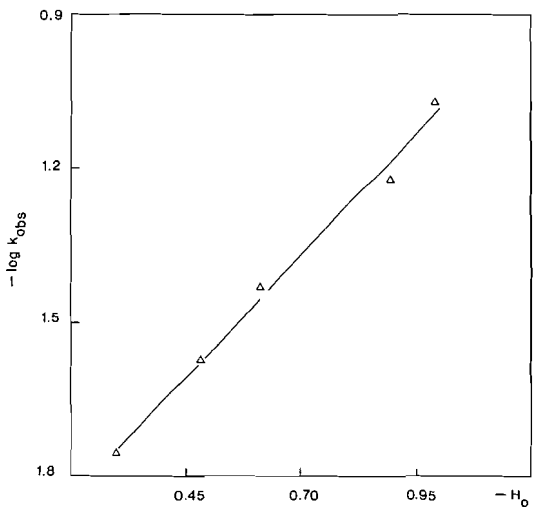

FIG. 2. Variation of the rate of appearance of the product **5**($R^1 = R^2 = Me$) with the acidity function H_0 (30 °C).

Can. J. Chem. Downloaded from www.nrcresearchpress.com by 210.87.254.42 on 09/05/12
For personal use only.

Can. J. Chem. Downloaded from www.nrcresearchpress.com by 210.87.254.42 on 09/05/12
For personal use only.

observe a slow decrease in bromine absorbance as the remaining bromine is consumed by **5** as rapidly as the latter is formed. Consistent with this interpretation, rate constants obtained by measuring the decreasing bromine absorption are, within experimental error, identical to those measured for the appearance of **5** in the absence of excess bromine.[2]

In the dehydration of the intermediate **4** it is envisaged that the slow step is the removal of the proton at the 5-position of **8**. To test this hypothesis 5-deuterio-**2** ($R^1 = R^2 = Me$, HSO_4^-) was prepared by isotopic exchange (3, 4), and the rate of its bromination was measured. In 0.5 *M* H_2SO_4 it gave $k_{obs} = 10.8 \times 10^{-4}$ min^{-1} from which $k_{obs}^H/k_{obs}^D = 5.9$. Such a large isotope effect is entirely consistent with the rate-determining rupture of C_5—H bond of the intermediate **8** (11).[3]

Work in progress also implicates covalent adducts similar to **4** in the bromination of other pyrimidine substrates.

Experimental

The melting points given below are uncorrected. Ultraviolet determinations were made on a Cary 14 instrument, n.m.r. spectra were obtained from a Varian A-60 spectrometer, and the mass spectrum was run on a Perkin-Elmer-Hitachi RMU-6E mass spectrometer. Elemental analyses were performed by Galbraith Labs. Inc., Knoxville, Tennessee, and by A. B. Gygli, Toronto, Ontario.

*2-Pyrimidinone Hydrochloride (**10**, $R^1 = R^2 = H$; $X = Cl$)*

This compound from Aldrich was recrystallized from ethanol–water before use.

*1-Methyl-2-pyrimidinone Hydrochloride (**10**, $R^1 = Me$; $R^2 = H$; $X = Cl$)*

This compound was prepared by literature methods (4, 13).

*1,2-Dihydro-1,3-dimethyl-2-oxopyrimidinium Hydrogen Sulfate (**10**, $R^1 = R^2 = Me$; $X = HSO_4$)*

Previously (4) this compound was made from the corresponding chloride by treatment with silver sulfate. It is more conveniently made by direct condensation.

1,3-Dimethylurea (8.8 g, 0.1 mol) in 40 ml absolute ethanol was added to 1,1,3,3-tetraethoxypropane (22 g, 0.1 mol) and the resulting solution was cooled in ice water. Upon dropwise addition of 95% sulfuric acid (20 g, 0.2 mol) the stirred solution became yellow and deposited an orange-yellow precipitate. The mixture was then heated at 50° for 30 min. Cooling to room temperature and filtration gave 21 g (95%) of pale yellow crystals. Recrystallization from ethanol–methanol–water afforded 18.3 g (83%) long colorless needles, m.p. 204–206°, reported (4) m.p. 200–205°. The n.m.r. spectrum agreed with literature values (4).

Anal. Calcd. for $C_6H_{10}N_2O_5S$: C, 32.43; H, 4.54; N, 12.61. Found: C, 32.54; H, 4.59; N, 12.72.

The 5-deuterated material was prepared by heating a sealed glass tube containing 2.2 g (0.01 mol) of the above crystals in 10 ml deuterium oxide at 100° for 10 days. The tube was cooled to 0°, opened, and the contents were decolorized by filtration through "Norite". Solvent removal and recrystallization from ethanol–water gave 1.82 g (81%) of long colorless needles. The n.m.r. spectrum in D_2O showed less than 3% protium at the 5-position of the pyrimidine ring.

*5-Bromo-2-pyrimidinone (**6**, $R^1 = H$)*

This was made in 84% yield by the method of Crosby and Berthold (14) but using 2-pyrimidinone hydrochloride in place of the free base.

*5-Bromo-1-methyl-2-pyrimidinone (**6**, $R^1 = Me$)*

To 1-methyl-2-pyrimidinone hydrochloride (0.5 g, 3.4 mmol) in 5 ml water was added saturated bromine water until color persisted. Removal of the solvent under reduced pressure gave a yellow material, which was recrystallized from ethanol to give white flakes, m.p. 237–239° (darkens at 180°), reported (15) m.p. 210–211° (darkens at 170°); n.m.r. (D_2O), δ 3.97 (s, 3, CH_3), 9.49 and 9.33 (AB "quartet" $J_{4,6} = 3$ Hz, 1 and 1, H_4 and H_6).

Anal. Calcd. for $C_5H_5N_2OBr$: C, 31.78; H, 2.65; N, 14.83; Br, 42.28. Found: C, 31.80; H, 2.75; N, 14.85; Br, 42.17.

*5-Bromo-1,2-dihydro-1,3-dimethyl-2-oxopyrimidinium Bromide (**5**, $R^1 = R^2 = Me$; anion = Br^-)*

To 1,2-dihydro-1,3-dimethyl-2-oxopyrimidinium chloride (4) or sulfate (1 mmol) was added 10 ml of 0.1 *M* bromine water. The resulting solution was reduced to dryness, and the pale yellow residue was recrystallized from ethanol to give 0.189 g (67%) bright yellow crystals, m.p. 267–268° (dec); n.m.r. (D_2O), δ 3.88 (s, 6, $N_{1,3}$—CH_3), 9.05 (s, 2, $H_{4,6}$); u.v. spectrum (9.5% H_2SO_4), λ_{max} (log ε) 222 (4.10), 346 (3.85).

Anal. Calcd. for $C_6H_8N_2OBr_2$: C, 25.38; H, 2.84; N, 9.87; Br, 56.28. Found: C, 25.59; H, 2.82; N, 9.76; Br, 56.06.

*5,5-Dibromo-4,6-dihydroxy-1,3-dimethylhexahydro-2-oxopyrimidine (**7**, $R^1 = R^2 = Me$)*

To 1 g (3.5 mmol) of the product of the previous preparation was added saturated bromine water until color persisted. A white material (0.97 g, 87%) immediately precipitated from solution, m.p. 135° (dec); n.m.r. (DMSO-d_6), δ 2.87 (s, 6, $N_{1,3}$—CH_3), 5.00 (s, 2, $H_{4,6}$), 3.40 (broad, 2, $O_{4,6}$—H); mass spectrum *m/e*, 316, 318, 320 (approximate ratio 1:2:1).

Anal. Calcd. for $C_6H_{10}N_2O_3Br_2$: C, 22.67; H, 3.15;

[2]For example, in 0.5 *M* H_2SO_4 at 25 °C the rate constant obtained by monitoring product increase in the absence of excess bromine was 3.45×10^{-3} min^{-1} (average of 10 runs). That obtained by monitoring bromine decrease was 3.62×10^{-3} min^{-1} (average of three runs), when initial bromine exceeded that of pyrimidine substrate.

[3]It should be noted that of the species **1**–**9** and **13** only **8** and **13** have not been directly observed.

TABLE 3. Ultraviolet spectral data and protonation pK_a's of the pyrimidine substrates and their 5-bromo derivatives

Pyrimidine	pK_a	pH or H_0	λ_{max} (log ε)		Reference
2-Pyrimidinone	2.24	6.21	298(3.67)	215(>4.0)	19
		0	309(3.75)	215(>3.2)	
1-Methyl-2-pyrimidinone	2.5	6.0	302(3.73)	215(4.0)	19
		0.3	313(3.85)	215(3.80)	
1,2-Dihydro-1,3-dimethyl-2-oxo-pyrimidinium hydrogen sulfate	7.03*	10.1	296(2.70)	239(3.93)	4†
		0.29	316(3.93)	215(>4.0)	
5-Bromo-2-pyrimidinone	0.44	4.0	322(3.54)	222(4.16)	20
		0.22	343(3.65)	222(4.19)	
5-Bromo-1-methyl-2-pyrimidinone	0.55	4.0	326(3.43)	225(4.0)	20
		−2.0	346(3.55)	224(3.96)	
5-Bromo-1,2-dihydro-1,3-dimethyl-2-oxopyrimidinium bromide	3.08‡	0.29	346(3.85)	222(4.10)	6†
		9.18	252(3.88)	<200(>4.00)	

*For the equilibrium 2 ⇄ 3, $K = [3][H^+]/[2] = 10^{-7.03}$ (4).
†This work.
‡For the equilibrium 5 ⇄ 9, $K = [9][H^+]/[5]$.

N, 8.81; Br, 50.27. Found: C, 22.63; H, 3.05; N, 8.86; Br, 50.13.

Kinetic Procedures (10)

Sulfuric acid and sodium thiosulfate solutions were prepared from commercial standard volumetric concentrates. Solutions of bromine in aqueous sulfuric acid were estimated by titration against sodium thiosulfate. This must be done frequently since bromine loss to the air is considerable.

The concentration of hydronium ion in dilute acid solutions was calculated assuming the second dissociation constant of sulfuric acid to be 1.2×10^{-2} (12). For stronger acid solutions values of H_0 were obtained from Johnson *et al.* (16) using "wt % H_2SO_4" calculated from "molarity" and the known density of sulfuric acid – water mixtures (17).

Rates of product formation were measured by monitoring a suitable wavelength in the region 365–375 nm using a Cary 14 spectrophotometer. Temperature control was maintained by circulating water through the cell holders from a Neslab TE9 constant temperature bath kept at 30.00 ± 0.02 °C. Solutions were kept at 30 °C prior to mixing and the start of kinetic measurements. Normally (>15) absorbance values were measured over at least 2 half-lives, and A_∞ values measured after at least 10 half-lives. Plots of ln $(A_\infty - A)$ *vs.* time gave good straight lines but only those having correlation coefficients >0.9998 were used to calculate rate constants. Such rate constants were independent of the initial concentrations of either bromine or pyrimidine substrates.

The rate data for the 5-deuterio substrate show initial curvature due to the preferential consumption of the small amount of protio material (<3%). Rate constants were obtained by the method of Brown and Fletcher (18) which utilizes the latter portions of the rate data which are very linear. The initial curvature corresponded to <3% protio material in agreement with the estimate from n.m.r. spectra. The rate constant for 5-deuterio substrate given in the text is the average of three determinations (1.05, 1.08, and 1.10×10^{-3} min^{-1}).

Ultraviolet spectral data for the pyrimidine substrates and their 5-bromo derivatives are presented in Table 3.

Appendix[4]

It is proposed that rates we have measured are for the reaction

$$4 + H^+ \overset{K}{\rightleftharpoons} 8 \underset{\text{slow}}{\overset{k}{\longrightarrow}} 9 \rightleftharpoons 5$$

For this scheme rate $= k_{obs}[5] = k[8]$, since $[5] \gg [9]$. However, the rate of appearance of **5** must equal the rate of the stoichiometric disappearance of **4**, and thus

$$\text{rate} = k_{obs}[4]_{st} = k[8],$$

and

$$k_{obs} = k[8]/[4]_{st}$$

where $[4]_{st} = ([4] + [8])$

For the equilibrium between **4** and **8**,

$$K = \frac{[4][H^+]}{[8]},$$

and so

$$\frac{[8]}{([4] + [8])} = \frac{[H^+]}{(K + [H^+])}$$

Therefore,

$$k_{obs} = \frac{k[H^+]}{(K + [H^+])}$$

a familiar result.

Also as long as the equilibrium lies in favor of **4**, *i.e.* $K \gg [H^+]$, then

$$k_{obs} = k[H^+]/K$$

and acid catalysis should be observed.

[4]The development of these equations was requested by a referee.

Can. J. Chem. Downloaded from www.nrcresearchpress.com by 210.87.254.42 on 09/05/12
For personal use only.

Our results require, therefore, that even in the strongest acid (2 *M* H_2SO_4), that **4** predominates over **8**. One might expect that the equilibrium formation of an iminium ion from a carbinolamine would be relatively complete in such a medium. In the present case, however, the iminium system of **8** is conjugated to a carbonyl and its equilibrium formation should be less facile. Furthermore, the observation of **4** (by n.m.r.), but not **8**, in solutions of 1–2 *M* acid is consistent with a value of $K \gg 1$.

The authors thank the National Research Council of Canada for financial support. Some of the preliminary experiments in this study were carried out in the laboratory of Prof. Keith Yates at the University of Toronto.

1. D. J. BROWN. The Pyrimidines. Vol. 16 *of* The chemistry of heterocyclic compounds. *Edited by* A. Weissberger. Interscience, New York. 1962.
2. D. J. BROWN. Supplement I. Wiley-Interscience, New York. The Pyrimidines 1970.
3. A. R. KATRITZKY, M. KINGSLAND, and O. S. TEE. Chem. Commun. 289 (1968).
4. A. KATRITZKY, M. KINGSLAND, and O. S. TEE. J. Chem. Soc. B, 1226 (1968).
5. C. D. JOHNSON, A. R. KATRITZKY, M. KINGSLAND, and E. F. V. SCRIVEN. J. Chem. Soc. B, 1 (1971).
6. O. S. TEE and S. BANERJEE. Chem. Commun. 1032 (1972).
7. W. BARBIERI, L. BERNARDI, G. PALAMIDESSI, and M. T. VENTURI. Tetrahedron Lett. 2931 (1968); W. BARBIERI, L. BERNARDI, F. LUINI, and G. PALAMIDESSI. Il Farmaco, Ed. Sci. **24**, 561 (1969); **25**, 694, 702 (1970).
8. A. M. MOORE and S. M. ANDERSON. Can. J. Chem. **37**, 590 (1959); S. Y. WANG. J. Org. Chem. **24**, 11 (1959).
9. C. BAUDISCH and D. DAVIDSON. J. Biol. Chem. **64**, 234 (1925).
10. S. BANERJEE. M.Sc. Thesis. Sir George Williams University, Montreal, Quebec. 1972.
11. K. B. WIBERG. Chem. Rev. **55**, 713 (1955); F. H. WESTHEIMER. Chem. Rev. **61**, 265 (1961).
12. J. G. DICK. Analytical chemistry. McGraw-Hill, New York. 1973. p. 665.
13. J. J. FOX and D. VAN PRAEG. J. Am. Chem. Soc. **82**, 486 (1960).
14. D. G. CROSBY and R. V. BERTHOLD. J. Org. Chem. **25**, 1916 (1960).
15. D. J. BROWN and R. V. FOSTER. Aust. J. Chem. **19**, 2321 (1966).
16. C. D. JOHNSON, A. R. KATRITZKY, and S. A. SHAPIRO. J. Am. Chem. Soc. **91**, 6654 (1969).
17. International critical tables, **3**, 56 (1928).
18. H. C. BROWN and R. S. FLETCHER. J. Am. Chem. Soc. **71**, 1845 (1949).
19. D. J. BROWN, E. HOERGER, and S. F. MASON. J. Chem. Soc. 211 (1955).
20. D. J. BROWN and T. C. LEE. Aust. J. Chem. **21**, 243 (1968).

Can. J. Chem. Downloaded from www.nrcresearchpress.com by 210.87.254.42 on 09/05/12
For personal use only.

Deuterium Isotope Effect on Shifts of ^{13}C Magnetic Resonance Signals of Sugars: Signal Assignment Studies[1]

PHILIP A. J. GORIN

Prairie Regional Laboratory, National Research Council of Canada, Saskatoon, Saskatchewan S7N 0W9

Received October 12, 1973

The ^{13}C chemical shifts of nuclei in several sugars undergo an isotope effect of 0 to -0.10 p.p.m. when a proton in the β position is substituted by a deuteron. The effect may be used for signal assignments in crowded spectra if it is taken into account that lower values are observed for ^{13}C nuclei which are attached to more electronegative groups. The β effect coupled with the elimination of the α-carbon signal have been used to assign signals in c.m.r. spectra of the α- and β-anomers of D-glucose, D-mannose, D-allose, and D-galactose.

Les déplacements chimiques du ^{13}C de plusieurs noyaux dans différents sucres subissent un effet isotopique de 0 à -0.10 p.p.m. lorsqu'un proton en position β est remplacé par un deutérium. Cet effet peut être utilisé lors de l'attribution des signaux d'un spectre complexe si l'on tient compte du fait que l'on observe les valeurs les plus basses pour les noyaux ^{13}C attachés aux groupes les plus électronégatifs. L'effet β en même temps que l'élimination du signal α-carbon, a été utilisée pour attribuer les signaux des spectres r.m.c. de l'αβ-D-glucose, de l'αβ-D-mannose, de l'αβ-D-allose et de l'αβ-D-galactose.
[Traduit par le journal]

Can. J. Chem., **52**, 458 (1974)

Signals of carbon-13 magnetic resonance (c.m.r.) spectra can be assigned following replacement of a given proton by a deuteron. The signal of the attached ^{13}C nucleus either disappears (1) or is converted to a triplet (2) at 0.1–0.5 p.p.m. higher field (3–6). Progressively smaller upfield shifts are observed for signals of the β-carbon (~0.1 p.p.m.; (3, 5–7)) and γ-carbon (~0.01 p.p.m.; (6)) nuclei. $^{13}C—C—^{2}H$ (5, 7) and $^{13}C—C—C—^{2}H$ (6) coupling can also occur.

In the carbohydrate field the $^{13}C—^{2}H$ effect, in which the ^{13}C signal is eliminated, has been used to assign c.m.r. signals (8). The current results show that the $^{13}C—C—^{2}H$ effect can also be used for assignment of certain sugar signals. For example, C-5 signals of hexose derivatives are identifiable using 6-$^{2}H_2$ derivatives which are more easily prepared than 5-^{2}H derivatives (9). The upfield shift of the C-5 signal is ~0.12 p.p.m. (measured to an accuracy of ±0.01 p.p.m.) (Table 1). The values were determined using mixtures of deuterated and undeuterated material in D_2O using conditions that do not detect differences of shift of <0.02 p.p.m. Assignments of C-5 signals for α- and β-anomers of D-mannose and D-galactose agree with previous ones obtained in H_2O (10, 11). Although shifts of C-5 signals of αβ-D-glucose in D_2O differ a little from those described in H_2O (8), the assignments essentially agree (see Experimental section).

The upfield shifts due to the $^{13}C—C—^{2}H$ effect in a number of monodeuterated hexoses were determined and recorded in Table 1. Their magnitude varied from approximately 0.01 to 0.10 p.p.m. per deuteron which is less than 0.09–0.15 p.p.m. observed with compounds having less electronegative substituents on the β-carbon (3, 5). (In contrast with nonoxygenated derivatives, $^{13}C—C—^{2}H$ and $^{13}C—C—C—^{2}H$ coupling (5–7) were not detected.) Similarly, an inverse relationship between the size of the shift and the deshielding on the ^{13}C nucleus was observed. The C-1 resonances of αβ-D-glucose-2-^{2}H and αβ-D-mannose-2-^{2}H are shifted 0–0.02 p.p.m. upfield, compared with the C-3 resonances of the methyl 2,3-di-*O*-methyl derivatives of α-D-glucopyranoside-4-^{2}H and α-D-galactopyranoside-4-^{2}H (0.04 p.p.m.), and the other β-CHOH derivatives (0.05–0.10 p.p.m.). No variation was noted on going from an axial to an equatorial ^{2}H nucleus.

It is possible, therefore, using the α- and β-carbon effects to assign the ^{13}C nuclei in spectra containing signals that are very close together, such as those of αβ-D-glucose and αβ-D-allose. The signal assignments obtained for αβ-D-glucose, αβ-D-mannose, and β-D-allose in D_2O agree essentially with those made by Perlin and co-workers (8, 10) and somewhat less with

[1]NRCC No. 13613.

Can. J. Chem. Downloaded from www.nrcresearchpress.com by 210.87.254.42 on 09/05/12
For personal use only.

TABLE 1. Upfield displacement of $^{13}C—C—^{2}H$ signals of sugars* compared with those of corresponding $^{13}C—C—^{1}H$ resonances in p.p.m.

Sugar	Displacement
αβ-D-Glucose-2-^{2}H	C_β-3 (0.06), C_α-3 (0.05); C_α-1, C_β-1 (0–0.02)
αβ-D-Glucose-3-^{2}H	C_β-2 (0.05), C_β-4 (0.06); C_α-2, C_α-4 obscured
αβ-D-Glucose-5-^{2}H	C_α-4, C_α-6, C_β-6 (0.06); C_α-4 obscured
αβ-D-Glucose-6-$^{2}H_2$	C_α-5, C_β-5 (0.12)
αβ-D-Mannose-6-$^{2}H_2$	C_β-5 (0.11), C_α-5 (0.13)
αβ-D-Galactose-6-$^{2}H_2$	C_α-5 (0.12), C_β-5 (0.10)
αβ-D-Galactose-4-^{2}H	C_β-5 (0.04), C_β-3 (0.06), C_α-5 (0.06), C_α-3 (0.10)
αβ-D-Allose-3-^{2}H	C_α-2, C_β-2 (0.09); C_α-4, C_β-4 (0.08)
αβ-D-Mannose-2-^{2}H	C_α-3, C_β-3 (0.06); C_α-1, C_β-1 (0–0.02)
Methyl 2,3-Di-*O*-methyl-α-D-galactopyranoside-4-^{2}H	C-3 (0.04), C-5 (0.08)
Methyl 2,3-Di-*O*-methyl-α-D-glucopyranoside-4-^{2}H	C-3 (0.04), C-5 (0.07)

*α and β subscripts refer to configuration of hexose.

those of Dorman and Roberts (11), who both used H_2O as solvent. In the case of αβ-D-galactose in D_2O, the present assignments of the six low-field signals agree with those of both groups of workers. However, the next four signals at δ_C 69.96, 69.81, 69.40, and 69.01 should be given different assignments of C_α-4, C_α-3, C_β-4, and C_α-2. Examination of the c.m.r. spectra of αβ-D-galactose-4-^{2}H and unmutarotated α-D-galactose served to assign the C_α-4 and C_β-4 signals. The remaining C_α-3 and C_α-2 signals were distinguishable since the spectrum of αβ-D-galactose mixed with its 4-^{2}H derivative contained C_α-3 as two signals with a 0.10 p.p.m. shift difference. Repetition of these experiments using aqueous solutions indicated a similar order of signals.

Three deuterated compounds were prepared for spectral examination. Methyl 6-*O*-benzoyl-2,3-di-*O*-benzyl-β-D-glucopyranoside (12) was oxidized with dimethyl sulfoxide – phosphorus pentoxide to the 4-keto derivative. Reduction with sodium borodeuteride followed by debenzylation gave a mixture containing methyl 2,3-di-*O*-benzyl-β-D-galactopyranoside-4-^{2}H. It was hydrogenolyzed using palladium on charcoal and the product hydrolyzed with acid. Chromatography on a column of cellulose provided the required galactose-4-^{2}H. In another reaction sequence methyl 2,3-di-*O*-methyl-α-D-glucopyranoside (13) was converted to its 6-benzoate, which was oxidized by dimethyl sulfoxide – acetic anhydride to the 4-keto derivative. Sodium borodeuteride reduction gave the 6-*O*-benzoyl-D-galacto isomer as the predominant one and a portion was debenzoylated to give required methyl 2,3-di-*O*-methyl-α-D-galactopyranoside-4-^{2}H. Another portion of the 6-*O*-benzoyl derivative was converted to its 4-*O*-*p*-toluenesulfonyl derivative which was treated with sodium benzoate in refluxing *N*,*N*-dimethylformamide to give methyl 4,6-di-*O*-benzoyl-2,3-di-*O*-methyl-α-D-glucopyranoside-4-^{2}H. Debenzoylation gave methyl 2,3-di-*O*-methyl-α-D-glucopyranoside-4-^{2}H.

Experimental

Carbon magnetic resonance spectra were obtained using a Varian XL-100-15 spectrometer with Fourier transform on D_2O solutions (0.5 ml) of compound (80 mg) contained in a coaxial cylinder within a 12 mm diameter × 8 in. tube maintained at 33°. The spectral width was 500 Hz (the total spectrum being thus obtained by combining two portions); the acquisition time 4 s, and the pulse width 117 μs, representing a 90° pulse. The number of transients used was approximately 18 000. In order to determine the extent of the $^{13}C—C—^{2}H$ shift, spectra of deuterated and undeuterated sugar were obtained and then a mixture of deuterated and undeuterated compound was prepared and examined. The latter spectrum was expanded by a factor of two which facilitated manual measurement of the shift difference. Chemical shifts are in p.p.m., based on the downfield difference of the resonance signal and that of external tetramethylsilane. Dioxane (δ_C 67.22) was used as internal standard.

Preparation of Deuterated Derivatives

α-D-Glucose-3-^{2}H, β-D-allose-3-^{2}H (8), α-D-glucose-2-^{2}H, α-D-mannose-2-^{2}H (14), and α-D-glucose-5-^{2}H (15) were prepared as described. The preparations of other deuterated derivatives are presented below.

α-D-*Glucose-6-*$^{2}H_2$

1,2-*O*-Isopropylidene-α-D-glucofuranose-6-$^{2}H_2$ was prepared from 1,2-*O*-isopropylidene-α-D-glucofuranurono-6,3-lactone using the same procedure as described for preparation of the 5,6,6′-$^{2}H_3$ derivative from 1,2-*O*-isopropylidene-α-D-xylohexofuranurono-6,3-lactone-5-ulose (8). Hydrolysis with 0.05 *M* H_2SO_4 at 100° for 1 h gave α-D-glucose-6-$^{2}H_2$ (from MeOH) with m.p. 144–145° and $[\alpha]_D^{25}$ +103 → +49° (*c*, 0.4 H_2O; constant value).

Can. J. Chem. Downloaded from www.nrcresearchpress.com by 210.87.254.42 on 09/05/12
For personal use only.

Can. J. Chem. Downloaded from www.nrcresearchpress.com by 210.87.254.42 on 09/05/12
For personal use only.

Anal. Calcd. for $C_6DH_{11}O_6$: C, 39.56; H + D, 7.74. Found: C, 39.3; H + D, 7.8.

α-D-*Galactose-6-*$^2H_2$

D-Galacturonic acid (0.40 g) was treated with refluxing 3% methanolic hydrogen chloride (10 ml) for 3 h, the solution neutralized (Ag_2CO_3), filtered, and evaporated to a sirup. Dissolution in 0.1 *M* $NaOCH_3$ in methanol (5 ml) was carried out and sodium borodeuteride (0.10 g) added. After 18 h the solution was evaporated, Na^+ removed with a suspension of Amberlite 1R120 (H^+ form) in water, and boric acid was removed as trimethyl borate by repeated evaporations of methanol. The resulting methyl galactosides were hydrolyzed in 0.5 *M* sulfuric acid (5 ml) at 100° for 6 h, the solution neutralized ($BaCO_3$), filtered, and the filtrate deionized with mixed bed resin. The residue obtained on evaporation crystallized from methanol giving α-D-galactose-6-$^2H_2$ with m.p. 159–161° and $[\alpha]_D^{25}$ +134 → +79° (*c*, 0.3 H_2O; constant value).

Anal. Calcd. for $C_6D_2H_{10}O_6$: C, 39.56; H + D, 7.74. Found: C, 39.6; H + D, 7.6.

α-D-*Mannose-6-*$^2H_2$

Using a procedure similar to that described above β-D-mannofuranurono-γ-lactone (200 mg; supplied by ICN-K&K Laboratories) was converted to α-D-mannose-6-$^2H_2$ (80 mg from EtOH) with m.p. 122° and $[\alpha]_D^{25}$ +25 → +15° (*c*, 0.3 H_2O; constant value).

Anal. Calcd. for $C_6D_2H_{10}O_6$: C, 39.56; H + D, 7.74. Found: C, 39.2; H + D, 7.8.

α-D-*Galactose-4-*^2H

Methyl 6-*O*-benzoyl-2,3-di-*O*-benzyl-β-D-glucopyranoside (1.90 g) was dissolved in dimethyl sulfoxide (50 ml) containing phosphorus pentoxide (7 g). After 1 week chloroform was added to the reaction mixture which was washed with water and evaporated. Thin-layer chromatography on silica gel (solvent, chloroform) showed the presence (spray, 50% sulfuric acid) of unchanged material and a faster moving spot corresponding to a ketone. After longer reaction times the relative amount of the faster spot did not increase. Use of the α-anomer as starting material was unsuccessful. The mixture was fractionated on a column of silicic acid (eluant, chloroform, 2:hexane, 3) to give the ketone (0.15 g) and a mixed fraction (1.12 g), from which the benzoate (0.35 g) crystallized. The mother liquor was evaporated and treated in methanol (10 ml) at −20° with sodium borodeuteride (0.20 g). After 1 h the product partitioned between water and chloroform. To the chloroform layer was added 0.1 *M* sodium methoxide in methanol (10 ml) in order to remove the benzoate group. The product was fractionated on a column of silicic acid, using as eluants chloroform followed by chloroform containing 2% methanol. Crystallization of the eluate from ether–hexane gave methyl 2,3-di-*O*-benzyl-β-D-glucopyranoside (0.27 g) and 0.13 g of sirupy material. The original sirupy ketone fraction (0.15 g) was reduced with $NaBD_4$ in a fashion similar to that described above, the product debenzoylated and combined with the above sirupy material (0.13 g). Hydrogenolytic debenzylation of the product with 5% palladium on charcoal in acetic acid gave a mixture of methyl β-D-glucopyranoside and methyl β-D-galactopyranoside (0.14 g). Hydrolysis with 0.5 *M* H_2SO_4 (5 ml) for 6 h at 100° gave galactose and glucose which were separated on a column of cellulose (eluant, *n*-butyl alcohol containing 5% water) providing a fraction containing galactose (60 mg). Crystallization from methanol gave α-D-galactose-4-^2H (36 mg) with m.p. 160–161° and $[\alpha]_D^{25}$ +127 → +76° (*c*, 0.1 H_2O; constant value).

Anal. Calcd. for $C_6DH_{11}O_6$: C, 39.68; H + D, 7.23. Found: C, 39.5; H + D, 7.4.

Methyl 2,3-Di-O-methyl Derivatives of α-D-*Galactopyranoside-4-*^2H *and* α-D-*Glucopyranoside-4-*^2H

Using benzoyl chloride (1.1 mol/mol) in pyridine as reagent methyl 2,3-di-*O*-methyl-α-D-glucopyranoside (3.60 g) was converted to its sirupy 6-benzoate (6.31 g). The product gave a single spot on t.l.c. (solvent, chloroform containing 4% methanol) and had $[\alpha]_D^{25}$ +108° (*c*, 0.5 EtOH); p.m.r. data (dimethyl sulfoxide-$^2H_6$; tetramethylsilane as external standard), δ 5.74 (*J* = 5 Hz, secondary OH).

Anal. Calcd. for $C_{16}H_{22}O_7$: C, 58.88; H, 6.80. Found: C, 58.4; H, 6.6.

The benzoate was dissolved in dimethyl sulfoxide (30 ml) containing acetic anhydride (20 ml). After 18 h the mixture was partitioned between chloroform and water and the material in the chloroform layer chromatographed on a column of silicic acid (eluant, chloroform, 1:hexane, 1). The product (5.9 g) gave two spots on t.l.c. (solvent, chloroform containing 3% methanol), the slower of which corresponded to the ketone. The mixture was reduced with sodium borodeuteride (for procedure see the above reduction of the di-*O*-benzyl derivative) and the product chromatographed on a column of silicic acid (eluant, chloroform) to give methyl 6-*O*-benzoyl-2,3-di-*O*-α-D-galactopyranoside-4-^2H which contained a trace of the α-D-glucopyranoside isomer.

Debenzoylation of a portion gave methyl 2,3-di-*O*-methyl-α-D-galactopyranoside-4-^2H, which had a c.m.r. spectrum that would be anticipated from that of authentic undeuterated material (16). Trace signals were present which corresponded to the deuterated gluco-derivative.

Anal. Calcd. for $C_9DH_{17}O_6$: C, 48.42; H + D, 8.58. Found: C, 48.0; H + D, 8.4.

The deuterated 6-benzoate fraction (1.32 g) was dissolved in pyridine (5 ml) containing *p*-toluenesulfonyl chloride (1.5 g). After 4 days at 37° the solution was added to water and the precipitate, which crystallized, was recrystallized from ethanol. The resulting methyl 6-*O*-benzoyl-2,3-di-*O*-methyl-4-*O*-*p*-toluenesulfonyl-α-D-galactopyranoside-4-^2H had m.p. 143–144° and $[\alpha]_D^{25}$ +86° (*c*, 0.8 $CHCl_3$).

Anal. Calcd. for $C_{23}DH_{27}O_9S$: C, 57.37; H + D, 6.07. Found: C, 57.3; H + D, 6.1.

The *p*-toluenesulfonate (0.30 g) was treated with refluxing *N*,*N*-dimethylformamide (60 ml) containing sodium benzoate (2.0 g). After 20 h the reaction mixture was partitioned between chloroform and water. The chloroform layer was evaporated and the residue crystallized from ether–hexane to give methyl 4,6-di-*O*-benzoyl-2,3-di-*O*-methyl-α-D-glucopyranoside-4-^2H (0.16 g) with m.p. 120–121° and $[\alpha]_D^{25}$ +92° (*c*, 0.5 EtOH); p.m.r. (dimethyl sulfoxide-$^2H_6$; tetramethylsilane as external standard); δ 7.85–8.42 (10 aromatic protons); 5.34 (*J* = 3.6 Hz, H-1), 3.68, 3.72, 3.74 (3 OCH_3's).

Anal. Calcd. for $C_{23}DH_{25}O_8$: C, 64.02; H + D, 6.31. Found: C, 63.8; H + D, 6.3.

Can. J. Chem. Downloaded from www.nrcresearchpress.com by 210.87.254.42 on 09/05/12
For personal use only.

Debenzoylation of the dibenzoate (0.12 g) with methanolic sodium methoxide gave methyl 2,3-di-*O*-methyl-α-D-glucopyranoside-4-^{2}H (52 mg from ether) with m.p. 77–78° and $[\alpha]_D^{25}$ +150° (*c*, 0.3 H_2O).

Anal. Calcd. for $C_9DH_{17}O_6$: C, 48.42; H + D, 8.58. Found: C, 48.2; H + D, 8.3.

Signal Assignments

Chemical shifts described below are those obtained in this laboratory.

αβ-D-*Mannose*. Assignments based on results of refs. 10 and 11 in H_2O: 94.60 (C_α-1), 94.24 (C_β-1), 76.75 (C_β-5), 73.65 (C_β-3), 73.02 (C_α-5), 71.83 (C_β-2), 71.31 (C_α-2), 70.83 (C_α-3), 67.50 (C_α-4), 67.22 (C_β-4), 61.63 ($C_{\alpha\beta}$-6), which are confirmed by the ^{13}C—C—^{2}H method.

αβ-D-*Glucose*. Assignments based on results of reference 10 in H_2O and present ^{13}C—C—^{2}H shift results which serve to distinguish C_β-5 from C_β-3, and C_α-2 from C_α-5 in D_2O: 96.50 (C_β-1), 92.70 (C_α-1), 76.59 (C_β-5), 76.43 (C_β-3), 74.80 (C_β-2), 73.45 (C_α-3), 72.14 (C_α-2), 72.10 (C_α-5), 70.36 (C_α-4), 70.28 (C_β-4), 61.47 (C_β-6), 61.31 (C_α-6).

αβ-D-*Galactose*. Assignments for the six lowest field signals of refs. 10 and 11 in H_2O agree with each other and those obtained by the ^{13}C—C—^{2}H method using the 6-^{2}H derivative: 97.02 (C_β-1), 92.90 (C_α-1), 75.71 (C_β-5), 73.45 (C_β-3), 72.54 (C_β-2), 71.07 (C_α-5), 69.96 (C_α-4), 69.81 (C_α-3), 69.40 (C_β-4), 69.01 (C_α-2), 61.81 (C_α-6), 61.63 (C_β-6). Signals at δ_C 69.96–69.01 were assigned using αβ-D-galactose-4-^{2}H (see theoretical section).

αβ-D-*Allose*. The results from the β-anomer were from ref. 10 in H_2O and confirmed (these disagreed with those of ref. 11). The partial results of ref. 11 for the α-anomer were confirmed and C_α-2 and C_α-5 assignments (120.9 or 121.4, respectively in ref. 11) made by the ^{13}C—C—^{2}H method: 93.97 (C_β-1), 93.37 (C_α-1), 74.17 (C_β-5), 72.26 (C_α-3), 71.87 (C_β-2), 71.75 (C_β-3), 67.62 (C_α-2), 67.50 (C_α-5), 67.42 (C_β-4), 66.71 (C_α-4), 61.83 (C_β-6), 61.35 (C_α-6). The spectrum of αβ-D-allose-3-^{2}H does not contain the C_β-3 signal but the C_β-2 signal is shifted upfield to occupy the approximate position of the C_β-3 signal of αβ-D-allose.

Methyl 2,3-Di-O-methyl-α-D-glucopyranoside. Assignment based on D-glucose in H_2O (10): 97.22 (C-1), 82.94 (C-3), 80.56 (C-2), 72.14 (C-5), 69.72 (C-4), 61.11 (C-6), 60.63, 58.73, 55.48 (3 OCH_3's).

Methyl 2,3-Di-O-methyl-α-D-galactopyranoside. Assignment based on above assignments for α-D-galactose and the ^{13}C—C—^{2}H method: 97.14 (C-1), 78.70 (C-3), 77.06 (C-2), 71.07 (C-5), 69.72 (C-4), 61.90 (C-6), 58.06, 56.43, 55.48 (3 OCH_3's).

The author wishes to thank Mr. M. Mazurek for preparation of c.m.r. spectra.

1. H. Spiesecke and W. G. Schneider. J. Chem. Phys. **35**, 731 (1961).
2. F. J. Weigert and J. D. Roberts. J. Am. Chem. Soc. **89**, 2967 (1967).
3. G. L. Lebel, J. D. Laposa, B. G. Sayer, and R. A. Bell. Anal. Chem. **43**, 1500 (1971).
4. Yu. K. Grishin, N. M. Sergeyev, and Yu. A. Ustynyuk. Mol. Phys. **22**, 711 (1971).
5. D. Doddrell and I. Burfitt. Aust. J. Chem. **25**, 2239 (1972).
6. R. A. Bell, C. L. Chan, and B. G. Sayer. J. Chem. Soc. Chem. Commun. 67 (1972).
7. G. E. Maciel, P. D. Ellis, and D. C. Hofer. J. Phys. Chem. **71**, 2160 (1967).
8. H. J. Koch and A. S. Perlin. Carbohydr. Res. **15**, 403 (1970).
9. J. Lehmann. Carbohydr. Res. **2**, 1 (1966).
10. A. S. Perlin, B. Casu, and H. J. Koch. Can. J. Chem. **48**, 2596 (1970).
11. D. E. Dorman and J. D. Roberts. J. Am. Chem. Soc. **92**, 1355 (1970).
12. D. M. Hall and T. E. Lawler. Carbohydr. Res. **16**, 1 (1971).
13. J. C. Irvine and J. P. Smith. J. Chem. Soc. **103**, 575 (1913).
14. P. A. J. Gorin. Can. J. Chem. **51**, 2105 (1973).
15. W. Mackie and A. S. Perlin. Can. J. Chem. **43**, 2921 (1965).
16. D. J. Bell and G. D. Greville. J. Chem. Soc. 1136 (1955).

Studies on the Biosynthesis of Antheridiol

C. R. POPPLESTONE AND A. M. UNRAU

Department of Chemistry, Simon Fraser University, Burnaby 2, British Columbia

Received July 30, 1973

Sexual reproduction in the aquatic fungus *Achlya bisexualis* is governed by antheridiol, a C_{29} sterol, secreted by the female plant and which initiates formation of antheridial hyphae on the male plant. Tracer studies showed that naturally occurring fucosterol supplied the necessary carbon skeleton for antheridiol. Labelling and trapping studies with a series of hypothetic sterol precursors have indicated the biological sequence involved in elaboration of the antheridiol side chain.

La reproduction sexuelle chez le champignon aquatique *Achlya bisexualis* est sous contrôle de l'anthéridiol, un stérol en C_{29}, secrété par l'espèce femelle et qui provoque la formation chez l'espèce mâle de l'anthéridial hyphae. Les études à l'aide de traceurs ont montré que le fucostérol, un produit naturel fournit le squelette carboné nécessaire à l'anthéridiol. Les études par marquage et par captage à l'aide d'une série de précurseurs hypothétiques du type stérol ont mis en évidence la séquence biologique impliquée lors de l'élaboration de la chaîne latérale de l'anthéridiol. [Traduit par le journal]

Can. J. Chem., **52**, 462 (1974)

The importance of sterols to permeability, reproduction and growth functions of many fungi has been well documented (1 and references therein). However, with the identification of antheridiol (**1**) as a sex hormone of *Achlya bisexualis* (2), it has been proposed that sterols which have previously been assigned hormonal activity in various fungi are, in fact, precursors of steroidal hormones analogous to antheridiol (3).

Our preliminary investigation of the sterols of *A. bisexualis* showed that fucosterol (**2**) was the major sterol and 7-dehydrofucosterol (**3**), a logical precursor to **2**, was also detected (4). It is reasonable to propose therefore, that fucosterol can provide the necessary carbon skeleton with subsequent modification of the side chain and nucleus for the production of antheridiol. With a view of establishing the biogenetic origin of antheridiol in *A. bisexualis* we have undertaken a biosynthetic study of this fungal sex hormone. The enzymatic conversion of fucosterol (**2**) to antheridiol (**1**) requires four general transformations:

(*1*) oxidation in the B-ring at C_7; (*2*) hydroxylation or oxidation at C_{22}, C_{23}; (*3*) oxidation at C_{29}; and (*4*) lactone formation.

A priori, these transformations could occur in any order. In order to simplify the overall picture and to reduce the total number of potential intermediates to a reasonable number, several reaction sequences were combined in one-step transformations. Also, previous biosynthetic studies of phytosterols have shown that enzymes responsible for steroidal modification have considerable latitude with respect to substrate structure (5). It seems likely therefore that the organism will modify the side chain regardless of the state of transformation of the nucleus. Based on these considerations Fig. 1 shows the possible alternative sequences that could conceivably operate in the elaboration of the antheridiol side chain.

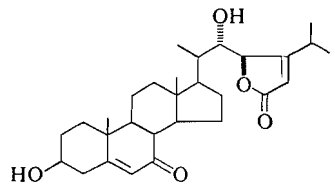

1

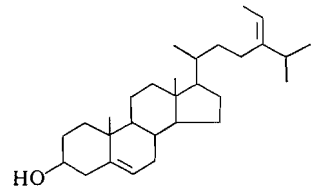

2

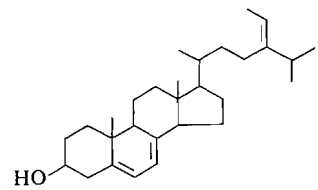

3

Can. J. Chem. Downloaded from www.nrcresearchpress.com by 210.87.254.6 on 09/05/12
For personal use only.

Can. J. Chem. Downloaded from www.nrcresearchpress.com by 210.87.254.6 on 09/05/12
For personal use only.

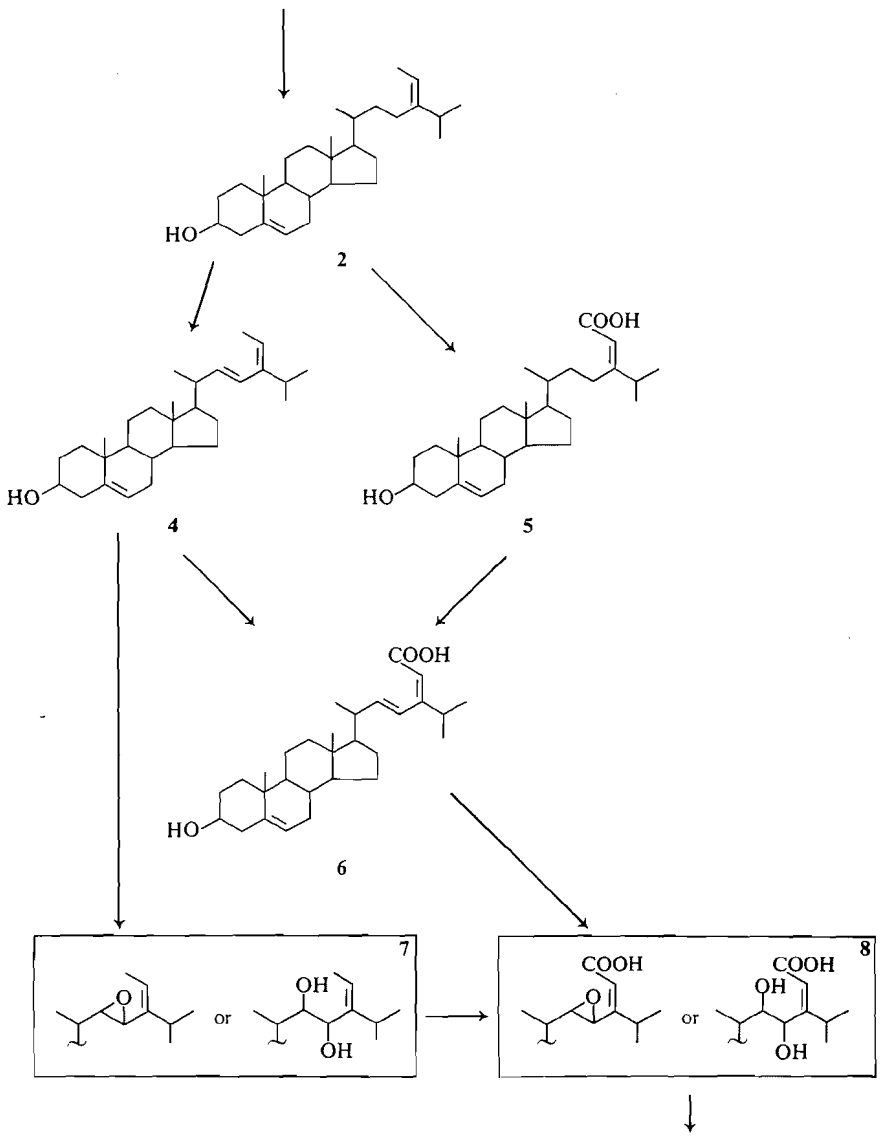

FIG. 1. Postulated intermediates involved in elaboration of the antheridiol side chain.

Using Fig. 1 as a model we approached the investigation of the biosynthesis of antheridiol by initially synthesizing the suspected intermediates (**4**–**6**). This was followed by tracer studies in order to obtain information on possible *in vivo* precursor–product relationships, and finally, we undertook trapping experiments to establish the involvement of individual intermediates in the biogenesis of antheridiol.

Synthesis of Intermediates (Fig. 2)

Synthesis of the intermediates was carried out after careful consideration as to the most favorable precursor to the required compounds **4** and **5**. Synthesis of **6** had been previously reported (6). The starting material chosen for the syntheses was the α,β-unsaturated ketone (**9**) derived from readily available stigmasterol (7). This C_{27} compound (**9**) was favored because it

Can. J. Chem. Downloaded from www.nrcresearchpress.com by 210.87.254.6 on 09/05/12
For personal use only.

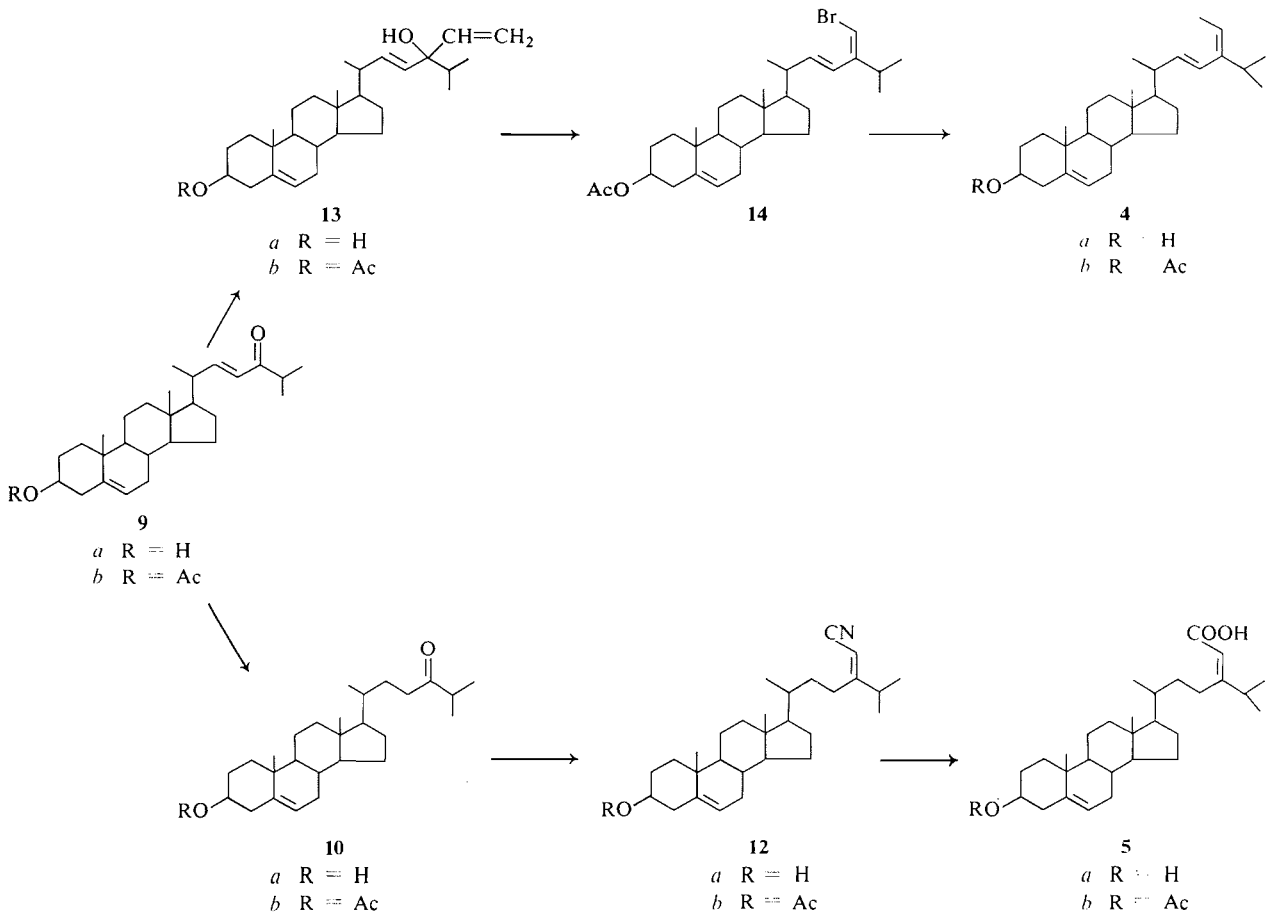

FIG. 2. Synthesis of intermediates.

Can. J. Chem. Downloaded from www.nrcresearchpress.com by 210.87.254.6 on 09/05/12
For personal use only.

possesses a Δ^{22} double bond required in **4**, and also, the carbonyl at C_{24} is suitably positioned for a Wittig reaction required to introduce the extra two carbon atoms in **5**.

$$(C_2H_5O)_2\overset{\overset{O}{\uparrow}}{P}—CH_2CN$$

11

Hydrogenation of the α,β-unsaturated ketone **9** with palladium catalyst poisoned with barium sulfate resulted in a >90% yield of **10** (8). A Wittig reaction (9) of the carbanion of diethyl cyanomethyl phosphonate (**11**) with **10** resulted in a yield of 68% of **12**. The 24(28)(*E*)-configuration was assigned to **12** based on the absence of C_{25}-proton resonance at δ 2.8 in the n.m.r. spectrum (10). Conversion of the nitrile (**12**) to the acid (**5**) was achieved by alkaline hydrolysis.

The C_{28}-isomer of **4** has previously been synthesized by a Wittig reaction between **9***b* and ethyl triphenyl phosphonium iodide (7). The authors reported the C_{25}-proton resonance at δ 2.8 indicative of the 24(28)(*Z*)-configuration (10). In order to synthesize the required *E*-isomer it was necessary to use the method described by Sucrow and Raduchel (11). The vinyl carbinols **13***a* and *b* were prepared from **9***a* and vinyl magnesium bromide in THF. Transformation of **13***b* under allylic rearrangement to the allyl bromide **14** by phosphorus tribromide followed by reduction with lithium aluminum hydride gave the required compound **4**.

Each of the above intermediates (**4**, **5**, and **6**) was also synthesized containing ^{14}C or ^{3}H label. Fucosterol (**2**), isolated from a species of *Fucus* (12), was exchange labelled with ^{3}H by the method of Thompson *et al.* (13). Labelled 7-dehydrofucosterol (**3**) was synthesized by allylic bromination of (^{3}H)-fucosterol with NBS followed by dehydrohalogenation in refluxing trimethylphosphite (7).

Labelling Studies

The finding of 7-dehydrofucosterol (**3**) and fucosterol (**2**) in *A. bisexualis* suggested the possibility that a precursor–product relationship might exist between the two since the normal sequence of double bond changes in the biosynthesis of phytosterols is [$\Delta^7 \rightarrow \Delta^{5,7} \rightarrow \Delta^5$] (14). At the outset of this biosynthetic study it was decided to confirm this relationship by a tracer experiment with ^{3}H-7-dehydrofucosterol. (2,4-$^{3}H_3$)-7-Dehydrofucosterol (11 mg, specific activity 5.3×10^4 c.p.m./mg) was distributed between thirty, 3 day old cultures of *A. bisexualis* and the sterols extracted from the mycelia as previously described after a further 3 day growth period (4). Fucosterol (100 mg) was added as carrier to the extract and after acetylation, separated by preparative thin-layer chromatography on silver nitrate impregnated silica gel, followed by recrystallization to constant activity (483 c.p.m./mg). Specific activity of fucosterol is therefore 483 × 100 c.p.m./mg based on carrier sterol. The complete results of this experiment are recorded in Table 1 and confirm that the transformation **3** → **2** occurs in this organism.

Antheridiol (**1**) has been isolated from culture liquids of *A. bisexualis* after a 3 day growth period (2). Barksdale has reported time course studies with this organism using a bioassay method and demonstrated that hormonal activity steadily increased between 24 and 72 h from time of inoculation after which it remained constant (15). Based on this information it was decided therefore to study the biosynthesis of antheridiol by administration of labelled precursors and work-up of the cultures within a 3 day period.

The mold cultures were grown in 500 ml of media as previously described (2). Radioactive sterol precursor (10–60 mg), emulsified in acetone–water with Tween 80, was equally distributed between sixty, 24 h old cultures of *A. bisexualis* under aseptic conditions and at the end of a 72 h growth period, the cultures worked-up as described previously (2). Since it was not possible to isolate antheridiol from 30 l of culture liquid, due to the small amount produced by the organism, it was necessary to perform a trapping experiment. Usually, synthetic antheridiol (50 mg) dissolved in methanol containing 1% Tween 80 was added to the culture filtrate before extraction with methylene chloride (2).

TABLE 1. Incorporation of 7-dehydrofucosterol into fucosterol

Total c.p.m. of precursor added	Number of recrystallizations	Specific activity* of fucosterol (c.p.m./mg)
5.83×10^5	1	488
	2	466
	3	483
	4	483

*Specific activity of fucosterol based on added carrier (100 mg) = 4.83×10^4 c.p.m./mg; incorporation, 8%.

TABLE 2. Incorporation of intermediates into antheridiol

Precursor	Specific activity (c.p.m./mg)	Total c.p.m. added	Specific activity of antheridiol (c.p.m./mg)	% incorporation
(2,4-$^3H_3$)-Fucosterol (**2**)	1.33×10^6	7.95×10^7	8.0×10^2	0.001
(23,24-$^3H_3$)-Stigmasta-5,22(*E*) 24(28)-triene-3β-ol (**4**)	6.37×10^4	1.91×10^6	2.0×10^2	0.01
(29-^{14}C)-3β-Hydroxystigmasta-5, 22(*E*)24(28)-triene-29-oic acid (**6**)	5.3×10^3	2.40×10^5	2.5×10^2	0.1
(23,25-$^3H_3$)-3β-Hydroxystigmasta-5(*E*)24(28)-diene-29-oic acid (**5**)	1.85×10^5	3.70×10^6	< 100	< 0.002

TABLE 3. Results of trapping experiments

Precursor	Total c.p.m. added	Intermediate	Specific* activity (c.p.m./mg)	% incorporation
^{3}H-Fucosterol (**2**)	3.99×10^7	Stigmasta-5,22,24(28)-triene-3β-ol (**4**)	3.0×10^2	0.07
^{3}H-Stigmasta-5,22,24(28)-triene-3β-ol (**4**)	1.91×10^6	3β-Hydroxystigmasta-5,22,24(28)-triene-29-oic acid (**6**)	1.2×10^2	0.06

*Based on added carrier.

The extract was chromatographed on silica gel with 1:1 ethyl acetate – petroleum ether and the antheridiol purified by preparative t.l.c. on silica gel with 6% MeOH–$CHCl_3$ before determination of the activity.

The antheridiol used as carrier was a mixture of two isomers and it was not possible therefore to recrystallize to constant activity. The two isomers did, however, chromatograph together in the solvent system used and the criteria of purity was therefore taken when rechromatography resulted in constant activity. Antheridiol was then acetylated and again purified by preparative t.l.c. using 1% MeOH–$CHCl_3$ and if the specific activity of the diacetate was found to be similar to that of the deacetylated material, this was taken as evidence that the precursor had been metabolized to antheridiol.

Each of the compounds **2**, **4**, **5**, and **6** was tested as precursor by the method just described and the results are summarized in Table 2, in which the specific activity of antheridiol is based on the amount of added carrier. The results show that compounds **2**, **4**, and **6** were metabolized by the organism to antheridiol.

Trapping experiments were then designed to determine the participation of compounds **4** and **6** as specific intermediates in the biosynthetic pathway. Labelled precursor of antheridiol was added to cultures and unlabelled intermediate (carrier) added during the work-up procedure. The intermediate was reisolated, assayed for radioactivity, and any radioactivity detected furnished strong evidence that the intermediate was involved in the biosynthetic pathway. The results of these studies are summarized in Table 3. In each experiment, the mycelium was subjected to base hydrolysis and the lipid fraction extracted with hexane (4). The respective intermediates were separated by chromatography and crystallized to constant activity.

Compounds **2** and **4** were not separated as their acetates under normal conditions of preparative t.l.c. on silica gel – $AgNO_3$ with benzene. Separation was achieved, however, by continuous t.l.c. over a 5 day period with 20% benzene–hexane in which **4** was slightly more polar. The extraction of **6** was carried out after the hydrolysate had been acidified with dilute HCl. Compound **6** was obtained from the extract by chromatography on a silica gel column and elution with increasing concentrations of methanol in chloroform and finally purified by preparative t.l.c. on silica gel with 8% MeOH–$CHCl_3$.

In order to determine whether the added

Can. J. Chem. Downloaded from www.nrcresearchpress.com by 210.87.254.6 on 09/05/12
For personal use only.

Can. J. Chem. Downloaded from www.nrcresearchpress.com by 210.87.254.6 on 09/05/12
For personal use only.

intermediates were degraded by the microorganism to simpler molecules (acetate) and then became reincorporated into steroids, fucosterol was isolated from the feeding experiment with compound **5**. After separation and purification, fucosterol was found to be devoid of activity thus indicating that compound **5** had not been catabolized by the organism. Based on this experiment, it is reasonable to assume that the other intermediates tested behaved likewise and that the transformations studied had indeed occurred.

The results of tracer experiments (Tables 2 and 3) indicate that the sequence of events leading to elaboration of the γ-lactone side chain of antheridiol involves dehydrogenation at $C_{22,23}$ followed by oxidation at C_{29}. Oxidation at C_{29} can be assumed to follow the sequence: $CH_3 \rightarrow CH_2OH \rightarrow CHO \rightarrow COOH$, similar to that which occurs in the removal of 4-dimethyl groups from lanosterol and cycloartanol (14). The nonincorporation of compound **6** into antheridiol indicates that oxidation at C_{29} does not precede dehydrogenation. Oxidation or hydroxylation at C_{22} and C_{23} to produce a side chain similar to that shown in **7** and **8** must subsequently occur. However, we have not been able to undertake tracer experiments to differentiate between these two possible alternatives because attempts were unsuccessful at synthesizing compounds of this structure. Nevertheless, cyclization in either **7** or **8** could result in γ-lactone formation.

Experimental

Materials and Instrumentation

Fucosterol was isolated from a species of *Fucus* (12) collected from the beach at Vancouver, B.C. Spectra were obtained on the following instruments: Perkin-Elmer 457 (i.r.), Unicam SP 800 (u.v.), Varian A56/60 and XL100 (n.m.r.), Hitachi-Perkin-Elmer RMU-7 double focussing mass spectrometer.

Growth of Fungus

Achlya bisexualis, 14524 obtained from the American Type Culture Collection, was grown on 500 ml of media as previously described (2) and stock cultures were maintained on agar slants (16).

Administration of Radioactive Precursors

The radioactive sterol of known activity (10–60 mg) was emulsified in Tween 80 (~500 mg) and dissolved in acetone. The mixture was diluted with distilled water to ~30 ml and distributed aseptically between the cultures.

Counting of Radioactive Compounds

Radioactivity measurements were made on a Beckman LS200B liquid scintillation counter. The sterol acetates were weighed into counting vials and dissolved in 15 ml of a toluene base scintillation solution containing 2,5-diphenyloxazole (4 g/l) and POPOP (50 mg/l). Antheridiol was dissolved in hot methanol (0.5 ml) before addition of 15 ml of scintillation solution.

Preparation of 3β-Acetoxystigmasta-5,22,(28)-triene-24-ol (13b)

To 2 ml of Grignard reagent prepared from magnesium turnings (1.20 g) and vinyl bromide (5.80 g) in dry THF (30 ml) was added dropwise a solution of **9***a* (500 mg) in THF (2 ml). The solution was left for 1 h with occasional warming to 50°. Excess reagent was decomposed with a saturated solution of ammonium chloride, the product extracted with ether, and dried over $MgSO_4$. Evaporation of the solvent gave **13***a* (32%), recrystallized from ether – petroleum ether, m.p. 150–155 °C.

Acetylation with acetic anhydride/pyridine gave **13***b* recrystallized from ether – petroleum ether, m.p. 138–140°; ν_{max} (KBr) 3470, 1730, 1368, 1260, 970, and 915 cm^{-1}; n.m.r. ($CDCl_3$) δ 0.70 (CH_3—C_{18}, s), 1.02 (CH_3—C_{19}, s), 2.01 (CH_3OCO—, s), 4.3–4.8 (H—C_3, broad m), 4.9–5.6 (5H, H—C_{23}, —CH=CH_2, H—C_6, m), 5.96 (H—C_{23}, d of d, J = 7 Hz and J = 17 Hz).

Mol. Wt. Calcd. for $C_{31}H_{48}O_3$: 468. Found (mass spectrum): 468.

Preparation of 3β-Acetoxystigmasta-5,22(E)24(28)-triene-29-bromide (14)

To a solution of phosphorus tribromide (0.2 ml) in petroleum ether (2 ml) was added pyridine (0.2 ml) and the mixture cooled to 0°. To this solution was added **13***b* (60 mg) and the resulting mixture stirred for 10 min at 0°, diluted with ether, and finally washed several times with H_2O. The extract was dried over $MgSO_4$ and the solvent removed to give **14** as a colorless oil; n.m.r. ($CDCl_3$) δ 0.75 (CH_3—C_{18}, s), 1.02 (CH_3—C_{19}, s), 1.01 (2 CH_3—C_{25}, J = 7 Hz), 2.01 (CH_3OCO—, s), 4.12, 4.17 (CH_3—C_{29}, 2 × d, J = 8.5 Hz), 4.5–4.8 (H—C_3, broad m), 5.42 (H—C_6, narrow m), 5.5–6.1 (3H, m; C_{22}—H, C_{23}—H, C_{28}—H).

Preparation of 3β-Acetoxystigmasta-5,22(E)24(28)-triene (4b)

To a solution of **14** (100 mg) in THF (3 ml) was added lithium aluminum hydride (80 mg) and the mixture refluxed for 2 h. The solution was diluted with ether, washed with H_2O, and dried over $MgSO_4$. The residue, after removal of the solvent, was acetylated, and purified by t.l.c. on silica gel – $AgNO_3$ (benzene). The product, **4***b*, was recrystallized from MeOH, m.p. 106–107°; ν_{max} (KBr) 2940, 1740, 1365, 1250, 1110, 1035, and 955 cm^{-1}; λ_{max} (EtOH) 236 nm (ε = 19 000); n.m.r. ($CDCl_3$) δ 0.72 (CH_3—C_{18}, s), 1.02 (CH_3—C_{19}, s), 1.01 (2CH_3—C_{25}, d, J = 7 Hz), 1.71 (CH_3—C_{29}, d, J = 7 Hz), 2.01 (CH_3OCO—, s), 4.3–4.8 (H—C_3, broad m), 5.2–6.5 (4H, H—C_{22}, C_{23}, C_{28}, and C_6).

Mol. Wt. Calcd. for $C_{31}H_{48}O_2$: 452. Found (mass spectrum): 452.

Preparation of 3β-Acetoxystigmasta-5(E)24(28)-diene-28-nitrile (12b)

A solution of diethyl cyanomethyl phosphonate (**11**) (1.8 g) in dry THF (4 ml) was added dropwise with stirring to a suspension of sodium amide (0.4 g) in dry THF (6 ml), at 0–5 °C. The resulting mixture was stirred at room temperature under a slow stream of N_2 for 3 h. To the

Can. J. Chem. Downloaded from www.nrcresearchpress.com by 210.87.254.6 on 09/05/12
For personal use only.

resulting yellowish-green solution was added **10***a* (2.5 g in THF, 4 ml), and the solution stirred for a further 20 h. The solvent was removed *in vacuo*, water added to the residue, and the aqueous solution extracted with ether followed by drying over $MgSO_4$ and evaporated to dryness. The residue was acetylated with acetic anhydride – pyridine to give **12***b* (68%) which was recrystallized from methanol, m.p. 108–109 °C; ν_{max} (KBr) 2940, 2210, 1715, 1480, 1370, and 1255 cm^{-1}; λ_{max} (EtOH) 222 nm (ε = 9000) and 260 nm (ε = 2800); n.m.r. ($CDCl_3$) δ 0.69 (CH_3—C_{18}, s), 1.02 (CH_3—C_{19}, s), 1.09 ($2CH_3$—C_{25}, d, J = 7 Hz), 1.12 (H—C_{21}, d, J = 7 Hz), 2.02 (CH_3OCO—, s), 4.3–4.8 (H—C_3, broad m), 5.10 (CN—CH=, d, J = 1 Hz), 5.38 (H—C_6, narrow m).

Mol. Wt. Calcd. for $C_{31}H_{47}O_2N$: 465. Found (mass spectrum): 465.

Preparation of 3β-Acetoxystigmasta-5(E)24(28)-diene-29-oic Acid (5b)

Hydrolysis of **12***b* (150 mg) was carried out by refluxing in 40% H_2O–MeOH for 4 h. After cooling, the solution was acidified with dilute HCl, extracted with ethyl acetate, and the combined extract dried over $MgSO_4$ and evaporated to dryness to give **5***a*, which upon recrystallization from acetone had m.p. 180–182°.

Acetylation of **5***a* in the same manner gave **5***b* m.p. 74–75°; ν_{max} (KBr) 3400, 2940, 1760, 1375, 1280, 1115, and 1032 cm^{-1}; λ_{max} (EtOH) 208 nm (ε = 5100); n.m.r. ($CDCl_3$) δ 0.69 (CH_3—C_{18}, s), 1.02 (CH_3—C_{19}, s), 2.02 (CH_3OCO—, s), 4.3–4.8 (H—C_3, broad m), 5.3–6.0 (2H, =CH—COO and H—C_6, narrow m).

Mol. Wt. Calcd. for $C_{31}H_{48}O_4$: 484. Found (mass spectrum): 484.

Preparation of Antheridiol

Antheridiol was synthesized by the method of McMorris *et al.* (17). The *erythro* isomers (*RS*) and (*SR*) were separated from the *threo* isomers, but since attempts at separation of the *erythro* isomers resulted in only small quantities of the required isomer (22*S*, 23*R*), it was decided to use the isomeric mixture (*erythro*) in trapping experiments. Both isomers had similar R_f values on silica gel in several solvent systems and cochromatographed with authentic antheridiol.[1]

Preparative t.l.c. of antheridiol was performed using silica gel "254" (20 × 20 cm, 1 mm thick) with 6% MeOH – $CHCl_3$.

Preparation of Tritium-labelled Compounds

(2,4-$^3H_3$)-Fucosterol was prepared by the method of Thompson *et al.* (13). The product was purified by t.l.c. (silica gel – $AgNO_3$ – benzene) and recrystallized from MeOH. It had a specific activity of 1.33×10^6 c.p.m./mg.

Tritium-labelled compounds **4** and **5** were prepared by the methods described above from the corresponding (23,25-$^3H_2$) ketone **9**, obtained by tritium exchange on basic alumina deactivated with tritiated water as described by Hofmann *et al.* (18). Compounds **4** and **5** had specific activities of 6.37×10^4 and 1.85×10^5 c.p.m./mg, respectively.

Preparation of (29-^{14}C)-3β-hydroxystigmasta-5,22(*E*)-24(28)-triene-29-oic acid (**6**) was carried out by the method of Edwards *et al.* (6). Thus, aldol condensation of 3β-acetoxy-22,23-bisnorchol-5-en-24-al with the anion of ethyl *trans*-3,4-dimethyl-2-pentenoate, prepared from acetic acid-1-^{14}C (1.0 mC) by the method described (19), resulted in the formation of (**6**) with a specific activity of 1.6×10^4 c.p.m./mg.

Synthesis of (2,4-$^3H_3$)-7-Dehydrofucosterol

(2,4-$^3H_3$)-Fucosterol (1.79×10^5 c.p.m./mg) (300 mg) was diluted with carrier fucosterol (700 mg) and benzoylated. A solution of fucosterol benzoate (1 g) in CCl_4 (25 ml) was heated to reflux and NBS (400 mg) added. The mixture was refluxed for 8 min, then cooled in ice and filtered. The filtrate was added dropwise to a boiling solution of trimethylphosphite (1.3 g) in xylene (8 ml). After refluxing for 90 min, the xylene was removed *in vacuo* and the residue hydrolyzed by refluxing for 1 h in alcoholic KOH (20 ml). The residue was acetylated and the product purified on a silica gel column impregnated with $AgNO_3$ and eluted with benzene–hexane 1:1. 7-Dehydrofucosterol acetate was further purified by preparative t.l.c. on silica gel – $AgNO_3$ and hydrolyzed by refluxing in 2% K_2CO_3 in 10% H_2O–MeOH for ½ h. Work-up in the usual way and recrystallization from MeOH gave 12 mg of 7-dehydrofucosterol, m.p. 120–121°, reported (20) m.p. 119–121°, with specific activity 5.3×10^4 c.p.m./mg.

Financial assistance from the National Research Council of Canada and Simon Fraser Research stipend (C.R.P.) are gratefully acknowledged.

1. C. G. Elliot, M. Hendrie, and B. A. Knights. J. Gen. Microbiol. **42**, 425 (1966).
2. T. C. McMorris and A. W. Barksdale. Nature, **215**, 320 (1967).
3. E. Heftmann. Lipids, **6**, 128 (1970).
4. C. R. Popplestone, and A. M. Unrau. Phytochemistry, **12**, 1131 (1973).
5. L. R. Lenton, J. Hall, A. R. H. Smith, E. L. Ghisalberti, H. H. Rees, L. J. Gioad, and T. W. Goodwin. Arch. Biochem. Biophys. **143**, 664 (1971).
6. J. A. Edwards, J. S. Mills, J. Sundeen, and J. H. Fried. J. Am. Chem. Soc. **91**, 1248 (1969).
7. M. Fryberg, A. C. Oehlschlager, and A. M. Unrau. Tetrahedron, **27**, 1261 (1971).
8. M. Fryberg, A. C. Oehlschlager, and A. M. Unrau. J. Am. Chem. Soc. **95**, 5747 (1973).
9. C. R. Popplestone and A. M. Unrau. Can. J. Chem. **51**, 1223 (1973).
10. D. J. Frost and J. P. Ward. Tetrahedron Lett. 3779 (1968).
11. W. Sucrow and B. Raduchel. Chem. Ber. **103**, 2711 (1970).
12. E. Reiner, J. Topliff, and J. D. Wood. Can. J. Biochem. Physiol. **40**, 1401 (1962).
13. M. J. Thompson, D. W. Berngruber, and P. D. Klein. Lipids, **6**, 233 (1970).
14. R. B. Clayton. Q. Rev. Lond. **19**, 201 (1965).
15. A. W. Barksdale. Mycol. **55**, 164 (1963).
16. A. W. Barksdale. Am. J. Bot. **49**, 633 (1962).
17. T. C. McMorris, T. Arunachalam, and R. Seshadri. Tetrahedron Lett. 2673 (1972).
18. A. F. Hoffmann, P. A. Szczepanik, and P. D. Klein. J. Lipid Res. **9**, 707 (1968).
19. W. S. Wadsworth and W. D. Emmons. J. Am. Chem. Soc. **87**, 5661 (1965).
20. W. R. Nes and P. A. Govinda Malya. J. Biol. Chem. **246**, 561 (1971).

[1]Kindly supplied by Dr. T. C. McMorris, The New York Botanical Garden, Bronx, N.Y.

The Specificity of the Nucleophilic Site of α-Chymotrypsin and its Potential for the Resolution of Alcohols. Enzyme-catalyzed Hydrolyses of Some (+)-, (—)-, and (±)-2-Butyl, -2-Octyl, and -α-Phenethyl Esters[1]

YONG YENG LIN, DAVID N. PALMER, AND J. BRYAN JONES[2]

Lash Miller Chemical Laboratories, Department of Chemistry, University of Toronto, Toronto, Ontario M5S 1A1

Received May 23, 1973

The α-chymotrypsin-catalyzed hydrolyses of a representative spectrum of (*R*)- and (*S*)-2-butyl, -2-octyl, and -α-phenethyl esters of *N*-acetyl-L-phenylalanine, *N*-acetylglycine, α-hydroxy-β-phenylpropionic, dihydrocinnamic, and hippuric acids have been examined. The kinetic studies were carried out in order to provide data on the practicability of exploiting the stereospecificity of the nucleophilic region of the active site of the enzyme for the resolution of racemic alcohols via selective hydrolysis of their esters. The data obtained indicate that the structure and chirality of the alcohol moieties affect both the catalytic and binding constants of the substrates and that the greatest differences between enantiomeric alcohol moieties are observed for nonspecific substrates of the dihydrocinnamate and hippurate series. For racemic esters of the latter type, the stereospecificity of the alcohol site is such that significant resolution of racemic esters and alcohols can be achieved via α-chymotrypsin-catalyzed hydrolyses on a preparative scale.

On a étudié l'hydrolyse catalysée par l'α-chymotrypsine d'une variété représentative d'esters (*R*) et (*S*), butyl-2, octyl-2 et α-phénetyl de la *N*-acétyl-L-phénylalanine, de la *N*-acétyl glycine et des acides α-hydroxy β-phénylpropionique, dihydrocinnamique et hippurique. Des études en cinétique ont été menées afin d'obtenir des données sur la possibilité d'exploiter le caractère stéréospécifique de la région nucléophilique du site actif de l'enzyme lors de la résolution d'alcools racémiques via une hydrolyse sélective de leur ester. Les données recueillies montrent que la structure et la chiralité des alcools modifient toutes deux les constantes catalytiques et de liaison des substrats; de même, elles montrent que les plus grandes différences entre les alcools énantiomériques sont observées pour des substrats nonspécifiques de la série dihydrocinnamate et hippurate. Pour les esters racémiques de ce dernier type, la stéréospécificité du site de l'alcool est telle qu'une résolution efficace d'esters et d'alcools racémiques peut être effectuée à l'échelle préparative via des hydrolyses catalysées par l'α-chymotrypsine.

[Traduit par le journal]

Can. J. Chem., **52**, 469 (1974)

The primary stereospecificity of α-chymotrypsin has been exploited extensively for the kinetic resolution of a broad structural range of racemic acids, usually via hydrolysis of their ester derivatives (1). In contrast, the secondary specificity of the enzyme with respect to chiral alcohol moieties of ester substrates, and its possible application to the resolution of racemic alcohols in an analogous manner, has received very little attention. The structural specificity of the alcohol site of α-chymotrypsin has been the subject of somewhat sporadic investigation and the data are generally indicative of a binding locus which is hydrophobic in character and which is moderately sensitive to both steric and electronic factors (2). Surprisingly, the stereospecificity of this site has been virtually ignored. However, the degrees of enantiomeric preferences observed during transesterification of acetylchymotrypsin with (±)-2-butanol (3) and hydrolyses of L-phenylalanyl esters of several racemic alcohols (4) demonstrate that the secondary stereospecificity of α-chymotrypsin in the nucleophilic region can be significant. Kinetic and preparative-scale studies on the α-chymotrypsin-catalyzed hydrolyses of (+)-, (−)-, and (±)-2-butyl, -2-octyl and -α-phenethyl esters **1–5** have now been carried out in order to evaluate the practicability of exploiting nucleophilic site stereospecificity for the resolution of racemic alcohols via selective enzymic hydrolysis of their esters and to delineate some of the factors involved. The results obtained establish that the method does have preparative potential and that the most favorable results are likely to be achieved using hippurate esters of hydrophobic alcohols.

[1]Abstracted in part from the M.Sc. Thesis of D.N.P., University of Toronto, 1972.

[2]To whom correspondence should be addressed.

Can. J. Chem. Downloaded from www.nrcresearchpress.com by 210.87.254.105 on 09/05/12
For personal use only.

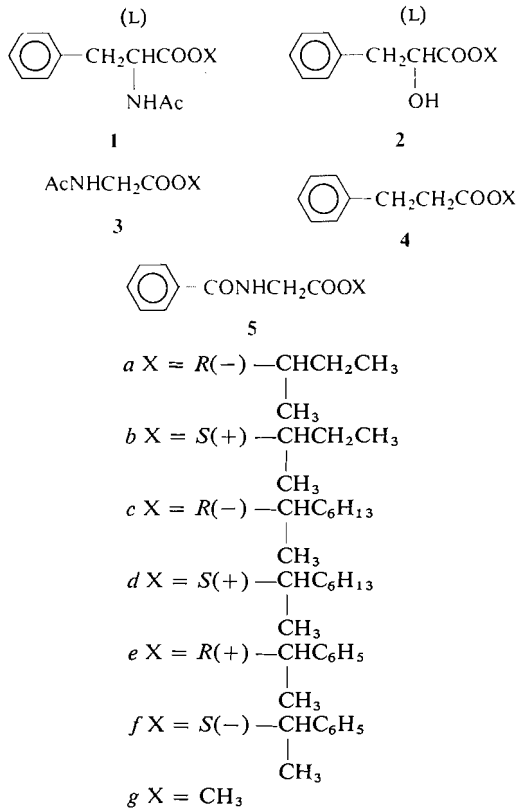

Results

The substrates studied, **1***a–f*, **2***a* and *b*, **3***a* and *b*, **4***a–f*, and **5***a–f*, were prepared from the appropriate *R* or *S* enantiomer of 2-butanol, 2-octanol, or α-phenethyl alcohol by Fischer esterification of the acids **1–3** (X = H) or via the acid chlorides of **4** and **5** (X = H). All chiral substrates were purified to constant optical rotation and in addition, for the diastereomeric esters **1***a–f* and **2***a* and *b*, that no racemization of the chiral center of the acid moiety had occurred was verified in each case using an α-chymotrypsin assay procedure.

The effect of the acyl moiety on the kinetic parameters[3] was evaluated on the representative 2-butyl esters **1***a* and *b* – **5***a* and *b*. The results obtained, which are included in Table 1, showed that the overall variations in the catalytic (k_{cat}), Michaelis (K_m), and specificity (k_{cat}/K_m) constants (5) were greatest for the enantiomeric dihydrocinnamates **4***a* and *b* and hippurates **5***a* and *b* and accordingly, the study was extended to their 2-octyl and α-phenethyl esters **4***c–f* and **5***c–f*. The corresponding *N*-acetyl-L-phenylalanine compounds **1***c–f* and the methyl esters **1***g*, **4***g*, and **5***g* were also evaluated.

The data obtained (Table 1) show that, except for **1***e* and *f*, k_{cat} and/or K_m vary significantly for the stereoisomers (with respect to the alcohol component) of each pair of esters. The largest differences occur with the non-specific (6) dihydrocinnamate and hippurate esters; with the analogous specific (6) substrates **1***a–f* the variations between the *R* and *S* alcohol derivatives are less marked. For dihydrocinnamate and hippurate alkyl esters acylation of the enzyme is considered to be the rate determining step (6, 7) under the kinetic conditions applied and the k_{cat} and K_m values of Table 1 therefore approximate closely the acylation $(k_2)^3$ and enzyme–substrate binding $(K_s)^3$ constants for the esters **4***a–g* and **5***a–g*. That this conclusion is valid for the hippurate series was confirmed as shown by Table 2. The k_2 and K_s values for **5***a*, *b*, *e–g*, were calculated using k_{cat} for the α-chymotrypsin-catalyzed hydrolysis of *p*-nitrophenyl hippurate as the deacylation rate constant $(k_3)^3$ for hippuryl–chymotrypsin (8, 9).

The total data confirm that the nucleophilic site of α-chymotrypsin is capable of considerable stereospecificity with respect to chiral, hydrophobic, alcohol moieties, particularly when they are attached to non-specific substrate acyl groups such as dihydrocinnamoyl or hippuryl. Although variations in the magnitudes of k_{cat}/K_m for enantiomeric esters do not exceed ~six-fold for any of the compounds examined in this study, the differences are sufficient to enable partial resolutions of racemic esters to be achieved in preparative-scale reactions in the more favorable cases. Representative resolution data are given in Table 3.

Discussion

The (*R*)- and (*S*)-2-butyl, -2-octyl, and -α-phenethyl alcohol moieties were selected for the initial study since their absolute configurations were known (10) and each enantiomer was commercially available. Preparation of the esters **1–5**

[3]The usual α-chymotrypsin steady state kinetics terminology outlined below has been used throughout this paper.

$$E + RCOOR' \overset{K_s}{\rightleftharpoons} ERCOOR' \xrightarrow[\text{(acylation)}]{k_2} ECOR + R'OH$$

$$k_3 \downarrow \text{(deacylation)}$$

$$E + RCOOH$$

For such situations $k_{cat} = k_2k_3/(k_2 + k_3)$; $K_m = k_3K_s/(k_2 + k_3)$.

Can. J. Chem. Downloaded from www.nrcresearchpress.com by 210.87.254.105 on 09/05/12
For personal use only.

Can. J. Chem. Downloaded from www.nrcresearchpress.com by 210.87.254.105 on 09/05/12
For personal use only.

TABLE 1. Kinetic parameters for the α-chymotrypsin-catalyzed hydrolysis of methyl, (*R*)- and (*S*)-2-butyl, -2-octyl, and -α-phenethyl esters of the series **1–5***

Substrate	Alcohol configuration	k_{cat} (s^{-1})	$K_m \times 10^3$ (M)	$\frac{k_{cat}}{K_m}$ ($M^{-1}\,s^{-1}$)
1*a*	*R*(−)	96.7 ±19.8	1.72 ±0.51	5.62×10^4
1*b*	*S*(+)	35.6 ± 2.9	0.91 ±0.13	3.91×10^4
1*c*†	*R*(−)	19.6 ± 1.4	0.49 ±0.06	4.00×10^4
1*d*†	*S*(+)	23.5 ± 3.8	0.53 ±0.13	4.43×10^4
1*e*	*R*(+)	104 ± 5	0.05 ±0.01	2.08×10^6
1*f*	*S*(−)	111 ± 5	0.06 ±0.01	1.85×10^6
1*g*	—	78.2 ± 3.9	0.77 ±0.07	1.02×10^5
2*a*	*R*(−)	13.9 ± 0.9	3.28 ±0.34	4.23×10^3
2*b*	*S*(+)	10.3 ± 1.4	4.18 ±0.86	2.46×10^3
3*a*	*R*(−)	—	—	—§
3*b*	*S*(+)	—	—	—§
4*a*†	*R*(−)	0.14 ± 0.04	1.44 ±0.56	97.2
4*b*†	*S*(+)	0.05 ± 0.01	0.97 ±0.41	51.5
4*c*†	*R*(−)	—	—	<0.8‖
4*d*†	*S*(+)	—	—	0.8‖
4*e*‡	*R*(+)	0.12 ± 0.01	0.016±0.002	7.5×10^3
4*f*‡	*S*(−)	0.014± 0.02	0.05 ±0.01	2.8×10^3
4*g*†	—	0.21 ± 0.02	2.57 ±0.43	81.7
5*a*	*R*(−)	0.24 ± 0.02	1.99 ±0.27	120.6
5*b*	*S*(+)	0.09 ± 0.01	1.12 ±0.20	80.4
5*c*†	*R*(−)	—	—	26.9‖
5*d*†	*S*(+)	—	—	60.5‖
5*e*	*R*(+)	0.25 ± 0.02	0.22 ±0.03	1.1×10^3
5*f*	*S*(−)	0.74 ± 0.05	0.17 ±0.02	4.4×10^3
5*g*	—	0.48 ± 0.04	4.43 ±0.62	108.4

*Kinetics were performed at p*H* 7.8 and 25° on aqueous solutions containing 0.1 *M* KCl and 3% DMSO.
†20% DMSO.
‡5% DMSO.
§Substrate activity too low to evaluate.
‖(v)/[S][E].

TABLE 2. Comparison of k_{cat} and k_2, and K_m and K_s, constants for methyl, and (*R*)- and (*S*)-2-butyl and -α-phenethyl hippurates **5***a,b,e–g**

Substrate	k_{cat} (s^{-1})	k_2 (s^{-1})	$K_m \times 10^3$ (M)	$K_s \times 10^3$ (M)	$\frac{k_{cat}}{K_m}$ ($M^{-1}s^{-1}$)
5*a*	0.11	0.12	9.11	9.85	12.1
5*b*	0.06	0.06	6.79	7.07	8.8
5*e*	0.08	0.08	1.22	1.28	65.6
5*f*	0.23	0.27	0.55	0.65	418.2
5*g*	0.25	0.3	6.35	7.61	39.4

*Kinetic measurements were carried out at p*H* 7.9 and 25°, on aqueous solutions containing 0.1 *M* KCl and 20% DMSO; k_2 and K_s were calculated[2] by taking the k_{cat} (1.52 s^{-1}) value for *p*-nitrophenyl hippurate as k_3.

TABLE 3. Partial kinetic resolutions of (*RS*)-2-butyl and -α-phenethyl dihydrocinnamates and hippurates via α-chymotrypsin-catalyzed hydrolysis*

Substrate	Alcohol (% optical purity)	Residual ester (% optical putity)
(*RS*)-2-Butyl dihydrocinnamate (**4***ab*)	*R*(−) (21)†	*S*(+) (24)
(*RS*)-2-Butyl hippurate (**5***ab*)	*R*(−) (33)†	*S*(+) (36)
(*RS*)-α-Phenethyl dihydrocinnamate (**4***ef*)	*R*(+) (11)	*S*(−) (7)
(*RS*)-α-Phenethyl hippurate (**5***ef*)	*S*(−) (38)	*R*(+) (35)
	S(−) (11)	*R*(+) (82)‡

*All experiments were carried out at 25° with heterogeneous mixtures of substrate and aqueous 0.1 *M* KCl solutions of p*H* 7.9 containing 1 mg/ml of α-chymotrypsin. The hydrolyses were terminated when ~50% hydrolysis of the ester had occurred.
†Isolated as 3,5-dinitrobenzoate.
‡After ~75% hydrolysis.

Can. J. Chem. Downloaded from www.nrcresearchpress.com by 210.87.254.105 on 09/05/12
For personal use only.

studied presented no difficulty except for the diastereomeric (+)- and (−)-α-phenethyl esters **1***e* and *f*. During Fischer esterification of *N*-acetyl-L-phenylalanine (**1**, X = H) with *R*(+)- and *S*(−)-α-phenethylalcohol, the facile, acid-catalyzed, conversion of the benzylic alcohols to their corresponding ethers was a major problem and low yields (~5%) only of the pure esters **1***e* and *f* were obtainable. Alternative approaches to **1***e* and *f* using thionyl chloride or dicylohexylcarbodiimide esterification methods were unsuccessful. Owing to the relative insolubility in aqueous solutions of all the esters surveyed, it was necessary to use dimethyl sulfoxide[4] (DMSO) as cosolvent in all the kinetic assays. In each case, the proportion of DMSO used was kept to the minimum required to obtain satisfactory steady state kinetic data.

For enzyme-catalyzed kinetic resolutions of racemic or diastereomeric esters to be practicable, the kinetic and binding differences between substrates derived from pairs of enantiomeric alcohols must be reasonably significant. Since the rates of ester hydrolyses are well known to be affected by the nature of the acyl and alcohol groups, the effects of structural and stereochemical variations of both moieties on the kinetic parameters were examined. The influence of chiral and achiral acyl groups on the enzymic catalyses was studied using the representative *R*(−)- and *S*(+)-2-butyl esters **1***a* and *b* – **5***a* and *b*. For the *N*-acetyl-L-phenylalanyl specific substrate esters **1***a* and *b* the rates of hydrolysis were high. However, the differences between the (+) and (−) esters, as reflected by the respective specificity constants (Table 1), were small. Replacement of the *N*-acetyl group of the phenylalanyl esters by hydroxyl reduces the degree of L-stereospecificity preference (12–14). As the data for **2***a* and *b* show, this reduction in the dominance of the stereospecificity of the aryl group on the catalytic process is reflected in a somewhat greater separation of the k_{cat}/K_m values. A further widening of the specificity constant differences within the R(−)- and S(+)-2-butyl series was observed when the substrate activities of the achiral dihydrocinnamoyl and hippuryl esters **4***a* and *b* and **5***a* and *b* were evaluated. Unfortunately, the *N*-acetylglycine esters **3***a* and *b*, for which only binding at the nucleophilic site should be important, were not substrates under the conditions investigated.[5] The overall kinetic data for the 2-butyl esters indicated that although the stereospecificity of the nucleophilic site was minor, it was not insignificant and was most marked for the substrates with achiral acyl groups. Accordingly, the studies were extended to the 2-octyl and α-phenethyl esters of dihydrocinnamic and hippuric acids. The corresponding *N*-acetyl-L-phenylalanyl esters were also investigated in order to provide representative specific substrate data for comparison purposes.

The results obtained (Table 1) confirm that kinetic differences between esters of *R* and *S* alcohols are greatest for the substrates possessing the non-specific achiral acyl groups and it appears that the dominance of the interaction of the L-acyl group of specific substrates tends to overwhelm the lesser stereospecificity of the nucleophilic site.[6]

The *N*-acetyl-L-phenylalanyl esters **1***a–g* were all rapidly hydrolyzed and for such substrates it is generally assumed (6) that deacylation is rate determining. Although the variations in k_{cat} for **1***a–g* are not considered overly meaningful since the data were obtained close to the experimental limit of the p*H* stat (16), the distinctly lower k_{cat} values of **1***b–d* do suggest that the structure and/or configuration of the alcohol moiety is interfering with binding and/or orientation of the substrate to the extent that the rate of acylation is markedly reduced. On the other hand, for the non-specific dihydrocinnamate and hippurate substrates, k_{cat} is expected to approximate (or be strongly influenced by) k_2 (6, 17) and a comparison of the k_{cat} values for **4***a*, *b*, *e*, *f* and **5***a*, *b*, *e*, *f* with those of the corresponding methyl esters **4***g* and **5***g* shows that the rates of enzyme acylation are being affected by both the structure and configuration of the alcohol to a considerable degree. Although the insolubility of **4***c* and *d* and **5***c* and *d* precluded their k_{cat} determinations, the (v)/[E][S] variations indicate that the situation is analogous for the 2-octyl moieties. When

[4]Of the organic cosolvents used in α-chymotrypsin studies, DMSO is the least disruptive in its effect on the kinetic parameters (11).

[5]The k_{cat} value for the methyl ester **3***g* is only 0.013 s^{-1} (15) and steric interactions of the 2-butyl groups of **3***a* and *b* at the nucleophilic site presumably (2) lower this value significantly.

[6]The L-phenylalanyl group of the esters surveyed by Halpern *et al.* (4) would not behave as a strongly α-chymotrypsin specific function under the p*H* 7.1 reaction conditions applied (14) and thus the influence of nucleophilic site stereospecificity remains significant.

Can. J. Chem. Downloaded from www.nrcresearchpress.com by 210.87.254.105 on 09/05/12
For personal use only.

acylation is rate determining, K_m approximates K_s (the enzyme–substrate dissociation constant)[3] and the K_m values for **4***a–g* and **5***a–g* show clearly that the more hydrophobic alcohols contribute significantly to substrate binding and that the nucleophilic site can exhibit marked stereospecificity. While for **1***a–g*, the magnitude of K_m does not reflect binding so directly, a similar trend is discernible.

The correspondence of k_{cat} and K_m with k_2 and K_s respectively was verified for the hippurate series (Table 2) using k_{cat} for *p*-nitrophenyl hippurate as the deacylation rate constant (8, 9). The enzymic hydrolysis of the latter proceeded extremely rapidly under the p*H* 7.8 reaction conditions and a steady state kinetics procedure could not be used. Accordingly, V_{max} was determined under turnover conditions (9) and corrections were made for the relatively rapid non-enzymic hydrolysis and 2-phenyloxazolin-5-one formation (18). Owing to solubility problems, k_{cat} for *p*-nitrophenyl dihydrocinnamate could not be measured under the same conditions.

Although the specificity constant differences between enantiomeric dihydrocinnamate and hippurate esters do not exceed ~six-fold for any of the pairs of enantiomers studied so far, considerable partial resolutions of the racemates can be achieved on the preparative-scale as shown by the results of Table 3. The initial preparative reactions were terminated after 50% hydrolysis for reference purposes. Since the stereospecificity was not absolute, complete resolution was not achieved at this point for any racemate. However, the degree of resolution of alcohol or residual ester could be increased by stopping the reaction at < or > 50% hydrolysis respectively. For example, after 75% hydrolysis of racemic **5***ef*, (*R*)-α-phenethyl hippurate (**5***e*) of 82% optical purity was isolated. Subjecting partially resolved esters to further α-chymotryptic hydrolysis has also been found to be effective in raising optical purities to high levels (19).

The data obtained support the previous evidence (2) regarding the hydrophobic nature of the alcohol binding site and of its structural specificity. The *R*(+)- and *S*(−)-α-phenethyl functions bind very strongly and the corresponding alcohols may well be capable of saturating the nucleophilic site (*cf.* ref. 2). In contrast, the 2-octyl group appears to exceed the structural tolerance of the site.

Contrary to the observations of Halpern and his co-workers (4) for racemic esters of the phenylalanine series, the stereospecificity of the nucleophilic site is seen to be fickle, particularly with respect to the enantiomeric alcohol moieties of the non-specific dihydrocinnamate and hippurate ester substrates. The 2-butyl esters, for which the *R*(−) enantiomers are always hydrolyzed more rapidly than the *S*(+), are the only substrates of Table 1 for which the stereospecificity remains constant.[7] The reversals in stereospecificity observed for the 2-octyl and α-phenethyl dihydrocinnamates and hippurates arise from variable and often opposite effects on the acylation and/or binding processes. For each of the series of esters **4** and **5** the variations in k_{cat} seem unrelated to the strength of binding of the various alcohol moieties and the efficiency of catalysis appears to reflect the precision of orientation and alignment of the ester carbonyl group and the serine-195 nucleophile at the active site rather than a distortion of the substrate (20).

The enantiomeric preferences observed in the preparative-scale hydrolyses of the racemic esters of Table 3 are in accord with those predicted by the k_{cat}/K_m ratios of Table 1 and this constant may be as useful for secondary stereospecificity predictions as it has been in primary stereospecificity studies. The current results confirm the earlier indications (3, 4) that resolution of racemic alcohols by selective α-chymotrypsin-catalyzed hydrolysis of their esters is practicable in favorable cases. On balance, hippurates seem the most suitable derivatives for preparative purposes and further studies on the scope of the method are in progress.[8]

Experimental

The general procedures followed and criteria of purity used were as outlined previously (21). Amino acid starting materials were purchased from Sigma or Mann Research Laboratories and chymotrypsin (three times crystallized) from Worthington Biochemical Corporation. The *R* and *S* alcohols used were obtained from Norse Laboratories. All optically active compounds prepared were purified to constant rotation. *N*-Acetyl-L-phenylalanine methyl ester (**1***g*), methyl dihydrocinnamate (**4***g*), methyl hippurate (**5***g*), and *p*-nitrophenyl hippurate were prepared by the standard literature methods (8, 16, 22).

---

[7]These results are in agreement with the preferred stereochemistry of transesterification of acetylchymotrypsin by (±)-2-butanol (3). They show that the same alcohol binding site is involved in both processes.

[8]NOTE ADDED IN PROOF: Other aspects of leaving group specificity have been reported recently (27).

TABLE 4. Physical and analytical data for all new compounds prepared

Ester*	Melting or boiling point (°C)	$[\alpha]_D^{22}$(*c*, $CHCl_3$)	Analysis (%) Calculated C	Calculated H	Found C	Found H
1*a*	75	+60.3° (0.5)	68.41	8.03	68.46	7.98
1*b*	55	+74.9° (0.5)	68.41	8.03	68.22	8.32
(*RS*) **1***ab*	56	—	68.41	8.03	68.26	8.09
1*c*	62	+49.6° (0.5)	71.43	9.15	71.44	9.07
1*d*	152 (0.005 Torr)	+53.3° (0.8)	71.43	9.15	71.37	9.02
1*e*	110 (0.006 Torr)	+102.9° (0.2)	73.28	6.79	73.38	6.96
1*f*	85	−31.4° (0.5)	73.28	6.79	73.42	6.92
2*a*	80 (0.002 Torr)	−32.2° (1.5)	70.24	8.16	70.05	8.35
2*b*	82 (0.005 Torr)	−17.6° (0.7)	70.24	8.16	70.05	8.17
(*RS*) **2***ab*	90 (0.03 Torr)	—	70.24	8.16	70.03	8.18
3*a*	92 (0.04 Torr)	−21.1° (1.0)	55.47	8.72	55.37	8.81
3*b*	100 (0.07 Torr)	+21.5° (1.6)	55.47	8.72	55.62	8.86
4*a*	85 (0.5 Torr)	−14.7° (1.5)	75.67	8.81	75.91	8.95
4*b*	85 (0.5 Torr)	+15.1° (1.5)	75.67	8.81	75.87	8.87
(*RS*) **4***ab*	60 (0.06 Torr)	—	75.67	8.81	75.85	8.80
4*c*	108 (0.004 Torr)	−11.7° (0.2)	77.81	9.98	77.99	10.15
4*d*	113 (0.05 Torr)	+12.1° (0.2)	77.81	9.98	77.71	9.96
4*e*	111 (0.004 Torr)	+48.8° (1.8)	80.28	7.13	80.42	7.10
4*f*	112 (0.005 Torr)	−47.9° (1.7)	80.28	7.13	80.34	7.28
(*RS*) **4***ef*	140 (0.003 Torr)	—	80.28	7.13	80.38	7.08
5*a*	120 (0.02 Torr)	−11.3° (1.5)	66.36	7.28	66.30	7.18
5*b*	120 (0.02 Torr)	+10.6° (1.5)	66.36	7.28	66.58	7.25
(*RS*) **5***ab*	140 (0.1 Torr)	—	66.36	7.28	66.28	7.31
5*c*	164 (0.025 Torr)	−7.8° (0.9)	70.07	8.64	70.19	8.71
5*d*	162 (0.001 Torr)	+8.1° (0.9)	70.07	8.64	70.27	8.66
5*e*	110	+92.2° (0.75)	72.06	6.04	71.93	6.07
5*f*	110	−91.5° (0.75)	72.06	6.04	72.06	6.04
(*RS*) **5***ef*	87	—	72.06	6.04	72.05	5.99

*The spectral data were as expected for each structure.

Preparation of N-Acetyl-L-phenylalanine and N-Acetyl Glycine (R)-, (S)-, and (R,S)-2-Butyl, 2-Octyl, and α-Phenethyl Esters

For each ester, the *N*-acetyl amino acid (**1**, **3**) in the appropriate *R*, *S*, or *RS* alcohol (2–10 ml) was saturated with dry hydrogen chloride at −5°. The mixture was then kept at 40° for 2 h, and, after rotary evaporation, the product was dissolved in ethyl acetate and washed with cold (0°) 1 *M* aqueous potassium carbonate and then with water. Evaporation of the dried ($MgSO_4$) ethyl acetate solution gave the expected ester which was purified by recrystallization from isopropyl ether – hexane or by vacuum distillation. The final yields were >50% except for the α-phenethyl esters in which cases silica gel chromatography was required to remove the large amount of di(α-phenethyl) ethers formed and ~5% yields only of the desired esters were obtained. Each compound was fully characterized; the data are summarized in Table 4. In addition, that no racemization of the diastereomeric *N*-acetyl-L-phenylalanyl esters had occurred was verified by assaying with α-chymotrypsin. Each of the esters **1***a–f* was hydrolyzed to the extent of 100%. In comparison, enzymic hydrolysis of the (*RS*)-2-butyl ester of *N*-acetyl-D,L-phenylalanine stopped when 50 ± 2% of the material had been hydrolyzed.

(R)-, (S)-, and (R,S)-2-Butyl-L-α-hydroxy-β-phenylpropionate

Esterifications of **2**, R = H (m.p. 123–124°, $[\alpha]_D^{22}$ −28.3° (*c*, 1.3 in acetone), prepared from L-phenylalanine by the method of Dakin and Dudley (23)), with (*R*)-, (*S*)- and (*RS*)-2-butanol were performed as described above for the amino acid derivatives. The physical and analytical data of **2***ab* are recorded in Table 4. The 100% hydrolysis of **2***ab* under α-chymotrypsin assay conditions showed that no racemization of the L-acid had occurred. (*RS*)-2-Butyl-D,L-α-hydroxy-β-phenylpropionate was only 50% hydrolyzed under the same conditions.

Preparation of (R)-, (S)-, and (RS)-2-Butyl, 2-Octyl, and α-Phenethyl Dihydrocinnamates and Hippurates

The esters were prepared by stirring 1 equiv. of each of dihydrocinnamoyl chloride or hippuryl chloride (24) and the appropriate alcohol in dry tetrahydrofuran at 20° for 12 h. The solvent was then removed and the residues dissolved in ether and washed with aqueous sodium bicarbonate solution. Evaporation of the dried ($MgSO_4$) ether

Can. J. Chem. Downloaded from www.nrcresearchpress.com by 210.87.254.105 on 09/05/12
For personal use only.

Can. J. Chem. Downloaded from www.nrcresearchpress.com by 210.87.254.105 on 09/05/12
For personal use only.

solution gave the desired esters in >90% yields. Each ester was purified by distillation except for the α-phenethyl hippurates which were recrystallized from aqueous methanol. The characterization data are summarized in Table 4.

α-Chymotrypsin-catalyzed Hydrolyses

Kinetic Studies

The kinetic studies were carried out at 25° under nitrogen using Radiometer p*H*-stat controlled addition of 5×10^{-2} to 5×10^{-3} *M* aqueous sodium hydroxide to maintain the p*H* at 7.8. Stock solutions of the enzyme (in 10^{-3} *M* HCl) and of the substrates (in aqueous DMSO) were made up and appropriate aliquots taken to enable 7–10 runs to be made under steady state conditions within the substrate concentration range 0.1–10 K_m and with enzyme concentrations 10^{-9}–10^{-6} *M*. A reaction volume of 10 ml of constant ionic strength (0.1 *M* KCl) was employed throughout. The final DMSO concentrations (3–20%) of the reaction mixtures were kept to the minimum required for adequate substrate solubility. Spontaneous hydrolysis at p*H* 7.8 was negligible for all substrates except in 20% DMSO when k_{OH^-} was determined in order to correct the initial velocities of the enzyme-catalyzed reactions. The enzyme concentration was determined spectrophotometrically (25) and the data were analyzed by the Lineweaver–Burk method and were subjected to least squares regression analysis (26). The K_m and k_{cat} values obtained are recorded in Table 1.

The V_{max} for the α-chymotrypsin-catalyzed hydrolysis of *p*-nitrophenyl hippurate was determined spectrophotometrically under turnover conditions (9) using a Cary 16 spectrophotometer. The kinetics were performed at 25° in 3 ml, 1 cm pathlength quartz cells on 20% aqueous DMSO solutions of p*H* 7.8 (THAM buffer). The substrate concentration was varied in the range 5×10^{-4} to 1×10^{-3} *M* (K_m ~2.5×10^{-5} *M* (8, 9)). All solutions were 0.1 *M* in KCl and the rate of *p*-nitrophenol formation in the presence of 5×10^{-6} *M* enzyme was monitored at both 340 and 350 mm, at which wavelengths Beer's Law was obeyed. The velocities were corrected for nonenzymic hydrolysis and a k_{cat} value of 1.52 ± 0.03 s^{-1} was obtained.

Partial Resolutions of (RS)-2-Butyl and -α-Phenethyl Dihydrocinnamates and Hippurates via α-Chymotrypsin-catalyzed Hydrolysis

The general procedure used was as described previously (21). The following conditions and isolation procedures are typical and have been applied to the partial resolution of up to 5 g of racemic esters. (*RS*)-α-Phenethyl hippurate (0.84 g) was suspended in 0.1 *M* aqueous KCl (40 ml) at 25° and a solution of α-chymotrypsin (50 mg) in water (10 ml) added all at once. The p*H* was maintained at 7.8 by the p*H*-stat procedure and at the 50% hydrolysis point (~5 h), the reaction mixture was continuously extracted with ether. The ether solution was then washed with aqueous sodium bicarbonate, dried ($MgSO_4$) and evaporated carefully. Column chromatographic or t.l.c. purification yielded (*S*)-α-phenethyl alcohol (0.21 g), b.p. 90° (10 Torr), $[\alpha]_D^{22°}$ −21° (*c*, 1.8 in $CHCl_3$, 38% optical purity) and (*R*)-α-phenethyl hippurate (0.34 g), m.p. ~100° after recrystallization from ether, $[\alpha]_D^{22°}$ +32.3° (*c*, 10 in $CHCl_3$, 35% optical purity). When the hydrolysis was allowed to proceed to the extent of ~75%, (*S*)-α-phenethyl alcohol and (*R*)-α-phenethyl hippurate of 11% and 82% optical purities respectively were obtained.

The conditions for the other racemic esters subjected to preparative-scale hydrolysis were similar except that for the dihydrocinnamates, half hydrolyses required 24–26 h and, owing to its volatility, it was necessary to isolate 2-butanol as its 3,5-dinitrobenzoate ester. In each case the spectral data of the partially resolved alcohols and esters were identical with those of the corresponding pure enantiomers and racemates and the overall results are summarized in Table 3.

The support of this work by the National Research Council of Canada is gratefully acknowledged.

1. S G. Cohen and L. W. Lo. J. Biol. Chem. **245**, 5718 (1970); T. N. Pattabiraman and W. B. Lawson. J. Biol. Chem. **247**, 3029 (1971); M. S. Silver, M. Stoddard, T. Sone, and M. S. Malta. J. Am. Chem. Soc. **92**, 3151 (1970); E. J. Corey, R. J. McCaully, and H. S. Sachdev. J. Am. Chem. Soc. **92**, 2476 (1970); J. H. Tong, C. Petitclerk, A. D'Iorio, and N. L. Benoiton. Can. J. Biochem. **49**, 877 (1971).
2. M. L. Bender and F. J. Kézdy. Annu. Rev. Biochem. **34**, 49 (1965); P. W. Inward and W. P. Jencks. J. Biol. Chem. **240**, 1986 (1965); A. J. Hymes, C. C. Cuppett, and W. J. Canady. J. Biol. Chem. **244**, 637 (1969); K. Martinek, A. V. Levashov, and I. V. Berezin. Mol. Biol. **4**, 517 (1970); C. Hansch and E. Coats. J. Pharm. Sci. **59**, 731 (1970); M. M. Werber and P. Greenzaid. Biochim. Biophys. Acta, **293**, 208 (1973).
3. N. S. Isaacs and C. Niemann. Biochim. Biophys. Acta, **44**, 196 (1960).
4. B. Halpern, J. Ricks, and J. W. Westley. Austr. J. Chem. **20**, 389 (1967).
5. F. E. Brot and M. L. Bender. J. Am. Chem. Soc. **91**, 7187 (1969).
6. M. L. Bender, F. J. Kézdy, and C. R. Gunter. J. Am. Chem. Soc. **86**, 3669 (1964).
7. G. H. Nelson, J. L. Miles, and W. J. Canady. Arch. Biochem. Biophys. **96**, 545 (1962).
8. A. Williams. Biochemistry, **9**, 3383 (1970).
9. R. E. Williams and M. L. Bender. Can. J. Biochem. **49**, 210 (1971).
10. V. Prelog and H. L. Meier. Helv. Chim. Acta, **36**, 320 (1953); V. Prelog and H. Scherrer. Helv. Chim. Acta, **42**, 2227 (1959); R. S. Cahn, C. K. Ingold, and V. Prelog. Experientia, **12**, 81 (1956).
11. Y. M. Azizov, I. B. Zverinskaya, A. N. Nikitina, V. Y. Roslyakov, and Y. I. Khurgin. Isv. Akad. Nauk. SSR., Ser, Khim. **12**, 2843 (1968).
12. J. C. Snoke and H. Neurath. Arch. Biochem. Biophys. **21**, 351 (1949).
13. M. L. Bender and B. W. Turnquest. J. Am. Chem. Soc. **77**, 4271 (1955).

14. F. J. KÉZDY, S. P. JINDAL, and M. L. BENDER. J. Biol. Chem. **247**, 5746 (1972).
15. J. P. WOLF and C. NIEMANN. Biochemistry, **2**, 82 (1963).
16. J. B. JONES and C. NIEMANN. Biochemistry, **2**, 498 (1963).
17. C. C. CUPPETT and W. J. CANADY. J. Biol. Chem. **245**, 1069 (1970).
18. J. DE JERSEY and B. ZERNER. Biochemistry, **8**, 1967 (1969) and previous papers.
19. P. W. MARR, Ph.D. Thesis, University of Toronto, Toronto, Ontario. 1972.
20. C. HANSCH. J. Org. Chem. **37**, 92 (1972).
21. J. B. JONES and Y. Y. LIN. Can. J. Chem. **50**, 2053 (1972); J. Org. Chem. **38**, 3575 (1973).
22. R. WILDNAUER and W. J. CANADY. Biochemistry, **5**, 2885 (1966).
23. H. D. DAKIN and H. W. DUDLEY. J. Biol. Chem. **18**, 46 (1914).
24. W. O. MCLURE. Biochem. Prep. **11**, 55 (1966).
25. L. W. CUNNINGHAM. J. Biol. Chem. **207**, 443 (1954).
26. G. N. WILKINSON. Biochem. J. **80**, 324 (1961).
27. A. R. FERSHT, D. M. BLOW, and J. FASTREG. Biochemistry, **12**, 2025, 2035 (1973).

Can. J. Chem. Downloaded from www.nrcresearchpress.com by 210.87.254.105 on 09/05/12
For personal use only.

The Preparation and Properties of 1-Cyano-2,3,4-triammine(ethylenediamine)cobalt(III) Chloride

ALBERT RICHARD NORRIS

Department of Chemistry, Queen's University, Kingston, Ontario

Received August 2, 1973

The i.r., u.v.–visible, and p.m.r. spectral characteristics of a cyanotriammine(ethylenediamine)cobalt(III) chloride are described and compared to the corresponding spectral characteristics of the related compounds *cis*-$[Coen_2NH_3CN]Cl_2$, *trans*-$[Coen_2NH_3CN]Cl_2 \cdot H_2O$, and $[Co(NH_3)_5CN]Cl_2$. Evidence is presented to support the formulation of the $[Coen(NH_3)_3CN]Cl_2$ complex as a 1-cyano-2,3,4-triammine(ethylenediamine)cobalt(III) chloride.

Les caractéristiques spectrales du chlorure de cyanotriammine (éthylènediamine) cobalt(III) obtenues en i.r., en u.v.–visible et en r.m.p. sont décrites et comparées aux caractéristiques spectrales correspondantes des composés apparentés, *cis*-$[Coen_2NH_3CN]Cl_2$, *trans*-$[Coen_2NH_3CN]Cl_2 \cdot H_2O$ et $[Co(NH_3)_5CN]Cl_2$. On présente des preuves visant à démontrer que la formulation du complexe $[Coen(NH_3)_3CN]Cl_2$ correspond au chlorure de cyano-1 triammine-2,3,4 (éthylènediamine) cobalt(III).

[Traduit par le journal]

Can. J. Chem., **52**, 477 (1974)

Introduction

In the course of studies of the hydrogen peroxide oxidation of coordinated thiocyanate ion in *cis*- and *trans*-$[Coen_2NH_3NCS]^{2+}$ (1) we required authentic samples of the corresponding cyanoammine- and diamminebis(ethylenediamine)cobalt(III) complexes for comparison purposes. Five early attempts to prepare *cis*-$[Coen_2NH_3CN]Cl_2$ according to a procedure reported by Ohkawa *et al.* (2) all led to a final cyanide ion-containing species which investigation showed to be the 1-cyano-2,3,4-triammine(ethylenediamine)cobalt(III) chloride. To our knowledge this particular complex has not been reported previously. We describe here some of the spectral and chemical properties of this complex and present the evidence upon which we base our conclusion regarding its configuration.

Experimental

Reagents

$NH_4[Co(SO_3)_2(NH_3)_4] \cdot 3H_2O$ was prepared according to the procedure reported by Bailar and Peppard (3). $[Co(NH_3)_5CN]Cl_2$ was prepared and recrystallized following Siebert's procedure (4). *trans*-$[Coen_2NH_3CN]Cl_2 \cdot H_2O$ was prepared and recrystallized as described previously (1). All other cobalt(III)-containing complexes were prepared following the procedures described by Ohkawa *et al.* (2, 5).

All reagents used were A.R. grade or better and were used without further purification.

Instruments

Ultraviolet–visible absorption spectra were recorded on a Cary 14 recording spectrophotometer using matched silica cells of 1.0 cm path length. The temperature in the cells was maintained at 25.0 °C by circulating water from a constant temperature bath through a specially designed cell holder in the spectrophotometer.

Infrared spectra were recorded on Beckman IR-10 and Perkin-Elmer 180 recording spectrophotometers operating in the double beam mode. Samples were prepared in potassium bromide or cesium iodide discs (1% w/w concentration) and spectra recorded *vs.* air or an attenuator in the reference beam path. Spectra were calibrated using a polystyrene film and all frequencies are believed to be accurate to within ± 5 cm^{-1}.

Proton magnetic resonance spectra were recorded on a Varian T-60 spectrometer. Samples normally contained about 20 mg of complex dissolved in 0.50 ml 1.8 *M* D_2SO_4. The sodium salt of 3-(trimethylsilyl)propane sulfonic acid (DSS) in 1.8 *M* D_2SO_4 was used as an external standard. Chemical shift values (τ) are given relative to the standard (τ = 10.00 p.p.m.).

Procedures

The techniques used in the ion-exchange, freeze-drying, and recrystallization procedures have been described previously (1).

Elemental analyses were carried out by Galbraith Laboratories, Inc. (Knoxville, Tenn.).

Results and Discussion

The reaction scheme outlined by Ohkawa *et al.* (2, 5) involves the reaction of either the dark yellow form of $Na_3[Co(CN)_2(SO_3)_2(NH_3)_2] \cdot 6H_2O$ or the orange-yellow form of $Na_3[Co(CN)_2(SO_3)_2(NH_3)_2] \cdot 5H_2O$ with aqueous ethylenediamine to yield *cis*-$[Coen_2CNSO_3]$, reaction of this complex with concentrated HBr to yield *cis*-

Can. J. Chem. Downloaded from www.nrcresearchpress.com by 210.87.254.5 on 09/05/12
For personal use only.

Can. J. Chem. Downloaded from www.nrcresearchpress.com by 210.87.254.5 on 09/05/12
For personal use only.

$[Coen_2BrCN]Br \cdot H_2O$, and ammonolysis of the latter compound to yield *cis*-$[Coen_2NH_3CN]Cl_2$.

We found that when the dark yellow form of $Na_3[Co(CN)_2(SO_3)_2(NH_3)_2] \cdot 6\ H_2O$ was heated with aqueous ethylenediamine, the solution changed color very slowly and, contrary to the observations of Ohkawa *et al.*, brown crystals did not appear within a few minutes. After 2 h heating on a steam bath and evaporation to approximately one-half volume, yellow-brown crystals were present in solution. These were collected by filtration of the hot solution and washed thoroughly with water, ethanol, and acetone.[1] Treatment of these yellow-brown crystals with concentrated HBr on a steam bath resulted in the formation of a deep purple solution from which a purple-red solid could be precipitated by the addition of absolute ethanol. Like *cis*-$[Coen_2BrCN]Br \cdot H_2O$ this solid possessed a visible absorption maximum at 514 nm and a strong, sharp C≡N stretch at 2130 cm^{-1}. Unlike *cis*-$[Coen_2BrCN]Br \cdot H_2O$ (5) it was very soluble in water and could not be recrystallized successfully from this solvent. Treatment of this purple-red solid with liquid ammonia as per Ohkawa *et al.* (2) gave an orange-yellow solid which, when dissolved in water and chromatographed on Dowex 50W-X2 ion-exchange resin, yielded at least four fractions: (*i*) unreacted starting material which was eluted with 0.50 *M* HCl, (*ii*) +2 charged species which were eluted with 1 *M* HCl, (*iii*) a +3 charged species which was eluted with 3 *M* HCl, and (*iv*) a species of unknown charge which was removed from the column with 6 *M* HCl (6). Only minor amounts of the total reaction product were in the 0.50, 3, and 6 *M* HCl fractions. The fractions from the column were freeze-dried and the solids obtained from the 1 *M* HCl fractions recrystallized from ethanol–water as previously described (1). The solid obtained by freeze-drying of the 1 *M* HCl fraction always contained a mixture of compounds as evidenced by the presence of at least three sharp bands of varying intensity in the 2100–2150 cm^{-1} region. On recrystallization from ethanol–water a yellow solid was obtained which possessed only a single, strong, sharp C≡N stretch at 2130 cm^{-1}.

After drying to constant weight *in vacuo* over phosphorus(V) pentoxide, the recrystallized yellow solid yielded the following elemental analysis.

Anal. Calcd. for $[Coen(NH_3)_3CN]Cl_2(C_3H_{17}N_7Cl_2Co)$: C, 13.50; H, 6.36; N, 31.50; Cl, 26.55. Found: C, 13.46; H, 6.31; N, 31.58; Cl, 27.01.

After recrystallization and drying in exactly the same manner *cis*-cyanoamminebis(ethylenediamine)cobalt(III) chloride yielded the anhydrous salt whereas the *trans* isomer yielded the monohydrate, *trans*-$[Coen_2NH_3CN]Cl_2 \cdot H_2O$ (1).

Assignments of configuration of *cis* and *trans* isomers using i.r. absorption spectra have frequently been recorded in the literature (7–12). The i.r. absorption characteristics of $[Coen(NH_3)_3CN]Cl_2$ were therefore examined in an effort to ascertain the geometrical arrangement of the ammonias and the cyanide ion in this complex. Like both *cis*-$[Coen_2NH_3CN]Cl_2$ and *trans*-$[Coen_2NH_3CN]Cl_2 \cdot H_2O$, $[Coen(NH_3)_3CN]Cl_2$ showed a single, strong, sharp C≡N stretch at 2130 cm^{-1}. In the 1580–1620 cm^{-1} region (8, 9) the absorption pattern of $[Coen(NH_3)_3CN]Cl_2$ was similar to that observed for *cis*-$[Coen_2NH_3CN]Cl_2$ but the midpoint of the major peak was, as in the case of *trans*-$[Coen_2NH_3CN]Cl_2 \cdot H_2O$, at 1610 cm^{-1}. In this region $[Co(NH_3)_5CN]Cl_2$ showed a single, strong, broad peak centered at 1600 cm^{-1}. Rigg and Sherwin (7) have assigned bands in the 1300 cm^{-1} region to the asymmetric deformation of NH_3 and have concluded that, in isomeric diacidodiammine(ethylenediamine)cobalt(III) complexes, the ammonia ligands are in a *trans* position if splitting is absent whereas, if splitting is present, no assignment of configuration can be made. In the 1300 cm^{-1} region, the absorption pattern of $[Coen(NH_3)_3CN]Cl_2$ was much less complex than that observed for either *cis*-$[Coen_2NH_3CN]Cl_2$ or *trans*-$[Coen_2NH_3CN]Cl_2 \cdot H_2O$. However, by comparison to $[Co(NH_3)_5CN]Cl_2$ which, in this region, showed single, sharp peaks at 1315 (s) and 1275 (w) cm^{-1}, splitting of the NH_3 bands was definitely present in $[Coen(NH_3)_3CN]Cl_2$. Chamberlain and Bailar (10) have attributed bands in the 1130–1150 cm^{-1} region to N—H vibrations and have stated that in diacidobis(ethylenedi-

[1]Treatment of these yellow-brown crystals with an excess of 10% aqueous ethylenediamine solution for 3 h at 100 °C resulted in a quantitative conversion to *cis*-cyanosulfitobis(ethylenediamine)cobalt(III). When the orange-yellow form of $Na_3[Co(CN)_2(SO_3)_2(NH_3)_2] \cdot 5H_2O$ was heated with aqueous ethylenediamine, *cis*-cyanosulfitobis(ethylenediamine)cobalt(III) chloride crystallized from the reaction mixture as indicated by Ohkawa *et al.* (2).

Can. J. Chem. Downloaded from www.nrcresearchpress.com by 210.87.254.5 on 09/05/12
For personal use only.

amine)cobalt(III) complexes *trans* isomers have one band in this region whereas *cis* isomers have two. Rigg and Sherwin (7) found the spectra of their isomeric diacidodiammine(ethylenediamine)cobalt(III) complexes in this region to be too complex to enable them to apply this rule to their complexes. $[Coen(NH_3)_3CN]Cl_2$ showed a single, sharp, strong band at 1150 cm^{-1}. In the 850–900 cm^{-1} region the spectrum of $[Coen(NH_3)_3CN]Cl_2$ showed a very weak shoulder at 885 cm^{-1} associated with a weak peak at 870 cm^{-1}. On the basis of Baldwin's (11) criterion and Rigg and Sherwin's (7) observations, $[Coen(NH_3)_3CN]Cl_2$ could be assigned a 1-cyano-2,3,4-triammine configuration. In the 610–500 cm^{-1} region the spectrum of $[Coen(NH_3)_3CN]Cl_2$ could be considered to possess four weak peaks if all shoulders were counted as peaks but the criterion advanced by Hughes and McWhinnie (12) to differentiate *cis* and *trans* isomers in the diacidobis(ethylenediamine)cobalt(III) series was very difficult to apply in this case. The overall absorption pattern of $[Coen(NH_3)_3CN]Cl_2$ in the 600–200 cm^{-1} region was more like the absorption pattern of *cis*-$[Coen_2NH_3CN]Cl_2$ than the absorption pattern of *trans*-$[Coen_2NH_3CN]Cl_2 \cdot H_2O$. In summary, i.r. data does no more than suggest a 1-cyano-2,3,4-triammine configuration for $[Coen(NH_3)_3CN]Cl_2$. Certainly there is no one criterion of the several proposed (7–12) that can be said to establish unequivocally the configuration of the compound.

In the u.v.–visible region $[Coen(NH_3)_3CN]Cl_2$ possessed absorption maxima (λ_{max}) at 437 (ε 69.0 M^{-1} cm^{-1}) and 327 nm (ε 65.0 M^{-1} cm^{-1}) and absorption minima (λ_{min}) at 373 ($\varepsilon \simeq 14.1$ M^{-1} cm^{-1}) and 280 nm ($\varepsilon \simeq 10.0$ M^{-1} cm^{-1}). The spectrum of the complex was unaffected by p*H* in the region p*H* 3.0–9.0. *cis*-$[Coen_2NH_3CN]Cl_2$ showed absorption maxima at 436 (ε 74.3 M^{-1} cm^{-1}) and 322 nm (ε 82.3 M^{-1} cm^{-1}) and minima at 371 (ε 19.5 M^{-1} cm^{-1}) and 282 nm (ε 22.0 M^{-1} cm^{-1}). *trans*-$[Coen_2NH_3CN]Cl_2 \cdot H_2O$ possessed absorption maxima at 434 (ε 56.0 M^{-1} cm^{-1}) and 322 nm (ε 59.9 M^{-1} cm^{-1}) and minima at 368 (ε 14.0 M^{-1} cm^{-1}) and 287 nm (ε 24.9 M^{-1} cm^{-1}) (1). $[Co(NH_3)_5CN]Cl_2$ had absorption maxima at 441 (ε 57.1 M^{-1} cm^{-1}) and 327 nm (ε 55.3 M^{-1} cm^{-1}) and absorption minima at 373 and 278 nm. The pattern observed for the λ_{max} and λ_{min} values of $[Coen(NH_3)_3CN]Cl_2$ suggests it is a 1-cyano-2,3,4-triammine species. Strong support for this formulation is provided by the magnitude of ε for $[Coen(NH_3)_3CN]Cl_2$ at the long wavelength maximum: it is clearly much closer to the corresponding value of ε for the *cis*-$[Coen_2NH_3CN]Cl_2$ complex than it is to the value of ε for the *trans*-$[Coen_2NH_3CN]Cl_2 \cdot H_2O$ complex.

The p.m.r. spectrum of $[Coen(NH_3)_3CN]Cl_2$ in 1.8 *M* D_2SO_4 showed resonance absorbances at 4.67, 5.00, and 7.10 τ. The 4.67 and 5.50 τ resonances were fairly broad and of equal intensity and the 7.10 τ resonance was very broad. Integrated areas were in the ratio of 1 (4.67 + 5.50 τ):3.1 (7.10 τ). On this basis the absorbances at 4.67 and 5.50 are associated with the NH_2 protons of the ethylenediamine while the broad resonance at 7.10 obviously contains the resonances of both the NH_3 and CH_2 protons. Under similar conditions *cis*-$[Coen_2NH_3CN]Cl_2$ showed resonance absorbances at 5.02, 5.49, 6.00 (very weak) and 7.23 τ; *trans*-$[Coen_2NH_3CN]Cl_2 \cdot H_2O$ showed resonance absorbances at 5.23, 5.64, 6.37, and 7.14 τ (1); and $[Co(NH_3)_5CN]Cl_2$ showed resonance absorbances at 6.00 and 6.95 τ (integrated ratio 1:4). A major observation here is that in $[Co(NH_3)_5CN]Cl_2$ the resonance absorbance of the protons on the ammonia *trans* to the cyanide ion is 57 Hz downfield from the resonance absorbance of the protons on the ammonias *cis* to the cyanide ion while the resonance absorbance of the protons on the ammonia in *trans*-$[Coen_2NH_3CN]Cl_2 \cdot H_2O$ is approximately 50 Hz downfield from the resonance absorbance of the protons on the ammonia in *cis*-$[Coen_2NH_3CN]Cl_2$. The proton resonance absorbance pattern for $[Coen(NH_3)_3CN]Cl_2$ clearly indicates the absence in this complex of an ammonia group *trans* to a cyanide ion. On this basis, the compound is 1-cyano-2,3,4-triammine(ethylenediamine)cobalt(III) chloride. This conclusion contradicts none of the spectral information previously presented and is in accord with the behavior of this compound on recrystallization.

The nature of the other products produced from the reaction of liquid ammonia with the purple-red bromocyanodiammine(ethylenediamine)cobalt(III) has not yet been clearly established. The solids obtained by freeze-drying of the 3 and the 6 *M* HCl fractions from the chromatography column both showed C≡N stretches in the 2130 (w) and 2190 (m) cm^{-1} region suggesting the presence of both terminal

and bridging cyanide groups in both complexes (13, 14). These compounds are undergoing further investigation.

Financial support by the National Research Council of Canada is acknowledged.

1. A. R. NORRIS and J. W. L. WILSON. Can. J. Chem. **51**, 4152 (1973).
2. K. OHKAWA, J. HIDAKA, and Y. SHIMURA. Bull. Chem. Soc. Japan, **40**, 2830 (1967).
3. J. C. BAILAR, JR. and D. F. PEPPARD. J. Am. Chem. Soc. **62**, 105 (1940).
4. H. SEIBERT. Z. Anorg. Allgem. Chem. **327**, 63 (1964).
5. K. OHKAWA, J. HIDAKA, and Y. SHIMURA. Bull. Chem. Soc. Japan, **39**, 1715 (1966).
6. D. A. BUCKINGHAM, I. I. OLSEN, A. M. SARGESON, and H. SATRAPA. Inorg. Chem. **6**, 1027 (1967).
7. J. M. RIGG and E. SHERWIN. J. Inorg. Nucl. Chem. **27**, 653 (1965).
8. P. E. MERRITT and S. E. WIBERLY. J. Phys. Chem. **59**, 55 (1955).
9. M. L. MORRIS and D. H. BUSCH. J. Am. Chem. Soc. **82**, 1521 (1960).
10. M. M. CHAMBERLAIN and J. C. BAILAR, JR. J. Am. Chem. Soc. **81**, 6412 (1959).
11. M. E. BALDWIN. J. Chem. Soc. 4369 (1960).
12. M. N. HUGHES and W. R. MCWHINNIE. J. Inorg. Nucl. Chem. **28**, 1659 (1966).
13. R. A. DE CASTELLÓ, C. PÍRIZ MAC-COLL, N. B. EGEN, and A. HAIM. Inorg. Chem. **8**, 699 (1969).
14. R. A. DE CASTELLÓ, C. PÍRIZ MAC-COLL, and A. HAIM. Inorg. Chem. **10**, 203 (1971).

Can. J. Chem. Downloaded from www.nrcresearchpress.com by 210.87.254.5 on 09/05/12
For personal use only.

Proton Magnetic Resonance Studies of Rotational Isomerism in Halotoluenes. X. Estimates of Conformational Preferences and Rotational Barriers in Benzal Fluoride and Some Dichloro Derivatives

J. Brian Rowbotham,[1] Alexander Frank Janzen, James Peeling,[2] and Ted Schaefer

Department of Chemistry, University of Manitoba, Winnipeg, Manitoba R3T 2N2

Received August 18, 1973

The synthesis of benzal fluoride and of its 2,6-, 3,5-, 3,4-, and 2,4-dichloro derivatives is followed by an analysis of their proton magnetic resonance spectra. The long-range spin–spin coupling constants are most consistent with a barrier to rotation about the sp^2–sp^3 carbon–carbon bond in benzal fluoride of less than 500 cal/mol, in semiquantitative agreement with an *ab initio* molecular orbital calculation. The 2,6-dichloro derivative has a conformation in which the C—H bond of the side chain lies in the plane of the aromatic ring. The 2,4-dichloro derivative favors a similar conformation, the C—H bond lying *cis* to the ring chlorine atom. In contrast to the long-range proton–proton couplings, the long-range proton–fluorine couplings are intrinsically sensitive to substituent effects from the ring chlorine atoms.

La synthèse du fluorure de benzyle et de ses dérivés -2,6, -3,5, -3,4 et -2,4 dichlorés est suivie de l'analyse de leurs spectres de résonance magnétique du proton. Les constantes de couplage à longue distance sont très cohérentes avec une barrière de rotation autour de la liaison carbone–carbone sp^2–sp^3 dans le fluorure de benzyle, inférieure à 500 cal/mol; elles sont en accord semiquantitatif avec les résultats d'un calcul théorique de type *ab initio*. Le dérivé -2,6 dichloré présente une conformation dans laquelle la liaison C—H de la chaine latérale se trouve dans le plan du cycle aromatique. Le dérivé -2,4 dichloré favorise une conformation similaire, la liaison C—H se trouvant dans une position *cis* par rapport à l'atome de chlore du cycle. Par apposition aux constantes de couplage à longue distance proton–proton, les constantes de couplage à longue distance proton–fluore sont intrinsèquement sensibles aux effets de substitution des atomes de chlore du cycle. [Traduit par le journal]

Can. J. Chem., **52**, 481 (1974)

Introduction

The long-range coupling constants between ring and methyl protons in toluene (1, 2), between ring fluorine nuclei and methyl protons in fluorotoluene derivatives (3, 4), and between ring protons and fluorine nuclei in benzotrifluoride (5) have been discussed in terms of σ and π electron contributions to the coupling mechanisms. The coupling over six bonds between protons, $^6J_p^{H,CH_3}$, and between ring fluorine nuclei and methyl protons, $^6J_p^{F,CH_3}$, are transmitted by a π electron mechanism (2, 6). The corresponding couplings over four and five bonds have substantial σ electron contributions. In toluene derivatives, the side-chain proton – ring proton coupling constants are highly stereospecific and relatively insensitive to the presence of ring substituents. These characteristics make them useful probes into the conformational preferences of these compounds. On the other hand, the couplings between side-chain fluorine nuclei and the ring protons in benzotrifluoride derivatives display a substantial dependence on substituents (5). In addition, little is known about their conformational dependence. In this paper such long-range couplings are measured in benzal fluoride and four of its derivatives containing two chlorine atoms as ring substituents, **1**–**5**.

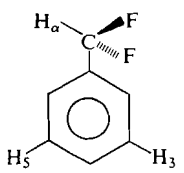

1

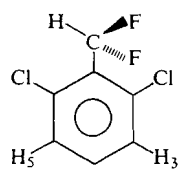

2

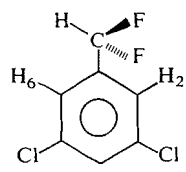

3

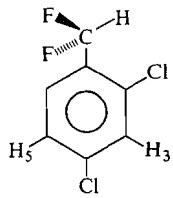

4*a*

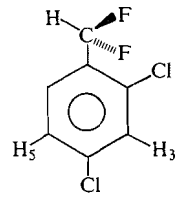

4*b*

[1]Postdoctoral fellow, 1971–1973.
[2]NRCC fellowship holder, 1971–1973.

Can. J. Chem. Downloaded from www.nrcresearchpress.com by 210.87.254.5 on 09/05/12
For personal use only.

TABLE 1. Conditions of synthesis for **1** to **5**

Product	Reactants (mmol)			Conditions		Yield (%)
	Aldehyde	SF_4	BF_3	Time (h)	Temp. (°C)	
1	31.3	63.2	—	6	150	80
2	15.6	31.6	—	10	150	< 5
	15.7	37.6	4.8	16	120	> 95
3	15.7	34.2	4.5	22	120	> 95
4	15.6	33.5	—	16	120	70
5	15.6	33.1	—	16	120	50

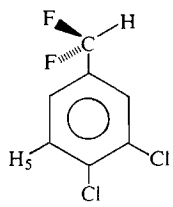

5a

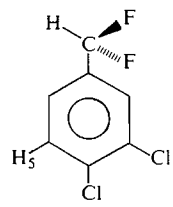

5b

It turns out that the long-range coupling constants are best interpreted in terms of almost free rotation about the sp^2–sp^3 carbon–carbon bond in benzal fluoride. A ground state conformation in which the C—H bond of the side chain lies in a plane perpendicular to the aromatic ring can be ruled out.

Experimental

Synthesis

Fluorination of the corresponding aldehydes (Aldrich) gave the benzal fluorides (7). Sulfur tetrafluoride (Matheson) was handled in a metal vacuum system and was condensed into a 75-cc stainless steel pressure reaction vessel containing the aldehyde. In some cases, boron trifluoride (Matheson) was added as a catalyst. No attempt was made to optimize yields. Compound **3** was used without purification, while the others were distilled under reduced pressure in a closed system. Details of the reaction conditions are given in Table 1. Highly characteristic p.m.r. spectra, particularly for the methine proton, left no doubt as to the identity of the products.

Proton Magnetic Resonance Spectra

Thoroughly degassed samples (freeze–pump–thaw) contained small amounts of tetramethylsilane as an internal reference. The solvents are given below. Spectral calibrations were performed on a HA100D spectrometer in the frequency sweep mode at sweep rates of 0.01 or 0.02 Hz/s and at a sweep width of 1 Hz/cm. Double resonance experiments (8) on **3**, **4**, and **5** gave the signs of the long-range coupling relative to those of the couplings between ring protons and of the two-bond coupling between fluorine and proton. Two different samples of **1** in C_6D_6 were calibrated in order to check the analysis of their complex spectra.

A solution of **2** in toluene-d_8 was cooled to below −100 °C but no evidence for slow rotation on the n.m.r. time scale was found. The spectral characteristics implied an upper limit of 8 kcal/mol to the free energy barrier to internal rotation about the C—C bond.

Results and Discussion

Spectral Analysis

The spectra of **2**–**5** approach first order and were analyzed using the computer program LAME (9). The 8-spin spectrum of **1** was rather complex and was analyzed in the iterative and noniterative modes of LACX (10). Spectral parameters were varied over generous ranges in a series of simulations to ensure that only the reported values gave a reasonable reproduction of the observed spectrum. A few impurity peaks caused minor difficulties; however, two different samples yielded almost identical parameter sets. In Fig. 1 the aromatic region of the spectrum of **1** is displayed, together with the calculated spectrum. The latter is obtained with the parameters given in column 2 of Table 2. All parameters except the shift of the methine proton, the shift of the fluorine nuclei, and $^2J^{H,F}$ were allowed to vary in the final iterations (for the other spectrum of **1** only the shift of fluorine was not allowed to vary). Of the 509 transitions of the aromatic protons having intensities greater than 0.01, 276 were assigned. Multiple near-degeneracies precluded more assignments. The r.m.s. deviation of calculated from observed transitions was 0.017 Hz; the standard deviations were very small, being as large as 0.007 Hz only for $^6J_p^{H,H}$ and $^6J_p^{H,F}$. The correlation coefficients were all less than 0.2 except that the shifts of the *ortho* and *meta* protons were correlated by 0.28, and $^3J^{H_2,H_3}$ was correlated to each of these shifts by 0.42.

The final spectral parameters for all compounds are given in Table 2.

Can. J. Chem. Downloaded from www.nrcresearchpress.com by 210.87.254.5 on 09/05/12
For personal use only.

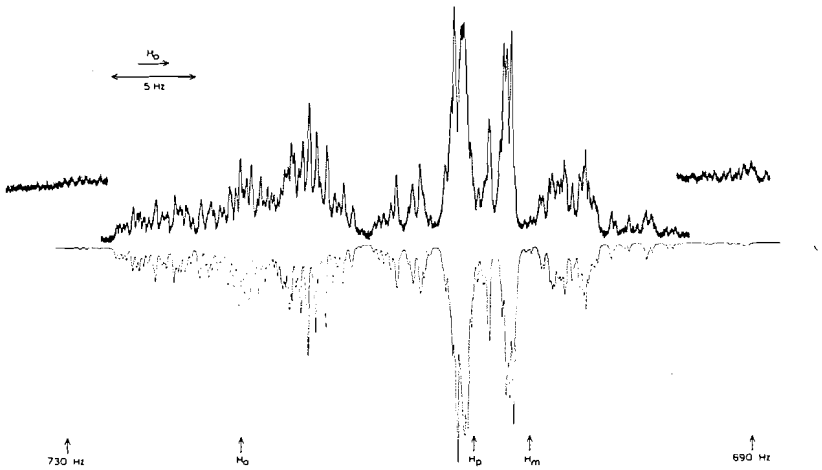

FIG. 1. The ring proton magnetic resonance spectrum at 100 MHz of a 15 mol % solution of benzal fluoride in benzene-d_6. The spectrum calculated with the parameters in Table 2 is shown below the observed spectrum. The experimental traces at the extremes of the figure were taken at higher gain. Some impurity peaks occur in the extreme high-field part of the observed spectrum in the region of 694–697 Hz.

TABLE 2. The chemical shifts* and coupling constants in Hz of benzal fluoride and some dichloro derivatives

Parameter	1†	1†	2†	3‡	4†	5§
ν_2	719.71	720.39	—	730.36	—	714.26
ν_3	702.98	703.68	678.03	—	696.73	—
ν_4	706.10	706.82	650.71	737.23	—	—
ν_5	702.98	703.68	678.03	—	677.47	695.25
ν_6	719.71	720.39	—	730.36	711.42	675.46
ν_α	618‖	619.18	706.28	645.71	654.01	596.43
$^2J^{H,F}$	56.5‖	56.44	53.00	56.05	54.76	56.01
$^3J_o^{H,H}$	7.80[2,3]	7.80	8.13	—	8.42	8.29
	7.54[3,4]	7.52	—	—	—	—
$^4J_m^{H,H}$	1.26[2,4]	1.26	—	1.89	2.05	2.05
	1.88[2,6]	1.89	—	—	—	—
	1.31[3,5]	1.31	—	—	—	—
$^5J_p^{H,H}$	0.63	0.63	—	—	0.36	0.37
$^4J_o^{H,CH_\alpha}$	−0.47	−0.46	—	−0.49	−0.45	−0.45[2] −0.48[6]
$^5J_m^{H,CH_\alpha}$	0.26	0.26	0.24	—	0.00[3] 0.48[5]	0.31
$^6J_p^{H,CH_\alpha}$	−0.24	−0.25	−0.01	−0.28	—	—
$^4J_o^{H,CF}$	−1.16	−1.17	—	−1.02	−0.91	−1.08[2] −1.08[6]
$^5J_m^{H,CF}$	0.92	0.92	1.06	—	1.20[3] 0.57[5]	0.95
$^6J_p^{H,CF}$	−1.16	−1.12	−1.25	−0.95	—	—

*In Hz at 100 MHz to low field from internal TMS.
†Approximately 15 mol % in C_6D_6.
‡Approximately 10 mol % in CS_2.
§Approximately 20 mol % in C_6D_6.
‖Not iterated on these parameters.

Can. J. Chem. Downloaded from www.nrcresearchpress.com by 210.87.254.5 on 09/05/12
For personal use only.

Can. J. Chem. Downloaded from www.nrcresearchpress.com by 210.87.254.5 on 09/05/12
For personal use only.

Long-range Couplings to the α Proton, Conformational Preferences, and Rotational Barriers

(a) Over Five Bonds, $^5J_m^{H,CH_\alpha}$

In 2,6-dichlorobenzal chloride the conformation analogous to **2** is about 15 kcal/mol more stable (11) than the high energy conformation (12) in which the C—H bond of the dichloromethyl group lies in a plane perpendicular to the aromatic ring. The long-range coupling $^5J_m^{H_3,CH_\alpha}$ is 0.50 ± 0.02 Hz in that compound while $^5J_m^{H_5,CH_\alpha}$ is less than 0.05 Hz. In **2** the barrier to rotation is probably less than 8 kcal/mol (see Experimental) and rapid conformational isomerism about the sp^2–sp^3 carbon–carbon bond could lead to the observed coupling of 0.24 Hz = $(^5J_m^{H_5,CH_\alpha} + {}^5J_m^{H_3,CH_\alpha})/2$. In **4** one observes $^5J_m^{H_5,CH_\alpha}$ as 0.48 Hz while $^5J_m^{H_3,CH_\alpha}$ is unobservable, implying that **4** exists predominantly as **4***a*. In **1** the coupling is 0.26 Hz, again suggesting equal populations of the isomers corresponding to conformation **1**. In **5** the observed coupling of 0.31 Hz then would suggest that **5***a* is populated to an extent of about 60%, this conformation having a somewhat smaller dipole moment than **5***b*, *i.e.*, a larger separation of negative halogen centers. These conclusions assume a negligible substituent dependence on $^5J_m^{H,CH_\alpha}$, in line with the data on the 2,4,6-trichlorobenzal chloride (12) and the 2,4,6-tribromobenzal chloride (13).

The $^6J_p^{H,CH_\alpha}$ values are interpreted below in terms of an almost free rotation about the C—C bond in **1**, **3**, and **5** (but not in **2**). The question therefore arises whether the five-bond couplings are also consistent with the latter model.

Calculations on $^5J_m^{H,CH_3}$ in toluene (2) suggest that the coupling is dominated by a σ electron mechanism which has a $(1 - \cos\theta)/2$ dependence and that a smaller contribution to the coupling originates in a π electron mechanism, depending on $\sin^2\theta$. From the measurement (6) of $^6J_m^{CH_3,CH_3}$ in a *m*-xylene derivative, it was suggested that the π contribution was given by 0.38 $\sin^2\theta$ in Hz. If, then, the π contribution to $^5J_m^{H,CH_\alpha}$ in benzal fluoride is reduced in proportion to $^6J_p^{H,CH_\alpha}$, *i.e.*, by $(-0.52 \times 0.38)/(-1.24)$, one may write

$$[1]\quad {}^5J_m^{H,CH_\alpha} = {}^5J^\sigma + {}^5J^\pi = 0.48\,(1 - \cos\theta)/2 + 0.15\sin^2\theta$$

For free rotation, an average from 0 to 2π radians yields $^5J_m^{H,CH_\alpha} = 0.24 + 0.07 = 0.31$ Hz. In other words, the π contribution raises $^5J_m^{H,CH_\alpha}$ somewhat from the value expected for rapid flips between coplanar conformations of type **1** or **2**. The calculated value of 0.31 Hz is a little larger than the 0.26 Hz observed in **1** but equal to that in **5**. The difference from **1** is too small to vitiate the model of nearly free rotation.

For **4** one may have an oscillation up to 30° about the C—C bond for conformation **4***a* and find that the calculated values are still within experimental error of the observed parameters, *i.e.*, eq. 1 averaged between $-\pi/6$ and $\pi/6$ yields 0.03 Hz (coupling to H_3) and yields 0.48 Hz when averaged between $5\pi/6$ and $7\pi/6$ (coupling to H_5). The free rotation model for **1** is, therefore, not disproved by the data on **4**.

(b) Over Six Bonds, $^6J_p^{H,CH_\alpha}$*, and Barrier to Rotation*

In **1** the barrier to rotation about the C—C bond may be rather small. *Ab initio* calculations (14) indicate **1** as more stable by 180 cal/mol than the form where the C—H bond lies in a plane perpendicular to the ring plane. Experimental data are unavailable. Such a low twofold barrier is only an order of magnitude larger than the sixfold barrier in toluene (15). If it is correct, then at room temperature the population of **1** is only 1.35 times the population of the perpendicular form. Classically, such a low barrier would entail large amplitudes of oscillation about the C—C bond in both **1** and the perpendicular conformation. Evidence for a substantial oscillation, at least in **1**, comes from the $^6J_p^{H,CH_\alpha}$ values in **1**, **2**, and **3**. Because this coupling is transmitted by a mechanism (2) in which σ–π interaction occurs between the C—H_α bond and the π electron system of the aromatic ring, it has a $\sin^2\theta$ dependence where θ is the angle between the plane of the aromatic ring and the plane containing the C—H_α bond. In **2** the coupling is effectively zero because θ is 0° and oscillations about this value of up to 15° will not increase the magnitude of the coupling significantly (16, 17). Quantum mechanically, a barrier to rotation in **2** of about 2 kcal/mol guarantees the same conclusion (17).

Now, in **1** and **3** the value of $^6J_p^{H,CH_\alpha}$ is −0.26 ± 0.02 Hz, indicating a substantial amplitude of oscillation in conformation **1** or a barrier lower than 2 kcal/mol. Unfortunately, no value of $^6J_p^{H,CH_\alpha}$ is available for θ = 90° for the difluoro-

Can. J. Chem. Downloaded from www.nrcresearchpress.com by 210.87.254.5 on 09/05/12
For personal use only.

methyl group. For *free* rotation, $\langle \sin^2 \theta \rangle = 0.5$, so that a *maximum* value of $^6J_p^{H,CH_\alpha}$ ($\theta = 90°$) would then be -0.52 ± 0.04 Hz. For the methyl group, the corresponding value is -1.24 Hz, while for the fluoromethyl group it is -0.64 Hz (16). For CH_2X groups the σ–π interaction decreases in magnitude in a roughly linear fashion as the electronegativity of X increases (16), so that a further decrease might well occur in going from CH_2F to CHF_2.

The first fluorine atom substituent decreases $^6J_p^{H,CH_\alpha}$ by a factor of two from its value in the methyl group. If, in fact, the second fluorine atom again halves $^6J_p^{H,CH_\alpha}$ ($\theta = 90°$), *i.e.*, to about -0.32 Hz, then the observed values of -0.26 ± 0.02 Hz in **1** and **3** are in agreement with neither a free rotation model nor a ground state conformation **1**. Rather one would need a perpendicular conformation with a substantial oscillation of near 30° about the C—C bond.

It is probably reasonable that substitution by a second fluorine atom does not have as large an effect on $^6J_p^{H,CH_\alpha}$ ($\theta = 90°$) as does substitution by the first fluorine atom into the methyl group. Then the value of -0.52 Hz above appears adequate as an estimate and is in agreement with the quantum mechanical model of Stone and Maki (17) for a barrier of 180 cal/mol, this value being hardly distinguishable from free rotation. In this model, if **1** is the ground state with a barrier to rotation of as much as 1 kcal/mol, the experimental value of -0.26 Hz implies a $^6J_p^{H,CH_\alpha}$ ($\theta = 90°$) of about -1.3 Hz, even larger than for the methyl group itself. Even a barrier of 0.5 kcal/mol entails a value of -0.74, greater in magnitude than the -0.64 Hz derived for the fluoromethyl group (16).

The present measurements, therefore, indicate a barrier of less than 0.5 kcal/mol for the barrier to internal rotation in benzal fluoride and also imply that the ground state is **1**. A microwave measurement of the barrier would be of interest, even though it may not indicate the ground state conformation if the barrier is very small.

(c) Coupling Over Four Bonds, $^4J_o^{H,CH_\alpha}$

To within experimental error, this coupling is the same in the four compounds where it occurs and since **4** exists predominantly in form **4***a*, it is apparently not suited to stereochemical deductions. The coupling presumably contains substantial contributions from both σ and π electrons (2, 6) and therefore its value need not vanish when the C—H_α lies in the plane of the aromatic ring. It would be useful to know whether $^4J_o^{H,CH_\alpha}$ has different values at $\theta = 0$ and 180°. Therefore, MO-INDO-FPT and MO-CNDO/2-FPT calculations were carried out on benzal fluoride.

(d) INDO and CNDO/2 Calculations of $^4J_o^{H,CH_\alpha}$, $^5J_m^{H,CH_\alpha}$ *and* $^6J_p^{H,CH_\alpha}$

These were performed on an IBM 360/65 computer in a manner described in detail for other molecules (2). Up to a hundred iterations were performed to achieve convergence in the coupling constants to about 10^{-3} Hz. The finite perturbation (18) was applied to the α proton for a standard geometry (20) and the angle was varied at intervals of 10 to 15°. Convergence was not obtained for some values of θ, which is defined by **6**. The computed couplings are given in Table 3.

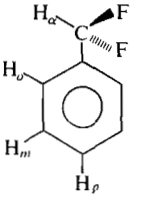

$\theta = 0°$ for H_o and H_m

6

(i) Over Four Bonds, $^4J_o^{H,CH_\alpha}$

In Fig. 2 the computed $^4J_o^{H,CH_\alpha}$ values are plotted as a function of the angle θ. The CNDO/2 predictions are clearly in disagreement with experiment, as expected if they do not take the σ–π mechanism into account (19). INDO predicts that the coupling is -0.3 Hz when $\theta = 180°$ and 0.13 Hz when $\theta = 0°$, suggesting **4***a* as the conformation for **4**, particularly if a sizeable oscillation occurs about the C—C bond.

The shape of the computed curve, with its maximum magnitude near $\theta = 90°$, implies a large π contribution to $^4J_o^{H,CH_\alpha}$ similar to that observed and calculated (2) for toluene. The average value over all angles in Table 3 is -0.48 Hz, in fortuitous quantitative agreement with the observed numbers for **1** and **3**. Thus, the INDO computations of $^4J_o^{H,CH_\alpha}$ agree with almost unhindered rotation about the C—C bond in **1** and **3**. For a large barrier to rapid rotation between identical forms **1**, INDO would indicate substantially different values in **1** and **4**, contrary to experiment.

TABLE 3. Computed long-range coupling constants in Hz in benzal fluoride

θ* (deg)	$^4J_o^{H,CH_\alpha}$		$^5J_m^{H,CH_\alpha}$		$^6J_p^{H,CH_\alpha}$	
	INDO	CNDO/2	INDO	CNDO/2	INDO	CNDO/2
5	0.112	0.276	0.038	0.075	−0.020	0.003
15	0.063	—	0.066	—	−0.071	—
30	−0.090	0.265	0.156	0.042	−0.226	0.003
45	−0.315	—	0.290	—	−0.440	—
60	−0.561	0.215	0.448	0.003	−0.653	0.002
75	−0.768	—	0.605	—	−0.808	—
85	−0.858	0.166	0.700	0.049	−0.858	0.002
95	−0.899	0.151	0.781	0.097	−0.858	0.002
105	−0.890	—	0.848	—	−0.808	—
120	−0.793	0.126	0.918	0.286	−0.653	0.002
135	−0.632	—	0.953	—	−0.440	—
150	−0.463	0.113	0.959	0.535	−0.226	0.003
165	−0.337	—	0.953	—	−0.071	—
175	−0.297	0.112	0.950	0.638	−0.020	0.003

*The angle θ is defined by 6 in the text and has the C—H_α bond in the plane of the ring and *cis* to the *ortho* proton when θ = 0°.

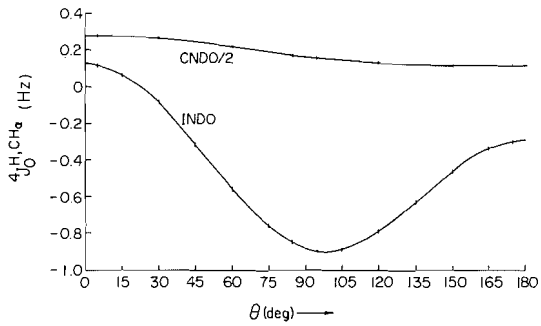

FIG. 2. The calculated coupling over four bonds between the α proton and the *ortho* ring protons as a function of the rotational angle θ in benzal fluoride. θ = 0° refers to the conformation in which the C—H_α bond lies in the plane of the ring and *cis* to the *ortho* proton.

(ii) Over Six Bonds, $^6J_p^{H,CH_\alpha}$

The INDO coupling in Table 3 closely follows $^6J_p^{H,CH_\alpha} = 0.87 \times \sin^2 \theta$ while the CNDO/2 result never rises above 0.0034 Hz, clearly indicating a π electron mechanism. The value of −0.87 Hz at θ = 90° is an overestimate in view of the experimental value of −0.64 Hz for the fluoromethyl group, discussed in a previous section, where a free rotation model implied −0.52 Hz at θ = 90° for the difluoromethyl group. If the calculated value were actually correct, simple averaging suggests an oscillation by 45° about the conformation **1** will also lead to an observed value of −0.26 Hz for $^6J_p^{H,CH_\alpha}$. Such a large oscillation implies a rather small barrier to internal rotation.

(iii) Over Five Bonds, $^5J_m^{H,CH_\alpha}$

The INDO and CNDO/2 values are plotted in Fig. 3. For toluene (2), benzaldehyde (21), and styrene (22), INDO substantially overestimates the magnitude of a five-bond coupling from an α proton. A similar situation exists for benzal fluoride, as can be seen in Fig. 3 where the values predicted by eq. 1 are also plotted. Comparison with the CNDO/2 curve indicates the π electron contribution to $^5J_m^{H,CH_\alpha}$ included in eq. 1, this contribution being substantially smaller than that clearly contained in the INDO curve. The experimental values in Table 2 suggest that neither the CNDO/2 nor the INDO curves are quantitatively correct. Reduction of the computed INDO values by a factor of two would produce a θ dependence of $^5J_m^{H,CH_\alpha}$ in

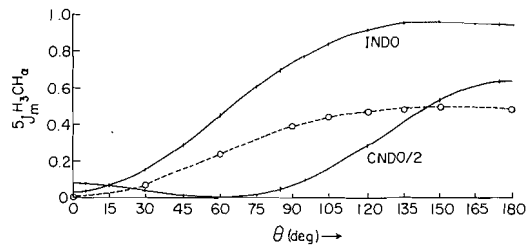

FIG. 3. The computed couplings over five bonds between the α proton and the ring proton as a function of rotational angle θ are plotted as solid lines. The dashed line refers to the couplings calculated from eq. 1 of the text. θ = 0° refers to the conformation in which the C—H_α bond lies in the plane of the ring and *cis* to the *meta* proton.

Can. J. Chem. Downloaded from www.nrcresearchpress.com by 210.87.254.5 on 09/05/12
For personal use only.

Can. J. Chem. Downloaded from www.nrcresearchpress.com by 210.87.254.5 on 09/05/12
For personal use only.

agreement with a free rotation model as well as with eq. 1.

Long-range Coupling from the Fluorine Nuclei

(a) Over Six Bonds, $^6J_p^{H,CF}$

In benzal fluoride $^6J_p^{H,CF}$ is -1.14 Hz. If the C—H_α bond lay in a plane perpendicular to the aromatic ring, the C—F bond would lie at 60° from the perpendicular, so that $^6J_p^{H,CF}$ ($\theta = 90°$ for F) would have a value of $-1.14/\sin^2 30° = -4.56$ Hz. In benzotrifluoride, however, the corresponding value is -1.28 Hz (5) and is -2.43 Hz in 2,6-dichlorobenzyl fluoride (23), *i.e.*, $^6J_p^{H,CF}$ decreases substantially in magnitude as more electronegative fluorine atoms are substituted into the methyl group (similar to the decrease in magnitude of $^6J_p^{H,CH_\alpha}$ on going from CH_3 to CHF_2 groups). Consequently, it is highly unlikely that the stable conformation of benzal fluoride is one in which the C—H_α bond lies perpendicular to the ring.[3]

On the other hand, if **1** is by far the most stable conformation of benzal fluoride it follows that $^6J_p^{H,CF}$ at 90° (C—F perpendicular to ring) is -2.28 Hz for benzal fluoride, -1.27 Hz for 3,5-dichlorobenzal fluoride, and -1.67 Hz for 2,6-dichlorobenzal fluoride ($\sin^2 60° = 0.75$). A substantial ring-substituent effect on $^6J_p^{H,CF}$ is clearly present. However, it is improbable that the chlorine atoms in the 3 and 5 positions should have a larger effect than in the 2 and 6 positions (because they are known not to affect $^6J_p^{H,CH_3}$). Therefore, the substituent effect must occur at the site where the C—F bonds undergo σ–π interaction with the π system of the ring, because the σ–π interaction at the C—H bond in the *para* position of the ring is no doubt much the same for 3,5-dichlorobenzal fluoride and 3,5-dichlorotoluene.

Now, if almost free internal rotation occurs about the C—C bond (180 cal/mol barrier (14)), the values of $^6J_p^{H,CF}$ at 90° (C—F perpendicular to ring) become -2.28 Hz for benzal fluoride, -1.90 Hz for the 3,5-dichloro derivative, and -1.76 Hz for the 2,6-dichloro derivative (because $\langle\sin^2\theta\rangle = 0.5$ for the first two, while the last compound exists in form **2**). The ring-substituent effect now increases in magnitude as the chlorine atoms more closely approach the difluoromethyl group, and there occurs a steady progression in the derived J values.[4]

The six-bond coupling to fluorine in benzal fluoride is therefore best interpreted in terms of an almost free rotation of the difluoromethyl group about the C—C bond.

(b) Over Five Bonds, $^5J_m^{H,CF}$

In **4**, $^5J_m^{H,CF}$ is 0.57 Hz to H_5 and 1.20 Hz to H_3, indicating form **4***a* if $^5J_m^{H,CF}$ follows an equation similar to eq. 1. Such an assumption implies two equations in $^5J_m^{H,CF}$. These yield a σ electron contribution of 1.26 Hz at $\theta = 180°$ (*trans*), 0.00 Hz at $\theta = 0°$, and 0.34 Hz for the π electron contribution to $^5J_m^{H,CF}$. But a ring-substituent effect is probably present here also so that a direct comparison with the other compounds is difficult. Thus, in **2** the average coupling over five bonds is 1.06 Hz, almost 0.2 Hz higher than the 0.89 Hz obtained from the average of the two couplings in **4**. Yet this average is nearly equal to the 0.92 Hz observed in **1**. In the absence of ring-substituent effects on $^5J_m^{H,CF}$, this equality would indicate that benzal fluoride exists in conformation **1**. If, then, the chlorine atoms reduce the π contribution to $^5J_m^{H,CF}$ in **2** (as they apparently do for $^6J_p^{H,CF}$), they must increase the σ electron contribution to this coupling in **2**. In order to reconcile all these observations with an "almost free rotation" in benzal fluoride, assume that the π electron contribution to $^5J_m^{H,CF}$ has the same ratio to $^6J_p^{H,CF}$ as for the corresponding couplings in toluene (**2**), namely, $-1/3$. One has $(2.28)/(3 \times 2) = 0.38$ Hz for $^5J^\pi$ for free rotation, leaving 0.54 Hz as $^5J^\sigma$. The latter is indeed smaller than the 0.63 Hz derivable from the 1.26 Hz deduced for $^5J^\sigma$ in **4**, as expected if the *ortho* ring-substituent increases $^5J^\sigma$; an increase being necessary to explain the value of $^5J_m^{H,CF}$ in **2**, as

[3]Our INDO and CNDO/2 calculations suggest the perpendicular form as more stable than the form **1** by 1.5 and 1.9 kcal/mol, respectively, contrary to the *ab initio* calculations (14). It appears likely that the reason for the error in the former lies in the fact that they favor more highly connected conformations, the two C—F bonds lying at 30° from the plane of the ring and, therefore, bringing the fluorine atoms closer to the ring atoms than when the C—H_α lies in the plane of the ring. Such an effect is particularly noticeable for calculations on carbonium ions (24). Of course, a proper optimization of geometry for each conformation of **1** may change substantially the energy calculated by both methods.

[4]Hence the value of $^6J_p^{H,CF}$ (at 90°) of -2.43 Hz in 2,6-dichlorobenzyl fluoride (23) is not necessarily the same as its value in benzyl fluoride.

was indicated above. Although the asymmetry in the substitution pattern in **4**, as compared to **2**, does not encourage quantitative comparisons once a ring-substituent effect on both the π and σ electron contributions to $^5J_m^{H,CF}$ is admitted, it is clear that the values of this coupling for the compounds in Table 2 do not disprove the "almost free rotation" model for benzalfluoride.

(c) Over Four Bonds, $^4J_o^{H,CF}$

A decrease in magnitude of this coupling as chlorine atoms are introduced on the ring (Table 2) is again explicable in terms of a ring-substituent effect on both σ and π contributions to $^4J_o^{H,CF}$ and cannot be used to contradict the "almost free rotation" model. Note that the magnitudes of $^4J_o^{H,CF}$ and $^6J_p^{H,CF}$ are nearly equal in a given compound and that substitution patterns can hardly be deduced from their comparison.

Conclusions

The long-range nuclear spin–spin couplings from the side-chain nuclei to the ring protons in benzalfluoride are best interpreted when the barrier to rotation about the sp^2–sp^3 carbon–carbon bond is less than 500 cal/mol. This result is consistent with an *ab initio* molecular orbital calculation which finds the conformation in which the C—H bond of the sidechain lies in the plane of the ring to be 180 cal/mol more stable than the conformation in which the C—H bond lies in a plane perpendicular to the ring. In contrast to the long-range proton–proton coupling constants, the long-range proton–fluorine couplings are sensitive to substituent effects from chlorine atoms in the ring.

We are grateful to the National Research Council of Canada for financial assistance.

1. M. P. Williamson, R. J. Kostelnik, and S. M. Castellano. J. Chem. Phys. **49**, 2218 (1968).
2. R. Wasylishen and T. Schaefer. Can. J. Chem. **50**, 1852 (1972).
3. D. J. Blears, S. S. Danyluk, and T. Schaefer. J. Chem. Phys. **47**, 5037 (1967).
4. R. Wasylishen and T. Schaefer. Can. J. Chem. **49**, 94 (1971).
5. R. J. Kostelnik, M. P. Williamson, D. E. Wisnosky, and S. M. Castellano. Can. J. Chem. **47**, 3313 (1969).
6. C. J. Macdonald and W. F. Reynolds. Can. J. Chem. **48**, 1002 (1970).
7. W. C. Smith. Angew. Chem. Int. Ed. **1**, 467 (1962).
8. W. A. Anderson and R. Freeman. J. Chem. Phys. **37**, 2053 (1962); **39**, 806 (1963).
9. C. W. Haigh and J. M. Williams. J. Mol. Spectrosc. **32**, 398 (1969).
10. C. W. Haigh. Private communication.
11. T. Schaefer, R. Schwenk, C. J. Macdonald, and W. F. Reynolds. Can. J. Chem. **46**, 2187 (1968).
12. B. J. Fuhr, B. W. Goodwin, H. M. Hutton, and T. Schaefer. Can. J. Chem. **48**, 1558 (1970).
13. J. Peeling, T. Schaefer, and C. M. Wong. Can. J. Chem. **48**, 2839 (1970).
14. W. J. Hehre, L. Radom, and J. A. Pople. J. Am. Chem. Soc. **94**, 1496 (1972).
15. H. Rudolph, H. Dreizler, A. Jaeschke, and P. Wendling. Z. Naturforsch. **22***a*, 940 (1967).
16. A. F. Janzen and T. Schaefer. Can. J. Chem. **49**, 1818 (1971).
17. E. W. Stone and A. H. Maki. J. Chem. Phys. **37**, 1326 (1962).
18. J. A. Pople, J. W. McIver, jr., and N. S. Ostlund. J. Chem. Phys. **49**, 2960, 2965 (1968).
19. J. A. Pople and D. L. Beveridge. Approximate molecular orbital theory. McGraw-Hill Book Company, New York, N.Y. 1970.
20. J. A. Pople and M. S. Gordon. J. Am. Chem. Soc. **89**, 4253 (1967).
21. R. Wasylishen and T. Schaefer. Can. J. Chem. **49**, 3216 (1971).
22. M. Barfield, C. J. Macdonald, I. R. Peat, and W. F. Reynolds. J. Am. Chem. Soc. **93**, 4195 (1971).
23. T. Schaefer, C. M. Wong, and K. C. Tam. Can. J. Chem. **47**, 3688 (1969).
24. V. Buss, P. von R. Schleyer, and L. C. Allen. Topics Stereochem. **7**, 253 (1973).

Can. J. Chem. Downloaded from www.nrcresearchpress.com by 210.87.254.5 on 09/05/12
For personal use only.

Methyl–Methyl Proton Spin–Spin Coupling Constants in Some Six-membered Ring Compounds. A Test for Delocalization in Borazine

J. BRIAN ROWBOTHAM[1] AND T. SCHAEFER

Department of Chemistry, University of Manitoba, Winnipeg, Manitoba R3T 2N2

Received August 13, 1973

Spin–spin coupling constants over five, six, and seven bonds between protons in different methyl groups are reported for the xylenes, derivatives of benzene, pyridine, pyrimidine, pyridinium salts, *p*-benzoquinone, and borazine. The coupling magnitudes are characteristic of the substitution pattern in the delocalized systems. Calculations at the INDO-MO-FPT level of methyl proton couplings in *N*- and *B*-methylborazines are in agreement with the available experimental evidence in indicating a relatively weak transmission of spin density information via the presumed π electron system of borazine.

Les constantes de couplage à travers cinq, six et sept liaisons entre des protons appartenant à des groupes méthyles différents sont rapportées pour les xylènes, des dérivés du benzène, de la pyridine, la pyrimidine, de sels de pyridinium, de la *p*-benzoquinone et de la borazine. La grandeur des couplages est caractéristique du schéma de substitution dans les systèmes délocalisés. Les calculs, par une méthode de type INDO-MO-FPT, des couplages des protons des méthyles dans les *N*- et *B*-méthlborazines montrent, en accord avec les preuves expérimentables disponibles, que la transmission de l'information de la densité de spin à travers le présumé système électronique π de la borazine est relativement faible.

[Traduit par le journal]

Can. J. Chem., **52**, 489 (1974)

Introduction

The spin–spin coupling constants between ring protons and methyl protons in toluene (1) and its derivatives, J^{H,CH_3}, and between the protons of different methyl groups in the xylenes and their derivatives (2), J^{CH_3,CH_3}, have been discussed in terms of the coupling mechanisms (1–3). Because their signs and magnitudes depend on the number of intervening bonds, their application to the determination of substitution patterns in aromatic systems is attractive. Furthermore, $^5J_m^{H,CH_3}$ and $^6J_p^{H,CH_3}$ are relatively insensitive to the presence of other substituents (3–7). Thus, the variations of $^5J_m^{H,CH_3}$ and $^6J_p^{H,CH_3}$ in a variety of toluene derivatives fall well within 10% of their respective values of $+0.36 \pm 0.02$ and -0.62 ± 0.02 Hz in toluene itself (1). On the other hand, $^4J_o^{H,CH_3}$ apparently depends on the mobile bond order of the intervening C⋯C bond in the ring (6, 8–11) and is -0.74 ± 0.02 Hz in toluene.

In some xylene derivatives, $^5J_o^{CH_3,CH_3}$, $^6J_m^{CH_3,CH_3}$, and $^7J_p^{CH_3,CH_3}$ have values of 0.40 ± 0.03, -0.19 ± 0.04, and 0.62 ± 0.03 Hz, respectively (2), indicating a substantial σ electron contribution to $^4J_o^{H,CH_3}$ and $^5J_m^{H,CH_3}$. Almqvist and co-workers (12) measured the methyl–methyl proton couplings to an accuracy of 0.1 Hz in the xylenes and in some of their derivatives. In *m*-xylene they found $^6J_m^{CH_3CH_3}$ as less than 0.3 Hz but could not detect the fine structure from this coupling.

In this paper we report the results of fairly accurate measurements of such couplings in the xylenes, in derivatives of pyridine and its salts, of pyrimidine, pyrazine, pyrone, and of *p*-benzoquinone. The latter compound is not aromatic and this fact is reflected in the magnitudes of the methyl–methyl proton couplings in its derivatives. In particular, $^7J_p^{CH_3,CH_3}$ arises purely from a π electron mechanism (3) and when these electrons are not delocalized the coupling becomes very small. It is suggested that this criterion of electron delocalization may be applicable to borazine, and its hexamethyl derivative is examined from this viewpoint.

Experimental

Proton Magnetic Resonance Spectra

All proton magnetic resonance measurements were made on an HA100D spectrometer, using internal tetramethylsilane for a locking material in degassed samples. Aqueous solutions were bubbled with nitrogen. Solvents and concentrations were chosen to facilitate decoupling experiments and to provide sufficient signal to noise ratios for the observation of the ^{13}C side bands from the methyl protons.

The decoupling frequencies were derived from HP-4204A and Wavetek VCG 114 audio oscillators. When the ring proton resonances occurred over a range of

[1]Postdoctoral fellow, 1971–1973.

Can. J. Chem. Downloaded from www.nrcresearchpress.com by 210.87.254.40 on 09/05/12
For personal use only.

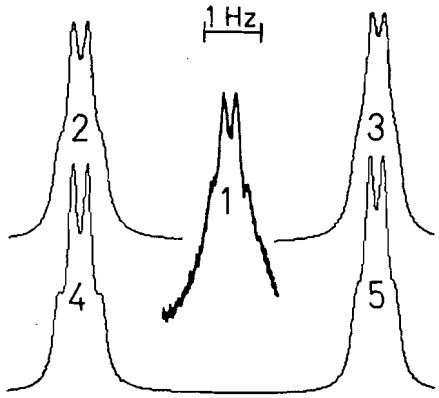

FIG. 1. The central spectrum, labelled *1*, is one ^{13}C side band of the methyl proton resonance in *m*-xylene under conditions where the ring protons are decoupled. The other peaks are calculated assuming lorentzian broadening of a symmetrical quartet with $^6J^{CH_3,CH_3}$ and the width of half-height, $\Delta\nu_{1/2}$, given, respectively, as: *2*, 0.25 and 0.25 Hz; *3*, 0.22 and 0.25 Hz; *4*, 0.25 and 0.20 Hz; *5*, 0.22 and 0.20 Hz.

frequencies the decoupling irradiation from the Wavetek oscillator was swept over this range in a manner designed to provide optimum peak widths in the methyl proton region.

Spectral Analysis

The methyl proton multiplets were simulated using the computer program LAME (13). A large number of simulations involved various combinations of peak widths and coupling constants to the protons of the other methyl group. The most difficulty occurred with the small coupling constants, about 0.2 Hz, between protons in methyl groups placed in *meta* positions. In Fig. 1 the unfavourable situation for *m*-xylene is displayed. The figure caption describes the details.

As a check on the accuracy of the coupling constants derived from experiments of this kind, they were applied to 4,6-dimethyl-2-fluoropyridine with the result that $|^6J_m^{CH_3,CH_3}| = 0.17 \pm 0.02$ Hz. Our previous value for this coupling was $\pm 0.19 \pm 0.02$ Hz, obtained from a total analysis of the proton resonance spectrum (14).

The signs of the coupling parameters could not be determined under the present experimental conditions. However, it is most unlikely that they differ from the signs determined by Macdonald and Reynolds for the xylene derivatives (2).

Borazine Derivatives

Hexamethylborazine as a saturated solution (~0.1 g/ml) in 1:1 DMSO–$CHCl_3$ gave an N—CH_3 peak which was 0.60 Hz wide at half-height while the B—CH_3 peak was 0.75 Hz wide. These widths are caused by partially relaxed coupling to boron and nitrogen and are smaller than in other solvents because the spin-lattice relaxation times of the quadrupolar boron and nitrogen nuclei are smallest in this solvent mixture. DMSO is probably the most efficient solvent in causing quadrupolar relaxation of nitrogen (15*a*) near ambient temperatures.

Strong irradiation of the B—CH_3 proton signals did not change the width of the N—CH_3 signal. Lineshape simulations, using various lorentzian peak widths and coupling constants in an A_9X_9 system, showed that $^5J_o^{CH_3,CH_3}$ and $^7J_p^{CH_3,CH_3}$ are both less than 0.1 Hz in magnitude. The A_9X_9 approximation is valid if $^5J_o^{CH_3,CH_3} = {}^7J_p^{CH_3,CH_3}$ and is not bad if both couplings are small and of the same sign. The value of 0.1 Hz is, in fact, very much of an upper limit because couplings of 0.06 Hz imply a line narrowing of 0.10 Hz on decoupling.[2] No line narrowing was observed. Also, the B—$^{13}CH_3$ peaks were no wider than the B—$^{12}CH_3$ peak, and the N—$^{13}CH_3$ and N—$^{12}CH_3$ peaks had the same widths as well. It follows that $^6J_m^{BCH_3,BCH_3}$ and $^6J_m^{NCH_3,NCH_3}$ are both less than 0.1 Hz in magnitude.

Results and Discussion

The methyl–methyl proton coupling constants are given in Tables 1 to 3.

Couplings over Five Bonds, $^5J_o^{CH_3,CH_3}$

To within experimental error the value of 0.45 ± 0.02 Hz in *o*-xylene is equal to those in the benzene derivatives and the dimethylpyridines, even when the latter are partially protonated. The effects of different solvents and of substituents, even when placed in the aromatic ring itself, are evidently quite small. In the pyridinium iodide, where one of the methyl groups is bonded to the nitrogen atom, the coupling does drop in magnitude but not enough to overlap with the magnitudes of the couplings over six bonds in other aromatic compounds (see Table 2).

Therefore $^5J_o^{CH_3,CH_3}$ is a sure indicator of the substitution pattern in cyclic six-membered molecules where delocalization of the π electrons occurs. In contrast, this coupling has a magnitude of 1.3 Hz in 2,3-dimethyl-1,4-benzoquinone (10) where delocalization of the π electrons is small. Similarly it is 1.20 ± 0.01 Hz in *cis*-butene-2 (16) where double bond localization is assured.

To a first approximation (11), a π electron

[2]On the slight possibility that ^5J_o and ^7J_p were larger but had opposite signs, giving a near zero average coupling, a series of simulations of an $[A_2X_2]_3$ system were run with the program NUMAR (15*b*) (it could not handle the true $[A_3X_3]_3$ system). J_{AX} and $J_{AX'}$ were set equal and negative while $J_{AX''}$ was positive and twice as large. As expected, if $J_{AA} = J_{XX} = 0$ a triplet of pentets was observed. When $J_{AA} = J_{XX} = 0.2$ Hz the spectrum was more complex but the envelope defined by the peaks had narrowed only slightly. Even when $J_{AA} = J_{XX} = 2.0$ Hz the envelope was considerably broadened. We thank A. R. Quirt and J. S. Martin for providing a copy of their program.

Can. J. Chem. Downloaded from www.nrcresearchpress.com by 210.87.254.40 on 09/05/12
For personal use only.

TABLE 1. Spin–spin coupling constants in Hz over five bonds between protons in methyl groups in *ortho* positions

Compound	State	$^5J_o^{CH_3,CH_3}$	Reference
o-Xylene	Neat*	0.45±0.02	—
		0.4	12
4,6-Dibromo-2,3-dimethylaniline	3 mol % in CS_2†	+0.40±0.03	2
2,3-Dimethylphenol	CCl_4	0.4	12
2-Hydroxy-4,5-dimethylacetophenone	CCl_4	0.4	12
3,4-Dimethylpyridine	Neat‡	0.43±0.01	—
	20% in TFA‡	0.42±0.01	—
2,3-Dimethylpyridine	Neat‡	0.47±0.03	—
	20% in TFA‡	0.47±0.03	—
1,2,6-Trimethylpyridinium iodide	20% in D_2O‡	0.32±0.03	—
Hexamethylborazine	~0.1 g/ml, 1:1 DMSO–$CHCl_3$	<0.1	—

*Decoupling of ring protons, observing ^{13}C side band.
†Total analysis of spectrum.
‡Decoupling of ring protons, TFA is trifluoroacetic acid.

TABLE 2. Spin–spin coupling constants in Hz over six bonds between protons in methyl groups in *meta* positions

Compound	State	$^6J_m^{CH_3,CH_3}$	Reference
m-Xylene	Neat*	0.23±0.02	—
		<0.3	12
Mesitylene	Neat*	0.23±0.02	—
3,4-Dibromo-2,6-dimethylaniline	6 mol % in CS_2†	−0.19±0.04	2
2,6-Dimethyl-3-fluoropyridine	24% in CS_2†	0.21±0.03	14
4,6-Dimethyl-2-fluoropyridine	17 mol % in CS_2	0.17±0.02†	14
		0.19±0.02‡	—
2-Hydroxy-4,6-dimethylacetophenone	CCl_4‡	<0.3	12
4,6-Dimethylpyrimidine	30% in CCl_4*	0.10±0.02	—
2,6-Dimethylpyrazine	30% in CCl_4*	0.22±0.02	—
4,6-Dimethyl-5-carboethoxy-2-pyrone	5% in CCl_4†	0.19±0.02	—
2,6-Dimethyl-*p*-benzoquinone	30% in CCl_4*	0.08±0.03	—
1,3,5-Trimethylpyridinium iodide	20% in D_2O‡	0.20±0.02 (1,3)	—

*Decoupling of ring protons, observing ^{13}C side band.
†Total analysis of spectrum.
‡Decoupling of ring protons.

TABLE 3. Spin–spin coupling constants in Hz over seven bonds between protons in methyl groups in *para* positions

Compound	State	$^7J_p^{CH_3,CH_3}$	Reference
p-Xylene	50% in CS_2*	0.60±0.03	—
	In CCl_4*	0.55	12
4,6-Dibromo-2,5-dimethylaniline	3 mol % in CS_2†	+0.62±0.03	2
2,5-Dimethylphenol	CCl_4‡	0.6	12
2,5-Dimethylaniline	CCl_4‡	0.6	12
2,5-Dimethylpyridine	Neat*	0.59±0.02	—
	20% in TFA*	0.55±0.02	—
1,4-Dimethylpyridinium iodide	20% in D_2O‡	0.53±0.02	—
2,5-Dimethylpyrazine	Neat*	0.66±0.03	—
2,5-Dimethyl-*p*-benzoquinone		0.0±0.04	—
Hexamethylborazine	~0.1g/ml, 1:1 DMSO–$CHCl_3$	<0.1	—

*Decoupling of ring protons, observing ^{13}C side band.
†Total analysis of spectrum.
‡Decoupling of ring protons.

Can. J. Chem. Downloaded from www.nrcresearchpress.com by 210.87.254.40 on 09/05/12
For personal use only.

Can. J. Chem. Downloaded from www.nrcresearchpress.com by 210.87.254.40 on 09/05/12
For personal use only.

transmitted coupling depends on the square of the mobile bond order of the intervening C⋯C bond and it is interesting to note that $1.20 \times 0.67 \times 0.67 = 0.53$ Hz, the mobile bond order in *cis*-butene-2 being taken as unity and that in *o*-xylene as 0.67. If the deviation of 0.08 Hz from the observed 0.45 Hz is significant, it may have its origin in the possibly different equilibrium conformations of the methyl groups in the two compounds. According to m.o. calculations at the INDO level (3), the stable conformation of *o*-xylene is **1**, and **2** is 4.8 kcal/mol less stable than **1**, which has been assumed as the stable form in u.v. work (17). On the other hand, *cis*-

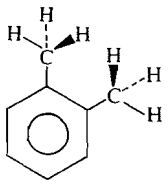

1

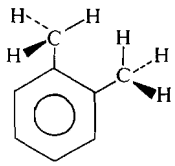

2

butene-2 has the stable form **3**, in which considerable strain arises from the repulsion of the two in-plane hydrogen atoms (18). In both molecules (3, 19) the coupling constants depend

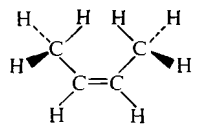

3

on the orientation of the methyl groups with respect to the π plane. Unfortunately, the calculated coupling constants are not reliable enough to resolve the question of the conformation of the methyl groups in *o*-xylene.

In **4** one has $^{2,5}J_o^{CH_3,CH_3} = 0.71 \pm 0.03$ Hz and the mobile bond order from INDO calcula-

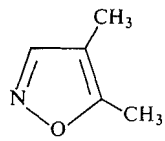

4

tions[3] is 0.826. Again, $1.20 \times 0.827 \times 0.827 = 0.82$ Hz which is 0.1 Hz larger than observed. Nevertheless, comparison of the three observed values of $^5J^{CH_3,CH_3}$ in *cis*-butene-2, *o*-xylene, and 4,5-dimethylisoxazole with the square of the mobile bond order of the intervening C⋯C bond, suggests that most of the coupling arises from a π electron mechanism.

The relatively small value of the coupling observed in the 1,2,6-trimethylpyridinium iodide, $^5J_o^{CH_3,CH_3} = 0.32$ Hz, would then result from either a large change in the double bond order of the C—N^+ bond in the ring or from an intrinsic change in the σ–π interaction integrals at the site of the nitrogen atom. However, a sizeable σ electron contribution to $^5J_o^{CH_3,CH_3}$ cannot be ruled out and the data in Table 2 for $^6J_m^{CH_3,CH_3}$ in a pyridinium iodide suggest a change in the σ electron contribution to $^5J_o^{CH_3,CH_3}$ in the salt. Of course, the counterion may exert a different influence in the two compounds and further discussion is hardly warranted.

Coupling over Six Bonds, $^6J_m^{CH_3,CH_3}$

This coupling is clearly diagnostic of the substitution pattern in those six-membered rings in Table 2 where substantial delocalization of π electrons occurs, except in 4,6-dimethylpyrimidine in which it is -0.10 ± 0.02 Hz. In general, substituent and solvent effects are not large, $^6J_m^{CH_3,CH_3}$ falling within -0.20 ± 0.03 Hz even in the pyridinium iodide, where one of the methyl groups is attached to the nitrogen atom. Because this coupling surely contains only a very small σ electron component, its unchanged magnitude in the iodide indicates that the explanation of the value of $^5J_o^{CH_3,CH_3}$ in an iodide in the previous section must involve a σ electron component.

Again, if $^6J_m^{CH_3,CH_3}$ is π electron transmitted, its small value in 4,6-dimethylpyrimidine must occur because the electronic effects of the two nitrogen atoms reinforce each other at C-2, -4, and -6, in contrast to the situation in 2,6-dimethylpyrazine, where $^6J_m^{CH_3,CH_3}$ has the same value as in *m*-xylene. As the C-5 environment in pyrimidine is often (20) said to be "more aromatic in character", measurement of $^5J_o^{CH_3,CH_3}$ and $^7J_p^{CH_3,CH_3}$ in the 4,5-dimethyl- and 2,5-dimethylpyrimidines would indicate how apposite the above interpretation really is.

A successful model for pyridine derivatives (14) in which the nitrogen atom does not affect the π electron contribution to coupling constants, acting only to polarize the σ core at C-2 and -6, is evidently inapplicable to pyrimidine. It is interesting that $^6J_m^{CH_3,CH_3}$ in 4,6-dimethylpyrimidine has half the value observed for it in

[3]Unpublished work in this laboratory.

Can. J. Chem. Downloaded from www.nrcresearchpress.com by 210.87.254.40 on 09/05/12
For personal use only.

the *m*-xylene and pyridine derivatives in Table 2. The coupling path via the nitrogen atoms involves eight bonds. If, in the absence of the nitrogen atoms, this path entailed the same contribution as that over six bonds, the observed magnitude would be rationalized.

The very small value of $^6J_m^{CH_3,CH_3}$ in 2,6-dimethyl-*p*-benzoquinone is expected if delocalization of π electrons is substantially suppressed.

Coupling over Seven Bonds, $^7J_p^{CH_3,CH_3}$

The value of 0.60 ± 0.03 Hz in *p*-xylene sinks to 0.53 ± 0.02 Hz in 1,4-dimethylpyridinium iodide, but the latter is still rather larger than those found for $^5J_o^{CH_3,CH_3}$ in Table 1. In 2,5-dimethyl-*p*-benzoquinone the coupling is undetectable by our methods, indicating negligible π electron delocalization, in agreement with the idea that $^7J_p^{CH_3,CH_3}$ is transmitted solely by the delocalized π electrons.

Hexamethylborazine

(a) Physical Evidence for Delocalization

Various physical and theoretical techniques estimate the π bond character in borazine to range from 15 to 79% of the value for benzene (21, 22). The overall picture appears to be one in which aromatic π bonds make relatively small contributions to the overall stability of the borazine ring.

More recently, photoelectron spectra (23, 24) have shown that the uppermost molecular orbitals of borazine are π rather than σ just as in benzene, in agreement with *ab initio* (25) and other calculations (26) of π, π, σ, π as the ordering of the orbitals but in disagreement with some semiempirical m.o. calculations (27, 28).

The chemical shifts of the protons in alkyl side chains (29) and the solvent effects on the proton shifts of benzene molecules dissolved in borazine derivatives (30) have been interpreted on the basis of an anisotropic susceptibility, $\Delta\chi$, of the borazine ring. If $\Delta\chi$ arises from a delocalization of π electrons then these data imply appreciable delocalization in the borazine ring. However, Benson and Flygare (31) show that in many cyclic molecules, including benzene, the observed $\Delta\chi$ values can be attributed partially or completely to local (atomic) contributions and therefore the data above need not be taken as proof of π electron delocalization in the borazine ring. Similar remarks may apply to the Faraday effect studies on borazine derivatives (32).

On the other hand, the chemical shift of the *para* N—H protons in *B*-monosubstituted borazines parallels the ^{13}C shifts in analogous benzenes and is consistent with electron delocalization (33). However, it cannot be used to deduce the extent of electron delocalization in borazine.

(b) Long-range Methyl–Methyl Couplings and INDO Calculations

The observation that these couplings in hexamethylborazine are smaller than 0.1 Hz indicates only a slight delocalization of π electrons in this compound. As stressed above, $^7J_p^{CH_3,CH_3}$ (but $^6J_p^{H,CH_3}$ also) arises from a π electron mechanism and INDO-MO-FPT calculations agree almost quantitatively with the observed magnitude of $^7J_p^{CH_3,CH_3}$ and of $^6J_p^{H,CH_3}$ in toluene, slightly overestimating the magnitude of the former coupling. Thus, INDO finds (3)

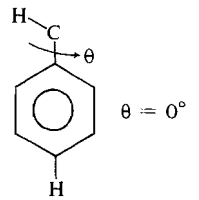

5

$^6J_p^{H,CH_3} = -1.22 \sin^2\theta$ where θ is indicated in **5**. For free rotation $\langle\sin^2\rangle\theta = 0.5$, and the predicted value of $^6J_p^{H,CH_3}$ becomes −0.61 Hz. The observed value is −0.62 Hz (1).

Because there are three C—H bonds in the methyl group, a preferred orientation of this group will still lead to observed and calculated values equal to that for free rotation. For example, if one C—H bond were fixed in the ring plane the above equation would predict $^6J_p^{H,CH_3} = -1.22\ (\sin^2 0° + \sin^2 60° + \sin^2 60°)/3 = -0.61$ Hz.

As the INDO calculations are so reliable for this long-range coupling but, because of their expense, they are here confined to the calculation of the coupling between methyl protons and the ring protons in *B*-methyl- and *N*-methylborazine. One additional calculation is performed on *p*-dimethylborazine for a conformation in which two C—H bonds lie in a plane perpendicular to the aromatic ring. The borazine bond angles were taken (34) as 120° with bond lengths: B—N, 1.44; B—H, 1.20; N—H, 1.02; N—C, 1.47; B—C, 1.56; and C—H, 1.09 Å. Up to 100 SCF cycles were performed (35) in the manner

TABLE 4. Computed long-range coupling constants in Hz of the methyl protons in *N*-methylborazine (N), B-methylborazine (B), and toluene (T)

θ* (deg)	$^4J_o^{H,CH_3}$			$^5J_m^{H,CH_3}$			$^6J_p^{H,CH_3}$		
	N	B	T	N	B	T	N	B	T
0	−0.655	−0.493	−0.345	−0.053	0.195	0.234	−0.012	0.028	−0.075
30	−0.507	−0.558	−0.606	−0.071	0.144	0.358	−0.031	−0.062	−0.357
60	−0.337	−0.687	−1.154	−0.079	0.066	0.646	−0.068	−0.245	−0.929
90	−0.282	−0.795	−1.467	0.001	0.095	0.889	−0.086	−0.339	−1.219
120	−0.214	−0.845	−1.264	0.180	0.277	0.946			
150	−0.140	−0.847	−0.806	0.374	0.511	0.876			
180	−0.115	−0.837	−0.575	0.458	0.619	0.831			

*For θ = 0° the C—H bond lies in the plane of the ring and *cis* to the coupled *ortho* or *meta* proton.

described previously (3) and were based on the parameterization of Pople and co-workers (36, 37). The calculated coupling constants converged to better than 0.001 Hz and are given in Table 4. In Fig. 2 the couplings are plotted *vs.* the angle θ for toluene (3), *N*-methyl-, and *B*-methylborazine.

$^6J_p^{H,CH_3}$ and $^7J_p^{CH_3,CH_3}$. It is apparent from Fig. 2 that $^6J_p^{H,CH_3}$ in *N*-methyl- and *B*-methylborazine has the θ dependence expected for a π electron transmitted coupling but that it is much smaller than in toluene. Thus, for rapid rotation about the B—C or N—C bonds INDO predicts $^6J_p^{H,CH_3} = \frac{1}{2}J(90°) = -0.043$ Hz for *N*-methylborazine and −0.170 Hz for *B*-methylborazine. For *p*-dimethylborazine INDO calculates $^6J_p^{CH_3,CH_3} = 0.272$ Hz for $\theta_1 = \theta_2 = 90°$ and therefore 0.272/4 = 0.063 Hz for free rotation of the methyl groups, in reasonable agreement with our observations. The calculations suggest more efficient transmission of spin density information when the methyl group is bonded to boron than when it is bonded to nitrogen, even though the π electron density on nitrogen is rather larger (Scheme 1). However, the

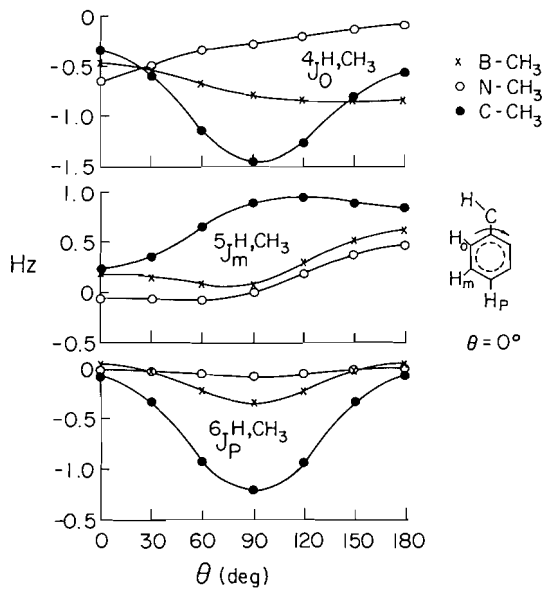

FIG. 2. The coupling constants in hertz computed by INDO-MO-FPT for coupling between methyl and ring protons in *N*-methylborazine, *B*-methylborazine, and toluene are plotted *vs.* the angle θ, defined in the diagram.

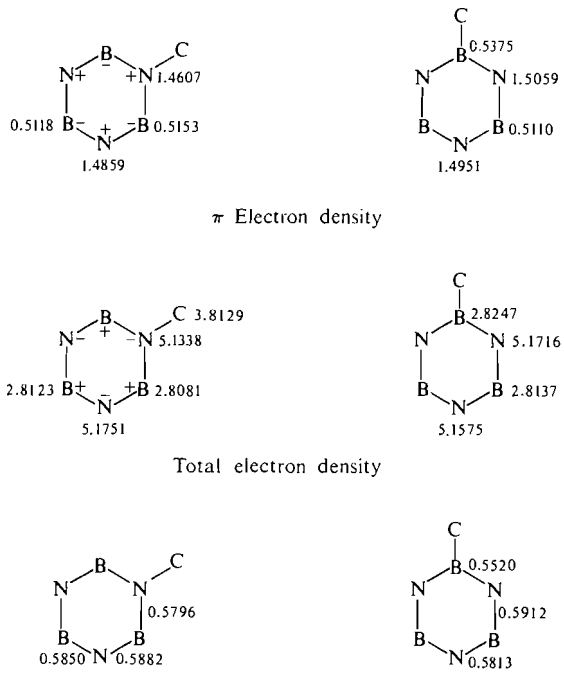

SCHEME 1

Can. J. Chem. Downloaded from www.nrcresearchpress.com by 210.87.254.40 on 09/05/12
For personal use only.

Can. J. Chem. Downloaded from www.nrcresearchpress.com by 210.87.254.40 on 09/05/12
For personal use only.

exchange interaction between p_z and σ orbitals may be larger for the N—H than for the B—H bonds at the other end of the coupling path.

The rather smaller decrease in $^7J_p^{CH_3,CH_3}$ observed when a positive charge is placed on nitrogen in 1,4-dimethylpyridinium iodide (Table 3) suggests that the alternation of total charge about the borazine ring is not the major reason for the very small observed and calculated $^6J^{CH_3,CH_3}$ in the methylborazines. Similarly, the transmission of spin density from the π system to the hydrogen orbitals in the free radical cations and anions of anthracene is altered but not strongly diminished on going from the negatively to the positively charged species (38), excess charge corrections amounting to at most $\pm 15\%$ of that occurring in neutral radicals. Again, the transmission of spin information from nitrogen π orbitals to the orbitals of attached hydrogen atoms in an N—H bond is, if anything, more efficient than for a C—H bond (39).

$^5J_m^{H,CH_3}$ in the Borazines. In toluene the available experimental and theoretical information can best be interpreted in terms of a predominant σ electron mechanism having a $(1 - \cos\theta)/2$ behavior, modified by a π electron mechanism of the same sign but with a $\sin^2\theta$ dependence (3). In consequence $^5J_m^{H,CH_3}$ has a maximum near 120° as in Fig. 2, the magnitude being overestimated substantially.

In *N*-methyl- and *B*-methylborazine the calculated values display a maximum at $\theta = 180°$, suggesting only small π electron contributions to this coupling. For free rotation the average values in Table 4 are 0.12 Hz for *N*-methyl- and 0.27 Hz for *B*-methylborazine, these being presumed overestimates.

$^4J_o^{H,CH_3}$ and $^5J_o^{CH_3,CH_3}$. The π electron contribution should cause a maximum in the magnitude of $^4J_o^{H,CH_3}$ near $\theta = 90°$, as illustrated in Fig. 2 for toluene but not calculated for the borazines. The calculated curves for the latter indicate a stereospecific σ electron mechanism, having a maximum magnitude at $\theta = 0°$ for *N*-methyl- and at $\theta = 180°$ for *B*-methylborazine.

In Scheme 1 the mobile bond orders in the monomethylborazines are reproduced as given by the total density matrix from the INDO computations. The bond order ranges from 0.55 to 0.59, not so very much less than the 0.67 in benzene. The ratio of the squares is about 0.7 so that one might expect a $^5J_o^{CH_3,CH_3}$ of about 0.45 $\times$ 0.7 $\sim$0.3 Hz.

The observed value of under 0.1 Hz is in agreement with the negligible π contribution to $^4J_o^{H,CH_3}$ calculated by INDO (methyl group replacement technique (40)). Apparently the formal mobile bond order in the borazine system need not necessarily indicate an appreciable ability to transmit a π electron effect.

Conclusions

The calculated and observed long-range proton coupling constants in methylborazines indicate a relatively weak transmission of spin density information via the presumed π electron system of borazine, in line with an m.o. comparison (41) of *N*- and *B*-, mono- and dimethylborazines with toluene and xylenes, which suggests that electronic effects can be transmitted around the borazine ring to only a small extent. The available coupling data on methylborazines should be extended by measuring methyl proton – ring proton and methyl proton – methyl proton couplings in appropriate borazine derivatives, preferably in the presence of ^{15}N, so that broadening from the ^{14}N quadrupole is eliminated. We are not equipped for the necessary synthetic procedures.

The J^{CH_3,CH_3} values for heterocyclic analogs of benzene indicate that the π electron contributions to these couplings can be noticeably altered if two heteroatoms reinforce one another at the sites of methyl substitution. Otherwise the J^{CH_3,CH_3} values are diagnostic of the substitution pattern even when the heteroatom bears a formal positive charge.

We are grateful to the National Research Council of Canada for financial assistance.

1. M. P. Williamson, R. J. Kostelnik, and S. M. Castellano. J. Chem. Phys. **49**, 2218 (1968).
2. C. J. Macdonald and W. F. Reynolds. Can. J. Chem. **48**, 1002 (1970).
3. R. Wasylishen and T. Schaefer. Can. J. Chem. **50**, 1852 (1972).
4. G. Kotowycz and T. Schaefer. Can. J. Chem. **44**, 2743 (1966).
5. D. Gagnaire and Trinh-Huu-Ich. Bull. Chem. Soc. Fr. 3763 (1966).
6. D. J. Blears, S. S. Danyluk, and T. Schaefer. J. Chem. Phys. **47**, 5037 (1967).
7. A. F. Janzen and T. Schaefer. Can. J. Chem. **49**, 1818 (1971).
8. H. M. McConnell. J. Chem. Phys. **30**, 126 1959).
9. J. B. Rowbotham and T. Schaefer Can. J. Chem. **51**, 953 (1973).

10. R. K. NORRIS and S. STERNHELL. Austral. J. Chem. **19**, 617 (1966).
11. K. D. BARTLE, D. W. JONES, and R. S. MATTHEWS. Rev. Pure Appl. Chem. **19**, 191 (1969).
12. S-O. ALMQVIST, A. J. AASEN, B. KIMLAND, and C. R. ENZELL. Acta Chem. Scand. **25**, 3186 (1971).
13. C. W. HAIGH and J. M. WILLIAMS. J. Mol. Spectrosc. **32**, 398 (1969).
14. J. B. ROWBOTHAM and T. SCHAEFER. Can. J. Chem. **50**, 2344 (1972).
15. (*a*) C. M. SHEPPERD, T. SCHAEFER, B. W. GOODWIN, and J. T'RAA. Can. J. Chem. **49**, 3158 (1971). (*b*) A. R. QUIRT and J. S. MARTIN. J. Magn. Resonance. **5**, 318 (1971).
16. F. H. A. RUMMENS and L. KASLANDER. Private communication to M. Barfield and S. Sternhell in ref. 19.
17. K. C. INGHAM and S. J. STRICKLER. J. Chem. Phys. **53**, 4313 (1970).
18. S. KONDO, X. SAKURAI, E. HIROTA, and Y. MORINO. J. Mol. Spectrosc. **34**, 231 (1970).
19. M. BARFIELD and S. STERNHELL. J. Am. Chem. Soc. **94**, 1905 (1972).
20. G. M. BADGER. The Chemistry of heterocyclic compounds. Academic Press. New York. 1961. p. 377.
21. H. R. ALLCOCK. Heteroatom ring systems and polymers. Academic Press. New York. 1967. Chapt. 3.
22. E. K. MELLON, JR. and J. J. LAGOWSKI. Adv. Inorg. Chem. Radiochem. **5**, 259 (1963).
23. D. R. LLOYD and N. LYNAUGH. Phil. Trans. Roy. Soc. London, **268A**, 97 (1970).
24. C. R. BRUNDLE, M. B. ROBIN, and N. A. KUEBLER. J. Am. Chem. Soc. **94**, 1451 (1972).
25. S. D. PEYERIMHOFF and R. J. BUENKER. Theor. Chim. Acta, **19**, 1 (1970).
26. J. GAYOSO, B. MAOUCHE, and A. BOUCEKKINE. C. R. Acad. Sc. Paris, **276C**, 257 (1973).
27. P. M. KUSNESOV and D. F. SHRIVER. J. Am. Chem. Soc. **90**, 1683 (1968).
28. D. W. DAVIES. Trans. Faraday Soc. **64**, 2881 (1968).
29. G. CROS, M. PASDELOUP, and J-P. LAURENT. Bull. Chem. Soc. Fr. 2601 (1969).
30. M. PASDELOUP, J.-P. LAURENT, and G. COMMENGES. J. Chim. Phys. **69**, 1024 (1972).
31. R. C. BENSON and W. H. FLYGARE. J. Chem. Phys. **58**, 2366 (1973).
32. M. PASDELOUP and J.-P. LAURENT. J. Chim. Phys. **70**, 199 (1973).
33. O. T. BEACHLEY, JR. J. Am. Chem. Soc. **92**, 5372 (1970).
34. V. M. SCHERR and D. T. HAWORTH. J. Inorg. Nucl. Chem. **35**, 660 (1973).
35. P. A. DOBOSH. Program 141. QCPE. University of Indiana, Bloomington, Indiana.
36. J. A. POPLE, J. W. MCIVER, JR., and N. S. OSTLUND. J. Chem. Phys. **49**, 2960, 2965 (1968).
37. J. A. POPLE and D. L. BEVERIDGE. Approximate molecular orbital theory. McGraw-Hill Book Co., New York, N.Y., 1970.
38. J. E. WERTZ and J. R. BOLTON. Electron spin resonance. McGraw-Hill Book Co., New York, N.Y., 1972, P. 123.
39. J. R. BOLTON *In* Radical Ions. *Edited by* E. T. Kaiser and L. Kevan. Interscience, New York, N.Y., 1968, p. 12.
40. R. A. HOFFMAN and S. GRONOWITZ. Acta Chem. Scand. **13**, 1477 (1959).
41. R. HOFFMANN. J. Chem. Phys. **40**, 2474 (1964).

Can. J. Chem. Downloaded from www.nrcresearchpress.com by 210.87.254.40 on 09/05/12
For personal use only.

A Nuclear Magnetic Resonance Study of Nucleoside Conformation in Solution. The Effect of Structure and Conformation on the Magnetic Nonequivalence of the 5′-Methylene Hydrogens

FRANK E. HRUSKA, DONALD J. WOOD, THOMAS N. MCCAIG, AND ANTHONY A. SMITH
Department of Chemistry, University of Manitoba, Winnipeg, Manitoba R3T 2N2

AND

ANTONIN HOLY
The Institute of Organic Chemistry and Biochemistry, Czechoslovak Academy of Science, Prague 6, Czechoslovakia

Received July 9, 1973

The relative chemical shift between the 5′-methylene hydrogens of a number of purine and pyrimidine nucleosides and nucleotides in solution are presented. For structurally related pyrimidine nucleosides in aqueous solution a good correlation between this relative shift and the sum of the 4′–5′ hydrogen–hydrogen vicinal coupling constants is noted. For this series of related molecules arguments are presented that the variation in the magnetic nonequivalence of this pair of hydrogens is a consequence of conformational changes about the C_4'—C_5' bond. Deviations from the correlation plot are observed for purine derivatives, nucleoside monophosphates etc. and discussed in terms of the effect of the specific chemical modification upon the nucleoside conformation and upon the intrinsic chemical shift nonequivalence of the 5′-methylene hydrogens.

On présente les déplacements chimiques relatifs des hydrogènes appartenant aux groupes méthylènes-5′ pour plusieurs nucléosides et nucléotides dérivés de la purine et de la pyrimidine en solution. On remarque un bon accord entre ce déplacement chimique relatif et la somme des constantes de couplage vicinal hydrogène–hydrogène 4′–5′ pour les nucléosides dérivés de la pyrimidine qui sont reliés par leur structure. On apporte des preuves visant à démontrer que la variation de la non-équivalence magnétique de cette paire d'hydrogènes est une conséquence de changements de conformation autour du lien C_4'—C_5' pour cette série de molécules. On observe et on discute des écarts par rapport à cette relation dans le cas des dérivés de la purine, des monophosphates de nucléoside etc. Ces écarts seraient dûs à l'effet de modification chimique spécifique au niveau de la conformation du nucléoside et au niveau de la non-équivalence intrinsèque des déplacements chimiques des hydrogènes appartenant aux groupes méthylènes-5′.
[Traduit par le journal]

Can. J. Chem., **52**, 497 (1974)

Introduction

A well-documented phenomenon (1–12) in proton magnetic resonance spectroscopy is the magnetic nonequivalence of the diastereotopic methylene hydrogens in molecules possessing a —CH_2—CXYZ fragment (where X, Y, and Z are different) as is manifested by a typical AB proton subspectrum. There seems to exist a general consensus that the differential chemical shift ($\delta_A - \delta_B$, henceforth $\Delta\delta$) can be discussed in terms of a temperature-dependent contribution, arising from unequal populations of the rotamers about the C—C bond, and a contribution due to "intrinsic molecular asymmetry" and attempts have been made to assess their relative contributions. Gutowsky (4), Raban (10), and Binsch and co-workers (11) have, for the purposes of quantitative discussions of the chemical shift difference, partitioned $\Delta\delta$ (eq. 1):

$$[1] \qquad \Delta\delta = \langle\Delta\rangle c + \langle\Delta\rangle i$$

where $\langle\Delta\rangle c$ represents the population-dependent conformational contribution and $\langle\Delta\rangle i$ the population-independent intrinsic contribution. In this work no attempt is made at any indepth analysis of their relative contributions; our purpose is simply to determine whether the magnetic nonequivalence observed for the diastereotopic 5′-hydrogens of a series of nucleosides and nucleotides can be related to their structural and conformational properties. Recently we reported (13–15) the complete analyses of the p.m.r. spectrum of β-pseudouridine (ψ), α-pseudouridine (αψ), and uridine (U) (Fig. 1) and commented on the observed magnetic nonequivalence of the 5′-hydrogens. In the present work it is demonstrated that the relative chemical shifts in a series of *structurally related pyrimidine nucleosides* in aqueous solution

Can. J. Chem. Downloaded from www.nrcresearchpress.com by 210.87.254.42 on 09/05/12
For personal use only.

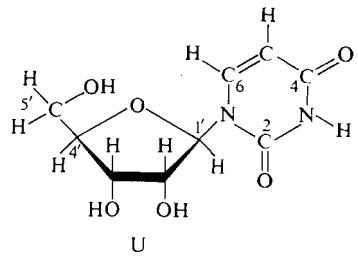

U

FIG. 1. Structure of uridine (U).

are correlated with the *sum* of the 4′–5′ vicinal H–H coupling constants and therefore must be directly related to the conformational preferences about the exocyclic $C_{4'}$—$C_{5'}$ bond. The observed correlation between shift and coupling constants argues that, *within this series of molecules*, variations in $\Delta\delta$ can be traced to variations in $\langle\Delta\rangle$c and that $\langle\Delta\rangle$i is essentially invariant. Deviations from the correlations are found for purine derivatives, for pyrimidine nucleosides with bulky and/or polar substitutions on the base at positions *ortho* to the *N*-glycosyl linkage, and for 3′- and 5′-nucleoside monophosphates. The deviations are attributed to highly specific effects of these alterations on the $\langle\Delta\rangle$i which lead to the observed deviations. Ambient and high temperature results are presented, as well as a limited number of results for nucleosides in dimethylsulfoxide. Though the results for the nonaqueous environment are limited, an interdependence of $\Delta\delta$ and the sum of the vicinal coupling constants parallel to that in the aqueous environment is indicated. These parallel dependences are taken as further evidence that the relative shifts are related to the exocyclic $C_{4'}$—$C_{5'}$ nucleoside conformation and can provide structural information which supplements that derived from coupling constant data.

Experimental

Nucleosides and nucleotides were purchased from Calbiochem or the Sigma Chemical Company and used without further purification. 6-Carboxyuridine (cU), 5-ethoxycarbonyluridine (eU), and 3-ribosyl-6-methyluracil (rmU) were prepared according to ref. 16. Solutions were 0.1 *M* or less in D_2O. 2,2,3,3,-Tetradeuterio-3-(trimethylsilylpropionic)acid sodium salt (TSP) was used as an internal p.m.r. reference (0.05 *M*) for the pyrimidine derivatives and tertiary butyl alcohol (OD) for the purine derivatives. TMS was used for DMSO solutions. The aqueous solutions were lyophilized three times from D_2O to reduce the HDO resonance. Spectra were recorded at 220 MHz at the Canadian 220 MHz Centre, Sheridan Park, Ontario and/or on a Varian 100 MHz spectrometer. Computer simulated spectra were generated as a final test of the derived chemical shift and coupling constant parameters. Some of the data are taken from the literature; the sources are indicated in Table 1. In this table are presented the data required for this study. All abbreviations for the compounds studied are given in the table.

Discussion

The Newman projection formulae (Fig. 2) facilitate discussion of nucleoside conformations about the $C_{4'}$—$C_{5'}$ bond.[1] The usefulness of Karplus treatments (17) of the vicinal coupling constants, $J_{4'5'}$ and $J_{4'5''}$, for monitoring changes in this exocyclic conformation has been demonstrated (13–15, 18). More recently we have approached this conformational problem in terms of the experimental sum, $\Sigma = J_{4'5'} + J_{4'5''}$ (18–22). This sum allows for a discussion of the fractional contribution of the *gauche–gauche* (*gg*) rotamer and the combined contribution from the *gauche–trans* (*gt*) and *trans–gauche* forms (Fig. 2). It has been argued (18, 19) that any perturbation resulting in an *increase* in the *gg* rotamer population should be manifest by a decrease in the experimental sum and con-

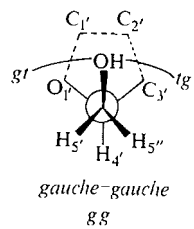

gauche–gauche
gg

FIG. 2. Newman projection formulae along the $C_{4'}$—$C_{5'}$ bond of a nucleoside indicating the *gauche–gauche* (*gg*), *gauche–trans* (*gt*), and *trans-gauche* (*tg*) conformers.

[1]It is important to point out that an absolute spectral assignment of the 5′,5″ protons has not been made in each instance. Recently a reasonable assignment was made for several pyrimidine nucleosides (ref. 65); the authors demonstrate that the hydrogen labelled 5′ occurs at high field from 5″ in the AB spectrum. There is no *a priori* justification for assuming that this labelling is appropriate for all molecules examined here but the linear correlation found (*vide infra*) for data of the structurally related molecules strongly suggests that at least for this series of molecules the assignments are identical. For the molecules deviating from the plots presented here the assignments could well be inverted in any one (or all) instances but our feeling is that in these cases as well the Remin and Shugar assignment can be assumed. In any case, because of our method of treating the data (which uses relative shifts and sums of coupling constants), possible misassignment in individual cases does not hamper our interpretation of the gross features of our plots.

Can. J. Chem. Downloaded from www.nrcresearchpress.com by 210.87.254.42 on 09/05/12
For personal use only.

TABLE 1. Relative chemical shifts of the 5′-methylene hydrogens ($\Delta\delta$) and the sum of the 4′–5′ vicinal coupling constants (Σ) for a series of purine and pyrimidine nucleosides and nucleotides in solution

Compound	Conditions*	$\delta_{5'}-\delta_{5''}(\Delta\delta)$ (p.p.m.)	$J_{4'5'}+J_{4'5''}(\Sigma)$ (Hz)	$J_{3'4'}$	Reference†
1. Uridine (U)	Ambient	0.104	7.3	5.4	54
	80°	0.092	7.9	5.1	54
	DMSO	0.069	6.6	3.6	This work
2. Cytidine (C)	Ambient	0.114	7.2	6.0	"
	65°	0.107	7.7	5.9	"
3. 5-Iodocytidine (IC)	Ambient	0.159	5.3	7.0	"
	65°	0.137	6.6	6.8	"
	DMSO	0.146	5.0	5.3	"
4. 5-Iodouridine (IU)	Ambient	0.137	6.2	6.3	"
	60°	0.120	6.9	5.8	"
	DMSO	0.110	5.1	4.4	"
5. 5-Bromouridine (BrU)	Ambient	0.125	6.3	6.2	"
	60°	0.114	7.1	5.9	"
6. 5-Chlorouridine (ClU)	Ambient	0.120	6.6	5.9	"
	60°	0.108	7.2	5.7	"
7. 5-Ethoxycarbonyluridine (eU)	5°	0.177	4.8	7.7	"
	Ambient	0.169	5.3	7.3	"
	55°	0.145	6.4	6.5	"
	DMSO	0.117	4.9	5.1	"
8. 5-Carboxyuridine (cU)	5°	0.113	6.8	5.4	"
	Ambient	0.105	7.2	5.4	"
	60°	0.098	7.9	5.2	"
9. 5-Azacytidine (5-azaC)	Ambient	0.153	6.9	7.1	"
10. β-Pseudouridine (ψ)	Ambient	0.114	7.8	5.2	13, 54
	70°	0.116	8.2	5.2	54
	DMSO	0.150	6.6	5.6	This work
11. 2′-*O*-Methyluridine (Um)	Ambient	0.109	7.2	5.9	59
	60°	0.105	7.4	5.6	59
12. 2′-*O*-Methylcytidine (Cm)	Ambient	0.117	7.2	6.7	59
	60°	0.109	7.6	6.3	59
13. Dihydrouridine (diHU)	Ambient	0.077	8.4	3.6	This work
	60°	0.078	8.1	4.2	"
14. 2′-Deoxyuridine (dU)	Ambient	0.075	8.5	4.1	"
	65°	0.074	9.1	4.0	"
15. 2′-Deoxycytidine (dC)	Ambient	0.080	8.7	4.0	"
	70°	0.074	9.2	4.0	"
	DMSO	0.043	7.5	3.2	"
16. 5-Bromo-2′-deoxyuridine (BrdU)	Ambient	0.081	8.0	4.1	"
	65°	0.079	8.6	4.2	"
17. 5-Bromo-2′-deoxycytidine (BrdC)	Ambient	0.093	8.0	4.1	"
	65°	0.086	8.7	4.1	"
18. 5-Iodo-2′-deoxycytidine (IdC)	Ambient	0.099	7.9	4.5	"
	65°	0.090	8.5	4.2	"
19. 2′-Deoxythymidine (dT)	18°	0.072	8.6	3.7	"
20. Adenosine (A)	Ambient	0.084	6.1	3.1	"
	55°	0.077	6.8	3.8	"
	DMSO	0.118	7.2	3.2	58

Can. J. Chem. Downloaded from www.nrcresearchpress.com by 210.87.254.42 on 09/05/12
For personal use only.

TABLE 1. (*Concluded*)

21. 2′-Deoxyadenosine (dA)	Ambient	0.063	7.3	3.0	This work
	60°	0.063	8.3	3.2	"
	DMSO	0.095	8.3	2.5	"
22. 2′-*O*-Methyladenosine (Am)	Ambient	0.066	5.7	3.0	60
23. 6-Azacytidine (azaC)	Ambient	0.125	8.9	5.8	This work
24. 8-Bromoadenosine (BrA)	DMSO	0.151	8.0	2.3	58
25. Inosine (I)	Ambient	0.074	7.1	4.0	This work
26. α-Pseudouridine (αψ)	Ambient (p*H* 6.7)	0.173	8.1	7.9	14
27. Arabinouridine (araU)	5°	0.083	7.6	5.7	61
	Ambient	0.080	8.8	5.5	61
	80°	0.073	9.3	5.4	61
	DMSO	0.034	10.0	3.6	58
28. Arabinocytidine (araC)	Ambient	0.077	9.0	5.3	This work
29. 6-Azauridine (azaU)	Ambient	0.123	8.8	5.8	20
30. Orotidine (O)	Ambient	0.111	9.1	7.0	27
	DMSO	0.168	9.4	6.0	58
31. 3-Ribosyl-6-methyluracil (rmU)	Ambient	0.134	9.1	7.0	This work
32. Ribosylcyanuric acid (RCA)	Ambient	0.13	9.4	6.7	47
33. Uridine-5′-monophosphate (UMP)	Ambient	0.052	5.5	3.9	20, 21
34. Uridine-3′-monophosphate (3′-UMP)	Ambient	0.046	7.0	5.5	54
35. 6-Azauridine-5′-monophosphate (azaUMP)	Ambient	0.078	10.7	5.4	20, 21
36. Adenosine-5′-monophosphate (AMP)	Ambient	~0.01	6.6	3.7	20
37. Adenosine-5′-diphosphate (ADP)	Ambient	~0.01	6.1	3.8	20
38. Guanosine-2′-monophosphate (2′-GMP)	Ambient	7.4	7.1	4.5	62
39. 2,2′-Anhydroarabinosyluracil (aU)	5°	0.001	7.6	1.8	61
	Ambient	0.023	8.2	1.9	61
	80°	0.062	9.3	2.3	61
40. 4-Thiouridine (sU)	Ambient	0.13	7.3	5.6	63
41. 1-Ribofuranosyl-2-pyrimidone (rPym)	Ambient	0.167	6.6	8.0	This work
	65°	0.145	7.3	7.3	"
42. 1-Ribofuranosyl-2-pyridone (rPy)	Ambient	0.124	6.7	6.5	"
	65°	0.110	7.8	6.4	"

*Ambient temperature 20–30 °C; unless otherwise indicated, all results are for D_2O solutions; all DMSO results are for 30 ± 1 °C.
†Numbers refer to literature sources; recorded at 100 or 220 MHz. Probable error: Δδ, ± 0.002 p.p.m.; Σ, ± 0.2 Hz.

versely any increase in the *gt* and/or *tg* population, at the expense of *gg*, should result in an increase in $\sum$. Equation 2 has been developed

$$[2] \qquad P_{gg} \simeq (13 - \sum)/10$$

(21*a*, *b*), relating P_{gg}, the *gg* fractional population, to the experimentally observed sum $\sum$ and shown to be useful for semiquantitative treatments of experimental data.

It is not possible to make quantitative estimates of Δδ for the 5′-hydrogens but it is safe to predict that changes in the $C_{4'}$—$C_{5'}$ conformational distribution brought about by changes in structure, solvent etc., will be manifest in variations in Δδ. Since we have argued that $\sum$ provides a means of monitoring these changes, then any empirical correlation between $\sum$ and Δδ would substantiate this prediction and provide support as well for our earlier contention that $\sum$ is a reliable probe for this particular conformational problem.

In Fig. 3 the experimentally determined $\sum$

Can. J. Chem. Downloaded from www.nrcresearchpress.com by 210.87.254.42 on 09/05/12
For personal use only.

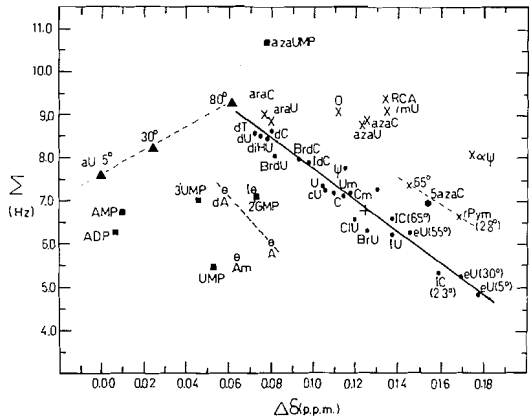

FIG. 3. Plot of Σ *vs.* $\Delta\delta$ for a series of pyrimidine and purine nucleosides and nucleotides in aqueous solution: (●), Correlating pyrimidine nucleosides; (×), noncorrelating pyrimidine nucleosides; (⊖), purine nucleosides; (■), mono- and diphosphates; (▲), 2,2′-anhydroarabinosyluracil (aU); (+), 1-ribofuranosyl-2-pyridone (rPy); (●), 5-azacytidine (5-azaC). Only ambient temperature (neutral p*H*) data from Table 1 are included except where indicated.

and $\Delta\delta$ values (in Hz and p.p.m., respectively) are plotted for a large number of purine and pyrimidine nucleosides and nucleotides in aqueous solution. The data span Σ values from 4.5 to 9.5 Hz and $\Delta\delta$ values from 0.0 to 0.18 p.p.m. with considerable scatter in the points and demonstrate that $\Delta\delta$ must be related to the chemical nature of the base and sugar ring. Moreover a reasonable linear correlation between Σ and $\Delta\delta$ is evident for a large number of *structurally related pyrimidine nucleosides* denoted by ●. The molecules lying close to this correlation line have, with only a few exceptions, the following common structural features: (*a*) They are ribosides, 2′-*O*-methylribosides, or 2′-deoxyribosides in the β-configuration. Thus in the entire series the furanose portion of the molecules is identical except for modifications at the 2′ position occurring to the side (*exo*) of the ring opposite to that on which the 5′-hydroxymethyl is located (*endo*). We choose for reasons given below to consider the arabinose derivatives araU and araC as exceptions; in these derivatives the change in configuration at $C_{2'}$ places the 2′-hydroxyl in the *endo* position and near to $C_{5'}$. (*b*) They have a C—H and a C=O group at the *ortho* positions of the pyrimidine base (relative to the *N*-glycosyl linkage). Thus base substitutions are limited to the 4 (*para*) and 5 (*meta*) positions for the correlating molecules. (*c*) They show a preference for the *anti* conformation in which the *ortho* C—H, rather than the *ortho* C=O, lies over the furanose ring and can approach the 5′-methylene group. One exception is dihydrouridine (diHU) which is *anti* and has a $-CH_2-$ group at the 6 position (23). Also available are data for 1-ribofuranosyl-2-pyridone (rPy, indicated by + on the diagram). This nucleoside, though neither a uracil nor a cytosine derivative, has feature *a*, possesses a C—H and C=O at the *ortho* position of the base, and for steric reasons is expected to prefer the *anti* conformation, feature *c*; it lies near to the correlation line as well.

Plotting above the correlation line are the α anomer of pseudouridine (αψ) and a collection of nucleosides with structural modifications at the 6 (or *ortho*) positions of the base. Thus, 6-azauridine (azaU) and 6-azacytidine (azaC) possess a nitrogen at the 6 position in place of the C—H in the parent compounds U and C. These modified compounds demonstrate a preference for the *anti* conformation (24–27) and thus will have the 6-aza nitrogen approaching the 5′-CH_2 moiety. β-Ribofuranosylcyanuric acid (RCA) and rmU have keto groups occupying both *ortho* positions and therefore one such group must be situated above the furanose and near the 5′ position. In this respect, they mimic the *syn* conformation of a normal pyrimidine nucleoside. The 6-carboxy derivative orotidine (O) is known to exist in the *syn* conformation (26, 28) and interestingly it plots near to the

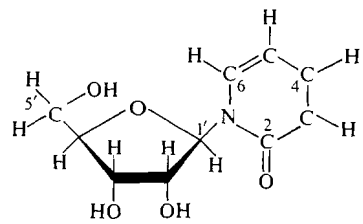

rPy

FIG. 4. Structure of 1-ribofuranosyl-2-pyridone (rPy).

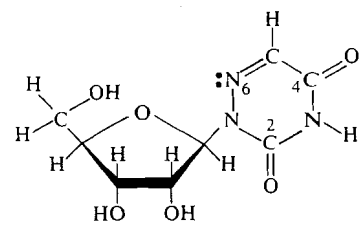

azaU

FIG. 5. Structure of 6-azauridine (azaU).

Can. J. Chem. Downloaded from www.nrcresearchpress.com by 210.87.254.42 on 09/05/12
For personal use only.

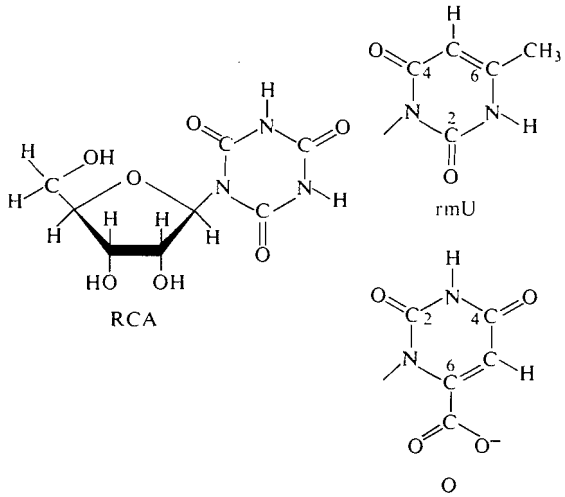

FIG. 6. Structure β-ribofuranosylcyanuric acid (RCA), 3-ribosyl-6-methyluracil (rmU), and orotidine (O).

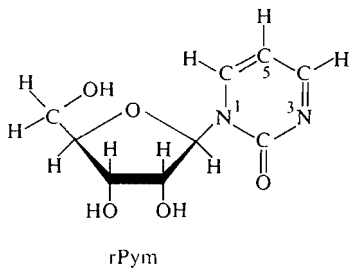

FIG. 7. Structure of 1-ribofuranosyl-2-pyrimidone (rPym).

points for RCA and rmU as well as to the aza derivatives. Also found above the line are points at two temperatures for 1-ribofuranosyl-2-pyrimidone (rPym, Fig. 7); rPym differs from U only at the 3 and 4 positions of base and thus is anomalous since it possesses features *a*, *b*, and *c* but deviates from the correlation plot. We find the 5′-monophosphate of 6-azauridine (azaUMP) plotting above the line.

Points lying distant from the correlation line but to the opposite side correspond to the adenine derivatives of ribose (A), 2′-deoxyribose (dA), and 2′-*O*-methyl ribose (Am). Also in this region are inosine (I), various mono- and diphosphates, and 2,2′-anhydroarabinosyluracil (aU, Fig. 8) at several temperatures.

From the distribution of points in Fig. 3, a number of qualitative conclusions regarding the origin of the magnetic nonequivalence may be drawn. First, the linear correlation between $\sum$ and $\Delta\delta$ suggests, that for the series of *structurally related* pyrimidine nucleosides, *variations* in $\Delta\delta$ can be traced to the variations in their conformational preferences about the $C_{4'}$—$C_{5'}$ bond. Furthermore, the monotonic variation in $\Delta\delta$ with $\sum$ suggests that the relative populations of the three conformers, within the span of the data obtained, are varying in a monotonic fashion. Estimates using eq. 2 indicate that a range from 35% *gg* ($\sum$ = 9.5 Hz) to 80% *gg* ($\sum$ = 5.0 Hz) is spanned by the line. Finally, the linear correlation of $\Delta\delta$ with $\sum$ suggests that *for the correlating series* variations in $\Delta\delta$ are due to variations in the $\langle\Delta\rangle$c term and that the $\langle\Delta\rangle$i term is essentially invariant to within, say, 0.015 p.p.m., the largest deviation from the line for a molecule with features *a*, *b*, and *c*.[2] In other words we are proposing that essentially identical magnetic environments are provided at the 5′-position by the furanose and base moieties in the correlating series, with the characteristic $\Delta\delta$ and $\sum$ values displayed by any given nucleoside in the series arising from a characteristic sampling of the three conformers. This does not seem to be an unreasonable suggestion since variations in structure in the series are restricted to positions distant from the 5′-position *i.e.* at the *exo* 2′-position and at the *meta* and *para* positions of the pyrimidine base. We are of course not suggesting that the base has no effect on the 5′-magnetic environment; we suggest only that for the correlating molecules the collection of pyrimidine bases make much the same magnetic contribution to $\langle\Delta\rangle$i but a contribution sensibly distinct from that of the 6-azauracil, orotic acid, purine, etc. bases of the noncorrelating molecules. That a β-linked base does contribute to $\langle\Delta\rangle$i is implied by the difference in $\Delta\delta$ values noted for

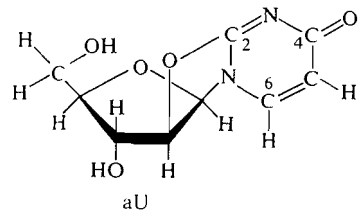

FIG. 8. 2,2′-Anhydroarabinosyluracil (aU).

[2]An alternative explanation for the linear correlation is that for this series of molecules changes in $\langle\Delta\rangle$c and $\langle\Delta\rangle$i are important but are proportional. However, in view of the diverse array of substituents (COO^-, I, S etc.) on, in particular, the base, this alternative seems unlikely.

Can. J. Chem. Downloaded from www.nrcresearchpress.com by 210.87.254.42 on 09/05/12
For personal use only.

Can. J. Chem. Downloaded from www.nrcresearchpress.com by 210.87.254.42 on 09/05/12
For personal use only.

the α and β anomers of pseudouridine and the displacement of αψ from the correlation plot.

The foregoing discussion has suggested that variations in the 2′-*exo* substituent of the (deoxy) furanose substituent and in the *meta* and *para* substituents of the base have little direct effect (*i.e.* through ⟨Δ⟩i) on Δδ and that the correlation of Δδ and ∑ argues for attributing variations in Δδ exclusively to ⟨Δ⟩c for molecules with features *a*, *b*, and *c*. Our interpretation of the sensitivity of Δδ and ∑ to structural variations in the molecules at these points which are distant from the $C_{4'}$—$C_{5'}$ bond is stimulated by suggestions in the literature of interdependences between, on the one hand, furanose ring puckering and the exocyclic conformation about the *N*-glycosyl (N—$C_{1'}$) linkage and between the furanose ring puckering and the exocyclic $C_{4'}$—$C_{5'}$ conformational distribution on the other. Thus several theoretical and experimental reports (29–34) have drawn attention to the apparent correlation between the nature of the ring puckering and rotation about the *N*-glycosyl linkage. X-Ray (30–35), p.m.r. (18–19), and theoretical calculations (36) consistently predict a correlation between puckering and the $C_{4'}$—$C_{5'}$ conformer population. (The consistent prediction is that for pyrimidine nucleosides with features *a*, *b*, and *c*, the *gg* conformation is favored if the ring assumes a $C_{3'}$ *endo* pucker but is destabilized by a $C_{2'}$ *endo* pucker.[3])

Bearing in mind this rather good agreement between X-ray, p.m.r. and theoretical data, we are inclined to propose that concomitant with variations in the 2′-*exo* substituent of the furanose, or at the *meta* and *para* positions of the base, are changes in the furanose ring puckering *i.e.* in the $C_{2'}$ *endo* ↔ $C_{3'}$ *endo* (S ↔ N) balance (18, 19, 38) which are sensed by the hydroxymethyl group and reflected in the *gg*, *gt*, and *tg* conformational weightings and manifest simultaneously in the correlated variations of ∑ and Δδ.

It is not surprising that variations in the 2′-*exo* substituent can result in perturbations in the sugar; differences in the pucker of ribosides and 2′-deoxyribosides have been known for some time at even the polynucleotide level (30, 32, 33, 39). Although we cannot make any but thoroughly speculative statements on the possible origin of the *meta* and *para* influences on ∑ and Δδ, it seems most likely that they are mediated by interactions involving the base and the unshared pair of electrons on the furanose ring oxygen *i.e.* through the so-called anomeric, or reverse anomeric effect (40–44). Our speculation, which incorporates the views of Lemieux (42) and the suggested interrelationships between the various conformational angles, is as follows: variations in the electronic structure of the base brought about by substitution modulate the interaction between the base and the ether oxygen which is reflected in a modulation of the $C_{2'}$ *endo* (S) ↔ $C_{3'}$ *endo* (N) equilibrium blend which in turn is sensed by the hydroxymethyl group and reflected simultaneously in the parameters dependent upon the conformation about the $C_{4'}$—$C_{5'}$ bond *i.e.* ∑ and Δδ. (It is sufficient to point out here that anomeric type interactions (repulsion between base and unshared pairs) will bias the ribose puckering towards $C_{3'}$ *endo* whereas the reverse anomeric type will introduce a bias towards $C_{2'}$ *endo*.)

To support the above interpretation of the regular progression of Δδ and ∑ for the correlating, structurally-related pyrimidine nucleosides we draw attention to the striking resemblance between the plotting pattern of points in Fig. 3 and those in Fig. 9 which, with a few additions, is taken from ref. 18. In the latter figure are plotted ∑ *vs.* $J_{3'4'}$ data for the same collection of molecules used in Fig. 3. Figure 9 is essentially a two-dimensional map of nucleoside(tide) conformation in aqueous solution. The ordinate (∑), of course, monitors changes in $C_{4'}$—$C_{5'}$ conformation whereas the abscissa ($J_{3'4'}$) relates information about the nature of the furanose ring puckering. This presentation of p.m.r. data follows the conformational mapping approach used by crystallographers (30) and theoreticians (36) for discussion of nucleoside conformation and facilitates comparison of crystal, n.m.r., and theoretical data. These coupling constant maps proved useful since they revealed the above-mentioned interdependence of the nucleoside $C_{4'}$—$C_{5'}$ conformation and the furanose puckering for *structurally similar pyrimidine nucleosides* (18, 19). From the plot, it is apparent that a decrease in the *gg* conforma-

[3]The authors realize that furanose ring conformations in solution are best discussed, not in terms of the conventional single puckered forms ($C_{3'}$ *endo*, $C_{2'}$ *endo* etc.), but rather in terms of significantly populated segments of the pseudorotational itinerary (37). Here the terms $C_{3'}$ *endo* and $C_{2'}$ *endo* are meant to stand for the N and S segments populated by (deoxy) ribosides (38).

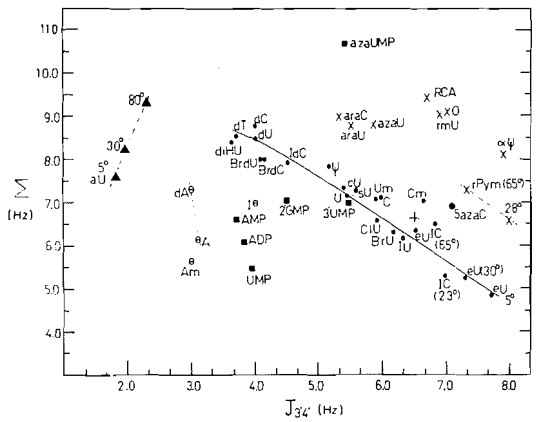

FIG. 9. Plot of Σ *vs.* $J_{3'4'}$ for a series of pyrimidine and purine nucleosides and nucleotides in aqueous solution: (●), correlating pyrimidine nucleosides; (×), noncorrelating pyrimidine nucleosides; (⊖), purine nucleosides; (■), mono- and diphosphates; (▲), 2,2′-anhydroarabinosyluracil (aU); (+), 1-ribofuranosyl-2-pyridone (rPy); (●), 5-aracytidine (5-azaC). Only ambient temperature data of neutral p*H* are included except where indicated.

tion is correlated with a decrease in the $C_{3'}$ *endo* contribution to the $C_{3'}$ *endo* (N) ↔ $C_{2'}$ *endo* (S) balance for a series of molecules connected by the solid line. However, and this is the important point, the molecules found to correlate in these two-dimensional Σ *vs.* $J_{3'4'}$ maps are (again with few exceptions) simply those correlating in the Σ *vs.* $\Delta\delta$ plot in Fig. 3. In addition, the locations of the points are qualitatively identical on the pair of plots. Thus, with U assumed to be central in both correlation plots, we find the pyrimidine 2′-deoxyribosides and dihydrouridine (diHU) displaced along the line toward larger Σ values while the halogenated pyrimidines and eU are displaced toward decreasing Σ. The plotting patterns of points lying off the line are also strikingly similar. Above the line we find, ordered with increasing $\Delta\delta$, or $J_{3'4'}$, values, 5′-azaUMP, the azapyrimidines and *syn*-like nucleosides (O, RCA, rmU) followed by αψ and rPym. Below the correlation line in each figure we find all of the purine derivatives and the 5′-mono- and diphosphates. Some trends other than the main correlations are also apparent. In both figures the effect of the base change from uracil to adenine results consistently in a displacement to smaller Σ and smaller $\Delta\delta$, or $J_{3'4'}$, values (compare the U–A, Um–Am, dU–dA pairs). Substitution of the 2′-hydroxyl by a hydrogen results in a displacement towards larger Σ and smaller $\Delta\delta$, or $J_{3'4'}$ values (compare the A–dA and U–dU pairs). In addition we see for aU that the effect of increasing temperature results in a displacement up and to the right in both figures. The most interesting trends must certainly be the almost vertical displacement of the points observed when the uracil base is substituted by the 6-azauracil base at *both* the nucleoside and 5′-mononucleotide levels (Compare the U–azaU and 5′-UMP–5′-azaUMP pairs). There are however some important differences in location. Thus in the $\Delta\delta$ plot 3′-UMP lies below the line but is found near the line in the $J_{3'4'}$ plot; araU and araC are found above the $J_{3'4'}$ correlation plot but near the $\Delta\delta$ plot. These dissimilarities shall be commented on later.[4]

Given then our large number of data for molecules with a diverse array of substituents it appears to us that the (virtually) identical plotting patterns for Σ *vs.* $\Delta\delta$ on the one hand and *vs.* $J_{3'4'}$, a parameter with no obvious relationship to $\Delta\delta$, on the other, are a consequence of something more than fortuity. The similarity argues strongly that $\Delta\delta$ and Σ are sensitive functions of the conformational preferences about $C_{4'}$—$C_{5'}$ which in turn can safely be said to depend upon the mode and extent of the furanose ring puckering. The apparent link between the $C_{4'}$—$C_{5'}$ conformational preferences and the ring puckering (though not direct evidence for) strongly supports our contention that the influence of base substitution on Σ and $\Delta\delta$, and $J_{3'4'}$, values can be mediated by interactions involving the unshared pairs of electrons on the furanose ring oxygen in the manner outlined by Lemieux (42). We do not feel sufficiently confident to suggest that our correlations are best discussed in either the anomeric or reverse anomeric context. At present it is sufficient to point out that variations along the Σ *vs.* $\Delta\delta$ and Σ *vs.* $J_{3'4'}$ plots towards increasing $J_{3'4'}$ and $\Delta\delta$ may be considered to reflect an increase in

[4]It is important to point out that in refs. 18 and 19 maps of Σ *vs.* $J_{1'2'}$ as well as Σ $J_{3'4'}$ maps were presented since both $J_{1'2'}$ and $J_{3'4'}$ reflect the $C_{3'}$ *endo* (*N*) ↔ $C_{2'}$ *endo* (*S*) balance. Both maps consistently point to the interrelationship between the ring pucker and exocyclic $C_{4'}$—$C_{5'}$ orientation. Although we have constructed a $\Delta\delta$ *vs.* $J_{1'2'}$ map it is not presented here for reasons of space but the same correlations and displacements are revealed.

Can. J. Chem. Downloaded from www.nrcresearchpress.com by 210.87.254.42 on 09/05/12
For personal use only.

Can. J. Chem. Downloaded from www.nrcresearchpress.com by 210.87.254.42 on 09/05/12
For personal use only.

repulsion between the base and the electron pairs. This statement becomes evident upon consideration of the relative disposition of the base and ether oxygen in the $C_{2'}$ *endo* and $C_{3'}$ *endo* puckered modes and the discussion given by Lemieux (42).

We now proceed to a discussion of temperature effects upon the $\sum$ *vs.* $\Delta\delta$ plot. The largest variations with temperature for the correlating molecules were noted for 5-iodocytidine (IC) and 5′-ethoxycarbonyluridine (eU); these are indicated on Fig. 3 with the appropriate symbol and with the temperature in parentheses. In each instance the influence of increasing temperature is identical; the points move toward increasing $\sum$ and decreasing $\Delta\delta$. These changes in $\sum$ with increasing temperature imply variations in the *gg*, *gt*, *tg* populations (18, 19) and interestingly the concomitant changes in $\Delta\delta$ are such that the points are displaced along the correlation plot. This certainly provides support for the contention that $\Delta\delta$ is a reflection of the conformational preference about $C_{4'}$—$C_{5'}$. In ref. 18 the temperature effects upon the $\sum$ *vs.* $J_{3'4'}$ maps were discussed; it is interesting to point out that the trends here are qualitatively identical, *i.e.* the points for IC and eU moved up (increasing $\sum$, decreasing *gg* population) and to the left (decreasing $J_{3'4'}$) corresponding to a shift towards $C_{2'}$ *endo* in the $C_{2'}$ *endo* (S) $\leftrightarrow$ $C_{3'}$ *endo* (N) balance).[5]

The data for nucleosides(tides) lying distant from the correlation line can be discussed in terms of the characteristic substitution on the molecule but we stress at the outset that in each instance the substitution occurs at a point in the molecule near to the 5′-hydrogens and thus is expected, unlike substitutions at the 2′-*exo*, *meta* or *para* positions of the molecules, to have a direct effect upon the $\langle\Delta\rangle$i term (over and above any effect on the $C_{4'}$—$C_{5'}$ conformational distribution) which results in the displacement from the line. Thus deviations from the plot for RCA, rmU, and O are reasonable in view of the keto oxygen of the base, located above the ring and near to the 5′-position, which is expected to have a direct influence upon $\langle\Delta\rangle$i nonequivalence of the 5′-group as well as to effect sterically the $C_{4'}$—$C_{5'}$ conformational preferences (18, 19, 27, 45–47). (A useful discussion by ApSimon and Bierbeck of the long-range shielding effects of C—H and C=O bonds has appeared (48).) It is not surprising to find the 6-aza derivatives, azaU and azaC, distant from the line since evidence has been provided for specific repulsive interactions between the 5′-group and the 6-aza bases (18–22, 49, 50) and since the lone pair of an sp^2 hybridized nitrogen atom has an appreciable magnetic anisotropy (51). In this regard it is relevant to point out that the point for 5-azacytidine (5-azaC) in which the insertion of the aza nitrogen occurs at the *meta* position falls nearer to the line and reasonably so since any direct effect of this alteration in the base on $\langle\Delta\rangle$i should be attenuated. A precise statement of the reason for the deviations of the purine derivatives is not possible but they do imply that the through-space influence of a purine base upon the magnetic environment of the 5′-region differs from that of a pyrimidine. This is not surprising since the large ring currents associated with purine bases are well known (52, 53). The displacement for $\alpha\psi$ is also reasonable since the base in an α-nucleoside is not expected to affect $\langle\Delta\rangle$i *directly*. The presence of rPym above the line is more difficult to rationalize since this β-nucleoside has features *a*, *b*, *c*. A possible rationale of this inconsistency may be based on the absence of the keto oxygen at the 4-position of the pyrimidine ring system. Since the keto group withdraws π density from the ring, it is safe to predict that the π structure of 2-pyrimidone differs from that of uracil, particularly in their C_5—C_6 bonds, and this difference is reflected in the influence of the base on $\langle\Delta\rangle$i. It is interesting, however, to point to the parallel effect of temperature (Figs. 3 and 9) for rPym and the correlating series.

The large deviations for 3′-UMP and 5′-UMP from the $\sum$–$\Delta\delta$ correlation are also expected

[5]In Fig. 3 we have presented some data which illustrate subtle temperature effects on $\Delta\delta$ for noncorrelating molecules. The data for 2,2′-anhydroarabinosyluracil (aU) are interesting since here we find one of the few instances where the effect of increasing temperature is to increase the magnetic nonequivalence of diastereotopic CH_2 hydrogens. aU is in several respects an unusual nucleoside. Molecular models indicate that the two point attachment of the base to the furanose ring locks the ring in an extreme $C_{2'}$ *endo*-like conformation (type *S* in the nomenclature of ref. 38), whereas the furanose ring systems in all other molecules undoubtedly undergo the pseudorotational motion characteristic of five membered ring systems. This unusual temperature behavior is undoubtedly related to the presence of the anhydro linkage between the base and the furanose and not simply to the presence of an *endo* 2′-oxygen since this unusual dependence is not noted for araU and araC (Table 1).

since the negative charges associated with the 3′- and 5′-linked phosphates should have a substantial direct influence on $\langle\Delta\rangle$i (see ref. 65). The presence of 3′-UMP on the $\sum$, $J_{3'4'}$ correlation, which contrasts with its displacement from the $\sum$–$\Delta\delta$, is not unexpected since it is known that substitution of a hydrogen by a phosphoryl group at the 3′-position has little influence on the ring puckering or exocyclic $C_{4'}$—$C_{5'}$ conformation (18, 54). However, the (downward) displacement for 5′-UMP from the $\sum$ *vs.* $J_{3'4'}$ plot is expected since recent studies by Wood *et al.* (21, 55) have revealed a marked influence of a 5′-phosphate on the exocyclic $C_{4'}$—$C_{5'}$ conformation as well as on the ring puckering.

There is a further feature of Fig. 3 which does not conform with our expectations. This is the presence of the arabinose derivatives, araU and araC, near to the correlation line. Examination of molecular models reveals the close approach of the *endo* 2′-hydroxyl group and the 5′-group, particularly when the molecule is puckered 2′-*endo*. This close approach is confirmed by X-ray work which reveals intramolecular hydrogen bonding[6] between the 2′- and 5′-positions in crystalline araU (56). No reason, other than fortuitous cancellation of effects, for the presence of these points near to the $\sum$, $\Delta\delta$ correlation is apparent. (In the following paragraph we present $\sum$, $\Delta\delta$ values obtained in DMSO and note a similar correlation plot from which araU deviates.)

Finally, in order to investigate the effect of solvent upon the magnetic nonequivalence of the 5′-methylene hydrogens and to test some of our conclusions in the preceding sections, data were also obtained for a number of nucleosides in DMSO. The DMSO data are presented in Table 1 and in Fig. 10 as a $\sum$ *vs.* $\Delta\delta$ plot. In order to facilitate comparison we have included on Fig. 10 the D_2O correlation plot (as a dashed line). Again we note considerable scatter in the values of $\Delta\delta$ and $\sum$. Furthermore, although the number of points is limited, there seems to be a roughly linear correlation for five points corresponding to nucleosides with features *a*, *b*, and *c* and

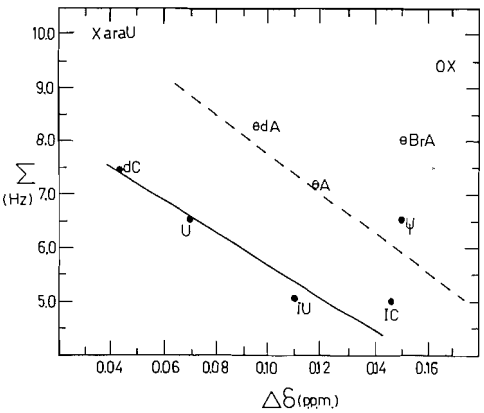

FIG. 10. Plot of Σ *vs.* $\Delta\delta$ for a series of purine and pyrimidine nucleosides in DMSO solution (30 °C): (●), pyrimidine nucleosides correlating in Figs. 3 and 9; (⊖), purine nucleosides; (×), pyrimidine nucleosides not correlating in Figs. 3 and 9. The dashed line corresponds to the Σ *vs.* $\Delta\delta$ correlation line for aqueous solution (Fig. 3.)

falling on the aqueous correlation plot. Moreover, the best straight line linking these points is essentially parallel to the dashed line representing the aqueous correlation. This correlation between $\Delta\delta$ and $\sum$ and the parallel behavior for D_2O and DMSO data is further evidence that variations in $\Delta\delta$ in each solvent are a consequence of conformational preferences about the $C_{4'}$—$C_{5'}$ bond.

In Fig. 11 we present a $\sum$ *vs.* $J_{3'4'}$ map for the available data in DMSO. As in the case for $\sum$ and $\Delta\delta$ we find for a series of molecules that a fair correlation exists between these parameters. Furthermore the correlation line is displaced from the $\sum$–$J_{3'4'}$ plot in D_2O and interestingly the displacement is in the same direction that the DMSO $\Delta\delta$–$\sum$ plot is displaced from its D_2O counterpart. In this case araU and O are displaced above the plot but now we find the purine derivatives (A and dA as well as 8-bromoadenosine, 8-BrA) near to the best straight line. We cannot offer any reasonable interpretation for the differences in the plotting patterns of the $\sum$ *vs.* $\Delta\delta$ and $J_{3'4'}$ maps but can only state the obvious, namely that the properties of the solvent can have subtle effects on the conformational properties (as well as the 5′-magnetic nonequivalence) of a nucleoside. Perhaps an important consideration insofar as an understanding of the maps in DMSO is concerned is the *syn–anti* balance of the nucleoside which is

[6]Though the X-ray work reveals a close approach between the 2′-OH and the 5′-position, it should be pointed out that this work (Fig. 9) as well as (18–19) reveals a repulsive interaction between these positions (compare Σ for the U–araU and C–araC pairs) and thus argues against the presence of hydrogen bonding between the 2′- and 5′-positions in *aqueous* solutions.

Can. J. Chem. Downloaded from www.nrcresearchpress.com by 210.87.254.42 on 09/05/12
For personal use only.

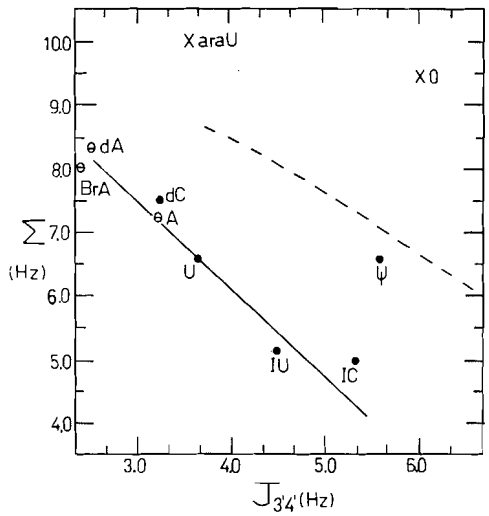

FIG. 11. Plot of Σ *vs.* $J_{3'4'}$ for a series of purine and pyrimidine nucleosides in DMSO solution (30 °C); (●), pyrimidine nucleosides correlating in Figs. 3 and 9; (⊖), purine nucleosides; (×), pyrimidine nucleosides not correlating in Figs. 3 and 9. The dashed line corresponds to the correlation line of Σ *vs.* $J_{3'4'}$ for aqueous solution (Fig. 9).

known to be influenced by the change from an aqueous to a DMSO environment (57).

In order to demonstrate one further class of molecules for which similar plotting patterns are observed, we present here the data for 2′-deoxythymidine-3′,5′-cyclicmonophosphate from ref. 64: $\Delta\delta$ = 0.155 p.p.m., Σ = 15.3 and $J_{3'4'}$ = 9.2. For reasons of space we have not constructed maps to allow their inclusion but obviously this molecule would lie at the extreme upper right of both the Σ *vs.* $\Delta\delta$, and Σ *vs.* $J_{3'4'}$ maps.

Conclusions

In the present study a correlation is observed between $\Delta\delta$ and Σ for a series of structurally related pyrimidine nucleosides. This is presented as evidence that $\Delta\delta$ is a reflection of the conformational preferences about the $C_{4'}$—$C_{5'}$ bond in these molecules. The correlations can be rationalized if the assumptions are made that the bases of the correlating molecules have a similar influence upon the magnetic environment of the 5′-CH_2 moiety and that an interdependency exists between the *N*-glycosyl linkage torsional angle, furanose puckering, and the $C_{4'}$—$C_{5'}$ conformation. Suggestions are made that interactions between the base and unshared pairs of electrons on the furanose oxygen play an important role in determining the furanose ring puckering and, indirectly, the exocyclic $C_{4'}$—$C_{5'}$ conformational preferences.

NOTES ADDED IN PROOF: One notes in Figs. 3 and 9 the proximity of the β-uridine (U) and β-pseudouridine (ψ) data which suggests that their conformational properties reflected in $\Delta\delta$, Σ, and $J_{3'4'}$ are similar in D_2O solution, consistent with earlier conclusions in refs. 13, 15, and 18. However a marked horizontal displacement is noted for ψ relative to U in Figs. 10 and 11 (DMSO solution) which indicates a larger proportion of the $C_{3'}$ *endo* (N) conformer in ψ relative to U (55 and 35% (N) according to the method of calculation in ref. 38*b*). These trends must reflect specific solution effects traceable to, perhaps, the presence of the pair of hydrogen donating N—H groups at the *meta* positions in ψ.

Insofar as our comments in footnote 6 concerning the apparent repulsion between the 2′-OH and 5′-hydroxymethyl groups of araU and araC are concerned, we should point out that recent work by Chwang and Sundaralingam (66) in conjunction with ref. 56 point to an attraction (hydrogen-bonding) between these groups whereas the work of Saenger (67) indicates no such attraction in the sulfur analog of araU, 1-β-D-arabinofuranosyl-4-thiouracil.

We are grateful for the support of the National Research Council of Canada, the Faculty of Graduate Studies of the University of Manitoba, and the Research Corporation of New York. We acknowledge Dr. A. A. Grey and Mrs. V. Robinson of the Canadian 220 MHz Centre. Valuable discussion with Drs. R. Wasylishen and T. Schaefer are also acknowledged. Special thanks go to Drs. W. Saenger, R. Sarma, M. Sundaralingam, M. Schweizer, and H. Wilson for making preprints available prior to publications. We thank Dr. H. Singh for a sample of 2′-O-methyladenosine.

1. J. A. POPLE, W. G. SCHNEIDER, and H. J. BERNSTEIN. High-resolution nuclear magnetic resonance. McGraw Hill, New York. 1959.
2. H. S. GUTOWSKY, G. G. BELFORD, and P. E. MCMAHON. J. Chem. Phys. **36**, 3353 (1962).
3. G. M. WHITESIDES, F. KAPLAN, K. NAGARAGAN, and J. D. ROBERTS. Proc. Natl. Acad. Sci. (U.S.), **48**, 1112 (1962).
4. H. S. GUTOWSKY. J. Chem. Phys. **37**, 2196 (1962).
5. E. I. SNYDER. J. Am. Chem. Soc. **85**, 2624 (1963).
6. (*a*) G. M. WHITESIDES and J. D. ROBERTS. J. Am. Chem. Soc. **86**, 2628 (1964). (*b*) G. M. WHITESIDES, J. J. GROCKI, D. HOLTZ, and J. D. ROBERTS. J. Am. Chem. Soc. **87**, 1058 (1965).
7. M. BUZA and E. I. SNYDER. J. Am. Chem. Soc. **88**, 1161 (1966).

Can. J. Chem. Downloaded from www.nrcresearchpress.com by 210.87.254.42 on 09/05/12
For personal use only.

Can. J. Chem. Downloaded from www.nrcresearchpress.com by 210.87.254.42 on 09/05/12
For personal use only.

8. (*a*) E. I. SNYDER. J. Am. Chem. Soc. **88**, 1155 (1966). (*b*) J. R. CAVANAUGH. J. Am. Chem. Soc. **89**, 1558 (1967).
9. M. VAN GORKOM and G. E. HALL. Q. Rev. (Lond.), **22**, 14 (1968).
10. M. RABAN. Tetrahedron Lett. 3105 (1966).
11. (*a*) G. R. FRANZER and G. BINSCH. J. Am. Chem. Soc. **95**, 175 (1973). (*b*) R. D. NORRIS and G. BINSCH. J. Am. Chem. Soc. **95**, 182 (1973). (*c*) G. BINSCH. J. Am. Chem. Soc. **95**, 191 (1973).
12. J. DRABOWSKI, A. EICHART, and W. BIERNACKI. Org. Magn. Resonance, **2**, 557 (1970).
13. F. E. HRUSKA, A. A. GREY, and I. C. P. Smith. J. Am. Chem. Soc. **92**, 214, 4088 (1970).
14. A. A. GREY, I. C. P. SMITH, and F. E. HRUSKA. J. Am. Chem. Soc. **93**, 1765 (1971).
15. B. J. BLACKBURN, A. A. GREY, I. C. P. SMITH, and F. E. HRUSKA. Can. J. Chem. **48**, 2866 (1970).
16. A. HOLY. Coll. Czech. Chem. Commun. **37**, 1555 (1972); M. PRYSTAS and F. SORM. Coll. Czech. Chem. Commun. **34**, 2316 (1969).
17. M. KARPLUS. J. Chem. Phys. **30**, 11 (1959).
18. F. E. HRUSKA. Conformations of biological molecules and polymers. Proceedings of the 5th Jerusalem symposium. *Edited by* E. D. Bergmann and B. Pullman. Academic Press, Jerusalem. 1973. p. 345.
19. F. E. HRUSKA, A. A. SMITH, and J. G. DALTON. J. Am. Chem. Soc. **93**, 4334 (1971).
20. R. H. SARMA, R. J. MYNOTT, F. E. HRUSKA, and D. J. WOOD. Can. J. Chem. **51**, 1843 (1973).
21. (*a*) F. E. HRUSKA, D. J. WOOD, R. J. MYNOTT, and R. H. SARMA. FEBS Lett. **31**, 153 (1973). (*b*) D. J. WOOD, F. E. HRUSKA, R. J. MYNOTT, and R. H. SARMA. Can. J. Chem. **51**, 2571 (1973). (*c*) R. H. SARMA, R. J. MYNOTT, D. J. WOOD, and F. E. HRUSKA. J. Am. Chem. Soc. **94**, 6457 (1973). (*d*) D. J. WOOD, F. E. HRUSKA, R. J. MYNOTT, and R. H. SARMA. FEBS Lett. **34**, 323 (1973).
22. D. J. WOOD, R. J. MYNOTT, F. E. HRUSKA, and R. H. SARMA. Submitted for publication.
23. R. DESLAURIERS, R. D. LAPPER, and I. C. P. SMITH. Can. J. Biochem. **49**, 1279 (1971).
24. C. H. SCHWALBE, W. SAENGER, and J. GASSMAN. Biochem. Biophys. Res. Commun. **44**, 57 (1971).
25. G. T. ROGERS and T. L. V. ULBRICHT. Eur. J. Biochem. **22**, 457 (1971).
26. F. E. HRUSKA. Can. J. Chem. **49**, 2111 (1971).
27. B. PULLMAN and H. BERTHOD. FEBS Lett. **20**, 341 (1972).
28. F. E. HRUSKA. J. Am. Chem. Soc. **93**, 1795 (1971).
29. A. E. V. HASCHMEYER and A. RICH. J. Mol. Biol. **27**, 369 (1967).
30. M. SUNDARALINGAM. Biopolym. **7**, 821 (1969).
31. S. KANG. J. Mol. Biol. **58**, 297 (1971).
32. H. R. WILSON, A. RAHMAN, and P. TOLLIN. J. Mol. Biol. **46**, 585 (1969).
33. S. ARNOTT and D. W. L. HUKINS. Nature, **224**, 886 (1969).
34. H. BERTHOD and B. PULLMAN. Biochem. Biophys. Acta, **232**, 595 (1971); **246**, 359 (1971).
35. H. R. WILSON and R. RAHMAN. J. Mol. Biol. **56**, 129 (1971).
36. A. SARAN, B. PULLMAN, and D. PERAHIA. Biochem. Biophys. Acta, **287**, 211 (1972).
37. L. D. HALL, P. R. STEINER, and C. PEDERSEN. Can. J. Chem. **48**, 1155 (1970).
38. (*a*) C. ALTONA and M. SUNDARALINGAM. J. Am. Chem. Soc. **94**, 8205 (1972). (*b*) C. ALTONA and M. SUNDARALINGAM. J. Am. Chem. Soc. **95**, 2333 (1973).
39. C. D. JARDETZKY. J. Am. Chem. Soc. **83**, 2919 (1961).
40. J. T. EDWARD. Chem. and Ind. (Lond.), 1102 (1955).
41. R. U. LEMIEUX, R. K. KULLNIG, H. J. BERNSTEIN, and W. G. SCHNEIDER. J. Am. Chem. Soc. **80**, 6098 (1958).
42. R. U. LEMIEUX. Pure Appl. Chem. **25**, 527 (1971).
43. S. WOLFE, A. RAUK, L. M. TEL, and I. G. CSIZMADIA. J. Chem. Soc. (B), 136 (1971).
44. G. A. JEFFREY, J. A. POPLE, and L. RADOM. Carbohydr. Res. **25**, 117 (1972).
45. W. SAENGER and K. H. SCHEIT. J. Mol. Biol. **50**, 153 (1970).
46. M. P. SCHWEIZER, J. T. WITKOWSKI, and R. K. ROBINS. J. Am. Chem. Soc. **93**, 277 (1971).
47. H. DUGAS, B. J. BLACKBURN, R. K. ROBINS, R. DESLAURIERS, and I. C. P. SMITH. J. Am. Chem. Soc. **93**, 3468 (1971).
48. J. W. APSIMON and H. BIERBECK. Can. J. Chem. **49**, 1328 (1970).
49. C. H. SCHWALBE, W. SAENGER, and J. GASSMAN. Biochem. Biophys. Res. Commun. **44**, 57 (1971).
50. W. SAENGER and D. SUCK. Nature, **242**, 610 (1973).
51. V. M. S. GIL and J. N. MURRELL. Trans. Faraday Soc. **60**, 248 (1964).
52. C. GIESSNER-PRETTRE and B. PULLMAN. C. R. Acad. Sci. Paris, **261**, 13 (1965).
53. P. O. P. Ts'O. *In* Fine structure of proteins and nucleic acids. *Edited by* G. D. Fasman and S. N. Timasheff. Marcel Dekker. 1970. Chapt. 2.
54. T. SCHLEICH, B. J. BLACKBURN, R. D. LAPPER, and I. C. P. SMITH. Biochemistry, **11**, 137 (1972).
55. D. J. WOOD, F. E. HRUSKA, R. J. MYNOTT, and R. H. SARMA. Unpublished results.
56. P. TOLLIN, H. R. WILSON, and D. W. YOUNG. Nature, **242**, 49 (1973).
57. D. W. MILES, L. B. TOWNSEND, M. J. ROBINS, W. H. INSKEEP, and H. EYRING. J. Am. Chem. Soc. **93**, 1600 (1971).
58. T. N. MCCAIG. M.Sc. Thesis. University of Manitoba, Winnipeg, Manitoba. 1973.
59. F. E. HRUSKA, A. MAK, H. SINGH, and D. SHUGAR. Can. J. Chem. **51**, 1099 (1973).
60. A. MAK. M.Sc. Thesis. University of Manitoba, Winnipeg, Manitoba. 1973.
61. J. G. DALTON. M.Sc. Thesis. University of Manitoba, Winnipeg, Manitoba. 1971.
62. S. TRANH-DINH, J. THIERY, W. GUSCHLBAUER, and J. DUNAND. Biochim. Biophys. Acta, **281**, 289 (1972).
63. F. E. HRUSKA, K. K. OGILVIE, A. A. SMITH, and H. WAYBORN. Can. J. Chem. **49**, 2449 (1971).
64. B. J. BLACKBURN, R. D. LAPPER, and I. C. P. Smith. J. Am. Chem. Soc. **95**, 2873 (1973).
65. M. REMIN and D. SHUGAR. Biochem. Res. Commun. **48**, 636 (1972).
66. A. K. CHWANG and M. SUNDARALINGAM. Nature, **243**, 78 (1973).
67. W. SAENGER. J. Am. Chem. Soc. **94**, 621 (1972).

Microwave Spectrum of Methoxyacetonitrile

ROGER KEWLEY

Department of Chemistry, Queen's University, Kingston, Ontario

Received August 22, 1973

The pure rotational spectrum of methoxyacetonitrile, CH_3OCH_2CN, has been investigated in the 8–40 GHz region. Spectra of the *gauche* and *trans* conformers, with respect to rotation about the O—CH_2 bond, have been assigned. The rotational constants for the ground vibrational state are (in MHz) *gauche*: $A = 11893.36(0.05)$, $B = 3423.26(0.02)$, and $C = 2871.53(0.02)$; *trans*: $A = 29610(90)$, $B = 2470.96(0.02)$, and $C = 2348.07(0.02)$. The centrifugal distortion parameters D_J and D_{JK} have also been determined for each conformer. The dipole moment components for the *gauche* conformer have been measured as (in D): $\mu_a = 2.40(0.03)$, $\mu_b = 1.37(0.10)$, $\mu_c = 1.11(0.11)$, and $\mu = 2.98(0.07)$. On the basis of relative intensity measurements at 25 °C the abundance of the *trans* form has been estimated as 4.8 ± 2.4% with the energy difference $E_{trans} - E_{gauche}$ having the value 5.7 ± 1.7 kJ mol^{-1} (1.3_5 ± 0.4 kcal mol^{-1}). From vibrational satellite intensities the frequency for the first excited state of skeletal torsion about the O—CH_2 bond has been found as (in cm^{-1}) *gauche*: 93(25) and *trans*: 74(32). From the observed values of the rotational constants the dihedral angle in the *gauche* conformer is found to be near to 69° from the *cis* position.

Le spectre de rotation pure du méthoxyacétonitrile, CH_3OCH_2CN, a été étudié dans la région 8-40 GHz. Les spectres des conformères *gauche* et *trans*, par rapport à la rotation autour de la liaison O—CH_2, ont été assignés. Les constantes de rotation pour l'état vibratoire fondamental sont (en MHz) *gauche*: $A = 11893.36(0.05)$, $B = 3423.26(0.02)$ et $C = 2871.53(0.02)$; *trans*: $A = 29610(90)$, $B = 2470.96(0.02)$ et $C = 2348.07(0.02)$. Les paramètres de déformation centrifuge D_J et D_{JK} ont aussi été déterminés pour chaque conformère. Les composantes du moment dipolaire du conformère *gauche* ont les valeurs mesurées (en D), $\mu_a = 2.40(0.03)$, $\mu_b = 1.37(0.10)$, $\mu_c = 1.11(0.11)$ et $\mu = 2.98(0.07)$. A partir des mesures des intensités relatives à 25° on a estimé que l'abondance de la forme *trans* est de 4.8 ± 2.4% avec une différence d'énergie $E_{trans} - E_{gauche}$ valant 5.7 ± 1.7 kJ mol^{-1} (1.3_5 ± 0.4 kcal mol^{-1}). A partir des intensités de satellites de vibration on a trouvé que la fréquence du premier état excité de torsion du squelette autour de la liaison O—CH_2 vaut (en cm^{-1}) 93(25) pour la forme *gauche* et 74(32) pour la *trans*. A partir des valeurs observées pour les constantes de rotation l'angle dièdre dans le conformère *gauche* s'est révélé proche de 69° par rapport à la position *cis*. [Traduit par le journal]

Can. J. Chem., **52**, 509 (1974)

Introduction

In earlier microwave spectroscopy papers dealing with *n*-propyl compounds the presence of both *gauche* and *trans* conformers was detected for each of the molecules C_3H_7F (1), C_3H_7CN (2), C_3H_7Cl (3), C_3H_7Br (4, 5), and C_3H_7I (5, 6). These studies support the general conclusion that the energy difference between the two conformers is about 1 kcal mol^{-1} or less. Only in the case of C_3H_7F, however, was it definitely stated that the *gauche* form is more stable, by 0.47 ± 0.31 kcal mol^{-1} (1). Other features of interest in these studies were the observation of strong vibrational satellites due to torsion about the central C—C bond and the possibility of determining the barrier height V_3 to methyl torsion. V_3 was determined as 2.6_9 kcal mol^{-1} for the *trans* form and as 2.8_7 kcal mol^{-1} for the *gauche* form of C_3H_7F (1).

There are three previous studies which have direct bearing on the conformation of methoxyacetonitrile, CH_3OCH_2CN. In an early Raman study, vibrational frequencies as low as 242 cm^{-1} were measured but not assigned (7). From their infrared study of the vapor and of solutions in CCl_4 and CS_2, Jones and Orville-Thomas (8) concluded, on the basis of a comparison of observed and calculated P–R separations, that the most stable state of the molecule is a slightly twisted *trans* conformation. They arrived at the same conclusion for the related molecule chloromethyl ether, CH_3OCH_2Cl (8). However, molecular polarizability considerations combined with dipole moment measurements (9, 10) give the result that the *gauche* conformer is the predominant one of each molecule. An electron diffraction study of CH_3OCH_2Cl also shows the *gauche* conformer to be present in large abundance (11).

In view of the discrepancies between the earlier investigations and general lack of structural information on the molecule it was considered worthwhile to undertake a microwave study of

Can. J. Chem. Downloaded from www.nrcresearchpress.com by 210.87.254.6 on 09/05/12
For personal use only.

methoxyacetonitrile with the objective of trying to clarify the situation regarding the number of conformers present and their relative energies.

Experimental

The methoxyacetonitrile sample was purchased from the Aldrich Chemical Company and used without further purification. Strong absorption due to the $J = 1 \rightarrow 2$ transition of CH_3CN was noticed near 36 795 MHz. This did not however interfere in any way with the recording or measurement of the CH_3OCH_2CN spectrum so no attempt was made to remove the impurity.

Observations in the 26.5 to 40 GHz region were made at Rice University using a Hewlett-Packard 8460A MRR spectrometer in the laboratory of Professor R. F. Curl. The Stark effect and frequency measurements on transitions involving lower J values were carried out at Queen's University using a conventional 100 kHz Stark modulation spectrometer described earlier (12, 13).

Rotational Spectrum

Initial Assignment, Ground Vibrational State

Preliminary calculations using structural parameters taken from the molecules dimethyl ether, $(CH_3)_2O$, (14) and acetonitrile, CH_3CN, (15) indicated that the *trans* conformer of CH_3OCH_2CN should be a very slightly asymmetric rotor with $\kappa \simeq -0.99$ while the *gauche* conformer should be more asymmetric with $\kappa \simeq -0.8$.

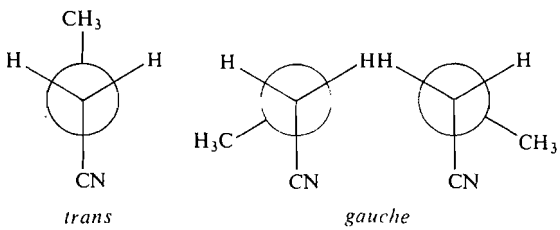

A scan of the 26.5 to 40 GHz region at a Stark field of about 1100 V cm^{-1} showed two prominent groups of lines which were quickly assigned to the high K_{-1} values of the *a*-type $J = 4 \rightarrow 5$ and $5 \rightarrow 6$ transitions of the *gauche* conformer. The remaining lines in these transitions were assigned without difficulty, see Table 1. The positions of the lines due to the *trans* conformer were not at all obvious on the initial scan. However it was found that at very low Stark fields, less than 5 V cm^{-1}, the lines of the *trans* conformer were far more prominent than those of the *gauche*. This technique allowed the assignment of the clumps of partially resolved high K_{-1} lines of the *a*-type $J = 5 \rightarrow 6$, $6 \rightarrow 7$, and $7 \rightarrow 8$ transitions of *trans* CH_3OCH_2CN.

TABLE 1. Observed lines of *gauche*-methoxyacetonitrile, ground vibrational state

Transition	ν_{obs} (MHz)	$\nu_{obs} - \nu_{calcd}$ (MHz)
a-type R-branch		
$2_{12} \rightarrow 3_{13}$	18 040.71	0.04
$2_{11} \rightarrow 3_{12}$	19 695.25	0.19
$2_{21} \rightarrow 3_{22}$	18 884.94	0.34
$2_{20} \rightarrow 3_{21}$	18 988.20	−0.35
$3_{03} \rightarrow 4_{04}$	24 920.99	−0.01
$3_{13} \rightarrow 4_{14}$	24 025.32	0.11
$3_{12} \rightarrow 4_{13}$	26 227.35	−0.12
$3_{22} \rightarrow 4_{23}$	25 159.32	0.48
$4_{04} \rightarrow 5_{05}$	30 967.71	0.15
$4_{14} \rightarrow 5_{15}$	29 987.39	0.29
$4_{13} \rightarrow 5_{14}$	32 729.42	−0.16
$4_{23} \rightarrow 5_{24}$	31 415.56	0.11
$4_{22} \rightarrow 5_{23}$	31 920.12	−0.09
$4_{32} \rightarrow 5_{33}$	31 556.56	0.18
$4_{31} \rightarrow 5_{32}$	31 572.43	−0.08
$4_{41} \rightarrow 5_{42}$	31 534.33	0.19
$4_{40} \rightarrow 5_{41}$	31 534.33	0.04
$5_{05} \rightarrow 6_{06}$	36 911.75	0.43
$5_{15} \rightarrow 6_{16}$	35 923.88	0.60
$5_{14} \rightarrow 6_{15}$	39 190.38	−0.45
$5_{24} \rightarrow 6_{25}$	37 650.17	0.06
$5_{23} \rightarrow 6_{24}$	38 503.81	−0.49
$5_{33} \rightarrow 6_{34}$	37 891.39	−0.05
$5_{32} \rightarrow 6_{33}$	37 934.03	−0.20
$5_{51} \rightarrow 6_{52}$	37 838.35	−0.09
$5_{50} \rightarrow 6_{51}$	37 838.35	−0.10
b-type		
$1_{10} \rightarrow 2_{21}$	38 551.87	−0.17
$1_{11} \rightarrow 2_{20}$	39 129.40	−0.45
$4_{04} \rightarrow 5_{15}$	36 296.14	−0.34
$9_{19} \rightarrow 9_{28}$	39 163.00	−0.51
$13_{2,11} \rightarrow 13_{3,10}$	34 022.50	−0.42
c-type		
$1_{10} \rightarrow 2_{20}$	38 577.84	−0.28
$1_{11} \rightarrow 2_{21}$	39 103.60	−0.16
$9_{27} \rightarrow 9_{37}$	38 605.55	0.71
Standard deviation* = 0.33		

*Defined as $(\Sigma (\nu_{obs} - \nu_{calcd})^2/(N - P))^{1/2}$; N = number of lines; P = number of parameters.

Rotational and Centrifugal Distortion Constants

Attempts to fit the ground vibrational state *gauche* spectrum using the three rigid rotor rotational constants gave discrepancies up to about 3 MHz between observed and calculated line frequencies. A satisfactory initial fit for the *a*-type lines, including those in the $J = 2 \rightarrow 3$ and $3 \rightarrow 4$ transitions, was obtained using the symmetric rotor centrifugal distortion constants D_J and

Can. J. Chem. Downloaded from www.nrcresearchpress.com by 210.87.254.6 on 09/05/12
For personal use only.

TABLE 2. Rotational and centrifugal distortion constants of *gauche*-methoxyacetonitrile

Constant*	Ground state		First excited state		Second excited state	
A (MHz)	11 893.36	±0.05	11 981.2	±2.0	12 100.1	±4.2
B (MHz)	3 423.26	±0.02	3 415.54	±0.04	3 406.46	±0.07
C (MHz)	2 871.53	±0.02	2 866.26	±0.03	2 860.50	±0.07
κ	−0.877690		−0.87948		−0.88182	
D_J (kHz)	2.93	±0.40	3.37	±0.42	3.39	±0.97
D_{JK} (kHz)	−23.3	±0.4	−26.0	±0.6	−28.4	±1.2
Watson parameters						
$\mathscr{A}$ (MHz)	11 893.02	±0.21				
$\mathscr{B}$ (MHz)	3 423.22	±0.07				
$\mathscr{C}$ (MHz)	2 871.61	±0.07				
d_J (kHz)	10.3	±7.5				
d_{JK} (kHz)	331	±268				
d_K (kHz)	874	±650				
$d_{EJ} \times 10^5$	−0.229	±0.244				
$d_{EK} \times 10^3$	−0.106	±0.078				

*Each uncertainty is one standard error of the parameter quoted.

D_{JK}. From this fit the frequencies of some of the *b*- and *c*-type lines were predicted and the lines located. These new lines were included in the final least-squares fit, see Tables 1 and 2. For the ground vibrational state of the *gauche* conformer a centrifugal distortion fit to Watson's parameters was also carried out with the aid of the computer program MB07, written by H. Møllendal. The resulting values of the eight parameters are given in the lower part of Table 2. The standard deviation of this fit was 0.27 MHz which is only slightly better than the value 0.33 MHz in the five-parameter fit. All of the five Watson centrifugal distortion parameters are highly correlated, with correlation matrix elements being in the range 0.95 to 1.00. To achieve a significantly better fit with the Watson parameters the millimeter wave spectrum of CH_3OCH_2CN should be studied and *a*-, *b*-, and *c*-type transitions involving $J \geqslant 15$ searched for. For the present data the D_J, D_{JK} fit is satisfactory.

An attempt to fit the observed spectrum of the *trans* conformer using five centrifugal distortion constants did not give meaningful results, as expected from the experiences of Marstokk and Møllendal with similar molecules having κ in the range −0.97 to −1 (16). The program attributed unreasonably large centrifugal distortion terms to the $K_{-1} = 1$ lines. The negative D_{JK} value for the *trans* conformer causes the high K_{-1} lines to appear in inverse order to that expected from asymmetry shifts alone. Once this was realized, which was the result of noticing that the structurally similar molecule *trans*-crotononitrile has a D_{JK} value of −12.6 kHz (17), there was no difficulty in making the correct assignment of the $K_{-1} = 2$ lines in the $J = 5 \rightarrow 6$, $6 \rightarrow 7$, and $7 \rightarrow 8$ transitions. The location of the widely spaced $K_{-1} = 1$ lines, which fall in regions of fairly high line density, presented some difficulty. The assigned lines are considered to be the true ones on the basis of the excellent fit, see Table 3, the observation of broad but correctly situated Stark lobes for the $5_{15} \rightarrow 6_{16}$ and $6_{16} \rightarrow 7_{17}$ transitions, and the value of the derived planar moment P_c, which is considered in more detail in the molecular structure discussion below. The rotational and centrifugal distortion constants of the *trans* conformer are given in Table 4.

For neither conformer has any resolved hyperfine structure due to coupling to the ^{14}N nucleus been observed. Quadrupole coupling constants for the molecule have been determined in the solid state (18).

Dipole Moment of Gauche Conformer

The electric dipole moment of the *gauche* conformer was determined by measuring the Stark shift for eight lobes of lines in the $J = 2 \rightarrow 3$ and $3 \rightarrow 4$ transitions. Effects of ^{14}N quadrupole hyperfine interaction were ignored since the splitting was unresolved. Linear plots of $\Delta\nu$ *vs.* E^2 were obtained for all the lobes, using field values in the range 200 to 1000 V cm^{-1}. The Stark coefficients and dipole moment components are given in Table 5. The Stark cell was calibrated on the basis

Can. J. Chem. Downloaded from www.nrcresearchpress.com by 210.87.254.6 on 09/05/12
For personal use only.

Can. J. Chem. Downloaded from www.nrcresearchpress.com by 210.87.254.6 on 09/05/12
For personal use only.

TABLE 3. Observed *a*-type R-branch lines of *trans*-methoxyacetonitrile

Transition	ν_{obs} (MHz)	$\nu_{obs} - \nu_{calcd}$ (MHz)
$5_{05} \rightarrow 6_{06}$	28 899.24	−0.03
$5_{15} \rightarrow 6_{16}$	28 542.10	0.01
$5_{14} \rightarrow 6_{15}$	29 279.38	0.02
$5_{24} \rightarrow 6_{25}$	28 913.24	0.41
$5_{23} \rightarrow 6_{24}$	28 927.22	−0.18
$5_{33} \rightarrow 6_{34}$	28 918.31	0.27
$5_{32} \rightarrow 6_{33}$	28 918.31	0.22
$5_{42} \rightarrow 6_{43}$	28 918.31	−0.38
$5_{41} \rightarrow 6_{42}$	28 918.31	−0.38
$5_{51} \rightarrow 6_{52}$	28 920.09	−0.16
$5_{50} \rightarrow 6_{51}$	28 920.09	−0.16
$6_{16} \rightarrow 7_{17}$	33 297.37	−0.02
$6_{15} \rightarrow 7_{16}$	34 157.56	0.06
$6_{25} \rightarrow 7_{26}$	33 730.72	0.30
$6_{24} \rightarrow 7_{25}$	33 753.63	−0.09
$6_{34} \rightarrow 7_{35}$	33 738.54	0.22
$6_{33} \rightarrow 7_{34}$	33 738.54	0.11
$6_{43} \rightarrow 7_{44}$	33 738.54	−0.19
$6_{42} \rightarrow 7_{43}$	33 738.54	−0.20
$6_{52} \rightarrow 7_{53}$	33 740.45	0.06
$6_{51} \rightarrow 7_{52}$	33 740.45	0.06
$6_{61} \rightarrow 7_{62}$	33 742.97	0.14
$6_{60} \rightarrow 7_{61}$	33 742.97	0.15
$7_{07} \rightarrow 8_{08}$	38 516.39	−0.08
$7_{17} \rightarrow 8_{18}$	38 051.93	−0.01
$7_{16} \rightarrow 8_{17}$	39 034.74	−0.07
$7_{26} \rightarrow 8_{27}$	38 547.48	0.02
$7_{25} \rightarrow 8_{26}$	38 582.56	0.16
$7_{35} \rightarrow 8_{36}$	38 558.89	0.02
$7_{34} \rightarrow 8_{35}$	38 558.89	−0.02
$7_{44} \rightarrow 8_{45}$	38 558.89	−0.01
$7_{43} \rightarrow 8_{44}$	38 558.89	−0.01
$7_{53} \rightarrow 8_{54}$	38 560.45	−0.14
$7_{52} \rightarrow 8_{53}$	38 560.45	−0.14
$7_{62} \rightarrow 8_{63}$	38 563.24	−0.03
$7_{61} \rightarrow 8_{62}$	38 563.24	−0.03
$7_{70} \rightarrow 8_{71}$	38 566.84	0.13
$7_{71} \rightarrow 8_{72}$	38 566.84	0.13

Standard deviation = 0.18

TABLE 4. Rotational and centrifugal distortion constants of *trans*-methoxyacetonitrile, ground vibrational state

Constant	Value
A (MHz)	29 610 ± 90
B (MHz)	2 470.96 ± 0.02
C (MHz)	2 348.07 ± 0.02
κ	−0.99100
D_J (kHz)	0.433 ± 0.096
D_{JK} (kHz)	−17.9 ± 0.2

of $\mu_{OCS} = 0.71512 \pm 0.00003$ D (19). The value of the total electric dipole moment may be compared to that found for a solution in carbon tetrachloride, 2.99 D (9), in which some *trans* conformer is also likely to be present. Because of the weakness of the lines of the *trans* conformer, it has not been possible to find Stark lobes suitable for shift measurements, so that no determination of the dipole components of the *trans* conformer has been possible as yet.

Energy Difference between Conformers

An idea of the relative intensities of the spectra of the two conformers may be gained from Fig. 1. From this and similar traces the intensity of the *trans* $7_{26} \rightarrow 8_{27}$ peak relative to the *gauche* $5_{23} \rightarrow 6_{24}$ peak was determined as 0.20 ± 0.02. To convert this intensity ratio to the relative abundance of the conformers it is necessary to assume a value for the μ_a dipole component of the *trans* conformer. Taking the COC group moment as 1.31 D, the dipole moment of dimethyl ether (20), and the CCN moment as 3.91 D, the dipole moment of methyl cyanide (21), together with the refined *trans* structure, see below, an estimate for μ_a of 4.05 ± 0.75 D can be made. The rather large value of the error estimate was arrived at by considering the discrepancies between the observed dipole moment components of the *gauche* conformer and those calculated using the above COC and CCN group moments and the refined *gauche* structure. Using this estimate together

TABLE 5. Stark effect coefficients and dipole moment components of *gauche*-methoxyacetonitrile

Transition	$\lvert M \rvert$	$10^6 \times \Delta\nu/E^2$ (MHz cm^2 V^{-2}) Observed	Calculated
$2_{12} \rightarrow 3_{13}$	1	19.7	21.1
$2_{12} \rightarrow 3_{13}$	2	93.4	92.2
$2_{11} \rightarrow 3_{12}$	1	−23.3	−23.4
$3_{13} \rightarrow 4_{14}$	2	7.41	7.48
$3_{13} \rightarrow 4_{14}$	3	22.7	22.4
$3_{03} \rightarrow 4_{04}$	2	6.69	6.99
$3_{03} \rightarrow 4_{04}$	3	21.0	20.2
$3_{12} \rightarrow 4_{13}$	1	10.0	10.2

Dipole component (D)	Value
μ_a	2.40±0.03
μ_b	1.37±0.10
μ_c	1.11±0.11
μ	2.98±0.07

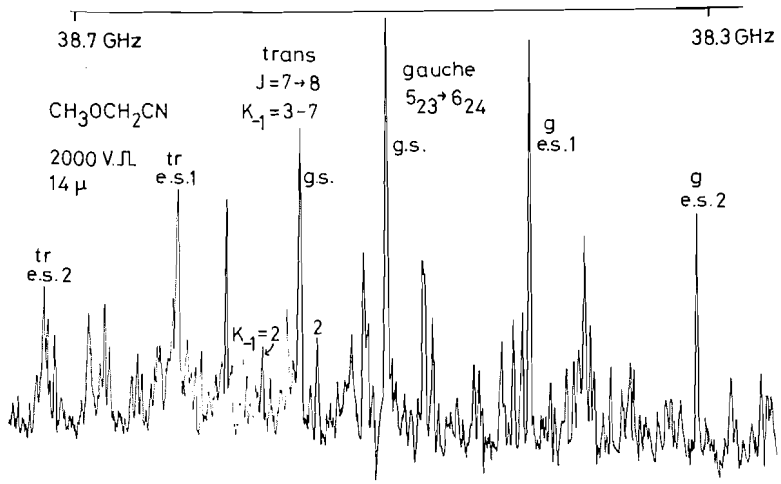

FIG. 1. Trace of a portion of the spectrum of methoxyacetonitrile. To the center and right of the figure may be seen the transition $5_{23} \rightarrow 6_{24}$ of *gauche*-CH_3OCH_2CN together with prominent vibrational satellites to lower frequency, designated g e.s. 1 and g e.s. 2. The clump of high K_{-1} lines in the $J = 7 \rightarrow 8$ transition of *trans*-CH_3OCH_2CN together with strong satellites tr e.s. 1 and tr e.s. 2 to higher frequency may be seen to the left of the trace. The designated satellites are due to skeletal torsion about the O—CH_2 bond. The lower frequency $K_{-1} = 2$ line of the *trans* conformer is the transition $7_{26} \rightarrow 8_{27}$ mentioned in the energy difference determination.

with the measured μ_a of the *gauche* conformer, see Table 5, the *trans* $7_{26} \rightarrow 8_{27}$ to *gauche* $5_{23} \rightarrow 6_{24}$ intensity ratio leads to a value of $4.8 \pm 2.4\%$ for the abundance of the *trans* conformer at room temperature. Allowing for the existence of two mirror-image *gauche* forms the energy difference $E_{trans} - E_{gauche}$ is calculated as 5.7 ± 1.7 kJ mol^{-1} ($1.3_5 \pm 0.4$ kcal mol^{-1}). This is compatible with estimates for the related molecules mentioned in the Introduction, although the present value appears to be somewhat larger. The abundance of the *trans* form of CH_3OCH_2CN is significantly lower than the figure 30% quoted for the abundance of *trans*-$CH_3CH_2CH_2CN$, which was deduced from the molar Kerr constant assuming a 60° dihedral angle for the *gauche* form (9). Possibly minimization of the interaction between the COC and CCN group moments favors a lower percentage of *trans* conformer in methoxyacetonitrile.

Excited Vibrational States

It may be seen from Fig. 1 that, in addition to the ground vibrational state peaks, there are intense satellites located towards higher frequency for the *trans* conformer and towards lower frequency for the *gauche* conformer. The intensity of these satellites strongly suggests that they are due to successive states of excitation of the skeletal torsion mode about O—CH_2. For the *gauche* form 16 transitions for the first excited state and 12 for the second excited state of this vibration were assigned and analyzed to give the rotational and centrifugal distortion constants, see Tables 2 and 6. For the *trans* conformer only the top of the peak of the central high K_{-1} cluster was measured to give $B + C$ values of 4828.9 and 4839.5 MHz, respectively, for the first and second excited states. Relative intensity measurements on 13 first excited state satellites within the $J = 4 \rightarrow 5$ and $5 \rightarrow 6$ transitions gave a frequency of 93 ± 25 cm^{-1} for this vibration of the *gauche* conformer. For the *trans* conformer nine satellite intensities were measured, in the $J = 5 \rightarrow 6$ and $7 \rightarrow 8$ transitions, yielding a value of 74 ± 32 cm^{-1} for the O—CH_2 skeletal torsion frequency. These frequencies are appreciably lower than those for the first excited state of skeletal torsion about the central C—C bond in *n*-propyl fluoride which are *gauche*: 161 cm^{-1} and *trans*: 98 cm^{-1} (1). The *gauche* skeletal torsion frequency of CH_3OCH_2CN is however similar to the value for CH_3OCH_2Cl, observed as 107 cm^{-1} in the Raman spectrum (8, 22).

For the *trans* conformer a low frequency satellite at $B + C = 4815.1$ was also easily seen at low Stark voltages. The intensity of this peak in the $J = 5 \rightarrow 6$ and $6 \rightarrow 7$ transitions gave a corre-

Can. J. Chem. Downloaded from www.nrcresearchpress.com by 210.87.254.6 on 09/05/12
For personal use only.

TABLE 6. Observed *a*-type R-branch lines of *gauche*-methoxyacetonitrile, first and second excited states of skeletal torsion

	ν (MHz)			
	First excited state		Second excited state	
Transition	Obs.	Obs. − Calcd.	Obs.	Obs. − Calcd.
$4_{04} \rightarrow 5_{05}$	30 911.65	−0.09	30 848.65	−0.06
$4_{14} \rightarrow 5_{15}$	29 929.91	−0.13	29 866.37	−0.10
$4_{13} \rightarrow 5_{14}$	32 661.00	0.12	32 581.23	0.09
$4_{23} \rightarrow 5_{24}$	31 351.48	−0.06		
$4_{22} \rightarrow 5_{23}$	31 847.20	0.20	31 763.20	0.28
$4_{32} \rightarrow 5_{33}$	31 490.10	0.08	31 414.19	0.02
$4_{31} \rightarrow 5_{32}$	31 505.42	−0.18	31 429.20	0.07
$4_{41} \rightarrow 5_{42}$	31 468.43	0.10	31 393.00	−0.09
$4_{40} \rightarrow 5_{41}$	31 468.43	−0.04	31 393.00	−0.23
$5_{14} \rightarrow 6_{15}$	39 109.90	−0.20		
$5_{24} \rightarrow 6_{25}$	37 574.60	0.34		
$5_{23} \rightarrow 6_{24}$	38 413.24	−0.21	38 308.61	−0.32
$5_{33} \rightarrow 6_{34}$	37 811.60	0.20	37 720.40	0.42
$5_{32} \rightarrow 6_{33}$	37 852.70	−0.03		
$5_{51} \rightarrow 6_{52}$	37 759.70	−0.04	37 669.70	−0.10
$5_{50} \rightarrow 6_{51}$	37 759.70	−0.05	37 669.70	−0.11
	Standard deviation = 0.19		Standard deviation = 0.29	

sponding vibrational frequency of 178 ± 23 cm^{-1}. In the Raman study of CH_3OCH_2Cl (8, 22) a frequency at 177 cm^{-1} has been assigned to methyl torsion so perhaps 178 cm^{-1} is the corresponding frequency for CH_3OCH_2CN. However taking an assumed I_r of 2.655 a.m.u. Å^2, obtained by taking the angles from the refined *trans* structure below with an assumed $I_\alpha(CH_3)$ of 3.200 a.m.u. Å^2, and using eq. 1 (23)

$$[1] \qquad V_3 = \frac{8}{9}\pi^2\nu^2 I_r$$

a frequency of 178 cm^{-1} leads to a threefold barrier V_3 of 6.7 kJ mol^{-1} (1.6 kcal mol^{-1}). This would seem to be too low in comparison to the value 2.72 kcal mol^{-1} for dimethyl ether (20). This height of barrier in eq. 1 gives a frequency of 230 cm^{-1}. So a possible explanation is that the satellite for ν = 178 cm^{-1} is due not to methyl torsion but to another skeletal vibration, such as the in-plane CCN bend. It therefore appears that in the present study methyl torsion satellites have not been assigned for either conformer. None of the observed *a*-, *b*-, or *c*-type lines of the *gauche* conformer or the *a*-type lines of the *trans* conformer exhibited any resolved splitting of the type that might arise from methyl torsion or, in the *gauche* form, from inversion. The lack of splitting in the ground state indicates a methyl torsion barrier of at least about 10.5 kJ mol^{-1} (2.5 kcal mol^{-1}) which is similar to the *n*-propyl fluoride values (1).

Discussion – Molecular Structure

A structural parameter that may be obtained quite precisely from the observed rotational constants of the *trans* conformer is c_H, usually referred to as the average distance of an out-of-plane hydrogen atom from the heavy atom, or, in this case, *ab* plane. There are four such hydrogens in *trans* CH_3OCH_2CN. The average distance is calculated from $c_H = (\sum_i m_i c_i^2/4m_H)^{1/2}$ where $\sum_i m_i c_i^2 = 1/2\,(I_a + I_b - I_c) = P_c$. The resulting value is 0.888 ± 0.004 Å. This may be compared with the values 0.883 Å for *trans*-CH_3CH_2-CH_2CN (2), 0.889 Å for *trans*-$CH_3CH_2CH_2F$ (1), and 0.894 Å for $(CH_3)_2O$ (20). The value obtained seems very reasonable and may be taken as confirmation of the $K_{-1} = 1$ assignment.

Although no isotopically substituted species have been examined it is of interest to attempt to use the observed rotational constants to estimate some of the angles in the heavy atom skeletons of the *trans* and *gauche* conformers. It was decided to limit these attempts to ∠COC, ∠OCC, and the dihedral angle between the OCC and

Can. J. Chem. Downloaded from www.nrcresearchpress.com by 210.87.254.6 on 09/05/12
For personal use only.

Can. J. Chem. Downloaded from www.nrcresearchpress.com by 210.87.254.6 on 09/05/12
For personal use only.

COC planes (taking the *cis* position as zero dihedral angle), since the rotational constants depend strongly on the values of these angles. The procedure adopted began with an assumed structure based on the known r_s structures of $(CH_3)_2O$ (20) and CH_3CN (15). In assessing the conclusions arrived at it is as well to bear in mind that r_s parameters do not exactly reproduce the observed rotational constants of the molecules from which they are taken, so an inherent error due to this cause will be present in the derived COC, OCC, and dihedral angles. In arriving at the initial assumed structure of CH_3OCH_2CN, one H atom is considered to be removed from the CH_3 of CH_3CN and the OC bond in the new structure is taken as being in the same direction as the original HC bond. The assumed structural parameters for the *trans* conformer are then:

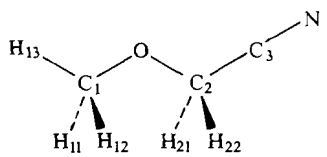

$C_1O = C_2O = 1.410$ Å	$\angle H_{13}C_1O = 107° 14'$
$C_2C_3 = 1.458$ Å	$\angle H_{11}C_1H_{12} = 108° 44'$
$C_3N = 1.157$ Å	$\angle H_{12}C_1O = 110° 50'$
$C_1H_{13} = 1.091$ Å	$\angle C_1OC_2 = 111° 43'$
$C_1H_{11} = C_1H_{12} = 1.100$ Å	$\angle OC_2C_3 = 109° 40'$
$C_2H_{21} = C_2H_{22} = 1.112$ Å	$\angle C_2C_3N = 180°$
	$\angle H_{21}C_2H_{22} = 109° 16'$
(dihedral angle 180°)	$\angle H_{22}C_2C_3 = 109° 40'$

The rotational constants calculated from this structure are (in MHz) $A = 29368$, $B = 2476.66$, and $C = 2353.52$, which are quite near to observed ones of Table 4. The angles C_1OC_2 and OC_2C_3 were then varied, keeping all other parameters fixed, to obtain the best least-squares fit to the observed A, B, and C of the *trans* conformer. This occurred at $\angle C_1OC_2 = 111° 15'$ and $\angle OC_2C_3 = 110° 17'$ and all three rotational constants were predicted to within 1.2 MHz of the observed values. Using the new values of these two angles and again keeping all other structural parameters fixed, the dihedral angle was varied until the closest fit to the *gauche* observed A, B, and C was reached. This happened at a dihedral angle of 68° 43′. The agreement between the observed and calculated A, B, and C for the *gauche* conformer was still not very good, the calculated value being about 42 MHz low for A and about 84 MHz low for B and C. Attempts to reach a better fit by simultaneously varying the dihedral angle and either the C_1OC_2 or OC_2C_3 angle did not lead to a significant improvement, suggesting that possibly one or more bond lengths have been assumed to have larger values than is actually the case. An estimate for the dihedral angle in the *gauche* conformer is 69 ± 5°. This value compares very well with that of 70° estimated from the observed dipole moment and molar Kerr constant in solution (9), although no allowance was made in that estimate for the presence of the small amount of *trans* conformer. The 69° angle is also very close to that estimated from the microwave study for CH_3OCH_2Cl (24), where an angle of 71° has been reported. Other estimates of the dihedral angle in chloromethyl ether are 74° from electron diffraction (11) and 78 ± 10° from the solution dipole moment (10). The angle in CH_3OCH_2CN appears to be a little larger than that of 63° in $CH_3CH_2CH_2F$ and possibly larger than that in $CH_3CH_2CH_2CN$, which was quoted as being slightly larger than 60° (2).

The author thanks Professor R. F. Curl of Rice University, Houston, Texas for the use of the Hewlett-Packard spectrometer and for stimulating and enjoyable discussions. The work at Rice University was supported by grant number C-071 from the Robert A. Welch Foundation. Support of the project by grant number A-2046 from the National Research Council of Canada is gratefully acknowledged. In addition the author wishes to thank Dr. R. E. Penn for providing a copy of the MB07 computer program and Messrs. N. Crowe, N. Berry, S. Tan, and H. Dodsworth for valuable assistance and advice concerning the use of various computer programs.

1. E. HIROTA. J. Chem. Phys. **37**, 283 (1962).
2. E. HIROTA. J. Chem. Phys. **37**, 2918 (1962).
3. T. N. SARACHMAN. J. Chem. Phys. **39**, 469 (1963).
4. T. N. SARACHMAN. Symposium on molecular structure and spectroscopy. Columbus, Ohio. 1968. Paper N7.
5. S. ARMSTRONG. Appl. Spectrosc. **23**, 575 (1969).
6. T. N. SARACHMAN. Symposium on molecular structure and spectroscopy. Columbus, Ohio. 1969. Paper U9.
7. K. W. F. KOHLRAUSCH and G. P. YPSILANTI. Z. Phys. Chem. **29**, (B) 290 (1935).
8. R. G. JONES and W. J. ORVILLE-THOMAS. J. Chem. Soc. 692 (1964).
9. R. J. W. LEFÈVRE, G. L. D. RITCHIE, and P. J. STILES. J. Chem. Soc. B, 819 (1967).
10. M. J. ARONEY, R. J. W. LEFÈVRE, and J. D. SAXBY. J. Chem. Soc. B, 414 (1966).
11. M. C. PLANJE, L. H. TONEMAN, and G. DALLINGA. Rec. Trav. Chim. **84**, 232 (1965).
12. V. M. RAO and R. KEWLEY. Can. J. Chem. **47**, 1289 (1969).
13. R. KEWLEY. Can. J. Chem. **50**, 1690 (1972).

14. P. H. KASAI and R. J. MYERS. J. Chem. Phys. **30**, 1096 (1959).
15. L. F. THOMAS, E. I. SHERRARD, and J. SHERIDAN. Trans. Faraday Soc. **51**, 619 (1955).
16. K.-M. MARSTOKK and H. MØLLENDAL. J. Mol. Struct. **8**, 234 (1971).
17. V. W. LAURIE. J. Chem. Phys. **32**, 1588 (1960).
18. A. COLLIGIANI, L. GUIBÉ, P. J. HAIGH, and E. A. C. LUCKEN. Mol. Phys. **14**, 89 (1968).
19. F. H. DE LEEUW and A. DYMANUS. Chem. Phys. Lett. **7**, 288 (1970).
20. U. BLUKIS, P. H. KASAI, and R. J. MYERS. J. Chem. Phys. **38**, 2753 (1963).
21. P. A. STEINER and W. GORDY. J. Mol. Spectrosc. **21**, 291 (1966).
22. M. HAYASHI. Nippon Kagaku Zasshi, **8**, 1073 (1959).
23. W. GORDY and R. L. COOK. Microwave molecular spectra. Wiley-Interscience, New York. 1970. p. 476.
24. T. IKEDA and R. F. CURL, JR. Symposium on molecular structure and spectroscopy. Columbus, Ohio. 1973. Paper T5.

Can. J. Chem. Downloaded from www.nrcresearchpress.com by 210.87.254.6 on 09/05/12
For personal use only.

Mass Spectra of some 5,6α-Cyclopropano-5α-cholestane Derivatives

J. F. TEMPLETON AND C. W. WIE

Faculty of Pharmacy, University of Manitoba, Winnipeg, Manitoba R3T 2N2

Received September 12, 1973

The mass spectra of the epimeric 3-substituted hydroxy and ethoxy derivatives of 5,6α-cyclopropano-5α-cholestane have been reported and on the basis of deuterium-labelled compounds the nature of some high molecular weight fragments are discussed. Together with the characteristic fragment ions of steroidal derivatives ions related to the presence of the 5,6α-cyclopropane ring occur at *m/e* 247, 301, 302, and 329.

On présente les spectres de masse des dérivés épimériques hydroxy et éthoxy substitués en position-3 du cyclopropano-5,6α cholestane-5α. En se basant sur des composés marqués par des deutériums, on discute de la nature de quelques fragments ayant des poids moléculaires élevés.

Les ions reliés au cycle cyclopropane-5,6α apparaissent à *m/e* 247, 301, 302 et 329 en même temps que les ions fragmentaires caractéristiques des dérivés de stéroides. [Traduit par le journal]

Can. J. Chem., **52**, 517 (1974)

Introduction

Recently, the preparation of a series of 5,6α-cyclopropano-5α-cholestane derivatives having a 3-oxygen function has been reported (1, 2). In general, the mass spectra of the epimeric 3α- and 3β-hydroxy and 3α- and 3β-ethoxy compounds (Figs. 1–4) show the expected fragmentations of saturated steroidal derivatives (3). In most cases, the basic fragmentations are similar, including the loss from the molecular ion of methyl, the side chain (C_8H_{17}), the side chain + 42, the oxygen function at C_3, and combinations of these. These fragmentations are all well-known electron-induced decompositions of substituted cholestane (4).

Three other fragments of moderate intensity appear in all the spectra at *m/e* 247 (10–45%), 301 (15–50%), and 302 (10–50%). A strong signal at *m/e* 329 appears in the spectrum of the 3β-alcohol (Fig. 2) and also in the spectra of the isomeric 3-ethers (Figs. 3 and 4), whereas in the spectrum of the 3α-alcohol (Fig. 1), this ion is much less abundant. The 3α-ether (Fig. 3) also has a prominent signal at *m/e* 384 not present in the other spectra.

The existence of these particular fragment ions in the mass spectrum of 5,6α-cyclopropano-5α-cholestane derivatives prompted us to study further the mechanism of their fragmentations in order to determine if there is any major involvement of the cyclopropane ring in the formation of their fragment ions. The cyclopropane ring may either stabilize the fragment ions and/or radicals formed or act as a directing function during the course of electron impact fragmentations. Several deuterium-labelled 5,6α-cyclopropano-5α-cholestane derivatives were prepared (**1**–**9**) for this study. Mass spectra of **3**–**7** and **9** were determined for comparison with the hydrogen analogs. Some mechanisms leading to these fragment ions are suggested and rationalized on the basis of mass spectrometric data of the unlabelled and deuterium-labelled derivatives.

Examination of the metastable ions present gave no information relevant to the fragmentation pathways discussed.

Results and Discussion

The fragment ion at *m/e* 247 present in all of the 5,6α-cyclopropano-5α-cholestane compounds (Figs. 1–4) was unshifted in the spectra of the deuterium-labelled derivatives (**3**–**7** and **9**) showing that loss of the hydrogen atoms at C_2, C_3, and C_4 had occurred. Cleavage of the C_7—C_8 and C_9—C_{10} bonds with migration of a hydrogen atom from C_{11} as outlined (Scheme 1) accounts for the formation of this fragment. The *m/e* 247 fragment in the spectrum of 3β-methoxy-5α-cholestane (5) and the corresponding ion of 3α-hydroxy-5α-cholestane (6) has been assigned to cleavage of the D-ring. The presence of a *m/e* 247 fragment in the mass spectra of 5-cholestene derivatives (3, 7) may be formed by an analogous process involving a cyclic five-membered transition state.

An ion of *m/e* 301 in the mass spectrum of 5-cholestene and the corresponding ion, *m/e* 205, in 3β,17β–dihydroxy-5-androstene has been re-

Can. J. Chem. Downloaded from www.nrcresearchpress.com by 210.87.254.5 on 09/05/12
For personal use only.

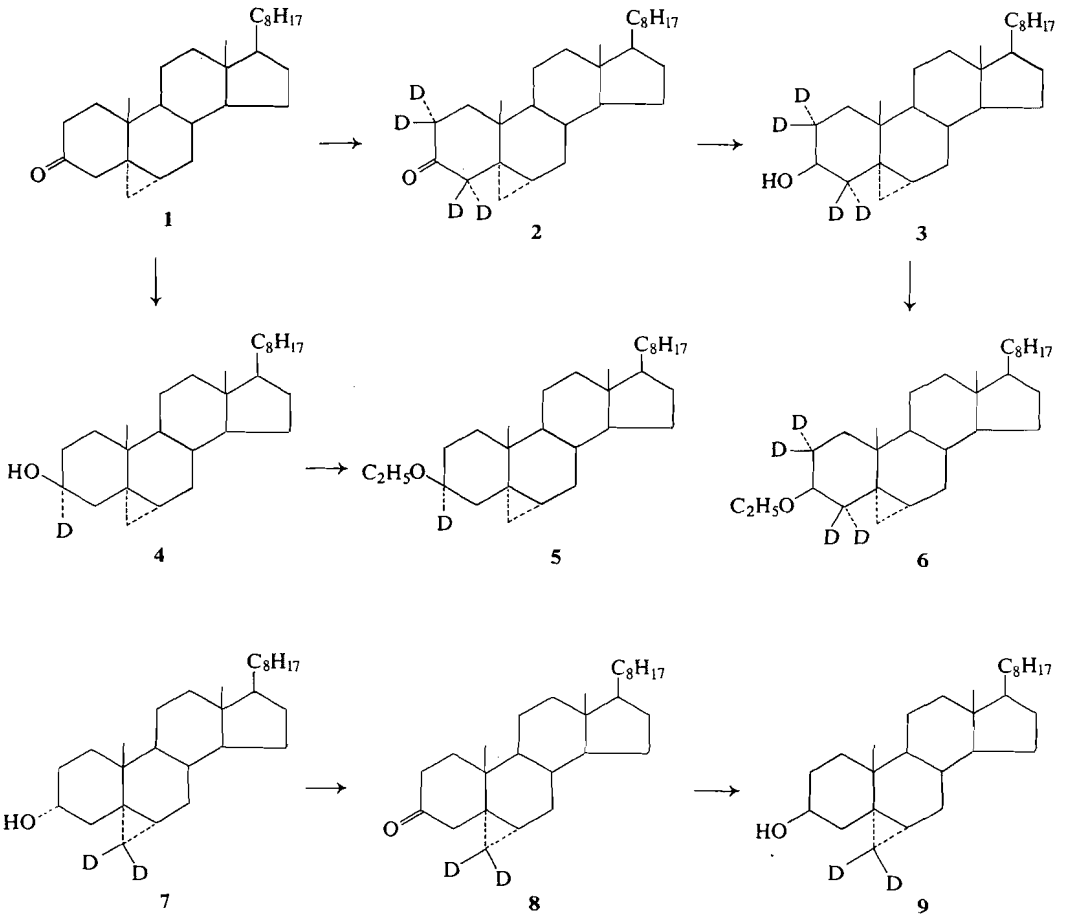

ported and a mechanism of formation proposed by Spiteller-Friedmann and Spiteller (3, 8). Deuterium labelling of the 5,6α-cyclopropano-5α-cholestane molecule shows that an analogous fragment is not formed from **3** and **6**. If the ion *m/e* 301 in the 5,6α-cyclopropano-5α-cholestane derivatives was identical with that proposed (8) for the above, **3** and **6** should give rise to an equivalent ion at *m/e* 303. The ion at *m/e* 303 present in **3** and **6** was calculated to be the ^{13}C isotopic contribution of the *m/e* 302 ion. Since ions at *m/e* 301 and 302 were unmoved in the mass spectra of the deuterium-labelled derivatives (**3–7** and **9**), fragmentation leading to their formation involving cleavage of the 5,6α-cyclopropane ring and ring A is proposed to occur (Scheme 2) with hydrogen transfer by route *a* or without hydrogen transfer by route *b*. Accurate mass determinations of the *m/e* 301 and 302 fragments in the 3β-alcohol (Fig. 2) show that these ions have a composition of $C_{22}H_{37}$ and $C_{22}H_{38}$, respectively, as expected from Scheme 2.

The presence of a *m/e* 329 ion in the mass spectra of the epimeric 3-alcohols (Figs. 1 and 2) and the corresponding 3-ethyl ethers (Figs. 3 and 4) implies loss of the C_3-oxygen function, possibly accompanied by cleavage of ring A. Compounds having a deuterium label at different positions show that the *m/e* 329 ion was increased by 1 a.m.u. in **3** and **6**, 1 a.m.u. in **4** and **5**, and 2 a.m.u. in **7** and **9**. These results show that the methylene protons of the three-membered ring remain with the positively charged portion during the fragmentation process. High resolution mass measurement of the *m/e* 329 ion in the 3β-alcohol (Fig. 2) and the 3α-ethyl ether (Fig. 3) gives a composition of $C_{24}H_{41}$ showing that loss of the oxygen atom at C_3 takes place. Cleavage of ring A followed by migration of the C_3-hydrogen atom and one of the two hydrogen atoms at either C_2 or C_4 toward the final positively charged fragment accounts for the fragment masses (Scheme 3).

The relative abundance of the *m/e* 329 ion is

Can. J. Chem. Downloaded from www.nrcresearchpress.com by 210.87.254.5 on 09/05/12
For personal use only.

Can. J. Chem. Downloaded from www.nrcresearchpress.com by 210.87.254.5 on 09/05/12
For personal use only.

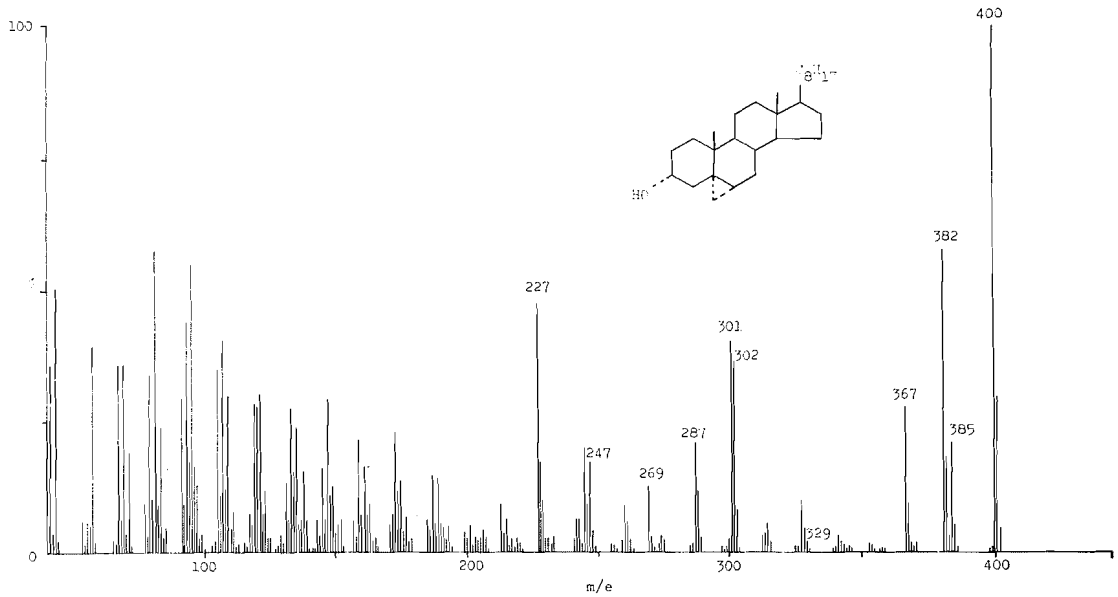

FIG. 1. Mass spectrum of 3α-hydroxy-5α,6-cyclopropano-5α-chloestane.

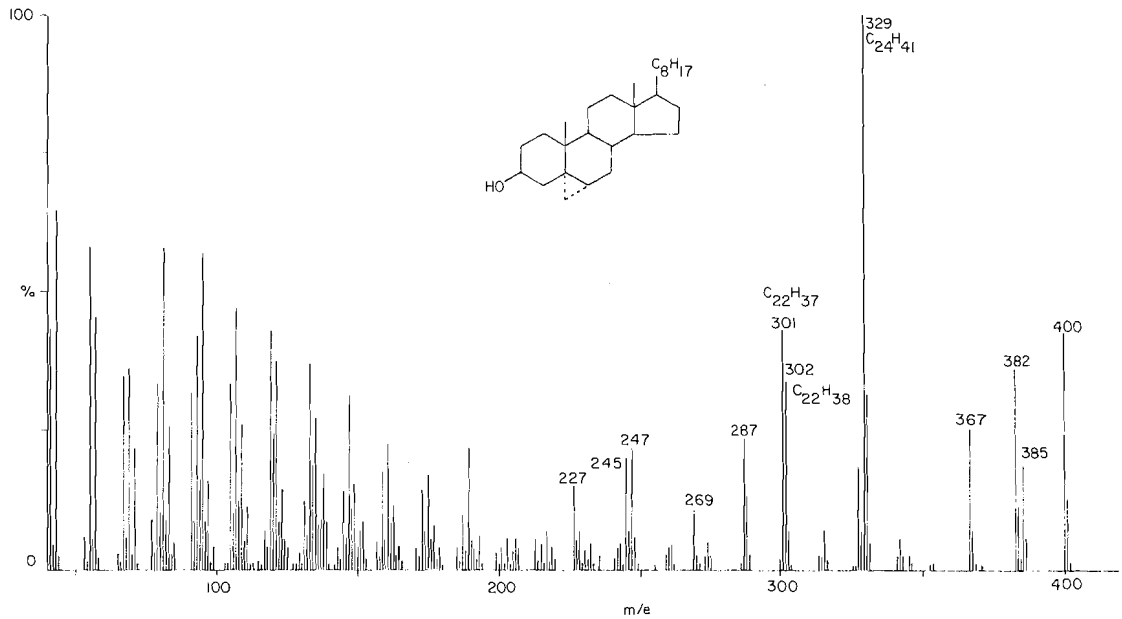

FIG. 2. Mass spectrum of 3β-hydroxy-5α,6-cyclopropano-5α-cholestane.

greater than 50% in the 3β-epimer (Fig. 2) and in compounds **3**, **4**, and **9**, and is less than 10% in the 3α-epimer (Fig. 1) and in **7**. This difference in relative abundance of the ion at *m/e* 329 shows that the configuration of the hydrogen atom next to the oxygen at C_3 affects the ease of formation of this ion. The mechanism shown in Scheme 3 accounts for all of the factors mentioned above for both epimeric 3-alcohols. Scheme 3 also accounts for the *m/e* 329 fragment present in the spectra of the epimeric 3-ethers (Figs. 3 and 4).

No structure has been assigned to the *m/e* 384 ($M^+ - 44$) fragment ion in the spectrum of the 3α-ethyl ether (Fig. 3) on the basis of the spectra

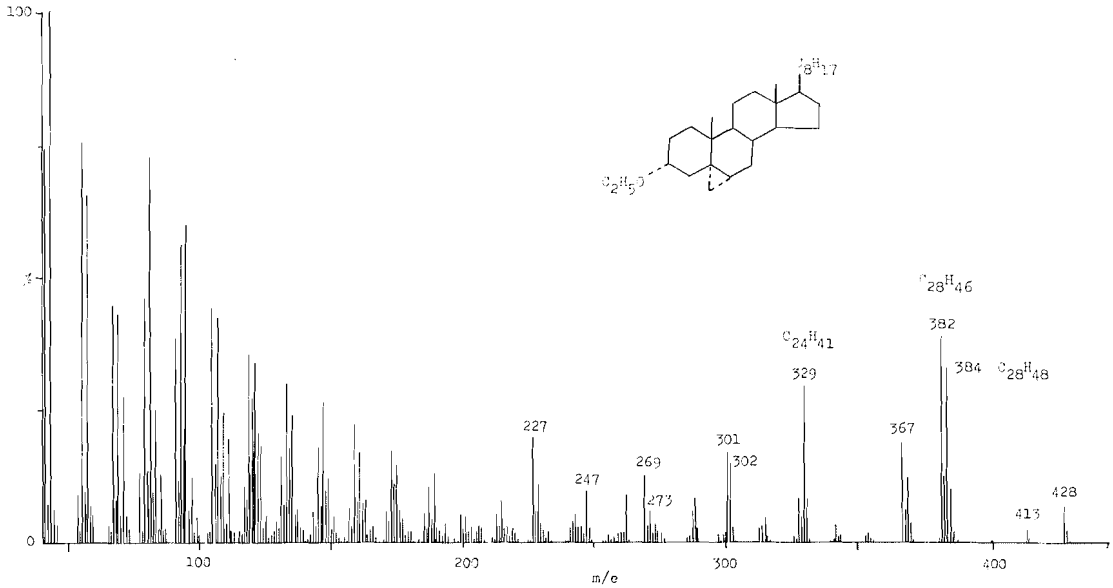

FIG. 3. Mass spectrum of 3α-ethoxy-5α,6-cyclopropano-5α-cholestane.

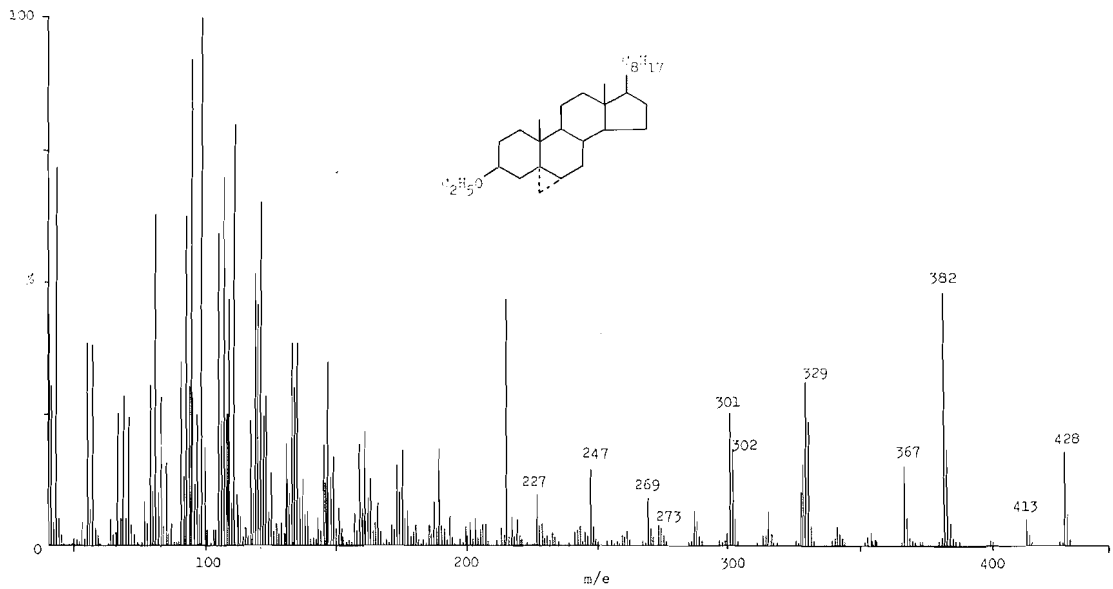

FIG. 4. Mass spectrum of 3β-ethoxy-5α,6-cyclopropano-5α-cholestane.

studied. However, accurate mass measurement shows that C_2H_4O has been lost from the molecular ion.

Besides the well-known fragment ions of steroidal derivatives (3, 4), mass spectrometric fragmentations of 5,6α-cyclopropano-5α-cholestane derivatives demonstrate the formation of additional characteristic fragment ions (*m/e* 247, 301, 302, 329) which have been related to the presence of the cyclopropane ring. In the case of the ions at *m/e* 247, 301, and 302, fragmentations appear to be directed by initial cleavage of the cyclopropane ring, whereas for the ion at *m/e* 329, the cyclopropane ring may stabilize the

Can. J. Chem. Downloaded from www.nrcresearchpress.com by 210.87.254.5 on 09/05/12
For personal use only.

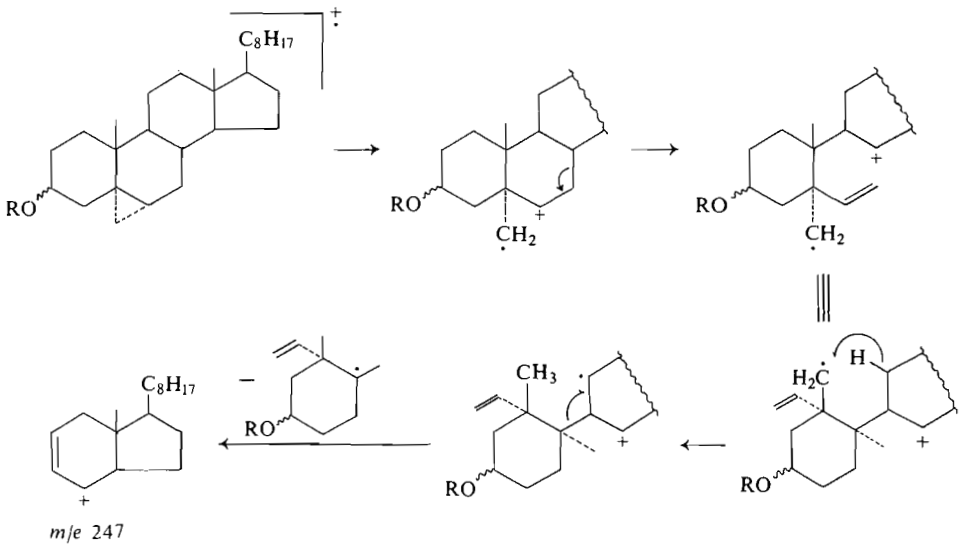

SCHEME 1

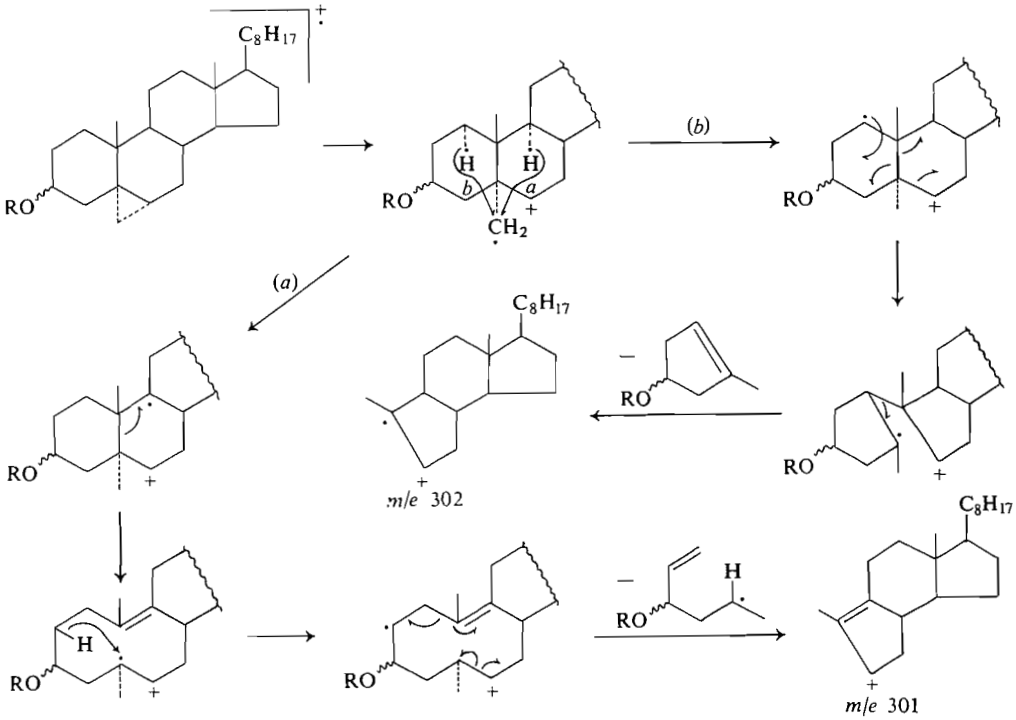

SCHEME 2

Can. J. Chem. Downloaded from www.nrcresearchpress.com by 210.87.254.5 on 09/05/12
For personal use only.

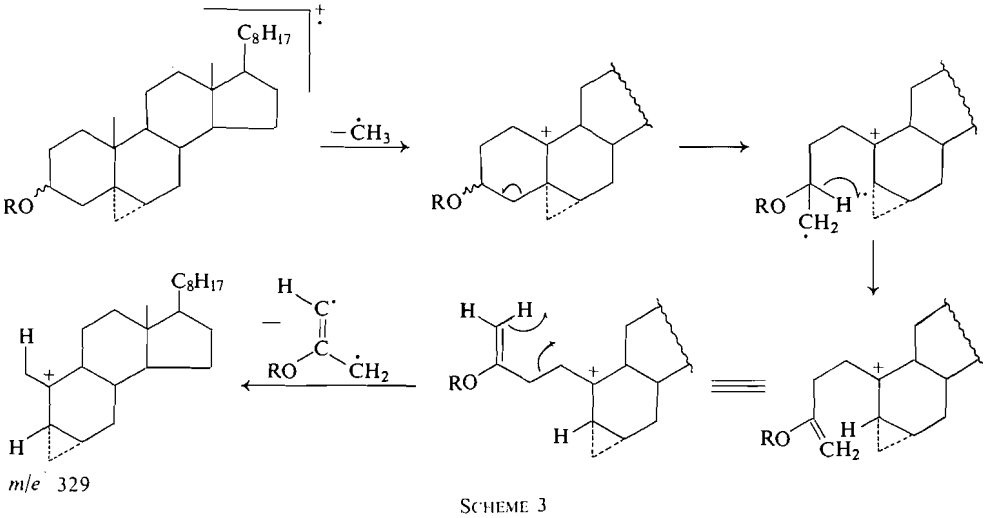

SCHEME 3

intermediate fragment ions and/or radicals leading to the *m/e* 329 ion or provide greater stability to the *m/e* 329 ion itself.

Experimental

General experimental details and apparatus are recorded in ref. 1. For the preparation of 3α- and 3β-hydroxy and 3α-ethoxy-5,6α-cyclopropano-5α-cholestane and the 3-ketone (**1**), and comparison of their physical properties with those of the deuterated analogs (**2**–**9**) see the experimental sections of refs. 1 and 2. Mass spectra were determined by the Mass Spectroscopy Laboratory, Chemistry Department, University of Alberta, Edmonton, using a Metropolitan-Vickers MS-2 (Figs. 1–2) at a source temperature of 125° and an AEI MS-9 (Figs. 3–4) at a source temperature of 155°. The mass spectrometers were operated at an accelerating voltage of 70 eV. Accurate mass measurements were carried out by the peak matching method.

3β-Ethoxy-5,6α-cyclopropano-5α-cholestane

To a solution of 3β-hydroxy-5,6α-cyclopropano-5α-cholestane (93 mg) in dry benzene (20 ml), potassium metal (280 mg) was added and the mixture refluxed for 1 h with vigorous stirring. Ethyl iodide (4 ml) was added and reflux continued for a further 4 h (9). Excess *t*-butanol was added to the cooled reaction mixture, and the slurry evaporated to dryness at reduced pressure. Water and dilute mineral acid were added to the residue and the resulting aqueous mixture extracted with ether. The crude reaction product was dissolved in petroleum ether and filtered through alumina. Recrystallization from acetone gave 3β-ethoxy-5,6α-cyclopropano-5α-cholestane, m.p. 53.5–54.5°; $[\alpha]_D$ −50° (*c*, 0.52 $CHCl_3$); i.r. ν_{max} (KBr) 3077 (cyclopropyl C—H), 1105 (C—O) cm^{-1}.

Anal. Calcd. for $C_{30}H_{52}O$: C, 84.04; H, 12.23. Found: C, 83.93; H, 12.11.

*5,6α-Cyclopropano-5α-cholestan-3-one-2,2,4,4-d_4 (**2**)*

Sodium metal (57 mg) was dissolved in dioxane (2 ml) and D_2O (0.5 ml). 5,6α-Cyclopropano-5α-cholestan-3-one (**1**) (100 mg) was added and the mixture was refluxed for 2 h. The reaction mixture was poured into an aqueous buffer solution (p*H* 6.5) and extracted with ether. The ether solution was washed with saturated sodium chloride solution, dried over anhydrous sodium sulfate, and evaporated at reduced pressure to give the deuterated derivative having 93% d_4, 7% d_3; isotope composition by mass spectrometric analysis.

*3β-Hydroxy-5,6α-cyclopropano-5α-cholestane-2,2,4,4-d_4 (**3**)*

5,6α-Cyclopropano-5α-cholestan-3-one-2,2,4,4-d_4 (**2**) (100 mg) was refluxed with lithium aluminum hydride (43 mg) in dry ether (10 ml) for 3 h. Excess hydride was destroyed with ethyl acetate. The reaction mixture was poured into water acidified with dilute hydrochloric acid, and extracted with ether. The crude product gave two spots on t.l.c. corresponding to the 3α- and 3β-alcohols. Chromatography on alumina gave **3** on elution with 75% benzene – petroleum ether, m.p. 156–156.5°; (82% d_4, 12% d_3, 5% d_2).

*3β-Hydroxy-5,6α-cyclopropano-5α-cholestane-3α-d_1 (**4**)*

A solution of 5,6α-cyclopropano-5α-cholestan-3-one (**1**) (150 mg) in dry ether (10 ml) was treated with lithium aluminum deuteride (57 mg) by the same method as **2**. Chromatography on alumina gave, on elution with 75% benzene – petroleum ether, 3β-hydroxy-5,6α-cyclopropano-5α-cholestane-3α-d_1 (**4**) (80 mg), recrystallized from petroleum ether, m.p. 155–156.5°; (97% d_1, 3% d_0).

*3β-Ethoxy-5,6α-cyclopropano-5α-cholestane-3α-d_1 (**5**)*

3β-Hydroxy-5,6α-cyclopropano-5α-cholestane-3α-d_1 (**4**) (37 mg) was treated in the same way as 3β-hydroxy-5,6α-cyclopropano-5α-cholestane. The crude reaction product was filtered through a column of alumina, and recrystallized from acetone to give **5**, m.p. 53–54°; (96% d_1, 4% d_0).

*3β-Ethoxy-5,6α-cyclopropano-5α-cholestane-2,2,4,4-d_4 (**6**)*

3β-Hydroxy-5,6α-cyclopropano-5α-cholestane-2,2,4,4-d_4 (**3**) (55 mg) was treated by the same method as

Can. J. Chem. Downloaded from www.nrcresearchpress.com by 210.87.254.5 on 09/05/12
For personal use only.

3β-hydroxy-5,6α-cyclopropano-5α-cholestane. The crude reaction product in petroleum ether was filtered through a column of alumina, and recrystallized from acetone to give **6**, m.p. 53–54°; (81% d_4, 12% d_3, 3% d_2).

3α-Hydroxy-5α,6-deuteriocyclopropano-5α-cholestane-d_2 (7)

A mixture of zinc dust (3.93 g) and cuprous chloride (595 mg) in dry ether (10 ml) was refluxed for 30 min. To this mixture CD_2I_2 (2.4 ml) was added and reflux continued for another 30 min (10). Epicholesterol (1.15 g) was added and the reaction mixture refluxed for 3 h. The reaction was poured into excess sodium bicarbonate and the products extracted with ether. The ether solution was washed with water, saturated sodium chloride solution, dried over sodium sulfate, and evaporated at reduced pressure. Chromatography of the crude product on alumina gave, on elution with benzene – petroleum ether, 3α-hydroxy-5α,6-deuteriocyclopropano-5α-cholestane-d_2 (**7**) (944 mg), which was recrystallized from acetone, m.p. 120–121°; (87% d_2, 7% d_1, 6% d_0).

5α,6-Deuteriocyclopropano-5α-cholestan-3-one-d_2 (8)

3α-Hydroxy-5α,6-deuteriocyclopropano-5α-cholestane-d_2 (**7**) (617 mg) was dissolved in acetone (40 ml) and oxidized with Jones reagent (11). Recrystallization of the crude product from methanol afforded **8**, 500 mg, m.p. 144°.

3β-Hydroxy-5α,6-deuteriocyclopropano-5α-cholestane-d_2 (9)

5α,6-Deuteriocyclopropano-5α-cholestan-3-one-d_2 (**8**) (490 mg) in dry ether (50 ml) was reduced with lithium aluminum hydride (250 mg) by the same method as **2**. Chromatography of the crude product gave, on elution with benzene – petroleum ether, **9**, (362 mg). Recrystallization from petroleum ether afforded 236 mg, m.p. 155–156°; (91% d_2, 5% d_1, 4% d_0).

We wish to thank Mr. R. Linklater for preparing compound **4** and Mrs. R. Redekop for normalizing the spectra. Financial assistance from the Research Board, University of Manitoba, and the Medical Research Council of Canada is gratefully acknowledged.

1. J. F. TEMPLETON and C. W. WIE. Can. J. Chem. **49**, 3636 (1971).
2. L. KOHOUT and J. FAJKOS. Collect. Czech. Chem. Commun. **37**, 3490 (1972); L. KOHOUT, J. FAJKOS, and F. SORM. Tetrahedron Lett. 3655 (1972).
3. M. SPITELLER-FRIEDMANN and G. SPITELLER. Forsch. Chem. Forsch. **12**, 440 (1969).
4. R. I. REED. Mass spectrometry of organic ions. *Edited by* F. W. McLafferty. Academic Press, New York. 1963. pp. 686–690.
5. C. R. NARAYANAN and A. K. LALA. Org. Mass Spectrom. **6**, 119 (1972).
6. J. KARLINER, H. BUDZIKIEWICZ, and C. DJERASSI. J. Org. Chem. **31**, 710 (1966).
7. D. R. IDLER, L. M. SAFE, and S. F. SAFE. Steroids, **16**, 251 (1970).
8. M. SPITELLER-FRIEDMANN and G. SPITELLER. Org. Mass Spectrom. **1**, 231 (1968).
9. C. R. NARAYANAN and K. N. IYER. J. Org. Chem. **30**, 1734 (1965).
10. R. J. RAWSON and I. T. HARRISON. J. Org. Chem. **35**, 2057 (1970).
11. K. BOWDEN, K. M. HEILBRON, E. R. H. JONES, and B. C. L. WEEDON. J. Chem. Soc. **39** (1946).

Can. J. Chem. Downloaded from www.nrcresearchpress.com by 210.87.254.5 on 09/05/12
For personal use only.

Can. J. Chem. Downloaded from www.nrcresearchpress.com by 210.87.254.42 on 09/05/12
For personal use only.

Restricted Rotation in α-Carbonyl Radicals

TERRY FOSTER, DIETER KLAPSTEIN, AND PAUL RONALD WEST
Department of Chemistry, University of Victoria, Victoria, British Columbia

Received August 31, 1973

Electron spin resonance spectra of tertiary α-carbonyl radicals, $R_1R_2\dot{C}COR_3$ ($R_1R_2R_3$ = H, alkyl), at 24 °C in aqueous solution show fully restricted rotation about the Ċ—CO bond. The effect is identified by differing h.f.s. constants for equivalent substituents R_1 and R_2. The radical intermediates are generated by direct abstraction, radical fragmentation, and reductive elimination processes.

Les spectres r.s.e. de radicaux tertiaries α-carbonylés, $R_1R_2\dot{C}COR_3$ ($R_1R_2R_3$ = H, alcoyle) à 24 °C en solution aqueuse ont révélés qu'*il* existe une rotation complètement empêchée autour du lien Ċ—CO. L'effet est identifié par différentiation des constantes h.f.s. pour substituants R_1 et R_2 équivalents. Les intermédiaires radicalaires sont formés par des processus d'abstraction directe de fragmentation radicalaire et d'élimination réductive. [Traduit par le journal]

Can. J. Chem., **52**, 524 (1974)

Considerable interest in the structure of α-carbonyl (2-alkanoyl) radicals has arisen over the question of the extent of delocalization of the unpaired electron over the C=O group (1–6). The normal magnitude of the α-hydrogen hyperfine splitting (h.f.s.) constants in the e.p.r. spectra of such species is consistent with minimal resonance interaction (1, 2), as is the failure to observe significant stabilization of the acetonyl radical in gas phase halogenation (3). However, restricted rotation in the acetonyl radical at low temperatures (−47.3 °C) (4, 5), and the magnitude of the ^{17}O and ^{13}C h.f.s. constants of the 2-cyclohexanoyl radical in the adamantane matrix (6) have been taken as evidence of some degree of allylic resonance.

In aqueous solution, α-carbonyl radicals result from the fragmentation of hydrogen abstraction radicals during the oxidation and radiolysis of a wide range of biologically important molecules including carbohydrates and sugar alcohols (7, 8), glycols (9, 10), and amino alcohols (11) (eq. 1).

[1] $$R_1R_2\dot{C}-CR_3(X)(OH) \xrightarrow{OH^-/H^+} R_1R_2\dot{C}-CR_3(=O)$$

1 **2**

$R_1R_2R_3$ = H, alkyl

In continuing studies on the oxidation of β-amino alcohols (X = NH_3^+),[1] we have now observed for the first time fully restricted rotation in α-carbonyl radicals at room temperature in aqueous solution (p*H* 6.0). In these examples, the radical center is tertiary, *i.e.* R_1R_2 = alkyl. Oxidation of 2-amino-2-methyl-1-propanol (**1**, R_1R_2 = CH_3; R_3 = H) gave the α-formyl radical **3**, with a_{CH_3-a} (3H) = 21.1 G, a_{CH_3-s}

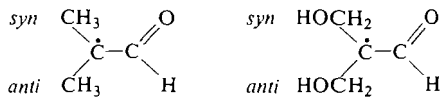

3 **4**

(3H) = 18.0 G, a_{CHO} (1H) = 3.0 G, and g = 2.0045. Similarly, oxidation of trishydroxymethylaminomethane (**1**, R_1R_2 = $HOCH_2$; R_3 = H) gave radical **4**: a_{CH_2OH-a} (2H) = 22.5 G, a_{CH_2OH-s} (2H) = 16.2 G, a_{CHO} (1H) = 2.0 G, g = 2.0045.

A strictly tentative assignment of the *syn* (s) and *anti* (a) disposition of the groups R_1 and R_2

[1]The β-amino alcohol (0.5 *M*) was added to a solution of H_2O_2 (0.1 *M*) and reacted with 0.02 *M* Ti(III) (EDTA) in a Varian E-6S E.P.R. spectrometer aqueous flow cell system (11). The flow rates (150 ml/min) and reacting volume (0.080 ml) yield an approximate dead time of 0.016 seconds.

Can. J. Chem. Downloaded from www.nrcresearchpress.com by 210.87.254.42 on 09/05/12
For personal use only.

relative to the carbonyl function in **3** and **4** can be made as follows. The h.f.s. constant of the necessarily *syn* α-hydrogen in the 2-cyclopentanoyl radical **5** is 17.9G, (ref. 9*a*), and in the

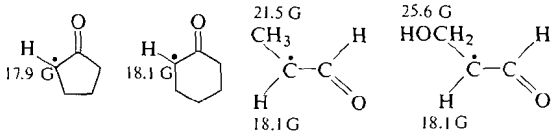

5 **6** **7** **8**

2-cyclohexanoyl radical **6**, 18.1 G, (ref. 6). These values can be taken in conjunction with the h.f.s. constants for the radicals **7** and **8** (9*a*) as being indicative of preferred (if not fixed) conformations of the latter radicals as shown.[2] Then by comparison with **7** and **8** one assigns the *anti* CH_3 and *anti* CH_2OH groups in **3** and **4** as indicated.

We have taken precautions to establish that metal complexing does not fix the conformation of the tertiary α-carbonyl radicals.[3] First, we have repeated the oxidation of isobutryaldehyde reported by Steven and Ward (13). In addition to confirming the presence of $(CH_3)_2CH\cdot$, a_{2CH_3} (6H) = 24.6 G, a_{CH}(1H) = 21.1 G, g = 2.0025, we observe **3** as the dominant species under both acidic (p*H* 1.4) and neutral (p*H* 6.0) conditions (eq. 2). Here, direct hydrogen abstraction as opposed to abstraction followed by fragmentation (reaction 1) produces **3**. As further confirma-

[2] 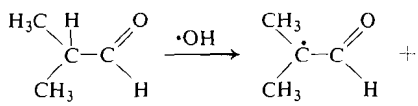

3

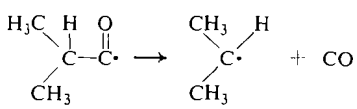

tion of the effect we have oxidized 3-methyl-2-butanone at p*H* 6.0, obtaining a complex spectrum dominated by the 1,1-dimethylacetonyl radical **9**. Identification was made possible by observation of **9** alone through reductive elimination of the bromoketone **10**[4] at p*H* 8.3 (eq. 3)(11). The assignment of the h.f.s. constants as a_{CH_3-a}(3H) = 21.3, a_{CH_3-s}(3H) = 19.0, a_{CH_3CO} (3H) = 2.0 has been based on the reported values for the 2-butanone abstraction radical **11** (2, 9*a*).

[3] 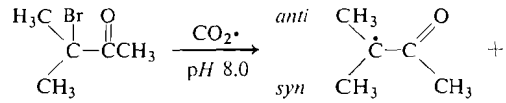

10 **9**

$Br^- + CO_2$ 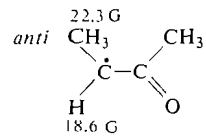

11

Generation of the radicals **3**–**5** by the use of three chemically distinct routes (eq. 1–3) is taken as strong indication that the species in all cases are observed free in aqueous solution. Therefore, in this type of α-carbonyl radical a fixed planar conformation must be adopted even at 24 °C, with delocalization (see structures **12**–**14**) suffi-

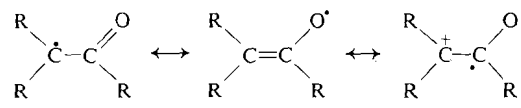

12 **13** **14**

R = H, alkyl

ciently stabilizing to overcome the substantial repulsive nonbonded interactions that occur between the *syn* substituents. We suspect the somewhat high values of the *H*—CO and *CH*$_3$—CO h.f.s. constants are just as likely to reflect twisting out of plane to accommodate these interactions, as they are to indicate increased (negative) spin density at the carbonyl carbon (2). The charge separation inferred by **14**, particularly when the α center is tertiary, is an attractive source of the additional resonance energy required to compensate for the steric requirements of the conformation. Such a distribution may be particularly favored in the polar hydroxylic medium. Indeed in our system the acetonyl radical

[2]Indeed apart from the close correspondance of a_{CH_2} values, one *a priori* expects the *transoid* conformations to dominate in **7** and **8** on steric grounds.

[3]Such interference is discounted by the close agreement in all instances of e.p.r. studies employing either this approach, or the alternative continuous radiolysis of aqueous solutions (12).

[4]Synthesized by the method of Pfleiderer and Zondler (14). Co-oxidation of formate ion (0.5 *M*) and bromoketone (0.05 *M*) effects the indicated reduction.

$\dot{C}H_2\overset{\overset{O}{\|}}{C}CH_3$ shows a fixed conformation at 11 °C with $a_{CH}(1H) = 20.0$ G, $a_{CH}(1H) = 19.5$ G, and $a_{CH_3}(3H) = 1.0$ G.[5] We note that in pure acetone the rotation becomes fixed only at −47 °C (4,5). The reported value of $a_{CH_3}(3H)$ of 0.27 G in these studies is consistent with a lesser delocalization being achieved in the nonpolar nonhydroxylic medium. However, solvation of the carbonyl group may well influence the barrier to rotation in α-carbonyl radicals providing an alternative explanation of such solvent dependance.

Generous support of this project by the National Research Council and the University of Victoria in the form of operating grants is acknowledged.

1. G. A. Russell and J. Lokensgard. J. Am. Chem. Soc. **89**, 5059 (1967).
2. P. H. Kasai and D. McLeod, Jr. J. Am. Chem. Soc. **92**, 7975 (1972).
3. K. D. King, D. M. Golden, and S. W. Benson. J. Am. Chem. Soc. 5541 (1970).
4. G. Golde, K. Möbius, and W. Kaminski. A. Naturforsch. A, **24**, 1214 (1969).
5. (*a*) R. Livingston and H. Zeldes. J. Am. Chem. Soc. **88**, 4333 (1966). (*b*) H. Zeldes and R. Livingston. J. Chem. Phys. **45**, 1946 (1966).
6. D. M. Camaioni, H. F. Walter, and D. W. Pratt. J. Am. Chem. Soc. **95**, 4057 (1973).
7. H. Scherz. Radiat. Res. **43**, 12 (1970).
8. R. O. C. Norman and R. J. Pritchett. J. Chem. Soc. B, 1329 (1967).
9. (*a*) A. L. Buley, R. O. C. Norman, and R. J. Pritchett. J. Chem. Soc. B, 849 (1966). (*b*) B. C. Gilbert, J. P. Larkin and R. O. C. Norman. J. Chem. Soc. Perkin II, 794 (1972).
10. C. E. Burchill and K. M. Perron. Can. J. Chem. **49**, 2382 (1971).
11. T. Foster and P. R. West. Can. J. Chem. **51**, 4009 (1973).
12. K. Eiben and R. W. Fessenden. J. Phys. Chem. **75**, 1186 (1971).
13. J. R. Steven and J. C. Ward. Aust. J. Chem. **20**, 2005 (1967).
14. W. Pfleiderer and H. Zondler. Chem. Ber. **99**, 3018 (1966).

[5]Hindered rotation persists even at room temperature as first reported by Norman and co-workers (9*a*).

Can. J. Chem. Downloaded from www.nrcresearchpress.com by 210.87.254.42 on 09/05/12
For personal use only.

Can. J. Chem. Downloaded from www.nrcresearchpress.com by 210.87.254.5 on 09/05/12
For personal use only.

Canadian Journal of Chemistry

Journal canadien de chimie

Published by
THE NATIONAL RESEARCH COUNCIL OF CANADA

Publié par
LE CONSEIL NATIONAL DE RECHERCHES DU CANADA

Volume 52 Number 4 February 15, 1974 Volume 52 numéro 4 15 février 1974

cis-Activation by Oxyanions Coordinated to Chromium(III): Aquation and Base Hydrolysis of Nitratopentaamminechromium(III) Ion

GIOVANNI GUASTALLA AND THOMAS WILSON SWADDLE

Department of Chemistry, The University of Calgary, Calgary, Alberta T2N 1N4

Received August 7, 1973

The aquation of $Cr(NH_3)_5NO_3^{2+}$ in acidic solutions yields not only $Cr(NH_3)_5OH_2^{3+}$ (33%) but also more highly aquated species including *cis*-$Cr(NH_3)_4(OH_2)_2^{3+}$ and $Cr(NH_3)_3(OH_2)_3^{3+}$. In 0.1 *M* $HClO_4$, several successive reactions of comparable rates are involved, but at p*H* 6 only the two competing initial reactions producing $Cr(NH_3)_5OH^{2+}$ and *cis*-$Cr(NH_3)_4(OH)NO_3^{+}$ are rate-controlling, so that the overall reaction rate is first-order in substrate with the apparent parameters $k_A = 2.4 \times 10^{-3}$ s^{-1} (25°), $\Delta H_A^* = 20.4$ kcal mol^{-1}, and $\Delta S_A^* = -2.1$ cal deg^{-1} mol^{-1}. In alkaline solutions, the pseudo-first-order rate of hydrolysis at a given $[OH^-]$ is governed by $k_{obs} = k_A + k_{OH}[OH^-]$, with $k_{OH} = 1.1 \times 10^{-2}$ M^{-1} s^{-1} (25°), $\Delta H_{OH}^* = 25.2$ kcal mol^{-1}, and $\Delta S_{OH}^* = 17.0$ cal deg^{-1} mol^{-1}. The path characterized by k_{OH} leads exclusively to $Cr(NH_3)_5OH^{2+}$. In both aquation and base hydrolysis, it is the Cr—ONO_2 bond that is broken. The production of more highly aquated species in the aquation reactions is attributed to transient chelation of NO_3^- at the expense of a ligand *cis* to it. The evidence for this mechanism, and for its operation when oxyanions other than nitrate are coordinated to Cr(III), is reviewed.

L'aquation du $Cr(NH_3)_5NO_3^{2+}$ dans des solutions acides a conduit non seulement au $Cr(NH_3)_5OH_2^{3+}$ (33%) mais aussi aux espèces "aquo" supérieures telles *cis*-$Cr(NH_3)_4(OH_2)_2^{3+}$ et $Cr(NH_3)_3(OH_2)_3^{3+}$. Dans le $HClO_4$ 0.1 *M*, plusieurs réactions successives de vitesses comparables sont impliquées alors qu'à p*H* 6, les deux réactions initiales conduisant au $Cr(NH_3)_5OH^{2+}$ et au *cis*-$Cr(NH_3)_4(OH)NO_3^{+}$ sont les seules à contrôler la vitesse. Par suite, dans ce dernier cas, la vitesse globale de la réaction obéit à une expression de vitesse du premier ordre par rapport au substrat dont les paramètres sont: $k_A = 2.4 \times 10^{-3}$ S^{-1} (25°), $\Delta H_A^* = 20.4$ kcal mol^{-1} et $\Delta S_A^* = -2.1$ cal deg^{-1} mol^{-1}. Dans des solutions alcalines, la vitesse d'hydrolyse obéit à une expression de vitesse du pseudo premier ordre pour une certaine concentration d'ions OH^- qui est traduite par $k_{obs} = k_A + k_{OH}[OH^-]$ avec $k_{OH} = 1.1 \times 10^{-2}$ M^{-1} s^{-1} (25°) $\Delta H_{OH}^* = 25.2$ kcal mol^{-1} et $\Delta S_{OH}^* = 17.0$ cal deg^{-1} mol^{-1}. Le mécanisme dépendant de k_{OH} conduit exclusivement au $Cr(NH_3)_5OH^{2+}$. La liaison Cr-ONO_2 est brisée dans les réactions d'aquation et d'hydrolyse basique. La production d'espèces "aquo" supérieures dans les réactions d'aquation est attribuée à la chélation intermédiaire de NO_3^- à la place d'un coordinat qui lui est *cis*. On passe en revue les preuves en faveur de ce mécanisme ainsi que de son application lorsque des oxyanions différents des nitrates sont coordonnés au Cr(III). [Traduit par le journal]

Can. J. Chem., **52**, 527 (1974)

Introduction

In a preliminary communication (1), we reported briefly that the nitrato-ligand in $Cr(NH_3)_5NO_3^{2+}$ strongly accelerates the aquation of ammine ligands in the *cis*-positions. This *cis*-activation phenomenon has some important consequences for the study of chromium(III) chemistry, since it requires the reassessment of kinetic studies involving chromium(III) complexes in nitrate-containing solutions (2), and furthermore it appears to occur with oxyanions other than nitrate (1). An earlier study by Monacelli (3) of the kinetics of the aquation of $Cr(NH_3)_5NO_3^{2+}$ was made on the assumption that only the nitrato-ligand

Can. J. Chem. Downloaded from www.nrcresearchpress.com by 210.87.254.5 on 09/05/12
For personal use only.

was replaced, and accordingly a reinvestigation of the hydrolysis kinetics is necessary; furthermore, there are no published data on the kinetics of the hydrolysis in alkaline solution.

The present article presents a full account of our studies of the reactions of nitratopentaamminechromium(III) ion and its salts, including the kinetics of base hydrolysis and the determination of the position of bond breaking. A survey of the evidence indicating that *cis*-activation is a characteristic property of oxyanions coordinated to Cr(III), and a rationale for our contention that the effect is due to transient chelation by the oxyanion (1), are also presented.

Experimental

Materials

All chemicals used were reagent grade. Distilled water was passed through Barnstead deionizing and organic removal cartridges before use. Spectroscopic measurements were made on a Cary Model 15 spectrophotometer.

Nitratopentaamminechromium(III) nitrate was prepared by thermal deaquation of $[Cr(NH_3)_5OH_2](NO_3)_3$ (4). The visible spectrum exhibited maxima at 485 (molar absorbancy index $\varepsilon = 39.3$) and 362 nm ($\varepsilon = 30.4\ M^{-1}\ cm^{-1}$).

Aquopentaamminechromium(III) perchlorate was made by addition of 70% $HClO_4$ to a filtered solution of $[Cr(NH_3)_5OH_2](NO_3)_3.NH_4NO_3$ (4), and *cis*-$[Cr(NH_3)_4(OH_2)_2](ClO_4)_3.H_2O$ by base hydrolysis of *cis*-$[Cr(NH_3)_4(OH_2)Cl]Cl_2$ with 1 *M* NaOH followed by precipitation with 70% $HClO_4$ (5). *cis*-$[Cr(NH_3)_4(OH)OH_2]S_2O_6.H_2O$ was also made from the latter complex (6), and its visible spectrum showed maxima at 518 ($\varepsilon = 40.7$) and 394 nm ($\varepsilon = 35.9\ M^{-1}\ cm^{-1}$).

The above compounds were shown to be authentic by microanalysis for N and H, and (where no spectral data are given) by comparison of their visible/ultraviolet solution spectra with those in the literature (7). The solids were stored in the dark over P_2O_5.

Two attempts were made to prepare *cis*-$[Cr(NH_3)_4(OH_2)NO_3](NO_3)_2$ according to a published procedure (8), but the visual appearance of the products suggested a mixture of compounds, as did the following analytical data.

Anal. Calcd. for $[Cr(NH_3)_4(OH_2)NO_3](NO_3)_2$: N, 30.3; H, 4.35. Found: (first preparation) N, 28.8; H, 4.89; (second preparation) N, 28.2; H, 4.90.

Determination of Reaction Stoichiometry

The various Cr(III) complexes produced in the hydrolysis reactions were separated by a standardized ion-exchange procedure. Typically, freshly-prepared $[Cr(NH_3)_5NO_3](NO_3)_2$ (0.201 g, 0.62 mmol) was dissolved in 100 ml of a solution of the desired composition (0.1 *M* in $HClO_4$, NH_4ClO_4 or NaOH for experiments representing acidic, neutral, or basic conditions respectively) at 25.0°, and, after at least 10 half-periods of the reaction of interest (100, 45, or 25 min respectively) the solution was cooled to 0° and treated with sufficient cold 10 *M* NaOH to bring the OH^- concentration in the resulting solution to 1.0 *M*. The solution was then passed through Dowex 50W-X2 resin (Na^+ form, 80 ml) in a jacketted column (2.5 cm i.d.) which was maintained at 0° with circulating water.

A fraction containing trihydroxotriamminechromium-(III) and possibly di- and mono-ammines was eluted from the resin with cold 0.1 *M* NaOH, and was identified by its spectrum after acidification (see below). The total amount of Cr present in this fraction was determined spectrophotometrically as CrO_4^{2-} by oxidizing the combined 0.1 *M* NaOH eluates with H_2O_2 (9).

Further elution with 1.5 or 2.0 *M* NaOH yielded a single red species which, on acidification, showed maxima at 495 ($\varepsilon = 35.5$) and 365 ($\varepsilon = 26.0$) and a minimum at 418 nm ($\varepsilon = 8\ M^{-1}\ cm^{-1}$), corresponding to *cis*-$Cr(NH_3)_4(OH_2)_2^{3+}$ (2, 6). The total Cr present in this fraction was determined as CrO_4^{2-} (9) or from the absorbance of the acidified solution at 454 nm, at which wavelength *cis*- and *trans*-$Cr(NH_3)_4(OH_2)_2^{3+}$ have an isosbestic point with $\varepsilon = 20.5\ M^{-1}\ cm^{-1}$.

The species remaining on the resin was evidently $Cr(NH_3)_5OH^{2+}$, and could not be conveniently eluted even with 5 *M* NaOH. It was shown that, when a prepared mixture of $Cr(NH_3)_5OH^{2+}$ and *cis*-$Cr(NH_3)_4(OH)_2^+$ in 1.0 *M* NaOH was subjected to ion-exchange chromatography in this way, the tetraammine was recovered in 97% yield, while no $Cr(NH_3)_5OH^{2+}$ was eluted.

The $Cr(NH_3)_5OH^{2+}$ yields were determined separately by adding 50 ml cold 70% $HClO_4$ to 100 ml portions of the hydrolyzed $[Cr(NH_3)_5NO_3](NO_3)_2$ solutions prepared as above. After 1 h, the precipitate was filtered, redissolved in 0.1 *M* $HClO_4$, identified spectroscopically as $[Cr(NH_3)_5OH_2](ClO_4)_3$ (2) and estimated as CrO_4^{2-} (9). A control experiment using a prepared solution of $Cr(NH_3)_5OH_2^{3+}$ and *cis*-$Cr(NH_3)_4(OH_2)_2^{3+}$ showed that the precipitation of $[Cr(NH_3)_5OH_2](ClO_4)_3$ was essentially quantitative, while $Cr(NH_3)_4(OH_2)_2^{3+}$ remained entirely in solution.

Spectrophotometric Kinetic Measurements

In general, these were made *in situ* in 2 cm cells in the thermostated (±0.1°) sample compartment of a Cary Model 15 spectrophotometer. The temperature of the solution in the cell was measured with an Atkins thermistor thermometer. The solutions were made from freshly-prepared $[Cr(NH_3)_5NO_3](NO_3)_2$ (3×10^{-3} *M*), and the ionic strength *I* and the p*H* were adjusted as required with $HClO_4$, $NaClO_4$ or NaOH/$NaClO_4$. In cases where the optical absorbance *A* changed as a function of time *t* according to first-order kinetics over at least two half-periods of the reaction, *A* was monitored continuously at a suitable wavelength (*e.g.*, 560 nm) and the first-order rate coefficient was derived from a plot of $\ln (A_t - A_\infty)$ *vs.* *t*. In the absence of first-order behavior, repeated wavelength scans were made over the visible region.

Kinetic Measurements Using Specific Ion Electrodes

The release of nitrate ion in the hydrolysis of $Cr(NH_3)_5NO_3^{2+}$ was followed potentiometrically using a Beckman Research p*H* Meter fitted with a double-junction calomel reference electrode and an Orion Model 92-07 nitrate-ion electrode. The electrodes dipped directly into the reaction mixture, which was thermostated at 25.0 ± 0.1°, and the assembly was calibrated against standard KNO_3 solutions (10^{-4} to 10^{-1} *M*) following each reading.

Can. J. Chem. Downloaded from www.nrcresearchpress.com by 210.87.254.5 on 09/05/12
For personal use only.

The release of ammonia (as NH_4^+) was followed in a similar fashion using a Beckman Selectlon ammonium electrode, Model N39626, the standards being solutions of NH_4Br.

The nitrate and ammonium electrodes were effective only within the p*H* range 2–10, and there was also the risk of interference from major concentrations of "inert" electrolytes such as perchlorates which might have been added to control p*H* and ionic strength. Accordingly, NO_3^- and NH_4^+ formation studies were made only on solutions prepared from $[Cr(NH_3)_5NO_3](NO_3)_2$ and pure water.

Establishment of Position of Bond-breaking

Nitratopentaamminechromium(III) nitrate (200–300 mg) was hydrolyzed at 25° for 20 min in 25 ml acidic (0.05 *M* $HClO_4$), neutral, and basic (0.1 *M* NaOH) water which contained ~1.3% $H_2{}^{18}O$. The $Cr(NH_3)_5OH_2{}^{3+}$ product was precipitated as the perchlorate by addition of 5 ml 70% $HClO_4$ at 0°, and the filtered precipitate was dried *in vacuo*. The coordinated water was removed on the vacuum line by fusing the salt in dry KNCS, and was converted to CO_2 and analyzed mass spectrometrically as described previously (10) except that a Varian/MAT CH-5 mass spectrometer was used. Reference samples of solvent were similarly analyzed as CO_2, relative to tank CO_2 of natural isotopic composition.

Results

Reaction Stoichiometry

The spectral changes accompanying aquation of $Cr(NH_3)_5NO_3{}^{2+}$ in 0.1 *M* NH_4ClO_4 (p*H* 6) at 25° are illustrated in Fig. 1. The spectrum of the final product (maxima at 517 and 395 nm, ε = 30 and 29 M^{-1} cm^{-1} respectively) corresponds fairly closely to that of *cis*-$Cr(NH_3)_4(OH)OH_2{}^{2+}$ (see above) but not $Cr(NH_3)_5OH_2{}^{3+}$ or $Cr(NH_3)_5OH^{2+}$ (6). Measurements with the specific ion electrode showed that these changes occurred concomitantly with the release of 0.96 ± 0.05 mol NO_3^- and 1.0 ± 0.1 mol NH_4^+ per mol Cr(III), while the p*H* remained constant at about 6 throughout the reaction.

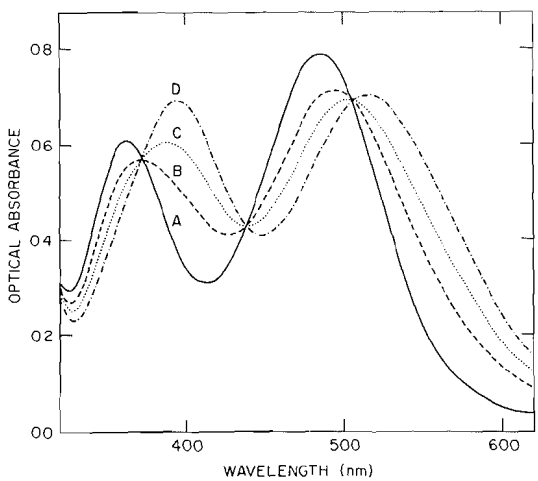

FIG. 1. Spectra of $Cr(NH_3)_5NO_3{}^{2+}$ undergoing aquation at 25.0° at p*H* 6 in 0.10 *M* NH_4ClO_4 (5 cm optical path length; [Cr] = 0.00402 *M*): (*A*), at zero time (pure $Cr(NH_3)_5NO_3{}^{2+}$); (*B*), after 3.0 min; (*C*), after 6.0 min; (*D*), after 23 min (final spectrum).

These results seemed, superficially, to indicate the formation of one NH_4^+ along with the release of NO_3^-, leaving *cis*-$Cr(NH_3)_4(OH)OH_2{}^{2+}$. However, examination of the products by ion-exchange chromatography showed that in reality the Cr(III)-containing species produced at p*H* 6 and 25° in the absence of added electrolytes were (after acidification) $Cr(NH_3)_5OH_2{}^{3+}$ (31%), *cis*-$Cr(NH_3)_4(OH_2)_2{}^{3+}$ (36%), and $Cr(NH_3)_3(OH_2)_3{}^{3+}$ (possibly with di- and mono-ammines) (33%); in 0.1 *M* NH_4NO_3 solution the corresponding percentages were 34, 35, and 31, and, in 0.1 *M* $HClO_4$, 33, 20, and 46. Thus, the closeness of the NH_4^+ yield to 1.00 per Cr, and of the final spectrum to that of the pure *cis*-tetraammine, were purely coincidental. Application of the relation

$$[1] \qquad \%\ cis = \frac{\varepsilon_{apparent} - \varepsilon_{trans}}{\varepsilon_{cis} - \varepsilon_{trans}} \times 100$$

to the spectrum of the 1.5 *M* NaOH eluate, as described elsewhere (2), showed that the tetraammine species present was the isomerically pure *cis* form (97 ± 3% *cis*).

The species which were eluted from the resin with 0.1 *M* NaOH were presumably those which can form complexes of zero charge in strong alkali, *i.e.*, the triammines and possibly di- and mono-ammines. The spectrum of the acidified 0.1 *M* NaOH eluate showed absorption maxima at 514 and 383 nm, with a peak height ratio of 1.03:1, and a minimum at 442 nm; these differ slightly but significantly from the corresponding features in the spectrum of *mer*-$Cr(NH_3)_3(OH_2)_3{}^{3+}$ (maxima at 507 and 373 nm, ratio 1.04:1, and minimum at 431 nm) (2, 7). The spectrum of authentic *fac*-$Cr(NH_3)_3(OH_2)_3{}^{3+}$ is a matter of some dispute (2, 7), but it seems that the characteristic which distinguishes it most clearly from the meridional isomer is its peak-height ratio of about 1.55:1, so that the spectrum of the acidified 0.1 *M* NaOH eluate cannot be accounted for entirely in terms of a mixture of the *fac*- and *mer*-triammines. It seems likely that a minor amount of $Cr(NH_3)_2(OH_2)_4{}^{3+}$ was present along with the triammines. Again, there is some uncer-

Can. J. Chem. Downloaded from www.nrcresearchpress.com by 210.87.254.5 on 09/05/12
For personal use only.

tainty concerning the spectra of the individual diammine isomers (2, 7); the maxima are evidently near 520 and 382 nm, with a peak height ratio of about 1.1:1 and a minimum near 440 nm, but these data are insufficiently precise to permit estimation of the diammine content of the 0.1 *M* NaOH eluate.

It was established empirically that the aquo- and hydroxo-forms of the penta-, tetra-, and triammine complexes do not decompose or isomerize significantly during the aquations (~1 h at 25°) or elutions (~1.5 h at 0°). This was verified by quantitative determinations of the appropriate hydrolysis rates (2).

When the hydrolysis of $Cr(NH_3)_5NO_3^{2+}$ was carried out in 0.1 *M* NaOH at 25°, the products were $Cr(NH_3)_5OH^{2+}$ (59%), *cis*-$Cr(NH_3)_4(OH)_2^{+}$ (20%) and lower hydroxoammines (21%), according to ion-exchange chromatography and precipitation studies; for 1.0 *M* NaOH, the corresponding percentages were 89, 6, and 5. Spectroscopic examination of the reaction mixtures themselves confirmed these data.

Reaction Kinetics

At p*H* 6, in either plain water or in 0.1 *M* NH_4ClO_4 solution, the spectrum of $Cr(NH_3)_5NO_3^{2+}$ changed in accordance with first-order kinetics throughout the first 80% at least of the aquation reaction, isosbestic points being accurately maintained at 372, 439, and 507 nm (Fig. 1). The appropriate first-order rate coefficients k_A are listed in Table 1, and are precise to within ±2%. A plot of $\ln(k_A/T)$ *vs.* $1/T$ is linear, within the experimental uncertainty, and gives $\Delta H_A^* = 20.4 \pm 0.4$ kcal mol^{-1} and $\Delta S_A^* = -2.1 \pm 1.2$ cal deg^{-1} mol^{-1}, which compare favorably with the values 21.0 kcal mol^{-1} and -3 cal deg^{-1} mol^{-1} reported by Monacelli (10) for the aquation of $Cr(NH_3)_5NO_3^{2+}$ in 0.0092 *M* $HClO_4$.

TABLE 1. Spectrophotometric first-order rate coefficients k_A for the aquation of $Cr(NH_3)_5NO_3^{2+}$ at p*H* 6

Temperature (°C)	Wavelength (nm)	[Cr] (m*M*)	$10^3 k_A$ (s^{-1})
15.0	560	3.0	0.67
25.0	560	13.0	2.40*
25.0	400	1.5	2.30
25.0	275	3.0	2.40
28.5	560	3.0	3.96
35.4	560	3.0	7.9
35.9	560	3.0	8.1
43.4	560	3.0	17.8
48.4	560	3.0	31.5

*No added electrolytes; in all other cases, $[NH_4ClO_4] = 0.1$ *M*.

The rate of NO_3^- release during the aquation of $Cr(NH_3)_5NO_3^{2+}$ at 25.0° in plain water (p*H* 6), as measured with the nitrate ion electrode, was first-order in the substrate, the corresponding rate coefficient being $(2.5 \pm 0.2) \times 10^{-3}$ s^{-1}. The corresponding datum for NH_3 release, obtained with the NH_4^+ electrode, was $(2.3 \pm 0.2) \times 10^{-3}$ s^{-1}. These data correspond excellently with the value $k_A = 2.4 \times 10^{-3}$ s^{-1} obtained spectrophotometrically with plain water as solvent.

In $NaClO_4$/NaOH media at $I = 1.0$ *M*, the spectrophotometric rate of disappearance of $Cr(NH_3)_5NO_3^{2+}$ was again first-order in substrate, and the corresponding rate coefficients k_{obs} are listed in Table 2. These values of k_{obs}, which are precise to ±2%, are accurately related to $[OH^-]$ by

$$[2] \qquad k_{obs} = k_0 + k_{OH}[OH^-]$$

and it will be seen from Table 3 that the intercepts k_0 can be identified with the coefficients k_A of Table 1, within the limitations imposed by the uncertainty in k_0 (~±5%) and the differences in ionic strength. A plot of $\ln(k_{OH}/T)$ *vs.* $1/T$ is linear, giving $\Delta H_{OH}^* = (25.2 \pm 0.5)$ kcal mol^{-1} and $\Delta S_{OH}^* = (17.0 \pm 1.5)$ cal deg^{-1} mol^{-1}.

TABLE 2. Spectrophotometric pseudo-first-order rate coefficients k_{obs} for the disappearance of $Cr(NH_3)_5NO_3^{2+}$ in alkaline solutions*

Temperature (°C)	$[OH^-]$ (*M*)	$10^3 k_{obs}$ (s^{-1})	$10^3 k_{calcd}$† (s^{-1})
15.0	0.20	1.18	1.15
	0.40	1.61	1.63
	0.60	2.10	2.11
	0.80	2.57	2.59
	1.00	3.09	3.07
25.0	0.10	3.62	3.60
	0.30	5.80	5.80
	0.40	6.80	6.80
	0.60	9.15	9.10
	0.80	11.2	11.3
	1.00	13.5	13.5
35.0	0.10	10.6	10.8
	0.20	15.1	15.2
	0.30	19.0	19.6
	0.40	24.3	24.0
	0.60	32.4	32.8
	0.80	42.0	41.6

*$I = 1.0$ *M* ($NaOH/NaClO_4$); [Cr] = 3.0 m*M*. Optical data obtained using 2 cm cell and 0.1 absorbance scale.
†Calculated from the parameters of Table 3.

Can. J. Chem. Downloaded from www.nrcresearchpress.com by 210.87.254.5 on 09/05/12
For personal use only.

TABLE 3. Rate coefficients for base-dependent (k_{OH}) and base-independent (k_o) hydrolysis of $Cr(NH_3)_5NO_3^{2+}$ at $I = 1.0\ M$

Temperature (°C)	$k_o(s^{-1})$	$k_{OH}(M^{-1}\,s^{-1})$
15.0	6.7×10^{-4}	2.4×10^{-3}
25.0	2.5×10^{-3}	1.1×10^{-2}
35.0	6.4×10^{-3}	4.4×10^{-2}

However, in acidic solutions such as 0.1 *M* $HClO_4$, the changes in the spectrum of $Cr(NH_3)_5NO_3^{2+}$ due to aquation took longer to complete than at p*H* 6 or higher, and isosbestic points were not maintained (Fig. 2). Thus, a series of at least two consecutive reactions with comparable rates was involved at p*H* 1, but, because the changes in the spectrum were complex and relatively small (Fig. 2, *cf.* Fig. 1) it was not possible to analyze these changes in terms of rate coefficients.

Position of Bond Cleavage

The ratio *R* of the peak heights for masses 46 and 45, which correspond to $^{12}C^{16}O^{18}O$ and $^{13}C^{16}O_2$, was used as a measure of the ^{18}O content of the $Cr(NH_3)_5OH_2^{3+}$ or $Cr(NH_3)_5OH^{2+}$ produced in the aquation or base hydrolysis of $Cr(NH_3)_5NO_3^{2+}$ in water enriched in $H_2{}^{18}O$, and the percentage Cr—ON bond cleavage (as opposed to CrO—N) was calculated from the formula

$$[3]\quad \%\,\text{Cr—O fission} = \frac{R_{aquo} - R_0}{R_{solvent} - R_0} \times 100$$

where R_0 is the 46:45 mass ratio obtained for CO_2 of natural ^{18}O abundance. For acidic or neutral solutions, the data indicated 95 ± 1% Cr—O fission (mean of 3 determinations), while the corresponding figure for base hydrolysis was 91%. It was not practicable to carry out similar experiments on the tetraammine or lower ammines which were also produced in the aquation reactions.

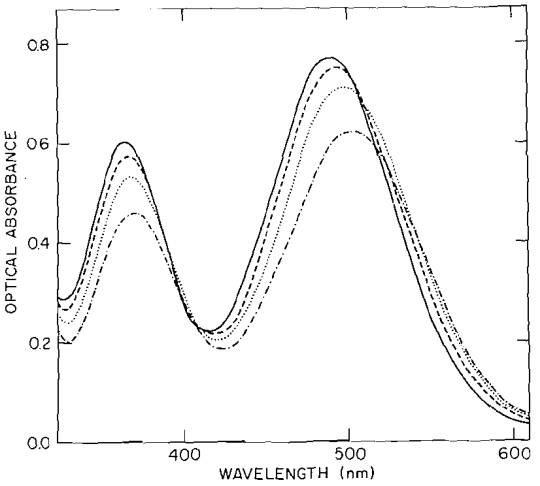

FIG. 2. Spectra of $Cr(NH_3)_5NO_3^{2+}$ undergoing aquation at 25.0° in 0.1 *M* $HClO_4$ (2 cm optical path length; [Cr] = 0.0130 *M*): solid line, zero time; dashes, after 15 min; dots, after 30 min; dots and dashes, after 90 min (final spectrum).

Related Observations

Dry, solid $[Cr(NH_3)_5NO_3](NO_3)_2$ decomposed slowly in the dark, changing color from flesh pink to sepia and developing an unmistakable odor of ammonia in about 3 weeks. By contrast, the comparable halopentaamminechromium(III) nitrates and perchlorates showed no evidence of decomposition after much longer periods, in the absence of light.

When a solution of aquopentaamminechromium(III) perchlorate was added to a sulfite/hydrogen sulfite buffer (p*H* 4) at 21°, an immediate change from orange to rose occurred, and this was followed over the next 4 h by a change to a lilac color. On acidification, $Cr(OH_2)_6^{3+}$ was shown to be present.

Aquopentaamminechromium(III) ion reacted slowly with sulfate in aqueous solution, but we were unable to isolate $Cr(NH_3)_5SO_4^+$ or its salts from these solutions, all products being unidentifiable mixtures. Attempts to prepare pure salts of $Cr(NH_3)_5SO_4^+$ by other means, notably thermal dehydration of solid $[Cr(NH_3)_5OH_2]_2(SO_4)_3$ followed by precipitation from solution with various monovalent anions, were also unsuccessful.

The acceleration of the aquation of aquoamminechromium(III) complexes by nitrate has been reported in detail elsewhere (2).

Discussion

The preceding data for the aquation of $Cr(NH_3)_5NO_3^{2+}$ at p*H* 6 and less are consistent with the following scheme of reactions 4 through 10. The competing initial reactions in 0.1 *M* $HClO_4$ are evidently

$$[4]\quad Cr(NH_3)_5NO_3^{2+} \xrightarrow{k_1} Cr(NH_3)_5OH_2^{3+} + NO_3^-$$

Can. J. Chem. Downloaded from www.nrcresearchpress.com by 210.87.254.5 on 09/05/12
For personal use only.

and

[5] $Cr(NH_3)_5NO_3^{2+} \xrightarrow{k_2(+H^+)}$ *cis*-$Cr(NH_3)_4(OH_2)NO_3^{2+} + NH_4^+$

with 33 ± 2% of the decomposition proceeding via reaction 4. The aquopentammine ion does not aquate detectably under the conditions of these experiments (2), but at high acidities reactions 6 through 8, and possibly 9 and 10, evidently occur at rates comparable to that governed by k_2.

[6] *cis*-$Cr(NH_3)_4(OH_2)NO_3^{2+} \xrightarrow{k_3'}$ *cis*-$Cr(NH_3)_4(OH_2)_2^{3+} + NO_3^-$

[7] *cis*-$Cr(NH_3)_4(OH_2)NO_3^{2+} \xrightarrow{k_4'(+H^+)}$ $Cr(NH_3)_3(OH_2)_2NO_3^{2+} + NH_4^+$

[8] $Cr(NH_3)_3(OH_2)_2NO_3^{2+} \xrightarrow{k_5'}$ $Cr(NH_3)_3(OH_2)_3^{3+} + NO_3^-$

[9] $Cr(NH_3)_3(OH_2)_2NO_3^{2+} \xrightarrow{k_6'(+H^+)}$ $Cr(NH_3)_2(OH_2)_3NO_3^{2+} + NH_4^+$

[10] $Cr(NH_3)_2(OH_2)_3NO_3^{2+} \xrightarrow{k_7'}$ $Cr(NH_3)_2(OH_2)_4^{3+} + NO_3^-$

About 30% of the product of reaction 5 at pH 1 (*i.e.*, 20% of the total of Cr complexes) decomposes via reaction 6. Difficulties in identifying the aquo-triammines and -diammines preclude a quantitative assessment of the relative importances and stereochemistries of reactions 8, 9, and 10, and indeed further reactions leading to the rather inert $Cr(NH_3)(OH_2)_5^{3+}$ (2) may occur to a small extent, but the proportion of complexed nitrate that would survive as far as reaction 9 must in any event be small. Even so, the involvement of several reactions of comparable rates leads to complex spectroscopic changes at low pH.

However, at pH 6, all the aquo-ions of reactions 4 through 10 will be present predominantly as monohydroxo-complexes (conjugate bases of aquo-species), since their pK_a values are typically near 5 (11). It is known (12, 13) that $Cr(OH_2)_4(OH)NO_3^+$ aquates much more rapidly than $Cr(OH_2)_5NO_3^{2+}$, and accordingly the conjugate base reaction corresponding to eq. 6 (rate coefficient now k_3, in the nomenclature of ref. 1) will now be rapid compared to reactions 4 and 5. The path governed by k_3 accounts for only 52% of the product of reaction 5 at pH 6, so that the rate coefficients k_4 and k_5 and possibly k_6 and k_7 (corresponding to the conjugate-base equivalents of reactions 7 through 10) must be of roughly the same order of magnitude as k_3. Reaction 4 is terminal and cannot be influenced by $[H^+]$; consequently, the yield of $Cr(NH_3)_5OH_2^{3+}$ or $Cr(NH_3)_5OH^{2+}$ is the same at pH 1 as at pH 6.

Thus, at pH 6, only the parallel reactions 4 and 5 are rate-determining, so that the overall hydrolysis reaction is cleanly first-order spectrophotometrically with well-defined isosbestic points, and is faster than at high acidities. The rate coefficient k_A is therefore equal to the sum of k_1 and k_2, so that $k_1 = 0.8 \times 10^{-3}$ and $k_2 = 1.6 \times 10^{-3}$ s^{-1} at 25° and ionic strengths up to 0.1 M at least. There is no detectable curvature of a plot of $\ln (k_A/T)$ *vs.* $1/T$, so that ΔH_1^* must be essentially equal to ΔH_2^* and so to ΔH_A^* (20.4 kcal mol^{-1}); if this were exactly so, then $\Delta S_1^* = -4.3$ and $\Delta S_2^* = -2.9$ cal deg^{-1} mol^{-1}, since $\Delta S_A^* = -2.1$ cal deg^{-1} mol^{-1}.

Monacelli (3) investigated the aquation of $Cr(NH_3)_5NO_3^{2+}$ on 0.004–0.025 M $HClO_4$, and reported first-order spectrophotometric rate coefficients which are substantially less than our k_A values. The first-order behavior observed by Monacelli may have been apparent rather than real, since k_3', k_4', and k_5' at least, as well as k_1 and k_2, can be expected to contribute to the control of the observed overall reaction rate at p$H \sim 2$. Indeed, Monacelli remarks that, at the highest acidities, the optical absorption continued to decrease slowly after the apparent first-order reaction had run to completion (3). Thus, there is no irreconcilable difference between Monacelli's observations and ours, and indeed his and our activation parameters for the disappearance of $Cr(NH_3)_5NO_3^{2+}$ are remarkably similar.

In alkaline solutions, the base hydrolysis pathway characterized by the rate-law term $k_{OH}[OH^-]$ competes with reactions 4 and 5. According to the data of Table 3, 66% of the reaction at $[OH^-] = 0.10$ M at 25° goes by the paths controlled by k_1 and k_2, which therefore provide only about 22% $Cr(NH_3)_5OH^{2+}$ in the products; the total yield of $Cr(NH_3)_5OH^{2+}$ was 59%, so that the base hydrolysis pathway must produce $Cr(NH_3)_5OH^{2+}$ exclusively. If this is so, then a similar calculation sets the yield of $Cr(NH_3)_5OH^{2+}$ in 1.0 M alkali at 25° at 88%; indeed, the observed yield was 89%. Thus, it is legitimate to compare k_{OH}, ΔH_{OH}^*, and ΔS_{OH}^* with the corresponding data for the base hydrolyses of other complexes of the type $Cr(NH_3)_5X^{2+}$, and in fact

Can. J. Chem. Downloaded from www.nrcresearchpress.com by 210.87.254.5 on 09/05/12
For personal use only.

the observed values for the nitrato-complex are in the ranges typical of these reactions (7).

The mass spectrometric data obtained for the hydrolyses using ^{18}O-enriched water as solvent show that *at least* 95% of reaction 4 and 91% of the base hydrolysis proceed with Cr—ONO_2 bond breaking. These percentages are lower limits, since any contamination of the ^{18}O-enriched product by compounds containing reactive oxygen atoms of natural isotopic composition would lead to low R values, and we believe that the hydrolyses proceed *exclusively* by Cr—ONO_2, rather than CrO—NO_2, bond breaking. Contamination by nitrate may be responsible for the deviation in the apparent degree of metal–oxygen bond-breaking from 100%, since a similar result was obtained for $Co(NH_3)_5NO_3^{2+}$ (14).

There is no detectable loss of NH_3 from bromo- or iodo-pentamminechromium(III) during aquation, and while some ammonia is formed before the aquation of the chloro-analog is complete, its rate of release certainly does not amount to as much as 10% of the chloride aquation rate (15). Thus, the first-order rate coefficient for ammonia release in typical $Cr(NH_3)_5X^{2+}$ ions at 25° must be considerably less than 1×10^{-6} s^{-1} (15), and the extrapolated value for $Cr(NH_3)_5OH_2^{3+}$ at 25° is only 1.8×10^{-7} s^{-1} (2). Similar values evidently apply for $Cr(NH_3)_5NCS^{2+}$ (16, 17), while for $Cr(NH_3)_5F^{2+}$ ammonia release is mainly from the aquation product rather than the fluoro-complex itself (18). Thus, the *cis*-ammine ligands in $Cr(NH_3)_5NO_3^{2+}$ are several thousand-fold more labile than expected.

The *cis*-activating effect of the nitrato-ligand could conceivably be due to some electronic effect such as π-donation from the nitrato-oxygen atom bound to Cr into the t_{1u} bonding orbitals of the central metal atom, as has been suggested for some similar systems (19). Such an effect might indeed explain why a Cr—N bond in *trans*-$Cr(en)_2F_2^+$ aquates more rapidly than Cr—F (20). However, this effect is not apparent in halo- or thiocyanato-pentaamminechromium(III) ions, nor yet in $Cr(NH_3)_5OH^{2+}$, which is perhaps a fairer analog for the O-bonded $Cr(NH_3)_5NO_3^{2+}$ and for which the rate coefficient for ammonia release can be calculated from the data of Yoneda (21) to be only about 2×10^{-7} s^{-1} in 1 M NaOH at 25°.

A more satisfying explanation is a "mechanical" one, in which the nitrato-ligand expels a ligand *cis* to it in an associative ring-closure movement leading to a transient bidentate species $Cr(NH_3)_4O_2NO^{2+}$, which would then aquate stereospecifically to *cis*-$Cr(NH_3)_4(OH_2)NO_3^{2+}$. The latter species could in turn aquate to *cis*-$Cr(NH_3)_4(OH_2)_2^{3+}$, or repeat the bidentate ring-closure process to give *fac*- and *mer*-$Cr(NH_3)_3(OH_2)_2NO_3^{2+}$, and so on. Conceivably, this could continue until $Cr(H_2O)_6^{3+}$ was produced, but little bound nitrate could remain sufficiently long, and furthermore the lower ammines are markedly more resistant toward ammonia loss than are the penta- and tetra-ammines (2).

Confirmation of this mechanism could come from the isolation of intermediates of the type $Cr(NH_3)_4O_2NO^{2+}$, but such species would be highly strained and so very susceptible to aquation, since the O—O distance in NO_3^- is only 2.11 Å (22), as against the 2.78 Å required for strain-free chelation (23). Indeed, we have been unable even to prepare the monodentate intermediate $Cr(NH_3)_4(OH_2)NO_3^{2+}$ as a pure salt, presumably because of the *cis*-activating properties of NO_3^-, and we are skeptical of earlier claims of success (8).

The transient-chelate mechanism is essentially an *associative* substitution process, *i.e.*, one which occurs with a substantial degree of bond-making in the transition state. This is fully in accordance with our contention (2, 10, 15, 24) that simple substitution processes at Cr(III) centers are normally associative. On the other hand, it is generally believed (25) that the base hydrolyses of metal ammine complexes involve aquation of intermediate amido-species (in the present case, $Cr(NH_3)_4(NH_2)NO_3^+$) which are relatively highly activated toward *dissociative* substitution; significantly, NH_3 activation by NO_3 does *not* occur in the base hydrolysis of $Cr(NH_3)_5NO_3^{2+}$.

The proposed mechanism predicts that any potentially bidentate oxyanion should behave similarly to NO_3^- when coordinated to Cr(III). Carbonate ion is a likely prospect for *cis*-activation, since it is isoelectronic with nitrate and, being dinegative, should be a more effective chelating agent. Indeed, Earley *et al.* (26) have shown that CO_2 acts as a powerful catalyst for the reaction of $Cr(NH_3)_5OH^{2+}$ with $EDTA^{4-}$, and they also suggest the formation of a chelated intermediate involving bidentate CO_3^{2-} to account for this. Similarly, Earley and Alexander (27) report that the decomposition of $Cr(NH_3)_5OH^{2+}$ at pH 4.9 is catalyzed by CO_2, the product being apparently a tetraammine, and they point out

Can. J. Chem. Downloaded from www.nrcresearchpress.com by 210.87.254.5 on 09/05/12
For personal use only.

that, although complexes such as $Co(NH_3)_5CO_3^+$ are well known, attempts to isolate carbonato-complexes of Cr(III) have always been unsuccessful and have usually produced $Cr(OH)_3$. Our inability to isolate $Cr(NH_3)_5SO_4^+$ may be explained in the same way, since Baldwin and Keen (28, 29) have found that the aquo-ligands of $Cr(OH_2)_5SO_4^+$ exchange unusually rapidly with solvent water, a fact which they, too, attribute to transient chelation by the sulfato-ligand.

Phatak *et al.* (30) report that the reaction of hexaaquo-chromium(III) with EDTA is catalyzed by nitrite and sulfite as well as carbonate, in accordance with Carlyle and King's report (31) that $Cr(OH_2)_5OSO_2^+$ reacts even more rapidly in substitution than does $Cr(OH_2)_5OH^{2+}$. Although *S*-bonded sulfite is known to cause *trans*-labilization, at least in cobalt(III) complexes (32), the sulfite ligand in sulfitochromium(III) species is evidently O-bonded, and Carlyle and King (31) showed that activation of Cr(III) complexes by sulfite cannot be exclusively a *trans*-effect; again, *cis*-activation via a transient sulfito-chelate seems likely.

Powerful *cis*-activation by coordinated NO_2^- has been reported by Fee *et al.* (33) for complexes of the type *cis*-$Cr(en)_2X(ONO)^{2+}$, and by Moore and co-workers for various aquo- and ammine-chromium(III) complexes (34–36). Moore and co-workers (34, 35) explain many of their results in terms of a direct attack of bound NO_2^- on the *cis*-ligand X^- itself, with the formation of XNO, but transient bidentate ring closure by NO_2^- is again a more likely reason for the relatively rapid loss of coordinated NH_3 from aqueous $Cr(NH_3)_5ONO^{2+}$ (36).

cis-Activation by coordinated carboxylate ions has been reported for $Cr(NH_3)_5OOCR^{2+}$ (R = CH_3, CH_2Cl, and $CHCl_2$) (37), and recently Olson (38) has attributed the relative rapidity of the reaction of EDTA with complexes of the type $Cr(OH_2)_5OOCR^{2+}$ to nucleophilic activation of the *cis*-aquo ligands by the unbound oxygen of the RCO_2^- ligand, much as we have proposed for nitrato-chromium(III) complexes. Similarly, Sykes and co-workers (39) report that the interconversions of the various aquochromium(III) EDTA complexes seem to involve marked *cis*-labilization by the coordinated carboxylate groups.

In summary, we conclude that an oxyanion coordinated to chromium(III) can cause strong activation of the ligands *cis* to it, apparently by transient chelation. This effect requires some degree of bond-formation between the activating ligand and the metal, at the *cis*-site, and so *cis*-activation is favored for chromium(III), for which associative activation is common (10, 15, 24), but not for typical spin-paired cobalt(III) complexes, since the latter apparently react exclusively by dissociative mechanisms (40, 41).

In practical terms, the occurrence of *cis*-activation by oxyanions coordinated to Cr(III) severely limits the prospects for preparing new mixed-ligand oxyanion complexes of Cr(III) in acceptable purity, and any solid salts of such complexes that might be prepared may be expected to decompose relatively rapidly on storage, as does $[Cr(NH_3)_5NO_3](NO_3)_2$. Furthermore, it is clear that studies of the aqueous physical chemistry of Cr(III) complexes may be carried out using perchlorate media (since ClO_4^- is a very poor complexing agent), but that solutions containing much nitrate or other oxyanions should be avoided; in addition to examples given previously (2) of activation of Cr(III) by oxyanionic supporting electrolytes, we may quote the acid cleavage of $(en)_2Cr(OH)_2Cr(en)_2^{4+}$, which, unlike its Co(III) analog, exhibits strong nitrate-ion catalysis, being some 100 times faster in 1 *M* HNO_3 than in 1 *M* $HClO_4$ (42).

We thank the National Research Council of Canada for financial support.

1. G. GUASTALLA and T. W. SWADDLE. J. Chem. Soc. Chem. Commun. 61 (1973).
2. G. GUASTALLA and T. W. SWADDLE. Inorg. Chem. In press.
3. F. MONACELLI. Ric. Sci. **37**, 781 (1967).
4. M. MORI. Inorg. Synth. **5**, 131 (1957).
5. D. W. HOPPENJANS and J. B. HUNT. Inorg. Chem. **8**, 505 (1969).
6. P. PFEIFFER. Ber. **40**, 3126 (1907).
7. C. S. GARNER and D. A. HOUSE. Transn. Met. Chem. **6**, 59 (1970).
8. A. BENRATH and H. STEINRATH. Z. anorg. allgem. Chem. **194**, 351 (1930).
9. G. W. HAUPT. J. Res. Natl. Bur. Stand. **48**, 414 (1952).
10. T. W. SWADDLE and D. R. STRANKS. J. Am. Chem. Soc. **94**, 8357 (1972).
11. L. G. SILLÉN and A. E. MARTELL. Stability constants of metal–ion complexes. Special Publication No. 17. The Chemical Society, London. 1964. p. 49.
12. T. W. SWADDLE. J. Am. Chem. Soc. **89**, 4338 (1967).
13. M. ARDON and N. SUTIN. Inorg. Chem. **6**, 2268 (1967).
14. W. E. JONES, R. B. JORDAN, and T. W. SWADDLE. Inorg. Chem. **8**, 2504 (1969).
15. G. GUASTALLA and T. W. SWADDLE. Can. J. Chem. **51**, 821 (1973).

16. D. L. GAY and G. C. LALOR. J. Chem. Soc. (A), 1179 (1966).
17. R. D. LINDHOLM, E. ZINATO, and A. W. ADAMSON. J. Phys. Chem. **71**, 3713 (1967).
18. T. P. JONES and J. K. PHILLIPS. J. Chem. Soc. (A), 674 (1968).
19. F. BASOLO and R. G. PEARSON. Mechanisms of inorganic reactions. 2nd ed. J. Wiley and Sons, Inc., New York, N.Y. 1967. p. 173.
20. S. C. PYKE and R. G. LINCK. Inorg. Chem. **10**, 2445 (1971).
21. H. YONEDA. Bull. Chem. Soc. Jap. **31**, 74 (1958).
22. R. L. SASS, R. VIDALE, and J. DONOHUE. Acta Cryst. **10**, 567 (1957).
23. J. E. FINHOLT, R. W. ANDERSON, J. A. FYFE, and K. G. CAULTON. Inorg. Chem. **4**, 43 (1965).
24. L. R. CAREY, W. E. JONES, and T. W. SWADDLE. Inorg. Chem. **10**, 1566 (1971).
25. F. BASOLO and R. G. PEARSON. Mechanisms of inorganic reactions. 2nd ed. J. Wiley and Sons, Inc., New York, N.Y. 1967. pp. 177–193.
26. J. E. EARLEY, D. J. SURD, L. CRONE, and D. QUANE. J. Chem. Soc. Chem. Commun. 1401 (1970).
27. J. E. EARLEY and W. ALEXANDER. J. Am. Chem. Soc. **92**, 2294 (1970).
28. H. W. BALDWIN. Private communication.
29. R. KEEN. Ph.D. Thesis. University of Western Ontario, London, Ontario. 1973.
30. G. M. PHATAK, T. R. BHAT, and J. SHANKAR. J. Inorg. Nucl. Chem. **32**, 1305 (1970).
31. D. W. CARLYLE and E. L. KING. Inorg. Chem. **9**, 2333 (1970).
32. P. H. TEWARI, R. W. GAVER, H. K. WILCOX, and W. K. WILMARTH. Inorg. Chem. **6**, 611 (1967).
33. W. W. FEE, J. N. MAC B. HARROWFIELD, and C. S. GARNER. Inorg. Chem. **10**, 290 (1971).
34. T. C. MATTS and P. MOORE. J. Chem. Soc. (A), 1632 (1971).
35. T. C. MATTS, P. MOORE, D. M. W. OGILVIE, and N. WINTERTON. J. Chem. Soc. Dalton, 992 (1973).
36. T. C. MATTS and P. MOORE. J. Chem. Soc. (A), 219 (1969).
37. E. ZINATO, C. FURLANI, G. LANNA, and P. RICCIERI. Inorg. Chem. **11**, 1746 (1972).
38. M. V. OLSON. Inorg. Chem. **12**, 1416 (1973).
39. R. N. F. THORNELEY, A. G. SYKES, and P. GANS. J. Chem. Soc. (A), 1494 (1971).
40. F. BASOLO and R. G. PEARSON. Mechanisms of inorganic reactions. 2nd ed. J. Wiley and Sons, Inc., New York, N.Y. 1967. pp. 158–177.
41. W. E. JONES, L. R. CAREY, and T. W. SWADDLE. Can. J. Chem. **50**, 2739 (1972).
42. M. M. DE MAINE and J. B. HUNT. Inorg. Chem. **10**, 2106 (1971).

Can. J. Chem. Downloaded from www.nrcresearchpress.com by 210.87.254.5 on 09/05/12
For personal use only.

Chemistry of Transition Metals. IV. Reactions of Alkyl Halides with the Metals of the First Transition Period

ROBERT W. EGAN[1] AND JOHN F. HARROD
Department of Chemistry, McGill University, Montreal, Quebec

Received July 24, 1973

The reactions of 1-chloropropane (**1**) and 1-chloro-2-methylpropane (**2**) with clean, polycrystalline films of the metals Ti through Cu were studied at ambient and elevated temperatures. At ambient temperature all of the metals exhibited a complex pattern of behavior. Titanium was uniquely different from other metals in that no catalytic hydrogenation of product olefin by product hydrogen was observed.

At elevated temperatures the two reactants exhibited the same dichotomy as previously reported for titanium in that **2** was catalytically dehydrochlorinated by all metals, whilst **1** underwent non-catalytic dehydrochlorination. Except in the cases of Ti and Mn, the halide deposited by reaction of **1** with the metal surfaces provided an effective diffusion barrier to further reaction. It is suggested that the rate-controlling step for both Ti and Mn in reactions with **1** is transport of metal atoms from the pure metal into the halide surface layer.

On a étudié à la température ambiante et aux températures élevées les diverses réactions du chloro-1 propane (**1**) et du chloro-1 méthyl-2 propane (**2**) avec des pellicules propres polycristallines de métaux (de Ti jusqu'à Cu). A la température ambiante, on a noté des comportements complexes pour tous les métaux. Dans un seul cas, soit celui du titanium, on n'a pas observé d'hydrogénation catalytique de l'oléfine produite par l'hydrogène produit.

Aux températures élevées, les deux réactifs réagissent avec la même dichotomie, laquelle a été déjà rapportée pour le titanium, à savoir que **2** était déhydrochloré catalytiquement par tous les métaux tandis que **1** subissait une déhydrochloration de façon non-catalytique. Sauf dans les cas du Ti et du Mn, l'halogénure déposé par la réaction de **1** avec les surfaces métalliques constitue une barrière de diffusion effective vis-à-vis des réactions subséquentes. On suggère que l'étape déterminante de la vitesse, dans le cas des réactions de Ti et Mn avec **1** implique le transport des atomes métalliques à partir du métal pur jusqu'à la couche de surface composée d'halogénures. [Traduit par le journal]

Can. J. Chem., **52**, 536 (1974)

Introduction

The earlier papers of this series described the reactions of a variety of simple aliphatic halides with evaporated, polycrystalline films of titanium (1). In all cases, the reactions involved dehydrohalogenation, but the stoichiometries and kinetic patterns differed for different classes of reactant and for different degrees of reaction of the metal surface. Clean titanium metal reacted too rapidly at ambient temperatures with all reactants to permit determination of kinetic parameters. Although all of these reactions resulted in deposition of halogen at the metal surface and liberation of alkene and/or alkane to the gas phase, the reactants behaved quite differently with respect to product composition and to the amount of hydrocarbon retained at the surface. With the exception of fluoride, the deposited halide poisoned the surface against further reaction, at something less than monolayer coverage.

The poisoned surfaces became active again at higher temperatures. Linear alkyl halides underwent continuous non-catalytic dehydrochlorination with deposition of all of the halide and part of the hydrogen at the surface and return of all hydrocarbon fragments to the gas phase as alkene, or alkane. The deposition of halide at higher temperatures did not result in diminished reactivity of the surface (1*a*). When the alkyl halide was branched at the 1- or 2-position, the halided titanium surface became catalytically active for dehydrochlorination, with return of hydrogen halide and alkene to the gas phase (1*b*).

The simplicity and reproducibility of the reactions described above encouraged further investigation of similar reactions on other transition metals. In particular, it was anticipated that the unique capacity of titanium to combine with hydrogen would make its behavior exceptional, at least amongst the metals of the first transition period. The reactants 1-chloropropane and 1-chloro-2-methylpropane were chosen, as representative of the non-catalytic and catalytic

[1]National Research Council of Canada Scholarship holder, 1969–1972.

Can. J. Chem. Downloaded from www.nrcresearchpress.com by 210.87.254.40 on 09/05/12
For personal use only.

Can. J. Chem. Downloaded from www.nrcresearchpress.com by 210.87.254.40 on 09/05/12
For personal use only.

classes of reactant on titanium, and their reactions on evaporated films of all the metals from titanium through copper were studied. The results of this study are reported in the present paper.

Experimental

The experimental techniques for studying reaction rates and products have been described previously (*1a*). Experimental films were all 10^{-5}–10^{-4} cm thick and 200 cm^2 in geometric area. The vacuum manifold used throughout this work had a capacity of 3.2×10^{17} molecules at 0.01 Torr.

The filament wires were all >99.9% pure and were purchased from A. D. Mackay Inc. Titanium, vanadium, iron, cobalt, and nickel were all successfully evaporated from multiple, parallel filaments of the pure metal and, with the exception of vanadium, the background during evaporation was always $< 10^{-9}$ Torr, provided the filaments were outgassed sufficiently. With vanadium, the background during evaporation was always in the range 10^{-8}–10^{-9} Torr during evaporation, even after 4 days of outgassing just below the melting point of the filaments.

Due to unavailability of suitable wires, or lack of suitable physical properties, chromium, manganese, or copper could not be directly evaporated from pure wires. Chromium and manganese were deposited electrolytically, as described by Moore (2), onto 3 in. lengths of 10 mil tungsten wire. About 0.1 g of metal was plated onto the filament. After degassing, chromium was easily evaporated with a background of *ca.* 10^{-9} Torr. Although manganese gave high initial backgrounds (*ca.* 10^{-7} Torr) the pressure quickly dropped to 10^{-9} Torr during evaporation.

Considerable problems were encountered with outgassing of copper. Pure wire filaments cannot be readily evaporated because of the low vapor pressure of copper at its melting point. Tungsten filaments wrapped with high purity copper wire, and plated with copper, were both used and both gave very high backgrounds after melting of the copper (*ca.* 10^{-6} Torr). Background pressure decreased slowly during evaporation.

Results

In the following, we shall use the expression "clean film" to indicate a film which has not been reacted with halocarbon. The mass balance of the reactions will be discussed in terms of "reactant", "product", and "retentively adsorbed" molecules. The first two terms will be applied to gas-phase species and the third is used to describe material lost to the surface in such a way as to reduce the number of molecules in the gas phase.

Although it is difficult to categorize all of the reactions to be described in any clear-cut, or unequivocal fashion, some system may be introduced as follows. Both halocarbons used in this work behave quite similarly on clean films at ambient temperatures and will be considered together. At higher temperatures, 1-chloropropane exhibited a consistent pattern of non-catalytic reactions with all metals, whilst 2-methyl-1-chloropropane gave consistent catalytic dehydrochlorination on each metal. Therefore, the two reactants will be treated separately for high temperature reactions.

Reactions on Clean Films at Ambient Temperature

Experiments on clean films were conducted as a consecutive sequence of reactions at 0.01 Torr initial pressure. After completion of each reaction the system was pumped to less than 10^{-6} Torr before addition of the next aliquot of reactant. The pattern of observed behavior was qualitatively similar for all metals and reactants and consisted of the following sequence of events: (*a*) A period of high retentive adsorption occurring rapidly, with products, if any, completely saturated, or even cracked. (*b*) A decline in the extent and rate of retention, accompanied by appearance of increasing amounts of alkene in the gas-phase products. (*c*) A period of isobaric dehydrochlorination to produce an alkene rich mixture of alkene and alkane. During this period, concurrent hydrogenation of alkene was generally observed, both before and after completion of dehydrohalogenation. (*d*) Declining reactivity, both with regard to rate and extent of reaction, until no further reaction could be observed. For a given metal, the number of molecules of 1-chloro-2-methylpropane reacted before complete deactivation of the surface was always considerably greater than that for 1-chloropropane. In general the number of doses of reactant required to complete the range of behavior described in (*a*)-(*d*) diminished on passing across the period from vanadium to copper. Titanium was anomalous with respect to the latter trend, reacting very much less than vanadium before complete loss of activity (see Table 2).

Vanadium

The results of a consecutive sequence of reactions of 1-chloro-2-methylpropane on vanadium are summarized in Table 1. The first six reactions were too rapid to follow by either the initial pressure drop due to retentive adsorption, or the appearance of hydrocarbon products resulting from dehydrochlorination. It was, however, possible to follow the slower hydrogenation of isobutene to isobutane which continued after the initial rapid reactions. The

TABLE 1. Initial reactions of 1-chloro-2-methylpropane with vanadium

Reaction No.	Initial pressure $\times 10^2$ Torr	Film temperature (°C)	% Retentively adsorbed	Product*
1	1.1	0	100	None
2	0.6	0	90	Trace MP† and CH_4
3	0.9	0	90	Trace MP and CH_4
4	1.1	0	80	87
5	1.0	0	80	65
6	1.0	0	80	64
7	1.0	0	80	38
8	0.5	0	30	—
9	0.4	0	30	—
10	1.1	0	95	38
11	1.0	30	70	39
12	1.0	73	40	28
13	1.1	73	25	17
14	1.1	30	60	—
15	1.1	71	25	10

*Percent methylpropane in mixture of methylpropane/methylpropene.
†Methylpropane.

TABLE 2. Some properties of reactions of alkyl halides with clean metals*

Metal/reactant	Initial P/O†	$\left[\frac{d(P/O)}{dt}\right]_D$‡	$\left[\frac{d(P/O)}{dt}\right]_H$§	Amount retentively‖ adsorbed mol $\times 10^{-17}$
Ti/C_4H_9Cl	0.68	—	—	0.5
V/C_3H_7Cl	0.60	2.9	1.7	13
V/C_4H_9Cl	—	—	—	32
Cr/C_3H_7Cl	—	—	—	1.6
Cr/C_4H_9Cl	0.67	5.9	3.4	5.8
Mn/C_4H_9Cl	—	—	—	0.4
Fe/C_3H_7Cl	—	—	—	0.5
Fe/C_4H_9Cl	—	—	—	3.2
Co/C_3H_7Cl	—	—	—	0
Co/C_4H_9Cl	—	—	—	0.9
Ni/C_3H_7Cl	—	—	—	0
Ni/C_4H_9Cl	—	—	—	0.7
Cu/C_3H_7Cl	—	—	—	0

*The paraffin:olefin numbers were obtained for the first reaction of a sequence in which olefin was observed as a product.
†Paraffin:olefin ratio.
‡Before completion of dehydrochlorination.
§After completion of dehydrochlorination.
‖Up to the point where the surface became completely inactive.

results for the hydrogenation following reactions 5 and 6 are shown in Fig. 1. Although reasonably straight lines were obtained with first order plots, little significance can be attached to this since the reactions were only followed to 20% conversion. On the other hand, it is clear that the activity of the film for hydrogenation declined considerably from run 5 to run 6.

Reactions 1 through 9 were carried out with only a short period between the end of one reaction and the beginning of the next (*ca.* 30 min). After reaction 9, the film was left for 3 h and in reaction 10 showed a considerably increased capacity for retentive adsorption. Reactions 10 through 15 were carried out with a short recovery time between runs (*ca.* 30 min) to establish the effects of temperature. Higher temperature diminished the amount of material retentively adsorbed, but temporarily regenerated the dehydrochlorination activity of the film.

1-Chloropropane behaved very similarly to 1-chloro-2-methylpropane. Less than half the number of molecules were adsorbed, or reacted, and the rate of dehydrochlorination in the later stages was slow enough to follow. Such a reaction was followed kinetically and gave apparent first

Can. J. Chem. Downloaded from www.nrcresearchpress.com by 210.87.254.40 on 09/05/12
For personal use only.

Can. J. Chem. Downloaded from www.nrcresearchpress.com by 210.87.254.40 on 09/05/12
For personal use only.

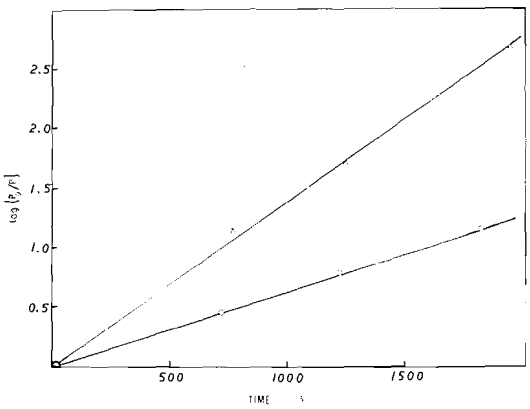

FIG. 1. Disappearance of methylpropene with time following completion of reactions of 1-chloro-2-methylpropane on vanadium at 0 °C. Initial pressure of methylpropene (P_0): △, 4.5×10^{-4} Torr (dose 5, Table 1); ○, 4.6×10^{-4} Torr (dose 6, Table 1).

order kinetics for the disappearance of reactant. This behavior was probably due to a superposition of a solid state diffusion controlled process on a surface dehydrochlorination with an order less than unity, as discussed below. Hydrogenation of product propene to propane was also observed subsequent to completion of dehydrochlorination. A graphical representation of the change in propene to propane ratio during and subsequent to dehydrochlorination is shown in Fig. 2. The sharp break in slope at complete reaction suggests that the changing ratio is due

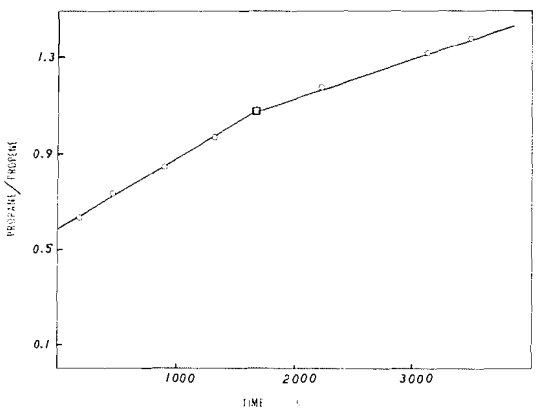

FIG. 2. Variation of paraffin:olefin ratio during and following a reaction of 1-chloropropane on vanadium at 0 °C: $P_0(C_3H_7Cl) = 0.01$ Torr; □, point at which dehydrochlorination was complete. The reaction depicted was the fourth dose in a sequence; the first three doses (0.01 Torr) reacted too rapidly to follow and gave only propane as product.

to two different processes, one of which is dependent on the presence of unreacted alkyl halide. This behavior was common to all of the hydrogenation reactions observed.

The Metals Chromium to Copper

Most of the features described for vanadium were common to all of the metals of the first transition period except titanium, at least qualitatively. The most important properties of reactions at ambient temperature are summarized in Table 2.

Reactions of 1-Chloropropane at Elevated Temperatures

Vanadium

When no further reaction of 1-chloropropane occurred on vanadium at ambient temperature, the film temperature was raised to *ca.* 150° and dehydrochlorination activity was again observed. At elevated temperature one mole of propene was produced per mole of 1-chloropropane reacted. Hydrogen was also released to the gas phase from the film at the same rate prior to, and subsequent to, completion of a given dehydrochlorination. Loss of reactivity occurred with each reaction, but the loss of reactivity could be offset by raising the temperature.

A series of five sequential reactions of *ca.* 1.3×10^{-3} Torr 1-chloropropane was studied at 230°. The initial slopes of the pressure/time plots, Fig. 3, were determined by an analytical curve-fitting procedure. Each reaction was carried to completion and a new reaction cycle was started as quickly as possible to minimize film recovery. A plot of the initial rates against

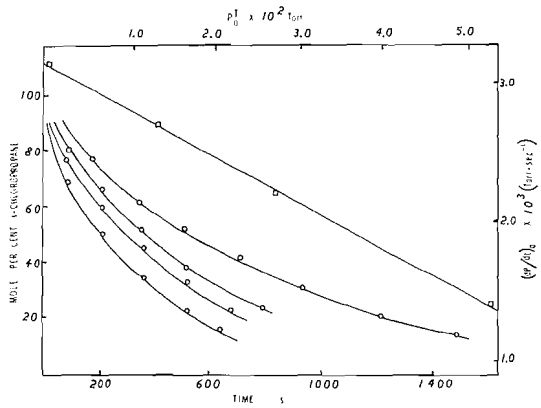

FIG. 3. ○, disappearance of 1-chloropropane with time on vanadium at 230° ($P_0 = 0.013$ Torr) for four consecutive doses; □, change in initial rate of reaction with total pressure reacted (P_0^T).

the total amount of 1-chloropropane reacted prior to the start of each run gave a straight line, Fig. 3, fitting the equation:

$$[1] \qquad -\left(\frac{dP}{dt}\right)_0 = 0.0031 - 0.033P_0{}^T$$

where $-(dP/dt)_0$ is the initial rate and $P_0{}^T$ is the total pressure of 1-chloropropane reacted. Although the film had already been reacted with 1.3×10^{-3} Torr of 1-chloropropane prior to this series of runs, the beginning of the series is chosen in Fig. 3 as an arbitrary zero of surface halide concentration. Inclusion of the additional halide would introduce a constant term to eq. 1.

First order plots of the data in Fig. 3 gave good straight lines. This apparent first order behavior was due to a superposition of the poisoning effect, expressed by eq. 1, upon a reactant concentration order of less than one. This behavior can be described by the expression

$$[2] \qquad -\left(\frac{dP}{dt}\right)_t = kP^n(0.0031 - 0.033P^T)$$

where $-(dP/dt)_t$ is the rate at time t, k is a constant, n is the reactant concentration order, and $P^T = P_0{}^T + (P_0 - P_t)$. P_0 is the initial reactant pressure for a given run and P_t is the pressure at time t. Insertion of $n = \frac{1}{2}$ and integration yields [3]

$$[3] \qquad t = \frac{2}{\alpha\beta^{1/2}}\{\tan^{-1}[(\beta/\alpha)^{1/2}P_0{}^{1/2}] - \tan^{-1}[(\beta/\alpha)^{1/2}P^{1/2}]\}$$

where $\alpha = k[0.0031 - 0.033(P_0{}^T + P_0)]$ and $\beta = 0.033k$. Plots of the right-hand side of [3] against time for the first and last runs of Fig. 3 are shown in Fig. 4. The linearity of these plots suggests that the true order of the surface reaction is 0.5. Similar treatments of the data for $n = 0.4$ and 0.6 show slight curvature. The 30% increase in slope between the first and fifth reactions may be due to a fundamental inadequacy of the model, but is more likely to be due to discrepancies between the poisoning rate as determined from initial reaction rates at constant pressure (eq. 1) and the poisoning rate in the dynamic, reacting system. The expression [3] also ignores film recovery between runs, which may not be entirely negligible. The non-zero intercepts in Fig. 4 are an artefact arising from the time lags between readings on the several mass-spectrometric peaks needed for analysis of reactant and products.

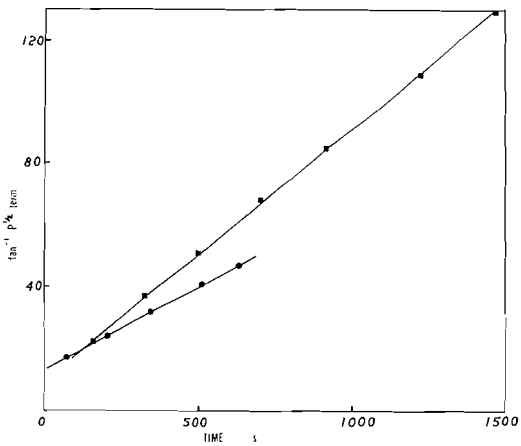

FIG. 4. Disappearance of 1-chloropropane on vanadium plotted as a combined half-order and surface poisoning limited reaction: $T = 230°$, $P_0 = 0.014$ Torr; ●, first reaction of Fig. 3. ■, fourth reaction of Fig. 3.

Although hydrogenation of product olefin was observed on vanadium during and following reaction with the first few aliquots of 1-chloropropane at ambient temperature, the hydrogenation activity was no longer evident at elevated temperature.

Chromium

When no further reaction was observed on chromium at ambient temperature, the film temperature was increased to 138°, liberating considerable amounts of hydrogen. Reaction of a 1.7×10^{-2} Torr aliquot of 1-chloropropane on this film gave complete dehydrochlorination in 380 s, yielding an equivalent amount of propene and a small amount of hydrogen. Subsequent to the completion of dehydrochlorination, the propene underwent slow hydrogenation to propane (half-life 5000 s) by a reaction that appeared to be first order in propene. A second aliquot of reactant also underwent rapid dehydrochlorination to an equivalent amount of propene and a small amount of hydrogen. No hydrogenation activity was observed after this reaction.

Further reactions were studied at 160° and 190°, and these consistently yielded *ca.* 70% propene and 30% hydrogen, according to [4].

$$[4] \qquad 2CH_3CH_2CH_2Cl + 2^* \rightarrow 2CH_3CH{=}CH_2 + H_2 + 2Cl^*$$

* is a reactive surface site.

Five consecutive reactions were followed to completion ($P_0 = 3 \times 10^{-3}$ Torr) at 180°. The

Can. J. Chem. Downloaded from www.nrcresearchpress.com by 210.87.254.40 on 09/05/12
For personal use only.

Can. J. Chem. Downloaded from www.nrcresearchpress.com by 210.87.254.40 on 09/05/12
For personal use only.

reactant disappeared by apparent first order kinetics within each experiment, but the initial rate fell by about 50% over the five runs. Thus the true concentration order was certainly less than one and may well have approached one-half, as observed with titanium, vanadium, and manganese.

Manganese

Six consecutive reactions at 0.01 Torr and 160° on a previously reacted surface caused no detectable decrease in the rate of dehydrochlorination of 1-chloropropane. A further reaction of 0.05 Torr did give a slight reduction in activity. The products were consistently an equivalent amount of propene and a lesser amount of hydrogen than required by eq. 4. Continued evolution of hydrogen during and between reactions made exact measurement of the amount arising from each dehydrochlorination sequence impossible.

The results of a sequence of six runs to completion at 0.01 Torr, at a series of temperatures between 160° and 200°, are summarized in Fig. 5. In these reactions 1-chloropropane disappeared according to a half-order rate law and an activation energy of 17.2 ± 0.6 kcal/mol was obtained from the Arrhenius plot in Fig. 6. The first and last runs in the temperature cycle were run at essentially the same temperature and showed negligible change in activity of the film.

No hydrogenation was observed in the above reactions either before or after completion of dehydrochlorination.

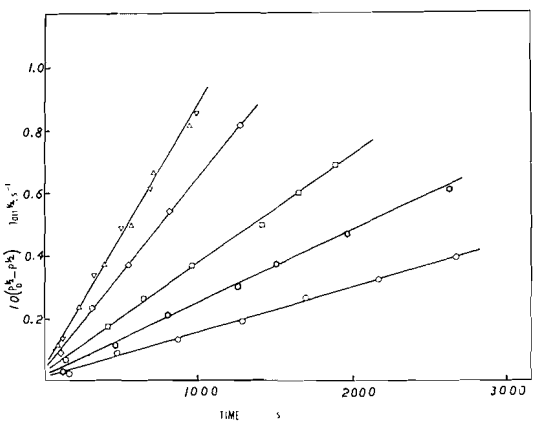

FIG. 5. Reaction of 1-chloropropane on manganese plotted as a half-order reaction: P_0 = 0.01 Torr; ○, 158°; ⬡, 169°; □, 177°; ◇, 189°; ▽, 198°; △, 200°. The last two runs were the first and last of the temperature scan.

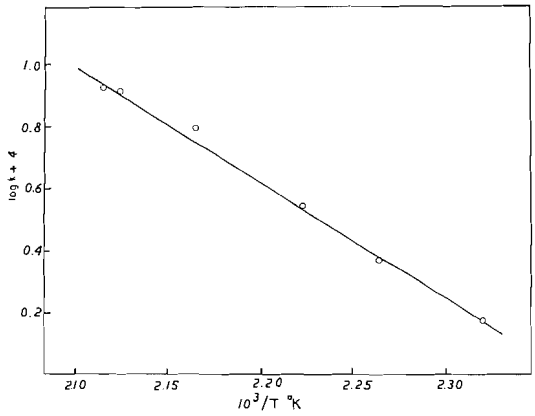

FIG. 6. Arrhenius plot of data from Fig. 5. k = slope of half-order plot.

Iron, Cobalt, and Nickel

High temperature reactions of 1-chloropropane with previously reacted iron, cobalt, and nickel were all characterized by rapid surface poisoning. Successive reactions were conducted at progressively higher temperatures betweeen 60 and 230°, until the metals became completely inactive. The gaseous products were consistently propene and hydrogen and all of the chloride was left at the surface. Each temperature rise induced hydrogen evolution from the surface. The poisoning rate was too rapid to allow measurement of meaningful kinetics with the experimental technique being used.

In each case the total pressure of 1-chloropropane reacted, by the time the surface became completely inactive at 230°, was *ca.* 0.05 Torr.

Reactions of 1-Chloro-2-methylpropane at Elevated Temperatures

At high temperature all of the reacted metal surfaces examined in this study became catalytically active for dehydrochlorination of 1-chloro-2-methylpropane to equimolar gaseous hydrogen chloride and 2-methylpropene. Between the initial low temperature reactions and the onset of catalytic behavior, the reactions passed through an intermediate phase of non-catalytic dehydrochlorination, very similar in character to the behavior of 1-chloropropane. During this intermediate phase, no hydrogen chloride was detected and the products were 2-methylpropene and progressively decreasing amounts of 2-methylpropane and hydrogen. The characteristic number of reactant molecules reacted during this period, the end of which was signalled by

TABLE 3. Summary of kinetic parameters for catalytic dehydrochlorination of 2-methyl-1-chloropropane

Metal	Temperature range (°C)	Initial pressure $\times 10^2$ Torr	E_a (kcal/mol)	log A*
Ti	160–210	1.0	12.6±0.3	2.4
Ti	140–180	5.0	15.5±0.5	4.1
V	180–220	1.0	8.1±0.3	1.1
Cr	150–200	1.0	6.6±0.2	0.3
Mn	175–235	1.0	2.9±0.2	−1.6
Mn	175–225	5.0	3.5±0.2	−1.4
Fe	210–240	1.0	6.2±0.4	−0.1
Co	200–245	1.0	8.3±0.4	1.5
Ni	190–240	1.0	7.6±0.4	0.3

*The apparent Arrhenius pre-exponential factor.

the appearance of hydrogen chloride in the gas phase, varied approximately in the sequence: Ti(50), V(15), Cr(15), Mn(25), Fe(6), Co(10), Ni(10). (Numbers are units of 10^{17} mol.) Since the walls of the vacuum manifold scavenge the initial product HCl, little quantitative significance can be attached to the latter figures, beyond the fact that titanium and manganese consistently required more reaction to achieve catalytic activity. The complexity of the rates and stoichiometries of reactions in this period precluded any attempt at detailed kinetic analysis.

At the conclusion of the intermediate phase described above, all reacted metal surfaces studied became consistently catalytically active, effecting dehydrochlorination according to a first order rate law up to conversions greater than 90%. Reaction temperatures could be cycled over at least a range of 50° without change in the activity of the surface. Some typical rate curves are shown in Fig. 7 and the activation parameters for all of the metals are summarized in Table 3.

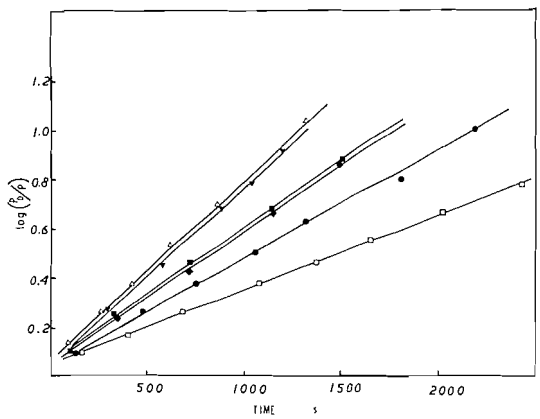

FIG. 7. Disappearance of 1-chloro-2-methylpropane on chromium plotted as a first-order reaction: □, 150°; ●, 171°; ■, ◆, 183°; △, ▼, 198°. $P_0 = 0.01$ Torr. Duplicate runs were performed on a rising temperature sweep after completion of the four runs on a downward temperature sweep.

Discussion

Reactions at Ambient Temperature

The reactions of alkyl halides with metals of the first transition period, although exhibiting consistent general features, are evidently very complicated. The early phases of the reaction, characterized by high rates of reaction, high levels of retention of organic radicals at the surface and traces of cracking as well as dehydrochlorination and disproportionation products, are probably representative of the reactivity of the unoxidized metal. This reactivity rapidly gives way to a second phase, characterized by fairly clean dehydrochlorination, little retention of organic radicals and, in some cases, catalytic hydrogenation of product alkene by product hydrogen. The latter catalytic activity is the most characteristic symptom of this intermediate phase, and the activity appeared to be constant in the absence of alkyl halide, but diminished with increasing contamination of the surface by halide. In view of the fact that higher temperatures renewed dehydrochlorination activity but not hydrogenation activity, it seems that hydrogenation and dehydrochlorination are characteristic of different surface species.

Can. J. Chem. Downloaded from www.nrcresearchpress.com by 210.87.254.40 on 09/05/12
For personal use only.

Can. J. Chem. Downloaded from www.nrcresearchpress.com by 210.87.254.40 on 09/05/12
For personal use only.

Although no quantitative analysis of the poisoning effect of halide deposited at the surface was undertaken at low temperature, it is most likely, in view of observations at high temperature discussed below, that the decline in rate was due to the build-up of a barrier against diffusion between the pure metal interface and the surface.

The behavior of titanium was notably different from the other metals, both at ambient and elevated temperatures, in that no gaseous hydrogen was ever liberated from the former and no catalytic hydrogenation was ever observed. Such behavior is consistent with the exceptional solubility of hydrogen in titanium if it is assumed that hydrogen, once incorporated into the bulk phase, is no longer available for either hydrogenation of alkene, or for desorption. In the cases of the other metals, hydrogen appeared to be readily available for release to the gas phase on heating the films. This hydrogen may have been present as weakly bound atomic hydrogen, or alternatively may have come from stripping of hydrocarbon radicals retentively adsorbed at the surface.

Reactions of 1-Chloropropene at Elevated Temperatures

Titanium and manganese behaved very similarly towards 1-chloropropene at high temperature, in that the deposited halide did not significantly impair the rate of transport of reactive intermediates between the surface of the bulk metal and the gas–solid interface. In a previous discussion (1*a*) this behavior was attributed, in the case of titanium, to the coincidence of a low lattice energy for the metal hydride/halide phase at the interface and a high sublimation energy for the metal. Thus, rate control was assumed to be due to migration of metal atoms out of the bulk metal surface into the hydride/halide phase and not to transport across the latter phase.

It is interesting to note that the lattice energies for the dichlorides of the metals from titanium to copper follow the sequence (3):

$$TiCl_2 < MnCl_2 < VCl_2 < CrCl_2 < FeCl_2 < CoCl_2 < NiCl_2 < CuCl_2$$

It can also be shown from thermodynamics that the most stable halide in equilibrium with the metal is the dihalide for all of the metals from titanium to copper.[2] Furthermore, all of these dihalides have essentially the same structure (either $CdCl_2$, or CdI_2 structure) (5). It is tempting, therefore to conclude that, although all of these metals react with 1-chloropropene by a common set of processes, a change from rate control by transfer of metal atoms from the bulk to rate control by diffusion across the halide occurs when the halide lattice energy becomes too high. That this comfortingly straightforward picture is probably a gross oversimplification is suggested by the fact that the heats of sublimation of Ti and Mn differ by the very substantial amount of 40 kcal per g atom (6), whilst the lattice energies of their dichlorides differ by only 10 kcal per mol.

The involvement of lattice energy in the rate-controlling process is also suggested by the greater reactivity of vanadium and chromium, relative to the metals beyond manganese. Although the linear decay law (eq. 1) observed with vanadium is different from others reported for thin film oxidation, or tarnishing, reactions (7), there is little doubt that the decay in reactivity is a diffusion phenomenon. The dramatic decline in reactivity beyond manganese is also in line with the steep rise in lattice energy for the dihalides.

Further speculation as to details of mechanism is not justified on the basis of the data obtained in this rather crude survey of behavior. It is already evident nonetheless that factors influencing corrosion by alkyl halides may well vary systematically with the known macroscopic physical properties of the reactant metal and the product surface layer.

Catalytic Dehydrochlorination of 1-Methyl-2-chloropropane

The surface catalyzed dehydrohalogenation of haloalkanes is a well-established and general phenomenon. In fact the ubiquitous catalytic

[2]Since the structures of the metals and the halides are very similar across the first transition period, it may be assumed that entropy differences are small and free energies of reaction follow enthalpy changes. Using published heats of formation (4), the heats of reaction for

$$nMCl_{(n+1)} + M \rightarrow (n+1)MCl_n$$

were calculated for $n = 1$ and 2 for several of the metals Ti to Cu. In each case the reaction for $n = 2$ was exothermic (Ti, −12 kcal/mol; V, −50 kcal/mol; Cr, −12 kcal/mol; Fe, −49 kcal/mol).

Can. J. Chem. Downloaded from www.nrcresearchpress.com by 210.87.254.40 on 09/05/12
For personal use only.

activity of surfaces is one of the major experimental problems in the study of such reactions homogeneously in the gas phase (8).

Schwab and Noller (9) and Noller and Ostermeier (10) studied the dehydrochlorination of alkyl chlorides on alkali metal halides. For these reactions, activation energies ranged from 8 kcal per mol (2-chloro-2-methylpropane on RbCl at 100°) to 53 kcal per mol (chloroethane on KCl at 400°). On the basis of such results, Noller suggested a relationship between lattice spacing in the crystal and the activation energy for the reaction (10). It was also proposed that effective catalysis required a good geometrical fit of the haloalkane to the active surface sites to facilitate a heterolytic cleavage of the C—Cl and C—H bonds. The mechanism proposed by Noller closely resembles the quasi-heterolytic model proposed by Maccoll and Thomas for homogeneous gas phase dehydrohalogenation (11). Swinbourne studied dehydrochlorination of cyclohexylchloride on the alkali chlorides and found activation energies of 11, 13, 17, and 25 kcal per mol for LiCl, NaCl, KCl, and RbCl (12).

Noller and Ostermeier studied reactions of a wide range of alkyl chlorides on transition metal oxides, nitrides, and carbides (13). Again, the activation energies ranged from a low of 11 kcal per mol (2-chloro-2-methylpropane on TaC) to a high of 50 kcal per mol (1-chloropropane on Ta_2O_5). The same mechanism as for the alkali chlorides was suggested, with the surface acting to facilitate heterolytic carbon–halogen bond breaking.

The results of the present study certainly are too complicated to be explained by any simple, one parameter model. In the series of halided metals Ti through Ni, the two outstanding features are the exceptionally high activation energy for titanium catalyzed dehydrochlorination of 1-chloro-2-methylpropane and the exceptionally low value for the corresponding manganese reaction. Although minor variations were observed between the activation energies for the remaining metals, these variations could not be taken as significant, and all of the values were roughly half-way between the extremes of the values for Ti and Mn.

The variable features of the surfaces that would most likely affect a heterolytic bond cleavage are the electron affinity of the metal ion and the internuclear separation between metal ion and chloride nuclei. Whatever the oxidation states involved (both thermodynamics and chemical intuition suggest a maximum of +2), titanium would have the lowest electron affinity and the largest interionic separation, so the extreme high value of the activation energy for the reaction on titanium can be rationalized. On the other hand, no such simple rationalization of the uniquely low energy of activation for manganese may be proposed. If the validity of the Noller geometric theory is accepted for the present reactions, the best that one can conclude is that the unusual position of manganese is a fortuitous optimum of interionic separation and electron affinity. It may be argued that, although the electron affinities of Cr^{II}, Fe^{II}, Co^{II}, and Ni^{II} are greater than that of Mn^{II}, there is a poorer geometric fit of the reactant to the surface lattice.

Although crystal field stabilization energy (CFSE) effects, due to changing coordination number of surface and metal atoms during reaction, are likely to be important, calculation of changes of CFSE between several pairs of reasonable geometries (14) showed no correlation with the sequence of activation energies.

The catalytic dehydrochlorination of branched alkyl chlorides on titanium was previously discussed in terms of a surface assisted, concerted *cis*-elimination (1*b*). In addition to the usual adsorption energy effects, it was proposed that the process of adsorption may reduce the energy barrier arising from the symmetry forbiddeness of the *cis*-elimination. The present experimental data do not permit an evaluation of the relative importance of geometric factors, symmetry factors, and electronic factors in the overall mechanism.

In conclusion, attention is drawn to the strong correlation between apparent activation energy and apparent frequency factor for all of the catalytic reactions studied so far. The apparent frequency factors contain undetermined variations in geometric surface area, roughness factor, and numbers of active surface sites, but these uncertainties do not exceed one order of magnitude. The linear correlation is shown in Fig. 8. Such linear correlations are not uncommon for reactions performed on a series of similar surfaces (15).

Conclusions

The non-catalytic reaction appears to depend on solid state transport of reducing species to, or oxidizing species from, the gas–solid interface.

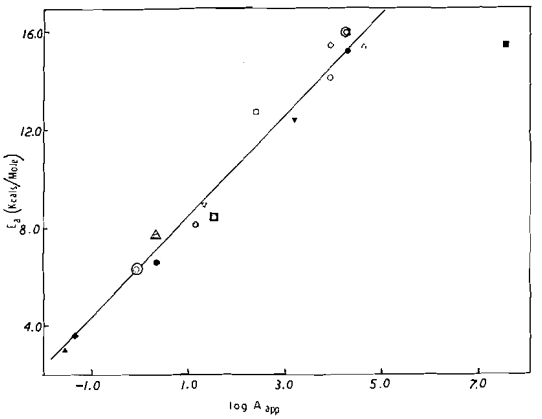

FIG. 8. Correlation between E_a and log A_{app} for catalytic dehydrochlorination of alkyl chlorides on transition metals: ▽, Ti (P_0 = 0.01 Torr); ▼, Ti (P_0 = 0.05 Torr); △, Ti (P_0 = 0.25 Torr). Latter three points for 2-chloropropane. ◇, Ti (P_0 = 0.01 Torr, 1-chloro-2-methylpropane); ◎, Ti (P_0 = 0.05 Torr, 1-chloro-2-methylpropane); ■, Ti (P_0 = 0.03 Torr, 2-chloro-2-methylpropane); ○, Ti (0.01 Torr, 1-chloro-2,2-dimethylpropane); ●, Ti (0.025 Torr, 1-chloro-2,2-dimethylpropane). Remaining points all for 2-chloro-2-methylpropane, 0.01 Torr except where otherwise noted. ⬡, V; ⬢, Cr; ▲, Mn; ◆, Mn (0.05 Torr); ◎, Fe; ⊡, Co; ⧋, Ni.

The transport processes are sufficiently facile in the cases of titanium and manganese to permit extensive reaction without diminution in rate. In all other cases studied, the slow diffusion of species through the surface product layer rapidly reduced the reaction rate to zero.

The catalytic reaction, always observed with 2-methyl-1-chloropropane, does not depend on solid state transport in the surface layers. Previous observations on the reactions of primary, secondary, and tertiary alkyl halides on titanium suggested that a low pre-exponential Arrhenius factor probably precluded the catalytic pathway for 1-chloropropane.

The presently available evidence does not permit any precise evaluation of the mechanism of the catalytic reactions.

Financial support for this work from the National Research Council of Canada is gratefully acknowledged.

1. J. F. HARROD and W. R. SUMMERS. (*a*) J. Am. Chem. Soc. **93**, 5051 (1971); (*b*) Can. J. Chem. **50**, 2167 (1972); (*c*) J. Oxid. Metals. **6**, 117 (1973).
2. A. S. MOORE. J. Sci. Inst. **22**, 101 (1945).
3. P. GEORGE and D. S. MCCLURE. Progress in inorganic chemistry. Vol. I. *Edited by* F. A. Cotton. Interscience Publishers, Inc., New York. 1959. p. 381.
4. F. P. ROSSINI, D. D. WAGMAN, W. H. EVANS, S. LEVINE, and I. JAFFE. Selected values of chemical thermodynamic properties. National Bureau of Standards. Circular No. 500.
5. R. W. G. WYCKOFF. Crystal structures. 2nd ed. Interscience Publishers, Inc., New York. 1963.
6. J. S. GRIFFITH. J. Inorg. Nucl. Chem. **3**, 15 (1956).
7. I. M. RITCHIE. Chemisorption and reactions on metallic films. Vol. II. *Edited by* J. R. Anderson. Academic Press, London and New York. 1971. p. 272.
8. D. V. BANTHORPE. Elimination reactions. Elsevier Publishing Co., Amsterdam. 1963. Chapt. 7.
9. G. M. SCHWAB and H. NOLLER. Z. Electrochem. **58**, 762 (1954).
10. H. NOLLER and K. OSTERMEIER. Z. Electrochem. **60**, 921 (1956).
11. A. MACCOLL and P. J. THOMAS. Nature, **176**, 392 (1955).
12. A. MACCOLL. *In* The chemistry of alkenes. *Edited by* S. Patai. Interscience Publishers, Inc., New York. 1964. Chapt. 3.
13. H. NOLLER and K. OSTERMEIER. Z. Electrochem. **63**, 191 (1959).
14. R. G. PEARSON. *In* Some aspects of crystal field theory. *Edited by* T. M. Dunn, D. S. McClure, and R. G. Pearson. Harper and Row, New York. 1965. p. 106.
15. J. S. CAMPBELL and P. H. EMMETT. J. Catal. **7**, 252 (1967).

Can. J. Chem. Downloaded from www.nrcresearchpress.com by 210.87.254.40 on 09/05/12
For personal use only.

An *Ab Initio* Study of the Effect of Substituents on Protonation of the Carbonyl Group

A. C. HOPKINSON
Department of Chemistry, York University, Downsview, Ontario M3J 1P3
AND
I. G. CSIZMADIA
Department of Chemistry, University of Toronto, Toronto 5, Ontario M5S 1A1

Received September 18, 1973

Ab initio calculations have been performed on a series of molecules HCOX, where X = CH_3, NH_2, OH, F, H, and also on the corresponding oxygen protonated cations. Rotational studies show the incoming proton to be *trans* to the substituent X except in formyl fluoride, where internal hydrogen bonding stabilizes the *cis* isomer. The geometries of the fluoro- and amino-substituted cations have been optimized along with that of oxygen protonated ketene. Proton affinities are found to be very dependent on substituents with the order of basicity being amide > carboxylic acid > acid fluoride ≃ acetaldehyde > ketene > formaldehyde, an order which closely follows the negative charge on the oxygen. Plots of the computed charge on the carbon atoms against the core binding energy are different for the cations and neutral compounds but can be made to fall on the same line by correcting the binding energy using "the charge potential model" for the K-shell electron which is removed.

Des calculs *ab initio* ont été effectués sur une série de molécules HCOX, où X = CH_3, NH_2, OH, F, H et aussi sur les cations correspondants où l'oxygène est protoné. Des études de rotation montrent que ce proton supplémentaire du cation est en position *trans* par rapport au substituent X excepté dans le fluorure de formyle où des liaisons hydrogènes internes stabilisent l'isomère *cis*. Les géométries des cations avec le fluor et l'amine ont été optimisées ainsi que celle du cétène protoné à l'oxygène. On a trouvé que les affinités pour le proton dépendent beaucoup des substituents et sont dans l'ordre de basicité amide > acide carboxylique > fluorure d'acide ≃ acétaldéhyde > cétène > formaldéhyde, ordre qui suit étroitement la charge négative sur l'oxygène. Les variations de la charge calculée sur les atomes de carbones en fonction de l'énergie de liaison de coeur sont différentes pour les cations et les composés neutres mais peuvent être rendues similaires en corrigeant l'énergie de liaison par le "modèle de charge potentielle" pour l'électron de la couche K qui est enlevé.

[Traduit par le journal]

Can. J. Chem., **52**, 546 (1974)

Protonated weak bases are important as intermediates in acid catalyzed hydrolysis reactions and also as indicators in the construction of acidity functions. Many such cations can be formed quantitatively in "magic acid" solutions and the most stable tautomers and rotational isomers (1–8), and the magnitude of rotational barriers (about the carbon–oxygen bond) have been deduced from low temperature n.m.r. measurements.

Several classes of weak bases contain a carbonyl group and vary markedly in basicity depending upon the substituent X. Amides

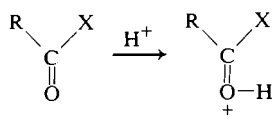

1 2

(X = NH_2) are the most basic carbonyl-containing compounds in solution and have been used to form an acidity function (9, 10). The generally recognised order of basicity in solution is amides > ketones > aldehydes > carboxylic acids > acid chlorides. For example, the pK_{BH^+} of benzamide (R = C_6H_5, X = NH_2) is −2.0, corresponding to half protonation in 34% H_2SO_4 while that of benzoic acid (R = C_6H_5; X = OH) is −7.2 with half protonation occurring in 82% H_2SO_4 (11). One possible explanation of this large difference is that the site of protonation may be different, the amino group of the amide and the hydroxy group of the acid being protonated. However both experimental (12–15) and theoretical data (16) point to carbonyl–oxygen protonation of both classes of compounds. Thus it appears that changing the amino group of an amide for a hydroxy group

Can. J. Chem. Downloaded from www.nrcresearchpress.com by 210.87.254.6 on 09/05/12
For personal use only.

Can. J. Chem. Downloaded from www.nrcresearchpress.com by 210.87.254.6 on 09/05/12
For personal use only.

decreases the basicity of the carbonyl–oxygen by more than five pK units.

As part of a continuing study of carbonyl-containing compounds we now report *ab initio* calculations on a series of formyl derivatives HCOX and $HC\overset{+}{O}HX$, where X = CH_3, NH_2, OH, F, and H. Oxygen protonated ketene has also been included. Some calculations have already been published for the molecules (17–21) and some of the ions (18, 22) but comparison of the different calculations is difficult as a variety of basis sets have been used. In the present work the same basis set has been maintained in all the calculations and the geometries of the conjugate acids have been optimized.

Both theoretical and experimental evidence indicate that, with the exception of ketene, all the compounds are carbonyl-oxygen protonated. Ketene protonates on the β-carbon atom to form the acetyl ion (**3**) rather than the hydroxyvinyl cation (**4**) (23). In the present work only protonation of the carbonyl oxygen is reported.

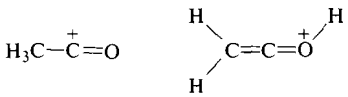

3 4

Computational Details

The calculations were carried out on an IBM 360–65 computer using IBMOL-IV (24). The Gaussian basis set consisted of 8^s and 3^p functions on carbon, nitrogen, oxygen, and fluorine and 3^s functions on hydrogen. These were contracted to 2^s, 1^p, and 1^s, respectively (25).

Microwave data provided geometries for all the neutral molecules (26–30). The geometries of three cations were taken from the optimization work by Ros (18); the others were optimized by first finding the best conformation for the incoming proton, then optimizing the C—O and C—X bond lengths in turn. All the bond angles in the conjugate acids were assumed to be ideal (120 or 180°) in accordance with Ros's work (18).

Results

Geometry Optimization

The most stable rotamer of acetaldehyde was computed to have one hydrogen of the methyl group eclipsing the oxygen atom (**5**). This was found to be more stable by 1.0 kcal/mol than the

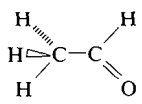

5

structure with two hydrogen atoms eclipsing. Structure **5** is also the experimentally observed conformation and the computed rotational barrier compares very favorably with the experimental value of 1.162 kcal/mol (27).

Both rotamers of acetaldehyde can protonate either *cis* or *trans* to the methyl group, leading to four possible tautomers. *Trans* protonation of the more stable rotamer of acetaldehyde produced the most stable conjugate acid (**6**). This

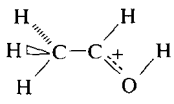

6

was computed to have a rotational barrier (about the C—C bond) of 0.9 kcal/mol and to be more stable than the *cis* protonated tautomer by 1.2 kcal/mol (the latter has a rotational barrier of 0.4 kcal/mol). Experimentally the *cis* and *trans* tautomers have been shown to be in equilibrium in SO_2—FSO_3H—SbF_5, with the *trans* tautomer being the more predominant by a factor of five (3) corresponding to a free energy difference of 0.95 kcal/mol at 298 °K. Thus these calculations, unlike the smaller basis set calculations of Ros (18), predict the experimentally observed *trans* isomer to be the more stable.

The remaining conjugate acids, with the exception of protonated ketene, were computed to be planar. As in protonated acetaldehyde the incoming proton in the conjugate acids of formic acid and formamide was found to be *trans* to the substituent. However in protonated formyl fluoride the hydrogen was predicted to be *cis* to the fluorine (see Table 1). The optimum conformation of a molecule or ion in the gas phase is determined by internal hydrogen bonds and steric interactions. Formic acid, formamide, and acetaldehyde all have weak hydrogen bonds between an in-plane hydrogen on the substituent and the carbonyl oxygen, leaving the other lone pair of electrons on the oxygen the more available. Protonation therefore occurs *trans* to the substituent. Formyl fluoride however has no hydrogen in the substituent, fluorine, and undergoes *cis* protonation to form the conjugate acid

TABLE 1. Optimized conformation and C—O and C—X bond lengths (Å) in

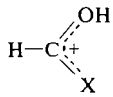

Conformation	C—O bond length[a]	C—X bond length[a]	Energy difference between *cis* and *trans* rotational isomers (kcal/mol)
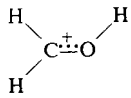	1.27[b] (1.21)	1.09[b] (1.12)	0.0
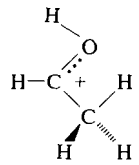	1.27[b] (1.216)	1.501[b] (1.501)	1.15
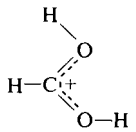	1.31[a] (1.245)	1.31[b] (1.312)	7.1[c]
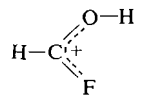	1.32 (1.185)	1.345 (1.345)	3.19
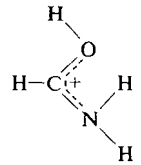	1.34 (1.193)	1.35 (1.376)	4.49
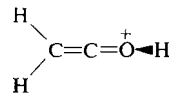	1.28 (1.16)	—	—

[a]Bond lengths of the corresponding free base are given in parentheses.
[b]Reference 18.
[c]Taken from ref. 22. The Gaussian basis set was $7^s\,3^p$; 3^s with no contraction.

in which internal hydrogen bonding is possible. Similar internal hydrogen bonds from fluorine to amino and hydroxy groups have been found in 1,2-disubstituted ethanes (31).

Finally a rotational study on oxygen-protonated ketene gave a large barrier (23.2 kcal/mol) with the incoming hydrogen atom 90° out of the plane (the COH bond angle was taken to be 120°) (32). This ion is isoelectronic with allene, a molecule which is known to have the hydrogen atoms on its terminal carbon atoms in planes which are perpendicular to one another.

After the optimum rotational conformations had been determined, the C—O and C—X bond lengths were optimized for the conjugate acids of formamide, ketene, and formyl fluoride. A typical optimization curve, for the C—O bond of protonated formyl fluoride, is given in Fig. 1. Geometries of protonated formaldehyde, acetaldehyde, and formic acid were taken from the literature (18). All the optimized geometries along with the barriers for rotation about C—O (prior to optimization of the bond lengths) are given in Table 1. All the optimized CO distances

Can. J. Chem. Downloaded from www.nrcresearchpress.com by 210.87.254.6 on 09/05/12
For personal use only.

Can. J. Chem. Downloaded from www.nrcresearchpress.com by 210.87.254.6 on 09/05/12
For personal use only.

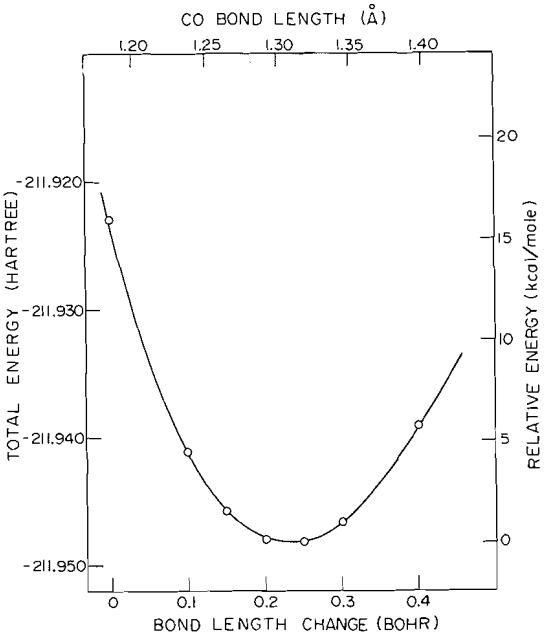

FIG. 1. Potential curve for optimization of carbon–oxygen bond length in protonated formyl fluoride.

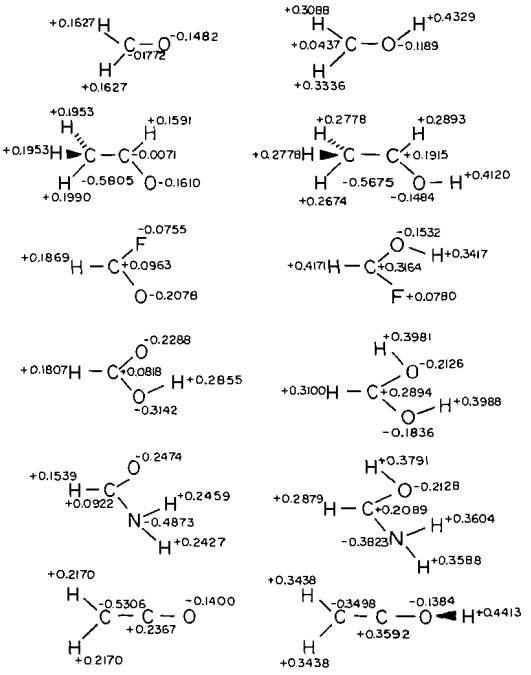

FIG. 2. Computed charge distributions.

are predictably longer than the experimental bond lengths of the free bases (given in parentheses) but deficiencies in the Gaussian basis set may result in the optimized geometries being slightly incorrect.

Protonation on oxygen results in the carbon–oxygen bond length increasing by at least 0.05 Å with the largest change occurring in formamide (0.147 Å). From this it may be interpreted that the resonance structure **7** is an important con-

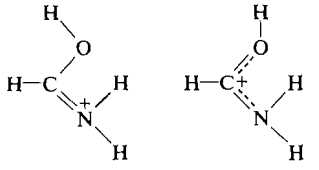

7 **8**

tributor, strengthening arguments for oxygen protonation of amides. However the C—N bond is considerably longer than in dimethylglyoxime (1.27 Å) (33) and the C—O bond is much shorter than in methanol (1.428 Å) (34) suggesting that the delocalized structure **8** best describes protonated formamide.

The carbon–oxygen bond length of formyl fluoride is also lengthened considerably on protonation, but unlike in the amide this is not accompanied by a shortening of the C—X bond. The C—F bond remains at 1.345 Å, longer than in fluoroethylenes (1.33 Å) and much longer than in CH_2F^+ (1.26 Å) (35).

Charge Densities

Charge densities obtained from a Mulliken population analysis (Fig. 2) show that the fluorine acquires some positive charge on protonation. However from the changes in the charge on group X, summarized in Table 2, it may be concluded that resonance structure **9** is

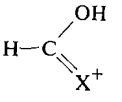

9

TABLE 2. Decrease in electron density on substituent-X on protonation of HCOX and computed and experimental dipole moments (Debye)

Substituent	Decrease in electron density	Dipole	
		Computed	Experimental[a]
H	0.1709	1.45	2.33
CH_3	0.2465	1.73	2.69
OH	0.2438	1.01	1.41
F	0.1535	1.46	2.02
NH_2	0.3357	2.7	3.73

[a]Reference 36.

Can. J. Chem. Downloaded from www.nrcresearchpress.com by 210.87.254.6 on 09/05/12
For personal use only.

least important for the fluoride and most important for the amide. Even formaldehyde, which cannot form a double bond with the substituent X (H), and acetaldehyde, which requires a structure involving hyperconjugation, have larger decreases in electron densities in their substituents on protonation.

Dipole moments of the parent molecules were compared with the experimental values from the literature (36) as a check on the reliability of the computed charge densities. These are listed in Table 2. All the computed dipole moments are smaller than the experimental ones, but exact agreement could not be expected from calculations using this medium size basis set. More importantly for comparative purposes there is a definite trend, with the calculations consistently predicting dipole moments which are too small by a third. It therefore seems that the changes in electron densities on protonation, although quantitatively inaccurate, should be valid for purposes of comparison.

Protonation Energies

The computed total energy for the molecules and cations are listed in Table 3 along with other literature values (17–22). Using the criterion of energy as a test for the accuracy of a wavefunction, it can be seen that better calculations are available for the bases. However for the cations, species for which geometries are not available and therefore have to be optimized, superior wavefunctions exist only for protonated formaldehyde (geometry assumed) and protonated formic acid (22).

Proton affinities, calculated by taking the difference in the total energies between a molecule and its conjugate acid and neglecting changes in zero-point vibrational energy (usually less than 5 kcal/mol), are listed in Table 4. The computed proton affinities are slightly larger than the experimental values, as expected, due to inadequacies in the basis set (22).

The predicted order of basicity in the *gas phase* is amide > carboxylic acid > acid fluoride ≃ acetaldehyde > ketene > formaldehyde. This closely follows the computed negative charge on the oxygen atom of the free base, with only ketene and formaldehyde being interchanged. In solution, however, the aldehydes are more basic than carboxylic acids and acyl fluorides, suggesting that their cations are stabilized more by solvation. The positive charges on the hydroxy protons of the protonated aldehydes (0.43 and 0.41) are computed to be slightly larger than in protonated formyl fluoride (0.34) and protonated formic acid (0.40) perhaps causing the protonated aldehydes to form stronger hydrogen bonds with the solvent and thereby producing more stable cations in solution. However, the differences in the charges are only small and this argument is clearly not very conclusive.

A different approach to considering the relative basicities of the carbonyl groups is to examine the binding energy of the oxygen "lone pair". In molecular orbital theory these orbitals are partly delocalized but are predominantly on the oxygen atom and are easily identified from the coefficient matrix. The order of availability of non-

TABLE 3. Computed total energies (hartrees)

Ion or molecule	Present calculations[a]	Previous calculations
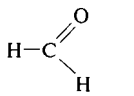	−113.3231	−113.8917[b]
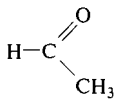	−152.2369	−148.5000[c]
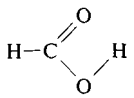	−187.8161	−188.6877[d]
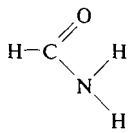	−168.1296 (planer) −168.1299 (experimental geometry)	−168.8684[d]
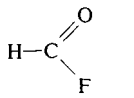	−211.5930	−212.6841[d]
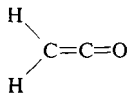	−151.0276	−151.5077[e]
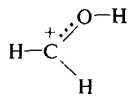	−113.6521	−110.8872[c] −113.8609[f]
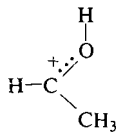	−152.5907	−148.8708[c]

TABLE 3(*Concluded*).

Ion or molecule	Present calculations[a]	Previous calculations
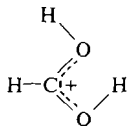	−188.1849	−188.5776[f]
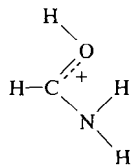	−168.5358	—
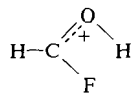	−211.9482	—
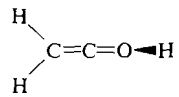	−151.3270	—

[a]Klessinger basis set.
[b]Reference 17.
[c]Reference 18.
[d]Reference 19.
[e]Reference 20.
[f]Reference 22.

TABLE 4. Computed proton affinities (kcal/mol)[a]

Molecule	Computed value	Experimental value
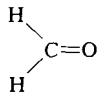	−206.6	−168[b]
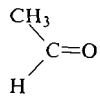	−221.0	−185[b]
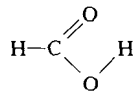	−231.5	−179[c]
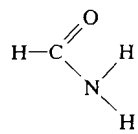	−254.8	—
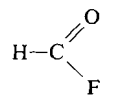	−223.0	—
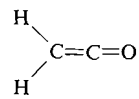	−216.8	—

[a]Not corrected for zero point energy changes or thermal energy.
[b]Reference 44.
[c]Reference 45.

bonding electrons is the *same* as the order of basicity in solution, *i.e.* formamide (9.86 eV) < acetaldehyde (10.09 eV) < formaldehyde (10.45 eV) < formic acid (10.56 eV) < formyl fluoride (11.09 eV). It therefore seems that a combination of availability of the lone pair for protonation and stabilization of the cation by solvation result in the aldehydes being more basic in solution than would be suggested by their proton affinities.

The Effect of Protonation on Orbital Energies

All the molecular orbitals of the cations are approximately 10 eV more stable than the corresponding ones of the base, as reported earlier (37). The shifts of the 1s core orbitals, although they are not formally included in the valence shell, are also of the same magnitude. Recently there has been considerable interest in the use of such "chemical shifts" of core orbitals (relative to an atom in some standard molecule) for the purpose of chemical analysis. Photoelectron spectroscopy provides accurate experimental ionization energies for ESCA (Electron Spectroscopy for Chemical Applications (or Analysis)) (38, 39). The core binding energies for an atom i can be related to the charge distribution in the molecule by eq. 1 (39), where E_0^i

$$[1] \qquad E^i = E_0^i + kq_i + \sum_{i \neq j} q_j/r_{ij}$$

is a reference level, q_i is the charge on atom i, and k is a proportionality constant depending on the electronegativity of the atom i, and also on the method of calculating the charge distribution. The last term represents the potential energy at atom i caused by the other atoms in the molecule.

Experimental binding energies for the cations and also for some of the free bases have not been measured experimentally. In order to use the above formula it was necessary to use Koopmans' approximation (40) that the binding energy equals the negative of the orbital energy. This method does not allow for the stabilization of the remaining electrons in the excited cation resulting from removal of one of the highly shielding inner electrons, and consequently overestimates ionization energies by as much as 21 eV for carbon atoms and 29 eV for oxygen atoms

Can. J. Chem. Downloaded from www.nrcresearchpress.com by 210.87.254.6 on 09/05/12
For personal use only.

TABLE 5. Potential energy terms provided by other atoms and 1s orbital energies

Compound	Base					Conjugate acid			
	$\sum_{i\neq j}^{c} \frac{q_i}{r_{ij}}$	Carbon 1s orbital energy	$\sum_{i\neq j}^{o} \frac{q_i}{r_{ij}}$	Oxygen 1s orbital energy		$\sum_{i\neq j}^{c} \frac{q_i}{r_{ij}}$	Carbon 1s orbital energy	$\sum_{i\neq j}^{o} \frac{q_i}{r_{ij}}$	Oxygen 1s orbital energy
	2.42	310.93	0.20	563.27		10.33	322.65	11.36	576.19
	(*a*) Carbonyl −1.46 (*b*) Methyl 7.62	311.06 308.77	−0.18	562.70		5.05 15.17	321.82 315.92	10.94	574.78
	−0.85	313.32	2.13	562.80		7.18	324.64	11.87	575.00
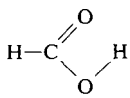	−0.89	312.36	(*a*) Carbonyl (*b*) Hydroxy	2.13 5.03	561.30 562.98	5.53	323.22	12.34 11.66	573.24 573.07
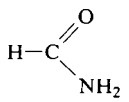	−2.66	311.76	1.64	561.11		5.18	321.58	11.04	571.71
$CH_2=C=O$	(*a*) Carbonyl −4.52 (*b*) Methylene 7.63	313.50 308.32	1.12	565.82		2.59 14.53	322.77 318.83	11.79	575.86

when near Hartree Fock wavefunctions are used (41). However the chemical shifts calculated by the *ab initio* method are of the right magnitude and vary in a predictable manner with the charge on the atom. The present calculations, using a medium size basis set, overestimate ionization energies by 17 eV for carbon and 23–25 eV for oxygen, but again the chemical shifts resulting from energy differences should be comparable with experimental values.

A plot of the charge on the carbon atom against the calculated core energy gives two separate lines, one for the neutral bases and the other for the positively charged species (Fig. 3). The least squares line for the free bases is

$$\Delta E_{\text{Koopmans'}} = 6.007q_i + 311.78 \text{ (correlation coefficient 0.958)}$$

and that for the protonated base

$$\Delta E_{\text{Koopmans'}} = 7.675q_i + 320.95 \text{ (correlation coefficient 0.939)}$$

It should be possible using eq. 1 to account for the difference in charge of the bases and conjugate acids, thereby correlating the binding energy, corrected for the potential provided by the other atoms in the molecule, with the charge on a particular carbon atom.

The appropriate Madelung potential terms and the core binding energies are listed in Table 5 and a plot of the corrected binding energies against the computed charge is shown in Fig. 4. The points for both the positive ions and neutral compounds do indeed now fall on the same line and there is considerably less scatter than on the plots of orbital energy against the charge. The least-squares line for the carbon atoms is

$$E_{\text{corrected binding energy}} = 20.5q_i + 312.23 \text{ (correlation coefficient 0.995)}$$

The equation for oxygen atoms, using data from Table 5, is

$$E_{\text{corrected binding energy}} = 44.6q_i + 570.31 \text{ (correlation coefficient 0.987)}$$

The values of k from eq. 1 were therefore

Can. J. Chem. Downloaded from www.nrcresearchpress.com by 210.87.254.6 on 09/05/12
For personal use only.

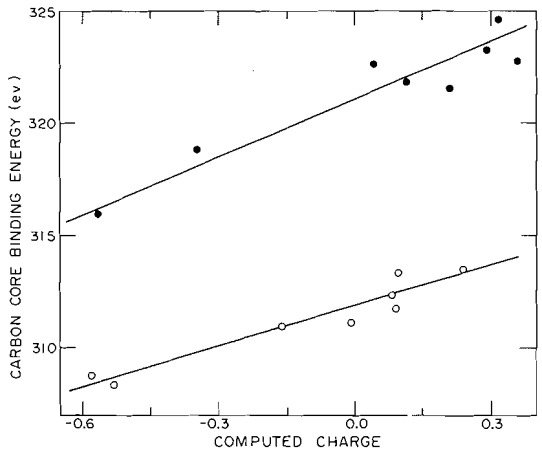

FIG. 3. Plot of binding energy (taken as negative of calculated orbital energy) against the computed charge for the carbon atom. ● indicates cations, ○ indicates neutral compounds.

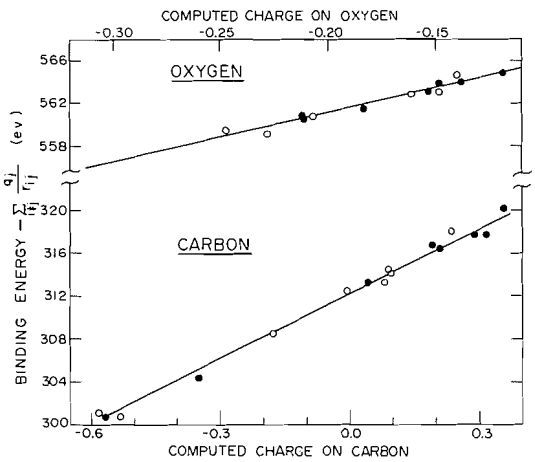

FIG. 4. Plot of binding energy corrected for potential of the other atoms against the computed charge. ● indicates cations, ○ indicates neutral compounds.

found to be 20.5 eV for carbon and 44.6 eV for oxygen. These compare with previously reported values of 21.9, 22.0 (39), 25.0 (42), and 20.46 (43) eV for carbon, and 25.8 and 30.7 eV for oxygen (39). k is dependent on the type and size of basis set used in SCF calculations and the surprisingly large value for the oxygen atom suggests that the Gaussian functions used to describe this atom may not be very well optimized.

The authors wish to thank the National Research Council of Canada for financial support.

1. G. A. OLAH, D. H. O'BRIEN, and A. M. WHITE. J. Am. Chem. Soc. **89**, 5692 (1967).
2. G. A. OLAH and A. M. WHITE. J. Am. Chem. Soc. **89**, 5072 (1967).
3. M. BROOKHART, G. C. LEVY, and S. WINSTEIN. J. Am. Chem. Soc. **89**, 1735 (1967).
4. H. HOGEVEEN, A. F. BICKEL, C. W. HILBERS, E. L. MACKOR, and C. MACLEAN. Rec. Trav. Chim. **86**, 867 (1967).
5. D. M. BROUWER. Rec. Trav. Chim. **86**, 879 (1967).
6. G. A. OLAH, D. H. O'BRIEN, and M. CALIN. J. Am. Chem. Soc. **89**, 3582 (1967).
7. H. HOGEVEEN. Rec. Trav. Chim. **86**, 696 (1967).
8. H. HOGEVEEN. Rec. Trav. Chim. **86**, 809 (1967).
9. K. YATES, J. B. STEVENS, and A. R. KATRITZKY. Can. J. Chem. **42**, 1957 (1964).
10. K. YATES and J. B. STEVENS. Can. J. Chem. **43**, 529 (1965).
11. E. M. ARNETT. Progress in physical organic chemistry. Vol. 1. Interscience Publishers, New York. p. 223.
12. R. J. GILLESPIE and T. BIRCHALL. Can. J. Chem. **41**, 148 (1963).
13. R. J. GILLESPIE and T. BIRCHALL. Can. J. Chem. **41**, 2642 (1963).
14. C. R. SMITH and K. YATES. Can. J. Chem. **50**, 771 (1972).
15. R. B. MARTIN. Chem. Commun. 73 (1972).
16. A. C. HOPKINSON and I. G. CSIZMADIA. Can. J. Chem. **51**, 1432 (1973).
17. D. B. NEWMAN and J. MOSKOWITZ. J. Chem. Phys. **50**, 2216 (1969).
18. P. ROS. J. Chem. Phys. **49**, 4903 (1968).
19. L. C. SNYDER and H. BASCH. J. Am. Chem. Soc. **91**, 2189 (1969).
20. J. H. LETCHER, M. L. UNLAND, and J. R. VAN WAZER. J. Chem. Phys. **50**, 2185 (1969).
21. R. DITCHFIELD, J. E. DEL BENE, and J. A. POPLE. J. Am. Chem. Soc. **94**, 703 (1972).
22. A. C. HOPKINSON, N. K. HOLBROOK, K. YATES, and I. G. CSIZMADIA. J. Chem. Phys. **49**, 3596 (1968); A. C. HOPKINSON, K. YATES, and I. G. CSIZMADIA. J. Chem. Phys. **52**, 1784 (1970).
23. G. A. OLAH, K. DUNNE, Y. K. MO, and P. SZILAGYI. J. Am. Chem. Soc. **94**, 4200 (1972).
24. A. VEILLARD. IBMOL: computation of wave functions for molecules of general geometry, version 4. IBM Research Laboratory, San Jose, California.
25. M. KLESSINGER. Theor. Chim. Acta, **15**, 353 (1969).
26. R. B. LAWRANCE and M. W. P. STRANDBERG. Phys. Rev. **83**, 363 (1951).
27. R. W. KILB, C. C. LIN, and E. B. WILSON. J. Chem. Phys. **26**, 1695 (1957).
28. I. G. CSIZMADIA, M. C. HARRISON, and B. T. SUTCLIFFE. Theor. Chim. Acta, **6**, 217 (1966).
29. C. C. COSTAIN and J. M. DOWLING. J. Chem. Phys. **32**, 158 (1960).
30. H. R. JOHNSON and M. W. P. STRANDBERG. J. Chem. Phys. **20**, 687 (1952).
31. L. RADOM, W. A. LATHAN, W. J. HEHRE, and J. A. POPLE. J. Am. Chem. Soc. **95**, 693 (1973).
32. A. C. HOPKINSON. J. Chem. Soc. Perkin II. In press.
33. L. MERRITT and E. LANTERMAN. Acta Cryst. **5**, 811 (1952).
34. J. D. SWALEN. J. Chem. Phys. **23**, 1736 (1955).

Can. J. Chem. Downloaded from www.nrcresearchpress.com by 210.87.254.6 on 09/05/12
For personal use only.

35. N. C. BAIRD and R. K. DATTA. Can. J. Chem. **49**, 3708 (1971).
36. Handbook of physics and chemistry. 49th ed. 1968–69.
37. A. C. HOPKINSON and I. G. CSIZMADIA. Theor. Chim. Acta. In press.
38. K. SIEGBAHN, C. NORDLING, A. FAHLMAN, R. NORDBERG, K. HAMRIN, J. HEDMAN, G. JOHANSSON, T. BERGMAN, S. E. KARLSSON, I. LINDGREN, and B. LINDBERG. ESCA – atomic, molecular and solid state structure studied by means of electron spectroscopy. Vol. 20. Nova Acta Regiae Soc. Sci. Upsaliensis Ser. IV. 1967.
39. K. SIEGBAHN, C. NORDLING, G. JOHANSSON, J. HEDMAN, P. F. HEDÉN, K. HAMRIN, U. GELINS, T. BERGMAN, L. O. WERME, R. MANNE, and Y. BAER. ESCA applied to free molecules. North-Holland, Amsterdam. 1969.
40. T. A. KOOPMANS. Physica, **1**, 104 (1933).
41. H. BASCH and L. C. SNYDER. Chem. Phys. Lett. **3**, 333 (1969).
42. D. T. CLARK and D. KILCAST. J. Chem. Soc. B, 2243, (1971).
43. D. T. CLARK and D. B. ADAMS. J. Chem. Soc. Faraday II, **68**, 1819 (1972).
44. K. M. A. RAFAEY and W. A. CHUPKA. J. Chem. Phys. **48**, 5205 (1967).
45. A. G. HARRISON, A. IVKO, and D. VAN RAALTE. Can. J. Chem. **44**, 1625 (1966).

Can. J. Chem. Downloaded from www.nrcresearchpress.com by 210.87.254.6 on 09/05/12
For personal use only.

An Electron Spin Resonance Study of the *tert*-Butylsulfinyl Radical[1]

JAMES A. HOWARD AND EDWARD FURIMSKY

Division of Chemistry, National Research Council of Canada, Ottawa, Canada K1A 0R9

Received September 5, 1973

The *tert*-butylsulfinyl radical, $(CH_3)_3CSO^{\cdot}$, can be prepared directly in the cavity of an e.p.r. spectrometer by photolysis of di-*tert*-butyl peroxide in a solution of *tert*-butylsulfenic acid in toluene or isopentane at low temperatures (−40° to −100°). The e.s.r. spectrum consists of a rather broad singlet ($\Delta H_{mls} \sim 1.9$ G) with the field center at $g = 2.0106$.

This radical undergoes self-reaction by a bimolecular process and a 2.5×10^{-7} *M* solution has a half-life of 0.07 s at −100 °C. It is, therefore, much shorter-lived than the iso-structural *tert*-butylperoxy radical, $(CH_3)_3COO^{\cdot}$.

Le radical *tert*-butylsulfinyle, $(CH_3)_3CSO^{\cdot}$, peut être préparé directement dans la cavité d'un spectromètre r.p.e. par photolyse du di-peroxyde de *tert*-butyle en solution avec de l'acide tertiobutylsulphénique dans le toluène ou l'isopentane à basse température (−40° à −100°). Le spectre r.p.e. consiste en un singulet plutôt large ($\Delta H_{mls} \sim 1.9$ G) avec un champ centré à $g = 2.0106$.

Ce radical réagit sur lui-même par un processus bimoléculaire à −100° C dans une solution 2.5×10^{-7} *M*, il a une demi-vie de 0.07 s. Il a donc une vie beaucoup plus courte que le radical iso-structural *tert*-butylperoxy, $(CH_3)_3COO^{\cdot}$. [Traduit par le journal]

Can. J. Chem., **52**, 555 (1974)

Our interest in the kinetics and mechanisms of the reactions of the *tert*-butylperoxy radical (1–3) has prompted us to prepare and investigate the stability of the iso-structural *tert*-butylsulfinyl radical, $(CH_3)_3CSO^{\cdot}$.

Kawamura, Krusic, and Kochi (4) have recently reported an electron spin resonance (e.s.r.) study of some alkylsulfinyl radicals prepared by several indirect methods. A simpler and more direct approach to the preparation of these radicals would be to react photochemically generated *tert*-butoxy radicals with the appropriate sulfenic acid (RSOH).

$$(CH_3)_3COOC(CH_3)_3 \xrightarrow{h\nu} 2(CH_3)_3CO^{\cdot}$$

$$(CH_3)_3CO^{\cdot} + RSOH \rightarrow (CH_3)_3COH + RSO^{\cdot}$$

Unfortunately very few alkylsulfenic acids are stable. Shelton and Davis (5) have, however, prepared *tert*-butylsulfenic acid in solution and report that in DMSO it has a half-life of about 1 week.

We found that photolysis of di-*tert*-butyl peroxide (DTBP) in a solution of *tert*-butylsulfenic acid in a solvent with a low melting point (such as toluene or isopentane) directly in the cavity of an e.p.r. spectrometer (Varian E-4) produced an e.s.r. spectrum which consisted of a rather broad single line ($\Delta H_{mls} \sim 1.9$ G) with the field center at $g = 2.0106$.

Photolysis of the acid in the absence of DTBP gave a much weaker signal while a spectrum was not obtained when a degassed solution of di-*tert*-butyl sulfoxide and DTBP in toluene was photolyzed.

The *g*-factor for $(CH_3)_3CSO^{\cdot}$ is similar to the value of 2.0096 found for methylsulfinyl (4) and is somewhat smaller than for the iso-structural *tert*-butylperoxy radical $g = 2.0146$ (6). *tert*-Butylsulfinyl and *tert*-butylperoxy radicals will have a bent structure with the unpaired electron localized in a S—O or O—O π-orbital (4). The lower *g*-factor for the sulfinyl radical is somewhat surprising because the spin–orbit coupling constant for sulfur is larger than it is for oxygen (7). The difference in *g*-factors must mean that, although the radicals have the same structure, their geometries are different.

When the initiating light was interrupted in the temperature range −34° to −100 °C the *tert*-butylsulfinyl radical decayed rapidly with bimolecular kinetics.

$$[1] \qquad 2(CH_3)_3CSO^{\cdot} \xrightarrow{2k_1} \text{Products}$$

and

$$\frac{-d[(CH_3)_3CSO^{\cdot}]}{dt} = 2k_1[(CH_3)_3CSO^{\cdot}]^2$$

At −100 °C a 2.5×10^{-7} *M* solution of this

[1]NRCC No. 13707.

Can. J. Chem. Downloaded from www.nrcresearchpress.com by 210.87.254.105 on 09/05/12
For personal use only.

Can. J. Chem. Downloaded from www.nrcresearchpress.com by 210.87.254.105 on 09/05/12
For personal use only.

radical has a half-life of 0.07 s and the bimolecular rate constant, $2k_1$, is $6 \times 10^7\ M^{-1}\ s^{-1}$.

Between -34 and $-100°$ *tert*-butylsulfinyl is considerably shorter-lived than the *tert*-butylperoxy radical, $(CH_3)_3COO^{\cdot}$. Thus at $-100°$ a $2.5 \times 10^{-7}\ M$ solution of $(CH_3)_3COO^{\cdot}$ would have a half-life of *ca.* $4\frac{1}{2}$ years (1). The *tert*-butylperoxy radical is remarkably long-lived because it exists in equilibrium with a rather unstable dimer, di-*tert*-butyl tetroxide, and only disappears by irreversible decomposition of the tetroxide (reaction sequence 2).

$$[2]\quad 2(CH_3)_3COO^{\cdot} \underset{b}{\overset{a}{\rightleftharpoons}} (CH_3)_3COOOOC(CH_3)_3 \xrightarrow{c} 2(CH_3)_3CO^{\cdot} + O_2$$

If a solution in which a significant concentration of $(CH_3)_3CSO^{\cdot}$ had decayed was heated in the cavity of the spectrometer from $-140°$ to $-30°$ there was no evidence for radical regeneration. This implies that, in this temperature range, an equilibrium analogous to reactions 2*a* and 2*b* does not exist for $(CH_3)_3CSO^{\cdot}$. Irreversible decay of $(CH_3)_3CSO^{\cdot}$ is rapid either because the dimer is not formed reversibly or because the dimer rapidly decomposes to products other than $(CH_3)_3CSO^{\cdot}$.

It is generally accepted (8) that alkylsulfinyl radicals dimerize by sulfur–oxygen coupling to give a sulfenyl sulfinate which is unstable and rearranges or decomposes to give a thiolsulfonate, $RS(O)_2SR$.

$$[3]\quad 2RSO \leftrightarrow 2RS^{+}\!-\!O^{-} \rightarrow RS(O)SR \rightarrow RS(O)_2SR$$

tert-Butylsulfinyl would appear to react by this mechanism since *tert*-butyl isobutanethiolsulfonate was the principal sulfur containing product formed when *tert*-butyl hyponitrite was decomposed thermally in the presence of a solution of *t*ert-butylsulfenic acid in toluene.

$$(CH_3)_3CON{=}NOC(CH_3)_3 \rightarrow 2(CH_3)_3CO^{\cdot} + N_2$$

$$(CH_3)_3CO^{\cdot} + (CH_3)_3CSOH \rightarrow (CH_3)_3COH + (CH_3)_3CSO^{\cdot}$$

$$2(CH_3)_3CSO^{\cdot} \rightarrow (CH_3)_3CS(O)_2SC(CH_3)_3$$

We have, of course no way of determining what fraction (if any) of the initial dimer involved oxygen-to-oxygen or sulfur-to-sulfur coupling.

Experimental

Materials

Di-*tert*-butyl sulfoxide was prepared by oxidation of di-*tert*-butyl sulfide with hydrogen peroxide in glacial acetic acid (m.p. 62–63°, lit. 63.5–65.0 (9)).

tert-Butylsulfenic acid was prepared by heating a solution of di-*tert*-butyl sulfoxide (0.02–0.5 *M*) in toluene under argon at 100° for about 15 min. For e.s.r. experiments this reaction was carried out in a Supracil tube (4 mm od). Di-*tert*-butyl peroxide (10% by vol) was then added and the resulting solution was flushed for about 10 min with argon.

tert-Butyl hyponitrite was prepared by the method of Kiefer and Traylor (10).

Kinetic Procedure

Absolute rate constants were determined from rates of disappearance of known concentrations of the radical (determined relative to a standard solution of DPPH) after the initiating light was interrupted. Decay curves were accumulated with the use of a rotating sector and a computer of average transients (11). Initial radical concentrations were varied by inserting neutral density filters between the cavity and the light source.

Products

tert-Butyl hyponitrite (0.2 *M*) was allowed to decompose completely in the presence of *tert*-butylsulfenic acid (~0.4 *M*) in deoxygenated toluene (50 h, dark, 50°). The principal sulfur containing reaction product was *tert*-butyl isobutanethiosulfonate identified by its infrared spectrum ($\nu_{S=O}$ = 1315 and 1110 cm^{-1}) (12) and its mass spectrum (*m/e* 210).

We thank the Chevron Research Company for financial support in the form of a Fellowship to one of us (E.F.) and Dr. J. R. Morton for determining the *g*-factor.

1. J. A. Howard. Adv. Free Radical Chem. **4**, 49 (1972).
2. S. Korcek, J. H. B. Chenier, J. A. Howard, and K. U. Ingold. Can. J. Chem. **50**, 2285 (1972).
3. E. Furimsky and J. A. Howard. J. Am. Chem. Soc. **95**, 369 (1973).
4. T. Kawamura, P. J. Krusic, and J. K. Kochi. Tetrahedron Lett. 4075 (1972).
5. J. R. Shelton and K. E. Davis. J. Am. Chem. Soc. **89**, 718 (1967).
6. J. A. Howard. Can. J. Chem. **50**, 1981 (1972).
7. D. S. McClure. J. Chem. Phys. **17**, 905 (1949).
8. J. L. Kice. Free Radicals. Vol. II. *Edited by* J. Kochi. J. Wiley, New York. 1973. Chapt. 24.
9. D. Barnard, L. Bateman, M. Cain, T. Colcough, and J. I. Cunneen. J. Chem. Soc. 2038 (1948).
10. H. Kiefer and T. G. Traylor. Tetrahedron Lett. 6163 (1966).
11. K. Adamic, D. F. Bowman, T. Gillan, and K. U. Ingold. J. Am. Chem. Soc. **93**, 902 (1971).
12. V. G. Bodyrev, L. P. Slesharchuk, E. E. Gatala, T. A. Trofimova, and E. Vasenko. Zh. Organ Khim. **2**, 96 (1966).

The Vapor Pressures and Enthalpies of Sublimation of Five Polycyclic Aromatic Hydrocarbons[1]

JOHN JAMES MURRAY AND ROSWELL FRANCIS POTTIE
Division of Chemistry, National Research Council of Canada, Ottawa, Canada K1A 0R9

AND

CHRISTIAN PUPP
Air Pollution Control Directorate, Department of the Environment, Ottawa, Canada K1A 0H3

Received September 18, 1973

The vapor pressures over benz[*a*]anthracene (B[*a*]A), benzo[*a*]pyrene (B[*a*]P), benzo[*e*]pyrene (B[*e*]P), benzo[*ghi*]perylene (B[*ghi*]P), and coronene have been measured using the Knudsen effusion weight loss method. The parameters A and B in the equation $\log_{10}[p(\text{atm})] = -(A/T) + B$ and the enthalpies of sublimation in kcal mol^{-1} derived therefrom are respectively: B[*a*]A, 5925 ± 36, 10.045 ± 0.099, 27.12 ± 0.54; B[*a*]P, 6181 ± 32, 9.601 ± 0.083, 28.29 ± 0.51; B[*e*]P, 6220 ± 33, 9.736 ± 0.085, 28.46 ± 0.55; B[*ghi*]P, 6674 ± 40, 9.519 ± 0.093, 30.54 ± 0.55; coronene, 7100 ± 69, 9.110 ± 0.149, 32.49 ± 0.55. The errors shown for the A and B values are standard deviations and for the enthalpies of sublimation are estimates of total probable error.

Les pressions de vapeur du benz[*a*]anthracène (B[*a*]A), benzo[*a*]pyrène (B[*a*]P), benzo[*e*]pyrène (B[*e*]P), benzo[*ghi*]pérylène (B[*ghi*]P) et coronène ont été mesurées à l'aide de la méthode de perte de poids par éffusion de Knudsen. Les paramètres A et B dans l'équation $\log_{10}[p(\text{atm})] = -(A/T) + B$ et les enthalpies de sublimation en kcal mol^{-1} ainsi dérivés sont respectivement: B[*a*]A, 5925 ± 36, 10.045 ± 0.099, 27.12 ± 0.54; B[*a*]P, 6181 ± 32, 9.601 ± 0.083, 28.29 ± 0.51; B[*e*]P, 6220 ± 33, 9.736 ± 0.085, 28.46 ± 0.55; B[*ghi*]P, 6674 ± 40, 9.519 ± 0.093, 30.54 ± 0.55; coronène, 7100 ± 69, 9.110 ± 0.149, 32.49 ± 0.55. Les erreurs obtenues sur les valeurs de A et B sont des déviations standards alors que pour les enthalpies de sublimation elles représentent des déviations de l'erreur totale probable.
[Traduit par le journal]

Can. J. Chem., 52, 557 (1974)

Introduction

Certain polycyclic aromatic hydrocarbons, p.a.h., which are generated principally during the incomplete combustion of fossil fuels, are present in the atmosphere as trace pollutants. These trace pollutants are of concern because some of them have been found to be carcinogenic (1). The five p.a.h. studied here (see Table 1), which include three carcinogenic substances, were chosen by a committee of the World Health Organization as the materials which should be analyzed in a program of monitoring the p.a.h. content of air samples (14).

A few studies of the vaporization of some p.a.h. have been made in the past (2, 3) and vapor pressures and enthalpies of vaporization, ΔH^0_{subl}, for some of the materials studied here have been obtained (see Discussion). However such studies, being parts of general surveys, were cursory and the scatter in the measurements and estimated accuracy of the data were not given. As well, the agreement among the various surveys is poor. Vapor pressures and ΔH^0_{subl} values are of general interest to physical chemists. In relation to the presence of p.a.h. as air pollutants, such data are useful for understanding how and in what state these materials are introduced into the atmosphere. The data can also be of value in devising effective means to reduce such introduction, and could be the basis for designing proper sampling procedures to determine the levels of these pollutants in stack gases, vehicle exhausts, the atmosphere, etc. The application of the present results to the latter purpose will be discussed elsewhere (15).

In this study the Knudsen weight loss effusion method (4, 5) was used in which the pressure p in atm is obtained from the equation

$$[1] \qquad p = \frac{W}{K_c A t}\left(\frac{2\pi R T}{M}\right)^{1/2} = 0.022557\,\frac{W}{K_c A t}\left(\frac{T}{M}\right)^{1/2}$$

[1]NRCC No. 13702.

Can. J. Chem. Downloaded from www.nrcresearchpress.com by 210.87.254.5 on 09/05/12
For personal use only.

TABLE 1. The polycyclic aromatic hydrocarbons which were studied

Compound	Supplier	Molecular weight	Structure	Melting point (°C) Measured*	Melting point (°C) Literature†
Benz[*a*]anthracene (B[*a*]A)	Schuchardt	228.3	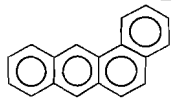	156.9	158–159
Benzo[*a*]pyrene (B[*a*]P)	Fluka	252.3	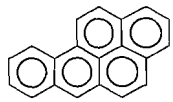	176.4	176.5–177.5
Benzo[*e*]pyrene (B[*e*]P)	K & K	252.3	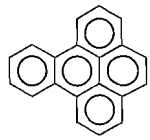	178.8	178–179
Benzo[*k*]fluoranthrene (B[*k*]F)	Paris‡	252.3	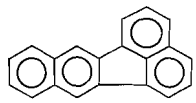	198–217	217
Benzo[*ghi*]perylene (B[*ghi*]P)	Fluka	276.3	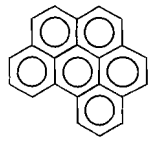	275–277	272–273
Coronene	Fluka	300.3	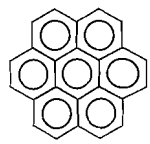	~440	438–440

*Single value m.p.'s obtained using a Mettler FP51 m.p. apparatus, ranges by using a Kofler m.p. microscope. The m.p. ranges for B[*a*]A, B[*a*]P, and B[*e*]P were 2° or less.
†All literature values were from ref. 9.
‡Police Department, Paris, Mme. Herot.

where W is the weight loss in grams occurring in t seconds due to the effusion of molecules of molecular weight M through an orifice of area A cm^2 in a Knudsen cell at T °K. R is the gas constant and K_c is the Clausing factor which corrects for the effect of the length of the orifice upon the rate of effusion (5, 6). By the strictest criterion (5) the method is valid as long as the mean free path of the vapor $\geqslant$ 10 times the diameter or "characteristic dimension" of the effusion orifice. In most instances this limitation restricts measurements to maximum pressures of about 5×10^{-4} to 10^{-3} atm.

Experimental

The apparatus is shown schematically in Fig. 1. A Sartorius 4104 electrobalance having a sensitivity of 1 μg, capacity of 25 g, and zero stability of better than 2 μg/24 h for $\Delta T \leqslant \pm 2$ °K was used. The flanges of the welded stainless steel vacuum manifold were sealed using Viton O-rings or copper gaskets. The system was pumped via a water cooled baffle and short 10 cm diameter line using a nominally 10 cm diffusion pump charged with a polyphenyl ether oil (Santovac 5, Monsanto Corp.). The vacuum obtained was about 10^{-9} atm being limited primarily by degassing from the furnace element. The 100 mm high by 38 mm i.d. furnace was made from two inductively wound semi-cylindrical heating units (Lindberg Hevi-Duty) supported on a stainless steel stand. The

Can. J. Chem. Downloaded from www.nrcresearchpress.com by 210.87.254.5 on 09/05/12
For personal use only.

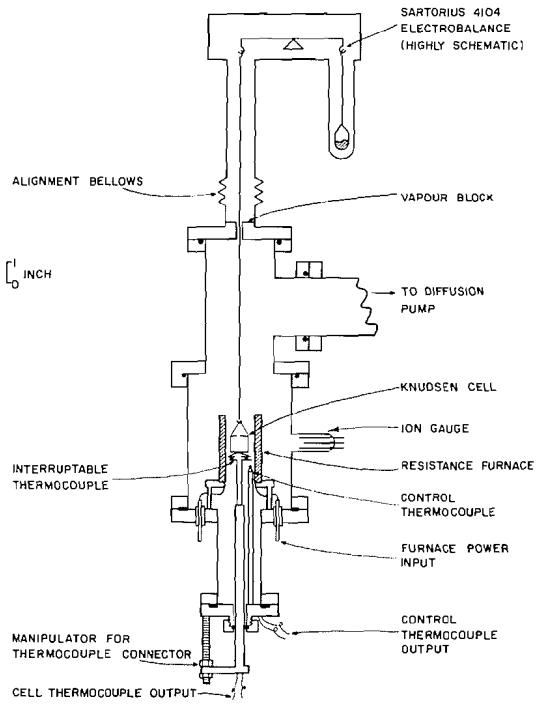

FIG. 1. Scale schematic of the Knudsen effusion weight loss apparatus.

Knudsen cells were 20 mm high by 20 mm diameter by 0.75 mm wall 304 stainless steel with an approximately 0.50 mm diameter by 0.50 mm long effusion orifice (Clausing factor typically 0.50). The orifice plate was press fitted into the lower section to form the cell thus ensuring no leakage except through the orifice. A new cell was used for each substance studied, the orifice lengths and diameter being determined by photomicrography. The ratio of the nominal vaporizing surface area to the cross-sectional area of the orifice was 1350:1.

The small mass of the furnace and of the Knudsen cell permitted re-equilibration after temperature changes to better than $\pm 1/2$ °K in 2 h or less. This interval was significantly shorter than if a tube furnace or temperature bath outside the vacuum enclosure had been used. The short hot zone which resulted from use of the 10 cm long internal furnace was expected to yield uniform cell temperature only at temperatures for which loss of energy by radiation from the top and bottom of the cell was negligible relative to the conductivity within the cell. This condition should be satisfied up to about 600 °K. Since this short hot zone did preclude the use of a dummy cell for temperature measurement, a technique of direct measurement of the temperature of the Knudsen cell was devised, as illustrated in Figs. 1 and 2. The thermocouple was chromel/alumel calibrated *in situ* against the freezing point of indium (429.76 °K). For rate of weight loss measurements, the connector B was in the lowered position so as not to touch the thermocouple assembly that was spot welded onto the Knudsen cell. To measure the temperature, the connector B was raised smoothly using the manipulator until contact with the fine wires of the assembly on the cell was achieved. The thermocouple output was measured with a null balance potentiometer. With care vibrations introduced into the balance system in the process of making and breaking contact with the cell were negligible. Vibrations from other sources were reduced by appropriate isolation of the entire vacuum manifold. An additional thermocouple below the cell provided the input signal for a proportional controller which triggered an SCR furnace power controller.

The apparatus and procedures were tested using arsenic trioxide of 99.7% purity obtained from Fisher Scientific Company. The p.a.h. samples from various sources (see below) were obtained via the bank of such materials maintained by the Air Pollution Control Directorate, Department of the Environment, Canada. The p.a.h. were used without further purification and their purity was checked using a mass spectrometer.

Results and Discussion

Test using Arsenic Trioxide

The uncertainties in the vapor pressures and enthalpy of vaporization of arsenic trioxide (arsenolite) have been substantially reduced by a recent careful study by Behrens and Rosenblatt

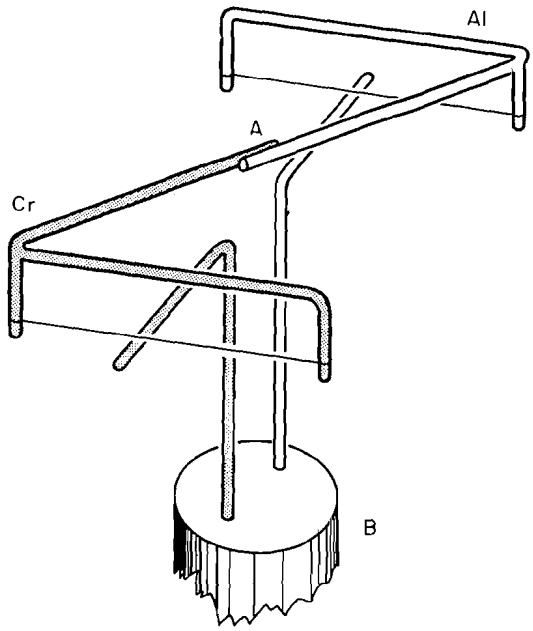

FIG. 2. Thermocouple arrangement. The junction A is spot welded to the bottom of the Knudsen cell. The part attached to the cell is made from 0.5 and 0.12 mm diameter wires. The part B which includes the 0.5 mm diameter connecting wires can be moved *in vacuo* along the vertical axis using a linear manipulator. Cr indicates chromel A; Al indicates alumel.

Can. J. Chem. Downloaded from www.nrcresearchpress.com by 210.87.254.5 on 09/05/12
For personal use only.

Can. J. Chem. Downloaded from www.nrcresearchpress.com by 210.87.254.5 on 09/05/12
For personal use only.

(7). As a result it was possible to use arsenic trioxide as a standard test material. For the vaporization

$$2As_2O_{3(c)} = As_4O_{6(g}$$

the present results over the temperature range 345–405 °K are described by the least squares fitted equation

$$[2] \quad \log_{10}[p(\text{atm})] = -\left[\frac{6077 \pm 18}{T}\right] + (9.944 \pm 0.048)$$

where the errors given are the standard deviations. This is in excellent agreement with the equation given in ref. 7 for 367–429 °K

$$[3] \quad \log_{10}[p(\text{atm})] = -\left[\frac{6067 \pm 125}{T}\right] + (9.905 \pm 0.319)$$

Using the pressure/temperature data of the present study and the free energy functions given by ref. 7, the following second and third law enthalpies of vaporization were derived

$$\Delta H^0 \text{ (298.15 °K, second law)} = (28.25 \pm 0.14) \text{ kcal mol}^{-1}$$

$$\Delta H^0 \text{ (298.15 °K, third law)} = (28.01 \pm 0.03) \text{ kcal mol}^{-1}$$

where the errors given are the standard deviations. The second law value was obtained using the Cubicciotti version of the Σ-plot method (8). Since eqs. 2 and 3 show good agreement, these enthalpy values also show excellent agreement with the second and third law results given in ref. 7 ((28.31 ± 0.56) and (28.13 ± 0.20) kcal mol^{-1}, respectively). In addition, within the 95% confidence limits (twice the standard deviations) the second and third law enthalpies agree with each other, which demonstrates the internal consistency of the data. Clearly, sources of systematic errors in this apparatus and procedure were small, and, indeed, as is clear from eq. 2 the reproducibility was excellent.

The Polycyclic Aromatic Hydrocarbons

The six compounds studied and the original sources of supply are listed in Table 1. B[*a*]P is highly carcinogenic, and B[*a*]A and B[*e*]P are also known to be carcinogenic (1). The suppliers purified these substances by column chromatography, repeated recrystallization, and/or fractional sublimation. The indicators of purity used were melting point range and u.v. absorption spectra. Based upon these indicators purities of 97% or better were claimed for all the compounds. All samples were pale yellow crystalline solids. These claimed purities were roughly confirmed by checking melting points (Table 1) and by using a Knudsen cell mass spectrometer with molar purity results as follows: B[*a*]A, 98.4%; B[*a*]P, 96.3%; B[*e*]P, 98.2%; B[*ghi*]P, 94.6%; and coronene 98.6%. B[*k*]F was found to be quite impure (about 10% impurity) and the results obtained are regarded as preliminary only. The most common impurities were 6 and 14 mass units above the principal component. Most probably these were principal component plus 6H and principal component with —CH_3 substituted for —H. B[*a*]A, B[*a*]P, and B[*k*]F were available in 25–30 mg quantities only; B[*e*]P, B[*ghi*]P, and coronene were available in 60–100 mg quantities. Such limited availability of material and, as discussed below, the minimum sample size requirement of the weight loss method precluded any attempt at further purification by fractional recrystallization or vacuum sublimation.

Vapor Pressures and Enthalpies of Sublimation

For each material the Knudsen cell was slowly heated maintaining the pressure below 3×10^{-9} atm until the rate of weight loss was about 0.1 μg s^{-1}. In all cases the rate of weight loss at constant temperature initially decreased rapidly with time. After about 1 mg of sample had been vaporized the rate of weight loss became time independent and reproducible. This suggests that a portion of the impurities in the samples had a higher vapor pressure than the principal component and, initially, was preferentially vaporized.

Having obtained reproducible rates of weight loss, data were collected in a random order with respect to temperature, each measurement requiring between ½ h and 3 d at fixed temperature. Pressures were calculated from the rates of weight loss via eq.1 using the measured orifice parameters. Mass spectra established that sublimation occurred to the monomer (intense molecular ion, all fragments derived logically from the molecular ion), so that the M in eq. 1 was the mole weight of the substance as given in Table 1. The results are presented in Figs. 3 and 4 and are described by least squares equations of the form

$$\log_{10}[p(\text{atm})] = -A/T + B$$

TABLE 2. The least squares parameters A and B in the equation $\log_{10}[p(\text{atm})] = -(A/T) + B$ and the temperature range of the measurements; errors given are standard deviations*

Compound	Temperature range (°K)	A (°K)	B (unitless)
B[*a*]A	330–390	5925 ± 36	10.045 ± 0.099
B[*a*]P	358–431	6181 ± 32	9.601 ± 0.083
B[*e*]P	359–423	6220 ± 33	9.736 ± 0.085
B[*ghi*]P	389–468	6674 ± 40	9.519 ± 0.093
Coronene	427–510	7100 ± 69	9.110 ± 0.149

*The preliminary values of A and B for B[*k*]F obtained at 363–430 °K are 6792 ± 68 and 10.885 ± 0.166, respectively.

with the parameters A and B as given in Table 2. The B[*k*]F results are also given in Fig. 3. However, because of the high impurity level these results are regarded as preliminary only and are presented only to show that the vapor pressure of B[*k*]F is about one-half to one-third that of B[*a*]P and B[*e*]P.

The weight loss equipment was designed to permit vapor pressure measurements with the small samples available. The sensitivity and zero stability of the electrobalance allowed pressures of 2×10^{-8} atm to be measured using the Knudsen cells described above with at least ±10% reproducibility, ±2% for 2×10^{-7} atm or above.

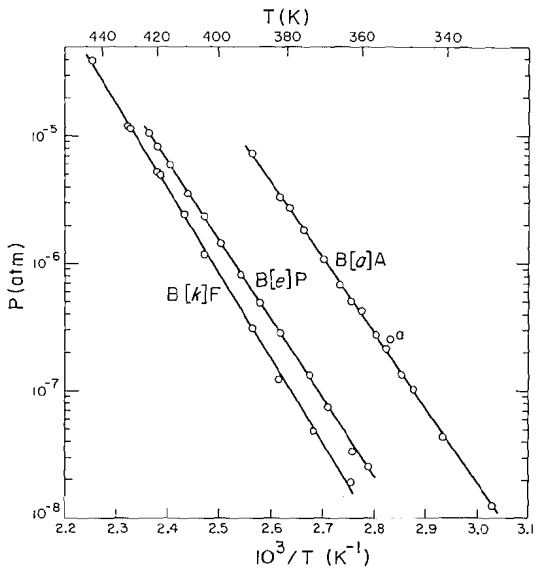

FIG. 3. Semilog plot of the vapor pressures of B[*a*]A, B[*e*]P, and B[*k*]F *vs.* T^{-1}. The point marked a was weighted to zero in the least squares analysis for B[*a*]A. The B[*k*]F results are based upon results obtained using a relatively impure sample and illustrate only that B[*k*]F has a pressure significantly below that of B[*a*]P and B[*e*]P.

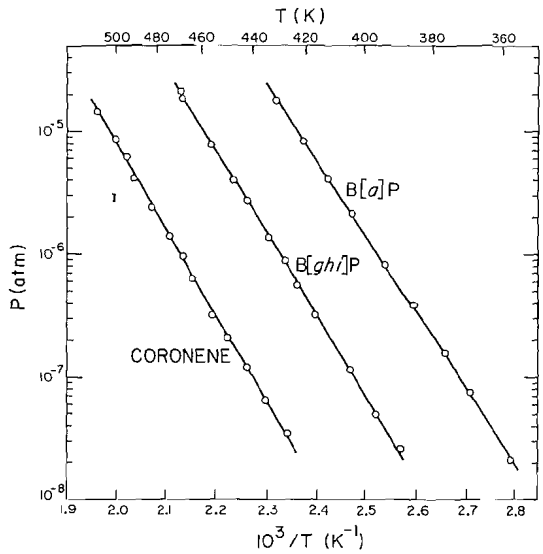

FIG. 4. Semilog plot of the vapor pressures of B[*a*]P, B[*ghi*]P, and coronene *vs.* T^{-1}.

Even with this sensitivity, together with the reasonably rapid rate of thermal equilibration of the system and the limitation of the maximum pressure measured to about 10^{-5} atm, vaporization of at least 5 mg of sample was needed to obtain the above statistically significant sets of data. Excessive sample depletion during the measurements would have resulted in failure to maintain the minimum sample size required for a close approximation to vapor equilibrium within the cell. A 5 mg weight loss amounted to 17 to 20% depletion of the 25 to 30 mg samples of B[*a*]A and B[*a*]P. No observable diminuation of apparent vapor pressure occurred with this amount of sample depletion. However further reduction of sample size would certainly have led to such effects.

Since virtually no physico-chemical data are

Can. J. Chem. Downloaded from www.nrcresearchpress.com by 210.87.254.5 on 09/05/12
For personal use only.

TABLE 3. The enthalpies and entropies of sublimation at the average temperature, T_{av}, of the vapor pressure measurements*

Compound	ΔH^0_{subl} (T_{av}) (kcal mol^{-1})	ΔS^0_{subl} (T_{av}) (cal mol^{-1} K^{-1})	ΔH^0_{subl}† (literature) (kcal mol^{-1})
B[*a*]A	27.12 ± 0.54	46.0 ± 1.5	28.6‡, 28.8§, 25.0‖
B[*a*]P	28.29 ± 0.51	43.9 ± 1.3	
B[*e*]P	28.46 ± 0.55	44.6 ± 1.3	
B[*ghi*]P	30.54 ± 0.55	43.5 ± 1.3	30.0§
Coronene	32.49 ± 0.75	41.7 ± 1.6	35.1‡, 30.7§

*The approximate values for ΔH^0 and ΔS^0 for B[*k*]F are 31.1 kcal mol^{-1} and 49.8 cal mol^{-1} K^{-1}, respectively.
†The literature values also apply to some T_{av} which may differ slightly from the T_{av} values for the present results.
‡Reference 2.
§Reference 3.
‖Reference 10.

available for these materials, the results can be analyzed only by the second law procedure, *i.e.*, by identifying the results with the expression

$$\log_{10}[p(\text{atm})] = -\frac{\Delta H^0}{4.576T} + \frac{\Delta S^0}{4.576}$$

where ΔH^0 is in cal mol^{-1} and ΔS^0 is in cal mol^{-1} K^{-1}. The ΔH^0 and ΔS^0 values so obtained pertain to the average temperature of the measurements, T_{av}, and are given in Table 3.

The total probable errors given in Table 3 were estimated taking account of the following. Twice the standard deviation in slope (A) and intercept (B) represent the reproducibility errors with 95% confidence. Experience with the balance shows that the accuracy of the measurements of the rate of weight loss equals the reproducibility. The effects of back effusion and condensation on the cell hang-down wire are trivial. However a systematic error of ±3% in the pressures arises from an estimated error of ±3% in the measurement of orifice area. The Clausing factor, K_c in eq. 1, may be in error because of error in the measurement of the orifice length to radius ratio (±5%) and because of error in using the tabulated Clausing factor. This latter error results from the possible partial invalidity of one of the assumptions made in the derivation of the Clausing factors. Based upon recent measurements (10) an error assignment of ±5% to this source of error is reasonable for orifices of the type used here. The accuracy of temperature measurement is estimated as ±1 °K, *c.f.* a reproducibility of better than ±0.5 °K; the accuracy of the measurement of the temperature interval of the measurements is estimated to be ±1 °K. The results for arsenic trioxide strongly suggest that these are overestimates of the temperature errors; however, considering the techniques used, such errors are possible and are presumed, therefore, to exist. Both of these temperature errors contribute to systematic error in A and B. Errors arising from the impurities are not included in the estimates of total error. Such errors are expected to be less than the measurement errors cited above because the impurities appear to be related hydrocarbons which would form essentially ideal solutions with the principal component. The errors given in Table 3 are valid for comparison with the results of others; for intra-comparison purposes twice the standard deviations given in Table 2 should be used.

As shown in Table 3, ΔH^0_{subl} has been measured previously for B[*a*]A, B[*ghi*]P, and coronene. With the exception of the value for B[*a*]A obtained by Kelley and Rice (11) all these results were obtained as part of survey studies. These surveys were done using modifications of the Knudsen method; in neither study was the scatter in the vapor pressure results given nor were estimates of the accuracies of the pressures or enthalpies given. Temperature measurement is often the most significant source of error in high vacuum studies such as these. In particular the technique of temperature measurement used by Wakayama and Inokuchi (3) could lead to substantial errors in T, ΔT, and hence ΔH^0_{subl}. The method of temperature measurement used by Hoyer and Peperle (2) was not specified. The sample purity in these previous studies was not clearly specified but was probably, at best, equal to that of the materials used here. The results of these two previous studies show poor agreement with each other (Table 3). In view of the above, the significance of these earlier results is difficult to assess and no meaningful comparison between

Can. J. Chem. Downloaded from www.nrcresearchpress.com by 210.87.254.5 on 09/05/12
For personal use only.

Can. J. Chem. Downloaded from www.nrcresearchpress.com by 210.87.254.5 on 09/05/12
For personal use only.

them and the present results is possible. The value of ΔH^0_{subl} obtained by Kelley and Rice (11) was obtained using a temperature range of only 23 °K, hence the ΔH^0_{subl} is subject to particularly large error.

A simple correlation of vapor pressures and ΔH^0_{subl} with the number of carbons in the molecule is to be expected for a homologous series. These p.a.h. do show decreasing vapor pressure at, say, 400 °K and increasing ΔH^0_{subl} as the number of carbons is increased. Since B[*a*]P and B[*e*]P are isomers having closely related structures, one might also expect these materials to have very similar vaporization behavior. In fact, as is clear from Table 2, their vapor pressure curves are indistinguishable within the scatter errors.

The preliminary results for B[*k*]F show that it does not fit this correlation. This is to be expected since B[*k*]F, unlike the other compounds studied, contains a five-membered ring.

There have been several attempts to quantify the correlation of ΔH^0_{subl} with the number of carbon atoms in the molecule. Inokuchi *et al.* (12) attempted to establish a simple linear relationship, each carbon being assigned a "vaporization energy" of 1.5 kcal mol^{-1}. Recent data shows such a correlation to be poor. Morawetz (13) has attempted to establish a better correlation by assigning bond parameters to eight different types of C—C bonds in aromatic molecules. Unfortunately the assignment of the parameters is rather suspect since the eight variables are established using only twelve ΔH^0_{subl} values. Nevertheless the ΔH^0_{subl} values predicted by the Morawetz correlation are, in kcal mol^{-1}: B[*a*]A, 28.3; B[*a*]P, 28.4; B[*e*]P, 29.3; B[*ghi*]P, 30.5; coronene, 33.4. These values agree with the present results within 1.2 kcal mol^{-1} or less,[2] which is well within the error of $\pm$2–3 kcal mol^{-1} generally assigned by Morawetz.

Conclusion

The present results for vapor pressures and ΔH^0_{subl} are the only known values for B[*a*]P and B[*e*]P. For B[*a*]A, B[*ghi*]P, and coronene they are the only results for which the scatter in the data is specified and the accuracy is estimated. In view of this and of the great care taken in the present study to obtain accurate temperature measurement, the present results are considered to be the most accurate available. The accuracy of the data is limited largely by errors inherent in the techniques as estimated above. Except for B[*k*]F improvement in sample purity would not appreciably affect the accuracy of the results. More accurate values for ΔH^0_{subl} may be obtainable by calorimetric methods, but these techniques generally require larger samples of higher sample purity than are currently available.

The authors thank J. L. Monkman, R. C. Lao, and R. J. Thomas of the Air Pollution Control group of the Department of the Environment for helpful discussions and for providing both the electrobalance and the samples.

1. D. Hoffman and E. L. Wynder. *In* Air pollution, Vol. 2, 2nd ed. *Edited by* A. C. Stern. Academic Press, New York. 1968. p. 187.
2. H. Hoyer and W. Peperle. Z Elektrochem. **62**, 61 (1958).
3. N. Wakayama and H. Inokuchi. Bull. Chem. Soc. Jap. **40**, 2267 (1967).
4. K. D. Carlson. *In* The characterization of high temperature vapors. *Edited by* J. L. Margrave. Wiley, New York. 1967. p. 115.
5. E. D. Cater. *In* Physicochemical measurements in metals research, Vol. IV, part 1. *Edited by* R. A. Rapp. Interscience, New York. 1970.
6. R. D. Freeman and J. G. Edwards. *In* The characterization of high temperature vapors. *Edited by* J. L. Margrave. Wiley, New York. 1967. p. 508.
7. R. G. Behrens and G. M. Rosenblatt. J. Chem. Thermodyn. **4**, 175 (1972).
8. D. Cubicciotti. J. Phys. Chem. **70**, 2410 (1966).
9. Dictionary of organic compounds. 4th edition and supplements. Eyre and Spottiswoode Publishers Ltd., London. 1965.
10. S. J. Wey and P. G. Wahlbeck. J. Chem. Phys. **57**, 2932 (1972).
11. J. D. Kelley and F. O. Rice. J. Phys. Chem. **68**, 3794 (1964).
12. H. Inokuchi, S. Shiba, T. Hauda, and H. Akamatu. Bull. Chem. Soc. Jap. **25**, 299 (1952).
13. E. Morawetz, J. Chem. Thermodyn., **4**, 461 (1972).
14. International Association for Research on Cancer, Internal Technical Report 71/002.
15. J. J. Murray, R. F. Pottie, C. Pupp, and R. C. Lao. To be published.

[2]The agreement is rather better than this since correction of the present results to 298.15 °K would probably increase the values by 0.5 to 1.0 kcal mol^{-1}.

Asymmetry in the ^{125}Te Mössbauer Spectra of Tellurium Thiourea Complexes: Sign of the Nuclear Quadrupole Moment of the $^3/_2$ State

B. M. CHEYNE AND C. H. W. JONES

Department of Chemistry, Simon Fraser University, Burnaby 2, British Columbia

Received August 1, 1973

Asymmetry in the Mössbauer spectra of Te(II) thiourea complexes is shown to be due predominantly, if not exclusively, to single crystal orientation effects. The asymmetry in $TeTu_4Cl_2 \cdot 2H_2O$ is consistent with a negative sign for the nuclear quadrupole moment of the $\frac{3}{2}$ excited state in ^{125}Te.

On montre que l'aspect asymétrique dans les spectres Mössbauer des complexes Te(II). Thiourée est dû principalement, sinon exclusivement, à des effets d'orientation d'un cristal unique. L'asymétrie dans le spectre du $TeTu_4Cl_2 \cdot 2H_2O$ est en accord avec un signe négatif du moment quadruplaire nucléaire de l'état excité $\frac{3}{2}$ du ^{125}Te. [Traduit par le journal]

Can. J. Chem., **52**, 564 (1974)

Can. J. Chem. Downloaded from www.nrcresearchpress.com by 210.87.254.5 on 09/05/12
For personal use only.

Introduction

In a previous Mössbauer study of tellurium thiourea complexes (1) a small asymmetry was observed in the quadrupole split spectra for microcrystalline samples of some of the Te(II) compounds. Since the tellurium is present in a square planar environment in these molecules (2), it was thought this effect may have been due to anisotropy of the recoil-free fraction (the Goldanskii–Karyagin effect). However, as will be described below, studies on single crystal and powdered samples have shown that the asymmetry observed in the quadrupole splitting arises predominantly, if not exclusively, from the orientation of single crystals in the absorber. The experiments on single crystal samples have allowed a further estimate of the sign of the nuclear quadrupole moment of the $\frac{3}{2}$ excited state in ^{125}Te.

Results and Discussion

Single Crystal and Powder Experiments

To establish the origin of the asymmetry in the line intensities, the ^{125}Te Mössbauer spectra of single crystal samples of $TeTu_4(SCN)_2$ (Tu = thiourea) and $TeEtu_4Cl_2$ (Etu = ethylenethiourea) were recorded. These two compounds were chosen because they yielded the largest asymmetry in the microcrystalline samples. $TeTu_4(SCN)_2$ crystallizes from aqueous solutions of thiourea as very thick needles (3), while $TeEtu_4Cl_2$ crystallizes as long, well-developed fine needles (4). In both cases the Mössbauer absorbers were prepared by aligning a large number of single crystals with their needle axes at right-angles to the γ-ray beam. Having recorded the single crystal spectra the samples were finely powdered with fine sand in an agate mortar and their Mössbauer spectra remeasured. Sample spectra are shown in Fig. 1 and the computed parameters are shown in Table 1. The large asymmetry observed in the single crystal samples was not present in the powdered samples and may be assigned to single crystal orientation effects. The small residual asymmetry present in the powdered samples could not be removed even on repeated grinding. However this was in all probability due to preferential orientation of microcrystallites in the absorber and this point will be discussed further later.

The Sign of the Nuclear Quadrupole Moment

Having established the presence of a single crystal effect, the study was extended to obtain an estimate of the sign of the nuclear quadrupole moment of the $\frac{3}{2}$ excited state in ^{125}Te.

General Discussion

While Pasternak and Bukshpan (5) have reported that the nuclear quadrupole moment Q is negative in sign, Kuzmin *et al.* (6) have arrived at the conclusion that Q is positive. Pasternak and Bukshpan interpreted the ^{129}I Mössbauer emission and ^{125}Te Mössbauer absorption of TeO_2 in terms of the Goldanskii–Karyagin effect. However, they did not observe an asymmetry in the $^{125}TeO_2$ absorption in their own experiments but instead referred to the earlier results of Stepanov *et al.* (7). An examination of the data of the latter authors clearly shows that their sample of TeO_2 contained more than one

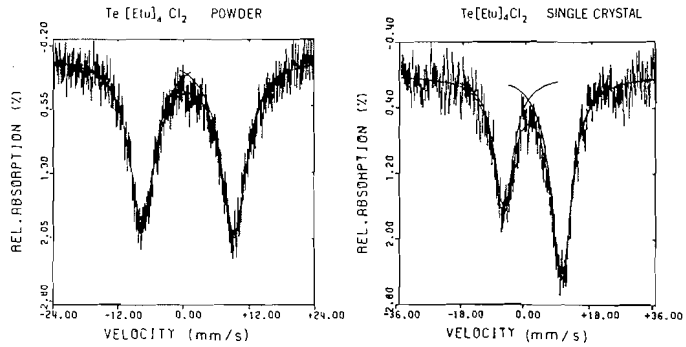

FIG. 1. Single crystal and powder spectra for $TeEtu_4Cl_2$.

TABLE 1.

Compound	Sample	δ* (mm s^{-1})	Δ (mm s^{-1})	2Γ† (mm s^{-1})	χ^2† 248 degrees of freedom	Peak intensities (%) Positive velocity	Negative velocity
$TeTu_4(SCN)_2$	Single crystal	0.74±0.06	16.3±0.1	6.3±0.3	286	62±3	38±3
	Powder	0.79±0.06	16.1±0.1	6.2±0.2	280	53±3	47±3
$TeEtu_4Cl_2$	Single crystal	0.74±0.08	15.8±0.1	6.5±0.5	155	60±3	40±3
	Powder	0.80±0.06	15.9±0.1	6.3±0.5	251	52±3	48±3
$TeTu_4Cl_2 \cdot 2H_2O$	Single crystal	0.70±0.06	15.0±0.1	6.8±0.2	270	46±1	54±1
	Powder	0.74±0.07	15.1±0.1	6.8±0.1	264	48±1	52±1
$TeTu_4Cl_2$	Single crystal	0.76±0.06	15.3±0.1	Mean of three measurements		49±2	51±2
(anhydrous)	Powder	0.76±0.06	15.6±0.1	6.5±0.3	231	51±1	49±1

*δ with respect to PbTe, source and absorber at 80 ± 1 °K.
†2Γ and χ^2 values are for the first half of each mirror image spectrum.

tellurium site and that the asymmetry of the lines in the spectrum cannot be assigned with any certainty to anisotropy of the recoil-free fraction in TeO_2. It must be noted, however, that subsequent experiments by Pasternak and Spijkervet (8) on $MnTe_2$ demonstrated, through the magnetic perturbation of the quadrupole coupling, that the sign of e^2qQ in the proposed Te_2^{2-} ion is negative and, assuming a simple model for the bonding in this ion, this must imply that Q is negative. There is some question however as to whether $MnTe_2$ can be considered an ionic solid containing discrete $[Te—Te]^{2-}$ ions. Thus the ^{125}Te quadrupole splittings (9) in $FeTe_2$ (3.32 mm s^{-1}), $CoTe_2$ (3.90 mm s^{-1}), and $RuTe_2$ (4.57 mm s^{-1}) are significantly different from those of $MnTe_2$ (7.8 mm s^{-1}). This is evidence of considerable covalent bonding between the tellurium $5p_x$ and $5p_y$ orbitals and the metal in the former compounds, and while such bonding may be less important in $MnTe_2$ as a result of the Mn d^5 configuration it would appear a considerable approximation to neglect it completely. In the di-antimonides such covalent bonding is predominant, leading to a negative sign for V_{zz} in comparison with the positive sign proposed for the ditelluride ion. Note that here V_{zz} is the maximum component of the electrostatic field gradient tensor and that $V_{zz} = eq$, where e is the charge on the proton. Kuzmin *et al.* (6) studied the asymmetry in the ^{125}Te Mössbauer absorption spectrum of oriented single crystals of elemental tellurium and concluded that e^2qQ was negative and hence, assuming that V_{zz} for tellurium is negative (10) in sign, that Q must be positive. However Boolchand *et al.* (11) have made a similar study and from their data concluded that e^2qQ is positive and that Q must therefore be negative. Aside from the problem of determining the sign of e^2qQ, this approach depends on a knowledge of the sign of V_{zz} in elemental tellurium. Given the complicated crystal structure of tellurium, the sign of V_{zz} is not immediately apparent and

Can. J. Chem. Downloaded from www.nrcresearchpress.com by 210.87.254.5 on 09/05/12
For personal use only.

Can. J. Chem. Downloaded from www.nrcresearchpress.com by 210.87.254.5 on 09/05/12
For personal use only.

the only estimate of this parameter has come through the calculations of Violet *et al.* (10) which in turn involved several assumptions.

The tellurium(II) thiourea complexes seem to be well suited to provide a further estimate of the sign of Q. Thus the molecules have a very large quadrupole splitting, leading to a wide separation of the naturally broad lines in the spectrum, and thus allowing a ready measurement of differences in the line intensities. Moreover the direction and sign of V_{zz} in these molecules is obvious from a consideration of the bonding. The tellurium in the $TeTu_4^{2+}$ cation is bonded to four sulfur atoms in a regular square-plane with a lone-pair of 5p electrons directed out of the plane (2). The asymmetry parameter in such a centro-symmetric molecule will be zero, the direction of V_{zz} will lie along the $5p_z$ orbital normal to the plane, and the sign of V_{zz} will be negative.

Orientation Studies on the Thiourea Complexes

An examination of the available crystal structure data shows that only preliminary measurements have been reported for $TeTu_4(SCN)_2$ (3) and $TeEtu_4Cl_2 \cdot 2H_2O$ (4), while full crystal structures have been carried out on $TeTu_4Cl_2$ and its dihydrate (12). Of the latter two compounds $TeTu_4Cl_2$ (anhydrous) appears at first glance to be the more promising one for single crystal orientation studies. The compound crystallizes from thiourea–methanol solutions as thin triclinic plates and with one molecule per unit cell. The crystal habit is a favorable one for orienting the single crystals with respect to the γ-ray beam in a Mössbauer experiment, while the presence of only one molecule in the unit cell simplifies the analysis of the data. However a computer analysis (see Appendix) of the position of the atoms in the unit cell (12) leads to the following conclusion. The square-planar $TeTu_4^{2+}$ ion is oriented in such a way that the axis normal to this plane (which also corresponds to the direction of V_{zz}) makes an angle of 56° 15′ with the c axis of the crystal, the latter being normal to the face of the platelets. Since the angular dependence of the relative intensities of the two transitions observed in the Mössbauer spectrum for a $\frac{1}{2} \rightarrow \frac{3}{2}$ transition is given by

$$\frac{I_{\frac{1}{2}-\frac{3}{2}}}{I_{\frac{1}{2}-\frac{1}{2}}} = \frac{1 + \cos^2\theta}{\frac{5}{3} - \cos^2\theta}$$

where θ is the angle between V_{zz} and the direction of the incident Mössbauer γ-ray beam; for θ = 56° 15′

$$I_{\frac{1}{2}-\frac{3}{2}}/I_{\frac{1}{2}-\frac{1}{2}} = 0.99$$

Thus it should be exceedingly difficult to observe an asymmetry for this compound with the platelets oriented at 90° to the beam and indeed this was found to be the case. Three independently prepared single crystal samples of $TeTu_4Cl_2$ were studied and no statistically significant asymmetry was observed in this orientation. Attempts to study this compound with the platelets aligned parallel to the γ-beam proved unsuccessful because of the difficulty of suitably mounting and aligning the large number of individual single crystals.

The dihydrate, $TeTu_4Cl_2 \cdot 2H_2O$, is monoclinic ($\beta = 98.5°$) and crystallizes from hot aqueous thiourea as needles which are extended along the crystallographic a axis. The two molecules in the unit cell are related by rotation through 180° about the b axis and translation by one half a unit cell along b, and thus are identical with respect to the orientation of V_{zz} and the direction of the incident γ-ray beam when the latter is incident at 90° to the a axis. An analysis of the position of the atoms in the unit cell (see Appendix) shows that the normal to the plane in which the $TeTu_4^{2+}$ ion lies subtends an angle of 15° with the crystallographic a axis. If in the Mössbauer experiment the $TeTu_4Cl_2 \cdot 2H_2O$ crystals are aligned in the absorber holder such that the needle axes are at right angles to the γ-ray beam, then rotation of the needles in the plane of the holder about the axis of the incident γ-rays would not influence θ. However rotation of the needles about the a axis would, as shown in Fig. 2. The angle between the direction of the γ-ray beam and the normal to the $TeTu_4^{2+}$ plane would then vary between 75 and 105°. Thus the minimum asymmetry would in theory be given by

$$\frac{I_{\frac{1}{2}-\frac{3}{2}}}{I_{\frac{1}{2}-\frac{1}{2}}} = \frac{1 + \cos^2 75^\circ}{\frac{5}{3} - \cos^2 75^\circ} = 0.66$$

and for any value of θ between 75 and 105° the $I_{\frac{3}{2}-\frac{1}{2}}$ transition should be the more intense of the two transitions.

In practise it was found difficult to obtain large single crystals of $TeTu_4Cl_2 \cdot 2H_2O$ on the preparative scale used in this work. The dihydrate is obtained on cooling hot, aqueous thiourea solutions of $TeTu_4Cl_2$, and to obtain large single

Can. J. Chem. Downloaded from www.nrcresearchpress.com by 210.87.254.5 on 09/05/12
For personal use only.

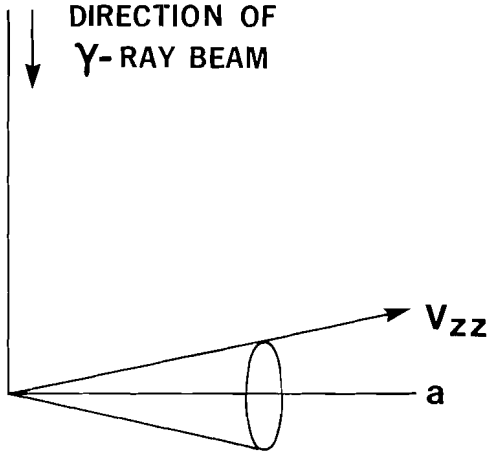

FIG. 2. The angle swept out by V_{zz} on rotation about the a axis.

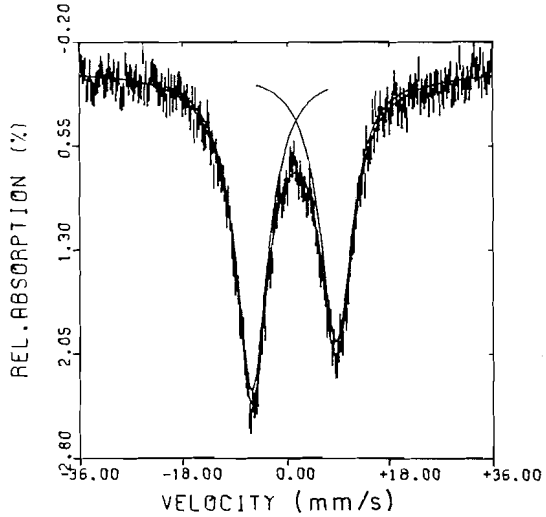

FIG. 3. The single crystal spectrum for $TeTu_4Cl_2 \cdot 2H_2O$.

crystals the solution should be cooled slowly. However, such hot solutions show a tendency to precipitate elemental tellurium, and a compromise had to be reached in the time taken to cool the solution. The larger single crystals obtained were selected for the Mössbauer experiment and were mounted in grease in the absorber holder with their needle axes at right angles to the γ-ray beam. However an asymmetry of only 8% was observed, *i.e.*

$$I_{\frac{1}{2}-\frac{3}{2}}/I_{\frac{1}{2}-\frac{1}{2}} = 0.81$$

and this relatively small asymmetry must reflect some randomization of the crystals in the absorber holder. A sample single crystal spectrum is shown in Fig. 3.

From the above discussion the more intense peak in Fig. 3 can be assigned to the $\frac{1}{2}-\frac{1}{2}$ transition and, since this lies at negative Doppler velocity of the source, the $m_I = \frac{1}{2}$ state must lie at lower energies than the $m_I = \frac{3}{2}$ state. Since, when $\eta = 0$

$$E_{m_I} = \frac{e^2qQ}{4I(2I-1)}[3m_I^2 - I(I+1)]$$

it follows that e^2qQ in $TeTu_4Cl_2 \cdot 2H_2O$ is positive and, since V_{zz} is negative for the $TeTu_4^{2+}$ ion, that Q must be negative. Thus the present experiments provide further support for the assignment of a negative nuclear quadrupole moment to the $\frac{3}{2}$ excited state in ^{125}Te.[1]

[1]We understand that N. E. Erickson (private communication) has made similar measurements to those reported in this paper and has also concluded that Q is negative.

The small residual asymmetry observed in the powdered samples had the same sign as that of the single crystal sample of each compound (see Table 1), having one sign for $TeTu_4(SCN)_2$ and $TeEtu_4Cl_2$, and the opposite sign for $TeTu_4Cl_2 \cdot 2H_2O$. In each of these compounds the tellurium is bonded in essentially the same square-planar environment, and anisotropy of the recoil-free fraction would be expected to result in a line asymmetry of the same sign in each case. Since this was not observed, this would suggest that the residual asymmetry was not due to the Goldanskii–Karyagin effect but due to preferential packing of the microcrystallites in the powdered samples. The different signs for the asymmetry observed in $TeTu_4(SCN)_2$ and $TeEtu_4Cl_2$ on the one hand and $TeTu_4Cl_2 \cdot 2H_2O$ on the other must reflect different values of θ in these two cases, both in the single-crystal and the microcrystalline samples.

A powdered sample of $TeTu_4Cl_2$ (anhydrous) was found, within the errors, to have no measurable asymmetry. In this case any preferential packing of micro-crystallites in the absorber would presumably occur such that V_{zz} and the γ-ray beam would subtend an angle of about 56° 15′, and would thus contribute nothing to the asymmetry. Thus any anisotropy of the recoil-free fraction would be less masked by single crystal orientation effects in $TeTu_4Cl_2$ (anhydrous) than in the case of the other compounds studied. Nevertheless, even here, no concrete evidence was found for asymmetry due

to anisotropy of the recoil-free fraction and it can only be concluded that such effects must be very small, if present at all, in these molecules. This finding is consistent with the results of previous Mössbauer investigations on the similar planar molecules $KICl_4 \cdot H_2O$ (13) and I_2Cl_6 (14) where no evidence was found for anisotropy of the recoil-free fraction.

Conclusions

Within the errors of the measurements, there is no evidence for anisotropy of the recoil-free fraction in these molecules. However, as in all Mössbauer measurements, some caution must be exercized in interpreting the relative intensities of the spectral lines for polycrystalline absorbers. Preferential packing of microcrystallites in the powdered absorber may lead to orientation effects masking possible anisotropy effects. Even in the case of $TeTu_4Cl_2$ (anhydrous) there is some uncertainty in the results, since, for example, preferential packing could occur at some angle other than 56° 15′. It can only be stated that any anisotropy of the recoil-free fraction must be very small.

The single crystal experiments on $TeTu_4Cl_2 \cdot 2H_2O$ support the assignment of a negative nuclear quadrupole moment to the tellurium $\frac{3}{2}$ excited state.

Experimental

The compounds were synthesized using 75% enriched ^{125}Te on the 100 mg scale and using the methods described by Foss (2). All absorbers were of comparable thickness containing *ca.* 10–15 mg cm^{-2} of ^{125}Te.

The Mössbauer spectra were recorded using the general methods previously described (1), but with several important differences. Instead of a Xe/CO_2 proportional detector, a Ge(Li) detector was used. As a result, higher count rates were attained in these experiments allowing the accumulation of spectra in shorter times. A cadmium absorber was used to attenuate the tellurium X-rays and ensure good resolution of the 35.5 keV γ-ray at high count rates. In all runs an iron foil standard spectrum was recorded simultaneously with the ^{125}Te spectrum using a $^{57}Co(Pd)$ source mounted on the rear of the transducer and utilizing a Nuclear Data dual input router in conjunction with the multi-channel analyzer. This form of calibration ensured a constant monitoring of the experiment and allowed a velocity calibration for each run. The standard parameters for iron given in ref. 15 were assumed. The ^{125}Te source used in these experiments, Pb ^{125m}Te, was obtained by irradiating $Pb^{124}Te$ (100 mg) at a thermal neutron flux of *ca.* 10^{14} neutrons cm^{-2} s^{-1} for a month at A.E.C.L. Chalk River Nuclear Laboratories. This source was found preferable to an $^{125}I/Cu$ source since it gave narrower linewidths.

Appendix

The analysis of the crystal structure data was performed using the program Xanadu (16). The required input data were the parameters of the atoms in the unit cell, and the lattice type of symmetry. The program calculates, among other things, bond-lengths, bond-angles, the equations of planes containing specified atoms, and the angles between specified lines and the normals to planes.

$TeTu_4Cl_2$

Triclinic, $a = 5.83$, $b = 7.77$, $c = 10.86$ Å, $\alpha = 95.5°$, $\beta = 90°$, $\gamma = 119.5°$, space group $C_i^1 - P\bar{1}$, and the equation of the plane describing the $TeTu_4^{2+}$ cation, expressed in terms of unit orthogonal axes XO, YO, and ZO, is $(0.8292)XO - (0.0594)YO + (0.5558)ZO = 0$ where XO, YO, and ZO are as defined in ref. 17. The angle between the c axis and the normal to the plane is 56.24°.

$TeTu_4Cl_2 \cdot 2H_2O$ is monoclinic, $a = 6.01$ Å, $b = 16.49$ Å, $c = 9.95$ Å, $\beta = 98.5°$, space group $C_{2h}^5 - P2_1/c$, and the equation of the plane describing the $TeTu_4^{2+}$ cation is $(0.9362)XO + (0.2389)YO + (0.2578)ZO = 0$.

The angle between the normal to the plane and (*i*) the b axis which also corresponds to the axis YO, is 103.82° and (*ii*) the a axis is 15.0°.

The authors acknowledge a grant in support of this research from the National Research Council of Canada. They wish to thank Dr. F. Brown, Head, Solid State Research Branch, Atomic Energy of Canada Limited, Chalk River, for arranging for the irradiation of the PbTe source and Dr. F. W. B. Einstein, Simon Fraser University, for many helpful discussions.

1. B. M. Cheyne, M.Sc. Thesis. Simon Fraser University, Burnaby, British Columbia. 1972. p. 49; B. M. Cheyne, C. H. W. Jones, and P. Vasudev. Can. J. Chem. **50**, 3677 (1972).
2. O. Foss. Pure Appl. Chem. **24**, 31 (1970).
3. O. Foss and S. Hauge. Acta Chem. Scand. **15**, 1616, (1961).
4. O. Foss and S. Fossen. Acta Chem. Scand. **15**, 1620, (1961).
5. M. Pasternak and S. Bukshpan. Phys. Rev. **163**, 297 (1967).
6. R. N. Kuzmin, A. A. Opalenko, V. S. Shpinel, and I. Avenarins. Sov. Phys. JETP, **29**, 94 (1969).
7. E. P. Stepanov, K. P. Aleshin, R. A. Manapov, B. N. Samoilov, V. V. Sklyarevsky, and V. G. Stankevich. Phys. Lett. **6**, 155 (1963).
8. M. Pasternak and A. L. Spijkervet. Phys. Rev. **181**, 574 (1969).
9. A. Kjekshus and D. G. Nicholson. Acta Chem. Scand. **26**, 3241 (1972).

Can. J. Chem. Downloaded from www.nrcresearchpress.com by 210.87.254.5 on 09/05/12
For personal use only.

10. C. E. VIOLET, R. BOOTH, and F. WOOTEN. Phys. Lett. **5**, 230 (1963).
11. P. BOOLCHAND, B. L. ROBINSON, and S. JHA. Phys. Rev. B, **2**, 3463 (1970).
12. K. FOSHEIM, O. FOSS, A. SCHEIE, and S. SOLHEIMSNES. Acta Chem. Scand. **19**, 2336 (1965).
13. G. J. PERLOW. *In* Chemical applications of Mössbauer spectroscopy. *Edited by* V. I. Goldanskii and R. H. Herber. Academic Press, New York, 1968. p. 390.
14. M. PASTERNAK and T. SONNINO. J. Chem. Phys. **48**, 2004 (1968).
15. A. H. MUIR, K. J. ANDO, and H. M. COOGAN. *In* Mössbauer effect data index 1958–65. Interscience, New York, 1966. p. 26.
16. P. ROBERTS and G. SHELDRICK. Private communication.
17. J. S. ROLLETT. Computing methods in crystallography. Pergamon, London. 1965. p. 22.

Can. J. Chem. Downloaded from www.nrcresearchpress.com by 210.87.254.5 on 09/05/12
For personal use only.

^{13}C Nuclear Magnetic Resonance Studies of Organometallic Compounds. III. *cis*-Methylplatinum(II) Derivatives[1]

H. C. CLARK AND J. E. H. WARD[2]

Department of Chemistry, The University of Western Ontario, London, Ontario N6A 3K7

Received September 18, 1973

Eight new *cis*-methylplatinum(II) derivatives of the type *DIARS*Pt(CH_3)X (*DIARS* abbreviates *o*-phenylenebis(dimethylarsine), where X is an anionic substituent, and $[DIARSPt(CH_3)L]^+PF_6^-$, where L is a neutral ligand, have been prepared. Data derived from the ^{13}C n.m.r. spectra of these complexes are discussed and compared with data derived from the ^1H n.m.r. spectra of the complexes. Comparisons with the ^{13}C n.m.r. parameters obtained from related series of *trans*-methylplatinum(II) derivatives reveal marked differences between the n.m.r. *cis*- and *trans*-influences. It appears that the n.m.r. *cis*-influence may in part be related to a ligand's "steric bulk".

On a préparé huit nouveaux dérivés *cis*-méthylplatine du type *DIARS*-Pt(CH_3)X (*DIARS* étant l'abréviation de *o*-phénylenebis (diméthylarsine)), où X est un substituant du type anionique, et du type $[DIARSPt(CH_3)L]^+PF_6^-$, où L est un coordinat neutre. On discute et l'on compare les données obtenues à partir des spectres r.m.n. du ^{13}C de ces complexes avec celles obtenues à partir des spectres r.m.n. du ^1H des complexes. La comparaison de ces données avec les paramèters obtenus de la r.m.n. du ^{13}C d'une série parente de dérivés *trans*-méthylplatine(II) a montré que l'influence des formes *cis* et *trans* sur les spectres r.m.n. était très différente. Il semble que l'influence de la forme *cis* sur les spectres r.m.n., soit imputable, en partie, à un encombrement stérique du coordinat. [Traduit par le journal]

Can. J. Chem., **52**, 570 (1974)

Introduction

While nuclear magnetic resonance studies of transition metal derivatives have yielded substantial information concerning the *trans*-influence (2), investigations (3, 4) of the n.m.r. *cis*-influence have been generally unrewarding. Our examination of series of *trans*-phenylplatinum(II) (1) and *trans*-methylplatinum(II) (5, 6) complexes has indicated that ^{13}C n.m.r. is an extremely powerful technique for the study of bonding in these and related derivatives. Thus, it appeared that the *cis*-influence might also be conveniently and successfully examined by ^{13}C n.m.r.

Accordingly, we have synthesized a number of new *cis*-methylplatinum(II) complexes of the type *DIARS*Pt(CH_3)X (where X is an anionic substituent) and $[DIARSPt(CH_3)L]^+PF_6^-$ (where L is a neutral ligand). We have specifically chosen the chelating ditertiary arsine *DIARS*-(*o*-phenylenebis(dimethylarsine) in order to preclude *cis–trans* isomerization in solution. In addition, we have selected the *cis* ligands L to encompass a wide range of the *trans*-influence, which some workers believe parallels a ligand's *cis*-influence.

The n.m.r. parameters of the platinum–methyl, arsenic–methyl, and aromatic carbons are discussed and compared with the n.m.r. parameters of related *trans*-methylplatinum derivatives. Finally, we note an interesting possible qualitative relationship between the n.m.r. *cis*-influence and the "steric bulk" of a ligand.

Experimental

The following chemicals were obtained commercially and used without further purification: diethylsulfide, *o*-phenylenebis(dimethylarsine), acetyl chloride, γ-picoline, triphenylphosphine, triphenylarsine, anisonitrile, and carbon monoxide. Methyllithium (1.50 *M* in ether) and silver hexafluorophosphate were purchased from Alfa Inorganics, Inc.

Potassium tetrachloroplatinite was prepared from platinum sponge by a modified method of Keller (7). Ethylisocyanide was obtained by the method of Casanova, Schuster, and Werner (8).

All reactions and recrystallizations were carried out using reagent grade or spectrograde solvents. Microanalyses were performed by Chemalytics Inc., Tempe, Arizona. The infrared spectrum was recorded on a Perkin–Elmer 621 spectrometer using 0.5 mm potassium bromide cells. Uncorrected melting points were determined on a Thomas Hoover "unimelt" capillary melting point apparatus.

The ^{13}C n.m.r. spectra were measured on a Varian XL-100-15 spectrometer operating in the pulsed Fourier transform mode at 25.2 MHz. All spectra were determined with noise-modulated proton decoupling. The spectra were taken on chloroform-*d* and/or methylene chloride-d_2 solutions in 5 mm sample tubes and were

[1]For the previous paper in this series see ref. 1.

[2]To whom correspondence should be addressed.

Can. J. Chem. Downloaded from www.nrcresearchpress.com by 210.87.254.105 on 09/05/12
For personal use only.

TABLE 1. Analytical data for the new complexes *DIARS*Pt(CH_3)R(**1–2**) and [*DIARS*Pt(CH_3)L]$^+PF_6^-$(**3–8**)

Complex	L or R	Calcd. (%) C	Calcd. (%) H	Found (%) C	Found (%) H	Yield (%)	Melting point (°C)
1	CH_3^-	28.2	4.34	28.5	4.33	44	171–172
2	Cl^-	24.9	3.60	24.9	3.46	80	281–283*
3	γ-$CH_3C_5H_4N$	27.8	3.57	27.9	3.41	72	212–213
4	$(C_6H_5)_3P$	38.6	3.79	38.7	3.66	98	242–245
5	ρ-$CH_3OC_6H_4CN$	29.5	3.38	29.4	3.20	74	187–188*
6	$(C_6H_5)_3As$	36.8	3.62	36.8	3.50	77	228–229
7	CH_3CH_2NC	24.2	3.47	24.1	3.27	83	151–155
8	CO†	21.5	2.86	21.7	2.78	75	197–200*

*Complex melts with decomposition.
†ν_{CO} = 2107(±2) cm^{-1} (CH_2Cl_2).

calibrated using the solvent resonances as secondary calibration standards (9).

^1H n.m.r. spectra were recorded on a Varian HA-100 spectrometer and the ^1H chemical shifts are reported with TMS as the internal standard.

A. Preparation of DIARSPtCl$_2$

This procedure was carried out using nitrogen saturated solvents and a nitrogen atmosphere. A solution of K_2PtCl_4 (5.0 g, 12.0 mmol) in 100 ml water was treated with $(CH_3CH_2)_2S$ (3.4 ml, 31.6 mmol). The reaction mixture was stirred for 3 h and then extracted with three 20 ml portions of methylene chloride. The combined methylene chloride extracts were added to a solution of *DIARS* (3.38 g, 11.8 mmol) in 100 ml methylene chloride. This was stirred for 16 h and then *ca.* 200 ml heptane were added. Evaporation of this solution to *ca.* 200 ml resulted in precipitation of a pale yellow solid which was recovered by filtration and vacuum dried, yielding *DIARS*PtCl_2 (6.1 g, 90%).

B. Preparation of DIARSPt(CH_3)$_2$(1)

Under a nitrogen atmosphere, a suspension of *DIARS*-PtCl_2 (6.1 g, 11.0 mmol) in 100 ml ether was cooled to 0°. Following the addition of 1.50 *M* methyllithium (40 ml, 60 mmol), the reaction mixture was stirred for 2 h at 0°. After hydrolysis with a saturated aqueous solution of ammonium chloride, and then water, the mixture was extracted with three portions of ether, and the combined extracts were dried over anhydrous magnesium sulfate. The ether layer was mixed with an equal volume of hexane and the solution was evaporated to *ca.* 50 ml. This caused precipitation of white crystals which were filtered and vacuum dried, yielding *DIARS*Pt(CH_3)$_2$(**1**) (4.20 g, 74%).

C. Preparation of DIARSPt(CH_3)Cl(2)

To a solution of *DIARS*Pt(CH_3)$_2$(**1**) (0.500 g, 0.98 mmol) in 50 ml ether was added acetyl chloride (70 μl, 0.98 mmol). While the solution was stirred 16 h, a white solid precipitated, presumably *DIARS*Pt(IV)(CH_3)$_2$-(CH_3CO)Cl.

Following evaporation of the ether, the solid was mixed with some methanol and the solution refluxed for 2 h. Evaporation of the methanol yielded a yellow solid which was purified by passing a methylene chloride solution of the substance through a short Florisil column. This afforded a colorless solution which was evaporated, yielding white crystals of *DIARS*Pt(CH_3)Cl(**2**) (0.416 g, 80%).

D. Preparation of [DIARSPt(CH_3)(γ-$CH_3C_5H_4N$)]$^+$-PF_6^- (3)

To a solution of *DIARS*Pt(CH_3)Cl (0.072 g, 0.136 mmol) in 10 ml acetone was added a solution of $AgPF_6$ (0.0344 g, 0.136 mmol) in 5 ml acetone. Silver chloride precipitated immediately and was removed by centrifuging the solution; next, γ-$CH_3C_5H_4N$ (13 μl, 0.136 mmol) was added, and the solution was stirred for 2 h. After removing the solvent on a rotary evaporator, the residual material was dissolved in methylene chloride and the solution was passed through a short Florisil column. White crystals precipitated from the solution on the addition of ether and these were washed with ether and then vacuum dried, yielding **3** (0.072 g, 72%).

E. Preparation of [DIARSPt(CH_3)CO]$^+PF_6^-$ (8)

To a solution of *DIARS*Pt(CH_3)Cl (0.150 g, 0.283 mmol) in 25 ml acetone was added a solution of $AgPF_6$ (0.072 g, 0.283 mmol) in 3 ml acetone. Silver chloride precipitated immediately and was removed by centrifuging the solution. After bubbling carbon monoxide through this solution for 0.5 h, the acetone was removed on the rotary evaporator. The solid residue was dissolved in methylene chloride and the solution was mixed with a small quantity of activated charcoal and passed through a short Florisil column. The addition of ether resulted in the formation of white crystals which were washed with ether and vacuum dried, yielding **8** (0.136 g, 75%).

The latter two procedures, *D* and *E*, are typical of those used for the preparation of all the cationic complexes described here. The analytical data for the new complexes **1–8** are summarized in Table 1.

Results

Preparation of the Complexes

*DIARS*PtX_2 (X = Cl^-, Br^-, I^-) has been reported only very recently. Hudson *et al.* (10) obtained this derivative in 18% yield by the following method:

Can. J. Chem. Downloaded from www.nrcresearchpress.com by 210.87.254.105 on 09/05/12
For personal use only.

TABLE 2. ^{13}C shieldings* for the complexes *DIARS*Pt(CH_3)R(**1–2**) and [*DIARS*Pt(CH_3)L]$^+PF_6^-$(**3–8**)

Complex	R or L	Solvent	Platinum methyl δC	Arsine methyls δC	Aromatic carbons† Quaternary δC	Ortho δC	Meta δC	Other
1	CH_3^-	CD_2Cl_2	−8.8	11.0	143.3	130.4	131.1	
		$CDCl_3$	−9.1	10.9	143‡	130.0	130.8	
2	Cl^-	CD_2Cl_2	−5.4	11.2	139.8	129.8	131.5	
				11.0	140.7	130.9	131.8	
3	γ-$CH_3C_5H_4N$	CD_2Cl_2	−4.0	10.6	138.1	130.0	132.1	δCH_3 21.0, $\delta C_{3,5}$ 127.8
				11.0	139.0	130.7	132.4	$\delta C_{2,6}$ 150.4, δC_4 151.5
		$CDCl_3$	−3.8	10.4	137.6	129.9	131.9	δCH_3 21.0, $\delta C_{3,5}$ 127.7
				11.0	138.6	130.4	132.3	$\delta C_{2,6}$ 150.1, δC_4 151.1
4	$(C_6H_5)_3P$	CD_2Cl_2	−8.0	10.6	137.7	§	§	δC_6H_5 and δC *DIARS*
				11.9	138.3	§	§	128.8–134.5
5	*p*-$CH_3OC_6H_4CN$	CD_2Cl_2	−8.5	10.9	137.5	130.1	132.4	δOCH_3 56.1, δC_1 99.8,
				12.5	138.6	130.9	132.8	$\delta C_{3,5}$ 115.6, δCN 124.4,
								$\delta C_{2,6}$ 135.5, δC_4 165.1
6	$(C_6H_5)_3As$	CD_2Cl_2	−10.9	10.8	137.3	§	§	δC_6H_5 and δC *DIARS*
				12.5	140.0	§	§	129.6–133.5
7	CH_3CH_2NC	CD_2Cl_2	−15.6	10.1	137.5	130.7	132.9	δCH_3 14.6, δCH_2 40.4
				13.1	139.1	130.9	132.9	δNC‖
		$CDCl_3$	−15.4	10.0	136.9	130.6	132.5	δCH_3 14.5, δCH_2 40.1,
				13.1	138.8	130.6	132.7	δNC‖
8	CO	CD_2Cl_2	−14.1	10.6	137.5	131.1	133.5	δCO‖
				14.2	137.5	131.1	133.8	

*In p.p.m. (±0.1) (downfield positive) from TMS.
†The ortho carbons are assigned to those having the largest ^{13}C–^{195}Pt coupling constants. We have observed (1) that three bond J_{PtC} values are frequently much larger than two or four bond J_{PtC} values.
‡Folded over signal; shielding estimated by extrapolation.
§Resonance obscured by $(C_6H_5)_3E$ signals (E = P or As).
‖Signal not observed.

$$[1]\qquad (C_6H_5CN)_2PtCl_2 + \textit{DIARS} \xrightarrow[CHCl_3]{\text{refluxing}} \textit{DIARS}PtCl_2 + 2C_6H_5CN$$

We now wish to report a vastly improved preparation in which the material may be obtained smoothly in *ca.* 90% yield

$$[2]\qquad ((C_2H_5)_2S)_2PtCl_2 + \textit{DIARS} \rightarrow \textit{DIARS}PtCl_2 + 2(C_2H_5)_2S$$

This method is analogous to that used by Whitesides *et al.* (11) to obtain dichloro[1,1′-bis(diphenylphosphino)ferrocene]platinum(II). All other derivatives reported here were prepared by standard procedures.

Nuclear Magnetic Resonance Results

The ^{13}C n.m.r. shieldings and coupling constants obtained from the spectra of **1–8** are summarized in Tables 2 and 3, respectively. Since we have not determined the relative signs of the ^{13}C–^{195}Pt coupling constants, the absolute values of these parameters are provided in Table 3. The use of their absolute values is adequate for the majority of the arguments we will present later.

In all cases the high field resonances of the spectra were assigned, on the basis of their relative intensities, to the carbons of the platinum methyl groups of **1–8**. The central resonances are flanked by widely spaced ^{195}Pt satellites of *ca.* one fourth intensity, whose separation appears to be sensitive to the nature of R or L.

The ^{13}C resonances of the arsenic methyl groups span a range (*ca.* 10–14 p.p.m.) similar to that (*ca.* 7–10 p.p.m.) observed for the series of related *trans*-methylplatinum(II) derivatives (1, 5). Together with this information and relative intensity observations, the assignments were readily carried out. As we had anticipated for the unsymmetrically substituted complexes **2–8** two sets of arsenic methyl signals were observed.

Assignments of the carbon resonances of the aromatic rings were carried out using similar arguments. The quaternary carbons could be

Can. J. Chem. Downloaded from www.nrcresearchpress.com by 210.87.254.105 on 09/05/12
For personal use only.

TABLE 3. ^{13}C–^{195}Pt coupling constants* for the complexes *DIARS*Pt(CH_3)R(1–2) and [*DIARS*Pt(CH_3)L]$^+PF_6^-$(3–8)

Complex	R or L	Solvent	Platinum methyl $\lvert^1J_{PtC}\rvert$	Arsine methyls $\lvert^2J_{PtAsC}\rvert$	Aromatic† carbons $\lvert^3J_{PtAsCC}\rvert$	Other
1	CH_3^-	CD_2Cl_2	690(±2)	27(±2)	‡	
		$CDCl_3$	678(±2)	28(±2)	‡	
2	Cl^-	CD_2Cl_2	555(±2)	80(±2)	27(±2)	
				10(±4)	10(±2)	
3	γ-$CH_3C_5H_4N$	CD_2Cl_2	575(±2)	70(±2)	26(±4)	$^2J_{PtNC_{2,6}}$17(±2), $^3J_{PtNCC_{3,5}}$40(±2)
				13(±2)	13(±2)	
		$CDCl_3$	575(±2)	68(±2)	25(±4)	$^2J_{PtNC_{2,6}}$18(±2), $^3J_{PtNCC_{3,5}}$40(±2)
				10(±4)	16(±4)	
4	$(C_6H_5)_3P$	CD_2Cl_2	533(±2)	45(±2)	‡	
				15(±2)	‡	
5	*p*-$CH_3OC_6H_4CN$	CD_2Cl_2	523(±2)	76(±4)	30(±4)	
				10(±2)	10(±4)	
6	$(C_6H_5)_3As$	CD_2Cl_2	508(±2)	54(±4)	‡	
				16(±4)	‡	
7	CH_3CH_2NC	CD_2Cl_2	500(±2)	55(±2)	20(±2)	
				15(±2)	10(±4)	
		$CDCl_3$	498(±2)	55(±2)	23(±2)	
				15(±2)	10(±4)	
8	CO	CD_2Cl_2	453(±3)	54(±3)	23(±3)	
				14(±6)	‡	

*In Hz.
†^{13}C–^{195}Pt coupling was not observed for any of the quaternary or meta aromatic carbons of **1–8**.
‡^{13}C–^{195}Pt coupling not observed.

distinguished from the ortho and meta carbons by their respective relative intensities. For **2–8**, the ortho and meta carbons were distinguished from one another on the basis of the relative magnitudes of their respective ^{13}C–^{195}Pt coupling constants. We anticipated that the *vicinal* $^3J_{PtAsCC}$ values are much larger than the $^4J_{PtAsCCC}$ values, since we have already observed a similar trend in a series of σ-bonded phenyl derivatives, *trans*-[$(C_6H_5)Pt(As(CH_3)_3)_2L]^+PF_6^-$ (1). In those complexes, $^3J_{PtC_{3,5}}$ (*ca.* 34–68 Hz) is significantly larger than $^4J_{PtC_4}$ (*ca.* 10 Hz).

The assignments of the quaternary, ortho, meta, and arsenic methyl *cis–trans* isomeric pairs require specific comment. Those carbons possessing platinum satellites may be generally divided into two classes, based on the relative magnitudes and ranges of the ^{13}C–^{195}Pt coupling constants. For example, for the arsenic methyl carbons, one of the $^2J_{PtAsC}$ values is large (*ca.* 45–80 Hz) and varies over a wide range, while the other $^2J_{PtAsC}$ value is small (*ca.* 10–16 Hz) and does not fluctuate so widely. On the basis of our observations on the relative sensitivities of *cis*- and *trans*-substituents to ligand variations (1, 2, 5), we have assigned the methyl carbons on the arsenic atoms *trans* to the ligand L, to the class with large $^2J_{PtAsC}$ values. A similar argument may be employed in assigning the stereochemistries of the ortho aromatic carbon atoms.

The signals arising from the ligands *cis* to the platinum methyl group were specifically assigned by comparing their ^{13}C n.m.r. parameters with those derived from the related *trans*-methylplatinum(II) derivatives (5).

The ^1H n.m.r. data for the new complexes **1–8** are assembled in Table 4. Assignments of the ^1H chemical shifts and J_{PtH} values were based on arguments similar to those used to assign the ^{13}C n.m.r. parameters.

Discussion

The cis- and trans-Influences

The *trans*-influence has been defined as the tendency of a ligand in a metal complex to weaken the bond *trans* to itself (12); it is believed to arise from the rehybridization of metal σ-orbitals in response to *trans*-ligand variations

Can. J. Chem. Downloaded from www.nrcresearchpress.com by 210.87.254.105 on 09/05/12
For personal use only.

TABLE 4. ^{1}H n.m.r. chemical shifts* and coupling constants† for the complexes *DIARS*Pt(CH_3)R(**1–2**) and [*DIARS*Pt(CH_3)L]$^+PF_6^-$(**3–8**)

Complex	R or L	Solvent	Platinum Methyl δ_{CH_3}	Platinum Methyl $\lvert^2J_{PtCH}\rvert$	Arsine Methyls δ_{CH_3}‡	Arsine Methyls $\lvert^3J_{PtAsCH}\rvert$	Arsine Methyls δ_{CH_3}§	Arsine Methyls $\lvert^3J_{PtAsCH}\rvert$	Other
1	CH_3^-	$CHCl_3$	0.670	78.5	1.545	12.5	1.545	12.5	δ_H (*DIARS*) 7.40–7.70
2	Cl^-	CD_2Cl_2	0.720	62.5	1.630	8.0	1.755	30.5	δ_H (*DIARS*) 7.52–7.71
3	γ-$CH_3C_5H_4N$	CD_2Cl_2	0.700	63.0	1.565	9.5	1.825	29.5	δ_H (*DIARS*) 7.54–7.95, δ_{CH_3} 2.48, $\delta_{C_5H_4N}$ 7.46, 8.54 $^3J_{HH}$ 6
		$CDCl_3$	0.645	62.5	1.550	9.0	1.805	30.0	δ_H (*DIARS*) 7.56–8.04 δ_{CH_3} 2.49, $\delta_{C_5H_4N}$ 7.53, 8.60 $^3J_{HH}$ 6
4	$(C_6H_5)_3P$	CD_2Cl_2	0.715	66.0	1.080	10.0	1.835	21.5	δ_H (*DIARS* and C_6H_5) 7.46–8.08
5	*p*-$CH_3OC_6H_4CN$	CD_2Cl_2	0.865	59.0	1.820	9.0	1.840	34.0	δ_H (*DIARS*) 7.63–8.00 δ_{CH_3O} 3.92, $\delta_{C_6H_4}$ 7.14, 7.68, $^3J_{HH}$ 9
6	$(C_6H_5)_3As$	CD_2Cl_2	0.830	63.5	1.150	9.0	1.885	26.0	δ_H (*DIARS* and C_6H_5) 7.33–8.08
7	CH_3CH_2NC	CD_2Cl_2	0.980	66.0	1.860	11.5	1.805	23.5	δ_H (*DIARS*) 7.56–8.00 δ_{CH_3} 1.545, δ_{CH_2} 3.91, $^3J_{HH}$ 6
		$CDCl_3$	0.935	68.5	1.875	11.0	1.780	23.5	δ_H (*DIARS*) 7.47–8.05 δ_{CH_3} 1.545, δ_{CH_2} 3.48. $^3J_{HH}$ 6
8	CO	CD_2Cl_2	1.235	65.5	1.995	11.0	1.880	25.5	δ_H (*DIARS*) 7.66–8.06

*In p.p.m. (downfield positive) from TMS. Those shifts given with three decimal places are accurate to *ca.* ±0.005 p.p.m., while those shown with two decimal places are likely accurate to ±0.01 p.p.m.
†In Hz (±0.5).
‡*trans* to the platinum methyl group.
§*cis* to the platinum methyl group.

(12, 13). Since one bond n.m.r. coupling constants are also thought to be mostly sensitive to the hybridization of the σ-bonding orbitals between adjacent atoms, many workers have commonly formulated relative *trans*-influence series from n.m.r. coupling constant data (2).

If we define the *cis*-influence in a similar manner, as the tendency of a ligand in a metal complex to weaken a bond *cis* to itself, we may also formulate *cis*-influence series via n.m.r. However, the nature of the relationships between the n.m.r. *cis*- and *trans*-influences of a particular ligand remain unknown (2). It has been shown experimentally that the n.m.r. *cis*-influence probably does not relate simply to the n.m.r. *trans*-influence (3, 4), in contrast with the theoretical findings of Drago and co-worker (13). Thus, it has been suggested that n.m.r. *cis*-influence series may not be dominated by σ-orbital rehybridization. Moreover, the relationships between the n.m.r. *cis*-influence and the *cis*-influence itself remain to be delineated.

The ^{13}C and ^1H N.m.r. Data: General

The symmetrically substituted dimethylplatinum(II) derivative **1** falls into a class by itself, and we will discuss it and its n.m.r. data elsewhere. The neutral chloro derivative **2** is also different from the six cationic complexes **3–8**. While we have previously shown (5) that certain relationships do not appear to depend on the charge of a complex, this feature remains to be demonstrated for the derivatives at hand.

The n.m.r. data obtained from complexes **2–8** reveal that with variations in the ligands *cis* to the platinum methyl group, substantial fluctuations in the ^{13}C and ^1H n.m.r. parameters may occur. For example, when γ-picoline is replaced by a carbonyl group, the platinum methyl carbon shielding increases from −4.0 to −14.1 p.p.m., while the one bond ^{13}C–^{195}Pt coupling constant decreases from 575(±2) to 453(±3) Hz. In addition, one of the $^2J_{PtAsC}$ values decreases from 70(±2) to 54(±3) Hz, while the other (*ca.* 13 Hz) remains constant. From the $^1J_{PtC}$ values of

Can. J. Chem. Downloaded from www.nrcresearchpress.com by 210.87.254.105 on 09/05/12
For personal use only.

Can. J. Chem. Downloaded from www.nrcresearchpress.com by 210.87.254.105 on 09/05/12
For personal use only.

the platinum methyl groups we may formulate an n.m.r. *cis*-influence series for the ligands used in **3–8**:

$$CO > CH_3CH_2NC > (C_6H_5)_3As > p\text{-}CH_3OC_6H_4CN > (C_6H_5)_3P > \gamma\text{-}CH_3C_5H_4N$$

This series follows the *trans*-influence series for these ligands with certain important exceptions: both anisonitrile and triphenylphosphine are centered in the series rather than occurring at opposite extremes.[3] Thus, at least qualitatively, the *cis*- and *trans*-influence series do not appear to have a simple relationship.

^{13}C and ^{1}H Coupling Constants

A. Platinum Methyl Groups

A plot of $^{1}J_{PtC}$ (**3–8**) *vs.* $^{1}J_{PtC}$ (*trans*-$[(CH_3)Pt(As(CH_3)_3)L]^+PF_6^-$) reveals only a wide scatter of points, confirming our qualitative conclusions concerning the relationship between the n.m.r. *cis*- and *trans*-influences: the two phenomena do not appear to share a common origin. The similarity of the $^{1}J_{PtC}$ values for the $(C_6H_5)_3P$(**4**) (533 Hz) and $(C_6H_5)_3As$(**6**) (508 Hz) complexes lends some support to our conclusion (5) that the *cis*-influences of arsine and phosphine ligands are alike and small compared to their *trans*-influences. The *DIARS* derivatives exhibit a difference of only 25 Hz in their $^{1}J_{PtC}$ values while the difference for the two analogous *trans*-methylplatinum derivatives is predicted[3] to be *ca.* 66 Hz.

A plot of δCH_3 (**3–8**) *vs.* δCH_3 (*trans*) for *trans*-methylplatinum(II) analogs where L equals p-$CH_3OC_6H_4CN$, γ-$CH_3C_5H_4N$, $(C_6H_5)_3As$, CH_3CH_2NC, and CO also consists of a scattered array of points. To a first approximation, neither $^{1}J_{PtC}$ values nor platinum methyl carbon shieldings bear simple relationships between like *cis* and *trans* derivatives.

Next, we considered the relationships between $^{1}J_{PtC}$ and $^{2}J_{PtCH}$ for the platinum methyl groups of **3–8**. We have previously shown (5) for series of *trans*-methylplatinum(II) complexes that there exists excellent linear correlations between these two coupling constants, and we have presented evidence which strongly indicates that both parameters provide a measure of the hybridization of the platinum σ-orbital in the platinum–carbon bond. In the complexes we are examining here, if the platinum σ-orbitals are rehybridizing *cis* to the ligand L, we might anticipate similar linear correlations. A plot of $^{1}J_{PtC}$ *vs.* $^{2}J_{PtCH}$ for the platinum methyl groups of **3–8** gives an apparently random array of points; hence we deduce that the major factor resulting in the variations of $^{1}J_{PtC}$ and $^{2}J_{PtCH}$ is *not* platinum σ-orbital rehybridization. While this effect may give rise partially to changes in the one and two bond coupling constants, any such contribution is seemingly masked. These conclusions are consistent with those of other workers (3,4) for series of similar platinum(II) derivatives.

It has been suggested that the magnitudes of one bond ^{1}H–^{13}C (15, 16) and ^{13}C–^{19}F (16) coupling constants are sensitive to steric effects. Changes in C=C—H and C=C—F bond angles, and thus the s characters of the C—H and C—F bonds, have been invoked to account for the observed coupling constant alterations in series of olefinic and aromatic organic compounds. Thus, it seemed possible that by increasing the "steric bulk" of a ligand *cis* to a platinum methyl group, similar variations in the $^{1}J_{PtC}$ values may occur, due to distortion of the C—Pt—L angle away from the ideal 90°. It is possible then, that one might observe a correlation between a measure of the "steric bulk" of a ligand and the $^{1}J_{PtC}$ values.

Tolman (17) has devised a method of deriving a measure of the "bulk" of a ligand by measuring "minimum cone angles" of various tertiary phosphines. He showed that steric effects are much more important than electronic effects, in determining the chemistries of a variety of zerovalent nickel derivatives. While a similar geometrical method may be applicable here, the lack of series of closely related ligands makes such a derivation unwise at this time. Nevertheless, we should point out that some of our results may be rationalized at least qualitatively on the basis of ligand size.

If we disregard the triphenylarsine and triphenylphosphine derivatives for the present, we

---

[3]For comparative purposes, it is convenient to know the $^{1}J_{PtC}$ value for *trans*-$[(CH_3)Pt(As(CH_3)_3)_2P(C_6H_5)_3]^+PF_6^-$ (**9**). While we have prepared this compound, we were not able to obtain a suitable ^{13}C n.m.r. spectrum of it, due to its limited solubility in common organic solvents. However, using the $^{2}J_{PtCH}$ value (60 Hz) of the platinum methyl group for the related derivative *trans*-$[(CH_3)Pt(P(CH_3)_2(C_6H_5))_2P(C_6H_5)_3]^+PF_6^-$ (**10**), (14) and the known relationships between $^{1}J_{PtC}$ and $^{2}J_{PtCH}$ for both types of compounds (5) we calculate the following coupling constants: $^{1}J_{PtC}$ (**9**) 446 Hz, $^{1}J_{PtC}$ (**10**) 484 Hz, and $^{2}J_{PtCH}$ (**9**) 59 Hz. Thus, the *trans*-influence series for the *trans*-methylplatinum derivatives is:

$$(C_6H_5)_3P > CO \approx CH_3CH_2NC > (C_6H_5)_3As > \gamma\text{-}CH_3C_5H_4N > p\text{-}CH_3OC_6H_4CN$$

TABLE 5. $^1J_{PtP}$* values and minimum cone angles for *cis*-$[PtCl_2(P(CH_2CH_2CH_2CH_3)_3)L]$

L	Minimum cone angle (deg)	$^1J_{PtP}(P(CH_2CH_2CH_2CH_3)_3)$
$(C_6H_5O)_3P$	121(±10)	3159
$(CH_3O)_3P$	107(±2)	3321
$(C_6H_5)_3P$	145(±2)	3348
$(CH_3)_2(C_6H_5)P$	†	3382
$(CH_3CH_2CH_2CH_2)_3P$	130(±4)	3500
$(C_2H_5)_3P$	132(±4)	3509

*In Hz.
†Not available.

may place the remaining ligands in the following order based on their respective "steric bulk", or "cone angle" assuming free rotation about the platinum-donor atom bond:

γ-picoline > anisonitrile > ethylisocyanide > carbon monoxide

Indeed, this is the approximate *decreasing* order of the $^1J_{PtC}$ values of the *cis*-methyl groups.

The triphenylarsine and phosphine ligands pose a more complicated problem. By appropriate "feathering" of the phenyl groups, the ligand as a whole may exist in a variety of conformations which have variable steric sizes. Thus it is difficult to place these two ligands in the above proposed scheme. In any event, we would anticipate for similar phenyl ring conformations of both $(C_6H_5)_3P$ and $(C_6H_5)_3As$ that the phosphine would have a greater "steric bulk" than the arsine, since the Pt—As bond is longer than the Pt—P bond. Again we observe the trend where the ligand with the greatest potential for steric interactions with the platinum methyl group has the higher $^1J_{PtC}$ value (533 Hz *vs.* 508 Hz).

At present, the mechanism by which the magnitude of such *cis* interactions can directly affect the $^1J_{PtC}$ values of the *cis*-methyl group is not clear. However, it would appear that rehybridization of the platinum σ-orbital in the platinum carbon bond is not a dominant consequence of this mechanism, since we would anticipate a good linear correlation between $^1J_{PtC}$ and $^2J_{PtCH}$ (5) if this were occurring.

Fortunately, Allen *et al.* (3) have presented n.m.r. data which may be used to test the validity of our hypothesis, that one bond coupling constants involving platinum are susceptible to steric effects. These authors have formulated the following n.m.r. *cis*-influence series for six tertiary phosphines in complexes of the type *cis*-$[PtCl_2(P(CH_2CH_2CH_2CH_3)_3)L]$:

$(C_6H_5O)_3P > (CH_3O)_3P > (C_6H_5)_3P) > (CH_3)_2(C_6H_5)P > (CH_3CH_2CH_2CH_2)_3P > (C_2H_5)_3P$

The appropriate $^1J_{PtP}$ values and "minimum cone angles" derived by Tolman (17) for five of these ligands are provided in Table 5.

It is immediately evident that the data as a whole do not follow the trend of decreasing one bond ^{31}P–^{195}Pt coupling constants with decreasing minimum cone angles. However, the opposite trends are followed within the two classes of ligands, phosphites, and phosphines. Since the changes in $^1J_{PtP}$ between these series are relatively small, it is reasonable to expect that the different electronic properties of these classes of ligands may well have an appreciable effect on $^1J_{PtC}$. In any event, while our steric effect hypothesis may have some merit, it is obvious that it does not provide a complete account for the n.m.r. *cis*-influence series of these neutral platinum derivatives or the cationic *DIARS* complexes examined here. Obviously further confirmation of this theory awaits the determination of the relative signs of one bond ^{13}C–^{195}Pt and ^{31}P–^{195}Pt coupling constants in these derivatives.

B. Arsenic Methyl Groups

In order to corroborate our stereochemical assignments of the arsenic methyl carbon resonances, we compared the $^2J_{PtAsC}$ values of the *trans* arsenic methyl groups with the $^1J_{PtC}$ values of the related *trans*-methylplatinum(II) derivatives *trans*-$[(CH_3)Pt(As(CH_3)_3)_2L]^+PF_6^-$. These data are plotted in Fig. 1 and a linear re-

Can. J. Chem. Downloaded from www.nrcresearchpress.com by 210.87.254.105 on 09/05/12
For personal use only.

Can. J. Chem. Downloaded from www.nrcresearchpress.com by 210.87.254.105 on 09/05/12
For personal use only.

gression analysis[4] of the data is shown in eq. 3.

[3] $^2J_{PtAsC} = 0.17(\pm 0.03)\ ^1J_{PtC}(trans\text{-methyl}) - 27.6(\pm 18.0)\ r = 0.980$

The relatively good linear fit affirms our association of the group of larger $^2J_{PtAsC}$ values with the arsenic methyl groups *trans* to the ligand L. In addition, the other group of $^2J_{PtAsC}$ values is much smaller in magnitude (*ca.* 10–16 Hz *vs.* 45–80 Hz) and spans a much smaller range (6 Hz *vs.* 35 Hz). These results are consistent with an assignment of the remaining arsino group *trans* to the platinum methyl group, which has a large *trans*-influence, yielding very low $^2J_{PtAsC}$ values. Moreover, the small range of values is consistent with the variation of ligands *cis* to the arsenic methyl groups. Finally the $^2J_{PtAsC}$ values observed for the arsenic methyl carbons *trans* to L are similar to those derived for mutually *trans* trimethyl arsino carbons (*ca.* 33–53 Hz) in a series of *trans*-methylplatinum derivatives.

Next, we sought possible relationships between the $^2J_{PtAsC}$ and $^3J_{PtAsCH}$ (*trans* to methyl), and $^2J_{PtAsC}$ and $^3J_{PtAsCH}$ (*cis* to methyl) values for the arsenic methyl groups of the *DIARS* derivatives **2–8**. This examination revealed an interesting linear correlation which is summarized in eq. 4 and Fig. 2

[4] $^2J_{PtAsC} = 2.78(\pm 0.45)\ ^3J_{PtAsCH} - 13.6(\pm 8.5)\ r = 0.990$

As has been found for a variety of platinum(II) systems (1, 5, 18) a reasonably good linear correlation results when two bond coupling constants are plotted against three bond J values for a group *trans* to a varied ligand. Interestingly, the tight cluster of points for the arsenic methyl groups *cis* to the ligand falls on the same line, although there does not appear to be a consistent trend within that sub-series. It should also be noted that the line falls reasonably close to the origin, thus supporting the notion that the Fermi contact mechanism dominates two and three bond coupling constants involving platinum(II).

[4]The average deviations of the slopes and intercepts for all the linear equations presented here are calculated on the basis of the maximum possible error due to the inherent uncertainty of the experimental measurements. These errors have already been cited in Tables 2 and 3. It is worthwhile noting that these variations represent the maximum error in *precision* and that as such they may be generous estimates.

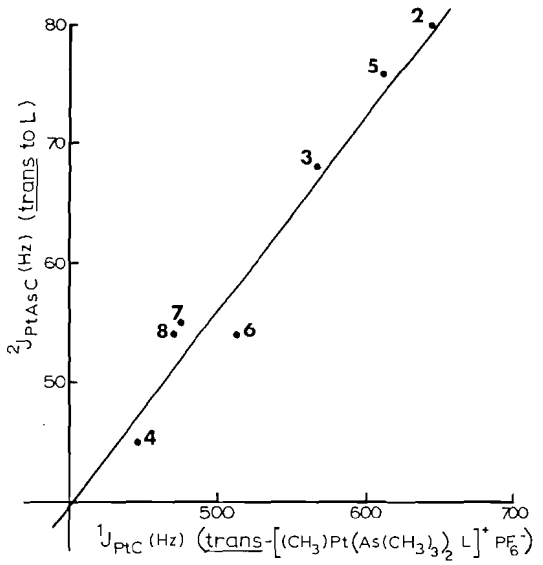

FIG. 1. Plot of $^2J_{PtAsC}$ (*trans* to L for **3–8**) *vs.* $^1J_{PtC}$ (*trans*-[$(CH_3)Pt(As(CH_3)_3)_2L]^+PF_6^-$) for complexes sharing common ligands.

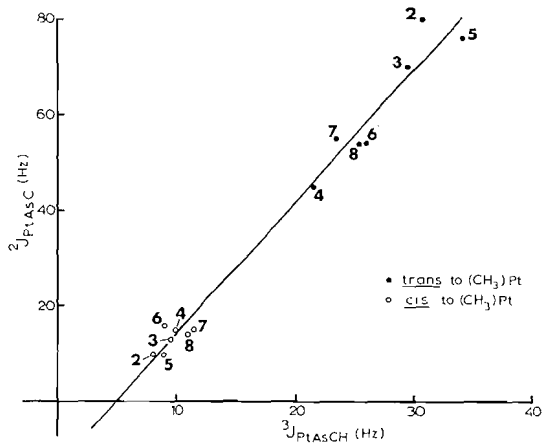

FIG. 2. Plot of $^2J_{PtAsC}$ *vs.* $^3J_{PtAsCH}$ for the arsenic methyl groups of **3–8**.

It is important to note that the data points used in eqs. 3 and 4 for the neutral chloride derivative **2**, appear to follow the same trends as the cationic complexes **3–8**. Thus, as we have shown for similar *trans*-methylplatinum(II) derivatives (5) the charge of the complex does not seem to have an appreciable bearing on the slopes or intercepts of these linear relationships.

C. Aromatic Carbons

Similar, but less marked trends appear to occur for the ^{13}C–^{195}Pt coupling constants of

the ortho carbons of the *DIARS* chelate ring. Due to the generally smaller coupling constants and hence the larger uncertainties in those parameters, we have not carried out any detailed analyses of those data.

We thank the National Research Council of Canada for financial support of this project and for an award to J.E.H.W.

1. H. C. CLARK and J. E. H. WARD. J. Am. Chem. Soc. Submitted for publication.
2. T. G. APPLETON, H. C. CLARK, and L. E. MANZER. Coord. Chem. Rev. **10**, 335 (1973).
3. F. H. ALLEN and S. N. SZE. J. Chem. Soc. (A), 2054 (1971).
4. M. J. CHURCH and M. J. MAYS. J. Chem. Soc. (A), 1938 (1970).
5. M. H. CHISHOLM, H. C. CLARK, L. E. MANZER, J. B. STOTHERS, and J. E. H. WARD. J. Am. Chem. Soc. In press.
6. M. H. CHISHOLM, H. C. CLARK, L. E. MANZER, and J. B. STOTHERS. Chem. Commun. 1627 (1971).
7. R. N. KELLER. Inorg. Synth. **2**, 247 (1946).
8. J. CASANOVA, R. E. SCHUSTER, and N. D. WERNER. J. Chem. Soc. 4280 (1963).
9. G. C. LEVY and J. D. CARGIOLI. J. Mag. Res. **6**, 143 (1972).
10. M. J. HUDSON, R. S. NYHOLM, and M. H. B. STIDDARD. J. Chem. Soc. (A), 40 (1968).
11. G. M. WHITESIDES, J. F. GAASCH, and E. R. STEDRONSKY. J. Am. Chem. Soc. **94**, 5258 (1972).
12. A. PIDCOCK, R. E. RICHARDS, and L. M. VENANZI. J. Chem. Soc. (A), 1707 (1966).
13. S. S. ZUMDAHL and R. S. DRAGO. J. Am. Chem. Soc. **90**, 6669 (1968).
14. H. C. CLARK and J. D. RUDDICK. Inorg. Chem. **9**, 1226 (1970).
15. K. L. SERVIS, W. P. WEBER, and A. K. WILLARD. J. Phys. Chem. **74**, 3960 (1970).
16. S. L. MANATT, M. A. COOPER, C. W. MALLORY, and F. B. MALLORY. J. Am. Chem. Soc. **95**, 975 (1973).
17. C. A. TOLMAN. J. Am. Chem. Soc. **92**, 2956 (1970).
18. T. G. APPLETON, M. H. CHISHOLM, H. C. CLARK, and L. E. MANZER. Can. J. Chem. **51**, 2243 (1973).

Can. J. Chem. Downloaded from www.nrcresearchpress.com by 210.87.254.105 on 09/05/12
For personal use only.

Strong Crystalline Field Perturbation Calculations for d^3, d^7 Penta-Coordinate Complexes. II.[1] The Square Pyramid

JUDITH A. VARGA AND CLIFFORD A. L. BECKER

Department of Chemistry, The University of Texas, Austin, Texas 78712

Received July 26, 1973

Crystal field calculations for d^3, d^7 square pyramidal complexes are carried out via the strong field formalism and in the limit of zero spin–orbit coupling. The field produced by the lone axial ligand is treated as an integral part of the crystal field potential. In the ionic model approximation the three crystal field parameters: *Dq*, *Ds*, and *Dt*; depend markedly on the angle of distortion, β, defined as that portion of the L_a—M—L_b bond angle in excess of 90°. The square pyramidal d^3 symmetry eigenfunctions are constructed from the one-electron crystal field eigenfunctions. Spin is only implicitly included, but both types of doublet wavefunctions are identified. The crystal field matrix in parametric form is strictly diagonal, but Coulombic interactions connect states arising from different strong field configurations. Coulombic calculations are performed in terms of the Slater–Condon–Shortley parameters: F_0, F_2, and F_4; then converted to the Racah parameters: *A*, *B*, and *C*. The complete (crystal field and Coulombic) perturbation matrices are used to interpret the spectroscopic properties of a strong field Co(II) square pyramidal complex. Both the symmetry and multiplicity of the ground state are dependent on β. An energy level diagram showing all doublets and quartets is calculated for β = 0°. Partial energy level diagrams are also given depicting behavior of the doublet and quartet states, individually, as functions of β. As β increases the crystal field bands shift to lower energy and become more clustered. Current experimental applications are also briefly cited.

Des calculs dans la théorie du champ cristallin ont été effectués pour des complexes pyramidaux à base carrée d^3 et d^7, par le formalisme du champ fort et dans le cadre du couplage -spin-orbite nul. Le champ produit par le seul ligand axial est traité comme partie intégrante du potentiel du champ cristallin. Dans l'approximation du modèle ionique les 3 paramètres du champ cristallin; *Dq*, *Ds* et *Dt* dépendent nettement de l'angle de déformation β, défini comme la partie de l'angle de valence L_a—M—L_b supérieure à 90°. Les fonctions propres de symétrie pyramidale à base carrée d^3 sont construites à partir des fonctions propres monoélectroniques du champ cristallin. Le spin n'intervient qu'implicitement mais les deux types de fonctions d'ondes sont identifiés. La matrice du champ cristallin, sous forme paramètrique est strictement diagonale mais les interactions coulombiennes relient les états provenant de configurations différentes du champ cristallin. Les calculs de ces interactions sont effectués en termes des paramètres de Slater–Condon–Shortley; F_0, F_2, et F_4 qui sont ensuite transformés en paramètres de Racah. Les matrices de perturbation complètes (champ cristallin et coulombienne) sont utilisées pour interpréter les propriétés spectroscopiques d'un complexe de Co(II), à champ fort de structure pyramidale à base carrée. La symétrie et la multiplicité de l'état fondamental dépendent tous les deux de β Un diagramme des niveaux d'énergie montrant que tous les doublets et les quartets est calculé pour β = 0°. Des diagrammes partiels des nivaux d'énergie décrivant la conduite des états doublets et quartets, individuellement, en fonction de β sont aussi donnés. Lorsque β augmente les bandes du champ cristallin se déplacent à des énergies plus basses et se regroupent davantage. Des applications expérimentales courantes sont aussi brièvement citées.

[Traduit par le journal]

Can. J. Chem., **52**, 579 (1974)

Introduction

Five-coordinate transition metal complexes are known to span two distinct (idealized) geometries: the trigonal bipyramid (D_{3h}), discussed in Part I (1), and the square pyramid (C_{4v}), to be treated in the present paper. Within the context of the strong crystalline field approximation and zero spin–orbit perturbation, the square pyramidal case can be approached in either of two ways. The field generated by the axial ligand can be treated as a perturbation on the major cubic potential or can be initially included as an integral part of the crystal field potential. The former approach is perhaps appropriate to mono- and di-substituted hexa-coordinate, basically octahedral, complexes; but the latter more closely approximates the situation in square pyramidal, as well as square planar and highly tetragonally-distorted octahedral, complexes. Available calculations for a metal ion in strong crystalline

[1]Taken in part from the dissertation submitted by Judith A. Varga in partial fulfillment of the requirements for the Ph.D. degree. Part I is ref. 1.

Can. J. Chem. Downloaded from www.nrcresearchpress.com by 210.87.254.40 on 09/05/12
For personal use only.

Can. J. Chem. Downloaded from www.nrcresearchpress.com by 210.87.254.40 on 09/05/12
For personal use only.

field of square pyramidal geometry treat the axial ligand as only a minor perturbative force.

Perumareddi (2) has discussed d^3, d^7 complexes in quadrate[2] (C_{4v}, D_{4h}), trigonal (*i.e.*, trigonally-distorted octahedral), and cylindrical ($C_{\infty v}$, $D_{\infty h}$) ligand fields. Since Perumareddi's calculations are based on cubically disposed wavefunctions properly decomposed on going to quadrate symmetry, the crystalline field parameters are not limited to diagonal entries in the perturbation matrices. Those states which belong to the same O_h irreducible representation but different representations in C_{4v} are connected by non-zero off-diagonal crystal field terms. These calculations, therefore, are not properly strong field square pyramidal in a strict sense, but, rather, strong field octahedral with a weak axial perturbation superimposed. Furlani (3) has qualitatively compared the experimental spectrum of $Ni(dtp)_2 \cdot C_2H_5OH$ ($dtp^- \equiv (C_2H_5O)_2PSS^-$) to that expected for both a trigonal bipyramid and a square pyramid.

Square pyramidal coordination has been established for a number of strong field Co(II) complexes and is suggested for many more. Complexes determined by X-ray crystallography include $[Co(ddc)_2NO]$ (ddc is dimethyldithiocarbamate) (4), [Co(tda)I]I (tda is tris(2-diphenylphosphinoethyl)amine) (5), $Co_2(Salen)_2$ (Salen is *N,N'*-ethylene-bis-(salicyladimine) (6), $[Co\{(C_6H_5)_2PCH_2CH_2P(C_6H_5)_2\}_2Cl]SnCl_3$ (18); and by analogy, presumably also $[Co(dmp)_2Cl]SnCl_3$, $[Co(dmp)_2Cl]B(C_6H_5)_4$, and $[Co(dmp)_2I]I$, where dmp is $(CH_3)_2PCH_2CH_2P(CH_3)_2$ (18). These complexes, however, are distorted square pyramidal, at best C_{2v} symmetry. More specifically these C_{4v} calculations have allowed characterization of the two isomers of $[Co(CNC_6H_5)_5](ClO_4)_2$ as true C_{4v} square pyramids (19). Spectral interpretation has also been extended to the $[Co(CNC_6H_5)_5](BF_4)_2$ complexes and to selected *p*-substituted phenylisocyanide complexes of Co(II) (20).

To interpret the electronic spectra of these Co(II) complexes it is necessary to consider the effect of the combined crystalline field-Coulombic Hamiltonian:

$$[1] \qquad H = V_{C_{4v}}{}^{CF}(r,\theta,\phi) + \sum_{i<j}^{3} \frac{e^2}{r_{ij}}$$

on the wavefunctions describing the d^3, d^7 strong field system. Neglect of spin–orbit perturbation in *first row* transition metal complexes can be justified on the basis of experimental expedience, if not on purely theoretical grounds. Parametric values necessarily assumed for strong field trigonal bipyramidal Ni(II) (7), for example, clearly illustrate that spin–orbit effects have essentially no influence on the energies of the perturbation levels. Spin–orbit coupling merely provides the mechanism through which perturbation levels of different multiplicity, placed in close proximity by the crystal field and Coulombic perturbations, can interact to allow the so-called spin-forbidden electronic transitions. Experimentally observed transitions of this nature are usually sufficiently weaker than the spin-allowed to be obscured by the latter if both should occur at similar energy. For a low-spin d^7 ion in a crystalline field of low symmetry it would seem unrealistic to expect to observe spin-forbidden transitions in the presence of as many symmetry-, spin-allowed transitions as are calculated to be present. Inclusion of spin–orbit perturbation would be a more complete theoretical treatment, but hardly seems merited by probable experimental application.

The three-electron square pyramidal strong field symmetry eigenfunctions are constructed from the one-electron crystal field eigenfunctions; *i.e.*, the one-electron states which diagonalize

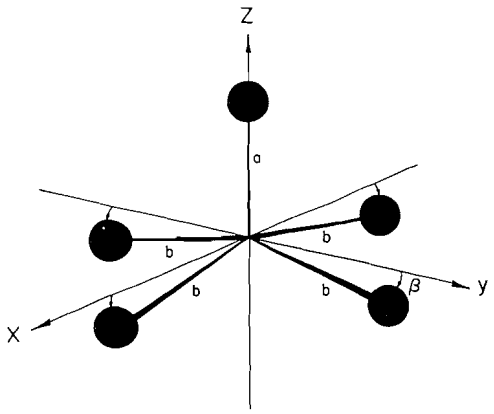

FIG. 1. The square pyramidal coordination sphere.

[2]Complexes of both C_{4v} and D_{4h} symmetry are often considered together under the heading "quadrate". This term is used, thus, to designate penta-coordinate square pyramidal and tetra-coordinate square planar complexes as well as mono- and *trans*-di-substituted hexa-coordinate octahedral complexes.

the crystal field perturbation under C_{4v} symmetry. Calculational procedures parallel those developed in Part I (1). In only those instances where the C_{4v} case differs markedly from the D_{3h} will details be given.

Definition of the Crystal Field Parameters

The square pyramidal coordination sphere is shown in Fig. 1. An electron placed therein finds itself subject to a potential, as expressed within the Ionic Model approximation (8),

$$[2]\quad V_{C_{4v}}{}^{CF}(r,\theta,\phi) = Ze^2\left(\frac{1}{a}+\frac{4}{b}+\frac{z}{a^2}-\frac{4z\sin\beta}{b^2}+\frac{3z^2-r^2}{2a^3}+\frac{5z^3-3zr^2}{2a^4}\right.$$
$$+\frac{3(x^2+y^2)\cos^2\beta+6z^2\sin^2\beta-2r^2}{b^3}$$
$$-\frac{15z(x^2+y^2)\cos^2\beta\sin\beta-10z^3\sin^3\beta+6zr^2\sin\beta}{b^4}+\frac{35z^4-30z^2r^2+3r^4}{8a^5}$$
$$+\frac{35(x^4+y^4)\cos^4\beta+70z^4\sin^4\beta+210z^2(x^2+y^2)\cos^2\beta\sin^2\beta}{4b^5}$$
$$\left.-\frac{30(x^2+y^2)r^2\cos^2\beta+60z^2r^2\sin^2\beta-6r^4}{4b^5}\right)$$

where a is the axial bond length; b, the basal bond length; and β, the L_a—M—L_b bond angle in excess of 90°. Under this potential three parameters arise in the calculation of the one-electron matrix elements:

$$[3a]\quad Dq = \frac{Ze^2\cos^4\beta}{6b^5}\langle r^4\rangle$$

$$[3b]\quad Dt = \frac{Ze^2}{21}\left(\frac{20\cos^2\beta-14\cos^4\beta-4}{b^5}-\frac{1}{a^5}\right)\langle r^4\rangle$$

$$[3c]\quad Ds = \frac{Ze^2}{7}\left(\frac{2-6\sin^2\beta}{b^3}-\frac{1}{a^3}\right)\langle r^2\rangle$$

In the limit of a regular square pyramid; *i.e.*, $a = b$ and $\beta = 0°$, then[3]

$$[4a]\quad Dq = \frac{Ze^2}{6b^5}\langle r^4\rangle \equiv Dq^0$$

$$[4b]\quad Dt = \frac{Ze^2}{21b^5}\langle r^4\rangle \equiv Dt^0 = \tfrac{2}{7}Dq^0$$

$$[4c]\quad Ds = \frac{Ze^2}{7b^3}\langle r^2\rangle \equiv Ds^0$$

For $\beta \neq 0°$ but keeping $a = b$, the parameters depend explicitly on the angle of distortion:

$$[5a]\quad Dq = (\cos^4\beta)\,Dq^0$$

$$[5b]\quad Dt = (20\cos^2\beta-14\cos^4\beta-5)\,Dt^0 = \tfrac{2}{7}(20\cos^2\beta-14\cos^4\beta-5)\,Dq^0$$

$$[5c]\quad Ds = (1-6\sin^2\beta)\,Ds^0$$

In Fig. 2*a* the parameters Dq and Dt are plotted as functions of β. As the angle of distortion increases; *i.e.*, the basal ligands bend down, away from the lone axial ligand, Dq decreases and Dt increases, until $Dt \simeq Dq$ at $\beta = 28°$. Hence Dq is not necessarily the dominant parameter. Similar results with weak field calculations have been observed by Gerloch *et al.* (9).

Figure 2*b* depicts the β dependency of the parameter Ds. Since Ds and Dq are different functions of the radial distribution, Ds cannot be related to Dq with the facility that Dt was so considered. The relation between the C_{4v} quartic and quadratic parameters, when attempted at all, is given in terms of the quantity (2*b*),

$$[6]\quad \kappa = Ds/Dt = 3\langle r^2\rangle/\langle r^4\rangle$$

Theoretical evaluation of the radial integrals

[3] To avoid confusion, it should be noted that $Dt(C_{4v}) = \frac{1}{2}\,Dt(D_{4h})$ and $Ds(C_{4v}) = \frac{1}{2}\,Ds(D_{4h})$, but $Dt^0 = \frac{2}{7}\,Dq^0(C_{4v}) = \frac{2}{7}\,Dq(O_h) = \frac{2}{7}\,Dq(D_{4h})$.

Can. J. Chem. Downloaded from www.nrcresearchpress.com by 210.87.254.40 on 09/05/12
For personal use only.

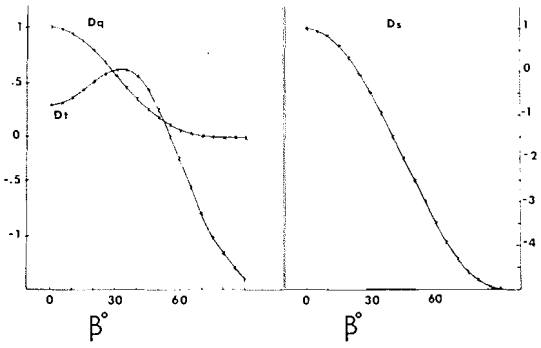

FIG. 2. Dependence of the square pyramidal crystal field parameters on β, the angle of distortion. (*a*) The quartic parameters *Dq* and *Dt*; (*b*) the quadratic parameter *Ds*.

using hydrogenic, Slater, and Hartree-Fock orbitals (10) yields $\kappa = 12/5$, whereas fitting experimental spectral data leads to $\kappa = 3$ (11). Perumareddi (2*b*, 12) has made equally satisfactory assignment of spectroscopic data using alternate values of κ. Hence whether the ratio $\langle r^2\rangle/\langle r^4\rangle$ is a constant or another empirical parameter remains open to question. In fact, the sign of *Ds* may even be opposite to that of *Dt*; *Ds* is negative for $\beta \geqslant 25°$, while *Dt* remains a positive quantity until $\beta \geqslant 57°$. The *Dq* is of course positive for all values of β.

In terms of the parameters *Dq*, *Dt*, and *Ds*, the square pyramidal one-electron symmetry eigenfunctions have the energies:

$$[7a]\quad \varepsilon[(b_1) \equiv 1/\sqrt{2}\,(\phi_2 + \phi_{-2})] = \varepsilon_0 + 6Dq - Dt + 2Ds$$

$$[7b]\quad \varepsilon[(a_1) \equiv \phi_0] = \varepsilon_0 + 6Dq - 6Dt - 2Ds$$

$$[7c]\quad \varepsilon[(b_2) \equiv 1/\sqrt{2}\,(\phi_2 - \phi_{-2})] = \varepsilon_0 - 4Dq - Dt + 2Ds$$

$$[7d]\quad \varepsilon[(e) \equiv (\phi_1, \phi_{-1})] = \varepsilon_0 - 4Dq + 4Dt - Ds$$

Construction of the Symmetry Eigenfunctions

Three d-electrons may occupy the one-electron C_{4v} energy levels in the seventeen different configurations: $[(a_1)^2(b_1)]$, $[(a_1)^2(b_2)]$, $[(a_1)^2(e)]$, $[(a_1)(b_1)^2]$, $[(b_1)^2(b_2)]$, $[(b_1)^2(e)]$, $[(a_1)(b_2)^2]$, $[(b_1)(b_2)^2]$ $[(b_2)^2\ (e)]$, $[(e)^3]$, $[(a_1)(e)^2]$, $[(b_1)(e)^2]$, $[(b_2)(e)^2]$, $[(a_1)(b_1)(b_2)]$, $[(a_1)(b_1)(e)]$, $[(a_1)(b_2)(e)]$, and $[(b_1)(b_2)\ (e)]$. Each of the first ten contains only one type of orbital symmetry state, which, by virtue of the Pauli principle, is a doublet. The remaining configurations contain both quartets and doublets. The symmetry direct product for $[(a_1)(b_1)(e)]$, $[(a_1)(b_2)(e)]$, and $[(b_1)(b_2)(e)]$ is E, that for $[(a_1)(b_1)(b_2)]$, A_2, so the strong field states must be ${}^4E + (2)^2E$ and ${}^4A_2 + (2)^2A_2$, respectively. Each of $[(a_1)(e)^2]$, $[(b_1)(e)^2]$, and $[(b_2)(e)^2]$, however, spans $A_1 + A_2 + B_1 + B_2$, and attempted correlation with the weak field limit indicates only that one of ${}^4A_2$, ${}^4B_1$, or ${}^4B_2$ is to be assigned to each configuration. Construction of the actual quartet wavefunctions from the one-electron levels appropriate to each configuration reveals that the ${}^4A_2$ belongs to $[(a_1)(e)^2]$; ${}^4B_1$, to $[(b_2)(e)^2]$; and ${}^4B_2$, to $[(b_1)(e)^2]$.

The strong field basis functions for the d^3 system are three-electron Slater determinants with spin implicitly included. The symmetry eigenfunctions are either identical to one of the basis functions or are some linear combinations thereof. Proper orbital transformation properties of the C_{4v} symmetry eigenfunctions are assured by use of the appropriate $D^2(\alpha,\beta,\gamma)$ rotation matrices (13). As in the D_{3h} calculations (1) two forms of doublets, termed Type I and Type II, occur for the square pyramidal d^3 system.

Two (orthogonal) sets of doublet wavefunctions are required for three particles of half-integral ($\pm 1/2$) spin whenever more than one distribution of spin among the three orbital functions is possible. For a configuration such as $[(a_1)(b_1)(b_2)]$ three basis functions are Pauli-allowed: $|b_1{}^+\phi_0{}^+b_2{}^-|$, $|b_1{}^-\phi_0{}^+b_2{}^+|$, $|b_1{}^+\phi_0{}^-b_2{}^+|$, where $b_1 \equiv (1/\sqrt{2})\ (\phi_2 + \phi_{-2})$ and $b_2 \equiv (1/\sqrt{2})\ (\phi_2 - \phi_{-2})$; each of which transforms as A_2. The two ${}^2A_2$ eigenfunctions result when these basis functions are linearly combined to yield a Type I doublet, $(1/\sqrt{6})|2i - j - k|$, and a Type II doublet, $(1/\sqrt{2})|j - k|$. Since each of the basis functions is of A_2 symmetry, i may be arbitrarily taken as any one of the three with j and k chosen accordingly. Configurations such as $[(e)^3]$ or $[(a_1)^2(e)]$, however, give rise to only one set of ${}^2E$ wavefunctions consistent with the Pauli principle. The C_{4v} strong field symmetry eigenfunctions of d^3 are given in Table 1.

The Perturbation Energy Matrices

The symmetry eigenfunctions listed in Table 1 are ultimately linear combinations of the products of the C_{4v} one-electron energy levels: a_1, b_1, b_2, and e. Since these one-electron symmetry eigenfunctions strictly diagonalize the crystal field matrix in its parametric form, all off-diagonal crystal field terms in the d^n case must

Can. J. Chem. Downloaded from www.nrcresearchpress.com by 210.87.254.40 on 09/05/12
For personal use only.

TABLE 1. The strong field C_{4v} symmetry eigenfunctions for a three-electron transition metal complex*

Quartets		
$^4A_2$	$\Psi_1(a_1)(e)^2$	$\lvert\phi_1^+\phi_0^+\phi_{-1}^+\rvert$
	$\Psi_2(a_1)(b_1)(b_2)$	$\lvert b_1^+\phi_0^+b_2^+\rvert$
$^4B_1$	$\Psi_4(b_2)(e)^2$	$\lvert\phi_1^+\phi_{-1}^+b_2^+\rvert$
$^4B_2$	$\Psi_3(b_1)(e)^2$	$\lvert b_1^+\phi_1^+\phi_{-1}^+\rvert$
^4E	$\Psi_5(b_1)(b_2)(e)$	$\lvert b_1^+\phi_{-1}^+b_2^+\rvert$, $\lvert b_1^+\phi_1^+b_2^+\rvert$
	$\Psi_6(a_1)(b_1)(e)$	$\lvert b_1^+\phi_1^+\phi_0^+\rvert$, $\lvert b_1^+\phi_0^+\phi_{-1}^+\rvert$
	$\Psi_7(a_1)(b_2)(e)$	$\lvert\phi_1^+\phi_0^+b_2^+\rvert$, $\lvert\phi_0^+\phi_{-1}^+b_2^+\rvert$
Doublets		
$^2A_1$	$\Psi_{11}(a_1)(b_1)^2$	$\lvert b_1^+b_1^-\phi_0^+\rvert$
	$\Psi_{14}(a_1)(b_2)^2$	$\lvert\phi_0^+b_2^-b_2^+\rvert$
	$\Psi_{17}(a_1)(e)^2$	$(1/\sqrt{2})[\lvert\phi_1^+\phi_0^+\phi_{-1}^-\rvert - \lvert\phi_1^-\phi_0^+\phi_{-1}^+\rvert]$
	$\Psi_{21}(b_1)(e)^2$	$(1/\sqrt{2})[\lvert b_1^+\phi_1^-\phi_1^+\rvert + \lvert b_1^+\phi_{-1}^-\phi_{-1}^+\rvert]$
	$\Psi_{26}(b_2)(e)^2$	$(1/\sqrt{2})[\lvert\phi_1^+\phi_1^-b_2^+\rvert - \lvert\phi_{-1}^+\phi_{-1}^-b_2^+\rvert]$
$^2A_2$	$\Psi_{18}(a_1)(e)^2$	$(1/\sqrt{6})[2\lvert\phi_1^+\phi_0^-\phi_{-1}^+\rvert - \lvert\phi_1^+\phi_0^+\phi_{-1}^-\rvert - \lvert\phi_1^-\phi_0^+\phi_{-1}^+\rvert]$
	$\Psi_{22}(b_1)(e)^2$	$(1/\sqrt{2})[\lvert b_1^+\phi_1^-\phi_1^+\rvert - \lvert b_1^+\phi_{-1}^-\phi_{-1}^+\rvert]$
	$\Psi_{25}(b_2)(e)^2$	$(1/\sqrt{2})[\lvert\phi_1^+\phi_1^-b_2^+\rvert + \lvert\phi_{-1}^+\phi_{-1}^-b_2^+\rvert]$
	$\Psi_{30}(a_1)(b_1)(b_2)$	$(1/\sqrt{2})[\lvert b_1^+\phi_0^-b_2^+\rvert - \lvert b_1^+\phi_0^+b_2^-\rvert]$
	$\Psi_{31}(a_1)(b_1)(b_2)$	$(1/\sqrt{6})[2\lvert b_1^-\phi_0^+b_2^+\rvert - \lvert b_1^+\phi_0^-b_2^+\rvert - \lvert b_1^+\phi_0^+b_2^-\rvert]$
$^2B_1$	$\Psi_8\ (a_1)^2(b_1)$	$\lvert b_1^+\phi_0^-\phi_0^+\rvert$
	$\Psi_{15}(b_1)(b_2)^2$	$\lvert b_1^+b_2^-b_2^+\rvert$
	$\Psi_{20}(a_1)(e)^2$	$(1/\sqrt{2})[\lvert\phi_1^+\phi_1^-\phi_0^+\rvert - \lvert\phi_0^+\phi_{-1}^-\phi_{-1}^+\rvert]$
	$\Psi_{23}(b_1)(e)^2$	$(1/\sqrt{2})[\lvert b_1^+\phi_1^-\phi_{-1}^+\rvert - \lvert b_1^+\phi_1^+\phi_{-1}^-\rvert]$
	$\Psi_{28}(b_2)(e)^2$	$(1/\sqrt{6})[2\lvert\phi_1^+\phi_{-1}^+b_2^-\rvert - \lvert\phi_1^+\phi_{-1}^-b_2^+\rvert - \lvert\phi_1^-\phi_{-1}^+b_2^+\rvert]$
$^2B_2$	$\Psi_9\ (a_1)^2(b_2)$	$\lvert\phi_0^+\phi_0^-b_2^+\rvert$
	$\Psi_{12}(b_1)^2(b_2)$	$\lvert b_1^+b_1^-b_2^+\rvert$
	$\Psi_{19}(a_1)(e)^2$	$(1/\sqrt{2})[\lvert\phi_1^+\phi_1^-\phi_0^+\rvert + \lvert\phi_0^+\phi_{-1}^-\phi_{-1}^+\rvert]$
	$\Psi_{24}(b_2)(e)^2$	$(1/\sqrt{2})[\lvert\phi_1^+\phi_{-1}^-b_2^+\rvert - \lvert\phi_1^-\phi_{-1}^+b_2^+\rvert]$
	$\Psi_{27}(b_1)(e)^2$	$(1/\sqrt{6})[2\lvert b_1^-\phi_1^+\phi_{-1}^+\rvert - \lvert b_1^+\phi_1^-\phi_{-1}^+\rvert - \lvert b_1^+\phi_1^+\phi_{-1}^-\rvert]$
^2E	$\Psi_{10}(a_1)^2(e)$	$\lvert\phi_1^+\phi_0^-\phi_0^+\rvert$, $\lvert\phi_0^+\phi_0^-\phi_{-1}^+\rvert$
	$\Psi_{13}(b_1)^2(e)$	$\lvert b_1^+b_1^-\phi_1^+\rvert$, $\lvert b_1^+b_1^-\phi_{-1}^+\rvert$
	$\Psi_{16}(b_2)^2(e)$	$\lvert\phi_1^+b_2^-b_2^+\rvert$, $\lvert\phi_{-1}^+b_2^-b_2^+\rvert$
	$\Psi_{29}(e)^3$	$\lvert\phi_1^+\phi_1^-\phi_{-1}^+\rvert$, $\lvert\phi_1^+\phi_{-1}^-\phi_{-1}^+\rvert$
	$\Psi_{32}(b_1)(b_2)(e)$	$\left\{\begin{array}{l}(1/\sqrt{2})[\lvert b_1^-\phi_1^+b_2^+\rvert - \lvert b_1^+\phi_1^+b_2^-\rvert] \\ (1/\sqrt{2})[\lvert b_1^-\phi_{-1}^+b_2^+\rvert - \lvert b_1^+\phi_{-1}^+b_2^-\rvert]\end{array}\right\}$
	$\Psi_{33}(b_1)(b_2)(e)$	$\left\{\begin{array}{l}(1/\sqrt{6})[2\lvert b_1^+\phi_1^-b_2^+\rvert - \lvert b_1^-\phi_1^+b_2^+\rvert - \lvert b_1^+\phi_1^+b_2^-\rvert] \\ (1/\sqrt{6})[2\lvert b_1^+\phi_{-1}^-b_2^+\rvert - \lvert b_1^-\phi_{-1}^+b_2^+\rvert - \lvert b_1^+\phi_{-1}^+b_2^-\rvert]\end{array}\right\}$
	$\Psi_{34}(a_1)(b_1)(e)$	$\left\{\begin{array}{l}(1/\sqrt{2})[\lvert b_1^-\phi_0^+\phi_{-1}^+\rvert - \lvert b_1^+\phi_0^-\phi_{-1}^+\rvert] \\ (1/\sqrt{2})[\lvert b_1^-\phi_1^+\phi_0^+\rvert - \lvert b_1^+\phi_1^+\phi_0^-\rvert]\end{array}\right\}$
	$\Psi_{35}(a_1)(b_1)(e)$	$\left\{\begin{array}{l}(1/\sqrt{6})[2\lvert b_1^+\phi_0^+\phi_{-1}^-\rvert - \lvert b_1^-\phi_0^+\phi_{-1}^+\rvert - \lvert b_1^+\phi_0^-\phi_{-1}^+\rvert] \\ (1/\sqrt{6})[2\lvert b_1^+\phi_1^-\phi_0^+\rvert - \lvert b_1^-\phi_1^+\phi_0^+\rvert - \lvert b_1^+\phi_1^+\phi_0^-\rvert]\end{array}\right\}$
	$\Psi_{36}(a_1)(b_2)(e)$	$\left\{\begin{array}{l}(1/\sqrt{2})[\lvert\phi_0^+\phi_{-1}^+b_2^-\rvert - \lvert\phi_0^-\phi_{-1}^+b_2^+\rvert] \\ (1/\sqrt{2})[\lvert\phi_1^+\phi_0^+b_2^-\rvert - \lvert\phi_1^+\phi_0^-b_2^+\rvert]\end{array}\right\}$
	$\Psi_{37}(a_1)(b_2)(e)$	$\left\{\begin{array}{l}(1/\sqrt{6})[2\lvert\phi_0^+\phi_{-1}^-b_2^+\rvert - \lvert\phi_0^+\phi_{-1}^+b_2^-\rvert - \lvert\phi_0^-\phi_{-1}^+b_2^+\rvert] \\ (1/\sqrt{6})[2\lvert\phi_1^-\phi_0^+b_2^+\rvert - \lvert\phi_1^+\phi_0^+b_2^-\rvert - \lvert\phi_1^+\phi_0^-b_2^+\rvert]\end{array}\right\}$

*$b_1 \equiv (1/\sqrt{2})(\phi_2 + \phi_{-2})$; $b_2 \equiv (1/\sqrt{2})(\phi_2 - \phi_{-2})$. For all the E wavefunctions the "a" component is listed first, the "b" component, second.

Can. J. Chem. Downloaded from www.nrcresearchpress.com by 210.87.254.40 on 09/05/12
For personal use only.

Can. J. Chem. Downloaded from www.nrcresearchpress.com by 210.87.254.40 on 09/05/12
For personal use only.

vanish identically. The diagonal crystal field energy of a given state is dependent only on the parent configuration and is straightforwardly obtained as the algebraic sum of the energies for the one-electron levels of that configuration. The Coulombic perturbation, however, connects states having like symmetry but arising from different configurations. Coulombic perturbation also factors the matrix of the (orbitally) doubly degenerate E states into two orthogonal blocks, designated as "a" and "b", which are identical or differ merely by phase factors in off-diagonal elements, the perturbation energies remaining unaffected. Given several wavefunctions of E symmetry, however, it is usually not possible to predict *a priori* which belongs to the respective sets. This is established by calculation of the matrix elements.

For d^3 the Coulombic perturbation is calculated via the operator,

$$[8] \qquad \sum_{i<j}^{3} \frac{e^2}{r_{ij}} = \frac{e^2}{r_{12}} + \frac{e^2}{r_{13}} + \frac{e^2}{r_{23}}$$

taken between two Slater determinants. So doing gives the Coulombic matrix elements as sums of two-electron elements, each of the form

$$[9] \qquad \left\langle \phi_a(i)\phi_b(j) \left| \frac{e^2}{r_{ij}} \right| \phi_c(i)\phi_d(j) \right\rangle = \delta(m_s^a, m_s^c)\delta(m_s^b, m_s^d)\delta(m_l^a + m_l^b, m_l^c + m_l^d) \cdot \sum_{k=0,2,4} c^k(2m_l^a, 2m_l^c)c^k(2m_l^d, 2m_l^b)F^k(n^a2, n^b2)$$

with the c^k being given in Table 1 of Condon and Shortley (14). The Coulombic matrix elements can alternately be expressed in terms of the Racah parameters (15), $A = F^0 - (1/9)F^4 = F_0 - 49F_4$, $B = (1/441)\ (9F^2 - 5F^4) = F_2 - 5F_4$, and $C = (5/63)F^4 = 35F_4$. This calculation is reported in terms of the latter parameters. The complete (crystal field and Coulombic) d^3 perturbation matrices are obtained by adding the diagonal crystal field energies of the appropriate configurations to the several Coulombic matrices; these composite matrices are listed in Table 2. Energy level diagrams can now be constructed.

The Energy Level Diagram

For illustration an energy level diagram for Co(II) square-pyramidally coordinated to five identical strong field ligands will be estimated. For CN^-, a typical (very) strong field ligand, $10Dq$ is measured as 32 200 cm^{-1} in $[Fe(CN)_6]^{4-}$ (16), so the value $Dq = 3000\ cm^{-1}$ was assumed for the Co(II) calculation. Since $10Dq = 32\,200\ cm^{-1}$ is also reported for $[Co(CN)_6]^{3-}$ (16), however, perhaps $Dq = 3000\ cm^{-1}$ represents a maximal, rather than a mean value for strong field ligands. With Dq specified, Dt follows as a function of β and Dq^0 (*i.e.*, $Dq|_{\beta=0} \equiv Dq^0$). A proportionality between the quadratic and quartic crystal field parameters is probably best not attempted in view of results obtained by Perumareddi (2*b*). In general it is simply observed that $Ds \ll Dq$. Accordingly Ds^0 has been taken as 300 cm^{-1}. The Coulombic parameters are taken as 70% their free ion value with C expressed in terms of B as $C/B = 4$, since $C_0/B_0 = 3.92$ (17).

Using these values of Dq^0, Ds^0, B, and C; *i.e.*, 3000, 300, 800, and 3200 cm^{-1}, respectively; the energy levels depicted in Figs. 3, 4, and 5 were calculated. (Since the ε_0 and A occur only along the diagonal and with the same numerical coefficients they cannot influence the transition energies.) Energies of the strong field states for Co(II) are shown in Fig. 3 for the case of a regular square pyramid (*i.e.*, $\beta = 0°$). The symmetry-allowed, spin-allowed transitions, assuming the $^2A_1[(b_2)^2(e)^4(a_1)]$ ground state, are indicated on the right-hand side of the diagram. Configurations giving rise to the excited states are also included. For $\beta = 0°$, a spectrum consisting of three groupings of absorption bands could be expected.

Since the crystal field parameters depend so dramatically on β, it is reasonable to expect the energies of the strong field states to vary as β increases. As long as the distortion remains less than 20°, the ground state possesses $^2A_1$ symmetry. For $\beta > 20°$, however, not only the symmetry, but also the multiplicity of the ground state can change, first to $^4E[(b_2)^2(e)^3(a_1)(b_1)]$ for $20° < \beta < 25°$, and then to $^4B_2[(b_2)^2(e)^2(a_1)^2(b_1)]$ for $\beta > 25°$. The energies of the doublet ground state and excited states to which symmetry-allowed electronic transitions are possible are plotted in Fig. 4 as a function of β.

Can. J. Chem. Downloaded from www.nrcresearchpress.com by 210.87.254.40 on 09/05/12
For personal use only.

TABLE 2. The complete C_{4v} perturbation energy matrices for a d^3, d^7 strong field transition metal complex

$^2A_1$

	Ψ_{11}	Ψ_{14}	Ψ_{17}	Ψ_{21}	Ψ_{26}
$\Psi_{11}[(a_1)(b_1)^2]$	$3\epsilon_o + 18Dq + 2Ds - 8Dt + 3A - 8B + 4C - E$	C	$\sqrt{2}\,(3B + C)$	$\sqrt{6}\,B$	0
$\Psi_{14}[(a_1)(b_2)^2]$	C	$3\epsilon_o - 2Dq + 2Ds - 8Dt + 3A - 8B + 4C - E$	$\sqrt{2}\,(3B + C)$	0	$\sqrt{6}\,B$
$\Psi_{17}[(a_1)(e)^2]$	$\sqrt{2}\,(3B + C)$	$\sqrt{2}\,(3B + C)$	$3\epsilon_o - 2Dq - 4Ds + 2Dt + 3A + 10B + 5C - E$	$5\sqrt{3}\,B$	$5\sqrt{3}\,B$
$\Psi_{21}[(b_1)(e)^2]$	$\sqrt{6}\,B$	0	$5\sqrt{3}\,B$	$3\epsilon_o - 2Dq + 7Dt + 3A - 6B + 3C - E$	$3B$
$\Psi_{26}[(b_2)(e)^2]$	0	$\sqrt{6}\,B$	$5\sqrt{3}\,B$	$3B$	$3\epsilon_o - 12Dq + 7Dt + 3A - 6B + 3C - E$

$= 0$

$^2A_2$

	Ψ_{18}	Ψ_{22}	Ψ_{25}	Ψ_{30}	Ψ_{31}
$\Psi_{18}[(a_1)(e)^2]$	$3\epsilon_o - 2Dq - 4Ds + 2Dt + 3A + 3C - E$	$3B$	$3B$	$3\sqrt{3}\,B$	$-3B$
$\Psi_{22}[(b_1)(e)^2]$	$3B$	$3\epsilon_o - 2Dq + 7Dt + 3A - 6B + 3C - E$	$3B$	$2\sqrt{3}\,B$	0
$\Psi_{25}[(b_2)(e)^2]$	$3B$	$3B$	$3\epsilon_o - 12Dq + 7Dt + 3A - 6B + 3C - E$	$\sqrt{3}\,B$	$-3B$
$\Psi_{30}[(a_1)(b_1)(b_2)]$	$3\sqrt{3}\,B$	$2\sqrt{3}\,B$	$\sqrt{3}\,B$	$3\epsilon_o + 8Dq + 2Ds - 8Dt + 3A - 2B + 3C - E$	$-2\sqrt{3}\,B$
$\Psi_{31}[(a_1)(b_1)(b_2)]$	$-3B$	0	$-3B$	$-2\sqrt{3}\,B$	$3\epsilon_o + 8Dq + 2Ds - 8Dt + 3A - 6B + 3C - E$

$= 0$

$^2B_1$

	Ψ_{8}	Ψ_{15}	Ψ_{20}	Ψ_{23}	Ψ_{28}
$\Psi_{8}[(a_1)^2(b_1)]$	$3\epsilon_o + 18Dq - 2Ds - 13Dt + 3A - 8B + 4C - E$	$-(4B + C)$	$\sqrt{6}\,B$	$-\sqrt{2}\,(B + C)$	0
$\Psi_{15}[(b_1)(b_2)^2]$	$-(4B + C)$	$3\epsilon_o - 2Dq + 6Ds - 3Dt + 3A + 12B + 4C - E$	0	$\sqrt{2}\,(3B + C)$	$-3\sqrt{6}\,B$
$\Psi_{20}[(a_1)(e)^2]$	$\sqrt{6}\,B$	0	$3\epsilon_o - 2Dq - 4Ds + 2Dt + 3A + 4B + 3C - E$	$-5\sqrt{3}\,B$	$3B$
$\Psi_{23}[(b_1)(e)^2]$	$-\sqrt{2}\,(B + C)$	$\sqrt{2}\,(3B + C)$	$-5\sqrt{3}\,B$	$3\epsilon_o - 2Dq + 7Dt + 3A + 5C - E$	$-3\sqrt{3}\,B$
$\Psi_{28}[(b_2)(e)^2]$	0	$-3\sqrt{6}\,B$	$3B$	$-3\sqrt{3}\,B$	$3\epsilon_o - 12Dq + 7Dt + 3A - 6B + 3C - E$

$= 0$

$^2B_2$

	Ψ_{9}	Ψ_{12}	Ψ_{19}	Ψ_{24}	Ψ_{27}
$\Psi_{9}[(a_1)^2(b_2)]$	$3\epsilon_o + 8Dq - 2Ds - 13Dt + 3A - 8B + 4C - E$	$4B + C$	$-\sqrt{6}\,B$	0	$-\sqrt{2}\,(B + C)$
$\Psi_{12}[(b_1)^2(b_2)]$	$4B + C$	$3\epsilon_o + 8Dq + 6Ds - 3Dt + 3A + 12B + 4C - E$	0	$-3\sqrt{6}\,B$	$-\sqrt{2}\,(3B + C)$
$\Psi_{19}[(a_1)(e)^2]$	$-\sqrt{6}\,B$	0	$3\epsilon_o - 2Dq - 4Ds + 2Dt + 3A + 4B + 3C - E$	$3B$	$5\sqrt{3}\,B$
$\Psi_{24}[(b_1)(e)^2]$	0	$-3\sqrt{6}\,B$	$3B$	$3\epsilon_o - 2Dq + 7Dt + 3A - 6B + 3C - E$	$3\sqrt{3}\,B$
$\Psi_{27}[(b_2)(e)^2]$	$-\sqrt{2}\,(B + C)$	$-\sqrt{2}\,(3B + C)$	$5\sqrt{3}\,B$	$3\sqrt{3}\,B$	$3\epsilon_o - 12Dq + 7Dt + 3A + 5C - E$

$= 0$

Can. J. Chem. Downloaded from www.nrcresearchpress.com by 210.87.254.40 on 09/05/12
For personal use only.

TABLE 2 *(Concluded)*

^2E

	Ψ_{10}	Ψ_{13}	Ψ_{16}	Ψ_{29}	Ψ_{32}	Ψ_{33}	Ψ_{34}	Ψ_{35}	Ψ_{36}	Ψ_{37}
$\Psi_{10}[(a_1)^2(e)]$	$3c_o + 8Dq - 5Ds - 8Dt + 3A + 7B + 4C - E$									
$\Psi_{13}[(b_1)^2(e)]$	$-(4B + C)$	$3c_o + 8Dq + 3Ds + 2Dt + 3A - 3B + 4C - E$								
$\Psi_{16}[(b_2)^2(e)]$	$-(4B + C)$	C	$3c_o - 12Dq + 3Ds + 2Dt + 3A - 3B + 4C - E$							
$\Psi_{29}[(e)^3]$	$-(B + C)$	$3B + C$	$3B + C$	$3c_o - 12Dq - 3Ds + 12Dt + 3A - 3B + 4C - E$						
$\Psi_{32}[(b_1)(b_2)(e)]$	0	$-\frac{3}{2}\sqrt{2}\,B$	$\frac{3}{2}\sqrt{2}\,B$	0	$3c_o - 2Dq + 3Ds + 2Dt + 3A - 3B + 3C - E$					
$\Psi_{33}[(b_1)(b_2)(e)]$	0	$\frac{3}{2}\sqrt{6}\,B$	$\frac{3}{2}\sqrt{6}\,B$	$3\sqrt{6}\,B$	0	$3c_o - 2Dq + 3Ds + 2Dt + 3A + 3B + 3C - E$				
$\Psi_{34}[(a_1)(b_1)(e)]$	$\frac{5}{2}\sqrt{6}\,B$	$-\frac{5}{2}\sqrt{6}\,B$	0	$-\sqrt{6}\,B$	$\frac{5}{2}\sqrt{3}\,B$	$-\frac{3}{2}\,B$	$3c_o + 8Dq - Ds - 3Dt + 3A - 2B + 3C - E$			
$\Psi_{35}[(a_1)(b_1)(e)]$	$\frac{3}{2}\sqrt{2}\,B$	$\frac{3}{2}\sqrt{2}\,B$	0	0	$-\frac{3}{2}\,B$	$\frac{3}{2}\sqrt{3}\,B$	$-\sqrt{3}\,B$	$3c_o + 8Dq - Ds - 3Dt + 3A - 6B + 3C - E$		
$\Psi_{36}[(a_1)(b_2)(e)]$	$\frac{5}{2}\sqrt{6}\,B$	0	$-\frac{5}{2}\sqrt{6}\,B$	$-\sqrt{6}\,B$	$-\frac{5}{2}\sqrt{3}\,B$	$-\frac{3}{2}\,B$	$\frac{3}{2}\,B$	$\frac{3}{2}\sqrt{3}\,B$	$3c_o - 2Dq - Ds - 3Dt + 3A - 2B + 3C - E$	
$\Psi_{37}[(a_1)(b_2)(e)]$	$\frac{3}{2}\sqrt{2}\,B$	0	$\frac{3}{2}\sqrt{2}\,B$	0	$\frac{3}{2}\,B$	$\frac{3}{2}\sqrt{3}\,B$	$\frac{3}{2}\sqrt{3}\,B$	$-\frac{3}{2}\,B$	$-\sqrt{3}\,B$	$3c_o - 2Dq - Ds - 3Dt + 3A - 6B + 3C - E$

$= 0$

$^4B_1$ $\quad \Psi_4[(b_2)(e)^2] \quad \left| 3c_o - 12Dq + 7Dt + 3A - 15B - E \right| = 0$

$^4B_2$ $\quad \Psi_3[(b_1)(e)^2] \quad \left| 3c_o - 2Dq + 7Dt + 3A - 15B - E \right| = 0$

$^4A_2$

$\Psi_1[(a_1)(e)^2]$	$3c_o - 2Dq - 4Ds + 2Dt + 3A - 3B - E$	$6B$
$\Psi_2[(a_1)(b_1)(b_2)]$	$6B$	$3c_o + 8Dq + 2Ds - 8Dt + 3A - 12B - E$

$= 0$

^4E

$\Psi_5[(b_1)(b_2)(e)]$	$3c_o - 2Dq + 3Ds + 2Dt + 3A - 6B - E$	$3\sqrt{3}\,B$	$-3\sqrt{3}\,B$
$\Psi_6[(a_1)(b_1)(e)]$	$3\sqrt{3}\,B$	$3c_o + 8Dq - Ds - 3Dt + 3A - 12B - E$	$-3B$
$\Psi_7[(a_1)(b_2)(e)]$	$-3\sqrt{3}\,B$	$-3B$	$3c_o - 2Dq - Ds - 3Dt + 3A - 12B - E$

$= 0$

Can. J. Chem. Downloaded from www.nrcresearchpress.com by 210.87.254.40 on 09/05/12
For personal use only.

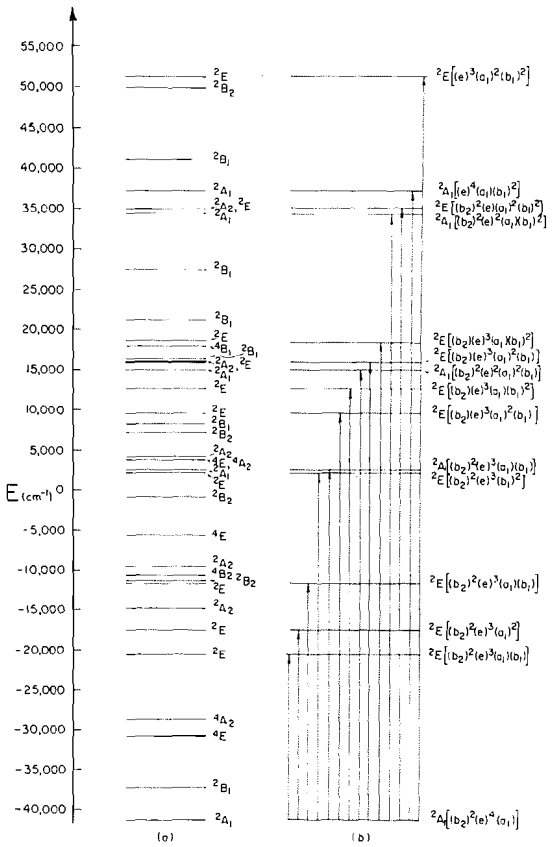

FIG. 3. The complete energy level diagram for a regular square pyramidal strong field d^7 complex. (*a*) The energies of the strong field states for $\beta = 0°$; (*b*) the symmetry-allowed, spin-allowed transitions.

Both stabilization of the various excited states and marked destabilization of the $^2A_1$ ground state shift the absorption bands to lower energy with increasing L_a—Co—L_b bond angle. Spacings between adjacent transitions decrease, leading to degeneracies and inversions. Figure 5 is the analog to Fig. 4, assuming a quartet ground state, which occurs only for $\beta > 20°$. Transitions to all quartet excited states are symmetry- and spin-allowed from the $^4E[(b_2)^2(e)^3(a_1)(b_1)]$ ground state, but from $^4B_2[(b_2)^2(e)^2(a_1)^2(b_1)]$ only transitions to a ^4E excited state are symmetry-allowed. In general, the number of allowed transitions becomes fewer as β increases, and the absorption bands shift to lower energy and become more clustered. The reader is cautioned, however, against using these illustrative energy level diagrams (*i.e.*, Fig. 3, 4, or 5) *per se*. To interpret specific electronic spectra requires use of the perturbation energy matrices (as listed in Table 2) with parameters adjusted to reflect experimental values.

Conclusion

By employing standard group theoretical methods in conjunction with time-independent perturbation theory, the parametric form of the complete (crystal field and Coulombic) energy matrices for the square pyramidal d^3, d^7 system is evaluated with quantitative accuracy. An energy level diagram for a Co(II) square pyramidal complex is then constructed from these matrices and the qualitative features of the expected absorption spectrum, noted. Recent experimental application of the C_{4v} energy matrices have treated the two isomers of $[Co(CNC_6H_5)_5](ClO_4)_2$ (21), fitting the liquid nitrogen temperature electronic spectra with the parameter values $Dq^0 = 2250$, $Ds^0 = 600$, $B = 700$, $C = 3000$ cm^{-1}, and $\beta = 14.0°$ or

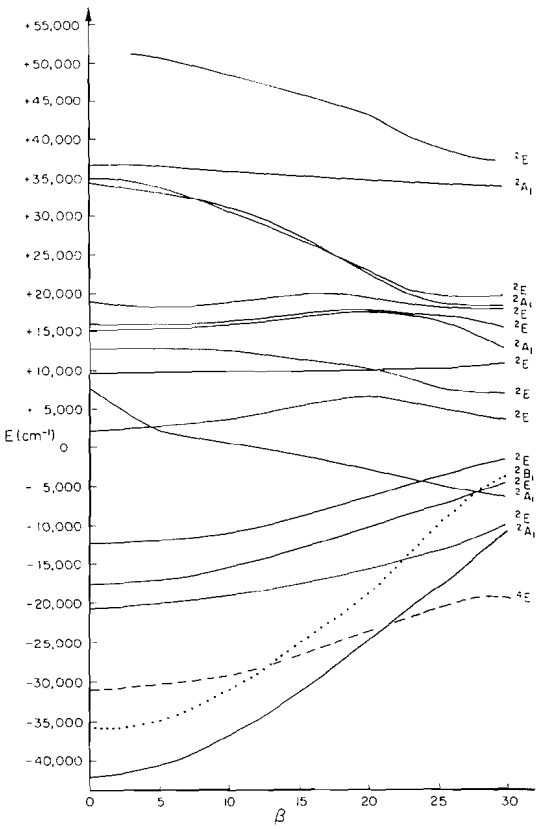

FIG. 4. The energies of the C_{4v} d^7 strong field doublet ground state and symmetry-accessible excited states as a function of β, the angle of distortion.

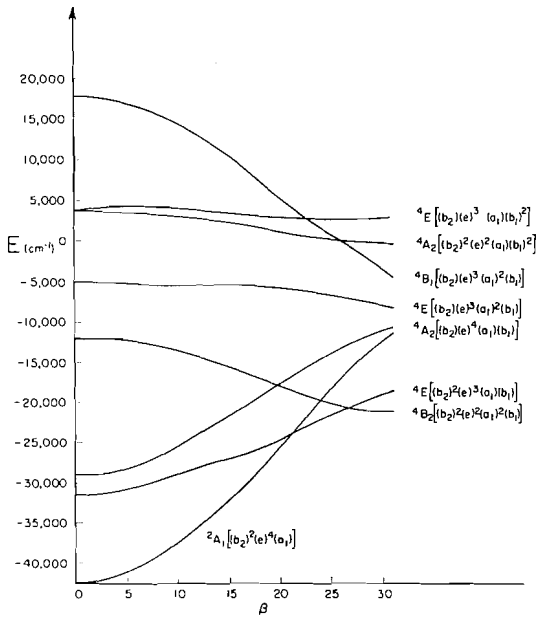

FIG. 5. The energies of the C_{4v} d^7 strong field quartets as a function of the angle of distortion, β.

11.0°, respectively (19). Strong dependence on initial reaction temperature for $[Co(CNC_6H_5)_5](BF_4)_2$ (prepared as $[Co(CNC_6H_5)_5](BF_4)_2 \cdot 1.0H_2O$ and easily dehydrated under strong vacuum), as reflected by systematic changes in both i.r. and electronic spectra, can be explained most satisfactorily in terms of a regularly decreasing β angle: 14.0° (for preparation at 0 °C), 13.0° (10 °C), 12.5° (20 °C), and 12.0° (30 °C); but otherwise the same crystal field parameters as for the perchlorate salt: $Dq^0 = 2250$, $Ds^0 = 600$, $B = 700$, and $C = 3000$ cm^{-1} (20). The effect of *para*-substitution on the phenylisocyanide is accommodated by slightly changing the Dq^0 value: $Dq^0 = 2150$ cm^{-1} for $[Co(CNC_6H_4F)_5](ClO_4)_2$, $Dq^0 = 2300$ cm^{-1} for $[Co(CNC_6H_4CH_3)_5](ClO_4)_2$ (20).

Acknowledgment is made to the donors of The Petroleum Research Fund, administered by the American Chemical Society, for partial support of this research; in particular, for making available a Wang Model 320 Electronic Calculator and Model 320E Electronics Package to this laboratory. The authors wish also to gratefully acknowledge The Robert A. Welch Foundation for financial support of this research and for a graduate fellowship to J. A. Varga.

1. J. A. VARGA and C. A. L. BECKER. J. Phys. Chem. **76**, 2907 (1972).
2. (*a*) J. R. PERUMAREDDI. J. Phys. Chem. **71**, 3144 (1967); (*b*) J. Phys. Chem. **71**, 3155 (1967).
3. C. FURLANI. Coord. Chem. Rev. **3**, 141 (1968).
4. P. R. H. ALDERMAN, P. G. OWSTON, and J. M. ROWE. J. Chem. Soc. A, 668 (1962).
5. P. L. ORIOLI and L. SACCONI. Chem. Commun. 1012 (1969).
6. S. BRÜCKNER, M. CALLIGARIS, G. NARDIN, and L. RANDACCIO. Acta Cryst. B**25**, 1671 (1969).
7. C. A. L. BECKER, D. W. MEEK, and T. M. DUNN. J. Phys. Chem. **74**, 1568 (1970).
8. T. M. DUNN, D. S. MCCLURE, and R. G. PEARSON. Some aspects of crystal field theory. Harper and Row, New York. 1965. Chapt. 1.
9. M. GERLOCH, J. KOHL, J. LEWIS, and W. URLAND. J. Chem. Soc. A, 3269, 3283 (1970).
10. (*a*) D. S. MCCLURE. J. Chem. Phys. **36**, 2757 (1962); (*b*) H. A. WEAKLIEM. J. Chem. Phys. **36**, 2117 (1962); (*c*) T. S. PIPER and R. L. CARLIN. J. Chem. Phys. **33**, 1208 (1960).
11. (*a*) W. E. HATFIELD and T. S. PIPER. Inorg. Chem. **3**, 841 (1964); (*b*) P. DAY. Proc. Chem. Soc. 18 (1964).
12. J. R. PERUMAREDDI. Coord. Chem. Rev. **4**, 73 (1969).
13. C. A. L. BECKER, D. W. MEEK, and T. M. DUNN. J. Phys. Chem. **72**, 3588 (1968).
14. E. U. CONDON and G. H. SHORTLEY. The theory of atomic spectra. Cambridge University Press, Cambridge. 1964. Chapt. 6.
15. G. RACAH. Phys. Rev. **61**, 186 (1942); Phys. Rev. **62**, 438 (1942); Phys. Rev. **63**, 367 (1943).
16. A. B. P. LEVER. Inorganic electronic spectroscopy. Elsevier Publishing Co., New York. 1968. Chapt. 9.
17. J. S. GRIFFITH. The theory of transition metal ions. Cambridge University Press, Cambridge. 1964. Appendix 6.
18. D. W. MEEK. Data reported in part, 162nd ACS National Meeting, Sept. 1971, Abstract No. 96 (Inorg. Div.).
19. C. A. L. BECKER and T. J. WEAVER. Data reported in part, 164th ACS National Meeting, Aug. 1972, Abstract No. 63 (Phys. Div.).
20. C. A. L. BECKER and C. G. JOHNSON. Data reported in part, 28th ACS Southwestern Regional Meeting, Dec. 1972, Abstract No. 138 (Inorg. Div.).
21. C. A. L. BECKER. Data reported in part, 25th ACS Southwestern Regional Meeting, Dec. 1969, Abstract No. 7 (Inorg. Div.); 162nd ACS National Meeting, Sept. 1971, Abstract No. 106 (Inorg. Div.).

Can. J. Chem. Downloaded from www.nrcresearchpress.com by 210.87.254.40 on 09/05/12
For personal use only.

Metals Intercalated in Graphite. II. The Friedel–Crafts Reactions with $AlCl_3$–Graphite

JEAN-MARC LALANCETTE, MARIE-JOSÉE FOURNIER-BREAULT, AND RAYMOND THIFFAULT

Département de chimie, Faculté des sciences, Université de Sherbrooke, Sherbrooke, Québec

Received September 12, 1973

Aluminum trichloride can be intercalated in the lattice of graphite. This intercalate is a milder catalyst than $AlCl_3$ for the alkylation reactions and gives less polysubstituted reaction products.

Le trichlorure d'aluminium peut être inséré dans le réseau du graphite. Ce produit d'insertion s'avère un catalyseur plus doux que $AlCl_3$ pur lors de réactions d'alkylation et donne moins de produits de polysubstitution.

Can. J. Chem., **52**, 589 (1974)

Can. J. Chem. Downloaded from www.nrcresearchpress.com by 210.87.254.42 on 09/05/12
For personal use only.

The intercalation of metals and salts in the lattice of graphite changes markedly the chemical behavior of the intercalated species (1). For example, the reaction of potassium intercalated in graphite with molecular hydrogen is extremely fast, even at room temperature, whereas metallic potassium shows very sluggish reaction with hydrogen below 200° (2). In some instances, the speed of the reaction may be retarded by the intercalation. In other cases, the selectivity of the reactions is improved as it was noted with CrO_3–graphite used as oxidizing agent for alcohols (3). It has been reported that aluminum trichloride can be intercalated in graphite, in an atmosphere of chlorine (4). We have compared the reactivity of this graphite aluminum chloride with that of pure $AlCl_3$ when used as catalyst for the Friedel–Crafts reaction. This study is in fact a comparison of the behavior of $AlCl_3$ inside and outside of the lattice of graphite, in the course of electrophilic substitutions, all the other experimental parameters being kept identical for a given system. The results are presented in Table 1.

From these results, it can be noted that the intercalation of $AlCl_3$ in the lattice of graphite decreases the speed of the reaction to some extent, but the reaction mixtures obtained with intercalated $AlCl_3$ indicate an important decrease of polysubstitution. Such a control over the degree of substitution by intercalation of $AlCl_3$ in the lattice of graphite offers interesting and new possibilities for the Friedel–Crafts reaction. The steps of the reaction between the organic substrate and the aluminum trichloride when intercalated remain an open question at the present time, since it has not been established if the organic substrate reacts at the edges, on the plane or inside the crystals of the $AlCl_3$–graphite intercalate.

Experimental

Reaction mixtures have been analyzed with a Varian Aerograph model 700 instrument. The column was of Carbowax 20M, 10 ft. The fractions have been condensed and identified by mass spectrometry using a Hitachi–Perkin–Elmer RMU-6 instrument.

(1) Preparation of $AlCl_3$–Graphite

The method used was in accordance with the description of Rudorff and Zeller (4). A mixture of 20 g of graphite and 40 g of $AlCl_3$ (Acheson type, 99.99% C, obtained from Fisher Co.) was introduced, in an atmosphere of helium, into an aluminum autoclave. The system was flushed with chlorine and a pressure of 2.8 atm of chlorine was built in the system. The inlet and outlet were then closed and the autoclave heated at 260° for 24 h. Upon heating, the pressure reached 17 atm. After cooling, the autoclave was opened. Some $AlCl_3$ was condensed on top of the autoclave. The solid mass was broken in a dry atmosphere and heated for 16 h under a pressure 0.1 mm, at 250°, with an acetone – Dry Ice trap in the system. This treatment removed the non-intercalated $AlCl_3$. By standard analytical procedure, this intercalate contained 6.0% Al and 24.0% Cl. The experiment could be easily reproduced and gave a concentration of $AlCl_3$ in the graphite in the range of 30–35%. This experimental method operates at higher pressure than other already reported procedures (5) but gives a lower Cl/Al ratio (6).

(2) Reaction in Sealed Tubes

In a thick wall test tube (1.5 × 12.5 cm), 1.00 g of $AlCl_3$–graphite (35% $AlCl_3$) was introduced with 0.500 g (4.1 mmol) of naphtalene and 1.330 g (12.3 mmol) of ethyl bromide. The mixture was frozen in Dry Ice and the tube sealed under vacuum. After a contact of 44 h, at room temperature, the tube was opened, after freezing, and the reaction mixture extracted with ethyl ether. A series of experiments was repeated using this technique and, for a given substrate the same amount of $AlCl_3$,

TABLE 1. Substitution with $AlCl_3$–graphite

System	Substrate (S)	Reagent (R)	Temperature (°C)	Duration (h)	Molar ratio (R/S)	Products*	with $AlCl_3$	with $AlCl_3$–graphite
Sealed tube	Benzene	Ethyl bromide	25	48	3	Benzene	2	29
						Monoethyl-	13	40
						Diethyl-	27	23
						Triethyl-	54	8
						Tetraethyl-	4	Traces
Sealed tube	Toluene	Ethyl bromide	25	24	3	Toluene	0	17
						Monoethyl-	Traces	52
						Diethyl-	41	31
						Triethyl-	60	Traces
Atmospheric	Toluene	Ethyl bromide	−10	24	2	Toluene	5	5
						Monoethyl-	Traces	33
						Diethyl-	30	52
						Triethyl-	65	10
Sealed tube	Naphtalene	Ethyl bromide	25	44	3	Naphtalene	26	77
						Monoethyl-	39	21
						Diethyl-tetrahydro-	2	Traces
						Diethyl-	17	1
						Triethyl-	16	0.5
Sealed tube	Biphenyl	Ethyl bromide	25	48	3	Biphenyl	26	81
						Diethyl-	16	15
						Tetra–hexa ethyl-	33	4
						Octaethyl-	25	0
Atmospheric	Benzene	Ethylene	75	24	—	Benzene	0	3
						Monoethyl-	Traces	19
						Diethyl-	1.1	47
						Triethyl-	25	22
						Tetraethyl-	53	6
						Pentaethyl-	18	2
						Hexaethyl-	4	1
Atmospheric	Benzene	Propylene	60	0.5	—	Benzene	23	44
						Monoisopropyl-	56	54
						Diisopropyl-	18	2
						Triisopropyl-	3	Traces
Atmospheric	Toluene	Ethylene	80	1.45	—	Toluene	8	17
						Monoethyl-	49	51
						Diethyl-	40	26
Atmospheric	Toluene	Propylene	80	2.50	–	Toluene	Traces	4
						Monoisopropyl-	Traces	33
						Diisopropyl-	42	59
						Triisopropyl-	46	Traces
Atmospheric	Toluene	Isobutylene	80	1.15	—	Toluene	20	35
						Monoisobutyl-	66	63
						Diisobutyl-	13	1

*Some minor components of the reaction mixtures have not been identified. The ratios reported are mass ratios. Most experiments have been repeated twice and could be reproduced within 1%.

Can. J. Chem. Downloaded from www.nrcresearchpress.com by 210.87.254.42 on 09/05/12
For personal use only.

either intercalated in graphite or free. The results are reported in Table 1.

(3) Reaction at Atmospheric Pressure

The procedure used was described by Norris and Rubinstein (7). Again, the relative amounts of $AlCl_3$, either intercalated or free, were maintained constant, for one given system. Results are reported in Table 1.

(4) Ethylation of Benzene

A 50 ml flask containing 20 g of dry benzene and 2.00 g of $AlCl_3$–graphite (30% $AlCl_3$) was kept at 75° for 24 h. In this mixture, a very slow stream of ethylene and HCl was circulated. After cooling, the organic phase was washed with bicarbonate and analyzed by preparative vapor phase chromatography. The experiment was repeated with the same amount of $AlCl_3$ not intercalated. Results are reported in Table 1.

1. (*a*) P. PASCAL. Nouveau traité de chimie minérale. Vol. VIII. Masson et Cie, Paris. 1968. p. 338. (*b*) H. PODALL and W. E. FOSTER. J. Org. Chem. **28**, 401 (1958).
2. H. REMY. Treatise on inorganic chemistry. Vol. I. Elsevier Publishing Co., N.Y. 1956. p. 168.
3. J. M. LALANCETTE, G. ROLLIN, and P. DUMAS. Can. J. Chem. **50**, 3058 (1972).
4. W. RUDORFF and R. ZELLER. Z. Anorg. Chem. **279**, 182 (1955).
5. J. G. HOOLEY. Carbon, **11**, 225 (1973).
6. M. L. DZURUS and G. R. HENNIG. J. Am. Chem. Soc. **79**, 1151 (1957).
7. J. F. NORRIS and D. RUBINSTEIN. J. Am. Chem. Soc. **61**, 1166 (1939).

Can. J. Chem. Downloaded from www.nrcresearchpress.com by 210.87.254.42 on 09/05/12
For personal use only.

Kinetics of Proton Transfer Reactions of Carbon Acids. IV. Primary Deuterium Isotope Effect in the Reaction of Di-(4-nitrophenyl)methane-d_2 with *t*-Butoxide

JAE-HANG KIM[1] AND KENNETH T. LEFFEK

Chemistry Department, Dalhousie University, Halifax, Nova Scotia

Received July 4, 1973

The primary deuterium isotope effect has been measured for the proton transfer reaction from di-(4-nitrophenyl)methane to *t*-butoxide ion in a solvent consisting of 10% v/v toluene in *t*-butanol at a series of temperatures between 20 and 45 °C. The isotopic rate ratio, k_H/k_D, is 7.3 at 25 °C. The activation parameters showed an enthalpy of activation difference ($\Delta H_D^{\ddagger} - \Delta H_H^{\ddagger}$) of only *ca.* $\frac{1}{2}$ kcal mol^{-1} and an entropy isotope effect ($\Delta S_D^{\ddagger} - \Delta S_H^{\ddagger}$) of -2.4 cal mol^{-1} deg^{-1}. The latter indicates, according to the theory of Bell, that tunnelling of the proton through the energy barrier is unimportant in this reaction. This result is compared to other reactions in the literature, in which tunnelling has been postulated to occur.

L'effet isotopique primaire du deutérium a été mesuré pour la réaction de transfert du proton du di(nitro-4 phényl) méthane à l'ion *t*-butoxide, dans un solvant constitué de 10% v/v de toluène dans le *t*-butanol et pour des températures variant entre 20 et 45 °C. Le rapport des vitesses isotopiques, k_H/k_D est de 7.3 à 25 °C. Les paramètres d'activation montrent une différence d'enthalpie d'activation de seulement ca. $\frac{1}{2}$ kcal mol^{-1} pour ($\Delta H_D^{\ddagger} - \Delta H_H^{\ddagger}$) et un effet isotopique d'entropie, ($\Delta S_D^{\ddagger} - \Delta S_H^{\ddagger}$) de -2.4 cal mol^{-1} deg^{-1}. Ce dernier résultat indique, selon la théorie de Bell, que l'effet tunnel du proton à travers la barrière énergétique n'est pas important dans cette réaction. Ces résultats sont comparés à ceux d'autres réactions de la littérature, où l'effet tunnel est supposé présent. [Traduit par le journal]

Can. J. Chem., **52**, 592 (1974)

Introduction

The investigation of primary deuterium isotope effects is of interest as one means of detecting proton tunnelling in organic reactions (1, 2). About a dozen examples have been treated by Caldin (2) using the appropriate mathematical expressions (3) to yield barrier widths and barrier heights for proton transfer, corrected for tunnelling. These reactions exhibited rate ratios, k_H/k_D, varying between 2.7 and 28.6 and within the reliability of the theory used, they showed significant tunnel effects. Nevertheless, isotopic rate ratios are not compelling manifestations of the tunnel effect unless k_H/k_D is greater than 17 at 25 °C, *i.e.* greater than the largest rate difference which can be accounted for by the loss of one stretching and two bending modes of vibration for the C—H and C—D bonds (4). Such large ratios have been observed by Lewis and co-workers (5–7). One of these examples, the proton transfer from 2-nitropropane to 2,6-dimethylpyridine, for which Lewis and co-workers (5, 6) reported $k_H/k_D = 24.1$ at 25 °C in aqueous *t*-butanol was confirmed by Bell and Goodall (8), $k_H/k_D = 19.5$ at 25 °C in water. However, from a temperature-dependence study of the isotope effect for the same reaction in aqueous ethanol Lehman (9) found that the frequency factor ratio A_H/A_D is much greater than unity, whereas Bell predicted (1) that the tunnel effect should be characterized by A_H/A_D ratios less than unity.

From a comparison of the rate ratios found for 2,6-dimethylpyridine and the unsubstituted base, Lewis suggested that a requirement for a large tunnel effect is that the reaction should have considerable steric hindrance, which would provide the necessary narrow energy barrier. The abstraction of a proton by the bulky *t*-butoxide ion in *t*-butanol is likely to be sterically hindered and large isotope effects have been measured for the reaction between *t*-butoxide and tri-(4-nitrophenyl)methane in *t*-butanol.[2] Therefore, the corresponding reaction with di-(4-nitrophenyl)methane-d_2 has been studied.

Results and Discussion

The rates and activation parameters for the proton transfer from di-(4-nitrophenyl)methane

[1]Postdoctoral Fellow 1971–1972.

[2]E. F. Caldin, personal communication.

Can. J. Chem. Downloaded from www.nrcresearchpress.com by 210.87.254.105 on 09/05/12
For personal use only.

TABLE 1. Rate constants and isotopic rate ratios for the reaction of di-(4-nitrophenyl)methane with sodium *t*-butoxide

Temperature (°C)	10^3 [ŌBu] (M)	$10^3 k_H$ (s^{-1})	$10^3 k_D$ (s^{-1})	k_{2H} ($l\ mol^{-1}\ s^{-1}$)	k_{2D} ($l\ mol^{-1}\ s^{-1}$)	k_{2H}/k_{2D}
20.0	0.80	3.55	1.80			
	2.05	5.26	2.04			
	3.80	7.66	2.39			
	8.60	13.7	3.31			
	16.20	22.5	4.32	1.23±0.02	0.164±0.009	7.50±0.02
25.0	0.80	4.19	2.11			
	2.05	6.06	2.51			
	3.80	9.35	2.80			
	8.60	15.7	3.75			
	16.20	27.2	5.29	1.48±0.03	0.202±0.004	7.33±0.02
30.0	0.80	4.82	2.78			
	2.05	7.01	3.10			
	3.80	11.2	3.84			
	8.60	19.0	5.17			
	16.20	33.1	6.66	1.82±0.04	0.253±0.019	7.19±0.03
35.0	0.80	5.66	3.42			
	2.05	8.32	3.71			
	3.80	12.3	4.37			
	8.60	23.3	5.97			
	16.20	38.2	8.01	2.12±0.04	0.303±0.01	7.00±0.03
40.0	0.80	6.88	4.11			
	2.05	10.1	4.61			
	3.80	15.1	5.31			
	8.60	28.3	7.24			
	16.20	47.8	9.85	2.66±0.03	0.374±0.009	7.11±0.02
45.0	0.80	8.82	5.04			
	2.05	12.3	5.82			
	3.80	18.8	6.69			
	8.60	34.1	8.72			
	16.20	57.2	12.1	3.15±0.04	0.450±0.01	7.00±0.03

NOTE: Initial concentration of substrate = $5 \times 10^{-5}\ M$; k_H and k_D are observed first-order rate constants for $(4\text{-}NO_2C_6H_4)_2CH_2$ and $(4\text{-}NO_2C_6H_4)_2CD_2$, respectively; k_{2H} and k_{2D} are second-order rate constants.

to *t*-butoxide in 10% v/v toluene in *t*-butanol have been reported in a previous paper (10), but the standard deviations obtained in that work were too large to allow those results to be incorporated in an isotope effect study. Therefore, the rates of reaction for the protium compound were redetermined along with those for the deuterated analogue, using the same experimental procedures as the earlier work (10).

The first-order rate constants were determined using a substrate concentration of $5 \times 10^{-5}\ M$ and *t*-butoxide concentrations varying between 8.0×10^{-4} and $1.6 \times 10^{-2}\ M$. The second-order rate constants were calculated from the slope of the plot of k_1 *vs.* *t*-butoxide concentration at each temperature studied between 20 and 45 °C. The rate constants are shown in Table 1, together with the isotopic rate ratios. The activation parameters and their isotopic dependence, calculated from the data in Table 1, are shown in Table 2.

For the protium compound the enthalpy of activation is slightly smaller and the entropy of activation slightly more negative than the previous measurement (10) but the two sets of parameters are in agreement within the quoted standard deviations.

The magnitude of the isotopic rate ratio of 7.0 to 7.5 looks quite normal for a primary deuterium kinetic isotope effect but its temperature dependence is unusual. For a number of proton transfer reactions from similar carbon acids, the isotope effects on the activation parameters are in the directions so as to partially cancel each other. $\Delta H_H^{\ddagger}$ is always less than $\Delta H_D^{\ddagger}$ as required by the lower zero point energy of the C—D bond compared to the C—H bond and the standard result up to now has been for

Can. J. Chem. Downloaded from www.nrcresearchpress.com by 210.87.254.105 on 09/05/12
For personal use only.

Can. J. Chem. Downloaded from www.nrcresearchpress.com by 210.87.254.105 on 09/05/12
For personal use only.

TABLE 2. Activation parameters for the proton and deuteron transfer reactions from di-(4-nitrophenyl)methane to *t*-butoxide

Compound	$\Delta H^{\ddagger}$ (kcal mol^{-1})	$\Delta S^{\ddagger}$ (cal mol^{-1} deg^{-1})	A (l mol^{-1} s^{-1})	$\Delta H_D^{\ddagger} - \Delta H_H^{\ddagger}$ (kcal mol^{-1})	$\Delta S_D^{\ddagger} - \Delta H_H^{\ddagger}$ (cal mol^{-1} deg^{-1})	A_H/A_D
H	6.41±0.16	−36.2±0.5	(2.1±0.5) × 10^5			
				0.46±0.17	−2.4±0.6	3.4±0.7
D	6.87±0.07	−38.7±0.3	(6.2±0.8) × 10^4			

Can. J. Chem. Downloaded from www.nrcresearchpress.com by 210.87.254.105 on 09/05/12
For personal use only.

$\Delta S_D^{\ddagger}$ to be more positive than the $\Delta S_H^{\ddagger}$. In collision theory terminology, this entropy effect is equivalent to the frequency factor A_H being less than A_D, and this fact, especially if $A_H/A_D < \frac{1}{2}$, together with activation enthalpy differences greater than 1 kcal/mol, has been cited as evidence of tunnelling through the energy barrier by the proton. The frequency factor ratio in Table 2, $A_H/A_D = 3.4$, indicates that tunnelling is unimportant in this reaction. Thus, if this theory is correct, we can conclude that the proton transfer between di-(4-nitrophenyl)methane to *t*-butoxide in 10% v/v toluene in *t*-butanol is characterized by a low broad barrier.

The frequency factor ratio of 3.4 is not only too large to indicate tunnelling through the barrier, it is also too large to be explained by any of the current models for primary deuterium isotope effects. Schneider and Stern (11), for example, have calculated preexponential factors for five model reactions and find that A_H/A_D lies between 0.7 and 1.2. The experimental error quoted in Table 2 indicates that there is only a very small chance that our A_H/A_D value is less than 2. The models used by Schneider and Stern, however, were chosen to test the lowest reasonable value of A_H/A_D and not the highest reasonable value and, in addition, their models contained no solvent. Since we already have evidence (10, 12) that solvent effects are important in the reaction of di-(4-nitrophenyl)methane with alkoxide bases, our abnormal frequency factor ratio may spring from this source.

Abnormal frequency factor isotope effects have been observed by others; Lehman (9) recorded a value of $A_H/A_D = 354$ for the proton transfer from 2-nitropropane to 2,6-dimethylpyridine in aqueous ethanol. While there are no apparent errors in his work, the fact that the activation energy for the deuterated 2-nitropropane is 2.1 kcal mol^{-1} *less* than that of the protium compound puts his results so far beyond the normal isotope effect theory that their authenticity must be doubted. On the other hand, Flanagan (13) found for the neutralization of nitrocyclobutane by hydroxide ion in 50% aqueous dioxane that $\Delta H_D^{\ddagger} - \Delta H_H^{\ddagger} = 0.8$ kcal mol^{-1} and $\Delta S_D^{\ddagger} - \Delta S_H^{\ddagger} = -1.3$ cal mol^{-1} deg^{-1}, corresponding to $A_H/A_D = 1.85$. It appears, therefore, that frequency factor ratios significantly greater than unity are experimentally possible.

The conclusion that tunnelling is unimportant in the present reaction, together with our earlier results on the isotope effect for the transfer of a proton from 4-nitrophenylnitromethane to the tertiary amine bases triethylamine and tri-*n*-butylamine, gives us two examples of proton transfer reactions which show no evidence of tunnelling against 11 reactions of similar type tabulated by Caldin (2), for which he was able to calculate a tunnelling correction to the activation energy ranging from 5 to 19%. The most obvious difference between the 2 reactions and the 11 reactions is that whereas the observed activation energies of the 11 reactions have values between 9.2 and 14.6 kcal mol^{-1}, the 2 reactions which show no evidence of a tunnel effect have E_H values of about 7 kcal mol^{-1}. Thus, there appears to be some circumstantial evidence that the tunnelling correction is related to the observed E_H, although the theory relates the tunnelling correction to the curvature at the top of the barrier and not to the barrier height itself. A least-squares calculation for a straight line relation between Caldin's tunnel correction (expressed as a percentage difference between E_H(obs) and E_H(corrected)) and E_H(obs) yields an E_H(obs) value of 9.3 kcal mol^{-1} as a figure below which tunnelling corrections are insignificant. This value has a standard deviation of 1.8 kcal mol^{-1}. However, the correlation coefficient for the data is only 0.42, which means that statistically the relation between the two quantities is essentially non-existent. However, the suspiciously minded will remember that both quantities are subject to considerable error and are somewhat removed mathematically from the original experimental observations. Thus, while there is no theoretical reason why a higher barrier should necessarily be narrower, and therefore more likely to show a tunnel effect than a low barrier, those who are looking for further examples of tunnelling might be advised to concentrate on proton transfer reactions with activation energies about 10 kcal mol^{-1} or more.

Experimental

Materials

Di-(4-nitrophenyl)methane was prepared and recrystallized as in the earlier work (10), m.p. 182–183 °C (lit. (14) 183°). Extensive deuteration of di-(4-nitrophenyl)-methane on the aliphatic hydrogens in NaOD–D_2O solution was reported by Bowden and Stewart (15). Our

method was similar, but used $NaOCH_3$–CH_3OD as the basic solution. The protium compound (0.2 g) was dissolved in dry toluene (30 ml) and sodium methoxide (1 mmol in 5 ml methanol-*d*) was added. After about ½ h the solution was neutralized with a few drops of concentrated DCl in D_2O. The mixture was evaporated to dryness at reduced pressure, redissolved in dry toluene (30 ml) and filtered through a sintered glass disk. The whole procedure was carried out under an atmosphere of dry nitrogen.

The exchange process was repeated twice, after which the deuterated material was more than 98% D on the aliphatic carbon judged from the n.m.r. spectrum.

Reagent grade *t*-butanol was dried over calcium hydride and fractionally distilled from dibutylphthalate. Toluene was dried with sodium metal and fractionally distilled.

Kinetic Measurements

The reaction was followed at 530 nm on a Unicam SP 800 spectrophotometer as previously described (10), except that an external slave recorder was used. Example runs have been quoted earlier (10).

The authors are grateful for financial support by the National Research Council of Canada.

1. R. P. BELL. The proton in chemistry. Cornell Univ. Press, Ithaca, N.Y. 1959.
2. E. F. CALDIN. Chem. Rev. **69**, 135 (1969).
3. R. P. BELL. Disc. Faraday Soc. **39**, 16 (1965).
4. L. MELANDER. Isotope effects on reaction rates. The Ronald Press Co., New York. 1960. p. 21.
5. L. H. FUNDERBURK and E. S. LEWIS. J. Am. Chem. Soc. **86**, 2531 (1964).
6. E. S. LEWIS and L. H. FUNDERBURK. J. Am. Chem. Soc. **89**, 2322 (1967).
7. H. WILSON, J. D. CALDWELL, and E. S. LEWIS. J. Org. Chem. **38**, 564 (1973).
8. R. P. BELL and D. M. GOODALL. Proc. Roy. Soc. A**294**, 273 (1966).
9. T. A. LEHMAN. Diss. Abstr. **28B**, 632 (1967).
10. A. JARCZEWSKI and K. T. LEFFEK. Can. J. Chem. **50**, 24 (1972).
11. M. E. SCHNEIDER and M. J. STERN. J. Am. Chem. Soc. **94**, 1517 (1972).
12. J-H. KIM and K. T. LEFFEK. Can. J. Chem. **51**, 2805 (1973).
13. P. FLANAGAN. Diss. Abstr. **18**, 1980 (1958).
14. Directory of organic compounds. Eyre and Spottiswoode Ltd., London, **4**, 2473 (1965).
15. K. BOWDEN and R. STEWART. Tetrahedron, **21**, 261 (1965).

Can. J. Chem. Downloaded from www.nrcresearchpress.com by 210.87.254.105 on 09/05/12
For personal use only.

Conformations of Bridged Diphenyls. V. A Nuclear Magnetic Resonance Comparative Study of the Conformations of Identically Substituted Diphenyl Ethers, Sulfides, Methanes, Ketones, Sulfoxides, and Sulfones

HARM BENJAMINS AND W. DAVID CHANDLER[1]

Department of Chemistry, University of Saskatchewan, Regina, Saskatchewan S4S 0A2

Received July 3, 1973

Using n.m.r. methods developed in earlier papers, the conformations of two series, one doubly *ortho*-substituted and one triply *ortho*-substituted, of six identically substituted bridged diphenyls were compared. The ethers, sulfides, and methanes have been shown to adopt the same conformation in which the di-*ortho*-substituted ring is perpendicular to the central bridge plane while the other ring lies in that plane and an *ortho* hydrogen takes up the "inside" or "proximal" position. The benzophenones and sulfoxides prefer a conformation in which the dihedral angle between each ring and the central plane is about 40–50° and an *ortho* hydrogen adopts the "outside" or "distal" position. The sulfones adopt a conformation in which the two rings are more nearly perpendicular to the central plane.

En utilisant les méthodes r.m.n. décrites dans les articles précédents on a comparé les conformations de deux séries de six diphényles pontés portant des substituants identiques, l'une doublement substituée en *ortho*, l'autre triplement substituée en *ortho*. On a montré que les éthers, les sulfures et les méthanes adoptent une même conformation où le cycle di-*ortho* substitué est perpendiculaire au plan du pont central, plan qui contient l'autre cycle, un hydrogène *ortho* occupant la position "intérieure" ou "la plus rapprochée". Les benzophénones et les sulfoxides préfèrent une conformation où l'angle dièdre entre chaque cycle et le plan central est environ 40–50°, un hydrogène *ortho* occupant la position "extérieure" ou "la plus éloignée". Les sulfones adoptent une conformation où les deux cycles sont pratiquement perpendiculaires au plan central. [Traduit par le journal]

Can. J. Chem., 52, 597 (1974)

Introduction

Extensive p.m.r. studies have shown that, for triply *ortho*-substituted diphenyl ethers, a skew or H-inside conformation (Fig. 1) is the lowest energy conformation (1–7). In solution the two rings may oscillate about the skew equilibrium angles ($\phi = 0°$, $\psi = 90°$)[2] by $\pm 20°$. Lehmann and co-workers (8–10), based on their dipole moment studies, have suggested that a twist conformation is lower in energy (Fig. 1). However, a definitive discrimination between skew and twist conformation is impossible to give using conventional techniques; the averaging of two twist conformations (Y = Z) must result in an apparent skew conformation.[3]

X-Ray diffraction studies on solids (11) have corroborated the p.m.r. results, where common ethers were used, and have shown values of ϕ and ψ close to 0 and 90°, respectively (7).

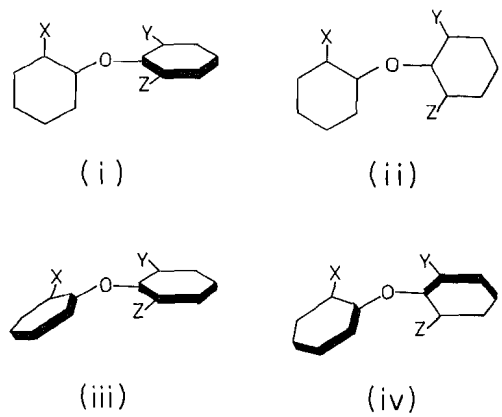

FIG. 1. Possible conformations of a triply *ortho*-substituted diphenyl ether; (*i*) skew, H-inside conformation $\phi = 0°$, $\psi = 90°$; (*ii*) planar conformation $\phi = \psi = 0°$; (*iii*) butterfly conformation $\phi = \psi = 90°$; (*iv*) twist, H-inside conformation ϕ, $\psi > 0°$.

It is clear that the triply *ortho*-substituted diphenyl ethers are forced into the skew, H-inside conformation as the result of a balance of competing forces: (*i*) the tendency of each phenyl ring to prefer a plane perpendicular to the un-

[1]Author to whom correspondence should be addressed.

[2]ϕ and ψ will be defined as the dihedral angles between the CGC plane and the two ring planes where G is the central atom of the bridge. This definition is different from the one used previously (5, 7) for ψ which is the angle between the CGC plane and the di-*ortho*-substituted ring.

[3]All ethers studied in this series of papers are symmetrically substituted in the one ring (5, 7, 11).

Can. J. Chem. Downloaded from www.nrcresearchpress.com by 210.87.254.6 on 09/05/12
For personal use only.

shared "p" electron pair on oxygen so that conjugation between oxygen and the ring may take place; (*ii*) steric repulsion among the four *ortho* substituents and the π-cloud of the rings. Conjugation alone makes a planar conformation lowest in energy while steric factors alone favor a more butterfly-like conformation (Fig. 1). With three large *ortho* substituents, the skew, H-inside conformation is the net result; the di-*ortho*-substituted ring is perpendicular to the COC plane for steric reasons while the mono-*ortho*-substituted ring is coplanar with the COC plane for reasons of conjugation and lower steric repulsion. The conjugation is increased if that ring is substituted with electron withdrawing groups (3, 8).

One would assume that if the bridge in another type of diphenyl were an electron donor like oxygen, the molecule would adopt a conformation similar to that shown by ethers. On the other hand, electron withdrawing bridges, through operation of a reversed mesomeric effect, should cause conformations somewhat different from the ethers. In fact, the p.m.r. studies of Montaudo and co-workers have been interpreted to mean that triply *ortho*-substituted diphenyl sulfides (3, 4) and methanes (12, 13) adopt conformations very similar to the ethers, whereas benzophenones (4, 14) adopt a twist conformation with the two rings approximately 20° from coplanarity, and sulfones (4, 53) take up a butterfly conformation. The limited data collected for the benzophenones were made harder to interpret by the known magnetic anisotropy of the carbonyl functional group.

In the work already done information was obtained for only one hydrogen per molecule and no common structure ran through the series of diphenyls. Thus it seemed advisable to investigate the effect of the bridge on the conformation of bridged diphenyls in a more quantitative and systematic way than had been done previously. To that end, the 24 compounds in series **1**, **2**, **3**, and **4** were obtained and their p.m.r. spectra were compared. The sulfoxides were chosen because of their obvious structural similarities to the benzophenones.

To analyze the p.m.r. data, the double-difference method, developed previously (5, 7) and applied with a fair amount of success to diphenyl ethers, was used. This method allows one to estimate that part of the chemical shift of ring protons that is due solely to conformation-

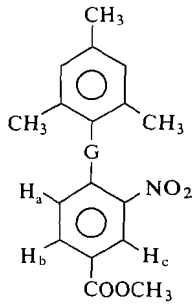

1

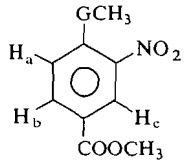

2

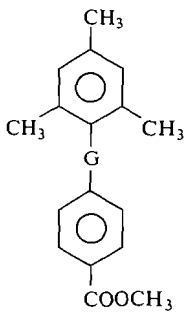

3

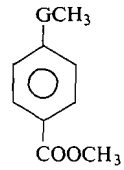

4

a G = O
b G = S
c G = CH_2
d G = CO
e G = SO
f G = SO_2

ally-dependent, ring anisotropic effects. Once this is known a comparison with values calculated using existing theories of ring anisotropy permits an estimate of the conformation of triply *ortho*-substituted diphenyls such as series **1**. To apply the double-difference analysis in this case, the chemical shifts of the ring protons, H_a, H_b, and H_c, were dissected to take account of the presence of the bridge G as follows: if $\delta_{DN}{}^j$ is the chemical shift of a particular ring proton, j = a, b, or c, in a member of series **1** and $\delta_{AN}{}^j$ is the chemical shift of the same proton in the corresponding member of **2**, then they may be written as

$$[1]\quad \delta_{DN}{}^j = \delta_\phi{}^j + \delta_{G\phi}{}^j + \delta_N{}^j + \delta_{\phi,G\phi}{}^j + \delta_{N,G\phi}{}^j + \delta_{\phi,N}{}^j + \delta_{\omega N}{}^j$$

$$[2]\quad \delta_{AN}{}^j = \delta_{Me}{}^j + \delta_{G\phi}{}^j + \delta_N{}^j + \delta_{Me,G\phi}{}^j + \delta_{N,G\phi}{}^j + \delta_{Me,N}{}^j$$

$\delta_\phi{}^j$ is the contribution to the total shift from the mesityl ring, $\delta_{Me}{}^j$ the contribution from the methyl on the bridge, $\delta_N{}^j$ the contribution from

Can. J. Chem. Downloaded from www.nrcresearchpress.com by 210.87.254.6 on 09/05/12
For personal use only.

Can. J. Chem. Downloaded from www.nrcresearchpress.com by 210.87.254.6 on 09/05/12
For personal use only.

the nitro group and $\delta_{G\phi}{}^j$ the contribution from the remainder of the molecule including the bridge itself. The $\delta_{X,Z}{}^j$ terms represent interactions between the contributors and $\delta_{\omega N}{}^j$ is the conformationally-dependent, mesityl ring shielding. Then

$$[3]\quad \delta_{DN}{}^j - \delta_{AN}{}^j = (\delta_\phi{}^j - \delta_{Me}{}^j) + (\delta_{\phi,G\phi}{}^j - \delta_{Me,G\phi}{}^j) + (\delta_{\phi,N}{}^j - \delta_{Me,N}{}^j) + \delta_{\omega N}{}^j = (\delta_\phi{}^j - \delta_{Me}{}^j) + (I_\phi{}^j - I_{Me}{}^j)I_{G\phi}{}^j + (I_\phi{}^j - I_{Me}{}^j)I_N{}^j + \delta_{\omega N}{}^j$$

where $I_Z{}^j$ represent interaction parameters (5, 7). Similarly

$$[4]\quad \delta_{DH}{}^j - \delta_{AH}{}^j = (\delta_\phi{}^j - \delta_{Me}{}^j) + (I_\phi{}^j - I_{Me}{}^j)I_{G\phi}{}^j + (I_\phi{}^j - I_{Me}{}^j)I_H{}^j + \delta_{\omega H}{}^j$$

where $\delta_{DH}{}^j$ and $\delta_{AH}{}^j$ are experimental chemical shifts for the corresponding compounds in series **3** and **4**, respectively. The double-difference, $\Delta_G{}^j$, is given by

$$[5]\quad \Delta_G{}^j = (\delta_{DN}{}^j - \delta_{AN}{}^j) - (\delta_{DH}{}^j - \delta_{AH}{}^j) = (I_\phi{}^j - I_{Me}{}^j)(I_N{}^j - I_H{}^j) + (\delta_{\omega N}{}^j - \delta_{\omega H}{}^j)$$

Since the term $(I_\phi{}^j - I_{Me}{}^j)(I_N{}^j - I_H{}^j)$ is a constant, independent of the bridge G, any variation in $\Delta_G{}^j$ with G can be attributed to changes in conformation which produce varying $\delta_{\omega N}{}^j$ or $\delta_{\omega H}{}^j$. In theory it should be possible to estimate the conformations of each member of **1** and **3** by looking at the $\Delta_G{}^j$ values. For each G there are three of these corresponding to j = a, b, and c, and these should be a self-consistent set for any particular conformation.

One defect in the double-difference analysis is that it fails to take into account the possibility that terms such as $\delta_{G\phi}{}^j$ and $\delta_N{}^j$ might not be the same in the corresponding diphenyl and monophenyl. This is likely to be a problem only if the bridge or nitro group has a different geometry relative to the common phenyl ring in the diphenyl–monophenyl pair. This was not a concern in the ethers (5, 7) but could be with bridges that do not have local spherical symmetry or if the conformation of the diphenyl is such that the nitro comes into close contact with the other ring.

Results and Discussion

The chemical shift, single and double differences are presented in Tables 1, 2, and 3. From [5] it is clear that the double-difference values can give $\delta_{\omega N}{}^j - \delta_{\omega H}{}^j$ only if the constant $(I_\phi{}^j - I_{Me}{}^j)(I_N{}^j - I_H{}^j)$ $(\equiv C^j)$ is corrected for. The values for $\delta_{\omega N}{}^j - \delta_{\omega H}{}^j$ are known for **5**, a series of diphenyl ethers with a trichlorophenyl ring rather than a mesityl ring so that it is pos-

TABLE 1. Single-difference chemical shifts for series **1** and **2***

	$\delta_{DN}{}^j - \delta_{AN}{}^j$ (p.p.m.)		
G	j = a	j = b	j = c
O	−0.51†	−0.18	0.12
S	−0.72	−0.27	0.05
CH_2	−0.58	−0.17	0.08
CO	0.00	−0.16	−0.32
SO	0.20	−0.06	−0.15
SO_2	0.03	−0.03	0.01

*In solution in chloroform-*d*.
†The negative sign means that the proton is more shielded in the diphenyl than in the monophenyl.

TABLE 2. Single-difference chemical shifts for series **3** and **4***

	$\delta_{DH}{}^j - \delta_{AH}{}^j$ (p.p.m.)	
G	j = a	j = b, j = c
O	−0.13†	−0.04
S	−0.31	−0.11
CH_2	−0.18	−0.06
CO	−0.13	−0.04
SO	−0.20	−0.12
SO_2	−0.19	−0.12

*In solution in chloroform-*d*.
†The negative sign means that the proton is more shielded in the diphenyl than in the monophenyl.

TABLE 3. Double-difference values

G	$\Delta_G{}^a$ (p.p.m.)	$\Delta_G{}^b$ (p.p.m.)	$\Delta_G{}^c$ (p.p.m.)
O	−0.38*	−0.14	0.16
S	−0.41	−0.16	0.16
CH_2	−0.40	−0.11	0.13
CO	0.13	−0.12	−0.28
SO	0.40	0.06	−0.04
SO_2	0.22	0.08	0.13

*The negative sign means that there is a net shielding effect at the proton in question.

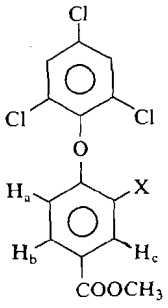

5

sible to estimate the constant in $\Delta_G{}^j$ (5).[4] For H_b and H_c in series **5**, $\delta_{\omega N} - \delta_{\omega H}$ is -0.14 and 0.14 p.p.m., respectively. Thus $C^b \simeq 0$ and $C^c \simeq 0.02$ p.p.m. For H_a in **5**, $\delta_{\omega N}{}^a - \delta_{\omega H}{}^a$ is -0.40 p.p.m. Since any correction in $\Delta_G{}^a$ is small compared to magnitude of the value and the uncertainty in the correction is large (5) C^a will be set equal to zero. With these corrections the values of $\delta_{\omega N}{}^j - \delta_{\omega H}{}^j$ for the six-bridged diphenyls are given in Table 4.

TABLE 4. Corrected experimental values for $\delta_{\omega N}{}^j - \delta_{\omega H}{}^j$

	$\delta_{\omega N}{}^j - \delta_{\omega H}{}^j$ (p.p.m.)		
G	j = a	j = b	j = c
O	−0.38*	−0.14	0.14
S	−0.41	−0.16	0.14
CH_2	−0.40	−0.11	0.11
CO	0.13	−0.12	−0.30
SO	0.40	0.06	−0.06
SO_2	0.22	0.08	0.11

*The negative sign means that there is a net shielding due to the "other ring".

Ethers, Sulfides, and Methanes

Table 4 shows clearly that the $\delta_{\omega N}{}^j - \delta_{\omega H}{}^j$ values are fairly constant for G = O, S, and CH_2 in spite of the fact that these bridges would have different bond angles and lengths. One must conclude that triply *ortho*-substituted diphenyl ethers, sulfides and methanes do adopt a similar conformation, which, for the ethers, has been shown to be the H_a-inside conformation with moderate librations (5, 7). For the doubly *ortho*-substituted analogs, **3**, there must be two identical H-inside conformations which equilibrate rapidly (5–7) to make the two *ortho* protons and the two *meta* protons magnetically equivalent in pairs. Since the free energy barrier to rotation of the *para*-disubstituted ring has been shown to be ~10 kcal/mol for ethers of type **3**, there has to be some conformational preference.

If the double-difference method is valid $\delta_{\omega N}{}^b - \delta_{\omega H}{}^b$ should be equal to $-(\delta_{\omega N}{}^c - \delta_{\omega H}{}^c)$. Table 4 shows that this identity holds with the exception of the bridges S and CO. The carbonyl case will be discussed later. S has been shown to be more effective in transmitting electronic effects in diphenyls than other bridges such as O, CH_2, SO, or SO_2 (15). It may be that the transmission of electronic charge is more geometry dependent for sulfur than it is for the other bridges so that different degrees of phenyl twist from the CSC plane in the diphenyl (**1***b*) and the monophenyl (**2***b*) would result in $\delta_{G\phi}{}^j$ not being a constant.

Sulfoxides

Those compounds with electron withdrawing bridges give quite different results from the ethers, sulfides, and methanes. For example, with G = SO the other-ring shielding values in Table 4 have changed sign. Since the single difference between corresponding members of series **3** and **4** is not greatly different regardless of the bridge, all of the doubly *ortho*-substituted diphenyl studies must adopt similar conformations (Table 2). The novelty in the sulfoxides must be due entirely to the single difference between **1***e* and **2***e*; H_a has become less shielded in the diphenyl sulfoxide **1***e* while H_c has become more shielded. That means that, unlike the ethers, a NO_2-inside or NO_2-proximal conformation must predominate. Assuming the same conformation for **3***e* and allowing for exchange of the equivalent *ortho* and *meta* protons, calculated values for $\delta_{\omega N}{}^j$ and $\delta_{\omega H}{}^j$ were arrived at (Table 5) using the ring current model of Johnson and Bovey (16).

If $\phi = 50°$ and $\psi = 40°$ the calculated values of $\delta_{\omega N}{}^j - \delta_{\omega H}{}^j$ are 0.37, 0.10, and -0.10 p.p.m. for j = a, b, and c, respectively. Although the calculated value for H_a is too low and that of H_b too high, a precise comparison of experimental and calculated other-ring shieldings (Tables 4 and 5) is difficult; if $\delta_{\omega N}{}^b - \delta_{\omega H}{}^b$ is lowered as the result of an assumed conforma-

[4]This assumes that $\delta_{\omega N}{}^j - \delta_{\omega H}{}^j$ is the same for all ethers of this type regardless of the nature of the two *ortho* substituents on the one ring. X-Ray studies have shown this to be approximately so (11). It has also been shown that the nature of the X-substituent in series **5** does not affect the conformation noticeably (5, 7).

Can. J. Chem. Downloaded from www.nrcresearchpress.com by 210.87.254.6 on 09/05/12
For personal use only.

Can. J. Chem. Downloaded from www.nrcresearchpress.com by 210.87.254.6 on 09/05/12
For personal use only.

TABLE 5. Values of $\delta_{\omega N}{}^{j} - \delta_{\omega H}{}^{j}$ calculated for NO_2-inside conformations of **1***e**

		$\delta_{\omega N}{}^{j} - \delta_{\omega H}{}^{j}$ (p.p.m.)		
ϕ (°)	ψ (°)	j = a	j = b	j = c
0†	90†	0.99	0.18	−0.18
10	80	0.95	0.17	−0.17
20	70	0.82	0.16	−0.16
30	60	0.67	0.15	−0.15
40	50	0.53	0.13	−0.13
50	40	0.37	0.10	−0.10
40	40	0.45	0.10	−0.10
50	50	0.40	0.12	−0.12
30	50	0.62	0.13	−0.13
30	40	0.51	0.07	−0.07
40	30	0.35	0.07	−0.07
50	30	0.30	0.07	−0.07
60	40	0.29	0.10	−0.10

*The CSC bond angle and the CS bond lengths were taken from Abrahams (17).
†The angles are defined in footnote 2.

tion, $\delta_{\omega N}{}^{a} - \delta_{\omega H}{}^{a}$ is lowered as well. For example, with $\phi = 40°$ and $\psi = 30°$ the calculated values become 0.35, 0.07, and −0.07 p.p.m. However, qualitative agreement can be obtained by assuming that the triply *ortho*-substituted sulfoxide **1***e* adopts a NO_2-inside, twist conformation with ϕ and $\psi = 40 \pm 10°$ (Fig. 2). A more detailed discussion of the validity of a method such as this for arriving at conformational angles has been presented in two previous papers (5, 7).

Although this work cannot tell, presumably the methyls and the "inside" nitro of **1***e* are as far from the sulfoxide oxygen as possible. The X-ray diffraction studies, to be published shortly, indicate that this is so.[5]

Further evidence supporting a twist conformation of the sort suggested comes from a comparison of the *ortho* methyl resonances in all the members of family **1** and the corresponding members of series **6** (Table 6). The increased shielding of the methyls in the diphenyl is more pronounced in the sulfoxide than in the ether, sulfide or methane. This would be true if the latter three adopt a conformation where the

[5]Of all the bridges SO is unique since there is no plane of symmetry including it and the two rings to which it is bonded. In the proposed conformation for the sulfoxides, when rotation of the mesityl ring becomes slow relative to n.m.r. relaxation times the methyl groups in the *ortho* positions lose their equivalence due to a lack of an average plane of symmetry in the molecule. It is not surprising that at −60° and 60 MHz the *ortho* methyls of both **1***e* and **3***e* become nonequivalent. These are the only diphenyls to exhibit this nonequivalence.

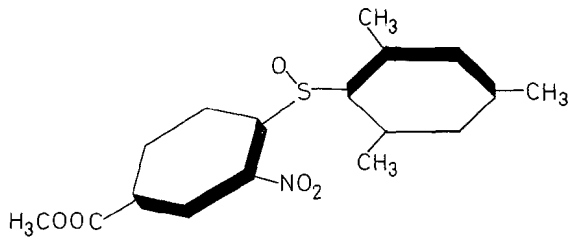

FIG. 2. Preferred NO_2-inside, twist conformation for the sulfoxide **1***e*.

TABLE 6. Chemical shift differences of *ortho* methyls in series **1** and **6***

G	$\delta_{DN}{}^{Me} - \delta_{6}{}^{Me}$ (p.p.m.)
O	−0.12†
S	−0.16
CH_2	−0.15
CO	−0.03
SO	−0.22
SO_2	−0.20

*In solution in chloroform-*d*.
†The negative sign means that the methyls are more shielded in the diphenyl than in the monophenyl.

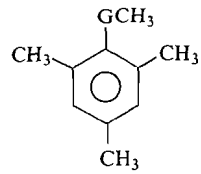

6

a G = O *d* G = CO
b G = S *e* G = SO
c G = CH_2 *f* G = SO_2

mesityl ring is more nearly perpendicular to the CGC plane while the sulfoxide has the mesityl ring twisted, thereby bringing the methyls further into the shielding region of the second ring.

Sulfones

The sulfones, **1***f* and **3***f*, present a different sort of problem. In **1***f*, H_a and H_c are slightly less shielded than in the corresponding monophenyl while H_b is more shielded (Table 1). This is possible if **1***f* were to take up an H-inside conformation with the two rings nearly perpendicular to the CSC plane (Fig. 3). In such a case, the net result of ring shielding and electronic effects on H_a would be a deshielding one relative to **2***f*. Since the single-difference results with **3***f* and **4***f*

TABLE 7. Calculated values for $\delta_{\omega N}{}^{j}$ and subsequently derived values for $\delta_{\omega H}{}^{j}$ in sulfones **1***f* and **3***f**

		$\delta_{\omega N}{}^{j}$ (p.p.m.)			$\delta_{\omega H}{}^{j}$ (p.p.m.)		
ϕ (°)	ψ (°)	j = a	j = b	j = c	j = a	j = b	j = c
90†	90†	0.13	−0.05	−0.05	−0.09	−0.13	−0.16
90	80	0.07	−0.07	−0.02	−0.15	−0.16	−0.13
90	70	0.02	−0.09	0.01	−0.21	−0.17	−0.10
80	90	0.12	−0.07	−0.03	−0.10	−0.16	−0.14
80	80	0.04	−0.10	−0.01	−0.19	−0.18	−0.12
80	70	−0.04	−0.11	0.02	−0.26	−0.19	−0.09
70	90	0.09	−0.10	−0.02	−0.14	−0.18	−0.13
70	80	−0.03	−0.13	0.00	−0.25	−0.21	−0.12

*The CSC bond angle and the CS bond lengths were taken from Abrahams (17). Values of $\delta_{\omega N}{}^{j}$ were calculated using the angles indicated. Values for $\delta_{\omega H}{}^{j}$ were obtained by subtracting experimental values for $\delta_{\omega N}{}^{j} - \delta_{\omega H}{}^{j}$ from $\delta_{\omega N}{}^{j}$.
†The angles are defined in footnote 2.

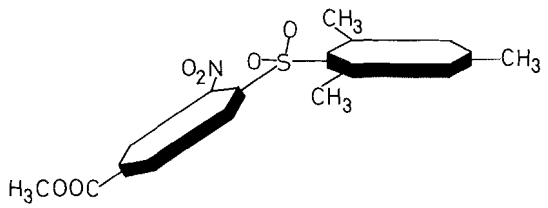

FIG. 3. Preferred butterfly conformation for the sulfone **1***f*.

(Table 2) are not much different from those using the other diphenyls it would seem reasonable to conclude that, for the sulfones, the triply and the doubly *ortho*-substituted members do not adopt the same conformation even allowing for averaging.

The approach that is most useful is to recognize that the calculated and experimental other-ring shielding values can be related by

[6] $\delta_{\omega H}{}^{j} = \delta_{\omega N}{}^{j} -$ experimental value

$\delta_{\omega H}{}^{j}$ and $\delta_{\omega N}{}^{j}$ are the calculated values of the other-ring shielding for the two sulfones and the experimental values, taken from Table 4, are 0.22, 0.08, and 0.11 p.p.m. for H_a, H_b, and H_c, respectively. Table 7 gives the $\delta_{\omega N}{}^{j}$ values calculated for a number of possible conformations and the values for $\delta_{\omega H}{}^{j}$ one would obtain using these and the experimental values in [6].

Since two identical conformations must be averaged in any calculation of $\delta_{\omega H}{}^{j}$, the values for $\delta_{\omega H}{}^{b}$ and $\delta_{\omega H}{}^{c}$ must be equal. As Table 7 indicates, that can be accomplished for a conformation of **1***f* having $\phi = \psi = 90 \pm 10°$ when $\delta_{\omega H}{}^{a} \simeq -0.12$ p.p.m. and $\delta_{\omega H}{}^{b} = \delta_{\omega H}{}^{c} \simeq -0.15$ p.p.m. To give these calculated values, the conformation of **3***f* would have to be such that $\phi \simeq 40°$ and $\psi \simeq 90°$. Thus the triply *ortho*-substituted sulfone **1***f* must be in a near-butterfly conformation with the nitro group slightly outside (Fig. 3) while the doubly *ortho*-substituted sulfone **3***f* does not have as large a rotation of the nonalkylated ring from the CSC plane.

Presumably these conformational differences in the two sulfones are largely sterically induced. The nitro group in **1***f*, to relieve interaction with the SO_2 oxygens, forces the ring to which it is attached to adopt a position nearly perpendicular to the CSC plane. The mesityl ring in both compounds is prevented from appreciable rotation by the two sulfone oxygens as well and, unlike the situation for the sulfoxides, is nearly perpendicular to the CSC plane. This is in agreement with previous suggestions made for similar diphenyl sulfones (4, 17, 53). It is interesting that the proposed butterfly conformation for **1***f* would bring the *ortho* NO_2 and a CH_3 on the other ring very close together.

Benzophenones

Structurally, the benzophenones and sulfoxides should be similar although the double-difference results of Table 4 do not indicate a similarity. The single difference between **3***d* and **4***d* follows the sort of trend observed for the other doubly *ortho*-substituted diphenyls but that between **1***d* and **2***d* is like the sulfoxide and then only qualitatively. It is impossible to suggest a conformation that by itself could give the results obtained experimentally. The source of the problem could be the well-known, magnetic anisotropy of the carbonyl functional group (18–20,

Can. J. Chem. Downloaded from www.nrcresearchpress.com by 210.87.254.6 on 09/05/12
For personal use only.

Can. J. Chem. Downloaded from www.nrcresearchpress.com by 210.87.254.6 on 09/05/12
For personal use only.

14) or effects produced by the twisting of the NO_2 out of coplanarity with the ring (10).

The question raised by Table 1 is how can H_b and H_c both be more shielded by a significant amount in the benzophenone **1***d* than in the acetophenone **2***d*. They both cannot be in the mesityl ring's shielding field nor can they both be in the CO shielding field. Although the purely electronic difference between a mesityl ring and a methyl group should affect the two *meta* protons equally, it is hard to account for the large shielding difference observed on this basis alone.

Based on the carbonyl anisotropy model of ApSimon *et al.* (19), in a nitro-inside conformation analogous to the sulfoxide (Fig. 4(*i*), $X = NO_2$), H_a would experience a large shielding effect, H_b would experience a smaller shielding, and H_c a deshielding due to the carbonyl alone. This effect would not be removed in the single- and double-difference data only if **1***d* and **2***d* had different conformations involving the direction of the CO and the dihedral angle between the planes of the phenyl ring and the carbonyl.

It is known that *ortho*-substituted acetophenones do appear to have preferred conformations (14, 21, 22). The suggestion for some of them is that conformation shown in Fig. 4(*ii*) ($R = CH_3$) (14, 22) although the carbonyl group is not coplanar with the phenyl (21). In no case has the conformation of an *ortho*-nitroacetophenone been studied although *meta*-nitroacetophenone appears to exist exclusively in a conformation analogous to Fig. 4(*i*) (22). Stothers and coworker have estimated the angle of twist of the carbonyl from the phenyl plane to be 24° in *ortho*-nitroacetophenone (21).

However, even if **1***d* and **2***d* were to adopt the conformations represented by Figs. 4(*i*) and (*ii*), respectively, the single and double differences, corrected for CO induced shielding, are not in keeping with a diphenyl nitro-inside conformation.[6] In fact, it is impossible to account for the single difference of Table 1 and the double difference of Table 4 on the basis of carbonyl magnetic anisotropy alone no matter what diphenyl and monophenyl conformations are assumed; there is no way to correct so that the double-difference values for H_b and H_c could be equal in magnitude but opposite in sign.[7]

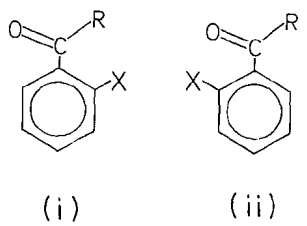

FIG. 4. The two planar conformations of an *ortho*-substituted phenyl ketone.

A more likely explanation involves the assumption that the *ortho* nitro becomes twisted out of planarity with the ring more in the benzophenone than in the acetophenone. As a result, the NO_2 in **1***d* would be less electron withdrawing so that the protons would appear to have become more shielded in the diphenyl compound. The greater NO_2-ring interplanar angle would be a likely consequence of **1***d* adopting the NO_2-inside conformation where that nitro would come close to the electron cloud of the other ring. The result of a correction for the twisted nitro could well be the making of $\delta_{\omega N}{}^b - \delta_{\omega H}{}^b$ positive and equal in magnitude to $\delta_{\omega N}{}^c - \delta_{\omega H}{}^c$ which could still be negative.[7] By the same argument, a correction for nitro twisting could make the other-ring shielding at H_a very much more positive, probably even greater than the 0.41 p.p.m. observed for the sulfoxides especially if CO anisotropic shielding is also corrected for.[8]

At this time it is impossible to separate the steric effect mentioned above and possible CO magnetic effects although the latter do not appear to be large in this case. We propose to discuss the NO_2 twisting in much more detail in future papers when X-ray diffraction data are presented for all the nitro-substituted diphenyls.

It has been suggested that changes in nitro

[6]Calculations were carried out using the model of ApSimon *et al.* (19) with the magnetic and electric dipoles of the carbonyl set at the bond's midpoint. Distances from the point dipoles to H_b and H_c were of the order of 4.7 and 5.0 Å. Placing the dipoles on the oxygen reduced the calculated shieldings to about half the values quoted.

[7]For example, adding 0.21 p.p.m. to both $\delta_{\omega N}{}^b - \delta_{\omega H}{}^b$ and $\delta_{\omega N}{}^c - \delta_{\omega H}{}^c$ would make them 0.09 and −0.09 p.p.m., respectively.

[8]Depending on the position of the electric and magnetic dipoles, as well as the relative conformations of **1***d* and **2***d*, the CO shielding difference for H_a could be as much as 1.2 p.p.m. However, because H_a is less than 3 Å from the dipoles in any conformation, the point dipole model is not particularly good.

Can. J. Chem. Downloaded from www.nrcresearchpress.com by 210.87.254.6 on 09/05/12
For personal use only.

group magnetic anisotropy (10) as the result of twisting might also play a role in the difficult interpretation of the chemical shift differences. Since H_b and H_c are at quite different distances from the NO_2 shielding cone, anisotropic effects could hardly be the same for them and yet the required corrections to the double-difference shifts would appear to have to be equal.

Since there seems to be absolutely no way to correct the double-difference values in Table 4 to accommodate an H_a-inside conformation, it is likely that the other-ring shieldings are similar to those of the corresponding sulfoxides and that **1***d* adopts a NO_2-inside, twist conformation as found for **1***e*.

A twist conformation would be in keeping with the evidence of other workers (4, 14, 23–25) for benzophenones although this work presents the first example of a conformation, for any bridged diphenyl, having an *ortho* substituent "inside". Even the very recent ^{13}C n.m.r. studies of Buchanan *et al.* (23) do not suggest such a conformation.

It is surprising that a NO_2-inside conformation would be preferred for the benzophenones and sulfoxides of series **1** in view of what must be a large steric interaction between the NO_2 and the π-cloud of the mesityl ring. The observation of an H_a-inside conformation for the corresponding ether, sulfide, and methane is more in keeping with expectation. However, it is possible that for the benzophenone and sulfoxide an electrostatic factor, repulsion between the partially negatively charged nitro and bridge oxygens more than offsets the apparent lower steric energy of an H_a-inside conformation. With the nitro "inside", its oxygens approach nearer to the positively charged carbonyl carbon or sulfoxide sulfur. For the sulfone the additional oxygen increases the "size" of the bridge considerably, adding new ring-oxygen steric interactions and making the butterfly-like conformation the stable one. It has been suggested that, although the rings are perpendicular to the CSC plane, there may still be considerable resonance interaction between the rings and the sulfur even in this conformation (4, 15, 53).

Experimental

The p.m.r. experimental procedure, including concentrations, spectral analysis, and estimation of errors, has been given previously (5). All lines in the aromatic three or four proton region of series **1–4** were reproduced to well within 0.2 Hz by means of ABC and AA′BB′ calculations respectively, making use of the program TWOSUM. Spectral assignments for **4***b*, *d*, *e*, and *f* were made unambiguously by analyzing the spectra of the monodeuterated analogs. The appropriate chemical shifts are given in Table 8. Melting points (m.p.) were determined on a Kofler, micro hot-stage apparatus and are reported uncorrected. Elemental analyses were carried out by Chemalytics Inc., 2330 S. Industrial Park Drive, Tempe, Arizona and by Galbraith Laboratories Inc., Box 4187, Knoxville, Tennessee.

Synthesis of Ethers

The preparation and properties of the following have been described previously: methyl 4-methoxybenzoate, **4***a* (1); methyl 4-methoxy-3-nitrobenzoate, **2***a* (1); 2-methoxy-1,3,5-trimethylbenzene, **6***a* (27); 2-(4′-carbomethoxy-2′-nitrophenoxy)-1,3,5-trimethylbenzene, **1***a* (26).

2-(4′-Carbomethoxyphenoxy)-1,3,5-trimethylbenzene (3a)

2-(4′-Carbomethoxy-2′-nitrophenoxy)-1,3,5-trimethylbenzene was reduced to the corresponding amine, m.p. 115–116°, using Raney nickel and hydrogen (7). Diazotization of the amine and the subsequent reduction of the diazonium salt with hypophosphorous acid were carried out by the method of Chandler and co-workers (1, 7). Recrystallization of the crude product from methanol

TABLE 8. Aromatic proton chemical shifts for series **1**, **2**, **3**, and 4

G	Compound	Chemical shift (p.p.m.)* H_a	H_b	H_c
O	**1***a*	6.63	8.03	8.60
	2*a*	7.14	8.21	8.48
	3*a*	6.78	7.95	7.95
	4*a*	6.91	7.99	7.99
S	**1***b*	6.71	7.90	8.88
	2*b*	7.43	8.18	8.85
	3*b*	6.93	7.82	7.82
	4*b*	7.24	7.93	7.93
CH_2	**1***c*	6.87	8.00	8.58
	2*c*	7.45	8.17	8.50
	3*c*	7.06	7.90	7.90
	4*c*	7.24	7.96	7.96
CO	**1***d*	7.50	8.20	8.40
	2*d*	7.50	8.36	8.72
	3*d*	7.83	8.11	8.11
	4*d*	7.97	8.15	8.15
SO	**1***e*	8.67	8.53	8.77
	2*e*	8.47	8.58	8.92
	3*e*	7.51	8.09	8.09
	4*e*	7.71	8.20	8.20
SO_2	**1***f*	8.31	8.37	8.44
	2*f*	8.28	8.40	8.42
	3*f*	7.82	8.14	8.14
	4*f*	8.01	8.25	8.25

*In solution in chloroform-*d* relative to tetramethylsilane.

Can. J. Chem. Downloaded from www.nrcresearchpress.com by 210.87.254.6 on 09/05/12
For personal use only.

yielded 1.92 g (80%), m.p. 83.5–88.5°. Repeated recrystallizations from methanol raised the m.p. to 87.5–89°.

Anal. Calcd. for $C_{17}H_{18}O_3$: C, 75.53; H, 6.71. Found: C, 75.49; H, 6.42.

Synthesis of Sulfides

The preparation and properties of the following have been described previously: methyl 4-methylthiobenzoate, **4***b* (29, 30) using potassium ethyl xanthate (28); 2-methylthio-1,3,5-trimethylbenzene, **6***b*, from mesitylenethiol (27); mesitylenethiol from mesitylenesulfonyl chloride (33–35).

*Methyl 4-Methylthio-3-nitrobenzoate (**2***b*)

This sulfide was prepared by a method described previously by Donleavy and Condit (32) except that the reaction had to be carried out in methanol and the methanethiol was obtained commercially. After one recrystallization from methanol **2***b*, m.p. 120–121° (70%) was obtained as bright yellow needles. The m.p. was raised to 122–123° as the result of several additional recrystallizations from methanol. The reported m.p. is 117° (32). When the reaction was carried out in ethanol a mixture of the methyl and ethyl esters resulted.

*2-(4′-Carbomethoxy-2′-nitrophenylthio)-1,3,5-trimethylbenzene (**1***b*)

The method used was similar to that described by Gilmand and Broadbent (36) for the synthesis of 1-(4′-nitrophenylthio)-3-methylbenzene. Equimolar amounts of sodium (0.457 g) and mesitylenethiol (3 g) were mixed in an Erlenmeyer flask equipped with a reflux condenser. Once the sodium had dissolved, a hot solution of methyl 4-chloro-3-nitrobenzoate (4.25 g) in methanol was added. Immediately a dark brown color appeared which changed in a few seconds to a bright yellow while a yellow precipitate began to form. After refluxing for 2 h more methanol was added until the yellow solid dissolved. The mixture was filtered to remove the NaCl and the filtrate was cooled. After two recrystallizations of the precipitated solid from methanol, 4.8 g (74%) of **1***b* was obtained, m.p. 123–125°. Two further recrystallizations from methanol gave the analytical sample, m.p. 125.5–126°.

Anal. Calcd. for $C_{17}H_{17}NO_4S$: C, 61.62; H, 5.17; S, 9.68. Found: C, 61.33; H, 5.06; S, 9.79.

2-(2′-Amino-4′-carbomethoxyphenylthio)-1,3,5-trimethylbenzene

The corresponding nitro compound, **1***b* (3.0 g), was reduced with W2 Raney nickel as described for the diphenyl ether **1***a*. The amine was obtained in 92% yield, m.p. 134–142° and after repeated recrystallizations from ethanol an analytical sample resulted, m.p. 139–142°.

Anal. Calcd. for $C_{17}H_{19}NO_2S$: C, 67.74; H, 6.35; N, 4.65. Found: C, 67.54; H, 6.50; N, 4.52.

*2-(4′-Carbomethoxyphenylthio)-1,3,5-trimethylbenzene (**3***b*)

2-(2′-Amino-4′-carbomethoxyphenylthio)-1,3,5-trimethylbenzene was diazotized and the diazonium salt reduced with hypophosphorous acid as described for the corresponding diphenyl ether and other ethers (1, 7). The crude, brown reaction product was very efficiently decolorized by sublimation (70%), m.p. 91–95°. After several recrystallizations from ethanol, an analytical sample was obtained, m.p. 96–98°.

Anal. Calcd. for $C_{17}H_{18}O_2S$: C, 71.30; H, 6.34; S, 11.20. Found: C, 71.12; H, 6.50; S, 10.98.

The direct nucleophilic substitution method described for **1***b* but using methyl 4-chlorobenzoate as the substrate gave only dimesityl sulfide, m.p. 127–128°. The literature m.p. for this sulfide is 123–124° (33).

Synthesis of Diphenylmethanes and Ethylbenzenes

The preparation and properties of the following have been described previously: methyl 4-ethylbenzoate, **4***c* (37); methyl 4-ethyl-3-nitrobenzoate, **2***c* (38, 39); 2-ethyl-1,3,5-trimethylbenzene, **6***c* (40, 41).

Methyl 4-Chloromethylbenzoate

Methyl *p*-toluate (83 g, m.p. 30–33°) was chlorinated in a quartz vessel equipped with a thermometer, condenser, and chlorine inlet tube. The reaction mixture was irradiated by means of a u.v. lamp at a temperature of 120° for 12 h with chlorine gas bubbling at a low rate through the mixture the entire time. Fractional distillation of the reaction mixture yielded, as the first fraction, the starting material (60 g) and as the second fraction, methyl 4-chlorobenzoate (19.9 g), b.p. 86–90°/1 mm Hg. The literature b.p. is 88–89°/0.7 mm Hg (42). A higher boiling fraction appeared to contain the dichloro compound.

*2-(4′-Carbomethoxybenzyl)-1,3,5-trimethylbenzene (**3***c*)

Methyl 4-chloromethylbenzoate (10 g) was added slowly to a mixture of mesitylene (10 ml) and aluminum chloride (6.5 g) at 10° with HCl gas evolved. The reaction mixture was heated after the initial addition for 1 h at 60°. At the end of this time it was poured onto ice and HCl (10 ml). The mixture was extracted with ether (3 × 25 ml), the ether evaporated and the residue refluxed with an excess of KOH (10% in water) for 4 h. The aqueous layer was separated, acidified with dilute HCl and the precipitate recrystallized from dilute ethanol to give 6.3 g of product, m.p. 175–180°. The crude acid was methylated with methanol, dichloroethane and sulfuric acid (31) giving 5.1 g of ester (35% overall), m.p. 75–78°. After several additional recrystallizations from dilute ethanol and a sublimation the analytical sample was obtained, m.p. 80–81°.

Anal. Calcd. for $C_{18}H_{20}O_2$: C, 80.56; H, 7.51. Found: C, 80.39; H, 7.27.

Methyl 4-Chloromethyl-3-nitrobenzoate

Methyl 4-chloromethylbenzoate was nitrated as described by Kamm and Segur (38) the only change being that the product was isolated by ether extraction since the product was a liquid. The ether extract was washed with water until neutral, dried over magnesium sulfate and the ether evaporated. The yellow oil remaining was distilled under reduced pressure and nitrogen, b.p. 126–128°/1 mm Hg (81%). The analytical sample was obtained after an additional distillation.

Anal. Calcd. for $C_9H_8NO_4Cl$: C, 47.08; H, 3.49; Cl, 15.44. Found: C, 46.97; H, 3.38; Cl, 15.70, 15.75.

This compound was very sensitive to light and high temperatures but when stored in the refrigerator no color change was observed.

*2-(4′-Carbomethoxy-2′-nitrobenzyl)-1,3,5-trimethylbenzene (**1***c*)

A Friedel–Crafts reaction, using anhydrous ferric chloride as catalyst (43), appeared to be the only route to

Can. J. Chem. Downloaded from www.nrcresearchpress.com by 210.87.254.6 on 09/05/12
For personal use only.

this diphenylmethane. Methyl 4-chloromethyl-3-nitrobenzoate (5 g) was dissolved in mesitylene (21 ml) and was added to a mixture of anhydrous ferric chloride (3 g) in mesitylene (25 ml). The mixture was heated at 80–90° for 2 h while HCl was evolving. The brown-black reaction mixture was then poured onto ice and hydrochloric acid (15 ml) prior to extraction with chloroform (3 × 75 ml). After evaporation of the chloroform, the mesitylene was removed by steam distillation and a small amount of 2,2′,4,4′,6′6′-hexamethylbiphenyl was isolated, with m.p. 100° as compared to the quoted m.p. of 100.5° (44). The black residue from the steam distillation was extracted with chloroform (3 × 75 ml) and dried over magnesium sulfate. The solution was filtered, the chloroform evaporated and the highly viscous, black product was distilled under nitrogen at reduced pressure. Early fractions yielded the ester starting material and 2,2′,4,4′,6,6′-hexamethylbiphenyl. The last fraction, b.p. 170–180°/1 mm Hg, contained mainly **1***c* as a thick, yellow oil. The oil was crystallized from ethanol as 1.0 g (15%) of a yellow solid, m.p. 104–105°. After three additional recrystallizations from ethanol an analytical sample was obtained, m.p. 104–105°.

Anal. Calcd. for $C_{18}H_{19}NO_4$: C, 69.00; H, 6.11. Found: C, 69.05; H, 6.11.

Synthesis of Ketones

*2-Acetyl-1,3,5-trimethylbenzene (**6***d*)

This compound was obtained commercially, b.p. 108–110°/8 mm Hg, and was used without further purification.

*Methyl 4-Acetylbenzoate (**4***d*)

4-Ethylbenzoic acid (1.5 g) (37) was dissolved in a solution of sodium dichromate (5 g) in water (400 ml) prior to being heated at 200° for 3 h in a pressurized reactor as described by Lee and Spitzer (45). After cooling to room temperature, the reaction mixture was filtered and the filtrate acidified with hydrochloric acid (6 *N*). The precipitate was collected and the filtrate extracted with ether (3 × 50 ml) to recover any dissolved reaction product which, after evaporation of the ether, was added to the rest of the product. In this way a total of 1.5 g of 4-acetylbenzoic acid was obtained which, without further purification, was esterified (31). The ester was purified by sublimation and a recrystallization from ethanol, 0.6 g (30%), m.p. 92–93°. The m.p. was raised to 96.5–97° after three further recrystallizations from ethanol. The quoted m.p. is 95.2–95.4° (37).

4-Carbomethoxy-2-nitrobenzoyl Chloride

Nitroterephthalic acid (10 g) was monoesterified with methanol (53 ml) and sulfuric acid (1 ml) by refluxing the mixture for 3 h (46). After cooling, sodium carbonate (150 ml, 10% in water) was added and the precipitated solid was collected. The filtrate was acidified with hydrochloric acid, cooled, and the solid filtered to give 7.0 g of crude 4-carbomethoxy-2-nitrobenzoic acid, m.p. 130–132°. The literature m.p. is 134–136° (46). The acid was refluxed with thionyl chloride (12 ml) for 3 h. The excess thionyl chloride was removed by distillation and the residue was distilled under reduced pressure, b.p. 127–129°/1 mm Hg, to give 6.0 g (60%) of the desired product. One recrystallization from cyclohexane–benzene produced a slightly yellow solid, m.p. 40–41°.

*Methyl 4-Acetyl-3-nitrobenzoate (**2***d*)

With some modifications, the method described by Reynolds and Hauser (47) for *o*-nitroacetophenone was used. In a 100 ml, three-necked flask, equipped with a stirrer, reflux condenser with drying tube and a dropping funnel the following were placed: magnesium (1.62 g), absolute methanol (15 ml), and CCl_4 (1.5 ml). After 5 min the magnesium began to react. Dried ether (15 ml) was added and after another 5 min a mixture of diethyl malonate (10.5 g, redistilled), dried ether (7.5 ml), and absolute methanol (6 ml) was added slowly. After the mixture had refluxed for 4.5 h, a solution of 4-carbomethoxy-2-nitrobenzoyl chloride (9.2 g) in ether (16 ml) was added just fast enough to maintain reflux. The solution was first yellow but turned green. After a further 4 h refluxing, the mixture was cooled and sulfuric acid (200 ml, 4 *N*) was added. The ether layer was separated and the water layer extracted with ether (2 × 50 ml) which was added to the original ether layer. The ether was evaporated and the liquid remaining refluxed with acetic acid (6 ml), sulfuric acid (1 ml), and water (4 ml) for 8 h. Again the mixture was extracted with ether and the ether evaporated. The resulting liquid was neutralized with an aqueous sodium carbonate solution to produce a white gum which solidified on cooling, 3.56 g, m.p. 62–75°. The crude solid was methylated (31) since partial hydrolysis had occurred during the reaction. The resulting solid ester was recrystallized from ethanol giving 1.4 g (17%) of **2***d*, m.p. 76–86°. Four additional recrystallizations raised the m.p. to 88.5–89.5°.

Anal. Calcd. for $C_{10}H_9NO_5$: C, 53.82; H, 4.07; N, 6.28. Found: C, 53.72; H, 3.95; N, 6.54.

*2-(4′-Carbomethoxybenzoyl)-1,3,5-trimethylbenzene (**3***d*)

4-Carbomethoxybenzoyl chloride (2.5 g, m.p. 54–55°) (49) dissolved in mesitylene (10 ml) and was added to a mixture of aluminum chloride (2.0 g) and mesitylene (10 ml). The mixture was heated at 100° for 1 h, was poured onto ice (20 g) with hydrochloric acid (2 ml) and the precipitate was collected. More product was obtained from the filtrate when the mesitylene was removed by steam distillation and the residue extracted with chloroform before evaporating the chloroform. After two recrystallizations from ethanol 1.2 g of **3***d* were obtained, m.p. 96–99°. Two further recrystallizations from the same solvent yielded the analytical sample, m.p. 97–98°.

Anal. Calcd. for $C_{18}H_{18}O_3$: C, 76.57; H, 6.43. Found: C, 76.83; H, 6.35.

*2-(4′-Carbomethoxy-2′-nitrobenzoyl)-1,3,5-trimethylbenzene (**1***d*)

This compound was prepared in the same way as **3***d*, using 4-carbomethoxy-2-nitrobenzoyl chloride and mesitylene. As catalyst, both aluminum chloride and ferric chloride were found successful. A representative procedure follows:

4-Carbomethoxy-2-nitrobenzoyl chloride (5.0 g) was added to a mixture of aluminum chloride (3.5 g) and mesitylene (20 ml). After the addition, the mixture was stirred for another hour without heating, then was poured over ice (100 g) and hydrochloric acid (10 ml). The solid was collected and recrystallized from 95% ethanol yielding 2.9 g (45%), m.p. 118–120°. After three recrystalliza-

Can. J. Chem. Downloaded from www.nrcresearchpress.com by 210.87.254.6 on 09/05/12
For personal use only.

TABLE 9. Synthesized sulfoxides and sulfones

Name	Formula	Melting Point (°C)	Analysis (%) C Found	C Calcd.	H Found	H Calcd.	N Found	N Calcd.	S Found	S Calcd.
2-(4′-Carbomethoxy-2′-nitrophenylsulfinyl)-1,3,5-trimethylbenzene (**1***e*)	$C_{17}H_{17}NO_5S$	168–169	58.64	58.78	4.76	4.93	3.87	4.03		
Methyl 4-methylsulfinyl-3-nitrobenzoate (**2***e*)	$C_9H_9NO_5S$	136–137 142–144	44.49	44.44	3.57	3.73	5.75	5.76		
2-(4′-Carbomethoxyphenylsulfinyl)-1,3,5-trimethylbenzene (**3***e*)	$C_{17}H_{18}O_3S$	125–126	67.76	67.52	5.93	6.00			10.57	10.60
Methyl 4-methylsulfinylbenzoate (**4***e*)	$C_9H_{10}O_3S$	122–124	54.58	54.53	4.97	5.09			16.34	16.17
Methyl 4-methylsulfinylbenzoate-3-*d*	$C_9H_9DO_3S$	122–123								
2-Methylsulfinyl-1,3,5-trimethylbenzene (**6***e*)	$C_{10}H_{14}OS$	56–57	66.04	65.89	7.55	7.74			17.48	17.59
2-(4′-Carbomethoxy-2′-nitrophenylsulfonyl)-1,3,5-trimethylbenzene (**1***f*)	$C_{17}H_{17}NO_6S$	169–170*	56.19	56.02	4.51	4.72	3.81	3.86		
Methyl 4-methylsulfonyl-3-nitrobenzoate (**2***f*)	$C_9H_9NO_6S$	121–122	41.72	41.70	3.40	3.50	5.35	5.40		
2-(4′-Carbomethoxyphenylsulfonyl)-1,3,5-trimethylbenzene (**3***f*)	$C_{17}H_{18}O_4S$	114–116	64.17	64.13	5.66	5.70			10.15	10.07
Methyl 4-methylsulfonylbenzoate (**4***f*)	$C_9H_{10}O_4S$	120–121†								
Methyl 4-methylsulfonylbenzoate-3-*d*	$C_9H_9DO_4S$	120–121								
2-Methylsulfonyl-1,3,5-trimethylbenzene (**6***f*)	$C_{10}H_{14}O_2S$	132–133	60.38	60.58	7.03	7.12			16.30	16.17

*The sulfone 1*f* and the sulfoxide 1*e* have virtually the same m.p. However, there is a large melting point depression when the two are mixed. In addition, the sulfone is a much lighter yellow color and the carbon analyses are different.
†Literature (52) m.p. 118–119 °C.

Can. J. Chem. Downloaded from www.nrcresearchpress.com by 210.87.254.6 on 09/05/12
For personal use only.

tions from ethanol an analytical sample was obtained, m.p. 121–122°.

Anal. Calcd. for $C_{18}H_{17}NO_5$: C, 66.05; H, 5.24; N, 4.28. Found: C, 66.14; H, 5.11; N, 4.14.

Synthesis of Sulfoxides

All the sulfoxides were prepared using the procedure outlined by Hyne and Greidanus (15). The corresponding sulfide and a molar equivalent amount of hydrogen peroxide (30%) were mixed. Enough glacial acetic acid was added to effect a solution and the reaction was allowed to proceed with stirring for 6–7 days. At the end of the reaction time, water was added and the mixture was extracted with chloroform from which the sulfoxide was isolated by evaporating the chloroform. The crude reaction product often contained some starting material or sulfone both of which could be removed by repeated recrystallization. **1***e* and **2***e* were recrystallized from ethanol; **3***e* was recrystallized from aqueous methanol; **4***e* was recrystallized from aqueous ethanol and **6***e* was recrystallized from petroleum ether (b.p. 30–60°). Typical yields were about 60%. **2***e* showed a double melting point, indicative of two crystal modifications. Table 9 lists all the synthesized sulfoxides along with their melting points and elemental analyses.

Synthesis of Sulfones

All the sulfones were synthesized by oxidation of the corresponding sulfide with excess hydrogen peroxide (30%) in refluxing glacial acetic acid for 0.5 to 1 h (15). Water was added and the product isolated by filtering the precipitated solid or by extraction with chloroform and evaporation of the chloroform. In general, the sulfones were very pure after isolation with typical yields about 90%. All the sulfones were recrystallized from ethanol except **1***f* which could be better recrystallized from either acetone–ethanol or ethyl acetate – ethanol. Table 9 lists all the synthesized sulfones, along with their melting points and elemental analyses.

Synthesis of Deuterated Analogs

Methyl 3-Amino-4-ethylbenzoate

Methyl 4-ethyl-3-nitrobenzoate (**2c**, 22.09 g), dissolved in absolute ethanol, was reduced with W2 Raney nickel and hydrogen at a pressure of 50 lb/in.^{2} in a pressurized Parr shaker for 48 h. After filtration of the nickel and evaporation of the ethanol the desired product was obtained, 18 g (95%), m.p. 53–55°. The reported m.p. is 53–54° (39).

Methyl 4-Ethyl-3-iodobenzoate

Methyl 3-amino-4-ethylbenzoate (17.4 g) was converted into the iodo compound by means of the diazotization and substitution method described by McCubbin *et al.* (50). The oil produced was distilled under reduced pressure, the fraction boiling at 111–117°/1 mm Hg being exclusively the desired product as indicated by the n.m.r. spectrum. An earlier fraction contained a lot of methyl 4-ethylbenzoate. For further identification, a small amount of the ester was saponified with aqueous KOH and the acid was recrystallized several times from aqueous ethanol, m.p. 195–196°. The reported m.p. for the acid is 191–192° (51).

4-Ethylbenzoic Acid-3-d

The 3-*d* compound was prepared by the method of McCubbin *et al.* (50). Methyl 4-ethyl-3-iodobenzoate (4.0 g) was refluxed for 24 h with zinc dust (6.0 g), NaOD (24 ml, 40% in D_2O), and D_2O (24 ml). The solid was removed by filtration, the filtrate acidified with hydrochloric acid and the white precipitate collected. The filtrate was extracted with ether, the solution dried over magnesium sulfate and the ether evaporated. The solid residue was combined with the filtered product to give a total of 2.0 g (97%) of the deuterated compound, m.p. 111–113°. There was no melting point depression when some of the product was mixed with an authentic sample of 4-ethylbenzoic acid.

Methyl 4-Acetylbenzoate-3-d

The oxidation of 4-ethylbenzoic acid-3-*d* with aqueous sodium dichromate under pressure was carried out exactly as described for the oxidation of the unlabelled acid in the synthesis of **4***d*. The crude acid was esterified with methanol, dichloroethane, and sulfuric acid (31). The m.p. 95–96° in this case was the same as for the unlabelled compound **4***d* and no melting point depression occurred when mixed with an authentic sample of **4***d*. The n.m.r. spectrum indicated that the labelling was successful.

Methyl 4-Methylthiobenzoate-3-d

Methyl 4-methylthio-3-nitrobenzoate (**2***b*) was reduced to the 3-amino compound with W2 Raney nickel in ethanol and hydrogen (50 lb/in.^{2}) in a pressurized Parr shaker for 24 h. The 3-amino compound was converted to the 3-iodo compound as described above for methyl 3-amino-4-ethylbenzoate, the only difference being that since methyl 3-iodo-4-methylthiobenzoate was a solid the distillation was omitted. The crude iodo compound (4.0 g) was treated with NaOD (24 ml, 40% in D_2O), zinc dust (6.0 g) and D_2O (24 ml). The solid was removed by filtration, the filtrate acidified with hydrochloric acid and the precipitate recovered and esterified with methanol (31). The methyl ester was recrystallized from methanol and sublimed giving 1.5 g, m.p. 80–81°. Compound **4***b* had a m.p. of 83–84° and no melting point depression was observed when the two were mixed. The n.m.r. spectrum confirmed the isolated compound as the monodeuterated one. Several attempts were made to synthesize the iodo compound by direct iodination (51) but only a small amount of impure product could be isolated.

Methyl 4-Methylsulfinylbenzoate-3-d and Methyl 4-Methylsulfonylbenzoate-3-d

Methyl 4-methylthiobenzoate-3-*d* was oxidized with hydrogen peroxide (30%) according to the general method outlined earlier in this section for the preparation of sulfoxides and sulfones (Table 8).

The authors wish to acknowledge the support of the National Research Council of Canada for grants in aid of research and for a scholarship to one of us (H.B.).

1. W. D. CHANDLER, W. MACF. SMITH, and R. Y. MOIR. Can. J. Chem. **42**, 2549 (1964).
2. P. A. LEHMANN and C. E. JORGENSEN. Tetrahedron, **21**, 363 (1965).
3. G. MONTAUDO, P. FINOCCHIARO, E. TRIVELLONE, F. BOTTINO, and P. MARAVIGNA. Tetrahedron, **27**, 2125 (1971).

4. G. MONTAUDO, P. FINOCCHIARO, F. BOTTINO, S. CACCAMESE, P. MARAVIGNA, and E. TRIVELLONE. Proc. XXIII Int. Cong. Pure and Appl. Chem. **II**, 1169 (1971).
5. J. J. BERGMAN, W. D. CHANDLER, and R. Y. MOIR. Can. J. Chem. **49**, 225 (1971).
6. J. J. BERGMAN and W. D. CHANDLER. Can. J. Chem. **50**, 353 (1972).
7. J. J. BERGMAN, E. A. H. GRIFFITH, B. E. ROBERTSON, and W. D. CHANDLER. Can. J. Chem. **51**, 162 (1973).
8. D. M. MCEACHERN and P. A. LEHMANN. J. Mol. Struct. **7**, 267 (1971).
9. P. A. LEHMANN and D. M. MCEACHERN. J. Mol. Struct. **7**, 277 (1971).
10. P. A. LEHMANN. Org. Magn. Res. **2**, 467 (1970).
11. E. A. H. GRIFFITH, W. D. CHANDLER, and B. E. ROBERTSON. Can. J. Chem. **50**, 2963 (1972); **50**, 2972 (1972); **50**, 2979 (1972).
12. G. MONTAUDO, S. CACCAMESE, P. FINOCCHIARO, and F. BOTTINO. Tetrahedron Lett. 877 (1970).
13. G. MONTAUDO, S. CACCAMESE, and P. FINOCCHIARO. J. Am. Chem. Soc. **93**, 4202 (1971).
14. G. MONTAUDO, P. FINOCCHIARO, and P. MARAVIGNA. J. Am. Chem. Soc. **93**, 4214 (1971).
15. J. B. HYNE and J. W. GREIDANUS. Can. J. Chem. **47**, 803 (1969).
16. C. E. JOHNSON and F. A. BOVEY. J. Chem. Phys. **29**, 1012 (1958).
17. S. C. ABRAHAMS. Quart. Rev. **10**, 407 (1956).
18. L. M. JACKMAN and S. STERNHELL. *In* Application of n.m.r. spectroscopy in organic chemistry. 2nd ed. Pergamon, Oxford. 1969. p. 88.
19. J. W. APSIMON, P. V. DEMARCO, D. W. MATHIESON, W. G. CRAIG, A. KARIM, L. SAUNDERS, and W. E. WHALLEY. Tetrahedron, **26**, 119 (1970).
20. J. W. APSIMON and H. BEIERBECK. Can. J. Chem. **49**, 1328 (1971).
21. K. S. DHAMI and J. B. STOTHERS. Can. J. Chem. **43**, 479 (1965).
22. A. R. KATRITSKY, M. V. SINNOTT, T. T. TIDWELL, and R. D. TOPSOM. J. Am. Chem. Soc. **91**, 628 (1969).
23. G. W. BUCHANAN, G. MONTAUDO, and P. FINOCCHIARO. Can. J. Chem. **51**, 1053 (1973).
24. R. F. REKKER and W. T. NAUTA. Rec. Trav. Chim. Pays-Bas, **80**, 747 (1961).
25. P. H. GORE, J. A. HOPKINS, R. J. W. LEFÈVRE, L. RADOM, and G. L. D. RITCHIE. J. Chem. Soc. B, 741 (1967).
26. W. D. CHANDLER, J. J. BERGMAN, and G. H. HAAS. Can. J. Chem. **49**, 583 (1971).
27. G. ILLUMINATI. J. Am. Chem. Soc. **80**, 4947 (1958).
28. A. I. VOGEL. A textbook of practical organic chemistry. Longmans Green, London. 1961. p. 499.
29. W. A. W. CUMMINGS. J. Chem. Soc. 2058 (1958).
30. R. GRICE and L. N. OWEN. J. Chem. Soc. 1947 (1963).
31. R. O. CLINTON and S. C. LASKOWSKI. J. Am. Chem. Soc. **70**, 3135 (1948).
32. J. J. DONLEAVY and P. C. CONDIT. J. Am. Chem. Soc. **69**, 1781 (1947).
33. C. WANG and S. G. COHEN. J. Am. Chem. Soc. **79**, 1924 (1957).
34. W. E. TRUCE and M. M. GUY. J. Org. Chem. **26**, 4331 (1961).
35. L. FIELD and F. A. GRUNWALD. J. Org. Chem. **16**, 946 (1951).
36. H. GILMAND and H. S. BROADBENT. J. Am. Chem. Soc. **69**, 2053 (1947).
37. W. S. EMERSON, J. W. HEYD, V. E. LUCAS, E. C. CHAPIN, G. R. OWENS, and R. W. SHORTRIDGE. J. Am. Chem. Soc. **68**, 674 (1946).
38. O. KAMM and J. B. SEGUR. *In* Organic syntheses. Coll. Vol. 1. Wiley, New York. 1941. p. 372.
39. D. S. NOYCE and L. J. DOLBY. J. Org. Chem. **26**, 1732 (1961).
40. M. CRAWFORD and J. H. MAGILL. J. Chem. Soc. 3275 (1957).
41. E. L. MARTIN. *In* Organic reactions. Vol. 1. Wiley, New York. 1957. p. 163.
42. British Patent No. 773,131 (April 24, 1957); Chem. Abstr. **52**, 434f (1958).
43. L. C. CASE. J. Appl. Polym. Sci. **8**, 533 (1964).
44. J. R. A. POLLOCK and R. STEVENS. Dictionary of organic compounds. 4th ed. Vol. 3. Oxford University Press, New York. 1965. p. 1604.
45. D. G. LEE and U. A. SPITZER. J. Org. Chem. **34**, 1493 (1969).
46. B. H. CHASE and D. H. HEY. J. Chem. Soc. 553 (1952).
47. G. A. REYNOLDS and C. R. HAUSER. *In* Organic syntheses. Coll. Vol. 4. Wiley, New York. 1963. p. 708.
48. R. C. WEAST. Handbook of chemistry and physics. 49th ed. Chemical Rubber Publishing Co., Cleveland. 1968. p. C-173, b 1029.
49. J. L. R. WILLIAMS, T. M. LAAKSO, K. R. DUNHAM, D. G. BORDEN, J. VANDEN BERGHE, I. A. VANALLEN, and D. D. REYNOLDS. J. Org. Chem. **25**, 817 (1960).
50. J. A. MCCUBBIN, R. Y. MOIR, and G. A. NEVILLE. Can. J. Chem. **48**, 945 (1970).
51. A. M. PLEIFEL. J. Org. Chem. **25**, 1024 (1960).
52. H. S. FORREST, A. T. FULLER, and J. WALKER. J. Chem. Soc. 1501 (1948).
53. G. MONTAUDO, P. FINOCCHIARO, E. TRIVELLONE, F. BOTTINO, and P. MARAVIGNA. J. Mol. Struct. **16**, 299 (1973).

Can. J. Chem. Downloaded from www.nrcresearchpress.com by 210.87.254.6 on 09/05/12
For personal use only.

Some Derivatives of 1-Benzazepine. Part II[1]

G. R. BIRCHALL[2] AND A. H. REES

Department of Chemistry, Trent University, Peterborough, Ontario K9J 7B8

Received July 16, 1973

We have investigated the ring expansion of some substituted 1,4-naphthoquinones by hydrazoic acid to yield new 1-benzazepine derivatives of the "azatropolone" type. Ring contraction of those products, which are 2,5-dihydro-3-hydroxy-2,5-dioxo-1-benzazepines, gives 4-quinolone-2-carboxylic acids. Some of the reactions of the new benzazepine system were investigated. Attempts to prepare substituted derivatives suitable for making 1-benzazatrop-5-one were not successful.

The effect of substituents on the ring expansion reaction is discussed and an anomalous ring expansion to a 2,5-dihydro-4-hydroxy-2,5-dioxo-1-benzazepine is described and explained mechanistically.

Nous avons étudié l'extension de cycle de quelques naphtoquinones-1,4 substituées en présence d'acide hydrazoique qui a conduit aux nouveaux dérivés benzazépine-1 du type "azatropolone". La contraction de cycle de ces composés, identifiés comme étant des dihydro-2,5 hydroxy-3 dioxo-2,5 benzazépines-1 a conduit aux acides quinolone-4 carboxyliques-2. On a aussi étudié quelques réactions du nouveau système benzazépine. Les essais de synthèse de dérivés substitués susceptibles de conduire au benzazatrop-1 one-5 furent infructueux.

On discute de l'effet des substituants sur la réaction d'extension de cycle. On décrit et on explique selon un mécanisme l'extension de cycle anormale conduisant au dihydro-2,5 hydroxy-4 dioxo-2,5 benzazépine-1. [Traduit par le journal]

Can. J. Chem., **52**, 610 (1974)

The reaction of naphthoquinones with hydrazoic acid has been reported (1) to give 2,5-dihydro-2,5-dioxo-1*H*-1-benzazepines (**1**), in accord with previous work (2, 3). This showed that attack took place predominantly at the less hindered carbonyl group of *p*-quinones, accompanied by migration of the larger substituent.

We have continued our studies in this field (4, 5) and now report the anomalous ring expansion reaction of 2-alkoxy-1,4-naphthoquinones.

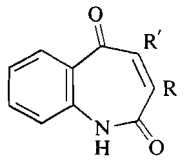

1 R and R′ = Alkyl
2 R = OH; R′ = H
3 R = H; R′ = OH
6 R = OMe; R′ = H
7 R = AcO; R′ = H
8 R = OH; R′ = Br

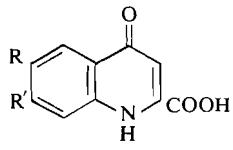

4 R = R′ = H
10 R = R′ = Me
21 R = HO; R′ = H

These expand following attack at the more hindered carbonyl group to give 3-alkoxy(or hydroxy)-2,5-dihydro-2,5-dioxo-1*H*-1-benzazepines. Thus, 2-methoxy-1,4-naphthoquinone gives 2,5-dihydro-3-hydroxy-2,5-dioxo-1*H*-1-benzazepine (**2**), in which the vinylic proton is a singlet, in sharp contrast to the isomer (**3**) where long range coupling of the NH with the vinyl proton at position 3 of the structure —NH—CO—CH=C— has been observed (6).

Proof of the structure **2** came from the alkaline ring contraction of a known type (5), which gave a quantititative yield of kynurenic acid (**4**), identical with a commercial sample. This also confirmed that the nitrogen atom was introduced adjacent to the benzene ring.

This ring expansion provides a short and easy synthesis of the biologically important kynurenic acid and certain analogs. That the reaction took place at the more hindered carbonyl group must be due to protonation of the ether, increasing the polarization of the adjacent carbonyl group, thus making it more susceptible to attack.

The same reaction was observed with 2-ethoxy- and 2-*n*-propoxy-1,4-naphthoquinone. With 2-isopropoxy-, 2-benzyloxy-, or 2-acetoxy-1,4-naphthoquinone, however, initial hydrolysis took place giving the known (6) reaction product (**5**) of 2-hydroxy-1,4-naphthoquinone and hydrogen azide.

Compound **2** gave the 3-methyl ether (**6**) with diazomethane and the 3-acetate (**7**) on acetyla-

[1]For Part I see ref. 4.

[2]Present address: Imperial Chemical Industries, Pharmaceutical Division, Alderley Park, Macclesfield, Cheshire, England.

Can. J. Chem. Downloaded from www.nrcresearchpress.com by 210.87.254.105 on 09/05/12
For personal use only.

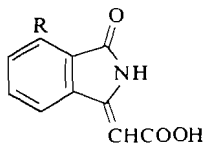

5 R = H
15 R = MeO

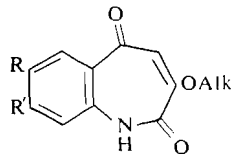

9

tion. Bromination of **2** gave the 4-bromo derivative (**8**). We also prepared some substituted derivatives, *e.g.* **9** where R = R′ = Me. This compound was dealkylated and ring contraction of the resulting enol gave 6,7-dimethylkynurenic acid (**10**).

We also attempted to expand the quinone **11** to the benzazepine which should lead to xanthurenic acid (8-hydroxykynurenic acid). An unexpected reaction took place giving a product with a different type of u.v. spectrum. Demethylation had occurred and the product was assigned structure **12**.[3] The loss of the other methyl group would result in cyanolactone **13** (7, 8), for which there was no spectroscopic evidence.

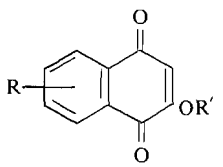

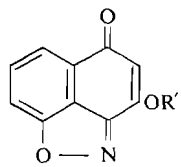

11 R = 8-MeO; R′ = Me
14 R = 8-MeO; R′ = H
16 R = 8-MeO; R′ = Et
22 R = 6-MeO; R′ = Alkyl

12 R′ = Me
17 R′ = Et

The reaction of quinone **14** with hydrogen azide gave only acid **15** but quinone **16** gave compound **17** with retention of the ethyl group. A similar result was found when R′ = isoBu.

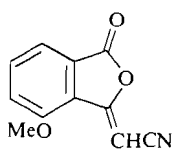

13

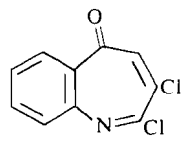

18

We attempted to produce the dichlorobenzazatropone **18** by treating compound **2** with phosphorus oxychloride. A trichloro compound, considered to be **19**, resulted but it readily lost hydrogen chloride to give an intermediate formulated as **18**. This was very reactive and rapidly hydrolyzed giving monochloro compound **20** as the only stable product isolated.

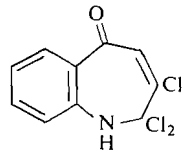

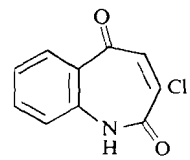

19 20

Satisfactory microanalysis results were obtained for **19** but on running the n.m.r. spectrum in DMSO-d_6 a reaction took place in the tube and the peaks shifted. The final product isolated was the chlorolactam **20**.

Attempts at dehydrohalogenation of **19** with pyridine, lithium chloride (9), or 1,5-diazabicyclo[5.4.0]undec-5-ene led, after work-up, to compound **20**. This suggests that the chloroimine **18** is very reactive. On steric grounds this is acceptable as there is considerable compression between the eclipsed chlorine atoms in **18** as compared with the staggered configuration of structure **19**. This is in part due to the increased strain in seven- over six-membered rings (5).

The confirmation for the structure of **20** came from its synthesis by the action of thionyl chloride on the corresponding hydroxy compound, **2**, as well as by comparison of its spectra with those of the corresponding bromo compound, prepared by a different route (10).

Since 6-hydroxykynurenic acid (**21**) is a natural product (11, 12), we decided to try to synthesize it via the benzazepine **9** where R = MeO and R′ = H. Accordingly, we prepared some 6-substituted 2-alkoxy-1,4-naphthoquinones, including in particular **22**, for ring expansion experiments. From this compound we obtained a product at first presumed to be **9**, R = MeO, R′ = Alkyl = H. However, the quinolone acid obtained by ring contraction was not 6-methoxykynurenic acid as it was not identical with a sample prepared by the literature method (13). Hence the benzazepine precursor was not of type **9**.

On considering the mechanism of the ring expansion of the protonated quinone, it is seen that one of the forms, **23**, is in equilibrium with another, **24**, which has the 4-carbonyl group as the logical site of azide attack. This would give the alternative 2,5-dihydro-4-hydroxy-8-methoxy-2,5-dioxobenzazepine (**25**). This type of

[3]We thank the referees for suggesting this structure for our product.

Can. J. Chem. Downloaded from www.nrcresearchpress.com by 210.87.254.105 on 09/05/12
For personal use only.

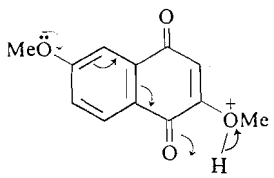

23

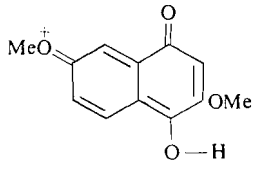

24

compound has been synthesized previously by two other routes (14, 6) and its ring contraction shown to give 2-quinolone-4-carboxylic acids. We therefore made the acid **26** from the appropriate *N*-acetylizatin (15) and found it was identical with the product obtained from quinone **23** via ring expansion. This confirms that the benzazepine intermediate had structure **25**.

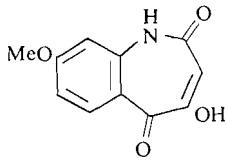

25

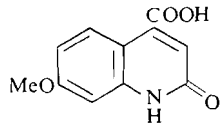

26

Hence the ring expansion of substituted *p*-quinones is influenced by subtle electronic effects.

We have not yet succeeded in synthesizing a simple benzazatropone and our work parallels that of Proctor and co-workers (9) in producing compounds of type **27**.

There is no evidence from our or from other work (16–18) for heteroaromaticity in benzazatropones or benzazatropolones. Therefore, we are investigating the monocyclic azepines **28** and **29**, obtained by ring expansion of alkoxybenzoquinones. An encouraging feature of compound **28** (R′ = H or Me) is that $J_{1,7}$ = 8 Hz, suggesting there is a ring current.

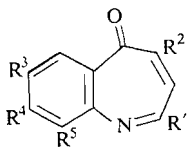

27

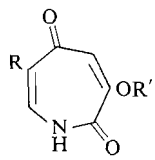

28

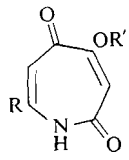

29

Results of this work, also the exploration of new routes to **2** will be reported later.

Experimental

Infrared spectra (Unicam S.P. 200) are in Nujol, quoting ν_{max} in cm^{-1}. Ultraviolet spectra (S.P. 800) are in ethanol quoting λ_{max} in nm (log ε). Nuclear magnetic resonance spectra (JeolCo. C60 HL) are in $CDCl_3$ unless stated and quote τ values relative to TMS (internal). Mass spectra (A.E.I. M.S. 12) are at 70 eV on the probe, quoting *m/e* (relative intensity). Recrystallization solvents are given in parentheses, immediately following the melting points.

2-Alkoxy-1,4-naphthoquinones

These were prepared according to the literature: methyl (19), ethyl (20), *n*-propyl (21), isopropyl (22), and benzyl (23). The i.r. showed carbonyls at *ca.* 1630 and 1680; u.v. 242, 247, 277, 328; n.m.r. showed the appropriate alkyl pattern, a vinyl proton (1H, s) at about 3.9 and two multiplets at around 1.9 (H5 and H8) and about 2.2 (H6 and H7).

2,5-Dihydro-3-hydroxy-2,5-dioxo-1H-1-benzazepine (2)

2-Methoxy-1,4-naphthoquinone, 11.4 g, in concentrated sulfuric acid, 75 ml, at 0° was treated portionwise with sodium azide, 4.2 g. The system was left to warm to 25°. After 2 days, the dark red solution was poured into ice water and the precipitate collected. 2,5-Dihydro-3-hydroxy-2,5-dioxo-1*H*-1-benzazepine formed colorless plates, 6.5 g (60%), m.p. 245–248° (aqueous alcohol); i.r. 3230, 3395, 3470, 1679, 1647, 1594, 1574, 1527; u.v. 239 (4.36), 272 (4.36); n.m.r. Table 1; mass spectrum 189 (100), 161 (70), 143 (18), 133 (28), 115 (18), 104 (19), 92 (18).

Anal. Calcd. for $C_{10}H_7NO_3$: C, 63.4; H, 3.7; N, 7.4. Found: C, 63.4; H, 3.85; N, 7.2.

When the reaction mixture was slowly poured onto stirred ice and the product triturated with sodium bicarbonate solution, the residue was the unhydrolyzed 3-methyl ether **6** (see below). Acidification of the alkaline solution gave compound **2**.

Reaction of 0.8 g of 2-ethoxy-1,4-naphthoquinone as above, gave, after separation of the neutral and acidic products, 0.2 g of **2** and 0.11 g of the ethyl ether, m.p. 219° (ethanol); i.r. 3300, 3150, 1679, 1645, 1612, 1515; u.v. 241 (4.38), 270 (4.38); mass spectrum 217 (90), 202 (32), 174 (36), 173 (36), 172 (42), 161 (100), 133 (52), 132 (60), 117 (40), 104 (30), 92 (40), 90 (45).

Anal. Calcd. for $C_{12}H_{11}NO_3$: C, 66.35; H, 5.1; N, 6.45. Found: C, 66.2; H, 5.1; N, 6.6

Reaction of 0.86 g of 2-*n*-propoxy-1,4-naphthoquinone as above gave 0.3 g of compound **2**.

Reaction of 2-acetoxy-1,4-naphthoquinone with Hydrogen Azide

The acetate (24), reacted in sulfuric acid at 0° as above, on work-up gave the acid **5**, identical with a sample made from the hydroxyquinone (6). This same product was similarly obtained from 2-isopropoxy- or 2-benzyloxy-1,4-naphthoquinone, indicating hydrolysis before the azide reaction.

Reactions of 2,5-Dihydro-3-hydroxy-2,5-dioxo-1-benzazepine

(*a*) Bromination. To 190 mg of **2** in 25 ml acetic acid, 180 mg bromine was added with stirring. After 20 h at 25°, the precipitate was collected and washed with ether giving 235 mg 4-bromo-2,5-dihydro-3-hydroxy-2,5-dioxo-1-benzazepine (**8**), buff prisms m.p. 260–265° dec. (ethanol); i.r. 3438, 1666, 1650, 1615, 1495; n.m.r. Table 1; mass spectrum 269 (100), 267 (100), 241 (80),

Can. J. Chem. Downloaded from www.nrcresearchpress.com by 210.87.254.105 on 09/05/12
For personal use only.

TABLE 1. Nuclear magnetic resonance spectra, in DMSO-d_6, except as indicated

	τ						
Compound	1	3	4	6	7	8	9
2	−1.6	Under aromatic	3.5s	1.7m		2.3 −2.8m	
6	−1.2	OMe, 3H 6.08s	3.6s	2.05m		2.4 −2.9m	
7	−1.63	OAc, 3H 7.58s	3.0s	2.05m		2.3 −2.8m	
8	−1.7	−0.1	Br	2.2m		2.4 −3.0m	
9	−1.4	OEt 2H 5.95q 3H 8.5t	3.62	1.45s	Me 7.65s	Me 7.65s	2.9s
19*	1.3	Cl	3.4s	1.25m		1.4 −3.3m	
20	−1.65	Cl	2.95s	2.0m		2.15–3.0m	
20*	0.25	Cl	2.6s	2.05m		2.25–3.0m	
20†	−0.5	Cl	2.6s	2.05m		2.15–3.0m	

*In $CDCl_3$.
†In $SOCl_2$.

239 (80), 213 (10), 211 (10), 160 (44), 132 (36), 120 (44), 104 (42), 103 (38), 92 (54), 90 (40), 77 (80), 76 (60).

Anal. Calcd. for $C_{10}H_6BrNO_3$: C, 44.8; H, 2.25; Br, 29.8; N, 5.2. Found: C, 45.0; H, 2.3; Br, 29.7; N, 5.1.

(*b*) Acetylation (pyridine – acetic anhydride) gave 3-acetoxy-2,5-dihydro-2,5-dioxo-1-benzazepine (**7**) as buff needles, m.p. 201–203° (aqueous ethanol); i.r. 1770, 1679, 1647, 1628, 1603, 1588, 1451; n.m.r. Table 1; mass spectrum 231 (30), 189 (65), 161 (100), 134 (25), 133 (11).

Anal. Calcd. for $C_{12}H_9NO_4$: C, 62.3; H, 3.9; N, 6.1. Found: C, 62.45; H, 3.9; N, 5.9.

(*c*) Methylation of the azepine **2**, 250 mg in 20 ml pure methanol, was effected by adding an ethereal solution of diazomethane in excess at 0°. 2,5-Dihydro-3-methoxy-2,5-dioxo-1-benzazepine (**6**), 250 mg, was precipitated, colorless plates, m.p. 255° (methanol); i.r. 3400, 3310, 1687, 1630, 1597, 1576, 1529; u.v. 241 (4.37), 269 (4.37); n.m.r. Table 1; mass spectrum 203 (100), 175 (52), 147 (12), 146 (56), 145 (30), 132 (56), 129 (20), 117 (32), 92 (30), 90 (32), 77 (32).

This compound was identical with the neutral ring expansion product from 2-methoxy-1,4-naphthoquinone, above.

Anal. Calcd. for $C_{11}H_9NO_3$: C, 65.0; H, 4.5; N, 6.9. Found: C, 64.9; H, 4.5; N, 6.8.

(*d*) Ring contraction of **2**, 100 mg, was effected by treatment with 10 ml of 2 *N* alkali solution at 90° for 45 min. Acidification precipitated 100 mg kynurenic acid (**4**), m.p. 250° (acetic acid – water, 20:1), identical (spectra, mixture m.p.) with a commercial sample (Fluka, A.G.); u.v. 247, 342, 360; n.m.r. H3 (NaOD), 3.33 (s); mass spectrum 189 (100), 145 (48), 143 (100), 115 (36), 105 (28), 89 (36).

Preparation and Ring Expansion of 2-Methoxy-6,7-dimethyl-1,4-naphthoquinone

6,7-Dimethyltetral-1-one (25) was oxidized (26) to 2-hydroxy-6,7-dimethyl-1,4-naphthoquinone, m.p. 168–170°, which was converted to the methyl ether, m.p. 167–168° (methanol) (lit. (27) m.p. 166°); n.m.r. 7.6 (2Me, s), 6.1 (OMe, s), 4.0 (H3, s), 2.33 (1H, s), 2.3 (1H, s).

The methoxyquinone, 0.86 g, when reacted as above gave 0.8 g of 2,5-dihydro-3-methoxy-7,8-dimethyl-2,5-dioxo-1-benzazepine, colorless needles, m.p. 295–298° (methanol); i.r. 3400, 1682, 1617, 1579, 1515; u.v. 247 (4.44), 273 (4.34); mass spectrum 231 (100), 203 (19), 202 (62), 174 (60), 173 (25), 160 (45).

Anal. Calcd. for $C_{13}H_{13}NO_3$: C, 67.5; H, 5.7; N, 6.1. Found: C, 67.5; H, 5.7; N, 6.15.

When the crude product was recrystallized from ethanol, exchange took place giving 3-ethoxy-2,5-dihydro-7,8-dimethyl-2,5-dioxo-1-benzazepine (**9**, R = R′ = Me; Alkyl = Et), m.p. 256°; i.r. 3400, 1676, 1650, 1617, 1589, 1567; n.m.r. Table 1; mass spectrum 245 (100), 202 (42), 201 (36), 189 (62), 174 (28), 160 (34).

Anal. Calcd. for $C_{14}H_{15}NO_3$: C, 68.5; H, 6.2; N, 5.7. Found: C, 68.5; H, 6.1; N, 5.5.

*Preparation of 6,7-Dimethylkynurenic Acid (**10**)*

The methyl ether **9**, above, 250 mg, was demethylated (hydrogen bromide – acetic acid) at 60° over 2 h. The precipitated enol was collected and washed with water giving colorless needles, m.p. 288° dec. (ethanol), 80 mg; i.r. 3480, 3250, 1671, 1647, 1584, 1517; u.v. 244 (4.48), 275 (4.44); mass spectrum 217 (100), 189 (100), 174 (24), 171 (14), 161 (12), 160 (16), 143 (12), 91 (20).

Anal. Calcd. for $C_{12}H_{11}NO_3$: C, 66.3; H, 5.1; N, 6.45. Found: C, 66.3; H, 5.1; N, 6.4.

Ring contraction of this azepine, as above, gave a high yield of 6,7-dimethylkynurenic acid, m.p. 278–280° (aqueous acetic acid 1:20); i.r. 3150, 1640, 1590, 810, 780; u.v. 220, 248, 344, 360; n.m.r. (NaOD) 7.8 (2Me, s), 3.3 (H3, s), 2.66 (H8, s), 2.3 (H6, s); mass spectrum 217 (13), 173 (21), 171 (15), 60 (100), 45 (100), 43 (100).

Anal. Calcd. for $C_{12}H_{11}NO_3.\frac{3}{4}CH_3COOH$: C, 62.25; H, 5.35; N, 5.44. Found: C, 62.3; H, 5.25; N, 5.4.

Preparation of 2-Alkoxy-8-methoxy-1,4-naphthoquinones and Reaction with Hydrogen Azide

8-Methoxy-2-tetralone (28) was oxidized to the known quinone **14** (26), which was methylated to give the dimethoxyquinone **11**, m.p. 195°.

Can. J. Chem. Downloaded from www.nrcresearchpress.com by 210.87.254.105 on 09/05/12
For personal use only.

Can. J. Chem. Downloaded from www.nrcresearchpress.com by 210.87.254.105 on 09/05/12
For personal use only.

2-Ethoxy-8-methoxy-1,4-naphthoquinone (**16**) was prepared in like manner, m.p. 178–179°; i.r. 1684, 1649, 1618, 1589; n.m.r. 8.53 (3H, t, J = 6 Hz), 6.27 (OMe, s), 6.02 (2H, q, J = 6 Hz), 4.07 (H3, s), 2.87 (H5, m), 2.43 (2H, m).

Anal. Calcd. for $C_{13}H_{14}O_4$: C, 67.2; H, 5.2. Found: C, 67.6; H, 5.1.

2-Isobutoxy-8-methoxy-1,4-naphthoquinone was prepared as above, m.p. 118° (aqueous ethanol); i.r. 1677, 1646, 1617, 1590; n.m.r. 8.98 (Me_2, d, J = 6 Hz), 7.83 (1H, m), 6.35 (CH_2, d, J = 6 Hz), 6.07 (OMe, s), 4.02 (H3, s), 2.4–2.9 (3H, m).

Anal. Calcd. for $C_{15}H_{16}O_4$: C, 69.2; H, 6.2. Found: C, 69.2; H, 6.1.

Quinone **11**, 160 mg, reacted with hydrogen azide as above, gave 60 mg product, m.p. 200–230° (ethanol); mass spectrum 201 M^+ (50), 117 (100).

Quinone **16** similarly gave a product, m.p. 160–165° (aqueous ethanol, charcoaled); i.r. 1646, 1606, 1568, 1517; u.v. 299 (4.3); n.m.r. (DMSO-d_6 at 60°) 8.17 (3H, t, J = 6 Hz, OCH_2CH_3), 5.5 (2H, q, J = 6 Hz, OCH_2CH_3), 3.77 (1H, s), 2.1 (3H, m); mass spectrum 215 M^+ (94), 200 (36), 187 (18), 159 (60), 146 (100), 145 (44).

Anal. Calcd. for $C_{12}H_9NO_3$: C, 67.0; H, 4.2; N, 6.5. Found: C, 66.8; H, 4.2; N, 6.5.

This compound is considered to be 3-ethoxy-5-oxo-5*H*-naphth[1,8-*cd*]isoxazole (**17**).

The corresponding 3-isobutoxy compound, 50 mg, was likewise prepared from 180 mg 2-isobutoxy-8-methoxy-1,4-naphthoquinone. The isoxazole had m.p. 131–133° (aqueous ethanol); i.r. 1655, 1610, 1572, 1522; u.v. 299 (4.3); mass spectrum 243 M^+ (24), 188 (43), 187 (100), 146 (63).

Quinone **14**, 150 mg, reacted with hydrogen azide to give 60 mg 4-methoxy-3-oxo-$\Delta^{1\alpha}$-isoindolineacetic acid (**15**), m.p. 218–220° dec. (aqueous ethanol); i.r. 3550, 1736, 1678, 1610, 1500; u.v. 286 (4.17), 348 (4.1); n.m.r. (DMSO-d_6) 6.12 (O*Me*, s), 4.19 (1H, s), 2.92 (1H, m), 2.35 (2H, m), 0.2 (OH, s), −2.5 (NH, br); mass spectrum 219 (100), 201 (76), 173 (95), 44 (79).

Anal. Calcd. for $C_{11}H_9NO_4$: C, 60.3; H, 4.1; N, 6.4. Found: C, 60.1; H, 4.0; N, 6.4.

*2,2,3-Trichloro-2,5-dihydro-5-oxo-1-benzazepine (**19**)*

2,5-Dihydro-3-hydroxy-2,5-dioxo-1-benzazepine (**2**), 1 g, was heated 1.5 h in 15 ml phosphorus oxychloride at 90°. The cooled mixture was poured onto ice and the solid collected and dried giving the trichloro compound **19**, colorless needles, m.p. 190° dec. (benzene – light petroleum); i.r. 1694, 1621, 1582; u.v. 209, 231, 261 (sh); n.m.r. Table 1; mass spectrum 265 (4), 263 (12), 261 (12), 228 (66), 226 (100), 200 (26), 198 (38), 164 (24), 163 (24), 162 (42).

Anal. Calcd. for $C_{10}H_6Cl_3NO$: C, 45.75; H, 2.3; Cl, 40.5; N, 5.3. Found: C, 45.9; H, 2.3; Cl, 40.3; N, 5.2.

*3-Chloro-2,5-dihydro-2,5-dioxo-1-benzazepine (**20**)*

The trichloro compound (**19**) gave an unstable spectrum in DMSO-d_6. Following t.l.c., the monochloro compound **20** was isolated, yellow needles, m.p. 204° (benzene – light petroleum); i.r. 1670, 1625, 1605; u.v. 215, 239, 264, 350; n.m.r. Table 1; mass spectrum 207 (60), 179 (100), 151 (86), 89 (63). Contrast the 2-chloro isomer (1).

Anal. Calcd. for $C_{10}H_6ClNO_2$: C, 57.85; H, 2.9. Found: C, 58.05; H, 3.0.

The trichloro compound, 50 mg in dry benzene, when treated overnight with 2.2 equiv piperidine at 25°, gave a precipitate of piperidine hydrochloride. This was filtered off and the filtrate was evaporated. On t.l.c. the monochloro compound **20**, 15 mg, was obtained from the residue.

The n.m.r. spectrum ($SOCl_2$) of hydroxy compound **2**, after gentle warming, was that of compound **20**, Table 1. After evaporation of the solvent, the residue was sublimed in vacuum and recrystallized, giving a product identical with **20**, above.

*Ring Expansion of 2,6-Dimethoxy-1,4-naphthoquinone (**22**)*

The quinone **29**, 0.65 g, reacted with hydrogen azide as above, gave only a few milligrams of neutral product, colorless needles, m.p. 278° (aqueous ethanol); i.r. 1675, 1640, 1610; u.v. 233, 253, 275, 345; mass spectrum 233 M^+ (20), 215 (100), 162 (70), 69 (40).

This compound is probably the methyl ether of compound **25**, below.

Preparation of 6-Benzyloxy-2-methoxy-1,4-naphthoquinone

6-Hydroxy-1-tetralone (30, 31), 0.35 g, as its crude oily tetrahydropyranyl ether, was oxidized (24). After acidification, the solution was left 72 h to hydrolyze the ether. Work-up gave 2,6-dihydroxy-1,4-naphthoquinone, 0.1 g orange needles, m.p. >300° dec. (aqueous ethanol).

Methylation (methanol – hydrochloric acid gas) gave 80 mg of 6-hydroxy-2-methoxy-1,4-naphthoquinone, m.p. 285–295° (methanol); n.m.r. (DMSO-d_6) 6.15 (OMe, s), 3.9 (H3, s), 2.85 (H5, d, J = 2 Hz), 3.0 (H7, q, $J_{5,7}$ = 2 Hz, $J_{7,8}$ = 8 Hz), 2.25 (H8, J = 8 Hz), −0.8 (OH, br).

Anal. Calcd. for $C_{11}H_8O_4$: C, 64.7; H, 3.95. Found: C, 64.5; H, 3.95.

The 6-acetyl derivative (acetic anhydride – pyridine), formed yellow needles, m.p. 187° (ethanol).

Anal. Calcd. for $C_{13}H_{10}O_5$: C, 63.4; H, 4.1. Found: C, 63.6; H, 4.05.

6-Hydroxy-2-methoxy-1,4-naphthoquinone, 0.5 g in acetone, was benzylated (benzyl bromide – anhydrous potassium carbonate). The benzyl ether, 0.5 g, had m.p. 160–162° (benzene – light petroleum).

Anal. Calcd. for $C_{18}H_{14}O_4$: C, 73.5; H, 4.1. Found: C, 73.5; H, 4.1.

A preliminary attempt at ring expansion of 6-hydroxy-2-methoxy-1,4-naphthoquinone failed. Because of other results, below, the benzyl ether was not utilized.

*Preparation and Ring Expansion of 2-Ethoxy-6-methoxy-1,4-naphthoquinone (**22**)*

6-Methoxy-2-hydroxy-1,4-naphthoquinone (29) was ethylated (ethanol – hydrogen chloride) giving the ether, m.p. 154–155° (aqueous ethanol).

Anal. Calcd. for $C_{13}H_{12}O_4$: C, 67.2; H, 5.2. Found: C, 67.2; H, 5.2.

The 2-ethoxy compound, 80 mg, was ring expanded as above, giving 5 mg of acidic product, slightly greenish needles, m.p. 260–262°; i.r. 1670, 1620, 1590; u.v. 222, 252, 276; mass spectrum 219 (60), 204 (6), 191 (31), 150 (100).

Ring contraction of the available material gave an acid, m.p. 290–310°; i.r. (KBr) 1740, 1660, 1620; u.v. 219, 344;

mass spectrum 219 (100), 204 (2), 176 (24), 147 (12), 104 (12).

This acid was compared with 6-methoxykynurenic acid and 7-methoxy-2-quinolone-4-carboxylic acid (**26**), below, and found to be identical with the latter.

The ring expansion product above was therefore 2,5-dihydro-4-hydroxy-8-methoxy-2,5-dioxo-1-benzazepine(25).

6-Methoxykynurenic Acid

The literature preparation (13) gave material with m.p. 282° dec.; i.r. 1740 (br), 1680, 1605; u.v. 215, 227, 258, 351; mass spectrum 219 (58), 175 (100), 173 (40), 132 (20).

Preparation of 7-Methoxy-2-quinolone-4-carboxylic Acid (26)

6-Methoxyisatin (32), 3.3 g, was acetylated (15) to give 2.4 g of *N*-acetyl derivative, m.p. 143–144° (toluene); mass spectrum 219 (17), 176 (100).

Alkaline rearrangement (15) of the acetyl derivative gave a 50% yield of acid **26**, whose i.r. spectrum (KBr, Perkin–Elmer 621) was superimposable with that of the material obtained by the azepine route. The pure acid had m.p. 313–314° (acetic acid).

Anal. Calcd. for $C_{11}H_9NO_4 \cdot \frac{1}{2}CH_3COOH$: C, 54.4; H, 4.9; N, 4.55. Found: C, 54.7; H, 4.9; N, 4.55.

We thank the National Research Council of Canada for financial support.

1. G. JONES. J. Chem. Soc. C, 1808 (1967).
2. R. W. RICKARDS and R. M. SMITH. Tetrahedron Lett. **22**, 2361 (1966).
3. G. R. BEDFORD, G. JONES, and B. R. WEBSTER. Tetrahedron Lett. **22**, 2367 (1966).
4. A. H. REES and K. SIMON. Can. J. Chem. **47**, 1227 (1969).
5. C. G. HUGHES and A. H. REES. Chem. Ind. 1439 (1971).
6. H. W. MOORE, H. R. SHELDON, and W. WEYLER. Tetrahedron Lett. 1243 (1969).
7. A. H. REES. Chem. Ind. 931 (1964).
8. A. H. REES. Chem. Ind. 1298 (1965).
9. A. CROMARTY, G. R. PROCTOR, and M. SHABBIR. J. Chem. Soc. (Perkin I), 2012 (1972).
10. R. A. JAMES. Thesis in progress.
11. P. K. MACNICOL. Biochem. J. **107**, 473 (1968).
12. M. SLAYTOR, L. COPELAND, and P. K. MACNICOL. Phytochemistry, **7**, 1779 (1968).
13. B. P. 942 524, 1963. Chem. Abstr. **60**, 5469b (1964).
14. A. H. REES. J. Chem. Soc. 3111 (1959).
15. Org. Synth. Coll. Vol. III, 456 (1955).
16. E. J. MORICONI and I. M. MANISCALCO. J. Org. Chem. **37**, 208 (1972).
17. R. G. COOKE and I. M. RUSSELL. Aust. J. Chem. **37**, 2421 (1972).
18. W. A. DENNE and M. F. MACKOY. Tetrahedron, **28**, 1795 (1972).
19. L. F. FIESER. J. Am. Chem. Soc. **48**, 2922 (1926).
20. L. HORNER and S. GOWECKE. Chem. Ber. **94**, 1291 (1961).
21. L. F. FIESER. J. Am. Chem. Soc. **50**, 459 (1928).
22. L. F. FIESER. J. Am. Chem. Soc. **70**, 3165 (1948).
23. L. F. FIESER. J. Am. Chem. Soc. **48**, 3201 (1926).
24. J. THIELE and A. WINTER. Ann. **311**, 347 (1900).
25. E. DE BARRY BARNETT and F. G. SANDERS. J. Chem. Soc. 434 (1933).
26. A. C. BAILLIE and R. H. THOMSON. J. Chem. Soc. C, 2184 (1966).
27. R. TRAVE, L. GARNATI, and M. PAVAN. Chim. Ind. (Milan) **41**, 19 (1959).
28. SANDOZ Ltd. Neth. Appl. 6 504 614. Chem. Abstr. **64**, 15771f (1966).
29. T. R. KASTURI and T. ARUNACHALAM. Can. J. Chem. **44**, 1086 (1966).
30. G. HABERLAND. Chem. Ber. **69**, 1380 (1936).
31. E. MOSETTIG and E. L. MAY. J. Org. Chem. **5**, 528 (1940).
32. P. W. SADLER. J. Org. Chem. **21**, 169 (1956).

Can. J. Chem. Downloaded from www.nrcresearchpress.com by 210.87.254.105 on 09/05/12
For personal use only.

Mercury(II) Complexation of Cysteine, Methyl Cysteineate, and *S*-Methylcysteine in Acidic Media

GEORGE A. NEVILLE[1] AND TORBJÖRN DRAKENBERG

The Institute of Hygiene, University of Lund, Magle Stora Kyrkogata 12, S-223 50 Lund, Sweden

and

Organic and Physical Chemistry 2, University of Lund, Chemical Center, Box 740, S-220 07 Lund, Sweden

Received August 21, 1973

Bis(cysteineato)mercury(II) hydrochloride hemihydrate, $(C_3H_6O_2NS)_2Hg\cdot HCl\cdot\frac{1}{2}H_2O$, was obtained by reaction of ethanolic solutions of L-cysteine hydrochloride with either $HgCl_2$ in 95% EtOH, $Hg(OAc)_2$ in MeOH, $Hg(NO_3)_2$ in HOAc, or by reaction of L-cysteine (free base) with $HgCl_2$. Reaction of L-cysteine (free base) with $Hg(OAc)_2$ gave a mercury(II) cysteineate with composition $(C_3H_6O_2NS)_5Hg_2$. Bis(*S*-methyl-L-cysteineate)mercury (II), $(C_4H_8O_2NS)_2Hg$, was obtained by reaction of *S*-methyl-L-cysteine with $Hg(OAc)_2$. ^1H- and ^{13}C-n.m.r. spectral data are reported and compared for acidic solutions of cysteine, methyl cysteineate, *S*-methylcysteine, and their mercury(II) complexes. The proton spectra for *S*-methyl-L-cysteine and L-cysteine hydrochloride have been analyzed as ABC systems and relative rotamer populations have been determined. In acidic solution, mercury bonding is localized to sulfur and the complexes appear to have an extended molecular configuration resulting from a *trans* orientation of the COOH group and the Hg site.

Le chlorhydrate hemihydraté de bis(cysteineato)mercure(II), $(C_3H_6O_2NS)_2\ Hg\cdot HCl\cdot\frac{1}{2}H_2O$, a été obtenu par réaction de solutions éthanoliques du chlorhydrate de la L-cysteine avec l'un des réactifs suivants $HgCl_2$ dans EtOH 95%, Hg $(OAc)_2$ dans MeOH, $Hg(NO_3)_2$ dans HOAC ou par réaction de la L-cysteine (base libre) avec $HgCl_2$. La réaction entre la L-cysteine (base libre) et $Hg(OAc)_2$ a conduit au cysteineate)mercure(II) correspondant à la composition $(C_3H_6O_2NS)_5Hg_2$. Le bis(*S*-méthyl-cysteineate)mercure(II), $(C_4H_8O_2NS)Hg$, a été obtenu à l'aide de la réaction entre la *S*-méthyl L-cysteine et $Hg(OAc)_2$. On rapporte et compare les données spectrales de la r.m.n. du ^1H et du ^{13}C obtenues pour des solutions acides de cysteine, de cysteineate de méthyle, de cysteineate de *S*-méthyle et leurs complexes de mercure(II). Les spectres du proton de la *S*-méthyl L-cysteine et du chlorhydrate de L-cysteine ont été analysés par rapport à un système du type ABC. Les populations relatives des rotamères ont aussi été déterminées. Dans une solution acide, le mercure est relié à l'atome de soufre et les complexes semblent posséder une configuration moléculaire étendue ce qui résulterait d'une orientation trans du groupe COOH par rapport à l'atome de Hg. [Traduit par le journal]

Can. J. Chem., **52**, 616 (1974)

Introduction

Because of the importance of L-cysteine in the chemistry of biological systems and because of its ability to complex with a wide variety of metal ions, metal complexation by cysteine and its derivatives has received considerable attention. This is particularly true for cobalt(III) and cobalt(II) complexes of cysteine whose coordination was elucidated by Neville and Gorin (1, 2) by means of spectrophotometric study some 30 years after the complexes had been isolated by Schubert (3). Perrin and Sayce (4) investigated zinc complexation with cysteine by p*H* titration and found evidence for formation of polynuclear and protonated species. More recently an ^1H-n.m.r. study of complexation of L-cysteine and *S*-methyl-L-cysteine with Ni^{2+}, Zn^{2+}, Cd^{2+}, Hg^{2+}, Ag^+, and Pb^{2+} as a function of p*H* was reported by Natusch and Porter (5) but no isolation of complexes was reported in either of these recent investigations.

Unfortunately, in the case of mercurial complexation, the investigations have tended to be sporadic and mainly devoted to the application of indirect methods for determining the nature of complex entities in solution. In spite of the early recognition of the affinity of mercuric ion for sulfhydryl groups (mercaptan reaction), few reports are available describing the isolation and characterization of mercurial derivatives of cysteine and its analogs. Stricks and Kolthoff (6) provided polarographic evidence for the formation of at least three mercurial complexes with cysteine (RSH): $Hg(RS)_2$, $Hg_2(RS)_2$, and Hg_3-

[1]1972 Centennial Fellow of the Medical Research Council of Canada. Present address: Health Protection Branch, Health and Welfare Canada, Tunney's Pasture, Ottawa, Canada K1A 0L2.

Can. J. Chem. Downloaded from www.nrcresearchpress.com by 210.87.254.6 on 09/05/12
For personal use only.

TABLE 1. Proton n.m.r. data (100 MHz) for D_2O solutions of cysteine hydrochloride, methyl cysteineate hydrochloride, *S*-methylcysteine, and their mercury(II) complexes

Compound	Concentration (*M*)	p*D*	δ_{CH_3}*	δ_{CH_3S}	δ_{CH_2}	δ_{CH}	J_{AB}†	J_{AC}	J_{BC}	$J_{a\beta}$
$HSCH_2CH(NH_3Cl)CO_2H$	0.50	1.4			3.50, 3.45	4.67	−15‡	5.35	4.51	
$(C_3H_6O_2NS)_2Hg\cdot HCl\cdot\frac{1}{2}H_2O$	0.21	0.7			3.85	4.67	—	5.10	5.10	
$HSCH_2CH(NH_3Cl)CO_2CH_3$	0.50	1.3	4.30		3.60	4.85				5.10
$(C_4H_9NO_2S)_2ClHgNO_3\cdot H_2O$	2.9	1.3	4.35		4.05	4.90				5.40
$(C_4H_9NO_2S)_2HgCl_2\cdot H_2O$	3.0	1.3	4.35		4.10	4.95				5.40
$CH_3SCH_2CH(NH_2)CO_2H$	0.5	2.2		2.63	3.54, 3.63	4.67	−15.02	4.31	7.64	
$(C_4H_8O_2NS)_2Hg$	0.21	1.9		2.92	3.87, 3.95	4.72	−14.24	5.34	6.32	

*δ measured in p.p.m. downfield from external TMS.
†*J* values measured to ±0.05 Hz.
‡Estimated from a 220 MHz spectrum.

$(RS)_2$. In the presence of much chloride ion, formation of $Hg_2(RS)_2$ and $Hg_3(RS)_2$ is suppressed by the complex $HgCl_4^{2-}$. Lenz and Martell (7) employed potentiometric titrimetry to study $HgCl_2$ complexation with L-cysteine and *S*-methyl-L-cysteine and concluded there is little or no involvement of substituted mercapto groups in chelation. Later, Porter, Perrin, and Hay (8), using potentiometry to investigate mercurial complexation of cysteine methyl ester, found that analysis of the mercury(II) system presented a number of problems (the best interpretation of data involved assuming that HgL^+ is completely formed at commencement of p*H* titrations at a 1:2 metal-to-ligand ratio) then the titration data could be satisfactorily described by the set of complexes HgL_2, $Hg_2L_3^+$, and $Hg_3L_4^{2+}$. Porter *et al.* isolated one complex in their study and characterized it as bis(methyl L-cysteineate)mercury(II) dihydrochloride sesquihydrate. Reinvestigation (9) has shown this complex to be a hydrochloride hydronitrate monohydrated salt. In an infrared study of complexes of L-cysteine and related compounds with zinc(II), cadmium(II), mercury(II), and lead(II), Shindo and Brown (10) reported empirical formulae (based on C, H, N, and Cl analysis only) for five mercurial complexes of cysteine but no details of preparation and isolation were reported. No proposals were advanced concerning the structure of any of the mercury complexes but the authors claimed that their findings were consistent with the indications from polarographic studies made by Stricks and Kolthoff (6). Recently, Natusch and Porter (11) provided evidence from ^{1}H-n.m.r. studies for "mercury–thio–ether" bonding in an *S*-methylcysteine complex in aqueous solution. It is the purpose of this paper to report the isolation and characterization of mercury(II) complexes of L-cysteine and *S*-methyl-L-cysteine under acidic conditions and the application of ^{1}H and ^{13}C-n.m.r. spectroscopy for the determination of ligand interaction and molecular conformation.

Results

Mercury complexes of L-cysteine, L-cysteine methyl ester, and *S*-methyl-L-cysteine were prepared and isolated under mildly acidic conditions which represent the simplest and most practical *in vitro* conditions that can be utilized in relation to *in vivo* mercurial complexation of molecules of biochemical interest. The stoichiometries of the complexes were determined by total elemental microanalyses and solid state characterization is reported in the Experimental.

The results of ^{1}H- and ^{13}C-n.m.r. spectral study of D_2O solutions of the complexes are summarized in Tables 1 and 2. For those complexes which would dissolve in water without the aid of acidification, spectra were obtained at solution p*D* and compared with spectra obtained following the addition of 2–3 drops of trifluoroacetic acid (TFA). Only small changes were observed between spectra following acidification of solutions with TFA due to the known p*H* effect (12). Accurate p*D* values were obtained from the expression, p*D* = p*H* scale reading + 0.4 of Glasoe and Long (13). In the case of the mercury complex of *S*-methylcysteine, it was necessary to add a few drops of TFA to obtain dissolution of the suspended solid in D_2O. The solution of this complex remained stable for weeks under ordinary refrigeration. In contrast, a suspension in water of the complex formed by cysteine and mercury(II) acetate decomposed

Can. J. Chem. Downloaded from www.nrcresearchpress.com by 210.87.254.6 on 09/05/12
For personal use only.

TABLE 2. ^{13}C-n.m.r. chemical shifts for D_2O solutions of cysteine hydrochloride, methyl cysteineate hydrochloride, *S*-methylcysteine, and their mercury(II) complexes

Compound	Concentration (*M*)	p*D*	Shifts (p.p.m. relative to TMS) CH_3	CH_3S	CH_2	CH	CO_2H	CO_2Me
$HSCH_2CH(NH_3Cl)CO_2H$	0.50	1.4			24.8	55.3	170.6	
$(C_3H_6O_2NS)_2Hg \cdot HCl \cdot \frac{1}{2}H_2O$	0.21	0.7			28.5	55.9	170.6	
$HSCH_2CH(NH_3 \cdot Cl)CO_2CH_3$	0.50	1.3	54.8		24.8	55.3		169.6
$(C_4H_9NO_2S)_2ClHgNO_3 \cdot H_2O$	2.9	1.3	55.3		29.0	56.8		169.8
$(C_4H_9NO_2S)_2HgCl_2 \cdot H_2O$	3.0	1.3	54.9		29.0	56.1		169.7
$CH_3SCH_2CH(NH_2)CO_2H$	0.5	2.2		15.5	34.6	53.3	172.6	
$(C_4H_8O_2NS)_2Hg$	0.21	1.9		18.5	37.5	51.8	174.5	

within minutes on treatment with TFA to form first a yellow solution which quickly darkened as a brownish-black sludge was deposited. In these studies, acidification was performed using TFA rather than HCl to avoid competitive complexation by formation of the highly stable $HgCl_4^{2-}$ ion (6).

Examination of ^{1}H-n.m.r. spectra of a 0.5 *M* aqueous solution of L-cysteine hydrochloride (p*D* 1.4) at 100 MHz revealed nonequivalent methylene protons. This is the first time such nonequivalence has been reported in proton spectra of cysteine in acidic media. Our analysis of the ABC pattern obtained for *S*-methyl-L-cysteine and for its mercury(II) complex (Figs. 1 and 2) provided chemical shifts and coupling constants which differ appreciably from published values (5, 14). The results from ^{1}H- and ^{13}C-n.m.r. studies (Tables 1 and 2) provide evidence for mercurial bonding to sulfur only in solution and an extended chain configuration in which preference is shown for the *trans* conformation.

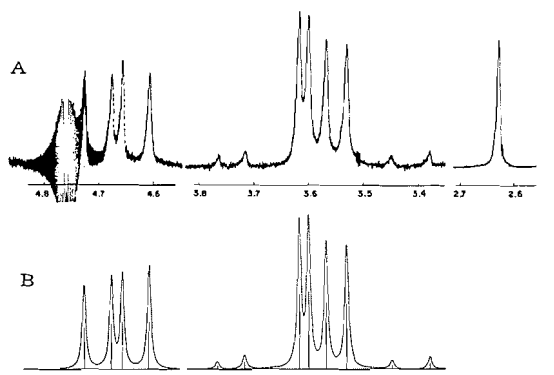

FIG. 1. 100 MHz ^{1}H-n.m.r. spectra of *S*-methyl-L-cysteine in D_2O at p*D* 2.2. Chemical shifts are relative to external TMS. (A) Experimental spectrum; (B) simulated spectrum.

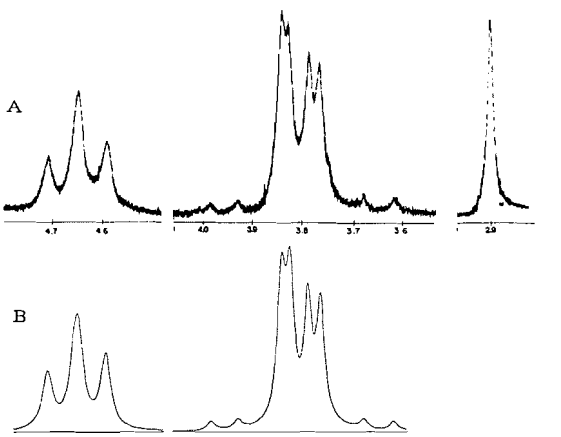

FIG. 2. 100 MHz ^{1}H-n.m.r. spectra of mercury(II) complex of *S*-methyl-L-cysteine in D_2O at p*D* 1.9. Chemical shifts are relative to external TMS. (A) Experimental spectrum; (B) simulated spectrum.

Discussion

Whereas other workers (5–8) sought to investigate the nature of mercurial complexation with sulfur containing amino acids in solution by varying p*H*, metal, and ligand concentrations, we have tackled the problem by placing an emphasis first on isolation and characterization of complexes before investigating their nature in the solvated state. One cannot overlook, however, the possibility of complex alteration during solvation. Further assurance for the interpretation of data may be obtained through comparison of the results from a variety of solvated complexes as well as uncomplexed parent substances. In this way we wished to minimize such difficulties as polynuclear complexation, multiple protonation, and the insolubility of certain complexes in particular p*D* regions experienced in earlier work as systems

Can. J. Chem. Downloaded from www.nrcresearchpress.com by 210.87.254.6 on 09/05/12
For personal use only.

Can. J. Chem. Downloaded from www.nrcresearchpress.com by 210.87.254.6 on 09/05/12
For personal use only.

were explored by indirect means while solution parameters were varied.

Cysteine

All previous investigators (14–17) have reported equivalent methylene protons and first order spectral features for the fully protonated form (LH_3^+) of cysteine in solution. At 100 MHz, we found evidence for nonequivalence of the methylene protons and at 220 MHz it was possible to analyze the ABC pattern to obtain coupling constants (Table 1) with greater accuracy as confirmed by spectral simulation (Fig. 3). It appears that the nearly similar methylene proton frequencies precluded the observation of this nonequivalence even with optimum resolution at 60 MHz by earlier workers thereby resulting in reports of equivalent protons and a first order system. The relative rotamer populations for L-cysteine hydrochloride are given in Fig. 4.

The ^{13}C-n.m.r. chemical shifts (Table 2) for bis(L-cysteineato)mercury(II) hydrochloride compared with L-cysteine hydrochloride indicate mercury bonding to sulfur and an extended molecular configuration. The downfield shift (~4 p.p.m.) for the methylene carbon signal of the complex relative to the uncomplexed molecule is the same order of magnitude observed in the mercurial complex of methionine (18). The small downfield shift (~1 p.p.m.) in the methine carbon and absence of effect to the carbonyl carbon frequencies support the extended molecular configuration in solution. Unfortunately, our cysteine mercurial complex shows equivalence of the methylene protons in aqueous solution ($pD = 0.7$) (Table 1) and it is not possible to describe the conformation in detail. In contrast, Natusch and Porter (5) provide ^1H-n.m.r. evidence for a mercury complex of cysteine which was found to give an ABC pattern and from which they were able to deduce rotamer populations. The ionic form of their complex is not clear; moreover, their complex has not been isolated and characterized and the pD of its n.m.r. solution is not known. Shindo and Brown (10) isolated five mercury–cysteine complexes which they examined by infrared spectroscopy. One of these complexes is a 1:2 complex formulated as $Hg[SCH_2CH(NH_3)CO_2]_2$ obtained at $pH = 2$ in the presence of excess cysteine. No other experimental details are given and no structural conclusions were reached.

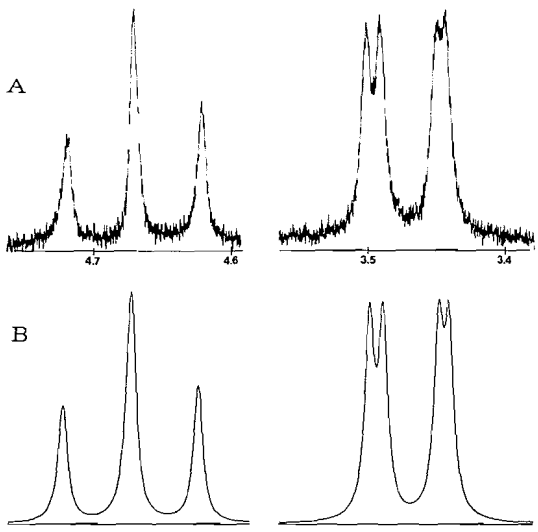

FIG. 3. 100 MHz ^1H-n.m.r. spectra of L-cysteine hydrochloride in D_2O at pD 1.4. Chemical shifts are relative to external TMS. (A) Experimental spectrum; (B) simulated spectrum.

Cysteine Methyl Ester

Unlike cysteine hydrochloride, a 0.5 *M* aqueous solution of cysteine methyl ester hydrochloride ($pD = 1.3$) shows equivalent methylene protons at 100 MHz. This finding agrees with that reported by Natusch and Porter (5). In an earlier communication (9) it was shown that cysteine methyl ester forms two complexes, bis(methyl L-cysteineato)mercury(II) hydrochloride hydronitrate monohydrate and bis(methyl L-cysteineato)mercury(II) dihydrochloride monohydrate. At $pD = 1.3$, each of these complexes shows equivalence of methylene protons, and ^{13}C-n.m.r. chemical shift data (Table 2) are consistent with an extended molecular configuration for these complexes as deduced for cysteine and its mercury complex.

S-Methylcysteine

Under the minimal acidic conditions utilized in this work for the preparation of a 0.5 *M* D_2O solution of *S*-methylcysteine ($pD = 2.2$), we obtained an ABC proton spectrum at 100 MHz which yielded the parameters in Table 1 following computer analysis and simulation (Fig. 1). The relative rotamer populations (Fig. 3) were calculated using standard relationships (5, 19). Natusch and Porter (5) reported equivalent methylene protons for the LH_2^+ form of *S*-

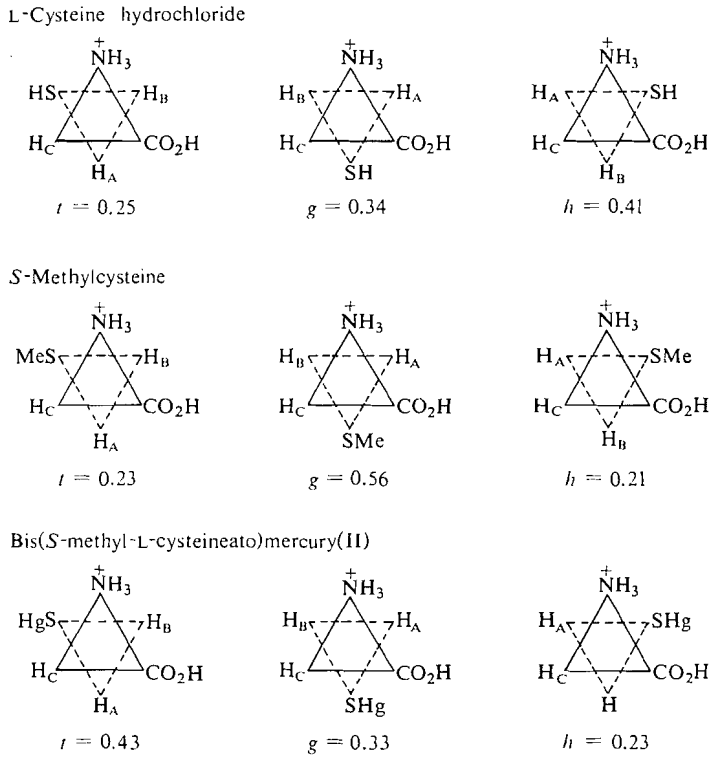

FIG. 4. Relative populations of the three staggered rotamers of L-cysteine hydrochloride, *S*-methyl-L-cysteine and its mercury(II) complex in D_2O at p*D* 1.9.

methylcysteine and nonequivalent methylene protons (ABC pattern) for *S*-methylcysteine in its zwitterionic form. In regard to the latter, the calculated rotamer populations do not agree with the published coupling data.

Upon complexation with mercury, the methyl and methylene protons of *S*-methylcysteine show similarly large downfield shifts (Table 1) indicative of mercurial bonding to sulfur. The very small change in the methine proton signal relative to the parent compound suggests no mercurial interaction in solution with either the ammonium or carboxylate groups. The ^{13}C chemical shift data (Table 2) confirm the proton evidence and support the view of an extended molecular configuration for the complex. Natusch and Porter (5) report ^1H-parameters for a solution with molar ratio of 1:2 with respect to $Hg(NO_3)_2$ and *S*-methylcysteine and 2.0 *M* in nitric acid. It appears from their structural representations (5, 11) and from the designation of ligands and ionic form (5) that they regard the complex in acidic solution as a triply, positively charged 1:1 species in which mercury bonding is localized to the sulfide group. Our evidence and that of Natusch and Porter (5) for mercurial complexation of *S*-methylcysteine is contrary to the conclusion reached by Lenz and Martell (7) that little or no involvement of substituted mercapto groups would occur in chelation of ethionine and *S*-methylcysteine. It is also interesting to note that Livingstone and Nolan (20) prepared Co, Ni, Pd, Pt, Cu, Zn, and Cd complexes of *S*-methylcysteine for infrared analysis but no mercury complexes of this amino acid were reported although a mercury complex of ethionine was prepared.

Relative Rotamer Populations

Relative populations for the three staggered rotamers of each of L-cysteine hydrochloride, *S*-methyl-L-cysteine, and bis(*S*-methyl-L-cysteineato)mercury(II) in D_2O solution have been calculated using the expressions $t = J_{BC} - J_g/J_t - J_g$, $g = J_{AC} - J_g/J_t - J_g$, and $h = 1 - (t + g)$ (5, 19). Values of 12.0 and 2.0 Hz for J_t and J_g, respectively, which were suggested by Martin and Mathur (14) for cysteine were used (Fig. 4). The rotamer distribution found for fully protonated cysteine is interesting for the

Can. J. Chem. Downloaded from www.nrcresearchpress.com by 210.87.254.6 on 09/05/12
For personal use only.

Can. J. Chem. Downloaded from www.nrcresearchpress.com by 210.87.254.6 on 09/05/12
For personal use only.

relatively high fraction (0.40) of the most sterically hindered rotamer. A similarly high fraction is found for one of the less hindered rotamers (*g*) and it is suggested that the dominant stabilizing factor for each of these rotamers of cysteine is the capability for intramolecular hydrogen bonding between the carboxylic proton and the S atom in a six-membered ring. Similar hydrogen bonding is believed to account for the relatively high population of the *S*-methylcysteine rotamer having adjacent —SMe and $-CO_2H$ groups where the presence of the electron donating methyl substituent enhances the Lewis basicity of the S atom. In the case of the mercury complex of *S*-methylcysteine, the increased steric repulsion of the —HgS— group and the reduced basicity of the S atom bonded to mercury together result in weaker hydrogen bonding and domination of steric effects; thus the rotamer with *trans* —HgS— and $-CO_2H$ groups is most highly populated as expected for bis(*S*-methyl-L-cysteineato)mercury(II).

Insofar as population calculations are concerned it is important to note, as a referee has emphasized, that the proton coupling data alone do not allow one to determine which one of a pair of populations should be assigned to one of the conformers with a methylene H *trans* to the methine or other (in this case *t* and *g*). This ambiguity in the interpretation of chemical shift and *J* data arises in general in any p.m.r. study of molecules involving a CH_2—CH— group unless an absolute assignment of the methylene H's can be made. In this study, it is the ^{13}C data which permit one to conclude that a complex is extended (*i.e.* which indicates a non-*gauche* orientation of the COOH and Hg site) and which justifies the spectral assignment.

Experimental

Instrumentation

^{13}C-n.m.r. spectra were obtained at 27 °C with a Varian XL-100 spectrometer at 25.2 MHz following accumulation and Fourier transformation of signals in both proton decoupled and coupled modes. Frequencies were measured relative to dioxane and converted to the TMS scale ($\delta_{TMS} = \delta_{dioxane} + 67.4$ p.p.m.) (21). Proton spectra were obtained at 35 °C at 100 MHz, and simulated spectra were calculated with the computer program UEAITR due to Johannessen *et al.* (22) by means of a UNIVAC 1108 computer.

Microanalyses

Microanalyses were performed by Alfred Bernhardt, Mikroanalytische Laboratorium, 5251 Elbach Uber Engelskirchen, Fritz-Pregl Strasse 14–16, W. Germany. Appropriate separatory processes were employed to eliminate the interference of mercury with C, H, and Cl determinations. Sulfur was analyzed by a reductive process.

Syntheses

Bis(L-cysteineato)mercury(II) Hydrochloride Hemihydrate

To a solution of L-cysteine hydrochloride hydrate (0.877 g, 0.005 mol, Sigma) in water (10 ml) diluted with 95% ethanol (10 ml), a solution of mercury(II) chloride (0.679 g, 0.0025 mol, BDH Analar) in 95% ethanol (10 ml) was added dropwise. After approximately 1 ml of the mercurial solution had been added, the reaction mixture became turbid and copious precipitation occurred during the remainder of the addition. Ethanol was used for rinsing. The mixture was stirred for 15 min, collected, washed with 95% ethanol (product slightly soluble in 95% ethanol), and dried over NaOH *in vacuo*. The yield was 1.10 g or 92%. Infrared spectra (4000–600 cm^{-1}) were rather similar to spectra of the parent substance with the exception of a new band near 1500 cm^{-1}.

Anal. Calcd. for $(C_3H_6O_2NS)_2Hg \cdot HCl \cdot \frac{1}{2}H_2O$ (mol. wt. 479.39): C, 14.78; H, 3.10; O, 14.77; N, 5.75; S, 13.16; Hg, 41.16; Cl, 7.28. Found: C, 14.90; H, 3.15; O, 14.82 and 14.91; N, 5.71; S, 13.97; Hg, 41.03; Cl, 7.32; and % drying loss (*RT*/2 mm), 0.23.

X-Ray diffraction patterns established the identity of this product with that obtained under each of the following conditions:

(*i*) From a solution of L-cysteine (free base) (0.606 g, 0.005 mol, Sigma) in glacial acetic acid – ethanol, prepared by first dissolving the cysteine in the acetic acid (15 ml) with heating and then adding 95% ethanol (10 ml), to which a solution of mercury(II) chloride (0.681 g, 0.0025 mol, BDH Analar) in 95% ethanol (10 ml) was added dropwise with magnetic stirring (yield, 68%).

(*ii*) From a solution of L-cysteine hydrochloride hydrate (0.877 g, 0.005 mol, Sigma) in 95% ethanol (20 ml) and water (10 ml) to which a warm solution (35°) of mercury(II) acetate (0.795 g, 0.0025 mol, Merck pro analysi) in methanol (10 ml) was added dropwise with stirring (yield, 92%).

(*iii*) From a solution of L-cysteine hydrochloride hydrate (0.877 g, 0.005 mol, Sigma) in water (10 ml) and 95% ethanol (10 ml) to which a hot solution (60°) of mercury(II) nitrate hydrate (0.858 g, 0.0025 mol, BDH Analar) in glacial acetic acid (10 ml) was added dropwise with stirring. Precipitation was so heavy in this reaction that additional ethanol (10 ml) was required for stirring (yield, 88%).

Mercury(II) Cysteineate

To a warm, magnetically stirred solution (50–60°) of L-cysteine (free base) (0.606 g, 0.005 mol, Sigma) in glacial acetic acid (15 ml) and 95% ethanol (10 ml), a solution of mercury(II) acetate (0.797 g, 0.0025 mol, Merck pro analysi) in methanol (10 ml) was added dropwise. Precipitation occurred immediately, resulting in a milky appearance and the deposition of a finely divided, white solid. The mixture was left stirring to cool to room temperature. The solid was collected, washed with 95% ethanol, and dried over NaOH *in vacuo*. X-Ray diffraction showed the product to be crystalline and infrared spectra suggested the presence of free carboxyl groups.

Anal. Calcd. for $(C_3H_6O_2NS)_2Hg_2$: C, 17.15; H, 3.05;

O, 16.13; N, 7.06; S, 16.16; Hg, 40.45. Found: C, 17.90; H, 3.15; O, 16.02 and 16.11; N, 6.82; S, 15.85; Hg, 39.81; and % drying loss (*RT*/2 mm) 0.19.

Bis(S-methyl-L-cysteineato)Mercury(II)

A warm solution (50–60°) of *S*-methyl-L-cysteine (0.608 g, 0.005 mol, Sigma) in 95% ethanol (20 ml) was prepared by the addition of just sufficient water (2–3 ml) to effect dissolution. To the magnetically stirred solution, a solution of mercury(II) acetate (0.795 g, 0.0025 mol, Merck pro analysi) in methanol (10 ml) was added dropwise. No "tail-effect" was seen upon addition of the mercurial solution but, towards the end of the addition, the mixture developed a turbidity and precipitation occurred. The mixture was stirred for 15 min and then left to stand at room temperature for 2 h. The precipitate (fraction A) was collected as a finely powdered, pale yellow solid, washed with 95% ethanol, and dried over NaOH *in vacuo*. The mother liquor was heated and treated with a few drops of water until clarified, then the warm solution was treated with acetone until just turbid. On standing at room temperature, the treated mother liquor produced a small quantity of solid (fraction B), which was handled as above.

X-Ray diffraction patterns showed the product to be crystalline and confirmed the identity of fractions A (0.75 g) and B (0.089 g). Infrared spectra showed (*i*) the absence of bands due to the acetate moiety, (*ii*) a ν(C=O) band little different from that of *S*-methyl-L-cysteine, and (*iii*) a ν(NH) band centered near 3200 cm^{-1} (~200 cm^{-1} higher than in the parent compound); yield, 80%.

Anal. Calcd. for $(C_4H_8O_2NS)_2Hg$ (mol. wt. 468.96): C, 20.49; H, 3.44; O, 13.65; N, 5.97; S, 13.67; Hg, 42.78. Found: C, 20.29; H, 3.28; O, 13.67; N, 5.80; Hg, 43.02; S, 13.48; and % drying loss (50°/HV) 0.10.

The interest of Prof. Maths Berlin, Institute for Hygiene, University of Lund, Sweden in encouraging structural studies related to mercurial toxicology and biotransformation is gratefully acknowledged. Special appreciation is extended to Prof. Börje Wickberg, Organic Chemistry 2, Chemical Center, University of Lund, Sweden for provision of laboratory space and resources. We are grateful to Dr. A. A. Grey, Canadian 220 MHz NMR Center, Ontario Research Foundation, Sheridan Park, Ontario, Canada for the 220 MHz proton spectrum of cysteine hydrochloride. The Medical Research Council of Canada is generously thanked for the provision of a Centennial Fellowship (G.A.N.) and research grant in support of this work. The Swedish Natural Science Research Council is thanked for financial support (T.D.).

1. R. G. NEVILLE and G. GORIN. J. Am. Chem. Soc. **78**, 4893 (1956).
2. R. G. NEVILLE. J. Am. Chem. Soc. **79**, 518 (1957).
3. M. P. SCHUBERT. J. Am. Chem. Soc. **53**, 3851 (1931).
4. D. D. PERRIN and I. G. SAYCE. J. Chem. Soc. (A), 53 (1968).
5. D. F. S. NATUSCH and L. J. PORTER. J. Chem. Soc. (A), 2527 (1971).
6. W. STRICKS and I. M. KOLTHOFF. J. Am. Chem. Soc. **75**, 5673 (1953).
7. G. R. LENZ and A. E. MARTELL. Biochemistry, **3**, 745 (1964).
8. L. J. PORTER, D. D. PERRIN, and R. W. HAY. J. Chem. Soc. (A), 118 (1969).
9. G. A. NEVILLE and M. BERLIN. Can. J. Chem. **51**, 3970 (1973).
10. H. SHINDO and T. L. BROWN. J. Am. Chem. Soc. **87**, 1904 (1965).
11. D. F. S. NATUSCH and L. J. PORTER. J. Chem. Soc. (D), 596 (1970).
12. W. J. HORSLEY and H. STERNLICHT. J. Am. Chem. Soc. **90**, 3738 (1968).
13. P. K. GLASOE and F. A. LONG. J. Phys. Chem. **64**, 188 (1960).
14. R. B. MARTIN and R. MATHUR. J. Am. Chem. Soc. **87**, 1065 (1965).
15. S. FUJIWARA and Y. ARATA. Bull. Chem. Soc. Jap. **36**, 578 (1963); **37**, 344 (1964).
16. K. G. R. PACHLER. Spectrochim. Acta, **19**, 2085 (1963).
17. F. TADDEI and L. PRATT. J. Chem. Soc. 1553 (1964).
18. B. BIRGERSSON, T. DRAKENBERG, and G. A. NEVILLE. Acta Chem. Scand. In press.
19. G. A. NEVILLE, R. DESLAURIERS, B. J. BLACKBURN, and I. C. P. SMITH. J. Med. Chem. **14**, 717 (1971).
20. S. E. LIVINGSTONE and J. D. NOLAN. Inorg. Chem. **7**, 1447 (1968).
21. L. F. JOHNSON and W. C. JANKOWSKI. *In* Carbon-13 n.m.r. spectra. Wiley, New York. 1972.
22. R. B. JOHANNESSEN, J. A. FERRETTI, and R. K. HAUIS. J. Magn. Res. **3**, 84 (1970).

Can. J. Chem. Downloaded from www.nrcresearchpress.com by 210.87.254.6 on 09/05/12
For personal use only.

Orientation in the Wallach Rearrangement for the Naphthyl Azoxy Series[1]

ALLAN DOLENKO[2] AND ERWIN BUNCEL

Department of Chemistry, Queen's University, Kingston, Ontario

Received March 14, 1973[3]

The acid-catalyzed Wallach rearrangement of azoxybenzenes has been extended to the naphthyl azoxy series in order to evaluate the effect of annelation of benzene rings on the course of rearrangement. The six known azoxy derivatives containing the α-naphthyl, β-naphthyl, and phenyl moieties, in various combinations, have been examined with respect to product orientation in moderately strong sulfuric acid solutions. The course of rearrangement (eqs. 2–6) is discussed on the basis of current mechanisms.

Le réarrangement de Wallach, sous catalyse acide, d'azoxybenzènes a été appliqué à la série d'azoxynaphtalène afin d'évaluer l'effet d'annellation d'anneaux benzéniques sur le mécanisme du réarrangement. Les six dérivés azoxy connus, contenant les groupes α-naphtyle, β-naphtyle et phényle dans des combinaisons différentes, ont été étudiés en fonction de l'orientation du produit dans des solutions d'acide sulfurique modérément fortes. On discute du processus de réarrangement (eqs. 2–6) en se basant sur les divers mécanismes connus. [Traduit par le journal]

Can. J. Chem., 52, 623 (1974)

The transformation of azoxybenzene (**1**) to *p*-hydroxyazobenzene (**2**) in strongly acidic media has been the subject of a number of investigations since its discovery by Wallach and Belli in 1880 (1). Studies related to this rearrangement

[1] 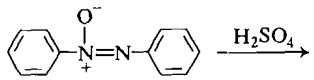

1

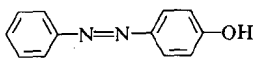

2

have included evaluation of the effect of substituents in one or both phenyls on the course of rearrangement (2, 3), the employment of isotopic tracers including ^{14}C (4), ^{15}N (5), and ^{18}O (6, 7), and kinetic investigations, performed on azoxybenzene and some substituted derivatives (2, 3, 8). As a result of these studies a number of mechanisms have been proposed (9), involving some rather unusual species as reaction intermediates. The postulated key intermediates are shown in structures **3**–**8**.

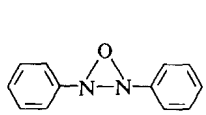

3

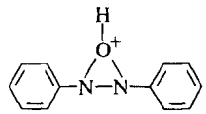

4

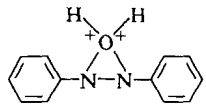

5

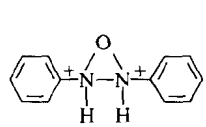

6

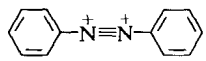

7

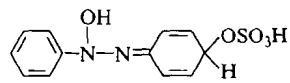

8

In order to broaden the scope of the previous studies, which until now have involved only azoxybenzene or its substituted derivatives, and to perhaps shed more light on the controversy surrounding the nature of the reactive intermediate, an investigation of the reactions of the series of azoxy compounds containing the naphthyl moiety has been undertaken. In the case of the benzidine rearrangement, extension of the studies from phenyl- to naphthyl-containing hydrazo compounds revealed new facets relating to product orientation which resulted in a better understanding of the reaction mechanism (10). Other aromatic rearrangements have received similar investigation (11).

[1]Part XII in the series on the Wallach Rearrangement. For Part XI see ref. 31. A portion of this work has appeared in a preliminary communication (ref. 14).

[2]Present address: Department of the Environment, Eastern Forest Products Laboratory, Montreal Road, Ottawa, Canada.

[3]Revision received October 15, 1973.

Can. J. Chem. Downloaded from www.nrcresearchpress.com by 210.87.254.40 on 09/05/12
For personal use only.

Can. J. Chem. Downloaded from www.nrcresearchpress.com by 210.87.254.40 on 09/05/12
For personal use only.

In this present study our objectives were to determine the effects of annelation of the benzene rings on the course of the Wallach rearrangement and to establish product orientation in these systems. To this end the transformation of the currently known phenyl–naphthyl and naphthyl–naphthyl azoxy derivatives (**9–14**) in moderately concentrated sulfuric acid has been investigated and the products identified.

Results

The naphthyl azoxy series investigated and the corresponding rearrangement products observed are summarized in eqs. 2–6. Thus β-1-phenylazoxynaphthalene (**9**) gives 4-phenylazo-1-naphthol (**15**), α-2-phenylazoxynaphthalene (**10**) and β-2-phenylazoxynaphthalene (**11**) yield 2-phenylazo-1-naphthol (**16**), 1,1′-azoxynaphthalene (**12**) gives rise to 4-naphthylazo-1-naphthol (**17**), β-1,2′-azoxynaphthalene (**13**) yields 4-(2′-naphthylazo)-1-naphthol (**18**), and 2,2′-azoxynaphthalene (**14**) gives 2-(2′-naphthylazo)-1-naphthol (**19**).

In determining the reaction products of this series it was necessary to accommodate certain experimental constraints. Previous studies with azoxybenzene have demonstrated that a number of other products (azobenzene, sulfonic acids, etc.) may be obtained when the reactions are run at high substrate and acid concentrations, high temperatures, and prolonged reaction times (12, 13). Subsequent work which has been carried out under controlled kinetic conditions, using low substrate concentrations ($\leqslant 10^{-3}\ M$), has shown the formation of a single primary product, the hydroxyazobenzene (8). The other products

[2] **9** → **15**

[3] **10** + **11** → **16**

[4] **12** → **17**

[5] **13** → **18**

[6] **14** → **19**

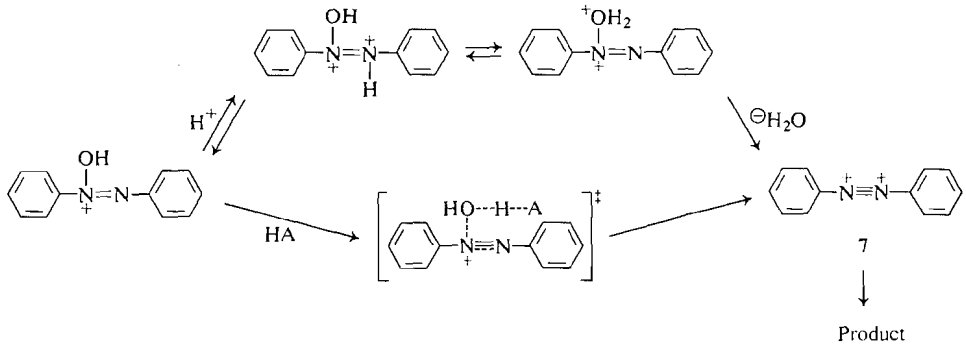

SCHEME 1

have apparently no relation to the actual Wallach rearrangement. Due to the very low solubility of the naphthyl azoxy compounds, complete solubilization in the acid concentrations of interest could only be achieved at very low substrate concentrations (*ca.* 10^{-5} *M*). Even so, the addition of organic cosolvents, 0.5% v/v ethanol for the phenyl–naphthyl azoxy compounds and 5.0% v/v dioxane in the case of the even less soluble naphthyl–naphthyl derivatives, was necessary to assist in solubilization. In view of these considerations, normal product isolation and characterization was quite impractical. Nevertheless this was carried out in two representative cases, the reactions of **9** and **12**.

The primary means of product identification was by quantitative comparison of the u.v.-visible spectra of the observed reaction product with the spectra of similar equimolar solutions of a number of authentic compounds considered to be among the most probable products. Repeated scanning of the spectra during reaction ensured that its course was known throughout and that the final spectra examined were representative of the primary rearrangement and not of some subsequent process. These spectral comparisons were carried out directly in the sulfuric acid reaction solutions and indirectly after quenching the reaction in an alcoholic base solution. In the case of each azoxy compound a preliminary survey was carried out to determine the optimum acid concentration for the study in terms of substrate solubility, reaction speed, and formation of side products, if any. With these precautions, and with the measurement of spectral characteristics under the various conditions of acidity–basicity (representative of different forms of ionization of the species concerned), identification of products could be satisfactorily accomplished.

Discussion

The studies described here have demonstrated that the main reaction pathway for the naphthyl azoxy compounds in moderately concentrated sulfuric acid solutions is rearrangement to hydroxyazo derivatives (eqs. 2–6). Moreover, for the phenyl–naphthyl azoxy compounds (**9–11**) it is found that rearrangement occurs preferentially to the naphthyl rather than to the phenyl ring. In the case of the azoxy substrates **10** and **11** this preference gives rise to instances of acid-catalyzed *ortho* rearrangements, of which only few are known (see ref. 14). In the case of the dinaphthyl azoxy compounds containing the 1- and/or 2-naphthyl ring systems, rearrangement occurs preferentially to the 4-position of the 1-naphthyl ring if such is available. If such a position is not available, as in the case of **14**, then *ortho* rearrangement to the 1-position of the 2-naphthyl ring system results, yielding the same product as obtained in the photochemically induced rearrangement (15).

Kinetic studies of the Wallach rearrangement have provided evidence concerning the reaction mechanism in establishing the form of the acid catalysis (2, 3, 8). The simultaneous measurement of the rate of rearrangement and the extent of monoprotonation of the substrate has revealed a continued dependence of rate on acidity beyond the monoprotonation stage (8). The reaction mechanism proposed to account for these data is given in Scheme 1 and involves a dicationic intermediate (**7**). It was argued that formation of the dication from the conjugate acid of azoxybenzene might occur by two possible reaction pathways, as shown in Scheme 1, and that the dication would then undergo nucleophilic attack by H_2O or HSO_4^- to give *p*-hydroxyazobenzene as the reaction product (8).

On the basis of similar studies on azoxyben-

Can. J. Chem. Downloaded from www.nrcresearchpress.com by 210.87.254.40 on 09/05/12
For personal use only.

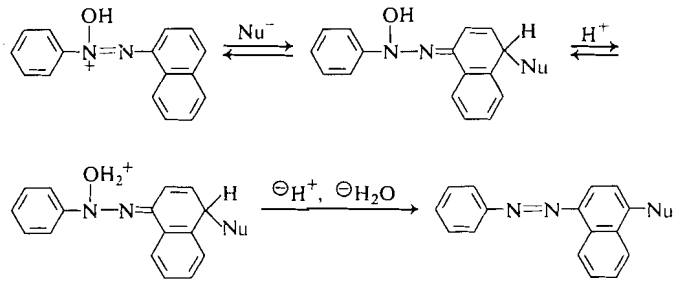

SCHEME 2

zene and a number of its substituted derivatives, Duffey and Hendley (3) have proposed a mechanism involving an unsymmetrical quinoid intermediate (**8**) formed by nucleophilic attack on the monoprotonated substrate. This mechanism is outlined in Scheme 2 as it would apply to the case of β-1-phenylazoxynaphthalene (**9**). The two reaction mechanisms, as given in Schemes 1 and 2, can both account satisfactorily for the rearrangement products observed in these systems. On the basis of resonance structures which may be written for the dicationic intermediates, the positions predicted to undergo nucleophilic attack are the same ones which are expected to give rise to the most stable quinoid type intermediates.

Previously we carried out a theoretical examination of the dicationic type of intermediate derived from azoxybenzene using the m.o. method (16) for both linear and bent configurations, which have different π-electron systems as shown in the orbital diagrams **20** and **21**, respectively. The calculations have been extended

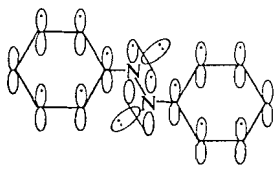

20

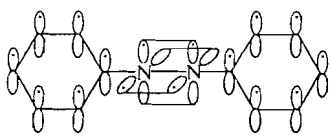

21

to the dications corresponding to the present series of azoxy compounds. Electron density values have been obtained by means of Hückel calculations (17) using the iterative ω technique (18, 19). In each case the observed product orientation corresponds to the entry of OH (through nucleophilic attack) at the carbon position (*ortho* or *para*) with the lowest π-electron density as determined for the corresponding linear dicationic structures. A typical example of the electron density values obtained is given below for the linear dicationic intermediate **22** pertaining to reaction 5.

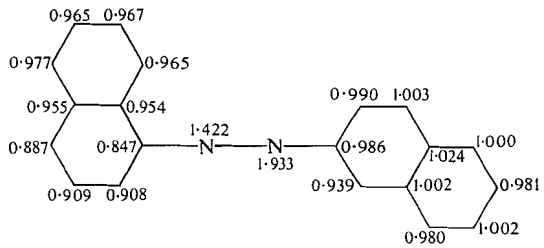

22

These results are interesting in terms of the correspondence which exists between the experimental results and the theoretical predictions based upon relatively simple calculations. They are also noteworthy in view of the fact that the dicationic intermediate derived from azoxybenzene has recently been observed by Olah *et al.* (20).

We will discuss in a future communication the consequences of the observed dependence of the rates of these rearrangements on solution acidity, as derived from a kinetic study of these reactions.

Experimental

Materials and Methods

Fisher certified grade dioxane was refluxed over sodium for 24 h and fractionally distilled prior to use. The fraction boiling at 101.5° and showing no absorption maxima at 261, 255, and 249 nm due to ethylene acetal was collected and stored in the dark. Sulfuric acid solutions of various concentrations were prepared by diluting Fisher or C.I.L. Reagent grade 96% sulfuric acid and analyzed by standard methods. A 1.0 *N* base quenching solution was prepared by dissolving 40 g of sodium hydroxide in

Can. J. Chem. Downloaded from www.nrcresearchpress.com by 210.87.254.40 on 09/05/12
For personal use only.

Can. J. Chem. Downloaded from www.nrcresearchpress.com by 210.87.254.40 on 09/05/12
For personal use only.

1.0 l of a solution of absolute ethanol – water (1:3). This solution was used immediately after preparation.

The reactions were carried out in aqueous sulfuric acid solutions containing a small amount of an organic co-solvent (0.5% v/v ethanol or 5% v/v dioxane) at 44.5 °C unless otherwise specified. Spectra of the acidic reaction media and of the base quenched solutions were obtained by the so-called "direct" and "indirect" techniques previously described (8), employing a Unicam model SP 800 B spectrophotometer.

Preparation of Compounds

The azoxy compounds were prepared by oxidation of the corresponding azo precursors as described previously (21). The hydroxyazo compounds of interest are itemized below with a brief statement concerning method of preparation. All compounds were purified by column chromatography, recrystallized to the highest level of purity which could be achieved and characterized. A detailed account may be found in ref. 22 along with the pertinent physical data.

4-Naphthylazophenol (**23**) was obtained by diazotization of 1-naphthylamine and coupling with phenol (23). 1-Phenylazo-2-naphthol (**24**) was prepared by coupling the diazonium salt of aniline with 2-naphthol (24). 4-Phenylazo-1-naphthol (**15**) was synthesized by coupling the diazonium salt of aniline with 1-naphthol (25). 4-(2′-Naphthylazo)phenol (**26**) was prepared by diazotization of 2-naphthylamine and coupling with phenol (26). 2-(2′-Naphthylazo)phenol (**27**) was obtained by condensing *o*-nitroanisole with 2-naphthylamine in the presence of alkali at elevated temperatures, followed by demethylation according to the procedure outlined by Badger and Buttery (15). 2-Phenylazo-1-naphthol (**16**) was prepared by coupling 2-naphthoquinone with phenylhydrazine in an acidic solution (27). 1-Naphthylazo-2-naphthol (**30**) was obtained by diazotization of 1-naphthylamine and coupling with 2-naphthol (28). Similarly 4-naphthylazo-1-naphthol (**17**) was synthesized by coupling with 1-naphthol (29). 2-(1′-Naphthylazo)-1-naphthol (**31**) was obtained by coupling 2-naphthoquinone and naphthylhydrazine in acid solution. 1-(2′-Naphthylazo)-2-naphthol (**32**) was prepared by diazotization of 2-naphthylamine and coupling with the 2-naphthol produced *in situ* by decomposition of the diazonium salt (30). 4-(2′-Naphthylazo)-1-naphthol (**18**) and 2-(2′-naphthylazo)-1-naphthol (**19**) were synthesized by diazotization of 2-naphthylamine hydrochloride and coupling with 1-naphthol.

Product Isolation From Reaction of β-1-Phenylazoxynaphthalene (9)

Due to the limited solubility of **9** in acidic media it was necessary to carry out the reaction in a large volume of acid in order to have a workable amount of substrate.

The reaction solution was prepared by dissolving **9** (0.1011 g) in 83.25% H_2SO_4 (490 ml) contained in a 1-l stoppered flask wrapped in aluminum foil and thermostatted at 25°. After 61 min, equivalent to 1 half-life, the reaction was halted by immersing the flask in an ice–methanol bath. The solution was then diluted to *ca.* 15% H_2SO_4 by the slow addition of the reaction mixture to 3.2 l water also cooled in an ice–alcohol bath. During the dilution the temperature did not rise above −2°. The resulting suspension was extracted with chloroform in a semicontinuous liquid–liquid extraction apparatus. The chloroform solution was dried ($MgSO_4$) and the solvent removed under vacuum. The residue was redissolved in 10 ml acetone and 2.5 ml of the solution was spotted on a large thin-layer plate (Eastman chromagram Sheets Type K301-R) along with the reference compounds **9**, **15**, **23**, **24**, and **25**. Development in petroleum ether (40–60°) – ethylacetate (20:1 v/v) gave two major bands which were cut separately and extracted with acetone until colorless. These solutions were filtered, evaporated to dryness, the residues dissolved in ethanol and their u.v.-visible spectra examined quantitatively. The composition of recovered material was 46.5% of **15** and 50.5% of **9**, based on amount of reactant used.

Product Isolation in the Reaction of 1,1′-Azoxynaphthalene (12)

The reaction solution was prepared by dissolving 0.075 g of **12** in dioxane and was added to a flask wrapped in aluminum foil containing 4.78 l of 67.95% sulfuric acid and 200 ml dioxane maintained at 25°. The dioxane content of the reaction solution was raised to 5% (v/v). The final substrate concentration was 5.0×10^{-5} *M*. After a period of time corresponding to 1 half-life (42 min) the reaction was stopped by cooling in an ice–methanol bath. The reaction mixture was then diluted to *ca.* 20% H_2SO_4 by slowly adding it to 11.5 l water contained in a 20 l flask which was cooled to 5°. The resulting suspension was extracted with 2 l of chloroform using a liquid–liquid extractor. After drying and removal of the solvent a portion of the residue was dissolved in acetone and spotted on a thin-layer plate together with **12**, **17**, **29**, and **30** as reference compounds and developed in the solvent system petroleum ether (40–60°) – 5% ethyl acetate (v/v). The remainder of the residue was purified on an alumina column and the u.v.-visible spectrum of each band examined. In addition, the i.r. spectrum (KBr disc) of the major product band was obtained and compared with those of **17** and **29**. The u.v.-visible and i.r. spectra confirmed that **17** is the major product by comparison with the authentic material. The minor product could not be identified though no trace of **29** was detected.

Spectral Identification

Rearrangement of 9

The reaction of **9** was followed to completion, (9 half-lives), in 77.00% H_2SO_4 – 0.5% EtOH and was characterized by the disappearance of a broad, low intensity band at *ca.* 450 nm due to **9** and the formation of an intense asymmetric band at 556 nm, ε 33 600, due to the product **15**. In base the formation of a strong asymmetric band at 494 nm, ε 25 600, was observed concurrently with the disappearance of a low intensity band at 380 nm (quenching after 3 half-lives). These spectral data correspond closely with those of **15** (λ_{max} 557 nm, ε 32 900, in acid and 494 nm, ε 28 100, in base) and indicate that the extent of formation of **15** is almost 100%. In separate experiments it was found that **15** is stable in this acid concentration for a period of time corresponding to at least 10 half-lives of reaction. Other compounds considered to be possible reaction products of **9** included 4-naphthylazophenol **23**, 1-phenylazo-2-naphthol **24**, and 1-phenylazonaphthalene **25**. Their spectra were determined in 77.00% H_2SO_4 – 0.5% ethanol and in base but showed no correspondence with the observed reaction product.

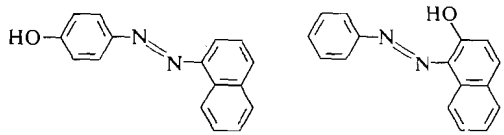

23 24

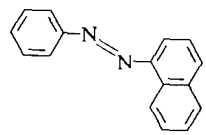

25

*Rearrangement of **10** and **11***

A comparison of the spectral data obtained in 77.00% H_2SO_4 – 0.5% ethanol and in base after almost complete reaction of the azoxy isomers **10** and **11** showed that **16** is the common product of both. Thus the positions of maximum absorbance of **16** (539 and 432 nm in acid, and 494 and 319 nm in base) coincide nicely with those of the product derived from **10** (539 and 432 nm in acid, and 495 and 320 nm in base) and from **11** (538 and 432 nm in acid, and 495 and 320 nm in base). However these spectral data also indicated that the extent of formation of **16** differs for the two azoxy isomers. For example, **16** is formed almost exclusively in the case of **10** as evidenced by the molar extinction values: ε_{539} 22 900, ε_{432} 19 300 after 4 half-lives reaction at this acid concentration, and ε_{495} 18 400, ε_{320} 15 800 after 3 half-lives as determined in base; this compares with actual values ε_{539} 24 700, ε_{432} 19 600, respectively, for **16** in acid and ε_{495} 20 800, ε_{320} 16 000 in base. In the case of **11** it appears that some other product(s) is being formed concurrently, ε_{538} 20 900 and ε_{432} 17 600 after 6 half-lives in acid and ε_{495} 17 600 and ε_{320} 14 400 after 10 half-lives as determined in base. The reaction of **11** in acid was also characterized by the formation of twin absorption bands of almost equal intensity at 258 and 263 nm. The intensity of these bands was found to increase with increasing acid concentration while at the same time the molar extinction at 538 nm due to **16** decreased. These bands were not due to **16**, which showed only a single band of low intensity at 255 nm in this region, nor were they due to any decomposition product of **16** since it was found to be completely stable at these acid concentrations. Compounds whose spectra were also characterized in acid and base were 4-(2′-naphthylazo)phenol (**26**), 2-(2′-naphthylazo)-phenol (**27**), and 2-phenylazonaphthalene (**28**), and were eliminated as possible reaction products on this basis.

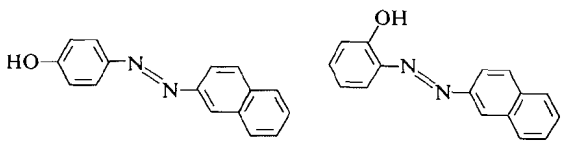

26 27

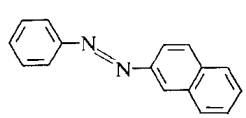

28

*Rearrangement of **12***

Spectral changes occurring during the reaction of **12** in 70.50% H_2SO_4 – 5.0% dioxane were characterized by the disappearance of a low intensity band at *ca.* 390 nm due to the substrate and the development of a single asymmetric band at 598 nm due to the formation of **17**. After 4.5 half-lives of reaction the molar extinction at 598 nm reached a maximum value of 21 300, or 81% of the theoretical value (26 400) given by **17** alone, and then began to decrease. This decrease was due, at least in part, to the fact that **17** is unstable in concentrated acid solution and undergoes a consecutive reaction resulting in a decrease in the molar extinction at 598 nm; *e.g.*, a 15% decrease in the molar extinction occurred at this acid concentration over a period of time corresponding to 3 half-lives of reaction. In base the spectrum of **12** after 2.7 half-lives reaction time in 67.95% H_2SO_4 – 5.0% dioxane showed a maximum at 505 nm with ε 15 600. This compared favorably with the spectrum of **17** which showed λ_{max} 505 nm, ε 18 500.

Other possible reaction products whose spectra were characterized included 1,1′-azonaphthalene, **29**, and 1-naphthylazo-2-naphthol, **30**. Of these compounds the

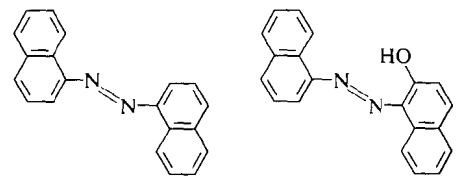

29 30

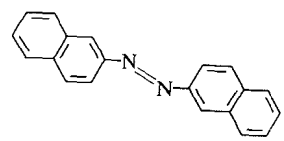

34

spectrum of **29** displayed some similarity to that of **17** in acidic media, λ_{max} 591 nm, ε 26 700. However, the spectrum of **29** in base, λ_{max} 400 nm, ε 11 800, was very different from **17**. This example demonstrates the utility of spectral characterization in both acidic and basic media.

*Rearrangement of **13***

The reaction of **13**, as followed by the direct method in 70.50% H_2SO_4 – 5.0% dioxane, was described by the formation of a strong asymmetric band at 582 nm with a shoulder at 622 nm due to the formation of the hydroxyazo product, **18**. The developing band at 582 nm reached a maximum molar extinction of 32 300 after 5 half-lives reaction time and then began to decrease in intensity, indicating that **18** undergoes a subsequent reaction in concentrated H_2SO_4 solution. An equimolar solution of **18** gave a molar extinction value of 42 500 at 582 nm. In basic solutions the reaction was characterized by the disappearance of a single weak band at 388 nm due to **13** and the formation of a maximum at 509 nm, ε 28 000, due to **18**. An equimolar solution of **18** in base gave λ_{max} 508 nm and ε 35 800. Among the compounds examined as possible reaction products were the following: 2-(1′-

Can. J. Chem. Downloaded from www.nrcresearchpress.com by 210.87.254.40 on 09/05/12
For personal use only.

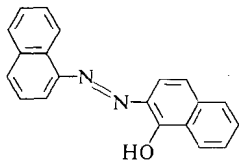

31

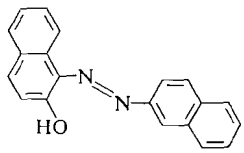

32

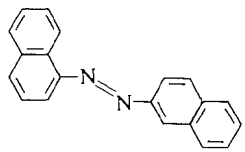

33

naphthylazo)-1-naphthol (**31**), 1-(2′-naphthylazo)-2-naphthol (**32**), and 1,2′-azonaphthalene (**33**). These compounds were excluded upon analysis of their spectra in acid and basic media.

Rearrangement of ***14***

The reaction of **14**, as followed directly in 77.00% H_2SO_4 – 5.0% dioxane, was characterized by the development of twin maxima of about equal intensity at 588 (ε 25 600) and 562 nm (ε 26 600), and a broad band at 430 nm (ε 12 200) after a period of time corresponding to 5 half-lives. Simultaneously, a slight decrease in the intensity of an absorption at *ca.* 410 nm was observed due to the disappearance of the substrate and this was accompanied by a shift to higher wavelength (430 nm, ε 12 700). These data correspond very closely to those of an equimolar solution of **19** at the same acid concentration, *i.e.*, λ_{max} 590 (ε 33 100), 564 (ε 32 900), and 429 nm (ε 14 900). However on the basis of these data it appears that **19** accounts for only about 75% of the original azoxy material. Contributing factors include the observations that **19** is not stable at this acid concentration (*e.g.*, the molar extinction coefficient of **19** decreases to 93% of its original value after a time equivalent to 3 half-lives) and that a competing reaction is occurring, manifested by the formation of twin maxima at 258 and 264 nm which are not due to decomposition of **19**. The nature of the material(s) responsible for these bands has not been determined. The spectral data obtained in base after 5 half-lives showed λ_{max} 505 nm (ε 20 200), compared with λ_{max} 507 (ε 27 000) and 328 nm (ε 18 900) given by an authentic sample of **19**. The spectral characteristics of 2,2′-azonaphthalene (**34**) were also determined in acid and base as a possible reaction product.

This research was supported by the National Research Council of Canada. Discussions with Professors I. G. Csizmadia and K. Yates are also acknowledged with thanks.

1. O. Wallach and L. Belli. Ber. **13**, 525 (1880).
2. C. S. Hahn, K. W. Lee, and H. H. Jaffé. J. Am. Chem. Soc. **89**, 4975 (1967).
3. D. Duffey and E. C. Hendley. J. Org. Chem. **33**, 1918 (1968); **35**, 3579 (1970).
4. L. C. Behr and E. C. Hendley. J. Org. Chem. **31**, 2715 (1966).
5. M. M. Shemyakin, V. I. Maimind, and B. K. Vaichunaite. Chem. Ind. 755 (1958); Zhur. Obshchei Khim. **28**, 1708 (1958). M. M. Shemyakin and V. I. Maimind. *In* Chemistry of natural and synthetic coloring matters. *Edited by* T. S. Gore. Academic Press, New York. 1962.
6. S. Oae, T. Fukumoto, and M. Yamagami. Bull. Chem. Soc. Japan, **36**, 601 (1963); **34**, 1873 (1961).
7. M. M. Shemyakin, T. E. Agadzhanyan, V. I. Maimind, and R. V. Kudryavtsev. Dokl. Akad. Nauk SSSR, **135**, 346 (1960); Izv. Akad. Nauk SSSR, Ser. Khim. 1339 (1963).
8. E. Buncel and B. T. Lawton. Can. J. Chem. **43**, 862 (1965). E. Buncel and W. M. J. Strachan. Can. J. Chem. **48**, 377 (1970).
9. E. Buncel. *In* Mechanisms of molecular migrations. Vol. 1. *Edited by* B. S. Thyagarajan. Wiley, N.Y. 1968.
10. D. V. Banthorpe. *In* Topics in carbocyclic chemistry. Vol. 1. *Edited by* D. Lloyd. Logos Press. London. 1969.
11. H. J. Shine. Aromatic rearrangements. Elsevier, Amsterdam. 1967.
12. P. H. Gore and G. R. Hughes. Aust. J. Sci. Res. A3, 136 (1950).
13. B. T. Newbold and M. H. Akhtar. Private communication.
14. E. Buncel and A. Dolenko. Tetrahedron Lett. No. 2, 113 (1971).
15. G. M. Badger and R. G. Buttery. J. Chem. Soc. 2243 (1954).
16. E. Buncel, A, Dolenko, I. G. Csizmadia, J. Pincock, and K. Yates. Tetrahedron, **24**, 6671 (1968).
17. A. Streitwieser, Jr. Molecular orbital theory for organic chemists. John Wiley, New York, N.Y. 1961.
18. G. W. Wheland and D. E. Mann. J. Chem. Phys. **17**, 264 (1949).
19. A. Streitwieser, Jr. and P. M. Nair. Tetrahedron, **5**, 149 (1959).
20. G. A. Olah, K. Dunne, D. P. Kelly, and Y. K. Mo. J. Am. Chem. Soc. **94**, 7438 (1972).
21. A. Dolenko, K. Mahendran, and E. Buncel. Can. J. Chem. **48**, 1736 (1970).
22. A. Dolenko. Ph.D. Thesis, Queen's University, Kingston, Ontario. 1969.
23. W. MacPherson and H. G. Gore. Am. Chem. J. **25**, 485 (1901).
24. A. I. Vogel. Practical organic chemistry. 2nd ed. Longmans, Green and Co. Ltd., London. 1964. p. 622.
25. O. N. Witt and J. Didichen. Ber. 2657 (1897).
26. E. Grandmorigin and H. Freiman. J. Für praktische chemie, **78**, 384 (1908).
27. T. Zincke and H. Bindewald. Ber. **17**, 3026 (1884).
28. R. Meldola and E. S. Hanes. J. Chem. Soc. **65**, 834 (1894).
29. P. F. Frankland. J. Chem. Soc. **37**, 752 (1880).
30. R. Nietzki and O. Goll. Ber. **19**, 1281 (1886).
31. R. A. Cox and E. Buncel. Can. J. Chem. **51**, 3143 (1973).

Can. J. Chem. Downloaded from www.nrcresearchpress.com by 210.87.254.40 on 09/05/12
For personal use only.

Structural Investigation of Sigma Complexes of Aromatic Amines with 1,3,5-Trinitrobenzene

ERWIN BUNCEL AND JOHN G. K. WEBB

Department of Chemistry, Queen's University, Kingston, Ontario

Received September 17, 1973

Reaction of the 1,3,5-trinitrobenzene (TNB) – methoxide ion adduct **1** with a series of substituted arylamines in dimethyl sulfoxide (DMSO) solution yields new 1,3,5-trinitrobenzene – aromatic amine σ-complexes (**2**). The parent TNB–anilide complex is also obtained in the reaction of TNB with potassium anilide in DMSO. Identification of the complexes is effected by n.m.r. and visible spectroscopy. The n.m.r. parameters of the complexes are influenced in characteristic manner by substituents in the arylamine moiety. An analysis of electronic and structural factors in these systems is given, with emphasis on the following aspects: structural implications of NH–$H_{\beta'}$ coupling; aromatic protons on the arylamine moiety; amino protons in free and complexed arylamines.

La réaction du complexe d'addition trinitro-1,3,5 benzène (TNB) – ion méthoxyde **1** avec une série d'arylamines substituées dans le sulfoxyde de diméthyle (DMSO) a conduit à de nouveaux complexes-σ (**2**) du type trinitro-1,3,5 benzène – amine aromatique. On a aussi obtenu les complexes TNB–anilide parents lors de la réaction du TNB avec l'anilide de potassium dans le DMSO. L'identification de ces complexes a été effectuée grâce à la spectroscopie dans le visible et à la r.m.n. Les paramètres r.m.n. des complexes sont influencés de façon particulière par les substituants de l'entité arylamine. On présente une analyse des facteurs électroniques et structuraux dans ces systèmes, en insistant sur les aspect suivants: conséquences structurales du couplage NH–$H_{\beta'}$; protons aromatiques sur l'entité arylamine; protons attachés à l'azote dans les arylamines libres et complexées. [Traduit par le journal]

Can. J. Chem., **52**, 630 (1974)

Introduction

Although Meisenheimer, or σ-complex, formation is well established for the interaction of polynitro aromatic compounds with a variety of bases (1–7), including aliphatic amines (8, 9), until now only one preliminary report of a σ-complex involving an arylamine has been given (10). Hitherto the interaction between aromatic amines and polynitroaromatics had been identified as characteristic of charge-transfer complex formation (11). This is surprising in view of the fact that arylamines are known to act as nucleophilic reagents toward nitro activated halobenzenes (12–14) and presumably form metastable σ-complex intermediates in those cases.

In a previous communication (10) we have presented spectral evidence which was strongly indicative of the formation of a σ-complex between 1,3,5-trinitrobenzene (TNB) and aniline. The complex resulted from the interaction between the TNB – methoxide ion adduct (**1**) and aniline in dimethyl sulfoxide (DMSO) solution.

A number of unusual aspects in the n.m.r. spectra of the TNB–anilide complex were previously noted (10). A downfield shift was observed for the amino proton peak on going from the free to the complexed aniline, which could be significant in providing information on the effect (*e.g.*, electronic) of replacing an amino proton by the 2,4,6-trinitrocyclohexadienate moiety. At present there are no n.m.r. data available in the literature to show this effect. Further, the NH–$H_{\beta'}$ fragment appears in the n.m.r. as a relatively sharp AB quartet with a large coupling constant; the observation of sharp doublets for N—H protons when coupled to C—H is a relatively rare occurrence (*vide infra*).

Thus it was believed that extension of the study to a series of arylamines could substantiate and clarify the origin of some of these unusual observations. Also it was anticipated that, with substituted arylamines, chemical shift analysis of the aromatic protons (which was not readily feasible with the unsubstituted aniline derivative due to the general complexity and overlap of peaks in the free and complexed aniline) should provide additional information on the nature of the 2,4,6-trinitrocyclohexadienate moiety. These expectations have largely been borne out in the study to be described.

Results

Reaction of complex **1** with the series of substituted arylamines can be represented by eq. 1.

Can. J. Chem. Downloaded from www.nrcresearchpress.com by 210.87.254.105 on 09/05/12
For personal use only.

[1] 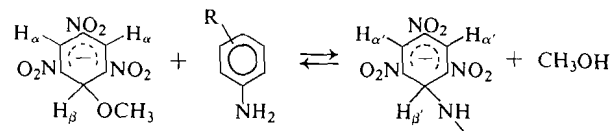

1

R = H, *p*-OCH_3, *p*-CH_3, *p*-Cl, *p*-Br, *m*-CF_3, *m*-NO_2, *p*-CH_3CO, *p*-CN, *p*-NO_2, 3,5-$(NO_2)_2$

2

A description of the n.m.r. and visible spectral changes which characterize this reaction is now presented.

Characterization of σ-Complexes by Nuclear Magnetic Resonance Spectra

The reaction of arylamines with **1** in DMSO-d_6 resulted in characteristic n.m.r. spectral changes with time, as follows. The absorptions for the H_α, H_β, and OCH_3 protons of **1**, and the peaks associated with the arylamine protons, decreased with time. Simultaneously, the peaks corresponding to $H_{\alpha'}$ and $H_{\beta'}$, and the protons in the arylamine moiety of **2**, as well as the absorptions due to methanol, were observed to increase with time. These changes were essentially complete within several hours.

The general description given above is illustrated in Fig. 1*a* and *b* for the reaction of **1** with *p*-chloroaniline. The spectrum shown in Fig. 1*a*, taken 10 min after mixing, exhibits basically the superposition of the spectra for **1** and *p*-chloroaniline, with a much smaller amount of **2**. The resonances at 8.48 (doublet, J = 1.2 Hz), 6.17 (triplet, J = 1.2 Hz), and 3.22 (singlet) p.p.m. correspond, respectively, to the H_α, H_β, and OCH_3 protons of **1**. The four main peaks of an AA'BB' multiplet centered at 6.8 p.p.m. and a broad peak at 5.1 p.p.m. are assigned, respectively, to the ring and amino protons of *p*-chloroaniline. In addition there is present a peak upfield by *ca.* 0.1 p.p.m. from H_α, assigned to $H_{\alpha'}$ of **2**, and signals due to methanol at 4.0 and 3.2 p.p.m. The remaining peaks expected for **2** are not readily discernible at this early stage of the reaction due to overlapping signals of the reactants.

The spectrum taken after 22 h is shown in Fig. 1*b* and exhibits further development of the $H_{\alpha'}$ peak at the expense of H_α, and an increase in intensity of the methanol signals, while the NH_2 signal has correspondingly decreased. In addition, the NH–$H_{\beta'}$ quartet anticipated for **2** has clearly emerged and is centered at 6.1 p.p.m. The signal positions of the *p*-chloroaniline ring protons in the complex are at lower field than in the uncomplexed aniline. The center of the AA'BB' multiplet in the complex is at 6.9 p.p.m.

The spectrum taken after addition of D_2O to the solution is shown in Fig. 1*c*. Collapse of the NH–$H_{\beta'}$ quartet to a slightly broadened singlet ($w_{1/2}$ = 2 Hz) at 6.2 p.p.m. results from deuteration of NH and at the same time a sharp OH signal at 4.0 p.p.m. has appeared. Integration of the peaks corresponding to $H_{\alpha'}$ and $H_{\beta'}$ in the deuterated complex yields integral values in the ratio of 2:1. In addition, a small amount of TNB–deuteroxide σ-complex, resulting from hydrolysis of **2**, was revealed on expansion of the spectrum to a sweep width of 1 Hz/cm. The resonances for the H_α and H_β type protons appeared at 8.4 (doublet, J = 1.2 Hz) and 6.25 p.p.m. (triplet, J = 1.2 Hz), respectively. Thus the chemical shift assignments for the σ-complex **2** (R = *p*-chloro) are: $H_{\alpha'}$ 8.40, $H_{\beta'}$ 6.20, NH 6.03 p.p.m.

The individual peaks in the NH–$H_{\beta'}$ quartet are relatively sharp, with apparent half-height widths of *ca.* 2 Hz. The coupling constant $J_{NH-H\beta'}$ was measured as 8.9 Hz. Coupling between $H_{\alpha'}$ and $H_{\beta'}$ was also revealed on expansion to sweep widths of 1.0 or 0.2 Hz/cm. A doublet was observed for $H_{\alpha'}$ with a coupling constant of *ca.* 0.4 Hz. Confirmation that the doublet structure arises from coupling of the spin states of $H_{\alpha'}$ and $H_{\beta'}$ was obtained by double resonance techniques. Irradiation of the signal for $H_{\beta'}$ eliminated the fine structure in $H_{\alpha'}$ signals, which then appeared as a sharp singlet with $w_{1/2}$ = 0.4 Hz.

The n.m.r. spectral features outlined above for the reaction of **1** with *p*-chloroaniline are typical for the series of reactions studied. Some pertinent n.m.r. parameters for the σ-complexes **2** are listed in Table 1. Amino proton chemical shifts (determined within a given reaction solution) are also provided for comparison.

Chemical shifts for aromatic protons on *para-*

Can. J. Chem. Downloaded from www.nrcresearchpress.com by 210.87.254.105 on 09/05/12
For personal use only.

Can. J. Chem. Downloaded from www.nrcresearchpress.com by 210.87.254.105 on 09/05/12
For personal use only.

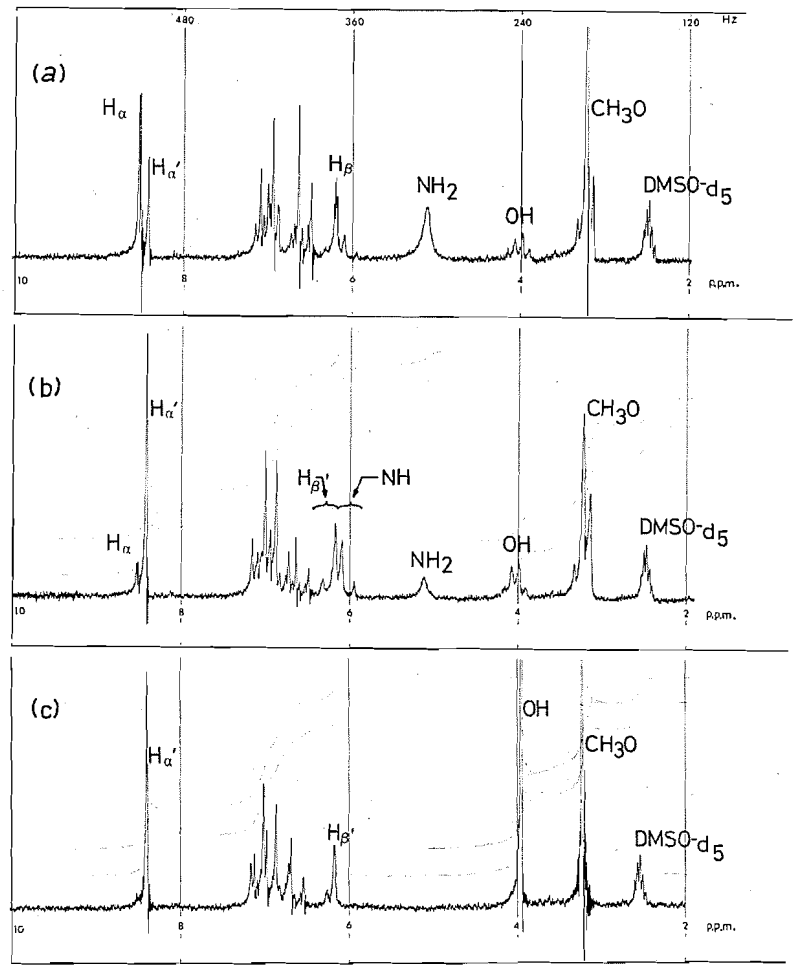

FIG. 1. Course of reaction of TNB–methoxide σ-complex **1** with *p*-chloroaniline: (*a*) n.m.r. spectrum taken after 10 min reaction time; (*b*) after 22 h; (*c*) n.m.r. spectrum of reaction product following deuteration. The designation of the various protons is given in eq. 1.

TABLE 1. Nuclear magnetic resonance parameters for the TNB–anilide σ-complexes **2**[a]

R	$\delta_{H_{\alpha'}}$[b] (p.p.m.)	$\delta_{H\beta'}$[b] (p.p.m.)	δ_{NH}[b] in p.p.m. (Hz)	δ_{NH_2}[b] in p.p.m. (Hz)	$J_{NH-H'}$ (Hz)	$J_{\alpha'\beta'}$ (Hz)
p-OCH_3	8.37	6.11	5.40 (323.8)	4.47 (268)	8.8	0.6
p-CH_3	8.38	6.18	5.58 (334.8)	4.65 (279)	8.8	0.6
H	8.39	6.24	5.81 (348.3)	4.88 (293)	8.8	0.6
p-Cl	8.40	6.20	6.03 (362.0)	5.12 (307)	8.9	0.4
p-Br	8.39	6.20	6.05 (363.2)	5.13 (308)	9.0	0.4
m-CF_3	8.43	6.35	6.35 (381.0)	5.45 (327)	—[c]	0.4
m-NO_2	8.45	6.36	6.65 (398.9)	5.72 (343)	8.8	0.5
p-CH_3CO	8.42	6.42	6.79 (407.3)	5.93 (356)	9.0	0.4
p-CN	8.42	6.39	6.89 (413.2)	6.03 (362)	9.1	0.5
3,5-$(NO_2)_2$	8.46	6.47	7.39 (442.8)	6.45 (387)	8.8	0.5
p-NO_2	8.45	6.50	7.41 (444.5)	6.62 (397)	8.8	0.5

[a]The data tabulated are obtained in reaction of the TNB–methoxide σ-complex **1** with the R-substituted anilines in DMSO-d_6. The amino proton chemical shifts, δ_{NH_2}, refer to the free arylamines present in the reaction solutions.

[b]Chemical shifts measured downfield relative to TMS as internal standard.

[c]AB quartet coalesced to A_2 system.

Can. J. Chem. Downloaded from www.nrcresearchpress.com by 210.87.254.105 on 09/05/12
For personal use only.

substituted arylamine moieties in the complexes are recorded in Table 2. For comparison purposes the aromatic proton chemical shifts of the corresponding uncomplexed arylamines, as measured internally, are also given. The aromatic proton signal pattern in both the free and complexed arylamines is of the AA'BB' type approximating to a simple AB system (15, 16). The simplicity of such patterns lends itself to facile chemical shift analysis.

An unambiguous assignment of the aromatic proton peaks in the free and complexed arylamines could be made from the progress of the reaction. Thus, as the reaction progressed, the four main peaks in the AA'BB' quartet of the complex increased at the expense of those belonging to the free arylamine. This allows for an internal comparison of chemical shifts which will reflect the effect of replacing a proton in an uncomplexed amine by the 2,4,6-trinitrocyclohexadienate moiety. The chemical shifts of the A and B protons in the free and complexed arylamines can be assigned on the basis of the known electronic properties of the substituents. Confirmation of the assignments was made by application of the method of additivity of substituent effects, which is described in more detail in the discussion.

It was evident in the n.m.r. spectra that a finite concentration of **1** still remained after the reaction with the various arylamines had ceased. The equilibrium constant for the reaction given by eq. 1 can be expressed as in eq. 2. Values of K

[2] $$K = [\mathbf{2}][CH_3OH]/[\mathbf{1}][ArNH_2]$$

were calculated for the series of reactions by obtaining the relative concentrations of **1** and **2** from integration of the peaks associated with H_α and $H_{\alpha'}$. Differences in the equilibrium constants so calculated were found to be small and somewhat random in the series of reactions. Thus an average equilibrium constant of 28 ± 4 appears to be applicable for the series. Uncertainty as to the degree of overlap in the H_α and $H_{\alpha'}$ signals, as well as the disparity in their relative magnitudes, precluded a more accurate determination of K by this method.

TABLE 2. Chemical shifts of aromatic protons in free and complexed arylamines (Y is the 2,4,6-trinitrocyclohexadienate moiety)

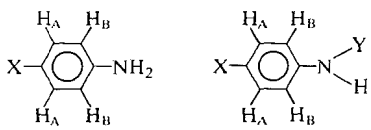

	δ_{H_A}[a]		δ_{H_B}[a]		δ_{H_A}[a]	δ_{H_B}[a]
X	Obs.	Calcd.[b]	Obs.	Calcd.[b]	Obs.	Obs.
OCH_3	6.64	(6.65)	6.54	(6.52)	6.70	6.70
CH_3	6.80	(6.91)	6.49	(6.50)	6.85	6.69
Cl	7.02	(7.15)	6.56	(6.58)	7.05	6.84
Br	7.10	(7.30)	6.50	(6.52)	7.15	6.75
CH_3CO	7.65	(7.72)	6.56	(6.72)	7.70	6.84
CN	7.35	(7.47)	6.62	(6.79)	7.42	6.89
NO_2	7.92	(8.05)	6.62	(6.85)	7.99	6.90

[a]Chemical shifts (in p.p.m.) measured downfield relative to TMS as internal standard in DMSO-d_6. The data for the free arylamines refer to measurements made in the reaction system.
[b]Calculated by method of additivity of substituent effects.

Characterization of σ-Complexes by Visible Spectra

The visible spectral changes accompanying the interconversion of **1** and **2** for the series of reactions studied constituted a decrease in the absorptions characteristic of the former with corresponding increase in those in the latter. Reasonably tight isosbestic points were maintained for the interconversion of species, as shown by the spectra in Fig. 2 for the reaction of **1** with aniline. The absorptions with maxima at 430 and 512 nm are characteristic of **1** while the complex **2** (R = H) exhibits maxima at 445 and 521 nm. The absorption maxima for the series of complexes **2** varied slightly within the range 439–445 and 521–527 nm. An estimate of the extinction coefficients at the maxima was made using the concentration of **2** as calculated from the equilibrium constant obtained by the n.m.r. method. The values so calculated were found to lie within ±5% of 32 000 M^{-1} cm^{-1} for the higher energy absorption and 18 500 M^{-1} cm^{-1} for the absorption at lower energy.

Acid–base reversibility is a characteristic of most σ-complexes of nitroaromatic compounds (1). In the present case, likewise, the absorption maxima associated with the complexes **2** disappear completely on addition of a slight excess of aqueous acid. On rebasification with aqueous sodium hydroxide two absorptions are restored with λ_{max} at 430 and 510 nm, arising from the hydroxide–TNB σ-complex.

Reaction of TNB with Potassium Anilide

On mixing solutions of potassium anilide in aniline and TNB in DMSO, a bright red color was observed immediately. Visible spectra were recorded following a 100-fold dilution of the

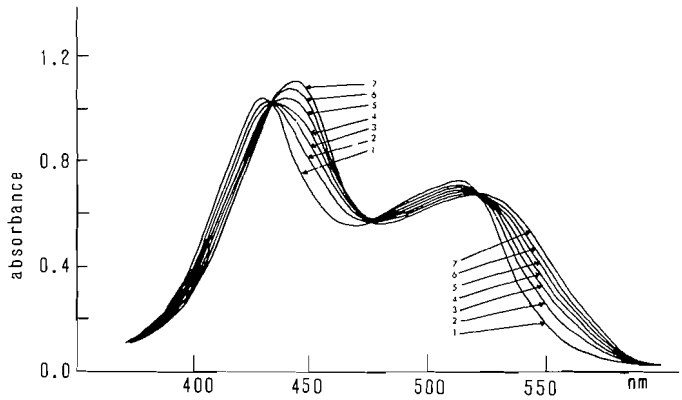

FIG. 2. Visible absorption spectra for reaction of TNB–methoxide complex **1** with aniline. Scan 1 taken after 5 min reaction time; scan 6 after 2 h; scan 7 after 24 h.

reaction solution (0.4 *M*) with DMSO. Two maxima were observed in the visible region, with ε (446 nm) 30 400 and ε (522 nm) 17 700. These spectral parameters are in satisfactory agreement with the values (ε_{445} 31 000, ε_{521} 17 700) obtained when the complex was produced by the less direct interaction of **1** with aniline.

The n.m.r. characteristics of the complex formed from the interaction of anilide ion with TNB are also in good agreement with those previously described. The following chemical shift assignments were made for the TNB–anilide complex as generated in DMSO–aniline (75:25 vol. %) solution: $H_{\alpha'}$ 8.45 (d, J = 0.6 Hz); $H_{\beta'}$ 6.28 (d, J = 8.8 Hz); NH 5.75 p.p.m. (d, J = 8.8 Hz). The slight differences in chemical shifts from those previously listed probably arise from the different reaction media in the two cases.

Discussion

General Conclusions from Spectral Studies of the Arylamine–TNB σ-Complexes

The evidence from n.m.r. and visible spectroscopy presented in the Results section is fully consistent with formation of the σ-complexes **2**, resulting from the interaction of **1** with the various arylamines. The double absorption maxima in the visible spectra of the reaction products are of course characteristic of σ-complexes of TNB (1–4). In the n.m.r. spectra, the peaks designated as $H_{\alpha'}$ are in the proper region for aromatic protons on a 2,4,6-trinitrocyclohexadienate moiety. The appearance of an AB quartet for the NH–$H_{\beta'}$ protons in the complexes, which can be collapsed to a singlet by deuteration of the amino nitrogen, is particularly strong support for our interpretation. Finally, the agreement between the n.m.r. and visible spectral characteristics in the products of the reaction of **1** with aniline, and in the interaction of TNB with potassium anilide, confirms the identity of **2**.

In a σ-complex, the chemical shift of a proton on the carbon where attachment of the nucleophile occurs is expected to reflect the electronegativity of the nucleophilic atom (1). In the present systems, this behavior is readily apparent on examination of the chemical shifts for $H_{\beta'}$ in the series of complexes listed in Table 1. A trend is observed such that, as the electron-withdrawing ability of the substituent in the arylamine ring increases, the chemical shift of the $H_{\beta'}$ proton also increases. Interestingly, the same sort of trend is observed for the signal positions of $H_{\alpha'}$ protons. However, as might be expected, the chemical shift range for $H_{\alpha'}$ on going from the least to the most electron-withdrawing substituent in the series is considerably less (4.6 Hz) than that for $H_{\beta'}$ (23.7 Hz). This attenuation is consistent with a change from sp^2 to sp^3 hybridization at the position of attachment on the TNB ring.

Structural Implications of NH–$H_{\beta'}$ Coupling

The appearance of a doublet for the NH protons in the complexes that is as well resolved as the doublet for $H_{\beta'}$ reveals that in DMSO-d_6 solution proton exchange is relatively slow and also that the rate of quadrupole relaxation is rapid. Slow proton exchange of the amino hydrogen in these complexes has several precedents. This effect is established for anilines (17),

Can. J. Chem. Downloaded from www.nrcresearchpress.com by 210.87.254.105 on 09/05/12
For personal use only.

Can. J. Chem. Downloaded from www.nrcresearchpress.com by 210.87.254.105 on 09/05/12
For personal use only.

alcohols (18), and phenols (19, 20) in DMSO solution and is attributed to the strong hydrogen bond acceptor properties of this solvent.

On the other hand, sharp peaks are seldom observed for protons attached to nitrogen because of quadrupole relaxation effects. Instances of relatively sharp NH doublets have been reported for amides of glycyl dipeptides in trifluoroacetic acid (21), *N*-substituted amides of carbohydrates in DMSO-d_6 (22), and alkylaminoanthraquinones in $CDCl_3$ (23). In these cases, as in the present work, quadrupole relaxation mechanisms must be especially effective (24). Presumably in the complexes this results from very inhomogeneous electric fields at the ^{14}N nucleus owing to the surrounding structure, and/or from the more effective coupling of the electric-field gradients to the nitrogen quadrupole arising from slower tumbling motions of the complexes in solution.

The observation of narrow peaks for $H_{\beta'}$ and NH allows for precise coupling constant determination in the complexes. The values of *ca.* 9 Hz for the NH–$H_{\beta'}$ vicinal coupling constants may be considered large when compared to values of 5–6 Hz which are reported for the spin–spin interaction between the amino and methyl protons in substituted *N*-methylanilines (25, 26). The relatively large values of $J_{NH-H\beta'}$ in the complexes imply that preferred conformations which have large coupling constants lend a strong weight to the observed coupling constant values.

The Karplus relationship, which can be expressed as in eq. 3, is often used to discern a relationship between molecular structure and vicinal coupling constants.[1] *A*, *B*, and *C* are positive coefficients with $A > C > 0$ and $A > 2B > 0$, and θ is the dihedral angle between protons on contiguous atoms. Ramachandran *et al.* (27) have recently obtained values for the constants *A*, *B*, and *C* for the fragment H—N—C—H. Values for *A*, *B*, and *C* were calculated from eq. 3 by utilizing the weighted average dihedral angle $\langle\theta\rangle$ in a number of simple amides and peptides for which the NHCH coupling constants were available. The values of $\langle\theta\rangle$ were determined from the probabilities of conformations of the structures at various dihedral angles as derived from the calculated potential energies of the conformations. The least-squares values for *A*, *B*, and *C* were calculated to be 7.9, 1.5, and 1.3, respectively. Application of eq. 3 to the present system, using the above values of *A*, *B*, and *C* in conjunction with the observed NH–$H_{\beta'}$ coupling constant, leads to a value of 168° for $\langle\theta\rangle$.

$$[3] \quad J_{vic} = A\cos^2\theta - B\cos\theta + C\sin^2\theta$$

[1]For recent evaluations of this relationship, pertaining to H—N—C—H, see refs. 27–29.

There is however some uncertainty as to the actual value of the dihedral angle. Bystrov *et al.* (28), in evaluating the peptide vicinal coupling constant, have given "refined" values of the coefficients *A*, *B*, and *C* in eq. 3, namely 9.4, −1.1, and 0.4, respectively. Use of these values together with the observed NH–$H_{\beta'}$ coupling constant yields $\langle\theta\rangle = 156°$. Fraser and coworkers (29) have similarly examined the dihedral dependence of H—N—C—H coupling constants in protonated amines, and these are found to be correlated by the expression $J = 9.8\cos^2\theta - 1.8\cos\theta$. Though less applicable to our case, use of the latter expression yields $\langle\theta\rangle = 150°$. Hence a more cautious appraisal of the dihedral angle in the complexes leads to $\theta = 150$–$170°$. Such a value would imply a *trans* orientation of the NH and $H_{\beta'}$ protons, as indicated in **3**. It is recognized however (*cf.* eq. 3 and refs. 28, 29) that a dihedral angle close to zero also leads to a large vicinal coupling constant. Thus a θ value in the range 0 to 10° is also permitted by our observed coupling constant, which would be in accord with the *cis* conformation, **4**. The latter structure is considered to be much less likely on steric grounds.

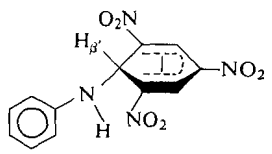

3

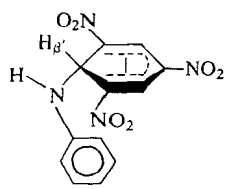

4

Aromatic Protons on the Arylamine Moiety

The chemical shift assignments for H_A and H_B in the free and complexed *para*-substituted arylamines were verified by the method of additivity of substituent effects (30, 31). The method as applied to *para*-disubstituted benzene rings is based on the premise that the chemical shift of an aromatic ring proton can be expressed as the sum of effects contributed by each substituent.

Can. J. Chem. Downloaded from www.nrcresearchpress.com by 210.87.254.105 on 09/05/12
For personal use only.

Hence for a *para*-disubstituted benzene C_6H_4XY, the chemical shift of protons *ortho* to X ($\delta_{o,X}$), and *ortho* to Y ($\delta_{o,Y}$) can be expressed as in eqs. 4 and 5. $S_{o,X}$ in eq. 4 is the contribution to the

$$\delta_{o,X} = S_{o,X} + S_{m,Y} \quad [4]$$

$$\delta_{o,Y} = S_{o,Y} + S_{m,X} \quad [5]$$

observed chemical shift $\delta_{o,X}$ made by the *ortho*-substituent X while $S_{m,Y}$ is the contribution made by the substituent Y. The chemical shift $\delta_{o,Y}$ can be similarly defined. Also the chemical shift of a proton which is *para* to a substituent, as in a 1,3-disubstituted benzene, can be expressed in terms of S values.

Smith (30) and van Meurs (31) have compiled tables of values of the n.m.r. substituent constants S for a large variety of substituents. Recently Ritchie and Spedding (32) have successfully applied the van Meurs data to chemical shift measurements in a number of *para*-substituted anilines and *N,N'*-disubstituted thioureas. In the present study we have found good agreement between the observed arylamine proton shifts and those calculated from van Meurs values of S. The constants appropriate to the present investigation are given in Table 3.

The chemical shifts which were calculated from eqs. 4 and 5 for H_A and H_B in the free arylamines have been given in Table 2. The differences between the observed and calculated chemical shifts range from +0.23 to −0.16 p.p.m. with an average difference of 0.10 p.p.m. This degree of agreement is comparable to that obtained by Ritchie and Spedding for substituted anilines where the average deviation was 0.08 p.p.m.

Application of the method of additivity to the determination of an S value for the 2,4,6-trinitrocyclohexadienate group (which shall be considered henceforth as a substituent Y in an *N*-substituted aniline) should provide information on the electronic properties of this substituent. Values of S_o and S_m for the group Y were calculated for each complex listed in Table 2. The best values for S_o and S_m are -0.53 ± 0.05 and -0.20 ± 0.01 p.p.m. respectively. An estimate for S_p of −0.53 p.p.m. could be obtained directly for the case of the TNB–3,5-dinitroanilide complex.

TABLE 3. Nuclear magnetic resonance substituent constants[a]

X	$S_{o,X}$	$S_{m,X}$	$S_{p,X}$[b]
NH_2	−0.75	−0.25	−0.63
OCH_3	−0.47	−0.10	−0.41
CH_3	−0.21	−0.12	−0.19
Cl	+0.03	−0.04	−0.09
Br	+0.18	−0.10	−0.05
CH_3CO	+0.60	+0.10	+0.18
CN	+0.35	+0.17	+0.28
NO_2	+0.93	+0.23	+0.37

[a]Values of S are in p.p.m. from the resonance peak of benzene. Negative values signify an upfield shift from benzene, while a positive value indicates a downfield shift (31).
[b]Values of $S_{p,X}$ were obtained from 1,3-disubstituted and 1,3,5-trisubstituted benzenes (31).

A comparison of the values obtained for S_o, S_m, and S_p for the group Y with the values in Table 3 places the NHY group between an amino and methoxyl group in electronic properties. Thus, although NHY is still electron releasing in nature, it is appreciably less so than an NH_2 group. Therefore, on the basis of the S values, it may be concluded that the 2,4,6-trinitrocyclohexadienate moiety is electron withdrawing relative to a proton. It was also noted by Crampton, from a study of equilibrium constants for σ-complex formation between TNB and substituted thiophenoxides, that Y is electron withdrawing relative to hydrogen (33).

In the treatment of the arylamine aromatic proton chemical shifts by the method of additivity of substituent effects, it has been assumed that other magnetic effects provide a less important contribution to the chemical shifts than the electronic effects of Y. This would appear to be a valid assumption with respect to the ring current effect of Y on the arylamine aromatic proton shifts. It has been well established that the negative charge resides largely in the *para*-nitro group of the 2,4,6-trinitrocyclohexadienate moiety (34–36). Hence a quinoid structure is a good representation for this moiety and its ring current should be small (37).

The through-space magnetic effect of the *ortho*-nitro groups on the chemical shifts of the arylamine aromatic protons is more difficult to assess. Such an effect may be expected to be important at the *ortho* positions in the arylamine ring but should be of minor significance at the *para* position. The greater downfield shift of the *ortho*-proton peaks on complex formation, relative to the shift in the *para*-proton peak position in the complex of 3,5-dinitroaniline, may perhaps arise from the effect of the *ortho*-nitro groups in the other ring. However the finding of a downfield shift for the *para*-proton reveals that the electron withdrawing ability of Y is likely to be

Can. J. Chem. Downloaded from www.nrcresearchpress.com by 210.87.254.105 on 09/05/12
For personal use only.

the predominant factor in determination of the aromatic proton chemical shifts in the arylamine ring in the complexes.

Amino Protons in Free and Complexed Arylamines

It is apparent that the amino proton chemical shifts for the complexed and free anilines given in Table 1 reflect the electronic properties of the substituents. The establishment of a linear relationship between amino proton shifts of substituted anilines and Hammett σ constants has already been clearly demonstrated (17, 38, 39). The slope of the line for *meta*- and *para*-substituted anilines in DMSO was calculated as 79.3 Hz/σ over a chemical shift range of 147 Hz by Lynch *et al.* (17).

We have extended the correlation between amino proton shifts and Hammett σ constants to the NH proton shifts in the complexes, **2**. A linear relationship is observed with a slope of 80.0 Hz/σ over a chemical shift range of 121 Hz. The plot is given in Fig. 3 and for comparison purposes includes the corresponding plot of NH_2 chemical shifts for the free amines. The two lines in Fig. 3 are observed to be parallel with a chemical shift separation of 54 Hz. This constant downfield shift in amino proton peak positions on complex formation reflects the effect of replacing a proton in the arylamine by the electron withdrawing group Y. It is also consistent with the observed downfield shift of the arylamine aromatic protons which are more remote from the electron withdrawing group Y than are the NH protons.

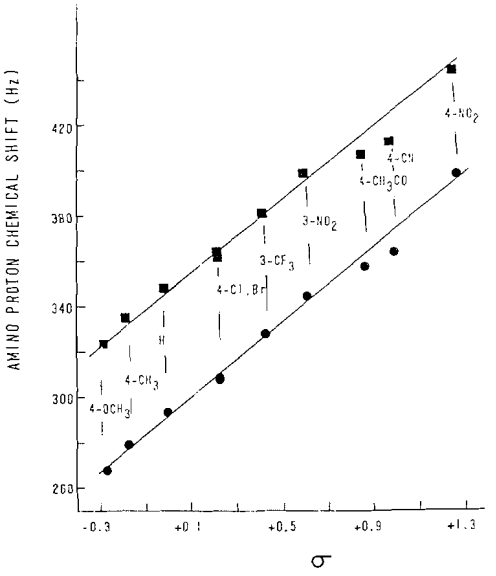

FIG. 3. Plot of amino proton chemical shifts in free (●) and complexed (■) anilines *vs.* Hammett σ-constants. In the case of the *p*-CN, *p*-$COCH_3$, and *p*-NO_2 substituents σ^- values are used.

A consideration of the amino proton chemical shifts in the free and complexed state may shed light on the question of a possible intramolecular hydrogen bonding between the amino proton and an *ortho*-nitro group in the complexes. Kinetic evidence is reported by Bernasconi for the existence of intramolecular hydrogen bonding in alkylammonium σ-complexes of TNB (40). It seems unlikely however that intramolecular hydrogen bonding exists for the complexes **2** in DMSO solution. It has been found that intramolecular hydrogen bonding in picramide complexes is accompanied in the n.m.r. spectrum by a large downfield shift of the proton peak involved (41). In our systems, the electron-withdrawing ability of the group Y would seem to accommodate the constant downfield shift experienced by the amino protons on complex formation. Thus intramolecular hydrogen bonding in the complexes does not appear likely under the conditions of observation. Instead an intermolecular hydrogen bond between NH and DMSO is considered as more probable.

In conclusion, we have established in this study the structures of the arylamine–trinitrobenzene σ-complexes, with regard to their overall features, and have also been able to discern the role played by electronic effects. In a future paper we will consider mechanistic aspects of the formation of the arylamine–TNB σ-complexes in these systems.

Experimental

Materials

TNB was recrystallized from ethanol and dried *in vacuo*, m.p. 123–123.5°. The substituted anilines were procured from commercial sources and either recrystallized to constant m.p. or distilled under nitrogen from zinc dust (42). DMSO (Fisher Certified Reagent) was distilled from barium oxide under nitrogen at reduced pressure, as recommended by Crampton and Gold (9). The middle fraction boiling at 44° was collected and stored in the dark. DMSO-d_6 (Stohler Isotope Chemicals) was treated twice with molecular sieves (Fisher 4A) before use.

Potassium 1-Methoxy-2,4,6-trinitrocyclohexadienate (**1**)

The substance **1** was prepared under nitrogen in a dry box using the basic procedure of Dyall (43). The product, which was collected by precipitation from solution by the addition of benzene, was washed with diethyl ether and

dried *in vacuo* for 48 h. The n.m.r. and visible spectra of the product, while consistent with that expected for the complex **1** (44), indicated the presence of methanol and water of crystallization. The total solvent content in the isolated complex was estimated as *ca.* 0.8 mol by means of a comparison of the visible spectra of the isolated complex **1** in DMSO–methanol solution and of the complex formed *in situ* from the interaction of methanolic potassium methoxide with TNB in DMSO solution. The water content could be estimated from the n.m.r. spectrum by integration as *ca.* 10 mol % of the methanol content. It may be noted that, in general, σ-complexes isolated by precipitation from solution contain solvent of crystallization in the range 0.3–1 mol (43, 45). In the present work the solvent of crystallization could not be removed by drying over P_2O_5 under vacuum (*ca.* 10^{-4} mm Hg) at room temperature for several days. Heating the salt while *in vacuo* up to 80° resulted in decomposition.

Potassium Anilide

A solution of potassium anilide in alinine was prepared by adding the amine (20 ml) to a 100-ml three-neck round bottom flask which contained freshly cut potassium metal (2.1 g). The mixture was heated at 80° until all the metal had reacted (*ca.* 3 h). The flask was flushed with dry nitrogen for the duration of the preparation. The concentration of anilide ion in the deeply colored violet solution was determined by titration with standard acid.

Apparatus for Spectral Measurements

The n.m.r. spectra were recorded using a Bruker 60 MHz HFX-60 spectrometer at a probe temperature of 36 ± 1°. Frequency shifts and coupling constants were measured on expanded sweep widths of 1.0 or 0.2 Hz/cm with a differential frequency counter having TMS as an internal lock. Proton signal positions were reproducible to ±0.1 Hz. Visible spectra were recorded with a Unicam SP800 spectrophotometer at 25°.

Reaction of **1** *with Arylamines*

Transfers of reagents were performed in a nitrogen-flushed dry box using apparatus which had been oven dried. In a typical experiment, the substance **1** (0.115 g) was placed in a 1-ml volumetric flask and was dissolved in 0.5 ml of DMSO-d_6. The arylamine in DMSO-d_6 was added and the volume brought up to mark with DMSO-d_6, yielding a resultant solution 0.38 *M* in complex and 0.45 *M* in arylamine.

The reaction solution was maintained at 36° and the course of reaction was monitored by recording the n.m.r. spectrum at various time intervals. After the reaction had been observed to be complete, precise n.m.r. characterizations of the new complex were carried out. Also at this time deuteration experiments were performed in anticipation of hydrogen–deuterium exchange at the amino nitrogen in the complexes. The method consisted of mixing 0.1 ml D_2O and 0.5 ml reaction solution in a small test tube fitted with a ground glass stopper. The deuteration process was followed by recording the n.m.r. spectra at various times.

The progress of the reaction of **1** with arylamines was also monitored by visible spectroscopy. Visible spectra were recorded in 0.1 mm cells following a 100-fold dilution of the reaction solution (maintained at 36° in an oil bath) with DMSO. The dilution was observed to quench the reaction. Acid–base reversibility of complex formation was tested by addition of excess dilute acid followed by rebasification with hydroxide ion. The visible spectra of the acidic and basic solutions were recorded.

Reaction of TNB with Potassium Anilide

For this reaction, about 0.25 ml of the solution of potassium anilide in aniline was added to a 1-ml volumetric flask containing 0.5 ml of a solution of TNB in DMSO. After making up to mark with DMSO, the solution was about 0.4 *M* in each component. The course of reaction was monitored as previously.

The award by the National Research Council of Canada of a scholarship to J.G.K.W. is gratefully acknowledged, as is the continued support via an operating grant.

1. M. J. Strauss. Chem. Rev. **70**, 667 (1970).
2. M. R. Crampton. Adv. Phys. Org. Chem. **7**, 211 (1969).
3. E. Buncel, A. R. Norris, and K. E. Russell. Quart. Rev. **22**, 123 (1968).
4. R. Foster and C. A. Fyfe. Rev. Pure Appl. Chem. **16**, 61 (1966).
5. C. F. Bernasconi. J. Am. Chem. Soc. **92**, 4682 (1970).
6. J. H. Fendler, E. J. Fendler, and L. M. Casilio. J. Org. Chem. **36**, 1749 (1971).
7. F. Terrier, F. Millot, and R. Schaal. J. Chem. Soc. Perkin II, 1192 (1972).
8. R. Foster and C. A. Fyfe. Tetrahedron, **22**, 1831 (1966).
9. M. R. Crampton and V. Gold. J. Chem. Soc. B, 23 (1967).
10. E. Buncel and J. G. K. Webb. Can. J. Chem. **50**, 129 (1972).
11. R. Foster. Organic charge transfer complexes. Academic Press, London. 1969.
12. J. F. Bunnett. Chem. Rev. **49**, 273 (1951); Quart. Rev. **12**, 1 (1958).
13. J. Miller. Aromatic nucleophilic substitution. Elsevier, Amsterdam. 1968.
14. F. Pietra. Quart. Rev. **23**, 504 (1969).
15. T. Schaeffer and W. G. Schneider. J. Chem. Phys. **32**, 1218 (1960).
16. B. Gestblom, R. A. Hoffman, and S. Rodmar. Mol. Phys. **8**, 425 (1964); Acta Chem. Scand. **18**, 1222 (1964).
17. B. M. Lynch, B. C. MacDonald, and J. G. K. Webb. Tetrahedron, **24**, 3595 (1968).
18. O. L. Chapman and R. W. King. J. Am. Chem. Soc. **86**, 1256 (1964).
19. R. J. Ouellette. Can. J. Chem. **43**, 707 (1965).
20. J. G. Traynham and G. A. Knesel. J. Org. Chem. **31**, 3350 (1966).
21. G. V. D. Tiers and F. A. Bovey. J. Phys. Chem. **63**, 302 (1959).
22. A. S. Cerezo. Chem. Ind. 96 (1971).
23. S. M. Hutton and R. F. Bloom. Tetrahedron Lett. 1993 (1963).
24. J. A. Pople, Mol. Phys. **1**, 168 (1958); J. A. Pople, W. G. Schneider, and H. J. Bernstein. High resolution nuclear magnetic resonance. McGraw Hill, New York. 1959.

Can. J. Chem. Downloaded from www.nrcresearchpress.com by 210.87.254.105 on 09/05/12
For personal use only.

25. J. HEIDBERG, J. A. WEIL, G. A. JANUSONIS, and J. K. ANDERSON. J. Chem. Phys. **41**, 1033 (1964).
26. I. D. RAE. Aust. J. Chem. **19**, 409 (1966).
27. G. N. RAMACHANDRAN. R. CHANDRASEKARAN, and G. D. KOPPLE. Biopolymers, **10**, 2113 (1971).
28. V. F. BYSTROV, V. T. IVANOV, S. L. PORTNOVA, T. A. BALASHOVA, and YU. A. OVCHINNIKOV. Tetrahedron, **29**, 873 (1973).
29. R. R. FRASER, R. N. RENAUD, J. K. SAUNDERS, and Y. Y. WIGFIELD. Can. J. Chem. **51**, 2433 (1973).
30. G. W. SMITH. J. Mol. Spectrosc. **12**, 146 (1964).
31. N. VAN MEURS. Rec. Trav. Chim. **87**, 145 (1968).
32. R. K. RITCHIE and H. SPEDDING. Spectrochim. Acta, **26** A, 1 (1970).
33. M. R. CRAMPTON. J. Chem. Soc. B, 2112 (1971).
34. H. HOSOYA, S. HOSOYA, and S. NAGAKURA. Theor. Chim. Acta, **12**, 117 (1968).
35. R. DESTRO, C. GRAMACCIOLI, and M. SIMONETTA. Acta Crystallogr. **24**, 1369 (1968).
36. P. CAVENG, P. B. FISHER, E. HEILBRONNER, A. L. MILLER, and H. ZOLLINGER. Helv. Chim. Acta, **50**, 848 (1967).
37. F. FIGENS and F. FLAMMANG. Mol. Phys. **12**, 581 (1967).
38. T. YONEMOTO, W. F. REYNOLDS, H. M. HUTTON, and T. SCHAEFER. Can. J. Chem. **43**, 2668 (1965).
39. L. K. DYALL. Aust. J. Chem. **17**, 419 (1964).
40. C. F. BERNASCONI. J. Am. Chem. Soc. **92**, 129 (1970); J. Phys. Chem. **75**, 3636 (1967).
41. M. R. CRAMPTON. J. Chem. Soc. B. 1341 (1967).
42. L. F. FIESER and M. FIESER. Reagents for organic synthesis. John Wiley and Sons Inc., New York. 1967. p. 41.
43. L. K. DYALL. J. Chem. Soc. 5160 (1960).
44. K. L. SERVIS. J. Am. Chem. Soc. **87**, 5495 (1965); **89**, 1508 (1967).
45. J. H. FENDLER, E. J. FENDLER, and C. E. GRIFFIN. J. Org. Chem. **34**, 689 (1969).

Can. J. Chem. Downloaded from www.nrcresearchpress.com by 210.87.254.105 on 09/05/12
For personal use only.

A Vinylogous Wagner Rearrangement in the Benzonorbornene Series

KAREL WIESNER, PAK-TSUN HO AND HIROYUKI OHTANI

Natural Products Research Center, University of New Brunswick, Fredericton, New Brunswick

Received October 29, 1973

A simple synthesis of compound **11** by a generally applicable novel method is described. This compound undergoes an acid-catalyzed rearrangement to the ketone **12** in high yield at room temperature.

On décrit une synthèse simple du composé **11** qui a été effectué par une méthode nouvelle d'application générale. Ce composé se réarrange avec un bon rendement à température de la pièce en milieu acide pour donner la cétone **12**. [Traduit par le journal]

Can. J. Chem., **52**, 640 (1974)

Introduction

Some time ago we proposed a simple sequence of reactions which appeared eminently suitable for the synthesis of the system present in anhydroryanodol (1).

In order to test this proposal we intended to perform the synthesis portrayed in Scheme 1. The key idea of the scheme was clearly the rearrangement **ii** → **iii** followed by the transformation of the double bond and cyclopentanol functions (**iii** → **iv**) to the lactone and hydroxyl needed in anhydroryanodol. It turned out however that the solvolysis of compound **ii** did not operate as we wished. Instead of the expected (or rather hoped for) product of a vinylogous Wagner rearrangement **iii** we obtained the much less interesting allylic rearrangement product **v**. The transformation of compound **v** to the hydroxylactone **iv** required a number of additional, not very efficient, steps.

Thus, it was clear that the scheme would be useful for a simple synthesis of anhydroryanodol only if the novel vinylogous rearrangement step **ii** → **iii** could be made to operate.

Since further transformation of compounds of the type **iv** to anhydroryanodol would require a methoxy substituent in the benzene ring, we at first hoped that methoxy substitution in the *para* position to the migrating bond could bring about the desired vinylogous rearrangement. It turned out however that a more efficient way to facilitate the rearrangement is to place a methoxyl at the bridgehead and that in fact both devices are needed to bring about the desired reaction in high yield. Since our methods for the synthesis of bridgehead substituted benzobicycloheptenes (*c.f.* ref. 2) and the successful vinylogous rearrangement are reactions of considerable synthetic utility, we wish to briefly describe in the present communication the synthesis of compound **11** and its rearrangement to compound **12** which proceeded smoothly and in a high yield.

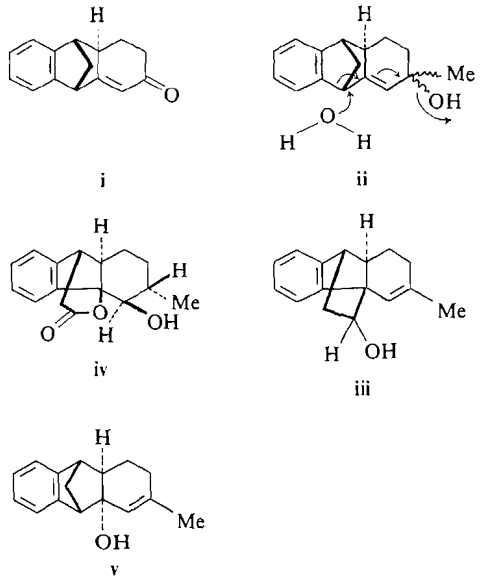

SCHEME 1

Discussion

The starting material for the preparation of compound **11** (Scheme 2) was the keto ester **1** which we have previously employed in our synthesis of songorine (2, 3). This compound was quantitatively converted by treatment with methyl orthoformate and hydrogen chloride into the oily enol ether **2**[1]. Addition of maleic anhydride to this material yielded a mixture of the crystal-

[1]For complete spectral characterization of all compounds see Experimental.

Can. J. Chem. Downloaded from www.nrcresearchpress.com by 210.87.254.42 on 09/05/12
For personal use only.

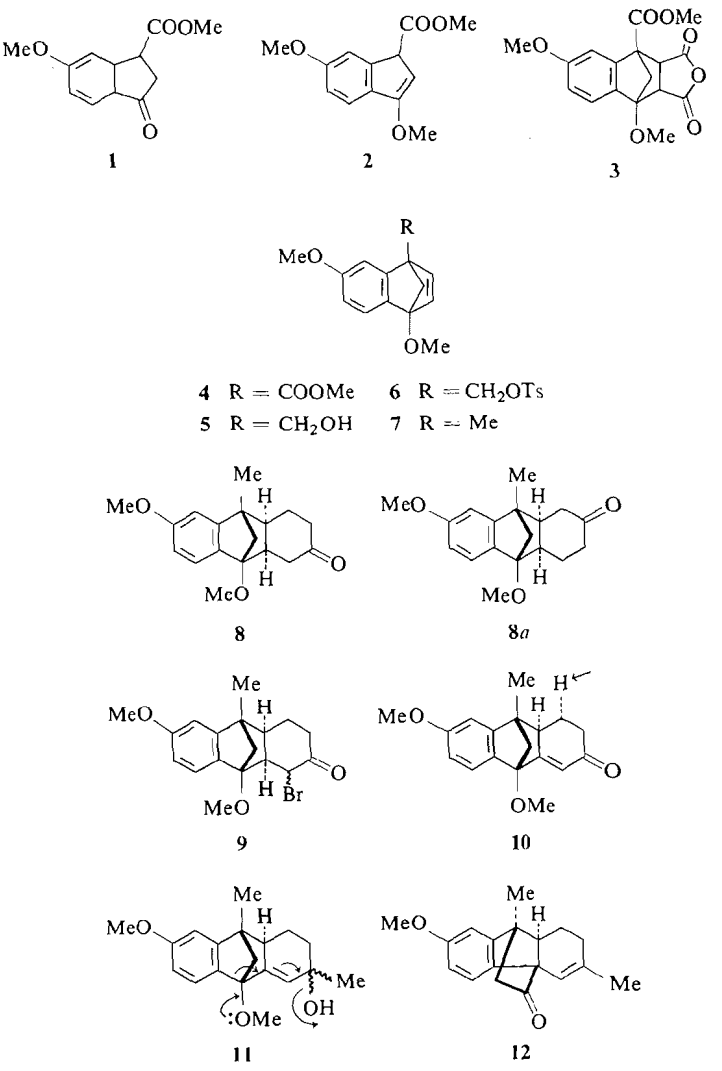

SCHEME 2

line *endo* and *exo* adducts **3** in a ratio approximately 6:1 (*c.f.* ref. 2). They were separated by crystallization from acetone and the yield of both compounds together after several recrystallizations was 72%. The configurations of the two adducts may be deduced from the chemical shift of the protons unshielded by the two anhydride carbonyls in the n.m.r. spectrum. In the *exo* adduct these two hydrogens are in the *endo* configuration and in the shielding field of the anisole ring. The quadruplet assigned to them (centered at $\tau = 6.63$ p.p.m.) is consequently shifted to higher field with respect to a similar quadruplet (centered at $\tau = 5.90$ p.p.m.) shown by the *endo* adduct. The mixture of the crystalline adducts **3** was next converted into the oily ester **4** by heating with bistriphenylphosphine nickel dicarbonyl in diglyme (2) in a yield of 70%. The modification of compound **4** into the dimethoxymethylnorbornene **7** via the intermediates **5** and **6** was accomplished by standard methods in high yield.

The norbornene **7** was now heated with an excess of 2-methoxybutadiene and the products of the diene addition were immediately hydrolyzed with methanolic oxalic acid. The two ketones **8** and **8***a* were obtained in a ratio 3:1 and the yield of the desired ketone **8** was 56%. In analogy to our previous study (1) the annelation

Can. J. Chem. Downloaded from www.nrcresearchpress.com by 210.87.254.42 on 09/05/12
For personal use only.

Can. J. Chem. Downloaded from www.nrcresearchpress.com by 210.87.254.42 on 09/05/12
For personal use only.

of the new ring was assumed to have occurred *exo*.

The ketone **8** was now brominated to the unstable bromoketone **9** and this material was immediately, without purification, subjected to dehydrobromination with lithium bromide and lithium carbonate in dimethyl formamide. The α,β-unsaturated ketone **10** was obtained as a homogeneous oil in a yield of 50% based on the saturated ketone **8**. The n.m.r. spectrum of compound **10** corroborated the *exo* annelation of the six-membered ring containing the keto group to the benzobicycloheptene system. We have shown in our previous work (1) that in the *endo* isomer the hydrogen marked by an arrow in formula **10** is located in the shielding region of the benzene ring and consequently its n.m.r. signal appears as a multiplet at very high field (τ = 8.8–9.5 p.p.m.). Compound **10** in agreement with the configuration assigned to it does not show any signal at all in this region. Its tertiary methyl group which is unshielded by the anisole ring appears as a singlet at τ = 8.53 p.p.m. Treatment of the ketone **10** with an excess of methyl magnesium iodide gave a quantitative yield of the oily alcohol **11** which behaved homogeneously in t.l.c., but probably was a mixture of epimers. The rearrangement of compound **11** to the final ketone **12** occurred under very mild conditions. A solution of formic acid in tetrahydrofuran at room temperature caused a complete conversion of compound **11** to the crystalline ketone **12** in 2 h. After several crystallizations the yield of the sharp melting product (m.p. 117 °C) was 80%. Compound **12** shows a carbonyl maximum in the i.r. spectrum at 1748 cm^{-1} in agreement with a somewhat strained five-membered ketone. The n.m.r. spectrum shows the vinylic methyl group as a singlet at τ = 8.20 p.p.m. and the vinylic hydrogen as a singlet at τ = 4.07 p.p.m. Thus, it is clear that the desired vinylogous rearrangement has in fact taken place.

The mechanism of this change is approximately indicated by the curved arrows in formula **11**. However, it is probable that the reaction is not concerted since it does not appear to be stereospecific. The formation of a delocalized allylic carbonium ion probably precedes bond migration and the development of the keto group. We feel that the methods, which we have in part developed for our terpene alkaloid work (2, 3) and used here in a quite facile synthesis of compound **12**, have general applicability in synthetic chemistry. It is clear that other approaches which come to mind for the synthesis of compounds of the type **12** are more complex.

Experimental

Preparation of the Enol Ether 2

Trimethyl orthoformate (21.6 g), absolute methanol (15 ml), and saturated methanolic hydrogen chloride (2.5 ml) were added in sequence to a solution of the keto ester **1**(4) (30 g) in anhydrous benzene (600 ml). The mixture was stirred at room temperature for 18 h, after which time trimethyl orthoformate (15 ml) and saturated methanolic hydrogen chloride (1 ml) were added and the solution was stirred for an additional 2 days. The solution was evaporated to dryness *in vacuo* and the enol ether **2** was isolated in quantitative yield as a colorless oil homogeneous in t.l.c.

Mol. Wt. Calcd. for $C_{13}H_{14}O_4$: 234. Found (*m/e*): 234.

Infrared (film): 1740, 1609 cm^{-1} (ester, enol ether); n.m.r. (CCl_4) τ = 4.93 (d, J = 2 Hz, 1H, vinylic proton), 5.82 (d, J = 2 Hz, 1H, benzylic proton), 6.15 (s, 3H, aromatic methoxyl), 6.20 (s, 3H, —OCH_3), 6.33 (s, 3H, —C(=O)—OCH_3).

The Diels–Alder Adducts 3

A solution of the enol ether **2** (31.5 g) and an excess of maleic anhydride (27 g) in xylene (70 ml) was heated under nitrogen to 175 °C (oil bath temperature) for 5 h. After removal of the solvent and excess of maleic anhydride *in vacuo*, the brown residue was subjected to column chromatography on silica gel using acetone–*n*-hexane (2:3, v/v) as solvent. The adduct **3** was isolated as white solid material and 7.03 g of the starting material **1** was recovered. The *endo* (21 g) and *exo* (3.67 g) adducts were separated by fractional crystallization from acetone. The yield was 72%. The *endo* adduct, m.p. 154.5°.

Anal. Calcd. for $C_{17}H_{16}O_7$ (mol. wt. 332): C, 61.44; H, 4.85. Found (*m/e*) 332: C, 61.50; H, 4.85.

Infrared (KBr): 1860, 1784 (anhydride), 1744 cm^{-1} (ester); n.m.r. ($CDCl_3$) τ = 5.90 (q, J = 9 Hz, 2H,

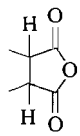

), 6.03 (s, 3H, aromatic methoxyl), 6.18 (s, 3H, ester), 6.40 (s, 3H, bridgehead methoxyl), 7.53 (q, J = 8 Hz, 2H, apex protons). The *exo* adduct, m.p. 194°.

Anal. Calcd. for $C_{17}H_{16}O_7$ (mol. wt. 332): C, 61.44; H, 4.85. Found (*m/e*) 332: C, 61.66; H, 4.90.

The mass spectra of both isomers were identical; i.r. (KBr): 1863, 1783 (anhydride), 1734 cm^{-1} (ester); n.m.r. ($CDCl_3$) τ = 6.03 (s, 3H, aromatic methoxyl), 6.17 (s, 3H, ester), 6.38 (s, 3H, bridgehead methoxyl), 6.63 (q, J = 9 Hz, 2H,

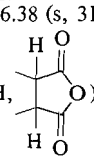

), 7.67 (q, J = 11 Hz, 2H, apex protons).

Can. J. Chem. Downloaded from www.nrcresearchpress.com by 210.87.254.42 on 09/05/12
For personal use only.

Preparation of the Olefin 4

The mixture of the Diels–Alder adducts **3** (27.41 g) was dissolved in anhydrous diglyme (550 ml) to which bistriphenylphosphine nickel dicarbonyl (52.7 g) was added. The mixture was heated under dry nitrogen at 210° for 3.5 h. The solvent was distilled off under reduced pressure. The residue was dissolved in methanol and the black precipitate was removed by filtration. After evaporation of the solvent, the product was isolated by chromatography on silica gel. Elution with benzene gave the oily olefin **4** (15.2 g, 70%), homogeneous in t.l.c.

Mol. Wt. Calcd. for $C_{15}H_{16}O_4$: 260.1049. Found (*m/e*): 260.1055.

Infrared (film): 1738 cm^{-1} (ester); n.m.r. (CCl_4) τ = 3.32 (broad s, 2H, vinylic protons), 6.17 (s, 3H, aromatic methoxyl), 6.28 (s, 3H, ester), 6.50 (s, 3H, bridgehead methoxyl), 7.38 (q, J = 6 Hz, 2H, apex protons).

Reduction of Compound 4 to the Corresponding Alcohol 5

A solution of **4** (603 mg) in anhydrous ether (10 ml) was added dropwise to a cold stirred suspension of $LiAlH_4$ (600 mg) in anhydrous ether (20 ml). The reaction mixture was stirred for 1 h at room temperature and worked up by careful addition of wet ether. The white precipitate was filtered and the filtrate was evaporated to give 540 mg of the alcohol **5** as an oil homogeneous by t.l.c.

Mol. Wt. Calcd. for $C_{14}H_{16}O_3$: 232.1099. Found (*m/e*): 232.1105.

Infrared (film): 3450 cm^{-1} (hydroxyl); n.m.r. (CCl_4) τ = 3.26 (m, 2H, vinylic protons), 5.83 (s, 2H, methylene of primary alcohol), 6.27 (s, 3H, aromatic methoxyl), 6.50 (s, 3H, bridgehead methoxyl), 7.61 (q, J = 6 Hz, 2H, apex protons).

Preparation of the Tosylate 6

The alcohol **5** (364 mg) was dissolved in anhydrous pyridine (5 ml) and *p*-toluenesulfonyl chloride (400 mg) was added. The reaction mixture was stirred at room temperature for 2 days and worked up in the usual manner. The product was crystallized from ether to a m.p. of 105°. The yield was 556 mg (92%).

Anal. Calcd. for $C_{21}H_{22}O_5S$ (mol. wt. 386): C, 65.27; H, 5.74. Found (*m/e*) 386: C, 65.42; H, 5.88.

Infrared (KBr): 1350, 1166 cm^{-1} (sulfonyl); n.m.r. (CCl_4) τ = 5.47 (s, 2H, —CH_2—O—SO_2—), 6.30 (s, 3H, aromatic methoxyl), 6.53 (s, 3H, bridgehead methoxyl), 7.53 (s, 3H, methyl), 7.68 (q, J = 6 Hz, 2H, apex protons).

Reduction of 6 to 7

An excess of $LiAlH_4$ (250 mg) was added in portions to a cold stirred solution of compound **6** (555 mg) in anhydrous ether (40 ml). The reaction mixture was stirred at room temperature for 15 h, after which time it was worked up in the usual manner. Evaporation of the solvent *in vacuo* gave 260 mg (82%) of 7 as an oil homogeneous by t.l.c.

Mol. Wt. Calcd. for $C_{14}H_{16}O_2$: 216.1150. Found (*m/e*): 216.1145.

Nuclear magnetic resonance (CCl_4) τ = 3.50 (m, 2H, vinylic protons), 6.28 (s, 3H, aromatic methoxyl), 6.52 (s, 3H, bridgehead methoxyl), 7.64 (q, J = 6 Hz, 2H, apex protons), 8.38 (s, 3H, tertiary methyl).

Preparation of the Ketones 8 and 8a

Compound **7** (202 mg) and excess 2-methoxy-1,3-butadiene in dry xylene (1 ml) were heated to 200 °C for 17 h in a sealed tube. Evaporation of the solvent and volatile material gave a residue which was dissolved in methanolic oxalic acid (200 mg in 10 ml of methanol). The solution was allowed to stand at room temperature for 1½ h. Most of the solvent was removed *in vacuo* and the residue was dissolved in ether. The ethereal solution was washed with water, dried over anhydrous sodium sulfate and evaporated to dryness. Analysis of the residue by t.l.c. showed the presence of two ketones **8** and **8***a* (ratio 3:1). Careful chromatography of the mixture on silica gel, eluting with benzene–chloroform (2:1, v/v), gave 146 mg (56%) of crystalline **8** and 48 mg (18%) of crystalline **8***a*. The ketone **8** was recrystallized from ether as white prisms, m.p. 109°; **8***a* was recrystallized from *n*-hexane also as white prisms, m.p. 86.5°.

Ketone 8

Anal. Calcd. for $C_{18}H_{22}O_3$ (mol. wt. 286): C, 75.49; H, 7.74. Found (*m/e*) 286: C, 75.65; H, 7.91.

Infrared (KBr): 1713 cm^{-1} (six-membered ketone); n.m.r. (CCl_4) τ = 6.22 (s, 3H, aromatic methoxyl), 6.59 (s, 3H, bridgehead methoxyl), 8.47 (s, 3H, tertiary methyl).

Ketone 8a

Mol. Wt. Calcd. for $C_{18}H_{22}O_3$: 286. Found (*m/e*): 286.

Infrared (KBr): 1716 cm^{-1} (six-membered ketone); n.m.r. (CCl_4) τ = 6.24 (s, 3H, aromatic methoxyl), 6.57 (s, 3H, bridgehead methoxyl), 8.68 (s, 3H, tertiary methyl).

Preparation of the Bromoketone 9

The ketone **8** (483 mg) was dissolved in ether (30 ml). Bromine (280 mg) in ether (20 ml) was added dropwise to the stirred solution at ice temperature. Evaporation of the solvent *in vacuo* gave 720 mg of the unstable bromoketone **9** with a small amount of the starting material **8**. This crude mixture had to be used immediately for further work.

Mol. Wt. Calcd. for $C_{18}H_{21}O_3Br$: 364 and 366. Found (*m/e*): 364 and 366.

Infrared (CCl_4): 1722 cm^{-1} (ketone); n.m.r. (CCl_4) τ = 5.33 (d, J = 4 Hz, 1H, proton unshielded by bromine atom), 6.27 (s, 3H, aromatic methoxyl), 6.60 (s, 3H, bridgehead methoxyl), 8.53 (s, 3H, tertiary methyl).

Preparation of the α,β-Unsaturated Ketone 10

The crude bromoketone **9** (720 mg), lithium bromide (350 mg) and lithium carbonate (460 mg) in anhydrous *N,N*-dimethylformamide (20 ml) were heated to 120° under nitrogen for 2 h. The solvent was distilled off *in vacuo* and the residue was dissolved in methylene dichloride (500 ml). The solution was washed with water, saturated sodium chloride solution, dried over anhydrous sodium sulfate, and evaporated to dryness. Chromatography of the residue on silica gel gave 207 mg (50%, based on **8** consumed) of the α,β-unsaturated ketone **10** as an oil homogeneous in t.l.c.

Mol. Wt. Calcd. for $C_{18}H_{20}O_3$: 284.1412. Found (*m/e*): 284.1403.

Infrared (film): 1666 cm^{-1} (unsaturated ketone); n.m.r. (CCl_4) τ = 4.15 (broad s, 1H, vinylic proton), 6.22 (s, 3H, aromatic methoxyl), 6.52 (s, 3H, bridgehead methoxyl), 8.53 (s, 3H, tertiary methyl).

Preparation of the Allylic Alcohol 11

A solution of the ketone **10** (185 mg) in absolute ether (4 ml) was added dropwise to a stirred Grignard solution prepared from excess methyl iodide (4 *M* equiv.) and

magnesium in ether (15 ml). The reaction mixture was maintained at 0 °C for 1 h. The mixture was poured into cold water (50 ml) and extracted with ether. The ethereal extract was washed with water, a saturated sodium chloride solution, and dried over anhydrous magnesium sulfate. Removal of the solvent *in vacuo* gave 187 mg (95%) of **11** as an oil.

Mol. Wt. Calcd. for $C_{19}H_{24}O_3 \cdot H_2O$: 282.1620. Found (*m/e*): 282.1613.

Infrared (CCl_4): 3617, 3490 cm^{-1} (hydroxyl); n.m.r. (CCl_4) τ = 4.62 (broad s, 1H, vinylic proton), 6.25 (s, 3H, aromatic methoxyl), 6.57 (s, 3H, bridgehead methoxyl), 7.50 (broad s, 1H, hydroxyl), 8.65 (s, 3H, tertiary methyl), 8.82 (s, 3H, tertiary methyl).

*Preparation of Rearranged Product **12** from Compound **11***

The allylic alcohol **11** (152 mg) was dissolved in anhydrous tetrahydrofuran (6 ml) and 97% formic acid (1.5 ml) was added. The reaction mixture was stirred at room temperature for 2 h. After removal of the solvent *in vacuo* at room temperature, the residue was chromatographed on silica gel. Elution with acetone–*n*-hexane (3:7, v/v) gave the crystalline product **12**. The product **12** was recrystallized from *n*-hexane to a m.p. of 117 °C. The yield was 105 mg (80%).

Anal. Calcd. for $C_{18}H_{20}O_2$ (mol. wt. 268): C, 80.56; H, 7.51. Found (*m/e*) 268: C, 80.72; H, 7.58.

Infrared (KBr): 1748 cm^{-1} (five-membered ketone); n.m.r. (CCl_4) τ = 4.07 (broad s, 1H, vinylic proton), 6.23 (s, 3H, aromatic methoxyl), 8.20 (broad s, 3H,

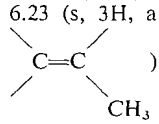

), 8.50 (s, 3H, tertiary methyl).

We wish to thank the National Research Council of Canada and the National Institutes of Health, Bethesda, Maryland, U.S.A., for generous support of this work.

1. B. G. Brownlee, Pak-tsun Ho, and K. Wiesner. Can. J. Chem. **50**, 4013 (1972).
2. K. Wiesner, Pak-tsun Ho, R. C. Jain, S. F. Lee, S. Oida, and A. Philipp. Can. J. Chem. **51**, 1448 (1973).
3. K. Wiesner, Pak-tsun Ho, D. Chang, Y. K. Lam, C. S. Pan, and W. Y. Ren. Can. J. Chem. **51**, 3978 (1973).
4. V. Askam and W. H. Linnel. J. Chem. Soc. 2435 (1954).

Can. J. Chem. Downloaded from www.nrcresearchpress.com by 210.87.254.42 on 09/05/12
For personal use only.

The Photochemical Isomerization of *N*-Bromo-α,β-unsaturated Lactams; An Intermolecular Allylic Bromination Process Involving a Probable Bromine Radical Chain

DENIS GRAVEL, JACQUES HEBERT,[1] JACQUES BILODEAU,[2] ERCOLE CAVALIERI, AND JEAN-PAUL DARIS

Department of Chemistry, University of Montreal, Montreal, Quebec

Received September 5, 1972[3]

The photochemical behavior of the *N*-bromo-α,β-unsaturated lactams **1***b* and **2***b* has been investigated with particular regard to their potential intramolecular reactions. In both cases the main product corresponds to an isomerization of bromine to the 5-position. A crossover experiment and free radical initiation by AIBN or benzoyl peroxide indicate that the reaction bears a close mechanistic analogy to the NBS reaction. It was furthermore observed that the allylic bromo derivatives prepared could be smoothly reduced to the corresponding β,γ-unsaturated lactam making available an efficient method of deconjugation of α,β-unsaturated lactams.

Le comportement photochimique des dérivés *N*-bromés des lactames α,β-insaturés **1***b* et **2***b* a été étudié avec une attention particulière quant à leur possibilité de donner des réactions intramoléculaires. Dans chaque cas, le produit principal correspond à une isomérisation du brome vers la position 5. Une expérience de compétition ainsi que l'initiation de la réaction par des sources de radicaux telles que l'AIBN et le peroxyde de benzoyle indiquent que le mécanisme de cette transformation est analogue à celui de la réaction du NBS. Il fut de plus observé que les dérivés bromés allyliques préparés pouvaient facilement être réduits à la lactame β,γ-insaturée correspondante rendant ainsi disponible une méthode efficace de déconjuguaison des lactames α,β-insaturées.

Can. J. Chem., **52**, 645 (1974)

Introduction

Our interest in the photochemistry of α,β-unsaturated lactams (1, 2) and a related synthetic problem prompted us to investigate the photochemical behavior of the *N*-bromo derivatives of lactams **1***a* and **2***a*. *A priori*, the u.v. irradiation of **1***b* and **2***b* might be expected to lead primarily to allylic bromination and/or, possibly, addition to the olefinic double bond (3–6).

In theory, the hydrogen abstraction step in the first process and the addition of an amidyl radical in the second process could occur essentially in an inter- or an intramolecular fashion. However, it

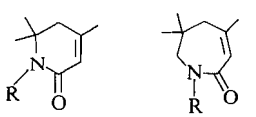

1 **2**

a R = H *a* R = H

b R = Br *b* R = Br

has been shown that intramolecular hydrogen abstraction by *saturated aliphatic amidyl radicals* is a highly selective reaction[4] which requires a six-membered ring transition state (3, 8–10) as is the case for aminium (11) and alkoxy (12) radicals in general. Furthermore, Edwards *et al.* (13) have recently observed that whereas saturated eight- and nine-membered ring *N*-chloro lactams transferred chlorine efficiently through intramolecular hydrogen abstraction, the seven-membered ring analog exclusively yields the parent lactam through intermolecular hydrogen abstraction from the solvent.

These considerations alone should therefore suffice to rule out the probability of any intramolecular hydrogen abstraction in an eventual allylic bromination process. On the other hand, in an intermolecular reaction, abstraction could be effected by an amidyl radical or a bromine atom as is the case for allylic brominations using *N*-bromosuccinimide (NBS) (14).

Regarding the possibility of an addition reaction, the intermolecular addition of simple *N*-halo carboxamides to isolated double bonds

[1]NRCC Scholarship Holder, 1969–1973.

[2]Jonquière CEGEP Scholarship Holder, 1967–1968.

[3]Revision received October 30, 1973.

[4]It is known from the work of Chow and Joseph (7) that the intramolecular hydrogen transfer occurs to nitrogen and not to oxygen in the potentially ambient radical.

Can. J. Chem. Downloaded from www.nrcresearchpress.com by 210.87.254.42 on 09/05/12
For personal use only.

Can. J. Chem. Downloaded from www.nrcresearchpress.com by 210.87.254.42 on 09/05/12
For personal use only.

generally does not take place (3)[5] and is even less likely in the case of *N*-alkyl-*N*-halo carboxamides (16) which are good analogs of *N*-halo lactams. The intramolecular "addition", on the other hand, which could conceivably result from interaction of the amidyl radical with the double bond, cannot totally be rejected especially in the case of the seven-membered ring lactam. Such a reaction would be somewhat analogous to the light catalyzed isomerization of *N*-chloroacetanilide to *o*- and *p*-chloroacetanilide (6*b*).

Irradiations and Structures of Photoproducts

Irradiation of N-Bromo Lactam 1b

The title compound (**1***b*) (m.p. 74–75°) was obtained by treating **1***a* with NBS in the absence of light. The product, a solid which decomposes slowly in the atmosphere or daylight, was characterized by its n.m.r. and i.r. spectra. Compounds **1***a* and **1***b* exhibit very similar spectra; however, the absence of a signal at δ 7.16 indicates that substitution of bromine for hydrogen has taken place on the nitrogen atom. Moreover, the remainder of the spectrum being identical to that of **1***a* except for a small downfield shift of most signals further substantiates the fact that bromine substitution has taken place on nitrogen only. Finally, a comparison of the i.r. spectra of **1***a* and **1***b* shows that N—H absorption at 3420 cm^{-1} has disappeared.

Due to its relative instability *N*-bromo lactam **1***b* was isolated for characterization purposes only. For photochemical studies **1***b* was prepared in dichloromethane and irradiated immediately *in situ* after eliminating the succinimide formed in the reaction.[6] Identical results were obtained using either a 450 W Hanovia lamp (Vycor filter), or a Rayonet Photochemical Reactor with 2537 Å light. (A 200 W incandescent bulb could also be used but with longer reaction times.) Generally, after 10 min of irradiation, an analysis of the reaction mixture by t.l.c. showed that all the starting material (**1***b*) had disappeared and that three new compounds were formed in unequal amounts. Separation of the crude mixture afforded three crystalline products: m.p. 163–164° (69%), m.p. 194–195 (3%), and m.p. 164–165° (1%). A mixture melting point of the two compounds melting at 163–164° and 164–165° gave a value of 130–155° and t.l.c. analysis showed that each substance was homogeneous.

The structures of the photoproducts were determined using physical methods. The elemental analysis of the compound having m.p. 163–164° suggested a molecular formula of $C_8H_{12}BrNO$ which was confirmed by a mass spectrum showing a molecular ion at *m/e* 217 accompanied by a peak of equal intensity at *m/e* 219. The main photoproduct was therefore isomeric with the starting *N*-bromo lactam **1***b*.

The position of the bromine atom was established from the n.m.r. spectrum which showed an absorption at δ 7.58 indicating the presence of one hydrogen on the nitrogen atom and also a one proton doublet at δ 4.25, ($J \cong 0.5$ Hz) replacing the allylic methylene at δ 2.50 in the starting *N*-bromo lactam **1***b*. The *gem*-dimethyl group appeared as a pair of singlets at δ 1.39 and 1.50 and the vinyl proton appeared as a singlet at δ 5.75 which is the same position as in **1***a* and **1***b*. Finally, the allylic methyl group gave rise to a doublet at δ 2.07 ($J = 1.5$ Hz). These results therefore agree with a bromine transfer from nitrogen to the allylic position of the ring to give lactam **3**.[7]

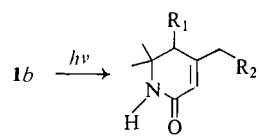

3 $R_1 = Br$; $R_2 = H$
4 $R_1 = H$; $R_2 = Br$
5 $R_1 = R_2 = Br$

The second product isolated (**4**) (m.p. 194–195°) gave an elemental analysis consistent with a molecular formula of $C_8H_{12}BrNO$ which was confirmed in the mass spectrum by a molecular ion

[5]See the case of *N*-bromoacetamide (NBA) which in refluxing carbon tetrachloride and under catalysis from light and peroxide adds to cyclohexene as observed by Wolfe and Awang (15). These authors, however, have shown that the reaction leads to *N,N*-dibromoacetamide which subsequently adds by an *ionic mechanism* to give 2-bromocyclohexyl-*N*-bromoacetimidate. In contrast with this behavior Touchard and Lessard (16) have found that irradiation of α-chlorinated *N*-chloro- or *N*-bromoacetamides leads to an efficient *radical addition* to cyclohexene yielding mainly the corresponding *cis*-mono-, -di-, or -trichloroacetamidocyclohexyl chloride or bromide.

[6]The n.m.r. spectrum was however recorded each time to ensure the purity of the solution.

[7]As expected, the same bromo compound (**3**) was obtained (73%) when lactam **1***a* was irradiated in the presence of NBS in dichloromethane.

Can. J. Chem. Downloaded from www.nrcresearchpress.com by 210.87.254.42 on 09/05/12
For personal use only.

peak at *m/e* 217 along with a P + 2 peak of equal intensity at *m/e* 219. The position of the bromine atom was deduced unambiguously by noting that the allylic methyl signal at δ 1.90 in the spectrum of **1***b* had been replaced by an allylic bromomethyl signal at δ 4.05; the remainder of the spectra were approximately superimposable with the exception of the N—H signal at δ 6.10 in the case of **4**.

The third compound isolated (**5**) (m.p. 164–165°) gave an elemental analysis suggesting a molecular formula of $C_8H_{11}Br_2NO$. This was confirmed by the mass spectrum which showed a molecular ion peak at *m/e* 295 along with peaks at *m/e* 297 and 299 in a 1:2:1 ratio. Once again, the position of the bromine atoms could easily be determined from the n.m.r. spectrum which exhibited two singlets at δ 1.45 and 1.55 for the *gem*-dimethyl protons and a doublet ($J \cong 0.5$ Hz) at δ 4.68 for the allylic hydrogen on carbon-5 bearing one bromine atom. These features had already been observed in the spectrum of the monobromo derivative **3**. The position of the second bromine atom could then be deduced unambiguously by observing an AB quartet at δ 4.21 ($J = 10.5$ Hz) characteristic of the allylic bromomethyl group. Finally, the vinyl proton and the amide proton were found at δ 6.00 and 7.42, respectively.

It may be of interest to note at this point that treatment of bromo lactam **3** with silver nitrate in aqueous dioxane yielded 50% of the known 4,5,6-trimethyl-2-pyridone (**6**) (17) via dehydrohalogenation accompanied by rearrangement.

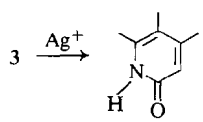

6

The spectral data obtained are fully in accord with the proposed structure **6**. In the mass spectrum a molecular ion is observed at *m/e* 137 and the elemental analysis suggests a molecular formula of $C_8H_{11}NO$. The n.m.r. spectrum shows four singlets at δ 1.95 (3H), 2.15 (3H), 2.32 (3H), and 6.26 (1H) with a broad signal at δ 13.3 (1H), the latter two protons appear at δ 6.58 and 12.05, respectively, in the unmethylated analog (18). The i.r. spectrum shows strong absorption in the 2400 to 3400 cm^{-1} region and a carbonyl band at 1650 cm^{-1} in accord with that of α-pyridone (19). Finally, the u.v. spectrum showed λ_{max} at 231 (ε 5891) and 307 nm (ε 5959) which agrees with the spectrum of α-pyridone (20).

Irradiation of N-Bromo Lactam 2b

As in the case of **1***a*, treatment of lactam **2***a* with NBS in the absence of light afforded the *N*-bromo derivative **2***b*. Irradiation of the latter[8] in carbon tetrachloride for 15 min led to incomplete consumption of the starting material and appearance of three new spots on t.l.c. Separation of the mixture, which proved very difficult, yielded a major product (38%), the structure of which is shown to be **7** and four other minor products: **8** (~10%), **9** (2.5%), **10** (~8%), and **11** (~2%).

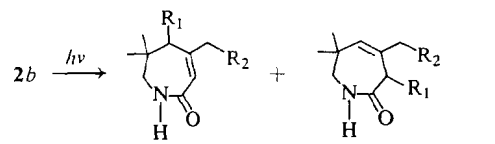

7 R_1 = Br; R_2 = H **10** R_1 = Br; R_2 = H
8 R_1 = H; R_2 = Br **11** R_1 = R_2 = Br
9 R_1 = R_2 = Br

The main compound (**7**) (38%) melting at 113° gave an elemental analysis suggesting a molecular formula of $C_9H_{14}BrNO$. This was confirmed by a molecular ion peak at *m/e* 231 accompanied by a peak of equal intensity at *m/e* 233. The n.m.r. spectrum showed two singlets at δ 1.12 and 1.20 for the *gem*-dimethyl group, a fine doublet at δ 2.07 ($J = 1.5$ Hz) for the allylic methyl, and an eight-line system in the δ 2.6–3.6 region for the AB portion of an ABX characteristic of the CH_2—NH moiety which collapses to a simple AB system centered at δ 3.13 ($J = 14.2$ Hz) upon exchange with D_2O. A sharp one proton singlet at δ 4.45 is characteristic of the brominated allylic methylene group, a singlet at δ 5.75 represents the vinyl proton, and a broad signal at δ 7.5 indicates the NH proton.

Compound **8** (~10%) was most difficult to purify from its isomer **7** and could not be obtained in a perfectly pure state. Its mass spectrum showed a molecular ion at *m/e* 231 along with a P + 2 peak at *m/e* 233 characteristic of a monobromo compound. The n.m.r. spectrum showed a six proton singlet at δ 1.04 for the *gem*-dimethyl group, a two proton singlet at δ 2.21 for the allylic

[8]As in the previous case, *N*-bromo lactam **2***b* was isolated once and characterized but for photochemical purposes the product was freed of succinimide and irradiated *in situ*.

Can. J. Chem. Downloaded from www.nrcresearchpress.com by 210.87.254.42 on 09/05/12
For personal use only.

methylene, a two proton doublet at δ 2.88 (J = 6 Hz) for the methylene α to nitrogen which collapses to a singlet upon addition of D_2O, a two proton singlet at δ 3.97 for the allylic bromomethyl group which replaces the allylic methyl, a vinyl proton singlet at δ 6.03, and an N—H absorption at δ 6.8.

Compound **9** (2.5%), m.p. 171–173°, showed a molecular ion peak at *m/e* 311 along with peaks at *m/e* 313 and *m/e* 315 in a 1:2:1 ratio characteristic of a dibromo compound. The n.m.r. spectrum showed a six proton singlet at δ 1.24 for the *gem*-dimethyl group, an eight line system in the δ 2.60–3.90 region for the AB portion of an ABX characteristic of the CH_2NH moiety which collapses to a simple AB system centered at δ 3.25 (J_{AB} = 15 Hz) upon exchange with D_2O. The allylic bromomethyl group also appears as an AB quartet centered at δ 4.16 (J_{AB} = 9.8 Hz). One proton singlets at δ 4.75 and 6.04 are characteristic of the brominated allylic methylene and the vinyl proton, respectively, and finally a broad singlet at δ 7.3 is typical of the amide proton.

Compound **10** (~8%) showed in the n.m.r. a six proton doublet at δ 1.03 for the *gem*-dimethyl group, a three proton doublet at δ 1.85 (J = 1.5 Hz) for the allylic methyl group, and an eight line system in the δ 2.55–4.35 region for the AB portion of an ABX characteristic of the CH_2NH moiety which collapses to a simple AB quartet centered at δ 3.45 (J_{AB} = 15 Hz) upon exchange with D_2O. Two one-proton singlets at δ 4.55 and 5.40 are characteristic of the brominated allylic methylene and the vinyl proton, respectively; finally, a broad one proton singlet appears at δ 7.2 for the amide proton.

Compound **11** (~2%) showed in the n.m.r. a six proton doublet at δ 1.08 for the *gem*-dimethyl group, an AB quartet centered at δ 4.03 (J_{AB} = 10.5 Hz) for the allylic bromomethyl group, and an eight line system in the δ 2.6–4.25 (overlapping with the above AB quartet) for the AB portion of an ABX system characteristic of the CH_2NH moiety which collapses to a simple AB quartet centered at δ 3.48 (J_{AB} = 15 Hz) upon exchange with D_2O. A doublet at δ 4.92 (J = 2 Hz) which collapses to a singlet upon exchange with D_2O indicates the CHBr group α to carbonyl and coupled through four bonds with the NH proton; a second doublet at δ 5.80 ($J \cong$ 1.5 Hz) is typical of the vinyl proton coupled through four bonds to the CH_2 group of the CH_2NH moiety (the 1.5 Hz splitting is visible in the AB portion of the ABX system). Finally, the NH proton which disappears upon exchange with D_2O is visible as a broad signal at δ 7.5.

In order to ascertain that the bromo compounds formed still retained the basic structure of **2***a* and were not the result of deep seated rearrangements, substances **7** and **10** were reduced with zinc in acetic acid (21) to yield 80% of the solid (m.p. 147–148°) β,γ-unsaturated lactam **13** characterized by physical methods.

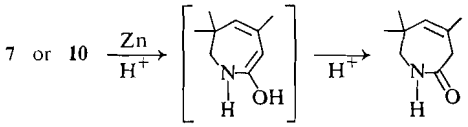

12 **13**

The elemental analysis suggested a molecular formula of $C_9H_{15}NO$ which was confirmed by a molecular ion at *m/e* 153 in the mass spectrum. In the n.m.r., the allylic methyl group appeared as a doublet at δ 1.80 ($J \cong$ 1.5 Hz) whereas it appeared at δ 1.92 in the corresponding α,β-unsaturated lactam **2***a*. The methylene α to carbonyl and the double bond gives rise to a singlet at δ 3.12 and the methylene α to nitrogen appears as a doublet at δ 3.14 (J = 6 Hz) and collapses to a singlet upon exchange with D_2O. The vinyl proton gives rise to a multiplet at δ 5.14 and the *gem*-dimethyl protons to a singlet at δ 1.01.

Formation of the β,γ-unsaturated lactam **13** at the expense of its conjugated isomer **2***a* is not unexpected[9] since it is in accordance with the Hughes–Ingold rule (22) for the kinetic protonation of **12** and since a similar behavior has already been observed in related intermediates (2, 23). Additional evidence to support this assertion was obtained by carrying out the reduction of **7** in deuterioacetic acid and showing that one deute-

[9]It is interesting to note that this same specificity is also observed in the case of bromo lactams **3** and **15** to produce the corresponding deconjugated analogs **16** and **17**. The sequence: allylic bromination followed by debromination with zinc dust in protic solvents which has been used with limited success for the deconjugation of α,β-unsaturated ketones (23*b*) seems to proceed remarkably well with α,β-unsaturated lactams and esters (23*e*) because of the ease of attaining kinetic control in this case.

16 R = H
17 R = CH_3

Can. J. Chem. Downloaded from www.nrcresearchpress.com by 210.87.254.42 on 09/05/12
For personal use only.

rium atom was incorporated and this at the 3 position only.

Mechanistic Aspects

In an effort to ascertain the intra- or intermolecular nature of the allylic hydrogen abstraction step, the photolysis of an equimolar mixture of *N*-bromo lactam **1***b* and *N*-methyl lactam **14** was carried out in dichloromethane. The resulting mixture of four products (t.l.c.) was chromatographed to yield three major fractions: the first containing a mixture of *N*-methyl lactam **14** and *N*-methyl-5-bromo lactam **15**; the second containing a mixture of the four products (**1***a*, **3**, **14**, and **15**) and the third containing a mixture of lactam **1***a* and 5-bromo lactam **3**. Fractional crystallization of the first fraction yielded pure *N*-methyl-5-bromo lactam **15** identical in all respects (n.m.r., i.r., m.p.) with an authentic sample prepared from *N*-methyl lactam **14** and NBS thus showing that the allylic hydrogen abstraction step is, at least in part, intermolecular.

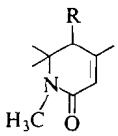

14 R = H
15 R = Br

The minimum extent to which the latter process is intermolecular was crudely estimated from the n.m.r. spectra of the three chromatographic fractions. The results show that the reaction mixture contains *approximately* 39% of 5-bromo-*N*-methyl lactam **15**, 17% of unreacted *N*-methyl lactam **14**, 15% of bromo lactam **3**, and 29% of lactam **1**. This means that at least 70% of the total allylic bromination observed was produced through an *intermolecular hydrogen abstraction mechanism*[10] which suggests a possible mechanistic analogy with the NBS allylic bromination reaction.

Evidence concerning an analogy with the NBS reaction was obtained by initiating in the dark the isomerization of *N*-bromo lactam **1***b* with trace amounts of AIBN or benzoyl peroxide, two well-known radical chain initiators in allylic halogenations (24). In both cases the reactions led to comparable product distributions with approximately 70% of the 5-bromo lactam **3** being formed. These results are identical to those obtained in the direct photolysis of *N*-bromo lactam **1***b* and in the photolysis of equimolar amounts of NBS and lactam **1***a*; they show conclusively that the photoisomerization described herein is mechanistically similar to the NBS allylic bromination reaction where a bromine atom is the chain carrying species (14).

Finally, an attempt was made to show that the reaction generates a low steady state concentration of free bromine which initiates a radical chain bromination. A refluxing carbon tetrachloride solution of *N*-bromo lactam **1***b* was irradiated with a 200 W incandescent lamp while the solvent was slowly being distilled (15, 25). After 3 h, the distillate showed no trace of bromine as evidenced by the total absence of a characteristic absorption at 400 nm (26). The remaining solution contained the 5-bromo lactam **3** (78%) along with minor amounts of the dibromo lactam **5** and the bromomethyl lactam **4** indicating that bromination was much too rapid to be intercepted.

Experimental

The silica gel used for chromatography was "Baker Analyzed Reagent". Melting points were taken on a "Büchi" apparatus and are uncorrected. The i.r. spectra were recorded in chloroform using a Beckman, Model IR-8 apparatus. The n.m.r. spectra were taken on a Varian Model A-60 apparatus or a Jeolco-60 apparatus using deuteriochloroform as solvent and TMS as internal reference. The u.v. spectra were recorded in methanol on a Bausch and Lomb Spectronic 505 spectrophotometer. The mass spectra were taken on a Hitachi-Perkin Elmer RMU 6-D spectrometer. Finally, the elemental analyses were carried out by Daesslé Organic Microanalyses, Montreal, and Midwest Microlab Inc., Indianapolis, U.S.A.

Preparation and Irradiation in situ of N-Bromo-5,6-dihydro-4,6,6-trimethyl-2(1H)-pyridone (1b)

A mixture of 5.56 g (4.0×10^{-2} mol) of dihydropyridone **1***a* (2, 27) and 7.12 g (4.0×10^{-2} mol) of NBS in 500 ml of dichloromethane was stirred in the dark for 2 h at room temperature. The reaction was monitored by t.l.c. on silica gel. The succinimide formed in the reaction was eliminated by washing the solution six times with ice water.[11] The dichloromethane solution was dried over anhydrous magnesium sulfate, filtered, and evaporated to give the *N*-bromo lactam **1***b* as a slightly yellow solid which decomposes after a few hours in the atmosphere or by exposure to light. When recrystallized from acetone–hexane at low temperature, the product showed a m.p. of

[10]The abstracting species being almost certainly an amidyl radical or/and a bromine radical since the irradiation of an equimolar mixture of the 5-bromo lactam **3** and the *N*-methyl lactam **14** did not yield any 5-bromo-*N*-methyl lactam **15** after the usual reaction time.

[11]Some *N*-bromo lactam **1***b* (10–20%) is lost during the washings.

Can. J. Chem. Downloaded from www.nrcresearchpress.com by 210.87.254.42 on 09/05/12
For personal use only.

74–75°. A bromine analysis showed 35.59% (Br) while the calculated value for $C_8H_{12}BrNO$ is 36.69%. The n.m.r. spectrum had δ 1.33 (s, 6H), 1.91 (s, 3H), 2.50 (s, 2H), and 5.75 p.p.m. (m, 1H). The i.r. spectrum showed absorptions at 1672 and 1630 cm^{-1}. The N—H band at 3420 cm^{-1} had disappeared.

The *N*-bromo lactam **1***b* was isolated only once in order to determine its characteristics. Normally, for photochemical experiments the dried methylene chloride solution of *N*-bromo lactam **1***b* was purged with oxygen-free nitrogen for 20 min and immediately irradiated for 10 min using a Hanovia 450 W lamp with a Vycor filter or a Rayonet Photochemical Reactor equipped with 2537 Å. The reaction was monitored by t.l.c. on silica gel.

Separation and Identification of Photoproducts

After evaporation of the dichloromethane, the residue crystallized from an acetone–hexane mixture to yield 4.6 g of a solid, m.p. 162–164°. Recrystallization from the same mixture gave a homogeneous product, m.p. 163–164°. Chromatography, using dichloromethane as eluent, of the mother liquors of the first recrystallization gave 1.4 g of the same product, 240 mg of a second compound, 274 mg of a third, and 604 mg of lactam **1***a*. The total weight of the major product (**3**) obtained was 6.0 g (69%); i.r. spectrum: 3420, 1670, and 1625 cm^{-1}; u.v. spectrum: λ_{max} 221 nm (ε 8720).

Anal. Calcd. for $C_8H_{12}BrNO$: C, 44.04; H, 5.50; Br, 36.69; N, 6.42. Found: C, 43.91; H, 5.55; Br, 37.51; N, 6.40.

The second compound isolated (**4**) (240 mg, 3%) was a solid, m.p. 194–195° after recrystallization from acetone–hexane; i.r. spectrum: 3420, 1675, and 1625 cm^{-1}.

Anal. Calcd. for $C_8H_{12}BrNO$: C, 44.04; H, 5.50; Br, 36.69; N, 6.42. Found: C, 43.94; H, 5.67; Br, 37.72; N, 6.30.

The third compound isolated (**5**) (275 mg, 1%) was a solid, m.p. 164–165° (dec.) after recrystallization from acetone–hexane; i.r. spectrum: 3420, 1675, and 1625 cm^{-1}.

Anal. Calcd. for $C_3H_{11}Br_2NO$: C, 32.32; H, 3.70; N, 4.71. Found: C, 32.48; H, 3.83; N, 4.79.

*Irradiation of 5,6-Dihydro-4,6,6-trimethyl-2(1H)-pyridone (**1a**) in the Presence of N-Bromosuccinimide*

A solution of 13.9 g (0.1 mol) of dihydropyridone **1***a* and 17.8 g (0.1 mol) of *N*-bromosuccinimide in 600 ml of dichloromethane was irradiated at 2537 Å for 15 min. The irradiated solution was then washed 10 times with 25-ml portions of ice-cold water to eliminate the succinimide formed. The organic layer was dried over anhydrous magnesium sulfate and evaporated under vacuum to give a solid residue which was chromatographed on silica gel using dichloromethane as eluent. Three compounds were thus separated: 5-bromo-5,6-dihydro-4,6,6-trimethyl-2(1H)-pyridone (**3**) (15.8 g, 73%), 4-bromomethyl-5,6-dihydro-6,6-dimethyl-2(1H)-pyridone (**4**) (0.9 g, 4%), and unreacted dihydropyridone (**1***a*) (1.4 g, 10%). Both bromo compounds were identical in all respects (m.p., i.r., n.m.r., mass spectrum) to authentic samples obtained in the previously described experiment.

Reaction of Bromo Lactam 3 with Silver Nitrate

To a solution of 5.01 g of bromo lactam **3** in 30 ml of dioxane was rapidly added a solution of 3.9 g (2.3×10^{-2} mol) of silver nitrate in 120 ml of distilled water. The mixture was heated slightly (30–40°) for 2–3 min. The nitric acid formed in the reaction medium was rapidly neutralized with a 3% aqueous solution of sodium carbonate and the mixture filtered over diatomaceous earth. The filtrate was saturated with ammonium sulfate and extracted three times with dichloromethane. The organic layer was dried over anhydrous magnesium sulfate and evaporated to yield a solid, m.p. 261–261.5° after recrystallization from acetone. The yield obtained was 1.5 g (50%) and the product was shown to be 4,5,6-trimethyl-2-pyridone (**6**) (lit. m.p. 252° (17*a*); 196° (17*b*)); i.r. spectrum: 3400–2400 cm^{-1}, 1650, and 1622 cm^{-1}; u.v. spectrum: λ_{max} 231 nm (ε 5891) and λ_{max} 307 nm (ε 5959).

Anal. Calcd. for $C_8H_{11}NO$: C, 70.07; H, 8.03; N, 10.22. Found: C, 70.34; H, 8.03; N, 9.96.

*Preparation and Irradiation in situ of N-Bromo-6,7-dihydro-4,6,6-trimethyl-2(5H)-azepinone (**2b**)*

A mixture of 1.04 g (6.8×10^{-3} mol) of dihydroazepinone **2***a* (28) and 2.42 g (13.6×10^{-3} mol) of NBS in 200 ml of dichloromethane was stirred for 90 min in the dark and at room temperature. The succinimide formed was removed by washing the solution six times with ice water. The organic layer was dried over anhydrous magnesium sulfate and the solvent evaporated to dryness. In order to separate the excess NBS present in the mixture, the residue was taken up with a few milliliters of carbon tetrachloride, in which NBS is insoluble, and the solid separated by filtration. Evaporation of the solvent then yielded a yellowish liquid (*N*-bromo lactam **2***b*) which decomposes in the atmosphere and when exposed to light. The purity obtained was 92% as calculated from the n.m.r. spectrum: δ 1.06 (s, 6H), 1.96 (d, $J = 1.5$ Hz, 3H), 2.09 (s, 2H), 3.55 (s, 2H), and 5.87 p.p.m. (m, 1H); i.r. spectrum: 1655 and 1615 cm^{-1}, the N—H band at 3420 cm^{-1} was no longer present. Normally, for photochemical purposes, the filtrate containing *N*-bromo lactam **2***b* in carbon tetrachloride, after elimination of the NBS, was diluted to 30 ml with the same solvent and immediately irradiated for 15 min (the reaction was monitored by t.l.c.) using a Hanovia 450 W lamp with a Vycor filter or a Rayonet Photochemical Reactor with 2537 Å light.

Separation and Identification of Photoproducts

After evaporation of the solvent, the oily residue was chromatographed on silica gel. Elution with dichloromethane gave 202 mg of a mixture of three products: **11**, **10**, and an unidentified compound.

Compound **11** (30 mg, 1.4%) was separated and purified by crystallization in carbon tetrachloride to a quasi pure state. Compound **10** (120 mg, 7.5%) was separated and purified by crystallization in petroleum ether 30–50° to a quasi pure state.

Further elution of the column with ether yields compound **9** (50 mg, 2.4%), m.p. 171–173°.

Finally, elution of the column with ether–acetone 1:1 gives 1.03 g of a mixture of three products: **7**, **8**, and starting lactam **2***a*.

Compound **7** (603 mg, 38%), m.p. 113°, was separated and purified by crystallization from acetone–hexane.

Anal. Calcd. for $C_9H_{14}BrNO$: C, 46.55; H, 6.03; Br, 34.48; N, 6.03. Found: C, 46.82; H, 6.16; Br, 34.34; N, 5.80.

Compound **8** (156 mg, 10%) was separated and purified

Can. J. Chem. Downloaded from www.nrcresearchpress.com by 210.87.254.42 on 09/05/12
For personal use only.

to a quasi pure state after numerous crystallizations from acetone–hexane.

Zinc in Acetic Acid Reduction of the 5- and 3-Bromodihydroazepinones 7 and 10 (21)

A solution of 173 mg of the 5-bromo compound **7** in 5 ml of glacial acetic acid was mixed with 1.2 g of powdered zinc and the mixture stirred for 2 h at 60° and overnight at room temperature. After filtration, most of the acetic acid was removed by distillation and the residue dissolved in dichloromethane. The resulting solution was neutralized with a 10% solution of sodium carbonate, washed twice with distilled water, dried over anhydrous magnesium carbonate, and evaporated to dryness to give 90 mg (80%) of a product identified as dihydroazepinone **13** after recrystallizing twice from acetone–hexane (m.p. 147–148°); i.r. spectrum: 3430, 1660, and 1615 cm^{-1}.

Anal. Calcd. for $C_9H_{15}NO$: C, 70.58; H, 9.80. Found: C, 70.19; H, 10.04.

The same reaction, when carried out on the 3-bromo compound **10** (110 mg), yielded a solid (56 mg, 78%) which after two recrystallizations from acetone–hexane had m.p. 147–148°. A mixture melting point with the product obtained in the previous reduction showed no depression. The n.m.r. and i.r. spectra were also superimposable with those obtained from the product of the previous reduction.

Zinc in Deuterioacetic Acid Reduction of the 5-Bromodihydroazepinone 7

Reduction of 232 mg (1×10^{-3} mol) of the 5-bromodihydroazepinone **7** by the above procedure using deuterioacetic acid gave 130 mg (84%) of product, m.p. 147–148°; mass spectrum: molecular ion at *m/e* 154; n.m.r. spectrum: δ 1.00 (s, 6H), 1.80 (d, $J \cong 1.5$ Hz, 3H), 3.07 (s, 1H), 3.14 (d, $J = 6$ Hz, 2H), 5.11 (m, 1H) and 7.4 p.p.m. (broad signal, 1H).

Zinc in Acetic Acid Reduction of 5-Bromo-5,6-dihydro-4,6,6-trimethyl-2(1H)-pyridone (3)

A solution containing 2.18 g (0.01 mol) of the 5-bromo lactam **3** and 12.0 g (0.2 mol) of powdered zinc in 25 ml of glacial acetic acid was treated as above to yield 1.30 g (95%) of a solid identified as the deconjugated lactam **12**, m.p. 110–111° after recrystallization from acetone–hexane; mass spectrum: molecular ion at *m/e* 139; n.m.r. spectrum: δ 1.30 (s, 6H), 1.73 (d, $J = 1.5$ Hz, 3H), 2.79 (s, 2H), 5.35 (m, 1H) and 7.40 p.p.m. (broad m, 1H); i.r. spectrum: 3410, 1690, and 1650 cm^{-1}.

Anal. Calcd. for $C_8H_{13}NO$: C, 69.03; H, 9.41; N, 10.06. Found: C, 69.37; H, 9.17; N, 9.83.

Preparation and Zinc in Acetic Acid Reduction of N-Methyl-5-bromo-5,6-dihydro-4,6,6-trimethyl-2-pyridone (15)

The 5-bromo-*N*-methyl lactam **15** was prepared from the parent *N*-methyl lactam (2) by the above NBS procedure. Compound **15** obtained in a 60–70% yield had m.p. 110–111° (acetone–hexane); mass spectrum: molecular ion at *m/e* 231 with P + 2 peak at *m/e* 233 (ratio 1:1); n.m.r. spectrum: δ 1.34 (s, 3H), 1.58 (s, 3H), 2.07 (d, $J = 1.5$ Hz, 3H), 3.00 (s, 3H), 4.33 (s, 1H), and 5.85 p.p.m. (s, 1H); i.r. spectrum: 1615 and 1670 cm^{-1}.

Treatment of the above compound (**15**) with zinc in acetic acid as described previously gave a 95% yield of the liquid (b.p. 55°/0.15 mm Hg) deconjugated lactam **17**. Mass spectrum: molecular ion at *m/e* 153; n.m.r. spectrum: δ 1.33 (s, 6H), 1.70 (s, 3H), 2.88 (s, 2H), 2.98 (s, 3H) and 5.34 p.p.m. (s, 1H); i.r. spectrum: 1620 cm^{-1}.

Rearrangement of N-Bromo-5,6-dihydro-4,6,6-trimethyl-2(1H)-pyridone (1b) Initiated with AIBN

A solution of freshly recrystallized *N*-bromo lactam **1***b* (1.09 g, 5×10^{-3} mol) and 2,2′-azobis(2-methylpropionitrile) (AIBN) (17 mg, 1×10^{-4} mol) in 50 ml of carbon tetrachloride was heated to reflux in the dark. After 1 h the starting *N*-bromo lactam **1***b* had completely disappeared as evidenced by t.l.c. The solvent was evaporated to dryness and the residue chromatographed on silica gel using dichloromethane as eluent. Three products were thus separated: 5-bromo lactam **3** (776 mg, 71%), 4-bromomethyl lactam **4** (64 mg, 6%), and dibromo lactam **5** (95 mg, 6%). All three compounds were identical in all respects (m.p., i.r., and n.m.r.) with authentic samples prepared by the photochemical method.

Rearrangement of N-Bromo-5,6-dihydro-4,6,6-trimethyl-2(1H)-pyridone (1b) Initiated with Benzoyl Peroxide

A solution of freshly recrystallized *N*-bromo lactam **1***b* (1.09 g, 5×10^{-3} mol) and benzoyl peroxide (14 mg, 1×10^{-4} mol) in 50 ml of carbon tetrachloride was heated to reflux in the dark. After 1 h the starting material had completely disappeared as evidenced by t.l.c. Addition of hexane to the solution caused the crystallization of 535 mg of the expected 5-bromo lactam **3**, identical in all respects (m.p., i.r., n.m.r.) with an authentic sample. The mother liquors were evaporated to dryness and an n.m.r. spectrum of the residue showed the presence of the three bromo lactams **3**, **4**, and **5**.

The authors gratefully acknowledge financial support from the National Research Council of Canada in the form of a grant to D.G. and a fellowship to J.H.; also from the CEGEP of Jonquière for a fellowship to J.B. We are also indebted to Professor J. Lessard for a fruitful discussion and for making available his manuscript before publication. Finally, we thank the referees for their useful comments and suggestions.

1. E. Cavalieri and D. Gravel. Tetrahedron Lett. 3973 (1967).
2. E. Cavalieri and D. Gravel. Can. J. Chem. **48**, 2727 (1970).
3. R. S. Neale. Synthesis, **1**, 1 (1971).
4. C. E. Boozer and J. W. Moncrief. J. Org. Chem. **27**, 623 (1962).
5. L. Horner and E. H. Winkelmann. Angew. Chem. **71**, 349 (1959).
6. (*a*) K. N. Ayad, C. Beard, R. F. Garwood, and W. J. Hickinbottom. J. Chem. Soc. 2981 (1957). (*b*) F. W. Hodges. J. Chem. Soc. 240 (1933) and references cited therein.
7. Y. L. Chow and T. C. Joseph. Chem. Commun. 490 (1969).
8. Y. L. Chow, N. S. Tam, and A. C. H. Lee. Can. J. Chem. **47**, 2441 (1969).
9. R. S. Neale, N. L. Marcus, and R. G. Schepers. J. Am. Chem. Soc. **88**, 3051 (1966).
10. D. H. R. Barton, A. L. J. Beckwith, and A. Goosen. J. Chem. Soc. 181 (1965).

11. E. J. COREY and W. R. HERTLER. J. Am. Chem. Soc. **82**, 1657 (1960).
12. (*a*) C. WALLING and A. PADWA. J. Am. Chem. Soc. **85**, 1597 (1963). (*b*) M. AKHTAR. *In* Advances in photochemistry. Vol. 2. Interscience Publishers Inc., New York. 1964. pp. 263–303.
13. O. E. EDWARDS, J. M. PATON, M. H. BENN, R. E. MITCHELL, C. WATANATADA, and K. N. VOHRA. Can. J. Chem. **49**, 1648 (1971).
14. (*a*) J. ADAM, P. A. GOSSELAIN, and P. GOLDFINGER. Nature, **171**, 704 (1953); Bull. Soc. Chim. Belges, **65**, 523 (1956); **65**, 533 (1956). (*b*) R. E. PEARSON and J. C. MARTIN. J. Am. Chem. Soc. **85**, 354, 3142 (1963). (*c*) G. A. RUSSELL, C. DEBOER, and K. M. DESMOND. J. Am. Chem. Soc. **85**, 366 (1963); G. A. RUSSELL and K. M. DESMOND. J. Am. Chem. Soc. **85**, 3139 (1963); G. A. RUSSELL and C. DEBOER. J. Am. Chem. Soc. **85**, 3136 (1963). (*d*) C. WALLING, A. L. RIEGER, and D. D. TANNER. J. Am. Chem. Soc. **85**, 3129 (1963); C. WALLING and A. L. RIEGER. J. Am. Chem. Soc. **85**, 3134 (1963). (*e*) J. H. INCREMONA and J. C. MARTIN. J. Am. Chem. Soc. **92**, 627 (1970).
15. S. WOLFE and D. V. C. AWANG. Can. J. Chem. **49**, 1384 (1971).
16. D. TOUCHARD and J. LESSARD. Tetrahedron Lett. 4425 (1971).
17. (*a*) M. P. OPARINA. Ber. **64**, 569 (1931). (*b*) A. DORNOV and O. HAHMANN. Arch. Pharm. **290**, 20 (1957).
18. R. H. COX and A. A. BOTHNER-BY. J. Phys. Chem. **73**, 2465 (1969).
19. (*a*) A. R. KATRITZKY. Physical methods in heterocyclic chemistry. Vol. 2. Academic Press, New York. 1963. p. 260. (*b*) G. H. KELLER, L. BAUER, and C. L. BELL. Can. J. Chem. **46**, 2475 (1968).
20. (*a*) H. SPECKER and H. GAWROSCH. Ber. **75**, 1338 (1942). (*b*) S. F. MASON. J. Chem. Soc. 5010 (1957).
21. H. O. HOUSE. Modern synthetic reactions. W. A. Benjamin Inc., New York. 1965. pp. 56–57.
22. C. K. INGOLD. Structure and mechanism in organic chemistry. 2nd ed. Cornell University Press, Ithaca, N.Y. 1969. p. 826; C. BROADDUS. Acc. Chem. Res. **1**, 231 (1968).
23. (*a*) J. F. WOLFE, G. B. TRIMITSIS, and D. R. MORRIS. J. Org. Chem. **34**, 3263 (1969). (*b*) A. L. NUSSBAUM, G. B. TOPLISS, T. L. POPPER, and E. P. OLIVETO. J. Am. Chem. Soc. **81**, 4574 (1959). (*c*) R. B. WOODWARD, F. E. BADER, H. BICKEL, A. J. FREY, and R. W. KIERSTEADT. Tetrahedron, **2**, 1 (1958). (*d*) T. G. HALSALL, W. J. RODEWALD, and D. WILLIS. Proc. Chem. Soc. 231 (1958). (*e*) C. E. MOPPETT and J. K. SUTHERLAND. J. Chem. Soc. C, 3040 (1968).
24. L. F. FIESER and M. FIESER. Reagents for organic synthesis. Vol. 1. John Wiley and Sons, Inc., New York. 1967. pp. 45, 90, and 197, and references cited therein.
25. R. E. BUCKLES, B. T. SIMPSON, and W. F. EDGELL. J. Org. Chem. **23**, 483 (1958).
26. A. I. POPOV, K. C. BRINKER, L. CAMPANARO, and R. W. RINEHART. J. Am. Chem. Soc. **73**, 514 (1951).
27. H. K. HALL, Jr. J. Am. Chem. Soc. **79**, 5444 (1957).
28. Y. H. MAZUR. J. Org. Chem. **26**, 1289 (1961).

Can. J. Chem. Downloaded from www.nrcresearchpress.com by 210.87.254.42 on 09/05/12
For personal use only.

Molecular Association of Hydrogen Bonding Solutes, *o*-, *m*-, and *p*-Cresol, in Carbon Tetrachloride

EARL M. WOOLLEY AND DENNIS S. RUSHFORTH

Department of Chemistry, Brigham Young University, Provo, Utah 84601

Received August 20, 1973

The intermolecular hydrogen-bonding self-association of the three cresols in CCl_4 solutions at 25 °C has been investigated by calorimetric means. Calorimetrically determined heats of dilution of each of the cresols in anhydrous CCl_4 are interpreted in terms of two different models: (*i*) dimerization and trimerization self-association reactions, and (*ii*) dimerization followed by stepwise polymerization self-association reactions. Values of K, ΔH^0, and ΔS^0 for these reactions are calculated using least-squares and other methods. Results show that *o*-cresol is clearly less associated in anhydrous CCl_4 solution at 25 °C than either *m*- or *p*-cresol. Values of K_2 and K_3 (both based on molar concentrations of solutes) and ΔH_2^0 and ΔH_3^0 (kcal) for the reactions $2C \rightleftharpoons C_2$ and $3C \rightleftharpoons C_3$, respectively, are *o*-cresol: 0.7, $1._3$, $-3._4$, $-12._5$; *m*-cresol: 0.8, $5._0$, $-5._0$, $-13._6$; *p*-cresol: 0.3_5, $6._5$, $-5._5$, $-13._4$. Values of K_2 and K_s (both based on molar concentrations of solutes) and ΔH_2^0 and ΔH_s^0 (kcal) for the reactions $2C \rightleftharpoons C_2$ and $C_{n-1} + C \rightleftharpoons C_n$ (all $n > 2$ with same K_s and ΔH_s^0), respectively, are *o*-cresol: 0.7, 1.6, $-4._2$, $-4._5$; *m*-cresol: 1.2, $4._0$, $-5._0$, $-4._3$; *p*-cresol: 1.0, $7._0$, $-3._3$, $-3._5$.

L'autoassociation par liaisons hydrogènes intermoléculaires des trois crésols dans des solutions de CCl_4 à 25 °C a été étudiée par des méthodes calorimétriques. Les chaleurs de dilution de chacun des crésols dans le CCl_4 anhydre, déterminées calorimétriquement, sont interprétées selon deux modèles différents: (*i*) réactions autoassociatives de dimérisation et trimérisation et (*ii*) dimérisation suivie par des réactions échelonnées autoassociatives de polymérisation. Les valeurs de K, ΔH^0 et ΔS^0 pour ces réactions sont calculées en utilisant les moindres carrés et d'autres méthodes. Les résultats montrent que l'*o*-crésol est nettement moins associé dans une solution de CCl_4 anhydre à 25 °C que le *m*-crésol ou le *p*-crésol. Les valeurs de K_2 et K_3 (toutes deux établies sur les concentrations molaires des produits dissous), de ΔH_2^0 et ΔH_3^0 (kcal) pour les réactions $2C \rightleftharpoons C_2$ et $3C \rightleftharpoons C_3$, sont, respectivement, *o*-crésol: 0.7, $1._3$, $-3._4$, $-12._5$; *m*-crésol: 0.8, $5._0$, $-5._0$, $-13._6$; *p*-crésol: 0.3_5, $6._5$, $-5._5$, $-13._4$. Les valeurs de K_2 et K_s (toutes deux établies sur les concentrations molaires des produits dissous) de ΔH_2^0 et ΔH_s^0 (kcal) pour les réactions $2C \rightleftharpoons C_2$ et $C_{n-1} + C \rightleftharpoons C_n$ (toutes pour $n > 2$ avec le même K_s et ΔH_s^0) sont, respectivement, *o*-crésol: 0.7, 1.6, $-4._2$, $-4._5$; *m*-crésol: 1.2, $4._0$, $-5._0$, $-4._3$; *p*-crésol: 1.0, $7._0$, $-3._3$, $-3._5$.

[Traduit par le journal]

Can. J. Chem., **52**, 653 (1974

Introduction

Many investigations have provided convincing evidence for self-association hydrogen bonding in substituted phenols but there is widespread disagreement concerning the extent of aggregation and a consequent lack of reliable data describing various association reactions (1, 2). Some of these investigations (cited in refs. 1–4) of phenols in CCl_4 and in other "inert" solvents have been interpreted in terms of monomer–dimer equilibrium. There is now evidence, however, that associated species larger than dimers are important in all but the most dilute solutions (3, 4).

Mecke (5) reviews i.r. data for phenol and *o*- and *p*-cresol in CCl_4 solutions. He has estimated values of ΔH^0 for hydrogen bond formation by evaluating temperature coefficients of $\varepsilon \times C$ (extinction coefficient times analytical concentration of cresol). In an earlier discussion (3) some of the difficulties of this approach to evaluating ΔH^0 values have been discussed.

Recently, Dearden (6) has carefully evaluated spectroscopic data for phenol and *m*- and *p*-cresols in cyclohexane solvent. He has interpreted the data in terms of dimers only, trimers only, and polymers of all sizes. We have previously discussed some of the advantages and disadvantages of these approaches for the phenol–cyclohexane and phenol–CCl_4 systems (4).

Davison (7) and more recently Vanderborgh, Armstrong, and Spall (8) have made freezing point depression measurements (sometimes complicated by solid solution formation) on the cresols in benzene solution. They have interpreted the data according to various reactions and mathematical models and have obtained thermodynamic values significant enough to try to interpret in terms of steric, resonance, and/or inductive effects.

Can. J. Chem. Downloaded from www.nrcresearchpress.com by 210.87.254.6 on 09/05/12
For personal use only.

TABLE 1. Relative apparent molar enthalpies of the cresols in CCl_4

Cresol concentration (F)	$-\phi_L$ (cal/mol)		
	o-Cresol	*p*-Cresol	*m*-Cresol
0.0100	27	60	32
0.0200	55	122	75
0.0300	82	187	127
0.0400	110	251	186
0.0500	137	315	252
0.0600	164	380	327
0.0700	191	445	402
0.0800	219	509	477
0.0900	249	572	552
0.1000	278	637	630
0.1100	306	699	700
0.1200	335	760	767
0.1300	363	819	840
0.1400	391	880	910
0.1500	420	940	978
0.1600	447	999	1047
0.1700	475	1056	1104
0.1800	502	1111	1162
0.1900	529	1163	1225
0.2000	557	1215	1278
0.2100	584	1265	1334
0.2200	611	1315	1390
0.2300	637	1363	1439
0.2400	664	1411	1485
0.2500	691	1456	1530
0.2600	719	1503	1572
0.2700	745	1548	1615
0.2800	773	1589	1654
0.2900	—	1624	1684
0.3000	—	1660	1714
0.3100	—	1693	—
0.3200	—	1725	—
0.3300	—	1752	—
0.3400	—	1777	—
1.4790	2100	—	—
2.0001	2135	—	—
1.8101	—	3340	—
2.0005	—	3360	—
1.4870	—	—	3180
2.0002	—	—	3280

We have undertaken the calorimetric measurements described in this paper to obtain data relevant to the identification and quantitative thermodynamic description of the principal self-association reactions of *o*-, *m*-, and *p*-cresol in CCl_4 solutions. These results will hopefully provide more complete insight into substituent effects on hydrogen bonding processes.

Experimental

Aldrich Gold Label cresols and Baker "Instra-Analyzed" GC-Spectrophotometric quality carbon tetrachloride were used. Considerable care was taken to prepare and keep all solutions and solvents free from water. All measurements were made at 25.0 ± 0.2 °C.

Calorimetric measurements of heats of dilution of the cresols in anhydrous CCl_4 were made with the Tronac 450 Adiabatic Titration Calorimeter (50 ml vessel) coupled to the Tronac 1040 Precision Temperature Controller and a Sargent–Welch SRG recorder. The calorimeter was modified to include a Metrohm Herisau Dosimat piston buret. All results are reported in terms of the calorie defined equal to 4.184 J. All solute concentrations are expressed in terms of molarities and activity coefficients are assumed to be unity (3, 4).

Results and Discussion

Our heat of dilution results are reported in Table 1 in the form of ϕ_L values. The relative apparent molar enthalpy, ϕ_L, is equal to the negative of the enthalpy of dilution of 1 mol of

Can. J. Chem. Downloaded from www.nrcresearchpress.com by 210.87.254.6 on 09/05/12
For personal use only.

Can. J. Chem. Downloaded from www.nrcresearchpress.com by 210.87.254.6 on 09/05/12
For personal use only.

solute from a solution of specified formal concentration to infinite dilution. Values of ϕ_L in Table 1 are taken from large scale plots of ϕ_L *vs.* formal cresol concentration, F, based on a very large number of experimental determinations of heats of dilution using titrant solutions 1.4790 and 2.0001 F in *o*-cresol, 1.8101 and 2.0005 F in *m*-cresol, and 1.4870 and 2.0002 F in *p*-cresol.

Following the methods developed earlier (3, 4) for phenol in "inert" solvents, we first consider interpretation of our ϕ_L results in terms of a single equilibrium represented by

$$[1] \qquad nC \rightleftharpoons C_n$$

with equilibrium constant expression

$$[2] \qquad K_n = (C_n)/(C)^n$$

in which parentheses indicate concentrations expressed in terms of molarities. Since at any finite formal concentration there will be both monomers and *n*-mers present, while at infinite dilution all *n*-mers are dissociated into monomers, we can express the ϕ_L values by the expression

$$[3] \qquad \phi_L = (\alpha/n)\Delta H_n^0$$

In eq. 3 α represents the fraction of monomeric cresol that is associated in the solution F formal in cresol and ΔH_n^0 represents the molar enthalpy of reaction 1. Using the material balance expression

$$[4] \qquad F = (C) + n(C_n)$$

and the equilibrium constant expression 2 we obtain

$$[5] \qquad K_n = \alpha/nF^{n-1}(1 - \alpha)$$

We have tested eqs. 3 and 5 with our ϕ_L results with a computer to find the value of K_n that leads to the most consistent value of ΔH_n^0 for each of the three cresols. This approach shows that the ϕ_L values in Table 1 do not fit eqs. 3 and 5 well for any n and K_n values when we consider only one possible *n*-mer reaction [1].

In an alternative approach we may take differences in ϕ_L values from Table 1 for each cresol and treat them according to eq. 6, which we obtain by combining two equations of the form of eq. 3.

$$[6] \qquad (\phi_L - \phi_L') = \Delta\phi_L = (\alpha - \alpha')\Delta H_n^0/n$$

Tabulated ϕ_L values are based on measured heats of dilution from one finite formal concentration to another, combined with an extrapolated heat of dilution to zero formal concentration. The use of eq. 6 eliminates any uncertainty that may arise in the ϕ_L values as a result of this extrapolation. However, the use of eq. 6 in analyzing the ϕ_L values in Table 1 also shows that the model of a single *n*-mer in equilibrium with monomer is not a good model for any n and K_n values over the range of concentrations studied here.

In an equation analogous to [3] but written in terms of (C_n) rather than α, we have

$$[7] \qquad \phi_L = \Delta H_n^0 (C_n)/F$$

Combination of eqs. 2, 4, and 7 leads to (3, 4)

$$[8] \qquad \phi_L = (\Delta H_n^0/n) + (1/n)(-\Delta H_n^0)^{(n-1)/n} \times (1/K_n)^{1/n}(-\phi_L/F^{n-1})^{1/n}$$

Values of ΔH_n^0 and K_n can be obtained from the slope and intercept of a plot of ϕ_L *vs.* $(-\phi_L/F^{n-1})^{1/n}$ for the correct value of n.

The approach based on eq. 8, as with the other approaches based on a *single* association reaction 1 between monomer and *n*-mer molecules, fails to fit the experimental ϕ_L results for the cresols satisfactorily, as illustrated in Figs. 1 and 2. If we ignore the low concentration parts (dimers?) of the curves in Fig. 2, we can estimate from the *approximately* linear left-hand portions

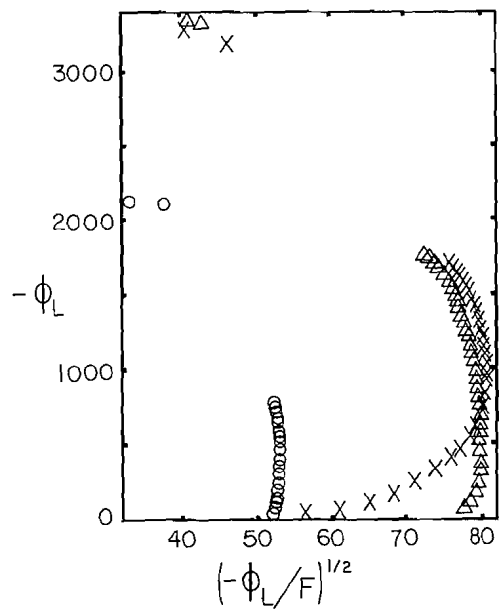

FIG. 1. Plots of $-\phi_L$ *vs.* $(-\phi_L/F)^{1/2}$ according to eq. 8 with $n = 2$ (monomer–dimer only) for *o*-cresol (○), *m*-cresol (△), and *p*-cresol (×) in CCl_4 at 25 °C.

TABLE 2. "Best" thermodynamic functions* for self-association of the cresols in carbon tetrachloride at 25 °C based on the monomer–dimer–trimer model (eqs. 1, 2, 9, and 10)

Parameter	Value		
	o-Cresol	*m*-Cresol	*p*-Cresol
$2C \rightleftharpoons C_2$			
K_2	$0.7(\pm 0.3)$	$0.8(\pm 0.3)$	$0.3_5(\pm 0.1_5)$
ΔG_2^0 (kcal)	$0.2(\pm 0.3)$	$0.1(\pm 0.3)$	$0.6(\pm 0.3)$
ΔH_2^0 (kcal)	$-3._4(\pm 1._0)$	$-5._0(\pm 1._0)$	$-5._5(\pm 1._0)$
ΔS_2^0 (cal/deg)	$-12(\pm 4)$	$-16(\pm 4)$	$-20(\pm 4)$
$3C \rightleftharpoons C_3$			
K_3	$1._3(\pm 0.4)$	$5._0(\pm 1._5)$	$6._5(\pm 1._5)$
ΔG_3^0 (kcal)	$-0.2(\pm 0.3)$	$-1.0(\pm 0.2)$	$-1.5(\pm 0.2)$
ΔH_3^0 (kcal)	$-12._5(\pm 1._0)$	$-13._6(\pm 0._9)$	$-13._4(\pm 0._8)$
ΔS_3^0 (cal/deg)	$-41(\pm 4)$	$-42(\pm 4)$	$-41(\pm 3)$

*The ± values listed are our estimates of total uncertainties in the various quantities (see Discussion in text). Values of K, ΔG^0, and ΔS^0 are based on molar concentrations of monomers, dimers, and trimers (3).

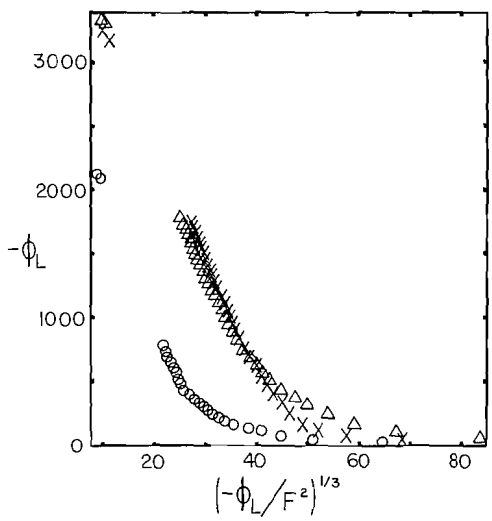

FIG. 2. Plots of $-\phi_L$ *vs.* $(-\phi_L/F^2)^{1/3}$ according to eq. 8 with $n = 3$ (monomer–trimer only) for *o*-cresol (○), *m*-cresol (△), and *p*-cresol (×) in CCl_4 at 25 °C.

of the graphs that $K_3 \sim 6$ and $\Delta H_3^0 \sim -8.6$ kcal for *o*-cresol and that $K_3 \sim 12$ and $\Delta H_3^0 \sim -12.5$ kcal for both *m*-cresol and *p*-cresol. These values lead to $\Delta S_3^0 \sim -25$ and -34 cal/deg for *o*-cresol and for *m*- and *p*-cresols. These results could erroneously indicate that phenol (3) and *o*-cresol trimers in CCl_4 are primarily linear (two H-bonds per trimer) whereas *m*- and *p*-cresol trimers in CCl_4 are primarily cyclic (three H-bonds per trimer).

All three of the above approaches show large systematic concentration-dependent deviations of the data from the single reaction model. We therefore conclude that the cresol–CCl_4 systems must be interpreted in terms of more than one equilibrium reaction.

To carry out analysis of our ϕ_L results in terms of both dimers and trimers ($n = 2$ and $n = 3$ in eq. 1) we write eq. 7 as

$$[9] \qquad \phi_L = \Delta H_2^0(C_2)/F + \Delta H_3^0(C_3)/F$$

Combination of this equation with the material balance equation

$$[10] \qquad F = (C) + 2(C_2) + 3(C_3)$$

and expressions for K_2 and K_3 from eq. 2 permits computer calculations that lead to the most consistent values of K_2, K_3, ΔH_2^0, and ΔH_3^0 in describing the ϕ_L values in Table 1. The thermodynamic quantities obtained in this manner are given in Table 2.

To assess uncertainties in the K_2, K_3, ΔH_2^0, and ΔH_3^0 values reported in Table 2 is a difficult problem. The following calculations illustrate some of the problems associated with estimating uncertainties in K_2, K_3, ΔH_2^0, and ΔH_3^0 values. If we use the K_2 and K_3 values in Table 2 and perform an *absolute* deviation least-squares analysis on the ϕ_L and F results in Table 1 according to eq. 9, we obtain least-squares standard deviations of 4.9, 15.3, and 6.3 cal/mol for *o*-, *m*-, and *p*-cresol when the titrant data are excluded. When the titrant data are included we obtain least-squares standard deviations of 15.2, 23.4, and 16.3 cal/mol for the *o*-, *m*-, and *p*-cresols. Alternatively, if we use the K_2 and K_3 values in Table 2 and perform a *relative* devia-

Can. J. Chem. Downloaded from www.nrcresearchpress.com by 210.87.254.6 on 09/05/12
For personal use only.

TABLE 3. Approximate contribution of dimers and trimers to formal concentrations and relative apparent molar enthalpies for representative data in Table 1 as calculated from K_2, K_3, ΔH_2^0, and ΔH_3^0 values given in Table 2

	o-Cresol	*m*-Cresol	*p*-Cresol
0.0500 *F* cresol solution			
% as monomer	93	90	93
% as dimer	6	7	3
% as trimer	1	3	4
% of ϕ_L from dimer	79	63	38
% of ϕ_L from trimer	21	37	62
0.2500 *F* cresol solution			
% as monomer	73	63	63
% as dimer	18	15	7
% as trimer	9	22	30
% of ϕ_L from dimer	47	32	14
% of ϕ_L from trimer	53	68	86
2.000 *F* cresol solution			
% as monomer	30	22	21
% as dimer	26	15	6
% as trimer	44	63	73
% of ϕ_L from dimer	21	14	6
% of ϕ_L from trimer	79	86	94

tion least-squares analysis (9) of the ϕ_L and F results in Table 1 according to eq. 9, we obtain least-squares standard deviations of 2.2, 2.3, and 3.8% without titrants and 2.3, 2.5, and 4.0% with titrants for the *o*-, *m*-, and *p*-cresols, respectively. In all four of these analyses we obtain slightly different ΔH_2^0 and ΔH_3^0 values. The absolute deviation approach tends to weight the high concentration data most heavily, and the relative deviation approach weights all data equally. The "best" values given in Table 2 are based upon the K_2 and K_3 values that give the smallest standard deviations in the least-squares fit of the data in Table 1 to eq. 9 according to all four of the above approaches.

The relative importance of monomers, dimers, and trimers is illustrated for three formal concentrations of each cresol in Table 3. The concentrations of each species are calculated from the K_2 and K_3 values in Table 2. Also illustrated in Table 3 are the relative importances of enthalpies of dilution due to the dimer and the trimer. These values are calculated using the K_2, K_3, ΔH_2^0, and ΔH_3^0 values listed in Table 2.

We now turn to consideration of interpretation of our ϕ_L results in terms of the monomer–dimer–*n*-mer stepwise association model which we have recently described (4) and used in attempting to interpret phenol association. Following this earlier treatment we write the dimerization reaction and further stepwise self-association reactions for the cresols as follows

$$[11] \qquad 2C \rightleftharpoons C_2$$

$$[12] \qquad C_{n-1} + C \rightleftharpoons C_n \text{ (all } n > 2)$$

Corresponding equilibrium constant expressions are

$$[13] \qquad K_2 = (C_2)/(C)^2$$

and

$$[14] \qquad K_s = (C_n)/(C_{n-1})(C) \text{ (all } n > 2)$$

In this treatment, as before, we take all stepwise equilibrium constants, K_s, to be equal so that there are only two independent equilibrium constants. It is also assumed that there are only two independent enthalpies of reaction, ΔH_2^0 and ΔH_s^0, for the reactions represented by eqs. 11 and 12. We may now obtain, from the material balance equation.

$$[15] \qquad F = \sum_{n=1}^{\infty} n(C_n)$$

and the equilibrium constant expressions in eqs. 13 and 14, the expression (4)

$$[16] \qquad F = \frac{K_2(C)^2[2 - K_s(C)]}{[1 - K_s(C)]^2} + (C)$$

Appropriate extension of eq. 9 gives (4)

Can. J. Chem. Downloaded from www.nrcresearchpress.com by 210.87.254.6 on 09/05/12
For personal use only.

TABLE 4. "Best" thermodynamic functions* for self-association of the cresols in carbon tetrachloride at 25 °C based on the monomer–dimer–stepwise polymer model. (eqs. 11–18)

Parameter	Value		
	o-Cresol	*m*-Cresol	*p*-Cresol
$2C \rightleftharpoons C_2$			
K_2	0.7(±0.2)	1.2(±0.3)	1.0(±0.3)
ΔG_2^0 (kcal)	0.2(±0.2)	−0.1(±0.2)	0.0(±0.2)
ΔH_2^0 (kcal)	−4.2(±0.6)	−5.0(±0.5)	−3.3(±0.5)
ΔS_2^0 (cal/deg)	−15(±2)	−16(±2)	−11(±2)
$C_{n-1} + C \rightleftharpoons C_n$ (all $n > 2$)			
K_s	1.6(±0.4)	4.0(±1.0)	7.0(±2.0)
ΔG_s^0 (kcal)	−0.3(±0.2)	−0.8(±0.2)	−1.2(±0.2)
ΔH_s^0 (kcal)	−4.5(±0.8)	−4.3(±0.5)	−3.5(±0.5)
ΔS_s^0 (cal/deg)	−14(±3)	−12(±2)	−8(±2)

*The ± values listed are our estimates of total uncertainties in the various quantities (see Discussion in text). Values of K, ΔG^0, and ΔS^0 are based on molar concentrations of monomers, dimers and polymers (3, 4).

$$[17] \quad F\phi_L = (C_2)\Delta H_2^0 + \sum_{n=3}^{\infty} \times (C_n)[\Delta H_2^0 + (n-2)\Delta H_s^0]$$

Combination of eqs. 13, 14, and 17 now leads to the expression (4)

$$[18] \quad \phi_L = \frac{K_2(C)^2}{F[1 - K_s(C)]} \times \left\{\Delta H_2^0 + \Delta H_s^0\left[\frac{K_s(C)}{1 - K_s(C)}\right]\right\}$$

Knowledge of values of K_2 and K_s would enable us to evaluate (C) from eq. 16 for each formal concentration of cresol in Table 1. Insertion of these K_2, K_s, and (C) values into eq. 18 would then enable us to evaluate ΔH_2^0 and ΔH_s^0. Since reliable values of K_2 and K_s are not available for the cresols in CCl_4, we have used an iterative computer method to find the values of K_2 and K_s which give the best least-squares fit of the ϕ_L results in Table 1 according to eq. 18. The results of this treatment are given in Table 4.

As in the analysis in terms of monomer–dimer–trimer discussed earlier in this paper, it is difficult to estimate uncertainties to be associated with the quantities listed in Table 4. An *absolute* deviation least-squares analysis of the ϕ_L and F results in Table 1 according to eq. 18 leads to least-squares standard deviations of about 2, 8, and 5 cal/mol for *o*-, *m*-, and *p*-cresol, respectively, when the titrant data are excluded. When the titrant data are included we obtain least-squares standard deviations of about 8, 15, and 15 cal/mol for the *o*-, *m*-, and *p*-cresol. Alternatively, using the K_2 and K_s values in Table 4 to perform a *relative* deviation least-squares analysis (9) of the ϕ_L and F results in Table 1 according to eq. 18, leads to least-squares standard deviations of about 0.4, 0.6, and 1% without titrants and 2, 2, and 2% with titrants for the *o*-, *m*-, and *p*-cresols, respectively.

If we assume that $\Delta H_2^0 = \Delta H_s^0$ in eq. 18 we obtain

$$[19] \quad \Delta H^0 = \phi_L F[1 - K_s(C)]^2/K_2(C)^2$$

Combination of eqs. 16 and 19 leads to values of ΔH^0 for each of the cresols if we know values of K_2 and K_s. By choosing K_2 and K_s so that ΔH^0 is as nearly constant as possible over the entire range of concentrations in Table 1, we obtain the values reported in Table 5. Standard deviations in ΔH^0 values calculated by eq. 19 with the data in Table 1 are about 30, 30, and 40 cal/mol for *o*-, *m*-, and *p*-cresols, respectively, when the titrant data are excluded. When the titrant data are included in the calculations we obtain standard deviations in ΔH^0 values of about 60, 80, and 70 cal/mol for the three cresols.

The relative importance of monomers, dimers, and higher *n*-mers ($n > 2$) is illustrated for three formal concentrations of each cresol in Table 6. The concentrations and relative importances of enthalpies of dilution due to dimers and higher *n*-mers are calculated from the K_2, K_s, ΔH_2^0, and ΔH_s^0 values in Table 4.

Although neither the monomer–dimer–trimer

Can. J. Chem. Downloaded from www.nrcresearchpress.com by 210.87.254.6 on 09/05/12
For personal use only.

TABLE 5. "Best" thermodynamic functions* for self-association of the cresols in carbon tetrachloride at 25 °C based on the monomer – dimer – stepwise polymer model with $\Delta H_2^0 = \Delta H_s^0 = \Delta H^0$ (eqs. 11–19)

	Value		
Parameter	*o*-Cresol	*m*-Cresol	*p*-Cresol
$2C \rightleftharpoons C_2$			
K_2	$0.7(\pm 0.2)$	$1._4(\pm 0.4)$	$0.9(\pm 0.2)$
ΔG_2^0 (kcal)	$0.2(\pm 0.2)$	$-0.2(\pm 0.2)$	$0.1(\pm 0.1)$
ΔH^0 (kcal)	$-4._0(\pm 0._5)$	$-4._3(\pm 0._5)$	$-3._4(\pm 0._5)$
ΔS_2^0 (cal/deg)	$-14(\pm 2)$	$-14(\pm 2)$	$-12(\pm 2)$
$C_{n-1} + C \rightleftharpoons C_n$ (all $n > 2$)			
K_s	$1._8(\pm 0.4)$	$4._0(\pm 1._0)$	$6._0(\pm 2._0)$
ΔG_s^0 (kcal)	$-0.3(\pm 0.1)$	$-0.8(\pm 0.2)$	$-1.1(\pm 0.2)$
ΔH^0 (kcal)	$-4._0(\pm 0._5)$	$-4._3(\pm 0._5)$	$-3._4(\pm 0._5)$
ΔS_s^0 (cal/deg)	$-12(\pm 2)$	$-12(\pm 2)$	$-8(\pm 2)$

*The ± values listed are our estimates of total uncertainties in the various quantities (see Discussion in text). Values of K, ΔG^0, and ΔS^0 are based on molar concentrations of monomers, dimers, and polymers (3, 4).

TABLE 6. Approximate contribution of dimers and higher polymers to formal concentrations and relative apparent molar enthalpies for representative data in Table 1 as calculated from K_2, K_s, ΔH_2^0, and ΔH_s^0 values given in Table 4

	o-Cresol	*m*-Cresol	*p*-Cresol
0.0500 *F* cresol solution			
% as monomer	93	86	88
% as dimer	6	10	8
% as *n*-mer ($n > 2$)	1	4	4
% of ϕ_L from dimer	91	86	74
% of ϕ_L from *n*-mer ($n > 2$)	9	14	27
0.2500 *F* cresol solution			
% as monomer	35	49	44
% as dimer	17	17	10
% as *n*-mer ($n > 2$)	48	34	46
% of ϕ_L from dimer	64	50	34
% of ϕ_L from *n*-mer ($n > 2$)	36	50	66
2.000 *F* cresol solution			
% as monomer	20	16	9
% as dimer	11	14	4
% as *n*-mer ($n > 2$)	69	70	87
% of ϕ_L from dimer	26	4	2
% of ϕ_L from *n*-mer ($n > 2$)	74	96	98

model nor the monomer – dimer – stepwise polymer model fits the data a great deal better than the other, we can say something, however, concerning the relative strengths and weaknesses of these two models. The monomer – dimer – stepwise polymer model constrains all K_s and ΔH_s^0 values to be the same regardless of polymer size. This is a reasonable assumption *if* the polymers assume linear conformations, but there is considerable evidence that this may not be the case (3, 4). The monomer–dimer–trimer model assumes only *negligible* amounts of higher polymers in solutions of the formal concentrations studied. This is most reasonable for low concentrations. The thermodynamic data given in Tables 2–6 do not appear to be unreasonable for either model.

We may use the data in Table 2 for the monomer–dimer–trimer model to estimate the relative importances of cyclic and linear dimers

Can. J. Chem. Downloaded from www.nrcresearchpress.com by 210.87.254.6 on 09/05/12
For personal use only.

in the following manner. If we assume that *o*-cresol is so sterically hindered near the —OH group that it forms *no* cyclic dimers, we may say that single bonded dimers contribute $-3._4$ kcal/mol of dimer formed. If it takes another $-3._4$ kcal/mol to form the cyclic dimer from the linear dimer, it can be shown that the ratios of cyclic dimer to linear dimer are 0, 0.9, and 1.7 for the *o*-, *m*-, and *p*-cresols, respectively.

We thank the Brigham Young University Research Division for support of part of this work.

1. M. M. DAVIS. Nat. Bur. Stand. (U.S.) Monogr. 105 (1968).
2. G. C. PIMENTEL and A. L. MCCLELLAN. The hydrogen bond. W. H. FREEMAN, San Francisco. 1960.
3. E. M. WOOLLEY, J. G. TRAVERS, B. P. ERNO, and L. G. HEPLER. J. Phys. Chem. **75**, 3591 (1971).
4. E. M. WOOLLEY and L. G. HEPLER. J. Phys. Chem. **76**, 3058 (1972).
5. R. MECKE. Disc. Faraday Soc. **9**, 161 (1950).
6. J. C. DEARDEN. Can. J. Chem. **41**, 2683 (1963).
7. J. A. DAVISON. J. Am. Chem. Soc. **67**, 228 (1945).
8. N. E. VANDERBORGH, N. A. ARMSTRONG, and W. D. SPALL. J. Phys. Chem. **74**, 1734 (1970).
9. K. P. ANDERSON and R. L. SNOW. J. Chem. Educ. **44**, 756 (1967).

Can. J. Chem. Downloaded from www.nrcresearchpress.com by 210.87.254.6 on 09/05/12
For personal use only.

2,3-Dioximes of Various Substituted Acetoacetamides and Their Metal Chelates

ANTONIUS KETTRUP AND KLAUS STRIEGLER

Department of Chemistry, Ruhr-University Bochum, 463 Bochum

and

Department of Chemistry, Gesamthochschule Paderborn, 479 Paderborn, Federal Republic of Germany

Received May 23, 1973

Methods of preparing 2,3-dioximes of various substituted acetoacetamides are presented. The dissociation constants of these compounds and the stability constants of their metal chelates were determined by potentiometric p*H* measurements. The influence of the substituents of the amide group on the change of stability is discussed.

Les méthodes pour préparer les 2,3-dioximes de divers acétoacétamides substitués sont présentées. Les constantes de dissociation de ces composés ainsi que les constantes de stabilité de ses chélates métalliques ont été déterminées par des p*H* mesurages potentiométriques. L'influence des substituantes du groupe amide sur le changement de la stabilité est discutée.

Can. J. Chem., **52**, 661 (1974)

Can. J. Chem. Downloaded from www.nrcresearchpress.com by 210.87.254.6 on 09/05/12
For personal use only.

In order to examine the relation between the structure of a chelating agent and its properties to form chelates, we prepared more than 300 various substituted acetoacetamides. The stability constants of metal chelates of acetoacetdialkylamides, as well as various substituted acetoacetarylamides, show that even substituents which are more distant from the chelate ring exercise a fundamental influence on the stability of metal chelates (1–3).

By substituting a hydrogen atom of the CH_2 group in central position we obtained 2-halo-, 2-nitro-, and 2-alkylacetoacetamides which differ fundamentally from the corresponding non-substituted chelating agents in their ability to form chelates (4, 5).

An oxime group was introduced into the 3-position of the acetoacetamides for preparing the 3-monoximes of the acetoacetamides, a group of compounds forming very stable metal chelates (6). Carrying on the previous work, the present study examines the 2,3-dioximes of the acetoacetamides and their employment as chelating agents.

Experimental

The Preparation of 2,3-Dioximes

The preparation of the chelating agents was based on two patent specifications which describe the production and use of fast pigments (7, 8).

Acetoacetanilide (0.1 mol) was dissolved in a mixture of 25 ml glacial acetic acid and 25 ml formic acid and 500 ml distilled water added. Sodium nitrite (0.11 mol) was added dropwise and the solution stirred for 1 h at 10°. The temperature was increased to 70°, 0.2 mol hydroxylammonium chloride added dropwise, and the solution neutralized with 0.2 mol sodium acetate. The dioxime **1** settles as a light yellow precipitate.

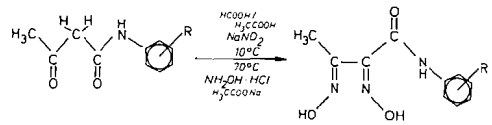

The Preparation of the Metal Chelates

The metal chelates were prepared in a mixture of methyl alcohol and water (50:50). The chelating agent was dissolved in methanol. An excess of sodium acetate was added to capture protons evolved during complex formation. The metallic salt was added at 55° in the form of an aqueous metal perchlorate solution. The Co(II) and Fe(II) chelates were prepared under nitrogen atmosphere. The metal chelates thus obtained are insoluble in nearly all organic solvents, especially the Ni(II), Co(II), and Cu(II) complexes; therefore, it is possible to remove an excess of the chelating agent by extraction with alcohol.

Nuclear Magnetic Resonance Spectra

The proton n.m.r. spectra were recorded at 60 MHz (Bruker-Spectrospin) in hexadeuteroacetone solution and chemical shifts are relative to internal tetramethylsilane.

Mass Spectra

The mass spectra were obtained with a SM 1 double-focusing mass spectrometer (Varian MAT) at 30 eV and calibrated with perfluorokerosene. The temperature of the ion source was 220° and the compounds were heated up to this temperature to produce an ion current of 10^{-11}–10^{-12}. The molecular masses were determined with an automatic comparator SAM 1 (Leitz-Varian-MAT) and in a final calculation (IBM 360/44) determined to 0.001 u.

TABLE 1. Elemental analyses, yields and melting points of acetoacetamide- and -anilide-2,3-dioximes

Dioxime	Melting point (°C)	Yield (%)	Elemental analyses (%) C Calcd.	C Found	H Calcd.	H Found	N Calcd.	N Found
Acetoacet-								
diethylamide	Subl. 178	55	47.75	47.68	7.56	7.52	20.90	20.83
dipropylamide	Subl. 180	57	52.41	52.84	8.30	8.73	18.35	18.89
dibutylamide	Subl. 147	37	56.01	55.78	8.95	9.66	16.35	16.35
N-benzylamide	Subl. 162	32	56.18	56.50	5.54	5.65	17.88	17.93
N-methyl-*N*-benzylamide	Subl. 183	61	57.78	57.76	6.03	6.50	16.85	16.59
p-nitranilide	127–128.5	40	45.20	45.48	3.76	4.06	21.03	20.85
m-nitranilide	148–149.5	52	45.20	45.23	3.76	4.01	21.03	20.83
p-amino-azobenzene	Subl. 155	76	59.25	59.34	4.65	4.75	21.53	21.73

Potentiometric Measurements

These were carried out with a super potentiograph E 436 (Metrohm) in a constant temperature (20 ± 0.5°) container. An electrode E 121 UX (Metrohm) (0–14 p*H*, 15–100°) was used as a surveyor's chain. The calibration was carried out in a standardized buffer solution. The accuracy of measurement was ± 0.02 p*H* units for the p*H* values 1–13. $HClO_4$ (1 mmol) and $NaClO_4$ (25 mmol) were mixed in 100 ml water–dioxane (50:50) for the titration. A solution of carbonate-free sodium hydroxide (1 *N*) was added in small amounts at a rate of 1 ml/5 min.

Magnetic Measurements

The magnetic moments were determined by the Gouy method with a research magnet B-E 10 C 8 (Bruker) at 294 °K and calibrated with $HgCo(SCN)_4$.

Infrared Spectra

The i.r. spectra were obtained on a Perkin-Elmer 225 spectrophotometer using CsJ plates of thickness 0.025 mm. The samples were measured as a Nujol mull and spectra recorded in the range 4000–200 cm^{-1}.

Results and Discussion

The new chelating agents are presented in Table 1. The compounds were analyzed mass spectroscopically. All mass spectra show the molecular peak. The line spectrum of 2,3-dioxime of acetoacetdibutylamide is given in Fig. 1. The molecular ion of this 2,3-dioxime has a mass of 257 and loss of a hydroxyl group gives an ion of mass 240. The fragmentation pattern may be interpreted as shown in Fig. 2.

The intensities (*I*) of the fragmentation ions of acetoacetdibutylamide-2,3-dioxime (A) and acetoacetbenzylamide-2,3-dioxime (B) are collected in Table 2. The fragment ions ($M - CH_3R$) probably indicate a McLafferty rearrangement as given in Fig. 3.

The fragmentation ions of acetoacetdibutyl-

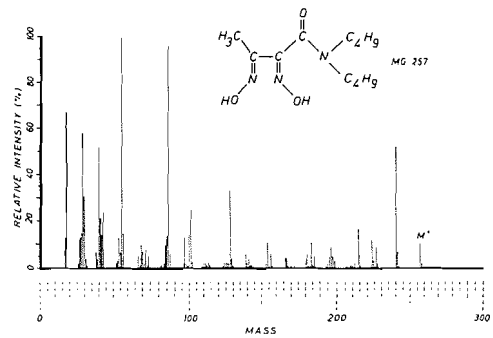

FIG. 1. Line spectrum of acetoacetdibutylamide-2,3-dioxime.

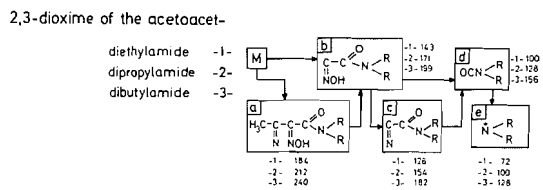

FIG. 2. Decay mechanism of acetoacetdialkylamide-2,3-dioximes.

amide-2,3-dioxime with the masses 214 and 86 show intensities of 17.70 and 96.98%. We will corroborate this possibility in further studies. Further fragmentation of acetoacetdialkylamides to give ions 86 (96.98%), 72 (8.62%), 58 (100%), 43 (24.64%), and 29 (58.81%) occurs in the same way as shown for acetoacetdibutylamide-2,3-dioxime. Up to the fragmention *c* the decay of acetoacetbenzylamide-2,3-dioximes and acetoacetarylamide-2,3-dioximes follows the same pattern as found with the decomposition of acetoacetdi-

Can. J. Chem. Downloaded from www.nrcresearchpress.com by 210.87.254.6 on 09/05/12
For personal use only.

TABLE 2. Relative intensities of peaks in fragmentation of acetoacetdibutylamide-2,3-dioxime (A) and acetoacetbenzylamide-2,3-dioxime (B)

Ion (A)	I(%)	Ion (B)	I (%)	Ion	I(%)	Remarks
M^+	11.01	M^+	3.78	85	4.24	C_4H_9CO
a	52.77	*a*	25.56	77	4.29	Decomposition
b	3.79	*b*	0.36	65	9.36	of the
c	1.49	*c*	0.64	51	3.35	phenyl ion
d	6.35	*d'*	4.80	39	4.05	
e	34.65	*e'*	18.97	58	1.89	CH_2=C(OH)—CH_3
		f	100.00	28	10.85	C_2H_4 or N_2

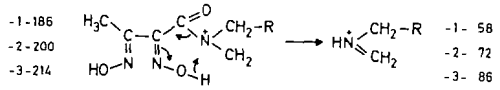

FIG. 3. McLafferty rearrangement.

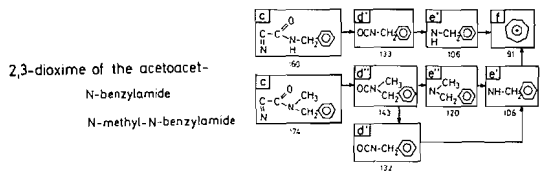

FIG. 4. Decay mechanism of acetoacet-*N*-benzylamide-2,3-dioxime.

alkylamide-2,3-dioximes. Further fragmentation of ions gives the results shown in Fig. 4.

With the aid of n.m.r. spectroscopy, the position of the oxime group in the molecule could be determined. By coupling the oxime groups with adjoining groups the resonance positions of these groups are displaced.

In comparison with the acetoacetarylamides, the n.m.r. spectrum of the dioxime as well as of the monoxime shows an upfield chemical shift of the methyl hydrogens. The chemical shifts in p.p.m. are: acetoacet-*p*-toluidide, 2.35; -*p*-toluidide-3-monoxime, 1.92; and -*p*-toluidide-2,3-dioxime, 1.97. The signals of the ring protons, however, are not influenced. These facts indicate that the oxime was formed in the 3-position. The absence of a signal of the hydrogen atoms of the methylene group on the one hand and the occurrence of the signal of a second hydroxyl proton (11.07 p.p.m.) on the other hand proves the oximation of the methylene group. Further evidence for the introduction of an oxime group in the 2-position is given by the displacement chemical shift of the amide proton to lower field, which can be explained by the introduction of an electron withdrawing oxime group instead of the electron donating methylene group: -3-monoxime, 9.15 p.p.m. and -2,3-dioxime, 9.25 p.p.m. Similarly, the oxime group, being adjacent to the methyl group, is displaced to lower field, compared with the corresponding monoxime: -3-monoxime, 9.77 p.p.m. and -2,3-dioxime, 10.21 p.p.m.

The n.m.r. and mass spectra, as well as the elemental analyses, thus confirm that the chelating agents are the 2,3-dioximes of the acetoacetamides.

The calculation of the dissociation constants of the chelating agents as well as the stability constants of the metal chelates was carried out by potentiometric analyses of the hydrogen ion concentration (1, 9–11). The trend of the titration curve shows that in aqueous solution the dioximes of the acetoacetamides form 1:2 chelates with bivalent ions. In Table 3 the dissociation constants pK_D of the chelating agents and the stability constants pK of some metal chelates are presented.

The values of the stability constants show that only Co(II) chelates have comparable values as has already been determined in previous work (1–6). The stability diminishes in the order 2,3-dioximes of the acetoacetanilide, -toluidide, -nitranilide, and -chloranilide; all these substituents have the same position in the ring. This phenomenon can be explained by the relation of the conjugation of the chelate ring to the electron density at the amide nitrogen. Substituents at the phenyl ring having a positive mesomeric effect, *e.g.* the ethoxy or methyl group, obviously favor mesomeric structures which increase electron density at the amide nitrogen.

The basicity constant pK_B of aniline is a measure for the electron density of the amino group nitrogen and in case of acetoacetanilide for the electron density of amide nitrogen.

When plotting the average stability constants

Can. J. Chem. Downloaded from www.nrcresearchpress.com by 210.87.254.6 on 09/05/12
For personal use only.

TABLE 3. Dissociation constants of the acetoacetamide- and -anilide-2,3-dioximes and the stability constants of some metal complexes (50% dioxane, $I = 0.048$)

Dioxime	pK_D	Co(II)			Cu(II)			Ni(II)			Zn(II)		
		pK_1	pK_{av}	pK_2	pK_1	pK_{av}	pK_2	pK_1	pK_{av}	pK_2	pK_1	pK_{av}	pK_2
Acetoacet-													
diethylamide	10.95	9.60	8.92	8.54	10.09	9.80	9.17	8.93	8.66	8.42	8.31	6.87	6.56
dipropylamide	11.00	9.61	8.95	8.60	10.17	9.89	9.34	9.14	8.78	8.63	8.46	7.01	6.70
dibutylamide	10.99	9.52	8.89	8.58	10.13	9.78	8.94	9.18	8.82	8.51	8.42	7.02	6.71
N-benzylamide	10.72	9.18	8.60	8.30	10.04	9.78	9.19	8.86	8.63	8.36	7.78	6.41	6.24
N-methyl-*N*-benzylamide	10.85	8.59	8.15	7.84	9.35	8.95	8.27	8.13	7.88	7.61	7.92	6.59	6.40
anilide	10.49	8.95	8.36	8.06	—	—	—	—	—	—	7.65	6.45	6.20
p-anisidide	10.09	9.44	8.43	8.12	—	—	—	—	—	—	7.31	6.03	5.74
m-anisidide	10.38	9.01	8.32	8.07	—	—	—	—	—	—	7.50	6.10	5.91
o-anisidide	10.08	8.96	8.35	7.92	—	—	—	—	—	—	7.19	5.76	5.59
p-toluidide	10.35	9.22	8.41	8.15	—	—	—	—	—	—	7.53	6.10	5.87
m-toluidide	10.65	8.88	8.46	8.13	—	—	—	—	—	—	7.74	6.90	6.28
o-toluidide	10.25	8.45	8.14	7.55	—	—	—	—	—	—	7.18	5.80	5.62
p-chloranilide	7.48	6.92	5.77	5.42	—	—	—	—	—	—	4.78	3.32	3.01
m-chloranilide	7.30	6.73	5.62	5.30	—	—	—	—	—	—	4.50	3.08	2.83
o-chloranilide	8.99	8.23	7.45	7.18	—	—	—	—	—	—	6.09	4.69	4.42
p-nitranilide	7.89	7.39	6.21	5.73	—	—	—	—	—	—	5.29	3.85	3.47
m-nitranilide	8.55	8.38	7.27	6.77	—	—	—	—	—	—	5.81	4.29	4.03

against the basicity constants of the corresponding anilines, only the 2,3-dioximes of the acetoacetanilides, substituted in *meta* position, have a linear relationship.

As shown in Fig. 5, a substituent which has a distinctly negative mesomeric effect, such as the nitro group, reduces the stability of the metal chelate. In addition, this substituent has a negative inductive effect, especially in the *ortho* or *meta* position.

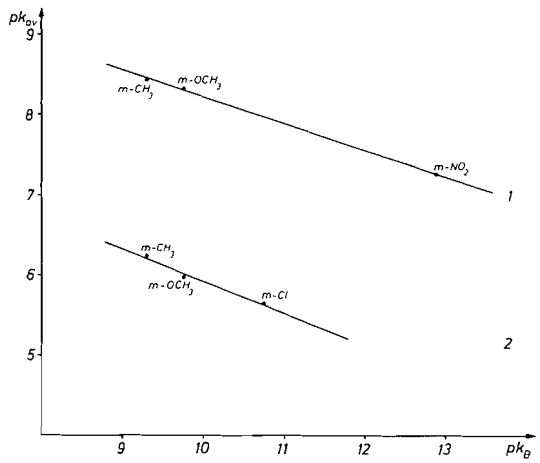

FIG. 5. Relationship between the stability constants pK_{av} of Co(II) complexes with acetoacetarylamide-2,3-dioximes (curve 1) and acetoacetarylamides (curve 2), and the basicity constants pK_B of the corresponding anilines.

Comparing the i.r. spectra of various similar compounds (12–16) we pointed out that the metal in the metal chelates of acetoacetamide-2,3-dioximes is coordinated to the nitrogens of the oxime groups. As an example from the compounds prepared for this study, the frequencies of the i.r. spectrum of acetoacet-*p*-toluidide-2,3-dioxime (HA) and its metal chelate (MeA_2) are collected in Table 4.

The frequencies of the C=N and the R—CO—NH vibrations in the i.r. spectra of the metal chelates are shifted to lower values in comparison to the i.r. spectra of the chelating compounds. This shift is related to the strength of the metal $\rightarrow$N=C donor π-bond.

The probability of the formation of a donor π-bond, and therefore the strength of a bond of this nature, depends on the energy difference between the d-electrons of the metal and the π-electrons of the ligand. The energy of the electrons participating in the formation of the donor π-bond can be characterized by the energy required for the further ionization of the metal ion in question (by the third ionization potential in the case of bivalent metals). The lower this latter value, the more probable is the formation of a donor π-bond in the case of the same ligand and,

Can. J. Chem. Downloaded from www.nrcresearchpress.com by 210.87.254.6 on 09/05/12
For personal use only.

TABLE 4. Frequencies of the i.r. spectra of the acetoacet-*p*-toluidide-2,3-dioxime and its metal chelates

Frequency (cm^{-1})	HA	CoA_2	NiA_2	CuA_2
ν(NH)	3280m	3170m	3200m	3210m
ν(OH)	3180w	3120m	2380w	2420m
δ(OH)	1730sh	1730w	1650m	1670w
ν(C=N)	1660s	1600s	1625m	1632s
ν′(C=N)	1603m	1550s	1585m	1600s
ν(CO—NH)	1548m	1520sh	1525m	1535m
ν(NO)	1160w	1155s	1120m	1150s
ν′(NO)	990w	980m	985w	990m
γ(OH)	905m	—	—	—
ν(Me—N)	—	588w	570w	556w
ν′(Me—N)	—	460m	410w	395m

thus, the more stable is the donor π-bond. This assumption has been presented in a simplified way, as ligand field effects and the symmetry of the orbitals in complexes were not taken into account. As the Co(II) complex of the acetoacet-*p*-toluidide-2,3-dioxime shows the lowest frequency of the C=N vibration, it can be seen that more conjugation takes place in the chelate ring of this complex.

Plotting the frequencies of the C=N vibration of the metal chelates against the third ionization potential of the metals gives a nearly linear correlation. The strength of the donor π-bond increases in the order Cu < Ni < Co.

The properties of the 2,3-dioximes of the acetoacetamides which differ in all other cases from the acetoacetamides, and from their corresponding 3-monoximes, can be explained by the following factors: instead of an oxygen atom the donor is a nitrogen atom, the distance of the donor atoms being much smaller, which causes the chelate ring to become smaller and not planar; the acid character of the acetoacetamides is dependent on the dissociation of the enol form corresponding to the keto–enol tautomerism (17). Although the enol form, in the monoxime, forms stable hydrogen chelates, this is not the case with the dioximes. Because of the fact that the measured K_D values do not correspond to the real dissociation constant K_E, the relatively low K_D values can be explained. The metal complex of the acetoacetamides holds two hexatomic chelates, compared to two pentatomic chelates for the corresponding 2,3-dioximes, whereby their stability can be further raised by formation of two additional hexatomic chelates which are formed by hydrogen bonds. The chelate rings do not possess a quasi-aromatic character. The dissociation and stability constants of the 2,3-dioximes show good agreement with the values reported by Banks and Anderson (18). In this context it has also been found that the stability of the metal chelates with an increasing volume is largely influenced by steric interferences. Increasing the length of the alkyl chain does not always lead to increased stability. The increase of electron density at the amide nitrogen, which is otherwise accompanied by an increasing stability, is exceeded by the steric influence.

On the basis of the present data the stability of the metal chelates decreases in the order

$$Cu > Co \gtrless Ni \gg Zn,$$

which corresponds to the rule of Irving and Williams about the stability of metal chelates (19).

Measurements of the magnetic properties of the complexes are of decisive importance for experiments concerning the structure and formation of chelates.

Nickel and palladium (both bivalent) have theoretically either two unpaired electrons with $\mu_{eff} = 2.83$ B.M. or no unpaired electrons with $\mu_{eff} = 0.0$ B.M. For the prepared Ni(II) complex, $\chi_M = -64$. This suggests that the complex is diamagnetic and possibly has a square-planar dsp^2 structure. Banks *et al.* (20) report similar values. The χ_M values of the Ni(II) complexes of various *vic*-dioximes are: $Ni(DMG)_2$ $\chi_M = -106$, bis(1,2-cyclohexadionoximato-*N*,*N*′)nickel(II) $\chi_M = -134$. The relatively small value of the molar susceptibility can probably be explained in terms of small amounts of the dimeric complex having a weakening effect on the magnetic susceptibility. A conclusive proof of the dimeric

Can. J. Chem. Downloaded from www.nrcresearchpress.com by 210.87.254.6 on 09/05/12
For personal use only.

complex of the prepared Ni(II) complex could not be found; however, the dimension of the spherical caps model indicates that this is generally possible. The X-ray structure analysis of this molecule remains to be done and shall furnish the conclusive proof of this hypothesis.

The Co(II) complex has a magnetic moment of $\mu_{eff} = 1.87$ B.M. There are numerous examples (21–23) for this typical low-spin complex: $Co(DMG)_2$, for instance, being quadruply square-planar coordinated, has a magnetic moment of $\mu_{eff} = 2.6$ B.M. Comparison with $Co(DMG)_2 \cdot H_2O$ ($\mu_{eff} = 1.92$ B.M.) gives an analogous value (23). The magnetic moment of the Cu(II) complex ($\mu_{eff} = 1.76$ B.M.) can be arranged among the first group of the Cu(II) complexes as postulated by Ray and Sen (24). In these cases the magnetic moments amount to 1.72–1.82 B.M., the bond being mainly covalent with a dsp^2 hybrid, the color being black, brown and red, or yellowish-green. Another possibility is that a dimeric complex impurity lowers the normal magnetic moment from $\mu_{eff} = 1.91$ to 1.76 B.M. (25–27). The magnetic moment of the Fe(III) complex with $\mu_{eff} = 5.15$ B.M. indicates a relatively normal high-spin complex (27). The magnetic moments of the Fe(II) complexes with acetoacetamide-2,3-dioximes were measured as a function of temperature. The values obtained point to a high-spin → low-spin transition. We will corroborate these measurements and publish the results in a subsequent paper.

1. A. KETTRUP and H. SPECKER. Z. Anal. Chem. **246**, 108 (1969); **246**, 183 (1969).
2. G. STÖCKELMANN, A. KETTRUP, and H. SPECKER. Z. Anorg. Allgem. Chem. **372**, 134 (1970); **372**, 144 (1970).
3. A. KETTRUP and W. RIEPE. Z. Anal. Chem. **252**, 1 (1970).
4. A. KETTRUP and J. ABSHAGEN. Z. Naturforsch. **25**, 1382 (1970); **25**, 1386 (1970).
5. A. KETTRUP and M. GROTE. Mh. Chem. **104**, 1333 (1973).
6. A. KETTRUP and T. NEUSTADT. Z. Naturforsch. **28***b*, 86 (1973).
7. P. DIMROTH, D. P. 1.252.341 (2.5.1968).
8. BASF. F. P. 1.527.379 (14.6.1967).
9. M. CALVIN and K. W. WILSON. J. Am. Chem. Soc. **67**, 2003 (1945).
10. G. VAN UITERT, W. FERNELIUS, and B. E. DOUGLAS. J. Am. Chem. Soc. **75**, 2736 (1953).
11. J. BJERRUM. Metal ammine formation in aqueous solution. P. Haase and Sohn, Kopenhagen. 1941.
12. R. C. VOTER, C. V. BANKS, V. A. FASSEL, and P. W. KEHRES. Anal. Chem. **23**, 1730 (1951).
13. S. SATPATHY and B. SAKOO. J. Inorg. Nucl. Chem. **33**, 1313 (1971).
14. R. BLINC and D. HADZI. J. Chem. Soc. 4536 (1958).
15. N. H. CROMWELL and D. J. CRAM. J. Am. Chem. Soc. **71**, 3337 (1949).
16. K. BURGER, J. RUFF, and F. RUFF. J. Inorg. Nucl. Chem. **27**, 179 (1965).
17. A. KETTRUP. Habilitationsschrift. Ruhr-Univ. Bochum. 1971.
18. C. V. BANKS and S. ANDERSON. Inorg. Chem. **2**, 112 (1963).
19. H. M. IRVING and R. WILLIAMS. Nature, **162**, 746 (1948).
20. C. V. BANKS, A. B. CARLSON, R. C. FERGUSON, W. SPRAIN, and R. C. VOTER. J. Am. Chem. Soc. **77**, 324 (1952).
21. M. GOEHRING, K. W. DAMM, and J. WEISS. Z. Naturforsch. **106**, 298 (1955).
22. G. BOOTH and M. KUBO. J. Chem. Soc. 2099 (1962).
23. A. G. SHARPE and D. B. WAKEFIELD. J. Chem. Soc. **25**, 281 (1957).
24. B. B. RAY and S. SEN. J. Indian Chem. Soc. **25**, 478 (1948).
25. M. KONDO and M. KUBO. J. Phys. Chem. **62**, 468 (1958).
26. R. L. MARTIN and A. WHITHEY. J. Chem. Soc. 1394 (1958).
27. A. EARNSHAW and J. LEWIS. J. Chem. Soc. 396 (1961).

Can. J. Chem. Downloaded from www.nrcresearchpress.com by 210.87.254.6 on 09/05/12
For personal use only.

The ^{19}F Nuclear Magnetic Resonance Spectra of Octahedral Fluorothiocyanato-N- and Fluorocyanato-N-Titanates(IV)

PHILIP A. W. DEAN AND BRIAN J. FERGUSON

Department of Chemistry, University of Western Ontario, London, Ontario N6A 3K7

Received July 30, 1973

The low temperature ^{19}F n.m.r. spectra of the mixtures TiF_6^{2-}–TiX_6^{2-} (X = Cl^-, Br^-, NCS^-, NCO^-) in sulfur dioxide solution have been examined. When X = Cl^- or Br^- rapid fluorine exchange is occurring even at the lowest accessible temperature, but when X = NCS^- or NCO^- the spectra of the individual mixed species $TiF_{6-x}X_x^{2-}$ are observed. In the latter two cases the solutions also contain fluorine-bridged dimers in stable equilibrium. The ^{19}F chemical shifts of $TiF_{6-x}X_x^{2-}$ (X = NCS^- or NCO^-) and of some related mixed complexes are reasonably represented by the equation $\delta = pC + qT$ where C and T are constants characteristic of the substituent X and p and q are the number of ligands X *cis* and *trans* respectively to the resonating fluorine. The constants T appear to be a measure of the π-donor ability of the ligand X in these complexes, supporting the idea that the chemical shift of a fluorine in fluorotitanates is determined largely by the extent to which fluorine-to-titanium back donation occurs.

Les spectres r.m.n. à basses températures du ^{19}F, des mélanges TiF_6^{2-}–TiX_6^{2-} (X = Cl^-, Br^-, NCS^-, NCO^-) dans des solutions d'anhydride sulfureux ont été examinés. Lorsque X = Cl^- ou Br^- l'échange rapide du fluore se produit même à la plus basse température accessible, par contre lorsque X = NCS^- ou NCO^- les spectres individuels des espèces mélangées $TiF_{6-x}X_x^{2-}$ sont observés. Dans ces deux derniers cas les solutions contiennent également en équilibre stable des dimères par pont fluor. Les déplacements chimiques du ^{19}F de $TiF_{6-x}X_x^{2-}$ (X = NCS^- ou NCO^-) et de quelques complexes mixtes apparentés sont assez bien décrits par l'équation $\delta = pC + qT$ où C et T sont des constantes caratéristiques du substituent X et p et q sont les nombres de ligands X en position *cis* et *trans* respectivement par rapport au fluor résonant. Les constantes T se révèlent comme des mesures du caractère π-donneur du ligand X dans ces complexes, ce qui prouve que le déplacement chimique de fluor dans les fluorotitanates est déterminé en grande partie par l'importance du transfert en retour fluor à titane.

[Traduit par le journal]

Can. J. Chem., **52**, 667 (1974)

Introduction

A number of ^{19}F n.m.r. studies of titanium(IV) fluorocomplexes have been reported (1–12). None of these studies, however, provide data for complete or near-complete series of species of the type $TiF_{6-x}X_x^{2-}$, where X is a monodentate ligand, although the spectra of complete series with the bidentate ligands oxalate and malonate are known (9).

We felt that it would be of interest to obtain the ^{19}F n.m.r. spectra of some representative series $TiF_{6-x}X_x^{2-}$, and to determine whether, in general, substituent effects on the fluorine chemical shifts in these series were additive. Additivity of substituent effects in octahedral fluorocomplexes was first noted for substituted fluorostannates (13), where, relative to SnF_6^{2-}, the chemical shift, $\delta(F)$, of any fluorine is related to p and q, the number of substituents *cis* and *trans* to it by eq. 1 in which C and T are empirical constants characteristic of the substituent. Among complexes of d^0 transition metal ions, this relationship has been found to hold loosely for fluorooxalato- and fluoromalonato-titanates (9), and for some fluoro compounds of hexavalent tungsten (14–16).[1]

$$\delta(F) = pC + qT \qquad [1]$$

The fluorine n.m.r. spectra of the series $TiF_{6-x}X_x^{2-}$ might also provide useful information regarding the extent and importance of fluorine-to-titanium π-bonding in titanium fluoro complexes. Ragsdale and his co-workers (2, 3, 7, 8) have provided two lines of evidence for back-bonding from the filled fluorine p_π orbitals into the empty titanium d_π orbitals. Firstly they find that, in the absence of bulky ligands,[2] the *cis* isomer of $TiF_4 \cdot 2B$ (where B is a neutral base) is greatly favored over the *trans*, though the *trans*/*cis* ratio increases as the base strength of B increases. These data are consistent with the occurrence of

[1] Brinckman and co-workers (17) have shown that the ^{19}F chemical shifts of the fluoromethoxytungsten(VI) series are best represented by separate parabolic functions for the cases where $q = 0$ or $q = 1$.

[2] The importance of steric effects due to the presence of bulky *donor atoms* has also been stressed (18).

Can. J. Chem. Downloaded from www.nrcresearchpress.com by 210.87.254.40 on 09/05/12
For personal use only.

Can. J. Chem. Downloaded from www.nrcresearchpress.com by 210.87.254.40 on 09/05/12
For personal use only.

fluorine-to-titanium back-bonding since such multiple-bonding is expected to favor the *cis* isomer if π-donation from fluorine exceeds π-donation from the other ligand (19). Secondly Ragsdale *et al.* find that, in TiF_4 complexes with substituted aromatic amine oxides (3, 7, 8), the chemical shift of a fluorine is particularly sensitive to the nature of the ligand *trans* to it; the shifts to lower field observed with decreasing electron availability on the *trans* ligand are suggested to reflect increasing fluorine-to-titanium π-bonding, such an interpretation being in agreement with the theoretical treatment of Karplus and Das (20).

In the present work we have used low temperature ^{19}F n.m.r. spectroscopy to study redistributions of TiF_6^{2-} with TiX_6^{2-} ($X = Cl^-$, Br^-, NCS^-, NCO^-) in liquid sulfur dioxide as solvent. The ^{19}F chemical shifts of the isothiocyanato- and isocyanato- complexes have been examined for the additivity of substituent effects, and the importance of fluorine-to-titanium π-bonding in these and some related complexes has been assessed.

Results and Discussion

Formation of the Complexes

The redistribution mixtures TiF_6^{2-}–TiX_6^{2-} were formed directly for $X = Cl^-$, Br^-, or NCS^-, but for $X = NCO^-$, the mixture was formed by treating TiF_6^{2-}–$TiCl_6^{2-}$ with a slight excess of silver cyanate.

Identification of, and Nomenclature used for, the Complexes

The species formed in the equilibrium mixtures were identified as described in ref. 13, *i.e.*, using a knowledge of the n.m.r. spectral pattern expected for each complex, coupled with the observed changes in intensities of the various signals as the *F/X* ratio was changed. In formulating the complexes, the conventional numbering scheme for an octahedron is followed, positions 1 and 6, 2 and 4, and 3 and 5 being *trans* to each other, and the numbers are presented in the formulae as right superscripts following the symbol for the ligand. The fluorines are not numbered in the formulae since their positions follow directly from the numbering of the other ligands.

^{19}F Nuclear Magnetic Resonance Spectra

At room temperature, the ^{19}F n.m.r. spectra of sulfur dioxide solutions of all the systems showed broad lines. For $X = Cl^-$ or Br^-, these broad lines persisted to the lowest temperature attainable (*ca.* −80°) so that no data on chlorofluoro- or bromofluoro-titanates were obtained. When $X = NCS^-$ or NCO^-, however, the low temperature n.m.r. spectra exhibited separate signals attributable to the expected redistribution products, as exemplified in Fig. 1 for TiF_6^{2-}–$Ti(NCS)_6^{2-}$. (The spectra of the system TiF_6^{2-}–$Ti(NCO)_6^{2-}$ were very similar but the amounts of dimeric ions (see below) formed in this case were smaller.) Details of the ^{19}F n.m.r. spectra of the fluorothiocyanato-*N*- and fluorocyanato-*N*-titanates(IV) are given in Table 1. In this table, the chemical shifts are referred to internal TiF_6^{2-} (these shifts varied over ~2 p.p.m. with concentration; mid-range values are given), and assignments in parentheses are those deduced from the empirical chemical shift correlations discussed later.

In addition to the resonances attributable to $TiF_{6-x}X_x^{2-}$, the n.m.r. spectra of TiF_6^{2-}–$Ti(NCS)_6^{2-}$ (see Fig. 1) and TiF_6^{2-}–$Ti(NCO)_6^{2-}$ solutions show signals due to dimeric fluorine-bridged fluoroanions of titanium (12). For instance in Fig. 1*a*, a spectrum consisting of a double-quintet, 1, a double-doublet, 2, and a high field multiplet, 3, is observed. This spectrum is due to the previously recognized (12) $Ti_2F_{11}^{3-}$ anion. Similarly, in Fig. 1*b*, resonances 3 and 4 are observed in the positions expected (12) for the $Ti_2F_{10}^{2-}$ ion, and resonance 7 is attributable (12) to the $Ti_2F_9^-$ anion.

The Mechanism of Redistribution

Polymeric fluoroanions of titanium have not previously been observed in redistributions involving titanium(IV) fluoro complexes. They have, however, been suggested as intermediates in such scrambling processes (2, 10). Formation and cleavage of a fluorine-bridge could result in the transfer of fluoride from one metal center to another, as shown by the following hypothetical sequence:

$$TiF_6^{2-} + TiX_6^{2-} \rightleftarrows F_5Ti—F—TiX_5^{3-} + X^-$$

$$X^- + F_5Ti—F—TiX_5^{3-} \rightleftarrows TiF_5X^{2-} + TiFX_5^{2-}$$

The existence of significant amounts of the dimeric fluorine-bridged species in stable equilibrium in the present systems is supportive evidence for such a transfer mechanism. The stability of the polymeric fluoroanions in these systems is probably a result of the acceptor ability of the sulfur dioxide which is being used as a solvent. SO_2 is known to form stable solvates with halide

Can. J. Chem. Downloaded from www.nrcresearchpress.com by 210.87.254.40 on 09/05/12
For personal use only.

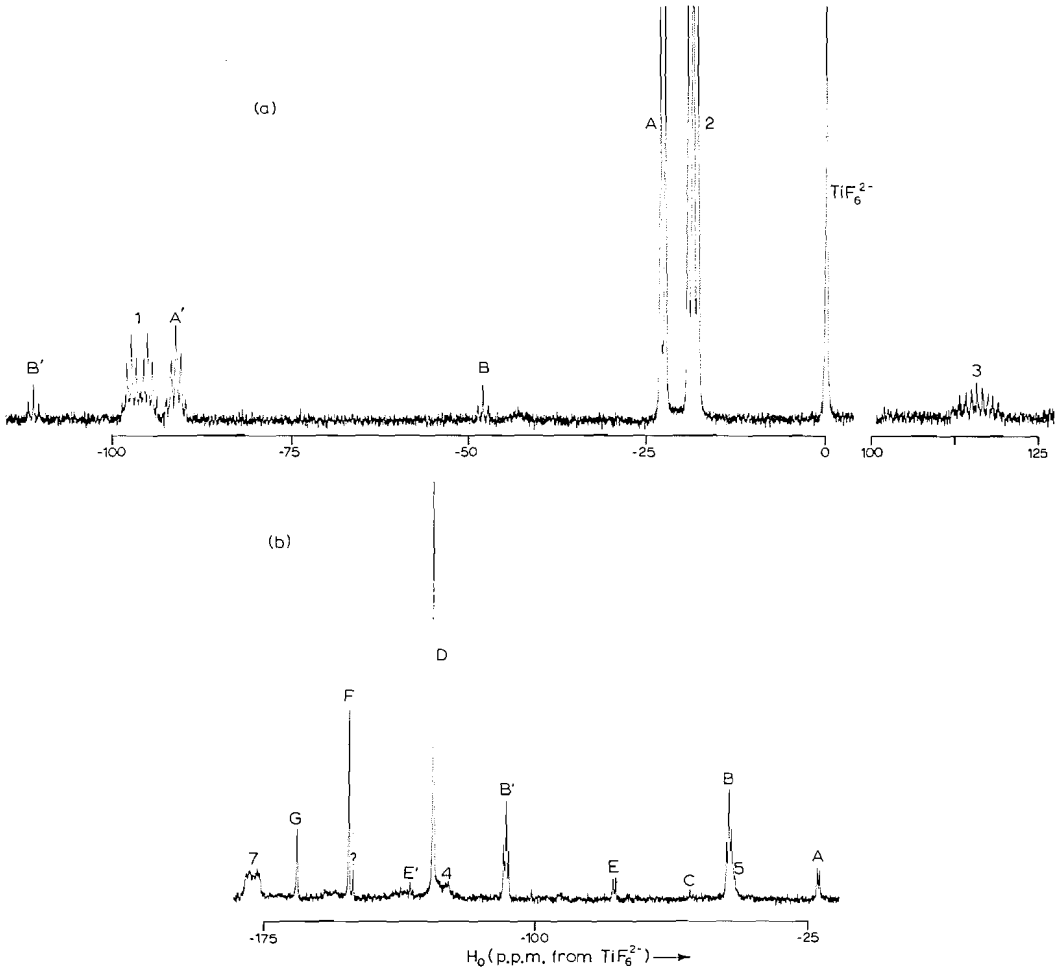

FIG. 1. The −60°, 58.3 MHz, ^{19}F n.m.r. spectra of solutions with (*a*) $(Pr^n{}_2NH_2)_2TiF_6/Bu^n{}_4N)_2Ti(NCS)_6/SO_2 = 9.14/1.00/118$, (*b*) $(Pr^n{}_2NH_2)_2TiF_6/(Bu^n{}_4N)_2Ti(NCS)_6/SO_2 = 1.00/1.06/28.3$. *A* = $[Ti(NCS)^1F_5]^{2-}$, F^{2-5}; *A'* = $[Ti(NCS)^1F_5]^{2-}$, F^6; *B* = $[Ti(NCS)_2{}^{1,2}F_4]^{2-}$, $F^{3,5}$; *B'* = $[Ti(NCS)_2{}^{1,2}F_4]^{2-}$, $F^{4,6}$; *C* = $[Ti(NCS)_2{}^{1,6}F_4]^{2-}$; *D* = $[Ti(NCS)_3{}^{1,2,3}F_3]^{2-}$; *E* = $[Ti(NCS)_3{}^{1,2,6}F_3]^{2-}$, $F^{3,5}$; *E'* = $[Ti(NCS)_3{}^{1,2,6}F_3]^{2-}$, F^4; *F* = $[Ti(NCS)_4{}^{1,2,3,4}F_2]^{2-}$; *G* = $[Ti(NCS)_5F]^{2-}$; *1,2,3* = $Ti_2F_{11}{}^{3-}$; *4,5* = $Ti_2F_{10}{}^{2-}$; *7* = $Ti_2F_9{}^-$.

and pseudohalide ions (ref. 21 and references therein), and the formation of these specific solvates would force an equilibrium such as

$$TiF_6{}^{2-} + TiF_5(NCS)^{2-} \rightleftarrows Ti_2F_{11}{}^{3-} + NCS^-$$

towards the right hand side.

^{19}F *Chemical Shifts*

If eq. 1 holds for the series $TiF_{6-x}X_x{}^{2-}$, then a plot of δ(F), the chemical shift of a fluorine relative to $TiF_6{}^{2-}$, *vs. p*, the number of substituents X *cis* to that fluorine, should give two parallel lines separated by a distance *T*. Figure 2 shows such plots for the thiocyanate and cyanate series. These plots exhibit the trends expected on the basis of eq. 1. The best fits to eq. 1 are represented by the solid lines in Fig. 2. $C = -21.9$ and $T = -80.4$ p.p.m. reproduce the 11 data points for the series $TiF_{6-x}(NCS)_x{}^{2-}$ with a mean deviation of 4.4 p.p.m., the range being 166 p.p.m.,[3] while for the series $TiF_{6-x}(NCO)_x{}^{2-}$ $C = -14.9$ and $T = -34.8$ p.p.m. reproduce the 12 data points (range 95 p.p.m.) with a mean deviation of 3.6 p.p.m. The agreement with eq. 1 is thus not

[3]The additivity provides evidence that the bonding mode of the NCS^- is constant in the series $TiF_{6-x}(NCS)_x{}^{2-}$, *i.e.*, it is N-bonded, as in $Ti(NCS)_6{}^{2-}$ itself (22).

TABLE 1. The ^{19}F n.m.r. spectra of fluorotitanate(IV) complexes in liquid sulfur dioxide solution at −60 °C

Complex	Assignment*	Chemical shift† (p.p.m.)	$J(^{19}F–^{19}F)$ (Hz)	*cis*/*trans* or *fac*/*mer* ratio
$[Ti(NCS)^1F_5]^{2-}$	F^{2-5}	−22	38 ± 1	
	F^6	−91		
$[Ti(NCS)_2^{1,2}F_4]^{2-}$	$(F^{3,5})$	−46	40 ± 1	
	$(F^{4,6})$	−108		
				~100
$[Ti(NCS)_2^{1,6}F_4]^{2-}$	F^{2-5}	−57		
$[Ti(NCS)_3^{1,2,3}F_3]^{2-}$	F^{4-6}	−129		
				10 ± 1
$[Ti(NCS)_3^{1,2,6}F_3]^{2-}$	$F^{3,5}$	−79	41 ± 2	
	F^4	−134		
$[Ti(NCS)_4^{1,2,3,4}F_2]^{2-}$(?)‡	$F^{5,6}$	−152		?
$[Ti(NCS)_5^{1,2,3,4,5}F]$	F^6	−166§		
$[Ti(NCO)^1F_5]^{2-}$	F^{2-5}	−14	42 ± 1	
	F^6	−46		
$[Ti(NCO)_2^{1,2}F_4]^{2-}$	$(F^{3,5})$	−34	43 ± 2	
	$(F^{4,6})$	−58		
				10 ± 1
$[Ti(NCO)_2^{1,6}F_4]^{2-}$	F^{2-5}	−39		
$[Ti(NCO)_3^{1,2,3}F_3]^{2-}$	F^{4-6}	−68		
				0.9 ± 0.1
$[Ti(NCO)_3^{1,2,6}F_3]^{2-}$	$F^{3,5}$	−53	42 ± 2	
	F^4	−70		
$[Ti(NCO)_4^{1,2,3,4}F_2]^{2-}$(?)‡	$F^{5,6}$	−81		
				10 ± 1
$[Ti(NCO)_4^{1,2,4,6}F_2]^{2-}$(?)‡	$F^{3,5}$	−69		
$[Ti(NCO)_5^{1,2,3,4,5}F]^{2-}$	F^6	−95		

*For numbering system, see text.
†Median values, relative to internal TiF_6^{2-} except where noted.
‡Query indicates assignment of isomer based on empirical chemical shift correlations (see text).
§Measured relative to internal $[Ti(NCS)_3^{1,2,3}F_3]^{2-}$ as primary reference, and referred to TiF_6^{2-} using $\delta(TiF_6^{2-}) = \delta(TiF_3(NCS)_3^{2-}) - 129$ p.p.m.

perfect, but it is certainly good enough to confirm the assignments made, and it is, in fact, comparable to the agreement obtained for the fluorostannates with the same ligands (13). Better reproduction of the data can be obtained by fitting the lines corresponding to $q = 0$ and to $q = 1$ separately (*c.f.* ref. 17): the dashed lines in Fig. 2 correspond to $q = 0$ and give mean deviations of 3.3 (NCS^-) and 1.7 (NCO^-) p.p.m., while the dot–dash lines correspond to $q = 1$, the mean deviations being 2.2 (NCS^-) and 0.8 (NCO^-). Unfortunately this "two-line" approach lacks the simplicity of eq. 1; it is not clear, for instance, how it could be extended to ternary mixtures such as the ether adducts of titanium chlorofluorides reported by Borden *et al.* (10, 11). The data for these systems can, however, be reproduced adequately using eq. 2, which is an obvious extension of eq. 1 (13). For example, the 12 data

$$[2] \qquad \delta(F) = \sum pC + \sum qT$$

points for 1,2-dimethoxyethane (DME) adducts of $TiF_{4-x}Cl_x$ in dichloromethane solution (11) can be reproduced to a mean deviation of 2.6 p.p.m. in a range of 273 p.p.m. using[4] $C_{DME} = -42.5$, $T_{DME} = -131.0$, $C_{Cl^-} = -33.3$, $T_{Cl^-} = -34.0$ and a chemical shift of -71ϕ (the value in $CHCl_3$ solution(9)) for TiF_6^{2-}.

It is evident that eq. 1 and the extension of it remain of considerable utility in making ^{19}F chemical shift assignments for substituted octahedral fluorocomplexes of titanium(IV).

[4]The parameters for DME correspond to ½ of that ligand.

Can. J. Chem. Downloaded from www.nrcresearchpress.com by 210.87.254.40 on 09/05/12
For personal use only.

Can. J. Chem. Downloaded from www.nrcresearchpress.com by 210.87.254.40 on 09/05/12
For personal use only.

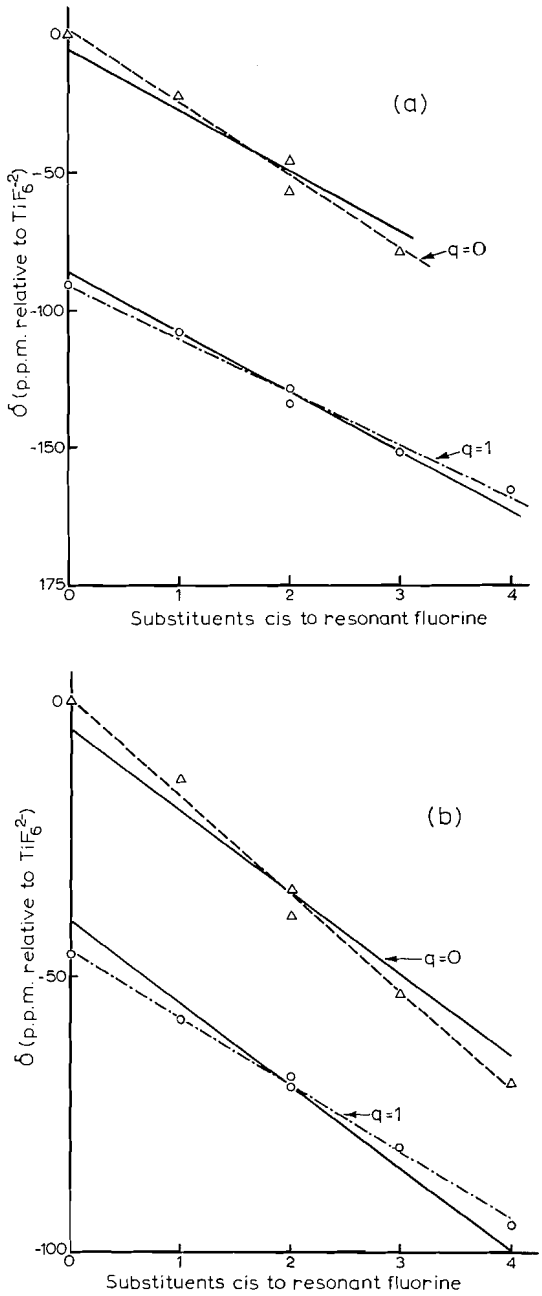

FIG. 2. (*a*) Fluorine chemical shift *vs.* number of *cis* substituents, *p*, for the system TiF_6^{2-}–$Ti(NCS)_6^{2-}$. The lines —, ---, and ····· correspond to $\delta(F) = p(-21.9) + q(-80.4) - 5.8$, $\delta(F) = p(-26.6) + 1.8$, and $\delta(F) = p(-19.4) - 91.2$ p.p.m., respectively. (*b*) Fluorine chemical shift *vs.* number of *cis* substituents, *p*, for the system TiF_6^{2-}–$Ti(NCO)_6^{2-}$. The lines —, ---, and ····· correspond to $\delta(F) = p(-14.9) + q(-34.8) - 5.0$, $\delta(F) = p(-17.7) + 0.6$, and $\delta(F) = p(-12.1) - 45.5$ p.p.m., respectively.

Fluorine-to-titanium π-Bonding in Titanium Fluorocomplexes

The data in Table 1 show that the distribution of geometrical isomers in the fluorothiocyanato-*N*- and fluorocyanato-*N*-titanates is not statistical. (For a statistical distribution we expect *cis*/*trans* = 4 and *fac*/*mer* = 2/3.) Rather, those isomers (*cis* or *fac*) having the maximum number of fluorines *trans* to —NCS or —NCO are preferred, this preference being stronger in the case of —NCS than in the case of —NCO. According to the arguments summarized earlier, the data suggest that the π-donor abilities of the ligands in these complexes are $F^- > NCO^- > NCS^-$.

If, as suggested by Ragsdale and co-workers (3, 7, 8), increasing back-donation from fluorine to titanium produces a downfield chemical shift and is caused by diminishing π-donor ability of the *trans* ligand, the parameter *T* derived from eq. 1 should be an approximate measure of the π-donor ability of a substituent in a titanium fluoro-complex. By this reasoning the values of *T* obtained above for NCO^- and NCS^- (*i.e.* −35 and −80 p.p.m.) lead to the π-donor abilities $F^- > NCO^- > NCS^-$, the same order obtained from the distribution ratios of the geometrical isomers.

In view of the apparently successful correlation of *T* and π-donor ability for the limited series of ligands F^-, NCO^-, NCS^-, it is of interest to determine whether the correlation is general. As noted earlier, data for few complete series have been obtained; nevertheless, approximate *C* and *T* parameters can be derived[5] from the chemical shifts of $TiF_5B^{(1\text{ or }2)-}$ and $TiF_4B_2^{(0\text{ or }2)-}$ relative to TiF_6^{2-}. In this way, approximate values of *T* for alkoxides (9), carboxylates (9), alcohols (2), water (5), substituted aromatic amine oxides (3, 7, 8), and TiF_6^{2-} (12) as ligands are obtainable, and comparison with the parameters for Cl^-, NCO^-, NCS^-, and DME (see earlier) is possible.

Figure 3 shows a plot of *T*, for various anionic ligands, as a function of the Hammett–Taft parameter, σ_R^0, of the ligand; σ_R^0 values are thought to be a measure of the π-donor abilities of the various substituents (23). An approximate relationship between *T* and σ_R^0 is evident in Fig. 3

[5]For $TiF_5B^{(1\text{ or }2)-}$, giving an AX_4 spectrum, $\delta(A) = T$, $\delta(X) = C$. *cis*-$TiF_4B_2^{(0\text{ or }2)-}$ gives an A_2X_2 spectrum: if A is shown to be *trans* to B, then $\delta(A) = C + T$, $\delta(X) = 2C$. *trans*-$TiF_4B_2^{(0\text{ or }2)-}$ gives a singlet with $\delta(F) = 2C$.

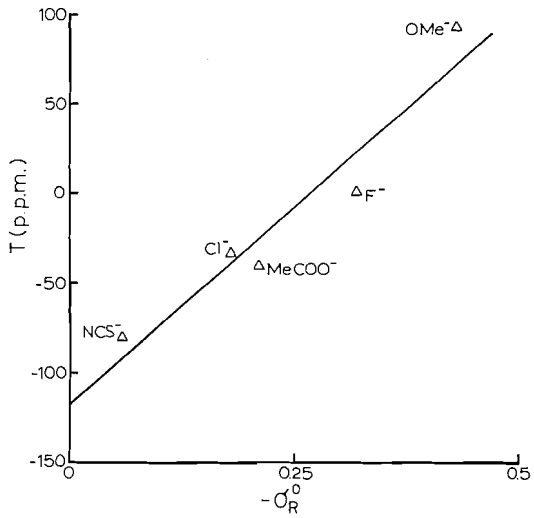

FIG. 3. The relationship between the empirical chemical shift parameter T (p.p.m.) and the Hammett–Taft parameter σ_R^0 (see text).

and the existence of such an approximate relationship is supported by two additional facts: (*i*) the observation that for fluorine-containing species of hexavalent tungsten, O^{2-} has a much more positive T value than OMe^- (15, 17, 24), while, consistently, σ_R^0 for O^{2-} is much more negative than σ_R^0 for OMe^- (23); (*ii*) the position of the intercept in Fig. 3 (*i.e.* −119 p.p.m. for the best straight line) which is in the region where the T values for ligands such as ROH, H_2O, DME, and TiF_6^{2-}, all expected to be poor π donors, fall.[6] (MeOH (2), H_2O (5), DME, and TiF_6^{2-} (12) have $T \approx -100$, −94, −131, and −103 p.p.m., respectively.)

Our results demonstrate, therefore, that a wide range of T values can be correlated at least approximately with the π-donor ability of the ligand. This observation in turn supports the suggestion (3, 7, 8) that fluorine chemical shifts in titanium fluorocomplexes depend upon the extent to which fluorine-to-titanium π-bonding occurs.

Experimental

Materials

Di-*n*-propylammonium hexafluorotitanate was prepared as reported earlier (4). The syntheses of tetra-*n*-butylammonium hexachlorotitanate and hexabromotitanate were according to refs. 25 and 26, respectively. Sulfur dioxide (Matheson anhydrous grade) was dried by standing in the gas phase over 3A Molecular Sieves.

Tetra-n-butylammonium Hexathiocyanato-N-titanate

A slight excess of silver thiocyanate was allowed to react with a sulfur dioxide solution of $(Bu^n_4N)_2TiCl_6$ or $(Bu^n_4N)_2TiBr_6$ in a previously described (27) apparatus. The mixture was stirred in the dark for *ca.* 1 h at room temperature, the deep red solution was filtered off, and the precipitate washed several times with SO_2. The SO_2 was removed from the solution leaving the deep red product which was pumped *in vacuo* to remove last traces of solvent.

Anal. Calcd. for $C_{38}H_{72}N_8S_6Ti$: C, 51.78; H, 8.24; N, 12.71; S, 21.82. Found: C, 51.89; H, 8.26; N, 12.52; S, 21.72.

$(Bu^n_4N)_2Ti(NCS)_6$ has recently been synthesized by an alternative route and shown from its vibrational spectrum to contain N-bonded thiocyanate (22).

Sample Preparation

The apparatus and mode of sample preparation were essentially as described for the preparation of TiF_4–TiF_6^{2-} mixtures (12). In the cases of TiF_6^{2-}–TiX_6^{2-} mixtures where X = Cl^-, Br, or NCS^-, the reactants were $(Pr^n_2NH_2)_2TiF_6$ and $(Bu^n_4N)_2TiX_6$. For TiF_6^{2-}–$Ti(NCS)_6^{2-}$ the reaction took several hours at room temperature to reach equilibrium. For the preparation of TiF_6^{2-}–$Ti(NCO)_6^{2-}$, $(Pr^n_2NH_2)_2TiF_6$, $(Bu^n_4N)_2TiCl_6$ and a slight excess of AgNCO were shaken in liquid SO_2 for 15–30 min before transferring the solution to the n.m.r. tube.

^{19}F Nuclear Magnetic Resonance Spectra

The methods of n.m.r. measurement have been described previously (28). Varian DP-60 and HA-100 spectrometers were used.

Microanalyses

These were performed by Alfred Bernhardt, Mikroanalytisches Laboratorium, West Germany.

We are grateful to the National Research Council of Canada for generous financial support of this work.

1. E. L. MUETTERTIES. J. Am. Chem. Soc. **82**, 1082 (1960).
2. R. O. RAGSDALE and B. B. STEWART. Inorg. Chem. **2**, 1002 (1963).
3. D. S. DYER and R. O. RAGSDALE. Inorg. Chem. **6**, 8 (1967).
4. P. A. W. DEAN and D. F. EVANS. J. Chem. Soc. A, 698 (1967).
5. YU A. BUSLAEV, D. S. DYER, and R. O. RAGSDALE, Inorg. Chem. **6**, 2208 (1967).
6. D. S. DYER and R. O. RAGSDALE. J. Phys. Chem. **71**, 2309 (1967).
7. D. S. DYER and R. O. RAGSDALE. Inorg. Chem. **8**, 1116 (1969).
8. C. E. MICHELSON, D. S. DYER, and R. O. RAGSDALE. J. Chem. Soc. A, 2296 (1970).
9. P. A. W. DEAN and D. F. EVANS. J. Chem. Soc. A, 2569 (1970).
10. R. S. BORDEN and R. N. HAMMER. Inorg. Chem. **9**, 2004 (1970).

[6]The plot in Fig. 3 suggests that aromatic amine oxides are moderate-to-poor π donors; *e.g.* use of $\delta(TiF_6^{2-}) = -71\phi$, and the data of ref. 8, gives T for pyridine-*N*-oxide as −54 p.p.m.

Can. J. Chem. Downloaded from www.nrcresearchpress.com by 210.87.254.40 on 09/05/12
For personal use only.

11. R. S. BORDEN, P. A. LOEFFLER, and D. S. DYER. Inorg. Chem. **11**, 2481 (1972).
12. P. A. W. DEAN. Can. J. Chem. In press.
13. P. A. W. DEAN and D. F. EVANS. J. Chem. Soc. A, 1154 (1968).
14. G. W. FRASER, C. J. W. GIBBS, and R. D. PEACOCK. J. Chem. Soc. A, 1708 (1970).
15. A. M. NOBLE and J. M. WINFIELD. J. Chem. Soc. A, 2574 (1970).
16. W. MCFARLANE, A. M. NOBLE, and J. M. WINFIELD. J. Chem. Soc. A, 948 (1971).
17. L. B. HANDY, K. G. SHARP, and F. E. BRINCKMAN. Inorg. Chem. **11**, 523 (1972).
18. R. F. ZAHROBSKY. J. Coord. Chem. **1**, 301 (1971).
19. I. R. BEATTIE. Q. Rev. **17**, 382 (1963).
20. M. KARPLUS and M. DAS. J. Chem. Phys. **34**, 1683 (1961).
21. D. F. BUROW. *In* The chemistry of non-aqueous solvents. Vol. III. *Edited by* J. J. Lagowski. Academic Press, New York, 1970. p. 137.
22. A. M. SYCH and V. P. DEM'YANENKO. Russ. J. Inorg. Chem. **16**, 1593 (1971).
23. R. W. TAFT, E. PRICE, I. R. FOX, I. C. LEWIS, K. K. ANDERSEN, and G. T. DAVIES. J. Am. Chem. Soc. **85**, 3146 (1963).
24. F. N. TEBBE and E. L. MUETTERTIES. Inorg. Chem. **7**, 172 (1968).
25. R. S. SANDHU, B. S. CHAKKAL, and G. S. SANDHU. J. Indian Chem. Soc. **37**, 329 (1960).
26. R. J. H. CLARK, L. MARESCA, and R. J. PUDDEPHATT. Inorg. Chem. **7**, 1603 (1968).
27. T. BIRCHALL, P. A. W. DEAN, and R. J. GILLESPIE. J. Chem. Soc. A, 1778 (1971).
28. P. A. W. DEAN and R. J. GILLESPIE. J. Am. Chem. Soc. **91**, 7260 (1969).

Can. J. Chem. Downloaded from www.nrcresearchpress.com by 210.87.254.40 on 09/05/12
For personal use only.

Thermodynamics and Spectroscopy of the Hydrogen Bonded Complex Formed between Hydrogen (Deuterium) Chloride and Dimethyl Ether in the Gas Phase by Raman Scattering[1]

A. S. GILBERT[2] AND H. J. BERNSTEIN

Division of Chemistry, National Research Council of Canada, Ottawa, Canada K1A 0R6

Received September 26, 1973

The equilibrium constant K_p has been obtained for the complex Cl—D···O(CH$_3$)$_2$ over a range of temperatures between 22 and 132 °C by monitoring the integrated intensity of the Raman scattered band from unassociated DCl in a mixture with dimethyl ether. By applying the relation $\ln K_p = -\Delta H/RT + \Delta S/R$ the quantities ΔH, ΔG, and ΔS have been evaluated.

Broad ν_{Cl-H} and ν_{Cl-D} complex bands have been observed and are found to be polarized.

Utilisant l'intensité intégrée de la raie diffusée dans le Raman par le DCl non-associé dans un mélange avec l'éther diméthylique, on a pu déterminer la constante d'équilibre K_p du complexe Cl—D···O(CH$_3$)$_2$ à diverses températures entre 22 et 132 °C. Utilisant $\ln K_p = \Delta H/RT + \Delta S/R$ on a pu évaluer les valeurs de ΔH, ΔG et ΔS.

On a pu observer des bandes larges et complexes pour ν_{Cl-H} et ν_{Cl-D} et on trouve qu'elles sont polarisées. [Traduit par le journal]

Can. J. Chem., **52**, 674 (1974)

Introduction

In order to gain information on the spectroscopic and thermodynamic properties of hydrogen bonds it is desirable to study such systems in the gas phase where nonspecific interactions such as solvent effects are minimized. However, relatively few such studies have been undertaken compared to the vast amount of published work on hydrogen bonding in liquid and solid phases.

When hydrogen (deuterium) chloride and dimethyl ether (DME) vapor are mixed together at room temperature a significant proportion of a complex, Cl—H···O(CH$_3$)$_2$, is formed as a gaseous component of the mixture in equilibrium with unassociated component molecules. Several studies of this system have been made using both spectroscopic (1–5) and nonspectroscopic (6) techniques. In this paper we report the results of an investigation into the spectroscopic and thermodynamic properties of the complex by utilizing Raman scattering.

The frequency separation of the $\nu_{Cl-H(D)}$ mode of the complex from the unassociated hydrogen chloride band suggests that the enthalpy of complex formation is in the region of a few kcal per mol. Values for the equilibrium constants of the system which have been obtained from vapor pressures (6), i.r. (3), and n.m.r. (5) measurements confirm this view and yield a range of values for ΔH of between $5\frac{1}{2}$ to $7\frac{1}{2}$ kcal mol^{-1}. This variation in published values is probably due to the unsuitability of the methods employed. For instance the method of vapor pressures does not distinguish between specific and nonspecific interactions in the gas mixture while, though the i.r. method allows the complex itself to be "seen", its bands are overlapped by those of the unassociated components.

Measurement of the Thermodynamic Values of the Deuterium Chloride – Dimethyl Ether System

If the self association of the gases is negligible, the equilibrium can be described as

$$A + B \leftrightarrows A\cdots\cdots B$$

with equilibrium pressures of $P_A - P_X$, $P_B - P_X$, and P_X. The equilibrium constant K_p is given by

$$K_p = P_X/(P_A - P_X)(P_B - P_X)$$

Assuming the gases behave ideally, the enthalpy of complexation is given by

$$\ln K_p = -\Delta H/RT + \Delta S/R$$

The enthalpy may thus be calculated from the

[1]NRCC No. 13680.

[2]N.A.T.O. Fellow 1972–1973. Present address: Department of Pure and Applied Chemistry, University of Strathclyde, Thomas Graham Building, 295 Cathedral Street, Glasgow G1 1XL, Scotland.

Can. J. Chem. Downloaded from www.nrcresearchpress.com by 210.87.254.5 on 09/05/12
For personal use only.

Can. J. Chem. Downloaded from www.nrcresearchpress.com by 210.87.254.5 on 09/05/12
For personal use only.

slope of a ln K_p *vs.* $-1/T$ plot, the intercept of which gives the entropy change. These quantities are related to the free energy by

$$\Delta G = \Delta H - T\Delta S$$

Though the shift of the Cl—D stretching mode of the complex is relatively large, it absorbs as a very broad and intrinsically very intense band which overlaps with both the rotational branches wherein resides all the vibrational intensity of the unassociated deuterium chloride. By contrast it is characteristic of Raman spectra that the major part of the intensity is from the central Q branches, and that hydrogenic modes of bonds involved in hydrogen bonding are intrinsically weak.

We have followed the equilibrium by monitoring the pure vibrational scattering (Q branch) of the unassociated deuterium chloride. The scattered intensity was assumed to be proportional to the molecular density of the component over the temperature range. Under the conditions of our experiment (*vide* experimental) self association of the gases can be ignored (5). We were able to examine the Q branch of deuterium chloride without significant overlapping from any other band. As it is desirable to use an internal intensity standard, we added nitrogen to our mixture. Thus several intensity values of the free DCl band $I_A - I_X$, proportional to $P_A - P_X$, (where P_A = partial pressure of free DCl, P_B = partial pressure for free DME) were measured by comparing the integrated scattered intensity with that of the N_2 vibrational band over a range of temperatures between 22 and 132 °C. To calculate I_X it was necessary to know I_A which was taken to be the limiting value of $I_A - I_X$ at high temperatures. This was estimated from a plot of $I_A - I_X$ *vs.* T. As the initial pressures of the constituents were known the quantities P_A, P_B, and P_X could be calculated with appropriate allowances for the Boyle's law variation of pressure with temperature. Thus K_p was evaluated and both ΔH and ΔS were obtained from a linear plot of ln K_p *vs.* $1/T$.

Experimental

The spectra were recorded using a Jarrell-Ash 25-102 dual monochromator with photoelectric detection (1TTFW130) and photon counting. Exciting source was a CRL Model 52 Ar ion CW laser delivering around 1W of power at either 4880 or 5145 Å. A multipassing device (8) was used to enhance the scattered light signal.

The samples were handled in a glass vacuum system, from which was filled a small quartz cell fitted with Brewster angle windows. For the measurement of the equilibrium constants, pressures of the gases were measured manometrically to within ±1 Torr and were taken to be 52, 754, and 304 Torr for DCl, DME, and N_2, respectively. No evidence of condensation was discovered at any temperature. For the observation of the Cl—H(D) stretching modes of the complex rather higher pressures of halide were used, typically 500 Torr along with a roughly equal pressure of ether.

Deuterium chloride was obtained from Merck, Sharp and Dohme; hydrogen chloride, dimethyl ether, and nitrogen from the Matheson Company, all with quoted minimum purities of 99%. No further purification of the gases was attempted.

The temperatures of the system were measured by a spectroscopic method. Originally it had been intended to use a thermocouple but the conclusion was that because of the experimental configuration, accurate readings might not be obtained. Instead the nitrogen gas was made to serve a dual purpose by recording its pure rotational spectrum at each temperature. The relative intensity of any line $I(J)$ in the pure rotational Raman spectrum of nitrogen is given (7) (rigid rotor approximation) by

$$I(J) = \nu^4 g(J) S(J) \exp\,[-BJ(J+1)hc/kT]$$

where ν = absolute frequency of the emitted line, $g(J)$ = nuclear spin factor which is 1 for even J and ½ for odd J, $S(J) = 3(J+1)(J+2)/2(2J+3)$ Stokes, $= 3(J-1)J/2(2J-1)$ Antistokes, h = Planck's constant, c = velocity of light, k = Boltzmann's constant, T = temperature. By rearrangement it is easily seen that

$$\ln \frac{I(J)}{g(J)S(J)} - 4 \ln (\nu) = -BJ(J+1)hc/kT$$

If $I(J)$ is measured for a number of bands, and the l.h.s. then plotted against $J(J+1)$, a straight line should be obtained whose slope is equal to $-Bhc/kT$. Thus a value for the temperature of the gas may be calculated. The advantage of this method is that the temperature measured is that of the part of the sample directly under investigation. Under the conditions of the experiment some interference was received from pure rotational transitions of the DCl and DME but this was not serious as the former was only present in small amounts while the latter's rotational transitions are closely spaced and were only visible as a change in background intensity.

Thermodynamics

A plot of ln K_p *vs.* $1/T$ is displayed in Fig. 1. A least squares fitted straight line through the best seven points yields a value of $\Delta H = -6.46$ kcal mol^{-1}. The corresponding entropy and free energy changes were found to be -24.7 cal deg^{-1} mol^{-1} and $+0.9$ kcal mol^{-1} at 25 °C. A more realistic value for ΔH is -6.7 ± 0.4 kcal mol^{-1}, and for ΔS it is -25.5 ∓ 1.5 cal deg^{-1} mol^{-1} again giving $\Delta G = +0.9$ kcal mol^{-1} at 25 °C. Comparison may be made with the values obtained for HCl and DME by other methods.

Method	Reference	ΔH (kcal mol^{-1})	ΔS (cal deg^{-1} mol^{-1})
Nuclear magnetic resonance	5	-7.1 ± 0.8	-25.7 ± 1.3
Vapor pressure	6	-7.4 or -6.25	-28.5 (no errors quoted)
Infrared	3	-5.6 ± 0.2	
Raman	This work	-6.7 ± 0.4	-25.5 ∓ 1.3

ΔH for HCl and DME is expected to be very similar to that for DCl/DME. The only difference is likely to be due to the difference in the change in zero point vibrational energy ($\Delta\omega$) of the H(D)—Cl stretching mode on complexation. By using i.r. data (1, 4) this may be calculated as follows:

$$\Delta\omega_{HCl} = \tfrac{1}{2}(2470 - 2885) = -207\tfrac{1}{2}\ cm^{-1}$$

$$\Delta\omega_{DCl} = \tfrac{1}{2}(1850 - 2090) = -120\ cm^{-1}$$

and thus $\Delta\omega_{HCl} - \Delta\omega_{DCl} = -87\tfrac{1}{2}\ cm^{-1} = -0.25$ kcal mol^{-1}.

Spectroscopy

Figures 2 and 3 illustrate the Cl—H and Cl—D Raman bands of the two isotopic forms of the complex. Both bands are very broad and intrinsically weak. The rotational lines of the unassociated halide gas can be seen superimposed upon them. In each case the position of maximum

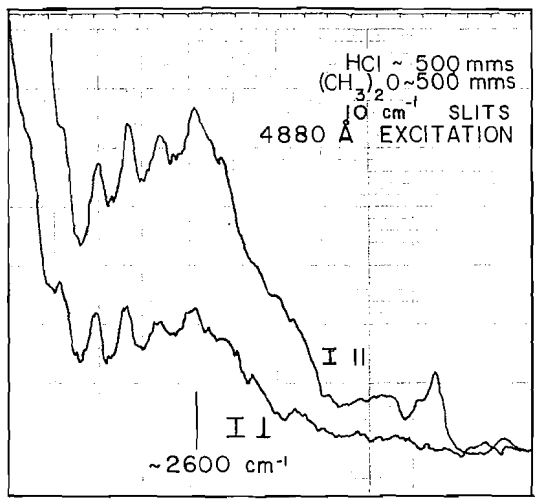

FIG. 2. The HCl stretching band in ClH...D(CH$_3$)$_2$ for both ∥ and ⊥ polarizations.

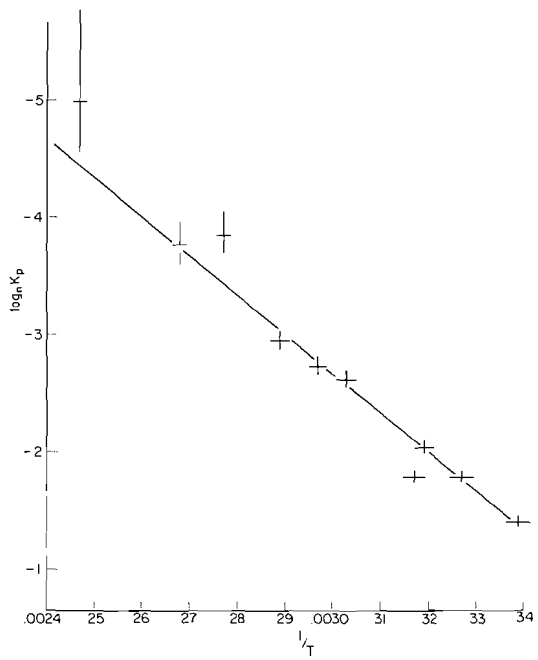

FIG. 1. $\log_n Kp$ vs. $1/T$.

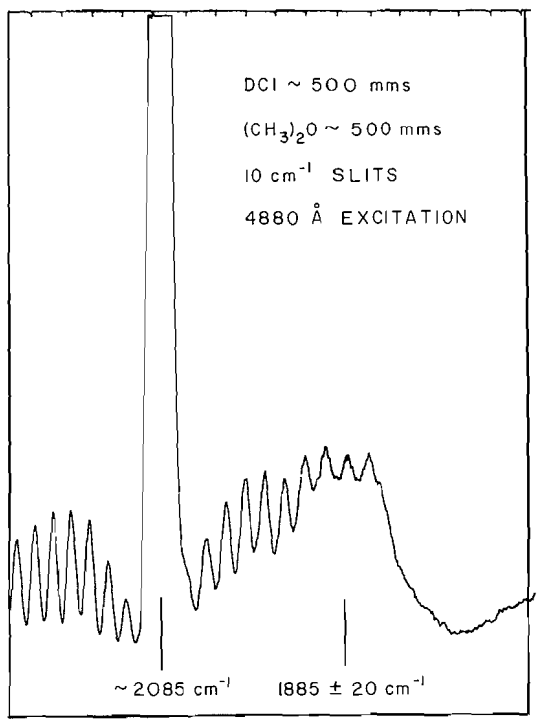

FIG. 3. The DCl band in ClD...O(CH$_3$)$_2$.

Can. J. Chem. Downloaded from www.nrcresearchpress.com by 210.87.254.5 on 09/05/12
For personal use only.

intensity of the broad complex band is very nearly the same as observed in the i.r. Figure 2 illustrates the polarization characteristics of the Raman band of the complex with HCl. Similar behavior is displayed by the complex with DCl. It is evident that the band due to the complex is polarized in each case.

The halfwidths of the complex bands are 200 ± 30 cm^{-1} (H) and 135 $\pm$ 20 cm^{-1} (D), which compare with the i.r. values of 275 $\pm$ 20 (4) and 135 $\pm$ 10 cm^{-1} (our estimate from the spectra of Bertie and Millen (1)), respectively. The difference in bandwidth for the hydrogen form may be connected with the fact that the side band structure observed in the i.r. does not appear in our Raman spectra.

The polarization characteristics of the complex bands and the diffuse nature of their envelopes suggest that the bandwidth is the result of the superposition of a number of vibrational components. Suitable candidates could be the intermolecular Cl···O stretching mode and the low frequency intermolecular bending vibrations.

One of us (A.S.G.) would like to thank the Science Research Council of the U.K. for the award of a N.A.T.O. Fellowship.

1. J. E. Bertie and D. J. Millen. J. Chem. Soc. 497 (1965); 514 (1965).
2. J. E. Bertie and M. V. Falk. Can. J. Chem. **51**, 1713 (1973).
3. L. P. Bilozerska and N. D. Shchepkin. Opt. Spectrosc. Suppl. **13**, 146 (1968).
4. J. C. Lassegues and P. V. Huong. Chem. Phys. Lett. **17**, 444 (1972).
5. G. Govil, A. D. H. Clague, and H. J. Bernstein. J. Chem. Phys. **49**, 2821 (1968).
6. A. T. Gladishev and Ya. K. Syrkin, C. R. Acad. Sci. URSS, **20**, 145 (1938).
7. G. Herzberg. Spectra of diatomic molecules. D. Von Nostrand, Inc., Princeton, New Jersey. 1961. p. 128.
8. W. Kiefer, H. J. Bernstein, H. Wieser, and M. Danyluk. J. Mol. Spectrosc. **43**, 393 (1972).

Can. J. Chem. Downloaded from www.nrcresearchpress.com by 210.87.254.5 on 09/05/12
For personal use only.

Synthesis of 4-*O*-α-D-Mannopyranosyl-L-rhamnopyranose

GWENDOLYN M. BEBAULT AND GUY G. S. DUTTON

Department of Chemistry, University of British Columbia, Vacouver, British Columbia V6T 1W5

Received June 18, 1973

4-*O*-α-D-Mannopyranosyl-L-rhamnopyranose has been synthesized in 55% yield by condensation of 2,3,4,6-tetra-*O*-benzoyl-α-D-mannopyranosyl bromide with methyl 2,3-*O*-isopropylidene-α-L-rhamnopyranoside using mercuric cyanide in acetonitrile (Helferich reaction). The disaccharide has m.p. 143–145°, $[\alpha]_D$ +53.0° → 60.3° (*c*, 1.0 water), and was characterized as the crystalline peracetates of the disaccharide (m.p. 149.5–150.5°, $[\alpha]_D$ −4.4° (*c*, 4.3 chloroform)) and of the derived alditol (m.p. 84–85°, $[\alpha]_D$ −4.4° (*c*, 1.9 chloroform)).

4-*O*-α-D-Mannopyrannosyle-L-rhamnose a été synthétisé avec un rendement de 55% par réaction du α-D-tetrabenzoylbromomannose avec le méthyl 2,3-*O*-isopropylidène-α-L-rhamnopyrannoside en utilisant le cyanure de mercure dans l'acétonitrile (réaction de Helferich). Le disaccharide est cristallin (p.f. 143–145°, $[\alpha]_D$ +53.0° → 60.3° (*c*, 1.0 eau)) et était caractérizé par les peracétates cristallins du disaccharide (p.f. 149.5–150.5°, $[\alpha]_D$ −5.5° (*c*, 4.3 chloroform)) et de l'alditol correspondant (p.f. 84–85°, $[\alpha]_D$ −4.4° (*c*, 1.9 chloroform)).

Can. J. Chem., **52**, 678 (1974)

The disaccharide unit 4-*O*-D-mannopyranosyl-L-rhamnopyranose occurs with the glycosidic linkage in both the α-D and β-D anomeric forms in the lipopolysaccharides of different *Salmonella* species. The two anomeric disaccharides isolated from natural sources were originally incorrectly identified owing to the lack of authentic standards (1). Synthetic disaccharides are also of use in determining the immunodominant site in antigenic lipopolysaccharides. We now report the synthesis of 4-*O*-α-D-mannopyranosyl-L-rhamnopyranose, a constituent of *Salmonella* types B and D_1 (1).

The general synthetic scheme was devised using the β-D-gluco analog (2) which, as stated there, served as a model for the D-manno compound. Since Gorin and Perlin have noted (3) that 2,3,4,6-tetra-*O*-benzoyl-α-D-mannopyranosyl bromide (**3**) gives higher yields and greater stereoselectivity than the more common acetyl derivative, **3** was condensed with methyl 2,3-*O*-isopropylidene-α-L-rhamnopyranoside (**1**) in mercuric cyanide and acetonitrile to give methyl 2,3-*O*-isopropylidene-4-*O*-(2,3,4,6-tetra-*O*-benzoyl-α-D-mannopyranosyl)-α-L-rhamnopyranoside (**4**) as a syrup. Debenzoylation and subsequent acetylation of **4** gave, in 76% yield based on **1**, crystalline methyl 2,3-*O*-isopropylidene-4-*O*-(2,3,4,6-tetra-*O*-acetyl-α-D-mannopyranosyl)-α-L-rhamnopyranoside (**5**), m.p. 119–120°. Hydrolysis with trifluoroacetic acid (2,4) of the isopropylidene group of **5** produced syrupy methyl 4-*O*-(2,3,4,6-tetra-*O*-acetyl-α-D-mannopyranosyl)-α-L-rhamnopyranoside (**6**) which, upon acetolysis (2,5), gave crystalline 1,2,3-tri-*O*-acetyl-4-*O*-(2,3,4,6-tetra-*O*-acetyl-α-D-mannopyranosyl)-α-L-rhamnopyranose (**10**) in 78% yield, m.p. 149.5–150.5°. Deacetylation of **10** with sodium methoxide gave crystalline 4-*O*-α-D-mannopyranosyl-α-L-rhamnopyranose (**11**), m.p. 143–145°. Reduction of **11** with sodium borohydride and subsequent acetylation gave crystalline 4-*O*-α-D-mannopyranosyl-L-rhamnitol octaacetate (**13**), m.p. 84–85°.

The α-D configuration of the mannopyranosyl moiety was confirmed by treatment of **11** with crude α-mannosidase prepared from jack bean meal (6). Using this preparation the disaccharide (**11**) and methyl α-D-mannopyranoside were cleaved but methyl β-D-mannopyranoside was not.

The presence of the 1 → 4 linkage was confirmed by periodate oxidation and methylation studies. Deacetylation of **6** with sodium methoxide gave syrupy methyl 4-*O*-α-D-mannopyranosyl-α-L-rhamnopyranoside (**7**). Oxidation of **7** with sodium periodate (7) showed it consumed 3 mol of sodium periodate; subsequent reduction with sodium borohydride, methanolysis, concentration, and acetylation with acetic anhydride gave 1-deoxy-D-erythritol triacetate and glycerol triacetate. Methylation (8) of **7** followed by hydrolysis with trifluoroacetic acid, reduction with sodium borohydride, and acetylation with acetic anhydride gave 1,4,5-tri-*O*-acetyl-2,3-di-*O*-methyl-L-rhamnitol and 1,5-di-*O*-acetyl-2,3,4,

Can. J. Chem. Downloaded from www.nrcresearchpress.com by 210.87.254.40 on 09/05/12
For personal use only.

Can. J. Chem. Downloaded from www.nrcresearchpress.com by 210.87.254.40 on 09/05/12
For personal use only.

6-tetra-*O*-methyl-D-mannitol as identified by g.l.c. and mass spectrometry (9).

Experimental

General experimental specifications were the same as for the β-D-gluco analog (2).

Methyl 2,3-O-Isopropylidene-α-L-rhamnopyranoside (1)

Prepared as in (2) except that the Amberlite IR-120 H^+ resin should be soaked in dry methanol and not acetone to avoid the formation of acetone polymers.

Methyl 2,3-O-Isopropylidene-4-O-(2,3,4,6-tetra-O-benzoyl-α-D-mannopyranosyl)-α-L-rhamnopyranoside (4)

1,2,3,4,6-Penta-*O*-benzoyl-α-D-mannopyranose (**2**) (10) was converted to 2,3,4,6-tetra-*O*-benzoyl-α-D-mannopyranosyl bromide (**3**) (11) 15 g of which, dissolved in acetonitrile (20 ml, distilled over CaH_2), was added with stirring during 2 h to a solution of methyl 2,3-*O*-isopropylidene-α-L-rhamnopyranoside (**1**) (4.0 g, 18.3 mmol) and dry mercuric cyanide (4.0 g) in acetonitrile (10 ml). After stirring for 3 h more the acetonitrile was removed from the reaction mixture under diminished pressure and the remaining syrup was dissolved in chloroform (100 ml). The chloroform solution was washed with 1 *N* potassium bromide (2 × 100 ml), water (100 ml), saturated sodium bicarbonate (100 ml), and water (2 × 100 ml). The chloroform was removed under diminished pressure leaving an impure amorphous solid (17.3 g) which showed a major component (~80%) on t.l.c. with R_f (solvent A) 0.71.

Methyl 2,3-O-Isopropylidene-4-O-(2,3,4,6-tetra-O-acetyl-α-D-mannopyranosyl)-α-L-rhamnopyranoside (5)

Compound **4** (impure amorphous solid, 17.3 g) was debenzoylated to yield a syrup (R_f (t.l.c. solvent B) 0.31) which on acetylation gave the acetate (**5**) which was crystallized from ethanol (25 ml); yield 7.6 g, 13.9 mmol, 76%. Recrystallization from ethanol gave pure **5**, m.p. 119–120°; $[\alpha]_D$ +30.7° (*c* 2.2, chloroform); R_f (t.l.c. solvent A) 0.53; p.m.r. ($CDCl_3$): τ 5.01 (1H, doublet, $J_{1',2'}$ = 1.7 Hz, H-1'), 5.14 (1H singlet, H-1), 6.63 (3H singlet, C-1, OCH_3), 7.84, 7.90, 7.97, 8.01 (3H singlets, OAc's), 8.48, 8.66 (3H singlets, isopropylidene CH_3's), 8.72 (3H doublet, $J_{5,6}$ = 6 Hz, CH_3).

Anal. Calcd. for $C_{24}H_{36}O_{14}$: C, 52.55; H, 6.62. Found: C, 52.38; H, 6.49.

Methyl 4-O-(2,3,4,6-Tetra-O-acetyl-α-D-mannopyranosyl)-α-L-rhamnopyranoside (6)

Compound **6** (1.83 g) was obtained as a syrup (t.l.c., R_f (solvent A) 0.17, (solvent B) 0.59) by deacetalation (2, 4) of **5** (2.0 g); p.m.r. ($CDCl_3$): τ 5.04 (1H doublet, $J_{1',2'}$ = 1.7 Hz, H-1') 5.31 (1H singlet, H-1), 6.62 (3H singlet, C-1, OCH_3), 7.85, 7.90, 7.95, 7.99 (3H singlets, OAc's), 8.67 (3H doublet, $J_{5,6}$ = 6 Hz, CH_3).

Methyl 4-O-α-D-Mannopyranosyl-α-L-rhamnopyranoside (7)

Deacetylation of **6** (1.83 g) gave **7**, R_f (solvent B) 0.03; yield 1.17 g; $[\alpha]_D$ +13° (*c* 2.2, water); $R_{glucose}$ (solvent C) 2.9; p.m.r. (D_2O, external TMS): τ 5.01 (1H doublet, $J_{1',2'}$ = 1.8 Hz, H-1'), 5.29 (1H doublet, $J_{1,2}$ = 1.5 Hz, H-1), 6.60 (3H singlet, C-1, OCH_3), 8.67 (3H doublet, $J_{5,6}$ = 6 Hz, CH_3).

Periodate Oxidation of Compound 7

Reaction of the methyl glycoside (7) (0.320 g, 0.94 mmol) with sodium metaperiodate (0.05 *M*, 120 ml) at 5° in the dark showed a rapid uptake of 2 mol with the consumption of periodate becoming constant (3.0 mol) in 30 h (7). Reduction of the polyaldehyde and methanolysis of the polyalcohol gave 1-deoxy-D-erythritol and glycerol (2).

Methylation of Compound 7

The methyl glycoside (**7**) (0.27 g) was methylated (2, 8) and the product (**8**) (0.2 g) gave one spot on t.l.c. (solvent A) with R_f 0.14; $[\alpha]_D$ +10° (*c* 1.0, chloroform); p.m.r. ($CDCl_3$): τ 4.93 (1H doublet, $J_{1',2'}$ = 1.6 Hz, H-1'), 5.27 (1H doublet, $J_{1,2}$ = 1.6 Hz, H-1), 6.46–6.63 (21H, OCH_3's), 8.72 (3H doublet, $J_{5,6}$ = 6 Hz, CH_3).

Hydrolysis of **8** (0.2 g, 2 *M* TFA, 20 ml, reflux, 15 h) gave 2,3,4,6-tetra-*O*-methyl-D-mannose and 2,3-di-*O*-methyl-L-rhamnose as shown by paper chromatography (solvent D) and by g.l.c.–m.s. (2, 9) of the alditol acetates prepared according to Albersheim and co-workers (12).

Methyl 2,3-Di-O-acetyl-4-O-(2,3,4,6-tetra-O-acetyl-α-D-mannopyranosyl)-α-L-rhamnopyranoside (9)

Methyl 4-*O*-(2,3,4,6-tetra-*O*-acetyl-α-D-mannopyranosyl)-α-L-rhamnopyranoside (**6**) (0.1 g) was acetylated with pyridine (4 ml) and acetic anhydride (4 ml); yield 0.11 g. A portion of the syrupy product was purified by preparative t.l.c. (13) for analytical purposes, $[\alpha]_D$ +4° (*c* 1.3, chloroform); R_f (t.l.c., solvent A) 0.41; p.m.r. ($CDCl_3$): τ 5.01 (1H doublet, $J_{1',2'}$ = 1.6 Hz, H-1'), 5.40 (1H doublet, $J_{1,2}$ = 1.5 Hz, H-1), 6.61 (3H singlet, C-1, OCH_3), 7.84–8.01 (18H, OAc's), 8.60 (3H doublet, $J_{5,6}$ = 6 Hz, CH_3).

1,2,3-Tri-O-acetyl-4-O-(2,3,4,6-tetra-O-acetyl-α-D-mannopyranosyl)-α-L-rhamnopyranose (10)

Methyl 4-*O*-(2,3,4,6-tetra-*O*-acetyl-α-D-mannopyranosyl)-α-L-rhamnopyranoside (**6**) (1.0 g) in acetic anhydride (5 ml) was shaken with concentrated sulfuric acid 2% (v/v) in acetic anhydride (10 ml) for 3 h (5). The reaction mixture was diluted with chloroform (100 ml) and the chloroform solution was washed with water (2 × 100 ml), saturated sodium bicarbonate (2 × 100 ml), and again with water (2 × 100 ml). Any remaining acetic anhydride or acetic acid was removed by distillation with ethanol. The remaining syrup was crystallized from ethanol (10 ml), yield 0.95 g. Recrystallization from ethanol gave pure **10**, m.p. 149.5–150.5°; $[\alpha]_D$ −5.5° (*c* 4.3, chloroform); R_f (t.l.c., solvent A) 0.39; p.m.r. ($CDCl_3$): τ 4.00 (1H doublet, $J_{1,2}$ = 1.5 Hz, H-1), 5.00 (1H doublet, $J_{1',2'}$ = 1.8 Hz, H-1'), 7.82–8.00 (21H, OAc's), 8.60 (3H doublet, $J_{5,6}$ = 6 Hz, CH_3).

Anal. Calcd. for $C_{26}H_{36}O_{17}$: C, 50.32; H, 5.85. Found: C, 50.37; H, 5.98.

4-O-α-D-Mannopyranosyl-α-L-rhamnopyranose (11)

The peracetate of the disaccharide (**10**) (1.2 g) was deacetylated and the product (0.6 g) crystallized neat after long standing. Pure **11** was obtained by recrystallization from a 1:1 mixture of methanol and 2-propanol (20 ml/g), m.p. 143–145°; $[\alpha]_D$ +53.0° mutarotating to +60.3° in 2 h (*c* 1.0, water); $R_{glucose}$ (solvent C) 1.0; p.m.r. (D_2O,

external TMS): τ 4.90 (0.6H doublet, $J_{1,2}$ = 1.5 Hz, H-1 of α-L form), 5.03 (1H doublet, $J_{1',2'}$ = 1.8 Hz, H-1'), 5.16 (0.4 H doublet, $J_{1,2}$ = 1.0 Hz, H-1 of β-L form), 8.71 (3H doublet, $J_{5,6}$ = 6 Hz, CH_3).

Anal. Calcd. for $C_{12}H_{22}O_{10}$: C, 44.17; H, 6.80. Found: C, 43.91; H, 6.86.

Gas–liquid chromatography of the per(trimethylsilyl) disaccharide (column a at 240°) gave one peak (80%) at 8.5 min and a second peak at 11.7 min (per(trimethylsilyl) sucrose 14.5 min) (14).

The free disaccharide (**11**) (0.1 g) was dissolved in sodium acetate buffer (0.3 *M*, p*H* 4.5, 2 ml) and incubated at 37° with 2 ml of crude α-mannosidase (6). The disaccharide (**11**) was 80% cleaved in 10 h and completely cleaved in 22 h as shown by paper chromatography (solvent C). Under these conditions methyl β-D-mannopyranoside (3) was not cleaved but methyl α-D-mannopyranoside (commercial preparation) was hydrolyzed. The products from the disaccharide were reduced, acetylated, and identified by g.l.c.–m.s. (2, 9) as an equimolecular mixture of L-rhamnitol pentaacetate and D-mannitol hexaacetate (m.p. 120–122°; lit. (15) m.p. 125°)

4-O-α-D-Mannopyranosyl-L-rhamnitol (12)

The free disaccharide (**11**) (0.5 g) was reduced with sodium borohydride (0.2 g) to give **12**; yield 0.5 g; $[\alpha]_D$ +57° (*c* 3.5, water); $R_{glucose}$ (solvent C) 0.5; p.m.r. (D_2O, external TMS): τ 4.89 (1H doublet, $J_{1',2'}$ = 1.9 Hz, H-1'), 8.73 (3H doublet, $J_{5,6}$ = 6 Hz, CH_3).

Gas–liquid chromatography of the per(trimethylsilyl) alditol (column a at 240°) gave one peak at 11.5 min (per(trimethylsilyl)sucrose, 12.9 min) (14).

The alditol **12** (0.3 g) was acetylated with pyridine (10 ml) and acetic anhydride (10 ml) to give 4-*O*-α-D-mannopyranosyl-L-rhamnitol octaacetate (**13**) (0.55 g, crystallized from ethanol (5 ml)). Recrystallization from ethanol gave pure **13**, m.p. 84–85°; $[\alpha]_D$ −4.4° (*c* 1.9, chloroform); R_f (t.l.c., solvent A) 0.33; p.m.r. ($CDCl_3$): τ 4.98 (1H doublet, $J_{1',2'}$ = 1.6 Hz, H-1'), 7.84–8.02 (24H, OAc's), 8.63 (3H doublet, $J_{5,6}$ = 6 Hz, CH_3).

Anal. Calcd. for $C_{28}H_{40}O_{18}$: C, 50.60; H, 6.07. Found: C, 50.39; H, 6.13.

Gas–liquid chromatography of the peracetylated alditol (**13**) (column a at 270°) gave one peak at 7.0 min (sucrose octaacetate, 10.0 min).

The authors thank the National Research Council of Canada for financial support and for the award of a scholarship to G.M.B.

1. M. Fukuda, F. Egami, G. Hämmerling, O. Lüderitz, G. Bagdian, and A. M. Staub. Eur. J. Biochem. **20**, 438 (1971).
2. G. M. Bebault and G. G. S. Dutton. Can. J. Chem. **50**, 3373 (1972).
3. P. A. J. Gorin and A. S. Perlin. Can. J. Chem. **39**, 2474 (1961).
4. A. J. Acher, Y. Rabinsohn, E. S. Rachaman, and D. Shapiro. J. Org. Chem. **35**, 2436 (1970).
5. G. O. Aspinall, R. Khan, and Z. Pawlak. Can. J. Chem. **49**, 3000 (1971).
6. Y. T. Li. J. Biol. Chem. **241**, 1010 (1966).
7. J. C. Rankin and A. Jeanes. J. Am. Chem. Soc. **76**, 4435 (1954).
8. P. A. Sandford and H. E. Conrad. Biochemistry, **5**, 1508 (1966).
9. H. Björndal, C. G. Hellerqvist, B. Lindberg, and S. Svensson. Agnew. Chem. Int. Ed. **9**, 610 (1970).
10. E. Fischer and R. Oetker. Ber. **46**, 4029 (1913).
11. R. K. Ness, H. G. Fletcher, Jr., and C. S. Hudson. J. Am. Chem. Soc. **72**, 2200 (1950).
12. P. Albersheim, D. J. Nevins, P. D. English, and A. Karr. Carbohydr. Res. **5**, 340 (1967).
13. D. Horton and T. Tsuchiya. Carbohydr. Res. **5**, 426 (1967).
14. E. Percival. Carbohydr. Res. **4**, 441 (1967).
15. L. Hough and A. C. Richardson. *In* Rodd's chemistry of carbon compounds. Vol. 1F. Elsevier, Amsterdam. 1967. p. 22.

Can. J. Chem. Downloaded from www.nrcresearchpress.com by 210.87.254.40 on 09/05/12
For personal use only.

The Synthesis of 4-*O*-α-D-Glucopyranosyl-L-rhamnopyranose

JOFFRE M. BERRY AND GUY G. S. DUTTON

Department of Chemistry, University of British Columbia, Vancouver, British Columbia V6T 1W5

Received June 13, 1973

4-*O*-α-D-Glucopyranosyl-L-rhamnose has been synthesized in 40% overall yield by condensation of 2-*O*-benzyl-3,4,6-tri-*O*-*p*-nitrobenzoyl-β-D-glucopyranosyl bromide with methyl 2,3-*O*-isopropylidene-α-L-rhamnopyranoside in nitromethane using mercuric cyanide as acid acceptor. The methyl glycoside hexaacetate was obtained crystalline.

4-*O*-α-D-Glucopyrannosyl-L-rhamnose a été synthétisé avec un rendement de 40% par condensation du bromo-2-*O*-benzyle-3,4,6-tri-*O*-*p*-nitrobenzoyl-β-D-glucopyrannose avec le méthyl 2,3-*O*-isopropylidène-α-L-rhamnopyrannoside en nitrométhane et le cyanure de mercure. Le glycoside méthyl hexaacétate a été obtenu sous forme cristallin.

Can. J. Chem., **52**, 681 (1974)

Can. J. Chem. Downloaded from www.nrcresearchpress.com by 210.87.254.42 on 09/05/12
For personal use only.

The importance of *cis*-glycosides in nature has led to many attempts to synthesize them (1–7). We now report the synthesis in 40% yield of 4-*O*-α-D-glucopyranosyl-L-rhamnose using an intermediate with a nonparticipating 2-*O*-benzyl group as suggested by the work of Ishikawa and Fletcher (6). This disaccharide is required for structural studies on capsular polysaccharides from *Klebsiella* and was originally thought to be an antigenic determinant in *Shigella* (8).

2-*O*-Benzyl-D-glucose (**1**) was prepared as described in the literature (10, 11) except that a higher yield in shorter time was obtained by using only 0.2 *M* excess of benzyl bromide, adding Drierite to the reaction and, in addition, using freshly prepared silver oxide (12).

Condensation of the derived 2-*O*-benzyl-3,4,6-tri-*O*-*p*-nitrobenzoyl-β-D-glucopyranosyl bromide (**2**) with methyl 2,3-*O*-isopropylidene-α-L-rhamnopyranoside (**3**) with mercuric cyanide as an acid acceptor in nitromethane at 40° and subsequent purification by column chromatography, gave the fully blocked disaccharide (**4**) in 80% yield. Deacylation of **4** gave crystalline methyl 4-*O*-(2-*O*-benzyl-α-D-glucopyranosyl)-2,3-*O*-isopropylidene-α-L-rhamnopyranoside (**5**). In addition, a small amount of β-linked disaccharide was detected which was conveniently identified as the trimethylsilyl derivative by p.m.r. (13) after removal of the benzyl group. Hydrogenolysis of **5** gave the debenzylated compound (**6**) which when reacted with trifluoroacetic acid, yielded methyl 4-*O*-α-D-glucopyranosyl-α-L-rhamnopyranoside as a syrup (**8**).

Acetylation of **8** gave the crystalline hexaacetate (**10**), m.p. 136–137°. Acetolysis of **10** gave the corresponding heptaacetate (**11**). Deacetylation then afforded 4-*O*-α-D-glucopyranosyl-L-rhamnopyranose (**12**) as a syrup, $[\alpha]_D$ +10° (water).

The structure of the disaccharide follows from the method of synthesis and was confirmed by the products obtained by periodate oxidation (14) and methylation (15) of **8**.

The nature of the anomeric linkage is confirmed by the p.m.r. spectra of compounds **5**, **6**, **8**, **9**, **12**, and **13**, all of which gave signals in the region τ 4.76–5.03 with a splitting of about 3.8 Hz, characteristic of the α-D-configuration. In addition **12** was hydrolyzed by maltase but not by β-D-glucosidase. This disaccharide (**12**) represents the first α-D-glycosyl-L-rhamnose to be synthesized.

Experimental

General methods and the preparation of several of the intermediates have been described previously (9). In some cases where only small quantities of material were available p.m.r. spectra were obtained on a Varian XL-100 instrument equipped with Fourier transform.

2-O-Benzyl-D-glucose (1)

3,4,6-Tri-*O*-acetyl-1-deoxy-1-piperidino-β-D-glucopyranose (16) (35 g), freshly prepared (12) powdered dry silver oxide (40 g) and ground Drierite (30 g) were stirred in dry benzene (250 ml) for 30 min in the dark at room temperature with exclusion of moisture. The mixture was cooled to about 15° and benzyl bromide (13 ml, 0.2 *M* excess) was added. After stirring at room temperature for 3½ h t.l.c. (solvent A) indicated that the reaction was complete. The mixture was filtered, the salts were washed with benzene, and the combined solvents were removed after which the product crystallized. Recrystallization from hot methanol (3 ml/g) and drying gave pure 3,4,6-tri-*O*-acetyl-2-*O*-benzyl-1-deoxy-1-piperidino-β-D-glucopyranose 38.7 g (89%), m.p. 99–100°; $[\alpha]_D$ +42° (*c* 2.2,

Can. J. Chem. Downloaded from www.nrcresearchpress.com by 210.87.254.42 on 09/05/12
For personal use only.

methanol) (lit. (10) m.p. 100°; $[\alpha]_D$ +41.5° (*c* 0.9, methanol)). The above compound (35 g) was treated with 2% sodium methoxide in anhydrous methanol and t.l.c. (solvent A) showed that the reaction was complete within 30 min. Molar sulfuric acid was added until the p*H* of the solution was about 3 and the mixture was refluxed for 1 h (11). After neutralization (barium carbonate) and concentration, 2-*O*-benzyl-D-glucose (**1**) crystallized. Recrystallization from hot methanol (10 ml/g) gave pure **1** (16 g), m.p. 176–177°; $[\alpha]_D$ +47° (*c* 2.0, methanol) (lit. (10, 11) m.p. 176–177°; $[\alpha]_D$ +47° (*c* 1.0, methanol)).

2-O-Benzyl-3,4,6-tri-O-p-nitrobenzoyl-β-D-glucopyranosyl Bromide (2)

This compound was prepared by the method of Ishikawa and Fletcher (6) in 25% overall yield from **1**, m.p. 142–143°; $[\alpha]_D$ +3° (*c* 2.0, dichloromethane) (lit. (6) m.p. 143–144°; $[\alpha]_D$ +2.4° (*c* 2.1, dichloromethane)).

Methyl 4-O-(2-O-Benzyl-3,4,6-tri-O-p-nitrobenzoyl-α-D-glucopyranosyl)-2,3-O-isopropylidene-α-L-rhamnopyranoside (4)

To a solution of methyl 2,3-*O*-isopropylidene-α-L-rhamnopyranoside (17) (**3**, 0.78 g, 3.58 mmol) and mercuric cyanide (1.08 g, 4.3 mmol) in nitromethane (50 ml, distilled from calcium hydride) was added the bromide (**2**) (3.4 g, 4.3 mmol) and the mixture was stirred at 40° with exclusion of moisture. After 5 h t.l.c. (benzene–ether (9:1) (7)) showed a small amount of unreacted **3** (R_f 0.06, no decrease on the addition of more bromide and cyanide) and a large yellow-brown spot (R_f 0.33) corresponding to the disaccharide (**4**). In addition, a faster running component (R_f 0.56, a monosaccharide tri-*p*-nitrobenzoate as indicated by p.m.r.) was detected. The reaction solvent was removed and the remaining syrup was dissolved in benzene (100 ml) and washed successively with water, sodium bicarbonate and water, then dried ($CaSO_4$). The syrup obtained after removal of the solvent was purified on a 25 cm × 7 cm silica gel pressure column (18) (180 g silica) using benzene–ether (9:1) as solvent. Fractions 50–70 (each fraction 20 ml, collected at 90 s intervals) contained the disaccharide. The combined fractions gave a syrup (**4**) (2.65 g, 80%) which was homogeneous on t.l.c., $[\alpha]_D$ +65° (*c* 2.0, chloroform); p.m.r. (CCl_4) τ 1.6–2.1 (12H, *p*-nitrobenzoates), 2.8–3.0 (5H, phenyl), 6.65 (3H singlet, C-1, OCH_3), 8.43, 8.67 (3H, singlets, isopropylidene CH_3), 8.70 (3H, doublet, $J_{5,6}$ = 6 Hz, CH_3).

Methyl 4-O-(2-O-Benzyl-α-D-glucopyranosyl)-2,3-O-isopropylidene-α-L-rhamnopyranoside (5)

Fully blocked disaccharide (**4**) (1.5 g) was refluxed in a mixture of potassium hydroxide (6 g) in water (15 ml) and ethanol (60 ml). After about 90 min (t.l.c., solvent B) the spot corresponding to starting material (R_f 0.84) was replaced by a large product spot (R_f 0.74) corresponding to **5** and a faint spot running slightly faster (R_f 0.76); this was more conveniently identified after hydrogenolysis. The cooled solution was neutralized with Dry Ice and the solvent was removed by evaporation. Residual water was removed by azeotroping with dry benzene or ethanol. The disaccharide was then extracted from the insoluble salts by refluxing with diethyl ether (300 ml × 3). The syrup obtained crystallized after seeding with a sample obtained by preparative t.l.c., yield 565 mg. Alternatively **5** was obtained by dissolving the fully blocked disaccharide (**4**) (1 g) in chloroform (50 ml) and adding 0.2 *M* sodium methoxide in methanol (40 ml). After 1 h at room temperature the solution was neutralized with Dry Ice or, while cold, with Amberlite IR 120 H^+ resin. In the latter case the resin must be removed as soon as the mixture is neutral to avoid deacetalation. Purification by preparative t.l.c. gave crystalline **5** which was recrystallized from 2-propanol (12 ml/g), m.p. 158–159°; $[\alpha]_D$ +71.5° (*c* 1.8, methanol); p.m.r. ($CDCl_3$) τ 2.68 (5H, phenyl), 5.04 (1H doublet, $J_{1',2'}$ = 3.7 Hz, H′-1), 5.18 (1H singlet, H-1), 6.67 (3H singlet, C-1, OCH_3), 8.50, 8.68 (3H singlets, isopropylidene CH_3), 8.70 (3H doublet, $J_{5,6}$ = 6 Hz, CH_3).

Anal. Calcd. for $C_{23}H_{34}O_{16}$: C, 58.69; H, 7.29. Found: C, 58.36; H, 7.34.

Methyl 4-O-α-D-Glucopyranosyl-2,3-O-isopropylidene-α-L-rhamnopyranoside (6)

Methyl 4-*O*-(2-*O*-benzyl-α-D-glucopyranosyl)-2,3-*O*-isopropylidene-α-L-rhamnopyranoside (**5**) (400 mg, m.p. 158–159°) was hydrogenated with 5% palladium-on-carbon (1 g) in absolute ethanol (15 ml) at 50 p.s.i. at room temperature for 16 h. After filtration, washing of the carbon with ethanol and removal of the solvent, a chromatographically pure syrup (320 mg) was obtained, $[\alpha]_D$ + 73° (*c* 2.0, methanol); p.m.r. τ 6.64 (3H singlet, C-1, OCH_3), 8.50, 8.68 (3H singlets, isopropylidene CH_3). The p.m.r. spectrum of the trimethylsilyl derivative (13) of (**6**) showed (benzene, external TMS) τ 5.03 (1H doublet, $J_{1',2'}$ = 4, H′-1), 5.11 (1H singlet, H-1), 7.0 (3H singlet, C-1, OCH_3), 8.40, 8.76 (3H singlets, isopropylidene CH_3), 8.56 (3H doublet, $J_{1,2}$ = 6 Hz, CH_3), 9.65, 9.68, 9.78, 9.90 (9H singlets, 4 trimethylsilyl groups).

Similarly, a sample of **5** (30 mg) containing a small amount of a faster running compound was hydrogenolyzed giving **6** (R_f 0.34, solvent B) and a second component (**7**) (R_f 0.43), which was isolated by preparative t.l.c. (1 mg obtained). The p.m.r. (Fourier transform) of **7** was similar to that of **6** but was unclear. The p.m.r. (Fourier transform) of the trimethylsilyl derivative of **7** showed (benzene-d_6, external TMS) τ 4.86 (1H doublet, $J_{1',2'}$ = 7.3, H′-1), 5.06 (1H, singlet, H-1), 6.92 (3H singlet, C-1, OCH_3), 8.43 (3H doublet, $J_{5,6}$ = 6 Hz, CH_3), 8.46, 8.76 (3H singlets, isopropylidene CH_3), 9.70, 9.71, 9.75, 9.84 (9H singlets, 4 trimethylsilyl groups) and was identical to the p.m.r. of the trimethylsilyl derivative of an authentic sample of methyl 4-*O*-β-D-glucopyranosyl-2,3-*O*-isopropylidene-α-L-rhamnopyranoside obtained by deacetylation of the crystalline tetraacetate (9).

Methyl 4-O-α-D-Glucopyranosyl-α-L-rhamnopyranoside (8)

The isopropylidene compound (**6**) (250 mg) in chloroform (10 ml) was treated at room temperature for 2½ h with trifluoroacetic acid (TFA, 1 ml) containing 1–2% water. The mixture was concentrated and small amounts of TFA removed by treatment with Duolite A-4 (OH^-) resin, or by evaporation with toluene. After filtration and evaporation a syrup (**8**) (211 mg) was obtained, $[\alpha]_D$ +43° (*c* 1.2, methanol), $R_{glucose}$ (solvent C) 2.1; p.m.r. (D_2O, external TMS) τ 4.97 (1H doublet, $J_{1',2'}$ = 3.3 Hz), 5.35 (1H doublet, $J_{1,2}$ = 1.7 Hz), 8.64 (3H doublet, $J_{5,6}$ = 6 Hz, CH_3), 6.64 (3H singlet, OCH_3).

Periodate Oxidation

The disaccharide methyl glycoside (**8**) consumed 3.0 mol of sodium metaperiodate and reduction of the product

Can. J. Chem. Downloaded from www.nrcresearchpress.com by 210.87.254.42 on 09/05/12
For personal use only.

followed by methanolysis gave 1-deoxy-D-erythritol and glycerol as determined by paper chromatography in solvent D or as acetates on column *b* (9).

Methylation

The glycoside (**8**) was methylated (9, 15) to give the permethylated compound **9** which, after purification by t.l.c. (R_f 0.13, solvent A; 0.61, solvent B), had $[\alpha]_D$ +80° (*c* 0.9, methanol); p.m.r. ($CDCl_3$) τ 4.97 (1H doublet, $J_{1',2'}$ = 3.7 Hz, H'-1), 5.27 (1H doublet, $J_{1,2}$ = 1.8 Hz, H-1), 6.35–6.65 (21H, 7-OCH_3), 8.65 (3H doublet, $J_{5,6}$ = 6 Hz, CH_3).

The sugars obtained on methanolysis or hydrolysis of **9** were characterized as 2,3-di-*O*-methyl-L-rhamnose and 2,3,4,6-tetra-*O*-methyl-D-glucose by g.l.c. and mass spectra (9).

*Methyl 2,3-Di-O-acetyl-4-O-(2,3,4,6-tetra-O-acetyl-α-D-glucopyranosyl)-α-L-rhamnopyranoside (**10**)*

The disaccharide methyl glycoside (**8**) (200 mg) was acetylated in pyridine (5 ml) and acetic anhydride (5 ml) at room temperature overnight to give **10** which was recrystallized from ethanol (6 ml/g), yield 290 mg, R_f 0.41 (solvent A); m.p. 136–137°; $[\alpha]_D$ +62.3° (*c* 2.6, chloroform); p.m.r. ($CDCl_3$) τ 6.62 (3H singlet, C-1, OCH_3), 7.90–8.02 (18H, OAc's), 8.60 (3H doublet, $J_{5,6}$ = 6 Hz, CH_3).

Anal. Calcd. for $C_{25}H_{36}O_{16}$: C, 50.65; H, 6.13; Found: C, 50.45; H, 6.11.

*4-O-(2,3,4,6-Tetra-O-acetyl-α-D-glucopyranosyl)-1,2,3-tri-O-acetyl-L-rhamnopyranose (**11**)*

To the hexaacetate (**10**) (80 mg) in acetic anhydride (1 ml) was added a solution of 2% (v/v) sulfuric acid in acetic anhydride (2 ml). After 3 h at room temperature, cold saturated sodium bicarbonate (15 ml) was added to the mixture and stirred for 35 min. The product was extracted with chloroform (2 × 15 ml) which was washed with water (2 × 5 ml) and dried ($CaSO_4$). Thin-layer chromatography (solvent A) showed one major spot (R_f 0.41, indistinguishable from starting material) and a small amount of cleavage products. Preparative t.l.c. gave chromatographically pure heptaacetate (**11**) as a syrup, yield 78 mg, $[\alpha]_D$ +55° (*c* 2.0, chloroform); p.m.r. ($CDCl_3$) τ 4.00 (1H doublet, $J_{1,2}$ = 1.6 Hz, H-1), 7.82–8.02 (21H, OAc's), 8.62 (3H doublet, $J_{5,6}$ = 6 Hz, CH_3).

*4-O-α-D-Glucopyranosyl-L-rhamnopyranose (**12**)*

The heptaacetate (**11**) (70 mg) was deacetylated in 0.2 *M* sodium methoxide in methanol (5 ml, 1 h, 20°) and passage through Amberlite IR-120 (H^+) resin gave the free disaccharide (**12**) as a syrup, 35 mg. Paper chromatography gave one component with $R_{glucose}$ 0.68 (solvent C) and $[\alpha]_D$ +10° (*c* 1.0, water); p.m.r. (D_2O, external TMS) τ 4.88 (1H doublet, $J_{1,2}$ = 1.3 Hz, H-1 of α-L-form), 5.14 (1H doublet, $J_{1,2}$ = 0.8 Hz, H-1 of β-L-form), 4.94 (1H doublet, $J_{1',2'}$ = 3.8 Hz, H'-1), 8.64 (3H doublet, $J_{5,6}$ = 6 Hz, CH_3).

Gas–liquid chromatography of the per(trimethylsilyl) disaccharide (column *a*, 250°) gave one peak (77%) at 6.4 min and a second peak at 8.7 min, (per(trimethylsilyl)sucrose, 9.0 min). Enzymatic hydrolysis of the disaccharide (2 mg) with maltase (2 mg) at p*H* 6.5 at 37° gave over 90% cleavage in 30 min as shown by paper chromatography. Incubation with β-glucosidase (19) at p*H* 5.1 gave only trace cleavage in 16 h.

*4-O-α-D-Glucopyranosyl-L-rhamnitol (**13**)*

The disaccharide (**12**) (15 mg) was reduced with sodium borohydride (30 mg) in water (2 ml) at room temperature overnight. Passage through IR-120 (H^+) cation exchange resin, concentration, and distillation with methanol gave a syrup (**13**), 14 mg, $R_{glucose}$ 0.58 (solvent C); p.m.r. (D_2O, external TMS) τ 4.76 (1H doublet, $J_{1',2'}$ = 3.8 Hz, H'-1), 8.70 (CH_3 doublet, $J_{5,6}$ = 6 Hz). Gas-liquid chromatography of the per(trimethylsilyl)alditol on column *a* at 250° gave one peak at 9.6 min, (per(trimethylsilyl)sucrose, 9.0 min). Acetylation of the alditol (12 mg, pyridine-acetic anhydride) gave a syrup $[\alpha]_D$ +56° (*c* 1.25, chloroform); p.m.r. ($CDCl_3$) τ 7.90–8.02 (24H, OAc's), 8.66 (CH_3 doublet, $J_{5,6}$ = 6 Hz). Injection of the alditol acetate onto column *a* at 275° gave one peak at 5.8 min (sucrose octaacetate, 7.2 min).

We are indebted to the National Research Council of Canada and the University of British Columbia for financial support of this work.

1. M. L. WOLFROM, K. IGARASHI, and K. KOIZUMI. J. Org. Chem. **30**, 3841 (1965).
2. R. U. LEMIEUX, K. JAMES, and T. L. MAGABHUSHAN. Can. J. Chem. **51**, 42 (1973).
3. R. J. FERRIER, R. W. HAY, and N. VETHAVIYASAR. Carbohydr. Res. **27**, 55 (1973).
4. P. A. GORIN and A. S. PERLIN. Can. J. Chem. **39**, 2474 (1961).
5. J. M. FRÉCHET and C. SCHUERCH. J. Am. Chem. Soc. **94**, 604 (1972).
6. T. ISHIKAWA and H. G. FLETCHER, JR. J. Org. Chem. **34**, 563 (1969).
7. H. M. FLOWERS. Carbohydr. Res. **18**, 211 (1971).
8. (*a*) D. A. R. SIMMONS. Immunology, **20**, 17 (1971). (*b*) B. LINDBERG, J. LÖNNGREN, U. RUDÉN, and D. A. R. SIMMONS. Eur. J. Biochem. **32**, 15 (1973).
9. G. M. BEBAULT and G. G. S. DUTTON. Can. J. Chem. **50**, 3373 (1972).
10. A. KLEMER. Chem. Ber. **96**, 634 (1963).
11. S. BRENNAN and P. A. FINAN. J. Chem. Soc. (C), 1742 (1970).
12. B. HELFERICH and W. KLEIN. Justus Liebigs Ann. Chem. **450**, 219 (1926).
13. G. M. BEBAULT, J. M. BERRY, G. G. S. DUTTON, and K. B. GIBNEY. Anal. Lett. **5**, 413 (1972).
14. G. O. ASPINALL and R. J. FERRIER. Chem. Ind. (London), 1216 (1957).
15. P. A. SANDFORD and H. E. CONRAD. Biochemistry, **5**, 1508 (1966).
16. J. E. HODGE and C. E. RIST. J. Am. Chem. Soc. **74**, 1498 (1952).
17. P. A. LEVENE and I. E. MUSKAT. J. Biol. Chem. **105**, 431 (1934).
18. B. J. HUNT and W. RIGBY. Chem. Ind. (London), 1863 (1967).
19. P. BARUAH and T. SWAIN. Biochem. J. **66**, 321 (1957).

The Structure of the Capsular Polysaccharide of *Klebsiella* K-type 72; Occurrence of 3,4-*O*-(1-Carboxyethylidene)-L-rhamnose

YUEN-MIN CHOY AND GUY G. S. DUTTON

Department of Chemistry, University of British Columbia, Vancouver, British Columbia V6T 1W5

Received September 10, 1973

Methylation and partial hydrolysis studies on the capsular polysaccharide of *Klebsiella* K72 show the structure to consist of a repeating unit

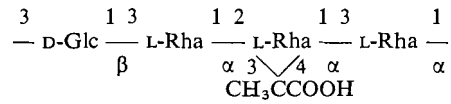

The anomeric linkages were determined in isolated oligosaccharides by p.m.r. spectroscopy which also showed the presence in the polysaccharide of one pyruvate ketal per four sugar residues.

Les méthodes de méthylation et hydrolyse partielle portées au polysaccharide capsulaire de *Klebsiella* K72 ont démontré que la structure se compose d'une unité qui se répéte

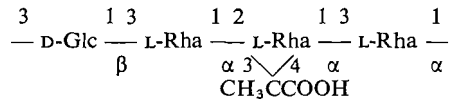

Les liaisons anomères ont été distinguées chez des oligosaccharides isolés par la spectroscopie r.m.n. qui a aussi mis en evidence la présence d'un cétal de l'acide pyruvique par rapport à quatre sucres.

Can. J. Chem., **52**, 684 (1974)

Many of the capsular polysaccharides of *Klebsiella* contain pyruvic acid (1–3), linked as a ketal (4), and in a few cases this may be the only acidic component; the capsule of *Klebsiella* K72 is one such example (5, 6). 4,6-*O*-(1-Carboxyethylidene)-D-galactose (7) and -D-glucose (8) were originally found in other contexts and the presence in nature of the D-*manno* analog was demonstrated for the first time (9) in *Klebsiella* K5. The capsular polysaccharide of *Klebsiella* K72 is now shown to have a structure composed of the repeat unit

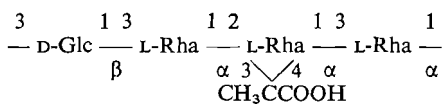

and thus to represent the first natural occurrence of 3,4-*O*-(1-carboxyethylidene)-L-rhamnose. The presence of *O*-(1-carboxyethylidene)-L-rhamnose in *Klebsiella* K32 has also been indicated but the precise linkage has not yet been verified (10).

Purified (4) capsular polysaccharide from *Klebsiella* K72 had $[\alpha]_D^{24}$ $-54°$ and the p.m.r. spectrum (11, 12) indicated the presence of pyruvate and deoxy sugar in the ratio of 1:3. The signals from the anomeric protons suggested three α- and one β-linkages (12, 13). Quantitative analysis, as alditol acetates, gave D-glucose and L-rhamnose in a ratio of 1:3 and the configurations were determined (14) by the sign of the circular dichroism (c.d.) spectra of the acetates. Methanolysis of the polysaccharide also gave crystalline methyl L-rhamnopyranoside.

Hydrolysis of the fully methylated (15, 16) polysaccharide gave 2,4-di-*O*-methyl-L-rhamnose, L-rhamnose, and 2,4,6-tri-*O*-methyl-D-glucose in the approximate ratio of 2:1:1. For the separation of the alditol acetates of the last two compounds only Apiezon L was found satisfactory. When the original polysaccharide was partially hydrolyzed to remove pyruvate (monitored by p.m.r.) and then methylated the hydrolyzate was shown to contain 3,4-di-*O*-methyl-L-rhamnose, in place of L-rhamnose, thus establishing the position of the 1-carboxyethylidene group (see Table 2, A and B).

As only one of the three L-rhamnose residues is linked through position 2 the location of this moiety identifies the position of the 3,4-*O*-(1-carboxyethylidene)-L-rhamnose unit in the polymer. This was achieved by examination of the oligosaccharides obtained on partial hydrolysis.

Can. J. Chem. Downloaded from www.nrcresearchpress.com by 210.87.254.6 on 09/05/12
For personal use only.

TABLE 1. Proton magnetic resonance data on *Klebsiella* K72 capsular polysaccharide and derived oligosaccharides

Repeating unit of compound	τ* (Hz)	Ratio of integrals	Proton assignment (D-glucose and L-rhamnose)
Glc(β 1→3) — Rha-OH	4.96	0.6	α-Rha-OH
	5.20	0.4	β-Rha-OH
	5.41(7)	1	β-Glc(1→3) — Rha
	8.76(6)	3	CH_3 of L-Rha
Glc(β 1→3) — Rha(α 1→2) — Rha-OH	4.63	1.0	α-Rha(1→2) — Rha
	4.90	0.7	α-Rha-OH
	5.13	0.3	β-Rha-OH
	5.38(7)	1.0	β-Glc(1→3) — Rha
	8.71(6)	6.0	CH_3 of L-Rha
Glc(β 1→3) — Rha(α 1→2) — Rha(α 1→3) — Rha-OH	4.63	1.0	α-Rha(1→2) — Rha
	4.91	0.7	α-Rha-OH
	4.95	1.0	α-Rha(1→3) — Rha
	5.13	0.3	β-Rha-OH
	5.39(7)	1.0	β-Glc(1→3) — Rha
	8.73(6)	9.0	CH_3 of L-Rha
—Glc(β 1→3) — Rha(α 1→2) — Rha(α 1→3) — Rha(α 1→) —	4.62	1.0	α-Rha(1→2) — Rha
	4.84	1.0	α-Rha(1→3) — Glc
	4.94	1.0	α-Rha(1→3) — Rha
	5.36(8)	1.0	β-Glc(1→3) — Rha
	8.70(5)	9.0	CH_3 of L-Rha
—Glc(β 1→3) — Rha(α 1→2) — Rha(α 1→3) — Rha(α 1→) — α 3,4 $CH_3CCOONa$	4.62	1.0	α-Rha(1→2) — Rha
	4.86	1.0	α-Rha(1→3) — Glc
	4.96	1.0	α-Rha(1→3) — Rha
	5.34†	1.0	β-Glc(1→3) — Rha
	8.42	3.0	CH_3 of pyruvate ketal
	8.71(5)	9.0	CH_3 of L-Rha

*Spectra run in D_2O with external tetramethylsilane (τ = 10) at 100 MHz.
†Broad signal, no distinct doublet.

Fragmentation of the capsular polysaccharide gave a di-, tri- and tetrasaccharide which were separated on a charcoal column (17) and by gel filtration. The identity of these oligosaccharides (see Experimental and Tables 1 and 2) is such that the 3,4-*O*-(1-carboxyethylidene)-L-rhamnose must be the center one of the three L-rhamnose units.

Can. J. Chem. Downloaded from www.nrcresearchpress.com by 210.87.254.6 on 09/05/12
For personal use only.

TABLE 2. Methylated sugars from *Klebsiella* K72

Sugars	Retention time (min)*	Sample† A	B	C	D	E
2,3,4,6-Me_4-Glc	19			1	1	1
2,4,6-Me_3-Glc	24	1	1			
2,4-Me_2-Rha	17	2	2	2	1	1
3,4-Me_2-Rha	15		1	1	1	
Rha	21	1				

*As alditol acetates on a column (8 ft × 0.25 in) of 20% Apiezon L on Diatoport S (60–80 mesh) at 218°; He flow rate 60 ml/min.
†A, original polysaccharide; B, depyruvylated polysaccharide; C, tetrasaccharide; D, trisaccharide; E, disaccharide; numbers give approximate molar ratios.

Experimental

General

Solvents for paper chromatography were as follows: (A) ethyl acetate – acetic acid – formic acid – water (18:3:1:4); (B) ethyl acetate – pyridine–water (4:1:1); (C) 1-butanol – acetic acid – water (2:1:1), (D) butanone –water azeotrope.

Other general methods were as described previously (4).

Preparation, Properties, and Analysis of K72 Capsular Polysaccharide

The bacteria were grown and harvested as previously described (9, 18) and the polysaccharide, purified by one precipitation with Cetavlon (19), had $[\alpha]_D^{24}$ −54° (*c* 0.275, water), neutralization equivalent 702 (by titration; theory 670). The p.m.r. spectrum (11, 12) of the sodium salt in D_2O at 95° showed a sharp singlet at τ 8.42 and a doublet at τ 8.71 (J = 5 Hz) in the ratio of 1:3. Signals from the anomeric protons appeared at τ 4.62, 4.86, 4.96, and 5.34 (Table 1).

The polysaccharide (40 mg) was hydrolyzed with trifluoroacetic acid (TFA, 2 *M*) for 4 h. Paper chromatography in solvent B showed the presence of D-glucose and L-rhamnose with a small amount of D-galactose and in solvent A the presence additionally of pyruvic acid (20). Quantitative analysis as alditol acetates showed the sugars to be present in the ratio of 1:3 and permitted the isolation of D-glucitol hexaacetate m.p. 96–98° and L-rhamnitol pentaacetate (syrup). Methanolysis (3% MeOH–HCl, 1 h, 0.1 g polysaccharide) gave methyl α-L-rhamnopyranoside m.p. 108–109° (from ethyl acetate) after t.l.c. separation in solvent D.

Methylation

Capsular polysaccharide (0.1 g) was methylated (15, 16) and hydrolyzed with 90% formic acid at 70° for 45 min and then with 2 *M* TFA at 95° for 4 h. Paper chromatography (solvent D) showed the presence of 2,4-di-*O*-methyl-L-rhamnose (R_f 0.64), 2,4,6-tri-*O*-methyl-D-glucose (0.49), and L-rhamnose (0.1) with a trace (*ca.* 2%) of 2,4,6-tri-*O*-methyl-D-galactose (0.38). Gas–liquid chromatography of the alditol acetates (21) gave the results shown in Table 2. Columns of BDS, ECNSS-M, or OS-138 were incapable of separating L-rhamnitol pentaacetate and 2,4,6-tri-*O*-methyl-D-glucitol triacetate. The identities of the methylated sugars were provisionally determined by comparison with standards by paper chromatography and confirmed by mass spectrometry of the alditol acetates (21).

Methylation of Depyruvylated Polysaccharide

Capsular polysaccharide (0.12 g) was hydrolyzed with 0.1 *M* TFA at 95° for 55 min and the product was recovered by dialysis and lyophilization. The p.m.r. spectrum of a 5% solution in D_2O at 95° confirmed the absence of pyruvic acid. The signal at τ 5.36 had J = 8 Hz and integration showed that L-rhamnose constituted three out of four sugar units; for detailed assignments see Table 1.

Methylation of the degraded polysaccharide (50 mg), hydrolysis (2 *M* TFA, 100°, 4 h) and examination of the alditol acetates showed the presence of 3,4-di-*O*-methyl-L-rhamnose in place of L-rhamnose. 2,4-Di-*O*-methyl-L-rhamnose (R_f 0.68) and the 3,4-isomer (0.67) are not distinguishable in solvent D by their R_f values but with *p*-anisidine the former gives a bluish-green and the latter a reddish-brown color. The mass spectra of the alditol acetates are unequivocal (21).

Characterization of Oligosaccharides

Capsular polysaccharide (0.3 g) was hydrolyzed (0.5 *M* TFA, 95°, 45 min) and the solution was passed through a charcoal column (Darco G 60, 10 × 3 cm). Monosaccharides were eluted with water (2 l) and 20% ethanol–water (1 l) gave 0.16 g of oligosaccharides a portion of which (0.1 g) was applied to a column (110 × 2 cm) of Sephadex G15. Irrigation with water at a flow-rate of 4–6 ml/h gave di- (10 mg), tri- (11 mg), and tetrasaccharides (15 mg) having $R_{glucose}$ 1.12, 0.99, and 0.88 in solvent C. Spectral data are recorded in Table 1 and the sugars obtained by hydrolysis of the methylated oligosaccharides are shown in Table 2. In addition, a portion (3 mg) of the disaccharide was reduced and acetylated. Gas–liquid chromatography (SE-30, 2 ft × 0.25 in., 260°) gave a retention time of 1.1 relative to scillabiitol octaacetate (22) and the peracetate had m.p. 50–54°.

We are indebted to Dr. I. Ørskov, Copenhagen, for a culture of *Klebsiella* K72 (1205) and to Dr. P. J. Salisbury of this department for growing the bacteria.

The financial support of the National Research Council of Canada and the award of a Killam Fellowship to Y.M.C. are gratefully acknowledged.

Can. J. Chem. Downloaded from www.nrcresearchpress.com by 210.87.254.6 on 09/05/12
For personal use only.

1. R. W. WHEAT, C. DORSCH, and G. GODOY. J. Bacteriol. **89**, 539 (1965).
2. B. J. GORMUS, R. W. WHEAT, and J. F. PORTER. J. Bacteriol. **107**, 150 (1971).
3. W. NIMMICH. Personal communication.
4. Y. M. CHOY and G. G. S. DUTTON. Can. J. Chem. **51**, 198 (1973).
5. W. NIMMICH. Z. Med. Mikrobiol. Immunol. **154**, 117 (1968).
6. W. NIMMICH. Acta Biol. Med. Ger. **26**, 397 (1971).
7. S. HIRASE. Bull. Chem. Soc. Jap. **30**, 75 (1957).
8. J. H. SLONEKER and D. G. ORENTAS. Can. J. Chem. **40**, 2188 (1962).
9. G. G. S. DUTTON and M. T. YANG. Can. J. Chem. **51**, 1826 (1973).
10. G. G. S. DUTTON and N. A. FUNNELL. Unpublished results.
11. Y. M. CHOY, G. G. S. DUTTON, A. M. STEPHEN, and M. T. YANG. Anal. Lett. **5**, 675 (1972).
12. G. M. BEBAULT, Y. M. CHOY, G. G. S. DUTTON, N. FUNNELL, A. M. STEPHEN, and M. T. YANG. J. Bacteriol. **113**, 1345 (1973).
13. J. M. VAN DER VEEN. J. Org. Chem. **28**, 564 (1963).
14. G. M. BEBAULT, J. BERRY, Y. M. CHOY, G. G. S. DUTTON, N. FUNNELL, L. D. HAYWARD, and A. M. STEPHEN. Can. J. Chem. **51**, 324 (1973).
15. S. HAKOMORI. J. Biochem. (Tokyo), **55**, 205 (1964).
16. P. A. SANDFORD and H. E. CONRAD. Biochemistry, **5**, 1508 (1966).
17. P. ANDREWS, L. HOUGH, and D. B. POWELL. Chem. Ind. (London), 658 (1956).
18. Y. M. CHOY and G. G. S. DUTTON. Can. J. Chem. **51**, 3021 (1973).
19. J. E. SCOTT. Methods Carbohydr. Chem. **5**, 38 (1965).
20. M. DUCKWORTH and W. YAPHE. Chem. Ind. (London), 747 (1970).
21. H. BJÖRNDAL, C. G. HELLERQVIST, B. LINDBERG, and S. SVENSSON. Agnew. Chem. Int. Ed. **9**, 610 (1970).
22. G. M. BEBAULT and G. G. S. DUTTON. Can. J. Chem. **50**, 3373 (1972).

Can. J. Chem. Downloaded from www.nrcresearchpress.com by 210.87.254.6 on 09/05/12
For personal use only.

The Quenching of Type II Photodecomposition of 2-Pentanone in *n*-Hexane Solution by Metal Chelates[1]

J. FLOOD AND K. E. RUSSELL
Department of Chemistry, Queen's University, Kingston, Ontario
AND
D. J. CARLSSON AND D. M. WILES
Division of Chemistry, National Research Council of Canada, Ottawa, Canada K1A 0R9

Received August 7, 1973

The effect of certain metal chelates on the yield of acetone from the photodecomposition of 2-pentanone in *n*-hexane solution has been studied. The chelates act as quenchers but the slopes of the Stern–Volmer plots are lower than the slope observed for *cis*-1,3-pentadiene. These additives protect solid polyolefins against photodegradation but it is unlikely that the mechanism primarily involves quenching of carbonyl triplets.

The quantum yield of acetone production in the type II decomposition of 2-pentanone in *n*-hexane solution is 0.20 ± 0.01; the triplet state lifetime of 2-pentanone is 2.3×10^{-8} s.

On a étudié l'effet de certains chélates métalliques sur le rendement en acétone formé par photodécomposition de la pentanone-2 dans une solution de *n*-hexane. Les chélates agissent comme extincteurs mais les pentes des courbes de Stern-Volmer ont plus basses que celles observées pour le *cis*-pentadiène-1,3. Ces additions protègent les polyoléfines solides contre la photodégradation mais il est improbable que le mécanisme implique principalement l'extinction des triplets de carbonyle.

Le rendement quantique de la production d'acétone dans une décomposition de type II de la pentanone-2 dans une solution de *n*-hexane est de 0.20 ± 0.01; le temps de vie de l'état triplet de la pentanone-2 est de 2.3×10^{-8} s. [Traduit par le journal]

Can. J. Chem., **52**, 688 (1974)

Introduction

The processing of polypropylene leads to the incorporation of oxygen-containing impurities which may be the source of photochemical degradation (1). The main oxidation products are believed to be polymeric ketones of the types $\sim CH(CH_3)CH_2COCH_2CH(CH_3)\sim$ and $\sim CH(CH_3)CH_2COCH_3$ (1). Photodegradation of polypropylene is reduced considerably by the incorporation of additives such as nickel(II) bis[2,2′-thiobis-(4-*t*-octyl) phenolate] (A), and it has been suggested that the additives function as quenchers of electronically excited carbonyl groups (2). Studies of the diethyl ketone-sensitized photooxidation of isopropylbenzene (3) showed that the reaction is retarded by the addition of A and the retardation was attributed to quenching of excited states of diethyl ketone by A.

In order to obtain further information on the effectiveness of additives in quenching excited ketones, we have studied the influence of chelate A, nickel(II) *n*-butylamine[2,2′-thiobis-(4-*t*-octyl) phenolate] (B), and zinc(II) di-*n*-butyldithiocarbamate (C) on the Norrish type II photodecomposition of 2-pentanone in *n*-hexane solution. The quenching abilities of the additives are compared with that of *cis*-1,3-pentadiene. 2-Pentanone decomposes to acetone and ethylene, the rate of formation of acetone being readily followed by gas–liquid chromatography. It was chosen for this study because it has a relatively long-lived triplet state and allows low concentrations of the additives to be studied. The nickel chelates A and B have high extinction coefficients at 313 nm and it was not possible to use them at concentrations greater than 4×10^{-3} *M*. The solvent *n*-hexane has a low viscosity and thus allows a relatively large rate of quenching if the process is subject to diffusion control.

Experimental

Materials

2-Pentanone was dried over magnesium sulfate and fractionally distilled. The middle fraction was found by g.l.c. analysis to be >99.9% pure; it was stored in the dark. *n*-Hexane and methylcyclohexane (99 mol %) and *cis*-1,3-pentadiene were used as supplied. The chelates A, B, and C were recrystallized and dried *in vacuo*. Potassium ferrioxalate was recrystallized three times

[1]NRCC No. 13726.

Can. J. Chem. Downloaded from www.nrcresearchpress.com by 210.87.254.40 on 09/05/12
For personal use only.

Can. J. Chem. Downloaded from www.nrcresearchpress.com by 210.87.254.40 on 09/05/12
For personal use only.

under dark-room conditions. It was dried and stored in the dark.

Procedure

The quantum yield for type II photodecomposition of the 2-pentanone in *n*-hexane solution was determined by photolysis of degassed solutions containing 0.2 *M* 2-pentanone and 0.01 *M* methylcyclohexane (g.l.c. internal standard). The solution was introduced into a Pyrex bulb attached to the photolysis cell and degassed; after being sealed off, the solution was transferred to the cylindrical cell of 1 mm pathlength. The photolysis was performed at 25 ± 3 °C using a 140 W Hanovia "Utility" medium pressure mercury lamp as u.v. source. The 313 nm line was isolated by means of a Pyrex plate (thickness 3.5 mm) and a filter solution of nickel and cobalt sulfates (thickness 2 cm) (4). Analysis by means of a Heath EU-700 scanning monochromator with 25 μ slit setting showed that less than 10% of the transmitted radiation came from lines at 302 and 334 nm. The photolysis time varied from 2 h in the absence of additive to as much as 18 h with the highest concentrations of nickel chelates. In all cases the resultant concentration of acetone was $1 - 2 \times 10^{-3}$ *M*. The intensity of the incident radiation was determined by means of potassium ferrioxalate actinometry (5) before and after photolysis of the 2-pentanone samples. The incident intensities were within ±2% of the average value which was used for quantum yield calculations. A continuous check of the intensity over a period of 12 h confirmed that maximum variations were considerably less than ±5%.

Analysis for acetone in the photolyzed samples was carried out by means of a Hewlett–Packard 5750B Series Research Gas Chromatograph with a flame-ionization detector. Separation was effected on a 4 ft column of Porapak Q at 190 °C. The ratio of the area of the acetone peak to that of the internal standard, methylcyclohexane, was determined by weighing. The concentration of acetone in the sample was obtained from a calibration graph of ratio of peak areas *vs.* concentration of acetone.

Extinction coefficients of 2-pentanone and the additives at 313 nm were determined by means of a Cary 14 spectrophotometer. The extinction coefficients of 2-pentanone, A, B, and C were found to be respectively 5.1, 7100, 5200, and 830 M^{-1} cm^{-1}. It was shown that absorbances of solutions of nickel chelates obey Beer's Law. These values were used to calculate the fraction of the incident radiation absorbed by the 2-pentanone in solutions containing the additives.

Results

Photolysis of 2-Pentanone

The extent of Norrish type II decomposition of 2-pentanone was determined *via* the rate of production of acetone. The quantum yield Φ_A^0 was 0.20 ± 0.01 at 25 °C in *n*-hexane. Conversions to acetone were maintained less than 1% (0.6 to 0.9%) because a significant decrease in rate of formation of acetone accompanies an increase in conversion of 2-pentanone (6). The data of Ausloos and Rebbert (7) lead to estimates of quantum yields for acetone production of 0.20 at 0 °C in the liquid phase and 0.22 at 76 °C. A recent detailed study of Golemba and Guillet (4) showed that Φ_A^0 for 2-hexanone in dodecane is 0.25 at 35 °C, and if the ratio of quantum yields for 2-pentanone and 2-hexanone in *n*-hexane is 0.84 (8), the estimated quantum yield for 2-pentanone is 0.21. Golemba and Guillet also concluded that type II quantum yields for a range of 2-alkanones are independent of both temperature and solution viscosity.

Quenching by cis- 1,3-Pentadiene

The quenching of the type II decomposition of 2-pentanone by *cis*-1,3-pentadiene was studied in order to provide a standard for comparison with the effects of the polymer additives. The results for the concentration range $0.9–4.4 \times 10^{-3}$ *M* *cis*-1,3-pentadiene are shown in Fig. 1. If Φ_A is the type II quantum yield in the presence of quencher, Q, the dependence of Φ_A on the concentration of Q is given by

$$[1] \qquad \Phi_A^0/\Phi_A = 1 + k_q\tau[Q]$$

where k_q is the rate constant for quenching and τ is the lifetime of the triplet state (the contribution of singlet state quenching is negligible at the low concentrations of *cis*-1,3-pentadiene used in this work (9)). The slope of the plot of Φ_A^0/Φ_A *vs.* [Q] is 680 ± 50 M^{-1}. Quenching in low viscosity solvents is probably not completely

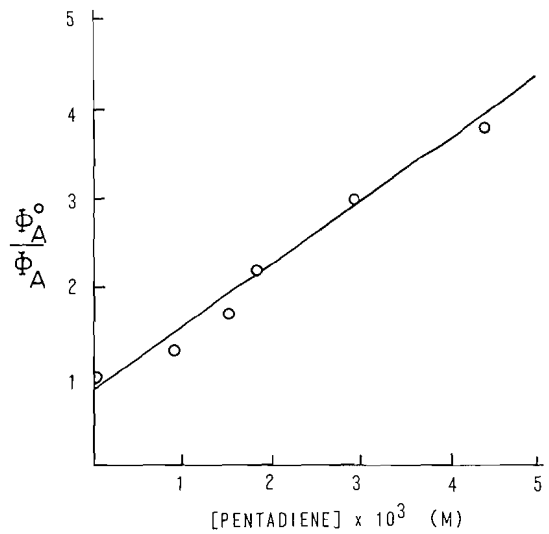

FIG. 1. Stern–Volmer plot for quenching of triplet 2-pentanone by *cis*-1,3-pentadiene at 25 °C. Solvent: *n*-hexane.

TABLE 1. Quenching of the type II reaction of 2-pentanone in *n*-hexane at 25 °C

Compound	Slope of Stern–Volmer plot (M^{-1})	Extinction coefficient at 313 nm (M^{-1} cm^{-1})
cis-1,3-Pentadiene	680 ± 50	—
Nickel(II) bis[2,2′-thiobis(4-*t*-octyl)phenolate] (A)	160 ± 50	7 100
Nickel(II) *n*-butylamine[2,2′-thiobis-(4-*t*-octyl)phenolate] (B)	195 ± 60	5 200
Zinc(II) di-*n*-butyldithiocarbamate (C)	260 ± 40	830
Nickel(II) di-*n*-butyldithiocarbamate	—	> 25 000

diffusion controlled (10), but assumption of diffusion control leads to an estimate of k_q in *n*-hexane, by means of the modified Debye equation of Osborne and Porter (11), of 2.9×10^{10} M^{-1} s^{-1} at 25 °C. The estimated lifetime of the triplet state of 2-pentanone is then 2.3×10^{-8} s. This compares with a lifetime of $1.56 \pm 0.06 \times 10^{-8}$ s estimated for 2-pentanone in *n*-heptane (6) from experiments in which the conversion to acetone was 3% or less.

Quenching by Metal Chelates

The stability of the metal chelates A, B, and C was first investigated by subjecting *n*-hexane solutions to photolysis for twenty hours and analyzing changes by means of u.v. spectroscopy and thin layer chromatography. There was no evidence for photochemical breakdown of the chelates under these conditions. The free ligand, 2,2′-thiobis(4-*t*-octyl)phenol decomposed slowly on irradiation, initially at about 4% h^{-1}, and analysis by t.l.c. showed that three products were formed, the major one having been identified earlier (3) as 4-*t*-octylphenol. It was thus not possible to use the free ligand in these studies.

The plot of Φ_A^0/Φ_A *vs.* concentration of chelate C is shown in Fig. 2. Least-squares analysis yields a slope of 260 ± 40 M^{-1}. The chelate C is thus about one third as effective as *cis*-1,3-pentadiene as a quencher of excited 2-pentanone in *n*-hexane solution. The corresponding slopes for chelates A and B are 160 ± 50 M^{-1} and 195 ± 60 M^{-1}, respectively, at 25 °C. The results are summarized in Table 1. It was hoped to determine the quenching ability of nickel(II) di-*n*-butyldithiocarbamate but its high extinction coefficient at 313 nm (>25 000 M^{-1} cm^{-1}) precluded its use in this study.

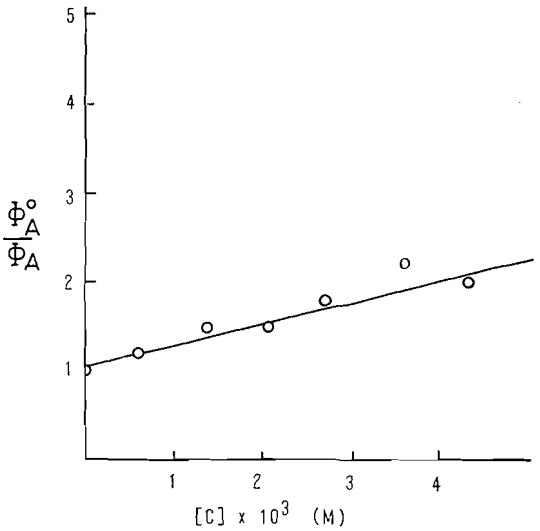

FIG. 2. Stern–Volmer plot for quenching of excited 2-pentanone by C (Zinc(II) di-*n*-butyldithiocarbamate) at 25 °C. Solvent: *n*-hexane.

Discussion

The results for the quenching of type II decomposition of 2-pentanone by *cis*-1,3-pentadiene show that it is possible to study the quenching effects of additives at concentrations as low as 10^{-3} *M* in *n*-hexane solution. Even at these concentrations, the metal chelates absorb a considerable fraction of the incident radiation at 313 nm, thus limiting the range of chelates which can be studied. The chelates A, B, and C are all capable of quenching the type II decomposition of 2-pentanone as measured by the formation of acetone. The slopes of the Stern–Volmer plots are smaller than the slope of 680 ± 50 M^{-1} observed for *cis*-1,3-pentadiene. The experimental results do not preclude some decomposition of the ketone via sensitization by the chelates. Such sensitization might however be expected to give rise to a curved Stern–Volmer plot for quenching by the nickel chelates and there is no positive evidence for such curvature.

The results of this study may be compared with those of a broader study of the type I and type II decompositions of 2,6-dimethyl-4-heptanone in decahydronaphthalene solution (12).

Can. J. Chem. Downloaded from www.nrcresearchpress.com by 210.87.254.40 on 09/05/12
For personal use only.

Can. J. Chem. Downloaded from www.nrcresearchpress.com by 210.87.254.40 on 09/05/12
For personal use only.

Carlsson *et al.* state that the nickel(II) chelates do not appear to quench either the type I or type II processes. They attribute the retardation of the 3-pentanone-sensitized photooxidation of isopropylbenzene by compound A, observed by Chien and Conner (3), to the ability of nickel chelates to quench singlet oxygen. Carlsson *et al.* found that the zinc chelate C gives a Stern–Volmer slope of $90 \pm 10\ M^{-1}$, as determined from the formation of 2-methyl-4-pentanone, which is comparable to the slope for *cis*-1,3-pentadiene ($70 \pm 10\ M^{-1}$). However, in both the type II decomposition of 2,6-dimethyl-4-heptanone in decahydronaphthalene solution (12) and of 2-pentanone in *n*-hexane solution (this work), the results found for triplet carbonyl deactivation by nickel chelates do not support the high k_q value (approximately $10 \times$ diffusion rate) found by Chien and Conner (3) who concluded that long range energy transfer occurred. Our work is in fair agreement with recent results of Guillory and Cook (13) which lead to k_q values of $\sim 1 \times 10^9$ for 4-methyl-2-pentanone quenching by chelates B and C.

Our studies have been confined to hydrocarbon solutions and the conclusions may not apply to quenching by nickel chelates in solid polymers such as polypropylene. However, Heskins and Guillet (13) have studied the energy transfer from excited states of carbonyl groups in solid ethylene – carbon monoxide copolymers to the triplet quencher *cis*-1,3-cyclooctadiene, and the quenching of naphthalene fluorescence by the copolymers. They conclude that the lifetime of the carbonyl triplet in the polymeric ketone is very short (1×10^{-8} s in the solid state as compared with 1.4×10^{-8} s in decahydronaphthalene solution) and that large stabilizer concentrations would be required in order to quench excited states of aliphatic ketones within the solid copolymer. The present study shows that if quenching by metal chelates has approximately the same characteristics in solid polymers as in *n*-hexane solution it is too weak to explain their high efficiency in protecting polyolefins. In fact the ketone photolysis rate can only be reduced a maximum of three-fold at nickel chelate concentrations up to 0.004 *M* (comparable to the concentration used to stabilize polyolefins), and oxygen dissolved in the polymer can be expected to be a more efficient scavenger of ketone triplets than these chelates (12).

The research at Queen's was performed under an operating grant from the National Research Council of Canada. We thank Dr. J. K. S. Wan for the loan of an apparatus and for discussion.

1. D. J. Carlsson and D. M. Wiles. Macromolecules, **2**, 587 (1969).
2. J. E. Bonkowski. Textile Res. J. **39**, 243 (1969).
3. J. C. W. Chien and W. P. Conner. J. Am. Chem. Soc. **90**, 1001 (1968).
4. F. J. Golemba and J. E. Guillet. Macromolecules, **5**, 63 (1972).
5. J. G. Calvert and J. N. Pitts, Jr. Photochemistry. John Wiley and Sons, New York, 1967. p. 783.
6. C. H. Bibart, M. G. Rockley, and F. S. Wettack. J. Am. Chem. Soc. **91**, 2802 (1969).
7. P. Ausloos and R. E. Rebbert. J. Am. Chem. Soc. **83**, 4897 (1961).
8. P. J. Wagner and G. S. Hammond. J. Am. Chem. Soc. **88**, 1245 (1966).
9. F. S. Wettack, G. E. Renkes, M. G. Rockley, N. J. Turro, and J. C. Dalton. J. Am. Chem. Soc. **92**, 1793 (1970).
10. P. J. Wagner and I. Kochevar. J. Am. Chem. Soc. **90**, 2232 (1968).
11. A. D. Osborne and G. Porter. Proc. R. Soc. London, A**284**, 9, (1965).
12. D. J. Carlsson, D. E. Sproule, and D. M. Wiles. Macromolecules, **5**, 659 (1972).
13. J. P. Guillory and C. F. Cook. J. Am. Chem. Soc. **95**, 4885 (1973).
14. M. H. Heskins and J. E. Guillet. Macromolecules, **3**, 224 (1970).

The Stereospecific Synthesis of Neutral and Cationic Tertiary Phosphine Complexes of Platinum(II)

KEITH R. DIXON, KENNETH C. MOSS, AND MARTIN A. R. SMITH

Department of Chemistry, University of Victoria, Victoria, British Columbia

Received July 23, 1973

Stereospecific synthetic methods for the preparation of complexes of the type *cis*- and *trans*-$[PtClL(PEt_3)_2]^+$ and *cis*-$[PtClX(PEt_3)_2]$ have been developed. Preparations of complexes where L = py, PPh_3, $PClPh_2$, or $P(OPh)_3$ and X = SCN, NO_2, NO_3, N_3, NCO, or Br are described and it is shown that bridge cleavage reactions in square planar platinum(II) complexes occur with retention of stereochemistry.

On a développé des méthodes de synthèse stéréospécifiques pour la préparation de composés du type *cis*- et *trans*-$[PtClL(PEt_3)_2]^+$ et *cis*-$[PtClX(PEt_3)_2]$. On décrit la préparation des complexes où L = py, PPh_3, $PClPh_2$ où $P(OPh)_3$ et X = SCN, NO_2, NO_3, N_3, NCO ou Br; on montre aussi que les réactions de coupure des ponts dans les complexes plan carré du platine(II) se font avec rétention de stéréochimie.

Can. J. Chem., **52**, 692 (1974)

In view of current emphasis on studies of the *cis* and *trans* influences of ligands in square planar complexes, we considered it of interest to develop stereospecific synthetic routes to complexes of the types $[PtClL(PEt_3)_2]^+$ and $[PtClX(PEt_3)_2]$ where Et = ethyl; L = neutral ligand, and X = anionic ligand. Such systems are potentially useful in that chloride substitution reactions can then be used to introduce "probe" ligands for studies of the *cis* and *trans* influences of the L and X groups.

The displacement of Cl^- from *cis*-$[PtCl_2(PEt_3)_2]$ by a series of neutral ligands in the presence of $NaClO_4$ to give $[PtClL(PEt_3)_2][ClO_4]$ has been described by Church and Mays (1). In all cases, except when L = triphenylphosphine (PPh_3) or pyridine (py), a *trans* product was obtained. The stereochemistry of $[PtCl(py)(PEt_3)_2]^+$ was uncertain whilst the PPh_3 compound was shown to be the *cis* isomer. Cherwinski and Clark (2) have utilized bridge cleavage of $[Pt_2Cl_2(PEt_3)_4][BF_4]_2$ by NaX (X = SCN, NO_3, or NO_2) to prepare *cis*-$[PtClX(PEt_3)_2]$ and we have previously reported the reactions of $[Pt_2Cl_2(PEt_3)_4][BF_4]_2$ with py and CO to give *cis*-$[PtCl(py)(PEt_3)_2][BF_4]$ (3) and *trans*-$[PtCl(CO)(PEt_3)_2][BF_4]$ (4) respectively. We now report the results of further investigation of the stereochemistry of these and related reactions and their use in stereospecific syntheses.

Results

The reactions studied are of three general types:

[1] $[Pt_2Cl_2(PEt_3)_4][ClO_4]_2 + 2L \rightarrow 2cis\text{-}[PtClL(PEt_3)_2][ClO_4]$

[2] $trans\text{-}[PtCl_2(PEt_3)_2] + L + NaClO_4 \rightarrow trans\text{-}[PtClL(PEt_3)_2][ClO_4] + NaCl$

[3] $[Pt_2Cl_2(PEt_3)_4][ClO_4]_2 + 2NaX \rightarrow 2cis\text{-}[PtClX(PEt_3)_2] + 2NaClO_4$

The products are formed in high yield under mild conditions and have the indicated stereochemistry for L = PPh_3, $P(OPh)_3$, or py and for X = SCN, NCO, NO_2, NO_3, N_3, or Br. We have found no examples where the reactions are not stereospecific except for the reported (4) preparation of *trans*-$[PtCl(CO)(PEt_3)_2][BF_4]$ from $[Pt_2Cl_2(PEt_3)_4][BF_4]_2$ (see discussion below). Reaction 2 is also successful for L = $PClPh_2$ but use of this ligand in reaction 1 causes transfer of chloride to platinum and production of *cis*-$[PtCl_2(PEt_3)_2]$.

The stereochemistry of the complexes was determined by established criteria using the infrared regions from 700–800 cm^{-1} and 400–450 cm^{-1} (5), the variation of ν(Pt—Cl) stretching frequencies with *trans* ligands (1), and the appearance of the methyl region in proton magnetic resonance spectra (ref. 6 and references therein). The methyl resonances show two coupling constants ($^3J_{H-H}$ = 7–8 Hz and $^3J_{H-P}$ = 17–18 Hz) directly[1] and the spectral type is determined by the relative magnitudes of $^2J_{P-P}$ and the chemical shift difference between the two

[1]All other couplings to the methyl protons are small (< 1 Hz), including those involving ^{195}Pt.

Can. J. Chem. Downloaded from www.nrcresearchpress.com by 210.87.254.105 on 09/05/12
For personal use only.

Can. J. Chem. Downloaded from www.nrcresearchpress.com by 210.87.254.105 on 09/05/12
For personal use only.

phosphorus atoms. If the phosphorus atoms are chemically equivalent then for small values of $^2J_{P-P}$ (*cis* PEt_3 ligands) the spectra appear as an overlapping doublet of triplets due to approximately first order coupling with the methylene protons and one phosphorus. For large values of $^2J_{P-P}$ (*trans* PEt_3 ligands) a "virtually coupled" spectrum having an overlapping triplet of triplets[2] is observed giving an apparent 1:4:6:4:1 quintet. Our *trans* complexes have chemically equivalent phosphines and give quintet spectra. The *cis* complexes have chemically non-equivalent phosphines but the chemical shift differences between the two sets of methyl protons are generally small and only one doublet of triplets is observed for all cases except *cis*-$[PtClL(PEt_3)_2]^+$ where L = PPh_3 or $P(OPh)_3$. For these two complexes there is the additional possibility of a "virtually coupled" spectrum arising from strong coupling between the *trans* phosphorus atoms of PEt_3 and L. However, when L = $P(OPh)_3$ the spectrum can be unambiguously assigned as two overlapping doublets of triplets arising from two chemically non-equivalent PEt_3 ligands and, although the case when L = PPh_3 is slightly more complex, the same basic pattern occurs. Thus in neither case is a "virtually coupled" spectrum observed, indicating that when the *trans* phosphorus atoms are in different phosphines the chemical shift difference is sufficiently large compared to $^2J_{P-P}$ to permit approximate first order analysis.

The stereochemistry of $[PtCl(py)(PEt_3)_2]^+$ prepared by Church and Mays from *cis*-$[PtCl_2(PEt_3)_2]$ was uncertain because of overlap of methyl and methylene resonances (1). However, we find that when both *cis*- and *trans*-$[PtCl(py)(PEt_3)_2]^+$ are available the slight overlap does not interfere with the assignment of stereochemistry. The occurrence of ν(Pt—Cl) at 340 cm^{-1} (*trans* to py) and 283 cm^{-1} (*trans* to PEt_3) in the *trans* and *cis* isomers respectively is further evidence for the correctness of our assignment and a repeat of Church and Mays' reaction shows the product to be stereospecifically *cis*-$[PtCl(py)(PEt_3)_2]^+$.

Discussion

Our reactions of type [2] lead specifically to *trans* products and it is therefore somewhat surprising that the analogous reactions of *cis*-$[PtCl_2(PEt_3)_2]$ gave mainly *trans* products (1), especially since it is generally accepted that substitution reactions at platinum(II) proceed with retention of stereochemistry (7). We have confirmed the previous results for L = $P(OPh)_3$ and find that even when careful control is exercised so that L is never in excess the products still have *trans* stereochemistry. However, attempted labilization of the *cis*/*trans* equilibrium by addition of ~10 mol % of L to 0.2 *M* solutions of *cis*-$[PtClL(PEt_3)_2][ClO_4]$ in dichloromethane shows that conversion to the *trans* isomer is essentially complete after 5 min at 35° for L = $P(OPh)_3$ whereas for L = PPh_3 the reaction takes 3 weeks and for L = py no isomerization is observed after 3 weeks. These results are unusual since the accepted order of nucleophilicity towards platinum is PPh_3 > $P(OPh)_3$ > py and the rates of isomerization might have been expected to follow the same order. However, they do suggest that, in the reaction of *cis*-$[PtCl_2(PEt_3)_2]$ with L, the rate of isomerization of the product is greater than the rate of substitution for L = $P(OPh)_3$ but is much slower for L = PPh_3 or py, thus giving *trans* and *cis* products respectively. Presumably a similar explanation holds for the other *trans* products described by Church and Mays (1).

Some examples of previous bridge cleavage reactions of platinum(II) complexes have been noted in the introduction and others involving $[Pt_2X_4(PR_3)_2]$ complexes with CO, olefins, and amines have been described by Chatt and coworkers (8). No consistent stereochemical pattern has been established but all the non-stereoretentive reactions were conducted for long reaction times with excess ligand and under these conditions isomerization of the initial products will be facilitated. Our results under more controlled conditions show that the bridge cleavage route to *cis* products (reactions 1 and 3) is applicable to ligands having a wide range of nucleophilicity and *trans* influence, *i.e.* PPh_3, $P(OPh)_3$, py, NCO^-, N_3^-, NO_2^-, SCN^-, and ONO_2^-. Attempts to extend the series at both ends of the range were unsuccessful. Strong nucleophiles (CN^- and CH_3^-) cause chloride substitution in addition to bridge cleavage and weak nucleophiles give only partial cleavage of the bridge (NO_3^-, *ca.* 90%; CH_3COO^-, *ca.* 50%; $AsPh_3$, no reaction). It is clear however that the bridge cleavage reaction is a versatile stereospecific synthetic route provided conditions are

[2] $^3J_{H-H}$ = 7–8 Hz, J_{H-P}(apparent) = $\frac{1}{2}|^3J_{H-P} + {}^5J_{H-P}|$ ≃ 7.5 Hz.

TABLE 1. Characterization data

Complex[a]	Melting point (°C)	Analyses %C Calcd.	%C Found	%H Calcd.	%H Found	^{1}H chemical shifts (τ) CH_2[b]	CH_3[c]	Infrared[d] ν(Pt—Cl) (cm^{-1})
$[Pt_2Cl_2(PEt_3)_4][ClO_4]_2$	220–225 dec.	25.4	25.6	5.3	5.4	7.9	8.75	*ca.* 300 (b)
cis-$[PtCl(py)(PEt_3)_2][ClO_4]$[e]	235–237	31.6	31.7	5.5	5.5	7.9	8.62	283
trans-$[PtCl(py)(PEt_3)_2][ClO_4]$[f]	184–188	31.6	31.7	5.5	5.5	8.4	8.85	340
cis-$[PtCl(PPh_3)(PEt_3)_2][ClO_4]$	178–180[g]	43.5	43.5	5.5	5.5	7.9	9.00 8.74	290
trans-$[PtCl(PPh_3)(PEt_3)_2][ClO_4]$	182–186	43.5	43.5	5.5	5.5	8.4	8.93	300
cis-$[PtCl(P(OPh)_3)(PEt_3)_2][ClO_4]$	150–152	41.1	40.8	5.2	5.2	7.9	9.00 8.90	286
trans-$[PtCl(P(OPh)_3)(PEt_3)_2][ClO_4]$	172–174	41.1	41.8	5.2	5.3	7.9	8.86	314
trans-$[PtCl(PClPh_2)(PEt_3)_2][ClO_4]$	145–147	36.6	36.8	5.1	5.2	8.3	8.93	300
cis-$[PtCl(N_3)(PEt_3)_2]$[h]	115–118	28.3	28.2	5.9	5.9	8.0	8.0	281[i]
cis-$[PtCl(NCO)(PEt_3)_2]$	134–138	30.7	30.7	5.9	5.7	8.1	8.76	284[j]
cis-$[PtClBr(PEt_3)_2]$	198–199	26.3	26.3	5.5	5.5	7.9	8.79	284
cis-$[PtCl(SCN)(PEt_3)_2]$[k]	154–156	29.7	29.4	5.8	5.7	8.0	8.76	280
cis-$[PtCl(NO_2)(PEt_3)_2]$[l]	188–191	28.1	27.9	5.9	5.9	8.0	8.75	287

[a]All complexes are colorless crystals.
[b]Broad complex resonances permitting only approximate determination of chemical shift. Resolution insufficient for meaningful analysis.
[c]See results section for coupling constants and multiplet structure.
[d]Medium intensity absorptions.
[e]%N: calcd. 2.2, found 2.1.
[f]%N: calcd. 2.2, found 2.0.
[g]Partial melting at *ca.* 140 suggests this complex may isomerize on heating.
[h]%N: calcd. 8.3, found 7.9.
[i]ν(Pt—N) = 380 (m), ν(N≡N) = 2045 (vs,b) cm^{-1}.
[j]δ(NCO) = 595 (m), ν(C≡N) = 2220 (vs,b) cm^{-1}.
[k]%N: calcd. 2.7, found 3.3.
[l]%N: calcd. 2.7, found 2.8.

controlled so as to prevent isomerization of the initial products.

In summary, our results demonstrate that, although product isomerization may occur, the substitution and bridge cleavage reactions at platinum(II) are themselves stereoretentive. This was well-known for substitution reactions (7), although the results of Church and Mays (1) appeared to provide some contrary examples, but had not been clearly established for bridge cleavage.

Experimental

Data relating to the characterization of the complexes are given in Table 1. Microanalyses were by D. L. McGillivray of this department. Infrared spectra were recorded from 4000–250 cm^{-1} with accuracy ±3 cm^{-1} on a Beckman IR 20 spectrophotometer calibrated against polystyrene film and water vapor. Solid samples were examined as Nujol mulls between cesium iodide plates. Nuclear magnetic resonance spectra were recorded in dichloromethane solution on a Perkin–Elmer R12A spectrometer using tetramethylsilane as external reference. Melting points were determined on a Reichert hot-stage apparatus and are uncorrected.

Solvents were of spectrograde quality and were dried and stored over type 4A molecular sieves. *cis*- and *trans*-$[PtCl_2(PEt_3)_2]$ were prepared as described elsewhere (9). $[Pt_2Cl_2(PEt_3)_4][ClO_4]_2$ was prepared by reaction of *cis*-$[PtCl_2(PEt_3)_2]$ with $AgClO_4$ under conditions similar to those described previously for preparation of $[Pt_2Cl_2(PEt_3)_4][BF_4]_2$ (3) and was recrystallized from dichloromethane by addition of diethyl ether until precipitation just began (cloud point).

cis-[PtClL(PEt$_3$)$_2$][ClO$_4$] Complexes (Reaction 1)

In a typical reaction, PPh_3 (0.129 g, 0.492 mmol) in acetone (3 ml) was added dropwise to a stirred solution of $[Pt_2Cl_2(PEt_3)_4][ClO_4]_2$ (0.290 g, 0.256 mmol) in acetone (10 ml). After stirring for 5 min at 25° the solution was evaporated under reduced pressure to *ca.* 3 ml. Dropwise addition of diethyl ether to the cloud point gave *cis*-$[PtCl(PPh_3)(PEt_3)_2][ClO_4]$ (0.354 g, 0.427 mmol) as colorless crystals.

Similar reactions gave the indicated yields for L = $P(OPh)_3$ (98%) and py (89%) except that the py reaction required reflux for 2 h.

trans-[PtClL(PEt$_3$)$_2$][ClO$_4$] Complexes (Reaction 2)

In a typical reaction, PPh_3 (0.154 g, 0.587 mmol) in acetone (3 ml) was added dropwise to a stirred solution of $NaClO_4 \cdot H_2O$ (0.088 g, 0.627 mmol) with *trans*-$[PtCl_2(PEt_3)_2]$ (0.300 g, 0.597 mmol) in acetone (15 ml). After stirring for 10 min at 25°, NaCl was removed by filtration and the filtrate evaporated under reduced pressure to give the crude product. Purification was achieved by extraction into dichloromethane, recovery by evaporation of solvent under reduced pressure, and recrystallization from acetone by dropwise addition of diethyl ether to the cloud point to

Can. J. Chem. Downloaded from www.nrcresearchpress.com by 210.87.254.105 on 09/05/12
For personal use only.

give *trans*-$[PtCl(PPh_3)(PEt_3)_2][ClO_4]$ (0.400 g, 0.483 mmol) as colorless crystals.

Similar reactions gave the indicated yields for L = $P(OPh)_3$ (98%), $PClPh_2$ (60%), and py (50%) after stirring for 30 min, 2 h, and 72 h respectively. No reaction was observed for L = $AsPh_3$.

cis-[PtClX(PEt$_3$)$_2$] Complexes (Reaction 3)

These were prepared from $[Pt_2Cl_2(PEt_3)_4][ClO_4]_2$ (0.300 g, 0.265 mmol) and NaX (0.530 mmol) by the method previously described (2). Products were recrystallized from ethanol containing 5–10% diethyl ether to give the indicated yields for X = SCN (82%), N_3 (85%), NCO (60%), NO_2 (84%), Br (70%). The reaction for X = NO_3 was only *ca.* 90% complete and the product (*ca.* 80%) could not be separated from unreacted starting material. For this reason detailed characterization is not included in Table 1 but the ^1H n.m.r. spectrum clearly showed a *cis* configuration for the product. A reaction with X = CH_3COO was only *ca.* 50% complete after reflux for 24 h.

We thank the National Research Council of Canada and the University of Victoria for research grants.

1. M. J. Church and M. J. Mays. J. Chem. Soc. A, 3074 (1968).
2. W. J. Cherwinski and H. C. Clark. Inorg. Chem. **10**, 2263 (1972).
3. K. R. Dixon and D. J. Hawke. Can. J. Chem. **49**, 3252 (1971).
4. H. C. Clark, K. R. Dixon, and W. J. Jacobs. Chem. Commun. 93 (1968).
5. G. W. Bushnell, K. R. Dixon, R. G. Hunter, and J. J. McFarland. Can. J. Chem. **50**, 3694 (1972); P. L. Goggin and R. J. Goodfellow. J. Chem. Soc. A, 1462 (1966).
6. H. C. Clark, K. R. Dixon, and W. J. Jacobs. J. Am. Chem. Soc. **90**, 2259 (1968); A. J. Rest. J. Chem. Soc. A, 2212 (1968); J. F. Nixon and A. Pidcock. Ann. Rev. N.M.R. Spectrosc. **2**, 380 (1969).
7. F. Basolo and R. G. Pearson. Mechanisms of inorganic reactions. 2nd ed. Wiley. 1967.
8. J. Chatt, N. P. Johnson, and B. L. Shaw. J. Chem. Soc. 1062 (1964); J. Chatt and L. M. Venanzi. J. Chem. Soc. 3852 (1955).
9. K. A. Jensen. Z. Anorg. Allgem. Chem. **229**, 238 (1936).

Can. J. Chem. Downloaded from www.nrcresearchpress.com by 210.87.254.105 on 09/05/12
For personal use only.

Can. J. Chem. Downloaded from www.nrcresearchpress.com by 210.87.254.105 on 09/05/12
For personal use only.

Canadian Journal of Chemistry

Published by
THE NATIONAL RESEARCH COUNCIL OF CANADA

Journal canadien de chimie

Publié par
LE CONSEIL NATIONAL DE RECHERCHES DU CANADA

Volume 52 Number 5 March 1, 1974

Volume 52 numéro 5 1 mars 1974

The Alkaline Hydrolysis of *N*-Acylthioureas

WAYNE I. CONGDON[1] AND JOHN T. EDWARD

Department of Chemistry, McGill University, Montreal, Quebec

Received May 8, 1973

N-Benzoylthiourea (pK_{HA} 10.9) and other *N*-acylthioureas ionize in alkaline solution, and then are rapidly hydrolyzed to thiourea and a carboxylic acid. The rates become independent of hydroxide ion concentration when this exceeds about 0.1 *M* and point to a mechanism in which hydrolysis takes place by attack of an hydroxide ion on the un-ionized molecule of *N*-acylthiourea. This mechanism accords with the Arrhenius parameters for the hydrolysis of *N*-benzoylthiourea in 0.2 *N* sodium hydroxide, and with the Hammett ρ value of 0.10 for the hydrolysis of *m*- and *p*-substituted *N*-benzoylthioureas in 1.0 *N* potassium hydroxide.

La *N*-benzoylthiourée (pK_{HA} 10.9) et les autres *N*-alcoylthiourées s'ionisent en milieux alcalins, puis s'hydrolysent rapidement en thiourée et en un acide carboxylique. La vitesse de ces réactions devient indépendante de la concentration de l'ion hydroxyde quand celle-ci est supérieure à 0.1 *M*, et indique un mécanisme dans lequel l'hydrolyse se produit par l'attaque d'un ion hydroxyde sur la molécule non-ionisée de la *N*-alcoylthiourée. Ce mécanisme est en accord avec les paramètres d'Arrhenius pour l'hydrolyse de la *N*-benzoylthiourée dans 0.2 *N* hydroxyde de sodium et aussi avec une valeur de 0.10 du paramètre ρ de Hammett pour l'hydrolyse dans 1.0 *N* d'hydroxyde de potassium des *N*-benzoylthiourées substituées en *méta* et *para*.

Can. J. Chem., **52**, 697 (1974)

2-Thiohydantoin (**1**) can be regarded as a cyclic *N*-acylthiourea (compare *N*-acetylthiourea (**2**)) and consequently it becomes of interest to see whether the kinetic features observed many years ago in the alkaline hydrolysis of 2-thiohydantoin (1) are also observed in the alkaline hydrolysis of *N*-acylthioureas.

N-Acylthioureas have a strong absorption peak at about 270 nm due to a $\pi \rightarrow \pi^*$ transition (2). In alkaline solution this peak shows a marked red shift due to formation of the conjugate base (A^-) (*e.g.* **3**) of the *N*-acylthiourea (HA) (*e.g.* **2**); however, at the same time rapid hydrolysis to a carboxylic acid and thiourea takes place, and the final spectrum is that expected for a mixture of these two compounds (see Fig. 1). The hydrolysis of *N*-benzoylthiourea was slow enough for absorbance curves to be obtained in solutions of p*H* 6.5 and 13.3 (corresponding to HA and A^-, respectively), and in five buffer solutions of ionic strength 0.5 and p*H* varying from 10.40 to 11.95. The curves passed through a well-defined isosbestic point, and analysis in the usual fashion (3) gave a pK_{HA} of 10.9 ± 0.1 in water at 25.3 °C (Table 1). The hydrolysis of *N*-acetylthiourea was too rapid for its pK_{HA} to be determined in this way.

The hydrolysis of *N*-acetylthiourea could be followed conveniently by observing the decrease in absorbance at 275 nm (see Fig. 1), and was found to follow pseudo first-order kinetics in the large excess of buffer or sodium hydroxide used. The results are given in Table 2, and show that a 22 000-fold increase in hydroxide ion concentration (from carbonate buffer to 1.00 *N* potassium hydroxide) causes only a 170-fold increase in k_ψ, the pseudo first-order rate constant, defined by eq. 1. Furthermore, the increase in this constant

[1]Holder of NRCC Scholarship, 1968–1970.

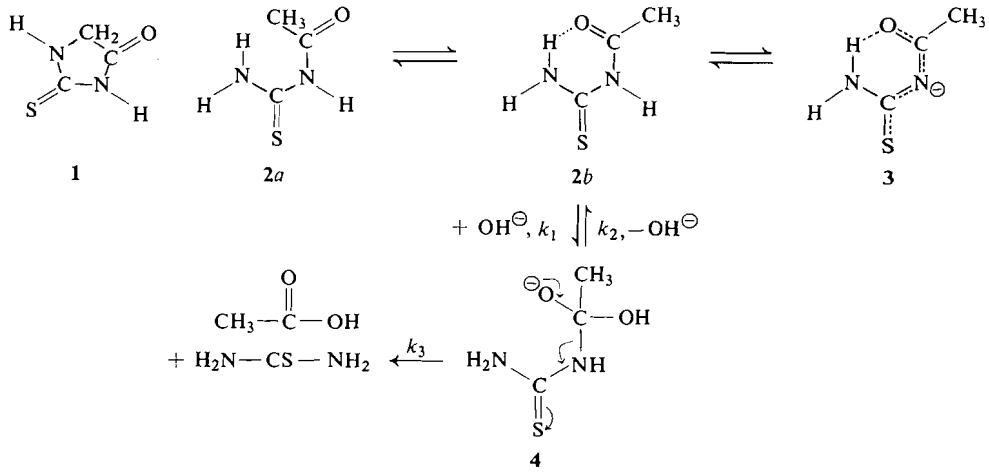

SCHEME 1

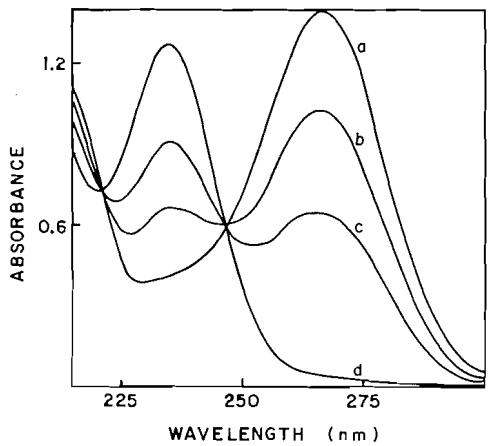

FIG. 1. Ultraviolet absorption spectra of 1.2×10^{-4} *M* *N*-acetylthiourea in aqueous phosphate buffer, p*H* 11.2, $I = 0.45$, at 25.3 °C after (*a*) 0 s (120 s after mixing); (*b*) 240 s; (*c*) 600 s; (*d*) 3600 s.

$$[1] \quad \text{Rate} = k_\psi[\text{HA}]_{\text{stoich}} = k_\psi([\text{A}^-] + [\text{HA}])$$

appears to level off at higher concentrations of hydroxide ion. These kinetic features are reminiscent of those already observed in the hydrolytic ring-opening of 2-thiohydantoin (1) and point to a mechanism in which hydrolysis occurs by reaction of hydroxide ion with the un-ionized molecule of *N*-acetylthiourea, without any significant contribution from reaction with the conjugate base. Application of the steady-state approximation then leads to eq. 2, where k_1, k_2, and k_3 are

$$[2] \quad k_\psi = k_1k_3([\text{HA}][\text{OH}^-])/(k_2 + k_3)([\text{A}^-] + [\text{HA}])$$

TABLE 1. Ionization of *N*-benzoylthiourea in phosphate buffers (ionic strength 0.5) at 25.3 °C, from absorbance measurements at 300 nm

p*H*	log ([HA]/[A⁻])	pK_{HA}
10.40	0.48	10.88
10.75	0.20	10.95
10.90	0.03	10.93
11.20	−0.28	10.92
11.95	−0.96	10.99

the rate constants indicated in Scheme 1. This equation may be simplified to eqs. 3*a* and *b*,

$$[3a] \quad k_\psi = \{k_1k_3K_w/K_{HA}(k_2 + k_3)\}\{[\text{A}^-]/([\text{A}^-] + [\text{HA}])\}$$

$$[3b] \quad = (k_1k_3K_w/(k_2 + k_3)([\text{H}^+] + K_{HA})$$

where K_W is the ionization constant for water and K_{HA} is the ionization constant for HA. Equation 3*a* indicates that the magnitude of the observed pseudo first-order rate constant k_ψ follows the fraction $[\text{A}^-]/([\text{A}^-] + [\text{HA}])$ of HA ionized: as ionization of HA becomes complete in strongly alkaline solutions, so k_ψ should level off to a constant value.[2] Indeed, the levelling-off of the observed rate of hydrolysis can be accommodated

[2]The kinetics do not distinguish between mechanisms involving attack of hydroxide ion on HA and attack of water on A^-. The latter mechanism has been advanced, from similar kinetic considerations, as a possibility for the hydrolysis of 5,6-dihydropyrimidines (4) and of trifluoroacetanilide (5). However, intuitively it seems less likely, and in the case of trifluoroacetanilide goes counter to further kinetic considerations (6).

Can. J. Chem. Downloaded from www.nrcresearchpress.com by 210.87.254.105 on 09/05/12
For personal use only.

Can. J. Chem. Downloaded from www.nrcresearchpress.com by 210.87.254.105 on 09/05/12
For personal use only.

TABLE 2. Rates of hydrolysis of *N*-acetylthiourea and *N*-benzoylthiourea in aqueous buffer and potassium hydroxide solutions

$[OH^-]^a$ (mol^{-1})	$10^4 k_\psi$ (s^{-1}) Exp.	Calcd.
N-Acetylthiourea		
4.47×10^{-5}[b]	0.71	0.68
1.78×10^{-4}[b]	2.51	2.67
2.88×10^{-3}	27.5	31.5
6.31×10^{-3}	44.2	52.1
7.94×10^{-3}	56.2	58.6
1.59×10^{-2}	74.1	77.7
7.94×10^{-2}	112.0	105.2
1.59×10^{-1}	118.0	110.1
3.98×10^{-1}	120.0	113.0
1.0	120.0	115.4
N-Benzoylthiourea		
1.74×10^{-4}[c]	0.96	0.91
10^{-3}	2.26	2.31
1.50×10^{-3}	2.80	2.71
1.86×10^{-3}[c]	2.94	2.91
3.00×10^{-3}	3.30	3.28
6.00×10^{-3}	3.97	3.67
10^{-2}	4.05	3.85
2.00×10^{-2}	4.10	4.00
10^{-1}	4.14	4.12
5.00×10^{-1}	4.18	4.15
1.0	4.15	4.15

[a]Rates were measured at 25.5 °C in potassium hydroxide – potassium chloride buffers of ionic strength of 1.0 unless otherwise noted.
[b]Carbonate buffers, $I = 1.0$, extrapolated to zero carbonate.
[c]Trimethylamine buffer, $I = 1.0$, extrapolated to zero amine. For the free base a second-order rate constant of 1.6×10^{-4} mol^{-1} s^{-1} was obtained.

fairly well by eq. 3, assuming a value of 1.3×10^{-12} mol l^{-1} (pK_{HA} 11.9) for K_{HA}[3] and a value of 1.5 l mol^{-1} s^{-1} for $k_1k_3/(k_2 + k_3)$. This is shown by the satisfactory agreement between experimental and calculated values of k_ψ in Table 2. Applying a similar analysis to the kinetic data (1) for the alkaline hydrolysis of 2-thiohydantoin (pK_{HA} 8.5 (7)) gives $k_1k_3/(k_2 + k_3) =$ 85.4 l mol^{-1} s^{-1}.

In the absence of oxygen-exchange studies to separate the kinetic terms, any interpretation of differences in $k_1k_2/(k_2 + k_3)$ must be very tentative. It seems likely that $k_3 > k_2$ because of the stability of the conjugate base of thiourea (pK_{HA} probably about 15 (8)) extruded from the tetrahedral intermediate **4** (8, 9), and in that case $k_1k_3/(k_2 + k_3) \simeq k_1$. In any case, it is evident that the acyl–thiourea bond is about 57 times more reactive in 2-thiohydantoin than it is in *N*-acetylthiourea, but is hydrolyzed more slowly because the greater acidity of 2-thiohydantoin (more than a thousandfold) causes it to be converted more completely into the inactive conjugate base A^- in alkaline solution.[4] Both the greater acidity and greater reactivity of 2-thiohydantoin may be a consequence of a less favorable orientation of dipoles (*cf.* Breslow (10) for discussion of an analogous case). Recent studies (11) make it likely that *N*-acetylthiourea has the conformation **2***b*; 2-thiohydantoin resembles the less stable conformation **2***a*. A similar difference in acidity and reactivity is found between cyclic and acyclic imides (12), and is probably to be explained in a similar fashion.

The rate of hydrolysis of *N*-benzoylthiourea also obeyed eq. 3; assuming $k_1k_3/(k_2 + k_3) =$ 0.52 l mol^{-1} s^{-1}, values of k_ψ in reasonable agreement with experiment for a wide range of hydroxide ion concentrations could be calculated, as shown in Table 2. Using a trimethylamine – trimethylammonium chloride buffer, general base catalysis (or nucleophilic catalysis (ref. 13, pp. 101–106)) by trimethylamine was noted, with a second-order rate constant of 1.6×10^{-4} mol^{-1} s^{-1}. General base catalysis of the decomposition of tetrahedral intermediates similar to **4** has been observed many times (see ref. 13, pp. 132 and 139 for a review of the literature).

The effect of *meta*- and *para*-substitution of *N*-benzoylthiourea on its rate of hydrolysis depends on the alkalinity of the hydrolyzing medium: in weakly alkaline solution (p*H* 9.02) the Hammett reaction constant ρ is about 1.20 and in strongly alkaline solution (1.0 *N* potassium hydroxide) it is about 0.10 (Table 3 and Fig. 2), although the scatter of the experimental points is rather great. The change in ρ with alkalinity of the medium can be accommodated by the mechanism of Scheme 1, as embodied in eq. 3. In weakly alkaline solution $[H^+] \gg K_{HA}$, and

[3]*N*-acetylthiourea would be expected to be a weaker acid than *N*-benzoylthiourea (compare acetic and benzoic acids) but not as much as indicated by this pK_{HA}.

[4]This analysis would indicate that in water at p*H* 5, when $[H^+] \gg K_{HA}$ and consequently when eq. 3*b* reduces to

$$[4] \qquad k_\psi = k_1[OH^-]$$

2-thiohydantoin should be hydrolyzed more rapidly than *N*-acetylthiourea. The slow hydrolysis of 2-thiohydantoin has been observed under these conditions (1); it would be interesting to observe whether *N*-acetylthiourea is stable under the same conditions.

Can. J. Chem. Downloaded from www.nrcresearchpress.com by 210.87.254.105 on 09/05/12
For personal use only.

TABLE 3. Pseudo first-order rate constants for the hydrolysis of substituted *N*-benzoylthioureas at 35.0 °C

Substituent	$10^5 k_\psi$[a] (s^{-1})	$10^4 k_\psi$[b] (s^{-1})
N-*p*-Methoxybenzoyl	1.62	7.05
N-*p*-Methylbenzoyl	2.34	9.30
N-*m*-Methylbenzoyl	3.92	9.20
N-Benzoyl	5.50	8.70
N-*p*-Chlorobenzoyl	6.60	8.20
N-*m*-Chlorobenzoyl	9.04	10.80

[a]Sodium borate buffer, 0.05 M, I = 1.0, pH = 9.02.
[b]Potassium hydroxide, 1.0 *N*.

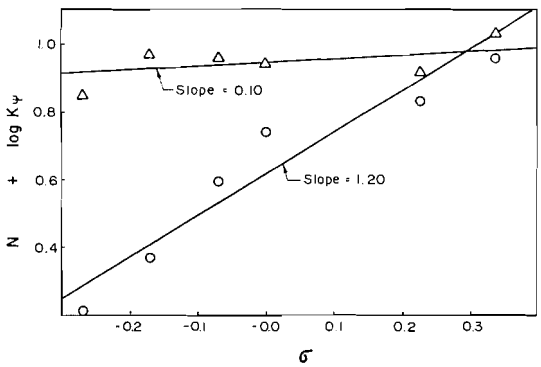

FIG. 2. Plot of log k_ψ against Hammett's substituent constant σ for the hydrolysis of *meta*- and *para*-substituted *N*-benzoylthioureas in borate buffer (○) and in 1.0 *N* potassium hydroxide (Δ).

making the assumption that $k_1k_3/(k_2 + k_3) \simeq k_1$, eq. 3 simplifies to

$$[4] \qquad k_\psi = k_1[OH^-]$$

Consequently, the plot of log k_ψ against σ (Fig. 2) is equivalent to a plot of log k_1 against σ and the slope should be designated ρ_1. This constant should be close to the reaction constant (1.055; ref. 14) for the alkaline hydrolysis of substituted benzamides, as is observed.

On the other hand, in strongly alkaline solution *N*-benzoylthiourea is almost completely ionized ($K_{HA} \gg [H^+]$), and eq. 3*b* simplifies to

$$[5a] \qquad k_\psi = k_1K_W/K_{HA}$$

$$[5b] \qquad \log k_\psi = \log k_1 + \log K_W - \log K_{HA}$$

Consequently, the Hammett reaction constant ρ_{ov} for the overall reaction is made up by the difference between the reaction constant ρ_1 for the k_1 step and the constant ρ_{HA} for the ionization

TABLE 4. Temperature dependence of the rate of alkaline hydrolysis of *N*-benzoylthiourea in 0.20 *M* sodium hydroxide

Temperature (°C)	k_ψ
25.3	3.65±0.15
35.1	9.28±0.30
44.8	20.60±0.01

of HA, as shown in eq. 6. ρ_{HA} would be expected

$$[6] \qquad \rho_{ov} = \rho_1 - \rho_{HA}$$

to be close to ρ (1.000) for the ionization of benzoic acids and so ρ_{ov} of 0.10 is reasonable.

A plot of log k_ψ against $1/T$ (Table 4) is linear and gives an entropy of activation $\Delta S_{ov}^{\ddagger}$ of -17 ± 2 e.u. This is considerably less than $\Delta S^{\ddagger}$ (-36 e.u.) for the alkaline hydrolysis of benzamide (15). However, in 0.2 *N* sodium hydroxide *N*-benzoylthiourea is almost completely ionized, and so in this case, the path to the activated complex involves two steps: $A^- + HOH \rightarrow HA + OH^-$; and $HA + OH^- \rightarrow$ tetrahedral intermediate. Hence

$$[7] \qquad \Delta S_{ov}^{\ddagger} = \Delta S_1^{\ddagger} - \Delta S^0_{\text{ionization}}$$

A possible model for the entropy change in the ionization step is furnished by the ionization of nitroethane, which has ΔS^0 of -18.3 e.u. (16).[5]

$$CH_3CH_2NO_2 + OH^- \leftrightarrows CH_3CH{=}NO_2^- + H_2O$$

Taking $\Delta S_1^{\ddagger}$ as equal to $\Delta S^{\ddagger}$ for the alkaline hydrolysis of benzamide, eq. 7 would yield $S_{ov}^{\ddagger} = -18$ e.u., in good agreement with the experimental value.

Thus a variety of results indicates that alkaline hydrolysis of *N*-acylthioureas involves reaction of the un-ionized molecule with hydroxide ion. In this respect the reaction is similar to the alkaline hydrolysis of many other weakly acidic substrates reported in the literature (1, 4–6, 17). Several of these hydrolyses (5, 6, 17) show second-order dependency on hydroxide ion concentration at low pH values. Our failure to observe second-

[5]A referee has objected that the ionization of nitroethane is not a good model for the ionization of an *N*-acylthiourea. However, if a large part of the entropy change comes from the replacement of the highly hydrated hydroxide ion by an organic ion having a delocalized charge and hence only lightly hydrated, the model may not be too inappropriate.

order dependency indicates perhaps the superiority of the conjugate base of thiourea as a leaving group, in comparison with the leaving groups in the reactions cited above. However, the observation of general base catalysis by trimethylamine indicates the need for further study of the reaction.

Experimental

The preparation of the *N*-acylthioureas has been described already (18) and kinetic methods are described in ref. 9.

The financial support of the National Research Council of Canada is gratefully acknowledged, as is the hospitality of Professor Myron L. Bender, in whose laboratory the experimental work was completed.

1. J. T. EDWARD and S. NIELSEN. J. Chem. Soc. 5075 (1957).
2. J. FABIAN, J. VIOLA, and R. MAYER. Tetrahedron, **23**, 4323 (1967).
3. L. A. FLEXSER, L. P. HAMMETT, and A. DINGWALL. J. Am. Chem. Soc. **57**, 2103 (1935).
4. E. G. SANDER. J. Am. Chem. Soc. **91**, 3629 (1969).
5. P. M. MADER. J. Am. Chem. Soc. **87**, 3191 (1965).
6. S. O. ERIKSSON and C. HOLST. Acta Chem. Scand. **20**, 1892 (1966).
7. J. T. EDWARD and S. NIELSEN. J. Chem. Soc. 5070 (1957).
8. J. T. EDWARD and I. C. WANG. Can. J. Chem. **40**, 399 (1962).
9. G. E. LIENHARD and W. P. JENCKS. J. Am. Chem. Soc. **81**, 3855 (1965). T. C. BRUICE and D. M. MCMAHON. Biochemistry, **11**, 1273 (1972).
10. R. BRESLOW. Organic reaction mechanisms. W. A. Benjamin, Inc., New York. 1966. p. 163.
11. C. M. LEE and W. D. KUMLER. J. Am. Chem. Soc. **83**, 4593 (1961); E. NOE and M. RABAN. J. Am. Chem. Soc. **95**, 6119 (1973).
12. J. T. EDWARD and K. A. TERRY. J. Chem. Soc. 3527 (1957).
13. M. L. BENDER. Mechanisms of homogeneous catalysis from protons to proteins. Wiley-Interscience, New York. 1971.
14. L. P. HAMMETT. Physical organic chemistry. McGraw-Hill Book Co. New York. 1940. p. 184.
15. J. PACKER, A. L. THOMSON, and J. VAUGHAN. J. Chem. Soc. 2601(1955).
16. R. G. PEARSON. J. Am. Chem. Soc. **70**, 204 (1948).
17. S. S. BIECHLER and R. W. TAFT. J. Am. Chem. Soc. **79**, 4927 (1957); M. T. BEHME and E. H. CORDES. J. Org. Chem. **29**, 1255 (1964); M. L. BENDER and R. J. THOMAS. J. Am. Chem. Soc. **83**, 4183 (1961); R. M. POLLACK and M. L. BENDER. J. Am. Chem. Soc. **92**, 7190 (1970).
18. W. I. CONGDON and J. T. EDWARD. J. Am. Chem. Soc. **94**, 6096 (1972).

Can. J. Chem. Downloaded from www.nrcresearchpress.com by 210.87.254.105 on 09/05/12
For personal use only.

Molluscicidal Saponins of *Phytolacca dodecandra*: Lemmatoxin

R. M. PARKHURST, DAVID W. THOMAS, AND W. A. SKINNER
Life Sciences Division, Stanford Research Institute, Menlo Park, California
AND
LEWIS W. CARY
Varian Associates, Palo Alto, California

Received October 27, 1972[1]

Lemmatoxin, one of the molluscicidal saponin components of the fruit of *Phytolacca dodecandra* (endod), has been found to be a derivative of oleanolic acid substituted in the 3 position with a branched trisaccharide containing two glucose units and one galactose unit. A structure is proposed.

On trouve qu'une des composantes des saponines molluscicides du fruit du *Phytolacca dodecandra* (endol), la lemmatoxine, est un dérivé substitué en position-3 de l'acide oléanolique par un trisaccharide ramifié contenant deux unités de glucose et une unité de galactose. Une structure est proposée.
[Traduit par le journal]

Can. J. Chem., **52**, 702 (1974)

Since the reported isolation and structure determination of the major biologically active saponin of endod, oleanoglycotoxin-A (1), further work has led to the isolation of another saponin. Although present in lesser amount in the crude saponin mixture, this component seems to be about twice as biologically active (LD_{90}, 1.5 p.p.m., 24 h, *Biomphalaria glabrata*) as the major component. The discovery of other biological activity of the saponin not related to its molluscicidal properties is also under investigation. We have designated this material lemmatoxin (R = OH; R′ = H) and present here evidence for our assignment of structure.

During the chromatographic isolation of oleanoglycotoxin-A as its acetyl derivative from the crude saponin acetates from endod, several less polar components were recovered as mixtures. Repeated chromatography of one of these mixtures on silica gel thick layer gave lemmatoxin acetate (R = Ac; R′ = H) as a noncrystalline, glassy material, which seemed to be homogeneous by virtue of its movement on thin-layer silica gel plates as a single spot in several solvent systems. Lemmatoxin acetate could be deacetylated to give a biologically active saponin and reacetylated (1) to give back lemmatoxin acetate identical to that of the originally isolated material. Comparison of the size of the spots of this material and the size of the corresponding spot in the t.l.c. of the crude saponin acetate mixture allowed us to estimate its approximate concentration in the crude material at 16%.

Acid hydrolysis of lemmatoxin gave oleanolic acid as in the case of oleanoglycotoxin-A and also glucose and galactose, in the ratio of 2:1, respectively, which were identified as their pertrimethylsilyl derivatives by gas chromatography. Gas chromatography of the total acid hydrolysis products of permethyl lemmatoxin (R = R′ = CH_3) as their pertrimethylsilyl derivatives showed 1 mol of 2,6-di-*O*-methyl-1,3,4-tri-*O*-(trimethylsilyl)-D-glucose, 1 mol of 2,3,4,6-tetra-*O*-methyl-1-*O*-trimethylsilyl-D-galactose, and 1 mol of 2,3,4,6-tetra-*O*-methyl-1-*O*-trimethylsilyl-D-glucose, which were identified by comparison of their mass spectra with those in the literature (2), indicating that a galactose and glucose unit are attached to a central glucose unit in the 3 and 4 positions, assuming the central glucose to be in its pyranose form.

Acid hydrolysis of lemmatoxin under mild conditions gave glucose and galactose in almost equal amounts, as identified by gas chromatography of their pertrimethylsilyl derivatives, and another saponin along with free oleanolic acid in almost equal amounts. The formation of free oleanolic acid would be accompanied by the release of twice as much glucose as galactose and we would expect that the new saponin formed would retain glucose in preference to galactose. The hydrolytic loss of sugars in the 3 position in preference to the 4 position would tend to indicate that the galactose is located at position 3 (3). The new saponin

[1]Revision received September 17, 1973.

Can. J. Chem. Downloaded from www.nrcresearchpress.com by 210.87.254.40 on 09/05/12
For personal use only.

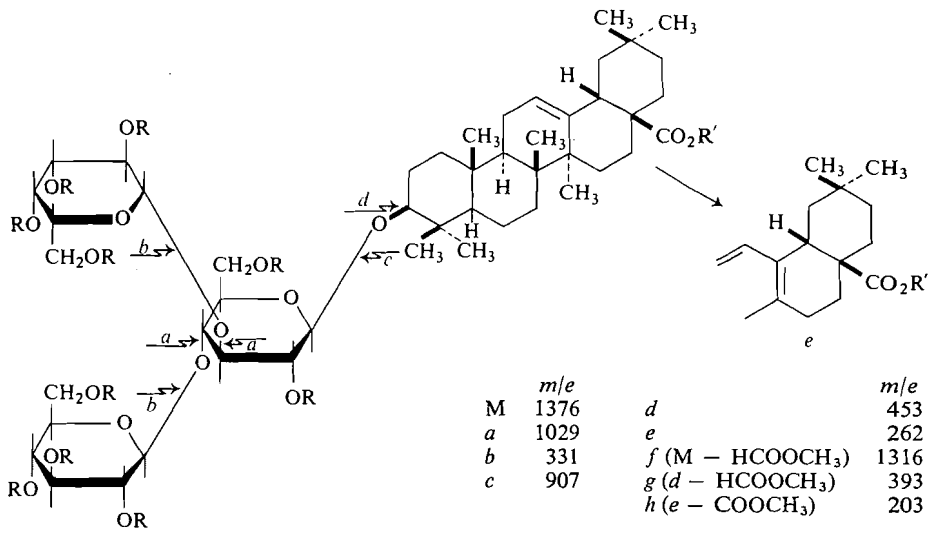

	m/e		m/e
M	1376	*d*	453
a	1029	*e*	262
b	331	*f* (M − $HCOOCH_3$)	1316
c	907	*g* (*d* − $HCOOCH_3$)	393
		h (*e* − $COOCH_3$)	203

FIG. 1. Interpretation of the mass spectrum of lemmatoxin acetate methyl ester (R = Ac; R′ = CH_3). The evidence for galactose and glucose being attached at positions 3 and 4, respectively, rather than 4 and 3, respectively, is not complete (see Text).

formed by this partial hydrolysis was not distinguishable from an authentic sample of oleanolic acid β-cellobioside by any of our thin-layer chromatographic systems when compared as either the peracetyl or permethyl derivative, further supporting our indication that galactose is located at the 3 position. Attempts to investigate the total hydrolysis products of the permethyl derivative of the new saponin formed by partial hydrolysis of lemmatoxin via gas chromatography – mass spectroscopy were inconclusive however, because the expected peaks for 2,3,4,6-tetra-*O*-methyl-1-*O*-trimethylsilyl-α- and β-D-glucose and 2,3,6-tri-*O*-methyl-1,4-di-*O*-trimethylsilyl-α- and β-D-glucose were very small due to the limited amount of sample available and the relatively high background of column bleed in the area of these peaks. This leaves still some doubt as to the position of attachment of the glucose and galactose units.

Mass spectra of lemmatoxin acetate and of its methyl ester (R = Ac; R′ = CH_3) gave added structural information. The molecular weight (1376) of the methyl ester could be seen by examination of this mass spectrum (Fig. 1).

That all three sugar units are contained within one single saccharide moiety is confirmed by the appearance of a peracetyl trihexose unit in the mass spectrum at *m/e* 907 (*c*). The appearance of fragment (*e*) at *m/e* 262, originating by a mechanism typical of Δ^{12}-unsaturated triterpenes, confirms that the carboxyl is present as a methyl ester, ruling out the possibility of the saccharide being bound to the carboxyl group.

A mass spectrum of peracetyl lemmatoxin was similar to the methylated compound with the exception that all fragments containing the carboxyl function appeared 14 mass units lower. Thus, the methyl ester of the derivative illustrated in Fig. 1 was introduced by treatment with diazomethane, and lemmatoxin therefore contains a free carboxylic acid.

The n.m.r. spectra of lemmatoxin acetate were taken in $CDCl_3$, C_6D_6:$CDCl_3$ (1:1), and two mixtures of these solvents. Two one-proton doublets δ ($CDCl_3$) 4.66, 4.70 p.p.m., (J = 8 Hz) each of which lean downfield and may be associated with the anomeric protons of two of the sugar units in the β configuration. The third anomeric proton is less well defined and partially covered by the C_6 protons, but can be detected via solvent shift as a doublet δ ($CDCl_3$) 4.37 p.p.m., (J = 8 Hz) indicating the β configuration.

Further upfield in the $CDCl_3$ spectra there are two multiplets δ 3.59 and 3.70 p.p.m., representing one and two protons, respectively. The fact that they lean downfield and their width suggest that these are three C_5 protons. The C_5 proton of galactose is only very weakly coupled to the C_4 proton and appears almost as a triplet (4). Spin decoupling at these multiplets causes the expected collapse of the minor splitting in the C_6 proton

Can. J. Chem. Downloaded from www.nrcresearchpress.com by 210.87.254.40 on 09/05/12
For personal use only.

quartets, confirming our previous assumptions. The triplet at δ 3.95 p.p.m. is collapsed by irradiation at 293 Hz downfield where we would expect the C_2 proton of the middle glucose unit; therefore this triplet must be assigned to the C_3 proton. The other triplet at δ 3.86 p.p.m. is therefore the C_4 proton of the middle glucose unit. The upfield shift of the C_3 and C_4 protons of the middle glucose is consistent with our proposed 3,4-di-*O*-substituted glucose structure.

Although the far less likely furanoid structure for the disubstituted glucose unit cannot be ruled out on the basis of the hydrolysis products, the appearance of the C_4 and C_5 protons of the central glucose unit in the n.m.r. suggests a splitting pattern of a pyranose form as does the large anomeric coupling (5). The low intensity of mass fragments resulting from the fission of the side chain from a five-membered furanose ring to give the planar oxinium ion also suggests the pyranose over the furanose form (6).

Since the anomeric configuration was clearly established by n.m.r., the unlikely possibility of L sugars can be ruled out by the optical rotation on the basis of Klyne's rule (7).

	$[\alpha]_D$ (deg)	M_D (deg)
Lemmatoxin acetate	+7.4±0.05	+101
Oleanolic acid	+83	+378
Sugar moiety required		−278
Methyl β-cellobioside acetate	−26	−169
Methyl β-D-galactoside acetate	−14	−51
Methyl β-cellobioside + methyl β-D-galactoside (acetates)		−218

The above data suggest that lemmatoxin is 3-*O*-[4′-*O*-(β-D-glucopyranosyl)-3′-*O*-(β-D-galactopyranosyl)-β-D-glucopyranosyl]olean-12-ene-28-oic acid (Fig.1).

Experimental

Mass spectra were determined with either a CEC Model 21-110B mass spectrometer or an LKB Model 9000 combination gas chromatograph – mass spectrometer. Quantitative gas chromatograms were obtained with a Varian-Aerograph Model 550-B instrument with flame ionization detector. Analyses were carried out with a 10 ft × 1/8 in column of 1% SE-30 on 100–120 mesh gas chrom Q at 170° and He flow of 20 ml/min for the TMS derivatives of unmethylated sugars. Analyses of TMS derivatives of methylated sugars were chromatographed similarly except that temperature was programmed and mass spectral comparison was used for identification rather than retention time.

Nuclear magnetic resonance spectra were determined with a Varian HR 300 nuclear magnetic resonance spectrometer employing a superconducting magnet at 70.5 kG. The sample was examined in a 5 mim sample tube at 35°.

All thin-layer and thick-layer chromatography was carried out using Mallinckrodt SilicAR-7GF plates and solvent systems *A*, chloroform; *B*, chloroform–ether (1:1); *C*, ether; *D*, ethyl acetate or; *E*, acetone.

Separation of Lemmatoxin Acetate

The crude saponin acetates from endod, 2 g, were chromatographed on a column (18 × 3 cm, 50 g, Malinckrodt SilicAR-CC7, 100–200 mesh) using chloroform–ether gradient elution and following the progress of the fractionation with t.l.c. A fraction, 1050 mg, eluted with 1% ether in chloroform was further purified by repetitive chromatography on thick plates (*B*) finally giving 20.9 mg of lemmatoxin acetate as a colorless glassy solid, R_f = 0.50–0.54 (*C*); $[\alpha]_D^{23}$ + 7.4 ± 0.05° (*c*, 1.26 chloroform); m.s. *m/e* 1362 (M^+), 1316, 1015, 907, 439, 393, 331, 248, 203; n.m.r. ($CDCl_3$) δ 0.72, 0.74 (CH_3), 0.89 ($3CH_3$), 0.92, 1.22 (CH_3), 1.95, 1.98, 2.00, 2.02 (CH_3CO), 2.08 ($3CH_3CO$), 2.09, 2.10, 2.13 (CH_3CO), 2.81 (C_{18}—H, m), 2.98 (C_3—H, m), 3.59 (C_5—H, m), 3.70 (C_5—2H, m), 3.86 (C_4—H, t), 3.95 (C_3—H, t) 4.05–4.50 (C_6—$3CH_2$, overlapping quartets), 4.37, 4.66, 4.70 (anomeric doublets, J = 8 Hz), 4.9–5.4 (complex series), 5.27 p.p.m. C_{12}—vinyl H, t).

Lemmatoxin Acetate Methyl Ester

Lemmatoxin acetate, 2 mg, was methylated with excess diazomethane in methanol–ether solution at room temperature overnight. Thin-layer chromatography showed the formation of a single new product, the methyl ester R_f = 0.62–0.67 (*C*); m.s. *m/e* 1376 (M^+), 1316, 1029, 907, 453, 393, 331, 262, 203.

Deacetylation of Lemmatoxin Acetate

Lemmatoxin acetate, 6.6 mg, was dissolved in 3 ml of methanol and 1 ml of concentrated ammonium hydroxide and maintained at 50° for 24 h. The solution was evaporated in a slow stream of nitrogen and extracted with 1-butanol. Evaporation of the butanol gave lemmatoxin as a colorless solid. This material could be reacetylated with excess acetic anhydride – pyridine at room temperature overnight to give back lemmatoxin acetate, R_f = 0.50–0.54 (*C*).

Total Hydrolysis of Lemmatoxin

Lemmatoxin, 1 mg, was dissolved in 2 ml of dioxane – 2 *N* HCl (1:1) and sealed in a glass tube. The sealed tube was placed in a steam bath for 15 h. The solid precipitate was centrifuged to one end; the liquid was decanted to the other end and the tube was cut in half. The precipitate was identified as oleanolic acid by comparison with an authentic sample via t.l.c. in two solvents, R_f = 0.70 (*D*); R_f = 0.90 (*E*). A drop of pyridine was added to the liquid portion before it was evaporated to dryness in a slow stream of nitrogen. The sugars remaining were pertrimethylsilylated in pyridine for gas chromatographic analysis. The retention times were compared with authentic samples of glucose and galactose treated similarly. The area of the peaks representing glucose (α-anomer, retention time 5.8 min; β-anomer, retention time 9.3 min)

Can. J. Chem. Downloaded from www.nrcresearchpress.com by 210.87.254.40 on 09/05/12
For personal use only.

and galactose (α-anomer, retention time 5.2 min; β-anomer, retention time 6.3 min) were in the ratio of 2 to 1.

Partial Hydrolysis of Lemmatoxin

Lemmatoxin, 1 mg, was dissolved in 4 ml of dioxane – 2% HCl (1:1) and heated on the steam bath for 3 h in a sealed tube. The solution was evaporated to a small volume in a slow stream of nitrogen; water and 1-butanol were added to separate the saponin from the free sugars. The butanol layer was evaporated and the solid remaining was acetylated and subjected to t.l.c. The t.l.c. showed only a trace of lemmatoxin acetate and about equal amounts of a new saponin acetate and oleanolic acid acetate by comparison of the areas of the spots. The saponin acetate was recovered and chromatographed in several solvent systems, R_f = 0.07–0.10 (*A*), R_f = 0.42–0.54 (*B*), R_f = 0.75–0.82 (*C*), R_f = 0.94—0.99 (*D*). The same values were obtained for authentic oleanolic acid β-cellobioside heptaacetate run on the same plate. The new saponin acetate was again recovered deacetylated and permethylated as described (8), R_f = 0.20–0.30 (*A*). The same R_f value was obtained for the standard compound treated similarly. The permethylated (8) new saponin was hydrolyzed in dioxane – 2 *N* HCl (1:1) as described for total hydrolysis above and the permethylated sugars pertrimethylsilylated for GC/MS.

Total Hydrolysis of Permethyl Lemmatoxin

Lemmatoxin, 1 mg, was permethylated and hydrolized in dioxane – 2 *N* HCl (1:1) as described above. The hydrolysis products were pertrimethylsilylated in pyridine and subjected to gas chromatography which showed 2,3,4,6-tetra-*O*-methyl-1-*O*-trimethylsilyl glucose, 2,3,4,6-tetra-*O*-methyl-1-*O*-trimethylsilyl galactose, and 2,6-di-*O*-methyl-1,3,4-tri-*O*-(trimethylsilyl) glucose in the ratio of 1:1:1. Peaks were doublets representing the two anomeric forms in each case. Mass spectrometry was used for identification and the area under the respective peaks used to determine the quantity.

The authors are indebted to Professor Aklilu Lemma for his interest and samples and to Percy Yau for biological testing. This work was supported by the Office of Naval Research Contract N00014-71-C-0123, Stanford Research Institute Research and Development funds, and General Research Support Grant RO-5522 from the National Institute of Health.

1. R. M. PARKHURST, D. W. THOMAS, W. A. SKINNER, and L. W. CARY. Phytochemistry, **12**, 1437 (1973).
2. G. PETERSSON and O. SAMUELSON. Svensk Papperstid. **71**, 731 (1968).
3. Z. WOJCIECHOWSKI, A. JELONKIEWICZ-KONADOR, M. TOMASZEWSKI, J. JANKOWSKI, and Z. KASPRZYK. Phytochemistry, **10**, 1121 (1971).
4. C. V. HOLLAND, D. HORTON, and M. J. MILLER. J. Org. Chem. **32**, 3077 (1967).
5. B. CAPON and D. THACKER. Proc. Chem. Soc. 369 (1964).
6. N. K. KOCHETKOV and O. S. CHIZHOV. *In* Advances in carbohydrate chemistry. Vol. 21. *Edited by* M. L. Wolfrom. Academic Press, New York and London. 1966. p. 62.
7. W. KLYNE. Biochem. J. **47**, xli (1950).
8. D. W. THOMAS. FEBS Lett. **5**, 53 (1969).

Can. J. Chem. Downloaded from www.nrcresearchpress.com by 210.87.254.40 on 09/05/12
For personal use only.

Ring C Functionalized Diterpenoids. Part III.[1] 12-Substituted *ent*-Beyeranes

JOHN CAIRNS FAIRLIE
Department of Chemistry, University of Glasgow, Glasgow, Scotland

AND

ALAN JAMES MCALEES, ROBERT MCCRINDLE,[2] AND ELI NEIDERT
Chemistry Department, University of Guelph, Guelph, Ontario N1G 2W1

Received September 19, 1973

On treatment with hot formic acid *ent*-16-kaurene (**4***a*) and the related ester **4***b* give a mixture containing 12-, 15- and 16-*ent*-beyerane derivatives (**10***a*, **1***a*; **7***a*, **12***a*; **9***a*, **11***a*) in which the last predominates, while *ent*-15-beyerene (**5***a*) gives mainly the C-15 formate **7***a*. In keeping with the anticipated longer lifetimes of the intermediate ions **2** and **3** in trifluoroacetic acid as compared with formic acid, reaction of **4***b* in the former medium at room temperature affords a mixture containing **1***c*, **11***c*, and **12***c*, in which the relative yield of the 12-substituted derivative (**1***c*) is markedly increased. Treatment of methyl *ent*-trachyloban-19-oate (**14**) or methyl *ent*-15-atisen-19-oate (**6***b*) under the same conditions gives a mixture similar to that obtained from **4***b*.

Après avoir réagi avec de l'acide formique chaud, l'*ent*-kaurène-16 (**4***a*) et son ester **4***b* ont conduit à un mélange comprenant les dérivés *ent*-beyerane-12, -15 et -16 (**10***a*, **1***a*; **7***a*, **12***a*; **9***a*, **11***a*) dans lequel le dernier dérivé prédomine alors que l'*ent*-beyerène-15 (**5***a*) a conduit principalement au dérivé formate en position C-15 (**7***a*). La réaction de **4***b* dans l'acide trifluoroacétique à température ambiante a conduit à un mélange comprenant les dérivés **1***c*, **11***c* et **12***c* dans lequel le rendement relatif du dérivé substitué en 12 (**1***c*) est, de façon marquée, plus élevé. Ce dernier résultat est en accord avec le temps de vie prévu des ions intermédiaires **2** et **3** qui semble plus long dans l'acide trifluoroacétique que dans l'acide formique. Lorsque l'on a fait réagir, dans les mêmes conditions, l'*ent*-trachylobanoate-19 de méthyle (**14**) ou l'*ent*-atisen-15 oate-19 de méthyle, on a obtenu un mélange semblable à celui obtenu avec **4***b*.
[Traduit par le journal]

Can. J. Chem., **52**, 706 (1974)

In earlier papers (1, 2), we have described procedures for the production of ring C functionalized *ent*-kauranes, phyllocladanes (13β-kauranes), and *ent*-atisanes. For rearrangement studies we also required 12-oxygenated beyeranes and although two routes to these compounds have been reported neither is entirely satisfactory. Methyl 12β-hydroxy-*ent*-beyeran-19-oate (**1***b*) has been prepared (3) from steviol in several steps and trachylobanes have been cleaved (4) by acetic acid – acetic anhydride – perchloric acid mixtures to products which include 12β-acetoxy-*ent*-beyeranes. The present article deals with the production of related derivatives by the acid-catalyzed rearrangement of readily available diterpenoid precursors and conditions which lead to optimum yields of these compounds.

Much work has been recorded (for leading references see ref. 5) on the generation of and products which emanate from the ions **2** and **3**.[3] Since direct precursors of ion **3**, which yields 12-derivatives of *ent*-beyerane on nucleophilic attack, are less available than precursors of ion **2**, namely *ent*-16-kaurenes (see *e.g.*, refs. 2 and 6), the latter ion represents a more accessible entry point provided that conditions which favor conversion of **2** into **3** can be found. However, there are only a few reports (5, 7, 8) of the crossover rearrangement ($C_{12} \rightleftharpoons C_{16}$ hydride shift) which interconverts **2** and **3** although this occurs readily in the absence of the C-13 methyl group (9) and in the parent bicyclooctane system (10). It seemed likely that production of the ion **2** in a medium of high solvating power and low nucleophilicity would allow it a longer lifetime and hence a greater opportunity to rearrange.

Our initial reactions were carried out on *ent*-

[1]For Part II see ref. 1.
[2]To whom correspondence should be addressed.
[3]Although nonclassical ion formulations are used we do not wish to rule out the possibility of equilibrating classical ions.

Can. J. Chem. Downloaded from www.nrcresearchpress.com by 210.87.254.42 on 09/05/12
For personal use only.

Can. J. Chem. Downloaded from www.nrcresearchpress.com by 210.87.254.42 on 09/05/12
For personal use only.

16-kaurene (**4***a*) with formic acid as the reaction medium, but since **4***a* is insoluble in formic acid alone we turned to various mixtures with chloroform, the most satisfactory results being obtained using 1:2 chloroform – formic acid. Small samples of **4***a* were heated in refluxing chloroform – formic acid for time intervals ranging from 30 min to 48 h. Analyses of the products by g.l.c. and t.l.c. indicated the presence of a mixture of formates and olefins, the former accumulating at the expense of the latter with increase in reaction time. Thus, after 6 and 24 h the olefin:formate ratio was 48:52 and 12:88, respectively. The relative amounts of individual components of the olefinic fractions were not determined but *ent*-16-kaurene (**4***a*), *ent*-15-kaurene, *ent*-15-beyerene (**5***a*), *ent*-15-atisene (**6***a*), and *ent*-16-atisene were separated from the mixtures and their identities established by t.l.c. on silver nitrate – silica gel and g.l.c. – mass spectroscopy. On the basis of both t.l.c. and g.l.c. the formate fractions appeared to contain only two components which were separated by preparative t.l.c. The n.m.r. spectra of the less polar component (**7***a*)[4] and the corresponding alcohol (**7***b*), obtained by treatment of **7***a* with lithium aluminum hydride, showed four quaternary *C*-methyl groups, suggesting the presence of the *ent*-beyerane skeleton, and a single low-field carbinyl proton. Their structures were established by comparison of the physical and spectral data of **7***a* and the derived ketone (**8***a*) with those published (11).

The n.m.r. spectrum of the material from the more polar t.l.c. band showed it to be a mixture. Accordingly, it was treated with lithium aluminum hydride to give a mixture of alcohols, **9***b* and **10***b*, separable by t.l.c. The formates (**9***a* and **10***a*) of each of these alcohols were prepared and their n.m.r. spectra compared with that of the material from the more polar t.l.c. band (above). This confirmed that the last had consisted of a mixture of the first two and that rearrangement had not accompanied the reductive cleavage. In addition, these spectra showed that **9***a* and **10***a* were, like **7***a*, secondary formates with *ent*-beyerane skeletons. Their structures rest on a comparison of the physical and spectral data obtained for the corresponding alcohols (**9***b*, **10***b*), derived ketones (**8***b*, **8***c*), and acetate (**10***c*) with published data (4, 11). Separation, as outlined above, of the formate fractions, obtained after various reaction times (0.5–24 h) indicated that the relative proportions of the three formates remained essentially constant (**7***a*:**9***a*:**10***a*, *ca.* 1:3:1). The obvious conclusion that **7***a*, **9***a*, and **10***a* are stable to the reaction conditions was confirmed by exposure of the individual formates, generated *in situ* from the alcohols, to refluxing formic acid – chloroform (2:1) for 24 h when each ester was recovered in an essentially pure state. While **9***a* and **10***a* are the expected products of trapping of the ions **2** and **3** respectively by solvent, the C-15 formate **7***a* may derive from **2** either by a $C_{15} \rightarrow C_{16}$ hydride shift or more likely by a deprotonation–reprotonation sequence via *ent*-15-beyerene (**5***a*) (see below). Notably, *ent*-beyerene was a major component of the olefin fraction.

ent-15-Beyerene (**5***a*) is another potential precursor (7) of the ions **2** and **3** and indeed, formolysis of the C-16 tosylate **11***d* has been reported (5) to give the formates **1***a*, **11***a*, and **12***a* (*ca.* 1:2:1). However, protonation of **5***a* may take place at C-15 to give the required ion **2** or at C-16. Since the former process introduces a severe nonbonded interaction between the C-15 α-hydrogen and the C-10 methyl group and since the secondary formate **7***a* is stable to the reaction conditions used above, it was anticipated that this compound, **7***a*, should be the principal product of treatment of *ent*-15-beyerene with formic acid – chloroform. Indeed, **5***a* in refluxing formic acid – chloroform was gradually converted into a mixture of formates, which consisted mainly (80%)[5] of **7***a* along with a minor amount (20%) of **9***a* and only a trace of **10***a*, and even after 22 h only substrate was detected in the recovered olefin fraction.

Our attention was next directed to methyl *ent*-16-kauren-19-oate (**4***b*) because of the availability of the parent acid from the common sunflower (2) and because of its greater solubility than *ent*-16-kaurene (**4***a*) in formic acid. Since the reaction of **4***b* in hot formic acid alone was complicated by extensive ester exchange, we turned to buffered formic acid (*cf.* 5) at 50–60° in which this side reaction was minimized. After 6 h, when the reaction appeared (t.l.c. and g.l.c.)

[4]In this paper the designation α or β for substituents on the α-bridge of rings C—D refers to orientations *syn* and *anti* to C-20, respectively.

[5]Yields are reported as a percentage by weight of recovered material.

Can. J. Chem. Downloaded from www.nrcresearchpress.com by 210.87.254.42 on 09/05/12
For personal use only.

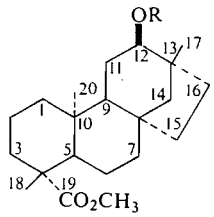

1

a R = CHO
b R = H
c R = $COCF_3$
d R = Ts

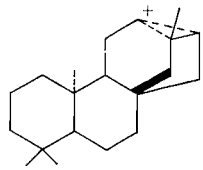

2

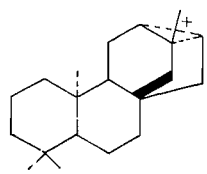

3

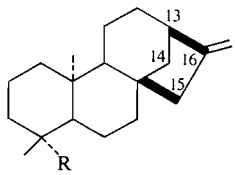

4

a R = CH_3
b R = CO_2CH_3

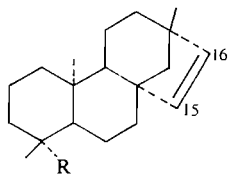

5

a R = CH_3
b R = CO_2CH_3

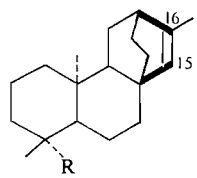

6

a R = CH_3
b R = CO_2CH_3

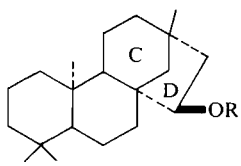

7

a R = CHO
b R = H

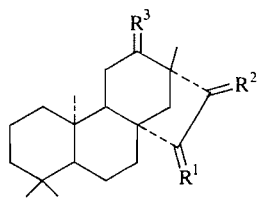

8

a R^1 = O; R^2 = R^3 = H_2
b R^2 = O; R^1 = R^3 = H_2
c R^3 = O; R^1 = R^2 = H_2

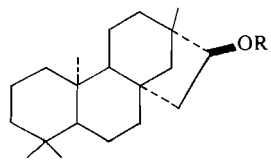

9

a R = CHO
b R = H

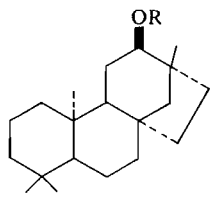

10

a R = CHO
b R = H
c R = $COCH_3$

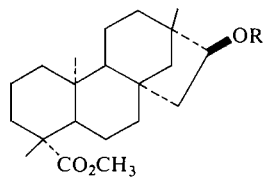

11

a R = CHO
b R = H
c R = $COCF_3$
d R = Ts

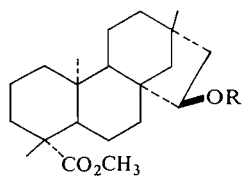

12

a R = CHO
b R = H
c R = $COCF_3$
d R = $COCH_3$

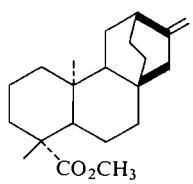

13

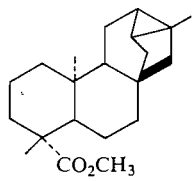

14

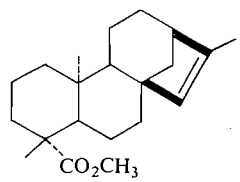

15

Can. J. Chem. Downloaded from www.nrcresearchpress.com by 210.87.254.42 on 09/05/12
For personal use only.

to have gone to completion, preparative t.l.c. gave an olefin (10%) and two formate (90%) fractions. Examination of the olefinic fraction (by analytical t.l.c. on silver nitrate – silica gel and g.l.c. only) suggested a mixture of components entirely analogous to those obtained from *ent*-16-kaurene (see above). Both the less polar (**1***a*; 17%) and the more polar (**11***a*; 73%) formate fractions appeared homogeneous by t.l.c., g.l.c., and n.m.r. However, they were not characterized directly but identified by conversion to the known (5) alcohols, **1***b* and **11***b*. No C-15 formate (**12***a*) was detected in the reaction mixture.

Since the yields of the desired 12-substituted *ent*-beyerane derivatives obtained under the above conditions were unacceptably low a reaction medium was sought which would allow even longer cationic lifetimes but yet have at least some nucleophilic capability. The recent results (5) on the solvolyses of **1***d* and **11***d* in sodium trifluoroacetate – trifluoroacetic acid suggested that this medium might satisfy these requirements. Thus the ester **4***b* was kept at 20° in this medium and after 18 h, when the reaction appeared complete, t.l.c. revealed the presence of at least four components of very similar mobility, which were separated by preparative t.l.c. The least polar fraction (12%) consisted of a mixture of olefins **5***b*, **6***b*, and **13** in which the first predominated. The remaining three components, in order of increasing polarity, were the C-15 (**12***c*; 8%), C-16 (**11***c*; 21%), and C-12 (**1***c*; 59%) trifluoroacetates. The first was identified by conversion, via the alcohol **12***b* into the known (5) acetate **12***d*, while the last two gave the known (5) alcohols **11***b* and **1***b*. Reaction of **4***b* in sodium trifluoroacetate – trifluoroacetic acid[6] thus leads to much more satisfactory yields of 12-substituted *ent*-beyeranes than exposure to formic acid.

Since the isolation of methyl *ent*-16-kauren-19-oate (**4***b*) from the common sunflower involves its separation from methyl *ent*-trachyloban-19-oate (methyl *ent*-13α,16-cycloatisan-19-oate; **14**) we were interested in the possibility of using the *mixture* of the two esters for the preparation of **1***c*. Accordingly, we have examined the reaction of **14** and **6***b*, the expected principal olefinic product (4, 7, 12) of acid-catalyzed opening of the cyclopropane ring in the former. While **14** gave a mixture of very similar composition (t.l.c.) to that obtained from methyl *ent*-16-kauren-19-oate (**4***b*) under the same conditions, **6***b* gave largely **1***c*. The latter result is not unexpected, since in this case conversion of **6***b* into **1***c* does not involve the hydride shift required for the conversion of the kaurene ester **4***b* into **1***c* (see above).

Since these results confirm that the lifetimes of the intermediate ions are longer in trifluoroacetic acid than in formic acid, methyl *ent*-15-beyeren-19-oate (**5***b*) was exposed to the former acid in the expectation that the slower capture of the kinetically favored C-15 ion would allow more extensive conversion to **2** and **3**. This was found (t.l.c.) to be the case, although the C-15 trifluoroacetate **12***c* was still the predominant product. In an attempt to induce more extensive conversion of the intermediate C-15 cation to **2** and thence **3**, the reaction was carried out at 60°. However, the relative amount of the C-12 ester (**1***c*) formed under these conditions was reduced compared with the other two (**11***c* and **12***c*). Indeed, when reaction of the methyl esters **4***b*, **6***b*, and **14** was repeated at this elevated temperature, the relative amounts of **11***c* and **12***c* also increased at the expense of **1***c*. This prompted us to test the stabilities of the secondary trifluoroacetates (**1***c*, **11***c*, and **12***c*) under the reaction conditions. This showed that whereas all three appeared to be relatively stable to sodium trifluoroacetate – trifluoroacetic acid at room temperature, the first (**1***c*) was converted to a mixture containing all three at 60°, while the last two showed (t.l.c.) little evidence of reaction at this temperature.

In conclusion, treatment of the diterpenoid esters **4***b* and **14**, which are readily available from the common sunflower, with sodium trifluoroacetate – trifluoroacetic acid at *room temperature*, represents a satisfactory route to the 12-substituted beyerane **1***c* which can be recovered from the product mixture in yields which exceed 50%, based on starting ester.

Experimental

Melting points were determined on a Kofler hot-stage apparatus and are uncorrected. For normal analytical and preparative t.l.c., chromatoplates were spread with Kieselgel G. (Merck), while silver nitrate – silica gel chromatoplates in addition contained 12% of the former. Gas–liquid chromatography was carried out with a Varian Aerograph 1200 gas chromatograph using a stainless steel column (⅛ in. × 10 ft packed with 5% SE-30) and nitrogen as carrier gas with a flow rate of

[6]Reaction in trifluoroacetic acid alone gave essentially the same mixture.

Can. J. Chem. Downloaded from www.nrcresearchpress.com by 210.87.254.42 on 09/05/12
For personal use only.

25 ml/min. Gas chromatography – mass spectral analyses were performed on an L.K.B. 9000A Gas Chromatograph – Mass Spectrometer using a glass column ($\frac{1}{4}$ in. × 10 ft) with a 1% SE-30 packing at 150° with helium as the carrier gas at a flow rate of 35 ml/min. Light petroleum was of b.p. 60–80°. Proton magnetic resonance spectra were run on a Varian Associates A-60A or HA 100 spectrometer in deuterochloroform using approximately 0.3 *M* solutions and tetramethylsilane as internal standard. Infrared spectra were recorded in carbon tetrachloride on a Perkin-Elmer 225 grating spectrophotometer.

Rearrangement of ent-16-Kaurene (4a) with Formic Acid

(−)-Kaurene (**4***a*, 35 mg) was heated in refluxing chloroform – formic acid (1:2, 3 ml), the progress of the reaction being monitored by working up (evaporation *in vacuo*) small aliquots after $\frac{1}{2}$, 1, 2, 4, 6, 12, 24, and 48 h and analyzing the resulting mixtures by g.l.c. at 208° and t.l.c. (ethyl acetate – light petroleum; 1:19). The results from the last two were very similar.

The reaction was repeated twice more with a larger quantity (150 mg) of (−)-kaurene. The first was worked up after 6 h and the products (158 mg) separated by preparative t.l.c. (ethyl acetate – light petroleum; 1:19) into three fractions. The major component of the least polar (olefin) fraction (74 mg) was identified by t.l.c. on silver nitrate – silica gel (benzene – light petroleum; 3:7) and g.c.–m.s. (7) as *ent*-15-kaurene. The fraction (14 mg) of intermediate polarity was essentially pure **7***a*; g.l.c. retention time 3.6 min at 208°; τ 1.93 (s, 1 H, —OCO*H*), 4.55 (br d, 1 H-15, J = 7.5 Hz), 7.65–8.15 (m, αH-16, J = 14.5, 7.5 Hz and $J_{16\alpha.13\beta}$ = 2 Hz), 9.01, 9.02, 9.17, and 9.21 (all s, 3H, quaternary C–CH_3's). The corresponding alcohol (**7***b*) was formed on treatment with lithium aluminum hydride. After crystallization from light petroleum it had m.p. 93–96° (lit. (11) m.p. 96–97°); τ 5.70 (br d, 1 H-15, J = 7 Hz), 7.75–8.20 (m, αH-16, J = 14, 7, and 2.5 Hz), 9.03, 9.05, 9.14, and 9.18 (all s, 3H, quaternary C—CH_3's). Oxidation of this alcohol with the Jones reagent furnished the ketone (**8***a*) which crystallized from light petroleum and had m.p. 86–88° (lit. (11) m.p. 88–89°); τ 7.97 (dd, αH-16, J = 18 and 3 Hz), 8.13 (d, βH-16, J = 18 Hz), 8.99, 9.18, 9.20, and 9.23 (all s, 3H, quaternary C—CH_3's); ν_{max} 1736 cm^{-1}.

The third fraction (62 mg) consisted of a mixture (n.m.r.) of **9***a* and **10***a* which gave one spot on t.l.c. (ethyl acetate – light petroleum; 1:19) and one peak on g.l.c., retention time 4.6 min at 208°. Treatment with lithium aluminum hydride furnished the corresponding alcohols which were separated by preparative t.l.c. (ethyl acetate – light petroleum; 1:19 (run thrice)). The less polar alcohol, **10***b* (13 mg), on crystallization from light petroleum had m.p. 100–102°; τ 6.52 (br s, 1 H-12, $w_{1/2}$ = 6 Hz), 9.01, 9.11, 9.16, and 9.20 (all s, 3H, quaternary C—CH_3's). The derived acetate **10***c* on crystallization from light petroleum had m.p. 146–148° (lit. (4) m.p. 150°); τ 5.28 (br s, 1 H-12), 7.96 (s, 3H, —OCOCH_3), 9.10, 9.11, 9.15, and 9.19 (all s, 3H, quaternary C—CH_3's). The derived ketone (**8***c*) crystallized from methanol and had m.p. 86–88° (lit. (4) m.p. 88–89°); τ 8.93, 9.02, 9.13, and 9.16 (all s, 3H quaternary C—CH_3's); ν_{max} 1710 cm^{-1}. The more polar alcohol **9***b* (41 mg) also crystallized from light petroleum and had m.p. 103–104° (lit. (11) m.p. 104–105°); τ 6.30 (br d, 1 H-16, J = 7 Hz), 7.15–7.60 (m, αH-15, J = 14, 7 Hz and $J_{15\alpha.13\beta}$ = 2 Hz), 9.09, 9.12, 9.15, and 9.20 (all s, 3H, quaternary C—CH_3's). Oxidation of this alcohol furnished the ketone **8***b*, m.p. 100–103° (lit. (11) m.p. 102–103°); τ 7.28 (dd, αH-15, J = 18 and 3 Hz), 8.21 (d, βH-15, J = 18 Hz), 8.98, 9.13 (both s, 3H, quaternary C—CH_3's), and 9.09 (s, 6H, quaternary C—CH_3's); ν_{max} 1742 cm^{-1}.

When the third batch of (−)-kaurene (150 mg) in refluxing chloroform – formic acid was worked up, on this occasion after 24 h using the procedure outlined above for the second batch, the following were recovered: an olefin fraction (20 mg), formate **7***a* (28 mg), and (after reduction with lithium aluminum hydride) alcohols **10***b* (27 mg) and **9***b* (82 mg).

Alcohols **9***b* and **10***b* on heating in refluxing chloroform – formic acid (1:2) for 30 min formed (t.l.c.) the corresponding formates **9***a* and **10***a*. These and the C-15 formate (**7***a*) on heating in the same medium for 6 h gave back essentially pure starting material in each case as shown by t.l.c., g.l.c. at 208°, and reconversion of each to the alcohol with lithium aluminum hydride and then t.l.c.

Treatment of ent-15-Beyerene (5a) with Formic Acid

ent-Beyerene (**5***a*, 150 mg) was exposed to refluxing chloroform – formic acid (1:2) for (*i*) 6 and (*ii*) 22 h. Work-up as above for the products from *ent*-kaurene gave (*i*) substrate (**5***a*; 88 mg) identified by t.l.c. on silver nitrate – silica gel (benzene – light petroleum; 3:7), g.l.c. at 180°, and n.m.r.; the C-15 formate **7***a* (57 mg); and after reduction with lithium aluminum hydride, the C-16 alcohol **9***b* (12 mg); and (*ii*) essentially pure substrate (**5***a*; 65 mg); the C-15 formate **7***a* (82 mg); the C-16 alcohol **9***b* (15 mg); and the C-12 alcohol **10***b* (< 1 mg).

Rearrangement of Methyl ent-16-Kauren-19-oate (4b) with Formic Acid

A solution of methyl *ent*-16-kauren-19-oate (**4***b*; 150 mg) in formic acid (15 ml) buffered with sodium carbonate (50 mg) was kept at 60° for 6 h. The products, recovered by evaporation of the solvent *in vacuo* and extraction into light petroleum, were separated by preparative t.l.c. (ethyl acetate – light petroleum; 1:9). The least polar fraction (16 mg) consisted of olefinic esters and was shown by t.l.c. on silver nitrate – silica gel (ethyl acetate – light petroleum; 2:23) to contain **15** (major component), **4***b*, **5***b*, **6***b*, and **13**. The component of intermediate polarity was the formate **1***a* (25 mg) which had τ 1.87 (s, 1H, —OCO*H*), 5.13 (br s, 1 H-12), 6.35 (s, 3H, —CO_2CH_3), 8.82, 9.06, and 9.28 (all s, 3H, quaternary C—CH_3's). The corresponding alcohol **1***b* prepared by hydrolysis of **1***a* with sodium hydroxide (1 *M*) in refluxing ethanol for 3 h, crystallized from light petroleum and had m.p. 101–101.5° (lit. (3) m.p. 104–105.5°); τ 6.35 (s, 3H, —CO_2CH_3), 6.47 (br s, 1 H-12), 8.82, 8.99, and 9.27 (all s, 3H, quaternary C—CH_3's). The most polar component was the formate **11***a* (110 mg) which had τ 1.93 (s, 1H, —OCO*H*), 5.13 (br d, 1 H-16, J = 7 Hz), 6.36 (s, 3H, —CO_2CH_3), 7.10–7.60 (m, αH-15, J = 15, 7, and 2 Hz), 8.83, 9.09 and 9.28 (all s, 3H, quaternary C—CH_3's). This formate on hydrolysis as above furnished the alcohol **11***b* which on crystallization from light petroleum had m.p. 108° (lit. (3) m.p. 109–111°); τ 6.36 (s + br d, 4H, 1H-16 + —CO_2CH_3),

Can. J. Chem. Downloaded from www.nrcresearchpress.com by 210.87.254.42 on 09/05/12
For personal use only.

7.20–7.70 (m, αH-15, J = 14.5, 7, and 2 Hz), 8.83, 9.06, and 9.28 (all s, 3H, quaternary C—CH_3's).

The C-15 formate **12***a* could not be detected in the reaction mixture by t.l.c., g.l.c. at 220° or n.m.r. It was prepared by heating methyl *ent*-beyeren-19-oate in refluxing formic acid – chloroform (2:1) for 22 h. It had τ 1.88 (s, 1H, —OCO*H*), 4.57 (br d, 1 H-15, J = 7.5 Hz), 6.35 (s, 3H, —CO_2CH_3) 7.65–8.15 (m, αH-16, J = 14, 7.5, and 2 Hz), 8.83, 9.00, and 9.18 (all s, 3H, quaternary C—CH_3's).

Rearrangements in Trifluoroacetic Acid

(*i*) Methyl *ent*-16-kauren-19-oate (**4***b*, 298 mg) was dissolved in trifluoroacetic acid (25 ml) to which had been added sodium carbonate (200 mg). After 18 h at 20° the solvent was evaporated *in vacuo* and the products recovered in light petroleum. These ran as four evenly spaced spots on t.l.c. (ethyl acetate – light petroleum; 1:24) and were separated by preparative t.l.c. (same solvent mixture). The least polar fraction (49 mg) which ran as one spot on analytical t.l.c. on silica gel consisted of olefinic esters. The major components were identified by t.l.c. on silver nitrate – silica gel (ethyl acetate – light petroleum; 2:23) and g.l.c. at 202° as **5***b* (*ca.* 55%; retention time, 3.7 min), **6***b* (*ca.* 30%; retention time, 4.4 min), and **13** (*ca.* 5%; retention time 4.9 min). The second fraction (31 mg) contained the 15-trifluoroacetate (**12***c*) which had τ 4.46 (br d, 1 H-15, J = 8 Hz), 6.38 (s, 3H, —CO_2CH_3), 8.84, 8.98, and 9.18 (all s, 3H, quaternary C—CH_3's). This compound was identified by hydrolysis with ethanolic sodium hydroxide (1 *M*) at reflux and acetylation (acetic anhydride – pyridine) to the known acetate **12***d*, which, after crystallization from methanol, had m.p. 122–124° (lit. (3) m.p. 122–123.5°); τ 4.70 (br d, 1 H-15, J = 7.5 Hz), 6.36 (s, 3H, —CO_2CH_3), 7.50–8.15 (m, αH-16, J = 14, 7.5, and 2 Hz), 7.95 (s, 3H, —OCOCH_3), 8.83, 9.01, and 9.18 (all s, 3H, quaternary C—CH_3's). The third fraction (82 mg) consisted of the 16-trifluoroacetate (**11***c*) which had τ 5.02 (br d, 1 H-16, J = 7 Hz), 6.36 (s, 3H, —CO_2CH_3), 7.05–7.65 (m, αH-15, J = 14.5, 7, and 2 Hz), 8.82, 9.07, and 9.27 (all s, 3H, quaternary C—CH_3's). This compound on hydrolysis formed the known (see above) alcohol **11***b*, m.p. 108°. The most polar fraction (232 mg) was essentially pure 12-trifluoroacetate **1***c*, which crystallized from methanol and had m.p. 123–124°; τ 5.03 (br s, 1 H-12), 6.35 (s, 3H, —CO_2CH_3), 8.82, 9.03, and 9.27 (all s, 3H, quaternary C—CH_3's). Hydrolysis afforded the known (see above) alcohol **1***b*, m.p. 102°.

(*ii*) Methyl *ent*-trachyloban-19-oate (**14**, 50 mg) on reaction with sodium trifluoroacetate – trifluoroacetic acid (10 ml) at 20° for 18 h and work-up as above afforded a product mixture which appeared essentially identical on t.l.c. to that from methyl *ent*-kauren-19-oate. The major product **1***c* (35 mg) was isolated and had m.p. 122–124°.

(*iii*) Methyl *ent*-15-atisen-19-oate (**6***b*, 12 mg) on reaction in the same medium at 20° for 18 h furnished a mixture giving a similar t.l.c. spot pattern, except that the intensity of the most polar spot (C-12 ester **1***c*) was enhanced relative to the products from (*i*) and (*ii*).

(*iv*) Methyl *ent*-15-beyerenoate (**5***b*, 10 mg) on reaction as above afforded products with a very similar t.l.c. spot pattern except that in this case, the second least polar spot (C-15 ester **12***c*) was more intense than the most polar spot (C-12 ester **1***c*).

(*v*) Portions (*ca.* 10 mg) of **4***b*, **5***b*, **6***b*, and **14** were exposed to the same medium for 6 h at 60°. In each case the products showed on t.l.c. a significantly reduced proportion of the C-12 ester **1***c* in comparison to the room temperature reactions.

(*vi*) The trifluoroacetates **1***c*, **11***c*, and **12***c* on exposure to the above reaction medium at 20° for 18 h were unchanged, as were the last two at 60° for 6 h. The first (**1***c*), at the higher temperature, gave a product mixture showing the typical four-spot t.l.c. pattern (see above).

We thank the Science Research Council of the U.K. for a maintenance award (to J.C.F.) and the National Research Council of Canada for an operating grant.

1. H. M. Campbell, P. A. Gunn, A. J. McAlees, and R. McCrindle. Can. J. Chem. **51**, 4167 (1973).
2. A. J. McAlees and R. McCrindle. Can. J. Chem. **51**, 4103 (1973).
3. R. M. Coates and E. F. Bertram. J. Org. Chem. **36**, 2625 (1971).
4. G. Hugel, L. Lods, J. M. Mellor, and G. Ourisson. Bull. Soc. Chim. Fr. 2894 (1965).
5. R. M. Coates and E. F. Bertram. J. Org. Chem. **36**, 3722 (1971).
6. B. E. Cross, R. H. B. Galt, J. R. Hanson, P. J. Curtis, J. F. Grove, and A. Morrison. J. Chem. Soc. 2937 (1963); C. A. Henrick and P. R. Jefferies. Aust. J. Chem. **17**, 578 (1964); C. H. Brieskorn and E. Pohlmann. Ber. **102**, 2621 (1969); R. A. Appleton, R. McCrindle, and K. H. Overton. Phytochem. **9**, 581 (1970); T. Anthonsen and S. Chantharasakul. Acta Chem. Scand. **25**, 1925 (1971); F. Piozzi, P. Venturella, A. Bellino, and M. L. Marino. J. Chem. Soc. Perkin Trans. I, 1164 (1973); J. R. Hanson. The tetracyclic diterpenes. Pergamon Press, Oxford. 1968. p. 12; J. R. Hanson. Specialist periodical reports: terpenoids and steroids. The Chemical Society, London, Vol. 1. 1971. p. 141; Vol. 2. 1972. p. 140.
7. R. A. Appleton, A. J. McAlees, A. McCormick, R. McCrindle, and R. D. H. Murray. J. Chem. Soc. 2319 (1966).
8. K. M. Baker, L. H. Briggs, J. G. St. C. Buchanan, R. C. Cambie, B. R. Davis, R. C. Hayward, G. A. S. Long, and P. S. Rutledge. J. Chem. Soc. Perkin Trans. I, 190 (1972); J. MacMillan and E. R. H. Walker. J. Chem. Soc. Perkin Trans. I, 1274 (1972).
9. R. A. Appleton, P. A. Gunn, and R. McCrindle. J. Chem. Soc. C, 1148 (1970).
10. R. A. Appleton, J. C. Fairlie, R. McCrindle, and W. Parker. J. Chem. Soc. C, 1716 (1968).
11. Y. Kitahara and A. Yoshikoshi. Tetrahedron Lett. 1771 (1964); R. R. Sobti and Sukh Dev. Tetrahedron Lett. 3939 (1966).
12. J. St. Pyrek. Tetrahedron, **26**, 5029 (1970).

Phase Transformation Studies in Silver and Thallium Chromates

MAHADEVA NATARAJAN AND ETALO A. SECCO

Department of Chemistry, St. Francis Xavier University, Antigonish, Nova Scotia

Received October 1, 1973

The existence of thermal transformations in silver and thallium chromate has been confirmed by differential thermal analysis, temperature-variable X-ray diffraction, and electrical conductivity measurements. The disputed transition ~330 °C in Tl_2CrO_4 has been shown to be due to lattice distortion. The subtle difference in behavior of the pre-annealed and unsintered samples is brought out by a variety of experimental measurements. The high temperature structure of these chromates is hexagonal. The presence of small amounts of Tl in Ag_2CrO_4 affects the transition temperature, enthalpy, and the order of the transformation.

L'existence de transformations thermiques dans le chromate d'argent et de thallium a été confirmée à l'aide d'analyse thermique différentielle, de la diffraction des rayons-X (à température variable) et de mesures de conductivité électrique. On montre que la transition controversée à 330 °C dans le Tl_2CrO_4 est attribuable à une distorsion du réseau. Les légères différences de comportement d'échantillons avant le recuit et non-frittés peuvent être décelées par une variété de mesures expérimentales. La structure de ces chromates est du type hexagonale à hautes températures. La présence de petites quantités de Tl dans le Ag_2CrO_4 modifie la température de transition, l'enthalpie et l'ordre de la transformation.

[Traduit par le journal]

Can. J. Chem., **52**, 712 (1974)

Introduction

Although silver chromate and thallium chromate both crystallize in orthorhombic structure with similar cell dimensions and in the same space group (1, 2), they are not isomorphous. Both chromates display semi-conducting properties up to their melting points; while thallium chromate shows n-type conductivity throughout the temperature range (3), the n-type mode changes to p-type at higher temperatures in silver chromate (4). The electrical conductivity and thermoelectric power studies by Sladky and others (3, 4) on these chromates indicated the existence of a structural phase transformation at ~490 °C in Ag_2CrO_4 and at ~520 °C in Tl_2CrO_4. Bashilova (5) reported a second phase transformation at ~330 °C in thallium chromate from differential thermal analysis experiments. However, Sladky (3) found no evidence for this latter transformation in his conductivity studies on Tl_2CrO_4.

Secondly, the samples of Ag_2CrO_4 and Tl_2CrO_4 behave differently depending upon their thermal history. The conductivity curves of these chromates reported by Sladky do not, however, indicate the differences between annealed and freshly prepared samples. We believe that annealing the samples might have precluded the observation of the phase change at 330 °C in Tl_2CrO_4, since the high temperature phase is known to persist even after cooling the samples to room temperature (3).

In this paper, we report the preparation and phase transformation studies of silver and thallium chromates employing differential thermal analysis, high-temperature X-ray diffraction and electrical conductivity measurements. A few solid solutions of thallium chromate in silver chromate have also been examined to study the effects of small amounts of thallium on the transformation of silver chromate.

Experimental

Samples of silver chromate and thallium chromate were prepared by precipitation from their respective nitrate solutions and potassium chromate (Alfa AR grade) solution. The precipitates were washed with water, alcohol, and ether, and finally dried at ~110 °C in air. Solid solutions were prepared similarly by taking a mixture of appropriate amounts of $AgNO_3$ (Engelhard, 99.98%) and $TlNO_3$ (Alfa AR grade) solutions; no direct analysis was made to confirm the compositions of the solid solutions. All the materials used in the preparation were of high purity (>99.98%). The pure chromates were characterized by their lattice constants (Ag_2CrO_4: $a_0 = 10.059$ Å, $b_0 = 7.025$ Å, $c_0 = 5.538$ Å; Tl_2CrO_4: $a_0 = 5.921$ Å, $b_0 = 10.724$ Å, $c_0 = 7.916$ Å, all values ± 0.002 Å) which agree very well with the data in refs. 1 and 2, respectively.

Specimens for electrical conductivity measurements were made in the form of compressed polycrystalline pellets (size 2 mm thick and 13 mm in diameter).

Differential thermal analysis curves were recorded on a DuPont 900 Thermo-analyzer at a constant rate of

Can. J. Chem. Downloaded from www.nrcresearchpress.com by 210.87.254.105 on 09/05/12
For personal use only.

heating (20° per min) using Al_2O_3 as the inert reference standard.

X-Ray diffraction patterns of samples were obtained on a 'Norelco' Philips Diffractometer employing MoK_α ($\lambda = 0.7107$ Å), following the procedure already described (6). The high temperature accessory was used for elevated temperatures and the temperature of the specimen stage (holder) was measured by using platinum/platinum–rhodium thermocouples and a millivolt potentiometer (Leeds and Northrup). The lattice constants at high temperatures were calculated (7) from positions of selected reflections. For example, in Ag_2CrO_4, the reflections 301, 121, and 002 were followed as a function of temperature. The observed and calculated $\sin^2\theta$ values (Tables 1 and 2) along with their relative intensities and *hkl* values for the high temperature phases of the chromates are placed with the Depository of Unpublished Data[1].

Electrical conductivity measurements were made on the pellet specimens in a stainless steel conductivity cell whose construction has already been described (8). The cell was heated in a cylindrical furnace at 30° an hour. The sample was held between two platinum discs by a spring-loaded support. The conductivity was measured in air at 1 kHz as a function of temperature employing a General Radio 1608-A Impedance bridge. Chromel–alumel thermocouples were employed to measure temperature.

Results and Discussion

Transformation in Silver Chromate

Differential thermal analysis curves are given in Fig. 1. The structural phase transformation for Ag_2CrO_4 at 490 °C is a sharp one and occurs over a narrow temperature range. The transformation is reversible at ~467 °C, and thus is accompanied by an appreciable thermal hysteresis. The transformation enthalpy, ΔH_{tr}, estimated from the area of the heating curve is ~1650 cal/mol. The existence of such a large thermal hysteresis and the magnitude of the transition enthalpy suggests that the transformation in silver chromate at ~490 °C is likely to be a first order one (9).

The lattice constants dependence on temperature of Ag_2CrO_4 are presented in Fig. 2(*a*). While c_o shows a slight increase with temperature, there are discontinuities in the b_o and a_o values with maxima between 200 and 280 °C; above 400 °C, b_o increases rapidly. These changes in the lattice constants do not, however, result in any change of structure, but do cause an anomalous increase in conductivity of silver

[1]Complete set of data is available, at a nominal charge, from the Depository of Unpublished Data, National Science Library, National Research Council of Canada, Ottawa, Canada K1A 0S2.

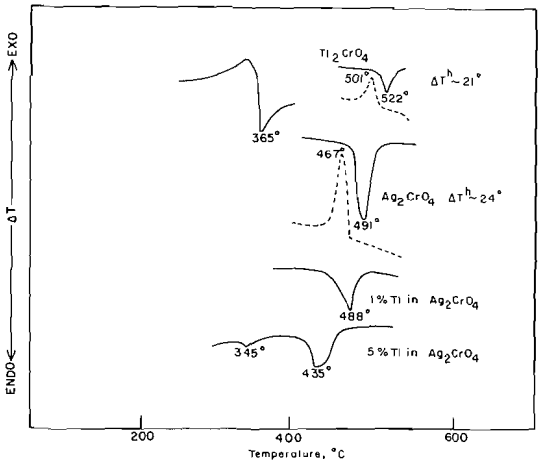

FIG. 1. Differential thermal analysis curves (dotted lines refer to cooling curves) of thallium chromate, silver chromate, and some solid solutions.

chromate. Thus, between 225 and 350 °C the lattice undergoes an appreciable amount of distortion without any change of crystal structure. The molar volume of silver chromate calculated from the lattice constants is shown as a function of temperature in Fig. 3(*a*). The molar volume increases slowly with temperature attaining a slight maximum at ~280 °C. Thereafter, the molar volume curve shows a slight dip at ~348 °C and then rises again. Just below the transformation, the molar volume shows an increase, ~430 °C. The high temperature structure appears to be hexagonal whose lattice constants, $a_o = 9.92 \pm 0.04$ Å and $c_o = 19.76 \pm 0.08$ Å at 506 °C, yield a molar volume of 63.39 cm^3 with 16 molecules per unit cell. Using the extrapolated value of the volume of the low temperature phase, we find the change in molar volume, ΔV, around 506 °C to be ~0.90 cm^3. This small increase in molar volume near the transition again suggests that the transition might be a first order one. An approximate estimate of dP/dT can be obtained for the Ag_2CrO_4 transition, by substituting the observed values of ΔH_{tr}, ΔV, and T_t in the Clapeyron–Clausius equation. The value thus obtained is 101 ± 10 bars deg^{-1}.

The logarithm of the electrical conductivity is plotted as a function of absolute temperature in Fig. 4, for two samples of silver chromate. In both the sintered and unsintered specimens the room temperature conductivity is almost the same. The unsintered sample shows a slight

Can. J. Chem. Downloaded from www.nrcresearchpress.com by 210.87.254.105 on 09/05/12
For personal use only.

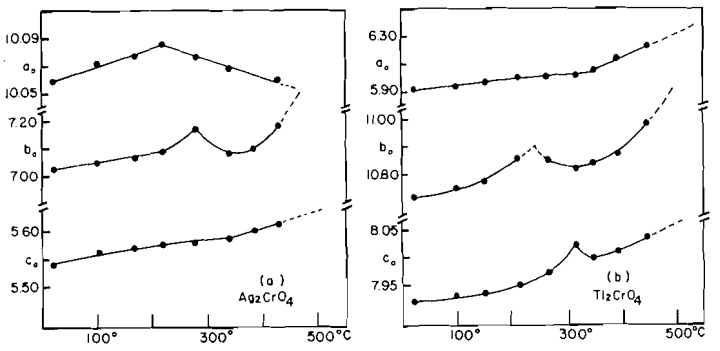

FIG. 2. Change in the orthorhombic lattice constants of (*a*) silver chromate and (*b*) thallium chromate, as a function of temperature.

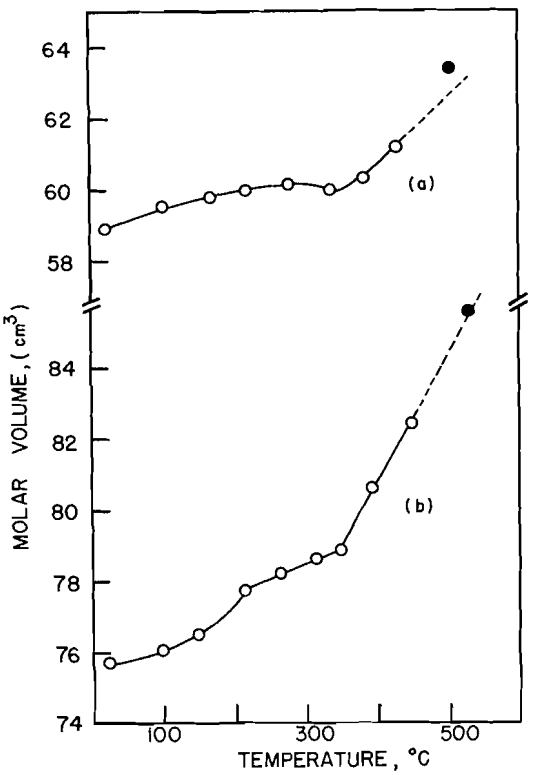

FIG. 3. Change in the molar volume in (*a*) silver chromate and (*b*) thallium chromate, as a function of temperature. The closed circles refer to the molar volumes of the high temperature structures.

increase in conductivity at ~125 °C, while in the sintered sample such an increase is noticeable at ~165 °C. In the vicinity of 225 °C, the slope of the log σ *vs.* $1/T$ plot gives a value of 0.18 eV as the energy for conduction, thus giving a value of 0.36 eV for the thermal band gap in Ag_2CrO_4. Above 225 °C there is a significant difference in the behavior of the two samples. In the unsintered sample the conductivity shows a large increase around 360 °C. This increase in conductivity may come at least in part from the lattice distortion as revealed by the anomalous trends in lattice constants up to 350 °C.

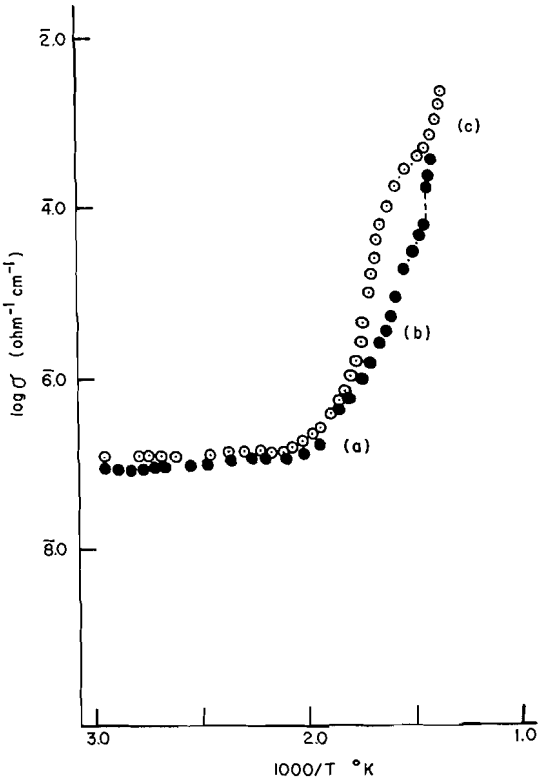

FIG. 4. Logarithm of the electrical conductivity of silver chromate for the two samples (sintered, filled circles; unsintered, open circles), as a function of reciprocal of absolute temperature. Energy values for the noted regions are (*a*) 0.18 ± 0.02 eV, (*b*) 1.1 ± 0.1 eV, (*c*) 1.9 ± 0.1 eV.

Can. J. Chem. Downloaded from www.nrcresearchpress.com by 210.87.254.105 on 09/05/12
For personal use only.

Can. J. Chem. Downloaded from www.nrcresearchpress.com by 210.87.254.105 on 09/05/12
For personal use only.

However, there is no change in the crystal structure in Ag_2CrO_4 at this temperature. It may be that silver chromate belongs to the class of superionic conductors recently described by Rice and Roth (10) where a free-ion like model has been suggested to explain the observed high conductivity in some of these solids. The high temperature structure of silver chromate where the conductivity increases very rapidly, may resemble a fluid-like state just as in the case of silver iodide. More experiments are, however, necessary before any definite conclusion can be made.

The conductivity of the sintered specimen shows almost a linear log σ *vs.* $1/T$ behavior in the low temperature region. The slope of the log σ *vs.* $1/T$ corresponds to an energy value of about 1.10 eV for the conduction. This is in excellent agreement with 1.10 eV reported by Sladky (4). This appears to be the intrinsic conductivity region in the low phase because of its excellent reproducibility in sintered samples.

The orthorhombic–hexagonal transformation is indicated by a small jump in the conductivity at ~498 °C. (In some samples the jump was preceded by an appreciable decrease in conductivity.) Above the transformation, the conductivity of both samples merges. The energy of activation for conduction, given by the slope, 1.90 eV, is in excellent agreement with known data (4). In our experiments, we observed that the conductivity jump at the transformation became less prominent in samples which were heated through the transition. This decreasing jump in conductivity suggested the possibility of the persistence of the high temperature structure in the heated specimens. Accordingly, the X-ray diffraction patterns of Ag_2CrO_4, cooled to room temperature, show clearly the reflections due to the hexagonal structure.

The decrease in conductivity prior to the transformation region, in some Ag_2CrO_4 samples might be expected since the small increase in molar volume around the transition does cause a decrease in conductivity (11). But, this decrease also vanishes as the sample is taken through the transformation in many cycles, for reasons mentioned above. These interesting observations would be missed if one started with a well sintered sample of silver chromate. The general features of the conductivity behavior of the sintered samples are in very good agreement with those reported by Sladky (4).

Transformations in Thallium Chromate

Although the room temperature structure of both Tl_2CrO_4 and Ag_2CrO_4 is orthorhombic, these two chromates are not isomorphous and they display distinct features with regard to thermal behavior and electrical conductivity. The differential thermal analysis curves for thallium chromate are shown in Fig. 1. The first endotherm at ~365 °C is most likely the transformation reported by Bashilova (5). This endothermic anomaly is not reversible and so it is possible that in their sintered samples of Tl_2CrO_4 Sladky and co-workers could not observe this transformation. The second endotherm at ~522 °C is a sharp one which is reversible at ~501 °C indicating an appreciable thermal hysteresis. This phase change resembles that in silver chromate. The transition enthalpy of ~70 cal/mol, estimated from the area of the heating curve, is much smaller than ~1650 cal/mol observed for silver chromate. The enthalpy for the change at 365 °C would be even smaller (~15 cal/mol).

The lattice constants of Tl_2CrO_4 at various temperatures, are presented in Fig. 2(*b*). The value of a_0 increases slowly up to 350 °C and then rises rapidly above this temperature. The values of b_0 and c_0 appear to go through a maximum at 225 and 315 °C, respectively. These trends in the lattice constants clearly establish anomalous changes in thallium chromate between 250 and 350 °C. We recall that the irreversible endothermic anomaly (Fig. 1) was observed within this region. The molar volume of thallium chromate also exhibits anomalous trends in the region 200–350 °C. Above 350 °C, the molar volume shows a very rapid increase and reaches a value of ~85.40 cm^3 (extrapolated) at 522 °C. The molar volume begins to show a marked increase in Tl_2CrO_4 much below the transformation temperature which is in contrast to the slight increase in Ag_2CrO_4. The high temperature structure is hexagonal whose lattice constants, $a_0 = 10.04 \pm 0.04$ Å and $c_0 = 16.28 \pm 0.08$ Å at 530 °C, yield a molar volume of 85.54 cm^3 (assuming 10 molecules per unit cell). We note the smaller molar volume change, *i.e.*, 0.14 cm^3, at the transition in thallium chromate, as compared with the change in molar volume (~0.90 cm^3) in silver chromate. These estimates of molar volume are compatible with the observed transition entropies in these two solids (0.09 cal per deg per mol for Tl_2CrO_4 and

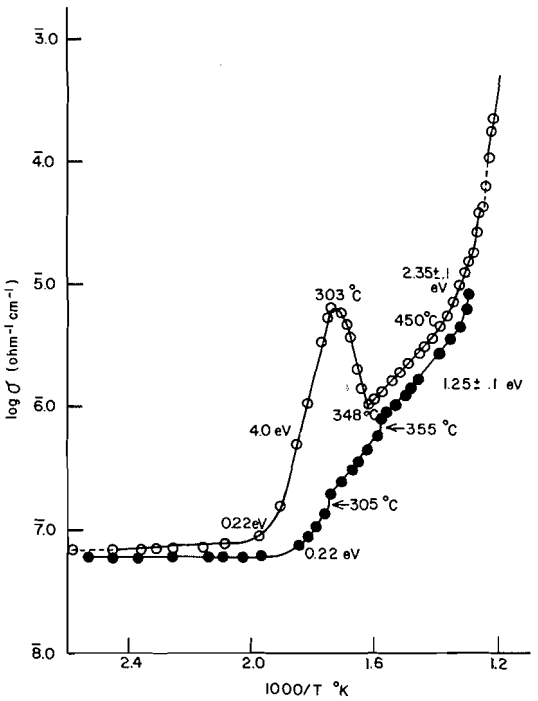

FIG. 5. Logarithm of the electrical conductivity of thallium chromate for the two samples (sintered, filled circles; unsintered, open circles), as a function of reciprocal of absolute temperature.

2.20 cal per deg per mol for Ag_2CrO_4). Using the observed values of ΔH_{tr}, ΔV, and T for the transition at ~520 °C in Tl_2CrO_4, the Clapeyron–Clausius equation yields a value of 26 ± 5 bars deg^{-1} for dP/dT.

Electrical conductivity measurements on sintered and fresh samples of thallium chromate are shown in Fig. 5. The room temperature conductivity of both samples is about the same. The unsintered sample shows a sudden increase in conductivity at ~225 °C. The activation energy for conduction in this region is 0.22 eV. This will give a thermal energy gap ε_g as 0.44 eV for thallium chromate. This value is ~25% higher than that in silver chromate ($\varepsilon_g \simeq 0.36$ eV). The conductivity rises sharply with an activation energy of 4.0 eV for conduction. This sharp increase in conductivity between 225–303 °C, results from the anomalous thermal behavior of Tl_2CrO_4. Above this temperature the conductivity starts to decrease to a minimum at ~348 °C. The anomalous conductivity behavior takes place over a temperature region where the lattice dimensions show irregular trends. These observations indicate clearly that in thallium chromate a change in crystal structure occurs between 300 and 350 °C. At 450 °C, there is a break in the conductivity curve. The activation energies 1.25 ± 0.10 eV (below the knee) and 2.35 ± 0.10 eV (above the knee) are in very good agreement with Sladký's (3) values. Below the transformation the conductivity rises sharply indicating a rapid movement of ions and other conducting species in the lattice. It is possible that thermally produced vacancies might start conducting, thus giving rise to an overall increase in the conductivity. It is pertinent to mention here that in both thallium and silver chromates there is appreciable ionic conduction even at low temperatures (~200 °C). The reversible phase change at 522 °C is indicated by a small jump in conductivity around 530 °C. Above 530 °C, the conductivity increases sharply. Again, the free-ion like model of Rice and Roth (10) might be applicable to thallium chromate as well. In our view, both the chromates may well belong to the class of superionic conductors where a fluid-like state has been postulated to account for the observed high conductivity in many of these solids.

The conductivity behavior of the sintered sample of Tl_2CrO_4 does not show the above-mentioned anomalous features in the temperature interval 225–350 °C. This is in line with the observation that the change at this interval is not a reversible one. But one can still see a slight deviation in the conductivity curve in samples sintered for a small interval of time. The sample shown in Fig. 5 was kept at about 580 °C for only 2 h and then cooled slowly to room temperature. However, in samples sintered for longer time intervals, the change will be hardly noticeable. Above 350 °C, the sintered and fresh samples show almost the same behavior. The knee at 450 °C suggests that the samples reported herein may be of higher purity than those employed by previous workers. The intrinsic conductivity region appears to be above 450 °C.

Solid Solutions of the Chromates

Solid solutions have been prepared up to ~40% thallium chromate in silver chromate. In Fig. 1, the differential thermal analysis curves for ~1% and 5% thallium chromate show that the transformation in silver chromate is modified by even small amounts of thallium. The transition temperature is lowered and the endothermic effect is broad over an extended temperature interval with increasing amounts of thallium. With 5% thallium, another small endotherm

Can. J. Chem. Downloaded from www.nrcresearchpress.com by 210.87.254.105 on 09/05/12
For personal use only.

appears at ~345 °C and with higher amounts of thallium both endotherms occur at still lower temperatures. The lattice constants of 5% thallium chromate give a molar volume of 59.92 cm^3 and this can be shown to be equal to the molar ratio additivity of the two individual molar volumes of the pure chromates. This suggests that the solid solutions formed up to ~5% thallium are substitutional ones. While the transformation in pure silver chromate is a first order change, in solid solutions with small amounts of thallium the order may not be the same. This was immediately suggested by the broad endotherms and the shape of the differential curves.

NOTE added in proof: The low temperature activation energy values, *viz.* 0.18 and 0.22 eV for Ag_2CrO_4 and Tl_2CrO_4, respectively, were erroneously stated as related to ε_g values. A low activation energy signifies an impurity-controlled conduction and not intrinsic conduction. The intrinsic region is identified with energy values of 1.10 and 1.25 eV for these compounds.

The authors are grateful to the National Research Council of Canada for financial support during this investigation and to Professor W. T. Foley for helpful discussions.

1. M. L. HACKERT and R. A. JACOBSON. J. Solid State Chem. **3**, 364 (1971).
2. R. L. CARTER and T. N. MARGULIS. J. Solid State Chem. **5**, 75 (1972).
3. J. SLADKÝ. Czech. J. Phys. B**19**, 123 (1969).
4. (*a*) J. SLADKÝ and F. KOSEK. Collection Czecholov. Chem. Commun. **31**, 3817 (1966). (*b*) J. SLADKÝ and Z. CIMPL. Ceskoslov. cas. Fys. **15**, 534 (1965).
5. N. J. BASHILOVA. J. Inorg. Chem. U.S.S.R. **9**, 57 (1964).
6. P. RAMAMURTHY and E. A. SECCO. Can. J. Chem. **47**, 1045 (1969).
7. B. D. CULLITY. Elements of X-ray diffraction. Addison-Wesley, U.S.A. 1959.
8. P. N. MEHROTRA. Ph.D. Thesis. Indian Institute of Technology, Kanpur, India. 1968.
9. C. N. R. RAO and K. J. RAO. Progress in solid state chemistry. Vol. 4. *Edited by* H. Reiss, Pergamon Press. 1967.
10. M. J. RICE and W. ROTH. J. Solid State Chem. **4**, 294 (1972).
11. M. NATARAJAN, B. PRAKASH, and C. N. R. RAO. J. Chem. Soc. (A), 2291 (1971).

Can. J. Chem. Downloaded from www.nrcresearchpress.com by 210.87.254.105 on 09/05/12
For personal use only.

Some Thermodynamic Properties of the Dimethylsulfoxide–Water and Propylene Carbonate–Water Systems at 25 °C

S. Y. Lam and R. L. Benoit

Département de chimie, Université de Montréal, Montréal 101, Québec

Received August 23, 1973

Molar excess free energies of the systems dimethylsulfoxide–water and propylene carbonate – water have been calculated from static vapor pressure measurements at 25 °C. Enthalpies of mixing at low water concentrations have also been determined. Possible association interactions in these systems are discussed.

Les énergies libres molaires d'excès des systèmes diméthylsulfoxyde–eau et carbonate de propylène – eau ont été calculées à partir de mesures statiques de pressions de vapeur à 25 °C. Les enthalpies de mélange ont aussi été déterminées pour de faibles concentrations d'eau. On examine les possibilités d'interactions par association dans ces systèmes.

Can. J. Chem., **52**, 718 (1974)

Can. J. Chem. Downloaded from www.nrcresearchpress.com by 210.87.254.5 on 09/05/12
For personal use only.

Introduction

This research is related to our study of hydration of ions at low water concentrations in some dipolar aprotic solvents (1). The determination of the thermodynamic properties of the binary systems water–dimethylsulfoxide (DMSO) and water – propylene carbonate (PC) is mandatory for comparing ionic hydration in these media as well as being a step in understanding the nature of the interactions between the components. As no vapor pressure data could be found for the PC–H_2O system and those for the DMSO–H_2O system directly determined (2) are values at 70 °C, vapor pressure measurements have been carried out at 25 °C over the whole range of compositions. Heats of mixing water with both solvents have also been measured at 25 °C and low water concentrations.

Experimental

Chemicals

The water used was conductivity water. Spectroscopic grade dimethylsulfoxide from Fisher was used without further purification. Propylene carbonate from Eastman Kodak was doubly distilled at a temperature below 100 °C and pressure under 10 mm Hg. The middle portion of the distillate, about 80%, was collected. Water contents in DMSO and PC determined by Karl Fisher titrations were 0.069% and 0.0059%, respectively.

Vapor Pressure

Vapor pressures were measured with a Texas Instruments quartz spiral gauge calibrated into millibars. To avoid condensation of vapor, the gauge was heated at 58 °C, and the tubing leading to it was kept at 40 °C with heating tapes. The bath temperature was calibrated by vapor pressure determinations on pure water against a new standard 23.78 mm Hg at 25.00 °C given by Stimson (3).

Binary mixtures were prepared by weighing known quantities of the components. Degassing was performed by repeated freezing and evacuation. Actual measurements were taken after equilibrium was attained. Compositions of the liquid were checked by reweighing; whenever correction was applicable, the loss in weight was assumed to be that of the more volatile component

Calorimetry

The apparatus and procedure for measuring heats have been given elsewhere (4).

Results and Discussion

The experimental total pressures for DMSO(1)–H_2O(2) and for the partially miscible binary PC(1)–H_2O(2) are given in Table 1 and Fig. 1. The values are believed to be accurate to within 0.01–0.04 mm Hg for pressures higher than 5 mm, 0.002 mm for pure propylene carbonate, and 0.002–0.01 mm for other pressures.

The vapor pressure for pure DMSO, 0.599 mm Hg, was obtained by measuring the pressures of wet DMSO with concentrations of water below about 0.1 *M*, as determined by Karl Fisher method, and extrapolating the results to zero water concentration. This value agrees well with that of Douglas, 0.600 mm Hg (5). The vapor pressure for pure propylene carbonate was obtained in the same manner. The miscibility gap for PC(1)–H_2O(2) was found to extend from $x_2 = 0.318$ to 0.960 as determined experimentally by mixing known masses of PC and water at 25 °C. These results agree with those quoted by Catherall and Williamson (6). The prevailing pressure over the two coexisting phases was found to be 23.35 mm Hg. Although DMSO and PC are dipolar aprotic solvents, both binary solvent–water systems exhibit contrasting non-

Can. J. Chem. Downloaded from www.nrcresearchpress.com by 210.87.254.5 on 09/05/12
For personal use only.

TABLE 1. Total vapor pressures of DMSO–H_2O and PC–H_2O Systems at 25 °C

DMSO(1)–H_2O(2)		PC(1)–H_2O(2)	
x_2	P(mm Hg)	x_2	P(mm Hg)
0.000	0.599	0.000	0.053
0.057	1.012	0.007	1.64
0.101	1.277	0.016	3.39
0.126	1.433	0.026	5.40
0.201	2.02	0.037	7.27
0.297	2.92	0.056	10.02
0.402	4.26	0.082	12.98
0.498	5.97	0.120	16.46
0.548	7.10	0.160	19.10
0.597	8.52	0.215	21.30
0.650	10.30	0.258	22.52
0.699	11.98	0.281	23.00
0.747	14.01	0.303	23.23
0.798	16.40	0.318 }	23.35
0.848	18.65	0.960 }	
0.898	20.73	0.979	23.50
0.950	22.43	1.000	23.78
1.000	23.78		

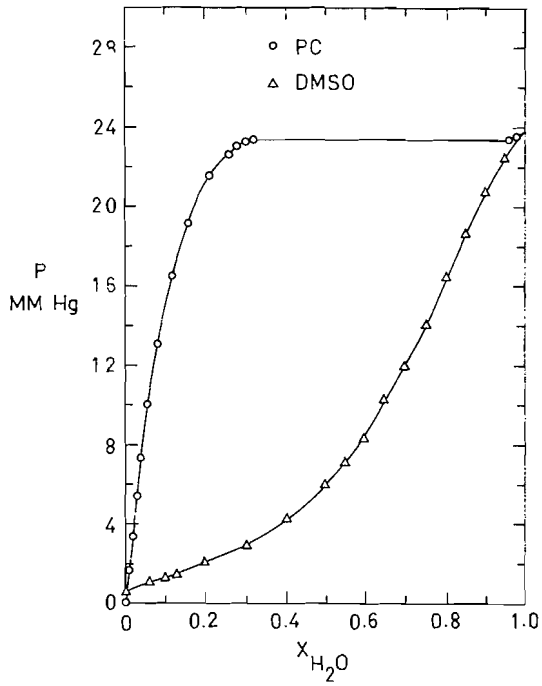

FIG. 1. Total vapor pressures of the systems DMSO–H_2O and PC–H_2O at 25 °C.

ideal behavior: DMSO-H_2O gives negative deviation and PC–H_2O gives positive deviation from Raoult's law.

Different methods (7–9) have been devised to resolve total pressures into partial pressures on the basis of the Gibbs–Duhem equation and on the assumption that the gaseous mixtures were ideal. The following procedure was adopted for our calculations. Partial pressures of water were evaluated by subtracting the Raoult's law contributions of PC and DMSO from the total pressures. These water pressures were used to calculate better values of partial pressures of other components by graphical integration of the Gibbs–Duhem equation

$$\ln P_1 = \ln P_1^{\,0} - \int_{x_2=0}^{x_2} \frac{x_2}{x_1}\, d \ln P_2$$

For PC–H_2O the first integration gave final values of pressures; for DMSO–H_2O, the second sufficed to yield converging results. A model calculation for $x_2 = 0.05$ for PC–H_2O is given below:

$$\frac{x_2}{0.05}\left|\frac{P}{9.15}\right|\frac{x_1P_1^{\,0}}{0.050}\left|\frac{P_2(\text{approx})}{9.10}\right|\frac{-\int_{x_2=0}^{x_2=0.05}\frac{x_2}{x_1}\,d\ln P_2}{-0.0449}\left|\frac{\ln P_1}{-2.982}\right|\frac{P_1(\text{final})}{0.051}\left|\frac{P_2(\text{final})}{9.10}\right|$$

Table 2 shows the partial pressures and the free energy functions for these systems. The excess Gibbs free energies, accurate to within 2 calories, are plotted in Fig. 2. Activity coefficients as calculated by means of the usual expression are > 1 for PC–H_2O and < 1 for DMSO–H_2O. The assumption of ideal gas behavior was examined by using Schiebel nomograph (10), which amounts to evaluating an activity coefficient correction factor Z that corrects the calculated activity coefficient for the departure from the ideal gas law. From the critical data available either in the literature or by estimation from the boiling points and the parachors, the correction factors obtained from the nomograph were between 1 to 1.002 for water, 0.997 to 1 for DMSO, and 0.996 to 1 for PC, and were therefore neglected.

The excess Gibbs free energies of mixing were fitted into the equation

$$[1]\quad \Delta G^E = 2.303\, RT\, x_1x_2\, [B + C(2x_1 - 1) + D(2x_1 - 1)^2]$$

with parameters B, C, and D, by employing a procedure given by Redlich and Kister (11). It was found that D values were very small and the terms associated with D could be absorbed into the preceding terms without loss of accuracy in representing the free energies. For that short range of excess quantities of mixing PC(1) and $H_2O(2)$ with small x_1 the expression used was:

$$[2] \qquad \Delta G^E = 2.303RT(Bx_1 + Cx_1^2)$$

The parameters chosen for these systems and the standard deviations of the calculated values from the experimental values are as follows

System	Parameter values B	C	σ
DMSO(1)–H_2O(2)	−0.86	0.38	2 cal/mol
PC(1)–H_2O(2) $x_1 > 0.682$	1.03	−0.54	1 cal/mol
$x_1 < 0.04$	1.86	−0.87	1 cal/mol
Eq. 2			

For the DMSO–H_2O system, the excess free energies ΔG^E are negative. Using Boissonnas' method for partial pressures, Kenttämaa and Lindberg (2) have calculated ΔG^E values at 25 °C on the basis of nine total pressure measurements at 70 °C ($0.09 \leqslant x_2 \leqslant 0.92$) and of heats of mixing at 70 and 25 °C (12). Our ΔG^E results are somewhat less negative and by some 11 cal/mol for $x_2 \leqslant 0.50$.

The heat of mixing per mole of added water with DMSO as deduced from eight measurements, at increasing water concentrations $0.003 < x_2 < 0.10$, was found to be -1.29 ± 0.01 kcal/mol and to be independent of the concentration, as already noted by some authors (12, 13) for $x_2 > 0.1$, but not by others (14, 15).

The ΔG^E and ΔH values suggest strong interactions between DMSO and water, in line with the known proton acceptor properties of DMSO. Structural interpretations of ΔS^E values have been advanced (12). For the PC–H_2O system, the partial pressures and the activity coefficients level off when concentrations approach the miscibility gap. The excess free energies are positive. The average heat of mixing $\Delta\bar{H}_W^\infty$ for three experiments at water concentrations $0.002 < x_2 < 0.012$ is $+1.93 \pm 0.02$ kcal per mol of added water. On the basis of $\Delta\bar{H}_W^\infty$, (kcal/mol), PC and DMSO can be compared with other dipolar aprotic solvents: nitromethane (2.4) < acetonitrile ~ PC (1.9) < sulfolane (1.6) < acetone (1.05) < DMSO (−1.29) (16). This reflects a "basicity" order among these solvents and suggests that high levels of acidity could be obtained in PC.

It is interesting to try to account for deviations of thermodynamic properties from ideality in terms of chemical equilibria (17). Recently the results of calorimetric studies of the systems $CHCl_3$ (A) + DMSO (B) (18) and $CHCl_3$ (A) + $(CH_3)_3N$(B) (17) were thus successfully interpreted in terms of species A, B, AB, and A_2B in the first case and A, B, and AB in the second one. However, when one considers binary systems

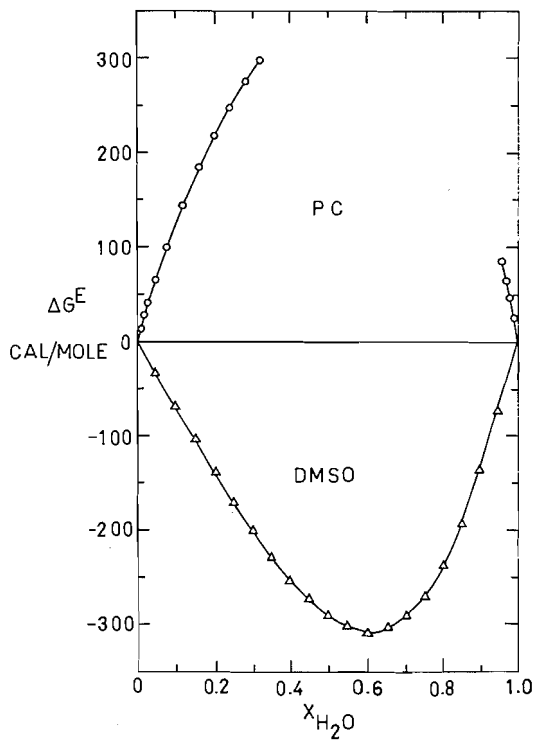

FIG. 2. Excess free energies of mixing for the systems DMSO–H_2O and PC–H_2O at 25 °C.

Can. J. Chem. Downloaded from www.nrcresearchpress.com by 210.87.254.5 on 09/05/12
For personal use only.

TABLE 2. Partial pressures, activity coefficients, and excess Gibbs free energies of the DMSO–H_2O and PC–H_2O systems at 25 °C

x_2	P(mm Hg)	P_1(mm Hg)	P_2(mm Hg)	γ_1	γ_2	ΔG^E(cal/mol)
DMSO(1)–H_2O(2)						
0.00	0.60	0.599	0.00	1.000	—	0
0.05	0.96	0.567	0.39	0.996	0.328	−36
0.10	1.27	0.538	0.73	0.998	0.307	−71
0.15	1.61	0.508	1.10	0.998	0.308	−105
0.20	2.02	0.472	1.55	0.985	0.326	−140
0.25	2.46	0.437	2.02	0.973	0.340	−172
0.30	2.95	0.400	2.55	0.954	0.357	−203
0.35	3.52	0.361	3.16	0.927	0.379	−230
0.40	4.23	0.317	3.91	0.882	0.411	−255
0.45	5.02	0.275	4.75	0.835	0.444	−275
0.50	6.00	0.231	5.77	0.771	0.485	−291
0.55	7.14	0.187	6.95	0.694	0.531	−303
0.60	8.63	0.142	8.49	0.594	0.595	−309
0.65	10.30	0.105	10.20	0.500	0.660	−304
0.70	12.00	0.0758	11.92	0.422	0.716	−292
0.75	14.18	0.0484	14.13	0.323	0.792	−272
0.80	16.54	0.0283	16.51	0.236	0.868	−238
0.85	18.78	0.0156	18.76	0.173	0.928	−194
0.90	20.82	0.0076	20.81	0.127	0.972	−137
0.95	22.43	0.0027	22.43	0.092	0.993	−75
1.00	23.78	0.0000	23.78	—	1.000	0
PC(1)–H_2O(2)						
0.00	0.053	0.0530*	0.00	1.000	—	0
0.01	2.23	0.0524	2.18	1.000	9.17	13
0.02	4.26	0.0520	4.21	1.000	8.85	26
0.03	6.07	0.0516	6.02	1.004	8.44	39
0.05	9.15	0.0510	9.10	1.013	7.65	64
0.08	12.76	0.0495	12.71	1.015	6.68	98
0.12	16.46	0.0484	16.41	1.038	5.75	143
0.16	19.10	0.0472	19.05	1.060	5.01	184
0.20	20.77	0.0463	20.72	1.092	4.36	216
0.24	22.05	0.0456	22.00	1.132	3.86	248
0.28	22.98	0.0449	22.94	1.177	3.45	275
0.318	23.35	0.0446	23.31	1.234	3.08	297
0.96	23.35	0.0446	23.31	21.05	1.021	84
0.97	23.45	0.0388	23.41	24.4	1.015	64
0.98	23.54	0.0344	23.51	32.5	1.009	46
0.99	23.65	0.0223	23.63	42	1.004	25
1.00	23.78	0.000	23.78	—	1.000	0

*A value 0.0530 mm Hg for propylene carbonate was used.

with water as a component, it is easier to restrict oneself to the water-poor mixtures because of water self-association. Thus, with PC–H_2O system, assuming that the non-linearity of our water partial pressure data, above 0.1 m water concentration, is due to water self-association, from the water monomer concentration given by the limiting slope of the water vapor pressure *vs.* water concentration, a water dimerization constant of 0.20 ± 0.03 is calculated below a 0.7 *M* ($x_2 \leqslant 0.06$) water concentration; above this concentration the dimerization constant increases (0.36 for $x_2 = 0.1$) suggesting more complex associations. Cogley *et al.* (19) interpreted their n.m.r. and infrared spectroscopic studies in terms of water monomer–dimer equilibria at moderately low water concentrations, with a dimer formation constant 0.15 ± 0.03 l per mol at 25 °C. The agreement is surprisingly good.

For the DMSO–H_2O system,[1] deviations from

[1]Three recent papers (20–22) quote numerous references dealing with both the nature of these widely studied mixtures and of DMSO itself.

Can. J. Chem. Downloaded from www.nrcresearchpress.com by 210.87.254.5 on 09/05/12
For personal use only.

ideality of many properties have been attributed by some authors to association interactions. Our vapor pressure data show that the water partial pressures of aqueous DMSO vary linearly with the water concentration up to 7 M ($x_2 \sim 0.35$), in sharp contrast to the behavior of aqueous PC solutions. The linear dependence of the water partial pressure and the constancy of the heat of mixing of water both with the water concentration, strongly suggest the presence of only one water species, in this concentration range, likely a monomer, either of the 1 : 1 or 1 : 2 (water : DMSO) type. The observed near constancy of the water proton chemical shift with the water concentration also implies that water hydrogen-bonding to DMSO dominates the interaction, rather than hydrogen bonded self-association.

The authors wish to express their gratitude to the National Research Council of Canada for a grant.

1. R. L. BENOIT and S. Y. LAM. 56th Canadian Chemical Conference, Montreal, June 4–6, 1973. Paper 319.
2. J. KENTTÄMAA and J. J. LINDBERG. Suom. Kemistil. B33, 98 (1960).
3. H. F. STIMSON. J. Res. Natl. Bur. Stand. 73A, 493 (1969).
4. R. L. BENOIT, M. RINFRET, and R. DOMAIN. Inorg. Chem. **11**, 2603 (1972).
5. T. B. DOUGLAS. J. Am. Chem. Soc. **70**, 2001 (1948).
6. N. F. CATHERALL and A. G. WILLIAMSON. J. Chem. Eng. Data, **16**, 335 (1971).
7. R. T. LATTEY. J. Chem. Soc. **91–2**, 1959 (1907).
8. CH.-G. BOISSONNAS. Helv. Chim. Acta, **22**, 541 (1939).
9. F. KOHLER. Monatsh. Chem. **82**, 913 (1951).
10. E. G. SCHIEBEL. Ind. Eng. Chem. **41**, 1076 (1949).
11. O. REDLICH and A. KISTER. Ind. Eng. Chem. **40**, 345 (1948).
12. J. KENTTÄMAA and J. J. LINDBERG. Suom. Kemistil. B33, 32 (1960).
13. W. DRINKARD and D. KIVELSON. J. Phys. Chem. **62**, 1494 (1958).
14. J. M. G. COWIE and P. M. TOPOROWSKI. Can. J. Chem. **39**, 2240 (1961).
15. H. L. CLEVER and S. P. PIGOTT. J. Chem. Thermodyn. **3**, 221 (1971).
16. R. L. BENOIT and G. CHOUX. Can. J. Chem. **46**, 3215 (1968).
17. L. G. HEPLER and D. V. FENBY. J. Chem. Thermodyn. **5**, 471 (1973).
18. R. PHILIPPE and P. CLÉCHET. J. Chem. Thermodyn. **5**, 430 (1973).
19. D. R. COGLEY, M. FALK, J. N. BUTLER, and E. GRUNDWALD. J. Phys. Chem. **76**, 855 (1972).
20. R. FUCHS and C. P. HAGAN. J. Phys. Chem. **77**, 1797 (1973).
21. T. K. COOPER, D. C. WALKER, H. A. GILLIS, and N. V. KLASSEN. Can. J. Chem. **51**, 2195 (1973).
22. J. B. KINSINGER, M. T. TANNAHILL, M. S. GREENBERG, and A. I. POPOV. J. Phys. Chem. **77**, 2444 (1973).

Can. J. Chem. Downloaded from www.nrcresearchpress.com by 210.87.254.5 on 09/05/12
For personal use only.

Crystal and Molecular Structure of 2-Deacylusnic Acid

ALISTAIR L. MACDONALD, STEVEN J. RETTIG, AND JAMES TROTTER
Department of Chemistry, University of British Columbia, Vancouver 8, British Columbia

Received April 30, 1973[1]

Crystals of the title compound are monoclinic $a = 9.801(2)$ $b = 9.120(1)$ $c = 8.026(2)$ Å, $\beta = 107.45(1)°$, $Z = 2$, space group $P2_1$. The structure was determined by direct methods, and refined by electron-density and full-matrix least-squares procedures to $R = 0.0325$ for 1363 observed reflections. An attempt to determine the absolute configuration by use of the anomalous scattering of oxygen and carbon atoms has been made. The most important structural feature is delocalization in the cyclohexadiene ring. There are two intramolecular O—H...O hydrogen bonds, O...O distances 2.532(3) and 2.712(2) Å. The crystal structure consists of molecules linked by intermolecular O—H...O hydrogen bonds, O...O = 2.625(2) Å, to form continuous spirals about the 2_1 axes.

Le composé cite dans le titre cristallise dans le système monoclinique, $a = 9.801(2)$, $b = 9.120(1)$, $c = 8.026(2)$ Å, $\beta = 107.45(1)°$, $Z = 2$, groupe spatial $P2_1$. La structure a été déterminée à l'aide de la procédure directe et a été affinee par un calcul de densité électronique et par la méthode de moindres carrés (matrice complète) jusqu'à un indice $R = 0.0325$ pour 1363 réflexions observées. On a essayé de déduire la configuration absolue à partir de la diffraction anormale des atomes d'oxygène et de carbone. La caractéristique principale de la structure concerne une délocalisation en dedans du cycle du cyclohexadiène. Il existe deux liaisons hydrogène intramoléculaires O—H...O, dont les distances O...O sont égales à 2.532(3) et 2.712(2) Å. Le cristal se compose des molécules enchaînées par des liaisons hydrogène intermoléculaires O—H...O, dont la distance O...O est égale à 2.625 Å, pour former des spirales continues autour des axes 2_1.

Can. J. Chem., **52**, 723 (1974)

Introduction

2-Deacylusnic acid has been obtained as a product of the biodegradation of usnic acid (**1**) by the fungi *Mortierella Isabellina* (1, 2). On the

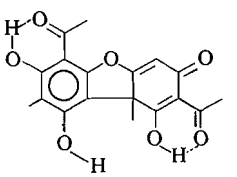

1

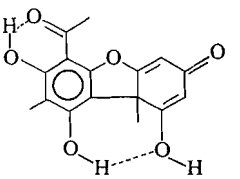

2

basis of spectral and analytical data, the structure (**2**) has been proposed for this compound (1). The object of this study was to determine the molecular structure of 2-deacylusnic acid, to aid in the understanding of the mechanism of the biodegradation of usnic acid.

Experimental

Crystals of 2-deacylusnic acid are thin pale-yellow plates. The crystals used for the data collection were mounted with b parallel to the goniostat axis and had dimensions of *ca.* 0.3 × 0.3 × 0.1 mm. Unit-cell and space group data were obtained from film and diffractometer measurements. The unit-cell parameters were refined by a least-squares treatment of $\sin^2\theta$ values for 30 reflections measured on a diffractometer with CuKα radiation. Crystal data are:

$C_{16}H_{14}O_6$ f.w. = 302.3

Monoclinic, $a = 9.801(2)$, $b = 9.120(1)$, $c = 8.026(2)$ Å, $\beta = 107.45(1)°$, $V = 684.4(2)$ Å^3, $Z = 2$, $\rho_{calc} = 1.466$ g cm^{-3}, $F(000) = 316$ (20 °C, CuKα, $\lambda = 1.5418$ Å, $\mu = 10$ cm^{-1}). Absent reflections: $0k0$, $k \neq 2n$, space group $P2_1(C_2^2$, No. 4.)

Intensities were measured on a Datex-automated General Electric XRD 6 diffractometer, with a scintillation counter, CuKα radiation (nickel filter and pulse height analyzer). Two crystals were used in the data collection due to instrument malfunction and possible decomposition of the first sample. The hkl reflections were measured using the first crystal, while the second crystal was used primarily to measure $hk\bar{l}$ reflections, with some overlap to provide a scale factor between the two sets of data. For the first crystal a θ–2θ scan at 1° min^{-1}, with 40 s background counts was used and for the second crystal the scan speed was increased to 2° min^{-1} and the backgrounds counted for 20 s. The scan range was (1.80 + 0.86 tan θ) degrees in 2θ for both crystals. Independent data were measured to $2\theta = 146°$ (minimum interplanar spacing 0.81 Å). A check reflection was monitored every 30 reflections throughout the data collection. The intensity of the check reflection dropped off by 15% of its starting value for the first crystal and for the second crystal it remained constant to within ±5% of the initial value. Lorentz and polarization corrections were applied, and structure amplitudes were derived. No absorption correction was made in view of the relatively small value of μ. Of 1502 independent reflections mea-

[1]Revision received October 26, 1973.

Can. J. Chem. Downloaded from www.nrcresearchpress.com by 210.87.254.105 on 09/05/12
For personal use only.

TABLE 1. Basic starting set of reflections for 2-deacylusnic acid

h	k	l	$\|E\|$	Phase (mc)
1	0	2	3.46	0
3	0	3	2.12	0 origin determining
8	1	$\bar{2}$	2.23	0
1	0	4	3.46	500 manual indication
8	1	$\bar{5}$	2.81	a
4	6	$\bar{2}$	2.44	b
8	4	$\bar{3}$	3.12	250 enantiomorph

TABLE 2. Results for the six starting sets in the phase determination procedure

Set	a(mc)	b(mc)	t	α	Q	R_K
1	0	200	0.624	195	0.355	0.192
2	0	400	0.736	206	0.287	0.300
3	0	600*	0.749	207	0.280	0.319
4	500	200	0.728	194	0.299	0.318
5	500	400	0.693	188	0.331	0.291
6	500	600*	0.683	194	0.334	0.282

*At input stage only; the final phases were normalized to lie in the range $-\pi < \phi(h) \leq \pi$.

sured 67 had intensities less than $3\sigma(I)$ above background, where $\sigma^2(I) = S + B + (0.03S)^2$ with S = scan count and B = background count. These reflections were classified as unobserved.

Structure Analysis

The space group was assumed to be $P2_1$ from absent reflections and number of molecules in the unit-cell ($Z = 2$). The structure was solved by direct methods, 300 reflections with normalized structure factor $|E| \geq 1.23$ being used in the symbolic addition procedure for non-centrosymmetric crystals (3). The phases of the 102, 303, and 812 reflections were fixed to define the origin. During a manual expansion carried out among those 80 reflections with highest $|E|$ values, symbol phases were assigned to the $81\bar{5}$, $46\bar{2}$, and $84\bar{3}$ reflections and the phase of the 104 reflection was strongly indicated to be 500 mc. These seven reflections comprise the basic starting set listed in Table 1.

The manual determination gave indications for a (0 or 500 mc) and $84\bar{3}$ ($\pm$250 mc). The enantiomorph was fixed by allowing $84\bar{3}$ to have only positive phases (*i.e.* using only +250 mc as a starting value for $84\bar{3}$). The basic set of reflections was split into six starting sets by allowing a either of its two values while b was given starting values of 200, 400, and 600 mc (see Table 2). The six sets were used as input to a computer program which determines phases using the tangent formula (4–7). The values of overall t, overall α, Q, and R_K(4–7) on the final cycle for each of the sets are given in Table 2. An E-map from set 1 gave the positions of all non-hydrogen atoms (22 atoms among the 23 highest peaks). Earlier attempts to obtain a solution using the 167 reflections with $|E| \geq 1.50$ failed to produce E-maps which could be easily interpreted, the final statistics after tangent formula refinement being very similar for many of the sets, and E-maps computed for several different phase combinations yielding only partial structures which could not be further expanded.

Two cycles of full-matrix least-squares refinement of the positional and isotropic thermal parameters of the carbon and oxygen atoms gave an R value of 0.156. The y coordinate of O(3) was fixed to define the origin. This was followed by two cycles of anisotropic refinement of the non-hydrogen atoms which reduced R to 0.106. A difference map at this stage revealed possible positions for some, but not all of the hydrogen atoms. One more cycle of refinement reduced R to 0.062 and all hydrogen positions were revealed in the subsequent difference map. All parameters, including hydrogen coordinates and temperature factors, were refined for one cycle resulting in an R value of 0.037.

Since the absolute configuration of this compound is of interest, an attempt to determine the absolute configuration has been made based on the anomalous scattering from oxygen ($\Delta f' = 0.05$, $\Delta f'' = 0.032$) and carbon atoms ($\Delta f' = 0.02$, $\Delta f'' = 0.010$) (see *e.g.* refs. 8 and 9). The problem in this case was twofold: first, to determine whether the second crystal was mounted about $+b$ or $-b$ (taking the first mounting as $+b$), and second, to determine the correct absolute configuration. To this end four separate refinements were carried out; the two enantiomorphs combined with each of the possible orientations of the second crystal. The final weighted R values for the four refinements are given in Table 3 and indicate that the second crystal was mounted about $+b$. R values calculated using reflections with $[F_{calc}(hkl) - F_{calc}(hk\bar{l})]/[F_{obs}(hkl)] > 0.01$ were in the same order as in Table 3 but showed larger differences. With the assumption that both crystals were mounted the same way, Hamilton's test (10) indicates that the hypothesis that the opposite enantiomorph is the correct one may be rejected at the 0.05 significance level. We may conclude that there is a 95% probability that the chosen enantiomorph is the correct absolute configuration, assuming the data to be free of systematic error. The final R value was 0.0325 for 1363 observed reflections.

Can. J. Chem. Downloaded from www.nrcresearchpress.com by 210.87.254.105 on 09/05/12
For personal use only.

TABLE 3. Weighted R factors

Enantiomorph*	Mounting axis of second crystal	Weighted R (%)
1	$+b$	4.1488
2	$+b$	4.1574
1	$-b$	4.1639
2	$-b$	4.1533

*Enantiomorph 1 is represented by the coordinates of Table 4 referred to a right-handed axial set.

The least-squares refinement was based on the minimization of $\Sigma w(F_o - F_c)^2$. The scattering factors of ref. 11 were used for the carbon and oxygen atoms, and those of ref. 12 for the hydrogen atoms. The anomalous scattering terms of ref. 9 have been used for carbon and oxygen. The anisotropic temperature factors employed in the refinement are U_{ij} in the expression:

$$f = f^\circ \exp [-2\pi^2(U_{11}h^2a^{*2} + U_{22}k^2b^{*2} + U_{33}l^2c^{*2} + 2U_{12}hka^*b^* + 2U_{13}hla^*c^* + 2U_{23}klb^*c^*)]$$

where f° is the tabulated scattering factor and f is that corrected for thermal motion. The weighting scheme: $\sqrt{w} = 1.0$ if $|F_o|$ 3.0, $\sqrt{w} = 3.0/|F_o|$ for $|F_o|$ 3.0, and $\sqrt{w} = 0.35$ for the unobserved reflections, gave satisfactory consistency of $w(F_o - F_c)^2$ over ranges of $|F_o|$, and was employed in the final stages of refinement. Five reflections (002, 011, 100, 101, and 102) were given zero weight in the final stages of refinement, due to suspected errors arising from extinction and counter overload.

On the final cycle of refinement, no parameter shift was greater than 0.25σ for carbon and oxygen atoms and 0.65σ for hydrogen atoms. The final positional and thermal parameters are given in Tables 4 and 5, respectively. Measured and calculated structure factors have been placed in the Depository of Unpublished Data.[2]

Thermal Motion and Correction of Molecular Geometry

The thermal motion ellipsoids for the carbon and oxygen atoms are shown in Fig. 1. The thermal motion has been analyzed in terms of the rigid-body modes of translation (**T**), libration (**L**), and screw (**S**) motion using the computer program MGTLS (13, 14). Two analyses were carried out; first only the 13 ring atoms, C(1)–C(12), O(3), were included in the rigid body and then all non-hydrogen atoms were included. The results for both analyses appear in Table 6.

The first analysis shows very good agreement between the derived and observed temperature factors; the r.m.s. deviation is 0.0017 Å^2 while the estimated standard deviations (see Table 5) range from 0.0006 to 0.0015 Å^2. The second analysis has an r.m.s. ΔU_{ij} of 0.0042 Å^2, still a reasonable agreement but indicative of some independent motion, particularly in the keto side chain, C(13), C(16), and O(4). Both analyses yielded physically reasonable modes of motion and there is good agreement between the two. The second analysis gave a better defined libration tensor (**L**) and more nearly intersecting principal axes of **L**, and was employed in calculating the corrected geometry. (The difference in corrected bond lengths for the two analyses was no more than 0.001 Å for any given bond.)

The principal axes of **L** correspond approximately to the principal moments of inertia of the molecule. L_1 corresponds to the long axis of the molecule, L_2 is parallel to the mean molecular plane and normal to L_1, and L_3 is nearly perpendicular to the mean plane of the molecule and passes through the five-membered ring. The unique origin (that which symmetrizes **S**) lies approximately centered in the five membered ring and slightly displaced toward C(15).

The intramolecular bond distances and angles have been corrected for libration by the method of Cruickshank (15, 16) using shape parameters q^2 of 0.08 for all atoms. Riding motion corrections based on the ΔU_{ij} (17, 18) have been applied to the bonds between ring atoms and terminal groups. Both the corrected and uncorrected bond distances and angles appear in Tables 7 and 8.

Results and Discussion

Intra-annular torsion angles defining the conformations of the rings appear in Table 9, the estimated standard deviations in these angles were calculated using the formula due to Huber.[3] Least-squares mean-planes appear in Table 10.

[2]The structure factor table is available, at a nominal charge, from the Depository of Unpublished Data, National Science Library, National Research Council of Canada, Ottawa, Canada K1A 0S2.

[3]P. Huber, appendix to ref. 19.

Can. J. Chem. Downloaded from www.nrcresearchpress.com by 210.87.254.105 on 09/05/12
For personal use only.

TABLE 4. Final positional parameters (fractional × 10^4) with estimated standard deviations in parentheses

Atom	*x*	*y*	*z*
O(1)	1102(2)	8249(2)	9013(2)
O(2)	778(2)	3092(3)	9253(3)
O(3)	4209(2)	5372	7108(2)
O(4)	8014(2)	6986(3)	6281(3)
O(5)	7248(2)	9527(3)	6907(2)
O(6)	2895(2)	10161(3)	8142(3)
C(1)	1392(2)	6964(3)	8642(3)
C(2)	832(2)	5688(3)	9143(3)
C(3)	1277(2)	4315(3)	8790(3)
C(4)	2415(3)	4091(3)	8000(4)
C(5)	2949(2)	5302(3)	7506(3)
C(6)	2295(2)	6796(3)	7414(3)
C(7)	3605(2)	7733(3)	7595(3)
C(8)	4624(2)	6843(3)	7253(2)
C(9)	5904(2)	7352(3)	7033(3)
C(10)	6084(2)	8899(3)	7166(3)
C(11)	5103(2)	9842(3)	7584(3)
C(12)	3847(2)	9242(3)	7789(3)
C(13)	7023(2)	6420(3)	6703(3)
C(14)	5381(3)	11464(3)	7778(4)
C(15)	1214(2)	6996(3)	5539(3)
C(16)	7013(3)	4806(4)	6935(4)
H(21)	165(38)	5687(46)	9740(43)
H(41)	2796(34)	3193(46)	7997(39)
H(141)	4713(48)	12040(59)	6872(62)
H(142)	5187(48)	11959(58)	8809(60)
H(143)	6309(45)	11629(47)	7796(51)
H(151)	1645(30)	6794(35)	4599(36)
H(152)	836(34)	8050(39)	5419(38)
H(153)	439(35)	6280(41)	5325(41)
H(161)	7080(52)	4527(66)	8094(69)
H(162)	7788(45)	4512(55)	6792(49)
H(163)	6151(44)	4259(53)	6130(53)
H(05)	7704(41)	8623(45)	6648(45)
H(06)	2202(39)	9627(47)	8269(44)
H(02)	225(67)	3172(69)	9946(74)

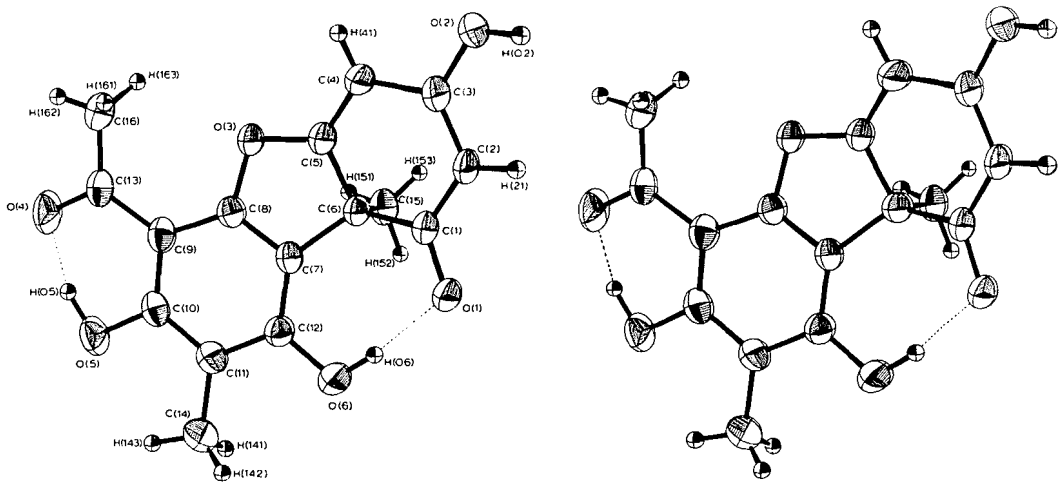

FIG. 1. A stereo view of the molecule; 50% ellipsoids are shown for oxygen and carbon atoms. The most probable absolute configuration is shown. Dotted lines indicate the intramolecular hydrogen bonds.

Can. J. Chem. Downloaded from www.nrcresearchpress.com by 210.87.254.105 on 09/05/12
For personal use only.

TABLE 5. Final thermal parameters and their estimated standard deviations

(*a*) Anisotropic thermal parameters (U_{ij} (Å^2) × 100)

Atom	U_{11}	U_{22}	U_{33}	U_{12}	U_{13}	U_{23}
O(1)	4.52(8)	3.57(8)	6.32(9)	0.10(6)	3.53(8)	−0.35(7)
O(2)	5.78(10)	3.52(8)	8.74(12)	−0.23(7)	5.18(10)	0.30(8)
O(3)	3.68(7)	3.68(8)	6.20(9)	−0.02(6)	3.19(7)	−0.19(7)
O(4)	3.83(8)	7.01(12)	8.25(11)	0.03(8)	3.71(8)	0.77(10)
O(5)	3.67(8)	5.53(10)	6.55(11)	−0.88(7)	2.33(7)	0.57(8)
O(6)	5.02(9)	3.51(8)	7.48(11)	−0.02(7)	3.63(8)	−0.35(7)
C(1)	3.08(9)	3.92(11)	4.40(9)	0.12(8)	2.01(8)	−0.12(9)
C(2)	3.66(9)	4.00(11)	4.87(10)	0.19(9)	2.78(8)	0.11(9)
C(3)	3.72(11)	3.93(11)	5.28(12)	−0.11(8)	2.59(9)	0.28(10)
C(4)	4.51(11)	3.13(10)	6.55(14)	0.18(9)	3.46(11)	−0.09(9)
C(5)	3.53(10)	3.65(11)	4.67(10)	0.08(8)	2.34(8)	−0.20(8)
C(6)	3.36(10)	3.29(10)	4.42(10)	−0.02(8)	2.24(8)	−0.03(8)
C(7)	3.26(9)	3.85(10)	4.18(10)	−0.19(8)	1.97(7)	0.02(8)
C(8)	3.51(10)	3.46(11)	4.25(9)	−0.12(8)	2.03(8)	0.15(8)
C(9)	3.04(9)	4.64(12)	4.24(10)	0.00(8)	1.76(8)	0.33(9)
C(10)	3.11(9)	4.55(12)	4.03(10)	−0.58(8)	1.42(8)	0.41(8)
C(11)	3.89(11)	3.89(11)	4.40(11)	−0.49(8)	1.51(9)	0.10(8)
C(12)	3.86(10)	3.52(11)	4.28(10)	0.11(8)	1.96(8)	0.12(8)
C(13)	3.08(10)	5.30(15)	4.16(10)	0.10(8)	1.70(8)	0.23(8)
C(14)	4.92(13)	3.90(12)	6.37(15)	−0.73(10)	1.96(12)	0.06(10)
C(15)	4.06(10)	5.28(13)	4.55(10)	−0.16(10)	1.99(9)	0.12(10)
C(16)	3.74(11)	5.29(15)	5.96(14)	0.70(10)	2.26(10)	−0.19(11)

(*b*) Isotropic thermal parameters

Atom	B (Å^2)	Atom	B (Å^2)
H(21)	5.4(8)	H(153)	5.0(7)
H(41)	4.5(7)	H(161)	8.4(11)
H(141)	7.1(10)	H(162)	6.7(9)
H(142)	7.4(10)	H(163)	6.2(9)
H(143)	6.3(9)	H(05)	5.2(7)
H(151)	3.7(5)	H(06)	4.8(7)
H(152)	4.2(6)	H(02)	8.8(13)

Details of the hydrogen-bonding and nonbonded interactions appear in Tables 11 and 12 respectively. Figures 2 and 3 show the molecular packing viewed down *c* and *b*.

The five-membered ring, C(5)–C(8) and O(3), is in the half-chair conformation with C(5) and C(6) displaced −0.09 and 0.23 Å from the C(7), C(8), O(3) plane. The mean angle in this ring is 107.2° and, as expected, is intermediate between the value of 108° for a planar ring and the values of 103.9–104.2° calculated for the minimum energy conformations of cyclopentanes (20). The dihedral angles in the ring have the same relative magnitudes as those calculated for the low energy conformation with $\omega_1 = 15°$ (20) although the inclusion of three trigonal carbon atoms in the ring make direct comparison impossible. The angles in the ring are all moderately but unequally strained, closures range from 3.1° at O(3) to 12.8° at C(7) (relative to the tetrahedral or trigonal planar angle). The O(3)—C(8) (1.399 Å) and C(6)—C(7) (1.515 Å) correspond to normal single bonds, while the remaining bonds in the rings are significantly shorter than expected (21). This shortening results from a combination of steric and electronic effects. A shortening of some, but not all of the bonds tends to ease the angular strain in the five-membered ring.

The aromatic ring, C(7)–C(12), is slightly, but significantly nonplanar. The conformation of the ring is that of an assymmetric boat with C(7) and C(10) displaced +0.015 and +0.022 Å from the mean plane of the ring. The mean angle in the aromatic ring is 120.0°, but there are significant deviations among the individual values. The angles at C(8) and C(10) are expanded to 124.1 and 123.3° while those at C(9)

Can. J. Chem. Downloaded from www.nrcresearchpress.com by 210.87.254.105 on 09/05/12
For personal use only.

TABLE 6. Rigid-body thermal parameters*

	Twelve ring atoms			All non-hydrogen atoms		
$L(\times 10^1 \text{deg}^2)$	10(14)	51(10)	−17(7)	82(9)	16(5)	−11(5)
		33(11)	−18(6)		48(7)	−9(5)
			38(5)			33(5)
Principal axes of L						
	r.m.s. amplitude	Direction cosines ($\times 10^3$)		r.m.s. amplitude	Direction cosines ($\times 10^3$)	
L_1	3.7°	854	464	−237	3.0°	−899	−374	227
L_2	1.9	331	−133	934	2.1	−425	867	−259
L_3	0.6	402	−876	−267	1.7	−101	−332	−938
Principle axes of reduced T						
	r.m.s. amplitude	Direction cosines ($\times 10^3$)		r.m.s. amplitude	Direction cosines ($\times 10^3$)	
	0.19 Å	−218	377	−901	0.21	−404	25	−914
	0.19	147	925	351	0.19	−85	−998	7
	0.15	965	−56	−256	0.15	−911	80	403
Displacements of axes from intersecting (Å)						
Parallel to L_1	−8.28			−1.06		
" L_2	−3.23			−0.07		
" L_3	−0.97			−0.81		
Effective screw translations (Å)						
Parallel to L_1	−0.001			0.003		
" L_2	−0.001			−0.029		
" L_3	0.007			0.031		
Fractional coordinates of unique origin ($\times 10^4$)						
x	3270			3557		
y	7238			7024		
z	7610			7683		
Fraction coordinates of center of gravity ($\times 10^4$)						
x	3445			3887		
y	6767			7108		
z	7754			7631		
$(\Delta U_{ij}^2)^{1/2}(\text{Å}^2)$	0.0017			0.0042		

*Axes of reference are a, b, c^*. E.s.d.'s of components of L are given after them in parentheses in units of the last place shown.

and C(11) are contracted to 114.5 and 118.5°. This is a result of fusion to the five-membered ring. The strain is taken up primarily by angular distortions and to a lesser extent by torsional strain (which is responsible for the nonplanarity of the system) and bond length distortion. Electronic effects, which will be discussed later, are also a contributing factor and influence the bond lengths most. Bond lengths in the ring average 1.401 Å which is slightly longer than normal. The C(9)—C(10) (1.424) and C(10)—C(11) (1.405 Å) bonds are significantly longer and C(7)—C(8) (1.379 Å) significantly shorter than the accepted mean of 1.394 Å (21). Remaining bonds are slightly, but not significantly, long. The phenolic C—O(H) bonds are 1.348 and 1.349 Å, both significantly less than the value of 1.40 Å expected for a $C(sp^2)$—$O(sp^3)$ bond. The mean plane of the aromatic ring makes an angle of 4.1° with that of the five-membered ring and 11.8° with that of the keto side chain at C(9).

The cyclohexadiene ring, C(1)–C(6), has the sofa conformation. Atoms C(1)–C(5) lie within 0.02 Å of their mean plane while C(6) is displaced 0.316 Å. The bond angle at tetrahedral C(6) is expanded to 112.6° and the mean angle at the trigonal atoms is 120.4° with individual values ranging from 115.7 to 124.6°. As with the aromatic ring, the fusion to the five-membered

Can. J. Chem. Downloaded from www.nrcresearchpress.com by 210.87.254.105 on 09/05/12
For personal use only.

TABLE 7. Bond distances (Å) with standard deviations in parentheses

Bond	Distance		Bond	Distance	
	Uncorrected	Corrected		Uncorrected	Corrected
O(1)—C(1)	1.262(3)	1.265*	C(9)—C(13)	1.473(3)	1.475*
O(2)—C(3)	1.315(3)	1.317*	C(10)—C(11)	1.403(3)	1.405
O(3)—C(5)	1.367(2)	1.369	C(11)—C(12)	1.402(3)	1.403
O(3)—C(8)	1.397(3)	1.399	C(11)—C(14)	1.503(3)	1.504*
O(4)—C(13)	1.233(3)	1.235*	C(13)—C(16)	1.484(4)	1.486*
O(5)—C(10)	1.348(3)	1.349*	O(2)—H(02)	0.89(6)	
O(6)—C(12)	1.346(3)	1.348*	O(5)—H(05)	0.99(4)	
C(1)—C(2)	1.396(3)	1.398	O(6)—H(06)	0.87(4)	
C(1)—C(6)	1.517(3)	1.519	C(2)—H(21)	0.92(4)	
C(2)—C(3)	1.383(3)	1.385	C(4)—H(41)	0.90(4)	
C(3)—C(4)	1.453(3)	1.455	C(14)—H(141)	0.97(5)	
C(4)—C(5)	1.333(3)	1.334	C(14)—H(142)	1.01(5)	
C(5)—C(6)	1.498(3)	1.500	C(14)—H(143)	0.92(4)	
C(6)—C(7)	1.513(3)	1.515	C(15)—H(151)	0.99(4)	
C(6)—C(15)	1.570(3)	1.572	C(15)—H(152)	1.03(4)	
C(7)—C(8)	1.377(3)	1.379	C(15)—H(153)	0.98(3)	
C(7)—C(12)	1.397(3)	1.398	C(16)—H(161)	0.95(5)	
C(8)—C(9)	1.398(3)	1.399	C(16)—H(162)	0.85(4)	
C(9)—C(10)	1.422(3)	1.424	C(16)—H(163)	1.03(4)	

*These distances have been corrected for riding motion as well as libration (see text).

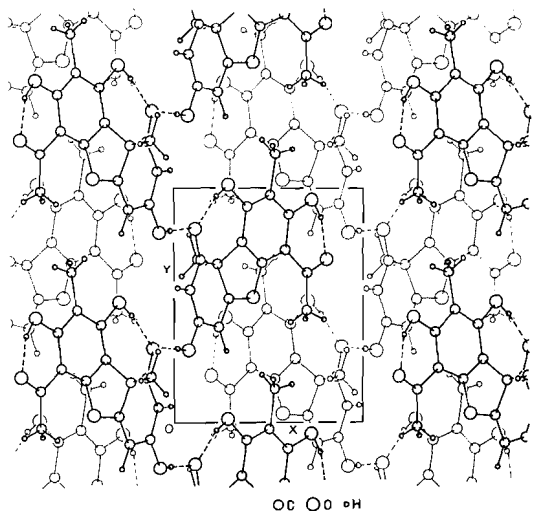

FIG. 2. The structure viewed down *c*; hydrogen bonds are represented by broken lines. Y = *b* and X = *a* sin β.

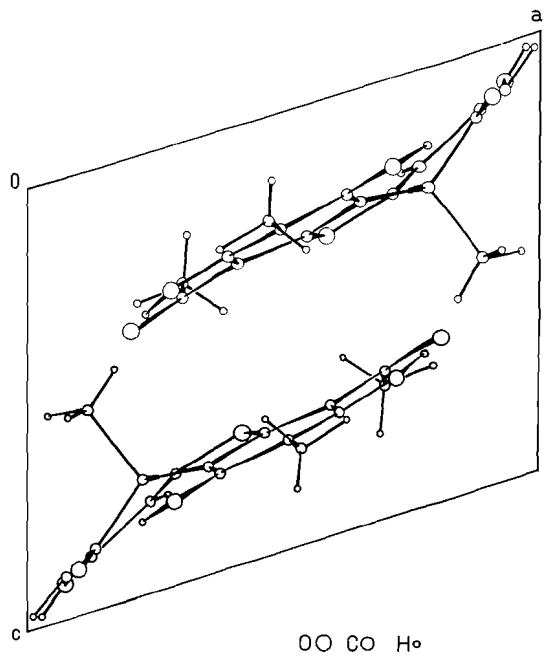

FIG. 3. The structure viewed down *b*.

ring introduces strain into the ring which is taken up by angular and torsional distortion (see *e.g.* Table 9). The greatest torsional strain occurs about the C(4)—C(5) double bond where the dihedral angle C(3)[C(4)—C(5)]C(6) is 11.5°. The C(1)—C(6) bond (1.519 Å) is a normal $C(sp^3)$—$C(sp^2)$ single bond and C(4)—C(5) (1.334 Å) is a normal double bond. The remaining bonds in the ring are significantly shorter than single bonds. The C(1)—O(1) bond (1.265 Å) and the C(3)—O(2) bond (1.317 Å) are intermediate in length between single and double bonds, indicating extensive delocalization in the O(1)—C(1)—C(2)—C(3)—O(2) portion of the molecule.

The C(6)—C(15) bond (1.572 Å) is signifi-

Can. J. Chem. Downloaded from www.nrcresearchpress.com by 210.87.254.105 on 09/05/12
For personal use only.

TABLE 8

(*a*) Bond angles involving non-hydrogen atoms with standard deviations in parentheses

Atoms	Angle (deg) Uncorrected	Corrected*	Atoms	Angle (deg) Uncorrected	Corrected*
C(5)—O(3)—C(8)	106.6(2)		C(8)—C(7)—C(12)	119.6(2)	
O(1)—C(1)—C(2)	124.8(2)	124.2	O(3)—C(8)—C(7)	111.9(2)	
O(1)—C(1)—C(6)	117.7(2)	118.0	O(3)—C(8)—C(9)	123.9(2)	
C(2)—C(1)—C(6)	117.3(2)	117.4	C(7)—C(8)—C(9)	124.2(2)	124.1
C(1)—C(2)—C(3)	121.4(2)	121.2	C(8)—C(9)—C(10)	114.5(2)	
O(2)—C(3)—C(2)	122.9(2)		C(8)—C(9)—C(13)	125.2(2)	
O(2)—C(3)—C(4)	113.8(2)	113.7	C(10)—C(9)—C(13)	120.3(2)	
C(2)—C(3)—C(4)	123.2(2)		O(5)—C(10)—C(9)	120.1(2)	
C(3)—C(4)—C(5)	115.7(2)		O(5)—C(10)—C(11)	116.7(2)	
O(3)—C(5)—C(4)	124.8(2)		C(9)—C(10)—C(11)	123.2(2)	123.3
O(3)—C(5)—C(6)	110.5(2)		C(10)—C(11)—C(12)	118.5(2)	
C(4)—C(5)—C(6)	124.6(2)		C(10)—C(11)—C(14)	120.7(2)	120.8
C(1)—C(6)—C(5)	112.6(2)		C(12)—C(11)—C(14)	120.8(2)	120.7
C(1)—C(6)—C(7)	121.6(2)	121.4	O(6)—C(12)—C(11)	118.0(2)	
C(1)—C(6)—C(15)	104.7(2)	104.9	O(6)—C(12)—C(7)	122.1(2)	122.2
C(5)—C(6)—C(7)	99.8(2)		C(11)—C(12)—C(7)	119.8(2)	
C(5)—C(6)—C(15)	108.0(2)		O(4)—C(13)—C(9)	119.8(2)	119.9
C(7)—C(6)—C(15)	109.6(2)		O(4)—C(13)—C(16)	119.0(2)	
C(6)—C(7)—C(8)	107.1(2)	107.0	C(9)—C(13)—C(16)	121.2(2)	121.1
C(6)—C(7)—C(12)	132.7(2)				

*Corrected angles are listed only if different from the uncorrected value.

(*b*) Angles involving hydrogen atoms

Atoms	Angle (deg)	Atoms	Angle (deg)
C(3)—O(2)—H(02)	117(4)	C(6)—C(15)—H(151)	113(2)
C(10)—O(5)—H(05)	98(2)	C(6)—C(15)—H(152)	109(2)
C(12)—O(6)—H(06)	107(3)	C(6)—C(15)—H(153)	111(2)
C(1)—C(2)—H(21)	124(3)	H(151)—C(15)—H(152)	109(3)
C(3)—C(2)—H(21)	115(3)	H(151)—C(15)—H(153)	103(3)
C(3)—C(4)—H(41)	120(2)	H(152)—C(15)—H(153)	112(3)
C(5)—C(4)—H(41)	124(2)	C(13)—C(16)—H(161)	113(4)
C(11)—C(14)—H(141)	113(3)	C(13)—C(16)—H(162)	105(3)
C(11)—C(14)—H(142)	108(3)	C(13)—C(16)—H(163)	116(3)
C(11)—C(14)—H(143)	117(3)	H(161)—C(16)—H(162)	104(4)
H(141)—C(14)—H(142)	97(4)	H(161)—C(16)—H(163)	107(4)
H(141)—C(14)—H(143)	111(4)	H(162)—C(16)—H(163)	111(4)
H(142)—C(14)—H(143)	110(4)		

cantly longer than a normal $C(sp^3)$—$C(sp^3)$ bond. The weakening of this bond is a consequence of steric distortion of the C(6) tetrahedron. The C(11)—C(14) distance of 1.504 Å corresponds to a normal for a $C(sp^2)$—$C(sp^3)$ single bond. The C(9)—C(13) distance of 1.475 Å is normal for a $C(sp^2)$—$C(sp^2)$ bond and C(13)—C(16) (1.486 Å) is somewhat shortened, but this is usual for a bond adjacent to a carbonyl group (21). The C(13)—O(4) bond length (1.235 Å) does not differ significantly from that expected for a double bond. The angle between the mean planes of the C(13) keto group and the aromatic ring (11.8°) represents a balance between steric effects, which are at a minimum when the planes are perpendicular, and formation of the intramolecular O(4)... H(05)—O(5) hydrogen bond, which is most favorable when the two groups are coplanar. The intramolecular van der Waals contact between the C(16) methyl group and ring atom O(3)...C(16), 2.840 Å and O(3)...H(163), 2.48 Å opens the C(9)—C(13)—C(16) angle to 121.1° with respect to O(4)—C(13)—C(16), 119.0°, and is partially responsible for the slight but significant nonplanarity of the keto group.

Can. J. Chem. Downloaded from www.nrcresearchpress.com by 210.87.254.105 on 09/05/12
For personal use only.

TABLE 9. Intra-annular torsion angles (ω°) with estimated standard deviations in parentheses

(*a*) Six membered rings

Ring 1: C(1)–C(6)		Ring 2: C(7)–C(12)	
Bond	Angle (deg)	Bond	Angle (deg)
C(1)—C(2)	−10.9(3)	C(7)—C(8)	1.8(3)
C(2)—C(3)	−4.6(3)	C(8)—C(9)	0.8(3)
C(3)—C(4)	4.8(3)	C(9)—C(10)	−3.5(2)
C(4)—C(5)	11.5(3)	C(10)—C(11)	3.5(3)
C(5)—C(6)	−25.5(3)	C(11)—C(12)	−0.7(3)
C(6)—C(1)	24.0(2)	C(12)—C(7)	−1.9(3)

(*b*) Five membered ring

Bond	Angle (deg)
O(3)—C(8)	4.9(2)
C(8)—C(7)	8.5(2)
C(7)—C(6)	−16.8(2)
C(6)—C(5)	20.6(2)
C(5)—O(3)	−16.7(2)

The significant differences between the corresponding exocyclic C—C—C and C—C—O angles at trigonal ring atoms C(1), C(3), C(9), and C(12) follow the trend that the larger angle is that involving the shorter C—C bond in the ring. The exceptions are the angles in the six-membered chelate ring formed by the O(4)... H(05)—O(5) hydrogen bond at C(10) and also at C(13) where O(4)—C(13)—C(9) would be expected to be larger than C(16)—C(13)—C(9). The mean $C(sp^3)$—H, $C(sp^2)$—H, and O—H distances of 0.99, 0.91, and 0.92 Å, as well as all angles involving hydrogen atoms, are generally as expected. The bond distances are shorter than those obtained spectroscopically indicating that the hydrogen electron has been pulled toward the atom to which it is bonded.

The crystal structure (Figs. 2 and 3) consists of molecules linked by intermolecular O—H...O hydrogen bonds (O...O, 2.625 Å) to form continuous spirals about the 2_1 axes. There are two intramolecular hydrogen bonds in the structure; O(4)...H(05)—O(5) and O(1)... H(06)–O(6) (O...O, 2.532 and 2.712 Å). Further details of the hydrogen-bonding scheme are given in Table 11. The closest intermolecular contacts and selected intramolecular non-bonded contacts are listed in Table 12. All intermolecular contacts correspond to normal van der Waals interactions, with the exception of the hydrogen bond.

The molecular geometry indicates that there are several resonance forms which are important contributors to the structure. The two most important are (**3**) and (**4**). Since a relatively

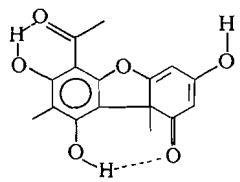

3

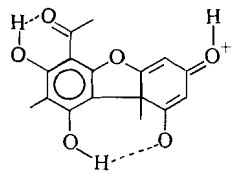

4

strong intermolecular hydrogen bond exists between O(1) and H(02) (see Table 11 and Fig. 2), **4** is essentially equivalent to the originally proposed structure **2**, proton transfer occurring via the O(2)—H(02)...O(1) hydrogen bond. The fully conjugated form **3** is slightly favored over the cross-conjugated **4**. Preliminary results of the structural study of aminousnic acid (22), indicate a similar situation occurs, the structure being best represented by **5** with important contributions from **6**. The delocalization in aminousnic acid probably occurs via proton transfer across an intramolecular N—H...O hydrogen bond. The C(10)—O(5) and C(12)—

Can. J. Chem. Downloaded from www.nrcresearchpress.com by 210.87.254.105 on 09/05/12
For personal use only.

O(6) distances indicate that electron density is being donated by the oxygen atoms to the aromatic ring. This indicates that phenolic type resonance structures also contribute to the structure. With the electron withdrawing keto group *ortho* to O(5) and *para* to O(6), the structure would be expected to indicate net

TABLE 10

(*a*) Distances (Å) of relevant atoms from mean planes through the molecule.

Atom	*d*	*d*/σ
Plane (*1*): aromatic ring, C(7)–C(12)		
C(7)	0.015	7.6
C(8)	−0.005	2.8
C(9)	−0.012	6.1
C(10)	0.022	10.7
C(11)	−0.012	5.7
C(12)	−0.008	3.8
C(6)	0.267	133.7
O(3)	0.016	10.7
C(13)	−0.062	28.5
O(5)	0.075	39.0
C(14)	−0.030	10.1
O(6)	−0.004	2.1
Plane (*2*): five membered ring		
C(5)	−0.139	67.3
C(6)	0.116	58.2
C(7)	−0.076	37.5
C(8)	−0.003	1.3
O(3)	0.028	18.1
C(4)	−0.544	202.5
C(9)	0.068	34.1
C(12)	−0.121	59.1
Plane (*3*): C(1)–C(5)		
C(1)	0.003	1.4
C(2)	−0.014	6.5
C(3)	0.021	9.1
C(4)	−0.020	7.3
C(5)	0.006	3.0
O(1)	−0.109	62.9
O(2)	−0.002	0.9
C(6)	0.316	156.2
H(21)	−0.065	1.9
H(41)	−0.168	5.5

(*b*) Equations of planes: $lX + mY + nZ = p$*

Plane†	*l*	*m*	*n*	*p*
(*1*)	−0.1714	0.1125	−0.9788	−5.2060
(*2*)	−0.1052	0.0866	−0.9905	−5.2385
(*3*)	−0.4486	−0.0220	−0.8934	−5.7331

*X, Y, and Z are orthonal angstrom coordinates derived as follows:

$$\begin{pmatrix} X \\ Y \\ Z \end{pmatrix} = \begin{pmatrix} a & 0 & c\cos\beta \\ 0 & b & 0 \\ 0 & 0 & c\sin\beta \end{pmatrix} \begin{pmatrix} x \\ y \\ z \end{pmatrix}$$

†Angles between planes: (*1*) – (*2*), 4.1°; (*1*) – (*3*), 18.4°; (*2*) – (*3*), 21.5°.

TABLE 11. Hydrogen bond data

Interaction A...H—B	Lengths (Å) A...H	A...B
O(1)...H(06)—O(6)	1.87(4)	2.712(2)
O(4)...H(05)—O(5)	1.57(4)	2.532(3)
O(1)...H(02)*—O(2)*	1.75(6)	2.625(2)

Bond	Angle (deg)
About A atoms	
C(1)—O(1)—H(06)	111(1)
C(1)—O(1)—O(6)	109.1(1)
C(1)—O(1)—H(02)*	109(2)
C(1)—O(1)—O(2)*	108.6(1)
H(06)—O(1)—H(02)*	140(2)
O(6)—O(1)—O(2)*	141.6(1)
C(13)—O(4)—H(05)	98(1)
C(13)—O(4)—O(5)	91.4(2)
About B atoms	
C(12)—O(6)—O(1)	101.4(1)
H(06)—O(6)—O(1)	10(2)
C(10)—O(5)—O(4)	87.5(1)
H(05)—O(5)—O(4)	10(2)
C(3)*—O(2)*—O(1)	118.9(1)
H(02)*—O(2)*—O(1)	7(4)
About H atoms	
O(1)—H(06)—O(6)	165(3)
O(4)—H(05)—O(5)	163(4)
O(1)—H(02)*—O(2)*	170(6)

*Atoms marked with asterisks are at positions $-x, \frac{1}{2}+y, 2-z$.

TABLE 12. Selected non-bonded contacts less than 3.4 Å

Atoms	Distance (Å)	Symmetry operation (B)		
O(1)...C(7)	3.035(2)			
O(1)...C(15)	3.046(3)			
O(3)...C(16)	2.840(3)			
O(4)...C(16)	2.345(4)			
O(5)...C(14)	2.780(4)			
O(6)...C(14)	2.804(3)			
O(1)...H(21)	2.64(4)			
O(2)...H(21)	2.50(4)			
O(2)...H(41)	2.48(3)			
O(5)...H(143)	2.33(4)			
O(1)...O(4)	3.364(3)	$x-1$	y	z
O(3)...O(5)	3.202(3)	$1-x$	$y-\frac{1}{2}$	$1-z$
O(2)...C(1)	3.254(3)	$-x$	$y-\frac{1}{2}$	$2-z$
O(2)...C(2)	3.190(3)	$-x$	$y-\frac{1}{2}$	$2-z$
O(2)...H(21)	2.60(4)	$-x$	$y-\frac{1}{2}$	$2-z$
O(6)...H(41)	2.77(4)	x	$1+y$	z
C(1)...H(02)	2.47(6)	$-x$	$\frac{1}{2}+y$	$2-z$
C(2)...H(02)	2.68(6)	$-x$	$\frac{1}{2}+y$	$2-z$

Can. J. Chem. Downloaded from www.nrcresearchpress.com by 210.87.254.105 on 09/05/12
For personal use only.

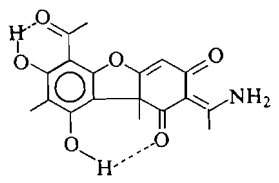

5

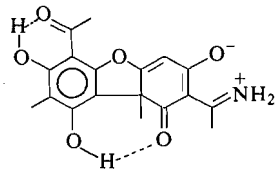

6

positive charges on O(5) and O(6), which is the case, and a net negative charge on O(4) which would be indicated by a lengthening of the C(13)—O(4) bond and a shortening of the C(9)—C(13) bond, neither of which were observed to a significant degree. The geometry of the aromatic ring indicates a net buildup of negative charge at ring carbon atoms, in the order C(9) > C(11) > C(10). A resonance form involving a positive charge on O(3), a negative charge on C(2), and a double bond between C(3) and C(4) is a minor contributor which accounts for the significant shortening of the O(3)—C(5) and C(3)—C(4) bonds.

The results of this analysis have provided evidence in support of the possible biodegradation sequence:

$$\mathbf{1} \xrightarrow{P} \mathbf{7} \xrightarrow{-Pi} \mathbf{8} \xrightarrow{-OAc} \mathbf{3} \xrightarrow{[H]} \mathbf{9}$$

A full account of the chemical work is in preparation (1).

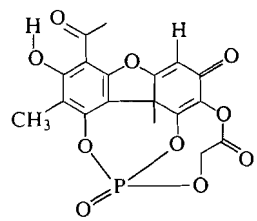

7

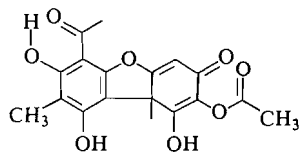

8

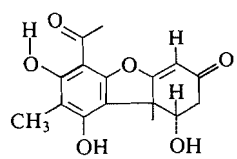

9

We thank Professor J. P. Kutney and Mr. I. Sanchez for the crystals and the discussion, the National Research Council of Canada for financial support, and the University of British Columbia Computing Centre for assistance.

1. I. H. Sanchez and J. P. Kutney. In preparation.
2. R. J. Bandoni and G. H. N. Towers. Can. J. Biochem. **45**, 1197 (1967).
3. J. Karle and I. L. Karle. Acta Cryst. **21**, 849 (1966).
4. J. Karle and I. L. Karle. Acta Cryst. **9**, 635 (1956).
5. (*a*) M. G. B. Drew. Personal communication; (*b*) M. G. B. Drew, D. H. Templeton, and A. Zalkin. Acta Cryst. B**25**, 261 (1969).
6. F. H. Allen and J. Trotter. J. Chem. Soc. B, 166 (1971).
7. W. Harrison, S. Rettig, and J. Trotter. J. Chem. Soc. Perkin II, 1036 (1972).
8. H. Hope, and U. de la Camp. Nature, **221**, 54 (1969).
9. H. Hope, U. de la Camp, and W. E. Thiessen. Acta Cryst. A**25**, S78 (1969).
10. W. C. Hamilton. Acta Cryst. **18**, 502 (1965).
11. International tables for X-ray crystallography. Vol. III. Kynoch Press, Birmingham. 1962.
12. R. F. Stewart, E. R. Davidson, and W. T. Simpson. J. Chem. Phys. **42**, 3175 (1965).
13. V. Schomaker and K. N. Trueblood. Acta Cryst. B**24**, 63 (1968).
14. P. K. Gantzel and K. N. Trueblood. Acta Cryst. **18**, 958 (1965).
15. D. W. J. Cruickshank. Acta Cryst. **9**, 757 (1956).
16. D. W. J. Cruickshank. Acta Cryst. **14**, 896 (1961).
17. W. R. Busing and H. A. Levy. Acta Cryst. **17**, 142 (1964).
18. C. K. Johnson. *In* Crystallographic computing. Munksgaard, Copenhagen. 1970.
19. E. Huber-Buser and J. D. Dunitz. Helv. Chim. Acta, **64**, 2027 (1961).
20. J. B. Hendrickson. J. Am. Chem. Soc. **83**, 4537 (1961); **85**, 4059 (1963).
21. Chem. Soc. Special Publ. No. 11, 1958 and No. 18, 1965.
22. J. C. Clardy. Private communication.

Can. J. Chem. Downloaded from www.nrcresearchpress.com by 210.87.254.105 on 09/05/12
For personal use only.

Crystal Structure of Bis[hexakis(dimethylamino)cyclotriphosphonitrilium] Tetrachlorocobaltate(II)

ALISTAIR L. MACDONALD AND JAMES TROTTER

Department of Chemistry, The University of British Columbia, Vancouver 8, British Columbia

Received June 21, 1973

Crystals of the title compound, $[N_3P_3(NMe_2)_6H]_2CoCl_4$, are orthorhombic, $a = 34.623$, $b = 13.964$, $c = 10.486$ Å, $Z = 4$, space group $P2_12_12_1$. The structure was determined by Patterson and electron-density methods and refined by full-matrix least-squares procedures to $R = 0.088$ for 2178 observed reflexions. Both rings are slightly non-planar, with three distinct pairs of NP bonds: commencing at the protonated nitrogen atom, 1.68, 1.56, and 1.58 Å. The $CoCl_4^{2-}$ ion is tetrahedral and is hydrogen bonded to both rings, N—H ... Cl = 3.32, 3.36 Å.

Le composé cité dans le titre cristallise dans le système orthorhombique, $a = 34.623$, $b = 13.964$, $c = 10.486$ Å, $Z = 4$, groupe spatial $P2_12_12_1$. La structure a été déterminée à l'aide des méthodes de Patterson et de la densité électronique, et a été affinée par la méthode de moindres carrés (matrice complète) jusqu'à $R = 0.088$ pour 2178 réflexions observées. Tous les deux cycles sont légèrement non-plans, et ont trois paires distinctes de liaisons NP: commencant à l'atome d'azote protoné, 1.68, 1.56, et 1.58 Å. L'ion de $CoCl_4^{2-}$ est tetrahedrique, et forme des liaisons hydrogènes, N—H ... Cl = 3.32, 3.36 Å.

Can. J. Chem., **52**, 734 (1974)

Introduction

The structures of several protonated phosphonitrilium ions have been investigated (1, 2), the only six-membered ring example being the unsymmetrically substituted $[N_3P_3Cl_2(NHPr^i)_4H]^+$ ion (2). We now describe the structure analysis of $[N_3P_3(NMe_2)_6H]_2CoCl_4$, comparison being possible with the recent accurate determination of the structure of the parent phosphazene (3).

Experimental

Crystals of $[N_3P_3(NMe_2)_6H]_2CoCl_4$ from $CCl_4/CHCl_3$ (4) are blue-green prisms elongated along c with (100) developed. Unit-cell and intensity data were measured as for the parent compound (3), but with MoKα radiation.

$C_{24}H_{74}Cl_4CoN_{18}P_6$ f.w. = 1002

Orthorhombic, $a = 34.623(20)$, $b = 13.964(7)$, $c = 10.486(7)$ Å, $V = 5070$ Å^3, $Z = 4$, $\rho_{calc} = 1.312$, $F(000) = 2116$ (20 °C, MoKα, $\lambda = 0.7107$ Å, $\mu = 8$ cm^{-1}). Space group $P2_12_12_1$ (D_2^4, No. 19).

Of 5027 reflexions with $2\theta(Mo) \leqslant 50°$, 2178 (43%) were observed.

Structure Analysis

The structure was determined from Patterson and electron-density syntheses, and was refined by full-matrix least-squares methods, with minimization of $\Sigma w(F_o - F_c)^2$, w being based on counting statistics. The final R value was 0.088 for the observed data. A final difference synthesis revealed positions for some of the hydrogen atoms, but the two acid hydrogens could not be located. Positional and thermal parameters are given in Table 1, and measured and calculated structure factors have been placed in the Depository of Unpublished Data.[1]

Discussion

The structure is shown in Fig. 1. Although the acid hydrogen atoms could not be directly located the bond lengths and likely hydrogen-bonding system (discussed below) indicated that the rings are protonated at N(3) and N(12). Both rings are slightly non-planar, as is the ring of the parent molecule. The first ring, P(1)—P(3) is a slight chair, with displacements of about 0.05 Å from a mean plane; the other ring, P(4)—P(6), has five atoms nearly in a plane, with N(10) displaced by about 0.2 Å. These small deviations from planarity can be ascribed to intra- and intermolecular steric effects (3).

The ring bond lengths show considerable variations from those in the parent molecule, the bonds to the protonated nitrogen being lengthened (Table 2) as a result of the use of the nitrogen lone-pair electrons in bonding to the hydrogen atom rather than in the ring π-system. The bond lengths are very similar to those in $N_3P_3Cl_2(NHPr^i)_4.HCl$ (2) and in the eight-membered $(NPMe_2)_4H^+$ ring (1*b*). The angles in

[1]The structure factor table is available, at a nominal charge, upon request from the Depository of Unpublished Data, National Science Library, National Research Council of Canada, Ottawa, Canada K1A 0S2.

Can. J. Chem. Downloaded from www.nrcresearchpress.com by 210.87.254.105 on 09/05/12
For personal use only.

Can. J. Chem. Downloaded from www.nrcresearchpress.com by 210.87.254.105 on 09/05/12
For personal use only.

TABLE 1. Final positional and thermal parameters

Atom	x	y	z	B (Å^2)
Co	0.1319(1)	0.1155(2)	0.2537(4)	
Cl(1)	0.0896(2)	0.0109(5)	0.1504(7)	
Cl(2)	0.1599(2)	0.2088(5)	0.1006(8)	
Cl(3)	0.1816(2)	0.0406(4)	0.3605(7)	
Cl(4)	0.0959(2)	0.1971(5)	0.4005(8)	
P(1)	−0.0273(2)	0.1074(4)	0.0839(7)	
P(2)	−0.0556(2)	0.2418(4)	−0.0967(6)	
P(3)	0.0249(2)	0.2048(4)	−0.1024(6)	
P(4)	0.2873(2)	0.2053(4)	0.4016(6)	
P(5)	0.3047(2)	0.3504(4)	0.5831(7)	
P(6)	0.2273(2)	0.2835(4)	0.5777(7)	
N(1)	−0.0589(6)	0.1696(13)	0.0193(19)	
N(2)	−0.0122(5)	0.2581(12)	−0.1383(15)	
N(3)	0.0159(5)	0.1354(12)	0.0238(17)	
N(4)	−0.0288(5)	0.1235(16)	0.2384(22)	
N(5)	−0.0316(6)	−0.0124(14)	0.0673(20)	
N(6)	−0.0759(5)	0.3471(15)	−0.0655(19)	
N(7)	−0.0816(5)	0.1983(17)	−0.2156(18)	
N(8)	0.0399(5)	0.1433(13)	−0.2226(18)	
N(9)	0.0614(6)	0.2642(13)	−0.0542(22)	
N(10)	0.3124(5)	0.2890(13)	0.4602(16)	
N(11)	0.2617(5)	0.3480(12)	0.6293(18)	
N(12)	0.2416(6)	0.2103(14)	0.4592(17)	
N(13)	0.2874(5)	0.2140(12)	0.2441(18)	
N(14)	0.2997(5)	0.0956(12)	0.4289(20)	
N(15)	0.3141(6)	0.4687(14)	0.5602(22)	
N(16)	0.3360(7)	0.3164(15)	0.6886(18)	
N(17)	0.2087(7)	0.2234(16)	0.6954(22)	
N(18)	0.1909(6)	0.3376(14)	0.5120(18)	
C(1)	−0.0043(9)	0.0651(19)	0.3202(28)	7.70(72)
C(2)	−0.0378(9)	0.2182(23)	0.2869(32)	8.49(89)
C(3)	−0.0652(7)	−0.0544(16)	0.1267(24)	7.42(57)
C(4)	−0.0117(8)	−0.0620(18)	−0.0417(27)	7.83(68)
C(5)	−0.0539(10)	0.4193(22)	0.0093(32)	6.88(93)
C(6)	−0.1207(8)	0.3548(17)	−0.0473(27)	6.27(69)
C(7)	−0.0946(8)	0.0979(21)	−0.2172(28)	8.08(75)
C(8)	−0.0844(8)	0.2522(19)	−0.3407(28)	6.43(69)
C(9)	0.0195(8)	0.1315(19)	−0.3504(28)	5.61(71)
C(10)	0.0746(8)	0.0813(20)	−0.2117(27)	6.36(75)
C(11)	0.0858(8)	0.3115(20)	−0.1492(30)	7.73(73)
C(12)	0.0612(8)	0.3127(20)	0.0766(31)	5.63(76)
C(13)	0.2698(9)	0.1410(22)	0.1711(31)	3.79(85)
C(14)	0.2899(7)	0.3098(18)	0.1833(24)	6.34(62)
C(15)	0.3380(9)	0.0629(21)	0.3833(33)	5.30(82)
C(16)	0.2847(10)	0.0427(22)	0.5484(33)	5.96(91)
C(17)	0.2846(10)	0.5305(23)	0.5081(32)	7.89(98)
C(18)	0.3586(8)	0.4920(18)	0.5554(27)	8.91(67)
C(19)	0.3539(8)	0.2168(22)	0.6938(27)	6.80(80)
C(20)	0.3334(9)	0.3638(21)	0.8238(32)	8.80(85)
C(21)	0.2331(9)	0.2034(21)	0.8041(29)	7.98(73)
C(22)	0.1731(11)	0.1629(24)	0.6799(33)	5.97(99)
C(23)	0.1653(9)	0.4000(22)	0.6103(35)	9.00(88)
C(24)	0.1856(9)	0.3650(21)	0.3754(32)	6.46(85)

TABLE 1 (*Concluded*)

Anistropic thermal parameters exp $-10^{-4}(b_{11}h^2 + ... + 2b_{12}hk + ...)$

Atom	β_{11}	β_{12}	β_{33}	β_{12}	β_{13}	β_{23}
Co	7(1)	53(2)	121(4)	2(1)	8(1)	8(3)
Cl(1)	10(1)	71(5)	136(9)	2(2)	8(2)	7(6)
Cl(2)	14(1)	84(5)	154(10)	2(2)	15(3)	41(7)
Cl(3)	10(1)	51(4)	131(10)	−1(1)	−3(2)	5(5)
Cl(4)	12(1)	88(5)	170(11)	6(2)	17(3)	20(8)
P(1)	8(1)	42(4)	82(8)	−3(2)	−2(2)	10(6)
P(2)	6(1)	34(4)	68(7)	2(1)	−2(2)	10(5)
P(3)	6(1)	50(4)	61(7)	0(1)	−2(2)	−9(5)
P(4)	6(1)	36(4)	60(7)	−3(1)	1(2)	5(5)
P(5)	8(1)	38(4)	86(8)	−5(1)	1(2)	−8(5)
P(6)	7(1)	48(4)	76(8)	1(2)	4(2)	7(6)
N(1)	6(2)	63(13)	133(28)	2(5)	−3(7)	10(16)
N(2)	3(2)	71(13)	53(19)	4(4)	−3(5)	29(13)
N(3)	10(2)	39(12)	75(23)	−6(4)	−3(6)	−8(14)
N(4)	12(2)	103(17)	43(32)	−4(5)	11(8)	44(22)
N(5)	6(3)	88(16)	159(27)	−4(5)	3(7)	43(18)
N(6)	6(2)	55(18)	67(26)	−1(5)	0(7)	6(19)
N(7)	14(2)	47(19)	128(25)	4(5)	−4(6)	−10(19)
N(8)	8(2)	90(14)	85(23)	4(4)	−1(6)	12(15)
N(9)	7(3)	88(12)	74(33)	−5(5)	11(9)	11(17)
N(10)	6(2)	51(12)	70(20)	2(4)	−2(5)	−15(4)
N(11)	9(2)	68(12)	79(26)	1(4)	2(6)	−16(15)
N(12)	9(3)	35(14)	83(20)	9(5)	−1(6)	19(16)
N(13)	10(2)	41(12)	98(21)	1(4)	7(7)	−9(17)
N(14)	3(2)	57(12)	102(26)	0(4)	12(7)	−21(16)
N(15)	9(3)	74(16)	168(35)	−5(5)	1(8)	−25(20)
N(16)	18(4)	63(17)	84(26)	−9(6)	1(8)	−19(16)
N(17)	11(3)	87(17)	76(33)	1(6)	−5(8)	10(20)
N(18)	12(3)	80(15)	121(24)	7(5)	1(7)	−9(16)

TABLE 2. Bond lengths (Å) and angles (deg.)

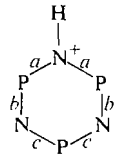

	Individual values	Mean	Parent molecule	$N_3P_3Cl_2(NHPr^i)_4.HCl$
P—N (ring) *a*	1.667, 1.669, 1.697, 1.683	1.68		1.666
b	1.555, 1.531, 1.581, 1.587	1.56	1.588	1.583
c	1.584, 1.582, 1.571, 1.568	1.58		1.558
∠ at N *a*–*a*	127.0, 124.2	126	123.0	131.7
b–*c*	129.9, 131.2, 129.0, 128.3	130		125.4
∠ at P *a*–*b*	109.6, 108.7, 110.1, 112.1	110	116.7	107.5
c–*c*	111.7, 113.8	113		120.1
P—N (exocyclic)	1.60–1.70	1.64	1.652	
Co—Cl	2.283, 2.286, 2.305, 2.336			
Cl—Co—Cl	106.3–107.8, 114.2, 114.9			

Can. J. Chem. Downloaded from www.nrcresearchpress.com by 210.87.254.105 on 09/05/12
For personal use only.

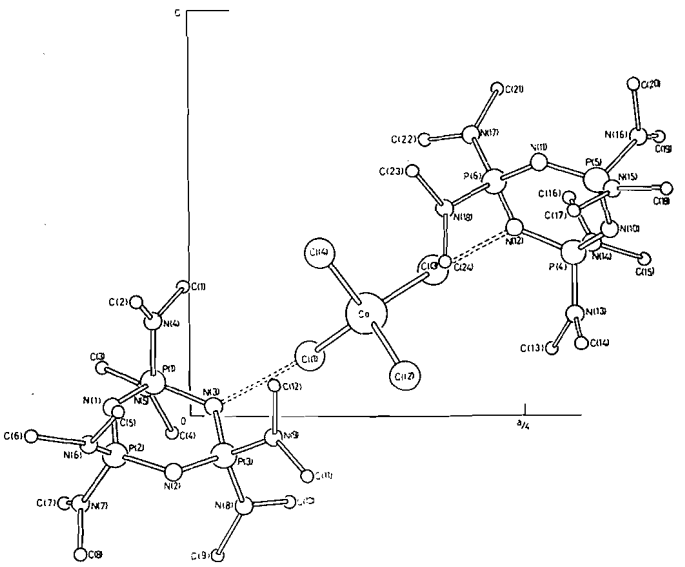

FIG. 1. Structure viewed along *b*.

the ring also differ somewhat from those in the parent compound. The exocyclic P—N bonds are in the range 1.60–1.70, mean 1.64 Å (parent 1.652 Å). The dimensions and general arrangement of the dimethylamino groups are similar to those in the parent molecule; the accuracy is poorer in the present case, so that no comment can be made on possible minor variations as observed in the parent (3).

The $CoCl_4^-$ ion is tetrahedral, with small deviations from exact tetrahedral geometry. Two of the chlorine atoms are involved in N—H ... Cl hydrogen bonding (Fig. 1, N ... Cl = 3.32 and 3.36 Å, P—N ... Cl = 114–119°), and the Co—Cl bonds average 2.32(1) Å. The other two Co—Cl bonds average 2.28(1) Å. These features were also observed in $[(NPMe_2)_4H]_2CoCl_4$ (*1b*). Other intermolecular distances correspond to van der Waals contacts.

We thank Professor N. L. Paddock for crystals and discussion, the National Research Council of Canada for financial support, and the University of British Columbia Computing Centre for assistance.

1. J. TROTTER and S. H. WHITLOW. J. Chem. Soc. (A), (*a*) 455 (1970); (*b*) 460 (1970).
2. N. V. MANI and A. J. WAGNER. Acta Cryst. **B27**, 51 (1971).
3. S. J. RETTIG and J. TROTTER. Can. J. Chem. **51**, 1295 (1973).
4. J. N. WINGFIELD and J. SERREQI. Private communication.

Can. J. Chem. Downloaded from www.nrcresearchpress.com by 210.87.254.105 on 09/05/12
For personal use only.

A Low Temperature Infrared Study on the Association of Thiols with Organic Oxygen Bases

R. BICCA DE ALENCASTRO[1]

Département de Chimie, Université de Montréal, Montréal, Québec

Received March 26, 1973[2]

The infrared spectra of mixtures of propane-1-thiol and several oxygen-containing weak organic bases have been measured between 2500 and 2650 cm^{-1}, in a 1:1 mixture of CCl_3F and $C_2F_4Br_2$ at temperatures ranging from 20 to −190 °C. Association of the S—H---O type was observed between propane-1-thiol and 2-methyl-tetrahydrofuran, or cyclopentanone. This association is less important between the thiol and hexachloropropanone. In the case of a thiol–furan mixture association of the S—H---π type is strongly indicated.

Les spectres infrarouges des mélanges entre le propanethiol-1 et plusieurs bases organiques faibles contenant de l'oxygène comme accepteur de proton ont été mesurés entre 2500 et 2650 cm^{-1}, dans un mélange 1:1 de CCl_3F et $C_2F_4Br_2$, à des températures allant de 20 à −190 °C. On observe des associations du type S—H---O chez les mélanges entre le thiol et le méthyle-2-tétrahydrofurane ou la cyclopentanone. L'association est moindre chez le mélange thiol–hexachloropropanone. Dans le cas d'un mélange thiol–furane la présence des liaisons hydrogène du type S—H---π est fortement indiquée.

Can. J. Chem., **52**, 738 (1974)

Introduction

It is well established that hydrogen bonding by O—H and N—H groups has an important place in many biochemical equilibria (1). This is not the case with S—H groups. Very little other than its existence (2) is known about hydrogen bonding of the S—H group in important biological molecules like proteins and coenzymes. Nevertheless, some work has been done on the association of sulfhydryl-containing compounds and a review of these is to be found in our previous work (3–6). The main objective of this series is to study by infrared spectroscopy the association in solution of S—H groups in simpler model systems over a wide temperature range. Some of the advantages of this are that at lower temperatures (*a*) some species not seen at room temperature can be formed; (*b*) the corresponding bands are narrower and easier to identify; and (*c*) in the less complicated cases values of equilibrium constants and enthalpies of formation can be obtained (7, 8).

Since the ketone and ether functional groups exist in important biological molecules (pyruvate-type molecules, sugars, etc.) we thought that it would be interesting to extend our work to the case of the association of mercaptans with simple ketones and ethers and to get some qualitative insight into the S—H---O type bonded species in these systems.

Some earlier studies have been made on the association of thiols with oxygen-containing acceptors. Copley, Marvel, and Ginzberg (9) have shown by cryoscopic studies the existence of a 1:1 S—H---O type hydrogen bonded complex between benzenethiol and ethyl ether or acetone. Gordy and Stanford (10) found, by i.r. spectroscopy at room temperature, very weak interactions between benzenethiol and isopropyl ether. This was confirmed by Josien, Dizabo, and Saumagne (11) and by David and Hallam (12). Lutskii and Sheremet'eva (13) studied the interaction of the X—H vibrator (X = O, N, S) with furan and tetrahydrofuran (THF). They have found hydrogen bonded species of the X—H---O type with THF and of the X—H---π type with furan. However, their work with S—H groups is not conclusive, since they could not observe any significant difference between thiophenol in THF or in furan.

In the present work we have studied by i.r. spectroscopy over a wide range of temperatures, the association of propane-1-thiol with 2-methyltetrahydrofuran (MTHF), furan, cyclopentanone (CP), and hexachloropropanone (HCP) as proton acceptors. A representative aliphatic thiol was chosen to prevent the ambiguity arising from S—H---π (self-associated) type species in an aromatic thiol. We hoped to be able to follow, as a function of the temperature, the changing pattern

[1]Present address: Instituto de Química, Universidade Federal do Rio de Janeiro, Caixa Postal 1573—ZC 00—Rio de Janeiro, Guanabara, Brazil.

[2]Revision received October 23, 1973.

Can. J. Chem. Downloaded from www.nrcresearchpress.com by 210.87.254.5 on 09/05/12
For personal use only.

Can. J. Chem. Downloaded from www.nrcresearchpress.com by 210.87.254.5 on 09/05/12
For personal use only.

of the fundamental S—H stretching vibration in the presence of the bases and to identify the various associated species.

Experimental

The technique and instruments we used have been fully described elsewhere (3–5). The sample of propane-1-thiol was the same as in our earlier works (3, 4). CCl_3F (Freon 11) and $C_2Br_2F_4$ (Freon 114B2) were obtained from E. I. Du Pont de Nemours Co., and were distilled and kept over phosphorus pentoxide. MTHF (b.p. 78–79 °C) and HCP (b.p. 202–204 °C) were purchased from Eastman Kodak Co., and CP (b.p. 129–132 °C) and furan (b.p. 30–31 °C) from the J. T. Baker Chem. Co. All products were dried over $CaSO_4$ and distilled twice before use. HCP boiled at 108–109 °C at 40 mm Hg. None of the i.r. spectra of these bases showed water absorption. They were handled under an inert atmosphere to avoid oxidation or moisture adsorption. The solutions were prepared gravimetrically and the concentrations were corrected for solvent contraction. They were used immediately after preparation. In the cases in which the bases showed little absorption in the 2500–2650 cm^{-1} region, we have presented only the spectra of the mixtures with the absorption due to the bases subtracted. However, in the case of furan where several bands are present in that spectral range, we give the spectra of the mixture, the spectra of furan and the subtracted spectra at different temperatures. Since the spectra of propane-1-thiol at similar concentrations and temperatures have been published already (3), we shall not reproduce them here. To prevent self-association the concentration of the base was kept at least twice that of the propane-1-thiol.

Results

Figure 1 shows the results that we obtained in a temperature-dependence study of a 1:2 solution of propane-1-thiol and MTHF in a 1:1 mixture of CCl_3F and $C_2Br_2F_4$ (FR). At room temperature the spectrum shows a band centered at 2558 cm^{-1}, with a shoulder on the high frequency side. This shoulder corresponds well with the free S—H band (3). The remaining band at lower frequencies is most likely to be assigned to the S—H---O type hydrogen bond since at this concentration no such band is observed in the absence of base (3). When the temperature is lowered it progressively shifts to lower frequencies (it is at 2520 cm^{-1} at −145 °C) and its intensity is increased. At low temperatures it is rather symmetric and its half-band width is roughly the same as at room temperature. This seems to indicate that we are dealing with a single species which is probably a 1:1 complex as has been suggested by other workers (9).

Figure 2 shows the results that we obtained with a mixture of 0.47 *M* propane-1-thiol and

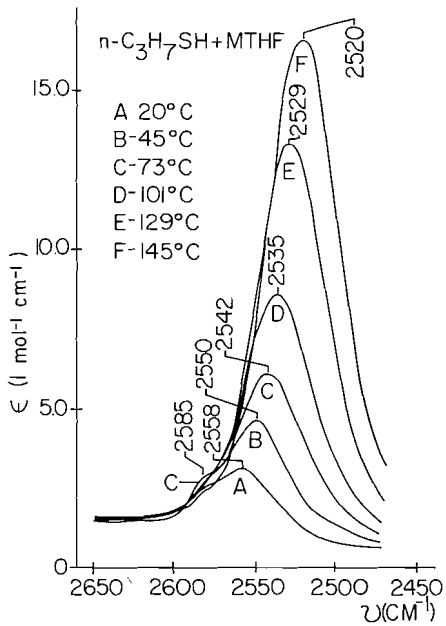

FIG. 1. The i.r. spectrum (2475–2650 cm^{-1}) of a mixture of 0.68 *M* propane-1-thiol and 1.39 *M* of 2-methyltetrahydrofuran in FR at different temperatures.

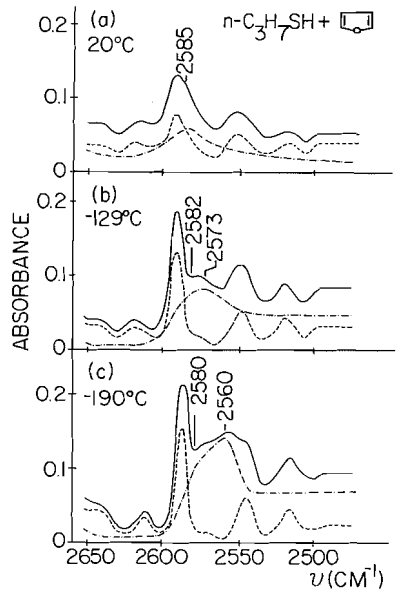

FIG. 2. The i.r. spectrum (2475–2650 cm^{-1}) of (---) a 1.26 *M* solution of furan in FR; (—) a mixture of 1.26 *M* furan and 0.47 *M* propane-1-thiol in FR; and (—.—.—) a mixture of 1.26 *M* furan and 0.47 *M* propane-1-thiol in FR with the absorption due to furan subtracted: (*a*) at 20 °C; (*b*) at −129 °C; (*c*) at −190 °C. Cell: 0.57 mm.

Can. J. Chem. Downloaded from www.nrcresearchpress.com by 210.87.254.5 on 09/05/12
For personal use only.

1.26 *M* furan. At room temperature (Fig. 2*a*) the spectrum is essentially that of a solution of pure propane-1-thiol in FR at a comparable concentration (see ref. 3). The free S—H band is at 2584 cm^{-1} (2585 cm^{-1} for propane-1-thiol in FR). As the temperature is lowered (Fig. 2*b*, *c*) the free band shifts to lower frequencies (the values for the free S—H bands in the figures are those of propanethiol in FR as quoted from ref. 3) and is seen as a shoulder on the more intense associated band. The position of this latter band and the magnitude of the shift with temperature are comparable with those of the S—H---π type hydrogen bonded species that we have found in our studies on the self-association of benzenethiol and α-toluenethiol (3) and in the association of propane-1-thiol with cumene (6). The shift is significantly smaller than that observed for the association between propane-1-thiol and MTHF (2573 cm^{-1} for furan and 2529 cm^{-1} for MTHF, at −129 °C). This low-temperature band is probably due to association of the S—H---π type rather than of the S—H---O type (see Discussion).

Figure 3 shows the variation with temperature of the spectrum of a 1:3 mixture of propane-1-thiol and CP. In this case the free band is not observed at 20 °C, probably due to overlap with the stronger band at 2569 cm^{-1} (free species are shown to be present at these concentrations by first overtone studies). At progressively lower temperatures this band shifts to lower frequencies and gains intensity. It is located at 2554 cm^{-1} at −101 °C and it is quite symmetric. We believe that this band is due to the 1:1 S—H---O type hydrogen bonded complex, since its position is comparable to that of the open dimer of the thiolic acids, at similar concentrations and temperatures (5).

Figure 4 shows the variation with temperature of the spectrum of a 1:2 mixture of propane-1-thiol and HCP in FR. Unlike the preceding case, practically no association is observed at room temperature. At lower temperatures some association occurs and the corresponding band is located at 2525 cm^{-1} at −180 °C. At −101 °C it is placed at about 2550 cm^{-1} and it is seen only as a shoulder on the free band. The position of this band is comparable to its position as in the case of propane-1-thiol and CP. The associated band is assigned to the S—H---O type hydrogen bonded 1:1 complex, but as it is very broad, the possibility of having more than one species is not excluded.

Discussion

One of the important conclusions of this work is that the oxygen bases form mainly 1:1 complexes with the aliphatic thiols. This is not true for the stronger bases pyridine and triethylamine where at least a 2:1 complex of the S—H---S—H---N type is present at lower temperatures (4). Whether this has some significant biochemical importance remains to be investigated. It is significant that, already at room temperature, association of the S—H---O type occurs. However, studies on the first overtone region show that, even at the lowest temperatures, free molecules

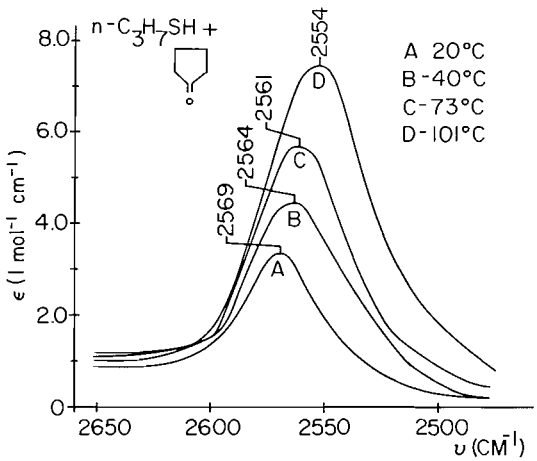

FIG. 3. The i.r. spectrum (2475–2650 cm^{-1}) of a mixture of 0.50 *M* propane-1-thiol and 1.66 *M* cyclopentanone in FR at different temperatures.

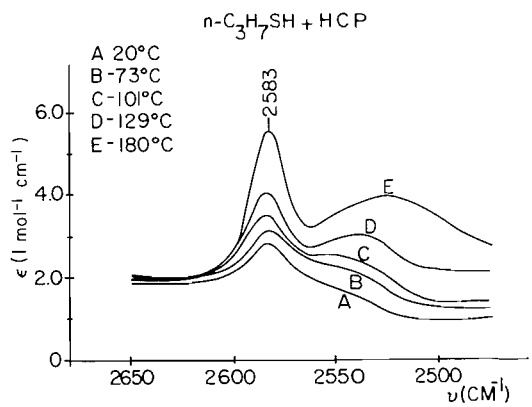

FIG. 4. The i.r. spectrum (2475–2650 cm^{-1}) of a mixture of 0.59 *M* propane-1-thiol and 1.32 *M* hexachloropropanone in FR at different temperatures.

Can. J. Chem. Downloaded from www.nrcresearchpress.com by 210.87.254.5 on 09/05/12
For personal use only.

still exist. For furan, the half-width position of the maximum and magnitude of the shift, are consistent with bonded species of the S—H---π type rather than of the S—H---O type. Lutskii and Sheremet'eva (13) have found a similar behavior with O—H and N—H containing molecules. This result is not surprising in view of the delocalization of the p-electrons of the oxygen which results in increased basicity of the π system and decreased basicity of the free pair. We have demonstrated that the formation of the S—H---π type hydrogen bonds is competitive even with the formation of the S—H---N type bonds at least in the case of benzenethiol (4) with strong bases such as pyridine. However, Fig. 2 shows that here, as in the case of the S—H---π type complex between propane-1-thiol and cumene (6), practically no bonded species are observed in the fundamental region at room temperature (or at higher concentrations of acceptor). To observe associated species is more difficult in the first overtone region where the related bands are weaker than the free band. This has proven to be a general fact in weak hydrogen bond type associations and it prevented us from making similar studies on the first overtone. The reason is thought to be linked to the mutual cancellation of some terms in the expressions for the intensity of the first overtone due to the large variation of the dipole moment with the normal coordinate upon hydrogen bond formation (14).

The intriguing fact that the "free" band seems to gain intensity when the temperature is lowered (Fig. 4) in the case of the mixture between propane-1-thiol and HCP merits some discussion at this point. In an earlier paper (3) we have found a similar phenomenon in connection with the self-association of mercaptans and have attributed it mainly to two factors. (The small variation of the integrated intensity coefficient with temperature as measured by Bourdéron (7) in the case of the association of 2,6-di-*tert*-butyl-*p*-cresol with cyclohexanone cannot account for the observed increase in our case.) The first, contributions of terminal S—H groups of open dimers and trimers of the S—H---S type obviously cannot apply here. The second, enhancement of the intensity of the "free" S—H band via a charge-transfer complex between the bromine atoms of the solvent and the sulfur in competition with the formation of hydrogen bonds, similarly to that observed with secondary amines (15), is more likely. That this effect is not seen in the other cases that we investigated can be explained as a consequence of the reduction of the basicity of the carbonyl caused by the chlorine atoms. The possibility that the increase in intensity may be caused by S—H---Cl species seems to be ruled out by the absence of a significant shift to lower frequencies. Josien, Dizabo, and Saumagne (11) have observed shifts of 10–20 cm^{-1} with S—H---X (X = halogen) hydrogen bonded 1:1 complexes in the case of benzenethiol and halogenated hydrocarbons.

It has been known for some time that the i.r. band corresponding to the ν_s vibration of hydrogen bonded species is temperature dependent. Asselin and Sandorfy (16) have discussed the matter and found that in the case of self-associated alcohols, the temperature variation of the anharmonicity coefficient has a significant influence on the shift. Moreover they found linear relationships between the temperature of the solution and the fundamental and overtone frequencies, the slope being about the same for both. Another important characteristic of $d\nu/dT$ is its mass dependence. A smaller value of $d\nu/dT$ was found with deuterated alcohols as compared with the nondeuterated corresponding alcohols (16). (The Buckingham theory on solvent effects (17–19) predicts a dependence of $d\nu$ on the square root of the reduced mass.) More recently, Rice and Wood (20, 21) have reexamined this effect. They have found no temperature shift in the gaseous phase using the 1:1 complex formed between trifluoroethanol and trimethylamine. Their results are consistent with a model where there is strong coupling between the ν(A—H) vibration and the "hydrogen bonding" vibration ν(A---B) in the complex A—H---B in solution. They have shown that the anharmonicity of the ν(A---B) vibration coupled with a contraction of the (A---B) distance in the upper vibrational levels of the stretching vibration ν(A—H) (caused by the contraction of the solvent cage or lattice with decreasing temperature) is responsible for a part of the observed shift.

In Table 1 we present the values of $d\nu/dT$ that we have found with some S—H systems. For comparison, some of the values of Asselin and Sandorfy (16) are included. Some interesting conclusions can be reached. The values for S—H associated species are generally smaller than those of the alcohols in part as a consequence of a mass effect. More important than this is the fact that the S—H---π type bonded species have a fairly

TABLE 1. The temperature dependence of the stretching vibration of associated hydrogen bonded species

Molecule	Solvent	dv/dT ($°K^{-1}$ cm^{-1})
i-C_3H_7OH*	FR	0.59
i-C_3H_7OD*	FR	0.48
t-C_4H_9OH*	FR	0.44
t-C_4H_9OD*	FR	0.28
n-C_3H_7SH†	FR	0.22
	Pure liquid	0.22
i-C_3H_7SH†	FR	0.18
	Pure liquid	0.20
C_6H_5SH‡	FR	0.09
$C_6H_5CH_2SH$‡	FR	0.09
n-C_3H_7SH + cumene‡	FR	0.09
n-C_3H_7SH + CP	FR	0.14
n-C_3H_7SH + THF	FR	0.24

*Reference 16.
†Dimer of the S—H---S type.
‡1 :1 complex of the S—H---π type.

constant value which is significantly different from the S—H---S and S—H---O type bonded 1 : 1 complex. This is probably due to the fact that in the case of the S—H---π type complex the ν(S—H) vibration is less coupled with the low frequency ν(S----π) vibration (this is in part also responsible for the characteristic small half-width of the S—H---π bands), and that the contraction of the (S---π) distance in the excited state is less important than in the case of the S—H---O and S—H---S type complexes. It is interesting to note that in the case of the S—H---π type band in the thiol–furan mixture the temperature dependence of the associated band is in agreement with the value of 0.09 cm^{-1} $°K^{-1}$ given in Table 1 for the S—H---π bonds, within the experimental errors caused by overlapping with the free band. This is an additional argument in favor of our assignment.[3]

[3]A referee has raised a question about the rather complicated matter of the increase in intensity of the associated bands with temperature. The spectra are presented in apparent intensity units (ε). However, it is well known that the band corresponding to the hydrogen bonded species has an intrinsic integrated intensity greater than that of the free band. This is known to be due to a large variation of the dipole moment upon formation of the hydrogen bond. Now, Herman and Shuler's expression for the intensity of the fundamental (22) (eq. 1) is

$$[1]\quad A^{1,0} = (8\pi^3 N_{v_0}/3hc)w^{1,0}\{\mu_1(1/\sqrt{2} - 3/2\sqrt{2}g + 11/4\sqrt{2}b^2) + \mu_2(-5b/\sqrt{2} + 88/\sqrt{2}bg - 715/12\sqrt{2}b^3)\}^2$$

where w is the wavenumber in cm^{-1}; $b = k_3/w_e$; $g = k_4/w_e$; N_{v_0} is the number of molecules per cm^3 in the lower vibrational level; $\mu_1 = (d\mu/dQ)_e$; $\mu_2 = (1/2)(d^2\mu/dQ^2)_e$; $\mu(Q) = \mu_e + \mu_1 Q + \mu_2 Q^2$; Q is the normal coordinate; k_3 and k_4 are the quartic potential constants.

In a condensed phase, due to changes in the solvent environment, N_{v_0}, μ_1, and μ_2 should be temperature dependent. This means that in a wide temperature range the intrinsic intensity is not constant for both free and associated species. The variation of N_{v_0} with temperature can be obtained assuming a Boltzmann distribution, but the dependence of μ_1 and μ_2 is not known. In some cases the experimental dependence of the intensity of the free band with temperature can be obtained, and so, equilibrium constants and enthalpy values can be found using classical procedures (7). In our case we cannot use a similar technique since the free band is very weak and overlapping with the associated band is extremely severe. We know of no similar procedures for the associated band. These problems prevented us from obtaining equilibrium constants and the values of the enthalpies of formation of the complexes in our systems.

We would like to express our thanks to the National Research Council of Canada for financial help, and to Professor C. Sandorfy for reading this manuscript and for his comments. The author would like also to express his gratitude to the Conselho Nacional de Pesquisas, Rio de Janeiro, Brazil, for a scholarship and to the Instituto de Química da Universidade Federal do Rio de Janeiro, Brazil, for a special leave of absence.

1. G. C. PIMENTEL and A. L. MCCLELLAN. The hydrogen bond. W. H. Freeman and Co. San Francisco 1960.
2. S. A. BERNHARD. The structure and functions of enzymes. W. A. Benjamin, Inc. N.Y. 1968.
3. R. BICCA de ALENCASTRO and C. SANDORFY. Can. J. Chem. **50**, 3594 (1972).
4. R. BICCA de ALENCASTRO and C. SANDORFY. Can. J. Chem. **51**, 985 (1973).
5. R. BICCA de ALENCASTRO and C. SANDORFY. Can. J. Chem. **51**, 1443 (1973).
6. R. BICCA de ALENCASTRO. Ph.D. Thesis. University of Montreal, Montreal, 1972.
7. C. BOURDÉRON. Can. J. Chem. **50**, 1199 (1972).
8. C. SANDORFY. Can. J. Spectrosc. **17**, 24 (1972).
9. M. J. COPLEY, C. S. MARVEL, and E. GINZBERG. J. Am. Chem. Soc. **61**, 3161 (1939).
10. W. GORDY and S. C. STANFORD. J. Am. Chem. Soc. **62**, 497 (1940).
11. M.-L. JOSIEN, P. DIZABO, and P. SAUMAGNE. Bull. Soc. Chim. Fr. 423 (1957).
12. J. G. DAVID and H. E. HALLAM. Trans. Faraday Soc. **60**, 2013 (1964).
13. A. E. LUTSKII and G. I. SHEREMET'EVA. Russ. J. Phys. Chem. (Engl. Transl.) **41**, 403 (1967).
14. T. DI PAOLO, C. BOURDÉRON, and C. SANDORFY. Can. J. Chem. **50**, 3161 (1972).

Can. J. Chem. Downloaded from www.nrcresearchpress.com by 210.87.254.5 on 09/05/12
For personal use only.

15. M.-C. BERNARD-HOUPLAIN, C. BOURDÉRON, J.-J. PÉRON, and C. SANDORFY. Chem. Phys. Lett. **11**, 149 (1971).
16. M. ASSELIN and C. SANDORFY. J. Mol. Struct. **8**, 145 (1971).
17. A. D. BUCKINGHAM. Proc. Royal Soc. (Lond.), **A248**, 169 (1958).
18. A. D. BUCKINGHAM. Proc. Royal Soc. (Lond.), **A255**, 32 (1960).
19. A. D. BUCKINGHAM. Trans. Faraday Soc. **56**, 753 (1960).
20. S. A. RICE and J. L. WOOD. J. Chem. Soc. Faraday Trans. II, 87 (1973).
21. S. A. RICE and J. L. WOOD. J. Chem. Soc. Faraday Trans. II, 91 (1973).
22. R. C. HERMAN and K. E. SHULER. J. Chem. Phys. **22**, 481 (1954).

Can. J. Chem. Downloaded from www.nrcresearchpress.com by 210.87.254.5 on 09/05/12
For personal use only.

A Carbon-13 Nuclear Magnetic Resonance Study of Cation Solvation in Alcohols

GERALD W. STOCKTON AND JOHN S. MARTIN

Department of Chemistry, University of Alberta, Edmonton, Alberta T6G 2G2

Received July 30, 1973

Natural abundance ^{13}C spectra of solvent coordinated to the cation have been observed in solutions of Mg(II) and Al(III) salts in alcohols. Carbon shielding changes induced by cations resemble those induced by electronegative substituents; a sign reversal between the β and γ positions is found in both instances. Solvent exchange rates correspond to those found by ^{1}H n.m.r.; this confirms that whole molecule exchange is dominant. Selective relaxation of the solvation shell signals at low temperatures reflects differences in conformational mobility within the solvation complex.

Utilisant les spectres du ^{13}C en abondance naturelle on a observé pour des solutions de sel Mg(II) et Al(III) dans des alcools que le solvant était coordonné au cation. Les changements dans les blindages du carbone qui sont induits par les cations ressemblent à ceux induits par des substituents électronégatifs; un renversement de signe entre les positions β et γ est trouvé dans chaque cas. Les taux d'échanges du solvant correspondent à ceux trouvé par r.m.n. ^{1}H; ceci confirme que l'échange de molécules entières est le processus dominant. Les relaxations sélectives des signaux de la micelle de solvatation à basse température indiquent des différences de mobilité conformationnelle dans le complexe de solvatation.

[Traduit par le journal]

Can. J. Chem., **52**, 744 (1974)

Introduction

The nuclear magnetic resonance (n.m.r.) spectra of solvent molecules coordinated to an ion may be observed directly if the residence time of the molecules in the solvation shell is long, compared to the inverse of the frequency difference between the n.m.r. signals of the bulk and solvation molecules. This condition is satisfied for the n.m.r. of hydroxyl group protons in alcohols and water bound to small, highly charged cations (1). ^{1}H n.m.r. spectra of these systems have yielded solvation numbers (2), exchange rates (3), and details of the structure of the solvation shell (4).

At this time, only one ^{13}C n.m.r. spectrum of a coordinated solvent has been reported: that of dimethylsulfoxide (DMSO) bound to Al(III) in a mixed D_2O–DMSO solvent (5). With the current development of sensitive high-field Fourier transform n.m.r. spectrometers (6), it has become possible to observe the natural abundance ^{13}C n.m.r. spectra of relatively dilute entities in solution. This has made the carbon resonances of relatively large solvation molecules accessible to study.

We report here the observation of solvation shell ^{13}C n.m.r. spectra of ethanol and *n*-propanol complexed to Mg(II) and Al(III) in single solvent systems. These experiments reveal interesting carbon shielding effects and define some of the constraints on this type of study.

Procedures

Fisher reagent grade *n*-propanol was Soxhlet extracted with 4A molecular sieve for 24 h and distilled, the middle 60% (boiling range less than 1°) being collected and stored over 4A molecular sieve. Ethanol from the U.S. Industrial Chemical Co. contained impurities (including water) at the level of 10^{-5} or less. The neat liquid at 20° gave a well-resolved OH proton n.m.r. triplet, indicating a very low concentration of acidic or basic impurities.

G. F. Smith Chemical Co. anhydrous magnesium perchlorate was initially dried by heating at 200° under vacuum. It was then recrystallized from a minimum of acetonitrile, using previously dried filter papers under a dry nitrogen atmosphere. The salt was then dried at 200° for several days. Anhydrous aluminum and gallium trichlorides and silver perchlorate from Alfa Inorganic Chemicals were used as received.

All chemicals were stored and handled in a glove box containing a positive pressure of dry nitrogen. Weighings were performed in the glove box on a Cahn DTL millibalance equipped with a radioactive source to dispel static charge. Samples prepared in the glove box were transferred in the box to 10-mm n.m.r. sample tubes which were capped to exclude air and water vapor.

Natural abundance ^{13}C n.m.r. spectra were obtained at 22.63 MHz using a Bruker HFX-90 spectrometer operating in the pulsed Fourier transform mode. An external deuterium lock was used. Spectra were normally obtained with incoherent decoupling of ^{1}H; these required accumulation of *ca.* 500 free induction decays to achieve adequate signal-to-noise ratio in the transformed

Can. J. Chem. Downloaded from www.nrcresearchpress.com by 210.87.254.42 on 09/05/12
For personal use only.

Can. J. Chem. Downloaded from www.nrcresearchpress.com by 210.87.254.42 on 09/05/12
For personal use only.

spectrum. Spectra taken without ^1H decoupling required *ca.* 3000 free induction decays.

Since this paper is concerned with effects on nuclear shielding, solvation shell shifts are reported as shielding changes in contrast to the usual convention in ^{13}C n.m.r. (7). A positive solvation shell shift thus means that a nucleus is more shielded in the solvation shell than in the bulk solvent. All such shifts reported here were measured directly, relative to the appropriate bulk solvent peak in the sample.

Peak areas were measured by planimeter, relative to an estimated smooth baseline. Their precision was limited by the reproducibility of the rather noisy spectra and was of the order of $\pm 15\%$.

Observations

Figure 1*a* shows the low-temperature ^{13}C n.m.r. spectrum of ethanol containing 0.72 *m* magnesium perchlorate. Each of the two major peaks, assigned to CH_2 and CH_3, respectively, develops a satellite at temperatures below about $-40°$. At any constant low temperature, the intensity of a satellite is proportional to the salt concentration. It is thus reasonable to assign the satellite peaks, by analogy to the ^1H n.m.r. (8), to solvent molecules coordinated to the cation.

Figure 1*b* is the ^{13}C n.m.r. spectrum of ethanolic $Mg(ClO_4)_2$ at $-70°$ without ^1H decoupling. The bulk and solvation shell ethanol spectra show identical coupling patterns. To the limit of the accuracy of our measurements (*ca.* 2 Hz), each one-bond C–H coupling constant is unchanged between the bulk and solvated states.

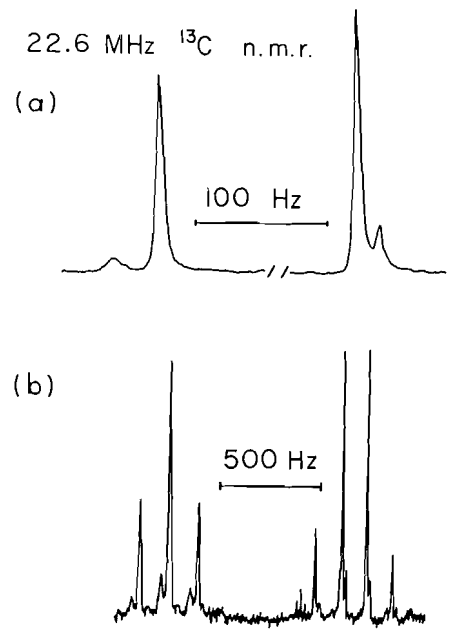

FIG. 1. The carbon-13 n.m.r. spectrum of 0.72 *m* ethanolic magnesium perchlorate at $-70°$: (*a*) with incoherent proton decoupling; (*b*) without decoupling. The two spectra are not to the same scale.

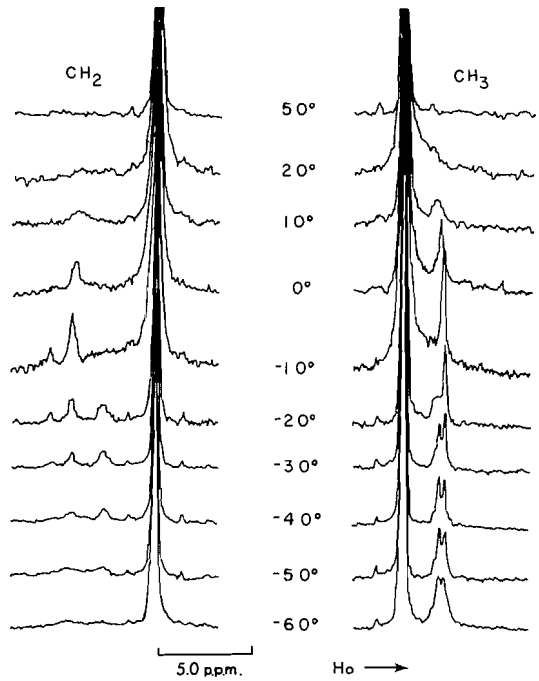

FIG. 2. The carbon-13 n.m.r. spectrum of 1.24 *m* ethanolic aluminium chloride as a function of temperature.

Careful measurement of the spectra indicates that the positions of the solvation shell peaks become invariant to temperature below $-50°$. Thus the exchange of molecules between bulk liquid and the solvation shell, which causes the merging of the signals at high temperatures, is so slow below $-50°$ that these spectra may be regarded as unaffected by exchange.

The carbon spectra of ethanolic aluminium chloride are shown in Fig. 2. Solvation shell signals first appear in the neighborhood of 0°. Below $-20°$, the CH_2 carbon shows three solvation shell signals. Their temperature dependencies and intensities correspond to those observed in the OH proton spectrum by Grasdalen (8). At least two CH_3 carbon solvation shell signals are discernible; a third may coincide with one of the others.

Ethanolic $AlCl_3$ was converted to aluminium perchlorate by reaction with an equivalent amount of silver perchlorate, the silver chloride precipitate being removed by centrifuge. The resulting solution showed only one solvation shell

Can. J. Chem. Downloaded from www.nrcresearchpress.com by 210.87.254.42 on 09/05/12
For personal use only.

signal for each carbon, indicating that the chloride ion must participate in the aluminium ion solvation shell. This experiment is not capable of determining whether chloride ion displaces solvent to form contact ion pairs or binds to solvation shell molecules to form solvent separated ion pairs.

Solutions of $AlCl_3$ in *n*-propanol showed solvation shell spectra for all three carbons. No multiple solvation shell spectra were observed, though Grasdalen has reported three OH proton signals (9). However, in the temperature range (0 to −40°) where multiple proton signals were observed, the carbon resonances were very broad and any multiplicity may have been masked.

In all cases, as the temperature was lowered further, the solutions became very viscous and the carbon n.m.r. lines broadened homogeneously. The solvation shell signals eventually disappeared into the baseline noise at very low temperatures, given in Table 1. In these spectra, solvation shell lines disappeared when their widths exceeded *ca.* 20 Hz. The bulk solvent signals did not broaden appreciably until the temperature fell below about −90°.

In all cases, the CH_2 carbon adjacent to oxygen showed the greatest broadening, beginning at the highest temperature. Because of this, it was not possible to observe the slow-exchange limiting shift of this CH_2 carbon in the solution of $AlCl_3$ in *n*-propanol. The shift was *ca.* −3 p.p.m. when the signal disappeared into the baseline noise. Its temperature dependence suggests a limiting shift of *ca.* − 5 p.p.m.

No solvation shell signals were observed in solutions of $Mg(ClO_4)_2$ in methanol or $CaCl_3$ in ethanol, in the range +30 to −90°. Hydroxyl proton solvation shell spectra have been observed in the former system (3). Presumably the homogeneous broadening of the carbon solvation shell signals occurs at such high temperatures in these systems that the slow-exchange spectra never appear.

TABLE 1. Approximate lower temperatures at which ^{13}C solvation shell signals disappeared, due to homogeneous broadening

System	Temperature (°C) β carbon*	γ carbon
$Mg(ClO_4)_2$ in EtOH, 0.72 *m*	−85	−100
$AlCl_3$ in EtOH, 1.24 *m*	−60	< −60
$AlCl_3$ in *n*-PrOH, 1.15 *m*	−30	−40

*Carbon "β" is bonded to the oxygen. See explanation in text.

TABLE 2. Carbon shieldings of coordinated solvent molecules, relative to those in bulk solvent

System	Shielding changes (p.p.m.) β carbon*	γ carbon	δ carbon
$Mg(ClO_4)_2$ in EtOH, −70°	−1.5	+0.8	
$Al(ClO_4)_3$ in EtOH, −30°	−5.6	+2.2	
$AlCl_3$ in EtOH, −50°	−5.5 −4.6 −2.8	+2.0 +1.7	
$AlCl_3$ in PrOH, −30°	*ca.* −5	+2.0	+0.1
$AlCl_3$ in DMSO, −70°		+1.9†	

*The designation of carbon positions is explained in the text.
†Taken from ref. 5.

Discussion

The Carbon Shieldings

Table 2 summarizes all the shielding changes of solvation shell carbons relative to bulk solvent that have been observed. If we regard the shifts in $Al(ClO_4)_3$ solutions as the "normal" ones for Al(III) in ethanol, certain regularities become apparent. At a given position in a solvent molecule, Al(III) induces shielding changes which are about two to three times those induced by Mg(II). The surface electrostatic fields, Ze/r^2, of the two ions are in the ratio 2.5 to 1. The relative magnitudes of the shielding effects are those to be expected of an electrostatic perturbation of the solvent molecule by the ion, as was the case for hydrogen shielding (10).

The magnitude of the shielding change decreases with increasing distance from the ion. Both positive and negative shielding effects occur, in contrast to the case of hydrogen, where all shielding changes induced by cations are negative (1, 10). The sign of the shift depends on the position of the carbon atoms in the molecule, in a regular way which becomes apparent when atoms are labelled as in Table 2. The complexed oxygen is designated α; β, γ, etc. denote successive non-hydrogenic atoms.

It is apparent that the cation-induced shifts of carbon are negative at the β position, and positive at γ, in all cases including that of DMSO (5). These solvation shifts, which involve a charge

Can. J. Chem. Downloaded from www.nrcresearchpress.com by 210.87.254.42 on 09/05/12
For personal use only.

shift toward the α-atom from the rest of the molecule, correspond in sign to those induced in hydrocarbons by electronegative substitution (11). Both perturbations characteristically produce deshielding of a carbon β, and shielding of a carbon γ to the point of substitution.

The appearance of the well known "γ effect" in the solvation shell spectra, in systems with one or two heteroatoms, may be of some significance in the theory of ^{13}C shielding. It is generally supposed that the γ effect arises from specific through space interactions (12). This may require reexamination in the light of evidence to be presented here that the γ carbon in a solvated alcohol is conformationally much more mobile than the β carbon.

Solvation Numbers

In principle, the integrated intensities of bound and bulk solvent signals, in the slow exchange limit, will yield the cation solvation number. In a carbon n.m.r. experiment, these intensities must be obtained from a spectrum in which proton decoupling is not used, since different relaxation processes of molecules in different environments may lead to different Overhauser enhancements (13). In the undecoupled spectra, the low signal to noise ratio made intensity measurements imprecise. Our solvation numbers were 5.5 ± 1 for $Mg(ClO_4)_2$ in ethanol, and 4 ± 1 for $AlCl_3$ in ethanol. These are consistent with previous determinations (2, 8).

Exchange Rates and Mechanisms

Because of the poor signal-to-noise ratios, no quantitative analysis of exchange rates was attempted. However, a rough order of magnitude estimate can be made at the upper temperature at which the solvation shell signal disappears: at this point, the lifetime of a molecule in the solvation shell is comparable to the inverse of the frequency separation between the bulk and solvation shell signals (14).

For $Mg(ClO_4)_2$ in ethanol, this occurs at about $-45°$, with frequency separation *ca.* 35 Hz; this implies a lifetime of *ca.* $(\pi \times 35)^{-1} = 9 \times 10^{-3}$ s. The proton lifetime observed by Alger (15) at $-45°$ was *ca.* 5×10^{-3} s. Similarly, for ethanolic $AlCl_3$ we estimate a solvation shell lifetime of 3×10^{-3} s at $+15°$; Grasdalen (8) observed two lifetimes, 0.3×10^{-3} and 12×10^{-3} s at this temperature. Our spectra suggest that there are different lifetimes in different sites, but the approximations and imprecision of measurement allow us only to note that the average carbon and proton lifetimes appear to be substantially identical.

Since carbon lifetimes must be those of the entire molecule, the agreement found here confirms the inference by previous workers that their proton exchange rates (3, 8) measure whole molecule exchange between the solvation shell and the bulk liquid.

Selective Relaxation in the Solvation Shell

In all cases where a solvation shell spectrum is visible, homogeneous broadening of the carbon signals occurs in the following order. The β-CH_2 signal of the solvating molecules broadens first, the other signals in the solvating molecules, and lastly at (*ca.* -90 to $-100°$) the signals of the bulk solvent. This is the order to be expected if the line broadening at low temperature is controlled by dipole–dipole relaxation of the carbons.

The linewidth of ^{13}C resonances, in the rapid reorientation limit is given by (16),

$$[1] \qquad \Delta\nu = (\pi T_2)^{-1} = (\pi T_1)^{-1} = \frac{N}{\pi} \hbar^2 \gamma_C^2 \gamma_H^2 r_{CH}^{-6} \tau_c$$

where N protons are at a distance r_{CH}. Since carbon relaxation is dominated by interaction with directly bonded hydrogens, r_{CH} is substantially constant and N is 2 or 3. Thus the major cause of variation in the linewidths should be differences in the reorientation correlation time τ_c.

The correlation time of a rigid spherical molecule of radius r is (17),

$$[2] \qquad \tau_c = \frac{4\pi}{3} \frac{\eta}{kT} r^3$$

The rapid increase of viscosity, η, of a hydrogen bonded solvent as the temperature decreases leads to an increase of all correlation times and linewidths. This is greatest for molecules involved in the solvation complex, whose effective radius is much greater than that of a single solvent molecule.

Within the solvation complex, one might expect that the carbon next to the site of ionic attachment would be rigidly bound, while carbons farther along the chain would have greater conformational mobility. This expectation is reinforced by examination of space filling molecular models. The rigidly bound β-CH_2 carbons share

in the relatively slow motion of the entire solvation complex, and show a greater linewidth than the more mobile γ and δ carbons. Similar behavior has been observed in 1-decanol, where the correlation time of the terminal methyl carbon is much shorter than those of carbons in the center of the chain, or near the hydrogen bonded OH group (16).

Conclusions

The ^{13}C spectra of alcohols coordinated to the small, highly charged cations Mg(II) and Al(III) are observable at temperatures low enough to retard solvent exchange with the bulk liquid, but not so low that the linewidth broadening brought about by increased viscosity causes the signals to disappear into the baseline. Apparently these limits overlap in the cases of $Mg(ClO_4)_2$ in methanol and $Ga(ClO_4)_3$ in ethanol; in neither case was any solvation shell signal observed.

Carbon shielding changes induced by formation of a cation complex appear to be related to the electrostatic field of the ion. In all cases, carbon β to the ionic attachment was deshielded, and carbon γ was shielded. This recalls the "γ effect" in substituted hydrocarbons.

Carbon n.m.r. spectra appear to yield solvation numbers and exchange rates similar to those observed by hydroxyl proton n.m.r. of the same systems. The latter agreement confirms that the reported proton n.m.r. exchange rates apply to whole molecule exchange.

Differences in the rates of homogeneous broadening at low temperatures are consistent with the reorientation correlation times which would arise from differences in conformational mobility to be expected in a solvation complex.

It appears likely that ^{13}C n.m.r. spectroscopy will be even more useful than proton n.m.r. as a probe of solvation phenomena. A given ion-induced electronic perturbation produces carbon shielding changes as large as or larger than those of hydrogen, and produces significant effects at more remote sites in the molecule. This should make possible solvation shell spectroscopy of many nonhydroxylic basic solvents, and give insight into the structure and dynamics of the solvation complex.

1. A. Fratiello, R. E. Lee, V. M. Nishida, and R. E. Schuster. J. Chem. Phys. **48**, 3705 (1968).
2. J. F. Hinton and E. S. Amis. Chem. Revs. **71**, 628 (1971).
3. S. Nakamura and S. Meiboom. J. Am. Chem. Soc. **89**, 1765 (1967).
4. R. N. Butler, J. Davies, and M. C. R. Symons. Trans. Faraday Soc. **66**, 2426 (1970).
5. J. C. Boubel, J. J. Delpuech, M. R. Khaddar, and A. Peguy. Chem. Commun. 1265 (1971).
6. E. D. Becker and T. C. Farrar. Science, **178**, 361 (1972).
7. J. B. Stothers. Carbon-13 n.m.r. spectroscopy. Academic Press, New York. 1972. p. 50.
8. H. Grasdalen. J. Magn. Reson. **5**, 84 (1971).
9. H. Grasdalen. J. Magn. Reson. **6**, 336 (1972).
10. G. W. Stockton and J. S. Martin. J. Am. Chem. Soc. **94**, 6921 (1972).
11. D. M. Grant and E. W. Paul. J. Am. Chem. Soc. **86**, 2984 (1964).
12. D. K. Dalling and D. M. Grant. J. Am. Chem. Soc. **94**, 5318 (1972).
13. A. J. Jones, D. M. Grant, and K. F. Kullmann. J. Am. Chem. Soc. **91**, 5013 (1969).
14. C. S. Johnson, Jr. Adv. Magn. Reson. **1**, 33 (1965).
15. T. D. Alger. J. Am. Chem. Soc. **91**, 2220 (1969).
16. D. Doddrell and A. Allerhand. J. Am. Chem. Soc. **93**, 1558 (1971).
17. J. A. Pople, W. G. Schneider, and H. J. Bernstein. High resolution nuclear magnetic resonance. McGraw-Hill, Toronto. 1959. p. 202.

Can. J. Chem. Downloaded from www.nrcresearchpress.com by 210.87.254.42 on 09/05/12
For personal use only.

Isotope Effect Studies on Elimination Reactions.[1] IX. The Nature of the Transition State for the E2 Reaction of 2-Arylethylammonium Ions with Ethoxide in Ethanol

P. J. SMITH[2] AND A. N. BOURNS

Department of Chemistry, McMaster University, Hamilton, Ontario

Received August 13, 1973

Kinetic isotope effects have been determined for the E2 reaction of some 2-arylethyltrimethylammonium ions with ethoxide in ethanol at 40°. The nitrogen effect, $(k^{14}/k^{15} - 1)100$, decreased with increasing electron-withdrawing ability of the *para* substituent; *i.e.* 1.37, 1.33, 1.14, and 0.88 for *p*-OCH_3, *p*-H, *p*-Cl, and *p*-CF_3, respectively. Furthermore, the primary hydrogen–deuterium isotope effects increased for the same substituents, respectively; *i.e.* k^H/k^D = 2.64, 3.23, 3.48, and 4.16. A large positive ρ value of 3.66 was found as well as a small secondary α-deuterium effect of 1.02 for *p*-H. In addition, the nitrogen isotope effect decreased with increasing strength of the abstracting base for the reaction of ethyltrimethylammonium ion; *i.e.* 1.86 and 1.41 at 60° for reaction with EtO^-–EtOH and *t*-BuO^-–*t*-BuOH, respectively. The results are discussed in terms of recent theoretical treatments of the effect of base, substituents, and nature of the leaving group on the nature of the transition state for an E2 process. The conclusion is reached that any structural change which causes one bond (C—H) to be weakened more at the transition state will have a corresponding effect on the other bond (C—$\overset{+}{N}$).

On a déterminé les effets isotopiques cinétiques pour les réactions E2 de quelques ions aryl-2 éthyltriméthylammonium avec l'éthylate dans l'éthanol à 40°. L'effet isotopique de l'azote $(k^{14}/k^{15} - 1)100$ diminue à mesure que le substituant en para est plus électroaffinitaire; *i.e.* 1.37, 1.33, 1.14 et 0.88 pour *p*-OCH_3, *p*-H, *p*-Cl et *p*-CF_3, respectivement. De plus les effets isotopiques primaires hydrogène–deutérium augmentent pour les mêmes substituants soit k^H/k^D = 2.64, 3.23, 3.48 et 4.16, respectivement. Une grande valeur positive de ρ de 3.66 a été trouvée de même qu'un petit effet isotopique secondaire α-deutérium de 1.02 pour *p*-H. De plus l'effet isotopique de l'azote diminue lorsque la basicité augmente dans la réaction de l'éthyltriméthylammonium soit 1.86 et 1.41 à 60° pour la réaction pour EtO^-–EtOH *t*-BuO^-–*t*-BuOH. On discute les résultats en terme des récents traitements théoriques de l'effet des bases de substituants et de la nature du groupe partant sur l'état de transition du processus E2. On arrive à la conclusion que tout changement qui amène un affaiblissement d'un lien (C—H) dans l'état de transition aura un effet semblable sur d'autre lien (C—$\overset{+}{N}$). [Traduit par le journal]

Can. J. Chem., 52, 749 (1974)

Introduction

An understanding of the effect of structural changes in reactants on the energy and structure of the transition state constitutes an important element in the detailed description of the pathway of many types of reactions. A number of studies of this kind have been carried out on the E2 elimination reaction, but conflicting theories and ambiguities in the interpretation of experimental results have led to considerable uncertainty.

One of the most direct ways of obtaining information on the transition state is by measuring the isotope effect associated with an atom whose bond is undergoing rupture in the reaction, since the magnitude of this effect is determined by the extent to which the force constants for this atom have changed at the transition state. Accordingly, a study has been made of the effect of structural changes on β-hydrogen and nitrogen isotope effects in the Hofmann elimination reaction of a series of β-substituted ethyltrimethylammonium salts.

In recent reports (2, 3) from this laboratory it has been shown that the reaction of 2-arylethyltrimethylammonium ion with sodium ethoxide in ethanol is a normal E2 process following the *anti*-elimination pathway. In addition, the low β-hydrogen isotope effect, k^H/k^D = 2.98 at 50°, found for the reaction of the parent compound, 2-phenylethyltrimethylammonium ion (4), the

[1]For Part VIII see ref. 1.

[2]Present address: Department of Chemistry and Chemical Engineering, University of Saskatchewan, Saskatoon, Saskatchewan. Author to whom correspondence should be addressed.

Can. J. Chem. Downloaded from www.nrcresearchpress.com by 210.87.254.40 on 09/05/12
For personal use only.

Can. J. Chem. Downloaded from www.nrcresearchpress.com by 210.87.254.40 on 09/05/12
For personal use only.

large positive Hammett ρ value of 3.67 at 40° (5) and the large secondary isotope effect, $k^{OD^-}/k^{OH^-} = 1.79$ at 80°, for the reaction of parent compound with OD^- in D_2O and OH^- in H_2O (6) all point to a transition state in which there has been extensive transfer of the β-hydrogen to base. That the carbon–nitrogen bond is also appreciably weakened is indicated by the substantial nitrogen isotope effect, $k^{14}/k^{15} - 1)100 = 1.17$ at 40°, reported by Bourns and co-workers (7) for the reaction with ethoxide in ethanol.

A theoretical treatment of the effect of substituents on transition state geometry was proposed some years ago by Thornton (8) in which changes in the vibrational potentials for motion along the reaction coordinate, designated as "parallel" motion, and for the normal modes of vibration, or "perpendicular" motion, of the transition state were examined. For motion along the reaction coordinate, the effect of a substituent change on bond length is exactly the opposite to its effect on the normal vibrational modes where the force constant is positive. Thornton suggests that the former effect usually will be dominant since the magnitude of the change in bond length is inversely proportional to the force constant which is determined by the curvature of the potential energy surface in the region of the energy maximum. In most systems this curvature is considerably smaller for parallel than for perpendicular motion. It follows that a substituent change which makes the cleavage of a bond easier will usually result in a decrease in the length of that bond at the transition state.

Applying this treatment to bimolecular elimination, Thornton considered the effect of substituents on the parallel motion, which can be depicted in Scheme 1.

$$\underset{\rightarrow}{B}\quad \underset{\leftarrow}{H}\quad \underset{\rightarrow}{C_\beta}\quad \underset{\leftarrow}{C_\alpha}\quad \underset{\rightarrow}{X}$$

SCHEME 1

An electron-withdrawing substituent will weaken the C_β—H bond and thus make the motion which extends this bond easier. It will also make the compression of the C_β—C_α bond more difficult. The B—H and the C_α—X bonds will "follow along" in the direction of the coordinate motion set by the C_β—H bond. It follows that the overall effect will be to make the transition state more reactant-like with both the C_β—H and the C_α—X bond rupture less advanced than in the absence of this substituent.

A somewhat different approach to predicting the effect of structural changes on transition state geometry in E2 reactions has been developed by O'Ferrall (9). Using a model in which reactants, products, and the transition state for concerted elimination are represented on a common potential energy surface with carbonium ion and carbanion intermediates of stepwise reaction paths, he examines the effect of changes in the energy of products and intermediates on the energy and structure of the E2 transition state. He concludes that structural changes that lead to a more stable olefin are transmitted along the reaction coordinate and, in agreement with the prediction of Thornton, result in a transition state which is more reactant-like, *i.e.*, less C_β—H and C_α—X bond weakening. On the other hand, the model predicts that the effect of structural changes which increase carbanion stability will ordinarily be exerted in a direction perpendicular to the reaction coordinate and will result in an E2 transition state which is more carbanion-like, *i.e.*, a longer C_β—H and a shorter C_α—X bond. This is in contrast to Thornton's view that structural influences on parallel motion can be expected to dominate.

In the present study β-deuterium and nitrogen isotope effects have been measured for the reaction of a series of *para*-substituted 2-phenylethyltrimethylammonium salts with ethoxide ion in ethanol. In addition, the nitrogen effect has been measured for the reaction of ethyltrimethylammonium ion and the α-deuterium isotope effect for 2-phenylethylammonium ion. Finally, the effect of a change in base strength has been determined by comparing the magnitude of the isotope effects in the reaction of 2-phenylethyl- and ethyltrimethylammonium ions with ethoxide ion in ethanol and *t*-butoxide ion in *t*-butanol.

Results

Hydrogen–Deuterium Isotope Effects

The rate constants for reaction of the series of *para*-substituted 2-phenylethyltrimethylammonium ions and their β-dideuterated analogs with ethoxide in ethanol are shown in Table 1. The primary hydrogen–deuterium effects calculated from the rate data are also given in this table. The rate constant for the α-dideuterated analog of the unsubstituted salt was found to be

TABLE 1. Rate constants and primary β-hydrogen–deuterium isotope effects in elimination reaction of $X—C_6H_4CY_2CH_2\overset{+}{N}(CH_3)_3$ ions with sodium ethoxide in ethanol

X	Y	Temperature ±0.03° (°C)	$k \times 10^4$ (l mol^{-1} s^{-1})	k^H/k^D[a]
OCH_3	H	40	0.420±0.003[b]	2.64±0.05
	D		0.159±0.003	
H	H	40	4.33±0.05	3.23±0.06
	D		1.34±0.02	
Cl	H	40	29.9±0.6	3.48±0.07
	D		8.60±0.06	
CF_3	H	40	1943.±6	4.16±0.07
	D		467.±8	
	H	25	198.±2	4.25±0.04
	D		46.6±0.2	
	H	15	46.9±0.2	4.30±0.08
	D		10.9±0.2	

[a]Ratio of rates of elimination; deviation $(\pm k^H/k^D)[(r^H/k^H)^2 + (r^D/k^D)^2]^{1/2}$, where r is the standard deviation in k.
[b]Standard deviation.

0.000425 ± 0.000003 l mol^{-1} s^{-1}. This value, when divided by the rate constant for the undeuterated substrate, gives a secondary α-deuterium isotope effect of 1.02 ± 0.01 at 40°.

The same concentration of base (0.1 *M*) was used in all of the experiments except for the *p*-CF_3 compound where the reaction was too fast at 40° to enable kinetic measurement. For this compound, the kinetics were determined at 25 and 15° with the same concentration of base as was used for the other compounds and the resultant hydrogen–deuterium effects were used to determine an extrapolated value at 40°. In this way, it was possible to compare isotope effects for all compounds under the same conditions of ionic strength. The extrapolated value for the *p*-CF_3 compound agrees well with the hydrogen–deuterium effect determined at 40° for this compound using a lower concentration of base.

Excellent Hammett plots of log k/k_0 *vs.* σ^- were obtained for the undeuterated and deuterated series. The slope, ρ, for the former is +3.66, with a correlation coefficient, *r*, of 0.998. This value agrees well with the value of +3.67 reported by Saunders (5) for reaction under the same conditions. The slope of the plot for the β-dideuterated series is +3.47, with a correlation coefficient of 0.999.

Nitrogen Isotope Effect Results

The results of the nitrogen isotope effect study on the reaction of 2-arylethyltrimethylammonium ions with sodium ethoxide in ethanol at 40° are shown in Table 2. Also shown are the nitrogen results obtained from the study of ethyltrimethylammonium ion with potassium hydroxide in 95% ethanol at 60° and with potassium *t*-butoxide in *t*-butanol at 60°.

The nitrogen isotope effect for the elimination reaction of the various substrates with base was obtained by comparing the $^{14}N/^{15}N$ ratio of the starting material of natural isotopic abundance with that of the trimethylamine formed in the reaction carried to some known extent of completion. Using the Kjeldahl procedure, the quaternary salts and the trimethylamine were converted to ammonium sulfate which was oxidized to nitrogen gas and purified prior to mass spectrometric analysis.

Discussion

Discussion of the Isotope Effects for the E2 Reaction of 2-Arylethyltrimethylammonium Ions with Ethoxide

The results of the nitrogen isotope effect study on the 2-arylethyl system, Table 2, show a relationship between the magnitude of the effect and the electron-withdrawing or -donating ability of the *para* substituent. Although the effects for the *p*-H and *p*-OCH_3 compounds are the same within experimental error there is a significant decrease in the magnitude of the

Can. J. Chem. Downloaded from www.nrcresearchpress.com by 210.87.254.40 on 09/05/12
For personal use only.

TABLE 2. Nitrogen isotope effects for the E2 reaction of $RCH_2CH_2\overset{+}{N}(CH_3)_3$ ions with base

Substituent(R)	Base–Solvent	Temp. (°C)	Extent of reaction (%)[a]	k^{14}/k^{15}[b]
p-CH_3O—C_6H_4—	EtO^-–EtOH	40	4.9	1.0125
			4.9	1.0135
			8.1	1.0141
			12.6	1.0137
			23.2	1.0133
			23.5	1.0153
				mean 1.0137±0.0009
p-H—C_6H_4—	EtO^-–EtOH	40	10.0	1.0133
			17.0	1.0131
			22.0	1.0134
			29.0	1.0133
			46.0	1.0136
				mean 1.0133±0.0002
p-Cl—C_6H_4—	EtO^-–EtOH	40	14.6	1.0118
			16.3	1.0098
			17.1	1.0113
			29.0	1.0118
			29.0	1.0122
				mean 1.0114±0.0009
p-CF_3—C_6H_4—	EtO^-–EtOH	40	17.3[c]	1.0088
			23.0[c]	1.0084
			43.6[c]	1.0093
			46.2[c]	1.0092
			60.0	1.0078
			70.0	1.0093
				mean 1.0088±0.0006
H	OH^-–EtOH[e]	60	8.3[d]	1.0190
			8.3[d]	1.0190
			8.3[d]	1.0181
			8.3[d]	1.0184
				mean 1.0186±0.0004
H	t-BuO^-–t-BuOH	60	13.4[c]	1.0145
			13.8[c]	1.0142
			27.6[c]	1.0139
			27.6[c]	1.0141
			60	1.0138
				mean 1.0141±0.0003

[a]Determined from the yield of trimethylamine.
[b]The limits shown are the standard deviation.
[c]The amount of base corresponding to the desired extent of reaction.
[d]The Kjeldahl digestion was carried out only on the trimethylamine after prior separation from the substitution product, dimethylethylamine.
[e]Essentially all of the base is ethoxide when KOH is dissolved in 95% ethanol (10).

effect when electron-withdrawing substituents are placed on the benzene ring, *i.e.*, $(k^{14}/k^{15} - 1)100$ is 1.33 and 0.88 for the p-H and p-CF_3 compounds, respectively. In fact, the magnitude of the nitrogen isotope effect is approximately linearly related to the effect of the *para* substituent on the free energy of activation for the elimination process as seen from the plot of $\log k^{14}/k^{15} - 1)100$ *vs.* $\log k$ for the reaction of the 2-arylethyltrimethylammonium ions with sodium ethoxide in ethanol at 40°, Fig. 1.

Since the magnitude of the nitrogen effect depends on the extent to which the composite force constant of the $C—\overset{+}{N}$ bond is decreased in going from the initial to the transition state, the effect will increase regularly in a reaction series with the extent of bond weakening at the transition state. Consequently, the experimental results show that the extent of carbon–nitrogen bond rupture in the transition state decreases as the *para* substituent becomes more electron withdrawing.

It is noteworthy that Katz and Saunders (11) have recently examined the problem of the interpretation of the leaving group isotope effect $(C—\overset{+}{S})$ in relation to the extent of bond rupture at the transition state. Their theoretical calculations suggest that the magnitude of the sulfur isotope

Can. J. Chem. Downloaded from www.nrcresearchpress.com by 210.87.254.40 on 09/05/12
For personal use only.

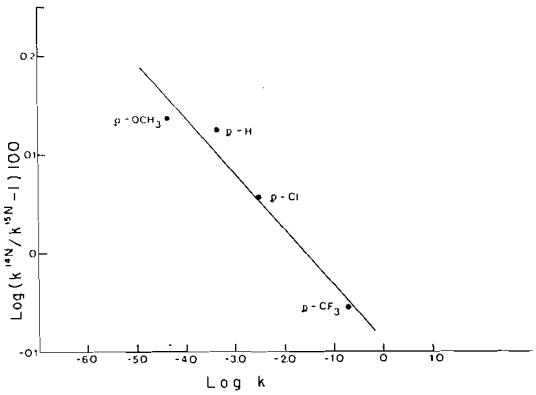

FIG. 1. Plot of log $(k^{14}/k^{15} - 1)100$ *vs.* log k for the reaction of 2-arylethyltrimethylammonium ions with sodium ethoxide in ethanol at 40°.

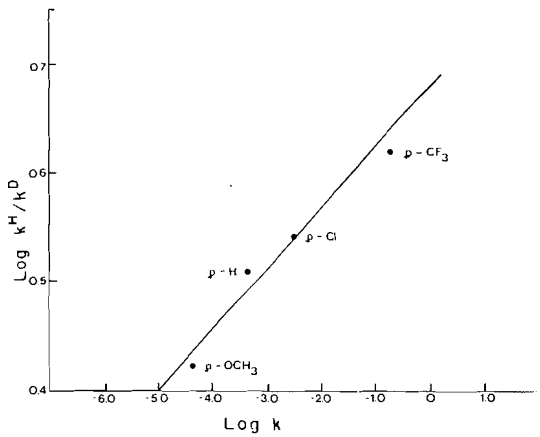

FIG. 2. Plot of log k^H/k^D *vs.* log k for the reaction of 2-arylethyltrimethylammonium ions with sodium ethoxide in ethanol at 40°.

effect can remain very small until the stretching force constant of the carbon–sulfur bond has decreased to less than one-half of its original value. If this conclusion is valid, small isotope effects for the leaving group may be associated with reactions in which C—X bond rupture is quite far advanced at the transition state.

Concerning the nitrogen effects in the present study, it is our opinion that qualitative interpretation of the effects in terms of the degree of bond rupture is justified since only systematic changes were made on the structure of the reactant by varying the *para* substituent. The approximate straight line obtained from the plot of log $(k^{14}/k^{15} - 1)100$ *vs.* log k gives some support to this belief. We feel, however, in agreement with Katz and Saunders (11), that care must be taken in a comparison of isotope effects obtained from different reaction systems.[3]

A clear trend is also shown in the magnitude of the hydrogen–deuterium isotope effects recorded in Table 1, where it is seen that the effect increases with increased electron-withdrawing ability of the *para* substituent, *i.e.*, 2.64 and 4.16 for p-OCH_3 and p-CF_3, respectively.[4] In fact, there is an approximate linear relationship between the effect of substituents on the free energy of activation for the elimination reaction and their effect on the free energy of activation difference between undeuterated and deuterated compounds. This is seen from a plot of log k^H/k^D *vs.* log k, as shown in Fig. 2.

An interpretation of the magnitude of the hydrogen–deuterium isotope effect in terms of the degree of bond rupture at the transition state is more difficult than the interpretation of the nitrogen effect since the reacting hydrogen is involved in a three-center displacement reaction. Westheimer (14) and others (15–17) have predicted on theoretical grounds that the magnitude of the hydrogen–deuterium effect should be at a maximum when the force constants associated with bonds being formed and broken are equal at the transition state. This prediction has been realized experimentally by several groups of workers (18–20) and, therefore, it is reasonable to interpret the trend in isotope effect in the present study in the light of this theory. Such an interpretation, however, requires a knowledge of the extent of proton transfer at the transition state, *i.e.*, whether the proton is more than or less than one-half transferred. This is provided by the calculations and experimental results of Steffa and Thornton (6) on the secondary isotope effect, k^{OD^-}/k^{OH^-}, for proton abstraction by DO^- in D_2O and HO^- in H_2O. For a reaction with complete proton transfer at the transition state, the theoretical value for this secondary isotope effect is 1.88 at 80°, while for half transfer the effect is the square root of this maximum value, or 1.37.

The secondary isotope effects, k^{OD^-}/k^{OH^-}, and primary β-deuterium isotope effects, k^H/k^D, for the bimolecular elimination reactions of 2-phenylethyltrimethylammonium bromide, 2-(*p*-chlorophenyl)ethyltrimethylammonium bromide, and 2-phenylethyldimethylanilinium bromide are

[3]For an illustration of the problem of comparing k^H/k^D values obtained from different reaction systems see Smith and Tsui (12).

[4]A similar trend has been observed for the reaction of 2-arylethylbromides with *t*-butoxide (13).

Can. J. Chem. Downloaded from www.nrcresearchpress.com by 210.87.254.40 on 09/05/12
For personal use only.

TABLE 3. Secondary and primary isotope effects in reaction of 2-phenylethyl derivatives

Substrate	k^{OD^-}/k^{OH^-}[a] at 80°	k^H/k^D[b] at 40°
$C_6H_5CH_2CH_2\overset{+}{N}(CH_3)_3$	1.79	3.23
p-Cl—$C_6H_4CH_2CH_2\overset{+}{N}(CH_3)_3$	1.73	3.48
$C_6H_5CH_2CH_2\overset{+}{N}(CH_3)_2C_6H_5$	1.62	4.50[c]

[a]Steffa and Thornton (6).
[b]Measured with ethoxide in ethanol.
[c]See ref. 21.

presented in Table 3. It is noted that the secondary effects are all greater than 1.37 suggesting that for reaction of the three substrates the proton is more than one-half transferred at the transition state. Furthermore, the magnitude of the secondary effect, k^{OD^-}/k^{OH^-}, decreases as one proceeds down the table, indicating a decrease in the extent of carbon–hydrogen bond rupture at the potential energy maximum. At the same time the value of the primary hydrogen–deuterium isotope effect increases. This relationship of the two effects clearly establishes that the proton is more than half transferred at the transition state since only in this circumstance can a decrease in the extent of proton transfer, as shown by the k^{OD^-}/k^{OH^-} values, result in an increase in the k^H/k^D ratios. It follows from the trend in the isotope effects reported in Table 1 that electron-withdrawing *para* substituents in the reaction of 2-arylethyltrimethylammonium ions result in a decrease in the extent of proton transfer to base at the transition state.

Theoretical Predictions on the Effect of Substituents on Transition State Geometry

The isotope effect results have shown for the reaction of 2-arylethyltrimethylammonium ions with ethoxide ion that electron-withdrawing substituents lead to a decrease in the extent of *both* carbon–hydrogen and carbon–nitrogen bond rupture at the transition state. This conclusion is in complete accord with the Thornton model for predicting the effect of a substituent on the nature of the activated complex. The removal of the β-hydrogen is made easier by placing electron-withdrawing substituents on the benzene ring and this effect, when considering motion along the reaction coordinate, should lead to a more reactant-like transition state, *i.e.*, less C—H and less C—$\overset{+}{N}$ bond weakening.

The relatively small k^H/k^D values in relation to the theoretical maximum, the large positive Hammett ρ of 3.77, and the large k^{OD^-}/k^{OH^-} value for reactions in water all point to a transition state which has considerable carbanion character. This also is in accord with the Thornton theory. As a leaving group $-\overset{+}{N}(CH_3)_3$ is relatively poor and, therefore, the transition state for onium salt eliminations can be expected to be more product-like than that for E2 reactions in general. Reference to Scheme 1 which depicts coordinate motion shows that by making H move much more relative to C_α, and C_β move more relative to X, more product-like transition states will have relatively more carbanion character at C_β than carbonium ion character at C_α. This may also account for the small α-deuterium secondary effect of 1.02 since this value is indicative of very little hybridization change at the α-carbon.[5]

The conclusions reached in the present study concerning the effect of *para* substituents on the extent of C—H and C—N bond rupture can also be examined in the light of the O'Ferrall model (9). The potential energy surface diagram of O'Ferrall is represented in Fig. 3 for an E2 process in which the transition state lies on the carbanionic side of centrality. This surface is considered to be of such flexibility as to transmit across its length and breadth the effect of energy changes at any point. It can be seen that an increase in the stability of the elimination product, R, will correspond to a "downward pull" at the top right-hand corner of the figure with the result that the energy of the transition state is decreased and its structure moves toward the bottom left-hand corner; that is, it becomes more reactant-like with decreased C—H and C—X bond rupture. On the other

[5]Asperger (22, 23) found an identical value for the reaction of the same substrate.

Can. J. Chem. Downloaded from www.nrcresearchpress.com by 210.87.254.40 on 09/05/12
For personal use only.

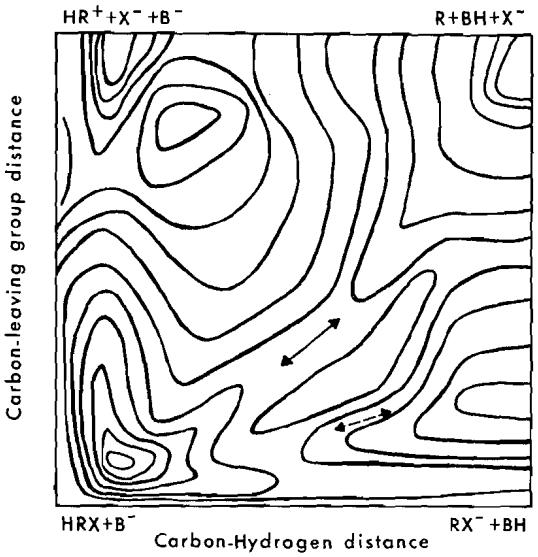

FIG. 3. Potential energy surface for an E2 transition state.

hand, an increase in the stability of the carbanion, R^-, means a downward pull at the bottom right-hand corner of the surface, and, therefore, would be expected to exert its effect mainly through the perpendicular vibrational mode. This would result in a lower transition state energy but a transition state structure which is closer to that of the carbanion; that is increased C—H but decreased C—X bond rupture, which is contrary to experimental findings.

A substituent change may, of course, affect the stability of more than one species. For example, electron-withdrawing substituents at the β-carbon may increase the stability of both the products and the carbanion intermediate, although intuitively the effect on the latter might be expected to outweigh the former. That this is so would seem to be indicated by the order of the substituent effects on the magnitude of k^H/k^D for the reaction of the 2-arylethyl salts with ethoxide, Table 2. Clearly, this order does not correspond at all to the order of product stability which, on the basis of λ_{max} values for the substituted styrenes,[6] would appear to be p-$CH_3O > p$-Cl $> p$-$CF_3 >$ H. On the other hand, the order of isotope effect values clearly does parallel the expected order of substituent effects on carbanion stability.

The O'Ferrall model can accommodate the results of the present study if the E2 transition states for quaternary ammonium salt eliminations are so carbanion-like that substituent effects on carbanion stability are felt more strongly along the reaction coordinate than perpendicular to it. (A potential energy surface such that the dotted double-headed arrow in Fig. 3 represents the direction of reaction coordinate motion would clearly be such a case.) A downward pull on the lower right hand corner would then give a transition state in which there is a decrease in both C—H and C—X bond rupture. As pointed out earlier, both the primary and secondary deuterium isotope effects and the Hammett ρ value do point to such a structure for the transition state.

Discussion of the Isotope Effects for the E2 Reaction of β-Substituted Ethyltrimethylammonium Ions with Ethoxide

The comparison of the isotope effects obtained for the E2 reaction of 2-phenylethyltrimethylammonium ion and ethyltrimethylammonium ion with ethoxide, Table 4, provides further evidence supporting the conclusion that β-substituents influence in a parallel way C_β—H C_α–$\overset{+}{N}$ bond rupture at the transition state. The significantly larger nitrogen isotope effect for reaction of the ethyl salt compared to that found for the 2-phenylethyl ion, 1.86 and 1.33, respectively, clearly establishes that there is greater C—$\overset{+}{N}$ bond weakening at the transition state for the former compound. A similar conclusion was reached by Simon and Mullhofer (24) who observed α-carbon isotope effects, $(k^{12}/k^{14} - 1)100$, of 6 and 3% for ethyl- and 2-(*p*-nitrophenyl)ethyltrimethylammonium ions, respectively.

Although the hydrogen isotope effects have not been measured under the same conditions, there is nevertheless a strong indication that the value is significantly smaller for the unsubstituted compound.[7] Since it has already been concluded that in these quaternary ammonium salt eliminations the proton is more than half trans-

[6] λ_{max}(nm) = 258, 253, 250, 248 for p-OCH_3, p-Cl, p-CF_3, and H, respectively.

[7] The value of 2 and 2.7 for the reaction of ethyl and 2-phenylethyl salts, respectively, are calculated from the intramolecular k^H/k^T values determined by Simon and Mullhofer (24). Their value of 2.7 at 60°, which includes a secondary isotope effect, and the intermolecular effect of 3.23 at 40° from the present study are in fairly good agreement if one takes the temperature difference into consideration.

Can. J. Chem. Downloaded from www.nrcresearchpress.com by 210.87.254.40 on 09/05/12
For personal use only.

TABLE 4. Hammett correlations and isotope effects in the reaction of ethyltrimethylammonium ion and 2-phenylethyltrimethylammonium ion with ethoxide ion and *t*-butoxide ion at 60°

Substrate	Base–Solvent	$(k^{14}/k^{15} - 1)100$	k^H/k^D	ρ
$CH_3CH_2\overset{+}{N}(CH_3)_3$	EtO^- – 95% EtOH	1.86	2[b]	—
$C_6H_5CH_2CH_2\overset{+}{N}(CH_3)_3$	EtO^-–EtOH	1.33[a]	3.23[a](2.7)[c]	+3.66[a]
$CH_3CH_2\overset{+}{N}(CH_3)_3$	*t*-BuO^-–*t*-BuOH	1.41	—	—
$C_6H_5CH_2CH_2\overset{+}{N}(CH_3)_3$	*t*-BuO^-–*t*-BuOH	—	7.03[d]	3.07[d]

[a]Measured at 40°.
[b]Calculated from intramolecular k^H/k^T value of 3.0 (24) determined with the basic hydrate (vacuum).
[c]Calculated from intramolecular k^H/k^T value of 4.2 (24) determined with methoxide–methanol.
[d]Saunders (5) at 30°.

ferred to base at the transition state and, therefore, that the smaller the isotope effect the greater the extent of this transfer, it follows that the transfer is more complete in the transition state of the ethyl compound.

The conclusion that there is decreased C—H and C—$\overset{+}{N}$ bond rupture at the transition state for the 2-phenylethyl salt compared with the ethyl compound is in agreement with Thornton's theory which predicts a more reactant-like transition state for the reaction which is facilitated by a substituent change at C_β, *i.e.* H replaced by phenyl. The results are also consistent with the O'Ferrall model since the greater stability of both the ethylenic product and carbanion derived from the phenyl-substituted compound would lead to a "pulling-down" of the entire side of the potential energy surface, Fig. 3, resulting in a more reactant-like transition state.

It is noteworthy that Fry (25), in a recent article, has arrived at a different conclusion with respect to the effect of a β-phenyl substitution on the degree of C—H and C—$\overset{+}{N}$ bond rupture for the same substrates. The discrepancy arises from the difference in k^H/k^D for the E2 reaction of the ethyl compound as measured by two different groups of workers; k^H/k^D at 60° $\simeq$2 (24) and $\simeq$6 (26), estimated from a higher temperature. There are several reasons for believing that the value of 2 determined by Simon and Mullhofer (24), which was used in the present discussion, is the more reliable. First, the isotope effects found for the reaction of the ethyl salt under two different reaction conditions are in agreement; k^H/k^T (intramolecular) = 3.0, as measured with the basic hydrate in vacuum, and 2.8, calculated from an experimental value of 1.23 at 130° when hydroxide was used in triethylene glycol. Second, Simon's data for a number of compounds form a consistent pattern: k^H/k^T of 3.0, 4.2, and 8.0 at 60° for reaction of ethyl-, 2-phenylethyl- and 2-(*p*-nitrophenyl)ethyltrimethylammonium ions, respectively. Finally, as mentioned in footnote 7, the Simon value for the 2-phenylethyl salt is in good agreement with our own as well as with the value of k^H/k^D = 2.98 determined by Saunders and Edison (4) for the same reaction at 50°.

The Effect of a Change in Abstracting Base on Transition State Geometry

The role of the abstracting base in determining the nature of the E2 transition state was examined by determining the nitrogen isotope effect for reaction of ethyltrimethylammonium ion with ethoxide ion in ethanol and *t*-butoxide in *t*-butanol. The results are shown in Table 4 along with the k^H/k^D, ρ and nitrogen isotope effect results for reaction of 2-phenylethyl ion with ethoxide. The Hammett ρ and k^H/k^D for reaction of this salt with *t*-butoxide as determined by Saunders *et al.* (5) are also included.

It is seen that the nitrogen effect associated with the reaction of ethyltrimethylammonium ion with the weaker base, ethoxide,[8] is significantly greater than when the base was *t*-butoxide, *i.e.*, 1.86 compared with 1.41% at 60°. Consequently, there is less C—$\overset{+}{N}$ bond weakening at the transition state for the reaction promoted by the stronger base. Furthermore, the large difference

[8]In a previous study in these laboratories, a nitrogen effect of 1.73% was determined for the reaction of ethyltrimethylammonium iodide with sodium ethoxide in ethanol at 60° (7). For the earlier determination the substitution product, dimethylethylamine, was not separated from the trimethylamine.

Can. J. Chem. Downloaded from www.nrcresearchpress.com by 210.87.254.40 on 09/05/12
For personal use only.

Can. J. Chem. Downloaded from www.nrcresearchpress.com by 210.87.254.40 on 09/05/12
For personal use only.

in the two hydrogen isotope effects show that the C_β—H bond also is weakened less at the transition state for the reaction of 2-phenylethyltrimethylammonium ion with *t*-butoxide ion. The ρ values are also in accord with this interpretation.

Once again, the conclusions reached from the isotope effects are in accord with Thornton's predictions. His theory predicts that increasing the base strength (making compression of the B—H bond easier) will increase the B—H bond length and shorten both the C_β—H and C_α—X bonds, making the transition state more reactant-like. In the O'Ferrall model, Fig. 3, an increase in base strength means an increased stability of the product BH which is common to both an E2 and a carbanion-forming process. This corresponds to a "pulling-down" of the right side of the potential energy surface. For a carbanion-like transition state the effect of this will be transmitted predominantly in the direction of the reaction co-ordinate and will result in a decrease of both C—$\overset{+}{N}$ and C—H bond rupture, *i.e.*, a more reactant-like transition state.

Comments in Relation to the Variable E2 Transition State Theory

The conclusions drawn from the present study are not in accord with a proposal by Bunnett (27, 28) that there will exist a continuum of E2 transition states in a reaction series extending from large C—H and small C—X bond rupture at one extreme to the reverse situation at the other. Bunnett reasons that a substituent change which makes the C—H bond cleavage easier at the transition state would have that bond weakened more and the C—X bond weakened less, and *vice versa*. Support for this concept has been provided by a series of studies by Bartsch and Bunnett (29) and Bartsch (30) on the reaction of alkyl halides with different bases.

The explanation for this apparent discrepancy between the findings of the present study on the elimination reaction of quaternary ammonium salts and those of Bunnett and co-worker on alkyl halides may lie in the relative extent to which the parallel and perpendicular modes of vibration of the transition state are affected by structural changes in the reactants in the two systems. Since halogen is a relatively good leaving "group", alkyl halides can be expected to undergo elimination with strong bases by way of a "central" transition state in which the extent of C—H and C—X bond rupture is approximately equal. Reference to Fig. 3 shows that substituents which increase the acidity of the β-hydrogen will exert their effect primarily through the perpendicular vibrational mode and, therefore, will move the transition state structure closer to that of the carbanion, *i.e.*, increase C—H and decrease C—X bond rupture. On the other hand, the transition states for the quaternary ammonium salt eliminations examined in the present study appear to be strongly carbanion-like. As a consequence, structural changes which influence carbanion stability may be transmitted to a greater extent along the reaction coordinate than in a direction perpendicular to it with the result that the transition state becomes more reactant-like, *i.e.*, less rupture of both C—H and C—X bonds. The apparent difference in the effect of changes in base strength on the structure of the transition state in the two systems may have a similar origin.

Experimental

All melting points are corrected.

2-Phenylethyltrimethylammonium Bromide

The sample was the same as used in an earlier study (2); m.p. 237–238° (lit. (5) m.p. 237.8–238.2°).

2-(p-Trifluoromethylphenyl)ethyltrimethylammonium Bromide

The sample was the same as used in an earlier study (2); m.p. 227.5–228°.

Anal.[9] Calcd. for $C_{12}H_{17}NBrF_3$: C, 46.18; H, 5.49; N, 4.49. Found: C, 46.18; H, 5.56; N, 4.56.

2-(p-Anisyl)ethyltrimethylammonium Bromide

A two-fold excess of methyl bromide (21 g, 0.22 mol), cooled to −30° in an acetone – Dry Ice bath was added to a similarly cooled solution of 19.3 g (0.11 mol) of dimethyl 2-(*p*-anisyl)ethylamine in 125 ml of nitromethane. The solution was allowed to stand for 1 day at room temperature and the solid product was filtered and recrystallized four times from ethanol–ether to give 27.3 g (92%) of product; m.p. 216.9–217.7 (lit. (5) m.p. 217.7–218.2°).

Dimethyl 2-(p-Anisyl)ethylamine

Cold anhydrous dimethylamine (13.0 g, 0.238 mol), was added to a cold solution of 36.0 g (0.118 mol) of 2-(*p*-anisyl)ethyl *p*-toluenesulfonate in 240 ml of anhydrous ether. The reaction was allowed to proceed for 9 days. After work-up there was obtained 19.3 g (91%) of product; b.p. 71–72°/0.05 mm. (lit. (5) b.p. 100°/2 mm).

2-(p-Anisyl)ethyl p-Toluenesulfonate

p-Toluenesulfonyl chloride (30.6 g, 0.16 mol) was added in three portions to an ice-cold solution of 22 g

[9]Elemental analyses were performed by Galbraith Laboratories Inc., Knoxville, Tennessee.

Can. J. Chem. Downloaded from www.nrcresearchpress.com by 210.87.254.40 on 09/05/12
For personal use only.

(0.145 mol) of 2-(*p*-anisyl)ethanol in 72 g of anhydrous pyridine. The solution was kept at 0° for 2 days. After work-up there was obtained 36.2 g (83%) of 2-(*p*-anisyl)-ethyl *p*-toluenesulfonate; m.p. 58.5–59.5° (lit. (31) 57–58°).

2-(p-Anisyl)ethanol

Ethyl 2-(*p*-anisyl)acetate (33.0 g, 0.17 mol), in 50 ml of anhydrous ether was reduced with 6.84 g (0.18 mol) of lithium aluminum hydride to give 22.1 g (88%) of 2-(*p*-anisyl)ethanol; b.p. 154.5–155°/21 mm (lit. (32) b.p. 110–113°/1 mm).

Ethyl 2-(p-Anisyl)acetate

A solution of 2-(*p*-anisyl)acetic acid, (32.0 g, 0.193 mol), in 100 ml of absolute ethanol containing 4 ml of concentrated sulfuric acid was refluxed for 7 h to give 33 g (88%) of ester; b.p. 158–158.5°/20 mm (lit. (33) b.p. 136–137°/10 mm).

2-(p-Anisyl)acetic Acid

A mixture of 84 g (0.56 mol) of *p*-methoxyacetophenone, 27 g of sulfur, and 60 ml of morpholine was refluxed for 13 h with stirring. After work-up 87 g (92%) of product was obtained; m.p. 87–90° (lit. (34) m.p. 86°).

2-(p-Chlorophenyl)ethyltrimethylammonium Bromide

A two-fold excess of methyl bromide (63 g, 0.66 mol) was added to 55 g of dimethyl 2-(*p*-chlorophenyl)ethylamine to produce 77.5 g (92%) of quaternary salt; m.p. 239.2–239.5° (lit. (5) m.p. 242.3–242.6°).

Dimethyl 2-(p-Chlorophenyl)ethylamine

2-(*p*-Chlorophenyl)ethyl *p*-toluenesulfonate (109.5 g, 0.35 mol), was treated with 38.4 g (0.85 mol) of anhydrous dimethylamine to produce 55.2 g (86%) of product; b.p. 63–65°/0.2 mm (lit. (5) b.p. 104–106°/1.2 mm).

2-(p-Chlorophenyl)ethyl p-Toluenesulfonate

2-(*p*-Chlorophenyl)ethanol (64.5 g, 0.41 mol), was treated with 86.2 g (0.45 mol) of *p*-toluenesulfonyl chloride to produce 109.4 g (86%) of tosylate; m.p. 79.5–80.0° (lit. (5) m.p. 79.5–80.1°).

2-(p-Chlorophenyl)ethanol

Ethyl 2-(*p*-chlorophenyl)acetate (90 g, 0.45 mol), was reduced with 17.2 g (0.45 mol) of lithium aluminum hydride to give 64.5 g (91%) of product; b.p. 86–87°/0.04 mm, (lit. (32) 98–100°/1 mm).

Ethyl 2-(p-Chlorophenyl)acetate

A solution of 76 g (0.5 mol) of *p*-chlorobenzyl cyanide, 120 ml of 95% ethanol, and 53 ml of concentrated sulfuric acid was refluxed for 8 h. After work-up the product, 90 g (90%), was collected at 96–98°/1 mm.

2-Phenylethyltrimethylammonium-2,2-d_2 Bromide

The sample was the same as used in an earlier study (2); m.p. 238–239°, (lit. (5) m.p. 237.8–238.2°). A deuterium analysis by Nemeth[10] indicated that this compound has 1.88 atoms D/mol.

2-Phenylethyltrimethylammonium-1,1-d_2 Bromide

The sample was the same as used in an earlier study (2); m.p. 237.5–238°, (lit. (5) m.p. 238–239°). A deuterium analysis by Nemeth indicated that this compound had 1.94 atoms D/mol.

2-(p-Trifluoromethylphenyl)ethyltrimethylammonium-2,2-d_2 Bromide

The sample was the same as used in an earlier study (2); m.p. 228–228.5°. A deuterium analysis by Nemeth indicated that this compound had 1.96 atoms D/mol.

2-(p-Anisyl)ethyltrimethylammonium-2,2-d_2 Bromide

This compound was prepared from diethyl *p*-anisylmalonate by the procedure described for the unsubstituted compound (2); m.p. 217.2–217.8, (lit. (5) m.p. 217.7–218.2). A deuterium analysis by Nemeth indicated that this compound had 1.92 atoms D/mol.

2-(p-chlorophenyl)ethyltrimethylammonium-2,2-d_2 Bromide

This compound was prepared by the lithium aluminum deuteride reduction of ethyl *p*-chlorobenzoate using the procedure described for the reduction of ethyl *p*-trifluoromethylbenzoate (2); m.p. 240–240.5°, (lit. (5) m.p. 242.3–242.6). A deuterium analysis by Nemeth indicated that this compound had 1.92 atoms D/mol.

Ethyltrimethylammonium Iodide

Ethyl iodide (25 g, 0.16 mol), in 25 ml of absolute ethanol was treated with 9.45 g (0.16 mol) of trimethylamine to give 16.5 g (49%) of product; m.p. 333.5–334 dec., (lit. (7) m.p. 336° dec.).

Ethyltrimethylammonium Nitrate

Ethyltrimethylammonium iodide (30 g, 0.14 mol), in 200 ml of water was treated with 23.8 g (0.14 mol) of silver nitrate in 100 ml of water to give 13 g (62%) of product; m.p. 263–264 dec., (lit. (35) m.p. 265° dec.).

Absolute Ethyl Alcohol

This solvent was dried by the method of Lund and Bjerrum (36) and stored under anhydrous conditions.

Absolute t-Butyl Alcohol

This solvent was dried by refluxing over and distilling from sodium metal. The process was repeated twice and the *t*-butyl alcohol was stored under anhydrous conditions.

Sodium Ethoxide and Potassium t-Butoxide

These bases were prepared by the action of the appropriate metal with the desired solvent under strictly anhydrous conditions in a nitrogen atmosphere.

Kinetic Measurements

A spectroscopic method described by Saunders *et al.* (5) was used to follow the rates of reaction of the deuterated and undeuterated 2-arylethyltrimethylammonium ions with sodium ethoxide in ethanol. Both λ_{max} and the molar extinction coefficient for the *para*-substituted styrenes were determined in the present study and these are shown in Table 5. For all the compounds studied a yield of 100 ± 1% of styrene was obtained for complete reaction.

The rate constants for all three of the deuterated and undeuterated 2-arylethyltrimethylammonium salts, except the *p*-trifluoromethyl compound, were determined using second-order conditions with the ethoxide component in approximately three-fold excess.

[10]Deuterium analyses were performed by Mr. J. Nemeth, 303 W. Washington Street, Urbana, Illinois.

TABLE 5. Ultraviolet absorption of *p*-substituted styrenes in 95% ethanol

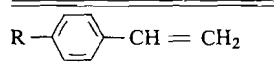

R	λ_{max}(nm)	Molar extinction coefficient $\times 10^{-4}$
H	248	1.38
OCH_3	258	1.92
Cl	253	1.97
CF_3	250	1.62

The reaction of the 2-(*p*-trifluoromethylphenyl)ethyltrimethylammonium ion and its deuterated analogue at 40° was too rapid to permit the measurement of rate constants under second-order conditions using the same concentrations for substrate and base as were used for the kinetics of the other *para*-substituted quaternary ammonium salts. These rate constants, therefore, were evaluated using second-order conditions with equal concentrations of the two reactants.

Nitrogen Isotope Effects

The procedure was essentially that as described by Ayrey *et al.* (7). Depending upon the reactivity of the compound under investigation, either of two methods was used to obtain the desired extent of reaction. For the 2-phenylethyltrimethylammonium ion, a salt of relatively low reactivity, the reaction was stopped by rapid cooling in liquid nitrogen and the trimethylamine was then removed by distillation under reduced pressure at ice-bath temperature. For the more reactive compound, 2(*p*-trifluoromethylphenyl)ethyltrimethylammonium ion, this method of quenching was unsatisfactory and the desired extent of reaction was achieved by adding the appropriate amount of base, corresponding to the extent of reaction required, and allowing the reaction to proceed for 20 half-lives. In these cases, the concentrations of the reactants were sufficiently low so that no more than 1% reaction occurred during the mixing of the reacting solutions.

The kinetic isotope effect was calculated as described previously (7) for all of the reactions except for that of the ethyltrimethylammonium iodide with ethoxide in ethanol where substitution was found to be a competing reaction. For this reaction the kinetic isotope effect was calculated by using the expression suggested by Baliga and Bourns (37).

$$\frac{k^{14}}{k^{15}} = \ln\left(1 - \frac{f^1(1-p)}{1-fp}\right) \Big/ \ln\left(1 - \frac{rf^1(1-p)}{1-f^1p}\right)$$

where f^1 is the mole fraction of the quaternary salt which has undergone reaction, p is the fraction of the reaction which is substitution and r is

$$(^{14}N/^{15}N)_{reactant}/(^{14}N/^{15}N)_{N(CH_3)_3}.$$

Separation of Trimethylamine and Dimethylethylamine Formed in the Reaction of Ethyltrimethylammonium Ion with Ethoxide in Ethanol at 60°

The reaction of ethyltrimethylammonium nitrate[11] in *t*-butanol gave only the elimination product trimethylamine. However, ethyltrimethylammonium ion with ethoxide in ethanol gave a mixture of trimethylamine and dimethylethylamine.

Ethyltrimethylammonium iodide (1.0 g) and the necessary amount of ethoxide in ethanol were allowed to react to completion in a constant temperature bath in a sealed tube. The tube was cooled in liquid air, opened, and the amine products were distilled into a 50 ml round-bottomed flask along with some ethanol.

One-half-milliliter amounts of this amine solution were injected directly on to a 10 ft × 3/8 in. Amines 220 Column (KOH treated 60–80 Chrom W) in an Aerograph Model A-700 gas chromatograph. A satisfactory separation was accomplished and the entire amount of trimethylamine was collected in dilute sulfuric acid and this solution was prepared for Kjeldahl digestion. The g.l.c. analyses indicated that trimethylamine was produced in the reaction mixture to an extent of 88.5% and that the remaining 11.5 % of the amine product was dimethylethylamine.

This work was supported by the National Research Council of Canada.

1. A. N. BOURNS and K. C. WESTAWAY. Can. J. Chem. **50**, 2332 (1972).
2. P. J. SMITH and A. N. BOURNS. Can. J. Chem. **48**, 125 (1970).
3. A. N. BOURNS and A. C. FROSST. Can. J. Chem. **48**, 133 (1970).
4. W. H. SAUNDERS JR. and D. H. EDISON. J. Am. Chem. Soc. **82**, 138 (1960).
5. W. H. SAUNDERS JR., D. G. BUSHMAN, and A. F. COCKERILL. J. Am. Chem. Soc. **90**, 1775 (1968).
6. L. J. STEFFA and E. R. THORNTON. J. Am. Chem. Soc. **89**, 6149 (1967).
7. G. AYREY, A. N. BOURNS, and V. A. VYAS. Can. J. Chem. **41**, 1759 (1963).
8. E. R. THORNTON. J. Am. Chem. Soc. **89**, 2915 (1967).
9. R. A. MORE O'FERRALL. J. Chem. Soc. B, 274 (1970).
10. R. E. BURNS and B. D. ENGLAND. Tetrahedron Lett. **24**, 1 (1960).
11. A. M. KATZ and W. H. SAUNDERS, JR. J. Am. Chem. Soc. **91**, 4469 (1969).
12. P. J. SMITH and S. K. TSUI. Tetrahedron Lett. **1**, 61 (1973).
13. L. F. BLACKWELL, P. D. BUCKLEY, K. W. JOLLEY, and A. K. H. MACGIBBON. J. Chem. Soc. Perkin II, 169 (1973).
14. F. H. WESTHEIMER. Chem. Rev. **61**, 265 (1961).
15. R. A. MORE O'FERRALL and J. KOUBA. J. Chem. Soc. B, 985 (1967).
16. R. P. BELL, W. H. SACHS, and R. L. TRANTER. Trans. Faraday Soc. **66**, 1995 (1970).
17. (*a*) J. BIGELEISEN. Pure Appl. Chem. **8**, 217 (1964). (*b*) L. MELANDER. Isotope effects on reaction rates. The Ronald Press Company, N.Y. 1960. pp. 24–32.

[11]It was necessary to use the nitrate salt in order to have sufficient solubility in *t*-butanol.

Can. J. Chem. Downloaded from www.nrcresearchpress.com by 210.87.254.40 on 09/05/12
For personal use only.

18. A. F. COCKERILL. J. Chem. Soc. B, 964 (1967).
19. R. P. BELL and B. G. COX. J. Chem. Soc. B, 783 (1971).
20. D. J. MCLENNAN and R. J. WONG. Tetrahedron Lett. **28**, 2887 (1972).
21. P. SCHMID. Private Communication.
22. S. ASPERGER, L. KLASINC, and D. PAVLOVIC. Croat. Chem. Acta, **36**, 159 (1964).
23. S. ASPERGER, N. ILAKOVAC, and D. PAVLOVIC. Croat. Chem. Acta, **34**, 7 (1962); S. ASPERGER, D. PAVLOVIC, K. KLASINC, D. STEFANOVIC, and I. MURATI. Croat. Chem. Acta, **36**, 209 (1964).
24. H. SIMON and G. MULLHOFER. Chem. Ber. **97**, 2202 (1964).
25. A. FRY. Chem. Soc. Revs. **1**, 163 (1972).
26. V. J. SHINER, JR. and M. L. SMITH. J. Am. Chem. Soc. **80**, 4095 (1958).
27. J. F. BUNNETT. Angew. Chem. Int. Ed. **1**, 225 (1962).
28. J. F. BUNNETT. Surv. Progr. Chem. **5** (1969).
29. R. A. BARTSCH and J. F. BUNNETT. J. Am. Chem. Soc. **91**, 1376 (1969); R. A. BARTSCH and J. F. BUNNETT. J. Am. Chem. Soc. **91**, 1382 (1969).
30. R. A. BARTSCH. J. Org. Chem. **35**, 1334 (1970).
31. S. WINSTEIN, C. R. LINDEGREN, H. MARSHALL, and L. L. INGRAHAM. J. Am. Chem. Soc. **75**, 147 (1953).
32. C. H. DEPUY and D. H. FROEMSDORF. J. Am. Chem. Soc. **79**, 3710 (1957).
33. R. S. LIVSHITS *et al.* J. Gen. Chem. **17**, 1671 (1947).
34. A. V. DOMBROVSKIĬ and A. P. TERENT'EV. Zhur Obsncheĭ Khim. **27**, 2000 (1947).
35. D. V. BANTHORPE, E. D. HUGHES, and C. K. INGOLD. J. Chem. Soc. 4054 (1960).
36. H. LUND and J. BJERRUM. Ber. 64B, 210 (1931).
37. B. T. BALIGA and A. N. BOURNS. Can. J. Chem. **44**, 363 (1966).

Can. J. Chem. Downloaded from www.nrcresearchpress.com by 210.87.254.40 on 09/05/12
For personal use only.

Carbon–Sulfur Bond Cleavage in the Reaction of Alkyllithiums with Sulfoxides

T. DURST, M. J. LEBELLE, RITA VAN DEN ELZEN, AND K.-C. TIN
Department of Chemistry, University of Ottawa, Ottawa, Canada K1N 6N5

Received September 18, 1973

When sulfoxides are reacted with alkyllithiums two competing reactions can occur: (*i*) abstraction of an α-hydrogen to give an α-lithiosulfoxide and (*ii*) carbon–sulfur bond cleavage according to $R_1S(O)R_2 + R_3Li \rightarrow R_1S(O)R_3 + R_2Li$. In the cleavage reaction the group which can best carry a negative charge is most readily displaced. The displacements occur with inversion of configuration at sulfur. *t*-Butyllithium racemizes optically active *t*-butyl aryl sulfoxides within a few minutes at −78° in tetrahydrofuran. The results show that in general *t*-butyllithium and *n*-butyllithium are unsatisfactory bases for the efficient generation of α-lithio sulfoxides. Methyllithium or lithium diisopropyl amide are better suited for this purpose.

Lorsque l'on fait réagir des sulfoxydes avec des alkyllithiens deux réactions compétitives peuvent se produire: (*i*) l'enlèvement d'un hydrogène-α pour donner un α-lithiosulfoxyde et (*ii*) la rupture du lien carbone-carbone suivant la réaction $R_1S(O)R_2 + R_3Li \rightarrow R_1S(O)R_3 + R_2Li$. Dans la réaction de coupure le groupe qui peut porter le plus facilement la charge négative est généralement déplacé. Ces réactions de substitutions se produisent avec inversion de configuration sur l'atome de soufre. A −78° dans le tétrahydrofuranne le *t*-butyllithium racémise les *t*-butyl aryl sulfoxydes optiquement actifs en quelques minutes. Les résultats obtenus montrent que le *t*-butyllithium et le *n*-butyllithium sont généralement des bases insatisfaisantes pour la formation efficace des α-lithio sulfoxydes. Le méthyllithium et l'amide diisopropyl lithium sont plus efficaces pour cette fin. [Traduit par le journal]

Can. J. Chem., **52**, 761 (1974)

Introduction

α-Lithio sulfoxides (α-sulfinyl carbanions) are routinely prepared by the reaction of the appropriate sulfoxides with a variety of alkyllithiums, mainly methyl, *n*-butyl-, and occasionally *t*-butyllithium (1). In our experiments in this area over the past several years we have noted that some alkyl group exchange, according to eq. 1, generally accompanies the carbanion forming reaction. Despite the widespread occurrence of this reaction and its potential detrimental effect in synthetic reactions, the exchange reaction has been mentioned but a few times in the chemical literature.[1] In this communication we report a relatively extensive study of the above alkyl group exchange reaction including factors which determine whether R_1 or R is displaced, variations in the amount of exchange with the alkyllithium, and the probable mechanism of the exchange.

[1] $$R{-}\overset{\overset{O}{\|}}{S}{-}R_1 + R_2Li \rightarrow R_1{-}\overset{\overset{O}{\|}}{S}{-}R_2 + RLi$$

The generality of eq. 1 with respect to dimethyl sulfoxide was briefly remarked upon by Franzen at the Organic Reaction Symposium, Cork, Ireland, 1964 (2), but no details have since appeared. Jacobus and Mislow (3) have studied in detail the mechanism of the racemization of optically active methyl phenyl sulfoxide (**1**) with both methyl- and phenyllithium. The conclusion of their study was that racemization of the sulfoxide (and exchange of the alkyl group) most probably occurred via a sulfine intermediate (see Scheme 1). In the racemization of phenyl-^{14}C methyl sulfoxide with phenyllithium some loss of the labelled phenyl group accompanied racemization. A second pathway for exchange involving a sulfoxide–phenyllithium adduct (sulfurane intermediate) **2** was proposed for the loss of the labelled phenyl group (see Scheme 2).

Andersen (4) has studied the reaction of di-*p*-tolyl sulfoxide with *p*-tolyllithium and has rationalized the formation of various products in terms of the decomposition (in the presence of excess *p*-tolyllithium) of an initially formed sulfurane **3** to an aryne (see Scheme 3).

[1]After submission of this paper a communication appeared pointing out the utility of the exchange reaction in the synthesis of optically active dialkyl sulfoxides starting from optically active aryl alkyl sulfoxides (see ref. 13). These authors also found that the exchange reaction occurred with inversion of configuration at sulfur.

Can. J. Chem. Downloaded from www.nrcresearchpress.com by 210.87.254.42 on 09/05/12
For personal use only.

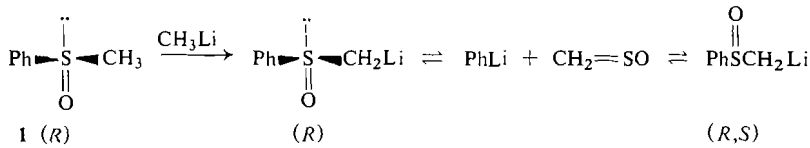

SCHEME 1. Racemization of optically active methyl phenyl sulfoxide via a sulfine intermediate.

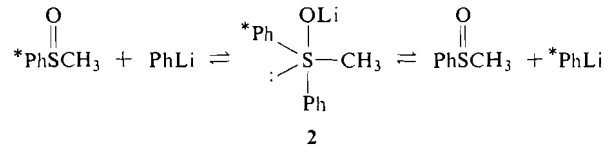

SCHEME 2. Exchange of labelled phenyl groups via a sulfurane intermediate.

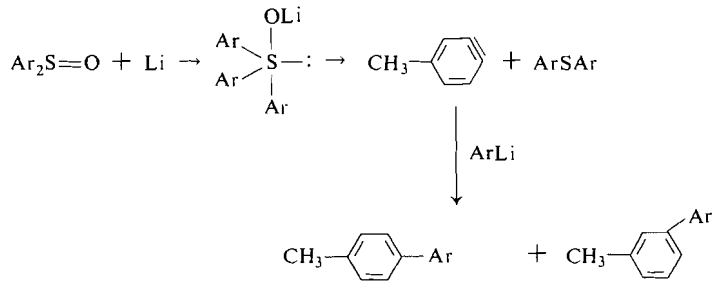

SCHEME 3

Our studies indicate that the sulfine mechanism is not an important pathway for the exchange of substituent on a reaction of a sulfoxide with alkyllithium. They point to a simple S_N2 displacement at sulfur, similar to that observed in the reaction of sulfinate esters with grignards (5) and sulfinamides with alkyllithiums (6), as the major pathway for exchange. No compelling evidence for the intermediacy of species such as **2** was found for the exchange reactions.

Discussion and Results

The reaction of the alkyllithiums with sulfoxides was carried out under N_2 in THF at acetone – Dry Ice temperatures for 10 min followed by addition of the reaction mixture to excess water. The product composition, *i.e.*, the amount of cleavage was determined from either n.m.r. integrations carried out on the total crude product and/or via oxidation of the total crude product with excess *m*-chloroperbenzoic acid in refluxing CH_2Cl_2 and determining the ratio of the sulfones thus produced by v.p.c. Good agreement was obtained when both methods were used to analyze a particular reaction. In general, reproducibility of the results was good, $\pm 4\%$, except when *t*-butyllithium was used as base. In this case the amount of displacement varied considerably with the rate of addition of the alkyllithium. Under the controlled conditions as outlined, the variations in the amount of cleavage was $\pm 10\%$.

Two concurrent reactions can occur when an alkyllithium is allowed to react with a sulfoxide: (*a*) abstraction of an α-hydrogen, *i.e.*, formation of an α-lithio sulfoxide (1) and (*b*) exchange of one of the alkyl groups of the sulfoxide for the alkyl group of the alkyllithium. The relative amounts of each reaction for any particular sulfoxide vary with both the structure of the sulfoxide (number of α-hydrogens and their acidity, the size of the two substituents bonded to the sulfoxide grouping and their leaving group characteristics) and that of the attacking alkyllithium (size and basicity). The variations due to each effect are considered individually below (see also Tables 1 and 2).

The reactions of methyl, ethyl, and isopropyl sulfoxides with methyl-, *n*-butyl-, and *t*-butyllithium illustrate several of the above points. Under the standard experimental conditions (THF solution, −78°, 10 min) methyllithium

Can. J. Chem. Downloaded from www.nrcresearchpress.com by 210.87.254.42 on 09/05/12
For personal use only.

TABLE 1. Reaction of sulfoxides with alkyllithiums

Expt. No.	Sulfoxide	Alkyllithium	Displacement product	Yield (%)
1	$PhS(O)CH_3$	*n*-BuLi	*n*-$BuS(O)CH_3$	30
2	$PhS(O)CH_3$	*t*-BuLi	*t*-$BuS(O)CH_3$	43
3	$PhS(O)CH_3$	*t*-BuLi[a]	*t*-$BuS(O)CH_3$	66
4	$PhS(O)CH_3$	CH_3Li	$CH_3S(O)CH_3$	<3[b]
5	$PhS(O)CH_2CH_3$	*n*-BuLi	*n*-$BuS(O)CH_3$	35
6	$PhS(O)CH_2CH_3$	*t*-BuLi	*t*-$BuS(O)CH_3$	50
7	$PhS(O)CH(CH_3)_2$	CH_3Li	—	0
8	$PhS(O)CH(CH_3)_2$	*t*-BuLi	*t*-$BuS(O)CH(CH_3)_2$	38
9	$PhS(O)CH_2Ph$	CH_3Li	$PhS(O)CH_3$	7
10	$PhS(O)CH_2Ph$	*n*-BuLi	PhS(O)*n*-Bu	40
11	$PhS(O)CH_2Ph$	*t*-BuLi	PhS(O)*t*-Bu	50
12	$PhS(O)CH_2Cl$	CH_3Li	$PhS(O)CH_3$	12
13	$PhS(O)CH_2Cl$	*n*-BuLi	PhS(O)*n*-Bu	4
14	$PhS(O)CH_2Cl$	*t*-BuLi	PhS(O)*t*-Bu	5
15	$PhS(O)CH(Cl)CH_3$	CH_3Li	$PhS(O)CH_3$	36
16	$PhS(O)CH(Cl)CH_3$	*n*-BuLi	PhS(O)*n*-Bu	22
17	$PhS(O)CH(Cl)CH_3$	*t*-BuLi	PhS(O)*t*-Bu	9
18	$PhS(O)CH_2(Li)$	*t*-BuLi	*t*-$BuS(O)CH_2Li$	33
19	$PhS(O)CH(Li)CH_3$	*t*-BuLi	*t*-$BuS(O)CH(Li)CH_3$	35
20	$C_4H_9S(O)C_4H_9$	*t*-BuLi	*t*-$BuS(O)C_4H_9$	7

[a]A 3:1 mol ratio of *t*-BuLi to sulfoxide was used.
[b]Estimated.

TABLE 2. Reaction of optically active sulfoxides with alkyllithiums

Sulfoxide	$[\alpha]_D$(°)	Alkyllithium	Displaced product	$[\alpha]_D$(°)
p-TolylS(O)CH_2Ph	245(8)	*t*-BuLi	*p*-TolylS(O)-*t*-Bu	0
p-TolylS(O)CH_3	145	*t*-BuLi	*t*-$BuS(O)CH_3$	−0.5
$PhCH_2S(O)Ph$	245(8)	CH_3Li	$PhS(O)CH_3$	−139
$PhCH_2S(O)Ph$	245	*t*-BuLi	*t*-$BuS(O)CH_3$	0°
p-TolylS(O)*t*-Bu	30(8)	*t*-BuLi	*p*-TolylS(O)-*t*-Bu	0

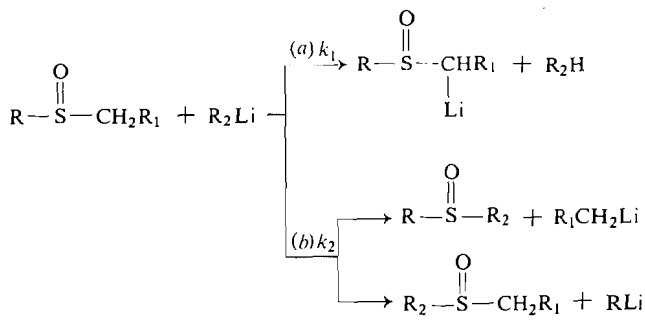

gave mainly carbanion formation and very little displacement with the above three sulfoxides (entries 4 and 7, Table 1). The stronger bases, *n*-BuLi and *t*-BuLi, on the other hand gave 30–50% of phenyl group displacement (entries 1, 2, 5, 6, 8). In general these bases are not suitable for the generation of α-sulfinyl carbanions for synthetic purposes. Methyllithium is sufficiently powerful to displace benzyl (~7%), chloromethyl (12%), and chloroethyl (36%) groups (entries 9, 12, 15). For these types of substances the use of lithium diisopropylamide is recommended for carbanion generation.

The variations in the amount of phenyl group

Can. J. Chem. Downloaded from www.nrcresearchpress.com by 210.87.254.42 on 09/05/12
For personal use only.

Can. J. Chem. Downloaded from www.nrcresearchpress.com by 210.87.254.42 on 09/05/12
For personal use only.

displacement involving the reaction of *t*-butyllithium with methyl, ethyl, and isopropyl sulfoxide (43, 50, and 38%, respectively) probably reflects an interplay of a variety of factors. Attack at sulfur is most favored for methyl phenyl and least favored for isopropyl phenyl sulfoxide on steric grounds. However, carbanion formation is also more favored for the methyl *vs.* isopropyl sulfoxide because of the greater number and greater acidity of the protons available for abstraction in the former compound. Ethyl phenyl sulfoxide represents an intermediate situation for both factors. The relative importance of the factors is such that the greatest amount of displacement occurs with the ethyl sulfoxide followed by the methyl and isopropyl derivatives.

Somewhat surprising is the observation that an exchange reaction is possible even for $PhS(O)CH_2Li$. This was suggested by the observation that addition of a two-fold excess of *t*-butyllithium increased the amount of phenyl group displacement from 43 to 67%. When $PhS(O)CH_2Li$ was generated from $PhS(O)CH_3$ with CH_3Li and then treated with *t*-butyllithium a 33% yield of *t*-butyl methyl sulfoxide was obtained (entry 18). Similarly, phenylsulfinyl ethide anion underwent a 38% displacement of the phenyl group upon exposure to *t*-BuLi (entry 19). The decrease in reactivity at sulfur due to the presence of an α-anion must be matched by a corresponding decrease in the acidity of the remaining α-hydrogens.

The exchange results indicate that the displaced group departs as an anion, *i.e.*, an alkyllithium. Thus, in the reactions of methyl phenyl sulfoxide with *n*-butyl- or *t*-butyllithium only displacement of the phenyl group was observed. Similarly, ethyl phenyl and isopropyl phenyl sulfoxides reacted with *t*-butyllithium to give *t*-butyl ethyl and *t*-butyl isopropyl sulfoxides, respectively, as the only exchange products. The observed ease of exchange, phenyl > alkyl is in agreement with the pK_a values of the conjugate acids (pK_a of benzene = 37, of CH_4 = 40, of C_2H_6 = 42) (7). Introduction of a chlorine atom in the α-position of the alkyl group apparently sufficiently enhances its pK_a to make CH_2Cl and $CH(Cl)CH_3$ better leaving groups than phenyl. The observed displacement of the benzyl group in both phenyl benzyl and methyl benzyl sulfoxide is also in agreement with the above postulate (pK_a of $PhCH_3$ = 35 (7)).

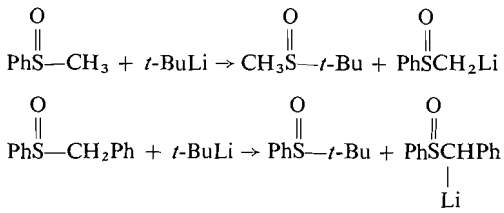

The effect of size of the alkyllithium was most apparent when one group on the sulfoxide was easily displaced such as in the reaction of α-chloroalkyl phenyl sulfoxides with methyl-, *n*-butyl- and *t*-butyllithium. As the size of the reagent increased the amount of displacement relative to proton abstraction is decreased. For example, in the reaction of $PhS(O)CH(Cl)CH_3$ with CH_3Li, *n*-BuLi, and *t*-BuLi the percentage displacement of the chloroethyl group decreased from 36 to 22 to 9, respectively. Similarly, the reaction of $PhS(O)CH_2Cl$ with methyl and *n*-butyllithium gave 12 and 4% displacement of CH_2Cl, respectively.

The reaction of a number of optically active sulfoxides with alkyllithium was also investigated. When methyl- or *n*-butyllithium was employed the displaced products were formed with essentially complete inversion of configuration. Thus, for example, (*R*)-benzyl phenyl sulfoxide $[\alpha]_D$ −245° (*c*, 0.4 acetone (8)) was reacted with 1 equiv. of methyllithium in THF at −78° for 10 min and then added to water. The crude product was separated by t.l.c. and gave recovered starting material (80% yield), $[\alpha]_D$ +241° (*c*, 0.4 acetone) ~98% optically pure, and 10% (*S*)-methyl phenyl sulfoxide, $[\alpha]_D$ −142° (*c*, 1.9 ethanol) (reported (3) $[\alpha]_D$ for the *R* isomer +147.5° (ethanol)). The exchanged product was therefore formed with greater than 95% inversion of configuration at sulfur. However, when *t*-butyllithium was used as base the optical purity of the exchanged products was variable and generally quite low (see Table 2). The residual rotations indicated net inversion of configuration at sulfur. In a control experiment it was shown that *t*-butyl phenyl sulfoxide undergoes rapid racemization upon exposure to *t*-butyllithium. The racemization of *t*-butyl alkyl or aryl sulfoxides upon exposure to *t*-butyllithium cannot proceed via a sulfine intermediate nor via repeated S_N2 displacements of the *t*-butyl group as an anion (all other groups, *e.g.*, phenyl or methyl would be expected to be displaced

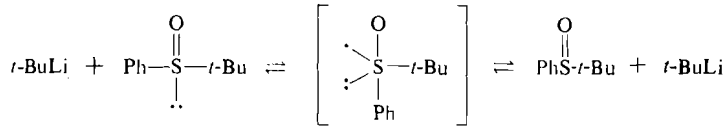

4

preferentially). One speculation which we would like to suggest at this time is that racemization might occur via a radical intermediate produced by a one electron transfer from *t*-butyllithium to the sulfoxide, *e.g.*, via **4**.

Several mechanisms for exchange of the alkyl groups in sulfoxides upon reaction with alkyllithium can be considered. As mentioned earlier, alkyl group exchange could occur via (*i*) a sulfine intermediate, (*ii*) by direct displacement, or (*iii*) via a pentacoordinate intermediate.

Alkyl group exchange via a sulfine can be eliminated in many of the reactions studied and thus must be considered highly unlikely except for possibly highly biased examples. Thus, for example, the exchange of the chloroalkyl groups in methyl, *n*-butyl, and *t*-butyl in chloromethyl and chloroethyl phenyl sulfoxides cannot occur via a sulfine intermediate. The only sulfines which could possibly be formed are CR(Cl)=SO (R = H or CH_3) and thus exchange via a sulfine would result in displacement of the phenyl group instead of the observed displacement of the chloroalkyl groups (see Scheme 4, and Table 1, entries 12–17). Similarly, the exchange of the benzyl group in benzyl phenyl (entries 9–11) and benzyl *p*-tolyl sulfoxide (Table 2) cannot involve a sulfine intermediate.

Our results are most readily explained in terms of an S_N2 mechanism. There is no evidence for the occurrence of a S(IV) intermediate capable of undergoing a pseudorotation (see below). Similar conclusions have been drawn by Tang and Mislow (9) for the base-catalyzed hydrolysis of *cis*- and *trans*-1-ethoxy-3-methyl thietanium hexachloroplatinates. Presented in Scheme 5 are trigonal bipyramidal intermediates which can be obtained from the reaction of (*R*)-benzyl methyl sulfoxide with methyllithium. In analogy with the pentacoordinate phosphorus chemistry (10), the possible intermediates are generated by attack on the edge of the sulfur tetrahedron (apical insertion) rather than attack on a face (equatorial insertion). A continuation of the analogy with the phosphorus compounds (11) and with compounds such as SF_4 (12) enables one to eliminate bipyramidal structures having an apical O^- or an apical lone pair. The above limitations allow only two possible initial bipyramidal species, **5** and **6**, and make pseudorotation of these species unlikely since such a process invariably produces structures having either a lone pair or the O^- (or both) in the unfavorable axial position.

Further consideration of Scheme 5 suggests that sulfuranes are not intermediates in these reactions. If they were, one would expect that species **5** and **6** would have been formed to approximately the same extent. If one also assumes apical departure then species **5** can lose either the CH_3 or the $PhCH_2$ leading to the starting materials or the observed product (*S*)-methyl sulfoxide, respectively, the latter being more likely because $PhCH_2$ is the better leaving group. From **6**, either CH_3 or Ph can be lost. In this case loss of the phenyl group (a viable leaving group) to give benzyl methyl sulfoxide should be the preferred pathway. Since none of this sulfoxide was obtained in the reaction, species such as **a** and **b** are probably not intermediates. The formation of phenyl methyl sulfoxide with inversion of configuration at sulfur from benzyl methyl sulfoxide and methyllithium is thus best explained in terms of **5** being a transition state, *i.e.*, partial bonds

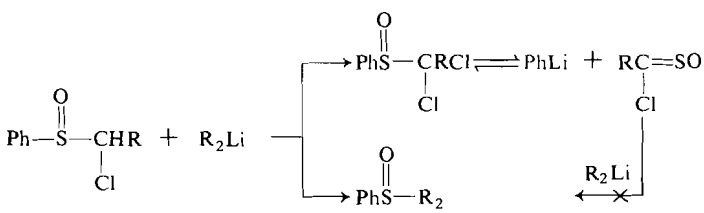

SCHEME 4. Reaction of chloroalkyl phenyl sulfoxides with alkyllithiums.

Can. J. Chem. Downloaded from www.nrcresearchpress.com by 210.87.254.42 on 09/05/12
For personal use only.

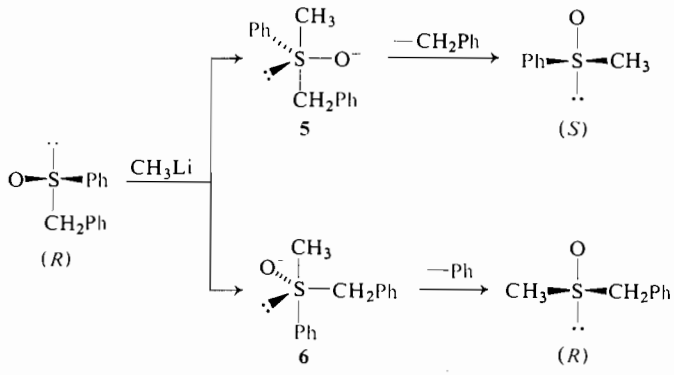

SCHEME 5

$H_3C\cdots\overset{|}{S}\cdots CH_2Ph$ instead of the full bonds shown in **5**.

Experimental

All sulfoxides and sulfones used in this study were known and prepared by standard procedures.

Reaction of Sulfoxides with Alkyllithiums

General Procedure

Approximately 300 mg of sulfoxide was dissolved in 15–20 ml of dry tetrahydrofuran in a two-neck flask equipped with a nitrogen inlet and a serum cap. The solution was cooled to −78° in a Dry Ice – acetone bath. The alkyllithium was added dropwise by means of a syringe. After the addition was complete, the reaction mixture was stirred for 10 min then poured into about 30 ml of H_2O. The product was extracted with three 30-ml portions of CH_2Cl_2. The combined organic phase was dried over magnesium sulfate and the solvent was evaporated. The product thus obtained was either analyzed directly by n.m.r. or oxidized with 1.5–2.0 equiv. of *m*-chloroperbenzoic acid in refluxing CH_2Cl_2 for about 6 h. The sulfones thus formed were isolated in the usual manner and crude product analyzed by v.p.c. The results are recorded in Table 1.

Reaction of Optically Active Sulfoxides with Alkyllithiums

Benzyl *p*-tolyl sulfoxide (450 mg) $[\alpha]_D$ +245° (*c*, 0.8 acetone) (reported (8) $[\alpha]_D$ +250° (acetone)) was dissolved in 20 ml of THF at −78°. To this solution was added 1.6 ml of *t*-BuLi (1.2 *M* in pentane). The reaction mixture was stirred for 10 min, then worked up as described for the inactive sulfoxides. An n.m.r. spectrum of the crude product indicated a 1 : 1 mixture of benzyl *p*-tolyl sulfoxide and *t*-butyl phenyl sulfoxide. The products were separated by preparative t.l.c. to give pure benzyl *p*-tolyl sulfoxide $[\alpha]_D$ +242° and *t*-butyl phenyl sulfoxide $[\alpha]_D$ 0°.

Benzyl Phenyl Sulfoxide and Methyllithium. Methyllithium (5.3 mol) was added dropwise to a solution of 950 mg (44 mmol) of sulfoxide, $[\alpha]_D$ 245° (*c*, 0.5 $CHCl_3$) (8). The reaction mixture was stirred for 2 min then poured into H_2O. Work-up yielded 0.88 g of crude product which was separated by preparative t.l.c. The recovered benzyl methyl sulfoxide had $[\alpha]_D$ +241°. The methyl phenyl sulfoxide prepared in this manner had $[\alpha]_D$ −142° (*c*, 1.9 ethanol). (Reported for (*R*)-methyl phenyl sulfoxide $[\alpha]_D$ +147°).

t-Butyl p-Tolyl Sulfoxide and t-Butyllithium. *t*-Butyl *p*-tolyl sulfoxide (180 mg), $[\alpha]_D$ 30°, 18.6% optically pure (8), was allowed to react with 1.0 equiv. of *t*-BuLi under the usual conditions. Work-up yielded 160 mg of *t*-butyl *p*-tolyl sulfoxide which was purified by sublimation. The purified product had $[\alpha]_D$ 0°.

Financial support by the National Research Council of Canada is gratefully acknowledged.

1. (*a*) E. J. COREY and M. CHAYKOVSKY. J. Am. Chem. Soc. **87**, 1345 (1965); (*b*) J. B. SIDALL, A. D. CROSS, and J. H. FRIED. J. Am. Chem. Soc. **88**, 862 (1966); (*c*) T. DURST. J. Am. Chem. Soc. **91**, 1034 (1969); (*d*) T. DURST, R. VIAU, and M. R. MCCLORY. J. Am. Chem. Soc. **93**, 3077 (1971).
2. V. FRANZEN. Special publication, No. 19. The Chemical Society, London. 1965. p. 172.
3. J. JACOBUS and K. MISLOW. J. Am. Chem. Soc. **89**, 5228 (1967).
4. K. K. ANDERSEN. Tetrahedron Lett. 2485 (1970).
5. (*a*) K. K. ANDERSEN. Tetrahedron Lett. 93 (1962); (*b*) K. MISLOW, M. M. GREEN, P. LAUR, J. T. MELILLO, T. SIMMONS, and A. TERNAY, JR. J. Am. Chem. Soc. **87**, 1958 (1965).
6. (*a*) C. R. JOHNSON and C. W. SCHROEK. J. Am. Chem. Soc. **90**, 6852 (1970); (*b*) J. JACOBUS and K. MISLOW. Chem. Commun. 253 (1968); (*c*) S. COLONNA, R. GIOVINI, and J. MONTANARI. Chem. Commun. 865 (1968).
7. D. J. CRAM. Fundamentals of carbanion chemistry. Academic Press, New York and London. 1965. p. 19.
8. B. J. AURET, D. R. BOYD, H. B. HENBEST, and S. Ross. J. Chem. Soc. C, 2371, 2374 (1968).
9. R. TANG and K. MISLOW. J. Am. Chem. Soc. **91**, 5644 (1969).
10. F. H. WESTHEIMER. Acc. Chem. Res. **1**, 70 (1968).
11. I. UGI and F. RAMIREZ. Chem. in Britain, **8**, 198 (1972).
12. F. A. COTTON, J. W. GEORGE, and J. S. WAUGH. J. Chem. Phys. **28**, 994 (1958).
13. J. P. LOCKARD, W. C. SCHROEK, and C. R. JOHNSON. Synthesis, 485 (1973).

Can. J. Chem. Downloaded from www.nrcresearchpress.com by 210.87.254.42 on 09/05/12
For personal use only.

Carbon-13 Nuclear Magnetic Resonance Studies of *ortho*-Substituted Anisoles and Diphenyl Ethers

GERALD W. BUCHANAN[1]
Department of Chemistry, Carleton University, Ottawa, Canada K1S 5B6
AND
GIORGIO MONTAUDO AND PAOLO FINOCCHIARO
Institute of Industrial Chemistry of the University, Viale A. Doria 8, Catania, Italy
Received September 5, 1973

Carbon-13 n.m.r. chemical shifts for 8 anisoles and 15 diphenyl ethers are reported. *para*-Carbon shieldings are found to be sensitive to the degree of steric interference to conjugative electron release by the ethereal oxygen atom. An empirical correlation between the *para*-carbon shifts and the average twist angle of the phenyl rings from a reference plane has been developed. Satisfactory agreement has been found between the angles of twist derived from carbon chemical shifts and those based on other physical measurements.

On rapporte les déplacements chimiques en r.m.n. du carbone-13 de 8 anisoles et de 15 éthers diphénylés. On a trouvé que le blindage des carbones en *para* est sensible au degré d'interférence stérique à la scission des électrons de l'atome d'oxygène de la fonction éthérée par conjugaison. On a développé une corrélation empirique entre les déplacements chimiques des carbones en *para* et les angles moyens de torsion du plan des noyaux phényles par rapport à un plan de référence. On a trouvé une corrélation satisfaisante entre les angles de torsion dérivés des déplacements chimiques du carbone et ceux basés sur d'autres méthodes physiques.
[Traduit par le journal]

Can. J. Chem., **52**, 767 (1974)

Introduction

In recent years considerable effort, using a variety of techniques, has been directed toward the elucidation of the geometries of substituted diphenyl ethers (DPO) in solution. As it would be expected, no single technique yields all the desirable information, rather the different methods appear complementary.

Several studies (1–6) indicate that the conformational preference of DPO can be reasonably established by ^{1}H n.m.r. only if it is of the H-inside type (1) (the two phenyls lying perpendicular to each other). In fact, the intramolecular ring current shielding effect is sizeable for the H-inside form but sharply decreases for the other skew conformations, which become practically undetectable by this method (7, 8). Skew conformations have been claimed at times (9–12) to be consistent with dipole moment data, but it has been recently (13, 7, 6) pointed out that dipole moments often do not provide unequivocal information about the conformational preferences of *ortho*-substituted DPO.

[1]Author to whom correspondence should be addressed.

Furthermore, semiempirical conformational energy calculations (8, 14) have shown that, except for the tri-*ortho* derivatives, there is a lack of conformational preference in *ortho*-methyl-substituted DPO; *i.e.*, there are several conformations with comparable populations or, in the case of a single conformation, the potential energy well is very shallow at its bottom so that the molecular population becomes distributed over a wide range of torsional angles.

Lately, ^{1}H n.m.r. (6) and X-ray diffraction (15) evidence has been produced showing that electron withdrawing groups (nitro) are able to induce a conformational preference in DPO by enhancing the conjugation between unshared electrons of the bridging atoms and the π electrons in the phenyl ring.

It is now well established that ^{13}C n.m.r. chemical shifts can be an order of magnitude more sensitive to steric factors than ^{1}H shifts in favorable cases (16, 17). Studies on *ortho*-substituted benzophenones (18) illustrate the potential of the method for conformational analysis of Ar—X—Ar compounds. It is clear from the results of Dhami and Stothers for

Can. J. Chem. Downloaded from www.nrcresearchpress.com by 210.87.254.40 on 09/05/12
For personal use only.

Can. J. Chem. Downloaded from www.nrcresearchpress.com by 210.87.254.40 on 09/05/12
For personal use only.

TABLE 1. ^{13}C n.m.r. chemical shifts for anisoles

Compound	Substituent position CH_3	NO_2	iso-Pr	δ_C (p.p.m. from TMS ±1)* C-1	C-2	C-3	C-4	C-5	C-6	OCH_3	2-CH_3	CH_3 ↓ CH CH_3	↓ CH_3 CH CH_3
1				159.2	113.8	128.9	120.1	128.9	113.8	55.1			
2	2			157.6	130.5	126.5	120.3	126.5	110.2	55.3	16.0		
3†	2, 6			156.2	129.3	127.6	122.6	127.6	129.3	57.9	15.0		
4		2		153.0	139.9	125.8	120.9	134.5	114.3	57.4			
5		4		163.8	113.6	125.1	141.0	125.1	113.6	55.9			
6		2, 4		157.0	(139.3)	122.2	(140.7)	129.8	114.7	58.8			
7			2	156.7	137.0	(126.3)	120.5	(125.9)	110.6	55.6		27.3	23.0
8			2, 6	154.7	141.4	123.9	123.3	123.9	141.4	61.6		26.8	23.8

*0.5 *M* solutions in $CDCl_3$.
†Saturated solution in CS_2 (ref. 19).

TABLE 2. ^{13}C n.m.r. chemical shifts for methyl and nitro substituted diphenyl ethers

Compound	Substituent position CH_3	NO_2	δ_C (p.p.m. from TMS ±1)* C-1	C-2	C-3	C-4	C-5	C-6	C-1′	C-2′	C-3′	C-4′	C-5′	C-6′	2-CH_3	6-CH_3
9			156.1	117.3	128.2	121.6	128.2	117.3								
10	2		154.5	131.1	126.8	121.8	129.7	119.6	157.8	117.4	129.3	122.1	129.3	117.4	16.0	
11	2, 2′		154.6	130.7	126.3	122.4	128.1	117.1							15.5	
12	2, 6		150.5	131.0	129.0	124.5	129.0	131.0	157.2	114.4	128.5	120.7	128.5	114.4		
13		2′	154.9	118.6	129.3	122.7	129.3	118.6	149.7	140.8	124.9	123.9	133.4	120.1		
14		4′	153.7	119.9	129.5	124.7	129.5	119.9	162.0	116.8	125.1	141.8	125.1	116.8		
15	2, 6	4′	150.3	130.3	128.9	126.0	128.9	130.3	162.6	114.8	126.0	142.8	126.0	114.8	16.0	16.0
16	2	4′	151.7	130.1	127.3	124.5	131.5	120.7	162.4	115.8	125.5	141.8	125.5	115.8	15.8	
17	2, 6	2′	150.1	130.5	128.9	125.5	128.9	130.5	149.1	138.4	125.7	120.7	133.4	114.8	16.2	16.2
18		2′, 4′	152.9	119.6	130.1	125.9	130.1	119.6	155.3	138.9	121.0	140.7	128.1	118.0		
19	2	2′, 4′	150.5	129.7	127.5	126.3	131.7	120.1	154.9	138.2	121.3	140.4	128.3	116.8	15.8	

*0.5 *M* solutions in $CDCl_3$.

Can. J. Chem. Downloaded from www.nrcresearchpress.com by 210.87.254.40 on 09/05/12
For personal use only.

substituted anisoles (19) that carbon shieldings reflect the degree of steric hindrance to electronic interactions in these molecules and it seems reasonable to expect that ^{13}C n.m.r. should have valuable application for the study of diphenyl ether conformations as well. Accordingly we have examined the ^{13}C n.m.r. spectra of 15 diphenyl ethers and compared the shieldings with those for related anisoles. The conformational implications of the data are discussed.

Results

To aid in the discussion of the diphenyl ether shielding trends, results for related anisoles are presented in Table 1. Tables 2 and 3 contain carbon chemical shifts for methyl and nitro substituted diphenyl ethers and isopropyl nitro diphenyl ethers, respectively.

Methods of assignment used for some anisoles have been published previously (19). For diphenyl ethers assignments for carbons bearing no directly bonded hydrogens are based on the retention of singlet structure for these resonances in the off-resonance decoupling experiment. In several compounds the *ortho* aromatic carbons were assigned from specific ^{1}H decoupling since it is known (6) that protons *ortho* to the oxygen of diphenyl ethers resonate at higher fields than those in *meta* and *para* positions. Remaining ring carbon assignments were made by analogy with anisoles (19) or by using well-established substituent effects on aromatic carbon shieldings (20). Characteristically, ring carbons directly bonded to nitrogen show low integrated intensity and additional line broadening due to the effect of the adjacent ^{14}N nucleus.

ortho-Methyl carbons can be clearly assigned and appear at 15.6 $\pm$ 0.6 p.p.m. These shifts are *ca.* 4 p.p.m. to higher field than those found in benzophenones (18) but they do not vary significantly with conformation. Isopropyl methine and methyl signals can be distinguished readily on the basis of off-resonance decoupling and empirically established trends of alkyl substitution (21) on ^{13}C n.m.r. shifts.

For anisoles **1**, **2**, **3**, and **5** present shifts are in good agreement with those reported earlier (19). No isopropyl methyl or methine shieldings for **7** and **8** were reported in the previous work (19) and for **8** the higher resolution now attainable allows observation of separate signals for the C-3,5 and C-4 ring carbons. The only published ^{13}C n.m.r. data available for diphenyl ethers are for the parent compound **9** (22), and agreement between shieldings observed herein and those previously reported is satisfactory.

A common practice in assignment of resonances for polysubstituted aromatics has been the use of additivity of substituent effects (19, 20). Providing the substituents are not *ortho*, good additivity relationships are generally found. Attempts to use additivity can, however, aid designation of resonances for ortho-substituted materials as well provided that proper caution is used. Consider 2-nitroanisole (**4**). Using nitrobenzene (**a**) and anisole (**b**) as models, the predicted shifts relative to that of benzene (128.7) are shown below (**c**).

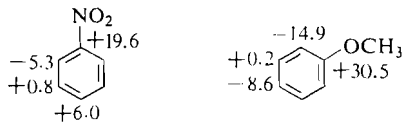

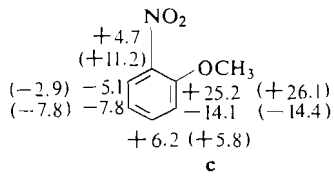

Observed values relative to benzene are shown in parenthesis. Only the C-2 value shows serious deviation from additivity but this resonance was clearly that due to a carbon bonded to nitrogen for spectral reasons outlined previously. For the 2,4-dinitroanisole **6**, chemical shifts can be predicted using the experimental values for **4** and assuming additivity effects from the 4-NO_2 function. Results are shown below, and with the

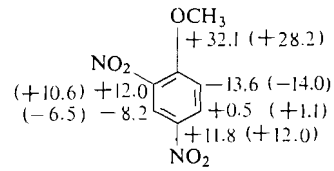

exception of C-1, predicted shifts based on additivity give reasonable (within 1.7 p.p.m.) agreement with those observed. These assignments in the anisoles were used as a basis for the more complex diphenyl ether systems to be discussed later.

Anisoles

The ^{13}C chemical shifts for anisole can be reasonably interpreted in terms of conjugative

Can. J. Chem. Downloaded from www.nrcresearchpress.com by 210.87.254.40 on 09/05/12
For personal use only.

TABLE 3. ^{13}C n.m.r. chemical shifts for isopropyl nitro diphenyl ethers

Compound	Substituent position		δ_C (p.p.m. from TMS ± 1)*													
	iso-Pr	NO_2	C-1	C-2	C-3	C-4	C-5	C-6	C-1′	C-2′	C-3′	C-4′	C-5′	C-6′	CH_3	CH_3 ↓ CH_3 CH
20	2, 6	4′	148.1	141.8	125.3	127.1	125.3	141.8	164.4	115.6	126.3	142.8	126.3	115.6	23.9	28.1
21	2	4′	151.3	140.3	(126.9)	124.8	(127.3)	109.8	163.2	116.2	125.5	142.4	125.5	116.2	23.1	27.5
22	2, 6	2′, 4′	147.0	140.8	125.7	128.2	125.7	140.8	155.8	138.4	122.5	141.4	130.2	116.5	{22.4, 24.1}	27.5
23	2	2′, 4′	150.5	140.6	(126.7)	126.4	(127.3)	111.9	155.9	139.0	121.6	141.0	128.1	117.2	22.9	27.9

*0.5 *M* solutions in $CDCl_3$.

Can. J. Chem. Downloaded from www.nrcresearchpress.com by 210.87.254.40 on 09/05/12
For personal use only.

electron release by the oxygen atom (19). Contributions from the resonance forms depicted below will increase the electron density at the *ortho* and *para* positions relative to benzene and

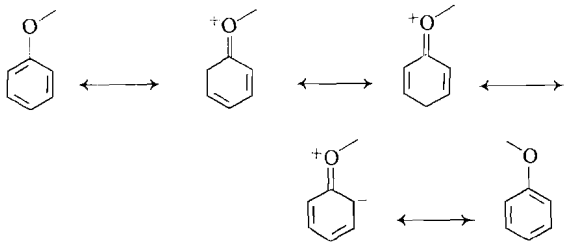

thus increase the shieldings. The resonance for the C-3,5 carbon (128.9) is nearly identical to that of benzene (128.7), an effect which appears to be general for mono-substituted aromatics (17). The methoxy carbon resonance at 55.1 p.p.m. is characteristic of such moieties (19).

When an alkyl group is substituted in the 2-position (*i.e.* compounds **2** and **7**) the most interesting effect is the upfield shift of *ca.* 3 p.p.m. observed at C-6. A possible rationale for this is a closer spatial approach of the methoxy carbon with C-6 as a consequence of the increased steric congestion at C-2. As a result a "γ" steric interaction will arise and an increased shielding at C-6 is expected (23). On this basis, one might

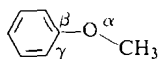

expect a shielding of the methoxy carbon as well, but no substantial difference is evident between **1**, **2**, and **7**. It may be that the *ortho* carbon shieldings are sensitive to the orientation of the lone pairs on oxygen, however the clear existence of such an effect remains to be demonstrated.

If there is a significant perturbation of the methoxy–aryl ring interaction, a deshielding of the *para*-carbon would be expected due to an attenuation of the conjugative electron release by oxygen. The C-4 shifts for **2** and **7** are nearly identical to **1** and thus there is no evidence for a steric inhibition of resonance in the mono-*ortho* derivatives. It is likely, however, that there is only one planar conformation (shown above) in which there is appreciable conjugation.

By contrast, in the 2,6-dialkyl derivatives **3** and **8** deshielding effects of *ca.* 3 p.p.m. are observed at the *para*-carbon. For an extensive series of anisoles, Dhami and Stothers have shown that the magnitude of this deshielding is dependent on the size of the *ortho* groups. It is reasonable to conclude, therefore, that there is steric interference of the *ortho* groups with the methoxy function in the 2,6-disubstituted materials, such that electron release by the oxygen is substantially reduced. The most populated conformation of these hindered materials is likely one in which the O—CH_3 group deviates from coplanarity with the aryl ring.

In the 2,6-diisopropyl compounds shieldings at C-2,6 and C-3,5 differ substantially from those for the 2,6-dimethylated materials. The downfield shift of *ca.* 11 p.p.m. at the C-2,6 carbon of the isopropyl ethers is in accord with the empirically established trends of β-alkyl substitution observed in hydrocarbons (21). The C-3,5 carbons of the 2,6-diisopropyl ethers are shielded by *ca.* 3 p.p.m. relative to the 2,6-dimethyl materials, an effect which is likely due to a γ steric interaction (23) between the isopropyl methyl groups and the C-3,5 carbon, which is not present in the methylated ethers.

The trends in methoxy carbon resonances for the anisoles indicate a deshielding in 2,6-dialkylated systems which is more pronounced as the steric bulk of the alkyl groups increase. As previously noted (19) this trend is opposite to that expected if the electron releasing tendency of oxygen is reduced in sterically hindered cases. Although we can offer no fundamental reason for the effect, there is now evidence for large steric *deshielding* effects between methyl groups which occupy a δ orientation in other compounds. A particular example is the 6.6 p.p.m. deshielding noted for the methyls of 1,8-dimethylnaphthalene relative to methylnaphthalene (24). For 2,6-dimethylanisole δ interactions

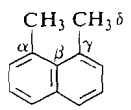

are possible between the *ortho*-CH_3's and the methoxy group, in a planar conformation. No

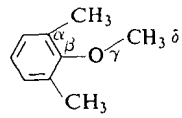

doubt the planar form will be populated to only a minor extent and thus the magnitude of the deshielding is smaller (*ca.* 2.5 p.p.m.) here than in 1,8-dimethylnaphthalene. In the 2,6-diiso-

Can. J. Chem. Downloaded from www.nrcresearchpress.com by 210.87.254.40 on 09/05/12
For personal use only.

propyl systems the interacting CH_3 groups are ε to each other and a further deshielding of the methoxy carbon by *ca.* 4 p.p.m. is noted. It is interesting that the methyl resonances of the 2,6-diisopropyl cases are *ca.* 0.8 p.p.m. lower field than the 2-isopropyl molecules, indicating a mutual methoxy-methyl deshielding in the di-*ortho*-substituted compounds. Clearly more work is needed to delineate the contributions to this phenomenon but it is now evident that considerable steric deshielding exists in favorable cases for interacting groups further apart than a γ orientation.

Diphenyl Ethers

It is useful to compare the ring carbon shifts of diphenyl ether **9** with anisole **1**. From the earlier discussion for anisole, one would expect (relative to benzene) an increase in the electron density at the *ortho* and *para* positions of diphenyl ether as well due to the conjugative electron release by oxygen. Shieldings for **9** are consistent with this suggestion. *Para*-carbon shieldings for **10** and **11** are close to that of **9**, a trend consistent with anisoles **1** and **2**. The downfield shift of C-6 in **10** is puzzling, however, and we can offer no rationale for this at present. With this exception, the *ortho*-methine carbon shifts of **9**, **10**, and **11** closely coincide.

For the 2,6-dimethyl derivative **12**, a deshielding of *ca.* 2.5 p.p.m. is observed at C-4 relative to **9**, **10**, and **11**. By analogy with the anisole trends it is suggested that this deshielding results from a steric inhibition of the conjugative electron release by oxygen into the substituted ring. Most interestingly, both the C-2′,6′ and C-4′ positions are shielded in **12** relative to **9** indicating that electron release into the unsubstituted aryl ring may be enhanced when both *ortho* positions are occupied in the adjacent aryl moiety. In fact the unsubstituted ring carbons of **12** are only slightly deshielded (except for C-1′) relative to anisole itself.

Shieldings for the 2′-nitrodiphenyl ether **13** were assigned using specific decoupling experiments and compound **4** as a model. Relative to **9**, the 2′-nitro group induces downfield shifts of *ca.* 1 p.p.m. for all carbons of the unsubstituted ring (except C-1). Introduction of methyl groups at C-2 and -6 as in **17** again produces appreciable deshielding (3 p.p.m.) at C-4 relative to **13**. Furthermore, C-2′, 4′, and -6′ of **17** are noticeably shielded (2–5 p.p.m.) relative to **13** or **14**, indicating that conjugative electron release by oxygen may be increased into the nitro substituted ring, while conjugation is decreased into the di-*ortho*-alkylated phenyl ring.

Compared to **9**, shieldings for the 4′-nitrodiphenyl ether (**14**) suggest that electron withdrawal by the NO_2 group from all positions of the remote phenyl ring (except C-1) as mirrored by downfield shifts of 1–3 p.p.m. A 2-methyl substituent as in **16** or a 2-isopropyl group (**21**) causes little change in the C-4 shift relative to **14**, a trend consistent with that for **9**, **10**, and **11**. For the 2,6-dialkylated compounds **15** and **20**, again substantial deshielding occurs at C-4 relative to **14**, **16**, and **21**. The deshielding is accentuated when the more bulky isopropyl functions are present in agreement with the suggested operation of steric interference to resonance. By contrast to the earlier cases, shieldings for C-2′, -4′, and -6′ of **14**, **15**, **16**, **20**, and **21** follow no clearly discernible pattern.

For **18**, the electron withdrawing power of the nitro groups is evident in the downfield shifts of the unsubstituted ring carbons, especially C-4 which now appears at 125.9 p.p.m. *i.e.*, 4.3 p.p.m. below C-4 of **9**. Shifts in the substituted ring follow patterns similar to the anisole **6**. Introduction of a 2-methyl (**19**) or a 2-isopropyl (**23**) moiety does not change the C-4 shift substantially from that of **18** but in the 2,6-diisopropyl derivative **22**, a deshielding of *ca.* 2.5 p.p.m. at C-4 is apparent. Again we suggest this has a conformational basis and is a result of sterically attenuated electron release by the ethereal oxygen.

The observation of separate isopropyl methyl resonances for **22** is consistent with the reports that the barrier to rotation about the aryl–oxygen bond is *ca.* 18 kcal/mol (4, 25). It is interesting to note that the shift difference between the diastereotopic methyl groups is 42 Hz for the carbons compared with only 7 Hz for the protons. Potentially, therefore, ^{13}C n.m.r. should yield more precise kinetic parameters for hindered rotation in these molecules.

Throughout this study no obvious carbon shielding trends as a function of substituents have been noticed at either C-1 or -1′ and accordingly no detailed discussion of these shieldings is included. Similar conclusions were reached in previous anisole work (19) regarding C-1 shifts.

Torsional Angles

The *para*-carbon shielding trends in anisoles

Can. J. Chem. Downloaded from www.nrcresearchpress.com by 210.87.254.40 on 09/05/12
For personal use only.

and DPO's suggest that an empirical correlation of these shifts with the average twist angle (θ) of the respective phenyl ring from the reference plane[2] may be possible. Initially, we make the reasonable assumption that the shift value of 120.1 for C-4 of **1** is indicative of a conformation with $\theta = 0°$.

From X-ray (15) and ^1H n.m.r. data (1–6), the tri-*ortho*-substituted compounds **17** and **22** are known to adopt an essentially perpendicular ($\theta = 90°$) conformation in both the solid state and in solution. In order to employ the C-4 shifts of **17** and **22** as models for compounds having $\theta = 90°$ however, correction for the inductive effects of the nitro groups on the remote phenyl ring must be made. Comparison of the 4′-NO_2 derivative **14** with diphenyl ether **9** indicates that C-4 of **14** is deshielded by 3.1 p.p.m. as a result of electron withdrawal by the 4′-NO_2 function. Applying this 3.1 p.p.m. "correction factor" to the C-4 shift of **22** yields a value of 125.1, which is in reasonable agreement with the value of 125.5 for C-4 of **17**. Accordingly we have used an average of these values, 125.3 p.p.m., to denote the C-4 shift for a compound in a perpendicular conformation. No correction factor for a 2′-NO_2 group is included due to the likelihood that this function in the *ortho* position will induce steric preferences.

Assuming complete absence of conjugation at $\theta = 90°$, the value of $\cos^2\theta$ should be proportional to the extent of conjugation present. From the equation:

$$\cos^2\theta = \frac{125.3 - \delta}{125.3 - 120.1}$$

where δ is the C-4 shift in p.p.m., θ values for some of the anisoles and all of the DPO's have been calculated. The anisole results in Table 4 indicate that only in the di-*ortho*-alkylated systems **3** and **8**, does θ vary substantially from that in **1**. Differential solvent effects ($CDCl_3$ *vs.* CS_2) however, may make the value for **3** somewhat uncertain.

For DPO's **14**, **15**, **16**, **18**, **19**, **20**, **21**, and **23**, the 3.1 p.p.m. "correction factor" has been used to adjust the C-4 shifts before substitution into the above equation. Except for perpendicular forms **17** and **22**, the largest interplanar angles (Table 5) are found in the di-*ortho*-alkylated compounds **12** and **20**. Mono-*ortho*-alkylated systems **10** and **21** show the smallest angles as expected.

TABLE 4. Average twist angle in anisoles

Compound	θ(°)
1	0
2	11
3	44
7	16
8	52

TABLE 5. Average interplanar angle in diphenyl ethers

Compound	θ(°)
9	33
10	35
11	41
12	67
13	45
14	33
15	47
16	30
17	90
18	46
19	50
20	60
21	34
22	90
23	52

Several other physical methods have been applied to the determination of θ in diphenyl ether **9**. X-Ray diffraction shows a twist angle of 17.5° (26) whereas Kerr constants have been interpreted in terms of a 37° angle (27). Ultraviolet spectral analysis furnished a value of 50° (6). Clearly our finding of $\theta = 33°$ for **9** compares favorably with estimates from other techniques. A recent extended Huckel m.o. treatment (28) suggests a twist angle of 52° in **9**.

Conclusions

para-Carbon shieldings in anisoles and diphenyl ethers can be rationalized on the basis of conjugative electron release into the aromatic rings by the ethereal oxygen atom. In di-*ortho*-alkylated materials there appears to be appreciable steric inhibition to conjugation with the congested aryl moiety. There is some evidence to indicate that in these cases the electron release into the adjacent benzene ring is enhanced. Correlation of the *para*-carbon shifts with molec-

[2]In anisoles, the reference plane is the $C_{ar}—O—CH_3$ plane.

ular conformation seems to indicate that these molecules adopt a helical conformation in solution, although the oscillation around the position of minimum energy is quite large.

Experimental

Spectra

The carbon n.m.r. spectra were obtained at 25.2 MHz using a Varian XL-100-12 n.m.r. spectrometer, most commonly under conditions of complete proton noise decoupling. Spectral accumulations were done with a Varian C-1024 time averaging computer. Samples were contained in 8 mm tubes and were examined as 0.5 *M* solutions in $CDCl_3$, containing 2% TMS as an internal standard. Off-resonance decoupling experiments were carried out with the proton frequency offset approximately 500 Hz from the center of the proton spectral region. During the specific proton decoupling experiments the noise modulation was turned off.

Compounds

The methods of preparation for the novel compounds discussed in this paper will be reported elsewhere. The remaining compounds were prepared according to the literature (1, 2, 4–6).

We thank the North Atlantic Treaty Organization and the National Research Council of Canada for generous financial support.

1. W. D. CHANDLER, W. MAC F. SMITH, and R. Y. MOIR. Can. J. Chem. **42**, 2549 (1964).
2. P. A. LEHMANN and C. E. JORGENSEN. Tetrahedron, **21**, 363 (1965).
3. P. A. LEHMANN. Org. Magn. Res. **2**, 467 (1970).
4. J. J. BERGMANN, W. D. CHANDLER, and R. Y. MOIR. Can. J. Chem. **49**, 225 (1971); **50**, 353 (1972).
5. J. J. BERGMANN, E. A. GRIFFITH, B. E. ROBERTSON, and W. D. CHANDLER. Can. J. Chem. **51**, 162 (1973).
6. G. MONTAUDO, P. FINOCCHIARO, E. TRIVELLONE, F. BOTTINO, and P. MARAVIGNA. Tetrahedron, **22**, 2125 (1971); G. MONTAUDO, F. BOTTINO, and E. TRIVELLONE, J. Org. Chem. **37**, 504 (1972).
7. G. MONTAUDO, S. CACCAMESE, and P. FINOCCHIARO. J. Am. Chem. Soc. **93**, 4204 (1971).
8. G. MONTAUDO and P. FINOCCHIARO. J. Mol. Struct. **14**, 53 (1972).
9. J. E. ANDERSON and C. P. SMYTH. J. Chem. Phys. **42**, 473 (1965); F. K. FONG. J. Chem. Phys. **40**, 132 (1964).
10. C. W. N. CUMPER, J. F. READ, and A. I. VOGEL. J. Chem. Soc. 5860 (1965).
11. G. C. PAPPALARDO and S. PISTARA. Tetrahedron, **28**, 1611 (1972).
12. P. A. LEHMANN and D. M. MCEACHERN. J. Mol. Struct. **7**, 253, 267, 277 (1971).
13. G. MONTAUDO, P. FINOCCHIARO, and S. CACCAMESE. J. Org. Chem. **38**, 170 (1973).
14. G. MONTAUDO and P. FINOCCHIARO. Unpublished observations.
15. E. A. H. GRIFFITH, W. D. CHANDLER, and B. E. ROBERTSON. Can. J. Chem. **50**, 2963, 2972 (1972).
16. G. W. BUCHANAN, D. A. ROSS, and J. B. STOTHERS. J. Am. Chem. Soc. **88**, 4301 (1966).
17. J. B. STOTHERS. Carbon-13 NMR spectroscopy. Academic Press, New York, N.Y. 1972.
18. G. W. BUCHANAN, G. MONTAUDO, and P. FINOCCHIARO. Can. J. Chem. **51**, 1053 (1973).
19. K. S. DHAMI and J. B. STOTHERS. Can. J. Chem. **44**, 2855 (1966).
20. P. C. LAUTERBUR. J. Am. Chem. Soc. **83**, 1846 (1961).
21. D. M. GRANT and E. G. PAUL. J. Am. Chem. Soc. **86**, 2984 (1964).
22. L. F. JOHNSON and W. C. JANKOWSKI. Carbon-13 n.m.r. spectra. John Wiley and Sons, New York, N.Y. 1972.
23. W. R. WOOLFENDEN and D. M. GRANT, J. Am. Chem. Soc. **88**, 1496 (1966).
24. S. H. GROVER, J. P. GUTHRIE, J. B. STOTHERS, and C. T. TAN. J. Magn. Res. **10**, 227 (1973).
25. H. KESSLER, A. RIEKER, and W. RUNDEL. Chem. Commun. 475 (1968).
26. H. HIGASI. Dipoles, molecules, and chemistry. Monograph Series of the Research Institute of Applied Electricity. No. 13. Hokkaido University, Sapporo. 1965.
27. R. J. W. LE FÈVRE, A. SUNDARAM, and K. M. S. SUNDARAM. Bull. Chem. Soc. Jap. **35**, 690 (1962).
28. V. GALASSO, G. DE ALTI, and A. BIGOTTO. Tetrahedron, **27**, 6151 (1971).

Can. J. Chem. Downloaded from www.nrcresearchpress.com by 210.87.254.40 on 09/05/12
For personal use only.

An Efficient and Selective Monohydrido Rhodium(I) Homogeneous Hydrogenation Catalyst Containing a Cyclic Phosphine

DONNA E. BUDD, DAVID G. HOLAH, ALAN N. HUGHES, AND BENJAMIN C. HUI

Department of Chemistry, Lakehead University, Thunder Bay, Ontario P7B 5E1

Received August 27, 1973

The preparation of the complex $RhH(DBP)_4$ (where DBP is a dibenzophosphole derivative) is described. It is a very effective and selective catalyst for the homogeneous hydrogenation of terminal olefins. Kinetic and mechanistic data for the hydrogenation of 1-hexene are presented.

On décrit la préparation du complexe $RhH(DBP)_4$ dans lequel DBP est un dérivé dibenzophosphole. Ce complexe est un catalyseur très efficace et très sélectif pour hydrogénation homogène des oléfines terminales. On présente des données cinétiques et méchanistiques pour l'hydrogénation de l'hexène-1. [Traduit par le journal]

Can. J. Chem., **52**, 775 (1974)

Can. J. Chem. Downloaded from www.nrcresearchpress.com by 210.87.254.6 on 09/05/12
For personal use only.

The wide use of phosphine complexes of rhodium as homogeneous hydrogenation catalysts is well documented (1, 2). We have previously noted that rhodium complexes of cyclic phosphines also catalyze the homogeneous hydrogenation of 1-hexene (3) although, so far, these systems have not been as effective as the triphenylphosphine analogs. Hydrido complexes of rhodium are known to be intermediates in hydrogenation processes, although relatively few systems involving monohydrido phosphine complexes (without CO) appear to be efficient catalysts *per se*. Hydrido phosphine complexes of Rh(I) of the type $RhHL_n$ ($n = 3$ or 4, L = PPh_3 (4), PPh_2Me (5), $P(OAr)_3$ (6), and PF_3 (7)) have been prepared, but only the complex $RhH(PPh_3)_4$ has been briefly studied as a homogeneous hydrogenation catalyst (8). In this paper we report the synthesis of a new, extremely active, hydrogenation catalyst $RhH(DBP)_4$ (where DBP = 5-phenyl-5*H*-dibenzophosphole (**1**)) and a study of the kinetics and mechanism of its use in the homogeneous hydrogenation of olefins.

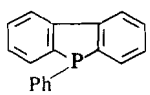

DBP

1

Results

The air stable, bright orange complex $RhH(DBP)_4$ can be prepared either by reduction of $RhCl_3(DBP)_3$ (3) with $NaBH_4$ or by reaction of the latter with $RhCl(CO)_2(DBP)$ (3) in the presence of an excess of DBP. Its i.r. spectrum has a band at 2070 cm^{-1} assignable to the Rh—H stretching frequency. A chloroform solution of the complex shows a broad n.m.r. signal at τ20.6 corresponding to the proton attached to the rhodium atom. Recrystallization of $RhH(DBP)_4$ from benzene/ethanol results in the loss of a ligand and the formation of $RhH(DBP)_3$ which has no detectable band in the 2000 cm^{-1} region of the i.r. spectrum nor could a reproducible n.m.r. signal for the hydrogen be found although the complex appears to be relatively stable in the solid state.

The orange-red oxygen-free benzene solutions of $RhH(DBP)_4$ are extremely effective in catalyzing the homogeneous hydrogenation of terminal olefins (C_6–C_{20}) at 20 °C and less than 1 atm of H_2 pressure (Table 1). Internal monoenes, conjugated dienes, and acetylenic bonds are hydrogenated at much slower rates. Cyclic monoenes, dienes, *trans*-olefins, together with functional groups such as —CN, —NO_2, and $>C{=}O$ are not hydrogenated under these conditions.

Benzene solutions of $RhH(DBP)_4$ do not react with hydrogen after stirring for several hours, nor with 1-hexene under a nitrogen atmosphere. Admission of more hydrogen gas into the reaction vessel after the initial hydrogen has been consumed by the 1-hexene increases the hydrogenation rate remarkably. Additional olefin can be reduced by introduction of more of the olefin and readjustment of hydrogen pressure at the end of a run.

Comparative rates of hydrogenation of 1-hexene in benzene using several rhodium(I)

Can. J. Chem. Downloaded from www.nrcresearchpress.com by 210.87.254.6 on 09/05/12
For personal use only.

TABLE 1. Relative rates of hydrogenation of unsaturated substances using $RhH(DBP)_4$ as catalyst in benzene at 20°. (0.5 m*M* $RhH(DBP)_4$, 0.5 *M* substrate, 60 cm partial H_2 pressure, 25 ml total volume).

Substrate*	Rate (ml of H_2 uptake per min)
1-Hexene	35.4
1-Heptene	26.8
1-Octene	47.3
1-Decene	42.4
1-Hexadecene	25.8
1-Docosene	13.0
2-Octene	0.9
1,3-Pentadiene†	0.2
1,5-Hexadiene	10.1
Styrene	7.4
Ethylene‡	6.0
Allyl cyanide	26.6
Allyl alcohol	7.4
Acrolein	2.4
Propargyl alcohol	0.2
2-Methyl-3-butyn-2-ol	9.9

*CH_3CN, $C_6H_5NO_2$, $(CH_3)_2C{=}O$, $CH_3(CH_2)_7CH{=}CH(CH_2)_7CO_2H$(oleic acid), 1,3-cyclooctadiene, cyclohexene, $HO_2C{-}C{\equiv}C{-}CO_2H$, *trans*-stilbene are not hydrogenated under these conditions.
†55 cm partial H_2 pressure.
‡Partial pressure of C_2H_4 = 26 cm; rate measured at total pressure of 66 cm.

TABLE 2. Relative rate of hydrogenation of 1-hexene (0.5 M) in C_6H_6 at 60 cm partial H_2 pressure and 20°

Catalyst*	Relative rate
$RhH(CO)(PPh_3)_3$	1
$RhH(PPh_3)_4$	2.8
$RhCl(PPh_3)_3$	3.5
$RhH(DBP)_4$	24.4

*Catalysts were 0.5 m*M* in concentration, except 1.0 m*M* for $RhH(CO)(PPh_3)_3$.

phosphine catalysts are listed in Table 2 and it can be seen that $RhH(DBP)_4$ is about 7 times as active as Wilkinson's catalyst, $RhCl(PPh_3)_3$, under similar conditions. Hydrido-tetrakis (triphenylphosphine)rhodium(I), $RhH(PPh_3)_4$, is also an efficient catalyst under similar conditions (rate = 1.2×10^{-4} *M* s^{-1} for a 0.5 m*M* catalyst solution, 0.5 *M* 1-hexene, 60 cm partial pressure of H_2 at 20°) although at a rate ~8 times slower than the DBP analog.

The ebullioscopically determined molecular weight of $RhH(DBP)_4$ in benzene (3.1 m*M* solution) is estimated at ~400. This is considered lower than the correct value for dissociation of one DPB ligand (~570) probably because of the extreme air sensitivity of benzene solutions of the complex and the relatively long times such solutions are exposed to the glove box atmosphere (N_2) during determinations.

The reaction kinetics for the hydrogenation of 1-hexene have been studied, the overall rates of hydrogenation being measured with variance of the alkene concentration, hydrogen pressure, catalyst concentration, and added ligand, DBP. The results obtained (shown in Table 3) indicate a good first order dependence on 1-hexene (0.2–0.6 *M*) (Fig. 1). The dependence on hydrogen which is first order at low pressure but tends to zero order at higher pressures, is shown in Fig. 2. The dependence on catalyst concentration (Fig. 3) is first order at very low concentrations, but becomes less than first order at higher catalyst concentration. Addition of DBP to the catalyst solution causes a marked decrease in reaction rates. Thus, a plot of the reciprocal of the rate against the added DBP is linear (Fig. 4).

Discussion

The results reported above indicate that $RhH(DBP)_4$ in benzene is an extremely efficient and highly selective catalyst for the hydrogenation of terminal olefins and other unsaturated molecules containing the grouping $RCH{=}CH_2$. The catalyst in solution is not as susceptible to

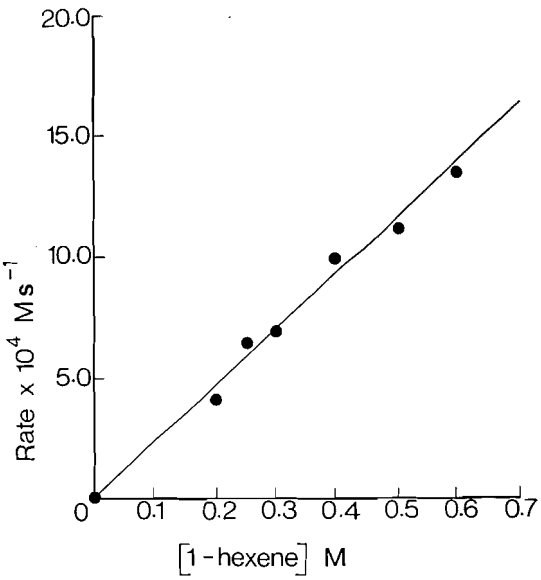

FIG. 1. Dependence of the rate of hydrogenation of 1-hexene in benzene at 20 °C on the concentration of 1-hexene (0.35 m*M* $RhH(DBP)_4$, 55 cm of H_2 pressure).

TABLE 3. Kinetic data for the hydrogenation of 1-hexene

$[RhH(DBP)_4]$ $\times 10^3$ (M)	P_{H2} (cm)	$[H_2]$ $\times 10^3$ (M)	[1-Hexene] (M)	[DBP] $\times 10^3$ (M)	Rate $\times 10^4$ ($M\ s^{-1}$)
0.35	55	3.60	0.20	—	4.16
0.35	55	3.60	0.25	—	6.40
0.35	55	3.60	0.30	—	6.88
0.35	55	3.60	0.40	—	9.80
0.35	55	3.60	0.50	—	11.18
0.35	55	3.60	0.60	—	13.48
0.35	62	4.06	0.25	—	6.22
0.35	38	2.50	0.25	—	5.42
0.35	30	1.98	0.25	—	4.39
0.35	20	1.34	0.25	—	3.22
0.05	55	3.60	0.25	—	2.95
0.10	55	3.60	0.25	—	4.23
0.20	55	3.60	0.25	—	5.10
0.30	55	3.60	0.25	—	6.11
0.43	55	3.60	0.25	—	6.98
0.54	55	3.60	0.25	—	8.55
0.60	55	3.60	0.25	—	7.48
0.35	55	3.60	0.25	0.02	1.61
0.35	55	3.60	0.25	0.04	0.63
0.35	55	3.60	0.25	0.09	0.39
0.35	55	3.60	0.25	0.18	0.19
0.35	55	3.60	0.25	0.34	0.11

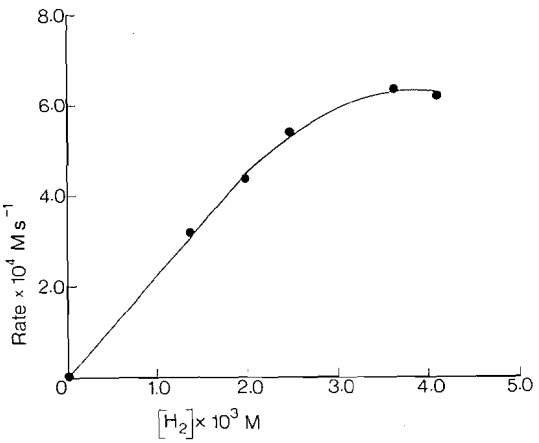

FIG. 2. Dependence of the rate of hydrogenation of 1-hexene in benzene at 20° on the concentration of hydrogen (0.35 mM $RhH(DBP)_4$, 0.25 M 1-hexene).

poisoning due to traces of oxygen (or peroxide) as is, for example, the excellent ruthenium catalyst, $RuHCl(PPh_3)_3$ (9). Under the conditions described here, $RhH(DBP)_4$ is clearly considerably more efficient than $RhH(CO)(PPh_3)_3$ (10), $RhCl(PPh_3)_3$ (11), and $RhH(PPh_3)_4$ in the catalytic hydrogenation of terminal olefins.

The crystal structure of $RhH(PPh_3)_4$ (12) shows the four phosphorus atoms occupying the tetrahedral positions about the metal and the hydrogen atom probably on a 3-fold axis. It is not unreasonable that $RhH(DBP)_4$ is isostructural with the triphenylphosphine analog because steric interactions between the DBP groups would probably be minimized in such an arrangement.

The specificity of some catalysts containing triphenylphosphine for the hydrogenation of 1-alkenes has been attributed to steric factors

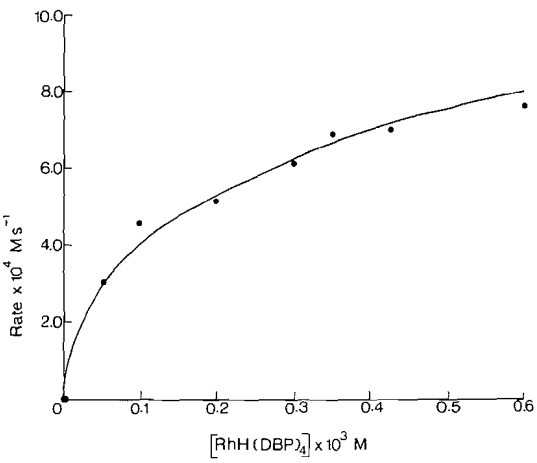

FIG. 3. Dependence of the rate of hydrogenation of 1-hexene in benzene at 20° on the concentration of $RhH(DBP)_4$ (0.25 M 1-hexene, 55 cm of H_2 pressure).

Can. J. Chem. Downloaded from www.nrcresearchpress.com by 210.87.254.6 on 09/05/12
For personal use only.

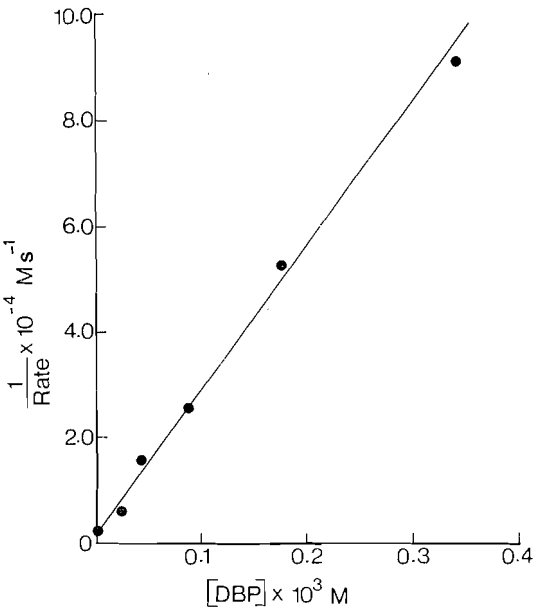

FIG. 4. Dependence of the reciprocal of the rate of hydrogenation of 1-hexene in benzene at 20° on the concentration of DBP (0.35 m*M* $RhH(DBP)_4$, 0.25 *M* 1-hexene, 55 cm of H_2 pressure).

associated with the triphenylphosphine ligands. The two phosphine ligands in the species, $RhH(CO)(PPh_3)_2$ or $RuHCl(PPh_3)_2$, formed by the dissociation of the trisphosphine complexes, are mutually *trans* and thus, formation of the intermediate square planar alkyl complex (see reaction 9) is seriously hindered (1). On this basis, the selectivity of the catalytic system described in this paper can easily be explained. Thus, molecular weight data are consistent with the complete dissociation of $RhH(DBP)_4$ in solution to form $RhH(DBP)_3$ which can be isolated by addition of ethanol to benzene solutions. Further slight dissociation to form $RhH(DBP)_2$ which is likely to have a square planar structure with a solvent molecule occupying one coordination site is then thought to occur. This would render the formation of the alkyl intermediates (except from 1-alkenes) sterically unlikely. Rhodium complexes of tertiary phosphines with very bulky substituents (*e.g.* PBu_3^t, $PBu^tPr_2^n$) have been reported (13) to be extremely active hydrogenation catalysts for 1-alkenes and this is consistent with the observation that $RhH(DBP)_4$ is more efficient than the analogous PPh_3 complex bearing in mind the rigid, bulky nature of DBP.

The kinetic data obtained for the hydrogenation of 1-hexene in benzene are consistent with reactions involving dissociated species formed in the equilibria.

$$[1] \qquad RhH(DBP)_4 \overset{K_1}{\rightleftharpoons} RhH(DBP)_3 + DBP$$

$$[2] \qquad RhH(DBP)_3 \overset{K_2}{\rightleftharpoons} RhH(DBP)_2 + DBP$$

Kinetic measurements (to be published) on the hydrogenation of 1-hexene using $RhH(DBP)_3$ as catalyst also show a similar dependence on the catalyst as presented in Fig. 3, and the slight dissociation of $RhH(DBP)_3$ to the catalytically active species $RhH(DBP)_2$ is thought to have taken place. Indeed the between first and zero order dependence on $RhH(DBP)_4$ and the marked inverse DBP dependence (Fig. 4) all point to equilibrium 2 lying mainly to the left, with K_2 small. A catalyst dependence of this form has been previously observed for systems such as $RhCl(PPh_3)_3$ (14) and $RhH(CO)(PPh_3)_3$ (10) and recently on $RhH(PPh_3)_4$ (8*b*), and the first two examples have been attributed to the equilibria

$$[3] \quad RhCl(PPh_3)_3 \overset{-PPh_3}{\rightleftharpoons} RhCl(PPh_3)_2 \overset{-PPh_3}{\rightleftharpoons} RhCl(PPh_3)$$

$$[4] \quad RhH(CO)(PPh_3)_3 \overset{-PPh_3}{\rightleftharpoons} RhH(CO)(PPh_3)_2 \overset{-PPh_3}{\rightleftharpoons} RhH(CO)(PPh_3)$$

The apparently higher pseudo first order rate constants at low catalyst concentrations have been attributed (10) to a change from one active species (monophosphine complex) to another less active one (bisphosphine complex).

Although there is uncertainty concerning the equilibria in [3] (14, 15), $RhH(CO)(PPh_3)_3$ has been found to dissociate extensively in solution (16) and the bisphosphine complex predominates at 10^{-3} *M*.

The observed dependence on hydrogen and olefin is consistent with either of the schemes:

$$[5] \quad A + \text{olefin} \underset{k_{-1}}{\overset{k_1}{\rightleftharpoons}} \text{alkyl complex} \xrightarrow[H_2]{k_2} \text{products}$$

$$[6] \quad A + H_2 \overset{K}{\rightleftharpoons} AH_2 \xrightarrow[\text{olefin}]{\text{slow}} \text{products}$$

where A is $RhH(DBP)_2$. The fact that the catalyst does not absorb hydrogen in the absence of olefin, together with the lack of color change in solutions during hydrogenations,

Can. J. Chem. Downloaded from www.nrcresearchpress.com by 210.87.254.6 on 09/05/12
For personal use only.

Can. J. Chem. Downloaded from www.nrcresearchpress.com by 210.87.254.6 on 09/05/12
For personal use only.

suggests that a trihydro species $RhH_3(DBP)_2$ is not formed. This evidence points to the first mechanism, [5], as the more likely, and kinetic data and observations are all satisfactorily explained on this basis. The inverse dependence of the rate on the added DBP concentration is consistent with a dissociation of $RhH(DBP)_3$ to give $RhH(DBP)_2$, which then reacts with the olefin to produce the intermediate alkyl complex, followed by a slow reaction with hydrogen according to the following scheme:

[7] $$RhH(DBP)_4 \rightarrow RhH(DBP)_3 + DBP$$

[8] $$RhH(DBP)_3 \overset{K}{\rightleftharpoons} RhH(DBP)_2 + DBP$$

[9] $$RhH(DBP)_2 + \text{olefin} \underset{k_{-1}}{\overset{k_1}{\rightleftharpoons}} Rh(\text{alkyl})(DBP)_2$$

[10] $$Rh(\text{alkyl})(DBP)_2 + H_2 \xrightarrow{k_2} RhH(DBP)_2 + \text{alkane}$$

Over the range of catalyst concentrations where the kinetics were studied, the tetrakis dibenzophosphole complex dissociates completely and thus

[11] $$\text{Total catalyst concentration} = [Rh]_T = [RhH(DBP)_4] = [RhH(DBP)_3] + [RhH(DBP)_2]$$

The equilibrium constant K for reaction 8 can be written as

[12] $$K = \frac{[RhH(DBP)_2][DBP]}{[RhH(DBP)_3]} = \frac{[RhH(DBP)_2]\{[Rh]_T + [RhH(DBP)_2]\}}{[Rh]_T - [RhH(DBP)_2]}$$

With K being small, and assuming a steady state concentration of $Rh(\text{alkyl})(DBP)_2$ the above mechanism would yield the rate law

[13] $$\text{Rate} = \frac{Kk_1k_2[Rh]_T[H_2][\text{olefin}]}{\{k_{-1} + k_2[H_2]\}\{K + [Rh]_T\}}$$

Since no reaction is observed with olefin in the absence of hydrogen, k_{-1} must be greater than k_1. If reaction 9 involves displacement of a solvent ligand, k_{-1} will be replaced by k_{-1} [solvent].

Equation 13 can be written in the form

[14] $$\frac{1}{\text{Rate}} = \frac{k_{-1} + k_2[H_2]}{k_1k_2[H_2][\text{olefin}]} \cdot \frac{1}{[Rh]_T} + \frac{k_{-1} + k_2[H_2]}{Kk_1k_2[H_2][\text{olefin}]}$$

Within experimental error, a plot of 1/rate against $1/[Rh]_T$ at constant [olefin] and $[H_2]$ yields a reasonably good straight line (Fig. 5). From the ratio of the slope to the intercept of the plot, K is estimated to be 8.9×10^{-5} M in agreement with our previous assumption.

Rearranging eq. 13 gives

[15] $$\frac{1}{\text{Rate}} = \frac{Kk_{-1} + k_{-1}[Rh]_T}{Kk_1k_2[Rh]_T[\text{olefin}]} \cdot \frac{1}{[H_2]} + \frac{K + [Rh]_T}{Kk_1[Rh]_T[\text{olefin}]}$$

Thus using data at constant $[Rh]_T$ and [olefin], a plot of 1/rate against $1/[H_2]$ should yield a straight line as is shown in Fig. 6. The ratio of the intercept to the slope of the plot gives $k_2/k_{-1} = 267\ M^{-1}$, and from the intercept with $K = 8.9 \times 10^{-5}$ M, k_1 is found to be 70.5 $M^{-1}\,s^{-1}$.

From the intercept of the plot of 1/rate against $1/[Rh]_T$ and with the values of k_1 and K obtained, k_2/k_{-1} is found to be 304 M^{-1} in good agreement with the above value.

Equation 13 can also be expressed in terms of [DBP] as

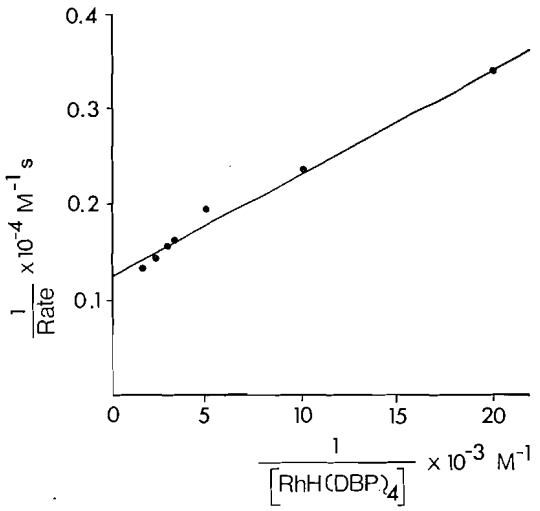

FIG. 5. Plot of 1/rate against $1/[RhH(DBP)_4]$ according to eq. 14.

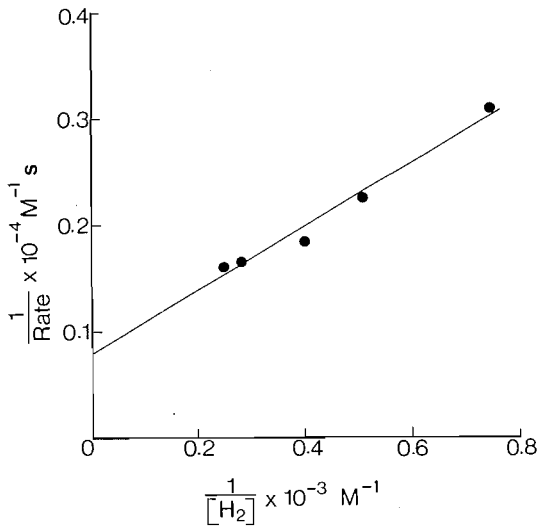

FIG. 6. Plot of 1/rate against $1/[H_2]$ according to eq. 15.

$$[16]\quad \text{Rate} = \frac{Kk_1k_2[\text{Rh}]_T[H_2][\text{olefin}]}{\{k_{-1} + k_2[H_2]\}\{K + [\text{DBP}]\}}$$

which can then be rearranged in the form

$$[17]\quad \frac{1}{\text{Rate}} = \frac{k_{-1} + k_2[H_2]}{Kk_1k_2[\text{Rh}]_T[\text{olefin}][H_2]} \cdot [\text{DBP}] + \frac{k_{-1} + k_2[H_2]}{k_1k_2[\text{Rh}]_T[\text{olefin}][H_2]}$$

Thus using data at constant $[\text{Rh}]_T$, [olefin], and $[H_2]$ an inverse dependence of the rate on [DBP] is anticipated, and is evident in Fig. 4. From the ratio of the intercept to the slope of the straight line K is estimated to be $1.6 \times 10^{-5}\ M$, the same order of magnitude as previously obtained.

It should be pointed out that the inverse phosphine dependence can also be satisfactorily explained by assuming a substitution reaction of the phosphine in $RhH(DBP)_3$ by olefin

$$[18]\quad RhH(DBP)_3 + \text{olefin} \rightleftharpoons RhH(DBP)_2(\text{olefin}) + DBP$$

$$[19]\quad RhH(DBP)_2(\text{olefin}) \rightleftharpoons Rh(\text{alkyl})(DBP)_2 + H_2 \rightarrow \text{product}$$

The between zero and first-order dependence on the catalyst can be attributed to the change from one species to a less active one. However kinetic studies (to be published) using $RhH(DBP)_3$ as the catalyst also shows a between first and zero-order dependence on the catalyst concentration with the Rh dependence approaching half-order at higher concentrations. Furthermore, the equilibrium constant for reaction 8 is estimated to be $7 \times 10^{-5}\ M$ in very good agreement with the value obtained from the $RhH(DBP)_4$ system. Hence a mechanism involving reactions 7 to 10 seems to be more reasonable.[1]

The catalyst $RhH(DBP)_4$ therefore resembles the ruthenium catalyst $RuHCl(PPh_3)_3$ (9) in activity and selectivity but has the advantage of being a more stable species in the solid state. No comparable rate data are available on other systems involving rhodium and ruthenium hydride complexes such as $RhH(PPh_3)_3$, $RhH(PPh_3)_4$, $RuH_2(PPh_3)_4$, $RuH_4(PPh_3)_3$, and $RuH_2(N_2)(PPh_3)_3$. $RhH(PPh_3)_4$ has been found (8) to hydrogenate 1-hexene, mesityl oxide, and acrylonitrile in the presence of an excess of PPh_3 at 80°. The ruthenium hydride complexes, $RuH_4(PPh_3)_3$ and $RuH_2(N_2)(PPh_3)_3$ have been reported (17) to catalyze the hydrogenation of 1-pentene in toluene at 25°. The complex $RuH_2(PPh_3)_4$ has also been used for the catalyzed hydrogenation of styrene and ethylene and probably involves styrene and ethylene complexes of Ru(0) as intermediates (18). Other rhodium(I) monohydrides *e.g.*, RhH(diphos)$_2$ (19), $RhH[P(OC_6H_5)_3]_4$ (6), and $RhH(PF_3)_4$ (7) are expected to be inefficient catalysts due to steric effects or high π-acidity of the ligands.

Experimental

Rhodium trichloride trihydrate was obtained from Engelhard Industries and DBP was prepared by the method of Hoffman (20). Solvents were dried by distillation over calcium hydride. Commercial olefins were shaken overnight with powdered iron(II) sulfate, then heated under reflux, and distilled over calcium hydride.

Microanalyses and physical measurements were carried out as previously described (3).

Syntheses

$RhCl(PPh_3)_3$ (11), $RhH(PPh_3)_4$ (4), $RhH(CO)(PPh_3)_3$ (10), and $RhCl(CO)_2(DBP)$ (3) were prepared as previously described. $RhH(DBP)_4$ can be prepared in two ways:

(*a*) $RhCl_3 \cdot 3H_2O$ (100 mg) was dissolved in ethanol (20 ml), the solution filtered, and the filtrate heated under reflux with a 6 molar excess of DBP until a yellow solid, $RhCl_3(DBP)_3$ (3), was formed (~½ h). A concentrated solution of $NaBH_4$ (200 mg) in ethanol (10 ml) was filtered and added to the mixture, producing an immediate color change from yellow to bright orange. The mixture was heated for ½ h and the resulting orange solid filtered off, washed successively with ethanol, 1:1 ethanol–water,

[1]We gratefully appreciate the careful work of a referee in helping us with the kinetic interpretation.

Can. J. Chem. Downloaded from www.nrcresearchpress.com by 210.87.254.6 on 09/05/12
For personal use only.

ethanol, and finally ether, and vacuum dried (yield 80%, m.p. 155°).

Anal. Calcd. for $RhH(DBP)_4$: C, 75.6; H, 4.6. Found: C, 74.8; H, 4.5.

(*b*) a mixture of $RhCl(CO)_2(DBP)\cdot CH_3OH$ (125 mg) and DBP (220 mg) in ethanol (40 ml) was heated under reflux for ¼ h. A concentrated ethanolic solution of $NaBH_4$ was added and the mixture heated for a further ½ h after which the product was separated as described above.

The red-orange complex $RhH(DBP)_3$ was prepared by dissolving $RhH(DBP)_4$ in the minimum amount of benzene, adding ethanol, and reducing the volume if necessary. The complex slowly decomposes in air (m.p. 179–181°, darkened ~170°).

Anal. Calcd. for $RhH(DBP)_3$: C, 73.7; H, 4.5. Found: C, 73.0; H, 4.5.

Catalytic Experiments

The reaction vessel was a 3-necked, 100 ml flask and was attached via condenser to a standard vacuum system. An external motor operated the stirrer, a Teflon coated magnet, at the gas–liquid interface. The catalyst was weighed into a small Teflon basket suspended from a side arm which, on rotation dropped the basket into the solvent. The olefin was placed in a burette (under nitrogen) in the third neck of the flask.

The solvent (25 ml benzene less the volume of olefin) was degassed twice and the system flushed at least three times with hydrogen which had been passed through a deoxo catalyst tube. The catalyst was dissolved, aided by stirring, producing a bright orange solution and was left under hydrogen for ~20 min. The stirring was stopped while the olefin was added and hydrogen was then admitted to the desired pressure. Absorption of hydrogen did not occur until stirring was begun. The vapor pressure of the system was measured after the run by removing the hydrogen and allowing the system to equilibrate. (The rate of hydrogenation was obtained from the tangent off the plot of hydrogen pressure against time.) The solubility of hydrogen in benzene was obtained from the literature (21). Alkanes obtained from the hydrogenation of 1-alkenes were identified by mass spectrometry.

We gratefully acknowledge the assistance of the personnel of the Science Instrumentation Laboratory in obtaining some physical data.

We also thank the Senate Research Committee of Lakehead University and the National Research Council of Canada for generous financial support.

1. B. R. JAMES. Homogeneous hydrogenation. John Wiley and Sons, Inc., New York. 1973.
2. R. E. HARMON, S. K. GUPTA, and D. J. BROWN. Chem., Rev. **73**, 21 (1973).
3. D. G. HOLAH, A. N. HUGHES, and B. C. HUI. Can. J. Chem. **50**, 3714 (1972).
4. J. J. LEVISON and S. D. ROBINSON. J. Chem. Soc. A, 2947 (1970).
5. K. C. DEWHIRST, W. KEIM, and C. A. REILY. Inorg. Chem. **7**, 546 (1968).
6. J. J. LEVISON and S. D. ROBINSON. Chem. Commun. 1405 (1968).
7. T. KRUCK. Angew. Chem. Int. Ed. **6**, 53 (1967).
8. (*a*) K. C. DEWHIRST. U.S. Pat. 3,480,659, through Chem. Abstr. **72**, 78105 (1970), (*b*) J. HJORTKJAER. 166th ACS Meeting, Chicago, 1973, Abstract INDE 10.
9. P. S. HALLMAN, B. R. MCGARVEY, and G. WILKINSON. J. Chem. Soc. A, 3143 (1968).
10. C. O'CONNOR and G. WILKINSON. J. Chem. Soc. A, 2665 (1968).
11. J. A. OSBORN, F. H. JARDINE, J. F. YOUNG, and G. WILKINSON. J. Chem. Soc. A, 1711 (1966).
12. R. W. BAKER and P. J. PAULING. Chem. Commun. 1495 (1969).
13. C. MASTERS, W. S. MCDONALD, G. RAPER, and B. L. SHAW. Chem. Commun. 210 (1971).
14. H. ARAI and J. HALPERN. Chem. Commun. 1571 (1971).
15. P. MEAKIN, J. P. JESSON, and C. A. TOLMAN. J. Am. Chem. Soc. **94**, 3242 (1972).
16. D. EVANS, G. YAGUPSKY, and G. WILKINSON. J. Chem. Soc. A, 2660 (1968).
17. F. PENNELLA, R. L. BANKS, and M. R. RYCHECK. Proceedings 14th International Conference on Coordination Chemistry. Toronto, Ontario. 1972. p. 78.
18. S. KOMIYA, A. YAMOMOTO, and S. IKEDA. J. Organomet. Chem. **42**, C65 (1972).
19. M. TAKESADA, H. YAMAZAKI, and N. HAGIHARA. Bull. Chem. Soc. Jap. **41**, 270 (1968).
20. H. HOFFMANN. Chem. Ber. **95**, 2563 (1962).
21. W. F. LINKE. (*Editor*). Solubilities of inorganic and metal organic compounds. Vol. 1, 4th ed. Am. Chem. Soc. Washington, D.C. 1958.

Can. J. Chem. Downloaded from www.nrcresearchpress.com by 210.87.254.6 on 09/05/12
For personal use only.

Spectroscopic Studies of Cationic h^5-Cyclopentadienyl Iron Carbonyl Derivatives

G. MICHAEL BANCROFT, K. DAVID BUTLER, LEO E. MANZER,
ALAN SHAVER, AND JOHN E. H. WARD
Department of Chemistry, The University of Western Ontario, London, Ontario N6A 3K7

Received September 17, 1973

Mössbauer, ^{13}C nuclear magnetic resonance and infrared spectroscopic studies of a series of cationic iron compounds of the type $[(h^5\text{-}C_5H_5)Fe(CO)_2L]^+X^-$ (L = CO, CH_3CN, C_2H_4, $(C_6H_5)_3P$, C_5H_4N; X = PF_6^-, BF_4^-) are described. The Mössbauer center shifts indicate that the σ donor plus π acceptor ability (σ + π) of these ligands increases in the order $CH_3CN \leqslant C_2H_4 < C_5H_5N < (C_6H_5)_3P < CO < CS$. The positive ^{57}Fe quadrupole splittings strongly suggest that the sign of the quadrupole splittings for the isovalent and isoelectronic Mn and Re compounds are also positive. The correlation between carbonyl infrared force constants and ^{13}C carbonyl shieldings is discussed in relation to a similar correlation previously reported in the literature for a series of neutral complexes $(h^5\text{-}C_5H_5)Fe(CO)_2Y$, where Y is an anionic ligand.

Les études par spectroscopie Mössbauer, résonance magnétique nucléaire du ^{13}C et infrarouge d'une série de composés cationiques du fer, du type $[(h^5\text{-}C_5H_5)Fe(CO)_2L]^+X^-$ (L = CO, CH_3CN, C_2H_4, $(C_6H_5)_3P$, C_5H_4N; X = PF_6^-, BF_4^-) sont décrites. Les déplacements de centre Mössbauer montrent que le caractère σ donneur plus π accepteur (σ + π) de ces ligands augmente dans l'ordre $CH_3CN \leqslant C_2H_4 < C_5H_5N < (C_6H_5)P < CO < CS$. Les couplages quadrupolaires positifs du ^{57}Fe suggèrent fortement que les signes des couplages quadrupolaires pour les composés isovalents et isoélectroniques du Mn et Re sont aussi positifs. La corrélation entre les constantes de force infrarouge du carbonyle et les constantes d'écran ^{13}C de ce groupement est discutée en fonction de corrélations semblables rapportées antérieurement dans la littérature pour des séries de complexes neutres $(h^5\text{-}C_5H_5)Fe(CO)_2Y$, où Y est un ligand anionique. [Traduit par le journal]

Can. J. Chem., 52, 782 (1974)

Introduction

A variety of spectroscopic investigations of the series of compounds $(h^5\text{-}C_5H_5)Fe(CO)_2Y$, where Y is an anionic substituent, have appeared in the literature (1–6), but considerably less attention has been directed towards the analogous cationic species of the type $[(h^5\text{-}C_5H_5)Fe(CO)_2L]^+$, where L is a neutral ligand (3, 4). In the case of the neutral complexes, studies using ^1H and ^{13}C n.m.r., ^{119}Sn and ^{57}Fe Mössbauer, and i.r. spectroscopies have led to a number of correlations which yield useful bonding information.

For such a system containing the π-bonding ligands $h^5\text{-}C_5H_5$ and CO, one of the principal objectives has been to evaluate σ and π effects in the bonding scheme. The relationship between carbonyl i.r. stretching frequencies, force constants, and intensities, and σ and π effects is still a matter of considerable controversy. For the neutral $(h^5\text{-}C_5H_5)Fe(CO)_2Y$ system, Nesmeyanov *et al.* (6) concluded that there is a linear relationship between Hammett σ parameters and ν(CO), implying that variations in ν(CO) are caused directly by variations in the σ-bonding character of the ligand Y. Gansow *et al.* (1) also suggested that their observed linear correlation between carbonyl i.r. force constants and ^{13}C carbonyl shieldings is due to changes in σ effects of X, except where X is a tri-organo–Group IV substituent.

In this investigation we have examined similar phenomena, utilizing ^{13}C n.m.r., i.r., and Mössbauer spectroscopic techniques in an attempt to obtain useful bonding information for the analogous complexes $[(h^5\text{-}C_5H_5)Fe(CO)_2L]^+X^-$; where L = CO, CH_3CN, C_5H_5N, $(C_6H_5)_3P$, and C_2H_4 and X = PF_6^- (for all cases) and BF_4^- (for L = C_2H_4).

In addition, using the results from ^{55}Mn, and ^{185}Re and ^{187}Re n.q.r. studies (7, 8), attempts have been made to rationalize the bonding in manganese and rhenium compounds which are isoelectronic and isostructural with the cationic iron derivatives examined here. However, without a knowledge of the signs of the appropriate quadrupole splitting parameters, discussions of bonding in the former derivatives, based on n.q.r. evidence, is necessarily specula-

Can. J. Chem. Downloaded from www.nrcresearchpress.com by 210.87.254.40 on 09/05/12
For personal use only.

Can. J. Chem. Downloaded from www.nrcresearchpress.com by 210.87.254.40 on 09/05/12
For personal use only.

tive. From our knowledge of the signs of the ^{57}Fe Mössbauer quadrupole splittings, the signs of the field gradients for the manganese and rhenium analogs can be deduced. A significant part of the small variations in the Mössbauer quadrupole splittings of the iron compounds, and $\nu(\pm\frac{5}{2} \leftrightarrow \pm\frac{3}{2})$ in the ^{55}Mn n.q.r. spectra, are ascribed to changes in η.

Experimental

All preparations were carried out under a pre-purified nitrogen atmosphere. Solvents were purged with nitrogen prior to their use.

$[(h^5\text{-}C_5H_5)Fe(CO)_3]^+PF_6^-$ (9), $[(h^5\text{-}C_5H_5)Fe(CO)_2(C_5H_5N)]^+PF_6^-$ (10), and $[(h^5\text{-}C_5H_5Fe(CO)_2(C_2H_4)]^+PF_6^-$ (11) were prepared by established literature methods.

The Mössbauer spectra were measured at 78 °K using an Austin Science Associates spectrometer with a 512 channel analyzer, and a ^{57}Co in copper source. All spectra were calibrated using iron foil; absorptions were in the 7–10% range. All spectra were fitted to Lorentzian line shapes by methods previously described (12).

The ^{13}C n.m.r. spectra were measured on a Varian XL-100-15 spectrometer operating in the pulsed Fourier transform mode at 25.2 MHz. All spectra were determined with noise-modulated proton decoupling. The spectra were taken in acetonitrile-d_3 solutions in 5 mm sample tubes and were calibrated using TMS as the internal reference.

The i.r. spectra of the complexes in the carbonyl region were measured on a Perkin–Elmer 621 spectrometer in acetonitrile. The scale was expanded to *ca.* 1 cm^{-1}/mm of chart paper. Each spectrum was calibrated by recording the spectrum of indene (13) in the region 2300 to 1900 cm^{-1} before the sample was run. Force constants for the carbon–oxygen stretching modes of the carbonyl groups were calculated by established methods (14).

(A) Preparation of $[(h^5\text{-}C_5H_5)Fe(CO)_2P(C_6H_5)_3]^+PF_6^-$ *(15)*

$Fe(ClO_4)_3 \cdot 6H_2O$ (4.22 g, 9.15 mmol) was dehydrated under high vacuum at 120 °C. The orange product was dissolved in 20 ml acetone and added to a solution of $[(h^5\text{-}C_5H_5)Fe(CO)_2]_2$ (1.0 g, 2.83 mmol), and $(C_6H_5)_3P$ (2.6 g, 10 mmol) was added to this solution. After 1.5 h, a yellow precipitate had formed which was collected and dissolved in acetone. Addition of ether caused precipitation of $[(h^5\text{-}C_5H_5)Fe(CO)_2P(C_6H_5)_3]^+ClO_4^-$ (1.07 g, 35%). The hexafluorophosphate salt was obtained by treating an acetone solution of the perchlorate salt with an aqueous solution of NH_4PF_6. Evaporation of the acetone by bubbling nitrogen through the solution caused the hexafluorophosphate salt to crystallize.

(B) Preparation of $[(h^5\text{-}C_5H_5)Fe(CO)_2(CH_3CN)]^+PF_6^-$ *(15)*

This complex was prepared by a procedure similar to (*A*) except that hydrated iron(III) perchlorate was used with acetonitrile as the solvent, since *a violent reaction occurred when anhydrous ferric perchlorate was dissolved in that solvent*. The crude product was precipitated by the addition of an aqueous solution of NH_4PF_6, and was purified by crystallization from acetone–water.

Results

The ^{57}Fe Mössbauer, ^{13}C n.m.r., and carbonyl i.r. data obtained from the six h^5-cyclopentadienylirondicarbonyl derivatives we have examined are summarized in Tables 1–3, respectively. For comparative purposes, Table 1 contains Mössbauer parameters for several related derivatives, which have been investigated by other workers.

The specific assignments of the ^{13}C resonances of the cationic iron derivatives merit brief comment. The intense signals arising from the *pentahapto*-cyclopentadienyl carbons were assigned on the basis of the similarity of their shieldings (*ca.* 88–91 p.p.m.) compared with those (*ca.* 81–88 p.p.m.) of the related neutral complexes (1). In a like manner, we readily assigned the carbonyl carbon resonances. The signals arising from the ^{13}C nuclei of the ligands L, were assigned by comparisons with the ^{13}C shieldings of the uncoordinated species (16). For example, the similar coordinated (uncoordinated) shieldings for the three types of carbons in pyridine are: $C_{2,6}$, 159.3(150.6); $C_{3,5}$, 127.3(124.5); and C_4, 140.0(136.4). Together with a knowledge of the expected relative intensities of the signals, this provides a firm foundation for our specific assignments. The ^{13}C shieldings of the ethylene ligand carbons (*ca.* 57 p.p.m.) are markedly shifted upfield from those of uncoordinated ethylene (*ca.* 123 p.p.m.). However, this highfield shift is anticipated on the basis of results we have obtained for series of π-olefinic platinum(II) derivatives (17).

Discussion

(A) Mössbauer Spectra

Center Shifts

As has been shown previously for Fe(II) compounds (18), the center shift, which has comparable sensitivity to both σ-donor and π-acceptor properties, decreases as the σ-donor and π-acceptor ability ($\sigma + \pi$) of the ligand(s) increases. Thus, H^- (a strong σ-donor) and NO^+ (a strong π-acceptor) give comparable decreases in iron(II) center shifts.

In the present series of compounds the center shifts (Table 1) vary substantially as L is changed. Hence, we may arrange the compounds (including the thiocarbonyl derivative (4)) in an

Can. J. Chem. Downloaded from www.nrcresearchpress.com by 210.87.254.40 on 09/05/12
For personal use only.

TABLE 1. Mössbauer parameters* for the derivatives $[(h^5\text{-}C_5H_5)Fe(CO)_2L]^+X^-$

L	X	Center shift†‡	Quadrupole splitting†	Reference
CS	PF_6^-	0.21	1.89	4
CO	PF_6^-	0.29	1.90	This work
		0.27	1.78	4
		0.31	1.88	3
$(C_6H_5)_3P$	PF_6^-	0.34	1.81	This work
	Cl^-	0.31	1.92	4
C_5H_5N	PF_6^-	0.41	1.86	This work
C_2H_4	PF_6^-	0.43	1.77	This work
	BF_4^-	0.42	1.71	This work
CH_3CN	PF_6^-	0.44	1.95	This work

*Full peak widths at half height in all cases were between 0.25 and 0.31 mm s^{-1}.
†± 0.01 mm s^{-1}.
‡With respect to $Na_2Fe(CN)_5NO{\cdot}2H_2O$ at room temperature.

TABLE 2. ^{13}C shieldings for the derivatives $[(h^5\text{-}C_5H_5)Fe(CO)_2L]^+X^-$*

L	X	δ(*C*O)	δ(C_5H_5)	Other
CO	PF_6^-	202.7	90.9	
CH_3CN	PF_6^-	209.1	87.5	*C*H_3 4.9, *C*N†
C_2H_4	PF_6^-	209.3	89.8	C_2H_4 56.9
	BF_4^-	209.4	89.9	C_2H_4 57.0
$(C_6H_5)_3P$	PF_6^-	210.1	89.2	C_6H_5 129.8–133.6‡
C_5H_4N	PF_6^-	210.8	88.1	C_5H_4N: $C_{3,5}$ 127.3, $C_{2,6}$ 159.3, C_4 140.0

*In p.p.m. (downfield positive) from TMS.
†Not observed.
‡Complex multiplet.

TABLE 3. Carbonyl infrared stretching frequencies* (cm^{-1}) and Cotton–Kraihanzel force constants (mdyn/Å) for the derivatives $[(h^5\text{-}C_5H_5)Fe(CO)_2L]^+X^-$

L	X	ν_1†	ν_2†	*k*‡	k_i
CO	PF_6^-	2125	2079	17.71	0.26
C_2H_4	PF_6^-	2082	2048	17.22	0.28
	BF_4^-	2081	2046	17.20	0.29
CH_3CN	PF_6^-	2078	2036	17.09	0.35
C_5H_5N	PF_6^-	2067	2020	16.87	0.39
$(C_6H_5)_3P$	PF_6^-	2057	2015	16.74	0.35

*Spectra obtained in CH_3CN solution.
†± 2 cm^{-1}.
‡± 0.02 mdyn/Å.

Can. J. Chem. Downloaded from www.nrcresearchpress.com by 210.87.254.40 on 09/05/12
For personal use only.

order of increasing ($\sigma + \pi$) properties of the ligands:

$$CH_3CN \leqslant C_2H_4 < C_5H_5N < (C_6H_5)_3P < CO < CS$$

The ordering of CH_3CN, $(C_6H_5)_3P$, and CO ligands is the same as that obtained from iron(II) six coordinate compounds (19, 20). The position of C_2H_4 is of special interest; in terms of its ($\sigma + \pi$) ability, C_2H_4 appears to be a very similar ligand to pyridine and acetonitrile. The carbonyl i.r. stretching frequencies are also consistent with this observation. From previous Mössbauer work, it is interesting to note that N_2 is also a very similar ($\sigma + \pi$) ligand to nitriles, although the quadrupole splitting data indicates that the former is an appreciably better π-acceptor and poorer σ-donor than the latter (20). However, as will be discussed in the ensuing part of this paper, the quadrupole splittings are not helpful in separating σ and π effects in this series of compounds.

Quadrupole Splittings for (h^5-C_5H_5)M(CO)$_2$L (M = Fe, Mn, Re) Analogs

On comparison with the quadrupole splittings in six-coordinate iron(II) low spin compounds of the type *trans*-[FeHL($(C_2H_5)_2PCH_2CH_2P(C_2H_5)_2)_2$)]$^+B(C_6H_5)_4^-$ (20), the quadrupole splittings in the present series of compounds are very insensitive to the nature of L. This is, perhaps, not surprising since, in the neutral complexes (h^5-C_5H_5)Fe(CO)$_2$Y (Y = halide$^-$, SnX_3^-, etc.) (3, 21–23), the quadrupole splittings are all 1.8 $\pm$ 0.1 mm s^{-1}, in the same range as our present splittings. It appears that the bonding properties of both CO and h^5-C_5H_5 change substantially with variations in L to effectively neutralize the changes in electron assymmetry about the iron atom. Thus, it has not been possible to rationalize the trends in previously obtained quadrupole splittings for either the neutral or cationic h^5-cyclopentadienylirondicarbonyl derivatives in terms of bonding properties of the ligands. Likewise, no distinct trends emerge from the quadrupole splitting data of our present series of complexes.

However, our iron quadrupole splittings are very useful for assigning the signs of the quadrupole splittings for analogous neutral manganese and rhenium compounds of the type (h^5-C_5H_5)M(CO)$_2$L (M = Mn or Re) (7, 8, 24, 25). The detailed method has been described in previous work (26–28). Considering isoelectronic, isostructural manganese and iron compounds, and assuming that the bonding in the two species is identical, we can write:

$$[1] \quad (e^2qQ)_{Mn} = \frac{\langle r^{-3}\rangle_{Mn}Q_{Mn}}{\langle r^{-3}\rangle_{Fe}Q_{Fe}}(e^2qQ)_{Fe} = K(e^2qQ)_{Fe}$$

Using literature values for $\langle r^{-3}\rangle$ and Q, K has been calculated to be +1.39 (28) (assuming Q_{Mn} is positive). The sign of $(e^2qQ)_{Fe}$ in (h^5-C_5H_5)-Fe(CO)$_2$SnCl$_3$ and (h^5-C_5H_5)Fe(CO)$_2$Sn(CH_2-$CH_2CH_2CH_3$)$_3$ is known to be positive (29), and the very small variation in quadrupole splitting for all h^5-cyclopentadienylirondicarbonyl type compounds strongly suggests that all of these neutral and cationic compounds have positive e^2qQ values. It is immediately apparent from eq. 1 that q and e^2qQ are also positive for the manganese compounds. This sign is opposite to the negative sign assumed in earlier manganese n.q.r. work (7, 8). Consequently, this result indicates that the bonding model chosen previously, and the ensuing discussion of variations in bonding were incorrect. It is also apparent that the signs of the rhenium e^2qQ values (24) can be assigned as positive.

More quantitatively, if we take the measured e^2qQ value for [(h^5-C_5H_5)Fe(CO)$_3$]$^+$ of (+)3.80 mm s^{-1} (= (+)44.2 MHz) and assume $\eta = 0$ (as measured in the manganese analog), the predicted value of $(e^2qQ)_{Mn}$, using $K = +1.39$ and eq. 1, is +61.4 MHz. This is in surprisingly good agreement with the measured value of 64.29 MHz, considering the assumptions inherent in the method, and possible errors in the Q and $\langle r^{-3}\rangle$ values.

In order to use the above method in a predictive sense, and to indicate that variations in η cause a substantial part of the variations in both Mössbauer quadrupole splittings [$\frac{1}{2}e^2qQ(1 + \eta^2/3)^{1/2}$], and in $\nu(\pm\frac{5}{2} \leftrightarrow \pm\frac{3}{2})$ in the ^{55}Mn n.q.r., we recalculate the multiplying factor K by using the measured values of e^2qQ for [(h^5-C_5H_5)Fe(CO)$_3$]$^+$ and (h^5-C_5H_5)Mn(CO)$_3$. This is the first analogous pair of iron and manganese compounds where $|e^2qQ|$ values have been *measured* for both. The calculated K becomes +1.45; which should be a more accurate value than +1.39 used

TABLE 4. Predicted quadrupole parameters* for isoelectronic $(h^5\text{-}C_5H_5)M(CO)_2L$ (M = Mn,Fe) derivatives

L	^{57}Fe data		^{55}Mn data			
	$e^2qQ\,(1+\eta^2/3)^{1/2}$ Observed	e^2qQ Predicted	$\nu(\pm\frac{5}{2}\leftrightarrow\pm\frac{3}{2})$ Observed	$\nu(\pm\frac{3}{2}\leftrightarrow\pm\frac{1}{2})$ Predicted	e^2qQ Predicted	η Predicted
CO	44.2	(+) 44.2	19.29	9.65†	+64.29†	0.0†
C_5H_5N	43.3	(+) 42.0	17.62	11.0	+60.9	0.45
CH_3CN	45.4	(+) 44.2	18.71	11.2	+64.3	0.40
$(C_6H_5)_3P$	42.1	~(+) 42.1	18.82	‡	‡	‡

*MHz.
†Observed values, ref. 7.
‡$\eta^2 < 0$, and values cannot be calculated.

earlier.[1] Using this factor and the measured ^{57}Fe quadrupole splittings, we can now predict η and the unmeasured $\nu(\pm\frac{3}{2}\leftrightarrow\pm\frac{1}{2})$ transition frequency in some manganese analogs of our iron compounds. These are summarized in Table 4.

The predicted e^2qQ and η values would not be expected to be more accurate than *ca.* ± 2 MHz and ± 0.2 respectively. (The results for the triphenylphosphine derivative (η^2(calculated) < 0) are indicative of these errors.) However, our results do indicate that the variation in both the ^{57}Fe Mössbauer quadrupole splittings and in the ^{55}Mn $\nu(\pm\frac{5}{2}\leftrightarrow\pm\frac{3}{2})$ is probably substantially due to variation in η. For example, the acetonitrile derivative has a larger ^{57}Fe quadrupole splitting than its carbon monoxide analog (and a smaller ^{55}Mn n.q.r. $\nu(\pm\frac{5}{2}\leftrightarrow\pm\frac{3}{2})$), yet their calculated e^2qQ values are identical within expected error.

We conclude, then, that even after the signs of the e^2qQ parameters have been assigned in such complexes, a substantial part of the variations in Mössbauer quadrupole splittings are due to changes in η. This places discussions concerning variations of quadrupole splittings with bonding properties of the ligands L in these systems on an even more tenuous footing.

(B) ^{13}C Nuclear Magnetic Resonance and Infrared Spectra

Gansow *et al.* (1) have noted interesting linear correlations between the ^{13}C shieldings of the carbonyl carbons and the carbonyl stretching frequencies (and their Cotton–Kraihanzel (C.K.) force constants) for a series of neutral derivatives of the type $(h^5\text{-}C_5H_5)Fe(CO)_2Y$, where Y is a predominantly σ-bonding anionic substituent. As the σ-donor ability of a ligand Y decreases they observed concomittant shifts of the carbonyl carbons to higher field and the carbonyl stretching frequencies (and C.K. force constants) to higher energies. However, this trend was not observed for triorgano–silicon, –germanium, and –tin groups, which are capable of π-bonding. Our examination of the ^{13}C n.m.r. and i.r. data for the cationic complexes reveals a similar trend between C.K. force constants and ^{13}C carbonyl carbon shieldings. These data, together with data from the neutral compounds with σ-bonding ligands, are plotted in Fig. 1.

First, it is important to note that the data points for the six cationic derivatives form an approximately linear extension to the high field – high energy end of the plot for the neutral $(h^5\text{-}C_5H_5)Fe(CO)_2Y$ complexes. Thus, a fairly consistent trend is followed whereby the withdrawal of electrons from iron is accompanied by an increase in the carbon–oxygen bond order and an increase in the screening of the

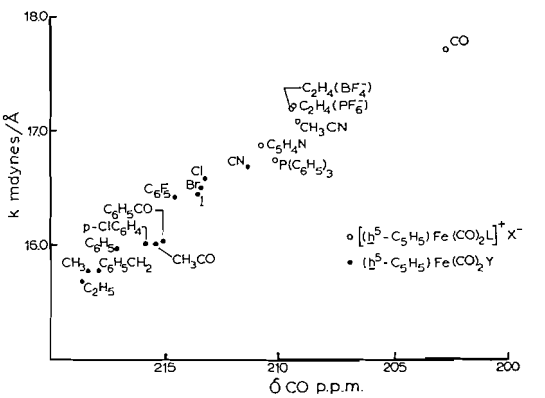

FIG. 1. Plot of carbon–oxygen stretching C.K. force constant (mdyn/Å) *vs.* δ_C (carbonyl (p.p.m.)) for complexes of the type $[(h^5\text{-}C_5H_5)Fe(CO)_2L]^+X^-$ and $(h^5\text{-}C_5H_5)Fe(CO)_2Y$.

[1]This change in K will have a very small effect on the $(e^2qQ)_{Mn}$ values calculated earlier (28).

Can. J. Chem. Downloaded from www.nrcresearchpress.com by 210.87.254.40 on 09/05/12
For personal use only.

^{13}C nucleus. The very short CO bond distances found recently in $[(h^5\text{-}C_5H_5)Fe(CO)_3]^+PF_6^-$ (30) compared with analogous neutral species is consistent with this trend. For a series of Group VIb derivatives, Braterman *et al.* (31) have reached a similar conclusion, that the total "charge donor" ability of a given ligand is directly related to the ^{13}C carbonyl shieldings. In that study, as in the work of Gansow *et al.*, it was concluded that consistent rationalization of the carbonyl carbon shieldings did not seem possible in terms of σ- and π-bonding arguments.

To determine possible relationships between the Mössbauer and ^{13}C n.m.r. parameters, we have compared the center shifts and carbonyl carbon shieldings for our cationic derivatives and a number of the neutral complexes (1, 3, 21). The examination revealed no consistent trend. This may be due to the differing sensitivities of these two physical techniques to variations in molecular parameters. In addition, such a possible relationship may also be masked by variations in parameters other than σ- and π-bonding.

We thank the National Research Council of Canada for financial support of this project and for awards of NRCC scholarships to K.D.B., L.E.M., A.S., and J.E.H.W.

1. O. A. GANSOW, D. A. SHEXNAYDER, and B. Y. KIMURA. J. Am. Chem. Soc. **94**, 3406 (1972).
2. P. C. LAUTERBUR and R. B. KING. J. Am. Chem. Soc. **87**, 3266 (1965).
3. R. H. HERBER, R. B. KING, and G. K. WERTHEIM. Inorg. Chem. **3**, 101 (1964).
4. K. BURGER, L. KORECZ, P. MAG, U. BELLUCO, and L. BUSETTO. Inorg. Chim. Acta **5**, 362 (1971).
5. R. B. KING. Inorg. Chim. Acta, **2**, 454 (1968).
6. A. N. NESMEYANOV, YU. A. CHAPOVSKII, L. I. DENISOVITCH, B. L. LOKSHIEN, and I. V. POLOVYANYUK. Dokl. Akad. Nauk SSR, **174**, 1342 (1967).
7. W. P. ANDERSON, T. B. BRILL, A. R. SCHOENBERG, and C. W. STANGER, JR. J. Organomet. Chem. **44**, 161 (1972).
8. T. B. BRILL and G. G. LONG. Inorg. Chem. **10**, 74 (1971).
9. L. BUSETTO and R. J. ANGELICI. Inorg. Chim. Acta, **2**, 391 (1968).
10. P. M. TREICHEL, R. L. SHUBKIN, K. W. BARNETT, and D. RICHARD. Inorg. Chem. **5**, 1177 (1966).
11. W. P. GIERING, M. ROSENBLUM, and J. TANCREDE. J. Am. Chem. Soc. **94**, 7170 (1972).
12. G. M. BANCROFT, W. K. ONG, A. G. MADDOCK, R. H. PRINCE, and A. J. STONE. J. Chem. Soc. A, 1966 (1967).
13. P. N. JONES and A. NODEAU. Spectrochim. Acta **20**, 1175 (1964).
14. F. A. COTTON and K. S. KRAIHANZEL. J. Am. Chem. Soc. **84**, 4432 (1962).
15. E. C. JOHNSON, T. J. MEYER, and N. WINTERTON. Inorg. Chem. **10**, 1673 (1971).
16. J. B. STOTHERS Carbon-13 N.M.R. spectroscopy. Academic Press, New York, N.Y. 1972.
17. M. H. CHISHOLM, H. C. CLARK, L. E. MANZER, and J. B. STOTHERS. J. Am. Chem. Soc. **94**, 5087 (1972).
18. G. M. BANCROFT, M. J. MAYS, and B. E. PRATER. J. Chem. Soc. A, 956 (1970).
19. G. M. BANCROFT and E. T. LIBBEY. J. Chem. Soc. Dalton, 2103 (1973).
20. G. M. BANCROFT, R. E. B. GARROD, A. G. MADDOCK, M. J. MAYS, and B. E. PRATER. J. Am. Chem. Soc. **94**, 647 (1972).
21. G. M. BANCROFT, H. C. CLARK, and A. T. RAKE. Unpublished results.
22. W. R. CULLEN, J. R. SAMS, and J. A. J. THOMPSON. Inorg. Chem. **10**, 843 (1971).
23. R. H. HERBER and Y. GOSCINNY. Inorg. Chem. **7**, 1293 (1968).
24. A. N. NESMEYANOV, G. K. SEMIN, E. V. BRYUCHOVA, T. A. BABYSHKINA, K. N. ANISIMOV, N. E. KALOBOVA, and YU. V. MAKAROV. Tetrahedron Lett. **37**, 3987 (1968).
25. M. D. FAYER and C. B. HARRIS. Inorg. Chem. **8**, 2792 (1969).
26. C. B. HARRIS. J. Chem. Phys. **49**, 1648 (1968).
27. G. M. BANCROFT. Chem. Phys. Lett. **10**, 449 (1971).
28. G. M. BANCROFT, H. C. CLARK, R. G. KIDD, A. T. RAKE, and H. G. SPINNEY. Inorg. Chem. **12**, 728 (1973).
29. B. A. GOODMAN, R. GREATREX, and N. N. GREENWOOD. J. Chem. Soc. A, 1868 (1971).
30. M. E. GRESS and R. A. JACOBSON. Inorg. Chem. **12**, 1746 (1973).
31. P. S. BRATERMAN, D. W. MILNE, E. W. RANDALL, and E. ROSENBERG. J. Chem. Soc. Dalton, 1027 (1973).

Can. J. Chem. Downloaded from www.nrcresearchpress.com by 210.87.254.40 on 09/05/12
For personal use only.

Excess Volumes of Binary Mixtures of Alcohols in Methylcyclohexane

MURARI VENKATA PRABHAKARA RAO AND P. RAMACHANDRA NAIDU

Chemical Laboratories, Sri Venkateswara University, Tirupati, S. India

Excess volumes of binary mixtures of alcohols in methylcyclohexane have been determined at 30.0 and 40.0 °C, using a modified dilatometer of Brown and Smith. The systems include: (*1*) 1-propanol – methylcyclohexane, (*2*) 1-butanol – methylcyclohexane, (*3*) 1-pentanol – methylcyclohexane, and (*4*) 1-hexanol – methylcyclohexane. The V^E values are found to be positive over the entire range of composition in all the four systems and the values are interpreted on the basis of the structure-breaking effect of methylcyclohexane.

Les volumes d'excès des mélanges binaires d'alcools dans le méthylcyclohexane ont été déterminés entre 30.0 et 40.0 °C en utilisant un dilatomètre modifié de Brown et Smith. Ces systèmes sont: (*1*) propanol-1 – méthylcyclohexane, (*2*) butanol-1 – méthylcyclohexane, (*3*) pentanol-1 – méthylcyclohexane. (*4*) hexanol-1 – méthylcyclohexane. On a trouvé que ces valeurs V^E sont positives dans tout le domaine de composition pour les quatre systèmes et on a interprété ces valeurs sur la base de l'effet de "bris de structure" du méthylcyclohexane.

[Traduit par le journal]

Can. J. Chem., **52**, 788 (1974)

Introduction

A survey of the literature relating to excess volumes of binary mixtures of normal alcohols has shown that aromatic solvents (1–4) and normal alkanes (5–7) have been used as solvents. By contrast only a few studies have been made using alicyclic compounds as solvents. Hence the present study has been devoted to the determination of excess volumes of binary mixtures of alcohols with methylcyclohexane. Methylcyclohexane has been chosen as a common solvent as it is less volatile than cyclohexane and hence errors arising due to evaporation of the solvent during the measurement of excess volume would be minimum.

Experimental

Mixing Cell

The cell used for measuring excess volumes was similar to that used by Brown and Smith (1) except for the detachable capillary arrangement. The cell was basically a U-tube with mercury at the bottom to separate the two components. One arm of the U-tube was closed with a ground glass stopper and the other arm was fitted with a capillary (1 mm i.d.), having a Teflon cap with small orifice at the top, which can be detached. Composition was determined directly by weighing. The cell was immersed in a thermostatic bath maintained at 30.0 and 40.0 ± 0.01 °C respectively. The change in liquid level after mixing in the capillary with reference to a fixed mark was read by a travelling microscope which had an accuracy of ±0.01 mm. Excess volumes were accurate to ±0.003 ml mol^{-1}. Three cells with different capacities were used to cover the mole fraction range from 0.1 to 0.9.

Purification of Materials

Methylcyclohexane (B.D.H.) was washed several times with a cold mixture of concentrated sulfuric acid and nitric acid until the acid layer gave no more yellow color. Then it was washed with dilute alkali solution to remove acid. After repeated washings with water it was dried over fused calcium chloride for 2 days and distilled. Finally it was refluxed with metallic sodium for 12 h and fractionated over sodium (d^{30} = 0.76019 g/ml; b.p. 100.7 °C).

1-Propanol (E. Merck) was refluxed over lime for 5 h and then distilled through a 1 m fractionating column. The fraction boiling at 97.0–97.2 °C was collected (d^{30} = 0.79596 g/ml; b.p. 97.0 °C).

1-Butanol (B.D.H.) was refluxed over freshly ignited calcium oxide for 4 h. The alcohol was decanted from the lime, refluxed with magnesium turnings and then fractionated. The middle fraction which had a boiling point 117.6 °C was collected (d^{30} = 0.80195 g/ml; b.p. 117.6 °C).

1-Pentanol (E. Merck) was dried over Drierite and fractionally distilled (d^{30} = 0.80760 g/ml; b.p. 138.0 °C).

1-Hexanol (B.D.H.) was fractionally distilled. (d^{30} = 0.81195 g/ml; b.p. 157.3 °C).

Densities were determined using a bicapillary type Pycnometer with an accuracy of 2 parts in 10^5. Values of the density and the boiling point agreed with those reported in the literature (8).

Results

The values[1] of V^E at 30.0 and 40.0 °C, as a function of composition for the four systems, are shown in Figs. 1, 2, 3, and 4. These data show

[1]Complete set of data is available at a nominal charge from the Depository of Unpublished Data, National Science Library, National Research Council of Canada, Ottawa, Canada K1H 0J2.

Can. J. Chem. Downloaded from www.nrcresearchpress.com by 210.87.254.40 on 09/05/12
For personal use only.

Can. J. Chem. Downloaded from www.nrcresearchpress.com by 210.87.254.40 on 09/05/12
For personal use only.

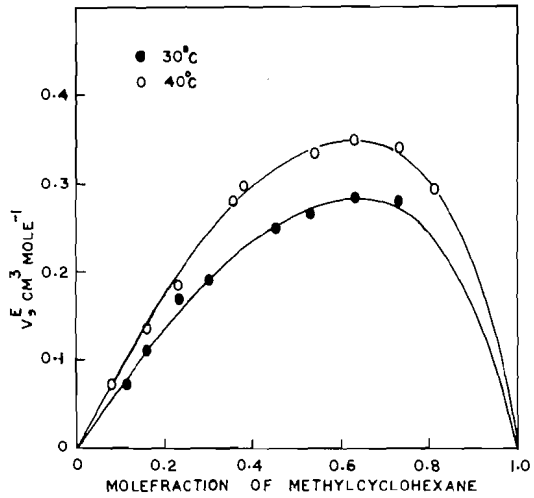

FIG. 1. Plot of V^E as a function of composition for methylcyclohexane and 1-propanol system.

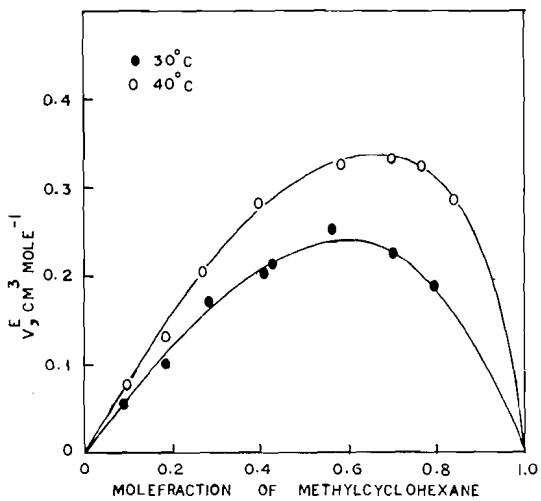

FIG. 2. Plot of V^E as a function of composition for methylcyclohexane and 1-butanol system.

that the values of V^E are positive over the whole range of composition. The maximum value of V^E occurs at about 0.7 mol fraction of methylcyclohexane in all the systems at 30.0 and 40.0 °C except in 1-butanol – methylcyclohexane at 30.0 °C. Further the volume change on mixing increases with increase in temperature.

Discussion

The positive values of V^E may be attributed to (*a*) depolymerization of alcohol polymers by methylcyclohexane and (*b*) interaction between the homomorphs of alcohols with methylcyclohexane. Since alcohols are associated in the pure state, addition of the non-polar solvent, methylcyclohexane, would be expected to depolymerize polymers into monomers and this would contribute to expansion in volume upon mixing, as the alcohol molecules occupy more space as monomers than as polymers. Furthermore, interaction between the homomorph of an alcohol and methylcyclohexane would also be expected to contribute to positive volume change. Hence the observed values of V^E for the systems support the above postulates.

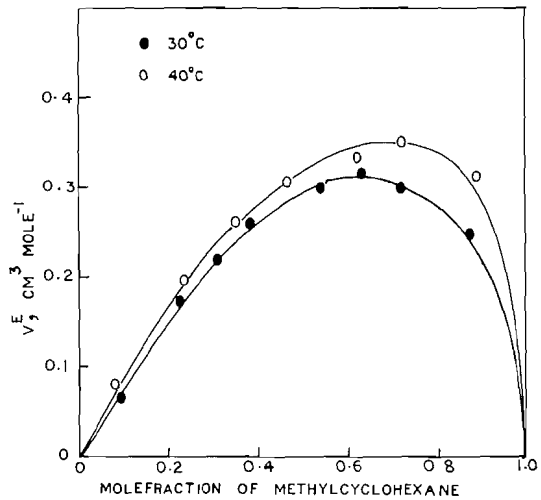

FIG. 3. Plot of V^E as a function of composition for methylcyclohexane and 1-pentanol system.

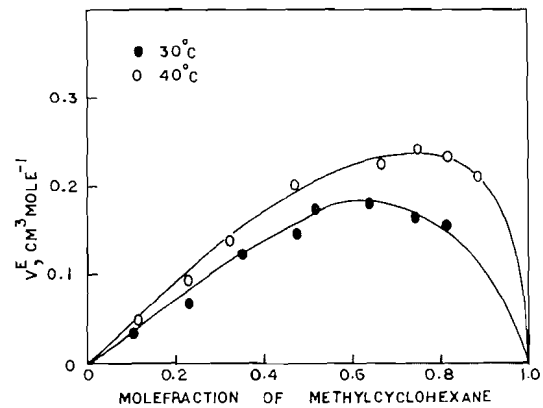

FIG. 4. Plot of V^E as a function of composition for methylcyclohexane and 1-hexanol system.

The differences in the values of V^E for the four systems may be ascribed to the effect of chain length on the degree of polymerization of alcohols in the pure state. An increase in chain length is expected to decrease the degree of polymerization in the pure state. Consequently when a homologous series of alcohols are diluted with a common solvent, the values of V^E would be expected to be large for the alcohol with the minimum chain length and small for the alcohol with the maximum chain length. The observed values of V^E for the four systems fall in this order, except in the case of 1-pentanol – methylcyclohexane. This anomaly indicates that in this case geometric factors also affect the values of V^E in addition to the structure-breaking effect of the solvent.

One of the authors (M. V. P. Rao) is thankful to the Council of Scientific and Industrial Research, New Delhi for the award of a Junior Fellowship.

1. I. Brown and F. Smith, Aust. J. Chem. **15**, 1 (1962).
2. H. Harms. Z. Physik. Chem. Ab. B, **53**, 280 (1943).
3. W. Jones, S. T. Bowden, W. W. Yarnold, and W. H. Jones. J. Phys. Chem. **52**, 753 (1948).
4. P. Huyskens and F. Cracco. Bull. Soc. Chim. Bulges. **69**, 422 (1960).
5. I. Brown, W. Fock, and F. Smith. J. Chem. Thermodyn. **1**, 273 (1969).
6. S. A. Levichev. Fiz. Kim. Svoistova Rastvoror. 219 (1964).
7. H. C. Van Ness, C. A. Soczek, G. L. Peloquin, and R. L. Machado. J. Chem. Eng. Data, **12**, 217 (1967).
8. J. Timmermans. Physico-chemical constants of pure organic compounds. Elsevier Publishing Co., Amsterdam. 1950.

Can. J. Chem. Downloaded from www.nrcresearchpress.com by 210.87.254.40 on 09/05/12
For personal use only.

Alchemists' Gold, $Hg_{2.86}AsF_6$; An X-Ray Crystallographic Study of A Novel Disordered Mercury Compound Containing Metallically Bonded Infinite Cations

I. David Brown, Brent D. Cutforth, Colin G. Davies, Ronald J. Gillespie, Peter R. Ireland, and John E. Vekris

Department of Chemistry, McMaster University, Hamilton, Ontario L8S 4M1

Received September 10, 1973

The compound $Hg_{2.86}AsF_6$ belongs to the tetragonal space group $I4_1/amd$ with lattice parameters $a = 7.538(4)$ Å, $c = 12.339(5)$ Å, and $Z = 4$. The structure was refined using 109 symmetry independent reflections by full matrix least-squares refinement to a final R value of 0.079. The structure may be described as consisting of octahedral AsF_6^- ions arranged on a lattice which contains linear, non-intersecting channels in two mutually perpendicular directions. Within these channels are infinite chains of mercury atoms, each with a formal charge of +0.35, and with a mercury–mercury distance of 2.64(1) Å.

Le composé $Hg_{2.86}AsF_6$ appartient au groupe d'espace tétragonal $I4_1/amd$ avec les paramètres de maille $a = 7.538(4)$ Å, $c = 12.339(5)$ Å, and $Z = 4$. En utilisant 109 réflexions symétrie indépendante la structure a été raffinée par une méthode de matrice complète des moindres carrés à une valeur finale du facteur R égal à 0.079. On peut décrire la structure comme si elle consiste des ions octaédrique AsF_6^- qui se trouvent sur un réseau qui contient les canaux linéaire en deux directions mutuellement perpendiculaire et qui ne se coupent pas. Dans ces canaux se trouvent les chaînes infinies d'atomes de mercure, dont chaque atome porte une charge formelle de +0.35, et qui ont une distance mercure–mercure de 2.64(1) Å.

Can. J. Chem., **52**, 791 (1974)

Introduction

It has been shown recently that compounds containing mercury in oxidation states lower than +1 can be obtained by treating mercury with AsF_5 in liquid SO_2. The compounds $Hg_3(AsF_6)_2$ (1) and $Hg_4(AsF_6)_2$ (2) have been isolated and characterized by spectroscopic techniques. X-Ray diffraction studies show that both compounds contain linear or almost linear polymercury cations. $Hg_3(AlCl_4)_2$ has also been prepared (3) by the reaction of mercury with a molten $HgCl_2$–$AlCl_3$ mixture, and a subsequent structural determination (4) showed that the cation is very nearly linear.

In the preparation of the compounds $Hg_3(AsF_6)_2$ and $Hg_4(AsF_6)_2$ by the reaction of liquid mercury with a solution of AsF_5 in SO_2 we observed that the liquid mercury is initially transformed to a golden crystalline mass. Unsatisfied with the obvious conclusion that the "sulfurous menstrue" contains the long sought after philosopher's stone (5), we subjected the material to chemical analysis, the results of which led to the conclusion that this remarkable material had the empirical formula Hg_3AsF_6. The material was found to be diamagnetic and by analogy with the other polymercury cations we concluded that the substance was $Hg_6^{2+}(AsF_6^-)_2$ (6). The X-ray crystallographic study reported here has however revealed that the true composition is $Hg_{2.86}AsF_6$ and, while confirming that the material is indeed not gold, has shown that mercury has, in fact, undergone a transformation almost as remarkable to give unique metallically bonded infinite polymeric cations which form part of an ionic crystal lattice.

Experimental Section

Preparation of $Hg_{2.86}AsF_6$

In a typical experiment, AsF_5 was condensed onto elemental mercury in liquid SO_2 at −196 °C and the mixture was allowed to warm to room temperature and slowly stirred. A slight excess of AsF_5 was used to ensure that no unreacted mercury contaminated the surface of the crystals. After the insoluble golden crystals had formed, they were filtered, washed several times with SO_2, and vacuum dried.

Anal. Calcd. for $Hg_{2.86}AsF_6$: Hg, 75.23; As, 9.82; F, 14.95. Found: Hg, 75.83; As, 9.52; F, 14.61.

Although the chemical analysis is somewhat closer to the empirical formula Hg_3AsF_6, crystallographic arguments (see below) show that the empirical formula must be $Hg_{2.86}AsF_6$.

Materials

Commercially available triply distilled mercury

Can. J. Chem. Downloaded from www.nrcresearchpress.com by 210.87.254.105 on 09/05/12
For personal use only.

TABLE 1. Structural parameters* for $Hg_{2.86}AsF_6$

	No. of positions and Wyckoff notations	x	y	z	B, Å^2
11.4Hg† in	16(h)	0	x(Hg)	0.000	B(Hg)
4As(1) in	4(b)	0	1/4	3/8	0 039(3)
8F(1) in	8(e)	0	1/4	0.245(5)	0.096(19)
16F(2) in	16(g)	0.659(7)	$x+1/4$	7/8	0.074(10)

*x, y, and z are fractional atomic coordinates. The isotropic temperature factor B is from the expression $\exp[-B(\sin^2\theta/\lambda^2)]$. Least squares estimated standard errors in the least significant digits are given in parentheses.
†To simulate a disordered chain, 0.179 Hg atoms were placed at each of x(Hg) = 0.03125, 0.09375, 0.15625, and 0.21875. Only the temperature factors were refined and these gave B(Hg) = 0.074(4), 0.075(6), 0.063(5), and 0.070(4), respectively.

(Shawinigan) was used without further purification. Anhydrous sulfur dioxide (Matheson) was stored as a liquid over P_2O_5 before use. Arsenic pentafluoride (Ozark–Mahoning) was used without purification after the purity had been checked by gas-phase infrared spectroscopy. All materials were handled in a very good dry box and transfer of solvents was carried out on a vacuum-line which had been thoroughly flame-dried before use.

Determination of the Structure of $Hg_{2.86}AsF_6$

Precession photographs showed the symmetry and systematic absences characteristic of the space group $I4_1/amd$ (No. 141, D_{4h}^{19}). In addition sheets of diffuse intensity were observed perpendicular to (100) and (010). Crystal data for $Hg_{2.86}AsF_6$ are as follows: tetragonal, $a = 7.538(4)$ Å, $c = 12.339(5)$ Å, $V = 701.1$ Å^3, $Z = 4$, $\mu(MoK_\alpha) = 685.5$ cm^{-1}. The experimental density was not measured as no satisfactory procedure was evolved for this very hygroscopic material. The unit cell parameters were found by full-matrix least-squares refinement of the Bragg angles and crystal orientation for 15 reflections in the region $5° < 2\theta < 20°$ measured on a Syntex $P\bar{1}$ four-circle autodiffractometer using $MoK_\alpha(\lambda = 0.71069$ Å) radiation.

An approximately spherical crystal (radius 0.08 mm) was sealed in a thin walled quartz capillary and used for intensity measurements of the Bragg peaks on the diffractometer. The θ–2θ scan technique was used with scan rates varying from 2 to 24°/min so that the weaker reflections were examined most slowly to minimize counting errors. Two standard reflections were recorded every 100 measurements to monitor the stability of the crystal and its orientation. No distinct time dependent trend was observed, the maximum intensity variation being of the order of 3%. Reflections within four symmetry related octants with $2\theta \leq 50°$ were measured resulting in 696 reflections, which were then corrected for Lorentz and polarization effects. The intensities were corrected for absorption assuming spherical geometry ($\mu R \simeq 5.5$). It was realized that this correction was not completely adequate but the poorly defined faces on the crystal used and the difficulties in handling the material made a more accurate correction impracticable. Symmetry equivalent reflections were averaged resulting in 109 independent reflections with intensities greater than 3 times the standard deviation based on counting statistics. Unobserved reflections were not included in the refinement.

Solutions and Refinement of the Structure

The prominent sheets of diffuse intensity perpendicular to the a^* and b^* axes corresponded to a spacing of 2.64(1) Å, a distance not commensurate with the lattice dimensions. Two orders of these sheets were visible in each direction. We assumed that the 2.64 Å spacing corresponded to a Hg—Hg interaction and that the mercury atoms were in some measure disordered. This was confirmed by the three-dimensional Patterson function which showed planes of high density at $w = 1/4$ and 3/4. A satisfactory solution to both the Patterson function and the diffuse reflections could be found by placing atoms in the positions given in Table 1. This model, refined with isotropic temperature factors and unit weights, converged at $R_1(= \Sigma\Delta/\Sigma|F_o|$ where $\Delta = ||F_o| - |F_c||) = 0.079$.

The atomic scattering factors for mercury, fluorine, and arsenic with corrections for anomalous dispersion for the mercury atoms were taken from ref. 7. All calculations were performed on a CDC 6400 computer using the series of programs in the XRAY 71 system (8) and local programs. The final atomic positional coordinates and temperature factors are given in Table 1, while a listing of the observed and calculated structure factors is available in Table 3.[1]

Results and Discussion

The structure consists of an array of octahedral hexafluoroarsenate anions conforming to the crystal space group symmetry, with the fluorine atoms occupying three-quarters of the points of a cubic close packed lattice (Fig. 1). Within this lattice there is an array of non-intersecting channels running along the a and b directions. Infinite chains of mercury atoms (Hg—Hg = 2.64(1) Å) lie within these channels but the Hg—Hg distance is not commensurate with the lattice dimensions. Thus whereas $a = 7.54$ Å, three Hg—Hg distances equal 7.92 Å

[1]Table 3 is available, at a nominal charge, from the Depository of Unpublished Data, National Science Library, National Research Council of Canada, Ottawa, Canada K1A 0S2.

Can. J. Chem. Downloaded from www.nrcresearchpress.com by 210.87.254.105 on 09/05/12
For personal use only.

Can. J. Chem. Downloaded from www.nrcresearchpress.com by 210.87.254.105 on 09/05/12
For personal use only.

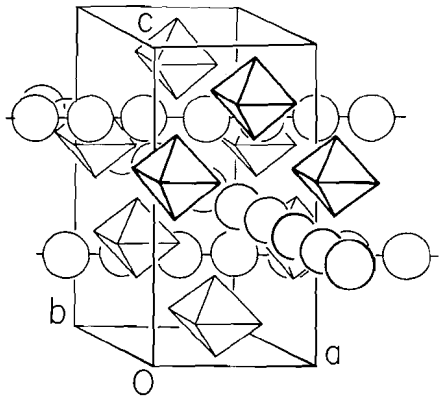

FIG. 1. An isometric view of $Hg_{2.86}AsF_6$ showing the infinite chains of Hg atoms (circles) running through the lattice of AsF_6^- ions (octahedra).

and therefore the empirical formula may be written as $Hg_{2.86}AsF_6$. The mercury atoms are in different positions in adjacent unit cells and each mercury atom has a different environment. The positions of the mercury atoms within a given chain are also disordered with respect to the positions in adjacent chains. To simulate the disorder of the mercury atoms, 0.179 atom was placed at x(Hg) = 0.03125, 0.09771, 0.15621, and 0.21875 thus giving 16 partial atoms along each chain in the unit cell, *i.e.*, an approximately continuous chain of mercury electron density. Selected bond distances and angles are given in Table 2. Two points appear worthy of note. Firstly the As—F distances are within the range found previously for AsF_6^-. The closest contact distance between the mercury atoms and a fluorine is 2.99(4) Å which is slightly greater than the sum of the Van der Waals' radii (2.85 Å). Thus it seems reasonable to conclude that the crystal contains AsF_6^- anions and mercury chains in which the average charge per mercury atom is 1/2.86 = +0.35 and that there is essentially ionic bonding between the positively charged mercury chains and the negative hexafluoroarsenate anions.

TABLE 2. Selected bond distances (Å) for $Hg_{2.86}AsF_6$*

Bond	Distance (Å)
As(1)—F(1)	1.61(7)
—F(2)	1.71(4)
Hg(2)—F(2)†	2.99(4)
Hg—Hg	2.64(1)

*Symmetry restricts the angles subtended by F(1)—As(1)—F(2) to 90° and angles subtended by Hg—Hg—Hg to 180°.
†Shortest distance.

The mercury–mercury distance of 2.64 Å is appreciably longer than that found in the mercurous halides (9) (2.49–2.54 Å) or in $Hg_3(AsF_6)_2$ (2.55 Å). This, coupled with the fact that the chains are electron deficient, leads us to believe that the chains have a "metallic character." The mercury–mercury distance is considerably shorter than in metallic mercury (3.005 Å) but it must be remembered that the coordination number in the metal is 12 whereas in the present compound it is only 2. It seems reasonable to suppose that the compound will display anisotropic conductivity, *i.e.*, it will be highly conducting along the *a* and *b* axes but not along the *c* axis. This is presently under investigation.

Recently Lokken and Corbett (10) have published the structural analysis of the compound Gd_2Cl_3 which contains infinite chains of metal atoms along one axis of the crystal. These chains are formed by the sharing of opposite edges of octahedra of gandolinium atoms. Both Gd_2Cl_3 and $Hg_{2.86}AsF_6$ contain infinite one-dimensional metal atom chains, and Lokken and Corbett have also predicted that their compound should display anisotropic conductivity.

1. B. D. CUTFORTH, C. G. DAVIES, P. A. W. DEAN, R. J. GILLESPIE, P. R. IRELAND, and P. K. UMMAT. Inorg. Chem. **12**, 1343 (1973).
2. B. D. CUTFORTH, R. J. GILLESPIE, and P. R. IRELAND. Chem. Commun. 723 (1973).
3. G. TORSI, K. W. FUNG, G. H. BEGUN, and G. MAMANTOV. Inorg. Chem. **10**, 2285 (1971).
4. R. D. ELLISON, H. A. LEVY, and K. W. FUNG. Inorg. Chem. **11**, 283 (1972).
5. E. ASHMOLE. Theatrum Chemicum Brittanicum. London. 1652. p. 125–127.
6. R. J. GILLESPIE and P. K. UMMAT. Chem. Commun. 1168 (1971).
7. International tables for X-ray crystallography. Kynock Press, Birmingham, England. 1962.
8. J. M. STEWART, F. A. KUNDELL, and J. C. BALDWIN. XRAY 71 system of crystallographic programs. Technical Report. University of Maryland, 1971.
9. E. DORM. Chem. Commun. 466 (1971).
10. D. A. LOKKEN and J. D. CORBETT. Inorg. Chem. **12**, 556 (1973).

Mechanism of Hydrogen Peroxide Pyrolysis

ANDRÉ TESSIER[1] AND WENDELL FORST
Department of Chemistry, Université Laval, Québec G1K 7P4

Received January 30, 1973[2]

The pyrolysis of hydrogen peroxide was followed mass spectrometrically, under conditions such that a steady-state concentration of the HO_2 radical equal to or exceeding 1/100th of the concentration of hydrogen peroxide would have been detected. The actual steady-state concentration of HO_2 in a reacting mixture was found to be below the detection limit, from which it is concluded that the simplest mechanism that provides an entirely adequate quantitative description of the pyrolysis is

$$H_2O_2 + M \rightarrow 2\,OH + M$$
$$OH + H_2O_2 \rightarrow HO_2 + H_2O$$
$$2\,HO_2 \rightarrow H_2O_2 + O_2$$

La pyrolyse du peroxyde d'hydrogène a été suivie par spectrométrie de masse, sous conditions telles qu'une concentration stationnaire du radical HO_2 égale ou supérieure à 1/100ème de la concentration du peroxyde était détectable. On trouve cependant que la concentration stationnaire de HO_2 dans le milieu réactionnel est en-dessous de la limite de détection, ce qui nous permet de conclure que le mécanisme le plus simple qui offre une description quantitative entièrement satisfaisante de la pyrolyse est

$$H_2O_2 + M \rightarrow 2\,OH + M$$
$$OH + H_2O_2 \rightarrow HO_2 + H_2O$$
$$2\,HO_2 \rightarrow H_2O_2 + O_2$$

Can. J. Chem., **52**, 794 (1974)

The thermal decomposition of hydrogen peroxide vapor in a suitably seasoned vessel is now established as a homogeneous non-chain gas phase reaction of order one with respect to peroxide (1). At total pressure below 1 atm the initiating step is pressure-dependent,

[1] $$H_2O_2 + M \rightarrow 2\,OH + M$$

(M = any heat bath molecule) and therefore [1] represents a unimolecular reaction at the low pressure limit (2). There is general agreement that reaction 1 is followed by

[2] $$OH + H_2O_2 \rightarrow HO_2 + H_2O$$

Since the overall reaction is $H_2O_2 \rightarrow H_2O + \frac{1}{2}O_2$, a reaction step producing oxygen is needed. One possibility (3)

$$HO_2 + H_2O_2 \rightarrow OH + H_2O + O_2$$

must be rejected because, contrary to experiment, it would (*i*) lead to order 3/2 in peroxide; and (*ii*) make the decomposition a chain reaction. A better alternative is

[3] $$OH + HO_2 \rightarrow H_2O + O_2$$

or

[4] $$2\,HO_2 \rightarrow H_2O_2 + O_2$$

A simple mechanism for the thermal decomposition of hydrogen peroxide would then consist of reactions 1, 2, and 3 (Mechanism A), or of reactions 1, 2, and 4 (Mechanism B); a more complicated mechanism would comprise all four reactions 1, 2, 3, and 4 (Mechanism C). If a stationary concentration of OH and HO_2 radicals is maintained throughout the reaction,[3] it is easy to show that all three mechanisms lead to $-d[H_2O_2]/dt = 2k_1[H_2O_2][M]$ (square brackets represent concentrations), which is fortunate insofar as the determination of k_1 from rate data is concerned, but at the same time this makes the three mechanisms kinetically indistinguishable if, as is usually the case, the reaction is followed by analysis for peroxide or manometrically.

[1]Present address: INRS-Eau, Université du Québec, C.P. 7500, Québec G1V 4C7.

[2]Revision received October 23, 1973.

[3]According to Troe (7), stationary concentration of OH and HO_2 is maintained at all temperatures below 1200 °K when $[H_2O_2]^0 \sim 10^{-4}$ mol/l.

Can. J. Chem. Downloaded from www.nrcresearchpress.com by 210.87.254.40 on 09/05/12
For personal use only.

Can. J. Chem. Downloaded from www.nrcresearchpress.com by 210.87.254.40 on 09/05/12
For personal use only.

In the absence of direct experimental evidence, the choice between the mechanisms has been made in the past on the basis of various uncertain arguments; thus one of the authors (2) has favored mechanism A at one time, while others (4, 5) have favored mechanism B, and still others (6, 7) have considered the more complicated mechanism C.

We have reported recently (8) on a mass-spectrometric study of the peroxide pyrolysis in the presence of M = water. The rate constant k_1 was obtained from the time dependence of mass peak at $m/e = 34$ (hydrogen peroxide), but in the process the whole mass spectrum was scanned, so that we could detect, in principle at least, every molecular species or radical in the reacting system if present in amounts exceeding its detection threshold.

The possibility of measuring radical concentrations in the course of the pyrolysis of H_2O_2 makes the mass spectrometric study particularly attractive for distinguishing among the mechanisms. While all three mechanisms lead to the same steady-state concentration of the OH radical ($\sim 10^{-11}$ mol/l at 754 °K), they lead to sufficiently different steady-state concentrations of the radical HO_2 to make the difference among the mechanisms detectable. It is not difficult to show that Mechanism A leads to a steady-state concentration of HO_2 given by

$$[5] \qquad [HO_2]_{s.s.} = k_2[H_2O_2]/k_3$$

while Mechanism B leads to

$$[6] \qquad [HO_2]_{s.s.} = \{(k_1[H_2O_2][M])/k_4\}^{1/2}$$

Mechanism C cannot be solved in closed form; it yields

$$[7] \qquad [HO_2]_{s.s.} = \{(k_1[H_2O_2][M][OH]_{s.s.} - k_2[H_2O_2])/k_4\}^{1/2}$$

where $[OH]_{s.s.}$ is the solution of

$$[8] \qquad 2k_1[H_2O_2][M] - \frac{k_3}{k_4^{1/2}}[OH](k_2[H_2O_2][OH] - k_1[H_2O_2][M])^{1/2} - k_2[H_2O_2][OH] = 0$$

which must be obtained numerically.

The various rate constants are reasonably well known; given below are their values in l mol^{-1} s^{-1} at 754 °K, a typical temperature of our experiments. From our previous work (8, eq. 18), we have $k_1(=a_2/2) = 42.9$ for M = water. The recommended expression for k_2 is (9) 10^{10} exp $(-1800/RT)$, which works out to 3×10^9. Two independent determinations (10, 11) give, at 300 °K, $k_4 \sim 2 \times 10^9$. This reaction is believed to have an activation energy of less than 2 kcal/mol (1), and therefore we have used $k_4 = 4.9 \times 10^9$, calculated from the 300 °K value on the assumption that the activation energy is 1 kcal/mol.

The value of k_3 is crucial to our argument, and therefore is discussed here at some length. Kaufman (12) estimated $k_3 \geqslant 6 \times 10^9$ at 300 °K, based on the work of Foner and Hudson (10) in which HO_2 was generated by an electrodeless discharge in H_2O_2. Troe (7) followed the u.v. absorption spectrum of HO_2 in the course of the thermal dissociation of H_2O_2 in a shock tube and found $10^9 < k_3 < 10^{10}$ at ~ 1400 °K. Peeters and Mahnen (13) determined by mass spectrometric sampling from lean methane–oxygen flames $k_3 \sim 5 \times 10^{10}$ at ~ 1600 °K, a value estimated to be good within a factor of two. Day, Thompson, and Dixon-Lewis (14) found from the kinetic analysis of burning velocities in hydrogen–oxygen flames $k_3 \leqslant 7 \times 10^{10}$ at 900 °K. Assuming, as seems reasonable, that reaction 3 has only a small activation energy (~ 1 kcal/mol or less), the three determinations of k_3 in the thermal systems are all compatible with the value $k_3 \sim 10^{10}$ at 754 °K. In sharp contrast, Hochanadel *et al.* (15) obtained $k_3 \sim 10^{11}$ at 298 °K in a photolytic system in which HO_2 was generated in the three-body process $H + O_2 + M \rightarrow HO_2 + M$. The reasons for the discrepancy between the values of k_3 obtained in thermal systems and in the photolytic system are not clear; possibly the high exothermicity of the HO_2-generating reaction in the photolytic system is at least partially responsible. Inasmuch as our own work concerns a thermal system, we shall use the thermal value $k_3 \sim 10^{10}$ at 754 °K. Finally, under our conditions,[4] $[M] \simeq [H_2O] = 30$ Torr $(=6.38 \times 10^{-4}$ mol/l) and $[H_2O_2] = 1.5$ Torr $(=3.2 \times 10^{-5}$ mol/l), which is actually

[4]For initial rates, [M] is actually a weighted sum of the concentrations of reactant and inert gas, but since the collisional efficiency of water is almost equal that of peroxide (2), we can put $[M] \simeq [H_2O]$ since under our conditions $[H_2O_2]^0 \ll [H_2O]$.

Can. J. Chem. Downloaded from www.nrcresearchpress.com by 210.87.254.40 on 09/05/12
For personal use only.

the initial concentration of peroxide, since our measurements refer essentially to initial rates. We can therefore replace $[H_2O_2]$ in eqs. 5 to 8 by $[H_2O_2]^0$, where the superscript 0 indicates initial concentration.

With the above numerical values of the various terms, the results for $[HO_2]_{s.s}$ (at 754 °K, in mol/l) calculated from eqs. 5–7 for the three mechanisms are

Mechanism A

$$[9] \qquad 1.92 \times 10^{-5} = 0.3\,[H_2O_2]^0$$

Mechanism B

$$[10] \quad 1.3 \times 10^{-8} = 4.2 \times 10^{-4}\,[H_2O_2]^0$$

Mechanism C

$$[11] \quad 1.3 \times 10^{-8} = 4.2 \times 10^{-4}\,[H_2O_2]^0$$

Two conclusions are immediately apparent: (*i*) Mechanism A leads to a very much larger stationary concentration of HO_2 than the other two; (*ii*) Mechanisms B and C yield similar values of $[HO_2]_{s.s.}$. The same conclusions apply throughout the temperature range of our experiments (717–754 °K). It is noteworthy that even if we had used Dixon-Lewis' (14) upper limit $k_3 \sim 7 \times 10^{10}$, $[HO_2]_{s.s.}$ in Mechanism A would still be some 10^2 times larger than the stationary concentration of HO_2 in Mechanism C, since the result [11] is quite insensitive to the value of the ratio $k_3/k_4^{1/2}$; the result [10] of course does not depend on k_3 at all. Hence the disparity of several orders of magnitude between $[HO_2]_{s.s.}$ in Mechanism A on the one hand, and in Mechanisms B and C on the other, is still true even if the uncertainty in the thermal value of k_3 is considered.

Insofar as the mass spectrometric analysis is concerned, the interesting species is therefore HO_2 which gives rise to a signal at $m/e = 33$. In a reacting mixture, the total signal at $m/e = 33$ arises from two sources: (*i*) by ionization of the HO_2 radical, and (*ii*) by fragmentation of the hydrogen peroxide ion. For a given adjustment of the mass spectrometer, the contribution from source (*ii*) is a fixed fraction of the signal at $m/e = 34$, characteristic of the mass spectrum of H_2O_2, and therefore is known if the mass spectrum of the *non-reacting* hydrogen peroxide is determined in a separate experiment under instrumental conditions identical to those used in studying reactive mixtures.

We have determined the mass spectrum of hydrogen peroxide at 42 °C, at which temperature the H_2O_2 does not measurably decompose, and found the signal at $m/e = 33$ to be $(6.8 \pm 0.1)\%$ (standard error) of the signal at $m/e = 34$ (8, Table 1); we assume that the ratio of the two signals at $m/e = 34$ and $m/e = 33$ remains the same in the temperature range 440–480 °C (717–754 °K) where the thermal decomposition of H_2O_2 was studied. On this assumption, any signal in a reactive mixture at $m/e = 33$ that exceeds 6.8% of the signal at $m/e = 34$ is assigned to HO_2 produced by the thermal decomposition of H_2O_2. The sensitivity of our apparatus was such that a signal at $m/e = 33$ that was 1% of the signal at $m/e = 34$ should be readily detectable. If we further assume that the cross-section for ionization of HO_2 is substantially the same as that for the ionization of H_2O_2, we could detect $[HO_2]_{s.s.} \gtrsim 0.01\,[H_2O_2]^0$.

A total of 45 experiments on reactive mixtures in the temperature range between 440–480 °C were analyzed, with $[H_2O]$ varied between 20 and 40 Torr. In each run the signals at $m/e = 34$ and $m/e = 33$ were recorded for the first minute or so, and their ratio calculated. In *no* case could we detect *any* increase in the signal at $m/e = 33$ above the 6.8% level of signal at $m/e = 34$, which rules out immediately Mechanism A which predict $[HO_2]_{s.s.}$ about 30 times higher than our detection limit. Even if the cross-section for ionization of HO_2 were ten times smaller than assumed, or if k_3 were 10 times larger, this would still make $[HO_2]_{s.s.}$ of Mechanism A about 3 times larger than our detection limit. The experimental finding is however, quite consistent with the result [10] or [11] which predicts $[HO_2]_{s.s.}$ well below our detection limit.

The radical OH yields a signal at $m/e = 17$, but in our system this could not be used for the measurement of $[OH]_{s.s.}$ because of interference from hydrogen peroxide and the omnipresent water.

The conclusion is therefore inescapable that, at least under our experimental conditions, Mechanism A leads to an unreasonably large steady-state concentration of HO_2, and therefore the pyrolysis of hydrogen peroxide is better described by Mechanisms B or C. In view of the very similar numerical results obtained for the last two mechanisms, it appears that even the very simple Mechanism B provides an entirely adequate quantitative description of the process.

Financial support for this work from the National Research Council of Canada and the Defence Research Board is gratefully acknowledged.

1. M. VENUGOPALAN and R. A. JONES. Chemistry of dissociated water vapor and related systems. Interscience–Wiley, New York. 1968. Chapt. 4.
2. W. FORST. Can. J. Chem. **36**, 1308 (1958).
3. C. N. SATTERFIELD and T. W. STEIN. J. Phys. Chem. **61**, 537 (1957).
4. D. E. HOARE, J. B. PROTHEROE, and A. D. WALSH. Trans. Faraday Soc. **55**, 548 (1959).
5. R. R. BALDWIN and D. BRATTAN. Eighth Symposium Int. on Combustion. The Williams and Wilkins Co., Baltimore. 1962. p. 110.
6. P. A. GIGUÈRE and I. D. LIU. Can. J. Chem. **35**, 283 (1957).
7. J. TROE. Ber. Bunsenges. **73**, 946 (1969).
8. A. TESSIER and W. FORST. Int. J. Mass Spectrom. Ion Phys. **7**, 281 (1971).
9. D. L. BAULCH, D. D. DRYSDALE, and A. C. LLOYD. Evaluated kinetic data for high temperature reactions, Vol. 1. The Chemical Rubber Co., Cleveland. 1972. p. 193.
10. S. N. FONER and R. L. HUDSON. Adv. in Chem. **36**, 42 (1962).
11. T. T. PAUKERT and H. S. JOHNSTON. J. Chem. Phys. **56**, 2824 (1972).
12. F. KAUFMANN. Ann. Geophys. **20**, 106 (1964).
13. J. PEETERS and G. MAHNEN. Fourteenth Symposium Int. on Combustion. The Combustion Institute, Pittsburgh, Pennsylvania. 1973. p. 133.
14. M. J. DAY, K. THOMPSON, and G. DIXON-LEWIS. Fourteenth Symposium Int. on Combustion. The Combustion Institute, Pittsburgh, Pennsylvania. 1973. pp. 47, 143.
15. C. J. HOCHANADEL, J. A. GHORMLEY, and P. J. OGREN. J. Chem. Phys. **56**, 4426 (1972).

Can. J. Chem. Downloaded from www.nrcresearchpress.com by 210.87.254.40 on 09/05/12
For personal use only.

Reactions of Functionalized 1,3-Dipoles

J. W. LOWN AND B. E. LANDBERG

Department of Chemistry, University of Alberta, Edmonton, Alberta

Received September 24, 1973

A new synthetic approach to the formation of 5–5, 5–6, 5–5–5, and 6–5–6 fused heterocycles employing cycloadditions with functionalized dipoles is described and its scope and utility explored through representative examples. The regiochemistry and stereochemistry of the additions is established by specific deuterium labelling, n.m.r. spectroscopy, and by chemical means.

On décrit une nouvelle approche synthétique à la formation des hétérocycles condensés 5–5, 5–6, 5–5–5 et 6–5–6; la généralité et l'utilité de cette méthode impliquant des cycloadditions de dipoles fonctionnalisés est examiné par l'intermédiaire d'exemples représentatifs. La régiosélectivité et la stéréochimie des additions est établie à l'aide de marquage par le deutérium de façon spécifique, par r.m.n. et par des moyens chimiques. [Traduit par le journal]

Can. J. Chem., **52**, 798 (1974)

The general 1,3-dipolar addition reaction developed and systematized by Huisgen (1) and illustrated in eq. 1 is of considerable utility for the rational synthesis of a wide variety of monocyclic heterocycles. We previously extended this

[1] 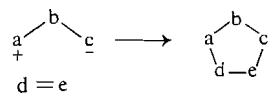

basic reaction to a scheme for the preparation of linked heterocycles (2) as illustrated in eq. 2 via consecutive condensation and 1,3-dipolar addition. A similar general synthetic scheme for the

[2] 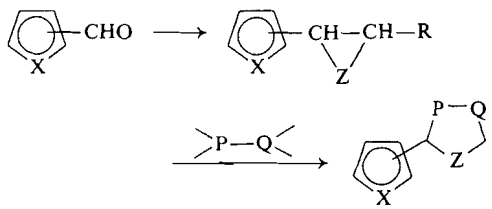

preparation of fused ring heterocycles would be a valuable extension of the general cycloaddition principle. One approach we wish to explore in this paper is the scope of the reactions of 1,3-dipoles bearing additional functionality (*i.e.* besides their basic 4π electron reactive system) to form bicyclic heterocycles, as shown in eq. 3. The additional functionalities f and g on the 1,3-dipole and dipolarophile, respectively, should give the potential second fused five- or six-membered ring provided the reaction has the desired regiochemistry and stereochemistry. Indications of the usefulness of this approach had been obtained during an examination of the

[3] 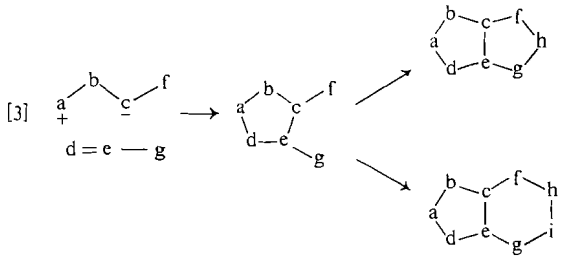

thermal decomposition of 3-aroylaziridines in acetonitrile (3, 4) and in their reaction with *p*-nitrosophenols (4) when 3,5-dihydro-2*H*-pyrrolo[3,4-*d*]oxazoles were obtained in good yield.

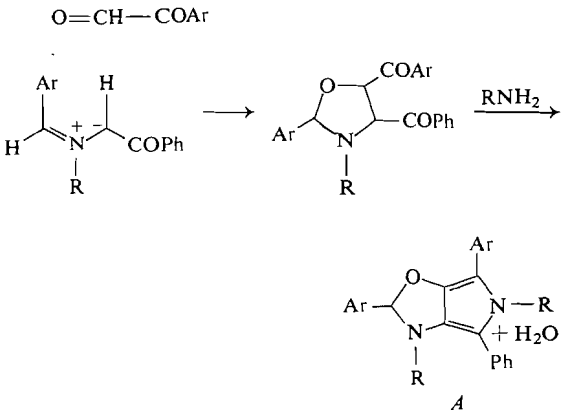

A

Our initial approach to systematize these findings has been to examine the reaction of aroylazomethine ylides (generated by the thermal electrocyclic cleavage of aziridines) with a range of suitably functionalized dipolarophiles). Exploratory reactions of azomethine oxides (nitrones) are also discussed in this context.

Can. J. Chem. Downloaded from www.nrcresearchpress.com by 210.87.254.105 on 09/05/12
For personal use only.

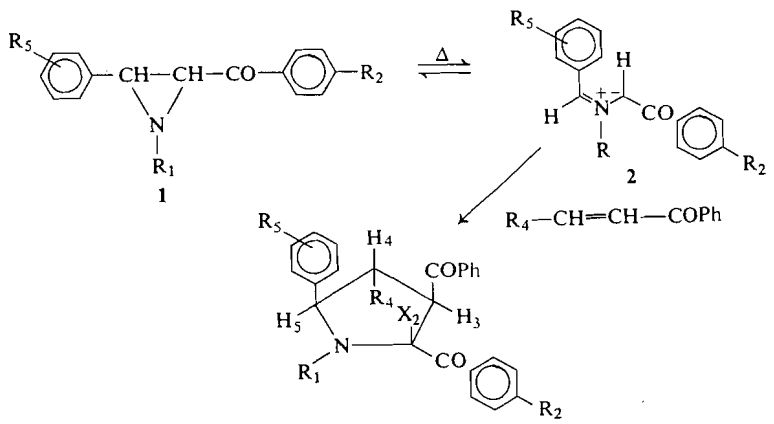

a	$R_1 = C_6H_{11}$;	$R_2 = OCH_3$;	$R_4 = mNO_2C_6H_4$;	$R_5 = H$;	$X_2 = H$
b	$R_1 = C_6H_{11}$;	$R_2 = OCH_3$;	$R_4 = C_6H_5$;	$R_5 = H$;	$X_2 = H$
c	$R_1 = C_6H_{11}$;	$R_2 = H$;	$R_4 = mNO_2C_6H_4$;	$R_5 = H$;	$X_2 = H$
d	$R_1 = (CH_3)_2CH—$;	$R_2 = H$;	$R_4 = mNO_2C_6H_4$;	$R_5 = mNO_2$;	$X_2 = H$
e	$R_1 = (CH_3)_2CH—$;	$R_2 = H$;	$R_4 = mNO_2C_6H_4$;	$R_5 = mNO_2$;	$X_2 = D$
f	$R_1 = (CH_3)_2CH—$;	$R_2 = H$;	$R_4 = pOCH_3C_6H_4$;	$R_5 = mNO_2$;	$X_2 = H$
g	$R_1 = (CH_3)_2CH—$;	$R_2 = H$;	$R_4 = C_6H_5$;	$R_5 = mNO_2$;	$X_2 = H$

SCHEME 1

Aroylazomethine Ylides and Aroylalkenes (Chalcones)

Regiochemistry of the Additions

Reaction of aziridine (**1***a*) with chalcone (**2***a*) in refluxing toluene afforded pyrrolidine (**3***a*) in 50% yield. The n.m.r. spectra of the pyrrolidines **1***a–g* showed the expected ABCD pattern for the methine protons, the chemical shifts and coupling constants of which were obtained by double irradiation experiments (see Table 1). These assignments received confirmation by a parallel experiment with specifically 3-deuterium labelled aziridine (5) (**1***e*). The n.m.r. methine pattern of the corresponding pyrrolidine (**3***e*) showed the 5.58 δ signal diminished (H_2) and the 4.01 δ signal simplified to a doublet confirming its assignment as H_3. The previous double irradiation experiments therefore confirmed 3.73 δ as H_4 and 5.15 δ as H_5.

Potassium carbonate catalyzed exchange of pyrrolidine (**3***a*) with deuterium oxide provided added confirmation in that the 4.01 δ (H_3) (α to a carbonyl group) was completely exchanged. As expected the 5.46 doublet became a singlet (H_2) after the exchange while the H_4 and H_5 signals were simplified to an AB quartet centered at 3.59 and 4.99, $J = 4$ Hz by this process. The preferential base catalyzed deuterium exchange of H_3 is characteristic of these pyrrolidines (8) (see also later examples).

The regiochemistry of the 1,3-dipolar additions indicated by the double resonance and deuterium labelling experiments received chemical confirmation by the cyclodehydration of (**3***c*) with polyphosphoric acid to the dihydrofuro-[3,4-*b*]pyrrole **4**, illustrating the potential for the synthesis of fused heterocycles, as shown in Scheme 2. All the 2,3-dibenzoylpyrrolidines gave mass spectral parent peaks of ($M - H_2O$) *i.e.* of ready loss of water to form the fused furan structure in the ion beam.

Stereochemistry of the Additions

It was necessary to establish the stereochemistry of the additions so that the relative positions of the reactive groupings at C_2 and C_3 may be known since this will dictate the method to be selected in constructing a fused six-membered ring.

Stereochemical assignment of the cycloadducts was made on the basis of chemical evidence in conjunction with p.m.r. spectroscopy; the observed coupling constants are consistent with the Karplus correlation (7) and with other model pyrrolidines (6).

Previous experience in the electrocyclic conrotatory generation of azomethine ylides from 3-aroylaziridines has established that the stereoisomeric azomethine ylides equilibrate to the more stable *trans* form prior to cycloadditon (8).

Can. J. Chem. Downloaded from www.nrcresearchpress.com by 210.87.254.105 on 09/05/12
For personal use only.

TABLE 1. Double irradiation experiments on pyrrolidines at 100 MHz

Compound	Proton irradiated	Decoupling frequency (Hz)	Lines collapsed: Original form	Lines collapsed: Final form	Measured remaining coupling (Hz)
3b	H_4	337	d 4.95(H_5)	s	—
	H_3	403	t 3.25(H_4)	d	J_{45} = 8.4
	H_3	403	d 5.66(H_2)	s	J_{34} = 7.5
	H_5	506	t 3.25(H_4)	d	J_{34} = 7.5
	H_2	576	d of d 3.96(H_3)	d	J_{23} = 3.4
5A	H_4	424	d of d 4.50(H_3)	d	J_{23} = 2.0
	H_4	424	d 5.05(H_5)	s	—
	H_3	454	d of d 4.19(H_4)	d	J_{45} = 5.0
	H_3	454	d 5.54(H_2)	s	J_{45} = 5.0
	H_5	511	d of d 4.19(H_4)	d	J_{34} = 3.5
	H_2	559	d of d 4.50(H_3)	d	J_{34} = 3.5
3a	H_5	509	t 3.68(H_4)	d	J_{34} = 7.5
	H_2	561	d of d 4.01(H_3)	d	J_{23} = 3.2
3d	H_4	316	d 5.15(H_5)	s	—
	H_3	405	d 5.58(H_2)	s	—
	H_5	519	t 3.73(H_4)	d	J_{43} = 6.5
	H_2	562	d of d 4.01(H_3)	d	J_{23} = 3.5

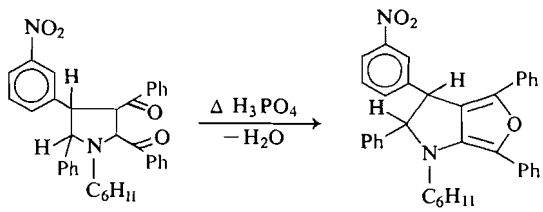

3c **4**

SCHEME 2

This combined with the *trans* geometry of the chalcones and the known regiochemistry provides for only two possible geometries **3***A* or **3***B*.

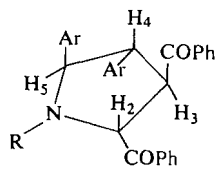

3A

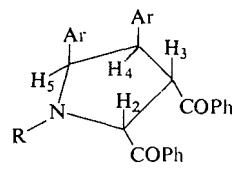

3B

The vicinal coupling constants determined from double irradiation are J_{23} = 3, J_{34} = 7.5, and J_{45} = 8.4 Hz. Other model pyrrolidines formed by reaction with *trans*-dibenzoylethylene (see below) in which J_{23} = 7 Hz was assigned a *cis* geometry because of the rapid and characteristic condensation with hydrazine to form fused dihydropyridazine structures. The lack of reaction of the pyrrolidines obtained in the present case combined with a J_{23} = 3 Hz established the *trans–trans–trans* structure **3***A* as the correct stereoisomer. The failure to epimerize upon treatment with sodium methoxide in methanol despite the rapid deuterium exchange indicates this is also the most stable stereoisomer.

Aroylazomethine Ylides with trans-Dibenzoylethylene

Reaction of aziridines with *trans*-dibenzoylethylene afforded two stereoisomeric pyrrolidines (**5***A* and *B*) which were separable by column

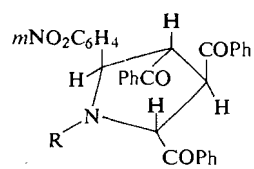

5A

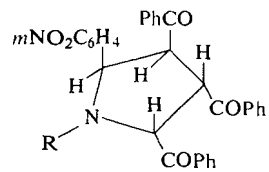

5B

a R = C_6H_{11}
b R = $(CH_3)_2CH$–

chromatography and recrystallization. One isomer shows an n.m.r. coupling constant of J_{23} = 7 Hz signifying a *cis* vicinal coupling in the *cis–trans–cis* structure (**5***B*). The second isomer displays a J_{23} = 2 Hz which is ascribed the *trans–trans–trans* structure (**5***A*). These assignments were confirmed chemically when pyrrolidine **5***B*, having the required *cis* arrangement for

Can. J. Chem. Downloaded from www.nrcresearchpress.com by 210.87.254.105 on 09/05/12
For personal use only.

Can. J. Chem. Downloaded from www.nrcresearchpress.com by 210.87.254.105 on 09/05/12
For personal use only.

the 2- and 3-benzoyl groups, reacted readily with hydrazine to form **6**. Both the mass spectrum and n.m.r. spectrum confirmed a composition of $C_{34}H_{32}N_4O_3$, *i.e.* corresponding to the addition of two hydrogens to the primary condensation product **7**. Since excess hydrazine was used in

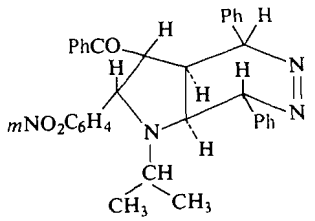

6

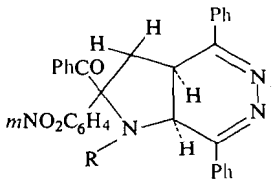

7

the reaction and since no NH absorption may be detected in the i.r. spectrum this indicates that the initial product **7** is further subject to a 1,4 reduction by hydrazine to give **6**. The stereoisomeric pyrrolidine **5***a*, having benzoyl groups in an all *trans* arrangement as expected failed to react with hydrazine.

Potassium carbonate catalyzed exchange with deuterium oxide resulted in the complete exchange of protons H_3 and H_4 only, when H_2 became a singlet at 5.58 and H_5 became a singlet

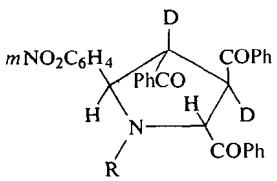

a R = C_6H_{11}
b R = $(CH_3)_2CH$—

5*c*

at 5.12 δ. Symmetrical 2,3-dibenzoylaziridines reacted with *trans*-dibenzoylethylene to give pyrrolidines **8***a* and *b*. In the case of **8***a* a single stereoisomeric pyrrolidine is obtained and assigned the *cis–trans–cis* stereochemistry (**8***aB*) since treatment with excess of hydrazine afforded **9**. In the case of **8***b* two stereoisomeric pyrrolidines were obtained, the major form of which, m.p. 183°, was assigned the

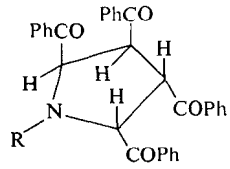

8*A*

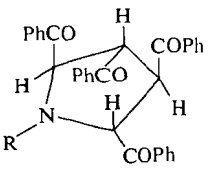

8*B*

a R = C_6H_{11}
b R = $CH_2C_6H_5$

cis–trans–cis stereochemistry because of the close similarity of the n.m.r. spectrum with that of **8***aB*, and the second minor isomer was ascribed the *trans–trans–trans* structure (**8***bA*). Treatment of the 2,3,4,5-tetrabenzoyl-1-benzylpyrrolidine with cyclohexylamine in methanol gave the tetraphenyldipyrrolo-[3,4-*b*:3′,4′-*d*]pyrrole (**10**) in 87% yield (4).

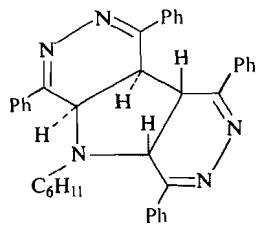

9

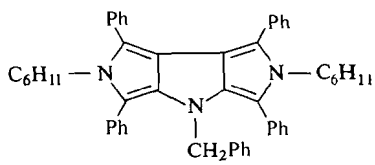

10

Aroylazomethine Ylides and Aroylalkynes

Aziridine **1***d* reacts with dibenzoylacetylene to give pyrroline **11***a* and (when the reaction is not carried out under nitrogen) some of the corresponding pyrrole **12**. Structure **11***a* is

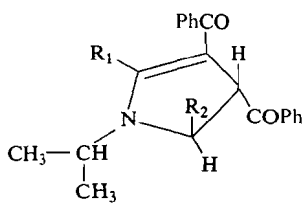

11

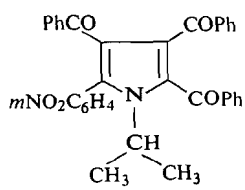

12

a R_1 = COPh, R_2 = $mNO_2C_6H_4$
b R_1 = $mNO_2C_6H_4$, R_2 = COPh

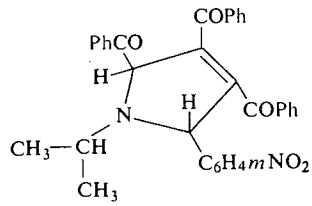

13

Ar = mNO$_2$C$_6$H$_4$

favored over the alternative 3-pyrroline form (**13**) since the compound is recovered unchanged after treatment with sodium methoxide in methanol indicating it is the more stable isomer (6). The isomeric 2-pyrroline structure **11***b* was also discounted because (*a*) the methine *trans* coupling constant 2.5 Hz is consistent with those found in analogous structures (6); (*b*) of the failure of an attempted Paal–Knorr reaction with cyclohexylamine in contrast to *e.g.* **3***c*, **8***b*; and (*c*) the position of the isopropyl methine 3.70 δ is also consistent with a 2-pyrroline structure, since the corresponding position for a 3-pyrroline *N*-isopropyl methine is found to be *ca.* 3 p.p.m. (2).

Although the n.m.r. spectrum of **11** shows a singlet for the methine protons at 4.93 δ, application of the Europium shift reagent resulted in the selective diamagnetic shift of one methine so that an AB pattern centered at 6.45 and 5.30 p.p.m., J = 2.5 Hz, resulted. This selective shift suggests the methines are in substantially different environments favoring pyrroline **11** over pyrroline **13** (*N.B.* contrast example **14**). The evident preference for formation of the 2-pyrroline isomer during cycloaddition is indicated by reaction of 1-isopropyl-2,3-dibenzoylaziridine with dibenzoylacetylene to form **14**. The structural assignment is supported by its lack of isomerization with sodium methoxide in methanol ruling out a 3-pyrroline structure (6) even though the methines appear as a singlet at 6.20 δ. Application of the Europium shift reagent resulted in complexing to the 4,5-carbonyls with a resultant shift of the methines *as a singlet* to δ 6.84. This result, in contrast to the previous case, points to the methines being in a closely similar chemical environment.

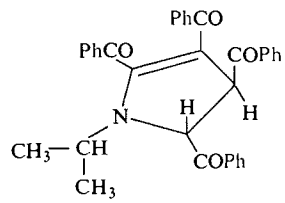

14

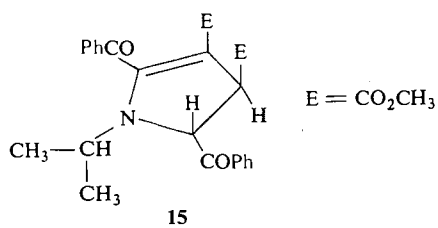

15

Another indication of the 2-pyrroline form is the characteristic position of the isopropyl methine at 4.25 δ. A similar formation of a 2-pyrroline is observed in the reaction of the same aziridine with dimethyl acetylenedicarboxylate to give pyrroline **15**. In the reaction of 1-isopropyl-2,3-dibenzoylaziridine with 1,3-diphenylpropynone preferential formation of the kinetically controlled cycloaddition product, the 3-pyrroline **16** was observed. Treatment of **16**

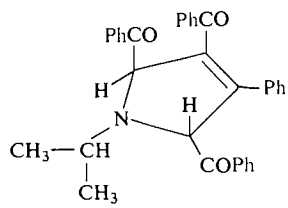

16

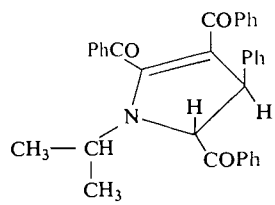

17

with sodium methoxide in methanol resulted in isomerization to the more stable 2-pyrroline **17**, assigned the *trans* geometry since the methines appeared as singlets. The question of the regiochemistry of unsymmetrical acetylenic dipolarophiles could be determined by examining the reaction of aziridine **1***d* with benzoylstyrene. In this case the initially formed pyrroline is oxidized *in situ* to the pyrrole **18**. The latter was related

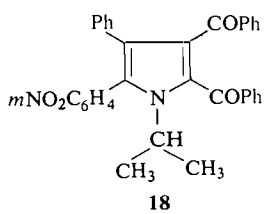

18

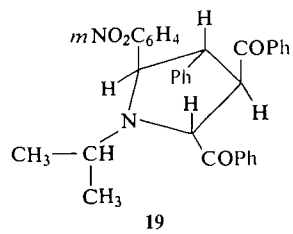

19

structurally to the corresponding chalcone adduct **19**, the regiochemistry and stereochemistry of which has previously been established. Controlled dehydrogenation of pyrrolidine **19** with *p*-chloranil (9) gave initially the pyrroline **20**. Further treatment of compound **20** with *p*-

Can. J. Chem. Downloaded from www.nrcresearchpress.com by 210.87.254.105 on 09/05/12
For personal use only.

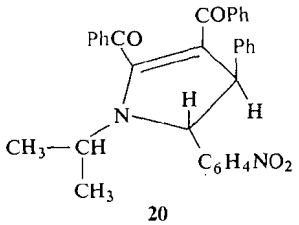

20

chloranil gave the pyrrole **18** obtained from benzoylstyrene.

Aroylazomethine Ylides with Imidodipolarophiles

Imine dipolarophiles are not normally very reactive, however when polarized by an adjacent group, say arylsulfonyl, we have found their 1,3-dipolar reactivity to be substantially enhanced (5). Thus reaction of aziridine **1***d* with the benzoylsulfonylimine gave the fused bicyclic structure **21** formed by spontaneous Paal–Knorr ring

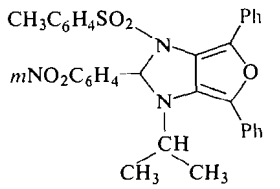

21

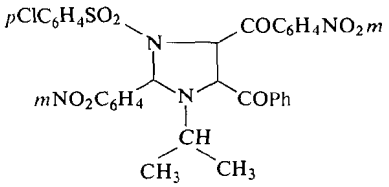

22

closure of the initially formed imidazolidine and the accompanying generation of water results in some hydrolysis of the sulfonylimine to the *p*-toluenesulfonamide.

Reaction of aziridine **1***d* with the *m*-nitrobenzoylsulfonylimine took a different course in that the product imidazolidine **22** had not cyclized but had suffered a partial base-catalyzed elimination of the arylsulfinic acid group, so the 2-imidazoline **23** is isolated as well.

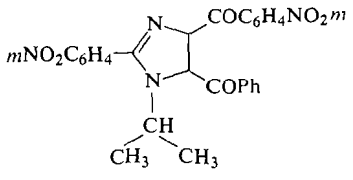

23

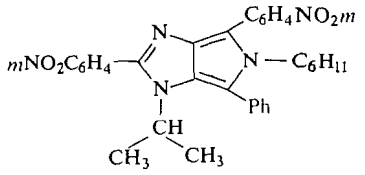

24

The regiochemistry of the addition and proposed structure of the imidazoline **21** was confirmed by the facile Paal–Knorr reaction with cyclohexylamine to give compound **22**. It may be noted that in the formation of fused heterocycles (*e.g.* **A**, **21**, **24**, **27**) by Paal–Knorr condensation, the reactions are considerably facilitated by having heteroatoms or other strongly polarizing groups adjacent to both aroyl groups. This is further exemplified in the following reactions with functionalized azomethine oxides. A second analogous set of examples is described in the Experimental section.

Aroylazomethineoxides with Dibenzoylethylene

The nitrone **25***a* readily underwent reaction with *trans*-dibenzoylethylene to give the isoxazolidine **26***a*. Paal–Knorr condensation took place

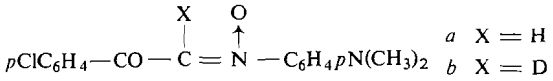

25

readily with isopropylamine to give the fused heterocycle **27**. The structural ambiguity with respect to this condensation was resolved by

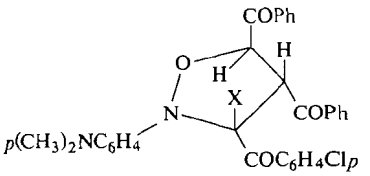

26

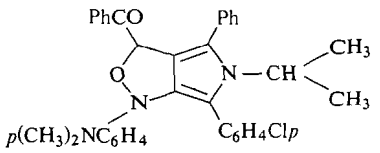

27

using specifically deuterium labelled nitrone **25***b* which reacted with *trans*-dibenzoylethylene to give the 3-*d* isoxazolidine **26***b*. Since treatment with isopropylamine also gave **27**, therefore the Paal–Knorr reaction occurs at positions 3 and 4

Can. J. Chem. Downloaded from www.nrcresearchpress.com by 210.87.254.105 on 09/05/12
For personal use only.

rather than positions 4 and 5. Hydrazine reacts readily with the *cis* vicinal aroyl groups of the isoxazolidine **26** (necessarily at positions 3 and 4) to give compound **28**. The representative ex-

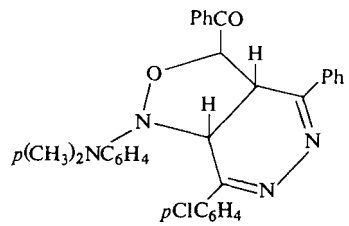

28

amples discussed in this paper serve to illustrate the potential of this approach towards a general synthesis of fused heterocycles. At present the principal limitation appears to be one of yield in many cases. However this is compensated for by the experimental convenience and simplicity and the accessibility of the starting materials.

Experimental

Melting points were determined on a Fisher-Johns apparatus and are uncorrected. The i.r. spectra were recorded on a Perkin-Elmer model 421 spectrophotometer and only the principal, sharply defined peaks are reported. The n.m.r. spectra were recorded on Varian A-60 and A-100 analytical spectrometers. The spectra were measured on approximately 10–15% (w/v) solutions in $CDCl_3$, with tetramethylsilane as a standard. Line positions are reported in p.p.m. from the reference. Mass spectra were determined on an Associated Electrical Industries MS-9 double focusing high resolution mass spectrometer. The ionization energy, in general, was 70 eV. Peak measurements were made by comparison with perfluorotributylamine at a resolving power of 15 000. Kieselgel DF-5 (Camag, Switzerland) and Eastman Kodak precoated sheets were used for t.l.c. Microanalyses were carried out by Mrs. D. Mahlow of this department.

Materials

(a) General Preparation of 3-Aroylaziridines

These compounds were prepared by established methods involving Aldol condensations to form chalcones followed by bromination to afford dibromochalcones and finally, treatment with primary amines to afford the aroylaziridines (10).

(b) Preparation of Aroyl N-Sulfonylimines

(*i*) *m*-Nitrophenylglyoxal methyl acetal was prepared by the method of Claisen (11) in 87% yield, b.p. 120°/2 mm (lit. b.p. 145–146°/9 mm).

(*ii*) The preparation of *N*-(*m*-nitrophenylglyoxal)-*p*-toluenesulfonamide is typical of the preparation of other aroyl *N*-sulfonylimines and the procedure is due to Kresze and co-workers (12).

A mixture of 7.30 g (32 mmol) of *m*-nitrophenylglyoxalmethyl acetal and 5.56 g (32.5 mmol) of *p*-toluenesulfonamide was heated with stirring to 150° for 1 h during which time methanol was evolved. Upon cooling the residual oil solidified and the product was purified by recrystallization from toluene–dioxan, m.p. 205–208°, 5.5 g (53% yield).

Anal. Calcd. for $C_{15}H_{12}N_2O_5S$ (mol. wt. 332.26): C, 54.22, H, 3.64; N, 8.43. Found (332, mass spectrum): C, 54.44; H, 4.3; N, 8.21.

The n.m.r. spectrum δ TMS ($CDCl_3$): 2.32 (3H, s, CH_3); 6.25 (1H, s, methine); 7–9 (8H, m, aryl protons).

(c) Preparation of Nitrones

N-Benzoylmethylene-4-dimethylaminoaniline-*N*-oxide and similar nitrones were prepared by the procedure of Krohnke and Borner (13) and in this case yield 55%, m.p. 109–111° (lit. (13) m.p. 110–111°).

Cycloadditions of Aroylazomethine Ylides with Chalcones

(a) Reaction of 3-p-Anisoyl-1-cyclohexyl-2-phenylaziridine with 3-m-Nitrophenyl-1-phenyl-2-propen-1-one

This reaction is typical of a series of six reactions of 3-aroylaziridines with chalcones to form pyrrolidines which are summarized in Table 2. A solution of 3.35 g (10 mmol) of the aziridine and 2.53 g (10 mmol) of the chalcone in 50 ml of benzene was heated under reflux for 12 h. The solvent was removed *in vacuo* and the residual oil subjected to chromatography on 100 g of B.D.H. grade I alumina with benzene eluant. The first fraction upon concentration gave pyrrolidine **3***a* purified by recrystallization from hexane–benzene, m.p. 140–142° 2.90 g, (50% yield).

Mol. Wt. Calcd. for $C_{37}H_{36}N_2O_5$: 588.2624. Found (mass spectrum): 588.2630.

The i.r. spectrum ν_{max} ($CHCl_3$): 1670 cm^{-1} (C=O). The n.m.r. spectrum TMS ($CDCl_3$): 3.62 (1H, t, J_{34} = 7.5 Hz, J_{23} = 3 Hz, H_3); 5.05 (1H, d, J_{45} = 8.4 Hz, H_5); 5.66 (1H, d, J_{23} = 3.0 Hz, H_2).

Double irradiation experiments are summarized in Table 1. Pyrrolidine **3***a* (0.1 g) was subjected to deuterium exchange by heating under reflux in a mixture of 10 ml anhydrous dioxan and 10 ml of deuterium oxide with 0.1 g of potassium carbonate. The n.m.r. spectrum showed almost complete exchange of the proton giving rise to the 4.01 δ doublet of doublets and ascribed to H_3 (see Table 2).

(b) Reaction of 3-Benzoyl-3-deuterio-1-isopropyl-2-m-nitrophenylaziridine with 3-m-Nitrophenyl-1-phenyl-2-propen-1-one

A solution of 1.48 g, (4.8 mmol) of the deuterated (or undeuterated) aziridine and 1.26 g (4.9 mmol) of the chalcone in 50 ml of toluene was heated under reflux overnight, then the usual work-up procedure afforded pyrrolidine (**3***e*), 2.0 g (72% yield), m.p. 131–133° (CH_3OH).

Anal. Calcd. for $C_{33}H_{29}N_3O_6$ (mol. wt. 563.2056): C, 70.32; H, 5.19; N, 7.46. Found (563.2070, mass spectrum): C, 69.58; H, 5.05; N, 7.55.

The i.r. spectrum ν_{max} ($CHCl_3$) 1670 cm^{-1}. The n.m.r. spectrum δ TMS ($CDCl_3$), 0.9 (6H, d of d, J = 6 Hz; $(CH_3)_2CH$); 3.0 (1H, m, $(CH_3)_2CH$); 4.01 (1H, d of d, J_{23} = 6.5, 3.0 Hz, H_3); 5.15 (1H, d, J = 8.5 Hz, H_5); 5.58 (1H, d, J = 3.5 Hz, H_2). The n.m.r. spectrum of the deuterated sample showed the doublet at 5.58 δ is diminished in intensity (therefore H-2) and the quartet at 4.01 δ became a doublet (J = 6.5 Hz) (therefore H_3).

(c) Paal–Knorr Reaction with 1-Cyclohexyl-2,3-dibenzoyl-4-m-nitrophenyl-5-phenylpyrrolidine. Formation of a Furo[3,4-b]pyrrole

1-Cyclohexyl-2,3-dibenzoyl-4-*m*-nitrophenyl-5-phenyl-

Can. J. Chem. Downloaded from www.nrcresearchpress.com by 210.87.254.105 on 09/05/12
For personal use only.

Can. J. Chem. Downloaded from www.nrcresearchpress.com by 210.87.254.105 on 09/05/12
For personal use only.

TABLE 2. Pyrrolidines

No.	Melting point (°C)	Yield (%)	Found C	Found H	Found N	Found Molecular ion (mass spectrum	Calculated C	Calculated H	Calculated N	Calculated Molecular ion (mass spectrum)	Nuclear magnetic resonance spectrum (methines) H_2	H_3	H_4	H_5	J_{23}	J_{34}	J_{45}	Infrared spectrum ($CHCl_3$) C=O
3*a*[a]	140–142	50	—	—	—	588.2635	—	—	—	588.2624	5.66d	4.01q	3.68t	5.05d	3.0	7.5	8.4	1670
3*b*[a]	Oil	62	—	—	—	543.2770	—	—	—	543.2773	5.66d	3.96q	3.25t	4.95d	3.4	7.5	8.3	1665
3*c*	176–178	83	79.86	5.99	5.20	558.2520	79.93	5.95	5.17	558.2518	5.51d	3.92q	3.62t	4.99d	3.0	7.0	8.0	1670
3*d*	131–133	72	69.58	5.05	7.55	563.2070	70.32	5.19	7.46	563.2056	5.58d	4.01q	3.73t	5.15d	3.0	6.5	8.5	1670
3*f*	138–139	25	74.14	5.86	5.10	548.2506	74.43	5.88	5.11	548.2510	5.75d	3.99q	3.17t	5.08d	3.0	7.0	8.0	1665
3*g*	Oil	52	—	—	—	518.2201	—	—	—	518.2205	5.75d	4.02q	3.39t	5.12d	3.5	7.5	8.0	1670
5*Ab*	128–130	56	74.64	5.53	5.31	546.2161	74.71	5.53	5.13	546.2153	5.50d	4.50q	4.29q	5.09d	2.0	3.5	5.0	1662
5*Aa*	Oil	10	—	—	—	481(—COPh)	—	—	—	585	5.54d	4.50q	4.19q	5.05d	2.0	3.5	5.0	1660
5*Bb*	198–199	16	74.36	5.29	5.18	546.2159	74.36	5.29	5.18	546.2153	5.65d	5.19q	5.19q	5.29d	8.0	1.5	7.0	1660
5*Ba*	183–185	48	75.59	5.92	4.77	481.2120 (—COPh)	75.75	5.84	4.78	481.2126	5.58d	5.19q	4.99q	5.31d	7.5	1.5	6.5	1660
8*Aa*	228–230	62	79.77	6.15	2.77	464.2220 (—COPh)	80.11	6.19	2.76	464.2226	—multiplet—		(5.15–5.78)		—	—	—	1670

[a]Decomposes rapidly in light or air.

Can. J. Chem. Downloaded from www.nrcresearchpress.com by 210.87.254.105 on 09/05/12
For personal use only.

TABLE 3. Pyrrolines and pyrroles

No.	Melting point (°C)	Yield (%)	Found				Calculated				Nuclear magnetic resonance spectrum (methines)				Infrared spectrum ($CHCl_3$) C=O
			C	H	N	Molecular ion (mass spectrum)	C	H	N	Molecular ion (mass spectrum)	H_4	H_5	J_{45}	R1 Methine	
11	183–184	56	74.80	5.20	5.80	544.1992	74.98	5.18	5.14	544.1998	4.93(s) 6.45d, with Eu agent	5.30d	2.5	3.68	1660
12	Oil	35	—	—	—	542.1841	—	—	—	542.1832	—		—	4.58	1645
14	201–203	60	79.57	5.48	2.61	527.2090	79.67	5.54	2.66	527.2096		6.20(s)	—	4.20	1660
15	196–197	58	68.65	5.55	3.14	435.1671	68.95	5.79	3.22	435.1682		4.48(m)[a]	—	4.20	1665 1735
16	132–134	36	81.48	5.81	3.01	499.2159	81.74	5.85	2.80	499.2147	6.21(d)	6.52(d)	3.5[d]	3.35	1662
17	Oil	46	—	—	—	499.2150	—	—	—	499.2147	4.30(d)	5.25(d)	7.0	3.62	1660
18[c]	189–190	77	76.92	5.05	5.31	514.1901	77.02	5.09	5.44	514.1893	—		—	4.50	1630
20	140–141	80	75.97	5.47	5.52	516.2062	76.72	5.46	5.42	516.2049	4.40(d)	4.86(d)	5.0	3.60	1660
3*c*[b]	Oil	76	—	—	—	556.2370	—	—	—	565.2361	4.52(d)	4.79(d)	5.0	3.62	1662

[a] H_6 not evident, apparently obscured by aromatic protons.
[b] Obtained from dehydrogenation of the corresponding pyrrolidine.
[c] Obtained as oxidation product from cycloaddition of aziridine and alkene.
[d] J_{25}.

Can. J. Chem. Downloaded from www.nrcresearchpress.com by 210.87.254.105 on 09/05/12
For personal use only.

pyrrolidine (0.4 g, 7.2 mmol) was heated with 20 ml of polyphosphoric acid at 150° for 2 h. The reaction mixture was poured into ice water, extracted with benzene, and the benzene extract dried (Na_2SO_4). Removal of the solvents *in vacuo* gave 4-cyclohexyl-5,6-dihydro-6-*m*-nitrophenyl-4*H*-furo[3,4-*b*]pyrrole (4), 0.11 g (30% yield).

Mol. Wt. Calcd. for $C_{36}H_{32}N_2O_3$: (540.2413). Found (mass spectrum): 540.2419.

The n.m.r. spectrum δ TMS ($CDCl_3$): 4.35 (1H, d, J_{56} = 5.0 Hz, H_5), 4.95 (1H, d, J_{56} = 5.0 Hz, H_6).

Reaction of 3-Benzoyl-1-isopropyl-2-m-nitrophenylaziridine with trans-Dibenzoylethylene

A solution of 1.48 g (5 mmol) of the aziridine and 1.18 g (5 mmol) of *trans*-dibenzoylethylene in 50 ml of benzene was heated under reflux overnight. Monitoring of the reaction by t.l.c. (silica gel – benzene) showed the presence of two products. Removal of the solvent *in vacuo* and trituration of the residual oil with methanol gave a first crop of yellow crystals 0.43 g (16% yield) m.p. 198–199°. Concentration of the mother liquor afforded a second crop 1.50 g (56% yield) m.p. 128–130°. The stereoisomeric pyrrolidines **5***A* and *B* could also be separated by column chromatography (B.D.H. alumina–benzene) when the lower melting isomer was eluted first. This isomer was assigned the structure and stereochemistry **5***A* *i.e.* *trans–trans–trans*-1-isopropyl-5-*m*-nitrophenyl-2,3,4-tribenzoylpyrrolidine based on the n.m.r. spectrum (see Table 2) and on the double irradiation experiments performed on a close analog (*i.e.*, *N*-substituent is cyclohexyl rather than isopropyl) (see Table 3).

The higher melting stereoisomer was assigned the *cis–trans–cis* structure **5***B* based upon its chemical reactivity towards hydrazine and upon its n.m.r. spectrum which shows two characteristically larger *cis* vicinal couplings of J = 6 and 7 Hz, respectively, for the methine absorptions.

Base Catalyzed Deuterium Exchange of trans–trans–trans-1-Isopropyl-5-m-nitrophenyl-2,3,4-tribenzoylpyrrolidine

A solution of 0.1 g of **5***A* and 0.1 g of potassium carbonate in 20 ml of 1:1 dioxan – deuterium oxide was heated under reflux for 2 h. Nuclear magnetic resonance examination of the recovered material showed complete exchange of H_3 and H_4 leaving H_2 and H_5 as singlets at 5.58 and 5.12 δ, respectively.

Reaction of cis–trans–cis-1-Isopropyl-5-m-nitrophenyl-2,3,4-tribenzoylpyrrolidine with Hydrazine

A solution of 0.2 g (0.37 mmol) of pyrrolidine **5***B* and 0.5 ml of 95% hydrazine hydrate in 20 ml of methanol was heated under reflux for 1 h. Cooling resulted in precipitation of 0.11 g (55% yield) of 7-benzoyl *cis–cis–cis*-(1,4) (4a, 7a) (6,7)-hexahydro-5-isopropyl-1,4-diphenyl-6-*m*-nitrophenyl-5*H*-pyrrolo[2,3-*d*]pyridazine (**6**) m.p. 85°.

Mol. Wt. Calcd. for $C_{34}H_{32}N_4O_3$: 544.2474. Found (mass spectrum): 544.2470.

The i.r. spectrum ν_{max} ($CHCl_3$) 1660 cm^{-1} (C=O). The n.m.r. spectrum δ TMS ($CDCl_3$): (methines) 4.33 (1H, d, J = 7.5 Hz), 4.52 (1H, d, J = 7 Hz); 4.82 (2H, s,); 5.29 (1H, d, J = 5.0 Hz), 5.49 (1H, d, J = 5.5 Hz).

Reaction of 1-Cyclohexyl-2,3,4,5-tetrabenzoylpyrrolidine with Hydrazine

A solution of 0.157 g (0.266 mmol) of pyrrolidine **8***A* and 0.03 ml (0.532 mmol) of hydrazine in 20 ml of methanol was heated under reflux for 2 h during which time a precipitate formed of 5-cyclohexyl-*cis-cis*-(1a,4a) (5a,9a)-tetrahydro-1,4,6,9-tetraphenyl-5*H*-dipyridazino-[4,5-6,4′,5′-*d*]pyrrole (**9**) 0.07 g (46% yield) m.p. 85–90°.

Anal. Calcd. for $C_{38}H_{35}N_5$ (mol. wt. 561.2892): C, 81.25; H, 6.28; N, 12.47. Found (561.2906, mass spectrum): C, 81.24; H, 5.91; N, 12.28.

The i.r. spectrum ν_{max} ($CHCl_3$) 1669 cm^{-1} (C=N); n.m.r. δ TMS ($CDCl_3$): 1–2 (1H, m, C_6H_{11}), 5.2 (4H, m, methines), 7–8 (20H, m, Ar-H).

Dehydrogenation of a Pyrrolidine to a Pyrroline with High Potential Quinone

A solution of 0.518 g (1 mmol) of 2,3-dibenzoyl-1-isopropyl-5-*m*-nitrophenyl-4-phenylpyrrolidine (**3***g*) and 0.246 g (1 mmol) of *p*-chloranil in 50 ml of toluene was heated under reflux for 2 days. The solvent was removed *in vacuo* and the residue subjected to column chromatography on 20 g of B.D.H. alumina with benzene as eluant. The first fraction gave 0.05 g (10%) of unreacted pyrrolidine and the second fraction gave 2,3-dibenzoyl-1-isopropyl-5-*m*-nitrophenyl-4-phenyl-2-pyrrolidine (**20**) 0.41 g (80% yield) as an oil.

Anal. Calcd. for $C_{33}H_{28}N_2O_4$ (mol. wt. 516.2049): C, 76.73; H, 5.46; N, 5.42. Found (516.2062, mass spectrum): C, 75.97; H, 5.47; N, 5.52.

The i.r. spectrum ν_{max} ($CHCl_3$) 1660 cm^{-1}. The n.m.r. spectrum δ TMS ($CDCl_3$) 1.0 (6H, d of d, J = 7 Hz, $(CH_3)_2CH$); 3.60 (1H, m, $(CH_3)_2CH$), 4.40 (1H, d, J_{23} = 5.0 Hz, H_3); 4.86 (1H, d, J_{23} = 5.0 Hz, H_2), 7–8.5 (19H, m, ArH). When 2 equiv. of *p*-chloranil were used, pyrroline **20** in 70% yield together with a small amount of pyrrole **18** (10%) when eluted with chloroform.

Dehydrogenation of 1-Isopropyl-5-m-nitrophenyl-2,3,4-tribenzoyl-2-pyrroline with p-Chloranil

A solution of 0.54 g (1 mmol) of pyrroline **20** and 0.25 g (1 mmol) of *p*-chloranil in 20 ml of toluene was heated under reflux for 14 h (10). Column chromatography on B.D.H. alumina with 1:1 benzene–chloroform afforded the pyrrole **18** 0.35 g (30% yield) (see Table 3).

Cycloadditions of Aroylazomethine Ylides with Acetylenes. Reaction of 1-Isopropyl-2-m-nitrophenyl-3-benzylaziridine with trans-Dibenzoylacetylene

A solution of 1.66 g (7.1 mmol) of *trans*-dibenzoylacetylene and 2.20 g (7.1 mmol) of the above aziridine in 50 ml of benzene was heated under reflux for 12 h. Hexane (50 ml) was added to the hot solution which was set aside at room temperature for 2 days when crystals of 1-isopropyl-5-*m*-nitrophenyl-2,3,4-tribenzoyl-2-pyrroline (**11**) separated, 1.1 g (30% total yield) m.p. 183–184°.

Anal. Calcd. for $C_{34}H_{28}N_2O_5$ (mol. wt. 544.1998): C, 74.98; H, 5.18; N, 51.4. Found (544.1992, mass spectrum): C, 74.80; H, 5.23; N, 5.0.

The i.r. spectrum ν_{max} ($CHCl_3$) 1660 cm^{-1} (C=O). The n.m.r. spectrum δ TMS ($CDCl_3$): 1.0 (6H, d of d, $(CH_3)_2CH$—); 3.7 (1H, m, $(CH_3)_2CH$—), 4.93 (2H, s, methine), 7–8.2 (19H, m, aryl). Upon treatment with Europium shift reagent, the H_2, H_3 singlet at 4.93 became an AB quartet centered at 5.30 and 6.45 δ, J = 2.5 Hz.

Chromatography of the mother liquor on B.D.H. alumina with benzene as eluent gave a further 1.0 g of the pyrroline **11** and 1.3 g of an oil which eluted with chloroform and which crystallized from hexane as

Can. J. Chem. Downloaded from www.nrcresearchpress.com by 210.87.254.105 on 09/05/12
For personal use only.

colorless prisms, m.p. 100–101°, 1-isopropyl-5-*m*-nitrophenyl-2,3,4-tribenzoylpyrrole (**12**).

Mol. Wt. Calcd. for $C_{34}H_{26}N_2O_5$: 542.1832. Found (mass spectrum): 542.1827.

The i.r. spectrum ν_{max} ($CHCl_3$) 1645 cm^{-1} (C=O); n.m.r. δ TMS ($CDCl_3$): 1.2 (6H, d of d, J = 7 Hz, $(CH_3)_2CH$—), 4.58 (1H, m, $(CH_3)_2CH$—), 7–9 (19H, m, aryl protons).

Base Catalyzed Deuterium Exchange

A solution of 0.1 g of compound **11** and 0.1 g of potassium carbonate in 50 ml of 1:1 dioxan – deuterium oxide was heated under reflux for 2 h. Examination of the n.m.r. spectrum of the recovered 2-pyrroline showed the 4.93 singlet had diminished to 1H due to exchange of H_4. No other structural changes had occurred indicating this to be the more stable 2-pyrroline isomer.

Base Catalyzed Isomerization of a 3-Pyrroline to a 2-Pyrroline

A solution of 1 g (2 mmol) 1-isopropyl-4-phenyl-2,3,5-tribenzoyl-3-pyrroline (**16**) (prepared from 1-isopropyl-2,3-dibenzoylaziridine and 1,3-diphenylpropynone) in methanol with a trace of sodium methoxide was stirred overnight at room temperature. Removal of the solvent *in vacuo* gave a substance (**17**) isomeric with the compound **16** (*i.e.* mass spectrum 499.2156. Calcd. for $C_{34}H_{29}NO_3$: 499.2147). The n.m.r. spectrum δ TMS ($CDCl_3$) 3.6 (1H, m, $(CH_3)_2CH$—), 4.1, 5.75 (1H each, s, H_4, H_5). On this basis the compound was assigned as 1-isopropyl-4-phenyl-2,3,5-tribenzoyl-2-pyrroline (**17**).

Cycloadditions of Aroylazomethine Ylides with Aroylsulfonylimines. Reaction of 1-Isopropyl-2-m-nitrophenyl-3-benzoylaziridine with Benzoyl-N-p-toluenesulfonylimine

A solution of 2.16 g (7 mmol) of the aziridine and 2.0 g (7 mmol) of the sulfonylimine in 50 ml of benzene–dioxan (10:1) or acetonitrile was heated under reflux for 12 h and the resulting precipitate was collected representing 4,5-dibenzoyl-1-isopropyl-2-*m*-nitrophenyl-3-*p*-toluenesulfonylimidazolidine, m.p. 272–273°, 0.4 g (7% yield).

Mol. Wt. Calcd. for $C_{33}H_{28}N_3O_4S$: 562. Found (mass spectrum): 562.

The i.r. spectrum ν_{max} ($CHCl_3$): 1635, (C=O) 1160, 1330 cm^{-1} (SO_2). The n.m.r. spectrum δ TMS ($CDCl_3$): 1.33 (6H, d, J = 7 Hz, $(CH_3)_2CH$—); 2.21 (3H, s, CH_3); 3.5 (1H, m, $CH(CH_3)_3$); 7–9 (20H, m, aryl).

The mother liquor was subjected to chromatography on B.D.H. alumina with benzene as eluent which gave some unreacted aziridine (0.3 g) and a second product 4,5-dibenzoyl-1-isopropyl-2-*m*-nitrophenyl-2-imidazoline, 0.25 g (9% yield) m.p. 205°.

Anal. Calcd. for $C_{26}H_{21}N_3O_4$ (M − 2H, 439.1532): C, 70.73: H, 5.25: N, 9.52. Found (439.1535, mass spectrum): C, 69.58; H, 4.95; N, 9.39.

The analogous 5-benzyl-3-*p*-chlorotoluenesulfonyl-1-isopropyl-4-*m*-nitrobenzoyl-2-*m*-nitrophenylimidazolidine (**22**), m.p. 278–279° and 5-benzoyl-1-isopropyl-4-*m*-nitrobenzoyl-2-*m*-nitrophenyl-2-imidazoline (**23**), m.p. 105° were prepared similarly in 12 and 20% yields, respectively.

Paal–Knorr Formation of a Pyrrolo[3,4-d]imidazole

A solution of 0.15 g of compound **23** and 1 ml of cyclohexylamine in 20 ml of methanol was heated for 1 h then set aside overnight. Chromatography of the resulting mixture on B.D.H. alumina with benzene gave 5-cyclohexyl-1,5-dihydro-2,4-di-*m*-nitrophenyl-1-isopropyl-6-phenylpyrrolo[3,4-*d*]imidazole (**24**), 0.08 g (60% yield).

Mol. Wt. Calcd. for $C_{32}H_{31}N_5O_4$: 549.2375. Found (mass spectrum): 549.2379.

The n.m.r. spectrum δ TMS ($CDCl_3$): 1.20 (10H, m cyclohexyl CH_2), 1.3 (6H, d, J = Hz, $(CH_3)_2CH$); 3.5 (2H, m, methines), 7–9 (13H, m, aryl protons).

Cycloadditions of Aroylazomethineoxides with Aroylalkenes

A solution of 1.18 g (5 mmol) of *trans*-dibenzoylethylene and 1.51 g (5 mmol) of the nitrone *N*-*p*-chlorobenzoylmethylene-4-dimethylaminoaniline-*N*-oxide in 100 ml of dry benzene was stirred overnight at room temperature. Most of the solvent was removed *in vacuo* and the resulting precipitate collected and purified by recrystallization from hexane–benzene to give 4,5-dibenzoyl-3-*p*-chlorobenzoyl-2-*p*-dimethylaminophenylisoxazolidine (**26**) 1.8 g (67% yield), m.p. 210–212°.

Paal-Knorr Formation of a Pyrrolo[3,4-c]isoxazole

(*a*) A solution of 0.2 g (3.7 mmol) of 4,5-dibenzoyl-3-*p*-chlorobenzoyl-2-*p*-dimethylaminophenylisoxazolidine (**26**) in 20 ml of methanol was treated with 2 ml of isopropylamine. A red color developed immediately and the solution was stirred overnight. Removal of the solvent *in vacuo* gave 3-benzoyl-6-*p*-chlorophenyl-3,5-dihydro-1-*p*-dimethylaminophenyl-5-isopropyl-4-phenyl-1*H*-pyrrolo-[3,4-*c*]isoxazole (**27**), 0.2 g as a red oil.

Mol. Wt. Calcd. for $C_{35}H_{32}N_3O_2Cl$: 561.2192. Found (mass spectrum): 561.2196.

The n.m.r. spectrum δ TMS ($CDCl_3$): 1.1 (3H, s, CH_3); 2.7 (3H, s, N-CH_3), 6.2–8 (20H, m, aryl H and methines).

(*b*) The assigned structure was confirmed by reacting the isoxazolidine (0.10 g) labelled with deuterium at the 3-position (75% replacement by n.m.r.) with isopropylamine to afford the same pyrrolo[3,4-*c*]isoxazole (0.1 g), (molecular ion 561, confirming loss of the label). The deuterated nitrone precursor was prepared from the pyridinium salt and *p*-nitrosodimethylamine, as before, but using CH_3OD instead of ethanol as solvent. The required deuterated acetophenone was prepared by base catalyzed deuterium exchange.

Formation of an Isoxazolo[3,4-d]pyridazine

A solution of 0.25 g (4.6 mmol) of 4,5-dibenzoyl-3-*p*-chlorobenzoyl-2-*p*-dimethylaminophenylisoxazolidine (**26**) in 10 ml of boiling ethanol was treated with 2 ml of 95% hydrazine. The solution was heated under reflux for 15 min, allowed to cool, and the yellow needles collected 0.15 g (75% yield) of 7-*p*-chlorophenyl-1-dimethylaminophenyl-4-phenyl-3-*cis*-(3a,7a)-trihydro-1*H*-isoxazolo-[3,4-*d*]pyridazine (**28**), m.p. 269–273°.

Anal. Calcd. for $C_{32}H_{25}N_4OCl$ (M − H_2O, 516.1717): C, 71.80; Cl, 6.63. Found (516.1694, mass spectrum): C, 71.11; Cl, 6.56. (Chemical ionization mass spectrometry shows the parent peak at 534.)

The n.m.r. spectrum δ TMS ($CDCl_3$): 2.90 (6H, s, N-CH_3), 4.18 and 4.49 (2H, AB quartet, J = 9 Hz, $C_6H_4N(Me)_2$).

This research was supported by a National Research Council of Canada grant to J.W.L. and by the Chemistry

Department, University of Alberta. We thank Mr. R. Swindlehurst and Dr. A. Hogg for the n.m.r. and mass spectra.

1. R. HUISGEN. Angew. Chem. Int. Ed. Engl. **2**, 565, 633 (1963).
2. J. W. LOWN and K. MATSUMOTO. Can. J. Chem. **48**, 3399 (1970).
3. J. W. LOWN and M. H. AKHTAR. Can J. Chem. **50**, 2236 (1972).
4. J. W. LOWN and M. H. AKHTAR. J. Chem. Soc. (Perkin I), 1459 (1972).
5. J. W. LOWN, J. P. MOSER, and R. WESTWOOD. Can. J. Chem. **47**, 4335 (1969).
6. P. B. WOLLER and N. H. CROMWELL. J. Org. Chem. **35**, 888 (1970).
7. M. KARPLUS. J. Chem. Phys. **30**, 11 (1959).
8. J. W. LOWN. Rec. Chem. Progr. **32**, 51 (1971).
9. J. W. LOWN, T. W. MALONEY, and G. DALLAS. Can. J. Chem. **48**, 584 (1970).
10. J. W. LOWN, G. DALLAS, and T. W. MALONEY. Can. J. Chem. **47**, 3557 (1969).
11. L. CLAISEN. Chem. Ber. **31**, 1010 (1898).
12. R. ALBRECHT, G. KRESZE, and B. MLAKER. Chem. Ber. **97**, 483 (1964).
13. F. KROHNKE and E. BORNER. Chem. Ber **69**, 2006 (1936).

Can. J. Chem. Downloaded from www.nrcresearchpress.com by 210.87.254.105 on 09/05/12
For personal use only.

Unsymmetric Cleavage of C_2—C_3 in 5β-Steroids

JOSEPH KENNETH PAISLEY, RONALD B. WARNEBOLDT, AND LARRY WEILER[1]

Department of Chemistry, University of British Columbia, Vancouver 8, British Columbia

Received September 20, 1973

A method to achieve the unsymmetric cleavage of C-2 and C-3 in 3-keto-5β-steroids is developed. This involves a *cine* substitution of 4-bromoketone to produce the 2-acetoxyketone. Possible mechanisms for this transformation are discussed and the route proceeding through the oxyallyl intermediate is considered most plausible. The 2-acetoxyketone is converted into the hydroxyoxime which undergoes a Beckmann fragmentation to yield the 2,3-seco-steroid. These products are useful intermediates for the synthesis of the salamander alkaloids.

On a développé une méthode pour couper préférentiellement entre les positions 2,3 les céto-3 stéroides-5β. Ceci implique une *ciné* substitution de la bromo-4 cétone pour obtenir l'acétoxy-2 cétone. Les mécanismes possibles pour cette transformation sont discutés et l'on considère que la route passant par un intermédiaire oxyallyle est la plus probable. L'acétoxy-2 cétone est transformé en hydroxyoxime qui subie un réarrangement de Beckmann pour fournir le stéroide coupé entre les positions 2,3. Ces produits sont des intermédiaires utiles pour la synthèse des alkaloides de la salamande. [Traduit par le journal]

Can. J. Chem., **52**, 810 (1974)

Can. J. Chem. Downloaded from www.nrcresearchpress.com by 210.87.254.5 on 09/05/12
For personal use only.

The European salamanders, *Salamandra maculosa taeniata* and *Salamandra maculosa maculosa*, produce a group of toxic defensive principles in their skin glands which have become known as the salamander alkaloids (1). These steroidal alkaloids have attracted attention because of their unusual structural, toxicological, and pharmacological properties. The toxicology and pharmacology studies of the major components of the salamander toxins have shown that these compounds have a dramatic effect on the central nervous system (2). These alkaloids also have unusual structures. They are the only known naturally occurring steroidal alkaloids in which the nitrogen forms an integral part of the steroidal ring system. There are three basic patterns found in the salamander alkaloids which are exemplified by samanine (**1**), cycloneosamandione (**2**), and samandarine (**3**). All of the alkaloids have a nitrogen atom inserted between carbons 2 and 3 of steroidal ring A and a 5β-hydrogen.

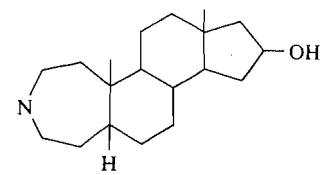

1

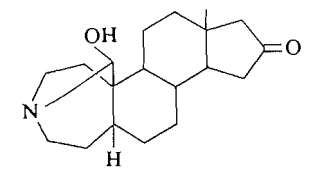

2

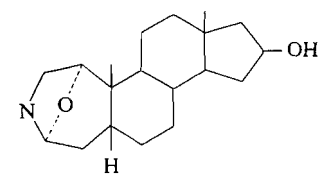

3

Because of these unusual and interesting properties we initiated a program to synthesize these alkaloids and structural variations and modifications of them. In 1967, Hara and Oka (3) reported the first synthesis of one of the salamander alkaloids, namely samandarine (**3**). Although the length of their synthetic sequence should not detract from its elegance and beauty, it does not appear to be a practical solution to our aims. During the course of our work two other syntheses of samandarine (**3**) have appeared (4,5). The work of Shimizu (4) is similar to our own in concept and execution and the synthesis of Benn and Shaw (5) is patterned more on the proposed biosynthesis of **3**. Cycloneosamandione (**2**) has been synthesized by Habermehl and Haaf (6) and there have been several

[1]Author to whom correspondence should be addressed.

Can. J. Chem. Downloaded from www.nrcresearchpress.com by 210.87.254.5 on 09/05/12
For personal use only.

syntheses of samanine (**1**) and related systems (7–9).

The key point in all of these methods is the cleavage of the bond between carbons 2 and 3 in a suitably substituted steroid (Scheme 1) to generate an unsymmetric compound of type **4**.

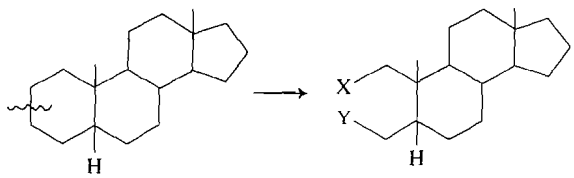

4

SCHEME 1

With the exception of the method of Shimizu (4) and our own (*vide infra* and ref. 10) the previous routes to effect this cleavage (Scheme 1) were either lengthy or nonstereospecific. Here we report our detailed results on this cleavage (10) and the chemistry of some of these derivatives.

The starting material for all our work is 17β-acetoxy-5β-androstan-3-one (**5**) which is readily available from testosterone (11).

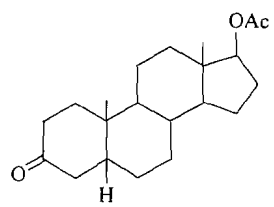

5

There are several oxidative methods available to cleave the carbon–carbon bond adjacent to a ketone. Beckmann rearrangement of the oximes from **5** gave a mixture of the two lactams **6** and **7** in a ratio of *ca.* 1:1 (Scheme 2) (7,12). The difficulty in separation of the isomeric lactams precluded using this method for the synthesis of large quantities of **6** (8,13). The *syn* and *anti* oximes of **5** have been separated and the individual oximes undergo a stereospecific Beckmann rearrangement to **6** or **7** (14). Here also the delicate chromatographic separation and ready equilibration of the two oximes was not compatible with our desired large scale reactions.

Originally it was reported that the Baeyer–Villiger oxidation of 3-oxo-5β-steroids gave a single lactone, namely, the 3-oxa-4-oxo-A-homo compound (15). However, later re-examination of this reaction showed that, in fact, the Baeyer–Villiger product was a mixture of the two possible lactones (16). We have found that action of *m*-chloroperbenzoic acid on **5** gave a 4:1 mixture of lactones **8** and **9** in 85% yield (Scheme 3). The two lactones could be separated by v.p.c. and their structures were proven as follows. The mixture of lactones was hydrolyzed, esterified, and tosylated to give a mixture of **10** and **11**. Treatment of **10** and **11** gave only the olefin **12** in 32% which indicates that the major lactone in the mixture has structure **8**. This was collaborated by synthesizing the known lactams **6** and **7** (14). These lactams were converted into the *N*-nitrosolactams (17) and pyrolysis of these *N*-nitrosolactams (18) gave the lactones **9** and **8**, respectively (19).

With this experience and the results reported above we felt that it would be essential to introduce a substituent at C-2 of **5** in order that the C_2—C_3 bond cleavage process would be favored. However, this approach is not totally free of obstacles since it is well known that most reactions of 3-keto-5β-steroids involve preferential enolization towards carbon 4 (11,20) and then reaction of this enol (or enolate) to generate mainly, if not exclusively, the C-4 substituted product (11,20,21). One exception to this is the formation of the 2-hydroxymethylene derivative of **5** (21*f*). Formylation is an equilibrium reaction and the 2-hydroxymethylene is more stable than the 4-hydroxymethylene because of the $A_{1,3}$ strain (22) in the latter isomer. This led us to the consideration of two possibilities, either we could obtain a 2-substituted derivative of **5** via a rearrangement of the 4-substituted derivative (Scheme 4) or we could trap an intermediate of type **15** preferentially at C-2 (*vide infra*) (Scheme 5). In the first possibility the reaction would be driven by the relief of the additional *gauche* interaction present in **13** but not in **14**. The work of Warnhoff and co-workers (23) on the rearrangement of α-acetoxyketones (Scheme 6) was a particularly relevant example of the anticipated rearrangement shown in Scheme 4. Although this specific example (Scheme 6) required rather high temperatures other similar rearrangements have been found to occur at lower temperatures (24).

Satoh and co-workers (25*a* and *b*) and Warnhoff and Wang (25*c*) have found that refluxing 4β-bromo-5β-cholestan-3-one in acetic acid containing sodium acetate yields 2β-acetoxy-5β-cholestan-3-one in good yield (Scheme 7).

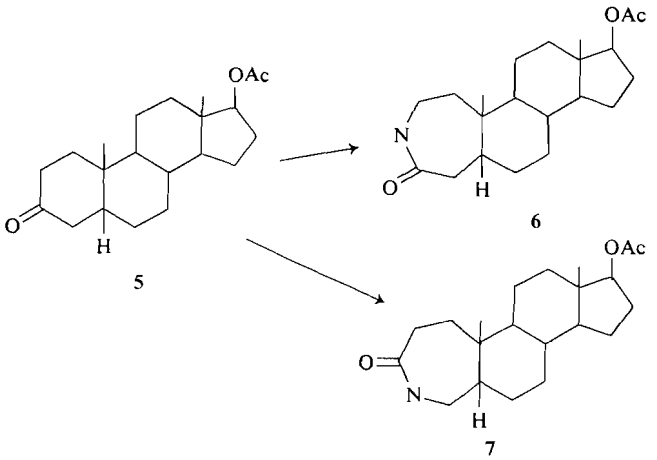

SCHEME 2. Beckmann rearrangement of a 5β-androstan-3-one.

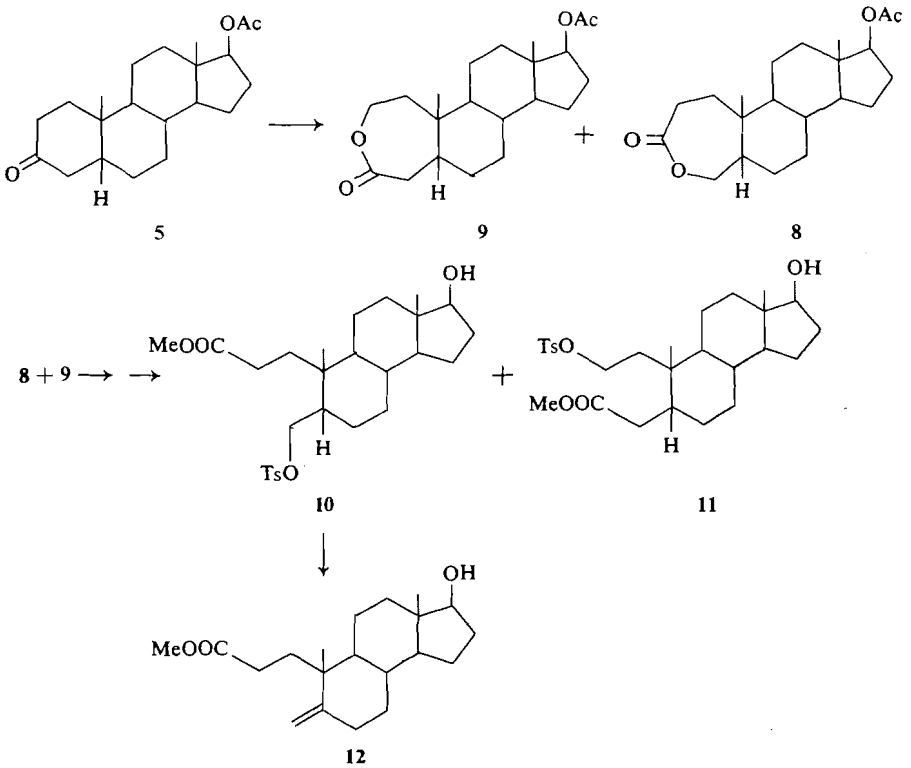

SCHEME 3. Baeyer–Villiger oxidation of a 5β-androstan-3-one.

It was not clear how this transformation occurred (*vide infra*) but it did appear to meet our objectives of introducing a substituent at C-2 in a 5β-steroid. Treatment of bromoketone **16** (26) under the same conditions as in Scheme 7 (25) gave 2β,17β-diacetoxy-5β-androstan-3-one (**17**) in *ca.* 70% yield. Either pure bromoketone **16** or the crude mixture of bromoketones from the bromination of **5** could be used with essentially the same overall results. Bromination of **5** gives a 4:1 mixture of two bromoketones, by v.p.c., and the major product is **16** and the minor product probably is 2β-bromoketone.

The structure **17** for the acetoxyketone derived

Can. J. Chem. Downloaded from www.nrcresearchpress.com by 210.87.254.5 on 09/05/12
For personal use only.

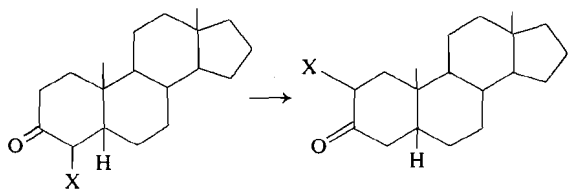

13 14

SCHEME 4

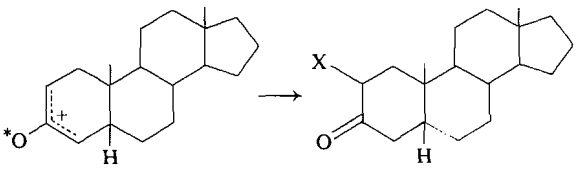

15 14

SCHEME 5

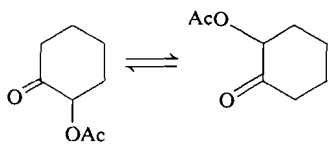

SCHEME 6

from **16** followed from its analytical and spectral properties. In particular the n.m.r. spectrum of the acetoxyketone had a double doublet (J = 6 and 14 Hz) at δ 5.15 which is assigned to the 2α-hydrogen, a broad triplet (J = 13 Hz) at δ 2.81 assigned to the 4α-hydrogen, and a double doublet (J = 5 and 13 Hz) at *ca.* δ 2.2 assigned to the 4β-hydrogen. Zinc – acetic acid reduction of the acetoxyketone gave **5** which indicates that no acyloxy–ketone exchange had occurred (23,25*c*). Also, bromination of the acetoxyketone gave a monobrominated derivative which had an n.m.r. spectrum consistent only with structure **18**. The salient features in the n.m.r. spectrum of

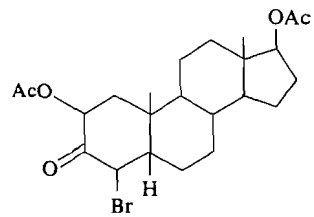

18

18 are a doublet (J = 13 Hz) at δ 4.98 assigned to the 4α-hydrogen and a double doublet (J = 5 and 13 Hz) at δ 5.21 assigned to the 2α-hydrogen. All of these physical and chemical properties are consistent only with structure **17** for the acetoxyketone; also this product is not unexpected in view of the previous *cine* substitution reactions of bromoketones (25,26).

The mechanism of this transformation has been the subject of several reports in recent years. There are several possible mechanisms for the reactions in Schemes 7 and 8. One possibility would involve direct displacement of the bromine at C-4 of **16** to give a 4-acetoxy compound which could rearrange to the 2-acetoxy isomer (Schemes 4 and 6). This possibility was

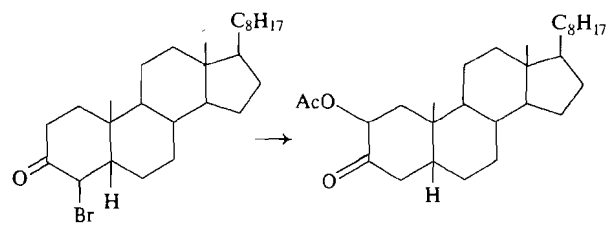

SCHEME 7

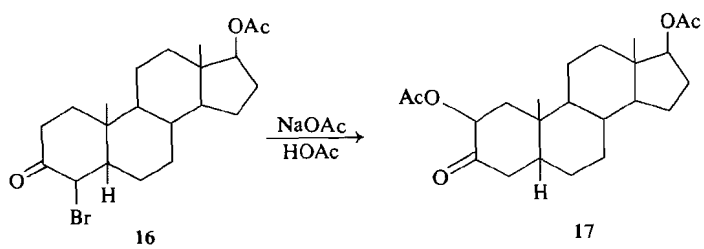

16 **17**

SCHEME 8

Can. J. Chem. Downloaded from www.nrcresearchpress.com by 210.87.254.5 on 09/05/12
For personal use only.

tested as follows. Ketone **5** was converted into the enol acetate **19** using the procedure of Liston (11). Compound **19** was contaminated with *ca.*

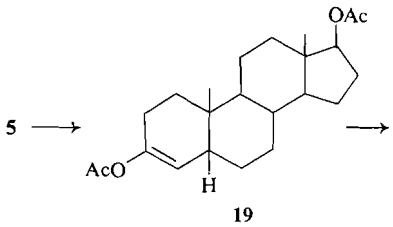

19

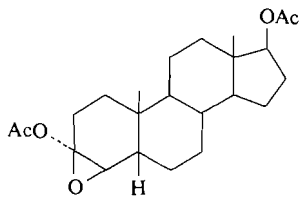

20

3% of the isomeric enol acetate but this did not interfere with the subsequent reactions. Enol acetate **19** was epoxidized with *m*-chloroperbenzoic acid – sodium bicarbonate (27) to give the β-epoxide **20** in over 80% yield. The configuration of the epoxidation product **20** was assigned as follows. The β-face of **19** appears to be the sterically more accessible direction for peracid attack (28). The n.m.r. spectrum of **20** has a singlet at δ 3.07 which is assigned to the C-4 hydrogen. Examination of the Dreiding model of **20** indicates that the dihedral angle between the hydrogens on C-4 and C-5 is *ca.* 100° and the dihedral angle between the hydrogens on C-4 and C-5 in the isomeric α-epoxide is *ca.* 50°. In an extensive study of steroidal epoxides and episulfides it was found that the coupling constant of these hydrogens on C-4 and C-5 could approach zero only for dihedral angles of 70–100° while a coupling constant of at least 2 Hz is expected for a dihedral angle of 50° (29). Furthermore, the chemical shift of the C-19 methyl hydrogens in **20** is δ 0.87 which agrees well with that of the C-19 hydrogens of 3β-4β-oxido-5β-cholestane at δ 0.87 (30).

Pyrolysis of **20** at 160° for 5 min gave 4α,17β-diacetoxy-5β-androstan-3-one (**21**) in good yield. The salient feature of the n.m.r. spectrum of **21** which suggested its structure was a one proton doublet (J = 8 Hz) at δ 5.41. This is assigned to the 4β-hydrogen of **21** which is probably in a boat conformation due to the severe interaction

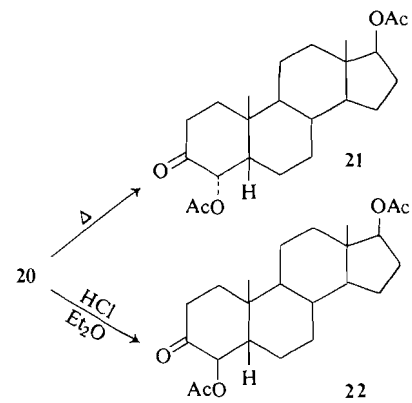

of the 4α-acetoxy group with C-7 and C-9 in the chair conformation. The 4β-isomer **22** was obtained by treating **20** with HCl in ether, and the n.m.r. spectrum of **22** has a one proton doublet (J = 12 Hz) at δ 5.52 which is assigned to the 4α-hydrogen. These epoxide rearrangements parallel those of 2α,3α-oxido-3β-acetoxycholestane (31). When the 4β-acetoxy isomer **22** was subjected to refluxing acetic acid containing sodium acetate, that is, the conditions for reaction in Scheme 8, the starting material was recovered unchanged. Also, the 4α-isomer **21** was cleanly converted into the 4β-isomer **22** on refluxing in acetic acid – sodium acetate. In neither case could any of the 2β-isomer **17** be detected. These experiments indicate that **21** and **22** are not intermediates in the *cine* substitution (Scheme 8). In fact, **21** or **22** did not rearrange to the 2-acetoxy compound even on thermolysis at 160°.

Satoh and Takahashi have detected an intermediate in this reaction in the cholestane system (Scheme 7) and they have suggested that this intermediate is the 2α-acetoxy isomer (32). The above results corroborate this suggestion. Satoh and Takahashi suggest that this involves a *trans* S_N2' displacement on the enol **23** as shown in Scheme 9 (32). Most S_N2' reactions involve a *cis* relation between the entering nucleophile and the leaving group. Also it would appear that the α-face of enol **23** would be more sterically shielded than the β-face, although Satoh and Takahashi suggest that ring B of **23** may be in a boat conformation.

We also considered the possibility of a S_Ni rearrangement of the enol **24** to **25** followed by a S_N2 reaction as shown in Scheme 10. However, Liston has found that the bromoketone **16**

Can. J. Chem. Downloaded from www.nrcresearchpress.com by 210.87.254.5 on 09/05/12
For personal use only.

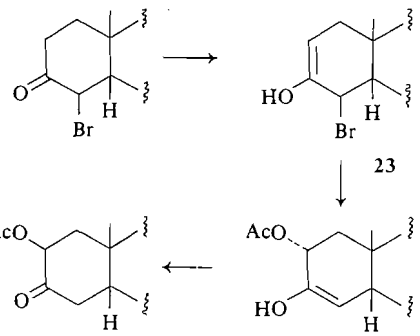

SCHEME 9. Proposed mechanism for *cine* substitution.

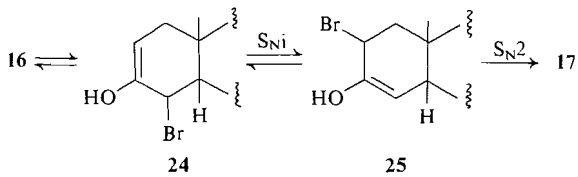

SCHEME 10. S_Ni and S_N2 routes for *cine* substitution.

and the 2β-bromo isomer **27** are not interchanged or equilibrated even in HBr—HOAc (11). This would suggest that the S_Ni rearrangement of **24** to **25** is not occurring under our reaction conditions. We have synthesized the 2β-bromo isomer **27** following the method

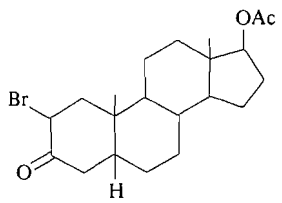

27

developed by Hanson and Organ (33), which involved bromination of the enolate of the 2-hydroxymethylene derivative of **5** and in this way the bromine was directed exclusively to the 2 position. Bromoketone **27** was converted to **17** in refluxing acetic acid – sodium acetate at a similar rate for reaction of **16** (Scheme 8). Detailed rate studies were not performed and only the appearance of product **17** was monitored but these results would suggest that **16** and **27** were going to a common intermediate which reacts with acetate in the slow step to give eventually **17**. This possibility is shown in Scheme 11. It is not clear if the intermediate **28** is the zwitterion or the protonated oxyallyl system. A similar mechanism has been previously proposed in the reaction of steroidal bromoenones (34), and more recently in the reaction of α,α'-dibromoketones with acetate in the presence of diiron nonacarbonyl (35) and for the reaction of a range of steroidal bromoketones with sodium acetate (25*c*).

If **28** is an intermediate in this reaction, then the presence of the three contiguous sp^2 carbons in ring A will substantially flatten this ring. Examination of molecular models of this system show that α-attack at C-4 is severely hindered by the C-7 methylene group, β-attack at C-4 introduces torsional strain as the nucleophile enters eclipsed to the C-5 hydrogen, β-attack at C-2 also introduces torsional strain, and attack at the α-face of C-2 is not as sterically or torsionally hindered as the other sites. Thus it is reasonable to expect that the 2α-isomer could result from reaction of **28** and it is subsequently isomerized to the 2β-isomer **17** under the reaction conditions.

Having introduced a substituent at C-2 of **5** we now examined methods to unsymmetrically cleave the C_2—C_3 bond. Mild basic hydrolysis of **17** gave a mixture of the two hydroxyketones **30** and **31** in *ca.* a 1:1 ratio, which precluded using oxidative cleavage of the hydroxyketone **30**. However, treatment of **17** with hydroxylamine in refluxing methanol gave the hydroxyoxime **32** in good yield. The molecular formula of this compound was established by mass

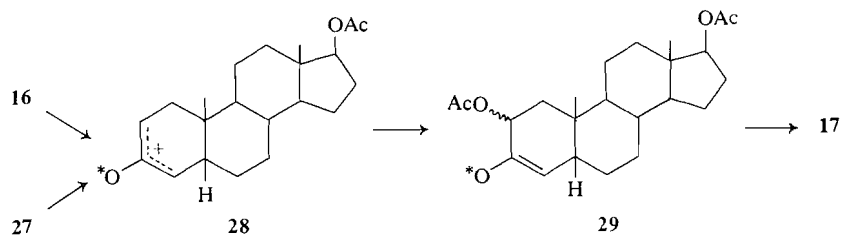

* = – or H

SCHEME 11. Proposed mechanism for *cine* substitution.

Can. J. Chem. Downloaded from www.nrcresearchpress.com by 210.87.254.5 on 09/05/12
For personal use only.

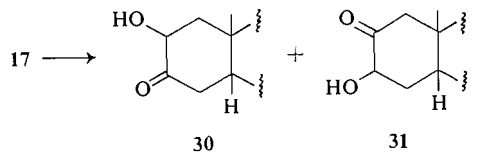

30 31

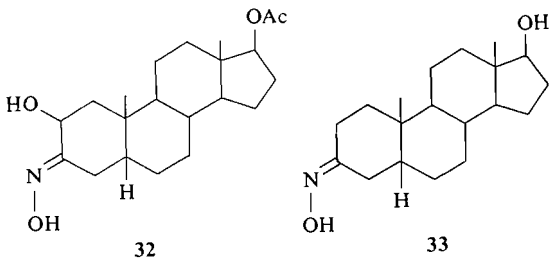

32 33

spectroscopy and analysis. The n.m.r. spectrum confirmed that the ring A acetate had been hydrolyzed and that the hydroxyl group was retained at C-2. A double doublet (J = 5 and 13 Hz) at δ 4.20 was assigned to the 2α-hydrogen and a second double doublet (J = 4 and 14 Hz) at δ 2.79 was assigned to the 4β-hydrogen. Oka and Hara (14*a*) have shown that the equatorial hydrogen *syn* to the OH of a number of steroidal oximes is deshielded and found at lower field than the methylene envelope. For example, the 4β-hydrogen in **33** is a double doublet (J = 5 and 15 Hz) at δ 2.93 (14*a*). The 4β-hydrogen of the isomeric oxime remains engulfed in the methylene envelope and the 2β-hydrogen is a double triplet ($J \simeq$ 4.5 and 14 Hz) at δ 3.08. This would suggest that our oxime has the stereochemistry shown in **32**. Since the acetoxy group at C-17 remained it would appear that the hydrolysis of the C-2 acetate is facilitated by the neighboring oximino group. It is also interesting to note that Autrey and Scullard found that oximation of ketone **34** gave the *anti*-oxime **35** which would appear to be more sterically crowded isomer (36).

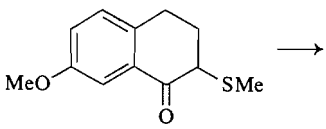

34

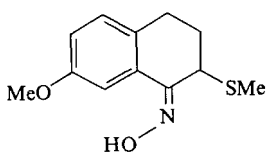

35

Beckmann fragmentation (37) of oxime **33** to give the cyanoaldehyde **36** was effected in low yield with tosyl chloride and pyridine, or better with thionyl chloride at −20° followed by treatment with 3 *N* potassium hydroxide (38). The n.m.r. spectrum of **36** has a double doublet

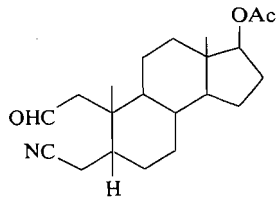

36

($J \simeq$ 1 and 3 Hz) at δ 9.85 due to the aldehyde proton, which is coupled to the two adjacent diastereotopic protons (39). An INDOR n.m.r. experiment was performed on this compound by monitoring the aldehyde peaks while sweeping a perturbing radio-frequency field through the steroidal methylene envelope. A pair of double doublets were found at δ 2.07 (J = 4.0 and 14.5 Hz) and δ 2.52 (J = 1.4 and 14.5 Hz) (40). This indicated that the OHC—CH_2 group was isolated by a quaternary carbon and was compatible only with structure **36** for the product from the Beckmann fragmentation. In this way we had achieved the desired cleavage of ring A in **5**.

The cyanoaldehyde **36** was the key intermediate in our synthesis of the salamander alkaloids. This compound can be converted into the samine family (**1**) by reduction of the aldehyde and nitrile of **36**, and cyclization (41). This material can also be converted to the olefin **37** which has been converted to samandarine (**3**) (4) and thus this would constitute a formal synthesis of the samandarine family. Several attempts to convert the alcohol **38**, readily

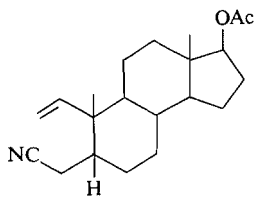

37

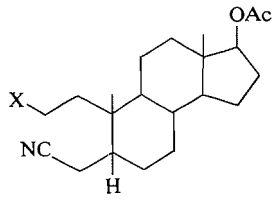

38

available from the sodium borohydride reduction of **36**, into **37** were unsuccessful (19). However, the aldehyde of **36** could be converted into the corresponding enol acetates **39**. The

Can. J. Chem. Downloaded from www.nrcresearchpress.com by 210.87.254.5 on 09/05/12
For personal use only.

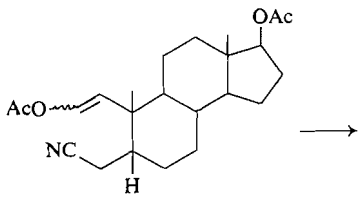

39

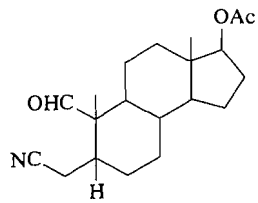

40

n.m.r. spectrum of the mixture of enol acetates suggested that the *cis* and *trans* isomers of **39** were present in *ca.* 1:1 ratio. Ozonolysis of **39** with a reductive work-up gave the cyanoaldehyde **40** in good yield and this compound was converted into **37** by Wittig reaction and subsequent reacylation of the C-17 hydroxyl. A more detailed discussion of the chemistry of intermediates **36–40** is anticipated at a later date.

Experimental

Melting points, which were determined on a Kofler hot stage, and boiling points are uncorrected. Optical rotations were recorded at the sodium D line using a Perkin-Elmer Model 141 Automatic Polarimeter. Ultraviolet spectra were measured in methanol solution on a Unicam model SP800 or Cary Model 14 spectrophotometer. The i.r. spectra were recorded on a Perkin-Elmer model 700 spectrophotometer and were calibrated using the 1601 cm^{-1} band of polystyrene. The ^1H n.m.r. spectra were recorded in deuteriochloroform solution on either a Varian T-60 or Varian HA-100 spectrometer. Line positions are given in the δ scale, with tetramethylsilane as internal standard; the multiplicity, coupling constant, integrated peak areas, and proton assignments are indicated in parentheses. The mass spectra were obtained using an Atlas CH-4 mass spectrometer and high resolution determinations were performed on an AEI MS-9 mass spectrometer. Microanalyses were performed by Mr. Peter Borda, University of British Columbia. The v.p.c. analyses were performed with a Varian Aerograph 90-P-3 using column *A*, 8 ft × ¼ in. column of 5% fluoro silicone (QF-1) on 60–80 mesh Diaport "S"; column *B*, 5 ft × ¼ in. column of 3% SE 30 on Chromosorb W; and column *C*, 5 ft × ¼ in. column of 10% carbowax on 60–80 mesh Chromosorb W; or with a Perkin-Elmer Model 900 using column *D*, 6 ft × ⅛ in. column of 8% SE 30 on 80–100 mesh Chromosorb W. The specific column used, along with the column temperature and carrier gas (helium) flow-rate (in ml/min) are indicated in parentheses. Silica gel GF-254 and a Woelm neutral alumina were used for t.l.c. Silica gel PF-254 and aluminum oxide F-254 were used for preparative-layer chromatography. Silica gel, Woelm alumina, and Fluorisil (100–200 mesh) were used for column chromatography.

17β-Acetoxy-5β-androstan-3-one (5) (11)

The hydrogenation of testosterone (5.0 g, 0.017 mol) was carried out by employing the procedure of Liston (11) to yield 4.98 g of a crystalline product, m.p. 123–127°. To a solution of this material (4.98 g) in dry pyridine (20 ml) was added acetic anhydride (5 ml). The solution was stirred at room temperature for 16 h, then diluted with water (200 ml), and shaken for 15 min. The precipitate was collected, washed with 1 *N* hydrochloric acid (100 ml) and with water (100 ml), and air dried. Vapor phase chromatographic analysis (column *A*, 225°, 60 ml/min) of the crude product indicated 75% of 17β-acetoxy-5β-androstan-3-one (**5**) and 25% of 17β-acetoxy-5α-androstan-3-one (retention times 7.5 and 8.6 min, respectively). Recrystallization from ether afforded 2.19 g (38%) of 17β-acetoxy-5β-androstan-3-one (**5**), m.p. 142–144°, $[\alpha]_D^{25}$ +43° (c, 1 MeOH) (lit. (42) m.p. 140–142°, $[\alpha]_D^{25}$ +45.2°); i.r. ($CHCl_3$), 1720 cm^{-1}; n.m.r. ($CDCl_3$), δ 0.78 (singlet, 3H, C-18 CH_3), 1.03 (singlet, 3H, C-19 CH_3), 2.03 (singlet, 3H, acetate), 4.63 (triplet, J = 9 Hz, 1H, C-17 $H\alpha$); mass spectrum *m/e* (relative intensity), 332(49), 272(85), 257(32), 230(16), 214(12), 160(20), 148(35), 42(100).

Anal. Calcd. for $C_{21}H_{32}O_3$: C, 75.86; H, 9.70. Found: C, 75.86; H, 9.52.

Baeyer–Villiger Oxidation of 5

To a solution of 17β-acetoxy-5β-androstan-3-one (**5**, 200 mg, 0.60 mmol) in chloroform (15 ml) was added *meta*-chloroperbenzoic acid (155 mg, 0.90 mmol). The reaction mixture was stirred in the dark at room temperature for 2 days. The solution was then poured into saturated sodium bicarbonate solution (30 ml) and extracted with chloroform (40 ml). The chloroform solution was washed with water (2 × 10 ml) and saturated sodium chloride solution (2 × 10 ml), dried over sodium sulfate, and filtered. The solvent was removed by evaporation under reduced pressure to afford 180 mg (85%) of a mixture of compounds **8** and **9** as a crystalline solid, m.p. 118–125°. Thin-layer chromatographic analysis of this product on silica gel with ethyl acetate as the eluant indicated the presence of two compounds, R_f 0.58 and R_f 0.61. Vapor phase chromatographic analysis (column *B*, 300°, 60 ml/min) of the crude product showed two peaks (retention times 18 and 31 min) in *ca.* a 1:4 ratio. An analytical specimen was obtained by three recrystallizations from methanol, m.p. 207–208°; i.r. ($CHCl_3$), 1720 cm^{-1}; n.m.r. ($CDCl_3$), δ 0.80 (singlet, 3H, C-18 CH_3), 1.03 (singlet, 3H, C-19 CH_3), 2.00 (singlet, 3H, acetate), 3.8–4.8 (multiplet, 3H, C-17 $H\alpha$ and C-2 H_2 **9**, C-4a H_2 **8**); mass spectrum *m/e* (relative intensity), 348(15), 288(25), 260(9), 94(100).

Anal. Calcd. for $C_{21}H_{32}O_4$: C, 72.30; H, 9.25. Found: C, 72.02; H, 9.48.

Hydrolysis and Esterification of 8 and 9

A solution of compounds **8** and **9** (100 mg, 0.258 mmol), obtained above, in 5% methanolic sodium hydroxide (30 ml) was heated to reflux. After 2 h of refluxing, the reaction mixture was cooled and the solvent

Can. J. Chem. Downloaded from www.nrcresearchpress.com by 210.87.254.5 on 09/05/12
For personal use only.

Can. J. Chem. Downloaded from www.nrcresearchpress.com by 210.87.254.5 on 09/05/12
For personal use only.

removed under reduced pressure. The residue was dissolved in water (30 ml) and carefully acidified with dilute acetic acid, and extracted with chloroform (2 × 30 ml). The combined chloroform extracts were washed with saturated sodium chloride (2 × 10 ml), dried over sodium sulfate, and filtered. The solvent was removed under reduced pressure to yield 100 mg of a crystalline solid, m.p. 185–189°. To a solution of this material (100 mg, 0.30 mmol) in methanol (30 ml) was added a solution of diazomethane in ether (0.35 mmol). After stirring the reaction mixture at room temperature for 5 min the solvent was removed under reduced pressure to yield 66 mg (75%) of a mixture of hydroxy methyl esters as an oil. Attempts to induce crystallization failed. The t.l.c. of this material on silica gel with ethyl acetate as the solvent system showed one broad spot, R_f 0.80; i.r. ($CHCl_3$), 3600, 3450, 1720 cm^{-1}; n.m.r. ($CDCl_3$), δ 0.73 (singlet, 3H, C-18 CH_3), 0.98 and 1.07 (singlets, 3H, C-19 CH_3), *ca.* 3.65 (multiplet, 3H, C-2 H_2 and C-17 $H\alpha$), 3.68 (singlet, 3H, methyl ester group); mass spectrum *m/e* (relative intensity), 338(8), 320(11), 306(76), 274(100), 263(65), 233(84).

Mol. wt. Calcd. for $C_{20}H_{34}O_4$: 338.2456. Found: 338.2442.

*Preparation of a Mixture of Methyl 17β-Hydroxy-2-tosyloxy-2,3-seco-5β-androstan-3-oate (**11**) and Methyl 17β-Hydroxy-2-tosyloxy-2,3-seco-5β-androstan-3-oate (**10**)*

To a pyridine solution of hydroxy esters from the previous experiment (30 mg, 0.088 mmol) was added *p*-toluenesulfonyl chloride (17.1 mg, 0.089 mmol). The reaction mixture was allowed to stand at 20° for 2 days. The pyridine was removed under reduced pressure and the resulting residue dissolved in ethyl ether (40 ml). The ethereal solution was washed with 1 *N* hydrochloric acid (4 × 10 ml), 1 *N* sodium hydroxide (4 × 10 ml), and saturated sodium chloride solution (2 × 10 ml), dried over sodium sulfate, and filtered. The solvent was removed under reduced pressure to yield 39.3 mg (88%) of a mixture of the tosyloxy methyl esters **10** and **11** as a clear oil. Attempts to induce crystallization failed. The t.l.c. of this material on silica gel with various solvent systems showed one broad spot; i.r. ($CHCl_3$), 3600, 3400, 1720, 1600, 1190 cm^{-1}; n.m.r. ($CDCl_3$), δ 0.71 and 0.73 (singlets, 3H, C-18 CH_3), 0.93 and 0.95 (singlets, 3H, C-19 CH_3), 2.45 (singlet, 3H, tosyl CH_3), 3.33 (singlet, 3H, methyl ester CH_3), *ca.* 3.6 (multiplet, 1H, C-17 $H\alpha$), 4.10 (multiplet, 2H, C-2 H_2 **11** and C-4 H_2 **10**), 7.32 and 7.80 (doublets, J = 9 Hz, 4H, tosylate group); mass spectrum *m/e* (relative intensity), 492(1), 474(1), 460(1), 305(3), 304(4), 288(3), 287(4), 234(12), 233(30), 215(30), 187(20), 91(100).

*Methyl 17β-Hydroxy-3,4-seco-androst-4-en-3oate (**12**)*

A mixture of compounds **10** and **11** (160 mg, 0.32 mmol) from the previous experiment was added to collidine (10 ml). The reaction mixture was refluxed for 4 h under an atmosphere of nitrogen. The solvent was removed by evaporation under reduced pressure to afford a brown oil which was dissolved in ethyl ether (35 ml). The ether solution was washed with saturated sodium bicarbonate (2 × 10 ml) and sodium chloride (2 × 10 ml) solutions, dried over sodium sulfate, and filtered. The solvent was removed under reduced pressure to yield a brown oil which was chromatographed on a 20 × 20 cm silica gel coated plate, adsorbant thickness 0.9 mm, using a mixture of benzene and ethyl acetate (1:1, v/v) as the eluant. After elution, the band lying in the region R_f 0.55–0.60 was removed and extracted with ethyl acetate (50 ml). The solvent was removed under reduced pressure to afford 35.5 mg (extrapolated yield, 32%) of methyl 17β-hydroxy-3,4-seco-5-androst-4-en-3-oate (**12**) as a clear oil. Attempts to induce crystallization failed; i.r. ($CHCl_3$), 3600, 3450, 1720, 1630, 900 cm^{-1}; n.m.r. ($CDCl_3$), δ 0.93 (singlet, 3H, C-18 CH_3), 1.03 (singlet, 3H, C-19 CH_3), *ca.* 3.5 (multiplet, 1H, C-17 $H\alpha$), 3.63 (singlet, 3H, ester group), 4.65 (doublet, 2H, C-4 H_2, J = 4 Hz); mass spectrum *m/e* (relative intensity), 320(5), 234(6), 233(25), 215(12), 205(6), 187(9), 160(10), 62(100).

Mol. wt. Calcd. for $C_{20}H_{32}O_3$: 320.2351. Found: 320.2327.

*17β-Acetoxy-4β-bromo-5β-androstan-3-one (**16**) (26)*

To a solution of 17β-acetoxy-5β-androstan-3-one (**5**, 9.197 g, 0.027 mol) in glacial acetic acid (50 ml) was added a solution of bromine (1.53 ml, 28.5 mmol) in acetic acid (40 ml) over a period of 20 min with vigorous stirring at 10°, decoloration of bromine was rapid, and 30 min later water (300 ml) was added and the mixture was allowed to stand for 1 h at 10°. The precipitated product was collected, washed with water (3 × 100 ml), and dissolved in ethyl ether (300 ml). The organic layer was washed with saturated sodium chloride (2 × 20 ml) solution, dried over sodium sulfate, and filtered. The solvent was removed under reduced pressure to give 10.44 g (92%) of a crystalline solid, m.p. 135–151°. Vapor phase chromatographic analysis (column *D*, 250°, 45 ml/min) of this product indicated the presence of two compounds (retention times 9.0 and 8.9 min) in *ca.* a 4:1 ratio. Two recrystallizations from ethyl ether gave compound **16** as a crystalline solid, m.p. 174–175°, $[\alpha]_D$ +43.0° (c, 1 MeOH) (lit. (26) m.p. 174–175°, $[\alpha]_D$ +44.7 ± 2° $CHCl_3$); i.r. ($CHCl_3$), 1730 cm^{-1}; n.m.r. ($CDCl_3$), δ 0.82 (singlet, 3H, C-18 CH_3), 1.10 (singlet, 3H, C-19 CH_3), 2.03 (singlet, 3H, acetate), 4.63 (triplet, J = 9 Hz, 1H, C-17 $H\alpha$), 5.0 (doublet, J = 12 Hz, 1H, C-4 H_{ax}); mass spectrum *m/e* (relative intensity), 412(30), 410(30), 353(70), 351(70), 333(100), 332(70), 273(100), 258(80), 245(70), 273(100).

*2β,17β-Diacetoxy-5β-androstan-3-one (**17**)*

A solution of crude 17β-acetoxy-4β-bromo-5β-androstan-3-one (**16**, 10.3 g, 0.025 mol) and anhydrous sodium acetate (50.2 g, 0.612 mol) in glacial acetic acid (730 ml) was refluxed for 2.5 h. After cooling the solution was poured into water (500 ml) and extracted with ethyl ether (2 × 200 ml). The combined ethereal extracts were washed with saturated sodium bicarbonate (4 × 50 ml) and saturated sodium chloride (2 × 50 ml) solutions, dried over sodium sulfate, and filtered. The solvent was removed under reduced pressure to afford a crystalline residue. Recrystallization of the residue from methanol gave 6.80 g (70%) of diacetate **17**, m.p. 170–173°. Vapor phase chromatographic analysis (column *D*, 250°, 45 ml/min) indicated the presence of one compound (retention time 16.8 min). The analytical specimen was obtained by two recrystallizations from methanol, m.p. 161–162°; i.r. ($CHCl_3$), 1720 cm^{-1}; n.m.r. ($CDCl_3$), δ 0.80 (singlet,

Can. J. Chem. Downloaded from www.nrcresearchpress.com by 210.87.254.5 on 09/05/12
For personal use only.

3H, C-18 CH_3), 1.05 (singlet, 3H, C-19 CH_3), 2.00 (singlet, 3H, acetate), *ca.* 2.2 (double doublet, J = 5 and 13 Hz, 1H, C-4 H_β), 2.81 (broad triplet, J = 13 Hz, 1H, C-4 $H\alpha$), 4.57 (triplet, J = 9 Hz, 1H, C-17 $H\alpha$), 5.15 (double doublet, J = 6 and 14 Hz, 1H, C-2 $H\alpha$); mass spectrum *m/e* (relative intensity), 390(4), 348(15), 346(9), 331(7), 330(30), 304(10), 288(14), 270(12), 55(100).

Anal. Calcd. for $C_{23}H_{34}O_5$: C, 70.74; H, 8.77. Found: C, 70.70; H, 8.82.

*Zinc – Acetic Acid Reduction of 2β,17β-Diacetoxy-5β-androstan-3-one (**17**)*

To a solution of diacetate **17** (100 mg, 0.25 mmol) in glacial acetic acid (30 ml) was added dry zinc dust (500 mg). The reaction mixture was refluxed for 30 h, then cooled, and poured into water (50 ml). The aqueous solution was extracted with ethyl ether (3 × 30 ml). The combined ethereal extracts were washed with water (3 × 10 ml), saturated sodium bicarbonate (3 × 10 ml), and sodium chloride (2 × 10 ml) solutions, dried over sodium sulfate, and filtered. The solvent was removed under reduced pressure to afford 72.5 mg of a yellow oil which was chromatographed on a 5 × 20 cm silica gel coated plate, adsorbant thickness 0.9 mm, using a mixture of chloroform and ethyl acetate (5:1, v/v) as the eluant. After elution, the band lying in the region R_f 0.52–0.59 was removed and extracted with ethyl acetate (50 ml). The solvent was removed by evaporation under pressure to yield 25.7 mg (extrapolated yield, 31%) of a clear oil. This material was identical (t.l.c., i.r., n.m.r., and mass spectrum) with 17β-acetoxy-5β-androstan-3-one (**5**).

*4β-Bromo-2β,17β-diacetoxy-5β-androstan-3-one (**18**)*

A solution of diacetate **17** (95 mg, 0.24 mmol) in 25 ml of glacial acetic acid was treated with bromine (12.4 μl, 0.23 mmol). The bromine color had disappeared after 2 h, and the acetic acid solution was poured into water (100 ml) and extracted with ethyl ether (150 ml). The ether was washed with saturated sodium bicarbonate (50 ml) and brine (50 ml), dried over sodium sulfate, filtered, and the solvent removed under reduced pressure to yield 120 mg of clear oil. This material was purified by t.l.c. on silica gel with chloroform development to yield 84 mg (74%) of **18** as a clear oil; i.r. ($CHCl_3$), 1735, 1720 cm^{-1}; n.m.r. ($CDCl_3$), δ 0.82 (singlet, 3H, C-18 CH_3), 1.15 (singlet, 3H, C-19 CH_3), 2.05 (singlet, 3H, acetate), 2.17 (singlet, 3H, acetate), 4.64 (triplet, J = 9 Hz, 1H, C-17 $H\alpha$), 4.98 (doublet, J = 13 Hz, 1H, C-4 $H\alpha$), 5.21 (double doublet, J = 5 and 13 Hz, 1H, C-2 $H\alpha$);

Mol. Wt. Calcd. for $C_{23}H_{33}O_5Br$: 468.1512 and 470.1492. Found: 468.1506 and 470.1501.

*3,17β-Diacetoxy-5β-androst-3-ene (**19**) (11)*

To a solution of 17β-acetoxy-5β-androstan-3-one (**5**, 250 mg, 0.75 mmol) in isopropenyl acetate (5 ml) was added hydroquinone (30 mg) and concentrated sulfuric acid (10 μl) under an atmosphere of nitrogen. The reaction mixture was heated to a gentle reflux and the acetone formed during the reaction was collected. Isopropenyl acetate was periodically added to maintain a solvent volume of *ca.* 5 ml. After refluxing under nitrogen for 2 h, the reaction mixture was cooled to 0° and diluted with ethyl ether (30 ml). This organic mixture was washed with saturated sodium bicarbonate (3 × 25 ml) and sodium chloride (15 ml) solutions, dried over sodium sulfate, and filtered. The solvent was distilled to afford 361 mg of a light yellow oil. Vapor phase chromatographic analysis (column *A*, 225°, 60 ml/min) of the crude product indicated the presence of 59% 3,17β-diacetoxy-5β-androst-3-one (**19**) and 23% 3,17β-diacetoxy-5β-androst-2-ene (retention times 12 and 14 min, respectively); i.r. ($CHCl_3$), 1750, 1725, 1685 cm^{-1}; n.m.r. ($CDCl_3$), δ 0.88 (singlet, 3H, C-18 CH_3), 2.02 and 2.10 (singlets, 6H, acetates), 4.64 (triplet, J = 9 Hz, 2H, C-17 $H\alpha$), 5.05 (singlet, C-4 H), 5.20 (multiplet, C-2 H).

Equilibration of Enol Acetates (11)

The enol acetate mixture from above (150 mg) was dissolved in benzene (12 ml), carbon tetrachloride (6 ml), and acetic anhydride (2.4 ml). To this solution was added 70% perchloric acid (30 μl) under an atmosphere of nitrogen. The reaction mixture was stirred under nitrogen at room temperature for 22 h. Then the reaction mixture was poured into ethyl ether (50 ml) and washed with water (25 ml), saturated sodium bicarbonate (4 × 20 ml), and sodium chloride (20 ml) solutions, dried over sodium sulfate, and filtered. The solvent was removed by evaporation under reduced pressure to yield 121 mg of a light yellow oil. Vapor phase chromatographic analysis (column *A*, 225°, 60 ml/min) of this product indicated 88% of 3,17β-diacetoxy-5β-androst-3-ene (**19**, retention time 12 min) and 2% of 3,17β-diacetoxy-5β-androst-2-ene (retention time 14 min); i.r. ($CHCl_3$), 1750, 1725, 1685, 1660 cm^{-1}; n.m.r. ($CDCl_3$), δ 0.88 (singlet, 3H, C-18 CH_3), 0.98 (singlet, 3H, C-19 CH_3), 2.03 (singlet, 3H, acetate), 2.11 (singlet, 3H, vinyl acetate), 4.64 (triplet, J = 9 Hz, 1H, C-17 $H\alpha$), 5.05 (singlet, 1H, C-4 H).

*3α,17β-Diacetoxy-3β,4β-oxido-5β-androstane (**20**)*

The equilibrated enol acetate mixture containing predominantly compound **19** (53 mg, 0.14 mmol) was dissolved in chloroform (5 ml). To this solution was added *m*-chloroperoxybenzoic acid (70 mg, 0.40 mmol) and sodium bicarbonate (50 mg). The reaction mixture was stirred at 0° for 4 h and then allowed to stand at −5° for 40 h. The reaction mixture was poured into cold saturated sodium bicarbonate solution (10 ml) and extracted with ethyl ether (3 × 10 ml). The organic layer was separated and washed with 20% sodium carbonate (3 × 15 ml) and saturated sodium chloride (10 ml) solutions, dried over sodium sulfate, and filtered. Removal of the solvent under reduced pressure afforded 46 mg (84%) of β-epoxide **20** as a light yellow oil, with no trace of the starting enol acetate **19** by v.p.c.; i.r. ($CHCl_3$), 1720–1745, 860 cm^{-1}; n.m.r. ($CDCl_3$), δ 0.80 (singlet, 3H, C-18 CH_3), 0.87 (singlet, 3H, C-19 CH_3), 2.03 (singlet, 3H, acetate), 2.07 (singlet, 3H, acetate), 3.07 (singlet, 1H, C-4 H), 4.64 (triplet, 1H, C-17 $H\alpha$).

Mol. Wt. Calcd. for $C_{23}H_{34}O_5$: 390.2406. Found: 390.2417.

*4β,17-Diacetoxy-5β-androstan-3-one (**21**)*

3α,17β-Diacetoxy-3β,4β-oxido-5β-androstan-3-one (**20**, 25 mg, 0.064 mmol) was pyrolyzed at 160° for 5 min under an atmosphere of nitrogen to afford 20.0 mg (80%) of compound **21**. Vapor phase chromatographic analysis (column *A*, 225%, 60 ml/min) of this product indicated one compound (retention time 24 min); i.r. ($CHCl_3$), 1740, 1725 cm^{-1}; n.m.r. ($CDCl_3$), δ 0.79 (singlet, 3H, C-18 CH_3), 1.10 (singlet, 3H, C-19 CH_3), 2.03 (singlet,

3H, acetate), 2.15 (singlet, 3H, acetate), 4.62 (triplet, J = 9 Hz, 1H, C-17 $H\alpha$), 5.41 (doublet, J = 8 Hz, 1H, C-4 H_β).

Mol. Wt. Calcd. for $C_{23}H_{34}O_5$: 390.2406. Found: 390.2400.

4β,17β-Diacetoxy-5β-androstan-3-one (22)

Hydrogen chloride was bubbled through a stirred solution of 3α,17β-diacetoxy-3β,4β-oxide-5β-androstane (**20**, 25 mg, 0.064 mmol) in ethyl ether at 12° for 5 min. The solution was stirred for 30 min, then allowed to stand at −5° for 20 h. The reaction mixture was diluted with ethyl ether (30 ml), washed with saturated sodium bicarbonate (3 × 20 ml), and sodium chloride (20 ml) solutions, dried over sodium sulfate, and filtered. The solvent was removed by evaporation under reduced pressure to afford 20.0 mg (80%) of crude compound **22**. Vapor phase chromatographic analysis (column *A*, 225°, 60 ml/min) of the crude product indicated the presence of one compound (retention time 24 min); i.r. ($CHCl_3$), 1740, 1725 cm^{-1}; n.m.r. ($CDCl_3$), δ 0.79 (singlet, 3H, C-18 CH_3), 1.07 (singlet, 3H, C-19 CH_3), 2.02 (singlet, 3H, acetate), 2.15 (singlet, 3H, C-4 acetate), 4.61 (triplet, J = 9 Hz, 1H, C-17 $H\alpha$), 5.52 (doublet, J = 12 Hz, 1H, C-4 $H\alpha$).

Mol. Wt. Calcd. for $C_{23}H_{34}O_5$: 390.2406. Found: 390.2409.

*Isomerization Studies of **21** and **22***

(*a*) To a solution of 4α,17β-diacetoxy-5β-androstan-3-one (**21**, 19 mg, 0.048 mmol) in hexamethylphosphoramide (1.5 ml) was added a crystal of *p*-toluenesulfonic acid and the reaction mixture was heated under nitrogen at 160° for 15 min. The reaction mixture was then cooled to room temperature and diluted with ethyl ether (25 ml). This organic layer was washed with water (3 × 20 ml), saturated sodium bicarbonate (2 × 15 ml), and sodium chloride (15 ml) solutions, dried over sodium sulfate, and filtered. The solvent was removed under reduced pressure to afford 12 mg of compound **22** with no trace of compound **21** detectable by n.m.r. spectroscopy or t.l.c.

(*b*) To a solution of 4α,17β-diacetoxy-5β-androstan-3-one (**21**, 30 mg, 0.076 mmol) in glacial acetic acid (4.5 ml) was added sodium acetate (300 mg, 3.65 mmol). The reaction mixture was refluxed under an atmosphere of nitrogen for 2 h. The reaction mixture was then cooled to 0°, diluted with cold water (25 ml), and extracted with ethyl ether (3 × 25 ml). The extracts were washed with saturated sodium bicarbonate (3 × 20 ml) and sodium chloride (2 ml) solutions, dried over sodium sulfate, and filtered. The solvent was removed under reduced pressure to afford 19 mg (63%) of 4β,17β-diacetoxy-5β-androstan-3-one (**22**).

(*c*) Compound **22** was recovered unchanged in 83% yield when subjected to conditions in *a* above and in 76% yield when subjected to conditions in *b* above.

2-Hydroxymethylene-5β-androstan-17β-ol-3-one (21f)

To a suspension of sodium hydride (31.2 mg, 1.3 mmol) in dry benzene (5 ml), under nitrogen, was added absolute methanol (40 ml). The mixture was stirred and heated briefly to boiling. After the mixture was cooled to room temperature, 17β-hydroxy-5β-androstan-3-one (200 mg, 0.68 mmol) and ethyl formate (50.3 mg, 0.68 mmol) were added. The mixture was stirred at room temperature under nitrogen for 30 h. After the careful addition of water (10 ml) to destroy the excess sodium hydride, the mixture was diluted with water (5 ml) and ethyl ether (25 ml). The ether–benzene layer was separated and re-extracted with water (10 ml). The combined aqueous layers were washed once with ethyl ether (10 ml) and then neutralized with carbon dioxide to p*H* 7. The mixture was filtered and the collected solid washed thoroughly with water (3 × 20 ml). Recrystallization of this material from acetonitrile gave 131 mg (60%) of the hydroxymethylene derivative as a crystalline solid, m.p. 153–159° (evacuated sealed tube), $[\alpha]_D^{25}$ +30.2° (c, 1 MeOH), λ_{max} 290 mμ (ε 8000) (lit. (21*f*) m.p. 157–163°, $[\alpha]_D$ +26.9°, λ_{max} 284 mμ (ε 7900)).

17β-Acetoxy-2β-bromo-5β-androstan-3-one (27)

Following the method of Hanson and Organ (33) an ethyl ether solution (20 ml) of the above hydroxymethylene derivative (200 mg, 0.63 mmol) was extracted with 0.05 *N* sodium hydroxide (3 × 10 ml). The aqueous extracts were combined and treated with a solution of bromine (100 mg, 0.63 mmol) and potassium bromide (*ca.* 200 mg) in 5 ml of water. The bromine color was discharged immediately. The reaction mixture was stirred at room temperature for ½ h, acidified with concentrated hydrochloric acid and extracted with methylene chloride (4 × 15 ml). The extracts were combined, dried over magnesium sulfate, filtered, and the solvent removed under reduced pressure to yield 82 mg of a white semisolid which was treated with acetic anhydride (1 ml) and pyridine (5 ml) overnight. This mixture was poured onto ice (10 g) and extracted with ethyl ether (3 × 15 ml). The ethereal extracts were washed with 10% hydrochloric acid, saturated sodium bicarbonate and water, dried over magnesium sulfate, filtered, and the solvents removed under reduced pressure to yield 80 mg of a pale yellow liquid which was chromatographed on sliica gel (25 g) using chloroform – ethyl acetate (6:1) as eluant. Fractions containing compound with R_f 0.7–0.8 on t.l.c. (silica gel, chloroform – ethyl acetate, 6:1) were combined and solvents removed under reduced pressure to yield a white solid which was recrystallized from acetone – isopropyl ether to yield 32 mg (12%) of **27**, m.p. 198–200° (lit. (11) m.p. 201–202°).

*Preparation of **17** from **27***

A solution of bromoketone **27** (15 mg, 0.036 mmol) and anhydrous sodium acetate (100 mg) in acetic acid (1 ml) was refluxed for 1.5 h and worked up as before for **17**, when no starting material could be detected by t.l.c. The yield of **17** was 11 mg (78%) of product m.p. 168–170°. A parallel reaction of bromoketone **16** gave 76% yield of **17** after 1.5 h. These products were compared with the previously prepared **17** by i.r., t.l.c., and v.p.c.

*Hydrolysis of **17***

To a solution of 2β,17β-diacetoxy-5β-androstan-3-one (**17**, 100 mg, 0.255 mmol) in methanol (4 ml) and water (1 ml) was added sodium bicarbonate (100 mg). The reaction mixture was heated at 50° for 30 min and then stirred for *ca*, 1 h at room temperature. The solvent was removed under reduced pressure and the resulting residue was dissolved in water (10 ml) and extracted with ethyl ether (2 × 10 ml). The combined ethereal extracts

Can. J. Chem. Downloaded from www.nrcresearchpress.com by 210.87.254.5 on 09/05/12
For personal use only.

Can. J. Chem. Downloaded from www.nrcresearchpress.com by 210.87.254.5 on 09/05/12
For personal use only.

were washed with saturated sodium chloride (2 × 5 ml), dried over sodium sulfate, and filtered. The solvent was removed under reduced pressure to afford 75 mg (84%, crude) of a mixture of 17β-acetoxy-2β-hydroxy-5β-androstan-3-one (**30**) and 17β-acetoxy-3α-hydroxy-5β-androstan-2-one (**31**). Thin-layer chromatographic analysis of the crude product on silica gel with a mixture of chloroform and ethyl acetate (5:1, v/v) as the eluant indicated the presence of two compounds, R_f 0.75 and R_f 0.78; i.r. ($CHCl_3$), 3350, 1720 cm^{-1}; n.m.r. ($CDCl_3$), 0.75 and 0.80, (singlets, 3H, C-18 CH_3), 1.03 and 1.10, (singlets, 3H, C-19 CH_3), 3.40–4.20 (multiplet, 1H, C-2 $H\alpha$, **30** and C-3 H_β, **31**), 4.60 (triplet, J = 9 Hz, 1H, C-17 $H\alpha$).

anti-17β-Acetoxy-2β-hydroxy-5β-androstan-3-one Oxime (32)

A solution of 2β,17β-diacetoxy-5β-androstan-3-one (**17**, 5.10 g, 0.013 mol), hydroxylamine hydrochloride (21.0 g, 0.302 mol), and sodium acetate trihydrate (27.5 g, 0.202 mol) in 90% methanol (400 ml) was refluxed for 48 h and then the methanolic solution was concentrated to 20 ml under reduced pressure. Water (100 ml) was added to the solution and the resulting suspension was extracted with ethyl ether (2 × 200 ml). The combined ethereal extracts were washed with aqueous sodium bicarbonate (2 × 30 ml), and saturated sodium chloride (2 × 20 ml) solutions, dried over Na_2SO_4, and filtered. The solvent was removed under reduced pressure to afford 4.01 g (85%) of hydroxyoxime **32**, m.p. 176–182°. Thin-layer chromatographic analysis of this material on silica gel, using a mixture of ethyl acetate and benzene (5:1, v/v) as eluant, indicated one major compound, R_f 0.78. The analytical specimen was obtained by three recrystallizations from methanol, m.p. 214–215°, $[\alpha]_D^{25}$ +21.42° (c, 0.7 MeOH); i.r. ($CHCl_3$), 3550, 3350, 1720, 1660 cm^{-1}; n.m.r. ($CDCl_3$), 0.75 (singlet, 3H, C-18 CH_3), 0.97 (singlet, 3H, C-19 CH_3), 2.79 (double doublet, J = 4 and 14 Hz, 1H, C-4 H_β), 4.20 (double doublet, J = 5 and 13 Hz, 1H, C-2 $H\alpha$), 4.60 (triplet, 1H, C-17 $H\alpha$); mass spectrum *m/e* (relative intensity), 363(1), 362(6), 347(3), 345(4), 344(5), 334(17), 333(78), 316(6), 303(3), 271(3), 43(100).

Anal. Calcd. for $C_{21}H_{33}NO_4$: C, 69.39; H, 9.15; N, 3.85. Found: C, 69.62; H, 9.37; N, 4.02.

17β-Acetoxy-2-oxo-2,3-seco-5β-androstane-3-nitrile (36)

(*a*) To a solution of *anti*-17β-acetoxy-2β-hydroxy-5β-androstan-3-one oxime (**32**, 1.0 g, 2.75 mmol) in pyridine (45 ml) was added *p*-toluenesulfonyl chloride (500 mg, 2.62 mmol). The reaction mixture was refluxed under an atmosphere of nitrogen for 5 h. The solution was cooled, poured into dilute sodium bicarbonate solution (50 ml), and extracted with ethyl ether. The organic layer was separated and washed with water (4 × 20 ml), saturated sodium bicarbonate (2 × 15 ml), and sodium chloride (2 × 10 ml) solutions, dried over sodium sulfate, and filtered. The solvent was removed by evaporation under reduced pressure to yield 985 mg of a brown oil. This material was chromatographed on a 20 × 20 cm silica gel coated plate, adsorbant thickness 0.9 mm, using a mixture of chloroform and ethyl acetate (5:1, v/v). After development, the band lying in the region R_f 0.62–0.68 was removed and extracted with ethyl acetate (100 ml). The solvent was removed by evaporation under reduced pressure to afford 190 mg (20%) of cyanoaldehyde **36** as a clear oil; i.r. ($CHCl_3$), 2750, 2250, 1720 cm^{-1}; n.m.r. ($CDCl_3$), δ 0.79 (singlet, 3H, C-18 CH_3), 1.32 (singlet, 3H, C-19 CH_3), 4.60 (triplet, 1H, C-17 $H\alpha$), 9.80 (double doublet, J = 1 and 3 Hz, 1H, CHO); mass spectrum *m/e* (relative intensity), 345(2), 318(5), 302(6), 301(11), 290(4), 258(7), 242(8), 241(16), 43(100).

Anal. Calcd. for $C_{21}H_{31}NO_3$: C, 73.01; H, 9.04; N, 4.06. Found: C, 72.82; H, 9.16; N, 3.88.

(*b*) *anti*-17β-Acetoxy-2β-hydroxy-5β-androstan-3-one oxime (**32**, 1.0 g, 2.75 mmol) was treated with distilled thionyl chloride (10 ml) at −20° (methanol–ice). After 1.5 min the resulting colorless solution was at once slowly poured into a mixture of 3 *N* potassium hydroxide (300 ml) and diethyl ether (100 ml) at 0°. The organic phase was separated and the aqueous solution was extracted with ethyl ether (2 × 50 ml). The combined ethereal extracts were washed with saturated sodium chloride (2 × 50 ml) solution, dried over sodium sulfate, and filtered. The solvent was removed under pressure to afford 1.10 g of an oily residue which was chromatographed on fluorisil (50 g). Elution with a mixture of chloroform and benzene (1:2, v/v) afforded 805 mg (85%) of cyanoaldehyde **36** as a clear oil which crystallized on standing, m.p. 110–112°, $[\alpha]_D^{20}$ +23.3° (c, 1 MeOH). Cyanoaldehyde **36** was also converted into its 2,4-DNP derivative, m.p. 238–240°, for analysis.

Anal. Calcd. for $C_{27}H_{35}N_5O_6$: C, 61.70; H, 6.71; N, 13.32. Found: C, 61.90; H, 6.84; N, 13.13.

17β-Acetoxy-2-hydroxy-2,3-seco-5β-androstane-3-nitrile (38, X = OH)

To a solution of 17β-acetoxy-2-oxo-2,3-seco-5β-androstane-3-nitrile (**32**; 80 mg, 0.23 mmol) in ethanol (10 ml) was added sodium borohydride (4.4 mg, 0.46 mmol), and the reaction mixture was stirred for 3 h at room temperature under an atmosphere of nitrogen. The solvent was removed under reduced pressure, water (20 ml) and ethyl ether (40 ml) were added to the residue. The organic layer was separated and the aqueous layer was extracted with ethyl ether (2 × 20 ml). The combined ethereal extracts were washed with 1 *N* hydrochloric acid (2 × 20 ml), saturated sodium bicarbonate (3 × 10 ml) and sodium chloride (10 ml) solutions, dried over sodium sulfate, and filtered. The solvent was removed under reduced pressure to yield 80.2 mg of a crystalline solid. Recrystallization of this material from methanol yielded 68.1 mg (85%) of compound **38** (X = OH), m.p. 139–144°. An analytical specimen was obtained by two recrystallizations from methanol, m.p. 138–140°, $[\alpha]_D^{20}$ +34° (c, 5 MeOH); i.r. ($CHCl_3$), 3450, 2250, 1720 cm^{-1}; n.m.r. ($CDCl_3$), δ 0.75 (singlet, 3H, C-18 CH_3), 1.03 (singlet, 3H, C-19 CH_3), 2.0 (singlet, 3H, acetate), 4.53 (triplet, J = 9 Hz, 1H, C-17 $H\alpha$), 3.70 (triplet, J = 10 Hz, 2H, C-2 H_2); mass spectrum *m/e* (relative intensity), 348(6), 347(23), 329(6), 332(5), 303(10), 302(39), 288(9), 287(24), 270(31), 260(14), 43(100).

Anal. Calcd. for $C_{21}H_{33}NO_3$: C, 72.58; H, 9.57; N, 4.03. Found: C, 72.43; H, 9.56; N, 3.88.

17β-Acetoxy-2-tosyloxy-2,3-seco-5β-androstane-3-nitrile (38, X = Ts)

To a solution of 17β-acetoxy-2-hydroxy-2,3-seco-5β-androstane-3-nitrile (**38**, X = OH; 200 mg, 0.57 mmol) in pyridine (15 ml) was added *p*-toluenesulfonyl chloride

Can. J. Chem. Downloaded from www.nrcresearchpress.com by 210.87.254.5 on 09/05/12
For personal use only.

(180.0 mg, 0.94 mmol). The reaction mixture was stirred at room temperature for 24 h and then cold saturated sodium bicarbonate (20 ml) solution and ethyl ether (40 ml) were added. The organic layer was separated and washed with 0.1 *N* hydrochloric acid (3 × 10 ml), saturated sodium bicarbonate (2 × 15 ml), and sodium chloride (10 ml) solutions, dried over sodium sulfate, and filtered. The solvent was removed under reduced pressure to afford 310 mg of a crystalline solid. This material was recrystallized from ethyl ether to give 232 mg (81%) of compound **38** (X = Ts) m.p. 128–129°. An analytical specimen was obtained by three recrystallizations from diethyl ether, m.p. 129–131°; $[\alpha]_D^{20}$ +37° (c, 1 MeOH); i.r. ($CHCl_3$), 2250, 1720, 1600, 1190 cm^{-1}; n.m.r. ($CDCl_3$), δ 0.76 (singlet, 3H, C-18 CH_3), 1.01 (singlet, 3H, C-19 CH_3), 2.0 (singlet, 3H, acetate), 2.48 (singlet, 3H, tosyl CH_3), 4.08 (triplet, J = 9 Hz, 2H, C-2 H_2), 4.60 (triplet, J = 9 Hz, 1H, C-17 $H\alpha$), 7.40 and 7.85 (doublets, J = 10 Hz, 4H, tosylate group); mass spectrum *m/e* (relative intensity), 501(10), 440(16), 346(15), 301(15), 269(35), 368(45), 241(29), 43(100).

Anal. Calcd. for $C_{28}H_{39}NO_5S$: C, 67.03; H, 7.83; N, 2.79; S, 6.39. Found: C, 67.02; H, 7.96; N, 2.89; S, 6.18.

*cis- and trans-2,17β-Diacetoxy-2,3-seco-5β-androst-1-ene-3-nitrile (**39**)*

To a solution of 17β-acetoxy-2-oxo-2,3-seco-5β-androstane-3-nitrile (**36**, 612 mg, 1.774 mmol) in isopropenyl acetate (15 ml) was added 2,5-di-*tert*-butyl-*p*-benzoquinone (60 mg) and 15 μl of concentrated sulfuric acid, and the mixture was heated to reflux. During addition and reflux a stream of nitrogen was passed through the solution. After 36 h of refluxing the mixture was cooled to room temperature, poured into dilute aqueous sodium bicarbonate (15 ml), and extracted with ethyl ether (2 × 100 ml). The combined ethereal extracts were washed with saturated sodium chloride (2 × 20 ml) solution, dried over sodium sulfate, and filtered. The solvent was removed under reduced pressure to afford 930 mg of a brown oil which was chromatographed on silica gel (45 g). Elution with chloroform gave 472 mg (68%) of a mixture of *cis* and *trans* enol acetates **39** as a colorless oil. Thin-layer chromatographic analysis of this material on a 20 × 5 cm silica coated plate, adsorbant thickness 0.1 mm, using chloroform as eluant indicated the presence of two compounds, R_f 0.81 and R_f 0.72, in *ca.* a 1:1 ratio; i.r. ($CHCl_3$), 1745, 1725, 1600 cm^{-1}; n.m.r. ($CDCl_3$), 0.80 (broad singlet, 3H, C-18 CH_3), 1.20 and 1.30 (singlets, 3H, C-19 CH_3), 1.98 (singlet, 3H, acetate), 2.07 and 2.14 (singlets, 3H, vinyl acetate), 4.58 and 5.26 (two doublets, J = 8 and 13 Hz, respectively, 1H, C_1H), 6.96 and 7.04 (two doublets, J = 8 and 13 Hz, respectively, 1H, C_2H); mass spectrum *m/e* (relative intensity), 387(25), 360(9), 359(35), 345(52), 344(45), 327(34), 318(22), 311(46), 303(36), 302(54), 301(23), 285(45), 49(100).

Mol. Wt. Calcd. for $C_{23}H_{33}NO_4$: 387.2409. Found: 387.2389.

*17β-Acetoxy-1-oxo-2,3-seco-A-nor-5β-androstane-3-nitrile (**40**)*

A solution of *cis*- and *trans*-2,17β-acetoxy-2,3-seco-5β-androst-1-ene-3-nitrile (**39**; 510 mg, 1.318 mmol) in ethyl acetate (20 ml) at Dry Ice – acetone temperature was treated with ozone (50 ml/min) for 20 min. The resulting dark blue solution was allowed to stand at Dry Ice – acetone temperature for 35 min and then the excess ozone was removed with a stream of nitrogen. The solvent was removed under reduced pressure to give an oily residue. Methanol (30 ml) and aqueous sodium sulfite (5%, 70 ml) were added to the residue. The mixture was allowed to stand at room temperature for 2.5 h and then concentrated (70 ml). The aqueous solution was then extracted with ethyl ether (3 × 50 ml). The combined etheral extracts were washed with saturated sodium chloride (2 × 50 ml) solutions, dried over sodium sulfate, and filtered. The solvent was removed under reduced pressure to afford 378 mg (86%) of compound **40** as a clear oil. Thin-layer chromatographic analysis of this material on silica gel with a mixture of chloroform and ethyl acetate as the eluant indicated one compound, R_f 0.73. Vapor phase chromatographic analysis (column *D*, 250°, 45 ml/min) indicated one compound (retention time, 9 min); i.r. ($CHCl_3$), 2725, 1720 cm^{-1}; n.m.r. ($CDCl_3$), δ 0.76 (singlet, 3H, C-18 CH_3), 1.03 (singlet, 3H, C-19 CH_3), 1.99 (singlet, 3H, acetate), 4.59 (triplet, 1H, C-17 $H\alpha$), 9.54 (singlet, 1H, CHO); mass spectrum *m/e* (relative intensity), 331(15), 330(8), 303(15), 302(20), 301(15), 270(12), 243(36), 242(70), 241(20), 202(15), 201(24), 200(15), 43(100). Compound **40** was converted into its 2,4-DNP derivative, m.p. 186–188°, for analysis.

Anal. Calcd. for $C_{26}H_{33}N_5O_6$: C, 61.04; H, 6.50; N, 13.68. Found: C, 60.90; H, 6.70; N, 13.48.

*17β-Acetoxy-2,3-seco-5β-androst-1-ene-3-nitrile (**37**)*

n-Butyllithium (2.1 *M*, 1.3 ml, 2.7 mmol) was added to methyltriphenylphosphonium bromide (1.00 g, 2.8 mmol) in dry benzene (50 ml) under an atmosphere of nitrogen. After 1.5 h, 17β-acetoxy-1-oxo-2,3-seco-A-nor-5-androstane-3-nitrile (**40**, 160 mg, 0.48 mmol) was added and the solution was stirred for 6 h at room temperature. Water (50 ml) was then added, and the organic layer separated. The aqueous phase was extracted with benzene (3 × 30 ml). The combined benzene extracts were washed with saturated sodium chloride (2 × 20 ml), dried over sodium sulfate, and filtered. The solvent was removed under reduced pressure to afford a brown oil (630 mg) which was chromatographed on silica gel (36 g). Elution with a mixture of chloroform ethyl acetate (3:1, v/v) afforded a clear oil which was dissolved in acetic anhydride (3 ml) and pyridine (0.4 ml). The solution was stirred at room temperature for 15 h, and then the solvent was removed under reduced pressure to give an oily residue which was taken up in ethyl ether (40 ml). The ether solution was washed with 1 *N* hydrochloric acid (2 × 10 ml), saturated sodium bicarbonate (2 × 20 ml) and sodium chloride (2 × 10 ml) solutions, dried over sodium sulfate, and filtered. The solvent was removed under reduced pressure to give 81.2 mg (51%) of compound **37** as a crystalline solid, m.p. 132–135°, which was sublimed at 125°, 0.1 mm pressure, to afford needles, m.p. 134–135°, $[\alpha]_D^{25}$ +31.2° (c, 8 MeOH); (lit. (4) m.p. 147–148°); i.r. ($CHCl_3$), 2250, 1720, 1630, 980, 920 cm^{-1}; n.m.r. ($CDCl_3$), δ 0.80 (singlet, 3H, C-18 CH_3), 1.17 (singlet, 3H, C-19 CH_3), 4.59 (triplet, 1H, C-17 $H\alpha$), 4.90–5.80 (multiplet, 3H, vinylic protons); mass spectrum *m/e* (relative intensity), 329(15), 303(10), 302(7), 301(20), 288(6), 287(11), 286(6), 254(10), 243(20), 242(16), 241(23), 43(100).

Anal. Calcd. for $C_{21}H_{31}NO_2$: C, 76.55; H, 9.48; N, 4.25. Found: C, 76.49; H, 9.54; N, 4.19.

Can. J. Chem. Downloaded from www.nrcresearchpress.com by 210.87.254.5 on 09/05/12
For personal use only.

17β-Hydroxy-2,3-seco-5β-androst-1-ene-3-nitrile

n-Butyllithium (2.4 *M*, 2 ml, 5.0 mmol) was added to methyltriphenylphosphonium bromide (1.80 g, 5.04 mmol) in dry tetrahydrofuran (20 ml) at 0° under an atmosphere of nitrogen. After 1.5 h the mixture was cooled to −78°, 17β-acetoxy-1-oxo-2,3-seco-A-nor-5β-androstane-3-nitrile (**40**, 360 mg, 1.08 mmol) in dry tetrahydrofuran (10 ml) was added, and the solution was stirred for 6.5 h at room temperature. Water (4 ml) was then added, the tetrahydrofuran was evaporated, and the residue was dissolved in ethyl ether (100 ml). The ether solution was washed with saturated sodium chloride (5 × 60 ml), dried over sodium sulfate, and filtered. Removal of the solvent under reduced pressure afforded 1.04 g of a brown oil which was chromatographed on silica gel (36 g). Elution with a mixture of chloroform ethyl acetate (3:1, v/v) gave 205 mg (65%) of compound which was sublimed at 125°, 0.1 mm pressure, to yield a crystalline solid, m.p. 129–131°; i.r. ($CHCl_3$), 3400, 2250, 1630, 920, 990 cm^{-1}; n.m.r. ($CDCl_3$), δ 0.77 (singlet, 3H, C-18 CH_3), 1.20 (singlet, 3H, C-19 CH_3), 3.66 (triplet, J = 9 Hz, 1H, C-17 $H\alpha$), 4.0–5.0 (multiplet, 3H, vinylic protons); mass spectrum *m/e* (relative intensity), 288(32), 287(100), 272(20), 269(15), 260(20), 245(25), 228(34).

Mol. Wt. Calcd. for $C_{19}H_{29}NO$: 287.2248. Found: 287.2254.

We are grateful to the British Columbia Heart Foundation and the National Research Council of Canada for financial support, and to Professor E. W. Warnhoff for preprints.

1. (*a*) C. Schöpf. Experientia, **17**, 285 (1961); (*b*) G. Habermehl. Naturwissenschaften, **53**, 123 (1966); (*c*) G. Habermehl. *In* The alkaloids. Vol. IX. *Edited by* R. H. F. Manske. Academic Press, Inc. New York, N.Y. 1967. p. 427; (*d*) G. Habermehl. *In* Progress in organic chemistry. Vol. VII. Butterworth, London. 1968. p. 35.
2. O. Gessner and G. Urban. Arch. Exptl. Pathol. Pharmakol. **187**, 378 (1937) and earlier papers.
3. (*a*) S. Hara and K. Oka. J. Am. Chem. Soc. **84**, 1041 (1967); (*b*) K. Oka and S. Hara. Tetrahedron Lett. 1987 (1969).
4. Y. Shimizu. Tetrahedron Lett. 2919 (1972).
5. M. H. Benn and R. Shaw. Chem. Commun. 288 (1973).
6. G. Habermehl and A. Haaf. Z. Naturforschg. **23b**, 1551 (1968).
7. G. Habermehl and A. Haaf. Liebigs Ann. Chem. **722**, 155 (1969).
8. (*a*) K. Oka and S. Hara. Tetrahedron Lett. 1193 (1969); (*b*) K. Oka and S. Hara. Tetrahedron Lett. 1189 (1969).
9. O. Jeger and H. Wehrli. Swiss Patent No. 482,721 (1970); Chem. Abstr. **72**, 121834 (1970).
10. J. K. Paisley and L. Weiler. Tetrahedron Lett. 261 (1972).
11. A. J. Liston. J. Org. Chem. **31**, 2105 (1966).
12. C. W. Shoppee and G. Kruger. J. Chem. Soc. 3641 (1961).
13. G. Habermehl and A. Haaf. Tetrahedron Lett. 3815 (1969).
14. (*a*) K. Oka and S. Hara. Chem. Ind. London, 911 (1968); (*b*) K. Oka and S. Hara. Chem. Ind. London, 168 (1969).
15. (*a*) V. Burchardt and T. Reichstein. Helv. Chim. Acta, **25**, 821 and 1434 (1942); (*b*) L. Ruzicka, V. Prelog, and P. Meister. Helv. Chim. Acta, **28**, 1251 (1945).
16. S. Hara, N. Matsumota, and M. Takeuchi. Chem. Ind. London, 2086 (1962).
17. M. Uskoković, J. Gutzwiller, and T. Henderson. J. Am. Chem. Soc. **92**, 203 (1970).
18. (*a*) E. H. White. J. Am. Chem. Soc. **77**, 6011 and 6014 (1955); (*b*) H. R. Nace and A. C. Watterson. J. Org. Chem. **31**, 2109 (1966).
19. J. K. Paisley. Ph.D. Thesis. University of British Columbia, Vancouver, British Columbia. 1973.
20. L. F. Fieser and M. Fieser. Steroids. Reinhold Publishing Corp. New York, N.Y. 1959. Chap. 8.
21. (*a*) E. Caspi, Y. Shimizu, and S. N. Balasubrahmanyam. Tetrahedron, **20**, 1271 (1964). (*b*) W. G. Dauben, R. A. Michili, and J. F. Eastman. J. Am. Chem. Soc. **74**, 3852 (1952); (*c*) L. F. Fieser and X. A. Dominguez. J. Am. Chem. Soc. **75**, 1704 (1953); (*d*) M. Rubin and B. H. Ambrecht. J. Am. Chem. Soc. **75**, 3513 (1953); (*e*) B. Camerino, B. Patelli, and R. Sliaky. Tetrahedron Lett. 554 (1961); (*f*) R. O. Clinton, R. L. Clarke, F. W. Stonner, A. J. Manson, K. K. Jennings, and D. F. Phillips. J. Org. Chem. **27**, 2800 (1962); (*g*) A. K. Rose, G. Mina, M. S. Manhas, and E. Rzucidlo. Tetrahedron Lett. 1467 (1963); (*h*) M. Garodetsky, E. Levy, R. D. Youssefyeh, and Y. Mazur. Tetrahedron, **22**, 2039 (1966).
22. F. Johnson. Chem. Rev. **68**, 375 (1968).
23. (*a*) I. S. Y. Wang and E. W. Warnhoff. Chem. Commun. 1158 (1969); (*b*) J. B. Stothers, I. S. Y. Wang, D. Ouchi, and E. W. Warnhoff. J. Am. Chem. Soc. **93**, 6702 (1971).
24. (*a*) J. C. Sheehan and R. M. Wilson. J. Am. Chem. Soc. **89**, 3457 (1967); (*b*) D. H. R. Barton, P. D. Magnus, and M. J. Pearson. Chem. Commun. 550 (1969).
25. (*a*) Y. Satoh, M. Mukoh, Y. Ogaki, T. Takahasi, T. Kimura, H. Aoki, and A. Hagitani. Chem. Pharm. Bull. Tokyo, **39**, 855 (1966); (*b*) T. Takahasi, Y. Satoh, and A. Hagitani, Nippon Kagaku Zasshi, **89**, 974 (1968); Chem. Abstr. **70**, 78247 (1969); (*c*) E. W. Warnhoff and I. S. Y. Wang. Personal communication. 1971.
26. L. F. Fieser and M. Romero. J. Am. Chem. Soc. **75**, 4716 (1953).
27. K. L. Williamson and W. S. Johnson. J. Org. Chem. **26**, 4563 (1961).
28. K. Takeda, T. Okanishi, H. Osaka, A. Shimaoka, and N. Aezono. Chem. Pharm. Bull. Tokyo, **9**, 388 (1961).
29. K. Tori, T. Komeno, and T. Nakagawa. J. Org. Chem. **29**, 1136 (1964).
30. R. F. Zurcher. Helv. Chim. Acta, **46**, 2054 (1967).
31. K. L. Williamson, J. I. Coburn, and M. F. Herr. J. Org. Chem. **32**, 3934 (1967).
32. J. Y. Satoh and T. T. Takahashi. Chem. Commun. 1714 (1970).
33. J. R. Hanson and T. D. Organ. J. Chem. Soc. C, 1065 (1970).
34. P. L. Julian, L. Bauer, C. L. Bell, and R. E. Hewitson. J. Am. Chem. Soc. **91**, 1690 (1969).

35. R. NOYORI, Y. HAYOKAUA, M. FUNAKURA, H. TAKAYA, S. MURAI, R. KOBAYASHI, and S. TSUTSUMI. J. Am. Chem. Soc. **94**, 7202 (1972).
36. R. L. AUTRY and P. W. SCULLARD. J. Am. Chem. Soc. **90**, 4924 (1968).
37. R. K. HILL. J. Org. Chem. **27**, 29 (1962).
38. C. W. SHOPPEE and S. K. ROY. J. Chem. Soc. 3774 (1963).
39. S. ITO, H. TAKESHITA, and M. HIRAMA. Tetrahedron Lett. 1181 (1971).
40. C. W. M. GRANT. Ph.D. Thesis, University of British Columbia, Vancouver, British Columbia. 1972.
41. R. B. RAO and L. WEILER. Tetrahedron Lett. 4971 (1973).

Can. J. Chem. Downloaded from www.nrcresearchpress.com by 210.87.254.5 on 09/05/12
For personal use only.

Metabolites of an Unidentified Fungus: a New 5,6-Dihydro-2-pyrone Related to Pestalotin

GEORGE M. STRUNZ, CHRISTOPHER J. HEISSNER, MASATOSHI KAKUSHIMA, AND MERLYN A. STILLWELL

Canadian Forestry Service, P.O. Box 4000, Fredericton, New Brunswick

Received September 28, 1973

Spectroscopic and chemical studies, including correlation with pestalotin (LL-P880α), show that a new metabolite isolated from cultures of an unidentified fungus is 5-hydroxy-3-methoxy-6-oxo-2-decenoic acid δ-lactone.

Les études spectroscopiques et chimiques, contenant une correlation avec la pestalotine (LL-P880α), démontrent qu'un nouveau métabolite, isolé de cultures d'un champignon non-identifié est le δ-lactone de l'acide 5-hydroxy-3-méthoxy-6-oxo-2-decenoique.

Can. J. Chem., **52**, 825 (1974)

Can. J. Chem. Downloaded from www.nrcresearchpress.com by 210.87.254.6 on 09/05/12
For personal use only.

Tamura and co-workers (1) recently described the isolation and structure elucidation of pestalotin (**1**), a new 5,6-dihydro-2-pyrone displaying gibberellin synergism, produced by the phytopathogenic fungus *Pestalotia cryptomeriaecola*. The same compound, designated LL-P880α, was isolated from an unidentified *Penicillium* species by Ellestad *et al.* (2), and these workers further demonstrated the configuration at C-6 and -1′ to be *S*. We report here on the closely related substance **2** isolated, together with **1**, from culture filtrates of an unidentified fungus.[1]

The new metabolite, $C_{11}H_{16}O_4$, displayed i.r. absorption (CCl_4) at 1728 and 1630 cm^{-1} and u.v. λ_{max} 233 nm (ε 10 600). These features, together with n.m.r. signals corresponding to an olefinic hydrogen at δ 5.17 (1H, s) and methyl ether protons at δ 3.78 (3H, s), suggested a 4-methoxy-5,6-dihydro-2-pyrone (1–5). In the mass spectrum, the base peak at *m/e* 127 ($M^+ - 85$) and an ion at *m/e* 85 ($C_5H_9O^+$) result from cleavage of an *n*-pentanoyl chain; further evidence for this structural element was found in the i.r. absorption at 1740 cm^{-1} (CO), and the appropriate methyl and methylene signals in the 220 MHz n.m.r. spectrum. A signal at δ 4.80 (1H, dd, $J_{AX} + J_{BX} \sim 14$ Hz) was attributed to the C-6 hydrogen by virtue of its low-field position and multiplicity,[2] and this assignment also defines the location of the side chain. These data are readily interpreted in terms of structure **2**.

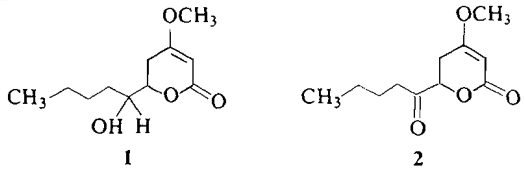

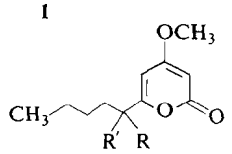

3 R=R′=O
4 R=H; R′=OH

Conversion of **2** into the corresponding pyrone, **3**, corroborated the assigned formulation. This transformation was effected directly (without isolation of a bromine-containing intermediate) by treatment of **2** with *N*-bromosuccinimide. To facilitate comparison with a simple model, 4-methoxy-6-methyl-2-pyrone, the carbonyl group in the side chain of **3** was reduced with sodium borohydride. The spectroscopic characteristics of the product, **4**, indeed showed a gratifying similarity to those of the model α-pyrone. Thus, **4** displayed (besides broad hydroxyl absorption at 3390 cm^{-1}) i.r. peaks (CCl_4) at 1737, 1650, and 1242 cm^{-1}; and u.v. λ_{max} (EtOH) 211 (ε 7420) and 282 nm

[1]The fact that the organism could not be induced to sporulate has rendered identification impossible so far but suggests that it is neither a *Pestalotia* nor a *Penicillium* species. We thank Dr. L. P. Magasi of this laboratory for providing the culture, IT-6, and for discussions relating to its identification.

[2]The signal for the C-6 proton changed in a manner consistent with the assigned structure on reduction of the ketone function.

Can. J. Chem. Downloaded from www.nrcresearchpress.com by 210.87.254.6 on 09/05/12
For personal use only.

(ε 6730) (6). In the n.m.r. spectrum of **4**, the C-3 and -5 hydrogens were manifested as doublets at δ 5.46 and 6.13 p.p.m. ($J \sim 2$ Hz) (5). These data establish **4** as an α-pyrone and confirm the formulation **2** for the new metabolite.

The second major metabolite, $C_{11}H_{18}O_4$, was identified as **1** on the basis of its spectroscopic characteristics and a correlation with **2** effected by oxidation with the Jones reagent (7). Direct comparison of the hydroxylic metabolite with a sample of LL-P880α[3] established their identity.

Experimental

The 220 MHz n.m.r. spectra were recorded for solutions in deuteriochloroform on a Varian HR-220 instrument at the Canadian 220 MHz NMR Center, Ontario Research Foundation. Microanalysis was performed by Spang Microanalytical Laboratory, Ann Arbor, Michigan.

Production and Isolation of Metabolities

Filtrates from a synthetic medium[4] that had supported growth of the fungus (liquid shake culture, temperature *ca.* 22°) for 6 weeks were extracted thoroughly with chloroform. After removal of the solvent *in vacuo*, t.l.c. analysis of the brown residue revealed two major components. The mixture was chromatographed on a column of silica gel (Davidson Grade 923) and elution with chloroform – methylene chloride (6:4) afforded **2**, slightly contaminated by other products. The second major metabolite **1**, again containing small amounts of impurities, was eluted with chloroform. The less polar compound **2**, was purified by preparative-layer chromatography on silica gel plates, using the solvent system benzene–*n*-hexane–acetone (10:9:1). Metabolite **2** ($R_f \sim 0.7$) crystallized from ether–cyclohexane as colorless needles, m.p. 83–84°; $[\alpha]_D^{22}$ −4.3° (*c*, 0.266 in CH_3OH); i.r. (KBr) 1710, 1620, 1248, and 1230 cm^{-1} (for i.r., (CCl_4), and u.v. spectra see text); n.m.r. ($CDCl_3$; 220 MHz) δ 0.92 (3H, t, $J \sim 7$ Hz), 1.34 (2H, sextet, slightly broadened, $J \sim 7$ Hz), 1.59 (2H, quintet, slightly broadened, $J \sim 7$ Hz), 2.75 (4H, m, simplified by irradiation at both δ 1.59 and δ 4.80), 3.78 (3H, s), 4.80 (1H, dd, $J_{AX} + J_{BX} \sim 14$ Hz), and 5.17 (1H, s); mass spectrum (see text) *m/e* 212 (M^+).

Anal. Calcd. for $C_{11}H_{16}O_4$: C, 62.25; H, 7.60; O, 30.15. Found: C, 62.44; H, 7.32; O, 30.20.

Material eluted with chloroform (*vide supra*) was further purified on a preparative-layer plate of silica gel (benzene–*n*-hexane–acetone (10:7:3), $R_F \sim 0.4$). Crystallization from benzene–cyclohexane yielded pure **1** as colorless rectangular platelets, m.p. 83–85°, spectra identical with published data (1, 2) (i.r. (CCl_4) 3580, 3410, 1724, 1630, and 1223 cm^{-1}). The m.p. was undepressed on admixture with a sample of LL-P880α.[3]

Mol. Wt. Calcd. for $C_{11}H_{18}O_4$: 214.1205. Found: 214.1200.

Preparation of Pyrone 3: N-Bromosuccinimide (NBS) Treatment of 2

NBS (28 mg) was added to a solution of **2** (38 mg) in carbon tetrachloride (7 ml). The mixture was heated under reflux for 2.5 h while being irradiated with a tungsten lamp. When cool, the mixture was filtered, and the filtrates were washed with water and dried over $MgSO_4$. Removal of solvent under reduced pressure afforded 34 mg of almost colorless crystalline **3**. A sample, recrystallized from ether–cyclohexane, had m.p. 129–132°; i.r. (KBr) 1721, 1702, 1639, 1569, 1273, and 1257 cm^{-1}; i.r. (CCl_4) 1746, 1711, 1638, and 1247 cm^{-1}; u.v. λ_{max} (EtOH) 223 (ε 18 100) and 309 nm (ε 5350); n.m.r. ($CDCl_3$; 60 MHz) δ 0.93 (3H, poorly resolved t, $J \sim 6$Hz), 1.2 to 1.9 (4H, m), 2.90 (2H, t, $J \sim 7$ Hz), 3.88 (3H, s) (a trace of unreacted **2** was evidenced by a small peak at δ 3.77), 5.71 (1H, d, $J \sim 2$ Hz), 6.76 (1H, d, $J \sim 2$ Hz); mass spectrum, *m/e* 210 (M^+), 168 $(M - C_3H_6)^+$, 125 (base peak) $(M - C_5H_9O)^+$, 69 $(C_4H_5O)^+$.

Mol. Wt. Calcd. for $C_{11}H_{14}O_4$: 210.0892. Found: 210.0897.

Reduction of 3 to 4

The α-pyrone **3** (13 mg) in methanol (5 ml) was treated with sodium borohydride (1 mg) at −3° for 30 min. Work-up yielded 12 mg of yellow oily product, purified by preparative t.l.c. (silica gel plates, benzene–chloroform (4:1)) to give **4** as a colorless oil; i.r. and u.v. see text; n.m.r. ($CDCl_3$; 60 MHz) δ 0.92 (3H, poorly resolved t, $J \sim 6$ Hz), 1.17–2.65 (> 7H, m), 3.84 (3H, s) 4.37 (1H, m), 5.46 (1H, d, $J \sim 2$ Hz), and 6.13 (1H, d, $J \sim 2$ Hz); mass spectrum, *m/e* 212 (M^+), 125 $(M - C_5H_{11}O)^+$ (base peak).

Mol. Wt. Calcd. for $C_{11}H_{16}O_4$: 212. Found: 212.

Correlation of Metabolities

Metabolite **1** (20 mg, 0.0933 mmol) in acetone (5 ml) was treated with Jones' reagent (7) (0.25 ml, 0.668 mmol CrO_3) at 15–20°. After 30 min, work-up and recrystallization yielded a crystalline product, m.p. 83–84°, identified as **2** by comparison of i.r., u.v., n.m.r., mass spectra, t.l.c. behavior, and mixture m.p.

We thank Mr. A. I. Budd, University of Alberta, Edmonton, for the accurate mass measurements, and Ms. G. Aarts, Ms. M. Austria, and Dr. K. T. Kan, University of New Brunswick, for mass spectra and optical rotation measurements.

[3]Kindly provided through the courtesy of Dr. E. L. Patterson, Lederle Laboratories, New York.

[4]The culture medium was the basal synthetic medium of Jennison *et al.* (8) with added KCl (0.1 g/l) and p*H* adjusted to 3.5 with HCl.

1. Y. Kimura, K. Katagiri, and S. Tamura. Tetrahedron Lett. 3137 (1971).
2. G. A. Ellestad, W. J. McGahren, and M. P. Kunstmann. J. Org. Chem. **37**, 2045 (1972).
3. R. Hänsel, H. Rimpler, and L. Langhammer. Fresenius' Z. Anal. Chem. **218**, 346 (1966).
4. M. Julia and J. Pilard. Bull. Soc. Chim. Fr. 651 (1964).
5. P. Beak and H. Abelson. J. Org. Chem. **27**, 3715 (1962).
6. J. D. Bu'Lock and H. G. Smith. J. Chem. Soc. 502 (1960).
7. K. Bowden, I. M. Heilbron, E. R. H. Jones, and B. C. L. Weedon. J. Chem. Soc. 39 (1946).
8. M. W. Jennison, M. D. Newcomb, and R. Henderson. Mycologia, **47**, 275 (1955).

Formation of the Radical Cations of Some Tetracyclic Aromatic Hydrocarbons in Boric Acid Glass

Z. H. KHAN AND B. N. KHANNA

Department of Physics, Aligarh Muslim University, Aligarh 202001, India

Received July 23, 1973

The radical cations of tetracene, chrysene, 1,2-benzanthracene, and 3,4-benzphenanthrene have been produced in boric acid glass by u.v. irradiation. Their electronic spectra are recorded in the region 200–1400 nm and show a close resemblance to the available data for the cations reported earlier.

Les radicaux cations du tétracène, du chrysène, du benzo[*a*]anthracène et du benzo[*c*]phénanthrène ont été générés par irradiation ultraviolette dans du verre à l'acide borique. Leur spectre électronique a été mesuré dans la région de 200–1400 nm et ils ressemblent tous aux spectres des cations rapportés antérieurement. [Traduit par le journal]

Can. J. Chem., **52**, 827 (1974)

Can. J. Chem. Downloaded from www.nrcresearchpress.com by 210.87.254.42 on 09/05/12
For personal use only.

A study of the electronic spectra of the tetracyclic aromatic hydrocarbons reveals that their electronic transitions show some systematic variations from one hydrocarbon to another (1). On the basis of this fact one may also think of some correlation in their ionic spectra as well; such correlation is hitherto unknown and may be very interesting and useful to investigate. However, at present this is not possible due to lack of theoretical and experimental data for these ions. Therefore, the present communication limits itself to a method of producing the radical ions of tetracyclic aromatic hydrocarbons and the recording of their complete electronic spectra which may in future be helpful in studying the correlation among their electronic transitions.

Although the formation of the radical ions of some tetracyclic hydrocarbons has been reported in certain matrices (2–4), their electronic spectra have not been recorded in detail and in many cases only the values of the absorption peaks are mentioned in the literature. In the present note we report the electronic absorption spectra of tetracene, chrysene, 1,2-benzanthracene, and 3,4-benzphenanthrene in boric acid glass after irradiation with the u.v. light of a high-pressure mercury lamp. These spectra are shown in Fig. 1. The boric acid glass is found to be the most suitable matrix for making studies in the region 200–1400 nm at room temperature, at which it forms a rigid solution. On irradiation, the tetracene-doped boric acid film retained its yellow color, while the colorless glass of chrysene acquired permanent yellow color and those of 1,2-benzanthracene and 3,4-benzphenanthrene became permanently brown. When the irradiated films were heated to about 110 °C, most of the bands which appeared after irradiation vanished and the films regained their original colors.

On the basis of the studies on optical and e.s.r. spectra of some aromatic hydrocarbons in boric acid glass irradiated with u.v. light, Hoijtink and co-workers (5) and other workers (6, 7) have drawn the conclusion that during irradiation the formation of monopositive ions of the hydrocarbons takes place. But the mechanism of photooxidation could be established only after extensive investigations carried out by Porter and coworkers (8), Joussot-Dubien and co-workers (9), Magat (10), Kieffer and co-workers (11), and Walentynowicz *et al.* (12) on the thermoluminescence of molecular solids in boric acid glass and other rigid matrices. It was found that the photooxidation in boric acid glass is a biphotonic process with the participation of the triplet state of the parent hydrocarbon. The photochemical reaction may be written as

$$[1] \qquad A \xrightarrow{h\nu_1} A^* \longrightarrow {}^3A$$

$$[2] \qquad {}^3A \xrightarrow{h\nu_2} A^{**} \longrightarrow \dot{A}^+ + e^-$$

where the single asterisk (*) corresponds to an excited singlet state of the molecule and the double asterisk (**) to the molecule excited to higher triplet states. From the thermoluminescence studies it has become evident that the free electron ejected in this process is removed far from the vicinity of the parent ion and neutralized as atomic or molecular hydrogen (9).

The optical absorption spectrum of tetracene monopositive ion in boric acid glass shows a striking resemblance to the spectra of its anions (2) and cations (13) reported earlier and the same

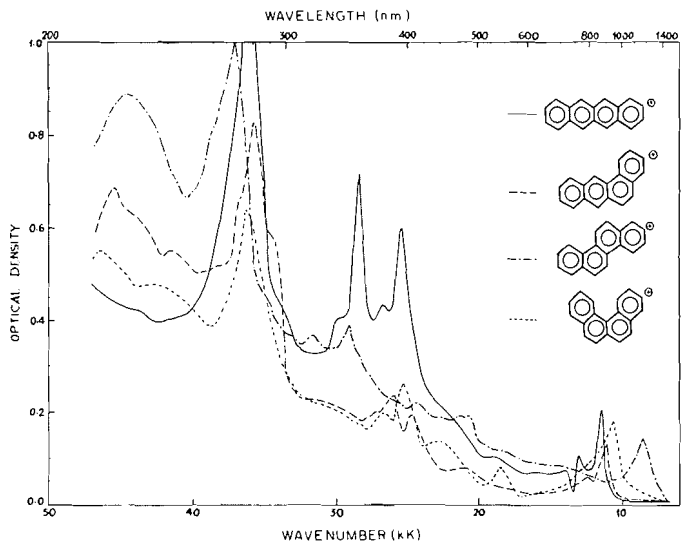

FIG. 1. Absorption spectra of the radical cations of tetracene — ; 1,2-benzanthracene --- ; chrysene ···· ; and 3,4-benzphenanthrene .... ; in boric acid glass irradiated with u.v. light at room temperature.

is expected on the basis of theoretical predictions also.

The positions of the absorption peaks of chrysene and 1,2-benzanthracene anions observed by Evans and Tabner (3) agree with our experimental results. Kira *et al.* (14) have recorded the transient spectrum of the monomer cation of 1,2-benzanthracene in benzonitrile solution in the region 11–14 kK which has a very strong band at 11.3 kK. This is very close to the band observed at 11.1 kK in the boric acid glass. Recently, Shida and Iwata (15) have produced the monopositive ions of tetracene, chrysene, and 1,2-benzanthracene in butyl chloride solution by γ-irradiation. Their spectra show a close resemblance to those recorded by us. The radical ions of 3,4-benzphenanthrene have not been produced so far and we are reporting here for the first time the electronic spectrum of its cation.

The spectra of all the monopositive ions under investigation have at least one thing in common: all of them show a very strong band in the near i.r. region. An extensive investigation of the spectra of all these cations is in progress.

The authors are thankful to Professor Rais Ahmed for his interest in this work and to Dr. Z. H. Zaidi for many fruitful discussions and suggestions. One of them (Z. H. K.) gratefully acknowledges the Council of Scientific and Industrial Research, India, for the award of a fellowship. We also thank Dr. T. Shida for sending us a preprint of his paper (ref. 15).

1. W. MOFFITT. J. Chem. Phys. **22**, 320 (1954); N. S. HAM and K. RUEDENBERG. J. Chem. Phys. **25**, 13 (1956).
2. P. J. ZANDSTRA. Ph.D. Thesis. Free University, Amsterdam. 1959; J. DIELEMAN and G. J. HOIJTINK. J. Chem. Phys. **42**, 1993 (1965).
3. A. G. EVANS and B. TABNER. J. Chem. Soc. 5560 (1963).
4. N. CHRISTODOULEAS and W. H. HAMILL. J. Am. Chem. Soc. **86**, 5413 (1964).
5. P. BENNEMA, G. J. HOIJTINK, J. M. LUPINSKI, L. J. OOSTERHOFF, P. SELLIER, and J. D. W. VAN VOORST. Mol. Phys. **2**, 431 (1959).
6. H. M. BUCK, W. TH. VAN DER LUGT, and L. J. OOSTERHOFF. Tetrahedron, **19** (Suppl. 2), 173 (1963).
7. G. VINCOW and P. M. JOHNSON. J. Chem. Phys. **39**, 1143 (1963).
8. W. GIBBSON, G. PORTER, and M. SAVADATTI. Nature, **206**, 1355 (1965).
9. R. LESCLAUX and J. JOUSSOT-DUBIEN. J. Chim. Phys. **61**, 1147 (1964); J. JOUSSOT-DUBIEN and R. LESCLAUX. J. Chim. Phys. **61**, 1631 (1964); R. LESCLAUX and J. JOUSSOT-DUBIEN. C.R. Acad. Sci. **263**, 1177 (1966); R. LESCLAUX and J. JOUSSOT-DUBIEN. J. Chim. Phys. **65**, 1313 (1968).
10. M. MAGAT. J. Chim. Phys. **63**, 142 (1966).
11. J. BULLOT, A. DEROULEDE, and F. KIEFFER. J. Chim. Phys. **63**, 150 (1966).
12. E. WALENTYNOWICZ. Acta Phys. Polon. **29**, 713 (1966); E. WALENTYNOWICZ. International Conference on Luminescence, Budapest. 1966; M. CZAJKOWSKI and E. WALENTYNOWICZ. Acta Phys. Polon. **34**, 633 (1968).
13. W. IJ. AALBERSBERG, G. J. HOIJTINK, E. L. MACKOR, and W. P. WEIJLAND. J. Chem. Soc. 3049, 3055 (1959); K. KIMURA, T. YAMAZAKI, and S. KATSUMATA. J. Phys. Chem. **75**, 1768 (1971).
14. A. KIRA, S. ARAI, and M. IMAMURA. J. Phys. Chem. **76**, 1119 (1972).
15. T. SHIDA and S. IWATA. J. Am. Chem. Soc. **95**, 3473 (1973).

Can. J. Chem. Downloaded from www.nrcresearchpress.com by 210.87.254.42 on 09/05/12
For personal use only.

A Selective Determination of the Proton Nuclear Relaxation Times of the Alkaloid Vindoline: An Extension via Fourier Transform Measurements[1]

L. D. HALL[2] AND CAROLINE M. PRESTON[3]

Department of Chemistry, The University of British Columbia, Vancouver 8, British Columbia

Received February 16, 1973[4]

A Fourier Transform method has been used to measure the spin–lattice relaxation times of essentially all the protons of the alkaloid, vindoline. It is shown that even for a molecule of this size substantial and potentially useful differences exist in the experimental relaxation times which reflect the degree of crowding of each proton by other protons.

On a utilisé la méthode de transformation de Fourier pour mesurer les temps de relaxation spin–réseau de pratiquement tous les protons de l'alkaloide vindoline. On montre que même pour une molécule de cette taille des différences appréciables et potentiellement utiles existent dans les temps de relaxation expérimentaux qui sont le reflet du degré d'encombrement de chaque proton par les autres protons. [Traduit par le journal]

Can. J. Chem., **52**, 829 (1974)

Can. J. Chem. Downloaded from www.nrcresearchpress.com by 210.87.254.5 on 09/05/12
For personal use only.

As part of a program to evaluate the diagnostic potential of proton nuclear relaxation times in organic chemistry, we previously studied (1) the alkaloid vindoline using the selective, audio-frequency-pulse technique. Although it proved possible to measure the T_1 and T_2 relaxation times of some of those protons that were clearly separated from all other resonances, it was found that the frequency selectivity of the technique used was insufficient for a detailed examination of all of the individual protons. We now show that the superior selectivity of the Fourier Transform method makes feasible a more comprehensive evaluation of longitudinal relaxation times (T_1 values).

Before discussing the results obtained for vindoline it is appropriate to mention briefly some of the difficulties associated with the measurement and subsequent interpretation of the longitudinal relaxation times of the protons of a complex organic molecule.

At the experimental level, the presence of cross-relaxation (*vide infra*) will often result in the individual transitions of a spin-coupled multiplet having different T_1 values. Even assuming that satisfactory procedures can be evolved to average these values and allow for nonexponential T_1 decays, any experimentally determined T_1 value is a composite one, containing contributions from a number of different relaxation sources; as a result, any *quantitative* interpretation of the significance of an individual T_1 value will generally be exceedingly difficult.

Fortunately for the organic chemist interested in using proton T_1 values as the basis of gross structural assignments, neither of the above sources of difficulty needs necessarily provide an insurmountable problem, although either may. If studies are made of an organic substance undergoing isotropic motion in a pure, dilute solution in a magnetically inert solvent, then the intramolecular dipole–dipole mechanism provides a major, and possibly exclusive, relaxation pathway. Since this mechanism has the form

$$\frac{1}{T_1} \propto \frac{1}{r^6}$$

meaningful intercomparisons can be made between the T_1 values of chemically similar protons (*i.e.*, CH with CH, CH_2 with CH_2, etc.) that may serve to assign molecular configuration. Another relaxation mechanism that can be operative involves the motion of the individual proton sites within a molecule; we shall discuss briefly later on the complication that this introduces.

The longitudinal relaxation times (T_1 values) of essentially all the protons of vindoline were

[1]Part III of a series entitled, "Applications of pulsed nuclear magnetic resonance spectroscopy." For Part II see ref. 7.

[2]Alfred P. Sloan Foundation Research Fellow, 1971–1973.

[3]Recipient of an NRCC 1967 Science Scholarship.

[4]Revision received October 31, 1973.

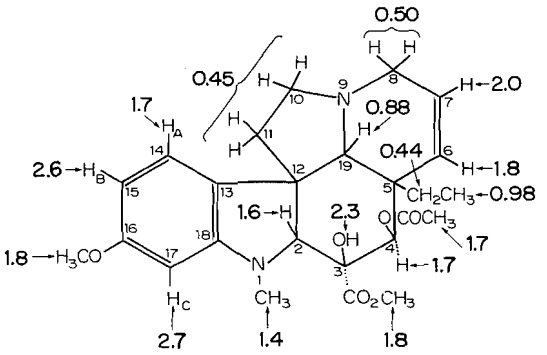

FIG. 1. Structural formula of vindoline showing the values (in seconds) of the longitudinal relaxation times (T_1 values) of the individual protons. The numerical values quoted are the mean of the values observed for the individual transitions. For a discussion of the values for H-14, H-15, and H-17 see the text.

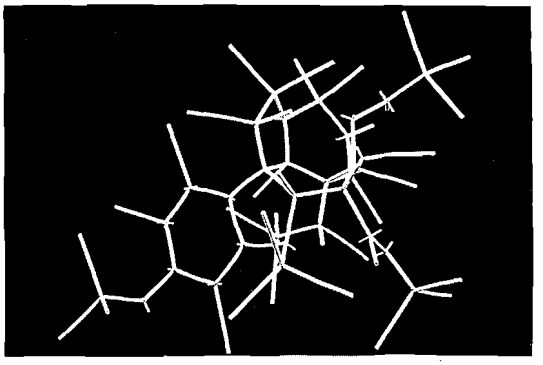

FIG. 2. A photograph of a molecular model of vindoline showing the overall spatial distribution of the proton substituents. Note that all of the methyl groups project towards the periphery of the molecule and that they and other peripheral protons generally have the longer relaxation times.

determined as described in the experimental section; these data are listed in Fig. 1. For many of the spin-coupled multiplets, the T_1 values of the individual transitions were identical within experimental error (±5%). However a notable exception to this generalization was observed for the protons of the aromatic ring: H-14, H-15, and H-17. These form part of a closely-coupled, ABC spectrum and the T_1 values of the multiplet components varied widely; for example, the T_1 values for the four transitions of the H-14 quartet were 2.55, 2.58, 3.17, and 3.16 s (in order from low, to high field). According to Freeman (3) this differential is due to cross-relaxation and is only significant for closely coupled spin systems (AB, ABC, etc.) for which each of the individual nuclei of this system have their principal relaxation *with different external* sources. For our particular system, the external relaxation of H-14 is likely with the methylene protons at position 11, whereas that of H-15 could be the methoxyl group at C-16 and that of H-17 the *N*-methyl group. The relaxation times given for H-14, H-15, and H-17 in Fig. 1 are the mean of the values obtained for the individual transitions.

It is interesting to note that the T_1 values for vindoline, given in Fig. 1 range from 0.5 to *ca.* 3.0 s; this significant differential bodes well for future studies of other large organic molecules.[5]

Inspection of molecular models of vindoline and of the photograph given in Fig. 2 serves to delineate some of the dependencies that are consistent with the effective operation of intramolecular dipole–dipole relaxation. Dealing first with the C—H protons, it is noteworthy that the protons near the center of the molecule, and hence nearest to other protons, have somewhat shorter relaxation times than those directed towards the periphery. Of those protons on the periphery, the ones having the shorter T_1 values are also the ones that have closer steric interactions with other protons. For example, H-14 is quite close to protons on positions 10 and 11 whereas H-15 and H-17 can only relax[6] via the protons of the methyl groups located at positions 1 and 16, and these groups are further away. A similar rationale can be proffered for the shorter T_1 value of H-6 compared with H-7; the former is rather close to the methyl protons of the C_5-ethyl moiety. The low values of the methylene protons at positions 8, 10, and 11 are also consistent with the fact that they are all in close array.

The situation for the four methyl resonances is more complex and illustrates nicely why any too ambitious interpretations of T_1 values on the sole basis of dipole–dipole interactions may be misleading. The resonances of the *N*-methyl and the acetate-methyl group had previously been assigned (4), but no distinction had been made between the methoxyl and carboxymethyl resonances. Although one of these resonances gave

[5]The fact that the four T_1 values previously reported for this compound are significantly smaller than those given here is due to a number of reasons. Importantly, the previous study was made in deuterochloroform solution, without degassing. It is also possible that some relaxation could have occurred during the rather long pulses used previously.

[6]Remember that these three protons show significant cross relaxation and hence their T_1 values are subject to appreciable systematic errors.

Can. J. Chem. Downloaded from www.nrcresearchpress.com by 210.87.254.5 on 09/05/12
For personal use only.

Can. J. Chem. Downloaded from www.nrcresearchpress.com by 210.87.254.5 on 09/05/12
For personal use only.

TABLE 1. Data concerning the proton longitudinal relaxation times (s) of the methyl resonances of vindoline

Resonance	T_1 value	Apparent T_1 values obtained from a semi-log plot for the time periods (s) listed below				
		0.8	1.3	2.0	2.4	3.6
—OCH_3	1.8	1.34	1.57	—	1.83	2.11
—OCH_3	1.8	1.68	1.69	1.76	1.80	1.89
—NCH_3	1.4	1.21	1.28	1.38	1.45	1.63
—$OCOCH_3$	1.7	1.37	1.45	—	1.69	2.03

a completely exponential T_1 decay curve, the other three showed decidedly nonexponential decays.[7] It was difficult to obtain any meaningful T_1 value for these resonances since the apparent value depended on how much of the decay curve was used (Table 1); the data given in Fig. 1 are for a plot out to 1.2 times the nominal T_1 value.

The numerical uncertainty of these data does not preclude any chemically useful comparisons simply because there are other serious problems. At the qualitative level it would, anyway, be difficult to simply compare the methyl values with those of the other protons attached directly to the skeleton of the molecule because allowance would have to be made for the extra degrees of motional freedom of the methyl groups. Furthermore, at the qualitative level there still appears to be some controversy as to the influence of the coupled motion of the three protons of a methyl group (5).

In spite of these many difficulties it is important to note that the measurements described here show that organic molecules of substantial molecular weight still have significant differentials between the relaxation times of individual protons. The enhanced frequency selectivity associated with the Fourier Transform method provides further encouragement that the diagnostic potential of proton T_1 values (2, 6, and 7) may be extended to quite complex molecules, in spite of the fact that explicit theory for interpreting such data is, as yet, unavailable. Other studies from this laboratory (7) have already shown that the method is most effective when several molecules are being compared, rather than when an isolated molecule is being studied.

[7]In an attempt to check whether this difference might lead to a means for distinguishing between the two methoxyl resonances a solution containing methyl benzoate, anisole, phenyl acetate, and acetone, each approximately 0.1 *M*, was studied. All of the methyl resonances gave nicely exponential T_1 decays and the T_1 values obtained in the standard way were, respectively, 10.9, 10.5, 10.7, and 20.6 s.

Experimental

All nuclear magnetic resonance measurements were made with a Varian XL-100 (15) Spectrometer, equipped with a Varian 620L (16K) computer programmed for a Fourier transform. The T_1 measurements were made with a standard programme that uses a 180°–90°–90° sequence and plots the spectra in the form $(M_0 - M_t)$. The sample of vindoline, kindly provided by Professor J. P. Kutney of this Department, was used as a 0.1 *M* solution in deuteriobenzene solution.

We have found that the following procedure leads to reliable values of the T_1 values. Initially all of the available data are plotted on a graph of "ln (peak height)" *vs.* "time", to give an approximate value of T_1. Then the part of the data obtained during the period up to about 1.2 times the estimated T_1 value is replotted and then the best, least-squares, slope taken. The advantage of this procedure is that it provides a sensible weight to the initial data points against the nonexponential components that sometimes occur during the later stages of the decay. Figure 3 shows a typical plot out to 2 times the T_1 value.

For most transitions the difference between this "initial slope" T_1 value and that obtained from a plot of the complete set of data is 10–20%. For those transitions that are part of a closely coupled spin system where cross-relaxation is significant the more difficult problem is the averaging of the T_1 values of the individual transitions; in the absence of any more fundamental method, the arithmetic mean is generally taken, but any intercomparisons involving that value are suitably discounted. In view of this and other difficulties, it is not sensible to make generalizations about the accuracy of T_1 values; indeed, for the purposes of most organo-chemical applications the experimental errors are almost irrelevant. Our own experience thus far suggests that the actual errors of the individual data points (*ca.* ± 5%) is of the same order, or is less than, the uncertainties arising from the complications of cross relaxation (10–20%). Thus we feel it is generally unwise to attempt to use T_1 values for any calculations that require an accuracy of ± 5% before they

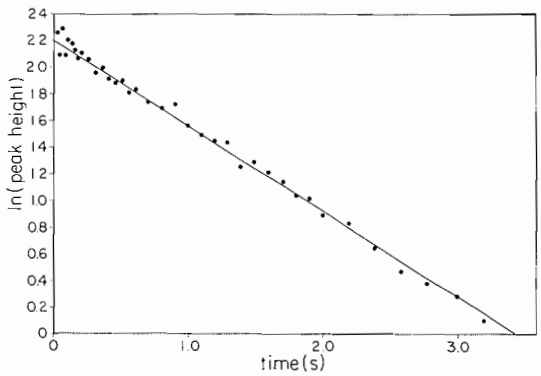

FIG. 3. Semi-log plot of the T_1 decay of the lower-field transition of the doublet resonance of H-14 of vindoline. The T_1 value assigned for this transition is 1.55 s.

are meaningful; if that high accuracy is required then extraordinary care is mandatory and the experiments must be repeated many times. Fortunately, all of the useful applications we have discovered thus far do not require this level of accuracy.

It is a pleasure to thank the National Research Council of Canada for their financial support of this work via operating grants (A-1905, to L.D.H.) and a 1967 Science Scholarship (to C.M.P.).

1. C. W. M. GRANT and L. D. HALL. Can. J. Chem. **50** 497 (1972).
2. T. L. PENDRED, A. M. PRITCHARD, and R. E. RICHARDS. J. Chem. Soc. (A), 1009 (1966).
3. R. FREEMAN. Personal communication. December 11, 1972; I. D. CAMPBELL and R. FREEMAN. J. Magn. Reson. **11**, 143 (1973).
4. M. GORMAN, N. NEUSS, and K. BIEMANN. J. Am. Chem. Soc. **84**, 1058 (1962).
5. L. G. WERBELOW and A. G. MARSHALL. J. Magn. Res. **11**, 299 (1973); J. Am. Chem. Soc. **95**, 5132 (1973).
6. L. D. HALL and C. M. PRESTON. Chem. Commun. 1319 (1972); Carbohydr. Reson. **27**, 286, 332 (1973).
7. L. D. HALL and C. M. PRESTON. J. Am. Chem. Soc. **95**, 7742 (1973).

Can. J. Chem. Downloaded from www.nrcresearchpress.com by 210.87.254.5 on 09/05/12
For personal use only.

Proton Spin–Spin Coupling Constants in Isothiazole, Isoxazole, and some of their Alkyl Derivatives

RODERICK E. WASYLISHEN,[1] J. BRIAN ROWBOTHAM,[2] AND TED SCHAEFER

Department of Chemistry, University of Manitoba, Winnipeg, Manitoba R3T 2N2

Received August 30, 1973

The signs and magnitudes of the spin–spin coupling constants over three to six bonds between protons in isothiazole, isoxazole, and in 10 of their alkyl derivatives are measured and discussed in terms of the coupling mechanisms. The chemical shifts of ring protons and methyl protons appear to arise from a common mechanism originating in the ring but are not simply related to electron densities calculated by molecular orbital theory at the CNDO/2 level of approximation.

On a évalué les signes ainsi que les grandeurs des constantes de couplage spin–spin incluant trois à six liaisons des protons dans l'isothiazole, l'isoxazole et dans dix de leurs dérivés alcoyles. On discute de ces données en fonction des mécanismes de couplage. Les déplacements chimiques des protons du cycle et des protons de groupes méthyles ne sont pas seulement reliés aux densités électroniques calculées à l'aide de la théorie des orbitales moléculaires (au niveau de l'approximation CNDO/2) mais aussi, semble-t-il, à un mécanisme commun provenant du cycle. [Traduit par le journal]

Can. J. Chem., **52**, 833 (1974)

Introduction

The signs and magnitudes of the proton–proton spin–spin coupling constants between ring protons and methyl protons, and between protons on different methyl groups are known for furan, thiophene, pyrrole, and a number of their derivatives (1–5). Similar data on five-membered rings containing two heteroatoms are relatively scarce and no signs are available (6–12). In this paper the signs and magnitudes of the three types of coupling constants are determined for isothiazole, **1**, and isoxazole, **2**, and for 10 of their alkyl derivatives. The data are discussed briefly in terms of coupling mechanisms.

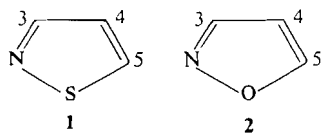

1 **2**

Experimental

Compounds

Isothiazole, isoxazole, and the three methylisothiazoles were obtained from Raylo Chemicals. The 3,5- and 4,5-dimethylisothiazoles were prepared by treating cold solutions of 3- and 4-methylisothiazoles in tetrahydrofuran, first with *n*-butyllithium and then with methyl iodide (13). Acidification and extraction with ether, followed by distillation of the dried extracts under reduced pressure, gave the products only slightly contaminated by starting materials.

The 4,5-dimethylisoxazole was prepared by condensing 2-butanone and ethyl formate with sodium metal in ether (14), followed by treatment of the collected salt with hydroxylamine hydrochloride (15). Extraction with carbon tetrachloride, followed by distillation of the extracts under reduced pressure, gave a mixture of the desired product with 5-ethylisoxazole. This mixture proved convenient for the p.m.r. studies. Previously (15) the second product had been identified as 3,4-dimethylisoxazole but we found no spectral evidence for it.

Trimethylisoxazole was prepared by the reaction between nitroethane and aqueous potassium carbonate (16, 17) and was isolated by distillation of the dried organic phase under reduced pressure.

5-Methylisoxazole and 3,5-dimethylisoxazole were obtained from Aldrich Chemical Co.

Proton Magnetic Resonance Spectra

The isothiazoles were prepared as degassed 10 mol % solutions in carbon disulfide, containing a small amount of tetramethylsilane as an internal reference material. Isoxazole, 13.7 mol %; 5-methylisoxazole, 10 mol %; 3,5-dimethylisoxazole, 21 mol %; and 3,4,5-trimethylisoxazole, 13.3 mol % were also dissolved in carbon disulfide. The approximately 50:50 mixture of 5-ethylisoxazole and 4,5-dimethylisoxazole contained a small amount of TMS and was degassed.

The p.m.r. spectra were repeatedly calibrated on HA-60-I or HA-100D spectrometers at sweep rates of 0.01–0.02 Hz/s in the frequency sweep mode. Double irradiation experiments were carried out in the usual way (18). The resonance of H_3 was always broad due to incompletely relaxed coupling to the ^{14}N nucleus, just as for H_2 in pyridine. Thus the coupling $^4J^{H_3,H_5}$ in isothiazole and in isoxazole could be shown to have the same sign as $^3J^{H_3,H_4}$ but the sign of the ratio $^3J^{H_3,H_4}/^3J^{H_4,H_5}$ could not be determined.

[1]NRCC scholarship, 1971–1972.
[2]Postdoctoral fellow, 1971–1973.

Can. J. Chem. Downloaded from www.nrcresearchpress.com by 210.87.254.6 on 09/05/12
For personal use only.

Can. J. Chem. Downloaded from www.nrcresearchpress.com by 210.87.254.6 on 09/05/12
For personal use only.

TABLE 1. Chemical shifts* and proton–proton coupling constants in Hz in isoxazole, isothiazole and some methyl derivatives

Compound†	X	ν_3	ν_4	ν_5	$^3J_{34}$	$^4J_{35}$	$^3J_{45}$	$^4J_o^{H,CH_3}$	$^5J_m^{H,CH_3}$	$^5J_o^{CH_3,CH_3}$	$^6J_m^{CH_3,CH_3}$
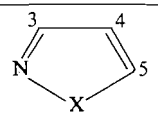	O	814.8	627.90	838.67	1.78	0.27	1.69	—	—	—	—
	S	841.2	719.01	859.90	1.66	0.15	4.66	—	—	—	—
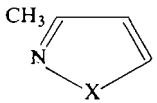	S	243.39	691.22	843.24	—	—	4.55	−0.27	0.51	—	—
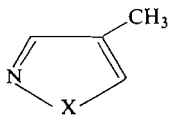	S	813.2	230.08	810.50	—	0.33	—	−0.44(3) −0.98(5)	—	—	—
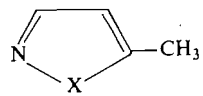	O	801.7	593.03	239.44	1.75	—	—	−0.89	0.64	—	—
	S	814.8	684.57	253.76	1.63	—	—	−1.00	0.55	—	—
	EtO	807.9	597.75	271.75‡	1.74	—	—	−0.91	0.59	—	—
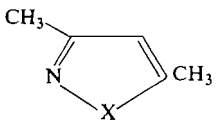	O	210.90	572.99	226.03	—	—	—	−0.33(3) −0.90(5)	—	—	−0.22
	S	231.56	659.87	247.68	—	—	—	−0.25(3) −1.00(5)	—	—	−0.23
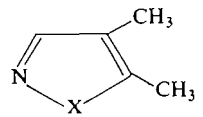	O	794.7	188.10	223.09	—	—	—	−0.43	0.63	0.71	—
	S	797.7	211.95	236.02	—	—	—	−0.45	0.59	0.60	—
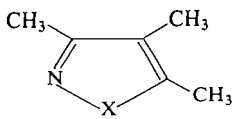	O	204.98	180.89	218.43	—	—	—	—	—	0.0±0.03 0.70(5)	−0.20

*In Hz at 100 MHz to low field of int ernal tetramethylsilane.
†In CS_2 solution at concentrations given unde r experimental, 5-methyl- and 5-ethylisoxazole as a 50:50 mixture.
‡ν_{CH_3} at 122.37 Hz; $^3J^{CH_2,CH_3}$ = 7.60 Hz.

Can. J. Chem. Downloaded from www.nrcresearchpress.com by 210.87.254.6 on 09/05/12
For personal use only.

Results and Discussion

Spectral Analysis

Spectra were analyzed with the computer program LAME (19). Only one or two transitions could be assigned in the broad resonance from H_3. All other transitions were assigned and the r.m.s. errors ranged from 0.0055 to 0.0184 Hz. The standard deviations in the spectral parameters ranged from 0.002 to 0.012 Hz but were generally well below 0.01 Hz. The spectral parameters are given in Table 1. The signs of the coupling constants in Table 1 rest on the assumption that $^3J_o^{H,H}$ is positive, as in thiophene and furan.

Molecular Orbital Calculations

The geometry of isoxazole was taken from an X-ray study of 5,5′-biisoxazole (20, 21) and was very close to that used by other workers (22). That of isothiazole was derived from a microwave study (23). Molecular orbital calculations at the CNDO/2 (24) and INDO level (25) were performed on an IBM 360/65 computer, using the parameterization of Pople and Beveridge (24). Calculations at the INDO level (24) cannot be made in the presence of a sulfur atom. The π bond orders and total charge densities are given in structures **3** to **6**. The observed dipole moment of isoxazole is 2.9 ± 0.1 D (26). A previous CNDO/2 calculation gave 3.17 D for **4** (27) and another calculation gave 3.11 D (28).

Chemical Shifts

The ring proton shifts in isoxazole correlate qualitatively with the total charges on the adjacent carbon atoms as given in **4**, the highest electron density at carbon being paired with the most shielded proton. However, the charges in the hydrogen 1s orbitals possess the opposite gradation (see **3**). For isothiazole, **5** and **6**, such correlations do not exist. Thus the charge at C-5 is negative, yet H_5 has the lowest shielding of the three protons and is even less shielded than H_5 in isoxazole.

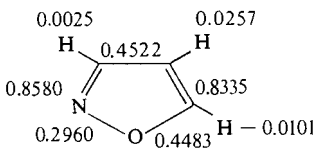

3

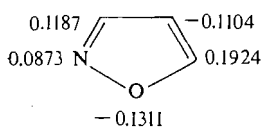

$\mu = 3.150$ (CNDO/2)
$\mu = 3.050$ (INDO)

4

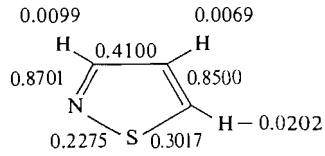

5

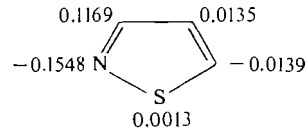

$\mu = 2.87$ D

6

The methyl proton shifts follow the order of the corresponding ring proton shifts; compare trimethylisoxazole with isoxazole, for example. The same shielding mechanism is presumably operative at both types of proton sites. The methyl proton shifts have a much lower range than the ring proton shifts, as expected if the intervening C—C bond attenuates an effect originating in the ring. The ring protons are more shielded in the presence of methyl groups, probably due to electron releasing or repelling properties of the latter.

The Coupling Constants

(a) Between Ring Protons

The values for $^3J_{45}$ of 1.69 Hz in **1** and 4.66 Hz in **2** differ little from those in furan, 1.75 Hz (29), and in thiophene, 4.90 Hz (29, 30). The presence of the electronegative nitrogen atom reduces $^3J_{34}$ substantially from its values of 3.30 and 3.50 Hz in furan and thiophene, respectively.

A marked decrease, from its values of 0.85 and 1.04 Hz in furan and thiophene, occurs for $^4J_{35}$, having values of 0.27 and 0.15 Hz in **1** and **2**. The methyl group replacement technique (31) indicates a π electron contribution to these couplings of -0.2 Hz (see last column of Table 1), so that a σ electron mechanism gives 0.5 and 0.3_5 Hz for $^4J_{35}$ in **1** and **2**, respectively.

Can. J. Chem. Downloaded from www.nrcresearchpress.com by 210.87.254.6 on 09/05/12
For personal use only.

(b) Between Ring Protons and Methyl Protons

(i) Over Four Bonds, $^4J_o^{H,CH_3}$

The values of $^4J_o^{H,CH_3}$ in Table 1 vary from -0.25 to -1.00 Hz. It is clear that the gross differences in magnitude depend on the difference in π bond order (32–34) of intervening C···C bonds of the ring (see **3** to **6**). For example, in 4-methylisothiazole $^4J_o^{H_5,CH_3} = -0.98$ Hz and $^4J_o^{H_3,CH_3} = -0.44$ Hz, corresponding to π bond orders of 0.85 and 0.41, respectively.[3] In toluene a π bond order of 0.67 corresponds to $^4J_o^{H,CH_3} = -0.75$ Hz (35) and in propene one has -1.7 Hz (36). The gross effects therefore arise from varying π electron contributions to the coupling.

Exhaustive studies of $^4J_o^{H,CH_3}$ in the methyl derivatives of the fluoropyridines (37) and molecular orbital calculations of $^4J_o^{H,CH_3}$ in toluene (38) indicate appreciable σ electron contributions to $^4J_o^{H,CH_3}$ in delocalized systems. The smaller differences in $^4J_o^{H,CH_3}$ in Table 1 can be rationalized in terms of the arguments developed for the pyridines (37). Thus, $^4J_o^{H,CH_3}$ is -0.27 Hz in 3-methylisothiazole but is -0.44 Hz in 4-methylisothiazole. An analogous situation exists in the 6-methyl and 5-methyl derivatives of the fluoropyridines and is attributable to the polarization of the σ electron core at C-6 by the nitrogen atom. The detailed arguments are given in ref. 37. The situation is somewhat analogous to propene where substitution by an electronegative substituent at C-2 causes a marked positive shift in ^4J but substitution at C-1 leaves the coupling unchanged (39).

If the nitrogen in **1** and **2** primarily polarizes the σ electron core at C-3 and reduces $^4J_o^{H,CH_3}$ when the methyl group is bonded to C-3 but not when it is bonded to C-4, then $^4J_o^{H,CH_3}$ in **7** and **8** should be similar in magnitude to $^4J_o^{H,CH_3}$ in **9** and **10**. In fact, all these couplings are equal to within experimental error (1, 2, 4). As it is relatively small anyway, the implied assumption that the π bond order of the intervening C···C bond is much the same in **7**–**10** is not crucial.

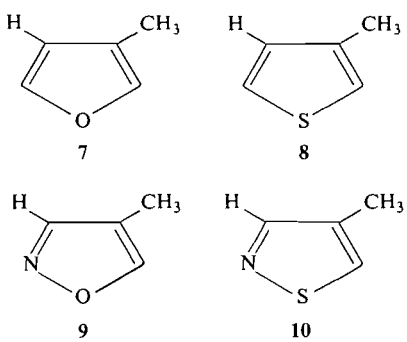

7 **8** **9** **10**

[3]The methyl group does not change the mobile bond order appreciably.

Again, if the oxygen and sulfur atoms serve mainly to polarize the σ core of the ring system, leaving the π electron contribution to the couplings unaffected, then $^6J_m^{CH_3,CH_3}$ should not vary for the compounds in Table 1, as observed. This coupling is presumably dominated by a π electron mechanism (40).

(ii) Over Five Bonds, $^5J_m^{H,CH_3}$

Varying from 0.51 to 0.64 Hz, this coupling is considerably larger in derivatives of **1** and **2** than of furan (1) and thiophene (4), in which it very nearly equals the 0.36 Hz observed in toluene (35). Now, the methyl group replacement technique (31) gives the π electron contribution to $^5J_m^{H,CH_3}$ as $|^6J_m^{CH_3,CH_3}|$. This magnitude is the same as in *m*-xylene (40) and in pyridine (37) derivatives. Consequently, in **1** and **2**, the larger magnitude of $^5J_m^{H,CH_3}$ may be assigned to a σ electron effect. The trend towards slightly larger values in the isoxazoles than in the isothiazoles may then arise from the higher electronegativity of oxygen, the presence of the electronegative nitrogen atom being responsible for the gross increase in the σ electron contribution to $^5J_m^{H,CH_3}$ on going from furan to **2** and from thiophene to **1**.

(c) Between Methyl Protons, $^5J_o^{CH_3,CH_3}$ *and* $^6J_m^{CH_3,CH_3}$

To a large extent $^5J_o^{CH_3,CH_3}$ is again dependent on the π bond order of the intervening C···C bond, as is particularly clear from the values of 0.10 and 0.70 Hz in the trimethylisoxazole (see also **3**). On the other hand, σ electron effects cannot be ruled out for a coupling over five bonds and these could possibly account for the difference of 0.1 Hz in $^5J_o^{CH_3,CH_3}$ for the 4,5-dimethyl derivatives of **1** and **2**, especially as the calculated π bond orders in **3** and **5** predict the larger value for the sulfur compound; contrary to observation. Nevertheless, the observed values of 1.2 Hz in *cis*-butene-2 (41), 0.40 Hz in a *m*-xylene derivative (40), and of 0.70 Hz in 2,3-dimethylthiophene (42) are in qualitative accord with a predominant π electron mechanism for $^5J_o^{CH_3,CH_3}$ in derivatives of **1** and **2**.

The values of $^6J_m^{CH_3,CH_3}$ have already been discussed above. For **1** and **2** we note that a coupling path via the heteroatoms would involve

seven bonds and would entail a positive coupling, as in a *p*-xylene derivative (4). However, in both **11** (3) and **12** (2), J^{CH_3,CH_3} is +0.55 Hz and the

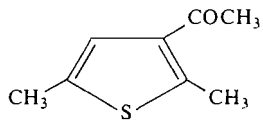

11

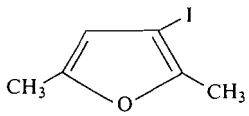

12

most efficient coupling path is apparently that over seven bonds via the carbon atom framework. We take this as a strong indication that in derivatives of **1** and **2** the coupling between protons in different methyl groups is transmitted to a negligible extent by the heteroatoms.

We are grateful to the National Research Council of Canada for financial assistance.

1. S. RODMAR, S. FORSÉN, B. GESTBLOM, S. GRONOWITZ, and R. A. HOFFMAN. Acta Chem. Scand. **19**, 485 (1965).
2. S. RODMAR, B. RODMAR, A. ALI KHAN, S. GRONOWITZ, and V. PAVULANS. Acta Chem. Scand. **20**, 2515 (1966).
3. B. GESTBLOM, S. GRONOWITZ, R. A. HOFFMAN, and B. MATHIASSON. Arkiv Kemi, **23**, 517 (1965).
4. H. J. JAKOBSEN and M. BEGTRUP. J. Mol. Spectrosc. **35**, 158 (1970); **40**, 276 (1971).
5. H. FUKUI, S. SHIMOKAWA, J. SHOMA, T. IWADARE, and N. ESUMI. J. Mol. Spectrosc. **35**, 521 (1971).
6. H. A. STAAB and A. MANNSCHRECK. Chem. Ber. **98**, 1111 (1965).
7. J. H. BOWIE, P. F. DONAGHUE, and H. J. RODDA. J. Chem. Soc. B, 1122 (1969).
8. P. HAAKE and W. B. MILLER. J. Am. Chem. Soc. **85**, 4044 (1963).
9. A. TAURINS and W. G. SCHNEIDER. Can. J. Chem. **38**, 1237 (1960).
10. A. PERICHARD, J-C. POITE, G. MILLE, and J-P. ROGGERO. Bull. Chem. Soc. Fr. 3830 (1972).
11. S. D. SOKOLOV, I. M. YUDINTSEVA, and P. V. PETROVSKII. Zh. Org. Khim. **6**, 2584 (1970).
12. R. C. ANDERSON. J. Heterocycl. Chem. **1**, 279 (1964).
13. M. P. L. CATON, D. H. JONES, R. SLACK, and K. R. H. WOOLDRIDGE. J. Chem. Soc. A, 446 (1964).
14. R. P. MARIELLA. J. Am. Chem. Soc. **69**, 2670 (1947).
15. R. JUSTONI. Rend. Ist. Lombardo Sci. **71**, 407 (1938); Chem. Abstr. **34**, 3268[3] (1940).
16. W. R. DUNSTAN and T. S. DYMOND. J. Chem. Soc. **59**, 410 (1891).
17. R. W. LOCKHART, K. W. NG, P. E. NOTT, and A. M. UNRAU. Can. J. Chem. **47**, 3107 (1969).
18. R. FREEMAN and W. A. ANDERSON. J. Chem. Phys. **37**, 2053 (1962).
19. C. W. HAIGH and J. M. WILLIAMS. J. Mol. Spectrosc. **32**, 398 (1969).
20. M. CANNAS and G. MARONGIU. Z. Krist. **127**, 388 (1968).
21. S. BIANGINI, M. CANVAS, and G. MARONGIU. J. Heterocycl. Chem. **6**, 901 (1969); Acta Cryst. **25**, 730 (1969).
22. R. D. BROWN, B. A. W. COLLER, and J. E. KENT. Theor. Chim. Acta, **10**, 435 (1968).
23. J. L. MEYER, J. DAVIDOVICS, J. CHOUTEAU, J-C. POITE, and J. ROGGERO. Can. J. Chem. **49**, 2254 (1971).
24. J. A. POPLE and D. L. BEVERIDGE. Approximate molecular orbital theory. McGraw-Hill Book Co., New York. 1970.
25. P. A. DOBOSH. Program No. 141. QCPE. Indiana University, Bloomington, Indiana.
26. W. C. MACKRODT, P. A. CURNUCK, A. WARDLEY, N. L. OWEN, and J. SHERIDAN. Chem. Commun. 692 (1966).
27. J. E. BLOOR and D. L. BREEN. J. Am. Chem. Soc. **89**, 6835 (1967).
28. D. W. DAVIES and W. C. MACKRODT. Chem. Commun. 345 (1967).
29. J. M. READ, C. T. MATHIS, and J. H. GOLDSTEIN. Spectrochim. Acta, **21**, 85 (1965).
30. D. M. GRANT, R. C. HIRST, and H. S. GUTOWSKY. J. Chem. Phys. **38**, 470 (1963).
31. R. A. HOFFMAN and S. GRONOWITZ. Arkiv Kemi, **16**, 563 (1960).
32. S. STERNHELL. Rev. Pure Appl. Chem. **14**, 15 (1964).
33. H. M. MCCONNELL. J. Mol. Spectrosc. **1**, 11 (1957).
34. K. D. BARTLE, D. W. JONES, and R. S. MATTHEWS. Rev. Pure Appl. Chem. **19**, 191 (1969).
35. M. P. WILLIAMSON, R. J. KOSTELNIK, and S. M. CASTELLANO. J. Chem. Phys. **49**, 2218 (1968).
36. A. A. BOTHNER-BY and C. NAAR-COLIN. J. Am. Chem. Soc. **83**, 231 (1961).
37. J. B. ROWBOTHAM and T. SCHAEFER. Can. J. Chem. **50**, 2344 (1972).
38. R. WASYLISHEN and T. SCHAEFER. Can. J. Chem. **50**, 1852 (1972).
39. M. BARFIELD. J. Am. Chem. Soc. **93**, 1066 (1971).
40. C. J. MACDONALD and W. F. REYNOLDS. Can. J. Chem. **48**, 1002 (1970).
41. R. K. HARRIS and R. R. HOWES. J. Mol. Spectrosc. **28**, 191 (1968).
42. S. GRONOWITZ, B. GESTBLOM, and R. A. HOFFMAN. Acta Chem. Scand. **15**, 1201 (1961).

Can. J. Chem. Downloaded from www.nrcresearchpress.com by 210.87.254.6 on 09/05/12
For personal use only.

Friedel–Crafts Condensations with Maleic Anhydrides. III.[1] The Synthesis of Polyhydroxylated Naphthoquinones

RICHARD HUOT AND PAUL BRASSARD

Département de Chimie, Université Laval, Québec, Québec

Received August 10, 1973

The condensation of hydroquinone ethers with an excess of dihalomaleic anhydrides has been found to give particularly good yields of dihalonaphthazarins. The etherification of the latter and the nucleophilic substitution of 2,3-dichloronaphthoquinones have been examined. Finally the structures of the products obtained from the Fries rearrangement of polyacetoxynaphthalenes have been definitively established.

La condensation d'éthers d'hydroquinones avec un excès d'anhydrides dihalogénomaléiques donne des rendements particulièrement élevés en dihalogénonaphtazarines. La méthylation de ces substances et la substitution nucléophile de dichloro-2,3 naphtoquinones ont été étudiées. Enfin la structure des produits obtenus lors de la transposition de Fries de polyacétoxynaphtalènes a été établie de façon définitive.

Can. J. Chem., **52**, 838 (1974)

Can. J. Chem. Downloaded from www.nrcresearchpress.com by 210.87.254.5 on 09/05/12
For personal use only.

Few methods exist for the formation of naphthazarins and none of these are very satisfactory. The syntheses of substituted compounds of this type (whether natural or otherwise), in spite of their apparent simplicity, are therefore usually quite tedious processes. We have attempted to improve the preparation of the basic structure and in principle render its derivatives more readily accessible.

The Preparation and Structure of Dihalonaphthazarins and of the Corresponding Ethers

Since its discovery by Zahn and Ochwat (1), the preparation of naphthazarins by the condensation of hydroquinones (or their ethers) (2) and maleic anhydrides in a molten mixture of aluminum and sodium chlorides has been frequently used. This method remains the most simple way of obtaining many naphthazarins but it suffers the serious inconvenience of giving rather low yields. We have found that the use of excess dichloromaleic anhydride can increase the yield quite spectacularly, in one case to 97%. Stoichiometric amounts of anhydride, dibromomaleic anhydride, and substituted hydroquinones give lower yields. Since the halogens can readily be removed (3), this modification also constitutes a convenient synthesis of some halogen-free naphthazarins.

The determination of oxidation–reduction potentials of quinones (4) and the analysis of the n.m.r. spectra of naphthazarins (5)[2] have shown that the latter exist mainly in the tautomeric form with the electron-withdrawing groups in the aromatic ring. These results suggest that the predominant tautomer of 2,3-dihalonaphthazarins should be **B** (Scheme 1). However the n.m.r. spectra of **2***a*, **2***b*, and **3** show only one signal at δ 7.33, 7.31, an 7.12, respectively, for ring protons and indicate that these compounds exist mainly with the halogens in the quinoid ring. (The spectrum of **3** could seem ambiguous but is in good agreement with other well established structures such as 6-ethyl-2-hydroxynaphthazarin, δ 7.13 (7-CH) (5).) The resonance effects which seem to predominate over other considerations in these cases apparently were not taken into account in earlier works.

The etherification of naphthazarins has not been studied extensively. Brass *et al.* (6) were not able to determine which isomer was isolated after the etherification of 2,3-dibromonaphthazarin. Bruce and Thomson (3) obtained two products by the methylation of chloronaphthazarin but the structure of only one was established. All other etherifications of naphthazarins yielded only one isomer. Hardegger *et al.* (7) however obtained both from javanicin but in this case the electronic effects of the substituents compete effectively.

We have methylated two 2,3-dihalonaphtha-

[1]For parts I and II see refs. 23 and 24, respectively.

[2]Halogenated naphthazarins are not specifically mentioned here.

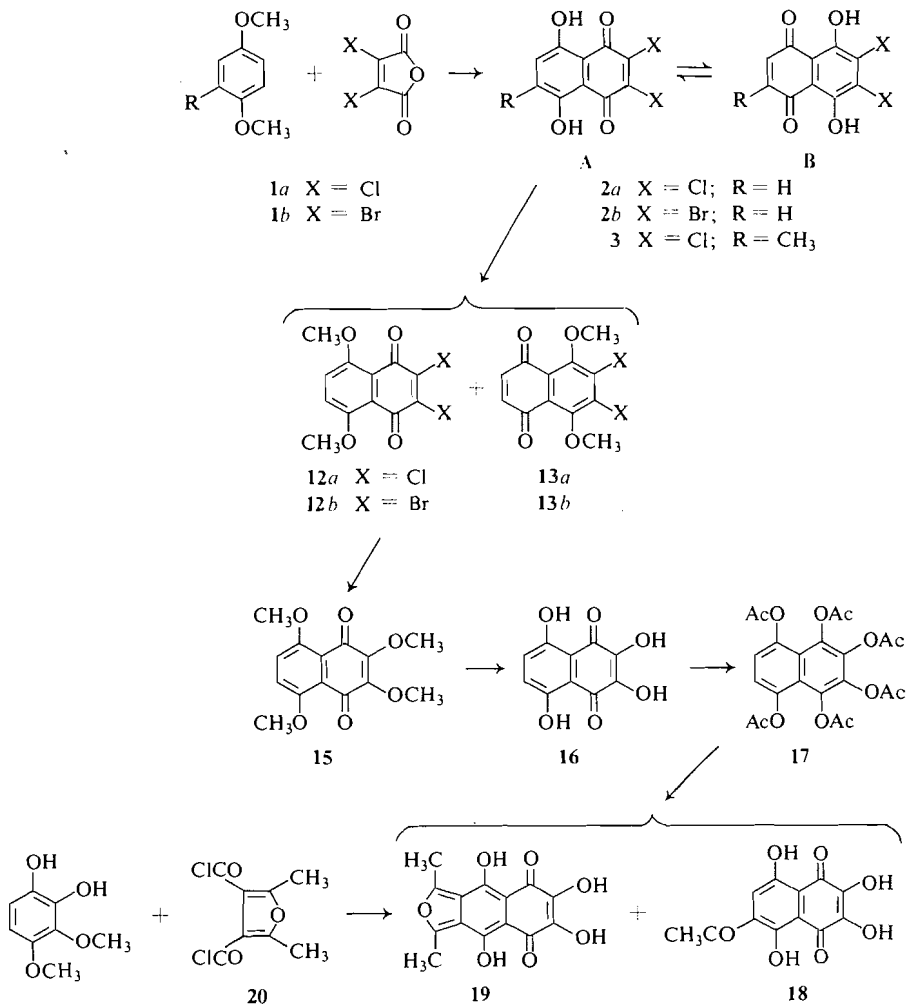

SCHEME I

zarins using methyl iodide and silver oxide and found that both isomers are formed. The main product invariably corresponds to the only discernible tautomer of the starting material. Furthermore these experiments established that a rapid etherification of the less stable tautomer plays an important role in this process.

Acetylation of a number of naphthazarins gives quite different results. This reaction with 2,3-dimethyl-, 2,3-dichloro-, 2,3-dibromo-, and 2,3-dibromo-6-methylnaphthazarins yields only the isomer corresponding to the most stable tautomer as shown by n.m.r. spectroscopy. Substrates with competing electronic effects such as 2-methyl-6- and 7-chloronaphthazarin give mixtures of isomers.

The Nucleophilic Substitution of Polyhalogenated Quinones

Since the main purpose in preparing the foregoing compounds was the synthesis of polyhydroxylated naphthoquinones, we have attempted, with various substrates, to find methods of improving the substitution of vicinal halogens.

The nucleophilic substitution of chloranil (**4**) even with strong bases (alkoxides and hydroxides) gives a mixture of the 2,5- and 2,6-disubstituted products (8). Although these undergo subsequent displacement to the completely substituted compound, the direct formation of tetramethoxybenzoquinone (**9**) using methoxide does not seem to have been recorded. The substitution of chloranil by methanol using potassium fluoride

Can. J. Chem. Downloaded from www.nrcresearchpress.com by 210.87.254.5 on 09/05/12
For personal use only.

Can. J. Chem. Downloaded from www.nrcresearchpress.com by 210.87.254.5 on 09/05/12
For personal use only.

as catalyst is claimed to yield only the 2,5-disubstituted product (9); we have repeated this procedure and found three products: trichloromethoxy- (**5**) (10%), 2,5-dichloro-3,6-dimethoxy- (**6**) (60%), and 2,6-dichloro-3,5-dimethoxybenzoquinone (**7**) (30%). When this reaction is carried out in a sealed tube at 110°, mixtures of chlorotrimethoxybenzoquinone (**8**) and tetramethoxybenzoquinone (**9**) are obtained. All of the foregoing substitution products are readily separated by column chromatography on silica gel (Table 1).

Although 2,3-dimethoxynaphthoquinone (**11**) is available from the dichloro compound **10** with sodium methoxide (10), a milder substitution was attempted. A direct displacement by methanol and potassium carbonate gave only 50% of the expected quinone **11** but when 2,3-dichloronaphthoquinone was converted to the diazido compound (11) (in a nearly quantitative yield) and the latter treated with potassium carbonate in boiling methanol, an 83% yield of **11** was obtained. The method is not applicable to chloranil as the substrate decomposes completely. Many attempts at direct substitution on dichloronaphthazarins confirmed the earlier findings as to the difficulty of this operation (12, 13). However the corresponding ether **12***a* was found to undergo efficient substitution in the presence of methoxide.

The Fries Rearrangement of Polyacetoxynaphthalenes

By diverse combinations of processes (reduction, nucleophilic and electrophilic substitution, etc.), a large number of polyhydroxynaphthoquinones are in principle readily accessible by the use of the foregoing intermediates. We have chosen the synthesis of 6-acetyl-2,3-dihydroxynaphthazarin (**18**) to illustrate the versatility of the method since this compound was once claimed to be a natural product (14) but was never adequately described (widely divergent m.p.'s have been attributed to the starting material, 1,2,3,4,5,8-hexaacetoxynaphthalene (15, 16); the end product gave an ambiguous analysis (16) and its m.p. was eventually found to indicate a mixture).

TABLE 1. The substitution of chloranil

Substrate	Conditions	Yield (%) 6 and 7	8	9
4	5 h at 95°	53	27	0
4	7 h at 110°	7	47	27
4	24 h at 110°	0	27	23
6	6 h at 105°	0	41	21
7	6 h at 105°	0	43	55

The hexaacetate of leucospinazarin (**17**) was subjected to various modifications of the Fries rearrangement and gave two products, one of which is undoubtedly the expected acetylspinazarin (**18**). The other appeared to be the furan resulting from a cyclization of the intermediate diacetyl derivative. An analogous structure has been proposed by Cort and Rodriguez (17) for a product obtained from 1,4,5,8-tetraacetoxynaphthalene. We have established both structures are correct by unambiguous syntheses. 1,3-Dimethylnaphtho[2,3-*c*]furan-4,9-quinone is prepared readily by the method of Nightingale and Sukornick (18) but the 5,8-dihydroxy derivative could be obtained only by condensing the substrates in a molten mixture of aluminum and sodium chlorides (Scheme 1).

Experimental

Dihalonaphthazarins

2,3-Dichloronaphthazarin (2a)

To a molten mass of $AlCl_3$ (142 g) and NaCl (28.3 g) at 140–150°, was added in portions a mixture of *p*-dimethoxybenzene (16.6 g) and dichloromaleic anhydride (**1***a*) (40.1 g). The temperature was then raised to 170–175° for 1–2 min and the dark red melt was allowed to cool, hydrolyzed with water (1.5 l) and concentrated HCl (100 ml), and allowed to stand overnight. 2,3-Dichloronaphthazarin (**2***a*) was then recovered by filtration and recrystallized from petroleum ether (b.p. 90–120°), m.p. 198–199° (97%) (lit. (19) m.p. 195°); ν_{max} (KBr) 1627, 1595 (sh), 1573 cm^{-1}; δ ($CDCl_3$) 7.33 s (6,7-CH), 12.36 s (5,8-OH).

Diacetate, m.p. 232–233° (lit. (3) m.p. 233°).

2,3-Dibromonaphthazarin (2b)

This compound was prepared as for the foregoing quinone using $AlCl_3$ (19.5 g), NaCl (3.90 g), *p*-dimethoxy benzene (1.60 g), and dibromomaleic anhydride (**1***b*) (6.16 g); m.p. 219–220° (petroleum ether) (77%) (lit. (19) m.p. 216.5°); ν_{max} (KBr) 1623, 1579, 1555 cm^{-1}; δ ($CDCl_3$) 7.31 s (6,7-CH), 12.43 s (5,8-OH).

2,3-Dichloro-6-methylnaphthazarin (3)

This quinone was obtained by the foregoing method using $AlCl_3$ (50 g), NaCl (10.0 g), 2,5-dimethoxytoluene (6.1 g), and dichloromaleic anhydride (13.4 g); m.p. 148–150° (petroleum ether) (75%); ν_{max} (KBr) 1630, 1573 cm^{-1}; δ ($CDCl_3$) 2.33 d (J = 1.3 Hz) (6-CH_3), 7.12 q (J = 1.3 Hz) (7-CH), 12.58 and 12.91 2 s (5,8-OH).

Anal. Calcd. for $C_{11}H_6O_4Cl_2$: C, 48.35; H, 2.21; Cl, 25.96. Found: C, 48.56; H, 2.29; Cl, 26.01.

Methylation of 2,3-Dichloronaphthazarin

A mixture of 2,3-dichloronaphthazarin (**2***a*) (5.2 g),

Can. J. Chem. Downloaded from www.nrcresearchpress.com by 210.87.254.5 on 09/05/12
For personal use only.

iodomethane (8 ml), freshly prepared silver oxide (8.0 g), and chloroform (100 ml) was stirred for 22 h at room temperature. The same amounts of iodomethane and silver oxide were added after 6 and 16 h. The residue after filtration and evaporation of the solvent was crystallized from a mixture of chloroform and carbon tetrachloride and gave 2,3-dichloro-5,8-dimethoxynaphthoquinone (**12***a*) (red needles), m.p. 237–238° (56%) (lit. (20) m.p. 237°; ν_{max} (KBr) 1671, 1646 (sh), 1600 cm^{-1}; δ ($CDCl_3$) 3.97 s (5,8-OCH_3), 7.37 s (6,7-CH).

Anal. Calcd. for $C_{12}H_8O_4Cl_2$: C, 50.20; H, 2.81; Cl, 24.70. Found: C, 50.16; H, 2.73; Cl, 24.59.

Chromatography on deactivated silica gel (21) (benzene–chloroform 1:1) of the mother liquor of the preceding crystallization gave 6,7-dichloro-5,8-dimethoxynaphthoquinone (**13***a*) (yellow needles), m.p. 203–203.5° (chloroform) (22%); ν_{max} (KBr) 1669, 1622 cm^{-1}; δ ($CDCl_3$) 3.96 s (5,8-OCH_3), 6.88 s (2,3-CH).

Anal. Found: C, 50.62; H, 2.89; Cl, 24.61.

Methylation of 2,3-Dibromonaphthazarin

The etherification was carried out as for 2,3-dichloronaphthazarin and gave two isomers.

2,3-Dibromo-5,8-dimethoxynaphthoquinone (**12***b*) (red needles), m.p. 212–213° (chloroform – carbon tetrachloride) (55%); ν_{max} (KBr) 1672, 1596 cm^{-1}; δ ($CDCl_3$) 3.96 s (5,8-OCH_3), 7.35 s (6,7-CH).

Anal. Calcd. for $C_{12}H_8O_4Br_2$: C, 38.32; H, 2.14. Found: C, 38.34; H, 2.06.

6,7-Dibromo-5,8-dimethoxynaphthoquinone (**13***b*) (yellow needles), m.p. 209–210° (benzene – petroleum ether) (17%); ν_{max} (KBr) 1668, 1622 cm^{-1}; δ ($CDCl_3$) 3.94 s (5,8-OCH_3), 6.87 s (2,3-CH).

Anal. Found: C, 38.34; H, 2.01.

The Nucleophilic Substitution of Haloquinones

Nucleophilic Substitution of Chloranil

Method A. A mixture of chloranil (**4**) (0.01 mol), anhydrous potassium fluoride (0.06 mol), and absolute methanol (50 ml) was heated in a sealed tube (Table 1). The cooled reaction mixture was filtered, evaporated under vacuum, diluted with water (200 ml), and extracted with benzene. After evaporation of the solvent, the residue was chromatographed on silica gel using a mixture of benzene and petroleum ether as eluant and gave two products.

Chlorotrimethoxybenzoquinone (**8**), m.p. 82–83° (methanol); ν_{max} (KBr) 1675, 1665, 1640, 1600 cm^{-1}; λ_{max} (ethanol) 298 nm (log ε 3.85); δ ($CDCl_3$) 4.04, 4.09 and 4.23 3 s (OCH_3).

Anal. Calcd. for $C_9H_9O_3Cl$: C, 46.67; H, 3.90; Cl, 15.24. Found: C, 46.59; H, 3.97; Cl, 15.18.

Tetramethoxybenzoquinone (**9**), m.p. 134.5–135.5° (methanol) (lit. (22) m.p. 135–136°); ν_{max} (KBr) 1670, 1610 cm^{-1}; λ_{max} (ethanol) 298 nm (log ε 3.86); δ ($CDCl_3$) 4.05 s (OCH_3).

Method B. Chloranil (0.01 mol) was added in small portions to a cooled solution of sodium methoxide (0.04 mol) in methanol (50 ml). The reaction mixture was then refluxed for 30 min and filtered hot. Tetramethoxybenzoquinone (**9**) crystallized on cooling, m.p. 134-135° (46%). 2,5-Dichloro-3,6-dimethoxybenzoquinone (**6**) could be recovered from the insoluble material (bishemiacetal salt) in the reaction mixture, m.p. 141–142° (methanol) (35%) (lit. (9) m.p. 141°).

*2,3-Dimethoxynaphthoquinone (**11**)*

A mixture of 2,3-diazidonaphthoquinone (0.6 g) (prepared in nearly quantitative yield from 2,3-dichloronaphthoquinone (**10**)) (11), anhydrous potassium carbonate (1.7 g), and absolute methanol (25 ml) was stirred at room temperature for 1.5 h and filtered. The residue was washed with methanol and the filtrates when concentrated and cooled in ice yielded 2,3-dimethoxynaphthoquinone (**11**), m.p. 116–117° (methanol) (83%) (lit. (10) m.p. 114–115°).

*2-Chloro-3,5,8-trimethoxynaphthoquinone (**14**)*

A mixture of 2,3-dichloro-5,8-dimethoxynaphthoquinone (**12***a*) (143 mg), anhydrous sodium acetate (100 mg), and absolute methanol (10 ml) was refluxed for 3 h, cooled and filtered, then concentrated and filtered again. The solid material was 2-chloro-3,5,8-trimethoxynaphthoquinone (**14**), m.p. 149–150° (benzene) (84%); ν_{max} (KBr) 1665, 1610 cm^{-1}; δ ($CDCl_3$) 3.95 s (5,8-OCH_3), 4.22 s (2-OCH_3), 7.30 s (6,7-CH).

Anal. Calcd. for $C_{13}H_{11}O_5Cl$: C, 55.23; H, 3.92. Found: C, 55.59; H, 3.74.

*2,3,5,8-Tetramethoxynaphthoquinone (**15**)*

2,3-Dichloro-5,8-dimethoxynaphthoquinone (**12***a*) (5.72 g) was added to a solution of sodium methoxide (1.4 g of sodium in 75 ml of methanol) and the mixture stirred at room temperature for 1 h and then cooled in ice. Upon filtration, 2,3,5,8-tetramethoxynaphthoquinone (**15**) was obtained, m.p. 139–139.5° (methanol) (86%); ν_{max} (KBr) 1656, 1624 cm^{-1}; δ ($CDCl_3$) 3.95 s (5,8-OCH_3), 4.05 s (2,3-OCH_3), 7.29 s (6,7-CH).

Anal. Calcd. for $C_{14}H_{14}O_6$: C, 60.43; H, 5.07. Found: C, 60.46; H, 5.14.

The Fries Rearrangement of 1,2,3,4,5,8-Hexaacetoxynaphthalene

*2,3-Dihydroxynaphthazarin (Spinazarin) (**16**)*

A solution of 2,3,5,8-tetramethoxynaphthoquinone (**15**) (4.2 g), $AlCl_3$ (50 g), and nitrobenzene (75 ml) was stirred for 24 h at 80° and then hydrolyzed with ice water (900 ml) and concentrated HCl (100 ml). The suspension was warmed until an orange precipitate was obtained, cooled and extracted with petroleum ether. Filtration of the aqueous phase gave spinazarin (**16**), (orange needles), m.p. 279–279.5° (acetic acid) (nearly quantitative) (lit. (15) m.p. 265°); ν_{max} (KBr) 3250, 1615 cm^{-1}; δ ($(CD_3)_2SO$) 7.65 s (6,7-CH).

*1,2,3,4,5,8-Hexaacetoxynaphthalene (**17**)*

A suspension of spinazarin (**16**) (0.55 g), zinc dust (2.5 g), anhydrous sodium acetate (1.5 g), and acetic anhydride (20 ml) was warmed slightly, then stirred at room temperature for 2 h and hydrolyzed. 1,2,3,4,5,8-Hexaacetoxynaphthalene (**17**) was extracted with chloroform and crystallized from acetic acid, m.p. 243–244° (83%) (lit. (15) m.p. 211.5–212°; (16) 245°); ν_{max} (KBr) 1792, 1778, 1766 cm^{-1}; δ (CF_3CO_2H) 2.40 s (2,3-OCOCH_3), 2.50 s (1,4,5,8-OCOCH_3), 7.30 s (6,7-CH).

The Fries Rearrangement of 1,2,3,4,5,8-Hexaacetoxynaphthalene (Table 2)

Method A. A mixture of the hexaacetoxynaphthalene **17** (240 mg) and $AlCl_3$ (500 mg) was heated at 160° for 1 h, hydrolyzed with ice and concentrated HCl and allowed to stand for 12 h. The products were separated by chromatography on silica gel using chloroform as eluant.

TABLE 2. The Fries rearrangement of **17**

Method	Conditions	Yield (%) **18**	**19**
A	$AlCl_3$; 1 h at 160°	16	20
B	$AlCl_3$; 20 min at 170°	50	25
C	$AlCl_3$ in CS_2; 30 min at 175°	20	20
D	BF_3 in acetic acid	0	44

Method B. As in method A, however the mixture was heated at 170° for 20 min.

Method C. As in ref. 6.

Method D. A solution of the hexaacetate **17** in acetic acid (3.0 ml) was saturated with BF_3 rapidly and without cooling.

6-Acetyl-2,3-dihydroxynaphthazarin (acetylspinazarin) (**18**), m.p. 227–228° (dioxan – petroleum ether) (lit. (16) m.p. 236°); ν_{max} (KBr) 3100, 1685, 1640, 1605 cm^{-1}; δ ($(CD_3)_2SO$) 2.61 s (6-$COCH_3$), 7.47 s (7-CH); *m/e* 264 (M^+).

Anal. Calcd. for $C_{12}H_8O_7$: C, 54.55; H, 3.05. Found: C, 54.94; H, 3.02.

1,3-Dimethyl-5,6,7,8-tetrahydroxynaphtho[2,3-*c*]furan-4,9-quinone (**19**), m.p. 305–310° (dec.) (methanol); ν_{max} (KBr) 3450, 1631, 1608 cm^{-1}; δ ($(CD_3)_2SO$) 2.61 s (1,3-CH_3); *m/e* 290 (M^+).

Anal. Calcd. for $C_{14}H_{10}O_7$: C, 57.94; H, 3.47. Found: C, 58.30; H, 3.36.

Tetraacetate of **19**, m.p. 212–213° (benzene – petroleum ether); ν_{max} (KBr) 1790, 1678, 1601 cm^{-1}; δ ($CDCl_3$) 2.31 s (6,7-$OCOCH_3$), 2.41 s (5,8-$OCOCH_3$), 2.63 s (1,3-CH_3).

6,7-Dimethyl ether of **19**, m.p. 218–219° (chloroform – petroleum ether); ν_{max} 1650, 1608 cm^{-1}; δ ($CDCl_3$) 2.68 s (1,3-CH_3), 4.08 s (6,7-OCH_3), 13.60 s (5,8-OH).

*1,3-Dimethyl-5,8-dihydroxynaphtho[2,3-c]furan-4,9-quinone (**21**)*

A solution of 2,5-dimethylfuran-3,4-dicarboxylic acid dichloride (**20**) (1.1 g) (19) and *p*-dimethoxybenzene (0.7 g) in methylene chloride (10 ml) was added dropwise to a suspension of $AlCl_3$ (4.5 g) in the same solvent (15 ml). After refluxing the mixture for 2 h, hydrolyzing it in the usual way and extracting with chloroform, 1,3-dimethyl-5,8-dihydroxynaphtho[2,3,-*c*]furan-4,9-quinone (**21**) was obtained, m.p. 260–260.5° (chloroform) (40%) (lit. (17) m.p. 258–258.5°); the i.r. and n.m.r. data were identical to those already published (17).

Diacetate, m.p. 229–229.5° (lit. (18) m.p. 226–226.5°).

*1,3-Dimethyl-5,6,7,8-tetrahydroxynaphtho[2,3-c]furan-4,9-quinone (**19**)*

A mixture of 2,5-dimethylfuran-3,4-dicarboxylic acid dichloride (**20**) (1.1 g) and 1,2-dihydroxy-3,4 dimethoxybenzene (0.9 g) was added in small portions to a molten mixture of $AlCl_3$ (4.5 g) and NaCl (1.0 g) at 140°. The cooled melt was hydrolyzed with ice and concentrated HCl, allowed to stand for 24 h and extracted repeatedly with chloroform. The crude extract, when chromatographed on silica gel using a mixture of chloroform and methanol (9:1) as eluant gave 1,3-dimethyl-5,6,7,8-tetrahydroxynaphtho[2,3-*c*]furan-4,9-quinone (**19**), m.p. and mixture m.p. 305–310° (dec.) (methanol) (22%). The i.r. and n.m.r. spectra were superimposable on those of the compound obtained from the Fries rearrangement.

1. K. ZAHN and P. OCHWAT. Ann. **462**, 72 (1928).
2. H. BROCKMANN and K. MUELLER. Ann. **540**, 51 (1939).
3. D. B. BRUCE and R. H. THOMSON. J. Chem. Soc. 1089 (1955).
4. L. F. FIESER and M. FIESER. Advanced organic chemistry. Reinhold Publishing Corp., New York. p. 847–851. 1962.
5. R. E. MOORE and P. J. SCHEUER. J. Org. Chem. **31**, 3272 (1966).
6. K. BRASS, R. PFLUGER, and K. HONSBERG. Chem. Ber. **69**, 80 (1936).
7. E. HARDEGGER, K. STEINER, E. WIDMER, and A. PFIFFNER. Helv. Chim. Acta, **47**, 2027 (1964).
8. K. WALLENFELS and K. FRIEDRICH. Chem. Ber. **93**, 3071 (1960).
9. K. WALLENFELS and W. DRABER. Chem. Ber. **90**, 2819 (1957).
10. L. F. FIESER and R. H. BROWN. J. Am. Chem. Soc. 71, 3609 (1949).
11. K. FRIES and P. OCHWAT. Chem. Ber. **56**, 1291 (1923).
12. J. F. GARDEN and R. H. THOMSON. J. Chem. Soc. 2483 (1957).
13. I. SINGH, R. E. MOORE, C. W. J. CHANG, R. T. OGATA, and P. J. SCHEUER. Tetrahedron, **24**, 2969 (1968).
14. L. MUSAJO and M. MINCHILLI. Boll. Sci. Facolta Chim. Ind. Bologna, **3**, 113 (1942).
15. C. KURODA. J. Sci. Res. Inst. (Tokyo), **46**, 188 (1952).
16. C. ANTONELLO. Atti Ist. Veneto Sci. Lettere Arti, Classe Sci. Mat. Nat. **122**, 1 (1964).
17. L. A. CORT and P. A. B. RODRIGUEZ. J. Chem. Soc. (C), 949 (1967).
18. D. V. NIGHTINGALE and B. SUKORNICK. J. Org. Chem. **24**, 497 (1959).
19. H. WALDMANN and E. ULSPERGER. Chem. Ber. **83**, 178 (1950).
20. A. J. SORRIE and R. H. THOMSON. J. Chem. Soc. 2243 (1955).
21. R. E. MOORE, I. SINGH, C. W. J. CHANG, and P. J. SCHEUER. J. Org. Chem. **31**, 3638 (1966).
22. B. EISTERT and G. BOCK. Chem. Ber. **92**, 1239 (1959).
23. P. C. ARORA and P. BRASSARD. Can J. Chem. **45**, 67 (1967).
24. P. C. ARORA and P. BRASSARD. Can. J. Chem. **49**, 3477 (1971).

Can. J. Chem. Downloaded from www.nrcresearchpress.com by 210.87.254.5 on 09/05/12
For personal use only.

Synthesis of 2,6-Naphthyridine, 4-Methyl-2,6-naphthyridine, and their Derivatives[1,2]

ALFRED TAURINS AND ROSITA TAN LI[3]

Department of Chemistry, McGill University, P.O. Box 6070, Station A, Montreal, Quebec H3C 3G1

Received February 27, 1973[4]

A detailed outline of the experimental procedures for the synthesis of 2,6-naphthyridine and 4-methyl-2,6-naphthyridine is given. Cyclization of 2-(4-cyano-3-pyridyl)propionitrile with anhydrous hydrogen bromide lead to 3-amino-4-methyl-2,6-naphthyridine which was transformed into 4-methyl-2,6-naphthyridine in a series of reactions. The u.v. spectra of 2,6- and 4-methyl-2,6-naphthyridine and their amino and halogen derivatives were recorded.

On décrit en détail les processus expérimentaux pour la synthèse de la naphthyridine-2,6 et de la méthyl-4 de la naphthyridine-2,6. La cyclisation de la (cyano-4 pyridyl-3)-2 propionitrile avec de l'acide bromhydrique anhydre conduit à l'amino-3 bromo-1 méthyl-4 naphthridine-2,6 par une série de réactions. Les spectres ultraviolets de la naphthyridine-2,6 de la méthyl-4 naphthyridine-2,6 ainsi que de leurs dérivés aminés et halogénés sont rapportés. [Traduit par le journal]

Can. J. Chem., **52**, 843 (1974)

Among the six isomeric naphthyridines, the chemistry of 2,6-naphthyridine has been comparatively little studied. The first synthesis of 2,6-naphthyridine (**1**) (1) involved the cyclization of β-homocinchomeronic acid diamide to form β-homocinchomeronimide, a compound possessing the structure of the desired ring system. Three additional steps were necessary to transform the latter compound into **1**. The second method for the preparation of 2,6-naphthyridine has been outlined in a preliminary report (2). The present paper has two objectives, first, to present detailed experimental procedures for the synthesis of the following compounds, not fully outlined in the previous article (2): ethyl 4-cyano-3-pyridylacetate (**2**), 1,3-dihydrazino-2,6-naphthyridine (**3**), 2,6-naphthyridine (**1**), 3-amino-1,4-dibromo- (**4**), 3-bromo-1-hydroxy- (**5**), 3-bromo-1-methoxy- (**6**), and 3-chloro-2,6-naphthyridine (**7**). The second objective of this paper is to describe the synthesis of 4-methyl-2,6-naphthyridine (**8**) (Scheme 1), a compound isolated by Harkiss and Swift (3) from a plant, *Antirrhinum majus*.

The starting material for the preparation of 4-methyl-2,6-naphthyridine (**8**) was 4-cyano-3-pyridylacetonitrile (**9**) which was methylated at the methylene group of the side chain to obtain 2-(4-cyano-3-pyridyl)propionitrile (**10**). Treatment of compound **10** with anhydrous hydrogen bromide in ethyl ether (4) gave 3-amino-1-bromo-4-methyl-2,6-naphthyridine (**11**) which was transformed into 1,3-dibromo- (**12**) and then to 1,3-dihydrazino-4-methyl-2,6-naphthyridine (**13**), respectively. The last step, the replacement of hydrazino groups by hydrogen, yielded 4-methyl-2,6-naphthyridine (**8**). The spectroscopic data of **8** are in agreement with those of the sample isolated by Harkiss and Swift (3), however, their melting point (78°) is considerably lower than that of our sample (94.5–95.5°) which we consider as being correct.

Derivatives of 2,6- and 4-Methyl-2,6-naphthyridine

Treatment of 3-amino-1-bromo-4-methyl-2,6-naphthyridine (**11**) with nitrous acid in hydrobromic acid solution produced 1,3-dibromo-4-methyl-2,6-naphthyridine (**12**). In the latter compound and in 1,3-dibromo-2,6-naphthyridine (2) only the bromine at position 1 is active in nucleophilic substitution reactions. Both compounds react readily with methanolic solution of sodium hydroxide to give 3-bromo-1-methoxy- (**6**) and 3-bromo-1-methoxy-4-methyl-2,6-naphthyridine (**17**). To show that the nucleophilic substitution had occurred at C-1,

[1]This work received financial assistance from the National Research Council of Canada, Ottawa.

[2]Preliminary report: ref. 2.

[3]Née Rosita Tan.

[4]Revision received October 30, 1973.

Can. J. Chem. Downloaded from www.nrcresearchpress.com by 210.87.254.5 on 09/05/12
For personal use only.

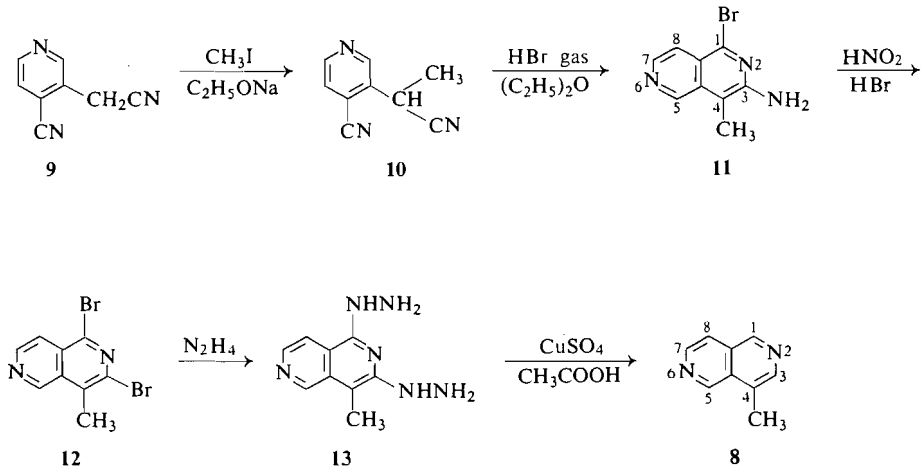

SCHEME I

compound **17** was synthesized also from 3-amino-1-bromo-4-methyl-2,6-naphthyridine (**11**), firstly, by replacing its bromine by treatment with sodium methoxide to form 3-amino-1-methoxy-4-methyl-2,6-naphthyridine (**15**) and, secondly, by exchanging the 3-amino group in compound **15** for bromine, by diazotization in hydrobromic acid. The similarity of compound **17** prepared by the two methods was proved by i.r. and n.m.r.

Hydrolysis of 1,3-dibromo-2,6-naphthyridine (2) and 1,3-dibromo-4-methyl-2,6-naphthyridine (**12**) with 6 *N* sulfuric acid gave 3-bromo-1-hydroxy- (**5**) and 3-bromo-1-hydroxy-4-methyl-2,6-naphthyridine (**16**), respectively. The latter compounds exist mainly in their tautomeric lactam forms as indicated by the C=O i.r. bands at 1670 cm^{-1}. The broad bands in the region 2800–2300 cm^{-1} indicated the presence of hydrogen bonded NH groups. The greater reactivity of bromine at C-1 compared to C-3 in these two dibromides is analogous to the relative reactivities of chlorine atoms in 1,3-dichloroisoquinoline.

Spectra

The u.v. absorption data published for all six naphthyridines (5) are incomplete because they do not cover the whole spectral range accessible with present day instruments. Thus in the u.v. spectrum of 2,6-naphthyridine (**1**) reported previously (1), the short-wave band at 207 nm (log ε 4.79) (Table 1) has not been detected and the band intensities were too low.

The u.v. spectrum of 4-methyl-2,6-naphthyridine (**8**) (Table 2) is very similar in band shapes and intensities to the spectrum of 2,6-naphthyridine (**1**).

It is interesting to note that the position of the β-band in 2,6-naphthyridine at 207 nm (log ε 4.79) (Table 1) is very close to the positions of this band in the spectra of 1,5-naphthyridine (206 nm, log ε 4.75) (6) and quinoline (203 nm, log ε 4.61) (7). The β- and p-bands of 1,5- and 2,6-naphthyridine are almost identical in their shapes, positions of λ_{max} and intensities. The α-bands are also similar, except that in 2,6-naphthyridine this band is shifted towards a longer wavelength.

The results in Table 1 and 2 show that in the substituted 2,6-naphthyridines the largest bathochromic shifts of the α-bands, in the order of 60–70 nm, are caused by the amino group in the 3-position. These shifts are about twice as large as the bathochromic shift of the α-band in 3-aminoisoquinoline compared with the unsubstituted isoquinoline. Apparently, in 3-amino-2,6-naphthyridines the determining factor in causing such large shifts is the nitrogen atom in the 6-position. The bathochromic shifts of the p-band in the u.v. spectra of 3-amino- and 3-amino-4-methyl-2,6-naphthyridine are only 25 and 29 nm, respectively.

The i.r. spectrum of 2,6-naphthyridine has been published (1) only in the form of a spectrogram in the region 1600–800 cm^{-1}, without giving exact band positions. In the present investigation the i.r. spectra of 2,6-naphthyridine (**1**) and 4-

Can. J. Chem. Downloaded from www.nrcresearchpress.com by 210.87.254.5 on 09/05/12
For personal use only.

TABLE 1. The u.v. absorption spectra and log ε values of 2,6-naphthyridine and its derivatives (in absolute methanol)

	α-band		p-band		β-band	
Compound	nm	log ε	nm	log ε	nm	log ε
2,6-Naphthyridine (**1**)	331	3.61	263	3.60	207	4.79
	317	3.61	254	3.69		
	305sh	3.42	246	3.62		
3-Acetamido-1-bromo- (2)	345	3.62	289	4.04	233	4.38
			278	4.04		
3-Amino- (2)	391	3.43	279	4.13	224	4.46
3-Amino-1-bromo- (2)	397	3.56	286	4.12	227	4.33
3-Amino-1,4-dibromo- (**4**)	399	3.70	292	4.13	234	4.39
3-Amino-1-ethoxy- (2)	385	3.54	295	4.26	222	4.33
3-Bromo-1-hydroxy- (**5**)	363sh	3.60	281	4.13		
	345	3.78				
3-Bromo-1-methoxy- (**6**)	342	3.65	282	4.02	214	4.51
	332	3.70	273	4.08		
3-Chloro- (7)	338	3.47	267	3.69	213	4.67
	327	3.47	258	3.76		
			250	3.66		
1,3-Dibromo- (2)	345	3.70	276	3.99	218	4.53
	334	3.70	268	3.98		
1,3,4-Tribromo- (2)	342	3.80	286	3.93	226	4.49
	335	3.82	276	3.93		

TABLE 2. The u.v. absorption spectra and log ε values of 4-methyl-2,6-naphthyridine and its derivatives (in absolute methanol)

	α-band		p-band		β-band	
Compound	nm	log ε	nm	log ε	nm	log ε
4-Methyl-2,6-naphthyridine (**8**)	331	3.69	268	3.57	210	4.74
	322.5	3.69	259	3.67		
			250	3.60		
3-Amino- (**14**)	395	3.62	283	4.15	228	4.60
3-Amino-1-bromo- (**11**)	398	3.65	294	4.13	230	4.38
3-Amino-1-methoxy- (**15**)	395	3.58	300	4.22	224	4.32
3-Bromo-1-hydroxy- (**16**)	350	3.74	286	4.05		
	330	3.70				
3-Bromo-1-methoxy- (**17**)	340	3.74	287	3.97	212	4.52
			278	4.02		
1,3-Dibromo- (**12**)	350	3.85	280	4.00	220	4.53
	338	3.84	271	4.01		

methyl-2,6-naphthyridine (**8**) were recorded in the region 3800–400 cm^{-1} (*cf.* Experimental).

Experimental

The melting points were determined on a Gallenkamp melting point apparatus and are corrected. The u.v. spectra were obtained on a Perkin-Elmer Model 350 Spectrophotometer using absolute methanol as a solvent. The n.m.r. spectra were determined on a Varian Model A-60 spectrometer. Solvents used were carbon tetrachloride, deuteriochloroform, and dimethyl sulfoxide-d_6. Tetramethylsilane was used as the internal standard. The n.m.r. peaks were designated as follows: s, singlet; d, doublet; t, triplet; q, quadruplet; m, multiplet. The i.r. spectra were measured on Perkin-Elmer Model 521 grating spectrometer. Elemental analyses were carried out by A. Bernhardt Laboratory, Germany.

Ethyl 4-Cyano-3-pyridylacetate (2)

Ethyl 3-pyridylacetate *N*-oxide (100 g; 0.552 mol) was placed in a 100 ml three-necked flask equipped with a mechanical stirrer, a thermometer, and a dropping funnel fitted with a calcium chloride drying tube. Dimethyl sulfate (47.5 ml; 0.552 mol) was added dropwise and the mixture was heated at 90–100° for 2 h on a steam bath.

Potassium cyanide (77 g; 1.175 mol) was dissolved in 187 ml of water and the solution flushed with nitrogen for

Can. J. Chem. Downloaded from www.nrcresearchpress.com by 210.87.254.5 on 09/05/12
For personal use only.

Can. J. Chem. Downloaded from www.nrcresearchpress.com by 210.87.254.5 on 09/05/12
For personal use only.

two hours; the *N*-methoxy salt dissolved in aqueous ethanol (180 ml ethanol and 270 ml water) was added dropwise to the potassium cyanide solution under nitrogen atmosphere at 23–25° for 9 h. After the addition was completed, the mixture was stirred for another 4 h. Chloroform (300 ml) was added and the resulting mixture was stirred for ½ h. The chloroform layer was separated and the aqueous layer was extracted twice with 100-ml portions of chloroform. The combined chloroform extract was washed with 1% sodium bicarbonate solution (100 ml), then with water (100 ml), and dried over anhydrous sodium sulfate. The solvent was evaporated leaving 65.6 g of a dark oil. Two products, ethyl 4-cyano- and ethyl 2-cyano-3-pyridylacetate, were obtained upon distillation. The yield of ethyl 4-cyano-3-pyridylacetate (**2**), the major product, which distilled at 128–131° (1.7 mm) was 39.2 g (36%); i.r. (KBr): 2232 cm^{-1} (CN). For elemental analysis see ref. 2.

1,3-Dihydrazino-2,6-naphthyridine

(*a*) 1,3-Dibromo-2,6-naphthyridine (2) (0.55 g; 1.91 mmol) was dissolved in 5 ml of dioxane and 2.5 ml of 85% hydrazine hydrate was added dropwise. The mixture was allowed to stand at room temperature for 2 days. The yellow needles were filtered off and dried to give 1,3-dihydrazino-2,6-naphthyridine in quantitative yield, m.p. 214–216°.

Anal. Calcd. for $C_8H_{10}N_6$: C, 50.5; H, 5.3; N, 44.2. Found: C, 50.7, H, 5.5; N, 44.0.

(*b*) One gram of 3-amino-1-bromo-2,6-naphthyridine (2) (4.45 mmol) was dissolved in 10 ml of dioxane and 5 ml of 85% hydrazine was added dropwise. The mixture was heated at 125° for 1 h and allowed to cool at room temperature. The yellow precipitate was filtered to give 0.74 g of 1,3-dihydrazino-2,6-naphthyridine (86.0% yield). The i.r. spectrum was identical in all respects with that of a sample obtained by method *a*. The mixture melting point with a sample obtained by method *a* showed no depression.

*2,6-Naphthyridine (**1**)*

One gram of 1,3-dihydrazino-2,6-naphthyridine (5.30 mmol) was dissolved in 15 ml of acetic acid and 30 ml of water. The mixture was poured slowly into 100 ml of 10% hot cupric sulfate solution. The resulting mixture was boiled for 15 min, made alkaline with 20% sodium hydroxide solution, and extracted several times with ether (600 ml). The ethereal solution was dried over anhydrous sodium sulfate and the solvent was evaporated leaving 0.35 g of pale yellow solid (53.0% yield). Chromatography and crystallization from hexane gave 2,6-naphthyridine (**1**) as colorless crystals, m.p. 118–119°, (lit. (1) 114–115°).

Anal. Calcd. for $C_8H_6N_2$: C, 74.1; H, 4.8; N, 21.5. Found: C, 73.8; H, 4.7; N, 21.5.

The i.r. spectrum (CS_2): 3055s, 3020m, 2980vw cm^{-1}; i.r. (KBr): 1665w, 1562s, 1481s, 1380s, 1298w, 1273s, 1247s, 1204m, 1128sh, 1115s, 1015s, 940s, 842vs, 804w, 800s, 660s + 650s (doublet), 447m cm^{-1}. Monopicrate of **1**, yellow needles, m.p. 222–224° (lit. (1) 206°). The dipicrate of **1**, prepared by treating the ethanolic solution of 2,6-naphthyridine with excess of ethanolic solution of picric acid, formed yellow needles, m.p. 207.5–209.5° (ethanol). Results of elemental analysis of the dipicrate were satisfactory.

*3-Amino-1,4-dibromo-2,6-naphthyridine (**4**)*

3-Amino-1-bromo-2,6-naphthyridine (2) (5.6 g; 25.4 mmol) was suspended in a mixture of 10 ml of hydrobromic acid and 20 ml of glacial acetic acid. Bromine (2.6 ml; 50.0 mmol) was added dropwise at −5 to 0°. The mixture was stirred for 12 h at room temperature and poured onto 500 g of crushed ice. It was made alkaline with 20% sodium hydroxide and the yellow precipitate, crystallized from benzene chloroform, gave 4.0 g of **4** (51.9% yield) as yellow needles, m.p. 212.5–213.5°.

Anal. Calcd. for $C_8H_5N_3Br_2$: C, 31.7; H, 1.7; N, 13.9; Br, 52.7. Found: C, 31.9; H, 1.8; N, 13.7; Br, 52.8.

The n.m.r. spectrum (DMSO-d_6): δ 6.92 (2H, broad, NH_2), 7.67 (1H, d, H-8), 8.45 (1H, d, H-7), 9.18 (1H, s, H-5); J_{78} = 5.8 Hz.

*3-Bromo-1-hydroxy-2,6-naphthyridine (**5**)*

1,3-Dibromo-2,6-naphthyridine (2) (0.4 g; 1.38 mmol) was refluxed in 10 ml of 6 *N* sulfuric acid for 1 h. The clear yellow solution was diluted with 50 ml of water, made alkaline with 20% sodium hydroxide solution, and then acidified with acetic acid. The precipitate on crystallization from dioxane yielded 0.19 g (61.3%) of **5**, m.p. 296–298° (pale yellow crystals).

Anal. Calcd. for $C_8H_5N_2BrO$: C, 42.7; H, 2.2; N, 12.5; Br, 35.5. Found: C, 42.8; H, 2.4; N, 12.2; Br, 35.4.

*3-Bromo-1-methoxy-2,6-naphthyridine (**6**)*

1,3-Dibromo-2,6-naphthyridine (2) (0.2 g, 0.69 mmol) in a methanolic solution of sodium hydroxide (0.06 g in 12 ml of methanol) was stirred at 20° for 1 h and the resulting mixture was poured onto 50 ml of ice water. Crystallization from hexane gave 0.14 g of **6** (80% yield) as colorless needles, m.p. 129–130°.

Anal. Calcd. for $C_9H_7N_2BrO$: C, 45.2; H, 2.9; N, 11.7; Br, 33.4. Found: C, 45.2; H, 3.2; N, 11.6; Br, 33.6.

The n.m.r. spectrum ($CDCl_3$): δ 4.17 (3H, s, OCH_3), 7.55 (1H, s, H-4), 7.94 (1H, d, H-8), 8.75 (1H, d, H-7), 9.17 (1H, s, H-5); J_{78} = 5.8 Hz.

*3-Chloro-2,6-naphthyridine (**7**)*

Cuprous chloride was prepared from sodium chloride (0.55 g), cupric sulfate (2.09 g), sodium bisulfite (0.45 g), and sodium hydroxide (0.30 g), and was dissolved in 10 ml of concentrated hydrochloric acid.

3-Amino-2,6-naphthyridine (2) (0.74 g; 0.0051 mol) was dissolved in 10 ml of concentrated hydrochloric acid (25 ml) cooled to −10°, and an aqueous solution of sodium nitrite (0.4 g; 0.0059 mol, in 1.5 ml water) was added dropwise. The resulting diazonium solution was poured slowly into the cuprous chloride solution at −2°.

The resulting mixture was made alkaline with 20% sodium hydroxide solution. The basic solution was extracted with three 100-ml portions of ether. The ethereal extract was dried over anhydrous sodium sulfate and the solvent was evaporated, leaving 0.35 g of a crude product. Extraction with hexane gave 0.14 g of 3-chloro-2,6-naphthyridine (**7**) (16.7% yield). Pale yellow needles, m.p. 149–150.5° (hexane).

Anal. Calcd. for $C_8H_5N_2Cl$: C, 58.4; H, 3.0; N, 17.0; Cl, 21.6. Found: C, 58.6; H, 3.2; N, 17.0; Cl, 21.4.

The n.m.r. spectrum ($CDCl_3$): δ 7.78 (1H, d, H-8), 7.85 (1H, s, H-4), 8.74 (1H, d, H-7), 9.17 (1H, s, H-5), 9.32 (1H, s, H-1).

Can. J. Chem. Downloaded from www.nrcresearchpress.com by 210.87.254.5 on 09/05/12
For personal use only.

*2-(4-Cyano-3-pyridyl)propionitrile (**10**)*

A solution of 4-cyano-3-pyridylacetonitrile (**9**) (4.0 g; 0.028 mol) in tetrahydrofuran–ether (10 ml:20 ml) was added dropwise to a sodium ethoxide solution (prepared from 0.64 g of sodium in 20 ml of ethanol) and kept at $-10°$ to $-5°$ over a period of 5 min. The resulting mixture was poured slowly into a solution of methyl iodide (3.4 ml; 0.053 mol) in 20 ml of ether and stirred at room temperature for 30 min. The mixture was poured into 300 ml of ice water and extracted with three 150-ml portions of chloroform. The chloroform extract was dried and the solvent was evaporated leaving 4.0 g of a dark viscous oil. Distillation at 152–156° (1.8 mm) gave 3.2 g (72.7% yield) of 2-(4-cyano-3-pyridyl)propionitrile (**10**), a colorless oil. It was analyzed in the form of a picrate; n.m.r. (**10**) ($CDCl_3$): δ 1.78 (3H, d, CH_3), 4.39 (1H, q, CH), 7.71 (1H, d, H-5), 8.93 (1H, d, H-6), 9.12 (1H, s, H-2); J_{56} = 5.0 Hz. The picrate of **10** formed yellow crystals, m.p. 107–108° (ethanol).

Anal. Calcd. for $C_9H_7N_3 \cdot C_6H_3N_3O_7$: C, 46.4; H, 2.6; N, 21.8. Found: C, 46.5; H, 2.8; N, 21.9.

*3-Amino-1-bromo-4-methyl-2,6-naphthyridine (**11**)*

2-(4-Cyano-3-pyridyl)propionitrile (**10**) (8.0 g; 0.051 mol) was dissolved in 100 ml of dry ether and cooled to $-5°$ to 0°. Anhydrous hydrogen bromide was bubbled through the mixture for 2 h and the resulting mixture was poured into a solution of excess sodium bicarbonate. The yellow precipitate obtained was washed with several small portions of water to yield 12.0 g of a crude product. Crystallization from methylene chloride – hexane gave 9.65 g of 3-amino-1-bromo-4-methyl-2,6-naphthyridine (**11**) (79.5% yield) as yellow needles, m.p. 197.5–198.5°.

Anal. Calcd. for $C_9H_8N_3Br$: C, 45.4; H, 3.4; N, 17.7; Br, 33.6. Found: C, 45.6; H, 3.6; N, 17.4; Br, 33.7.

The n.m.r. spectrum (DMSO-d_6): δ 2.38 (3H, s, CH_3), 5.53 (3H, broad, NH_2), 7.63 (1H, d, H-8), 8.30 (1H, d, H-7), 9.26 (1H, s, H-5); J_{78} = 5.8 Hz.

3-Acetamido-1-bromo-4-methyl-2,6-naphthyridine

3-Amino-1-bromo-4-methyl-2,6-naphthyridine (**11**) was acetylated with acetic anhydride in the presence of pyridine. The acetyl derivative forms pale crystals, m.p. 147.5–148.5° (hexane – methylene chloride).

Anal. Calcd. for $C_{11}H_{10}N_3O$: C, 47.5; H, 3.6; N, 15.0; Br, 28.5. Found: C, 47.1; H, 3.7; N, 15.2; Br, 28.2.

*1,3-Dibromo-4-methyl-2,6-naphthyridine (**12**)*

3-Amino-1-bromo-4-methyl-2,6-naphthyridine (**11**) (1.52 g; 6.40 mmol) was dissolved in 25 ml of 48% fuming hydrobromic acid. Solid sodium nitrite (0.7 g; 1.0 mmol) was added in small portions over a 15 min period with constant stirring at $-4°$ to $-2°$. After the addition was completed, the mixture was stirred for 30 min at 0° and allowed to stand for 12 h at room temperature. The mixture was then poured onto 400 g of crushed ice, made alkaline with 20% sodium hydroxide solution, extracted with three 200-ml portions of chloroform and the extract was dried. The solvent was evaporated leaving 1.2 g of a pale yellow solid. Crystallization from benzene–hexane gave 0.91 g of 1,3-dibromo-4-methyl-2,6-naphthyridine (**12**) (47.2% yield) as pale yellow needles, m.p. 150.5–151.5°.

Anal. Calcd. for $C_9H_6N_2Br_2$: C, 35.8; H, 2.0; N, 9.3; Br, 52.9. Found: C, 35.9; H, 1.9; N, 9.1; Br, 53.0.

The n.m.r. spectrum ($CDCl_3$): δ 2.82 (3H, s, CH_3), 8.03 (1H, d, H-8), 8.91 (1H, d, H-7), 9.59 (1H, s, H-5); J_{78} = 6.0 Hz.

*1,3-Dihydrazino-4-methyl-2,6-naphthyridine (**13**)*

1,3-Dibromo-4-methyl-2,6-naphthyridine (**12**) (2.36 g; 7.80 mmol) was dissolved in 20 ml of dioxane and 30 ml of 85% hydrazine hydrate was added dropwise. The mixture was heated at 125° for 1 h. The yellow precipitate was filtered off and washed with a small amount of water to give 1.3 g (81.2% yield) of 1,3-dihydrazino-4-methyl-2,6-naphthyridine (**13**), m.p. 197.5–198.5°.

Anal. Calcd. for $C_9H_{12}N_6$: C, 52.9; H, 5.9; N, 41.2. Found: C, 53.1; H, 6.1; N, 41.2.

*4-Methyl-2,6-naphthyridine (**8**)*

One gram of 1,3-dihydrazino-4-methyl-2,6-naphthyridine (**13**) (4.90 mmol) was dissolved in 15 ml of acetic acid and 30 ml of water. The solution was poured slowly into 100 ml of 10% hot copper sulfate solution. The resulting mixture was boiled for 15 min, made alkaline with 20% sodium hydroxide solution, and extracted with three 200-ml portions of chloroform. The combined chloroform extract was dried over anhydrous magnesium sulfate and the solvent was evaporated leaving 0.64 g of a pale yellow solid (90.1% yield). Crystallization from hexane gave 4-methyl-2,6-naphthyridine (**8**) as colorless crystals, m.p. 94.5–95.5°.

Anal. Calcd. for $C_9H_8N_2$: C, 75.0; H, 5.7; N, 19.4. Found: C, 75.2; H, 5.7; N, 19.3.

The n.m.r. spectrum ($CDCl_3$): δ 2.70 (3H, s, CH_3), 7.71 (1H, d, H-8), 8.71 (1H, d, H-7), 8.48 (1H, s, H-3), 9.20 (1H, s, H-1), 9.46 (1H, s, H-5); J_{78} = 5.5 Hz; i.r. (CS_2): 3057s, 3034s, 2977m, 2950m, 2927w; i.r. (KBr): 1565s, 1484s, 1399m, 1384s, 1314m, 1271s, 1229s, 1168m, 1098m, 1036s, 970w, 945m, 886vs, 816vs, 801s, 723vs, 650vs, 576m, 538m, 417w. The picrate of **8** forms yellow crystals, m.p. 186–187° (ethanol). Results of the elemental analysis of the picrate were satisfactory.

*3-Amino-4-methyl-2,6-naphthyridine (**14**)*

3-Amino-1-bromo-4-methyl-2,6-naphthyridine (**11**) (1.44 g; 6.05 mmol) was dissolved in absolute ethanol (160 ml). Alcoholic potassium hydroxide (0.9 g in 20 ml) and 10% palladium-on-charcoal (0.30 g) were added and the resulting mixture was hydrogenated for 1 h at 30 p.s.i. The catalyst was filtered off and the filtrate was diluted with 500 ml of water. It was extracted with three 250-ml portions of methylene chloride and the extract was dried over anhydrous sodium sulfate. The solvent was evaporated and the residue was crystallized from methylene chloride – benzene to give 0.63 g of 3-amino-4-methyl-2,6-naphthyridine (**14**) (65% yield) as yellow needles, m.p. 197.5–198.5°.

Anal. Calcd. for $C_9H_9N_3$: C, 67.9; H, 5.7; N, 26.4. Found: C, 67.5; H, 5.6; N, 26.3.

The n.m.r. spectrum (DMSO-d_6): δ 2.46 (3H, s, CH_3), 5.21 (2H, s, NH_2), 7.61 (1H, q, H-8), 8.27 (1H, d, H-7), 8.83 (1H, s, H-1), 9.32 (1H, t, H-5).

*3-Amino-1-methoxy-4-methyl-2,6-naphthyridine (**15**)*

3-Amino-1-bromo-4-methyl-2,6-naphthyridine (**11**) (2.40 g; 0.010 mol) and sodium methoxide (prepared from 0.46 g of sodium in 50 ml of methanol) were refluxed for 30 min. The mixture was poured into 100 ml of ice water. The precipitate was filtered off and crystallized to obtain yellow needles, m.p. 195–197° (benzene).

Anal. Calcd. for $C_9H_9N_3O$: C, 61.7; H, 5.2; N, 24.0. Found: C, 61.9; H, 5.3; N, 23.8.

3-Bromo-1-hydroxy-4-methyl-2,6-naphthyridine (16)

1,3-Dibromo-4-methyl-2,6-naphthyridine (**12**) (0.3 g; 1.0 mmol) was obtained in the same way as compound **5**. Crystallization from dioxane–ethanol gave 0.18 g (83.3% yield) of **16** as colorless crystalline flakes, m.p. 296° (dec.).

Anal. Calcd. for $C_9H_7N_2BrO$: C, 45.2; H, 3.0; N, 11.7; Br, 33.4. Found: C, 45.1; H, 3.2; N, 11.5; Br, 33.7.

3-Bromo-1-methoxy-4-methyl-2,6-naphthyridine (17)

(*a*) 1,3-Dibromo-4-methyl-2,6-naphthyridine (**12**) (0.25 g; 8.10 mmol) was transformed into **17** by a method similar to that used for the preparation of compound **6**. Crystallization from hexane gave 0.19 g (95% yield) of **17** as colorless needles, m.p. 145.5–146°.

Anal. Calcd. for $C_{10}H_9N_2OBr$: C, 47.5; H, 3.6; N, 11.1; Br, 31.6. Found: C, 47.5; H, 3.7; N, 10.9; Br, 31.7.

(*b*) 3-Amino-1-methoxy-4-methyl-2,6-naphthyridine (**15**) (1.0 g; 5.30 mmol) was dissolved in 30 ml of 48% fuming hydrobromic acid and cooled to $-5°$ to $-2°$. Solid sodium nitrite (0.7 g; 10.0 mmol) was added in small portions over a 5-min period. The mixture was stirred at 0° for 30 min and for 6 h at 20°. It was poured onto 200 g of crushed ice and made alkaline with 20% sodium hydroxide solution. The solution was extracted with three 100-ml portions of methylene chloride and the combined extract was dried. The solvent was evaporated to give 0.7 g of a pale yellow solid. Crystallization from hexane yielded 0.55 g of 3-bromo-1-methoxy-4-methyl-2,6-naphthyridine (**17**) (41.0% yield) as colorless needles. The i.r. and n.m.r. spectra were identical in all respects with those of a sample obtained by method *a*. The mixture melting point of **17** with the sample obtained by method *a* showed no depression.

1. G. GIACOMELLO, F. GUALFIERI, F. M. RICCIERI, and M. L. STEIN. Tetrahedron Lett. 1117 (1965).
2. R. TAN and A. TAURINS. Tetrahedron Lett. 2737 (1965).
3. K. J. HARKISS and D. SWIFT. Tetrahedron Lett. 4773 (1970).
4. F. JOHNSON and W. A. NASUTAVICUS. J. Org. Chem. 27, 3953 (1962).
5. W. W. PAUDLER and T. J. KRESS. *In* Advances in heterocyclic chemistry. Vol. 11. *Edited by* A. R. Katritzky and A. J. Boulton. Academic Press, New York. 1970. p. 131.
6. S. F. MASON. Spectrum No. H. 18/27. DMS UV Atlas of organic compounds. Butterworth, London and Verlag Chemie, Weinheim. 1968.
7. H. BRUNS. Spectrum No. H 1/1. DMS UV Atlas of organic compounds. Butterworth, London and Verlag Chemie, Weinheim. 1968.

Can. J. Chem. Downloaded from www.nrcresearchpress.com by 210.87.254.5 on 09/05/12
For personal use only.

Proton Magnetic Resonance Studies of Rotational Isomerism in Halotoluene Derivatives. XI. Experimental and Theoretical Barriers to Rotation in α,α,2,4,6-Pentabromo-, α,α-Dibromo-2,4,6-trichloro-, and α,α-Dibromo-2,6-dichlorotoluene

JAMES PEELING,[1] LUDGER ERNST,[2] AND TED SCHAEFER

Department of Chemistry, University of Manitoba, Winnipeg, Manitoba R3T 2N2

Received September 12, 1973

Using rate constants determined from an analysis of the p.m.r. lineshape of the ring protons as a function of temperature, the activation parameters for the hindered rotation about the sp^2–sp^3 carbon–carbon single bond in α,α,2,4,6-pentabromotoluene dissolved in perchlorobutadiene are determined. Values of ΔG^* for the analogous hindered rotations in α,α-dibromo-2,6-dichlorotoluene in toluene-d_8, and for α,α-dibromo-2,4,6-trichlorotoluene in solutions of toluene-d_8 and methylcyclohexane are also given. The results are compared with semiempirical potential energy barrier calculations employing partial geometry optimization. The agreement is satisfactory.

A l'aide des constantes de vitesse déterminées en fonction de la température par l'analyse du signal des protons du cycle en r.m.n., on a déterminé les paramètres d'activation pour les rotations empêchées autours de la liaison simple carbone–carbone de type sp^2–sp^3, dans le pentabromo-α,α,2,4,6 toluène dissout dans le perchlorobutadiène. Les valeurs de ΔG^* sont aussi rapportées pour les rotations empêchées analogues du dibromo-α,α dichloro-2,6 toluène en solution dans le toluène-d_8, et du dibromo-α,α trichloro-2,4,6 toluène en solution dans le toluène-d_8 et le méthylcyclohexane. Les résultats sont comparés avec les calculs empiriques de la barrière d'énergie potentielle en utilisant la géométrie partielle d'optimalisation. L'accord est satisfaisant. [Traduit par le journal]

Can. J. Chem., **52**, 849 (1974)

Introduction

Proton magnetic resonance (p.m.r.) studies of the hindered rotation of the dichloromethyl group in α,α,2,4,6-pentachlorotoluene (PCT) (1) and α,α-dichloro-2,4,6-tribromotoluene (DCTBT) (2) have been presented in previous papers of this series. A similiar study of the hindered rotation of the dibromomethyl group about the sp^2–sp^3 carbon–carbon single bond in α,α,2,4,6-pentabromotoluene (PBT), α,α-dibromo-2,4,6-trichlorotoluene (DBTCT), and in α,α-dibromo-2,6-dichlorotoluene (DBDCT) is presented in this paper. The results are compared with semiempirical calculations in which the sp^2–sp^3 carbon–carbon bond length and the bond angles involving the halogen substituents are optimized for each rotational arrangement (3).

Experimental

Preparation of PBT

2,4,6-Tribromotoluene (prepared by following Lock and Schreckeneder (4)) was treated in a quartz flask with a large excess of bromine at 200–250 °C under u.v. radiation for 6 days. The reaction mixture was extracted with ether. The solution was then filtered, washed successively with aqueous sodium hydrogen sulfite and water, dried over magnesium sulfate, and the solvent was evaporated. The residue was dissolved in petroleum ether and stored at −20 °C. A brown oil which separated was discarded and the petroleum ether was evaporated. The product was a yellow oil. The p.m.r. spectrum at room temperature displayed the expected ABX pattern and a number of impurity peaks. Repeated attempts to purify the product by distillation under reduced pressure, by t.l.c., and by dry column chromatography failed to reduce the intensities of the impurity peaks significantly.

Preparation of DBTCT

2,4,6-Trichlorotoluene (prepared as described previously (1)) was treated with an excess of bromine in a quartz flask at 150–220 °C under u.v. radiation for 3 days. The reaction mixture was treated as above (PBT), leaving a yellow-brown oil containing about 80% DBTCT and 20% α-bromo-2,4,6-trichlorotoluene. Repeated attempts to purify the product by the methods above were unsuccessful.

Preparation of DBDCT

2,6-Dichlorobenzyl bromide (Aldrich) in carbon tetrachloride was treated with an excess of bromine under u.v. radiation. The bromination was monitored by observation of the proton chemical shift of the side-chain protons. The product was purified by vacuum sublimation.

Proton Magnetic Resonance Spectra

A 10 mol % solution of PBT in perchlorobutadiene, containing a small amount of hexamethyldisilane as a

[1]NRCC Scholarship, 1972–1973.

[2]Postdoctorate fellow, 1971–1972.

Can. J. Chem. Downloaded from www.nrcresearchpress.com by 210.87.254.42 on 09/05/12
For personal use only.

Can. J. Chem. Downloaded from www.nrcresearchpress.com by 210.87.254.42 on 09/05/12
For personal use only.

lock and reference signal, was prepared and carefully degassed by the freeze–pump–thaw technique. Fourteen p.m.r. spectra were recorded at different temperatures from 18.9–125.9 °C in a manner described previously (2). In the case of DBTCT, two degassed solutions, 10 mol % in methylcyclohexane and 10 mol % in toluene-d_8, each containing tetramethysilane as a lock and reference material, were prepared. Spectra were recorded at five temperatures from −9.7 to 82.6 °C for the former solution and at four temperatures from 21.0–78.5 °C for the latter solution. Spectra were recorded at five temperatures from −10.0 to 80.0 °C for DBDCT as a 15 mol % solution in toluene-d_8 containing a small amount of tetramethylsilane. All spectra were taken on a HA100D spectrometer.

For all samples the homogeneity of the external magnetic field was monitored by the appearance of impurity peaks and of the methine proton peaks, whose widths are independent of the preexchange lifetimes (1). Temperatures were measured as described previously (2) and are believed to be accurate to ±0.5 °C.

Determination of Preexchange Lifetimes

The computer program for an ABX spectrum in which A and B undergo mutual exchange (1) was used to fit the experimental spectra of PBT and DBTCT. Rate constants for the internal rotation in DBDCT were determined by matching spectra with the computer program DNMR2 (5, 6). The usual precautions (2) concerning linewidth corrections, aromatic solvent shifts (7), and impurity peaks were taken.

Results and Discussion

Spectral Parameters in the Region of Slow Exchange

Below about 45 °C the mean lifetime of **1** before exchange to its mirror image isomer is relatively long, and the p.m.r. spectra of PBT show no sign of broadening. There is no noticeable broadening in the spectra of DBTCT or DBDCT below about 30 °C, indicating that the preexchange lifetime of **2** is relatively long below this temperature. The spectra of PBT and DBTCT

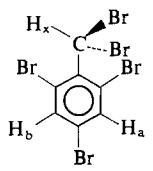

1

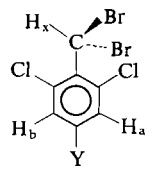

2

Y = Cl, H_c

are similar to those of PCT (1) and DCTBT (2), except that in the case of PBT the H_x resonance lies to high field of H_a and H_b. Figure 1 displays the spectrum of PBT at ambient temperature.

The chemical shifts and coupling constants were determined from the spectra using the iterative computer program LAME (8). The values obtained at a representative temperature for each sample are given in Table 1. The errors are standard deviations in the computer analyses.

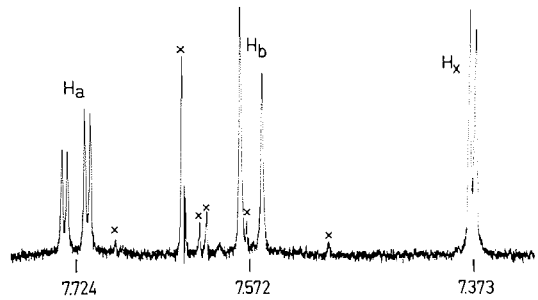

FIG. 1. The p.m.r. spectrum of a 10 mol % solution of α,α,2,4,6-pentabromotoluene (PBT) in perchlorobutadiene at 100 MHz at ambient temperature. The chemical shift scale is in p.p.m. to low field of internal hexamethyldisilane. The structural formula is given as **1** in the text. The splitting of the H_x resonance is 0.50 Hz. Impurity peaks are marked by crosses.

Proton Magnetic Resonance Spectra Under Conditions of Exchange

Preexchange lifetimes, τ, for PBT were determined at 10 temperatures from 54.8–125.9 °C and are listed in Table 2. The two values of τ for each temperature are the limits of τ which give reasonable fits to the observed line shapes. Some representative calculated and experimental spectra are given in Fig. 2. Coalescence of the signals from H_a and H_b occurred at about 98 °C. Above 125 °C the magnetic field homogeneity decreased to such an extent that really accurate fitting of calculated to experimental spectra was not possible.

Coalescence of the H_a and H_b signals of DBTCT and DBDCT occurred at about 75 °C. Preexchange lifetimes were determined at 72.6 and 82.6 °C for the sample of DBTCT in methylcyclohexane, at 70.0 and 78.5 °C for the toluene-d_8 solution of DBTCT, and at 70.9 and 80.0 °C for DBDCT in toluene-d_8 solution, in order to calculate $\Delta G^{\ddagger}$ at these temperatures.

Activation Parameters for the Hindered Rotations

(a) Experimental Values

Table 3 gives the activation parameters determined in this work with the results for PCT and DCTBT included for comparison. The values of E_a, log A, $\Delta H^{\ddagger}$, and $\Delta S^{\ddagger}$ and their respective errors given in Table 3 are the results

TABLE 1. Proton chemical shifts[a] and coupling constants in Hz for α,α,2,4,6-pentabromotoluene; α,α-dibromo-2,4,6-trichlorotoluene, and α,α-dibromo-2,6-dichlorotoluene

Parameter[b]	PBT[c]	DBTCT[d]	DBTCT[e]	DBDCT[f]
ν_A	772.446(5)	731.913(5)	680.900(4)	684.802(14)
ν_B	757.236(5)	719.190(5)	658.262(4)	665.611(14)
ν_C	—	—	—	639.467(15)
ν_X	737.263(5)	738.234(5)	726.714(4)	743.955(14)
$^3J^{H,H} \equiv J_{AC}$	—	—	—	8.226(21)
$^3J^{H,H} \equiv J_{BC}$	—	—	—	8.186(20)
$^4J^{H,H} \equiv J_{AB}$	1.998(7)	2.140(7)	2.166(6)	1.251(19)
$^5J^{H,H} \equiv J_{AX}$	0.500(7)	0.540(7)	0.532(6)	0.551(19)
$^5J^{H,H} \equiv J_{BX}$	−0.003(7)	−0.009(7)	−0.002(6)	0.000(20)
$^6J^{H,H} \equiv J_{CX}$	—	—	—	−0.010(21)
Root mean square error	0.007	0.007	0.006	0.032
Largest error	0.012	0.015	0.009	0.076
Lines assigned	12	12	12	32

[a]In Hz at 100 MHz downfield from internal hexamethyldisilane for PBT and from internal tetramethylsilane for the others.
[b]The bracketed numbers give the standard deviation in the last significant figure.
[c]10 mol % in perchlorobutadiene at 32.4 °C.
[d]10 mol % in methylcyclohexane at 17.1 °C.
[e]10 mol % in toluene-d_8 at 21.0 °C.
[f]15 mol % in toluene-d_8 at 22.3 °C.

TABLE 2. Preexchange lifetimes, τ, from fitted spectra at various temperatures for the compounds studied in this work[a]

Compound	Temperature (°K)	τ(s)
PBT	328.0	0.95–1.25
	329.9	0.65–0.85
	340.1	0.32–0.35
	349.4	0.14–0.16
	359.2	0.068–0.074
	367.4	0.040–0.043
	373.2	0.025–0.027
	376.9	0.0182–0.0188
	391.2	0.0069–0.0073
	399.1	0.0043–0.0046
DBTCT(in C_7H_{14})	345.8	0.055–0.062
	355.8	0.027–0.030
DBTCT(in C_7D_8)	343.2	0.045–0.065
	351.7	0.024–0.036
DBDCT	344.1	0.063–0.083
	353.2	0.032–0.040

[a]The limits given for τ represent those values which yield computed spectra in clear disagreement with observation.

of a standard error propagation treatment (10) of the experimental rate data for each compound. Rate constants for DBDCT and for the two samples of DBTCT were measured at only two temperatures in each case, so only $\Delta G^{\ddagger}$ values are given. All values of $\Delta G^{\ddagger}$ listed in Table 3 were calculated from rate constants determined by total lineshape analysis at temperatures (given in the table) very near the coalescence temperatures of the respective compounds. In this temperature region rate constants can be determined very precisely, resulting in highly accurate values of $\Delta G^{\ddagger}$. The errors in $\Delta G^{\ddagger}$ given in Table 3 are the linearized statistical errors, considering the errors contributed by uncertainties in both the rate constants and the temperatures.

Solvent effects on the activation parameters for internal rotation in PCT have been shown to be small (1, 9) and that this is the rule for molecules of this type is confirmed by the values of $\Delta G^{\ddagger}$ for DBTCT in methylcyclohexane and toluene-d_8 solutions (Table 3). Furthermore, comparison of the $\Delta G^{\ddagger}$ values for DBTCT and

Can. J. Chem. Downloaded from www.nrcresearchpress.com by 210.87.254.42 on 09/05/12
For personal use only.

Can. J. Chem. Downloaded from www.nrcresearchpress.com by 210.87.254.42 on 09/05/12
For personal use only.

TABLE 3. Activation parameters and the results of semiempirical barrier calculations for some halotoluenes

Compound	E_a(kcal/mol)	log A (s^{-1})	$\Delta H^{\ddagger}$(kcal/mol)	$\Delta S^{\ddagger}$(eu)	$\Delta G^{\ddagger}$(kcal/mol)	T(°K)	Calculated barrier(kcal/mol)
PCT (1,9)[a]	14.56±0.50	12.19±0.88	13.97±0.50	−4.7±1.7	15.33±0.05	300.4	13.26
DBTCT (in C_7H_{14})	—	—	—	—	18.39±0.05	345.8	
					18.44±0.05	355.8	
DBTCT (in C_7D_8)	—	—	—	—	18.21±0.13	343.7	16.20
					18.26±0.15	351.7	
DBDCT	—	—	—	—	18.44±0.11	344.1	
					18.46±0.09	353.2	
DCTBT (2)[a]	16.33±0.42	11.76±0.28	15.68±0.42	−7±2	18.14±0.05	347.2	16.35
PBT	19.85±0.22	13.23±0.13	19.13±0.22	−0.4±0.6	19.30±0.05	373.2	19.68

[a]References 1, 2, and 9 used $\kappa = \frac{1}{2}$: the values given here use $\kappa = 1$. The values for the activation parameters of PCT are obtained from the program ACTPAR (10) using the data from the three solutions combined.

Can. J. Chem. Downloaded from www.nrcresearchpress.com by 210.87.254.42 on 09/05/12
For personal use only.

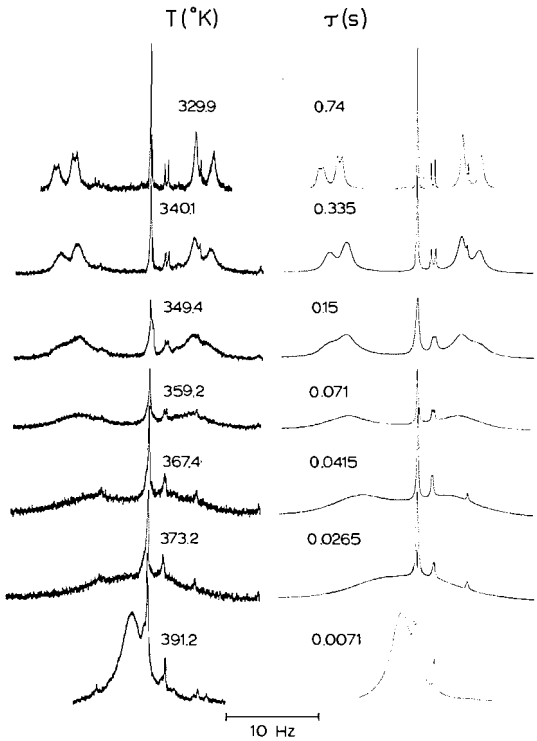

FIG. 2. Experimental and observed p.m.r. spectra of α,α,2,4,6-pentabromotoluene in perchlorobutadiene solution at a few representative temperatures and preexchange lifetimes τ.

DBDCT shows that a substituent *para* to the dihalomethyl group has a negligible effect on the barrier height. These conclusions are perhaps expected for barriers originating primarily in steric interactions between substituents *ortho* to the dihalomethyl group and the substituents on this group.

The entropies of activation for the hindered rotations are small and negative, indicating perhaps a loss of vibrational contribution to the entropy in the more sterically crowded, and hence rigid, transition state conformations.

The free energy of activation, $\Delta G^{\ddagger}$, increases by about 3 kcal/mol when the chlorine atoms in the α positions or in the *ortho* positions of PCT are replaced by bromine atoms. On replacing the other chlorine atoms by bromine atoms to give PBT, $\Delta G^{\ddagger}$ increases by 1 kcal/mol. The smaller increase on going to PBT possibly means that this molecule has a more crowded, and hence less stable, ground state conformation.

(b) Semiempirical Calculations of Conformational Energies

To obtain a deeper insight into the nature of the conformations involved in the rotation about the sp^2–sp^3 bond, Westheimer's classical model (11–13) was used for calculating conformational energies of DBTCT, DCTBT, and PBT. The energy minimization procedure has been described previously (3). The only parameters that are not included in reference 3 are the three force constants for bond angle deformations[3] at the dibromomethyl group (see 3): $k(C_1—C_\alpha—Br)$ 0.032, $k(Br—C_\alpha—Br)$ 0.030, and $k(Br—C_\alpha—H)$ 0.026 kcal/mol/deg^2; and the f_{ij} and g_{ij} values for nonbonded interactions given in Table 4.

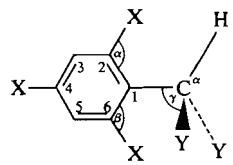

3

For all four compounds it was evident from the calculations that the most stable conformation is **a** with $\omega = 0°$, *i.e.* the C^α—H bond is coplanar with the aromatic ring. This is in accord with the experimental findings, *viz.* the large long-range spin–spin coupling between the methine and one of the *meta* protons, the zero coupling between the methine and *para* protons in compounds where there is no substituent in the 4-position, and the downfield shift of the methine proton.

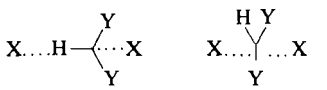

a (ω = 0°) **b** (ω = 30°)

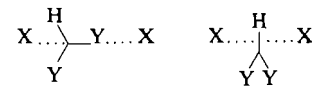

c (ω = 60°) **d** (ω = 90°)

The calculations show that the sum of the two repulsive X...Y interactions in **d** over dihedral angles of 30° is more severe than the

[3]These force constants were estimated by comparison with related compounds (3, 14).

TABLE 4. Constants f_{ij} and g_{ij} describing the nonbonded interaction between atoms i and j for a 6–12 potential

i	j	$10^{-4} f_{ij}$ (kcal mol^{-1} Å^{12})	g_{ij} (kcal mol^{-1} Å^{6})
Cl	Br_{aliph}	401.03	3563
Cl	Br_{arom}	449.75	3563
Br_{arom}	Br_{aliph}	716.85	5109

single interaction in **c** over a dihedral angle of 0°. A very large portion of the strain that would occur in **c** for rigid rotation is actually avoided by opening of bond angles.

The calculated barriers should be compared to $\Delta H^{\ddagger}$ because the Westheimer method does not take into account entropy effects. As can be seen from Table 3 the right order of magnitude is reproduced by the calculations: PCT has the lowest barrier; DBTCT and DCTBT have almost identical activation parameters and lie in the middle; PBT is the highest one. In all of the compounds the shape of the barrier to internal rotation from 0 to 180° is of a very simple type with a single maximum at 90° and minima at 0 and 180°. The type of energy curve having maxima at 60 and 120°, low minima at 0 and 180°, and a high energy minimum at 90° can be ruled out (see **a**–**d**). This finding demands the use of a transmission coefficient of unity in the determination of experimental activation parameters.

1. B. J. FUHR, B. W. GOODWIN, H. M. HUTTON, and T. SCHAEFER. Can. J. Chem. **48**, 1558 (1970).
2. J. PEELING, T. SCHAEFER, and C. M. WONG. Can. J. Chem. **48**, 2839 (1970).
3. A. MANNSCHRECK and L. ERNST. Chem. Ber. **104**, 228 (1971).
4. G. LOCK and R. SCHRECKENEDER. Ber. **72**, 511 (1939).
5. G. BINSCH. J. Am. Chem. Soc. **91**, 1304 (1969).
6. G. BINSCH and D. A. KLEIER. Computer program DNMR. QCPE. Chemistry Department, Indiana University, Bloomington, Indiana. No. 140.
7. P. LASZLO. Progr. NMR Spectrosc. **3**, 231 (1968).
8. C. W. HAIGH and J. M. WILLIAMS. J. Mol. Spectrosc. **32**, 398 (1969).
9. H. G. GYULAI, B. J. FUHR, H. M. HUTTON, and T. SCHAEFER. Can. J. Chem. **48**, 3877 (1970).
10. A. STEIGEL, J. SAUER, D. A. KLEIER, and G. BINSCH. J. Am. Chem. Soc. **94**, 2770 (1972).
11. H. A. SCHERAGA. *In* Advances in physical organic chemistry. Vol. 6. *Edited by* V. Gold. Academic Press, New York. 1968. p. 103.
12. J. E. WILLIAMS, P. J. STANG, and P. v. R. SCHLEYER. *In* Annual review of physical chemistry. Vol. 19. *Edited by* H. Eyring, C. J. Christensen, and H. S. Johnston. Annual Reviews, Inc., Palo Alto. 1968. p. 531.
13. E. L. ELIEL, N. L. ALLINGER, S. J. ANGYAL, and G. A. MORRISON. Conformational analysis. Interscience Publishers, New York. 1965. Chapt. 7.
14. H. A. STUART. Molekülstruktur. Springer, Berlin – Heidelberg – New York. 1967. p. 166.

Can. J. Chem. Downloaded from www.nrcresearchpress.com by 210.87.254.42 on 09/05/12
For personal use only.

Can. J. Chem. Downloaded from www.nrcresearchpress.com by 210.87.254.6 on 09/05/12
For personal use only.

COMMUNICATIONS

The Trishomocyclopropenyl Cation. I. Direct Observation

S. MASAMUNE,[1] M. SAKAI, A. V. KEMP-JONES, AND T. NAKASHIMA
Department of Chemistry, University of Alberta, Edmonton, Alberta T6G 2G2

Received August 17, 1973

The trishomocyclopropenyl cation has been prepared for the first time and is shown to be a remarkably stable, highly charge-delocalized species. The large $J_{^{13}C-H}$ value associated with the carbons formally carrying the positive charge, the high-field chemical shift of these carbons, and the absence of hydride shift, all are significant and are consistent with the formulation of **1** subject to the limit of the n.m.r. time scale.

On a préparé le cation trishomocyclopropényle pour la première fois et démontré que c'est une espèce d'une stabilité remarquable et où la charge est hautement délocalisée. Le fait que la valeur de $J_{^{13}C-H}$ soit grande pour les carbones portant la charge positive, de même que le grand déplacement chimique vers les champs élevés de ces carbones, ainsi que l'absence de transfert d'hydrure sont tous significatifs et en accord avec la formulation de **1** dans les limites de l'échelle de temps de la r.m.n. [Traduit par le journal]

Can. J. Chem., **52**, 855 (1974)

We record herein the first direct observation of the trishomocyclopropenyl cation (**1**). Since Winstein proposed the involvement of **1** in the solvolysis of *cis*-3-bicyclo[3.1.0]hexyl tosylate, first in 1959 (1), there have been presented experimental data that argue against its intermediacy in some related reaction systems (2). Repeated attempts to prepare **1** in superacid media have met with no success (3,4). Thus, despite Broser's seemingly valid spectral evidence to favor the existence of triaryl substituted trishomocyclopropenyl cations (*5a*), it has recently been concluded (4) that the inability to observe **1** even at low temperatures shows that "the initially formed bicyclic cation (**1**) must be so unstable that either hydride shift or ring contraction occurs immediately" to provide 1-methyl-2-cyclopentenyl cation (**2**) at $-60°$. This note provides a definite answer to the above enduring, controversial problems associated with **1** and demonstrates clearly that an energy minimum of the remarkably stable system (**1**) corresponds to the conformation in which the positive charge is highly delocalized.

Our previous experience (6) and simple reasoning have led us to choose *cis*-3-chlorobicyclo[3.1.0]hexane (**3**) as a precursor of **1** rather than the corresponding hydroxy compound (**4**). Mixing a CD_2Cl_2 solution of **3** (*2b*)[2] with a 1:5 mixture of SbF_5–SO_2ClF at *ca.* $-120°$ provided a bright orange lower layer which exhibited the ^1H and ^{13}C n.m.r. spectra shown in Figs. 1 and 2. Apart from line broadening due to viscosity, these spectra remained unchanged between -110 and $-40°$, at which temperature new, as yet unidentified, signals slowly appeared. In a ^1H-coupled ^{13}C spectrum, the singlets at δ 17.3 (A) and 4.7 (B) in Fig. 1 became a triplet and a doublet, respectively, showing that the latter (B) is ascribed to the carbons (C-1, -3, and -5) formally carrying the positive charge. The $J_{^{13}C-H}$ values are shown in Scheme 1. Since the proton assignment by means of selective decoupling was inconclusive, trideuterio compound *3a* with the stereochemistry indicated in Scheme 1 was prepared from cyclopentadiene oxide (**5**) with $LiAlD_4$ (7) and then CD_2I_2 (Simmons–Smith) (1,9). The *trans* ring opening of the epoxide ensures that the deuterium atom at C-2 is *trans* to the chlorine atom. When deuterated cation **1** was generated from *3a* the relative intensity of the signals X, Y, and Z became

[1]The author is grateful to the National Research Council and Hoffmann-LaRoche, Inc. for financial support.

[2]The preparation of **3** has been improved greatly by first preparing the chlorosulfite of **4** and then converting it into **3** in refluxing CH_2Cl_2.

Can. J. Chem. Downloaded from www.nrcresearchpress.com by 210.87.254.6 on 09/05/12
For personal use only.

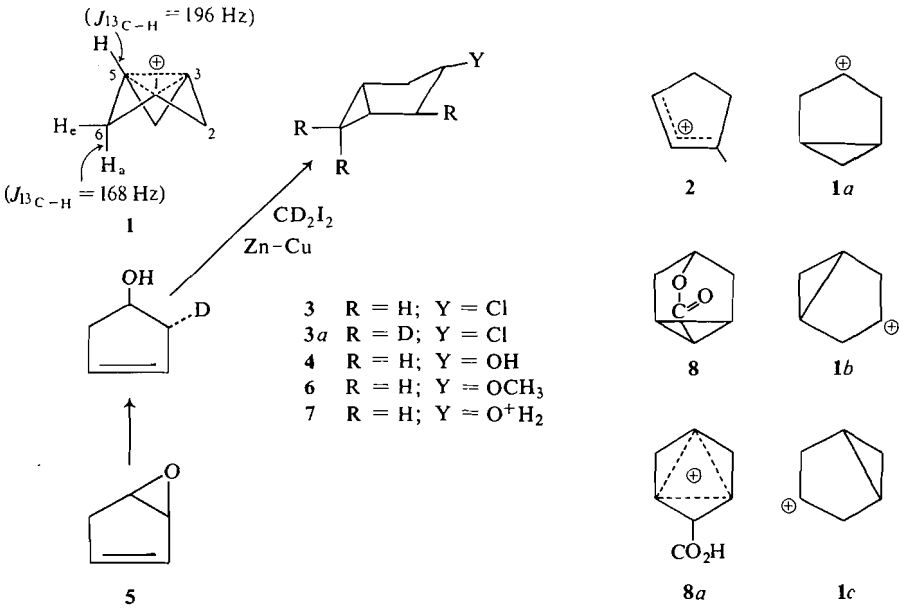

SCHEME 1

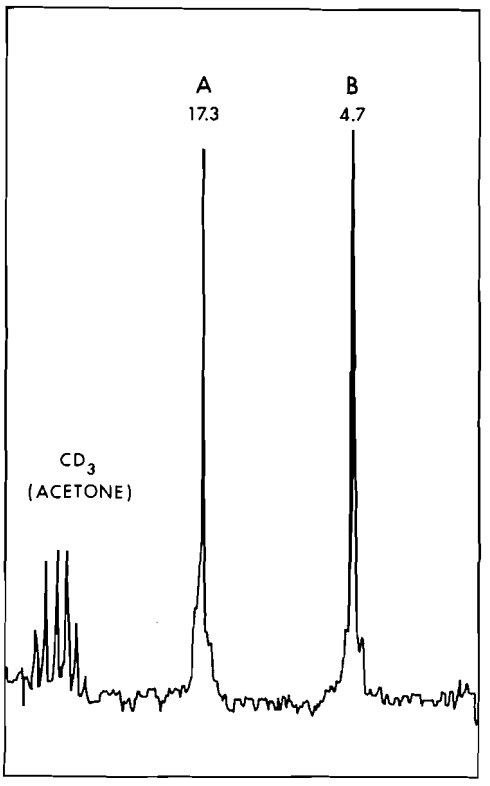

FIG. 1. A ^{13}C n.m.r. spectrum (22.63 MHz) of **1** in SbF_5–SO_2ClF at −90°. External deuterioacetone was used to lock the spectrometer and its signal taken as δ 31.2 from TMS.

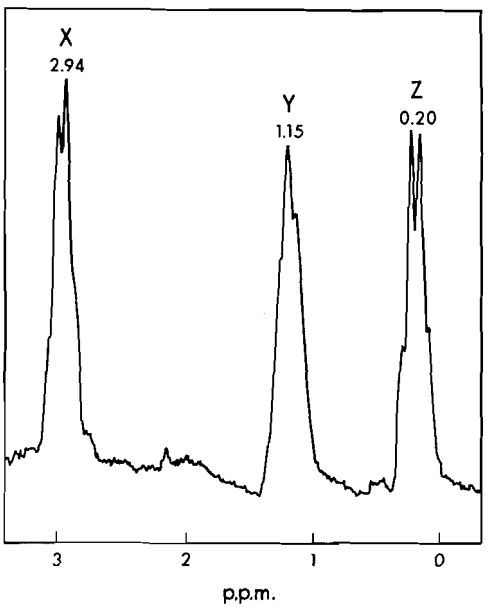

FIG. 2. A p.m.r. spectrum (100 MHz) of **1** in SbF_5–SO_2ClF at −80°. External *cis*-1,2-dichloroethylene was used to lock the Varian HA-100 spectrometer (622 Hz from TMS).

1:3:2. Thus signal Y is assigned to H(1,3,5), X to H_e, and Z to H_a. This experiment also demonstrates that **1** has formed directly from **3** without undergoing hydride shift, and that the stereochemical integrity of all the hydrogen atoms of **3** has been preserved. The high-field

absorption of the protons H_a, especially relative to H_e, is consistent with a substantial shielding contribution due to the *pseudo*-cyclopropane rings (9) of **1**. The c.m.r. spectrum of trideuterio-**1** also confirms these conclusions. Quenching the solution of **1** with methanol containing excess Na_2CO_3 provided a bicyclomethoxy compound (**6**) in *ca.* 50% yield, a result again consistent with the formation of **1**.

Some comments on earlier reports are now in order. The choice of **4** (4) to generate **1** in superacid media was inappropriate and the mechanistic interpretation (4) for the formation of **2** from **1** in $DF–SbF_5–SO_2ClF$ at $-78°$ (or $-60°$) appears to be inconsistent with the observed thermal stability of **1**. The protonated alcohol **7** is very likely to undergo rearrangement (intramolecular hydride shift) before **7** ionizes. However, it is not inconceivable that **1** was less stable in these media and rearranged faster than it was formed. While the claim by Broser and Rahn (*5a*) seems plausible, the spectrum of lactone **8** in sulfuric acid (10) may be simply that of the protonated lactone, rather than **8***a* as reported. There is a need of further evidence (11).

In conclusion, the evidence presented above clearly shows that cation **1** is an extensively charge-delocalized species and excludes the possibility of an equilibrium mixture of **1***a*, *b*, and *c*. The large J_{13c-H} value associated with C-1, -3, -5 (12), the high-field ^{13}C chemical shift of these carbons (12), and the absence of hydride shift, a process frequently observed in unstabilized cations (*e.g.*, cyclopentyl) even at $-130°$ (13), all are particularly significant and are consistent with the formulation of **1** subject to the limit of the n.m.r. time scale. We are more concerned at present with a subtle, intriguing question of whether or not the true energy minimum of the system corresponds to the geometry (**1**) with C_{3v} symmetry implied originally (1). A future note will elaborate on this point.

1. S. WINSTEIN. J. Am. Chem. Soc. **81**, 6524 (1959); S. WINSTEIN, J. SONNENBERG, and L. DEVRIES. J. Am. Chem. Soc. **81**, 6523 (1959); S. WINSTEIN and J. SONNENBERG, J. Am. Chem. Soc., **83**, 3235 and 3244 (1961); S. WINSTEIN, E. C. FREDERICK, R. BAKER, and Y-I LIU. Tetrahedron, **22**, S621 (1966).
2. (*a*) E. J. COREY and R. L. DAWSON. J. Am. Chem. Soc. **85**, 1782 (1963); E. J. COREY and H. UDA. J. Am. Chem. Soc. **85**, 1788 (1963); (*b*) P. K. FREEMAN, F. A. RAYMOND, and M. F. GROSTIC. J. Org. Chem. **32**, 24 (1967).
3. N. C. DENO. Prog. Phys. Org. Chem. **2**, 129 (1964); P. M. WARDER. Ph.D. Thesis, University of California, Los Angeles, Calif. (1970); G. A. OLAH and W. S. TOLGYESI. J. Am. Chem. Soc. **83**, 5031 (1961).
4. G. A. OLAH, G. LIANG, and Y. K. MO. J. Am. Chem. Soc. **94**, 3544 (1972).
5. (*a*) W. BROSER and D. RAHN. Chem. Ber. **100**, 3472 (1967); (*b*) P. K. FREEMAN and D. M. BALLS. Tetrahedron Lett. 437 (1967).
6. S. MASAMUNE, M. SAKAI, A. V. KEMP-JONES, H. ONA, A. VENOT, and T. NAKASHIMA. Angew. Chem. **85**, 829 (1973).
7. J. K. CRANDALL, D. B. BANKS, R. A. COLYER, R. J. WATKINS, and J. P. ARRINGTON. J. Org. Chem. **33**, 423 (1968).
8. C. D. POULTER and S. WINSTEIN. J. Am. Chem. Soc. **94**, 2297 (1972).
9. C. D. POULTER, R. S. BOIKESS, J. I. BRAUMAN, and S. WINSTEIN. J. Am. Chem. Soc. **94**, 2291 (1972).
10. R. R. SAUERS. Tetrahedron Lett. 1015 (1962).
11. G. A. OLAH and A. T. KU. J. Org. Chem. **35**, 3917 (1970).
12. G. A. OLAH. Angew. Chem. Intern. Ed. Engl. **12**, 173 (1973).
13. G. A. OLAH and J. LUKAS. J. Am. Chem. Soc. **90**, 933 (1968).

Can. J. Chem. Downloaded from www.nrcresearchpress.com by 210.87.254.6 on 09/05/12
For personal use only.

The Trishomocyclopropenyl Cation. II. An Ethano-bridged Derivative

S. MASAMUNE,[1] M. SAKAI, AND A. V. KEMP-JONES
Department of Chemistry, University of Alberta, Edmonton, Alberta T6G 2G2

Received September 28, 1973

An ethano-bridged trishomocyclopropenyl carbonium ion has been generated in superacid media from 8-chlorotricyclo[3.2.1.$0^{2,4}$]octane and/or 4-chlorotricyclo[3.3.0.$0^{2,8}$]octane. The ^{1}H and ^{13}C n.m.r. spectra of this new stable carbonium ion compare well with those of the parent trishomocyclopropenyl carbonium ion and yet show some indication that the degree of charge delocalization is more extensive than that originally implied.

On a produit un ion carbonium éthano-ponté du trishomocyclopropènyle dans un milieu superacide à partir du chloro-8 tricyclo[3.2.1.$0^{2,4}$]octane et/ou du chloro-4 tricyclo[3.3.0.$0^{2,8}$]-octane. Les spectres r.m.n. du ^{1}H et du ^{13}C de ce nouveau carbocation stable se comparent bien avec ceux de l'ion carbonium parent du trishomocyclopropènyle. Cependant ces spectres montrent que le degré de délocalisation de charge est plus élevé qu'il n'était prévu à l'origine.
[Traduit par le journal]

Can. J. Chem., **52**, 858 (1974)

The successful preparation of the parent trishomocyclopropenyl cation (**1**) of C_{3v} symmetry (1) has encouraged us to generate the carbocation (**2**) in superacid media from now available 8-chlorotricyclo[3.2.1.$0^{2,4}$]octane (**3**) (2) and/or 4-chlorotricyclo[3.3.0.$0^{2,8}$]octane (**4**) (3).[2] We expected that this structural modification (by means of an ethano-bridge) introduced into **1** would only slightly perturb the electronic structure of **1** but yet, in view of our recent work on the related systems (4–6), would provide further information on the degree of electron delocalization in the entire system of **4**. Results are summarized below (Scheme 1).

As noted previously (1, 4, 6), chlorides appear to serve as the best precursors for the generation of cations in the present case. Thus, extraction of the chlorides **3** or **4** in CD_2Cl_2 with SbF_5–SO_2ClF at $-120°$ provided yellow solutions which exhibited identical, clearly resolved ^{13}C and ^{1}H n.m.r. spectra as shown in Figs. 1 and 2. All the signals remained virtually unchanged up to $-40°$ and quenching the solutions with Na_2CO_3 in methanol at $-80°$ yielded a methoxy compound, almost certainly **5**, identical with material obtained by solvolysis of **6** in a K_2CO_3–methanol mixture (3). These experiments demonstrate that there was formed a stable, spectrally well-characterized carbocation.

In order to define the structure of the new cation, the unambiguous assignment of the n.m.r. signals to the nuclei is of prime importance and calls for the preparation of two deuterated precursors, **7** and **8**. While the synthesis of **7** was readily accomplished through reduction of ketone **9** with deuterium over platinum (CH_3OD) (3*a*) and then treatment of the resulting monodeuterated hydroxy compound (**10**-d_1) with $SOCl_2$,[2] the four deuterium atoms in **8** were incorporated at an early stage of the reaction sequence (3*a*), *i.e.*, reduction of chloroketal **11** using sodium in a $(CH_3)_3COD$–tetrahydrofuran mixture.

The ^{1}H and ^{13}C spectra of the new cation both show the presence of two-fold symmetry in this species and can be in accord with the formulation of **2**. The proton-decoupled ^{13}C spectrum consists of five lines at δ(TMS) 0.00(d),[3] 5.88(t), 19.58(d), 25.45(t), and 29.67(d). The approximate relative intensities (1:1:2:2:2+) and the multiplicities of these signals in the off-resonance spectrum permit the δ 0.00 peak to be assigned to C-8 and the δ 5.88 and 25.45 peaks to C-3, and to C-6 and -7, respectively. The cation derived from **8** showed that only the two peaks at 29.67 and 25.46 collapsed with a slight upfield shift and this information leads to the assignment of the δ 19.58 and 29.67 peaks to C-2 and -4, and to C-1 and -5, respectively (7). The ^{1}H signals shown in Fig. 3 are assigned in the following manner. The spectrum of **2***a* lacks the

[1]The author is grateful to the National Research Council and Hoffmann-LaRoche, Inc. for financial support.

[2]Compound **4** was prepared by treating **10** with $SOCl_2$.

[3]The letter in parentheses after each figure indicates that the peak becomes a doublet (d) or triplet (t) in the off-resonance spectrum.

Can. J. Chem. Downloaded from www.nrcresearchpress.com by 210.87.254.42 on 09/05/12
For personal use only.

Can. J. Chem. Downloaded from www.nrcresearchpress.com by 210.87.254.42 on 09/05/12
For personal use only.

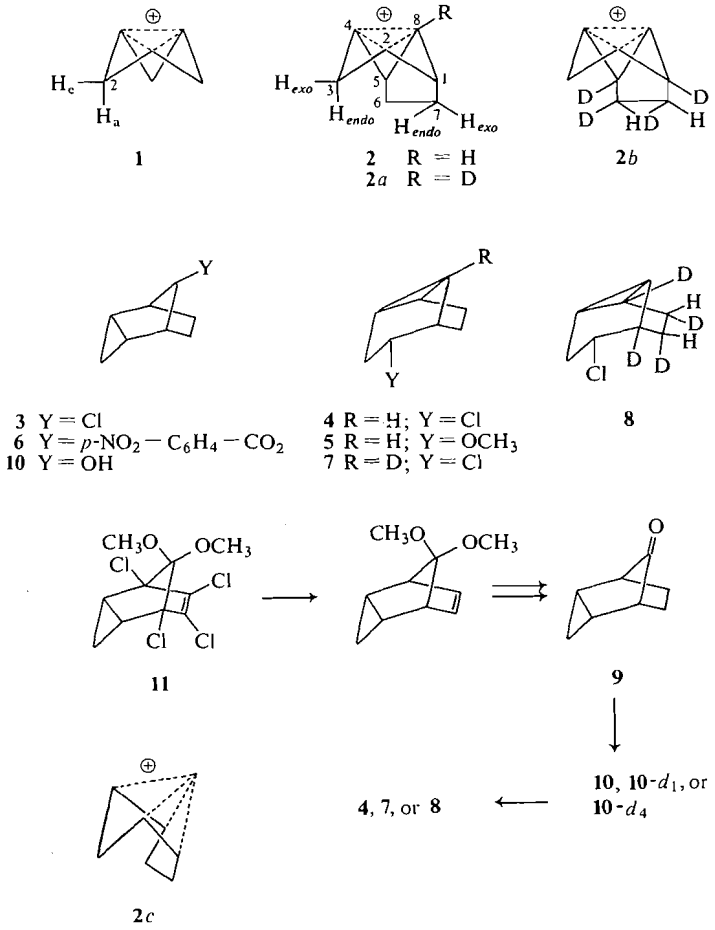

SCHEME 1

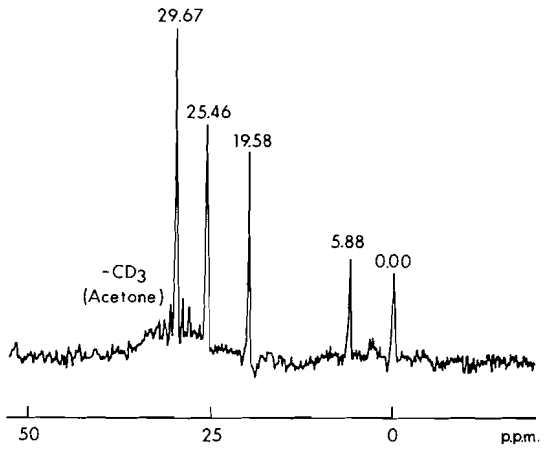

FIG. 1. A ^{13}C n.m.r. spectrum (22.63 MHz) of **2** in SbF_5–SO_2ClF at −90°. External deuterioacetone was used to lock the spectrometer and its signal taken as δ 31.2 from TMS.

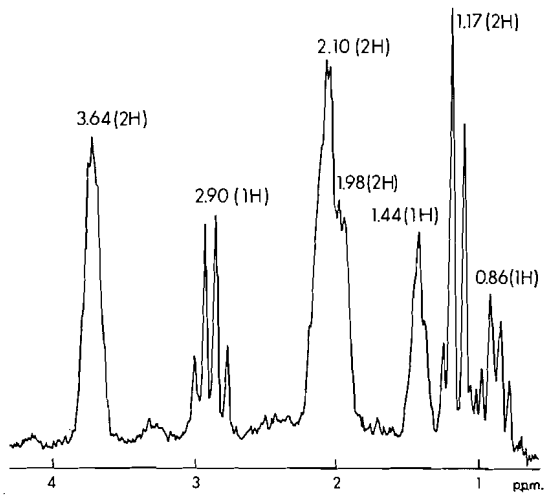

FIG. 2. A p.m.r. spectrum (100 MHz) of **2** in SbF_5–SO_2ClF at −80°.

δ 1.44 peak, which readily leads to the assignment of this peak to H-8. The appearance of two approximate quartets at δ 0.86 and 2.90 suggested that these are a part of an AXM_2 system (confirmed by decoupling experiments) and the chemical shift values compare very well with those observed for Ha and He of **1** (1). Furthermore, these signals are virtually unaffected in the spectrum of **2***b* which showed no absorption at δ 1.17 and 3.64, and sharp and broad singlets at δ 1.98 and 2.10, respectively. These results permit the assignment of (*i*) the peaks at δ 0.86 and 2.90 to H-3 *endo* and H-3 *exo* in that order, and (*ii*) those at 3.64 and 1.17 to H-1 and -5, and H-6 and -7 *endo*, respectively. The reverse assignment of the last two signals appears to be inconsistent with the chemical shift (*ca.* δ 0.65) of the H-6 and -7 *endo* protons of **10** (3*a*). The peak at 1.98 (sharp singlet in the spectrum of **2***b*, *vide supra*) is reasonably assigned to H-6 and -7 *exo* because of the absence of coupling with other protons and finally the δ 2.10 peak to H-2 and -4.

Comparison of the ^1H n.m.r. spectra of **1** and **2** readily discloses several common features, except that the protons attached to the carbons 2, 4, and 8, formally carrying partial charge in formula **2** absorb at lower fields than those in **1**. The chemical shift values of H-3 *endo* and *exo* have already been commented on. The protons at C-1 and -5 correspond to He of **1** but are tertiary (instead of secondary). Also, H-1 and -5 are attached to carbons next to those formally positively charged and the chemical shift (δ 3.64) of these protons represents a 1.7 δ unit downfield shift, compared with those of **10** (3*a*, 8). Thus the value δ 3.64 appears quite reasonable. ^{13}C spectra are generally quite sensitive to a change of geometry and charge density and these factors apparently bring about an upfield shift for carbon 8 and a downfield shift for C-2 and -4, compared with those of the corresponding carbons in **1**, although the magnitude of the chemical shift change is not large. Thus, at present we may conclude that the cation derived either from **3** or **4** can safely be represented by **2**, but the above departure in the ^{13}C chemical shift is in line with the trend we have observed for the square pyramidal carbocation (4, 5, 6) and the structure **2***c* might make some contribution. In either case, the charge is delocalized so extensively that it is not even clear at which carbon atom most of the charge resides.

1. S. MASAMUNE, M. SAKAI, A. V. KEMP-JONES, and T. NAKASHIMA. Can. J. Chem. This issue.
2. P. K. FREEMAN, R. S. RAGHAVAN, and G. L. FENWICK. J. Am. Chem. Soc. **94**, 5101 (1972).
3. (*a*) J. S. HAYWOOD-FARMER and R. E. PINCOCK. J. Am. Chem. Soc. **91**, 3020 (1969); (*b*) M. A. BATTISTE, C. L. DEYRUP, R. E. PINCOCK, and J. S. HAYWOOD-FARMER. J. Am. Chem. Soc. **89**, 1954 (1967); (*c*) H. TANIDA, T. TSUJI, and T. IRIE. J. Am. Chem. Soc. **89**, 1953 (1967).
4. S. MASAMUNE, M. SAKAI, A. V. KEMP-JONES, H. ONA, A. VENOT, and T. NAKASHIMA. Angew. Chem. **85**, 829 (1973).
5. S. MASAMUNE, M. SAKAI, H. ONA. J. Am. Chem. Soc. **94**, 8955 (1972); S. MASAMUNE, M. SAKAI, H. ONA, and A. J. JONES. J. Am. Chem. Soc. **94**, 8956 (1972).
6. A. V. KEMP-JONES, NOBUO NAKAMURA, and S. MASAMUNE. Chem. Commun. In press.
7. J. B. STOTHERS, C. T. TAN, A. NICKON, F. HUANG, R. SRIDHAR, and R. WEGLEIN. J. Am. Chem. Soc. **94**, 8581 (1972); D. H. HUNTER, A. L. JOHNSON, J. B. STOTHERS, A. NICKON, J. L. LAMBERT, and D. F. COVEY. J. Am. Chem. Soc. **94**, 8582 (1972).
8. E. I. SNYDER and B. FRANZUS. J. Am. Chem. Soc. **86**, 1166 (1964); M. BROOKHART, A. DIAZ, and S. WINSTEIN J. Am. Chem. Soc. **88**, 3135 (1966); C. U. PITTMAN, JR. and G. A. OLAH. J. Am. Chem. Soc. **87**, 5123 (1965).

Can. J. Chem. Downloaded from www.nrcresearchpress.com by 210.87.254.42 on 09/05/12
For personal use only.

Intrinsic Acidities of α, β, γ Chlorosubstituted Aliphatic Acids from Gas Phase Equilibrian Mesurements

R. YAMDAGNI AND P. KEBARLE

Chemistry Department, University of Alberta, Edmonton, Alberta

Received November 19, 1973

Measurements of the proton transfer equilibria: $A_1^- + A_2H = A_2^-$ with a pulsed electron beam high pressure mass spectrometer were extended to α, β, γ chlorosubstituted aliphatic acids. The equilibrium constants were used to evaluate ΔG^0 for the proton transfer reactions. Assuming $\Delta G \approx \Delta H$ and using standard acids AH for which the difference between the bond dissociation energy D(A—H) and the electron affinity of A, EA(A) was known one could evaluate the corresponding difference for the newly measured acids and place them on an absolute acidity scale. The gas phase acidity was observed to increase in the order: acetic, propionic, butyric, γ-Cl butyric, β-Cl butyric, β-Cl propionic, α-Cl butyric, α-Cl propionic, α-Cl acetic. The gas phase acidities are compared with those observed in aqueous solution. The effects of the Cl substituent parallel those in solution but are much larger. The attenuation occurring in solution is attributed to weaker hydrogen bonding of the chloro stabilized acid anions to water molecules.

Les mesures de l'équilibre de transfert de protons: $A_1^- + A_2H = A_1H + A_2^-$ avec un spectromètre de masse à haute pression et à faisceau d'électrons à impulsions sont étendues aux acides aliphatiques chlorosubstitués en α, β, et γ. Les constantes d'équilibre sont utilisées pour évaluer ΔG^0 pour les réactions à transfert de protons. Admettant que $\Delta G \approx \Delta H$ et utilisant des acides standard AH pour lesquels la différence entre l'énergie de dissociation de liaison D(A—H) et l'affinité électronique de A, EA(A) sont connues, on pourrait évaluer la différence correspondante pour les acides nouvellement mesurés et les classer sur une échelle d'acidité absolue. L'acidité en phase gazeuse augmente selon l'ordre: acétique, propionique, butyrique, γ-Cl butyrique, β-Cl butyrique, β-Cl propionique, α-Cl butyrique, α-Cl propionique, α-Cl acétique. Les acidités en phase gazeuse sont comparées à celles observées en solution aqueuse. Les effets du substituant Cl sont analogues à ceux en solution mais sont plus grands. L'atténuation qui apparait en solution est attribuée à un plus faible enchaînement par liaison d'hydrogène des anions chlorures d'acides stabilisés aux molécules d'eau. [Traduit par le journal]

Can. J. Chem., **52**, 861 (1974)

Recently (1, 2) it has become possible to determine acidities of carboxylic acids AH in the absence of solvent by measuring the gas phase proton transfer equilibria (1).

$$[1] \qquad A_1^- + A_2H = A_1H + A_2^-$$

The measurements are made with a pulsed electron beam high pressure mass spectrometer under conditions where the residence time of the ions A^- in the ion source is much longer than the time required for establishment of the equilibrium (1). The ion intensities A_1^- and A_2^- are measured with the mass spectrometer. Since the concentrations of the neutrals AH are also known the equilibrium constant K_1 and $\Delta G_1^0 = -RT \ln K_1$ can be evaluated. In favorable cases the temperature dependence of K_1 can also be determined and ΔH_1^0 and ΔS_1^0 obtained from Van't Hoff plots. The earlier two publications (1, 2) described results for several unsubstituted and α halosubstituted aliphatic acids.

The present work examines the change of acidity occurring when a halosubstituent (Cl) is moved progressively farther away from the carboxylic group. The work thus parallels the early researches (3) on effects of halosubstituents in aqueous solution, but gives for the first time the changes on a molecular level, *i.e.*, in the absence of solvent.

The directly measured equilibria are summarized in Fig. 1. The equilibria were measured in the presence of some 3–5 Torr CH_4 or N_2 gas. The weaker acid was generally at some 50–200 mTorr, the stronger at 10–50 mTorr. Collisions with the buffer gas should lead to thermalization of the reactants. The measurements were done at 600 °K. Formation of the proton bound dimers $(AHA)^-$ and higher clusters $A^-(HA)_n$ interfered with measurements at lower temperatures while thermal decomposition of the acids occurred at higher temperatures. On the basis of earlier measurements (2, 4), we expect that the proton transfer reactions proceed with small entropy changes which rarely exceed 2 e.u.

Can. J. Chem. Downloaded from www.nrcresearchpress.com by 210.87.254.40 on 09/05/12
For personal use only.

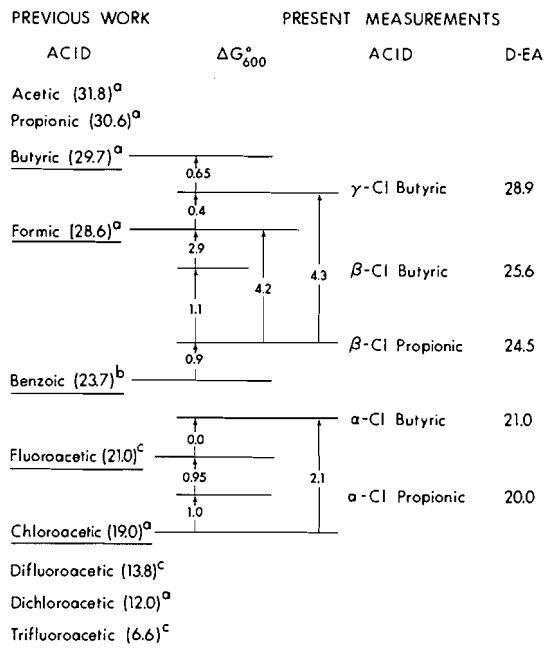

FIG. 1. Gas phase acidities of aliphatic acids: ΔG_{600}° values for gas phase equilibria: $A_1^- + A_2H = A_1H + A_2^-$ measured in present work shown connected by an arrow. The upper acid is the weaker one (A_2H). $D - EA$ refers to the difference between bond dissociation energy D(A—H) and electron affinity of A. Figures given in parentheses besides previously measured acids correspond to values for $D - EA$. The acids used as standards for the present work have been underlined. Other previously measured acids are given for comparison. Acidity increases from top to bottom of the figure: (*a*) ref. 1; (*b*) R. Yamdagni, T. B. McMahon, and P. Kebarle, to be published; (*c*) ref. 2.

Therefore $\Delta G_{600}^0 \approx \Delta G_{300}^0$ and $\Delta G^0 \approx \Delta H^0$ within about 1 kcal. Shown in Fig. 1 are the measured ΔG_1^0 values for proton transfer from the stronger acid (below) to the conjugate base of the weaker acid (above).

$$\Delta G_1^0 = D(A_2 - H) - D(A_1 - H) + EA(A_1) - EA(A_2)$$

if one assumes $\Delta G^0 = \Delta H^0$. D(A—H) and EA(A) are the bond dissociation energy and the electron affinity. Thus if D(A—H) − EA(A) for one (standard) acid is known, the corresponding difference for the other can be evaluated. The standard acids are shown on the left of Fig. 1. Their values of D(A—H) − EA(A) (given in parentheses) were determined in earlier work (1, 2). Some cross checks of the data are possible if one uses thermodynamic cycles. Thus the $\Delta G^0 = 4.3$ kcal for proton transfer from β-Cl, propionic to γ-Cl, butyric can also be obtained via β-Cl, propionic → β-Cl, butyric → formic → γ-Cl, butyric. These differences add up to 4.4 kcal. Two other similar checks are evident in Fig. 1.

The relative acidities of the chlorosubstituted acids in gas phase and aqueous solution are compared in Table 1*a*. Introduction of an α-Cl substituent leads to a large increase of acidity. The ΔG^0 value for the gas phase is around 10 kcal and only 2.5 for the aqueous acids. Removal of the substituent to β position reduces the acidity increase by a factor of about two for both gas and aqueous phase and a similar decrease is observed for β → γ. In general, the gas phase substituent effects are attenuated by a factor of four in aqueous solution. Similarly large attenuations have been observed also in other comparisons between gas phase and aqueous substituent effects (5, 6). Studies of the strongly hydrogen bonded adducts A^-HR and particularly A^-HOH observed in the gas phase have shown (7) that the hydrogen bond energy increases with the (gas phase) basicity of A^-. Since A^- is the conjugate base of AH, this means that the hydrogen bond decreases when the acidity of AH increases. The formation of the adduct A^-HOH is the first and most important step in the hydration sequence and since a similar effect is expected for further additions of water molecules it follows that a substituent which increases the acidity of AH automatically decreases the hydration energy of A^- and thus attenuates the acidity increase in aqueous solution.

Some interesting smaller effects are also evident from Table 1. Shown in part *b* are the acidities of the unsubstituted acids measured earlier (1). These increase, in the order: acetic, propionic, butyric, which is opposite to that observed in aqueous solution. Following Brauman and Blair (8), we assumed (1) that the gaseous increase is due to the increasing polarizability which stabilizes the charge. The present results show that the effect of the α-chloro substituent decreases in the order: acetic, propionic, butyric, for which Table 1*a* gives ΔG^0 of 12.8, 10.6, and 8.7 kcal relative to the unsubstituted acid. This probably means that the more polarizable larger alkyl groups attenuate the influence of the C—Cl dipole and thus the stabilizing effect of Cl on the acid

Can. J. Chem. Downloaded from www.nrcresearchpress.com by 210.87.254.40 on 09/05/12
For personal use only.

TABLE 1. ΔG^0 (kcal/mol) for proton transfer reactions in acids*

(*a*) $RHCOOH + RClCOO^- = RHCOO^- + RClCOOH$

	ΔG^0					
	Gas phase			Aqua†		
Acid	α	β	γ	α	β	γ
Acetic	12.8	—	—	2.6	—	—
Propionic	10.6	6.1	—	2.7	1.2	—
Butyric	8.7	4.1	0.8	2.5	1.1	0.4

(*b*) $CH_3COOH + RCOO^- = CH_3COO^- + RCOOH$‡

	ΔG^0	
Medium	C_2H_5	C_3H_7
Gas phase	+1.2	+2.1
Aqua	−0.16	−0.09

*ΔG^0 values measured at 600 °K, α, β, γ are positions of Cl substituent.
†From ref. 3.
‡From ref. 1, measured between 500–600 °K.

anion. It is worth noting that the counter effect of the alkyl groups is considerable and leads to the following gas phase acidity order for α chloro substituted acids: acetic > propionic > butyric. (From combined ΔG^0 data of Table 1*a* and 1*b*.)

1. R. YAMDAGNI and P. KEBARLE. J. Am. Chem. Soc. **95**, 4050 (1973).
2. K. HIRAOKA, R. YAMDAGNI, and P. KEBARLE. J. Am. Chem. Soc. **95**, 6833 (1973).
3. C. K. INGOLD. Structure and mechanism in organic chemistry. Cornell University Press, Ithaca and London, 1969. p. 114.
4. J. P. BRIGGS, R. YAMDAGNI, and P. KEBARLE. J. Am. Chem. Soc. **94**, 5128 (1972).
5. M. TAAGEPERA, W. G. HENDERSON, R. T. C. BROWNLEE, J. L. BEAUCHAMP, D. HOLTZ, and R. W. TAFT. J. Am. Chem. Soc. **95**, 1369 (1972).
6. A. G. HARRISON, P. KEBARLE, and F. P. LOSSING. J. Am. Chem. Soc. **83**, 777 (1961).
7. R. YAMDAGNI and P. KEBARLE. J. Am. Chem. Soc. **93**, 7139 (1971).
8. J. I. BRAUMAN and L. K. BLAIR. J. Am. Chem. Soc. **93**, 4315 (1971).

Can. J. Chem. Downloaded from www.nrcresearchpress.com by 210.87.254.40 on 09/05/12
For personal use only.

The EPR Spectra of Hydrazyl and Some 1-Substituted Hydrazyl Radicals in Solution[1]

V. MALATESTA,[2] D. LINDSAY, E. C. HORSWILL, AND K. U. INGOLD

Division of Chemistry, National Research Council of Canada, Ottawa, Canada K1A 0R9

Hydrogen atom abstraction by *tert*-butoxy radicals from hydrazine, methyl-, benzyl- and carboethoxy-hydrazine yields the hydrazyl radical and the appropriate 1-substituted hydrazyls, $R\dot{N}NH_2$. The radical structures are assigned on the basis of their e.p.r. spectral parameters. It has been shown by ^{15}N labelling that in 1-alkylhydrazyls the larger nitrogen splitting is produced by the divalent nitrogen that formally bears the unpaired electron. This result contrasts with the behavior of 2,2-dialkylhydrazyls (1).

Les radicaux *tert*-butoxyle enlevant des atomes d'hydrogène de l'hydrazine ainsi que de la méthyle, de la benzyle et de la carboéthoxy hydrazine fournissent les radicaux hydrazyles et les hydrazyles substitués en position 1 appropriés, $R\dot{N}NH_2$. Les structures radicalaires ont été attribuées en se basant sur les paramètres de leur spectre rpe. On a démontré par marquage avec ^{15}N que dans les alkyl-1 hydrazyle le couplage plus grand de l'azote est dû à l'azote divalent qui porte formellement l'électron non-pairé. Les résultats obtenus sont inattendus si l'on considère les propriétés attribuées (1) aux dialkyl-2,2 hydrazyles. [Traduit par le journal]

Can. J. Chem., 52, 864 (1974)

The solution e.p.r. spectra of a great many trisubstituted hydrazyls have been known for many years, but it is only very recently that we reported the first solution spectra of some 2,2-di-substituted-hydrazyls (1). We have now extended our studies to hydrazyl itself, $H\dot{N}NH_2$, and to some mono-substituted hydrazyls.

The radicals were generated by photolysis of solutions of the parent hydrazines in benzene containing about 25% by volume di-*tert*-butyl peroxide. Although the structures of mono-substituted hydrazyls cannot be unequivocally assigned there is no such structural ambiguity with hydrazyl nor with 2,2-dialkyl-hydrazyls. Comparison of the various hyperfine splittings leads us to conclude that the mono-substituted hydrazyls are all 1-substituted, *i.e.*, $R\dot{N}NH_2$. The e.p.r. parameters are recorded in Table 1.

Hydrazyl, $H\dot{N}NH_2$

The hydrogens on the H_2N group are not equivalent at 0°. Their splitting changes with temperature and these changes will be examined in order to determine the barrier to rotation about the N—N bond. The spectral parameters are similar to those found for the hydrazyl radical adsorbed in the pores of a zeolite molecular sieve, *viz.*, $a^N = 11.7$ and 8.8 G, $a^H = 18.8$ G (1H) and 2.3 G (2H, average value, the NH_2 hydrogens were not equivalent even at 90°) (2) and for the hydrazyl radical imbedded in an adamantane matrix (3). The spectrum at 0° is shown in Fig. 1.

1-Methylhydrazyl, $Me\dot{N}NH_2$

The hydrogens on the NH_2 group are again non-equivalent and produce only small splittings comparable to those found in $H\dot{N}NH_2$. There is no large (> 13 G) splitting due to a unique hydrogen and the splitting due to the CH_3 protons is more than twice as large as that found for the CH_3 groups in $(CH_3)_2N\dot{N}H$. For these reasons, we rule out the alternate 2-methylhydrazyl structure. The spectrum at 0° is shown in Fig. 2.

1-Benzylhydrazyl, $C_6H_5CH_2\dot{N}NH_2$

The splittings and hence the structural assignment for this radical are essentially the same as for $CH_3\dot{N}NH_2$. The assignment of the hydrogens in the CH_2 and NH_2 groups was confirmed by replacement of the hydrazine's labile hydrogen atoms by deuterium.

In 2,2-dialkylhydrazyls, $R'_2N\dot{N}H$, we have shown by ^{15}N labelling that the smaller nitrogen splitting comes from the divalent, $N_{(1)}$, nitrogen (1). This was rationalized[3] as being due to the inductive effect of the alkyl groups which stabilizes resonance structure **b** relative to **a**, and so

[1]NRCC No. 13775.

[2]NRCC Postdoctoral Fellow 1972–1973.

[3]The alkyl groups may also affect a^N by changing the degree of planarity of $N_{(1)}$ and $N_{(2)}$.

Can. J. Chem. Downloaded from www.nrcresearchpress.com by 210.87.254.6 on 09/05/12
For personal use only.

TABLE 1. Electron spin resonance parameters for some hydrazyl radicals, $R\dot{N}_{(1)}N_{(2)}H_2$, in solution*

Hydrazyl	Temperature (°C)	g	$a^{N(1)}$	$a^{N(2)}$	$a^{H}(N_{(1)})$	$a^{H}(N_{(2)})$	a^{H} (other)
$H\dot{N}NH_2$	0	2.00369	11.7†	8.8†	16.3	4.3, 1.6	
$CH_3\dot{N}NH_2$	0	2.00378	14.0	7.9		2.8, 1.3	17.7 (3H)
$H\dot{N}N(CH_3)_2$(ref. 1)	25	2.00381	9.6	11.5	13.7		6.9 (6H)
$C_6H_5CH_2\dot{N}NH_2$	25	2.00378	13.5	7.9		2.6, 1.3	19.1 (2H)
$C_6H_5CH_2\dot{N}ND_2$	25		13.5	7.9		2D not resolved	19.1 (2H)
$C_6H_5CH_2\dot{N}^{15}NH_2$	25		13.5	11.1‡		2.8, 1.3	19.1 (2H)
$CH_3CH_2OC(O)\dot{N}NH_2$	0	2.00385	7.8§	10.2§		9.6 (2H)	1.3 (2H)
$CH_3CH_2OC(O)\dot{N}ND_2$	0	2.00385	7.8§	10.2§		1.5 (2D)	1.3 (2H)
$CH_3CH_2OC(O)\dot{N}NH_2$	30		8.0§	9.8§		9.8 (2H)	1.3 (2H)

*Hyperfine splittings, in G, were obtained by computer simulation.
†Assignment of reference (2).
‡^{15}N splitting (*i.e.*, a doublet splitting with the expected value of 1.4 for $a^{15}N/a^{14}N$).
§Tentative assignment, see text.

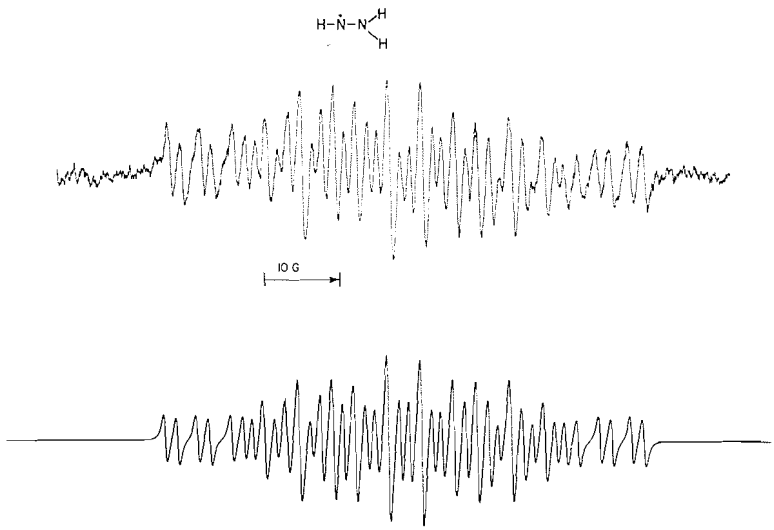

FIG. 1. Electron paramagnetic resonance spectra (top) and simulation (bottom) for $H\dot{N}NH_2$ at 0°.

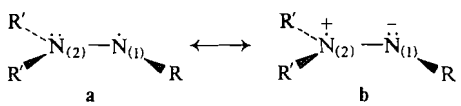

a b

increases the spin density on $N_{(2)}$. By the same argument we concluded that in 1-alkylhydrazyls, $H_2N\dot{N}R$, the +I effect of the alkyl group should reverse the nitrogen splittings. That is, **a** should be stabilized relative to **b** and so the smaller nitrogen coupling should come from $N_{(2)}$ which bears the two hydrogens. This was confirmed by ^{15}N labelling of the NH_2 groups in the radical (see Table 1). The $C_6H_5NH^{15}NH_2$ was prepared by *N*-nitrosation of *N*-benzylglycine with $Na^{15}NO_2$ followed by preparation and thermal decomposition of *N*-benzylsydnone (4).

1-Carboethoxyhydrazyl, $CH_3CH_2OC(O)\dot{N}NH_2$

Deuterium labelling shows that the 1.3 G splitting by two equivalent hydrogens is due to the CH_2 group. The two equivalent hydrogens that produce the 9.6 G splitting are assigned to the NH_2 group, rather than to a fortuitous equivalence in a 2-carboethoxyhydrazyl radical. The electron-withdrawing carboethoxy group should stabilize resonance structure **b** relative to **a**. This suggests that $N_{(2)}$ will now produce the larger splitting and, as a consequence of its increased

Can. J. Chem. Downloaded from www.nrcresearchpress.com by 210.87.254.6 on 09/05/12
For personal use only.

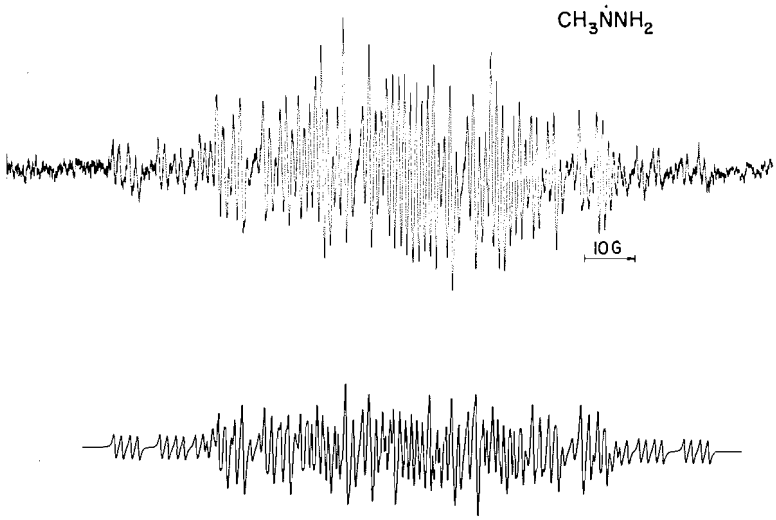

FIG. 2. Electron paramagnetic resonance spectra (top) and simulation (bottom) for $CH_3\dot{N}NH_2$ at 0°.

spin density, the splitting by the hydrogens attached to $N_{(2)}$ will also increase. This assignment of the two nitrogens must, however, be considered as very tentative, since in 1,1-diphenyl-2-picrylhydrazyl it has been shown that it is the divalent nitrogen (attached to the strongly electron withdrawing picryl group) that has the larger coupling (5, 6).

The equivalence of the two hydrogens on $N_{(2)}$ at 0° implies either that the barrier to rotation about the $N_{(1)}$—$N_{(2)}$ bond is less in CH_3CH_2-$OC(O)\dot{N}NH_2$ than in $H\dot{N}NH_2$ and $CH_3\dot{N}NH_2$ or that inversion at $N_{(1)}$ is more rapid. On lowering the temperature to −30° there are some spectral changes but the intensity was too low to justify analysis. On raising the temperature to 30° various lines in the spectrum shift slightly and there is a coalescence to give a spectrum of fewer lines. This does not appear to be due to line broadening but rather to changes in some of the coupling constants (see Table 1). These changes might arise from an increase in the rate of rotation or inversion. The spectrum did not change on further warming to 60°.

The apparently exclusive formation of 1-substituted hydrazyls from mono-substituted hydrazines is rather surprising. It may reflect either differences in the rates of formation of 1- and 2-substituted hydrazyls or differences in their rates of decay.

1. V. MALATESTA and K. U. INGOLD, J. Amer. Chem. Soc., **95**, 6110 (1973).
2. R. FANTECHI and G. A. HELCKE, J. Chem. Soc. Faraday II, **68**, 924 (1972).
3. D. E. WOOD. Private communication.
4. J. FUGGER, J. M. TIEN, and I. M. HUNSBERGER, J. Amer. Chem. Soc. **77**, 1843 (1955).
5. R. W. HOLMBERG, R. LIVINGSTON, and W. T. SMITH, J. Chem. Phys. **33**, 541 (1960).
6. M. M. CHEN, K. V. SANE, R. I. WALTER, and J. A. WEIL, J. Phys. Chem. **65**, 713 (1961).

Can. J. Chem. Downloaded from www.nrcresearchpress.com by 210.87.254.6 on 09/05/12
For personal use only.

Can. J. Chem. Downloaded from www.nrcresearchpress.com by 210.87.254.105 on 09/05/12
For personal use only.

Canadian Journal of Chemistry

Published by
THE NATIONAL RESEARCH COUNCIL OF CANADA

Journal canadien de chimie

Publié par
LE CONSEIL NATIONAL DE RECHERCHES DU CANADA

Volume 52 Number 6 March 15, 1974

Volume 52 numéro 6 15 mars 1974

The Ion Kinetic Energy Spectra of Benzyl Fluoride and the Isomeric Fluorotoluenes[1]

S. SAFE,[2] W. D. JAMIESON, AND D. J. EMBREE

Atlantic Regional Laboratory, National Research Council of Canada, Halifax, Nova Scotia

Received November 19, 1973

One of the classical problems in mass spectrometry is the structure and formation of the $C_7H_7^+$ and $XC_7H_6^+$ ions which are generated in the mass spectra of alkylbenzenes and many other aromatic compounds. The intermediacy of both symmetrical tropylium ion structures and unsymmetrical benzyl ions has been postulated using a number of different approaches. We have investigated this problem using ion kinetic energy spectroscopy, a relatively new technique, with the isomeric fluorobenzenes and benzyl fluoride as model compounds. Our results indicated incomplete substituent (*i.e.* fluorine) scrambling in the first field-free region of the mass spectrometer and thus incomplete equilibration in the decomposing $FC_7H_6^+$ ions and these conclusions are in contrast to results obtained using other techniques.

Un des problèmes classiques en spectrométrie de masse consiste en la formation et la détermination de structure des ions $C_7H_7^+$ et $XC_7H_6^+$ formés dans les spectres de masse des alcoyles de benzène et de plusieurs autres composés aromatiques. En utilisant différentes approches, une structure intermédiaire a été proposée entre l'ion tropylium symétrique et l'ion benzyle asymétrique. Nous avons étudié ce problème sur des composés modèles tels les isomères du fluorobenzène et le fluorure de benzyle par une méthode spectroscopique relativement nouvelle basée sur l'énergie cinétique de l'ion. Nos résultats ont montré une distribution incomplète au hazard du substituant (*i.e.* fluor) dans la région sans champ du spectromètre de masse, donc un équilibre incomplet dans la décomposition des ions $FC_7H_6^+$. Les conclusions sont donc en désaccord avec les résultats obtenus par d'autres techniques. [Traduit par le journal]

Can. J. Chem., **52**, 867 (1974)

The electron impact-induced rearrangements of toluene, substituted toluenes, and alkylbenzene derivatives invariably leads to the formation of the ubiquitous tropylium $[C_7H_7]^+$ or substituted tropylium $[XC_7H_6]^+$ ions (1, 2). The structures of these ions have been probed using specifically labelled (^2H, ^{13}C) precursors (3–7), ionization and appearance potential data (8–10), and studies of the energetics of the formation and decomposition of these ionic species (11–13). In most cases the results have indicated that the structures of the decomposing $[C_7H_7]^+$ and $[XC_7H_6]^+$ ions were best represented as a cyclic tropylium ion species (*i.e.* *m/e* 109 (*b*), Scheme 1).

Ion kinetic energy (IKE) spectrometry (14) permits a study of those decomposition reactions which occur in the first field-free region of the mass spectrometer in front of the electric sector. The IKE spectrum is obtained by varying the electric sector voltage (at constant accelerating voltage) from 100% V (or 1.0 *E*) to zero. The main ion beam is transmitted at 100% electric sector

[1]Issued as NRCC 13758.

[2]Present address: Department of Chemistry, University of Guelph, Guelph, Ontario, and to whom enquiries should be addressed.

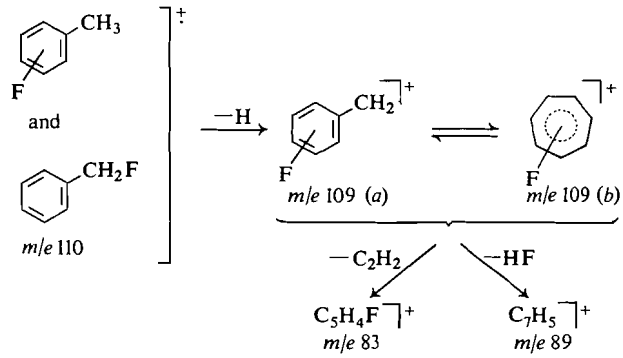

SCHEME 1

voltage (V) and this can be defined as 1.0 E; (as the electric sector voltage is scanned from 400 to 0 V the E values correspondingly decrease from 1.0–0 E). At voltages less than 100% V (*i.e.*, at E values less than 1.0) the "less energetic" ionic decomposition peaks (or daughter ions) are transmitted and these can be duly detected and recorded and constitute the low energy (*i.e.*, 0–1.0 E) IKE spectrum (14). In a unimolecular reaction (*e.g.*, $m_1^+ \rightarrow m_2^+ + (m_1 - m_2)$) occurring in the first field-free region the daughter ions for this reaction will appear at m_2/m_1 E and only daughter ions possessing that fractional energy are transmitted at this fractional energy value. Thus the IKE spectrum gives a series of peaks at specific E values which are directly related to the masses of their corresponding daughter and parent ions. We have used this technique to study the electron impact-induced fragmentations of the isomeric fluorotoluenes which are reported to decompose via the intermediacy of a symmetrical FC_7H_6 fluorotropylium ion (*i.e.* Scheme 1, *m/e* 109 (*b*)), (8, 13). The (IKE) spectra of benzyl fluoride and the isomeric fluorotoluenes confirm the fragmentation scheme with ionic decomposition peaks at 0.822 and 0.761 E corresponding to the *m/e* 109 → *m/e* 89 and *m/e* 109 → *m/e* 83 reactions, respectively. The IKE results are shown in Table 1 and the relative peak intensities are the average results obtained from 4–5 scans in which the standard deviation was less than ±0.01. Since the $[M - 1]^+$ ion (*m/e* 109) decomposes in two different pathways the ratio 0.822:0.761 E is a measure of the relative rates of these two decomposition modes for the decomposing *m/e* 109 ion. The ratios measured for the isomeric fluorotoluenes and benzyl fluoride were significantly different and, moreover, the relative intensities of the ionic decomposition peaks with respect to the main ion beam (at 1.0 E) were also significantly different. Thus the IKE data suggest that the decomposing $FC_7H_6^+$ ions derived from the isomeric fluorotoluenes and benzyl fluoride have different internal energies (15) and/or structures implying some retention of the substituent (fluorine) identity in these ions. This would imply that equilibration in the molecular ion or in the $[M - 1]^+$ ion between alternate structures (*i.e.*, *m/e* 109 (*a*) → *m/e* 109 (*b*)) is incomplete with a portion of non-equilibrated benzyl species *m/e* 109 (*a*) undergoing decomposition prior to equilibration. These results therefore contrast with some of the previous data and the technique provides a sensitive and useful probe into the study of ionic decomposition reactions and the structures of the decomposing ions.

TABLE 1. Ion kinetic energy data

Compound	Ionic decomposition peak × 10^3*		
	0.822 E	0.761 E	(0.822 E)/(0.761 E)
2-Fluorotoluene	3.10	9.10	0.34
3-Fluorotoluene	3.20	10.5	0.30
4-Fluorotoluene	3.25	9.10	0.36
Benzyl fluoride	3.40	12.1	0.28

*The 1.0 E peak was taken as the base (100%) peak.

Experimental

Mass and ion kinetic energy spectra were recorded on a Dupont CEC 21-110B double focussing mass spectrometer at 70 eV. The samples were introduced with a temperature controlled probe (16) to avoid thermal reactions and so that the sample temperature could be readily controlled and a constant ion beam maintained.

The electric sector voltage was varied from 400 (1.0 E) to 0 V. The relative peak areas and peak heights were the

Can. J. Chem. Downloaded from www.nrcresearchpress.com by 210.87.254.105 on 09/05/12
For personal use only.

average values obtained from 4–5 scans with a standard deviation in the peak areas being less than ± 0.01. The toluenes were purified by chromatography prior to use.

1. H. M. GRUBB and S. MEYERSON. Mass spectrometry of organic ions. *Edited by* F. W. McLafferty. Academic Press, New York. 1963. Chapt. 10.
2. D. A. LIGHTNER, G. B. QUISTAD, and E. IRWIN. Appl. Spectrosc. **25**, 253 (1971).
3. S. MEYERSON and P. N. RYLANDER. J. Chem. Phys. **27**, 901 (1957).
4. K. L. RINEHART, A. C. BUCHHOLZ, G. E. VAN LEAR, and H. L. CANTRILL. J. Am. Chem. Soc. **90**, 2983 (1968).
5. A. S. SIEGEL. J. Am. Chem. Soc. **92**, 5277 (1970).
6. T. K. BRADSHAW, J. H. BOWIE, and P. Y. WHITE. Chem. Commun. 537 (1970).
7. T. AST, J. H. BEYNON, and R. G. COOKS. J. Am. Chem. Soc. **94**, 1834 (1972).
8. A. N. H. YEO and D. H. WILLIAMS. Chem. Commun. 886 (1970).
9. S. MAJETI and D. A. LIGHTNER. Tetrahedron Lett. 20 (1970).
10. J. M. S. TAIT, T. W. SHANNON, and A. G. HARRISON. J. Am. Chem. Soc. **84**, 4 (1962).
11. P. BROWN. J. Am. Chem. Soc. **90**, 2694 (1968).
12. M. K. HOFFMAN and M. M. BURSEY. Tetrahedron Lett. **27**, 2539 (1971).
13. K. R. JENNINGS and A. WHITING. Org. Mass Spectrom. **6**, 917 (1972).
14. J. H. BEYNON and R. G. COOKS. Res. Devel. **22**, 26 (1971).
15. M. K. HOFFMAN and J. C. WALLACE. J. Am. Chem. Soc. **95**, 5064 (1973).
16. W. D. JAMIESON and F. G. MASON. Rev. Sci. Instr. **41**, 778 (1970).

Can. J. Chem. Downloaded from www.nrcresearchpress.com by 210.87.254.105 on 09/05/12
For personal use only.

^{13}C Nuclear Magnetic Resonance Studies. 38.[1] Examination of the Long-range Shielding Effects of the Hydroxyl Group in Alicyclic Systems

S. H. GROVER[2] AND J. B. STOTHERS

Department of Chemistry, University of Western Ontario, London, Ontario N6A 3K7

Received September 10, 1973

The substituent effects of the hydroxyl group on the ^{13}C shieldings of the *trans*-decalols and the 10-methyl-*trans*-decalols have been determined. The shifts for the carbons three and four bonds from the site of substitution depend strongly on their orientation with respect to the hydroxyl group. While the latter have not been widely recognized, these δ effects are valuable for spectral analysis and stereochemical assignments since these range up to 3.4 p.p.m. In direct contrast to the well established trends for γ effects, steric crowding of δ nuclei causes marked downfield shifts. The corresponding effects in several steroids are illustrated.

On a déterminé les effets de substituent du groupe hydroxyle sur le blindage du ^{13}C des *trans*-décalols et des méthyl-10 des *trans*-décalols. Le déplacement des carbones qui se trouve à trois et quatre liens du site de la substitution montre une grande dépendance sur l'orientation par rapport au groupe hydroxyle. Même si ces derniers effets n'ont pas été reconnus d'une façon générale jusqu'à maintenant les effets sont très utiles pour l'analyse spectrale et la détermination stéréochimique puisqu'ils ont des valeurs allant jusqu'à 3.4 p.p.m. L'encombrement stérique des noyaux cause un déplacement chimique marqué vers les bas champs et ceci en opposition directe avec les tendences bien établies pour les effets γ. On illustre enfin des correspondents dans plusieurs stéroides. [Traduit par le journal]

Can. J. Chem., **52**, 870 (1974)

Introduction

One of the earliest findings in ^{13}C n.m.r. investigations of organic compounds was the discovery of remarkably consistent shielding effects exerted by an array of substituents within families of compounds (1). Because of their reproducibility, a knowledge of these substituent effects for a given system often can permit the direct assignment of ^{13}C signals in the spectra of related compounds (2). While the early work with aromatic systems showed that these effects clearly reveal the presence of steric inhibition of resonance (3), it was not until the results for alicyclic systems were available that the existence of pronounced steric effects in σ-bonded systems was established (4, 5). For example, the effect of a substituent group separated by three bonds from a given carbon depends on its relative orientation; if *gauche* or eclipsed, the carbon is shielded relative to that in the corresponding *anti* arrangement. This general behavior has been utilized for stereochemical purposes in a wide variety of systems (6) and a theoretical model rationalizing the geometrical features in terms of interacting proximate hydrogen atoms for hydrocarbons has been presented (7).

The general conclusion that ^{13}C shieldings increase as the extent of steric crowding increases appears to have no exceptions for interactions be-

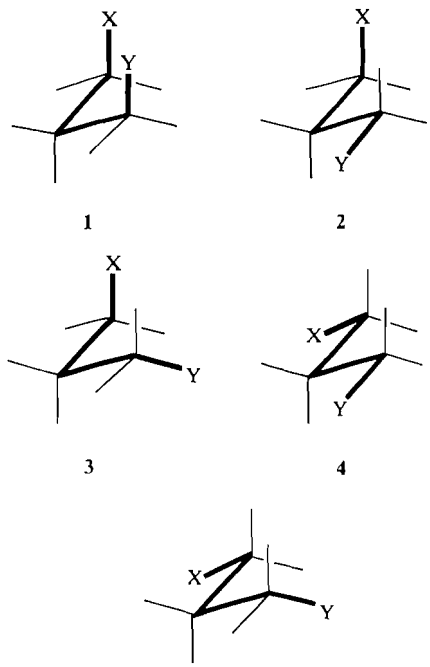

1 2 3 4 5

[1]Part 36, ref. 34; Part 37, ref. 35.

[2]Holder of NRCC scholarship, 1968–1971.

Can. J. Chem. Downloaded from www.nrcresearchpress.com by 210.87.254.42 on 09/05/12
For personal use only.

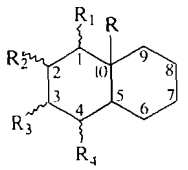

Compound	R	R_1	R_2	R_3	R_4
6	H	β-OH	H	H	H
7	H	α-OH	H	H	H
8	H	H	α-OH	H	H
9	H	H	β-OH	H	H
10	CH_3	β-OH	H	H	H
11	CH_3	α-OH	H	H	H
12	CH_3	H	α-OH	H	H
13	CH_3	H	β-OH	H	H
14	CH_3	H	H	β-OH	H
15	CH_3	H	H	α-OH	H
16	CH_3	H	H	H	α-OH
17	CH_3	H	H	H	β-OH

tween substituents and carbons *separated by three bonds*. Appreciable longer range effects have been found in cyclohexane systems (5, 8) and these were also found to be shielding (*i.e.* producing upfield shifts) and have been interpreted in terms of inductive parameters with negligible steric contributions. For groups separated by four bonds, however, a variety of orientations may be adopted and the initial work did not involve examinations of all possibilities **1–5**. Of these, the *syn*-axial **1** (with either or both X and Y = C) is particularly interesting since the separation of X and Y is comparable to that for *gauche* interactions. The overwhelming majority of cyclic model systems examined, however, lack cases having *syn*-axial **1** interactions. For acyclic systems, these represent only minor contributors to the observed shifts since more stable orientations are favored. In the initial report of the effects of molecular symmetry on ^{13}C shieldings (9) it was noted that significant *deshielding* effects occur over four bonds and in the course of a structural elucidation using ^{13}C n.m.r. (10) it was found that *syn*-axial methyl–methyl interactions were accompanied by marked downfield shifts.

A systematic study, therefore, seemed warranted to include examples having each of the arrangements **1–5**. For this purpose we have determined the ^{13}C spectra of the *trans*-decalols **6–9**, the eight 10-methyl-*trans*-decalols **10–17**,[3] a few substituted cyclohexanols **18–21**, as well as the cholestan-3β,6-diols **22** and **23**. Comparison of these data with those for the corresponding hydrocarbons permitted the assessment of the shielding effects of the hydroxyl group at the neighboring carbons. In this way definitive evidence of appreciable downfield shifts for *syn*-axial interactions was obtained. This finding is in striking contrast to the general trend for *gauche* interactions and clearly violates the general premise which associates steric crowding with upfield shifts. These examples were chosen because unequivocal assignments for most of the nuclei are straightforward and, since the general equivalence of the effects of hydroxyl and methyl groups has been recognized (11), the trends should be indicative of 1,5 Me···Me interactions which are commonly encountered in more complex systems. A preliminary report of some of these results has appeared (12).

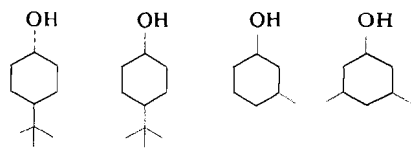

18 **19** **20** **21**

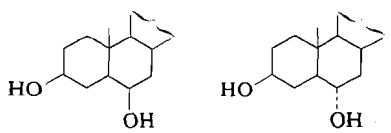

22 **23**

[3]The numbering scheme given in **10** has been employed to simplify comparisons with related systems such as steroids.

Experimental

Materials

The parent hydrocarbons and most of the steroids examined are commercially available compounds. The

Can. J. Chem. Downloaded from www.nrcresearchpress.com by 210.87.254.42 on 09/05/12
For personal use only.

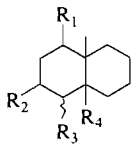

Compound	R_1	R_2	R_3	R_4
24	=O	H	H	α-H
25	H	=O	H	α-H
26	H	=O	=	
27	H	H	α-OH	β-H
28	H	H	β-OH	β-H
29	H	H	=O	H

trans-decalols were prepared by combinations of published procedures as outlined below.

trans-1- and -2-Decalols (6–9)

Stereospecific reductions of *trans*-1-decalone, which was obtained by treatment of a commercial mixture of *cis*- and *trans* isomers with MeO^-–MeOH (13), were employed to prepare the *trans*-1-decalols. The $LiAlH_4$–$AlCl_3$ method of Eliel and Nasipuri (14) furnished **6** while the $IrCl_4$ reagent (15) gave 7. By fractional distillation of a commercial mixture of *trans*-2-decalyl acetates, a sample rich in the 2β isomer was obtained. Hydrolysis gave crude **9** which was purified by recrystallization from petroleum ether and sublimation. The equatorial isomer was obtained by mixed hydride equilibrium (14) of the alcohols from hydrolysis of the *trans*-2-decalyl acetates; recrystallization from petroleum ether gave pure **8**. The physical properties of the four decalols agreed well with published data (16).

10-Methyl-trans-decal-1-ols (10 and 11)

The preparation of 10-methyl-*trans*-decal-1-one (**24**) from *trans*-1-decalone via the 2-furfurylidene derivative (17) gave crude 10-methyl-*trans*-decal-1α-ol (**11**) before the oxidation step. A portion of this material crystallized on standing in the cold and recrystallization from petroleum ether gave **11**, m.p. 56–57°. $LiAlH_4$ reduction of **24** gave a 4:1 mixture of **10** and **11**, from which the required spectral data were readily obtained since pure **11** was available.

10-Methyl-trans-decal-2-ols (12 and 13)

These alcohols were prepared from 10-methyl-*trans*-decal-3-one (**25**) which was obtained from 2-methylcyclohexanone and methyl vinyl ketone via published procedures (18, 19). Bromination (20) of **25** gave the 3α-bromo derivative which with $LiAlH_4$ furnished 2β,3β-oxido-10-methyl-*trans*-decalin (21) and, subsequently, **13** (22) which was purified by recrystallization from pentane, m.p. 56–59° (lit. (22), m.p. 57.5–58.5°).

Oxidation of **13** with Jones' reagent followed by mixed hydride reduction (14) gave **12**, m.p. 44–47° (lit. (22), b.p. ~ 140°/0.4 m).

10-Methyl-trans-decal-3-ols (14 and 15)

Reduction of **25** with the $IrCl_4$ reagent (15) gave **15** in 75% yield, m.p. 86–88°. In the preparation of **25**, the reduction of 10-methyl-Δ^4-octal-3-one (**26**) with Li–NH_3 gave a mixture of **25** and the corresponding decalols. A second treatment with Li–NH_3 converted the mixture entirely to alcohols which were oxidized by Jones' reagent to **25**. It was found that partial oxidation, with insufficient reagent, furnished a mixture from which **14** was readily separated by fractional distillation. Recrystallization of this material from petroleum ether gave **14**, m.p. 71–73°.

10-Methyl-trans-decal-4-ols (16 and 17)

Since attempts to isolate pure samples of each of these alcohols were unsuccessful, mixtures of different compositions were prepared using different procedures. Detailed comparisons of the n.m.r. spectra of these mixtures, together with the knowledge of their mode of formation, permitted the characterization of each.

Hydroboration (23) of 10-methyl-Δ^4-decalin, prepared from **26** via its ethylene thioketal (19) gave a mixture of three decalols whose methyl protons absorbed at 0.85, 0.96, and 1.03 p.p.m. A mixture containing only two of these was produced by catalytic hydrogenation of 10-methyl-Δ^5-decal-4α-ol (24). The major component, having methyl shieldings of δ_H 0.96 and δ_C 27.9, and the minor component with methyl shieldings of δ_H 0.85 and δ_C 16.8, are the *cis*- and *trans*-alcohols **27** and **16**, respectively; the methyl ^{13}C shieldings clearly identify each isomer since the geometry of the ring junction markedly affects angular methyl shieldings (25). Thus, the third decalol from hydroboration, the major product, with methyl shieldings of δ_H 1.03 and δ_C 28.1, is **28**. It is interesting that both hydrogenation and hydroboration preferentially occur at the 4-(5-)double bond on the same side as the methyl group.

To obtain mixtures containing **17**, the *trans*-axial isomer, the mixture from hydroboration was oxidized with Jones' reagent to obtain a mixture of 10-methyl-4-decalones (**29**), in which the *cis*-isomer was predominant. Treatment with the $IrCl_4$ reagent proceeded to only a limited extent but the major component of the alcohol fraction exhibited methyl absorption at δ_H 1.07 and δ_C 19.1, values different from each of the other isomers, and its carbinyl proton signal at 3.80 p.p.m. had a width at half-height of 8.0 Hz, consistent with the equatorial orientation expected for **17**. $LiAlH_4$ reduction of **29** afforded a mixture of the four decalols **16**, **17**, **27**, and **28**, with **16** present in the smallest amounts but readily identified by its methyl n.m.r. absorptions.

Cholestan-3β,6-diols (22 and 23)

Hydrogenation of cholestan-3β-ol-6-one over platinum oxide (26) gave, after recrystallization from methanol, **22** in 68% yield, m.p. 189–192° (lit. (26) m.p. 188–190°). Reduction of the same cholestanone with sodium in alcohol (27) gave **23**, from methanol, m.p. 219–221° (lit. (27) m.p. 216–217°).

Spectra

The proton spectra were obtained with Varian T60 and HA100 spectrometers using $CDCl_3$ solutions. The ^{13}C spectra were determined on a Varian XL-100-15 system operating in the Fourier transform mode as described previously (28). All shieldings were measured relative to internal TMS with 20% (w/v) solutions in $CDCl_3$ using either 5 or 10 mm sample tubes and the appropriate receiver inserts. The precision of the individual shielding values is ±0.05 p.p.m.

Results and Discussion

The shielding data for the *trans*-decalols **6–17** are listed in Table 1 together with the results for *trans*-decalin and 10-methyl-*trans*-decalin. The

Can. J. Chem. Downloaded from www.nrcresearchpress.com by 210.87.254.42 on 09/05/12
For personal use only.

TABLE 1. ^{13}C Shieldings[a] of *trans*-decalin, 10-methyl-*trans*-decalin, and the *trans*-decalols **6–17**

Compound	C-1	C-2	C-3	C-4	C-5	C-6	C-7	C-8	C-9	C-10	Me
trans-Decalin	34.3	26.9	26.9	34.3	43.7	34.3	26.9	26.9	34.3	43.7	
6	74.6	35.8	24.1	(33.5)	41.2	(33.7)	(26.4)	(26.2)	29.1	50.4	
7	70.4	34.3	20.0	(33.8)	35.6	33.9	(26.8)	(26.4)	29.6	47.4	
8	43.0	70.2	35.6	32.0	42.3	(33.8)	(26.5)	(26.3)	(33.3)	41.2	
9	40.4	66.6	(33.9)	27.6	43.2	(33.8)	26.7	26.7	32.9	36.4	
10-Methyl-*trans*-decalin	42.1	22.1	27.2	29.3	45.8	29.3	27.2	22.1	42.1	33.9	15.7
10	79.6	30.4	24.4	28.1	44.2	28.1	26.8	21.7	37.3	39.2	9.8
11	75.2	(28.5)	20.4	(28.8)	37.5	(28.8)	26.7	21.8	34.8	38.3	16.1
12	50.9	66.9	36.4	27.9	44.9	28.1	26.9	21.2	41.6	34.7	16.6
13	47.8	67.6	34.1	24.0	45.9	28.7	27.0	21.2	41.9	33.5	17.9
14	40.0	31.2	71.0	38.1	43.1	28.8	26.7	21.9	41.1	33.0	15.7
15	35.6	28.6	66.6	36.0	37.8	28.8	27.0	21.9	41.5	33.7	14.7
16	41.2	20.4	36.6	70.0	52.4	23.0	26.7	21.7	41.9	34.8	16.8
17	43.7	16.9	34.1	71.8	48.5	26.0	27.3	21.9	41.7	33.7	19.1

[a]In p.p.m. from TMS in $CDCl_3$ solutions. Similar values in parentheses may be interchanged.

TABLE 2. ^{13}C Shieldings[a] of some cyclohexanols, sterols, and the related hydrocarbons

Compound	C-1	C-2	C-3	C-4	C-5	C-6	C-7	C-8	C-9	C-10	Me
t-Butylcyclohexane											
18	70.9	36.0	25.6	47.2	25.6	36.0					27.6[b]
19	65.7	33.4	20.9	48.1	20.9	33.4					27.5[b]
Methylcyclohexane	32.9	35.6	26.6	26.5	26.6	35.6					22.9
20	70.6	44.6	31.4	34.1	24.2	35.4					22.3
21	70.0	44.0	30.8	41.2	30.8	44.0					22.3
Cholestane	38.7	22.2	26.9	29.1	47.1	29.1	32.3	35.6	54.9	36.3	12.3[c]
Pregnane	38.9	22.3	26.9	29.2	47.2	29.2	32.4	35.7	55.3	36.4	12.3[c]
Androstane	38.8	22.2	26.9	29.1	47.1	29.1	32.6	36.0	55.1	36.4	12.3[c]
Cholestan-3β-ol (**30**)	37.1	31.6	71.2	38.3	45.0	28.8	32.1	35.6	54.4	35.5	12.4[c]
Pregnan-3β-ol-20-one (**31**)	37.0	32.0	71.0	38.1	44.8	28.6	31.4	35.4	54.2	35.4	12.3[c]
Pregnan-3β,20-diol (**32**)	37.5	32.5	70.5	39.2	45.3	29.2	32.5	35.7	54.8	35.8	12.5[c]
Androstan-3β-ol-17-one (**33**)	36.9	31.4	70.9	38.0	44.8	28.4	30.9	35.0	54.4	35.6	12.3[c]
Androstan-3β,17β-diol (**34**)	37.5	(32.0)	70.5	39.2	45.3	29.1	(32.3)	35.8	54.9	35.8	12.5[c]
Androstan-3α,17β-diol (**35**)	32.1	29.8	65.5	36.9	39.5	29.1	32.1	36.0	55.0	36.6	11.6[c]
Androstan-3α-ol-17-one (**36**)	30.9	29.0	66.3	36.3	39.2	28.3	32.2	35.1	54.5	35.8	11.2[c]
22	38.5	31.5	71.5	35.4	47.3	71.9	39.6	30.4	54.2	35.4	15.8[c]
23	37.3	31.3	71.1	32.3	51.6	69.3	41.7	34.3	53.7	36.2	13.5[c]

[a]In p.p.m. from TMS in $CDCl_3$ solutions. Values in parentheses may be interchanged.
[b]Quaternary carbons appeared at 32.2 p.p.m.
[c]C-19.

shieldings for the cyclohexanols **18–21**, the cholestanediols **22** and **23**, and the steroids **30–36** are given in Table 2. Since the reason for including these steroids was for comparison with the decalols, the data are limited to those for the A and B rings in these systems. The results for the parent hydrocarbons of the alcohols in Table 2 are also included. Although the results for some of these materials have been reported by other workers, the data were remeasured in $CDCl_3$ solutions to obtain results for a common solvent for more precise comparisons of the hydroxyl substituent effects.

Signal Assignments

The present results for *trans*-decalin and 10-methyl-*trans*-decalin agree reasonably well with those recently reported (29). Although most of the deviations are ~0.3 p.p.m., the differences between the two sets of data range from 0.05–0.8

Can. J. Chem. Downloaded from www.nrcresearchpress.com by 210.87.254.42 on 09/05/12
For personal use only.

Can. J. Chem. Downloaded from www.nrcresearchpress.com by 210.87.254.42 on 09/05/12
For personal use only.

TABLE 3. Substituent effects[a] of the hydroxyl group in cyclohexanols **18–21** and decalols **6–17**

	A Ring				B Ring			
Compound	α	β	γ	δ	γ	δ	ε	ζ
6	40.3	8.9, $6.7_{(CH)}$	-2.8, $-2.5_{(CH)}$	-0.8	-5.2	-0.6, -0.7	-0.5	
7	36.1	7.4, 3.7	-6.9, -8.1	-0.4	-4.7	-0.4, -0.5	-0.1	
8	43.3	8.7, 8.7	-2.3, $-2.5_{(CH)}$	$-1.4_{(CH)}$		-1.0	-0.5, -0.6	-0.4
9	39.7	6.1, 7.0	-6.7, -7.3	-0.5		-1.4	-0.5, -0.2	$a-0.2$
10	37.5	8.3, $5.3_{(C)}$	-2.8, $-1.6_{(CH)}$ $-5.9_{(Me)}$	-1.2	-4.8	-1.2, -0.4	-0.4	
11	33.1	6.4, 4.4	-6.8, -8.3 $+0.4$	-0.5	-7.3	-0.5, -0.3	-0.5	
12	44.8	8.8, 9.2	-1.4, $+0.8_{(C)}$	$-0.9_{(CH)}$ $+0.9_{(Me)}$		-0.5	-1.2, -0.9	-0.3
13	45.5	5.7, 6.9	-5.3, -0.4	$+0.1$ $+2.2$		-0.2	-0.6, -0.9	-0.2
14[b]	43.8	9.1, 8.8	-2.1, $-2.7_{(CH)}$	-0.9[c]		-0.5	-0.5, -1.0	-0.2
15[b]	39.4	6.5, 6.7	-6.5, -8.0	-0.2		-0.5	-0.2, -0.6	-0.2
16	40.7	9.4, $6.6_{(CH)}$	-1.7, $+0.9_{(C)}$	-0.9, $+1.1_{(Me)}$	-6.3	-0.5, -0.2	-0.4	
17	42.5	6.6, 2.7	-5.2, -0.2	$+1.6$, $+3.4$	-3.3	$+0.1$, -0.4	-0.2	
18								
19								
20[c]	44.0	9.0, 8.9	-1.5(CH), -2.4	-1.5, -0.6(Me)				
21[c]	(44.5)[d]	(10.5)[d]	(-1.0)[d]	(-2.3)[d]				

[a]Values represent $\delta_C^{ROH}-\delta_C^{RH}$ for corresponding carbons in each case; the carbon with the lower number is listed first in the tabulation for the same effects. Carbons other than methylenes are noted.
[b]The ε effects at the methyl carbon are 0.0 (**14**) and -1.0 p.p.m. (**15**).
[c]Comparing C-1 in **20** with C-3 in methylcyclohexane, C-2 (**20**) *vs.* C-2, -3 (**20**) *vs.* C-1, etc.
[d]Shieldings for *cis*-1,3-dimethylcyclohexane estimated from methyl substituent effects from methylcyclohexane assuming simple additivity.

Can. J. Chem. Downloaded from www.nrcresearchpress.com by 210.87.254.42 on 09/05/12
For personal use only.

p.p.m., indicating the existence of small solvent effects and the necessity of employing a common solvent in the present study.

With the results for the parent hydrocarbons and the cyclohexanols (11), the problem of individual assignments for the decalols was reduced. The signals of methylene carbons were distinguished from the others by off-resonance decoupling and then assigned by consideration of the expected substituent effects of the hydroxyl group. It had been established that the hydroxyl group deshields both the carbon to which it is bonded and its immediate neighbors; these have been termed α and β effects, respectively. Carbons three and four bonds removed from the oxygen atom tend to experience upfield shifts (8, 11) with the most pronounced effects found for *gauche* arrangements of γ carbons. More remote carbons are expected to be little affected by the hydroxyl group and this series permits characterization of the ε and ζ effects.

For decalols **6–9**, the carbinyl signal was readily identified as the lowest field signal, while the signals for C-6, -7, and -8 were taken as those closest to the values for the corresponding carbons in *trans*-decalin, although C-7 and -8 could not be uniquely identified in **6–8**. Of the remaining methylene signals, those at lowest field were assigned to the β carbons, *i.e.* C-2 in **6** and **7** and C-1, -3 in **8** and **9**. The 29 p.p.m. signal for each of **6** and **7** was assigned to C-9 since this carbon is *gauche* to the hydroxyl group and a shift of *ca.* −5 p.p.m. is expected to result. The pair of methylene signals remaining for **6–9** were assigned directly from their observed positions relative to the corresponding carbons in *trans*-decalin taking into account the upfield shift expected for those *gauche* to the axial hydroxyl group in **7** and **9**. For **6** and **7** the less shielded methine signal must arise from C-10 while the more shielded methine signal for **9** is from C-10 because of the γ effect of the axial hydroxyl. For **8** the methine signals were assigned from the fact that equatorial hydroxyl groups shield the γ carbon more than the δ carbon (8, 11). Thus, the assignments were completed.

For the methyldecalols **10–17**, the carbinyl, methyl, methine, and quaternary signals were easily identified. For **12–15**, the methylene carbons of the unsubstituted ring should be little affected by the hydroxyl group and so were assigned as listed. The assignments for C-7, -8, and -9 in **16** and **17** and C-6, -7, and -8 in **10** and **11** were based on similar grounds; for the latter the least shielded methylene signal arises from C-9, leaving only C-2, -3, and -4 unassigned. Since C-2 and -4 will be most and least affected, respectively, by the hydroxyl group, the assignments in Table 1 follow. The expected β-effect of *ca.* 10 p.p.m. permitted assignment of the β-methylene carbons for **12–17** and the remaining methylene signals were readily associated with specific carbons, with the distinctive differences for the γ carbons in the axial and equatorial cases taken into account.

The results for cholestane and androstane are in good agreement with those reported (30, 31) and the data for pregnane are very similar, as one would expect since detailed study of several steroids has established that substitution at C-17 has little effect on the A and B ring carbon shieldings (30). As in the case of the decalols, consideration of the shielding trends found for the cyclohexanols led to the assignments listed in Table 2. The five 3β-hydroxy derivatives exhibited closely similar patterns as did the pair of 3α-hydroxyandrostane derivatives. For each steroid the methine (C-5, -8, and -9), quaternary (C-10), and methyl (C-19) signals were identified by off-resonance decoupling and the carbinyl signals were characteristically shifted to the region, 65–72 p.p.m. Comparison of the cholestanediol spectra with that for cholestan-3β-ol led to the assignments listed with no apparent ambiguities.

Shielding Trends

With these assignments in hand, the observed trends can be considered in more detail. The consistency of the trends lends strong support to the present assignments, but, in any event, the emphasis is directed toward those centers for which the assignments are certain. In complex spectra a complete analysis may not be possible without an array of suitable model compounds for comparison but signals arising from methyl, carbinyl, quaternary, and, often, methine carbons are readily distinguished. To simplify discussion, the observed substituent effects in the decalols and cyclohexanols have been collected in Table 3; for each epimeric pair, the equatorial epimer is listed first.

Some general trends are apparent from comparison of the results for each epimeric pair. The α effects of equatorial hydroxyl groups are larger, unless the axial hydroxyl is *syn*-axial with the 10-methyl group (**13** and **17**). In all cases, the β effects produced by the equatorial hydroxyls are consistently larger than those found for their axial

Can. J. Chem. Downloaded from www.nrcresearchpress.com by 210.87.254.42 on 09/05/12
For personal use only.

counterparts and the magnitude of the downfield shifts depends on the degree of substitution of the affected carbon with methylene carbons undergoing greater shifts. This tendency was initially noted in a detailed examination of several norbornyl derivatives and possible interpretations of the trend were proposed (32). As already noted, greater upfield shifts were anticipated and are exhibited by the skeletal γ carbons in the axial epimers. The opposite trend for the methyl carbon in **12** and **13** is a consequence of the fact that it is γ *gauche* with respect to the equatorial hydroxyl (**12**) and *anti* relative to the axial hydroxyl (**13**). The attenuated α and β effects and enhanced upfield γ shifts found for the axial epimers are exactly analogous to the trends exhibited by a variety of substituents (2) and it is precisely this trend which led to the generalization that steric crowding enhances the shieldings of the carbons involved in the fragment containing the γ *gauche* groups.

The γ effects operative at the methylene carbon in the unsubstituted ring of **6**, **7**, **10**, **11**, **16**, and **17** are interesting since these vary from −3.3 to −7.3 p.p.m. although each arises from a similar γ *gauche* interaction with the hydroxyl group. Presumably the variation in these shifts results from different degrees of skeletal twisting associated with minimizing the steric interactions between the methyl and hydroxyl groups. The fact that the γ effects at C-9 in **6** and **7** are comparable lends credence to this interpretation since **6** and **7** would be expected to have very similar geometries. For the other two pairs, the γ effect at this methylene is smaller in the epimer having *syn*-axial methylhydroxyl interactions, *e.g.* **17** *vs.* **16**, and **10** *vs.* **11**. A consistent variation in the γ effects experienced by methylene and methine carbons is also apparent for **7**, **9**, **11**, and **15** with the methine carbon more strongly affected. It seems reasonable to propose that this tendency results from the somewhat greater freedom of the methylenes to minimize *gauche* interactions with the hydroxyl group since these alcohols are presumably less flexible at the ring junction. Similar variations in γ effects for methyl *vs.* methylene carbons have been noted in a series of methylcyclohexanes (33).

The results in the last few columns of Table 3 show that even the more remote carbons are slightly affected by the hydroxyl group. It seems reasonable to attribute the ε and ζ effects to slight geometrical alterations of the decalyl skeleton and it is interesting that the general tendency is toward higher field for these nuclei. A particularly striking example is the difference found for the methyl carbons in **14** and **15**. Although the hydroxyl and methyl groups are separated by five bonds and are on opposite faces of the molecule in **15**, its methyl carbon exhibits the larger shift. Perhaps the twist associated with minimizing the interactions of the hydroxyl group on the α face of the molecule tends to increase the γ *gauche* interactions experienced by the β-methyl carbon.

Within the series **6–17**, each of the arrangements **2–5**, with X = oxygen and Y = carbon, occurs several times while **1** occurs only twice. With few exceptions, the arrangements **2–5** are associated with upfield shifts while **1** produces relatively large (2–3 p.p.m.) downfield shifts. This deshielding influence is in direct contrast to the trend normally associated with sterically crowded carbons although of the possible arrangements **1–5** for δ groups, these groups are closest in **1**. Clearly, the interpretation relating steric crowding with upfield shifts through steric polarization of the interacting bonds (7) is inadequate to account for these *syn*-axial effects. It should be noted that the exceptions to the general trend for the α effects, mentioned earlier, are those having *syn*-axial OH···Me interactions, **13** and **17**. In each of these, the α effect is accentuated such that the axial hydroxyl group deshields the carbinyl carbon more than its equatorial counterpart. Thus, the generalization regarding attenuated α effects for axial hydroxyls, proposed earlier (4), is shown to have exceptions. The magnitude of the δ effects for *syn*-axial arrangements of substituents, however, is sufficiently large to render these useful for stereochemical analysis. At the same time, these trends show that the interpretation of small shifts in the spectra of complex molecules in conformational terms may be difficult since steric crowding can produce both upfield *and* downfield shifts.

To obtain additional examples of the hydroxyl substituent effects in related polycyclic systems, the sterols **22**, **23**, **30–36** were examined and the substituent effects observed are listed in Table 4. The data for **30–34** demonstrate both the general consistency of these effects and the fact that each varies by *ca.* ±0.5 p.p.m. These results are expected to be comparable to those for **14** while the data for **35** and **36** compare favorably with those for **15**. In these sterols it is again apparent that the more remote carbons in the **B** ring experience small effects of the hydroxyl group. As in the decalols, the methine carbons exhibit slightly

TABLE 4. Substituent effects[a] of 3- and 6-hydroxyl groups in some steroids

	A Ring							B Ring			
Compound	α (C-3)	β (C-2, C-4)		γ (C-1, C-5)		δ (C-10)	ε (C-19)	δ (C-6)	ε (C-7, C-9)		ζ (C-8)
30	44.3	9.4	9.2	−1.6	−2.1	−0.8	0.1	−0.3	−0.2	−0.5	0.0
31	44.1	9.7	8.9	−1.9	−2.4	−1.0	0.0	−0.6	−1.0	−1.1	−0.3
32	43.6	10.2	10.0	−1.4	−1.9	−0.6	0.2	0.0	0.1	−0.5	0.0
33	44.0	9.2	8.9	−1.9	−2.3	−0.8	0.0	−0.7	−1.7	−0.7	−1.0
34	43.6	9.8	10.1	−1.3	−1.8	−0.6	0.2	0.0	−0.3	−0.2	−0.2
35	38.6	7.6	7.8	−6.7	−7.6	0.2	−0.7	0.0	−0.5	−0.1	0.0
36	39.4	6.8	7.2	−7.9	−7.9	−0.6	−1.1	−0.8	−0.4	−0.6	−0.9

	B Ring							A Ring			
	α (C-6)	β (C-5, C-7)		γ (C-8, C-10)		δ (C-9, C-19)		γ (C-4)	δ (C-1, C-3)		ε (C-2)
23[b]	40.5	6.6	9.6	−1.3	0.7	−0.7	1.1	−6.0	0.2	−0.1	−0.3
22[b]	43.1	2.3	7.5	−5.2	−0.1	−0.2	3.4	−2.9	1.4	0.3	−0.1

[a]Values obtained from $\delta_C^{ROH} - \delta_C^{RH}$ for the corresponding carbons in each case.
[b]Values obtained by comparing **22** and **23** with cholestan-3β-ol.

greater γ effects than the methylene carbons and the angular methyl carbons in **35** and **36** are shielded relative to the C-19 absorption for androstane even though the hydroxyl group is five bonds away and on the opposite face of these molecules. The angular methyl absorptions for **22** and **23**, relative to **30**, exhibit the same shifts as those for **16** and **17** indicating the consistency of the δ effect of the hydroxyl group. It is interesting that the methyl shifts for **23**, **16**, and **12** are downfield since the orientation of the methyl and hydroxyl groups corresponds to **2**, X = CH_3, Y = OH. Similar orientations for methylene and hydroxyl groups in the other decalols lead to upfield shifts but it may be unwise to compare the effects for skeletal methylene carbons with those for methyl carbons since there are two bonded pathways between the hydroxyl and methylene groups. The somewhat smaller δ effect at the methyl carbon in **13** may be due to the greater ease with which the *syn*-axial Me···OH interaction can be reduced by skeletal twist. It may be noted that the other individual hydroxyl effects in **22** and **23** agree remarkably well with those for **16** and **17**, in particular, the γ effects at C-4 and the α, β, and γ effects in the substituted rings.

In summary, the hydroxyl group exerts comparable effects at the neighboring carbons in the *trans*-decalols, 10-methyl-*trans*-decalols, and sterols. Although the individual effects at the α, β, γ, and δ carbons can vary by *ca.* 0.5 p.p.m., the shifts are sufficiently distinctive to identify specific centers and should be valuable for signal assignments in a wide variety of terpenes and steroids. The steric dependence of the γ and δ effects clearly characterizes sterically crowded carbons and even though a theoretical interpretation of the opposite effects of γ *gauche* and *syn*-axial interactions is lacking these trends are qualitatively useful. From these and other results (12) the general tendency for downfield shifts arising from *syn*-axial arrangements of substituents shows that conformational interpretations of differences for complex systems must be approached cautiously. The sensitivity of carbon shieldings to minor changes in molecular geometry is illustrated by the small, but readily measurable, shifts found for centers five and six bonds removed from the hydroxyl group.

We are grateful to the National Research Council of Canada for financial support of this work.

1. P. C. LAUTERBUR. J. Am. Chem. Soc. **83**, 1838, 1846 (1961); Tetrahedron Lett. 274 (1961); H. SPIESECKE and W. G. SCHNEIDER. J. Chem. Phys. **35**, 722, 731 (1961); Tetrahedron Lett. 468 (1961).
2. (*a*) G. C. LEVY and G. L. NELSON. ^{13}C Nuclear magnetic resonance for organic chemists. Wiley-Interscience, New York. 1972; (*b*) J. B. STOTHERS. Carbon-13 NMR spectroscopy. Academic Press, New York. 1972.
3. P. C. LAUTERBUR. J. Chem. Phys. **38**, 1406, 1415, 1432 (1963). K. S. DHAMI and J. B. STOTHERS. Tetrahedron Lett. 631 (1964); Can. J. Chem. **43**, 479, 498 (1965).

Can. J. Chem. Downloaded from www.nrcresearchpress.com by 210.87.254.42 on 09/05/12
For personal use only.

4. G. W. BUCHANAN, D. A. ROSS, and J. B. STOTHERS. J. Am. Chem. Soc. **88**, 4301 (1966); G. W. BUCHANAN and J. B. STOTHERS. Can. J. Chem. **47**, 3605 (1969).
5. D. K. DALLING and D. M. GRANT. J. Am. Chem. Soc. **89**, 6612 (1967).
6. N. K. WILSON and J. B. STOTHERS. *In* Topics in stereochemistry. Vol. 8. *Edited by* E. L. Eliel and N. L. Allinger. Wiley-Interscience, New York. 1973. Chapt. 1.
7. D. M. GRANT and B. V. CHENEY. J. Am. Chem. Soc. **89**, 5315 (1967).
8. T. PEHK and E. LIPPMAA. Org. Mag. Res. **3**, 679 (1971).
9. J. I. KROSCHWITZ, M. WINOKUR, H. J. REICH, and J. D. ROBERTS. J. Am. Chem. Soc. **91**, 5927 (1969).
10. K. R. STEPHENS, J. B. STOTHERS, and C. T. TAN. *In* Mass spectrometry and NMR in pesticide chemistry. *Edited by* F. J. Biros and R. A. Haque. Plenum Press, New York. 1974.
11. J. D. ROBERTS, F. J. WEIGERT, J. I. KROSCHWITZ, and H. J. REICH. J. Am. Chem. Soc. **92**, 1338 (1970).
12. S. H. GROVER, J. P. GUTHRIE, J. B. Stothers, and C. T. TAN. J. Mag. Res. **10**, 227 (1973).
13. A. C. COPE, R. J. COTTER, and G. G. ROLLER. J. Am. Chem. Soc. **77**, 3594 (1955).
14. E. L. ELIEL and D. NASIPURI. J. Org. Chem. **30**, 3809 (1965).
15. E. L. ELIEL, T. W. DOYLE, R. O. HUTCHINS, and E. C. GILBERT. Org. Syn. **50**, 13 (1970).
16. W. HÜCKEL. Ann. **441**, 31 (1925).
17. W. S. JOHNSON, I. A. DAVID, H. C. DEHM, R. J. HIGHET, E. W. WARNHOFF, W. D. WOOD, and E. T. JONES. J. Am. Chem. Soc. **80**, 661 (1958).
18. J. A. MARSHALL and W. I. FANTA. J. Org. Chem. **29**, 2501 (1964).
19. F. SONDHEIMER and D. ROSENTHAL. J. Am. Chem. Soc. **80**, 3995 (1958).
20. M. YANAGITA and A. TAHARA. J. Org. Chem. **18**, 792 (1953).
21. J. A. MARSHALL, N. COHEN, and K. R. ARENSON. J. Org. Chem. **30**, 762 (1965).
22. J. A. MARSHALL and R. D. CARROLL. J. Org. Chem. **30**, 2748 (1965).
23. F. SONDHEIMER and S. WOLFE. Can. J. Chem. **37**, 1870 (1959).
24. G. I. BIRNBAUM, S. H. GROVER, A. STOESSL, and J. B. STOTHERS. Can. J. Chem. In press.
25. J. L. GOUGH, J. P. GUTHRIE, and J. B. STOTHERS. J. Chem. Soc. Chem. Commun. 979 (1972).
26. R. E. MARKER and J. KRUEGER. J. Am. Chem. Soc. **62**, 79 (1940).
27. P. A. PLATTNER and W. LANG. Helv. Chim Acta, **27**, 1872 (1944).
28. J. B. STOTHERS, C. T. TAN, and K. C. TEO. Can. J. Chem. **51**, 2893 (1973).
29. D. K. DALLING, D. M. GRANT, and E. G. PAUL. J. Am. Chem. Soc. **95**, 3718 (1973).
30. H. J. REICH, M. JAUTELAT, M. T. MESSE, F. J. WEIGERT, and J. D. ROBERTS. J. Am. Chem. Soc. **91**, 7445 (1969).
31. B. BALOGH, D. M. WILSON, and A. L. BURLINGAME. Nature, **233**, 261 (1971).
32. J. B. GRUTZNER, M. JAUTELAT, J. B. DENCE, R. A. SMITH, and J. D. ROBERTS. J. Am. Chem. Soc. **92**, 7107 (1970).
33. D. K. DALLING and D. M. GRANT. J. Am. Chem. Soc. **94**, 5318 (1972).
34. G. W. BUCHANAN, J. B. STOTHERS, and G. WOOD. Can. J. Chem. **51**, 3746 (1973).
35. P. A. W. DEAN, D. G. IBBOTT, and J. B. STOTHERS. Chem. Commun. 626 (1973).

Can. J. Chem. Downloaded from www.nrcresearchpress.com by 210.87.254.42 on 09/05/12
For personal use only.

Routes to *N*-Aryl-*N'*-thioaroylhydrazines and Related *sym*- and *unsym*-Hydrazonyl Sulfides, and a Note on the So-called *N*-Phenyl-*N'*-thiobenzoyldiimide

P. WOLKOFF AND S. HAMMERUM

Chemical Laboratory II (General and Organic Chemistry), The H. C. Ørsted Institute, University of Copenhagen, Universitetsparken 5, DK-2100 Copenhagen, Denmark

AND

P. D. CALLAGHAN AND M. S. GIBSON

Department of Chemistry, Brock University, St. Catharines, Ontario[1]

Received August 15, 1973

Aromatic hydrazonyl halides (**1**), treated successively with triethylamine and hydrogen sulfide – triethylamine, give *N*-aryl-*N'*-thioaroylhydrazines (**3**) as primary products, which can be isolated in many cases. Depending on conditions, further reaction may occur to give *sym*-hydrazonyl sulfides.

Both *sym*- and *unsym*-hydrazonyl sulfides are available from reaction of appropriate hydrazonyl halides and *N*-aryl-*N'*-thioaroylhydrazines in presence of triethylamine.

The product of oxidation of *N*-phenyl-*N'*-thiobenzoylhydrazine under various conditions is confirmed as the corresponding hydrazonyl disulfide rather than *N*-phenyl-*N'*-thiobenzoyldiimide.

Des halogénures d'hydrazonyle aromatiques (**1**), traités successivement avec de la triéthylamine et un mélange de sulfure d'hydrogène et de triéthylamine, donnent principalement des *N*-aryl-*N'*-thioaroylhydrazines (**3**) qui peuvent être isolées dans plusieurs cas. Selon les conditions, une autre réaction peut donner lieu à la formation des *sym*-sulfures d'hydrazonyle.

Ces deux *sym*- et *asym*-sulfures d'hydrazonyle sont obtenus à l'aide de la réaction d'halogénures d'hydrazonyle appropriés et de *N*-aryl-*N'*-thioaroylhydrazines en présence de triéthylamine.

L'oxydation sous diverses conditions de la *N*-phényl-*N'*-thiobenzoylhydrazine conduit à un produit identifié comme étant le disulfure d'hydrazonyle correspondant, plutôt que le *N*-phényl-*N'*-thiobenzoyldiimide. [Traduit par le journal]

Can. J. Chem., **52**, 879 (1974)

Walter and Reubke have reported that bromination of araldehyde dialkylhydrazones followed by successive treatment with triethylamine (NEt_3) and hydrogen sulfide – triethylamine (H_2S–NEt_3) in chloroform gives *N*,*N*-dialkyl-*N'*-thioaroylhydrazines (1), see eq. 1.

[1] $ArCH{=}NNR_2 \rightarrow [ArCBr{=}NNR_2] \rightarrow ArCSNHNR_2$

This report is of considerable interest in connection with current work in our respective laboratories on 1,3,4-thiadiazol-2-enes (2), 4*H*-1,3,4-benzothiadiazines, and hydrazonyl sulfides (3) and has prompted the investigation of a corresponding synthesis of *N*-aryl-*N'*-thioaroylhydrazines (**3**) and, from these compounds and hydrazonyl halides (**1**), a synthesis of hydrazonyl sulfides (**4**) (see Scheme 1).

[1]Address for correspondence.

The hydrazonyl halides used in this study were all known compounds (3–11) and initially, in examining reaction 2, the order of addition of reagents corresponded with that used by Walter and Reubke (1). Typically (Procedure *A*), NEt_3 (1 equiv.) in $CHCl_3$ was added to **1***d* in $CHCl_3$. After 25 s, a solution of H_2S–NEt_3 in $CHCl_3$, prepared by saturating NEt_3 (2 equiv.) in $CHCl_3$ with H_2S, was added. After 2 h, acidification gave **3***d* in 82% yield. However, if the interval between addition of the NEt_3 and H_2S–NEt_3 solutions was extended to 4 min, the product isolated was the hydrazonyl sulfide (**4***d*) (93% yield). Mixtures of **3***d* and **4***d* were obtained after intermediate intervals in the range 25 s to 4 min. Similar patterns were observed with other hydrazonyl halides, though in yet other cases the product distribution was not detectably time dependent in the intervals examined. For example, **1***a* (intervals, 25 s to 3 min) gave **4***a* in nearly quantitative yield

Can. J. Chem. Downloaded from www.nrcresearchpress.com by 210.87.254.105 on 09/05/12
For personal use only.

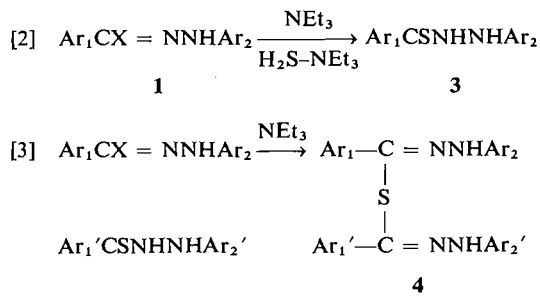

a $Ar_1 = Ph$; $Ar_2 = Ph$; X = Cl
b $Ar_1 = Ph$; $Ar_2 = 2,4\text{-}Br_2C_6H_3$; X = Br
c $Ar_1 = 4\text{-}MeOC_6H_4$; $Ar_2 = 2,4\text{-}Br_2C_6H_3$; X = Br
d $Ar_1 = 4\text{-}BrC_6H_4$; $Ar_2 = 2,4,6\text{-}Br_3C_6H_2$; X = Br
e $Ar_1 = 3\text{-}NO_2C_6H_4$; $Ar_2 = 4\text{-}BrC_6H_4$; X = Br
f $Ar_1 = 3\text{-}NO_2C_6H_4$; $Ar_2 = 2,4\text{-}Br_2C_6H_3$; X = Br
g $Ar_1 = Ph$; $Ar_2 = 2\text{-}ClC_6H_4$; X = Cl
h $Ar_1 = 4\text{-}NO_2C_6H_4$; $Ar_2 = Ph$; X = Cl
i $Ar_1 = Ph$; $Ar_2 = 4\text{-}NO_2C_6H_4$; X = Br
j $Ar_1 = 4\text{-}MeOC_6H_4$; $Ar_2 = Ph$
k $Ar_1 = 4\text{-}Me_2CHC_6H_4$; $Ar_2 = Ph$
l $Ar_1 = Ph$; $Ar_2 = 2,4\text{-}FIC_6H_3$; X = Cl
m $Ar_1 = Ph$; $Ar_2 = 2,4\text{-}Br(Me_2NSO_2)C_6H_3$; X = Br
n $Ar_1 = Ph$; $Ar_2 = 2,4\text{-}BrIC_6H_3$; X = Cl
o $Ar_1 = Ph$; $Ar_2 = 2,4\text{-}IBrC_6H_3$; X = Cl
p $Ar_1 = Ph$; $Ar_2 = C_{10}H_7$ (1-naphthyl)

(For *sym*-Sulfides, $Ar_1 = Ar_1'$; $Ar_2 = Ar_2'$)

SCHEME 1

(crude), necessitating an alternative procedure for preparing **3***a*, while **1***b* (intervals, 25 s to 5 min) gave a mixture of **3***b* and **4***b* from which **4***b* could be isolated in 5–7% yield. In two cases, triethylammonium salts of thiohydrazides were isolated rather than the thiohydrazides by omitting the acidification stage during the work-up.

When **1***a* was treated with H_2S–NEt_3 without prior addition of NEt_3 (Procedure *C*), a somewhat sluggish reaction ensued giving **3***a* (24% after 4 h, the remainder of **1***a* being recovered); **1***b* under these conditions gave **3***b* (60%) and **4***b* (27%). In a modification, **1***a* was treated with H_2S–NEt_3, followed after 30 min by NEt_3, to give **3***a* in 92% yield.

These results may be considered in terms of alternative routes from **1** to **3** and **4**. Substitution mechanisms, implicit for the cases examined by Walter and Reubke (1), are possible for conversions **1** → **3** and **1** + **3** (anion) → **4** (3) or, alternatively, dehydrohalogenation of **1** by NEt_3 to the nitrilimine **2** may occur, as proposed earlier by Huisgen (12); addition of HS^- to **2** would give the anion of **3** and addition of this anion to **2**, followed by protonation, would give the *sym*-hydrazonyl sulfide **4** (eqs. 4–6). In either event, **4** is seen as arising from reactions involving successful competition between anion of **3** and HS^- (present in excess) for substrate **1** or **2** derived from **1**. Circumstances favoring reaction via **2** would include a high rate of conversion **1** → **2** relative to substitution reactions of **1**, or high initial concentration of **2** (possibly occurring in the interval dependent cases). Conversely a low rate of conversion **1** → **2** relative to substitution reactions of **1** would favor a substitution mechanism (possibly occurring when preliminary addition of NEt_3 to **1** is omitted). In given circumstances, the product ratio **3**:**4** would thus be dependent on the relative importance of the two pathways: **1** → **3**, **1** + **3** → **4** and **1** → **2** → **3**, **2** + **3** → **4**.

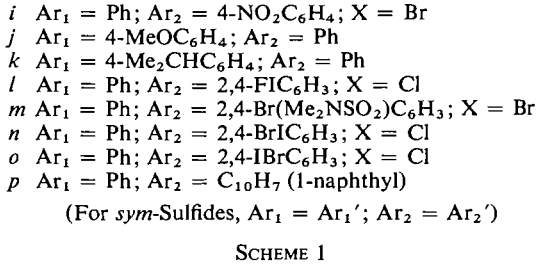

Attention was next directed to the preparation of hydrazonyl sulfides from thiohydrazides and hydrazonyl halides in $CHCl_3$ (as in the foregoing synthesis) or CH_3CN (as in reactions of hydrazonyl halides with thioacetate ion reported previously (3)) using NEt_3 as base (reaction 3), and in case of **4***b* from **1***b* and the triethylammonium salt of **3***b* in benzene. Hydrazonyl sulfides were readily obtained under these circumstances, consistent with the view that thiohydrazides (or derived anions) are intermediates in the formation of hydrazonyl sulfides in these reactions. This synthesis was also extended to *unsym*-hydrazonyl sulfides not available previously. Formulation **4** is still preferred for these compounds as, at least for the *sym*-sulfides, n.m.r. and i.r. spectra show the aryl substituents and NH groups to be pairwise equivalent. The mass spectra are complicated by skeletal rearrangements but the presence of weak molecular ions (detectable at 14 eV) and ions corresponding to loss of H_2S, Ar_2N_2H, Ar_1NCS, and Ar_2NSH_2 together with Ar_1CS^+, $Ar_1CSNAr_2^+$, and $Ar_1CNNAr_2^{+\cdot}$ fragment ions are compatible with the structural assignment.

A number of thiohydrazides required for purposes of correlation and for syntheses of hydra-

Can. J. Chem. Downloaded from www.nrcresearchpress.com by 210.87.254.105 on 09/05/12
For personal use only.

Can. J. Chem. Downloaded from www.nrcresearchpress.com by 210.87.254.105 on 09/05/12
For personal use only.

zonyl sulfides were prepared by the method of Jensen and co-workers (13). In cases where it was necessary to modify the procedure by heating to effect reaction, it was noted that small amounts of colored by-products were generated, rendering purification difficult. The possibility that these by-products might include the hydrazonyl disulfide (**5**) (from oxidation of the thiohydrazide (14)) was briefly examined. Compound **3***l* was oxidized using hydrogen peroxide to **5***l*; **5***l* was not apparently (t.l.c.) the by-product present in the sample of **3***l* prepared by the carboxymethyl dithiobenzoate method. A similar oxidation of **3***a* has been reported to give **6** (15). This has been reexamined and the product confirmed as **5***a* (mol. wt., i.r. spectrum, n.m.r. spectrum, N—H exchangeable with D_2O), identical with the disulfide previously reported by Wuyts and Lacourt (14).

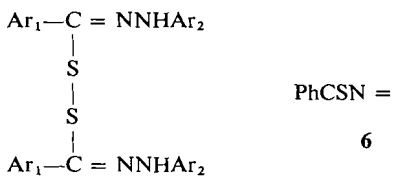

5

PhCSN = NPh

6

The present work provides an indirect method for thioaroylation of arylhydrazines, supplementing the direct procedures of Jensen and coworkers (13) and of Walter and Badke (16).

Experimental

Mass spectra were determined with an AE1-MS902 mass spectrometer; results are quoted as *m/e* values for the lowest isotopic species with relative intensities (% of base peak) in parentheses.

Thiohydrazides and Hydrazonyl Sulfides

Thiohydrazides were normally crystallized from benzene–hexane. Triethylammonium salts of thiohydrazides were crystallized from cyclohexane or benzene but could be crystallized from ethanol–triethylamine; crystallization from ethanol gave the thiohydrazide through dissociation.

Hydrazonyl sulfides were normally crystallized from benzene or chloroform and in all cases melted with decomposition.

Procedure A

Thiohydrazides

A solution of NEt_3 (0.26 ml, 1.86 mmol) in $CHCl_3$ was added with stirring and cooling to a suspension of α,4-dibromobenzaldehyde 2,4,6-tribromophenylhydrazone (**1***d*) (1.00 g, 1.7 mmol) in $CHCl_3$ (65 ml). After 25 s interval, a stirred solution of NEt_3 (0.52 ml, 3.7 mmol) in $CHCl_3$ (25 ml) saturated at 0° with H_2S was added. After 2 h at room temperature, the solution was washed with aqueous acetic acid and water, dried, and evaporated to give **3***d* (0.54 g, 82%); after crystallization, **3***d* (71%) had m.p. 160–163°.

Anal. Calcd. for $C_{13}H_8Br_4N_2S$: C, 28.71; H, 1.48; N, 5.15; S, 5.89. Found: C, 28.85; H, 1.54; N, 5.15; S, 6.12.

Compound **1***b* (25 s to 5 min intervals) gave **3***b* (60%), m.p. and mixture m.p. 118–119° and **4***b* (5–7%), m.p. and mixture m.p. 194–195°.

Anal. Calcd. for $C_{13}H_{10}Br_2N_2S$: C, 40.44; H, 2.61; N, 7.26; S, 8.30. Found: C, 40.32; H, 2.67; N, 7.36; S, 8.42.

Compound **1***e* (20 s interval) gave **3***e* (50%), m.p. 155–157°.

Anal. Calcd. for $C_{13}H_{10}BrN_3O_2S$: C, 44.33; H, 2.86; N, 11.93; S, 9.10. Found: C, 44.58; H, 2.96; N, 11.79; S, 9.07.

Compound **1***f* (2 min interval) gave **3***f* (79%), m.p. 124–126°.

Anal. Calcd. for $C_{13}H_9Br_2N_3O_2S$: C, 36.22; H, 2.10; N, 9.75; S, 7.44. Found: C, 36.65; H, 2.13; N, 9.80; S, 7.67.

Compound **1***g* (3 min interval) gave **3***g* (89%), m.p. 111–113°.

Anal. Calcd. for $C_{13}H_{11}ClN_2S$: C, 59.42; H, 4.22; N, 10.66; S, 12.20. Found: C, 59.58; H, 4.39; N, 10.76; S, 12.18.

Triethylammonium Salts of Thiohydrazides

The foregoing experiment was repeated for **1***b* but the washing with aqueous acetic acid was omitted; the *triethylammonium salt* of **3***b* (67%), m.p. *ca.* 80° (from cyclohexane), was isolated.

Anal. Calcd. for $C_{19}H_{25}Br_2N_3S$: C, 46.83; H, 5.17; N, 8.62. Found: C, 46.69; H, 5.11; N, 8.74.

Under these conditions, **1***c* (20 s interval) gave a crude product which was crystallized from benzene to give *bis(α-(2,4-dibromophenylhydrazono)-4-methoxybenzyl) sulfide* (**4***c*) (24%), m.p. 208–210°.

Anal. Calcd. for $C_{28}H_{22}Br_4N_4O_2S$: C, 42.13; H, 2.78; N, 7.02; S, 4.02. Found: C, 42.35; H, 2.79; N, 6.94; S, 4.11.

The mother liquor was concentrated, whereupon the *triethylammonium salt* of **3***c* (32%), m.p. 108–110°, crystallized.

Anal. Calcd. for $C_{20}H_{27}Br_2N_3OS$: C, 46.43; H, 5.26; N, 8.12; S, 6.20. Found: C, 46.32; H, 5.44; N, 8.15; S, 6.18.

From the salt, **3***c*, m.p. 134–136°, was recovered.

Anal. Calcd. for $C_{14}H_{12}Br_2N_2OS$: C, 40.41; H, 2.91; N, 6.73; S, 7.70. Found: C, 40.05; H, 2.98; N, 6.71; S, 7.78.

Hydrazonyl Sulfides

The foregoing experiment was repeated for **1***d* except that the interval between addition of the solutions of NEt_3 in $CHCl_3$ and H_2S–NEt_3 in $CHCl_3$ was 4 min. This gave **4***d* (93%; 80% after crystallization). Compound **4***d* crystallized from benzene as a solvate, m.p. 168–170°.

Anal. Calcd. for $C_{26}H_{14}Br_8N_4S \cdot C_6H_6$: C, 33.96; H, 1.78; Br, 56.48; N, 4.95; S, 2.83. Found: C, 33.07; H, 1.92; Br, 56.65; N, 5.10; S, 3.17.

Compound **4***d* also crystallized from chloroform in a solvated form, m.p. 108–111°.

Anal. Calcd. for $C_{26}H_{14}Br_8N_4S \cdot 2CHCl_3$: C, 27.53;

Can. J. Chem. Downloaded from www.nrcresearchpress.com by 210.87.254.105 on 09/05/12
For personal use only.

H, 1.32; N, 4.58; S, 2.82. Found: C, 27.57; H, 1.32; N, 4.85; S, 3.01.

Compound **1***a* (3 min interval) gave **4***a* (75%), m.p. 158–160°; mass spectrum (70 eV) *m/e* 388 (4) (M − H_2S), 316 (12) ($C_{20}H_{16}N_2S$), 297 (7) ($C_{20}H_{15}N_3$), 287 (6) ($C_{19}H_{17}N_3$), 239 (6), 213 (6), 212 (7) ($C_{13}H_{10}NS$), 196 (6), 195 (6), 194 (22) ($C_{13}H_{10}N_2$), 181 (11), 180 (65) ($C_{13}H_{10}N$), 137 (5) (C_7H_7NS), 121 (29) (C_7H_5S), 110 (19), 108 (19), 104 (38), 103 (100) (C_7H_5N), 93 (32), 92 (30), and 91 (81) (C_6H_5N).

Anal. Calcd. for $C_{26}H_{22}N_4S$: C, 73.95; H, 5.25; N, 13.26; S, 7.59. Found: C, 73.52; H, 5.45; N, 13.05; S, 7.37.

Compound **1***h* (3 min interval) gave **4***h* (12%), m.p. 174–175°.

Anal. Calcd. for $C_{26}H_{20}N_6O_4S$: C, 60.93; H, 3.93; N, 16.40; S, 6.26. Found: C, 61.00; H, 4.07; N, 16.43; S, 6.32.

Procedure B

N-Phenyl-N′-thiobenzoylhydrazine (3a)

Compound **1***a* (5.8 g, 25 mmol), powdered or dissolved in a few ml of $CHCl_3$, was added to a stirred solution of NEt_3 (7.0 ml, 50 mmol) in $CHCl_3$ (100 ml) saturated with H_2S at 0°. After 30 min, NEt_3 (14.0 ml, 100 mmol) was introduced dropwise. The reaction mixture was left at room temperature for 2 h and then worked up as described above. Compound **3***a* (5.2 g, 92%), after crystallization from benzene–hexane, had m.p. 87–89°; mixture m.p. with an authentic sample showed no depression (13).

Significant reduction of H_2S concentration, *e.g.* by adding **1***a* in 100 ml $CHCl_3$ resulted in formation of **3***a* and **4***a*.

Procedure C

Hydrazonyl Sulfide (4i)

A saturated solution of H_2S in a mixture of NEt_3 (0.43 ml, 3.1 mmol), and $CHCl_3$ (20 ml) was added to a stirred solution of **1***i* (0.50 g, 1.6 mmol) in $CHCl_3$ (25 ml). After 1 h, the dark red solution was filtered and the precipitate crystallized from nitromethane to give **4***i* (50 mg, 6%), m.p. 185–186°.

Anal. Calcd. for $C_{26}H_{20}N_6O_4S$: C, 60.93; H, 3.93; N, 16.40. Found: C, 59.17; H, 3.99; N, 16.40.

Under these conditions, **1***b* gave a mixture of **3***b* and **4***b* (t.l.c.), whereas **1***a* did not appear to react; after 4 h, **1***b* gave **3***b* (60%) and **4***b* (27%) while **1***a* gave **3***a* (24%, estimated by subsequent conversion to **4***a*).

Procedure D

sym- and unsym-Hydrazonyl Sulfides from Hydrazonyl Halides and Thiohydrazides

(i) In $CHCl_3$

Triethylamine (0.14 ml, 1.1 mmol) was added to a solution of α-bromobenzaldehyde 2,4-dibromophenylhydrazone (**1***b*) (0.43 g, 1.0 mmol) and *N*-(2,4-dibromophenyl)-*N′*-thiobenzoylhydrazine (**3***b*) (0.39 g, 1.0 mmol) in $CHCl_3$ (45 ml). The precipitated material was isolated after 5 h and crystallized from benzene to give **4***b* (0.40 g), m.p. 194–195°. The mother liquor was washed with aqueous acetic acid and water, dried, and evaporated. Crystallization from benzene gave another 50 mg of **4***b* (total yield, 61%).

Under similar conditions, **1***a* and **3***a* gave **4***a* (80%), m.p. 158–160°.

Compounds **1***f* and **3***f* gave **4***f* (46%) which crystallized from benzene as a solvate, m.p. 187–189°.

Anal. Calcd. for $C_{26}H_{16}Br_4N_6O_4S \cdot C_6H_6$: C, 42.69; H, 2.46; N, 9.34; S, 3.56. Found: C, 42.59; H, 2.50; N, 9.26; S, 3.71.

Compounds **1***b* and **3***a* gave the *unsym-sulfide* **4***ab* (90%), m.p. 167–168°.

Anal. Calcd. for $C_{26}H_{20}Br_2N_4S$: C, 53.81; H, 3.47; N, 9.65; S, 5.53. Found: C, 53.62; H, 3.51; N, 9.76; S, 5.49.

Compounds **1***f* and **3***a* gave **4***af* (59%), m.p. 165–166°.

Anal. Calcd. for $C_{26}H_{19}Br_2N_5O_2S$: C, 49.94; H, 3.06; N, 11.20; S, 5.13. Found: C, 50.33; H, 3.12; N, 11.34; S, 5.22.

Compounds **1***f* and **3***b* gave **4***bf* (83%), m.p. 167–169°.

Anal. Calcd. for $C_{26}H_{17}Br_4N_5O_2S$: C, 39.87; H, 2.19; N, 8.94; S, 4.09. Found: C, 40.15; H, 2.28; N, 8.95; S, 4.25.

Compounds **1***g* and **3***a* gave **4***ag* (86%), m.p. 138–140°.

Anal. Calcd. for $C_{26}H_{21}ClN_4S$: C, 68.33; H, 4.63; N, 12.26; S, 7.02. Found: C, 67.91; H, 4.67; N, 12.33; S, 6.96.

Compounds **1***a* and **3***j* (17) gave **4***aj* (84%), m.p. 157–158°; mass spectrum (70 eV) *m/e* 419 (10) (M − HS), 346 (16) ($C_{21}H_{18}N_2OS$), 327 (13), 316 (6), 287 (13), 269 (4), 243 (8), 242 (6), 237 (4), 226 (4), 225 (6), 224 (11), 213 (9), 212 (11), 211 (7), 210 (33), 196 (4), 195 (8), 194 (26), 181 (11), 180 (60), 167 (27), 151 (27), 137 (7), 134 (29), 133 (65), 121 (29), 110 (24), 108 (37), 104 (30), 103 (98), 93 (57), 92 (50), and 91 (100).

Anal. Calcd. for $C_{27}H_{24}N_4OS$: C, 71.66; H, 5.35; N, 12.38; S, 7.09. Found: C, 71.45; H, 5.35; N, 12.30; S, 7.16.

Compounds **1***a* and **3***k* gave **4***ak* (81%), m.p. 147–148°.

Anal. Calcd. for $C_{29}H_{28}N_4S$: C, 74.97; H, 6.07; N, 12.06; S, 6.90. Found: C, 74.70; H, 6.16; N, 12.13; S, 6.97.

(ii) In CH_3CN

Compounds **1***l* (0.40 g, 1.1 mmol) and **3***l* (0.40 g, 1.1 mmol) were dissolved, with warming, in acetonitrile (10 ml). Triethylamine (2 ml, 14.3 mmol) was added when a precipitate immediately appeared. The warm mixture was stirred for 10 min and then left to cool (20 min). Filtration gave **4***l* (0.60 g, 78%), m.p. (after crystallization) 194–195°, identical with a reference sample (3).

Compounds **1***m* and **3***m* (in boiling acetonitrile) gave **4***m* (62%), m.p. 203.5–205° (from toluene), identical with a reference sample (3).

Compounds **1***n* and **3***l* gave the *unsym-sulfide* **4***ln* (80%), m.p. 185–186°.

Anal. Calcd. for $C_{26}H_{18}BrFI_2N_4S$: N, 7.26; S, 4.15. Found: N, 7.3; S, 4.0; C, H discrepant.

Compounds **1***o* and **3***l* gave **4***lo* (33%), m.p. 165–167°.

Anal. Calcd. for $C_{26}H_{18}BrFI_2N_4S$: C, 40.47; H, 2.33; N, 7.26. Found: C, 41.0; H, 2.4; N, 7.3.

Compounds **1***a* and **3***p* gave **4***ap* (almost quantitative), m.p. 165°.

Anal. Calcd. for $C_{30}H_{24}N_4S$: C, 76.27; H, 5.08; N, 11.86; S, 6.78. Found: C, 76.5; H, 5.1; N, 11.9; S, 6.6.

(iii) From 1b and Triethylammonium Salt of 3b

Compound **1***b* (0.56 g, 1.3 mmol) and the triethylammonium salt of **3***b* (0.59 g, 1.3 mmol) were dissolved in dry benzene (13 ml). After 1 h at room temperature, the mixture was heated to boiling. Benzene (5 ml) was added,

Can. J. Chem. Downloaded from www.nrcresearchpress.com by 210.87.254.105 on 09/05/12
For personal use only.

and the solid was filtered off, washed well with hot benzene, and dried, yielding triethylammonium bromide (0.22 g, 97%). The filtrates provided **4***b* (0.86 g, 93%), m.p. 198–201°.

Thiohydrazides from Carboxymethyl Dithioaroates

Yields are quoted for crude compounds in this section.

Phenylhydrazine and carboxymethyl *p*-isopropyldithiobenzoate gave, under standard conditions, compound **3***k* (92%), m.p. 103–105°.

Anal. Calcd. for $C_{16}H_{18}N_2S$: C, 71.07; H, 6.71; N, 10.36; S, 11.86. Found: C, 71.15; H, 6.82; N, 10.39; S, 11.87.

Compound **3***b* (98%) (warming preferable to start reaction) had m.p. 118–119°.

Anal. Calcd. for $C_{13}H_{10}Br_2N_2S$: C, 40.44; H, 2.61; N, 7.26; S, 8.30. Found: C, 40.32; H, 2.67; N, 7.36; S, 8.42.

The following thiohydrazides were prepared by the same general procedure, with heating as necessary, but were not purified, (m.p. data refer to crude compounds): compound **3***l* (97%), m.p. 100–105°; **3***m* (almost quantitative), m.p. 184–185°; **3***p* (78%), m.p. 144–148°. These thiohydrazide samples contained colored by-products which were difficult to remove by crystallization and the crude products were therefore used for the above preparations of hydrazonyl sulfides.

Oxidation of Thiohydrazides

(i) Compound **3***a* was oxidized using hydrogen peroxide according to ref. 15 to give bis(α-phenylhydrazonobenzyl) disulfide (**5***a*), m.p. 141° (lit. (15) m.p. 135° for compound reported as *N*-phenyl-*N'*-thiobenzoyldiimide (**6**)); ν_{max} 3270 cm^{-1} (N—H).

Mol. Wt. Calcd. for $C_{26}H_{22}N_4S_2$: 454. Found (vapor pressure, benzene): 455.

Compound **5***a* was also prepared by oxidation of **1***a* using potassium ferricyanide and sodium bicarbonate in aqueous solution, and is identical with the disulfide (lit. (14) m.p. 149°) obtained previously by oxidation of **1***a* with iodine and sodium bicarbonate in aqueous solution.

(ii) To a solution of **3***l* (1.0 g, 2.7 mmol) in ethanol (5 ml) was added 3% hydrogen peroxide solution (1.5 ml). The mixture was boiled for 2 min, cooled, and the red solid was collected, washed, and dried. Crystallization from ethyl acetate gave *bis(α-(2-fluoro-4-iodophenylhydrazono)benzyl) disulfide* (**5***l*) (0.54 g) as orange prisms, m.p. 138–139°; a further 0.15 g crystallized from the mother liquor (total yield 69%); ν_{max} 3270 cm^{-1} (N—H).

Anal. Calcd. for $C_{26}H_{18}F_2I_2N_4S_2$: C, 42.05; H, 2.43; N, 7.55; S, 8.63. Found: C, 42.2; H, 2.5; N, 7.4; S, 8.5.

Compound **5***l* was not apparently the by-product present in **3***l* prepared by the carboxymethyl dithiobenzoate procedure above (t.l.c.).

1. W. WALTER and K. J. REUBKE. Tetrahedron Lett. 5973 (1968).
2. P. WOLKOFF and S. HAMMERUM. Org. Mass Spectrom. In press.
3. I. T. BARNISH and M. S. GIBSON. J. Chem. Soc. C, 854 (1970): P. D. CALLAGHAN and M. S. GIBSON. J. Chem. Soc. C, 2106 (1970): I. T. BARNISH, P. D. CALLAGHAN, and M. S. GIBSON. J. Chem. Soc. Perkin I, In press.
4. R. HUISGEN, M. SEIDEL, G. WALLBILLICH, and H. KNUPFER. Tetrahedron, **17**, 3 (1962).
5. F. D. CHATTAWAY and A. J. WALKER. J. Chem. Soc. 975 (1925).
6. R. CIUSA and P. MEGA. Gazz. Chim. Ital. **58**, 836 (1928).
7. J. M. BURGESS and M. S. GIBSON. J. Chem. Soc. 1500 (1964).
8. F. D. CHATTAWAY and A. J. WALKER. J. Chem. Soc. 1687 (1925).
9. R. HUISGEN, R. SUSTMANN, and G. WALLBILLICH. Chem. Ber. **90**, 1786 (1967).
10. F. L. SCOTT and J. B. AYLWARD. Tetrahedron Lett. 841 (1965).
11. V. V. KOSOVTSEV, V. N. CHRISTOKLETOV, AND A. A. PETROV. Zh. Obshch. Khim. **41**, 2649 (1971).
12. R. HUISGEN. Angew. Chem. Int. Ed. Engl. **2**, 565 (1963); *cf.* A. F. HEGARTY, M. P. CASHMAN, and F. L. SCOTT. J. Chem. Soc. Perkin II, 44 (1972), and references cited.
13. K. A. JENSEN, H. R. BACCARO, O. BUCHARDT, G. E. OLSEN, C. PEDERSEN, and J. TOFT. Acta Chem. Scand. **15**, 1109 (1961).
14. M. H. WUYTS and A. LACOURT. Bull. Soc. Chim. Belg. **48**, 193 (1939).
15. G. CORSI. Ann. Chim. (Rome), **56**, 1203 (1966).
16. W. WALTER and M. BADKE. Liebigs Ann. Chem. **739**, 201 (1970).
17. G. SHEROWSKY. Tetrahedron Lett. 4985 (1971).

Mechanism and Stereochemistry of the Hydrolysis of 4-Arylamino-1,2,3,4-tetrahydroquinaldines

T. P. FORREST, G. A. DAUPHINEE, AND W. F. MILES
Chemistry Department, Dalhousie University, Halifax, Nova Scotia

Received August 20, 1973

Rates of acid-catalyzed hydrolysis of the benzylic amino group in stereoisomers of 4-arylamino-1,2,3,4-tetrahydroquinaldines have been determined by n.m.r. spectroscopy. Those isomers which have a pseudo-axial leaving group react more rapidly than those with a pseudo-equatorial leaving group, forming in each case the isomer with a pseudo-axial hydroxyl group as the kinetically controlled product. This product is converted in time to an equilibrium mixture of the two stereoisomeric alcohols. The reaction is inhibited by excess acid and appears to proceed through an intermediate carbonium ion which is stabilized by the heterocyclic nitrogen atom.

On a déterminé par spectroscopie r.m.n. les vitesses d'hydrolyse catalysé par les acides du groupe aminobenzylique des stéréoisomères de l'arylamino-4 de tétrahydro-1,2,3,4 de quinaldines. Les isomères dans lesquels le groupe nucléofuge est pseudo-axial réagissent plus rapidement que ceux dans lesquels le groupe nucléofuge est pseudo-équatorial et dans chaque cas le produit formé le plus rapidement est l'isomère ayant un groupe hydroxyle pseudo-axial. Ce produit se transforme avec le temps pour donner à l'équilibre un mélange des deux alcools stéréoisomères. La réaction est inhibée par un excès d'acide et il semble qu'il se produise par l'intermédiaire d'ion carbonium qui est stabilisé par l'atome d'azote de l'hétérocycle. [Traduit par le journal]

Can. J. Chem., **52**, 884 (1974)

Can. J. Chem. Downloaded from www.nrcresearchpress.com by 210.87.254.42 on 09/05/12
For personal use only.

Although benzylamines do not normally undergo acid-catalyzed substitution reactions, the acid-catalyzed displacement of an arylamino group from the benzylic position of 1,2,3,4-tetrahydroquinolines by water (1) or hydroxylamine (2) occurs very readily. We wish to report on the determination of the mechanism and stereochemistry of this type of substitution reaction by an investigation of the reactivity of some 4-aminotetrahydroquinaldines in which the conformation of the heterocyclic ring is controlled by the methyl group.

The conformations of the *cis*- and *trans*-4-anilino-1,2,3,4-tetrahydroquinaldines (**1** and **2**), formed by the reaction of aniline with acetaldehyde, have been established (3, 4) and are shown in projection formulae **1***a* and **2***a*. In both cases the methyl group assumes the pseudo-equatorial orientation thus yielding two isomers with different orientations of the amine group. An analogous pair of bases, *cis*- and *trans*-2,6-dimethyl-4-(*p*-toluidino)-1,2,3,4-tetrahydroquinoline (**3** and **4**), with the same stereochemistry is formed from the reaction of *p*-toluidine with acetaldehyde. The conformations are readily established from the coupling constants of the heterocyclic ring protons (see Experimental).

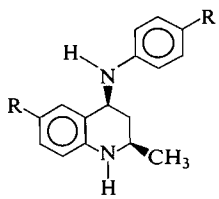

1 R = H
3 R = CH_3

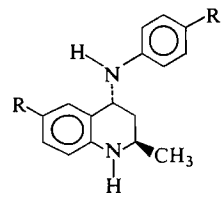

2 R = H
4 R = CH_3

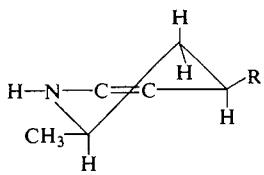

1*a* R = NHAryl or OH

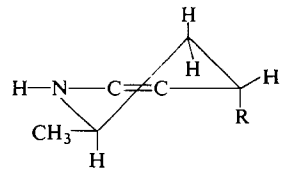

2*a* R = NHAryl or OH

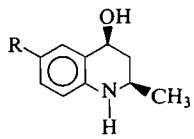

5 R = H
7 R = CH_3

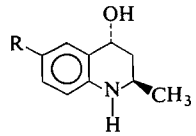

6 R = H
8 R = CH_3

Can. J. Chem. Downloaded from www.nrcresearchpress.com by 210.87.254.42 on 09/05/12
For personal use only.

The rates of the conversion of these four diamines to the amino alcohols were determined by monitoring the reaction in $DCl \cdot D_2O$ solutions by n.m.r. spectroscopy. In some cases the signals due to the C-4 protons were well separated from other signals permitting an accurate integration. In all of these cases, plots of the logarithm of concentrations of diamines against time gave linear plots indicating the reaction is first-order with respect to 4-aminotetrahydroquinaldine. In other cases where the peak due to HOD interfered with the C-4 proton signals, an estimate of the half-life of the reaction was obtained from the time required to obtain equivalent peak heights of the methyl groups of the substrate and product.

In all cases the kinetically controlled product was the *trans* hydroxy compound. The stereochemistry of the alcohols could be readily determined from the splitting pattern of the heterocyclic ring protons (see Experimental). The *cis* alcohols, **5** and **7**, have conformation **1***a* and the *trans* alcohols, **6** and **8**, have conformation **2***a*.

The fact that the same kinetically controlled product is obtained from the *cis* or *trans* diamine indicates that the same intermediate is formed in each case and that the reaction is S_N1 rather than S_N2. The lack of exchange of the protons on C-3 shows that the reaction does not proceed by an elimination–addition mechanism.

A comparison of the half-lives of the reactions shows that the *trans* isomer reacts more rapidly than the *cis* isomer in each case. It is unlikely that the greater reactivity of the *trans* isomer is due to the greater steric interaction of the pseudo-axial arylamino group. There appears to be little difference in the steric crowding of the arylamino group in the pseudo-axial and pseudo-equatorial positions since the conformation of both the *cis* and *trans* isomers is controlled by the single methyl group at C_2. In the equilibrium mixture of the alcohols the *trans* isomer with a pseudo-axial hydroxyl group is the predominant isomer.

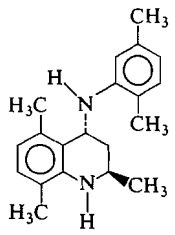

10

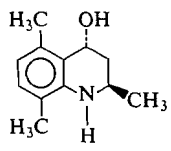

9

The rate difference is most likely due to the better orientation of the pseudo-axial arylamino group as a leaving group. In the *trans* isomer the bond being broken can maintain better overlap with the π orbitals of the aromatic ring which stabilizes the incipient carbonium ion. This conclusion is supported by the formation of the *trans* alcohol as the kinetic product indicating a lower-energy transition state for addition in the pseudo-axial manner. This principle of maintenance of maximum overlap of orbitals has been applied in a similar case by Eliel and Nader to explain the reactivity and product stereochemistry of 2-alkoxy-1,3-dioxanes (5).

The *cis* and *trans* alcohols (**7** and **8**) have been shown to be converted on standing in acid to an equilibrium mixture of the two (6). This equilibration was also observed in this investigation. The kinetically controlled *trans* products, **6** and **8**, are converted on standing in acid to an equilibrium mixture of the *cis* and *trans* isomers (*trans–cis* = 3:2). In the case of 2,5,8-trimethyl-4-hydroxy-1,2,3,4-tetrahydroquinoline (**9**), formed from the diamine **10**, only the kinetically controlled *trans* product was detected. This may be due to the steric interaction of the 5-methyl group and the pseudo-equatorial hydroxyl group which makes the *trans* isomer much more stable than the *cis* isomer.

Although the substitution is catalyzed by acid, the rate is decreased as the concentration of acid is increased from 0.5 to 3 *M* (Table 1). This behavior is in accord with a mechanism which requires resonance stabilization of the intermediate carbonium ion by the lone pair of the heterocyclic nitrogen (Scheme 1). The benzylic amino group would be converted to a better leaving

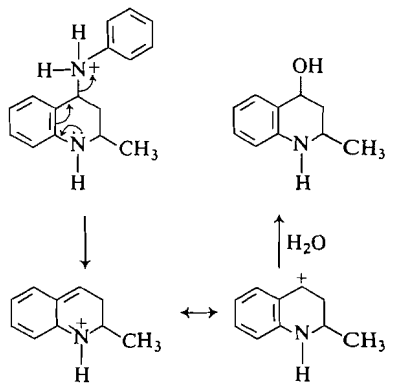

SCHEME 1

TABLE 1. Half-lives of diamines

Compound	Half-life: Acid concentration (*M*) 3	2	1	0.5
1 (*trans*)	22 min*	5 min*	63 s*	
2 (*cis*)	2.5 h	50 min*	18 min	<1 min
3 (*trans*)	30 min	9 min	<2 min	
4 (*cis*)	6 h	3 h	40 min	4.5 min*

*Obtained from plot of log concentration *vs.* time.

group upon protonation but the reaction would be inhibited if both nitrogens were protonated.

The bases **3** and **4** which have methyl groups on the aromatic ring are seen to react slower than their analogs **1** and **2** (Table 1). This may be explained by the difference in basicity of the amines in the two series. The inductive effect of the methyl group would make **3** and **4** stronger bases so that the rate of reaction, in conditions of excess acid as employed here, would be decreased because of a higher concentration of the diprotonated species.

Experimental

Nuclear magnetic resonance spectra were recorded at 35 °C on a Varian T 60 spectrometer. Mass spectra were recorded on a DuPont model 21-110 mass spectrometer. Melting points are uncorrected.

cis- and trans-2-Methyl-4-hydroxy-1,2,3,4-tetrahydroquinoline (5 and 6)

cis-2-Methyl-4-anilino-1,2,3,4-tetrahydroquinoline (**1**) (4) (13.3 g, 0.05 mol) was dissolved in 2 *N* HCl (100 ml) and allowed to remain at room temperature for 8 h. The solution was then made basic with 2 *N* NaOH and steam distilled to remove the aniline. The residue from the distillation was cooled and extracted with benzene. The benzene was removed *in vacuo* and the *cis–trans* mixture of alcohols separated by chromatography on silica gel using benzene – petroleum ether (30–60°).

cis Isomer **5**: yield 2.9 g, 36%; m.p. 124 °C; n.m.r. ($CDCl_3$) δ 1.18, (d, J = 6 Hz, CH_3), 1.53 (H_{3a}), 2.10 (H_{3e}), 3.46 (H_2), 4.84 (H_4) ($J_{3e,3a}$ = 12.5 Hz, $J_{3e,2a}$ = 3 Hz, $J_{3e,4a}$ = 6 Hz, $J_{2a,3a}$ = 11 Hz, $J_{4a,3a}$ = 10 Hz), 6.34–7.45 (m, aromatic H's), 2.87 (bs, OH, NH). Mass spectrum, 163(44), 148(36), 146(18), 144(28), 130(100).

trans Isomer **6**: yield 4.1 g, 50%; m.p. 78 °C, n.m.r. ($CDCl_3$) 1.20 (d, J = 6 Hz, CH_3), 1.47 (H_{3a}), 1.92 (H_{3e}), 3.50 (H_2), 4.64 (H_4) ($J_{3e,3a}$ = 12.5 Hz, $J_{3e,2a}$ = 2.5 Hz, $J_{3e,4e}$ = 2.5 Hz, $J_{3a,4e}$ = 3 Hz, $J_{3a,2a}$ = 11 Hz), 6.40–7.20 (m, aromatic H's), 3.10 (bs, OH, NH). Mass spectrum 163(40), 148(30), 146(20), 144(30), 130(100).

cis- and trans-2,6-Dimethyl-4-(p-toluidino)-1,2,3,4,-tetrahydroquinoline 3 and 4.

Acetaldehyde (4.9 g, 0.11 mol) was added to *p*-toluidine (10.7 g, 0.1 mol) in ethanol (100 ml) and allowed to sit at room temperature for 16 h. The ethanolic solution was decanted from the oily precipitate which had formed. Crystallization of the oily residue in benzene yielded the *cis* isomer (3 g, 23%). Chromatography of the mother liquors on silica gel using petroleum ether (30–60°) as eluant yielded the *trans* isomer as a yellow oil (4 g, 30%).

cis Isomer **3**: m.p. 114 °C; n.m.r. ($CDCl_3$) δ 1.20 (d, J = 6 Hz, CH_3), 2.22 (s, CH_3), 2.28 (s, CH_3), 1.43 (H_{3a}), 2.40 (H_{3e}), 3.56 (H_2), 4.76 (H_4) ($J_{3e,3a}$ = 12.5 Hz, $J_{3e,2a}$ = 2.5 Hz, $J_{3e,4a}$ = 6 Hz, $J_{3a,4a}$ = 11 Hz, $J_{3a,2a}$ = 11 Hz), 6.36–7.40 (m, aromatic H's), 3.40 (bs, NH's). Mass spectrum 266(14), 223(2), 160(100), 144(23).

trans Isomer **4**: n.m.r. ($CDCl_3$) δ 1.17 (d, J = 6 Hz, CH_3), 2.10 (s, CH_3), 2.16 (s, CH_3), 1.50 (H_{3a}), 2.14 (H_{3e}), 3.38 (H_2), 4.43 (H_4) ($J_{3e,3a}$ = 13 Hz, $J_{3e,2a}$ = 2.5 Hz, $J_{3e,4e}$ = 2.5 Hz, $J_{3a,4e}$ = 3.5 Hz, $J_{3a,2a}$ = 11 Hz), 6.40–7.10 (m, aromatic H's), 3.80 (bs, NH's). Mass spectrum 266(10), 233(2), 160(100), 144(30).

cis- and trans-2,6-Dimethyl-4-(hydroxy)-1,2,3,4-tetrahydroquinoline 7 and 8

These compounds were prepared following the procedure of Edwards *et al.* (6).

cis Isomer, m.p. 165°; n.m.r. ($CDCl_3$) δ 1.22 (d, J = 6, CH_3), 2.25 (s, CH_3), 1.57 (H_{3a}), 2.27 (H_{3e}), 3.48 (H_2), 4.90 (H_4) ($J_{3e,3a}$ = 12 Hz, $J_{3e,2a}$ = 3 Hz, $J_{3e,4a}$ = 6 Hz, $J_{3a,4a}$ = 11 Hz, $J_{3a,2a}$ = 11 Hz), 6.32–7.23 (m, aromatic H's), 2.2 (bs, OH, NH). Mass spectrum 177(64), 162(52), 160(12), 158(16), 144(100).

trans Isomer, m.p. 110°; n.m.r. ($CDCl_3$) δ 1.17 (d, J = 6, CH_3), 2.22 (s, CH_3), 1.43 (H_{3a}), 1.88 (H_{3e}), 3.37 (H_2), 4.55 (H_4) ($J_{3e,3a}$ = 13 Hz; $J_{3e,2a}$ = 2.5 Hz; $J_{3e,4e}$ = 2.5 Hz; $J_{3a,4e}$ = 3.5 Hz; $J_{3a,2a}$ = 11 Hz), 6.30–7.10 (m, aromatic H's), 3.05 (bs, NH, OH). Mass spectrum, 177(64), 162(52), 160(12), 158(16), 144(100).

trans-2,5,8-Trimethyl-4-hydroxy-1,2,3,4-tetrahydroquinoline 9

trans-2,5,8-Trimethyl-4-(2,5-dimethylanilino)-1,2,3,4-tetrahydroquinoline (**10**) (3 g, 0.01 mol), prepared as previously described for **3** and **4**, was dissolved in 6 *N* HCl (5 ml) and after dissolution the solution diluted with water to 2 *N*. After remaining at room temperature for 16 h, the solution was made basic and extracted with benzene. After removal of the benzene the residue was crystallized from benzene – petroleum ether (30–60°). Yield 1.7 g, 90%, m.p. 106°; n.m.r. ($CDCl_3$) δ 1.31 (d, J = 6 Hz, CH_3), 2.08 (s, CH_3), 2.35 (s, CH_3), 1.46 (H_{3a}), 2.03 (H_2), 4.85 (H_4) ($J_{3e,3a}$ = 13 Hz, $J_{3e,2a}$ = 3 Hz, $J_{3e,4e}$ = 2.5 Hz, $J_{3a,4e}$ = 3 Hz, $J_{3a,2a}$ = 12 Hz), 6.45 (d, J = 8 Hz, aromatic H),

Can. J. Chem. Downloaded from www.nrcresearchpress.com by 210.87.254.42 on 09/05/12
For personal use only.

6.88 (d, $J = 8$ Hz, aromatic H). Mass spectrum, 191(55), 176(22), 174(10), 172(33), 158(100).

Determination of Reaction Rates

The diamine under investigation was dissolved in $DCl{\cdot}D_2O$ solution in order to make a solution 0.25 *M* in diamine. The spectra were then determined at various time intervals. In those cases which yielded well separated H_4 peaks, integrals of these peaks were used to calculate the concentration of diamine substrate at any particular time. The plots of the logarithm of this concentration against time gave straight lines, the slopes of which were used to calculate half-lives. In other cases the half-life was estimated from the time required to obtain equal peak heights for the signals due to the methyl peaks of substrate and product.

The formation of the *trans* alcohols as the initial hydrolysis product was indicated by the splitting pattern of the C_4 proton. The signal developed initially as a triplet typical of the *trans* isomer and then changed to a mixture of the triplet and a double doublet typical of the mixture.

The financial assistance of the National Research Council of Canada is acknowledged.

1. G. A. DAUPHINEE and T. P. FORREST. Chem. Commun. 327 (1969).
2. L. P. ZALUKAEV and L. YA. SPITSYNA. Zhurnal Obshchii Khimie, **33**, 3776 (1963).
3. T. P. FORREST, G. A. DAUPHINEE, and W. F. MILES. Can. J. Chem. **47**, 2121 (1969).
4. M. FUNABASHI, M. IWAKAWA, and J. YOSHIMIRRA. Bull. Chem. Soc. Jap. **42**, 2885 (1969).
5. E. L. ELIEL and F. W. NADER. J. Am. Chem. Soc. **92**, 584 (1970).
6. M. G. EDWARDS, R. E. GARROD, and H. O. JONES. J. Chem. Soc. 1376 (1912).

Can. J. Chem. Downloaded from www.nrcresearchpress.com by 210.87.254.42 on 09/05/12
For personal use only.

Reductive Cleavage of Acetals and Ketals by Borane

BRUCE FLEMING AND HENRY I. BOLKER

Pulp and Paper Research Institute of Canada, and Department of Chemistry, McGill University, Montreal, Quebec H3C 3G1

Received October 9, 1973

Borane in tetrahydrofuran was found to reduce acetals and ketals to ethers, generally in good yield and under mild and convenient conditions. Cyclic acetals and ketals were converted by this reagent into hydroxy ethers. The mechanism appeared to resemble that of reduction with $LiAlH_4$–$AlCl_3$.

On a observé que le borane dans le tétrahydrofuranne réduit les acétals et les cétals en éther généralement avec de bon rendement et dans des conditions simples et douces. Les acétals et les cétals cycliques sont transformés par ce réactif en hydroxy éthers. Il semble que le mécanisme de cette réaction ressemble à celui de la réduction par $LiAlH_4$–$AlCl_3$. [Traduit par le journal]

Can. J. Chem., **52**, 888 (1974)

A number of reagents are known, notably diisobutylaluminum hydride (1), decaborane (2), trialkyl silanes (3), and lithium aluminum hydride – Lewis acid mixtures (mixed hydrides), which can effect homogeneous reductive cleavage of acetals and ketals. The Lewis acids used in the mixed hydrides have been either boron trifluoride (4, 5) with a hydridoboron fluoride (5) postulated as the active species, or aluminum chloride (6–8), which is believed to be active as a hydridoaluminum chloride (9, 10).

We have now found that borane in tetrahydrofuran (THF) is also an effective agent for the reductive cleavage of acetals and ketals at room temperature or slightly above (Table 1). Borane may prove to have practical advantages over the mixed hydride systems: in its readily available form as a 1 *M* solution in THF, the reagent is stable over long periods of time in the refrigerator, and thus, no preparation is required; the boric acid product is readily separated by water extraction or by volatilization as its trimethyl ester. In reactions with mixed hydride systems, either dilute acid must be used to decompose the aluminum complexes, or if water is used, then the aluminum hydroxide must be filtered off.

In each of the experiments described in Table 1, an excess of borane was used and conditions were chosen so that unreacted starting material was generally no longer detectable at the end of the reaction. Except for acetophenone diethyl ketal (experiment 2), from which a large amount of nondistillable oily residue was obtained, yields of ethers and hydroxyethers were good.

Table 2 illustrates how some substituents at C_4 on the dioxane and dioxolane rings influence the position of cleavage. The results presented in both tables are strikingly similar to those obtained by other workers (7, 8) with the $LiAlH_4$–$AlCl_3$ reagent and indicate that the course of cleavage by borane may closely resemble the oxocarbonium ion mechanism postulated for the mixed hydride reagent. For example, preferential attack of borane at O_1 of the dioxane and dioxolane rings to give the most stabilized oxocarbonium ion (Scheme 1) would explain the results of experiments 8, 9, and 11.

The cleavage at O_3 which predominated in the reduction of 2,2-dimethyl-4-chloromethyl-1,3-dioxolane (**1**) (experiment 12) is explicable by noting that the inductive effect of the substituent at C_4 is opposite to that of the corresponding substituents in the previous examples. Under the influence of an electron-attracting group, the most stable carbonium ion would be obtained as illustrated in Scheme 2. Thus it appears that electronic factors control the direction of cleavage, at least when steric hindrance is not extreme, for, had steric factors been important in the reaction of **1**, the preferred attack would have been at O_1, as in experiment 11, but the preference would have been even greater because of the bulk of the chlorine atom near O_3.

Although no special measurements were made of the effect of substituents on the rate of reduction, the conditions required for completion give some general indications. Thus, comparing experiments 4 and 5 with experiment 7 (Table 1) shows that the presence at C_2 of substituents

Can. J. Chem. Downloaded from www.nrcresearchpress.com by 210.87.254.105 on 09/05/12
For personal use only.

TABLE 1. Reductive cleavage of simple acetals and ketals with borane

Expt. No.	Compound reduced	Product	Yield (%)	Reaction time (h)*
1	$C_6H_5CH(OMe)_2$	$C_6H_5CH_2OMe$	100† (90)‡	24
2	$C_6H_5C(OEt)_2Me$	$C_6H_5CH(OEt)Me$	40† (35)	1¶
3	$(Me)_2C(OC_4H_9\text{-}n)_2$	$Me_2CHOC_4H_9\text{-}n$	58†	48
4	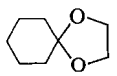	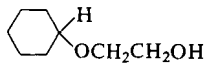	90§ (80)	15 (at 35°)
5	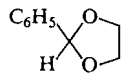	$C_6H_5CH_2OCH_2CH_2OH$	94§ (85)	19
6	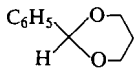	$C_6H_5CH_2O(CH_2)_3OH$	96§ (92)	40
7		$MeOCH_2CH_2OH$	16†‖	24 (at 57°)

*At ambient unless otherwise stated.
†Yield obtained by gas chromatographic analysis of the crude reaction mixture after excess borane was decomposed.
‡The figures in parentheses represent yields obtained after distillation.
§Yields obtained by gas chromatographic analysis of the ether extract before distillation.
‖78% starting material remains.
¶Reaction mixture became hot (50°) immediately after mixing. Mixing at −78 °C and allowing to warm slowly to ambient did not produce better yields.

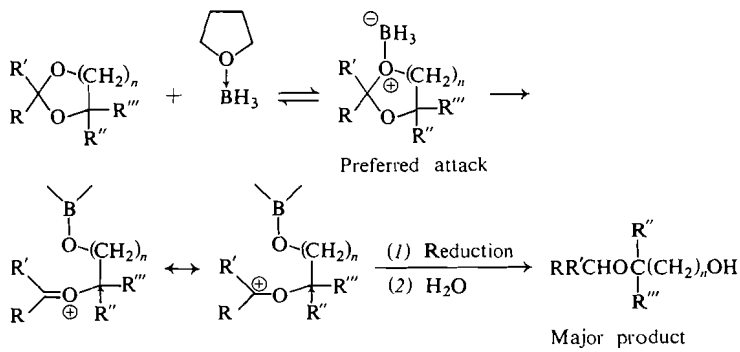

SCHEME 1

which can stabilize a carbonium ion increases the reaction rate. Further, the reduction of 2,2,4-trimethyl-1,3-dioxolane (experiment 11) was complete in 2 h at 40 °C, whereas reduction of **1** (experiment 12) conducted at 50 °C, required 41 h for completion. Hence, electron-withdrawing substituents at C_4 slow the reaction.

The very small influence observed here of a phenyl group at C_4 (experiment 10) has also been noted in the mixed hydride reactions (8).

The behavior of the borane moiety may be visualized by considering that as the C—O bond breaks, the boron atom receives a greater share of the electrons from the hitherto strongly polarized O—B bond and thus tends to become an alkoxyborohydride ion. It is unlikely, however, that such a species could exist uncoordinated in presence of excess borane, for Brown (11*a*) has observed that borohydride ion reacts with the diborane in diglyme solution to give a complex

Can. J. Chem. Downloaded from www.nrcresearchpress.com by 210.87.254.105 on 09/05/12
For personal use only.

TABLE 2. Reductive cleavage of C_4-substituted dioxane and dioxolane

Expt. No.	Compound reduced	Products obtained	Yield (%)*	Total recovery of product (%)
8	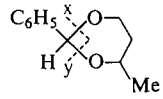	$C_6H_5CH_2OCHCH_2CH_2OH$ (Me) (cleavage at x)	82	92
		$C_6H_5CH_2OCH_2CH_2CHOH$ (Me) (cleavage at y)	18	
9	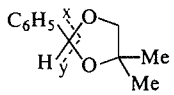	$C_6H_5CH_2OCCH_2OH$ (Me, Me) (cleavage at x)	97	89
		$C_6H_5CH_2OCH_2COH$ (Me, Me) (cleavage at y)	3	
10	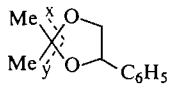	$C_6H_5CHCH_2OH$ (O-*i*Pr) (cleavage at x)	58	88
		$C_6H_5CHCH_2O$-*i*Pr (OH) (cleavage at y)	42	
11	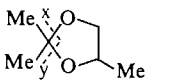	*i*PrOCHCH$_2$OH (Me) (cleavage at x)	80	75
		*i*PrOCH$_2$CHOH (Me) (cleavage at y)	20	
12	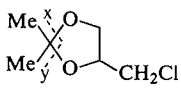	*i*PrOCHCH$_2$OH (CH_2Cl) (cleavage at x)	15	88
		*i*PrOCH$_2$CHOH (CH_2Cl) (cleavage at y)	85	

*The percentage of the isolated reduction product that is primary or secondary (tertiary) alcohol, as analyzed by gas chromatography.

Can. J. Chem. Downloaded from www.nrcresearchpress.com by 210.87.254.105 on 09/05/12
For personal use only.

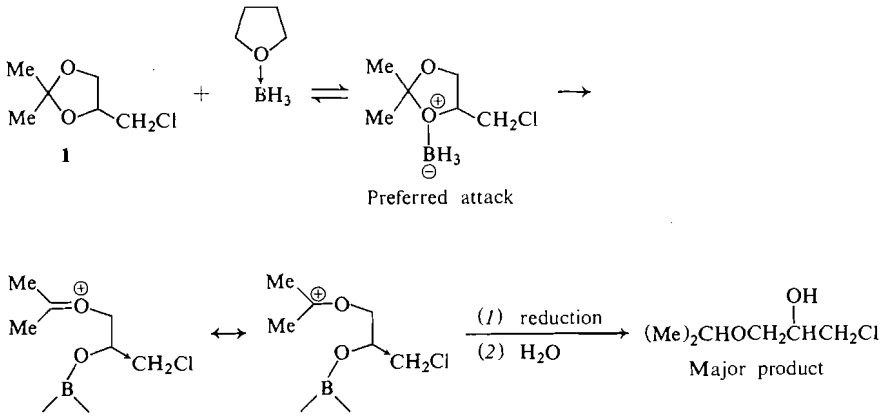

SCHEME 2

ion, $B_2H_7^-$. Since alkoxyborohydride ions are more powerful nucleophiles than borohydride (11*b*), one expects reduction of borane by $ROBH_3^-$ species to proceed to a greater extent than reduction by BH_4^-. During acetal cleavage, energetically favorable complex formation (or complete hydride transfer) between the incipient alkoxyborohydride ion and neighboring borane molecules will reduce the activation energy required for C—O cleavage and the two processes should occur simultaneously. Kinetic studies are in progress to investigate this hypothesis.

Experimental

Boiling and melting points are uncorrected.

Gas chromatographic analyses of the products were done on a Hewlett-Packard F & M model 402 instrument, equipped, in most cases, with 120-cm glass column packed with 4% SE-30 on Chromosorb WAWDMCS. The products of experiment 11 required a 180-cm column for adequate separation and the volatile product of experiment 7 could only be separated from the THF solvent by using a 120-cm Porapak R column.

All products shown in Table 1 were first quantitatively analyzed by g.l.c. using bracketing standards of authentic samples dissolved in THF. The ethers and hydroxyethers were then separated from the solvent, where possible, by distillation and their properties (b.p., refractive index, n.m.r. spectrum) were compared with those of authentic samples.

Reduction products obtained from the acetals shown in Table 2 were distilled similarly and the mixed isomeric hydroxyethers were analyzed by g.l.c. using authentic samples for identification. In some cases, small amounts of the isomers were separated by silica-gel chromatography (Mondray silica, 0.08 mm) and thus could be characterized as above. Proton magnetic resonance spectroscopy was used to confirm the g.l.c. analysis, as the isomers had distinctly different p.m.r. spectra. These spectra were measured in carbon tetrachloride solution on a Varian HA-100 spectrometer. Chemical shifts are given in p.p.m. relative to the tetramethylsilane internal standard.

General Procedure

The reduction of 2-phenyl-4-methyl-1,3 dioxane (experiment 8, Table 2) is representative of the general experimental procedure. The acetal (3.56 g, 20 mmol) was cooled to 0° and borane in THF (30 ml of 1 *M* solution (Alfa Inorganics), ~30 mmol), previously cooled to −10°, was pipetted in. The mixture was swirled, kept for 10 min in an ice bath then allowed to warm to room temperature. After 24 h, the extent of the reaction was tested as follows: 3 drops of solution were removed, treated with an equal volume of water,[1] and the mixture was shaken with a little benzene. A gas chromatogram of the benzene layer showed that some starting material remained. To complete the reaction the mixture was heated at 40 ± 5° for 24 h, when gas chromatography showed all starting material to have reacted.[2] Next the reaction mixture was cooled and water was added dropwise causing effervescence. Slow addition of water was continued until effervescence ceased and then more water (30–40 ml) was added to dissolve the precipitated boric acid and to hydrolyze the boric esters. The aqueous solution was extracted several times with ether and the combined extracts were washed with water, dried (Na_2SO_4), and evaporated. A little dry methanol was added and the mixture was evaporated, this procedure being repeated to remove any remaining traces of boric acid. The residue was distilled, yielding 3.3 g (92%) of mixed alcohols, b.p. 107–110° at 1 mm.

Analysis by g.l.c., with calibration standards prepared from authentic samples of the isomeric hydroxyethers, gave the results shown in Table 2. Complete separation of the isomers was not achieved but a small amount of each in pure form was obtained by chromatography on silica gel. The p.m.r. spectra and refractive indices of the pure

[1]Acetone *n*-butyl ketal (experiment 3) was completely hydrolyzed by this procedure.

[2]All cyclic acetals except 2-phenyl-1,3-dioxolane required a heating period to complete the reaction.

Can. J. Chem. Downloaded from www.nrcresearchpress.com by 210.87.254.105 on 09/05/12
For personal use only.

Can. J. Chem. Downloaded from www.nrcresearchpress.com by 210.87.254.105 on 09/05/12
For personal use only.

fractions so obtained confirmed the identification of the g.l.c. peaks.

Source of the Acetals and Ketals

Benzaldehyde Dimethyl Acetal. This was prepared in 35% yield according to Fischer and Giebe (12); b.p. 97.5° at 30 mm (lit. (12) b.p. 198–199° at 762 mm).

Acetophenone Diethyl Ketal. This was prepared according to Fuson and Burness (13); b.p. 103° at 16 mm; n_D^{20} 1.4781 (lit. b.p. (13) 101.5° at 15 mm; n_D^{20} 1.4773).

Acetone Di-n-butyl Ketal. The method of Howard and Lorette (14) was used, yield 70%; b.p. 80–80.5° at 10 mm; $n_D^{23.5}$ 1.4117 (lit. (14) b.p. 88° at 18 mm; n_D^{25} 1.4105 and lit. (15) b.p. 64–64.5° at 3 mm; n_D^{20} 1.4120).

Cyclohexanone Ethylene Ketal. This and the following four compounds were all synthesized by Salmi's method (16); b.p. 69–70° at 12 mm, n_D^{20} 1.4592 (lit. (16) b.p. 73° at 16 mm; n_D^{20} 1.4583).

2-Phenyl-1,3-dioxolane. Yield 66%, b.p. 123–124° at 26 mm; n_D^{22} 1.5264 (lit. (8) b.p. 116° at 20 mm; lit. (17) b.p. 129° at 25 mm; n_D^{18} 1.5285).

2-Phenyl-1,3-dioxane. Yield 85%, b.p. 126–127° at 15 mm; m.p. 46–48° (lit. (18) b.p. 125° at 14 mm; m.p. 49–51°).

2-Phenyl-4-methyl-1,3-dioxane. Boiling point 134–135° at 18 mm; n_D^{25} 1.5145 (lit. (19) b.p. 134–135° at 15 mm; lit. (17) b.p. 162° at 40 mm; n_D^{18} 1.5165). The p.m.r. spectrum indicates that this compound is a single pure isomer (presumably *cis* e,e). The methyl group appears as a sharp doublet at δ 1.2 and the proton at C_2 is a singlet at δ 5.3.

2-Phenyl-4,4-dimethyl-1,3-dioxolane. Yield 93%, b.p. 99.5–101.5° at 10 mm; n_D^{25} 1.5005 (lit. (8) b.p. 85° at 5 mm; n_D^{25} 1.5015). Whereas the alcohols used for the previous syntheses were commercially available, in this case it was necessary to synthesize 2-methyl-1,2-propanediol. The method of Leggetter and Brown (8) was employed.

2,2-Dimethyl-4-phenyl-1,3-dioxolane. This and the following two compounds were prepared according to the method of Fischer and Pfähler (20). Yield 85%, b.p. 104–105° at 13 mm; n_D^{22} 1.5016 (lit. (21) b.p. 95–96° at 10 mm).

2,2,4-Trimethyl-1,3-dioxolane. Yield 14%, b.p. 98–100° at 758 mm; n_D^{22} 1.3952 (lit. (8) b.p. 99° at 700 mm; lit. (22) b.p. 98–99° at 760 mm).

2,2-Dimethyl-4-chloromethyl-1,3-dioxolane. Yield 42%, b.p. 76-77° at 38 mm; n_D^{22} 1.4341 (lit. (8) b.p. 78° at 40 mm; lit. (20) n_D^{15} 1.4375).

1,3-Dioxolane. This was obtained from Eastman Kodak Co.

Source of Authentic Samples of Reduction Products

Benzyl Methyl Ether, 2-Benzyloxyethanol, and 2-Methoxyethanol. These were obtained from Eastman Kodak Co.

α-Methylbenzyl Ethyl Ether. This was prepared according to Mislow (23).

Isopropyl n-Butyl Ether. This was synthesized by the method of Henstock (24), b.p. 109° at 763 mm (lit. (24) b.p. 108° at 738 mm).

2-Cyclohexyloxyethanol. The synthesis of Eliel *et al.* (25) was employed. Overall yield 18%; b.p. 115–118° at 28 mm; n_D^{22} 1.4602 (lit. (25) b.p. 100° at 14 mm; n_D^{25} 1.4605).

3-Benzyloxy-1-propanol. This was made according to ref. 26; b.p. 130° at 10 mm; n_D^{26} 1.5110, (lit. (26) b.p. 114° at 0.9 mm; n_D^{20} 1.5184; lit. (27) b.p. 155° at 23 mm).

3-Benzyloxy-1-butanol. This was prepared according to Stork *et al.* (28). Since these authors did not give details, the procedure employed is described. Sodium was added to benzyl alcohol (10.8 g, 0.1 mol) in 50 ml of xylene. When the reaction terminated, excess sodium was removed, ethyl crotonate (5.7 g, 0.05 mol) was added with stirring, and the mixture was heated for 5 h at 90°. The pasty mixture was cooled in ice water and acidified with a slight excess of 5% sulfuric acid. Ether (60 ml) was added and the mixture was stirred until all solid had dissolved. Gas–liquid chromatography of the ether extract showed two major products which were assumed to be the benzyl and ethyl esters of 3-benzyloxybutanoic acid. Fractional distillation of the extract yielded a fairly pure fraction of the benzyl ester, b.p. 100–105° at 0.35 mm; n_D^{25} 1.5370; λ_{max} 1740 cm^{-1}; p.m.r. spectrum shows two types of benzyl protons: δ 5.0 (s, 2H) and 4.4 (m, 2H). This material was reduced with $LiAlH_4$ and yielded benzyl alcohol (identified by g.l.c.) and 3-benzyloxy-1-butanol (1.5 g, 17%), b.p. 108–109° at 1 mm; n_D^{24} 1.5095. The p.m.r. spectrum of the benzyl protons showed an AB pattern, (lit. (28) b.p. 98–107° at 1 mm).

4-Benzyloxy-2-butanol. This was obtained in 82% yield by $LiAlH_4$ reduction of 4-benzyloxy-2-butanone (Fluka) as described by Eliel *et al.* (25). The product was purified by chromatography on silica gel after which i.r. spectroscopy showed no trace of carbonyl absorption; n_D^{26} 1.5051 (lit. (25) n_D^{20} 1.5080).

2-Benzyloxy-2-methyl-1-propanol. This and the following two compounds were prepared according to Leggetter and Brown (8), b.p. 132–134° at 9 mm; n_D^{25} 1.5115 (lit. (8) b.p. 102° at 3.5 mm; n_D^{25} 1.5088).

1-Benzyloxy-2-methyl-2-propanol. b.p. was 106–107° at 7 mm; n_D^{25} 1.4997 (lit. (8) b.p. 106° at 6 mm; n_D^{25} 1.4997).

2-Isopropoxy-2-phenylethanol. The b.p. was 122–123.5° at 13 mm; n_D^{25} 1.5030 (lit. (8) b.p. 94° at 3 mm; n_D^{25} 1.4982).

2-Isopropoxy-1-phenylethanol. This was obtained as a gift from Dr. R. K. Brown.

2-Isopropoxy-1-propanol. This and the following compound were made by the method of Chitwood and Freure (29), b.p. 145–146° at 763 mm; n_D^{23} 1.4149 (lit. (29) b.p. 143–144° at 760 mm; n_D^{20} 1.4094).

1-Isopropoxy-2-propanol. The b.p. was 144–144.5° at 764 mm; $n_D^{23.5}$ 1.4070 (lit. b.p. 137–138° at 760 mm; n_D^{20} 1.4070).

3-Chloro-2-isopropoxy-1-propanol. This was obtained as a gift from Dr. Brown.

1-Chloro-3-isopropoxy-2-propanol. Synthesis of this compound according to Leggetter and Brown (8) failed but success was achieved via a different set of conditions (30), b.p. 90–92° at 23–24 mm; n_D^{23} 1.4398 (lit. (30) b.p. 87–87.5° at 20 mm; n_D^{25} 1.4370).

We wish to thank Dr. R. K. Brown for supplying comparison samples of cleavage products obtained in experiments 9, 10, and 12. This work was supported by the National Research Council of Canada.

1. L. I. ZAKHARKIN and I. M. KHORLINA. Izv. Akad. Nauk. SSSR, Otd. Khim. Nauk. 2255, 1959.
2. L. I. ZAKHARKIN, V. I. STANKO, and Y. A. CHAPOVS-

KII. Izv. Akad. Nauk. SSSR, Otd. Khim. Nauk. 1118, 1962.
3. E. FRAINNET, R. CALAS, and A. BAZOUIN. Bull. Soc. Chim. Fr. 1480 (1960).
4. A-R. ABDUN-NUR and C. H. ISSIDORIDES. J. Org. Chem. **27**, 67 (1962).
5. E. L. ELIEL, B. E. NOWAK, R. A. DAIGNAULT, and V. G. BADDING. J. Org. Chem. **30**, 2441 (1965).
6. E. L. ELIEL. Rec. Chem. Prog. **22**, 129 (1961).
7. E. L. ELIEL, V. G. BADDING, and M. N. RERICK. J. Am. Chem. Soc. **84**, 2371 (1962).
8. B. E. LEGGETTER and R. K. BROWN. Can. J. Chem. **42**, 990 (1964).
9. E. C. ASHBY and J. PRATHER. J. Chem. Soc. **88**, 729 (1966).
10. U. E. DINER, H. A. DAVIS, and R. K. BROWN. Can. J. Chem. **45**, 207 (1967).
11. H. C. BROWN. Hydroboration. W. A. Benjamin, New York. 1962. (*a*) p. 86; (*b*) p. 246.
12. E. FISCHER and G. GIEBE. Ber. **31**, 545 (1898).
13. R. C. FUSON and D. M. BURNESS. J. Am. Chem. Soc. **68**, 1270 (1946).
14. W. L. HOWARD and N. B. LORETTE. J. Org. Chem. **25**, 521 (1960).
15. H. B. DYKSTRA. J. Am. Chem. Soc. **57**, 2255 (1935).
16. E. J. SALMI. Ber. **71B**, 1803 (1938).
17. P. MASTAGLI, Z. ZAFIRIADIS, and G. LAGRANGE. C.R. **237**, 187 (1953).
18. E. FISCHER. Ber. **27**, 1537 (1894).
19. J. KOVAR and J. JARY. Collect. Czech. Chem. Commun. **30**, 2793 (1965).
20. E. FISCHER and E. PFÄHLER. Ber. **53**, 1606 (1920).
21. F. G. PONOMAREV. Dokl. Akad. Nauk. SSSR, **108**, 648 (1956).
22. J. BOESEKEN and P. H. HERMANS. Rec. Trav. Chim. **42**, 1104 (1923).
23. K. MISLOW. J. Am. Chem. Soc. **73**, 4043 (1951).
24. H. HENSTOCK. J. Chem. Soc. 372 (1931).
25. E. L. ELIEL, L. A. PILATO, and V. G. BADDING. J. Am. Chem. Soc. **84**, 2371 (1962).
26. J. D. GENZER, C. P. HUTTERER, and G. C. VAN WESSEM. J. Am. Chem. Soc. **73**, 3159 (1951).
27. G. BENNETT and A. L. HOCK. J. Chem. Soc. 472 (1927).
28. G. STORK, H. J. E. LOEWENTHAL, and P. C. MUKHARJI. J. Am. Chem. Soc. **78**, 501 (1956).
29. H. C. CHITWOOD and B. FREURE. J. Am. Chem. Soc. **68**, 680 (1946).
30. H. FLORES-GALLARDO and C. R. POLLARD. J. Org. Chem. **12**, 831 (1947).

Can. J. Chem. Downloaded from www.nrcresearchpress.com by 210.87.254.105 on 09/05/12
For personal use only.

The Radiochemistry of Organoiron Compounds. IV. $FeCp(CO)_2$

W. KANELLAKOPULOS-DROSSOPULOS AND D. R. WILES

Institut für Heisse Chemie, Kernforschungszentrum Karlsruhe, 75 Karlsruhe, Germany and Department of Chemistry, Carleton University, Ottawa, Canada K1S 5B6

Received September 4, 1973

The radiochemical yields of $[Cp^{59}Fe(CO_2]\cdot$ in neutron-irradiated $[CpFe(CO)_2]_2$ and $[CpFe(CO)_2]I$ are 6.9 and 14.8%, respectively. Other prominent products are $[CpFe(CO)_2]_2$-^{59}Fe, $^{59}Fe(CO)_5$, and $^{59}FeCp_2$, in both target compounds.

Thermal treatment at 75 °C increases the yields of $^{59}Fe(CO)_5$, and of the radioactive target compound in both cases, and does not affect the yields of the other two products. The radioactive radical $[Cp^{59}Fe(CO)_2]\cdot$ is stable to 75° in the solid $[CpFe(CO)_2]_2$, and on dissolution is rapidly scavenged by iodine transfer from carrier $[CpFe(CO)_2]I$.

It is suggested that complex molecular products are not reformed following the nuclear activation, but are rather preserved during and despite the nuclear reaction. An effective "hot zone" need not contain more than two or three molecules.

Production of $[Cp^{59}Fe(CO)_2]\cdot$ and $[Cp^{59}Fe(CO)_2]_2$ is observed in neutron irradiated solutions of $Fe(CO)_5$ and benzene with either $FeCp_2$ or C_5H_6.

Dans le cibles solides de $[CpFe(CO)_2]_2$ et de $[CpFe(CO)_2]I$, irradiées par des neutrons, les rendements radiochimiques de $[Cp^{59}Fe(CO)_2]I$ sont respectivement 6.9% et 14.8%. D'autres produits importants sont $[CpFe(CO)_2]_2$-^{59}Fe, $^{59}Fe(CO)_5$ et $^{59}FeCp_2$, dans les deux composés visés.

Le traitement thermique à 75 °C augmente les rendements de $^{59}Fe(CO)_5$ et du composé visé radioactif dans les deux cas, et n'affecte par les rendements des deux autres produits. Le radical radioactif $[Cp^{59}Fe(CO)_2]\cdot$ est stable jusqu'à 75° dans le solide $[CpFe(CO)_2]_2$ et est rapidement purifié par le transfert de l'iode du porteur $[CpFe(CO)_2]I$ par dissolution.

Il est suggéré que les produits moléculaires complexes ne sont pas regénérés suivant l'activation nucléaire, mais sont plutôt conservés au cours et malgré la réaction nucléaire. Une "zone chaude" eventuelle efficace n'a pas besoin de contenir plus de deux ou trois molécules.

La formation de $[Cp^{59}Fe(CO)_2]\cdot$ et $[Cp^{59}Fe(CO)_2]_2$ est observée par irradiation à l'aide de neutrons de solutions de $Fe(CO)_2$ et benzène avec du $FeCp_2$ ou du C_5H_6.

[Traduit par le journal]

Can. J. Chem., **52**, 894 (1974)

Our earlier work in this series (1–3) has shown a number of significant things about the chemical behavior of iron atoms which have captured neutrons. In dimeric $[CpFe(CO)_2]_2$, it is found that $^{59}Fe(CO)_5$ and $^{59}FeCp_2$ are formed in a ratio of approximately 5:2. These proportions of the radioactive atoms in ferrocene and iron pentacarbonyl are such as to suggest that the reaction is not one of local pyrolysis and rearrangement. The preponderance of the $Fe(CO)_5$ supported once again our hypothesis (4) that the metal atom is able to accumulate more carbonyls as ligands than the overall stoichiometry of the target would justify. The increase of radiochemical yield of the $Fe(CO)_5$ from 3.2 to 5.4% on thermal treatment indicates that carbonyl radicals are available and are also thermally reactive with such moieties as $Fe(CO)_4$

[1] $$Fe(CO)_4 + CO \rightarrow Fe(CO)_5$$

At the same time, however, failure of the $FeCp_2$ yield to increase during thermal treatment suggests that the ferrocene is formed at a quite early stage in the reaction sequence, and that Cp groups are not further thermally reactive. The high yield of the parent dimer, $[FeCp(CO)_2]_2$, violated once again the simplistic hypothesis (5) that structurally simpler molecules should be easier to re-form and thus should have higher yields. This high yield suggested that the molecule was *preserved* rather than *re-formed*. The increase, on thermal annealing, of the yield of this parent dimer once again suggested reaction of available CO groups with species such as $Cp_2Fe_2(CO)_3$

[2] $$Cp_2Fe_2(CO)_3 + CO \rightarrow [CpFe(CO)_2]_2$$

although it also raised the question of possible recombination of $CpFe(CO)_2$ fragments.

Can. J. Chem. Downloaded from www.nrcresearchpress.com by 210.87.254.5 on 09/05/12
For personal use only.

Can. J. Chem. Downloaded from www.nrcresearchpress.com by 210.87.254.5 on 09/05/12
For personal use only.

In subsequent work, we have found that ^{59}Fe atoms, produced by neutron bombardment of $Fe(CO)_5$ and of $FeCp_2$, are able to react with nearby ligand molecules, specifically with cyclopentadiene, when the ligand is in a reactive form. These reactive forms evidently include Cp present either in a neighboring $FeCp_2$ molecule (2) or in solution as the monomeric C_5H_6, but do not include the dimeric $C_{10}H_{12}$ (3).

The present study is a continuation of previous work, and is intended to investigate the extent to which the radioactive $\cdot CpFe(CO)_2$ radical is found in neutron-irradiated $[CpFe(CO)_2]_2$, and to determine the yields[1] of ^{59}Fe-$[CpFe(CO)_2]_2$ and other products in neutron-irradiated $CpFe(CO)_2I$. A further objective was to learn about the behavior of the radical monomer on thermal treatment: whether it decomposes on being heated

[3] $\cdot Cp^*Fe(CO)_2 \rightarrow \cdot Cp^*Fe(CO) + CO$

whether it reacts in one way or another to regenerate the dimer

[4a] $2\cdot Cp^*Fe(CO)_2 \rightarrow [Cp^*Fe(CO)_2]_2$

[4b] $\cdot Cp^*Fe(CO)_2 + [CpFe(CO)_2]_2 \rightarrow [Cp^*Fe(CO)_2]_2 + \cdot CpFe(CO)_2$

[4c] $\cdot Cp^*Fe(CO)_2 + CpFe(CO)_2I \rightarrow [CpFe(CO)_2]_2 + \cdot I$

or whether it may itself be built up by local reactions

[5] $\cdot Cp^*Fe(CO) + CO \rightarrow \cdot CpFe(CO)_2$

Experimental

The experiments were carried out essentially as has already been described (1–3). The dimeric $[CpFe(CO)_2]_2$ was obtained from Atomergic Chemicals Co. and was repurified by crystallization from pentane. The $CpFe(CO)_2I$ was prepared from the dimer by treatment with a stoichiometric quantity of iodine in chloroform solution (6). After removal of the chloroform, the compound was purified by extraction and crystallization from boiling pentane. The i.r. spectrum and mass spectrum showed the compound to be free of impurities. Targets for neutron irradiation were either (*a*) crystalline $[CpFe(CO)_2]_2$, or (*b*) crystalline $[CpFe(CO)_2]I$, or (*c*) ~30 mg $FeCp_2$ + 500λ $Fe(CO)_5$ + 250λ benzene (prepared as described earlier (2)), or (*d*) 500λ $Fe(CO)_5$ + 250λ benzene + 300λ monomeric cyclopentadiene (prepared as described earlier (3)). These samples, after being degassed *in vacuo*, were sealed in quartz vials under vacuum. Neutron irradiations were done in the FR-2 reactor in Karlsruhe, in the Rohrpost position at a thermal neutron flux of 9×10^{13} cm^{-2} s^{-1} or in the thermal column at a flux of 3×10^{11} cm^{-2} s^{-1}.

Chemical separations following neutron irradiation involved the use of $FeCp_2$, $Fe(CO)_5$, and $[CpFe(CO)_2]I$ (or $[CpFe(CO)_2]_2$) as carriers. The irradiated targets along with the solid carriers were dissolved in a mixture of 0.1 ml petroleum ether and 2.0 ml $CHCl_3$. $Fe(CO)_5$ was added immediately. After dissolution, the solution was transferred to a silica gel column, and the compounds eluted initially with petroleum ether and subsequently with a 1:1 mixture of pentane and diethyl ether. The quantities used were usually about 30 mg $[CpFe(CO)_2]_2$ (or $[CpFe(CO)_2I$) as target, 15 mg $FeCp_2$, 20 mg $CpFe(CO)_2I$, and 30λ $Fe(CO)_5$. Radioactivity measurements were made by counting the γ radiation of ^{59}Fe using a well-type NaI scintillation counter.

Some further experiments have been done to check the extent of formation of $\cdot Cp^*Fe(CO)_2$ and $[Cp^*Fe(CO)_2]_2$ from their separate components; that is, in neutron-irradiated benzene solutions of $FeCp_2$ and $Fe(CO)_5$ and of $Fe(CO)_5$ with monomeric cyclopentadiene (Cp_1).

Results and Discussion

$[CpFe(CO)_2]_2$ Irradiations

The experiments showed that a considerable radioactivity accompanied the $CpFe(CO)_2I$ carrier, and is presumably in the same chemical form as the carrier molecule. This fact, along with the observation that the data were internally quite consistent, leads us to believe that the $CpFe(CO)_2I$ molecule is acting efficiently as a scavenging carrier for the $\cdot CpFe(CO)_2$ radical, according to the exchange reaction

[6] $CpFe(CO)_2I + \cdot Cp^*Fe(CO)_2 \rightleftarrows Cp^*Fe(CO)_2I + \cdot CpFe(CO)_2$

where the asterisk designates the radioactive atom. This same type of exchange scavenging has been used successfully in several other cases to convert trapped radicals into chemically stable species. Thus, the radioactive species $\cdot Mn(CO)_5$, $\cdot Mn(CO)_4$, $\cdot Tc(CO)_5$, and $\cdot Re(CO)_5$ have been detected and their yields measured in this way (4, 7–9). While the occurrence of this scavenging reaction does not prove conclusively that the scavenged species is a free radical, it seems quite likely to be so, and has been independently confirmed in at least one instance (10). It is probable, then, that the radioactive iron atoms are present in the solid in reasonable yield as the $\cdot CpFe(CO)_2$ radical.

The results of neutron bombardment of $[CpFe(CO)_2]_2$ are given in Table 1. The lack of

[1]Note that the "yields" referred to in this paper are radiochemical yields. The chemical yields will, of course, be extremely small. An asterisk will be used to indicate that the following atom is radioactive, and does not imply chemical excitation.

TABLE 1. Radiochemical yields of $\cdot CpFe(CO)_2$ from neutron irradiation of $[CpFe(CO)_2]_2$, as a function of irradiation time and thermal annealing. Irradiations were done at −78 °C. The data represent some 85 separate determinations

Irradiation time (min)	Yield (%)	Annealing Temperature (°C)	Annealing Time (min)	Yield (%)
1	7.2	45	15	6.9
2	7.7	55	15	6.7
3	7.4	60	15	6.7
4	7.3	65	15	7.0
5	6.8	75	5	7.5
6	7.8	75	10	6.5
7	8.0	75	15	6.6
8	7.1			7.5
9	7.9			
10	6.5			

influence of the irradiation time shows the absence of γ-radiation effects over these short times, and indicates that the presence of radiolytically-produced CO groups in the target compound is not important, either to the instantaneous reaction or to any subsequent thermal reaction. Experiments done with the neutron irradiation conducted at reactor temperature (about 55°) gave the same value for the yield as those done at −78°, indicating that slow thermal annealing reactions during the irradiation are not important. Thermal annealing at temperatures up to 75° is seen to have little effect. The main reactions, then, seem not to depend on the ambient temperature. It is interesting to note that this behavior indicates that the radical $\cdot CpFe(CO)_2$ is reasonably stable in the target matrix, and contrasts with the abrupt decrease in yield of $\cdot *Mn(CO)_5$ in neutron-irradiated $Mn_2(CO)_{10}$ under similar treatment (4).

It was concluded earlier (1) that the annealing reactions in $[CpFe(CO)_2]_2$ were due to the migration of CO groups rather than Cp groups. It seems that a parallel annealing reaction

[7] $$\cdot CpFe(CO) + CO \rightarrow \cdot CpFe(CO)_2$$

does not occur in this matrix unless it is able to proceed rapidly below −78°.

Thermal recombination of the $\cdot Cp^*Fe(CO)_2$ groups to reform the dimer, as in reactions 4*a* and *b*, ought to appear as a decrease in the yield of $Cp^*Fe(CO)_2I$, corresponding to the increase in the yield of $[CpFe(CO)_2]_2$. This latter amounts (1) to some 4.1% of the total ^{59}Fe (16.0% at 25°, 20.1% at 75°). Such a decrease could scarcely be concealed in the present data, and it is concluded that reactions 4*a* and *b* are not prominent in the thermal annealing of this target compound if, indeed, they occur at all.

In a few experiments all of the carriers were collected, purified, and measured. The yield values found in these experiments were in good agreement with those found previously (1) with the exception of $*Fe(CO)_5$, which was 0.62% compared with the previous value of 2.5%. We do not understand this discrepancy, but feel that it may be some chemical artifact, so that the previous value should be regarded as the more reliable value.

$CpFe(CO)_2I$ Irradiations

Table 2 gives the result of neutron irradiation of the "monomeric" $CpFe(CO)_2I$ with subsequent thermal treatment. It is seen that, although the data are somewhat scattered, the nature of the results is unambiguous. No pronounced thermal effect is seen, except for $*Fe(CO)_5$, which increases steadily from 2.6 to 4.2% as the annealing temperature is increased from room temperature to 75°. This behavior is closely similar to that observed for $*Fe(CO)_5$ produced by neutron bombardment of the dimeric $[CpFe(CO)_2]_2$ (1). The same interpretation seems applicable here, namely, that fragments $*Fe(CO)_x$ react progressively with available CO groups to produce the final product. These groups could be either nearby labile bound ligands or fragments of nearby molecules destroyed during the nuclear event.

The ferrocene yield of roughly 0.7% is, as before, essentially unaffected by thermal treatment of up to 15 min at 75°. Again, the earlier interpretation is applicable; that the Fe—Cp bonds are formed in hot reactions rather than by thermal, diffusive processes. The fact that the radio-ferrocene yield in the monomer is just half that in the dimer may perhaps signify that intramolecular reactions are favored over intermolecular ones, but there is no other evidence to support this speculation.

The dimeric $[CpFe(CO)_2]_2$ is formed in low yield which is not increased by thermal treatment. This fact confirms the conclusion described above, that the $\cdot CpFe(CO)_2$ radicals do not react to form the dimer, and shows also that the exchange reaction 4*c* does not occur. This preponderance of reaction 6 over 4*c* is exactly

Can. J. Chem. Downloaded from www.nrcresearchpress.com by 210.87.254.5 on 09/05/12
For personal use only.

TABLE 2. Radiochemical yields from neutron irradiation of $CpFe(CO)_2I$ at $-78\,^{\circ}C$[a]

Annealing temperature (°C)	Radiochemical yields			
	$\cdot CpFe(CO)_2$	$[CpFe(CO)_2]_2$	$Fe(CO)_5$	$FeCp_2$
~22	14.5	2.7	2.6	0.63
45	15.0	1.8	3.6	0.71
55	14.7	2.2	3.6	0.64
65	15.4	2.3	3.7	0.60
75	16.8	2.7	4.2	0.69

[a]Each value is the average from at least four separate determinations.

TABLE 3. Radiochemical yields from the given mixed targets

Target[a]	Product compound	Yield (%)[b]	
		25 °C	−78 °C
30 mg $FeCp_2$	$*FeCp_2$	0.25	0.62[a]
+0.50 ml $Fe(CO)_5$		5.6[c]	14[c]
+0.25 ml C_6H_6	$[Cp*Fe(CO)_2]_2$	1.57	0.25
	$[Cp*Fe(CO)_2]I$	0.58	0.58
0.30 ml C_5H_6	$*FeCp_2$	1.20	0.48
+0.50 ml $Fe(CO)_5$	$[Cp*Fe(CO)_2]_2$	40.4	0.49
+0.25 ml C_6H_6	$[Cp*Fe(CO)_2]I$	11.4	0.40

[a]Irradiation times were: target no. 1, 4 h; target no. 2, 24 h at 25 °C or 16 h at −78 °C.
[b]Yields are calculated with reference to the total ^{59}Fe radioactivity, except as noted.
[c]Yield with reference to the ^{59}Fe radioactivity from $FeCp_2$ only.

parallel to the behavior of $\cdot Mn(CO)_5$ (7)

[8] $\cdot *Mn(CO)_5 + IMn(CO)_5 \rightarrow I*Mn(CO)_5 + \cdot Mn(CO)_5$
$\cdot *Mn(CO)_5 + IMn(CO)_5 \not\rightarrow *Mn_2(CO)_{10} + \cdot I$

The dimer which is observed must presumably be found by an epithermal reaction, although again this must be regarded as conjecture.

The high yield of the parent compound, $Cp*Fe(CO)_2I$, which increases slightly on thermal annealing at 75°, is approximately the same as the parent yield in the $[CpFe(CO)_2]_2$ (n,γ) reaction (1). As in the earlier case, it is not likely that such a complex structure would be re-formed through hot-zone recombination, and it seems more likely that the origin of the high yield is through preservation of the essential structure of the molecule through the nuclear transition and de-excitation.

$Fe(CO)_5$ Irradiations

The results of iron carbonyl irradiations in solution with either $FeCp_2$ or Cp_I are given in Table 3. The data are somewhat difficult to compare quantitatively, but some interesting observations may be made. We note that the reference used for the experiments in Table 3 is the total ^{59}Fe activity of the target irrespective of the chemical form of the iron in the target. When this initial form is taken into account, the yield value of 0.62% for the $^{59}FeCp_2$ at −78° in Table 3 becomes 14.2% of the ^{59}Fe produced from ferrocene in the target, and is consistent with an observation made previously (2) that the $FeCp_2$ seemed to have segregated during the freezing, and thus gives yields characteristic of the pure crystalline ferrocene: 12% (11), 14.6% (12). It is also noteworthy that small but significant yields of both the monomeric $\cdot Cp*Fe(CO)_2$ and the dimeric $[Cp*Fe(CO)_2]_2$ are found.

In the presence of monomeric cyclopentadiene, all the expected compounds are found at low temperatures, albeit in very low yields. At reactor temperatures (~25°) the yields of the $Cp*Fe(CO)_2I$ and $[Cp*Fe(CO)_2]_2$ are considerably higher than can be accounted for by any hot reaction, and clearly these high yields must be the result of some radiolytic reaction in the liquids.

It is seen that, although the more complex molecules can, in fact, be synthesized from the simpler components (especially in the liquid state, presumably by radiolysis) large yields are

Can. J. Chem. Downloaded from www.nrcresearchpress.com by 210.87.254.5 on 09/05/12
For personal use only.

obtained in the solid state only when the target molecule is itself one of the complex molecules. The formation of $[CpFe(CO)_2]^{\cdot}$ in $[CpFe(CO)_2]_2$ gives much larger yield than the formation of $[CpFe(CO)_2]_2$ from $[CpFe(CO)_2]I$ even though the parent yields are very similar.

This supports the view that in those 15–16% of the events leading to formation of the radioactive parent in each case, the essential structure is preserved through the nuclear transformation, rather than reconstituted subsequently.

The occurrence of mild damage to the individual molecule would be consistent with the reasonably high yield of the monomer from dimer targets. Formation of dimer from monomer targets, on the other hand, requires the disruption to be more extensive, and extend at least to the next molecule. The probability of such selective intermolecular excitation is evidently lower than for intramolecular reaction.

The fact that the yields of parent compound in the monomer and dimer targets are so similar suggests that the dissipation of nuclear energy in these events does not involve distribution kinetic energy of recoil among available degrees of vibrational freedom, since the one molecule has far more vibrational modes than the other.

The formation of the smaller molecules, $FeCp_2$ and $Fe(CO)_5$, clearly involves yet greater damage to the molecule. Most simply, the initial reactive intermediates must be *FeCp and $*Fe(CO)_2$, respectively. In both cases further ligands must be available by virtue of excitation of or damage to adjacent molecules. There is no evidence of thermal influences on the $FeCp_2$ yield, so the addition of a second Cp must be a fast, hot reaction involving an adjacent molecule in the monomer targets, but possibly the other end of the same molecule in the case of dimer targets. This latter seems to be supported by the somewhat higher yields of $*FeCp_2$ from the dimer targets. In both targets thermal annealing gives an increase in the yield of $*Fe(CO)_5$. This is clear evidence of the occurrence of reaction, as in reaction 1. The fact that even at $-78°$ without thermal treatment a significant yield of $*Fe(CO)_5$ is observed shows that some of the molecules reach their final configuration by fast, hot reaction with adjacent excited or damaged molecules. In the case of monomer targets, this requires two disrupted adjacent molecules in addition to the target molecule.

The thermal annealing effects on the two complex molecules are interesting in that increased yields are found in both cases for the target compound only. It has been argued earlier (1) and supported here that there seem to be available and reactive CO groups but not Cp groups. Thus, the CO transfer reactions between similar molecules occur

$$[9]\quad Cp^*Fe(CO) + CpFe(CO)_2I \rightarrow Cp^*Fe(CO)_2 + CpFe(CO)I$$

$$[10]\quad Cp_2^*Fe_2(CO)_3 + [CpFe(CO)_2]_2 \rightarrow [Cp^*Fe(CO)_2]_2 + Cp_2Fe_2(CO)_3$$

while the cross reactions

$$[11]\quad Cp^*Fe(CO) + [CpFe(CO)_2]_2 \not\rightarrow Cp^*Fe(CO)_2 + Cp_2Fe_2(CO)_3$$

$$[12]\quad Cp_2^*Fe_2(CO)_3 + CpFe(CO)_2I \not\rightarrow [Cp^*Fe(CO)_2]_2 + CpFe(CO)I$$

evidently do not occur. The reason for this is not at present obvious. Since $\cdot Cp^*Fe(CO)_2$ and $Cp^*Fe(CO)_2I$ are chemically indistinguishable in our procedure, nothing can be implied about iodine transfer in reaction 9.

Much has been written about the occurrence of "hot zones" in reactions such as these, and estimates of size, shape, and duration have been published. To date there is little agreement, and vigorous bodies of published and unpublished opinion both for and against hot zones. It must be admitted that the opinion of the present authors has substantially altered (*cf.* ref. 5) in the face of the evidence of the past few years.

If the results of the present work and its immediate antecedents are being correctly interpreted, the "hot zone" need not contain more than two or three molecules including the primary target molecule. The amount of kinetic energy deposited in this volume is evidently small and in many cases leads to no effective disruption of the target molecule. Although the quantitative data are slightly different for the Cp–Mn–CO series of compounds, the principal conclusions above apply unaltered: that the complex molecules are preserved rather than reformed, and that formation of other molecules need not involve more than an additional one or two adjacent molecules of the matrix.

Recent work (13) involving both (n,γ) recoils on manganese and (n,p) recoils on iron, both producing high energy ^{56}Mn in $[CpFe(CO)_2]_2$

Can. J. Chem. Downloaded from www.nrcresearchpress.com by 210.87.254.5 on 09/05/12
For personal use only.

targets show these high energy recoils to be ineffective in giving molecular ^{56}Mn products.

The question of why there is an evident preference for formation of metal carbonyls rather than π-ring–metal sandwich compounds as side products remains unanswered. Whether it involves a selective bond breaking or a selective bond reformation is not yet clear.

The authors wish to express their gratitude to Professor F. Baumgärtner for his continued interest and support, and to Mrs. E. Rauch for experimental assistance.

1. W. KANELLAKOPULOS-DROSSOPULOS and D. R. WILES. Can. J. Chem. **49**, 2977 (1971).
2. W. KANELLAKOPULOS-DROSSOPULOS and D. R. WILES. Radiochem. Acta, **16**, 179 (1971).
3. W. KANELLAKOPULOS-DROSSOPULOS and D. R. WILES. Can. J. Chem. **51**, 215 (1973).
4. I. G. DEJONG, S. C. SRINIVASAN, and D. R. WILES. Can. J. Chem. **47**, 1327 (1969).
5. S. R. NARAYAN and D. R. WILES. Can. J. Chem. **47**, 1019 (1969).
6. T. S. PIPER, F. A. COTTON, and G. WILKINSON. J. Inorg. Nucl. Chem. **3**, 104 (1956); **1**, 165 (1955).
7. I. G. DEJONG and D. R. WILES. Can. J. Chem. **50**, 961 (1972).
8. I. G. DEJONG and D. R. WILES. Inorg. Chem. **12**, 2519 (1973).
9. I. WEBBER. Unpublished results.
10. A. WOJCICKI. Personal communication; S. A. Hallock and A. Wojcicki. J. Organomet. Chem. **54**, C27 (1973).
11. N. SUTIN and R. W. DODSON. J. Inorg. Nucl. Chem. **6**, 91 (1958).
12. M. HILLMAN and A. J. WEISS. Unpublished results.
13. D. R. WILES. To be published.

Can. J. Chem. Downloaded from www.nrcresearchpress.com by 210.87.254.5 on 09/05/12
For personal use only.

A Nuclear Magnetic Resonance Investigation of Molecular Motion in Solid *cis*-Diaquotetramminecobalt(III)sulfate

B. A. DUNELL, J. F. NATTRASS, AND S. E. ULRICH

Chemistry Department, University of British Columbia, Vancouver, British Columbia V6T 1W5

Received September 6, 1973

The second moment and spin lattice relaxation times have been obtained for *cis*-diaquotetramminecobalt(III)sulfate between 77 and 310 °K. The results suggest that one of the ammine ligands is unique, reorienting more slowly at a given temperature than the others. Both water ligands undergo C_2-jumps. Although whole ion rotation does not occur libration does, and the second moment is interpreted in terms of such a torsional motion.

On a évalué pour le composé *cis*-diaquotétramminecobalt(III)-sulfate, le moment secondaire et les temps de relaxation spin-reseau entre 77 et 310 °K. Les résultats montrent qu'un seul des coordinats "ammine" peut se réorienter plus lentement que les autres à une température donnée. Les deux coordinats, H_2O subissent des transitions C_2. Même si la rotation entière de l'ion ne se produit pas, un balancement de ce dernier peut se produire; on interprète alors le moment secondaire en fonction d'un tel mouvement de torsion.

[Traduit par le journal]

Can. J. Chem., **52**, 900 (1974)

Can. J. Chem. Downloaded from www.nrcresearchpress.com by 210.87.254.5 on 09/05/12
For personal use only.

In previous studies of molecular motion (1–3) in cobalt ammine complexes, two types of motion were observed between 77 and 400 °K. In most complexes studied the ammine groups were reorienting about their Co—N axes at not less than 10^5 Hz even at 77 °K, and reorientation of the whole complex ion was observed for the hexammine and *trans*-tetrammine complexes above 250 °K. In this work we have studied the ammine group and the water group motions in *cis*-diaquotetramminecobalt(III)sulfate using continuous wave and pulsed n.m.r. techniques. We wish to compare our results for the reorientation of the water ligands with those obtained for gypsum by Holcomb and Pedersen (4).

Experimental

cis-$[Co(NH_3)_4(H_2O)_2]_2[SO_4]_3$ was prepared according to Glemser (5). The samples were evacuated for 48 h to insure removal of water of hydration and promote desorption of oxygen.

Proton continuous wave spectra were obtained at 16 MHz using a spectrometer described elsewhere (6). T_1 values were obtained at 30 MHz as described previously (7). The calculated points shown in Fig. 2 were computed using a Non-Linear Least Squares program (BMD) written by Paul Sampson at the UCLA Health Sciences Computing Facility. The observed T_1 was assumed to be the sum of two separate, and uncorrelated, relaxation times, that is, $(T_{1\,obs})^{-1} = (T_{1A})^{-1} + (T_{1B})^{-1}$. Each T_1 was described by the Bloembergen, Purcell, Pound (B.P.P.) expression (8). The calculated curve was fit to the experimental curve by an iterative procedure where there were three variable parameters in each B.P.P. term (6 total parameters). The variable parameters were $P(1)$, determined from the depth of the T_1 minimum, $P(2)$, the pre-exponential term in $A = A_0 \exp(E/RT)$ where $A = \omega_0\tau_c = 0.6158$ at the minimum and $A_0 = \omega_0\tau_c^0$, and $P(3)$, the activation energy, estimated from the slope of the experimental curves (9).

Results and Discussion

Second Moments

Figure 1 shows the experimental second moments for *cis*-$[Co(NH_3)_4(H_2O)_2]_2[SO_4]_3$. Table 1 lists the theoretical second moments for possible motions and shows for comparison experimental values at selected temperatures.

The rigid lattice second moments were calculated from the following parameters: r(H—H) in $NH_3 = 1.67 \pm 0.03$ Å, r(N—H) $= 1.02 \pm 0.02$ Å, r(Co—N) and r(Co—O) $= 1.97$Å, and r(H—H) in $H_2O = 1.58 \pm 0.05$ Å (1, 3, 10). All the bond

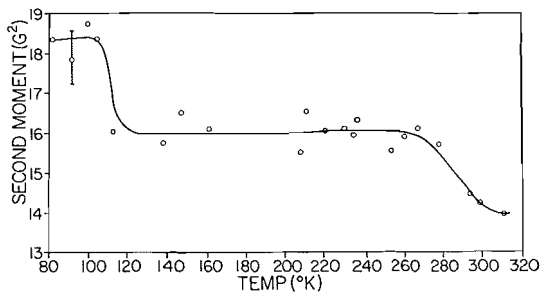

FIG. 1. Second moment (G^2) as a function of temperature.

TABLE 1. Theoretical and experimental second moments (in G^2)

Motion*			Second moment contribution				
			Theoretical				
NH_3	H_2O	Ion	Intra-ionic	Inter-ionic	Total	Experimental	Temperature (°K)
R	R	R	36.0 ± 3.7	4 ± 1	40.0 ± 4.7		
$3\times C_3$	R	R	20.7 ± 2.1	1.6 ± 0.8	22.3 ± 2.9		
$3\times C_3$	$1\times C_2$	R	18.4 ± 1.9	1.6 ± 0.8	20.0 ± 2.7		
$4\times C_3$	R	R	15.6 ± 1.7	1.6 ± 0.8	17.2 ± 2.5	18 ± 1	77
$4\times C_3$	$1\times C_2$	R	13.3 ± 1.5	1.6 ± 0.8	14.9 ± 2.3	16.0 ± 0.7	120–260
$4\times C_3$	$2\times C_2$	R	11.1 ± 1.0	1.6 ± 0.8	12.7 ± 1.8		

*R = rigid, $n \times C_3$ = number of ammine ligands rotating, $n \times C_2$ = number of water groups rotating.

angles at cobalt have been assumed to be 90°. Little error is introduced by assuming that all Co—N and Co—O bond lengths are the same and that all bond angles at cobalt are 90°, since the largest contributions to the second moment are intraligand. In this compound only the complex cation contributes significantly to the second moment. From previous arguments (3) we assume a value of 4 ± 1 G^2 for the rigid lattice interionic contribution to the second moment.

The experimental second moment below about 105 °K (18.3 ± 1 G^2) is consistent with either of the following motional processes: reorientation of all 4 ammine groups about their C_3 axes with rigid water molecules, or reorientation of 3 ammine groups and one water molecule freely rotating about its C_2 axis. The results of spin–lattice relaxation measurements indicate the situation is one in which all 4 ammine groups are reorienting. This point will be discussed further in the next section.

The plateau region of 16 G^2 above 130 °K does not clearly correspond to any of the calculated values shown in Table 1. We believe the observed value is consistent with C_2 jumps (180° flips) of the water molecules about their C_2 axes. Andrew and Brookeman (11) have shown there is no reduction in intra-group contribution to the second moment for 180° jumps about a C_2 axis normal to the internuclear vector. The only reduction occurs for the intergroup contribution. For this system, containing 16 spins, it would be very difficult to estimate the magnitude of this reduction. We cannot state with certainty whether the change in second moment between 105 and 125 °K represents the C_2 jumping motion of one or both water molecules. We tend to favor, however, the notion of simultaneous motion of both waters as it seems unlikely that the waters would be so dissimilar in environment that the motion of one water would be four orders of magnitude faster than that of the other water. Since the shapes of the second moment changes at 110 and 270 °K differ, we believe the changes represent different processes. The gradual change in second moment at 270 °K is consistent with that observed for torsional oscillation of the whole molecule in other cobalt complexes (12).

Spin–Lattice Relaxation

Figure 2 shows the spin–lattice relaxation curve for *cis*-$[Co(NH_3)_4(H_2O)_2]_2(SO_4)_3$. The two minima were resolved by the procedure outlined in the Experimental section. The values of best fit are: minimum 1 at 95 °K with a depth of 75 ± 4 ms and an activation energy of 904 ± 65 cal mol^{-1}; minimum 2 at 150 °K with a depth of 180 ± 16 ms and E_{act} = 3.32 ± 0.58 kcal mol^{-1}.

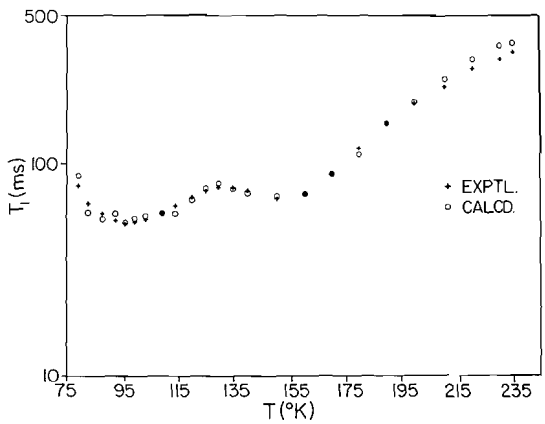

FIG. 2. T_1 (ms) as a function of temperature.

Can. J. Chem. Downloaded from www.nrcresearchpress.com by 210.87.254.5 on 09/05/12
For personal use only.

Can. J. Chem. Downloaded from www.nrcresearchpress.com by 210.87.254.5 on 09/05/12
For personal use only.

In the following discussion we refer to both reorientation and smooth rotation. In the case of smooth rotation the motion of the molecular group is such that all angular orientations must be considered in determining the time average behavior of the system and implies that some fraction of the molecules possess energy greater than the barrier height. In the case of reorientation or jumping about an axis it is assumed the molecular group spends an infinitesimally small time between equilibrium positions and hence has discrete angular descriptions. When the motional process involves potential barriers which are three-fold or greater the analytical description of the two processes is identical. In the case of a two-fold potential barrier the analytical expressions differ. For reorientation, or jumping, between two equilibrium positions separated by 180° about a C_2 axis normal to the internuclear vector there is no intra-group relaxation as there would be in the case of smooth rotation. Hence the only relaxation for a group undergoing a C_2 jump is intermolecular.

The predicted depth of a T_1 minimum arising solely from intra-group contribution for one ammine group reorienting would be 60 ms, while the corresponding quantity for both waters would be 63 ms on the assumption of a smooth rotation of the water molecules. However, if both water molecules are jumping about their C_2 axes the relaxation would be via inter-group mechanisms only and the predicted depth of minimum would be less than 540 ms. This value was arrived at from the work of Holcomb and Pedersen (4) for $CaSO_4 \cdot 2H_2O$. As the two waters in gypsum are coplanar Holcomb and Pedersen used only spectral densities at $2\omega_0$ to calculate a value for T_1. Since this constraint does not hold for our compound we must conclude the calculated value of $T_{1\ min}$ must be somewhat less than 540 ms in a system where the motion of 4 spins in 16 is relaxing the whole.

Since the value of T_1 at the higher temperature minimum is too large to correspond to any ammine group motion (and the second moment is too large for whole molecule motion), one must conclude that the minimum at 95 °K is due to the reorientation of one ammine group which is more hindered than the other three, for which $\omega_0\tau_c$ is already much less than one at 95 °K. The position of the minimum and the activation energy are consistent with ammine group motion observed in similar systems (9, 12). If the low temperature minimum is assigned to motion of one ammine group, then the change in second moment for this motion should occur at about 40 °K and thus the value of the second moment at 77 °K is consistent with four reorienting ammine groups and two rigid waters.

An activation energy of 4 kcal mol^{-1} obtained from the second moment transition at 115 °K is in agreement with the value of 3.3 kcal mol^{-1} obtained from the T_1 curve for the minimum at 150 °K. We can then conclude with reasonable assurance that the second moment change at 115 °K and the T_1 minimum at 150 °K can be accounted for by a C_2-jump reorientation of both water molecules. The 3.3 kcal mol^{-1} activation energy is consistent with a large hindering potential needed for jump motions.

This work has been supported by a grant-in-aid from the National Research Council of Canada.

1. G. R. MURRAY, JR. and J. S. WAUGH. J. Chem. Phys. **29**, 207 (1958).
2. S. S. DHARMATTI, V. SARASWATI, and R. VIJAYARAGHAVEN. Proc. Colloq. Ampere, XIII, 133 (1965).
3. S. E. ULRICH and B. A. DUNELL. Inorg. Nucl. Chem. Lett. **9**, 85 (1973).
4. D. F. HOLCOMB and B. PEDERSEN. J. Chem. Phys. **36**, 3270 (1962).
5. O. GLEMSER. Handbook of preparative inorganic chemistry. Vol. II. *Edited by* G. Brauer. Academic Press, New York. 1965.
6. B. A. DUNELL, C. A. FYFE, C. A. MCDOWELL, and J. RIPMEESTER. Trans. Faraday Soc. **65**, 1153 (1969).
7. S. E. ULRICH and B. A. DUNELL. J. Chem. Soc. Faraday Trans. II, **68**, 680 (1972).
8. N. BLOEMBERGEN, E. M. PURCELL, and R. V. POUND. Phys. Rev. **73**, 679 (1948).
9. B. A. DUNELL, M. D. PACHAL, and S. E. ULRICH. Can. J. Chem., **51**, 1107 (1973).
10. Interatomic distances. Chem. Soc. Spec. Publ. No. 11, 1958 and No. 18, 1965.
11. E. R. ANDREW and J. R. BROOKEMAN. J. Magn. Reson. **2**, 259 (1970).
12. S. E. ULRICH and B. A. DUNELL. J. Chem. Soc. Faraday Trans. II., **69**, 1609 (1973).

Model Calculations of Kinetic Isotope Effects in Nucleophilic Substitution Reactions

JAN BRON

Department of Chemistry, University of Natal, Durban, South Africa

Received August 2, 1973

The results of calculations indicate that a previously proposed model for the transition state in "borderline" substitution reactions can be generalized and, as a result, the observed differences in the carbon-13 and deuterium isotope effects of S_N1, S_N2, and "borderline" reactions rationalized. Although the conclusions may apply more generally, the standard reaction investigated is the solvolysis of benzyl bromide. The importance of resonance interaction with the phenyl ring, the significance of the product- or reactant-like character of the transition state, and the influence of the magnitude of force constants in determining isotope effects are examined. The temperature dependence of kinetic isotope effects in solvolysis is also investigated.

Les résultats des calculs indiquent que le modèle proposé antérieurement pour l'état de transition dans les réactions de substitutions "limites" peut être généralisé. En conséquence, les différences observées dans les effets isotopiques du carbone-13 et du deutérium dans les réactions S_N1, S_N2 et les réactions "limites" peuvent être rationalisées. La réaction standard que l'on a étudiée est la solvolyse du bromure de benzyle, bien que les conclusions peuvent être généralisées. On examine l'importance de l'interaction de résonance avec le cycle du phényle, du caractère de l'état de transition en fonction de sa ressemblance avec le produit initial ou final et l'influence de la grandeur des constantes de force lors de la détermination des effets isotopiques. On examine de plus la dépendance entre la température et les effets isotopiques sur la cinétique de solvolyse. [Traduit par le journal]

Can. J. Chem., **52**, 903 (1974)

Introduction

The mechanism of solvolytic reactions with characters between the two extremes of S_N1 and S_N2 (1), the "borderline" cases, is still not clearly resolved. Reaction schemes of varying complexity have been proposed (2–6).

The simplest mechanism involves a single transition state with a high degree of charge separation (7). The other more complex mechanisms for the borderline cases supposedly follow a mixture of two competing reaction paths. The first path leads via the traditional (1) S_N2 transition state to products while the second may involve several carbonium ion-like species (2, 5).

The kinetic isotope effect method has been used extensively to obtain information about the mechanism of nucleophilic substitution reactions (8–11), mainly because the effects may provide details about the bonding and geometry of the transition state (12). If the reaction path involves several transition states and intermediates the observed isotope effect may become a complex quantity which is difficult to interpret unambiguously. For example, if the formation of products is preceded by a rapid equilibrium, as in ion pair formation (2), the overall isotope effect is the product of an equilibrium and a kinetic isotope effect and unless one of the isotope effects can be calculated or measured separately, the overall isotope effect becomes a less useful parameter.

To explain experimental observations a model for the transition state may be proposed. An example is Ingold's (1) model for second order nucleophilic substitution reactions.

By use of well known computational methods (12–19) a suitable model of reasonable geometry and bonding (force field) should then reproduce the observed isotope effects (12–14). For large transition states it has been shown (12) that parts of the molecule which are not directly involved in the reaction may be ignored and the molecule "abbreviated".

As in essence proposed previously (20, 21), the S_N1 and S_N2 transition states can be represented by essentially the same model if the sum of the bond orders, n_t, between the incoming nucleophile, the leaving group, and the carbon atom at the seat of displacement is zero and unity respectively. Borderline mechanisms may then

Can. J. Chem. Downloaded from www.nrcresearchpress.com by 210.87.254.42 on 09/05/12
For personal use only.

Can. J. Chem. Downloaded from www.nrcresearchpress.com by 210.87.254.42 on 09/05/12
For personal use only.

TABLE 1. Definition of geometry, internal coordinates, and force field of initial and transition states in the solvolysis of benzyl bromide

State	Geometry*	Internal coordinates	Force field†
Initial state	$r_{12} = 1.10$	$S_1 = \Delta r_{12}$, $S_2 = \Delta r_{13}$,	$f_{11} = 4.40$
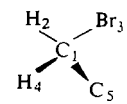	$r_{13} = 1.94$, $r_{14} = 1.10$,	$S_3 = \Delta r_{14}$, $S_4 = \Delta r_{15}$,	$f_{22} = 2.14$, $f_{33} = 4.40$
	$r_{15} = 1.52$	$S_5 = \Delta\alpha_{213}$, $S_6 = \Delta\alpha_{314}$	$f_{44} = 3.68$
	Tetrahedral structure	$S_7 = \Delta\alpha_{214}$, $S_8 = \Delta\alpha_{415}$	$f_{55} - f_{10,10} = 0.40$
		$S_9 = \Delta\alpha_{215}$, $S_{10} = \Delta\alpha_{315}$	
Transition state			
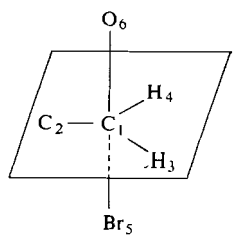	$r_{12} = 1.52 - 0.6 \log (1.6 - 0.6n_t)$	$S_1 = \Delta r_{12}$, $S_2 = \Delta r_{13}$	$f_{11} = 3.68(1.6 - 0.6n_t)$
	$r_{13} = r_{14} = 1.10$	$S_3 = \Delta r_{14}$, $S_4 = \Delta r_{15}$	$f_{22} = f_{33} = 4.40$
	$r_{15} = 1.94 - 0.6 \log n_1$	$S_5 = \Delta r_{16}$, $S_6 = \Delta\alpha_{213}$	$f_{44} = -2.14n_1$, $f_{55} = 5.72n_2$
	$r_{16} = 1.43 - 0.6 \log n_2$	$S_7 = \Delta\alpha_{214}$, $S_8 = \Delta\alpha_{314}$	$f_{45} = 4n_t - 2$
	$\alpha_{213} = \alpha_{314} = \alpha_{214} = 120°$	$S_9 = \Delta\alpha_{216}$, $S_{10} = \Delta\alpha_{316}$	$f_{66} - f_{88} = 0.50$
	$\alpha_{216} = \alpha_{416} = 90°$	$S_{11} = \Delta\alpha_{416}$, $S_{12} = \Delta\alpha_{215}$	$f_{99} - f_{11,11} = 0.283n_2$
	Trigonal bipyramidal structure	$S_{13} = \Delta\alpha_{315}$, $S_{14} = \Delta\alpha_{415}$	$f_{12,12} - f_{14,14} = 0.283n_1$

*Bond distances in Å; r_{IJ} is the distance between atom i and j; α_{IJk} is the angle defined by atoms i, j, and k.
†Units of stretching force constants are mdyn/Å, bending . mdyn Å/rad². The force constant f_{IJ} is defined by $(\partial^2 V/\partial S_i \partial S_j)_0$.

Can. J. Chem. Downloaded from www.nrcresearchpress.com by 210.87.254.42 on 09/05/12
For personal use only.

involve a transition state where n_t is between zero and unity and with the same planar configuration around the central carbon atom (1).

For this collective model to be acceptable it should at least be able to reproduce the observed trends in carbon-13 and α-deuterium isotope effects in nucleophilic substitution reactions. Therefore, by assigning a reasonable geometry and bonding which change continuously with changing bond orders, the model has been investigated in detail. It must be emphasized, however, that all discussions will be limited to reactions unlikely to involve unstable intermediates.

The Calculation of Carbon-13 and Deuterium Isotope Effects

Calculations based on a suitable model for the initial and transition states of kinetic isotope effects in nucleophilic substitution reactions should confirm the following observations concerning carbon-13 and deuterium isotope effects:

(*1*) Near room temperature the ^{13}C kinetic isotope effect, k_{12}/k_{13}, of typical S_N2 reactions is about 1.05, while nucleophilic displacement reactions exhibiting considerable carbonium ion character can have k_{12}/k_{13} less than unity (11).

(*2*) The value of k_{12}/k_{13} for S_N2 reactions decreases with increasing temperature and increases with increasing temperature for reactions believed to proceed through an S_N1 mechanism (11).

(*3*) Near room temperature the α-deuterium isotope effect, k_H/k_D, of typical S_N2 reactions is approximately 1.0, while k_H/k_D for S_N1 reactions is about 1.15 (8).

Furthermore, it is reasonable to assume (22) that the variation of bond lengths and force constants with changing bond order follow the relationships given by Johnston (23) and Pauling (24) and that the model representing the transition state should be a statistical average over all states available to the transition state (25).

An abbreviated model for the transition state in the solvolysis of benzyl bromide (11) that reproduces the above experimental observations and follows these bond order – force constant and bond order – bond length relationships is given in Table 1 together with that for the initial state. The bond lengths, internal coordinates, and force fields for these states are also included in Table 1. The phenyl group in the initial and transition states is represented by a single carbon atom, labelled C_5 and C_2 respectively, and the solvent molecule in the transition state by an oxygen atom (O_6). Sims *et al.* (27) proposed a similar transition state in which, however, the bond order around the carbon atom at the seat of displacement was kept constant.

In the transition state the bond order of the C_1—Br_5 bond is n_1, the bond order of the C_1—O_6 bond n_2 and the sum of n_1 and n_2 is n_t. In the calculations, n_t has been varied from 0 to 1 to give a series of transition states with varying degrees of carbonium ion character. If n_t is zero the central carbon atom has a full positive charge, which may be delocalized into the phenyl ring. The corresponding negative charge will then be on the leaving group (the bromide ion). Also, for values of n_t smaller than one, the central carbon atom can carry a fractional positive charge of $(1 - n_t)e^+$, which, similarly may be delocalized into the phenyl ring. If the percentage of delocalization is p, then the bond order of the C_1–C_5 bond in the transition state will be $(1 + p(1 - n_t)/100)$.

If the force constant of the single C—C bond is 3.68 mdyn/Å, then f_{11}, the stretching force constant of the C_1—C_5 bond in the transition state, will be $3.68(1 + p(1 - n_t)/100)$. The expression for f_{11} in Table 1 corresponds to p equals 60%.

The transition state in Table 1 with $n_t = 0$ is taken as a model for a limiting S_N1 process. The transition states with a value of n_t between 0 and 1 will correspond to processes with characters intermediate between pure S_N1 and S_N2 mechanisms.

The choice of internal coordinates deserves additional comment. A set of $3N - 6$ linearly independent internal coordinates is sufficient to describe the vibrational motion of the atoms in a molecule-fixed coordinate system (27). One must choose, however, the most significant set of internal coordinates (28, 29) and the best choice is not always easy. Although bond stretching coordinates never form a linearly dependent set, valence angle bending internal coordinates can easily form such a set, such as the non-linear valence angle bending coordinates in the initial state in Table 1 (29). Since calculations showed that k_H/k_D is strongly dependent upon the choice of bending coordinates while

Can. J. Chem. Downloaded from www.nrcresearchpress.com by 210.87.254.42 on 09/05/12
For personal use only.

k_{12}/k_{13} is unaffected, a redundancy of coordinates has been used to be sure that the most important coordinates were included. If there are i redundant coordinates, and the molecule is stable, $3N - 6$ non-zero frequencies will be obtained from the secular determinant and i zero ones. Therefore the redundancy is easily removed by neglecting the zero frequencies. For non-linear transition states 3N − 7 non-zero, real frequencies are obtained. The force field that fits best is that described in Table 1. The force field for the initial state is diagonal. Except for the interaction force constant $f_{45}(=f_{54})$ all off-diagonal **F** matrix elements for the transition state are also zero. All force constants of the single bonds have been determined by Badger's rule (23).

The theoretical expression for kinetic isotope effects [1], using transition state theory and statistical mechanics, is

$$[1]\quad \frac{k_1}{k_2} = \frac{\left[\left(\frac{M_2}{M_1}\right)^{\frac{3}{2}}\left(\frac{(I_A I_B I_C)_2}{(I_A I_B I_C)_1}\right)^{\frac{1}{2}}\prod_{i=1}^{3n-6}\left(\frac{\sinh(u_i/2)_1}{\sinh(u_i/2)_2}\right)\right]_{IS}}{\left[\left(\frac{M_2}{M_1}\right)^{\frac{3}{2}}\left(\frac{(I_A I_B I_C)_2}{(I_A I_B I_C)_1}\right)^{\frac{1}{2}}\prod_{j=1}^{3m-7}\left(\frac{\sinh(u_j/2)_1}{\sinh(u_j/2)_2}\right)\right]_{TS}}$$

In this expression the subscript 1 refers to the lighter isotope, while 2 refers to the heavier one. M_i is the molecular weight, I_x the principal moment of inertia, ω_i the normal frequency, n the number of atoms in the initial state (IS), m the number of atoms in the transition state (TS) and

$$u_i = (hc\omega_i)/(kT)$$

A computer program has been written to calculate the isotope effect. The normal frequencies ω_i have been evaluated from the matrix equation (29).

$$[2]\quad \mathbf{GFL} = \mathbf{L}\Lambda$$

The **G** matrix elements have been determined by use of the expression

$$[3]\quad \mathbf{G} = \mathbf{BM}^{-1}\mathbf{B}^t$$

The **B** matrix elements have been evaluated using the method of Pariseau *et al.* (30). Although there are other ways (12, 31, 32) to obtain a zero or an imaginary frequency for the transition state, the force field in Table 1 was found the most satisfactory.

Results and Discussion

The primary purpose of these model calculations is to investigate a collective representation of the transition state in nucleophilic substitution reactions in the condensed phase for which there is no direct experimental evidence for unstable intermediates. Therefore, it is suggested, that the model should not be considered to represent the transition state of benzyl bromide in nucleophilic substitution reactions only, but should be interpreted similarly to Fry's (21) "symbolic model". The force constants in the initial state and transition state vary from system to system and are not necessarily equal to those in Table 1. However, by a systematic study of the importance of a force constant or a set of force constants some insight can be gained into their role in the determination of the magnitude of kinetic isotope effects.

Figure 1 shows the dependence of k_{12}/k_{13} and k_H/k_D on n_t, the sum of the bond orders of the C—O and C—Br bonds. For $n_t = 0$, S_N1, the carbon-13 isotope effect is about 0.98 and the deuterium isotope effect 1.18, while for $n_t = 1$, S_N2, the carbon-13 isotope effect is 1.05 and the deuterium isotope effect 1.00. The temperature is 300 °K and n_1 is equal to $0.4n_t$. The results are in agreement with experimental trends (8, 11) and it is particularly worth noting that the relationship between isotope effect and n_t is almost linear.

Calculations showed that k_{12}/k_{13} may be quite dependent upon the relative magnitudes of n_1 and n_2, or, phrased differently, whether the transition state is reactant- or product-like. Figure 2 shows the dependence to be greatest

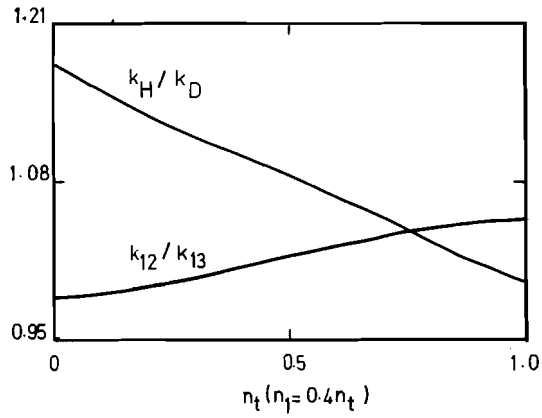

FIG. 1. The dependence of k_{12}/k_{13} and k_H/k_D on n_t, with n_1 equal to $0.4n_t$.

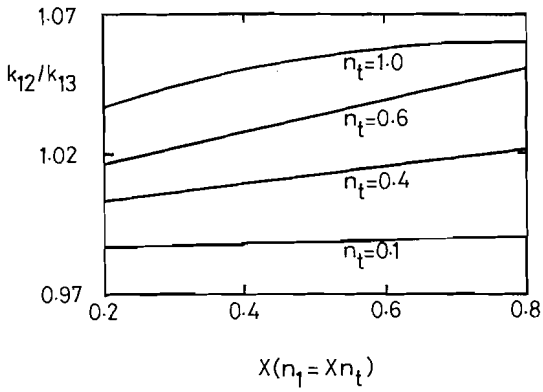

FIG. 2. k_{12}/k_{13} as a function of the product or reactant like character of the transition state ($n_1 + n_2 = n_t$).

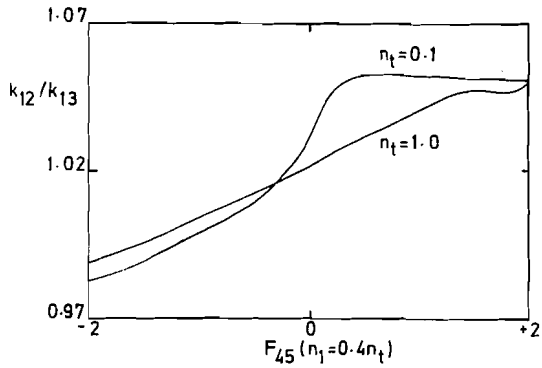

FIG. 3. k_{12}/k_{13} *vs.* the interaction force constant, f_{45}, of f_{44} and f_{55}.

for $n_t = 0.6$ and smallest for $n_t = 0.1$. The decrease in importance of the product- or reactant-like character of the transition state with decreasing n_t follows from the force constant relationships used to define the force field of the transition state and the first quantum correction (12, 23). However, the maximum at $n_t = 0.6$ is not readily explained without ambiguity and deserves further investigation.

The plots in Fig. 2 are linear for $n_t < 0.6$ and become curved for larger values of n_t. Since curvature is largest for $n_t = 1$, only this curve has been shown to represent $n_t > 0.6$. Contrary to the results reported by Sims *et al.* (26) the curve corresponding to $n_t = 1$ does not show a maximum. The reasons for this difference are not clear because the required details of their calculations have not been included in their paper. The deuterium isotope effect is insensitive towards relative changes in n_1 and n_2; even for $n_t = 0.6$ the effect changes by less than 0.01 if n_1 is varied from 0.2 to 0.8. This result is not surprising since it can be readily shown by means of the first quantum correction, in terms of **F** and **G** matrix elements and the high temperature limit (12), that the deuterium isotope effect should be almost insensitive towards changes in n_1 for a particular value of n_t and for the investigated model for the transition state.

Figure 3 shows the dependence of k_{12}/k_{13} upon f_{45}, the interaction force constant of the internal coordinates of the transition state that are defined by the change in the C—O and the C—Br bonds. A clear trend can be noted. As f_{45} increases, k_{12}/k_{13} increases for both $n_t = 0.1$ and $n_t = 1.0$. If f_{45} is equal to zero, however, the force field predicts that S_N1 and S_N2 reactions exhibit nearly equal isotope effects, which, by changing the force constants, cannot be made to agree with experimental ^{13}C and ^{2}H isotope effects at the same time. Therefore f_{45} may play an important role in determining the magnitude of kinetic isotope effects. The deuterium isotope effect is remarkably insensitive towards f_{45}, and indeed in all calculations it has been found that k_H/k_D, as a rule, is almost exclusively dependent upon all bending force constants ($f_{99} - f_{14,14}$) and shows little dependence upon f_{44}, f_{55}, and f_{45}. The situation is entirely different for k_{12}/k_{13} which shows a strong dependence upon the reaction coordinate, defined by f_{44}, f_{55}, and f_{45}, and a smaller dependence upon the bending and stretching force constants. The calculations suggest that, experimentally, k_H/k_D gives information about changes in the bending force constants with respect to some standard reaction, which is in agreement with the findings of other workers (34), while k_{12}/k_{13} supplies details about the reaction coordinate defined above.

It has been proposed (11) that overlap of a vacant p orbital with the phenyl ring in the transition states in solvolytic reactions of benzyl halides may explain the large difference in k_{12}/k_{13} for S_N1 and S_N2 reactions. These model calculations suggest that f_{11} (C—C bond) is much less important than previously suspected (21). In fact k_{12}/k_{13} decreases linearly by less than 0.02 ($n_t = 0.1$; $n_1 = 0.04$) when f_{11} is varied from 3 to 7 mdyn/Å, while the deuterium isotope effect is insensitive towards changes in f_{11}.

It was found, in general, that the explanation of isotope effects in terms of a single force constant or set of equivalent force constants, like $f_{99} - f_{14,14}$ and $f_{66} - f_{88}$, may not be sufficient.

Can. J. Chem. Downloaded from www.nrcresearchpress.com by 210.87.254.42 on 09/05/12
For personal use only.

Can. J. Chem. Downloaded from www.nrcresearchpress.com by 210.87.254.42 on 09/05/12
For personal use only.

To explain an isotope effect a comparison of force constants in the transition state with force constants in the initial state is not possible, because the transition state does not generally contain the same number of atoms. Therefore, except in unimolecular decompositions, the transition state does not have the same number of internal coordinates and force constants (29).

It has been suggested (11) that the temperature dependence of k_{12}/k_{13} may be used to distinguish between S_N2 reactions and reactions that proceed through or approach a limiting S_N1 mechanism. The present calculations clearly support this notion. Figure 4 shows a non-linear increase for k_{12}/k_{13} with increasing temperature when n_t is equal to 0.1. For $n_t = 1$ the trend is in the opposite direction since k_{12}/k_{13} decreases with increasing temperature. For $n_t = 0.3$, k_{12}/k_{13} only changes from 1.000 to 1.003 by raising the temperature from 200 to 500 °K. An inversion of the temperature dependence takes place if n_t is about 0.3. At this value for n_t, k_{12}/k_{13} is almost temperature independent.

The temperature dependence of the calculated deuterium isotope effect is shown in Fig. 5 for $n_t = 0.1$. Clearly the deuterium isotope effect decreases rapidly with increasing temperature. For $n_t = 1$, however k_H/k_D is 1.002 at 200 and 0.998 at 500 °K. The temperature dependence of the α-deuterium isotope effect suggests that it may be ambiguous to deduce from a single measurement of k_H/k_D at a particular temperature the detailed mechanism of a given reaction without measuring the temperature dependence of the isotope effect. This, of course, also holds for the carbon-13 isotope effects and for the isotopic method in general (31).

The calculations show that the replacement of

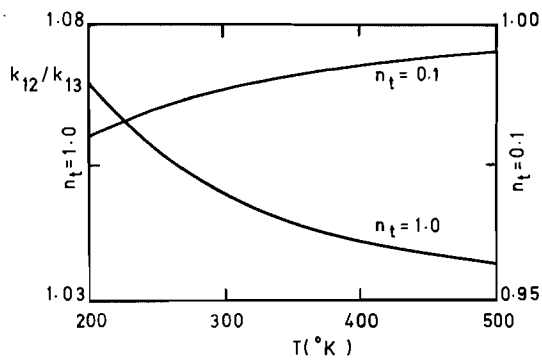

FIG. 4 The change of k_{12}/k_{13} with temperature.

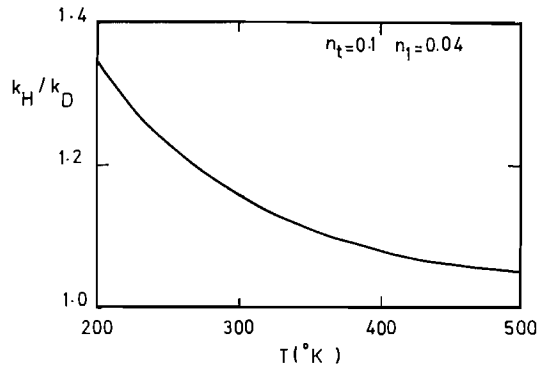

FIG. 5. k_H/k_D as a function of temperature.

Br by Cl in the initial and transition states increases k_{12}/k_{13} by 0.009 for $n_t = 0.1$ and 0.006 for $n_t = 1$. The deuterium isotope effect decreases by less than 0.002 for all values of n_t. The geometry and force field are basically the same in both cases with only the relevant bond length and force constant changed. The bond order n_1 is, again, 0.4 n_t and the temperature 300 °K. This result suggests that for solvolytic reactions k_{12}/k_{13} and k_H/k_D may not be particularly sensitive to the halide leaving group, if the geometry and force field of the initial and transition states (or reaction mechanism) are basically the same. The effect of the leaving group on the magnitude of α-deuterium isotope effects for solvolytic reactions believed to have a limiting mechanism has been discussed by Shiner *et al.* (34).

1. C. K. INGOLD. Q. Rev. **11**, 1 (1957).
2. S. WINSTEIN and G. C. ROBINSON. J. Am. Chem. Soc. **80**, 169 (1958).
3. E. R. THORNTON. Solvolysis mechanism. The Ronald Press Company, New York. 1964.
4. R. A. SNEEN and J. W. LARSEN. J. Am. Chem. Soc. **91**, 362, 6031 (1969).
5. V. J. SHINER, JR. and R. D. FISHER. J. Am. Chem. Soc. **93**, 2553 (1971).
6. R. A. SNEEN, G. R. FELT, and W. C. DICKASON. J. Am. Chem. Soc. **95**, 638 (1973).
7. G. J. FRISONE and E. R. THORNTON. J. Am. Chem. Soc. **90**, 1211 (1968).
8. V. J. SHINER, JR., W. E. BUDDENBAUM, and G. LAMATY. J. Am. Chem. Soc. **90**, 418 (1968).
9. J. M. HARRIS, R. E. HALL, and P. v. R. SCHLEYER. J. Am. Chem. Soc. **93**, 2551 (1971).
10. B. L. MURR and M. F. DONNELLY. J. Am. Chem. Soc. **92**, 6688 (1970).
11. J. BRON and J. B. STOTHERS. Can. J. Chem. **47**, 2506 (1969) and papers cited therein.
12. M. WOLFSBERG and M. J. STERN. Pure Appl. Chem. **8**, 225 (1964).

13. J. BIGELEISEN and M. G. MAYER. J. Chem. Phys. **15**, 261 (1947).
14. A. V. WILLI. Z. Phys. Chem. Neue Folge. **66**, 317 (1969).
15. I. SAFARIK and O. P. STRAUSZ. J. Phys. Chem. **76**, 3613 (1972).
16. J. S. SHAPIRO and R. E. WESTON, JR. J. Phys. Chem. **76**, 1669 (1972).
17. M. E. SCHNEIDER and M. J. STERN. J. Am. Chem. Soc. **94**, 1517 (1972).
18. R. C. WILLIAMS and J. W. TAYLOR. J. Am. Chem. Soc. **95**, 1710 (1973).
19. F. J. TORRE, M. CZUCZAK, and E. U. MONSE. J. Chem. Phys. **58**, 1804 (1973).
20. G. J. FRISONE and E. R. THORNTON. J. Am. Chem. Soc. **90**, 1211 (1968).
21. A. FRY. Pure Appl. Chem. **8**, 409 (1964).
22. B. D. NEELY and H. CARMICHAEL. J. Phys. Chem. **77**, 307 (1973).
23. H. S. JOHNSTON. Gas phase reaction rate theory. Ronald Press Company, New York. 1966.
24. L. PAULING. J. Am. Chem. Soc. **69**, 542 (1947).
25. T. L. HILL. An introduction to statistical thermodynamics. Addison-Wesley Publishing Company, Inc., Reading, Massachusetts. 1960.
26. L. B. SIMS, A. FRY, L. T. NETHERTON, J. C. WILSON, K. D. REPPOND and S. W. CROOK. J. Am. Chem. Soc. **94**, 1364 (1972).
27. H. H. NIELSEN. Rev. Mod. Phys. **23**, 90 (1951).
28. J. C. DECIUS. J. Chem. Phys. **17**, 1315 (1949).
29. E. B. WILSON, J. C. DECIUS, and P. C. CROSS. Molecular vibrations. McGraw–Hill, Toronto. 1955.
30. M. A. PARISEAU, I. SUZUKI, and J. OVEREND. J. Chem. Phys. **42**, 2335 (1965).
31. P. C. VOGEL and M. J. STERN. J. Chem. Phys. **54**, 779 (1971).
32. W. J. KASS and P. E. YANKWICH. J. Phys. Chem. **73**, 3722 (1969).
33. M. WOLFSBERG and M. J. STERN. Pure Appl. Chem. **8**, 325 (1964).
34. V. J. SHINER, JR., M. W. RAPP, E. A. HALEVI, and M. WOLFSBERG. J. Am. Chem. Soc. **90**, 7171 (1968).

Can. J. Chem. Downloaded from www.nrcresearchpress.com by 210.87.254.42 on 09/05/12
For personal use only.

The Kinetic Activation Volumes for the Binding of Iodide to Cobalamin (Vitamin B_{12}) Studied on a High Pressure Laser Temperature Jump Apparatus[1]

BRIAN B. HASINOFF[2]

University Chemical Laboratory, University of Kent at Canterbury, Canterbury, Kent, England

Received August 7, 1973

The relaxation kinetics of the reaction of iodide with cobalamin (vitamin B_{12}) were studied on a high pressure laser temperature jump apparatus in aqueous solution at 25° and ionic strength 0.2 *M*. Analysis of the pressure dependence of the formation and dissociation rate constants gave their respective volumes of activation to be: $\Delta V_f^* = 5.5 \pm 0.8$ cm^3 mol^{-1} and $\Delta V_d^* = 11.5 \pm 1.6$ cm^3 mol^{-1}. The positive activation volume for formation of the complex, ΔV_f^*, after appropriate correction for the volume change due to formation of an outer sphere complex, is consistent with a dissociative type mechanism in which the metal ion – water bond is stretched in the activated complex.

Les relaxations cinétiques de la réaction d'iodure avec la cobalamine (vitamine B_{12}) ont été étudiées sur un appareil laser à haute pression à température discontinue en solution aqueuse à 25° et à une concentration ionique de 0.2 *M*. L'analyse de la dépendance de la pression suivant les constantes des vitesses de formation et de dissociation donne leur volume respectif d'activation : $\Delta V_f^* = 5.5 \pm 0.8$ cm^3 mol^{-1} et $\Delta V_d^* = 11.5 \pm 1.6$ cm^3 mol^{-1}. Le volume d'activation positif pour la formation du complexe ΔV_f^*, après correction appropriée pour le changement du volume dû a la formation d'un complexe de sphère externe, est conforme à un mécanisme type dissociant où la liaison l'ion du métal – eau est allongée dans le complexe activé. [Traduit par le journal]

Can. J. Chem., **52**, 910 (1974)

Introduction

The macrocyclic corrin compound confers unusual properties to the ligand substitution kinetics of the Co(III) derivative. For example, the second order rate constant for ligand substitution is about 10^7 faster on cobalamin (vitamin B_{12}) than on other simple Co(III) compounds (1). Previous work has measured the kinetics of the reaction of cobalamin with N_3^-, OCN^-, and SCN^- (2, 3) as well as more recently the kinetics and activation parameters for I^-, Br^-, $S_2O_3^{2-}$, HSO_3^-, and SO_3^{2-} (4, 5).

The benzimidazole side chain on cobalamin coordinates with the Co^{3+} in one of the axial positions preventing formation of 2:1 complexes with small ligands; this is often a complicating factor in studying the ligand substitution kinetics on other metal ion macrocyclic complexes such as porphyrins (1).

By measuring the influence of pressure on the rate constant of a reaction,

$$[1] \qquad (\partial \ln k/\partial P)_T = -\Delta V^*/RT$$

it is possible to obtain the activation volume, ΔV^*, the difference between the molar volume of the transition state and the ground state of the reactants. From ΔV^* inferences can be made about the mechanism of ligand substitution (6–8). Previous pressure studies on the kinetics of substitution on labile metal ions, including Ni^{2+}, Co^{2+}, Zn^{2+}, and Cu^{2+} (9, 10) with ligands including NH_3, PADA (pyridine-2-azodimethylaniline), and glycinate$^-$, gave activation volumes that were consistent with the generally accepted dissociative mechanism (11). That is, in the activated complex, ligand bound water dissociates from the metal ion.

Experimental

Materials

All reagents used, cobalamin (vitamine B_{12b}, cryst. puriss, Fluka A.G.), KNO_3 (Fisons AR), KI (Fisons Lab R, 99% min), and Napthol Green B (BDH Stains), were of highest purity available. All solutions were prepared with triply distilled water on a molar concentration scale. For the purposes of the pressure work, the rate and equilibrium constants are on a molality scale reduced to molarity at 1 bar (6–8); that is, no correction was made for the compression of the solvent. The total ionic strength was kept constant at 0.2 *M* by the addition of appropriate

[1]This work has been supported by the Science Research Council (Great Britain) by Research Grant B/SR/8667.

[2]Present address: Department of Physical Sciences, Notre Dame University of Nelson, Nelson, British Columbia.

Can. J. Chem. Downloaded from www.nrcresearchpress.com by 210.87.254.5 on 09/05/12
For personal use only.

Can. J. Chem. Downloaded from www.nrcresearchpress.com by 210.87.254.5 on 09/05/12
For personal use only.

amounts of KNO_3. Generally, kinetic relaxation experiments were conducted on solutions within 1 h of preparation.

Kinetic and Equilibrium Measurements

The high pressure laser temperature jump apparatus used in previous studies (9, 10) has been described in some detail (12). It is sufficient to say that the relaxation kinetics of I^- substitution on cobalamin were followed spectrophotometrically at 570 nm (13) on a Tektronix 549 storage oscilloscope. The ruby laser pulse was 90% complete in 500 μs and was much faster than the observed chemical relaxation.

The sample solution was contained in a cylindrical Pyrex spectrophotometric cell sealed by a KEL-F piston and a rubber O-ring (12).

The exponential traces, obtained upon perturbation of the equilibrium between cobalamin and I^-, were measured by a trace matching method to obtain τ^{-1}, the reciprocal relaxation time (12). The temperature of the stainless steel pressure vessel was maintained constant to within 0.1° and was such that the final temperature of the solution was 25.0° after the application of the temperature perturbation from the ruby laser.

All reaction solutions contained equal concentrations of the inert dye, Napthol Green B, to absorb the light energy from the laser pulse and produce a 4.2° temperature jump (12). The concentration of Napthol Green B, which was present at a very low concentration, was such that its absorbance at 694 nm, the wavelength at which the ruby laser emits light, was 1.14 cm^{-1}. Differential spectrophotometric measurements, conducted with a tandem cell arrangement in a thermostatted recording spectrophotometer (Perkin–Elmer 402), indicated that the spectra of Napthol Green B was not measurably affected by the presence of cobalamin, KI or KNO_3. Similarly, the spectra of cobalamin or its equilibrium with I^- was also not measurably affected by the presence of the dye absorber.

The concentration of cobalamin in all kinetic experiments was kept constant at 5.9×10^{-5} *M*; that of I^- was much larger, in the range 0.01 to 0.2 *M*. The measured p*H* of all solutions was 5.5 or slightly lower so that the concentration of the hydroxide complex of cobalamin was kinetically insignificant (4).

Equilibrium measurements for the reaction of cobalamin and I^- were conducted on the recording spectrophotometer thermostatted at 25.0° and at a wavelength of 560 nm in the manner described by Pratt and Thorp (13).

Results

The reaction of cobalamin (CBM) with I^- is given by

$$[2] \qquad \mathrm{CBM} + \mathrm{I}^- \underset{k_d}{\overset{k_f}{\rightleftharpoons}} \mathrm{CBM{-}I}$$

where k_f is a second order formation rate constant and k_d is a first order dissociation rate constant (2–5). The relaxation expression for reaction 2 is (4)

$$[3] \qquad \tau^{-1} = k_f([\mathrm{CBM}] + [\mathrm{I}^-]) + k_d$$

where [ ] represents an equilibrium concentration. However, under the conditions of this study, $[I^-] \gg [CBM]$ so that

$$[4] \qquad \tau^{-1} = k_f[\mathrm{I}^-] + k_d$$

Hence a plot of τ^{-1} *vs.* $[I^-]$ gives k_f as the slope and k_d as the intercept. Results, obtained at a series of constant pressures, are shown in Fig. 1; the straight lines are those calculated from weighted linear least squares analyses of eq. 4. The value of k_f is with its standard deviation $(2.6 \pm 0.2) \times 10^3\ M^{-1}\ s^{-1}$ at 1 bar, 25.0°, and ionic strength 0.2 *M*. This compares to the value of k_f previously determined of $1.4 \times 10^3\ M^{-1}\ s^{-1}$ at 1 bar, 25.5°, and ionic strength 0.5 *M*, which is in good agreement if allowance is made for the effect of ionic strength on the rate constant (4). Similarly, the value of k_d is $42 \pm 6\ s^{-1}$ which also compares well to the previously determined value of $35\ s^{-1}$ obtained under slightly different conditions (4).

The formation equilibrium constant for reaction 2,

$$K = [\mathrm{CBM{-}I}]/[\mathrm{CBM}][\mathrm{I}^-],$$

was determined to have a value of $53\ M^{-1}$ at 1 bar under the conditions that the kinetic experiments were conducted. Since from reaction 1 $K = k_f/k_d$, the kinetically determined value of *K* from the plot of the data of Fig. 1 (slope/intercept) is calculated to be $61 \pm 10\ M^{-1}$ at 1 bar, in good agreement with that determined spectrophotometrically.

Generally, the pressure dependence of log *k* is analyzed with either of two equations (6–8):

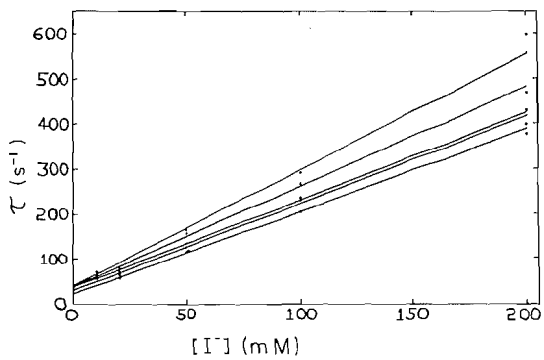

FIG. 1. τ^{-1} as a function of $[I^-]$ at 25.0° and ionic strength 0.2 *M*. Best fit linear least squares calculated lines are from the top, at constant pressures of: 0.001, 0.34, 0.69, 1.03, and 1.38 kbar respectively. Slopes and intercepts give k_f and k_d.

$$\log k = a + bP$$

or

$$\log k = a + bP + cP^2$$

The latter equation assumes that a plot of log k is curved with pressure; that is ΔV^* itself is a linear function of pressure. In cases where there is little curvature or the curvature is only poorly determined, it is common to use the equation that is linear in P only. In the analysis of both the log k_f and log k_d pressure data the parabolic equation gives a better fit than the linear equation. There are substantial grounds, however, for rejecting the more complex three parameter fit over the simpler two parameter linear fit. The standard deviation in log k_f and log k_d are for the linear fits: 0.020 and 0.028 respectively. By comparison the parabolic fit gives for the standard deviation in log k_f and log k_d values of 0.011 and 0.010 respectively. The standard deviations of log k_f and log k_d at each pressure were measured independently from the slopes and intercepts obtained by linear least squares analysis of the plots of τ^{-1} *vs.* $[I^-]$ at each successive pressure. The average standard deviations from these results are 0.026 and 0.055, respectively. These values are more comparable in size to the values obtained from the linear fit than from the parabolic fit. This indicates that even though the parabolic equation provides a better fit to the data there is no justification for going to the more complex model to rationalize the data.

Further, the values calculated for the change in compressibility of the transition state,

$$\Delta\beta^* = -(\partial\Delta V^*/\partial P)_T(1/\Delta V^*)$$

from the parameters b and c in the parabolic equation are for the formation and dissociation reaction: $(5.8 \pm 3.5) \times 10^{-4}$ bar^{-1} and $(-165 \pm 418) \times 10^{-4}$ bar^{-1}. Since the standard deviations on these parameters are as large as the parameters themselves they are only very poorly determined. It should be noted in the latter case the sign of the change in the compressibility of the transition state is inconsistent with the reasonable physical model in which the molecular species become more incompressible at higher pressures. The best fit weighted linear least squares analyses of the data, plotted as log k_f, log k_d, and log K *vs.* P., are shown in Fig. 2.

Values of the activation volumes determined, are with their standard deviations

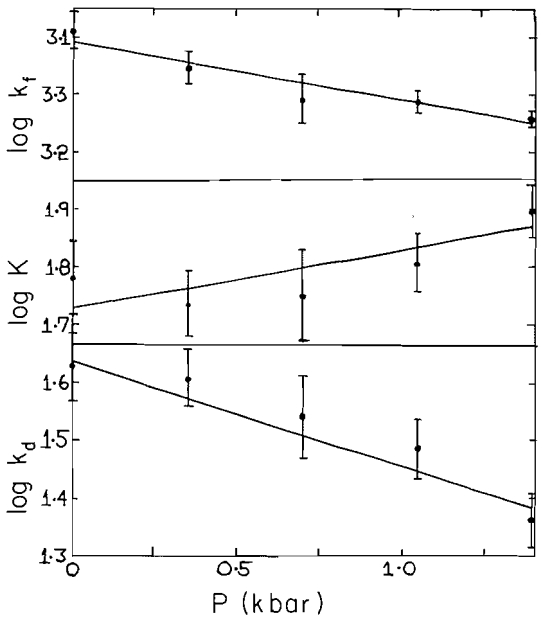

FIG. 2. log k_f, log K, and log k_d as a function of P at 25.0° and ionic strength 0.2 M. The straight lines are those calculated from linear least squares analyses. Error bars are standard deviations calculated from the linear least squares analyses of the data in Fig. 1. The slopes of the straight lines give ΔV_f^*, ΔV^0, ΔV_d^*, respectively, from eq. 1.

$$\Delta V_f^* = 5.5 \pm 0.8 \text{ cm}^3 \text{ mol}^{-1}$$

$$\Delta V_d^* = 11.5 \pm 1.6 \text{ cm}^3 \text{ mol}^{-1}$$

and

$$\Delta V^0 = -5.8 \pm 2.3 \text{ cm}^3 \text{ mol}^{-1}$$

As was the case with the systems studied by Thusius (4), a fast prior change in absorption (here observed to be complete in less than 500 μs, the resolution time of the laser temperature jump apparatus, and of amplitude comparable to the chemical relaxation) was observed in addition to the single chemical relaxation, τ, for the binding of I^- to cobalamin. The origin of this fast absorption change (which was determined to be faster than 20 μs for CBM–SCN on Thusius' modified joule heating temperature jump apparatus (4)) has not been satisfactorily resolved but could be due to either temperature dependent molar absorptivities of cobalamin or a fast intramolecular transformation in the corrin ring.

Discussion

It appears that a number of ligand substitution reactions on metal ions are consistent with

Can. J. Chem. Downloaded from www.nrcresearchpress.com by 210.87.254.5 on 09/05/12
For personal use only.

Can. J. Chem. Downloaded from www.nrcresearchpress.com by 210.87.254.5 on 09/05/12
For personal use only.

Eigen and Wilkins' mechanism (11) in which after prior formation of an outer sphere complex, ligand water dissociates from the metal ion in the transition state. There is some evidence to indicate that cobalamin contains water in its sixth axial coordination position (1, 4). This mechanism would be:

[5] $$CBM{-}OH_2^+ + I^- \overset{K_{os}}{\rightleftharpoons} CBM{-}OH_2^+,I^- \overset{k_{H_2O}}{\underset{k_d}{\rightleftharpoons}} CBM{-}I$$

where $CBM{-}OH_2^+$ is cobalamin now shown as the aquo complex with its overall charge and $CBM{-}OH_2^+,I^-$ is an outer sphere complex. This mechanism predicts (11) when $K_{os}[I^-] \ll 1$ that:

[6] $$k_f = K_{os}k_{H_2O}$$

where K_{os} is the equilibrium constant for formation of the outer sphere complex and k_{H_2O} is the first order rate constant for the dissociation of water from cobalamin in the outer sphere complex (11). From eq. 6 it is apparent that

[7] $$\Delta V_f^* = \Delta V_{os}^0 + \Delta V_{H_2O}^*$$

Hemmes (14) developed a theoretical expression for ΔV_{os}^0 which gave reasonable agreement with experiment,

[8] $$\Delta V_{os}^0 = RT[(z_+z_-e^2/aDkT)(\partial \ln D/\partial P)_T - \beta],$$

where R is the gas constant; z_+ and z_- are the charges on the two ions; a is the distance of closest approach, D is the dielectric constant; k is Boltzmann's constant, and β is the solution compressibility. There is some ambiguity in choosing a value of z_+z_- appropriate for the outer sphere complex between cobalamin and I^-. When all charges on cobalamin are taken into account, at the pH at which this study was conducted, cobalamin formally has a charge of +1; obtained from the sum of +3 from the Co(III) ion, −1 from the corrin ring, and −1 from a phosphate ester side group. Following previous work (10), and taking a as 0.5 nm; for $z_+z_- = -1$, eq. 8 predicts that $\Delta V_{os}^0 = 1.1$ cm^3 mol^{-1}. Since the phosphate group is quite distant from the site of the metal ion where the outer sphere complex is presumably formed, it may be more reasonable to treat the outer sphere complex as having a z_+z_- effectively equal to −2. Equation 8 now predicts that $\Delta V_{os}^0 = 3.2$ cm^3 mol^{-1}. It should be noted that either value of ΔV_{os}^0 chosen does not change the qualitative nature of the following discussion.

From eq. 7 $\Delta V_{H_2O}^*$ is calculated to be (5.5 − 3.2) = 2.3 cm^3 mol^{-1} when $z_+z_- = -2$. The positive value of $\Delta V_{H_2O}^*$ so calculated is consistent with a dissociative type mechanism in which in the activated complex there is stretching of the metal ion – water bond (6–8).

The positive value of ΔV_f^* is consistent with a dissociative mechanism even if the simple Eigen mechanism is inoperative for this complex Co(III) cation.

Values of $\Delta V_{H_2O}^*$ and ΔV_f^* for ligand substitution on a number of other metal ions, assuming a dissociative type mechanism, are given in Table 1 for comparison.

It is interesting to note that $\Delta V_{H_2O}^*$ for the cobalamin reaction is similar in magnitude to that for solvent water exchange on $Co(NH_3)_5OH_2^{3+}$. The mechanism of substitution on this Co(III) complex is presumed to proceed through a dissociative interchange mechanism (15, 16).

The small value of $\Delta V_{H_2O}^*$ for cobalamin may indicate that H_2O in cobalamin is only weakly co-ordinated to the central cobalt ion, necessitating only a small volume change for formation of the transition state. This might also explain, in part, why the activation enthalpies for ligand binding to cobalamin are anomalously low for a Co(III) complex.

It is likely that it is the presence of the corrin ring that increases the reactivity of Co(III) towards ligand substitution. In this regard, the activation volume, $\Delta V_{H_2O}^*$, for CO binding to heme, a Fe(II) protoporphyrin IX complex, is similar to that for cobalamin (Table 1). This shows that there may be a common effect due to the presence of a highly conjugated ring system. Ligand substitution on heme was presumed to proceed through an activated complex in which water was, at best, only loosely bound to the central metal ion.

The kinetically determined value of ΔV^0 of -5.8 ± 2.3 cm^3 mol^{-1} cannot be explained in terms of volume changes expected on simple electrostatic models for reactions between simple oppositely charged ions (6–8). Generally, charge neutralization is accompanied by an increase in volume due to the release of electrostricted sol-

TABLE 1. Calculated values of $\Delta V_{H_2O}^*$ assuming a dissociative mechanism for ligand substitution

Metal complex	Metal	Ligand	$\Delta V_{H_2O}^*$ ($cm^3\ mol^{-1}$)	ΔV_f^* ($cm^3\ mol^{-1}$)
Cobalamin$^+$	Co(III)	I^-[a]	2.3 ± 0.8	5.5 ± 0.8
$Co(NH_3)OH_2^{3+}$	Co(III)	H_2O[b]	1.2 ± 0.1	—
Co^{2+}	Co(II)	PADA[c]	7.2 ± 0.2	7.2 ± 0.2
		NH_3[c]	4.8 ± 0.7	4.8 ± 0.7
		Glycinate$^-$[d]	5 ± 2	8 ± 2
$Heme^{2-}$	Fe(II)	CO[e]	2.0 ± 0.4	2.0 ± 0.4
$FeOH^{2+}$	Fe(III)	Cl^-[f]	4.3 ± 1.0	7.8 ± 1.0
Ni^{2+}	Ni(II)	PADA[c]	7.7 ± 0.3	7.7 ± 0.3
		NH_3[c]	6.0 ± 0.3	6.0 ± 0.3
		Glycinate$^-$[d]	7 ± 1	10 ± 1
Cu^{2+}	Cu(II)	Glycinate$^-$[d]	9 ± 1	12 ± 1
Zn^{2+}	Zn(II)	Glycinate$^-$[d]	4 ± 1	7 ± 1

[a]This work. Overall charge on cobalamin indicated.
[b]Reference 15.
[c]Reference 9.
[d]Reference. 10.
[e]E. F. Caldin and B. B. Hasinoff. Submitted for publication. Reaction medium: 80% v/v ethylene glycol – water.
[f]B. B. Hasinoff. In preparation.

vent water about the ions. The failure of $Cr(H_2O)_5OH^{2+}$ and $Co(NH_3)_5OH^{2+}$ in reaction with H^+ to likewise give values of ΔV^0 expected on the basis of simple application of electrostatic theory have been pointed out (17) and attributed to the effective spreading out of the +3 charge over the surface of a large sphere.

If there is in fact a fast intramolecular process in cobalamin, the anomalous volume change observed for the reaction of cobalamin and I^- could be due to this process occurring in addition to a simple ligand substitution. If this were the case eq. 7 would then become: $\Delta V_f^* = \Delta V_{os}^0 + \Delta V_{int.mol.}^0 + \Delta V_{H_2O}^*$, where $\Delta V_{int.mol.}^0$ is the volume change for the presumed intramolecular process. If $\Delta V_{int.mol.}^0$ were comparable in size to $\Delta V_{H_2O}^*$, then the interpretation of ΔV_f^* is more complex than indicated.

I would like to acknowledge the advice and encouragement of Professor E. F. Caldin in the course of this work. I am also grateful for helpful discussions with Dr. M. Grant.

1. J. M. PRATT. Inorganic chemistry of vitamin B_{12}. Academic Press, London. 1972.
2. W. C. RANDALL and R. A. ALBERTY. Biochem. **5**, 3189 (1966).
3. W. C. RANDALL and R. A. ALBERTY. Biochem. **6**, 1520 (1967).
4. D. THUSIUS. J. Am. Chem. Soc. **93**, 2629 (1971).
5. D. THUSIUS. Chem. Commun. 1183 (1968).
6. G. KOHNSTAM. Prog. React. Kinet. **5**, 335 (1970).
7. W. J. LE NOBLE. Prog. Phys. Org. Chem. **5**, 207 (1965).
8. E. WHALLEY. Adv. Phys. Org. Chem. **2**, 93 (1964).
9. E. F. CALDIN, M. W. GRANT, and B. B. HASINOFF. J. Chem. Soc. Faraday Trans. I, **3**, 560 (1973).
10. M. W. GRANT. Faraday Trans. I, **3**, 560 (1973).
11. M. EIGEN and R. G. WILKINS. Mechanisms of inorganic reactions. Adv. Chem. Ser. **49**. American Chemical Society, Washington. 1965. p. 55.
12. E. F. CALDIN, M. W. GRANT, B. B. HASINOFF, and P. A. TREGLOAN. J. Phys. E, **6**, 349 (1973).
13. J. M. PRATT and R. G. THORP. J. Chem. Soc. (A), 187 (1966).
14. P. HEMMES. J. Phys. Chem. **76**, 895 (1972).
15. H. R. HUNT and H. TAUBE. J. Am. Chem. Soc. **80**, 2642 (1958).
16. W. E. JONES, L. R. CAREY, and T. W. SWADDLE. Can. J. Chem. **50**, 2739 (1972).
17. T. W. SWADDLE and P. KONG. Can. J. Chem. **48**, 3223 (1970).

Can. J. Chem. Downloaded from www.nrcresearchpress.com by 210.87.254.5 on 09/05/12
For personal use only.

Etude comparée des spectres d'absorption dans le proche infrarouge des complexes 1–1 entre l'eau et les bases, en mélanges ternaires[1]

ANDRÉ BURNEAU ET JACQUES CORSET

Laboratoire de Spectrochimie Moléculaire, Bâtiment F, Université de Paris VI, 75230 Paris Cédex 05, et Laboratoire de Chimie Physique, C.N.R.S., 2 rue Henri Dunant, 94320 Thiais, France

Reçu le 29 octobre 1973

Les spectres des complexes entre une molécule d'eau et une molécule d'accepteur de proton sont obtenus à partir de mélanges ternaires eau – base – tétrachlorure de carbone. L'attribution vibrationnelle de ces spectres est faite en s'aidant d'un calcul réalisé antérieurement et en examinant la forme des absorptions et leur fréquence suivant la base. Avec les complexes HOH . . . B, on observe que les bandes correspondant aux combinaisons $\nu(011)$, qui mettent en jeu le vibrateur OH libre, sont plus étroites que $\nu(110)$ et ont toujours un coefficient d'extinction plus grand. Au contraire, dans la région 7000–7300 cm^{-1}, l'absorption la plus intense est la combinaison $\nu(101)$ avec les bases faibles, et l'harmonique $\nu(002)$ avec les bases fortes.

The spectra of the complexes involving a water molecule and a proton acceptor molecule are obtained by using ternary mixtures water – base – carbon tetrachloride. The vibrational assignment of these spectra is performed through a prior calculation and by examining the shape of the absorptions and their frequencies according to the base. With the complexes HOH . . . B, it is observed that the bands related to the $\nu(011)$ combinations, which involve the free OH group, are narrower than $\nu(110)$ and have always a larger extinction coefficient. In the 7000–7300 cm^{-1} region, the most intense absorption is the $\nu(101)$ combination with the weak bases, but the $\nu(002)$ overtone with the strong ones.

Can. J. Chem., **52**, 915 (1974)

Introduction

On sait que dans un mélange eau – base(B) – tétrachlorure de carbone suffisamment dilué en eau, la molécule d'eau peut être soit quasi libre, soit engagée dans des complexes 1–1 (HOH...B) ou 1–2 (B...HOH...B) (1–3); la proportion des espèces dépend de la nature de la base et de sa concentration dans le mélange ternaire. Le but de cette étude est de généraliser les analyses que nous avons faites antérieurement en utilisant l'hexaméthylphosphorotriamide (2) et l'acétone (3), et de préciser l'interprétation des spectres des complexes 1–1 en fonction de la force de la base.

Afin de connaître la gamme de concentrations où le complexe 1–1 prédomine, il faut analyser l'évolution du spectre de l'eau en fonction de la proportion de base dans chaque mélange ternaire.[2]

Les spectres des complexes DOD...B, HOD...B et B...HOD ont été étudiés en faisant varier le taux isotopique de l'eau suivant une méthode qui permet, dans certains cas, d'attribuer le spectre malgré la coexistence de 10 espèces (2).

Conditions experimentales

Les solvants organiques utilisés comme accepteurs de protons ainsi que leurs provenances sont indiqués ci-après: **1**: acétonitrile (Prolabo, pour spectrophotométrie); **2**: acétone (Prolabo, pour spectrophotométrie); **3**: méthyl-isoamyl-cétone (MIC) ou méthyl-5 hexanone-2 (Light et Co, redistillée); **4**: *p*-dioxanne (Merck, Uvasole); **5**: tétrahydrofuranne (THF) (Carlo Erba, pur); **6**: tétrahydropyranne (THP) (Fluka, purum); **7**: eucalyptol (Prolabo, pur); **8**: *N*,*N*-diméthylacétamide (DMA) (Fluka, puriss); **9**: diméthylsulfoxyde (DMSO) (Prolabo, pour chromatographie en phase gazeuse); **10**: hexaméthylphosphorotriamide (HMPT) (Prolabo, pour chromatographie en phase gazeuse). En outre nous avons utilisé le tétrachlorure de carbone pour spectrophotométrie, de chez Prolabo. Ces solvants ont été desséchés sur tamis moléculaire 4A. L'hydroquinone utilisée pour stabiliser le THF, à un taux de 0.05% environ, était en fait totalement oxydée en quinone; nous avons observé la réduction de la quinone dans le mélange H_2O–THF–CCl_4: une bande vers 7064 cm^{-1}, caractéristique de l'hydroquinone, apparaissait en effet avec le temps. Pour cette raison les spectres discutés ici ont été enregistrés immédiatement après préparation de la solution, avant la formation de traces appréciables d'hydroquinone.

Les solvants deutériés, utilisés à cause de leur trans-

[1]Avec la collaboration technique de Jean Limouzi.

[2]L'ensemble de ce travail a été résumé sous forme de figures dans la réf. 4; il ne sera pas repris ici.

Can. J. Chem. Downloaded from www.nrcresearchpress.com by 210.87.254.105 on 09/05/12
For personal use only.

Can. J. Chem. Downloaded from www.nrcresearchpress.com by 210.87.254.105 on 09/05/12
For personal use only.

TABLEAU 1. Fréquences des transitions $\nu(v_1v_2v_3)$ observées*

			HOH		HOH...B									
v_1	v_2	v_3	Vapeur†	CCl_4‡	Acétonitrile-d_3	Acétone	MIC	*p*-Dioxanne	THF	THP	Eucalyptol	DMA	DMSO-d_6	HMPT
0	1	0	1 595		1 617	1 621		1 619	1 620	1 620	1 624		1 627	1 630
0	2	0	3 151	(3 160)								3 215	3 211	3 216
1	0	0	3 657	3 619	3 554	3 530	3 535	3 515	3 490	3 492	3 474	3 464	3 443	3 385
0	0	1	3 756	3 710	3 688	3 689	3 692	3 690	3 689	3 689	3 689	3 687	3 686	3 684
0	3	0	4 667										(4 745)	4 760
1	1	0	5 235	5 198	5 148	(5 139)	5 135	5 117	5 093	5 099	5 084	5 080	5 059	5 008
0	1	1	5 331	5 283	5 283	5 288	5 287	5 284	5 288	5 287	5 288	5 291	5 289	5 297
0	2	1	6 871	6 824	6 842	6 850	6 850	6 843	6 852	6 849	6 848	6 855	6 855	6 866
2	0	0	7 201	(7 121)										
1	0	1	7 250	7 163	7 149	7 150	7 151	7 142	7 133	7 134	7 124	7 118	7 118	(7 070)
0	0	2	(7 445)						7 224	7 228	7 216	7 209	7 202	7 203
2	1	0		(8 660)										
1	1	1	8 807	8 717	(8 723)	(8 725)	(8 727)	(8 718)	(8 718)				(8 711)	
0	1	2			8 838			(8 820)	8 808				8 793	8 802
			10 613 11 032	10 483	(10 494)	(10 499)	(10 499)	(10 492)	(10 499)				(10 496)	(10 497)

*Fréquences en cm^{-1}; les valeurs approchées sont indiquées entre parenthèses.
†Références 7, 11-14.
‡Référence 2.

TABLEAU 2. Fréquences des transitions $\nu(v_1v_2v_3)$ observées*

			DOD		DOD...B				
v_1	v_2	v_3	Vapeur†	Solution CCl_4‡	Acétonitrile	Acétone	THF	DMSO-d_6	HMPT
0	2	0							2 375
1	0	0	2 672	2 644	(2 602)	2 597	2 565	2 536	2 496
0	0	1	2 788	2 753	2 730	2 731	2 731	2 724	2 722
0	1	1	3 956	3 921	3 912		3 912	3 909	3 913
0	2	1	5 105	5 071	5 073	(5 081)	5 077	5 072	5 076
2	0	0	5 292	5 237					
1	0	1	5 374	5 312	5 279	5 270	5 255	5 235	(5 207)
0	0	2			(5 388)	(5 382)	5 374	5 360	5 361
1	1	1	6 533	6 469	6 456				
0	1	2							6 541

*Fréquences en cm^{-1}; les valeurs approchées sont indiquées entre parenthèses.
†Référence 7.
‡Référence 2.

parence, ont été fournis par C.E.A. France (taux isotopique 99.3 à 99.8%). Nous n'avons pas étudié le mélange H_2O–$(CD_3)_2CO$–CCl_4 parce qu'il s'y produit assez rapidement un échange isotopique entre l'eau et l'acétone. Les fréquences portées dans les tableaux 2 et 3 pour les mélanges D_2O–$(CH_3)_2CO$–CCl_4 et HOD–$(CH_3)_2CO$–CCl_4 ne sont donc données qu'à titre indicatif.

Les spectres ont été enregistrés à l'aide de spectromètres Perkin–Elmer 225, Beckman IR 12 et Cary 14, celui-ci étant équipé d'un potentiomètre d'échelle 0–2 ou 0–0.2 unités d'absorbance. En outre nous avons utilisé un dispositif permettant l'observation du spectre sous une épaisseur équivalente à 100 cm (5) pour montrer que les absorptions vers 8 710 – 8 730 et 10 490 – 10 500 cm^{-1} n'impliquent pas seulement les molécules H_2O libres, mais aussi les complexes 1–1(4).

La température d'équilibre des solutions dans les faisceaux du Cary 14 est d'environ 30 °C. La largeur de fente spectrale a généralement été maintenue à une valeur égale au dixième de la largeur à mi-hauteur de la bande observée.

La précision de la mesure du nombre d'ondes au maximum d'absorption est estimée, sauf indication contraire, de 1 à 5 cm^{-1}, suivant la forme de la bande. Mais, quand il y a recouvrement de bandes, ou quand ces dernières sont larges, il est possible que le maximum d'absorption ne corresponde que de façon approchée à la position de la transition étudiée. De plus, la fréquence du maximum de certaines bandes, faisant intervenir un vibrateur associé, varie avec la concentration du mélange.

Resultats

Les tableaux 1 à 3 résument l'attribution vibrationnelle pour les complexes HOH...B, DOD...B, HOD...B et DOH...B. Les spectres les plus caractéristiques des complexes HOH...B sont rassemblés dans la figure 1; nous avons choisi ceux qui présentent des traces de complexes 1–2, contribuant relativement peu à la région 6400–7400 cm^{-1}, plutôt que ceux où existe une quantité notable d'eau libre qui complique l'interprétation. De ce fait, ces spectres comportent en général une absorption entre les transitions $\nu(011)$ et $\nu(110)$ du complexe 1–1, dans la région 5000–5300 cm^{-1}: cette absorption doit être attribuée aux complexes 1–2 (2).

Les coefficients d'anharmonicité x_{ss} et $x_{ss'}$ ont été évalués en utilisant les relations déjà définies (6). Pour utiliser celles-ci dans les meilleures conditions, il faudrait connaître les fréquences purement vibrationnelles des transitions, corrigées des résonances éventuelles, ce qui est difficile pour les phases condensées. Il y a cependant cohérence entre les valeurs calculées à partir de relations mettant en jeu des transitions différentes (tableaux 4 et 5): la précision des coefficients d'anharmonicité est d'autant meilleure qu'ils sont obtenus à partir de bandes impliquant le vibrateur libre, relativement étroites et peu sensibles à l'environnement.

Discussion

L'ensemble des résultats obtenus permet de généraliser la plupart des remarques faites à partir des complexes 1–1 entre l'eau et le HMPT ou l'acétone (2, 3, 6).

Pour tous les complexes HOD...B et DOH...B étudiés, les coefficients d'anharmonicité x_{33} sont voisins respectivement de 83 et 43 cm^{-1}, valeurs observées à l'état gazeux (7)[3]; l'anharmonicité des vibrateurs OH ou OD restés libres dans ces

[3]En ce qui concerne les notations, rappelons que la coordonnée normale q_3 met essentiellement en jeu le groupement OH ou OD libre (2).

Can. J. Chem. Downloaded from www.nrcresearchpress.com by 210.87.254.105 on 09/05/12
For personal use only.

Can. J. Chem. Downloaded from www.nrcresearchpress.com by 210.87.254.105 on 09/05/12
For personal use only.

TABLEAU 3. Fréquences des transitions $\nu(v_1v_2v_3)$ observées*

			HOD		B...HOD					HOD...B				
v_1	v_2	v_3	Vapeur†	Solution CCl_4‡	Acétonitrile	Acétone	THF-d_8	DMSO-d_6	HMPT	Acétonitrile	Acétone	THF-d_8	DMSO-d_6	HMPT
0	1	0	1 403	1 405	(1 438)			(1 457)		1 410		1 403	1 404	1 400
1	0	0	2 724	2 694	3 575		3 506	3 460	3 387	(2 626)				2 500
0	0	1	3 707	3 665	(2 700)	(2 703)	2 703	2 704	2 705	3 673	3 675	3 677	3 675	3 676
0	3	0	4 146	4 134										
1	1	0	4 100	4 080	5 002	4 995	4 950	4 915	4 860	(4 029)				
0	1	1	5 090	5 045	4 128		4 144	(4 150)		5 053	5 056	5 054	5 052	5 053
0	2	1	6 452	(6 405)										6 406
2	0	0	5 364	(5 285)										
1	0	1	6 416	6 347										
0	0	2		7 165	(5 313)	(5 321)	(5 316)	(5 318)	5 323	7 180	7 184	7 185	7 182	7 188

*Fréquences en cm^{-1}; les valeurs approchées sont indiquées entre parenthèses.
†Références 7, 15.
‡Référence 2.

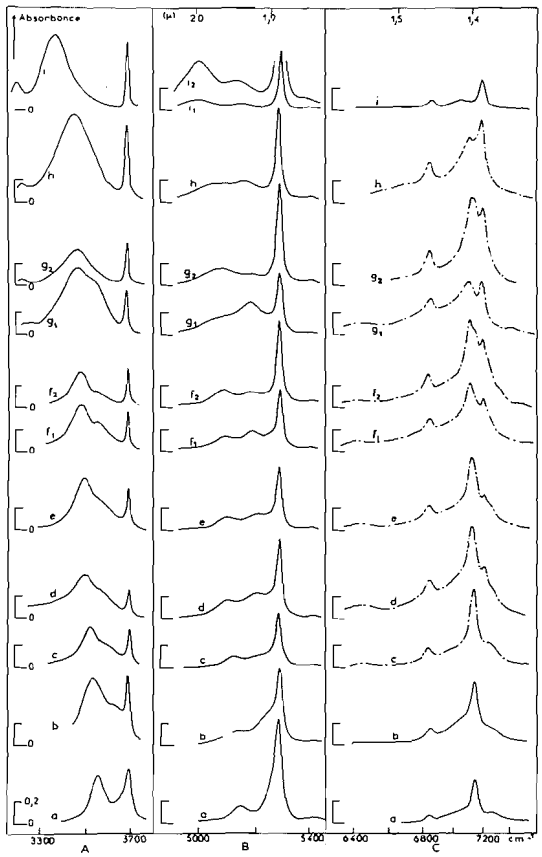

FIG. 1. Spectres de la molécule H_2O engagée dans des complexes 1–1 avec les bases dans des mélanges base – tétrachlorure de carbone.

Courbes	Base	Fraction molaire en base	Concentration en eau (M)			Epaisseur de cuve (cm)		
			A	B	C	A	B	C
a	Acétonitrile	0.17	0.03	0.05	0.05	0.2	5	10
b	Acétone	0.25	0.04	0.04	0.12	0.2	5	10
c	*p*-Dioxanne	0.14	0.025	0.025	0.025	0.2	5	5
d	THF	0.28	0.05	0.05	0.05	0.1	5	5
e	THP	0.24	0.06	0.03	0.03	0.1	5	5
f_1	Eucalyptol	0.37	0.075	0.075	0.075	0.06	2	2
f_2	Eucalyptol	0.16	0.04	0.04	0.04	0.1	5	5
g_1	DMA	0.21	0.1	0.1	0.1	0.06	2	2
g_2	DMA	0.04	0.02	0.02	0.02	0.2	10	10
h	DMSO	0.038	0.02	0.02	0.02	0.5	10	10
i_1, *i*	HMPT	0.03	0.03	0.01	0.05	0.2	20	20
i_2	HMPT	0.03		0.05			20	

Les ordonnées à gauche de chaque courbe correspondent à 0.2 ou 0.02 unité d'absorbance pour les courbes — ou - - - respectivement. Ces courbes ont été obtenues en soustrayant le spectre du solvant mixte du spectre de la solution ternaire, dans les régions où le solvant n'absorbe que modérément. Les parties de courbes douteuses sont indiquées par des tirets (---).

Can. J. Chem. Downloaded from www.nrcresearchpress.com by 210.87.254.105 on 09/05/12
For personal use only.

Can. J. Chem. Downloaded from www.nrcresearchpress.com by 210.87.254.105 on 09/05/12
For personal use only.

TABLEAU 4. Coefficients d'anharmonicité $x_{ss'}$ (en cm^{-1})*

		HOH	HOH...B									
$x_{ss'}$	Relation†	Vapeur‡	Acétonitrile-d_3	Acétone	MIC	*p*-Dioxanne	THF	THP	Eucalyptol	DMA	DMSO-d_6	HMPT
x_{11}		43										
x_{22}	[1]	17										22
	[3]										(24)	21
	[4]		18	18, 5	16	17, 5	17, 5	18	19, 5	20	18, 5	22
x_{33}	[1]	48					77	75	81	82, 5	85	82, 5
	[4]		56			64, 5	74					81
x_{12}	[6]	16	23	(12)§		17	17	13	14			7
	[7]		(21)	(24)	(19)	(18)	(14)				(10)	
	[9]						(17)				(21)	
x_{13}	[6]	166	93	69	76	63	46	47	39	33	11	(−1)
	[7]		(91)	(81)§		(64)	(43)					
	[9]										(15)	
x_{23}	[6]	20	22	22		25	21	22	25			17
	[7]		(20)	(34)§	(24)	(26)	(18)				(23)	
	[8]						18			23, 5	21	15, 5 et 17

*Les valeurs approchées sont indiquées entre parenthèses.

†Pour les molécules d'eau en solution, il s'agit des coefficients apparents; le chiffre entre parenthèses carrées indique alors celle des relations [1] à [9] de la réf. 6 ayant servi à calculer les coefficients figurant sur la ligne.

‡Coefficients corrigés des résonances éventuelles d'après réf. 7.

§Pour le complexe 1–1 avec l'acétone, le désaccord entre les valeurs obtenues à partir des relations [6] et [7] peut provenir de l'imprécision de la fréquence ν(110) (tableau 1); pour les coefficients x_{12}, x_{13} et x_{23}, nous adoptons les valeurs (24), 69 et 22 cm^{-1}; ils indiquent en effet que la fréquence mesurée pour la transition ν(110) pourrait être 12 cm^{-1} trop grande, à cause de la bande 3 νCO de l'acétone.

TABLEAU 5. Coefficients d'anharmonicité $x_{ss'}$* (en cm^{-1})

		Valeur					
			DOD...B				
$x_{ss'}$	Relation†	DOD	Acétonitrile	Acétone	THF	DMSO	HMPT
x_{11}		23					
x_{22}	[4]	9	10, 5		8	11	14
x_{33}	[1]	(26)	(36)	(40)	44	44	42
x_{12}	[7]	8	5				
x_{13}	[6]	87	(53)	58	41	25	(11)
x_{23}	[8]	11					10, 5

		Valeur					
			HOD...B				
$x_{ss'}$	Relation†	HOD	Acétonitrile	Acétone	THF	DMSO	HMPT
x_{11}		43					
x_{22}	[4]	12					12
x_{33}	[1]	83	83	83	84, 5	84	82
x_{12}	[6]	9	(7)				
x_{13}		13					
x_{23}	[6]	20	30		26	27	23

		Valeur, B...HOD				
$x_{ss'}$	Relation†	Acétonitrile	Acétone	THF	DMSO	HMPT
x_{33}	[1]	(44)	(43)	45	45	44
x_{12}	[6]	(11)			(2)	
x_{23}	[6]	(10)			(11)	

*Les valeurs approchées sont indiquées entre parenthèses.
†Pour les molécules d'eau en solution, il s'agit des coefficients apparents; le chiffre entre parenthèses carrées indique alors celle des relations [1] à [9] de la réf. 6 ayant servi à calculer les coefficients sur la ligne.
‡Coefficients corrigés des résonances éventuelles d'après réf. 7.

complexes est donc bien à peu près indépendante de la complexation sur l'autre liaison (6). Cependant l'interaction d'une molécule de base avec HOD entraîne toujours, par rapport aux valeurs dans le tétrachlorure de carbone, une augmentation de fréquence d'une dizaine de cm^{-1} pour l'élongation du vibrateur resté libre (tableau 3). Pour chaque complexe HOH...B, la transition ν(011), mettant en jeu le vibrateur libre a un coefficient d'extinction beaucoup plus grand que la transition ν(110) (fig. 1). Mais la résonance entre les niveaux (v_1, v_2, v_3) et $(v_1 + 1, v_2 - 2, v_3)$ n'est pas observée avec les solvants moins basiques que le DMA (tableau 1).

La validité du calcul effectué (8) pour prévoir l'influence de la formation du complexe 1–1 sur les fréquences des transitions et les coefficients d'anharmonicité, en fonction de la force de la liaison hydrogène, est confirmée.[4] La fig. 2 montre que l'évolution des valeurs observées pour ν_3, x_{33} et x_{13} est en bon accord avec celle que prévoit le calcul. Les courbes calculées pourraient être raffinées en tenant compte des variations de longueur de liaison, d'angle et de constante d'interaction f_{rr} qui modifient le découplage des vibrateurs et les coefficients d'anharmonicité (8); mais déjà l'ensemble de la fig. 2 apparaît assez significatif, surtout si l'on tient compte de la précision des mesures: pour H_2O et D_2O, la diminution de symétrie entraîne le découplage des deux vibrateurs OH ou OD,

[4]Pour définir la diminution de constante de force f_r associée à chaque liaison hydrogène, les fréquences expérimentales ont été placées sur la courbe calculée pour ν_1, dans les figs. 2 et 3 (9).

Can. J. Chem. Downloaded from www.nrcresearchpress.com by 210.87.254.105 on 09/05/12
For personal use only.

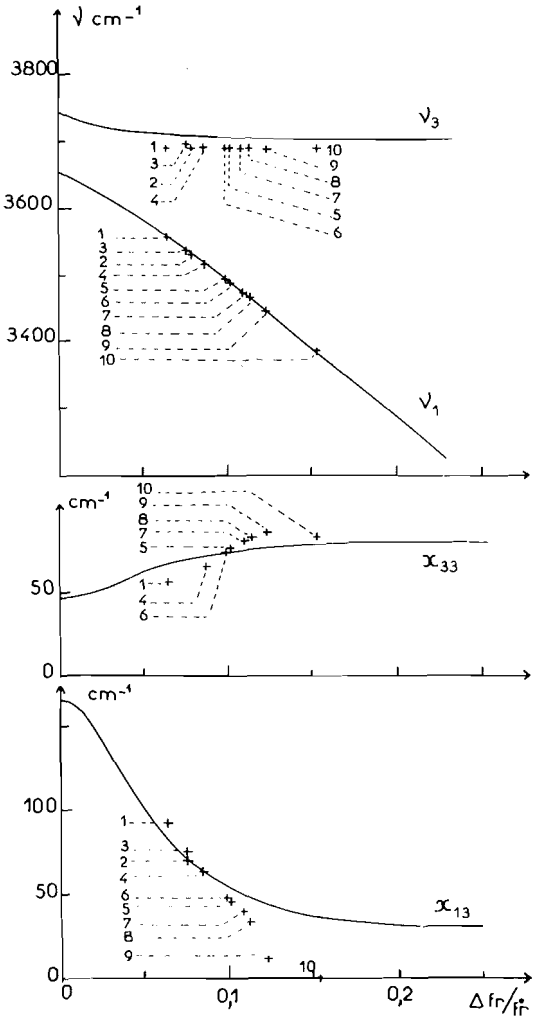

FIG. 2. Evolution des fréquences fondamentales et des coefficients d'anharmonicité de la molécule H_2O engagée dans des complexes 1–1 en fonction de la diminution relative de constante de force du vibrateur associé. + : points expérimentaux; —: courbes calculées (8).

qui se traduit par la diminution de x_{13} et l'augmentation de x_{33}, ce dernier coefficient prenant à la limite la valeur caractéristique d'un vibrateur OH ou OD isolé (tableaux 4 et 5).

L'absorption vers 7150 cm^{-1} du complexe $HOH...O{=}C(CH_3)_2$ doit être attribuée à la combinaison ν(101) et non pas à l'harmonique ν(002) comme nous l'avions d'abord fait (3) en généralisant directement les résultats obtenus avec une base forte telle que le HMPT (2). Pour le complexe HOH...B, il convient en effet d'analyser la région 6800–7300 cm^{-1} avec une attention particulière (fig. 1). La bande vers

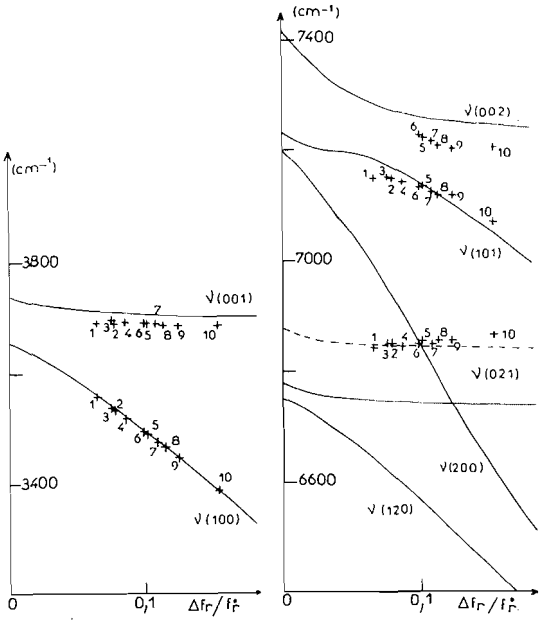

FIG. 3. Evolution de diverses transitions fondamentales et harmoniques de la molécule H_2O engagée dans des complexes 1–1, en fonction de la diminution relative de constante de force du vibrateur associé. + : points expérimentaux; —: courbes calculées en négligeant la correction due à l'énergie cinétique d'interaction vibration-rotation; ---: courbe obtenue en admettant pour le complexe 1–1 la correction calculée pour l'état vapeur (10).

6850 cm^{-1} est commune à tous les spectres et est attribuée à la combinaison ν(021). En opposition au-dessus de 7000 cm^{-1}, le profil du spectre du complexe 1–1 dépend de la nature de la base. Avec le DMSO comme avec le HMPT (2), l'intensité de la transition ν(002) vers 7200 cm^{-1} est plus grande que celle de ν(101) vers 7100 cm^{-1}; elle lui est égale avec le DMA. Avec les solvants moins basiques que le THP ou le THF, c'est ν(101) qui prédomine, ν(002) n'étant plus distinguée. L'évolution du rapport d'intensité des transitions ν(101) et ν(002) peut être interprétée de la façon suivante. Lorsque la diminution de constante de force $\Delta f_r/f_r^0$ est supérieure à 11%, valeur observée avec le DMA (fig. 2), le découplage entre les vibrateurs est suffisant pour que les coordonnées normales q_1 et q_3 n'aient pratiquement plus leur caractère de symétrie A_1 et B_1: les bandes ν(002) impliquent essentiellement le vibrateur libre et sont étroites comme ν(001). En opposition, pour une diminution de constante de force inférieure à 8% environ, cas du dioxanne, la molécule H_2O conserve un

Can. J. Chem. Downloaded from www.nrcresearchpress.com by 210.87.254.105 on 09/05/12
For personal use only.

Can. J. Chem. Downloaded from www.nrcresearchpress.com by 210.87.254.105 on 09/05/12
For personal use only.

TABLEAU 6. Coefficients d'extinction estimés pour les complexes HOH...B: 100 × ε (en l mol^{-1} cm^{-1})

B	ν(101)	ν(002)
HMPT	11	33
DMSO	29	37
DMA	28	30
Eucalyptol	48	38
THP	50	10
p-Dioxanne	50	—
Acétone	60	—

certain caractère de symétrie C_{2v}, et les transitions les plus intenses sont alors virtuellement de type B_1: la transition ν(002) ne peut plus être distinguée dans le spectre à cause de l'augmentation importante du coefficient d'extinction de ν(101) (tableau 6), et du recouvrement des bandes. Le rapport d'intensité des transitions ν(002) et ν(101) varie de la même façon pour les complexes DOD...B.

Cette attribution est confirmée par la comparaison des fréquences des absorptions ν(101) et ν(002) avec celles prévues par le calcul (8) (fig. 3). L'évolution des fréquences est plus significative que leurs valeurs propres à cause de certaines hypothèses de calcul. La constante de force du vibrateur libre dans les complexes 1–1 expérimentalement étudiés est voisine de la valeur $f_r^0 = 8.275$ mdyn/Å, évaluée pour l'eau en solution dans le tétrachlorure de carbone (6), alors que le calcul a été fait avec la valeur $f_r^0 = 8.453$ mdyn/Å, associée à la molécule d'eau à l'état vapeur. En outre, la correction due à la partie énergie cinétique de l'hamiltonien (10) a été négligée; pour la molécule H_2O à l'état gazeux, cette correction est nulle pour ν(100) et faible pour ν(001) et ν(101); elle contribue un peu plus à ν(002), et de façon importante à ν(021) dont les valeurs calculées doivent être environ 100 cm^{-1} trop faibles (8). Cet écart est confirmé en attribuant à ν(021) la bande vers 6850 cm^{-1} peu sensible à la force de la liaison hydrogène: on peut donc appliquer la même correction pour la molécule d'eau isolée ou dans le complexe 1–1, correction à partir de laquelle a été obtenue la courbe en pointillés (fig. 3). Remarquons enfin que la fréquence de la transition ν(101) est moins abaissée que celle de ν(100): cette différence provient des modifications d'anharmonicité des vibrations normales lorsque la molécule H_2O devient dissymétrique (8).

En résumé, lorsque les molécules H_2O et D_2O sont dans un environnement tel qu'elles n'ont plus exactement la symétrie C_{2v}, les deux vibrateurs OH ou OD sont partiellement découplés. Ce découplage intervient à la fois pour définir la valeur des coefficients d'anharmonicité, donc la fréquence des transitions, et l'intensité de ces transitions.

Nous exprimons notre gratitude à Mademoiselle Josien, Professeur à l'Université de Paris VI, pour l'intérêt avec lequel elle a suivi l'ensemble de ce travail.

1. P. SAUMAGNE et M. L. JOSIEN. Bull. Soc. Chim. Fr. 813 (1958). P. SAUMAGNE. Thèse d'Etat, Bordeaux, 1961. S. C. MOHR, W. D. WILK et G. M. BARROW. J. Am. Chem. Soc. **87**, 3048 (1965). G. V. YUKNEVICH, A. V. KARYAKIN et A. V. PETROV. Zh. Prikl. Spektrosk. **3**, 142 (1965). D. N. GLEW et N. S. RATH. Can. J. Chem. **49**, 837 (1971).
2. A. BURNEAU et J. CORSET. J. Chim. Phys. Physicochim. Biol. **69**, 142 (1972).
3. A. BURNEAU et J. CORSET. J. Phys. Chem. **76**, 449 (1972).
4. A. BURNEAU. Thèse d'Etat, C.N.R.S. A.O. 6526, Paris VI, 1973.
5. A. BURNEAU, J. CORSET et J. LIMOUZI. Méth. Phys. Analyse (G.A.M.S.), **7**, 33 (1971).
6. A. BURNEAU et J. CORSET. J. Chim. Phys. Physicochim. Biol. **69**, 171 (1972).
7. W. S. BENEDICT, N. GAILAR et E. K. PLYLER. J. Chem. Phys. **24**, 1139 (1956).
8. A. BURNEAU et J. CORSET. J. Chim. Phys. Physicochim. Biol. **69**, 153 (1972).
9. J. LAURANSAN, J. CORSET et M. T. FOREL. Ann. Chim. (Paris), **3**, 109 (1968).
10. B. T. DARLING et D. M. DENNISON. Phys. Rev. **57**, 128 (1940). W. F. LIBBY. J. Chem. Phys. **11**, 101 (1943).
11. G. HERZBERG. Infrared and Raman spectra. Van Nostrand, New York. 1945.
12. W. S. BENEDICT et E. K. PLYLER. J. Res. Natl. Bur. Stand. **46**, 246 (1951).
13. O. C. MOHLER et W. S. BENEDICT. Phys. Rev. **74**, 702 (1948).
14. R. C. NELSON et W. S. BENEDICT. Phys. Rev. **74**, 703 (1948).
15. N. M. GAILAR et F. P. DICKEY. J. Mol. Spectrosc. **4**, 1 (1960).

A Carbon-13 Nuclear Magnetic Resonance Study of Binding of Copper(II) to Pyrimidine Nucleotides and Nucleosides[1]

GEORGE KOTOWYCZ

Department of Chemistry, University of Alberta, Edmonton, Alberta T6G 2G2

Received September 19, 1973

The influence of paramagnetic Cu^{2+} ions on the proton decoupled ^{13}C n.m.r. spectra of pyrimidine nucleosides and nucleotides has been studied. For 5′-CMP, the C5 resonance is broadened first on the addition of Cu^{2+} ions followed by the C2, C4, and C1′ resonances. From a comparison of the transverse and longitudinal relaxation rates of the base carbon nuclei due to the presence of Cu^{2+} ions, binding of Cu^{2+} to the N3 nitrogen of 5′-CMP is predicted. A similar broadening behavior is observed for 5′-UMP, 5′-TMP, cytidine, and uridine. This indicates that the Cu^{2+} ion is located near the N3 nitrogen in these Cu^{2+}-nucleoside and -nucleotide complexes.

On a étudié l'influence des ions Cu^{2+} paramagnétiques sur les spectres r.m.n. du ^{13}C de nucléosides de pyrimidine et de nucléotides dans lesquels les protons étaient découplés. Dans le cas du 5′-CMP, l'addition des ions Cu^{2+} élargit premièrement la résonance en C5 suivie par les résonances en C2, C4 et C1′. En se basant sur les temps de relaxation transversale et longitudinale du carbone de la base dû à la présence d'ion Cu^{2+} on prédit que la fixation du Cu^{2+} se fait sur l'azote N3 du 5′-CMP. On observe un élargissement semblable des bandes pour les 5′-UMP, 5′-TMP, pour la cytidine et l'uridine. Ceci indique que les ions Cu^{2+} se localisent près de l'azote N3 dans ces complexes entre Cu^{2+} et les nucléosides et les nucléotides. [Traduit par le journal]

Can. J. Chem., **52**, 924 (1974)

Copper(II) ions have significant and different effects on polyribonucleotides and deoxyribonucleic acid (DNA). Polyribonucleotides are degraded into small oligonucleotides when heated with copper ions (1) by the cleavage of phosphate bonds. Cu^{2+} ions have an influence on the mean temperature of denaturation of DNA (2). The effect of Cu^{2+} ions on DNA melting has now been extensively studied (3–11). Cu^{2+} ions interact with DNA in two places, namely the phosphate groups and nitrogen bases.

^{31}P n.m.r. shows the binding of Cu^{2+} ions to the phosphate portion of the nucleotides (12–15). Metal interactions with the base portion of the nucleotides have also been extensively studied. Cu^{2+} ions preferentially broaden the H5 resonance of -5′CMP and 5′-*d*CMP (13) indicating a binding to N3. The p.m.r. spectrum of 5′-TMP was not affected leading to the interpretation that Cu^{2+} is not bound to this deoxyribonucleotide. Proton magnetic resonance spectra have also been obtained for a series of deoxyribonucleosides in DMSO-d_6 (13). The effect of Cu^{2+} ions on the carbon-bound protons was generally the same as with the deoxyribonucleotides in D_2O. The NH and NH_2 resonances are relatively unaffected suggesting that the amino group is not involved in the binding in deoxycytidine or cytidine. The N3 proton was unaffected in deoxythymidine indicating no binding to this nucleoside. These studies were extended to an investigation of Cu^{2+} ion interactions with uridine in DMSO-d_6 and 5′-UMP in D_2O (16). Broadening of the N3 and C5 proton resonances of uridine and the H5 proton resonance of 5′-UMP was interpreted in terms of Cu^{2+} ions binding to the base near N3 and C5 and possibly to the oxygen at C4.

Since Cu^{2+} ions produce such interesting effects on nucleic acids, we wished to study the nature of the Cu^{2+}–nucleotide interaction. A shortcoming of studying these interactions by means of p.m.r. measurements is that in D_2O solutions only the H5, H6, and H1′ resonances are clearly observed. In the present study, the Fourier transform, natural abundance, ^{13}C n.m.r. approach is used. Thus we have a large number of nuclear probes which can be used to yield information about the metal binding site.

[1]Paper number 4 in a series on nuclear magnetic resonance studies of nucleoside– and nucleotide–metal interactions.

Can. J. Chem. Downloaded from www.nrcresearchpress.com by 210.87.254.40 on 09/05/12
For personal use only.

TABLE 1. Values of $1/T_{1p}$ and $1/T_{2p}$ (s^{-1}) for the base carbon nuclei of 5′-CMP*

Carbon	$1/T_{1,obs}$	$1/T_{1,O}$	$1/T_{1p}$	$1/T_{2,obs}$	$1/T_{2,O}$	$1/T_{2p}$
C2	7.7	0.14	7.6	30	5.3	25 ± 3
C4	7.1	0.22	6.9	20	6.0	14 ± 3
C5	8.3	5.6	2.7	135	13	122 ± 15

*The measurements were made on a 0.87 *M* 5′-CMP sample containing 2.5×10^{-4} *M* Cu^{2+} ions in a D_2O solution at a p*D* of 7.4. $T = 35$ °C. All measurements were carried out at 25.15 MHz.

Experimental

All nucleotides and nucleosides were obtained from Sigma Chemical Company and were used without further purification. The solutions for the ^{13}C n.m.r. experiments were prepared in D_2O (obtained from Columbia Organic Chemicals) and the p*H* was adjusted to 7.0 (p*D* = 7.4) (17). The nucleotides 5′-CMP, 5′-UMP, and 5′-TMP and nucleosides cytidine and uridine were studied at concentrations between 0.75 to 0.80 *M*. Stock solutions of $CuCl_2$ were prepared and were added to the above solutions using H. E. Pedersen micropipettes. The nucleotide solutions for the ^{31}P n.m.r. experiments were prepared in distilled water and were adjusted to a p*H* of 7.0.

The proton decoupled ^{13}C n.m.r. spectra for the concentration and temperature experiments were obtained using a Bruker HFX-90 n.m.r. spectrometer (22.63 MHz) operating in the Fourier transform mode and equipped with a Nicolet 1085 computer. The deuterium resonance from the solvent D_2O was used for the heteronuclear lock signal. The free induction decay signals were accumulated in 16K data points of the computer and 1024 accumulations were carried out. The frequency range of the Fourier transformed spectra was 3000 Hz for cytidine, uridine, 5′-CMP, and 5′-UMP (0.37 Hz/point) and 5000 Hz for 5′-TMP (0.61 Hz/point). The ^{13}C chemical shifts are calibrated with respect to the internal dioxane resonance and are accurate to ± 0.1 p.p.m. For resonances with a line width at half height less than 10 Hz, the line width measurements are accurate to ± 1 Hz. However, for resonances with a line width greater than 10 Hz, the line width measurements are accurate to ± 3 Hz. The ^{31}P n.m.r. spectra were measured at 36.43 MHz and the proton resonance from the solvent H_2O was used for the heteronuclear lock. The free induction decay signals were accumulated in 8K data points and the frequency range of the Fourier transformed spectra was 5000 Hz (1.2 Hz/point). The temperature for all measurements as a function of Cu^{2+} ion concentration was maintained at 28 °C. The temperature for all experiments was determined directly using the Bruker temperature control unit.

The spin–lattice relaxation times were determined from proton decoupled partially relaxed Fourier transform spectra using the $(-180°-\tau-90°-T-)_n$ pulse sequence (18–25). These experiments were obtained using the Varian HA-100-15 NMR spectrometer (25.15 MHz) interfaced with a Digilab FTS/NMR-3 data system, FTS/NMR 400-2 pulse unit, and a Nova 1200 computer. The deuterium resonance of the solvent D_2O was used for the lock signal. Least squares analyses of the data were carried out on 8 to 12 different values of τ from which T_1 values were obtained. This technique yields T_1 values which are accurate to about 10%. The experimental details have been described elsewhere (50). Spin–spin relaxation times were also obtained from the line widths at half height from normal proton decoupled ^{13}C Fourier transform spectra with a resolution of 0.31 Hz/point at a frequency of 25.15 MHz at 35 °C. The error limits are given in Table 1.

Results

The proton-decoupled ^{13}C n.m.r. spectrum of 5′-CMP and the effect of progressive addition of Cu^{2+} ions on the spectrum is shown in Fig. 1. The results of the line broadening experiments on 5′-CMP, 5′-UMP, and 5′-TMP are shown in Fig. 2 and those of cytidine and uridine are shown in Fig. 4. These figures illustrate the selective broadening of the ^{13}C resonances which closely follows a linear dependence on the concentration of Cu^{2+} ions. The ^{13}C n.m.r. line assignments are based on those reported in the literature for nucleosides (26–28), 5′-nucleotides (29), uridine monophosphates and polyuridylic acid (30). The ^{13}C chemical shifts with respect to internal dioxane have been reported previously (31, 32) together with the observed ^{31}P—^{13}C coupling constants (29–33). The ^{13}C chemical shifts were not affected by the presence of the Cu^{2+} ions. The ^{31}P n.m.r. chemical shifts for all the nucleotides occur at 109.2 ± 0.5 p.p.m. to high field of the external P_4O_6 capillary. The ^{31}P n.m.r. linewidths increase linearly from 15 ± 3 Hz for the pure nucleotide solutions to about 190 ± 20 Hz for solutions with a metal concentration about 2×10^{-4} *M*.

The temperature dependence of $\Delta\nu_{1/2}$ metal for the base carbon nuclei that are affected by the presence of Cu^{2+} ions is seen in Fig. 3. Values of the spin–lattice and spin–spin relaxation times obtained at 25.15 MHz are tabulated in Table 1.

Discussion

The influence of paramagnetic ions on nuclear relaxation times has been extensively studied (34–38). For Cu^{2+} complexes, the spin–lattice relaxation rate $1/T_{1M}$ and spin–spin relaxation

Can. J. Chem. Downloaded from www.nrcresearchpress.com by 210.87.254.40 on 09/05/12
For personal use only.

Can. J. Chem. Downloaded from www.nrcresearchpress.com by 210.87.254.40 on 09/05/12
For personal use only.

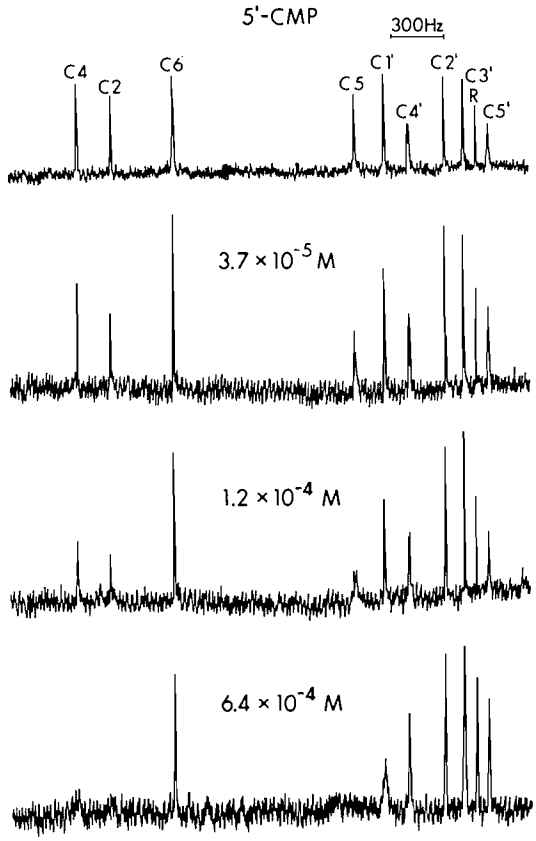

FIG. 1. The effect of Cu^{2+} ions on the natural abundance, Fourier transform, proton decoupled ^{13}C n.m.r. spectra of 5′-CMP in D_2O (p*D* 7.4) at 25 °C. The top spectrum is for the metal-free solution and the Cu^{2+} ion concentration is indicated for the remaining spectra. The recycle time for the experiment is 2.6 s. The operating frequency is 22.63 MHz. R is the reference dioxane resonance.

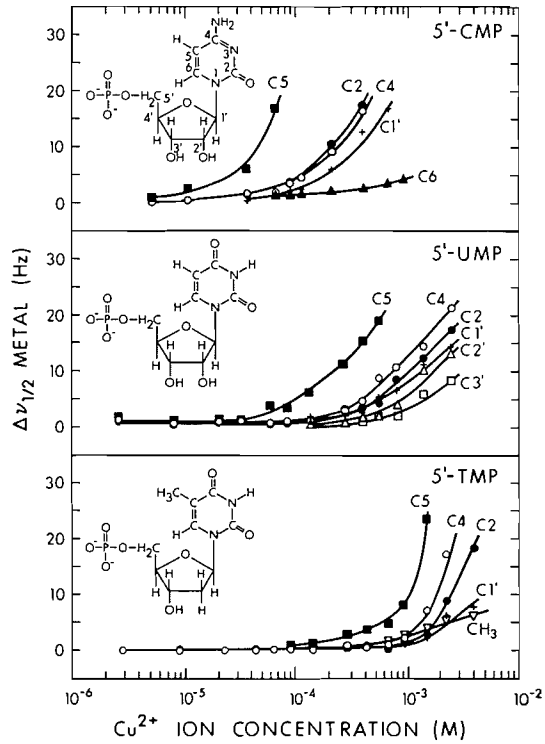

FIG. 2. The dependance of $\Delta\nu_{1/2}$ metal on the Cu^{2+} ion concentration for the carbon nuclei of 5′-CMP, 5′-UMP, and 5′-TMP that are affected by the presence of Cu^{2+} ions.

rate $1/T_{2M}$ due to the presence of paramagnetic ions are given by (36)

$$[1]\quad \frac{1}{T_{1M}} = \frac{4}{30}\frac{S(S+1)\gamma_I^2 g^2\beta^2}{r^6} \times \left(3\tau_c + \frac{7\tau_c}{1+\omega_s^2\tau_c^2}\right)$$

$$[2]\quad \frac{1}{T_{2M}} = \frac{4}{60}\frac{S(S+1)\gamma_I^2 g^2\beta^2}{r^6} \times \left(7\tau_c + \frac{13\tau_c}{1+\omega_s^2\tau_c^2}\right) + \tfrac{1}{3}S(S+1)\frac{A^2}{\hbar^2}\tau_e$$

where r_i is the average electron nuclear separation, γ_I is the nuclear magnetogyric ratio, S the electron spin, $A/\hbar$ is the contact coupling constant in radians per second, g is the g value of the electron, β is the value of the Bohr magneton, τ_c and τ_e are the correlation times for the dipolar and contact interactions, respectively. The electron paramagnetic resonance frequency is designated by ω_s. In deriving these equations, it is assumed that $\omega_s^2\tau_e^2 \gg 1$. The first term in the above equations represents the dipolar relaxation rate. For the transverse relaxation rate $1/T_{2M}$ the second term is the relaxation rate due to hyperfine interactions. For the dipole–dipole interaction, relaxation times are extremely sensitive to the distance between the metal ion and the nucleus under study. The scalar interaction is sensitive to the nature of the intervening bonds. If the dipole–dipole interaction is predominant, the measurement of $1/T_{1M}$ and $1/T_{2M}$ will yield important information about the location of the metal ion binding site.

The line widths and therefore the transverse relaxation rates of each ^{13}C and ^{31}P resonance

Can. J. Chem. Downloaded from www.nrcresearchpress.com by 210.87.254.40 on 09/05/12
For personal use only.

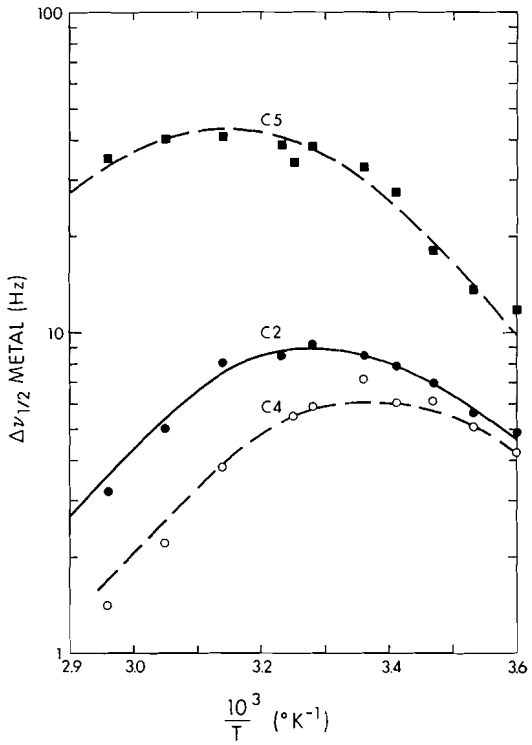

FIG. 3. The temperature dependence of $\Delta\nu_{1/2}$ metal for the C2, C4, and C5 carbon nuclei of 5′-CMP. The concentration of 5′-CMP is 0.87 *M* in D_2O (p*D* 7.4) whereas the Cu^{2+} ion concentration is 2.5×10^{-4} *M* for a [nucleotide]/[metal ion] ratio of 3.5×10^3. The free induction decay signals are accumulated in 16K data points of the computer (1024 accumulations) and the frequency range of the Fourier transformed spectra is 3000 Hz. For $\Delta\nu_{1/2}$ (metal) < 10 Hz, the error limits are ±1 Hz. When $\Delta\nu_{1/2}$ (metal) increases to 10–20 Hz, the error limits are ±3 Hz and increase to ±10 Hz for $\Delta\nu_{1/2}$ (metal) > 20 Hz.

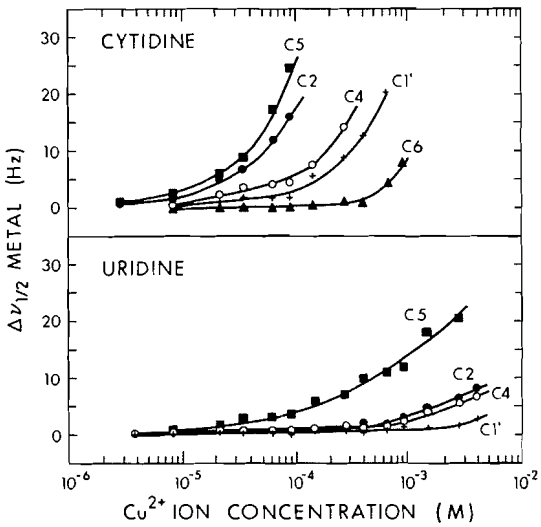

FIG. 4. The dependance of $\Delta\nu_{1/2}$ metal on the Cu^{2+} ion concentration for the carbon nuclei of cytidine and uridine that are affected by the presence of Cu^{2+} ions.

were studied with the progressive addition of the Cu^{2+} ions (39). The Cu^{2+} ion concentration is much less than that of the nucleotide and the rapid exchange of molecules in solution causes all nucleotides to be equally affected by the metal ions.

As seen from the ^{31}P line broadening results, Cu^{2+} ions definitely bind to the phosphate groups of the nucleotides under study. In addition, the metal interaction with the ring must be considered. As has been previously observed (31, 32), ^{13}C n.m.r. linewidths are very sensitive to the presence of Mn^{2+} ions in solution. Specific line broadening effects were observed that depend on the nature of the Mn^{2+} ion binding site. Specific line broadening effects have now also been observed with Cu^{2+} ions. When Cu^{2+} ions were added to 5′-CMP (Figs. 1 and 2) the C5 resonance broadened first followed by the C2, C4, and C1′ resonances at higher Cu^{2+} ion metal concentrations, indicating a metal ion interaction with the base portion of the nucleotide. The C6 base carbon resonance, the remainder of the ribose carbon resonances as well as the dioxane reference signal are unaffected.

The increase in line width measured at half height due to paramagnetic metal ions, $\Delta\nu_{1/2}$ metal, may be expressed as

$$[3]\quad \Delta\nu_{1/2}\,\text{metal} = \Delta\nu_{1/2,\text{obs}} - \Delta\nu_{1/2,\text{o}} = \frac{1}{\pi T_{2\text{p}}} = \frac{1}{\pi T_{2,\text{obs}}} - \frac{1}{\pi T_{2,\text{o}}}$$

where $\Delta\nu_{1/2,\text{obs}}$ $(1/\pi T_{2,\text{obs}})$ is the observed line width at half height when metal ions are present, $\Delta\nu_{1/2,\text{o}}$ $(1/\pi T_{2,\text{o}})$ is the line width at half height for the same resonance without metal ions, and $1/T_{2\text{p}}$ is the total transverse relaxation rate of a nucleus due to the presence of the paramagnetic ions. In Fig. 2, $\Delta\nu_{1/2}$ metal is plotted *vs.* the Cu^{2+} ion concentration for the carbon resonances which showed an appreciable broadening for 5′-CMP, 5′-UMP, and 5′-TMP.

A temperature study of $\Delta\nu_{1/2}$ metal of the base ^{13}C resonances of 5′-CMP in the presence of Cu^{2+} ions was carried out and the results are shown in Fig. 3. The temperature dependence of

Can. J. Chem. Downloaded from www.nrcresearchpress.com by 210.87.254.40 on 09/05/12
For personal use only.

$\Delta\nu_{1/2}$ metal in the presence of the metal ion is determined by the temperature dependence of the average lifetime of a molecule coordinated at any site (τ_M) and the relaxation time of the nuclei when the nucleotide is coordinated to the metal ion ($1/T_{2M}$) (40). At high temperatures the positive slope of the curves for all three nuclei indicates that $1/T_{2p}$ is controlled by the nuclear relaxation rate $1/T_{2M}$. At lower temperatures the negative slope indicates that this is the exchange controlled region τ_M.

From Fig. 3, the values of $1/T_{2p}$ at 35 °C for nuclei C2 and C4 are in the $1/T_{2M}$ region whereas both $1/T_{2M}$ and τ_M contribute to $1/T_{2p}$ for C5. Then it is also true that $1/T_{1p} = 1/T_{1M}$ for nuclei C2 and C4 (41). $1/T_{1p}$ is defined as

$$[4] \qquad \frac{1}{T_{1p}} = \frac{1}{T_{1,obs}} - \frac{1}{T_{1,O}}$$

where $1/T_{1,obs}$ is the observed longitudinal relaxation rate for a nucleus in the presence of metal ions and $1/T_{1,O}$ is the longitudinal relaxation rate for the same resonance without metal ions, and $1/T_{1p}$ is the total longitudinal relaxation rate of a nucleus due to the presence of the paramagnetic ions. The values of $1/T_{1p}$ and $1/T_{2p}$ evaluated at 35 °C are tabulated in Table 1. From an analysis of the data in Table 1, $T_{1p}/T_{2p} = 3.3$ for C2 and 2.0 for C4. For such small ratios, the dipole–dipole relaxation process is the predominant relaxation mechanism for these two nuclei (36). In addition, from eq. 1, $T_{1p}(C2)/T_{1p}(C4) = r^6(C2)/r^6(C4)$ so that $r(C2)/r(C4) = 1.01$, indicating that the Cu^{2+} ion is equidistant from both C2 and C4 and binds to N3. This implies that τ_c (C2) = τ_c (C4) which is expected when the binding is at N3. This is in excellent agreement with the structure determined for the cupric chloride complex of cytosine (42) in which Cu^{2+} forms a strong bond to N3. The binding of Cu^{2+} ions to the N3 nitrogen of 5′-CMP was also postulated from p.m.r. studies (13).

The strong broadening of the C5 resonance of 5′-CMP is due to the hyperfine interaction. The C5 nucleus is much further removed from the binding site than are C2 and C4. Proton magnetic resonance measurements (13) on 5′-*d*CMP showed that the H5 resonance is greatly broadened by the presence of Cu^{2+} ions whereas the H6 resonance is only slightly broadened and the coupling between the H5 and H6 nuclei is still apparent from the splitting observed for H6. Hence H5 is seeing a change in the transverse relaxation time with little change in its longitudinal relaxation time since a significant change in the longitudinal relaxation time would cause the doublet H6 structure to broaden and coalesce. Therefore the transverse relaxation is controlled by the contact interaction at H5 and hence at C5. This is also illustrated by the $1/T_{1p}$ and $1/T_{2p}$ data in Table 1. $1/T_{1p}$ for C5 is 2.8 s^{-1} whereas the line width of C5 increases by a factor of ten on adding the Cu^{2+} ions ($1/T_{2p} = 122 \pm 15\ s^{-1}$). Miller and McClung (43) observed that the effect of the paramagnetic vanadyl ion is larger on the distant N—CH_3 protons than on the neighboring C—CH_3 protons for solutions of vanadyl ions in dimethylacetamide. It was found that the N—methyl protons are predominantly relaxed by hyperfine interactions while the major contribution to C—methyl proton relaxation is dipolar.

Similar line broadening behavior for the three nucleotides 5′-UMP, 5′-TMP, and 5′-CMP (Fig. 2) indicates that Cu^{2+} ions bind to the base portion of these nucleotides at the same position. In addition, the line broadening behavior observed for cytidine and uridine (Fig. 4) is similar to that observed for the nucleotides. This indicates that the metal ion is located near the N3 position of the nucleosides. Cu^{2+} ions have broadened the C2′ and C3′ ribose resonances of 5′-UMP, indicating a metal ion interaction with the ribose hydroxyl groups also. Cu^{2+} complexes with 5′-TMP have previously not been detected using p.m.r. (13) and i.r. (44) techniques.

Proton magnetic resonance measurements (13) as well as ^{13}C n.m.r. measurements have been carried out on highly concentrated solutions of nucleotides and nucleosides. In the present work, the nucleotide – metal ion ratio is about 5,000 : 1. Under these conditions, the nucleosides and nucleotides stack in aqueous solution (45, 46). In addition, the presence of metal(M)–ligand(L) complexes of the type ML, ML_2, M_2L_2 could be considered (47, 48). Unfortunately, stability constants are not known for the complexes under study and hence it is not possible to know the solution compositions as have been tabulated for Mn^{2+}–ATP complexes (49).

The spectra in Fig. 1 indicate an additional interesting feature. As the Cu^{2+} ion concentration increases, the C4′ and C5′ resonances become sharp and the ^{31}P—^{13}C couplings disappear. As the Cu^{2+} ions bind to the phos-

phate groups, they shorten the phosphorus nuclei longitudinal relaxation time and the coupling to the ^{13}C nuclei is removed. This effect has previously been observed with Mn^{2+} ions (31, 32).

Thanks are extended to Dr. Tom Nakashima and Mr. Yiu-Fai Lam for their assistance with the T_1 measurements, to Dr. O. Suzuki for his assistance with several of the ^{13}C measurements, to Dr. G. P. P. Kuntz and Mr. F. Lluch for valuable discussions, and to the National Research Council of Canada for financial assistance.

1. J. J. BUTZOW and G. L. EICHHORN. Biopolymers, **3**, 95 (1965).
2. G. L. EICHHORN. Nature, **194**, 474 (1962).
3. G. L. EICHHORN and P. CLARK. Proc. Natl. Acad. Sci. U.S. **53**, 586 (1965).
4. S. HIAI. J. Mol. Biol. **11**, 672 (1965).
5. H. VENNER and C. ZIMMER. Biopolymers, **4**, 321 (1966).
6. J. H. COATES, D. O. JORDAN, and V. K. SRIVASTAVA. Biochem. Biophys. Res. Commun. **20**, 611 (1965).
7. G. L. EICHHORN and Y. A. SHIN. J. Am. Chem. Soc. **90**, 7323 (1968).
8. D. C. LIEBE and J. E. STUEHR. Biopolymers, **11**, 145 (1972).
9. D. C. LIEBE and J. E. STUEHR. Biopolymers, **11**, 167 (1972).
10. L. R. HOLMAN and D. O. JORDAN. Biopolymers, **11**, 1661 (1972).
11. H. RICHARD, J. P. SCHREIBER, and M. DAUNE. Biopolymers, **12**, 1 (1973).
12. M. COHN and T. R. HUGHES, JR. J. Biol. Chem. **237**, 176 (1962).
13. G. L. EICHHORN, P. CLARK, and E. D. BECKER. Biochemistry, **5**, 245 (1966).
14. L. S. KAN and N. C. LI. J. Magn. Reson. **7**, 161 (1972).
15. A. W. MISSEN, D. F. S. NATUSCH, and L. J. PORTER. Aust. J. Chem. **25**, 129 (1972).
16. N. A. BERGER and G. L. EICHHORN. Biochemistry, **10**, 1857 (1971).
17. P. K. GLASOE and F. A. LONG. J. Phys. Chem. **64**, 188 (1960).
18. R. L. VOLD, J. S. WAUGH, M. P. KLEIN, and D. E. PHELPS. J. Chem. Phys. **48**, 3831 (1968).
19. R. FREEMAN and H. D. W. HILL. J. Chem. Phys. **51**, 3140 (1969).
20. R. FREEMAN and H. D. W. HILL. J. Chem. Phys. **53**, 4103 (1970).
21. A. ALLERHAND, D. DODDRELL, V. GLUSHKO, D. W. COCHRAN, E. WENKERT, P. J. LAWSON, and F. R. N. GURD. J. Am. Chem. Soc. **93**, 544 (1971).
22. R. FREEMAN and H. D. W. HILL. J. Chem. Phys. **54**, 3367 (1971).
23. A. ALLERHAND, D. DODDRELL, and R. KOMOROSKI. J. Chem. Phys. **55**, 189 (1971).
24. T. C. FARRAR and E. D. BECKER. Pulse and Fourier transform NMR. Academic Press, New York. 1971. pp. 20–22.
25. G. C. LEVY and G. L. NELSON. Carbon-13 nuclear magnetic resonance for organic chemists. Wiley–Interscience, New York. 1972. Chapt. 9.
26. A. J. JONES, D. M. GRANT, M. W. WINKLEY, and R. K. ROBINS. J. Am. Chem. Soc. **92**, 4079 (1970).
27. A. J. JONES, D. M. GRANT, M. W. WINKLEY, and R. K. ROBINS. J. Phys. Chem. **74**, 2684 (1970).
28. A. J. JONES, M. W. WINKLEY, D. M. GRANT, and R. K. ROBINS. Proc. Natl. Acad. Sci. U.S. **65**, 27 (1970).
29. D. E. DORMAN and J. D. ROBERTS. Proc. Natl. Acad. Sci. U.S. **65**, 19 (1970).
30. H. H. MANTSCH and I. C. P. SMITH. Biochem. Biophys. Res. Commun. **46**, 808 (1972).
31. G. KOTOWYCZ and K. HAYAMIZU. Biochemistry, **12**, 517 (1973).
32. G. KOTOWYCZ and O. SUZUKI. Biochemistry, **12**, 3434 (1973).
33. R. D. LAPPER, H. H. MANTSCH, and I. C. P. SMITH. J. Am. Chem. Soc. **94**, 6243 (1972).
34. I. SOLOMON. Phys. Rev. **99**, 559 (1955).
35. N. BLOEMBERGEN. J. Chem. Phys. **27**, 572 (1957).
36. R. A. BERNHEIM, T. H. BROWN, H. S. GUTOWSKY, and D. E. WOESSNER. J. Chem. Phys. **30**, 950 (1959).
37. N. BLOEMBERGEN and L. O. MORGAN. J. Chem. Phys. **34**, 842 (1961).
38. A. CARRINGTON and A. D. MCLACHLAN. Introduction to magnetic resonance. Harper and Row Publishers, Inc., New York. 1967. pp. 225–229.
39. N. C. LI, R. L. SCRUGGS, and E. D. BECKER. J. Am. Chem. Soc. **84**, 4650 (1962).
40. T. J. SWIFT and R. E. CONNICK. J. Chem. Phys. **37**, 307 (1962).
41. R. A. DWEK. Adv. mol. relaxation processes, **4**, 1 (1972).
42. M. SUNDARALINGAM and J. A. CARRABINE. J. Mol. Biol. **61**, 287 (1971).
43. G. A. MILLER and R. E. D. MCCLUNG. J. Chem. Phys. **58**, 4358 (1973).
44. H. FRITZSCHE and C. ZIMMER. Europ. J. Biochem. **5**, 42 (1968).
45. P. O. P. TS'O. Fine structure of proteins and nucleic acids. *Edited by* G. D. FASMAN and S. N. TIMASHEFF. Marcel Dekker, New York, N.Y. p. 49.
46. P. O. P. TS'O, M. P. SCHWEIZER, and D. P. HOLLIS. Ann. N.Y. Acad. Sci. **158**, 256 (1969).
47. N. A. BERGER and G. L. EICHHORN. Biochemistry, **10**, 1847 (1971).
48. C. M. FREY and J. E. STUEHR. J. Am. Chem. Soc. **94**, 8898 (1972).
49. M. S. ZETTER, H. W. DODGEN, and J. P. HUNT. Biochemistry, **12**, 778 (1973).
50. Y. F. LAM, G. P. P. KUNTZ, and G. KOTOWYCZ. J. Am. Chem. Soc. In press.

Can. J. Chem. Downloaded from www.nrcresearchpress.com by 210.87.254.40 on 09/05/12
For personal use only.

Anodic Charging of Electrodes at Low Temperatures Studied by Electron Spin Resonance[1]

C. L. GARDNER AND E. J. CASEY

Electrical Power Sources Division, Defence Research Establishment, Ottawa, Canada K1A 0Z4

Received October 18, 1973

A study of anodic oxidation processes at several electrodes at low temperatures in KOH solutions is presented. The techniques of electron spin resonance have been used to identify intermediates. From a detailed kinetic analysis of the information obtained, the role of the formation and decay of O_3^- and certain metallic oxide radicals in the anodic charging of metal (hydr)oxide electrodes has been deduced.

The formation of O_3^- and/or O_2^-, or neither, during anodic oxygen evolution seems to be controlled by the tightness of binding of OH to the surface (hydr)oxide which changes with the metal in the (inferred) order of increasing binding strength Cd, Pb, Ni, Pt.

Once formed in solution, O_3^- decays slowly below 0 °C, slower the higher the KOH concentration. Primary dissociation, influenced by ion pair formation and by hydrolysis, controls the rate.

Le produit O_3^- se dégage de plusieurs métaux dans l'électrolyte KOH_{aq} durant l'oxidation anodique à basses températures. On peut mesurer la quantité d'O_3^- par la r.p.e., et ensuite faire une analyse cinétique des réactions lorsqu'il se détruit. Le comportement varie selon les métaux utilisés durant les expériences. L'ion CuO_2^{2-} se produit du cuivre, et l'O_2^- ou l'O_3^- se produit du cadmium selon les conditions expérimentales. L'O_3^- est le seul produit qui peut être détecté par la r.p.e. de l'argent.

En frais de résultats, on propose que l'énergie d'adsorption de l'OH détermine les produits, soit l'oxide bien chargé soit les radicaux libres dans l'electrolyte. Il nous semble que l'ordre de lier l'OH serait Cd < Ag < Pb < Ni < Pt, une fonction de la structure des (hydr)oxides à la surface. Pour emmagasiner plus de charge anodique sur les électrodes il faut supprimer la formation de l'O_3^- et l'O_2^-.

L'O_3^- se détruit lentement à basses températures (<0 °C). La vitesse baisse si la concentration de KOH est plus forte. Un modèle théorique est proposé pour décrire les résultats.

Can. J. Chem., **52**, 930 (1974)

Introduction

Problems such as the slow rate of charge acceptance encountered in the electrical recharging of aqueous battery systems at low temperatures are due to a number of causes. First, a decrease in temperature causes relative changes in the reversible electrode potentials of the reactions possible. Secondly, increased polarizations and higher potentials at the anode and cathode occur, because of kinetic and compositional barriers, increase in electrolyte viscosity, etc. As a result, alternate side reactions, such as oxygen evolution and even oxidation of the anions of the electrolyte, can more easily occur (1–3). To improve the low temperature recharge properties of a battery system it is necessary to find ways to decrease the polarizations of the electrodes and/or to inhibit the unwanted side reactions.

The present work was directed towards a better understanding of the processes which can and do occur during some anodic oxidations (positive-plate charging reactions) at low temperature. Fortunately, certain free-radical intermediates which are produced during the anodic oxidation at low temperatures in aqueous KOH electrolyte decay rather slowly and can be detected and their concentration followed by e.s.r. techniques. Thus in an earlier note (4) we indicated identification of O_3^- as a radical produced anodically on silver and gave some of its properties in cold aqueous KOH.

Since the problem of slow recharge of positive active material is closely related to the relative ease with which the alternative reaction, oxygen evolution, can take place, we have now made a detailed study, using electrochemical and e.s.r. techniques combined, of anodic reactions on several metals under a variety of conditions at

[1]DREO Report No. 69, October, 1973.

Can. J. Chem. Downloaded from www.nrcresearchpress.com by 210.87.254.105 on 09/05/12
For personal use only.

Can. J. Chem. Downloaded from www.nrcresearchpress.com by 210.87.254.105 on 09/05/12
For personal use only.

low temperatures, following the radical concentration changes where possible.

From a detailed analysis some tentative conclusions have been drawn about the anodic oxidation process at low temperatures.

Methods and Results

Electron Spin Resonance and Electrochemical Measurements

The potassium hydroxide used in these experiments was Fisher certified 45% KOH solution. In most of the experiments this solution was used without further dilution or purification. The metals used as electrodes were all of high purity (99.99% or better) with the exception of the copper which was of a commercial grade. All of the glass apparatus used in these experiments was constructed of Pyrex glass (7740) which has a low transition metal content (<0.1%). In addition, in all experiments the KOH used was cold (−40 to −20 °C) and kept in contact with glass during preparation and experiment at most 2–3 h. There was little likelihood of impurities affecting the principal results.

A Varian V-4500 e.s.r. spectrometer equipped with a Varian fieldial was used to record the e.s.r. spectra. The *g*-values were determined with reference to a DPPH sample for which $g = 2.0036$.

For some of the e.s.r. measurements at 77 °K, a sample cell of the design shown in Fig. 1 was used. In this case a silver or platinum wire was anodized at ~25 mA/cm^2 in 45% KOH solution which had been cooled to −40 °C. During this oxidation, oxygen evolution occurred and, in the case of silver, a yellow color could be observed streaming away from the anode, and eventually the whole anode compartment became yellow. After several minutes' oxidation, the e.s.r. sample tube (Fig. 1) was cooled with liquid nitrogen and the solution tipped into this tube and frozen at 77 °K as rapidly as possible. The liquid nitrogen Dewar containing the sample was then inserted into the microwave cavity and the spectrum measured.

In other experiments measurements were made by plunging a cooled, open-ended 4-mm quartz sampling tube close to the anode of a cell in which a foil electrode was being anodized at −40 °C. The solution contained in the sampling tube was then removed and frozen by direct immersion in liquid N_2.

The apparatus used to obtain e.s.r. spectra of the species in solution during and after anodic oxidation is shown in Fig. 2. In these experiments the electrodes were continuously anodized in an upper reservoir containing KOH, at about 90 mA/cm^2 in 45% KOH at −20°, for example. A portion of this solution was then allowed to transfer rapidly (forced by a syringe) to or through a Scanlon low temperature aqueous cell mounted in the Varian variable temperature accessory that fitted inside the e.s.r. cavity. The e.s.r. spectrum of the electrolyte sample was then measured. In some experiments a reference electrode was added close to the anode so that the onset of formation of the species could be correlated with oxidation potential.

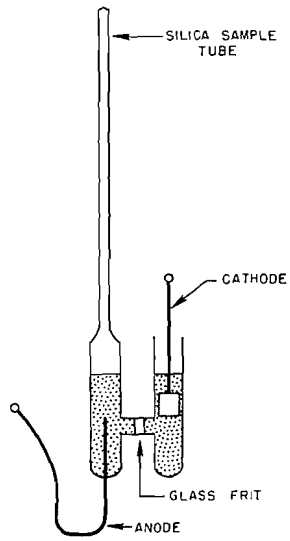

FIG. 1. Apparatus used to anodize metals in aqueous KOH at temperatures 25 to −40 °C and to trap and quick-freeze a sample of the anolyte for e.s.r. measurements.

Silver Electrodes

Anodic oxidation of a silver foil electrode in 45% KOH at −20 °C and high (~90 mA/cm^2) current densities resulted in the formation of a paramagnetic yellow species that was stable for several minutes and that could be easily detected using e.s.r. Continued anodization of silver at high current densities resulted in dissolution of the electrode and formation of the very stable, yellow species that has been assigned (5) to the tetrahydroxyargentite ion. (This second species is not paramagnetic.)

The e.s.r. spectrum of a sample prepared by the first experimental method, and recorded at 77 °K, is shown in Fig. 3. The spectrum can be

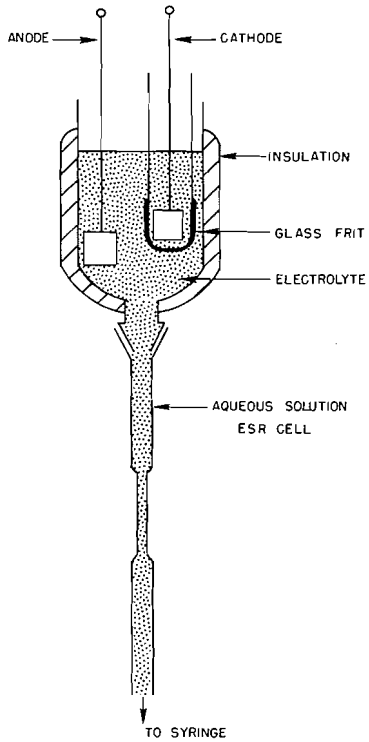

FIG. 2. Apparatus used to measure the e.s.r. spectra of samples of the anolyte at various temperatures.

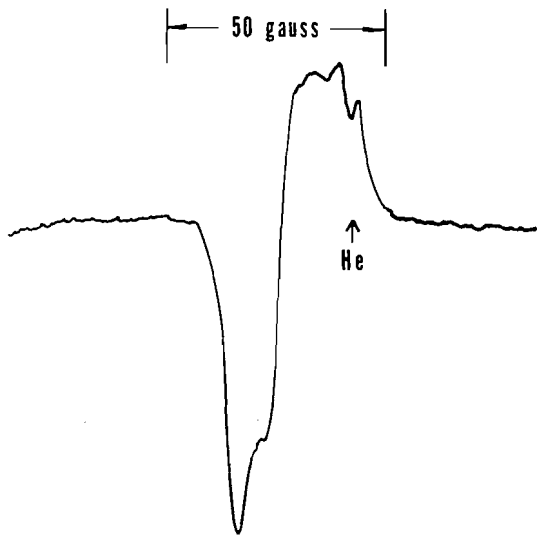

FIG. 3. Electron spin resonance spectrum of O_3^- at 77 °K, produced anodically on Ag in 45% KOH at −40 °C. H_e indicates the free electron field value.

TABLE 1. Electron spin resonance spectral parameters of O_3^- formed anodically compared with those from different sources

Matrix	g_{xx}	g_{yy}	g_{zz}
$KClO_4$ (7)	2.0174	2.0113	2.0025
$KClO_4$ (7)	2.018	2.011	2.0034
NaO_3 (6)	2.015	2.015	2.003
This work	2.0181	2.0112	2.0019

described in terms of a species having an anisotropic **g**-tensor with principal values as shown in Table 1. The species can be identified as the ozonide ion (O_3^-) by comparison with the spectra of alkali metal ozonides (6), of γ-irradiated $KClO_4$,(7) of u.v.-irradiated alkaline glasses containing H_2O_2 (8), and of O_3^- formed on an MgO surface (9).

An intense signal was also obtained for O_3^- in solution, using the apparatus shown in Fig. 2, during anodic oxidation at −20 °C. The spectrum consisted of a single symmetrical line with $g = 2.0108 \pm 0.0010$. This is in agreement with the value of $g_{iso} = 1/3(g_{xx} + g_{yy} + g_{zz}) = 2.0104 \pm 0.0010$ obtained from the spectrum of O_3^- at 77 °K.

In order that a correlation could be made between oxidation potential and the appearance of the e.s.r. signal for O_3^-, the silver electrode was maintained at a constant potential while the sample was monitored for the appearance of the e.s.r. signal. It was found that the O_3^- was not formed at potentials lower than that corresponding to the onset of visible oxygen evolution (1.40 V *vs.* Hg/HgO reference electrode at −20 °C). Methanol, a good scavenger for OH, suppressed the appearance of O_3^- at the silver anode, even at high potentials.

In almost all of the spectra observed at 77 °K an additional sharp peak called species X, was observed at $g = 2.003$. This peak showed different saturation behavior from the O_3^- and is thought probably to be due to conduction-electron resonance (10) in small colloidal metal particles produced during the electrolysis. However, it could be due to an impurity in the KOH, or possibly due to solvated (trapped) electrons (11). More work is needed to obtain a positive identification.

A kinetic study was made of the decay of O_3^- in several KOH concentrations and at several temperatures. In all cases the decay was found to be closely first order. Thus as illustrated by

Can. J. Chem. Downloaded from www.nrcresearchpress.com by 210.87.254.105 on 09/05/12
For personal use only.

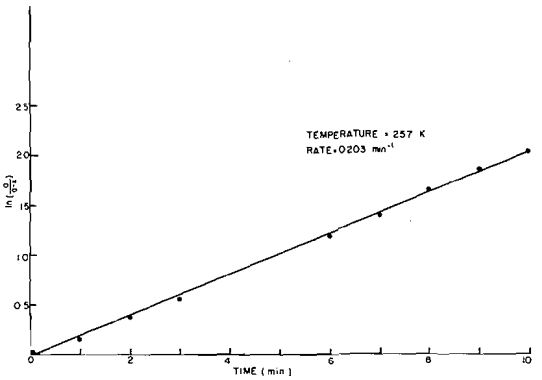

FIG. 4. Typical decay rate measurement of O_3^-: exponential loss of intensity of e.s.r. signal with time at −15 °C.

Fig. 4 for one case, the standard deviation from linearity, as obtained from a least-squares fit of the data, is 0.01. The decay-rate was also found to depend approximately exponentially on KOH concentration (Fig. 5). The results of certain self-consistent, carefully performed experiments (such as those shown in Fig. 6) seemed to indicate that the activation energy for the decay increased with increasing KOH concentration, but the results were not sufficiently reproducible to demonstrate unequivocally this effect.

Since carbonate is likely to be the most important impurity in the KOH, the effect of carbonate concentration on the decay kinetics was

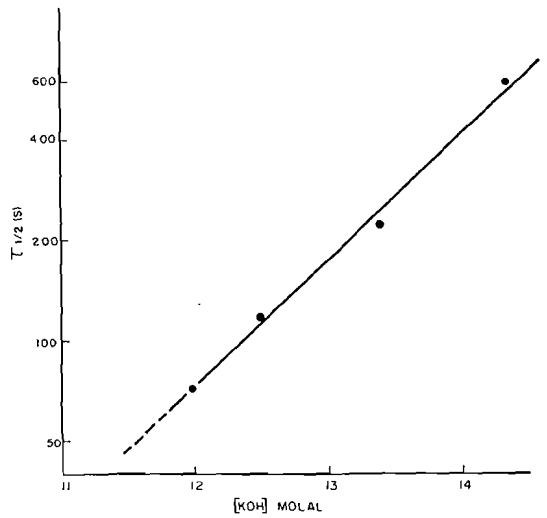

FIG. 5. Dependence of rate of loss of O_3^- (half-life) on KOH concentration: log $\tau_{1/2}$ (in s) *vs.* molality.

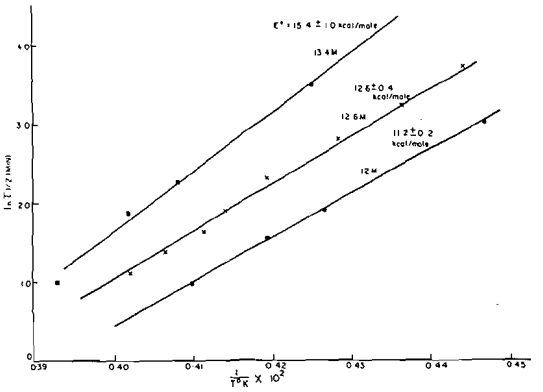

FIG. 6. Temperature dependence of rate of loss of O_3^- at different concentrations: ln $\tau_{1/2}$ (in min) *vs.* $1/T$ °K.

measured. Results of measurements made on solutions with carbonate concentration up to 6 equiv.% (equiv. CO_3^-/total equiv. basicity) indicated that, in this range of concentration, the carbonate has little or no effect on the formation or rate of decay of the O_3^-.

Lead, Nickel, and Platinum Electrodes

Anodic oxidation of the above metals in 45% KOH at low temperatures gave rise to the formation of small amounts of O_3^- and/or the species X as indicated in Table 2. Also indicated in this table are the relative concentrations of the species produced. The decay of species X formed on Ni or Pt was found to be quite rapid (half-life a few seconds), whereas formed on Ag it sometimes persisted for hours. The *g*-value, 2.003, is consistent with X being solvated electrons, but it could be a metal colloid equally well. Distinguishing quantitative measurements have not yet been made.

Copper Electrodes

During the anodic oxidation of copper a

TABLE 2. Relative amounts of O_3^- and species X formed anodically on different metal hydr(oxide) surfaces

Anode material	Species detected*
Silver	O_3^-(s) ; X(w)
Cadmium	O_3^-(s) ; X(w)
Lead	O_3^-(w); X(w)
Nickel	X(w)
Platinum	X(w)
Copper	CuO_2^{2-}(s); X(w)

*w = weak; s = strong e.s.r. signal.

Can. J. Chem. Downloaded from www.nrcresearchpress.com by 210.87.254.105 on 09/05/12
For personal use only.

Can. J. Chem. Downloaded from www.nrcresearchpress.com by 210.87.254.105 on 09/05/12
For personal use only.

soluble, blue species could be observed forming at the anode below the oxygen evolution potential. This phenomenon has been reported previously (12) and assigned to the cuprite ion ($HCuO_2^-$ in weak base or CuO_2^{2-} in strong base). Electron spin resonance measurements made on this blue solution have an intense e.s.r. spectrum shown in Fig. 7. A sample of this solution frozen at 77 °K gave rise to the spectrum shown in Fig. 8. Spin Hamiltonian parameters, obtained by computer simulation of the spectrum, for this species are given in Table 3. The species can be identified as a Cu^{2+}-containing species having non-axial symmetry, which is consistent with the assignment to CuO_2^{2-}, but not to a planar or tetrahedral hydroxy species such as $Cu(OH)_4^{2-}$. However measurements made at various KOH concentrations failed to elicit the expected e.s.r. spectra changes due to a shift in the following equilibrium.

$$HCuO_2^- + OH^- \rightleftharpoons CuO_2^{2-} + H_2O$$

It is possible that the equilibrium was already shifted far to the right even at the lowest concentration measured, ~ 1 *M*. The CuO_2^{2-} species is very stable and will last for days even at room temperature.

When anodic oxidation was carried out at much higher current densities so that oxygen evolution occurred, a fairly stable yellow solution resulted. Electron spin resonance measurements indicated only the presence of a lesser quantity of CuO_2^{2-}, as well as species X. It is tentatively suggested that the yellow coloration might result from the formation of a non-paramagnetic Cu^{3+} species such as $Cu(OH)_4^-$ (13) in solution,

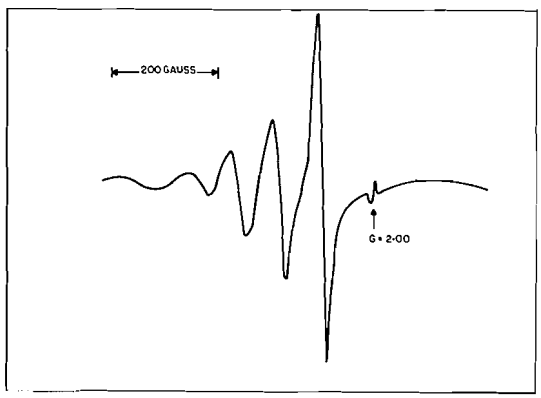

FIG. 7. Electron spin resonance spectrum of paramagnetic species (CuO_2^{2-}) formed anodically on Cu in KOH at room temperature.

FIG. 8. As in Fig. 7, but frozen to 77 °K. Weaker low-field lines shown at a gain 8 × that of lines in $g = 2$ region.

TABLE 3. Electron spin resonance spectral parameters of CuO_2^{2-} formed anodically

$g_x = 2.27$	$A_x = 186.4$ gauss
$g_y = 2.06$	$A_y = 26.1$
$g_z = 2.00$	$A_z = 2.0$

analogous to the tetrahydroxyargenite ion, $Ag(OH)_4^-$, obtained from oxidation of silver at high current densities (5). Like Ag^{3+}, Cu^{3+} forms stable complexes with certain organic ligands (14).

Cadmium Electrodes

Anodic oxidation of cadmium in 45% KOH at low temperatures produced large amounts of O_3^- as well as the species X. The rate of decay of the O_3^- was found to be the same as that produced from the anodic oxidation of silver in 45% KOH at the same temperature.

The decay of O_3^- formed on cadmium in 30% KOH, even at −40°, must be very rapid because the species could not be detected using the apparatus for kinetic measurements. If, however one takes a sample by plunging a cooled sample tube into the electrolyte in the vicinity of the anode and freezes this sample at 77 °K as rapidly as possible, reasonably intense e.s.r. signals for O_3^- can be obtained. Figure 9 shows a series of samples taken in this way at different temperatures of the anolyte between −40 and −10 °C. Notice that the major product changes from O_3^- at −40 °C to a species with the parameters (Table 4) of O_2^- at −10 °C. Spectra at intermediate temperature show an overlap of the two species.

We were unable to detect O_2^- during the anodic oxidation of Ag, Pb, Ni, and Pt in 30% KOH

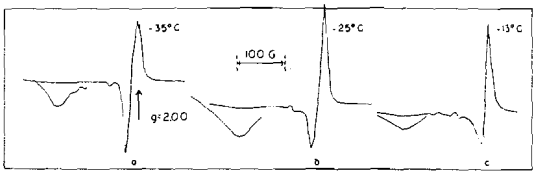

FIG. 9. Spectra showing O_3^- and O_2^- formed during anodic oxygen evolution from cadmium at different temperatures in 30% KOH: (*a*) −35 °C: O_3^-; (*b*) −25 °C: O_3^- and O_2^-; (*c*) −13 °C: O_2^-. High-gain (6.4×) traces of low-field region also shown.

TABLE 4. Electron spin resonance spectral parameters of O_2^- formed anodically on Cd at −13 °C, compared with those from different sources

Matrix	g_x	g_y	g_z	Reference
KNO_3	1.958	1.958	2.408	28
Adsorbed on BaY zeolite	2.005	2.009	2.057	29
Adsorbed on MaY zeolite	2.002	2.007	2.113	29
NaO_2	2.000	2.000	2.175	8
This work	2.01	2.01	2.11	

Formation and Decay of O_3^-

Anodic Formation

The controlled-potential measurements indicate that O_3^- is formed during the oxygen evolution process. The mechanism of oxygen evolution (15) in alkaline solution is generally considered to involve discharge of adsorbed hydroxyl ions as the primary step.

[1] $$OH^- \rightarrow OH + e^-$$

In strong alkali, other steps could follow:

[2] $$OH + OH^- \rightarrow O^- + H_2O$$

[3] $$O^- \rightarrow O + e^-$$

[4] $$2O \rightarrow O_2$$

All these species are adsorbed except O_2 which disengages.

The O_3^- formed in our system could arise (9) from the reaction of adsorbed O^- with O_2

[5] $$O^- + O_2 \rightarrow O_3^-$$

or alternatively O_3^- could be produced by dissociation of HO_3 to O_3^- in strong base following the reaction of oxygen with adsorbed OH

[6] $$OH + O_2 \rightarrow HO_3$$

This scheme of reactions is very similar to that postulated (16, 17) for the formation of O_3^- in the radiolysis of oxygenated alkali solutions, where the primary step is thought to be

[7] $$OH^- \rightsquigarrow OH + e^-$$

reactions 2 and 5 then following to yield O_3^-.

This type of mechanism, involving either OH or O^-, is supported by the observation that addition of a small amount of methanol almost completely eliminates the signal due to O_3^-. Since it is well known (16) that the formation of O_3^- during the radiolysis of alkaline solutions can be suppressed by the addition of a hydroxyl-radical scavenger such as methanol, this observation provides strong evidence that hydroxyl radicals are a precursor to the anodic formation O_3^- as well.

The mechanism of oxygen evolution on many metals can be considered (18) to involve the formation and decomposition of unstable surface oxides. The general case (18) and the case of silver (19) have been reviewed in some depth elsewhere. For silver, one scheme proposed is as follows: an unstable higher silver oxide, Ag_2O_3 is produced by the reaction

[8] $$2AgO + 2OH^- \rightarrow Ag_2O_3 + H_2O + 2e^-$$

involving intermediate steps such as

[8*a*] $$AgO + OH^- \rightarrow AgO(OH) + e^-$$

[8*b*] $$AgO(OH) + OH^- \rightarrow AgO(O^-) + H_2O$$

[8*c*] $$AgO + AgO(O^-) \rightarrow Ag_2O_3 + e^-$$

The Ag_2O_3 then decomposes to liberate oxygen as follows in the decomposition reaction

[9] $$Ag_2O_3 \rightarrow 2AgO + \tfrac{1}{2}O_2$$

Alternatively, adsorbed O^- could be oxidized anodically directly to adsorbed O

[10] $$AgO(O^-) \rightarrow AgO(O) + e^-$$

with oxygen being then formed by combination of oxygen atoms on the AgO surface

[11] $$2AgO(O) \rightarrow O_2 + 2AgO$$

Taub's oxygen-tracer studies discussed in ref. 18 seem to support a mechanism of this type. However, recent photoelectrochemical work (20) suggests two adjacent AgO sites on which an extra oxygen atom is shared do indeed rearrange to form the phase-oxide Ag_2O_3. Thus it can then disproportionate according to reaction 9. Probably [9] *and* [10] both occur, even on the same sample of active material undergoing anodic

Can. J. Chem. Downloaded from www.nrcresearchpress.com by 210.87.254.105 on 09/05/12
For personal use only.

Can. J. Chem. Downloaded from www.nrcresearchpress.com by 210.87.254.105 on 09/05/12
For personal use only.

oxygen evolution. In any case it is easy to see that the surface oxides are probably well charged with the species necessary for the formation of O_3^- by reactions 3 to 6.

Kinetics of Decay

The mechanism of decay of O_3^- formed by radiolysis in alkaline solutions has been studied by several workers and was recently reviewed by Czapski (21). For low concentrations of O_3^- the decay has been found to be first order (17). All the results that we obtained concerning anodically formed O_3^- are in agreement with this finding. (At high concentrations of radiolytically formed O_3^-, the decay has been found (22) to be mixed first and second order.) The first order rate constant has been found (22) to be inversely proportional to $[O_2]$, the oxygen concentration in solution as inferred through Henry's law from the partial pressure above the solution. It has also been observed (16, 17) that the rate of decay decreases markedly with increasing hydroxyl ion concentration.

Felix *et al.* (22) have suggested that O_3^- decays by unimolecular dissociation of the ozonide ion by the reverse of reaction 5

[12] $$O_3^- \rightarrow O_2 + O^-$$

the active species O^- being then removed by reaction with an unspecified scavenger S:

[13] $$O^- + S \rightarrow \text{Products}$$

These reactions enabled them to describe the first-order decay and the inverse dependence of the rate constant on oxygen pressure. The deviation from first-order at high concentrations of O_3^- was ascribed by them to

[14] $$O^- + O_3^- \rightarrow O_2 + O_2^{2-} \text{ (or } 2O_2^-)$$

But we have never observed the deviation in our studies on anodically formed O_3^-.

The above mechanism does not explain the observed decrease in decay rate with increasing KOH concentration. If however one considers that the following reactions also contribute to the decay of O_3^- then the decay can become pH dependent.

[15] $$O^- + H_2O \rightleftharpoons OH + OH^-$$

[16] $$OH + S \rightarrow \text{Products}$$

The general rate equation in this case can be written (21)

[17] $$\frac{-d[O_3^-]}{dt} = \frac{\left\{k_{13} + \frac{k_{16}[H^+]}{k_{OH}}\right\}[S]k_{-5}[O_3^-]}{k_5[O_2] + \left\{k_{13} + \frac{k_{16}[H^+]}{K_{OH}}\right\}[S]}$$

where

$$K_{OH} = [OH][OH^-]/[O^-][H_2O]$$

Under certain conditions (*i.e.* $[O_2]$ high), the observed approximate linear relation between log $\tau_{1/2}$ and m_{KOH} can be explained in terms of [17] since it is known (23, 24) that a_{KOH}, a_{H_2O}, and $[O_2]$ all have an approximate exponential dependence on m_{KOH} in the concentration range used even at the low temperatures of this investigation (25).

It should be noted however that it has been found by Landi and Heidt (26) that the rate constant k_5 (for the reaction $O_3^- \rightarrow O_2 + O^-$) decreases markedly with increasing NaOH concentration. These workers suggested that this decrease in k_5 is caused by the formation of stable ion pairs NaO_3, the decay of O_3^- occurring only through free O_3^-.

In treating our data then we assume that, because of the salting out effect, the concentration of oxygen was sufficiently low in the concentrated KOH solutions used that the decay rates we have measured are unaffected by $[O_2]$, the rate controlling reaction being simply the unimolecular decay rate for the process $O_3^- \rightarrow O_2 + O^-$ (see eq. 17). Following Landi and Heidt we assume that the stabilization of O_3^- with increasing [KOH] is a result of the formation of stable ion pairs.

[18] $$KO_3 \rightleftharpoons K^+ + O_3^-$$

The rate of decay can then be written

[19] $$-\frac{d[KO_3]}{dt} = K[O_3^-] = \frac{kK_{eq}[KO_3]}{[K^+]\gamma_\pm^2}$$

where

$$K_{eq} = a_{K^+}a_{O_3^-}/a_{KO_3}$$

Figure 10 shows that the decay rate has an approximate linear dependence on $[K^+]\gamma_\pm^2$. In this analysis and apparently in that of Landi and Heidt γ_{KO_3} has been assumed to be independent of [KOH].

The mechanism proposed by Kazarnovskii *et al.* (27), namely, the hydrolysis of O_3^-, was also

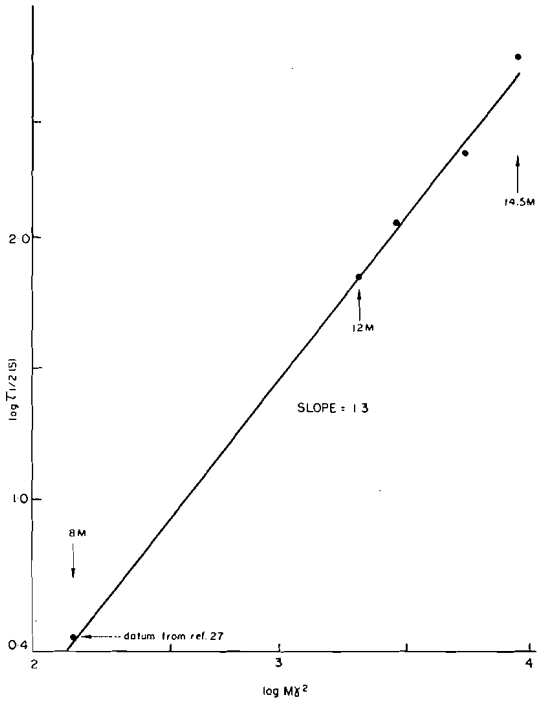

FIG. 10. Linear dependence of log $\tau_{1/2}$ (in s) on log $M\gamma_{\pm}^2$ at -20 °C: a test of expression 19 in text.

considered

[20] $O_3^- + H_2O \rightleftharpoons OH + OH^- + O_2$

It of course leads to a similar quantitative description of the mechanism, since it is a combination of processes 2 and 3 above. Although less explicit it promoted considerable thought about possible molecular arrangements during the decomposition step.

General Inferences

The observation that O_3^- is formed during oxygen evolution of "active" metals such as silver and cadmium, but weakly or not at all on copper, nickel, and platinum can be explained on the basis of the relative strengths of binding of O^- and/or OH to the surface (hydr)oxides. If the O^- formed in reaction 8*b* is weakly bound, it can leave the surface accompanied by O_2 to form O_3^- by reaction 5; but if it is strongly bound then it is discharged to O_{ads} instead, [10] for example, and little or no O_3^- can be produced, although higher phase-oxides could be formed. Similar arguments hold for OH. The evidence for anodically formed higher oxides on nickel and platinum is better than for their formation on silver or cadmium. The conclusion is that O_{ads}^- and OH_{ads} are strongly bound on nickel and platinum (hydr)-oxide surfaces during oxygen evolution but are weakly bound on the silver and cadmium. Lead is intermediate.

The formation of O_2^- on cadmium is ascribed to the high concentration of OH at the surface as indicated by the high concentration of O_3^- produced. Under these conditions the formation of hydrogen peroxide via the bimolecular reaction 21 becomes more probable.

[21] $2OH \rightarrow H_2O_2$

O_2^- can then be formed as follows (21)

[22] $H_2O_2 + OH^- \rightarrow HO_2^- + H_2O$

[23] $HO_2^- + OH \rightarrow O_2^- + H_2O$

The general inference is that OH_{ads} is the key actor. Its binding strength to the surface (hydr)-oxides during anodic oxygen seems to vary with the metallic component, increasing qualitatively in the series Cd, Ag, Pb, Cu, Ni, and Pt. The more tightly OH and O are held the greater the possibility of their incorporation into higher-valence phase-oxides.

It is probably no coincidence that the order given above is the order of increasing passivity of the metal as well. Thus Cd and Ag, and Cu too, anodically oxidize to considerable depths in aqueous KOH, but Pt and Ni little or not at all. Many authors (30, 31) have inferred that the final closure of the surface of a metal to (further) anodic oxidation is caused by anodically formed OH_{ads}. Unfortunately, so far no one has been able to produce any direct evidence of its existence on the surface.

In this paper we have been very cautious about identity of species X which appears, sometimes strongly, in many spectra, as a simple sharp absorption band at $g = 2.003$. As has been mentioned previously, it is thought possible that this peak could be due to conduction electron resonance in small colloidal metal particles, it could be due to solvated electrons (although there is disagreement (32, 33) currently over the evidence that electrons can be produced anodically in aqueous solutions), or possibly due to a KOH impurity. The single, sharp band alone simply provides too little information to permit identification.

Can. J. Chem. Downloaded from www.nrcresearchpress.com by 210.87.254.105 on 09/05/12
For personal use only.

1. T. R. BECK and R. W. MOULTON. J. Electrochem. Soc. **103**, 4 (1956).
2. A. A. YAKOVLEVA and V. I. VESELOVSKII. Electrokhimiya, **7**, 683 (1971).
3. L. EBERSON. Acta Chem. Scand. **17**, 2004 (1963).
4. C. L. GARDNER and E. J. CASEY. Can. J. Chem. **49**, 1782 (1971).
5. G. L. COHEN and G. ATKINSON. J. Electrochem. Soc. **115**, 1236 (1968).
6. J. E. BENNETT, D. J. E. INGRAM, and D. SCHOULAND. Proc. Phys. Soc. Lond. A**69**, 556 (1956).
7. P. W. ATKINS, J. A. BRIVATI, N. KEEN, M. C. R. SYMONS, and P. A. TREVALION. J. Chem. Soc. 4785 (1962).
8. A. D. MCLACHLAN, M. C. R. SYMONS, and M. G. TOWNSEND. J. Chem. Soc. 952 (1959).
9. A. J. TENCH and T. LAWSON. Chem. Phys. Lett. **8**, 177 (1971).
10. G. FEHER and A. F. KIP. Phys. Rev. **98**, 337 (1955).
11. L. KEVAN. J. Am. Chem. Soc. **87**, 1481 (1965).
12. A. M. SHAMS EL DIN and F. M. ABD EL WAHAB. Electrochem. Acta, **9**, 113 (1964).
13. B. MILLER. J. Electrochem. Soc. **116**, 1675 (1969).
14. J. KLEINBERG. Unfamiliar oxidation states and their characterisation. University of Kansas press. Lawrence, Kansas. 1950.
15. J. O'M BOCKRIS. J. Chem. Phys. **24**, 817 (1956).
16. G. E. ADAMS, J. W. BORG, and B. O. MICHAEL. Proc. R. Soc. Lond. A**289**, 321 (1966).
17. G. CZAPSKI and L. M. DORFMAN. J. Phys. Chem. **68**, 1169 (1964).
18. J. P. HOARE. Electrochemistry of oxygen. Interscience Publishers. New York. 1968.
19. G. D. NAGY and E. J. CASEY. Zinc – silver oxide batteries. *Edited by* A. Fleischer and J. J. Lander. J. Wiley and Sons Inc., New York. 1971. pp. 143–146.
20. R. G. BARRADAS. Private communication.
21. G. CZAPSKI. Ann. Rev. Phys. Chem. **22**, 171 (1971).
22. W. D. FELIX, B. L. GALL, and L. M. DORFMAN. J. Phys. Chem. **71**, 384 (1967).
23. G. C. AKERLOF and P. BENDER. J. Am. Chem. Soc. **70**, 2366 (1948).
24. T. MORRISON. J. Chem. Soc. 3814 (1952).
25. P. BRO and H. Y. KANG. J. Electrochem. Soc. **118**, 1430 (1971).
26. V. R. LANDI and L. J. HEIDT. J. Phys. Chem. **73**, 2361 (1969).
27. I. A. KAZARNOVSKII, D. S. GARBENKO-GERMANOV, and I. V. KOZLOVA. Izv. Akad. Nauk SSSR. Ser. Khim, **1**, 197 (1969).
28. W. KANZIG. J. Phys. Chem. Solids, **17**, 88 (1960).
29. P. H. KASAI. J. Chem. Phys. **43**, 3322 (1965).
30. P. E. LAKE and E. J. CASEY. J. Electrochem. Soc. **105**, 52 (1958).
31. M. BREITER. Electrochemistry of fuel cells. Springer-Verlag, New York. 1969.
32. D. C. WALKER. Can. J. Chem. **45**, 807 (1967); J. Electronal. Chem. Interf. Sci. **42**, App. 17 (1973).
33. A. BEWICK, B. E. CONWAY, and A. M. TUXFORD. J. Electronal. Chem. Interf. Sci. **42**, App. 11 (1973).
34. A. V. DUBOVITSKII and G. B. MANDELIS. Kin. Katal. **6**, 828 (1965).

Can. J. Chem. Downloaded from www.nrcresearchpress.com by 210.87.254.105 on 09/05/12
For personal use only.

The Master Equation for the Dissociation of a Dilute Diatomic Gas. XI. Vibrational Freezing in a Nozzle Flow

NABIL I. LABIB AND HUW O. PRITCHARD

Centre for Research in Experimental Space Science, York University, Downsview, Ontario M3J 1P3

Received September 17, 1973

A previously reported calculation on a model expansion in a nozzle flow is extended to the point where the whole vibrational energy "freezes" and the behavior of the vibrational relaxation time is examined. Starting with the high levels, each individual vibrational energy level becomes decoupled from the ground state in sequence, down to and including $v = 1$; under these conditions, all measures of the vibrational relaxation time fail, but perhaps surprisingly the rate constant for recombination remains well defined.

Un calcul préalablement décrit sur une expansion modèle dans une "buse de courant" est développé au point où toute l'énergie vibrationnelle "gèle" et le comportement du temps de relaxation vibrationnelle est examiné. Partant des niveaux élevés, chaque niveau particulier d'énergie vibrationnelle devient découplé, en série, de l'état fondamental diminuant jusqu'à $v = 1$ inclusivement; dans ces conditions, toutes les mesures du temps de relaxation vibrationnelle font défaut mais, ce qui peut être surprenant, la constante de vitesse de recombinaison reste bien définie. [Traduit par le journal]

Can. J. Chem., **52**, 939 (1974)

Can. J. Chem. Downloaded from www.nrcresearchpress.com by 210.87.254.6 on 09/05/12
For personal use only.

In an earlier paper (1), we reported the results of a calculation on a model flow in which a H_2/He mixture was cooled by a nozzle expansion from 3900 to 1500 °K; we now report the extension of this model calculation down to 685 °K because it demonstrates three interesting features.

We had found in earlier model calculations on the vibration–dissociation coupling in a shock wave (2) that the second eigenvalue (d_{n-2}) of the relaxation matrix was related to the vibrational relaxation time through

$$[1] \qquad \tau_{vib}^{-1} = -d_{n-2}$$

Furthermore, at low temperatures, this eigenvalue relation was equivalent to the ordinary harmonic-oscillator formula

$$[2] \qquad \tau_{vib}^{-1} = Z[\mathrm{M}](P_{01} - P_{10})$$

although above about 1500 °K, these two diverged somewhat because of increasing complexity of the relaxation process (2, 3): this is apparent in Fig. 1. In the nozzle calculation, however, it was found (1) that one could not define a vibrational relaxation time using the conventional concept of a vibrational temperature because of the severity of the flow conditions and the rapidity of the resulting vibrational population changes; on the other hand, the well-known formula

$$[3] \qquad \tau_{vib}^{-1} = (\tilde{\varepsilon}_{vib} - \varepsilon_{vib})^{-1} \frac{d\varepsilon_{vib}}{dt}$$

which defines the relaxation time in terms of the rate of loss of vibrational energy remained in acceptable agreement with eq. 1, although the

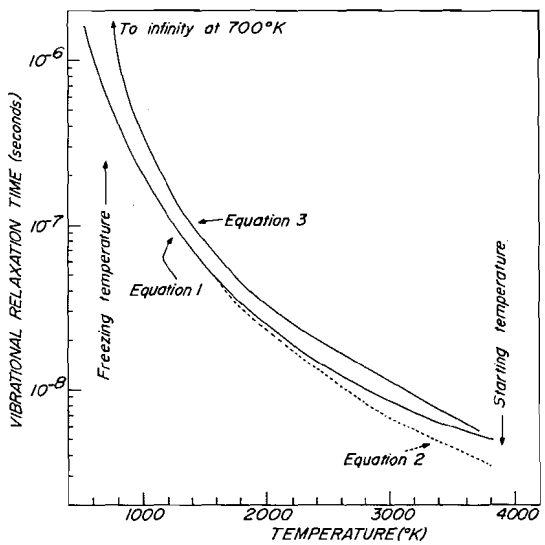

FIG. 1. Comparison of vibrational relaxation times for the model flow calculated from the rate of loss of vibrational energy (eq. 3) with the correct values (eq. 1); numerical values refer to a constant density, see ref. 1 for further details.

Can. J. Chem. Downloaded from www.nrcresearchpress.com by 210.87.254.6 on 09/05/12
For personal use only.

agreement in fact became poorer as the flow progressed (1). The recent implementation of quadruple-length arithmetic on our IBM 370 computing machine has enabled us to continue this calculation with good accuracy down to 790 °K, and with limited accuracy (*c.a.* 2 decimal places on most populations) down as far as 685 °K, confirming in fact that this divergence between eqs. 1 and 3 is caused by the onset of "freezing" and not by computational deficiencies.

We may summarize the results of this extended calculation[1] under the following three headings.

(i) The Recombination Rate Constant

The flow continues to be virtually frozen in respect of recombination, and the top-most vibrational levels continue to be in good equilibrium with the local atom concentration, which is in fact decreasing mainly because of the expansion, but partly also because of a small amount of recombination. Throughout the calculation, the phenomenological rate constant for recombination, calculated from the net recombination flux remains in excellent agreement with that calculated from the smallest eigenvalue (d_{n-1}) of the system of relaxation equations. It may seem surprising that even though the vibrational relaxation time becomes ill-defined as described below, the rate constant remains well behaved: in fact the reaction is very far from equilibrium in respect of recombination, and this behavior can be understood in terms of Boyd's recent analysis of the rate-quotient law (4).

(ii) Consecutive Freezing

As the flow progresses, the upper vibrational level populations cease to be coupled to the ground-state population in monotonic succession. We had suggested previously that the over-population of a particular level by a factor of about three with respect to the ground state could be regarded as a reasonable criterion for the freezing of that level in a vibrational relaxation (1): Table 1 shows such freezing points for each vibrational level in the column headed "criterion 1". However, because in this calculation we have the upper vibrational levels strongly coupled to a source of new molecules through recombination of atoms, a second more dramatic criterion for freezing arises: shortly after a particular level becomes essentially decoupled from the ground state according to criterion 1, the supply of molecules from the reservoir of newly formed highly excited molecules causes the population of that level to cease falling and to rise again. Thus the level is completely and absolutely decoupled from the ground state as its population is now rising although the translational temperature is falling: these absolute freezing points are listed in Table 1 under the heading "criterion 2" and it is seen that this behavior also progresses monotonically downwards in v until it reaches the $v = 1$ state; criterion 2, however, is not applicable to the high vibrational levels where the dominating trend is a fall in population related to the fall in atom concentration caused by the expansion.

TABLE 1. Freezing points of individual vibrational energy levels in the nozzle flow

Vibrational level v	T(°K) Criterion 1	T(°K) Criterion 2
14	3560	—
13	3550	—
12	3530	—
11	3475	—
10	3380	(1930)
9	3250	(2425)
8	3075	2435
7	2860	2345
6	2610	2200
5	2330	2005
4	2025	1760
3	1690	1415
2	1190	960
1	1005	700

(iii) The Vibrational Relaxation Time

It is clear that as soon as the populations of *all states* are rising whereas the translational temperature is falling, which happens at about 700 °K in this experiment, calculation of the vibrational relaxation time via eq. 3 must also fail, since $d\varepsilon_{vib}/dt$ passes through zero and therefore τ_{vib}^{-1} becomes negative! Figure 1 compares the behavior of the practical vibrational relaxation time, calculated according to eq. 3, with the other two theoretical measures, *i.e.* eqs. 1 and 2. Equation 3 departs soon after the

[1]Tables of the gasdynamic properties of this flow and the population distributions can be obtained, at a nominal charge, from The Depository of Unpublished Data, National Science Library, National Research Council of Canada, Ottawa, Canada, K1A 0S2.

commencement of the expansion at 3900 °K from the true relaxation time (eq. 1), and although it is not ideally apparent from the logarithmic plot shown in Fig. 1, the disagreement between the two equations becomes progressively greater as the flow evolves: the error becomes a factor of 2 near 1000 °K, and eq. 3 finally diverges to infinity at 700 °K.

1. N. I. LABIB, D. L. S. MCELWAIN, and H. O. PRITCHARD. Can. J. Chem. **50**, 3832 (1972). Part VII.
2. D. L. S. MCELWAIN and H. O. PRITCHARD. Thirteenth Symposium (International) on Combustion. The Combustion Institute. 1971. p. 37. Part III.
3. A. G. GAYDON and I. R. HURLE. The shock tube in high-temperature chemical physics. Chapman and Hall, London. 1963. p. 196.
4. R. K. BOYD. J. Chem. Phys. To be published.

Can. J. Chem. Downloaded from www.nrcresearchpress.com by 210.87.254.6 on 09/05/12
For personal use only.

The Microwave Spectrum of Trifluoromethyl Hypofluorite

P. BUCKLEY AND J. P. WEBER

Département de Chimie et Centre de Recherches sur les Atomes et les Molécules, Université Laval, Québec 10, Québec G1K 7P4

Received February 5, 1973[1]

The microwave spectrum of trifluoromethyl hypofluorite (CF_3OF) has been analyzed in the region 8–40 GHz. Only μ_a R-type transitions were observed despite a careful search and using double-resonance techniques. These determine the following rotational constants: $A = 5600 \pm 100$, $B = 3108.13 \pm 0.02$, $C = 3049.25 \pm 0.02$ MHz. The dipole moments determined from Stark effect measurements are $\mu_a = 0.30 \pm 0.02$, $\mu_b = 0.10 \pm 0.06$, $\mu_c = 0$ D. The $v = 1$ state of the CF_3 torsion has also been measured; relative intensity measurements lead to a potential barrier of 3.9 kcal/mol, somewhat higher than the electron diffraction results.

On a analysé le spectre du trifluorométhyl hypofluorite dans la région de 8 à 40 GHz. Seules des transitions de type R μ_a ont pu être observées malgré un balayage minutieux et l'emploi de la technique de double résonance. Les constantes rotationnelles sont les suivantes: $A = 5600 \pm 100$, $B = 3108.13 \pm 0.02$, $C = 3049.25 \pm 0.02$ MHz. Les moments dipolaires obtenus par effet Stark sont: $\mu_a = 0.30 \pm 0.02$, $\mu_b = 0.10 \pm 0.06$, $\mu_c = 0$ D. Le spectre de l'état $v = 1$ de la torsion CF_3 a également été mesuré; les mesures d'intensité relative conduisent à une barrière de potentiel de 3.9 kcal/mol, ce qui est un peu plus élevé que les résultats obtenus par diffraction des électrons.

Can. J. Chem., **52**, 942 (1974)

Introduction

Trifluoromethyl hypofluorite (CF_3OF) is an important reagent in the synthesis of organic and inorganic fluorine compounds and its properties and reactions have been extensively studied (1). Prior to undertaking this microwave investigation, the only structural data available were based on the i.r. and Raman spectra (2–4). These medium-resolution studies included a band contour analysis from which an accidentally symmetric prolate top structure was derived. A band at 56 cm^{-1} was assigned as the $1 \leftarrow 0$ transition of the CF_3 torsion and a potential barrier of 395 cm^{-1} (1.13 kcal/mol) was determined with an assumed geometry. While our work was in progress, the structure of the molecule was determined by electron diffraction (5). The results indicated a CF_3 group tilt of $4.1 \pm 0.8°$ and a potential barrier of 2.5 ± 0.5 kcal/mol.

Experimental

The microwave spectrum was observed on a conventional 100 kHz square-wave Stark modulation spectrometer built in this laboratory. The source was a Hewlett–Packard model 8690A sweep oscillator using appropriate plug-in RF units, covering the range 8 to 40 GHz. Precise frequency measurements were achieved by phase-locking the oscillator to a Microwave Systems Frequency Stabilizer model MOS-V. Markers were derived from the electronic counter. The frequencies are accurate to 50 kHz.

A sample of CF_3OF was purchased from Peninsular Chem Research Inc. Impurities detected by gas chromatography included small amounts of CF_4 and COF_2. Initially, only the spectrum of COF_2 could be observed. This source of COF_2 could be eliminated by keeping the sample in contact with water for long periods (several days); CF_3OF itself undergoes only very slow hydrolysis. However, the intensity of the COF_2 lines increased with time indicating that the CF_3OF was decomposing in the cell, the probable reaction being: $CF_3OF \rightarrow COF_2 + F_2$. Upon cooling to Dry Ice temperature, the rate of decomposition was slowed down appreciably, especially after the cell had been filled repeatedly with large quantities of CF_3OF.

Results and Discussion

Ground State Spectrum

Preliminary calculations using an assumed structure (2) indicated that CF_3OF is a nearly symmetric prolate top with rotational constants $A \simeq 5700$ MHz, $B \simeq C \simeq 3100$ MHz. From the assumed structure and tabulated bond moments (6), the principal dipole moments were evaluated as $\mu_a = 0.4$ D, $\mu_b = 0.2$ D, and $\mu_c = 0.0$ D.

Transition frequencies were calculated from the assumed moments of inertia using an asymmetric rotor program written in APL/360. An a-type R branch was predicted, with J's between 1 and 5 in the region 12 to 36 GHz.

The observed spectrum is characteristic of a

[1]Revision received October 26, 1973.

Can. J. Chem. Downloaded from www.nrcresearchpress.com by 210.87.254.5 on 09/05/12
For personal use only.

Can. J. Chem. Downloaded from www.nrcresearchpress.com by 210.87.254.5 on 09/05/12
For personal use only.

prolate asymmetric rotor with *a*-type selection rules. Only the R(0,1) type transitions were observed. They were readily identified by their characteristic pattern, and Stark effect of the $K = 1$ ($K \equiv K_{-1}$) lines.

Fitting the observed lines to rigid rotor theory through a least-squares procedure produced the rotational constants shown in Table 1. The low J, R-branch transition frequencies are nearly independent of A, thus only B and C could be calculated with great accuracy. Variations of 0.04 MHz in the value of B or C affected the calculated spectrum as much as variations of 100 MHz in A. A comparison of observed and calculated transition frequencies for the ground state is given in Table 2. Small differences for higher J's and K's are due to centrifugal distortion. These differences are too small for calculation of centrifugal constants.

To determine A more precisely a thorough search was carried out for other transitions, especially μ_b Q-type transitions, but none were found using conventional techniques.

Double-resonance experiments were performed using an experimental arrangement similar to that described by Cox *et al.* (7). The pumping source was the HP sweep oscillator with 4–8 and 8–12.5 GHz plug-in units yielding power levels of approximately 50 mW. An OKI 24V10 reflex klystron was phase-locked on the peak of selected R μ_a lines. The resultant signal was recorded while the pumping source was swept through the appropriate frequency region. Resonance would be indicated by a dip or rise in the recorded trace. Rotational constant A being known within 200 MHz it was possible to calculate the frequency domain of the Q μ_b transitions as shown in Table 3. The absence of any observable resonances indicated that the μ_b is extremely small such that much higher pumping powers are necessary.

Although no structural information can be obtained from the present results, the inertial constants are consistent with the structure determined by electron diffraction (5). Using structural parameters obtained from electron diffraction we calculated the following rotational constants: $A = 5640 \pm 50$, $B = 3070 \pm 50$, $C = 3040 \pm 50$ MHz. It must be mentioned, however, that these constants are derived from r_g parameters whereas ours are ground rotational state constants.

TABLE 1. Rotational constant of CF_3OF (in MHz)

v	A	B	C
0	5600±100	3108.11±0.02	3049.24±0.02
1	5530±100	3100.49±0.03	3048.87±0.03

TABLE 2. Ground state spectrum of CF_3OF

Transition	ν_{obs} (MHz)	$\nu_{obs} - \nu_{calc}$ (MHz)
$1_{11} \rightarrow 2_{12}$	12 255.85	0.02
$1_{01} \rightarrow 2_{02}$	12 313.75	0.07
$1_{10} \rightarrow 2_{11}$	12 373.69	0.11
$2_{12} \rightarrow 3_{13}$	18 383.17	0.06
$2_{02} \rightarrow 3_{03}$	18 468.03	0.08
$2_{21} \rightarrow 3_{22}$	18 472.02	−0.03
$2_{20} \rightarrow 3_{21}$	18 476.18	0.02
$2_{11} \rightarrow 3_{12}$	18 559.76	0.04
$3_{13} \rightarrow 4_{14}$	24 509.60	−0.04
$3_{03} \rightarrow 4_{04}$	24 619.09	−0.06
$3_{22} \rightarrow 4_{23}$	24 628.57	−0.04
$3_{31} \rightarrow 4_{32}$	24 631.26	−0.17
$3_{30} \rightarrow 4_{31}$	24 631.26	−0.23
$3_{21} \rightarrow 4_{22}$	24 638.89	0.03
$3_{12} \rightarrow 4_{13}$	24 745.09	0.03
$4_{14} \rightarrow 5_{15}$	30 635.01	−0.18
$4_{32} \rightarrow 5_{33}$	30 789.96	−0.21
$4_{13} \rightarrow 5_{14}$	30 929.40	0.08

TABLE 3. Some double-resonance schemes for CF_3OF

Observed transition	Pumped transition	ν(MHz)*
$3_{13} \rightarrow 4_{14}$ (24 509.60)	$4_{14} \rightarrow 4_{23}$	7560–8160
	$3_{13} \rightarrow 3_{22}$	7441–8040
$3_{12} \rightarrow 4_{13}$ (24 745.09)	$4_{13} \rightarrow 4_{22}$	6987–7586
	$3_{12} \rightarrow 3_{21}$	7094–7692
$3_{30} \rightarrow 4_{31}$ (24 631.26)	$3_{21} \rightarrow 3_{30}$	12 102–13 102

*Frequency range with $A = 5500$ to $A = 5700$ MHz.

Excited State Spectrum

Each ground state line was accompanied by a satellite line having a relative intensity of about 0.4 at −79 °C (Dry Ice). Several transitions in the vibrationally excited state were measured and the derived rotational constants listed in Table 1. Observed transitions are shown in Table 4.

The lowest frequency vibration is expected to be the torsion about the C—O axis. That torsion was assigned to a very weak band in the i.r. spectrum of the vapor (2). Such a frequency corresponds to a relative intensity of 0.65 at the temperature of our measurements. Careful relative

TABLE 4. First excited state spectrum of CF_3OF

Transition	ν_{obs} (MHz)	$\nu_{obs} - \nu_{calc}$ (MHz)
$2_{12} \rightarrow 3_{13}$	18 370.19	0.04
$2_{21} \rightarrow 3_{22}$	18 448.55	0.40
$2_{20} \rightarrow 3_{21}$	18 451.23	−0.11
$2_{11} \rightarrow 3_{12}$	18 524.97	−0.03
$3_{13} \rightarrow 4_{14}$	24 492.58	−0.03
$3_{22} \rightarrow 4_{23}$	24 596.93	0.12
$3_{31} \rightarrow 4_{32}$	24 598.80	−0.25
$3_{21} \rightarrow 4_{22}$	24 604.65	−0.30
$3_{12} \rightarrow 4_{13}$	24 699.06	−0.02
$4_{14} \rightarrow 5_{15}$	30 614.15	−0.10
$4_{13} \rightarrow 5_{14}$	30 872.20	0.01

TABLE 5. Stark coefficients and dipole moment of CF_3OF*

		$\Delta\nu/E^2 \times 10^5$ MHz (V/cm)^2	
Transition	M	Observed	Calculated
$2_{12} \rightarrow 3_{13}$	1	0.343 ± 0.002	0.315
	2	1.287 ± 0.01	1.268
$2_{11} \rightarrow 3_{12}$	1	−0.328 ± 0.002	−0.315
		−1.193 ± 0.05	−1.253
$3_{13} \rightarrow 4_{14}$	2	0.160 ± 0.002	0.144
	3	0.359 ± 0.01	0.326
$3_{12} \rightarrow 4_{13}$	2	−0.160 ± 0.002	−0.144
	3	−0.359 ± 0.01	−0.322

*$\mu_a = 0.30 \pm 0.02$ D, $\mu_b = 0.10 \pm 0.06$ D, $\mu_c = 0$ D (assumed).

intensity measurements on the $J = 2, 3$, $K = 1$ lines yielded an average value of 0.4. The difficulties of relative intensity measurements are well known (8) but the experimental errors are not large enough to explain this discrepancy. Our results correspond to a torsional frequency of approximately 120 cm^{-1}. Using the electron diffraction structure to determine the reduced moment of inertia for internal rotation, rI_α, together with $1 \leftarrow 0$ frequency of 120 cm^{-1}, we obtain a potential barrier of about 3.9 kcal/mol which is somewhat higher than the value $V_3 = 2.5 \pm 0.5$ kcal/mol from electron diffraction.

Intensities of torsional bands are notoriously weak because of the small changes in dipole moment for such motions. Moreover, measurements in the far i.r. region are difficult and spurious absorptions are often detected.

The next highest vibrational frequencies are those of the A' and A'' CF_3 rocking modes at 227 and 250 cm^{-1}, respectively. A second, much weaker satellite is observed for the more intense transitions. This may be the second excited state of the torsion or one of the rocking modes. This question was not further explored.

Dipole Moment

Stark effect measurements were carried out on the $M = 1, 2$ lobes of the $J = 2$, $K = 1$ lines and on the $M = 2, 3$ lobes of the $J = 3$, $K = 1$ lines. (The $M = 1$ lobes on the latter pair of lines were too small for their frequency displacement to be followed with accuracy.) The electric field was calibrated before and after measurements with the $2 \leftarrow 1$ transition of OCS, μ(OCS) being taken as 0.71521 D (9). The frequency displacement for each lobe was measured as a function of the field at intervals of approximately 100 V/cm, from 400 V/cm to the point where the resulting field inhomogeneity so broadened the lobe that it became lost in the background noise. We thus obtained between six and twenty experimental points for each lobe. Maximum displacements achieved were of the order of 20 MHz for the $J = M = 2$ lobes and 5–8 MHz for the others. The second-order Stark coefficients were calculated by performing a linear least-squares fit on the frequency displacement as a function of the square of the electric field. These coefficients are given in Table 5 along with the standard error of estimate and the derived dipole moments. The deviations appear to be large enough to warrant a fourth-order perturbation calculation, but this has not been attempted here.

The symmetry of the molecule is such that one of the components of the dipole moment is necessarily zero. For most molecular models (including those obtained by electron diffraction), it would appear that the c-component vanishes. However it is difficult to positively locate axes b and c since corresponding moments of inertia are almost identical. Setting μ_b at 0 led to an imaginary μ_c, therefore we set μ_c at 0. The very small dipole moment obtained for μ_b explains why it was impossible to observe transitions other than a-type.

The authors wish to thank Professor L. Bartell for communicating his results before publication. One of us (J.W.) wishes to thank the National Research Council of Canada for a bursary and we are grateful to the NRCC and DRBC for operating grants.

Can. J. Chem. Downloaded from www.nrcresearchpress.com by 210.87.254.5 on 09/05/12
For personal use only.

1. C. J. HOFFMANN. Chem. Rev. **64**, 91 (1964).
2. P. M. WILT and E. A. JONES. J. Inorg. Nucl. Chem. **30**, 2933 (1968).
3. P. M. WILT and E. A. JONES. J. Inorg. Nucl. Chem. **29**, 2108 (1967).
4. R. T. LAGEMANN, E. A. JONES, and P. J. H. WOLTZ. J. Chem. Phys. **20**, 1768 (1952).
5. F. P. DIODATI and L. S. BARTELL. J. Mol. Struct. **8**, 395 (1971).
6. C. P. SMYTH. Dielectric behavior and structure. McGraw Hill, New York. 1965. p. 244.
7. A. P. COX, G. W. FLYNN, and E. B. WILSON. J. Chem. Phys. **42**, 3094 (1965).
8. A. S. ESBITT and E. B. WILSON. Rev. Sci. Instrum. **34**, 901 (1963).
9. J. S. MUENTER. J. Chem. Phys. **48**, 4544 (1968).

Can. J. Chem. Downloaded from www.nrcresearchpress.com by 210.87.254.5 on 09/05/12
For personal use only.

Drop Calorimetry of the Complex Compounds $CsMnCl_3$, Cs_2MnCl_4, and Cs_2ZrCl_6

A. S. KUCHARSKI AND S. N. FLENGAS

Department of Metallurgy and Materials Science, University of Toronto, Toronto, Ontario M5S 1A4

Received October 22, 1973

Enthalpies of fusion, heat contents, and heat capacities, for the compounds $CsMnCl_3$, Cs_2MnCl_4, and Cs_2ZrCl_6 have been determined by drop calorimetry. The following results were obtained for the enthalpies of fusion:

$CsMnCl_3$	$\Delta H_F = 15.70 \pm 0.41$ kcal/mol^{-1} at 866 K
Cs_2MnCl_4	$\Delta H_F = 6.29 \pm 0.80$ kcal/mol^{-1} at 811 K
Cs_2ZrCl_6	$\Delta H_F = 17.53 \pm 0.58$ kcal/mol^{-1} at 1082 K

The heat capacities were determined as

$CsMnCl_3$	$C_{p(s)} = 34.587$	for $866 \geq T\,K > 437$
	$C_{p(s)} = 37.937$	$1076 > T\,K \geq 866$
Cs_2MnCl_4	$C_{p(s)} = 23.091$	for $811 \geq T\,K > 592$
	$C_{p(l)} = 27.354$	$1059 > T\,K \geq 811$
Cs_2ZrCl_6	$C_{p(s)} = 56.717 + 13.586T$	for $1082 \geq T\,K > 537$
	$C_{p(l)} = 73.426$	$1180 > T\,K \geq 1082$

Les enthalpies de fusion, les enthalpies et les capacités calorifiques des composés $CsMnCl_3$, Cs_2MnCl_4 et Cs_2ZrCl_6 ont été établies par abaissement calorimétrique. Les résultats suivants sont obtenus pour les enthalpies de fusion:

$CsMnCl_3$	$\Delta H_F = 15.70 \pm 0.41$ kcal/mol^{-1} à 866 K
Cs_2MnCl_4	$\Delta H_F = 6.29 \pm 0.80$ kcal/mol^{-1} à 811 K
Cs_2ZrCl_6	$\Delta H_F = 17.53 \pm 0.58$ kcal/mol^{-1} à 1082 K

Les capacités calorifiques ont été évaluées à:

$CsMnCl_3$	$C_{p(s)} = 34.587$	pour $866 \geq T\,K > 437$
	$C_{p(l)} = 37.937$	$1076 > T\,K \geq 866$
Cs_2MnCl_4	$C_{p(s)} = 23.091$	pour $811 \geq T\,K > 592$
	$C_{p(l)} = 27.354$	$1059 > T\,K \geq 811$
Cs_2ZrCl_6	$C_{p(s)} = 56.717 + 13.586T$	pour $1082 \geq T\,K > 537$
	$C_{p(l)} = 73.426$	$1180 > T\,K \geq 1082$

[Traduit par le journal]

Can. J. Chem., **52**, 946 (1974)

Introduction

Recently a model has been developed to account for the enthalpies of mixing for charge asymmetrical systems of the type MCl_2–ACl (1), where M and A are the transition metal and alkali metal cations, respectively. The free energies, enthalpies, and entropies of mixing for the $MnCl_2$–ACl systems where A = Li, Na, K, and Cs have been reported (2) as well as the electrical conductivities and molar volumes of these systems (3).

The interpretation of these results has been based on the formation of a tetrahedrally coordinated chloride complex via the reaction

[1] $$MCl_2 + 2ACl \rightarrow A_2MCl_4$$

where A = Li, Na, K, Rb, and Cs.

Also, the formation of the octahedrally coordinated chloride complexes with tetravalent transition metal cations has been shown to decrease the activity of MCl_4 vapor (4) by reactions of the type

[2] $$MCl_{4(v)} + 2ACl \rightarrow A_2MCl_6$$

Can. J. Chem. Downloaded from www.nrcresearchpress.com by 210.87.254.40 on 09/05/12
For personal use only.

Can. J. Chem. Downloaded from www.nrcresearchpress.com by 210.87.254.40 on 09/05/12
For personal use only.

where A = Li, Na, K, and Cs and M = Ti or Zr.

The thermal properties for the Li_2ZrCl_6, Li_2HfCl_6, Na_2ZrCl_6, and K_2ZrCl_6 have been measured in this laboratory (5). However, accurate heat capacity and heat of fusion data for cesium complexes of these types are generally lacking.

Experimental

The design and operation of the calorimeter used in this work has been reported from this laboratory (6). The preparation of anhydrous $MnCl_2$, KCl, and CsCl used in the present investigation has also been described previously (2). The $ZrCl_4$ was purified by sublimation and the Cs_2ZrCl_6 complex compound was formed by reacting $ZrCl_4$ vapor with a weighed amount of CsCl in a closed system (10).

The manganese complexes were formed by weighing out the salts in the correct stoichiometric proportions into fused silica capsules. The silica capsule was sealed under vacuum. The salts were always handled in a dry box in order to avoid contact with moisture.

Calibration

The drop calorimeter was recalibrated using the method employed previously (6). Synthetic sapphire obtained from the U.S. Bureau of Standards was used as a standard.

The synthetic sapphire was enclosed in a fused silica capsule. The silica and the sapphire were separated by a thin platinum foil liner to prevent their reaction. Thus, the silica, platinum, and sapphire contribute to the total heat content of the capsule. To separate these effects, the silica portion was determined by dropping a pure solid silica slug. The data were fitted by least squares to equation

$$[3]\quad V_{SiO_2} = -4.0744 \times 10^{-2} + 8.7551 \times 10^{-5}T + 6.8865 \times 10^{-9}T^2 + 4.1816T^{-1}$$

where V_{SiO_2} is the thermopile signal in mV per g of silica and T is the temperature in K. The standard deviation for the data is 0.474×10^{-3} mV/g.

Similarly, the part of the signal due to the heat content of platinum was determined as

$$[4]\quad V_{Pt} = -3.3756 \times 10^{-3} + 1.1604 \times 10^{-5}T + 1.4084 \times 10^{-10}T^2$$

with a standard deviation of 0.978×10^{-4} mV/g. These results for the silica and the platinum vary from the previously reported results (6) at 1000 K by only 2.8 and 0.3%, respectively.

The calorimeter constant was determined from the accurate known enthalpy content of sapphire given as

$$[5]\quad H_T - H_0 = 148.5704T - 1.7106 \times 10^{-3}T^{-2} - 46994.87 \log T + 82146.1$$

The average calorimetric constant from eleven sapphire determinations was computed to be 2945.4 ± 143 cal/mV.

TABLE 1. The enthalpy content of SiO_2 and Pt at 1000 K (1 cal_{th} = 4.184 J)

Compound	$H_{1000} - H_{298}{}^0$ (cal/mol)	Reference
SiO_2	10 260	This work
	10 280	7
Pt	4 808	This work
	4 660	7

The previous constant (6) was determined as 2885 ± 35 cal/mV. The molar enthalpy content relative to 25 °C for pure fused SiO_2 and Pt was calculated at 1000 K using eqs. 3 and 4 incorporating the new calorimetric constant. The calculated and literature values (7) are compared in Table 1. The enthalpy contents for SiO_2 and Pt differ from the literature values (7) by 0.2 and 3.2%, respectively.

Results and Discussion

The enthalpy contents of the compounds at the corresponding temperatures are shown in Table 2 and plotted in Fig. 1. These data were fitted by least square analysis to enthalpy functions of the type

$$[6]\quad H_T - H_{298} = a_0 + a_1T + a_2T^2$$

Equation 6 corresponds to the heat capacity given by eq. 7 where T represents temperature in K.

$$[7]\quad C_p = a_1 + 2a_2T$$

The standard deviation for these fits were calculated using the equation

$$[8]\quad \sigma = \left[\frac{s}{N - M}\right]^{\frac{1}{2}}$$

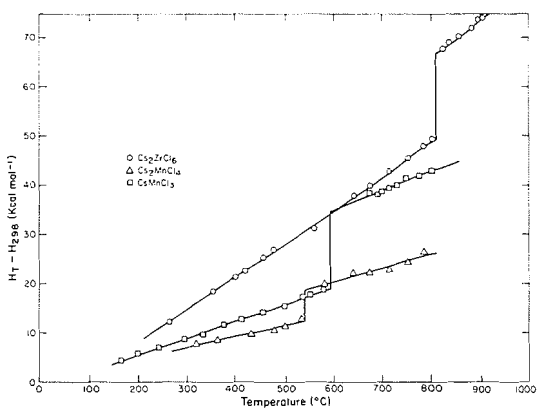

FIG. 1. $H_T - H_{298}$ as a function of temperature for the compounds Cs_2ZrCl_6, Cs_2MnCl_4, and $CsMnCl_3$.

TABLE 2. Enthalpy contents of $CsMnCl_3$, Cs_2MnCl_4, and Cs_2ZrCl_6 (1 cal_{th} = 4.184 J)

Cs_2ZrCl_6		$CsMnCl_3$		Cs_2MnCl_4	
t (°C)	$H_T - H_{298}$ (cal/mol)	t (°C)	$H_T - H_{298}$ (cal/mol)	t (°C)	$H_T - H_{298}$ (cal/mol)
Solid					
264	12 210	164	4 490	319	7 630
355	18 430	200	5 720	365	8 400
401	21 400	243	6 980	432	9 980
422	22 580	296	8 610	475	10 500
455	25 420	335	9 560	500	11 450
476	26 740	379	11 650	533	12 860
559	31 160	415	12 890		
642	37 560	455	14 090		
675	39 690	498	15 540		
716	42 930	535	17 410		
755	45 320	549	17 600		
788	47 950	578	18 790		
802	49 010				
Liquid					
822	67 560	693	38 270	575	19 930
853	70 070	676	38 220	642	22 110
894	73 720	700	38 840	675	22 080
833	69 060	716	39 200	716	22 980
880	71 610	733	39 860	755	24 170
907	73 850	751	41 270	786	26 450
		779	41 750		
		803	42 700		

where s is the sum of squares, N is the number of data points, and M is the number of coefficients. Thus, the standard deviation reflects the number of coefficients used in the function to fit the data.

The standard deviation for the heat of fusion was determined by taking the square root of the sum of squares of the standard deviation for liquid and solid lines. The coefficients determined by the least square fits are shown in Table 3 along with the enthalpies and entropies of fusion for the cesium compounds.

For systems of the type $MnCl_2$–CsCl it has been suggested (1–3) that the compound Cs_2MnCl_4 is formed in the molten state according to reaction 1. Hence for liquid compositions $X_{MnCl_2} \leq 1/3$, the only species that can exist in the melt are $MnCl_4^{2-}$, Cs^+, and excess Cl^- ions. For compositions $X_{MnCl_2} \geq 1/3$, only the $MnCl_4^{2-}$, Mn^{2+}, and Cs^+ ion species are possible. Thus upon fusion the $CsMnCl_3$ and the Cs_2MnCl_4 complexes each form 3 moles of ions. The entropy of fusion can be estimated by using the general rule that upon fusion each particle contributes 2 to 4 entropy units to account for the total of 6 to 12 entropy units. It is apparent from Table 3 that the entropy of fusion for the Cs_2MnCl_4 complex lies within this range. The fact that the entropy of fusion for the $CsMnCl_3$ complex is somewhat higher and outside this range can be attributed to the different solid state crystal structure of this complex. The solid state crystal structure of $CsMnCl_3$ and Cs_2MnCl_4 has been reviewed by Papatheodorou (8). The $CsMnCl_3$ complex is hexagonal with the Mn^{2+} ion octahedrally coordinated while the β-Cs_2MnCl_4 complex is orthorhombic and tetrahedrally coordinated. This solid state structural evidence indicates that the fusion process for the $CsMnCl_3$ complex breaks more bonds on fusion than the Cs_2MnCl_4 complex and thus has a more profound effect on entropy of fusion.

The drop calorimetry results for the $MgCl_2$–ACl system (A = K, Rb, Cs) reported by Holm *et al.* (9) are compared with this study in Table 4. It is seen that the entropy of fusion for the Cs_2MgCl_4 and $CsMgCl_3$ compounds parallels the trends for the analogous $MnCl_2$ compounds.

The enthalpies for alkali chlorozirconates taken from the work of Dutrizac and Flengas (5) are listed in Table 5 along with the enthalpy for

Can. J. Chem. Downloaded from www.nrcresearchpress.com by 210.87.254.40 on 09/05/12
For personal use only.

TABLE 3. Least square fit for enthalpy functions $H_T - H_{298} = a_0 + a_1T + a_2T^2$ (1 cal_{th} = 4.184 J)

Compound	a_0	a_1	$a_2 \times 10^3$	Standard deviation	t_f (°C)	ΔH_f (kcal/mol)	ΔS_f (cal/mol K)
Cs_2ZrCl_6 (solid)	−19 985	56.717	6.793	300	808.7	17.53±0.58	15.9
Cs_2ZrCl_6 (liquid)	−12 579	73.426		460			
$CsMnCl_3$ (solid)	−10 890	34.587		280	593	15.70±0.41	18.0
$CsMnCl_3$ (liquid)	1 911	37.937		300			
Cs_2MnCl_4 (solid)	−6 269	23.091		390	538	6.29±0.80	7.8
Cs_2MnCl_4 (liquid)	−3 433	27.354		700			

TABLE 4. Enthalpies of fusion for the 1:1 and 2:1 congruent compounds formed in the $MgCl_2$–ACl and $MnCl_2$–ACl systems (A = K, Rb, or Cs) (1 cal_{th} = 4.184 J)

Compound	ΔH_f (kcal mol^{-1})	ΔS_f (e.u.)	Structure
K_2MgCl_4	10.75*	15.3	Tetragonal
Rb_2MgCl_4	12.04*	16.3	Tetragonal
Cs_2MgCl_4	9.40*	11.6	Orthorhombic
$KMgCl_3$	10.30*	13.7	Hexagonal
$RbMgCl_3$	12.30*	14.9	Hexagonal
$CsMgCl_3$	13.70*	15.5	Hexagonal
Cs_2MnCl_4	6.29†	7.8	Orthorhombic§
$KMnCl_3$	10.98‡	14.2	
$CsMnCl_3$	15.70†	18.0	Hexagonal

*Reference 9.
†This work.
‡Reference 11.
§Reference 8.

TABLE 5. Enthalpy and entropies of transformation for the alkali chlorozirconate compounds (1 cal_{th} = 4.184 J)

Compound	Type of transformation	Temperature (°C)	Enthalpy (kcal mol^{-1})	Entropy (e.u.)
Li_2ZrCl_6*	Solid–liquid	535	9.3 ±1.6	11.5
Na_2ZrCl_6*	α-Solid–β-solid	351–385	7.0 ±1.0	10.9
	β-Solid–liquid	646	4.0 ±1.3	4.4
K_2ZrCl_6*	α-Solid–β-solid	614–631	4.5 ±1.5	5.0
	β-Solid–liquid	800	5.5 ±2.0	5.1
$CsZrCl_6$†	Solid–liquid	808.7	17.53±0.58	15.9

*Reference 5.
†This work.

Cs_2ZrCl_6 complex determined in the present work. No solid state transformation was observed in Cs_2ZrCl_6 compound in contrast to other alkali chlorozirconates shown in Table 5. This result is substantiated by the phase diagram studies on CsCl–Cs_2ZrCl_6 systems (10) in this laboratory.

The financial assistance to one of the authors (A.S.K.) by the National Research Council of Canada is gratefully acknowledged.

1. S. N. FLENGAS and A. S. KUCHARSKI. Can. J. Chem. **49**, 24 (1971).
2. A. S. KUCHARSKI and S. N. FLENGAS. J. Electrochem. Soc. **119**, 1170 (1972).

Can. J. Chem. Downloaded from www.nrcresearchpress.com by 210.87.254.40 on 09/05/12
For personal use only.

3. A. S. KUCHARSKI and S. N. FLENGAS. J. Electrochem. Soc. In press.
4. S. N. FLENGAS and P. PINT. Can. Met. Q. **8** (2), 151 (1969).
5. J. E. DUTRIZAC and S. N. FLENGAS. Can. J. Chem. **45**, 2313 (1967).
6. W. T. THOMPSON and S. N. FLENGAS. Can. J. Chem. **49**, 1550 (1971).
7. C. E. WICKS and F. E. BLOCK. U. S. Bureau of Mines Bulletin 605. 1963.
8. G. N. PAPATHEODOROU. J. Inorg. Nucl. Chem. **35**, 465 (1973).
9. J. L. HOLM, B. J. HOLM, and B. RINNAN. J. Chem. Thermodyn. **5**, 97 (1973).
10. P. PINT. PH.D. Thesis. University of Toronto, Toronto, Ontario. 1972.
11. J. M. SCULLY. B.A.Sc. Thesis. University of Toronto, Toronto, Ontario. 1970.

Can. J. Chem. Downloaded from www.nrcresearchpress.com by 210.87.254.40 on 09/05/12
For personal use only.

Quaternary Nitrogen Heterocycles. IV.[1] The 1-Methyl-4-nitroquinolinium and 4,4-Diiodo-1,1-dimethyl-1,4-dihydroquinolinium Cations, Two Methylation Products of 4-Nitroquinoline and their Reactions in Aqueous Solutions

JOHN W. BUNTING AND WILLIAM G. MEATHREL

Department of Chemistry, University of Toronto, Toronto, Ontario M5S 1A1

Received August 30, 1973

Methylation of 4-nitroquinoline wth methyl fluorosulfonate ("magic methyl") gives the expected 1-methyl-4-nitroquinolinium fluorosulfonate. However, methylation with methyl iodide gives an unexpected product ($C_{11}H_{12}I_3N$) which is shown to be 4,4-diiodo-1,1-dimethyl-1,4-dihydroquinolinium iodide. This latter salt readily loses a molecule of methyl iodide in aqueous alkaline solution and forms 4-hydroxy-4-iodo-1-methyl-1,4-dihydroquinoline. This latter product reacts in aqueous solution with excess silver iodide or bromide in the presence of silver nitrate to give 3-iodo-1-methyl-4-quinolone or the corresponding 3-bromo derivative. The 1-methyl-4-nitroquinolinium cation readily forms a pseudobase in aqueous solution ($pK_{ROH} = 5.31$; $pK_{RO^-} = 10.95$). Kinetic and spectroscopic data are consistent with the predominant neutral pseudobase species being 4-hydroxy-1-methyl-4-nitro-1,4-dihydroquinoline, while the predominant pseudobase anion is the alkoxide ion of 2-hydroxy-1-methyl-4-nitro-1,2-dihydroquinoline.

La méthylation du nitro-4 quinoléine avec du méthyle fluorosulfonate ("méthyle magique") donne, comme prévu, le sulfonate fluoré du méthyl-1 nitro-4 quinoléinium. Pourtant, la méthylation avec de l'iodure de méthyle donne un produit inattendu ($C_{11}H_{12}I_3N$) qui est l'iodure du diiodo-4,4 diméthyl-1,1 dihydro-1,4 quinoléinium. Ce dernier sel perd aisément une molécule d'iodure de méthyle dans une solution aqueuse alcaline et forme du hydroxy-4 iodo-4 méthyl-1 dihydro-1,4 quinoléine. Ce dernier produit, dans une solution aqueuse avec de l'iodure ou du bromure d'argent en excès, réagit en présence du nitrate d'argent pour donner l'iodo-3 méthyl-1 quinolone-4 ou le dérivé bromo-3 correspondant. Le cation méthyl-1 nitro-4 quinoléinium forme aisément une pseudobase dans une solution aqueuse ($pK_{ROH} = 5.31$; $pK_{RO^-} = 10.95$). Les données cinétiques et spectroscopiques sont en accord avec l'espèce de pseudobase neutre prédominante qui est l'hydroxy-4 méthyl-1 nitro-4 dihydro-1,4 quinoléine alors que l'anion pseudobase prédominant est l'ion alcoolate du hydroxy-2 méthyl-1 nitro-4 dihydro-1,2 quinoléine. [Traduit par le journal]

Can. J. Chem., **52**, 951 (1974)

We wish to report a dramatic difference between the methylation products obtained upon treatment of 4-nitroquinoline with methyl iodide and methyl fluorosulfonate ("magic methyl"). Each of these products undergoes an interesting series of facile reactions in aqueous solution and we also report a detailed study of these transformations.

Treatment of 4-nitroquinoline with methyl fluorosulfonate gave a product whose p.m.r. spectrum in trifluoroacetic acid could be assigned to the 1-methyl-4-nitroquinolinium cation (**1**): δ 4.97 (N—CH_3, s, 3H), 8.24–8.73 (H−3+H−5+H−6+H−7+H−8, m, 5H), 9.60 H-2, d, 1H, J_{23} = 6.5 Hz). This spectrum is very similar to that of 4-nitroquinoline in trifluoroacetic acid, *i.e*

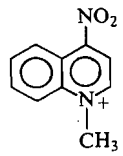

1

the 4-nitroquinolinium cation (Table 1). Furthermore, the u.v. spectrum of **1** in water is also very similar to that of the 4-nitroquinolinium cation (λ_{max} 325 and 322 nm, respectively).

Treatment of 4-nitroquinoline with methyl iodide, either neat or in acetone solution, produced quite a different product. Elemental analysis indicated the presence of 3 atoms of iodine per quinoline moiety ($C_{11}H_{12}I_3N$). Titration of a suspension of this product with silver nitrate solution in *neutral* aqueous solution indicated that

[1]For Part III, see ref. 16.

Can. J. Chem. Downloaded from www.nrcresearchpress.com by 210.87.254.5 on 09/05/12
For personal use only.

Can. J. Chem. Downloaded from www.nrcresearchpress.com by 210.87.254.5 on 09/05/12
For personal use only.

TABLE 1. Proton magnetic resonance spectra of some quinoline derivatives

Structure	Solvent	Chemical shift δ (p.p.m.) H_2	H_3	H_5–H_8	N—CH_3
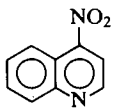	$CDCl_3$	8.70 (d,J=4.5 Hz)[a]	[a]	7.6–8.3(m)	—
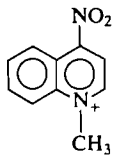	CF_3CO_2H	9.60 (d,J=6.5 Hz)	[b]	8.24–8.73(m)	4.97(s)
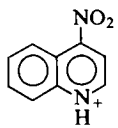	CF_3CO_2H	9.65 (d,J=6 Hz)	[b]	8.24–8.89(m)	—
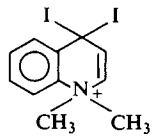	CF_3CO_2H	8.89 (d,J=7 Hz)	7.32 (d,J=7 Hz)	7.9–8.4(m),8.7(m)	4.44(s),4.52(s)
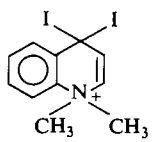	Acetone	9.40 (d,J=7 Hz)	7.73 (d,J=7 Hz)	8.0–8.4(m),8.7(m)	4.54(s),4.74(s)
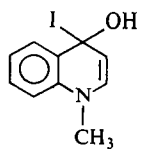	$NaOD$–D_2O	7.78 (d,J=7.5 Hz)	6.20 (d,J=7.5 Hz)	7.2–8.0(m)	3.74(s)

Can. J. Chem. Downloaded from www.nrcresearchpress.com by 210.87.254.5 on 09/05/12
For personal use only.

TABLE 1. (*Concluded*)

Structure	Solvent	Chemical shift δ (p.p.m.) H_2	H_3	H_5–H_8	N—CH_3
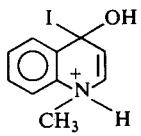	Acetone	9.02 (d,J=7.5 Hz)	7.36 (d,J=7.5 Hz)	7.8–8.3(m),8.7(m)	4.57(s)
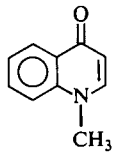	$CDCl_3$	7.58 (d,J=7.5 Hz)	6.27 (d,J=7.5 Hz)	7.3–7.7(m),8.5(m)	3.83(s)
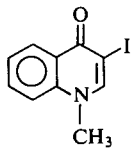	Acetone	8.25(s)	—	7.4–7.8(m),8.4(m)	4.00(s)
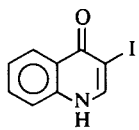	Acetone	8.27(s)	—	7.4–7.8(m),8.4(m)	—

[a]One of these signals is hidden in the multiplet (δ 7.6–8.3) which integrates for five protons. The doublet δ 8.70 may be due to either the H_2 or H_3 proton.
[b]Hidden in the H_5—H_8 multiplet which integrates for five protons.

Can. J. Chem. Downloaded from www.nrcresearchpress.com by 210.87.254.5 on 09/05/12
For personal use only.

only one of these iodine atoms was present as iodide ion. The p.m.r. spectrum in both trifluoroacetic acid (Fig. 1 and Table 1) and acetone (Table 1) indicated the presence of two nonequivalent methyl groups. The chemical shifts of both of these methyl groups are typical of quaternary *N*-methyl protons in a heterocyclic cation (for 1-methylquinolinium cation N—CH_3 δ 4.67 (D_2O)). In both solvents a pair of one-proton doublets (coupling constant 7 Hz) is evident, one at higher field and the other at lower field than the four-proton multiplet for the protons on the aromatic homocyclic ring. The chemical shifts of these doublets show a considerable solvent dependence. We assign this spectrum to the 4,4-diiodo-1,1-dimethyl-1,4-dihydroquinolinium cation, **2**, with the downfield doublet (δ 8.70 in trifluoroacetic acid) being assigned to the proton on C-2 and the higher field doublet (δ 7.35 in trifluoroacetic acid) to the proton on C-3. The positively charged nitrogen atom would be expected to cause the signal from C_2—H to occur at much lower field than that from C_3—H. The coupling constant, J_{23} = 7 Hz, is consistent with similar values for other 1,4-dihydroquinolines (1, 2). We assume that the nonequivalent *N*-methyl groups are a reflection of the conformation taken up by the 1,4-dihydropyridine ring.

An attractive route for the formation of the 4,4-diiodo-1,1-dimethyl-1,4-dihydroquinolinium cation (**2**) from the methylation of 4-nitroquinoline is outlined in Scheme 1. This route assumes the formation of the 1-methyl-4-nitroquinolinium cation (**1**) as the initial product which can then undergo subsequent reactions as indicated. To test this proposal, we have refluxed 1-methyl-4-nitroquinolinium fluorosulfonate with methyl iodide, both in the absence and presence of potassium iodide as a source of iodide ions. However, the only product that could be isolated from these reaction mixtures was 1-methyl-4-quinolone, to which the above fluorosulfonate salt is rapidly degraded even at room temperature. In the absence of a detailed investigation of this reaction, it is not clear at present whether the cation **1** is not an intermediate in this reaction or whether the fluorosulfonate salt of **1** decomposes too rapidly under the reaction conditions to allow the formation of significant amounts of **2**.

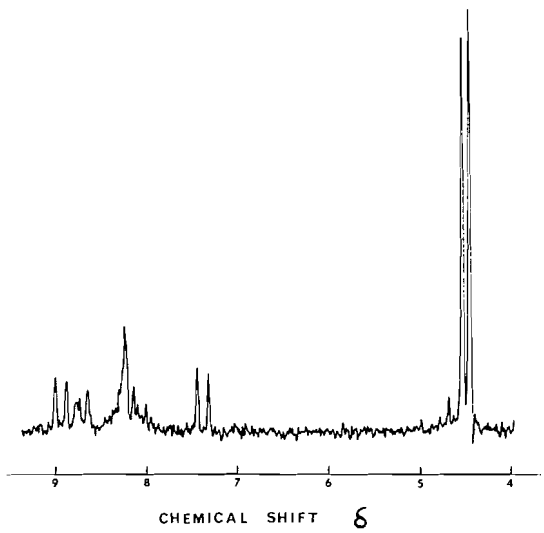

FIG. 1. Proton magnetic resonance spectrum (in trifluoroacetic acid) of the product from the methylation of 4-nitroquinoline with methyl iodide – 4,4-diiodo-1,1-dimethyl-1,4-dihydroquinolinium iodide.

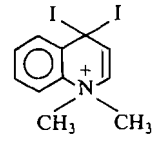

2

Reactions of the 4,4-Diiodo-1,1-dimethyl-1,4-dihydroquinolinium Cation in Aqueous Solution

During attempts to confirm chemically the presence of two iodine atoms on C-4 in **2**, we have observed that this cation undergoes a series of facile reactions in aqueous solution. Although **2** is relatively insoluble in water, when a suspension is heated in dilute aqueous sodium hydroxide

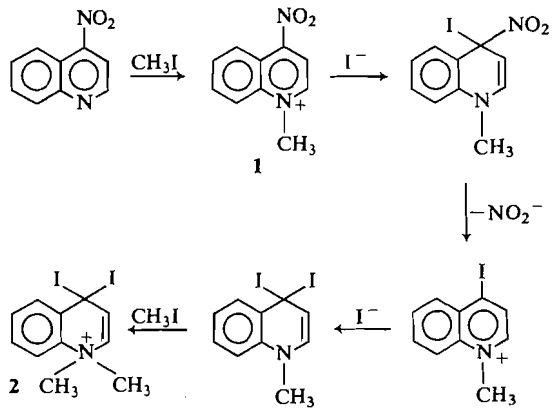

SCHEME 1

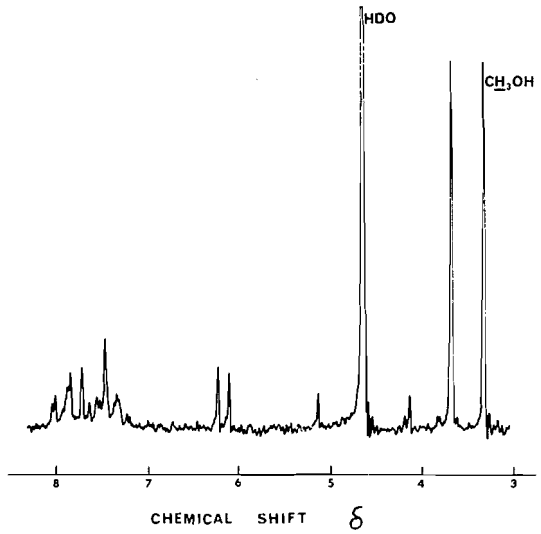

FIG. 2. Proton magnetic resonance spectrum immediately after dissolution of 4,4-diiodo-1,1-dimethyl-1,4-dihydroquinolinium iodide in NaOD–D_2O.

(0.03 *M*) a clear yellow solution is obtained. The p.m.r. spectrum of this solution (NaOD–D_2O) (Fig. 2 and Table 1) is consistent with the presence of a 4,4-disubstituted 1-methyl-1,4-dihydroquinoline (**3**). However, there is an additional

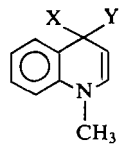

3

three-proton singlet (δ 3.37) in the p.m.r. spectrum which has the same chemical shift as the methyl protons of methanol in this solvent. The upfield shift of the C-2, C-3, and *N*-methyl protons relative to the corresponding protons in **2** indicates that the nitrogen atom no longer bears a positive charge. This is consistent with nucleophilic attack by hydroxide ion (or water) on one of the methyl groups in **2** to produce methanol and thus the singlet at δ 3.37.

Neutralization of such an alkaline solution gives a suspension of a brown solid. Careful titration of this solid with standard silver nitrate solution, and using the complete solution of the brown solid as an end point, indicates the presence of 2 iodide ions per molecule of iodide salt of **2** originally present. One of these iodide ions is, of course, the counterion that is originally present with **2**, whereas the second must arise by displacement from C-4 in alkaline solution. Extraction of the brown suspension into chloroform gave a product with p.m.r. spectrum (Table 1) quite similar to that of **2**, except that only one *N*-methyl signal is present. We formulate this product as the hydroiodide salt, **4**, of the pseudobase of the 4-iodo-1-methylquinolinium cation. This suggests that in alkaline solution, the species present is **3** (X = OH or O^-; Y = I).

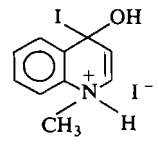

4

Addition of a small amount of potassium chromate solution as indicator, after the addition of 2 equiv. of silver nitrate in the above titration, allows the titration of a third equivalent of iodide ion to the Mohr end point (4). After filtering off silver iodide and silver chromate and basifying, extraction with chloroform gave a mixture of two products which could be separated chromatographically. Blank experiments indicated that the presence of the chromate ion did not influence the formation of these products. One of the products was readily identified as 1-methyl-4-quinolone. The second product contained 1 atom of iodine per quinoline moiety and had similar u.v. (λ_{max} 288, 303, 334, 348 in ethanol) and p.m.r. (Table 1) spectra to 1-methyl-4-quinolone (λ_{max} 281, 291, 326, 340 in ethanol). However, the C-2 and C-3 proton doublets in the p.m.r. spectrum of the latter compound were replaced by a one-proton singlet at δ 8.00 in the iodine-containing product. This product was believed to be either 2-iodo- or 3-iodo-1-methyl-4-quinolone, **5** and **6**, respectively.

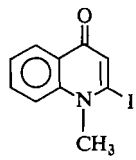

5

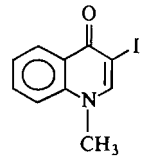

6

3-Iodo-4-quinolone has previously been synthesized by treatment of 4-quinolone with iodine monochloride and has been unambiguously shown to be the 3-iodo rather than the 2-iodo derivative (5). We therefore treated 1-methyl-4-quinolone with iodine monochloride under the

Can. J. Chem. Downloaded from www.nrcresearchpress.com by 210.87.254.5 on 09/05/12
For personal use only.

Can. J. Chem. Downloaded from www.nrcresearchpress.com by 210.87.254.5 on 09/05/12
For personal use only.

same reaction conditions and isolated an iodine-containing product identical with the compound obtained above from the degradation of **2**. By analogy with the iodination product from 4-quinolone, this is expected to be the 3-iodo derivative, **6**. This is borne out by a comparison of the p.m.r. spectra of this product and 3-iodo-4-quinolone (Table 1). The chemical shifts for the C-2 protons are almost identical (δ 8.25 and 8.27). Furthermore, the chemical shift for the C-3 proton in a 2-iodo-4-quinolone would be expected to be at considerably higher field (by more than 1 p.p.m.)[2] than that for the C-2 proton in a 3-iodo derivative. Thus **6** is firmly established as the second product from the degradation of **2**.

The ratio of 1-methyl-4-quinolone to 3-iodo-1-methyl-4-quinolone in the product mixture varied to some extent from run to run, between 2:1 and 1:3 based on the relative intensities of the C_2—H proton of **6** and the C_3—H proton of 1-methyl-4-quinolone in the p.m.r. spectrum of the mixture. This ratio was somewhat sensitive to a number of experimental variables, particularly the time that the solution of **2** was maintained basic prior to neutralization. Prolonged treatment of **2** in basic solution resulted in complete conversion to 1-methyl-4-quinolone by loss of hydrogen iodide from the pseudobase, **3** (X = OH; Y = I).

The formation of a substantial amount of iodine-containing organic product appears to be inconsistent with the titration with silver nitrate solution of 3 atoms of iodine per molecule of the iodide salt of **2**. Collection of the silver iodide produced in the above titration with 3 equiv. of silver nitrate indicated the formation of only 2.4 ± 0.1 equiv. of silver iodide per mol of **2**, assuming all the precipitate to be silver iodide. Thus 0.6 equiv. of the three equivalents of silver ion used in the titration (to the Mohr end point) are unaccounted for in the gravimetric analysis. The gravimetric analysis is consistent, however, with the conversion of approximately 60% of **2** to 3-iodo-1-methyl-4-quinolone, **6**. It appears that the silver ion is involved in this very facile rearrangement of **3** (X = OH; Y = I) to **6** and the reaction may be *formally* written as eq. 1. We

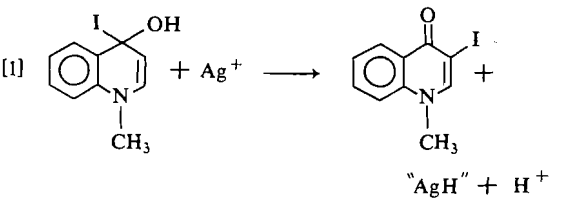

assume that the ultimate fate of the silver ion in eq. 1 is as a deposit of silver on the walls of the reaction vessel. This is not obvious to the eye, however, at the concentrations at which we have been able to work.

We have been able to show that the rearrangement of iodine from C-4 to -3 is not mechanistically a totally intramolecular reaction as might be inferred from eq. 1. Thus, treatment of **4** with silver nitrate in the presence of a large excess of silver bromide gave a mixture of **6** and the corresponding 3-bromo-1-methyl-4-quinolone. This ability to replace iodine with bromine clearly indicates that at least some of **6** arises by attack of iodine (chemical form unspecified) from solution rather than by an intramolecular migration of iodine from C-4 to -3. Treatment of 1-methyl-4-quinolone with silver nitrate and excess silver iodide did not produce any **6**, so that pathways for formation of **6** which involve the iodination of 1-methyl-4-quinolone can be eliminated. The rearrangement of **3** (X = OH; Y = I) to **6** may possibly be formulated as an electrophilic attack by iodine at C-3, followed by elimination of hydrogen iodide (Scheme 2). The electrophilic species is assumed to be a silver–iodine complex[3] of unknown structure which is concomitantly reduced to silver. This assumption is consistent with our observation that it is possible to introduce bromine by the use of excess silver bromide.

Although the detailed mechanism of the involvement of silver ion in this reaction is not known at present, it is clear that it is not a case of a silver ion catalyzed rearrangement similar to reactions of the type that have recently been studied in considerable detail by Paquette (7). The requirement for equimolar amounts of silver

[2]Compare the chemical shifts of C_3—H (δ 6.27) and C_2—H (δ 7.58) in 1-methyl-4-quinolone (in $CDCl_3$). The effect upon the chemical shift of the remaining proton, of individually replacing one of these protons by an iodine atom should be independent of whether iodine is introduced at C-2 or -3, since in each case the iodine atom can be considered to be a *cis*-olefinic substituent to the proton under observation (6). Thus the difference of approximately 1.3 p.p.m. between the chemical shifts of the C-2 and C-3 protons in 1-methyl-4-quinolone should be retained in the iodo derivatives.

[3]Species such as Ag_2I^+ are known to be formed by the interaction of silver iodide with silver ions (14, 15). The reaction of $Ag_2I^+ \rightarrow 2Ag + I^+$ is formally consistent with our current suggestions.

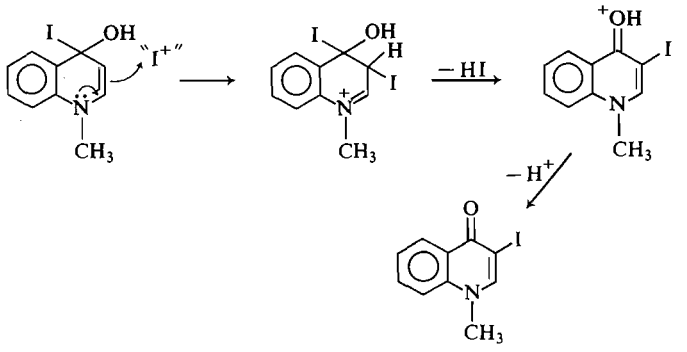

SCHEME 2

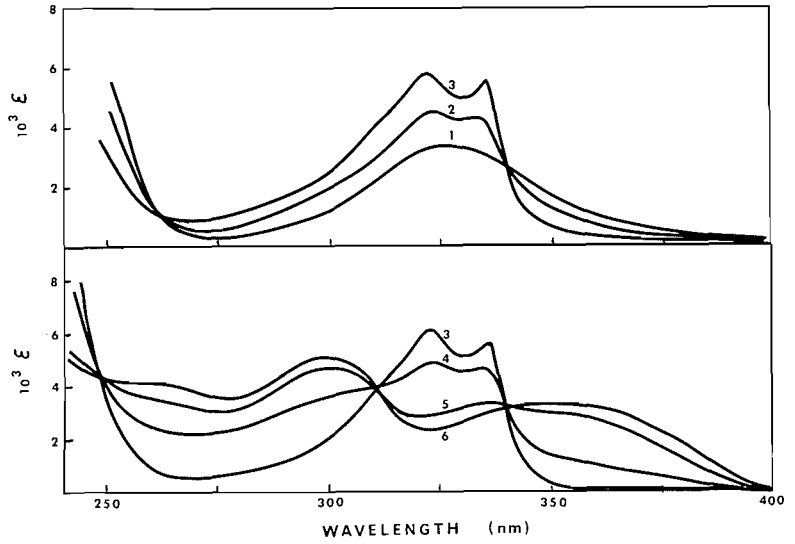

FIG. 3. The p*H* dependence of the u.v. spectrum of the 1-methyl-4-nitroquinolinium cation (**1**) in aqueous solution: *1*, p*H* 3.0; *2*, p*H* 5.3; *3*, p*H* 9.5; *4*, p*H* 10.3; *5*, p*H* 11.3; *6*, p*H* 13.0.

ion consumed, and 3-iodo-1-methyl-4-quinolone produced, clearly distinguishes the present reaction from those rearrangements which require only the presence of a trace of silver ion as a catalyst.

Reactions of the 1-Methyl-4-nitroquinolinium Cation (1) in Aqueous Solution

The u.v. spectrum of **1** in aqueous solution is p*H* dependent (Fig. 3). These spectral changes are reversible upon acidification, and from the p*H* dependence of these spectra pK_a values of 5.31 ± 0.06 and 10.95 ± 0.06 have been measured at 25°.

The p.m.r. spectrum of **1** in aqueous alkaline solution (0.5 *N* NaOD–D_2O) seems to indicate the presence of a mixture of two products: δ 3.05(s), 3.80(s), 4.92 (d, J = 3 Hz), 6.27 (d, J = 8 Hz), 7.0–8.5(m). The relative intensity of the singlets at δ 3.05 and 3.80 is time dependent and eventually the signals at δ 3.05 and 4.92 disappear. One of these products can readily be assigned as 1-methyl-4-quinolone (*cf.* Table 1), while the other we assign as 1,2-dihydro-2-hydroxy-1-methyl-4-nitroquinoline (**7**) or more likely its alkoxide anion: δ 3.05 (N—Me, s), 4.92

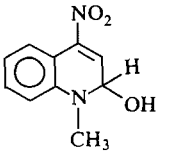

7

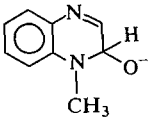

8

(H-2, d, J_{23} = 3 Hz), 7.0–8.0 (H−3+H−5+H−6+H−7+H−8, m). Such an assignment is in good agreement with the spectrum of the anion of 1,2-dihydro-2-hydroxy-1-methylquinoxaline

Can. J. Chem. Downloaded from www.nrcresearchpress.com by 210.87.254.5 on 09/05/12
For personal use only.

(**8**): (NaOD–D_2O) δ 3.05 (N—Me, s), 5.15 (H-2, d, J_{23} = 3 Hz), 6.7–7.3 (H−5+H−6+H−7 +H−8, m), 7.67 (H-3, d, J_{23} = 3 Hz) (8). The 1-methyl-4-quinolone is presumably formed through loss of nitrite ion and a proton from the pseudobase, 1,4-dihydro-4-hydroxy-1-methyl-4-nitroquinoline (**9**). Thus appreciable amounts

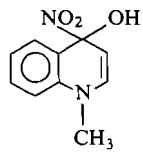

9

of the pseudobases from both C-2 and -4 attack by hydroxide ion appear to be formed in aqueous solutions of **1**.

Pseudobase formation proved to be too rapid to allow observation by the stopped-flow technique upon mixing solutions of the 1-methyl-4-nitroquinolinium cation with aqueous buffers in the p*H* range 5–9.5. This in itself is not surprising, since numerous other examples of the attainment of pseudobase–cation equilibria so rapidly that the reaction cannot be observed by the stopped-flow technique, have been documented (9); however, at higher p*H* values relatively slow attainment of equilibrium is observable by the stopped-flow technique. The dependence of the observed first-order rate constants on p*H* is indicated in Fig. 4*A*. Since the reaction in this region seems to be related to the observed pK_a = 10.95, this pK_a value cannot be merely associated with the ionization of the pseudobase to an alkoxide ion since such proton transfer reactions are too rapid to allow observation by the stopped-flow technique. The observed rates suggest that this ionization must also be associated with some form of molecular rearrangement.

Further evidence that this ionization constant does not merely reflect a deprotonation was obtained from studies of the conversion of the species present in solutions of p*H* 8 and p*H* 13 respectively back to the cation **1** by rapid acidification in the stopped-flow apparatus. Thus, acidification of a p*H* 8 solution resulted in an instantaneous (not observable by stopped-flow) formation of **1**, whereas acidification of a p*H* 13 solution led to an observable reaction in the stopped-flow spectrophotometer ($t_{1/2}$ = 71 ms at p*H* 1.53) and the u.v. spectrum of the product is that of cation **1**.

We suggest that these phenomena arise from differences in the relative stabilities of the pseudobases **7** and **9**, and their corresponding alkoxide ions. The presence of the alkoxide ion of **7** in strongly alkaline solutions of **1** as is indicated by the p.m.r. spectral data discussed above, suggests that this is the predominant pseudobase anion that is present in such solutions. The gradual conversion of this anion to 1-methyl-4-quinolone is then consistent with the presence of smaller amounts of the alkoxide anion from **9** which would be expected to undergo rapid elimination of nitrite ion. We further suggest that in solutions of the neutral pseudobase, species **9** predominates. Thus, the changes in u.v. spectrum that are associated with pK_a = 10.95 seem to be too great to be merely reflecting alkoxide ion formation. The longer wavelength absorption in more alkaline solution is also consistent with the well established differences in the spectra of isomeric 1,2- and 1,4-dihydroquinolines (1–3).

These ideas are summarized in Scheme 3. The two measured pK_a values then correspond to

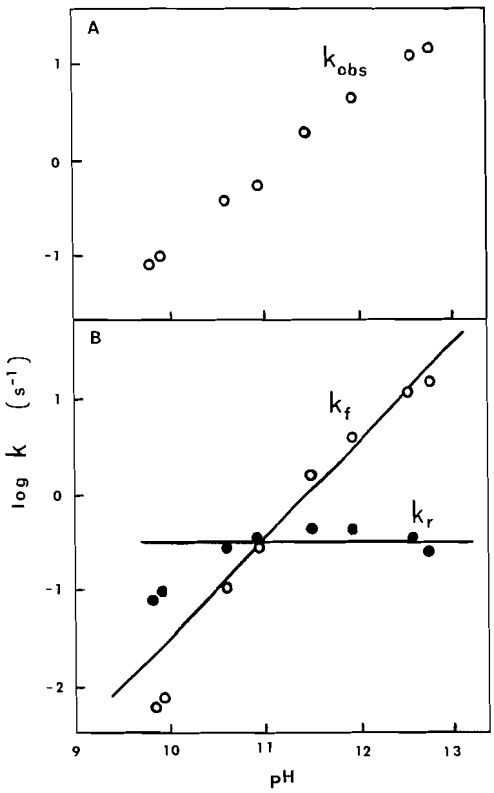

FIG. 4. (*A*) The p*H* dependence of the observed pseudo first-order rate constant, k_{obs}, upon mixing a solution of the 1-methyl-4-nitroquinolinium cation (**1**) with various buffer solutions. (*B*) The p*H* dependence of k_f and k_r which are calculated from k_{obs} as described in the text.

Can. J. Chem. Downloaded from www.nrcresearchpress.com by 210.87.254.5 on 09/05/12
For personal use only.

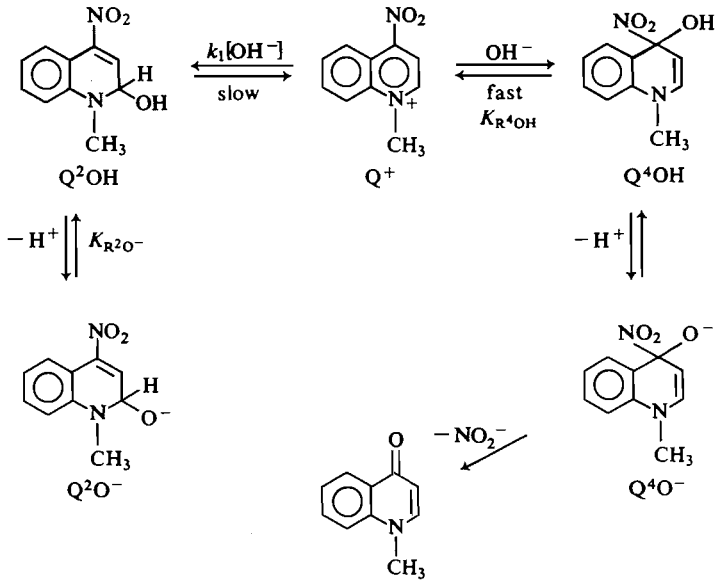

SCHEME 3

$pK_{R^4OH} = 5.31$ for formation of pseudobase **9** (Q^4OH) (predominantly) from cation **1** and $pK^{app}_{RO^-} = 10.95$ which is a composite equilibrium constant, defined by

$$K^{app}_{RO^-} = \frac{[H^+]([Q^2O^-] + [Q^4O^-])}{[Q^2OH] + [Q^4OH]} \approx \frac{[H^+][Q^2O^-]}{[Q^4OH]}$$

if the neutral pseubodase **9** and the alkoxide anion of **7** predominate in neutral and basic solution, respectively.

Our kinetic studies seem to support the above interpretations; thus the rearrangement of **9** to the isomeric pseudobase, 1,2-dihydro-2-hydroxy-1-methyl-4-nitroquinoline, presumably via the cation **1**, would provide the relatively slow molecular rearrangement required prior to deprotonation, and so account for the observable kinetic changes that are associated with the $pK_a = 10.95$.

If in Scheme 3 we assume that the equilibrium between Q^4OH and Q^+ is attained much more rapidly than the equilibrium between Q^2OH and Q^+ and also that Q^4OH and Q^2O^- predominate in neutral and alkaline solutions, respectively, then the observed rate constants in the region $pH > 9.5$ in Fig. 4*A* refer to the attainment of equilibrium between Q^4OH (**9**) and Q^2O^- (**7**)

i.e. $$Q^4OH \underset{k_r}{\overset{k_f}{\rightleftarrows}} Q^2O^- + H^+$$

where k_f and k_r are pseudo first-order rate constants. Thus, $k_{obs} = k_f + k_r$, and since at equilibrium

$$k_f[Q^4OH] = k_r[Q^2O^-]$$

$$\frac{k_f}{k_r} = \frac{[Q^2O^-]}{[Q^4OH]} = \frac{K^{app}_{RO^-}}{[H^+]}$$

Therefore

$$k_f = \frac{k_{obs}}{1 + [H^+]/K^{app}_{RO^-}}$$

and

$$k_r = \frac{k_{obs}}{1 + K^{app}_{RO^-}/[H^+]}$$

Values of k_f and k_r calculated in this way are given in Fig. 4*B*.

For Scheme 3

$$\frac{d}{dt}(Q^2O^-) = \frac{K_{R^2O^-}}{[H^+]}\frac{d}{dt}(Q^2OH) = \frac{K_{R^2O^-}}{[H^+]}k_1[OH^-][Q^+] = \frac{K_{R^2O^-}k_1}{K_w}[OH^-]^2[Q^+]$$

Also

$$\frac{d}{dt}(Q^2O^-) = k_f([Q^+] + [Q^4OH]) = k_f[Q^+]\left(1 + \frac{K_{R^4OH}}{[H^+]}\right)$$

Can. J. Chem. Downloaded from www.nrcresearchpress.com by 210.87.254.5 on 09/05/12
For personal use only.

Can. J. Chem. Downloaded from www.nrcresearchpress.com by 210.87.254.5 on 09/05/12
For personal use only.

Hence

$$k_f\left(1 + \frac{K_{R^4OH}}{[H^+]}\right) = \frac{K_{R^2O^-}k_1}{K_w}[OH^-]^2$$

$$i.e.\ k_f = \frac{K_{R^2O^-}k_1[OH^-]^2}{K_w\left(1 + \frac{K_{R^4OH}}{[H^+]}\right)}$$

$$\approx \frac{K_{R^2O^-}k_1}{K_{R^4OH}}[OH^-]$$

for $pH \gg pK_{R^4OH}$

Thus Scheme 3 predicts that in alkaline solution k_f should be linearly dependent on $[OH^-]$ which is consistent with the observed dependence in Fig. 4*B*. Further, since $k_r = k_f[H^+]/K^{app}_{RO^-}$, Scheme 3 predicts that in alkaline solution

$$k_r \approx \frac{K_{R^2O^-}k_1K_w}{K_{R^4OH}K^{app}_{RO^-}}$$

i.e. p*H* independent, in agreement with the experimental data in Fig. 4*B*.

4-Nitroquinoline

Ochiai (10*a*) describes a procedure based on the report of Nakayama (11) which is claimed to give 4-nitroquinoline in quantitative yield from the deoxygenation of 4-nitroquinoline-1-oxide with phosphorus tribromide in chloroform. By this procedure, we have consistently obtained a product that has a similar melting point to 4-nitroquinoline, but on the basis of its mass spectrum this product is clearly a mixture of 4-nitroquinoline (M^+ 174) and a dibromoquinoline (M^+ 285, 287, and 289). A number of other workers have observed the formation of 2,4-dibromoquinoline from this reaction under similar reaction conditions (12, 13), although Filippi has obtained pure 4-nitroquinoline by carrying out the reaction below $-10°$ (13). Even at this temperature we have obtained a contaminated product, from which we have been unable to obtain pure 4-nitroquinoline by recrystallization or chromatography. However, treatment of 4-nitroquinoline-1-oxide with phosphorus tribromide in *ethyl acetate* below 10° did consistently give uncontaminated 4-nitroquinoline (compare ref. 3 and 12) and we recommend this procedure for the most efficient deoxygenation of this *N*-oxide.

Experimental

4-Nitroquinoline

4-Nitroquinoline-1-oxide (4.7 g) (10*b*) was dissolved in ethyl acetate (100 ml) and cooled to 5°. Phosphorus tribromide (6 ml) in ethyl acetate (30 ml) was added dropwise with stirring while the temperature of the reaction mixture was maintained below 5°. After stirring for a further 15 min, the reaction mixture was poured into ice water (200 ml). The ethyl acetate layer was removed, and the aqueous solution was extracted with further ethyl acetate (2 × 100 ml) .The combined ethyl acetate solutions were washed with 10% aqueous sodium sulfite (2 × 75 ml), 5% aqueous sodium hydroxide (2 × 75 ml) and water (2 × 100 ml) and then dried over anhydrous magnesium sulfate. After removal of the solvent (rotary evaporation) the residue was recrystallized from petroleum ether to yield 4-nitroquinoline (2.9 g, 67%) m.p. 83–84° (lit. (13) m.p. 87°).

1-Methyl-4-nitroquinolinium Fluorosulfonate

4-Nitroquinoline (300 mg) was dissolved in a mixture of anhydrous ether (10 ml) and chloroform (10 ml). Methyl fluorosulfonate (2 ml) was added and after 20 min at room temperature, the yellow product was filtered and washed with anhydrous ether. Yield 164 g (33%), m.p. 110°. This salt is relatively unstable, even at room temperature, and gradually decomposes to 1-methyl-4-quinolone.[4] Only relatively poor analytical data could be obtained.

Anal. Calcd. for $C_{10}H_9FN_2O_5S$: C, 41.7; H, 3.12; N, 9.72. Found: C, 40.5; H, 3.77; N, 9.32.

4,4-Diiodo-1,1-dimethyl-1,4-dihydroquinolinium Iodide

4-Nitroquinoline (1.0 g) was refluxed in methyl iodide (5 ml) either neat or in acetone solution for 24 h. After cooling, the acetone and methyl iodide were removed on the rotary evaporator and the residue was recrystallized from ethanol, 1.67 g (54%), m.p. 142–143°.

Anal. Calcd. for $C_{11}H_{12}I_3N$: C, 24.5; H, 2.23; N, 2.60; I, 70.7. Found: C, 23.5; H, 2.05; N, 2.81; I, 70.8.

Attempted Conversion of 1-Methyl-4-nitroquinolinium Fluorosulfonate to the Iodide Salt of 2

A freshly prepared sample of 1-methyl-4-nitroquinolinium fluorosulfonate (50 mg) was treated with methyl iodide as described above for 4-nitroquinoline both in the absence and presence of potassium iodide (100 mg). In each case, the only identifiable product obtained was 1-methyl-4-quinolone.

3-Iodo-1-methyl-4-quinolone

1-Methyl-4-quinolone (500 mg) was dissolved in 3 ml glacial acetic acid and heated to 75 °C. Iodine monochloride (1 ml) was added and the solution was heated to approximately 85 °C for 5 min. Aqueous sodium hydroxide (5 ml; 10 *N*) was added (causing a dark red precipitate to form). The cooled basic solution was extracted with chloroform (3 × 20 ml). The $CHCl_3$ extracts were evaporated and the residue was chromatographed on silica gel eluting with acetone to yield 3-iodo-1-methyl-4-quinolone, 760 mg (85%), m.p. 197–199°.

Anal. Calcd. for $C_{10}H_8INO$: C, 42.1; H, 2.81; N, 4.92; I, 44.6. Found C, 42.8; H, 3.11; N, 4.99; I, 43.7.

Degradation of 4,4-Diiodo-1,1-dimethyl-1,4-dihydroquinolinium Iodide

The iodide salt (100 mg) was heated in aqueous sodium

[4]This decomposition seems to involve the interaction of the fluorosulfonate anion with the very electron-deficient 1-methyl-4-nitroquinolinium cation. Prolonged storage (1 week or longer) of samples of this salt resulted in considerable etching of the glass vial and also a strong odor of sulfur dioxide upon removal of the stopper.

Can. J. Chem. Downloaded from www.nrcresearchpress.com by 210.87.254.5 on 09/05/12
For personal use only.

hydroxide (25 ml; 0.03 *M*) until dissolved. Upon neutralization with nitric acid, a brown solid separated which was removed by extraction into chloroform. After removal of the chloroform on the rotary evaporator, the p.m.r. spectrum of the residue in acetone could be assigned to 4-hydroxy-4-iodo-1-methyl-1,4-dihydroquinolinium iodide (Table 1).

In another experiment, excess silver nitrate solution (10 ml; 0.1 *M*) was immediately added to the suspension obtained upon neutralization. Precipitated silver iodide was filtered off and the aqueous filtrate was extracted with chloroform (2 × 15 ml). The chloroform was removed, and the residue was chromatographed on a silica gel column, eluting with acetone. 3-Iodo-1-methyl-4-quinolone (identical to the authentic material prepared as described above) was eluted first, followed by 1-methyl-4-quinolone. Repetition of this experiment in a blackened flask gave the same result, and so it is unlikely that the formation of 3-iodo-1-methyl-4-quinolone involves a photochemical reaction.

Argentimetric Titration

An alkaline solution of the iodide salt of **2** was prepared and neutralized as described above. This stirred suspension was then carefully titrated with standard silver nitrate solution (0.1 *M*) until the brown precipitate had dissolved. Although this is a somewhat difficult end point, repetitive experiments indicated the requirement for 2.0 ± 0.1 equivalents of silver ions. A few drops of potassium chromate solution were added, and the titration continued to the Mohr end point, which required a further 1.0 ± 0.1 equivalents of silver ions.

Gravimetric Analysis

A sample of the iodide salt of **2** of known mass, was treated as described above under "Degradation". The precipitated silver iodide was isolated by filtration through a tared sintered-glass funnel (medium porosity) and washed with water and dilute nitric acid. The funnel and contents were dried to constant weight. Repeated analyses indicated the presence of 2.4 ± 0.1 mol of silver iodide per mol of iodide salt of **2**. The product was completely soluble in aqueous potassium cyanide, and hot aqueous sodium thiosulfate.

Blank experiments on the determination of iodide ion in 1-methylquinolinium iodide gave gravimetric iodine analyses that were 98–100% of the titrimetric values.

*Degradation of **4** in the Presence of Silver Bromide*

The iodide salt of **2** (100 mg) was heated in aqueous sodium hydroxide (25 ml; 0.03 *M*) until dissolved. After neutralization with nitric acid, the brown precipitate was filtered off and washed with water. This product (50 mg) was suspended in water (50 ml) containing sodium bromide (~100 mg). Excess aqueous silver nitrate solution was added. After filtering off the silver salts, the filtrate was extracted with chloroform. Evaporation of the chloroform gave a solid residue which consisted of a mixture of 3-iodo-1-methyl-4-quinolone (**6**) and 3-bromo-1-methyl-4-quinolone. The presence of the bromo derivative was established from the mass spectrum of the mixture. The mass spectrum of **6** consists of a molecular ion peak (*m/e* 285) and a series of peaks for fragments which do not contain iodine. The mass spectrum of the mixture obtained above consisted of this same set of peaks plus twin peaks at masses 237 and 239 (each of approximately the same intensity as the 285 peak) which are assigned as the molecular ion peaks for 3-bromo-1-methyl-4-quinolone containing the two predominant isotopes of bromine (^{79}Br and ^{81}Br). The assignment of these peaks to the bromine derivative corresponding to **6** is consistent with the occurrence of the same fragments lacking halogen in the mass spectrum, and almost identical p.m.r. and u.v. spectra for the mixture and an authentic sample of **6**.

Proton magnetic resonance spectra were recorded on a Varian T-60 instrument using tetramethylsilane as internal reference in $CDCl_3$, acetone, and trifluoroacetic acid and sodium 2,2-dimethyl-2-silapentane-5-sulfonate in D_2O.

Stopped-flow kinetic studies were carried out on a Durrum–Gibson stopped-flow spectrophotometer at 25° and using buffers of ionic strength 0.1 as previously described (9); λ_{anal} = 296 nm; concentration, 4.1 × 10^{-5} *M*.

This research was supported by an operating grant from the National Research Council of Canada, and by the award of an Ontario Graduate Fellowship to W.G.M.

1. R. Bramley and M. D. Johnson. J. Chem. Soc. 1372 (1965).
2. J. W. Bunting and W. G. Meathrel. Tetrahedron Lett. 133 (1971).
3. M. Hamana. J. Pharm. Soc. Jap. **75**, 135 (1955); Chem. Abstr. **50**, 1818 (1956).
4. D. A. Skoog and D. M. West. Fundamentals of analytical chemistry. 2nd ed. Holt, Rinehart and Winston, Inc., New York. 1969. p. 225.
5. A. R. Surrey and R. A. Cutler. J. Am. Chem. Soc. **68**, 2570 (1946).
6. D. J. Pasto and C. R. Johnson. Organic structure determination. Prentice-Hall, Inc., Englewood Cliffs, N.J. 1969. p. 174.
7. L. A. Paquette. Acc. Chem. Res. **4**, 280 (1972).
8. J. W. Bunting and W. G. Meathrel. Can. J. Chem. **50**, 917 (1972).
9. J. W. Bunting and W. G. Meathrel. Can. J. Chem. **51**, 1965 (1973).
10. E. Ochiai. Aromatic amine oxides. Elsevier Publishing Co., Amsterdam. 1967. (*a*) p. 195; (*b*) p. 225.
11. I. Nakayama. J. Pharm. Soc. Jap. **71**, 1088 (1951); Chem. Abstr. **46**, 5046 (1952).
12. M. Hamana, Y. Hoshide, and K. Kaneda. J. Pharm. Soc. Jap. **76**, 1337 (1956); Chem. Abstr. **51**, 6639 (1957).
13. J. Filippi. Bull. Soc. Chim. Fr. 259 (1968).
14. K. H. Lieser. J. Inorg. Nucl. Chem. **26**, 1571 (1964).
15. D. C. Luehrs and K. Abate. J. Inorg. Nucl. Chem. **30**, 549 (1968).
16. J. W. Bunting and W. A. Meatrel. Can. J. Chem. **52**, 303 (1974).

Quaternary Nitrogen Heterocycles. V.[1] Substituent Effects on the Equilibrium Constants for Pseudobase Formation from Quinolinium and Isoquinolinium Cations

JOHN W. BUNTING AND WILLIAM G. MEATHREL

Department of Chemistry, University of Toronto, Toronto, Ontario M5S 1A1

Received October 5, 1973

Equilibrium constants (pK_{ROH}) have been measured for pseudobase formation from the 1-methyl-*x*-nitroquinolinium cations (x = 5–8), the *N*,*N*[1]-dimethyl-1,5-, -1,6-, and -2,7-naphthyridinium dications and various *N*-substituted quinolinium, isoquinolinium, 5-nitroisoquinolinium, and 1,8-naphthyridinium cations. The pK_{ROH} values for *N*-substituted 5-nitroisoquinolinium and 1,8-naphthyridinium cations are correlated by the equations $pK_{ROH} = -3.7\sigma^* + 11.6$ and $pK_{ROH} = -4.9\sigma^* + 12.5$, respectively ($\sigma^*$ is Taft's substituent constant for the substituent on nitrogen).

Proton magnetic resonance and u.v. spectral data have been used to assign the structures of the pseudobases formed from each of the above cations. In several cases ylide formation rather than pseudobase formation has been observed. The *N*,*N*[1]-dimethylnaphthyridinium dications are shown to form zwitterionic alkoxide ions in strongly basic aqueous solution, rather than undergoing attack by a second hydroxide ion.

Equilibration between cation and pseudobase occurs at rates near or beyond the limit of the stopped-flow technique for all the above cations, except the 2-cyanomethyl-5-nitroisoquinolinium cation. An analysis of the p*H*-rate profiles for reversible pseudobase formation from this latter cation is given.

On a déterminé les constantes d'équilibre (pK_{ROH}) pour la formation de pseudobases à partir des cations méthyl-1 nitro-*x* quinoléiniums (x = 5–8) des dications *N*,*N*′-diméthyl naphtyridiniums-1,5, -1,6, -2,7, et de divers cations *N*-substitués quinoléiniums, isoquinoléiniums, nitro-5 isoquinoléiniums et naphtyridiniums-1,8. On a relié les valeurs de pK_{ROH} des cations *N*-substitués nitro-5 isoquinoléiniums et naphtyridiniums-1,8 par les équations suivantes: $pK_{ROH} = -3.7\sigma^* + 11.6$ et $pK_{ROH} = -4.9\sigma^* + 12.5$ (σ^* est la constante de substituant de Taft pour le substituant sur l'azote).

On a utilisé les spectres r.m.n. et u.v. pour attribuer les structures des pseudobases obtenues de chaque cation mentionné ci-haut. Dans plusieurs cas on a observé la formation d'ylides plutôt que de pseudo-bases. On a montré que les cations *N*,*N*′-diméthyl naphtyridiniums forment, dans des solutions fortement basiques, des alcoolates ampholytes au lieu de subir une attaque par un second ion hydroxyde.

Pour tous les cations étudiés, excepté le cation cyanométhyl-2 nitro-5 isoquinoléinium, l'équilibre se fait à une vitesse proche ou au-delà de la limite de la technique à débit arrêté. On mentionne une analyse de la courbe de p*H* pour la formation réversible de pseudobase à partir de ce cation. [Traduit par le journal]

Can. J. Chem., **52**, 962 (1974)

As a further extension of our quantitative studies (1, 2) of pseudobase formation from heteroaromatic cations, we now wish to present equilibrium data for some substituent effects on pseudobase formation from substituted quinolinium, isoquinolinium, and related cations. In addition to measuring pK_{ROH} values for each cation, in each case we have investigated the reaction by u.v. and p.m.r. spectroscopy to ensure that pseudobase formation is the predominant reaction that is under observation. In a number of cases competing reactions were observed, and the products of these reactions are interpreted from the spectroscopic data.

Cooksey and Johnson (3) have previously studied the effects of substituents in the homocyclic ring on the pK_{ROH} value for pseudobase formation from 1-cyanoquinolinium cations and have also reported some very approximate values for a few similarly substituted 1-methylquinolinium cations. Apart from this comparison of pairs of similarly substituted *N*-methyl and *N*-cyano cations; there has been no attempt to define the dependence of pK_{ROH} on the nature of the substituent on nitrogen in these systems. The present study reports such an investigation for

[1]For Part IV, see ref. 19.

Can. J. Chem. Downloaded from www.nrcresearchpress.com by 210.87.254.105 on 09/05/12
For personal use only.

TABLE 1. Proton magnetic resonance spectra of 1-methyl-*x*-nitroquinolinium cations in basic methanol-d_4 (0.1 *M* $NaOCD_3$)

	δ					
x	H-2	H-3	H-4—H-8	N—CH_3	J_{23}	J_{24}
5	5.56	6.00	7.17–7.38	3.25	5	10
6	5.69	5.94	6.79–7.04, 7.97	3.24	5	10
7	5.62	6.00	6.95–7.62	3.25	5	9.5
8	5.34	5.97	6.87–7.77	3.07	5	9.5

TABLE 2. pK_{ROH} and u.v. spectral data for 1-methyl-*x*-nitroquinolinium cations

x	pK_{ROH}	λ_{max}(nm) (0.1 *M* NaOH–H_2O)	λ_{max}(nm) (0.1 *M* $NaOCH_3$–CH_3OH)
5	12.04±0.05[a]	306, 405	294, 380
6	10.80±0.09	294, 403	285, 378
7	11.78±0.03	258, 323, 398	260, 316, 405
8	9.67±0.06	260, 302, 416	262, 290, 396

[a]Reference 3 reports 12.3.

various substituents on nitrogen and also accurate pK_{ROH} values for the 1-methyl-*x*-nitroquinolinium ions (x = 5–8). In addition, we have investigated the effects upon pseudobase formation of a second positive charge in a bicyclic system, by measuring pK_{ROH} values for the N,N'-dimethyl dications of 1,5-, 1,6-, and 2,7-naphthyridines.

For most of these heterocyclic cations, equilibration between the cation and pseudobase was found to occur too rapidly to allow a study of the kinetics of these reactions by the stopped-flow technique. In only one case, namely the 2-cyanomethylisoquinolinium cation, could a detailed p*H*–rate profile be obtained.

Results and Discussion

1-Methyl-x-nitroquinolinium Cations

Proton magnetic resonance spectral data for the 1-methyl-*x*-nitroquinolinium cations (x = 5–8) in basic methanol-d_4 (0.1 *M* $NaOCD_3$) are given in Table 1.[2] These spectra are consistent with the C-2 methoxide adducts **1** (R = CD_3)

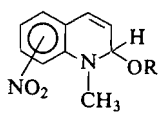

1

being the predominant species present in these solutions for each of these cations. In particular, the coupling constants J_{34} ~10 Hz and J_{23} ~5 Hz are typical of 1,2-dihydroquinolines, and the chemical shifts of the various protons are consistent with those previously observed (1) for 2-methoxy-1-methyl-1,2-dihydroquinoline (δ 5.70 (H-2), 5.66 (H-3), 6.6–7.3 (H-4—H-8), 3.12 (N—CH_3)) when allowance is made for the influence of the nitro groups.

Reversible u.v. spectral changes are observed when aqueous solutions of these cations are basified.[3] The u.v. spectra in basic aqueous and methanolic solutions (Table 2) are quite similar in each case and together with the p.m.r. spectral data in Table 1, this indicates that the pseudobases **1** (R = H) are the predominant species in these aqueous solutions.

From the p*H* dependence of the u.v. spectrum, the value of pK_{ROH} has been calculated for each ion and these are also included in Table 2. These pK_{ROH} values are somewhat similar to those of the corresponding *N*-methyl-1,*x*-naphthyridinium cations (1), which is consistent with the general observation that a pyridine-type ring nitrogen atom has approximately the same electronic effect as a nitro group in a homocyclic

[2]A direct p.m.r. investigation of pseudobase species in basic aqueous solution is not possible, because solids and/or oils (including products from irreversible reactions) separate from such solutions at p.m.r. spectral concentrations (*cf.* ref. 1).

[3]Contrary to an earlier report (3) that "the product of methylation of 6-nitroquinoline . . . reacts irreversibly with alkali," we observe reversible p*H*-dependent u.v. spectra for the 1-methyl-6-nitroquinolinium cation up to p*H* 14.

Can. J. Chem. Downloaded from www.nrcresearchpress.com by 210.87.254.105 on 09/05/12
For personal use only.

TABLE 3. Equilibrium and u.v. spectral data for naphthyridinium cations in aqueous solutions

Cation	pK_{ROH}	pK_{RO^-}	λ_{max}nm(log ε)	p*H*
1,5-Dimethyl-1,5-naphthyridinium	4.93±0.06	11.75±0.06	272(3.73), 309(4.03), 321(4.16)	1
			268(3.98), 374(3.82)	8
			274(3.98), 390(3.63)	14
1,6-Dimethyl-1,6-naphthyridinium	2.15±0.08	11.72±0.02	259(3.52), 315(3.70)	0
			297(3.95)	7
			306(3.96)	14
2,7-Dimethyl-2,7-naphthyridinium	3.84±0.07	10.9±0.1	313, 327	1
			328, 392	9
			347, 400	13
2-Methyl-2,7-naphthyridinium	10.52±0.04		315(3.35)	6
			346(3.64)	12

ring (*cf.* σ_p = 0.78 (for NO_2) (4) and 0.83 (for —N=) (5)). For the 1-methyl-1,5-naphthyridinium and 1-methyl-5-nitroquinolinium cations which are directly comparable, the pK_{ROH} values are 12.67 (1) and 12.04 respectively. The greatest deviation from this generalization arises with the 1-methyl-1,8-naphthyridinium (pK_{ROH} = 12.44 (1)) and the 1-methyl-8-nitroquinolinium (pK_{ROH} = 9.67) cations. Thus, this latter cation is considerably more susceptible to pseudobase formation than one might predict from its naphthyridine analog. We feel that this arises from the unfavorable *peri*-interactions between the 8-nitro and 1-methyl substituents in the cation which are considerably relieved upon pseudobase formation. The observation of Cooksey and Johnson (3) that an 8-methoxy substituent increases the susceptibility of the 1-cyanoquinolinium cation to pseudobase formation, whereas methoxy substituents in other positions have the opposite effect is consistent with this hypothesis.

The effects of some substituents other than nitro groups in the homocyclic ring of the 1-methylquinolinium cation were investigated to some extent but in general pK_{ROH} values were not sufficiently low to allow their measurement in a p*H* range where subsequent irreversible reactions do not occur. Thus, the u.v. spectra of each of the 6-halo(Cl, Br, I)-1-methylquinolinium cations were p*H* independent below p*H* 14, which is consistent with an estimate that the pK_{ROH} values for these cations are $\geqslant$ 15 (3).

N,N^1-*Dimethylnaphthyridinium Dications*

To further illustrate the effect of strongly electron-withdrawing substituents on pseudobase formation we have investigated the reactions of the *N,N*^{1}-dimethyl dications of 1,5-, 1,6-, and 2,7-naphthyridine in aqueous solution. While this work was in progress, Pokorny and Paudler (6) reported a p.m.r. spectral investigation of these and other *N,N*^{1}-dimethylnaphthyridinium dications. They concluded that the p.m.r. spectra of 0.5 *M* NaOD–D_2O solutions of these cations are consistent with the presence of the pseudobases **2**, **3**, and **4** being predominantly present but did not attempt to measure equilibrium constants for the reactions.

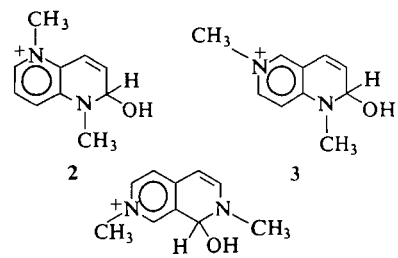

2 **3**

4

The p*H* dependences of the u.v. spectra of the *N,N*^{1}-dimethyl dications of each of the 1,5-, 1,6-, and 2,7-naphthyridines indicate that two reactions occur over the p*H* range 0–14. pK_a values for each of these reactions have been measured and are indicated in Table 3, along with u.v. spectral data for each pure species. The pK_{ROH} value and u.v. spectral data for pseudobase formation from the 2-methyl-2,7-naphthyridinium cation are also included in Table 3 since these data have not been previously reported.

Proton magnetic resonance spectral data for the 1,5- and 1,6-naphthyridinium dications in unbuffered D_2O, D_2O buffered at p*D* 10, and 1 *M* NaOD–D_2O are presented in Table 4. The

Can. J. Chem. Downloaded from www.nrcresearchpress.com by 210.87.254.105 on 09/05/12
For personal use only.

TABLE 4. Proton magnetic resonance spectral data for 1,5- and 1,6-naphthyridinium dications

Dication	Solvent	δ H-2	H-3	H-4	H-5	H-6	H-7	H-8	N—CH_3	J_{23}	J_{34}
1,5-Dimethyl-1,5-naphthyridinium	D_2O	9.90	8.80	9.80	—	9.90	8.80	9.80	4.99, 4.99		
	D_2O–pD 10	5.76	6.65	7.30	—	7.50 ⟷		8.05	3.30, 4.28	5.5	10
	1 M NaOD–D_2O	5.50	6.62	6.98	—	7.45 ⟷		7.92	3.16, 4.17	5	10
	0.1 M $NaOCD_3$–CD_3OD	5.68	6.60	7.68	—	7.49 ⟷		8.18	3.33, 4.34	5.5	10
	[a]	—	6.90	7.36	—	—	6.90	7.36	3.75, 3.75	—	10
1,6-Dimethyl-1,6-naphthyridinium	D_2O	9.87	8.57	9.63	10.30	—	9.19	9.00	4.75, 4.85		
	D_2O–pD 10	5.75	6.45	6.82	8.19	—	8.19	7.20	3.40, 4.10	5	10
	1 M NaOD–D_2O	5.60	6.10	6.50	7.48	—	7.88	6.79	3.20, 3.92	5	10
	0.1 M $NaOCD_3$–CD_3OD	5.80	6.20	6.97	8.24	—	8.24	7.19	3.34, 4.07	5	10
	[a]	—	6.62	7.40	—	—	8.21	6.30	3.57, 3.60	—	9.5

[a]Product from oxidation of dication with aqueous alkaline $K_3Fe(CN)_6$.

spectrum of the 1,5-dimethyl-1,5-naphthyridinium dication at pD 10 is readily interpreted as that of the monopseudobase **2** that is produced by addition of hydroxide ion to C-2 of one of the equivalent pyridinium rings of the parent dication. This spectrum is in good agreement with that assigned previously to the C-2 methoxide adduct of the 1-methyl-1,5-naphthyridinium cation (1), when suitable allowance is made for the downfield shifts due to the presence of the positive charge on N-5 of **2**. Thus, the observed ionization with $pK_a = 4.93$ is in fact the pK_{ROH} value for this dication. In more strongly alkaline solutions (1 M NaOD–D_2O) the p.m.r. spectrum is little different from that at pD 10. The small downfield shifts of some signals in the more basic solution are consistent with the second ionization constant being that for the ionization of the pseudobase **2** to its alkoxide ion (*i.e.* $pK_{RO^-} = 11.75$) (actually a zwitterion) rather than the addition of a second hydroxide ion at C-6 (as in **5**), or elsewhere, to give a dipseudobase. The slight change in u.v.

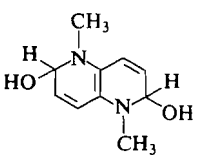

5

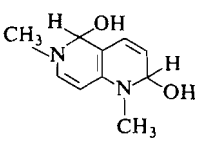

6

spectrum between pH 8 and 14 is also consistent with this interpretation. The other p.m.r. and u.v. spectral data in Tables 3 and 4 can likewise be used to assign the equilibrium constants for the N,N^1-dimethyl-1,6- and -2,7-naphthyridinium dications as being pK_{ROH} and pK_{RO^-} values for the formation of **3** and **4**, respectively, and their alkoxide zwitterions.

The data in Table 4 in 1 M NaOD–D_2O agree well with the data for these two dications in 0.5 M NaOD–D_2O as reported by Pokorny and Paudler (6). The ionization of each of the pseudobases in the present study with $pK_{RO^-} < 12$, suggests that all the data in Table 2 of reference (6) actually refer to the pseudobase alkoxide ions (zwitterions) rather than to the pseudobases themselves.

The spectral data in Tables 3 and 4 indicate that dipseudobase species such as **5** and **6** must be relatively minor components of these solutions even at pH 14. This further confirms the inherent stability of pyridinium cations towards pseudobase formation.[4] The presence of **5** and **6** as minor components of alkaline solutions of the 1,5-dimethyl-1,5-naphthyridinium and 1,6-dimethyl-1,6-naphthyridinium dications may be inferred, however, from the isolation of **7** and **8** (p.m.r. spectra in Table 4) when such alkaline

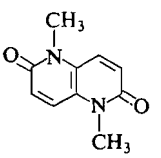

7

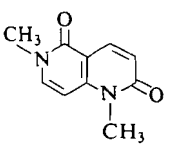

8

solutions are oxidized with potassium ferricyanide.[5] The isolation of **7** and **8**, from solutions

[4]In 1 M $NaOCD_3$–CD_3OD the p.m.r. spectra indicate that only monomethoxide adducts are formed.

[5]Compound 7 has also been obtained by Rapoport and Batcho (7) by oxidation of the 5-methyl cation of 1-methyl-2-naphthyridone with aqueous alkaline potassium ferricyanide solution.

Can. J. Chem. Downloaded from www.nrcresearchpress.com by 210.87.254.105 on 09/05/12
For personal use only.

TABLE 5. pK_{ROH} and u.v. spectral data (1 *M* NaOD–D_2O) for some *N*-alkyl heterocyclic cations

N-Alkyl substituent	5-Nitroisoquinolinium cations		1,8-Naphthyridinium cations		8-Nitroquinolinium cations	
	pK_{ROH}	λ_{max}(nm)	pK_{ROH}	λ_{max}(nm)	pK_{ROH}	λ_{max}(nm)
Methyl	11.7 ±0.1	325, 430	12.44±0.03	335	9.67±0.03	260, 302, 422
Ethyl	11.8 ±0.1	326, 429	12.81±0.05	335	9.83±0.06	260, 304, 418
n-Propyl	11.84±0.09	328, 429	12.81±0.04	337		
Isopropyl			13.7 ±0.1	330		
sec-Butyl	12.61±0.01	330, 410				

which we have shown can contain only very minor amounts of **5** and **6**, further emphasizes the caution that is necessary in accepting the products from oxidation studies as being representative of the major pseudobase species that are present in solution (1).

The pK_{ROH} values for the N,N^1-dimethyl-1,5-, -1,6-, and -2,7-naphthyridinium dications are much lower than those for the corresponding *N*-methyl monocations (12.67 (1), 12.33 (1), and 10.52, respectively). Thus the presence of a second positive charge in these ions increases the equilibrium constants for pseudobase formation by factors of 10^7–10^{10} relative to the corresponding monocations, and clearly strongly activates these systems towards nucleophilic attack.

Influence of the N-Substituent on Pseudobase Formation

The pK_{ROH} values for various *N*-alkyl 5-nitroisoquinolinium, 1,8-naphthyridinium, and 8-nitroquinolinium cations and also u.v. spectral data for each cation in aqueous alkaline solution are listed in Table 5. The similarity of the u.v. spectra of the pseudobases of all *N*-alkyl cations of each heterocycle indicates that predominant hydroxide attack occurs at the same position irrespective of the nature of the alkyl substituent. From detailed studies on the *N*-methyl cations of each heterocycle, these positions have been identified as C-2 for 1,8-naphthyridine (1) and 8-nitroquinoline (Table 1) and C-1 for 5-nitroisoquinoline (Table 8). The data in Table 5 indicate that increasing the size of a primary alkyl *N*-substituent has less effect on the pK_{ROH} value than replacing a primary alkyl group by a secondary alkyl substituent (isopropyl or *sec*-butyl). In all cases the pseudobase formation is less favored upon replacement of an *N*-methyl group by any other alkyl substituent which is consistent with the relative electronic effects of various alkyl groups. However, the much larger difference between primary and secondary alkyl groups must be attributed to steric and/or solvation effects. The increase in pK_{ROH} for the secondary alkyl groups is consistent with these bulkier *N*-alkyl substituents being more effective than the primary alkyl groups in shielding the α-carbon atom from hydroxide ion attack. Differences in solvation of the cation and pseudobase will also be influenced by the nature of the substituent on nitrogen but the probable magnitude of these effects is difficult to estimate.

Further evidence for the importance of *peri*-interactions which were postulated above to be important in the destabilization of 1,8-disubstituted quinolinium cations was obtained in attempts to extend the series of *N*-alkyl-substituted 8-nitroquinolinium cations. Thus attempts to produce 1-isopropyl-8-nitroquinolinium iodide by treatment of 8-nitroquinoline with isopropyl iodide were unsuccessful, and considerably longer reaction times were necessary for the quaternization of 8-nitroquinoline with ethyl iodide than for methyl iodide. Corresponding differences were not apparent in the alkylation of the electronically similar 1,8-naphthyridine.

In order to study a wider range of *N*-substituents, quinoline, isoquinoline, 5-nitroisoquinoline, and 1,8-naphthyridine were quaternized with each of iodoacetonitrile, bromoacetophenone, benzyl and *p*-nitrobenzyl bromides, and iodoacetamide. No identifiable quaterization products could be obtained for the reactions of quinoline and 1,8-naphthyridine with iodoacetonitrile. The pK_{ROH} values calculated from the p*H* dependence of the u.v. spectra of these various *N*-substituted cations are collected in Table 6 and relevant u.v. and p.m.r. spectral data for these cations are given in Tables 7 and 8.

The *N*-(2′,4′-dinitrophenyl)quinolinium and isoquinolinium and *N*-(2′,4′,6′-trinitrophenyl)-

Can. J. Chem. Downloaded from www.nrcresearchpress.com by 210.87.254.105 on 09/05/12
For personal use only.

TABLE 6. pK_{ROH} values for *N*-substituted heterocyclic cations in aqueous solutions

N-Substituent	Quinolinium cations	Isoquinolinium cations	5-Nitroisoquinolinium cations	1,8-Naphthyridinium cations
CH_3	(~16.5)[a]	(~15.3)[a]	11.7 ±0.1	12.44±0.03
$C_6H_5CH_2$	⩾14	⩾14	10.93±0.06	
p-$NO_2C_6H_4CH_2$	11.91±0.02	11.94±0.06	9.34±0.06	10.88±0.05
NH_2COCH_2	11.54±0.03	12.1 ±0.1[b]	9.77±0.07	9.83±0.05
$C_6H_5COCH_2$	10.35±0.07[c]	9.91±0.09[c]	~8.1	7.98±0.05
$CNCH_2$		10.04±0.06	7.26±0.07	
CN	−1.05[d]	−2.0[e]		

[a]Estimated values from ref. 1.
[b]Possibly for formation of an intramolecular adduct (see text).
[c]Ylide formation (see text).
[d]From ref. 3.
[e]From ref. 16.

quinolinium cations were also prepared. However, in aqueous solution each of these cations immediately decomposed to the neutral heterocycle and corresponding di- or trinitrophenol. Thus, the p*H* dependence of the u.v. spectrum of each of these cations was identical with that of a 1:1 mixture of the corresponding heterocycle and phenol. It is clear that in these cases hydroxide attack on the highly electron-deficient phenyl substituent on nitrogen predominates over attack in the heterocyclic ring. The result is an aromatic nucleophilic substitution via the Meisenheimer complex (**9**) (8–11). These reactions are quite analogous to the conversion of 2,4-dinitrochlorobenzene to 2,4-dinitrophenol (12).

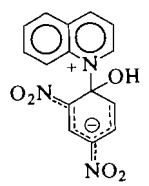

9

N-Substituted 5-Nitroisoquinolinium Cations

The p.m.r. spectrum of the 2-methyl-5-nitroisoquinolinium cation in basic methanol-d_4 solution (Table 8) is readily assigned to the C-1 methoxide adduct (**10**) by comparison with the

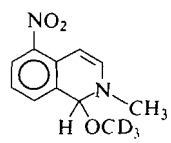

10

corresponding data for the 2-methylisoquinolinium cation (1). The similarities in the u.v. spectra of the other 5-nitroisoquinolinium cations in Table 7 to that of the *N*-methyl cation suggest that in each case similar nucleophilic addition reactions occur at C-1.

The p.m.r. spectra of the 2-carbamoylmethyl-, 2-benzyl-, and 2-*p*-nitrobenzyl-5-nitroisoquinolinium cations in basic methanol-d_4 are consistent with methoxide attack at the C-1 position of each of these cations (Table 8). The chemical shifts and coupling constants (J_{34} = 7.5 Hz) for these 2-substituted 5-nitroisoquinolinium cations in basic methanol are similar to the p.m.r. spectral assignments for 1,2-dihydro-2-methyl-1-trideuteromethoxy-5-nitroisoquinoline.

A red precipitate formed when alkali was added to solutions of the 5-nitro-2-phenacylisoquinolinium cation. This red precipitate was not sufficiently soluble in deuterochloroform to allow a p.m.r. spectral identification. Similar insoluble precipitates formed when alkali was added to the *N*-phenacylquinolinium and isoquinolinium cations. For these latter two cations, on the basis of u.v. and p.m.r. spectral evidence, the product is suggested (see later discussion) to be the ylide which is formed by proton abstraction from the methylene group of the phenacyl moiety. The red solid formed from the 5-nitro-2-phenacylisoquinolinium cation is possibly the analogous ylide **11**, and this is supported by its dissolution in acid to regenerate a p.m.r. spectrum which is identical with that of the cation except for the absence of the methylene protons which have undergone deuterium exchange. However, the similarity of the u.v. spectra of this

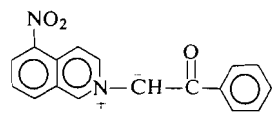

11

Can. J. Chem. Downloaded from www.nrcresearchpress.com by 210.87.254.105 on 09/05/12
For personal use only.

Can. J. Chem. Downloaded from www.nrcresearchpress.com by 210.87.254.105 on 09/05/12
For personal use only.

TABLE 7. Ultraviolet maxima for *N*-substituted cations in aqueous alkali and basic methanol

	Quinoline		Isoquinoline		5-Nitroisoquinoline		1,8-Naphthyridine	
N-Substituent	Water[a]	Methanol[b]	Water[a]	Methanol[b]	Water[a]	Methanol[b]	Water[a]	Methanol[b]
$-CH_3$		263, 330		277, 326, 334	266, 324, 450	276, 322, 433	330	265, 330
$-CH_2\overset{O}{\overset{\|}{C}}-C_6H_5$	314, 455	280, 491	328, 414	307, 455	325, 450	278, 321, 434	325	240, 325
$-CH_2\overset{O}{\overset{\|}{C}}NH_2$	276, 315(s)	265, 271(s), 328	311	300	271, 314(s), 440	270, 320, 422	326	328
$-CH_2-C_6H_5$		320[c]		305[c]	259, 322, 430	279, 323, 434		
$-CH_2-C_6H_4-NO_2$	269, 298, 311.5	267, 325	270, 306, 320	260, 302(s), 317(s)	277, 313, 436	277, 321, 438	277, 310	272, 325
$-CH_2CN$			315	293	273, 308, 419	274, 312, 404	277, 310	

[a] 1 *M* $KOH-H_2O$.
[b] 0.05 *M* $NaOCH_3-CH_3OH$.
[c] Cation; little methoxide adduct formed in 0.05 *M* $CH_3ONa-CH_3OH$.

TABLE 8. Proton magnetic resonance spectral data for *N*-substituted heterocyclic cations in basic methanol-d_4 (0.1 *M* $NaOCD_3$)

N-Substituent	Product	δ H-1	H-2	H-3	H-4	H-5—H-8	Other H
	(*i*) *Quinolinium cations*						
$C_6H_5CH_2$	C-2 adduct	—	5.70	5.70	[a]	6.52–7.23	4.75(s, 2H)[b], 7.23(s, 5H)[c]
p-$NO_2C_6H_4CH_2$	C-2 adduct	—	5.84	5.84	[a]	6.59–7.08	[d], 7.36[e], 8.00[e]
	(*ii*) *Isoquinolinium cations*						
NH_2COCH_2	**17**	4.27	—	6.05	5.44	7.0–7.7	[d]
p-$NO_2C_6H_4CH_2$	C-1 adduct	5.91	—	6.63	5.61	7.1–7.3	[d], 7.53[e], 8.20[e]
	(*iii*) 5-*Nitroisoquinolinium cations*						
NH_2COCH_2	C-1 adduct	5.80	—	6.77	6.40	7.2–8.0	[f]
$C_6H_5CH_2$	C-1 adduct	5.92	—	6.95	6.27	7.3–8.0	[a,f]
p-$NO_2C_6H_4CH_2$	C-1 adduct	6.04	—	6.89	6.32	7.1–8.1	[a,f]
	(*iv*) 1,8-*Naphthyridinium cation*						
p-$NO_2C_6H_4CH_2$	C-2 adduct	—	5.62	[g]	[g]	[g]	5.75[b,g]

[a]Hidden under H-5—H-8 multiplet.
[b]Benzylic CH_2 protons.
[c]Phenyl protons of benzyl group.
[d]CH_2 protons readily exchange with solvent deuterium.
[e]Phenyl protons of *p*-nitrobenzyl group; both signals are 2H doublet (J = 9 Hz).
[f]CH_2 protons obscured by solvent signal (δ 4.7–5.2).
[g]δ 7.89–8.15 (H-5 + H-7 + H-3',5', m, 4H), 7.32–7.52 (H-4 + H-2',6', m, 3H), 6.56–6.95 (H-3 + H-6, m, 2H).

cation in basic methanol and water to those of species which have been definitely established as C-1 adducts (Table 7) suggests that *in solution* the pseudobase (**12**: R = H) and methoxide adducts (**12**: R = CH_3) are formed preferentially to the ylide **11**.

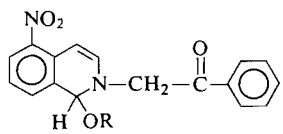

12

No solid separated from alkaline solutions of the 2-cyanomethyl-5-nitroisoquinolinium cation at p.m.r. spectral concentrations; however, no signals were present in the p.m.r. spectrum of this alkaline solution and this suggests that unidentified radical species may be present. Nevertheless, there is little doubt that at u.v. spectral concentrations, the predominant species present is the C-1 pseudobase (Table 7).

N-Substituted Quinolinium Cations

The u.v. spectra of the 1-carbamoylmethyl- and 1-*p*-nitrobenzylquinolinium cations in basic methanol (Table 7) are similar to the u.v. spectrum of the C-2 methoxide adduct of the 1-methylquinolinium cation. The u.v. spectra of aqueous alkaline and basic methanolic solutions of the 1-phenacylquinolinium cation are quite different to those of the other *N*-substituted quinolinium cations and have long wavelength maxima in the visible region of the spectrum (455 and 491 nm, respectively).

The p.m.r. spectra of the 1-benzyl- and 1-*p*-nitrobenzylquinolinium cations in basic methanol-d_4 are consistent with methoxide attack at the C-2 position. The chemical shifts of these C-2 methoxy adducts are similar to the chemical shifts for 1,2-dihydro-1-methyl-2-trideuteromethoxyquinoline (1). The u.v. spectra of the 1-*p*-nitrobenzylquinolinium cation in basic methanol and in aqueous alkaline solutions are similar and therefore indicate that the C-2 pseudobase of the 1-*p*-nitrobenzylquinolinium cation predominates in aqueous alkaline solution.

A red precipitate was collected from alkaline solutions of the 1-phenacylquinolinium cation ($\lambda_{max}(CH_3O^-–CH_3OH)$ 491 nm). This precipitate was insufficiently soluble in p.m.r. solvents to allow structure identification by p.m.r. spectroscopy. When a sample of this precipitate from $NaOD–D_2O$ was dissolved in acid, the p.m.r. spectrum of the starting cation was regenerated, except for the absence of the peak corresponding to the methylene protons of the phenacyl moiety. This suggests that these protons have undergone

Can. J. Chem. Downloaded from www.nrcresearchpress.com by 210.87.254.105 on 09/05/12
For personal use only.

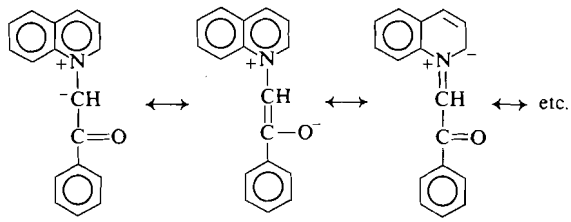

13

hydrogen–deuterium exchange in basic solution, and a likely route for such an exchange would be via the resonance-stabilized ylide **13**. It is possible that the red product from basic solutions is this highly conjugated ylide species, and such an ionic structure is also consistent with the insolubility of this product in organic solvents.

Yellow precipitates were produced from basic aqueous and methanolic solutions of the 1-carbamoylmethylquinolinium cation, and again these products were not soluble in suitable p.m.r. solvents. In light of the above discussion, the ylide structure **14** should be considered, although

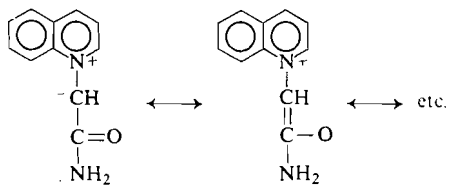

14

the zwitterion **15** is also possible. The u.v. spectra (Table 8) suggest however that *in solution* the C-2 adducts predominate.

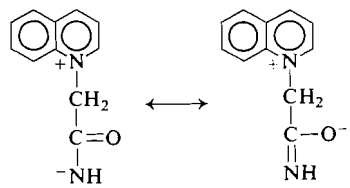

15

N-Substituted Isoquinolinium Cations

The u.v. spectra of the 2-substituted isoquinolinium cations in aqueous alkali and basic methanol solutions indicate greater differences than the corresponding spectra of the 2-substituted 5-nitroisoquinolinium cations (Table 7). The C-1 methoxide adduct of the 2-methylisoquinolinium cation has u.v. maxima similar to those observed for basic methanolic solutions of the 2-*p*-nitrobenzylisoquinolinium cation. The u.v. spectrum of basic methanolic solutions of the 2-benzylisoquinolinium cation (λ_{max} 305 nm) is identical to that of the cation in neutral methanol and indicates that methoxide attack does not occur on this cation in 0.05 *M* sodium methoxide solutions. This result is consistent with the pK_{ROH} value being >14 (Table 5) for this cation. The long wavelength u.v. maximum observed in alkaline solutions of the 2-phenacylisoquinolinium cation (Table 7) (λ_{max} 414 nm) (H_2O) and 455 nm (CH_3OH) is analogous to that observed for the corresponding quinolinium cation, and so suggests that the ylide **16** is formed preferentially to nucleophilic attack in these solutions also.

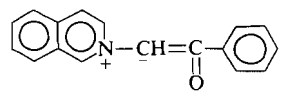

16

The p.m.r. spectra of the 2-benzyl- and 2-*p*-nitrobenzylisoquinolinium cations in basic methanol-d_4 are consistent with methoxide attack at the C-1 position of these cations (Table 8). The chemical shifts and coupling constant (J_{34} = 7.5 Hz) are typical of a 1,2-dihydroisoquinoline structure and are similar to the p.m.r. spectral assignments for 1,2-dihydro-2-methyl-1-trideuteromethoxyisoquinoline (1). As was the case for the 2-cyanomethyl-5-nitroisoquinolinium cation in alkali, no p.m.r. spectrum could be observed for alkaline solutions of the 2-cyanomethylisoquinolinium cation.

The p.m.r. spectrum of the 2-carbamoylmethylisoquinolinium cation in basic methanol-d_4 is characteristic of a 1,2-dihydroisoquinoline structure with the doublets (J_{34} = 7.5 Hz) for H-3 and H-4 readily assigned with chemical shifts (CD_3OD) δ 6.05 and 5.44, respectively. However, the peak for the C-1 proton occurs at abnormally high field (δ 4.27) in comparison with the chemical shift for the C-1 proton of 1,2-dihydro-1-methoxy-2-methylisoquinoline (δ 6.10). We suggest that the p.m.r. spectrum of the 2-carbamoylmethylisoquinolinium cation in basic methanol-d_4 is consistent with structure **17** which results from intramolecular cyclization by nucleophilic attack by the amide nitrogen atom (presumably as the anion) at the C-1 position of the isoquinoline ring followed by ionization of the amide in

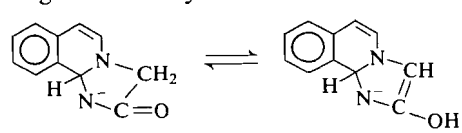

17

Can. J. Chem. Downloaded from www.nrcresearchpress.com by 210.87.254.105 on 09/05/12
For personal use only.

Can. J. Chem. Downloaded from www.nrcresearchpress.com by 210.87.254.105 on 09/05/12
For personal use only.

strong alkali. This is analogous to the report by Finch and Gemenden (13) that the *N*-3′-aminopropylisoquinolinium cation reacts in aqueous base to give a 95% yield of the intramolecular cyclization product **18**.

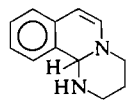

18

N-Substituted 1,8-Naphthyridinium Cations

The u.v. spectra of the 1-substituted 1,8-naphthyridinium cations in aqueous alkali and in basic methanol are similar and have u.v. maxima in the region of 330 nm which is typical of a 1,2-dihydro-1,8-naphthyridine structure (1).

The p.m.r. spectra of the 1-carbamoylmethyl- and 1-*p*-nitrobenzyl-1,8-naphthyridinium cations in basic methanol-d_4 (Table 8) are consistent with a 1,2-dihydro-1,8-naphthyridine structure and have been assigned to the C-2 methoxide adducts. The chemical shifts for these 1,2-dihydro-1,8-naphthyridine structures are similar to the chemical shifts for 1,2-dihydro-2-methoxy-1-methyl-1,8-naphthyridine (1). No p.m.r. spectrum was recorded for the 1-phenacyl-1,8-naphthyridinium cation in basic methanol-d_4 since an oily black solid separated from the basic solution.

Correlation of pK_{ROH} with Substituent Effects

Lindquist and Cordes (14) have reported that the association constants for *N*-substituted 3-carbamoylpyridinium cations with cyanide ion to give the 1,4-dihydro adducts are linearly correlated with Taft's σ^* substituent constants (15) with $\rho^* = -3.7$. We have therefore sought a similar correlation of pK_{ROH} with σ^* for the *N*-substituted 5-nitroisoquinolinium and 1,8-naphthyridinium cations using the data in Tables 5 and 6. Plots of pK_{ROH} for these two series of cations against σ^* are shown in Fig. 1. In each case reasonable linear correlations are apparent. Least squares fitting of the data gives: 5-nitroisoquinolinium cations, $pK_{ROH} = -3.7\ \sigma^* + 11.6$ (correlation coefficient 0.982 for nine substituents); 1,8-naphthyridinium cations, $pK_{ROH} = -4.9\ \sigma^* + 12.5$ (correlation coefficient 0.977 for seven substituents). These correlations are surprisingly good in view of the fact that σ^* reflects only electronic inductive effects of the substituents and thus steric and solvation effects are ignored.

The large negative ρ^* values in these two correlations clearly indicate the expected strong sensitivity of nucleophilic attack on these heterocyclic systems to electron-withdrawing substituents. A further striking indication of this effect is obtained from a comparison of the pK_{ROH} values for the 2-cyanomethylisoquinolinium (10.14) and 2-cyanoisoquinolinium cations (−2.0 (16)). Thus the insertion of a methylene group between the ring-nitrogen atom and its substituent in the latter cation reduces its susceptibility to pseudobase formation by a factor of 10^{12}.

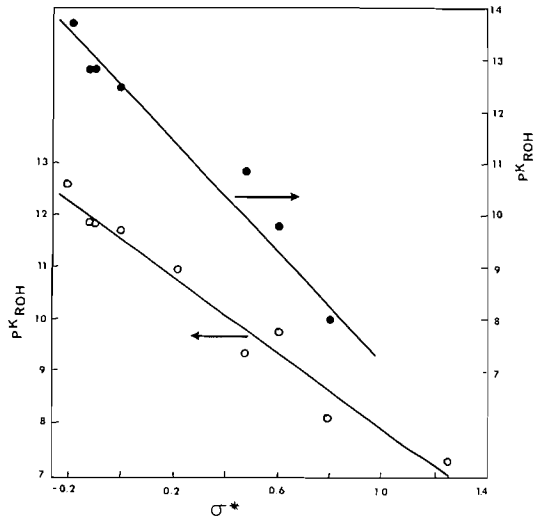

FIG 1. Dependence of pK_{ROH} on σ^* for *N*-substituted 5-nitroisoquinolinium (○) and 1,8-naphthyridinium (●) cations. Values of σ^* are from ref. 17 except for *p*-nitrobenzyl, estimated from $\sigma^*_{(XC_6H_4CH_2)} = 0.326\ \sigma^n_{(X)} + \sigma^*_{(C_6H_5CH_2)}$ (18); carbamoylmethyl and phenacyl, estimated from $\sigma^*_{R-CH_2} = 0.360\ \sigma_R^*$ (15).

Kinetic Studies

For many of the cations that are included in this study, the pseudobase–cation equilibrium was established too rapidly to allow a kinetic study by the stopped-flow technique. In some cases, the equilibration was sufficiently slow that the rate could be measured at p*H* values in the vicinity of pK_{ROH}, where the p*H*–rate profiles for these reactions typically pass through minima (2), but detailed kinetic studies were still not possible. The limited data available for all the cations in these two classes are summarized in Table 9.

For the 2-cyanomethyl-5-nitroisoquinolinium cation, reaction was sufficiently slow to allow a more detailed study. The p*H*-dependence of the first-order rate constant, k_{obs}, for attainment of

TABLE 9. Rapid cation–pseudobase equilibration

Cation	pH	$k_{obs}(s^{-1})$
1-Methyl-5-nitroquinolinium	11.6	>200
1-Methyl-6-nitroquinolinium	10.6	117
1-Methyl-7-nitroquinolinium	12.0	>200
1-Methyl-8-nitroquinolinium	10.0	>200
2-Methyl-5-nitroisoquinolinium	12.0	>200
1,5-Dimethyl-1,5-naphthyridinium	5.15	48
1,6-Dimethyl-1,6-naphthyridinium	2.45	170
1-Phenacylquinolinium	10.4	171
1-Carbamoylmethylquinolinium	12.0	>200
1-(*p*-Nitrobenzyl)quinolinium	12.0	>200
2-Phenacylisoquinolinium	9.95	151
2-Carbamoylmethylisoquinolinium	12.0	>200
2-(*p*-Nitrobenzyl)isoquinolinium	12.0	>200
2-Cyanomethylisoquinolinium	10.0	>200
2-Phenacyl-5-nitroisoquinolinium	8.56	50
2-Carbamoylmethyl-5-nitroisoquinolinium	9.94	55
2-Benzyl-5-nitroisoquinolinium	11.0	162
2-(*p*-Nitrobenzyl)-5-nitroisoquinolinium	9.41	15
1-Phenacyl-1,8-naphthyridinium	7.48	>200
1-(*p*-Nitrobenzyl)-1,8-naphthyridinium	11.1	58

equilibrium between this cation and its pseudobase is indicated in Fig. 2. The rate constant, k_{obs}, is the sum of the pseudo first-order rate constants, k_f and k_d respectively, for the formation and decomposition of the pseudobase. The individual rate constants, k_f and k_d, may be evaluated (2) from:

$$k_f = \frac{k_{obs}}{1 + [H^+]/K_{ROH}}$$

$$k_d = \frac{k_{obs}}{1 + K_{ROH}/[H^+]}$$

The pH dependences of k_f and k_d evaluated in this way are also indicated in Fig. 2. These curves are of somewhat different shape to those previously observed for other cations (2). Despite the scatter in the data (possibly arising from buffer effects (2)), the k_{obs} and k_d appear to be pH independent at low pH compared with a linear dependence on $[H^+]$ in this region that is observed in other cases, whereas k_f is inversely proportional to $[H^+]$ rather than the more usual pH independence at low pH (2). The pH profiles in Fig. 2 are consistent, however, with the reactions outlined in Scheme 1.

Since k_f and k_d have been individually evaluated, we may consider pseudobase formation and decomposition individually in Scheme 1. Thus

$$\frac{d[Q^+]}{dt} = k_2[QOH] + k_1{}^1[QOH_2{}^+]$$
$$= (k_2 + k_1[H^+])[QOH]$$

where

$$k_1 = k_1{}^1/K_a{}^0$$

Also $$\frac{d[Q^+]}{dt} = k_d([QOH] + [HQOH^+])$$
$$= k_d\left[1 + \frac{[H^+]}{K_a{}^N}\right][QOH]$$

Hence $$k_d\left[1 + \frac{[H^+]}{K_a{}^N}\right] = k_2 + k_1[H^+]$$

At low pH, $[H^+]/K_a{}^N \gg 1$, $k_1[H^+] \gg k_2$, and $k_d \approx k_1 K_a{}^N$ *i.e.* pH independent as is observed in Fig. 2.

Also

$$\frac{d}{dt}([QOH] + [HQOH^+])$$
$$= (1 + [H^+]/K_a{}^N)\, d[QOH]/dt$$
$$= (k_4 + k_3[OH^-])[Q^+]$$

and

$$d[QOH]/dt = k_f[Q^+]$$

hence $$k_f = \frac{k_4 + k_3[OH^-]}{1 + [H^+]/K_a{}^N}$$

$$\approx k_4 K_a{}^N/[H^+] \text{ for low p}H$$

$$([H^+]/K_a{}^N \gg 1, k_4 \gg k_3[OH^-])$$

For high pH, the dependences of k_f and k_d on pH simplify to $k_f = k_3[OH^-]$ and $k_d = k_2$. Thus $k_2 = 0.54\ s^{-1}$ and $k_3 = 1.9 \times 10^6\ M^{-1}\ s^{-1}$ may be evaluated.

Can. J. Chem. Downloaded from www.nrcresearchpress.com by 210.87.254.105 on 09/05/12
For personal use only.

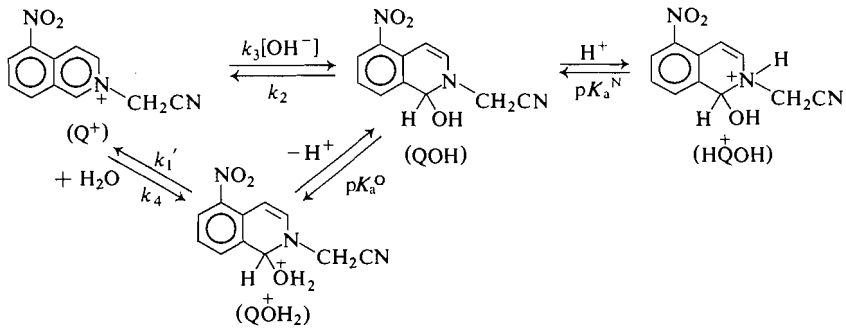

SCHEME 1

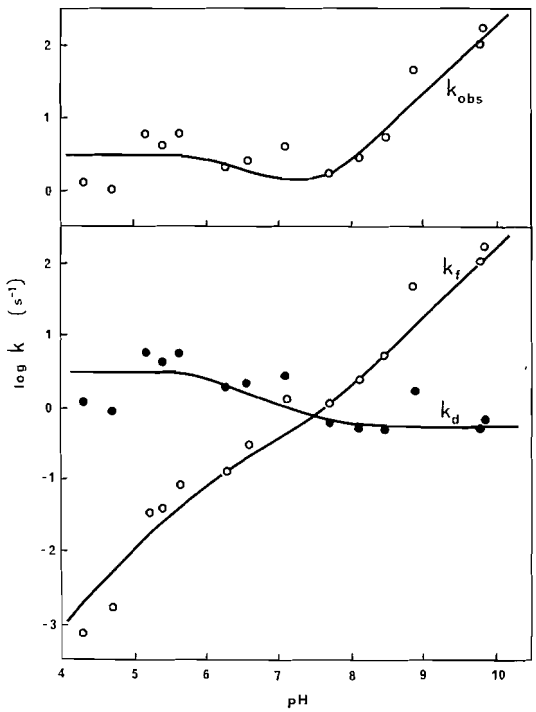

FIG. 2. p*H*–rate profiles for reversible pseudobase formation from the 2-cyanomethyl-5-nitroisoquinolinium cation (25°; ionic strength 0.1).

From the low p*H* data, $k_1K_a^N = 3.2\ s^{-1}$ and $k_4K_a^N = 1.1 \times 10^{-7}\ M\ s^{-1}$ may also be estimated. The parameters k_1, k_4, K_a^N cannot be individually evaluated from the available data. However, if we assume that k_3/k_4 for this cation is similar to the value previously found for the related 2-methyl-4-nitroisoquinolinium cation (8.8×10^6 (2)), then $k_1 = 6.4 \times 10^6\ M^{-1}\ s^{-1}$, $k_4 = 0.22\ s^{-1}$ and $K_a^N = 5.0 \times 10^{-7}\ M$ are obtained. Thus pK_a^N for *N*-protonation of the pseudobase QOH in Scheme 1 is estimated to be 6.30 which seems a reasonable value for such a substituted amine. The lines in Fig. 2 are calculated using the above values for the various parameters, and give a reasonable fit to the experimental data.

Thus the differences in the p*H*–rate profiles for the 2-cyanomethyl-1-nitroisoquinolinium cation and those species studied earlier (2) arise from the greater basicity of the pseudobase towards *N*-protonation in the present case. In the earlier study (2), species equivalent to $HQOH^+$ would not be expected to be present in significant amounts in the experimentally observable p*H* ranges.

Experimental

Materials

Unless specifically discussed below, quaternary salts were prepared by refluxing the parent heterocycle with an appropriate alkyl halide, either neat or in a suitable solvent (acetone or ethanol). After recrystallization, compounds were obtained which had melting points consistent with literature data and p.m.r. spectra (D_2O or TFA) in accord with the expected cation structure.

Naphthyridinium Dications

Each of 1,5-, 1,6-, and 2,7-naphthyridine was heated with excess dimethyl sulfate for approximately 4 h. After addition of water, excess dimethyl sulfate was removed by extraction with chloroform. The methyl sulfate anion was exchanged for iodide ion by passing the aqueous solution of the dication through a column of Dowex 2-X8 anion exchange resin which had previously been saturated with sodium iodide. The aqueous solvent was evaporated to dryness to yield the solid diiodide salt with the exception of the 2,7-dimethyl-2,7-naphthyridinium dication which could not be obtained solid, and so was handled as an aqueous solution. The p.m.r. spectral data for these naphthyridinium dications in D_2O were in agreement with the data given by Pokorny and Paudler (6).

1-Phenacylquinolinium Bromide

Quinoline (2 ml) was refluxed in acetone (10 ml) with excess bromoacetophenone for 1 h. After removal of the solvent, the residue was dissolved in absolute ethanol, and anhydrous ether was added to give red crystals which were recrystallized from absolute ethanol. Yield 3.8 g (68%), m.p. 193–195°; p.m.r. (TFA): δ 9.16–9.42 (H-2 + H-4, m, 2H), 7.33–8.53 (all other aromatic protons, m, 10H), 6.94 (CH_2, s, 2H).

Can. J. Chem. Downloaded from www.nrcresearchpress.com by 210.87.254.105 on 09/05/12
For personal use only.

Can. J. Chem. Downloaded from www.nrcresearchpress.com by 210.87.254.105 on 09/05/12
For personal use only.

Anal. Calcd. C, 62.2; H, 4.27; N, 4.27. Found: C, 62.1; H, 4.12; N, 4.26.

1-Phenacyl-1,8-naphthyridinium Bromide

This was similarly prepared. Yield 1.5 g (25%), viscous gum; p.m.r. (TFA): δ 7.7–9.8 (all aromatic protons, m, 11H), 7.07 (CH_2, s, 2H).

2-Phenacylisoquinolinium Bromide

Isoquinoline (2 ml) was mixed with excess 2-bromoacetophenone in acetone (10 ml). After 10 min, a white solid separated from solution; recrystallization from ethanol gave 4 g (72%), m.p. 210–212°; p.m.r. (TFA): δ 9.79 (H-1, s, 1H), 7.6–8.6 (all other aromatic protons, m, 11H), 6.70 (CH_2, s, 2H).

Anal. Calcd. C, 62.2; H, 4.27; N, 4.27; Br, 24.4 Found: C, 62.4; H, 4.83; N, 4.38; Br, 24.2.

2-Phenacyl-5-nitroisoquinolinium Bromide

This was similarly prepared. Yield 3.4 g (55%), m.p. 190–191°; p.m.r. (TFA): δ 10.01 (H-1, s, 1H), 7.6–9.5 (other aromatic protons, m, 10H), 6.79 (CH_2, s, 2H).

Anal. Calcd. C, 54.7; H, 3.51; N, 7.51. Found: C, 54.2; H, 3.74; N, 7.39.

1-Carbamoylmethylquinolinium Iodide.

Yield 58%, m.p. 226–228°; p.m.r. (TFA): δ 9.18–9.43 (H-2 + H-4, m, 2H), 8.04–8.53 (other aromatic protons, m, 5H), 6.25 (CH_2, s, 2H).

Anal. Calcd. C, 42.0; H, 3.50; N, 8.92. Found: C, 42.2; H, 3.70; N, 8.73.

2-Carbamoylmethylisoquinolinium Iodide

Yield 48%, m.p. 194–196°; p.m.r. (TFA): δ 9.90 (H-1, s, 1H), 8.34–8.67 (other aromatic protons, m, 6H), 6.10 (CH_2, s, 2H).

Anal. Calcd. H, 3.81; N, 8.92; I, 40.5. Found: H, 3.66; N, 8.92; I, 40.5.

2-Carbamoylmethyl-5-nitroisoquinolinium Iodide

Yield 31%, m.p. 233°; p.m.r. (TFA): δ 8.3–9.6 (aromatic protons, m, 5H), 7.86 (H-7, m, 1H), 6.90 (CH_2, s, 2H).

Anal. Calcd. C, 36.8; H, 2.81; N, 11.70. Found: C, 36.8; H, 3.20; N, 11.78.

1-Carbamoylmethyl-1,8-naphthyridinium Iodide

Yield 18%, m.p. 210°; p.m.r. (TFA): δ 8.1–9.6 (aromatic protons, m, 6H), 6.33 (CH_2, s, 2H).

1-(p-Nitrobenzyl)quinolinium Bromide

Yield 31%, m.p. 168°; p.m.r. (TFA): δ 9.29–9.58 (H-2 + H-4, m, 2H), 8.19–8.54 (other quinoline protons + H-3′, 5′, m, 7H), 7.60 (H-2′,6′, d, 2H, J = 9 Hz), 6.60 (CH_2, s, 2H).

2-(p-Nitrobenzyl)isoquinolinium Bromide

Yield 25%, m.p. 201–202°; p.m.r. (TFA): δ 9.87 (H-1, s, 1H), 8.32–8.62 (other isoquinoline protons + H-3′,5′, m, 8H), 7.63 (H-2′,6′, d, 2H, J = 9 Hz), 6.24 (CH_2, s, 2H).

Anal. Calcd. H, 3.80; N, 8.12; Br, 23.2. Found: H, 3.97; N, 7.78; Br, 22.9.

2-(p-Nitrobenzyl)-5-nitroisoquinolinium Bromide

Yield 27%, m.p. 203–204°; p.m.r. (TFA): δ 10.30 (H-1, s, 1H), 8.29–9.65 (other isoquinoline protons + H-3′,5′, m, 7H), 7.86 (H-2′,6′, d, 2H, J = 9.5 Hz), 6.35 (CH_2, s, 2H).

Anal. Calcd. C, 49.25; H, 3.10; N, 10.77. Found: C, 49.10; H, 3.46; N, 10.55.

1-(p-Nitrobenzyl)-1,8-naphthyridinium Bromide

Yield 9%, m.p. 217–218°; p.m.r. (TFA): 8.05–9.89 (naphthyridine protons + H-3′,5′, m, 8H), 7.84 (H-2′,6′, d, 2H, J = 9 Hz), 6.74 (CH_2, s, 2H).

Anal. Calcd. C, 52.0; H, 3.50; N, 12.13; Br, 23.1. Found: C, 51.7; H, 3.95; N, 11.93; Br, 23.1.

2-Cyanomethylisoquinolinium Iodide

Yield 17%, m.p. 161–162°; p.m.r. (TFA): δ 9.70 (H-1, s, 1H), 8.39–8.57 (other aromatic protons, m, 6H), 5.86 (CH_2, s, 2H).

Anal. Calcd. C, 44.6; H, 3.06; N, 9.47; I, 43.2. Found: C, 44.6; H, 3.44; N, 9.52; I, 43.0.

2-Cyanomethyl-5-nitroisoquinolinium Iodide

Yield 12%, m.p. 169–170°; p.m.r. (TFA): δ 10.00 (H-1, s, 1H), 8.21–9.57 (other aromatic protons, m, 5H), 6.00 (CH_2, s, 2H).

Anal. Calcd. H, 2.36; N, 12.32. Found: H, 2.72; N, 12.17.

Methods

Equilibrium and kinetic studies were performed as previously described (1,2). All equilibrium constants were measured spectrophotometrically at 25°, ionic strength 0.01. Kinetic data were obtained at 25° in buffers of ionic strength 0.1.

We appreciate the continued support of this work by a grant from the National Research Council of Canada, and the award of a University of Toronto Open Fellowship to W.G.M.

1. J. W. Bunting and W. G. Meathrel. Can. J. Chem. **50**, 917 (1972).
2. J. W. Bunting and W. G. Meathrel. Can. J. Chem. **51**, 1965 (1973).
3. C. J. Cooksey and M. D. Johnson. J. Chem. Soc. B, 1191 (1968).
4. H. H. Jaffe. Chem. Rev. **53**, 191 (1953).
5. D. D. Perrin. J. Chem. Soc. 5590 (1965).
6. D. J. Pokorny and W. W. Paudler. Can. J. Chem. **51**, 476 (1973).
7. H. Rapoport and A. D. Batcho. J. Org. Chem. **28**, 1753 (1963).
8. M. J. Strauss. Chem. Rev. **70**, 667 (1970).
9. M. R. Crampton. Adv. Phys. Org. Chem. **7**, 211 (1969).
10. P. Buck. Angew. Chem. Int. Ed. Engl. **8**, 120 (1969).
11. E. Buncel, A. R. Norris, and K. E. Russel. Quart. Rev. Chem. Soc. **22**, 123 (1968).
12. S. D. Ross. J. Am. Chem. Soc. **80**, 5319 (1958).
13. N. Finch and G. W. Gemenden. J. Org. Chem. **38**, 437 (1973).
14. R. N. Lindquist and E. H. Cordes. J. Am. Chem. Soc. **90**, 1269 (1968).
15. R. W. Taft. Steric effects in organic chemistry. *Edited by* M. S. Newman. John Wiley and Sons Inc. N.Y. 1956. pp. 607–610.
16. B. J. Huckings and M. D. Johnson. J. Chem. Soc. 5371 (1964).
17. P. R. Wells. Linear free energy relationships. Academic Press, New York. 1968. p. 38.
18. C. D. Ritchie and W. F. Sager. Prog. Phys. Org. Chem. **2**, 323 (1964).
19. J. W. Bunting and W. G. Meathrel. Can. J. Chem. **52**, 303 (1974).

Quaternary Nitrogen Heterocycles. VI.[1] Equilibria and Kinetics of Pseudobase Formation from some Heteroaromatic Dications

JOHN W. BUNTING AND WILLIAM G. MEATHREL

Department of Chemistry, University of Toronto, Toronto, Ontario M5S 1A1

Received October 5, 1973

Equilibrium constants (pK_{ROH}) and the kinetics of cation–pseudobase equilibration have been measured for pseudobase formation by the 5,6-dihydropyrazino[1,2,3,4-*lmn*]-1,10-phenanthrolinium (**1**; pK_{ROH} = 9.54), 5*H*-6,7-dihydro-1,4-diazepino[1,2,3,4-*lmn*]-1,10-phenanthrolinium (**2**; pK_{ROH} = 9.17), and pyrazino[1,2,3,4-*lmn*]-1,10-phenanthrolinium (**3**; pK_{ROH} = 6.22) dications. Ultraviolet and p.m.r. spectral studies indicate that in strongly basic methanolic solutions **1** and **2** form bismethoxide adducts whereas in aqueous alkaline solutions these cations form the monopseudobase alkoxide ions (zwitterions) rather than the dipseudobases. The lower pK_{ROH} value for **2** than for **1** is suggested to arise from strain in the dication **2**, which is relieved upon pseudobase formation.

Les constantes d'équilibre (pK_{ROH}) et la cinétique de l'équilibration cation–pseudobase ont été mesurées lors de la formation de la pseudobase à partir des dications, dihydro-5,6 pyrazino-[1.2.3.4-*lmn*] phénantrolium-1,10 (**1**:pK_{ROH} = 9.54), 5*H*-dihydro-6,7 diazepino-1,4[1,2,3,4-*lmn*] phénanthrolinium-1,10 (**2**; pK_{ROH} = 9.17) et pyrazino [1,2,3,4-*lmn*] phénanthrolinium-1,10 (**3**; pK_{ROH} = 6.22). Des études à l'aide de la spectroscopie u.v. et r.m.p. ont montré que dans des solutions méthanoliques fortement basiques, **1** et **2** conduisent à des composés d'addition bisméthoxyde alors que dans des solutions alcalines aqueuses ces cations conduisent aux ions alkoxydes monopseudobasiques (zwitterions) plutôt qu'aux dipseudobases. On suggère que la valeur de pK_{ROH} plus faible pour **2** que pour **1** provient de contraintes à l'intérieur de dication **2** qui sont perdues lors de la formation de la pseudobase. [Traduit par le journal]

Can. J. Chem., **52**, 975 (1974)

During the course of our studies (1, 2) on the dependence of pK_{ROH} values for pseudobase formation upon the structure of the heterocyclic cation, we recently noted (2) that *N*,*N*[1]-dimethylnaphthyridinium dications are more susceptible to pseudobase formation by factors of 10^7–10^{10} than the corresponding *N*-methylnaphthyridinium monocations. This strong activation of heteroaromatic cations to nucleophilic attack by the presence of a second positive charge elsewhere in the molecule has prompted us to extend these studies to other heteroaromatic dications. In the present study, we report equilibrium, kinetic, and spectral data for pseudobase formation from the dications **1**, **2**, and **3** which are derived from 1,10-phenanthroline, and also more limited studies on some other related cations.

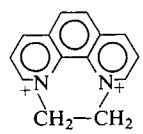

1

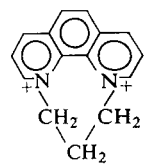

2

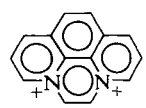

3

Results and Discussion

The u.v. spectrum of the 1-methyl-1,10-phenanthrolinium cation **4** is p*H* independent in aqueous solutions below p*H* 14. This indicates that the pK_{ROH} value for pseudobase formation by this cation is $\geqslant 15$. The p.m.r. spectrum of **4** in basic methanol-d_4 (0.1 *M* $NaOCD_3$) is readily assignable to the methoxide adduct **5** as

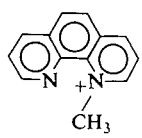

4

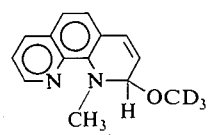

5

[1]For Part V, see ref. 2.

Can. J. Chem. Downloaded from www.nrcresearchpress.com by 210.87.254.40 on 09/05/12
For personal use only.

Can. J. Chem. Downloaded from www.nrcresearchpress.com by 210.87.254.40 on 09/05/12
For personal use only.

the predominant species present in this solution: δ 3.88 (N—CH_3, s, 3H); 5.60 (H-2, d, 1H, J_{23} = 5.5 Hz), 6.01 (H-3, dd, 1H, J_{23} = 5.5 Hz, J_{34} = 9 Hz), 7.00 (H-4, d, 1H, J_{34} = 9 Hz), 7.24–7.45 (H-5 + H-6 + H-8, m, 3H), 8.09 (H-7, m, 1H), 8.77 (H-9, m, 1H). Thus nucleophilic attack on **4** occurs predominantly at C-2 as in the 1-methylquinolinium cation and the N-10 nitrogen atom is apparently sufficiently removed from the nucleophilic center that it has little effect on the susceptibility of C-2 to nucleophilic attack (for the methylquinolinium cation $pK_{ROH} \sim 16.5$ (1)). This result may be compared to the *N*-methylnaphthyridinium cations in which the presence of a nitrogen atom in the adjacent aromatic ring activates C-2 to nucleophilic attack to such an extent that pK_{ROH} values of 12.67 and 12.44 are observed for the 1-methyl-1,5- and -1,8-naphthyridinium cations, respectively (1).

The p*H* dependence of the u.v. spectrum of the 5,6-dihydropyrazino[1,2,3,4-*lmn*]-1,10-phenanthrolinium dication (**1**) indicates the occurrence of two successive equilibria in basic solutions. We assign these u.v. spectral changes to formation of the pseudobase **6** (R = H) (pK_{ROH} = 9.54 ± 0.03) and its ionization to an alkoxide ion (actually a zwitterion) ($pK_{RO^-} \sim 13.5$) on the basis of the following spectral evidence.

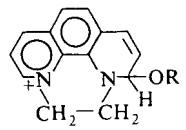

6

The p.m.r. spectrum of a basic methanol-d_4 (0.01 *M* $NaOCD_3$) solution of this dication is consistent with the formation of a monomethoxide adduct (**6**; R = CD_3): δ 4.15 (N^1—CH_2—, t, 2H), 5.10 (N^{10}—CH_2—, t, 2H), 5.88 (H-2, d, 1H, J_{23} = 5.5 Hz), 6.30 (H-3, dd, 1H, J_{23} = 5.5 Hz, J_{34} = 9.5 Hz), 7.22 (H-4, d, 1H, J_{34} = 9.5 Hz), 7.67–8.10 (H-5 + H-6 + H-8, m, 3H), 8.97–9.20 (H-7, H-9, m, 2H). The u.v. spectrum of the monomethoxide adduct (λ_{max} 303 nm) is similar to the u.v. spectrum of a p*H* 10 solution of this 1,10-phenanthrolinium dication (λ_{max} 302 nm).

The p.m.r. spectrum of this dication in more basic methanol-d_4 solution (1.5 *M* $NaOCD_3$) is consistent with the formation of the dimethoxide adduct (**7**; R = OCD_3): δ 3.82 (—CH_2—CH_2—, s, 4H), 5.84 (H-3, H-8, d, 2H, $J_{34} = J_{78}$ = 10 Hz), 6.75 (H-5 + H-6, s, 2H), 6.99 (H-4 + H-7, d, 2H, $J_{34} = J_{78}$ = 10 Hz). It is evident that the H-2 and -9 protons have exchanged with solvent

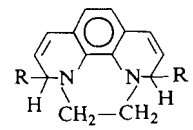

7

deuterium. The p.m.r. spectrum of the product from the lithium aluminum hydride reduction of this 1,10-phenanthrolinium dication is consistent with the formation of a 1,2,9,10-tetrahydro reduction product (**7**; R = H): (in $CDCl_3$) δ 3.20 (—CH_2—CH_2—, s, 4H), 3.75 (H-2 + H-8, dd, 4H, $J_{23} = J_{89}$ = 4 Hz, $J_{24} = J_{79}$ = 1.8 Hz), 5.57–5.82 (H-3 + H-8, m, 2H), 6.19–6.39 (H-4 + H-5 + H-6 + H-7, m, 4H).

The u.v. spectrum of the dimethoxide adduct (**7**; R = OCH_3) (λ_{max} (1.5 *M* $NaOCH_3$) 260, 310, 323, 380 nm) differs from the u.v. spectrum of a p*H* 14 solution of this 1,10-phenanthrolinium dication (λ_{max} 312 nm). A bathochromic shift of 10 nm from λ_{max} (p*H* 10) 302 nm to λ_{max} (p*H* 14) 312 nm would be consistent with ionization of the initially formed pseudobase rather than the addition of a second hydroxide ion. This result is similar to the ionization of the pseudobase of the naphthyridinium dications rather than the addition of a second hydroxide ion to the remaining quaternized ring (2). However, even in strongly basic methanolic solution (1 *M* $NaOCH_3$), the naphthyridinium dications form only a monomethoxide adduct, whereas the 5,6-dihydropyrazino[1,2,3,4-*lmn*]-1,10-phenanthrolinium dication forms a dimethoxide adduct by methoxide ion attack at both the C-2 and -9 positions. These results can be rationalized in terms of the greater susceptibility of the quinolinium system (in **6**; R = OCH_3) than the pyridinium moiety (in **8**) to nucleophilic attack by methoxide ion.

For the 5*H*-6,7-dihydro-1,4-diazepino[1,2,3,4-

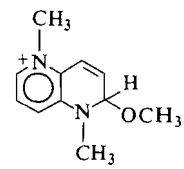

8

Can. J. Chem. Downloaded from www.nrcresearchpress.com by 210.87.254.40 on 09/05/12
For personal use only.

lmn]-1,10-phenanthrolinium dication (**2**) a pK_{ROH} value of 9.17 ± 0.03 was calculated from the p*H* dependence of the u.v. spectrum. The p.m.r. spectrum of a basic methanol-d_4 solution (0.01 *M* $NaOCD_3$) of this dication is consistent with the formation of a monomethoxide C-2 adduct **9** (R = CD_3): δ 2.87 (—CH_2—, m, 2H), 3.92 (N^1—CH_2—, m, 2H), 5.12 (N^{10}—CH_2—, m, 2H), 5.59 (H-2, d, 1H, J_{23} = 5.5 Hz), 6.30 (H-3, dd, 1H, J_{23} = 5.5 Hz, J_{34} = 9.5 Hz), 7.14 (H-4, d, 1H, J_{34} = 9.5 Hz), 7.79–8.04 (H-5 + H-6 + H-8, m, 3H), 8.95–9.30 (H-7 + H-9, m, 2H).

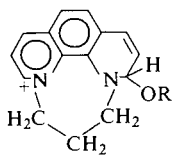

9

The u.v. spectra of **9** (R = CH_3) in methanol and a p*H* 10 aqueous solution of this dication are similar (λ_{max} 303.5 and 303 nm, respectively). These u.v. spectral maxima are also similar to those observed for the C-2 mono adducts of the 5,6-dihydropyrazino[1,2,3,4-*lmn*]-1,10-phenanthrolinium dication (**1**) (λ_{max} (0.01 *M* $NaOCH_3$) 303 nm and λ_{max} (p*H* 10) 302 nm).

In more basic methanol-d_4 (1 *M* $NaOCD_3$), the dimethoxide adduct (**10**; R = OCD_3) is formed as evident by its p.m.r. spectrum. It is evident that the C-2 and -9 protons, the sites of methoxide attack, have exchanged in this strongly basic deuterated solvent (1): δ 2.18 (—CH_2—, m, 2H), 3.94 (N—CH_2—, m, 4H), 5.90 (H-3 + H-8, d, 2H, J_{34} = J_{78} = 10 Hz), 6.78–7.14 (H-4 + H-5 + H-6 + H-7, m, 4H).

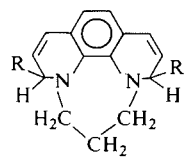

10

The u.v. spectrum of this dimethoxide adduct (λ_{max} (1 *M* $NaOCH_3$) 268, 316, 380 nm) differs from the u.v. spectrum of a 1 *M* potassium hydroxide solution of this dication (λ_{max} 308 nm). This result indicates that the initially formed pseudobase is ionized in strongly alkaline solution more readily than the addition of a second hydroxide ion to the cation. The bathochromic shift in the u.v. spectral maxima of aqueous solutions of p*H* 11.7 and 14 from 303 to 308 nm would be consistent with such an ionization. This result is also consistent with the ionization of the pseudobase from the naphthyridinium dications and the 5,6-dihydropyrazino-[1,2,3,4-*lmn*]-1,10-phenanthrolinium dication which were discussed earlier.

When the 5*H*-6,7-dihydro-1,4-diazepino[1,2,-3,4-*lmn*]-1,10-phenanthrolinium dication was reduced with lithium aluminum hydride, the 1,2,9,-10-tetrahydro reduction product **10** (R = H) was obtained as evident by its p.m.r. spectrum: (in $CDCl_3$) δ 1.57–1.97 (—CH_2—, m, 2H), 3.27–3.87 (—CH_2—N, t, 4H), 3.87 (H-2 + H-9, dd, 4H, J_{23} = J_{89} = 4 Hz, J_{24} = J_{79} = 1.8 Hz), 5.52–5.82 (H-3 + H-8, m, 2H), 6.24–6.45 (H-4 + H-5 + H-6 + H-7, m, 4H).

Comparison of the pK_{ROH} values for **1** (9.54) and **2** (9.17) indicates that the latter cation is slightly more susceptible to pseudobase formation than the former. In such systems, the electronic effect of a positive charge in one pyridinium ring is transmitted to the other ring through both the aromatic system and the saturated bridge. One would predict that electronic effects transmitted via the aromatic ring should be the same for each cation, while the relative effects transmitted via the saturated bridge would be greater in **1** than in **2** as a result of the insulating effect of the additional methylene group in **2**. Thus the pK_{ROH} value for **2** would be predicted to be greater than for **1** which is contrary to the present observations. An explanation of this apparent anomaly can be suggested on the basis of model building studies of these two dications. Thus, for a trimethylene bridge (**2**), space-filling Corey–Pauling–Koltun models suggest that it is not possible to insert three methylene groups between the nitrogen atoms of 1,10-phenanthroline without seriously distorting the three rings of the aromatic system out of coplanarity. No such distortion is indicated when only two methylene groups (**1**) are inserted. The models indicate that the interactions that produce this effect in **2** are considerably relieved upon pseudobase formation and so the unusually high susceptibility of this dication to pseudobase formation is apparently due to the strained nature of the dication. The effects of the strain induced upon inserting an additional methylene

group into the saturated bridge in **1** apparently outweigh the decrease in transmission of electronic charge through the saturated bridge as discussed above.[2]

To illustrate further the importance of this effect we have compared the pK_{ROH} values of the two cations (**11**; $n = 2$, 3) as a model for the transmission of charge through dimethylene and trimethylene bridges. From the p*H*-

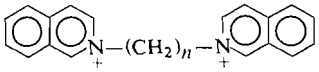

11

dependence of the u.v. spectrum of **11** ($n = 2$) a pK_{ROH} value of 10.84 ± 0.06 was calculated. This is consistent with pK_{ROH} values observed for other isoquinolinium cations that have strongly electron-withdrawing substituents on the nitrogen atom (2) and is considerably less than the value (15.3) estimated for the 2-methylisoquinolinium cation (1). Unfortunately, aqueous alkaline solutions of **11** ($n = 3$) rapidly become turbid and an accurate determination of pK_{ROH} is not possible for this cation, but can only be estimated as $\geqslant 12$. Thus, **11** ($n = 3$) is at least 10 times less susceptible to pseudobase formation than **11** ($n = 2$) which is consistent with the greater attenuation of charge for a trimethylene than a dimethylene bridge in these strain-free systems.

From the p*H*-dependence of the u.v. spectrum of the pyrazino[1,2,3,4-*lmn*]-1,10-phenanthrolinium dication (**3**) a pK_{ROH} value of 6.22 ± 0.05 was calculated. Black and Summers have previously proposed that this dication forms the pseudobase (**12**) by hydroxide ion attack at the C-5 position of the pyrazine ring (3).

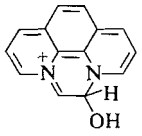

12

[2]Attempts to synthesize the 1,10-phenanthrolinium dication, in which the N-1 and -10 hetero atoms are coupled through a single methylene group, by condensation of 1,10-phenanthroline with methylene iodide were unsuccessful. Space-filling models of the 1,10-phenanthrolinium dications also indicate that a single methylene bridge cannot be placed between the two hetero atoms without severely distorting the aromatic ring system out of planarity.

The p.m.r. spectra of solutions of this dication in basic methanol-d_4 and basic deuterium oxide have peaks of low intensity due to the low solubility of the basic product(s) in the p.m.r. solvents. Thus identification of the pseudobase **12** in alkaline solutions by p.m.r. spectroscopy was not possible. Pseudobase formation by hydroxide attack in the pyrazine ring yields a highly conjugated nonaromatic system which is consistent with the u.v. spectrum of aqueous alkaline solutions of this dication having an absorbance maximum in the visible region ($\lambda_{max} \sim 500$ nm) of the spectrum. The carbon atoms of the pyrazine ring of **3** are extremely electron deficient due to the presence of the two positively charged nitrogen atoms. Nucleophilic attack in the pyrazinium rather than one of the pyridinium rings to give an adduct analogous to **6** and **9** is also consistent with the observation that quinoxalinium cations are approximately 10^8 times more susceptible to pseudobase formation than the corresponding quinolinium cations (1).

In view of this latter fact, it is noteworthy that the pK_{ROH} value for **3** is only 3.5 units lower than for **1**. However, an important offsetting factor in the formation of **12** compared with **6** or **9** is the loss of aromatic character in all four rings of **3** upon pseudobase formation.

Kinetic Studies

The equilibration of each of the cations **1**, **2**, and **3** with their respective pseudobases followed pseudo first-order kinetics over the p*H* ranges examined. The individual pseudo first-order rate constants for formation (k_f) and decomposition (k_d) of the pseudobases are plotted as a function of p*H* in Figs. 1–3. These p*H*-rate profiles may be fitted by equations of the form

$$k_d = k_1[H^+] + k_2$$

$$k_f = k_3[OH^-] + k_4$$

and the evaluated parameters k_1, k_2, k_3, and k_4 for each cation are listed in Table 1. Equations of this form have also been observed for cation–pseudobase equilibration for a number of other cations (4) and the mechanistic implications of the parameters have previously been considered in some detail. In particular, k_3 and k_4 refer to attack on the heterocyclic cation by hydroxide ion and neutral water molecules, respectively. Comparison of the data for **1** and **3** indicates

Can. J. Chem. Downloaded from www.nrcresearchpress.com by 210.87.254.40 on 09/05/12
For personal use only.

TABLE 1. Kinetic parameters for reversible pseudobase formation[a]

Cation	pK_{ROH}	k_1 (M^{-1} s^{-1})	k_2 (s^{-1})	k_3 (M^{-1} s^{-1})	k_4 (s^{-1})
1	9.54	2.6×10^8	25	5.5×10^5	0.059
2	9.17	1.9×10^8	14	9.4×10^5	0.12
3	6.22	1.9×10^5	0.032	1.5×10^6	0.115

[a]At 25°, buffer ionic strength 0.1.

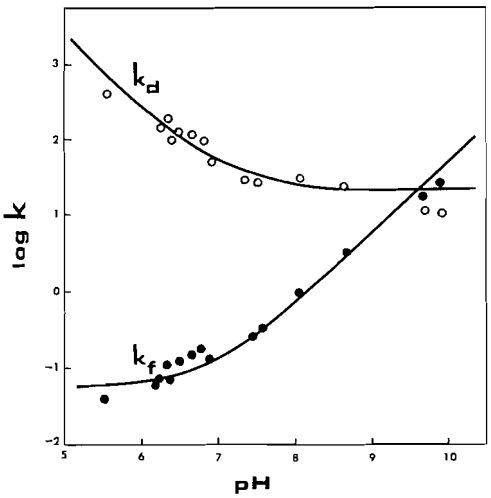

FIG. 1. The pH dependence of the pseudo first-order rate constants for formation (k_f) and decomposition (k_d) of the pseudobase of the 5,6-dihydropyrazino-[1,2,3,4-*lmn*]-1,10-phenanthrolinium dication (**1**) (k_d, k_f in s^{-1}).

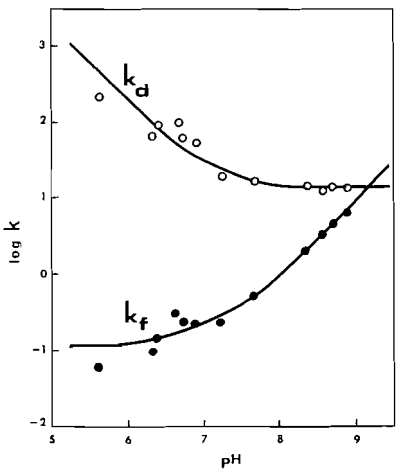

FIG. 2. The pH dependence of the pseudo first-order rate constants for formation (k_f) and decomposition (k_d) of the pseudobase of the 5*H*-6,7-dihydro-1,4-diazepino[1,2,3,4-*lmn*]-1,10-phenanthrolinium dication (**2**) (k_d, k_f in s^{-1}).

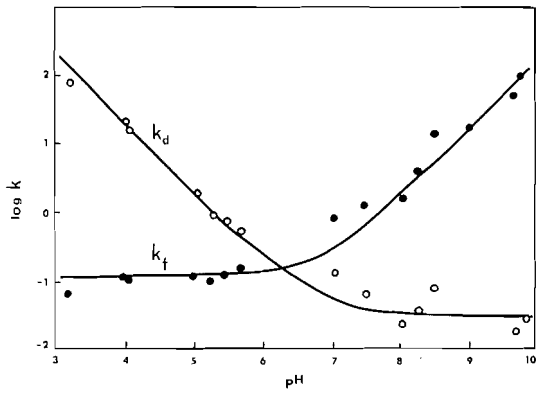

FIG. 3. The pH dependence of the pseudo first-order rate constants for the formation (k_f) and decomposition (k_d) of the pseudobase of the pyrazino[1,2,3,4-*lmn*]-1,10-phenanthrolinium dication (**3**) (k_d, k_f in s^{-1}).

that although the equilibrium constant for hydroxide addition to **3** is approximately 2000 times greater than for **1**, the rate constant for hydroxide attack on **3** is only three-fold greater than for **1**. Such a lack of correspondence between rate and equilibrium effects is not unusual in cation–anion combination reactions (5,6). Comparison of the rates of hydroxide and water attack on these cations gives log k_3/k_4 = 7.0, 6.9, and 7.1 for **1**, **2**, and **3**, respectively. This ratio is similar to that previously observed for the 2-methyl-4-nitroisoquinolinium cation (6.9 (4)) but considerably greater than Ritchie's N_+ value (4.5) for the hydroxide ion (5,6).

Experimental

Materials

5,6-Dihydropyrazino[1,2,3,4-*lmn*]-1,10-phenanthrolinium dibromide (**7**), 5*H*-6,7-dihydro-1,4-diazepino[1,2,-3,4-*lmn*]-1,10-phenanthrolinium dibromide (**7**), and pyrazino[1,2,3,4-*lmn*]-1,10-phenanthrolinium dibromide (**3**) were prepared as described in the literature.

Dimethylenebis-2,2'-isoquinolinium Dibromide

Isoquinoline (13 ml) was refluxed with 1,2-dibromoethane (4.3 ml) in absolute ethanol (20 ml) for 16 h. The solvent was evaporated to yield a dark brown residue which was recrystallized from ethanol and washed with

Can. J. Chem. Downloaded from www.nrcresearchpress.com by 210.87.254.40 on 09/05/12
For personal use only.

anhydrous ether to yield light brown crystals (10.3 g, 46%), m.p. 260–262° (lit. (8) 268°).

Trimethylenebis-2,2′-isoquinolinium Dibromide

This was similarly prepared (83% yield), m.p. 241° (lit. (8) 244°).

Methods

Equilibrium and kinetic measurements were made as previously described (1,4). The rate constants k_f and k_d were calculated (4) from

$$k_f = k_{obs}/(1 + [H^+]/K_{ROH})$$

and

$$k_d = k_{obs}/(1 + K_{ROH}/[H^+])$$

Analytical wavelengths used were **1**, 302 nm; **2**, 303 nm; **3**, 282 nm.

We appreciate the continued support of this work by an operating grant from the National Research Council of Canada and the award of a University of Toronto Open Fellowship to W.G.M.

1. J. W. BUNTING and W. G. MEATHREL. Can. J. Chem. **50**, 917 (1972).
2. J. W. BUNTING and W. G. MEATHREL. Can. J. Chem. **52**, 303 (1974).
3. A. L. BLACK and L. A. SUMMERS. Tetrahedron, **24**, 6453 (1968).
4. J. W. BUNTING and W. G. MEATHREL. Can. J. Chem. **51**, 1965 (1973).
5. C. D. RITCHIE. Acc. Chem. Res. **5**, 348 (1972).
6. C. D. RITCHIE and P. O. I. VIRTANEN. J. Am. Chem. Soc. **94**, 4966 (1972).
7. L. A. SUMMERS. Tetrahedron, **24**, 5433 (1968).
8. J. L. HARTWELL and M. A. POGORELSKIN. J. Am. Chem. Soc. **72**, 2040 (1950).

Can. J. Chem. Downloaded from www.nrcresearchpress.com by 210.87.254.40 on 09/05/12
For personal use only.

Quaternary Nitrogen Heterocycles. VII.[1] Reactions of some Tricyclic Heteroaromatic Cations in Basic Solutions

JOHN W. BUNTING AND WILLIAM G. MEATHREL
Department of Chemistry, University of Toronto, Toronto, Ontario M5S 1A1

Received October 5, 1973

Pseudobase formation and methoxide ion addition have been investigated spectroscopically for some *N*-methylacridinium, -phenanthridinium, and -benzoquinolinium cations. Susceptibility to nucleophilic attack decreases in the order 10-methylacridinium ($pK_{ROH} = 9.86$) > 5-methylphenanthridinium ($pK_{ROH} = 11.94$) > 1-methyl-5,6-benzoquinolinium ≈ 1-methyl-7,8-benzoquinolinium ($pK_{ROH} > 14$). A qualitative correlation of pK_{ROH} with loss of resonance energy upon pseudobase formation is shown to exist. For the 9,10-dimethylacridinium cation, the C-9 pseudobase (or methoxide adduct) is the kinetically preferred product in basic solutions but this is subsequently converted to the thermodynamically more stable anhydrobase. With the corresponding 9-ethyl- and 9-benzyl-10-methylacridinium cations, the pseudobase, rather than the anhydrobase, seems to predominate at equilibrium.

On a examiné à l'aide de la spectroscopie la formation de pseudobases et l'addition d'ion méthylate pour quelques cations tels *N*-méthylacridinium, phénanthridinium et benzoquinoléinium. La susceptibilité de l'attaque nucléophile diminue dans l'ordre méthyl-10 acridinium ($pK_{ROH} = 9.86$) > méthyl-5 phénanthridinium ($pK_{ROH} = 11.94$) > méthyl-1 benzoquinoléinium-5,6 ≈ méthyl-1 benzoquinoléinium-7,8 ($pK_{ROH} > 14$). On a montré qu'une relation existe entre le pK_{ROH} et la perte d'énergie de résonnance lors de la formation de pseudobases. En solution basique, la pseudobase C-9 (ou l'addition de méthylate sur) du cation diméthyl-9,10 acridinium est obtenue par contrôle cinétique, mais elle est transformée en anhydrobase thermodynamiquement plus stable. Parcontre la pseudobase plutôt que l'anhydrobase semble être majoritaire à l'equilibre pour les cations éthyl-9 et benzyl-9 méthyl-10 acridiniums. [Traduit par le journal]

Can. J. Chem., **52**, 981 (1974)

Although Hantzsch and Kalb (1) first recognized the formation of the pseudobase (**2**; R = H) by hydroxide ion addition to the 10-methylacridinium cation (**1**; R = H) in 1899, it was not

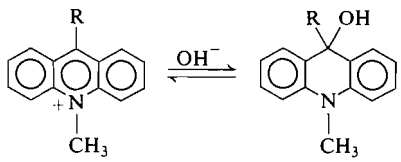

1 **2**

until 1949 that Goldacre and Phillips (2) measured the equilibrium constant ($pK_{ROH} = 9.75$) for this reaction. We obtained (3) a similar value ($pK_{ROH} = 9.86$; ionic strength 0.01 and 25°) during the course of our studies of the dependence of the equilibrium constant for pseudobase formation upon the structure of the heterocyclic cation and we later measured (4) the rates of pseudobase formation and decomposition for both this cation and the 10-methyl-9-phenylacridinium cation (**1**; R = C_6H_5).

Magrath and Phillips (5) have also reported equilibrium constants for pseudobase formation from the 5-methylphenanthridinium (**3**; R = H; $pK_{ROH} = 10.4$) and 5,6-dimethylphenanthridinium (**3**; R = CH_3; $pK_{ROH} = 10.1$) cations which suggest that the *N*-methylphenanthridinium cation is only slightly less susceptible to pseudobase formation than its acridinium isomer.

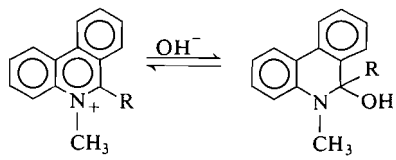

3 **4**

We have now extended these studies to a series of 9-substituted-10-methylacridinium cations and some other tricyclic cations that are isomeric with **1** (R = H). Owing to the general insolubility of the pseudobases in aqueous solution at p.m.r. spectral concentrations, we have again employed

[1]For Part VI, see preceding paper.

Can. J. Chem. Downloaded from www.nrcresearchpress.com by 210.87.254.42 on 09/05/12
For personal use only.

Can. J. Chem. Downloaded from www.nrcresearchpress.com by 210.87.254.42 on 09/05/12
For personal use only.

TABLE 1. The u.v. spectra and pK_{ROH} values of some *N*-methyl tricyclic cations

Cation	pK_{ROH}[a]	p*H*	λ_{max} (log ε) Aqueous solution	λ_{max} (log ε) 0.1 *M* $NaOCH_3$–CH_3OH
10-Methylacridinium	9.86±0.06	7	341.5(3.97), 358(4.28), 396(3.72), 414(3.72)	
		13	281(4.21)	280(4.30), 324(3.57)
9,10-Dimethylacridinium	[b]	7	342(3.41), 360(3.70), 400(3.16), 420(3.16)	
		12[d]	283(3.51), 395(3.13)	289(3.74), 303(3.75), 375(3.66)[d]
9-Ethyl-10-methylacridinium	9.99±0.06[c]	7	341(3.93), 357(4.23), 398(3.65), 4.16(3.65)	
		12	283(4.12)	283(4.19), 315(3.58)
9-Benzyl-10-methylacridinium	[b]	7	346(3.67), 361(3.97), 400(3.46), 420(3.47)	
		12	285(3.96)	284(4.07), 320(3.43)
10-Methyl-9-phenylacridinium	11.03±0.04	7	344(3.37), 362(3.69), 406(s) (3.13), 424(3.21)	
		12	285(3.56)	285(3.65)
5-Methylphenanthridinium	11.94±0.06	7	316.5(3.87), 358(3.58)	
		14	263(4.04), 273(4.03), 325(3.75)	260(s), 327
5-Methyl-6-phenylphenanthridinium	~13.5[b]	7	321(3.87), 376(3.74)	
		14	270(s) (3.80), 345(3.69)	275, 349

[a]At 25°, ionic strength 0.01.
[b]Solution turbidity prevents accurate measurement.
[c]At 25°, ionic strength 0.1.
[d]Equilibrium spectrum.

Can. J. Chem. Downloaded from www.nrcresearchpress.com by 210.87.254.42 on 09/05/12
For personal use only.

the strategy (3) of assigning structures to the methoxide adducts in basic methanol on the basis of their p.m.r. spectra and then comparing the u.v. spectra of corresponding methoxide adducts and pseudobases to ascertain that the predominant adducts in methanol and water arise by nucleophilic attack at the same site in the heterocyclic cation.

Results and Discussion

Acridinium Cations

The u.v. spectra of the *N*-methylacridinium cations that were examined were p*H* dependent. For each cation these p*H*-dependent spectral changes were readily reversible upon acidification, and, where possible, equilibrium constants (pK_{ROH}) have been calculated and are given in Table 1. In some cases rapid precipitation of the pseudobase did not allow the measurement of an accurate equilibrium constant. The u.v. spectra of each cation in neutral and basic aqueous solutions and also in basic methanol (0.1 *N* $NaOCH_3$) are also compared in Table 1. In all cases there is a close correspondence between the spectra in basic aqueous and methanolic solutions; it should be noted that the maxima which occur in the vicinity of 320 nm in basic methanolic solutions of the acridinium cations occur only as broad shoulders of similar intensity in aqueous base. The intense peak in the vicinity of 280 nm which occurs in the spectra of the basic solutions of all of the acridinium ions, except the 9,10-dimethylacridinium cation, is typical of a 9,10-dihydroacridine structure (*e.g.* 9,10-dihydro-10-methylacridine; λ_{max} (ethanol) = 284 nm (log ε = 4.1) (6)). Thus these u.v. spectral data indicate that the C-9 methoxide and hydroxide adducts (**2**) are present in basic solutions of these cations. The u.v. spectra of the 9,10-dimethylacridinium cation (**1**; R = CH_3) in basic aqueous and methanolic solutions at equilibrium differ from those of the other acridinium ions in Table 1, in that the maximum at 283 nm is less intense than expected and furthermore a long-wavelength absorption maximum (395 nm in water; 375 nm in methanol) is also present. This long-wavelength absorption maximum suggests a more highly conjugated species than the 9,10-dihydroacridine system.

A closer investigation of the u.v. spectrum of the 9,10-dimethylacridinium cation in basic solution revealed that in both methanol and water time-dependent spectral changes were observable before the final establishment of the equilibrium spectra that are given in Table 1. This phenomenon is illustrated in Fig. 1 for the 9,10-dimethylacridinium cation in 0.04 *M* sodium methoxide in methanol. Initially the spectrum has a high absorbance maximum at 282 nm (log ε = 4.05) typical of a 9,10-dihydroacridine, as discussed above, and it seems reasonable to assign this spectrum to the usual C-9 methoxide adduct of these acridinium cations. This maximum gradually decreases in intensity over a period of 1 h and is replaced by a very broad maximum in the region 289–303 nm and much longer wavelength maximum at 375 nm. The time-dependent spectra in Fig. 1 have three clearly defined isosbestic points (264, 299, and 327 nm) which suggests an equilibration between two species, with a half-time of approximately 7 min for their interconversion under these conditions. Similar time-dependent u.v. spectral changes occur in basic aqueous solutions of this cation. The initial spectrum suggests the presence of the C-9 pseudobase and the half-time for equilibration of the pseudobase with the final species is approximately 2.5 min at p*H* 12.

The p.m.r. spectra of basic methanolic solutions (0.1 *M* $NaOCD_3$–CD_3OD) of the 10-methylacridinium cations are given in Table 2. Solids separated when sodium methoxide was added to methanolic solutions of the 9,10-dimethyl- and 10-methyl-9-phenylacridinium cations, and the spectra in Table 2 in these two cases are for these solids in chloroform solution. The p.m.r. spectrum of the 10-methylacridinium cation in basic methanol-d_4 is readily reconciled with the C-9 methoxide adduct: δ 3.54 (N–CH_3, s, 3H), 5.40 (H-9, s, 1H), 6.87–7.55 (aromatic protons, m, 8H). The spectra of the 9-ethyl- and 9-benzyl-substituted cations in Table 2, and also of the solid obtained from the 10-methyl-9-phenylacridinium cation are also quite consistent with the analogous C-9 methoxide adducts. With the latter cation, the *O*-methyl protons appear as a three-proton singlet (δ 3.00) if the experiment is carried out in methanol rather than methanol-d_4, and this further confirms these assignments. The spectrum of the solid obtained from the 9,10-dimethylacridinium cation contains a two-proton singlet at δ 5.26 which cannot be rationalized with the C-9 methoxide adduct of this cation. The C-9 methyl protons of such an adduct would be expected to have a chemical shift $\delta \sim 1.5$

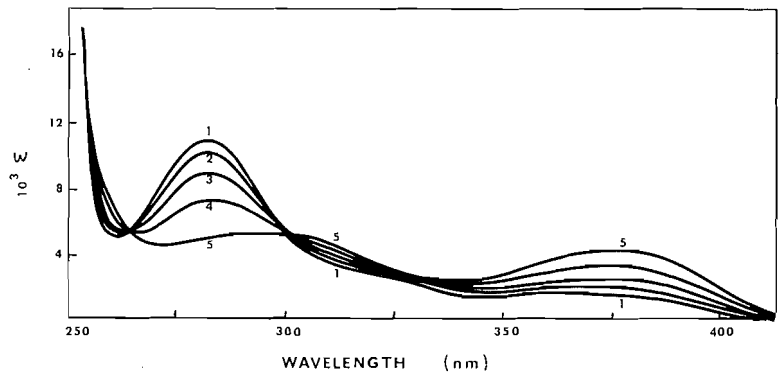

FIG. 1. The time-dependent u.v. spectrum of the 9,10-dimethylacridinium cation in 0.04 *M* $NaOCH_3$ in methanol: (1) 0.25 min; (2) 2 min; (3) 5 min; (4) 10 min; (5) 65 min (scan time, 30 s).

TABLE 2. The p.m.r. spectral data for some tricyclic monocations in basic methanol-d_4

Cation	δ (p.p.m.)[a] N—CH_3		Aromatic protons
10-Methylacridinium	3.54	5.40(H-9)	6.87–7.55
9,10-Dimethylacridinium[b]	3.47	5.26(=CH_2)	6.78–7.70
9-Ethyl-10-methylacridinium	3.40	1.87(CH_2)0.45(CH_3)	6.90–8.25
9-Benzyl-10-methylacridinium	2.74[d]	3.03(—CH_2)	6.75–7.89
10-Methyl-9-phenylacridinium[b]	3.54		6.78–7.44
[c]	3.54	3.00(O—CH_3)	6.78–7.44
5-Methylphenanthridinium	3.23	5.64(H-6)	6.80–7.97
5-Methyl-6-phenylphenanthridinium[b]	2.70		6.70–8.04
[c]	2.70	2.94(O—CH_3)	6.70–8.04

[a]In 0.1 *M* $NaOCD_3$–CD_3OD.
[b]Spectrum (in $CDCl_3$) of solid from basic methanol-d_4 solution.
[c]Spectrum (in $CDCl_3$) of solid from basic methanol solution.
[d]Models suggest that the protons of the *N*-methyl group in this case will be shielded by the aromatic ring of the 9-benzyl substituent.

(*cf.* δ 1.87 for the methylene protons of the corresponding 9-ethyl derivative (Table 1)), and furthermore no additional singlet for *O*-methyl protons is observed if methanol is used in place of methanol-d_4. We suggest that the product from the 9,10-dimethylacridinium cation is the anhydrobase **5** and this is consistent with the two-proton singlet (δ 5.26) arising from the exocyclic methylene protons.

The u.v. spectral data discussed above for the 9,10-dimethylacridinium cation in basic aqueous and methanolic solutions can also be rationalized in terms of the anhydrobase **5** being the predominant species that is present in these solutions at equilibrium. Thus, the time dependence of these spectra (*e.g.* Fig. 1) can be rationalized in terms of the pseudobase (or methoxide adduct) being the kinetically controlled product, whereas the anhydrobase is the thermodynamically more

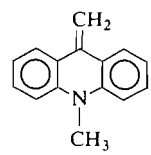

5

stable product. Thus, the equilibration in Fig. 1 is of the C-9 methoxide adduct to the anhydrobase. It is reasonable that anhydrobase formation should be slower than pseudobase formation, since the former involves a relatively slow C—H ionization (7), whereas pseudobase formation has been established to be quite rapid in these systems (4). Furthermore, the increased conjugation that is present in **5** from the presence of an additional C=C chromophore is also consistent with the observed long-wavelength absorption in these solutions.

Can. J. Chem. Downloaded from www.nrcresearchpress.com by 210.87.254.42 on 09/05/12
For personal use only.

Can. J. Chem. Downloaded from www.nrcresearchpress.com by 210.87.254.42 on 09/05/12
For personal use only.

The concept of anhydrobase formation by proton abstraction from a *C*-alkyl group of a heteroaromatic cation is well-established in heterocyclic chemistry (8–10) and this reaction must be considered as a possible competitor with pseudobase formation when an alkyl group is present on a carbon atom that is also susceptible to nucleophilic attack. Furthermore, our data on the 9,10-dimethylacridinium cation suggest that the kinetically and thermodynamically controlled products may be quite different in such systems. It is interesting that we have only observed anhydrobase formation for the 9-methyl cation, although the corresponding 9-ethyl and 9-benzyl cations might also be expected to form anhydrobases. It is not clear whether in these two cases the pseudobases are thermodynamically favored over the anhydrobases or alternatively the pseudobase – anhydrobase equilibrium is established much more slowly than for the 9,10-dimethylacridinium cation. In this regard, it should be noted that we have not been able to establish the equilibrium anhydrobase–pseudobase ratio for this latter cation but can only say that a significant proportion of anhydrobase is present at equilibrium. The fact that the solid obtained from basic solutions of this cation is essentially all anhydrobase (by p.m.r. spectroscopy) may be dictated by solubility considerations, and does not necessarily reflect the situation *in solution*.[2] Replacement of one of the exocyclic methylene hydrogen atoms by a larger substituent may result in unfavorable nonbonded interactions with the C-1 and -8 hydrogen atoms of the acridine system and so sufficiently reduce the stability of the anhydrobase relative to the corresponding pseudobase, that the latter predominates in the 9-ethyl and 9-benzyl systems. Similar interactions may be invoked to explain the observation that the plane of the phenyl ring in 9-phenylacridine makes an angle of greater than 40° with the plane of the acridine system (16).

Phenanthridinium Cations

The u.v. and p.m.r. spectral data for the 5-methylphenanthridinium (**3**; R = H) and 5-methyl-6-phenylphenanthridinium (**3**; R = C_6H_5) cations are included in Tables 1 and 2. Oxidation of the 5-methylphenanthridinium cation to 5-methyl-6-phenanthridone has previously been observed (12, 13) and indicates the presence of at least some of the pseudobase **4** (R = H) in basic aqueous solutions of this cation (14). The p.m.r. spectral data for this cation in Table 2 are consistent with the corresponding methoxide adduct being the predominant species in basic methanolic solutions, and the similar u.v. spectra in basic methanolic and aqueous solutions (Table 1) further substantiate **4** (R = H) as the predominant species present in aqueous alkaline solutions of this cation. The p.m.r. spectrum of the product that precipitates from basic methanolic solutions of the 5-methyl-6-phenylphenanthridinium cation (Table 2) is also quite consistent with the methoxide adduct corresponding to **4** (R = C_6H_5) and in fact, a solid which precipitated from basic aqueous solutions of this cation had the same p.m.r. spectrum as the trideuteriomethoxy adduct and so can be readily assigned to the pseudobase **4** (R = C_6H_5).

We have measured a pK_{ROH} value of 11.94 for the 5-methylphenanthridinium cation. This value is considerably higher than a value (10.4) reported some years ago by Magrath and Phillips (5)[3] and suggests that the phenanthridinium system is approximately 100 times less susceptible to pseudobase formation than the corresponding acridinium system. We have been unable to measure an accurate pK_{ROH} value for the 5-methyl-6-phenylphenanthridinium cation because of the insolubility of the pseudobase but have estimated $pK_{ROH} \sim 13.5$. The influence of the phenyl substituent in this system is thus somewhat similar to that previously observed in the acridinium cations (Table 1).

Other Cations

The u.v. spectra of both the 1-methyl-5,6-benzoquinolinium (**6**) and 1-methyl-7,8-benzoquinolinium (**7**) cations are p*H* independent below p*H* 14. Thus, the pK_{ROH} values for each of these two cations are > 14, and they are comparable with the 1-methylquinolinium cation

[2]In an early study, Decker and Hock (11) reported the isolation of the anhydrobase of the 9-benzyl-10-methylacridinium cation, under somewhat different reaction conditions.

[3]Magrath and Phillips (5) also reported $pK_{ROH} = 10.1$ for the 5,6-dimethylphenanthridinium cation. However, since their pK_{ROH} value for the 5-methylphenanthridinium cation appears to be in considerable error, their value for the 5,6-dimethylphenanthridinium cation is also in doubt. Furthermore, it is also possible that the predominant species in basic aqueous solutions of this latter cation is the anhydrobase, rather than the pseudobase.

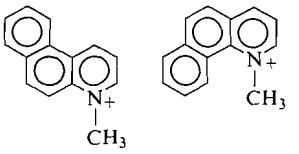

6 7

($pK_{ROH} \sim 16.5$ (3)) in this regard. This is consistent with our recent observations on the 1-methyl-1,10-phenanthrolinium (**8**) cation which has $pK_{ROH} \geq 14$ (15).

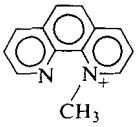

8

The p.m.r. spectrum of the residue from a basic methanol-d_4 (1 *M* $NaOCD_3$) solution of **6** is consistent with methoxide attack at C-2 to give **9**: (in $CDCl_3$) δ 3.12 (N—CH_3, s, 3H), 4.72 (H-2, d, 1H, J_{23} = 4 Hz), 5.94 (H-3, dd, 1H, J_{23} = 4 Hz, J_{34} = 9.5 Hz), 7.04–8.19 (aromatic protons + H-4, m, 7H). Under the same conditions **7** gives **10**: (in $CDCl_3$) δ 3.45 (N—CH_3, s, 3H), 4.72 (H-2, d, 1H, J_{23} = 6 Hz), 5.89 (H-3, dd, 1H, J_{23} = 6 Hz, J_{34} = 9 Hz), 6.89 (H-4, d, 1H, J_{34} = 9 Hz), 7.11–8.20 (aromatic protons, m, 6H). Thus the presence of an additional annelated aromatic ring on the 1-methylquinolinium cation does not appear to influence the preference for nucleophilic attack at C-2 rather than C-4 in these quinolinium systems.

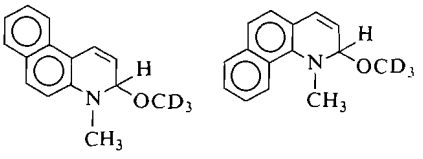

9 10

It is clear that the tricyclic 10-methylacridinium (**1**; R = H) (pK_{ROH} = 9.86) and 5-methylphenanthridinium (**3**; R = H) (pK_{ROH} = 11.94) cations are considerably more susceptible to pseudobase formation than the isomeric *N*-methylbenzoquinolinium cations (**6** and **7**) ($pK_{ROH} >$ 14). The loss in resonance energy upon pseudobase formation is expected to be one of the major factors involved in considerations of the relative susceptibilities of heterocyclic cations to pseudobase formation. In this regard, it should be noted that the resonance energy of the pseudobases of **1** and **3** can reasonably be approximated by the resonance energies of two isolated benzene rings (*i.e.*, 2 × 36 = 72 kcal/mol), while the resonance energies of species such as **9** and **10** are probably somewhat similar to the resonance energy of naphthalene (61 kcal/mol (17)). If it is assumed that these isomeric tricyclic cations have approximately equal resonance energies, this suggests that **6** and **7** lose about 10 kcal/mol more in resonance energy upon pseudobase formation than do **1** and **3**. The above assumptions are clearly crude approximations, but do allow a rationalization of the observed susceptibilities to nucleophilic attack.

Experimental

Materials

Acridine, phenanthridine and the benzoquinolines were obtained commercially. 6-Phenylphenanthridine was synthesized as described by Stackun (18). The 9-substituted acridines were synthesized by condensation of diphenylamine with the appropriate carboxylic acid by the method described by Albert (19). Each of these heterocyclic bases (except 9-ethyl- and 9-benzylacridine) was methylated by refluxing with methyl iodide in ethanol. Methylation with methyl iodide was slow with these latter two bases, and it was found more convenient to methylate with methyl fluorosulfonate (Magic Methyl) in 1:1 chloroform – anhydrous ether. All salts were recrystallized to constant melting point, and their identity confirmed by p.m.r. spectroscopy.

Methods

pK_{ROH} values were measured spectrophotometrically as previously described (3). Reported values are averages of at least eight values and the error quoted is the maximum deviation from the average. Proton magnetic resonance spectra were obtained on a T-60 spectrometer using tetramethylsilane as internal standard in both $CDCl_3$ and CD_3OD. The u.v. spectra were recorded on a Unicam SP-8 spectrophotometer and absorption maxima were checked manually on a Beckman DU-2 spectrophotometer.

We appreciate the continued support of this research by the National Research Council of Canada, and the award of a University of Toronto Open Fellowship to W.G.M. We thank Mr. E. P-C. Wong and Mr. J. Duran for the synthesis of the 9-substituted acridines.

1. A. HANTZSCH and M. KALB. Chem. Ber. **32**, 3109 (1899).
2. R. J. GOLDACRE and J. N. PHILLIPS. J. Chem. Soc. 1724 (1949).
3. J. W. BUNTING and W. G. MEATHREL. Can. J. Chem. **50**, 917 (1972).
4. J. W. BUNTING and W. G. MEATHREL. Can. J. Chem. **51**, 1965 (1973).
5. D. MAGRATH and J. N. PHILLIPS. J. Chem. Soc. 1940 (1949).
6. A. KELLMAN. J. Chim. Phys. **54**, 468 (1957).

Can. J. Chem. Downloaded from www.nrcresearchpress.com by 210.87.254.42 on 09/05/12
For personal use only.

7. M. EIGEN. Angew. Chem. Int. Ed. Engl. **3**, 1 (1964).
8. A. E. TCHITCHIBABINE. Bull. Soc. Chim. Fr. **3**, 1607 (1936).
9. O. MUMM and R. PETZOLD. Ann. Chem. **536**, 1 (1938).
10. M. J. COOK, A. R. KATRITZKY, P. LINDA, and R. D. TACK. J. Chem. Soc. Perkin II, 1080 (1973).
11. H. DECKER and T. HOCK. Chem. Ber. **37**, 1564 (1904).
12. A. PICTET and E. PATRY. Chem. Ber. **26**, 1962 (1893).
13. T. HASE. Acta Chem. Scand. **18**, 1806 (1964).
14. C. K. TINKLER. J. Chem. Soc. **89**, 856 (1906).
15. J. W. BUNTING and W. G. MEATHREL. Can. J. Chem. This issue.
16. C. W. N. CUMPER, R. F. A. GINMAN, and A. I. VOGEL. J. Chem. Soc. 4518 (1962).
17. G. M. BADGER. Aromatic character and aromaticity. University Press, Cambridge. 1969. p. 45.
18. B. STACKUN. J. Org. Chem. **29**, 2856 (1964).
19. A. ALBERT. The acridines. 2nd ed. Edward Arnold Ltd., London. 1966. p. 100.

Can. J. Chem. Downloaded from www.nrcresearchpress.com by 210.87.254.42 on 09/05/12
For personal use only.

Base Catalyzed Isomerization of Epoxides to Bicyclic Allylic Alcohols, Potential Intermediates for the Total Synthesis of the DL-Aldohexoses

KURUPATI RANGANAYAKULU,[1] UDAI P. SINGH,[2] THOMAS P. MURRAY,[3] AND ROBERT K. BROWN

Department of Chemistry, University of Alberta, Edmonton, Alberta

Received September 28, 1973

Treatment of the epoxide 2-deoxy-1,6:3,4-dianhydro-β-DL-*ribo*-hexopyranose (**3**) with *n*-butyllithium, and the epoxides 2-deoxy-1,6:3,4-dianhydro-β-DL-*lyxo*-hexopyranose (**5**) and 4-deoxy-1,6:2,3-dianhydro-β-DL-*lyxo*-hexopyranose (**7**) with lithium diethylamide has provided 1,6-anhydro-2,3-dideoxy-β-DL-*erythro*-hex-2-enopyranose (**4**), 1,6-anhydro-2,3-dideoxy-β-DL-*threo*-hex-2-enopyranose (**6**), and 1,6-anhydro-3,4-dideoxy-β-DL-*threo*-hex-3-enopyranose (**8**) in yields of 65, 50, and 20%, respectively. These allylic alcohols are potential intermediates for the synthesis of the various DL-aldohexoses.

La réaction de l'époxyde déoxy-2 dianhydro-1,6:3,4-β-DL-*ribo* hexopyrannose (**3**) avec le *n*-butyllithium de même que les réactions des époxydes déoxy-2 dianhydro-1,6:3,4 β-DL-hexopyrannose (**5**) et déoxy-4 dianhydro-1,6:2,3-β-DL-hexopyrannose (**7**) avec l'amidure diéthyl lithium ont conduit respectivement à l'anhydro-1,6 didéoxy-2,3-β-DL-*érythro*-hex-éno-2 pyrannose (**4**) anhydro-1,6 didéoxy-2,3-β-DL-*thréo*-hex-éno-3 pyrannose (**6**) et anhydro-1,6 didéoxy-3,4-β-DL-*thréo*-hex-éno-3 pyrannose (**8**) avec des rendements 65, 50 et 20%. Ces alcools allyliques sont des intermédiaires possibles pour les synthèses de divers aldohexose-DL.
[Traduit par le journal]

Can. J. Chem., **52**, 988 (1974)

Introduction

Recent reports from this laboratory (1, 2*a*) have shown that *n*-butyllithium effected the conversion of 4-deoxy-1,6:2,3-dianhydro-β-DL-*ribo*-hexopyranose (**1**) to the allylic alcohol 1,6-anhydro-3,4-dideoxy-β-DL-*erythro*-hex-3-enopyranose (**2**). The latter could be converted to DL-glucose (1, 2*a*) and to DL-allose and DL-galactose (2*b*). We have now explored the feasibility of a

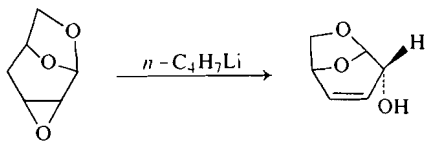

1 2

similar conversion of the isomeric epoxides **3**, **5**, **7** to the corresponding allylic alcohols **4**, **6**, **8**, compounds which could be used as intermediates for the preparation of most if not all of the eight isomeric DL-aldohexoses, as well as several mono- and dideoxy-DL-aldohexoses. This paper describes the results of our work on the preparation of these allylic alcohols.

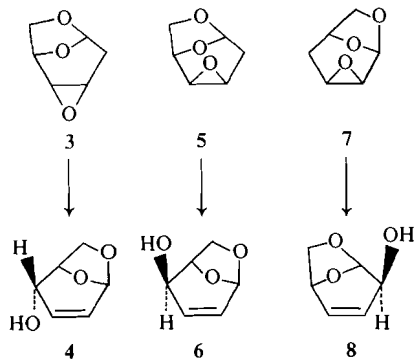

The oxide, **3**, previously synthesized (3), and the oxides **5** and **7**, both prepared by advantageous modifications of the procedure reported for the preparation of the D isomer of **7** (4), were first each subjected to treatment with *n*-butyllithium according to the directions which had been used for the conversion of **1** to **2** (1, 2*a*). This procedure was successful for **3**, giving **4** in 65% yield. However for both **5** and **7**, *n*-butyllithium was quite unsatisfactory since apparently

[1]Postdoctoral Fellow; present address: the Department of Chemistry at Banares Hindu University, Varanasi-5, U.P. India.

[2]Postdoctoral Fellow; present address: Rohm and Haas, Philadelphia, Pennsylvania.

[3]Postdoctoral Fellow; present address: the Department of Science, Florence State University, Florence, Alabama, 35630.

Can. J. Chem. Downloaded from www.nrcresearchpress.com by 210.87.254.6 on 09/05/12
For personal use only.

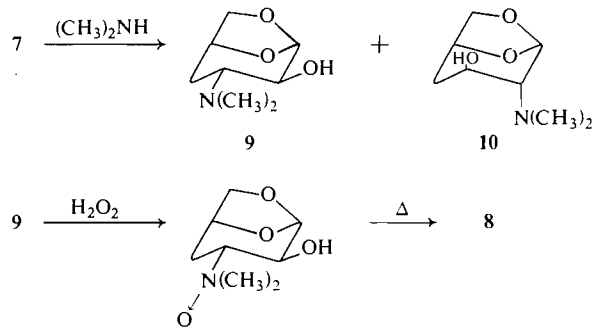

SCHEME I

the attack by the *n*-butyl carbanion on the epoxide ring itself competed successfully, and little if any of the allylic alcohols **6** or **8** could be isolated. The reagent lithium diethylamide, however, provided **6** and **8** from **5** and **7** in yields of 50 and 20%, respectively.

The use of sodium hydride on benzene, toluene, or 1,2-dimethoxyethane solutions of the oxides or the application of the strong base 1,5-diazabicyclo[4.3.0]non-5-ene (5) was in each case quite unsuccessful.

Since pyrolysis of amine oxides has been used to prepare similar allylic alcohols in carbohydrate syntheses (6–8) we attempted a similar sequence of reactions on the epoxide **7** in order to obtain a better yield of **8**. Amination of **7** gave two products, **9** and **10**, isolable in yields of 60 and 30% respectively, based on **7** (Scheme 1). Conversion of the amine **9** to the amine oxide **11** (not isolated), followed by pyrolysis of the latter, gave **8** in 10% yield based on **9**. The bulk of **11** appeared to decompose to a charred mass. It is clear that the reaction of lithium diethylamide with **7** is preferred over the amination and pyrolysis route.

Experimental

All melting points and boiling points are uncorrected. Elemental analyses were made by Mrs. D. Mahlow of this department. The p.m.r. spectra and decoupling experiments were made with a Varian Associates HR 100 Spectrometer by Mr. Glen Bigam of this department. Tetramethylsilane was used as the internal standard. Observed couplings are reported.

The g.l.c. analyses were made with a Wilkins Autoprep Model A 700 using a column $\frac{1}{8}$ in. × 10 ft packed with a 1:1 mixture of butanediol succinate and silicone rubber SE 30 (F and M Scientific Corp., Avondale Pa.), total 20%, on Carbowax 4000 (W. H. Curtin and Co., Houston, Texas). Helium was the carrier gas at a flow rate of 60–90 ml/min.

The i.r. spectra were obtained with a Perkin-Elmer 421 Grating Spectrophotometer, by Mr. Robert Swindlehurst of this department.

Solvents were removed by rotary evaporator under water pump vacuum. Organic solutions were dried with magnesium sulfate.

Preparation of the Epoxides 3, 5, 7

2-Deoxy-1,6:3,4-dianhydro-β-DL-*ribo-hexopyranose (3)*

This compound was prepared according to published directions (3).

2-Deoxy-1,6:3,4-dianhydro-β-DL-*lyxo-hexopyranose (5)*

Conversion of 7.16 g (0.4 ml) of the epoxide, **3**, to 1,6-anhydro-2-deoxy-β-DL-*arabino*-hexopyranose was accomplished by using the reported procedure (3), modified as follows to obtain a better yield of product in a much shorter time (1/2 day rather than 3 days). After the reaction mixture was neutralized to p*H* 8, the resulting aqueous solution was freed from water and the residue was dissolved in 100 ml of methanol. Precipitated sodium chloride was removed and the solution freed from methanol. The oily residue was dissolved in 100 ml of methanol again and the second precipitate of sodium chloride was removed. The methanol was distilled from the filtrate and the residue dissolved in 200 ml of chloroform. The solution was dried, freed from solid and solvent, and the residue purified by sublimation as previously described (3), giving a 90% yield of pure *1,6-anhydro-2-deoxy*-β-DL-*arabino-hexopyranose.*

The above *arabino*-hexopyranose was converted to a mixture of the mono- and ditosylated derivatives using the following modification of a reported tosylation procedure (9). A stirred mixture of 15.95 g (0.11 mol) of 1,6-anhydro-2-deoxy-β-DL-*arabino*-hexopyranose, 300 ml of dry pyridine, and 400 ml of dry acetone, cooled to 10° was treated with a total of 29.38 g (0.13 mol) of *p*-toluenesulfonyl chloride, added in small portions. When addition was complete, the mixture was allowed to stand for 5 days at 10–12° and then at room temperature for an additional 2 days. This temperature and time minimized the formation of the ditosylated product and allowed completion of reaction. The mixture was then reduced to $\frac{2}{3}$ its volume, and the residue was diluted with 400 ml of water and allowed to stand. The precipitate of ditosylated byproduct was removed. The mother liquor, on standing for 2 h in a refrigerator, deposited additional ditosylated product. The combined ditosylate, dissolved in chloroform, was washed thoroughly with cold 1% aqueous hydrochloric

Can. J. Chem. Downloaded from www.nrcresearchpress.com by 210.87.254.6 on 09/05/12
For personal use only.

Can. J. Chem. Downloaded from www.nrcresearchpress.com by 210.87.254.6 on 09/05/12
For personal use only.

acid (to remove pyridine) and then with water. The dried solution was freed from solid and solvent, and provided a colorless amorphous solid which was crystallized from ethanol to give 4 g (8%) of pure *1,6-anhydro-2-deoxy-3,4-di-O-p-toluenesulfonyl*-β-DL-*arabino-hexopyranose*, m.p. 146–148°.

Anal. Calcd. for $C_{20}H_{22}O_8S_2$: C, 52.85; H, 4.88; S, 14.1. Found: C, 52.80; H, 4.85; S, 13.81.

Both the i.r. and p.m.r. spectra agreed completely with the structure designated.

The mother liquor from the ditosyl compound above was extracted repeatedly with chloroform and the combined chloroform solutions were freed from solvent.The residue, again dissolved in 300 ml of chloroform, was washed carefully several times with cold 1% aqueous hydrochloric acid. After a final water wash, the solution was dried. Removal of the drying agent and solvent gave a residue which solidified on standing. This crude *1,6-anhydro-2-deoxy-4-O-p-toluenesulfonyl*-β-DL-*arabino-hexopyranose* (yield, 76%) melted at 58–60° but contained a small amount of pyridine (odor) probably as part of the crystalline structure. Attempts at further purification by repetition of the washing procedure produced a syrupy material which gave unsatisfactory elemental analyses. A similar observation has been reported for an analogous compound (9). However the crude material was quite satisfactory for the subsequent epoxide formation.

The 100 MHz p.m.r. spectrum of this crude material in $CDCl_3$ was surprisingly clean and clearly verified the structure. Signals occurred at δ 7.84 and 7.36 (two doublets as an AB quartet for 4H, aromatic), 5.55 (narrow multiplet for H-1, $w_{1/2} \sim 4$ Hz, $J_{1,5} < 0.5$ Hz, $J_{1,2endo} \sim 2$ Hz, $J_{1,2exo} < 0.5$ Hz); 4.48 (complex doublet for H-5); 4.42 (narrow multiplet for H-4, $w_{1/2} \sim 5.0$ Hz); 4.19 (doublet of narrow doublets for H-6_{endo}, $J_{6exo,6endo} \sim 7.5$ Hz, $J_{6endo,5} \sim 1$ Hz); 3.95–3.65 (complex multiplet for H-3); 3.62 (quartet for H-6_{exo}, $J_{6exo,5} \sim 5$ Hz); 3.28 (doublet for C_3—OH, $J_{3,OH} \sim 6$ Hz); 2.41 (singlet for CH_3); 2.08 (doublet of quartets for H-2_{endo}, $J_{1,2endo} \sim 2$ Hz, $J_{2endo,2exo} \sim 15$ Hz, $J_{2endo,3} \sim 6$ Hz); 1.82 (doublet for H-2_{exo}).

The crude monotosyl compound above (22.5 g) in 300 ml of chloroform was added with stirring to 100 ml of dry methanol, previously treated with 4 g of sodium metal. The solution was kept at room temperature and stirred for 12 h, then poured into cold water (200 ml). The organic layer was separated and the aqueous layer was extracted repeatedly with chloroform. The combined chloroform extracts and organic layer were dried, then freed from solid and solvent. The residue on distillation gave pure *2-deoxy-1,6:3,4-dianhydro*-β-DL-*lyxo-hexopyranose*, b.p. 45° at 0.3 mm. Yield, 8 g (83%).

Anal. Calcd. for $C_6H_8O_3$: C, 56.25; H, 6.29. Found: C, 56.32; H, 6.44.

The 100 MHz p.m.r. spectrum in $CDCl_3$ showed signals nearly identical to those reported for the same compound obtained as a minor product and contaminated with a small amount of the *ribo* isomer (3).

4-Deoxy-1,6:2,3-dianhydro-β-DL-*lyxo-hexopyranose (7)*

The epoxide 4-deoxy-1,6:2,3-dianhydro-β-DL-*ribo*-hexopyranose (10), (7.1 g, 0.4 mol) was converted to *1,6-anhydro-4-deoxy*-β-DL-*xylo-hexopyranose* following the modified procedure described above for the reaction of epoxide **3** to form 1,6-anhydro-2-deoxy-β-DL-*arabino*-hexopyranose. The *xylo* isomer, identical to that described previously (10), was obtained in a much shorter time and in ~90% yield.

The 1,6-anhydro-4-deoxy-β-DL-*xylo*-hexopyranose (3.6 g) was converted to a mixture of mono- and ditosylated derivatives according to the method used above for the *arabino* isomer, but with the following modification, required because of the different solubility and melting point properties. After the reacting mixture had stood for 5 days, it was diluted with water (100 ml) and then extracted thoroughly with chloroform. The combined chloroform extracts were washed carefully with cold 1% aqueous hydrochloric acid, then with water, and finally dried. Removal of the solid and solvent provided a crude product which showed only two spots on t.l.c. (chloroform – ethyl acetate, 2:1). Separation was carried out by chromatography on a silica gel column using chloroform – ethyl acetate, 2:1, as solvent. The first fraction gave a solid which when crystallized from dichloromethane–*n*-hexane produced 5.5 g (75%) of pure *1,6-anhydro-4-deoxy-2-O-p-toluenesulfonyl*-β-DL-*xylo-hexopyranose* as colorless needles, m.p. 123–124°.

Anal. Calcd. for $C_{13}H_{16}O_6S$: C, 52.0; H, 5.33; S, 10.66. Found: C, 51.97; H, 5.27; S, 11.04.

The 100 MHz p.m.r. spectrum in $CDCl_3$ showed signals at δ 7.82 and 7.34 (AB quartet for 4H, aromatic, $J \sim 8$ Hz); 5.27 (narrow multiplet for H-1, $w_{1/2} \sim 5$ Hz, $J_{1,2} \sim 1.0$ Hz); 4.68–4.50 (triplet for H-5, $J_{5,4exo} \sim 5$ Hz, $J_{5,4endo} \sim 1.0$ Hz, $J_{5,6endo} < 1.0$ Hz, $J_{5,6exo} \sim 5.0$ Hz); 4.25 (narrow multiplet for H-2, $w_{1/2} \sim 4.5$ Hz); 4.21 (doublet for H-6_{endo}, $J_{6endo,6exo} \sim 7.0$ Hz); 3.94 (multiplet for H-3, $J_{3,4exo} \sim 5.0$ Hz); 3.73 (triplet of doublets for H-6_{exo}, $J_{4,6exo} \sim 1.5$ Hz); 2.98 (singlet for OH, $w_{1/2} \sim 2.5$ Hz); 2.53 (singlet for CH_3); 2.31 (multiplet for H-4_{exo}, $J_{4exo,4endo} \sim 15.0$ Hz); 1.70 (doublet of narrow doublets for H-4_{endo}).

The second fraction, eluted with a 1:1 mixture of chloroform and ethyl acetate, gave *1,6-anhydro-4-deoxy-di-O-p-toluenesulfonyl*-β-DL-*xylo-hexopyranose*; colorless needles from dichloromethane-*n*-hexane; m.p. 46–47°; yield, 0.51 g (4.5%).

Anal. Calcd. for $C_{20}H_{22}O_8S_2$: C, 52.85; H, 4.88; S, 14.1. Found: C, 53.11; H, 4.97; S, 14.29.

The 100 MHz p.m.r. spectrum in $CDCl_3$ showed signals at δ 7.80 and 7.40 (a doublet of quartets for 8H, aromatic); 5.27 (singlet for H-1, $w_{1/2} \sim 4$ Hz, $J_{1,2} \sim 1.0$ Hz); 4.74 (doublet of triplets for H-3, $J_{3,4exo} \sim 4.5$ Hz, $J_{3,4endo} \sim 1.5$ Hz, $J_{3,2} \sim 1.5$ Hz); 4.56 (multiplet for H-5, $J_{5,6exo} \sim 5.0$ Hz, $J_{5,6endo} \sim 1.0$ Hz, $J_{5,4exo} \sim 4.0$ Hz); 4.28 (narrow doublet for H-2, $w_{1/2} \sim 4.5$ Hz); 4.15 (doublet for H-6_{endo}, $J_{6endo,6exo} \sim 7$ Hz); 3.75 (two overlapping quartets for H-6_{exo}); 2.57 (singlet for two CH_3, overlapping signal for H-4_{exo}); 2.48 (doublet of triplets for H-4_{exo}, $J_{4exo,4endo} \sim 15.0$ Hz, $J_{4exo,6exo} \sim 1.5$ Hz); 1.95 (doublet for H-6_{endo}).

The monotosylated compound (7.8 g) from the first fraction was converted to the epoxide **7** by the same procedure used above to obtain epoxide **5** from the corresponding monotosylated compound. The pale yellow syrup obtained after removal of the chloroform solvent was purified by sublimation at 90–95° at 0.3–0.5 mm. There was obtained 3.0 g (94%) of **7** as colorless needles, m.p. 73–74° (lit. (4) m.p. for the D-enantiomer, 69–70°).

Can. J. Chem. Downloaded from www.nrcresearchpress.com by 210.87.254.6 on 09/05/12
For personal use only.

Anal. Calcd. for $C_6H_8O_3$: C, 56.25; H, 6.29. Found: C, 56.18; H, 6.11.

The 100 MHz p.m.r. spectrum of **7** in $CDCl_3$ showed signals at δ 5.70 (doublet for H-1, $J_{1,2} \sim 3.0$ Hz); 4.47 (complicated quartet for H-5, $J_{5,4exo} \sim 5.5$ Hz, $J_{5,6exo} \sim 3.5$ Hz, $J_{3,5} < 1.0$ Hz, $J_{4endo,5} < 1.0$ Hz); 3.75 (apparent singlet for H-6_{endo}, $w_{1/2} \sim 1.5$ Hz, $J_{6exo,6endo} \sim 0.0$ Hz); 3.73 (doublet for H-6_{exo}, $J_{6exo,5} \sim 3.5$ Hz); 3.42 (triplet for H-2, $J_{1,2} \sim 3$ Hz, $J_{2,3} \sim 4$ Hz); 3.20 (triplet for H-3, $J_{3,4exo} \sim 3.0$ Hz, $J_{2,3} \sim 4$ Hz, $J_{3,5} < 1.0$ Hz); 2.32 (doublet of quartets for H-4_{exo}, $J_{5,4exo} \sim 5.5$ Hz, $J_{4exo,4endo} \sim 16$ Hz, $J_{3,4exo} \sim 3$ Hz); 2.03 (doublet of narrow doublets for H-4_{endo}, $J_{5,4endo} < 1.0$ Hz).

*Preparation of the Allylic Alcohols **4**, **6**, and **8***

*1,6-Anhydro-2,3-dideoxy-*β-DL-*erythro-hex-2-enopyranose (**4**)*

A solution of 7.68 g (0.06 mol) of 2-deoxy-1,6:3,4-dianhydro-β-DL-*ribo*-hexopyranose (**3**) (3) in 50 ml of dry ether was treated with *n*-butyllithium (0.123 mol) according to published directions (2*a*), but with the following modification. The oil left after the removal of the solvent from the dried solution, was fractionally distilled to give 5 g (65%) of pure *1,6-anhydro-2,3-dideoxy-*β-DL-*erythro-hex-2-enopyranose (**4**)* b.p. 69° at 0.3 mm.

Anal. Calcd. for $C_6H_8O_3$: C, 56.25; H, 6.29. Found: C, 55.08; H, 6.39.

The 100 MHz spectrum in $CDCl_3$ agreed completely with the assigned structure and showed signals at δ6.02 (doublet of doublets for H-2, $J_{2,3} \sim 10$ Hz, $J_{1,2} \sim 3.5$ Hz); 5.82 (complicated doublet of doublets for H-3, $J_{3,4} \sim 4.0$ Hz, $J_{3,5} \sim 1.5$ Hz, $J_{1,3} \sim 1.0$ Hz); 5.51 (narrow doublet of doublets for H-1, $J_{1,2} \sim 3.5$ Hz, $J_{1,3} \sim 1.0$ Hz); 4.65 (multiplet for H-5, $J_{5,6exo} \sim 6.5$ Hz, $J_{5,6endo} \sim 2.0$ Hz, $J_{5,4endo} \sim 2.0$ Hz); 3.92 (doublet of doublets for H-6_{exo}, $J_{6exo,6endo} \sim 8.0$ Hz); 3.75–3.52 (multiplet for H-4); 3.43 (doublet of doublets for H-6_{endo}); 3.30–2.90 (broad signal for OH).

*1,6-Anhydro-2,3-dideoxy-*β-DL-*threo-hex-2-enopyranose (**6**)*

A solution of 1.28 g (0.01 mol) of 2-deoxy-1,6:3,4-dianhydro-β-DL-*lyxo*-hexopyranose (**5**) in 10 ml of dry benzene, was added all at once to a stirred solution of lithium diethylamide, previously prepared by the addition of 10.5 ml of 22.3% *n*-butyllithium to a solution of 2.25 g of diethylamine in a mixture of 10 ml of dry benzene and 10 ml of dry hexane (11). All operations were carried out under nitrogen. The stirred solution stood for 18 h at room temperature, and then was heated under reflux for 1 h. The solution was cooled and treated with 10 ml of water. The aqueous layer was extracted with methylene chloride (3 × 50 ml) and then continuously extracted with methylene chloride for 24 h to remove the somewhat water-soluble allylic alcohol. The combined extracts and organic layer were dried. Removal of the solid and solvent gave a brown oil which was fractionally distilled to provide 0.64 g (50%) of pure *1,6-anhydro-2,3-dideoxy-*β-DL-*threo-hex-2-enopyranose*, **6**, b.p. 65–60° at 0.05 mm.

Anal. Calcd. for $C_6H_8O_3$: C, 56.25; H, 6.25. Found: C, 56.13; H, 6.46.

The p.m.r. spectrum in $CDCl_3$ agreed with the proposed structure, showing signals at δ 5.87 (doublet of quartets for H-2, $J_{2,1} \sim 3$ Hz, $J_{2,3} \sim 10$ Hz, $J_{2,4} \sim 1.5$ Hz); 5.67 (double of multiplets for H-3, $J_{3,1} \sim 1.0$ Hz, $J_{3,4} \sim 2.0$ Hz, $J_{3,5} \sim 2.0$ Hz); 5.48 (doublet for H-1, $J_{1,2} \sim 3.0$ Hz, $J_{1,3} \sim 1.0$ Hz); 4.73 (multiplet for H-4, $J_{3,4} \approx J_{2,4} \approx J_{4,6exo} \sim 1.5$ Hz, $J_{4,5} \sim 5.0$ Hz); 4.48 (multiplet for H-5 $J_{5,3} \approx J_{5,6endo} \sim 2.0$ Hz); 4.18 (doublet of quartets for H-6_{endo}, $J_{6endo,6exo} \sim 8.0$ Hz, $J_{5,6endo} \sim 2.0$ Hz, $J_{1,6endo} \sim 0.5$ Hz); 3.86 (doublet of quartets for H-6_{exo}, $J_{6exo,4} \sim 1.5$ Hz, $J_{6exo,5} \sim 6.0$ Hz); 3.34 (singlet for OH, $w_{1/2} \sim 3$ Hz).

*1,6-Anhydro-3,4-dideoxy-*β-DL-*threo-hex-3-enopyranose (**8**)*

This compound was prepared by the following two methods.

Procedure A

The epoxide 4-deoxy-1,6:2,3-dianhydro-β-DL-*lyxo*-hexopyranose (**7**) (1.28 g, 0.01 mol) was converted to **8** by the same procedure used to obtain **6** above. After a second distillation to remove traces of contaminating epoxide **7**, 0.26 g (20%) of *1,6-anhydro-3,4-dideoxy-*β-DL-*threo-hex-3-enopyranose (**8**)* was obtained boiling at 43–44° at 0.1 mm. This was about 98% pure. An analytical sample was prepared by preparative g.l.c. on a column packed with butanediol succinate and S.E. 30, operating at 160 °C with a helium gas flow rate of 60 ml/min.

Anal. Calcd. for $C_6H_8O_3$: C, 56.25; H, 6.25. Found: C, 55.94; H, 6.10.

The 100 MHz p.m.r. spectrum in $CDCl_3$ verified the assigned structure, showing signals at δ 6.14 (doublet of doublets for H-4, $J_{4,5} \sim 4.0$ Hz, $J_{4,3} \sim 10.0$ Hz, $J_{4,2} \sim 1.0$ Hz); 5.72 (doublet of triplets for H-3, $J_{3,1} \sim J_{3,2} \sim 2.0$ Hz, $J_{3,5} < 1.0$ Hz); 5.53 (narrow multiplet for H-1, $w_{1/2} \sim 6.5$ Hz, $J_{1,2} \sim 3.5$ Hz, $J_{1,3} \sim 2.0$ Hz); 4.66 (triplet for H-5, $J_{4,5} \sim 4.0$ Hz, $J_{5,6exo} \sim 4.0$ Hz); 4.33 (narrow multiplet for H-2, $w_{1/2} \sim 6.5$ Hz, $J_{2,1} \sim 3.5$ Hz, $J_{2,3} \sim 2.0$ Hz, $J_{2,4} < 1.0$ Hz); 3.85 (doublet for H-6_{endo}, $J_{6endo,6exo} \sim 6.5$ Hz, $J_{6endo,5} < 1.0$ Hz); 3.73 (doublet of doublets for H-6_{exo}); 2.31 (singlet for OH, $w_{1/2} \sim 2.5$ Hz).

Procedure B

A mixture of 2.56 g (0.02 mol) of 4-deoxy-1,6:2,3-dianhydro-β-DL-*lyxo*-hexopyranose and 20 ml of 20% dimethylamine in water was allowed to stand for 72 h at room temperature. The water and excess dimethylamine were then removed. The residue solidified on standing. The 100 MHz p.m.r. spectrum of this crude material showed two signals in the anomeric proton region, of area ratio ~1:2, indicative of two products. The two substances were separated by repeated crystallization using dry ether as solvent and provided the two amines **9** and **10**. Compound **9** was purified by sublimation at 0.1 mm, bath temperature 80–90°. There was obtained 2.1 g (60% based on **7**) of pure *1,6-anhydro-3,4-dideoxy-3-dimethylamino-*β-DL-*arabino-hexopyranose*, **9**, melting at 108–109°.

Anal. Calcd. for $C_8H_{15}O_3N$: C, 55.47; H, 8.73; N, 8.09. Found: C, 55.27; H, 8.76; N, 7.86.

The 100 MHz p.m.r. spectrum in $CDCl_3$–acetone-d_6 showed signals at δ 5.23 (narrow doublet for H-1, $J_{1,2} \sim 2.0$ Hz); 4.66–4.48 (multiplet for H-5); 3.78 (doublet for H-6_{endo}, $J_{6endo,5} \sim 1$ Hz, $J_{6endo,6exo} \sim 7.0$ Hz); 3.65 (doublet of doublets for H-$6_{exo,5} \sim 5.0$ Hz); 6.57 (doublet of doublets for H-2, $J_{2,3} \sim 9.0$ Hz); 3.00–2.50 (multiplet for H-3, $J_{3,4eq} \approx J_{3,4ax} \sim 8$ Hz); 2.27 (singlet for $(CH_3)_2N$); 1.50–1.90 (multiplet for H-4_{exo} and H-4_{endo}, $J_{4eq,5} \approx J_{4ax,5} \sim 2$ Hz).

Can. J. Chem. Downloaded from www.nrcresearchpress.com by 210.87.254.6 on 09/05/12
For personal use only.

The second product was purified by distillation and gave 1.0 g (30%) of pure *1,6-anhydro-2,4-dideoxy-2-dimethylamino*-β-DL-*xylo-hexopyranose*, ***10***, b.p. 45–47° at 0.15 mm, m.p. 94–95°.

Anal. Calcd. for $C_8H_{15}O_3N$: C, 55.47; H, 8.73; N, 8.09. Found: C, 55.40; H, 8.94; N, 7.85.

The 100 MHz p.m.r. spectrum in $CDCl_3$–acetone-d_6 showed signals at 5.47 (singlet for H-1, $w_{1/2} \sim 3$ Hz, $J_{1,2} \approx J_{1,3} < 1$ Hz); 4.51 (complicated triplet for H-5, $J_{5,6endo} < 0.5$ Hz, $J_{5,6exo} \sim 5.0$ Hz, $J_{5,4ax} \sim 5$ Hz, $J_{5,4eq} \sim 1$–2 Hz); 4.04 (doublet for H-6_{endo}, $J_{6endo,6exo} \sim 6.5$ Hz); 3.97–3.80 (multiplet for H-3, $J_{3,2} \sim 2$ Hz, $J_{3,4eq} \sim 3$ Hz, $J_{3,4ax} \sim 6.0$ Hz, $J_{3,5} \sim 1$ Hz); 3.55 (multiplet for H-6_{exo}, $J_{6exo,4ax} \sim 2$ Hz); 2.50–2.28 (multiplet for overlapping signals for H-2 and $(CH_3)_2N$); 2.28–2.05 (multiplet for H-4_{ax}, $J_{4ax,4eq} \sim 15$ Hz).

A quantity (1.0 g) of the amine **9** was treated with 10 ml of 30% hydrogen peroxide and the mixture was allowed to stand at room temperature for 2½ weeks. The length of time was necessary to ensure completion of the slow reaction. The bulk of the excess hydrogen peroxide was removed carefully by rotary evaporator at room temperature under vacuum, and the residual peroxide removed under 0.1 mm vacuum at a bath temperature not exceeding 40° to avoid decomposition. The crude glassy *N*-oxide was then subjected directly to pyrolysis under vacuum (0.1 mm) using an oil bath heated at first to 130–140° at which temperature pyrolysis begins and the product **8** distills, and then finally to 170° at which temperature pyrolysis is considered to be complete and the residue is black. The distillate was dissolved in chloroform and dried. The solid and solvent were removed and the residue was distilled and purified following the directions in procedure A above. Yield of pure **8**, based on the amine **9** is 10%.

Pyrolysis of the quaternary ammonium salt obtained by the reaction of **9** with methyl iodide gave only the epoxide **7**.

1,6-Anhydro-3,4-dideoxy-2-O-methyl-β-DL-*threo-hexopyranose*

The allylic alcohol **8** was methylated according to reported procedure (12). The product, obtained in good yield, boiled at 42° at 0.1 mm; η_D^{25} 1.4759.

Anal. Calcd. for $C_7H_{10}O_3$: C, 59.14; H, 7.09. Found: C, 58.98; H, 7.26.

1,6-Anhydro-2,3-dideoxy-4-O-methyl-β-DL-*threo-hexopyranose*

The allylic alcohol **6** was methylated by the procedure noted immediately above; b.p. 35° at 0.1 mm; η_D^{25} 1.4695.

Anal. Calcd. for $C_7H_{10}O_3$: C, 59.14; H, 7.09. Found: C, 58.55; H, 7.39.

The authors thank the National Research Council of Canada for financial support throughout the course of this work.

1. U. P. SINGH and R. K. BROWN. Can. J. Chem. **48**, 1791 (1970).
2. U. P. SINGH and R. K. BROWN. Can. J. Chem. (*a*) **49**, 3342; (*b*) **49**, 1179 (1971).
3. T. P. MURRAY, U. P. SINGH, and R. K. BROWN. Can. J. Chem. **49**, 2132 (1971).
4. M. CERNÝ and J. PACÁK. Coll. Czech. Chem. Commun. **27**, 94 (1962).
5. H. OEDIGER, H-J. KABBE, F. MÖLLER, and K. EITER. Chem. Ber. **99**, 2012 (1966).
6. W. D. CELMER. J. Am. Chem. Soc. **87**, 1797 (1965).
7. P. H. JONES and E. K. ROWLEY. J. Org. Chem. **33**, 665 (1968).
8. A. BANASZEK and A. ZAMOJSKI. Carbohydr. Res. **25**, 453 (1972).
9. M. CERNÝ, L. KALVODA, and J. PACÁK. Coll. Czech. Chem. Commun. **33**, 1143 (1968).
10. F. SWEET and R. K. BROWN. Can. J. Chem. **46**, 2289 (1968).
11. J. K. CRANDALL. J. Org. Chem. **29**, 2830 (1964).
12. R. M. SRIVASTAVA and R. K. BROWN. Can. J. Chem. **48**, 2334 (1970).

The Complete Stereostructure of Capsidiol. X-Ray Analysis and ^{13}C Nuclear Magnetic Resonance of Eremophilane Derivatives Having *trans*-Vicinal Methyl Groups[1,2,3]

GEORGE I. BIRNBAUM
Division of Biological Sciences, National Research Council of Canada, Ottawa, Canada
AND
A. STOESSL
Research Institute, Canada Agriculture, University Sub Post Office, London, Ontario
AND
S. H. GROVER AND J. B. STOTHERS
Department of Chemistry, University of Western Ontario, London, Ontario

Received November 30, 1973

To define the stereochemistry of capsidiol (**1**), an antifungal sesquiterpene isolated from sweet peppers, a detailed ^{13}C n.m.r. investigation was carried out. From the results for **1** and a series of its derivatives (**2–6**) compared with those for several well-defined model compounds (**7–21**) it has been established that the vicinal methyl groups are *trans*, in contrast to all other previously described eremophilanes. This was confirmed by an X-ray structure analysis of **1** which also established the stereochemistry of the isopropenyl group as well as the detailed conformations of the two rings.

The ^{13}C spectra for the series **1–21** have been completely analyzed and these results are discussed in terms of the observed substituent effects. Further evidence of deshielding *syn*-axial δ effects is presented.

On a réalisé une étude détaillée par r.m.n. de ^{13}C afin de définir la stéréochimie du capsidiol (**1**), un sesquiterpene fongicide extrait des piments doux. Par comparaison des résultats obtenus avec **1** et une série de ses dérivés (**2–6**) avec ceux obtenus pour plusieurs composés modèles bien définis (**7–21**) on a pu établir que les groupes méthyles vicinaux sont *trans* et ceci en opposition avec tous les érémophilanes décrits antérieurement. Ce résultat a été confirmé par une analyse structural aux rayons-X de **1** qui a aussi établi la stéréochimie du groupe isopropényle de même que les conformations détaillées des deux noyaux.

Les spectres ^{13}C pour tous les composés **1–21** ont été complètement analysés et ces résultats sont discutés en termes des effets de substituents qui ont été observés. On présente des preuves supplémentaires au sujet des effets de déblindages *syn*-axial δ. [Traduit par le journal]

Can. J. Chem., **52**, 993 (1974)

The gross structure of capsidiol (**1**) and of several derivatives (**2**, **4–6**) had been determined and, as described in the earlier report (1), the proton spectral data indicated that this series of antifungal sesquiterpenes differed from all previously described eremophilanes in that the vicinal methyl groups (C-14 and -15) are in a *trans* disposition. The key assumption, on which this interpretation was based, requires that the saturated ring exist in a chair conformation, although undoubtedly somewhat flattened because of its sp^2 center at C-10. Since alternative conformations for **1** could not be rigorously excluded with the available data, conclusive evidence was sought from a detailed analysis of the ^{13}C spectra of this series of compounds. It is well established that the shieldings of methyl carbons are remarkably sensitive to their spatial orientation with respect to their γ neighbors (2). More recently it has been demonstrated that similarly distinctive, although directionally opposed, effects are observed for methyl carbons in *syn*-axial orientations relative to their δ neighbors (3). Thus, it appeared that a comparison of the methyl shieldings for **1–6** with the corresponding data for the model compounds (**7–21**) of known stereochemistry would provide definitive evidence to confirm or refute our earlier interpretation.

[1]Issued as NRCC No. 13769; Contribution No. 565 from the Research Institute.

[2]Part VIII in the series Post-infectional Inhibitors from Plants; for Part VII, see ref. 28.

[3]Part 40 in the series ^{13}C NMR Studies; for Part 39, see ref. 29; for Part 38, see ref. 15.

Can. J. Chem. Downloaded from www.nrcresearchpress.com by 210.87.254.5 on 09/05/12
For personal use only.

Can. J. Chem. Downloaded from www.nrcresearchpress.com by 210.87.254.5 on 09/05/12
For personal use only.

In this report we wish to present the methyl shielding data which establish that the vicinal methyl carbons, C-14 and -15, in **1–6** are *trans*-diaxial; consequently, the saturated ring must exist in the chair conformation. As the ^{13}C n.m.r. study was completed, an X-ray examination of **1** was undertaken to confirm this conclusion unequivocally and to establish the stereochemistry of the isopropenyl group, a feature which could be inferred but not established from the ^{13}C n.m.r. data. Another result of the X-ray study is the precise description of the conformations of the two rings and the distortions caused by some of the substituents. Since the series **8–21** permitted detailed comparison of substituent effects in closely related compounds, the ^{13}C results provide further evidence of the consistency of these trends which should prove useful for signal assignments in related systems. Similarly the results for **1–7** provide reference data for the spectral analysis and structural elucidation of other eremophilane derivatives.

Experimental

Materials

With the exception of epicapsidiol (**3**), the capsidiol derivatives have been described previously (1). The model compounds included in this study were known materials but slightly modified preparations for **10** and **16** are described below. All separations by thin-layer chromatography (t.l.c.) were done on silica gel (Camag DF5). Elemental analyses were performed by C. Daesslé, Montreal, Quebec.

Epicapsidiol (3)

A stirred solution of **4** (122 mg) in *i*-PrOH (12 ml) at room temperature was treated dropwise with sodium borohydride solution (0.07 *M* in *i*-PrOH) until reduction was complete (2 h; 13 ml reagent) as judged by t.l.c. The reaction mixture was poured into water (30 ml), just acidified with 6 *M* acetic acid, and the product extracted with ether. Recrystallization from chloroform by the addition of carbon tetrachloride gave pure **3**, m.p. 151–152°; $[\alpha]_D^{22}$ + 24° (*c*, 1.0 in $CHCl_3$); ν_{max} (KBr) 3520, 3450, 1650, 1460, 1380, 1318, 1135, 1129, 1075, 1050, 1041, 1015 and 889 cm^{-1}. ^1H n.m.r. ($CDCl_3$): 0.93 (3H, H-14) J = 7.1 Hz; 1.12 (3H, H-15); 1.73 (3H, H-13); 4.24 (1H, H-3) J = 4.6, 4.6, 12.4 Hz; 4.34 (1H, H-1) J = 1.9, 2.7, 5.2, 11.4 Hz; 5.94 (1H, H-9) J = 1.9, 1.9, 6.3 Hz; 4.69, 4.72 (1H each, H-12) J = 2 Hz. A small amount of **1** was detected by t.l.c. in the mother liquors of crystallization.

Anal. Calcd. for $C_{25}H_{24}O_2$: C, 76.22; H, 10.24. Found: C, 76.30; H, 10.14.

Decalol 10

Reduction of **9** (104 mg) with sodium borohydride as above afforded a single isomer of **10** (65 mg) having the expected physical properties (4). The ^{13}C spectrum showed it to be the equatorial isomer as discussed below.

Octalol 18

Crude racemic 2-bromo-*trans*-10-methyldecal-3-one (5) (500 mg) was converted to (±)-Δ^5-10-methyldecal-4-one as described for the (−)-isomer (6). The octalone product (173 mg), isolated by preparative t.l.c. (ether – light petroleum, 1:3) and identified by ^1H and u.v. spectra, was reduced as described for **3**. Octalol **18** was isolated by ether extraction and purified by preparative t.l.c. (ether – light petroleum, 1:1) to furnish a liquid, ν_{max} (liquid film) 3380, 3080, 1092, and 1070 cm^{-1}; *m/e* 168 (M^+, 5%), 153 (M − 15, 11%), 150 (M − 18, 75%) and 135 (M − (15 + 18), base peak). The ^{13}C and ^1H spectra indicated the presence of a single isomer. The proton spectrum contained a diffuse doublet (4.18 p.p.m.) for one proton, with the largest J = 12 Hz, and also coupled to the lone olefinic proton (5.65 p.p.m.) with J = 2 Hz. A single methyl singlet appeared at 1.03 p.p.m.

Spectra

The proton spectra were determined in $CDCl_3$ solutions with Varian A60A and HA100 spectrometers. The ^{13}C spectra were obtained by Fourier transform operation with a Varian XL-100-15 system using 5- or 10-mm sample tubes and 50–100 mg of material in $CDCl_3$ solutions. Capsidiol (**1**) was also examined in CD_3OD solution. In most cases one or two thousand transients sufficed to produce spectra with good signal-to-noise ratio. Off-resonance spectra were obtained by off-setting the decoupler frequency from the optimum value by 1 kHz without noise modulation and usually doubling the number of transients. Single frequency, selective decoupling experiments were performed for **1** to correlate its methyl signals with specific proton absorptions; these were done with CD_3OD solutions.

X-Ray Analysis of Capsidiol

The material was crystallized from ethyl acetate to give colorless prisms, m.p. 152–153°. Precession photographs showed the following systematic absences: *h*00 when $h = 2n + 1$, 0*k*0 when $k = 2n + 1$, 00*l* = $2n + 1$; the space group was, therefore, unambiguously determined to be $P2_12_12_1$. A crystal fragment with dimensions 0.30 × 0.35 × 0.50 mm was mounted along the prism (*c*) axis on an automated Picker four-circle diffractometer and the following crystal data were obtained.

$C_{15}H_{24}O_2$ Mol. wt. = 236.3

Orthorhombic, a = 16.043 ± 0.002, b = 12.406 ± 0.002, c = 6.968 ± 0.003 Å, V = 1386.8 Å^3, D_m = 1.13 g cm^{-3}, Z = 4, D_x = 1.132 g cm^{-3} (21 °C; CuKα_1, λ = 1.54051 Å; CuKα_2, λ = 1.54433 Å), F(000) = 520, μ(CuKα) = 5.78 cm^{-1}.

Monochromatization was achieved by a nickel filter and a pulse-height analyzer. The moving-crystal – moving-counter (θ–2θ scan) method was employed with 2° scans for $0 < 2\theta \leq 100°$ and 3° scans for $100 < 2\theta \leq 130°$. There was no indication of any deterioration of the crystal during the data collection. Of the 1386 reflections with $2\theta \leq 130°$, 1346 (97%) were considered observed. A net count of 90 or 5% of the background, whichever was higher, were determined to be threshold intensities.

The structure was solved by direct methods developed for noncentrosymmetric space groups (7). The procedure was similar to that described by Kennard *et al.* (8). An *E* map calculated with the phases obtained from the tangent

Can. J. Chem. Downloaded from www.nrcresearchpress.com by 210.87.254.5 on 09/05/12
For personal use only.

refinement of one of the starting sets revealed the positions of all 17 nonhydrogen atoms.

The block diagonal approximation of the least-squares method was used to refine the atomic parameters. The quantity $\Sigma w(F_o - F_c)^2$ was minimized and a shift factor of 0.8 was used throughout. The atomic scattering factors of Hanson *et al.* (9) were used for C and O and those of Stewart *et al.* (10) for bonded H. All but one hydrogen atoms were located on subsequent difference Fourier maps; the missing atom was one of those attached to the strongly vibrating C-13. The contributions of the 23 hydrogen atoms were included in structure-factor calculations but their parameters were not refined. The refinement converged to a conventional agreement index $R = 0.052$ and a weighted factor $R'(= \Sigma w(\Delta F)^2/\Sigma w F_o^2)^{1/2} = 0.062$ for 1340 observed reflections. The average coordinate shift at the end of the last cycle was 0.10 σ and the maximum shift equalled 0.55 σ. The final difference Fourier map showed no significant features.

The final atomic coordinates and temperature parameters are listed in Table 1. The estimated standard deviations (shown everywhere in parentheses and referring always to the last digit) were derived from the inverse of the least-squares matrix. Table 2 lists the observed and calculated structure factors.[4]

Results and Discussion

The ^{13}C shieldings for the sesquiterpenes **1–7** are collected in Table 3 and the data for the model compounds **8–21** appear in Table 4. For each compound off-resonance decoupled spectra were determined to distinguish between quaternary, methine, methylene, and methyl signals. Assignments for specific signals were then obtained by comparison of the results for closely related compounds throughout the series from the simpler systems to the most highly substituted cases. In this manner a consistent set of assignments followed readily with little ambiguity for all of the skeletal carbons. The well-established substituent effects of carbonyl, hydroxyl, and methyl groups (2) and those of the olefinic bond (2) in cyclohexane systems are evident throughout the series and further examples of downfield shifts associated with *syn*-axial interactions of neighboring groups (3) are discussed. Since the methyl protons in capsidiol (**1**) have significantly different shieldings (1), selective decoupling experiments were carried out to identify the methyl carbons unequivocally. These spectra were obtained for CD_3OD solutions because of the higher solubility of **1** thereby reducing the sampling time required.

[4]Table 2 may be obtained at a nominal charge from the Depository of Unpublished Data, National Science Library, National Research Council of Canada, Ottawa, Canada K1A 0S2.

Comparison of the methyl shieldings for **1–6** with those in a variety of related compounds clearly establishes the relative orientation of the vicinal methyls (C-14 and -15). These data are discussed in the following section while the trends found for the skeletal carbons are presented in a second section.

The preparation and characterization of epicapsidiol (**3**), isomeric with **1**, is described in the Experimental Section. It may be noted that these two diols are nearly indistinguishable from their m.p., $[\alpha]_D$, and i.r. spectra but are easily identified from their n.m.r. spectra. The absorption pattern for the C-1 proton contained a 11.4 Hz coupling to one of the vicinal methylene protons, an allylic coupling of 1.9 Hz and a homoallylic coupling of 2.7 Hz. These data clearly establish its axial orientation. The angular methyl proton absorptions for **1** and **3** differ by 0.25 p.p.m. and the 3-protons by 0.35 p.p.m. (To be consistent with popular usage the numbering scheme employed for **1–7** in this paper has been altered from that used in our earlier report (1).) In their ^{13}C spectra, the olefinic methyl carbons are the only centers exhibiting identical shieldings. While the change in orientation of the 1-hydroxyl group from axial (**1**) to equatorial (**3**) was expected to produce marked differences in the shieldings of the carbons within three bonds of this group, significant differences were found for more remote carbons. The differences for all centers range from 0.1 to 9.9 p.p.m. illustrating the remarkable sensitivity of carbon shieldings to molecular geometry and conformation.

(a) Methyl Carbon Shieldings

In **1**, the methyl carbons at 8.9, 21.0, and 32.1 p.p.m. arise from C-14, -13, and -15, respectively, as was established by selective decoupling. From these data, the olefinic methyl absorptions at 20.9 ± 0.1 p.p.m. for **3–7** were identified; the position is unexceptional (2). The vicinal methyl carbons (C-11, -12) in **8** were also distinguished by selective decoupling from which the consistent appearance of methyl absorption at 15.5 ± 0.2 p.p.m. for **7–10** and **12** led to its assignment to C-11. The structural variations at C-3, -4, and -5 in **8–10** would not be expected to have significant effects on the shielding of an equatorial methyl carbon at C-9 nor would the change in geometry at the ring junction in **12**. The methyl signal near 30 p.p.m. in the spectra of **3–6** was assigned to C-15. In this way the individual methyl assign-

Can. J. Chem. Downloaded from www.nrcresearchpress.com by 210.87.254.5 on 09/05/12
For personal use only.

TABLE 1. Final fractional coordinates and thermal parameters (Å²)

Nonhydrogen atoms[a]

	10^5x	10^5y	10^5z	10^4U_{11}	10^4U_{22}	10^4U_{33}	$10^4(2U_{23})$	$10^2(2U_{13})$	$10^4(2U_{12})$
C(1)	62648(15)	37150(23)	47705(38)	374(10)	589(14)	359(12)	134(23)	−120(21)	−52(21)
C(2)	66171(15)	37763(24)	27466(38)	334(10)	600(14)	391(12)	−106(24)	27(20)	62(22)
C(3)	63445(14)	47978(22)	17432(31)	349(10)	575(13)	238(9)	−53(21)	48(17)	−193(20)
C(4)	53877(14)	48635(22)	15636(36)	347(10)	521(13)	342(11)	198(21)	−39(18)	−152(19)
C(5)	49727(14)	47774(18)	35892(34)	321(9)	356(10)	368(10)	−32(19)	40(18)	−104(17)
C(6)	40085(14)	46843(21)	34219(42)	317(10)	441(12)	514(13)	−110(24)	74(20)	−2(18)
C(7)	36680(14)	35328(21)	33530(38)	329(10)	476(12)	419(12)	−131(22)	123(20)	−187(19)
C(8)	39199(17)	29687(23)	52041(43)	473(13)	515(13)	479(14)	43(25)	147(24)	−328(23)
C(9)	48528(17)	30451(22)	54290(36)	490(13)	494(13)	359(11)	158(22)	−12(22)	−122(22)
C(10)	53234(14)	38203(20)	46801(32)	361(10)	444(12)	256(10)	−60(19)	18(17)	−86(18)
C(11)	27346(16)	35071(25)	29512(46)	357(10)	596(15)	547(15)	−72(27)	106(23)	−238(22)
C(12)	24387(20)	29078(31)	14879(57)	499(14)	815(21)	676(20)	−195(36)	−153(32)	−299(30)
C(13)	21889(19)	41109(41)	41868(86)	334(13)	1085(30)	1312(41)	−1069(63)	234(37)	−175(31)
C(14)	50693(17)	40508(31)	980(36)	406(12)	1018(22)	268(10)	−118(28)	−35(20)	−431(28)
C(15)	51340(17)	58308(23)	47065(53)	433(12)	490(13)	743(19)	−373(30)	188(28)	−214(22)
O(1)	66659(12)	45578(21)	58298(24)	422(8)	960(15)	268(7)	34(18)	−84(14)	−410(20)
O(2)	66978(11)	48749(22)	−1344(25)	416(9)	1078(16)	275(7)	59(21)	93(15)	−441(20)

Hydrogen atoms[b]

	10^3x	10^3y	10^3z	10^3U_{iso}		10^3x	10^3y	10^3z	10^3U_{iso}
H(11)	642	279	521	51	H(122)	283	258	62	63
H(21)	642	312	220	43	H(131)	241	473	521	76
H(22)	723	371	292	43	H(132)	173	416	359	76
H(31)	646	537	258	45	H(141)	449	411	−19	53
H(41)	532	575	124	49	H(142)	509	317	53	53
H(61)	382	502	459	46	H(143)	536	403	−105	53
H(62)	384	500	225	46	H(151)	567	594	474	56
H(71)	399	304	230	45	H(152)	478	650	383	56
H(81)	380	223	478	49	H(153)	488	583	612	56
H(82)	364	344	622	49	H(O1)	656	450	694	46
H(91)	509	245	617	50	H(O2)	724	479	17	54
H(121)	179	285	120	63					

[a]The thermal vibration parameters are expressed as exp $[-2\pi^2 (U_{11}h^2a^{*2} + U_{22}k^2b^{*2} + U_{33}l^2c^{*2} + 2U_{23}klb^*c^* + 2U_{13}hla^*c^* + 2U_{12}hka^*b^*)]$.
[b]Coordinates from difference Fourier maps.

TABLE 3. ^{13}C shieldings[a] of capsidiol, its derivatives and aristolochene

Carbon	1[b]	1	2	3	4	5	6	7
1	75.4	75.0	75.2	(67.2)	200.8	145.8	189.3	32.6
2	36.8	36.3	36.3	39.8	(43.0)	122.9	127.4	27.9
3	65.8	65.3	65.4	(67.0)	66.4	202.7	154.0	(31.2)
4	48.9	47.7	47.7	47.1	46.4	55.2	44.7	44.1
5	40.0	39.1	38.8	38.7	38.8	39.7	39.5	38.7
6	46.4	44.9	43.7	44.3	(44.4)	41.4	41.5	43.3
7	41.4	40.2	39.3	39.4	40.6	41.4	40.0	37.7
8	31.4	30.4	29.2	29.9	30.3	31.2	30.5	(31.3)
9	128.9	128.8	129.1	118.9	134.8	135.4	135.4	122.9
10	141.2	140.3	140.2	140.6	141.4	138.8	139.6	144.3
11	150.3	149.1	32.8	149.4	148.0	148.3	148.3	150.3
12	109.0	108.7	19.9	108.6	109.4	109.4	109.2	108.2
13	21.1	21.0	20.0	21.0	20.9	21.0	20.8	20.9
14	9.5	8.9	9.1	9.4	8.9	14.8	16.7	15.7
15	32.4	32.1	32.4	30.1	30.9	30.7	31.0	18.1

[a]In p.p.m. from TMS, $CDCl_3$ solutions (5–15% w/v). Values in parentheses may be interchanged.
[b]Measured in CD_3OD solution.

ments were completed. The nonequivalence of the isopropyl methyl carbons of **2** is typical (2).

The shieldings of the vicinal methyl carbons in the sesquiterpenes are instructive. By comparison with the results for **7–21**, the angular methyl absorption near 32 p.p.m. for **1** and **2** is remarkably low. Since the shieldings of vicinal methyl groups depend markedly on their relative orientation (2, 11) and the angular methyl carbons in **7–10** and **12** are substantially upfield from the C-15 signals in **1–6**, it follows that C-14 and -15 must be *trans*-diaxial in capsidiol and its derivatives (**1–6**). The magnitude of the shielding associated with a *gauche* arrangement of vicinal methyls in these systems is indicated by the angular methyl shieldings in **8** *vs.* **14**, **9** *vs.* **15**, **10** *vs.* **13**, and **8** *vs.* **11**. An angular methyl carbon is also shielded by its *gauche* interactions with the ring carbons (2, 12, 13) as shown by the 6 p.p.m. shifts found for **8** *vs.* **9** and **10**; the olefinic bond in **8** eliminates one of these interactions relative to the situation in **9** and **10**. Two *gauche* interactions are lacking in **12** relative to **9** and the downfield shift of 11.4 p.p.m. is typical for this change in geometry (14). The deshielding influence of the axial 1-hydroxyl group in **1** and **2** is shown by the results for **3**; a comparable difference was found for **16** and **17**. These are examples of the deshielding trends caused by *syn*-axial interactions of groups separated by four bonds (3). Because of the flexibility of the unsaturated ring in **7**, the favored conformation will be that having an equatorial isopropenyl group and, therefore, this group should have little effect on the angular methyl shielding. The 2 p.p.m. difference for this carbon in **7** and **8** may be ascribed to the carbonyl group in the latter since 3-oxo groups shield C-19 in steroids (2). From these comparisons, it is clear that C-15 in capsidiol must be well separated from C-14 and therefore a *trans*-diaxial orientation is required. With this point established the relative orientation of the hydroxyl groups are as indicated with the ring in a chair conformation as had been concluded from the proton results (1). Possible twist forms are inconsistent with the n.m.r. data.

From the angular methyl shielding of **7**, the C-15 shielding in **1** can be estimated on the basis of the data for the model compounds. From the trends noted above and the results for **11**, a change in the C-14 configuration from *cis* to *trans* should lead to a downfield shift of the angular methyl carbon of 6–8 p.p.m. Since the axial 1-hydroxyl group presumably causes a shift of $\sim$2 p.p.m. and the equatorial 3-hydroxyl deshields C-15 by $\sim$1 p.p.m., from the results for **19** and **20**, the net effect at C-15 is estimated as 9–11 p.p.m., assuming additivity of these three contributions in **1** relative to **7**. Thus, the predicted shielding for C-15 in **1** is 27–29 p.p.m., somewhat upfield from that observed. An additional feature, however, requires consideration. Because of the flexibility of the unsaturated ring in **1**, structures **22** and **23** are possible, differing in the configuration of the isopropenyl group with respect to C-15. Aristolochene (7) corresponds to **23** and with its angular methyl as the base value the predicted shielding for C-15 in **1** is upfield from the observed value.

Can. J. Chem. Downloaded from www.nrcresearchpress.com by 210.87.254.5 on 09/05/12
For personal use only.

Can. J. Chem. Downloaded from www.nrcresearchpress.com by 210.87.254.5 on 09/05/12
For personal use only.

TABLE 4. ^{13}C shieldings[a] of the decalin derivatives[b] **8–21**

Compound	C-1	C-2	C-3	C-4	C-5	C-6	C-7	C-8	C-9	C-10	C-11	C-12
8	35.5	34.0	199.4	123.9	171.0	33.3	26.5	30.5	43.1	39.0	15.3	16.0
9	(38.1)	(38.5)	211.6	44.6	46.2	29.4	26.3	30.6	42.5	36.0	15.6	9.8
10	38.3	31.6	71.4	37.1	43.0	29.1	26.8	30.9	44.5	35.9	15.5	10.6
11	32.1	34.3	199.2	126.0	170.0	31.8	20.8	28.6	39.5	39.4	16.4	23.8
12	(36.3)	(37.3)	212.8	42.5	43.2	27.4	20.6	30.6	30.1	34.9	15.5	21.2
13	40.0	31.2	71.0	38.1	43.1	28.7	26.7	21.8	41.1	33.0	15.7	
14	38.1	34.0	199.1	123.9	170.2	32.8	27.2	21.8	41.6	36.0	22.1	
15	40.3	38.1	210.6	44.8	44.6	29.0	26.0	21.6	41.0	33.1	14.9	
16	(41.2)	20.4	36.6	70.0	52.4	23.0	26.7	21.7	(41.9)	34.8	16.8	
17	43.7	16.9	34.1	71.8	48.5	26.0	27.3	21.9	41.7	33.7	19.1	
18	40.2	18.8	25.7	115.6	145.3	69.4	37.9	20.5	41.4	35.6	25.1	
19	50.9	66.9	36.4	(27.9)	44.9	(28.1)	26.9	21.2	41.6	34.7	16.6	
20	42.1	22.1	27.2	29.3	45.8	29.3	27.2	22.1	42.1	33.9	15.7	
21	40.2	19.1	26.0	119.2	143.6	32.8	28.7	22.5	42.3	34.8	24.4	

[a]In p.p.m. from TMS, $CDCl_3$ solutions (5–10% w/v). Values in parentheses may be interchanged.
[b]For ease of comparison, the steroid numbering scheme has been employed for these derivatives.

Can. J. Chem. Downloaded from www.nrcresearchpress.com by 210.87.254.5 on 09/05/12
For personal use only.

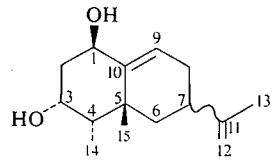

1

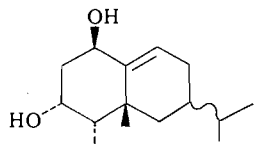

2

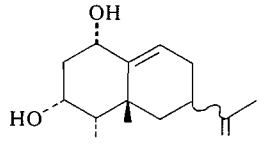

3

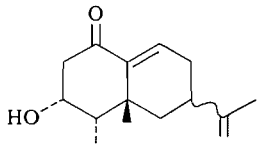

4

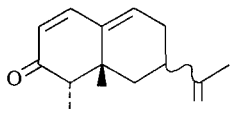

5

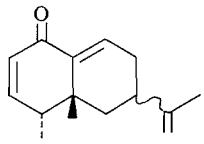

6

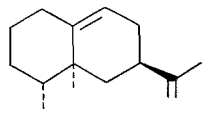

7

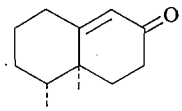

8

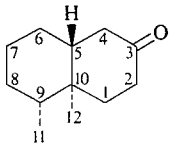

9

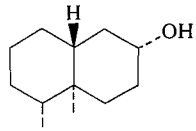

10

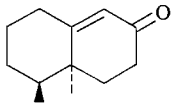

11

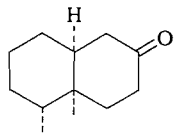

12

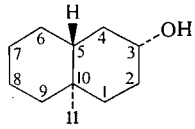

13

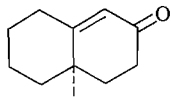

14

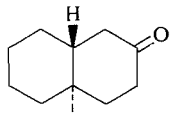

15

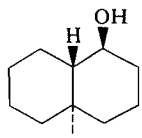

16

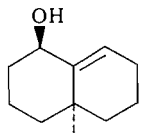

18

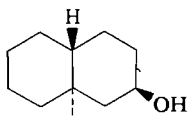

19

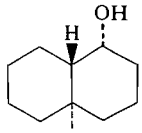

17

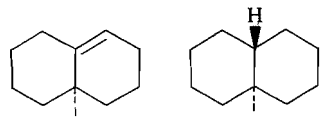

21 20

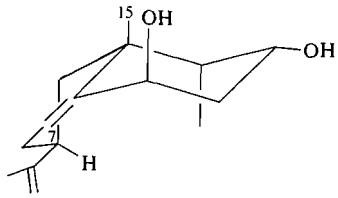

22

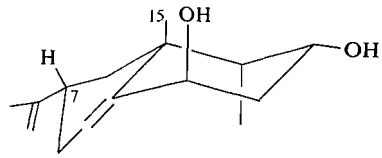

23

A comparison of **22** with **23**, however, shows that the relative orientation of C-7 and -15 is different in each and the angular methyl carbon for these should exhibit different shieldings with that in **22** at lower field. On this basis, it may be proposed that **1** is best represented by **22** with the isopropenyl group *cis* with respect to C-15. Although this interpretation is permissive rather than compelling, the results of the X-ray examination have established that **22** is indeed the correct representation of **1** in the crystal.

The relatively high field position of C-14 in **1–4** compared with the results for C-11 in **8–10** is undoubtedly due, in large part, to the neighboring *gauche* hydroxyl group. It may be noted that the angular methyl shieldings in the isomeric 10-methyl-*trans*-decal-1-ols are 9.8 and 16.1 p.p.m. (15) for *gauche* and *anti* arrangements of the hydroxyl and methyl groups, respectively. The *gauche* interactions of axial and equatorial methyl carbons at C-4 in **1–4** would not be expected to be greatly different since the C-14 · · · C-2 interaction for the former is replaced by the *gauche* Me · · · Me interaction for the latter. The C-14 shieldings in **5** and **6**, therefore, seem unexceptional.

(b) Skeletal Carbons

The consideration of specific assignments for the skeletal carbons in these compounds began with the saturated monomethyldecalin derivatives **13**, **15–17**, and **19** since the shieldings of the individual methylene carbons in the unsubstituted ring, C-6 to -9 should be comparable to those in **20** for which the assignments were known (12). For ease of comparison within the series and with related materials the steroidal numbering scheme has been adopted for **8–21**. The average shieldings for these centers were found to be: C-6, 28.8 ± 0.4 (excluding **16** and **17**); C-7, 26.8 ± 0.3; C-8, 21.7 ± 0.2 and C-9, 41.6 ± 0.3 p.p.m. In the 4-decalols **16** and **17**, C-6 is more shielded because of the γ *gauche* effect of the 4-hydroxyl group. The greater shielding of C-6 in **16** relative to that in **17** may be indicative of some distortion in the latter compound arising from the *syn*-axial interaction between the methyl and hydroxyl groups. The remaining methylene signals were assigned from the characteristic substituent effects of the carbonyl and hydroxyl groups (2); the α-methylene carbons exhibit downfield shifts of ~ 15 and ~ 9 p.p.m., respectively, as expected. Further confirmation of some of the methylene assignments was provided by considerations of the γ effects of hydroxyl groups. Equatorial hydroxyls tend to shield γ-carbons by *ca.* -2 p.p.m. (16) (*e.g.* C-1 in **13**), while axial hydroxyls shield these centers by *ca.* -5 p.p.m. (2) (C-2 in **17**). From the off-resonance decoupled spectra, the methine and quaternary signals were identified and the carbonyl and carbinyl absorptions distinguished by their characteristic shieldings. It is interesting that the carbinyl carbon bearing the axial hydroxyl in **17** is *deshielded* relative to the corresponding carbon bearing an equatorial hydroxyl in **16**. This is the opposite trend to that generally observed in less hindered cyclohexanols (17) and decalols (15) but arises from the *syn*-axial interaction of the methyl and hydroxyl groups in **17** as shown for a variety of model systems (3).

With these assignments complete, the methylene shieldings for **9** and **10** were next considered. The additional equatorial methyl group at C-9 was expected to affect the shieldings of C-1 and -8

Can. J. Chem. Downloaded from www.nrcresearchpress.com by 210.87.254.5 on 09/05/12
For personal use only.

Can. J. Chem. Downloaded from www.nrcresearchpress.com by 210.87.254.5 on 09/05/12
For personal use only.

appreciably on the basis of the results for a variety of methyldecalins (12) whereas the remaining methylene carbons should be comparable to the corresponding centers in **15** and **13**, respectively. The appropriate data (12) for *trans*-decalin, its 1-methyl, 2-methyl and 1,3-dimethyl derivatives indicated that in **9** and **10** C-1 should be shielded by *ca.* −3 p.p.m. with C-8 deshielded by *ca.* 10 p.p.m. On this basis, the methylene assignments given in Table 4 follow. The signals for the remaining skeletal carbons were assigned from off-resonance decoupled spectra. The *cis*-decalone **12** was only examined in a mixture with **9** and the high field region of the decoupled spectrum contained 20 separately resolved signals indicating two overlapping signals at 30.6 and 42.5 p.p.m. From the shifts observed for the A and B ring carbons in a series of isomeric 5α and 5β steroids (14), the assignments for **12** followed by comparison with the data for **9**, since similar shifts may be anticipated. The observed shifts **9** → **12**, together with the corresponding results for the steroid series, in parentheses, were: C-1, −1.8 (−1.5); C-2, −1.1 (−1.0); C-3, +1.2 (+1.3); C-4, −2.1 (−2.3); C-5, −3.0 (−2.4); C-6, −2.0 (−3.3); C-7, −5.7 (−4.5); C-8, 0.0 (0.0); C-9, −12.4 (−13.0); C-10, −1.1 (−0.8) p.p.m.

The assignments for the methylene signals in the saturated ring of **14** and **21** were made by comparison with the data for 2,2-dimethylmethylenecyclohexane (18) in which C-6 absorbs at 33.2 p.p.m., C-5 at 28.8, C-4 at 22.7, and C-3 at 41.6 p.p.m. The values listed in Table 4 for C-6 to -9 in **14** and **21** agree nicely with these as expected. The methylene signals near 40 p.p.m. were assigned to C-1, since the lowest field methylene signal in **8** and **11** is near 35 p.p.m. and the absence of a C-9 methyl in **14** and **21** will deshield this position. The remaining methylene signals for **21** were assigned by comparison with **20**. The methylene assignments for **8** followed from the characteristic shifts produced by the introduction of an equatorial methyl at C-9 as discussed above for the saturated series. Specifically, C-9 and -8 will be deshielded by *ca.* 2 and 9 p.p.m., respectively, and C-1 shielded by *ca.* −3 p.p.m. relative to the results for **14**, while the remaining methylenes should be little affected. An axial methyl group at C-9 in this skeleton would be expected to shield C-7 appreciably because of the *gauche* effect thus the signal at 20.8 p.p.m. in the spectrum of **11** was readily assigned. Since C-2 and -7 should be little affected by the axial 9-methyl while C-1 should be comparable to that in **8**, the methylene assignments for **11** were completed. The remaining skeletal signals observed were readily assigned from off-resonance decoupled spectra and their characteristic absorption positions.

For **18**, the methylene signals at 18.8 and 20.5 p.p.m. were assigned to C-2 and -8, respectively, since the latter value agrees nicely with that for C-2 in **16**, while those at 40.2 and 41.4 p.p.m. were assigned to C-1 and -9. For each of these pairs the more shielded signal arises from carbon in the unsaturated ring as anticipated for the homoallylic shielding effect exerted by the olefinic bond as first recognized in terpene spectra (19). The methylene signal at 37.9 p.p.m. fits nicely for C-7 since the neighboring hydroxyl group should deshield this position by *ca.* 10 p.p.m. Finally, C-3 must give rise to the 25.7 p.p.m. signal, in good agreement with the C-3 absorption for cyclohexene, as expected, since alkyl substitution on the cyclohexene ring has been shown to have little effect at carbons two or more bonds from the site of substitution (2). The remaining signals were readily assigned from the peak positions. The similarity of the carbinyl carbon shielding with that in **16** indicates an equatorial hydroxyl group as confirmed by the carbinyl proton absorption for **18** (see Experimental Section) which contained a diaxial vicinal coupling of 12 Hz and an allylic coupling of 2 Hz, consistent only with an axial carbinyl proton. Additional evidence of an equatorial hydroxyl group is provided by the marked upfield shifts of the olefinic methine (C-4) signal relative to that in **21** (see below).

From the foregoing results the assignments of the skeletal carbons in the sesquiterpenes **1**–**7** were made. Beginning with aristolochene (**7**) the lowest field methylene signal, 43.3 p.p.m., was assigned to C-6 since this methylene carbon is expected to experience the strongest deshielding effects. In each of **1**–**6**, a similarly shielded carbon was observed in support of this assignment since substitution differences at C-1 – -3 should have minimal effects at C-6. For similar reasons, the methylene signal in the range 29.9–31.2 p.p.m. was assigned to C-8 in each of **1**–**7**. The assignments for C-1, -2, and -3 in **7** followed from those for the corresponding carbons in **8**. The two methine signals at 37.7 and 44.1 p.p.m. were assigned to C-7 and -4, respectively, since analogous signals appeared in the ranges 39.3–40.6

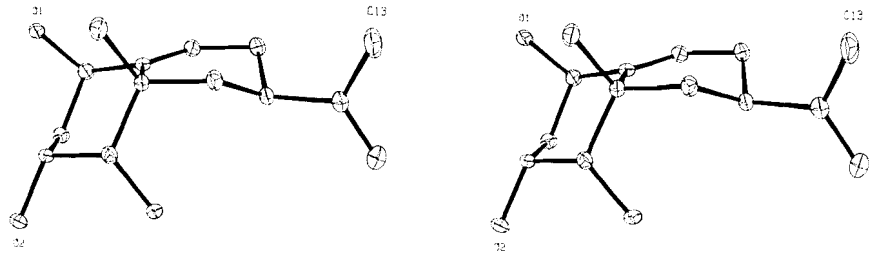

FIG. 1. Stereoscopic view of the structure; the ellipsoids include 50% probability.

and 46.4–47.7 p.p.m. for **1**–**4**. Introduction of an equatorial hydroxyl at C-3 is expected to deshield C-4 in **1**–**4** relative to that in **7** but the shift is small (*ca.* 3 p.p.m.) because of the *gauche* interaction of the hydroxyl with the axial 4-methyl group. The quaternary olefinic carbons (C-10, -11) were distinguished for **1**–**7** from the spectrum of **2** which lacks the exocyclic double bond. Off-resonance decoupling readily identified C-12 for the series. The remaining methylene signal in the spectra of **1**–**4** arises from C-2 whose shieldings agree well with those reported for the 1,3-cyclohexanediols (20) after allowance for the γ effect of the axial 4-methyl group (*ca.* −6 p.p.m.). The remaining sp^3-methine signals for **5** and **6** are those of C-4. In this series, the quaternary C-5 signals were uniquely defined by off-resonance decoupling.

Of the two carbinyl signals for **1** and **2**, the lower field peak at 75 p.p.m. was assigned to C-1 by comparison with **17**; the 3 p.p.m. downfield shift is readily ascribed to the neighboring double bond. The second carbinyl signal for **1** and **2**, near 65 p.p.m., is shielded relative to that in **19** indicating that the γ effect of the axial 1-hydroxyl group is greater than the β effect of the axial 4-methyl. Although axial methyls exhibit β effects of *ca.* 5.5 p.p.m. (13), the *gauche* interaction between the 4-methyl and 3-hydroxyl groups will attenuate the β effect of the methyl. The downfield shift found for C-3 in **3**, relative to **1** and **2**, together with the fact that this shielding is comparable to that in **19**, indicates that the β effect of the 4-methyl group is *ca.* 2.5 p.p.m.; the equatorial 1-hydroxyl group may be expected to shield C-3 by *ca.* −2.5 p.p.m. (16). The much more shielded C-1 carbinyl carbon in **3** compared to **1** and **2** appears contrary to the general tendency for carbinyl carbons bearing axial and equatorial hydroxyls (17), as noted earlier for **16** and **17**. The rather large shift for the change **1** → **3** presumably arises from the combined effects of the *syn*-axial Me · · · OH interaction in **1**, tending to deshield C-1, and the *gauche* eclipsed interaction between the hydroxyl and C-9 in **3**, increasing the deshielding of C-1. A clear indication of an appreciable steric interaction for the latter centers is the −10 p.p.m. shift found for C-9 in **3** relative to **1**. The carbonyl shieldings for **4** and **6** are typical of conjugated and cross-conjugated systems in six-membered rings (2). The protonated olefinic carbons in **5** and **6** were assigned by analogy with simpler cyclohexenones (2) with the signals near 135 p.p.m. in each case assigned to C-9 from its shielding in **4**.

A stereoscopic diagram of capsidiol is shown in Fig. 1. Ring A has a chair conformation which is slightly distorted owing to a 1,3-interaction, the presence of the sp^2-hybridized C-10, and the fact that ring B is in sofa form. The hydroxy group attached to C-3 is in equatorial orientation while the other three substituents are in axial positions. The structure analysis has thus confirmed the novel anti-periplanar orientation of the two methyl groups. Ring B has a somewhat distorted sofa conformation with C-7 displaced from the mean plane through the other atoms in the ring. The isopropylene group is in an equatorial orientation.

It may be of interest to assess the distortions in the two rings, and this can be best done on the basis of torsional angles. The fact that C-5, -6, -9, and -10 are coplanar within 0.01 Å causes a flattening of that part of ring A which is adjacent to ring B. This is evidenced by decreased absolute values of three torsional angles (Fig. 2) which may be compared with the value ±55.9° obtained from an electron diffraction study of gaseous cyclohexane (21). An additional flattening may have been expected as a result of the presence of three axial substituents. From an electron diffraction study of 1,1-dimethylcyclohexane Geise *et al.* (22) determined an average endocyclic torsional angle of 51.7° and they attributed the flattening pri-

Can. J. Chem. Downloaded from www.nrcresearchpress.com by 210.87.254.5 on 09/05/12
For personal use only.

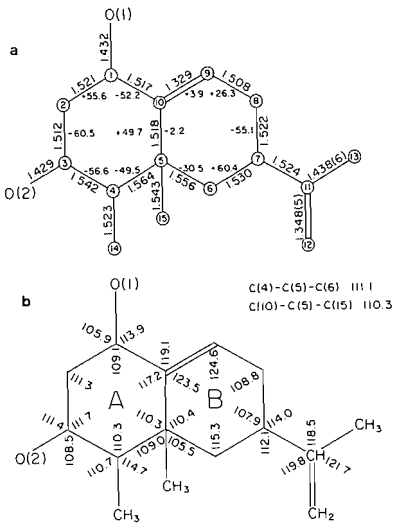

FIG. 2. (*a*) Bond lengths and torsional angles. Unless otherwise indicated the e.s.d.'s are 0.003–0.004 Å and 0.3°, respectively. (*b*) Bond angles. All e.s.d.'s are 0.2° except at C(11) where they are 0.3°.

marily to the axial substituent. In view of these considerations the extent of puckering in ring A, indicated by an average torsional angle of 54.0°, is surprisingly high. There is a strong interaction between the two *syn*-axial substituents on ring A which may be assessed by considering the following intramolecular distances: C(1) · · · · C(5) 2.591(3), O(1) · · · · C(15) 3.024(4) Å. This repulsion affects not only the conformation of ring A, but it also distorts the B ring.

Theoretical calculations have indicated (23, 24) that the energy of the sofa conformation of cyclohexene is only 1–2 kcal/mol higher than that of the most stable half-chair form. As a consequence of being fused to ring A, the B ring in capsidiol differs substantially from the half-chair form but only slightly from the sofa form. This observation has a bearing on the discussion of conformations of many natural products, such as Δ^4-steroids, which incorporate the $\Delta^{1,9}$-octalin system (25). The distortion from the sofa form is due to the nonplanarity of the endocyclic double-bond system, a feature for which precise structural data are rare (26), and a rotation about the C(5)—C(10) bond. The latter serves to increase the short distance between O-1 and C-15. The four carbon atoms in the exocyclic double-bond system are coplanar and that plane forms a dihedral angle of 82.2° with the mean plane through ring B. The conformation of this substituent is shown in a Newman projection (Fig. 3).

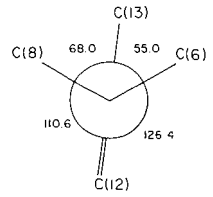

FIG. 3. Newman projection along the C(7)—C(11) bond.

Most bond lengths and bond angles (Fig. 2) agree with expected values. The abnormally short value for the C(11)—C(13) bond undoubtedly reflects the strong vibration of the latter atom. The fact that all bonds involving C-5 appear longer than normal can be ascribed to the full substitution of that atom. Several other bonds are also elongated as a result of steric effects. Such bond stretching is well known and occasionally gives rise to extreme values, such as the C—C bond of 1.628(2) Å which was recently encountered (27). Apart from the necessary increase at C-10 the bond angles in ring A agree fairly well with those in a chair-shaped cyclohexane ring. It is more difficult to assess the angles in ring B since the calculated values for a sofa conformation (23, 24) differ by as much as 3.2°. Nevertheless, it appears that the angle at C-5 is smaller than normal while that at C-6 is larger than normal. The abnormally small angles C(2)—C(1)—O(1) and C(6)—C(5)—C(15) are further manifestations of the repulsion between the two *syn*-axial substituents. Similarly, the angle C(5)—C(4)—C(14) indicates that C-14 is bent away from ring B, thus increasing its distance to C-7 to 3.257(4) Å.

There are two intermolecular hydrogen bonds in the crystal structure (Table 5). The hydroxyl group attached to C-1 donates a proton to O-2 in the molecule related by a **c** translation. It also accepts a proton from O-2 in the molecule related by a twofold screw axis parallel to *z*. The latter bond is indicated in the packing diagram (Fig. 4). The crystal structure may be described as consisting of ribbons parallel to *z*, formed by hydrogen-bonded molecules. Apart from the hydrogen bonds, there are no intermolecular distances between nonhydrogen atoms which are shorter than 3.5 Å.

Conclusions

On the basis of these ^{13}C n.m.r. data for the entire series, **1–21**, the stereochemistry of the vicinal methyl groups (C-14 and -15) in **1–6** must

Can. J. Chem. Downloaded from www.nrcresearchpress.com by 210.87.254.5 on 09/05/12
For personal use only.

TABLE 5. Geometry of hydrogen bonds

	O(1)—H(O1) · · · · O(2[I])[a]	O(2)—H(O2) · · · · O(1[II])[a]
O—H (Å)	0.80	0.90
H · · · · O (Å)	2.10	1.99
O · · · · O (Å)	2.840	2.800
O—H · · · · O (deg)	154	149
O · · · · O—H (deg)	19	21
O · · · · O · · · · H (deg)	7	9

[a]I: $x, y, 1 + z$; II: $3/2 - x, 1 - y, -1/2 + z$.

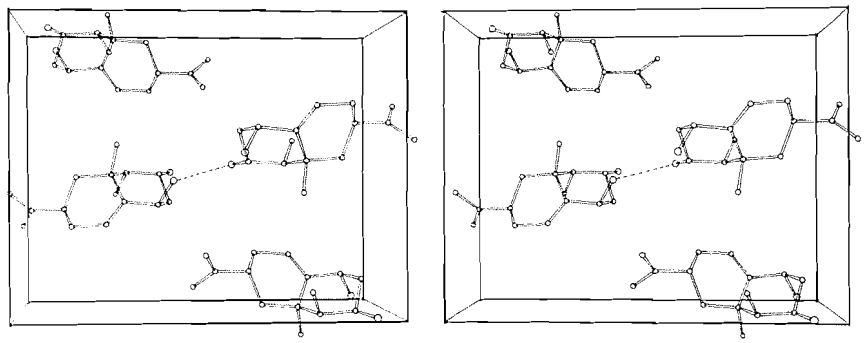

FIG. 4. Stereoscopic view along z of the contents of a unit cell. The directions of the axes are $x \rightarrow$ (0.25–1.25), $y \uparrow$ (0–1.0) and $z \odot$.

be *trans*. This feature in conjunction with the earlier proton results requires that the saturated ring adopt a chair conformation as in **22**. Comparison of the angular methyl shielding in **1** with that for **7**, together with the trends accompanying the structural variations in **8–21**, indicated that the isopropenyl group is *cis* with respect to the angular methyl, as subsequently proved by X-ray results. A detailed examination of the skeletal carbon shieldings for the entire series provided further evidence of the essential additivity of substituent effects in these systems and the results should be useful in the investigation of related sesquiterpenes.

We thank the National Research Council of Canada for financial support of this work through an Operating Grant (J.B.S.) and Scholarships (S.H.G.). We are grateful to R. Lazier for mass spectra and Ms. J. L. Gough for technical assistance. Samples of some of the model compounds were kindly supplied by Dr. P. C. Parthasarathy, CIBA Research Centre (**7**), Prof. E. Piers, University of British Columbia (**8**, **9**, and **12**), and Prof. A. R. Pinder, Clemson University (a mixture of **8** and **11**); their assistance is most appreciated. Figures 1 and 4 were drawn with the help of the ORTEP program by C. K. Johnson. All other crystallographic computations were performed with programs written by Ahmed, Hall, Pippy, and Huber.

1. M. GORDON, A. STOESSL, and J. B. STOTHERS. Can. J. Chem. **51**, 748 (1973).
2. For general discussion see G. C. LEVY and G. L. NELSON. ^{13}C Nuclear magnetic resonance for organic chemists. Wiley-Interscience, New York. 1972; J. B. STOTHERS. Carbon-13 NMR spectroscopy. Academic Press, New York. 1972; N. K. WILSON and J. B. STOTHERS. *In* Topics in stereochemistry. Vol. 8. *Edited by* E. L. Eliel and N. L. Allinger. Wiley-Interscience, New York. 1973. Chap. 1.
3. S. H. GROVER, J. P. GUTHRIE, J. B. STOTHERS, and C. T. TAN. J. Mag. Res. **10**, 227 (1973); K. R. STEPHENS, J. B. STOTHERS, and C. T. TAN. *In* Mass spectrometry and NMR in pesticide chemistry. Plenum Press, New York. 1973.
4. E. PIERS, R. W. BRITTON, and W. DE WAAL. Can. J. Chem. **47**, 4307 (1969).
5. M. YANAGITA and A. TAHARA. J. Org. Chem. **18**, 792 (1953).
6. C. DJERASSI and D. MARSHALL. J. Am. Chem. Soc. **80**, 3987 (1958).
7. J. KARLE and I. L. KARLE. Acta Crystallogr. **21**, 849 (1966).
8. O. KENNARD, N. W. ISAACS, W. D. S. MOTHERWELL, J. C. COPPOLA, D. L. WAMPLER, A. C. LARSON, and D. G. WATSON. Proc. Roy. Soc. A, **325**, 401 (1971).
9. H. P. HANSON, F. HERMAN, J. D. LEA, and S. SKILLMANN. Acta Crystallogr. **17**, 1040 (1964).
10. R. F. STEWART, E. R. DAVIDSON, and W. T. SIMPSON. J. Chem. Phys. **42**, 3175 (1965).
11. J. B. STOTHERS, C. T. TAN, and K. C. TEO. Can. J. Chem. **51**, 2893 (1973).
12. D. K. DALLING, D. M. GRANT, and E. G. PAUL. J. Am. Chem. Soc. **95**, 3718 (1973).

Can. J. Chem. Downloaded from www.nrcresearchpress.com by 210.87.254.5 on 09/05/12
For personal use only.

13. D. K. DALLING and D. M. GRANT. J. Am. Chem. Soc. **89**, 6612 (1967); **94**, 5318 (1972).
14. J. L. GOUGH, J. P. GUTHRIE, and J. B. STOTHERS. J. Chem. Soc. Chem. Commun. 979 (1972) and unpublished results.
15. S. H. GROVER and J. B. STOTHERS. Can. J. Chem. **52**, 0000 (0000).
16. T. I. PEHK and E. T. LIPPMAA. Org. Mag. Res. **3**, 679 (1971).
17. G. W. BUCHANAN, D. A. ROSS, and J. B. STOTHERS. J. Am. Chem. Soc. **88**, 4301 (1965); G. W. BUCHANAN and J. B. STOTHERS. Can. J. Chem. **47**, 3605 (1969).
18. S. H. GROVER. Ph.D. Thesis. University of Western Ontario, London, Ontario. 1974.
19. G. LUKACS, F. KHUONG-HUI, C. R. BENNETT, B. L. BUCKWALTER, and E. WENKERT. Tetrahedron Lett. 3515 (1972); E. WENKERT and B. L. BUCKWALTER. J. Am. Chem. Soc. **94**, 4367 (1972).
20. A. S. PERLIN and H. J. KOCH. Can. J. Chem. **48**, 2639 (1970).
21. H. R. BUYS and H. J. GEISE. Tetrahedron Lett. 2991 (1970).
22. H. J. GEISE, F. C. MIJLHOFF, and C. ALTONA. J. Mol. Struct. **13**, 211 (1972).
23. R. BUCOURT and D. HAINAUT. Bull. Soc. Chim. Fr. 1366 (1965).
24. G. FAVINI, G. BUEMI, and M. RAIMONDI. J. Mol. Struct. **2**, 137 (1968).
25. G. I. BIRNBAUM. Acta Crystallogr. Sect. B, **29**, 54 (1973).
26. O. ERMER and S. LIFSON. J. Am. Chem. Soc. **95**, 4121 (1973).
27. G. I. BIRNBAUM. Acta Crystallogr. Sect. B, **28**, 1248 (1972).
28. E. W. B. WARD, C. H. UNWIN, and A. STOESSL. Can. J. Bot. **51**, 2327 (1973).
29. V. DAVE, E. W. WARNHOFF, and J. B. STOTHERS. Tetrahedron Lett. 4229 (1973).

Can. J. Chem. Downloaded from www.nrcresearchpress.com by 210.87.254.5 on 09/05/12
For personal use only.

The Near-ultraviolet Absorption Spectrum of Diimide Vapor[1]

R. A. BACK AND C. WILLIS

Division of Chemistry, National Research Council of Canada, Ottawa, Canada K1A 0R6

AND

D. A. RAMSAY

Division of Physics, National Research Council of Canada, Ottawa, Canada K1A 0R6

Received September 5, 1973

Absorption spectra of N_2H_2 and N_2D_2 in the gas phase have been obtained in the region 3000–4300 Å, consisting of about 30 diffuse bands for each compound. Long progressions in the spectra are attributed to excitation of the H—N=N bending mode, ν_2', in the upper state, with much shorter progressions arising from the N=N stretching mode, ν_3'; values of $\nu_2' = 1215$ and 910 cm^{-1} and $\nu_3' = 1550$ and 1440 cm^{-1} were estimated for N_2H_2 and N_2D_2 respectively.

The spectra are attributed to the $^1B_g \leftarrow {}^1A_g$ ($\pi^* \leftarrow n_+$) transition of *trans* diimide, probably made allowed by vibronic interaction. From Franck–Condon calculations the H—N=N angle in the upper state was estimated to be 132 ± 2°, an increase of 25° from the ground-state value; the increase in the N=N bond length was estimated to be about 0.05 Å.

Les spectres d'absorption de N_2H_2 et N_2D_2 en phase gazeuse ont été obtenus dans la region spectrale 3000–4300 Å, ceux-qui presentent environ 30 bandes diffuses pour chaque produit. Les progressions longues dans les spectres sont attribuées à l'excitation du mode de déformation angulaire H—N=N, ν_2', dans l'état excité; les progressions plus courtes venant du mode de valence N=N, ν_3'; les valeurs de $\nu_2' = 1215$ et 910 cm^{-1}, et $\nu_3' = 1550$ et 1440 cm^{-1} ont été estimées pour N_2H_2 et N_2D_2 respectivement.

Les spectres sont attribués à la transition $^1B_g \leftarrow {}^1A_g$ ($\pi^* \leftarrow n_+$) de la diimide *trans*, probablement permise par l'interaction vibronique. Après des calculs de type Franck–Condon, l'angle H—N=N de l'état excité a été estimé être 132 ± 2°, une augmentation de 25° par rapport à la valeur pour l'état fondamental; l'augmentation dans la longueur de la liaison N=N a été estimée être environ 0.05 Å.

Can. J. Chem., **52**, 1006 (1974)

Introduction

The absorption spectrum of diimide vapor has been studied in some detail in the infrared (1–3) and vacuum ultraviolet (2) regions. A partial rotational analysis of the latter system suggested a ^3B_g ground-state (2), but there is now substantial evidence, summarized recently (4), for a singlet rather than a triplet ground-state. This conclusion is supported by a recent rotational analysis of the N—H and N—D stretching bands in the high-resolution infrared spectrum of N_2H_2 and N_2D_2 (3), which shows clearly that the molecule has a *trans* structure and that the electronic ground-state is totally symmetric (^1A_g).

Considerable work has also been done on the infrared spectrum of diimide in solids and matrices, recently reviewed by Bondybey and Nibler (5). Much of the interpretation has been inaccurate because of the failure to recognize that diimide is usually hydrogen-bonded except in very dilute matrices. Rosengren and Pimentel (6) have identified the H—N=N bending frequency by careful work with ^{15}N substitution, while Bondybey and Nibler have observed the Raman spectrum (5). All the ground-state frequencies except the torsional frequency are now reasonably well established (5).

Trombetti, in addition to his observations in the infrared and vacuum ultraviolet, reported a very weak absorption near 3500 Å in diimide vapor generated at low pressures in a flow system (2). This absorption appeared continuous but was too weak to permit closer investigation. In a recent study of the chemistry of diimide, much higher pressures of the vapor were obtained, and the near ultraviolet absorption was shown to have a strongly banded structure (4). There has been much interest recently in the photochemistry and electronic structure of simple azo compounds, particularly with regard

[1]NRCC No. 13562.

Can. J. Chem. Downloaded from www.nrcresearchpress.com by 210.87.254.6 on 09/05/12
For personal use only.

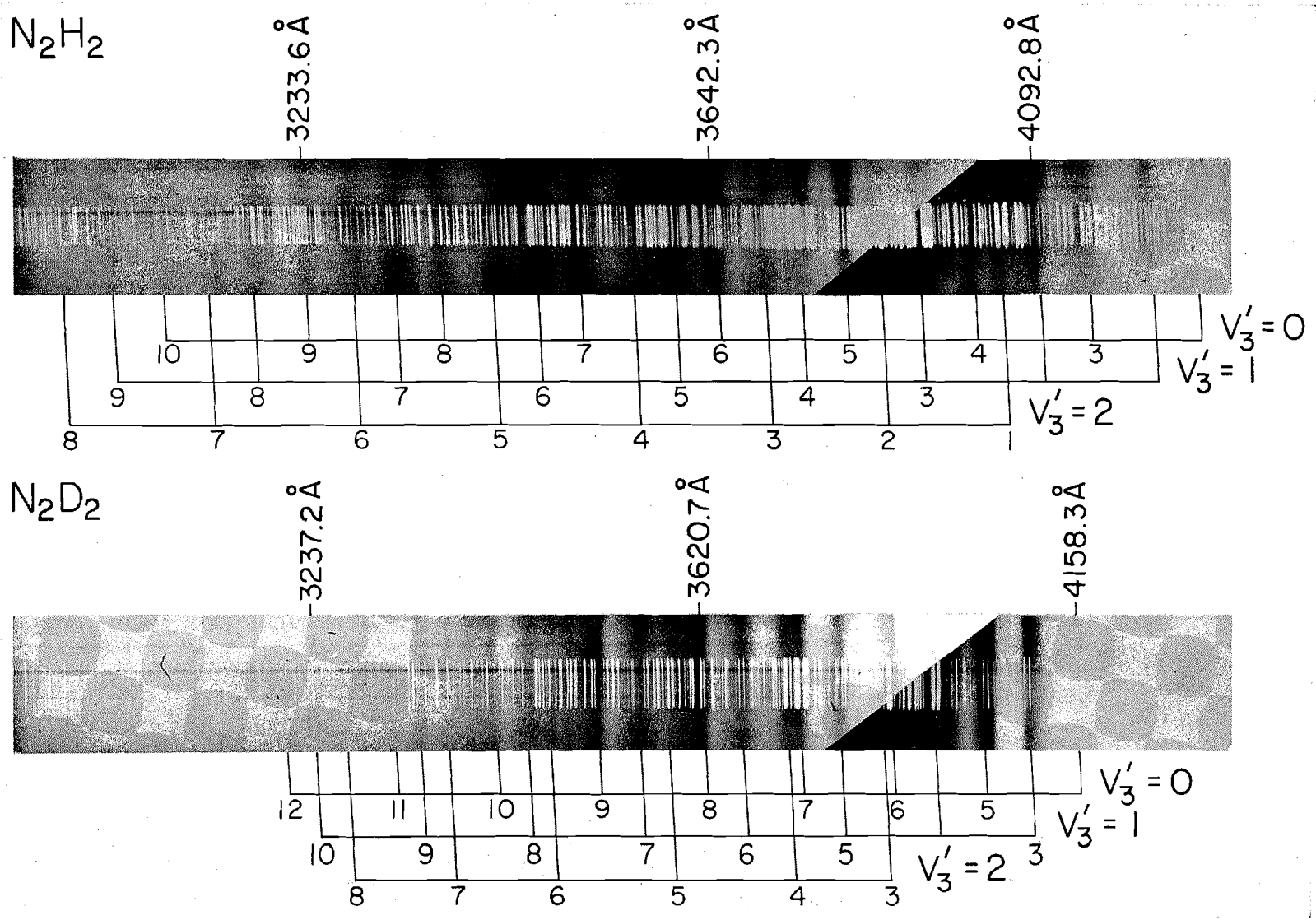

FIG. 1. These absorption spectra were photographed using a medium-dispersion Hilger quartz spectrograph with a path length of 72 m. The long wavelength features were photographed at a high initial diimide pressure (~50 Torr). The main parts of the spectra were obtained after the diimide concentration had been reduced by ~90%. An Fe hollow cathode spectrum is superimposed on each plate.

Can. J. Chem. Downloaded from www.nrcresearchpress.com by 210.87.254.6 on 09/05/12
For personal use only.

Can. J. Chem. Downloaded from www.nrcresearchpress.com by 210.87.254.6 on 09/05/12
For personal use only.

Can. J. Chem. Downloaded from www.nrcresearchpress.com by 210.87.254.6 on 09/05/12
For personal use only.

to the weak transition in the near ultraviolet. The corresponding transition in diimide, the prototype azo compound, is of obvious interest, especially as it is the first azo compound to show sufficiently well-developed structure in its spectrum to permit a complete vibrational analysis and thence to provide information about the upper state of the transition. The present paper gives a detailed account of the spectrum and the vibrational analysis.

Experimental

The preparation and handling of diimide have been described (4). N_2H_2 was prepared from anhydrous N_2H_4 (Matheson, Coleman, and Bell), and N_2D_2 from anhydrous N_2D_4 obtained from Merck, Sharp, and Dohme of Canada Ltd. with 99 at. % D content.

Spectra were obtained with a medium-dispersion Hilger quartz spectrograph, using an absorption cell 2 m long equipped with multiple-reflection aluminum mirrors to give a total light path of 72 m. A large sample of diimide, together with a 10-fold excess of ammonia, was rapidly vaporized into the 7 liter cell to give a total pressure of about 500 Torr. The diimide decomposed over a period of minutes and spectra were photographed at intervals during the decay.

Results

Spectra of N_2H_2 and N_2D_2 are shown in Fig. 1, and corresponding microdensitometer traces in Figs. 2 and 3. Both spectra are strongly banded, with apparently little or no underlying continuous absorption. The bands appear to be completely diffuse, and spectra taken at higher resolution confirm the absence of rotational fine structure.

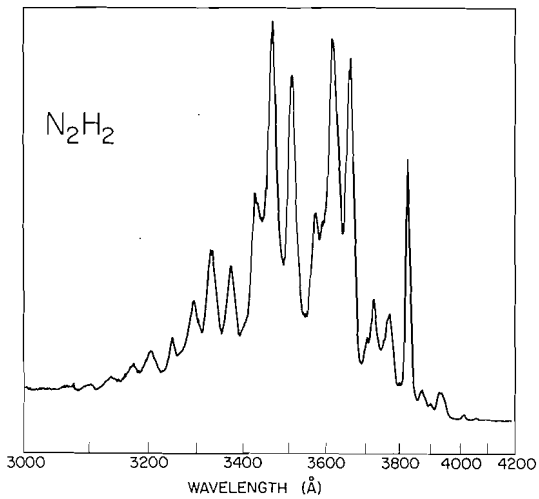

FIG. 2. Microdensitometer trace of N_2H_2 spectrum. Vertical scale is arbitrary.

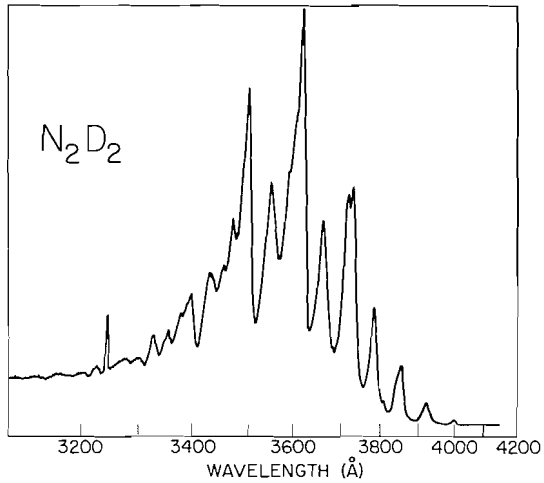

FIG. 3. Microdensitometer trace of N_2D_2 spectrum. Vertical scale is arbitrary.

The bands in both spectra fall fairly obviously into three main progressions as shown, the first two about equally strong and the third rather weak. In Tables 1 and 2 are listed wavenumbers of the band centers, the vertical columns corresponding to the three main progressions. Wavenumber differences are tabulated and vibrational assignments presented. The only unusual feature is an apparent doubling of the higher members of the third progression in the N_2D_2 spectrum.[2] The data show considerable scatter, particularly in the weaker third progressions, which can be attributed to the uncertainty in locating the centers of the rather broad and often overlapping absorption bands.

Vibrational Analysis

The six fundamental vibrations of *trans* diimide are:[3] $\nu_1(a_g)$ N—H stretching, $\nu_2(a_g)$ H—N=N bending, $\nu_3(a_g)$ N=N stretching, $\nu_4(a_u)$ torsion, $\nu_5(b_u)$ N—H stretching, and $\nu_6(b_u)$ H—N=N bending. The frequencies for these vibrations in the ground state are summarized by Bondybey and Nibler (5).

The main progressions in the near ultraviolet spectrum are assigned to the H—N=N symmetric bending mode ν_2' in the excited state on the basis of the magnitudes of the vibrational

[2]A possible cause of this splitting is the near coincidence of the sum of the ν_2' and ν_3' frequencies (Table 3) with that of ν_1' the N—D stretching vibration.

[3]There is still some uncertainty concerning the assignments for ν_2 and ν_3 in the ground state, so the numberings of these vibrations are provisional.

TABLE 1. Wavenumbers of band centers and vibrational assignments for the 3000–4300 Å band system of N_2H_2*

v_2' \ v_3'	0		1		2
0	—		—		[23 622]
1	—		23 296	(1616)	24 912
			(1137)		(1061)
2	[22 794]		24 433	(1540)	25 973
			(1096)		(1012)
3	23 840	(1689)	25 529	(1456)	26 985
	(1233)		(1102)		(1208)
4	25 073	(1558)	26 631	(1562)	28 193
	(1189)		(1170)		(1160)
5	26 262	(1539)	27 801	(1552)	29 353†
	(1193)		(1191)		(1194)
6	27 455†	(1537)	28 992†	(1555)	30 547
	(1185)		(1168)		(1146)
7	28 640	(1520)	30 160	(1533)	31 693
	(1166)		(1147)		(1166)
8	29 806	(1501)	31 307	(1552)	32 859
	(1119)		(1112)		
9	30 925	(1494)	32 419		—
	(1108)				
10	32 033		—		—
Average differences	(1170)	(1548)	(1140)	(1546)	(1135)

*All wavenumbers in cm^{-1} *in vacuo*. Wavenumber differences are given in parentheses. v_2' values are taken from Fig. 4, as discussed in text. Values in square brackets are less certain.
†Denotes strongest band in each main progression.

frequencies and the deuterium isotope effect. In a similar manner the short progressions are assigned to the N=N stretching mode ν_3'. In the short progressions the intensity distribution indicates quite clearly that the first bands in each progression can be assigned the quantum number $v_3' = 0$. In the longer progressions the numbering is less certain, and depends on the nature of the electronic transition which is discussed below. The lengths of the progressions indicate that there is a fairly large change in the H—N=N angle, but a small change in the N=N bond length, between the ground and excited states. The values of the vibrational frequencies in the two states, and also in the upper state of the vacuum ultraviolet bands, are summarized in Table 3.

It appears that no transitions from vibrationally excited levels of the ground-state are observed in the present spectra. Such "hot bands" might be expected through favorable Franck–Condon factors arising from the large change in geometry, but the magnitude of the ν_2 quanta apparently makes the Boltzman term prohibitive at room temperature (the spectrum of N_2H_2 was also obtained at 160 °C and was essentially unchanged from that at 25 °C). There are no bands of significant intensity unaccounted for, which also appears to rule out excitation of any vibrational modes in the upper state other than ν_2' and ν_3'.

Nature of the Electronic Transition

According to the simple molecular-orbital considerations of Walsh (7) the electron configuration and term type for the ground state of *trans* diimide should be

$$\cdots \sigma_{N-H}(2a_g)^2 \cdot \sigma_{N-H}(2b_u)^2 \cdot \sigma_{N-N}(3a_g)^2 \cdot n_-(3b_u)^2 \cdot \pi(1a_u)^2 \cdot n_+(4a_g)^2,\ ^1A_g$$

Walsh's prediction of the relative energies of the three highest orbitals for the observed H—N=N angle of 107° is not clear, but more recent calculations (8–10) show that the n_+ orbital is undoubtedly the highest, with the n_- orbital probably lying at a lower energy than the π orbital. The lowest excited singlet state should then be

$$\cdots n_-(3b_u)^2 \cdot \pi(1a_u)^2 \cdot n_+(4a_g) \cdot \pi^*(1b_g),\ ^1B_g$$

The first singlet–singlet transition, $\pi^* \leftarrow n_+$, will be of the type $^1B_g \leftarrow {}^1A_g$, and should lead to a

Can. J. Chem. Downloaded from www.nrcresearchpress.com by 210.87.254.6 on 09/05/12
For personal use only.

TABLE 2. Wavenumbers and vibrational assignments for the 3200–4300 Å band system of N_2D_2*

v_2' \ v_3'	0		1		2
0	—		—		—
1	—		—		—
2	—		23 601		—
			(976)		
3	23 168	(1409)	24 577	(1368)	25 945
	(895)		(891)		(911)
4	24 063	(1405)	25 468	(1388)	26 856
	(881)		(897)		(993)
5	24 944	(1421)	26 365	(1483)	{27 816 {27 881
	(913)		(897)		(990)
6	25 857	(1405)	27 262	(1577)	{28 777 {28 900
	(875)		(902)		(856)
7	26 732	(1432)	28 164†	(1530)	{29 593 {29 796
	(904)		(945)		(729)
8	27 636†	(1473)	29 109	(1314)	{30 368 {30 478
	(902)		(914)		
9	28 538	(1485)	30 023		—
	(871)		(851)		
10	29 409	(1465)	30 874		—
	(842)				
11	30 251		—		—
	(832)				
12	31 083		—		—
Average differences	(880)	(1437)	(909)	(1443)	(896)

*All wavenumbers in cm^{-1} *in vacuo*. Wavenumber differences are given in parentheses. v_2' values are taken from Fig. 4, as discussed in text.
†Denotes strongest band in each main progression.

TABLE 3. Vibration frequencies for diimide (cm^{-1})

	ν_2 (symmetric H—N=N bending mode)	ν_3 (symmetric N=N stretching mode)	Reference
Upper state, near-u.v. transition, (gas phase)			
N_2H_2	1215 ± 15	1550 ± 20	
N_2D_2	910 ± 10	1440 ± 20	Present work
Ground state (low-temperature matrices)			
N_2H_2	1583	1529	Bondybey and
N_2D_2	1215	1539	Nibler (5)
Upper state, vacuum-u.v. transition, (gas phase)			
N_2H_2	1192	1874	
N_2D_2	955	—	Trombetti (2)

Can. J. Chem. Downloaded from www.nrcresearchpress.com by 210.87.254.6 on 09/05/12
For personal use only.

Can. J. Chem. Downloaded from www.nrcresearchpress.com by 210.87.254.6 on 09/05/12
For personal use only.

large increase in the H—N=N bond angle and a small increase in the N=N bond length (7). The transition is forbidden by the electric dipole selection rules, but can become active by vibronic mixing with allowed transitions. Alternatively, it is permitted as a magnetic dipole transition; magnetic dipole bands have been seen in the near-ultraviolet spectrum of formaldehyde under similar conditions of path length and pressure, although they were considerably weaker than the vibronically induced bands (11, 12). Detailed calculations by Robin, Hart, and Kuebler (8) and by Ditchfield, Del Bene, and Pople (9) confirm that the first singlet–singlet transition should be $\pi^* \leftarrow n_+$, and predict energies of 3.92 and 3.37 eV respectively. Robin *et al.* also predicted that the next singlet–singlet transitions, $\pi^* \leftarrow \pi$ and $\pi^* \leftarrow n_-$, should lie higher than 7 eV, and there seems little doubt that the near ultraviolet bands described in the present paper arise from the $\pi^* \leftarrow n_+$, $^1B_g \leftarrow {}^1A_g$ transition of *trans* diimide.[4]

Geometry of the Excited State

In the absence of rotational fine structure, the only deductions which can be made concerning the geometry of the excited state must be derived from the magnitudes of the vibrational frequencies and from Franck–Condon considerations. For N_2H_2 and N_2D_2 the N=N stretching frequencies in the excited state are 1550 and 1440 cm^{-1} respectively; the isotope shift is similar to that for the C=C stretching frequencies of C_2H_2 and C_2D_2 in the *trans* bent excited state, 1385 and 1299 cm^{-1} respectively (14). Comparison with the ground-state N=N stretching frequencies (5) for N_2H_2 (1529 cm^{-1}) and N_2D_2 (1539 cm^{-1}) is complicated by an anomalous isotope effect,[5] and it can be said only that the frequency in the excited state is similar to that in the ground state. The $v_3' = 0$ and $v_3' = 1$ progressions are of comparable intensity, while that for $v_3' = 2$ is considerably weaker[6] and the $v_3' = 3$ progression is not observed. From Franck–Condon considerations, using a simplistic diatomic model and the convenient tables of Bates (15), a change in the N=N bond length of about 0.05 Å may be estimated, in reasonable agreement with the increase predicted in a recent *ab initio* calculation by Baird and Swenson (10).

The length and intensity distribution of the main progressions point to a large change in the H—N=N angle, presumably an increase, as predicted (7, 10), since a large decrease from the ground-state value of 107° seems unlikely. To determine the magnitude of the change it is first necessary to establish the origins of these progressions. If the transition is allowed (*e.g.*, as a magnetic dipole transition), this is done by a simple extrapolation of the $v_3' = 0$ progressions for N_2H_2 and N_2D_2 to near convergence (shown in Fig. 4), so that the difference in the frequencies of the 0—0 bands corresponds to the net difference in the zero-point energies. The 0—0 band for the deuterated species usually lies at a slightly higher frequency; for example, in the first ultraviolet band system of acetylene (14) $\nu_{0,0}'(C_2D_2) - \nu_{0,0}'(C_2H_2) = 62\ cm^{-1}$. On this basis the values of v_2' shown in Fig. 4 were obtained. The relative positions of the plots for N_2H_2 and N_2D_2 in Fig. 4 are somewhat arbitrary, since the N_2D_2 data could be shifted by one or more quantum numbers to the left or right relative to the N_2H_2 data, leading to other near convergences at higher or lower frequencies. The former is impossible since it would lead to negative quantum numbers for some of the observed bands; the latter (shown as the dashed line in Fig. 4) would lead to quantum numbers larger by 3 and 4 for N_2H_2 and N_2D_2 respectively, which seems unlikely.

If the transition is electronically forbidden but

[4]It should be noted that the corresponding transition in *cis* diimide (point group C_{2v}) is $^1B_1 \leftarrow {}^1A_1$, and is allowed by the electronic selection rules (8). The *trans* isomer is known to be the predominant form of diimide as prepared in the present experiments and there is no evidence for the presence of even low concentrations of the *cis* isomer in the gas phase. The close similarity of the extinction coefficient of diimide in the near ultraviolet to that of *trans* azomethane (4) also suggests that *trans* diimide is the absorbing species. However, we cannot rigorously exclude the possibility that a small fraction of the *cis* isomer, with an extinction coefficient 10 or 20 times that of the *trans* isomer (*cf.* azomethane (13)), is responsible for the bands.

[5]This has been explained in terms of an interaction between v_2 and v_3 (5), but may reflect an error in one or both of the assignments.

[6]Relative intensities of the 3 progressions should be compared at the strongest bands in each progression, as the relative intensities appear to depend on the value of v_2'.

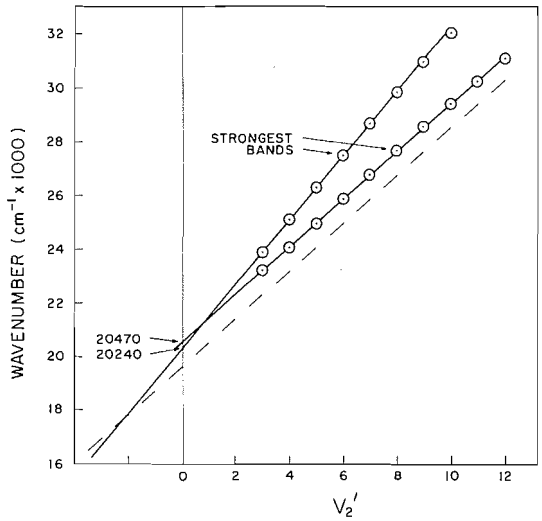

FIG. 4. Extrapolation of first ν_2' progressions in N_2H_2 and N_2D_2 spectra, to establish vibrational quantum numbers and positions of origins. The dashed line shows an alternative plot of the N_2D_2 data.

permitted by the vibronic selection rules, the $v_3' = 0$ progressions in N_2H_2 and N_2D_2 must be extrapolated to their respective vibronic origins. The separation, then, between the $v_2'=0$ bands must take into account not only the difference in the zero-point energies but also the isotope shift in the $v' = 1$ level of the inducing mode. For the $\pi^* \leftarrow n_+$, $^1B_g \leftarrow {}^1A_g$ transition of *trans* diimide, the possible inducing modes are $\nu_4'(a_u)$, $\nu_5'(b_u)$, and $\nu_6'(b_u)$. For ν_5' and ν_6', isotope shifts of about 800 and 300 cm^{-1} can be estimated. The frequency of the torsional mode, ν_4', is not known but the isotope shift should probably not exceed 300 cm^{-1} and may well be very much less than this. If ν_5' is the inducing mode, reasonable vibronic origins are obtained if the quantum numbers for N_2H_2 shown in Fig. 4 are retained while those for N_2D_2 are increased by one, as shown by the dashed line. If ν_6' is the inducing mode, a decrease of one in the quantum numbers for both species appears most reasonable: a less likely possibility is an increase of one and two respectively for N_2H_2 and N_2D_2. If ν_4' is the inducing mode, for an isotope shift of 300 cm^{-1}, a decrease of one in the quantum numbers for both species is reasonable while, if the torsional frequency is low, the numbers remain unchanged from those shown in Fig. 4.

From the discussion above it is seen that there is a probable uncertainty in the v_2' numbering for N_2H_2 of ± 1 and that the origin (0—0 band or vibronic origin) lies at 20 240 $\pm$ 1 200 cm^{-1}. Thus in the strongest band of the $v_3' = 0$ progression which lies near 27 450 cm^{-1}, there is a vibrational excitation ΔE in the ν_2' mode of the upper state of 7 200 $\pm$ 1 200 cm^{-1}. Assuming that the strongest band corresponds to a transition vertical with respect to the H—N=N angle, ΔE can be equated to $2 \times \frac{1}{2} f_{HNN} (\Delta\theta)^2$, where f_{HNN} is the bending force constant in the excited state and $\Delta\theta$ is the difference in the H—N=N angle between the ground and excited states. Using the equations given by Kohlrausch (16) for the a_g vibrations of a *trans* HAAH molecule, and taking $\nu_1' = 3130\ cm^{-1}$ (assumed), $\nu_2' = 1215\ cm^{-1}$, and $\nu_3' = 1550\ cm^{-1}$, a value for f_{HNN} can be obtained. In the initial calculation the geometrical parameters in the excited state were assumed to be the same as for the ground state, *viz.* $r_{N-H} = 1.028$ Å, $r_{N=N} = 1.252$ Å, H—N=N = 106° 51′ (3), and a value for $\Delta\theta$ obtained. The value for the H—N=N angle in the excited state was then revised and the calculation repeated until no further change was obtained. In this way, a value of $\Delta\theta = 25 \pm 2°$ was determined, corresponding to an H—N=N angle in the excited state of 132 $\pm$ 2°. The Franck–Condon calculation was repeated for N_2D_2 and a similar change in angle was obtained. Calculations were also made assuming a *cis* configuration and gave a value of $\Delta\theta = 22 \pm 2°$. These can be compared to the recent calculations of Baird and Swenson (10) who predicted values for $\Delta\theta$ of 12 and 18°, and H—N=N angles of 121 and 133°, for the first excited singlet states of *trans* and *cis* diimide, respectively.

Finally, it must be considered whether diimide in the excited state retains the planar configuration of the ground state, as has been tacitly assumed in the foregoing discussion, or becomes non-planar. Both ethylene and formaldehyde become non-planar in their first excited singlet states (11, 17, 18), and for reasons discussed by Walsh (7) one might expect a similar tendency in isoelectronic diimide. If the excited state of diimide in the present system were non-planar, one would expect to observe progressions in the spectra corresponding to excitation of the ν_4' torsional vibration, but as noted earlier there are no unassigned bands of significant intensity. It

Can. J. Chem. Downloaded from www.nrcresearchpress.com by 210.87.254.6 on 09/05/12
For personal use only.

might be argued that the long progressions assigned to ν_2' should in fact be assigned to ν_4', but then the absence of bending progressions must be explained; the frequencies also appear high for a molecule in which the double bond is weakened sufficiently to permit a twisted structure (*cf.* ethylene (17)). The lack of any features in the spectra which can reasonably be attributed to excitation of the torsional vibration suggests that the excited state is planar. Baird and Swenson have in fact predicted a planar structure (10), but with a rather flat potential curve corresponding to a low torsional frequency. If the torsional frequency is very low, it is possible that the bands involving the torsional vibration might be obscured in the rather broad band structures of the present spectrum.

Concluding Remarks

While there is some uncertainty in the precise interpretation of the near-ultraviolet spectrum of diimide, the main features are clear. The assignment to the $^1B_g \leftarrow {}^1A_g$ ($\pi^* \leftarrow n_+$) transition of *trans* diimide appears reasonably certain, and the transition is probably induced through vibronic interaction. There is a large increase (25 $\pm$ 2°) in the H—N=N angle and a small change ($\sim$0.05 Å) in the N=N bond length in the transition, and the excited state probably remains planar although this is less sure.

The diffuseness of the N_2H_2 and N_2D_2 spectra indicates that the individual rotational lines are broad, probably >1 cm^{-1} in width, and that the lifetime in the excited state is very short, $<5 \times 10^{-12}$ s. It is not clear whether this can be attributed to a true predissociation or to a rapid intersystem crossing, perhaps to the $\pi^* \leftarrow n_+$ triplet state; there is some evidence for the latter process in the photochemistry of the azoalkanes (19). If a true predissociation is involved, the dissociation energy must be less than that of the first observed band at 22 794 cm^{-1}, *i.e.* $<$65 kcal/mol or 2.83 eV. The photodissociation process to which this limit applies is not known; dissociation to H + N_2H or 2H + N_2 could be expected by analogy with the azoalkanes, but a molecular decomposition (to N_2 + H_2) might well occur in diimide as it does in formaldehyde.

We are indebted to M. Barnett and W. Goetz for assistance with the spectroscopic work. We are also grateful to Dr. A. Trombetti and Dr. N. C. Baird for communicating results to us prior to publication.

1. E. J. Blau and B. F. Hochheimer. J. Chem. Phys. **41**, 1174 (1964).
2. A. Trombetti. Can. J. Phys. **46**, 1005 (1968).
3. M. Carlotti, J. W. C. Johns, and A. Trombetti. Can. J. Phys. **52**, 340 (1974).
4. C. Willis and R. A. Back. Can. J. Chem. **51**, 3605 (1973).
5. V. E. Bondybey and J. W. Nibler. J. Chem. Phys. **58**, 2125 (1973).
6. K. Rosengren and G. C. Pimentel. J. Chem. Phys. **43**, 507 (1965).
7. A. D. Walsh. J. Chem. Soc. 2288 (1953).
8. M. B. Robin, R. R. Hart, and N. A. Kuebler. J. Am. Chem. Soc. **89**, 1564 (1967).
9. R. Ditchfield, J. E. Del Bene, and J. A. Pople. J. Am. Chem. Soc. **94**, 703 (1972).
10. N. C. Baird and J. R. Swenson. Can. J. Chem. **51**, 3097 (1973).
11. J. H. Callomon and K. K. Innes. J. Mol. Spectrosc. **10**, 166 (1963).
12. J. R. Lombardi, D. E. Freeman, and W. Klemperer. J. Chem. Phys. **46**, 2746 (1967).
13. R. F. Hutton and C. Steel. J. Am. Chem. Soc. **86**, 745 (1964).
14. C. K. Ingold and G. W. King. J. Chem. Soc. 2740 (1953); 2746 (1953); G. Herzberg. Electronic spectra of polyatomic molecules. D. Van Nostrand. New York. 1966. p. 517.
15. D. R. Bates. Roy. Astronomical Soc. Monthly Notices, **112**, 614 (1952).
16. K. W. F. Kohlrausch. Der Smekal-Raman effekt. Julius Springer, Berlin. 1938. pp. 68, 69.
17. P. G. Wilkinson and R. S. Mulliken. J. Chem. Phys. **23**, 1895 (1955).
18. J. C. D. Brand. J. Chem. Soc. 858 (1956); G. W. Robinson. Can. J. Phys. **34**, 699 (1956); A. D. Walsh. J. Chem. Soc. 2306 (1953).
19. I. I. Abram, G. S. Milne, B. S. Solomon, and C. Steel. J. Am. Chem. Soc. **91**, 1220 (1969).

Can. J. Chem. Downloaded from www.nrcresearchpress.com by 210.87.254.6 on 09/05/12
For personal use only.

Influence of Lewis Acids on the Diels–Alder Reaction. VII. The Reaction of Furan with Ethyl Propiolate[1]

A. W. McCulloch, D. G. Smith, and A. G. McInnes

Atlantic Regional Laboratory, National Research Council of Canada, Halifax, Nova Scotia B3H 3Z1

Received October 3, 1973

Reaction of furan and ethyl propiolate at 130° affords a low yield of 2,6-dicarbethoxy-9-oxatetracyclo[3.2.1.1.^{3,8}0^{2,4}]non-6-ene (**4**). This structure was confirmed by ^{1}H and ^{13}C n.m.r. spectroscopy. In the presence of $AlCl_3$ the same addends give only a mixture of the Diels–Alder *endo–endo* **10** and *endo–exo* **11** diadducts. Isomer **11** is decomposed by $AlCl_3$, the rate of decomposition, and therefore the product ratio **10**:**11**, being as expected dependent on time, temperature, and reactant concentrations.

La réaction du furanne avec le propiolate d'éthyle à 130° conduit avec un mauvais rendement au dicarbéthoxy-2,6 oxa-9 tetracyclo[3.2.1.1^{3,8}0^{2,4}] nonène-6 (**4**). La structure de ce composé est confirmée par spectroscopie r.m.n. du ^{1}H et du ^{13}C. En présence du $AlCl_3$ les deux réactifs conduisent à un mélange des composés de double addition de Diels–Alder à savoir les produits *endo–endo* (**10**) et *endo–exo* (**11**). L'isomère **11** se décompose en présence de $AlCl_3$; le taux de décomposition et donc le rapport des produits **10**:**11** varie en fonction du temps de la température et de la concentration des réactifs. [Traduit par le journal]

Can. J. Chem., **52**, 1013 (1974)

Introduction

In a previous communication we discussed the reaction of furan with dimethyl acetylenedicarboxylate (DMAD) (1). Studies on the corresponding reaction of furan with ethyl propiolate (EP), described in this article, reveal significant differences in the two reactions.

Results and Discussion

Thermal Reaction

The uncatalyzed combination of furan with EP is very slow: no reaction was observed in 6 months at 25°. The only recognizable product isolated after 20 h reaction at 130° was 2,6-dicarbethoxy-9-oxatetracyclo[3.2.1.1.^{3,8}0^{2,4}]non-6-ene (**4**) (9%). No Diels–Alder addition products (**1**, **2**, or **3**) were detected. This is in direct

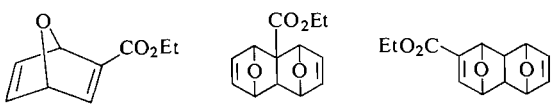

1 2 3

contrast to the thermal reaction of furan and DMAD which under the same conditions affords a monoadduct, three diadducts, and four triadducts, but no product of type **4** (1).

Formation of **4** would be expected to involve homoconjugate addition of EP to **1**. However, our studies on the analogous compound **5**, a product of the thermal reaction of 2,5-dimethylfuran and EP, indicate that this compound does not arise by direct addition, but is formed chiefly by dimerization of adduct **6** and subsequent retrocleavage of 2,5-dimethylfuran (Scheme 1) (2). The same mechanism may apply to the formation of **4** from **1**, as well as to the formation of compound **7** which was isolated by Solo *et al.* from the reaction of methyl propiolate with methyl bicyclo[2.2.1]heptadiene-2-carboxylate at 107° (3).

$AlCl_3$-promoted Reaction

The reaction of furan and DMAD in the presence of $AlCl_3$ gave essentially two products, the monoadduct **8** and *endo–exo* diadduct **9** (1).

In contrast, reaction of furan and EP under the same conditions afforded a *mixture* of the *endo–endo* diadduct **10** and *endo–exo* diadduct **11**, and *no* monoadduct **1** was detected. Compounds **10** and **11** are formed by Diels–Alder additions of furan to the activated double bond of **1**, the steric course of both additions being controlled by the dienophile (1, 4, 5).

The product ratio **10**:**11** is dependent on the reaction temperature and reactant concentrations (Table 1). This can be rationalized in terms of the unexpected instability of the *endo–exo*

[1]NRCC No. 13765.

Can. J. Chem. Downloaded from www.nrcresearchpress.com by 210.87.254.6 on 09/05/12
For personal use only.

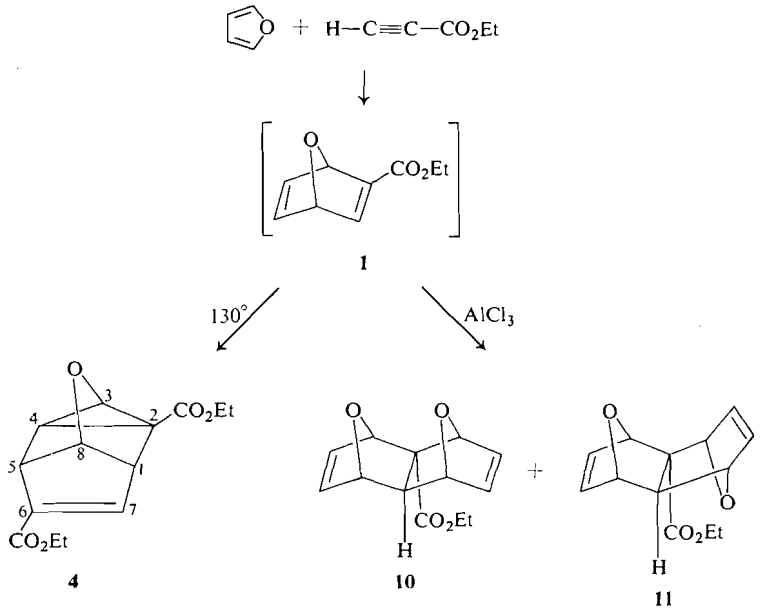

product **11** towards the Lewis acid (see Experimental).

Since **11** is labile towards $AlCl_3$ it follows that the product ratio **10**:**11** will increase under any conditions where increasing concentrations of the Lewis acid are present. Use of an excess of EP, which forms a complex with $AlCl_3$, leads to a reduction in the concentration of $AlCl_3$ available to catalyze the decomposition. Under such conditions the ratio **10**:**11** decreases dramatically and indeed isomer **11** can be made to predominate.

The rate of decomposition is markedly enhanced by a relatively small increase in temperature. The ratio **10**:**11** is of course also time dependent (see Experimental). Use of a high concentration of the diene has little effect on the product ratio, indicating that it does not compete favorably for $AlCl_3$.

The reason for the contrasting stabilities of **10** and **11** is not clear. Perhaps the proximity of the bridge and ester carbonyl oxygen atoms in **11** favors the formation of a complex with the ester carbonyl which could initiate the decomposition pathway shown in Scheme 2.[2] Such assistance to complex formation would not occur with **10**. In the case of **9**, although the complex might be favored, retrogression would be inhibited by the electron-withdrawing substituent at the second ring-juncture position. In accord with this, both **9** and **10** are quite stable to $AlCl_3$ under the conditions used.

The isolation of **9** as essentially the only diadduct from the catalyzed reaction of furan and DMAD was in fact attributed to the formation of a stable diadduct–$AlCl_3$ complex which prevented retrogression and equilibration (1). Although this is not the case in the furan–EP reaction, the *endo–exo* isomer **11** is still the kinetically favored product. Catalyzed decomposition of **11** and recombination of the addends (furan and **1**) may lead to the more stable *endo–endo* isomer **10**.

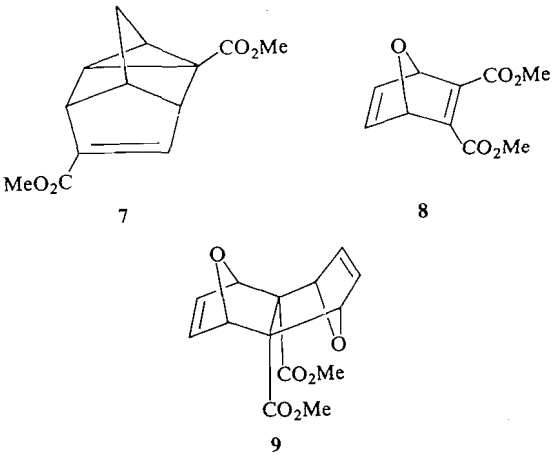

[2]The resultant diene is of course susceptible to polymerization: the monoadduct can again react as a dienophile to give **10** or **11**.

Can. J. Chem. Downloaded from www.nrcresearchpress.com by 210.87.254.6 on 09/05/12
For personal use only.

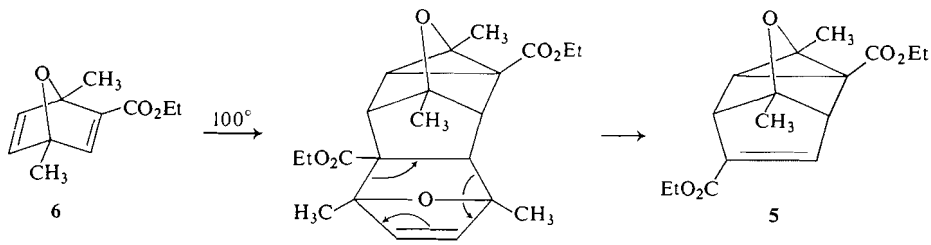

SCHEME 1

TABLE 1. Effect of temperature and reactant concentrations*

Reactant ratios furan–EP–$AlCl_3$	Temperature (°C)	Overall yield (%)	Product ratio† **10**:**11**
Reaction mixture 0.2 M in EP‡			
2:1:1	−10	19	1.8
2:1:1	0	31	2.0
2:1:1	12	33	2.3
2:1:1	27	27	6.7
1:1:1	0	24	1.9
2:1:1	0	31	2.0
3:1:1	0	31	1.6
2:1:0.5	0	20	1.1
2:1:1	0	31	2.0
2:1:1.5	0	30	2.4
2:1:2	0	22	2.6
Reaction mixture 0.2 M in furan§			
1:1:1	0	48	1.9
1:2:1	0	62	0.9
1:5:1	0	53	0.5

*All reactions were carried out in CH_2Cl_2 and were terminated after 30 min.
†Determined from integrated intensities of p.m.r. signals for ring-juncture hydrogens.
‡Yields based on EP.
§Yields based on furan.

A distinguishing feature of the reaction (thermal or $AlCl_3$ catalyzed) between furan and EP is the failure to isolate the adduct **1**. This is due in part to the lesser reactivity of EP as a dienophile compared to DMAD (6). A second contributing factor is the enhanced reactivity of **1**, which is a substituted acrylate, and therefore a more powerful dienophile than the corresponding maleate **8** (6).

Nuclear Magnetic Resonance Spectroscopy

*Diadducts **10** and **11***

The parameters (Table 2), confirmed by spectral simulation, are entirely consistent with the assigned structures. The two isomers could be differentiated on the basis of symmetry considerations and the multiplicity of the signal for the ring-juncture hydrogen. Absence of coupling between the latter and the adjacent bridgehead hydrogens is observed when the ring-juncture proton is *endo* (1, 7, 8). Irradiation of H_4 and H_5 in **10** produced a 13% enhancement (nuclear Overhauser effect) in the signal for H_{4a} and thus allowed unambiguous assignment of the chemical shift of these protons.

*Compound **4***

The 100 MHz spectrum of **4** (Table 3) showed, as expected, resonances for two carbethoxyl groups and for six single hydrogens. Multiple irradiation experiments established the coupling parameters. The shifts of four of the hydrogens (2.34, 2.97, 3.12, and 7.05 δ) and the couplings between them are very similar to the corresponding parameters (2.30, 2.97, 3.02, and 7.09 δ) for the four ring hydrogens of the 3,8-

Can. J. Chem. Downloaded from www.nrcresearchpress.com by 210.87.254.6 on 09/05/12
For personal use only.

TABLE 2. Proton magnetic resonance parameters for **10** and **11** (60 MHz, solvent $CDCl_3$)

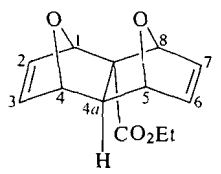

10

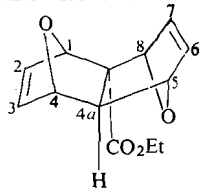

11

Parameter*	Value	Parameter*	Value	Parameter	Value
$\nu_1 = \nu_8$	11.0	ν_1	8.9	ν_8	111.7
$\nu_2 = \nu_7$	86.7	ν_2	112.7	ν_7	201.9
$\nu_3 = \nu_6$	105.6	ν_3	125.6	ν_6	204.5
$\nu_4 = \nu_5$	0.0† (δ 4.87)	ν_4	0.0† (δ 4.45)	ν_5	109.9
ν_{4a}	(δ 2.36)	ν_{4a}	(δ 3.05)	ν_{4a}	0.0† (δ 3.05)
$J_{1,2} = J_{7,8}$	1.6	$J_{1,2}$	1.6	$J_{7,8}$	1.9
$J_{1,3} = J_{6,8}$	0.0	$J_{1,3}$	0.0	$J_{6,8}$	0.2
$J_{1,4} = J_{5,8}$	0.8	$J_{1,4}$	0.7	$J_{5,8}$	0.8
				$J_{8,4a}$	0.0
$J_{2,3} = J_{6,7}$	5.8	$J_{2,3}$	5.7	$J_{6,7}$	5.8
$J_{2,4} = J_{5,7}$	0.0	$J_{2,4}$	0.0	$J_{5,7}$	0.4
				$J_{7,4a}$	0.1
$J_{3,4} = J_{5,6}$	1.7	$J_{3,4}$	1.7	$J_{5,6}$	1.5
				$J_{6,4a}$	0.1
				$J_{5,4a}$	4.8
$-OCH_2CH_3(\delta)$	4.07(q)	$-OCH_2CH_3(\delta)$	4.18(q)		
$-OCH_2CH_3(\delta)$	1.22(t)	$-OCH_2CH_3(\delta)$	1.28(t)		

*In these cases the spectra were analyzed as four-spin ($H_1H_2H_3H_4$) systems. The couplings $J_{1,4a}$ and $J_{4,4a}$ were of the order of 0.2 Hz.
†For computer purposes the chemical shift of the highest field proton (or protons when chemically equivalent) was empirically given a value of 0.0 Hz and all others were measured relative to it.

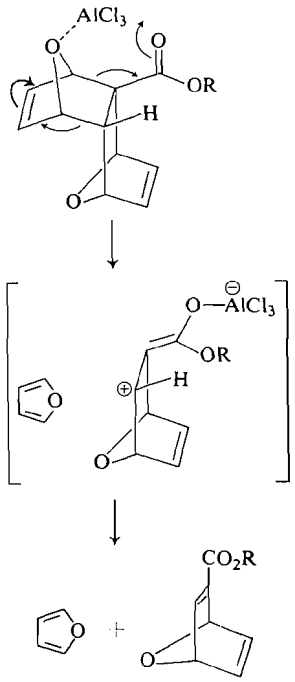

SCHEME 2

dimethyl analog **5** (2). The p.m.r. data are consistent with those reported for structurally related compounds (3, 9, 10).

Carbon-13 n.m.r. spectroscopy was used to confirm the structure of **4**, and the availability of **5** for comparison purposes simplified spectral assignments (Table 4). The carbonyl, olefinic, and ethoxy carbons were readily assigned. The high-field shifts (11*a*, 12–14) and high $J_{^{13}C-H}$ values (11*b*, 12) characteristic of cyclopropyl ring carbons facilitated unequivocal assignment of C-2, -3, and -4. The data for the remaining carbons were consistent with those obtained for similarly located carbons in other polycyclic systems (11*b*, 14).

Experimental

Proton magnetic resonance spectra were recorded on a Varian A-60A (V-6058 A spin-decoupler) spectrometer and a Varian HA-100 spectrometer equipped with a Spectrosystem 100. The tetramethylsilane resonance was used to provide the field-frequency lock for the HA-100.

^{13}C n.m.r. spectra at 25.16 MHz were obtained on a Varian XL-100-15 spectrometer equipped with a VT-100 data system (16 K). Samples (500 mg) in benzene-d_6

Can. J. Chem. Downloaded from www.nrcresearchpress.com by 210.87.254.6 on 09/05/12
For personal use only.

TABLE 3. Proton magnetic resonance (100 MHz; solvent benzene-d_6) parameters for **4**

Chemical shifts		Coupling constants			
Hydrogens	δ	J_{pq}	Value (Hz)	J_{pq}	Value (Hz)
H-1	2.97	$J_{1,3}$	<0.1	$J_{3,8}$	1.1
H-3	4.88	$J_{1,4}$	<0.3	$J_{4,5}$	2.1
H-4	2.34	$J_{1,5}$	0.9	$J_{4,7}$	0.0
H-5	3.12	$J_{1,7}$	3.5	$J_{4,8}$	0.6
H-7	7.05	$J_{1,8}$	2.6	$J_{5,7}$	1.1
H-8	4.01	$J_{3,4}$	3.7	$J_{5,8}$	2.8
OCH_2CH_3	3.90(q)	$J_{3,5}$	<0.2	$J_{7,8}$	0.0
	4.03(q)	$J_{3,7}$	0.0		
OCH_2CH_3	0.93(t)				
	1.06(t)				

TABLE 4. ^{13}C n.m.r. data for **4** and **5** (25.16 MHz; solvent benzene-d_6)

	4		5	
Carbons	δ_C (TMS)† (p.p.m.)	$^1J_{C-H}$* (Hz)	δ_C (TMS)† (p.p.m.)	$^1J_{C-H}$* (Hz)
CH_3	—	—	11.4 (q)	127.2
CH_3	—	—	12.7 (q)	128.3
$-OCH_2CH_3$	14.1 (q)	127.1	14.2 (q)	126.9
$-OCH_2CH_3$	14.2 (q)	127.1	14.2 (q)	126.9
C-4	34.8 (d)	184.9	41.9 (d)	181.5
C-2	41.4 (s)	—	47.6 (s)	—
C-5 and	48.8 (d)	152.8	54.4 (d)	152.3
C-1	50.1 (d)	152.0	55.8 (d)	151.9
$-OCH_2CH_3$	60.3 (t)	147.3	60.3 (t)	147.7
$-OCH_2CH_3$	60.5 (t)	147.3	60.4 (t)	147.7
C-3	71.3 (d)	204.2	78.1 (s)	—
C-8	91.4 (d)	170.0	99.2 (s)	—
C-6	138.6 (s)	—	139.9 (s)	—
C-7	142.5 (d)	175.7	143.7 (d)	174.8
EtO—CO—C=CH	163.5 (s)	—	163.9 (s)	—
—C—CO—OEt	169.6 (s)	—	169.7 (s)	—

*The coupling constants are judged to have an accuracy of ±0.7 Hz.
†s = singlet, d = doublet, t = triplet, q = quartet.

were contained in 12 mm tubes. The deuterium resonance from the solvent was used for the field-frequency lock. Spectral width was 5120 Hz, with an acquisition time of 0.8 s, and using an 8 K transform. In addition to proton noise decoupled spectra, off resonance single frequency decoupled spectra were recorded to assist in signal assignments. Coupling constants ($J_{^{13}C-^1H}$) were measured from high resolution spectra enhanced by gated noise decoupling.

The i.r. absorptions were measured on a Perkin–Elmer 521 spectrometer, and the mass spectra recorded using a Dupont-C.E.C. 21-491 instrument. Chromatographic separations were carried out on Mallinckrodt silicic acid (100–150 mesh).

Reaction of Furan with EP

Thermal Reaction

(*i*) Equimolar amounts of furan and EP contained in a sealed n.m.r. tube were allowed to stand at room temperature. Monitoring by p.m.r. revealed no reaction during 6 months.

(*ii*) A mixture of furan (21.0 g, 0.31 mol) and EP (10.0 g, 0.10 mol) was heated for 20 h in a Baskerville high pressure autoclave at 130°. The brown glassy product was chromatographed ($CHCl_3$). Early fractions yielded **4** as a pale yellow oil (2.28 g, 9%). Ion of highest mass at *m/e* 264 (14%) ($C_{14}H_{16}O_5$ requires 264); base peak at *m/e* 235; strong ions at *m/e* 219 (71%), 218 (81%), 207 (55%), 191 (45%), 190 (67%), 179 (38%), 163 (26%), 162 (48%), 145 (38%), 118 (33%), 105 (19%), and 89 (38%); ν_{max} (liquid film) 1725 cm^{-1}. Full n.m.r. data (^1H and ^{13}C) for **4** is detailed in Tables 3 and 4.

$AlCl_3$-promoted Reaction

(*i*) A solution containing $AlCl_3$ (5.32 g, 0.04 mol) and EP (7.84 g, 0.08 mol) in CH_2Cl_2 (140 ml) was cooled to

Can. J. Chem. Downloaded from www.nrcresearchpress.com by 210.87.254.6 on 09/05/12
For personal use only.

0°. To this was added a pre-cooled solution of furan (2.72 g, 0.04 mol) in CH_2Cl_2 (60 ml). The mixture was allowed to stand at 0° for 30 min and was then washed with water. Separation of the organic layer, followed by drying (Na_2SO_4), and evaporation of solvent gave a brown gummy residue which was chromatographed ($CHCl_3$).

Early fractions yielded a cream-colored solid (899 mg). Further purification by preparative t.l.c. on silica gel G (5% CH_3OH–$CHCl_3$) gave pure *endo–exo* diadduct **11** as a colorless solid (732 mg, 16% based on furan), m.p. 108–109°. Very weak parent ion (4%) at *m/e* 234 ($C_{13}H_{14}O_4$ requires 234), base peak at *m/e* 68 ($C_4H_4O^+$); strong ions at *m/e* 188 (17%), 160 (20%), 138 (30%), 121 (27%), 110 (33%), 95 (23%), 66 (25%); ν_{max} (CCl_4) 1740, 1708 cm^{-1}.

Intermediate fractions gave a colorless solid (0.239 g), shown by p.m.r. to be a 1:1 mixture of **10** and **11**. Later fractions afforded a cream-colored solid (1.11 g), p.m.r. of which showed it to be predominantly **10** (see below).

(*ii*) The reaction was repeated under the same conditions as in *i* above, but using $AlCl_3$ (2.66 g, 0.02 mol), EP (2.00 g, 0.02 mol), and furan (1.36 g, 0.02 mol) in CH_2Cl_2 (100 ml). In this case early chromatographic fractions (289 mg) were rich in **11**.

Later fractions were purified by preparative t.l.c. (see above) to give the *endo–endo* diadduct **10** as a colorless solid (399 mg, 17% based on furan), m.p. 165–166°. Weak molecular ion (15%) at *m/e* 234 ($C_{13}H_{14}O_4$ requires 234); base peak at *m/e* 68 ($C_4H_4O^+$); strong ions at *m/e* 166 (20%), 138 (23%), 121 (30%), 110 (30%), 66 (20%); ν_{max} (CCl_4) 1738, 1710 cm^{-1}.

(*iii*) *Effect of Reaction Temperature and Reactant Ratios.* The following standard procedure was adopted and used throughout. Solutions of furan and of EP-$AlCl_3$ complex were maintained for 10 min at the desired reaction temperature before mixing. Unit concentration (of either furan or EP) was taken as 0.2 *M*, and the concentrations of the other reactants adjusted accordingly. All reactions were allowed to proceed for 30 min and were then stopped by addition of water. The residue obtained by evaporation of solvent from the dried organic phase was in each case applied to a 20 × 8 in. t.l.c. plate coated with silica gel G (1.5 mm layer), which was then developed with 5% CH_3OH–$CHCl_3$. A broad band, R_f 4–8, which was thoroughly extracted with warm $CHCl_3$, gave a residue containing only diadducts **10** and **11**. The relative amounts of the two isomers were determined by measurement of the p.m.r. integrals for the ring-juncture hydrogens (for **10** a singlet at δ 2.36; for **11** a doublet at δ 3.05). Reactions were carried out using a furan–EP–$AlCl_3$ ratio of 2:1:1 at −10, 0, 10, and 27° to determine the effect of temperature. The effect of varying the reactant ratios was determined by reactions at 0°. The results (overall yields, product ratios) are detailed in Table 1.

(*iv*) *Effect of Reaction Time.* Standard reactions as in *iii* above employing a reactant ratio of 2:1:1 were carried out at 0 and 27°. Aliquots of each reaction mixture were withdrawn at regular intervals, worked up in the usual way and assayed for **10** and **11** by p.m.r. These showed that the ratio **10**:**11** increased slowly during the first 60 min reaction at 0° (from *ca.* 1.3 during the first 3 min to *ca.* 1.8 after 60 min). After 5 min reaction at 27° the ratio **10**:**11** was *ca.* 3:1, whereas only a small amount of **11** could be detected after 1 h.

*Stability of Compounds **10** and **11** Towards $AlCl_3$*

(*i*) A solution of **10** (234 mg, 1 mmol) in CH_2Cl_2 (5 ml) was added to a suspension of $AlCl_3$ (155 mg, 1.15 mmol). The mixture was allowed to stand with occasional shaking for 1 h at room temperature and was then washed with water. Separation of the organic layer, drying, and evaporation gave a pale yellow solid (230 mg); p.m.r. showed almost totally unreacted **10**.

(*ii*) Under identical conditions to *i* above isomer **11** yielded a brown gummy material; p.m.r. showed no recognizable products.

(*iii*) When the reaction described in *ii* above was carried out at 0°, the material recovered after 1 h was mainly unreacted **11**, although some decomposition had obviously occurred.

We wish to acknowledge the excellent technical assistance of Mrs. M. G. Flack. Our thanks are also due to Dr. J. A. Walter for measurement of the ^{13}C n.m.r. spectra.

1. A. W. McCulloch, D. G. Smith, and A. G. McInnes. Can. J. Chem. **51**, 4125 (1973).
2. A. W. McCulloch and A. G. McInnes. Unpublished work.
3. A. J. Solo, B. Singh, and J. N. Kapoor. Tetrahedron, **25**, 4579 (1969).
4. J. G. Martin and R. K. Hill. Chem. Rev. **61**, 537 (1961).
5. K. L. Williamson and Y.-F. Li Hsu. J. Am. Chem. Soc. **92**, 7385 (1970).
6. J. Sauer, H. Wiest, and A. Mielert. Chem. Ber. **97**, 3183 (1964).
7. F. A. L. Anet. Can. J. Chem. **39**, 789 (1961).
8. J. D. Slee and E. Legoff. J. Org. Chem. **35**, 3897 (1970).
9. T. Sasaki, S. Eguchi, M. Sugimoto, and F. Hibi. J. Org. Chem. **37**, 2317 (1972).
10. B. Franzus, S. Wu, W. C. Baird, and M. L. Scheinbaum. J. Org. Chem. **37**, 2759 (1972).
11. J. B. Stothers. Carbon-13 NMR spectroscopy. Academic Press, New York. 1972. (*a*) Chapt. 3. (*b*) Chapt. 10.
12. G. C. Levy and G. L. Nelson. Carbon-13 nuclear magnetic resonance for organic chemists. Wiley-Interscience, New York. 1972. Chapt. 3.
13. J. B. Grutzner, M. Jautelat, J. B. Dence, R. A. Smith, and J. D. Roberts. J. Am. Chem. Soc. **92**, 7107 (1970).
14. E. Lippmaa, T. Pehk, and J. Paasivirta. Org. Mag. Resonance, **5**, 277 (1973).

Can. J. Chem. Downloaded from www.nrcresearchpress.com by 210.87.254.6 on 09/05/12
For personal use only.

Chemistry of Aminochromes. Part XVIII. The Effects of p*H* and Substituents on some Aminochrome–Thiol Reactions[1,2]

W. S. POWELL[3,4,5] AND R. A. HEACOCK[6]

Chemistry Department, Dalhousie University, Halifax, Nova Scotia and Atlantic Regional Laboratory, National Research Council of Canada, Halifax, Nova Scotia

Received April 5, 1973[7]

Aminochromes react with thiols in the p*H* range *ca.* 3–4 to give mainly 4-thiosubstituted-5,6-dihydroxyindoles (or the corresponding 5,6-dihydroxyindolines) along with reduction products (5,6-dihydroxyindoles or 5,6-dihydroxyindolines). There is also some evidence, in this p*H* range, for the formation of an addition product involving one of the aminochrome carbonyl groups directly. Under somewhat less acidic conditions (p*H* 5–6), however, the major products formed initially are, in general, 3*a*-thiosubstituted-3*a*,4-dihydroaminochromes. These products, which are formed reversibly, are gradually replaced in the reaction mixture by the indolic products, which are formed irreversibly. The increased rate of formation of the 4-thiosubstituted-5,6-dihydroxyindoles at lower p*H*'s is probably due to the increased protonation of the C-6 carbonyl oxygen. The 3*a*-thiosubstituted-3*a*,4-dihydroaminochromes may be formed more readily at higher p*H*'s due to the increased ionization of the thiol.

Les aminochromes réagissent avec les thiols dans la région de p*H* 3 à 4 pour donner principalement les dihydroxy-5,6 indoles thiosubstitués en position 4 (ou les dihydroxy-5,6 indolines correspondant) ainsi que les produits de réduction (dihydroxy-5,6 indoles ou dihydroxy-5,6 indolines). Il y a aussi quelques évidences, dans cet intervalle de p*H*, pour la formation d'un produit d'addition concernant directement un des groupes carbonyles de l'aminochrome. Dans des conditions quelque peu moins acides (p*H* 5–6), les principaux produits formés initialement sont, en général, des thio-3*a* dihydro-3*a*,4 aminochromes. Ces produits, formés réversiblement, sont graduellement remplacés dans le mélange réactionnel par les produits indoliques, formés irréversiblement. La vitesse élevée de formation des dihydroxy-5,6 indoles thiosubstitués en position 4 à des p*H* plus bas, est probablement due à une augmentation de la protonation de l'oxygène du carboxyle C-6. Les thio-3*a* dihydro-3*a*,4 aminochromes peuvent être formés plus aisément à des p*H* plus élevés par une ionisation augmentée du thiol.

[Traduit par le journal]

Can. J. Chem., **52**, 1019 (1974)

Aminochromes have been shown to react with thiols to give three major types of products. Almost all aminochromes react with these reagents at intermediate p*H* values (p*H* 4–6) to give addition products (*i.e.* a 3*a*-thiosubstituted-3*a*,4-dihydroaminochrome (1, 2)). Aminochromes which have either a hydroxyl or an alkoxyl substituent in the 3-position also react with thiols to give 4-thiosubstituted-5,6-dihydroxyindoles (3, 4) and 5,6-dihydroxyindoles (5, 6); with no such group in this position (*e.g.* as in the case of epinochrome), 4-thiosubstituted-5,6-dihydroxyindolines and 5,6-dihydroxyindolines are formed (7).

An attempt has been made to determine the effects of p*H* and of some of the structural features of both the animochrome and the thiol upon the overall rates of several aminochrome–thiol reactions. This has been done by following the decrease in the absorbance at *ca.* 490 nm, due to the aminochrome, in the visible region of the spectrum of the reaction mixture. The absorbances were then plotted against the reaction time and the half times of the reactions were determined. The reciprocals of the half times were plotted against the p*H* of the reaction mixture for each of the reactions investigated (see Figs. 1 and 4). The absorbances of the reaction mixtures in the region of 360 nm due to the addition prod-

[1]For Part XVII, see ref. 2.

[2]Issued as NRCC No. 13745.

[3]Taken from the Ph.D. Thesis of W. S. Powell, Dalhousie University 1972.

[4]Holder of NRCC Scholarship (1967–1971).

[5]Present address: Dept. of Chemistry, Karolinska Institutet, S 104 01 Stockholm 60, Sweden.

[6]Correspondence and reprint requests should be sent to this author (R.A.H.) at the Atlantic Regional Laboratory.

[7]Revision received November 21, 1973.

Can. J. Chem. Downloaded from www.nrcresearchpress.com by 210.87.254.105 on 09/05/12
For personal use only.

Can. J. Chem. Downloaded from www.nrcresearchpress.com by 210.87.254.105 on 09/05/12
For personal use only.

ucts were also measured as the reactions progressed. Since these compounds (*i.e.* the addition products) have never been isolated (other than as their arylhydrazone derivatives (1, 2)) it was impossible to determine their actual concentrations in the reaction mixture.

All the reactions were carried out with a ratio of thiol to aminochrome of 2:1 in the p*H* range 2.7–5.9. At p*H* values lower than this, dark colored insoluble products, probably melanins, are formed and at higher p*H*'s aminochromes undergo a rearrangement reaction (*cf.* ref. 8). A ratio of thiol to aminochrome of 2:1 was chosen in order to minimize the effects due to competing reactions (*e.g.* rearrangements of the aminochromes) and to optimize the conditions for the aminochrome–thiol reactions.

It can be seen from Fig. 1 that the reaction between adrenochrome (**1**) and *N*-acetylcysteine[8] is slowest in the p*H* range 4.0–4.5, but is faster at either lower (*i.e.* p*H* 3–4) or higher p*H*'s (*i.e.* p*H* 5–6). At low p*H*'s the peak due to adrenochrome (**1**) at 301 nm was replaced by a peak at 308 nm (see Fig. 2), probably due mainly to 4-*S*-(*N*-acetylcysteinyl)-5,6-dihydroxy-1-methylindole (**2**) (*cf.* ref. 11) along with some 5,6-dihydroxy-1-methylindole (**3**). An extract containing the acid fraction of the reaction mixture, which consisted mainly of **2** along with *N*-acetylcysteine and its disulfide (*i.e.* *N*,*N*′-diacetylcysteine) also exhibited a λ_{max} at 308 nm in aqueous solution (*cf.* ref. 11).

An addition product (or products) appeared to be formed fairly rapidly in the initial stages of the reactions carried out at lower p*H*'s, but after about 4 min its concentration began to decline (see Figs. 2 and 3). This was presumably due to a shift in the equilibrium caused by the removal of adrenochrome (**1**) as a result of the irreversible formation of **2** and **3**. This addition product is probably not identical to that (*i.e.* **4**) which is formed at higher p*H*'s (*cf.* refs. 1, 2) since the λ_{max} of the former compound is in the region of 376 nm (when the reaction was carried out at p*H* 2.80) whereas the λ_{max} of **4** was found to be 357 nm (see Table 2). It is unlikely that the λ_{max} value of the addition product **4** would undergo a bathochromic shift of this magnitude due to the low p*H* of the reaction mixture, since no such shift is observed in the spectrum of sodium 3*a*,4-dihydroadrenochrome-3*a*-sulfonate (*i.e.* the adrenochrome – sodium bisulfite addition product (**5**)) in acidic solutions.

Although the structure of the second type of

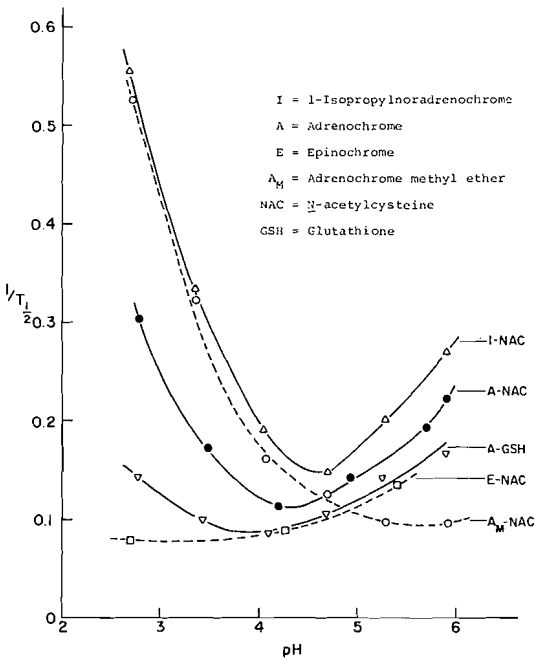

FIG. 1. Effect of p*H* upon the reciprocals of the half times of some aminochrome–thiol reactions. The concentrations of the reactants were increased fourfold in the case of the epinochrome–*N*-acetylcysteine reaction.

[8]*N*-Acetylcysteine was used in these studies, instead of the simpler thiol cysteine, after preliminary experiments had shown that very complex mixtures of products were obtained by the interaction of cysteine with the aminochromes studied. This may have been due to additional reactions involving the amino group of cysteine, leading to the formation of more complex cyclic structures (*cf.* refs. 9, 10).

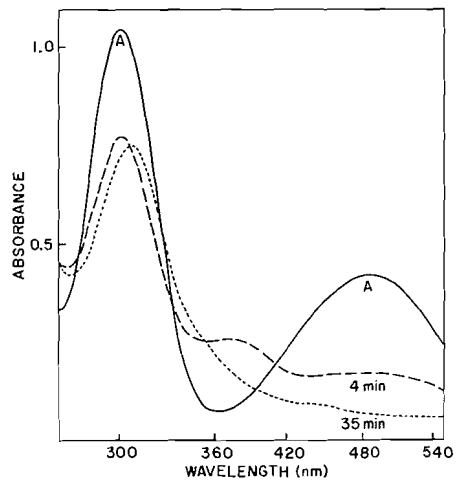

FIG. 2. Ultraviolet–visible spectra of adrenochrome (A) and the products of the adrenochrome–*N*-acetylcysteine reaction (p*H* 2.8) after 4 min and after 35 min.

Can. J. Chem. Downloaded from www.nrcresearchpress.com by 210.87.254.105 on 09/05/12
For personal use only.

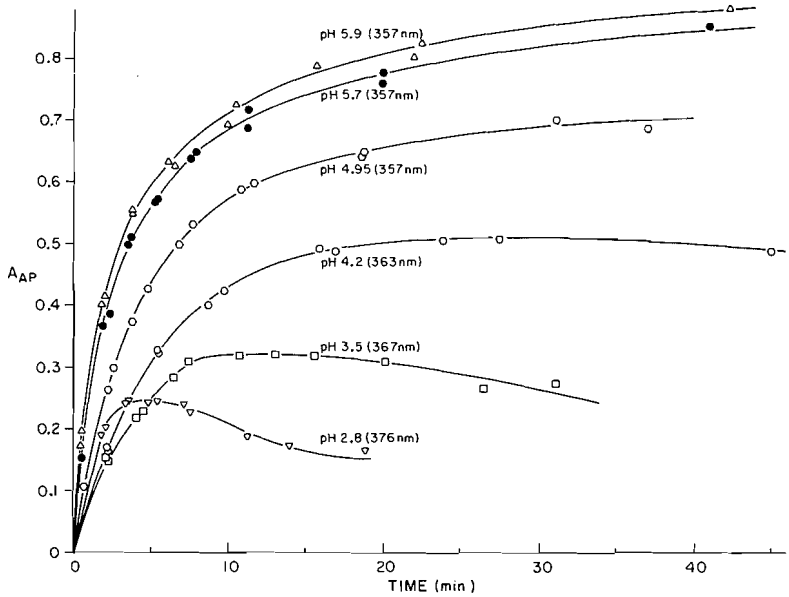

FIG. 3. Absorbances (corrected for adrenochrome absorption) of the addition product(s) *vs.* reaction time for the reactions between adrenochrome and *N*-acetylcysteine at various p*H*'s (see Experimental section for details of procedure) (A_{AP} = corrected absorbance of addition product).

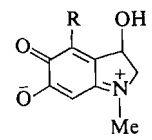

1 R = H
6 R = Me

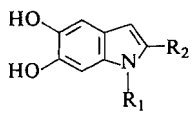

3 R_1 = Me; R_2 = H
22 R_1 = H; R_2 = Me

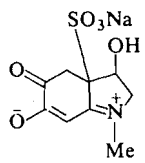

5

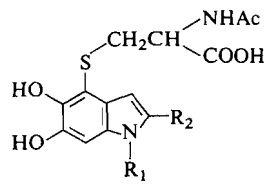

2 R_1 = Me; R_2 = H
11 R_1 = isoPr; R_2 = H
21 R_1 = H; R_2 = Me

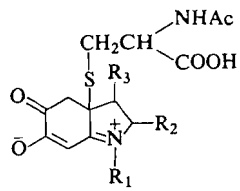

4 R_1 = Me; R_2 = H; R_3 = OH
15 R_1 = Me; R_2 = H; R_3 = OMe_3
19 R_1 = Me; R_2 = H; R_3 = H
23 R_1 = H; R_2 = Me; R_3 = OH

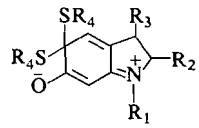

7 R_1 = Me; R_2 = H; R_3 = OH; R_4 = $CH_2CH(NHAc)COOH$
13 R_1 = isoPr; R_2 = H; R_3 = OH; R_4 = $CH_2CH(NHAc)COOH$
16 R_1 = Me; R_2 = H; R_3 = OMe; R_4 = $CH_2CH(NHAc)COOH$

addition product has not yet been established with certainty, the following arguments suggest that it may be formed by addition of the thiol to the C-5 carbonyl group of the aminochrome. Addition of the thiol to C-7*a* is unlikely since this carbon is part of a vinylogous amide system. Moreover, addition products are not formed with 4-methyladrenochrome (**6**), the 4-methyl group of which would not greatly influence the reactivity of the 7*a* carbon atom. Addition to C-7 would be expected to lead to the formation of a 7-thiosubstituted-5,6-dihydroxyindole. Such products do not appear to be formed in aminochrome–thiol reactions (3). Addition to either C-3*a* or C-4 can be eliminated since the products formed by such reactions have already been isolated and identified. This leaves the C-5 and C-6 carbonyl groups as the only possible points of attack by the thiol. Since C-6 is also part of the vinylogous amide system, addition at this position is unlikely. As a result of the above process of elimination C-5 remains the most likely position where addition could have occurred.

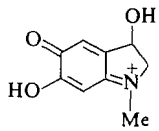

8

This conclusion is supported by the fact that 4-methyladrenochrome (**6**) reacts extremely slowly with *N*-acetylcysteine at all the p*H* values investigated (*cf.* ref. 3). No product having a λ_{max} value in the range 370–380 nm could be detected, as would have been expected (if addition had occurred at the C-5 carbonyl group) due to the proximity of the C-4 methyl group. The second type of addition product may therefore be the mercaptal 7, the formation of which would be acid catalyzed (*cf.* ref. 12).[9]

The acceleration of the reaction rate at lower p*H*'s would appear to be largely due to an increase in the rate of formation of the indole thioether **2**. This can be explained by an increase in the concentration of the conjugate acid **8**, although this species would only be present in very low concentrations[10] it would be much more reactive than the unprotonated form **1**. The positive charge at C-4 would be considerably greater in **8** than that on the corresponding carbon atom in the unprotonated species **1**, thus the rate of formation of the 4-thiosubstituted-trihydroxyindoline **9** would be enhanced. 3,5,6-Trihydroxyindolines of this type are known to dehydrate to the corresponding 5,6-dihydroxyindoles very readily (*cf.* ref. 8) and in the case of **9** this tendency would be increased by the electron donating thiol substituent. This dehydration reaction (*i.e.* **9** → **2**) would also be acid catalyzed (see Scheme 1).

Under less acidic conditions (*i.e.* p*H* 5–6), however, the peaks due to adrenochrome (**1**) at 301 and 489 nm were supplanted by a peak at 357 nm, due to the formation of the addition product **4** (*cf.* ref. 2). Although this product was eventually replaced in the reaction mixture by the indolic products (λ_{max} 310 nm) its lifetime under these conditions was much longer than that of the addition product which was produced in more acidic solutions (see Fig. 3). This is presumably due to the much slower rate of formation of the indole thioether **2** under less acidic conditions. The increased rate of disappearance of adrenochrome (**1**) which is observed in this p*H* range (see Fig. 1) would thus appear to be almost completely due to an enhancement in the rate of formation of **4**. This may be explained by the greater degree of ionization of the thiol at relatively higher p*H* values.[11] Since the degree of protonation of the C-6 carbonyl group would be very small under these conditions, the rate of formation of **2** would be much reduced. In summary it can be postulated that the formation of the 4-thiosubstituted-5,6-dihydroxyindole derivative (*i.e.* **2**) at low p*H* values involves attack of the thiol on the protonated aminochrome, which is more reactive in the 4-position than in the 3*a*-position. Formation of the addition product (*i.e.* **4**) at higher p*H* values, on the other hand, involves interaction of the thiol with the unprotonated aminochrome which is more reactive in the 3*a*-position than in the 4-position.

The effect of p*H* upon the overall rate of the reaction between adrenochrome and glutathione (GSH) was found to be quite similar to that

[9]The formation of the more stable mercaptal from the unstable hemimercaptal requires a lower p*H* than the formation of the hemimercaptal from the ketone (*cf.* ref. 12).

[10]The u.v.–visible spectrum of adrenochrome (**1**) and of other aminochromes does not change appreciably in the p*H* range investigated.

[11]The attacking species would almost certainly be RSH at low p*H*'s (*i.e.* 3–4) but at higher p*H* values (4 or 5–6) it may be RS^-, which, although present in very low concentrations, would be much more reactive than the unionized thiol.

Can. J. Chem. Downloaded from www.nrcresearchpress.com by 210.87.254.105 on 09/05/12
For personal use only.

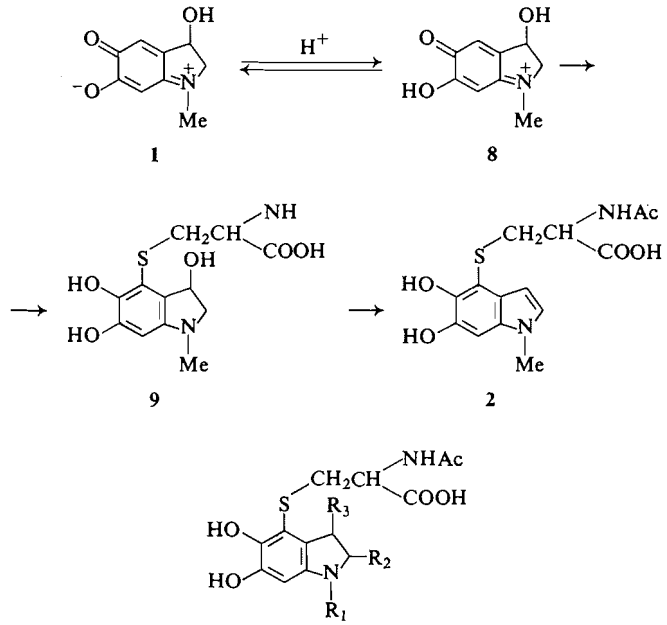

12 R_1 = isoPr; R_2 = H; R_3 = OH
18 R_1 = Me; R_2 = H; R_3 = H
25 R_1 = H; R_2 = Me; R_3 = OH

SCHEME 1

TABLE 1. The λ_{max} values and extinction coefficients in the visible spectra of aminochromes in 0.1 *M* citrate buffer (p*H* 2.7–6.0)*

Aminochrome	λ_{max} (nm)	ε
Adrenochrome (**1**)	489	4170
1-Isopropylnoradrenochrome (**10**)	495	4300
Adrenochrome methyl ether (**14**)	491	4270
Epinochrome (**17**)†	476	4070
2-Methylnoradrenochrome (**20**)	488	3490

*No changes were observed in the spectra of these aminochromes in the p*H* range under investigation.
†Spectrum in 0.25 *M* citrate buffer.

which was observed for the adrenochrome–*N*-acetylcysteine reaction (see Fig. 1). The rate was minimal at a p*H* of *ca.* 4 and was faster at p*H* values both above and below 4. Adrenochrome reacted more slowly with GSH than with *N*-acetylcysteine at all the p*H*'s investigated, probably due to the greater bulk of the GSH molecule. The addition product (*cf.* **7**) was formed to a lesser extent with GSH and the λ_{max} observed for the addition product at low p*H*'s was only 6 nm higher than that observed for the addition product formed at higher p*H*'s (see Table 1). This may indicate that a greater proportion of the addition product formed at low p*H*'s in the adrenochrome–GSH reaction is the one involving the 3*a*-carbon of adrenochrome (*cf.* **4**), rather than the second type of addition product (*cf.* **7**) which is formed in the reaction between adrenochrome and *N*-acetylcysteine. The formation of the mercaptal would be expected to be more sensitive to the bulk of the thiol than that of the 3*a*-thiosubstituted addition product, since formation of the former involves the addition of two thiol molecules. The increase in the overall reaction rate at higher p*H*'s was due to an increase in the rate of formation of the addition product involving the 3*a*-carbon of adrenochrome (*cf.* **4**). The rate of formation of this compound increased with increasing p*H* in the range investigated and apparently does not form optimally at a p*H* of *ca.* 4.7 as had been reported earlier (13).

Adrenochrome reacted very slowly with thioglycollic acid in the p*H* range 2.8–5.9 at the concentrations employed (*i.e.* 1×10^{-2} *M* adrenochrome and 2×10^{-2} *M* thioglycollic acid) and the half times could not be readily determined. The slower reaction rate at lower p*H*'s is probably due to a decrease in the nucleophilicity of the thiol group in thioglycollic acid due to the electronegative effect of the α-carboxylic acid group. At higher p*H*'s, on the other hand,

Can. J. Chem. Downloaded from www.nrcresearchpress.com by 210.87.254.105 on 09/05/12
For personal use only.

Can. J. Chem. Downloaded from www.nrcresearchpress.com by 210.87.254.105 on 09/05/12
For personal use only.

ionization of the thiol group would be repressed by the proximity of the ionized carboxyl group.[12]

The reaction between 1-isopropylnoradrenochrome (**10**) and *N*-acetylcysteine was considerably faster than that of adrenochrome (**1**) with this thiol, especially at low p*H*'s (see Fig. 1). This is probably due to an increase in the rate of formation of the 5,6-dihydroxyindole thioether **11**. This may be due to the relief in the steric interaction between the 1-isopropyl group and the 7-proton which would occur in going from the planar vinylogous amide system of the aminochrome to the tetrahedral nitrogen of the thiosubstituted indoline **12**. This relief would be greater in the case of **10** than with adrenochrome (**1**) which has a 1-methyl group rather than a 1-isopropyl group. An alternate explanation of the increased reactivity of **10** could be the poorer solvation of its amino group. Thus the conversion of **10** to the thiosubstituted indoline **12** with its uncharged amino group would be more favorable than the conversion of an aminochrome with a more highly solvated amino group to the corresponding indoline. A compound (*cf.* **13**) analogous to the addition product (*cf.* **7**) formed between adrenochrome (**1**) and *N*-acetylcysteine at low p*H*'s was also observed when the reaction between 1-isopropylnoradrenochrome (**10**) and *N*-acetylcysteine was carried out at similar p*H* values.

Adrenochrome methyl ether (**14**) reacted much more rapidly with *N*-acetylcysteine at lower p*H*'s than did adrenochrome (**1**), but much more slowly at higher p*H*'s due to an increase in the rate of formation of the indole thioether **2** and a decrease in the rate of formation of the addition product **15**. It is rather difficult to explain the increased rate of formation of **2** in this case. The decrease in the rate of formation of **15** would be due to the steric interaction between the attacking thiol molecule and the methoxyl group. There was also evidence for the formation of the second addition product (*cf.* **16**) at low p*H* values.

The reaction between epinochrome (**17**) and *N*-acetylcysteine was much slower than the one involving adrenochrome (**1**) and consequently the concentrations of both the aminochrome and the thiol had to be increased fourfold to obtain meaningful results. The formation of the indoline

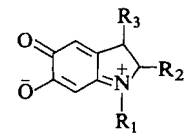

10 R_1 = isoPr; R_2 = H; R_3 = OH
14 R_1 = Me; R_2 = H; R_3 = OMe
17 R_1 = Me; R_2 = H; R_3 = H
20 R_1 = H; R_2 = Me; R_3 = OH

thioether **18** would be less favored since the partial positive charge on the 4-carbon atom of epinochrome would be reduced due to: (*a*) the replacement of the electronegative hydroxyl group by a proton and (*b*) the greater hyperconjugative effect of the C-3 methylene group. The formation of the addition product **19** would be less favored due to a decrease in the partial positive charge on the 3*a*-carbon atom, which can also be explained by the effect of the C-3 methylene group as has been discussed above. The unfavorable electronic effects caused by the absence of the hydroxyl (or alkoxyl) group in the 3-position of epinochrome would appear to outweigh the advantage of the low steric effect of the 3-methylene group of this compound.

2-Methylnoradrenochrome (**20**) reacts with *N*-

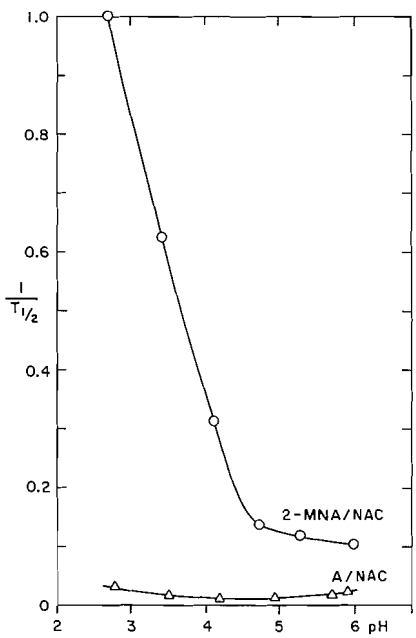

FIG. 4. Effect of p*H* upon the reciprocals of the half times of the reactions between (*a*) adrenochrome and (*b*) 2-methylnoradrenochrome with *N*-acetylcysteine. 2-AMN = 2-Methylnoradrenochrome; A = Adrenochrome; NAC = *N*-acetylcysteine.

[12]The pK_a values for the —SH groups of thioglycollic acid, glutathione, and *N*-formylcysteine are 10.4, 8.65–8.93, and 9.5, respectively (*cf.* ref. 14).

TABLE 2. The λ_{max} values of the addition products formed in some aminochrome–thiol reactions at various p*H*'s

Reaction	p*H*	λ_{max} (nm)	p*H*	λ_{max} (nm)
Adrenochrome–*N*-acetylcysteine	2.80	376	4.95	357
	3.50	367	5.70	357
	4.20	363	5.91	357
Adrenochrome–glutathione	2.79	360	4.70	356
	3.44	356	5.26	355
	4.10	356	5.90	354
1-Isopropylnoradrenochrome–*N*-acetylcysteine	2.70	382	4.71	363
	3.37	378	5.29	360
	4.06	367	5.92	359
Adrenochrome methyl ether–*N*-acetylcysteine	2.74	374	4.70	365
	3.38	374	5.30	362
	4.08	370	5.93	361
Epinochrome–*N*-acetylcysteine*	2.71	365 (sh)		
	4.28	360 (sh)		
	5.42	360 (sh)		
2-Methylnoradrenochrome–*N*-acetylcysteine	2.7	378	4.74	362
	3.4	377	5.30	358
	4.12	375	5.98	357

*The concentration of the reactants were increased fourfold in this case.

acetylcysteine much more rapidly in the p*H* range covered by this investigation than any other aminochrome studied (see Fig. 4). The major product was quite soluble in aqueous sodium bicarbonate but could be extracted from acid solution by ethyl acetate, suggesting that it contained a free carboxylic acid group. It behaved like an indole and a phenol with chromogenic reagents (positive reactions with Ehrlich's and Gibb's reagents and the Folin–Ciocalteu reagent) and had a λ_{max} at 310 nm with a shoulder at 300 nm. It would appear therefore, that this product is 4-*S*-(*N*-acetylcysteinyl)-5,6-dihydroxy-2-methylindole (**21**). A small amount of the reduction product, 5,6-dihydroxy-2-methyindole (**22**), was also produced. This was identified on the basis of the similarity of its u.v. spectroscopic, chromatographic, and chemical properties with those of the ether soluble product of the reaction between **20** and ascorbic acid. An addition product (*i.e.* **23**) (λ_{max} 357 nm) was produced at higher p*H*'s but was replaced fairly rapidly by **21**. The reason for the rapidity of the reaction of **20** with *N*-acetylcysteine is the increase in the rate of formation of the indole thioether **21**. It is somewhat difficult to explain the observed magnitude of the increase in the rate of reaction of this aminochrome with *N*-acetylcysteine over the rates of the reactions of *N*-alkylaminochromes with this thiol. Although the vinylogous amide system of **20** (which contains a secondary nitrogen atom) would be protonated less readily than those of the other aminochromes studied (which contain tertiary nitrogen atoms), the reactivity of the protonated species **24** would be greater than those of the other protonated aminochromes. The positive charge on the nitrogen of **23** would be relatively greater, leading to a greater partial positive charge on the 4-carbon and therefore to an increase in the rate of formation of **25**, which would immediately lose the elements of water to give **21**.

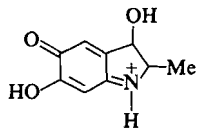

24

Experimental

General

Adrenochrome (15), 4-methyladrenochrome (16), adrenochrome methyl ether (17), 1-isopropylnoradrenochrome (17), epinochrome (7), 2-methylnoradrenochrome (18), and sodium 3*a*,4-dihydroadrenochrome-3*a*-sulfonate (19) were prepared by methods described in the literature.

The u.v.–visible absorption spectra were measured on a Beckman DK-2 recording spectrophotometer and the p*H* values were determined using a Fisher Accumet 320 expanded scale research p*H* meter.

Can. J. Chem. Downloaded from www.nrcresearchpress.com by 210.87.254.105 on 09/05/12
For personal use only.

Rate Studies

All reactions were carried out in duplicate in a water bath maintained at 27°. The aminochrome (10^{-4} mol) was dissolved in 0.1 *M* citrate buffer[13] (5 ml) at the required p*H*. A solution of the thiol (2×10^{-4} mol) in 0.1 *M* citrate buffer (5 ml) at the same p*H* was immediately added. Aliquots (0.5 ml) were taken from the reaction mixture at various time intervals and were diluted to 50 ml with the corresponding buffer.

For the experiments with epinochrome, however, the concentrations of epinochrome and of *N*-acetylcysteine were greater by a factor of four and 0.25 *M* citrate buffer was used. Aliquots (0.125 ml) were taken from the reaction mixture and were diluted to 50 ml with buffer.

The absorbances of the diluted samples at the λ_{max} of the aminochrome (*ca.* 490 nm) and at the λ_{max} of the addition product (*ca.* 360 nm) were measured as quickly as possible. The λ_{max} and extinction coefficient in the visible spectrum of each of the aminochromes investigated were found not to change noticeably with respect to the p*H* of the solution within the range studied. Consequently, for each aminochrome, the same value could be used in the calculation of its concentrations at different p*H*'s (see Table 2).

The λ_{max} values for the addition products were determined by carrying out a preliminary reaction at each p*H* and scanning the spectra of the samples diluted at varying time intervals. The λ_{max} values found for the addition products formed in each of the reactions at different p*H*'s are given in Table 2. The absorbance for each of the addition products at its λ_{max} was determined by subtracting the absorbance due to the unreacted aminochrome at the corresponding wavelength from the total absorbance at that wavelength. This correction was only significant in the early stages of the reaction.

The half times of the reactions were determined by plotting the concentration of the aminochrome in the reaction mixture against the reaction time and determining the time at which the aminochrome concentration was equal to one half of its original value.

[13]The decomposition of each of the aminochromes studied, in buffer alone at every p*H* investigated, was found to be sufficiently slow so as not to compete with the reaction of the aminochrome with the thiol.

1. W. S. Powell and R. A. Heacock. Experientia, **28**, 124 (1972).
2. W. S. Powell and R. A. Heacock. J. Chem. Soc. Perkin I, 509 (1973).
3. W. Powell, R. A. Heacock, G. L. Mattok, and D. L. Wilson. Can. J. Chem. **47**, 467 (1969).
4. W. Powell and R. A. Heacock. Can. J. Chem. **47**, 2102 (1969).
5. R. A. Heacock and B. D. Laidlaw. Chem. Ind. London, 1510 (1958).
6. R. A. Heacock and B. D. Scott. Can. J. Biochem. Physiol. **37**, 1087 (1959).
7. W. S. Powell and R. A. Heacock. Can. J. Chem. **50**, 3360 (1972).
8. R. A. Heacock and W. S. Powell. Prog. Med. Chem. **9**, 275 (1972).
9. G. Prota, G. Scherillo, E. Napolano, and R. A. Nicolaus. Gazz. Chim. Ital. **97**, 1451 (1967).
10. G. Prota, G. Scherillo, and R. A. Nicolaus. Gazz. Chim. Ital. **98**, 495 (1968).
11. W. S. Powell and R. A. Heacock. Bioorg. Chem. **2**, 191 (1973).
12. E. Campaigne. *In* Organic sulfur compounds. Vol. 1. *Edited by* N. Kharasch. Pergamon Press, New York. 1961. p. 134.
13. G. L. Mattok and R. A. Heacock. Can. J. Chem. **43**, 119 (1965).
14. P. C. Joceyln. Biochemistry of the SH group. Academic Press, New York. 1972. p. 51.
15. R. A. Heacock, C. Nerenberg, and A. N. Payza. Can. J. Chem. **36**, 853 (1958).
16. R. A. Heacock and O. Hutzinger. Can. J. Chem. **43**, 2535 (1965).
17. R. A. Heacock and B. D. Scott. Can. J. Chem. **38**, 516 (1960).
18. W. S. Powell, R. A. Heacock, D. G. Smith, and A. G. McInnes. Can. J. Chem. **51**, 776 (1973).
19. R. L. Tse and M. J. Oesterling. Clin. Chim. Acta, **8**, 393 (1963).

Can. J. Chem. Downloaded from www.nrcresearchpress.com by 210.87.254.105 on 09/05/12
For personal use only.

The Isolation of an Episelenurane from the Reaction of 4-Tolueneselenenyl Chloride with Ethylene[1]

DENNIS G. GARRATT AND GEORGE H. SCHMID

Department of Chemistry, University of Toronto, Toronto, Ontario M5S 1A1

Received November 19, 1973

The structure of the first product from the addition of 4-tolueneselenenyl chloride to 1–90% ^{13}C ethylene in methylene chloride or chloroform has been assigned as 1-chloro-1-(4′-tolyl)selenocyclopropane (**1**) on the basis of its n.m.r. and c.m.r. data. In particular the chemical shifts and ^{13}C–^{77}Se spin–spin coupling constants serve to distinguish it from its isomer 2-chloroethyl 4-tolyl selenide (**2**) which is slowly formed from **1**.

En se basant sur les spectres r.m.n. du proton et du ^{13}C on attribue la structure chloro-1 (tolyl-4′)-1 sélénocyclopropane (**1**) au premier produit qui se forme lorsque le chlorure de *p*-toluènesélényle est additionné à de l'éthylène (contenant 30% de ^{13}C en position 1) en solution dans le chlorure de méthylène ou le chloroforme. On utilise en particulier les déplacements chimiques et les constantes de couplage spin–spin ^{13}C–^{77}Se pour distinguer le premier produit de son isomère le sélénure de chloroéthyl-2 et de tolyl-4 (**2**) qui se forme lentement à partir de **1**. [Traduit par le journal]

Can. J. Chem., **52**, 1027 (1974)

The addition of 4-tolueneselenenyl chloride to ethylene in methylene chloride or chloroform at 25° in an atmosphere of anhydrous, deoxygenated nitrogen yields quantitatively the 1:1 adduct **1** as a fine white powder, m.p. 103° (dec.) (Anal. Calcd. for $C_9H_{11}SeCl$: C, 46.28; H, 4.75. Found: C, 46.25; H, 4.57), mol wt 234 by electron impact and chemical ionization. Upon standing for a few days at 25° **1** isomerizes to **2**, a tan solid, m.p. 35° (dec.) (Anal. Found: C, 46.32; H, 4.45). The structures of **1** and **2** have been assigned as 1-chloro-1-(4′-tolyl)selenocyclopropane and 2-chloroethyl 4′-tolyl selenide, respectively, on the basis of the n.m.r. data in Table 1.

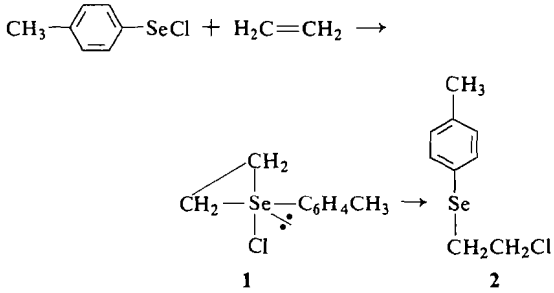

1 **2**

The p.m.r. spectrum of **2** is almost superimposable on that of 2-chloroethyl 4′-tolyl sulfide in accord with previous results (1). This firmly establishes that **2** is the selenium analog of the usual arenesulfenyl chloride adduct to alkenes (2). The methylene protons of **1** appear as a tightly coupled AA′BB′ system in contrast to the two distinct groups observed in **2** which arise from protons adjacent to chlorine or selenium. In general the chemical shifts of the protons in **1** are deshielded relative to those in **2**. These downfield shifts are consistent with oxidation of Se^{II} to Se^{IV} (3). A similar result is found by comparing the ^{13}C n.m.r. spectra of **1** and **2**.

Further structural information is available from the ^{13}C–^{77}Se spin–spin coupling constants obtained from the spectrum of a sample of **1** prepared from 1–90% ^{13}C ethylene. Both methylene carbons of **1** show ^{13}C–^{77}Se spin–spin coupling while **2** shows ^{13}C–^{77}Se coupling only for the carbon attached to selenium. No ^{77}Se–C–^{13}C coupling is observed. This result strongly supports the cyclic structure of **1**.

The ^{13}C–H spin–spin coupling constants are in accord with the proposed structures of **1** and **2**. The magnitude of J_{C-H} for the carbon attached to Se in **2** is quite similar to those of reported acyclic

[1]Organo selenium chemistry, Part II. For Part I, see ref. 9.

TABLE 1. Calculated n.m.r. chemical shifts and coupling constants for 1-chloro-1-(4′-tolyl)selenocyclopropane and 2-chloroethyl 4′-tolyl selenide*

Compound	Chemical shifts δ_H	$\delta_{H'}$	$\delta_{H(Ar)}$	$\delta_{H(CH_3)}$	δ_C	$\delta_{C'}$	Spin–spin coupling constants (Hz)
	4.37	4.53	7.89 7.38	2.40, s	65.20, t(t)	38.06, t(t)	J_{SeC}, ±59.25; $J_{SeC'}$, ±18.54; $J_{CC'}$, 37.25; J_{CSeC}, 13.84; $J_{H(Ar)}$, 9.0
	AA′BB′		A_2B_2				J_{CH}, 152.03; $J_{C'H'}$, 155.23; $J_{CC'H}$, 3.18; $J_{C'CH}$, 4.38; $J_{HH'}$, 8.0, 4.5, 1.5
$Cl'CH_2'CH_2SeAr$	3.10	3.63	7.46 6.97	2.28, s	29.28, t(dd)	43.29, t(dd)	J_{SeC}, ±66.32; $J_{SeCC'}$, <8; $J_{CC'}$, 28.8; $J_{H(Ar)}$, 7.8
	AA′BB′		A_2B_2				J_{CH}, 145.55; $J_{CH'}$, 155.60; $J_{CC'H'}$, 4.22, 6.84; $J_{C'CH}$, 4.80, 7.80

*Chemical shifts δ p.p.m. relative to TMS; s = singlet, t = triplet, dd = doublet of doublets; $t(t) = J_{CH,triplet}, J_{CCH,triplet}$.

selenides (4). For example $(CH_3)_2Se$, 140.3; CH_3SeH, 142.7; and $(CH_3)_3Se^+$ 145.8 Hz. Similarly the value of J_{CH} for the carbon bonded to chlorine is of the normal magnitude. The similarity of the values of J_{C-H} for both carbons in **1** rules out an acyclic structure. The increase in the value of J_{C-H} for carbons bonded to selenium in **1** relative to the one in **2** is consistent with the change of oxidation state of the selenium in **2** as can be seen from the relative magnitudes of J_{C-H} in the S, Se, and P analogs. For example $(CH_3)_2S$, 138; $(CH_3)_3S^+$, 146 Hz; and $P(CH_3)_3$ 127; $P^+(CH_3)_4$ 134 Hz (5).

It is thus our belief that this data is in agreement with a cyclic structure for **1**, which contains nonequivalent positions in the three-membered ring. On the basis of the known stereochemistry about selenium in Se^{IV} compounds (6), the structure of **1** may be tentatively assigned as a triagonal bipyramid. If the assumption is made that those factors which govern the stability of isomeric trigonal bipyramidal phosphoranes (7) are also applicable for selenuranes the three-membered ring will prefer to span an apical–equatorial position and the electronegative chlorine atom the remaining apical position.

The results reported here suggest that in the analogous addition of arenesulfenyl chlorides to alkenes, an episulfurane may be the first formed intermediate. Evidence for such an intermediate has recently been claimed (8).

Continued financial support from the National Research Council of Canada is gratefully acknowledged. The technical assistance of Mr. Nick Plavac is greatly appreciated as is a University of Toronto Special Open Fellowship to D. G. G.

1. (*a*) W. JENNY. Helv. Chim. Acta, **41**, 317 (1958); (*b*) W. JENNY. Helv. Chem. Acta, **41**, 331 (1958).
2. (*a*) D. R. HOGG and J. H. SMITH. Mech. React. Sulfur Compd. **3**, 63 (1968); (*b*) G. H. SCHMID, V. M. CSIZMADIA, V. J. NOWLAND, and D. G. GARRATT. Can. J. Chem. **50**, 2457 (1972); (*c*) D. GARRATT and G. H. SCHMID. Can. J. Chem. **51**, 2463 (1973).
3. (*a*) K. J. WYNNE and J. W. GEORGE. J. Am. Chem. Soc. **91**, 1649 (1969); (*b*) H. J. REICH. J. Am. Chem. Soc. **95**, 964 (1973).
4. (*a*) H. DREESKAMP and G. PFISTERER. Mol. Phys. **14**, 295 (1968); (*b*) W. MCFARLANE. Mol. Phys. **12**, 243 (1967); (*c*) J. B. STOTHERS. Carbon-13 NMR spectroscopy. Academic Press, New York, London. 1972. p. 375.
5. (*a*) H. W. DOUGLAS. J. Chem. Phys. **45**, 3465 (1966); (*b*) P. HEAKE, W. B. MILLER, and D. A. TYSSEE. J. Am. Chem. Soc. **86**, 3577 (1964).
6. I. L. KERLE and J. KARLE. *In* Organic selenium compounds, their chemistry and biology. *Edited by* D. L. Klayman and W. H. H. Gunther. John Wiley and Sons. 1973. Chapt. XVH, p. 989.
7. (*a*) D. GORENSTEIN and F. H. WESTHEIMER. J. Am. Chem. Soc. **92**, 634 (1970); (*b*) D. GORENSTEIN. J. Am. Chem. Soc. **92**, 644 (1970).
8. D. C. OWSLEY, G. K. HELMKAMP, and M. F. RETTIG. J. Am. Chem. Soc. **91**, 5239 (1969).
9. D. G. GARRATT, I. G. CSIZMADIA, and G. H. SCHMID. J. Mol. Struct. In press.

8417

Can. J. Chem. Downloaded from www.nrcresearchpress.com by 210.87.254.5 on 09/05/12
For personal use only.

Canadian Journal of Chemistry

Published by
THE NATIONAL RESEARCH COUNCIL OF CANADA

Journal canadien de chimie

Publié par
LE CONSEIL NATIONAL DE RECHERCHES DU CANADA

Volume 52 Number 7 April 1, 1974

Volume 52 numéro 7 1 avril 1974

Infrared Studies of Water in Crystalline Hydrates: $K_2CuCl_4 \cdot 2H_2O$[1]

GWEN H. THOMAS[2] AND MICHAEL FALK

Atlantic Regional Laboratory, National Research Council of Canada, Halifax, Nova Scotia

AND

OSVALD KNOP

Department of Chemistry, Dalhousie University, Halifax, Nova Scotia

Received August 20, 1973

Infrared spectra of polycrystalline $K_2CuCl_4 \cdot 2H_2O$ at different degrees of deuteration were recorded, between 4000 and 300 cm^{-1}, at temperatures from −160 to 90 °C. The spectra confirm the existence of only one crystallographically distinct type of water molecule in the structure, on sites of symmetry C_{2v}. Vibrational coupling of the bending fundamentals of the water molecule has been analyzed in detail. It is shown that the existence and magnitude of such coupling may be used to predict, from the spectrum of a hydrate, the manner in which a water molecule participates in the crystal structure. The structure and the vibrational spectra of $K_2CuCl_4 \cdot 2H_2O$ are compared with those of the closely related $CuCl_2 \cdot 2H_2O$.

Les spectres infrarouges de $K_2CuCl_4 \cdot 2H_2O$ ont été enregistrés entre 4000 et 300 cm^{-1} à différentes températures et différents degrés de deutération. Ces spectres confirment l'existence, dans la structure cristalline de ce composé, d'un seul type distinct de molécule d'eau sur des sites de symétrie C_{2v}. L'analyse détaillée du couplage vibrationnel des déformations fondamentales de la molécule d'eau a été réalisée. L'existence et l'ordre de grandeur d'un tel couplage peuvent servir à prevoir, à partir du spectre de l'hydrate, de quelle manière la molécule d'eau participe à la structure cristalline. On compare la structure et les spectres vibrationnels de $K_2CuCl_4 \cdot 2H_2O$ avec ceux du composé apparenté, $CuCl_2 \cdot 2H_2O$.

Can. J. Chem., **52**, 1029 (1974)

Potassium tetrachlorocuprate(II) dihydrate (PTD), $K_2CuCl_4 \cdot 2H_2O$, is the best known member of the isostructural series of tetragonal compounds $M_2CuX_4 \cdot 2H_2O$, where M = K, NH_4, Rb, Cs and X = Cl or Br (1–3). It occurs also in nature as the mineral *mitscherlichite*. The crystal structure of PTD has been determined both by X-ray (1, 2, 4) and neutron (5) diffraction (Table 1, Fig. 1), and there are also n.m.r. studies (11–13). The water molecules in PTD are all crystallographically equivalent and occupy sites of the undiminished symmetry of the free water molecule, C_{2v}.

In the structure of PTD the nearest neighbors of each Cu atom (B, Fig. 1) are two Cl(1) atoms (C, D) at *ca.* 2.28 Å and the oxygen atoms (C, D) of two water molecules at *ca.* 1.97 Å. The resulting coordination groupings $CuCl(1)_2(H_2O)_2$ of symmetry *mmm* are arranged in a linear chain located in a vertical mirror plane which also contains the Cl(2) atoms (A, B). The chains, which are parallel to the *c* axis, are not cross-linked by "short bonds"; their positions relative

[1]NRCC No. 13375.
[2]Summer student assistant in 1968 and 1969.

Can. J. Chem. Downloaded from www.nrcresearchpress.com by 210.87.254.5 on 09/05/12
For personal use only.

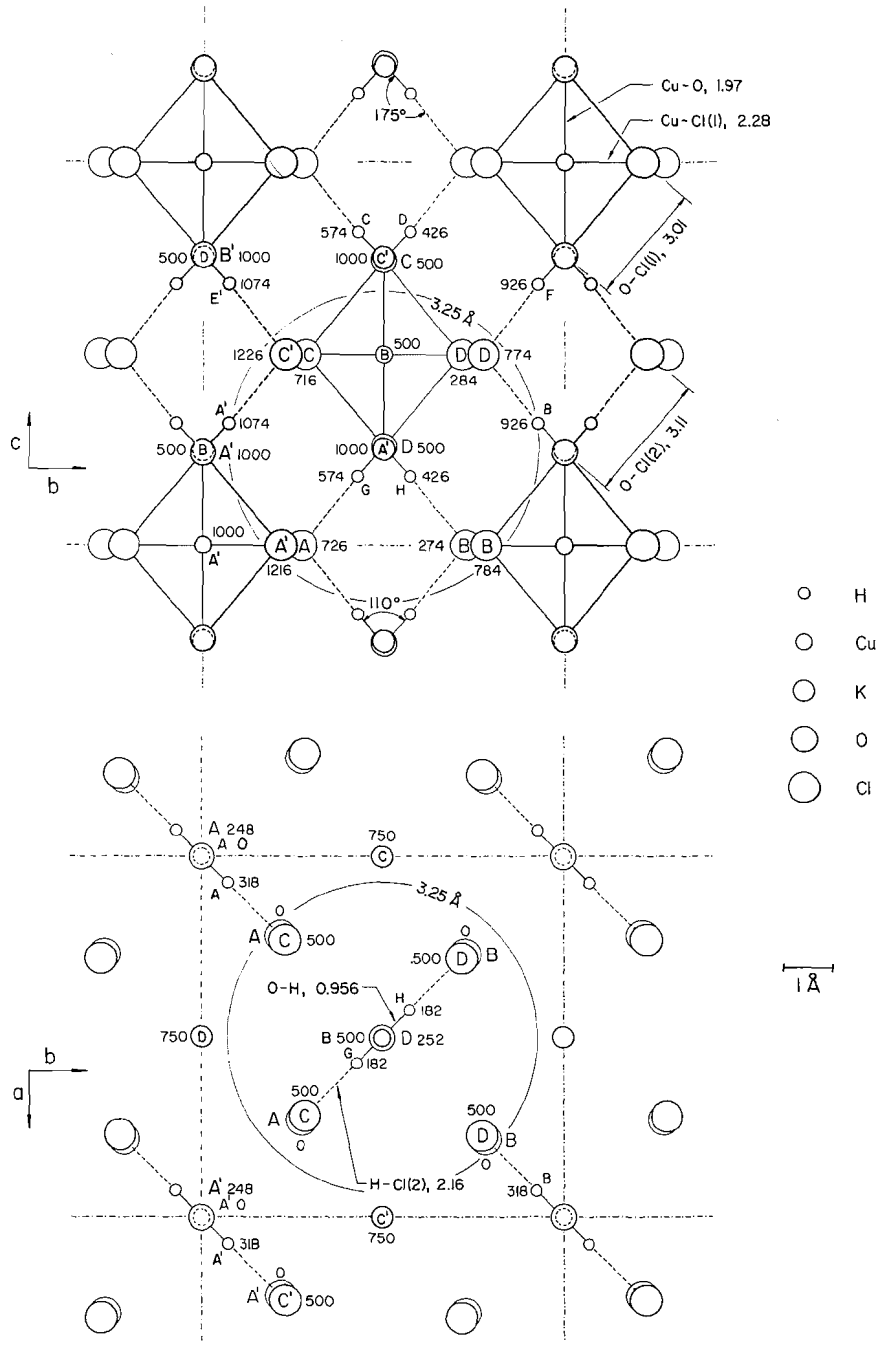

FIG. 1. Projection of a portion of the crystal structure of $K_2CuCl_4 \cdot 2H_2O$ (as reported in ref. 5) on the 100 (top) and 001 (bottom) planes. The fractional coordinates have been multiplied by 1000. Atoms with coordinates as listed in Table 1 are labelled A (A′ when in a neighboring unit cell); atoms in positions derived from A by symmetry operations are labelled B, C etc. The distances and angles are not corrected for thermal motion.

Can. J. Chem. Downloaded from www.nrcresearchpress.com by 210.87.254.5 on 09/05/12
For personal use only.

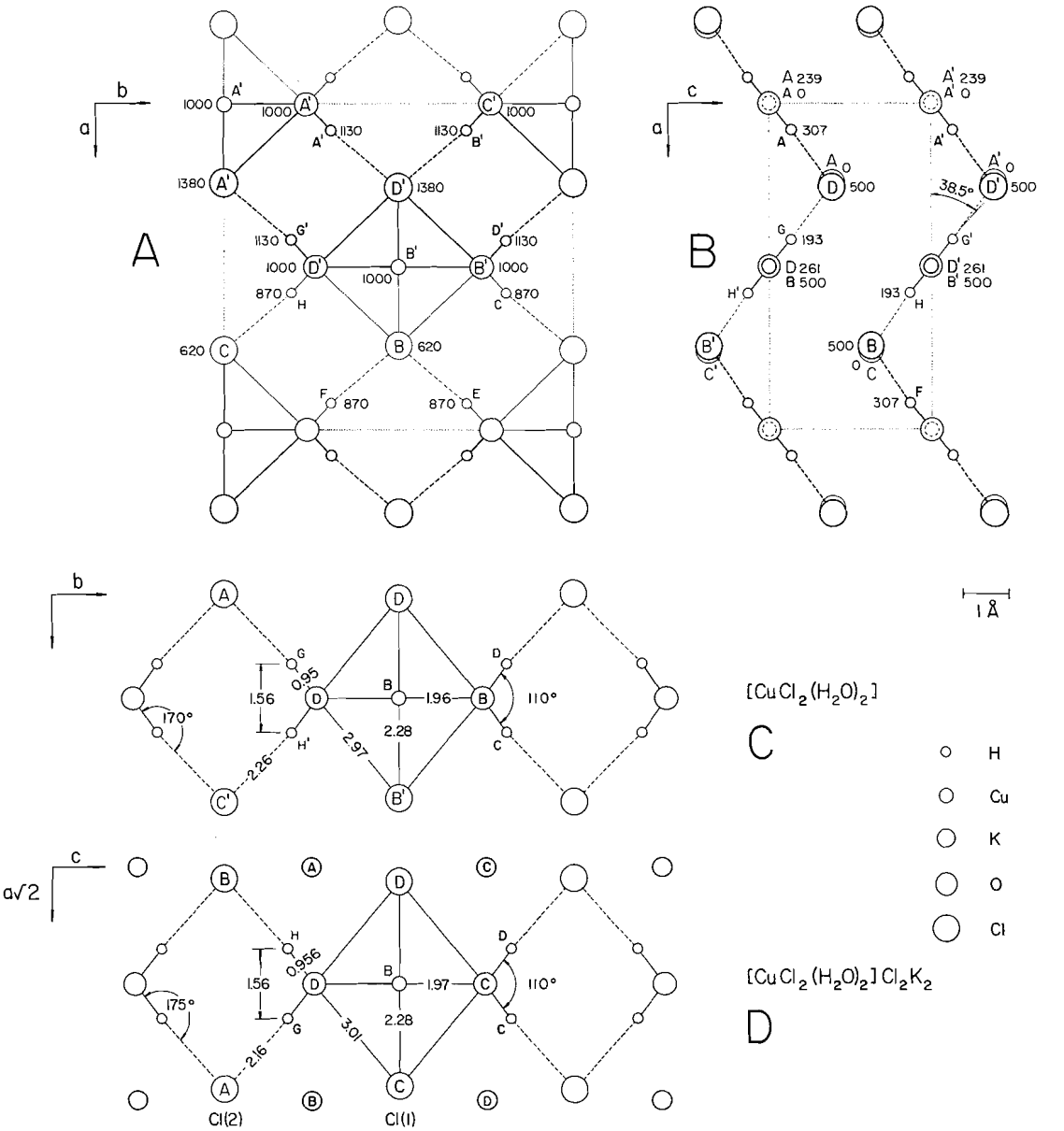

FIG. 2. Projection of a portion of the crystal structure of $CuCl_2 \cdot 2H_2O$ (as reported in refs. 6 and 8) on the 001 (*A*) and 010 (*B*) planes. The projection in *C* is essentially along $Cl^D—O^D—Cl^{B'}$ of *B*. The coordination of the Cu atom in $K_2CuCl_4 \cdot 2H_2O$ is shown for comparison (*D*); the projection is along the $Cl(2)^D—O^D—Cl(2)^C$ section of Fig. 1 (bottom). In *C* the uncorrected distances and angles are based on positional and lattice parameter values of ref. 8 (Table 1).

to one another are shown in the *xy* projection of Fig. 1. The smallest interatomic distance between chains is Cu—Cl(2), *ca.* 2.90 Å, the two Cl(2) atoms C and D at $z = \frac{1}{2}$ completing the coordination octahedron $CuCl(1)_2Cl(2)_2O_2$ about the Cu atom.

The trigonal coordination of the water molecule, $Cl(2)_2^{A,B}—H_2^{G,H}O^D—Cu^B$ (Fig. 2*D*), and the arrangement of atoms within the planar chains are remarkably similar to those in $CuCl_2 \cdot 2H_2O$ (CCD; the mineral *eriochalcite*) (Fig. 2*C*). In CCD the chains are not completely planar,

TABLE 1. Positional parameters and site symmetries of atoms in $K_2CuCl_4 \cdot 2H_2O$ (neutron diffraction, ref. 5) and $CuCl_2 \cdot 2H_2O$ (neutron (6) and X-ray (8) diffraction)

Atom	Equipoint	Site symmetry	x	y	z	
		$K_2CuCl_4 \cdot 2H_2O$* ($P4_2/mnm$, No. 136)				
Cu	2(*a*)	*mmm*	0	0	0	
K	4(*d*)	$\bar{4}$	0	$\frac{1}{2}$	$\frac{1}{4}$	
Cl(1)	4(*f*)	*mm*	0.2161(3)	0.2161(3)	0	
Cl(2)	4(*g*)	*mm*	0.7262(3)	0.2738(3)	$\frac{1}{2}$	
O	4(*e*)	*mm*	0	0	0.2484(5)	
H	8(*j*)	*m*	0.0739(10)	0.0739(10)	0.3178(6)	
		$CuCl_2 \cdot 2H_2O$† (*Pbmn*,‡ No. 53)				
Cu	2(*a*)	2/*m*	0	0	0	
Cl	4(*h*)	*m*	0.2402	0	0.3804	(6)
			0.2402(2)	0	0.3800(5)	(8)
O	4(*e*)	2	0	0.2390	0	(6)
			0	0.2408(4)	0	(8)
H	8(*i*)	1	0.0822	0.3065	0.1295	(6)

*$Z = 2$; $a = 7.477(13)$ Å, $c = 7.935(19)$ Å (5); $a = 7.454(1)$ Å, $c = 7.909(1)$ Å (7).

†$Z = 2$; $a = 7.440(14)$ Å, $b = 8.126(16)$ Å, $c = 3.764(10)$ Å. These are the lattice parameters (with twice the uncertainty quoted by the author) used in ref. 8 to calculate interatomic distances and bond angles. It is not clear whether the values used for this purpose by Peterson and Levy (6) were those of ref. 9 or of ref. 10, both of which are significantly smaller than those of ref. 8. In particular, they lead to an (uncorrected) Cu—O distance about 0.02 Å shorter than the values of ref. 8.

‡This is the setting used in ref. 6. The tabulated standard setting *Pmna* used by Engberg (8) has been converted to *Pbmn* for convenience of comparison.

consistent with the lower site symmetry of the oxygen atom (Table 1), but the deviation from planarity is slight (Fig. 2B).[3] The main difference between the dimeric groupings in the two compounds appears to be in the (uncorrected) H...Cl distance, which is 2.16(4) Å in PTD and 2.26 Å in CCD, and in the O—H—Cl angle, *ca.* 175° in PTD and *ca.* 170° in CCD (Fig. 2 *C*, *D*). The other distances and angles are the same within the limits of the experimental accuracy.[4]

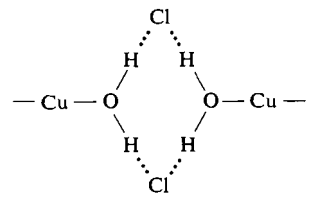

Such planar chains are also a common feature of the crystal structures of $MX_2 \cdot 2H_2O$ dihalides of the first transition-element series. In the Mn—Cl (15), Mn—Br (16), Fe—Cl (15), Co—Cl (17, 18), Co—Br (16), and Cu—F (19) members of the isostructural (*C*2/*m*) series the chains are of the type present in CCD; a less symmetric arrangement exists in $NiCl_2 \cdot 2H_2O$ (20). The variations, with *M*, in the two (unequal) *M*—*X* distances and in the *M*—O distance appear to reflect the 3d-orbital occupancy in the *M* atoms.

The similarity of the surroundings of the water molecule in these dihydrates and its participation as a link in the planar chains lends special interest to the study of the vibrational frequencies of H_2O in these structures. Owing to their high crystallographic symmetry, PTD and its isostructural cognates are particularly suited for a detailed analysis. The full symmetry of the free water molecule is retained in these structures, and the vibrational coupling between equivalent water molecules can be expected to be very simple, all the water molecules in the unit cell being of the same type and each related to the others by several symmetry operations. Investigation of the effective range of coupling interactions within and between the planar chains is thus not ruled out from the outset by complexities of the experimental spectra, which is important for an understanding of the "typical" situation encountered in these hydrate structures.

The Raman spectra of CCD and PTD have

[3]The angle of inclination the H–H vector makes with the *a* axis (38.5° (6), Fig. 2*B*) agrees with the value estimated from n.m.r. measurements (11, 12).

[4]There are significant differences between the two sets of unit-cell dimensions available for PTD, and likewise for CCD (*cf.* Table 1). Proper attention will have to be paid to the factors responsible for this variation (*cf.* ref. 8) if a closer comparison of bond distances and angles is to be made, the variation being a major source of uncertainty in these quantities. The same probably applies to the other $MX_2 \cdot 2H_2O$ compounds.

Can. J. Chem. Downloaded from www.nrcresearchpress.com by 210.87.254.5 on 09/05/12
For personal use only.

Can. J. Chem. Downloaded from www.nrcresearchpress.com by 210.87.254.5 on 09/05/12
For personal use only.

been studied by several authors (21, 22), as have their far-infrared spectra (23–27). Fifer and Schiffer (28–30) have reported the mid-infrared spectra of CCD at different degrees of deuteration. We have now examined the mid-infrared spectra of unoriented polycrystalline PTD, with particular attention to the spectrum of isotopically dilute H_2O, HDO, and D_2O, to see how much of the information of interest in the above context can be obtained from this type of spectroscopic evidence.[5]

Experimental

Crystals of PTD were grown, as in refs. 1 and 2, by allowing an aqueous solution of stoichiometric quantities of KCl and $CuCl_2 \cdot 2H_2O$ (Mallinckrodt, analytical grade) to evaporate at room temperature. The turquoise crystals, which appeared after 3 days, were authenticated by their X-ray powder diffraction pattern and their i.r. spectra were recorded using Nujol mull and KCl pellet techniques. No differences were observed between the spectra of mulls and pellets, or between the spectra of different samples of PTD, including a commercial sample (J. F. Baker Chemical Co.). The spectra were also identical with the survey spectrum published by Nyqvist and Kagel (31).

Pellets of PTD in KCl were also prepared directly by pressing $CuCl_2$ with a large excess of KCl. Anhydrous $CuCl_2$ and KCl were ground together in proportion of 1:100, exposed to water vapor for about 5 min and pressed into pellets at 90 000 p.s.i. in the usual manner. The spectrum of such pellets was identical with that of pellets prepared with PTD and KCl (Fig. 3 *A*, *B*), no residual bands being detected. This rapid method was particularly convenient for the preparation *in situ* of a series of samples with different deuterium contents (Fig. 3 *C–H*).

When PTD or CCD crystals (or the pale brown anhydrous $CuCl_2$) are ground with KCl, a very pale yellow powder results. Pellets pressed from this powder are pale honey-colored. This change in color initially caused some concern. Investigation showed, however, that the pale blue PTD *itself* turns pale green to pale brown on grinding in an agate mortar in atmospheric air. This color change appears to be caused by partial, reversible dehydration to the brown anhydrous K_2CuCl_4 at the surface of the PTD particles. The freshly ground pale green PTD powder still analyzed to 11.4% H_2O (11.3% required for $K_2CuCl_4 \cdot 2H_2O$), and X-ray powder photographs of the pale brown material were visually indistinguishable from those of any other PTD sample. On exposure to water vapor the color of the ground powder reverted to very pale blue. A similar color change from pale blue to rich reddish brown is observed, after several days, in PTD crystals on standing in *dry* air; even though the dehydration may affect the bulk of the crystal, the original PTD color is restored eventually on exposure to atmospheric air.

On grinding PTD or CCD with KBr the powder turns brown. The dark-brown pellets pressed from it gradually darken to brown-black and their i.r. spectra show features different from those observed with PTD mulls. Here the color change is undoubtedly due to *chemical* interaction and seems to be common to Cu^{2+} in the presence of solid KBr; the color of $KCuBr_3$, for example, ranges from red to black. This has been observed for other cupric salts (32), and we have had a similar experience with $CuSO_4 \cdot 5H_2O$.

Spectra were recorded on a Perkin–Elmer model 521 spectrophotometer from 4000 to 350 cm^{-1} for KCl pellets and to 300 cm^{-1} for Nujol mulls, at 30 and −160 °C; a few were recorded also at 90 °C. Lowering of temperature caused a considerable narrowing of most bands, but no new bands appeared. Frequency shifts were very small, averaging about +0.02 cm^{-1} deg^{-1} for the bending and only about +0.01 cm^{-1} deg^{-1} for the stretching fundamentals. The frequencies quoted in the text are for 30 °C.

The approximate H:D ratio was determined from the integrated intensities of the bands in the OH and OD stretching regions (*cf.* ref. 33).

Results and Discussion

Stretching Vibrations

The vibrationally isolated OH and OD stretching fundamentals of isotopically dilute HDO gave rise to sharp single bands at all temperatures studied (Fig. 3 *C*, *H*). The frequencies at room temperature are 3262 and 2428 cm^{-1}, respectively. The singlets confirm the equivalence of the two hydrogens, consistent with the C_{2v} site symmetry of the water molecule as determined by crystallography.

At intermediate isotopic concentrations the spectrum in the stretching region shows evidence of coupled vibrations of HDO–HDO pairs which give rise to shoulders on the sides of the peaks due to the vibrationally isolated HDO. A detailed analysis of this coupling is difficult. The broad shoulders observed include a contribution from vibrations of isotopically dilute H_2O (or D_2O in the OD stretching region), and further complications arise from possible Fermi resonance of the latter with the overtone of the H_2O (or D_2O) bending vibration. For undeuterated or fully deuterated PTD, on the other hand, the rules of factor-group splitting (Fig. 4) apply and the spectrum becomes tractable.

The observed Raman and i.r. features in the OH stretching region can be assigned on the assumption that $\nu_3 > \nu_1$ (Table 2). The Raman band at 3250 cm^{-1} is of E_g species and must therefore belong to ν_3 (Fig. 4),[6] along with the

[5]A partial account of our results has been included in a recent review (14).

[6]Our designation of symmetry species follows the convention of Adams and Newton (26). The designations used by Mathieu and Couture-Mathieu (21), in which the B_1 and B_2 modes are interchanged, have been converted to the usage of ref. 26.

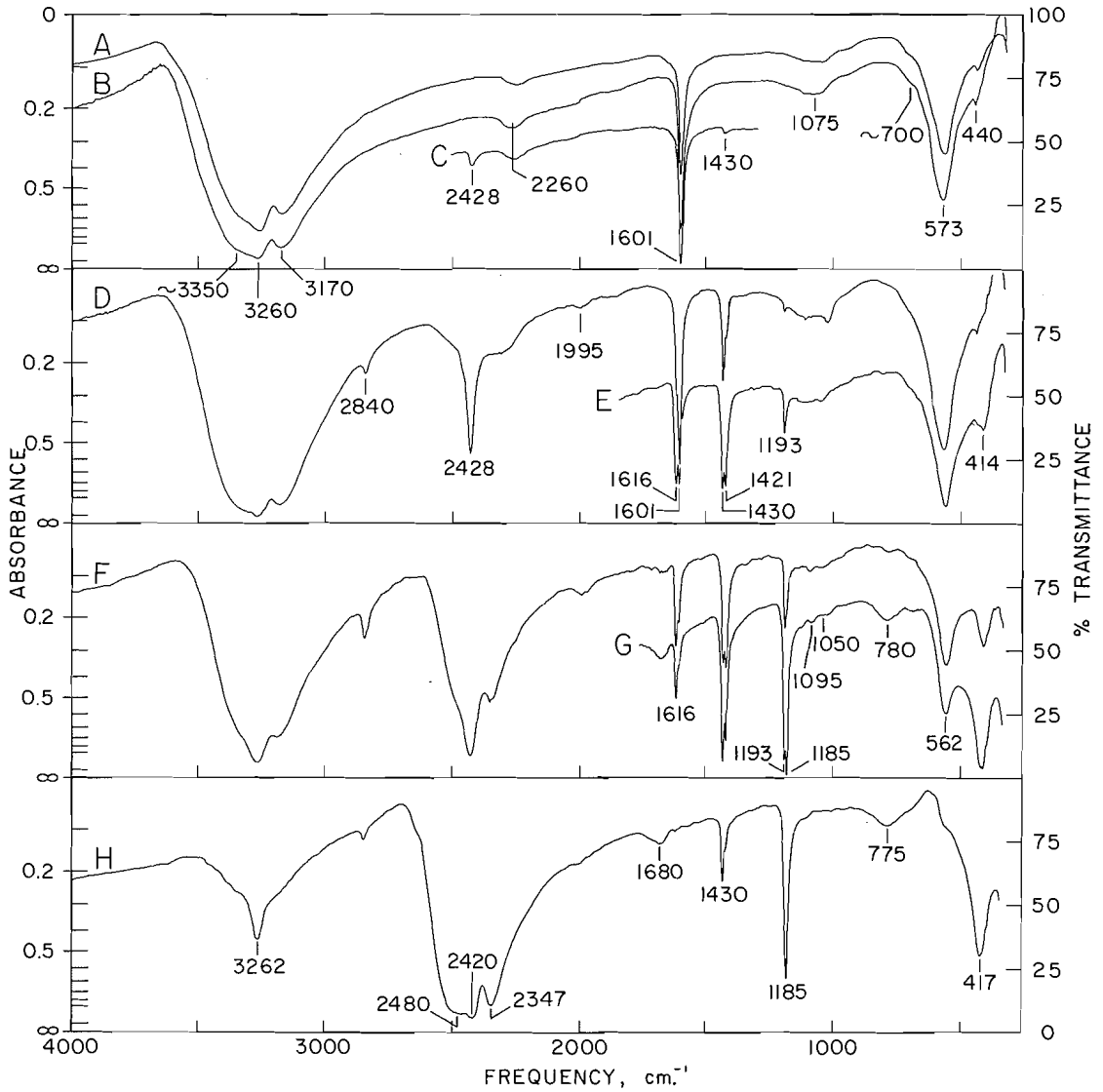

FIG. 3. Infrared spectra of $K_2CuCl_4 \cdot 2H_2O$ (KCl pellets) at different deuterium contents. *A* and *B*, 0% D; *C*, 0.6% D; *D*, 16% D; *E*, 39% D; *F*, 51% D; *G*, 73% D; *H*, 91% D. Sample *A* was obtained by dispersing $K_2CuCl_4 \cdot 2H_2O$ in KCl; samples *B* to *H* were obtained by pressing anhydrous $CuCl_2$ with excess KCl after exposure to water vapor of appropriate D content.

i.r. feature at 3350 cm^{-1} which we assign to the E_u species. The remaining Raman and i.r. bands must then belong to factor-group components of ν_1, in Fermi resonance with the overtones and other binary combinations of the factor-group components of ν_2.

Group-theoretical considerations of direct products of irreducible representations of the group D_{4h} lead to the distribution of species, after Fermi resonance, shown in Table 3: a total of eight Raman components (four observed, all of them A_{1g} species), three i.r. components (two observed), and three inactive and unobservable components. The undetected Raman components could probably be made visible by a low-temperature single-crystal study.[7]

Bending Vibrations: Partially Deuterated Crystals

At low isotopic concentrations the bending fundamentals of H_2O, HDO, and D_2O give

[7]The Raman spectra reported in ref. 21 were recorded at room temperature.

Can. J. Chem. Downloaded from www.nrcresearchpress.com by 210.87.254.5 on 09/05/12
For personal use only.

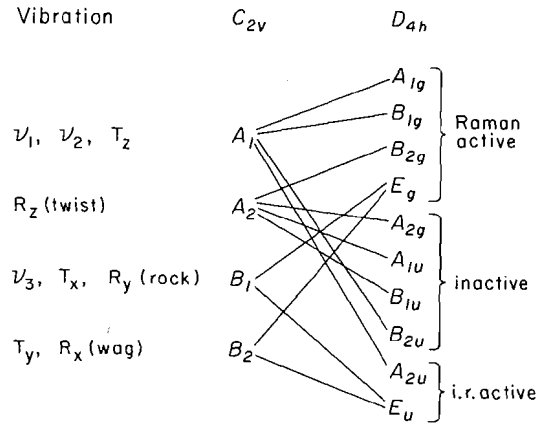

FIG. 4. Correlation of the symmetry species of the molecular (C_{2v}), site (C_{2v}), and factor (D_{4h}) groups of H_2O fundamentals in $K_2CuCl_4 \cdot 2H_2O$ (see footnote 6).

rise to single bands at 1616, 1430, and 1193 cm^{-1}, respectively (Fig. 3). These frequencies are due to the nearly independent motions of water molecules whose nearest molecular neighbors belong to other isotopic species. The fact that these vibrationally isolated bending fundamentals are singlets, even at liquid-nitrogen temperatures, confirms the existence of only one crystallographically distinct type of water molecule in PTD.

At somewhat higher concentrations of a given isotopic species one may expect additional peaks due to coupled vibrations of H_2O–H_2O (or HDO–HDO or D_2O–D_2O) pairs. In principle, every possible type of pair of water molecules of like isotopic species should couple vibrationally. However, the magnitude of the coupling should diminish rapidly with the inter-pair distance; it should also depend on the relative orientation of the molecules in a given pair as well as on the details of intermolecular bonding. The water–water pairs in PTD which correspond to the six shortest O—O distances can be seen in Fig. 5.[8]

Coupling to several types of neighboring molecules may be expected to give rise to broadened bands with many unresolved or partially resolved features changing in a complicated manner with increasing isotopic concentration as triplets, and larger groupings, of

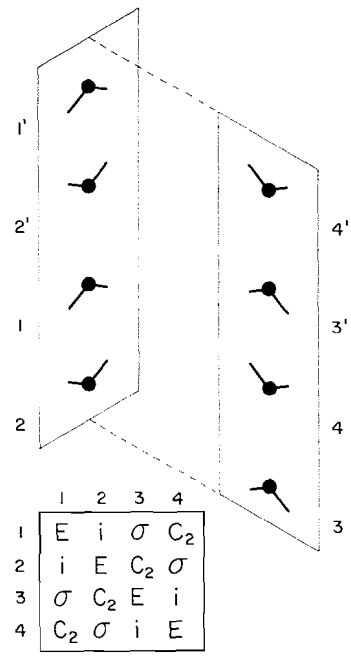

FIG. 5. Orientation of the four water molecules *1*, *2*, *3*, *4* (*cf.* footnote 8) in the unit cell of $K_2CuCl_4 \cdot 2H_2O$. The *modulo translations* E, C_2, i, σ relating these molecules form a group isomorphic with C_{2h}. They arise from coalescence of the 16 symmetry operations of the space group D_{4h}^{14} (no. 136): $\{E, C_2(z), \sigma_d(110), \sigma_d(\bar{1}\bar{1}0)\} \rightarrow E$; $\{C_2(x), C_2(y), S_4^1(z), S_4^3(z)\} \rightarrow C_2$; $\{i, \sigma_h(xy), C_2(\perp 110), C_2(\perp \bar{1}\bar{1}0)\} \rightarrow i$; $\{\sigma_v(xz), \sigma_v(yz), C_4^1(z), C_4^3(z)\} \rightarrow \sigma$.

vibrationally coupled molecules begin to occur. However, for the bending fundamentals in PTD the spectra at intermediate concentrations of each isotopic species are extremely simple: only one additional peak appears, at 1601 cm^{-1} for H_2O, 1421 cm^{-1} for HDO, and 1185 cm^{-1} for D_2O. The intensity of this peak, relative to the peak belonging to the respective vibrationally isolated molecule, increases with the concentration of the isotopic species, while its frequency is independent of the concentration. This indicates that appreciable vibrational coupling arises from *only one* type of water pair.

The relatively large inter-pair distances rule out from consideration inter-chain pairs such as *1–4*, *1–3*, and *1–3′*, as well as second-nearest neighbors within a chain such as *1–1′* and certainly more distant pairs. The vibrationally interacting pairs may thus be identified with the intra-chain pairs of type *1–2 or 1–2′*. Both types possess centers of symmetry,[9] hence the

[8] In Fig. 5 the oxygen atoms *1*, *2*, *3*, *4* correspond to oxygens B (or B′), A (or A′), D, C respectively of Fig. 1. The approximate O—O distances are *1–2′*, 3.93 Å; *1–2*, 3.99 Å; *1–4*, 5.28 Å; *1–3*, 6.60 Å; *1–3′*, 6.61 Å; *1–1′*, 7.92 Å.

[9] One half of the HDO–HDO pairs do not possess centers of symmetry.

Can. J. Chem. Downloaded from www.nrcresearchpress.com by 210.87.254.5 on 09/05/12
For personal use only.

TABLE 2. Vibrational frequencies of water in $K_2CuCl_4 \cdot 2H_2O$ between 350 and 4000 cm^{-1} at room temperature

	H_2O		HDO	D_2O
	Raman (21)	I.r.	I.r.	I.r.
OH stretch	3340 ν_1 A_{1g}* 3275 ν_1 A_{1g}* 3250 ν_3 E_g 3235 ν_1 A_{1g}* 3170 ν_1 A_{1g}*	~3350 ν_3 E_u†‡ 3260 ν_1 A_{2u}*†‡ 3170 ν_1 A_{2u}*†‡	3262§	
$2\nu_2$			2840	
OD stretch			2428§	2480 ν_3 E_u†‡ 2420 ν_1 A_{2u}*†‡ 2347 ν_1 A_{2u}*†‡
$\nu_2 + \nu_L$		2260	1995	1680
ν_2 (isolated)		1616§	1430§	1193§
ν_2 (coupled)	1630 B_{1g} 1628 A_{1g}	1601 A_{2u}† (1605 B_{2u})‖	1421	1185 A_{2u}†
$2\nu_L$, $\nu_T + \nu_L$, $2\nu_T$		1075 950	~1095 ~1050 ~780	775
ν_L Rock	685 E_g	~700 E_u†?		
ν_L Wag	633 E_g	573 E_u†	562**	417 E_u†
ν_L Twist	~550 B_{2g}¶		414††	
ν_T (Cu—O stretch)	404 A_{1g} (25) 395 B_{1g} (25)	440 A_{2u}	(428)‡‡	(417)‡‡

*In Fermi resonance with overtones and binary combinations of ν_2.
†Symmetry species assigned from vibrational analysis.
‡Assignment based on the assumption that $\nu_3 > \nu_1$.
§Isotopically isolated spectra.
‖Inactive component; frequency estimated on the assumption that the mean frequency of the four factor-group components equals the isotopically isolated frequency.
¶In ref. 21 this band was observed more clearly for $Rb_2CuCl_4 \cdot 2H_2O$ and $(NH_4)_2CuCl_4 \cdot 2H_2O$.
**Largely out-of-plane H motion.
††Largely out-of-plane D motion.
‡‡Calculated value; region blocked by more intense HDO and D_2O bands. The corresponding Raman A_{1g} frequency is 387 cm^{-1} (26).

TABLE 3. Factor-group components of ν_1 and $2\nu_2$ which may undergo Fermi resonance

Components of "$2\nu_2$"	Components of ν_1
Overtones	
$A_{1g} \times A_{1g} = A_{1g}$ $B_{1g} \times B_{1g} = A_{1g}$ $B_{2u} \times B_{2u} = A_{1g}$ $A_{2u} \times A_{2u} = A_{1g}$	A_{1g} (Raman)
Combinations	
$A_{1g} \times B_{1g} = B_{1g}$ $A_{2u} \times B_{2u} = B_{1g}$	B_{1g} (Raman)
$A_{1g} \times A_{2u} = A_{2u}$ $B_{1g} \times B_{2u} = A_{2u}$	A_{2u} (i.r.)
$A_{1g} \times B_{2u} = B_{2u}$ $A_{2u} \times B_{1g} = B_{2u}$	B_{2u} (inactive)

in-phase coupled vibration can be expected to be i.r.-inactive while the out-of-phase coupled vibration would give rise to a single i.r. peak, as observed.

Bending Vibrations: Isotopically Pure Crystals

For crystals containing only H_2O or only D_2O, factor-group analysis (Fig. 4) predicts the bending fundamental to split into one i.r. active component, A_{2u}, two Raman-active components, A_{1g} and B_{1g}, and one inactive component, B_{2u}. For H_2O bending, the three active frequencies are known (Table 2) and the inactive B_{2u} frequency may be estimated by assuming that the average of the frequencies of the four coupled components equals the frequency of the isolated fundamental (*cf.* ref. 30). These four coupled bending vibrations involve the following in-phase (+) and out-of-phase

Can. J. Chem. Downloaded from www.nrcresearchpress.com by 210.87.254.5 on 09/05/12
For personal use only.

(−) vibrations of the molecules in two neighboring chains (two unit cells shown, as in Fig. 5):

+ +	+ −	+ +	+ −
+ +	+ −	− −	− +
+ +	+ −	+ +	+ −
+ +	+ −	− −	− +
A_{1g}	B_{1g}	A_{2u}	B_{2u}
1628	1630	1601	1605 cm^{-1}

In the two *g* vibrations the motions of neighboring water molecules in each chain are in phase, while in the two *u* vibrations they are out of phase. The frequency difference between the B_{1g} and A_{1g} motions (2 cm^{-1}), or between the B_{2u} and A_{2u} motions (4 cm^{-1}) is small. By contrast, there is a 26 cm^{-1} difference between the mean of the frequencies of the two *g* vibrations and the mean for the two *u* vibrations. We conclude that appreciable vibrational coupling only occurs for the intra-chain pairs *1–2* and *1–2′* (=*3–4*), whereas inter-chain pairs such as *1–3* and *1–4* appear to vibrate nearly independently. This agrees with the independent conclusion from the analysis of the i.r. spectra of partially deuterated PTD samples. An analogous situation appears to exist in CCD, whose spectra also show large frequency differences between the *g* and *u* motions, but much smaller differences between the *A* and *B* motions (30).

Unfortunately there seems to be no way of determining which of the two pairs *1–2* and *1–2′* is actually responsible for the main coupling of the bending motions, either in PTD or CCD. Fifer and Schiffer (30) carried out a calculation of the intermolecular force constants for the coupling of the bending motions of the four water molecules in the unit cell of CCD. However, as in PTD, a single coupling force constant F_{12} includes contributions from both *1–2* and *1–2′* interactions, and there appears no way to estimate the individual magnitudes of these two interactions. It may be added that F_{12} must be equal to F_{34} since by definition (30) each measures the coupling between a water molecule and all the water molecules related to it by inversion in centers of symmetry. As all water molecules in these crystals are equivalent, F_{12} and F_{34} are equal by symmetry and cannot be different as has been implied by Fifer and Schiffer (ref. 30, footnote 16).

Rotatory and Translatory Vibrations

In the region between 350 and 700 cm^{-1} one expects bands due to the three rotational vibrations (librations) of the H_2O molecule and the highest translatory vibration, that corresponding to Cu—O stretching. Under the factor-group selection rules these four vibrations should yield a total of twelve components, five of which are Raman active and three i.r. active.

Earlier assignments for PTD show discrepancies (Table 5) stemming in part from the failure of the authors of refs. 23–26 to make use of the complete Raman study of PTD published in 1953 (21) and to examine spectra of fully and partially deuterated samples. While assignments in this region are notoriously difficult, our assignment (Table 2 and discussion below) is the best that can be made on the basis of the evidence available at present.

The translational vibration should be distinguishable by the H_2O/D_2O frequency ratio of about $(20/18)^{1/2} = 1.05$, in contrast to the ratio of 1.35–1.41 for the librations. If the i.r. band at 440 cm^{-1} were due to a libration, one would expect the corresponding D_2O band near 320 cm^{-1}; if it were due to a translational vibration, the D_2O band would be expected near 417 cm^{-1} and the HDO band, near 428 cm^{-1}. Since there are no detectable bands near 320 cm^{-1} in the i.r. spectrum of the deuterated hydrate (Fig. 3), we must conclude that the 440 cm^{-1} band cannot arise from a libration. Its assignment to the translatory vibration, on the other hand, is consistent with the effect of deuteration, the spectrum near 417 and 428 cm^{-1} showing strong absorption due to D_2O and HDO respectively. The two Raman bands in this region (both at 396 cm^{-1} in ref. 21 and at 395 and 404 cm^{-1} in ref. 26) are unequivocally assigned to components of the *z*-axis (‖*c*-axis of the crystal) translation on the basis of their symmetry species A_{1g} and B_{1g}. The assignment of the 440 cm^{-1} i.r. band to the A_{2u} component (26) leads to a reasonable value for the maximal factor-group splitting of 440 − 395 = 45 cm^{-1}.

The Raman band at about 550 cm^{-1} in the spectrum of ref. 21 has the symmetry species B_{2g} and can therefore be unequivocally assigned to the twisting libration. This libration has no i.r. active component.

The remaining two Raman bands at 633 and 685 cm^{-1} in the spectrum of ref. 21 belong clearly to the rocking and wagging librations. However, as they both are of the same species, E_g, they cannot be distinguished by symmetry,

Can. J. Chem. Downloaded from www.nrcresearchpress.com by 210.87.254.5 on 09/05/12
For personal use only.

TABLE 4. Vibrational assignments by previous authors in the 350–700 cm^{-1} region of $K_2CuCl_4 \cdot 2H_2O$

Mode		Raman (ref. 21)	I.r. (refs. 23, 24)	I.r. (ref. 25)	Raman (ref. 26)	I.r. (ref. 26)
H_2O librations	Rock, Wag, Twist	*685 E_g, 633 E_g, 550 B_{2g}		395 E_u, 575 E_u		
Cu—O stretch		396 A_{1g}, 396 B_{1g}	573 A_{2u}	445 A_{2u}	404 A_{1g}, 395 B_{1g}	445 A_{2u}

*Order uncertain.

and some other consideration must be employed. The order of their frequencies, or of their relative intensities in the i.r. or Raman spectra, is not a useful guide in the assignment, for both the frequency and the intensity of the absorptions due to these two modes seem to depend on details of the force field about the water molecule. For example, in vibrational assignments reported to-date the rocking frequency has been placed about as often *above* the wagging frequency (34–39) as *below* it (22, 25, 40–43). It may be commented in passing that many of the assignments in these references are far from conclusively proven.

One means of distinguishing between the rocking and wagging vibrations depends on the cation effect. As suggested by Adams and Lock (25), in hydrate structures related to PTD the wagging frequency may be expected to be sensitive to replacement of the cation, while the rocking frequency should be relatively insensitive to such change. The Raman spectra of ref. 21 clearly show that in the series $(NH_4)_2CuCl_4 \cdot 2H_2O - K_2CuCl_4 \cdot 2H_2O - Rb_2CuCl_4 \cdot 2H_2O$ the lower-frequency band shifts from 625 to 633 to 635 cm^{-1}, while the higher-frequency band remains stationary at 685 cm^{-1}. Adams and Lock's suggestion would lead to the assignment of the 633 cm^{-1} band to wagging and the 685 cm^{-1} to rocking.

The intense i.r. band at 573 cm^{-1} has previously been assigned, incorrectly, to Cu—O stretching (Table 4). This interpretation rested on an assignment of the i.r. band at 562 cm^{-1} to the corresponding D_2O band (24). Our study shows, however, that this band disappears at high deuterium contents, hence it belongs to HDO. The corresponding D_2O band is actually at 417 cm^{-1} and the ratio of 573/417 = 1.374 requires this band to be assigned to a libration. It could correspond either to the wagging or to the rocking mode. Comparison with the HDO spectrum leads us to assign this band to the E_u component of the wagging libration. This assignment agrees far better with the expected relations between frequencies and intensities of the librational modes (Fig. 6). Assignment of the 573 cm^{-1} band to wagging also yields a reasonable value for the correlation-field splitting of this mode, 633 − 573 = 60 cm^{-1}. The alternative assignment to the rocking would have led to an unexpectedly large value of the correlation-field splitting of 685 − 573 = 112 cm^{-1}. The HDO frequencies at 562 (observable at high deuterations) and 414 cm^{-1} (observable at low deuterations) correspond clearly to the H and D out-of-plane motions respectively (*a* and *b*, Fig. 6).

Finally, the assignment of the very weak shoulder at 700 cm^{-1} to the E_u component of the H_2O rocking frequency is less certain than the other assignments.

In the above discussion we have neglected mixing of the wagging and rocking vibrations, which is in principle possible, as the factor-group components of these two librations belong to the same symmetry species (Fig. 4). We note, however, that of the two Raman-active E_g bands one exhibits a very pronounced cation effect while the other does not: appreciable mixing of the two librations would have led to two bands with comparable cation effects. Furthermore, there is only one i.r. active band of appreciable intensity, whereas mixing of the two librational modes would tend to give rise to a pair of bands of comparable intensity.

Combination Modes Involving Librations

The factor-group components of the three librational modes of H_2O can, in principle, appear as combination modes with various factor-group components of the bending vibra-

Can. J. Chem. Downloaded from www.nrcresearchpress.com by 210.87.254.5 on 09/05/12
For personal use only.

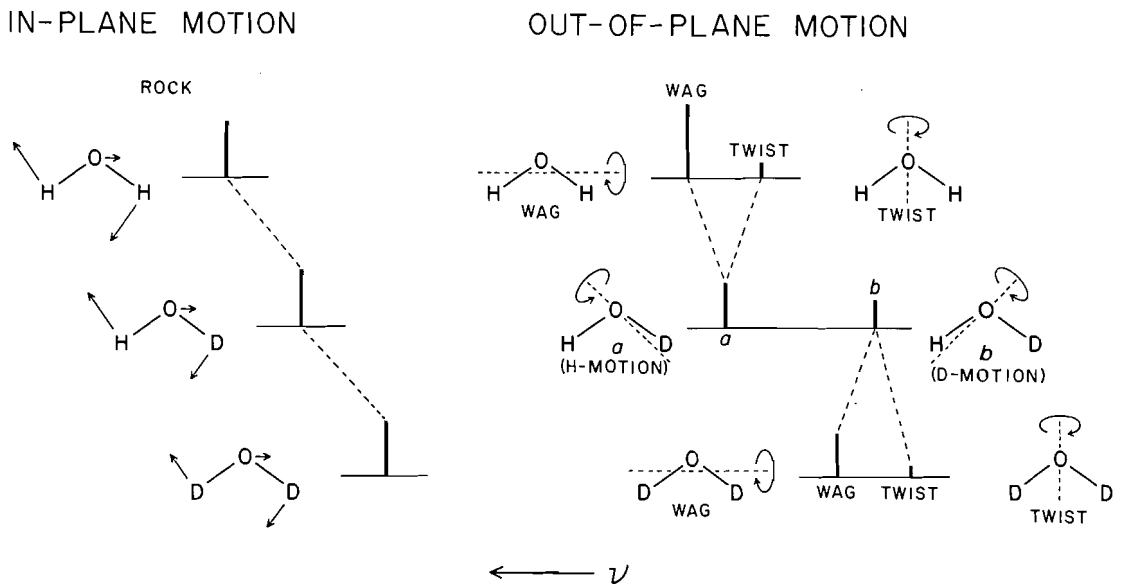

FIG. 6. Relation between the motions and the frequencies of the librational modes of H_2O, HDO, and D_2O in $K_2CuCl_4 \cdot 2H_2O$. The frequencies shown could refer either to the mean frequencies of factor-group components or to those of vibrationally isolated water molecules.

tion, $\nu_2^i + \nu_L^j$, with components of the translatory modes, $\nu_T^i + \nu_L^j$, or with themselves, $\nu_L^i + \nu_L^j$.[10]

The observed band at 2260 cm^{-1} for H_2O corresponds clearly to the combination $\nu_2 + \nu_L$. As there are four factor-group components of the bending vibration ν_2 ($A_{1g} + A_{2u} + B_{1g} + B_{2u}$) and eight factor-group components of the various librations ($A_{1u} + A_{2g} + B_{1u} + B_{2g} + 2E_g + 2E_u$), 32 distinct combinations of the type $\nu_2^i + \nu_L^j$ are possible. Eight of these modes belong to E_u and are in principle i.r. active. The calculated frequencies of these eight modes are 2201, 2203, 2234, 2238, 2286, 2290, 2328, and 2330, with a mean frequency of 2263 cm^{-1}. The observed band, centered at 2260 cm^{-1}, does not correspond to any of the individual calculated frequencies, but seems to represent a superposition of many, or most, of the allowed components.

The observed broad bands in the region 1075–950 cm^{-1} for H_2O correspond to the combinations $\nu_L + \nu_L$ and $\nu_T + \nu_L$. There are 36 distinct combinations of the type $\nu_L^i + \nu_L^j$, of which eight are true overtones ($i = j$). Considering the representation of the direct product shows that these 36 combinations give rise to 66 distinct components, of which 14 are i.r. active, $6A_{2u} + 8E_u$. The 64 possible combinations of the type $\nu_T^i + \nu_L^j$ give rise to 112 components, 24 of which are i.r. active, $8A_{2u} + 16E_u$. The values of many of these combination frequencies cannot be estimated, since the frequencies of three components of the fundamental librations, and five of the translations, are not available. The observed bands, with their complex shapes and complicated changes upon deuteration, appear to be the superpositions of many of the allowed components.

Comparison of the Structural Environment and of the Vibrational Spectrum of Water in PTD and CCD

The fundamental frequencies of water in PTD and CCD are compared in Table 5. The lower OH and OD stretching frequencies in PTD are consistent with the stronger hydrogen bonding in this hydrate. The O...Cl distance estimated from the correlation of stretching frequency and O...Cl separation (14) is 3.21(3) Å for CCD and 3.14(3) Å for PTD; the difference, 0.07(5) Å, agrees with the value derived from the neutron diffraction studies, 0.08(1) Å.

[10]The superscripts refer to the individual factor-group components.

Can. J. Chem. Downloaded from www.nrcresearchpress.com by 210.87.254.5 on 09/05/12
For personal use only.

TABLE 5. Comparison of the stretching, bending, and librational frequencies (cm^{-1}) of water in $K_2CuCl_4 \cdot 2H_2O$ and $CuCl_2 \cdot 2H_2O$

Mode	Frequencies	
	$K_2CuCl_4 \cdot 2H_2O$*	$CuCl_2 \cdot 2H_2O$
Stretching		
OH of HDO	3262	3385 (30)
OD of HDO	2428	2511 (30)
Bending		
HOH	1616	1602 (30)
HOD	1430	1419 (30)
DOD	1193	1187 (30)
H_2O librations		
Rock (Raman)	685	778 (22)
Wag (Raman)	633	693 (22) 669 (22)
Wag (i.r.)	573†	719‡ 685‡
Average	630	709

*See Table 2.
†The most intense component.
‡From Nujol mulls of CCD in this work.

If other effects can be neglected, stronger hydrogen bonding would be expected to raise the bending and librational frequencies. The bending frequencies in PTD are indeed higher than in CCD. The librational frequencies, on the other hand, are lower in PTD by an average of about 80 cm^{-1}.[11] This shows that the frequencies of the librational motions must depend strongly on details of inter-chain packing in the two structures. A qualitative consideration of bonding about the Cl atoms that are ligated to the water molecule (Figs. 1 and 2) shows that movement of these atoms to follow the motions of the hydrogens in the wag and twist librations is opposed by the force constant of the Cu—Cl bond in CCD, whereas in PTD it is essentially unopposed. This could explain the higher frequency, in CCD, of the wag and possibly also of the rock, since the wag and rock librations in CCD are of the same symmetry species and some mixing of the two motions can be expected.

While there is no simple relation between librational frequencies and hydrogen bonding about water in hydrate structures in general (14), the stretching and librational frequencies of H_2O may be correlated in isostructural series of compounds. This is observed, for example, in $MSO_4 \cdot H_2O$ sulfates of the kieserite type (44). However, as the present results show, outside such series the correlation fails even for structures in which the nearest-neighbor environments of the water molecule are as similar as those in CCD and PTD. The libration frequencies of water are thus seen to depend significantly on details of crystal structure beyond the nearest hydrogen-bonded neighbors.

Coupling of Bending Vibrations in Crystalline Hydrates

It appears that in PTD and CCD appreciable coupling of bending, and very likely also of stretching, vibrations of water molecules may be limited to fairly near H_2O neighbors. We have surveyed the small number of hydrates for which spectroscopic information on coupling of the bending vibrations exists. Although the evidence available to-date is scant, in all the cases where the existence of such coupling has been demonstrated the water molecules are "connected" either directly, through a hydrogen bond, or indirectly, by hydrogen or water–metal "bonds" to a common atom. If additional investigations confirm that coupling of bending vibrations is limited to "connected" water molecules, the

[11]Several of the factor-group components are not known, and the twist mode has not been clearly observed for CCD. Nevertheless, it seems unlikely that omission of inactive and unobserved frequencies can reduce the average librational frequency in CCD below that of PTD.

Can. J. Chem. Downloaded from www.nrcresearchpress.com by 210.87.254.5 on 09/05/12
For personal use only.

presence or absence of the coupling will be of value in making structural predictions from vibrational spectra.

We thank Mr. P. F. Seto for assistance with the experimental work and Dr. D. A. Othen for helpful comments on the manuscript.

1. S. B. HENDRICKS and R. G. DICKINSON. J. Am. Chem. Soc. **49**, 2149 (1927).
2. L. CHROBAK. Z. Krist. **88**, 36 (1934).
3. T. O. KLAASSEN and N. J. POULIS. J. Phys. **32**, CI-1157 (1971).
4. R. W. G. WYCKOFF. Crystal structures. Vol. 3. 2nd ed. Interscience, New York. 1965.
5. R. CHIDAMBARAM, Q. O. NAVARRO, A. GARCIA, K. LINGGOATMODJO, S.-C. LIN, I.-H. SUH, A. SEQUEIRA, and S. SRIKANTA. Acta Cryst. B, **26**, 827 (1970).
6. S. W. PETERSON and H. A. LEVY. J. Chem. Phys. **26**, 220 (1957).
7. H. E. SWANSON, H. F. MCMURDIE, M. C. MORRIS, E. H. EVANS, B. PARETZKIN, J. D. DEGROOT, and S. J. CARMEL. Natl. Bur. Std. Monogr. **25**, sect. 9. p. 34. December 1971.
8. Å. ENGBERG. Acta Chem. Scand. **24**, 3510 (1970).
9. D. HARKER. Z. Krist. **93**, 136 (1936).
10. C. H. MACGILLAVRY and J. M. BIJVOET. Z. Krist. **94**, 231 (1936).
11. J. ITOH, R. KUSAKA, Y. YAMAGATA, R. KIRIYAMA, and H. IBAMOTO. Physica, **19**, 415 (1953).
12. J. ITOH, R. KUSAKA, R. KIRIYAMA, and Y. SAITO. Mem. Inst. Sci. Ind. Res. Osaka Univ. **14**, 1 (1957).
13. S. H. CHOH and C. V. STAGER. Can. J. Phys. **49**, 144 (1971).
14. M. FALK and O. KNOP. *In* Water: a comprehensive treatise. Vol. 2. *Edited by* F. Franks. Plenum Press, New York. 1973. Chapt. 2.
15. B. MOROSIN and E. J. GRAEBER. J. Chem. Phys. **42**, 898 (1965).
16. B. MOROSIN. J. Chem. Phys. **47**, 417 (1967).
17. B. MOROSIN and E. J. GRAEBER. Acta Cryst. **16**, 1176 (1963).
18. B. MOROSIN. J. Chem. Phys. **44**, 252 (1966).
19. E. PRINCE. J. Chem. Phys. **56**, 4352 (1972).
20. B. MOROSIN. Acta Cryst. **23**, 630 (1967).
21. J.-P. MATHIEU and L. COUTURE-MATHIEU. J. Chim. Phys. **50**, 573 (1953).
22. I. R. BEATTIE, T. R. GILSON, and G. A. OZIN. J. Chem. Soc. A, 534 (1969).
23. J. T. R. DUNSMUIR and A. P. LANE. J. Chem. Soc. A, 2724 (1971).
24. D. M. ADAMS and P. J. LOCK. J. Chem. Soc. A, 620 (1967).
25. D. M. ADAMS and P. J. LOCK. J. Chem. Soc. A, 2801 (1971).
26. D. M. ADAMS and D. C. NEWTON. J. Chem. Soc. A, 3507 (1971).
27. K. FUKUSHIMA and T. YANAGIDA. Bull. Chem. Soc. Jap. **45**, 2285 (1972).
28. R. A. FIFER and J. SCHIFFER. J. Chem. Phys. **50**, 21 (1969).
29. R. A. FIFER and J. SCHIFFER. J. Chem. Phys. **52**, 2664 (1970).
30. R. A. FIFER and J. SCHIFFER. J. Chem. Phys. **54**, 5097 (1971).
31. R. A. NYQVIST and R. O. KAGEL. Infrared spectra of inorganic compounds. Academic Press, New York. 1971.
32. F. BRÉHAT, B. WYNCKE, and A. HADNI. C. R. Acad. Sc. Paris, B, **267**, 778 (1968).
33. V. SEIDL, O. KNOP, and M. FALK. Can. J. Chem. **47**, 1361 (1969).
34. G. SARTORI, C. FURLANI, and A. DAMIANI. J. Inorg. Nucl. Chem. **8**, 119 (1958).
35. T. MIYAZAWA. J. Chem. Soc. Jap. **34**, 202 (1961).
36. I. NAKAGAWA and T. SHIMANOUCHI. Spectrochim. Acta, **20**, 429 (1964).
37. H. J. PRASK and H. BOUTIN. J. Chem. Phys. **45**, 3284 (1966).
38. G. CHOTTARD, J. FRAISSARD, and B. IMELIK. Bull. Soc. Chim. Fr. 4331 (1967).
39. H. D. LUTZ, H.-J. KLÜPPEL, M. FEHÉR, and S. BURSIAN. Ber. Bunsenges. Phys. Chem. **75**, 583 (1971).
40. J. VAN DER ELSKEN and D. W. ROBINSON. Spectrochim. Acta, **17**, 1249 (1961).
41. I. GAMO. Bull. Chem. Soc. Jap. **34**, 1430 (1961).
42. J. GUILLERMET and A. NOVAK. J. Chim. Phys. **66**, 68 (1969).
43. K. FUKUSHIMA and H. KATAIWA. Bull. Chem. Soc. Jap. **43**, 690 (1970).
44. H. R. OSWALD. Helv. Chim. Acta, **48**, 590 (1965).

Can. J. Chem. Downloaded from www.nrcresearchpress.com by 210.87.254.5 on 09/05/12
For personal use only.

A Stereospecific Synthesis of the Denudatine Skeleton: Stereospecificity of the C/D Ring Construction by Diene Addition

KAREL WIESNER, PAK-TSUN HO, AND SADAO OIDA

Natural Products Research Center, University of New Brunswick, Fredericton, New Brunswick

Received November 14, 1973

The diene **20** synthesized by the aziridine rearrangement method was shown to add maleic anhydride with complete stereospecificity to yield the adduct **21**. The causes of this stereospecificity and its implications for the synthesis of denudatine type compounds are discussed.

On montre que le diène **20** synthétisé par la méthode du réarrangement de l'aziridine donne par réaction avec l'anhydride maléique, une addition complètement stéréospécifique conduisant au produit **21**. On discute des causes de cette stéréospécificité et de ses implications pour la synthèse de composés du type dénatudine.

[Traduit par le journal]

Can. J. Chem., **52**, 1042 (1974)

Introduction

A stereospecific synthesis of the denudatine skeleton is quite important. It may lead not only to the synthesis of denudatine (**i**) itself, but also to the synthesis of polysubstituted compounds such as **ii**. Ejection of the leaving group X from **ii** may in turn lead by a biogenetic type rearrangement to the product **iii** which is a simple functional derivative of the alkaloid chasmanine.

Such a rearrangement was realized for the first time experimentally when Johnston and Overton (1) converted the atisine derivative **iv** to the product **v** in excellent yield by pyrolysis. A short time later similar rearrangements were accomplished by Ayer and Deshpande (2).

Recently we have worked out synthetic methods for the aromatic intermediates **vi** and **vii** (3, 4). In these syntheses all the substituents materialized automatically in the desired positions simultaneously with the stereospecific construction of the skeleton. Consequently the functional group system of compounds **i** and **ii** should pose no problem.

However, it is first necessary to find an efficient conversion of the benzene ring in the aromatic intermediates to the substituted C/D ring system of compounds **i** and **ii**.

Discussion

The most obvious possibility by which this might be accomplished very simply is the addition of a suitable dienophile to a diene of the type **20**.

However, fundamental knowledge for the reliable planning of such a synthesis is lacking. It is not quite clear what the stereochemistry of the adduct between diene **20** and a dienophile would be. If the Diels–Alder addition is governed by steric hindrance to the approach of the dienophile, inspection of the model reveals that both possible adducts might be formed. On the other hand, the well known preference of the bicycloheptene system for *exo* attack in ionic reactions gives one, in spite of the lack of precedent, the feeling that the Diels–Alder reaction would be stereospecific and that the dienophile would approach the diene from the β side.

In order to solve this preliminary but crucial stereochemical problem we have decided to synthesize the unsubstituted diene **20** and to investigate the stereospecificity of the Diels–Alder reaction between this compound and maleic anhydride.

The starting material for the synthesis of the diene **20** was compound **1**. We have described in a recent publication (4) the synthesis of this material, which is in principle a mixture of four diastereoisomers, and its conversion to the aromatic intermediate **vi**. Since the alcoholic group of compound **1** was not needed in the present synthesis, it was mesylated and the mesylate **2** was reduced with lithium aluminum hydride to compound **3** which behaved as homogeneous material in thin-layer chromatography. This last product was now converted to the aromatic compound **15** via the intermediates **4**–**14**. This synthesis is only formally new as it is precisely analogous to the synthesis

Can. J. Chem. Downloaded from www.nrcresearchpress.com by 210.87.254.105 on 09/05/12
For personal use only.

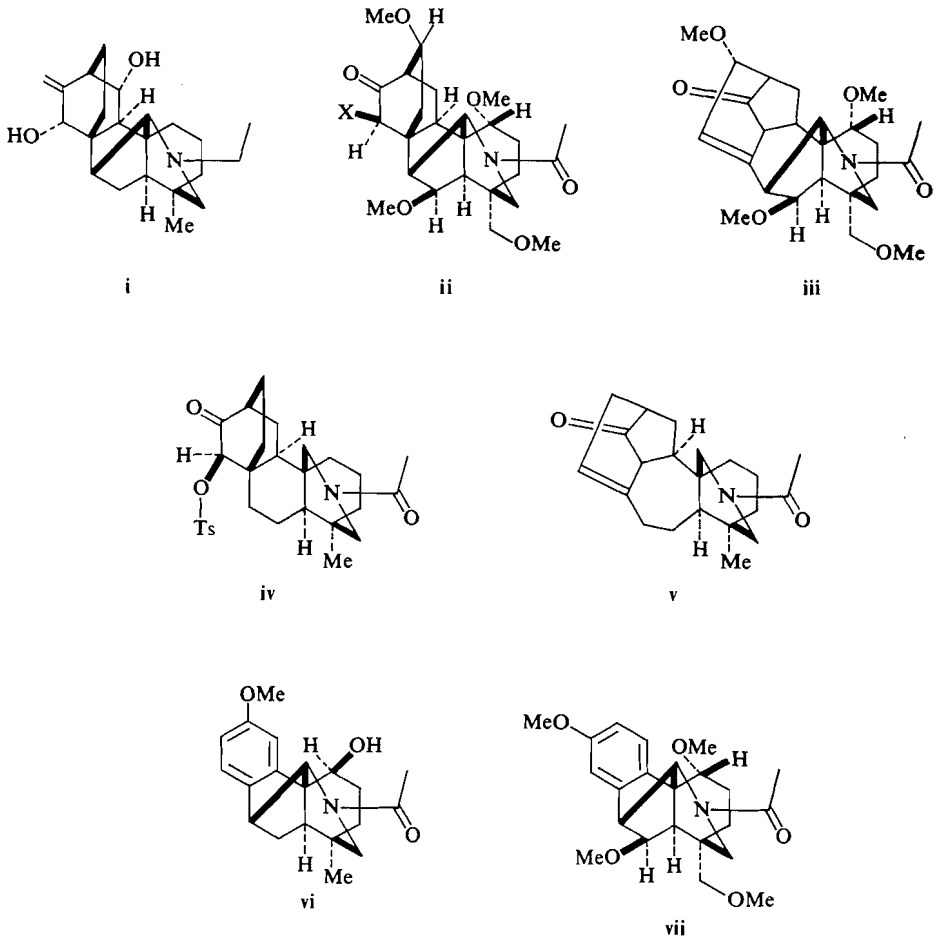

SCHEME 1

of **vi** (4) and we record the preparation of the relevant intermediates in the Experimental. The advantage of removing the future ring A functional group at an early stage rather than reducing simply the alcoholic group in compound **vi** is the greater simplicity of several work-ups since all the intermediates starting with compound **7** are sterically homogeneous. Compound **15** was now subjected to a Birch reduction followed by a reacetylation and the resulting dihydroderivative **16** was hydrolyzed with dilute oxalic acid to the crude β,γ-unsaturated ketone **17** in a yield of 95%. This relatively unstable product was immediately reduced with sodium borohydride to the alcohol **18**.

Mesylation of this last material gave the oily mesylate **19** which on treatment with potassium *t*-butoxide in dimethyl sulfoxide yielded the unstable diene **20**. The diene showed the expected u.v. spectrum (λ_{max}^{EtOH} = 274 nm, log ε 4.06) and molecular ion in mass spectrometry but it had to be used immediately in the next step. Thus, the diene was fully characterized as its beautifully crystalline Diels–Alder adduct **21** which was the final product of the present synthesis.

The Diels–Alder addition between the diene **20** and maleic anhydride in refluxing benzene gave a single homogeneous product, which after chromatography and recrystallization, was obtained in a yield of 60%. The configuration of this product is portrayed by the structure **21**. The dienophile has added to the β face of the molecule with complete stereospecificity and as expected the anhydride was orientated *endo* with respect to the diene system. The correctness of this configuration follows from the n.m.r. signal

Can. J. Chem. Downloaded from www.nrcresearchpress.com by 210.87.254.105 on 09/05/12
For personal use only.

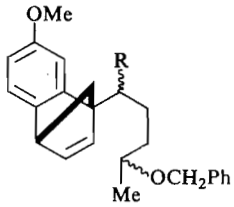

1 R = OH

2 R = O—S(=O)(=O)—Me

3 R = H

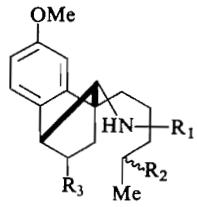

4 R_1 = SO_2Ph; R_2 = OCH_2Ph; R_3 = OAc

5 R_1 = C(=O)—Me; R_2 = OCH_2Ph; R_3 = OH

6 R_1 = C(=O)—Me; R_2 = R_3 = OH

7 R_1 = C(=O)—Me; R_2 = R_3 = =O

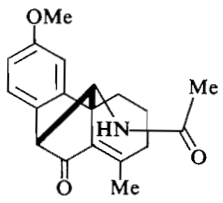

8

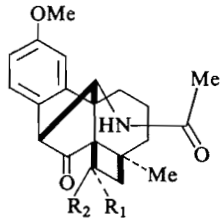

9*a* R_1 = OAc; R_2 = H

9*b* R_1 = H; R_2 = OAc

SCHEME 2

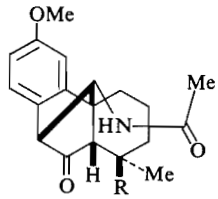

10 R = CH_2CHO

11 R = 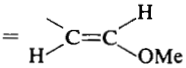

12 R = COOMe

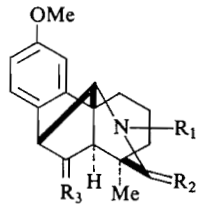

13 R_1 = H; R_2 = R_3 = O

14 R_1 = H; R_2 = O; R_3 = H_2

15 R_1 = C(=O)—Me; R_2 = R_3 = H_2

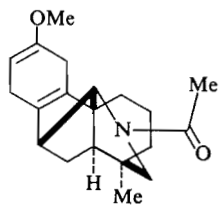

16

SCHEME 3

Can. J. Chem. Downloaded from www.nrcresearchpress.com by 210.87.254.105 on 09/05/12
For personal use only.

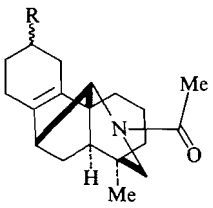

17 R = =O
18 R = OH

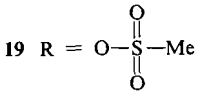

19 R = O—S(=O)(=O)—Me

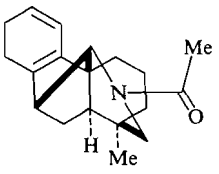

20

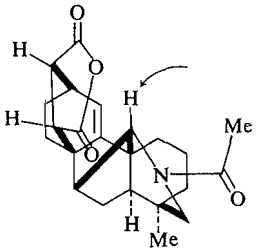

21

SCHEME 4

of the apex hydrogen marked with an arrow in formula **21**. This hydrogen is experiencing the deshielding field of the anhydride group and consequently its signal which is a broad singlet is shifted significantly downfield (τ = 6.48 p.p.m.) in comparison with, for example, the same hydrogen in compound **18** (τ = 6.87 p.p.m.).

In view of the importance of this result both fundamentally and for the planning of our synthetic work, we had hoped to corroborate the configuration of compound **21** by an X-ray structure determination. However, in spite of crystallizing beautifully compound **21** refused to yield to X-ray methods. Fortunately, a second project which proceeded in our laboratories simultaneously made this corroboration unnecessary. In an attempt to work out an alternative synthesis of the C/D ring system of songorine Dr. R. C. Jain performed the synthesis of compound **xii** starting with the diene **viii** via the intermediates **ix**, **x**, and **xi**. The configuration of **xii** was determined by Dr. J. F. Blount, Hoffmann-La Roche, Nutley, New Jersey, by single crystal X-ray analysis. The step **viii** → **ix** of this synthesis was a Diels–Alder addition of acetoxyacrylo nitrile followed by hydrolysis. Also, in this case complete stereospecificity was observed and Dr. Blount's analysis proved rigorously that the dienophile added to the β or *exo* face of the molecule.

The preference of bicycloheptenes for reaction from the *exo* side was discussed a few years ago by Schleyer (5). In the case of carbonium ions derived from the 1,2,2-bicycloheptane system this preference is usually ascribed to bond delocalization resulting in the nonclassical character of such ions. However, this clearly cannot be the whole story since the same selectivity is also observed in the preferential base catalyzed exchange of the *exo* hydrogen in norcamphor (*cf.* ref. 5). We feel that whatever directional forces are at work in all these cases (and Schleyer's explanation seems to us to be at least a part of the truth) are also responsible for the stereospecific outcome of the Diels–Alder additions described in this article.

The significance of the present work for the planning of syntheses of denudatine type compounds is clear. The α branch of the 2,2,2-bicyclooctane system in compounds **i** or **ii** must be derived from the ring containing the diene system and the β branch from the dienophile. Consequently, it is necessary to place into the ring containing the diene functions which are capable of a simple elaboration into the functionality of the final product.

In this connection the ingenious device discovered by Deslongchamps (6) comes to mind. The aromatic intermediate **xiii** can be converted by the Deslongchamps method in one step to the quinonoid diene **xiv** which seems to be an eminently suitable candidate for our purposes.

Experimental

Preparation of the Mesylate 2

The alcohol **1** (14.0 g) was dissolved in anhydrous pyridine (50 ml) and methane sulfonyl chloride (6.0 g) was added at 0 °C. The mixture was stirred at this temperature for 2 h and worked up in the usual manner. The mesylate **2** was obtained in quantitative yield as a colorless oil, homogeneous in t.l.c.

Mol. Wt. Calcd. for $C_{25}H_{30}O_5S$: 442. Found (*m/e*): 442.

Infrared ($CHCl_3$): 1340, 1175 cm^{-1} (sulfonyl); n.m.r. ($CDCl_3$): τ 4.42 (m, 1H, proton deshielded by mesylate), 6.18 (s, 3H, aromatic methoxyl), 6.95 (s, 3H, $—SO_3CH_3$), 8.77 p.p.m. (d, 3H, methyl).

Preparation of Compound 3

An excess of $LiAlH_4$ (2.0 g) was added in one portion to a stirred solution of the mesylate **2** (16.5 g) in anhydrous ether (300 ml). The mixture was stirred at room temperature overnight and the excess of hydride was decomposed

Can. J. Chem. Downloaded from www.nrcresearchpress.com by 210.87.254.105 on 09/05/12
For personal use only.

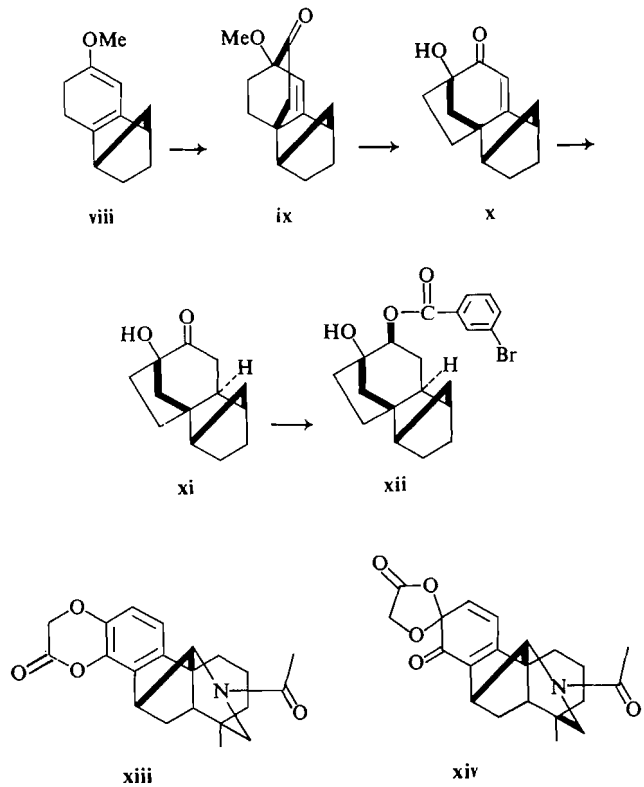

SCHEME 5

by addition of methanol (15 ml). The white precipitate was removed by filtration and washed with ether. The combined filtrates were evaporated to give 12.8 g of the reduction product **3**.

Mol. Wt. Calcd. for $C_{24}H_{28}O_2$: 348. Found (*m/e*): 348.

Infrared (CCl_4): 1600 cm^{-1} (double bond); n.m.r. ($CDCl_3$) τ 3.22 (m, 2H, vinylic protons), 6.25 (s, 3H, aromatic methoxyl), 8.78 p.p.m. (d, 3H, methyl protons).

Preparation of the Rearranged Product 4

A mixture of the olefin **3** (12.5 g) and an excess of benzenesulfonyl azide (10 g) in dry benzene (15 ml) was stirred at room temperature for 2 days. Glacial acetic acid (10 ml) was then added and the reaction mixture was kept at room temperature for an additional 2 days. Benzene and most of the acetic acid were removed *in vacuo*. The residue was dissolved in benzene–hexane and the rearranged product **4** crystallized on standing. Recrystallization from benzene yielded 14.5 g (74%) of **4**, m.p. 158 °C.

Anal. Calcd. for $C_{32}H_{37}O_6NS$ (mol. wt. 563): C, 68.19; H, 6.62; N, 2.49. Found (*m/e* 563): C, 68.21; H, 6.55; N, 2.41.

Infrared ($CHCl_3$): 3375 (NH), 1742 cm^{-1} (acetate); n.m.r. ($CDCl_3$): τ 4.53 (d, J = 11 Hz, 1H, —N(H)—), 5.33 (m, 1H, proton unshielded by acetoxyl), 6.27 (s, 3H, aromatic methoxyl), 7.12 (broad s, 1H, benzylic bridgehead proton), 7.90 p.p.m. (s, 3H, acetoxy methyl).

Conversion of 4 to the Acetamide 5

A mixture of compound **4** (13.0 g) and $LiAlH_4$ (9.0 g) in anhydrous dioxane (450 ml) was refluxed under nitrogen for 20 h. When the mixture was cooled to ice temperature, methanol (5 ml) and water (3 ml) were added dropwise. The white precipitate was filtered and washed with tetrahydrofuran (4 × 100 ml). The combined filtrates were evaporated to dryness and the residue was acetylated with acetic anhydride (5 ml) in methanol (50 ml) at room temperature for ½ h. The mixture was diluted with water and extracted with chloroform. The combined extracts were washed with dilute aqueous sodium bicarbonate and water. After drying over anhydrous sodium sulfate, evaporation gave a light yellow residue which was chromatographed on silica gel. Elution with benzene–ether (1:1) recovered 3.9 g (32%) of hydroxy sulfonamide and further elution with benzene–acetone (1:1) yielded 6.3 g (65%) of the acetamide **5** as a thick oil homogeneous in t.l.c. The yield was 91% (based on the starting material consumed).

Mol. Wt. Calcd. for $C_{26}H_{33}O_4N$: 423.3725. Found: (high resolution mass spectroscopy): 423.3713.

Infrared ($CHCl_3$): 3610, 3410 (hydroxyl, NH) 1669 cm^{-1} (amide); n.m.r. ($CDCl_3$): τ 5.48 (s, 2H, benzylic protons), 6.27 (s, 3H, aromatic methoxyl), 6.93 (broad s, 1H, benzylic bridgehead proton), 8.14 p.p.m. (s, 3H, —N(C=O)—CH_3).

Can. J. Chem. Downloaded from www.nrcresearchpress.com by 210.87.254.105 on 09/05/12
For personal use only.

Can. J. Chem. Downloaded from www.nrcresearchpress.com by 210.87.254.105 on 09/05/12
For personal use only.

Preparation of the Diol **6**

Compound **5** (9.0 g) was dissolved in methanol (50 ml) and 10% palladium-on-charcoal (1.0 g) was added. The mixture was hydrogenated at atmospheric pressure and room temperature for 1½ h. The catalyst was removed by filtration through Celite and the solvent was evaporated *in vacuo*. The crude product was crystallized from ethyl acetate and gave pure **6** (6.54 g, 97%), m.p. 170 °C.

Anal. Calcd. for $C_{19}H_{27}O_4N$: C, 68.44; H, 8.16; N, 4.19. Found: C, 68.41; H, 8.22; N, 4.21.

Infrared ($CHCl_3$): 3610, 3400 (hydroxyl, NH), 1670 cm^{-1} (amide); n.m.r. ($CDCl_3$): τ 2.23 (d, J = 9 Hz, 1H, —N—H), 6.24 (s, 3H, aromatic methoxyl), 6.89 (broad s, 1H, benzylic bridgehead proton), 8.03 (s, 3H, —N—C(=O)—CH_3), 8.83 p.p.m. (d, 3H, methyl).

Preparation of the Diketone **7**

The diol **6** (5.0 g) in pyridine (40 ml) was added to a stirred solution of chromium trioxide – pyridine complex (7.5 g) in pyridine (50 ml). The mixture was stirred at room temperature overnight. It was then dissolved in chloroform and the brown precipitate was removed by filtration. The filtrate was washed with dilute hydrochloric acid, dilute aqueous sodium bicarbonate, and finally with water. Removal of the solvent and filtration through a short neutral alumina column gave the crystalline diketone **7**. The compound melted at 149.5–150 °C (3.95 g, 80%) after recrystallization from benzene.

Anal. Calcd. for $C_{19}H_{23}O_4N$: C, 69.27; H, 7.04; N, 4.25. Found: C, 69.29; H, 7.11; N, 4.24.

Infrared ($CHCl_3$): 3440 (NH), 1750 (five-membered ketone), 1715, 1675 cm^{-1} (ketone, amide); n.m.r. ($CDCl_3$): τ 6.14 (s, 3H, aromatic methoxyl), 6.41 (broad s, 1H, benzylic bridgehead proton), 7.82 (s, 3H, —C(=O)—CH_3), 8.00 p.p.m. (s, 3H, —N—C(=O)—CH_3).

Aldol Condensation of **7** *to* **8**

A solution of compound **7** (4.4 g) and potassium hydroxide (2.0 g) in methanol (200 ml) was refluxed in a nitrogen atmosphere for 5 h, after which time it was neutralized with dilute hydrochloric acid. Most of the solvent was removed *in vacuo* and the residue was extracted with chloroform. The extract was washed with water, dried over anhydrous magnesium sulfate, and evaporated to dryness. The crude product was crystallized from benzene and gave the α,β-unsaturated ketone **8** (3.67 g, 89%), m.p. 191 °C.

Anal. Calcd. for $C_{19}H_{21}O_3N$: C, 73.29; H, 6.80; N, 4.50. Found: C, 73.34; H, 6.75; N, 4.49.

Infrared ($CHCl_3$): 3430 (NH), 1725 (conjugated five-membered ketone), 1680, 1660 cm^{-1} (amide and conjugated double bond); u.v.: λ_{max}^{EtOH} = 236 nm (log ε 4.04); n.m.r. ($CDCl_3$) τ 3.88 (d, J = 9 Hz, 1H, —N—H), 6.45 (broad s, 1H, benzylic bridgehead proton), 7.87 (s, 3H, >C=C(CH3)<), 8.00 p.p.m. (s, 3H, —N—C(=O)—CH_3).

Photoaddition of Vinyl Acetate to Compound **8**

A solution of the α,β-unsaturated ketone **8** (700 mg) and excess vinyl acetate (21 ml) in freshly distilled tetrahydrofuran (21 ml) was irradiated with a 100 W Hanovia Mercury lamp (Pyrex was used as filter) at −10 °C for 20 h under nitrogen. After removal of the vinyl acetate and solvent, the crude product was crystallized from benzene and yielded 560 mg of the pure photoadduct **9*a*** (m.p. 246 °C). Chromatography of the mother liquor by preparative t.l.c. on silica gel with benzene – ethyl acetate (1:4) gave another 69 mg of **9*a*** and 142 mg of **9*b*** (crystallized from benzene, m.p. 241 °C). The ratio of these two epimers was 4.5:1 and the total yield was 90%.

Photoadduct **9*a***

Anal. Calcd. for $C_{23}H_{27}O_5N$: C, 69.50; H, 6.85; N, 3.52. Found: C, 69.37; H, 6.77; N, 3.62.

Infrared ($CHCl_3$): 3420 (NH), 1740 (ketone and acetate), 1680 cm^{-1} (amide); n.m.r. ($CDCl_3$): τ 4.63 (q, J = 8 Hz, J = 4 Hz, 1H, proton unshielded by acetoxyl), 6.19 (s, 3H, aromatic methoxyl), 6.23 (broad s, 1H, benzylic bridgehead proton), 7.82 (s, 3H, acetoxy methyl), 8.08 (s, 3H, —N—C(=O)—CH_3), 9.65 p.p.m. (s, 3H, methyl shielded by benzene ring).

Photoadduct **9*b***

Anal. Calcd. for $C_{23}H_{27}O_5N$: C, 69.50; H, 6.85; N, 3.52. Found: C, 69.46; H, 6.79; N, 3.60.

The mass spectra of both epimers were identical; i.r. ($CHCl_3$): 3420 (NH), 1740 (ketone and acetate), 1680 cm^{-1} (amide); n.m.r. ($CDCl_3$): τ 4.81 (t, J = 8 Hz, 1H, proton unshielded by acetoxyl), 6.19 (s, 3H, aromatic methoxyl), 6.38 (broad s, 1H, benzylic bridgehead proton), 7.86 (s, 3H, acetoxy methyl), 8.08 (s, 3H, —N—C(=O)—CH_3), 9.60 p.p.m. (s, 3H, methyl shielded by benzene ring).

Hydrolysis of Compounds **9*a*** *and* **9*b*** *to the Aldehyde* **10**

The photoadduct **9*a*** (2.74 g) was hydrolyzed in 1% methanolic potassium hydroxide (60 ml) for 30 min at 0 °C. After this time the mixture was poured into water, extracted with chloroform, the extract was washed with water, dried over anhydrous magnesium sulfate and evaporated to dryness. The product crystallized from benzene and gave 2.38 g (97%) of the aldehyde **10**, m.p. 180 °C.

Anal. Calcd. for $C_{21}H_{25}O_4N$: C, 70.96; H, 7.09; N, 3.94. Found: C, 70.86; H, 7.04; N, 3.91.

Infrared ($CHCl_3$): 3440 (NH), 2720 (aldehydic C—H), 1740 (five-membered ketone), 1720 (aldehyde), 1680 cm^{-1} (amide); n.m.r. ($CDCl_3$): τ 0.16 (t, 1H, aldehydic proton), 6.53 (broad s, 1H, benzylic bridgehead proton), 8.00 (s, 3H, —N—C(=O)—CH_3), 9.50 p.p.m. (s, 3H, methyl shielded by benzene ring).

Under the same conditions, hydrolysis of **9*b*** (225 mg) gave the identical compound **10** in quantitative yield.

Preparation of the Enol Ether **11**

A solution of compound **10** (2.10 g), trimethyl orthoformate (2 ml), methanol (2 ml) and *p*-toluenesulfonic

Can. J. Chem. Downloaded from www.nrcresearchpress.com by 210.87.254.105 on 09/05/12
For personal use only.

acid (15 mg) in dioxane (40 ml) was stirred at room temperature for 2 h, after which time two drops of pyridine were added and the solution was evaporated to dryness *in vacuo*. The residue was heated under reflux for 45 min in xylene (60 ml). The solution was diluted with ether, washed with water, dried over anhydrous magnesium sulfate and evaporated to dryness. The crude product crystallized from benzene to give 1.52 g (80%) of pure **11**, m.p. 214–215 °C.

Mol. Wt. Calcd. for $C_{22}H_{27}O_4N$: 369.1940. Found (high resolution mass spectroscopy): 369.1949.

Infrared ($CHCl_3$): 3450 (NH), 1740 (five-membered ketone), 1680, 1660 cm^{-1} (amide and enol ether); n.m.r. ($CDCl_3$): τ 3.75 (d, J = 13 Hz, 1H, vinylic proton), 4.67 (d, J = 13 Hz, 1H, vinylic proton), 6.17 (s, 3H, aromatic methoxyl), 6.47 (s, 3H, methoxyl), 7.96 (s, 3H, —N—C(=O)—CH_3), 9.53 p.p.m. (s, 3H, methyl shielded by benzene ring).

*Cleavage of Compound **11** to the Keto Ester **12***

A solution of compound **11** (1.72 g) in acetone (100 ml) was added to a stirred solution of sodium metaperiodate (5.0 g), potassium permanganate (50 mg) and potassium carbonate (1.0 g) in water (150 ml) (7). The reaction mixture was stirred at room temperature overnight. The solution was poured into ice water, acidified with dilute hydrochloric acid and extracted with chloroform (5 × 100 ml). The combined extracts were washed with water, dried and evaporated to dryness. The residue was dissolved in methanol (25 ml) and treated with excess diazomethane. After removal of the solvent, crystallization of the crude product from benzene gave the pure keto ester **12** (1.39 g, 80%), m.p. 235–236 °C.

Anal. Calcd. for $C_{21}H_{25}O_5N$: C, 67.90; H, 6.78; N, 3.77. Found: C, 67.99; H, 6.67; N, 3.69.

Infrared ($CHCl_3$): 3440 (NH), 1745 (five-membered ketone), 1720 (ester), 1680 cm^{-1} (amide); n.m.r. ($CDCl_3$): τ 6.19 (s, 3H, aromatic methoxyl), 6.30 (s, 3H, methyl ester), 7.97 (s, 3H, —N—C(=O)—CH_3), 9.41 p.p.m. (s, 3H, methyl shielded by benzene ring).

*Cyclization of **12** to the Keto Lactam **13***

The keto ester **12** (1.46 g) dissolved in 5% methanolic potassium hydroxide (100 ml) was allowed to stand at room temperature under nitrogen for a week. The reaction mixture was diluted with water and extracted with chloroform (3 × 150 ml). The extracts were washed with water, dried over anhydrous magnesium sulfate and evaporated to dryness. The solid residue was crystallized from chloroform – ethyl acetate to yield 1.06 g (89%) of the keto lactam **13**, m.p. 280–281 °C.

Mol. Wt. Calcd. for $C_{18}H_{19}O_3N$: 297.1365. Found (high resolution mass spectroscopy): 297.1362.

Infrared ($CHCl_3$): 3410 (NH), 1750 (five-membered ketone), 1670 cm^{-1} (lactam); n.m.r. ($CDCl_3$): τ 6.18 (s, 3H, aromatic methoxyl), 6.25 (broad s, 1H, benzylic bridgehead proton), 8.65 p.p.m. (s, 3H, tertiary methyl).

*Wolff–Kishner Reduction of Compound **13** (8)*

A solution of the keto lactam **13** (863 mg), 95% hydrazine (7.0 g), hydrazine dihydrochloride (1.7 g) in triethylene glycol (70 ml) was heated at 140 °C with stirring for 2 h, after which time potassium hydroxide pellets were added in portions with stirring. The temperature was gradually raised to 210 °C (oil bath temperature) and the solution was maintained at this temperature for 2 h. The reaction mixture was cooled and extracted with ether (3 × 100 ml). The ethereal extract was washed, dried and evaporated to dryness. Crystallization of the crude product from chloroform – ethyl acetate gave 695 mg (85%) of **14**, m.p. 217–218 °C.

Anal. Calcd. for $C_{18}H_{21}O_2N$: C, 76.29; H, 7.47; N, 4.94. Found: C, 76.18; H, 7.24; N, 4.93.

Infrared ($CHCl_3$): 3410 (NH), 1660 cm^{-1} (lactam); n.m.r. ($CDCl_3$): τ 3.41 (broad s, 1H, —N—H), 6.20 (s, 3H, aromatic methoxyl), 6.80 (m, 1H, benzylic bridgehead proton), 8.78 p.p.m. (s, 3H, tertiary methyl).

*Reduction of Compound **14** to **15***

The secondary lactam **14** (200 mg) was dissolved in anhydrous dioxane (10 ml). An excess of lithium aluminum hydride (160 mg) was added and the resulting suspension was refluxed under a nitrogen atmosphere for 22 h. The excess of hydride was destroyed with methanol and the milky solution was diluted with ether (200 ml). The precipitate was filtered off and washed with ether. The filtrate was evaporated to dryness under reduced pressure. The oily residue was acetylated with acetic anhydride (0.5 ml) in methanol (3 ml) at room temperature for 20 min. Removal of the solvent and volatile material *in vacuo* left the crude product (230 mg) which was purified by preparative t.l.c. on silica gel with acetone–hexane (1:2) as solvent. 198 mg (84%) of the pure **15** was obtained as a thick oil, homogeneous in t.l.c.

Mol. Wt. Calcd. for $C_{20}H_{25}O_2N$: 311.2435. Found (high resolution mass spectroscopy): 311.2439.

Infrared ($CHCl_3$): 1625 cm^{-1} (tertiary lactam); n.m.r. ($CDCl_3$): τ 6.17 (s, 3H, aromatic methoxyl), 7.90 (s, 3H, —N—C(=O)—CH_3), 9.01 p.p.m. (s, 3H, tertiary methyl).

*Birch Reduction of Compound **15** to the Diene **16***

A solution of **15** (330 mg) in tetrahydrofuran (8 ml) and *t*-butanol (8 ml) was added dropwise to a stirred solution of lithium metal (600 mg) in distilled liquid ammonia (60 ml). The mixture was stirred at acetone – Dry Ice temperature for 16 h, after which time methanol was added until the blue color disappeared. The ammonia was allowed to evaporate and the mixture was worked up by the standard procedure. The oily residue (305 mg) was acetylated immediately with acetic anhydride (0.4 ml) in pyridine (1 ml). After work-up in the usual manner, the pure diene **16** (238 mg, 72%) was obtained by preparative t.l.c. on neutral alumina as an oil homogeneous in t.l.c.

Mol. Wt. Calcd. for $C_{20}H_{27}O_2N$: 313. Found (*m/e*): 313.

Infrared ($CHCl_3$): 1622 cm^{-1} (tertiary lactam); n.m.r. ($CDCl_3$): τ 5.31 (m, 1H, vinylic proton), 6.42 (s, 3H, methoxyl), 7.89 p.p.m. (s, 3H, —N—C(=O)—CH_3).

*Conversion of Compound **16** to the Alcohol **18***

Compound **16** (238 mg) was dissolved in methanol (20 ml). Oxalic acid (200 mg) in water (5 ml) was added

Can. J. Chem. Downloaded from www.nrcresearchpress.com by 210.87.254.105 on 09/05/12
For personal use only.

and the mixture was stirred at 0 °C for 1 h. The mixture was neutralized with aqueous sodium bicarbonate and extracted with ether. The extract was washed with water and dried over anhydrous magnesium sulfate. Evaporation of the solvent gave the crude ketone **17** (214 mg, 95%) which was used immediately without purification for the subsequent step.

Mol. Wt. Calcd. for $C_{19}H_{25}O_2N$: 299. Found (*m/e*): 299.

Infrared ($CHCl_3$): 1715 (six-membered ketone), 1624 cm^{-1} (lactam).

The crude ketone **17** (214 mg) was dissolved in methanol (10 ml). Sodium borohydride (200 mg) was added and the mixture was stirred at 0 °C for ½ h. After work-up in the usual manner, chromatography of the crude product by preparative t.l.c. on silica gel (30% acetone in *n*-hexane) yielded the pure alcohol **18** (149 mg, 70%) as a colorless syrup, homogeneous in t.l.c.

Mol. Wt. Calcd. for $C_{19}H_{27}O_2N$: 301.2437. Found: (high resolution mass spectroscopy): 301.2416.

Infrared ($CHCl_3$): 3400 (hydroxyl), 1620 cm^{-1} (lactam); n.m.r. ($CDCl_3$): τ 6.19 (m, 1H, proton deshielded by hydroxyl), 6.87 (broad s, 1H, apex proton), 7.92 (s, 3H, —N—C(=O)—CH_3), 9.03 p.p.m. (s, 3H, tertiary methyl).

*Preparation of the Mesylate **19***

The alcohol **18** (146 mg) and methane sulfonyl chloride (150 mg) dissolved in pyridine (2 ml) was stirred at 0 °C for 3 h. The reaction mixture was diluted with ether and the solution was washed with dilute hydrochloric acid, then with water, dried over anhydrous magnesium sulfate and evaporated to dryness *in vacuo*. The mesylate **19** was obtained in quantitative yield as an oil homogeneous in t.l.c.

Mol. Wt. Calcd. for $C_{20}H_{29}O_4NS$: 379. Found (*m/e*): 379.

Infrared ($CHCl_3$): 1625 (lactam), 1310, 1155 cm^{-1} (sulfonyl); n.m.r. ($CDCl_3$): τ 6.85 (broad s, 1H, apex proton), 6.97 (s, 3H, $—SO_3CH_3$), 7.91 (s, 3H, —N—C(=O)—CH_3), 9.01 p.p.m. (s, 3H, tertiary methyl).

*Preparation of the Diene **20***

Freshly sublimed potassium *t*-butoxide (300 mg) was added to a stirred solution of the mesylate **19** (162 mg) in anhydrous dimethyl sulfoxide (5 ml). The solution was stirred at room temperature under nitrogen for 1 h. After addition of ice water (50 ml), the mixture was extracted with ether. The ethereal extract was washed with water and dried over anhydrous magnesium sulfate. Evaporation of the solvent *in vacuo* gave the unstable conjugated diene **20** (102 mg, 85%) which had to be used immediately without purification for the subsequent step.

Mol. Wt. Calcd. for $C_{19}H_{25}ON$: 283. Found (*m/e*): 283.

Ultraviolet: λ_{max}^{EtOH} = 274 nm (log ε 4.06).

*The Diels–Alder Adduct **21***

A mixture of the crude diene **20** (102 mg) and maleic anhydride (200 mg) in anhydrous benzene (2 ml) was refluxed under nitrogen for 24 h. After removal of the solvent and excess maleic anhydride *in vacuo*, the solid residue was purified by preparative t.l.c. on silica gel (30% acetone in *n*-hexane) to yield the highly crystalline adduct **21**. Recrystallization from chloroform–acetone gave pure **21** (79 mg, 60%), m.p. 300 °C.

Anal. Calcd. for $C_{23}H_{27}O_4N$: C, 72.42; H, 7.13; N, 3.67. Found: C, 72.38; H, 7.01; N, 3.68.

Infrared ($CHCl_3$): 1870, 1780 (anhydride), 1625 cm^{-1} (lactam); n.m.r. ($CDCl_3$): τ 4.04 (d, J = 6.5 Hz, 1H, vinylic proton), 6.48 (broad s, 1H, apex proton), 7.87 (s, 3H, —N—C(=O)—CH_3), 9.09 p.p.m. (s, 3H, tertiary methyl).

We thank the National Research Council of Canada, Ottawa, and the Hoffmann-La Roche Company, Nutley, New Jersey, (U.S.A.) and Dorval, Quebec, for the generous support of these studies. We also gratefully acknowledge the extremely valuable X-ray work of Dr. J. F. Blount (Hoffmann-La Roche, Nutley).

1. J. P. JOHNSTON and K. H. OVERTON. J. Chem. Soc. 1490 (1973).
2. W. A. AYER and P. D. DESHPANDE. Can. J. Chem. **51**, 77 (1973).
3. K. WIESNER, PAK-TSUN HO, R. C. JAIN, S. F. LEE, S. OIDA, and A. PHILIPP. Can. J. Chem. **51**, 1448 (1973).
4. K. WIESNER, PAK-TSUN HO, DING CHANG, YIU KUEN LAM, CONNIE SHII JEOU PAN, and WU YUN REN. Can. J. Chem. **51**, 3978 (1973).
5. P. VON R. SCHLEYER. J. Am. Chem. Soc. **89**, 699, 701 (1967).
6. D. BERNEY and P. DESLONGCHAMPS. Can. J. Chem. **47**, 515 (1969).
7. R. V. LEMIEUX and E. VON RUDLOFF. Can. J. Chem. **33**, 1701 (1955).
8. W. NAGATA and H. ITAZAKI. Chem. and Ind. 1194 (1964).

Kinetics of the Nitrosation of Pyrrolidine and Proline

A. OKANY, T. F. MASSIAH, AND L. J. RUBIN

Canada Packers Limited, Research and Development Laboratories, 2211 St. Clair Avenue West, Toronto, Ontario M6N 1K4

AND

K. YATES

Department of Chemistry, University of Toronto, 80 St. George Street, Toronto, Ontario M5S 1A1

Received May 29, 1973[1]

The kinetics of the nitrosation of pyrrolidine and proline have been investigated in buffer solutions of mildly acidic p*H*'s in the temperature range 40–100 °C. The rate constants were determined and the enthalpy and the entropy of activation were calculated for both reactions. Examples are presented in which are estimated the maximum amounts of nitroso compounds formed under conditions relevant to meat processing.

Les cinétiques de la nitrosation de la pyrrolidine et de la proline ont été étudiées dans des solutions tamponnées à des p*H*s faiblement acides et à des températures entre 40 et 100 °C. Les constantes de réactions étaient déterminées et l'enthalpie et l'entropie d'activation étaient calculées pour les deux réactions. On a présenté des exemples dans lesquels on a estimé les quantités maximum des composés nitroso formés sous les conditions qui existent durant la traitement de la viande.

Can. J. Chem., **52**, 1050 (1974)

Introduction

Since the reported (1, 2) carcinogenic effect of certain nitrosamines (in animal experiments), there has been a surge of interest in *N*-nitroso compounds. The occurrence of nitrosamines in food products (3–6), the conditions necessary for their formation (7–9), their stability (10, 11), and their biological effect (12–15) have been studied.

Earlier work on the kinetics of nitrosation was mainly in connection with diazotization. This work has been reviewed by Turney and Wright (16) and also by Ridd (17). Recently, Mirvish investigated the kinetics of the nitrosation of dimethylamine (18) and the formation of some nitrosamides (19). Fan and Tannenbaum gave an account on the kinetics of the nitrosation of morpholine (20). Schweinsberg and Sander (21) studied the kinetics of the reactions between tertiary amines and nitrite.

Small amounts of *N*-nitrosopyrrolidine (<0.1 p.p.m.) have recently been reported to be present in samples of fried bacon (3, 4). This fact prompted us to investigate the kinetics of the formation of *N*-nitrosopyrrolidine, under conditions relevant to cured meat processing.

This paper reports kinetic results, obtained for the reaction between pyrrolidine and nitrite, under mildly acidic conditions (p*H* 4.15, 5, and 6), in the temperature range of 40–100 °C. Kinetic data on the nitrosation of proline are also given. Proline was selected since it seemed to be the most likely precursor of *N*-nitrosopyrrolidine in cured meat products.

[1]Revision received December 7, 1973.

Experimental

Materials

Pyrrolidine (BDH), proline (NBCo), sodium nitrite (Fisher), and *N*-nitrosopyrrolidine (K & K Laboratories Inc.) were of analytical purity. *N*-Nitrosoproline was prepared from proline by the method of Sander (22).

Buffer Solutions

Acetate buffers at a 0.25 *M* sodium acetate level were used in all experiments.

Nitrosation of Pyrrolidine

The reactions up to 70 °C were performed in a constant-temperature water bath (±1 °C) in Erlenmeyer flasks equipped with pressure-release tubes. The reactions at the boiling point were carried out in Erlenmeyer flasks equipped with reflux condensers.

Aliquots (49 ml) of the pyrrolidine solutions of the specified concentrations were equilibrated in the water bath for 1 h; the required concentrations of sodium nitrite were pipetted, in 1 ml volume, into the pyrrolidine solutions and the flasks were shaken. After the required time had elapsed, the solutions were made 3 *N* in sodium hydroxide and 75% of the alkaline solution was distilled. Under these conditions an average of 90% of the *N*-nitrosopyrrolidine distilled over.

Can. J. Chem. Downloaded from www.nrcresearchpress.com by 210.87.254.6 on 09/05/12
For personal use only.

Can. J. Chem. Downloaded from www.nrcresearchpress.com by 210.87.254.6 on 09/05/12
For personal use only.

Nitrosation of Mixtures of Proline and Pyrrolidine

Pyrrolidine (0.25 mol/l) and proline (0.25 mol/l) were dissolved in acetate buffer. Aliquots (49 ml) of the solution were equilibrated in the water bath for 1 h (or were brought to boiling under reflux), then sodium nitrite solution (1 ml) was introduced to give a 0.05 mol/l concentration in the reaction mixture. The solutions were left in the water bath (or under reflux) for the specified time period. Sodium hydroxide (6 g) or sodium chloride (10 g) was added and 75% of the volume of the solution was distilled. Recovery of *N*-nitrosopyrrolidine in the distillate from the sodium hydroxide solution was 90%, and in the distillate from the sodium chloride solution 66%. *N*-Nitrosoproline was recovered from the distillation residues in 57 and 66% yields, respectively. All reaction mixtures were prepared in duplicate and the two samples were processed by the two different methods.

Determination of N-Nitrosopyrrolidine

N-Nitrosopyrrolidine was determined in the acidified distillates spectrophotometrically at 230 nm (7) against the distillate of a blank experiment. A standard absorption curve was prepared using the commercial *N*-nitrosopyrrolidine sample.

Determination of N-Nitrosoproline

The distillation residues were dissolved in water. The resulting solutions were acidified to pH = 1.4 with 3 *N* sulfuric acid and the volume was made up to 100 ml. Aliquots (2 ml) of the solution were extracted with distilled ethyl acetate (10 ml) in a stoppered centrifuge tube. The aqueous layer was removed, and the ethyl acetate solution was washed with water (1 ml). An appropriate aliquot of the ethyl acetate layer was transferred into another stoppered tube and the ethyl acetate was removed under a stream of nitrogen. The residue was dissolved in water and diluted to the proper concentration for optical density measurement, at 235 nm, against a blank treated similarly. The *N*-nitrosoproline concentrations were estimated from a calibration curve and were corrected for the recovery values determined previously.

Results

The kinetic order of the reaction between pyrrolidine and sodium nitrite at pH 4.15 was determined by the Ostwald isolation method (23). The reaction followed first-order kinetics with respect to pyrrolidine and was second order with respect to nitrite. The overall third-order character of the reaction was confirmed by the constancy of the rate constant with time, as calculated from the integrated form of the third-order rate equation for a reaction of the type A + B → product (24).

The rate constants for the nitrosation of pyrrolidine at different pH's and temperatures are shown in Table 1. It is known (17) that the nitrosation of amines takes place between unprotonated amine and free nitrous acid. Our calculations, therefore, were based on the actual concentrations of the reactive species of both pyrrolidine and nitrite at a given pH, estimated from their stoichiometric concentrations, and pk_a values of 11.27 for pyrrolidine and 3.37 for nitrous acid (25). (The temperature dependence of pk_a was neglected.)

TABLE 1. Rate constants for the nitrosation of pyrrolidine in acetate buffers ([CH_3COONa] = 0.25 mol/l). $[Py]_0$ = 0.2 mol/l; $[NaNO_2]_0$ = 0.05 mol/l

Temperature (°C)	pH	k (mol^{-2} l^2 min^{-1})	
40	4.15	2.3×10^7	2.3×10^7
	5.05	2.1×10^7	
	6.00	2.5×10^7	
50	4.15	4.8×10^7	4.5×10^7
	5.05	4.0×10^7	
	6.00	4.8×10^7	
70	4.15	2.2×10^8	2.1×10^8
	5.05	1.8×10^8	
	6.00	2.1×10^8	
	6.05	2.2×10^8	
102	6.00	4.4×10^9	4.4×10^9

The rate constant for the nitrosation of proline was determined by simultaneous nitrosation of proline and pyrrolidine in a reaction mixture containing less than the stoichiometric amount of sodium nitrite.[2] The amounts of *N*-nitrosoproline and *N*-nitrosopyrrolidine formed under different conditions and their ratios are shown in Table 2.

Discussion

The rate constants for the nitrosation of pyrrolidine are independent of the pH in the range studied; their value depends only on the temperature at constant salt concentrations (Table 1).

Based on the foregoing results and in accordance with earlier publications on the nitrosation of dimethylamine (18) and morpholine (20) the reaction mechanism shown in eqs. 1–3 is suggested for the nitrosation of pyrrolidine.

The concentrations of the reactive species are determined by the hydrogen ion concentration, according to the equilibria 1*a* and *b*. The rate-determining step is probably the attack of the nitrosating agent (nitrous anhydride formed from nitrous acid) on the unshared electron pair of the non-protonated pyrrolidine molecule. Conse-

[2]The competition method was used because the presence of unreacted nitrite complicated the method of *N*-nitrosoproline analysis.

TABLE 2. Rate constants for the nitrosation of proline, as determined by simultaneous nitrosation of proline and pyrrolidine (acetate buffers [CH_3COONa] = 0.25 mol/l), [Py]$_0$ = 0.25 mol/l; [Pro]$_0$ = 0.25 mol/l; and [$NaNO_2$]$_0$ = 0.05 mol/l

Temperature (°C)	pH	Nitroso compounds (mol/l) [NNPro] × 10^2	[NNPy] × 10^3	[NNPro]/[NNPy]	k (mol^{-2} l^2 min^{-1})	
40	4.15	4.4	3.0	14.7	7.2×10^7	
	5.00	4.0	4.7	8.5	4.2×10^7	3.95×10^7
	6.00	3.5	4.6	7.6	3.7×10^7	
50	4.15	4.3	4.1	10.5	10.0×10^7	
	5.00	3.9	5.3	7.4	7.1×10^7	7.1×10^7
	6.00	2.2	3.0	7.3	7.1×10^7	
70	5.00	3.6	6.2	5.8	2.6×10^8	2.45×10^8
	6.00	2.8	5.5	5.1	2.3×10^8	
102	6.00	1.8	7.3	2.5	2.1×10^9	

[1] (*a*) 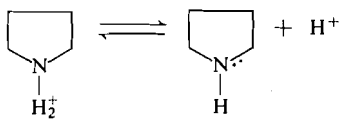

(reactive)

[1] (*b*) $NaNO_2 + H^+ \rightleftharpoons HNO_2 + Na^+$

(reactive)

[2] $2\ HNO_2 \rightleftharpoons N_2O_3 + H_2O$

[3] 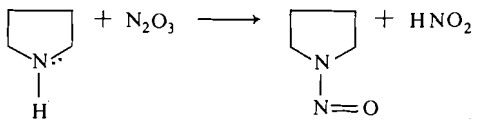

quently, the amount of nitrosopyrrolidine formed in a given time is proportional to the product [$Py_{reactive}$] [HNO_2]^2 at any pH and reaches a maximum at pH 3.4 as was suggested by Fan and Tannenbaum for amines of pk_a values greater than 5 (20).

The rate constant for the nitrosation of proline was determined by the competition method (23). The assumption was made that the reaction follows a kinetic order similar to that for the nitrosation of pyrrolidine. If, therefore, the concentration of nitrite is kept sufficiently low in the reaction mixture with proline and pyrrolidine, the quotient of the rate equations for the two competitive reactions approximates the form: [NNPy]/[NNPro] = k_1[Py_r]/k_2[Pro_r] where [NNPy] and [NNPro] are the concentrations of the two nitroso compounds, k_1 and k_2 are the rate constants for the nitrosation of pyrrolidine and proline, respectively, and [Py_r]/[Pro_r] represent the concentration ratio of the reactive species of pyrrolidine to that of proline, as calculated from their stoichiometric concentrations and their pk_a values (pk_{a1} = 1.95 and pk_{a2} = 10.60 for proline (25)).

The *N*-nitrosoproline to *N*-nitrosopyrrolidine ratios and the rate constants for the nitrosation of proline, determined at different temperatures and pH's, are shown in Table 2.

The pH independence of the rate constant, for the nitrosation of proline, is observed only at pH 5 and 6. At pH 4.15, the values are somewhat higher and a different mechanism may be operative; the possibility of nitrosyl acetate, as a nitrosating agent, in acetate buffers has been suggested by Hughes *et al.* (26).

The values of the kinetic parameters obtained from the Arrhenius plot for the nitrosation reactions are: $\Delta H^{\ddagger}$ = 19.3 kcal mol^{-1}, $\Delta S^{\ddagger}$ = 28.5 cal mol^{-1} deg^{-1} for pyrrolidine, and $\Delta H^{\ddagger}$ = 14.5 kcal mol^{-1}, $\Delta S^{\ddagger}$ = 14.6 cal mol^{-1} deg^{-1} for proline.

From the foregoing kinetic results we can estimate the maximum amounts of *N*-nitrosopyrrolidine or *N*-nitrosoproline which would be formed under a variety of conditions of temperature and pH.

For example, it is estimated that, assuming a 50 p.p.m. proline and a 150 p.p.m. sodium nitrite concentration in a medium of pH 6 containing 2% inorganic salt at 54 °C (processing conditions for bacon), less then 0.9 p.p.b. of *N*-nitrosoproline will form in 4 h; it was estimated that, assuming 100 p.p.m. pyrrolidine and 150 p.p.m. sodium nitrite in a medium of pH 5.7 containing 2% inorganic salts at 71 °C (processing condition for ham), less than 2.36 p.p.b. *N*-nitrosopyrrolidine would form in 3 h.

Can. J. Chem. Downloaded from www.nrcresearchpress.com by 210.87.254.6 on 09/05/12
For personal use only.

We wish to thank Miss T. R. Khomasurya for calculating the values of the rate constants.

1. P. N. MAGEE and J. N. BARNES. Adv. Cancer Res. **10**, 163 (1967).
2. H. DRUCKREY, R. PREUSSMANN, S. IVANKOVIC, D. SCHMÄHL. Z. Krebsforsch. **69**, 103 (1967).
3. T. G. ALLISTON, G. B. COX, and R. S. KIRK. Analyst, **97**, 915 (1972).
4. N. T. CROSBY, J. K. FOREMAN, J. F. PALFRAMAN, and R. SAWYER. Nature, **238**, 342 (1972).
5. N. P. SEN. Food Cosmet. Toxicol. **10**, 219 (1972).
6. T. FAZIO, J. N. DAMICO, J. W. HOWARD, R. H. WHITE, and J. O. WATTS. J. Food Agr. Chem. **19**, 250 (1971).
7. F. ENDER and L. CEH. Z. Lebensmittel-Untersuch. Forsch. **145**, 133 (1971).
8. J. SANDER, F. SCHWEINSBERG, and H. P. MEINZ. Z. Physiol. Chem. **349**, 1691 (1968).
9. E. BOYLAND, E. NICE, and K. WILLIAMS. Food Cosmet. Toxicol. **9**, 639 (1971).
10. D. T. BURNS and G. V. ALLISTON. J. Food Technol. **6**, 433 (1971).
11. T. Y. FAN and S. R. TANNENBAUM. J. Food Sci. **37**, 274 (1972).
12. V. M. CRADDOCK. J. Nat. Cancer Inst. **47**, 899 (1971).
13. A. E. ROSS, L. KEEFER, and W. LIJINSKY, J. Nat. Cancer Inst. **47**, 789 (1971).
14. P. F. SWANN and P. N. MAGEE. Biochem. J. **110**, 39 (1968).
15. D. SCHMÄHL and H. OSWALD. Experientia, **23**, 497 (1967).
16. T. A. TURNEY and G. A. WRIGHT. Chem. Revs. **59**, 497 (1959).
17. J. H. RIDD. Quart. Rev. Chem. Soc. **15**, 418 (1961).
18. S. S. MIRVISH. J. Nat. Cancer Inst. **44**, 633 (1970).
19. S. S. MIRVISH. J. Nat. Cancer Inst. **46**, 1183 (1971).
20. T. Y. FAN and S. R. TANNENBAUM. J. Agr. Food Chem. **21**, 237 (1973).
21. F. SCHWEINSBERG and J. SANDER. Z. Physiol. Chem. **353**, 1671 (1972).
22. J. SANDER. Z. Physiol. Chem. **348**, 852 (1967).
23. R. LIVINGSTONE. *In* Investigation of rates and mechanisms of reactions, technique of organic chemistry VIII. *Edited by* S. L. Friess and A. Weissberger. Interscience Publishers Inc., N.Y. 1953. pp. 185 and 107.
24. A. A. FROST and R. G. PEARSON. Kinetics and mechanism. 2nd ed. J. Wiley & Sons, N.Y. 1961. p. 21.
25. Handbook of chemistry and physics. The Chemical Rubber Co., Cleveland, Ohio. 1969.
26. E. D. HUGHES, C. K. INGOLD, and J. H. RIDD. J. Chem. Soc. 88 (1958).

Can. J. Chem. Downloaded from www.nrcresearchpress.com by 210.87.254.6 on 09/05/12
For personal use only.

Nitrogen–Sulfur Ligand Systems via Reduction of Schiff's Base – Zinc Complexes Derived from Benzothiazolines[1]

JAMES L. CORBIN[2] AND DALE E. WORK

Charles F. Kettering Research Laboratory, Yellow Springs, Ohio 45387

Received October 4, 1973

The coordinated imine groups of the Schiff's base – zinc complexes derived from various 2-substituted benzothiazolines are easily reduced with sodium borohydride to the corresponding amines. Removal of the metal ion from these reduced complexes yields the free ligands, providing a simple route to novel aminomercaptan chelating agents. Compounds of bi-, tri-, and tetradentate types were prepared in this manner.

Evidence is given for a disproportionation of 2,2′-dimethyl-2,2′-bibenzothiazolinyl into 2-methylbenzothiazoline and 2-methylbenzothiazole in chloroform solution.

Les groupes imines de bases de Schiff coordonnés avec des complexes de zinc dérivés de plusieurs benzothiazolines substitués en position 2 sont facilement réduits par le borohydrure de sodium en amines correspondantes. L'élimination de l'ion métallique de ces complexes réduits fournit les ligands libérés et assure ainsi une route simple pour obtenir des aminomercaptans qui peuvent agir comme agents chélatants. Des composés du type bi-, tri- et tétradentate ont été préparés de cette manière.

On fournit des preuves pour supporter l'idée qu'une disproportionnation du diméthyl-2,2′ bibenzo-2′ thiazolinyle en méthyl-2 benzothiazoline et méthyl-2 benzothiazole se produit en solution chloroformique. [Traduit par le journal]

Can. J. Chem., **52**, 1054 (1974)

We were interested in preparing the unknown bis(2-mercaptoanilino)ethanes, **1**, as a part of our studies on novel nitrogen–sulfur tetradentate chelating agents. Potentially, the most attractive route appeared to be through the formation of the corresponding coordinated Schiff's bases (**2**), which if reducible, would yield the desired compounds upon removal of the metal ions. The free Schiff's bases of this type are not isolatable compounds. However they apparently exist as equilibrium amounts in solutions of the isolatable bibenzothiazolinyls (**3**), as evidenced by their behavior in alkaline solution or with metal ions.[3]

The appropriate metal complexes are well known for **2***a* and **2***b* (M = Zn or Cd (2–4) and Ni (5, 6)) and more recently were reported for **2***c* (M = Ni, Zn (7)). Except for **2***c*, they are prepared by reaction of the metal ion with the corresponding benzothiazoline (**3**).

While reduction of the coordinated imine group to a secondary amine has been carried out with sodium borohydride for another type of ligand (8), the nickel complex of **2***a*, unfortunately, has been reported (9) to give only a partially-reduced, oxygen-sensitive product with this reagent. However, we wish to report that the highly colored zinc complexes, **2***a* and **2***b*, are smoothly reduced with sodium borohydride in DMF–ethanol or as a slurry in ethanol to the colorless complexes, **4***a* and **4***b*, in good yield. These compounds were sufficiently soluble in DMSO-d_6[4] for n.m.r. spectra to be obtained, which supported the assigned structures. The zinc was readily removed from the reduced complexes by treatment with 2 mol of NaOH (DMF–H_2O) and filtration of the precipitated $Zn(OH)_2$. Acidification of the filtrate gave the desired tetradentates **1***a* and **1***b*, characterized by n.m.r., i.r., molecular weight, and elemental analysis.

Some insight into the lack of stereospecificity of the reduction step is provided by the complex **4***b* in which two asymmetric carbons are formed. The methyl region of the n.m.r. spectrum consists of two sets of doublets of *ca.* equal intensity, probably corresponding to a mixture of *dl* and *meso* diasteroeisomers. Although the n.m.r. data

[1]Contribution No. 508 from the Charles F. Kettering Research Laboratory.

[2]To whom correspondence should be addressed.

[3]A general discussion including the influence of metal ions appears in review form (1).

[4]**4***a*, **4***b*, and also **3***b* could be recovered (>90%) unchanged from DMSO. This precludes possible oxidation by this solvent, a point raised by one of the referees.

Can. J. Chem. Downloaded from www.nrcresearchpress.com by 210.87.254.105 on 09/05/12
For personal use only.

Can. J. Chem. Downloaded from www.nrcresearchpress.com by 210.87.254.105 on 09/05/12
For personal use only.

and narrow boiling point range of the free ligand **1***b* appear to argue against this conclusion, use of a lanthanide shift reagent gives results that agree with it. Thus, $Eu(FOD)_3$ shifts the methyl doublet of **1***b* downfield and splits it into two doublets of about equal area.

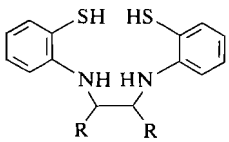

1

a R = H
b R = CH_3
c R = Ph

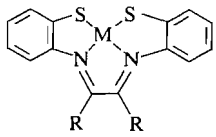

2

a R = H
b R = CH_3
c R = Ph

3

a R = H
b R = CH_3
c R = Ph

4

a R = H
b R = CH_3

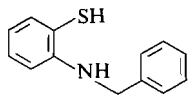

5

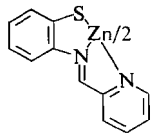

6

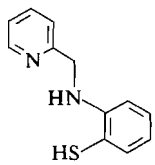

7

The orange zinc complex, purportedly **2***c* (7), was also reduced but the gummy product would not crystallize. Removal of the zinc as above gave the bidentate *N*-benzyl-2-mercaptoaniline (**5**) as the only product. Because the expected tetradentate was not obtained, the original formulation for **2***c* must have been incorrect or else carbon–carbon bond cleavage occurred during the reduction. The latter was not particularly likely in view of the mild conditions and reducing agent employed. In addition, the method cited for preparation of **2***c* involves only refluxing 2-phenylbenzothiazoline and the metal ion in methanol,[5] which might be expected to yield a complex containing two of the bidentate imines instead of the tetradentate Schiff base. Jadamus *et al.* (3) had earlier tried to make **2***c* using what they thought was the corresponding benzothiazoline (**3***c*), but with no success. Their starting material was later shown to be 2-phenylbenzothiazole by Bayer and Breitmaier (10).

A number of other complexes of the zinc–mercaptoimine type are reported (1, 11) and application of our procedure to these could provide a route to other novel chelating agents. We selected one of these (**6**) of the tridentate type to explore this possibility. The reduction went as expected, yielding the previously unknown tridentate **7** after removal of the zinc from the intermediate reduced complex. It seems reasonable to assume the general utility of this reaction sequence for related preparations.

During the course of these studies a pertinent observation was made concerning one of the bibenzothiazolinyls used as a precursor. Bayer and Breitmaier (4) questioned the structure of the benzothiazoline **3***b* based on n.m.r. data in $CDCl_3$ solution and inferred an equilibrium between several isomeric species. We found that a freshly prepared, recrystallized sample of this compound was only slightly soluble in this solvent, but that slow solution occurred (*ca.* 24 h under argon, much faster in air). The n.m.r. spectrum of this solution eventually stabilized (Fig. 1*b*) and resembled that published by Bayer and Breitmaier (4) but with different peak ratios. The singlet at 2.80 p.p.m. and the doublet at 1.53 and 1.62 p.p.m. were in a 1:1 ratio and this ratio did not change further in the absence of air. Also, spectra at intermediate times (Fig. 1*a*) contained an additional singlet (1.80 p.p.m.) which decreased as the others increased, eventually disappearing. This signal probably arises from the methyl of real **3***b* (see below). Further examination of the spectrum indicated the results would be easily explained by formation of a 1 : 1 mixture of 2-methylbenzothiazoline and 2-methylbenzothiazole (Scheme 1). This was confirmed using a 1:1 mixture of the authentic compounds as well as g.l.c. examination. In the presence of air the thiazoline methyl doublet (1.53, 1.62) slowly disappears as oxidation to the thiazole occurs.

[5]The reaction time to be used was not clear; *i.e.*, ref. 7*b* cites "prolonged heating" while ref. 7*a* says "briefly heated." We used both 30 min and 70 h reaction times and got identical products (see Experimental).

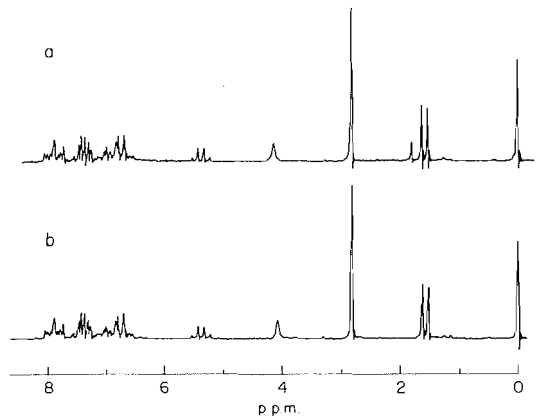

FIG. 1. Nuclear magnetic resonance spectrum of **3***b* ($CDCl_3$) at *ca.* (*a*) 35 h and (*b*) 48 h after mixing.

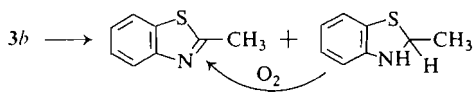

SCHEME 1

Therefore, it appears that some type of disproportionation of **3***b* occurs in chloroform. Inhibition of this reaction by adding Galvinoxyl suggests a free radical mechanism, perhaps induced by traces of oxygen. 2-Alkylbenzothiazolines are known to decompose to the thiazole and corresponding alkane (12) but only at elevated temperatures. The nature of the disproportionation products from **3***b* would tend to support the thiazoline structure questioned by Bayer and Breitmaier and also explains their n.m.r. data. Compound **3***a* does not exhibit this phenomenon. Disproportionation of **3***b* evidently does not occur in DMSO-d_6, and only a single methyl peak is seen (1.79 p.p.m.) and is not affected by air. This signal probably corresponds to the decaying 1.80 p.p.m. peak seen in $CDCl_3$.

Experimental

Nuclear magnetic resonance spectra were obtained with a Varian A-60 instrument (35°) and tetramethylsilane was the internal standard. A Hewlett-Packard 302B vapor pressure osmometer (37°) was used for molecular weight data. The H-P Model 185 C,H,N Analyzer was used for the elemental microanalyses. Gas–liquid chromatography was performed on an H-P 5750 dual flame instrument. Infrared spectra were run as KBr pellets on a Beckman IR-20A. All evaporations were done at or near room temperature on a rotary vacuum evaporator. 2-Methylbenzothiazoline was prepared according to Larivé *et al.* (13) and 2-phenylbenzothiazoline was synthesized by the method described by Lankelma and Sharnoff (14). All other chemicals were reagent grade.

2,2′-Bibenzothiazolinyls (3a and b)

These compounds were prepared by the reaction of 2-aminobenzenethiol and glyoxal or 2,3-butanedione as described by Bayer and Breitmaier (4). The reactions as well as the recrystallizations were conducted under argon and the products were used as soon as possible.

Glyoxal- and 2,3-Butanedionebis(2-mercaptoanil)–Zinc(II) (2a and b)

The general procedure of Bayer and Breitmaier (4) was followed except that the solvent was altered to allow for larger scale preparations without the inconvenience of very large volumes, *i.e.*, 0.10 mol of the appropriate bibenzothiazolinyl (**3**) was dissolved in 400 ml of 1:1 dioxane–methanol at reflux (argon) and then 0.10 mol of zinc acetate (dihydrate) in 175 ml of methanol added. Yields were typically 2–4% lower using this mixed solvent instead of methanol only.

"Benzilbis(2-mercaptoanil)–Zinc(II) (2c)"

The orange complex reported by Kochin *et al.* (7) was obtained by adding 0.01 mol of zinc acetate (30 ml methanol) to a refluxing solution of 0.02 mol of 2-phenylbenzothiazoline (14) in 35 ml of methanol. The yield was 67% (m.p. 252–255° corrected; lit. (7) m.p. 249–250°) and the product was the same (i.r., m.p.) with 30 min or 70 h reaction time.

2,3-Bis(2-mercaptoanilino)butane–Zinc(II) (4b)

A slurry of **2***b* (14.9 g, 0.0407 mol) in 50 ml of dimethylformamide and 13 ml absolute ethanol was cooled in ice and a solution of sodium borohydride (0.875 g, 0.023 mol) in 7 ml of DMF was dropped in over 5–10 min. Stirring was continued for 30 min at room temperature and the light orange-brown solution was filtered and 140 ml of methanol added. After chilling (freezer) overnight, the nearly white crystals of the product were filtered and washed with methanol to give 12.0 g (80.2%) after vacuum drying; n.m.r. (DMSO-d_6): 1.10, 1.18 (two doublets, J = 7, 6 Hz, 6H, CH_3—), *ca.* 3.0 (m, 2H, —CH—), 6.25 (b-d, 2H, exchangeable with D_2O, —NH), 6.8–7.5 p.p.m. (m, 8H, ArH). An analytical sample was vacuum dried for 2 h at 100°. Some residual DMF was still evident (n.m.r.).

Anal. Calcd. for $C_{16}H_{18}N_2S_2Zn$: C, 52.25; H, 4.93; N, 7.61. Found: C, 52.48; H, 5.14; N, 7.61.

1,2-Bis(2-mercaptoanilino)ethane–Zinc(II) (4a)

The above procedure gave a very dark reaction mixture and tan-brown product in only 60% yield when applied to **2***a*. A better method was to add solid $NaBH_4$ (1.5 g) to a stirred suspension of **2***a* (10.0 g, 0.030 mol) in 100 ml absolute ethanol. After stirring overnight the gray to purple-gray product was filtered off and washed with ethanol. To remove any remaining color, this product was dissolved in *ca.* 45 ml of DMF at 50–60° (filtering if necessary) and more $NaBH_4$ added to give a pale yellow solution. The product was recovered by the addition of methanol (4 volumes) to give an overall yield of 80–85% of white solid; n.m.r. (DMSO-d_6): 2.95 (b-d, 4H, —CH_2—), 6.42 (b-t, 2H, D_2O exchangeable, NH), 6.8–7.6 p.p.m. (m, 8H, ArH). For analysis 1 g was recrystallized (4 ml DMF and 5 ml isopropanol) and vacuum dried at 100° (2 h).

Anal. Calcd. for $C_{14}H_{14}N_2S_2Zn$: C, 49.49; H, 4.15; N, 8.24. Found: C, 49.88; H, 4.45; N, 8.27.

Can. J. Chem. Downloaded from www.nrcresearchpress.com by 210.87.254.105 on 09/05/12
For personal use only.

Can. J. Chem. Downloaded from www.nrcresearchpress.com by 210.87.254.105 on 09/05/12
For personal use only.

Bis[N-(2-picolyl)-2-mercaptoanilino]-Zinc(II)

Reduction of the known (15) complex **6** (45.4 mmol in 100 ml of DMF) by the procedure used for **4***b* gave an 83.8% yield of the white zinc complex. An analytical sample was recrystallized (DMF–methanol) and vacuum-dried (100°); n.m.r. (DMSO-d_6): 4.25 (b, 2H, —CH_2—), 6.07 (b, 1H, D_2O exchangeable, NH), 6.50–8.55 p.p.m. (m, 8H, Ar—H).

Anal. Calcd. for $C_{24}H_{22}N_3S_2Zn$: C, 58.12; H, 4.47; N, 11.30. Found: C, 57.76; H, 4.63; N, 11.33.

Removal of the Zinc from the Reduced Complexes

The reduced complex (0.05 mol) was dissolved in DMF (*ca.* 75 ml) and then 50 ml of 2.0 *N* NaOH was dropped in with stirring. After addition of 100 ml of H_2O, the zinc hydroxide was filtered (Celite) and the filtrate neutralized with 100 ml of 1.0 *N* HCl. After standing a few minutes the supernate could be decanted from the gummy product. This was taken up in 100 ml of methylene chloride, washed twice with H_2O, and dried (Na_2SO_4). Final purification of the product is given below under the individual compounds.

1,2-Bis(2-mercaptoanilino)ethane (1a)

The methylene chloride solution was evaporated and the residue was recrystallized from absolute ethanol (64 ml) and chloroform (16 ml) to yield 9.80 g (71%) of yellow prisms, m.p. 84–86° (corrected); n.m.r. ($CDCl_3$): 3.47 (s, 4H, —CH_2CH_2—), 5.6–7.5 (m, 8H, Ar—H), 2.5–4.5 p.p.m. (extremely broad, 4H by exchange with D_2O, NH and SH); i.r.: 3495 (NH), 2515 (SH), 750 cm^{-1} (1,2-disubstituted benzene). An analytical sample was recrystallized and vacuum dried at 25°.

Anal. Calcd. for $C_{14}H_{16}N_2S_2$ (mol. wt. 276): C, 60.83; H, 5.83; N, 10.13. Found (mol. wt. 288, 1,2-dichloroethane): C, 60.69; H, 5.99; N, 10.13.

2,3-Bis(2-mercaptoanilino)butane (1b)

The solvent was removed from the dried methylene chloride solution and the residual golden oil distilled (no column) to give 11.2 g (83%) of light yellow oil (178–182°/0.05 mm); n.m.r. ($CDCl_3$): 1.20, 1.30 (6H, CH_3—),[6] 3.73 (m, 2H, —CH), 2.0–5.0 (extremely broad, 4H by exchange with D_2O, NH and SH), 6.4–7.4 p.p.m. (m, 8H, ArH); i.r. 3390 (NH), 2520 (SH), 750 cm^{-1} (1,2-disubstituted benzene).

Anal. Calcd. for $C_{16}H_{20}N_2S_2$ (mol. wt. 304): C, 63.12; H, 6.62; N, 9.20. Found (mol. wt. 289, 1,2-dichloroethane): C, 62.92; H, 6.70; N, 9.17.

N-(2-Picolyl)-2-mercaptoaniline (7)

The methylene chloride solution was evaporated and the residual oil distilled (no column) to give 14.2 g (65%) of yellow oil (146–156°/0.04 mm). A thiol determination (iodine) gave 99% of the expected value; n.m.r. ($CDCl_3$): 4.47 (s, 2H, —CH_2—), 4.30 (b, 2H, D_2O exchangeable, NH and SH), 6.47–8.67 p.p.m. (m, 8H, Ar—H); i.r. 3390 (NH), 2540 (SH), 750 cm^{-1} (1,2-disubstituted benzene).

Anal. Calcd. for $C_{12}H_{12}N_2S$ (mol. wt. 216): C, 66.63; H, 5.59; N, 12.95. Found (mol. wt. 227, 1,2-dichloroethane): C, 66.41; H, 5.37; N, 12.99.

[6]Addition of $Eu(FOD)_3$ (Aldrich Chemical Co.) caused a downfield shift and appearance of two doublets (J = 6, 7 Hz).

N-Benzyl-2-mercaptoaniline (5) from "2c"

The orange zinc complex thought to be **2***c* (8.69 g, 0.0178 mol) in 45 ml DMF and 18 ml absolute ethanol was reduced according to the above procedure. No solid could be obtained, even with addition of 400 ml of methanol, so the solvent was evaporated and the metal ion was removed as follows: the residual pale yellow gum was dissolved (readily) in 50 ml methanol,[7] 17.8 ml of 2.0 *N* NaOH was added slowly, and the precipitated zinc hydroxide filtered off (Celite); 17.8 ml of 2.0 *N* HCl was added to neutralize the filtrate and the solvent was removed. The residue was dissolved by swirling with 75 ml of chloroform and 25 ml of H_2O. The organic layer was washed with H_2O (25 ml), dried (Na_2SO_4), the solvent removed, and the residual oil subjected to simple distillation (139–145°/0.5 mm; 3.61 g of colorless oil). This material was shown to be *N*-benzyl-2-mercaptoaniline (16) by n.m.r. ($CDCl_3$): 4.33 (s, 2H, —CH_2—), *ca.* 2.6–4.7 (extremely broad, 2H by exchange with D_2O, —NH and —SH), 7.28 (s, 5H, phenyl); 6.5–7.4 p.p.m. (m, 4H, Ar—H). A molecular weight of 198 (theory 215) was found (1,2-dichloroethane) and supported by a thiol determination with iodine.

Disproportionation of 2,2'-Dimethyl-2,2'-bibenzothiazolinyl (3b)

A sample of **3***b* (101 mg) was placed in an n.m.r. tube, stoppered with a serum cap, and flushed well with argon by evacuation. $CDCl_3$ (1.0 ml) was added through the serum cap and the contents mixed by continual inversion on a slowly rotating wheel. After *ca.* 24 h no solid remained and the colorless solution was monitored by n.m.r. (Fig. 1). After *ca.* another 24 h the spectrum showed no further change. The same spectrum was obtained from a 1:1 mixture of 2-methylbenzothiazole and 2-methylbenzothiazoline. The n.m.r. solution was examined by g.l.c. (6 ft. × $\frac{1}{8}$ in. column, 10% silicone gum on Chromosorb W, 161°, 25 ml/min of He), and showed two peaks corresponding to the above two compounds (retention times 4.6 and 6.8 min respectively) in *ca.* 1:1 ratio.

In a parallel experiment in the presence of Galvinoxyl (17) (25 mg) most of the solid still remained after 50 h.

1. L. F. LINDOY. Coord. Chem. Revs. **4**, 41 (1969).
2. H. JADAMUS, Q. FERNANDO, and H. FREISER. Inorg. Chem. **3**, 928 (1964).
3. H. JADAMUS, Q. FERNANDO, and H. FREISER. J. Am. Chem. Soc. **86**, 3056 (1964).
4. E. BAYER and E. BREITMAIER. Chem. Ber. **101**, 1579 (1968).
5. E. I. STIEFEL, J. H. WATERS, E. BILLIG, and H. B. GRAY. J. Am. Chem. Soc. **87**, 3016 (1965).
6. M. S. ELDER, G. M. PRINZ, P. THORNTON, and D. H. BUSCH. Inorg. Chem. **7**, 2426 (1968).
7. (*a*) S. G. KOCHIN, A. D. GARNOVSKII, V. A. KOGAN, O. A. OSIPOV, and T. G. SUSHKO. Russian J. Inorg. Chem. (Eng. Transl.), **14**, 748 (1969); (*b*) Chem. Abstr. **71**, 45218j (1969).
8. N. F. CURTIS. J. Chem. Soc. 2644 (1964); 924 (1965).
9. F. LALOR, M. F. HAWTHORNE, A. H. MAKI, K. DARLINGTON, A. DAVISON, H. B. GRAY, Z. DORI, and E. I. STIEFEL. J. Am. Chem. Soc. **89**, 2278 (1967).

[7]In contrast, the other reduced complexes (**4***a* and *b*) were insoluble in methanol.

10. E. BAYER and E. BREITMAIER. Tetrahedron Lett. (15), 1689 (1966).
11. L. F. LINDOY and D. H. BUSCH. Chem. Commun. 683 (1972).
12. R. C. ELDERFIELD and E. C. MCCLENACHAN. J. Am. Chem. Soc. **82**, 1982 (1960).
13. H. LARIVÉ, A. J. CHAMBONNET, and J. METZGER. Bull. Soc. Chim. Fr. **30**, 1675 (1963).
14. H. P. LANKELMA and P. X. SHARNOFF. J. Am. Chem. Soc. **53**, 2654 (1931).
15. L. F. LINDOY and S. E. LIVINGSTONE. Inorg. Chim. Acta, **1**, 365 (1967).
16. K. FUJII. J. Pharm. Soc. Japan, **77**, 3 (1957); Chem. Abstr. **51**, 8756i (1957).
17. L. F. FIESER and M. FIESER. Reagents for organic synthesis. Vol. 1. Wiley, New York. 1967. p. 409.

Can. J. Chem. Downloaded from www.nrcresearchpress.com by 210.87.254.105 on 09/05/12
For personal use only.

The Rate of Ionization of Some Aromatic Hydrocarbons in Ethanolic Dimethyl Sulfoxide

A. ALBAGLI, J. R. JONES, AND ROSS STEWART

Department of Chemistry, University of British Columbia, Vancouver, British Columbia

Received October 22, 1973

The rates of detritiation of triphenylmethane, 9-phenylxanthene, fluorene, 9-ethylfluorene, 9-phenylfluorene, and 2,3-benzofluorene have been measured in ethanolic dimethyl sulfoxide (DMSO) containing sodium ethoxide. When the logarithm of the ionization rate is plotted against the logarithm of the ionization rate of DMSO a straight line of near-to-unit slope is obtained in each case. There are significant differences, however, between relative ionization rates and equilibrium acidities.

Les taux d'éliminations du tritium du triphénylméthane, du phényl-9 xanthène, du fluorène, de l'éthyl-9 fluorène, du phényl-9 fluorène et du benz-[2,3] fluorène ont été mesurés dans un mélange d'éthanol et de diméthyle sulfoxide (DMSO) contenant de l'éthylate de sodium. Quant on porte le logarithme de la vitesse d'ionisation en abcisse et le logarithme de la vitesse d'ionisation du DMSO en ordonné on obtient dans chaque cas une ligne droite ayant une pente près de l'unité. On note toutefois des différences nettes entre les vitesses relatives d'ionisation et les acidités d'équilibre.

[Traduit par le journal]

Can. J. Chem., **52**, 1059 (1974)

Can. J. Chem. Downloaded from www.nrcresearchpress.com by 210.87.254.6 on 09/05/12
For personal use only.

In connection with earlier work on the rate of ionization of dimethyl sulfoxide (DMSO) in aqueous and alcoholic DMSO mixtures (1) we had occasion to measure the rates of ionization of several hydrocarbons. Some recent work on the equilibrium acidities of these compounds (2–4) has induced us to report briefly the results of our earlier study. Despite its somewhat fragmented character several interesting points emerge from the work.

Results and Discussion

The ionization of DMSO in aqueous and alcoholic DMSO mixtures containing a fixed amount of base (HO^-, CH_3O^-, or $C_2H_5O^-$) is linear in H_- (based on the ionization of aromatic amines) with near-to-unit slope over a remarkable range (some 8 powers of 10 in the rate and some 8.6 powers of 10 in the equilibrium acidity) (1*a*). The great variation in rates meant that measurements in concentrated DMSO had half-lives of seconds while those in very dilute DMSO had half-lives of many years.

The ionization rates of several hydrocarbons in ethanolic DMSO (Table 1) can be correlated with the rate of ionization of DMSO itself, as shown in Fig. 1. The slopes of the lines vary (randomly) in the range 0.90–1.03 and are linear to a fairly high degree of precision. If we use the average slope (0.944) and assume it remains constant outside the convenient range of concentrations in which each compound was studied we can make estimates of the rates of ionization of hydrocarbons of widely varying strengths. On this basis the range of rates between the strongest acid studied, 9-phenylfluorene ($pK_{HA} = 18.5$) (2) to the weakest, triphenylmethane ($pK_{HA} = 31.5$) (2) is 7.2 powers of 10, compared to the ΔpK of 13.0.

Discrepancies between the order of equilibrium and kinetic acidities soon reveal themselves, however. For example, 9-ethylfluorene and fluorene have almost the same acid strengths (3, 4) but the 9-ethyl compound is ionized some 10 times more slowly than the parent compound. (There is a six-fold difference in methanolic methoxide (5)). A more striking inconsistency appears when DMSO itself is compared to triphenylmethane. There is evidence to indicate that their equilibrium acidities are fairly near one another in most media, with DMSO being the weaker of the two (1*a*, 2, 6). Yet DMSO reacts with base about 200 times faster than does triphenylmethane. This probably has two causes: a smaller change in geometry at the acidic carbon atom accompanying the ionization of DMSO, and more ready access of the base to the ionizing proton in the case of DMSO, the smaller molecule. A corollary of these results is that protonation of the triphenylmethide anion is much slower than diffusion-controlled in ethanolic DMSO. (See ref. 7 for a general discus-

TABLE 1. Rate of detritiation of various hydrocarbons at 25° in mixtures of ethanol and DMSO containing sodium ethoxide

Compound	Mol % DMSO	$[OEt]^-$ (M)	$l\ mol^{-1}\ s^{-1}$
9-Phenylfluorene	0.0	0.0100	7.68×10^{-3}
	5.0	0.0098	2.33×10^{-2}
	10.0	0.0100	4.60×10^{-2}
	14.6	0.0105	8.73×10^{-2}
	20.4	0.0100	1.84×10^{-1}
2,3-Benzofluorene	0.0	0.0100	1.54×10^{-3}
	5.0	0.0087	3.51×10^{-3}
	33.5	0.0103	1.25×10^{-1}
	39.2	0.0086	2.52×10^{-1}
Fluorene	10.0	0.0102	2.72×10^{-3}
	12.5	0.0112	4.19×10^{-3}
	20.2	0.0100	8.75×10^{-3}
	24.4	0.0095	1.52×10^{-2}
	30.3	0.0100	2.77×10^{-2}
	35.0	0.0103	4.81×10^{-2}
	39.2	0.0086	7.44×10^{-2}
	44.6	0.0100	2.08×10^{-1}
9-Ethylfluorene	12.5	0.0107	3.24×10^{-4}
	29.9	0.0091	2.58×10^{-3}
	35.0	0.0095	4.22×10^{-3}
	39.2	0.0090	7.56×10^{-3}
	44.5	0.0091	1.63×10^{-2}
	49.1	0.0100	2.93×10^{-2}
	54.6	0.0085	5.54×10^{-2}
	59.6	0.0090	8.88×10^{-2}
	64.9	0.0092	1.81×10^{-1}
9-Phenylxanthene	49.1	0.0094	3.51×10^{-4}
	64.9	0.0100	2.96×10^{-3}
	70.3	0.0140	6.53×10^{-3}
	75.0	0.0150	1.64×10^{-2}
	94.0	0.0100	5.53×10^{-1}
Triphenylmethane*	83.5	0.0100	6.45×10^{-4}
	87.0	0.0100	1.28×10^{-3}
	90.6	0.0100	5.99×10^{-3}

* A referee has kindly drawn our attention to the possibility of tritium being introduced into the rings of triphenylmethane as a consequence of the tritiation method employed for this compound. The low residual activity observed at late stages of the detritiation reaction suggests that this was not a serious source of error in determining reaction rates.

sion of solvent effects on rate of protonation of carbanions.)

The activation parameters for the ionization of four of the carbon acids are given in Table 2. It can be seen that the weaker the acid the larger is $\Delta H^{\ddagger}$. Changes in $\Delta S^{\ddagger}$ are less important and in most cases, they oppose the change in enthalpy. In previous work with carbon acids (8) it was also found that changes in $\Delta H^{\ddagger}$ were more important than changes in $\Delta S^{\ddagger}$ in determining relative ionization rates. The increased exchange rate that accompanies an increase in the DMSO content

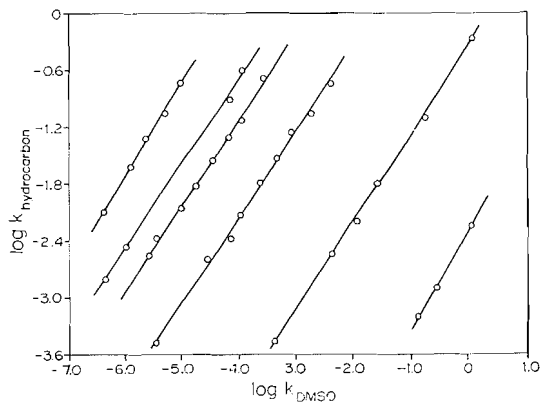

FIG. 1. Plot of $\log k$ (detritiation of hydrocarbon) against $\log k$ (DMSO exchange) in DMSO–ethanol containing 0.01 M sodium ethoxide; rate constants in units of $l\ mol^{-1}\ s^{-1}$. The compounds are, from left to right, 9-phenylfluorene, 2,3-benzofluorene, fluorene, 9-ethylfluorene, 9-phenylxanthene, and triphenylmethane. The slopes and correlation coefficients (in parentheses) are, respectively, 0.983(0.999), 0.904(0.999), 0.914(0.999), 0.908(0.998), 0.928(0.999), and 1.029(0.999).

of the solution is likewise caused chiefly by a change in enthalpy.

The activation of hydroxide that results from the use of polar aprotic solvents is usually attributed to the inability of the solvent molecules to form hydrogen bonds with the small anion, a further factor being the increased solvating ability of polar aprotic solvents towards large, charge-dispersed anions (9). Both factors would lead one to expect $\Delta H^{\ddagger}$ to decrease as the DMSO content increases, as is observed.

Experimental

Materials

The unlabelled hydrocarbons were obtained from commercial sources, except for 9-ethylfluorene, which was prepared by the method of Cuvigny and Normant (10) and 9-phenylxanthene, which was prepared as follows. Treatment of xanthenone with phenylmagnesium bromide in dry benzene gave 9-phenylxanthenol, which was reduced by a formic acid – sodium formate mixture to give 9-phenylxanthene. The product was recrystallized from benzene–ethanol and then sublimed and recrystallized, m.p. 144.5–145°, (lit. (11) 145°).

The tritiated hydrocarbons were prepared by the method of Jones (12), except for triphenylmethane-*t*. This compound was made by treating triphenylcarbinol with acetyl chloride in benzene followed by treatment with sodium amalgam in ether to give triphenylmethylsodium; addition of HTO gave the tritiated hydrocarbon. After filtering off the precipitate of sodium hydroxide the solvent was evaporated, the product was redissolved in ether and refiltered. This procedure was repeated once more and the product then recrystallized from ethanol.

Can. J. Chem. Downloaded from www.nrcresearchpress.com by 210.87.254.6 on 09/05/12
For personal use only.

TABLE 2. Activation parameters for the detritiation of hydrocarbon in mixtures of ethanol and DMSO containing 0.01 *M* sodium ethoxide

Compound (p*K*)*	Mol % DMSO	$\Delta H^{\neq}$ (kcal mol^{-1})	$\Delta S^{\neq}$ (e.u.)
Triphenylmethane (31.5)	62.5	23.3	−2.3
9-Phenylxanthene (28.5)	62.5	21.1	0.5
9-Ethylfluorene (22.2; 22.6)	62.5	16.7	−5.9
	35.0	18.6	−7.1
Fluorene (22.1; 22.7)	62.5	14.4	−10.2
	10.0	17.2	−12.4

*References 2–4.

Exchange Measurements

A weighed amount (20–30 mg) of tritiated hydrocarbon was dissolved in 100 ml of the appropriate DMSO–ethanol solution in a glass-stoppered 125 ml flask immersed in a thermostatted bath. After thermal equilibration was reached 1.0 ml of a 1 *M* solution of sodium ethoxide in ethanol was added. Aliquots were withdrawn at appropriate time intervals and introduced into a 125 ml separatory funnel containing 50 ml of cold water and 15 ml of liquid scintillator (3.5 g of 2,5-diphenyloxazole per liter of toluene). The funnel was shaken, the layers separated, and the toluene layer dried over anhydrous magnesium sulfate. An aliquot (10 ml) of the dried toluene solution was transferred to a counting vial and counted for 20 min in a Nuclear Chicago Mark 1 model 6860 liquid scintillation counter.[1] The counting efficiency was roughly determined for each sample by the external standard technique utilizing the built-in ^{133}Ba source. All vials which did not have close to the average efficiency were discarded. The usual count at time zero was around 500 000 counts per min. In general the reactions were taken to about 70% completion. However, for each hydrocarbon at least one run was allowed to proceed to greater than 90% completion.

[1]We thank Professor J. P. Kutney for the use of this equipment.

The financial support of the National Research Council of Canada is gratefully acknowledged.

1. (*a*) A. ALBAGLI, R. STEWART, and J. R. JONES. J. Chem. Soc. B, 1509 (1970). (*b*) R. STEWART and J. R. JONES. J. Am. Chem. Soc. **89**, 5069 (1967).
2. A. STREITWIESER, J. R. MURDOCH, G. HAFELINGER, and C. J. CHANG. J. Am. Chem. Soc. **95**, 4248 (1973).
3. A. STREITWIESER, C. J. CHANG, and D. M. E. REUBEN. J. Am. Chem. Soc. **94**, 5730 (1972).
4. K. BOWDEN and A. F. COCKERILL. J. Chem. Soc. B, 173 (1970).
5. A. STREITWIESER, A. P. MARCHAND, and A. M. PUDJAATMAKA. J. Am. Chem. Soc. **89**, 693 (1967).
6. E. C. STEINER and J. M. GILBERT. J. Am. Chem. Soc. **87**, 383 (1965).
7. C. D. RITCHIE. *In* Solute-solvent interactions. *Edited by* J. F. Coetzee and C. R. Ritchie. Marcel Dekker, New York. 1969. p. 219.
8. A. STREITWIESER, W. B. HOLLYHEAD, G. SONNICKSEN, A. H. PUDJAATMAKA, C. J. CHANG, and T. L. KRUGER. J. Am. Chem. Soc. **93**, 5096 (1971).
9. E. GRUNWALD and E. PRICE. J. Am. Chem. Soc. **86**, 4517 (1964).
10. T. CUVIGNY and H. NORMANT. Bull. Soc. Chim. Fr. 1872 (1965).
11. F. ULLMANN and G. ENGI. Ber. **87**, 2367 (1904).
12. J. R. JONES. J. Labelled Compounds. **IV**, 197 (1968).

Can. J. Chem. Downloaded from www.nrcresearchpress.com by 210.87.254.6 on 09/05/12
For personal use only.

Chemistry of 2-Substituted Adamantanes. V.[1] Photolysis of 2-Adamantyl Azidoformate

J. W. GREIDANUS

Department of Chemistry, School of Natural Sciences, University of Zambia, P.O. Box 2379, Lusaka, Zambia

Received March 6, 1973[2]

In an attempt to prepare adamanto[1,2-*d*]oxazolidin-2-one (**2**), 2-adamantyl azidoformate was subjected to photolysis in cyclohexane. The main product **8** (yield 41%) is formed by intermolecular insertion of the nitrene in the solvent. The only other pure compound isolated (yield 15%) is a product of intramolecular insertion. The i.r. spectrum of the latter supports the presence of a five-membered cyclic carbamate. The fact that intermolecular insertion is the main reaction is unexpected in view of the results reported by others.

Afin de préparer l'adamantano [1,2-*d*]oxazolidinone-2 (**2**) on a soumis l'azydoformate d'adamantyle-2 en solution dans le cyclohexane à une photolyse. Le produit principal de la réaction, **8**, (rendement 41%) est formé par une insertion intermoléculaire du nitrène dans le solvant. Le seul autre produit pur isolé (rendement 15%) est un produit d'insertion intramoléculaire. Le spectre infrarouge de ce dernier indiquerait la présence d'un carbamate dans un cycle à cinq membres. Le fait que l'insertion intermoléculaire est la réaction principale est inattendue considérant les résultats rapportés par d'autres autours. [Traduit par le journal]

Can. J. Chem., **52**, 1062 (1974)

Insertion reactions of nitrene intermediates, especially of carbonylnitrenes, can lead to synthetically useful processes and the topic has been thoroughly reviewed (1). The photolytic decomposition of 1-adamantyl azidoformate in cyclohexane (2,3) gives a 45% yield of adamanto-[2,1-*d*]oxazolidin-2-one (**1**). Intermolecular insertion of the intermediate carbalkoxynitrene into the solvent is a minor process giving only 4% of 1-adamantyl *N*-cyclohexylcarbamate and the three methylene groups adjacent to the substituted bridgehead in the azidoformate compete effectively with those in cyclohexane for the nitrene.

We were interested in the isomeric adamanto-[1,2-*d*]oxazolidin-2-one (**2**) and decided to attempt its synthesis in a way completely analogous to that used for **1** (2,3). Solely on statistical grounds the chances for the formation of **2** are one-third those for the cyclization leading to **1** (assuming that **3** is not formed).

Cyclization of the intermediate nitrene to the tetrahydro-1,3-oxazin-2-one derivative **3** is also a possibility, as several examples of the formation of this ring system by acylnitrene insertion have been reported (4). The considerable preference of ethoxycarbonylnitrene for insertion

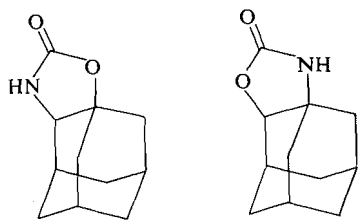

1

2

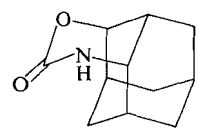

3

into the bridgehead C—H bond of adamantane has been demonstrated clearly[3] and it was hoped that this would be the dominant factor and would result in a good yield of **2**.

As will be shown below, the photolysis of 2-adamantyl azidoformate was highly disappointing from the standpoint of satisfactorily preparing **2**.

Results

The compound 2-adamantyl *p*-nitrophenyl carbonate (**4**) and the carbazate **5** were prepared

[1]For Part IV see ref. 15.

[2]Revision received November 12, 1973.

[3]The relative reactivity of the tertiary C—H bond in adamantane was found to be more than six times that of a secondary C—H bond in its reaction with ethoxycarbonylnitrene (5).

Can. J. Chem. Downloaded from www.nrcresearchpress.com by 210.87.254.40 on 09/05/12
For personal use only.

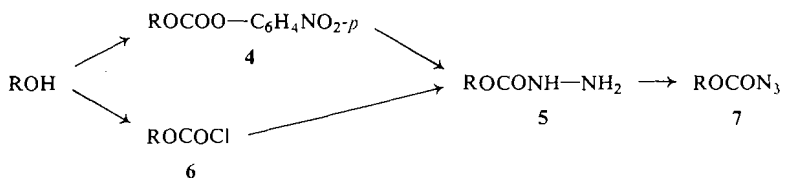

R = 2-Adamantyl

SCHEME 1

(yields, respectively, 66 and 89%) following the procedures reported for the corresponding 1-adamantyl isomers (3) but with some experimental modifications. The carbazate **5** could also be prepared (yield 82%) from 2-adamantyl chloroformate (**6**). The crude chloroformate **6** was obtained from 2-adamantanol and phosgene[4] but the yields were variable and low (28–42%).

The carbazate **5** was treated with nitrous acid and gave 2-adamantyl azidoformate (**7**), as shown in Scheme 1, with a yield of 78%.[5] The photolysis of **7** was carried out in a quartz tube at 253.7 nm and was found to be complete after 90–100 min.

Two pure products could be isolated. The first and most easily obtained product $C_{11}H_{15}NO_2$, m.p. 135–136°, has like its isomer **1** a rather low solubility in cyclohexane (3) and is obtained by filtration with a maximum yield of 15%. Although its i.r. spectrum seems to indicate the presence of a five-membered cyclic carbamate we cannot at this stage assign structure **2** to it with certainty (see Discussion).

[1] 7 $\xrightarrow[\text{cyclohexane}]{h\nu \text{ in}}$ $C_{11}H_{15}NO_2$ +

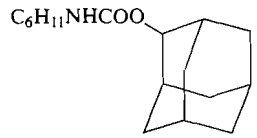

+ Unknown products

8

Insertion of the nitrene intermediate into the solvent appeared to be the main reaction, giving a 41% yield of 2-adamantyl *N*-cyclohexylcarbamate (**8**), isolated after chromatography on alumina (eluent benzene). Continued elution with more polar solvents gave a variety of small and mostly very viscous residues, the i.r. spectra of which indicated the presence of amide-like compounds as well as some 2-adamantanol. These were not further investigated.

Discussion

In the absence of skeletal rearrangements[6] intramolecular insertion of the nitrene intermediate from **7** will give rise to a 2-oxazolidinone ring, as in **2**, or to a tetrahydro-1,3-oxazin-2-one ring, as in **3**.[7]

A photolysis product $C_{11}H_{15}NO_2$ resulting from intramolecular nitrene insertion and isolated with a yield of 15%, shows in its i.r. spectrum a split carbonyl absorption band with maxima at 1715 and 1755 cm^{-1} (both very strong). Compound **1** shows also two maxima, at 1724 and 1754 cm^{-1} (3), and a double band has been reported for other five- and six-membered cyclic carbamates (9,10). The carbonyl absorption in five-membered carbamate rings occurs about 40 wavenumbers higher than in six-membered rings (9–11). In the case of 2-oxazolidinone, the values 1724 (12) and 1730 cm^{-1} (10) have been reported; the six-membered cyclic carbamate tetrahydro-1,3-oxazin-2-one absorbs at 1699 cm^{-1}, while 2-oxa-4-azabicyclo-[3.3.1]nonan-3-one absorbs at 1686 and 1646 cm^{-1} (10). The last compound, especially, is of interest as its bicyclic structure is part of **3**. A

[4]Compare with the preparation of 1-adamantyl chloroformate (6,7).

[5]It is not necessary to isolate **7** for the next photolysis step (compare with ref. 3) but we often did so in order to get more accurate information about the yield of the photolysis products.

[6]The possibility of a skeletal rearrangement has been suggested by one of the referees and can of course not be ruled out, although it seems unlikely to the present author. 1-Adamantyl cations and free radicals appear to have considerable stability and skeletal isomerizations of adamantane compounds (including degenerate isomerizations) are interpreted as reactions of the 2-adamantyl carbonium ion (8).

[7]The author is not aware of any intramolecular carbalkoxynitrene insertion leading to a four-membered cyclic carbamate and considers its formation from **7** also very unlikely.

Can. J. Chem. Downloaded from www.nrcresearchpress.com by 210.87.254.40 on 09/05/12
For personal use only.

Can. J. Chem. Downloaded from www.nrcresearchpress.com by 210.87.254.40 on 09/05/12
For personal use only.

five-membered ring is indicated by the i.r. spectrum of $C_{11}H_{15}NO_2$.

Compound **3** should show two one-proton absorptions in its n.m.r. spectrum for hydrogen at C-2 and -4. The n.m.r. spectrum of the product $C_{11}H_{15}NO_2$ ($CDCl_3$) does not show these peaks but neither does it all by itself prove structure **2**. In addition to a massive multiplet (δ 1.1–2.6, 13 protons) four minor peaks occur at δ 6.22, 5.14, 4.78, and 4.11, together representing two protons. The peaks at δ 6.22 and 5.14 amount together to one proton, they can be removed by exchange with D_2O–NaOD, have the broad shape of an amide proton, and appear to have aromatic solvent-induced shifts of opposite sign in perdeuteriobenzene. These data would be compatible with structure **2** only if we were dealing with a mixture of invertomers. As the barrier to nitrogen inversion in amides is generally low,[8] this explanation would be sufficiently unusual to require confirmation which is outside the scope of the original project and at present not yet available.

Our finding that intermolecular insertion of the nitrene intermediate into the solvent cyclohexane competes so effectively with intramolecular insertion in the photolysis of 2-adamantyl azidoformate is unexpected in view of the behavior of its 1-adamantyl isomer under identical reaction conditions (3) and because of the observation (5) that, in its reaction with ethoxycarbonylnitrene, the tertiary C—H bond in adamantane is much more reactive than the secondary.

Intermolecular insertion of nitrene in cyclohexane appeared to be the main reaction in the photolysis of 1-adamantyl carbamoyl azide (14) and it is clear that the conditions for successful intramolecular nitrene insertion in adamantane derivatives are not well understood and will require further investigation.

Experimental

Photolyses were carried out in a quartz reaction tube in a Rayonet photochemical reactor equipped with eight low-pressure mercury lamps giving 84% of their emission at 253.7 nm. Melting points were determined in sealed capillary tubes and are uncorrected. The i.r. spectra were run in KBr pellets unless otherwise specified and were recorded on a Perkin-Elmer spectrophotometer, model 337, or a Unicam SP 200G instrument. Mass spectral data were obtained with a Varian-Mat CH-15 instrument at an ionization energy of 70 eV. The n.m.r. spectra were recorded on Varian A-60 and HA-100 spectrometers of the Department of Chemistry, University of Calgary and on the Varian A-60 D instrument of the National Council for Scientific Research of Zambia in the Chemistry Department of the University of Zambia. Tetramethylsilane was used as an internal standard (δ = 0 p.p.m.) in the indicated solvent. Elemental analyses were carried out by the Analytical Laboratory of the Department of Chemistry or the Analytical Service of the Department of Chemical Engineering, both of the University of Calgary.

2-Adamantyl p-Nitrophenyl Carbonate (4)

A solution of *p*-nitrophenyl chloroformate (24.0 g, 119 mmol) in dichloromethane (60 ml) was added dropwise in 1 h to a well-stirred solution of 2-adamantanol (18.0 g, 118 mmol) and quinoline (15.5 g, 120 mmol) in dichloromethane (180 ml). The reaction mixture was left standing at 25° for 3 days, extracted with water (twice, 600 ml), with 0.25 *N* HCl (twice, 600 ml), and dried (anhydrous $MgSO_4$). After evaporation of the solvent the residue (38.4 g) was redissolved in boiling dichloromethane (100 ml), treated with charcoal, and filtered. Petroleum ether (150 ml) was added to the filtrate and after cooling to 0° 2-adamantyl *p*-nitrophenyl carbonate (**4**) (24.6 g, 65.5%), m.p. 124–127°, was obtained. After repeated recrystallization the m.p. was unchanged.

Anal. Calcd. for $C_{17}H_{19}NO_5$: C, 64.35; H, 6.04; N, 4.41. Found: C, 63.99; H, 6.01; N, 4.47.

The i.r. spectrum ν_{max}: 1765 (C=O), and 1525 and 1350 cm^{-1} (NO_2), all very strong; n.m.r. δ ($CDCl_3$): 7.86 (4H, center of aromatic quartet), 4.96 (broad singlet, 1H at C-2), 1.45–2.35 (massive multiplet, 14H).

2-Adamantyl Carbazate (5)

Procedure A. 2-Adamantyl *p*-nitrophenyl carbonate (32.2 g, 101 mmol) was added to a mixture of hydrazine (20.0 g, 0.62 mol) and dry methanol (800 ml). The reaction mixture was stirred for 65 h, then heated to reflux for 3 h. After removal of the solvent (under reduced pressure), ether (900 ml) was added which dissolved part of the red oily residue. The ethereal solution was extracted with 10% NaOH (six times, 600 ml) and water (three times, 600 ml), dried (anhydrous $MgSO_4$), and after evaporation gave a residue of 2-adamantyl carbazate (18.9 g, 89%), m.p. 69–70°. Recrystallization from ether–hexane (1:2) gave an analytical sample with unchanged m.p.

Anal. Calcd. for $C_{11}H_{18}N_2O_2$: C, 62.83; H, 8.63; N, 13.32. Found: C, 63.03; H, 8.79; N, 13.00.

The i.r. spectrum ν_{max}: 1720 cm^{-1} (C=O); n.m.r. δ ($CDCl_3$): 6.16 (1H, broad singlet, —NH—), 4.87 (1H at C-2), 3.55 (2H, broad singlet, $—NH_2$), 1.30–2.85 (massive multiplet, 14H).

Procedure B. Following a published method for the preparation of 1-adamantyl chloroformate (6), 2-adamantanol (8.0 g, 53 mmol) was allowed to react at 0–5° with a mixture of liquid phosgene (30 g, 0.3 mol) and benzene (200 ml) in the presence of pyridine. After washing, drying, and evaporation of the solvent at 25° under reduced pressure (CAUTION: large quantities of excess phosgene escape), crude 2-adamantyl chlorofor-

[8]Ring strain and a hetero atom bonded to nitrogen are normally required for the stabilization of the nitrogen pyramid in order to give stable invertomers (13).

Can. J. Chem. Downloaded from www.nrcresearchpress.com by 210.87.254.40 on 09/05/12
For personal use only.

mate (**6**) (7.2 g) was obtained, m.p. 40–42°. After recrystallization from petroleum ether at −20°, 4.8 g (42%), m.p. 42–44° was obtained. A small sample of **6**, repeatedly recrystallized, had a m.p. 44–45°, but no fully satisfactory elemental analysis could be obtained for this chloroformate for which the following spectral data were recorded; i.r. ν_{max}: 1775 (C=O) and 1170 cm^{-1} (broad, C—O); n.m.r. δ (CCl_4): 4.95 (singlet, 1H at C-2), 1.3–2.4 (massive multiplet, 14H).

Reaction of **6** with anhydrous hydrazine in *tert*-butyl alcohol – benzene according to the published procedure (6) for 1-adamantyl carbazate gave an 82% yield of **5**, identical with the product obtained in Procedure A.

2-Adamantyl Azidoformate (7)

2-Adamantyl carbazate (1.05 g, 5.0 mmol) was dissolved in a mixture of acetic acid (15 ml), water (50 ml), and concentrated hydrochloric acid (3.3 ml). To this solution, cooled to 0°, was added dropwise a solution of sodium nitrite (0.37 g, 5.4 mmol) in cold water (4 ml). The reaction mixture was extracted with cyclohexane (three times, 50 ml). The extract was washed with water, 5% aqueous $NaHCO_3$, water again, and dried ($MgSO_4$). Evaporation of the solvent at 20° gave a residue of 2-adamantyl azidoformate (0.86 g, 78%), m.p. 52–54°. Two recrystallizations from ethanol (at −20°) raised the m.p. to 55–56°.

Anal. Calcd. for $C_{11}H_{15}N_3O_2$: C, 59.71; H, 6.83; N, 18.99. Found: C, 59.58; H, 7.05; N, 18.68.

The i.r. spectrum ν_{max}: 2420(w), 2200(s), and 2145 (s, $—N_3$), 1730(vs, C=O), 1238 cm^{-1} (vs, C—O in ester); n.m.r. δ ($CDCl_3$): 5.09 (s, 1H at C-2), 1.40–2.20 (massive multiplet, 14H).

Photolysis of 2-Adamantyl Azidoformate (7) in Cyclohexane

A solution of 2-adamantyl azidoformate (3.51 g, 15.9 mmol) in cyclohexane was subjected to photolysis for 100 min, when it was found that no azidoformate was present any more. Most of the solvent was evaporated under reduced pressure (rotary evaporator) and an oily semisolid residue (4.6 g) was obtained. When some cyclohexane (15 ml) was added to this material not all redissolved at 20° and after filtration 473 mg of product with m.p. 133–134.5° was obtained. Recrystallization from ethyl acetate gave an analytical sample (m.p. 135–136°) of $C_{11}H_{15}NO_2$.

Anal. Calcd. for $C_{11}H_{15}NO_2$: C, 68.37; H, 7.82; N, 7.25. Found: C, 68.30; H, 8.07; N, 7.27.

The i.r. spectrum ν_{max}: 3400(m), 3320(w), 3255(m) with weak shoulder at 3130 (NH, free and bonded), 1755 and 1715 (vs, C=O), and the following major peaks below 1700 cm^{-1}: 1625(m), 1465(m), 1412(s), 1375(s), 1340(s), 1248(m), 1213(m), 1142(s), 1100(m), 1060(s), 1030(m), 980(m), and 948(m) cm^{-1}. Mass spectrum *m/e* 193 (M^+). For the n.m.r. spectrum (10% solution in $CDCl_3$) see text.

The concentrated filtered solution from which the product $C_{11}H_{15}NO_2$ had been obtained was subjected to chromatography on an alumina column. Elution with benzene yielded 2-adamantyl *N*-cyclohexylcarbamate (**8**) (1.81 g, 41%), m.p. 119–120.5°. After crystallization from 95% aqueous methanol m.p. 121–122°.

Anal. Calcd. for $C_{17}H_{27}NO_2$: C, 73.61; H, 9.81; N, 5.05. Found: C, 73.75; H, 9.49; N, 5.18.

The i.r. spectrum ν_{max}: 3310(s) and 3060(w, NH), 1695(vs, C=O), 1545(s, "amide II"); n.m.r. δ ($CDCl_3$): 4.80(s, 1H at C-2 of adamantane), 4.54(s, broad, 1H, NH, exchangeable), 3.48(s, broad, 1H, adjacent to NH), 1.0–2.4(massive multiplet, 24H).

The author thanks the Central Research Fund of the University of Zambia for financial support. During the early stages of this investigation at the University of Calgary he received a grant from the National Research Council of Canada which enabled him to employ Mr. B. Jennings (Summer Research Assistant, 1970), whose skillful and enthusiastic assistance he is pleased to acknowledge.

1. W. Lwowski (*Editor*). Nitrenes. Interscience Publishers, New York. 1970.
2. W. V. Curran and R. B. Angier. Chem. Commun. 563 (1967).
3. W. V. Curran and R. B. Angier. J. Org. Chem. **34**, 3668 (1969).
4. O. E. Edwards. *In* Nitrenes. *Edited by* W. Lwowski. Interscience Publishers, New York. 1970. Chapt. 7.
5. D. S. Breslow, E. I. Edwards, R. Leone, and P. v. R. Schleyer. J. Am. Chem. Soc. **90**, 7097 (1968).
6. W. L. Haas, E. V. Krumkalns, and K. Gerzon. J. Am. Chem. Soc. **88**, 1988 (1966).
7. D. N. Kevill and F. L. Weitl. J. Am. Chem. Soc. **90**, 6416 (1968).
8. M. L. Sinnott, H. J. Storesund, and M. C. Whiting. Chem. Commun. 1000 (1969). J. R. Alford and M. A. McKervey. Chem. Commun. 615 (1970). Z. Majerski, S. H. Liggero, and P. v. R. Schleyer. Chem. Commun. 1596 (1970).
9. R. Gompper and H. Herlinger. Chem. Ber. **89**, 2825 (1956).
10. H. K. Hall, Jr. and R. Zbinden. J. Am. Chem. Soc. **80**, 6428 (1958).
11. L. J. Bellamy. Advances in infrared group frequencies. Methuen, London. 1968. p. 134.
12. R. Mecke, R. Mecke, and A. Luttringhaus. Chem. Ber. **90**, 975 (1957).
13. H. Kessler, Angew. Chem. Int. Ed. Engl. **9**, 219 (1970).
14. D. Lenoir, R. Glaser, P. Mison, and P. v. R. Schleyer. J. Org. Chem. **36**, 1821 (1971).
15. J. W. Creidanus. Int. J. Sulfur Chem. **3**, 243 (1973).

Reactivity of Organophosphates. IV. Acid-catalyzed Hydrolysis of Triethyl Phosphate: a Comparison with Ethyl Acetate[1]

EDWARD P. LYZNICKI, JR., KIYOTAKA OYAMA, AND THOMAS T. TIDWELL
Department of Chemistry, University of Toronto, Scarborough College, West Hill, Ontario M1C 1A4

Received May 1, 1973[2]

The hydrolysis of triethyl phosphate in water and in 35% dioxane – 65% water has been examined. Hydrolysis in neutral water proceeds with a rate constant of 8.35×10^{-6} s^{-1} at 101°, $\Delta H^* = 23.4$ kcal/mol, $\Delta S^* = -20$ e.u., a solvent isotope effect k_{H_2O}/k_{D_2O} of 1.3, C—O bond cleavage as shown by ^{18}O labeling, and no catalysis by 0.5 *M* sulfuric acid. These results are consistent with the $B_{AL}2$ mechanism of hydrolysis and the same pathway is indicated for the reaction in neutral 35% dioxane – 65% water. Perchloric acid catalyzes the reaction in dioxane–water with C—O bond cleavage in 0.904 *M* acid, $\Delta H^* = 24.1$ kcal/mol, $\Delta S^* = -17$ e.u., and the solvent isotope effect $k_{H_2O}/k_{D_2O} = 0.6$ in 0.556 *M* acid. These results indicate that the $A_{AL}2$ pathway of hydrolysis is followed under these conditions. The reactivity of triethyl phosphate is compared with that of ethyl acetate.

On a examiné l'hydrolyse du phosphate de triéthyle dans l'eau et dans un mélange contenant 35% de dioxanne et 65% d'eau. En milieu neutre l'hydrolyse se produit avec une constante de vitesse de 8.35×10^{-6} s^{-1} à 101°, un $\Delta H^* = 23.4$ kcal/mol, un $\Delta S^* = -20$ u.e., avec un effet isotopique de solvant K_{H_2O}/K_{D_2O} de 1.3, avec un bris du lien C—O tel que démontré par marquage avec ^{18}O et sans catalyse par l'acide sulfurique 0.5 *M*. Ces résultats sont en accord avec un mécanisme d'hydrolyse du type $B_{AL}2$ et il apparait que la réaction se produit de la même manière dans le mélange 35% dioxanne – 65% d'eau à un p*H* neutre. L'acide perchlorique catalyse la réaction dans le mélange dioxanne–eau et la réaction se produit avec rupture du lien C—O dans de l'acide de 0.904 *M* et avec un $\Delta H^* = 24.1$ kcal/mol, un $\Delta S^* = -17$ u.e. et un effet isotopique de solvant $K_{H_2O}/K_{D_2O} = 0.6$ dans de l'acide 0.556 *M*. Ces résultats indiquent que l'hydrolyse se produit dans ces conditions par l'intermédiaire d'un mécanisme $A_{AL}2$. On compare la réactivité du phosphate d'éthyle avec celle de l'acétate d'éthyle. [Traduit par le journal]

Can. J. Chem., **52**, 1066 (1974)

Ester hydrolysis has perhaps received more mechanistic study than any other organic reaction, and this attention is justified in view of the pervasive importance of this reaction in organic chemistry and biochemistry. Carboxylate esters have received the most attention (1) but phosphate esters have also been examined by many investigators (2). Study of the phosphates is of importance because of the biological significance of these materials and also because the comparison of phosphate and carboxylate esters has been instructive (3). Ethyl acetate hydrolysis has been examined intensively and is the reference to which many other compounds have been compared. Triethyl phosphate is a suitable model in the phosphate series for comparison but, although there have been several studies of the neutral and acid-catalyzed reactivity of this compound (4), the mechanism of its hydrolysis is still not clear. The reasons for this deficiency are the low susceptibility of the compound to acid-catalyzed hydrolysis, the lack of good analytical methods for examining the kinetics of triethyl phosphate reactivity (particularly in strong acids), and the failure to apply isotopic labeling techniques to elucidate the position of bond cleavage in the hydrolysis reaction. Accordingly we have examined the reactivity of this compound in more detail to establish its mechanism of hydrolysis, with particular emphasis on the comparison with ethyl acetate.

Results

Rate constants were obtained for the hydrolysis of triethyl phosphate in various solvents by titration of the liberated diethyl phosphoric acid and

[1]This investigation was initiated at the University of South Carolina and was supported by U.S. Public Health Service Research Grant No. 1 R01 GM 16818 from the National Institute of General Medical Sciences. Present research support from the National Research Council of Canada is gratefully acknowledged. For Part III, see ref. 3*c*.

[2]Revision received December 17, 1973.

Can. J. Chem. Downloaded from www.nrcresearchpress.com by 210.87.254.6 on 09/05/12
For personal use only.

Can. J. Chem. Downloaded from www.nrcresearchpress.com by 210.87.254.6 on 09/05/12
For personal use only.

TABLE 1. Hydrolysis of triethyl phosphate in water

Temperature	$[H_2SO_4](M)$	Solvent	$k(s^{-1} \times 10^6)^a$
101.0	—	H_2O	8.35
101.0	—	D_2O	6.76
101.0	0.25	H_2O	11.4
101.0	0.50	H_2O	8.17
79.6	—	H_2O	1.27

[a]Rate constants were reproducible to ±3% for neutral reactions and ±10% for acid-catalyzed reactions.

TABLE 2. Hydrolysis of triethyl phosphate in 35% dioxane – 65% water

Temperature	$[HClO_4](M)$	Solvent	k_{obs} $(s^{-1} \times 10^6)^a$
115.0	0.234	H_2O	13.1
115.0	0.370	H_2O	22.4
115.0	0.908	H_2O	48.5
101.0	—	H_2O	1.88
101.0	—	D_2O	1.83
101.0	0.066	H_2O	2.30
101.0	0.124	H_2O	2.80
101.0	0.165	D_2O	3.70[b]
101.0	0.234	H_2O	4.40
101.0	0.370	H_2O	7.14
101.0	0.537	H_2O	8.22
101.0	0.556	D_2O	13.3[b]
101.0	0.791	H_2O	10.3
101.0	0.904	H_2O	13.0
79.7	—	H_2O	0.293
79.7	0.234	H_2O	0.499
79.7	0.904	H_2O	1.91

[a]Rate constants were reproducible to ±5%, with the exception of the runs at 0.904 *M* acid, which were reproducible to ±10%.
[b]For comparison the rate constants for reaction in H_2O-containing solvent at 0.165 and 0.556 *M* HClO were interpolated from a plot of *k vs.* $[HClO_4]$, and were found to be 3.70 and $8.45 \times 10^{-6}\ s^{-1}$, respectively.

are tabulated in Tables 1 and 2. Rates were followed for only about 20% reaction to avoid complications due to the further hydrolysis of diethyl phosphoric acid. Below 0.3 *M* acid rates were reproducible to ±5%; at higher concentrations of acid, where relatively larger amounts of base were needed to neutralize the acid catalyst, reproducibility was ±10%. Activation parameters derived from rate measurements for fixed acidities at different temperatures are reported in Table 3. Rate constants for the acid-catalyzed hydrolysis in 35% dioxane – 65% water corresponding to 0.165 and 0.556 *M* $HClO_4$ were obtained from a plot of the observed rate constants versus acid concentration for comparison with the corresponding measured rates in deuterated solvent.

Isotope labeling experiments on the position of bond cleavage using ^{18}O labeled water are recorded in Table 4. Analyses were carried out by first making the solution basic and extracting with ether. Ethanol was isolated from the ether extracts by distillation and v.p.c. The aqueous layer was acidified, extracted with ether, and treated with diazomethane. Vapor phase chromatography separation yielded methyl diethyl phosphate. The ethanol and the phosphate were analyzed for ^{18}O content by mass spectrometry. A control experiment showed that exchange of diethyl phosphoric acid with the solvent under these conditions was negligible.

The reaction of ethyl acetate in pure water at 101° was monitored by titration of the liberated acetic acid. When these data were plotted as a first-order reaction a curved line was obtained due to autocatalysis by the product acetic acid. Extrapolation of the rate curve to zero time gave an initial rate constant of $5 \times 10^{-7}\ s^{-1}$.

Discussion

The absence of a systematic increase in the rate of hydrolysis of triethyl phosphate in water with increasing concentration of acid indicates that the reaction is not acid catalyzed at the concentrations used. Higher concentrations of acid could not be used to obtain titrimetric rates and attempts to measure the rate by monitoring the u.v. absorption were not successful. The isotopic labeling experiments show that C—O bond cleavage is involved, indicating that the reaction in pure water proceeds by an S_N2 displacement ($B_{AL}2$ in the terminology of ester hydrolysis (1*a*)) as depicted in eq. 1. The entropy of activation,

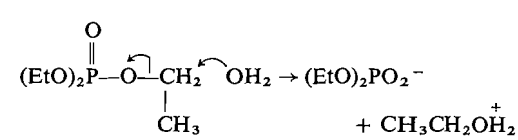

[1] $(EtO)_2P(=O)-O-CH_2(CH_3)-OH_2 \rightarrow (EtO)_2PO_2^- + CH_3CH_2O\overset{+}{H}_2$

−20 e.u., and the solvent isotope effect, $k_{H_2O}/k_{D_2O} = 1.3$, are also in the range expected for such a reaction (5, 6). This is the same mechanism proposed for the neutral hydrolysis of trimethyl phosphate (7), which has a reported rate constant at 100° of $4.23 \times 10^{-5}\ s^{-1}$, compared to the value of 0.835×10^{-5} for triethyl phosphate at 101°, leading to a calculated rate ratio of 5.0 for trimethyl phosphate – triethyl phosphate.

In aqueous dioxane solution the rate of reaction increased markedly with increasing acid concentration, as anticipated from the previous

TABLE 3. Activation parameters for triethyl phosphate hydrolysis

Solvent	$[HClO_4]$ (M)	ΔH^* (kcal/mol)[b]	ΔS^*(e.u.)[b]
H_2O[a]	—	23.4	−20
35% dioxane – 65% water	—	24.6	−19
35% dioxane – 65% water	0.234	24.6	−18
	0.370	22.8	−22
	0.904	24.1	−17

[a]Includes the data in Table 1, as well as that reported in ref. 4*a* and *c*.
[b]Standard deviations did not exceed 0.05 kcal/mol for ΔH^* and 0.1 e.u. for ΔS^*.

TABLE 4. Isotopic content of products of reaction of $(EtO)_3PO$ with $H_2{}^{18}O$

% excess ^{18}O content (solvent H_2O)	Solvent	Acid	% excess ^{18}O content	
			$(EtO)_2PO_2H$	EtOH
3.5±0.2	H_2O	—	0.0±0.1	4.0±0.3
3.52±0.20	35% dioxane – 65% water	1.02 M $HClO_4$	0.0±0.2	3.58±0.04

report (4*a*) of a five-fold increase in the rate of triethyl phosphate in 60% aqueous dioxane on the addition of 0.27 N $HClO_4$.

The emergence of the acid-catalyzed reaction in the presence of an organic cosolvent has been examined for the case of trimethyl phosphate (7*b*) and was attributed to a combination of a diminution of the water activity and an enhancement of the proton activity by the organic cosolvent. In contrast, ethyl dihydrogen phosphate has an acid-catalyzed component to the overall hydrolysis which is observable in completely aqueous solutions (8).

A plot of k_{obs} *vs.* the concentration of $HClO_4$ is shown in Fig. 1. The scatter of the points suggests that a comparison of the rate dependence on $[H^+]$ and the H_0 acidity function would not provide a reliable criterion of mechanism in this case, especially since the higher acidities at which the H_0 scale becomes significantly different from $-\log [H^+]$ are not accessible for triethyl phosphate by our rate measurements. By contrast, for ethyl acetate plots of $\log k_{obs}$ *vs.* $-\log [H^+]$ are close to linear with unit slope in water (9*a*) and aqueous dioxane (9*b*), supporting an A2 mechanism for this compound.

The decisive criterion of mechanism for the acid-catalyzed hydrolysis of triethyl phosphate is the isotope labeling experiments (Table 4) which show exclusive C—O bond fission. The possibility of a unimolecular reaction to form an ethyl cation under these conditions is negligible (10), so the isotope labeling results combined with the observed acid-catalysis require unambiguously the $A_{AL}2$ pathway for hydrolysis. It is also known that triethyl phosphate undergoes preferential protonation on phosphoryl oxygen in acid (11), so that the overall pathway shown in eqs. 2 and 3 is indicated.

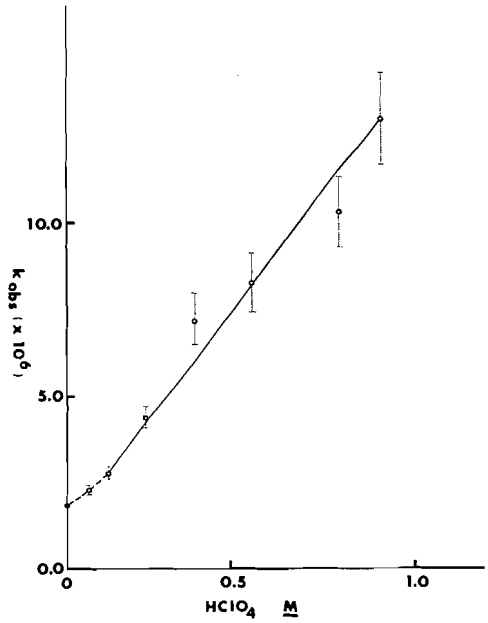

FIG. 1. Hydrolysis of triethyl phosphate in 35% dioxane – 65% water catalyzed by $HClO_4$ at 101°. Error bars represent estimated precision of measured rate constants.

Can. J. Chem. Downloaded from www.nrcresearchpress.com by 210.87.254.6 on 09/05/12
For personal use only.

Can. J. Chem. Downloaded from www.nrcresearchpress.com by 210.87.254.6 on 09/05/12
For personal use only.

[2] $(EtO)_3PO + H^+ \overset{K}{\rightleftharpoons} (EtO)_3\overset{+}{P}OH$

[3] $(EtO)_2\overset{+}{P}(OH)-O-CH_2-\overset{+}{O}H_2 \xrightarrow[\text{slow}]{k} (EtO)_2PO_2H + CH_3CH_2\overset{+}{O}H_2$

The negative activation entropies at various acidities and the solvent isotope effect $k_{H_2O}/k_{D_2O} = 0.6$ at 0.556 *M* perchloric acid are also supportive of an A2 mechanism (6), but these parameters cannot be used as the primary indicators of mechanism due to the imprecise data from which they are derived.

The initial curvature in the k_{obs} *vs.* $[H^+]$ plot is felt to be genuine and to represent a decrease in the neutral hydrolysis due to decreased water activity on addition of the electrolyte perchloric acid. Similar effects have been established for trimethyl phosphate (7*b*).

Several informative comparisons may be made between the reactivities of triethyl phosphate and ethyl acetate. Whereas the phosphate reaction with neutral water proceeds by S_N2 displacement (eq. 1), the uncatalyzed reaction of ethyl acetate presumably (12) occurs by a $B_{AC}2$ pathway (eq. 4). Even though these compounds react by

[4] $CH_3COEt + H_2O \rightarrow CH_3C(OH)(OH)OEt \rightarrow CH_3CO_2H + EtOH$

different pathways, the difference in their reactivity is not great. The rate constant for hydrolysis of ethyl acetate by neutral water has been reported (13) as 2.4×10^{-10} s^{-1} at 25°, and the neutral rate for triethyl phosphate extrapolated to this temperature is 2.4×10^{-9} s^{-1}, giving a ratio $k_{(EtO)_3PO}/k_{EtOAc}$ of 10 for neutral hydrolysis in pure water. The corresponding ratio from the data reported herein at 101° is 16. The phosphate is a better leaving group and promotes displacement on the ethyl group, whereas attack at phosphorus is not favored, as discussed below.

No acid catalysis of triethyl phosphate hydrolysis was observed in water, so the upper limit for this rate constant, corresponding to the observed rate in 1 *N* sulfuric acid at 101°, is 8.2×10^{-6} M^{-1} s^{-1}, as compared to the value for ethyl acetate[3] of 2.40×10^{-2} under the same conditions. Thus the acid-catalyzed hydrolysis of ethyl acetate in water is calculated to be at least 4100 times that of triethyl phosphate. Furthermore the phosphoryl group is known to be more basic than the carbonyl group: measurements of the heats of protonation of ethyl acetate and triethyl phosphate in fluorosulfuric acid give pK_a values for ionization of the corresponding conjugate acids of −6.5 and −4.5, respectively (14). Thus triethyl phosphate is 100 times more basic than ethyl acetate, and hence the rate-determining attack of water on the protonated carbonyl group in the hydrolysis of ethyl acetate (eq. 5) must be at least 4.1×10^5 times as favorable as the corresponding step in the hydrolysis of triethyl phosphate (eq. 6).

[5] $CH_3CO_2Et + H^+ \overset{k}{\rightleftharpoons} CH_3\overset{+}{C}(OH)OEt \xrightarrow[\text{slow}]{k_{H_2O}} CH_3C(OH)(\overset{+}{O}H_2)OEt \xrightarrow{\text{fast}} \text{Products}$

[6] $(EtO)_3PO + H^+ \overset{k}{\rightleftharpoons} (EtO)_3\overset{+}{P}OH \xrightarrow[\text{slow}]{k_{H_2O}} (EtO)_3\overset{+}{P}O_2H_3 \xrightarrow{\text{fast}} \text{Products}$

Experimental

Materials

Commercial samples of triethyl phosphate were purified by distillation, b.p. 99–100° (20 mm). Dioxane was purified by a literature method (15). Solutions of perchloric acid in aqueous dioxane were prepared from concentrated $HClO_4$ (70%) (Baker Reagent) and standardized with dilute potassium hydroxide to a phenolphthalein end point. Solvent isotope effects were measured using either 99.7% D_2O or 99.7% D_2O in dioxane, acidified as necessary with 70% $HClO_4$. Water containing 3.5% ^{18}O was obtained from ICN Corporation and Miles Laboratory, and was acidified as necessary with 70% $HClO_4$. Dilution of the enriched solvent by the H_2O in the $HClO_4$ amounted to 5%, and values were corrected accordingly. Ether was distilled from sodium to remove any ethanol present.

Kinetics

Solutions of 0.06 *M* triethyl phosphate in the solvents specified were divided into 4-ml aliquots which were sealed in ampoules under nitrogen. Ten minutes were allowed for thermal equilibrium after placing the samples in a constant temperature bath. Samples were removed at intervals and calibrated amounts (3.76 ml) were removed with a constant volume pipet and titrated with dilute potassium hydroxide solution. Reactions were carried only to a point representing 20% reaction to avoid complications from further hydrolysis. Exclusion of air from the ampoules is necessary to prevent oxidation of dioxane at these temperatures. Activation parameters (Table 3) were derived from the rate constants in Tables 1 and 2

[3]Calculated from the data of Tommila and Hella quoted on p. 533 of ref. 1*b*.

Can. J. Chem. Downloaded from www.nrcresearchpress.com by 210.87.254.6 on 09/05/12
For personal use only.

without correction for the neutral reaction and in view of this fact and the relatively low precision of the rate constants the low standard deviations of these parameters must be partly fortuitous.

Product Analysis from Triethyl Phosphate

Neutral Hydrolysis

A solution of 0.857 g (4.7 mmol) triethyl phosphate in 6.0 ml of 3.5 at. % ^{18}O water was sealed in an ampoule under nitrogen and heated at 101° for 46 h. The solution was cooled and brought to p*H* 11 with dilute KOH, and was extracted with five 50-ml portions of ether. The combined extracts were dried over $MgSO_4$ and concentrated to a volume of 5 ml by distillation through a 30 cm Vigreaux column. Ethanol was separated by v.p.c. (25 ft × $\frac{1}{4}$ in. 20% Carbowax 20 M on Chromosorb W at 165° and 100 ml/min of He) at a retention time of 11.5 min and analyzed by mass spectrometry. The aqueous layer from the extraction was acidified with HCl to p*H* 2 and was subjected to continuous ether extraction. The ether extract was dried over $MgSO_4$ and evaporated leaving 0.112 g of crude diethyl hydrogen phosphate which was treated with excess ethereal diazomethane. The ether was evaporated and the residue purified by v.p.c. (10 ft × $\frac{3}{8}$ in. SE-52 on Chromosorb W at 155° and 120 ml/min of He) to give 0.025 g of diethyl methyl phosphate which was analyzed by mass spectrometry.

Acid Hydrolysis

A solution of 0.867 g (4.8 mmol) triethyl phosphate in 5.0 ml of 3.5 at. % ^{18}O water (acidified to 1.02 *N* with 70% $HClO_4$) and 2.7 ml dioxane was sealed in an ampoule and heated to 101° for 12.0 h. Products were isolated as in the neutral hydrolysis.[4]

In a control experiment diethyl hydrogen phosphate was prepared by hydrolysis of diethyl chlorophosphate and was treated with ^{18}O water as in the acid hydrolysis procedure. Mass spectral analysis of the resultant diethyl methyl phosphate revealed the presence of 0.0% excess ^{18}O. For mass spectral comparison a sample of 1.00 g diethyl chlorophosphate was hydrolyzed by 1.0 ml of ^{18}O water. The product was isolated by dissolving in ether, extracting with water and drying over $MgSO_4$. Evaporation of the ether and treatment with diazomethane gave diethyl methyl phosphate.

Mass Spectral Studies

These were carried out using a Perkin-Elmer RMU instrument. Isotopic compositions were calculated from the ratio of the mass spectral ions $M^+ + 2/M^+$ by the procedure of Swain *et al.* (16). At least four determinations were made for each sample. More accurate results for ethanol from acid-catalyzed hydrolysis were obtained with an AEI-MS902 instrument.

[4]Ethanol is not expected to exchange with the medium under these conditions, since *n*-butanol, which should be approximately as reactive as ethanol, has a rate of exchange in 0.9 *N* sulfuric acid at 125° of 5.6×10^{-7} s^{-1} (17).

1. (*a*) C. K. INGOLD. Structure and mechanism in organic chemistry. 2nd ed. Cornell University Press, Ithaca, New York. 1969. Chap. 15; (*b*) E. K. EURANTO *In* The chemistry of carboxylic acids and esters. *Edited by* S. Patai. Interscience, New York, N.Y. 1969. Chap. 11; (*c*) K. YATES. Acc. Chem. Res. **4**, 136 (1971).
2. For reviews see C. A. Bunton, Acc. Chem. Res. **3**, 257 (1970). Also S. J. BENKOVIC. *In* Comprehensive chemical kinetics. Vol. 10. *Edited by* C. H. BAMFORD and C. F. H. TIPPER, Elsevier Publishing Co., London. 1972. Chap. 1.
3. (*a*) R. D. FRAMPTON, T. T. TIDWELL, and V. A. YOUNG. J. Am. Chem. Soc. **94**, 1271 (1972); (*b*) E. P. LYZNICKI, JR., and T. T. TIDWELL. J. Am. Chem. Soc. **94**, 3676 (1972); (*c*) E. P. LYZNICKI, JR., and T. T. TIDWELL. J. Am. Chem. Soc. **95**, 4935 (1973).
4. (*a*) E. M. THAIN. J. Chem. Soc. 4694 (1957); (*b*) J. MASSE and L. DOMANGE. C. R. Acad. Sci. Ser. C, **250**, 4177 (1960); (*c*) V. E. BELSKII, A. N. PUDOVIK, M. V. EFREMOVA, V. N. ELISEENKOV, and A. R. PANTELEEVA. Dokl. Akad. Nauk SSSR, **180**, 351 (1968); (*d*) F. W. LICHTENTHALER and F. CRAMER. Chem. Ber. **95**, 1971 (1962).
5. R. E. ROBERTSON and P. M. LAUGHTON. Can. J. Chem. **35**, 1319 (1957).
6. (*a*) C. A. BUNTON and V. J. SHINER, JR. J. Am. Chem. Soc. **83**, 3207 (1961); (*b*) A. R. BUTLER and V. GOLD. Proc. Chem. Soc. 15 (1960); Chem. Ind (London), 1218 (1960).
7. (*a*) P. W. C. BARNARD, C. A. BUNTON, D. R. LLEWELLYN, C. A. VERNON, and V. A. WELCH. J. Chem. Soc. 2670 (1961); (*b*) P. T. MCTIGUE and P. V. RENOWDEN. Aust. J. Chem. **23**, 297 (1970).
8. L. KUGEL and M. HALMANN. J. Org. Chem. **32**, 642 (1967).
9. (*a*) R. P. BELL, A. L. DOWDING, and J. A. NOBLE. J. Chem. Soc. 3106 (1955); (*b*) C. A. BUNTON, J. B. LEY, A. J. RHIND-TUTT, and C. A. VERNON. J. Chem. Soc. 2327 (1957).
10. I. L. REICH, A. DIAZ, and S. WINSTEIN. J. Am. Chem. Soc. **91**, 5635 (1969).
11. G. A. OLAH and C. W. MCFARLAND. J. Org. Chem. **36**, 1374 (1971).
12. J. P. GUTHRIE. J. Am. Chem. Soc. **95**, 6999 (1973).

13. (*a*) A. SKRABAL and A. ZAHORKA. Monatsch. Chem. **53**, 562 (1929); (*b*) J. F. KIRSCH and W. P. JENCKS. J. Am. Chem. Soc. **86**, 837 (1964).
14. (*a*) E. M. ARNETT, R. P. QUIRK, and J. J. BURKE. J. Am. Chem. Soc. **92**, 1260 (1970); (*b*) E. M. ARNETT, R. P. QUIRK, and J. W. LARSEN. J. Am. Chem. Soc. **92**, 3977 (1970); (*c*) E. M. ARNETT and E. J. MITCHELL. J. Am. Chem. Soc. **93**, 4052 (1971).
15. A. I. VOGEL. A textbook of practical organic chemistry. 3rd ed. John Wiley and Sons, New York. 1956. p. 177.
16. C. G. SWAIN, G.-I. TSUCHIHASHI, and L. J. TAYLOR. Anal. Chem. **35**, 1415 (1963).
17. I. DOSTROVSKY and F. S. KLEIN. J. Chem. Soc. 4401 (1955).

Can. J. Chem. Downloaded from www.nrcresearchpress.com by 210.87.254.6 on 09/05/12
For personal use only.

The Low Temperature Oxidation of Humic Substances[1]

MORRIS SCHNITZER AND STEWART I. M. SKINNER

Soil Research and Chemistry and Biology Research Institutes, Agriculture Canada, Ottawa, Canada K1A 0C6

Received October 4, 1973

In attempts to uncover a relatively mild method for the oxidative degradation of humic substances, a humic and a fulvic acid were oxidized with peracetic acid at 40 °C for 8 days. The oxidation products were extracted into organic solvents, methylated, separated by column-, thin layer-, and preparative gas-chromatography, and identified by matching their mass and micro-i.r. spectra with those of authentic specimens.

The major humic acid oxidation products were phenolic acids (isolated in fully methylated forms, 8.4%), benzenecarboxylic acids (as methyl esters, 16.0%), and aliphatic acids (as methyl esters, 3.4%). The fulvic acid yielded 11.5% phenolic compounds, 8.4% benzenecarboxylic acids (as methyl esters), and 2.6% aliphatic acids (as methyl esters). These data indicated a more phenolic character for the fulvic acid than for the humic acid. In addition, small amounts of 2-methyl-3,4-furandicarboxylic acid were tentatively identified as dimethyl esters among humic and fulvic acid oxidation products. As far as total yields of oxidation products were concerned, peracetic acid oxidation at 40 °C of untreated humic and fulvic acids compared favorably with permanganate oxidation of methylated humic materials at about 100 °C, but was more time consuming.

The results of this and earlier oxidative degradation studies show that the oxidation of humic substances produces phenolic and benzenecarboxylic acids as major products in addition to smaller amounts of aliphatic dicarboxylic acids. Whether these products arise from more complex structures of lignin or microbial origin or whether they occur in the forms in which they were isolated but held together by hydrogen-bonding or Van der Waal's forces requires further investigation.

Dans le but de trouver une méthode douce de dégradation par voie d'oxydation des substances humiques, un acide humique et fulvique ont été oxydés par l'acide peracétique à 40 °C pendant 8 jours. Les produits d'oxydation furent extraits par des solvants organiques, puis méthylés et séparés par chromatographie sur colonne, sur couche mince et par chromatographie préparative en phase gazeuse. Ils ont été identifiés en comparant leurs masses et leurs spectres micro-infrarouges avec ceux de composés connus.

Les principaux produits obtenus de l'oxydation des acides humiques sont des acides phénoliques (isolés à l'état complètement méthylé, 8.4%), des acides carboxyliques dérivés du benzène (sous forme d'esters méthyliques, 16.0%) et des acides aliphatiques (sous forme d'esters méthyliques, 3.4%). On obtient 11.5% de composés phénoliques lors de l'oxydation des acides fulviques, ainsi que 8.4% d'acides carboxyliques dérivés du benzène (sous forme d'esters méthyliques) et 2.6% d'acides aliphatiques (sous forme d'esters méthyliques). Ces données montrent que l'acide fulvique possède un caractère phénolique plus grand que l'acide humique. De plus, on a tenté d'identifier de petites quantités d'acide méthyl-2 dicarboxylique-3,4 furanne sous forme d'esters diméthyliques lors de l'oxydation des acides humiques et fulviques. Les quantités de produits obtenus par l'oxydation directe des acides humiques et fulviques, à l'aide de l'acide peracétique à 40 °C peuvent être comparées avantageusement avec celles obtenus par l'oxydation des acides humiques méthylés à l'aide du permanganate à 100 °C, bien que la première réaction soit plus lente.

Ces résultats et les récentes études de dégradation par voie d'oxydation montrent que l'oxydation des substances humiques donnent, comme produits principaux, des acides phénoliques, des acides dérivés du benzène et des diacides aliphatiques en plus petites quantités. D'autres recherches seraient utiles pour expliquer si ces produits résultent de structures plus complexes de la lignine ou de souches microbiennes; ou si ces substances se trouvent sous leurs formes isolées, mais liées ensemble par des liaisons hydrogène ou des forces de Van der Waal. [Traduit par le journal]

Can. J. Chem., **52**, 1072 (1974)

[1]Contribution No. 469. Soil Research Institute.

Can. J. Chem. Downloaded from www.nrcresearchpress.com by 210.87.254.42 on 09/05/12
For personal use only.

Can. J. Chem. Downloaded from www.nrcresearchpress.com by 210.87.254.42 on 09/05/12
For personal use only.

Introduction

To throw light on the chemical structure of humic substances, which are complex organic materials widely occurring in soils and waters, oxidative, reductive, and biological degradation methods have been used (1). The intention in each instance was to produce simpler compounds that could be identified and whose chemical structures would be related to those of the initial materials. So far oxidative methods have been more useful for this purpose than reductive and biological ones (1). The principal oxidative degradation methods that have been used are oxidation with: (*a*) alkaline nitrobenzene; (*b*) CuO–NaOH; (*c*) alkaline $KMnO_4$; (*d*) HNO_3; (*e*) H_2O_2; and (*f*) CuO–NaOH and $KMnO_4$ oxidations of methylated humic materials (1). Most of these procedures are usually done in alkaline solutions and at elevated temperatures (100 to 170 °C). These somewhat drastic conditions could lead to serious alterations in the chemical structures of the initial humic materials and to the formation of artifacts. Thus, the use of oxidants that operate under milder conditions and that would most likely minimize the extent of undesirable chemical modifications and so provide more comprehensive information on the chemical structure of humic substances seemed worthy of investigation. One reagent that appeared to be suitable for this purpose was peracetic acid, which has been used for many years for the oxidation of ethylenic compounds to oxiranes and α-glycols (2*a*). Aqueous peracetic acid has also been employed by wood chemists for the preparation of holocellulose and fibrous pulps (2*b*). Reactions of known phenols and phenolic ethers lead first to ring hydroxylation, then to oxidation to *ortho*- and *para*-quinones, and finally, by oxidative ring opening to muconic acid and ester structures (2*c*). With some phenols, maleic and fumaric acid derivatives are the final products (2*c*). The peracetic oxidation of lignin leads to the oxidative ring opening of aromatic rings and to the formation of muconic acid derivatives and lactones (2*c*). Recently, Meneghel *et al.* (2*d*) oxidized a peat humic acid with peracetic acid at 40 °C for 8 days. Five amino acids and five sugars were isolated as oxidation products but no phenolic or otherwise aromatic compounds were found (2*d*). Since the experimental conditions employed by Meneghel *et al.* were relatively mild (low temperature, acidic solutions) and since only ten simple aliphatic compounds were identified among the oxidation products, we thought it worthwhile to re-examine the possible usefulness of peracetic acid oxidation for humic substances. Thus, we set out to oxidize a humic acid (HA) and a fulvic acid (FA) with peracetic acid, using the conditions employed by Meneghel *et al.* (2*d*). Following oxidation, the products were separated by column-, and thin layer-, and preparative gas chromatography and identified by matching their mass and micro-i.r. spectra with those of authentic specimens.

Experimental

Humic Acid and Fulvic Acid

The HA was extracted from the Ah horizon (0–25 cm) of the Beaverhills, a Black Chernozemic soil (6.1% C, p*H* (H_2O) 6.4) in Central Alberta. The FA originated from the Bh horizon (15–21 cm) of the Armadale, a poorly drained Podzol (4.2% C, p*H* (H_2O) 4.0) in Prince Edward Island. Methods of extraction, fractionation, and purification of the HA and FA as well as a number of analytical characteristics have been described previously (3). The two humic preparations mentioned above were selected for this investigation because (*a*) they are considered by most soil scientists to be the best developed naturally occurring (almost "ideal") HA and FA, respectively, and (*b*) we have assembled a considerable amount of analytical data (3) on these two preparations, and this, we hoped, would help us in interpreting the results obtained.

Peracetic Acid Oxidation

To 110 ml of glacial acetic acid in a 500 ml 3-necked ground glass flask, equipped with a reflux condenser, dropping funnel, and stirrer and submerged in a water bath maintained at 40 ± 0.1 °C, 1.0 g of HA or FA was added. Ten ml of 30% H_2O_2 was then added dropwise over a period of 3 h while the solution was stirred gently. Another 10 ml of 30% H_2O_2 was added 24 h later. Two more 10 ml aliquots of 30% H_2O_2 were added after 120 and 144 h. The reaction was allowed to proceed for 192 h. At the end of this period of time, the supernatant solutions were separated from the residues (Ii and IIi, see Fig. 1) by filtration. The supernatant solutions were freeze-dried and yielded yellowish gums (Is and IIs). After dissolution in small volumes of CH_3OH, fractions Is and IIs were methylated with an ether solution of diazomethane.

Separation and Identification of Degradation Products

Methylated fractions Is and IIs were separated over Al_2O_3 (grade I, 40.0 g), using the following sequence of solvents (100 ml of each): hexane (I*a* and II*a*), benzene (I*b* and II*b*), ethyl acetate (I*c* and II*c*), and methanol (I*d* and II*d*). Because they were still too complex, fractions I*d* and II*d* were further separated by t.l.c. on Al_2O_3 with toluene – ethyl acetate (1 : 1) to give fractions I*d*1 to I*d*3 and II*d*1 to II*d*3. The fractionation procedure is summarized in Fig. 1.

The gas chromatographic, mass spectrometric, and micro-i.r. spectrophotometric methods used for the identification of the oxidation products were the same as those described earlier (4).

Can. J. Chem. Downloaded from www.nrcresearchpress.com by 210.87.254.42 on 09/05/12
For personal use only.

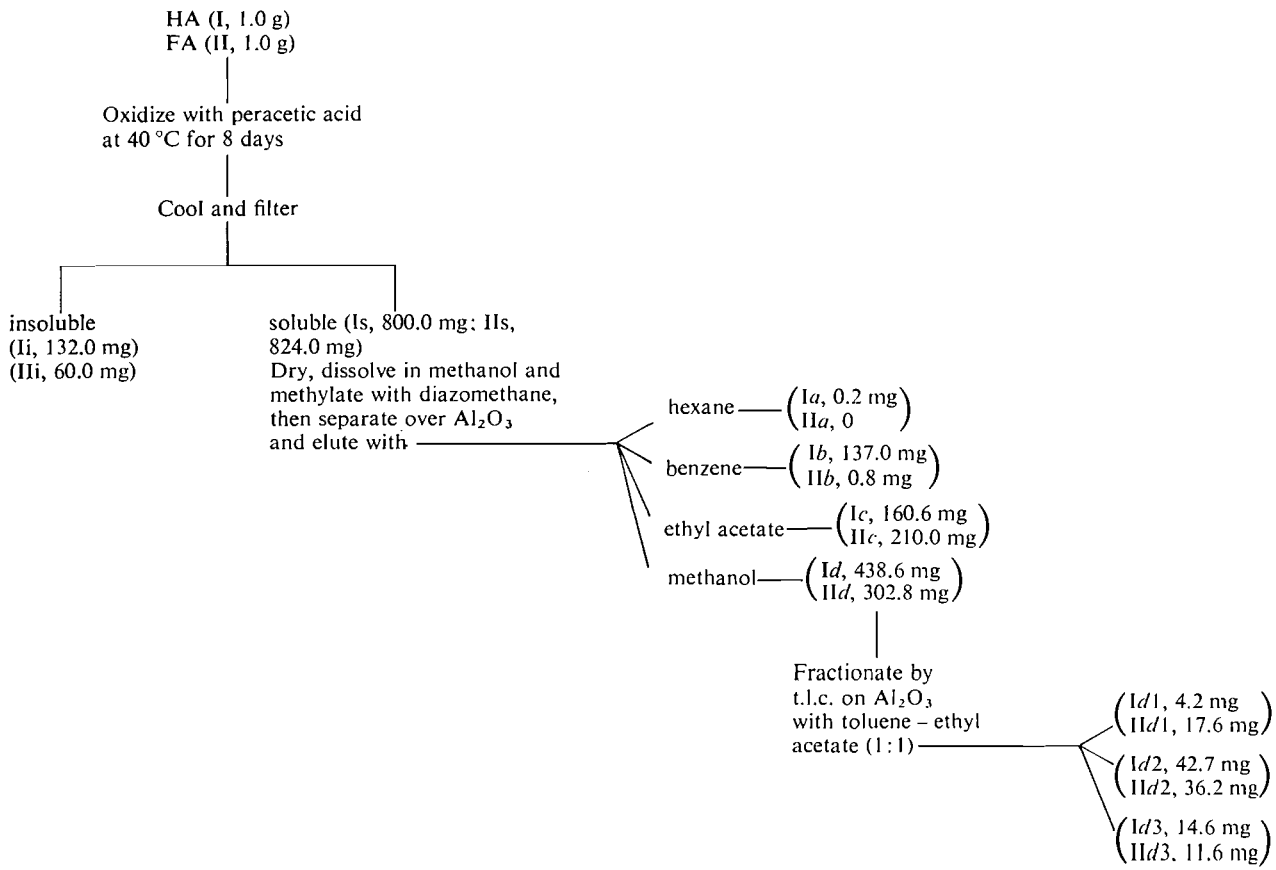

FIG. 1. Fractionation scheme.

Can. J. Chem. Downloaded from www.nrcresearchpress.com by 210.87.254.42 on 09/05/12
For personal use only.

Results

Types and Yields of Oxidation Products

Yields and chemical structures of the HA and FA oxidation products identified are listed in Tables 1 and 2 and in Fig. 2, respectively.

As shown in Table 1, the most abundant aromatic compounds isolated from the HA oxidation products were benzenecarboxylic acid methyl esters **22**, **9**, and **27**. Major fully methylated phenolic acids identified were **25**, **19**, and **14**. The most prominent aliphatic compounds were **4**, **7**, and **13**. Aliphatic compounds accounted for only 11.6% of the compounds identified, phenolic compounds for 25.3%, and benzenecarboxylic ones for 58.1%. The identification of compound **8** (5.0%) was tentative only since we were unable to obtain an authentic specimen for comparative purposes. The mass spectrum of **8** showed a molecular ion (M^+) at *m/e* 198. The base peak was at *m/e* 167 ($M^+ - OCH_3$). Major fragment ions appeared at *m/e* 166 ($M^+ - CH_3OH$), 139 ($M^+ - CO_2CH_3$), 137, 133, 109, 107, 82, 81, 80, 79, 59, 54, 53, 52, 51, 44, 43, 42, 41, 40, 39. The mass spectrum was very similar to that of 2-methyl-3,4-furandicarboxylic acid dimethyl ester (5). The identity of **8** was also confirmed by i.r. spectrophotometry. The i.r. spectrum (KBr pellet) showed the following bands: 3570 (w), 3480 (w), 2900 (m), 2500 (m), 1730 (str), 1640 (str), 1610 (m), 1590 (m), 1490 (str), 1470 (m), 1400 (m), 1390 (m), 1280 (m), 1235 (str), 1110 (m), 1085 (w), 1025 (w), 950 (m), 890 (w), 795 (m), 780 (m), and 712 (m), where m stands for medium, str for strong, and w for weak. This spectrum strongly resembled Sadtler Standard Spectra No. 26082 (2,5-dimethyl-3,4-furandicarboxylic acid dimethyl ester).

The most prominent benzenecarboxylic acid methyl esters produced by the oxidation of FA (Table 2) were **29**, **27**, and **22**. The most abundant fully methylated phenolic acids were **25**, **19**, and **28**, whereas among aliphatic compounds **3**, **4**, and **13** were isolated in highest yields. Aliphatic compounds accounted for 11.2%, phenolic compounds for 50.0%, benzenecarboxylic acid methyl esters for 36.1%, and furan derivative **8** for 2.7% of the compounds identified. From the FA oxidation products we isolated also small amounts of methyl palmitate and methyl stearate.

Discussion

Major Oxidation Products

Since the oxidation products were methylated prior to chromatographic separations (see Fig. 1), and in view of the low OCH_3-content of the untreated HA (0.9%) and FA (0.3%), it is likely that most of the CO_2H and OH groups occurred in the original humic materials as carboxyls and phenolic hydroxyls rather than as esters and ethers. It may, therefore, be more realistic to refer, in the context of this discussion, to the compounds isolated as benzenecarboxylic and phenolic acids rather than as esters and ethers.

As shown in Tables 1 and 2, benzenecarboxylic acids were the major oxidation products formed by the HA, whereas the FA yielded phenolic acids as major products. Aliphatic compounds accounted for only about 11% of the compounds identified from the two humic materials. There were some differences in the types and yields of products isolated from the HA and from the FA. Thus, the peracetic acid oxidation of the HA yielded substantial amounts of the di-, penta-, and tetra-forms of benzenecarboxylic acids. The FA, by contrast, yielded large amounts of hydroxylated benzenetetracarboxylic acids and, in general, more phenolic acids than did the HA. Weight ratios of benzenecarboxylic to phenolic acids isolated were 1.9 for the HA (see Table 3, column 4) but only 0.7 for the FA (Table 4, column 4), indicating a more phenolic character for the FA. Weight ratios of aromatic to aliphatic compounds were similar (7.7 for the HA *vs.* 7.2 for the FA). Of special interest was the isolation of **7**, **13**, and **8**. Compound **7** has been isolated as an oxidation product of HCl-lignin or cuproxam lignin (6) and may originate from cyclolignans or α-conidendin-type structures (6). The origins of **13** and **8** are difficult to assess at this time. To the best of our knowledge this is the first time that furan derivative **8** has been tentatively identified among oxidation products resulting from humic substances. In addition to aliphatic dicarboxylic acids, small amounts of *n*-fatty acid methyl esters (n-C_{16} and n-C_{18}) were isolated from the FA oxidation products. It is likely the fatty acids are adsorbed on the large FA surface (7) and are not structural components.

Varying the Conditions of Oxidation

To better understand the degradative action of peracetic acid at 40 °C, it may be instructive to compare the types and yields of products resulting from oxidation under a variety of conditions. The data in Table 3 shows that peracetic acid oxidation at 40 °C of untreated HA produced greater amounts of aliphatic and benzene-

Can. J. Chem. Downloaded from www.nrcresearchpress.com by 210.87.254.42 on 09/05/12
For personal use only.

TABLE 1. Compounds produced by the oxidation of 1.0 g of HA

Component number	Compound	Isolated from fractions (mg)				Total (mg)
		Ia	Ib	Ic	Id1 to Id3	
1	*n*-C_{12} to *n*-C_{20} fatty acid methyl esters	0.2	0	0	0	0.2
2	Dimethyl malonate	0	0	0	5.4	5.4
3	Dimethyl succinate	0	0	0	2.2	2.2
4	Dimethyl glutarate	0	0	0	9.6	9.6
5	Dimethyl adipate	0	0	0	1.8	1.8
7	1,2,3-Propanetricarboxylic acid trimethyl ester	0	3.6	4.2	0.2	8.0
8	Methyl-3,4-furandicarboxylic acid dimethyl ester	0	6.0	8.6	0	14.6
9	1,2-Benzenedicarboxylic acid dimethyl ester	0	13.0	10.6	6.8	30.4
10	1,3-Benzenedicarboxylic acid dimethyl ester	0	0	0.4	1.6	2.0
11	2-Carbomethoxy-phenylacetic acid methyl ester	0	2.6	1.8	0.4	4.8
12	3-Methoxy-1,2-benzenedicarboxylic acid dimethyl ester	0	5.0	0	0	5.0
13	1,2,3,4-Butanetetracarboxylic acid tetramethyl ester	0	4.0	2.4	0.2	6.6
14	2-Methoxy-1,5-benzenedicarboxylic acid dimethyl ester	0	6.4	3.6	0	10.0
15	1,2,3-Benzenetricarboxylic acid trimethyl ester	0	12.0	5.6	1.2	18.8
16	1,2,4-Benzenetricarboxylic acid trimethyl ester	0	0	0	0.2	0.2
17	1,3,5-Benzenetricarboxylic acid trimethyl ester	0	0	0	0.2	0.2
18	3,4-Dimethoxy-1,5-benzenedicarboxylic acid dimethyl ester	0	2.4	0	0	2.4
19	3-Methoxy-1,2,4-benzenetricarboxylic acid trimethyl ester	0	12.8	10.8	0	23.6
20	2-Methoxy-1,3,5-benzenetricarboxylic acid trimethyl ester	0	1.8	1.4	0	3.2
21	5-Methoxy-1,2,4-benzenetricarboxylic acid trimethyl ester	0	2.8	3.0	0	5.8
22	1,2,3,4-Benzenetetracarboxylic acid tetramethyl ester	0	17.2	19.0	0.4	36.6
23	1,2,4,5-Benzenetetracarboxylic acid tetramethyl ester	0	3.2	6.4	0.8	10.4
24	1,2,3,5-Benzenetetracarboxylic acid tetramethyl ester	0	1.4	14.8	1.2	17.4
25	5-Methoxy-1,2,3,4-benzenetetracarboxylic acid tetramethyl ester	0	8.0	4.4	12.4	24.8
26	2-Methoxy-1,3,4,5-benzenetetracarboxylic acid tetramethyl ester	0	0	0	1.2	1.2
27	Benzenepentacarboxylic acid pentamethyl ester	0	10.0	19.0	0.2	29.2
28	Methoxybenzenepentacarboxylic acid pentamethyl ester	0	5.6	2.4	0.2	8.2
29	Benzenehexacarboxylic acid hexamethyl ester	0	6.0	4.0	0.1	10.1
	Total identified (mg)	0.2	123.8	122.4	46.3	292.7
	Weight of methylated fractions	0.2	137.00	160.6	61.5	359.3
	% identified	100.0	90.2	76.2	75.3	81.5

Can. J. Chem. Downloaded from www.nrcresearchpress.com by 210.87.254.42 on 09/05/12
For personal use only.

TABLE 2. Compounds produced by the oxidation of 1.0 g of FA

Component number	Compound	Isolated from fractions (mg)			Total (mg)
		IIb	IIc	IId1 to IId3	
3	Dimethyl succinate	0	0.4	6.4	6.8
4	Dimethyl glutarate	0	0.6	6.0	6.6
5	Dimethyl adipate	0	0.4	1.4	1.8
6	Dimethyl pimelate	0	0.4	0.6	1.0
7	1,2,3-Propanetricarboxylic acid trimethyl ester	0	4.4	0	4.4
8	Methyl-3,4-furandicarboxylic acid dimethyl ester	0	6.2	0	6.2
9	1,2-Benzenedicarboxylic acid dimethyl ester	0	0	1.6	1.6
	Methyl palmitate	0.2	0	0	0.2
12	3-Methoxy-1,2-benzenedicarboxylic acid dimethyl ester	0	0.6	1.0	1.6
13	1,2,3,4-Butanetetracarboxylic acid tetramethyl ester	0	4.8	0	4.8
14	2-Methoxy-1,5-benzenedicarboxylic acid dimethyl ester	0	5.4	0	5.4
	Methyl stearate	0.2	0	0	0.2
15	1,2,3-Benzenetricarboxylic acid trimethyl ester	0	3.8	0.8	4.6
16	1,2,4-Benzenetricarboxylic acid trimethyl ester	0	0	0.8	0.8
17	1,3,5-Benzenetricarboxylic acid trimethyl ester	0	0	0.8	0.8
18	3,4-Dimethoxy-1,5-benzenedicarboxylic acid dimethyl ester	0	0	0.8	0.8
19	3-Methoxy-1,2,4-benzenetricarboxylic acid trimethyl ester	0	20.2	0	20.2
20	2-Methoxy-1,3,5-benzenetricarboxylic acid trimethyl ester	0	3.4	0	3.4
21	5-Methoxy-1,2,4-benzenetricarboxylic acid trimethyl ester	0	2.0	0.8	2.8
22	1,2,3,4-Benzenetetracarboxylic acid tetramethyl ester	0	7.0	0.2	7.2
23	1,2,4,5-Benzenetetracarboxylic acid tetramethyl ester	0	5.0	0.2	5.2
24	1,2,3,5-Benzenetetracarboxylic acid tetramethyl ester	0	0	0.2	0.2
25	5-Methoxy-1,2,3,4-benzenetetracarboxylic acid tetramethyl ester	0	34.2	20.0	54.2
26	2-Methoxy-1,3,4,5-benzenetetracarboxylic acid tetramethyl ester	0	8.6	0	8.6
27	Benzenepentacarboxylic acid pentamethyl ester	0.2	19.0	3.0	22.2
28	Methoxybenzenepentacarboxylic acid pentamethyl ester	0	15.2	3.2	18.4
29	Benzenehexacarboxylic acid hexamethyl ester	0	39.6	1.5	41.1
	Total identified (mg)	0.6	181.2	49.3	231.1
	Weight of methylated fractions	0.8	210.0	65.4	276.2
	% identified	75.0	86.3	75.4	83.7

Can. J. Chem. Downloaded from www.nrcresearchpress.com by 210.87.254.42 on 09/05/12
For personal use only.

1. $CH_3(CH_2)_{12}CO_2CH_3$ to $CH_3(CH_2)_{18}CO_2CH_3$

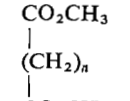

2. $n = 1$
3. $n = 2$
4. $n = 3$
5. $n = 4$
6. $n = 5$

7.

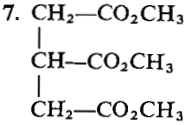

8.

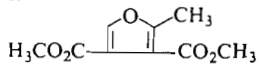

13.

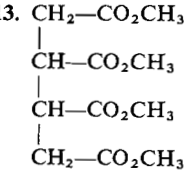

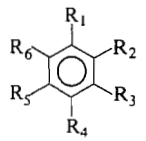

9. $R_1 = R_2 = CO_2CH_3$; $R_3 = R_4 = R_5 = R_6 = H$
10. $R_1 = R_3 = CO_2CH_3$; $R_2 = R_4 = R_5 = R_6 = H$
11. $R_1 = CH_2CO_2CH_3$; $R_2 = CO_2CH_3$; $R_3 = R_4 = R_5 = R_6 = H$
12. $R_1 = R_2 = CO_2CH_3$; $R_3 = OCH_3$; $R_4 = R_5 = R_6 = H$
14. $R_1 = R_5 = CO_2CH_3$; $R_2 = OCH_3$; $R_3 = R_4 = R_6 = H$
15. $R_1 = R_2 = R_3 = CO_2CH_3$; $R_4 = R_5 = R_6 = H$
16. $R_1 = R_2 = R_4 = CO_2CH_3$; $R_3 = R_5 = R_6 = H$
17. $R_1 = R_3 = R_5 = CO_2CH_3$; $R_2 = R_4 = R_6 = H$
18. $R_1 = R_5 = CO_2CH_3$; $R_3 = R_4 = OCH_3$; $R_2 = R_6 = H$
19. $R_1 = R_2 = R_4 = CO_2CH_3$; $R_3 = OCH_3$; $R_5 = R_6 = H$
20. $R_1 = R_3 = R_5 = CO_2CH_3$; $R_2 = OCH_3$; $R_4 = R_6 = H$
21. $R_1 = R_2 = R_4 = CO_2CH_3$; $R_5 = OCH_3$; $R_3 = R_6 = H$
22. $R_1 = R_2 = R_3 = R_4 = CO_2CH_3$; $R_5 = R_6 = H$
23. $R_1 = R_2 = R_4 = R_5 = CO_2CH_3$; $R_3 = R_6 = H$
24. $R_1 = R_2 = R_3 = R_5 = CO_2CH_3$; $R_4 = R_6 = H$
25. $R_1 = R_2 = R_3 = R_4 = CO_2CH_3$; $R_5 = OCH_3$; $R_6 = H$
26. $R_1 = R_3 = R_4 = R_5 = CO_2CH_3$; $R_2 = OCH_3$; $R_6 = H$
27. $R_1 = R_2 = R_3 = R_4 = R_5 = CO_2CH_3$; $R_6 = H$
28. $R_1 = R_2 = R_3 = R_4 = R_5 = CO_2CH_3$; $R_6 = OCH_3$
29. $R_1 = R_2 = R_3 = R_4 = R_5 = R_6 = CO_2CH_3$

FIG. 2. Chemical structures of compounds identified.

carboxylic acids than did permanganate oxidation (p*H* 10) of methylated HA. On the other hand, oxidation with 10% (v/v) aqueous peracetic acid solution at 80 °C (8) yielded approximately equal amounts of benzenecarboxylic acids but smaller quantities of phenolic and aliphatic acids than did peracetic acid oxidation at 40 °C. As far as total yields of oxidation products were concerned, peracetic acid oxidation at 40 °C was the most effective procedure. Table 4 presents com-

TABLE 3. Compounds produced by the oxidation of 1.0 g of HA with alkaline $KMnO_4$ (3) and peracetic acid at 80 °C (8) and 40 °C

Types of compounds	$KMnO_4$* (mg)	Peracetic acid (mg)	
		80 °C	40 °C
Aliphatic	15.8	13.4	34.0
Phenolic	96.4	43.4	84.2
Benzenecarboxylic	137.4	152.4	160.1
Total	249.6	209.2	278.3
Weight ratio of benzenecarboxylic to phenolic	1.4	3.5	1.9

*Oxidation of methylated HA.

TABLE 4. Compounds produced by the oxidation of 1.0 g of FA with CuO–NaOH (8), $KMnO_4$ (3) and peracetic acid at 80 °C (8) and at 40 °C

Types of compounds	CuO–NaOH* (mg)	$KMnO_4$* (mg)	Peracetic acid (mg)	
			80 °C	40 °C
Aliphatic	5.7	1.0	23.1	25.8
Phenolic	115.0	88.5	40.6	115.4
Benzenecarboxylic	25.1	114.9	72.5	83.7
Total	145.8	204.4	136.2	224.9
Weight ratio of benzenecarboxylic to phenolic	0.2	1.3	1.8	0.7

*Oxidation of methylated FA.

parisons of the types and quantities of major compounds produced by $KMnO_4$ (3) and CuO–NaOH (8) oxidations of methylated FA and peracetic acid oxidation of untreated FA at 40 and 80 °C. Both types of peracetic acid oxidations yielded greater amounts of aliphatic compounds than did the alkaline methods. Peracetic acid oxidation at 40 °C and CuO–NaOH oxidation produced equal amounts of phenolic compounds; $KMnO_4$ was less effective in forming phenolic products and peracetic acid at 80 °C was the least effective reagent for this purpose. $KMnO_4$ oxidation produced the highest yield of benzenecarboxylic acids, with the two types of peracetic oxidations forming smaller but approximately equal amounts, and CuO–NaOH being the least effective reagent in this respect. Again, peracetic acid at 40 °C produced the highest yield of oxidation products per g of initial material. From the relatively low yields of phenolic compounds resulting from the peracetic acid oxidation at 80 °C (compared with peracetic acid oxidation at 40 °C, see Tables 3 and 4), it appears that phenolic compounds were degraded by the peracetic acid at the higher temperature. This is also indicated by the weight ratios of benzenecarboxylic to phenolic compounds isolated which are shown in Tables 3 and 4.

The data reported in this paper are not in accord with the findings of Meneghel *et al.* (2) who failed to detect aromatic compounds among peracetic acid oxidation products from a peat humic acid. It is possible that their peat humic acid was less aromatic than the humic substances that we have oxidized and which we extracted from inorganic soils.

We were unable to detect muconic acid-type compounds nor maleic or fumaric acid derivatives, which have been reported to result from the peracetic acid oxidation of known phenols, phenolic ethers, and lignins (2). It is unlikely that these compounds were formed in more than trace amounts. The data shown herein suggest that mechanistically the attack of peracetic acid on the humic materials is similar to that of $KMnO_4$, that is, it is electrophilic, depending on the electrophilic character of the peroxy oxygen atom and the ease with which this oxygen can be transferred to the nucleophilic humic materials (9).

Experimentally, peracetic acid oxidation of humic substances is a mild but lengthy procedure which provides valuable information on the

Can. J. Chem. Downloaded from www.nrcresearchpress.com by 210.87.254.42 on 09/05/12
For personal use only.

chemical structure of these materials. In this respect it compares favorably with the permanganate oxidation of methylated humic substances. The latter procedure, however, is less time-consuming.

The Chemical Structure of Humic Substances

The results in Tables 3 and 4 and other oxidative degradation studies done in our laboratory over a period of many years (10) show that the oxidation of humic substances produces three types of compounds: (*a*) phenolic acids; (*b*) benzenecarboxylic acids; and (*c*) aliphatic dicarboxylic acids, which are formed in much smaller amounts than the compounds listed under (*a*) and (*b*). The phenolic and benzenecarboxylic acids could have originated from lignin, condensed lignin, or complex aromatic products of microbial synthesis. On the other hand, it is also possible that the phenolic and benzenecarboxylic acids occur in the humic substances in the forms in which they were isolated, but joined by relatively weak bonds such as hydrogen-bonding or Van der Waal's forces to form polymeric structures of considerable stability. Support for the latter view comes from long time observations which have shown that humic substances are readily dispersed or aggregated by changes in p*H*, salt concentration, and valence of cations. If the hypothesis that phenolic and benzenecarboxylic acids are the "building blocks" of humic substances is correct, the next problem to be solved is to find out how the "building stones" fit together and what type of structural arrangement is formed. If, however, the degradation products originate from more complex chemical structures, further research in this field should be concerned with the development of degradative procedures that would permit the isolation and characterization of larger fragments of the humic molecules or molecular associations. It is possible that both types of structural arrangements coexist in humic substances.

We thank E. Vendette and D. Dobson for technical assistance.

1. M. SCHNITZER and S. U. KHAN. Humic substances in the environment. Marcel Dekker, New York. 1972. pp. 137–161.
2. (*a*) D. SWERN. *In* Organic reactions. VII. *Edited by* R. Adams. John Wiley and Sons, Inc., New York. 1953. p. 379; (*b*) N. THOMPSON and O. KAUSTINEN. Tappi, **47**, 157 (1964); (*c*) H. M. CHANG and G. G. ALLAN. *In* Lignins. *Edited by* K. V. Sarkanen and C. H. Ludwig. Wiley Interscience, New York. 1971. pp. 457–463; (*d*) R. MENEGHEL, C. PETITSARLOTTE, and J. M. BLOCK. Bull. Soc. Chim. Fr. **7**, 2997 (1972).
3. (*a*) S. U. KHAN and M. SCHNITZER. Can. J. Soil Sci. **52**, 43 (1972); (*b*) G. OGNER and M. SCHNITZER. Can. J. Chem. **49**, 1053 (1971).
4. M. SCHNITZER and M. I. ORTIZ DE SERRA. Can. J. Chem. **51**, 1554 (1973).
5. R. I. REED and W. K. REID. J. Chem. Soc. 5933 (1963).
6. K. FREUDENBERG and A. C. NEISH. Constitution and biosynthesis of lignin. Springer Verlag, New York. 1968. pp. 81, 89.
7. S. U. KHAN and M. SCHNITZER. Geochim. Cosmochim. Acta, **36**, 745 (1972).
8. (*a*) M. SCHNITZER and S. I. M. SKINNER. Soil Sci. In press. (*b*) M. SCHNITZER. Soil Biol. Biochem. In press.
9. R. STEWART. Oxidation mechanisms. W. A. Benjamins, New York. 1964. pp. 119–120.
10. (*a*) M. SCHNITZER and J. R. WRIGHT. Trans. 7th Int. Congr. Soil Sci. Madison, Wisconsin. II, 112 (1960); (*b*) E. H. HANSEN and M. SCHNITZER. Soil Sci. Soc. Am. Proc. **31**, 79 (1967); (*c*) K. MATSUDA and M. SCHNITZER. Soil Sci. **114**, 185 (1972).

Can. J. Chem. Downloaded from www.nrcresearchpress.com by 210.87.254.42 on 09/05/12
For personal use only.

Far Infrared Spectra of Crystalline Iodine Monobromide and Iodine Monochloride

HSIAO-CHIAN LEUNG AND ANTHONY ANDERSON

Department of Physics, University of Waterloo, Waterloo, Ontario N2L 3G1

Received October 4, 1973

Infrared spectra, in the range 20–400 cm^{-1}, of thin polycrystalline films (at 80 °K) of iodine monobromide and the β-form of iodine monochloride have been recorded. For IBr, the intramolecular stretching region shows two peaks separated by 16 cm^{-1} and shifted appreciably from the gas phase value, indicating strong intermolecular interactions. Four lattice modes are also observed and assigned in accordance with group theoretical predictions. For β-ICl the spectrum of the stretching region confirms the presence of two distinct molecules with different bond lengths. The complexity of the ICl structure prevents an assignment of the ten observed lattice absorptions.

Les spectres infrarouge, dans l'intervalle de 20–400 cm^{-1} de fines pellicules polycrystallines (à 80 °K) du monobromure d'iode et de la forme β du monochlorure d'iode ont été enregistrés. Pour IBr, la région d'élongation intramoléculaire montre deux pics espacée par 16 cm^{-1} et déplacés appréciablement par rapport à la valeur en phase gazeuse indiquant de fortes interactions intramoléculaires. Quatre modes de réseaux sont aussi observés et attribués selon les prévisions théoriques de groupe. Pour β-ICI le spectre de la région d'élongation confirme la présence de deux molécules distinctes avec des longueurs de liaison différentes. La complexité de la structure de ICI empêche l'attribution des dix absorptions des réseaux observés.

[Traduit par le journal]

Can. J. Chem., **52**, 1081 (1974)

Introduction

Recently obtained Raman spectra of the halogen crystals, Cl_2, Br_2, and I_2 (1) have shown evidence for strengthening of the intermolecular forces with increase of mass. In iodine, this is manifested by a measurable increase in the molecular bond length in the crystal (2). Even for the chlorine crystal, there is evidence that the normal Van der Waals type of interaction is inadequate to describe the dynamical properties of the molecules in the crystal, and a charge transfer process had to be invoked (3) in order to obtain reasonable agreement with the experimentally observed lattice frequencies.

There is thus considerable interest in obtaining further experimental data on the nature of the forces between the nonbonded halogen atoms in crystals, and spectroscopic studies of the diatomic interhalogen compounds promise to be useful in this respect. Previous work has been confined to the electronic excitations (4–6), and the i.r. absorption in various solvents (7). Raman spectra of these crystals, at least with conventional techniques, are very difficult to obtain because of their strong absorption of visible radiation and their high volatility and tendency to dissociate. The i.r. spectra, however, should be relatively straightforward to obtain, and moreover, because of the polar nature of the molecules, these spectra should provide data on both the translations and librations, in contrast to those for the pure halogens where only the translations are i.r. active (8).

The crystal structure of IBr is orthorhombic, with space group $Ccm2_1$ (C_{2v}^{12}) (9). There are two molecules in the primitive unit cell on sites of C_s symmetry, which form planar zig-zag chains as shown in Fig. 1. This structure is isomorphous to the low temperature phase of HCl and HBr (10) and differs from that of the halogen crystals (Cl_2, Br_2, and I_2) only in the absence of a center of symmetry (11, 12, 2). The correlation diagram (Fig. 3, left) indicates that there are 7 i.r. active modes composed of 2 intramolecular stretches, 3 librations, and 2 non-acoustic translations.

There are two forms of crystalline ICl, both monoclinic with space group $P2_1/c$ (C_{2h}^5) and 8 molecules in the unit cell. In both structures, there are chains of ICl molecules in zig-zag formation, but these differ from those in crystals of the halogens and IBr in two important respects: firstly, there are chlorine atoms branching from the main chains (*cis* in the α-form (13) and *trans* in the β-form (14)), as shown in Fig. 2; and secondly, the chains are non-planar, the degree of puckering being greater in the α-form. In both

Can. J. Chem. Downloaded from www.nrcresearchpress.com by 210.87.254.40 on 09/05/12
For personal use only.

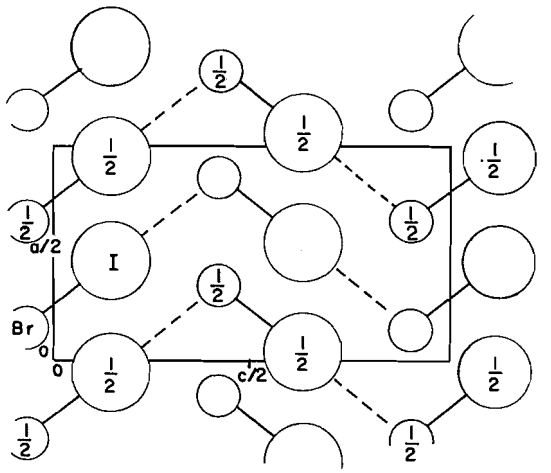

FIG. 1. Crystal structure of IBr (from ref. 9). Projection on *ac* plane, showing two adjacent mirror planes.

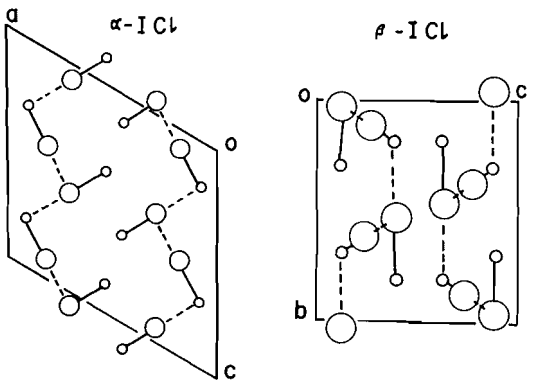

FIG. 2. Crystal structures of α-ICl (left) and β-ICl (right) (from ref. 14). Projections on *ac* and *bc* planes respectively.

structures there are unusually short distances between non-bonded atoms in the same chain, and the strong intermolecular forces result in marked differences between the bond lengths of molecules in the main chains (2.44 Å) and those in the branches (2.37 Å in α-ICl, 2.35 Å in β-ICl). Both sets of 4 molecules are on general sites, and the correlation diagram for ICl (α or β) is shown on the right of Fig. 3. This indicates that 21 modes are i.r. active, of which 4 are stretches, 8 librations, and 9 non-acoustic translations. Appreciable mixing between lattice modes of like symmetry and similar frequency is to be expected.

Experimental

Far i.r. spectra were obtained with a Fourier Spectrophotometer (RIIC Beckman 620), using a Mylar beam divider (thickness 0.00025 or 0.005 in.) and Golay cell detector. The interferogram signal was led directly through an A/D converter to a Hewlett Packard 2116 computer for processing. Spectra in the higher frequency range ($>200\ cm^{-1}$) were also checked with a grating spectrometer (Beckman IR 12). Substrates of crystal quartz and polyethylene were mounted in a conventional glass cryostat fitted with polyethylene outer windows, and cooled with liquid nitrogen. Temperatures were measured by a copper–constantan thermocouple on the substrate.

Samples of ICl and IBr were obtained from Research Organic/Inorganic Corp. and were stated to be of better than 99% purity. These were vacuum distilled onto the substrate until the overall absorption (which is directly measured by the interferometer) reached a predetermined value. The samples were subsequently annealed before spectra were recorded. Observations on ICl, as it was warmed after the spectra were obtained, showed that its melting point was close to 13 °C, thus indicating the β-form. The α-form, which melts at 27 °C, could not be obtained in these experiments either by annealing, recrystallizing, or variation of the deposition rate or substrate temperature. It appears that the small amount of iodine liberated by dissociation at room temperature (0.42% at 25 °C) is instrumental in stabilizing the β-form (15).

Spectra of solutions of IBr and ICl in CCl_4 and C_6H_6 were also obtained. Standard liquid cells with polyethylene windows and a 1 mm Teflon spacer were used.

Results

Absorption spectra of polycrystalline IBr and β-ICl at 80 °K in the range 40–400 cm^{-1} are shown in Figs. 4 and 5 respectively. These are from samples absorbing approximately 50% of the overall radiation, and the spectral resolution is about 2.5 cm^{-1}. Spectra at higher resolution and of thicker samples were also recorded but showed no new features.

Frequencies of maximum absorption, estimated accurate to $\pm 1\ cm^{-1}$ except for very broad bands or shoulders, are listed in Tables 1 and 2 with the widths at half intensity indicated in parentheses. Data from gas phase and solution studies are also included.

Discussion

IBr

In the stretching region, two strong peaks are observed separated by 16 cm^{-1}, with the band center displaced to lower frequency by about 55 cm^{-1} from the gas phase value. The separation of the components from the different bromine isotopes is calculated to be less than 1.5 cm^{-1} with approximately equal intensities, and was not seen either in solution or crystalline state. The observed splitting is a result of coupling between the two molecules in the unit cell, and its magni-

Can. J. Chem. Downloaded from www.nrcresearchpress.com by 210.87.254.40 on 09/05/12
For personal use only.

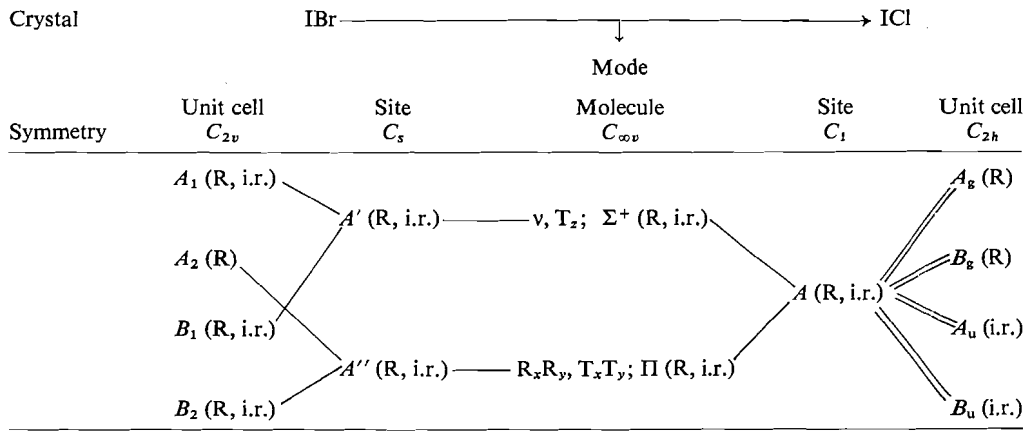

FIG. 3. Correlation diagrams for IBr (left) and ICl (right) (R = Raman active, i.r. = infrared active). The double lines for ICl represent the two distinct sets of four molecules.

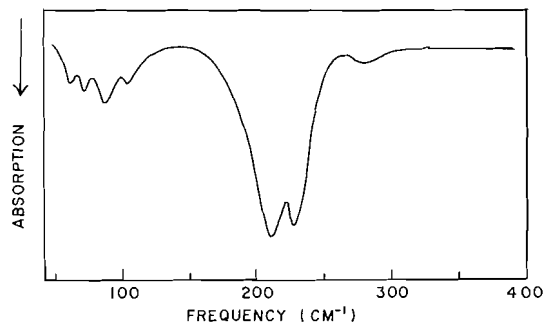

FIG. 4. Far i.r. spectrum of crystalline IBr at 80 °K.

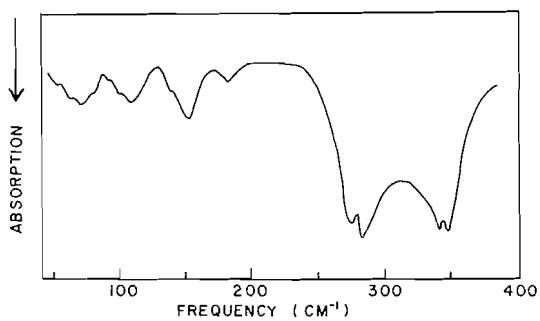

FIG. 5. Far i.r. spectrum of crystalline β-ICl at 80 °K.

tude is an indication of very strong intermolecular interactions. For comparison, the observed splittings for the halogen stretching modes are 1, 5, and 8 cm^{-1}, and the displacements from the gas phase values are 16, 23, and 33 cm^{-1} for Cl_2, Br_2, and I_2 respectively (1). The fact that the values for IBr do not lie between those for Br_2 and I_2 is probably a consequence of the additional interaction between the permanent dipoles of the interhalogen molecules. As in iodine, an increase of about 0.05 Å in the bond length of the molecule in the crystal has been found by X-ray diffraction (9), further evidence of the unusually strong interaction between adjacent molecules in the same chain.

The orientation of the dipoles ($\sim \pm 35°$ to the chain axis) leads to the result that the in-phase mode (A_1) involves the larger dipole moment change for a given amplitude and hence absorbs more strongly by a factor of about 2, ($\cot^2 35$). This identifies the lower frequency band as the A_1 mode and the higher frequency one as the out-of-phase B_1 mode. A much weaker peak at 280 cm^{-1} is probably a combination of the A_1 stretching mode and a libration.

In the lattice region, 4 peaks are observed instead of the 5 predicted from group theory, although in several spectra an additional shoulder was resolved. For molecules with a permanent dipole moment, one expects the librational modes in general to absorb more strongly than the translations, as for example in the isomorphous hydrogen halides (16). In addition, from considerations of the changes in separations between neighboring non-bonded atoms in the same chain for given angular displacements about the centers of mass, one can deduce that the frequency sequence of the librations (from low to high) will be as follows: A_2 (out-of-plane, out-of-phase); A_1 (in-plane, out-of-phase); B_2 (out-of-plane, in-phase); and B_1 (in-plane, in-phase). Similarly for the translations, one expects the sequence A_2, A_1, and B_1 where the non-acoustic modes all involve out-

Can. J. Chem. Downloaded from www.nrcresearchpress.com by 210.87.254.40 on 09/05/12
For personal use only.

TABLE 1. Frequencies of maximum absorption in IBr (with widths at half intensity in parentheses)

Mode	State	Temperature (°K)	Frequency (cm^{-1})
Stretch (ν_1)	Gas*	295	265
Stretch (ν_1)	Solution CCl_4	295	261
Stretch (ν_1)	Solution C_6H_6	295	251
Stretch (ν_1)	Solid	80	210, 226 (53) A_1, B_1
Libration (ν_L)	Solid	80	85(24)A_1 + B_2; 103(16)B_1
Translation (ν_T)	Solid	80	60(12)A_1; 71(12)B_1
Combination ($\nu_1 + \nu_L$)	Solid	80	280(5)

*From ref. 18.

TABLE 2. Frequencies of maximum absorption in ICl (with widths at half intensity in parentheses)

Mode	State	Temperature (°K)	Frequency (cm^{-1})†
Stretch (ν_1)	Gas*	295	381
Stretch (ν_1)	Solution CCl_4	295	375
Stretch (ν_1)	Solution C_6H_6	295	355
Stretch (ν_1)	β-Solid	80	275, 282 (54) 342, 348 (32)
Libration (ν_L)	β-Solid	80	100(sh), 110(20), 140(sh), 153(28), 182(16)
Translation (ν_T)	β-Solid	80	55(sh), 63(sh), 73(20)
Mixed modes (?)	β-Solid	80	81(sh), 91(sh)

*From ref. 18.
†sh = shoulder.

of-phase displacements along the directions y, x, and z respectively. On the basis of these qualitative arguments (which in the case of the hydrogen halides have been confirmed by lattice dynamics calculations (17)), the assignments given in Table 1 are proposed, where it is assumed that the broadest and strongest lattice absorption band includes contributions from two librations, A_1 and B_2 (in a few spectra, an additional shoulder at 91 cm^{-1} is observed). An alternative assignment consistent with these ideas is that the higher frequency translation (B_1) has been obscured by the stronger libration (A_1) at 71 cm^{-1}. Lattice dynamics computations on IBr have been initiated in this laboratory to check these tentative assignments.

β-ICl

Two well separated partly resolved doublets are observed in the stretching region of this molecule. It seems clear that the main splitting is due to the presence of two distinct molecules with different bond lengths. The higher frequency pair is assigned to the molecules in the branches of the chain (bond length 2.35 Å), and the lower frequency pair to those in the main chain (bond length 2.44 Å). The latter is over 100 cm^{-1} lower than the stretching frequency in the gas phase, where the bond length is 2.32 Å (18). There are two possible causes of the smaller splittings: the presence of the different isotopes ^{35}Cl and ^{37}Cl in a 3:1 proportion should lead to peaks separated by about the magnitude observed, although the splitting of the higher frequency doublet would be expected to be slightly larger. The observed intensity ratios are much less than 3:1, but the accuracy for such broad, incompletely resolved, bands is perhaps not too reliable; the other possible explanation is that the splittings are due to couplings between molecules in the unit cell, which as discussed above, is the dominant effect in IBr. However, in β-ICl, the nearest neighbors of any given molecule are those of different bond length and different "natural" frequency, and hence the resonant interaction will be much reduced. An approximate analysis of coupled pendulums (19,

Can. J. Chem. Downloaded from www.nrcresearchpress.com by 210.87.254.40 on 09/05/12
For personal use only.

20) predicts that the splitting will be slightly larger for the lower frequency doublet. Although this has been experimentally observed, the differences are small, and since the measured splittings may be appreciably influenced by overlap of the broad components, no firm conclusion can be reached.

Ten absorptions in the lattice region are observed, but because of the complexity of the crystal structure and possible mixing allowed by its low symmetry, it is extremely difficult to make even tentative assignments. One would again expect the librational modes to be more intense, and if the pattern of the halogens and IBr is followed to be at higher frequencies. This is consistent with the observed spectra. The peaks above 100 cm^{-1} probably originate from librational motions, those below 75 cm^{-1} from translations, with those between these values being of uncertain or mixed origin. It is rather doubtful whether conventional lattice dynamics calculations can throw light on these assignments, since it is unlikely that any model potential, such as the Lennard–Jones or Buckingham type, can be realistically used for the very strong interactions between adjacent nonbonded atoms in the same chain. Polarized Raman spectra of a single crystal of ICl would be useful for resolving this problem, but the experimental difficulties involved in such a study are formidable.

We express our thanks to Drs. J. W. Leech and D. E. Irish for helpful discussions, to Dr. J. L. Ord for assistance in setting up the computational system, and to the National Research Council of Canada for financial support.

1. A. Anderson and T. S. Sun. Chem. Phys. Lett. **6**, 661 (1970).
2. A. I. Kitaigirodskii, T. L. Khotsyanora, and Y. T. Struchov. J. Phys. Chem. Mosc. **27**, 780 (1951).
3. P. S. English. Ph.D. Thesis, University of Waterloo, Waterloo, Ontario. 1972.
4. R. M. Bodger and D. M. Yost. Phys. Rev. **37**, 1548 (1931).
5. H. Cordes. Z. Phys. **74**, 34 (1932).
6. W. G. Brown. Phys. Rev. **42**, 355 (1932).
7. W. B. Person, R. E. Humphrey, W. A. Deskin, and A. I. Popov. J. Am. Chem. Soc. **80**, 2049 (1958).
8. S. H. Walmsley and A. Anderson. Mol. Phys. **7**, 411 (1964).
9. L. N. Swink and G. B. Carpenter. Acta Cryst. B**24**, 429 (1968).
10. E. Sandor and R. F. C. Farrow. Nature, **213**, 171 (1967); **215**, 1265 (1967).
11. R. L. Collin. Acta Cryst. **5**, 431 (1952); **9**, 537 (1956).
12. B. Vonnegut and B. E. Warren. J. Am. Chem. Soc. **58**, 2459 (1936).
13. K. H. Boswijk, J. van der Heide, Aafje Vos, and E. H. Wievenga. Acta Cryst. **9**, 274 (1956).
14. G. B. Carpenter and Stephanie M. Richards. Acta Cryst. **15**, 360 (1962).
15. W. Stortenbeker. Zeit. Phys. Chem. **3**, 11 (1889); Rec. Trav. Chim. Pays-Bas, **7**, 152 (1889).
16. A. Anderson, H. A. Gebbie, and S. H. Walmsley. Mol. Phys. **7**, 401 (1964).
17. T. S. Sun and A. Anderson. Chem. Phys. Lett. **17**, 104 (1972).
18. G. Herzberg. Spectra of diatomic molecules. Van Nostrand, Princeton, N.J. 1950. p. 542.
19. A. Sommerfeld. Mechanics. Academic Press, New York. 1952.
20. H. C. Leung. M.Sc. Thesis, University of Waterloo, Waterloo, Ontario. 1973.

Can. J. Chem. Downloaded from www.nrcresearchpress.com by 210.87.254.40 on 09/05/12
For personal use only.

A Kinetic Study of Isotopic Exchange Between Terbium Ion and its EDTA Complex in Aqueous Buffer Systems and the Possible Role of Buffer Anion

R. E. JERVIS[1] AND K. NEELAKANTAN

Department of Chemical Engineering and Applied Chemistry, University of Toronto, Toronto, Ontario M5S 1A4

Received July 31, 1973

The nature of the species undergoing exchange and the role of the buffer anion in the medium are not known precisely from previous investigations on the isotopic exchange of rare earth metal ions with their EDTA complexes confined to acetate medium only.

Using terbium-160 as radiotracer, the kinetics of self-exchange of Tb(III) in $TbEDTA^-$ has been studied in detail in 0.025 *M* acetate buffer. The exchange has also been investigated in various other concentrations of acetate and phthalate buffer solutions, and also in benzoate buffer.

In 0.025 *M* ammonium acetate solution the rate of exchange (R in mol l^{-1} s^{-1}) is expressed by

$$R = k_1[TbEDTA^-][H^+] + k_2[TbEDTA^-][H^+]^2 + k_3[TbEDTA^-][H^+][Tb^{3+}]$$

over the concentration ranges employed. The predominant mode of exchange is the decomposition of the protonated complex TbHEDTA.

It is concluded that the complex $TbEDTA^-$ is the only species undergoing exchange, although it is possible that mixed complexes formed between $TbEDTA^-$ and acetate ion may be present in the medium. Increasing charge on the buffer anion species accelerates the rate of exchange, while the effect of the buffer anion size is relatively insignificant. A small positive effect observed for the ionic strength on exchange has also been interpreted.

La nature des espèces subissant l'échange et le rôle de l'anion-tampon dans le milieu ne sont pas précisément connus par les recherches antérieures sur l'échange isotopique d'ions métalliques des terres rares avec leurs complexes d'EDTA limitées en milieu acétate seulement.

Utilisant le terbium-160 comme traceur-radio, la cinétique du libre-échange du Tb(III) en $TbEDTA^-$ a été étudiée en détail dans un tampon acétate de 0.025 *M*. L'échange a aussi été examiné dans divers autres concentrations de solutions tampon d'acétate et de phtalate, et aussi dans le tampon benzoate.

Dans la solution 0.025 *M* d'acétate d'ammonium la vitesse d'échange (R en mol l^{-1} s^{-1}) est exprimée par:

$$R = k_1[TbEDTA^-][H^+] + k_2[TbEDTA^-][H^+]^2 + k_3[TbEDTA^-][H^+][Tb^{3+}]$$

pour les intervalles de concentrations utilisés. Le mode prédominant d'échange est la décomposition du complexe TbHEDTA protoné.

Il a été conclu que le complexe $TbEDTA^-$ est la seule des espèces subissant l'échange, bien qu'il soit possible que des complexes mixtes formés entre $TbEDTA^-$ et l'ion acétate soient présents dans le milieu. L'augmentation de la charge sur les types d'anions de tampon accélère la vitesse d'échange tandis que l'effet de la grosseur de l'anion du tampon est relativement insignifiant. Un petit effet positif observé pour la force ionique sur l'échange a aussi été interprété. [Traduit par le journal]

Can. J. Chem., **52**, 1086 (1974)

Introduction

There have been several investigations on the isotopic exchange reactions of rare earth metal ions (M^{3+}) with their ethylenediaminetetraacetate complexes (ML^-) in aqueous acetate solutions, *viz.* La(III), Nd(III), Dy(III), and Yb(III) (1), Ce(III) and Pr(III) (2); Ce(III) (3), Ce(III), and Lu(III) (4); Nd(III) (5), Eu(III) (6, 7), Ho(III) (8), Lu(III) (9–11), and Tb(III) (12). The exchange of metal ions with their ML^- complexes has been carried out in the studies published under the following range of experimental conditions (1–12): p*H*, 4–6; concentrations of M^{3+} and ML^-, less than millimolar. One of the areas of current

[1]To whom all correspondence should be addressed.

Can. J. Chem. Downloaded from www.nrcresearchpress.com by 210.87.254.5 on 09/05/12
For personal use only.

Can. J. Chem. Downloaded from www.nrcresearchpress.com by 210.87.254.5 on 09/05/12
For personal use only.

interest in the chemistry of rare earths is the investigation of possible mixed complex formation resulting from "coordination unsaturation" exhibited by the rare earth metal ions with their relatively high coordination number. Several reports have appeared recently in the literature on mixed complex formation by rare earth-polyaminopolycarboxylates with additional ligands present in the medium. It is important to examine the nature of the rare earth complex or complexes in the medium specified for the exchange reactions (1–12) and characterize precisely the species participating in exchange. This aspect of the exchange reaction ($M(III)/ML^-$) has apparently not been given enough consideration so far in the studies reported on this topic.

Nature of the Rare Earth Complex Species in the Reaction Medium

Although solid rare earth compounds of the type M_4L_3 (13) are reported to have been prepared under suitable experimental conditions, it appears doubtful that these species exist in solution at the concentration ranges of the reactants used for most isotopic exchange studies. The same consideration seems to rule out the possible formation (14) of the cationic species M_2L^{2+}. In addition to studies on the formation (15) of hydroxy complexes of ML^-, complexes of (M^{3+}—L^{4-}) containing more than one ligand molecule have also been reported (16) in the literature. The hydroxy complexes are formed in basic media (15), and the higher EDTA complexes of rare earth metal ions are formed only in the presence of an excess of the ligand (16). Since the exchange experiments are conducted only in acidic medium, and since the complexing agent itself is never present in excess at any time, the possibility of the presence of $MOHL^{2-}$ and $M_nL_m^{(4m-3n)-}$ for ($m > n$) does not have to be considered.

In addition to mixed complexes of the type mentioned above, there are several reports in the literature of complex formation between ML^- and other ligands such as citric acid (17), tartaric acid (18), iminodiacetic acid (19), nitrilotriacetic acid (19), 8-oxyquinoline-5-sulfonate (19), etc. It is evident from these studies on the formation of mixed complexes that neither the size nor the charge on the second ligand appears to be a hindrance in the formation of mixed complexes. Also, it appears (20) that complex formation with a second ligand takes place by replacement of the coordinated water molecule and not by the sites that could be available due to the loosening of bonds (21) between the metal ion and the first ligand.[2]

Further Galaktinov and Astakhov (23) have studied mixed complex formation between NdH(HMDTA) (HMDTA is hexamethylenediaminetetraacetic acid) and acetate $(OAc)^-$. These authors have reported a value of 16 for the stability constant for the mixed complex species $[NdH(HMDTA)(OAc)]^-$ under experimental conditions comparable to those in most exchange reactions. Recently, Ryhl (21) has deduced from p.m.r. studies of LaL^- in basic media the presence and dissociation of the species $LaL(OH)^{2-}$ contributing to the decomposition of the chelate LaL^-. With respect to the bonding abilities of hydroxide and acetate as ligands in lanthanide complexation reactions, Karraker (24) states "the added stability of the resonating structures allows these ligands (*viz.*, bidentate acetate ligands) to compete successfully with OH^- or H_2O in the coordination sphere of the lanthanide ion". As a result of these considerations, the possibility of a mixed complex species formed between ML^- and acetate ions in the exchange reaction medium has to be reckoned in considering the mechanism of exchange in the $M(III)/ML^-$ reaction. The possible role of the mixed complex, if any, in acetate medium becomes even more a relevant consideration in the light of the findings by Janes and Margerum (25) in multidentate kinetics that mixed complex formation between a multidentate chelate and other anions in the medium can result in an increased rate of the proton-assisted decomposition of the multidentate chelate. Although Glentworth *et al.* (3) report that the rate of metal ion exchange in the $Ce(III)/CeL^-$ reaction is catalyzed by acetate ion in the medium, it does not appear that enough consideration has been given in their investigation as to the nature of the chemical species undergoing exchange.

[2]Lee (22) has carried out an X-ray crystallographic investigation of solid NaTbEDTA and it is suggested by this author that the dominant species of the EDTA complex of terbium in aqueous solutions of $pH \sim 4$ is the nine coordinated $TbEDTA(OH_2)_3^-$ type (EDTA is a sexadentate in this species) as observed in solid NaTbEDTA. In the latter compound the entire chelating ligand is relegated to one hemisphere with the metal ion in the center, leaving ample space for three water molecules in the other hemisphere (22).

Can. J. Chem. Downloaded from www.nrcresearchpress.com by 210.87.254.5 on 09/05/12
For personal use only.

Moreover, the previous exchange studies of M(III)/ML^- reactions have been confined to acetate medium only. Therefore an investigation of exchange in other suitable buffer media (benzoate, phthalate, etc.) will be of interest *per se* and may even provide information on the effect of size and charge of the buffer anion on the rate of exchange.

The predominant mode of exchange in M(III)/ML^- reactions is the decomposition of the protonated complex MLH under the experimental conditions studied (1–12). It has been reported in some of the published investigations (3, 7, 9) that the rate-determining step during exchange by the predominant mode is the formation of the protonated complex. However, an examination of the available evidence (3, 7, 9) on the mechanism of exchange does not appear to justify this conclusion, and it seemed therefore important to obtain further evidence concerning the mechanism of exchange in these reactions.

For the reasons discussed above we have undertaken a comprehensive investigation of the exchange behavior of terbium in TbL^- in aqueous medium as well as mixed solvent media consisting of acetone–water, and 1-propanol–water. The choice of terbium as the element for this study was made for the reason that while there is relatively more information on the exchange behavior of light and heavy rare earth elements, those from the mid region of the series have not been investigated in detail.[3] This publication presents results of a detailed study of the exchange behavior of terbium in TbL^- in aqueous acetate solutions, and also in two other buffer systems, *viz.*, phthalate and benzoate. The exchange behavior of terbium with TbL^- in mixed solvent media will be reported separately.

Experimental

Materials

Reagent grade chemicals and deionized water only were used in the preparation of all solutions for use in exchange experiments.

Terbium Chloride Solutions

The purity of the terbium oxide sample (Tb_4O_7, BDH Reagent Grade) used in the preparation of terbium chloride solution for exchange experiments was confirmed by a nuclear activation technique. Stock solutions of terbium chloride were suitably prepared by dissolving weighed amounts of the oxide in a slight excess of dilute hydrochloric acid. No further standardization was made of these solutions. Aliquots of the stock terbium chloride solution were evaporated to dryness and the residue was dissolved in buffer solutions of the composition required for exchange experiments.

Buffer Solutions

Ammonium acetate buffer solutions of the desired concentration and p*H* were obtained by potentiometric titration of standard acetic acid against standard ammonium hydroxide. Measurements of p*H* were made with a Beckman Expanded Scale p*H* Meter to an accuracy of ± 0.015 p*H* unit. Potassium hydrogen phthalate and benzoic acid (both of BDH Analar Grade) were used in the preparation of buffer solutions for exchange experiments in phthalate and benzoate media respectively. Potassium nitrate (BDH Analar Grade) was used as the supporting electrolyte in exchange experiments carried out under constant ionic strength conditions.

Solutions of the Chelating Agent EDTA

The disodium salt of the ethylenediaminetetraacetic acid (BDH Analar Grade) was used in the preparation of solutions of the complexing agent EDTA. The solution obtained by dissolution in deionized water of a weighed amount of the salt was standardized by titration against standard zinc solution using eriochrome black T indicator (26).

Cation Exchange Resin

Dowex 50W-X8 cation exchange resin (Baker Analyzed Reagent) in the hydrogen form and 100–200 mesh size was water-graded to remove very fine particles and converted to the ammonium form before use in the exchange experiments.

The Exchange Reaction

Solutions of the complex TbL^- were made essentially by mixing stoichiometric amounts of the complexing agent and the metal ion in the buffer solution. Solutions preequilibrated for many hours and which contained the specified amounts of the complex and metal ion for the exchange reaction in appropriate buffer solutions were brought to the required temperature in a thermostat controlled to ± 0.01 °C. Isotopic exchange was initiated by adding $^{160}Tb^{3+}$ tracer of high specific activity in about 10 μl of the same buffer solution. At suitable time intervals, aliquots of the reaction mixture were withdrawn and separation of the anionic TbL^- from the metal ion was carried out by using the Dowex 50-X8 cation exchange resin in a suitably designed column of size 25 × 7.5 mm i.d. The resin bed had been pre-treated with the appropriate buffer solution. The reaction mixture was forced rapidly through the resin column and the column was washed with the buffer solution (complete separation of the products was achieved in about 10–20 s and it was ascertained that the amount of further exchange in this time interval was insignificant under the experimental conditions). The volume of the effluents was all combined in the counting vials and was adjusted to a common level

[3]Following a preliminary communication by the authors on some of the findings of this work on the exchange of terbium in TbL^- (12*a*), Szarvas and Brucher (12*b*) have reported on the Tb(III)/TbL^- reaction. However their investigation has not taken into account the following: (*i*) the nature of the chemical species undergoing exchange, (*ii*) the precise role of buffer anion during exchange and the effect of charge and size of buffer anion on the exchange, (*iii*) the mechanism of exchange, and (*iv*) the effect of ionic strength on the exchange rate.

Can. J. Chem. Downloaded from www.nrcresearchpress.com by 210.87.254.5 on 09/05/12
For personal use only.

before assaying its radioactivity. The isotopic exchange was followed for about three to four half-times (*i.e.* to more than 90% completion) and an infinite time sample was also taken the next day in most of the exchange experiments. The radiometric assay of the tracer was done using a NaI(Tl) scintillation well-type counter and all samples were counted to 1% standard deviation.

Results and Discussion

The rate of exchange R was calculated by using the McKay equation (27)

$$[1] \quad R = -\frac{2.303}{t} \times \frac{ab}{a+b} \times \log(1-F)$$

where F is the fraction of exchange at time t and a and b are the molar concentrations of the initially unlabelled complex TbL^- and the metal ion respectively. The fraction of exchange is given by the Norris equation (28)

$$[2] \quad F = \frac{\text{activity per ml associated with } TbL^-}{\text{total activity per ml of reaction mixture}} \times \frac{a+b}{a}$$

when the exchange was initiated by adding the labelled metal ion. The fraction of exchange at zero time was found to be negligible within the limits of experimental error. A principal source of error in the exchange experiments was the uncertainty in the measurements of pH ($\pm$0.015 pH unit) which is a sensitive variable, and other errors of lesser significance such as inaccuracies in counting, volume measurements, sample timings, and separation of the exchanged species. A variation of 0.015 in pH can cause an error of 3–4% in the exchange rate depending on the order of the latter with respect to the hydrogen ion concentration (see the discussion following). The magnitude of the errors from the other sources are estimated to less than about 2–3%. Exchange rates were reproducible with an average deviation of about 3% and with a maximum deviation not exceeding 5% in most of the duplicate experiments. The reversibility of exchange in the $Tb(III)/TbL^-$ reaction was checked by initiating the exchange instead with the terbium tracer in the labelled chelate form. The exchange rate obtained in this case agreed within the experimental precision with those for exchange experiments using labelled terbium ions but otherwise done under identical conditions.

At constant buffer concentration the rate of exchange in these reactions is known to depend (1) on the concentration of the complex, the metal ion, and H^+. Using 0.025 M acetate solution as buffer the rate of exchange was studied over a range of concentration of each of these species and the results obtained from these experiments are summarized in Table 1.

Ionic Strength in Exchange Experiments

It was necessary for the exchange study in the mixed solvent media to keep the concentration of external electrolytes to a minimum. Since the exchange behavior of $Tb(III)/TbL^-$ in the aqueous medium and the mixed solvent media were to be correlated in our investigation, it was desirable to study the exchange reaction in the aqueous medium in the absence of any external electrolyte, wherever possible. When the ionic strength is not kept constant by the addition of a supporting electrolyte, the degree of dissociation of acetic acid will vary with the hydrogen ion concentration of the medium. This will result in changes in the ionic strength and the consequences of these changes in ionic strength were considered in the following manner.

(*i*) The effect of changes in ionic strength on the activity of hydrogen ion and hence its concentration was taken into account by the following procedure.

As an initial approximation, the hydrogen ion concentration was obtained from the instrumental pH meter reading, $pH = -\log_{10}[H^+]$. Using this value for $[H^+]$ and the dissociation constant for acetic acid at infinite dilution (29), the concentration of the acetate ion was calculated and hence the ionic strength of the medium. The activity coefficient f of the single univalent ion (*e.g.* f_{H^+}) was determined at this ionic strength by using the Davies equation (29). With the initial value for f_{H^+} a more accurate value for $[H^+]$ was obtained from the relationship (30, 31)

$$[3] \quad \log_{10}[H^+] = pH + \log f_{H^+}$$

The corresponding concentration dissociation constant K_c (29) at this particular ionic strength was also calculated. Using the values for K_c and $[H^+]$ calculations were continued to obtain new values for OAc^-, μ, f_{H^+}, H^+, and K_c. This process of refining these parameters was reiterated until a constant set of values was obtained for them. The difference between the instrumental pH value and the pH_c calculated from the pro-

TABLE 1. Tb(III)/TbL^- exchange at 20.5 °C; [Acetate] = 0.025 *M*

$[TbL^-] \times 10^4$ (*M*)	$[Tb^{3+}] \times 10^4$ (*M*)	pH_c*	$R \times 10^8$ Observed	$R \times 10^8$ Calculated (eq. 6)
0.25	1.00	5.37	0.60	0.62
0.50	1.00	5.37	1.30	1.23
1.00	1.00	5.37	2.35	2.46
2.50	1.00	5.37	6.18	6.16
5.00	1.00	5.37	12.46	12.33
7.50	1.00	5.37	18.78	18.47
1.00	0.50	5.37	2.20	2.39
1.00	2.50	5.37	2.83	2.68
1.00	5.00	5.37	3.07	3.02
1.00	7.50	5.37	3.57	3.39
1.00	10.00	5.37	3.48	3.72
1.00	15.00	5.37	4.12	4.42
1.00	1.00	5.00	6.68	6.64
1.00	5.00	5.00	7.67	7.94
1.00	7.00	5.00	8.70	8.59
1.00	1.00	5.96	0.52	0.57
1.00	1.00	5.76	0.96	0.92
1.00	1.00	5.70	1.03	1.08
1.00	1.00	5.57	1.32	1.49
1.00	1.00	5.21	3.38	3.74
1.00	1.00	4.87	9.25	9.66
1.00	5.00	5.44	2.63	2.55
1.00	5.00	5.74	1.15	1.19
8.00	1.00	5.68	8.13	9.09
4.00	1.00	5.74	3.60	3.93
1.00	2.00	5.35	2.97	2.72

*p$H_c = -\log_{10}[H^+]$.

cedure outlined above was significant even in the light of the uncertainty in the measurement of the instrumental readings themselves. Therefore the exchange rates in this study are referred in Table 1 to the pH_c values obtained in the calculation described above.

The difference between the maximum and minimum of the ionic strength values in the reaction mixtures (0.025 *M* in total acetate) with the hydrogen ion concentration range in Table 1 is about 0.008 *M*; this is not of a sufficient magnitude to cause its own effect on exchange, as demonstrated by a few separate experiments for studying the effect of ionic strength on exchange. The variations in acetate concentrations of the buffer (0.025 *M*) corresponding to different hydrogen ion concentrations of the medium are also not sufficiently large in most of the experiments to affect the rate of exchange to any appreciable extent.

Dependence of Exchange Rate on the Concentration of H^+, TbL^-, and Tb^{3+}

To elucidate the dependence of exchange rate on the concentration of the reactants the rate can be expressed as

$$[4] \qquad R = k[H^+]^a[TbL^-]^b[Tb^{3+}]^c$$

at constant buffer concentration. Using the *R* values in Table 1 obtained by independently varying the concentrations of H^+, TbL^-, and Tb^{3+} the exponents *a*, *b*, and *c* were determined by the method of least squares. For the ranges of concentrations of the reactants indicated in Table 1 the rate of exchange is best fitted to the equation by

$$[5] \quad R = k[H^+]^{1.13 \pm 0.05}[TbL^-]^{1.00 \pm 0.02} \times [Tb^{3+}]^{0.13 \pm 0.02}$$

and the values for the exponents are expressed at 99% confidence limits. The variation of the rate with the concentration of each of the reactants is shown separately in Figs. 1–3. Below a pH_c value of about 5.2 hydrogen ion dependence of the rate appears to be of a higher order than unity (Fig. 1). Within the ranges of concentration investigated the rate appears to be exactly first

Can. J. Chem. Downloaded from www.nrcresearchpress.com by 210.87.254.5 on 09/05/12
For personal use only.

Can. J. Chem. Downloaded from www.nrcresearchpress.com by 210.87.254.5 on 09/05/12
For personal use only.

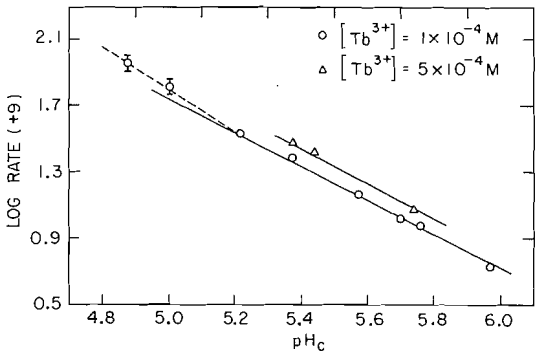

FIG. 1. Variation of log rate with pH_c for the Tb(III)/TbL^- reaction at 20.5 °C ([Acetate] = 0.025 *M*, [TbL^-] = 1×10^{-4} *M*). ○ and △ represent the experimental results. The solid lines correspond to a slope of −1.

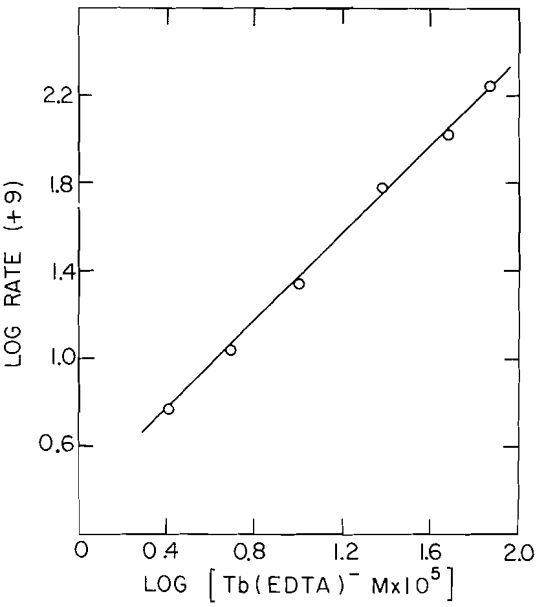

FIG. 2. Variation of rate with [TbL^-] for the Tb(III)/TbL^- reaction at 20.5 °C ([Acetate] = 0.025 *M*, [Tb^{3+}] = 1×10^{-4} *M*, pH_c = 5.37). ○ represents experimental results; the solid line is obtained by using the rate equation (eq. 6).

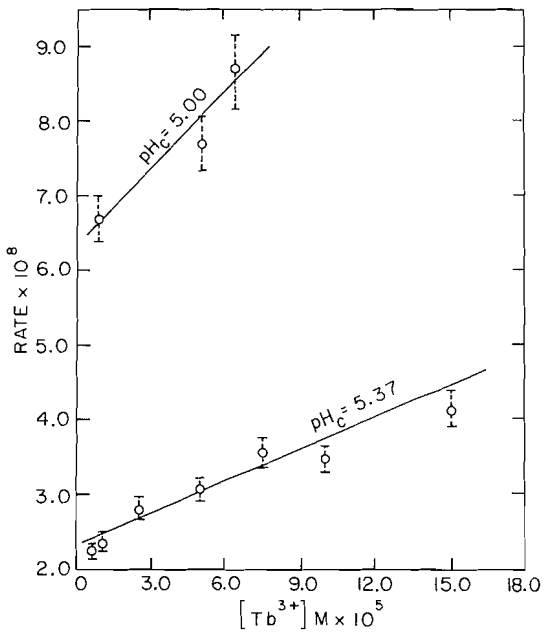

FIG. 3. Variation of rate with [Tb^{3+}] for the Tb(III)/TbL^- reaction at 20.5 °C ([Acetate] = 0.025 *M*, [TbL^-] = 1×10^{-4} *M*). ○ represents experimental results; the solid lines are obtained by using the rate equation (eq. 6).

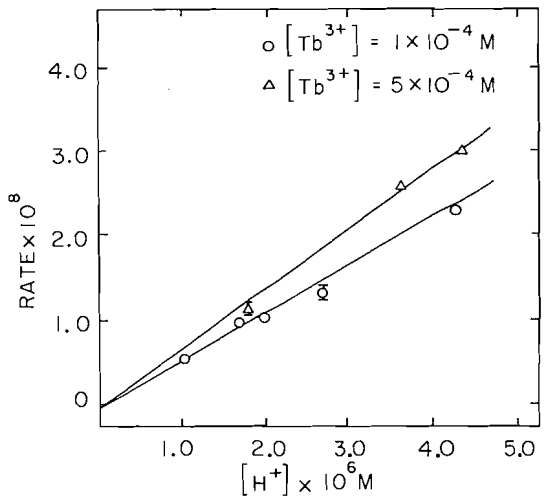

FIG. 4. Variation of rate with [H^+] concentration for the Tb(III)/(TbL^- reaction at 20.5 °C ([Acetate] = 0.025 *M*, [TbL^-] = 1×10^{-4} *M*). The straight lines in Fig. 4 drawn by inspection are extrapolated to zero [H^+] concentration.

order in the concentration of the complex (Fig. 2) while only a slight dependence of the rate on the concentration of Tb^{3+} is observed (Fig. 3).

In Fig. 4 the rate *R* is shown as a function of hydrogen ion concentration in the medium. The best fitting straight line, drawn by inspection in this case, when extrapolated to zero hydrogen ion concentration appears to indicate that, within experimental precision, there is no exchange at zero hydrogen ion concentration and therefore no other acidic species protonates the complex. A similar conclusion has been reported also for the exchange of Eu(III) between La(III) and LaL^- (7).

Can. J. Chem. Downloaded from www.nrcresearchpress.com by 210.87.254.5 on 09/05/12
For personal use only.

Rate Equation for Exchange in 0.025 M Acetate

The most suitable rate equation leading to a plausible kinetic scheme for exchange was determined by a regression analysis with the kinetic data for exchange in Table 1. The following rate equation was found to be most suitable to fit all the exchange data for the reaction Tb(III)/TbL^- in 0.025 *M* acetate in this study

$$[6] \quad R = k_1[TbL^-][H^+] + k_2[TbL^-][H^+]^2 + k_3[TbL^-][H^+][Tb^{3+}]$$

where $k_1 = 47.0 \pm 2.2\ l\ mol^{-1}\ s^{-1}$, $k_2 = 1.7 \pm 0.4 \times 10^6\ l^2\ mol^{-2}\ s^{-1}$, and $k_3 = 3.4 \pm 0.7 \times 10^4\ l^2\ mol^{-2}\ s^{-1}$. The *R* values were calculated by using best fitting constants and the actual concentrations for the reactants and the calculated *R* values are compared with the observed values in Table 1. The mean percent deviation between the observed rates and the calculated ones is about 5.5% which is comparable in magnitude to the uncertainties in the rate measurements themselves. The constants k_1, k_2, and k_3 can be associated with the following modes of exchange.

Mode 1

$$[7] \quad TbL^- + H^+ \underset{k_{-1}'}{\overset{k_1'}{\rightleftharpoons}} TbLH$$

$$[8] \quad TbLH \xrightarrow{k_2'} \text{Products}$$

Mode 2

$$[9] \quad TbLH + H^+ \underset{k_{-3}'}{\overset{k_3'}{\rightleftharpoons}} TbLH_2^+$$

$$[10] \quad TbLH_2^+ \xrightarrow{k_4'} \text{Products}$$

Mode 3

$$[11][4] \quad TbLH + Tb^{3+} \underset{k_{-5}'}{\overset{k_5'}{\rightleftharpoons}} TbLHTb^{3+}$$

$$[12] \quad TbLHTb^{3+} \xrightarrow{k_6'} \text{Products}$$

Although the predominant contribution to exchange arises from mode 1, experimental conditions have been varied sufficiently for exchange to discern significant contributions to exchange from modes 2 and 3 as indicated in Table 2.

Role of Buffer Anion during Exchange

(i) Exchange Experiments in Acetate Buffer

The results obtained with variations in acetate concentration and at constant ionic strength (0.1*M*) are shown in Fig. 5. Since there were variations in the concentrations of the reactant species so that rate measurements can be made conveniently, the normalized quantity $(R/[TbL^-][H^+][Tb^{3+}]^{0.13})$ is shown in Fig. 5 as a function of buffer concentration.[5] The increase in exchange rate with increasing buffer concentration may not be due to any effect on the lability of aquo metal ion arising from the presence of the buffer anion. This can be attributed to the observation that complex formation between M^{3+} and EDTA, or the ligand replacement reaction between any mono or bidentate complex of rare earth metal ion and EDTA is an extremely rapid process (33) compared to the half-time for metal ion exchange in the (M^{3+}–ML^-) system. Possibly, the increase in the rate with increasing buffer concentration is due either to the formation of a labile mixed complex between the chelate and the buffer anion or to an increase in the catalytic effect of the buffer anion on the decomposition of the chelate. The variation of exchange rate with buffer concentration can be analyzed as below for the presence and effect of such mixed complex, if any, on the exchange.

Now, let R_1, R_2, ..., R_i...R_n be the rates of isotopic exchange in experiments with the same molar concentrations of the complex TbL^-, Tb^{3+}, and H^+ but in varied concentrations b_i of buffer B, at constant ionic strength. The rate of exchange R_0 at zero buffer concentration may be obtained by extrapolating to zero buffer concentration the linear graph for the variation of rate

[4]The formation of M_2L^{2+} by direct reaction between ML^- and M^{3+} is reported to take place only in media more basic than the condition of these experiments (15). The possibility (mode 3) of direct reaction between the neutral TbLH and Tb^{3+} may be justified by the following considerations: (*i*) regression analysis of the kinetic data does imply the association of hydrogen ion with exchange by mode 3, and (*ii*) the labile nature of the carboxylate–metal ion bonds in these chelates as observed by Ryhl (21), (*iii*) and evidence for the formation of a binuclear complex is also available from chemical shift data obtained by Brucher (32) on the n.m.r. spectra of ML^- complexes in the presence of excess metal ions.

[5]pH_c values for these experiments were above 5.2 (Fig. 1). Also the exchange rates obtained as a function of $[H^+]$ indicate that the protonation of the complex TbL^- by other acidic species (*e.g.* [HOAc]) is negligible, if any (Fig. 4). The latter conclusion appears to be further supported by the investigation of Glentworth *et al.* (3) on the effect of acetate concentration on the exchange of Ce(III) with its multidentate chelates.

TABLE 2. Exchange modes and exchange rates at 20.5 °C; [Acetate] = 0.025 *M*

Experimental conditions			*R*		Percent contribution of *R* calculated for exchange modes		
pH_c	$[TbL^-] \times 10^4$ (*M*)	$[Tb^{3+}] \times 10^4$ (*M*)	Observed $\times 10^8$	Calculated (eq. 6) $\times 10^8$	1	2	3
4.87	1.00	1.00	9.25	9.66	65	30	5
5.00	1.00	5.00	7.67	7.94	59	21	20
5.00	1.00	7.00	8.70	8.59	55	19	26
5.38	1.00	2.50	2.83	2.68	76	11	13

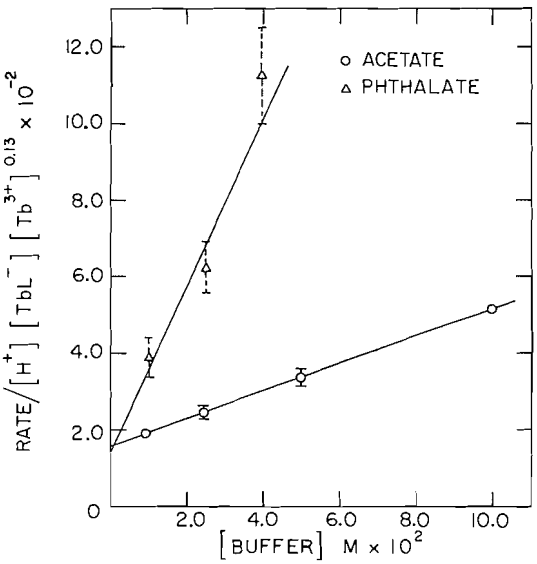

FIG. 5. Variation of rate with buffer concentration for the Tb(III)/TbL^- reaction at 20.5 °C (ionic strength = 0.1 *M*).

with the buffer concentration (in Fig. 5 the normalized quantity corresponding to R_0 will be obtained). Therefore, the quantity ΔR_i (defined as $\Delta R_i = R_i - R_0$) is the net exchange rate due to effect of buffer of concentration b_i.

Since the exchange experiments are considered under identical concentration conditions of all species except buffer, ΔR_i at buffer concentration b_i should be proportional to the molar concentration of the rate-determining mixed complex species $TbHLB^-$, if any, prevailing at the buffer concentration b_i, *i.e.*

$$[13] \qquad \Delta R_i = k_m[TbHLB^-]_i$$

where k_m is some rate constant. Similarly,

$$[14] \qquad \Delta R_j = k_m[TbHLB^-]_j$$

at another buffer concentration b_j, and

$$[15] \qquad \frac{\Delta R_i}{\Delta R_j} = \frac{[TbHLB^-]_i}{[TbHLB^-]_j} = \frac{m_i}{m_j}$$

where m represents the molar concentration of the mixed complex species $TbHLB^-$. Under the experimental conditions $b_i \gg [TbHLB^-]_i$ (since $b_i \gg [TbL^-] > \{[TbHL] + [TbHLB^-]\}$). The formation of a mixed complex between the buffer anion and TbHL can be represented by the equation

$$[16] \qquad TbHL + B^- \rightleftharpoons TbHLB^-$$

If C is the molar concentration of the complex TbHL and K is the formation constant for the mixed complex

$$[17] \qquad K = \frac{m_i}{(C - m_i)b_i}$$

(at buffer concentration b_i)

and

$$[18] \qquad K = \frac{m_j}{(C - m_j)b_j}$$

(at buffer concentration b_j)

Equating [17] and [18]

$$[19] \qquad \frac{b_i m_j(C - m_i)}{b_j m_i(C - m_j)} = 1$$

Eliminating m_i from eq. 19 in terms of eq. 15 and rearranging terms, the following quadratic equation is obtained

$$[20] \qquad \frac{\Delta R_i}{\Delta R_j} m_j^2(b_i - b_j) + m_j C\left(\frac{\Delta R_i}{\Delta R_j} b_j - b_i\right) = 0$$

Solving eq. 20 for m_j

$$[21] \qquad m_j = \frac{C\left(b_i - \frac{\Delta R_i}{\Delta R_j} b_j\right)}{\frac{\Delta R_i}{\Delta R_j}(b_i - b_j)} = CY$$

where

Can. J. Chem. Downloaded from www.nrcresearchpress.com by 210.87.254.5 on 09/05/12
For personal use only.

$$[22] \qquad Y = \frac{b_i - \frac{\Delta R_i}{\Delta R_j} b_j}{\frac{\Delta R_i}{\Delta R_j}(b_i - b_j)}$$

Substituting eq. 21 in eq. 18

$$[23]^6 \qquad K = \frac{Y}{(1 - Y)b_j}$$

Using eqs. 23 and 22, values for $\Delta R_i/\Delta R_j$ at buffer concentrations b_i and b_j can be calculated for different values of the formation constant K. With b_i and b_j taken as 0.04 and 0.02 M respectively, the results of these calculations are recorded in Table 3 for the formation constant values of interest in this discussion.

In Table 3 the upper limit for an estimate of K was chosen as comparable in magnitude to the formation constants for mixed complexes reported (17–19) in the literature, and the value of 10^{-6} for K is also included as a corresponding lower limit. A value of 15 is the approximate magnitude of the formation constant for the mixed complex between NdHHMDTA and acetate ion in the pH_c region of interest in the exchange experiments (23). Since the experimental exchange rates are normalized to identical concentration conditions of the reactants in the medium with exception of buffer concentration, values for $\Delta R_i/\Delta R_j$ can be obtained from the ordinate in Fig. 5 for the buffer concentrations under consideration or analytically by the method of least squares. A value of 2 ± 0.20 is found for the ratio $\Delta R_i/\Delta R_j$ when b_i and b_j are 0.04 and 0.02 M respectively (*cf.* Table 3) and it indicates that there is no contribution to exchange by any labile mixed complex over the region of buffer concentration where the rate of exchange increases with increasing acetate concentration. These results can be confirmed by choosing any suitable buffer concentration for this purpose. Since a very significant amount of exchange takes place at zero buffer concentration (see Fig. 5) and contribution to exchange of a labile mixed complex is not indicated over the region of acetate concentration investigated the only species participating in exchange is TbL^-. Glentworth *et al.* (3) have studied the effect of acetate concentration on the exchange of Ce(III) with CeHyEDTA (HyEDTA:*N'*-(2-hydroxyethyl)ethylenediamine-*N,N,N'*-triacetate), CeDCTA (DCTA:1,2-diaminocyclohexane-*N,N,N',N'*-tetraacetate) and CeL^-, although no definite conclusion is indicated in their investigation regarding the possible contribution to exchange from a mixed complex (formed between the multidentate chelate and acetate ion), if any, in the medium. We have applied quantitative formulations on the possible participation of a mixed complex in the exchange reaction in our paper to the experimental data on acetate concentration effect on Ce(III) exchange with CeHyEDTA, $CeDCTA^-$, and CeL^- (the results in Fig. 11 of ref. 3 were used for this purpose with the help of a Ruscom Logics Graph Digitizer-Model 214-1). From this consideration we are led to conclude that there is no mixed complex (formed between acetate ion and the multidentate chelate concerned) that contributes to exchange, thereby indicating similarities in the role of buffer anion in these exchange reactions. It has been reported (20) that when mixed complex formation takes place with rare earth multidentate chelates it is by replacement of the water molecule or molecules coordinated to the metal ion. Presumably, in the case of the protonated multidentate chelates under discussion the chelate itself is labilized during the formation of a mixed complex by the acetate ion.

TABLE 3. Dependence of $\Delta R_i/\Delta R_j$ on the formation constant value for the mixed complex;* ($b_i = 0.04$ M and $b_j = 0.02$ M)

K	Y	$\Delta R_i/\Delta R_j$
10^6	0.0	0.010
15	0.23	0.016
10^{-6}	2×10^{-8}	0.020

*$\Delta R_i/\Delta R_j$ was calculated from eqs. 23 and 22.

(ii) Exchange in Benzoate and Phthalate Buffer Media

Since a detailed and thorough investigation of exchange in these buffer media has not been carried out as in the acetate medium, it is assumed that the role of buffer anion during exchange in phthalate and benzoate buffer media would be similar to that of acetate ion in labilizing the species undergoing exchange. Benzoic acid is a stronger acid than acetic acid (29) and therefore the benzoate anion (the conjugate base

[6]If the mixed complex is formed directly between TbL^- and B^- without the initial protonation of the former, the resulting expression for the stability constant will be the same as eq. 23.

Can. J. Chem. Downloaded from www.nrcresearchpress.com by 210.87.254.5 on 09/05/12
For personal use only.

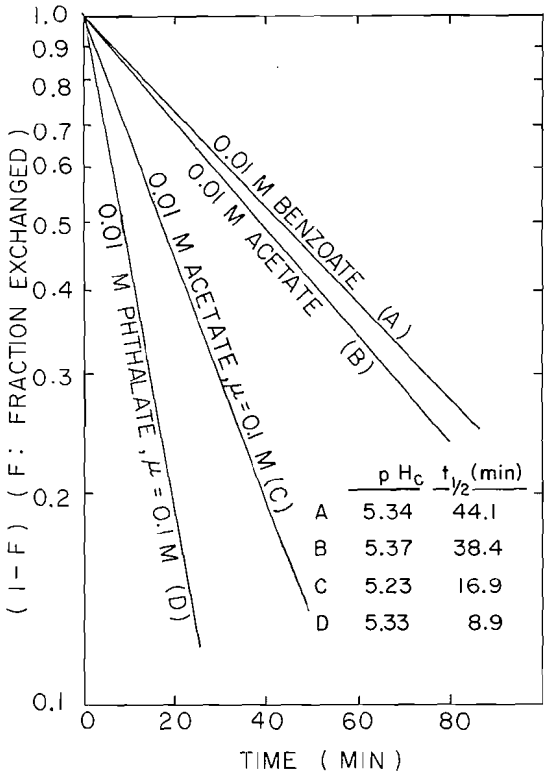

FIG. 6. Comparison of exchange rates and half-times ($t_{1/2}$) for the Tb(III)/TbL^- reaction in different buffer systems at 20.5 °C ($[Tb^{3+}] = 1 \times 10^{-4}$ *M*, $[TbL^-] = 1 \times 10^{-4}$ *M*).

of the former acid) will be relatively less basic than acetate ion. Hence the possibility of a mixed complex formed between TbL^- and benzoate participating in the exchange reaction will be rather limited relative to the role of mixed complex, if any, in the acetate medium in which it has been proved that there is no mixed complex contributing to exchange. Therefore it is assumed that, under identical concentrations of buffer and other reactants in the medium, any difference in exchange behavior observed for acetate and benzoate media may possibly be attributed to the effect of different sizes of the buffer anions under consideration (it is to be noted that the molar concentration of benzoate anion is slightly greater than acetate under the same pH_c and total acid concentration). From the comparison of exchange in acetate and benzoate media in Fig. 6 it appears that the size of buffer anion does not influence significantly the rate of exchange. In isomolar phthalate and acetate solutions at the same pH_c value and ionic strength, the total molar concentration of anionic species in phthalate buffer (HPh^- and Ph^{2-}) is greater than in acetate solution (in 0.01 *M* phthalate solution at 0.1 *M* ionic strength with a pH_c of 5.32, the concentration of Ph^{2-} and HPh^- are about 0.007 and 0.003 *M* respectively; in a 0.01 *M* solution of acetate under the same conditions the concentration of acetate ion is about 0.008 *M* (29)). However, a comparison of exchange in phthalate and acetate buffer media as in Fig. 6 does seem to indicate that the rate of exchange is accelerated by increasing the charge on the buffer anion. This conclusion is also strengthened by the variation observed for the rate with phthalate concentration in Fig. 5. But it is to be noted that the same rate law is assumed in the latter case as in the acetate medium; also, since the exchange rates are rather high in phthalate medium ($t_{1/2}$ is about 10 min or less), the error in the *R* values is relatively greater.

Slow Step During Exchange by the Predominant Mode

It has been postulated in the literature (3, 7, 9) that the rate-determining step during exchange by the predominant mode (proton-assisted decomposition of the chelate ML^-, mode 1) is the formation of the protonated complex MLH. However the experimental data in the studies cited do not appear to justify this conclusion. From our study of the exchange of terbium with TbL^- in mixed solvent media we have established clearly that the rate-determining step during exchange by the predominant mode is the decomposition of the protonated complex and not its formation.[7] Szarvas and Brucher (12*b*) have stated that some significant change takes place on protonation of the complex and presumably this change occurs after pre-equilibration of the complex with the proton. The concentration of the structurally changed protonated intermediate undergoing decomposition may be very small indeed and the exchange appears to be better considered in terms of the steady-state theory. By applying the steady-state considerations to the concentrations of the species TbLH, $TbLH^{2+}$, and $TbLHTb^{3+}$ it can be shown that

$$[24] \quad R = K_1k_2'[TbL^-][H^+] + K_1K_3k_4'[TbL^-][H^+]^2 + K_1K_5k_6'[TbL^-][H^+][Tb^{3+}]$$

[7]NOTE ADDED IN PROOF: This has recently appeared in ref. 38.

Can. J. Chem. Downloaded from www.nrcresearchpress.com by 210.87.254.5 on 09/05/12
For personal use only.

where k_2', k_4', and k_6' are the relevant rate constants (*cf.* eqs. 7–12) and K_1, K_2, and K_3 are the ratios of the rate constants for opposing reactions leading to the formation and dissociation of the steady-state species TbLH, $TbLH_2^+$, and $TbLHTb^{3+}$, respectively. A comparison of eq. 24 with eq. 6 will indicate the nature of the empirical rate constants in eq. 6. If the species involved in exchange through modes 2 and 3 is different from that in mode 1, which is a possibility, it can be shown that the resulting steady-state equation will have the same form as eq. 2 with the appropriate "equilibrium constants" in this case.

Influence of Ionic Strength on Exchange

In order to examine the effect of ionic strength on the exchange the overall rate was expressed in the form

$$[25] \qquad R = k'[TbL^-][H^+][Tb^{3+}]^{0.13}$$

for the pH_c region 5.2–6.0 (*cf.* dependence of rate on $[H^+]$, Fig. 1). It is assumed here that eq. 25 is valid at all ionic strength values (Asano *et al.* (9)). The experimental conditions maintained in this investigation for observing the effect of ionic strength on exchange were in favor of the exchange taking place predominantly by mode 1. Therefore, it may be valid if the effect of ionic strength observed is considered as mainly due to the same on the rate constant k_1 in eq. 6 or k_2' in the steady-state equation for exchange (eq. 24).[8] Since the decomposition of the uncharged protonated complex is the rate-determining step during exchange by the predominant mode, it is appropriate to consider the effect of ionic strength on the activity coefficient f of the neutral species TbLH (*c*). Using the Debye–McAulay (35) equation for this purpose

$$[26] \qquad \log f_c = b_c\mu$$

where b is a constant. The activated complex must have the same net charge as *c*, and its activity coefficient $f_\ddagger$ will be therefore given by an equation of the same form as eq. 26 but involving a constant $b_\ddagger$ in this case. The rate constant k_1 at ionic strength μ is related to the rate constant k_1^0 at infinite dilution by the equation (36)

[8]In eq. 24 the value of K_1 associated with k_2' would normally decrease (34) to a small extent with increasing ionic strength; this assumption implies that the quotient K_1 arising from steady-state consideration of exchange behaves as the conventional formation constant in this aspect.

TABLE 4. Ionic strength and Tb(III)/TbL^- exchange; [Acetate] = 0.025 *M*, T = 20.5 °C

M	$k' \times 10^{-2}$
0.02	1.82
0.06	2.24
0.10	2.31

$$[27] \qquad \log k_1 = \log k_1^0 + \log f_c/f_\ddagger$$

Substituting in eq. 27 the values for f in terms of eq. 26

$$[28] \qquad \log k_1 = \log k_1^0 + (b_c - b_\ddagger)\mu$$

The b values are known to be in the order of the sum of reciprocals of radii of the species involved (37). Also, since the distance of separation between the product components in the activated complex would be larger than in the reactant molecule it is reasonable to expect the term $(b_c - b_\ddagger)$ to have a positive value resulting in an increase in the rate of reaction with increasing ionic strength. Thus the slight positive effect observed for ionic strength on the exchange (see Table 4) is in agreement with the conclusion from mixed solvent media that the rate-determining step is the decomposition of the protonated complex.[5] The effect of ionic strength on exchange appears thus to arise from activity coefficient considerations in addition to the possible catalytic effect of the nitrate anion (present in the supporting electrolyte KNO_3) on the decomposition of the protonated complex as reported by Asano *et al.* (9). Interestingly, the latter authors associate the activation energy calculated from the effect of temperature on k' with the initial protonation of the complex. In this case the protonation step becomes rate-determining, and therefore, the catalytic effect of NO_3^- ion on the decomposition of MLH may not have any effect on the rate of exchange.

We thank the National Research Council of Canada for financial support of this work.

1. R. H. BETTS, O. DAHLINGER, and D. M. MUNRO. Proc. 1st. UNESCO Conf. Vol. II. Pergamon Press, Oxford. 1958. p. 363.
2. T. SHIOKAWA, H. KUDO, and T. OMORI. Bull. Chem. Soc. Jap. **38**, 1340 (1965); T. SHIOKAWA and T. OMORI. Bull. Chem. Soc. Jap. **38**, 1892 (1965).
3. P. GLENTWORTH, B. WISEALL, C. L. WRIGHT, and A. J. MAHMOOD. J. Inorg. Nucl. Chem. **30**, 967 (1968).

Can. J. Chem. Downloaded from www.nrcresearchpress.com by 210.87.254.5 on 09/05/12
For personal use only.

4. P. SZARVAS and E. BRUCHER. Acta Chim. Acad. Sci. Hung. **50**, 279 (1966).
5. E. BRUCHER and P. SZARVAS. Magy. Kem. Foly. **73**, 376 (1967).
6. V. V. FOMIN, E. P. MAIOROVA, and G. A. LEMAN. Russ. J. Inorg. Chem. **14**, 1000 (1969).
7. W. D'OLIESLAGER, G. R. CHOPPIN, and K. R. WILLIAMS. J. Inorg. Nucl. Chem. **32**, 3605 (1970); W. D'OLIESLAGER and G. R. CHOPPIN. J. Inorg. Nucl. Chem. **33**, 127 (1971).
8. YU. A. MAKASHEV, I. E. MAKASHEVA, and V. A. MELINIKOV. Radiokhimia, **8**, 371 (1966).
9. T. ASANO, S. OKADA, K. SAKAMOTO, S. TANIGUCHI, and Y. KOBAYASHI. J. Inorg. Nucl. Chem. **31**, 2127 (1969).
10. T. ASANO, S. OKADA, K. SAKAMOTO, S. TANIGUCHI, and Y. KOBAYASHI, Radioisotopes, **14**, 363 (1965).
11. E. BRUCHER and P. SZARVAS. Magy. Kem. Foly. **75**, 139 (1969).
12. (*a*) K. NEELAKANTAN and R. E. JERVIS. Inorg. Nucl. Chem. Lett., **7**, 131 (1971); (*b*) P. SZARVAS and E. BRUCHER. Monatsh. Chem. **101**, 1321 (1970).
13. T. MOELLER, F. MOSS, and R. MARSHALL. J. Am. Chem. Soc. **77**, 3182 (1955); L. I. MARTYNENKO. Russ. J. Inorg. Chem. **6**, 1366 (1961).
14. L. I. MARTYNENKO. Russ. J. Inorg. Chem. **8**, 799 (1963).
15. E. J. GUSTALT. J. Am. Chem. Soc. **74**, 3773 (1952).
16. N. A. KOSTROMINA, T. V. TERNOVAYA, and K. B. YATSIMIRSKII. Russ. J. Inorg. Chem. **14**, 80 (1969).
17. L. I. MARTYNENKO, G. A. ARTYUKHINA, and V. I. SPITSYN. Dokl. Akad. Nauk. SSSR, **185**, 243 (1969).
18. N. A. DOBRYNINA, L. I. MARTYNENKO, L. V. AGEEVA, and V. I. SPITSYN. Dokl. Akad. Nauk SSSR, **193**, 466 (1970).
19. G. GEIER and U. KARLEN. *In* Progress in coordination chemistry, proceedings of the eleventh international conference on coordination chemistry, Haifa, Jerusalem. Edited by M. Cais. Elsevier, New York. 1968. p. 159.
20. L. C. THOMPSON and J. A. LORRAS. Inorg. Chem. **2**, 89 (1963); N. A. KOSTROMINA, K. B. YATSIMIRSKII, T. V. TERNOVAYA, and N. N. TANANAEVA. *In* Proc. Sym. Coord. Chem. (3rd), **1**, 425 (1970). *Edited by* M. T. BECK. Akad. Kiado, Budapest.
21. TORSTEN RYHL. Acta Chem. Scand. **26**, 4001 (1972).
22. B. LEE. Ph.D. Thesis, Cornell University, Ithaca, New York. 1967.
23. YU.P. GALAKTINOV and K. V. ASTAKHOV. Russ. J. Inorg. Chem. **8**, 1309 (1963).
24. D. G. KARRAKER. J. Chem. Educ. **47**, 424 (1970).
25. D. L. JANES and D. W. MARGERUM. Inorg. Chem. **5**, 1135 (1966).
26. H. FLASCHKA. EDTA titrations: an introduction to theory and practice. Pergamon Press, Oxford. 1964.
27. H. A. C. MCKAY. Nature, **142**, 997 (1938).
28. T. H. NORRIS. J. Phys. Colloid Chem. **54**, 777 (1950).
29. J. N. BUTLER. Ionic equilibrium. Addison–Wesley, Reading, Mass. 1964.
30. R. G. BATES. Determination of p*H*. Wiley, New York, N.Y. 1964.
31. I. FELDMAN. Anal. Chem. **28**, 1859 (1956).
32. E. BRUCHER. Magy. Kem. Foly. **78**, 571 (1972).
33. K. B. YATSIMIRSKII and L. I. BUDARIN. Dokl. Akad. Nauk. SSSR, **170**, 1107 (1966).
34. L. G. SILLEN and A. E. MARTELL. Stability constants of metal–ion complexes. Special Publication No. 17, Chemical Society, London. 1964.
35. P. DEBYE and J. MCAULAY. Phys. Z. **26**, 22 (1925).
36. K. J. LAIDLER. Chemical kinetics. McGraw–Hill, New York, N.Y. 1965. Chapt. 5.
37. H. S. HARNED and B. B. OWEN. The physical chemistry of electrolytic solutions. 3rd ed. Reinhold Publishing Corporation, New York, N.Y. 1958. p. 534.
38. K. NEELAKANTAN and R. E. JERVIS. Inorg. Nucl. Chem. Lett., **10**, 67 (1974).

Can. J. Chem. Downloaded from www.nrcresearchpress.com by 210.87.254.5 on 09/05/12
For personal use only.

Thermodynamics of Transfer of Organic Molecules from Water to Acid Solutions. The Effects of Nitro Substitution

KEITH YATES AND ROBERT A. MCCLELLAND

Lash Miller Chemical Laboratories, University of Toronto, Toronto, Ontario M5S 1A1

Received August 23, 1973

The free energies, enthalpies, and entropies of transfer for a series of neutral aromatic solutes from water to aqueous sulfuric and perchloric acids have been determined by measuring the "medium effect" activity coefficient over a range of temperatures. The more negative free energies of transfer (salting-in) into perchloric acid relative to sulfuric acid are due to more favorable entropy terms, although enthalpies of transfer to perchloric acid solutions are similar to or more positive than those for sulfuric acid solutions. The generally observed salting-in caused by substitution of a nitro group in a neutral solute (the nitro-group effect) results from a more favorable enthalpy of transfer, with a small amount of compensation from the entropy term. A brief discussion of the solute–solvent interactions responsible for these observations is presented.

Les énergies libres, les enthalpies et les entropies de transfert d'une série de solutés aromatiques neutres dans l'eau et jusque dans les acides sulfurique et perchlorique aqueux ont été déterminées par mesure du coefficient d'activité "d'effet moyen" sur un intervalle de températures. Les plus négatives des énergies libres de transfert (anti-relargage) dans l'acide perchlorique relativement à l'acide sulfurique sont dues à des termes d'entropie plus favorables, bien que les enthalpies de transfert aux solutions d'acide perchlorique sont similaires ou plus positives que celles des solutions d'acide sulfurique. L'anti-relargage, généralement observé, causé par la substitution d'un groupement nitro dans un soluté neutre (L'effet du groupe-nitro) résulte d'une enthalpie de transfert plus favorable, avec une petite quantité de compensation provenant du terme entropique. Une brève discussion des interactions soluté–solvant, responsables de ces observations est présentée. [Traduit par le journal]

Can. J. Chem., 52, 1098 (1974)

Can. J. Chem. Downloaded from www.nrcresearchpress.com by 210.87.254.40 on 09/05/12
For personal use only.

In a recent article (1) we reviewed the considerable body of data that has accumulated concerning the activity coefficient behavior of organic molecules and ions in aqueous mineral acids. This topic has considerable importance for an understanding of protonation equilibria and acid-catalyzed reactions in these generally non-dilute solutions, since outside the pH region, activity coefficient variation cannot be neglected in any quantitative treatment.

The type of activity coefficient being discussed in these terms is defined by the following equation for the chemical potential of a solute species i in an acid solution s.

$$[1] \quad {}_s\mu_i(C_i,C_s) = {}_w\mu_i^0(C_i = 1, C_s = C_w^0) + RT \ln y_i \cdot C_i$$

In this equation C_i is the molar concentration of i and C_s refers to the acid composition; the activity coefficient y_i and the standard chemical potential ${}_w\mu_i^0$ refer to a hypothetical standard state of an ideal 1 M solution of i in pure water, C_w^0.

This chemical potential can also be written in terms of a standard state in the acid solution itself.

$$[2] \quad {}_s\mu_i(C_i,C_s) = {}_s\mu_i^0(C_i = 1, C_s = C_s^0) + RT \ln {}_sy_i \cdot C_i$$

In this equation the standard chemical potential ${}_s\mu_i^0$ and the activity coefficient ${}_sy_i$ refer to a hypothetical standard state of an ideal 1 M solution of i in the pure solvent C_s^0. Since we are generally concerned with very dilute solutions of organic solutes in these acids, the assumption is made that solute–solute interactions are negligible and that the solution is not far from ideality when referred to this standard state (*i.e.* ${}_sy_i \doteq 1$). On this basis, subtracting eq. 2 from eq. 1 gives

$$[3] \quad RT \ln y_i = {}_s\mu_i^0 - {}_w\mu_i^0$$

Thus the activity coefficient y_i is dependent only on the difference in the standard chemical potentials of i in the acid solution and water, and for this reason can be described as a

Can. J. Chem. Downloaded from www.nrcresearchpress.com by 210.87.254.40 on 09/05/12
For personal use only.

"medium effect" activity coefficient since it is determined largely by solute–solvent interactions and not solute–solute interactions.

Another way of regarding y_i in eq. 3 is in terms of the free energy change in transferring one mole of i from a solution in water to a solution in the acid solvent s, where both solutions are in their respective standard states, that is the hypothetical ideal 1 *M* solution in the pure solvents. We will define this free energy term as $[\Delta G_{tr}^0(w,s)]_c$, *i.e.*

$$[4] \qquad RT \ln y_i = [\Delta G_{tr}^0(w,s)]_c$$

where the subscript *c* indicates the concentration units (molarity) used in defining the standard states.

In this paper we wish to report an analysis of this free energy of transfer in terms of the enthalpy and entropy components.

$$[5] \quad [\Delta G_{tr}^0(w,s)]_c = \Delta H_{tr}^0(w,s) - [T\Delta S_{tr}^0(w,s)]_c$$

The enthalpy term is independent of the concentration units employed, and in fact is the enthalpy change in transferring one mole of the solute species from an infinitely dilute solution in water to an infinitely dilute solution in the acid. This term was estimated from the temperature dependence of the free energy (*i.e.* activity coefficient). Although the result is not as precise as that obtained using other thermodynamic methods, one advantage of this method is that it permits a study of sparingly soluble substrates. Furthermore, this method is quite suitable for the present study, the objective of which is not to report a number of highly precise heats of transfer, but rather to examine the structural trends, if any exist, for a series of related compounds to see if further useful information can be obtained concerning the problem of organic activity coefficient variation in mineral acids.

This sort of thermodynamic analysis was recently reported by Arnett and co-workers for a small number of compounds, both electrolytes and nonelectrolytes, for transfer from water to sulfuric acid solutions (2). These workers determined the enthalpy of transfer from the difference in the partial molar heats of solution in the acid and pure water as measured using a calorimetric method. This work suggested that activity coefficient variation in sulfuric acid solutions is mainly enthalpy controlled, particularly in the more concentrated acids. Entropy contributions were found to be more important in dilute acids but acted in the opposite direction to the enthalpy, to produce a moderating effect on the free energy.

In this report two particular aspects of the activity coefficient variation of neutral solutes in acid solutions have been explored. Firstly a comparison of the thermodynamics of transfer from water to two different mineral acid systems, sulfuric acid and perchloric acid, has been carried out, in order to investigate the origin of the well-known salting-in[1] effect of perchloric acid relative to sulfuric acid for neutral substrates (1, 3).

Secondly, through the study of a series of progressively substituted nitrobenzenes, an investigation was undertaken into "the nitro-group" effect (1, 4), that is, the pronounced and progressive salting-in effect of nitro-substitution in neutral aromatic substrates. This effect is of the utmost importance for the study of acidity functions and related protonation equilibria, since such studies usually involve the use of nitro-substituents to produce progressively weaker indicator bases (5), leading to some concern over the validity of such acidity function scales (1).

Experimental

Materials

Sulfuric and perchloric acid solutions were prepared by diluting either CIL reagent grade concentrated sulfuric acid or BDH Analar grade concentrated perchloric acid with distilled water. Concentrations were determined from densities at 25.0 °C (6, 7), measured with an Anton Paar Precision Density Meter, Model No. DMA 02C. Fisher Certified A.C.S. grade cyclohexane was used, with no further purification.

All compounds used in this study were commercially available. Liquids were dried using an appropriate agent and distilled before use. Solids were recrystallized and dried in a vacuum desiccator.

Equipment

A "LABCONCO" Fiberglass Glove Box was converted to a constant temperature controlled box. This was done by fitting the built-in circulation duct with a "Muffin Fan" by Rotron Manufacturing Co., Glendale, California, which has a specified circulating capacity of 100 cu ft per min. A 100-Watt wire heater was placed in front of the fan, and the box was thermostatically controlled by means of the heater which was connected to a thermoregulator through a solid-state relay box. The

[1]The terms salting-in and salting-out derive from the solubility changes in these systems, which are directly related to the activity coefficient variation and thus free energy of transfer. In general terms, "salting-in" implies a more negative free energy of transfer.

Can. J. Chem. Downloaded from www.nrcresearchpress.com by 210.87.254.40 on 09/05/12
For personal use only.

exterior of the box was packed with insulating material to lower heat losses at the higher temperatures. At lower temperatures cooling coils were found to be necessary to maintain constant temperature. With these modifications the temperature could be controlled to ± 0.1 °C at 25 °C, ranging up to ± 0.2 °C at 55 °C. Although better temperature control would be desirable for this type of study, the advantage of the glove box lies in the fact that the mechanical separations required can be conveniently carried out at the same temperature as the equilibrations.

Benzene Solubilities

Mixtures of 5 ml of aqueous acid solution and 0.2–0.5 ml of benzene were shaken for 2–4 h using a mechanical shaker, and allowed to separate overnight. Portions of the aqueous phases were then carefully removed and placed in stoppered u.v. cells of suitable path length. These were immediately transferred to a Unicam SP 800 spectrophotometer thermostatted at the same temperature as the glove box, and the spectra recorded in the wavelength range 245–265 nm. The concentrations of the saturated aqueous solutions were then determined from the absorbances at the maxima at 247, 254, and 263 nm. The extinction coefficients at the appropriate temperature were determined from the absorbances of a standard solution in water. At 25.0 °C no medium effect on the spectra was observed on substituting aqueous acid for water and this was assumed to be the case at the other temperatures as well.

Nitrobenzene Partition Coefficients

Mixtures of 5 ml of aqueous acid solution and 5 ml of a solution of nitrobenzene in cyclohexane were shaken for 2–4 h and allowed to separate overnight. Portions of the two phases were then placed in u.v. cells of suitable path length, and the spectra recorded at the same temperature as the partitioning. The initial concentrations of nitrobenzene in the cyclohexane phase and the pathlengths of the u.v. cells were chosen so that the absorbances in the two phases could be conveniently measured without dilution. The former ranged from 4×10^{-4} to 2×10^{-3} *M*. Concentrations in the two phases were determined from the absorbances at the maxima in the two phases (253 nm in cyclohexane, 269–273 nm in aqueous acids). Extinction coefficients in the appropriate solutions at the appropriate temperature were determined from standard solutions. The partition coefficients were calculated from ratios of the concentrations in the aqueous phases to the concentrations in cyclohexane.

Solid Solubilities

Mixtures of the aqueous acid solutions and an excess of solid were shaken overnight, and filtered through sintered glass. The aqueous phases were diluted by a known amount with water and the u.v. spectra recorded in 1 cm cells at 25.0 °C. The concentrations of the saturated aqueous phases were determined from the absorbances at the maxima and the known dilution factors, taking into account the density differences of the acid solution at 25 °C and at the temperature of equilibration. The extinction coefficients used were those in water at 25.0 °C. This is justified since the large dilution used (factors of at least twenty) ensures that there is virtually no medium effect on the spectra. Wavelengths used were: for *m*-dinitrobenzene, 254 nm; 1,3,5-trinitrobenzene, 245 nm; 4-nitrotoluene, 275 nm; and benzhydrol, 220 nm.

Precision of Measurements

Three separate measurements were usually made in any acid at any temperature. In general an agreement of $\pm 1\%$ was found. The nitrobenzene partition coefficients were more precise; some of the measurements involving benzene and 4-nitrotoluene showed poorer agreement.

Results

Activity Coefficients

Activity coefficients for a number of neutral aromatic solutes in sulfuric acid and perchloric acid solutions were determined at a series of temperatures over the range 25–55 °C. Solutes involved in sulfuric acid were benzene, nitrobenzene, *m*-dinitrobenzene, 1,3,5-trinitrobenzene, benzyhydrol, and 4-nitrotoluene. In perchloric acid, benzene, nitrobenzene, and *m*-dinitrobenzene were studied. Values of the activity coefficients have been placed in the Depository of Unpublished Data.[2] With the exception of nitrobenzene, the activity coefficients were determined from the ratio of the solubility of the solute in water (S^0) to the solubility in the acid solution (S) (1),

$$[6] \qquad \log y_i = \log S^0/S$$

with the solubilities expressed in molarity units. With nitrobenzene a distribution method with cyclohexane as the organic phase was employed. The activity coefficient is then the ratio of the distribution coefficient in water (D^0) to the distribution coefficient in the acid solution (D) (1),

$$[7] \qquad \log y_i = \log D^0/D$$

where the distribution coefficients represent the ratios of the molar concentrations of the solute in the aqueous phases to the molar concentrations in cyclohexane. The solubilities or distribution coefficients in water are also stored in the Depository of Unpublished Data.

The validity of these activity coefficients depends upon the assumption that the solutions involved are dilute enough that solute–solute interactions are negligible (8). There is no direct way of testing this assumption based only on these measurements. In general concentrations

[2]Photocopies are available at a nominal charge from the Depository of Unpublished Data, National Science Laboratory, National Research Council of Canada, Ottawa, Canada K1A 0S2.

TABLE 1. Thermodynamics of transfer of benzene from water to sulfuric acid and perchloric acid solutions at 25 °C

Sulfuric Acid				Perchloric Acid			
$\%H_2SO_4$	$[\Delta G_{tr}^0(w,s)]_c$[a]	$\Delta H_{tr}^0(w,s)$[a]	$[T\Delta S_{tr}^0(w,s)]_c$[a]	$\%HClO_4$	$[\Delta G_{tr}^0(w,s)]_c$	$\Delta H_{tr}^0(w,s)$	$[T\Delta S_{tr}^0(w,s)]$
10.0	0.22	0.51±0.24[b]	0.29	9.8	−0.04	0.53±0.06	0.57
20.0	0.37	0.98±0.13	0.61	19.8	−0.07	1.07±0.06	1.14
29.9	0.50	1.34±0.18	0.84	30.4	−0.09	1.52±0.15	1.61
39.9	0.56	1.46±0.13	0.90	40.0	−0.10	1.75±0.13	1.85
50.1	0.57	1.55±0.09	0.98	48.7	−0.05	1.88±0.14	1.93
60.1	0.56	1.39±0.08	0.83	59.3	+0.04	2.25±0.13	2.21
69.5	0.54	1.15±0.13	0.61				

[a]Units of kcals/mol.
[b]Standard deviation in the slope of the plot of $2.303R \log_{10} f_i$ *vs.* $1/T$.

TABLE 2. Thermodynamics of transfer of nitrobenzene from water to sulfuric acid and perchloric acid solutions at 25 °C

Sulfuric acid				Perchloric acid			
$\%H_2SO_4$	$[\Delta G_{tr}^0(w,s)]_c$[a]	$\Delta H_{tr}^0(w,s)$[a]	$[T\Delta S_{tr}^0(w,s)]_c$[a]	$\%HClO_4$	$[\Delta G_{tr}^0(w,s)]_c$	$\Delta H_{tr}^0(w,s)$	$[T\Delta S_{tr}^0(w,s)]_c$
10.0	0.09	0.18±0.06[b]	0.09	10.0	−0.26	0.05±0.04	0.31
20.0	0.15	0.49±0.07	0.34	19.7	−0.47	0.38±0.10	0.85
29.9	0.16	0.89±0.09(1.05)[c]	0.73	30.1	−0.66	0.42±0.06	1.08
39.9	0.02	0.58±0.05(0.65)[c]	0.56	39.6	−0.82	0.62±0.09	1.44
50.1	−0.25	−0.28±0.04(0.30)[c]	−0.03	49.3	−0.98	0.46±0.10	1.44
60.1	−0.53	−0.74±0.14(−0.10)[c]	−0.21	59.2	−1.13	0.62±0.10	1.75
69.5	−0.83	−0.94±0.08(−0.38)[c]	−0.11				

[a]Units of kcals/mol.
[b]Standard deviation in the slope of the plot of $2.303R \log_{10} f_i$ *vs.* $1/T$.
[c]Enthalpies of transfer from ref. 2.

TABLE 3. Thermodynamics of transfer of *m*-dinitrobenzene from water to sulfuric and perchloric acid solutions at 25 °C

Sulfuric acid				Perchloric acid			
$\%H_2SO_4$	$[\Delta G_{tr}^0(w,s)]_c$[a]	$\Delta H_{tr}^0(w,s)$[a]	$[T\Delta S_{tr}^0(w,s)]_c$[a]	$\%HClO_4$	$[\Delta G_{tr}^0(w,s)]_c$	$\Delta H_{tr}^0(w,s)$	$[T\Delta S_{tr}^0(w,s)]_c$
10.0	0.00	0.01±0.03[b]	0.01	9.8	−0.47	−0.38±0.07	0.09
20.0	−0.07	−0.09±0.02	−0.02	19.8	−0.87	−0.36±0.04	0.51
29.9	−0.24	−0.19±0.05	0.05	30.4	−1.26	−0.36±0.08	0.90
39.9	−0.59	−1.11±0.11	−0.52	40.0	−1.62	−0.43±0.07	1.19
50.1	−1.01	−2.28±0.05	−1.27	49.7	−1.92	−0.73±0.06	1.19
60.1	−1.40	−2.44±0.18	−1.04	59.3	−2.27	−0.80±0.02	1.47
69.5	−1.74	−2.72±0.05	−0.98				

[a]Units of kcals/mol.
[b]Standard deviation in the slope of the plot of $2.303R \log_{10} f_i$ *vs.* $1/T$.

of the saturated solutions involved in the solubility measurements were less than 0.05 *M*. The concentrations involved in the distribution measurements were $10^{-3} - 10^{-4}$ *M*.

The standard deviation in log y_i is 0.006, based on an assignment of one percent as the error in the solubilities or distribution coefficients.

Thermodynamics of Transfer

Tables 1–6 list the thermodynamic functions ($[\Delta G_{tr}^0(w,s)]_c$, $\Delta H_{tr}^0(w,s)$, and $[T\Delta S_{tr}^0(w,s)]_c$) for the transfer of one mole of solute from pure water to the acid solutions at 25 °C, the standard states being defined in concentration units of molarity.

The values for $[\Delta G_{tr}^0(w,s)]_c$ were determined

Can. J. Chem. Downloaded from www.nrcresearchpress.com by 210.87.254.40 on 09/05/12
For personal use only.

Can. J. Chem. Downloaded from www.nrcresearchpress.com by 210.87.254.40 on 09/05/12
For personal use only.

TABLE 4. Thermodynamics of transfer of 1,3,5-trinitrobenzene from water to sulfuric acid solutions at 25 °C

%H_2SO_4	$[\Delta G_{tr}^0(w,s)]_c$[a]	$\Delta H_{tr}(w,s)$[a]	$[T\Delta S_{tr}^0(w,s)]_c$[a]
10.0	−0.13	−0.23±0.10[b]	−0.10
20.0	−0.35	−0.62±0.11	−0.27
29.9	−0.65	−1.40±0.06	−0.75
39.9	−1.08	−2.63±0.04	−1.55
50.1	−1.54	−3.42±0.09	−1.88
60.1	−1.90	−3.81±0.08	−1.91
69.5	−2.14	−3.93	−1.79

[a]Units of kcal/mol.
[b]Standard deviation in the slope of the plot of $2.303R \log_{10} f_i$ *vs.* $1/T$.

TABLE 5. Thermodynamics of transfer of 4-nitrotoluene from water to sulfuric acid solutions at 25 °C

%H_2SO_4	$[\Delta G_{tr}^0(w,s)]_c$[a]	$\Delta H_{tr}^0(w,s)$[a]	$[T\Delta S_{tr}^0(w,s)]_c$[a]
10.0	0.13	1.39±0.44[b]	1.26
20.0	0.25	2.47±0.29	2.22
29.9	0.30	3.92±0.25	3.62
39.9	0.07	2.00±0.24	1.93
50.1	−0.22	1.82±0.37	2.04
60.1	−0.59	1.09±0.25	1.68
69.5	−1.04	−0.34±0.34	0.70

[a]Units of kcal/mol.
[b]Standard deviation in the slope of the plot of $2.303R \log_{10} f_i$ *vs.* $1/T$.

TABLE 6. Thermodynamics of transfer of benzhydrol from water to sulfuric acid solutions at 25 °C

%H_2SO_4	$[\Delta G_{tr}^0(w,s)]_c$[a]	$\Delta H_{tr}^0(w,s)$[a]	$[T\Delta S_{tr}^0(w,s)]_c$[a]
10.0	0.30	0.82±0.15[b]	0.52
20.0	0.55	1.52±0.26	0.97
29.9	0.71	1.99±0.22	1.28
39.9	0.67	1.54±0.17	0.87

[a]Units of kcal/mol.
[b]Standard deviation in the slope of the plot of $2.303R \log_{10} f_i$ *vs.* $1/T$.

directly from the activity coefficients at 25 °C (eq. 4). Errors in these terms are consequently of the order of ±0.01 kcal/mol.

The enthalpies of transfer were obtained via the temperature variation in the activity coefficients. In order to do this the molarity activity coefficients were first converted to a mole fraction scale using the relationship

$$\log f_i = \log y_i + \log M_{H_2O}\, d/\overline{M}_s\, d^0$$

where d^0 and d are the densities of pure water and acid solution, M_{H_2O} is the molecular weight of water, and $\overline{M}_s$ is the average molecular weight in the acid solution,

$$\overline{M}_s = 100 \Big/ \left(\frac{100 - s}{M_{H_2O}} + \frac{s}{M_s}\right)$$

where M_s is the molecular weight of the acid, and s is the percent by weight of the acid in the acid solution. Re-writing eq. 4 in terms of mole fraction concentration units, the following expression can be derived upon application of the Gibbs–Helmholtz equation:

$$\Delta H_{tr}^0(w,s) = 2.303R[\mathrm{d} \log_{10} f_i/\mathrm{d}(1/T)]$$

Thus plots of $\log_{10} f_i$ *vs.* $1/T$ allow the determination of $\Delta H_{tr}^0(w,s)$. If this were temperature dependent the plots would be curved and the enthalpy term would have to be estimated from the tangent to the curve at the appropriate temperature (9). However for the data obtained here, no significant curvature can be observed outside the range of experimental error, and thus the values of $\Delta H_{tr}^0(w,s)$ listed in Tables 1

Can. J. Chem. Downloaded from www.nrcresearchpress.com by 210.87.254.40 on 09/05/12
For personal use only.

to 6 were determined from the least squares slopes of plots of $2.303R \log_{10} f_i$ *vs.* $1/T$. The least squares standard deviations in these slopes are listed alongside. Standard deviations of 0.10–0.15 kcal/mol are expected, based on the precision of the solubilities and distribution coefficients and the temperature range involved. In Fig. 1, representative plots of $\log_{10} f_i$ *vs.* $1/T$ using data for *m*-dinitrobenzene in sulfuric acid are illustrated.

The entropies of transfer $[T\Delta S_{tr}^0(w,s)]_c$ were then obtained from the difference in the free energy and enthalpy terms. The error in this term is essentially the same as that in the enthalpy, since the free energy is much more precisely determined.

Included in Table 2 are the enthalpies of transfer obtained by Arnett and co-workers for nitrobenzene (2). Although the two sets of values display a similar trend, there are considerable differences, particularly in the more concentrated acids; differences which are outside the range of experimental uncertainty involved in the two methods. No obvious reason for this discrepancy is evident. Possibly certain errors were introduced in the direct measurements of the heats of solution due to the low solubility of nitrobenzene in these aqueous solutions (approximately 0.02 *M*). Interestingly the large decrease in $\Delta H_{tr}^0(w,s)$ from 40% H_2SO_4 to 50% H_2SO_4 found in this study, which is the major difference in the two sets of results, was also observed with *m*-dinitrobenzene and 1,3,5-trinitrobenzene.

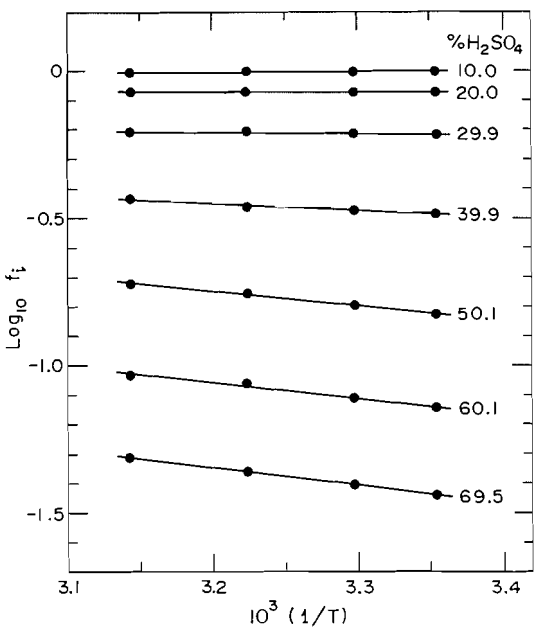

FIG. 1. Temperature variation of $\log_{10} f_i$ with $(1/T)$ for *m*-dinitrobenzene in sulfuric acid.

Discussion

Sulfuric Acid

The thermodynamics of transfer from water to sulfuric acid solutions for four neutral solutes are shown in Fig. 2. In this and all following figures the entropy term is plotted in a negative sense $(-[T\Delta S_{tr}^0(w,s)]_c)$, to aid visualization of its contribution to the total free energy of transfer. The free energy changes in sulfuric acid are apparently enthalpy controlled processes; that is, the direction of the free energy is generally the same as that of the enthalpy. This is true for all the solutes studied, from benzene, which has positive enthalpies and free energies, to 1,3,5-trinitrobenzene, which has negative enthalpies and free energies. Even with nitrobenzene, where the sign of the free energy term changes at

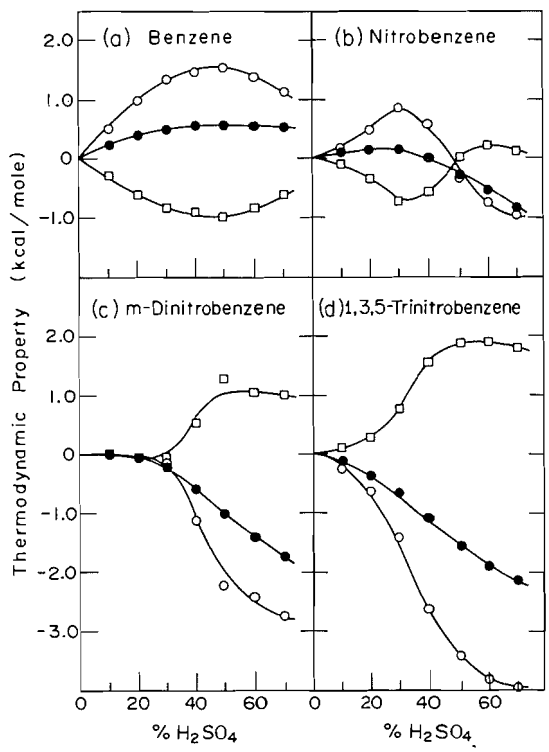

FIG. 2. Thermodynamics of transfer as a function of sulfuric acid concentration: $[\Delta G_{tr}^0(w,s)]_c$ (●); $\Delta H_{tr}^0(w,s)$ (○); $[-T\Delta S_{tr}^0(w,s)]_c$ (□).

moderate acidity, the enthalpy term shows the same behavior. The free energy change, however, is never as great as the enthalpy contribution, since the entropy term is not small and acts in the opposite direction. This compensation of enthalpy and entropy is a very commonly observed phenomenon for aqueous solutions (9–11), and is shown very strongly in this system. It has been suggested to arise because of the unusual structural properties of aqueous solutions (11).

These results extend those of Arnett and coworkers (2). The general conclusion remains the same, namely that activity coefficient behavior in sulfuric acid solutions is enthalpy controlled. However, contrary to Arnett's statement (2) that the enthalpy and free energy are nearly equivalent at concentrations above 25% H_2SO_4, what is obvious from this study is that the importance of the entropy term in moderating the overall free energy cannot be neglected at any acidity.

Perchloric Acid

Figure 3 depicts the variation of the thermodynamic properties for the three solutes studied in perchloric acid. Strikingly different behavior from that in sulfuric acid is observed. Benzene shows a very small change in the free energy term, due to an almost complete compensation of the enthalpy and entropy. For nitrobenzene there is a substantially negative free energy of transfer throughout; this is entropy controlled, with a small amount of compensation by the enthalpy term. For *m*-dinitrobenzene there is again a large negative free energy of transfer, but with this solute the enthalpy and entropy terms act to augment each other. Of the nine systems investigated in this study, this is the only example where there is no compensation effect. As will be seen shortly, this system is not really anomalous, and does show the pattern which would be expected for it on the basis of substitution and mineral acid. In summary no general observation can be made regarding the thermodynamics of transfer to perchloric acid, except that again the entropy variation cannot be neglected at any acidity.

The Nitro-group Effect

Figures 4 and 5 show the thermodynamic properties as a function of nitro-substitution. The two acids (Fig. 4, sulfuric acid; and Fig. 5, perchloric acid) show qualitatively the same behavior. The free energies of transfer become

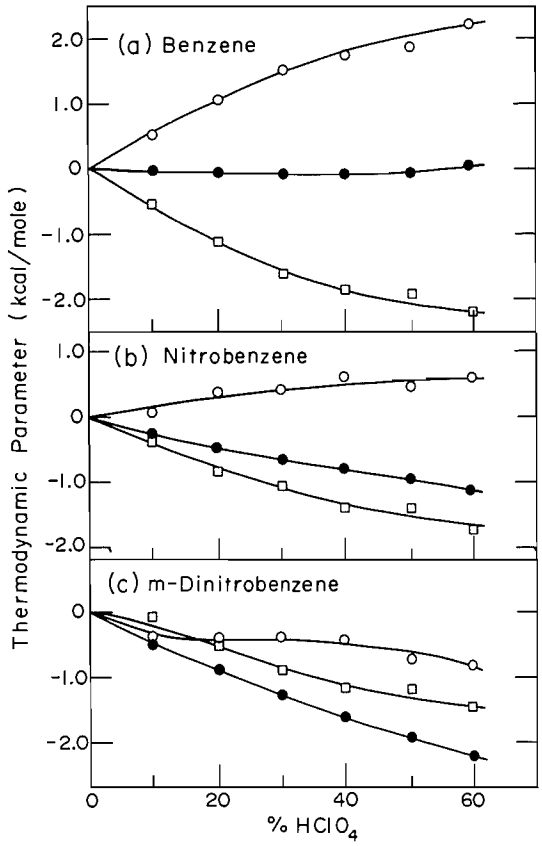

FIG. 3. Thermodynamics of transfer as a function of perchloric acid concentration: $[\Delta G_{tr}^{0}(w,s)]_c$ (●); $\Delta H_{tr}^{0}(w,s)$ (○), $[-T\Delta S_{tr}^{0}(w,s)]_c$ (□).

increasingly more negative in a regular manner as the number of nitro substituents on the aromatic ring increases, as has been found to be the general effect of nitro substitution in other neutral aromatic solutes (1). The enthalpies show the same pattern. The entropies change in the opposite direction with nitro-substitution. Thus the nitro-group effect is an essentially enthalpy controlled phenomenon. There is a small amount of compensation from the entropy terms so that the free energy change caused by introduction of the nitro-substituents is never as great as the enthalpy changes.

This enthalpic origin of the nitro-group effect is consistent with previous suggestions (1, 12) that the cause is a hydrogen-bonding interaction between the nitro-group acting as a hydrogen-bond acceptor and some acid species acting as a hydrogen-bond donor. This type of interaction also results in a more ordered situation so that

Can. J. Chem. Downloaded from www.nrcresearchpress.com by 210.87.254.40 on 09/05/12
For personal use only.

Can. J. Chem. Downloaded from www.nrcresearchpress.com by 210.87.254.40 on 09/05/12
For personal use only.

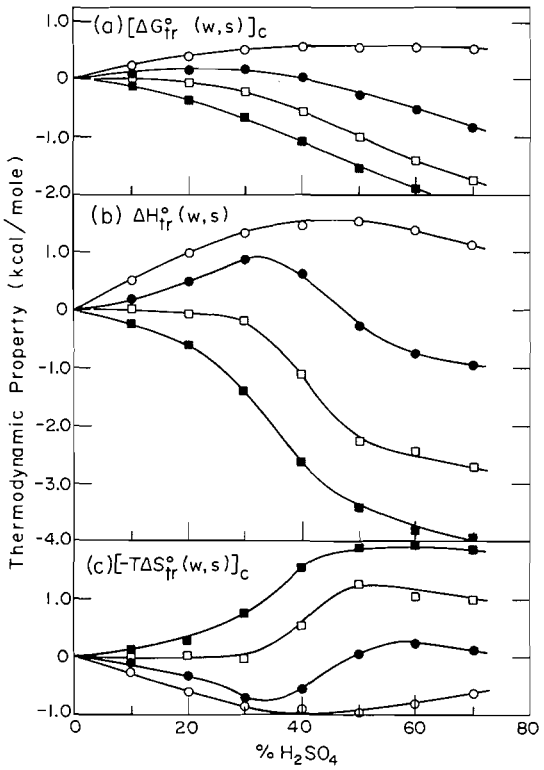

FIG. 4. The effect of nitro substitution on the thermodynamics of transfer from water to sulfuric acid solutions: benzene (○), nitrobenzene (●), *m*-dinitrobenzene (□), 1,3,5-trinitrobenzene (■).

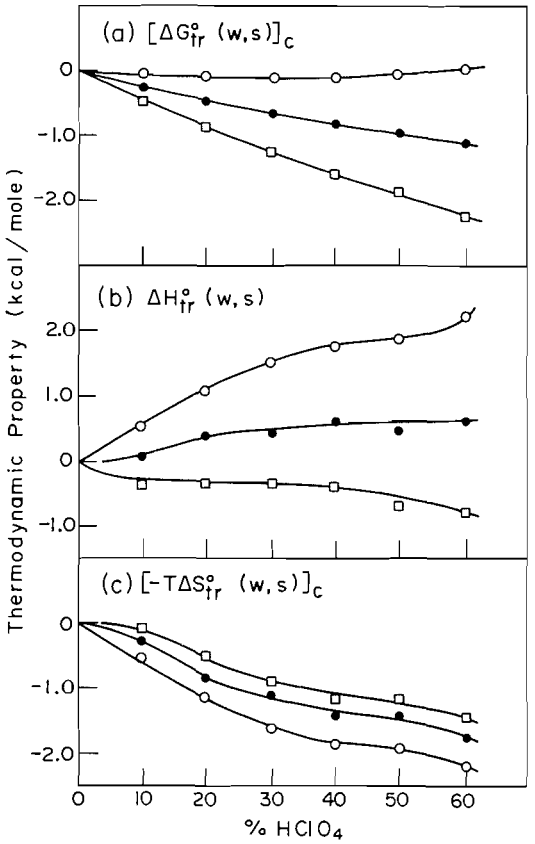

FIG. 5. The effect of nitro substitution on the thermodynamics of transfer from water to perchloric acid solutions: benzene (○), nitrobenzene (●), *m*-dinitrobenzene (□).

on the basis of this interpretation the more unfavorable entropy of transfer resulting from nitro-substitution is not surprising. One unexpected aspect of the nitro-group effect is that the two acid systems show qualitatively the same trends in all three thermodynamic functions with the addition of the nitro-substituents, despite the fact that for each individual solute there is a considerable difference in each of these functions. This suggests that the interactions giving rise to the nitro-group effect must have a similar origin in the two acids, a conclusion that is also consistent with the interpretation in terms of a hydrogen-bonding interaction, since in gross terms the two systems contain similar acid species.

Effect of Different Mineral Acids

The data for benzene, nitrobenzene, and *m*-dinitrobenzene (Tables 1–3) allow a comparison of the three thermodynamic properties of transfer in the two different acids. The three solutes show similar behavior. At the same acid concentration the free energy of transfer is more negative in the perchloric acid solution, as is expected on the basis of previous studies (1, 3). This study shows this to be an entropy effect; entropies of transfer are substantially more positive in perchloric acid as compared with sulfuric acid. In dilute acids up to 30–40%, the enthalpies of transfer for benzene are approximately the same in the two acids, and for nitrobenzene and *m*-dinitrobenzene slightly more negative in perchloric acid. At concentrations above 40% however the enthalpy of transfer to a perchloric acid solution actually is more positive than to a sulfuric acid solution, acting in the opposite direction to the free energy and thus showing some compensation to the entropy effect.

This order of entropies in the two different acids probably has its origin in some solvent structuring effect. Neutral solutes such as those

Can. J. Chem. Downloaded from www.nrcresearchpress.com by 210.87.254.40 on 09/05/12
For personal use only.

investigated here tend to make structure in water (13) and the fact that the entropies of transfer from water to the acid solutions are not generally large and positive suggests that they are making structure there as well. Thus the more favorable entropy of transfer to perchloric acid relative to sulfuric acid implies that the neutral solutes are not able to make structure in perchloric acid solutions to the same extent as in sulfuric acid solutions. Because of the similar acidities of the two systems this effect probably originates with the anion.

The perchlorate anion has been suggested to be a very strong structure breaker (14). If perchlorate does break solvent structure to a greater extent than bisulfate, it may be that in the perchloric acid solutions the neutral solutes are not able to make structure as well as they can in sulfuric acid solutions. This explanation requires that the degree to which a solute can make structure in an aqueous acid solution is proportional to the structure already present. Studies are currently being undertaken to investigate this problem.

One final observation comes from Figs. 4*c* and 5*c* where the effect of nitro-substitution on the entropy of transfer to the two acids is shown. Both show a less favorable entropy as the number of nitro-substituents is increased, but this effect is less pronounced in perchloric acid, again consistent with a greater difficulty of forming ordered solute–solvent interactions in this system.

Other Solutes

In addition to the four compounds used to investigate the nitro-group effect, two additional solutes, benzhydrol and 4-nitrotoluene were studied in sulfuric acid. Measurements on the former could only be made up to 40% H_2SO_4 before decomposition became too severe. However, the data obtained show that the presence of the hydroxyl group does not alter the qualitative pattern of the three thermodynamic functions significantly; the data in fact are quite similar to those obtained for benzene.

The nitrotoluene was studied for comparison with nitrobenzene. Although the free energies of transfer for the pair are very similar, the addition of the methyl substituent causes a dramatic increase in the enthalpy term, with of course an opposing effect on the entropy term. This effect is difficult to understand. On the basis of the nitro-group effect a more favorable enthalpy might be expected since the methyl substituent should increase the capacity of the nitro-group to act as a hydrogen-bond acceptor. Consequently the explanation may lie in the effect of the methyl substituent on solvent structure.

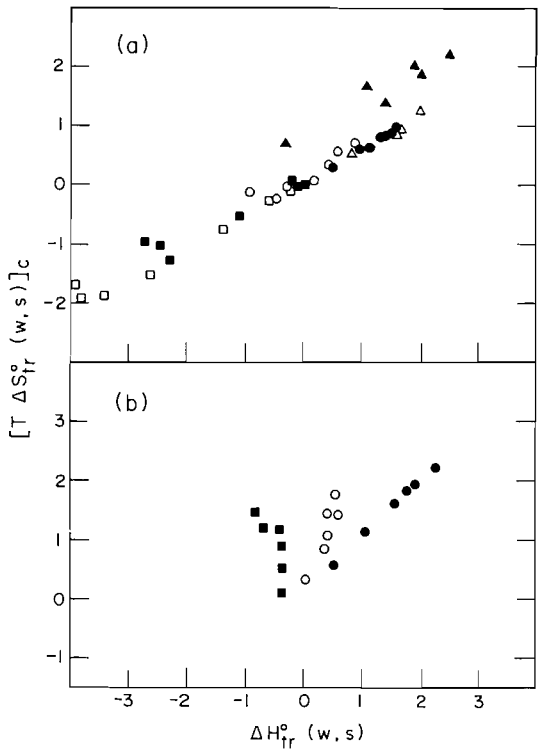

FIG. 6. Plots of $[T\Delta S_{tr}{}^0(w,s)]$ *vs.* $\Delta H_{tr}{}^0(w,s)$ for the transfer of solute to acid solutions: (*a*) sulfuric acid solutions, (*b*) perchloric acid solutions; (●), benzene; (○), nitrobenzene; (■), *m*-dinitrobenzene; (□), 1,3,5-trinitrobenzene; (▲), 4-nitrotoluene; (△), benzhydrol.

Compensation

In recent years many linear plots of the entropy contribution to some free energy change *vs.* the enthalpy contribution have been observed (11). Figure 6 plots $[T\Delta S_{tr}{}^0(w,s)]_c$ *vs.* $\Delta H_{tr}{}^0(w,s)$ for the systems of this study. In sulfuric acid, the points for all the compounds except 4-nitrotoluene do lie near a common line, although some points in the more concentrated acids deviate. In perchloric acid no such common line exists for the three compounds studied. In fact even the plots for the individual solutes are not especially linear. In summary then a linear compensation effect does exist for some of the

solutes in sulfuric acid, but this is not general for acid solutions.

The continued financial support of the National Research Council of Canada is gratefully acknowledged.

1. K. YATES and R. A. McCLELLAND. Progr. Phys. Org. Chem. In press.
2. E. M. ARNETT, J. J. BURKE, J. V. CARTER, and C. F. DOUTY. J. Am. Chem. Soc. **94**, 7837 (1972).
3. C. A. BUNTON and J. H. FENDLER. J. Org. Chem. **31**, 3764 (1966); C. A. BUNTON, J. H. CRABTREE, and L. ROBINSON. J. Am. Chem. Soc. **90**, 1258 (1968); K. YATES, H. WAI, G. WELCH, and R. A. McCLELLAND. J. Am. Chem. Soc. **95**, 418 (1973).
4. L. P. HAMMETT and R. CHAPMAN. J. Am. Chem. Soc. **56**, 1282 (1934).
5. R. H. BOYD. *In* Solute–solvent interactions. *Edited by* J. F. COETZEE and C. D. RITCHIE. Marcel Dekker, New York. 1969. pp. 97–218.
6. International critical tables. Vol. 3. McGraw-Hill Book Co., Inc., New York. 1928. p. 56.
7. Perchlorates. *Edited by* J. C. SCHUMACHER. Reinhold Publ. Corp., New York. 1960. p. 16.
8. R. H. BOYD. J. Am. Chem. Soc. **85**, 1555 (1963).
9. D. B. WETLAUFER, S. K. MALIK, L. STOLLER, and R. L. COFFIN. J. Am. Chem. Soc. **86**, 508 (1964).
10. W-Y. WEN and J. H. HUNG. J. Phys. Chem. **74**, 170 (1970). E. M. ARNETT, M. Ho, and L. L. SCHALEGER. J. Am. Chem. Soc. **92**, 7039 (1970).
11. R. LUMRY and S. RAJENDER. Biopolym. 1125 (1970).
12. N. C. DENO and C. H. SPINK. Private communication.
13. H. S. FRANK and M. W. EVANS. J. Chem. Phys. **13**, 507 (1945).
14. H. S. FRANK and W-Y. WEN. Discuss. Faraday Soc. **24**, 133 (1957).

Can. J. Chem. Downloaded from www.nrcresearchpress.com by 210.87.254.40 on 09/05/12
For personal use only.

The Preparation of *cis*-1,3-Bis(dimethylarsino)-2,2,4,4-tetramethylcyclobutane and its Group VIB Metal Carbonyl Derivatives

WILLIAM R. CULLEN[1] AND JOHN T. PRICE

Contribution from the Chemistry Department, University of British Columbia, Vancouver 8, British Columbia V6T 1W5

Received September 28, 1973

The addition of tetramethyldiarsine to 2,2,4,4-tetramethylbicyclo[1.1.0]butane forms predominantly *cis*-1,3-bis(dimethylarsino)-2,2,4,4-tetramethylcyclobutane, L. The compound can behave as either a bridging or chelating ligand with group VIB metal carbonyls depending upon the reaction conditions affording $LM(CO)_4$ and $LM_2(CO)_{10}$ (M = Cr, Mo, W). The structures of these derivatives are discussed.

L'addition du tétraméthyldiarsine au tétraméthyl-2,2,4,4, bicyclo[1.1.0] butane conduit principalement au *cis* bis(diméthylarsino)1,3-tétraméthyl-2,2,4,4 cyclobutane, L. Dépendant des conditions de la réaction ce composé peut agir soit comme pont ou agent de chélation avec les carbonyles de métaux du groupe VIB pour fournir soit $LM(CO)_4$ ou $LM_2(CO)_{10}$ (M = Cr, Mo, W). On discute des structures de ces dérivés.

[Traduit par le journal]

Can. J. Chem., **52**, 1108 (1974)

Introduction

The photolytic addition of tetramethyldiarsine to acetylenic and olefinic compounds has been useful for the preparation of ditertiary arsine ligands (1, 2).

Bicyclic and cyclic compounds with strained rings are unsaturated systems and have properties similar to olefinic compounds reflected by the acidic nature of their C—H bonds, the stability of the carbanions formed, and the large $J_{^{13}C-H}$ observed (3). Highly strained ring systems also have high rates of reactivity (3–6), large heats of combustion, and a tendency to undergo facile thermolytic rearrangements (5, 7). In particular, bicyclobutane has an exceptionally high ring strain energy (63.9 kcal/mol) and very large $J_{^{13}C-H}$ values which indicate a high percentage of s character in the bonding throughout the carbon skeleton (5). Thus bicyclobutane and substituted bicyclobutanes could be expected to behave like olefins and be excellent reagents for the preparation of new 1,3-ditertiary arsine ligands by the addition of tetramethyldiarsine.

In this work we have prepared 1,3-bis(dimethylarsino)-2,2,4,4-tetramethylcyclobutane (L) by the photolytic addition of tetramethyldiarsine to 2,2,4,4-tetramethylbicyclo-[1.1.0]butane. Group VIB tetracarbonyl and pentacarbonyl derivatives of L have been prepared and their structures are discussed.

[1]To whom correspondence should be addressed.

Experimental

A standard vacuum system was used for the manipulation of volatile reactants. Ultraviolet irradiations were performed using a 200 W Hanovia lamp situated ~20 cm away from the reactants. Unless otherwise indicated all reactions were carried out in sealed Carius tubes. Microanalyses were made by Mr. Peter Borda of this department.

Melting points were determined using a Gallenkamp melting point apparatus and are uncorrected. The i.r. spectra of samples dissolved in cyclohexane were recorded on a Perkin–Elmer 457 spectrometer and calibrated using polystyrene film. The n.m.r. spectra were measured on samples dissolved in $CDCl_3$ with ~10% by volume TMS using a Varian T-60 instrument. The variable temperature n.m.r. experiment was performed using a Varian XL-100 instrument. Chemical shifts are reported in p.p.m. downfield from TMS. Osmometric measurements were made on samples dissolved in $CHCl_3$ using a Mechrolab Model 301 A osmometer. Mass spectra were recorded on an AEI MS9 spectrometer.

All solvents were degassed by bubbling nitrogen through them prior to use. The petroleum ether boiled in the range 30–60°.

The Preparation of 1,3-Bis(dimethylarsino)-2,2,4,4-tetramethylcyclobutane

Tetramethyldiarsine (5 g) (8) and 2.5 g of 2,2,4,4-tetramethylbicyclo[1.1.0]butane (9, 10) were irradiated with a 200 W u.v. lamp for 48 h. The tube was opened to a vacuum system and the volatile contents removed leaving an air sensitive residue which was dissolved in ether (10 ml). Cooling the ether solution to −78°, gave 5.5 g (73%) of the colorless solid ditertiary arsine. This was used directly to make the group VIB carbonyl complexes and no further attempt was made to purify it. The n.m.r. spectrum showed major signals at 2.10, 2.07, 1.30, 1.23, 1.13, and 0.88 p.p.m.

Can. J. Chem. Downloaded from www.nrcresearchpress.com by 210.87.254.6 on 09/05/12
For personal use only.

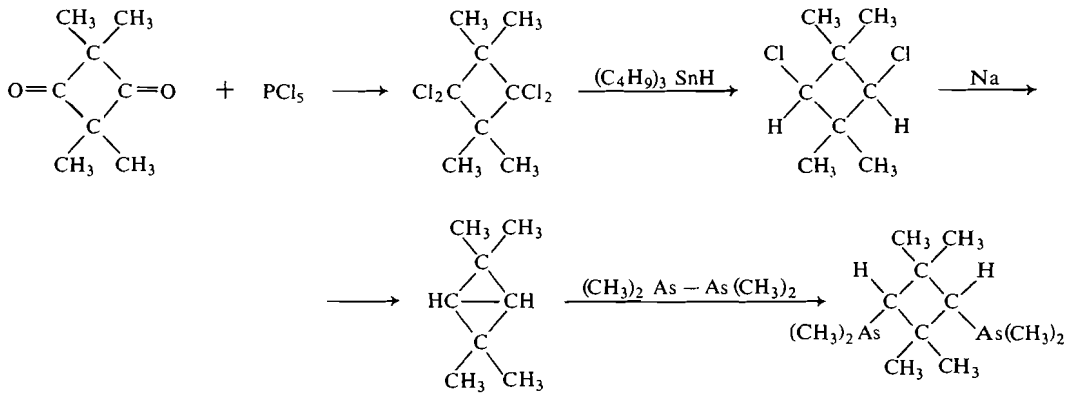

SCHEME 1

The Preparation of $LM_2(CO)_{10}$ Complexes (L = 1,3-Bis(dimethylarsino)-2,2,4,4-tetramethylcyclobutane; M = Cr, Mo, W)

Equimolar quantities of chromium hexacarbonyl (0.5 g) and L (0.75 g) in benzene (10–15 ml) were heated to 150° for 15 h. The tube was opened and unreacted metal hexacarbonyl was removed by filtration. The filtrate was evaporated to dryness under vacuum. (An n.m.r. spectrum of this residue indicated that a number of products were present.) Chromatography on a column of Florisil using petroleum ether/ether (95:5) as the eluent gave only one yellow colored fraction. This was evaporated to dryness and recrystallized from methylene chloride/hexane. The yield of the chromium complex was 0.4 g (47%).

The molybdenum and tungsten analogs were similarly prepared except two moles of metal carbonyl were used for every mole of ligand.

The Preparation of $LM(CO)_4$ (M = Cr, Mo, W)

The ligand L (1.0 g) was added to an equimolar quantity of norbornadiene metal tetracarbonyl $C_7H_8M(CO)_4$ (11, 12) dissolved in methylcyclohexane (25 ml) and stirred under a nitrogen atmosphere at 90° for approximately 10 min. The hot solution was filtered under nitrogen to remove the insoluble and polymeric materials that had precipitated. The filtrate was cooled in ice to precipitate the product. The chromium and molybdenum compounds were recrystallized directly from chloroform. The precipitate of the tungsten compound was found to be oily and initial purification was achieved by sublimation (140°, 0.01 mm) before recrystallization from chloroform.

Results and Discussion

Scheme 1 shows the route used to prepare tetramethylbicyclo[1.1.0]butane (9, 10) and the final reaction shows the expected 1,3 addition of tetramethyldiarsine to afford 1,3-bis(dimethylarsino)-2,2,4,4-tetramethylcyclobutane, L. Although the air sensitive L was not fully characterized the isolation and complete characterization of derivatives of formula $LM_2(CO)_{10}$ and $LM(CO)_4$ (M = Cr, Mo, W) (*vide infra*) leaves little doubt that the reaction goes as indicated. Furthermore, the X-ray structure of $LCr(CO)_4$ (Fig. 2) confirms the 1,3 addition.

Cyclobutane has been shown to have a puckered structure by electron diffraction (13, 14), spectroscopic, and thermodynamic measurements (15). The nonplanarity of the ring introduces two kinds of positions in cyclobutane analogous to the axial and equatorial positions found in cyclohexanes.

In 1,3 substituted cyclobutanes both *cis* and *trans* isomers are possible. The *trans* isomer has an axial–equatorial (ae) arrangement while the *cis* isomer can be either diequatorial (ee) or diaxial (aa). Simple Van der Waals calculations indicate that a methyl group would prefer an equatorial position to an axial position, analogous to cyclohexanes, and that the *cis* arrangement of 1,3 substituted cyclobutanes is more stable than the *trans* configuration (16).

The 1,3 addition of tetramethyldiarsine to the bicyclobutane can therefore, in theory, form a product L that has *cis* and *trans* isomers and each isomer could be involved in a conformational equilibrium involving inversion of the ring. Unlike the two *cis* conformers which are different (aa and ee) the two *trans* isomers are identical (ae) and therefore of equal energy.

The n.m.r. spectrum of a locked *trans* conformer should show two ring methyl signals and two arsenic methyl signals; however, if rapid interconversion between conformers occurs, then only one ring methyl and one arsenic methyl signal would be expected. The *cis* isomer should show two ring methyl signals and one arsenic methyl signal with or without ring inversion.

The n.m.r. spectrum of the ditertiary arsine, L,

Can. J. Chem. Downloaded from www.nrcresearchpress.com by 210.87.254.6 on 09/05/12
For personal use only.

Can. J. Chem. Downloaded from www.nrcresearchpress.com by 210.87.254.6 on 09/05/12
For personal use only.

TABLE 1. Analytical and spectra data of metal complexes

Compound	Molecular weights			Melting point (°C)*	Analysis				Carbonyl region of infrared (cm^{-1})	Chemical shifts from n.m.r. spectra†		
					Carbon		Hydrogen					
	Calcd.	Osmom.	M.S.		Calcd.	Found	Calcd.	Found		Ring protons	Ring methyls	Arsenic methyls
$LCr(CO)_4$	484	465	484	d. 150	39.70	39.42	5.38	5.24	2006(w) 1912(w) 1891(s) 1888(m)	2.23(2)	1.61(6) 1.51(6)	1.36(12)
$LMo(CO)_4$	528	498	528	d. 115	36.38	36.26	4.97	4.78	2020(w) 1918(w) 1903(s) 1897(m)	2.24(2)	1.60(12,br)	1.38(12)
$LW(CO)_4$	616			d. 210	31.10	31.06	4.25	4.28	2015(w) 1912(w) 1893(s) 1890(s)	2.28(2)	1.60(12)	1.48(12)
$LCr_2(CO)_{10}$	748	724		d. 170	37.51	37.19	3.72	3.79	2060(w) 1943(s) 1936(s)	2.56(2)	1.58(6) 1.40(6)	1.53(12)
$LMo_2(CO)_{10}$	792	765	792	d. 145	33.35	33.35	3.31	3.16	2067(w) 1945(s) 1939(s)	2.51(2)	1.58(6) 1.38(6)	1.51(12)
$LW_2(CO)_{10}$	968	1000		183	27.29	27.15	2.71	2.86	2077(w) 1934(s) 1931(s)	2.56(2)	1.60(6) 1.38(6)	1.66(12)

*d. = decomposition.
†Relative areas given in parentheses.

Can. J. Chem. Downloaded from www.nrcresearchpress.com by 210.87.254.6 on 09/05/12
For personal use only.

showed major signals at 2.10, 2.07, 1.30, 1.23, 1.13, and 0.88 p.p.m. Only one signal (0.88 p.p.m.) can be assigned to the arsenic methyl groups suggesting that either the *cis* and *trans* isomers have arsenic methyl groups that give accidentally degenerate resonance signals (unlikely) or only one of the isomers is obtained from the reaction.

It seems reasonable to suggest that the major product of the photolytic addition is probably the *cis* isomer whose n.m.r. spectrum would show one ring proton signal (2.10 p.p.m.), two ring methyl signals (1.30 and 1.13 p.p.m.), and one arsenic methyl signal (0.88 p.p.m.). In view of the bulk of the dimethylarsino groups this should be predominantly (ee) in solution.

Support for this comes from the finding that the addition of iodine to bicyclobutane (5) or 1,3-dimethylbicyclobutane (17) gives 1,3-substituted products having predominantly *cis* configurations. A four center reaction mechanism has been proposed (5) and the predominant conformation of the *cis* product has been found to be (ee).

The reaction of the group VIB hexacarbonyls with the 1,3-bis(dimethylarsino)cyclobutane affords complexes of formula $LM_2(CO)_{10}$ (Table 1). The compounds are monomeric and the carbonyl stretching frequencies are characteristic of $M(CO)_5$ moieties (18). The n.m.r. spectra of these complexes (Table 1) have one ring proton signal, two ring methyl signals, and one arsenic methyl signal (area ratio 1:6:6) and indicates these compounds are the *cis* isomers regardless of the conformer. The repulsive effect of the large metal pentacarbonyl groups presumably causes the conformational equilibrium to lie well toward the (ee) conformer.

The n.m.r. spectrum for the *trans* isomer of a $LM_2(CO)_{10}$ complex would have two ring methyl and two arsenic methyl signals for an (ae) conformer. If ring inversion occurred then only one ring methyl and one arsenic methyl signal would be observed. No spectrum corresponding to these types was observed. The n.m.r. spectrum of the impure product (before chromatography) showed evidence for a second product which appeared to have uncoordinated arsenic methyl groups. This material may have been an unstable metal complex of the *trans* diarsine ligand and was not isolated although more likely it was an intermediate such as **1** (*vide infra*).

The i.r. spectra showed no evidence for any metal tetracarbonyl product when the diarsine ligand was reacted with metal hexacarbonyl thus chelation does not occur via this synthetic route. However, since a stepwise mechanism is probably involved (19), the intermediate **1** (Y = CO)

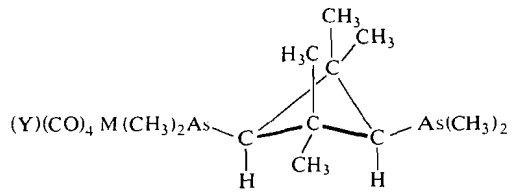

1

being formed first, the absence of chelation cannot be taken as evidence for a predominance of the (ee) conformer of the *cis* ligand in solution, since **1** would be even more likely to exist in this conformation.

Chelate $LM(CO)_4$ complexes *are* obtained when the norbornadiene derivatives $C_7H_8M(CO)_4$ are heated with L in an inert solvent, the easy displacement of this diene affording conditions ideal for the formation of such complexes. Chemical analysis, mass spectra, and osmometric molecular weights (Table 1) confirm the formulation. Again little can be said about the (ee) $\rightleftharpoons$ (aa) equilibrium in solutions of L on the basis of these results, even though chelation involves complex formation by the (aa) form, because little is known about the mechanism of displacement of dienes by ditertiary arsines (19). It is conceivable that if intermediates such as **1** are involved with, in this case, Y being a monocoordinated diene, products such as $L_2M(CO)_4$, $(LM(CO)_4)_2$, or even $(LM(CO)_4)_n$ could be expected. These were not observed.

The chelation of the *cis* ligand to a metal carbonyl forms complexes that have two six membered rings as well as the cyclobutane ring inherent in the ligand. All atoms in the rings except the metal are four coordinate and should, ideally, have tetrahedral symmetry. The atoms of a six membered cyclohexane ring can attain tetrahedral symmetry in chair, boat, or skew boat conformers (16). Puckered chair conformers have been found to predominate in six membered ring – metal complexes of diamines (20, 21 and references therein) and other ditertiary arsine complexes (22). The presence of the cyclobutane ring in this complex precludes the existence of skew boat conformers and results in one of the six membered rings having an unstable (distorted) boat conformation if the other six membered ring is in the more stable (distorted chair) conformer (Fig. 1).

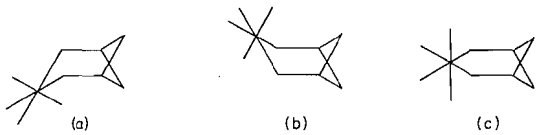

FIG. 1. (*a*) and (*b*) two equivalent conformers, (*c*) intermediate conformer having C_{2v} symmetry.

The n.m.r. spectrum of our $LCr(CO)_4$ complex shows only one arsenic methyl resonance and two ring methyl resonances. The analogous molybdenum and tungsten complexes have only one arsenic methyl resonance and one (broad) ring methyl resonance, the two ring methyl resonances being probably accidentally degenerate.

If the complexes are effectively locked in one of the equivalent conformers (*a*) or (*b*) (Fig. 1) in solution two arsenic methyl resonances and four ring methyl resonances would be expected. Our n.m.r. results could indicate that the molecules interconvert between the equivalent conformers (*a* and *b*) in solution. (Conformational equilibria between equivalent chair conformers have been shown to occur in group VIB tetracarbonyl complexes of 1,3-bis(dimethylarsino)-propane (22).) However, it is possible that the molecules have a structure that has a plane of symmetry which passes through the C—As—M—As—C portion of the complex (giving it C_{2v} symmetry) (Fig. 1*c*). Nuclear magnetic resonance spectra of the molybdenum complex run at temperatures between 35° and −60° showed no significant temperature changes and suggest that the symmetric (C_{2v}) structure may predominate in solution. Models of the complex indicate such a structure might be favored because it lessens the repulsive force between the ring methyl groups and the axial metal carbonyl groups. In such a structure, however, the arsenic atoms might be expected to show a large deviation from tetrahedral symmetry.

The i.r. spectra are of little value in assigning a structure to the molecules in solution since four carbonyl bands are expected for the C_{2v} structure as well as any structure of lower symmetry.

The crystal structure of our $LCr(CO)_4$ complex has recently been determined at −150° (23) (Fig. 2). The compound has a structure with the arsenic atoms in an (aa) position relative to the cyclobutane ring which enables the ligand to chelate to the metal carbonyl, and this chelation has had little effect upon the folding of the

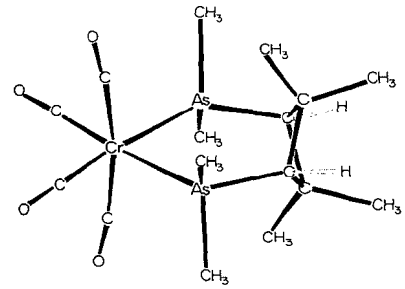

FIG. 2. Crystal structure of $(CH_3)_2AsCHC(CH_3)_2CHAs(CH_3)_2C(CH_3)_2Cr(CO)_4$ (23).

cyclobutane ring. The dihedral angle is 31.9° compared with 35° for cyclobutane and 33° for halogenated cyclobutanes (24).

The bite of the ligand (the As–As distance) is 3.36 Å and is not significantly larger than the As–As distance in other diarsine – metal carbonyl complexes that contain 5 and 6 membered rings (25–27).

The C—As—Cr—As—C portion of the complex is nearly planar; the maximum deviation of any atom is 0.10 Å. The molecule in the solid state, however, has only a two-fold axis of symmetry. The two methyl groups on each arsenic atom are different and have quite different Cr—As—CH_3 bond angles (113.9° *vs.* 118.5°). The molecule has only C_2 symmetry in the solid state and not C_{2v} symmetry as suggested by our n.m.r. results. Movement of atoms in solution probably causes the arsenic methyl groups to become equivalent on a time averaged basis.

The chemical shifts of the ring protons and ring methyl groups show little variation with a change in metal substituent for either the pentacarbonyl or tetracarbonyl series of complex (although there are differences between the two series). The arsenic methyl groups have chemical shifts at lower field in the tungsten (pentacarbonyl and tetracarbonyl) complexes than in the chromium or molybdenum analogs.

We wish to thank the National Research Council of Canada for financial support of this work in the form of an operating grant to W.R.C. and a Postdoctoral Fellowship to J.T.P.

1. W. R. CULLEN and N. K. HOTA. Can. J. Chem. **42**, 1123 (1964).
2. W. R. CULLEN, L. D. HALL, and J. E. H. WARD. J. Am. Chem. Soc. **94**, 5702 (1972).
3. L. N. FERGUSON. J. Chem. Educ. **47**, 46 (1970).
4. C. S. FOOTE. J. Am. Chem. Soc. **86**, 1853 (1964).

Can. J. Chem. Downloaded from www.nrcresearchpress.com by 210.87.254.6 on 09/05/12
For personal use only.

5. K. B. WIBERG, G. M. LAMPMAN, R. P. CIULA, D. S. CONNOR, P. SCHERTLER, and J. LAVANISH. Tetrahedron, **21**, 2749 (1965).
6. H. C. BROWN, R. S. FLETCHER, R. B. JOHANNESON. J. Am. Chem. Soc. **73**, 212 (1951).
7. G. H. SCHMID and A. A. WOLKOF. J. Org. Chem. **32**, 254 (1967).
8. V. AUGER. C. R. **142**, 151 (1906).
9. H. G. GILCH. J. Org. Chem. **30**, 4392 (1965).
10. H. K. HALL, C. D. SMITH, E. P. BLANCHARD, S. C. SHERKOFSKY, and J. B. SIEJA. J. Am. Chem. Soc. **93**, 121 (1971).
11. R. B. KING. Organometallic synthesis, Vol. 1. Academic Press, New York. 1965.
12. R. B. KING and A. FRONZAGLIA. Inorg. Chem. **5**, 1837 (1966).
13. A. ALMENNIGIN, O. BASTIANSEN, and P. N. SKANCKE. Acta Chem. Scand. **15**, 711 (1961).
14. J. D. DUNITZ and V. SCHOMAKER. J. Chem. Phys. **20**, 1703 (1952).
15. G. W. RATHJEN, N. K. FREEMAN, W. D. GWINN, and K. S. PITZER. J. Am. Chem. Soc. **75**, 5634 (1953).
16. E. L. ELIEL, N. L. ALLINGER, S. J. ANGYAL, G. MORRISON. Conformational analysis. Wiley–Interscience, New York, N.Y. 1965.
17. R. B. TURNER, P. GOEBEL, W. v. E. DOERING, and J. F. COBURN. Tetrahedron Lett. 997 (1965).
18. G. R. DOBSON, I. W. STOLZ, and R. K. SHELINE. Adv. Inorg. Chem. Radiochem. **8**, 1 (1966).
19. D. A. BROWN. Inorg. Chim. Acta Rev. **1**, 35 (1967); A. Z. RUBEZHOV and S. P. GUBIN. Adv. Organomet. Chem. **10**, 347 (1973); R. J. ANGELICI. Organomet. Chem. Rev. **3**, 173 (1968).
20. W. R. CULLEN and J. T. PRICE. Unpublished results.
21. T. G. APPLETON and J. R. HALL. Inorg. Chem. **11**, 117 (1972).
22. W. R. CULLEN, L. D. HALL, J. T. PRICE, and G. SPENDJIAN. J. Am. Chem. Soc. **96**, 410 (1974).
23. F. W. B. EINSTEIN and R. D. G. JONES. Inorg. Chem. **12**, 1148 (1973).
24. P. ANDERSON, O. BASTIANSEN, and S. FURBERG. (Editors). Selected topics in structure chemistry. Universitetsfolaget. Oslo. 1967.
25. C. BEAR and J. TROTTER. J. Chem. Soc. Dalton, 673 (1973).
26. P. J. ROBERTS and J. TROTTER. J. Chem. Soc. A, 1501 (1971).
27. I. W. NOWELL, S. RETTIG, and J. TROTTER. J. Chem. Soc. Dalton, 2381 (1972).

Can. J. Chem. Downloaded from www.nrcresearchpress.com by 210.87.254.6 on 09/05/12
For personal use only.

Competition between Acid Catalyzed Interconversion and Solvolysis of Adducts of Dimethyl Azodicarboxylate and 2,5-Dimethyl-3,4-diphenylcyclopentadienone

DONALD MACKAY AND CHARLES W. PILGER

Department of Chemistry, University of Waterloo, Waterloo, Ontario

Received August 27, 1973

Trifluoroacetic acid catalyzes the conversion of each of the isomers, the Diels–Alder adduct **1***a*, the 1,3,4-oxadiazine **2***a*, and the 1,2-diazetidine **3***a* into the others, with the exception of **3***a* → **1***a*. The isomerizations compete with solvolysis to the common end products, the 1,3,4-oxidiazinone **4***a* and methyl trifluoroacetate, directly in the case of **1***a* and **2***a*, but perhaps only by way of **2***a* in the case of **3***a*. The isomerization and solvolysis rates increase with acid concentration in dilute acid but in concentrated acid there is evidence that all the isomers are converted into a (probably) multi-protonated form of **2***a*, which is stable to isomerization and whose solvolysis rate decreases with increasing acid concentration.

A l'exception de la transformation **3***a* vers **1***a*, l'acide trifluoroacétique catalyse la conversion de chacun des isomères soit le produit d'addition de Diels–Alder **1***a*, l'oxadiazine-1,3,4 **2***a* et la diazétidine-1,2 **3***a* dans tous les autres. Les isomérisations sont en compétition avec la solvolyse vers des produits finals identique, dans tous les cas l'oxydiazinone-1,3,4 **4***a* et le trifluoroacétate de méthyle qui se produiraient directement dans le cas de **1***a* et de **2***a* mais peut être seulement par l'intermédiaire de **2***a* dans le cas de **3***a*. Les vitesses d'isomérisation et de solvolyse augmentent avec la concentration d'acide en milieu dilué mais en milieu concentré il semble que tous les isomères sont transformés en une forme multi-protonée de **2***a* qui est stable vis à vis de l'isomérisation et dont la vitesse de solvolyse diminue avec une augmentation de la concentration de l'acide. [Traduit par le journal]

Can. J. Chem., **52**, 1114 (1974)

Previous work has established that the thermal isomerization of the adducts of azodiacyls and cyclic 1,3-dienes to 1,3,4-oxadiazine derivatives is a reaction of some generality (1–3) and that the isomerization is extremely sensitive to catalysis by strong protic acids or Lewis acids (4). More recently (5) we have shown that the analogous adducts **1** of azo esters and 2,5-dimethyl-3,4-diphenylcyclopentadienone could also be thermally isomerized to the corresponding oxadiazines **2** but that the isomerization was reversible, and furthermore that a competing, apparently irreversible, isomerization of **1** to the diazetidines **3** made the latter in fact the final thermal end product (Scheme 1)

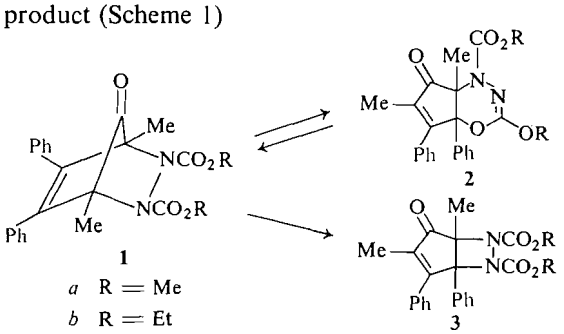

SCHEME 1

The present work shows that the processes of Scheme 1 are also sensitive to catalysis by acid but that the isomerizations compete with a solvolytic dealkylation which probably occurs by more than one pathway.

Our early attempts to obtain structural information on the stable thermal isomers, which showed some puzzling spectroscopic features (5), included hydrolysis with aqueous ethanolic hydrochloric acid. Refluxing **3***a* with 2*N* acid gave a 93% yield of a compound with m.p. 232.5–234°; a simpler synthesis involved keeping a solution of **3***a* in trifluoroacetic acid (TFA) at room temperature for several hours, in which case the yield was quantitative. The elemental analysis and mass spectrum (M^+ 392) required the formula $C_{22}H_{20}N_2O_5$, corresponding to the loss of CH_2, and along with spectroscopic evidence showed the product to be the 1,3,4-oxadiazin-2-one **4***a*, a relatively uncommon heterocyclic type (6, 7).

The i.r. spectrum ($CHCl_3$) had NH absorption at 3400 and three carbonyl peaks at 1780, 1750, and 1712 cm^{-1}. The u.v. absorption maximum at 281 nm was indicative of survival of the β-phenyl-α-methyl enone chromophore present in

Can. J. Chem. Downloaded from www.nrcresearchpress.com by 210.87.254.105 on 09/05/12
For personal use only.

Can. J. Chem. Downloaded from www.nrcresearchpress.com by 210.87.254.105 on 09/05/12
For personal use only.

the parent compound and its isomer **2***a* (8). The n.m.r. spectrum ($CDCl_3$) contained an absorption for one easily exchangeable proton at 3.1 and vinylic and *tert*-methyl singlets at 7.86 and 9.06 τ, respectively, but only one methoxy singlet, at 6.25 τ. In particular the anomalously high field methoxy absorption found in **3***a* (5) was absent. Since the reaction had not involved simple *N*-ester hydrolysis, which would have been accompanied by decarboxylation, a more profound structural alteration must have occurred in which the diazetidine ring had been destroyed. The presence of an amide, rather than an amine, NH was indicated by the chemical shift of the exchangeable proton in the n.m.r. spectrum and by the fact that the compound could be dissolved in aqueous sodium hydroxide and reprecipitated unchanged with acid; there was no salt formation with strong acids.

The chemical and spectroscopic evidence was accommodated reasonably only by the bicyclic structures **4***a* or **5***a*. The carbonyl bands at 1712 and 1750 cm^{-1} are readily identified with the enone and exocyclic urethane carbonyl groups respectively. The absorption at 1780 cm^{-1} does not unambiguously distinguish between the 5- or 6-membered ring forms (9).

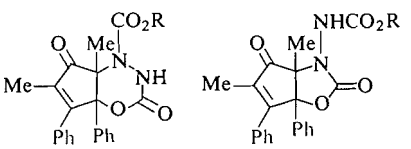

4 **5**

a R = Me
b R = Et

A decision between **4***a* and **5***a* by chemical means was reached by conversion of the amide into its *N*-methoxycarbonyl derivative. No reaction occurred on treatment with methyl chloroformate in pyridine, even after long reflux. However, conversion of the amide into the anion with sodium hydride in dimethoxyethane, followed by addition of methyl chloroformate at room temperature gave a nearly quantitative yield of the urethane. It resisted crystallization but could be purified as an amorphous solid of satisfactory elemental analysis by letting a solution of it slowly evaporate. Its n.m.r. spectrum had two sharp methoxy singlets at 6.19 and 6.28 τ (CCl_4) and was therefore that of the derivative of **4***a*, in which chemical shift difference in the methoxy groups is expected. The analogous derivative of **5***a* would have isochronous methoxy groups, as a result of combinations of rotation and inversion at nitrogen.

The diazetidine **3***b* likewise gave the oxadiazinone **4***b*, m.p. 166–167°, on treatment with aqueous hydrochloric acid or with TFA. The ethoxycarbonyl derivative of **4***b* was a glass, whose n.m.r. spectrum showed chemical shift difference in its ethoxy groups, both in the methylene quartets and the methyl triplets.

Since the solvolysis product of **3***a* had the same basic ring structure as the oxadiazine **2***a*, isomeric with **3***a*, we examined the reaction of **2***a* and the other isomer **1***a* with TFA at room temperature. Again **4***a* was formed quantitatively in each case. We accordingly decided to investigate systematically the competition between isomerization and solvolysis of all the isomers **1***a*–**3***a* with TFA. Analysis by n.m.r. was especially suitable since the aliphatic portion of the spectrum of mixtures of all the isomers and the product **4***a* contained only methyl singlets, no two of which were coincident in chloroform-*d* except the methoxy peaks of **2***a*. The high-field (tertiary) methyl peaks were routinely used in the analysis, peak heights being used as a measure of concentration.

The reactions were run in chloroform-*d*, using 0.25 *M* solutions of each of the isomers, in the presence of increasing amounts of TFA, from 0.2% (v/v; 0.11 equiv.) up to 100%. The extent of the reaction with limited amounts of TFA in commercial chloroform-*d* was found to depend on the trace amounts of water present in the solvent. The reactions with 0.2 and 1% TFA were therefore run in dry[1] chloroform and with chloroform-*d* saturated with D_2O.

The % molar compositions of the reaction mixtures are shown in each case for various times up to completion of the reaction (Tables 1 and 2). Clearly the ratio of total isomerization to solvolysis for both **1***a* and **2***a* is always at a maximum at the beginning of the reaction (since the isomerization products themselves solvolyze). To obtain this maximum the ratios were plotted against time for the early stages of the reaction and extrapolated to zero time. These

[1]This is a difficult solvent to dry rigorously. An easier choice in this regard is benzene, but the methyl peaks of the mixtures of products in benzene were not as well separated as in chloroform, making a quantitative analysis difficult. Furthermore the amide **4***a* was rather insoluble in benzene and began to separate out in the n.m.r. tube at any early stage in the reaction.

Can. J. Chem. Downloaded from www.nrcresearchpress.com by 210.87.254.105 on 09/05/12
For personal use only.

TABLE 1. Product composition (%) with limited amounts of TFA in dry (wet) chloroform

Starting isomer	TFA (%)	Products	Time (min) 0.5	1	1.5	2	3	5	8	12	17	25	40	70	∞		$r^0_{1/5}$
1*a*	0.2	**1***a*				91(94)	89(94)	87(90)	83(86)	81(80)	78(75)	76(69)	73(62)	71(66)	71(44)	[b]	2.8±0.4
		2*a*				3 (2)	4 (2)	4 (3)	5 (4)	6 (5)	7 (6)	7 (6)	8 (6)	8 (7)	8 (8)		(2.4±0.4)
		3*a*				3 (2)	3 (2)	4 (3)	6 (4)	6 (6)	7 (7)	7 (9)	8(12)	8(14)	8(17)		
		4*a*				3 (2)	4 (2)	5 (4)	6 (6)	7 (9)	8(12)	10(16)	11(20)	13(23)	13(31)		
	1	**1***a*	71(78)	58(65)	50(48)	44(43)	37(35)	29(26)	23(18)	20(12)	16 (8)	13 (6)	11 (6)	9 (1)		[a c]	1.4±0.3
		2*a*	4 (4)	4 (4)	4 (4)	4 (4)	4 (3)	3 (2)	1 (0)								(1.4±0.3)
		3*a*	11 (6)	15(13)	18(18)	20(20)	23(22)	26(26)	28(30)	30(32)	31(33)	32(34)	32(34)	32(34)	35		
		4*a*	14(12)	23(18)	28(30)	32(33)	36(40)	42(46)	48(52)	50(56)	53(59)	55(60)	57(60)	59(65)	65		
2*a*	0.2	**1***a*				1 (1)	1 (2)	1 (2)	1 (3)	1 (3)	1 (3)	(3)	(3)	(3)	1 (4)	[d]	1.0±0.2
		2*a*				84(95)	82(88)	80(83)	80(78)	80(74)	80(71)	(69)	(65)	(62)	80(59)		(0.9±0.2)
		3*a*				6 (1)	6 (2)	6 (3)	5 (3)	5 (4)	5 (4)	(4)	(4)	(4)	5 (5)		
		4*a*				9 (3)	11 (8)	13(12)	14(16)	14(19)	14(22)	(24)	(28)	(31)	14(32)		
	1	**1***a*	1 (2)	2 (2)	2 (2)	2 (2)	2 (2)	2 (2)	3 (2)	3 (2)	3 (2)	3 (2)	(2)	(2)	3	[a e]	0.5±0.1
		2*a*	63(55)	50(33)	46(28)	43(25)	38(22)	35(18)	33(16)	32(13)	32(12)	31(11)	(10)	(9)	31		(0.6±0.1)
		3*a*	9(10)	9(11)	9(11)	9(11)	9(11)	9(11)	9(10)	9(11)	9(11)	9(11)	(11)	(11)	9		
		4*a*	27(33)	39(54)	43(59)	46(52)	51(65)	54(69)	55(72)	56(74)	56(75)	57(76)	(77)	(78)	57		

[a]Separation of solid 4*a* occurred.
[b]Final ester to methanol mol ratio = 0.54.
[c]Final ester to methanol mol ratio = 2.0.
[d]Final ester to methanol mol ratio = 0.45.
[e]Final ester to methanol mol ratio = 0.20.

Can. J. Chem. Downloaded from www.nrcresearchpress.com by 210.87.254.105 on 09/05/12
For personal use only.

maximum values, $r^0_{i/s}$, are also shown in the Tables.[2]

In the presence of 0.2% TFA in dry chloroform solvolysis occurred at about the same rate as isomerization for **1***a* as starting material, but solvolysis was much more rapid than isomerization in the case of **2***a*. In both experiments reaction ceased near the point where the theoretical amount of **4***a* (11%) had been formed. The formation of methyl trifluoroacetate was indicated by a peak at 6.03 τ, authentic ester being prepared for comparison in the n.m.r. tube, from methanol and trifluoroacetic anhydride in chloroform.

The presence of water had little effect on the partitioning of either **1***a* or **2***a* between isomerization and solvolysis in the early stages of the reaction. However, hydrolysis could evidently compete with trifluoroacetolysis, so that consumption of acid was not as fast as in the dry reaction, thus allowing more starting material to react by isomerization. The occurrence of hydrolysis was confirmed by the presence of a methanol CH_3 peak at 6.51 τ. The amount of solvolysis at the end of each reaction in conjunction with the ester to methanol peak ratio (Table 1) was indicative of complete consumption of the acid.

In dry chloroform containing 1% TFA both **1***a* and **2***a* reacted rapidly. **1***a* was completely converted into **3***a* and **4***a*, but solvolysis of **2***a* greatly exceeded isomerization, the resulting consumption of acid thus stopping reaction before isomerization was complete.[3]

Water had little effect on the reaction of **1***a* in 1% acid, **3***a* being stable to isomerization or solvolysis at low acid concentration, but as expected it caused extensive hydrolysis of **2***a*.

Even at a starting concentration of 1% TFA the diazetidine was only slowly solvolyzed (33% in 2 days, after which reaction ceased); there was no detectable isomerization.

At acid levels higher than 1% there was an increase in both the $r^0_{i/s}$ (contrast the trend in dilute acid) and the overall rate of reaction of **1***a*, which was undetectable in acid of 4% strength or greater after the time taken (~30 s) for addition of the acid and rapid scanning of the spectrum. The isomerization to **2***a* and **3***a* went increasingly in favor of the former and with 8–100% acid, only **2***a* and the solvolysis product **4***a* were observable when the spectrum was first run. The solvolyses thereafter were first order but the rates *decreased* markedly with increasing acid concentration.

With the oxadiazine **2***a* as starting material isomerization to **3***a*, but not to **1***a*, was noted in 2 or 4% TFA. In 8–100% acid only solvolysis occurred, the behavior being just that noted for **1***a*.

The stability to acid of the diazetidine **3***a*, compared with **1***a* or **2***a*, still persisted in 2% TFA ($t_{\frac{1}{2}}$ ~ 70 m), solvolysis but no isomerization being observed. At acid levels >4% TFA, isomerization, to **2***a* only, became the dominant process, followed by solvolysis, increasingly retarded by acid as before.

The reactions of **1***a*, **2***a*, and **3***a* in concentrated acid, after initial rapid isomerization in the case of **1***a* and **3***a*, followed a common solvolytic pathway. We have described the precursor to **4***a* in each case as **2***a* but the spectra of the solutions suggested that the latter is not present in the free unprotonated form. While all absorptions in **2***a* and **4***a* showed the expected downfield shift in neat TFA, their relative positions remained unchanged,[4] except that one of the methoxy peaks derived from **2***a*, coincident in the absence of acid or in dilute acid, was shifted 0.71 p.p.m. from the other, down to 5.26 τ. It seems most reasonable that this signal was due to the methoxy group on the protonated imidate function of the oxadiazine.

The rapid formation of protonated **2***a* in the reactions of either **1***a* or **3***a* with TFA suggested an alternative synthesis of **2***a* from either of these starting materials, which can each be easily made in one step from the cyclone and dimethyl azodicarboxylate (5). However, attempts to

[2]The ratio in the early stages was of course subject to the largest errors since the composition of the mixture was changing rapidly, but the trends in the limiting value at zero time for both **1***a* and **2***a* in the presence of different amounts of acid and water were both clear and informative.

[3]The theoretical amount of **4***a* is 54%. The value for the reaction of **1***a* is high. The acid was introduced into the n.m.r. tubes using a microsyringe and errors of 2 or 3% are to be expected. However, the discrepancy here was due to inadvertent inclusion of moisture; a small methanol peak was observed in the spectrum.

[4]The *tert*-methyl peaks in **2***a* and **4***a* used in the kinetic analysis not only had the same relative line positions but had exactly the same chemical shift difference in neat TFA as in chloroform. This superimposability was also found in the vinyl and the ester methyls.

TABLE 2. Product composition (%) with excess of TFA in chloroform

Starting isomer	%TFA	Products	Time (min) 0.5	1	1.5	2	3	4	5	7	9	13	$r^0_{i/s}$
1*a*	2	**1***a*	20	5									1.8±0.3
		2*a*	16	10	3								
		3*a*	27	30	30	30	30	29	29	28	28		
		4*a*	37	55	67	70	70	71	71	72	72		
2*a*	2	**2***a*	22	6	3	1							0.6±0.3
		3*a*	17	13	12	12	12	11	11				
		4*a*	61	81	85	87	88	89	89				
3*a*	2	**3***a*		99	97	96	94	91	89	86	83	78[a]	
		4*a*		1	3	4	6	9	11	14	17	22	
1*a*	4	**2***a*	33	25	19	13	7	4	2				2.0±0.3
		3*a*	27	23	20	17	13	12	9	6	2		
		4*a*	40	52	61	70	80	84	89	94	98	100	
2*a*	4	**2***a*	45	18	10	3							0.7±0.3
		3*a*	13	13	12	11	9	8	7	5	4	3	
		4*a*	42	69	78	86	81	92	93	95	96	97	
3*a*	4	**2***a*	6	10	12	13	10	9	7	3	1		1.1±0.2
		3*a*	88	79	72	65	58	51	45	38	32	24	
		4*a*	6	11	16	22	32	40	48	59	67	76	
3*a*	8	**2***a*	43	48	46	41	28	19	10				11±3
		3*a*	50	37	26	16	6						
		4*a*	7	15	28	43	66	81	90	100			
1*a*	8	**2***a*	→	**4***a*	First-order $t_{\frac{1}{2}}$ = 1.2 m								
2*a*	8	**2***a*	→	**4***a*	First-order $t_{\frac{1}{2}}$ = 1.1 m								
	20	**2***a*	→	**4***a*	First-order $t_{\frac{1}{2}}$ = 8.8 m								
1*a*	100	**2***a*	→	**4***a*	First-order $t_{\frac{1}{2}}$ = 30 m								
2*a*	100	**2***a*	→	**4***a*	First-order $t_{\frac{1}{2}}$ = 31 m								
3*a*	100	**2***a*	→	**4***a*	First-order $t_{\frac{1}{2}}$ = 28 m								

[a]Reaction not run to completion.

quench the solutions obtained by adding TFA to **3***a* with excess of aqueous base (sodium hydrogen carbonate) or organic bases (triethylamine or pyridine) lead only to the isolation of **4***a*. Demethylation to the stable amide linkage is thus faster than deprotonation.

Control reactions showed that acid was necessary for hydrolysis, **2***a* being stable to chloroform saturated with water or to 0.001 *M* TFA over 3 days. Methyl trifluoroacetate was also stable to water under the reaction conditions but the rate of esterification of TFA by methanol was significant. The above reactions in the presence of water are thus slightly retarded due to loss of acid by esterification. Finally the solvolysis reactions were irreversible: **4***a* did not react with either methyl trifluoroacetate or methanol in the presence of TFA.

The figures in the tables and the above discussion are reconcilable with the following qualitative facts.

(*i*) **1***a*, **2***a*, and **3***a* can each isomerize directly to either of the others, except for **3***a* → **1***a*; isomerization of **2***a* → **1***a* is slight in dilute acid but detectable. These results contrast markedly with the thermal isomerizations, in which the process **2***a* → **3***a* could not be confirmed and to which **3***a* was inert (5).

(*ii*) The overall isomerization rates of **1***a*, **2***a*, and **3***a* and, in particular, the isomerization rates of **1***a* and **3***a* to **2***a* increase with TFA concentration; the isomerization of **3***a* is, however, only significant at high acid levels.

(*iii*) The trifluoroacetolysis rates of the isomers show the trend **2***a* > **1***a* ≫ **3***a*; hydrolysis of **2***a* is also much more efficient than that of the others.

(*iv*) In dilute acid the trifluoroacetolysis rates of **1***a* and **2***a* increase with concentration and more rapidly than the isomerization rates; $r^0_{i/s}$ thus decreases.

(*v*) In concentrated acid **2***a* undergoes pro-

Can. J. Chem. Downloaded from www.nrcresearchpress.com by 210.87.254.105 on 09/05/12
For personal use only.

Can. J. Chem. Downloaded from www.nrcresearchpress.com by 210.87.254.105 on 09/05/12
For personal use only.

tonation close to the solvolysis site. The species formed resists isomerization, and its solvolysis rate *decreases* with increasing acid concentration. The combined effects of this and *iv* cause $r^0_{i/s}$ for **1***a* to pass through a minimum.

(*vi*) Solvolysis of **1***a* and **2***a* to **4***a* occurs directly;[5] solvolysis of **3***a* to **4***a* probably occurs only through **2***a*.

In the thermal interconversions of **1***a*, **2***a*, and **3***a* we proposed as a common intermediate the dipolar species **6** (5). In the present series of acid catalyzed reactions it seems reasonable to suggest an analogous protonated intermediate either **7** or **8**, the tautomeric forms of a bisurethane which

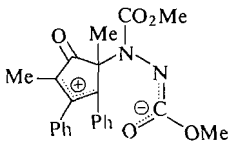

6

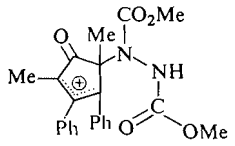

7

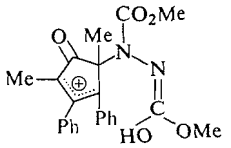

8

could arise formally by protonation of the isomers on nitrogen or oxygen followed by ring opening. A decision between nitrogen and oxygen as the site of protonation is clear only in the case of **2***a* which has a recognizably basic nitrogen. In **1***a* and **3***a* protonation on an amide carbonyl oxygen leading to **8** may be preferred.[6] Either **7** or **8** can isomerize to the protonated isomers, **1***a*–H^+ (by cyclization of Me—C^+ to N), **2***a*–H^+ (Ph—C^+ to O), or **3***a*–H^+ (Ph—C^+ to N) or give **4***a* by solvolytic demethylation with the appropriate nucleophile (the counter-ion TFA^-, TFA itself, or water) at the ester function together with cyclization.

Alternatively **4***a* might be obtained by direct solvolysis of **9**, the protonated oxadiazine (Scheme 2), a pathway consistent with the rapid formation of **4***a* in dilute acid by TFA or water, since it does not involve ring opening and could thus occur in one step.

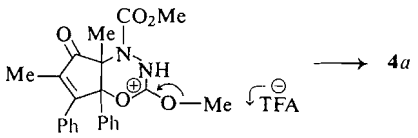

9

SCHEME 2

Indeed solvolysis of all the isomers could proceed through **9**, this in no way conflicting with our earlier conclusion (point *vi* above) that **1***a* solvolyzes directly to **4***a*. The sequence **1***a* → **8** → **9** → **4***a* does not involve the free oxadiazine.

The low-field methoxy absorption in the spectra from solution of **2***a* in concentrated acid belongs to a species protonated on an imidate nitrogen but it is unlikely that this is the monoprotonated form **9**, which we have judged to be very labile. At high acid levels multiprotonation may become important since there are a number of potential sites available in the isomers or their ring-opened intermediates, both in the enone and the azo derived portions.

The increase in catalytic efficiency of TFA with its concentration in the isomerization reactions was expected (4) but there is no clear reason for the negative effect in solvolysis of the oxadiazine.[7]

A comment on the stereochemistry of the ring junction in the oxadiazines **2** and their solvolysis products **4** is in order. We have tacitly assumed (5) that the thermal reaction of **1** gave the *cis*-oxadiazines, by analogy with the isomerization of the adduct of azodibenzoyl and cyclopentadiene to an oxadiazine in which the *cis* stereochemistry was established by chemical degradation and which the concerted nature of the isomerization in any event dictated (1). No such structural proof has been provided for the oxadiazines **2**.

The formation of the *trans* isomer of **2***a* merely requires that the lifetime of the open structure **6** be long enough to allow free conformational rotation. Our belief in the *cis* stereochemistry of both **2** and **4** rests entirely, and we feel con-

[5]The build-up of **4***a* from **1***a* seems too rapid to be explicable on the basis of the sequence **1***a* → **2***a* → **4***a* exclusively.

[6]While protonation of simple amides is now well established as occurring on oxygen (10), the general question of oxygen *vs.* nitrogen protonation is not a fully resolved one in complex systems like these. Though we are showing **7** and **8** as the free protonated forms it is possible that in a medium such as dry chloroform only coordination of the amide group to the acid hydrogen occurs and that the acid OH bond is never broken.

[7]A referee has pointed out that if the solvolysis requires TFA^- the nucleophilic activity of the latter would be reduced in excess of TFA by acid to anion hydrogen bonding. The occurrence of free TFA^- in dry chloroform, however, is not certain.

Can. J. Chem. Downloaded from www.nrcresearchpress.com by 210.87.254.105 on 09/05/12
For personal use only.

vincingly, on the chemical shift values of their *tert*-methyl groups.

The absorptions of the *tert*-methyl groups in the diazetidine **3***a*, in **2***a*, and in **4***a* occur very close together, at 8.86, 8.96, and 9.06 τ. Since all three methyl groups are attached to carbon atoms with identical nearest neighbor atoms they must also all have the same stereochemistry with respect to the nearest phenyl group, that is, **2***a* and **4***a*, like **3***a*, must have a *cis* ring junction.

A *cis*-phenyl group is expected to have a strong shielding effect on the adjacent methyl. The methyl groups in the *trans* isomers of **2***a* and **4***a* would resonate at much lower fields than in the *cis* isomers. The magnitude of the effect can be gauged from the spectra of the *cis* and *trans* alcohols **10**, both of which are formed when diethyl ketone and benzil are condensed with Triton B as catalyst (5). Separation by fractional crystallization gave the *cis* and *trans* epimers with m.p. 129–129.5° and 153–154° respectively, and *tert*-methyl doublets at 9.28 and 8.78 τ, a shift too large to be reconcilable with any stereochemical difference in the ring junctions of compounds **1***a*–**4***a*.[8]

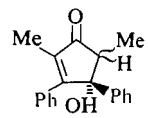

10

Experimental

The i.r. spectra were obtained on a Beckman IR10 and the u.v. spectra on a Coleman EPS-3T Hitachi spectrometer. All n.m.r. routine and kinetic analyses were done on a Varian T60 spectrometer against tetramethylsilane as internal standard (abbreviations: s, singlet; d, doublet; t, triplet; q, quartet; m, multiplet). For mass spectra a Perkin Elmer RM-U6E Hitachi spectrometer was used.

Anhydrous magnesium sulfate was used as drying agent for solutions in organic solvents. Melting points are uncorrected.

cis-4-Carbomethoxy-4a,6-dimethyl-7,7a-diphenyl-2,3,4,4a,5,7a-hexahydrocyclopenta-1,3,4-oxadiazin-2,5-dione (4a)

From Diazetidine 3a

A solution of **3***a* (122 mg, 0.30 mmol) in 12 *N* hydrochloric acid and methanol (1:5, 3 ml) was refluxed for 2 h and evaporated to near dryness. Water was added and the product (93%) collected. Its i.r. spectrum was identical with that of material obtained as almost colorless prisms, m.p. 232.5–234°, from methanol or aqueous methanol.

Alternatively, a solution of **3***a* (100 mg) was kept in TFA (1 ml) at room temperature for 6 h and then evaporated. Addition of a few drops of methanol induced crystallization and the precipitate was collected and washed with very dilute ammonia, the yield being essentially quantitative.

The *oxadiazinone* had ν ($CHCl_3$) 3400 (NH), 1780, 1750, and 1712 cm^{-1} (endocyclic and exocyclic urethane and enone C=O, respectively); λ_{max} (EtOH) 282 nm; τ ($CDCl_3$) 2.3–3.0 (10 phenyl H), 3.25 (broad, NH), 6.23 (s, OMe), 7.86 (s, vinyl Me), 9.06 p.p.m. (s, *tert*-Me); *m/e* 392 (P^+, 16%), 348 ($C_{21}H_{20}N_2O_3^+$, 100%).

Anal. Calcd. for $C_{22}H_{20}N_2O_5$: C, 67.33; H, 5.15; N, 7.14. Found: C, 67.09; H, 5.28; N, 6.82.

A sample of the product was dissolved by warming it in 1 *N* aqueous sodium hydroxide – methanol (1:1). Most of the methanol was removed by evaporation. Addition of dilute hydrochloric acid reprecipitated **4***a* in pure form.

From Isomers 1a or 2a

The TFA method was used on the same scale and with the same work-up procedure; the yields were quantitative. The identity of the product as **4***a* was confirmed in each case by its spectra and its mixed m.p. with the product from **3***a*.

The 4-Carboethoxy Derivative 4b

Either of the above methods on the same scale gave excellent yields (> 90%) of **4***b* which formed colorless prisms from methanol, m.p. 166–167°; ν (CCl_4) 3420, 1796, 1758, and 1712 cm^{-1} (assignments as for **4***a*); λ_{max} (EtOH) 282 nm (ε 12 600); τ ($CDCl_3$) 2.3–3.2 (10 phenyl H), 3.53 (broad, NH), 5.76 (q, 2 methylene H, J = 7.5 Hz), 7.86 (s, vinyl Me), 8.78 (t, 3 methyl H), 9.05 p.p.m. (s, *tert*-Me); *m/e* 406 (P^+, 16%), 362 ($C_{22}H_{22}N_2O_3^+$, 100%).

Anal. Calcd. for $C_{23}H_{22}N_2O_5$: C, 67.96; H, 5.46; N, 6.89. Found: C, 67.42; H, 5.39; N, 7.13.

cis-3,4-Dicarbomethoxy-4a,6-dimethyl-7,7a-diphenyl-2,3,4,4a,5,7a-hexahydrocyclopenta-1,3,4-oxadiazin-2,5-dione (Carbomethoxy Derivative of 4a)

The compound **4***a* (100 mg) was recovered quantitatively after refluxing for 12 h in pyridine (5 ml) containing methyl chloroformate (0.5 ml), evaporating, and adding water.

Addition of **4***a* (98 mg, 0.25 mmol) to a suspension of 50% sodium hydride – mineral oil (26 mg, 0.55 mmol) in dry dimethoxyethane (2 ml) caused vigorous effervescence of hydrogen and formation of a yellow solution. Methyl chloroformate (29 μl, 0.37 mmol) was injected with a microsyringe, causing the solution to become colorless, and the formation of a precipitate of sodium chloride. After 3 h at room temperature ether and water were added, the ether layer was shaken out several times with water, then dried, and evaporated. The residue was washed with several portions of hexane to remove the mineral oil (it was then of 90–95% purity as estimated by n.m.r. analysis) and then dissolved in ethyl acetate. The solution was filtered, 2-methylheptane was added until a second phase just appeared which was then removed by addition of a drop of ethyl acetate. The clear solution was allowed to evaporate slowly at room temperature. The

[8]Work with related cyclopentene derivatives epimeric at these two carbons indicates that this large shift difference in the methyl groups is quite general: for example 0.57 p.p.m. in 2,5-dimethyl-3,4-diphenylcyclopent-2-enone and 0.40 p.p.m. in 2,5-dimethyl-3,4-diphenyl-1,4-dihydroxycyclopent-2-ene (C_1 stereochemistry not known).

Can. J. Chem. Downloaded from www.nrcresearchpress.com by 210.87.254.105 on 09/05/12
For personal use only.

amorphous material which separated slowly became brittle; it was ground up, filtered, washed liberally with 2-methylheptane, and kept for a day in an evacuated desiccator over paraffin wax. It had ν (CCl_4) 1801, 1790 (sh), 1762, and 1724 cm^{-1} (three urethane and enone C=O); λ_{max} (EtOH) 286 nm; τ (CCl_4) 2.3–3.1 (10 phenyl H), 6.19 (s, OMe), 6.28 (s, OMe), 7.94 (s, vinyl Me), 9.16 p.p.m. (s, *tert*-Me).

Anal. Calcd. for $C_{24}H_{22}N_2O_7$: C, 64.00; H, 4.92; N, 6.22. Found: C, 64.21; H, 5.15; N, 6.39.

The Carboethoxy Derivative of 4b

The method and scale were the same as those used for **5***a*. The glassy product had ν (CCl_4) 1804, 1782, 1752, and 1722 cm^{-1} (three urethane and enone C=O); λ_{max} (EtOH) 286 nm; τ (CCl_4) 2.3–3.1 (10 phenyl H), 5.73 (q, 2 methylene H, J = 8.0 Hz), 5.80 (q, 2 methylene H, J = 7.5 Hz), 7.93 (s, vinyl Me), 8.69 (t, 3 methyl H), 8.73 (t, 3 methyl H), 9.16 p.p.m. (s, *tert*-Me).

Kinetic Determinations

Materials

The trifluoroacetic acid used was Baker Reagent grade.

Chloroform was dried by refluxing over phosphorous pentoxide for 2 h, fractionating and then stirring for 2 days over molecular sieves (Type 4A, BDH). "Wet" chloroform-*d* was obtained by shaking with D_2O, removing the chloroform layer after all cloudiness had disappeared, and filtering it through a cotton wool plug.

The purification of the isomers **1***a*, **2***a*, and **3***a* has been described previously (5); **1***a* and **2***a* were recrystallized till each was free of traces of the other.

Nuclear Magnetic Resonance Measurements

Solutions of the isomers (50.0 mg, 0.25 *M*) in dry chloroform or wet chloroform-*d* (500 μl) were allowed to warm to the n.m.r. probe temperature (35°) and the TFA added with a microsyringe. The 2, 4, and 8% solutions were made by injecting 10, 20, and 40 μl, respectively, of neat TFA; for the 20% solution containing **2***a*, 400 μl of chloroform were put in the tube and 100 μl of prewarmed neat TFA added. The 0.2 and 1% solutions were obtained by adding 10 and 50 μl, respectively, of a 10% solution of TFA in the appropriate chloroform.

Spectra of the *tert*-methyl region were recorded immediately and repeatedly after injection of the acid and mixing, first at rapid (10 Hz s^{-1}) and later at slow (2 Hz s^{-1}) scan. Other regions of the spectrum were also examined as necessary. Radio frequency values were optimized to prevent saturation.

Calculation of Composition of Mixture

Analysis of suitable mixtures of **1***a*, **2***a*, **3***a*, and **4***a* showed that the *tert*-methyl peak heights (times a factor of one half for the symmetrical adduct **1***a*) could be used as a measure of concentration (±3%) except in the case of **4***a* whose peak was consistently less intense by about 10%. This was corrected for when necessary. The peak positions for the compounds **1***a*–**4***a* in chloroform-*d* were respectively 8.18, 8.96, 8.86, and 9.06 τ.

The percentage of each compound in a given run, as determined by peak heights, was plotted against time and a smooth curve drawn through the points. The % composition of the mixture at representative times, as shown in Tables 1 and 2, was read off the curves by interpolation.

The results for the reactions in concentrated or neat TFA involving only the process **2***a*–H^+ → **4***a* gave a first-order rate plot.

Control Reactions

Stability of 2a to Water or Very Dilute Acid. A solution of **2***a* (50 mg) in chloroform (0.50 ml) containing 1.2 μl D_2O (0.13 *M*) showed no change in its spectrum over 12 days. Similarly addition of 1.5 μl of aqueous TFA (40:1 v/v) to a solution of **2***a* (50 mg) in chloroform (0.50 ml; hence 0.001 *M* in acid) was without effect over 3 days).

Esterification of Methanol by Aqueous TFA. A solution 0.13 *M* in each reagent was made by adding TFA (5 μl, 1%), water (1.2 μl), and methanol (2.7 μl) to chloroform (0.50 ml) in the n.m.r. sample tube. The extent of esterification was 24% in 2.5 h and 70% in 24 h.

Stability of Methyl Trifluoroacetate to Aqueous TFA. A solution 0.13 *M* in each reagent was made by adding trifluoroacetic anhydride (9.5 μl) and methanol (2.7 μl) to chloroform (0.05 ml) in the n.m.r. tube. Esterification was complete in 20 h (90% in 5 h). Water (1.2 μl, 0.13 *M*) was then added; over a period of 30 h no methanol could be detected.

Irreversibility of Solvolysis. A solution of **4***a* (50 mg) in chloroform (0.50 ml) was made 0.13 *M* in TFA, water and methanol (as in *b*). Over a 24-h period only esterification, and no reaction of **4***a*, was observed. Enough trifluoroacetic anhydride to destroy the water, and generate fresh acid and more ester, was then added. No trace of the isomers **1***a*, **2***a*, **3***a* could be detected after 15 h.

Attempted Synthesis of 2a from 3a with TFA

Samples of **3***a* (about 30 mg) were dissolved in TFA (0.2 ml) and treated as follows.

(*i*) Methylene chloride and a large excess of aqueous sodium hydrogen carbonate were added and the organic layer was separated.

(*ii*) Methylene chloride containing an excess of pyridine was added, followed by a large volume of water, and the organic layer was separated.

(*iii*) An excess of pyridine was added directly, with cooling and the salt which precipitated was filtered off from the pyridine solution.

In each case the n.m.r. spectrum of the organic solution showed the presence only of **4***a*.

2,5-Dimethyl-3,4-diphenyl-4-hydroxycyclopent-2-enone (Cis- and Trans-10)

To a solution of benzil (20 g, 0.095 mol) in diethyl ketone (20 ml) was added 10 ml of a 40% solution in methanol of benzyltrimethylammonium hydroxide (Triton B). There was an exothermic reaction and the whole was then refluxed for 0.5 h and poured into an excess of cold dilute hydrochloric acid. The product crystallized (>95%) but its n.m.r. spectrum indicated the presence of both epimers in about equal amounts. Crystallization from aqueous ethanol gave the *trans*-alcohol, m.p. 153–154°, as prisms (lit. (11) m.p. 150°). Repeated crystallization of the soluble fraction, with working-up of the mother liquors in each case, gave the *cis*-alcohol, which formed prisms, m.p. 129–129.5°, from benzene–hexane.

The *trans*-alcohol had τ ($CDCl_3$) 2.3–3.2 (10 phenyl H), 7.35 (q, *tert*-H, J = 11 Hz), 7.4 (s, OH), 8.02 (s, vinyl Me), 8.78 p.p.m. (d, *tert*-Me).

The *cis*-alcohol had τ ($CDCl_3$) 2.3–3.2 (10 phenyl H), 7.07 (q, *tert*-H, J = 11 Hz), 7.5 (s, OH), 8.00 (s, vinyl Me), 9.28 p.p.m. (d, *tert*-Me).

We thank the National Research Council of Canada for support of this work.

1. D. MACKAY, J. A. CAMPBELL, and C. P. R. JENNISON. Can. J. Chem. **48**, 81 (1970).
2. J. A. CAMPBELL, D. MACKAY, and T. D. SAUER. Can. J. Chem. **50**, 371 (1972).
3. C. Y-J. CHUNG, D. MACKAY, and T. D. SAUER. Can. J. Chem. **50**, 3315 (1972).
4. C. Y-J. CHUNG, D. MACKAY, and T. D. SAUER. Can. J. Chem. **50**, 1568 (1972).
5. D. MACKAY, C. W. PILGER, and L. L. WONG. J. Org. Chem. **38**, 2043 (1973).
6. M. ROSENBLUM and H. MOLTZAN. Chem. and Ind. (London) 1480 (1956); M. ROSENBLUM, V. NAYAK, S. K. DASGUPTA, and A. LONGROY. J. Am. Chem. Soc. **85**, 3874 (1963); M. ROSENBLUM, A. LONGROY, M. NEVEU, and C. STEEL. J. Am. Chem. Soc. **87**, 5716 (1965); B. FUCHS and M. ROSENBLUM. J. Am. Chem. Soc. **90**, 1061 (1968).
7. D. L. TREPANIER, J. N. EBLE, and G. H. HARRIS. J. Med. Chem. **11**, 357 (1968); D. L. TREPANIER and G. H. HARRIS. U.S. Patent 3,377,345. Chem. Abstr. **69**, 59293a (1968) and U.S. Patent 3,428,632. Chem. Abstr. **70**, 78026 (1969).
8. C. F. H. ALLEN, T. DAVIS, D. W. STEWART, and J. A. VANALLAN. J. Org. Chem. **20**, 310 (1955).
9. L. J. BELLAMY. *In* Advances in infrared group frequencies. Methuen, London. Chap. 5.
10. G. A. OLAH, A. M. WHITE, and D. H. O'BRIEN. Chem. Rev. **70**, 561 (1970).
11. F. R. JAPP and A. N. MELDRUM. Trans. Chem. Soc. **79**, 1024 (1901).

Can. J. Chem. Downloaded from www.nrcresearchpress.com by 210.87.254.105 on 09/05/12
For personal use only.

The Conformational Requirements for the Transition State of Bogert–Cook–Bardhan–Sengupta Cyclizations

FRANÇOIS BRISSE AND ALAIN LECTARD
Département de Chimie, Université de Montréal, Montréal, Québec

AND

CIRILL SCHMIDT
Chemistry Department, University of Prince Edward Island, Charlottetown, Prince Edward Island

Received October 16, 1973

It is shown that the cyclizations discussed proceed through twist-boat shaped carbonium ions, *e.g.* **9**. Due to structural rigidity such a conformation cannot be assumed in a *trans*-fused decalin system and the reaction is arrested at the olefinic stage such as **9**. The structure of ketoalcohol **9***c* is elucidated by X-ray crystallography.

On démontre que les cyclisations discutées se produisent par l'intermédiaire d'ions carboniums ayant la forme bateau-croisé. A cause de la rigidité du système décalinique lié en *trans* une telle conformation n'est pas possible et la réaction s'arrête au niveau d'une oléfine telle que **9**.

On a élucidé la structure du cétoalcool **9***c* par diffraction des rayons-X.

Can. J. Chem., **52**, 1123 (1974)

Can. J. Chem. Downloaded from www.nrcresearchpress.com by 210.87.254.40 on 09/05/12
For personal use only.

The title reactions (1, 2) designate the acid catalyzed cyclodehydration of phenylethylcyclohexanols **1** to mainly octahydrophenanthrene derivatives **2** accompanied by spiranes **3**.

An ample number of synthetic examples are known in the literature with various substituents in the cyclohexane ring and the aromatic nucleus. Recently the subject has been excellently reviewed (2). In most of the cyclohexanols studied the hydroxyl group is located at position 1 or 2 (formula **1**).

Perhaps the most controversial aspect of all mechanistic considerations has been the question whether or not olefins are intermediates in these reactions.

Undeniably the most convincing evidence against the participation of olefins has been presented by Barnes and Olin (3) demonstrating that the cyclodehydration of optically active alcohol **4** led to the formation of optically active phenanthrene derivative **5**.

Yet it has been shown by Haworth and coworkers (4) that olefins might be implicated at least in some of these reactions since olefin **6** could actually be cyclized to the octahydrophenanthrene **7**. The stereochemistry of **7** is represented as assigned recently by the reviewer (2).

It should be stated that the retention of stereochemical entity in Barnes' reaction **4** → **5** can be considered as evidence against the participation of an olefin only in those reactions where the OH is located at C-2 and the cyclohexane ring carries a minimum number of substituents. The cyclodehydrations of those compounds which carry the hydroxyl group at position 1 (in formula **1**) are more heavily substituted in the cyclohexane ring and might belong mechanistically to an entirely different class of reactions.

In the course of our synthetic work in the terpene field we encountered an interesting case which might be quite revealing with respect to the stereochemical requirements of the transition state of cyclodehydrations involving 1-(2-phenylethyl)-cyclohexanols.

Our intention was to cyclize ketoalcohol **8** to compound **10** in an acidic medium. Refluxing compound **8** in 85% formic acid led to the formation of olefin formate **9***a* as expected (5). However, the cyclization of the latter compound to phenanthrene derivative **10** did not take place under any conditions. Heating formate **9***a* in a solution of acetic acid and sulfuric acid for 8 h as applied by Haworth for compound **6** (4) led to the formation of a mixture of the formate **9***a* and the corresponding acetate **9***b*. The latter products were both converted to the readily isolable alcohol **9***c* by treatment with sodium methylate in methanol. In subsequent experiments it was found that refluxing in 85% formic acid for 8 h

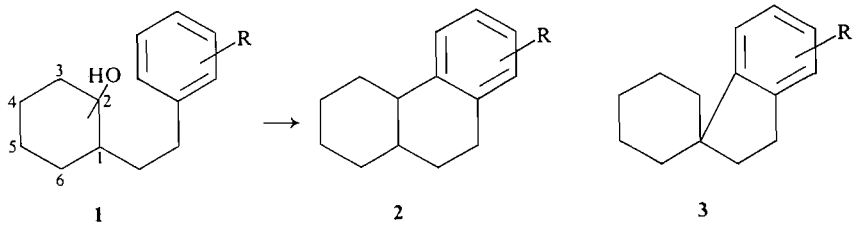

1 2 3

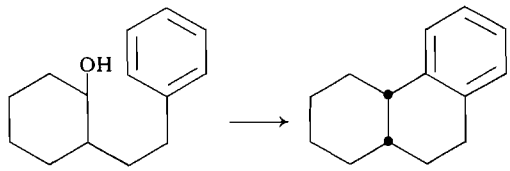

4 5

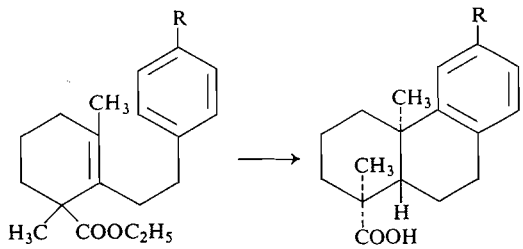

6 7

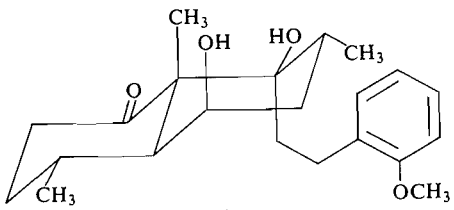

8

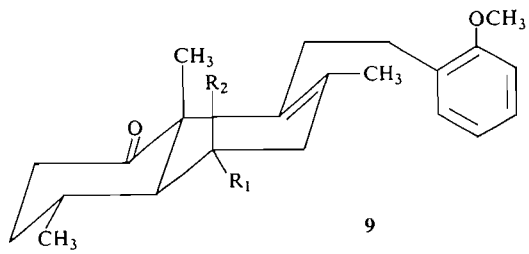

9

a $R_1 = H$; $R_2 = O-\overset{O}{\overset{\|}{C}}-H$
b $R_1 = H$; $R_2 = OCOCH_3$
c $R_1 = H$; $R_2 = OH$
d $R_1 = R_2 = O=$

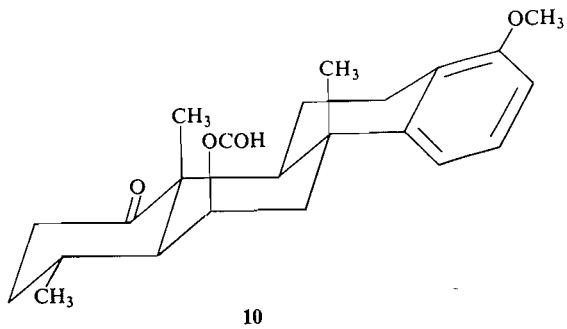

10

Can. J. Chem. Downloaded from www.nrcresearchpress.com by 210.87.254.40 on 09/05/12
For personal use only.

Can. J. Chem. Downloaded from www.nrcresearchpress.com by 210.87.254.40 on 09/05/12
For personal use only.

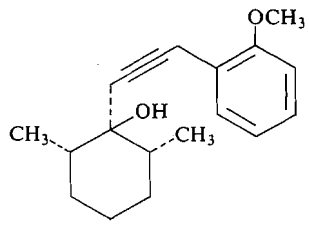

11

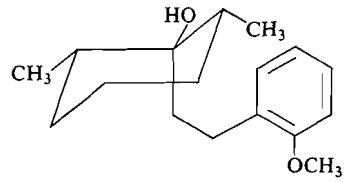

12

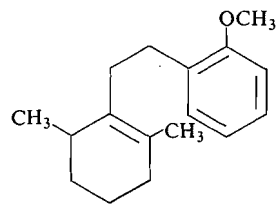

13

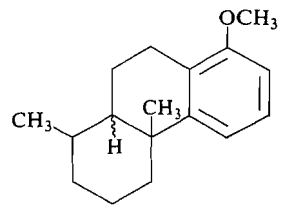

14

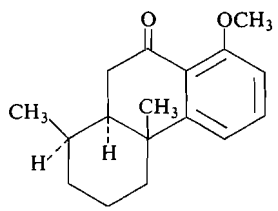

15

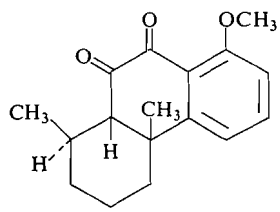

16

was equivalent to and less damaging than the acetic acid – H_2SO_4 treatment. But even under these conditions no cyclization to **10** took place and merely the starting material was recovered in 85%. Heating olefin **9***c* with polyphosphoric acid led to unidentifiable polymers only.

The failure of converting **9***a* to **10** was quite unexpected. Yet it was believed that our negative results could illuminate the mechanism of the Bogert–Cook reaction provided that our stereochemical assignment of compound **9***a* was ascertained beyond doubt and the circumstances of the reaction were supported by a closely related positive example.

In the second part of this paper the crystallographic analysis of **9***c* is described proving that our previous assignment was correct (5).

It was surmised that the inability of olefin **9** to cyclize might be attributable to 1,3-diaxial interactions in the transition state. Consequently we prepared tertiary alcohol **12** from the known acetylene **11** (6). Compound **12** is essentially analogous to **8** but must be devoid of 1,3-diaxial interactions in the transition state of its cyclization.

Tertiary alcohol **12** could be cyclized under very mild conditions to a 3 : 1 *cis–trans* mixture of octahydrophenanthrene **14** in 85% formic acid at room temperature. The same isomer ratios were found when the cyclization of **12** was carried out in a solution of acetic acid and sulfuric acid at room temperature.

From the n.m.r. of the cyclized product **14** it was apparent that a mixture was formed. Since all attempts to separate the two components by preparative v.p.c. were unsuccessful the product was subjected to Wenkert oxidation. The latter reaction is known to convert *cis*-fused octahydrophenenanthrenes to α-diketones whereas the corresponding *trans* isomer furnishes a monoketone (7). Thus the cyclized material **14** was oxidized with chromic acid in CH_3COOH–H_2O to a mixture of monoketone **15** and diketone **16**, which were readily separated by preparative thick-layer chromatography.

Since monoketone **15** was not crystalline it was

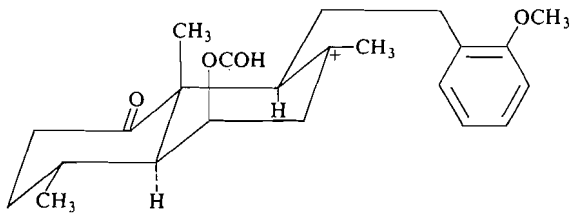

17

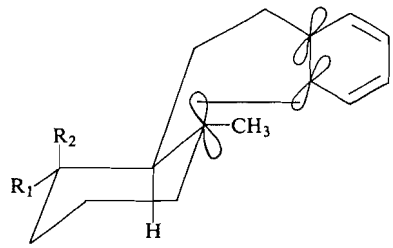

18

a $R_1 = CH_3$; $R_2 = H$
b $R_1 = COOC_2H_5$; $R_2 = CH_3$

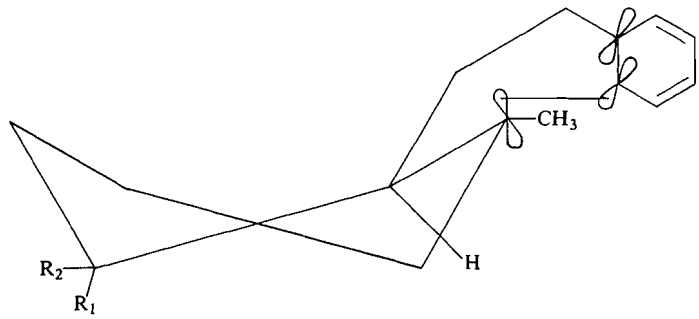

19

a $R_1 = CH_3$; $R_2 = H$
b $R_1 = COOC_2H_5$; $R_2 = CH_3$

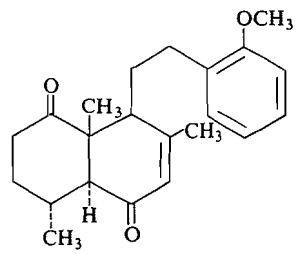

20

subsequently converted to the crystalline diketone **16** by oxidation with SeO_2 in dioxane in terms of which it was characterized. Apparently the *trans* ring junction in **15** must have isomerized to the *cis* isomer during the oxidation.

It is believed that this reaction **12** → **14** also involves an olefin, since the related cyclization **6** → **7** starts with an olefin and the attempted ring closure **8** → **10** is arrested at the olefin stage, **9***a*. Unfortunately in the cyclization **12** → **14** we have not been able to isolate an olefin.

We postulate that the cyclizations discussed here all proceed through a carbonium ion formed by the protonation of the corresponding olefin which appears to be the primary intermediate. The combined consideration of these three reactions permits the following mechanistic rationalization.

Due to conformational inflexibility, the equatorial and axial directions in structure **17** must be defined clearly. While the axial approach by the benzene ring to carbonium ion **17** is quite hindered due to two 1,3-diaxial interactions the equatorial attack to the same carbonium ion **17** should be as free as on carbonium ion **18***a* derived by the protonation of olefin **13**. On the basis of the unsuccessful reaction **17** → **10**, it is concluded that the Bogert–Cook reaction cannot take place from an equatorial direction. Furthermore carbonium ion **18***a* is not attacked from a distinct equatorial direction either.

It might be suggested that the failure of the ring closure **8** → **10** from the axial direction on carbonium ion **17** could be attributed to steric interference of the angular methyl and the formyloxy group against the approaching phenyl group in the transition state. However, such an interaction must also have been involved in the cyclization **6** → **7** (4). Since the latter reaction under the same conditions was successful this assumption is not justified.

An examination of a Dreiding model of transition state **18***b* shows that the overlap of the p orbital of carbonium ion with the electrons of the benzene ring leads to a demanding 1,3-diaxial interaction between the methyl and the approaching phenyl group. A large proportion of this steric strain could be avoided by the assumption of a twist form relieving the 1,3-diaxial interaction and at the same time providing a better geometry for the σ complex.

Therefore in the authors' opinion the failure

Can. J. Chem. Downloaded from www.nrcresearchpress.com by 210.87.254.40 on 09/05/12
For personal use only.

Can. J. Chem. Downloaded from www.nrcresearchpress.com by 210.87.254.40 on 09/05/12
For personal use only.

of **17** to cyclize is attributable to the conformational rigidity of the *trans*-decalin system which prevents the attainment of a twist-shaped transition state. Correspondingly the facile conversion **12** → **14** and the moderate conditions applied for **6** → **7** are explained by the fact that both systems are flexible enough to assume a twist conformation such as **19**.

The argument[1] could be raised that the cyclization of **9*a*** to **10** failed since an axial attack in carbonium ion **17** was impeded by two 1,3-diaxial interactions as compared to only one in the cyclization **6** → **7**. This possibility however, is quite unlikely since we found that diketone **9*d*** lacking the 4-axial OH is recovered unchanged after standing in 90% formic acid at room temperature for 18 h. Under the same conditions the cyclization **12** → **14** readily proceeded. In refluxing formic acid the β,γ-unsaturated diketone **9*d*** merely isomerized to the α,β-unsaturated diketone **20**. An attempt was made to cyclize diketone **20** in polyphosphoric acid; however, only an unidentifiable polymeric substance was formed.

In most of these cyclizations as in **12** → **14** a *cis–trans* mixture is formed. This could be understood from the fact that the twist conformation of the carbonium ion could also be approached from the quasiequatorial direction as well as from the quasiaxial direction.

The preponderance of the *cis* isomer over the *trans* indicates that the quasiaxial approach is favored due to the stereoelectronic reasons.

Synthetic Work

All melting points were taken on a Fisher-John melting point apparatus and are uncorrected. The elemental analyses were carried out by Pascher Mikroanalytical Laboratorium, Bonn, West Germany and Schwarzhopf Mikroanalytical Laboratory, Woodside, N.Y. The i.r. spectra were recorded on a Perkin-Elmer Model 137B infracord spectrophotometer. The u.v. spectrograms were taken on a Coleman Hitachi Model 124 double-beam grating spectrophotometer. The n.m.r. spectra were recorded on a Varian Associates 56.4 MHz spectrophotometer. The mass spectra were obtained with a Hitachi Perkin-Elmer Model RMS-4 spectrometer.

trans-1α-(2-O-Methoxyphenylethyl)-1β, 4β-dihydroxy-2α,5α,9β-trimethyl-8-decalone (8)

Ten grams of the previously described acetylene *trans*-1α-(O-methoxyphenylethynyl)-1β,4β-dihydroxy-8,8-ethylenedioxy-2α,5α,9β-trimethyldecalin (**5**) dissolved in methanol (200 ml) was hydrogenated for 18 h in the presence of 5% Pd-on-charcoal (100 mg). After filtration 20 ml of water and 300 mg of *p*-toluenesulfonic acid was added to the filtrate and the solution was stirred at room temperature for 18 h. The reaction mixture was then diluted with water (300 ml) and extracted with chloroform (4 × 300 ml). The combined extracts were washed with water, dried ($MgSO_4$), and evaporated to dryness furnishing 8.5 g (80%) of crystalline homogeneous product, m.p. 165°.

An analytical sample was prepared by recrystallizing from benzene–chloroform, m.p. 171°. Mass spectrum (70 eV) *m/e* (relative intensity) no parent peak, 342 (30), 324 (20), 309 (10), 219 (100), 203 (80); i.r. ($CHCL_3$) 3500, 2950, 1690,[2] 1480, 1460, 1240, 1040, 960, 910, 840 cm^{-1}; u.v.$_{max}$ (96% C_2H_5OH) 221 nm (ε 6700), 272 (2230), 278 (2000); n.m.r. at 60 MHz ($CDCl_3$) τ 9.00 (d, 3, J = 6 Hz), 8.70 (d, 3, J = 6 Hz), 8.50 (s, 3, angular methyl), 6.13 (s, 3, CH_3O), 5.75 (m, 1, C*H*OH), 3 (m, 4, aromatic protons).

Anal. Calcd. for $C_{22}H_{32}O_4$: C, 73.30; H, 8.95. Found: C, 73.13; H, 9.01.

*Dehydration of Alcohol **8** to olefin **9a***

One gram of alcohol **8** dissolved in 20 ml of 85% formic acid was refluxed for 4 h. The reaction mixture was poured on water (100 ml). The ether extracts were washed successively with saline, 5% sodium bicarbonate and saline. The dried ($MgSO_4$) ether extracts were evaporated to dryness. The residue was recrystallized from benzene–pentane furnishing 720 mg (70%) of crystalline olefin formate, m.p. 120°, which was previously characterized (5).

trans-1-(2-O-Methoxyphenylethyl)-4β-hydroxy-2, 5α, 9β-trimethyl-1-octal-8-one (9c)

A solution of 2.1 g of formate **9*a*** in methanol (20 ml) was allowed to stand for 3 h in the presence of sodium methylate (200 mg of Na dissolved in 5 ml of methanol). The reaction mixture was poured on water (50 ml) and extracted with ether (4 × 50 ml). The combined ether extracts were washed with water then dried ($MgSO_4$) and evaporated to dryness resulting in 1.95 g of t.l.c. homogeneous crystalline product (yield, 90%) m.p. 161°.

An analytical sample was prepared by recrystallization from benzene–pentane, m.p. 168°. Mass spectrum (70 eV) *m/e* (relative intensity) 342 (35, parent peak), 324 (60), 309 (40) 291 (30), 281 (15), 221 (100), 203 (80); i.r. ($CHCl_3$) 3500, 2950, 1710, 1600, 1490, 1480, 1240, 1110, 1030, 960, 920, 860 cm^{-1}; u.v.$_{max}$ (96% C_2H_5OH) 224 nm (ε 6980), 273 (2325), 278 (1995); n.m.r. at 60 MHz, ($CDCl_3$) τ 9.02 (d, 3, J = 6 Hz, 5-methyl), 8.26 (s, 3, angular methyl), 8.13 (s, 3; 2-methyl), 6.13 (s, 3, CH_3O), 5.60 (m. 1, C*H*OH), 3.00 (m, 3, aromatic protons).

Anal. Calcd. for $C_{22}H_{30}O_3$: C, 77.16; H, 8.83. Found: C, 77.01; H, 8.71.

*Cyclization Experiments with **9a***

(*a*) One gram of formate **9*a*** was refluxed for 5 h with glacial acetic acid (15 ml) and concentrated sulfuric acid (½ ml). The reaction mixture was poured on water (250 ml) and extracted with ether (4 × 100 ml). The combined extracts were washed with $NaHCO_3$ solution until neutrality and dried ($MgSO_4$). After evaporation the

[1]This possibility was also suggested by one of our referees. In the meantime we prepared compounds **9*d*** and **20** and thus excluded the alternative explanation. Nevertheless we thank the referee for the suggestion.

[2]The unusually low C=O stretching is probably due to hydrogen bonding.

Can. J. Chem. Downloaded from www.nrcresearchpress.com by 210.87.254.40 on 09/05/12
For personal use only.

residue was found to be a two-component mixture by t.l.c. The n.m.r. of the product revealed the presence of acetate **9***b* as well as formate **9***c*.

The mixture was dissolved in methanol (15 ml) and treated with sodium methylate (200 mg in 5 ml of methanol) for 18 h. After the same work-up as applied for **9***c*, 900 mg of alcohol **9***c* (85%) was recovered.

(*b*) Refluxing 500 mg of formate **9***a* in 10 ml of 85% formic acid for 8 h resulted in the recovery of the starting material only (420 mg).

*1-(2-O-Methoxyphenylethyl)-2, 6-dimethylcyclohexanol (**12**)*

A solution of acetylene **11** (6) (9.5 g) in methanol (200 ml) was hydrogenated overnight in the presence of 400 mg of 5% palladium-on-charcoal. After filtering the catalyst and evaporation to dryness of colorless oil was obtained (8.7 g, 92%); t.l.c. examination showed the presence of one component. Mass spectrum (70 ev) *m/e* (relative intensity) 262 (10, parent) 244 (95), 205 (11), 135 (21), 134 (21), 123 (24), 122 (100), 109 (20), 91 (80); i.r. ($CHCl_3$) 3571, 2900, 1595, 1486, 1456, 1238, 1046, 1028, 952, 941 cm^{-1}; u.v.$_{max}$ (95% C_2H_5OH) 278 nm (ε 2132), 271.5 (2234), 221 (9784): n.m.r. ($CDCl_3$) τ 9.07 (d, 6, J = 6 Hz, methyls), 8.57 (cyclohexane protons), 6.23 (s, 3, OCH_3), 3.1 (m, 4, aromatic). The product was characterized in terms of crystalline diketone **16**.

*1,2,3,4,4a,9,10,10a-Octahydro-1,4a-dimethyl-8-methoxyphenanthrene (**14**)*

(*a*) *Preparation*

Tertiary alcohol **12** (8.7 g) was stirred magnetically with 200 ml of 80% formic acid overnight at room temperature. The product was diluted with water and extracted with ether (3 × 200 ml). The organic layer was washed in succession with 10% sodium bicarbonate until neutrality, then with saline. The dried solution ($MgSO_4$) was evaporated to dryness (7 g, 86%). Thin-layer chromatography examination showed the product to be homogeneous: however, n.m.r. revealed the presence of *cis* and *trans* isomers. Mass spectrum (70 ev) *m/e* (relative intensity) 244 (51, parent) 229 (30), 201 (13); i.r. ($CHCl_3$) 2817, 1575, 1450 (broad), 1242 (broad), 1059 cm^{-1}; u.v.$_{max}$ (96% C_2H_5OH) 280 nm (ε 1635), 272 (1561) 222 (7700); n.m.r. ($CDCl_3$) τ 9.13 (broad, 3, CH-CH_3), 8.87 (2 peaks, 3, angular methyl), 6.27 (s, 3, OCH_3), 3.07 (m, 3, aromatic protons). The product was characterized in terms of crystalline diketone **16**.

(*b*) *Oxidation of **14** to **15** and **16***

A sample of tricyclic hydrocarbon **14** (1.2 g) was dissolved in glacial acetic acid (10 ml) and cooled with ice water. To this solution 1.8 g of chromium trioxide dissolved in 10 ml of 4:1 acetic acid – water was dripped in 10 min. The reaction mixture was stirred at room temperature for 24 h. After dilution with water to 50 ml the products were extracted with methylene chloride (3 × 20 ml). The organic layer was washed in succession with 10% sodium bicarbonate, and saline. The dried ($MgSO_4$) solution was evaporated to dryness (1.067 g, 82%). Thin-layer chromatography analysis distinguished two components.

The mixture was separated on silica gel preparative plates. Diketone **16** was isolated in crystalline form as the more polar component (420 mg). Its characterization is described below.

The less polar component (130 mg) is monoketone **15** as identified by the following data. Mass spectrum (70 ev) *m/e* (relative intensity) 258 (60 parent), 229 (52), 225 (50), 201 (64), 187 (52), 161 (100); i.r. ($CHCl_3$) 2800 (broad), 1660, 1587, 1450, 1258, 1053 cm^{-1}; u.v.$_{max}$ (95% C_2H_5OH) 320 nm (ε 3791), 259 (8055), 217 (15, 606); n.m.r. ($CDCl_3$) τ 8.95 (d, 3, J = 6 Hz, Ch—CH_3), 8.53 (s, 3, angular methyl), 6.13 (s, 3, OCH_3), 3.0 (m, 3, aromatic). Monoketone **15** was oxidized to the crystalline diketone **16***a* in terms of which its composition was characterized.

*1,2,3,4,4a,10aα-Hexahydro-1α,4aα-dimethyl-8-methoxyphenanthrenequinone (**16**)*

A solution of monoketone **15** (350 mg) in dioxane (20 ml) was refluxed with sublimed selenium oxide (300 mg) and a drop of water for 5 h. When the oxidation was complete (t.l.c.), the product was filtered, diluted with ether and washed with saline. Thin-layer chromatography examination showed the presence of one major and two minor products, which were separated by preparative chromatography on silica gel plates using 1:4 ether–benzene for development. The yellow α-diketone **16***a* (210 mg) was recrystallized from ether, m.p. 113–114 °C. The minor components could not be recovered in sufficient quantities. Mass spectrum (70 ev) *m/e* (relative intensity) 272 (22, parent), 257 (5), 244 (48), 229 (100), 201 (51); i.r. ($CHCl_3$) 2800, 1724, 1667, 1587, 1450, 1307, 1264, 1503 cm^{-1}; u.v.$_{max}$ (95% C_2H_5OH) 353 nm (ε 3497), 290 (6476) 250 (3238), 217 (9590), 207 (11, 916); n.m.r. ($CDCl_3$) τ 9.18 (d, 3, J = 8 Hz, 1-methyl), 8.75 (s, 3, angular methyl) 7.45 (d, 1, J = 10 Hz, proton at C-10a), 6.03 (s, 3, OCH_3), 2.73 (m, 3, aromatic ring).

Anal. Calcd. for $C_{17}H_{20}O_3$: C, 75.07; H, 7.41. Found: C, 74.91; H, 7.38.

*trans-1-(2-O-Methoxyphenylethyl-2,5α,9β-trimethyl-1-octal-4,8-dione (**9d**)*

A solution of 2.5 g of keto alcohol **9***c* in acetone (50 ml) was magnetically stirred at room temperature and titrated until the appearance of permanent brown color with Jones' reagent. The reaction mixture was poured on 150 ml of water and extracted with chloroform (4 × 50 ml). The combined extracts were washed in succession with water, 5% sodium bicarbonate solution and water. After drying ($MgSO_4$) and evaporation the crystalline residue was found homogeneous (yield, 2.1 g; 85%), m.p. 131°. An analytical sample was obtained by recrystallizing from benzene–pentane, the crystals were washed with methanol, m.p. 135°. Mass spectrum (70 ev) *m/e* relative intensity) 340 (30, parent peak), 322 (70), 307 (100), 218 (70); i.r. ($CHCl_3$) 2950, 1710, 1490, 1460, 1380, 1240, 1150, 1110, 1030 cm^{-1}; u.v.$_{max}$ (96% C_2H_5OH) 222 nm (ε 7020), 273 (2210), 278 (2010); n.m.r. at 60 MHz ($CDCl_3$) τ 9.25 (d, 3, J = 6 Hz, CH—CH_3), 8.75 (s, 3, angular methyl), 8.23 (s, 3, =C—CH_3), 6.27 (s, 3, CH_3O), 3.00 (m, 3, aromatic protons).

Anal. Calcd. for $C_{22}H_{28}O_3$: C, 77.61; H, 8.29. Found: C, 77.59; H, 8.3.

*An Attempt to Cyclize Diketone **9d***

A solution of β,γ-unsaturated ketone **9***d* (100 mg) in 90% formic acid (5 ml) was stirred at room temperature for 18 h. After dilution with water the product was extracted with chloroform (4 × 50 ml). The organic layer was washed with 5% $NaHCO_3$ solution and dried

TABLE 1. Statistical averages of the normalized structure factors

	Observed	Theoretical*	
		Centrosymmetric	Noncentrosymmetric
$\langle\|E\|\rangle$	0.772	0.798	0.886
$\langle\|E^2 - 1\|\rangle$	1.029	0.968	0.736
$\langle\|E\|^2\rangle$	1.016	1.000	1.000

*See ref. 9.

Can. J. Chem. Downloaded from www.nrcresearchpress.com by 210.87.254.40 on 09/05/12
For personal use only.

($MgSO_4$). After evaporation a crystalline material was obtained which proved to be identical with the starting material **9***d*.

*trans-1-(2-O-Methoxyphenylethyl-2,5α,9β-trimethyl-2-octal-4,8-dione (**20**)*

A solution of β,γ-unsaturated ketone **9***d* (300 mg) was refluxed for 8 h in 90% formic acid (15 ml). The reaction mixture was poured on water (100 ml) and extracted with chloroform (4 × 50 ml). After washing with 5% $NaHCO_3$ solution and drying ($MgSO_4$) the chloroform solution was concentrated. The oily t.l.c. homogeneous solution resisted all attempts of crystallization. It was therefore microdistilled at 135°/0.2 mm Hg (yield, 200 mg; 66%). Mass spectrum (70 ev) *m/e* (relative intensity) 340 (100, parent), 322 (30), 312 (35); i.r. ($CHCl_3$) 2950, 1700, 1685, 1600, 1480, 1350, 1220, 1100, 1020, 900, 850 cm^{-1}; u.v.$_{max}$ (96%, C_2H_5OH) 223 nm (ε 7500), 235 (8100), 275 (2100), 278 (1900); n.m.r. at 60 MHz ($CDCl_3$) τ 8.65 (s, 3, angular methyl), 8.57 (d, 3, J = 6 Hz, CH—CH_3), 7.93 (s, 3, =C—CH_3), 6.13 (s, 3, OCH_3), 4.23 (s, 1, olefinic), 3.00 (m, 4, aromatic protons).

Anal. Calcd. for $C_{22}H_{28}O_3$: C, 77.61; H, 8.29. Found: C, 77.98; H, 8.05.

A sample of diketone **20** (200 mg) was heated with polyphosphoric acid for 25 min at 120°. After the usual work-up only a polymeric substance was recovered devoid of carbonyl stretching (i.r.) having a molecular weight higher than 600.

Crystallographic Studies

Well developed prismatic crystals of **9***c* were obtained by slow evaporation from a methanol solution. Precession photographs revealed that the crystals belonged to the orthorhombic system, space group *Pbca*. The unit cell dimensions were obtained at 20(1) °C by a least-squares refinement of the angular measurements of 12 reflections centered on the Picker diffractometer. The wavelength for the CuKα$_1$ radiation, λ = 1.54056 Å, was taken from Bearden (8).

Crystal data.

$C_{22}H_{30}O_3$ f.w. = 342.48

a = 10.254(2), b = 15.740(3), c = 24.164(4) Å, V = 3899.8 Å^3, D_x = 1.167 g cm^{-3}, Z = 8, $F(000)$ = 1488 (CuKα = 5.73 cm^{-1}). Space group, *Pbca*.

Three dimensional intensity data were collected with an automatic Picker diffractometer using a graphite monochromator and CuKα radiation with a take off angle of 2°. Intensity data were collected by the θ–2θ scan technique, with scan width varying from 1.70 to 2.80° as θ increased. Backgrounds of 20 s were measured at both scan limits. The three nearly orthogonal standard reflections, remeasured every 30 reflections, indicated that there was no sign of deterioration of the crystal over the duration of the data collection. All the intensities were corrected for background and placed on a common scale. The standard deviation for the net intensity of a reflection was calculated according to $\sigma(I) = [T + (t/80)^2B + (0.03\ N)^2]^{1/2}$, T being the total count, B the total background count, N the net count, and t the scanning time over one reflection. Of the 3128 independent reflections measured up to 2θ = 125°, only 2075 reflections (66.0%) were considered observed, *i.e.* $N/\sigma(I) > 1.96$. Lorentz and polarization corrections were made, but since the crystal was of small dimensions (0.17 × 0.20 × 0.30 mm^3), no absorption correction was applied.

*Structure Determination of Compound **9***c*

A set of normalized structure factors $|E|$ was obtained after isotropic temperature factor correction. The statistical averages of the normalized structure factors, shown in Table 1, indicate a centrosymmetrical distribution in agreement with the space group determination. The signs of 329 reflections with $|E| \geqslant 1.65$ were determined using the MULTAN symbolic addition program of Main *et al.* (10). The *E*-map, calculated with the set of signs with the highest absolute figure of merit of 1.168 and an *R*-Karle value (11) of 0.252, revealed 17 peaks forming a bonded fragment constituted of two fused six-membered rings. There were some other relatively strong peaks visible on the *E*-map but they were not considered since they did not seem to belong to the expected structure. The set of structure factors calculated with the coordinates of the 17 "carbon" atoms and an overall temperature factor of 3.48 Å^2 gave an *R*-value of 0.53 which decreased to 0.48 in two cycles of isotropic refinement. A Fourier difference map indicated peaks at the positions already observed in the first *E*-map but not taken into account then. A critical look at the peak distribution and at the synthesis reactions led us to the conclusion that the 25 peaks corresponded to a structure very close to **9***c*. In retrospect, these peaks were among the first 26 strongest peaks of the original *E*-map.

Two cycles of isotropic refinement of the coordinates of 25 heavy atoms gave an *R*-factor of 0.186. The three oxygen atoms were identified from the behavior of their temperature factors. Two more cycles with anisotropic temperature factors decreased *R* to 0.143.

Seventeen hydrogen atoms were located on a Fourier difference map computed at this stage. When these atoms were included in the refinement, the *R* factor dropped in four cycles to 0.080. A succession of Fourier difference maps and structure factor calculations finally yielded most of the H atoms. For each of the three methyl groups C(20), C(21), and C(22), (see Fig. 2 for numbering) only one hydrogen could be found; the positions of the two others were calculated assuming sp^3 geometry and a

TABLE 2. Positional and thermal parameters of the heavy atoms in olefin **9c***

Atom	X	Y	Z	U_{11}	U_{22}	U_{33}	U_{12}	U_{13}	U_{23}
O(1)	28695(13)	32811(7)	13167(5)	576(9)	284(7)	639(8)	32(3)	38(3)	53(3)
O(2)	17853(13)	65508(7)	10564(5)	664(9)	276(7)	659(9)	41(3)	−79(4)	−0(3)
O(3)	−25993(14)	32733(9)	18499(5)	706(10)	823(11)	453(8)	−118(4)	41(4)	−11(4)
C(1)	30385(17)	38939(11)	10188(7)	364(11)	283(10)	394(10)	5(4)	−4(4)	−15(4)
C(2)	41897(19)	39551(12)	6345(8)	437(12)	358(11)	627(14)	47(5)	68(5)	−1(5)
C(3)	50503(19)	47108(13)	8073(8)	337(11)	536(13)	611(14)	7(5)	69(5)	24(5)
C(4)	43090(18)	55353(12)	8992(8)	358(12)	377(11)	511(12)	−19(5)	16(5)	10(5)
C(5)	31554(17)	53607(10)	12874(7)	319(11)	282(9)	351(10)	3(4)	−20(4)	8(4)
C(6)	24465(19)	61413(11)	15041(7)	378(11)	314(10)	508(12)	0(5)	−38(5)	−36(4)
C(7)	15281(19)	58766(12)	19578(8)	396(11)	450(12)	490(12)	33(5)	−16(5)	−80(5)
C(8)	7458(18)	50833(12)	18420(7)	342(11)	435(12)	387(11)	10(5)	13(4)	−16(5)
C(9)	10081(18)	45569(10)	14265(7)	297(10)	293(10)	361(10)	9(4)	0(4)	14(4)
C(10)	21801(17)	46910(10)	10487(6)	313(10)	221(8)	328(10)	3(4)	1(4)	0(4)
C(11)	1123(18)	38160(11)	12839(7)	327(11)	357(10)	428(11)	−25(4)	13(4)	9(4)
C(12)	−12103(18)	40940(12)	10378(7)	369(12)	404(11)	517(12)	−15(5)	−27(5)	12(5)
C(13)	−20840(17)	33488(11)	9095(7)	291(10)	347(11)	483(12)	0(4)	−7(4)	−0(4)
C(14)	−22450(19)	30460(12)	3774(7)	438(12)	454(12)	466(12)	5(5)	21(5)	1(5)
C(15)	−30434(19)	23629(13)	2571(8)	510(13)	477(13)	601(13)	−1(6)	−20(6)	−70(5)
C(16)	−36875(19)	19639(13)	6786(9)	401(13)	417(12)	847(16)	−38(5)	10(6)	−58(6)
C(17)	−35515(19)	22434(13)	12179(8)	361(12)	514(13)	641(14)	−38(5)	33(5)	39(6)
C(18)	−27645(18)	29371(12)	13329(7)	338(11)	434(11)	495(12)	−12(5)	3(5)	−6(5)
C(19)	16698(18)	49024(11)	4609(7)	406(11)	326(11)	394(11)	0(5)	−5(5)	12(4)
C(20)	52329(22)	62164(15)	11251(10)	499(14)	642(15)	947(19)	−138(6)	38(7)	−11(7)
C(21)	−3534(22)	49539(16)	22443(9)	586(16)	961(20)	571(14)	−62(7)	114(6)	−90(7)
C(22)	−33156(29)	29157(19)	22963(10)	1299(25)	1093(23)	586(16)	−129(11)	109(9)	22(8)

*The coordinates are in fractions of unit cell edges × 10^5. The thermal parameters are given × 10^4. The standard deviations refer to the least significant digits. The temperature factor is of the form $T = \exp(-2\pi^2(U_{11}h^2 - A^{*2} + ... + 2U_{12}hkA^*B^* + ...)$.

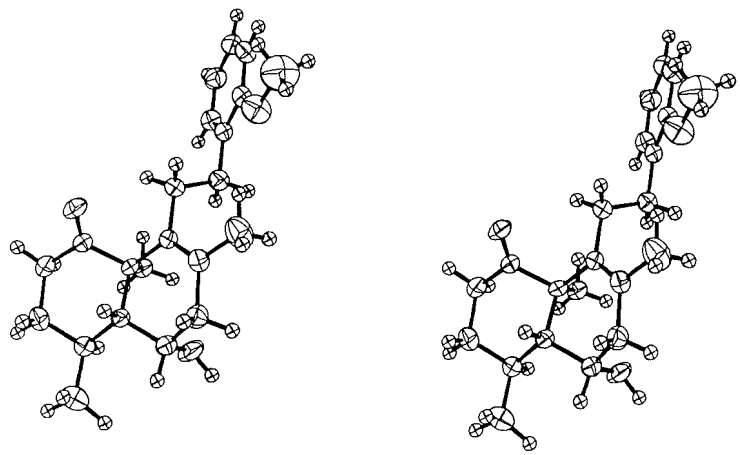

FIG. 1. Stereoscopic pair of drawing showing the molecule.

Can. J. Chem. Downloaded from www.nrcresearchpress.com by 210.87.254.40 on 09/05/12
For personal use only.

Can. J. Chem. Downloaded from www.nrcresearchpress.com by 210.87.254.40 on 09/05/12
For personal use only.

TABLE 3. Positional and thermal parameters of the hydrogen atoms in olefin 9c*

Atom	X	Y	Z	$U_{(ISO)}$
H(21)	3866(18)	4037(11)	233(7)	625(61)
H(22)	4641(14)	3405(10)	652(6)	404(50)
H(31)	5523(16)	4570(10)	1175(6)	449(53)
H(32)	5744(15)	4777(10)	538(6)	386(50)
H(41)	3949(15)	5751(10)	543(6)	413(53)
H(51)	3541(15)	5068(9)	1631(6)	294(46)
H(61)	3141(14)	6552(10)	1658(6)	351(47)
H(71)	2035(15)	5768(9)	2316(6)	403(51)
H(72)	921(15)	6360(10)	2040(6)	486(54)
H(111)	552(14)	3424(9)	988(6)	333(47)
H(112)	−64(15)	3455(10)	1610(6)	413(51)
H(121)	−1035(16)	4424(10)	695(6)	439(53)
H(122)	−1658(17)	4516(10)	1314(6)	549(58)
H(141)	−1758(16)	3304(11)	84(6)	562(58)
H(151)	−3150(17)	2187(12)	−143(7)	696(65)
H(161)	−4279(17)	1493(11)	615(7)	623(62)
H(171)	−4011(17)	1975(10)	1504(6)	505(55)
H(191)	1063(15)	5354(10)	483(6)	402(50)
H(192)	1192(15)	4400(10)	300(6)	424(52)
H(193)	2369(17)	5060(10)	200(6)	424(51)
H(201)	6027(19)	6221(13)	897(8)	836(73)
H(202)	4831(21)	6855(14)	1119(8)	1040(85)
H(203)	5536(21)	6026(13)	1507(9)	1041(85)
H(211)	−858(19)	4395(13)	2209(7)	833(76)
H(212)	−1030(24)	5331(16)	2168(9)	1246(96)
H(213)	−71(24)	5085(14)	2618(10)	1182(91)
H(221)	−3089(22)	2315(15)	2320(9)	1356(91)
H(222)	−4229(24)	2948(17)	2207(9)	1457(97)
H(223)	−2994(22)	3217(15)	2620(10)	1394(93)
OH(1)	1648(23)	7079(15)	1150(8)	1106(90)

*The coordinates are in fractions of unit cell edges × 10^4. The thermal parameters are given × 10^4. The standard deviations refer to the least significant digits. The temperature factor is of the form

$$T = \exp(-8\pi^2 U_{iso} \sin^2\theta/\lambda^2).$$

C—H bond distance of 1.00 Å. When all atomic coordinates and temperature factors were allowed to vary, R decreased to 0.067. This value is for observed reflections only, each having unit weight. In three more cycles, using weights $w = 1/\sigma^2(F)$ and reduced parameter shifts, R decreased to 0.048 and R_w was found to be 0.038. For all measured reflections $R = 0.081$ and $R_w = 0.042$. The overall standard deviation $\sigma(F) = [\Sigma_H w_H \Delta F^2/(n-m)]^{1/2}$, where n is the number of reflections and m the number of parameters, was 1.38 at the end of the refinement and the final secondary extinction parameter g was $0.288(6) \times 10^{-4}$. A final difference electron density map showed no significant residual density, the maximum density being 0.17 $e/Å^3$, the minimum -0.21 $e/Å^3$.

The scattering factors for the heavy atoms were those of Cromer and Waber (12) and those of Stewart *et al.* (13) for H. The programs used in this work were the NRC set of crystallographic programs of Ahmed *et al.* (14) and NUCLS, originally ORFLS, modified by Doedens and Ibers.

Results and Discussion[3]

The atomic coordinates, the vibrational parameters and their standard deviations are listed in Table 2 for the heavy atoms and in Table 3 for the hydrogen atoms. The molecular structure is represented by the pair of stereoscopic drawings in Fig. 1.

The two steroid rings are *trans* fused and the C(20) and C(21) methyl groups are in equatorial positions while the C(19) methyl and O(2) hydrogen are attached in axial positions.

Bond Distances and Angles

The interatomic distances and angles between nonhydrogen atoms are summarized in Figs. 2*a* and *b* respectively. The distances and angles, calculated from the final refined coordinates, are not corrected for thermal motion. The estimated standard deviations have been doubled to allow for the block-diagonal approximation; they are of the order of 0.006 Å and 0.4° for the distances and angles respectively, for non-hydrogen atoms.

The average distances in the molecule are compared below with the value given by Sutton (15).

Bond type	Number	Average distance (Å)	Sutton's values (Å)
$C(sp^3)$—$C(sp^3)$	9	1.534	1.537(5)
$C(sp^3)$—$C(sp^2)$	7	1.515	1.506(5)
$C(sp^2)$—$C(sp^2)$ (benzene)	6	1.383	1.394(5)
$C(sp^2)$—$C(sp^2)$	1	1.329	1.335(5)
$C(sp^2)$=O	1	1.216	1.215(5)
$C(sp^2)$—O—CH_3	1	1.367	1.358(5)
$C(sp^3)$—O—	2	1.426	1.426(5)

Some of the bond distances of the $C(sp^3)$—$C(sp^3)$ type (C(5)—C(10) = 1.563, C(6)—C(7) = 1.504, C(10)—C(19) = 1.550 Å) deviate by more than 3 standard deviations from the average

[3]The structure factor table is available, at a nominal charge, from the Depository of Unpublished Data, National Science Library, National Research Council of Canada, Ottawa, Canada K1A 0S2.

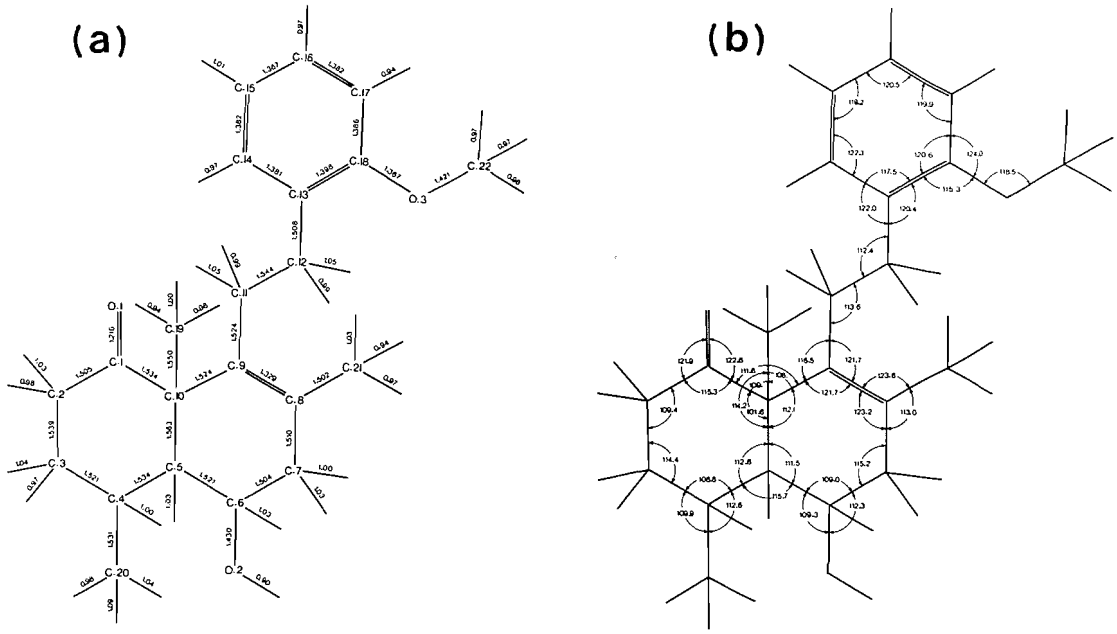

FIG. 2. (*a*) Bond distances. (*b*) Bond angles.

TABLE 4. Comparison of bond distances in a number of steroids

C(5)—C(10) (Å)	C(10)—C(19) (Å)	C(10)—C(9) (Å)	Reference
1.563(6)	1.550(6)	1.524(6)*	This work
1.567(8)	1.546(8)	1.559(8)	16
1.562(11)	1.550(11)	1.567(11)	16
1.546(9)	1.557(9)	1.553(9)	17
1.520(6)*	1.562(6)	1.562(6)	18
1.525(5)*	1.564(5)	1.566(5)	19
1.526(5)*	1.553(6)	1.571(6)	20

*One of the atoms of the bond is of the C(sp^2) type.

TABLE 5. Torsion angles* in the steroid part of the molecule

Ring A		Ring B	
Bond	θ(M—N)	Bond	θ(M—N)
C(1)—C(2)	−57.6°	C(5)—C(6)	−60.2°
C(2)—C(3)	48.9	C(6)—C(7)	+42.8
C(3)—C(4)	−50.6	C(7)—C(8)	−12.7
C(4)—C(5)	60.1	C(8)—C(9)	3.4
C(5)—C(10)	−63.5	C(9)—C(10)	−13.0
C(10)—C(1)	62.9	C(10)—C(5)	+45.0

*θ(M—N) is the torsion angle L—M—N—P, when the two other atoms L and P are in the ring in question.

value quoted by Sutton. The C(9)—C(10) bond, of the C(sp^2)—C(sp^3) type, is also longer than expected. Such a lengthening of the bonds around C(10) has already been observed in a number of steroids. For comparison purpose some of these values are presented in Table 4.

The average bond angle around C(sp^3) atoms is 111.2°; the individual angles vary in the range 101.6–115.7°. The average bond angles around C(sp^2) atoms is 120.0° with a range of 113.0–124.0°.

The distances and angles for bonds involving hydrogen atoms have also been calculated. The standard deviations are estimated to be 0.06 Å for the C—H distances for the C(20), C(21), C(22) methyl groups, and O(2)—H, and 0.04 Å for all the other C—H bond distances. A summary of the distances involving hydrogen atoms is shown below.

Bond type	Number	Average distance (Å)	Extreme distances (Å)
C(sp^3)—H	25	1.00	0.94–1.09
C(sp^2)—H	4	0.97	0.94–1.01
O—H	1	0.90	

Can. J. Chem. Downloaded from www.nrcresearchpress.com by 210.87.254.40 on 09/05/12
For personal use only.

TABLE 6. Mean planes

Plane I				Plane II	
Atom	Deviation	Atom	Deviation	Atom	Deviation
O(3)	0.021 Å	C(22)†	0.093 Å	C(9)	−0.006 Å
C(12)	−0.012	H(141)†	−0.03	C(11)	0.006
C(13)	−0.003	H(151)†	−0.04	C(12)	0.006
C(14)	0.006	H(161)†	0.03	C(13)	−0.006
C(15)	0.013	H(171)†	−0.01	H(111)†	0.86
C(16)	−0.003	H(221)†	−0.67	H(112)†	−0.77
C(17)	−0.018	H(222)†	0.89	H(121)†	0.81
C(18)	−0.004	H(223)†	0.02	H(122)†	−0.82

Equations for least-squares planes*

Plane I $0.3892X - 0.0446Y - 0.9201Z + 3.0835 = 0$

Plane II $-0.7736X + 0.6187Y - 0.1369Z - 4.6165 = 0$

*The planes are in the form $lX + mY + nZ - p = 0$, where X, Y, Z and p are in Å units. The X, Y and Z axes are parallel to the a, b, and c axes, respectively.
†Atoms not included in the least-squares plane calculation.

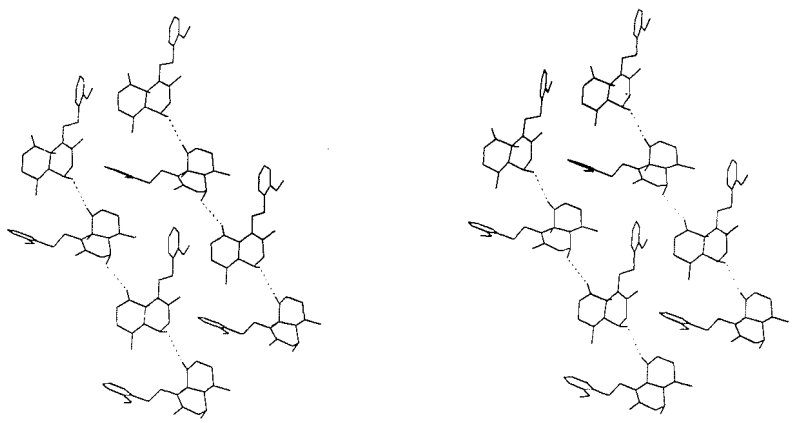

FIG. 3. Molecular packing projected on (001) showing the hydrogen bonding of the molecules.

Torsional Angles

Some of the torsional angles calculated for the steroid part of the molecule are listed in Table 5. In ring A (atoms C(1) through C(5) and C(10)) the average absolute value of the torsional angles, 57.3°, remains close to the expected value for the symmetrically staggered configuration. The distortion due to the double bond between C(1) and O(1) is reflected in θ(2,3) and θ(3,4) while θ(1,2) and θ(1,10) are seemingly not affected. In ring B (atoms C(5) through C(10)) the double bond at C(8)—C(9), which causes the torsional angle θ(8,9) to assume nearly an eclipsed configuration, also affects very significantly θ(7,8) and θ(9,10).

The C(19) and (C20) methyl groups deviate by an average of 16 and 20°, respectively, from the staggered configuration.

Mean Planes

As can be observed in Table 6, the methoxy phenyl group is very nearly planar (Plane I). The hydrogen atoms are slightly farther away from this ring mainly because of more important errors in the determination of their coordinates. It is interesting to note that H(221) and H(222) of the C(22) methyl group are located on either side of Plane I although not exactly equidistant from the plane since (C22) is off by about 0.1 Å. H(223) is itself in Plane I, pointing away from H(171) to reduce H—H interaction.

The four carbon atoms making up Plane II

Can. J. Chem. Downloaded from www.nrcresearchpress.com by 210.87.254.40 on 09/05/12
For personal use only.

form a planar zigzag chain as found in polyethylene with hydrogen atoms symmetrically placed on either side of the chain.

Molecular Packing

The molecular packing projected on (001) is shown in Fig. 3. None of the carbon–carbon or carbon–oxygen contacts is shorter than 3.30 Å. However there is one short O—O contact at 2.817(6) Å. The oxygen atoms involved are O(1) in the symmetry position (XYZ) and O(2) in the position ($\frac{1}{2} - X$, $\frac{1}{2} + Y$, Z). The O(1) . . . H-(OH 1) distance is 2.00(5) Å and the O(1) . . . H(OH 1)—O(2) angle is 154.8°.

In the solid state the molecules are held together in chains by hydrogen bonding.

The financial assistance of the National Research Council of Canada and the Research Corporation are gratefully acknowledged, special thanks are due Dr. R. Duffy and the Senate Research Committee of University of Prince Edward Island for promoting this research. Dr. R. Rigney is thanked for encouraging this work. We also thank Dr. H. Dugas at the University of Montreal for his help and attention.

1. (*a*) J. C. BARDHAN and S. C. SENGUPTA. J. Chem. Soc. 2520, 2798 (1932). (*b*) D. PERLMAN, D. DAVIDSON, and M. T. BOGERT. J. Org. Chem. 288, 300 (1936). (*c*) J. W. COOK, C. L. HEWETT, and A. M. ROBINSON. J. Chem. Soc. 168 (1939).
2. L. R. C. BARCLAY. Cyclialkylation of aromatics. *In* G. Olah's Friedel-Crafts and related reactions. Vol. II. Part 2. Interscience Publishers, New York. 1971. p. 785.
3. R. A. BARNES and A. D. OLIN. J. Am. Chem. Soc. **78**, 3830 (1956).
4. (*a*) R. D. HAWORTH and R. L. BARKER. J. Chem. Soc. 1299 (1939). (*b*) R. D. HAWORTH and B. P. MOORE. J. Chem. Soc. 633 (1946).
5. C. SCHMIDT. Can. J. Chem. **51**, 3989 (1973).
6. C. SCHMIDT and J. THAZHUTHAVEETIL. Can. J. Chem. **51**, 3620 (1973).
7. E. WENKERT and W. G. JACKSON. J. Am. Chem. Soc. **80**, 211 (1958).
8. J. A. BEARDEN. X-Ray wavelengths. U.S. Atomic Energy Commission, Division of Technical Information Extension, Oak Ridge, Tennessee (1964).
9. F. HANIC. Acta Cryst. **21**, 332 (1966).
10. P. MAIN, M. N. WOOLFSON, and G. GERMAIN. A computer program for the automatic solution of crystal structures. CECAM Meeting, Parma, Italy, 1970.
11. J. KARLE and I. L. KARLE. Acta Cryst. **21**, 847 (1966).
12. D. T. CROMER and J. T. WABER. Acta Cryst. B**24**, 337 (1965).
13. R. F. STEWART, E. R. DAVIDSON, and N. T. SIMPSON. J. Chem. Phys. **42**, 3175 (1965).
14. F. R. AHMED, S. R. HALL, M. E. PIPPY, and C. P. HUBER. NRC Crystallographic Programs for the IBM System. World List of Crystallographic Programs. 2nd ed. Appendix. 1966. p. 52.
15. L. E. SUTTON. Tables of Interatomic Distances and Configuration in Molecules and Ions. Supplement 1956–1959. The Chemical Society, London. (1965).
16. I. L. KARLE. Acta Cryst. B**28**, 2000 (1972).
17. J. M. OHRT, A. COOPER, and D. A. NORTON. Acta Cryst. B**25**, 41 (1969).
18. B. BUSETTA, C. COURSEILLE, F. LEROY, and M. HOSPITAL. Acta Cryst. B**28**, 3293 (1972).
19. L. DUPONT, O. DIDEBERG, and H. CAMPSTEYN. Acta Cryst. B**28**, 3023 (1972).
20. E. M. GOPALAKRISHNA, A. COOPER, and D. A. NORTON. Acta Cryst. B**25**, 639 (1969).

Can. J. Chem. Downloaded from www.nrcresearchpress.com by 210.87.254.40 on 09/05/12
For personal use only.

Spectra and Decay of Trichloromethyl Radicals in Aqueous Solution

B. LESIGNE, L. GILLES, AND R. J. WOODS[1]

Section de Recherches et Interaction du Rayonnement avec la Matière, CEN SACLAY, B.P. 2, Gif-sur-Yvette 91190, France

Received November 15, 1973

Trichloromethyl radicals ($\lambda_{max} < 230$ nm, $\varepsilon_{230\ nm} = 2300 \pm 450\ M^{-1}\ cm^{-1}$) are formed by the pulse radiolysis of aqueous carbon tetrachloride solutions. At concentrations of the order of 10^{-4} M and pH 5.5–12.4, CCl_3 disappears by a second-order process with $2k = (7.4 \pm 1.8) \times 10^8\ M^{-1}\ s^{-1}$ and without detectable hydrolysis. Both CCl_3 and $CHCl_2$ are believed to be formed by the pulse radiolysis of aqueous chloroform solutions but at wavelengths greater than 230 nm only absorption attributable to CCl_3 was observed.

Les radicaux trichlorométhyles ($\lambda_{max} < 230$ nm, $\varepsilon_{230\ nm} = 2300 \pm 450\ M^{-1}\ cm^{-1}$) sont formés par la radiolyse à impulsion des solutions aqueuses de tétrachlorure de carbone. A des concentrations de l'ordre de 10^{-4} M et de pH 5.5–12.4, CCl_3 disparaît par un procédé du second ordre avec $2k = (7.4 \pm 1.8) \times 10^8\ M^{-1}\ s^{-1}$, et sans hydrolyse décelable. On considère que ces deux produits CCl_3 et $CHCl_3$ sont formés par la radiolyse à impulsion de solutions aqueuses de chloroforme, mais à des longueurs d'onde supérieures à 230 nm, seule une absorption attribuable au CCl_3 est observée. [Traduit par le journal]

Can. J. Chem., **52**, 1135 (1974)

The reactions of photochemically produced trichloromethyl radicals have been studied extensively in the gas phase (1) and, to a lesser extent, in organic solvents but have received little attention in aqueous media, where hydrolysis may be one of the processes involved. Trichloromethyl radicals can be produced in aqueous solution by the radiolysis of carbon tetrachloride solutions (2), taking advantage of the efficient reaction between aliphatic chlorine compounds and hydrated electrons (3),

$$[1]\quad e_{aq}^- + CCl_4 \rightarrow CCl_3 + Cl^- \qquad k_1 = 3.0 \times 10^{10}\ M^{-1}\ s^{-1}\ (4)$$

Dichloromethyl radicals will be formed via the corresponding reaction with chloroform,

$$[2]\quad e_{aq}^- + CHCl_3 \rightarrow CHCl_2 + Cl^- \qquad k_2 = 3.0 \times 10^{10}\ M^{-1}\ s^{-1}\ (4)$$

The present paper describes the pulse radiolysis of aqueous carbon tetrachloride solutions and reports absorption in the 230–280 nm region which is attributed to CCl_3. The decay of the absorbing species from 2 to 90 μs after the pulse is consistent with CCl_3 dimerization without hydrolysis. Pulse radiolysis of aqueous chloroform solutions appears to produce the same absorbing species, which decays by a second-order process but more rapidly than when formed by the radiolysis of CCl_4 solutions.

Experimental

Saturated solutions were prepared by shaking reagent grade carbon tetrachloride (Prolabo) or chloroform (Merck) with triple-distilled water (discarding the first five washings) and were purged with argon saturated with the solute and water vapor. Solutions were irradiated as described previously (5) in 2.5 or 5 mm thick silica cells (optical path length, 2.5 cm) by 12 ns pulses of 1.8 MeV electrons from a modified (6) Febetron 707. The system included a Zeiss M4 QIII prism monochromator for which the scattered light at 230–300 nm was less than 0.1% (makers specification, confirmed by experiment). At 230 nm with a slit width of 0.9 mm (the largest used) the bandwidth of the monochromator was 2.3 nm. Absorbed dose (5–100 krad per pulse) was estimated using 0.1 M potassium ferrocyanide solutions saturated with nitrous oxide taking $\varepsilon = 600\ M^{-1}\ cm^{-1}$ at 440 nm (7) and $G = 5.5$ (8) for ferricyanide.

Results

Absorption spectra of transient species present in 5×10^{-3} M CCl_4 solutions (initial pH 5.5) ~30 ns (curve A) and 2 μs (curve B) after an electron pulse are plotted in Fig. 1. The absorption spectrum of hydroxyl radicals (9) formed during the pulse ($G_{OH} = 2.75$), assuming that none have disappeared by subsequent reaction, is also shown. Transitory absorption which decayed with a half-life of less than 10 ns was observed at 550 nm and attributed to the hydrated electron but no longer-lived absorption was found at

[1]On leave from the Department of Chemistry and Chemical Engineering, University of Saskatchewan, Saskatoon, Saskatchewan, 1972–1973.

Can. J. Chem. Downloaded from www.nrcresearchpress.com by 210.87.254.5 on 09/05/12
For personal use only.

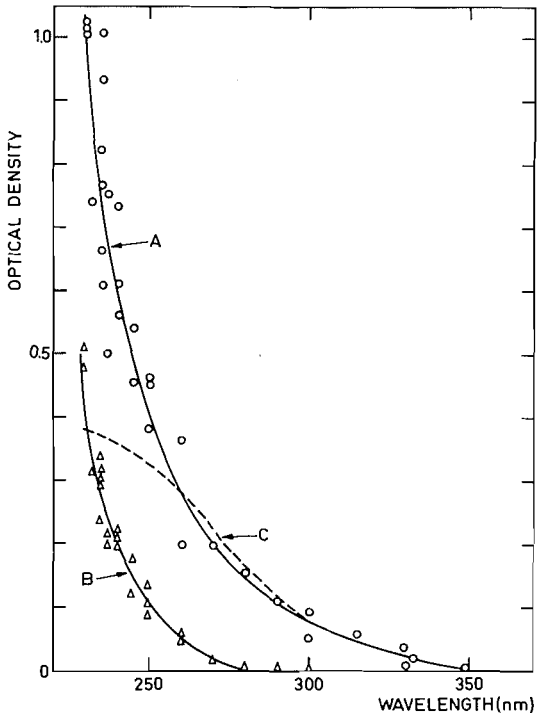

FIG. 1. Transient spectra in 5×10^{-3} M aqueous CCl_4 solution; initial pH 5.5, 100 krad/pulse. Curve A, at ~30 ns; curve B at 2 μs. Curve C, predicted absorption of 2.85×10^{-4} M OH (9).

wavelengths above 350 nm. The absorption at 230–250 nm decayed rapidly during the first 1–2 μs following the pulse (Fig. 2*a*), then more slowly by a second-order process (Fig. 3) having $2k/\varepsilon = 3.2 \times 10^5$ cm s^{-1} at 230 ± 1 nm.

An extinction coefficient of 2300 ± 450 M^{-1} cm^{-1} at 230 ± 1 nm was estimated for the longer lived transient in a separate series of experiments in which the absorbed dose for each pulse was monitored using a Faraday cup coupled with a capacitive shunt and placed immediately behind the silica irradiation cell; the value of the shunt was calibrated in terms of absorbed dose using the ferrocyanide dosimeter. This system was not available for the experiments depicted in Figs. 1 and 4, for which a mean absorbed dose was determined by dosimetry before and after a series of runs with CCl_4 or $CHCl_3$ solutions. In calculating the extinction coefficient it was assumed that the initial absorption was due to OH and a longer-lived transient formed with G values of 2.75 and 2.7, respectively (10). Small corrections were made to these G values to allow for radical reactions occurring during the first 30 ns following the pulse; calculations were carried out with a Hewlett-Packard 9100B calculator equipped with a 9101A Extended Memory and were based on a mechanism made up of reaction 1 and reactions 3–6.

[3] $e_{aq}^- + OH \rightarrow OH^-$
$k_3 = 3.0 \times 10^{10}\ M^{-1}\ s^{-1}$ (3)

[4] $e_{aq}^- + e_{aq}^- \rightarrow H_2 + 2OH^-$
$2k_4 = 6 \times 10^9\ M^{-1}\ s^{-1}$ (3)

[5] $OH + OH \rightarrow H_2O_2$ $2k_5 = 6 \times 10^9\ M^{-1}\ s^{-1}$ (11)

[6] $OH + CCl_3 \rightarrow$ Products
$k_6 = 2 \times 10^9\ M^{-1}\ s^{-1}$ (estimated below)

The mechanism includes only the more important reactions influencing the G values but is adequate since the corrections are small, *e.g.*, for a 20 krad electron pulse (the median dose in this set of experiments), $G(OH)_{30\ ns} = 2.70$ and $G(e_{aq}^- + CCl_4)_{30\ ns} = 2.64$. A small correction was made for absorption due to hydrogen peroxide formed during (G = 0.7) and after the pulse.

If it is assumed that curve B of Fig. 1 relates to a single species with $\varepsilon = 2300 \pm 450\ M^{-1}$ cm^{-1} at 230 nm, the mean rate constant for the slower decay measured from 230 to 245 nm (pH 5.5) is $2k = (7.4 \pm 1.8) \times 10^8\ M^{-1}\ s^{-1}$ independent of wavelength.

Data for 7×10^{-2} M $CHCl_3$ solutions (initial pH 5.3) are plotted in Fig. 4. With these solutions the absorption observed in the 230–250 nm region decayed in an essentially uniform, second order, manner (Fig. 2*b*) without the more rapid initial decay found with CCl_4 solutions (Fig. 2*a*); at 230 nm, the slope of a second-order decay plot (corresponding to $2k/\varepsilon$ for a single species) was 6×10^5 cm s^{-1}.

Discussion

The initial absorption in the 230–300 nm region for CCl_4 solutions (Fig. 1, curve A) is attributed to CCl_3 formed by reaction 1 and OH produced during the pulse. The latter disappear largely by reaction 5, whose rate constant sets a maximum half-life of ~600 ns for OH in the present system, although this will be reduced by the occurrence of other hydroxyl radical reactions, *e.g.*, 3 and 6. Additional CCl_3 will be produced if hydrogen atoms produced by irradiation abstract chlorine from CCl_4,

[7] $H + CCl_4 \rightarrow CCl_3 + HCl$
$k_7 = 4.8 \times 10^7\ M^{-1}\ s^{-1}$ (12)

Can. J. Chem. Downloaded from www.nrcresearchpress.com by 210.87.254.5 on 09/05/12
For personal use only.

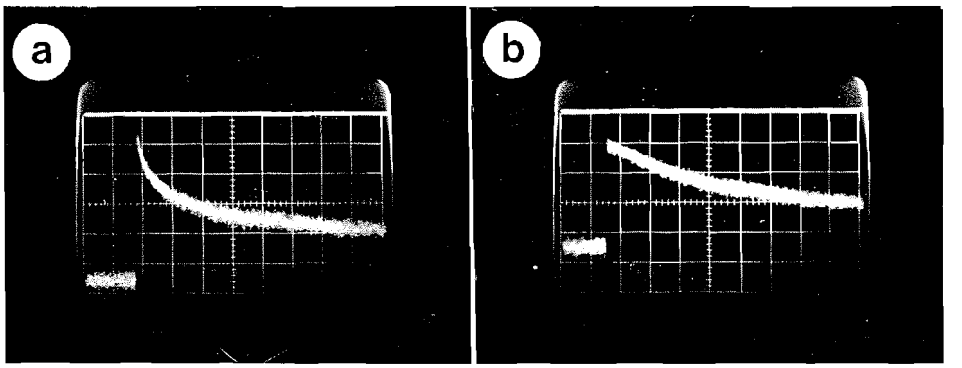

FIG. 2. Transient absorption produced in (*a*) 5×10^{-3} *M* aqueous CCl_4, (*b*) 7×10^{-2} *M* aqueous $CHCl_3$ solution by electron irradiation (initial p*H* 5.3–5.5, ~100 krad/pulse, 230 nm, 20 mV per vertical division, 2 μs per horizontal division).

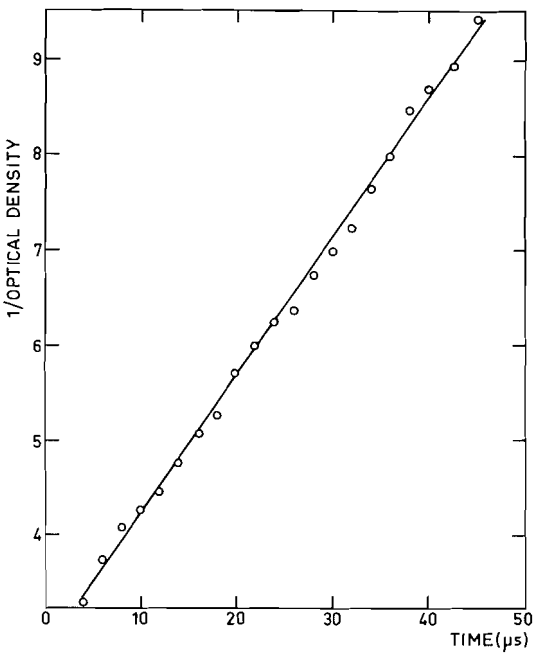

FIG. 3. Second-order decay plot for the longer-lived transient produced by electron irradiation of aqueous CCl_4 solutions (230 nm).

However, the relatively low rate constant for reaction 7 and the lower optical densities which we observe at p*H* 1.1 (Table 1), where 90% of the hydrated electrons are converted to H by reaction with H_3O^+, suggest that only a small proportion (<5%) of the hydrogen atoms formed react with CCl_4. The remainder probably dimerize or react with the relatively high concentration of OH present,

[8] $H + OH \rightarrow H_2O \qquad k_8 = 2 \times 10^{10}\ M^{-1}\ s^{-1}$ (11)

Thus, apart from a small contribution from hydrogen peroxide amounting to 2–4% of the total absorption, curve *B* of Fig. 1 is believed to represent the absorption spectrum of CCl_3 in water.

In aqueous solution CCl_3 might be expected to undergo hydrolysis in a similar manner to $CFCl_2$, CF_2Cl, and CF_3 (13, 14). However, it

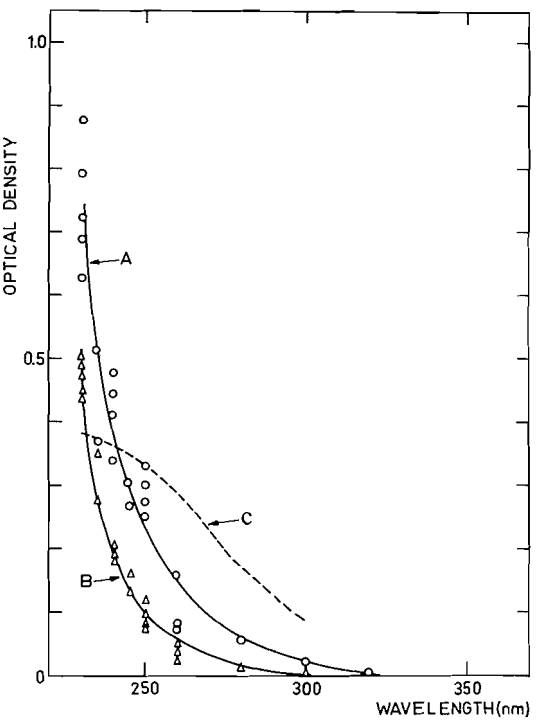

FIG. 4. Transient spectra in 7×10^{-2} *M* aqueous $CHCl_3$ solution; initial p*H* 5.3, 100 krad/pulse. Curve *A*, at ~30 ns; curve *B* at 2 μs. Curve *C*, predicted absorption of 2.85×10^{-4} *M* OH (9).

Can. J. Chem. Downloaded from www.nrcresearchpress.com by 210.87.254.5 on 09/05/12
For personal use only.

TABLE 1. Effect of pH on the pulse radiolysis of CCl_4 solutions*

Initial pH	Mean optical density† ~30 ns	Mean optical density† 2 μs	Mean $2k/\varepsilon$† ($cm^{-1}s^{-1}$)
1.1	0.27	0.12	9.6×10^5
5.5	1.1	0.49	3.2×10^5
9.8	0.81	0.40	6.9×10^5
11.8	0.97	0.70	2.2×10^5
12.4	0.94	0.71	4.3×10^5

*5×10^{-3} M CCl_4, pH adjusted with $Ba(OH)_2$ or $HClO_4$; 100 krad/pulse.
†230 nm. Values are the mean for three determinations except for those at pH 5.5, which are the mean for 14 experiments.

appears that CCl_3 disappears predominantly by combination under our conditions (radical concentration $\sim 2 \times 10^{-4}$ M) since the decay follows closely a second-order law (*e.g.* Fig. 3). The second-order rate constant, $(7.4 \pm 1.8) \times 10^8$ M^{-1} s^{-1}, is of the same order of magnitude as values determined by the rotating sector technique for the dimerization of CCl_3 in organic media which range from (0.5–14) $\times 10^7$ (15) to $(\sim 1\text{–}3) \times 10^9$ M^{-1} s^{-1} (16). The rate constant for reaction 9 (13) must be less than 5×10^4 s^{-1} or our second-order decay plots (*e.g.* Fig. 3) would show a significant deviation from linearity.

$$[9] \qquad CCl_3 + H_2O \rightarrow CCl_2OH + H^+ + Cl^-$$

An upper limit of $\sim 10^6$ M^{-1} s^{-1} is established for k_{10} by the observation that CCl_3 decay at pH 11.8–12.4 (Table 1) is second order with, within experimental limits, the same rate constant as at pH 5.5.

$$[10] \qquad CCl_3 + OH^- \rightarrow CCl_2OH + Cl^-$$

The order of magnitude of k_6 is estimated to be $\sim 2 \times 10^9$ M^{-1} s^{-1} from the decrease in absorption at 230 nm between 30 ns and 2 μs after the electron pulse, *i.e.* from the difference between curves A and B of Fig. 1. In making the estimate it is assumed that all OH will have reacted in 2 μs and that CCl_3 will have reacted in part by reaction 6 and by dimerization ($2k = 7.4 \times 10^8$ M^{-1} s^{-1}).

At high pH, an increase was observed in the optical density 2 μs after the pulse (Table 1) which is too great to be due entirely to scavenging reactions in the spurs. Furthermore, the decay of absorption is essentially uniform (as in Fig. 2*b*) and cannot be broken down into faster and slower components as is the case in neutral and acid solutions; the rate of decay is that found after 2 μs at lower pH and attributed to CCl_3 dimerization. The range of pH in which the optical density increases is that in which reaction 11 becomes significant,

$$[11] \qquad OH + OH^- \underset{b}{\overset{f}{\rightleftharpoons}} O^- + H_2O$$
$$k_{11f} = 1.2 \times 10^{10}\ M^{-1}\ s^{-1} \text{ (17)}$$
$$k_{11b} = 9.2 \times 10^7\ s^{-1} \text{ (17)}$$

and the increased absorption may be due to O^- (λ_{max} 240 nm with $\varepsilon = 240\ M^{-1}\ cm^{-1}$ (18)), which decays more slowly ($2k = 9 \times 10^8\ M^{-1}\ s^{-1}$) (11) than OH or, possibly, to the formation of additional CCl_3 by,

$$[12] \qquad O^- + CCl_4 \rightarrow CCl_3 + OCl^-$$

A reaction of this type has been proposed to account for an increase in the yield of $Cl^- + OCl^-$ from aqueous chloroform solutions irradiated at high pH (19).

Aqueous chloroform solutions were examined in the expectation, based on published rate constants for reactions 2 and 13, that the initial absorption spectrum obtained upon pulse radiolysis would be due to OH and $CHCl_2$. However

$$[13] \qquad OH + CHCl_3 \rightarrow CCl_3 + H_2O$$
$$k_{13} = 8.5 \times 10^{-6}\ M^{-1}\ s^{-1} \text{ (20)}$$

the spectra observed strongly suggest that k_{13} has a higher value than reported, probably above 10^8 M^{-1} s^{-1}, since the initial absorption between 240–300 nm (Fig. 4, curve *A*) is lower than expected if most of the OH have not yet reacted, and since the rapid decay associated with reactions such as 5 and 8 is absent. Within experimental limits, the absorption spectra (Fig. 4) are identical with that found after 2 μs with CCl_4 solutions and attributed to CCl_3, although the rate of decay is about 1.9 times as great as in CCl_4 solution. These observations are most readily explained if reactions 2 and 13 are both essentially complete within 30 ns, giving a mixture of $CHCl_2$ and CCl_3, and if $CHCl_2$ absorbs only weakly between 230 and 280 nm (the CCl_3 formed would be sufficient to account for the absorption observed). Decay of CCl_3 would be more rapid than in CCl_4 solution, although still second order, because of the additional possibility of reaction with $CHCl_2$ present in approximately equal concentration.

Can. J. Chem. Downloaded from www.nrcresearchpress.com by 210.87.254.5 on 09/05/12
For personal use only.

1. J. M. TEDDER and J. C. WALTON. Progress in reaction kinetics. Vol. 4. *Edited by* G. Ponter, K. R. Jennings, and B. Stevens. Pergamon Press, Oxford. 1967. p. 37.
2. R. KÖSTER and K.-D. ASMUS. Z. Naturforsch. **26**b, 1104 (1971).
3. E. J. HART and M. ANBAR. The hydrated electron. Wiley-Interscience, New York. 1970. p. 138.
4. E. J. HART, S. GORDON, and J. K. THOMAS. J. Phys. Chem. **68**, 1271 (1964).
5. F. BARAT, L. GILLES, B. HICKEL, and B. LESIGNE. J. Phys. Chem. **76**, 302 (1972).
6. B. LESIGNE and R. SAUNEUF. To be published.
7. S. R. COHEN and R. A. PLANE. J. Phys. Chem. **61**, 1096 (1957).
8. E. D. BLACK and E. HAYON. J. Phys. Chem. **74**, 3199 (1970).
9. P. PAGSBERG, H. CHRISTENSEN, J. RABANI, G. NILSSON, J. FENGER, and S. O. NIELSEN. J. Phys. Chem. **73**, 1029 (1969).
10. M. S. MATHESON and L. M. DORFMAN. Pulse radiolysis. M.I.T. Press, Cambridge, Mass. 1969. p. 64.
11. M. ANBAR and P. NETA. Int. J. Appl. Radiat. Isot. **18**, 493 (1967).
12. P. NETA, R. W. FESSENDEN, and R. H. SCHULER. J. Phys. Chem. **75**, 1654 (1971).
13. T. I. BALKAS, J. H. FENDLER, and R. H. SCHULER. J. Phys. Chem. **75**, 455 (1971).
14. J. LILIE, D. BEHAR, R. J. SUJDAK, and R. H. SCHULER. J. Phys. Chem. **76**, 2517 (1972).
15. D. J. CARLSSON and K. U. INGOLD. J. Am. Chem. Soc. **89**, 4891 (1967) and references cited therein.
16. D. J. CARLSSON, K. U. INGOLD, and L. C. BRAY. Int. J. Chem. Kin. **1**, 315 (1969).
17. G. V. BUXTON. Trans. Faraday Soc. **66**, 1656 (1970).
18. J. RABANI. Advances in chemistry series. Vol. 81. *Edited by* R. F. Gould. American Chemical Society, Washington, D.C. 1968. p. 131.
19. B. J. REZANSOFF, K. J. MCCALLUM, and R. J. WOODS. Can. J. Chem. **48**, 271 (1970).
20. M. ANBAR, D. MEYERSTEIN, and P. NETA. J. Chem. Soc. B, 742 (1966).

Can. J. Chem. Downloaded from www.nrcresearchpress.com by 210.87.254.5 on 09/05/12
For personal use only.

Structure cristalline et moléculaire du cyclopentadiényle-carbonyle-bistriphénylphosphine-manganèse (benzénate), $MnC_5H_5CO[P(C_6H_5)_3]_2 \cdot C_6H_6$

CLAUDE BARBEAU ET RAM JANAM DUBEY

Département de Chimie, Université Laval, Québec, Québec

Reçu le 30 août, 1973

La structure cristalline et moléculaire du cyclopentadiényle-carbonyle-bistriphénylphosphine-manganèse (benzénate), $MnC_5H_5CO[P(C_6H_5)_3]_2 \cdot C_6H_6$, a été obtenue après analyse de données tridimensionnelles de rayons X recueillies sur films de chambre de précession. Les cristaux rectangulaires rouges sont tricliniques, groupe d'espace $P\bar{1}$, avec les paramètres de la maille unitaire $a = 9.83(2)$ Å, $b = 14.79(1)$ Å, $c = 11.36(2)$ Å, $\alpha = 69.44(8)°$, $\beta = 66.48(8)°$, $\gamma = 67.57(10)°$, et $z = 2$. Le facteur de désaccord final est 0.087 pour 4554 réflexions indépendantes utilisées dans l'affinement par moindres carrés. La structure consiste en des molécules individuelles de $MnC_5H_5CO[P(C_6H_5)_3]_2$. La distance Mn—$C_{C_5H_5}$ est de 2.16(1) Å. Le coordinat CO (Mn—C: 1.748(9) Å, C—O: 1.172(11) Å) se situe perpendiculairement au plan des phosphores et du manganèse.

La caractéristique importante est l'angle P—Mn—P de 104(1)° (Mn—P: 2.237(3) Å). L'ouverture angulaire de 14° est vue comme une conséquence d'une répulsion électrostatique entre les deux atomes donneurs P.

The crystal and molecular structure of cyclopentadienylcarbonyl-bis(triphenylphosphine)-manganese(benzenate), $MnC_5H_5CO[P(C_6H_5)_3]_2 \cdot C_6H_6$, has been obtained from analysis of three dimensional X-ray data obtained with a precession camera. The red, rectangular crystals are triclinic, space group $P\bar{1}$, and have a unit cell with the following parameters: $a = 9.83(2)$ Å, $b = 14.79(1)$ Å, $c = 11.36(2)$ Å, $\alpha = 69.44(8)°$, $\beta = 66.48(8)°$, $\gamma = 67.57(10)°$, and $z = 2$. The final residual factor is 0.087 for the 4554 independent reflections used in the least squares refinement. The structure consists of individual molecules of $Mn(C_5H_5)CO[P(C_6H_5)_3]_2$. The distance Mn—$C_{C_5H_5}$ is 2.16(1) Å. The coordinate CO (Mn—C: 1.748(9) Å, C—O: 1.172(11) Å) is perpendicular to the plane of the phosphorous and manganese atoms.

The important characteristic is the angle P—Mn—P of 104(1)° (Mn—P: 2.237(3) Å). The angular opening of 14° is considered to be a consequence of an electrostatic repulsion between the two donor P atoms. [Journal translation]

Can. J. Chem., **52**, 1140 (1974)

Introduction

Lors de l'étude structurale du composé $MnC_5H_5(CO)_2P(C_6H_5)_3$ (1), nous avons constaté que les paramètres atomiques communs de $MnC_5H_5(CO)_3$ (2) et du monosubstitué avaient subi très peu de changements. Pour faire suite à cette première étude, nous présentons la structure cristalline et moléculaire du composé bisubstitué $MnC_5H_5CO[P(C_6H_5)_3]_2$ dont les caractéristiques tel que stabilité, moment dipolaire et fréquences vibrationnelles (3) sont différentes de celles du monosubstitué.

Partie Expérimentale

Le composé $MnC_5H_5CO[P(C_6H_5)_3]_2$ (4) s'obtient sous forme de poudre lors de l'irradiation à 3360 Å (lampe à mercure) d'une solution de 1 mmol de $MnC_5H_5(CO)_3$ et de 5 mmol de $P(C_6H_5)_3$ dans 70 ml d'éthanol. Une solution du précipité dans le benzène est soumise à une diffusion lente d'isopentane pour donner des cristaux rouges de forme rectangulaire. Le composé cristallise avec une molécule de solvant comme l'indique l'analyse élémentaire ($C_{calculé}$: 76.7%, C_{obtenu}: 76.3%) et ainsi que l'a prouvé l'élucidation de la structure. Données cristallines:

$C_{42}H_{35}MnOP_2 \cdot C_6H_6$ m.m. 750.4
Triclinique $P\bar{1}$, $a = 9.83(2)$, $b = 14.79(1)$, $c = 11.36(2)$ Å; $\alpha = 69.44(8)$, $\beta = 66.48(8)$, $\gamma = 67.57(10)°$.[1] $\mu = 4.6$ cm^{-1}, $V = 1923$ Å^3, $\rho_o = 1.25(1)$, $z = 2$, $\rho_c = 1.29$ (20 °C, MoK$\bar{\alpha}$, $\lambda = 0.71069$ Å).

La mesure de la densité s'est faite selon la méthode de flottaison dans un mélange iodobutane-méthanol. Les paramètres cristallins ont été mesurés sur trois clichés de niveau zéro obtenus avec l'aide d'une chambre à précession de Buerger (après calibrage avec un cristal de chlorure de sodium). Le composé se désintégrant rapidement sous les rayons X, nous avons utilisé, en moyenne, un cristal par strate étudiée. Trois temps d'exposition (0.5, 4 et 8 h) pour chacune des trente-deux strates (4 le long de a, 6 le long de b, 6 le long de c, 6 le long de [011], 9 le long de [0$\bar{1}$1] et [012]) ont permis de recueillir plus de 18 000 intensités. La mesure des intensités s'est faite à l'aide d'un microdensitomètre du type Wooster Mark IV. Les cristaux employés,

[1] Les dimensions de la maille réduite selon Delaunay (5) sont: $a = 9.83$ Å, $b = 14.97$ Å, $c = 15.12$ Å, $\alpha = 97.18$, $\beta = 103.08$ et $\gamma = 112.43°$.

Can. J. Chem. Downloaded from www.nrcresearchpress.com by 210.87.254.5 on 09/05/12
For personal use only.

Can. J. Chem. Downloaded from www.nrcresearchpress.com by 210.87.254.5 on 09/05/12
For personal use only.

ayant comme dimension moyenne 0.4 × 0.3 × 0.2 mm et le coefficient d'absorption linéaire μ étant inférieur à 5 cm^{-1}, seules les corrections résultant des facteurs de Lorentz et ceux de polarisation ont été apportées aux intensités mesurées. La mise sur échelle commune a été réalisée selon la méthode de Hamilton, Rollet, et Sparks (6). Des 7723 réflexions indépendantes obtenues, 4568 possédaient une intensité mesurable. Les calculs ont été effectués sur ordinateur IBM 360/50 à l'aide des programmes du système X-RAY-70 de Stewart, Kundell et Baldwin (7) en employant exclusivement les réflexions observées.

Détermination de la structure

Après avoir localisé la position de l'atome de manganèse grâce à la fonction tridimensionnelle de Patterson, deux synthèses de Fourier ont été suffisantes pour mettre en évidence le reste de la molécule (indice résiduel $R = \sum||F_o| - |F_c||/\sum|F_o| = 0.35$).

L'affinement des paramètres atomiques et des coefficients d'agitation thermique s'est effectué selon la méthode des moindres carrés (matrice complète). La quantité minimisée est la suivante: $S = \sum w(|F_o| - |F|_c)^2$. L'indice résiduel R a été amené à 0.134 en quatre cycles d'affinement avec des poids w unitaires et des coefficients de température isotropes. Le poids arbitraire w a été dès lors exprimé en termes de σ ($w = 1/\sigma^2$) selon l'expression $\sigma = 0.115\,F_o + 1.063 + 3.000/F_o$. L'attribution de ce nouveau poids à chaque réflexion observée n'a apporté aucun changement au facteur de désaccord R. A ce stade, une synthèse de Fourier-différence a fait apparaître six pics de densité variant entre 2.0 et 2.7 e/Å^3 et formant un hexagone régulier. L'affinement du nombre de molécules de benzène en la position de l'hexagone a donné 0.75 molécule et a amené R à 0.098. Une deuxième synthèse de Fourier-différence a montré un autre hexagone régulier (ρ = 1.2 e/Å^3) très voisin du premier. Un nouvel affinement du degré d'occupation a donné 0.25 molécule en cette position et un facteur résiduel de 0.092. Après le rejet des 14 réflexions observées qui présentaient un écart $|F_o| - |F_c|$ supérieur à 3σ, deux cycles d'affinement en isotropie thermique pour les carbones des groupements phényles et de la molécule incluse C_6H_6 et en anisotropie thermique pour les dix autres atomes non-hydrogène, ont amené le facteur de désaccord à 0.087 et 0.087. Les coefficients d'agitation thermique et les coordonnées atomiques n'ont pas été modifiés par plus de 0.1σ lors de ces deux dernières itérations. Une synthèse de Fourier-différence n'a révélé aucun pic supérieur à 0.76 e/Å^3.

Les facteurs de diffusion atomique utilisés proviennent de la réf. 8. Les coordonnées et les facteurs d'agitation thermique affinés sont présentés dans le Tableau 1. La liste des facteurs de structure observés et calculés a été versée au dépôt des données nonpubliées.[2]

Description de la structure

La Fig. 1 schématise la disposition des molécules dans la maille. Les molécules du solvant occupent l'espace libre. Dans les deux positions préférentielles tracées, la distance minimale entre un atome de benzène et un atome du composé $MnC_5H_5CO[P(C_6H_5)_3]_2$ est de 3.6 Å et elle implique deux atomes de carbone. La plus courte distance intermoléculaire est de 3.5 Å (C—C). Les deux atomes Mn sont distants de 7.5 Å.

La Fig. 2 montre les molécules $MnC_5H_5(CO)_x[P(C_6H_5)_3]_{3-x}$ (x = 3, 2, 1) projetées sur un plan parallèle au cycle cyclopentadiényle. Le Tableau 2 contient les longueurs de liaison et les angles de valence et le Tableau 3 présente les équations des plans et les distances des atomes à leur plan.

Dans $MnC_5H_5CO[P(C_6H_5)_3]_2$ (II), les groupements phényles C et F sont parallèles l'un à l'autre, distants de 4 Å, et presque perpendiculaires au cycle C_5H_5. Ce cycle forme un plan distant de 1.77(2) Å de l'atome central Mn. Les carbones de C_5H_5 présentent des coefficients d'agitation thermique uniformes, contrairement à ceux des composés $MnC_5H_5(CO)_2P(C_6H_5)_3$ (I) et $MnC_5H_5(CO)_3$ (III) où une libration importante du cycle conférait des valeurs d'agitation thermique anisotropes variables et élevées. Les distances Mn—$C_{C_5H_5}$ et $C_{C_5H_5}$—$C_{C_5H_5}$ sont cependant les mêmes dans les trois composés et la position du cycle est demeurée inchangée par rapport à C(2). Ce dernier aspect est conforme avec l'approche de Bennett *et al.* (9) concernant la localisation des liaisons qui se forment entre le coordinat C_5H_5 et un métal.

La distance moyenne Mn—P (2.237(3) Å) et les paramètres structuraux de la triphénylphosphine sont les mêmes dans II et I. La distance intramoléculaire minimale entre un atome de phosphore et un atome de carbone est de 2.9 Å et elle se manifeste à l'intérieur du groupement

[2]On peut obtenir la série complète des tableaux à un prix nominal, en s'adressant au Dépôt des données non publiées, Bibliothèque scientifique national, Conseil national de recherches du Canada, Ottawa, Canada K1A 0S2.

TABLEAU 1. Coordonnées atomiques ($\times 10^4$) et coefficients d'agitation thermique†

Atome	x	y	z	B(Å^2)
Mn	3780(2)	3137(1)	2300(1)	*
P(1)	5276(3)	1891(2)	1567(2)	*
P(2)	5194(3)	3183(2)	3072(2)	*
O(2)	2232(10)	1768(7)	3875(6)	*
C(2)	2927(10)	2284(7)	3248(6)	*
C(4)	3852(13)	4567(7)	1305(8)	*
C(5)	2762(13)	4716(8)	2208(8)	*
C(6)	1578(14)	4276(9)	2435(9)	*
C(7)	1971(13)	3815(9)	1648(9)	*
C(8)	3340(13)	4020(7)	0991(7)	*
C(9)	4093(12)	1591(8)	1094(7)	3.6(2)
C(10)	2730(14)	1380(9)	1705(8)	4.5(2)
C(11)	1799(18)	1168(11)	1350(11)	5.9(3)
C(12)	2214(20)	1216(13)	0416(12)	6.7(3)
C(13)	3516(19)	1471(12)	−0190(11)	6.3(3)
C(14)	4508(16)	1656(10)	0114(9)	5.0(2)
C(15)	6186(11)	0645(7)	2216(6)	3.0(2)
C(16)	7632(13)	0459(8)	2277(8)	3.8(2)
C(17)	8362(14)	−0470(9)	2766(8)	4.3(2)
C(18)	7641(16)	−1209(11)	3200(10)	5.3(3)
C(19)	6174(18)	−1027(11)	3162(10)	5.7(3)
C(20)	5465(16)	−0138(10)	2667(9)	4.9(2)
C(21)	6965(11)	2039(7)	0525(7)	3.3(2)
C(22)	7958(13)	1234(8)	0121(7)	3.7(2)
C(23)	9233(16)	1347(10)	−0645(9)	5.1(3)
C(24)	9543(15)	2272(9)	−1046(9)	4.7(2)
C(25)	8616(13)	3041(9)	−0651(8)	4.1(2)
C(26)	7315(12)	2947(7)	0135(7)	3.3(2)
C(27)	4130(10)	3605(7)	4167(6)	2.8(1)
C(28)	4954(14)	3666(9)	4702(8)	4.2(2)
C(29)	4168(16)	3911(10)	5549(9)	5.1(3)
C(30)	2543(17)	4156(10)	5905(10)	5.3(3)
C(31)	1748(16)	4115(10)	5412(9)	4.9(2)
C(32)	2538(13)	3821(8)	4542(8)	3.9(2)
C(33)	6548(10)	2056(6)	3570(6)	2.7(2)
C(34)	8123(12)	1934(8)	3376(7)	3.5(2)
C(35)	9017(13)	1070(9)	3834(8)	4.0(2)
C(36)	8371(13)	0337(8)	4466(8)	3.9(2)
C(37)	6810(13)	0457(8)	4663(7)	3.8(2)
C(38)	5914(12)	1303(8)	4222(7)	3.6(2)
C(39)	6327(11)	4081(7)	2397(7)	3.0(2)
C(40)	7625(12)	3871(8)	1649(7)	3.4(2)
C(41)	8424(15)	4582(9)	1043(9)	4.5(2)
C(42)	7836(17)	5554(11)	1215(10)	5.6(3)
C(43)	6580(15)	5775(9)	1962(9)	4.7(2)
C(44)	5805(13)	5048(8)	2554(8)	4.0(2)
C(45)′‡	2583(22)	7595(22)	2533(14)	6.3(4)
C(46)′	1730(29)	7038(18)	3217(19)	7.6(5)
C(47)′	1374(23)	7046(15)	4124(15)	7.1(4)
C(48)′	1637(19)	7852(12)	4335(11)	5.8(3)
C(49)′	2352(24)	8474(17)	3584(19)	7.3(4)
C(50)′	2895(28)	8339(18)	2670(19)	7.5(5)
C(51)′′§	2363(79)	7190(48)	2806(51)	5.3(9)
C(52)′′	2066(35)	6706(22)	3578(22)	2.9(5)
C(53)′′	1728(43)	7137(28)	4401(26)	5.3(6)
C(54)′′	2470(55)	8039(38)	3978(35)	5.8(7)
C(55)′′	2663(89)	8551(51)	3024(65)	7.5(9)
C(56)′′	2576(51)	8113(42)	2457(30)	5.0(7)

Can. J. Chem. Downloaded from www.nrcresearchpress.com by 210.87.254.5 on 09/05/12
For personal use only.

TABLEAU I (*Conclu*).

Atome	U_{11}	U_{22}	U_{33}	U_{12}	U_{13}	U_{23}
Mn	25(1)	30(1)	30(1)	−5(1)	−11(1)	−6(1)
P(1)	31(1)	34(1)	34(1)	−10(1)	−12(1)	−7(1)
P(2)	31(1)	31(1)	31(1)	−10(1)	−9(1)	−7(1)
O(2)	53(5)	74(5)	57(5)	−31(4)	−12(4)	4(4)
C(2)	28(4)	48(5)	37(4)	−16(3)	−11(4)	1(4)
C(4)	59(6)	34(4)	51(5)	−8(4)	−31(5)	−6(4)
C(5)	50(6)	36(5)	53(6)	2(4)	−16(5)	−6(5)
C(6)	54(7)	53(6)	59(7)	9(5)	−22(6)	−13(5)
C(7)	40(5)	56(6)	63(7)	−1(5)	−28(5)	−4(5)
C(8)	52(6)	38(5)	49(5)	−5(4)	−26(5)	−4(4)

*Le facteur de température de chacun de ces atomes est de la forme exp. $\{-2\pi^2(a^{*2}h^2U_{11} + b^{*2}k^2U_{22} + c^{*2}l^2U_{33} + 2a^*b^*hkU_{12} + 2a^*c^*hlU_{13} + 2b^*c^*klU_{23})\}$. Chaque coefficient U est multiplié par 10^3.
†Les écarts-types sont donnés entre parenthèses.
‡Atome de solvant en position A (75%).
§Atome de solvant en position B (25%).

TABLEAU 2. Distances interatomiques et angles de valence*

Liaison	Distance (Å)	Liaison	Angle (deg)
Mn—C(2)	1.748(9)	C(2)—Mn—P(1)	89.96(36)
Mn—P(1)	2.239(3)	C(2)—Mn—P(2)	91.98(32)
Mn—P(2)	2.234(3)	P(1)—Mn—P(2)	104.32(11)
		P(1)—Mn...O(2)	91.34(22)
C(2)—O(2)	1.172(11)	P(2)—Mn...O(2)	93.49(21)
Mn—C(4)	2.163(10)	Mn—C(2)—O(2)	174(1)
Mn—C(5)	2.138(10)		
Mn—C(6)	2.161(11)	C(4)—C(5)—C(6)	109(1)
Mn—C(7)	2.156(10)	C(5)—C(6)—C(7)	106(1)
Mn—C(8)	2.161(10)	C(6)—C(7)—C(8)	107(1)
		C(7)—C(8)—C(4)	110(1)
C(4)—C(5)	1.451(16)	C(8)—C(4)—C(5)	107(1)
C(5)—C(6)	1.409(18)		
C(6)—C(7)	1.491(18)	C(9)—P(1)—C(15)	102.98(45)
C(7)—C(8)	1.403(16)	C(15)—P(1)—C(21)	98.37(43)
C(8)—C(4)	1.401(15)	C(21)—P(1)—C(9)	101.08(45)
P(1)—C(9)	1.846(10)	C(27)—P(2)—C(33)	95.06(40)
P(1)—C(15)	1.849(9)	C(33)—P(2)—C(39)	104.52(42)
P(1)—C(21)	1.846(10)	C(39)—P(2)—C(27)	101.89(42)
P(2)—C(27)	1.838(9)		
P(2)—C(33)	1.846(9)	Mn—P(1)—C(9)	109.13(27)
P(2)—C(39)	1.825(10)	Mn—P(1)—C(15)	120.22(25)
		Mn—P(1)—C(21)	122.19(25)
		Mn—P(2)—C(27)	116.72(24)
		Mn—P(2)—C(33)	123.85(24)
		Mn—P(2)—C(39)	112.10(25)
C—C:†	1.34–1.43	C—C—C:†	118–122
	1.39(1)		120(1)

*Les écarts-types sont donnés entre parenthèses.
†Valeurs extrêmes et valeur moyenne des carbones des groupements C_6H_5.

Can. J. Chem. Downloaded from www.nrcresearchpress.com by 210.87.254.5 on 09/05/12
For personal use only.

Can. J. Chem. Downloaded from www.nrcresearchpress.com by 210.87.254.5 on 09/05/12
For personal use only.

TABLEAU 3. Plans moyens

(*a*) Coefficients des équations des plans: $lX + mY + nZ - p = 0$*

Plan	*l*	*m*	*n*	*p*	χ^2
A	−0.4462	0.7702	−0.4558	−1.0883	0.9
B	−0.2263	0.9615	−0.1559	−0.9494	5.7
C	−0.0453	−0.5569	−0.8293	3.9035	2.5
D	−0.7917	0.1193	−0.5992	6.7013	2.2
E	0.1118	0.8759	−0.4694	−3.7565	4.5
F	−0.2596	−0.6359	−0.7268	8.8535	0.3
G	−0.7962	0.1665	−0.5817	8.9423	1.8

*Le système orthonormé des axes de référence comprend *X* le long de *a*, *Y* dans le plan *ab* et *Z* le long de *c**.

(*b*) Distances (Å) de chacun des atomes à leur plan

Plan A		Plan B		Plan C		Plan D		Plan E		Plan F		Plan G	
C(4)	0.0033	C(9)	−0.0112	C(15)	−0.0006	C(21)	0.0071	C(27)	0.0020	C(33)	0.0017	C(39)	0.0047
C(5)	−0.0063	C(10)	0.0189	C(16)	−0.0045	C(22)	−0.0016	C(28)	0.0100	C(34)	0.0000	C(40)	−0.0026
C(6)	0.0081	C(11)	−0.0123	C(17)	0.0039	C(23)	−0.0125	C(29)	−0.0187	C(35)	−0.0037	C(41)	−0.0066
C(7)	−0.0050	C(12)	−0.0143	C(18)	0.0058	C(24)	0.0148	C(30)	0.0047	C(36)	0.0039	C(42)	0.0179
C(8)	0.0008	C(13)	0.0199	C(19)	−0.0173	C(25)	−0.0039	C(31)	0.0129	C(37)	−0.0010	C(43)	−0.0083
		C(14)	0.0042	C(20)	0.0118	C(26)	−0.0053	C(32)	−0.0122	C(38)	−0.0021	C(44)	−0.0023

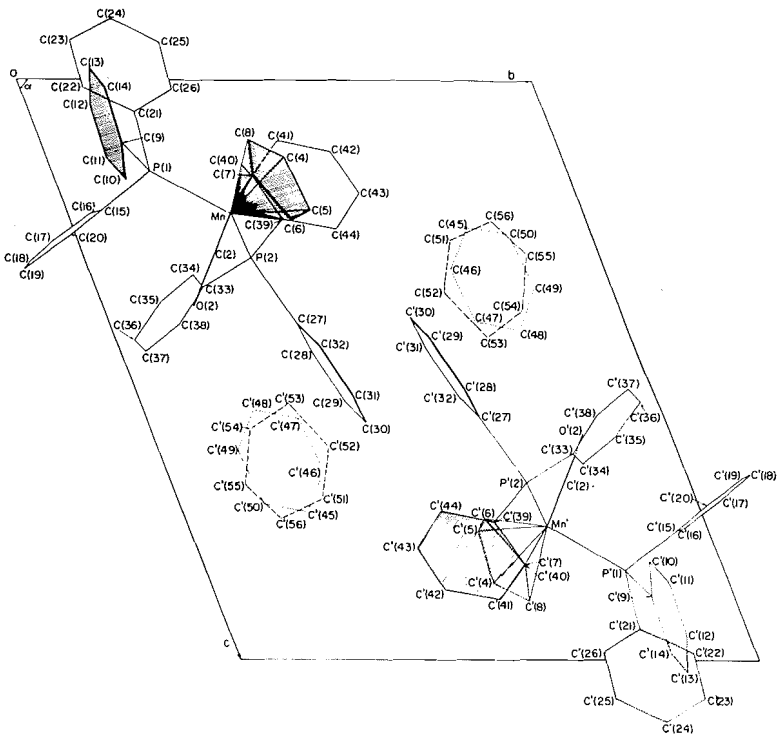

FIG. 1. Disposition des molécules dans la maille selon une projection dans le plan *bc*.

$P(C_6H_5)_3$. Aussi, sauf pour la distance P(1)—P(2) qui est inférieure de 0.3 Å à la somme des rayons van der Waals, aucun empêchement stérique semble résulter de la présence, en position *cis*, des deux coordinats $P(C_6H_5)_3$.

La différence majeure entre les composés II et I apparaît au niveau des angles de liaison impliquant l'atome central et le coordinat $P(C_6H_5)_3$. Considérant trois axes orthogonaux dont le point commun est Mn, on constate (Fig. 2) que les coordinats CO se situent le long des axes, que $P(C_6H_5)_3$ dans I forme la liaison Mn—P le long d'un axe mais que les atomes P(1) et P(2) de II s'écartent, dans le plan P—Mn—P, de 7° de la direction axiale. Cette ouverture angulaire pourrait constituer le facteur déterminant dans la faible stabilité du composé bisubstitué, tant en solution qu'à l'état solide, comparée à la grande stabilité du composé monosubstitué. La cause de cette ouverture d'angle ne peut résider uniquement dans l'empêchement stérique du type van der Waals. En effet, les distances C—C des coordinats CO dans I et III sont inférieures de 0.7 Å à la somme des rayons de van der Waals sans que l'angle C—Mn—C s'accroisse de plus de 2°, tandis que la distance P(1)—P(2) serait, elle aussi, inférieure de 0.7 Å à la somme des rayons de van der Waals si l'angle P—Mn—P était de 90°.

Dans les complexes donneur-accepteur, les liaisons ont un caractère polaire élevé, comme en font foi les moments dipolaires des composés dérivés des métaux carbonyle (10). Les charges résiduelles portées par les atomes donneurs de coordinats tel que $P(C_6H_5)_3$ entraînent certainement des répulsions électrostatiques qui s'ajoutent, sous la forme de forces de Keesom, aux répulsions électrostatiques normales de van der Waals. La présence de dipôles élevés, résultant de fortes liaisons L→M, pourrait provoquer des répulsions importantes si les atomes donneurs sont en position *cis* comme c'est le cas des atomes P dans le composé $MnC_5H_5CO[P(C_6H_5)_3]_2$.

Conclusion

Le remplacement de groupements CO dans $MnC_5H_5(CO)_3$ par $P(C_6H_5)_3$ n'entraîne aucune modification importante impliquant le cycle C_5H_5. L'apparition d'une ouverture angulaire de

Can. J. Chem. Downloaded from www.nrcresearchpress.com by 210.87.254.5 on 09/05/12
For personal use only.

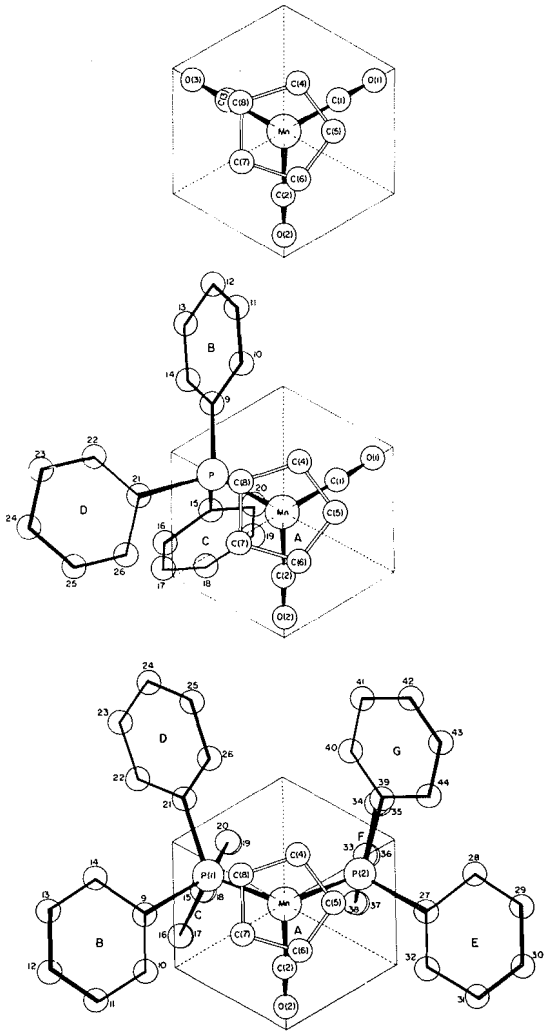

FIG. 2. Projection orthogonale dans un plan parallèle à celui du cycle C_5H_5 des composés $MnC_5H_5(CO)_3$, $MnC_5H_5(CO)_2P(C_6H_5)_3$ et $MnC_5H_5CO[P(C_6H_5)_3]_2$.

14° dans le composé bisubstitué dans le plan P—Mn—P laisse entrevoir des répulsions électrostatiques impliquant les atomes donneurs comme facteurs importants dans la stabilité du composé $MnC_5H_5CO[P(C_6H_5)_3]_2$.

Nous sommes reconnaissants au Ministère de l'Education du Québec et au Conseil national de recherches du Canada d'avoir supporté financièrement ce projet. Les auteurs remercient également Monsieur K.S. Dichmann pour sa contribution aux calculs.

1. C. BARBEAU, K. S. DICHMANN et L. RICARD. Can. J. Chem. **51**, 3027 (1973).
2. A. F. BERNDT et R. E. MARSH. Acta Cryst. **16**, 118 (1963).
3. C. BARBEAU. Can. J. Chem. **45**, 161 (1967).
4. W. STROHMEIER et C. BARBEAU. Z. Naturforsch. **17b**, 848 (1962).
5. International tables for X-ray crystallography. Vol. I. Kynoch Press, Birmingham. 1965. p. 530.
6. W. C. HAMILTON, J. S. ROLLETT, et R. A. SPARKS. Acta Cryst. **18**, 129 (1965).
7. J. M. STEWART, F. A. KUNDELL, et J. C. BALDWIN. The X-RAY-70 System. Univ. of Maryland (1970).
8. International tables for X-ray crystallography. Vol. III. Kynoch Press, Birmingham. 1965.
9. M. J. BENNETT, M. R. CHURCHILL, M. GERLOCH, et R. MASON. Nature, **201**, 1318 (1964).
10. A. D. GARNOVSKII, O. S. OSIPOV, et V. I. MINKIN. Russ. Chem. Rev. **37**, 763 (1968).

Can. J. Chem. Downloaded from www.nrcresearchpress.com by 210.87.254.5 on 09/05/12
For personal use only.

The State of Hydrogen Desorbing from Intermediates Formed by Ammonia Interaction with Tungsten Surfaces

Y. K. PENG AND P. T. DAWSON[1]

Department of Chemistry and Institute for Materials Research, McMaster University, Hamilton, Ontario, L8S 4M1

Received September 27, 1973

Ammonia interaction with a tungsten surface can generate dense adlayers containing nitrogen and hydrogen, *i.e.* an η-species of surface stoichiometry $W^s_2N_3H$. In thermal desorption mass spectrometry experiments, hydrogen desorbing from the η-species interacts with the glass wall in a manner similar to that previously observed for atomic hydrogen. This paper describes two mass spectrometric techniques designed to confirm this conclusion directly. The first method uses a line-of-sight geometry between the tungsten filament and the ionization source of the mass spectrometer and the results indicate that, at least, part of the hydrogen desorbing from the η-species does so atomically. In the second method a multiple wall collision geometry is used but prior saturation of the wall with D atoms will result in an HD^+ ion current for desorbing H atoms. The results suggest that 26% of the hydrogen desorbs atomically. Hydrogen atom desorption from the η-species occurs at tungsten filament temperatures below those required for hydrogen atom evaporation from a pure hydrogen adlayer. It is proposed that a reduced binding energy for adsorbed hydrogen atoms and a reduced mobility of these adatoms arises from the presence of a large surface concentration of nitrogen. This will result in the rates of atomic hydrogen desorption and bimolecular recombination becoming comparable at temperatures lower than is the case for pure hydrogen interaction with tungsten. The implications of these results for the ammonia synthesis reaction are discussed.

L'interaction de l'ammoniac avec une surface de tungstène peut produire des couches adsorbantes denses contenant de l'azote et de l'hydrogène c'est-à-dire une η-variété de stoechiométrie de surface $W^s_2N_3H$. Dans les expériences de spectrométrie de masse de désorption thermique, l'hydrogène désorbant du η-variété agit sur la paroi en verre d'une manière similaire à celle antérieurement observée pour l'hydrogène atomique. Cette publication décrit deux techniques de spectrométrie de masse conçues pour confirmer directement cette conclusion. La première méthode utilise une géométrie à rayon visuel entre le filament de tungstène et la source d'ionisation du spectromètre de masse et les résultats montrent que, au moins, une partie de l'hydrogène qui se désorbe du η-variété se fait atomiquement. Dans la seconde méthode, une géométrie de collision multiple sur les parois est utilisée mais une saturation préalable des parois avec des atomes D conduit à un courant d'ions HD^+ pour les atomes H qui désorbent. Les résultats suggèrent que 26% de l'hydrogène désorbe atomiquement. La désorption d'atomes d'hydrogène du η-variété se produit à des températures du filament de tungstène en-dessous de celles nécessaires pour l'évaporation d'atomes d'hydrogène d'une pure couche adsorbante d'hydrogène. Il est suggéré qu'une énergie de liaison réduite pour les atomes d'hydrogène adsorbés et une mobilité réduite de ces atomes adsorbés résultent de la présence d'une grande concentration de surface d'azote. Ceci conduira aux vitesses de désorption d'hydrogène atomique et une recombinaison bimoléculaire devenant comparable aux températures plus basses qu'est le cas de l'interaction de l'hydrogène pur avec le tungstène. Les conséquences de ces résultats pour la réaction de la synthèse de l'ammoniac sont examinées. [Traduit par le journal]

Can. J. Chem., **52**, 1147 (1974)

Introduction

The catalytic decomposition of ammonia on tungsten surfaces is an approximately zero order reaction (1–3) with a large hydrogen isotope effect (4, 5) and therefore a process of considerable interest. The application of modern techniques has shown (6–10) that the simple interpretation by a Langmuir–Hinshelwood mechanism (11) is inadequate. Ammonia interacts in a complex fashion with tungsten to produce surface species of estimated stoichiometry $W^s_2N(\beta)$, $W^sN(\delta)$, and $W^s_2N_3H(\eta)$. At low reactant pressure the overall reaction kinetics will correspond to those for a δ-nitrogen adlayer and there should be no isotope effect, whereas at high reactant pressure η-formation and desorption will represent the decomposition mechanism (8–10). Most studies of the overall

[1]To whom all correspondence should be addressed.

Can. J. Chem. Downloaded from www.nrcresearchpress.com by 210.87.254.105 on 09/05/12
For personal use only.

kinetics have been determined at pressures where an η-species will be formed. The η-species contains hydrogen and thus one can readily understand the observed isotope effect as a consequence of N—H bond breaking in the rate limiting step (8–10).

[1] $W^s{}_2N_3H(\eta) \rightarrow W^s{}_2N(\beta) + N_2(g) + H(g)$

The conclusion that hydrogen desorption occurs in the atomic state is based on the mode of interaction of the desorbed hydrogen with the glass walls of the reaction vessel (8). While the evidence is fairly conclusive, it is indirect. This paper describes experiments designed to test these observations directly. In view of the principle of microscopic reversibility it is important to establish whether for ammonia synthesis the only route to the formation of the η-species is via atomic hydrogen, *viz.* does all, or only a fraction, of the hydrogen desorb in the atomic state?

Experimental Methods

Two different approaches have been used in this investigation. The first is a direct method using an experimental arrangement with line-of-sight between the sample filament and the ionization chamber of the mass spectrometer. In this experiment the fraction of desorbed species detected before interacting with the reaction vessel walls can be large, in contrast with the previous experimental method (8) which necessitated multiple wall collisions for all desorbing particles before detection. In the second method a multiple wall collision geometry was again used but, by prior saturation of the wall with deuterium atoms, any hydrogen atom desorption followed by wall interaction to produce molecules should result in an HD^+, mass 3, component in the desorption spectrum.

Line-of-Sight Experiment

The bakeable ultra-high vacuum apparatus used is shown in Fig. 1. The sample filament, F, was a 12 cm length of 0.025 cm diameter tungsten wire (Phillips Elmet) mounted as a coil, 1.2 cm in length, parallel to the ionization chamber opening, 0.4 cm in diameter, of the mass spectrometer, M, and 0.5 cm distant from it. The quadrupole mass spectrometer was an Ultek/EAI Quad 150, modified to permit variation of the electron accelerating voltage; the ionizer was operated at 60 eV and 50 μA emission current. The mass spectrometer and ion gauge, G, were both provided with low work function emitters to minimize their operating temperatures. The system was pumped by a 20 l s^{-1} ion pump through a 1 in. metal valve, V_1. Purified ammonia, hydrogen, and deuterium could be introduced from storage bulbs via the 1/2 in. metal valve, V_2. Anhydrous ammonia (Matheson) was further purified by vacuum distillation whereas hydrogen and deuterium (99.5% D; Matheson) were purified by diffusion through palladium.

Thermal desorption spectra were obtained using a linear heating rate obtained by using a motorized potentiometer as the comparison resistor in an automatic Kelvin double-bridge temperature control circuit. A mechanical switch allowed alternate monitoring of the mass 1 and mass 2 ion currents by changing the d.c. voltage to the quadrupole. This switch simultaneously changed the sensitivity of the recording system so that the mass 1 ion current was monitored at 10 times the sensitivity of mass 2.

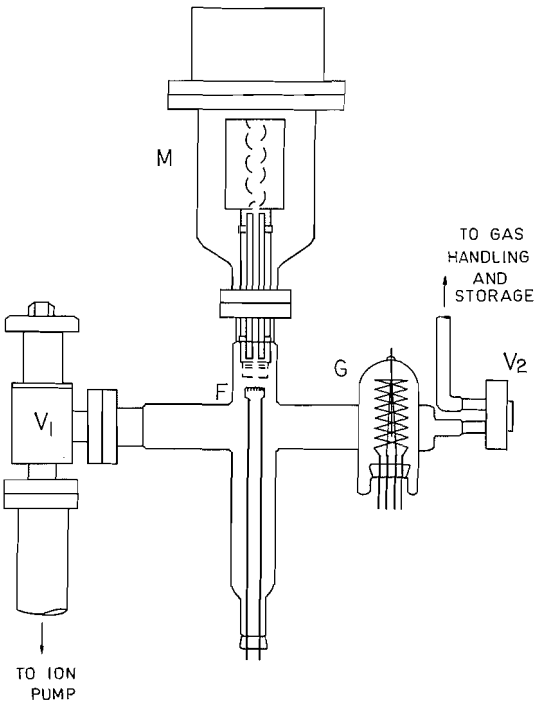

FIG. 1. Ultra-high vacuum apparatus with line-of-sight between the sample filament and ionization source of the quadrupole mass spectrometer.

Deuterium Saturated Wall Method

The experimental arrangement used ensures multiple wall collisions by desorbing particles prior to detection by separating the mass spectrometer from the reaction vessel, and has been described previously (9). The glass wall of the freshly-baked system was saturated with deuterium atoms by allowing deuterium gas to flow through the reaction vessel for several hours at a pressure of 2×10^{-6} Torr with the sample filament maintained at about 2000 °K to atomize the gas. After the deuterium gas flow was stopped, the system was evacuated overnight before allowing ammonia gas to interact with the filament. The reactant gas was pumped out to a pressure of 5×10^{-7} Torr and then desorption spectra were generated as described previously, monitoring the mass 2, 3, and 4 ion currents simultaneously.

Results

Effect of Varying Heating Rate on the Desorption Spectra for the η-Species

The hydrogen and nitrogen desorption spectra shown in Fig. 2 (full lines) were obtained after a

Can. J. Chem. Downloaded from www.nrcresearchpress.com by 210.87.254.105 on 09/05/12
For personal use only.

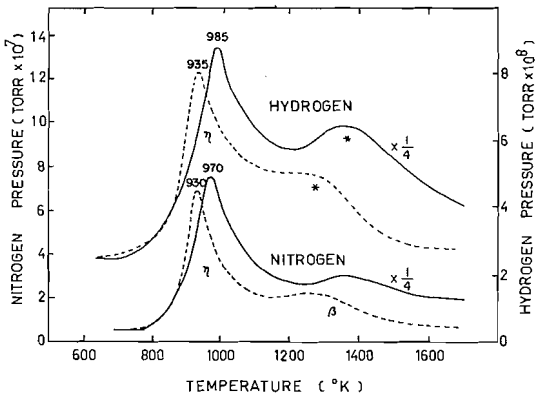

FIG. 2. Hydrogen and nitrogen desorption spectra following adsorption of ammonia at 10^{-2} Torr for 10 min at 700 °K. The heating rates were 50 deg s^{-1} (full line) and 10.5 deg s^{-1} (broken line). The high temperature hydrogen peaks (*) arise from interaction of a small residue of ammonia gas in the reaction vessel with the hot filament and do not represent a primary desorption process for the η-adlayer.

10 min interaction of ammonia at 10^{-2} Torr with the tungsten filament at 700 °K, using a heating rate of 50 deg s^{-1}. As discussed previously (8), the areas of the first order desorption peaks at 970 °K (mass 14) and 985 °K (mass 2) suggest that the desorption process for the η-species has the stoichiometry indicated by reaction 1. The observation that the mass 2 peak was much reduced when the reaction vessel wall was freshly baked, or maintained at 77 °K, led to the conclusion that the hydrogen desorbed atomically (8). The η-hydrogen desorption peak lags that for η-nitrogen by 15 deg for a heating rate of 50 deg s^{-1} and this can be attributed to the greater residence time on the reaction vessel walls for hydrogen in the atomic state. This conclusion is supported by the observation that with a slower heating rate of 10.5 deg s^{-1} (broken lines, Fig. 2) the delay in the hydrogen peak is reduced from 15 deg to 5 deg. Thus the lag times in the two experiments, 0.30 and 0.48 s, are the same within experimental error. Taken with a value of 7.5×10^{-4} for the surface recombination efficiency (12), the lag time suggests a binding energy for H atoms on the wall of ~13 kcal; this does not seem unreasonable.

Line-of-Sight Experiment

Since the cracking pattern of molecular hydrogen has a mass 1 component, with a magnitude which could depend on the experimental conditions, this experiment was carried out in a comparative way. The mass 2 and mass 1 ion currents were monitored simultaneously during desorption from adlayers generated by ammonia interaction with the filament first at 300 °K, for which the hydrogen desorption shows no peculiarities and is expected to be molecular, and then at 700 °K. Typical desorption spectra are shown in Fig. 3. Clearly there is a greater mass 1 component in the desorption of the η-species (700 °K interaction) than in the low temperature hydrogen desorption peak. Unfortunately the results were not reproducible, forcing us to repeat the experiment many times to obtain a statistically meaningful result. The experiment was repeated 30 times at 700 °K and 22 times at 300 °K and the mass 2 to mass 1 peak height ratio determined for each experiment. The probability of occurrence of a given (mass 2)/(mass 1) ratio is shown in Fig. 4 as a function of (mass 2)/(mass 1) ratio. It can be seen that for interaction at 300 °K over 80% of these ratios range between 80 and 140. Since the ratio obtained from the cracking pattern of molecular hydrogen gas is 110, it can be concluded that the hydrogen desorbing from the surface species produced at 300 °K does so in the molecular state. The (mass 2)/(mass 1) ratio in the hydrogen desorbing from the η-species formed by interaction at 700 °K does have considerably lower values; approximately 80% of the (mass 2)/(mass 1) ratios fall in the range from 20 to 80. Thus, at least, a substantial fraction of the hydrogen desorbs in the atomic state.

The (mass 2)/(mass 1) ratio observed will depend on (*a*) the fraction of desorbing particles which can enter the ionization chamber directly,

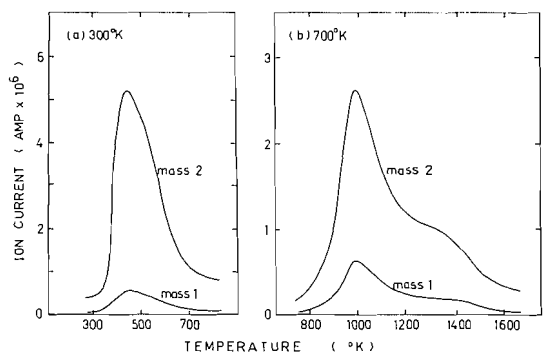

FIG. 3. Atomic and molecular hydrogen desorption spectra obtained with line-of-sight geometry after adsorption of ammonia at 10^{-2} Torr for 10 min at (*a*) 300 °K and (*b*) 700 °K. Mass 1 was recorded at 10 times higher sensitivity than mass 2.

Can. J. Chem. Downloaded from www.nrcresearchpress.com by 210.87.254.105 on 09/05/12
For personal use only.

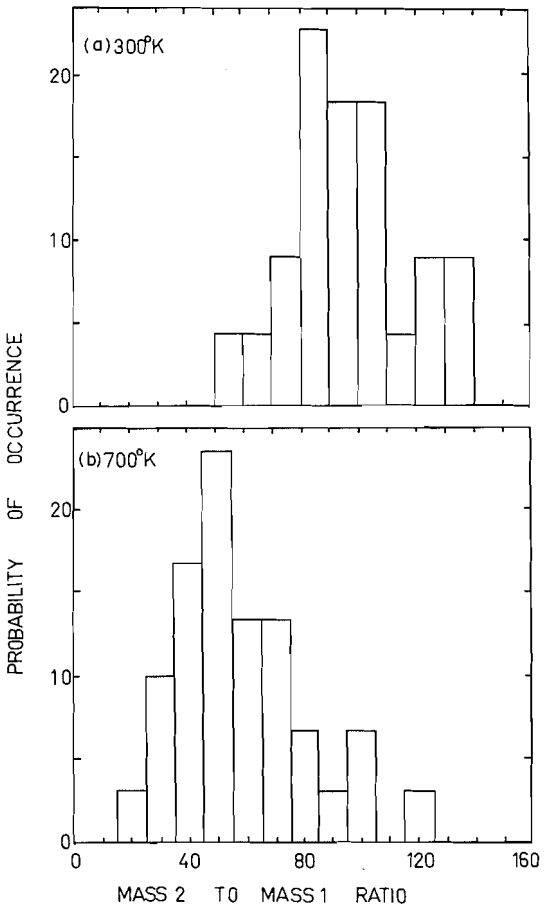

FIG. 4. Histograms for (mass 2)/(mass 1) ratios obtained from the peak maxima in desorption spectra typified by those shown in Fig. 3. (*a*) At 300 °K the mean value observed is 94 with a standard deviation of 20; (*b*) At 700 °K the mean value is 57 with a standard deviation of 23.

0.021 for the present geometry, (*b*) the ratio of the mass 2 and mass 1 sensitivities, which is approximately 1.5 (13) and (*c*) on the pumping speeds for molecules and atoms from the ionization chamber. Since the pumping speeds cannot be determined with sufficient precision, it is impossible to calculate the fraction desorbing atomically from these experiments. An experimental geometry in which *all* desorbing particles not passing directly through the ionization chamber were efficiently pumped (*i.e.* a molecular beam) would permit such a calculation.

Deuterium Saturated Wall Method

This experiment was also carried out in a comparative manner. With the reaction vessel walls saturated with deuterium as described earlier, ammonia gas at 10^{-2} Torr was allowed to interact for 10 min with the tungsten filament at 300 °K and 700 °K, *i.e.* the same conditions as used in the line-of-sight experiment. Desorption spectra were obtained by monitoring the mass 2, 3, and 4 ion currents simultaneously and are shown in Fig. 5. This experiment was then repeated and the (mass 3/(mass 2) ion current ratios were determined for each of the four sets of desorption spectra. The (mass 3/(mass 2) ratios for hydrogen desorbing from the 300 °K adlayer were 0.08 in both cases whereas those determined for the η-species, 700 °K adlayer, were 0.38 and 0.31. This experiment again establishes conclusively that part of this hydrogen desorbs atomically. The mass 3 peak cannot arise from a molecular desorption followed by atomization on the hot tungsten filament since this effect becomes appreciable only at temperatures in excess of 100 °K (14).

Hickmott has shown (15) that bimolecular surface recombination of H atoms adsorbed on a glass surface is very slow, particularly when compared with recombination by reaction of an adsorbed H atom with an H atom colliding from

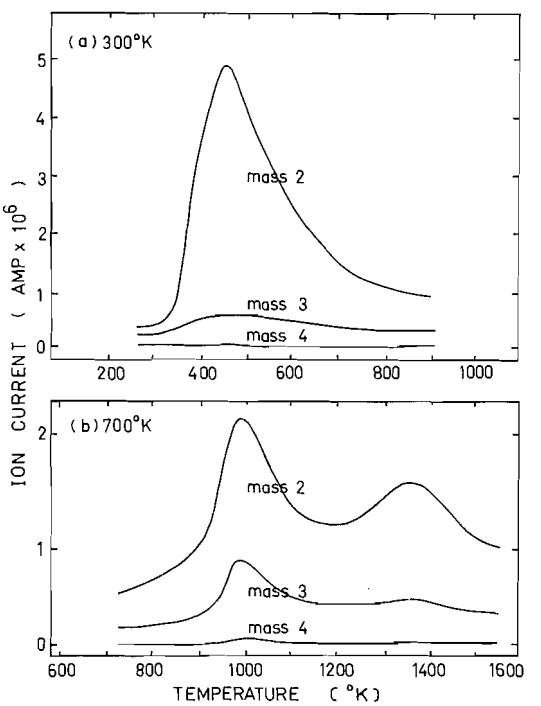

FIG. 5. Mass 2, 3, and 4 desorption spectra obtained simultaneously following NH_3 adsorption at 10^{-2} Torr for 10 min at (*a*) 300 °K and (*b*) 700 °K, in a reaction vessel with the wall saturated with deuterium.

Can. J. Chem. Downloaded from www.nrcresearchpress.com by 210.87.254.105 on 09/05/12
For personal use only.

Can. J. Chem. Downloaded from www.nrcresearchpress.com by 210.87.254.105 on 09/05/12
For personal use only.

the gas phase. Thus H atoms colliding with a glass wall can either stick if they collide with a vacant site or recombine if they collide with an adsorbed H atom. Since both adsorption and removal of adsorbed H atoms will be first order in the gas phase H atom concentration, the saturation coverage of hydrogen atoms on the wall will be such that the overall recombination probability for impacting H atoms will be one-half, independent of the H atom pressure. In the present experiments, the deuterium concentration on the wall will reach a steady state value during preparation such that the probability of recombination for impacting atoms will be one-half. Thus H atoms desorbing from the η-species will also have an equal chance of sticking and recombining with wall deuterium.

If the η-hydrogen desorbed completely in the atomic state, we would predict that it would be detected completely as HD, mass 3, since the number of deuterium atoms on the wall far exceeds the number of H atoms in the η-species. Experimentally, the mass 3 signal represents only about 35% of the H_2, mass 2 signal. If a fraction, f, of the η-hydrogen desorbs as atoms, the observed (mass 3)/(mass 2) ratio will be $(f/2)/((1 - f)/2)$, since half the desorbing H atoms will stick on the wall. Thus the observed (mass 3)/(mass 2) ratios indicate that approximately 26% of the η-hydrogen desorbs atomically. There are experimental uncertainties which could make this calculated fraction too small.

First the glass wall may not be saturated with deuterium. Based on Hickmott's results (15), the method employed in this experiment generates more than enough D atoms to saturate the glass walls. However, after saturation with deuterium the system was evacuated overnight during which time the slow surface recombination of deuterium atoms could reduce the wall concentration and make the overall recombination probability less than one-half. Calculations show that this effect will be small (15). A fraction of the hydrogen on the wall will be H, rather than D, because of the 0.5% hydrogen in the deuterium gas and also because hydrogen is a large component in the residual gases following bakeout. Also, since ammonia can be adsorbed strongly on the walls, the introduction of NH_3 to generate the η-species could lead to an exchange process and the replacement of adsorbed D by H,

$$NH_3(g) + D(a) \rightleftarrows NH_2D(g) + H(a)$$

It has been reported (16) that a random distribution of hydrogen over ND_3 molecules was observed when ND_3 was introduced into a mass spectrometer operating at a sufficiently low electron-energy that only the parent ion peak was observed in the spectrum. The observed randomization was interpreted as the result of an exchange reaction between ND_3 and H trapped in the system. In additional experiments, not reported here, in which a nickel film was present in the reaction system, such a randomization was observed in the ammonia mass spectrum; however, in the experiments described in this paper, *i.e.* Fig. 5, no nickel film was present and such an effect was not detected. This should not be construed to indicate that the only species on the wall with which H atoms can interact is D. Ammonia is quite strongly bound to the glass wall and exchange reactions could take place without desorption of isotopic ammonia. Furthermore, it is quite possible for the impacting H atoms to interact directly with adsorbed NH_3 to produce molecular hydrogen. No data is available for this process to establish its efficiency.

A second effect which can lead to low values for the fraction of hydrogen desorbing as atoms is isotopic scrambling of hydrogen itself, *i.e.* masses 2, 3, and 4. This can occur on the hot filament in the mass spectrometer, the grid of the ionization gauge and the metal walls of the system. Such an effect was observed, as shown in Fig. 6. When hydrogen and deuterium were allowed to flow through the system from separate reservoirs, an HD^+, mass 3, peak was

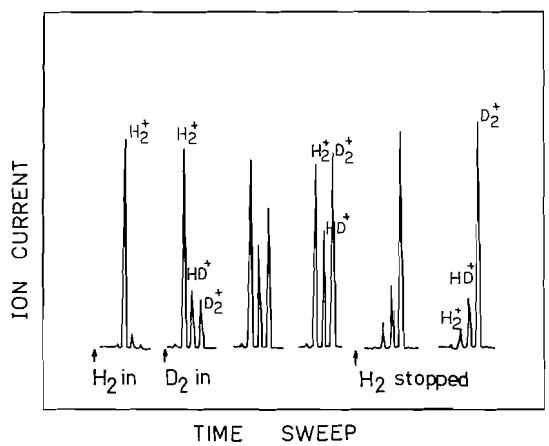

FIG. 6. Relative mass 2, 3, and 4 ion current observed when hydrogen and deuterium gases were flowed through the system from separate gas reservoirs. The sweep rate was 1 s per mass number.

observed instantaneously. Consequently, any HD resulting from a recombination of H atoms desorbing from the η-species with D atoms on the wall would give rise to mass 2 and mass 4 peaks and a reduction in the amount of HD. As can be seen in Fig. 5*b*, the mass 4 spectrum is detectable, though quite small; the peak height is only ~10% of that for mass 3. No correction has been applied for this effect since an opposite effect of comparable magnitude was observed in the 300 °K spectra; *i.e.* a mass 3 signal equal to 8% of that for mass 2. It cannot be assumed that a similar mass 3 signal will not be generated in the 700 °K experiment.

The results described in this paper establish conclusively that an appreciable fraction of the hydrogen desorbing from the η-species, generated from ammonia interaction with a tungsten surface, does so in the atomic state.

Discussion

The equilibrium concentration of atomic hydrogen in the gas phase can be calculated. At 298 °K, the equilibrium concentration is trivial; even at a pressure as low as 10^{-7} Torr the mole fraction of atomic hydrogen, x_H, calculated from the free energy of formation is 1.55×10^{-12}. This corresponds to two atoms per liter of gas. Even for the gas at 1 000 °K and 10^{-7} Torr $x_H = 2 \times 10^{-5}$, as calculated from the equilibrium constant (17). Clearly, if the gas desorbs at equilibrium the fraction desorbing atomically will be negligible. Conversely, if the gas desorbs atomically it is to be expected that a step in the surface recombination process is sufficiently slow to prevent the attainment of equilibrium.

Adsorption, Desorption, and Atomization of Pure Hydrogen on Tungsten

Hydrogen interaction with tungsten has been extensively investigated for a long time and with a recent increase in interest. The binding states, populated at room temperature, β-states, are currently considered to be almost exclusively atomic (18, 19) which is consistent with the low binding energy anticipated for adsorbed molecular hydrogen. Desorption of adsorbed atomic hydrogen from polycrystalline tungsten filaments occurs between 300 and 700 °K (19, 20) and there exists no evidence to suggest that the desorbing gas is not molecular. Desorption from the (100), (110), and (111) single crystal planes of tungsten also occurs in this same temperature interval and nearly all the desorption peaks show the characteristic features for second order desorption processes (19). This is again to be expected for adsorbed adatoms which field electron emission studies have shown to be mobile at temperatures above 200 °K (21). The rate of recombination of migrating adatoms to form hydrogen molecules is faster than the desorption rate of hydrogen atoms.

The general features of the adsorption–desorption of pure hydrogen would seem to be well understood; hydrogen adsorbs dissociatively and desorbs associatively. Atomic hydrogen desorption from a pure hydrogen adlayer can occur when hydrogen gas interacts with a tungsten surface at temperatures in excess of 1050 °K (14). The rate of formation of atomic hydrogen varies with the square root of the hydrogen pressure at high pressures but linearly at low pressure, reflecting a transition from adatom recombination to impingement rates being rate limiting respectively (14, 22, 23). A relatively straightforward interpretation emerges. Hydrogen atom evaporation only occurs from a sufficiently dilute surface layer that the rate of recombination by collision of migrating adatoms becomes sufficiently reduced that the rate of evaporation of atomic hydrogen can become significant.

Desorption of Hydrogen following Interaction of Ammonia with Tungsten

The stoichiometry (8) and kinetic parameters (9, 24) for the reactions of ammonia with tungsten have been reported. The reactions which occur with desorption of hydrogen and production of adlayers of steadily increasing density can be represented as

$$[2] \quad 2W^s + NH_3(g) \rightarrow W^s{}_2N(\beta) + \tfrac{3}{2} H_2(g)$$

$$[3] \quad W^s{}_2N(\beta) + NH_3(g) \rightarrow 2W^sN(\delta) + \tfrac{3}{2} H_2(g)$$

$$[4] \quad 2W^sN(\delta) + NH_3(g) \rightarrow W^s{}_2N_3H(\eta) + H_2(g)$$

The hydrogen atom remaining in the η-species is lost in the η-desorption process, reaction 1.

Ammonia will adsorb to the equivalent of a half-monolayer of nitrogen, $W^s{}_2NH_3$, at 200 °K (6–8). Field electron emission microscope observations show that surface dissociation of hydrogen from chemisorbed ammonia occurs over the temperature interval 200–400 °K, being more rapid on crystallographic planes of low electron affinity (6). The adsorbed hydrogen

Can. J. Chem. Downloaded from www.nrcresearchpress.com by 210.87.254.105 on 09/05/12
For personal use only.

Can. J. Chem. Downloaded from www.nrcresearchpress.com by 210.87.254.105 on 09/05/12
For personal use only.

starts to desorb, reaction 2, at 285 °K (8) and is thus indistinguishable from the desorption of pure β-hydrogen from a polycrystalline tungsten surface. Desorption of the β-nitrogen left behind does not commence until 1150 °K. Thus the surface dissociation of the hydrogen from chemisorbed ammonia requires little activation energy up to this coverage and, moreover, surface diffusion and recombination of hydrogen adatoms is inappreciably restricted by the presence of a half-monolayer of nitrogen.

As the temperature of interaction is progressively raised the nitrogen coverage steadily increases, reaction 3, and the desorption of hydrogen progressively shifts to higher temperatures (8). The increasing stability of the surface phase towards hydrogen desorption could be caused by a decreased efficiency of hydrogen adatom recombination as the nitrogen coverage increases. Alternatively, a reduction in the ability of adjacent tungsten atoms to participate in transition states could increase the stability of the adsorbed NH_x intermediates towards N—H bond breaking. Nevertheless, reaction 3 is rapid at 700 °K in contrast to reaction 4 which has an initial reaction probability of only 10^{-6} (8) and requires an activation energy of 12 kcal mol^{-1} (24). It is tempting to consider that the mobility of hydrogen adatoms and, possibly, the ability of adjacent tungsten atoms to participate in transition states, is so reduced that desorption of hydrogen in reaction 4 is essentially a localized process; the hydrogen molecule which desorbs originates from a single ammonia molecule. The remaining hydrogen atom per adsorbed ammonia molecule is incorporated into the η-species and its desorption, reaction 1, is depicted in the spectra of Fig. 2. Two possible structures have been proposed (8, 10) for the η-species, $W^sN_2H\cdot W^sN$ and $W^sN_2\cdot W^sNH$; both structures can account for the thermal desorption results but the magnitude of the hydrogen isotope effect involved in this reaction supports the first of these structures (10). In this case, the η-desorption process can be represented as

$$[1'] \quad W^sN_2H\cdot W^sN(\eta) \rightarrow W^s{}_2N(\beta) + N_2(g) + H(g)$$

The activation energy for the η-desorption process is 35 kcal mol^{-1} (24), the same as that observed for the overall decomposition process (1, 2, 4). It is possible to account for the desorption of hydrogen in the atomic state by assuming that the ability of adjacent tungsten atoms to participate in the breaking of the N—H bond is reduced to zero at this adatom density. This would leave the hydrogen atom no alternative but to dissociate directly into the gas phase. Since such a process would be expected to require an activation energy approaching the N—H bond energy, *i.e.* much greater than 35 kcal mol^{-1}, we propose an additional mechanism involving an intermediate adsorbed state for hydrogen

$$[1a] \quad W^sN_2H\cdot W^sN(\eta) \rightarrow WN^s{}_2\cdot W^sN + H(a)$$

$$[1b] \quad W^sN_2\cdot W^sN + H(a) \rightarrow W^sN_2\cdot W^sN + H(g)$$

$$[1c] \quad W^sN_2\cdot W^sN + 2H(a) \rightarrow W^sN_2\cdot W^sN + H_2(g)$$

$$[1d] \quad W^sN_2\cdot W^sN \rightarrow W^s{}_2N(\beta) + N_2(g)$$

The desorption of hydrogen as atoms, reaction 1*b*, and by bimolecular recombination as molecules, reaction 1*c*, are both assumed to take place from a surface crowded by co-adsorbed nitrogen. At large nitrogen coverages we would expect that the binding energy of co-adsorbed hydrogen atoms would be less than that for a pure hydrogen adlayer at the same hydrogen coverage; this will lead to an enhancement in the desorption rate of hydrogen atoms, [1*b*]. It is also to be expected that for steric reasons the surface migration of hydrogen atoms will be retarded in adlayers crowded by co-adsorbed nitrogen; this will reduce the rate of bimolecular recombination, [1*c*]. In this way it is possible for the rates of reactions 1*b* and 1*c* to be comparable at temperatures much below those required in the absence of adsorbed nitrogen.

The experimental results reported here suggest that only one-quarter of the adsorbed hydrogen desorbs atomically. The desorption spectra shown in Figs. 2 and 3 suggest a constant fraction desorbing atomically, independent of surface coverage. With decreasing coverage of nitrogen and hydrogen the rates of migration will increase but the collision rate may decrease because of the decrease in concentration of diffusing hydrogen atoms. It is thus quite possible that the rates of reactions 1*b* and 1*c* both decrease to a comparable extent as a result of a decrease in surface concentration.

Role of Absorbed Hydrogen in Desorption of the η-Species

We have recently observed (25) that the ammonia decomposition reaction is 1/3 order

Can. J. Chem. Downloaded from www.nrcresearchpress.com by 210.87.254.105 on 09/05/12
For personal use only.

in the ammonia pressure over such a wide range in pressure that a Langmuir–Hinshelwood mechanism involving progressive saturation of the surface with the η-species seems unlikely. It was proposed (25) that absorbed hydrogen, H(*), in equilibrium with gaseous ammonia, participates in desorption of the η-species,

$$[5]\quad H(^*) + W^s{}_2N_3H(\beta) \rightarrow W^s{}_2N(\beta) + N_2(g) + H_2(g)$$

to account for these observations. Such hydrogen absorption accompanies nitriding of the tungsten, but only at higher temperatures and pressures than used to form the η-species in these experiments (8, 24). Thus reaction 5 does not account for the fraction which desorbs molecularly in the present experiments; however, it is impossible to distinguish surface and sub-surface hydrogen atom migration in the bimolecular recombination process [1*c*].

The Ammonia Synthesis Reaction

If the hydrogen desorbing from the η-species did so exclusively in the atomic state, then, by the principle of microscopic reversibility, one would deduce that ammonia synthesis would occur by the reverse path, *i.e.* interaction of atomic hydrogen gas with a dense nitrogen adlayer. Since the concentration of atomic hydrogen in the gas phase is minute under synthesis conditions, *i.e.* moderate temperature and high pressure, it would be concluded that the η-species played a negligible role in the ammonia synthesis reaction. That is, unless the catalyst were polyfunctional (polycrystalline or with added promoters) such that some portion of the catalyst surface were to dissociate adsorbed molecular hydrogen and the resulting hydrogen atoms diffused to the active surface where the η-species could be generated. The observation that only one-quarter of the hydrogen desorbs atomically obviates this involved process; molecular hydrogen gas can generate the η-species. However, this result is subject to considerable uncertainty. Therefore, it is worth noting that even if the fraction desorbing molecularly in the thermal desorption experiments were so small as to be undetectable, though not zero, molecular hydrogen can still generate the η-species. If the rate of reaction 1*b* was orders of magnitude less than the rate of 1*c* then a negligible fraction of molecular hydrogen would be detected in a thermal desorption experiment. However, in a totally different situation, such as during ammonia synthesis, where the gas phase hydrogen atom concentration was negligible compared to the concentration of molecules, the rate of the reverse of 1*c* could become orders of magnitude greater than that for the reverse of 1*b*, and possibly large enough to sustain the η-species on the surface. The role of the η-species in the ammonia synthesis process could best be determined directly, by identifying the surface species which are generated by nitrogen and hydrogen gas mixtures under synthesis conditions.

The authors wish to thank the National Research Council of Canada for their support of this research.

1. C. N. HINSHELWOOD and R. E. BURK. J. Chem. Soc. (Lond.), **127**, 1105 (1925).
2. C. H. KUNSMAN. J. Am. Chem. Soc. **50**, 2100 (1928).
3. H. R. HAILES. Trans. Faraday Soc. **27**, 601 (1931).
4. J. C. JUNGERS and H. S. TAYLOR. J. Am. Chem. Soc. **57**, 679 (1935).
5. R. M. BARRER. Trans. Faraday Soc. **32**, 490 (1936).
6. P. T. DAWSON and R. S. HANSEN. J. Chem. Phys. **48**, 623 (1968).
7. K. MATSUSHITA and R. S. HANSEN. J. Chem. Phys. **52**, 4877 (1970).
8. Y. K. PENG and P. T. DAWSON. J. Chem. Phys. **54**, 950 (1971).
9. P. T. DAWSON and Y. K. PENG. Surface Sci. **33**, 565 (1972).
10. P. T. DAWSON and Y. K. PENG. J. Phys. Chem. **77**, 135 (1973).
11. S. J. THOMSON and G. WEBB. Heterogeneous catalysis. J. Wiley, New York. 1968. pp. 83–86.
12. B. J. WOOD and H. WISE. J. Chem. Phys. **29**, 1416 (1958).
13. W. L. FITE and R. T. BRACKMANN. Phys. Rev. **112**, 1141 (1958).
14. T. W. HICKMOTT. J. Chem. Phys. **32**, 810 (1960).
15. T. W. HICKMOTT. J. Appl. Phys. **31**, 128 (1960).
16. K. MIYAHARA, A. OZAKI, and T. KIMURA. J. Res. Inst. Catal. Hokkaido Univ. **11**, 124 (1963).
17. D. R. STULL and G. C. SINKE. Thermodynamic properties of the elements. American Chemical Society, Washington. 1956. p. 104.
18. T. E. MADEY. Surface Sci. **36**, 281 (1973).
19. P. W. TAMM and L. D. SCHMIDT. J. Chem. Phys. **54**, 4775 (1971).
20. L. J. RIGBY. Can. J. Phys. **43**, 1020 (1965).
21. R. GOMER, R. WORTMAN, and R. LUNDY. J. Chem. Phys. **26**, 1147 (1957).
22. D. BRENNAN and P. C. FLETCHER. Proc. Roy. Soc. (Lond.), **A250**, 389 (1959).
23. G. EHRLICH. J. Chem. Phys. **31**, 1111 (1959).
24. Y. K. PENG. Ph.D. Thesis. McMaster University, Hamilton, Ontario, 1973.
25. P. T. DAWSON. J. Catal. In press.

Crystal Structure of Synthetic Mg-Whitlockite, $Ca_{18}Mg_2H_2(PO_4)_{14}$

RAMANATHAN GOPAL AND CRISPIN CALVO
Institute for Materials Research, McMaster University, Hamilton, Ontario L8S 4MI
JUN ITO
Department of Geological Sciences, Harvard University, Cambridge, Massachusetts 02138
AND
W. K. SABINE
Department of Orthopaedic Surgery, Children's Hospital Medical Center, Boston, Massachusetts 02115

Received September 10, 1973

Crystals of synthetic Mg-whitlockite, $Ca_{18}Mg_2H_2(PO_4)_{14}$, have been grown by hydrothermal techniques and their structure refined by full-matrix least-squares methods, using 1626 unique reflections measured with a Syntex $P\bar{1}$ automatic diffractometer, to a final R value of 0.046. The crystals have space group $R3c$ with $Z_R = 1$, $a = 13.765(8)$ Å and $\alpha = 44.25(5)°$ with the equivalent hexagonal parameters $a = 10.350(5)$, $c = 37.085(12)$ Å and $Z_H = 3$. The structure, although similar to that of $\beta Ca_3(PO_4)_2$, differs significantly. The structure contains interconnected infinite chains of polyhedra paralleling the hexagonal c axis with links in the chains consisting of three CaO_8 polyhedra separated by two PO_4 tetrahedra. Six of these chains surround a chain of MgO_6 octahedra and PO_4H groups which lie on the three-fold axes. These chains however contain only half the formula unit density of the calcium containing ones and a proton, presumably disordered, is attached to the oxygen atom on the triad axes.

Des cristaux de Mg-whitlockite synthétique $Ca_{18}Mg_2H_2(PO_4)_{14}$ ont été développés par des techniques calorimétriques et leur structure raffinée par une matrice complète des méthodes de moindres carrés, utilisant la réflection unique 1626 mesurée par un diffractomètre automatique Syntex $P\bar{1}$, à une valeur finale R de 0.046. Les cristaux ont un groupe d'espace $R3c$ avec $Z_R = 1$, $a = 13.765(8)$ Å et $\alpha = 44.25(5)°$ avec les paramètres hexagonaux équivalents $a = 10.350(5)$, $c = 37.085(12)$ Å et $Z_H = 3$. La structure, bien que similaire à celle de $\beta Ca_3(PO_4)_2$, en diffère grandement. La structure contient des chaînes infinies réticutées de polyèdres parallèles à l'axe hexagonal c avec des maillons de chaînes qui consistent en trois polyèdres de CaO_8 séparés par deux tétraèdres de PO_4. Six de ces chaînes entourent une chaîne de MgO_6 octaédrique et des groupes de PO_4H qui reposent sur les axes d'ordre 3. Pourtant on trouve dans ces chaînes seulement la moitié de la densité unitaire en calcium des formules qui en contiennent et un proton, probablement désordonné, est attaché à l'atome d'oxygène sur les axes ternaires.
[Traduit par le journal]

Can. J. Chem., **52**, 1155 (1974)

Introduction

The problem of the structure and stoichiometry of whitlockite, originally posed by Frondel (1, 2) has only recently been resolved. Gopal and Calvo (3) showed that the mineral from Palermo Quarry is, in fact, a solid solution of essentially $Ca_{18}(Mg,Fe)_2Ca(PO_4)_{14}$ and $Ca_{18}(Mg,Fe)_2H_2(PO_4)_{14}$ in a ratio of about 1 to 4. The primary structural difference between the two end-members involves a reorientation of the PO_4 groups on the triad axes, one in every seven, to permit the replacement of a phosphate oxygen atom bonded to three calcium ions with a P—O—H group.

Because of the similarities in the Debye–Scherrer patterns, the name "whitlockite" and "β calcium orthophosphate" ($\beta Ca_3P_2O_8$) have been used interchangeably to characterize the structures of the entire range of compositions. Prior to this study the structure of synthetic whitlockite had not been reported, although Keppler (4) prepared Fe-whitlockite and he suggested that the name X-whitlockite be reserved for $Ca_{18}X_2H_2(PO_4)_{14}$. Since "whitlockite" has been found in abnormal human and animal calcification (5) and dental caries (6, 7) a detailed resolution of the structural parameters would be important in understanding the stability field and perhaps the role of impurities in the stabilization of this phase. Because of the solid solution nature of the mineral the synthetic system offers a more suitable framework for this investigation.

Can. J. Chem. Downloaded from www.nrcresearchpress.com by 210.87.254.40 on 09/05/12
For personal use only.

TABLE 1. A chemical analysis of Mg-whitlockite ($Ca_{18}Mg_2H_2(PO_4)_{14}$) in weight percent compared with the mineral*

	Synthetic Mg-whitlockite		Whitlockite‡	
	Theory	Found	Chemical analysis	Structure analysis
CaO, SrO	48.03	47.0†	47.15	47.77
P_2O_5, SiO_2	47.28		46.87	46.53
MgO, FeO, MnO	3.84	3.93†	3.95	3.76
H_2O+	0.86	0.96(5)	0.65(4)	0.68
H_2O-		0.08(1)	0.04(1)	

*For the mineral the various oxides are calculated as the oxide, in italics.
†Courtesy of Dr. D. Walker, Department of Geological Sciences, Harvard University, Cambridge, Mass.
‡C. Calvo and R. Gopal (1974), ref. 17.

A nomenclature which would distinguish the structures of the end members of the whitlockite solid solution, $Ca_{18}Mg_2H_2(PO_4)_{14}$ and $Ca_{18}Mg_2Ca(PO_4)_{14}$, would be useful since it is anticipated that the proton in the former would be biologically important. In this paper the former will be referred to as having the synthetic Mg-whitlockite structure and the latter will be said to have the $\beta Ca_3P_2O_8$ structure.

Experiments

Crystals of Mg-whitlockite up to 0.5 mm on a side were grown hydrothermally by heating an amorphous phosphate gel in a stainless steel bomb with a capacity of 25 ml. The gel was precipitated from a slightly acidic solution (150 ml) containing 14 m*M* of $NH_4H_4PO_4$, 18 m*M* of $Ca(NO_3)_2$, and 2 m*M* $Mg(NO_3)_2$, by rapidly adding 25 ml of concentrated ammonia. The resulting precipitate, a gel, was separated by centrifuging, then spread on filter paper and dried in air at 110 °C. The crushed dried gel half-filled a gold tube, 6 mm in diameter and 10 cm long, with one end welded. The remaining space was filled with distilled water and the top crimped shut. The optimum conditions for the synthesis of coarse crystalline Mg-whitlockite are 300 °C, 1.5 kb for 2 weeks. Mixtures with other stoichiometries, but with Ca and Mg in a molar ratio maintained at 9 to 1, afforded single phase compounds but always with very small crystals.

A chemical analysis of the synthetic Mg-whitlockite demonstrated that it is a compound consisting of $Ca_9MgH(PO_4)_7$. Its composition is compared to that of the mineral in Table 1. The Mg to Ca ratio was determined by microprobe analysis through the kindness of Dr. D. Walker.[1] The water content of both materials was determined by the electrolytic method described by Wilkins and Sabine (8). This method was also used to determine their thermal dehydration curves. As shown in Fig. 1, both undergo the same two major dehydration events centered at about 780 and 1035 °C. All the water released at these high temperatures is undoubtedly essential and is designated as H_2O+ while the minor amount released below 560 °C is considered non-essential (H_2O-). These results constitute the first direct evidence that hydrogen occurs in both natural and synthetic whitlockite as an integral part of their structures although the structural studies of the mineral strongly suggested its presence (9).

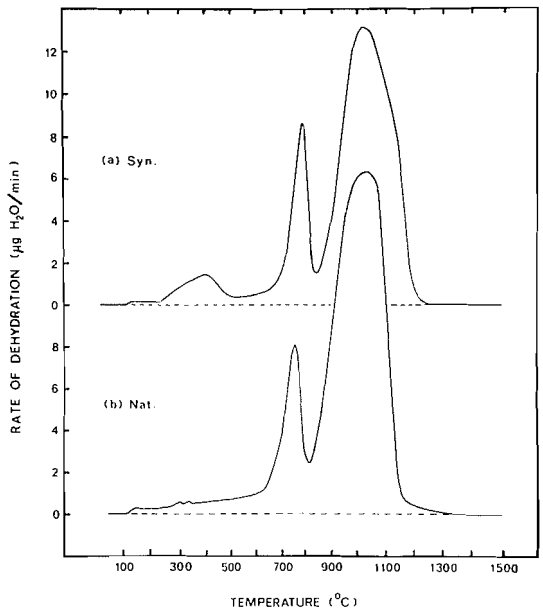

FIG. 1. Thermal dehydration curves of (*a*) synthetic Mg-whitlockite and (*b*) natural whitlockite from the Palermo Quarry, New Hampshire. Both curves were obtained using a heating rate of 15 °C/min, a dry nitrogen carrier gas at 4 psig pressure, and an electrolytic P_2O_5 detector. The total amount of water released by each sample, or the amount released over a given temperature range, is directly proportional to the area under its curve.

Complete dehydration of the synthetic whitlockite, however, produced only small changes in its unit cell dimensions. The following values for the hexagonal cell parameters were obtained from a least-squares refinement of powder diffraction data (CuKα = 1.5432 Å) using a program written by Evans, Appleman, and Handwerker (10):

[1]Details are available from Dr. D. Walker, Department of Geological Sciences, Harvard University, Cambridge, Mass. 02138.

Can. J. Chem. Downloaded from www.nrcresearchpress.com by 210.87.254.40 on 09/05/12
For personal use only.

Composition	a (Å)	c (Å)	Volume (Å^3)
$Ca_{18}Mg_2H_2P_{14}O_{56}$ (before dehydration)	10.347(1)	37.099(5)	3440.2(6)
$Ca_{18}Mg_2P_{14}O_{55}$ (after dehydration)	10.303(1)	37.272(5)	3426.8(7)

Preliminary results of structure analysis of Mg-whitlockite at room temperature after heating to 900 °C and again after heating to 1200 °C indicates that it has adopted the the $\beta Ca_3P_2O_8$ structure (11).

Equidimensional crystals, with mean diameters of about 0.20 mm were chosen for X-ray examination. The data were taken with graphite monochromatized MoKα radiation on a Syntex P$\bar{1}$ automatic diffractometer. 3548 reflections were recorded from the first crystal and an additional 1675 were taken from the second crystal to check the reproducibility of the crystals and measurements. These data sets were combined since the deviations between the sets were of the same order as the deviations between symmetry equivalent reflections within a set. Peaks were scanned at a rate between 2 and 24° per min, a value dependent upon peak intensity, and a scan range from 1° below the α_1 to 1° above the α_2 peak. Backgrounds were determined at either side and 1° removed from the peak. Resultant intensities greater than three times the estimated standard deviations derived from counting statistics were considered observed and the remainder as unobserved. Amongst the latter those whose intensity measure was less than zero after correction for background were dropped from the refinement to save computing cost. The remaining 1626 reflections were used in the refinement and of these 1157 were observed. All the data were corrected for Lorentz, polarization, absorption, ($\mu R = 0.33$) based upon a spherical crystal shape, and extinction, using the procedure of Larson (12). Symmetry equivalent reflections in each set were averaged with the average discrepancy in structure factor of 2%.

15 reflections were accurately centered and their 2θ values, measured with MoKα radiation ($\lambda = 0.71069$ Å) at 21 °C, fitted by a least-squares method to obtain the lattice parameters.

Crystal data
$Ca_{18}Mg_2H_2(PO_4)_{14}$
Rhombohedral, $a_R = 13.765(8)$ Å, $\alpha = 44.25(5)°$,
$Z_R = 1$, $V = 1154.5$ Å^3.
Hexagonal, $a_H = 10.350(5)$, $c_H = 37.085(11)$ Å, $Z_H = 3$.
Space group $R3c$, $\rho_x = 3.033$ g/cm^3.

The positional parameters for the mineral, given by Gopal (9), were used as initial atomic parameters. Weights, ω, were chosen so that $\omega|F_o - F_c|^2$ would locally be independent of F_o and the function obtained was $\omega = [14.9 - 0.077F_o + 0.0005F_o^2]^{-1}$. This distribution paralleled the curve obtained by plotting the difference in the structure factors for the two sets of observed data *vs.* F_o. The atomic parameters, including isotropic thermal parameters, were refined to a minimum in ωR and then the anisotropic components were varied together with the positional parameters. Atomic scattering factors were chosen from Cromer and Waber (13) and corrected for dispersion using the values of Cromer (14). When all the calculated shifts were less than 0.2 of the estimated standard deviations the refinement was terminated. The final R value is 0.049 and includes all reflections. The value of $\omega R = (\Sigma\omega|F_o - F_c|^2/\Sigma\omega F_o^2)^{1/2}$ is 0.039. The observed and calculated structure factors are in Table 2 and the final positional and thermal parameters are in Tables 3 and 4.[2]

Description of the Structure

The structure of Mg-whitlockite can easily be related to that of $Ba_3P_2O_8$ (15) (Fig. 2). The latter structure is composed of chains, paralleling the c axis, with links consisting of three Ba ions in a row terminated at either end with tetrahedral PO_4 groups. The chain has $3m$ symmetry with the central barium ion, Ba(I), lying at a center of symmetry.[3] Three O(II) atoms of each phosphate group lie on mirror planes while the fourth, O(I), also lies on the three-fold axis. Each chain is surrounded by six others, related to it by the rhombohedral centering. Ba(I) is coordinated octahedrally to six O(II) atoms, contributed by six PO_4 groups lying on neighboring chains. In this structure the O(I) atoms on these phosphate groups are too far away to form significant bonds (3.22 Å). Each Ba(II) ion shares a face with one of these Ba(I)—$O(II)_6$ octahedra, an O(I) atom with a phosphorus atom in the same chain and three O(II)—O(II) edges with phosphate groups lying on neighboring three-fold axes. The atoms of the O(II)—O(II) edge and the O(II) shared between a given Ba(II) and Ba(I) arise from PO_4 groups in an adjacent chain.

Mg-whitlockite has two types of chains in a cell with axes about double those in $Ba_3P_2O_8$ and thus about eight times the volume. The A chains contain $MgHPO_4$ units alternating with empty sites, when compared with the chains in $Ba_3P_2O_8$ while the B chains are much as those just described. Each A chain is surrounded by six B chains while each B chain has two A chains on opposite sides in addition to four B chains as neighbors, as shown in Fig. 3.

If the present compound were structurally like

[2]Table 2 is available, at a nominal charge, from the Depository of Unpublished Data, National Science Library, National Research Council of Canada, Ottawa Canada, K1A 0S2.

[3]Roman numerals have been used instead of the arabic ones of Süsse and Buerger (20) in describing the isotypic $Ba_3V_2O_8$ and the analogous atoms are labelled similarly in the present compound.

Can. J. Chem. Downloaded from www.nrcresearchpress.com by 210.87.254.40 on 09/05/12
For personal use only.

Can. J. Chem. Downloaded from www.nrcresearchpress.com by 210.87.254.40 on 09/05/12
For personal use only.

TABLE 3. Atomic positions for $Ca_{18}Mg_2H_2(PO_4)_{14}$ with estimated standard deviations in parentheses

Atom	x*	y	z
Ca(IB)	0.2951(1)	0.1580(1)	0.6720(1)
Ca(IIB1)	0.2810(1)	0.1468(1)	0.5648(1)
Ca(IIB2)	0.3880(1)	0.1800(1)	0.7676(1)
Mg	0	0	0
P(A)	0	0	0.7531(1)
P(B1)	0.3180(2)	0.1433(2)	0.8641(1)
P(B2)	0.3511(2)	0.1578(2)	0.9674(1)
O(IA)	0	0	0.7957(2)
O(IIA)	−0.0219(5)	0.1290(4)	0.7407(1)
O(IB1)	0.2758(5)	0.0910(5)	0.8250(1)
O(IIB1)	0.2477(5)	0.2334(5)	0.8773(2)
O(IIB3)	0.2736(4)	0.0025(4)	0.8866(1)
O(IIB5)	0.4892(4)	0.2421(5)	0.8685(2)
O(IB2)	0.4063(4)	0.1980(4)	0.0065(1)
O(IIB2)	0.3994(4)	0.0477(5)	0.9539(1)
O(IIB4)	0.4151(5)	0.3037(5)	0.9460(1)
O(IIB6)	0.1781(4)	0.0782(5)	0.9643(1)

*Coordinates are based upon a hexagonal cell.

TABLE 4. Thermal parameters for $Ca_{18}Mg_2H_2(PO_4)_{14}$ with estimated standard deviations in parentheses*

Atom	U_{11}	U_{22}	U_{33}	U_{12}	U_{13}	U_{23}
Ca(IB)	0.0251(6)	0.0147(5)	0.0141(3)	0.0145(5)	−0.0098(3)	−0.0070(4)
Ca(IIB1)	0.0089(5)	0.0084(4)	0.0078(3)	0.0044(4)	−0.0010(3)	−0.0013(4)
Ca(IIB2)	0.0091(5)	0.0079(5)	0.0081(3)	0.0040(4)	−0.0018(3)	0.0002(4)
Mg	0.0068(9)	U_{11}	0.0080(8)	$1/2U_{11}$	—	—
P(A)	0.0079(7)	U_{11}	0.0113(9)	$1/2U_{11}$	—	—
P(B1)	0.0070(6)	0.0062(6)	0.0061(4)	0.0032(5)	0.0003(4)	0.0000(5)
P(B2)	0.0056(5)	0.0055(5)	0.0055(4)	0.0019(5)	0.0006(4)	0.0011(4)
O(IA)	0.031(4)	U_{11}	0.008(2)	$1/2U_{11}$	—	—
O(IIA)	0.017(2)	0.009(2)	0.018(2)	0.009(1)	0.007(1)	0.005(1)
O(IB1)	0.017(2)	0.016(2)	0.006(1)	0.009(2)	0.001(1)	−0.001(1)
O(IIB1)	0.012(2)	0.011(2)	0.011(1)	0.009(1)	0.000(1)	−0.001(1)
O(IIB3)	0.011(2)	0.008(2)	0.008(1)	0.004(1)	−0.000(1)	0.001(1)
O(IIB5)	0.005(2)	0.010(2)	0 014(1)	0.005(2)	0.004(1)	0.002(1)
O(IB2)	0.012(2)	0.011(2)	0.006(1)	0.005(1)	−0 002(1)	−0.001(1)
O(IIB2)	0.007(2)	0.014(2)	0.009(1)	0.007(1)	0 000(1)	−0.000(1)
O(IIB4)	0.013(2)	0.010(2)	0.011(1)	0.003(1)	0.000(1)	0.002(1)
O(IIB6)	0.010(2)	0.012(2)	0.008(1)	0.008(2)	−0.000(1)	−0.001(1)

*Thermal factor equals $\exp -2\pi^2 [b^2h^2U_{11} + \ldots + 2b_1b_2hkU_{12} + \ldots]$ and the b_i's are reciprocal lattice vectors of the hexagonal cell.

$Ba_3P_2O_8$, except for doubled axes lengths, it would have twenty-four divalent cations, with $2H^+$ taken as equivalent to one Ca^{2+}, and sixteen phosphate groups rather than twenty-one cations and fourteen phosphate groups. The smaller radius of Ca^{2+}, compared with Ba^{2+}, introduces instabilities in the $Ba_3P_2O_8$ structure because of the repulsion between cation (I) and cation (II) on the same chain since they share three O(II) atoms (16). Further, the reduction in the average cation – oxygen atom bond length enhances the repulsion between the oxygen atoms of the three O(II)—O(II) edges of the PO_4 groups shared with type II cations.

The loss of $3Ca^{2+}$ and 2 phosphate groups from the A chains of every rhombohedral cell relieves some of these repulsive interactions yielding Ca(IB), Ca(IIB1) and Ca(IIB2) coordinated to 5, 9, and 8 oxygen atoms. This results from the loss of one of the three O(II) shared between Ca(IB) and Ca(IIB1) and one of the three O(II)—O(II) edges about Ca(IIB2). Coordinations of 8 are obtained for these cations, as shown in Fig. 4, by the rotation of the $P(A)O_4$ group so

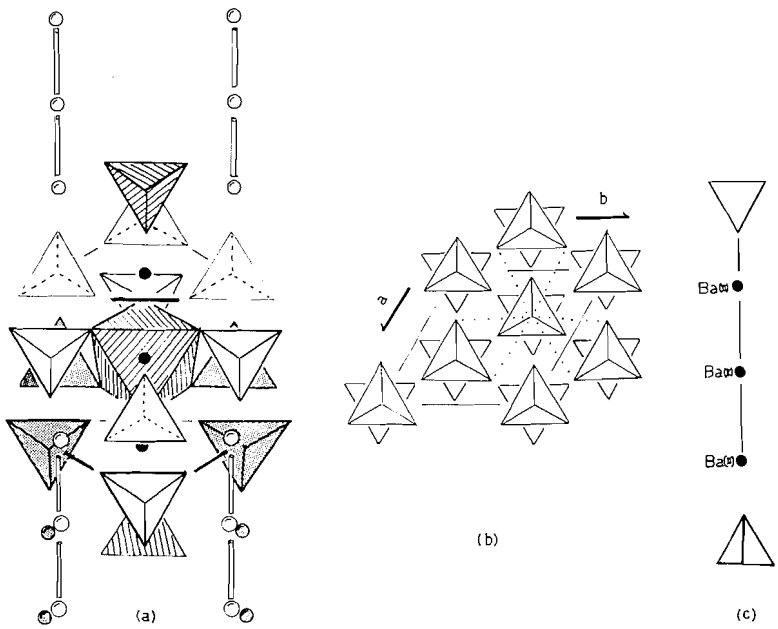

FIG. 2. (*a*) A view of the $Ba_3P_2O_8$ structure. The circles represent Ba ions and the tetrahedra are PO_4 groups. The cross hatched tetrahedra and the filled circles are on the same chain and surrounded by six other chains. The octahedron about Ba(I) is shown. The Ba(II) ion lies in a hexagon and shares one edge with each of the three neighboring PO_4 groups. (*b*) The $Ba_3(PO_4)_2$ structure is shown projected down the hexagonal axis. The PO_4 groups are shown. The dotted lines indicate the Ba(II)—O(II) bonds of the Ba(II)—O_6 hexagon indicated in (*a*). (*c*) The chain structure in the $Ba_3(PO_4)_2$ structure is shown.

that it shares a corner, rather than an edge, with Ca(IIB1) and the formation of three Ca(IB)—O(I) bonds with O(I) atoms from phosphate groups on neighboring chains. The bonds in $Ba_3V_2O_8$ comparable to these latter ones are very weak.

Mg occupies the cation site in the A chain as shown in Fig. 5 and is octahedrally coordinated showing two unique Mg—O bond lengths of 2.057(5) and 2.077(5) Å. The octahedron is elongated parallel to its three-fold axis, as seen by the deviation of the O(IIB5)—Mg—O(IIB6) angles from 90° and 180° (Table 5). The P(A)O_4 groups are inverted through a plane perpendicular to the *c* axis relative to the tetrahedron's configuration in $Ca_3V_2O_8$ (16), permitting the hydrogen atom to bond strongly to O(IA) and weakly to O(IB1) (O(IA)—O(IB1) = 2.774(7) Å). In $Ca_3V_2O_8$ O(IA) is bonded to three Ca(IB) ions. The P(A)—O(IA) and P(A)—O(IIA) bond distances, at 1.580(9) and 1.532(6) Å, are comparable to those reported in the mineral (17). It is of interest to note that Sutor (18) recently reported a P—O(—H) bond lengths of 1.588(5) Å in $MgHPO_4 \cdot 3H_2O$.

The P(B1)—O_4 and P(B2)—O_4 tetrahedra have average P—O bond lengths of 1.537 and 1.535 Å. The P—O(IB) bonds of these tetrahedra subtend angles of 29.0 and 29.5° with the *c* axis and their centers are displaced from the 1/3,1/6,*z* axis by 0.21 and 0.24 Å for the P(B1)O_4 and P(B2)O_4 groups, respectively. The P(A)O_4 group is distorted as if the effect of the hydrogen atom, assumed to be bonded to O(IA), is to repel the phosphorus atom by about 0.04 Å along the *c* axis towards the plane of the three O(IIA) oxygen atoms. The Ca ions have moved from colinearity in order to accommodate the displacements and rotations of the PO_4 groups in the structure. Each of the Ca(IIB) ions shares two edges with two PO_4 groups on neighboring B chains. Unlike the situation in the $Ba_3P_2O_8$ structure, each Ca(I) share three O(I)—O(II) edges with phosphate groups in neighboring chains.

Discussion

The existence of hydrogen atoms in the structure is clearly shown by the results of our chemical analysis and thermal dehydration studies.

Can. J. Chem. Downloaded from www.nrcresearchpress.com by 210.87.254.40 on 09/05/12
For personal use only.

Can. J. Chem. Downloaded from www.nrcresearchpress.com by 210.87.254.40 on 09/05/12
For personal use only.

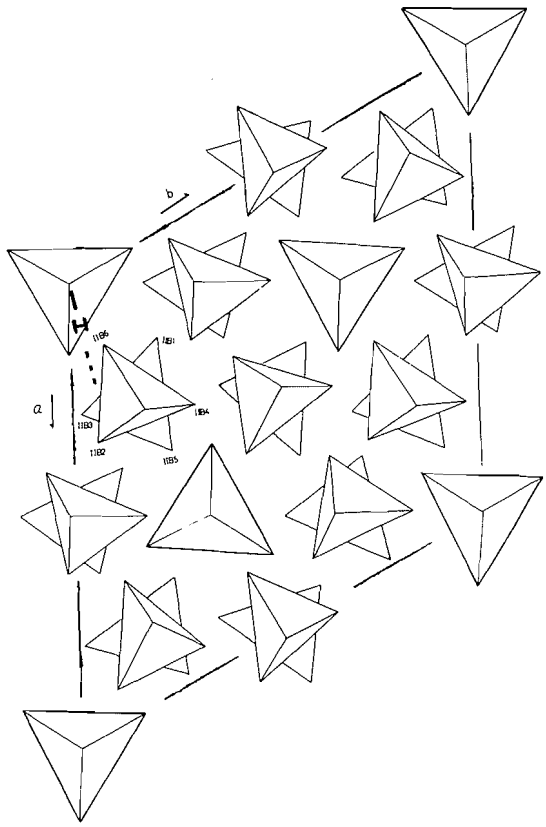

FIG. 3. The PO_4 groups upper half cell of Mg whitlockite are shown in projection down the hexagonal c axis. The oxygen atoms about P(B1) and P(B2) are labelled. The three-fold axes pass through the non-superimposed PO_4 groups. One of the three possible assumed hydrogen atom positions is shown bonded to the PO_4 group at the origin.

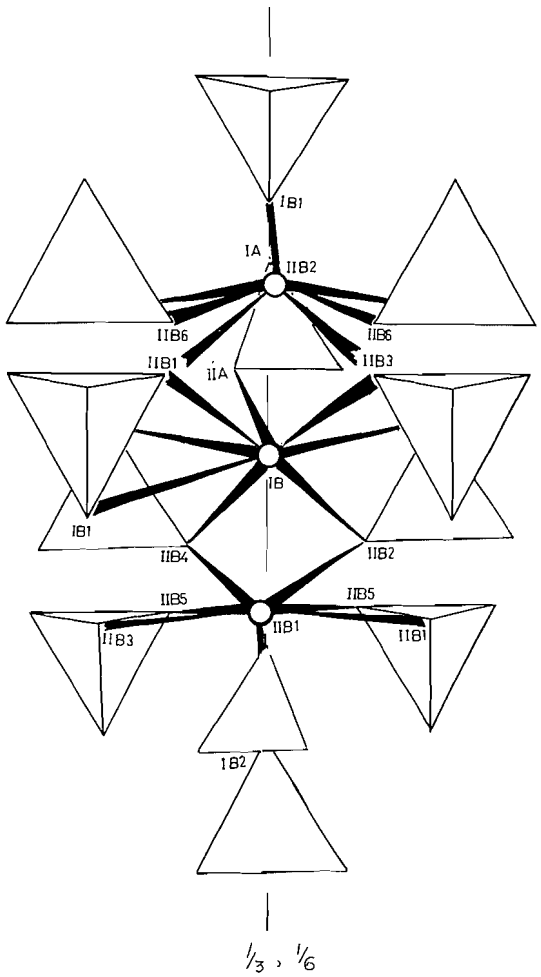

FIG. 4. The environment of a B chain in Mg-whitlockite viewed along [$\bar{2}\bar{1}0$]. The circles are calcium ions and the PO_4 groups are shown as tetrahedra. The Ca—O bonds are shown and the oxygen atoms at the corners of the tetrahedra are labelled.

The role of the hydrogen atom in the structure, as can be seen in the difference between the whitlockite and $\beta Ca_3P_2O_8$ structures (isostructural with $Ca_3V_2O_8$), is to invert the $P(A)O_4$ group so as to allow hydrogen bonding between O(IA) and O(IB1). The structural changes upon heating, particularly caused by the loss of 20% of the hydrogen near 780 °C and the remainder near 1035 °C is not known. However, the stoichiometry of the transformation

$$Ca_{18}Mg_2H_2(PO_4)_{14} \rightarrow Ca_{18}Mg_2(PO_4)_{12}P_2O_7 + H_2O$$

suggests that P_2O_7 should result from this change. Figure 1 shows that the changes of the same magnitude occur at the same temperatures in the mineral as in synthetic whitlockite. Although the composition after the initial water loss in Mg-whitlockite is similar to that of the mineral, the structure of Mg-whitlockite above 780 °C is not the same as the mineral at room temperature. Thus, these studies do not permit one to conclude the special conditions which leads to the solid solution in the naturally occurring mineral. However, further chemical syntheses may resolve this problem. Because the water evolution profile is so characteristic, it should be possible to show whether the "whitlockite" occurring in vivo has the present structure, that of $\beta Ca_3P_2O_8$ or a solid solution as in the mineral, but perhaps with a different component ratio.

The geometry of the PO_4 groups in the mineral

Can. J. Chem. Downloaded from www.nrcresearchpress.com by 210.87.254.40 on 09/05/12
For personal use only.

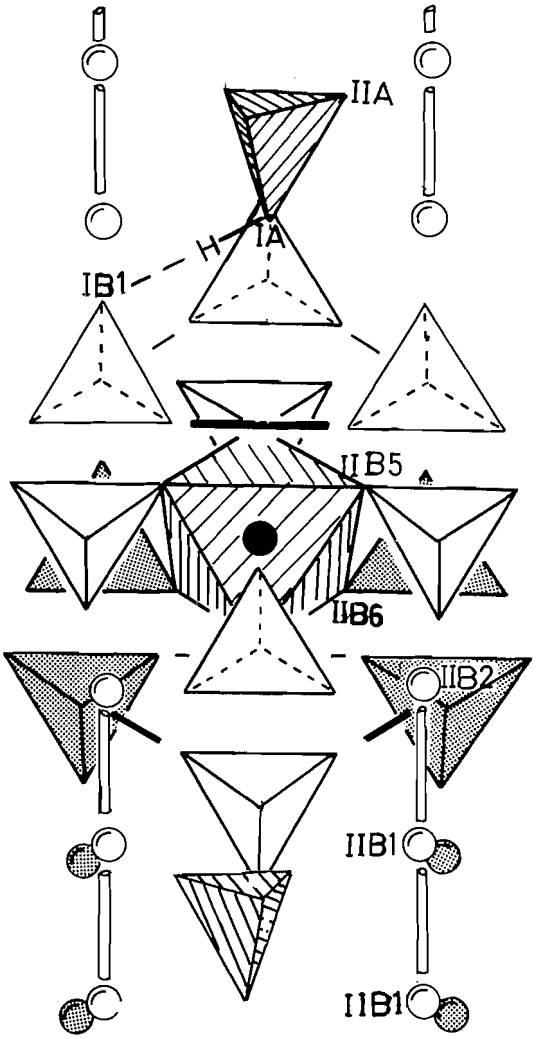

FIG. 5. The environment of the A chain in Mg-whitlockite is shown. The Mg is represented as filled circles and the Ca ions as open circles. The phosphate groups are shown as tetrahedra. The octahedron about the Mg is shown as is one of the ordered hydrogen atom positions.

and the Mg-whitlockite are similar with most bond lengths differing by less than 2σ. In particular, the P(B1)—O(IIB1) is the shortest in both cases and may be related to the long bond this oxygen atom shares with Ca(IIB1). The P(A)—O(IA) bond differ between these structures.

Each oxygen atom in the structure, except O(IA), is bonded to three cations and a phosphorus atom, with the proton considered as a cation and assumed bonded weakly to O(IB1). O(IIA) is bonded weakly to Ca(IB) but does seem to have compensated for this by an exceptionally strong bond to the other cations.

A detailed comparison of the bond lengths in Mg-whitlockite with other structures in this series will appear elsewhere (17). However, a few points should be made here. All the individual Ca—O bond lengths are the same within 5σ in the $Ca_{18}(Mg,Fe)_2H_2(PO_4)_{14}$ portion of the mineral and the present structure save for Ca(IB1)—O(IB1). This bond is 2.550(4) Å in the former case compared with 2.503(4) Å in the present case. Generally, as with other structures in this series, those Ca—O bond lengths nearly in the equatorial plane of the cation, that is, those of the type Ca(IB)—O(I) and those of the type Ca(IIB)—O(II), where the oxygen atoms are part of the shared PO_4 edge system, are longer than the others. This is expected from the O(II)–O(II) repulsions. Unlike the $Ba_3P_2O_8$-type structure case the Ca(IIB)—O(I) bonds are normal suggesting that it was the underbonding of O(I) which was responsible for the short Ba(II)–O(I) interaction.

The M—O_6 octahedron is elongated along c as is the case in $Pb_3P_2O_8$ (19), $Ba_3V_2O_8$ (20), and the $Ca_3X_2O_8$ systems. Some of this elongation is attributable to repulsion between cations which share the octahedral face, but in the present structure and in the $Ca_3X_2O_8$ compounds the effect persists albeit somewhat diminished. The Mg-whitlockite differs from the mineral in that the Mg—O(IIB5) bond length is shorter than the Mg—O(IIB6) bond, whereas the analogous distances are 2.088(5) and 2.077(5) Å in the mineral. In the latter case, this site contains almost as much Fe^{2+} and Mn^{2+} as Mg^{2+}, but it is not certain that the composition effects the reversal in these lengths.

It is clear that Mg is analogous to the type I cation in $Ba_3P_2O_8$ since it is nearly half a rhombohedral axis length from Ca(IB). The P(A)O_4 group, however, is translated by about 1.6 Å from the predicted position based upon the B chain structure. Thus the A chain has room for substitution of suitably charged ions. Thus for example, sodium ions can occur in the structure near either $0,0,\pm z$ with $z \sim 0.10$ in compensation for tetravalent ions substituted for P, in lieu of Mg^{2+} or both if trivalent ions substitute for divalent cations. In this regard it should be noted that the mineral contains some sodium (2) while some whitlockite meteorites, presumably with the $\beta Ca_3P_2O_8$

Can. J. Chem. Downloaded from www.nrcresearchpress.com by 210.87.254.40 on 09/05/12
For personal use only.

TABLE 5. Bond lengths and angles in synthetic whitlockite with standard errors in parentheses*

Bond	Distance (Å)	Bond	Distance (Å)	Bond	Distance (Å)
Ca(IB)—O(IIB3)*r*	2.394(6)	Ca(IIB1)—O(IIB3)*h*	2.499(6)	Ca(IIB2)—O(IIB3)*r*	2.368(6)
—O(IIB2)*h*	2.365(6)	—O(IIB5)*h*	2.479(4)	—O(IIB2)*r*	2.646(6)
—O(IIB4)*i*	2.662(7)	—O(IIB5)*i*	2.452(6)	—O(IIB4)*r*	2.626(5)
—O(IIB1)*p*	2.394(6)	—O(IIB2)*h*	2.472(6)	—O(IIB1)*p*	2.469(7)
—O(IB1)*r*	2.503(4)	—O(IIB4)*i*	2.316(7)	—O(IB1)*a*	2.379(6)
		—O(IIB1)*l*	2.753(5)		
—O(IIA)*c*	2.933(6)	—O(IB2)*e*	2.436(6)	—O(IIA)*c*	2.383(5)
—O(IB2)*h*	2.544(4)	—O(IIA)*a*	2.472(4)	—O(IIB6)*p*	2.479(6)
—O(IB2)*i*	2.467(6)			—O(IIB6)*r*	2.444(5)

Bonds	Angle (Deg)	Bonds	Angle (Deg)	Bonds	Angle (Deg)
O(IIB3)*r*—Ca(IB)—O(IIB2)*h*	159.9(2)	O(IIB3)*h*—Ca(IIB1)—O(IIB5)*h*	59.2(2)	O(IIB3)4—Ca(IIB2)—O(IIB2)*r*	66.1(2)
—O(IIB4)*i*	115.3(2)	—O(IIB5)*i*	125.1(2)	—O(IIB4)*r*	141.2(2)
—O(IIB1)*p*	72.4(2)	—O(IIB2)*h*	67.0(2)	—O(IIB1)*p*	71.5(2)
—O(IIB1)*r*	60.2(2)	—O(IIB4)*i*	138.9(2)	—O(IB1)*a*	140.8(2)
		—O(IIB1)*l*	148.4(2)		
—O(IIA)*c*	69.2(2)	—O(IB2)*e*	76.2(2)	—O(IIA)*c*	80.1(2)
—O(IB2)*h*	131.0(2)	—O(IIA)*a*	100.5(2)	—O(IIB6)*p*	131.4(2)
		O(IIB5)*h*—Ca(IIB1)—O(IIB5)*i*	68.0(2)	—O(IIB6)*r*	85.5(2)
—O(IB2)*i*	77.6(2)	—O(IIB2)*h*	93.8(2)	O(IIB2)*r*—Ca(IIB2)—O(IIB4)*r*	147.8(2)
O(IIB2)*h*—Ca(IB)—O(IIB4)*i*	67.8(2)	—O(IIB4)*i*	121.9(2)	—O(IIB1)*p*	137.0(2)
		—O(IIB1)*j*	85.4(2)		
—O(IIB1)*p*	98.0(2)	—O(IB2)*e*	76.2(2)	—O(IB1)*a*	77.4(2)
—O(IB1)*r*	106.4(2)	—O(IIA)*a*	153.4(2)	—O(IIA)*c*	93.1(2)
—O(IIA)*c*	123.5(1)	O(IIB5)*i*—Ca(IIB1)—O(IIB2)*h*	133.1(2)	—O(IIB6)*p*	122.7(2)
—O(IB2)*h*	60.4(2)	—O(IIB4)*l*	81.7(2)	—O(IIB6)*r*	58.5(2)
		—O(IIB1)*j*	56.5(1)		
—O(IB2)*i*	117.1(2)	—O(IB2)*e*	86.2(2)	O(IIB4)*k*—Ca(IIB2)—O(IIB1)*p*	71.5(2)
O(IIB4)*i*—Ca(IB)—O(IIB1)*p*	158.7(2)	—O(IIA)*a*	123.0(2)	—O(IB1)*a*	71.0(2)
—O(IB1)*r*	68.6(2)	O(IIB2)*h*—Ca(IIB1)—O(IIB4)*l*	72.0(2)	—O(IIA)*c*	80.0(2)
		—O(IIB1)*j*	138.9(2)		
—O(IIA)*c*	136.4(2)	—O(IB2)*e*	137.1(2)	—O(IIB6)*p*	58.3(2)
—O(IB2)*h*	107.1(2)	—O(IIA)*a*	93.0(2)	—O(IIB6)*r*	124.9(2)
—O(IB2)*i*	57.6(2)	O(IIB4)*i*—Ca(IIB1)—O(IIB1)*j*	70.9(2)	O(IIB1)*p*—Ca(IIB2)—O(IB1)*a*	139.9(2)
		—O(IB2)*e*	142.1(2)		

Can. J. Chem. Downloaded from www.nrcresearchpress.com by 210.87.254.40 on 09/05/12
For personal use only.

TABLE 5. (*Concluded*)

Bonds	Angle (Deg)	Bonds	Angle (Deg)	Bonds	Angle (Deg)
O(IIB1)*p*—Ca(IB)—O(IB1)*r*	102.3(2)	—O(IIA)*a*	84.6(2)	—O(IIA)*c*	72.8(2)
—O(IIA)*c*	64.5(2)	O(IIB1)*j*—Ca(IIB1)—O(IB2)*e*	72.5(2)	—O(IIB6)*p*	90.5(2)
—O(IB2)*h*	77.0(2)	—O(IIA)*a*	66.7(2)	—O(IIB6)*r*	125.3(2)
—O(IB2)*i*	142.2(3)	O(IB2)*e*—Ca(IIB1)—O(IIA)*a*	72.3(2)	O(IB1)*a*—Ca(IIB2)—O(IIA)*c*	88.4(2)
O(IB1)*r*—Ca(IB)—O(IIA)*c*	129.2(2)			—O(IIB6)*p*	80.2(2)
—O(IB2)*h*	166.2(2)			—O(IIB6)*r*	87.5(2)
—O(IB2)*i*	81.6(2)			O(IIA)*c*—Ca(IIB2)—O(IIB6)*p*	138.2(2)
O(IIA)*c*—Ca(IB)—O(IB2)*h*	63.3(2)			—O(IIB6)*r*	151.5(2)
—O(IB2)*i*	83.7(2)			O(IIB6)*p*—Ca(IIB2)—O(IIB6)*r*	68.5(2)
O(IB2)*h*—Ca(IB)—O(IB2)*i*	107.5(1)				

Bond	Distance (Å)	Bond	Distance (Å)	Bond	Distance (Å)
Mg—O(IIB5)	2.057(5) 3×	P(A)—O(IA)	1.580(9)	P(B1)—O(IIB3)	1.537(5)
—O(IIB6)	2.077(5) 3×	—O(IIA)	1.532(6) 3×	—O(IIB5)	1.549(4)
				—O(IIB1)	1.522(6)
		P(B2)—O(IIB2)	1.539(6)	—O(IB1)	1.533(7)
		—O(IIB4)	1.533(5)		
		—O(IIB6)	1.533(4)		
		—O(IB2)	1.538(6)		

Bonds	Angle (Deg)	Bonds	Angle (Deg)	Bonds	Angle (Deg)
O(IIB5)—Mg—O(IIB5)	84.1(2)	O(IA)—P(A)—O(IIA)	107.5(3)	O(IB1)—P(B1)—O(IIB2)	112.4(4)
—O(IIB6)	97.7(2)	O(IIA)—P(b)—O(IIA)	111.4(3)	—O(IIB3)	106.4(3)
—O(IIB6)	177.6(2)	O(IB2)—P(B2)—O(IIB2)	107.0(3)	—O(IIB5)	111.3(3)
—O(IIB6)	94.5(2)	—O(IIB4)	107.6(3)	O(IIB1)—P(B1)—O(IIB3)	113.5(3)
O(IIB6)—Mg—O(IIB6)	83.7(2)	—O(IIB6)	112.7(3)	—O(IIB5)	107.5(3)
		O(IIB2)—P—O(IIB4)	114.9(4)	O(IIB3)—P(B1)—O(IIB5)	105.6(3)
		—O(IIB6)	107.3(3)		
		O(IIB4)—P—O(IIB6)	107.4(3)		

*Symmetry transformations *a*, *b* ..., *r*: x, y, z; $-y, x-y, z$; $y-x, -x, z$; $-y, -x, 1/2+z$; $x, x-y, 1/2+z$; $y-x, y, 1/2+z$; $1/3+x, 2/3+y, 2/3+z$; $1/3-y, 2/3+x-y, 2/3+z$; $1/3+y-x, 2/3-x, 2/3+z$; $1/3-y, 2/3-x, 1/6+z$; $1/3+x, 2/3+x-y, 1/6+z$; $1/3+y-x, 2/3+y, 1/6+z$; $2/3+x, 1/3+y, 1/3+z$; $2/3-y, 1/3+x-y, 1/3+z$; $2/3+y-x, 1/3-x, 1/3+z$; $2/3-y, 1/3-x, 5/6+z$; $2/3+x, 1/3+x-y, 5/6+z$; $2/3+y-x, 1/3+y, 5/6+z$.

structure, have both Mg and two Na in their structure (21, 22) and a lunar whitlockite contains a considerable amount of trivalent rare earth ions (23). It is not surprising that Mg and other small radii divalent ions, stabilizes the whitlockite phase (5) because of its solubility in the octahedral site. Further studies will be needed to ascertain the role of the other impurities in the structure.

The research has been supported by a grant from the National Research Council of Canada to C.C. and by grants from The John A. Hartford Foundation, Inc. and N.I.H. Grant AM15671 to W.K.S.

1. C. FRONDEL. Am. Mineral, **26**, 145 (1941).
2. C. FRONDEL. Am. Mineral, **28**, 215 (1943).
3. R. GOPAL and C. CALVO. Nature Physical Sciences, **237**, 30 (1972).
4. U. KEPPLER. Neues. Jahrb. Mineral. Monatsch, **6**, 171 (1965).
5. S. L. ROWLES. Bull. Soc. Chem. France, 1797 (1968).
6. M. W. JOHNSON, B. R. TAYLOR, and D. S. BERMAN. Caries Res. **3**, 348 (1969).
7. J. VAHL, H. J. HÖHLING, and R. M. FRANK. Arch. Oral. Biol. **9**, 315 (1964).
8. R. W. T. WILKINS and W. K. SABINE. Am. Mineral. **58**, 508 (1973).
9. R. GOPAL. Ph.D. Thesis, McMaster University, Hamilton, Ontario. 1972.
10. H. T. EVANS, D. E. APPLEMAN, and P. S. HANDWERKER. Amer. Cryst. Assoc. Annual Meeting, Cambridge, Mass., 42 (1963).
11. C. CALVO. Unpublished results.
12. A. C. LARSON. Acta Cryst. **23**, 664 (1967).
13. D. T. CROMER and J. T. WABER. Acta Cryst. **18**, 104 (1965).
14. D. T. CROMER. Acta Cryst. **18**, 17 (1965).
15. W. H. ZACHARIASEN. Acta Cryst. **1**, 263 (1948).
16. R. GOPAL and C. CALVO. Z. Krist. **137**, 67 (1973).
17. C. CALVO and R. GOPAL. Amer. Mineral. To be published.
18. D. J. SUTOR. Acta Cryst. **23**, 418 (1967).
19. U. KEPPLER. Z. Krist. **132**, 228 (1970).
20. P. SÜSSE and M. J. BUERGER. Z. Krist. **131**, 161 (1970).
21. W. R. SCHMUS and P. H. RIBBE. Geochemica et Cosmochimica Acta, **33**, 637 (1968).
22. L. H. FUCHS. Science, **139**, 425 (1962).
23. A. L. ALBEE, D. S. BURNETT, A. A. CHODES, O. J. EUGSTER, J. C. HUNCKE, D. A. PAPANASTASSIOU, F. A. PODOSEK, RUSS II, G. PRICE, H. G. SANZ, F. TERA, and G. J. WASSERBURG. Science, **169**, 463 (1970).

Can. J. Chem. Downloaded from www.nrcresearchpress.com by 210.87.254.40 on 09/05/12
For personal use only.

^{13}C Nuclear Magnetic Resonance Studies of Organometallic Compounds. IV. *cis*-Dimethylplatinum(II) Derivatives[1]

HOWARD CHARLES CLARK, LEO ERNEST MANZER,[2] AND JOHN EDWARD HENRY WARD[3]

Department of Chemistry, The University of Western Ontario, London, Ontario N6A 3K7

Received October 19, 1973

Data derived from the ^{13}C n.m.r. spectra of seven neutral *cis*-dimethylplatinum(II) derivatives of the type *cis*-$(CH_3)_2PtL_2$ and *cis*-$(CH_3)_2Pt(L—L)$ (where L and L—L are neutral donors) are discussed and compared with data derived from the ^1H n.m.r. spectra of the complexes. Simultaneous variations in L or L—L reveal that the n.m.r. *trans*-influence rather than the n.m.r. *cis*-influence is dominant. The suggestion that the n.m.r. *cis*- and *trans*-influences may be additive is discussed. In contrast with data obtained by other workers, it is shown that the $^1J_{CH}$ values of the platinum methyl groups are essentially insensitive to variations in the remaining ligands.

On discute les résultats obtenus par r.m.n. du ^{13}C de sept dérivés neutres du type *cis* $(CH_3)_2PtL_2$ et *cis* $(CH_3)_2Pt(L—L)$ (dans lesquels L et L—L sont des donneurs neutres) et l'on compare ces données avec celles obtenues par r.m.n. du proton de ces complexes. Des variations simultanées dans L ou L—L montrent que l'influence *trans* de la r.m.n. prédomine plutôt sur l'influence *cis*. On discute de la suggestion selon laquelle les influences *cis* et *trans* de la r.m.n. peuvent être additives. Par opposition avec les résultats obtenus par d'autres chercheurs on a démontré que les valeurs $^1J_{CH}$ entre le platine et les groupes méthyles sont essentiellement insensibles aux variations dans les autres ligands. [Traduit par le journal]

Can. J. Chem., **52**, 1165 (1974)

Introduction

As part of a general study of the *cis*- and *trans*-influences (2, 3) by ^{13}C nuclear magnetic resonance spectroscopy, we have examined several series of methylplatinum(II) derivatives. For complexes of the type *trans*-$[(CH_3)Pt(Q_2)L]^+PF_6^-$ (4, 5), where Q is $As(CH_3)_3$ or $P(CH_3)_2(C_6H_5)$ and L is a neutral ligand, and *trans*-$[(C_6H_5)Pt(As(CH_3)_3)_2L]^+PF_6^-$ (6) we presented substantial evidence supporting the theory that the n.m.r. *trans*-influence is governed by the rehybridization of platinum σ-orbitals in the two *trans* bonds. In particular, for the trimethylarsine series of *trans*-methylplatinum derivatives, it was found that substitution of the ligand *trans* to the methyl group resulted in large parallel changes in $^1J_{PtC}$ and $^2J_{PtCH}$ while $^1J_{CH}$ was invariant. This evidence supports the notion that changes in α_{Pt}^2, the s character of the hybrid platinum σ-bonding orbitals in the Pt—C bonds, are mainly responsible for alterations in $^1J_{PtC}$ and $^2J_{PtCH}$.

In contrast, our ^{13}C n.m.r. studies of *cis* substituted methylplatinum(II) derivatives (1) of the type $[DIARSPt(CH_3)L]^+PF_6^-$ (*DIARS* is *o*-phenylenebis(dimethylarsine), where L is also a neutral ligand, have revealed a significantly different behavior. A plot of $^1J_{PtC}$ (*trans* to L) *vs.* $^1J_{PtC}$ (*cis* to L) for the analogous *trans*-$[(CH_3)Pt(As(CH_3)_3)_2L]^+PF_6^-$ and *cis*-$[DIARSPt(CH_3)L]^+PF_6^-$ derivatives produced a wide scatter of points. Furthermore, a plot of $^1J_{PtC}$ *vs.* $^2J_{PtCH}$ for the methyl group of $[DIARSPt(CH_3)L]^+PF_6^-$ also failed to yield a discernible relationship. This evidence supports the idea that the n.m.r. *cis*-influence is not strongly related to the n.m.r. *trans*-influence, and that it is not clearly related to the rehybridization of platinum σ-orbitals in the platinum–carbon bonds.

In order to derive further information about the relationships of the n.m.r. *cis*- and *trans*-influences, we have obtained the ^{13}C n.m.r. spectra of neutral platinum(II) derivatives of the type *cis*-$(CH_3)_2PtL_2$ and *cis*-$(CH_3)_2Pt(L—L)$, where L and L—L are neutral donors. In this series, a given platinum methyl group will undergo variations of ligands *cis* and *trans* to itself, so that results will reflect a simultaneous variation in both the n.m.r. *cis*- and *trans*-influences.

[1]For the previous paper in this series see ref. 1.

[2]Present address: Central Research Department, Experimental Station, E. I. DuPont de Nemours and Co., Wilmington, Delaware 19898, U.S.A.

[3]To whom correspondence should be addressed.

Can. J. Chem. Downloaded from www.nrcresearchpress.com by 210.87.254.40 on 09/05/12
For personal use only.

Can. J. Chem. Downloaded from www.nrcresearchpress.com by 210.87.254.40 on 09/05/12
For personal use only.

TABLE 1. ^{13}C shieldings* and coupling constants† for the *cis*-dimethylplatinum(II) derivatives **1–7**

Complex	L	Solvent	δ_{PtCH3}	$\lvert^1J_{PtC}\rvert$	$\lvert^1J_{CH}\rvert$	Other	$^2J_{PtCH}$‡	^{1}H n.m.r. reference
1	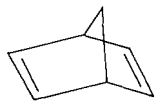	$CDCl_3$	+5.9	816(±2)	125(±2)	$\delta_{C1,4}$49.4, J_{PtC}38(±2) $\delta_{C2,3,5,6}$88.3, J_{PtC}46(±2) δ_{C7}73.2, J_{PtC}38(±2)	91.2(±0.5)	10
2	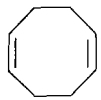	$CDCl_3$	+4.7	773(±2)	126(±2)	δ_{CH}98.8, J_{PtC}55(±2) δ_{CH2}29.9	83.4(±0.5)	9
		CD_2Cl_2	+4.8	777(±2)		δ_{CH}99.0, J_{PtC}55(±2); δ_{CH}30.3		
		$(CD_3)_2CO$	+4.4	783(±2)		δ_{CH}98.8, J_{PtC}58(±2) δ_{CH2}29.9		
3	*DIARS*	$CDCl_3$	−9.1	678(±2)	124(±2)	§	78.5(±0.5)	1
		CD_2Cl_2	−8.8	690(±2)				
4	$(As(CH_3)_3)_2$	$CDCl_3$	−4.6	668(±2)	123(±2)	$\delta_{As(CH3)3}$ + 11.6, $^2J_{PtC}$18(±2)	76.0(±0.2)	12
		$(CD_3)_2CO$	−4.0	689(±1)		$\delta_{As(CH3)3}$ + 11.1, $^2J_{PtC}$19(±1)		
5	$(p\text{-}CH_3C_6H_4NC)_2$	$CDCl_3$	−5.7	590(±2)	123(±2)	δ_{CH3}21.2, δ_{C6H4} and NC 124.7, 125.1, 129.8, 139.2, 147.7	73.6(±0.5)‖	9
6	$(As(CH_3)_2(C_6H_5))_2$	CH_2Cl_2	+3.0	685(±5)	125.9(±0.2)		77.2(±0.2)	7
7	$(P(CH_3)_2(C_6H_5))_2$	CH_2Cl_2	−3.3	594(±5)	132.0(±0.2)		67.1(±0.1)	7

*In p.p.m. (±0.1) (downfield positive) from TMS.
†In Hz.
‡The errors in $^2J_{PtCH}$ were taken to be ±0.5 Hz unless otherwise noted.
§See ref. 1.
‖^{1}H n.m.r. spectrum recalibrated.

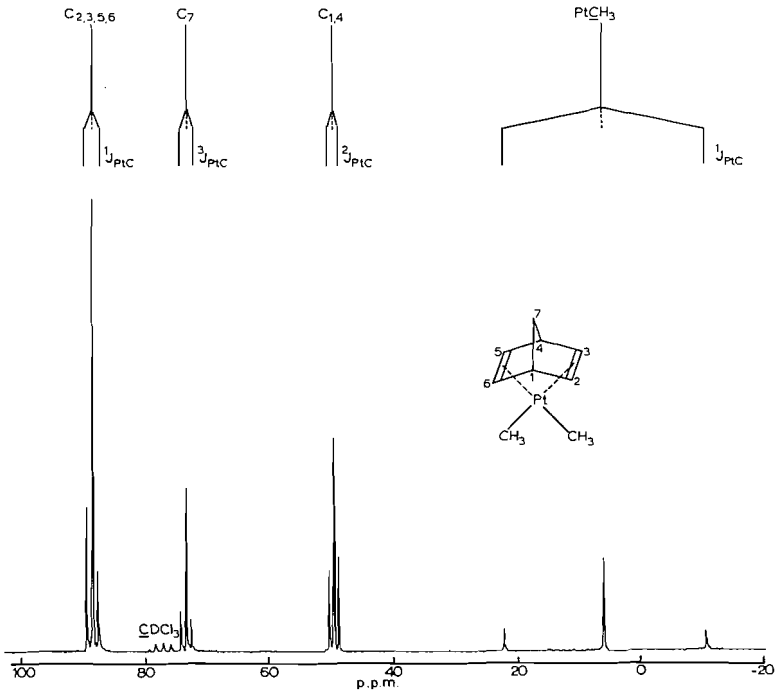

FIG. 1. ^{13}C n.m.r. spectrum (25.2 MHz) of $(CH_3)_2Pt$ (norbornadiene) **1** in chloroform-*d* solution.

Cheney *et al.* (7) have already examined two derivatives of this type, where L is dimethylphenylphosphine and dimethylphenylarsine. Their results indicate, in contrast with those derived from our *trans*-methylplatinum(II) derivatives, that σ-orbitals in the C—H bonds of the methyl groups may be rehybridizing, since $^1J_{CH}$ as well as $^1J_{PtC}$ and $^2J_{PtCH}$ vary on changing from the phosphorus to arsenic donors. Thus, we have also obtained the $^1J_{CH}$ values of the *cis*-dimethylplatinum derivatives examined here, with the hope of rationalizing and resolving the apparently contradictory observations.

Experimental

All the *cis*-dimethylplatinum(II) derivatives, $(CH_3)_2Pt(As(CH_3)_3)_2$ (8), $(CH_3)_2PtDIARS$ (1), $(CH_3)_2Pt(p\text{-}CH_3C_6H_4NC)_2$ (9), $(CH_3)_2Pt$(1,5-cyclooctadiene) (9), and $(CH_3)_2Pt$(norbornadiene) (10) were obtained by established procedures. The ^{13}C n.m.r. spectra were measured on a Varian XL-100-15 spectrometer operating in the pulsed Fourier transform mode at 25.2 MHz. All spectra were determined with noise-modulated proton decoupling, and proton-coupled spectra were obtained by off-setting the decoupling frequency by *ca.* 30 kHz. The spectra were taken on chloroform-*d*, methylene chloride-d_2, and/or acetone-d_6 solutions in 5 mm sample tubes and were calibrated using the solvent resonances as secondary standards (11).

Results

The ^{13}C shieldings and ^{195}Pt–^{13}C coupling constants obtained from the spectra of the *cis*-dimethylplatinum(II) derivatives are summarized in Table 1. For comparative purposes, this table also includes the relevant data presented by Cheney *et al.* (7). The ^{13}C n.m.r. spectrum of the norbornadiene derivative **1** is a typical example, which is shown in Fig. 1. Since we have not determined the relative signs of the ^{13}C–^{195}Pt coupling constants, the absolute values of these parameters, which are adequate for the arguments that we will present later, are provided in Table 1.

In all cases, the high field resonances in the spectra were assigned to the carbons of the platinum methyl groups of **1**–**5**, on the basis of their similarity with a host of related methylplatinum(II) derivatives (1, 4, 5). These platinum methyl resonances are flanked by widely spaced ^{195}Pt satellites of *ca.* one-fourth intensity, whose separation appears to be sensitive to the nature of L or L—L.

In certain instances, assignments of the ^{13}C resonances of the ligands were carried out by comparing the shieldings of the coordinated and

Can. J. Chem. Downloaded from www.nrcresearchpress.com by 210.87.254.40 on 09/05/12
For personal use only.

Can. J. Chem. Downloaded from www.nrcresearchpress.com by 210.87.254.40 on 09/05/12
For personal use only.

uncoordinated species and from off-resonance ^{13}C—$\{^1H\}$ experiments. For example, the similar coordinated (uncoordinated) shieldings of the saturated carbons of norbornadiene (13, 14) are $C_{1,4}$ 49.4 (50.9) and C_7 73.2 (75.4) p.p.m. These data, together with the relative intensities of the signals, provide the basis for the specific assignments. The intense signals arising from the four unsaturated carbons, $C_{2,3,5,6}$ 88.3 (143.4) are shifted considerably upfield; this is consistent with our observations on a series of metal-coordinated olefinic and acetylenic systems (15). The signals arising from the 1,5-cyclooctadiene ligand were assigned by similar arguments. The specific assignments of the *DIARS* and trimethylarsine carbons have been discussed previously (1, 4, 6). Finally, there have apparently been no reports of ^{13}C n.m.r. data for aromatic isocyanide derivatives, such as phenylisocyanide or *p*-tolylisocyanide. Thus, we have been unable to specifically assign the carbon resonances of the latter ligand in **5**.

Discussion

The n.m.r. data for **1**–**7** reveal that with variations in the ligands, relatively large fluctuations in the ^{13}C n.m.r. parameters may occur. For example, when norbornadiene is replaced by two *p*-tolylisocyanide donors, the methyl carbon shieldings shift upfield from +5.9 to −5.7 p.p.m., while the $^1J_{PtC}$ values decrease from *ca.* 816 to 590 Hz, and the $^1J_{CH}$ values remain constant (*ca.* 124 (±2) Hz).

From the $^1J_{PtC}$ values of the platinum methyl groups, we may formulate a combined n.m.r. *cis*- and *trans*-influence series for the ligands used in **1**–**7**:

$$2P(CH_3)_2(C_6H_5) \approx 2p\text{-}CH_3C_6H_4NC > 2As(CH_3)_3 \approx DIARS \approx 2As(CH_3)_2(C_6H_5) >$$

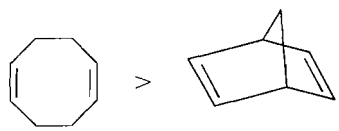

This series approximately follows the trend

phosphine > isocyanide > arsine > olefin

which we have observed for complexes of the sort *trans*-$[(CH_3)Pt(P(CH_3)_2(C_6H_5))_2L]^+PF_6^-$ (4). Hence there appears to be some relationship between the *combined* n.m.r. *cis*- and *trans*-influences and the n.m.r. *trans*-influence for the ligands we are considering here. However, it differs from the order

isocyanide ≈ arsine > phosphine

which we have observed for the n.m.r. *cis*-influence of related ligands (1). Nevertheless, since the n.m.r. *cis*-influence series is formulated from $^1J_{PtC}$ values falling within a much smaller range than those values used to derive analogous n.m.r. *trans*-influence series, such a *cis* trend may well be effectively masked.

If the n.m.r. *cis*- and *trans*-influences are additive in the *cis*-dimethylplatinum(II) derivatives here, we may algebraically manipulate some of these $^1J_{PtC}$ values in order to determine the expected ordering of the ligands in the combined *cis*- and *trans*-influence series. For example, the $^1J_{PtC}$ value for the platinum methyl group in *trans*-$[(CH_3)Pt(As(CH_3)_3)_2L]^+PF_6^-$ (4) increases by 29 Hz, (from 446 to 475 Hz)[4] when a triphenylphosphine donor is replaced by ethylisocyanide. On the other hand, when the same two ligands are considered in the *cis-DIARS* derivatives (1), a decrease of 33 Hz is observed (from 533 to 500 Hz). Thus, there is an effective mutual cancelling of the combined *cis*- and *trans*-influences of these two ligands. If we can extend a similar argument to the *p*-tolylisocyanide and dimethylphenylphosphine derivatives examined here, we may well anticipate that the $^1J_{PtC}$ values will be very similar, and indeed, this is the case. Our additivity argument would predict a difference of −4 Hz on replacing a phosphine by an isocyanide donor, while the actual difference is also −4 Hz, in embarrassingly good agreement. This agreement may be fortuitous, since directly analogous compounds were not considered.

All the $^1J_{CH}$ values of the platinum methyl groups of the *cis*-dimethylplatinum(II) derivatives lie within the experimental error of 124 Hz, except that for the dimethylphenylphosphine derivative **7**, reported by Cheney *et al.* (7). Therefore, it seems that these derivatives are behaving similarly to the *trans*-$[(CH_3)Pt(As(CH_3)_3)_2L]^+PF_6^-$ (4) complexes we have already examined. While the platinum σ-orbital of the Pt—C bond appears to undergo rehybridization with ligand variations, the hybridizations of the σ-bonding C—H orbitals appear to remain constant. The $^1J_{CH}$ value of 132.0 Hz for the bis(dimethylphenyl-

[4]For the value of 446 Hz, see footnote in ref. 1.

Can. J. Chem. Downloaded from www.nrcresearchpress.com by 210.87.254.40 on 09/05/12
For personal use only.

phosphine) complex **7** thus seems anomalous, and the observation that both $^1J_{PtC}$ and $^1J_{CH}$ values change with ligand variations does not seem to have any generality.[5]

Next, we examined the relationship of the $^1J_{PtC}$ and $^2J_{PtCH}$ values for the derivatives **1–7**. A plot of those data is shown in Fig. 2 and a linear regression analysis[6] of the data is given in eq. 1.

$$[1] \quad {}^1J_{PtC} = 10.5(\pm 0.6)\,{}^2J_{PtCH} - 135.8(\pm 44.6)\,r = 0.949$$

The reasonable linear correlation indicates that the n.m.r. *trans*-influence of a given ligand outweighs its n.m.r. *cis*-influence, since the latter does not yield a linear relationship in an analogous comparison with *cis*-methylplatinum derivatives (1). The distinctly poorer correlation coefficient for this series ($r = 0.949$) compared with those derived from data obtained from series (4) in which only the *trans* ligand is varied ($r = 0.997$, 0.994, and 0.986) probably reflects the superimposition of the non-linearly related *cis*-influence components. In addition, the fact that the plot here of $^1J_{PtC}$ *vs.* $^2J_{PtCH}$ does not pass through the origin adds further evidence to this proposal, since similar plots for *trans*-methylplatinum(II) analogs (4) pass much closer to the origin.

Finally, we should comment on our brief examination of the solvent dependences of the ^{13}C n.m.r. parameters. In contrast with results we obtained for series of *trans*- (4) and *cis*- (1) methylplatinum derivatives, the $^1J_{PtC}$ values vary over a considerably greater range than that encompassed by the inherent experimental error. For example, the bis(trimethylarsino) derivative **4** yields a $^1J_{PtC}$ value of 668 (±2) Hz in chloroform-*d*, which increases to 689 (±1) Hz when the spectrum is obtained in acetone-d_6. The other derivatives **2** and **3** whose spectra were determined in a number of solvents exhibit similar, but less marked behavior. In addition, the ^{13}C shieldings of the methylplatinum carbons also vary in ranges greater than that dictated by the experimental uncertainty of measurement. Thus, an effort should be made to evaluate the solvent dependence of ^{13}C n.m.r. parameters before quantitative relationships are considered. It would be particularly appropriate to use data derived from spectra determined in a single solvent.

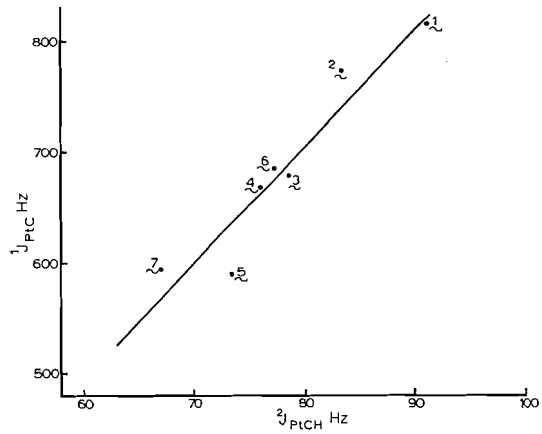

FIG. 2. Plot of $^1J_{PtC}$ *vs.* $^2J_{PtCH}$ for the *cis*-dimethylplatinum(II) derivatives **1–7**.

We thank the National Research Council of Canada for financial support of this project, for the award of an N.R.C.C. postdoctoral fellowship to J.E.H.W., and for the award of an N.R.C.C. scholarship to L.E.M.

[5]A referee has pointed out that the $^1J_{CH}$ values (124 (±2) Hz) for **1–6** are consistently lower than those values (131(±2) Hz) (16) obtained by ^1H n.m.r. for the platinum methyl groups of the series *trans*-[$^{13}CH_3Pt((C_6H_5)_3P)_2X$]. That higher $^1J_{CH}$ values are observed only for the bis(triphenylphosphine) complexes and for the bis(dimethylphenylphosphine) complex 7 leads us to speculate that the presence of phenyl substituted phosphines *cis* to a platinum methyl group may be important in causing these differences. For example, we have indicated (1) that "steric" interactions of ligands with a *cis* platinum methyl group may have a bearing on the magnitude of $^1J_{PtC}$ for that group. Perhaps a similar behavior may be invoked to account for the higher $^1J_{CH}$ values observed for the bis(phosphine) derivatives.

[6]The average deviations of the slope and intercept for the linear equation presented here are calculated on the basis of the maximum possible error due to the inherent uncertainty of the experimental measurements. These errors have already been cited in Table 1. It is worthwhile noting that these variations represent the maximum error in *precision* and that as such they may be generous estimates. All the data points are derived from ^{13}C and ^1H n.m.r. data obtained in $CDCl_3$ solutions except for those of **6** and **7** which were run in CH_2Cl_2.

1. H. C. CLARK and J. E. H. WARD. Can. J. Chem. **52**, 570 (1974).
2. T. G. APPLETON, H. C. CLARK, and L. E. MANZER. Coord. Chem. Rev. **10**, 335 (1973).
3. A. PIDCOCK, R. E. RICHARDS, and L. M. VENANZI. J. Chem. Soc. A, 1707 (1966).
4. M. H. CHISHOLM, H. C. CLARK, L. E. MANZER, J. B. STOTHERS, and J. E. H. WARD. J. Am. Chem. Soc. **95**, 8574 (1973).
5. M. H. CHISHOLM, H. C. CLARK, L. E. MANZER, and J. B. STOTHERS. Chem. Commun. 1627 (1971).

6. H. C. CLARK and J. E. H. WARD. J. Am. Chem. Soc. To be published.
7. A. J. CHENEY, B. E. MANN, and B. L. SHAW. Chem. Commun. 431 (1971).
8. H. C. CLARK and R. J. PUDDEPHATT. Inorg. Chem. **9**, 2670 (1970).
9. H. C. CLARK and L. E. MANZER. J. Organomet. Chem. **59**, 411 (1973).
10. H. C. CLARK and L. E. MANZER. Unpublished results.
11. G. C. LEVY and J. D. CARGIOLI. J. Magn. Reson. **6**, 143 (1972).
12. H. C. CLARK and J. E. H. WARD. Unpublished results.
13. J. B. STOTHERS. Carbon-13 N.M.R. spectroscopy. Academic Press, New York, N.Y. 1972.
14. J. B. GRUTZNER, M. JAUTELAT, J. B. DENCE, R. A. SMITH, and J. D. ROBERTS. J. Am. Chem. Soc. **92**, 7107 (1970).
15. M. H. CHISHOLM, H. C. CLARK, L. E. MANZER, and J. B. STOTHERS. J. Am. Chem. Soc. **94**, 5087 (1972).
16. C. D. COOK and K. Y. WAN. J. Am. Chem. Soc. **92**, 2595 (1970).

Can. J. Chem. Downloaded from www.nrcresearchpress.com by 210.87.254.40 on 09/05/12
For personal use only.

Shock Tube Studies of the Reactions of Hydrogen Atoms. I. The Reaction $H + NH_3 \rightarrow H_2 + NH_2$

JOHN E. DOVE AND WING S. NIP

Department of Chemistry, University of Toronto, Toronto, Ontario M5S 1A1

Received August 23, 1973

The partial equilibrium state following the branched-chain explosion of shock-heated rich H_2/O_2/diluent mixtures contains a high concentration of H atoms. The conditions under which this state can be used as a source of H atoms for the study of elementary reactions have been investigated. A small amount of NH_3 was added to H_2/O_2/inert gas mixtures in order to measure the rate of the reaction $H + NH_3 \rightarrow H_2 + NH_2$. The pseudo-first order decay of NH_3 in an approximately ten-fold excess of H atoms was followed by a time-of-flight mass spectrometer which sampled from the reflected shock region in a shock tube. The rate coefficient for this reaction, determined over the temperature range 1500–2150 °K, is $10^{13.44\pm0.10}$ exp $-(17\,400 \pm 1\,300$ cal mol$^{-1})/RT$ cm^3 mol^{-1} s^{-1}.

It is pointed out that, under certain stated conditions, the method can also be extended to study the rates of elementary reactions involving O atoms and OH radicals. From our experiments, upper limits on the rate coefficients of the reactions $OH + NH_3 \rightarrow H_2O + NH_2$ and $O + NH_3 \rightarrow OH + NH_2$ over the temperature range 1620–1920 °K are $8 \times 10^9 T^{0.68}$ exp $(-1100/RT)$ and 1×10^{13} exp $(-6600/RT)$, respectively.

L'état d'équilibre partiel résultant de l'explosion en chaîne multiple de mélanges riches en H_2/O_2/diluant à la suite d'un effet choc-chaleur, contient une concentration élevée en atomes d'hydrogène. On a étudié des conditions expérimentales permettant l'utilisation de cet état comme source d'atomes d'hydrogène pour l'étude de réactions élémentaires. Une faible quantité de NH_3 fut ajoutée à des mélanges H_2/O_2/gaz inerte afin de mesurer la vitesse de la réaction $H + NH_3 \rightarrow H_2 + NH_2$. La décroissance du pseudo-premier ordre de NH_3 dans un excès (d'environ dix fois) d'atomes d'hydrogène a été suivie à l'aide d'un spectromètre de masse, mesurant la durée de la trajectoire, dont la source d'échantillons correspond à la région de réflexion des chocs dans un tube à ondes de chocs. Le coefficient de vitesse pour cette réaction, déterminé pour des températures allant de 1500 à 2150 °K, est $10^{13.44\pm0.10}$ exp $-(17\,400 \pm 1\,300$ cal mol$^{-1})/RT$ cm^3 mol^{-1} s^{-1}.

Il est à remarquer que, dans certaines conditions, la méthode peut être utilisée pour l'étude des vitesses de réactions élémentaires impliquant des atomes O et des radicaux OH. A partir de nos expériences, les limites supérieures des coefficients de vitesse des réactions $OH + NH_3 \rightarrow H_2O + NH_2$ et $O + NH_3 \rightarrow OH + NH_2$ sont évaluées à $8 \times 10^9\ T^{0.68}$ exp $(-1\,100/RT)$ et 1×10^{13} exp $(-6\,600/RT)$ respectivement pour des températures allant de 1620 à 1920 °K. [Traduit par le journal]

Can. J. Chem., **52**, 1171 (1974)

Introduction

The elementary reaction

[9] $$H + NH_3 \rightarrow H_2 + NH_2$$

almost certainly plays a role in the high temperature chemistry of ammonia. However, the importance of this role is a subject of dispute (1–3) because so little is known about the rate of reaction 9. There have been no measurements of k_9 at high temperatures, and there is disagreement among the various low temperature data.

Early attempts (4–6) to study the reaction at room temperature failed to detect any reaction at all. More recent work (7, 8) has used e.s.r. detection to study $H + NH_3$ in flow systems at temperatures up to 800 °K, but the rate of reaction was found to be too low to measure, and only upper limits on k_9 could be given. However, values of k_9 have been deduced from studies of explosion limits (9) and radiolysis (10), but these values are substantially higher than the upper limits obtained by the more direct e.s.r. method. The only data on reaction 9 above 1000 °K come from a computer simulation of ammonia pyrolysis (3) in which the proposed value of k_9 was calculated from simple collision theory using an

Can. J. Chem. Downloaded from www.nrcresearchpress.com by 210.87.254.42 on 09/05/12
For personal use only.

Can. J. Chem. Downloaded from www.nrcresearchpress.com by 210.87.254.42 on 09/05/12
For personal use only.

TABLE 1. Mechanism and rate expressions used in the computer simulation*

	Reaction	Rate expression	Equilibrium constant expression	Reference for rate expression
[1]	$H_2 + O_2 \rightarrow OH + OH$	$1.70 \times 10^{13} \exp(-48\,150/RT)$	$2.63 \times 10^{1} \exp(-17\,770/RT)$	17
[2]	$H_2 + OH \rightarrow H_2O + H$	$2.19 \times 10^{13} \exp(-5\,150/RT)$	$2.60 \times 10^{-1} \exp(+14\,950/RT)$	18
[3]	$H + O_2 \rightarrow OH + O$	$1.38 \times 10^{13} \exp(-16\,400/RT)$	$1.125 \times 10^{1} \exp(-15\,513/RT)$	19
[4]	$O + H_2 \rightarrow H + OH$	$1.74 \times 10^{14} \exp(-9\,450/RT)$	$2.370 \exp(-2150/RT)$	18
[5]	$O + H_2O \rightarrow OH + OH$	$5.75 \times 10^{13} \exp(-18\,000/RT)$	$9.204 \exp(-16\,800/RT)$	18
[6]	$H_2O + M \rightarrow H + OH + M$	$5.01 \times 10^{14} \exp(-105\,000/RT)$	$1.60 \times 10^{1} \exp(-119\,200/RT)$	20
[7]	$H_2 + M \rightarrow H + H + M$	$2.23 \times 10^{12} T^{1/2} \exp(-92\,600/RT)$	$2.233 \times 10^{4} T^{-1} \exp(-108\,821/RT)$	21
[8]	$O_2 + M \rightarrow O + O + M$	$3.60 \times 10^{18} T^{-1} \exp(-118\,000/RT)$	$1.151 \times 10^{5} T^{-1} \exp(-121\,940/RT)$	22
[9]	$H + NH_3 \rightarrow NH_2 + H_2$	$2.46 \times 10^{13} \exp(-17\,071/RT)$	$4.554 \exp(+3\,853/RT)$	This work
[10]	$NH_2 + NH_2 \rightarrow N_2 + 2H_2$	$3.981 \times 10^{13} \exp(-12\,000/RT)$	$3.296 T^{-1} \exp(76\,970/RT)$	23

*Concentration units mol cm^{-3}. Activitaion energies in cal mol^{-1}. All equilibrium constants are from ref. 35.

Can. J. Chem. Downloaded from www.nrcresearchpress.com by 210.87.254.42 on 09/05/12
For personal use only.

empirically-obtained activation energy. Though a qualitative explanation of the experimental pyrolysis data was achieved, there seems to be no direct quantitative justification of this value of k_9.

While working on the interpretation of recent shock-tube data (11) on the pyrolysis of NH_3, we needed to have a high temperature value of k_9. Because of doubts about the validity of literature data on reaction 9, we sought to measure k_9 independently by as direct a method as possible. For such a measurement, the reaction between hydrogen and oxygen is a possible source of hydrogen atoms. Baldwin *et al.* (12–14) have shown that the concentrations of H, O, OH, and HO_2 in slowly reacting hydrogen–oxygen mixtures can be accurately calculated, and they have made use of this fact to study the reactions of these reactive species with small amounts of added substances. Unfortunately their particular methods can only be applied below 800 °K, well below the temperature of our NH_3 pyrolysis experiments. However, a related possibility is that of using the large quasi-stationary concentration of hydrogen atoms in the "partial equilibrium" mixture (15) formed by the high temperature branched-chain explosion of hydrogen–oxygen mixtures. Gardiner *et al.* (16) have recently used such a mixture in a study of the reaction $H + CO_2 \rightarrow OH + CO$. In the present work we have investigated conditions under which the partial equilibrium of hydrogen–oxygen mixtures can be used to study reactions of H, O, and OH in shock waves and we have applied the results of this investigation to a measurement of the rate of reaction 9.

Partial Equilibria in Hydrogen-Oxygen Mixtures

If a mixture of hydrogen and oxygen is heated to a suitably high temperature, *e.g.* in a shock tube, a branched-chain explosion occurs in which the main elementary reactions are [1]–[5] (Table 1). The reaction proceeds rapidly to a partial equilibrium (p.e.) state in which the forward and reverse processes of reactions 1–5 are balanced, but the concentrations of the species H, O, and OH greatly exceed their true equilibrium values. Complete thermodynamic equilibrium can only be attained through three-body recombination processes such as [−6] to [−8] (Table 1). However under conditions typical of our experiments, *i.e.* temperatures of 1500–2100 °K, reactant concentrations 10^{-9} to 10^{-7} mol cm^{-3}, and total gas concentrations about 10^{-6} mol cm^{-3}, the three-body recombinations (including the formation of HO_2) are very slow. Thus, after the explosion, the concentrations of H, O, and OH remain almost constant at their p.e. values for a considerable time.

The branched-chain explosion, attainment of partial equilibrium, and subsequent recombination, can be simulated by numerical integration of the reaction rate equations (*cf.* Table 1 and Fig. 1). The typical behavior is an initiation phase followed by exponential growth of radical and product concentrations until a transition occurs to the almost constant concentrations of the p.e. state. The basic experimental method that we have used is to add a small amount of another molecular species to the initial reaction mixture. The reaction between the added species and the known constant p.e. concentrations of free radicals can then be studied, provided of course that the added species does not significantly perturb the p.e. state and is not destroyed before p.e. is attained.

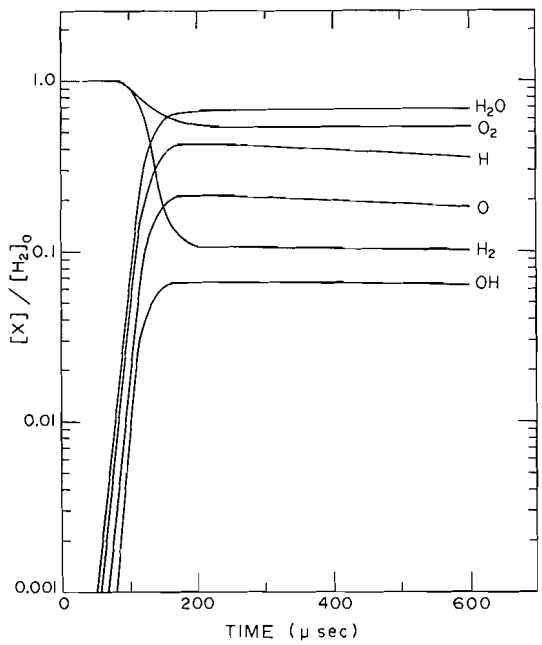

FIG. 1. Concentration profiles of a shock-heated hydrogen – oxygen – diluent mixture simulated by computer integration of the rate equations for reactions 1 to 8 and the corresponding reverse reactions in Table 1. $H_2/O_2/Kr$ = 5.5/5.5/89; temperature = 1500 °K; pressure = 300 Torr; total gas concentration = 3.2×10^{-6} mol cm^{-3}.

Can. J. Chem. Downloaded from www.nrcresearchpress.com by 210.87.254.42 on 09/05/12
For personal use only.

Atom and radical concentrations in the p.e state can be calculated from the rate equations or from thermodynamic data (15); the latter method was used in most of our work that is described below. Incidentally, it can be shown that (neglecting recombination effects) the composition of the p.e. state depends only on the temperature and the initial ratio of hydrogen to oxygen concentrations, and not on the concentration of inert diluents or the total concentration.

Besides the fact that high concentrations of radicals can be achieved, two other features of the p.e. state make the high temperature H_2/O_2/diluent system a useful medium for the study of reactions between an added species and H, O, or OH. Firstly, a large range of relative concentrations of the reactive species is attainable. A hydrogen-rich mixture will produce a high concentration of H atoms but much lower concentrations of O and OH. In oxygen-rich mixtures, on the other hand, O atoms are the most abundant reactive species. Figure 2 illustrates the wide range of concentrations of H, O, and OH that can be obtained by simply varying the initial H_2 to O_2 ratio in the test gas. Thus in principle, by using three different mixtures, the rate coefficients for the reactions of H, O, and OH with an added species can be determined. Secondly, since the p.e. state concentrations are known through thermodynamics (15), they are within reason independent of uncertainties in the rate coefficients of individual elementary reactions.

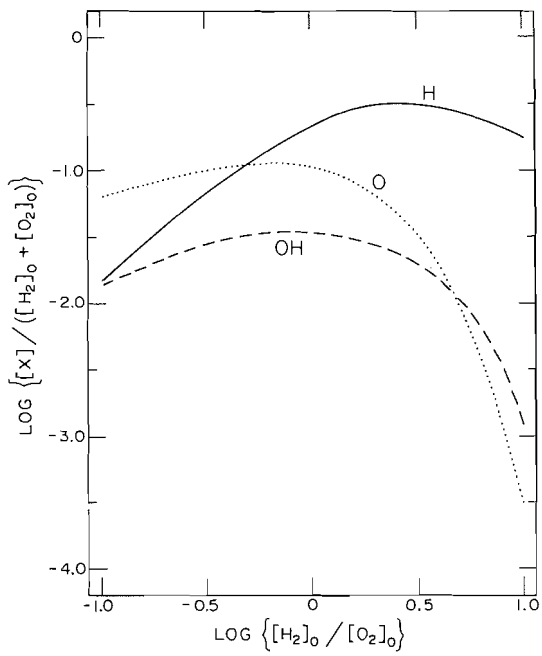

FIG. 2. Calculated partial equilibrium concentrations of H, O, and OH expressed as a fraction of initial reactant concentration and plotted against the logarithm of the initial hydrogen:oxygen ratio, $T = 1500$ °K. The corresponding plot for 2000 °K shows very similar features.

There are, however, some limitations to the method. The reactions of the added species with H, O, and OH must be substantially slower than the chain propagation or branching steps. Otherwise much of the consumption of the added species will occur during the explosion and transition periods; a detailed knowledge of elementary reaction rates in H_2/O_2 will be needed in order to make a meaningful analysis of this consumption. However, if the reaction of added species is very slow, there will not be any observable change in the concentration of additive within the available test time in a shock tube. The rate of reaction of added species can be enhanced by increasing the concentrations of other reactants. This has the additional advantage of reducing the H_2/O_2 induction period which is "dead time" as far as measurement of the reaction of added species is concerned. There is however a limit to this increase in concentration since third order recombination reactions of radicals will eventually become important and partial equilibrium will not be well maintained. Also, even though the relative concentrations of H, O, and OH can be varied over a wide range, the fact that all three species are always present introduces some complications.

Experimental

The apparatus consisted of a 2.5 cm i.d. stainless steel shock tube mounted into the ion source of a Bendix time-of-flight mass spectrometer. Reacting gas mixtures were continuously sampled from behind reflected shock waves by expansion through a 0.1 mm orifice in the end wall of the shock tube. Details of this apparatus have been given previously (24).

Matheson UHP hydrogen and oxygen and research grade neon, krypton, and argon were used. Anhydrous ammonia, also from Matheson, was further purified by fractional distillation from liquid nitrogen and a Dry Ice – acetone bath (about −40 °C). The stated purity of all gases used was better than 99.99%. Two reaction mixtures were used: mixture A: 0.99% O_2, 8.96% H_2, 0.19% NH_3, 18.94% Kr, 68.89% Ne, 2.05% Ar; mixture B: 1.09% O_2, 5.46% H_2, 0.19% NH_3, 0.18% Ar, 20.06% Kr, 73.01% Ne.

Experiments were carried out at two different total concentrations, about 1.0×10^{-6} and 3.3×10^{-6} mol

TABLE 2. Mole fraction of H, OH, and O in gas mixtures A and B in the partial equilibrium state. [M] = total gas concentration

	1500 °K		2000 °K	
Ratio	Mixture A	Mixture B	Mixture A	Mixture B
$\frac{[H]}{[M]}$	1.95×10^{-2}	2.02×10^{-2}	1.91×10^{-2}	1.87×10^{-2}
$\frac{[OH]}{[M]}$	1.64×10^{-4}	4.55×10^{-4}	5.40×10^{-4}	1.29×10^{-3}
$\frac{[O]}{[M]}$	4.69×10^{-5}	3.39×10^{-4}	1.22×10^{-4}	6.82×10^{-4}

cm^{-3}, at temperatures of 1500–2100 °K. The chosen compositions of mixtures A and B give about the same H atom concentration but very different O atom and OH radical concentrations (Table 2). Each mixture produced about 2% H atoms in the p.e. state. Under our conditions, the calculated effects of atom recombination and of temperature change during the course of reaction were small.

We also made experiments to examine the attainment of partial equilibrium in the absence of added NH_3. Two mixtures were used: mixture C: 1.00% O_2, 8.96% H_2, 19.99% Kr, 68.81% Ne, 1.23% Ar; mixture D: 1.00% O_2, 9.01% H_2, 88.96% Kr, 1.03% Ar. Mixture C was similar to mixture A but without added NH_3. Mixture D was used to check whether a change of noble gas altered the observed kinetic behavior. Argon was used as a mass spectrometric internal standard in all mixtures.

Results and Discussion

Induction Period Kinetics

The induction period kinetics in H_2/O_2 are mainly determined by reactions 1 to 5. Although a knowledge of individual reaction rates is not needed for a calculation of the p.e. state, we wanted to check that k_1 to k_5 correctly predicted the observed induction kinetics. There were two reasons for making this check, (*i*) we wanted to use k_1 to k_5 to calculate the time of establishment of p.e. which is also the starting time for measuring NH_3 consumption, and (*ii*) we later used k_1 to k_5 and other rate coefficients in a computer simulation of NH_3 profiles in order to check our measured value of k_9. Accordingly we measured the time dependence of $[H_2O]$ in mixtures C and D at two different total concentrations, 1.0×10^{-6} and 3.3×10^{-6} mol cm^{-3}, at temperatures of 1550–2390 °K.

The observed H_2O concentration profiles were similar to the calculated profile of Fig. 1. We defined an induction period τ as the time taken for $[H_2O]$ to reach 5% of its p.e. value. Our measurements are plotted as log $([O_2]_0\tau)$ against $1/T$ in Fig. 3. It is known (25) that under the conditions of our experiments such a plot produces a linear relationship. The rate equations corresponding to reactions 1 to 6 in Table 1 were then numerically integrated to simulate H_2O concentration profiles of several experiments. (Reaction 6 was actually included, but other calculations showed that it and other recombination reactions had no significant effect on the results.) An induction period, as defined above, was determined from each computation. The plot of the computed values of log $([O_2]_0\tau)$ against $1/T$ is shown as the solid line in Fig. 3.

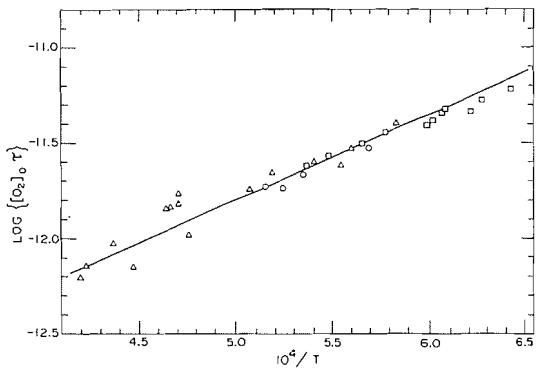

FIG. 3. Plot of log $([O_2]_0\tau)$ *vs.* $10^4/T$. $[O_2]_0\tau$ in mol cm^{-3} s. Points are experimental values: ○, mixture C, total gas concentration $\sim1\times10^{-6}$ mol cm^{-3}; □, mixture C, total gas concentration $\sim3.3\times10^{-6}$ mol cm^{-3}; △, mixture D, total gas concentration $\sim1\times10^{-6}$ mol cm^{-3}. The solid line represents values computed using the rate equations for reactions 1 to 6 in Table 1.

It can be seen that the experimentally observed and the computer simulated induction periods agree very well, especially at 1550–2100 °K, approximately the temperature range of our experiments with added NH_3. This result gave us confidence in the use of the rate coefficients k_1 to k_5. Comparison of mixtures C and D indicated that the induction kinetics are independent of the diluent under our conditions.

Can. J. Chem. Downloaded from www.nrcresearchpress.com by 210.87.254.42 on 09/05/12
For personal use only.

Can. J. Chem. Downloaded from www.nrcresearchpress.com by 210.87.254.42 on 09/05/12
For personal use only.

Measurement of the Rate of Reaction of Hydrogen Atoms with NH_3

Figure 4 is a first order plot of the measured NH_3 concentration from one of our experiments. The graph can be divided into three regions. Initially there is an induction period in which the NH_3 concentration remains fairly constant. This induction period agrees well with that calculated for the same mixture but without NH_3. There then occurs a relatively rapid decay which corresponds to the pseudo-first order reaction between NH_3 and the excess of H atoms in the p.e. state. Finally there is a region in which the plot tends to level off. We attribute this levelling off to the occurrence of a significant amount of the back reaction [−9] $NH_2 + H_2 \rightarrow NH_3 + H$ in the large excess of H_2.

The approximately linear slope immediately following the induction period, in the first order plot, represents the rate of reaction of NH_3 with a concentration of H atoms closely equal to the p.e. concentration of H atoms in the absence of ammonia. Since the quantity $[H]_{p.e.}/[H_2]_0$ was almost independent of temperature in mixture A, its value was set at 0.21 throughout the whole temperature range. (The kinetic calculations described later indicated that in the absence of NH_3 the quantity $[H]/[H_2]_0$ reached a value of 0.214 at 1923 °K and 0.217 at 1620 °K; the corresponding values with NH_3 added were 0.202 and 0.207.) The rate coefficient of reaction 9 was found from the maximum slope, using the relationship

$$2.303\ \mathrm{d}\log[NH_3]/\mathrm{d}t = k_9[H] = 0.21 \times k_9[H_2]_0$$

An Arrhenius plot of k_9 for mixture A is shown in Fig. 5. It will be seen that there is good agreement between the high concentration and low concentration experiments. This agreement indicates that our assumption of pseudo-first order kinetics is correct; it also confirms the conclusion from our computations that the effects of H atom recombination, which should be enhanced at the higher concentration, were not important under our experimental conditions. A least squares fit to the Arrhenius plot over the temperature range 1500–2150 °K gives k_{9A} for mixture A

$$k_{9A} = 10^{13.39\pm0.21} \exp -(17\,100 \pm 1\,700)/RT\ \mathrm{cm^3\ mol^{-1}\ s^{-1}}$$

with the activation energy in cal mol^{-1}. The quoted uncertainties are standard deviations.

We next considered whether the small p.e. concentrations of O and OH could have significantly affected our observed rates of NH_3 removal. Because of the lack of literature data on the reactions

[11] $OH + NH_3 \rightarrow$ products

and

[12] $O + NH_3 \rightarrow$ products

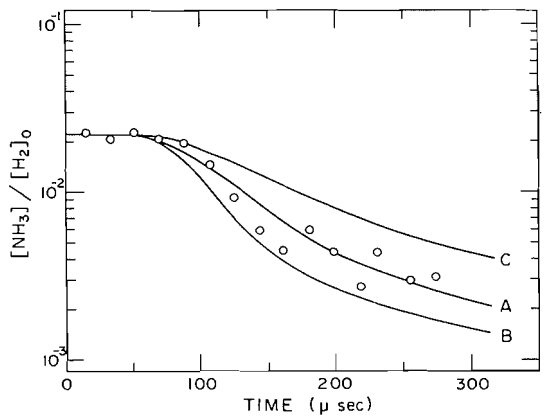

FIG. 4. Comparison of experimentally observed and computer simulated $[NH_3]/[H_2]_0$ profiles. Circles represent observed $[NH_3]/[H_2]_0$ ratios in an experiment with mixture A. Temperature = 1923 °K; total gas concentration = 3.7×10^{-6} mol cm^{-3}. Line A represents computer simulation of $[NH_3]/[H_2]_0$ profile in above experiment using reaction rate coefficients given in Table 1. Lines B and C are calculated in the same way as line A except that rate coefficient for reaction 9 was doubled and halved respectively.

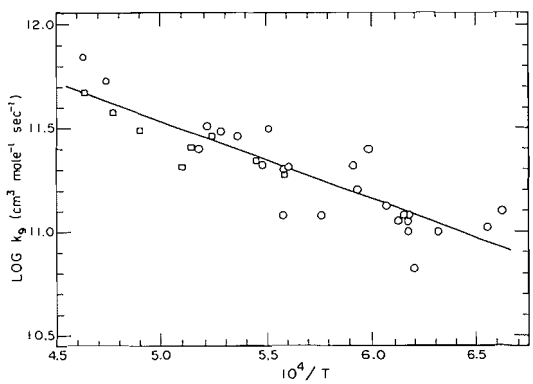

FIG. 5. Arrhenius plot of values of k_9 obtained with mixture A. □, higher density experiments (total gas concentration about 3.3×10^{-6} mol cm^{-3}); ○, lower density experiments (total gas concentration ~1×10^{-6} mol cm^{-3}).

Can. J. Chem. Downloaded from www.nrcresearchpress.com by 210.87.254.42 on 09/05/12
For personal use only.

in our temperature range, we had to estimate the range of likely values of k_{11} and k_{12}. From these estimates we concluded that, while reactions 11 and 12 were probably unimportant, there was some possibility that they contributed significantly to our observed rates. We therefore decided to examine the effects of these radicals experimentally. To do this, mixture B was used. The calculated p.e. concentrations of O and OH for this mixture were each several times larger than for mixture A (Table 2).

The same experimental procedure and analysis as described above for mixture A were then repeated with mixture B. Figure 6 shows an Arrhenius plot of the results. The solid line represents a least squares fit to the data, giving

$$k_{9B} = 10^{13.62\pm0.28} \exp -(18\,800 \pm 2\,300)/RT$$

k_{9A} is also shown in Fig. 6 as a dashed line. It will be seen that the agreement between k_{9A} and k_{9B} is very close, indicating that the larger concentration of O and OH in mixture B had a negligible effect on the observed rate of removal of NH_3. We conclude that the measured k_9 does indeed represent the rate coefficient of reaction 9. A least squares fit to the combined data from mixtures A and B then gave

$$k_9 = 10^{13.44\pm0.16} \exp -(17\,400 \pm 1\,300)/RT \text{ cm}^3 \text{ mol}^{-1} \text{ s}^{-1}$$

From our results we have also estimated upper limits for the rates of reactions 11 and 12. We find that in the temperature range 1620–1923 °K k_{11} must be less than $8 \times 10^9 T^{0.68} \exp(-1\,100/RT)$ cm^3 mol^{-1} s^{-1} which is only 20% of the value from a Johnston and Parr calculation (26). Similarly an upper limit on k_{12} in the same temperature range was found to be $1 \times 10^{13} \exp(-6600/RT)$. This is about two and one-half times the extrapolated low temperature result of Kurylo *et al.* (8).

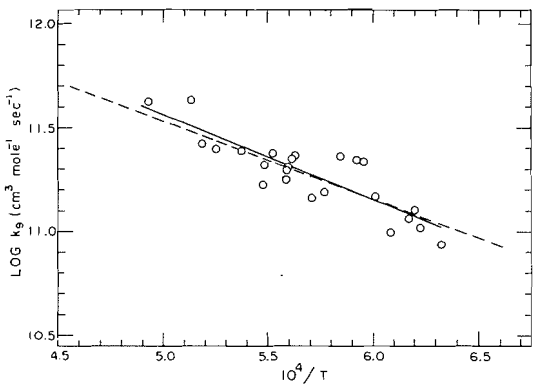

FIG. 6. Arrhenius plot of values of k_9 obtained with mixture B. The solid line is the least squares fit for this mixture, and the dashed line is k_9 from the experiments with mixture A.

Reaction Products

The principal nitrogen-containing products which we detected were NO and N_2. NO accounted for about 10% of the NH_3 consumed in mixture A and about 25% in mixture B. Both NO and N_2 became detectable at the end of the induction period. We have not investigated the mechanism of formation of NO and N_2, but we have assumed that they are produced in secondary reactions which do not significantly affect the rate of NH_3 removal.

Computer Simulation of Reaction Profiles of NH_3

In order to test for consistency of the complete profiles of observed NH_3 concentration against time with the value of k_9 deduced from parts of those profiles, the full profiles were simulated by numerical integration of the reaction rate equations using the kinetic data in Table 1. Reaction 10 was included as a termination step to remove NH_2. The agreement between computed and experimental profiles was found to be satisfactory, as illustrated by Fig. 4.

Since the experimentally measured quantity in these experiments was the slope of the pseudo-first order decay plot of ammonia, we felt that it was very important to make sure that this characteristic of the profile does depend strongly on the value of k_9 and is only weakly dependent on the other rate coefficients. The effect of changing the rate coefficients by factors of two on the maximum slope in the computer simulated plot of log $[NH_3]$ against time is shown in Fig. 7. Each rate expression from k_1 to k_{10} was individually changed by a factor of 2 and then by $\frac{1}{2}$ and the ammonia concentration profile simulated in each case by a computer. It can be seen that the maximum slope is very sensitive to the numerical value of k_9 whereas small uncertainties in the other rate coefficients are of only secondary importance.

Comparison with Literature Data

Figure 8 is an Arrhenius plot showing our results and the rather sparse data on k_9 reported by other workers.

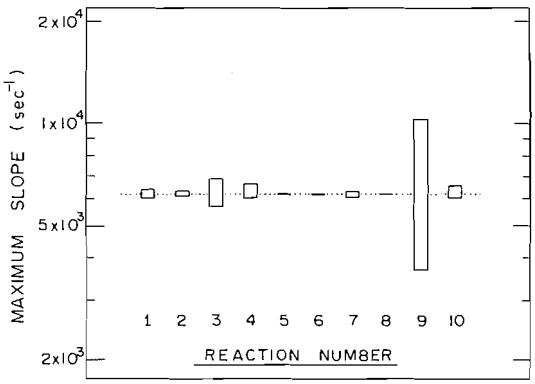

FIG. 7. Sensitivity of the pseudo-first order NH_3 decay rates, computed using the reaction scheme in Table 1, to variation of individual rate coefficients. To test the sensitivity of the decay rate, each of the reaction rate coefficients in Table 1 was individually halved and then doubled. The length of each bar represents the total resulting change in the maximum slope of a plot of log $[NH_3]$ against time. The horizontal dotted line represents the slope using the unchanged rate coefficients of Table 1. Temperature = 1923 °K. Total concentration = 3.7×10^{-6} mol cm^{-3}.

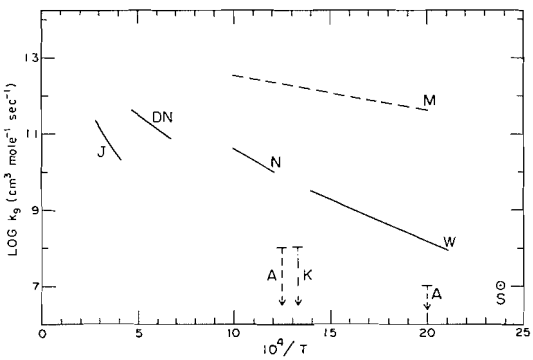

FIG. 8. Comparison of various calculated and experimental values of k_9. J, ref. 3; A, upper limits from ref. 7; K, upper limit from ref. 8; N, ref. 9; W, ref. 10; M, calculated value from ref. 26; S, ref. 29; DN, present work.

A theoretical value of k_9 has been calculated by Mayer and co-worker (26, 27). However this value must surely be wrong since it is in such serious conflict with all of the experiments.

Our values of k_9 are considerably larger than the extrapolated high temperature results of Johnson (3). However, for the reasons mentioned in the Introduction, we are doubtful about the quantitative significance of Johnson's value. We therefore believe that our result is the first quantitative determination of k_9 above 1000 °K.

The rate of the related isotopic reaction

[−9′] $NH_2 + D_2 \rightarrow NH_2D + D$

has been deduced by Lifshitz *et al.* (28) from studies of the exchange reaction between NH_3 and D_2 at 1150–1450 °K. Their rate coefficients, when extrapolated to the temperature range of our experiments, are about 2.5 times those deduced, from our results, for the isotopic analog

[−9] $NH_2 + H_2 \rightarrow NH_3 + H$

However we note that in Lifshitz' analysis it was assumed that the reaction

[13] $D + NH_3 \rightarrow NH_2D + H$

is very much slower than

[9″] $D + NH_3 \rightarrow HD + NH_2$

whereas recent work (8) has indicated that in reality reaction 13 is rapid and would be substantially faster than reaction 9″ at 1150–1450 °K. We therefore believe that the data of Lifshitz give only an upper limit to the rate of reaction −9′ and are not in conflict with our value of k_9.

It is interesting to consider what insight our results can give into the conflicting data below 1000 °K. Our extrapolated k_9 is substantially smaller than the value obtained by Agnesyan and Nalbandyan (9) from a study of the effect of NH_3 on H_2/O_2 explosion limits. However we note that their value of k_9 depends on the correctness of an assumed mechanism for a fairly complex reaction. Their analysis assumes that reaction 9 is responsible for the observed inhibition of explosion. However since they used stoichiometric hydrogen–oxygen, substantial amounts of OH and O would be present. It therefore seems very possible that reactions other than [9] were contributing appreciably to the observed inhibition, and that their value of k_9 should more properly be considered an upper limit.

Further extrapolation of our results to 800–750 °K gives a value very close to the upper limits observed by Albers *et al.* (7) and Kurylo *et al.* (8). Extrapolation to still lower temperatures does not produce any conflict with Albers' (7) upper limit value at 500 °K but does appear to conflict with the value of Schiavello and co-worker (29). However this extrapolation is much too long to be made with any confidence.

The low temperature value of Willis *et al.* (10), when extrapolated, intersects with our results but our activation energy is considerably larger than theirs.

One possibility that should be considered is

Can. J. Chem. Downloaded from www.nrcresearchpress.com by 210.87.254.42 on 09/05/12
For personal use only.

Can. J. Chem. Downloaded from www.nrcresearchpress.com by 210.87.254.42 on 09/05/12
For personal use only.

that the Arrhenius plot for k_9 is curved. Several authors have recently reported (30–34), in both experimental and theoretical studies, non-Arrhenius behavior in hydrogen abstraction reactions. However, if we propose a smooth curve joining our results to those of Willis *et al.*, and agreeing approximately with our Arrhenius activation energy as well as theirs, we have to assume that the upper limit estimates of Albers *et al.* and Kurylo *et al.* are grossly wrong. We thus conclude that our results, considered alone, do not permit a clear choice among the conflicting data at lower temperatures. Nevertheless it is hard to see how, using the relatively direct e.s.r. method, both Albers *et al.* and Kurylo *et al.* could have failed to find a measurable rate at about 800 °K if k_9 at that temperature is indeed as large as stated by Agnesyan and Nalbandyan. Therefore, taking all factors into account, we are inclined to think that the available data may be best interpreted by proposing an Arrhenius line which passes close to our results and to the upper limiting values of Albers *et al.* and Kurylo *et al.* at about 800 °K, and which may show some concave upwards curvature. However further work on this interesting reaction, particularly at low and intermediate temperatures, is clearly desirable.

Conclusions

The present work has demonstrated that the large concentration of H atoms in the partial equilibrium state of a shock-heated hydrogen-rich H_2/O_2/diluent mixture can be used to study the elementary reaction between H and a small concentration of added NH_3. The method should be applicable to other elementary reactions of O and OH as well as H, provided that certain conditions are met.

For the temperature range 1500–2150 °K a least squares fit of the results from two different $H_2/O_2/NH_3$/diluent mixtures gave the following rate coefficient for reaction 9, $H + NH_3 \rightarrow H_2 + NH_2$

$$k_9 = 10^{13.44 \pm 0.16} \exp -(17\,400 \pm 1\,300)/RT \text{ cm}^3 \text{ mol}^{-1} \text{ s}^{-1}$$

Our results appear to be first direct measurement of the rate of reaction 9 above 1000 °K. The observed value of k_9 was also found to be: (*i*) independent of initial $H_2:O_2$ ratio over the range studied by us (5:1 to 9:1), and (*ii*) independent of total gas concentration over the range 1.0×10^{-6} to 3.3×10^{-6} mol cm^{-3}.

From our experimental results, an upper limiting value for the rate coefficient of reaction

[11] $OH + NH_3 \rightarrow$ products

over the temperature range 1620 to 1923 °K is

$$k_{11} = 8 \times 10^9 T^{0.68} \times \exp(-1100/RT) \text{ cm}^3 \text{ mol}^{-1} \text{ s}^{-1}$$

For reaction

[12] $O + NH_3 \rightarrow$ products

over the same temperature range, the upper limit is

$$k_{12} = 1 \times 10^{13} \times \exp(-6600/RT) \text{ cm}^3 \text{ mol}^{-1} \text{ s}^{-1}$$

These upper limits of course apply equally to the elementary processes

[11*a*] $OH + NH_3 \rightarrow H_2O + NH_2$,

and

[12*a*] $O + NH_3 \rightarrow OH + NH_2$,

respectively.

This work was supported by grants from the National Research Council of Canada and Imperial Oil Limited. W.S.N. thanks the National Research Council of Canada for the award of a Scholarship. We are grateful to Dr. T. C. Clark for helpful discussions.

1. J. N. Bradley, R. N. Butlin, and D. Lewis. Trans. Faraday Soc. **63**, 1 (1967).
2. M. Haluk. Ph.D. Thesis. University of Toronto, Toronto, Ontario. 1970.
3. D. N. Johnson. D.Sc. Thesis, Washington University, St. Louis, Missouri. 1966.
4. J. K. Dixon. J. Am. Chem. Soc. **54**, 4262 (1932).
5. H. W. Melville. Trans. Faraday Soc. **28**, 885 (1932).
6. J. C. Jungers and H. S. Taylor. J. Chem. Phys. **2**, 452 (1934).
7. E. A. Albers, K. Hoyermann, H. Gg. Wagner, and J. Wolfrum. 12th Symposium (International) on Combustion. The Combustion Institute, Pittsburgh, Pennsylvania. 1969. p. 313.
8. M. J. Kurylo, G. A. Hollinden, H. F. LeFevre, and R. B. Timmons. J. Chem. Phys. **51**, 4497 (1969).
9. K. T. Agnesyan and A. B. Nalbandyan. Dokl. Phys. Chem. **160**, 18 (1965).
10. C. Willis, A. W. Boyd, and O. A. Miller. Can. J. Chem. **47**, 3007 (1969).
11. J. E. Dove and W. S. Nip. Unpublished results.
12. R. R. Baldwin, D. Jackson, R. W. Walker, and S. J. Webster. Trans. Faraday Soc. **63**, 1665, 1676 (1967).
13. R. R. Baldwin, D. E. Hopkins, and R. W. Walker. Trans. Faraday Soc. **66**, 189 (1970).

14. R. R. BALDWIN and R. W. WALKER. Essays in chemistry. Vol. 3. Academic Press, New York. 1972.
15. G. SCHOTT and J. L. KINSEY. J. Chem. Phys. **29**, 1177 (1958).
16. W. C. GARDINER, M. MCFARLAND, K. MORINAGA, T. TAKEYAMA, and B. F. WALKER. Proc. 8th Internat. Shock Tube Symp. Paper no. 23. Chapman and Hall, London. 1971.
17. C. J. JACHIMOWSKI and W. M. HOUGHTON. Combust. Flame **17**, 25 (1971).
18. D. L. BAULCH, D. D. DRYSDALE, and A. C. LLOYD. High temperature reaction rate data No. 2. Leeds University, Dept. of Physical Chemistry. 1968.
19. T. A. BRABBS and F. E. BELLES. Proc. 8th Internat. Shock Tube Symp. Paper no. 24. Chapman and Hall, London. 1971.
20. H. A. OLSCHEWSKI, J. TROE, and H. GG. WAGNER. 11th Symposium (International) on Combustion. The Combustion Institute, Pittsburgh, Pennsylvania. 1967. p. 155.
21. A. L. MYERSON and W. S. WATT. J. Chem. Phys. **49**, 425 (1968).
22. M. CAMAC and A. VAUGHN. J. Chem. Phys. **34**, 460 (1961).
23. K. W. MICHEL. 10th Symposium (International) on Combustion. The Combustion Institute, Pittsburgh, Pennsylvania. 1965. p. 351.
24. S. C. BARTON and J. E. DOVE. Can. J. Chem. **47**, 521 (1969).
25. D. R. WHITE and G. E. MOORE. 10th Symposium (International) on Combustion. The Combustion Institute, Pittsburgh, Pennsylvania 1965. p. 785.
26. S. W. MAYER and L. SCHIELER. Aerospace Corp. Rept. TR-669(9210-02)-3. 1966.
27. G. S. BAHN. Reaction rate compilation for the H–O–N system. Gordon and Breach, New York. 1968.
28. A. LIFSHITZ, P. SCHECHNER, and A. BURCAT. Proc. 7th Internat. Shock Tube Symp. University of Toronto Press, Toronto, Ontario. 1970. p. 644.
29. M. SCHIAVELLO and G. VOLPI. J. Chem. Phys. **37**, 1510 (1962).
30. F. DRYER, D. NAEGELI, and I. GLASSMAN. Combust. Flame **17**, 270 (1971).
31. T. C. CLARK and J. E. DOVE. Can. J. Chem. **51**, 2147, 2155 (1973).
32. P. D. PACEY and J. H. PURNELL. J. Chem. Soc. Faraday Trans. I. **68**, 1462 (1972).
33. W. C. GARDINER, W. G. MALLARD, M. MCFARLAND, K. MORINAGA, J. H. OWEN, W. T. RAWLINS, T. TAKEYAMA, and B. F. WALKER. 14th Symp. (Internat.) on Combustion. The Combustion Institute, Pittsburgh, Pennsylvania. 1973. p. 61.
34. A. A. WESTENBERG and N. DE HAAS. J. Chem. Phys. **58**, 4066 (1973).
35. JANAF thermochemical tables, 2nd ed. NSRDS-NBS 37. 1970. National Bureau of Standards, Washington, D.C.

Can. J. Chem. Downloaded from www.nrcresearchpress.com by 210.87.254.42 on 09/05/12
For personal use only.

Radiolysis of Liquid Di-*n*-propyl Ether: Alcohol Formation and Solvated Electrons[1]

REBECCA ARRIETA VERMEER AND GORDON R. FREEMAN
Chemistry Department, University of Alberta, Edmonton, Alberta T6G 2G2

Received October 29, 1973

In the γ radiolysis of pure di-*n*-propyl ether at 296 K, G(*n*-propanol) = 2.5 ± 0.1. The propanol yield was reduced by the addition of an electron scavenger (SF_6) or proton scavenger ($C_3H_7NH_2$), but was not affected by the addition of hydrogen chloride or propylene. In the absence of additives the geminate neutralization reaction [7] $R_2OH^+ + e_{solv}^- \rightarrow ROH + R$ gave 1.8 G units of alcohol. The charge scavenging reactions of SF_6 and $C_3H_7NH_2$ were consistent with the nonhomogeneous kinetics model reported earlier. The optical absorbance of solvated electrons in di-*n*-propyl ether increased with wavelength up to 1.6 μ, the practical limit of the detector, at all temperatures in the liquid range, including the liquid supercooled to 140 K (f.p. = 151 K). The kinetics of electron reactions could be measured by observing the absorption at 0.9 μ. The optical absorbance observed as a function of time t at all temperatures was consistent with the kinetics model and had the general form: absorbance = $b(t^{-1/2} + c)e^{-kt}$, where b is a proportionality constant, c is related to the free ion yield and k is a first order decay constant that describes the decay of the solvated electron free ions. At 273 K, $k(e_{solv}^- + SF_6) = 4.5 \times 10^{10}\ M^{-1}\ s^{-1}$ and the activation energy is 3.2 ± 0.3 kcal/mol.

Le rendement en *n*-propanol, G(*n*-propanol) = 2.5 ± 0.1, provenant de l'irradiation gamma du di-*n*-propyle éther à 296 K, diminue par l'addition d'un capteur d'électrons (SF_6) ou de protons ($C_3H_7NH_2$), mais n'est pas influencé par l'addition d'acide chlorhydrique ou de propylène. Dans l'éther pur, la neutralisation [7] $R_2OH^+ + e_{solv}^- \rightarrow ROH + R$ a un rendement en alcool de 1.8 unité G. Les réactions de capture de charges dûes au SF_6 et $C_3H_7NH_2$ sont compatibles avec un modele de cinétique nonhomogène proposé précedemment. L'absorption optique pour l'électron solvaté dans le di-*n*-propyle éther liquide augmente en fonction de la longueur d'onde jusqu'à 1.6 μ, la limite pratique du spectrophotomètre, et ce même dans le liquide surfondu à 140 K (la température de fusion est 151 K). La cinétique des réactions de l'électron est suivie par l'observation a 0.9 μ de son absorption optique. La variation de celle-ci en fonction du temps t est en accord avec le modele de cinétique non homogène, et est de la forme: absorbance = $b(t^{-1/2} + c)e^{-kt}$, où b est une constante de proportionnalité, c une grandeur liée au rendement en ion libres, et k une constante de vitesse du premier order caractérisant la disparition des électrons libres solvatés. A 273 K, $k(e_{solv}^- + SF_6) = 4.5 \times 10^{10}\ M^{-1}\ s^{-1}$; l'énergie d'activation de la réaction est 3.2 ± 0.3 kcal/mol.

Can. J. Chem., **52**, 1181 (1974)

Introduction

The alcohol ROH is one of the major products of γ radiolysis of an ether R_2O (1, 2), although the mechanism of its formation is uncertain. Ethanol formation during the radiolysis of diethyl ether was reduced to one half by the addition of 1,3-pentadiene (2), but it was not certain whether the inhibition was due to reactions of free radicals or of solvated electrons. To obtain more information about this mechanism, the formation of *n*-propanol in di-*n*-propyl ether has been studied. It now appears that the effect of 1,3-pentadiene in diethyl ether was due to the scavenging of electrons.

The absorption spectrum of e_{solv}^- in the ether, and the value of the rate constant and activation energy for reaction with sulfur hexafluoride, were also determined.

Experimental

Materials

Di-*n*-propyl ether was obtained from Eastman Organic Chemicals and from Aldrich Chemical Co. (Gold Label quality). The main impurities were peroxide, propionaldehyde, *n*-propanol, and 1,1-dipropoxypropane, each at a concentration of $\sim 10^{-3}\ M$. The liquid was passed through a 14 in. × 3/4 in. column of neutral Woelm alumina to remove peroxide, then refluxed for 20 h with 1.5 g of 2,4-dinitrophenylhydrazine and 2 ml of concentrated sulfuric acid per 700 ml of ether. It was then fractionally distilled through a 24 in. column packed with glass beads. About 300 ml of the prime distillate was passed through two 14 in. × 3/4 in. columns of neutral Woelm alumina.

[1]Supported by the National Research Council of Canada.

Can. J. Chem. Downloaded from www.nrcresearchpress.com by 210.87.254.5 on 09/05/12
For personal use only.

Can. J. Chem. Downloaded from www.nrcresearchpress.com by 210.87.254.5 on 09/05/12
For personal use only.

No impurities ($< 10^{-4}$ *M*) could be detected in the resultant ether, which was then degassed and stored under vacuum in contact with a sodium mirror.

Sulfur hexafluoride from Matheson of Canada was purified by sublimation under vacuum.

Anhydrous hydrogen chloride (Matheson of Canada) was passed over copper foil to remove chlorine, then sublimed under vacuum.

Propylene (Matheson of Canada) was thoroughly degassed prior to use.

n-Propylamine (Eastman Organic) was purified by fractional distillation, followed by thorough degassing. It was stored in a Pyrex reservoir fitted with a Hoke valve (stainless steel needle and Teflon seat).

1,1-Dipropoxypropane was prepared by putting 10 g of anhydrous copper sulfate into 500 ml of a solution containing 25% propionaldehyde and 75% *n*-propanol. The solution was shaken and then allowed to stand overnight. The copper sulfate was removed by centrifugation, and the excess alcohol by rotary evaporation. The crude product was fractionally distilled at about 60 μ pressure, with the pot at room temperature and the receiver at −78 °C. The final material was 96% pure.

Anhydrous copper sulfate was prepared by heating copper sulfate hydrate to 200 °C under vacuum, until colorless.

Sulfuric acid (C.I.L.), *n*-propanol (Fisher Scientific, Certified Reagent), and propionaldehyde (Eastman Organic) were used as received.

Procedures for Steady State Radiolysis and Product Analysis

Two ml samples were prepared by standard vacuum techniques. Most additives were measured in the vapor phase. Sulfuric acid was delivered quickly into the cell from a syringe with a stainless steel needle. The acid was frozen with liquid nitrogen, then degassed by successive pump–thaw–freeze cycles. A known amount of degassed ether was then distilled into the cell and the cell sealed off.

The radiation source was a ^{60}Co Gammacell-220 (Atomic Energy of Canada). The dose was 4×10^{19} eV/g and the temperature 296 K.

Products were analyzed by gas chromatography, using a flame ionization detector. Calibrating solutions were used daily. A 6 ft × 1/8 in. stainless steel column packed with 10 wt% 1,2,3-tris(2-cyanoethoxy)propane (TCEP) on Chromosorb W.A.W. was used at 338–373 K to measure propanol and 1,1-dipropoxypropane in all samples except those containing a high concentration of *n*-propylamine or hydrogen chloride. A 2 ft × 1/8 in. glass column packed with Porapak Q was used at 393 K for the former and a 4 ft × 1/8 in. stainless steel column packed with Porapak T at 408 K for the latter. Acid was removed from samples by injection onto a 1 in. × 1/4 in. pre-column packed with potassium hydroxide pellets. Propionaldehyde was analyzed on a 6 ft × 1/8 in. stainless steel column containing 10 wt% Carbowax 1540 on Porapak P, at 358 K.

The relative density of di-*n*-propyl ether was measured at 161, 186, 231, and 273 K. Using $d = 0.766$ g/cm^3 at 273 K (3) one obtains $dd/dt = -9.1 \times 10^{-4}$ g/cm^3 deg over the entire range.

The Ostwald absorption coefficient α of sulfur hexafluoride in di-*n*-propyl ether was measured at 197, 273, and 298 K (4). The respective values obtained were 9.4, 2.2, and 1.7. All of the sulfur hexafluoride was assumed to be dissolved in the supercooled liquid ether at 140 K.

Pulse Radiolysis Procedures

The equipment used for pulse radiolysis (1 μs pulses of 1.7 MeV electrons, $\sim 6 \times 10^{16}$ eV/g) and optical spectroscopy has been described elsewhere (5), with the following exceptions.

Two Bausch and Lomb grating monochromators were used, one to cover the range 350–800 nm and the other 700–1600 nm. Corning filters #3-74, 3-66, and 7/56 were used to remove higher order diffractions with wavelengths below 400, 560, and 800 nm, respectively. The gratings were calibrated with a He–Ne laser, using the first order 632.8 nm and second order 1265.5 nm lines.

The photodetectors were EG & G model SGD444 (silicon) for 400–1000 nm and ENL type 653 (germanium) for 700–1600 nm. The response time of the former was 70 ns. The response from the latter occurred in two steps, the first in < 1 μs and the second over many μs. Four ENL653 detectors were purchased and the one with the largest first step (0.58 of the final signal) was used. The measurements with the ENL653 were then normalized by dividing them by 0.58. The normalization was checked by matching the results with those from the SGD444 in the overlapping range 700–1000 nm.

All studies of absorbance decay rates were done with the fast detector, SGD444.

Results

Alcohol Formation

In samples that contained acid, part of the alcohol reacted with the product aldehyde to form the acetal 1,1-dipropoxypropane. In pure ether the yields were $G(n\text{-propanol}) = 2.5 \pm 0.1$, $G(\text{propionaldehyde}) = 0.3$, and $G(1,1\text{-dipropoxypropane}) = 0.01$; the irradiated samples were stable for many hours. In samples that contained sulfur hexafluoride, the measured amounts of alcohol and aldehyde decreased over a period of hours, while that of the acetal increased by a corresponding amount. Acetal formation was presumably catalyzed by hydrogen fluoride produced by reaction of sulfur hexafluoride with electrons.

$$[1]\quad C_2H_5CHO + 2C_3H_7OH \xrightarrow{H^+} C_2H_5CH(OC_3H_7)_2 + H_2O$$

The initial alcohol yield was therefore taken as $G(n\text{-}C_3H_7OH)_i = G(n\text{-}C_3H_7OH)_{obs} + 2G(C_2H_5\text{-}CH(OC_3H_7)_2)_{obs}$, where the observed yields were measured at the same time.

The initial yield of propanol decreased with increasing sulfur hexafluoride concentration reaching a lower limit of about 0.7 units at > 0.1 *M* sulfur hexafluoride (Fig. 1).

Hydrogen chloride had no effect on the radiol-

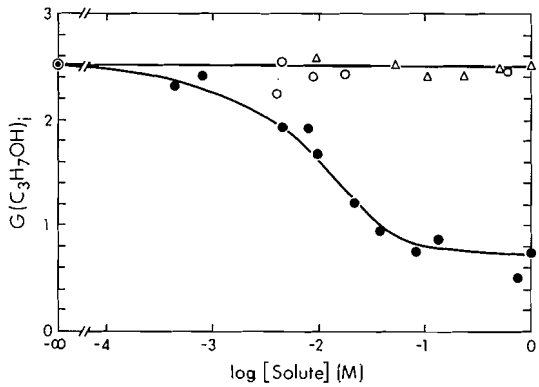

FIG. 1. Yield of *n*-propanol as a function of solute concentration. $T = 296$ K. Solute: ●, sulfur hexafluoride; ○, hydrogen chloride; △, propylene. The curve through the sulfur hexafluoride points was calculated using eq. 9 and $\beta = 9 \times 10^{14}$ V/cm².

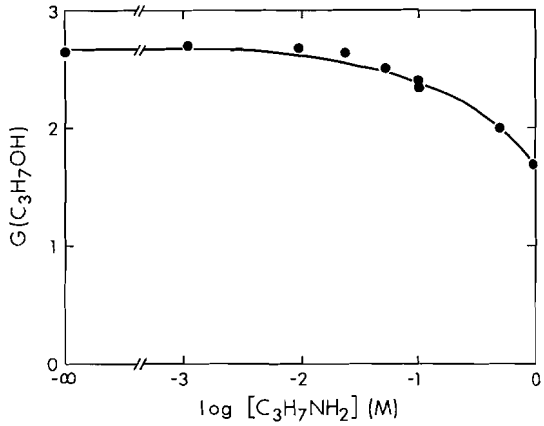

FIG. 2. Yield of *n*-propanol as a function of *n*-propylamine concentration at 296 K. The curve was calculated using eq. 9 and $\beta = 1.0 \times 10^{13}$ V/cm².

ysis yield of propanol (Fig. 1). At [HCl] > 0.1 *M* the acid catalyzed decomposition of the ether to propanol and chloropropane was appreciable. In this case the amount of chloropropane was subtracted from the amount of alcohol before calculating the radiolysis yield of the latter. The correction was 15% at 0.6 *M* hydrogen chloride.

[2] $(C_3H_7)_2O + HCl \rightarrow C_3H_7OH + C_3H_7Cl$

Sulfuric acid dissolved in the ether but reacted relatively rapidly to form propanol and propyl hydrogen sulfate. It therefore could not be used in the radiolysis study. Propyl hydrogen sulfate was identified by its physical characteristics: denser than ether and only slightly soluble in ether, so it precipitated and settled to the bottom as a colorless, very viscous liquid; it was very soluble in water, and acidic. It decomposed upon gentle heating, presumably to form dipropyl sulfate and water.

Addition of up to 0.02 *M* *n*-propylamine had no effect on propanol formation, but higher concentrations decreased the alcohol yield (Fig. 2).

Propylene had no effect on the yield of alcohol (Fig. 1).

Solvated Electron Spectrum

The optical absorption spectrum of the liquid was measured at the end of 1 μs pulses of electrons. The spectra recorded at 273, 200, and 140 K are shown in Fig. 3. The rate of decay of the absorbance was greatly increased by the addition of 10^{-4} *M* sulfur hexafluoride, an efficient electron scavenger (Fig. 4). The absorbance was attributed to solvated electrons. Similar spectra have been observed in other ethers (6).

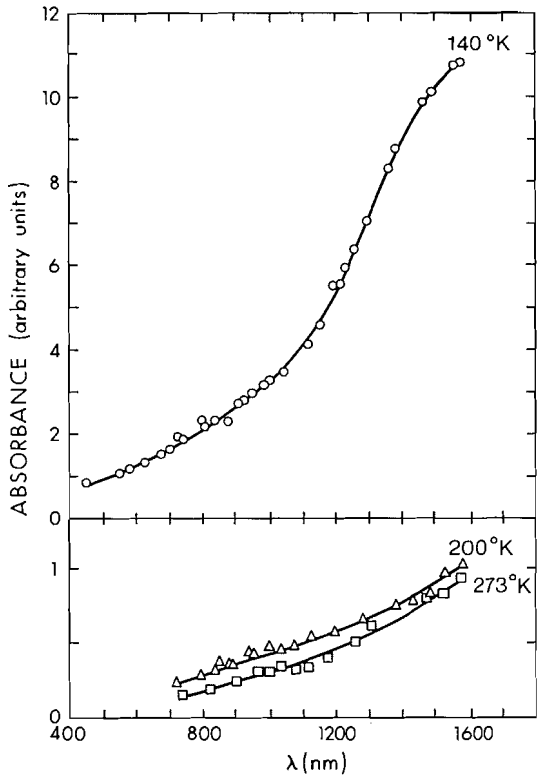

FIG. 3. Optical absorption spectra of solvated electrons in liquid di-*n*-propyl ether. The liquid at 140 K was supercooled by 11°.

The absorbance observed at the end of a 1 μs pulse increased only slightly when the ether was cooled from 273 to 200 K, but increased greatly

Can. J. Chem. Downloaded from www.nrcresearchpress.com by 210.87.254.5 on 09/05/12
For personal use only.

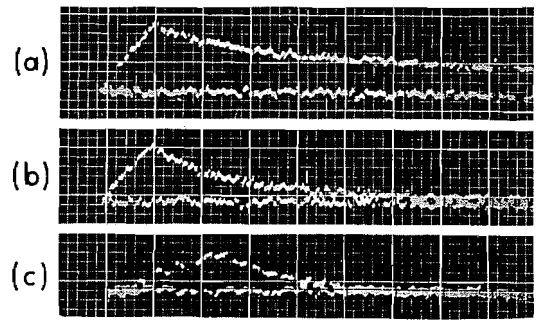

FIG. 4. Optical absorbance at 920 nm as a function of time in propyl ether at 200 K: (*a*) no additive, time = 1 μs/main div.; (*b*) $[SF_6] = 0.5 \times 10^{-4}$ *M*, time = 1 μs/main div.; (*c*) $[SF_6) = 1.1 \times 10^{-4}$ *M*, time = 0.5 μs/main div.

when the liquid was cooled further to 140 K (Fig. 3). Absorbance is given in arbitrary units because there is uncertainty about the infrared detector response. However, one arbitrary unit $\approx 1 \times 10^4$ units of $G\varepsilon$, e_{solv}^- $M/100$ eV cm.

The normal freezing point of di-*n*-propyl ether is 151 K, so the liquid at 140 K was supercooled. Sudden freezing of the supercooled liquid caused the light signal to disappear; thawing such a sample usually broke the cell.

At 273 K the absorption spectrum decayed by simple first order kinetics within the time resolution of the apparatus (Fig. 5). The order of the decay at 200 K (Fig. 5) and 149 K (Fig. 6) was complex, presumably due to the observation of

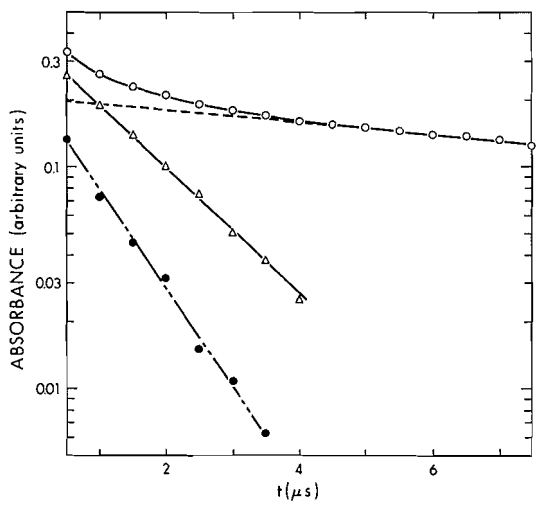

Fig. 5. Optical absorbance at 900 nm as a function of time in propyl ether: △, observed at 273 K; ○, observed at 200 K; ---, approximate first order line; ●, difference between observed and approximate first order values. The full lines were calculated from eq. 15.

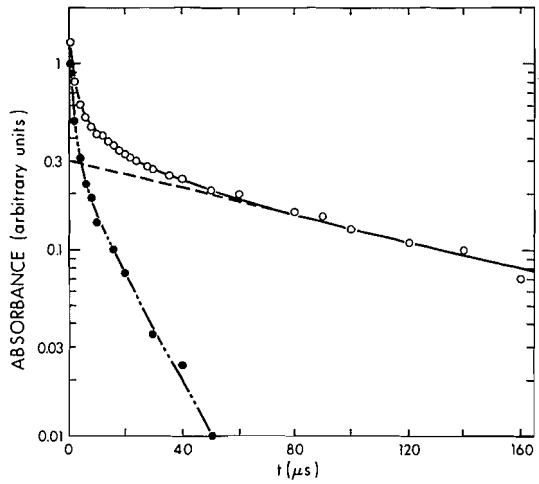

FIG. 6. Optical absorbance at 900 nm as a function of time in propyl ether at 149 K. ○, observed; ---, approximate first order line; ●, difference between observed and approximate first order values. The full line was calculated from eq. 15.

the final portion of the geminate neutralization reaction.

$k(e_{solv}^- + SF_6)$

The first order decay of the free-ion solvated-electrons in the absence of sulfur hexafluoride was presumably due to reaction with an impurity S:

[3] $$e_{solv}^- + S \rightarrow S^-$$

At low temperatures the final part of the geminate neutralization reaction was also observed:

[4] $$e_{solv}^- + M^+ \rightarrow \text{products}$$

Reaction with added sulfur hexafluoride was superimposed upon [3] and [4]:

[5] $$e_{solv}^- + SF_6 \rightarrow SF_6^-$$

The value of the rate constant k_5 of reaction 5 was determined from the difference in the observed rates in the presence and absence of sulfur hexafluoride.

[6] $$k_5 = \left\{\left(\frac{-dA}{dt}\right)_{\text{with } SF_6} - \left(\frac{-dA}{dt}\right)_{\text{no } SF_6}\right\}[SF_6]^{-1}A^{-1}$$

where A = absorbance.

Measurements were made at 273, 200, and 140 K. An Arrhenius plot of the values of k_5 is shown in Fig. 7. At 273 K, $k_5 = 4.5 \times 10^{10}$ M^{-1} s^{-1}.

Can. J. Chem. Downloaded from www.nrcresearchpress.com by 210.87.254.5 on 09/05/12
For personal use only.

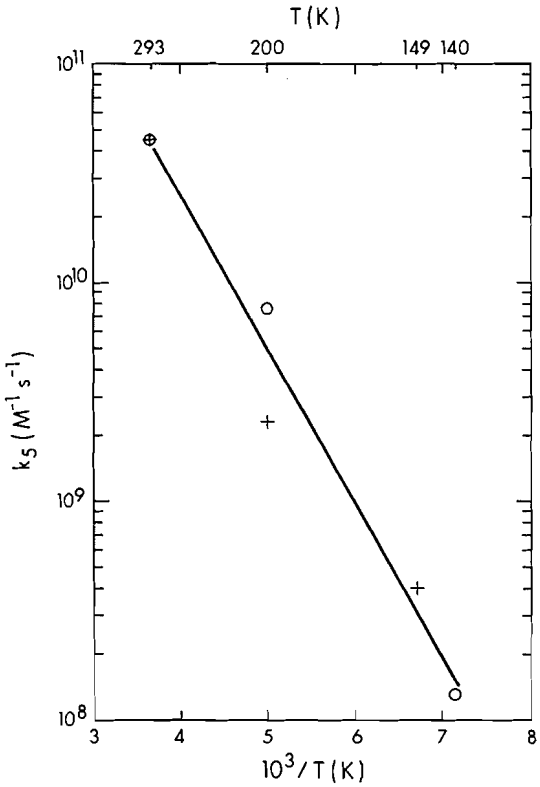

FIG. 7. Arrhenius plot of k_5, (○). Values of $k = k_3$[S] from eq. 15, multiplied by 7×10^4 to make the point at 273 K coincide with k_5, and corrected for the change in density so that [S] remains at the 273 K value, are shown for comparison, (+).

Values of k_3[S], normalized to the value of k_5 at 273 K and to constant [S] with change in density, are also shown in Fig. 7 for comparison. The activation energies of [5] and [3] are $E_3 \approx E_5 = 3.2 \pm 0.3$ kcal/mol.

Discussion

Alcohol Formation

Approximately 70% of the alcohol formation is inhibitable by the addition of the electron scavenger sulfur hexafluoride (Fig. 1). Thus electrons are precursors of about 1.8 G units of alcohol, probably by way of reaction 7.

[7] $$R_2OH^+ + e_{soln}^- \rightarrow ROH + R$$

This reaction would not be inhibited by the addition of an acid or an olefin, in agreement with the behavior of the alcohol yields (Fig. 1). The inhibition caused by the addition of propylamine (Fig. 2) may be ascribed to [8].

[8] $$RNH_2 + R_2OH^+ \rightarrow RNH_3^+ + R_2O$$

For the present treatment the total ionization yield in the liquid ether is assumed to equal that in the gas phase, although ionization yields in liquids might in general be somewhat greater than those in the corresponding gases (7). The gas phase ionization yields in di-ethyl and di-isopropyl ether are each G(ionization) = 4.3 (8), so that in di-*n*-propyl ether is taken to be the same. The scavengeable yield of alcohol indicates that only about 40% of the ions and electrons lead to alcohol formation; the rest may form other products, such as hydrogen (2, 9).

The free ion yield in propyl ether should be in the vicinity of $G_{fi} = 0.3$ (2, 10, 11) which could contribute 0.1 units to the alcohol yield. However, the free-ion solvated-electrons were probably scavenged by a trace of impurity in the absence of additive, so reaction 7 can be assumed to have occurred exclusively in the spurs.

The sulfur hexafluoride curve in Fig. 1 was calculated using a stochastic model of nonhomogeneous kinetics (12). The decrease in alcohol yield is given by [9].

[9] $$\Delta G(\text{ROH}) = -G_7 \sum F(y)\,(1 - e^{-r/y})\phi$$

where $G_7 = 1.8$ is the yield of [7] in the absence of additive, $F(y)$ is fraction of thermalized electron–ion pairs that have an initial intrapair separation distance y, $r = \xi^2/\varepsilon kT$, ξ is the charge on an electron, ε is the dielectric constant of the liquid, k is Boltzmann's constant, T is the absolute temperature, and ϕ is the probability that reaction 5 occurs before [7].

[10] $$\phi = 1 - (1 - f N_s)^{\beta\nu}$$

where f is the encounter efficiency of [5] (assumed to be unity), N_s is the mole fraction of scavenger, β is an adjustable parameter that indicates the scavenging efficiency and

[11] $$\nu = 1.4 \times 10^7 \varepsilon y^3$$

The distribution $F(y)$ was assumed to be the same as that in *n*-hexane, adjusted for the difference in densities (12).

The best value of β was 9×10^{14} V/cm^2, which is slightly larger than the value 6×10^{14} V/cm^2 obtained for electron scavenging by nitrous oxide in cyclohexane (13) and methylcyclopentane (14).

The curve for positive ion scavenging in Fig. 2 was also calculated from eq. 9, with ϕ representing the probability that reaction 8 occurs before 7. Assuming $f = 1$, the best value of β was $1.0 \times$

Can. J. Chem. Downloaded from www.nrcresearchpress.com by 210.87.254.5 on 09/05/12
For personal use only.

10^{13} V/cm^2. The analogous value for positive ion scavenging by ND_3 in methylcyclopentane was somewhat larger, 4×10^{13} V/cm^2 (14). The greater scavenging efficiency by ND_3 in the hydrocarbon might be related to a greater difference in proton affinities between the ND_3 and alkyl radical than between the amine and ether (15).

Decay of e_{solv}^- Spectrum

The decay of the optical absorption at 900 nm was simple first order at 273 K (Fig. 5). This was verified by showing that the absorption did not fit a second order plot, which would have been a linear variation of absorbance^{-1} with time. The decay is attributed to reaction 3.

At 200 and 149 K the decay was neither simple first nor second order (Figs. 5, 6, 8, and 9). The downward curvature of these lines in Figs. 8 and 9 does not imply that the order of the reaction was greater than two, but that more than one decay mechanism was occurring (12). The absorbance above the approximate first order line at short times in Figs. 5 and 6 was due to electrons that were undergoing geminate neutralization [4]. The rate of [4] is such that the final portion of it in a pure system follows eq. 12 (12, 16).

$$[12] \qquad [e_{solv}^-]_{gn}^t = at^{-1/2}$$

where $[e_{solv}^-]_{gn}^t$ is the concentration of solvated

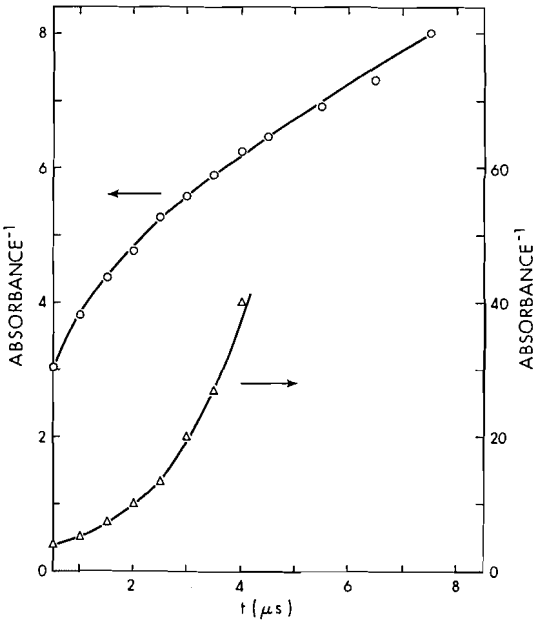

FIG. 8. Plot of absorbance^{-1} *vs.* time. The data and symbols are the same as those in Fig. 5. The lines were calculated from [15].

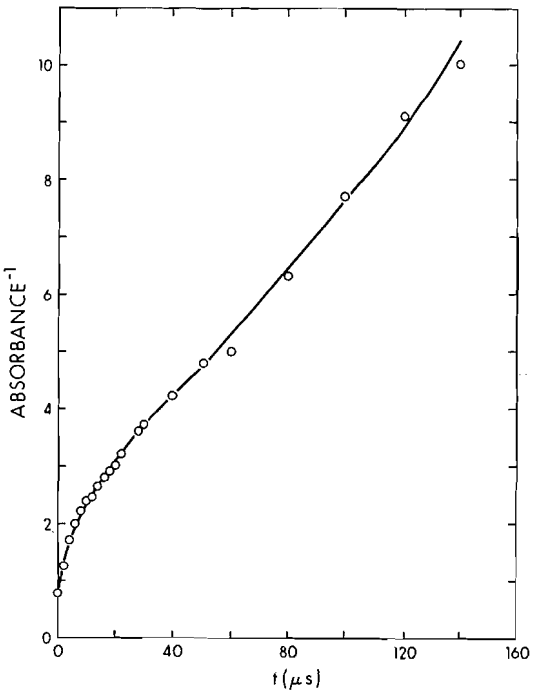

FIG. 9. Plot of absorbance^{-1} *vs.* time at 149 K. The data are the same as those in Fig. 6. The line was calculated from [15].

electrons that will undergo geminate neutralization but have not yet done so at time t, and a is a constant. The total electron concentration in the system would be:

$$[13] \qquad [e_{solv}^-]_{tot}^t = at^{-1/2} + [e_{solv}^-]_{fi}$$

where $[e_{solv}^-]_{fi}$ represents the free ions. The occurrence of a first order reaction, such as a reaction with the solvent or the pseudo first order [3], would cause the time dependence of the total electron concentration to be:

$$[14] \qquad [e_{solv}^-]_{tot}^t = \{at^{-1/2} + [e_{solv}^-]_{fi}\}e^{-kt}$$

where k is the first order decay constant and presumably equals $k_3[S]$.

In dipropyl ether neither the free ion yield nor the optical extinction coefficient of solvated electrons is known, so to test whether the observed absorbance decay was consistent with [14] a general form of the equation was used:

$$[15] \qquad \text{absorbance} = b(t^{-1/2} + c)e^{-kt}$$

where b and c are constants that depend on the temperature.

The decay at all temperatures did indeed agree with [15]. Using μs as the unit of t and arbitrarily

Can. J. Chem. Downloaded from www.nrcresearchpress.com by 210.87.254.5 on 09/05/12
For personal use only.

TABLE 1. Electron mobilities and liquid viscosities

Solvent	T(K)	u_e (cm^2/V s)	η (mP)	ηu_e
NH_3	240	0.0091[a]	2.5	0.023
Pr_2O	273	0.004[b]	5.2	0.021
H_2O	298	0.0020[c]	8.9	0.016
MeOH	298	0.003[d]	5.4	0.016[e]
EtOH	298	0.001_5[d]	10.8	0.016[e]

[a]Calculated from results of Burns (22).
[b]Present work.
[c]Reference 23.
[d]Estimated from ηu_e.
[e]Assumed.

taking $t = 0$ at the center of the pulse, the full curves in Figs. 5 and 6 were calculated from [15] with the following parameter values: $T = 273$, $bc = 0.36$, $c \gg 1$, $k = 0.64$; $T = 200$, $b = 0.17$, $c = 0.6$, $k = 0.036$; $T = 149$, $b = 0.97$, $c = 0.16$, $k = 0.0066$.

It should be noted that the observed absorbance decay at 200 K could be empirically divided into two simple first order portions (Fig. 5), and the decay at 149 K could be divided into three approximately first order portions (Fig. 6). Such a subdivision into a series of first order contributions has no theoretical significance. Furthermore, the decay constant obtained in this way for the solvated electron free ions may be too large due to incomplete separation of the geminate neutralization reaction.

$k(e_{solv}^- + SF_6)$ and the Electron Mobility

The value $k_5 = 4.5 \times 10^{10}\ M^{-1}\ s^{-1}$ at 273 K corresponds to a diffusion controlled reaction with the sum of the diffusion coefficients ($D_{SF_6} + D_e$) $= 12 \times 10^{-5}$ cm^2/s, assuming a reaction radius of 5 Å: $k = 4\pi DrN/1000$, where $N =$ Avogadro's number. The viscosity of propyl ether at 273 K is 0.5 cP (17), so one may assume $D_{SF_6} \approx 2 \times 10^{-5}$ cm^2/s, whence $D_e \approx 10 \times 10^{-5}$ cm^2/s. The electron mobility at 273 K is therefore $u_e \approx 0.004$ cm^2/Vs.

It is interesting that the product of the electron mobility and the liquid viscosity is approximately constant for the polar liquids ammonia, propyl ether, and water (Table 1). By assuming the product to have about the same value for the alcohols one obtains $u_e \approx 0.003$ cm^2/V s in methanol and 0.001_5 in ethanol at 298 K (Table 1). These values are five-fold larger than those estimated (18) from results of Fowles (19) and data from Conway (20). Thus the electron mobility in an alcohol at 298 K appears to be several-fold larger than that of the alkoxide ion. The same conclusion has been reported for higher alcohols (21).

The activation energy of [5] is 3.2 ± 0.3 kcal/mol, which is greater than that of viscosity, 1.9 kcal/mol (17).

The authors wish to express their gratitude to the staff of the Radiation Research Center for aid with the electronics.

1. A. S. NEWTON. J. Phys. Chem. **61**, 1485 (1957).
2. M. K. M. NG and G. R. FREEMAN. J. Am. Chem. Soc. **87**, 1635 (1965).
3. J. TIMMERMANS. Physico-chemical constants of pure organic compounds. Vol. 1. Elsevier, Amsterdam. 1950.
4. R. A. VERMEER. M. Sc. Thesis. University of Alberta, Edmonton, Alberta. 1972.
5. K. N. JHA, G. L. BOLTON, and G. R. FREEMAN. J. Phys. Chem. **76**, 3876 (1972).
6. F. Y. JOU and L. M. DORFMAN. J. Chem. Phys. **58**, 4715 (1973).
7. M. G. ROBINSON and G. R. FREEMAN. Can. J. Chem. **51**, 641 (1973).
8. R. M. LEBLANC and J. A. HERMAN. J. Chim. Phys. **63**, 1055 (1966).
9. K. BANSAL and S. RZAD. J. Phys. Chem. **74**, 2888 (1970).
10. G. R. FREEMAN and J. M. FAYADH. J. Chem. Phys. **43**, 86 (1965).
11. W. F. SCHMIDT and A. O. ALLEN. J. Chem. Phys. **52**, 2345 (1970).
12. G. R. FREEMAN. J. Chem. Phys. **46**, 2822 (1967).
13. M. G. ROBINSON and G. R. FREEMAN. J. Chem. Phys. **48**, 983 (1968).
14. E. D. STOVER and G. R. FREEMAN. J. Chem. Phys. **48**, 3902 (1968).
15. G. R. FREEMAN. Radiat. Res. Rev. **1**, 1 (1968).
16. G. R. FREEMAN. Int. J. Radiat. Phys. Chem. **4**, 237 (1972).
17. R. W. GALLANT. Physical properties of hydrocarbons. Vol. 2. Gulf Publishing Co. Houston, Texas. 1968.
18. J.-P. DODELET and G. R. FREEMAN. Can. J. Chem. **50**, 2667 (1972).
19. P. FOWLES. Trans. Faraday Soc. **67**, 428 (1971).
20. B. CONWAY. Electrochemical data. Elsevier Publishing Co. Amsterdam. 1952. p. 162.
21. A. V. RUDNEV, A. V. VANNIKOV, and N. A. BAKH. High Energy Chem. **6**, 416 (1972), Engl. trans.
22. D. S. BURNS. Adv. Chem. Ser. **50**, 82 (1965).
23. K. SCHMIDT and M. ANBAR. J. Phys. Chem. **73**, 2846 (1969).

Can. J. Chem. Downloaded from www.nrcresearchpress.com by 210.87.254.5 on 09/05/12
For personal use only.

Comment: On the Whiteway–Smith–Masson and Flory–Stockmayer Theories of Polymerization

R. F. T. STEPTO

Department of Polymer and Fibre Science, The University of Manchester Institute of Science and Technology, Manchester, England

Received July 11, 1973

An error in the Whiteway–Smith–Masson (W.S.M.) theory of random polymerization is noted. The application of the W.S.M. theory and the Flory–Stockmayer (F.S.) theory to experimental data is discussed, and no grounds for the rejection of the F.S. theory are found. A method of simulating the self-polymerization of RA_f monomers is proposed which should be capable of resolving differences between the two theories.

On note une erreur dans la théorie de la polimérisation au hasard développée par Whiteway–Smith–Masson (W.S.M.). On discute de l'application de la théorie W.S.M. et de la théorie de Flory–Stockmayer (F.S.) aux résultats expérimentaux et on ne trouve aucune raison de rejeter la théorie F.S. On propose une méthode pour simuler la polimérisation sur eux-mêmes de monomère RA_f et cette méthode devrait permettre de résoudre les différences entre les deux théories. [Traduit par le journal]

Can. J. Chem., **52**, 1188 (1974)

Recently a series of papers have been published by Whiteway, Smith, and Masson (W.S.M.) (1–4) which challenge the established Flory–Stockmayer (F.S.) theory of the distribution of molecular sizes in polycondensations (5–11). Both theories refer to reactions in which functional groups are of equal reactivity, and in which no intramolecular reaction occurs. In the F.S. theory the latter condition is relaxed when the gel point is reached. That is, in the self-polycondensation of RA_f monomers, when the extent of reaction $\alpha = 1/(f-1)$. In contrast, the W.S.M. theory perpetuates the misconception that gelation, or network formation occurs only when all the monomer units have combined to form a single molecule. That is, when $\alpha = 2/f$, this being the maximum reaction allowed. Such a growth towards a large single molecule before complete reaction ($\alpha = 1$) is contrary to the assumption of equal reactivity of the unreacted groups. Equal reactivity must require that the larger molecules grow at the expense of smaller molecules, and therefore that unlimited molecules, or gel, form before the combination of all molecules into a single species.

There has been much discussion concerning the W.S.M. theory, some unpublished and some published (12, 13). Quite rightly the arguments have been concerned with the basis of the theory itself rather than its ability to explain experimental data. However the latter aspect should not be neglected, and it is with the application of the W.S.M. and of the F.S. theories to experimental data that the present communication is concerned.

Whiteway, Smith, and Masson (2, 4) have shown that data on silicate melts are not consistent with the F.S. gel point, $\alpha = 1/(f-1)$. However, it may be noted that they are also not consistent with the W.S.M. concept of maximum reaction at $\alpha = 2/f$. The continuation of reaction beyond this point is attributed by Whiteway, Smith, and Masson to intramolecular reaction. Such reaction may well be significant, but if so the data cannot prove or disprove the F.S. theory. What should be tested is one of the later developments of the F.S. theory which account for ring formation, at least approximately (14–17).

Contrary to the statements of Whiteway *et al.* (1), the occurrence of a gel point in organic polymers and the effects of intramolecular reaction caused by the dilution of reactive groups, are well-documented (5, 8, 18–22). In general, with sufficient dilution, it is possible to delay gelation to beyond complete reaction ($\alpha = 1$), so that the gel point is not observed. Only in the limit of infinite concentration of reactive groups is the F.S. theory obeyed. Further, it has been shown (22) that the experimental gel point is the point at which insoluble polymer is first formed.

In view of the results with organic polymers it

Can. J. Chem. Downloaded from www.nrcresearchpress.com by 210.87.254.42 on 09/05/12
For personal use only.

would seem feasible that the properties of silicate melts are explicable in terms of the F.S. theory and any peculiarities of the systems (*e.g.* ease of ring formation, unequal reactivities).

It must be recognized that there is a basic difficulty in attempting to distinguish rigorously between the two theories on the basis of data from actual polymerizations as both are limiting theories in the sense that they neglect intramolecular reaction. However, it should be possible to simulate the polymerization of RA_f monomers with ring formation excluded, and to use the resulting distribution of molecular sizes to distinguish between them. Such a simulation could be conducted by having a large array of numbers each member of which represents a reactive —A group. If the polymerization of RA_3 monomers is being considered then numbers 1, 2, 3 are taken to represent the reactive groups of one monomer, 4, 5, 6 those of another, and so on. A pair of numbers is chosen randomly to represent a pair of groups about to react. A record of the pairs which have reacted previously is kept, and provided the groups about to react do not belong to the same molecule their reaction is allowed. In this way intramolecular reaction can be excluded. Once a pair has reacted it is removed from the population, and the polymerization continues by the choosing of a further pair of groups. Periodically, at chosen extents of reaction, the record of reactions is analyzed to find the distribution of molecular sizes.

To ensure that the results of such a simulation are statistically significant a large population (say 10^4 numbers) would be required, and the simulation would have to be repeated several times. A computer would be needed.

The preceding method of simulating a polymerization is offered as a means by which the distribution of molecular sizes can be calculated based on premises common to both theories, namely, equal reactivity (random choice of pairs of groups) and exclusion of intramolecular reaction. Provided the simulation is restricted to the range of values of α in which both theories predict only finite species ($0 \leqq \alpha < 1/(f-1)$), the results should show in an unbiased fashion which theory correctly describes the distribution of molecular sizes. This would be in contrast to some calculations and simulations attempted by Whiteway, Smith, and Masson (1), which were restricted to the point $\alpha = 2/f$.

1. S. G. WHITEWAY, I. B. SMITH, and C. R. MASSON. Can. J. Chem. **48**, 33 (1970).
2. C. R. MASSON, I. B. SMITH, and S. G. WHITEWAY. Can. J. Chem. **48**, 201 (1970).
3. S. G. WHITEWAY. Can. J. Chem. **48**, 1432 (1970).
4. C. R. MASSON, I. B. SMITH, and S. G. WHITEWAY. Can. J. Chem. **48**, 1456 (1970).
5. P. J. FLORY. J. Am. Chem. Soc. **63**, 3083 (1941).
6. P. J. FLORY. J. Am. Chem. Soc. **63**, 3091 (1941); **63**, 3096 (1941).
7. W. H. STOCKMAYER. J. Chem. Phys. **11**, 45 (1943).
8. P. J. FLORY. Chem. Rev. **39**, 137 (1946).
9. P. J. FLORY. J. Amer. Chem. Soc. **69**, 30 (1947), **74**, 2718 (1952).
10. W. H. STOCKMAYER. J. Polymer Sci. **9**, 69 (1952).
11. P. J. FLORY. Principles of polymer chemistry, Cornell Univ. Press, Ithaca, 1953. Chapt. IX.
12. M. GORDON and M. JUDD. Nature, **234**, 96 (1971).
13. C. R. MASSON, I. B. SMITH, and S. G. WHITEWAY. Nature, **234**, 97 (1971).
14. F. E. HARRIS. J. Chem. Phys. **23**, 1518 (1955).
15. H. L. FRISCH. Presented at 128th Meeting Amer. Chem. Soc. (Polymer Division), Minneapolis. 1955.
16. R. W. KILB. J. Phys. Chem. **62**, 969 (1958).
17. W. B. TEMPLE. Makromol. Chem. **160**, 277 (1972).
18. R. H. KIENLE, P. A. VAN DER MEULEN, and F. E. PETKE. J. Am. Chem. Soc. **61**, 2258, (1939); **61**, 2268 (1939); R. H. KIENLE and F. E. PETKE. J. Am. Chem. Soc. **62**, 1053 (1940); **63**, 481 (1941).
19. W. H. STOCKMAYER and L. L. WEIL. *In* Advancing fronts in chemistry. *Edited by* S. B. Twiss. Reinhold Publ. Corp., New York. 1945. Chapt. 6.
20. F. P. PRICE, J. H. GIBBS, and B. H. ZIMM. J. Phys. Chem. **62**, 972 (1958); F. P. PRICE. J. Phys. Chem. **62**, 977 (1958); B. H. ZIMM, F. P. PRICE, and J. P. BIANCHI. J. Phys. Chem. **62**, 979 (1958).
21. R. H. PETERS and R. F. T. STEPTO. *In* The chemistry of polymerisation processes. Monograph No. 20., Soc. Chem. Ind. London. 1965. p. 157.
22. R. F. BATES and G. J. HOWARD. J. Polymer Sci. Part C, **16**, 921 (1967).

Can. J. Chem. Downloaded from www.nrcresearchpress.com by 210.87.254.42 on 09/05/12
For personal use only.

Reply to Comment: On the Whiteway–Smith–Masson and Flory–Stockmayer Theories of Polymerization[1]

C. R. MASSON AND S. G. WHITEWAY

Atlantic Regional Laboratory, National Research Council of Canada, Halifax, Nova Scotia B3H 3Z1

Received November 1, 1973

A computer simulation of random polymerization reveals that the Flory–Stockmayer expression describes a model where functional groups are of equal reactivity and all chain and ring configurations are allowed. The Whiteway–Smith–Masson expression describes a model in which rings are formally forbidden by a technique that requires departure from the principle of equal reactivity. The apparent conflict between the two theories thus is resolved, and each appears to have application in describing various real systems.

Une simulation ordinateur de la polymérisation au hasard montre que l'équation de Flory–Stockmayer décrit un modèle dans lequel les groupes fonctionnels sont tous de réactivité égale et dans lequel toutes les chaines et toutes les configurations de cycle sont permises. Par ailleur l'équation de Whiteway–Smith–Masson décrit un modèle dans lequel les cycles sont prohibés d'une manière formelle par une technique qui dévie du principe de la réactivité égale de tous les groupes fonctionnels. On élimine ainsi les conflits apparents entre les deux théories et il semble que chacune permet de décrire divers systèmes réels. [Traduit par le journal]

Can. J. Chem., 52, 1190 (1974)

The preceding comment (1) serves to reveal a difference in concept and applicability between the Flory–Stockmayer (F.S.) theory and ours. The source of the difficulty is that in real systems it is impossible to satisfy simultaneously the requirements of (*a*) no rings and (*b*) equal reactivity of functional groups over the range $0 < \alpha < 2/f$, where α is the fraction of functional groups which have condensed. Thus in the computer simulation proposed by Stepto some pairs of groups chosen as candidates for reaction are declared unreacted when it is discovered they belong to the same molecule. Although this is necessary in order to preserve the characteristics of the model, it is obviously contary to the requirement of equal reactivity of groups.

In the F.S. theory, the use of α to denote the probability that a group has reacted implies that no restriction is imposed on the system and that therefore intramolecular condensation (including, it may be noted, self-condensation of groups on the same monomer or dimer) is *allowed*. Our method adheres to the principle of no ring formation and, it is now recognized, does so at the partial expense of the principle of equal reactivity. It is no longer surprising therefore that the two methods yield different results or that each appears to have application in describing various real systems.

Computer simulations similar to the one suggested by Stepto have been in progress in our laboratory for some time (2). Results for the weight fraction of monomer and dimer in the self-polymerization of RA_3, in the limit of an infinite population of groups, are shown in Fig. 1. The following points are observed: (*a*) in the region $0 < \alpha < 1/(f-1)$ the results agree with the F.S. expression rather than ours; (*b*) in the region $1/(f-1) < \alpha < 2/f$ the results lie intermediate between the two expressions. Agreement with the F.S. expression in the region $0 < \alpha < 1/(f-1)$ is a consequence of the fact that, for an infinite population, intramolecular condensation does not occur in this region.

Other simulations, details of which will be published separately, show that for an infinite number of groups, (*a*) the F.S. results can be reproduced over the entire range $0 < \alpha < 2/f$ when ring formation is *allowed* and (*b*) our result can be reproduced over the same range when an artifice is introduced which, in effect, prohibits the choice of functional groups on the same molecule as candidates for reaction, and thus forbids ring-formation.

Our result was derived to interpret the behavior of silicate melts and evolved from an

[1]NRCC No. 13784.

Can. J. Chem. Downloaded from www.nrcresearchpress.com by 210.87.254.105 on 09/05/12
For personal use only.

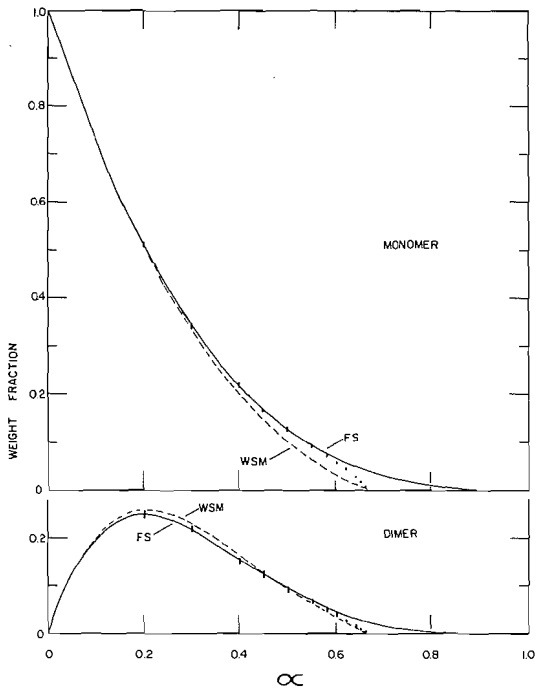

FIG. 1. Weight fraction of monomer (upper curve) and dimer (lower curve) for $f = 3$. Solid curves according to Flory–Stockmayer; dashed curves according to Whiteway, Smith, and Masson; the bars are the results of the computer simulation and their height represents the standard error.

earlier approach (3) in which silicate melts were discussed in terms of the sol and gel fractions required by the F.S. theory. Our expressions appear particularly useful for describing the features of silicate polymerization in the region approaching $\alpha = 2/f$. It is possible that, due to their polyelectrolyte nature, silicates exhibit a smaller tendency towards cyclization than uncharged organic polymers. This appears to be true also for phosphates.

Finally, it should be mentioned that we have never expressed the view that gelation occurs at $\alpha = 2/f$. Our theory predicts that, for a system in which ring formation is excluded, the probability of branching is $1/(f - 1)$ when $\alpha = 2/f$. But, as we have also pointed out (4), this is not within the physically realizable range of α allowed by our theory and cannot be equated with experimental gel points.

We are grateful to Dr. M. Falk who kindly allowed us to quote the results of his computer simulations prior to publication.

1. R. F. T. STEPTO. Can. J. Chem. This issue.
2. M. FALK and R. THOMAS. Unpublished results.
3. C. R. MASSON. J. Am. Ceram. Soc. **51**, 134 (1968).
4. S. G. WHITEWAY, I. B. SMITH, and C. R. MASSON. Can. J. Chem. **48**, 33 (1970).

Can. J. Chem. Downloaded from www.nrcresearchpress.com by 210.87.254.105 on 09/05/12
For personal use only.

Juvenile Hormone Analogs in Conifers. II.[1] Isolation, Identification, and Biological Activity of *cis*-4-[1′(*R*)-5′-Dimethyl-3′-oxohexyl]-cyclohexane-1-carboxylic Acid and (+)-4(*R*)-[1′(*R*)-5′-Dimethyl-3′-oxohexyl]-1-cyclohexene-1-carboxylic Acid from Douglas-fir Wood

I. H. ROGERS[2] AND J. F. MANVILLE[3]

Department of the Environment, Canadian Forestry Service, Western Forest Products Laboratory, Vancouver, British Columbia

AND

T. SAHOTA

Department of the Environment, Canadian Forestry Service, Pacific Forest Research Centre, Victoria, British Columbia

Received November 5, 1973

The petroleum ether extract from the whole-wood meal of a number of British Columbia Interior-Intermediate variety Douglas-fir trees have yielded two carboxylic acids (+)-todomatuic acid (**3***b*) and *cis*-dihydrotodomatuic acid (**4***b*) which as their methyl esters are potentially useful juvenile hormone analogs. These compounds possess the *R,R* and *R* stereoconfigurations, respectively. The configuration at C-1′ is opposite to that reported by others for "(+)-juvabione" isolated from *Abies balsamea* grown in Czechoslovakia. Whereas (+)-juvabione naturally occurs as and is the methyl ester of (+)-todomatuic acid (**4***b*), in this variety of Douglas-fir these compounds appear as the free acids. Results of biological assays on certain insects indicate that the methyl ester derivatives of these acids are effective ovicides and juvenilizing hormones.

L'extraction par l'éther de pétrole d'une farine de bois entier d'un certain nombre de sapin Douglas de la Colombie Britannique variété intérieure intermédiaire fourni deux acides carboxyliques soit l'acide (+)-todomatuique (**3***b*) et l'acide *cis*-dihydrotodomatuique (**4***b*) dont les esters méthyliques sont des analogues d'hormones juvéniles qui pourraient s'avérer utiles. Ces composés possèdent respectivement les stéréoconfigurations *RR* et *R*. La configuration en C-1′ est l'inverse de celle rapportée par d'autres pour la "(+)-juvabione" qui a été isolé de l'Abies balsamea cultivé en Tchécoslovaquie. Alors que la (+)-juvabione se retrouve dans la nature comme, et est, l'ester méthylique de l'acide (+)-todomatuique (**4***b*) ces composés existeraient dans le sapin de Douglas sous forme d'acides libres. Les résultats des essais biologiques sur certains insectes indiquent que les esters méthyliques dérivés de ceś acides sont des ovicides et des hormones juvéniles efficaces. [Traduit par le journal]

Can. J. Chem., **52**, 1192 (1974)

Although there is widespread current research activity by chemists interested in insect juvenile hormones, most efforts are directed towards the synthesis of analogs which mimic the activity of the naturally occurring compounds. Such substances may eventually have utility as third-generation insecticides, active against selected insect pests and with the advantage of full biodegradability. The natural occurrence of such compounds in wood of coniferous species and the biological implications of their presence to forestry has effectively been ignored since the discoveries of juvabione (**1***a*) and "dehydrojuvabione" (**2**) in balsam fir [*Abies balsamea* (L.) Miller] grown in North America (2) and Czechoslovakia (3) respectively. This also applies to the much earlier isolation (4) of (+)-todomatuic acid (**1***b*) from bisulfite-treated pulp oil of a Japanese fir (*Abies sachalinensis* Schmidt).

This paper describes the structural identification and biological activity of the methyl esters of two compounds, *cis*-dihydro- (**3***b*) and (+)-todomatuic (**4***b*) acids present in the whole wood of Interior-Intermediate variety (9) Douglas-fir

[1]Presented at the Northwest Regional Meeting of the American Chemical Society at Corvallis, Oregon, June, 1972. A preliminary report (1) has been published.

[2]Present address: Pacific Environment Institute, West Vancouver, B.C.

[3]To whom inquiries should be sent.

Can. J. Chem. Downloaded from www.nrcresearchpress.com by 210.87.254.42 on 09/05/12
For personal use only.

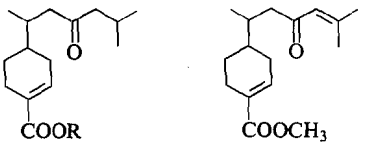

1 2

a R = CH_3
b R = H

trees [*Pseudotsuga menziesii* var. *glauca* (Beissn.) Franco] grown in British Columbia.

Subsequent to the completion of our own work, two preliminary communications by Sakai and Hirose (5) have appeared. Their work confirms our assignments[1] of structure and stereoconfiguration for **3***b* and **4***b*. Moreover they have reversed the [*R*,*S*] stereoconfigurational assignments (6, 7) of "natural (+)-juvabione" back to the [*R*,*R*] stereoconfiguration, as originally assigned by Nakazaki and Isoe (8). We accept this correction pointing out that the names assigned to those compounds isolated by others (3) from "*Abies balsamea* grown" in Czechoslovakia and the naming of the four stereoisomers of juvabione, synthesized by Pawson and co-workers (6, 7), are incorrect. It is now evident that Bowers and co-workers (2) isolated the compound responsible for the "paper factor" and named it (+)-juvabione. They correctly identified it as the methyl ester of (+)-todomatuic acid which was subsequently and correctly assigned the *R*,*R* stereoconfiguration (8). The compound isolated by Cerny and co-workers (3) and identified as the *R*,*S* isomer by Pawson and co-workers (7) was mistakenly named and assumed to be (+)-juvabione. Evidently it is (+)-epijuvabione [*R*,*S*]. Thus there must exist in nature at least two epimers of juvabione the *R*,*R* form being found in North America and the *R*,*S* form in Europe.

Sakai and Hirose (5) also reported the finding of other related sesquiterpenes,[4] including the methyl ester analogs of **3***b* and **4***b*, in the volatile oil of the whole wood from a Coastal variety of Douglas-fir grown in British Columbia.

Isolation

The petroleum ether soluble fraction from an Interior-Intermediate variety of Douglas-fir whole-wood meal was a mobile, pale-yellow oil. This was partially separated by ion-exchange chromatography on DEAE-Sephadex A-25 according to the method of Zinkel and Rowe (10), resulting in the removal of the neutrals fraction from the mixed resin and fatty acids. Separation of the resin acids from the fatty acid methyl esters was achieved by partial esterification of the acidic fraction with methanol and sulfuric acid. Gas chromatographic analysis revealed the presence of two major components (compounds **3***a* and **4***a*) which did not correspond to any of the common fatty acids (11). These two compounds were recovered as a pair by use of the familiar Girard-T reaction and were clearly the methyl esters of two keto acids. The keto esters were finally separated from each other by preparative thick-layer argentative chromatography and were colorless oils which distilled easily under reduced pressure.

Compound 3a

The more abundant compound, which emerged first from the gas chromatographic column, had the empirical formula $C_{16}H_{28}O_3$ as determined by elemental analysis and mass spectrometry. The i.r. spectrum contained a broad unresolved band in the region 1730 to 1700 cm^{-1}, apparently arising from an ester and a ketone function. No signals attributable to hydroxyl or olefinic groupings were observed.

The p.m.r. spectrum measured at 220 MHz [$(CD_3)_2CO$] (Fig. 1) was most informative. The numbers and magnitudes (quintet, *ca.* 4 Hz) of the vicinal couplings, observed in the lowest field multiplet and assigned to H_1, indicated that the carboxylic acid methyl ester group was in an axial orientation. Thus, it is most probable that **3***a* has a *cis* configuration with the bulky side chain in an equatorial position. It unfortunately was not possible to confirm this assumption by observing the couplings in H_4, since H_4 was hidden amongst the ring hydrogens; however, this was proven by chemical synthesis (*vide infra*). The two methylene protons, resonating at δ 2.41 and 2.18, assigned to $H_{2'_1}$ and $H_{2'_2}$, respectively, were observed to be magnetically nonequivalent, indicating that the asymmetric center was adjacent. The remaining side-chain methylene protons ($H_{4'_1}$ and $H_{4'_2}$), also deshielded by a carbonyl group, resonated together as a doublet, indicating the remoteness of the asymmetric

[4]It was most fortuitous that no chemical transformations of these labile molecules occurred inside these logs that were exposed for more than one year while enroute to or part of British Columbia's Expo '70 pavilion at Osaka.

Can. J. Chem. Downloaded from www.nrcresearchpress.com by 210.87.254.42 on 09/05/12
For personal use only.

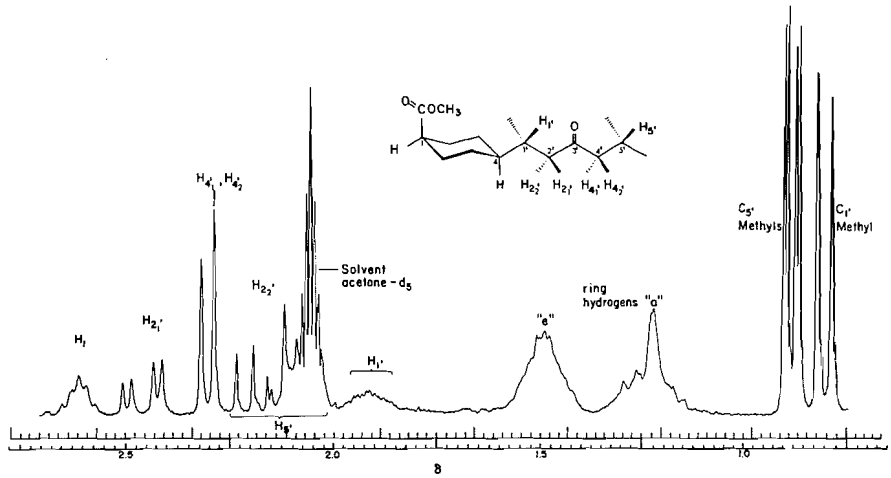

FIG. 1. Partial 220 MHz p.m.r. spectrum of **3***a* in $(CD_3)_2CO$ solution.

center. The two methine protons $H_{1'}$ and $H_{5'}$ were assigned on the basis of the magnitude of their observed and estimated vicinal couplings. Nuclear magnetic double resonance experiments (100 MHz) confirmed that $H_{1'}$ was at δ 1.95, $H_{5'}$ at δ 2.13, and that the C-1′ methyl group protons resonated at δ 0.81. Interestingly, the two methyl groups on C-5′ were magnetically nonequivalent, possibly due to the asymmetric center at C-1′. This nonequivalence indicated to us that this molecule in solution adopts a conformation in which these methyl groups approach more closely C-1′ than does C-4′.

Much structural information was gleaned from consideration of the mass spectral fragmentation behavior of the ester which included an abundant crop of metastable ions. The molecular ion (*m/e* 268) underwent homolytic cleavages in the carbomethoxy group to yield satellite ions of low abundance at *m/e* 237 (M − 31) and 209 (M − 59). Fragments at *m/e* 226 (M − 42), 211 (M − 57), 183 (M − 85), and the base peak at *m/e* 168 (M − 100) were associated with various cleavages within an eight-carbon side chain containing a carbonyl group. Further evidence supporting the presence of this structural feature includes an abundant fragment (twin base peak) at *m/e* 127 comprising the entire side chain and various ionic species in which side-chain cleavages are combined with scissions within the carbomethoxy group (*m/e* 179, 151, 136, 123, and 108). The interrelationships of the various cleavage products are rationalized in Scheme 1 in which structure **3***a* has been assumed. Although no deuterium labelling studies were performed, most of the cleavages indicated were supported by the presence of the appropriate metastable ions.

The mass spectral fragmentation of "juvabione" (epijuvabione) has been discussed by Cerny and co-workers (3). Besides the molecular ion *m/e* 266, abundant fragments were observed at *m/e* 207, 177, 167, 166, 127, 85, 79, 59, and 57. These were all present in the spectrum of **3***a* except that the first five species listed were displaced by two additional mass units.

Base catalyzed epimerization of compound **3***a* yielded a mixture of two compounds in the ratio 1 to 2. Upon methylation the less plentiful component eluted faster from the g.l.c. column and had the same retention time as the starting material. It was therefore anticipated that **3***b* has the side chain in the *cis* configuration relative to the carboxyl group, since *cis* isomers in general have shorter retention times than *trans* isomers and epimerization generally favors formation of the more thermodynamically stable *trans* form.

Hydrogenation of an authentic sample of "(±)-juvabione" proceeded smoothly and the reaction product contained two components in the ratio 3 to 7, with retention times identical with those of the two components arising from the epimerization reaction. Application of the epimerization reaction to this mixture caused a shift in concentration to 1 to 4 in favor of the isomer with longer retention time. This was

Can. J. Chem. Downloaded from www.nrcresearchpress.com by 210.87.254.42 on 09/05/12
For personal use only.

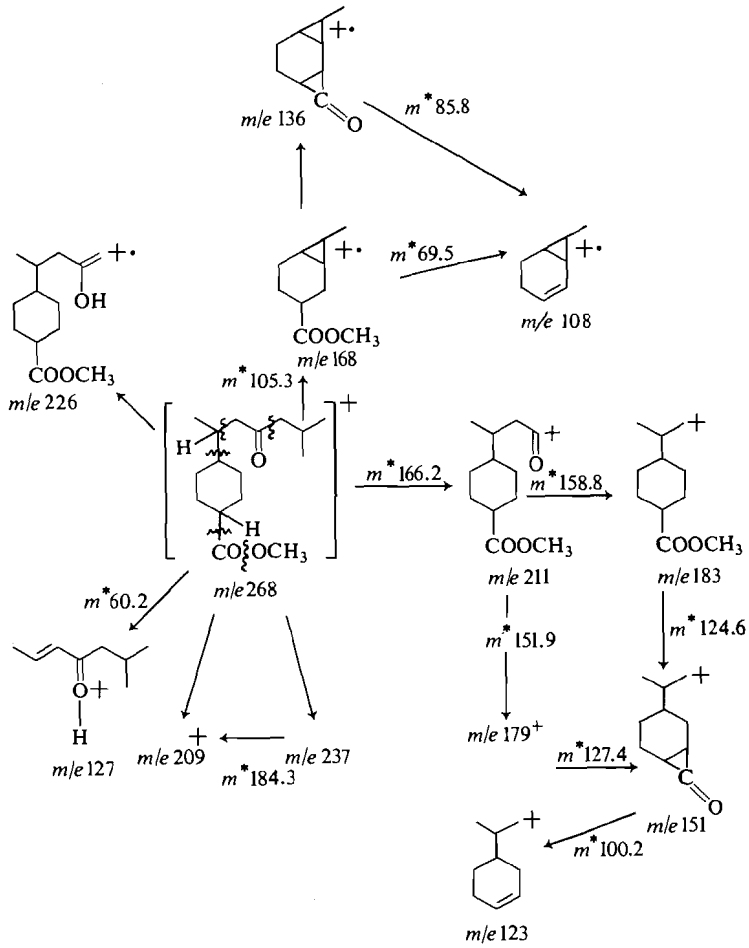

SCHEME 1

considered proof that **3***b* contains the juvabione skeleton and that the side chain is arranged *cis* to the carboxyl group.

The optical rotary dispersion (o.r.d.) curve measured on compound **3***a* is illustrated in Fig. 2. The negative Cotton effect was quenched very slowly in the presence of mineral acid, indicating a considerable degree of steric hindrance in the neighborhood of the carbonyl group. Of major significance was the observation that the mixture of epimers, derived from **3***b* by treatment with base, possessed the o.r.d. curve identical in shape and amplitude with that of the starting material. This can only happen if the point of attachment of the side chain is the 4 position with respect to the carboxyl group, in which case this center lies in a plane of symmetry. We therefore ascribe the following structure to **3***b* which may be described

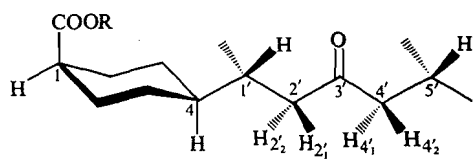

3

a R = CH_3

b R = H

as the *cis*-dihydro analog of (+)-todomatuic acid and is *cis*-4-[1′(*R*)-5′-dimethyl-3′-oxohexyl]cyclohexane-1-carboxylic acid. It is the first example of a naturally occurring hydrogenated analog of (+)-juvabione.

Compound 4a

This compound had the empirical formula $C_{16}H_{26}O_3$ as determined by elemental analysis

Can. J. Chem. Downloaded from www.nrcresearchpress.com by 210.87.254.42 on 09/05/12
For personal use only.

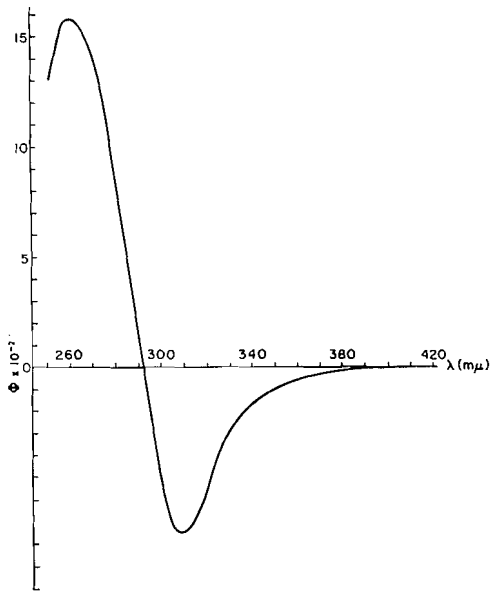

FIG. 2. Optical rotatory dispersion curve for **3***a*.

and mass spectrometry. The p.m.r. spectrum indicated the presence of a trisubstituted olefinic double bond, a methyl ester, two terminal methyls (isopropyl) and one other secondary methyl group. The mass spectrum contained a series of prominent fragments similar to those reported by other authors for juvabione (2) and its various diastereoisomers (3, 7), and it was thus tempting to consider that **4***a* is the parent unsaturated analog of **3***a*.

Hydrogenation of **4***a* yielded a mixture of *cis*- and *trans*-dihydroisomers, the o.r.d. curve of which was identical with that observed for **3***a*. Thus these two compounds isolated from Douglas-fir have the identical configuration at C-1′. The structural elucidation of **4***b* was completed by measuring the c.d. curve of its methyl ester (**4***a*) which was identical to that reported by Pawson *et al.* (7) for "(+)-epijuvabione" (*R*,*R*). It should be noted (*vide infra*) that the corrected (5) name for this *R*,*R* (**4***b*) isomer is (+)-todomatuic acid and not (+)-epitodomatuic acid (7). Compound **4***b* is therefore (+)-4(*R*)-[1′(*R*)-5′-dimethyl-3′-oxohexyl]-1-cyclohexene-1-carboxylic acid.

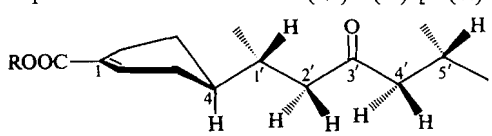

4

a R = CH_3

b R = H

Bioassays

The existence of these juvabione-related compounds in Douglas-fir, the host tree for the Douglas-fir beetle (*Dendroctonus pseudotsugae*), coupled with the variability in the resistance by these trees to beetle attack, prompted us to test **3***a* for possible female sterilizing effects. Certain juvenile hormone analogs have been shown (12) to cause female sterility in some insects; however, in this case there was an appreciable *increase* in fecundity of treated beetles (Table 1). A number of other juvenile hormone analogs have caused similar effects on Douglas-fir beetles tested at the Pacific Forest Research Centre. However the same juvenile hormone analogs, when made available to larval stages of Douglas-fir beetles by direct application to the phloem, interfere with the larval development and cause appreciable larval mortality. Thus, the result of the present experiments, where **3***a* was applied only to female parent adults, does not necessarily mean that this compound is not involved in reducing the brood production of Douglas-fir beetles in Douglas-fir trees. Therefore, **3***a* will be tested for its activity against all life-history stages of Douglas-fir beetles. Testing of the naturally occurring free acids (**3***b* and **4***b*) will also be undertaken to ascertain if esterification altered the activities of these substances. Thujic acid is more active as a juvenile hormone analog than its methyl ester (13). It is anticipated that the free acids present in Douglas-fir wood will also be more active and therefore effect a diminished brood production of Douglas-fir beetles.

Tests with the eggs of *Christoneura fumiferana*, a lepidopteran pest, demonstrated that **3***a* reduced the percentage hatch of these eggs (Table 1).

In *Tenebrio molitor*, application of 0.25 μl/pupa of **4***a* caused morphogenetic deformity in 90% of the adults emerging from the treated pupae. Similar doses of the methyl ester of (+)-todomatuic acid resulted in 80% of the adults being deformed. Thus these two compounds were very similar in their activity. Compound **3***a* was not quite as active, causing deformities in only 60% of the adults when applied at the above dosage. When tested[5] on

[5]C. M. Williams. Private communication.

Can. J. Chem. Downloaded from www.nrcresearchpress.com by 210.87.254.42 on 09/05/12
For personal use only.

TABLE 1. Bioassay results

Compound	Dose/insect or egg mass	Test material (insect or eggs)	No. of observations	Type of activity tested	Quantitative expression of activity
4*a**	0.25 µl	*T. molitor* pupae	10	Morphogenetic	80% deformity
4*a*	0.25 µl	*T. molitor* pupae	20	Morphogenetic	90% deformity
3*a*	0.25 µl	*T. molitor* pupae	20	Morphogenetic	60% deformity
3*a*	10 µg	*C. fumiferana* eggs	264	Ovicidal	0% reduction in egg hatch
3*a*	50 µg	*C. fumiferana* eggs	260	Ovicidal	80% reduction in egg hatch
3*a*	100 µg	*C. fumiferana* eggs	254	Ovicidal	82% reduction in egg hatch
3*a*	100 µg†	*D. pseudotsugae* adults	9 pairs	Female sterility	81% *increase* in fecundity over the controls

*Methylated (CH_2N_2) sample of natural (+)-todomatuic acid (**4***b*).
†Results for smaller doses are not reported because the highest doses used in these experiments failed to produce any female sterility.

Pyrrhocoris apterus, 0.5 ± 0.2 µg of **3***a* and 0.6 ± 0.2 µg **4***a* per insect caused 50% morphogenetic deformity. Similar effects were produced[5] by 10 µg of **4***a* on *Oncopeltus fasciatus*. Both compounds were ineffective[5] when applied to the lepidopteran pupae of *Manduca sexta* and *Antheraea polyphemus*. Juvabione has been shown to be effective on *P. apterus*, *O. fasciatus* (14), and *T. molitor* (15). Thus both compounds reported in this paper show typical juvabione-type activities.

Results of the biological assays indicate that the methyl ester derivatives of these acids are effective ovicides and juvenilizing hormones. Moreover, the results also indicate a profound selectivity in their action on the various insects tested. The naturally occurring Douglas-fir wood acids may have practical significance in terms of being able to control insect pests selectively.

Experimental

Most p.m.r. spectra were determined in deuteriochloroform using a Varian HA-100 spectrometer with tetramethylsilane as internal standard. Also, the p.m.r. spectrum of **3***a* was obtained in acetone-d_6 and $CDCl_3$ at the Canadian 220 MHz Centre, Ontario Research Foundation, Sheridan Park, Ont. Mass spectra were recorded in the Department of Chemistry and Chemical Engineering, University of Saskatchewan, using an AEI-MS-12 spectrometer. Samples for i.r. spectra were prepared as liquid films on the surface of KBr disks and were recorded on a Perkin-Elmer 521 spectrophotometer. The o.r.d. curves were measured on a JASCO Model ORD/UV-5 spectropolarimeter. Circular dichroism (c.d.) measurements were made with a JASCO J-20 automatic recording spectropolarimeter calibrated against a standard solution of (+)-10-camphorsulfonic acid. These two instruments were kindly made available to us by the Departments of Biochemistry and Chemistry, respectively, of the University of British Columbia. Elemental analyses were conducted by M-H-W Laboratories, Inc., Garden City, Mich. Gas–liquid chromatographic analyses were performed on a Hewlett Packard Model 7620A equipped with flame ionization detector. The column used was 6 ft × 1/8 in. o.d. stainless steel packed with 10% EGSS-X on 100–120 mesh Gas Chrom P purchased from Applied Science Laboratories, Inc. The column was held isothermally at 185°. The nitrogen carrier-gas flow rate was 48 ml/min. The injector port was maintained at 270°.

Isolation and Purification

A 12-in.-diameter butt log was obtained from a 164-year-old Interior-Intermediate variety Douglas-fir tree grown near Savona, British Columbia. The tree was felled in late May, 1971. Debarked whole wood was air dried and ground in a Wiley mill to pass a 3-mm screen. The wood meal (6420 g, air-dry) was extracted 24 h in an all-glass Soxhlet apparatus with petroleum ether (b.p. 65–110°). Recovered 56.05 g yellow oil (yield 1.60% on oven-dry wood). Methylation of an aliquot with diazomethane followed by g.l.c. showed the presence of fatty acids, resin acids and two unknown major components ($R_{\text{methylstearate}}$ 2.42 and 6.00, respectively) (11). The oil was redissolved in ether–methanol (9:1) and chromatographed on a column of DEAE-Sephadex-A25 according to an established procedure (10). Elution with the starting solvent yielded a neutrals fraction (30.45 g).[6] Saturation of this solvent with carbon dioxide followed by further elution of the column yielded a mixed acid fraction (23.82 g, yield 0.68% on oven-dry wood). This fraction was treated under reflux in methanol (1100 ml) containing H_2SO_4 (20 ml) for 1 h. The solution was neutralized with NaOH and evaporated to dryness under reduced pressure. Water (500 ml) was added to the residue,

[6]Detailed g.l.c. examination of the neutrals fraction, following Sephadex-A25 chromatographic separation, revealed two very minor peaks with the retention times corresponding to **3***a* and **4***a*. AGC-MS was not available for confirmation. The amount represented by these peaks would, however, be in the range 0.001–0.0001% of oven-dry wood, whereas **3***b* and **4***b* are major extractives and are as abundant as the resin or fatty acids (11). Unfortunately Sakai and Hirose (5) did not list relative amounts for these and related compounds isolated in their studies.

Can. J. Chem. Downloaded from www.nrcresearchpress.com by 210.87.254.42 on 09/05/12
For personal use only.

Can. J. Chem. Downloaded from www.nrcresearchpress.com by 210.87.254.42 on 09/05/12
For personal use only.

p*H* adjusted to 10, and the fatty acid ester fraction extracted with petroleum ether. Yield was 6.415 g. Analysis by g.l.c. confirmed the presence of **3***a* and **4***a*. This fraction was treated under reflux 1.5 h with Girard's T reagent (3 g), acetic acid (5 ml), and ethanol (50 ml) and the reaction mixture diluted with water and extracted three times with ether. The aqueous phase was then acidified with HCl to p*H* 2, heated on the steam cone 10 min to decompose the complex, and the mixture (**3***a* and **4***a*, 2:1) of two keto esters recovered by ether extraction (yield 1.45 g). Separation was achieved at about 40% recovery by preparative thick-layer chromatography on silica gel impregnated with 12% silver nitrate. Thick-layer plates were developed in chloroform, sprayed with Rhodamine-6G for band visualization, and the bands scraped off and extracted with chloroform. The individual esters were finally purified by reduced-pressure distillation using a hot oil bath (b.p. 150° at 0.5 mm Hg).

Compound 3a

Compound **3***a* was a colorless oil, b.p. 150 °C at 0.5 mm, $[\alpha]_D^{23}$ (*c* 1.0 $CHCl_3$) $\simeq$ 0°. The o.r.d. (*c* 1.0, MeOH, 23°) $[\Phi]_{350}$ −107, $[\Phi]_{308}$ −749, $[\Phi]_{292}0$, $[\Phi]_{260}$ +1584, and $[\Phi]_{230}$ +780°; molecular amplitude −23.3. Addition of 1 drop HCl gave rise to 31% quenching of amplitude of Cotton effect after 70 min. The u.v$_{max}$ showed no hydroxyl or olefinic bands, 1700–1730 (unresolved carbonyl and ester bands) cm^{-1}. The p.m.r. (220 MHz, $CDCl_3$) δ 3.66 (3H, singlet, methyl ester), 2.61 (1H, quintet, $J \simeq 4$ Hz, H_1), 2.41 (1H, quartet, $J_{2'_1,2'_2} = 15.8$ Hz, $J_{2'_1,1'_1} = 4.5$ Hz, $H_{2'_1}$), 2.26 (2H, doublet, $J_{vic} = 6.7$ Hz, $H_{4'_1}$ and $H_{4'_2}$), 2.41 (1H, quartet, $J_{2'_1,2'_2} = 15.8$ Hz, $J_{2'_1,1'_2} = 9.0$ Hz, $H_{2'_2}$), 2.13 (1H, multiplet, $H_{5'}$), 1.95 (1H, multiplet, $H_{1'}$), 1.5 (5H, broad band, ring protons), 1.2 (4H, broad band, ring protons), 0.91_4 (3H, doublet, $J = 6.7$ Hz, C-5′ methyl), 0.90_9 (3H, doublet, $J = 6.7$ Hz, C-5′ methyl), and 0.83 (3H, doublet, $J = 6.7$ Hz, C-1′ methyl). Mass spectrum (*m/e*) 268(4%)[M], 237(8)[M − 31], 211(50) [M − 57], 209(5)[M − 59], 168(100)[M − 100], 179(20), 169(26), 151(18), 137(22), 136(53), 133(15), 127(100), 109(58), 108(94), 85(34), 79(15), 69(12), 67(34), 57(70), 43(18), and 41(46). Metastable ions observed are listed in Scheme 1.

Anal. Calcd. for $C_{16}H_{28}O_3$ (mol. wt. 268): C, 71.64; H, 10.44; O, 17.91. Found (268, mass spectrum): C, 71.85; H, 10.59; O, 17.68.

Epimerization of Compound 3a

Compound **3***a* (25 mg) was epimerized by treatment under reflux (1 h) with Na metal (20 mg) in methanol (2 ml). Upon cooling, a solution of KOH (150 mg) in water (1 ml) was added to the reaction flask and refluxing continued an additional 3 h. The methanol was removed by distillation, the residue acidified with HCl, and the product extracted into ether. After esterification with excess diazomethane, g.l.c. analysis showed two peaks (R_t 583 and 810 s) in the ratio 1 to 2.

Hydrogenation and Epimerization of "(±)-juvabione"

A standard sample of "(±)-juvabione" (48 mg) was dissolved in methanol (9 ml) in the presence of palladium-on-charcoal (10% Pd, 90 mg). Hydrogenation was conducted at room temperature at 100 p.s.i. in a Parr bomb for 3 h. After removal of the catalyst by filtration, the product was recovered. Gas–liquid chromatography showed complete reaction with two products (R_t 564 and 815 s) in the ratio 3 to 7 (compound **3***a*, R_t 570 s). The reduction product (50 mg) was epimerized as described above to yield a mixture of the same two compounds but in a different ratio (1 to 4).

Compound 4a

Compound **4***a* was a colorless oil, b.p. 150° at 0.5 mm, $[\alpha]_D^{23}$ (*c* 1.01 $CHCl_3$) + 65.9°. The o.r.d. (*c* 1.5 and 0.3, methanol, 23°) $[\Phi]_{400}$ +355, $[\Phi]_{340}$ +443, $[\Phi]_{315}$ +320, $[\Phi]_{255}$ +3260, $[\Phi]_{240}$ +3901. The c.d. (*c* 1.96, methanol, 23°) $[\Phi]_{330}$ O, $[\Phi]_{290}$ −994, $[\Phi]_{262}$ O, $[\Phi]_{230}$ +2686, $[\Phi]_{215}$ +7253, $[\Phi]_{205}$ +5642. The p.m.r. (100 MHz) δ 6.96 (1H, multiplet, H_2) 3.72 (3H, singlet, methyl ester), 0.90 (6H, doublet, $J = 6$ Hz, C-5′ methyls), 0.86 (3H, doublet, $J = 6$ Hz, C-1′ methyl), 2.8–1.1 (13H). Mass spectrum (*m/e*): 266(3%) [M], 234(13.5) [M − 32], 206(6) [M − 60], 167(21) [M − 99], 166(24) [M − 100], 139(19), 135(14), 134(100), 127(12.5), 107(29), 105(14), 91(18), 85(27), 79(47), 77(26), 69(7), 67(10), 57(15), 43(17), and 41(20).

Anal. Calcd. for $C_{16}H_{26}O_3$ (mol. wt. 266): C, 72.18; H, 9.77; O, 18.04. Found (266, mass spectrum): C, 72.35; H, 9.86; O, 18.24.

Hydrogenation of 4a

Compound **4***a* was hydrogenated as described above for "(±)-juvabione". Gas–liquid chromatography showed complete reaction with two products (R_t 568 and 812 s) in the ratio 3 to 8. The o.r.d. curve of this mixture was the same as that observed for compound **3***a*.

Bioassays

Bioassays were mainly conducted on insects which have been routinely used (14, 15) by others for testing morphogenetic activity of juvabione. Insects included in this group were *P. apterus*, *O. fasciatus*, *A. polyphemus*, *M. sexta* (14), and *T. molitor* (15). Tests were also conducted on adult female, *D. pseudotsugae* for possible sterilizing and ovicidal effects, and on eggs of *C. fumiferana* for possible ovicidal effects.

Test compounds were delivered to the insects or egg masses in acetone solution. Doses of test compounds delivered to various insects are listed in bioassay results or in Table 1. For testing morphogenetic activity of these compounds, methods described by Bowers and Thompson (15) and Slama and Williams (14) were used. When treated insects moulted into the next instar, percentage morphogenetic deformity was determined and compared to controls. In *D. pseudotsugae*, test material was delivered to adult females. The number of eggs laid per female and percentage hatching of eggs was determined. In *C. fumiferana*, test material was applied to egg masses and their percentage hatch was recorded.

We wish to thank B. A. Pawson for a sample of "(±)-juvabione", W. S. Bowers for a sample of natural (+)-todomatuic acid, and A. Retnakaran, of the Insect Pathology Research Institute, for testing **3***a* on the eggs of *C. fumiferana*.

1. I. H. Rogers and J. F. Manville. Can. J. Chem. **50**, 2380 (1972).
2. W. S. Bowers, H. M. Fales, M. J. Thompson, and E. C. Uebel. Science, **154**, 1020 (1966).

3. V. CERNY, L. DOLEJS, L. LABLER, F. SORM, and K. SLAMA. Coll. Czech. Chem. Commun. **32**, 3926 (1967).
4. R. TUTIHASI and T. HANAZAWA. J. Chem. Soc. (Japan), **61**, 1041 (1940); Chem. Abstr. **37**, 258 (1943).
5. T. SAKAI and Y. HIROSE. Chem. Lett. (Japan), 491 (1973); 825 (1973).
6. J. F. BLOUNT, B. A. PAWSON, and G. SAUCY. J. Chem. Soc. Chem. Commun. 715 (1969).
7. B. A. PAWSON, H. C. CHEUNG, S. GURBAXANI, and G. SAUCY. J. Am. Chem. Soc. **92**, 336 (1970).
8. M. NAKAZAKI and S. ISOE. Bull. Chem. Soc. (Japan), **36**, 1198 (1963).
9. E. VON RUDLOFF. Can. J. Bot. **50**, 1025 (1972).
10. D. F. ZINKEL and J. W. ROWE. Anal. Chem. **36**, 1160 (1964).
11. I. H. ROGERS, A. G. HARRIS, and L. R. ROZON. Can. For. Serv. Western For. Prod. Lab. Inf. Rep. VP-X-57 (revised), Vancouver, B.C. (1972).
12. P. MANSER, K. SLAMA, and V. LANDA. Nature, **219**, 395 (1968).
13. G. M. BARTON, B. F. MACDONALD, and T. SAHOTA. Can. For. Serv. Bi-Mon. Res. Notes, **28** (4) 22 (1972).
14. K. SLAMA and C. M. WILLIAMS. Biol. Bull. **130**, 235 (1966).
15. W. S. BOWERS and M. J. THOMPSON. Science, **142**, 1469 (1963).

Can. J. Chem. Downloaded from www.nrcresearchpress.com by 210.87.254.42 on 09/05/12
For personal use only.

Surface Area Effects on the Sorption of Hydrogen by Palladium[1]

MICHAEL J. B. EVANS

Department of Chemistry and Chemical Engineering, Royal Military College of Canada, Kingston, Ontario K7L 2W3

Received September 6, 1973

Pressure–composition isotherms for dilute solutions of hydrogen in palladium have been measured at temperatures between 100 and 240 °C at pressures of up to 1000 Torr using a conventional volumetric technique. For palladium foil the isotherms are consistent with data over lower temperature ranges and with existing theoretical isotherms. With samples having appreciable surface area, however, a higher sorptive capacity is found which, it is suggested, is due to the formation of a layer of adsorbed hydrogen on the metal surface. It is demonstrated that correction can be made for this effect, to some extent, giving better agreement between the experimental data and the theoretical isotherm.

The variation of partial molar enthalpy of absorbed hydrogen with hydrogen content is also affected by this surface phenomenon, although the data available at present are not sufficiently accurate for a detailed discussion.

Les isothermes de pression–composition pour des solutions diluées d'hydrogène dans du palladium ont été mesurées à des températures entre 100 et 240 °C et des pressions allant jusqu'à 1000 Torr à l'aide d'une technique volumétrique classique. Pour la lame de palladium les isothermes sont compatibles avec les données pour des intervalles de températures plus basses et avec les isothermes théoriques existant. Avec des échantillons ayant une surface appréciable, cependant, une capacité d'adsorption supérieure est trouvée qui, croit-on, est due à la formation d'une couche d'hydrogène absorbé sur la surface du métal. Il est montré qu'une correction, dans une certaine mesure, peut être faite pour cet effet, donnant un meilleur accord entre les données expérimentales et les isothermes théoriques.

La variation de l'enthalpie molaire partielle de l'hydrogène adsorbé avec la teneur en hydrogène est aussi influencée par le phénomène de surface, bien que les données disponibles actuellement ne sont pas suffisamment précises pour une discussion détaillée.

[Traduit par le journal]

Can. J. Chem., **52**, 1200 (1974)

Introduction

The palladium + hydrogen system has been the most extensively studied of all metal + hydrogen systems. Despite the attention the system has received, there are a number of aspects of its behavior that are not clearly understood. This, plus the fact that increasing use is being made of palladium and palladium alloy membranes to produce high purity hydrogen in industry, accounts for the continued interest in the system.

At low hydrogen concentrations pressure–composition isotherms (1–6) obey Sieverts' law reasonably well, the amount of hydrogen absorbed by the metal being proportional to the square root of the pressure, suggesting that hydrogen is in a dissociated state in the metal. Magnetic (7) and electrical properties (8) of the system lead to the conclusion that the hydrogen is dissociated into protons, the electrons from the hydrogen being accommodated in the unfilled d-band of the metal. Some doubt has, however, been expressed concerning the latter conclusion (9).

Deviations from Sieverts' law as the concentration of absorbed hydrogen increases can be explained if there is an attractive interaction between the absorbed species. This assumption is used in deriving Lacher's equation (10), which, if it is also assumed that the maximum hydrogen content corresponds to the hydride PdH, can be expressed in the form

$$[1] \qquad \frac{1}{2}\ln p = \ln\left(\frac{r}{1-r}\right) + A + \frac{Br}{T}$$

where r is the amount of hydrogen absorbed, expressed as the atomic ratio H/Pd, in equilibrium with hydrogen gas at pressure p. A is a temperature dependent parameter and B a constant proportional to the attractive interaction between

[1]Presented, in part, at the 56th Canadian Chemical Conference, Montreal, June 1973.

Can. J. Chem. Downloaded from www.nrcresearchpress.com by 210.87.254.40 on 09/05/12
For personal use only.

TABLE 1. Palladium samples

Sample No.	Form of metal	Purity (%)	Surface area ($m^2\ g^{-1}$)	r_{ads} (H/Pd)
I	Powder	99.999	0.2	0.0004
II	Sintered black		2.4	0.0051
III	Sponge	>99	0.2	0.0004
IV	Foil	99.999	6.5×10^{-4}*	0

*Geometric area.

neighboring absorbed species. Subsequent theoretical treatments of the system (11–13) yield similar equations which can be expressed in the form given in eq. 1, at least at low hydrogen concentrations in the α-phase.

Published data for low concentrations of hydrogen fit the above equation reasonably well but there are instances of considerable differences between the results obtained by various workers in this α-phase region. Hydrogen absorption isotherms obtained using palladium samples of high surface area (14–17) indicate that the amount of hydrogen adsorbed on the surface of the metal can make a significant contribution to the total amount of hydrogen taken up by the metal and should be considered when analyzing isotherms. An investigation of this effect on isotherms in the α-phase region has been made in this study.

Experimental

Materials

Palladium black (British Drug Houses Ltd.) was sintered by prolonged heating *in vacuo* at 320 °C to prevent any further change in surface area while degassing the sample at 300 °C prior to the measurement of absorption isotherms. Palladium sponge (Fluka A.G.) was sieved to remove large and small particles. The sample used was 50–80 mesh. Palladium powder (< 60 mesh) and 1 sq in. of 10 mil palladium foil (both from Alfa Inorganics) were used as received. Details of the samples are summarized in Table 1.

Hydrogen gas (high purity grade) was purified by passage through a heated palladium–silver diffusion thimble and stored in a grease-free section of the apparatus. High purity helium and nitrogen were used in dead space calibrations and surface area determinations.

Apparatus and Techniques

The volumetric apparatus and experimental techniques employed were essentially similar to those used by Everett and Nordon (18) except that greaseless metal valves (Hoke bellows-sealed valve) were used to admit hydrogen into the gas measuring buret and into the sample bulb, and a quartz spiral gauge manometer (Texas Instruments Inc., Model No. 144) was used to measure the pressure in the absorption section.

Pressure–composition isotherms were measured for the four palladium samples in the pressure range 0–1000 Torr at temperatures between 100 °C and 240 °C. Prior to each isotherm the metal was degassed for several hours until the pressure fell below 10^{-5} Torr, equilibrated with about 150 Torr of hydrogen gas to remove any surface oxygen and finally evacuated for 3 h, all at 300 °C.

B.E.T. surface areas were measured using the conventional low temperature nitrogen adsorption method.

Results and Discussion

At low pressures (< 100 Torr) the experimental data follow Sieverts' law fairly closely, as expected for dilute solutions of hydrogen in palladium. Deviations from Sieverts' law occur as the concentration of absorbed hydrogen increases as can be seen in Fig. 1, where isotherms obtained at several temperatures using palladium foil (sample IV) are shown.

The statistical equation derived by Lacher (10) assuming that an attraction exists between neighboring protons in the lattice, eq. 1, can be rearranged to give

$$[2] \qquad \ln p^{1/2}\left(\frac{1-r}{r}\right) = A + \frac{Br}{T}$$

which, at low values of r, can be reduced to

$$[3] \qquad \ln p^{1/2}/r = A + \frac{Br}{T}$$

The experimental data obtained in this study have been compared with this approximate form of Lacher's equation. Figures 2 and 3 show the results for samples IV and II plotted as $\log_{10} p^{1/2}/r$ against r. The data in Fig. 2 fit eq. 3 well over the range shown. At higher values of r, deviations from straight line behavior would be expected since the term $\ln(1-r)$ has been neglected in going from eq. 2 to eq. 3. However, the data for sintered palladium black shown in Fig. 3 deviate considerably from eq. 3 at very low values of r, indicating that the sample has a greater sorptive capacity for hydrogen at very low pressures than is predicted by Lacher's equation. Similar behavior was found for samples I and III, although the deviations were smaller.

Can. J. Chem. Downloaded from www.nrcresearchpress.com by 210.87.254.40 on 09/05/12
For personal use only.

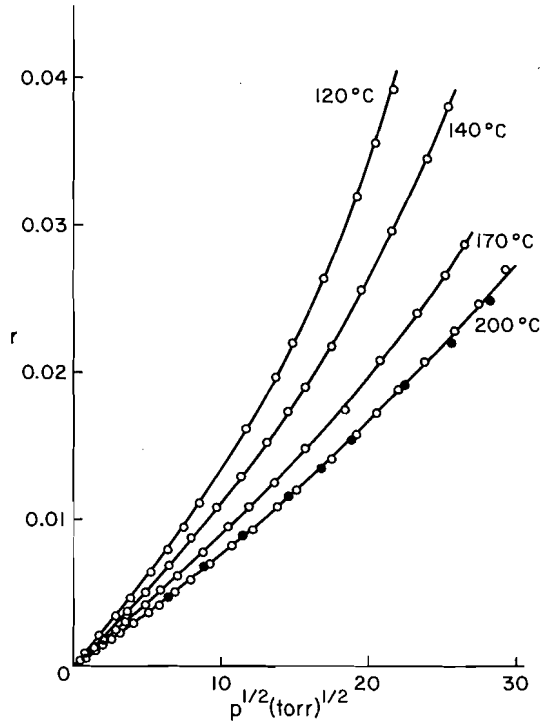

FIG. 1. Variation in hydrogen concentration, r(H/Pd), as a function of the square root of the hydrogen pressure for sample IV at various temperatures. Filled circles denote a second run at 200 °C.

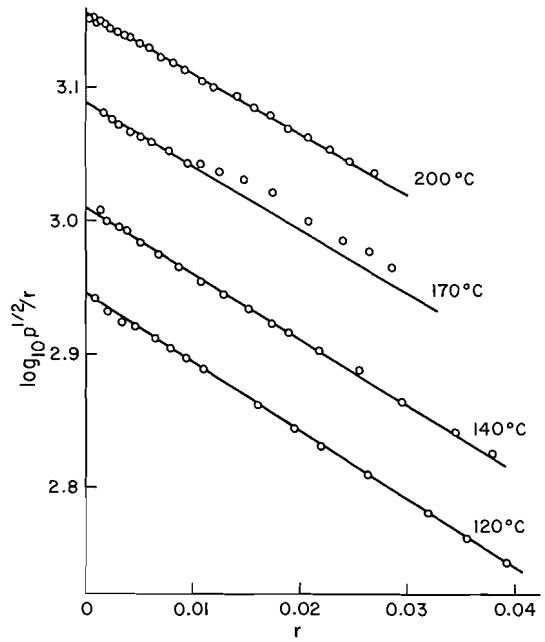

FIG. 2. Plot of $\log_{10} p^{1/2}/r$ against r for sample IV to test eq. 2.

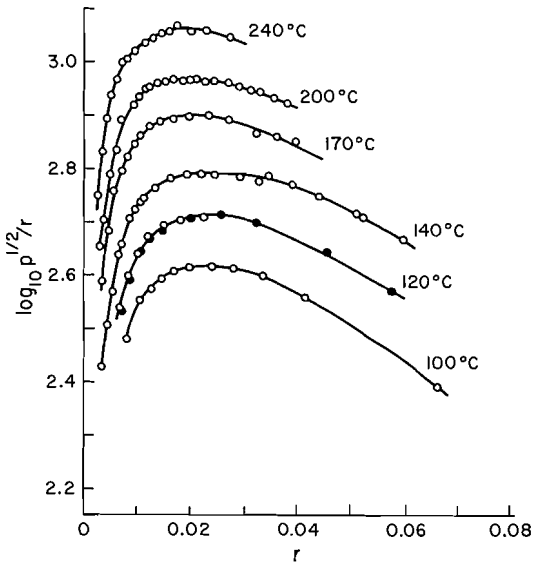

FIG. 3. Plot of $\log_{10} p^{1/2}/r$ against r for sample II to test eq. 2.

From the study of supported palladium catalysts and palladium black, Aben (19) concluded that a number of hydrogen atoms approximately equal to the number of surface metal atoms was adsorbed by the metal at 70 °C and 1 Torr pressure of hydrogen. Both Aben and, more recently, Sermon (16), using a slightly different approach, determined surface areas of palladium samples based on this conclusion which were in good agreement with B.E.T. surface areas.

Taking Aben's estimate of the average density of surface palladium atoms, 1.21×10^{15} atoms/cm^2, the atomic ratio of adsorbed hydrogen on a surface of area $\sum$ m^2 g^{-1} will be $0.00212 \times \sum$ if the surface is completely covered. If it is assumed that the surface layer is complete even at the lowest pressures at which isothermal data were obtained, subtracting this amount from the total hydrogen uptake should give the amount of hydrogen absorbed into the metal lattice. It is this value of r that should be used in Lacher's equation.

For the foil sample the amount of hydrogen adsorbed is negligible if the surface area is not much greater than the geometric area of the sample (6.5 cm^2 g^{-1}). However, this is not the case for the other three samples whose surface areas are given in Table 1. The data for sample II plotted in Fig. 3 are re-plotted in Fig. 4 for r values below 0.04 after subtracting the amount

Can. J. Chem. Downloaded from www.nrcresearchpress.com by 210.87.254.40 on 09/05/12
For personal use only.

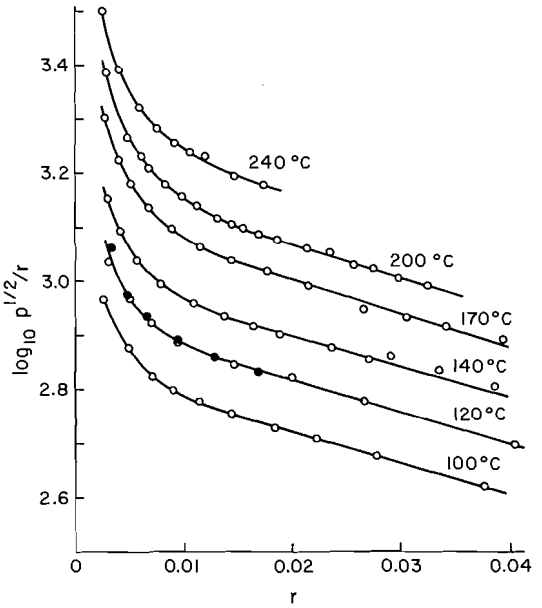

FIG. 4. Plot of $\log_{10} p^{1/2}/r$ against r for sample II in which r is the total hydrogen uptake less r_{ads} given in Table 1. Note that the range of r shown is half that in Fig. 3.

of hydrogen adsorbed given as r_{ads} in Table 1. It can be seen that agreement with eq. 3 is improved down to r values of about 0.01, below which deviations in the opposite direction now occur. Extrapolation of the linear portions of the graphs in Fig. 4 to zero hydrogen content gives intercepts which agree closely with those found for the foil sample. Table 2 gives the values of the intercepts obtained in this way for all the samples. The temperature dependence of this parameter is shown in Fig. 5.

It would appear from Fig. 4, and from similar graphs obtained with data for samples I and III, that the metal surface is not completely saturated at the lowest pressures measured at these temperatures. If one were to assume that the adsorption of hydrogen by palladium followed the Langmuir isotherm, for instance, the data could be made to follow Lacher's equation even more closely at low pressures. However, as there is considerable uncertainty in the surface area and in the number of hydrogen sites on the polycrystalline metal surface, further analysis was not considered worthwhile.

The slopes of the graphs in Fig. 2, B/T, give an almost constant value of B for the foil sample over the temperature range studied. For sample I, palladium powder, slightly lower B values were

TABLE 2. Intercepts, A, of graphs of $\log_{10} p^{1/2}/r$ against r

Temperature (°C)	Sample number I	II	III	IV
100	2.82	2.84		
110	2.86			
120	2.89	2.93		2.946
130	2.93			
140	2.99	3.01		3.010
170		3.13		3.087
180			3.14	
200		3.20		3.155
240		3.30		

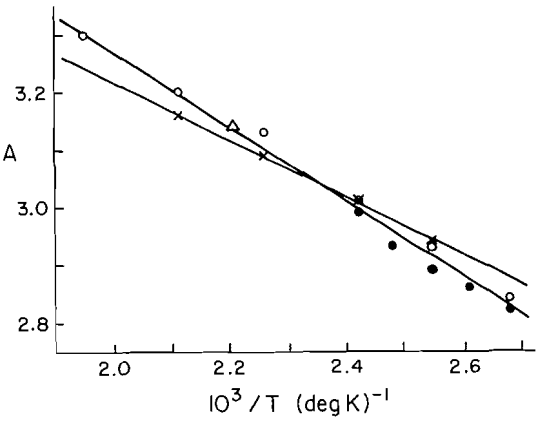

FIG. 5. Temperature dependence of A (eq. 2, using $\log_{10}$ instead of natural logarithms) for all samples: ●, sample I; ○, sample II; △, sample III; ×, sample IV.

obtained while for sample III, sintered palladium black, significantly higher values of B were found. Using the average value of B for the foil sample and the equation of the line drawn in Fig. 5 for the variation of A for the foil with temperature, the isotherms for this sample are closely described up to values of r of at least 0.04 H/Pd by the equation

$$[5] \quad \log_{10}(p/\text{Torr})^{1/2} = \log_{10} r + 4.31 - \frac{545}{T} - \frac{2090}{T} r$$

where r is the total hydrogen uptake. Written in the form used by Simons and Flanagan (5), who measured isotherms at temperatures ranging from 0 to 90 °C using an electrochemical technique with palladium foil, eq. 5 becomes

$$[6] \quad \ln(p/\text{atm}) = 13.19 - \frac{2510}{T} - \frac{9625r}{T} + 2\ln\left(\frac{r}{1-r}\right)$$

Can. J. Chem. Downloaded from www.nrcresearchpress.com by 210.87.254.40 on 09/05/12
For personal use only.

Can. J. Chem. Downloaded from www.nrcresearchpress.com by 210.87.254.40 on 09/05/12
For personal use only.

which agrees fairly closely with equation of Simons and Flanagan

$$[7]\quad \ln(p/\text{atm}) = 13.04 - \frac{2327}{T} - \frac{11110r}{T} + 2\ln\left(\frac{r}{1-r}\right)$$

The agreement between these equations and the results of Wicke and Nernst (6), who used a volumetric technique with palladium foil between −78 °C and +75 °C, is also good and demonstrates that consistent data can be obtained over a wide temperature range for palladium foil samples. However, although it has been shown that the data for the other samples can be made to follow Lacher's equation more closely by correcting for the amount of hydrogen held on the surface, the resulting fitted equations still differ significantly from eq. 6. For sample I the best fit is found using the equation

$$[8]\quad \ln(p/\text{atm}) = 14.4 - \frac{2980}{T} - \frac{8500r}{T} + 2\ln\left(\frac{r}{1-r}\right)$$

while for sample II

$$[9]\quad \ln(p/\text{atm}) = 14.4 - \frac{2980}{T} - \frac{11510r}{T} + 2\ln\left(\frac{r}{1-r}\right)$$

In both equations r is the total hydrogen uptake less the amount given as r_{ads} in Table 1. The best straight line through the values of A for samples I and II shown in Fig. 5 was used to calculate the variation of A with T.

It appears that in addition to the surface adsorption effect, other factors are involved which result in different forms of the metal having different sorptive properties in the α-phase. If the surface effect were alone responsible for the observed differences in behavior, a single isotherm would be obtained when correction was made for the amount of hydrogen adsorbed, which is clearly not the case here. The much higher sorptive capacity of a sample of palladium sponge used by Lambert and Gates (20) and subsequently by Everett and Nordon (18) and Evans (4) cannot be explained in terms of a surface adsorption effect either. The possibility that lattice strain influences the absorption process has been discussed by Burch and Lewis (13, 21). These authors suggest that deviations from behavior predicted by Lacher's model (10), which assumes a random occupation of interstitial sites by hydrogen, occur because strain energy in the system may be reduced by the pairing of occupied sites. MacQuillan (22) has also demonstrated that deviations from predicted behavior of dilute solutions of hydrogen in body-centered cubic metals can be explained by pair formation. The existence of pairs in this case was argued on electronic grounds. Further studies, particularly in the $\alpha \rightarrow \beta$ phase transition region, are planned to investigate such effects.

Applying the Clausius–Clapeyron equation to Lacher's equation, an expression for the partial molar enthalpy of absorbed hydrogen is obtained. The equation predicts that this quantity should become more negative (higher isosteric heat of absorption) as the concentration of absorbed hydrogen increases. From eq. 6 it is found that for sample IV

$$[10]\quad \Delta\bar{H}_{H_2} = -4988 - 19127r \quad \text{cal/mol } H_2$$

Thus, as r increases from 0 to 0.04, $\Delta\bar{H}_{H_2}$ changes from −4988 to −5753 cal/mol H_2. This function can also be calculated from the variation of $\ln p$ with $1/T$ obtained directly from the isotherms. A similar change is found although there is some scatter in the points. The data of Simons and Flanagan (5) and Wicke and Nernst (6) give similar variations of $\Delta\bar{H}_{H_2}$ with r but their values at zero hydrogen content are about 7% lower. Closer agreement is found with the more recent results of Clewley *et al.* (17), who measured isochores for the system using massive palladium samples over a large temperature range. The partial molar enthalpy was found to show little variation between 200 and 500 °K for dilute solutions containing up to 0.003 H/Pd hydrogen, the average value being −4774 cal/mol H_2.

For samples I and II, the partial molar enthalpy of absorbed hydrogen calculated from eqs. 8 and 9 is −5922 cal/mol H_2 at zero uptake, falling to −6598 cal/mol H_2 for sample I and −6837 cal/mol H_2 for sample II at $r = 0.04$ H/Pd. Values obtained by plotting $\ln p$ against $1/T$ for the various isotherms are in reasonable agreement for sample I, but for sample II $\Delta\bar{H}_{H_2}$ is considerably more negative than predicted at very low r, reaches a maximum when r is approximately 0.02 H/Pd and then falls as predicted above in the range 0.02 to 0.04 H/Pd. It is believed that the more negative enthalpy values for these two samples, and the anomalous variation with uptake found for sample II, are a consequence of

the heat of adsorption of hydrogen which makes a considerable contribution to the isosteric heat unless the surface area of the metal sample is low.

Summary and Conclusions

The absorption of hydrogen by palladium foil is well described in Lacher's equation at concentrations of up to at least 0.04 H/Pd in the temperature range 120–240 °C. Agreement with earlier studies at lower temperatures is good.

For samples having larger surface area, agreement between data obtained and Lacher's equation is poor but can be greatly improved if allowance is made for the amount of hydrogen adsorbed on the surface. Deviations which still exist at very low concentrations presumably indicate that the surface is not completely covered by adsorbed hydrogen under these conditions.

For palladium foil and a powder sample having a low surface area, the partial molar enthalpy of absorbed hydrogen increases in magnitude as the hydrogen content increases, as predicted by Lacher's equation. However, the sorption process is apparently more exothermic for the powder sample than for the foil. For a sample of sintered palladium black having a much larger surface area than the powder, the isosteric heat is even more exothermic at very low hydrogen content, the heat falling rapidly to a minimum as the hydrogen uptake is increased before showing an increase similar to that found for the powder sample. It is suggested that these effects are a result of a high heat of adsorption of hydrogen on the metal surface.

The assistance of Miss J. de Zoete and J. Priestley with computer analysis of data is gratefully acknowledged, as is the financial assistance under DRB Grant No. 9530–122 provided by the Defence Research Board of Canada.

1. L. J. GILLESPIE and F. P. HALL. J. Am. Chem. Soc. **48**, 1207 (1926).
2. L. J. GILLESPIE and L. S. GALSTAUN. J. Am. Chem. Soc. **58**, 2565 (1936).
3. H. BRUNING and A. SIEVERTS. Z. phys. Chem. A, **163**, 409 (1933).
4. M. J. B. EVANS. PH.D. Thesis. University of Bristol, England, 1962.
5. J. W. SIMONS and T. B. FLANAGAN. J. Phys. Chem. **69**, 3773 (1965).
6. E. WICKE and G. H. NERNST. Ber. Bunsenges. physik. Chem. **68**, 224 (1964).
7. A. SIEVERTS and W. DANZ. Z. phys. Chem. **38B**, 46, 61 (1937).
8. C. WAGNER and G. HELLER. Z. phys. Chem. **46B**, 242 (1940).
9. R. BURCH. Trans. Faraday Soc. **66**, 736 (1970).
10. J. R. LACHER. Proc. R. Soc. (Lond.), A, **161**, 525 (1937).
11. H. BRODOWSKY. Z. phys. Chem. (N.F.), **44**, 129 (1965).
12. T. B. FLANAGAN and J. W. SIMONS. Can. J. Chem. **43**, 1665 (1965).
13. R. BURCH. Trans. Faraday Soc. **66**, 749 (1970).
14. I. YASUMORI, T. KOMORITA, and S. SUZUKI. Bull. Chem. Soc. Jap. **34**, 588 (1961).
15. S. SUZUKI and T. SUZUKI. Bull. Tokyo Inst. Tech. **64**, 21 (1965).
16. P. A. SERMON. J. Catal. **24**, 460 (1972).
17. J. D. CLEWLEY, T. CURRAN, T. B. FLANAGAN, and W. A. OATES. J. Chem. Soc. Faraday Trans. I. **69**, 449 (1973).
18. D. H. EVERETT and P. NORDON. Proc. R. Soc. (Lond.), A, **259**, 341 (1960).
19. P. C. ABEN. J. Catal. **10**, 224 (1968).
20. B. LAMBERT and S. F. GATES. Proc. R. Soc. (Lond.), A, **108**, 456 (1925).
21. R. BURCH and F. A. LEWIS. Platinum Metal. Rev. **15**, 21 (1971).
22. A. D. MCQUILLAN. J. Chem. Phys. **53**, 156 (1970).

Can. J. Chem. Downloaded from www.nrcresearchpress.com by 210.87.254.40 on 09/05/12
For personal use only.

Structure of Radicals Produced by γ-Radiolysis. Part 3. Radicals Derived from Adamantane, Adamantyl Derivatives, and Diamantane

GEORGE J. HYFANTIS, JR. AND A. CAMPBELL LING[1]

Department of Chemistry, West Virginia University, Morgantown, W. Virginia, 26506

Received November 13, 1973

The effects of γ-radiolysis on adamantane, perdeuterated adamantane, diamantane, 1- and 2-chloroadamantane, 1- and 2-bromoadamantane, 1-cyanoadamantane, 1- and 2-adamantanol, 1- and 2-adamantylamine have been examined via electron spin resonance techniques, and the nature of the predominant species produced is discussed. Spin-scavenging experiments using 2-methyl-2-nitrosopropane have been used, together with previously reported Br_2 scavenging experiments, to identify the nature of the predominant species produced when purified solid adamantane is subjected to radiolysis. Data indicate that this is the 1-adamantyl radical. A possible reason for the controversial nature of data on this subject reported previously by other investigators is given.

Les effets de radiolyse γ de l'adamantane, de l'adamantane perdeutérié, de la diamantane, du chloro-1 et -2 adamantane, du bromo-1 et -2 adamantane, du cyano-1 adamantane, de l'adamantanol-1 et -2, de l'adamantylamine-1 et -2 ont été examinés par les techniques de résonnance de spin électronique et la nature d'espèces prédominantes produites est discutée. Des expériences de balayage de spin utilisant le méthyl-2 nitroso-2 propane ainsi que l'expérience de balayage de Br_2 mentionnée précédemment, furent utilisées afin d'identifier la nature des espèces prédominantes produites lorsque l'adamantane solide purifié est radiolysée. Les données indiquent que c'est le radical de l'adamantyl-1. Une cause probable de la nature de contreverse des données à ce sujet, mentionnées précédemment par d'autres chercheurs, est traitée.

[Traduit par le journal]

Can. J. Chem., **52**, 1206 (1974)

Introduction

The use of adamantane as an isolation matrix is now well established but considerable controversy has occurred in the recent literature as to the nature of the radiolysis process in adamantane itself (1–8). The success, or failure to resolve adequately the hyperfine splitting from e.s.r. studies of pure phase adamantane samples has led to a variety of claims and counter claims concerning the identity of the majority species produced.

The most recent reports from Filby and Gunther (6) and Filby[2] favor formation of the 1-adamantyl radical. This postulation was based on data obtained from well resolved e.s.r. spectra taken over a wide range of temperature (77–400 °K) and from both high LET (electron beam) and low LET (Co-60 γ-source) radiolysis of carefully purified adamantane samples. However, their reported hyperfine coupling constants do not agree with those reported by Krusic and co-workers (9) for authentic 1-adamantyl radicals generated by photochemical means, a point already commented on by Marx (7). In opposition to this assignment, Ferrell *et al.* (3) postulate formation of the 2-adamantyl radical, a hypothesis supported by Lloyd and Rogers (8) via consideration of data obtained by double-resonance ENDOR techniques. As an alternate to either of these postulations, Bonnazola and Marx (2) have suggested that a substituted cyclohexadienyl radical may be formed by C—C bond cleavage, rather than a radical resulting from the more usual C—H bond cleavage exhibited by the majority of hydrocarbons. That C—C bond cleavage on radiolysis of adamantane is possible is shown by product analyses by Hattenbach and vom Baur (10). We have reported recently (11) the results of preliminary experiments utilizing classical radiation chemistry techniques to determine the nature of the predominant species produced by radiolysis of solid adamantane and concluded that the 1-adamantyl radical was the most probable species. We report here additional data supporting this assignment and further details pertinent to that communication.

Experimental

Radiolyses were performed using a 150 Ci Co-60 water-well source, dose rates were *ca.* 3×10^{16} eV g^{-1} min^{-1} (Fricke dosimetry) and total doses varied between

[1]To whom correspondence should be addressed.

[2]W. G. Filby. Personal communication.

Can. J. Chem. Downloaded from www.nrcresearchpress.com by 210.87.254.42 on 09/05/12
For personal use only.

Can. J. Chem. Downloaded from www.nrcresearchpress.com by 210.87.254.42 on 09/05/12
For personal use only.

10^{17} and 10^{19} eV g^{-1}. Photolyses were performed using a Bausch and Lomb 200 W high pressure Hg arc monochromator source yielding *ca.* 5×10^{16} photons/s (potassium ferrioxalate actinometry).

Adamantane, perdeuterated adamantane,[3] diamantane,[4] 1- and 2-adamantanol, 1- and 2-adamantylamine hydrochlorides, 1- and 2-chloroadamantane, and 1- and 2-bromoadamantane, were obtained from commercial sources. All compounds were recrystallized from purified cyclohexane (benzene and methylcyclohexane were also used, to check that no solvent had been introduced by the recrystallization process) and then transferred to a vacuum line. The adamantylamine derivatives were liberated from their hydrochloride compounds by dissolving them in water, adding stoichiometric quantities of NaOH to liberate the free base, extracting the free base with cyclohexane, and evaporating to dryness under reduced pressure using a rotary evaporator. The solid amine was then recrystallized from cyclohexane and transferred to a vacuum line as above. The samples were pumped and gently warmed to remove traces of excess solvent, and except where indicated in the text below, used directly in this form. As previously noted (see ref. 12, p. 3983), cyclohexane does not lead to any characteristic e.s.r. signal when adamantane recrystallized from this solvent is subjected to radiolysis. This technique provides a convenient method of preliminary purification for commercially supplied samples. 2-Methylpentane (2MP) was used as an isolation matrix for studies at 77 °K. Purification of 2MP was effected by multiple passages of the liquid through a column (12 in. × ½ in.) of activated silica gel containing approximately 10% w/w $AgNO_3$ crystals, followed by distillation from a sodium mirror surface under vacuum into a storage vessel containing a further sodium mirror, and subsequent degassing to remove O_2 and CO_2. This latter component is adequately removed by extensive pumping over the surface of the cooled, but liquid, hydrocarbon at temperatures up to 273 °K. Repetitive "freeze–pump thaw–pump" cycles, together with renewal of the Na mirror at frequent intervals during the degassing led to a 2MP sample with an optical density of 1.0 at 194 nm.

Samples were prepared for irradiation in several ways. Adamantane and adamantane derivatives were prepared by simply irradiating the compounds as polycrystalline solids in stoppered Pyrex vials under normal atmospheric conditions[5] and the irradiated samples transferred to silica e.s.r. tubes (⅛ in. i.d. "suprasil" quartz) for monitoring. A second set of samples was prepared by adding the solid to an e.s.r. cell (*ca.* 10–16 in. in length overall), degassing the sample and sealing off the cell via conventional vacuum-line techniques under pressures of $< 10^{-3}$ Torr. The tube was inverted and the sample irradiated at the Pyrex end of the tube. Prior to monitoring the sample in an e.s.r. spectrometer, the sample tube was returned to the upright position with the quartz e.s.r. cell at the bottom allowing the solid sample to fall back down into the quartz cell. This method minimized interference from cell signals generated by radiolysis of the quartz envelope. All cells were initially flamed extensively to remove any trapped color centers generated in previous radiolyses before use in succeeding experiments. Irradiation temperatures were 77 °K, 195 °K, or room temperature. Matrix isolation samples using 2MP as the glassy matrix were prepared by standard techniques, solute concentrations were in the range 10^{-1} mol % to saturation (*ca.* 10 mol %). All samples were degassed and evacuated to a pressure of $< 10^{-3}$ Torr prior to sealing. Electron spin resonance signals generated via γ-radiolyses were compared to signals generated in control samples prepared and irradiated under identical conditions, and containing only 2MP, in order to eliminate possible contributions from the cell and/or matrix itself. 2-Methyl-2-nitrosopropane ("*t*-nitroso" trap) dimer was prepared by the following sequence of reactions as described in the literature. *N*-Benzylidine-*t*-butylamine prepared by the method of Emling *et al.* (13) was reacted with peracetic acid to form 2-butyl-3-phenyloxazirane (14). The oxazirane was then hydrolyzed to the hydroxylamine followed by formation of the *t*-nitrosobutane dimer (15). The dimer is "activated" (conversion to the monomer) via u.v. light, mild heating, or by the radiolysis process itself (16). The *t*-nitroso spin-trap was purified by preparative gas chromatography.

Samples for spin trapping were prepared by two different methods. One method utilized a "break-seal" tube with an e.s.r. quartz cell attached to the lower part of the seal into which was transferred approximately 0.5 ml of degassed solvent (*n*-hexane) containing the *t*-nitroso spin-trap at 10^{-2} *M*. The lower part of the cell was then sealed off under a pressure of *ca.* 10^{-3} Torr. The top part of the "break-seal" cell was utilized to irradiate a small quantity of purified solid adamantane, or adamantane derivative. After the top section had been degassed and sealed off at $< 10^{-3}$ Torr pressure, the Pyrex top-half of this composite cell, containing the solid adamantane, was irradiated at room temperature and the cell mounted in the e.s.r. cavity with the solid sample section uppermost, the e.s.r. cell containing solvent and spin trap in the e.s.r. resonant cavity at the bottom. After the solvent had been cooled to −80 °C the "break-seal" device could be broken to allow mixing between the irradiated solid and the solution; the resultant scavenging of the free radicals by the spin trap could then be monitored via e.s.r. spectrometry. The second method used in the spin-trap experiments required that the adamantane or adamantane derivative be dissolved (saturation) in *n*-hexane containing 10^{-2} *M* spin trap. The solution was degassed and sealed at a pressure of $< 10^{-3}$ Torr. The cell was then irradiated at 195 °K and monitored via e.s.r. at *ca.* 195 °K to room temperature. A control sample containing only *n*-hexane solvent and spin-trap was used to identify data resulting from spin-trapping of radicals derived from the solvent molecules.

Similar techniques were used for scavenger studies with bromine. Bromine (0.1 mol %) was dissolved in purified

[3]We thank Professor J. K. S. Wan of Queen's University, Ontario, for the gift of perdeuterated adamantane.

[4]We thank Professor P. v. R. Schleyer of Princeton University, New Jersey, for the gift of a sample of diamantane.

[5]Work in progress on radiolysis processes in adamantane, and radiolyses of solutes held in adamantane, while under controlled atmospheres of various gases, both before and after radiolysis, will be reported at a later date. No gross qualitative differences in e.s.r. spectra of radicals were detected when samples were irradiated *in vacuo* relative to irradiation under atmospheric pressure or even pressures of O_2 gas up to *ca.* 2 atm.

Can. J. Chem. Downloaded from www.nrcresearchpress.com by 210.87.254.42 on 09/05/12
For personal use only.

cyclohexane and placed in the lower half of a "break-seal" cell. Enough adamantane was placed in the upper portion of the cell to make its concentration when dissolved approximately 1 mol %. The inverted cell was irradiated as in the spin-trapping technique but the seal was broken at ambient temperature and suitable aliquots withdrawn (through a septum) and subjected to analyses via g.l.c. techniques. A second method involved direct irradiation of a three-component system (solvent–scavenger–solute). A third method of sample preparation used for bromine scavenging experiments was to irradiate approximately 1 g of the adamantane in a Pyrex vial while open to atmospheric pressure and at room temperature and then add this irradiated solid to approximately 5 ml of 0.1 mol % Br_2 in cyclohexane to allow any radicals to be scavenged by the bromine.

Photolyses were performed directly on polycrystalline samples, glassy matrix isolated samples, and spin-trap solutions, together with photolyses of pressed pellets of the polycrystalline solids as described by Volman and co-workers (17). Solid adamantyl derivatives were incorporated into adamantane matrices by co-evaporation; various concentrations of each solid were mixed with solid adamantane and the whole dissolved in cyclohexane; the solution was then evaporated to dryness using a rotary evaporator under slightly reduced pressures.

Electron spin resonance spectra were obtained via a Varian E.3 spectrometer utilizing a Varian gas-flow variable temperature controller; gas chromatographic analyses were carried out using a Bendix ChromaLab 2100 instrument (f.i.d., with either a $\frac{1}{8}$ in. × 6 ft stainless steel column, 5% w/w SE-30 on 60–80 mesh Chromo-Sorb G, or $\frac{1}{8}$ in. × 12 ft glass column with 5% w/w diisodecylphthalate on 100–120 mesh ChromoSorb G). Computer simulations were obtained via an IBM-360/75 Computer and CalComp accessory using a program written by one of us (18).

Results and Discussion

Radiolyses of Adamantane and Diamantane[6]

Adamantane has been used successfully by many groups as an isolation matrix to study both qualitative and quantitative properties of radicals derived from various solute molecules. Radical lifetimes vary between approximately 10 min to 100 h at room temperature and radicals appear to decay by a pure second-order process over more than 5 half-lives, although no evidence was found for any new radical growing in as the other decayed.[7] While resolution of e.s.r. signals in adamantane does not compare with that from liquid phase studies, line-widths are sufficiently small[8] to allow adequate structural assignments to be made and are far superior to standard glassy or polycrystalline matrix isolation methods. Unfortunately, this resolution is inadequate to resolve the controversy concerning the nature of the radical generated from adamantane itself. We have shown already (11) that line-widths of *ca.* 1.4 G or larger for the adamantyl radical in adamantane matrices lead to serious degeneration of the 448 closely spaced lines (9) and that at only 1.8 G or so, the envelope of the e.s.r. spectrum is essentially a broad singlet with little or no discernible features. The experimentally derived spectrum from γ-irradiated adamantane that has been purified by multiple recrystallization from cyclohexane is shown in Fig. 1*a*. We utilized zone refining techniques, but have been unable to duplicate the results obtained by Bonnazola and Marx (2) or those of Filby and co-workers (4–6).[2] Use of preparative gas chromatography, particularly multiple passages of the collected fraction back through the separation cycle, and collection of only the central 50% of the product at each cycle, led to slightly improved resolution (or at least, the appearance of distinguishable fine structure). However, this did not allow any reasonable assignment of radical structure to be made and spectra resembled those obtained from adamantane samples by irradiation and monitoring at 77 °K (11). Radiolysis of perdeuterated adamantane, purified by recrystallization techniques only, led to the spectra shown in Figs. 1*b* and *c* but we have been unable to simulate spectra matching these in any respects using either 1-adamantyl parameters or 2-adamantyl parameters.[9] Similarly, radiolysis of diamantane leads to a featureless singlet envelope with parameters almost

[6]Also known as "congressane", pentacycl[7.3.1.1.^{4,12}.-$0^{2,7}$.$0^{6,11}$] tetradecane, m.pt. 244–245 °C.

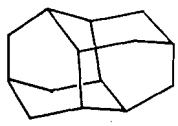

[7]M. E. Manzuk and A. C. Ling. Unpublished work.

[8]We have found that the majority of radicals exhibit a FWHM Lorentzian line width of *ca.* 1.1–1.3 G, with a lower limit of 0.7 G for N,N,N′,N′-tetramethyl-*p*-phenylenediamine cation (Wurster's Blue Cation) in adamantane and *ca.* 0.4 G for $C_6H_5\dot{C}H_2$ in perdeuterated adamantane, at room temperatures.

[9]Primary efforts were directed towards 1-adamantyl, using values from Krusic *et al.* (9) for protonated adamantane reduced by a factor of *ca.* 0.15; typical parameters used were: 1-adamantyl (perdeuterated), a_β^D(6) 1.1 G, a_α^D(3) 0.7 G, and a_α^D(3) 0.5 G; 2-adamantyl (perdeuterated), a_α^D(1) 3.5 G, a_β^D(2) 1.1 G, a_α^D(4) 0.5 G. Line widths were varied from 1–4 G, and hyperfine coupling constants by *ca.* ± 50%.

Can. J. Chem. Downloaded from www.nrcresearchpress.com by 210.87.254.42 on 09/05/12
For personal use only.

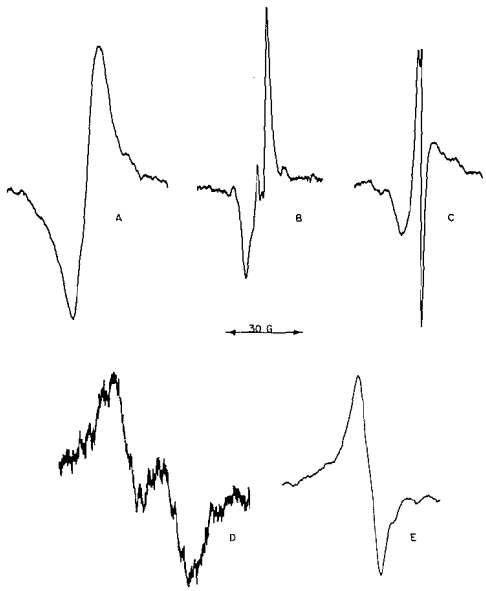

FIG. 1. First derivative e.s.r. spectral envelopes following radiolysis of adamantane and diamantane. (*a*) Radiolysis and monitoring at room temperature of adamantane. (*b*) Radiolysis and monitoring of perdeuterated adamantane at room temperature. (*c*) Radiolysis and monitoring of perdeuterated adamantane at 78 °K. (*d*) Radiolysis and monitoring of adamantane at room temperature after a prolonged radiolysis to *ca.* 10^{19} eV g^{-1} dose. (*e*) Radiolysis and monitoring of diamantane at room temperature. The γ-dose to samples *a* through *c*, and *e*, was *ca.* 10^{18} eV g^{-1}.

identical to those obtained for adamantane (Fig. 1*e*). Diamantane has basically two different bridgehead positions, one of which has an identical environment to that in adamantane; it is not surprising, therefore, that the e.s.r. signal from diamantane resembles that from adamantane when both systems are subjected to radiolysis under similar conditions.[10] In view of the controversy concerning the nature of this radical derived from the adamantyl skeleton, classical radiation chemistry techniques of scavenger studies, and comparative radiolyses, were used to support the postulation that the 1-adamantyl radical (bridgehead position) was formed as the predominant species (11). Comparative radiolyses of a variety of adamantyl derivatives, reported below, do support this postulation, and in addition to the bromine scavenger work already reported, we have further data from spin-scavenging experiments.

Finally, with regard to radiolyses of adamantane itself, we offer a possible reason for the controversy concerning the identity of the radical produced and in particular for the conflicting experimental data. We have already reported that bromine scavenging experiments appear to show production of both 1-adamantyl *and* 2-adamantyl species in an approximate ratio of 3:1, respectively (11). However, e.s.r. data from samples subjected to approximately 10^{18} eV g^{-1} absorbed dose (Fig. 1*a*) indicate formation of the 1-adamantyl radical with no discernible contribution from the 2-adamantyl spectrum. Prolonged radiolysis of adamantane samples (recrystallized from cyclohexane) to an absorbed dose of 10^{19} eV g^{-1} (5–6 h) leads to the e.s.r. spectrum shown in Fig. 1*d*. This is similar to that reported by Wood and co-workers (3) and identical to the spectra obtained from 2-adamantyl derivatives that are thought to yield 2-adamantyl radicals (see below). In contrast to the report by Wood and co-workers (3), however, the radical found by us is definitely stable at room temperature, albeit with a lifetime of *ca.* 10 min, compared to approximately 60 min for the radical producing the "singlet" e.s.r. spectrum. This effect does not appear to be a dose-rate phenomenon, since Filby *et al.* (4–6) report essentially identical results from both electron-beam and γ-source radiolyses of adamantane. Since previous workers have not reported their absorbed doses, we merely offer this as a possible explanation for the reported data but, in view of the fact that the 1-adamantyl radical is more stable than the 2-adamantyl species (19,20), we have no explanation as to why prolonged radiolysis will enhance the population of the less stable species at the expense of the more stable entity.

Radiolyses of Various Solid Adamantyl Derivatives

Various solid adamantyl derivatives were subjected to γ-radiolysis (*ca.* 10^{18} eV g^{-1}) at room temperature in an attempt to obtain comparative e.s.r. spectra that would aid in determining the processes occurring in adamantane itself. In view of the well-substantiated dissociative electron attachment reactions of alkyl halides, initial experiments were directed at the 1- and 2-chloro- and bromoadamantanes. Data

[10]Diamantane may be utilized as an isolation matrix in the same manner as adamantane, but resolution is either comparable or inferior to adamantane, and cost factors are significantly higher.

Can. J. Chem. Downloaded from www.nrcresearchpress.com by 210.87.254.42 on 09/05/12
For personal use only.

obtained were both distinctive and very characteristic of the 1- or 2-substituted derivatives, and appear to substantiate the dissociative electron attachment mode even for moieties as large as the adamantyl residue. A broad singlet, overall width approximately 50 G, and with an apparent peak-to-peak "line width" of the first derivative spectrum of *ca.* 12 G, was obtained from the 1-adamantyl derivative (1-Cl, 1-Br, and 1-CN). This compares favorably with the parameters reported by Krusic *et al.* (9), since using their reported coupling constants for authentic 1-adamantyl radicals produced photochemically, and peak-to-peak first derivative line widths for individual lines of 1.8 G or greater (FWHM line widths of 1.6 G or greater for a Lorentzian line shape), a reasonable match can be obtained between computer-simulated spectra and the experimental spectral envelope observed. Electron spin resonance spectra from polycrystalline 2-adamantyl derivatives (2-Cl and 2-Br) display a "doublet" pattern, characteristic of a strong coupling to one proton, and thus suggesting that 2-adamantyl radicals had been formed by dissociative electron attachment reactions, the α-hydrogen providing the necessary single species of spin $\frac{1}{2}$. In an attempt to improve resolution of the e.s.r. signals from the 1- and 2-adamantyl halides, experiments were tried where adamantyl derivatives were held in adamantane matrices (rather than a matrix of the halide itself, since these may be sufficiently asymmetric and/or polar as to inhibit free isotropic rotation) and then subjected to radiolysis. Varying concentrations of 1-chloroadamantane (between 1–5 mol %) in adamantane were prepared by dissolving both components in cyclohexane, and then removing the solvent by rotary evaporation under reduced pressures. Electron spin resonance signals following radiolysis from samples prepared by co-evaporation were virtually identical to those from pure-phase adamantyl derivatives. However, signal levels were significantly higher with the co-evaporattion samples compared to adamantane itself, indicating clearly the presence of the dissociative electron attachment mode of reaction for these cases.

Examination of the data from radiolyses of other derivatives further substantiates these findings. For example, previous reports on the radiolyses of alkyl amines and alkyl alcohols indicate that the α-carbon is the most probable site for attack. Thus, if this reaction mode obtains for adamantyl species 2-adamantanol should lead to a radical whose e.s.r. fine structure will resemble that for the 1-adamantyl radical. This is exactly the experimental result found. On the other hand, 2-adamantylamine will be expected to yield an α-carbon radical, and although there will undoubtedly be some form of coupling to the nitrogen atom, it is not expected that the resulting equal intensity triplet will be resolved. This would lead to a broad singlet envelope for the e.s.r. spectrum, as was found experimentally.[11]

In contrast to the relatively simple assignments and/or predictions possible for the 2-adamantyl derivatives, both 1-adamantanol and 1-adamantylamine provide an increased degree of complication. Excluding C—C bond cleavage, which we discount in view of the restrictive cage effects operating and the relatively strong adamantyl frameworks involved, there are four probable modes of radical formation in these 1-substituted derivatives.

A. Loss of Functional Group

This would lead immediately to 1-adamantyl radicals from both systems and a predicted broad singlet e.s.r. envelope; in general terms this is an unusual reaction, and is not substantiated here by the experimental results. It is therefore eliminated from further consideration.

B. Loss of a Hydrogen Atom from a Site Removed from the Vicinity of the Functional Group

This is tantamount to radiolysis of adamantane itself, the functional group playing no part

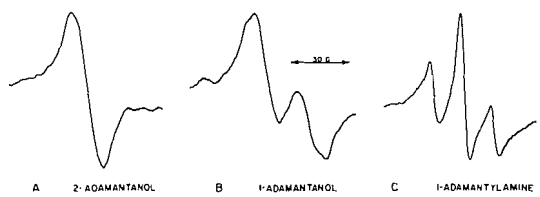

FIG. 2. First derivative e.s.r. spectral envelopes following radiolysis of some adamantyl derivatives. Radiolysis and monitoring at room temperature (dose *ca.* 10^{18} eV g^{-1}) of (*a*) 2-adamantanol, (*b*) 1-adamantanol, (*c*) 1-adamantylamine.

[11]Radiolyses of 1-adamantylamine-hydrochloride and 2-adamantylamine-hydrochloride as pure-phase polycrystalline solids at room temperature did not lead to the development of any characteristic or distinctive e.s.r. signals.

Can. J. Chem. Downloaded from www.nrcresearchpress.com by 210.87.254.42 on 09/05/12
For personal use only.

in the overall radical formation process. This is unusual. Moreover, if this were so, we would expect the same results from 1-adamantanol, 1-adamantylamine, and adamantane itself. This is manifestly untrue, since comparison of e.s.r. spectra in Figs. 2*b* and *c*, and 1*a*, show obvious differences immediately. We therefore eliminate this mode of radical formation from further consideration.

C. Loss of a Hydrogen Atom from the Functional Group Itself

This would lead to a radical $\rangle\dot{C}—O\cdot$ or $\rangle\dot{C}—\dot{N}H$. This mode of reaction for adamantanol can be discounted, since in general it is an unusual reaction mode for aliphatic alcohols, and because the e.s.r. signal observed cannot easily be correlated with the structure postulated. However, for the imino radical postulated, although the basic structure resembles that of the radical obtained by radiolysis of 2-adamantylamine (*cf.* $\rangle\dot{C}—NH_2$), the spin density at the nitrogen is probably sufficiently high to lead to a significant coupling constant that may be resolvable under the conditions of these experiments. Computer simulations using a^N coupling constants of 10 ± 5 G with $a_{NH}{}^H$ coupling constants of 10 ± 5 G, and $a_{CH}{}^H$ of 3 G for the six equivalent hydrogen atoms adjacent to the functional group, showed that for line widths in the range 1.5–4.0 G, no reasonable agreement could be found between the experimental spectrum and the simulations. A three-peak envelope is obtained from spectra with $a^N = 15$ G, $a_{NH}{}^H = 5$ G, $a_{CH}{}^H = 3$ G, line widths $\geqslant 3.5$ G, but the relative intensities of each "line" of the envelope are in the ratios of approximtely 2:1:2 rather than 1:2:1 as observed.

D. Loss of a Hydrogen Atom Adjacent to the Functional Group

This would lead to the formation of 2-adamantyl radicals directly, and should lead to a doublet envelope pattern seen already in the dissociative electron attachment reactions of 2-Cl and 2-Br derivatives. This is seen to be the case for 1-adamantanol and provides a reasonable interpretation of the observed spectrum. However, the data from 2-adamantylamine do not fit this hypothesis and the explanation offered above in *C* is preferred at this time.

The results of γ-radiolyses in adamantyl derivatives are summarized in Table 1, and typical e.s.r. spectral envelopes are displayed in Fig. 2. In addition, spectra were obtained for all derivatives after radiolysis and monitoring at 77 °K, and at various temperatures between 77 and 273 °K, but no significant data were obtained over and above that from the room temperature experiments already described.

Matrix Isolation Studies and Photolyses Experiments

In view of the rewarding results obtained by Volman and co-workers (17,21) via photolysis of solutes held in adamantane matrices, it was felt to be of interest to investigate this technique for adamantane derivatives themselves. Accordingly, samples were prepared by the following methods. (*a*) Solid adamantyl derivatives (1- and 2- chloro- and -bromoadamantanes) were recrystallized from cyclohexane and sealed under vacuum in standard e.s.r. cells. (*b*) Solid derivatives were recrystallized as above, the excess solvent removed by pumping the gently warmed solid, and then pressed into pellets as per the technique described by Volman and co-worker (17) via a hand press at *ca.* 7 kbars pressure (which is lower than the *ca.* 10 kbar pressure utilized by Volman and co-workers). (*c*) Conventional glassy matrix isolated samples in 2-methylpentane (2MP)[12] were prepared, using solute concentrations in the range 2 mol% to saturation (*ca.* 20 mol % at 78 °K), and data were compared to control samples containing only 2MP photolyzed under identical conditions. Methods *a* and *b* gave no distinguishable e.s.r. signals after several hours exposure at room temperature and method *c* produced a weak spectrum that appeared to consist of contributions from the matrix molecule and a broad envelope similar to those already reported. Equally, radiolysis of glassy matrix isolated samples did not lead to any significant results, e.s.r. spectra being obtained that were directly attributable to radicals derived from the 2MP matrix with an unresolved singlet envelope

[12]Preferred to 3-methylpentane (3MP) matrices, since 2MP is below its glass transition region (*ca.* 80 °K) and approximately one order of magnitude harder than 3MP at customary experimental temperatures (22,23) (liquid nitrogen at 77.5–78 °K), thus leading to an additional stabilization factor for trapped radical species compared to 3MP (T_g at *ca.* 77 °K).

TABLE 1. Summary of results obtained from γ-radiolysis of 1- and 2-adamantyl derivatives as polycrystalline solids at room temperatures

Derivative	Radical expected	Electron spin resonance: Spectrum expected	Electron spin resonance: Spectrum found experimentally
1-Chloroadamantane 1-Bromoadamantane 1-Cyanoadamantane	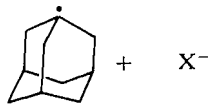 + X^- X = Cl, Br, CN	A broad singlet	Type A of fig. 2
2-Chloroadamantane 2-Bromoadamantane	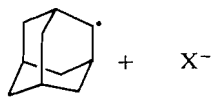 + X^- X = Cl, Br	A broad doublet	Type B of fig. 2
2-Adamantanol 2-Adamantylamine	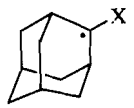 X = OH, NH_2	A broad singlet	Type A of fig. 2
1-Adamantanol	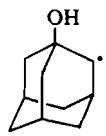	A broad doublet	Type B of fig. 2
1-Adamantylamine	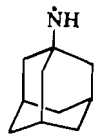		Type C of fig. 2

superimposed on top. Photolysis of 1- and 2-chloroadamantane in liquid *n*-hexane in the presence of spin trap at temperatures down to 173 °K did not lead to any radical scavenging by any of the spin traps utilized.

Spin-scavenging Experiments

We have already reported (11) on the successful use of classical Br_2 scavenging experiments with irradiated adamantane. Williams and co-worker (16) have shown that the spin-scavenging techniques described by Janzen (23) and McConnell and co-worker (24) can be successfully applied to radiation chemistry uses and we have utilized similar techniques in an attempt to clarify the controversy concerning the nature of the adamantyl radical produced by radiolysis. Various spin scavengers were investigated (2,2-dimethylpropionitrile oxide, 2,4,6-trimethylbenzonitrile oxide, and 2-methyl-2-nitrosopropane, all prepared by conventional techniques) but only 2-methyl-2-nitrosopropane gave any evidence of spin scavenging on radiolysis. The data from spin-scavenging experiments with 1-chloro- and 2-chloroadamantane are shown in Fig. 3, data from adamantane and diamantane in Fig. 4, and expanded views of the central line from spin-scavenging experiments with 1-chloroadamantane, adamantane, and diamantane, are shown in Fig. 5.

The data clearly indicate that the radical from adamantane and diamantane are almost certainly identical, and that this radical is similar to, if not identical with, the radical seen by radiolysis of 1-chloroadamantane. The nitrogen hyperfine constant ($a^N = 14.85 \pm 0.1$ G) is similar to that

Can. J. Chem. Downloaded from www.nrcresearchpress.com by 210.87.254.42 on 09/05/12
For personal use only.

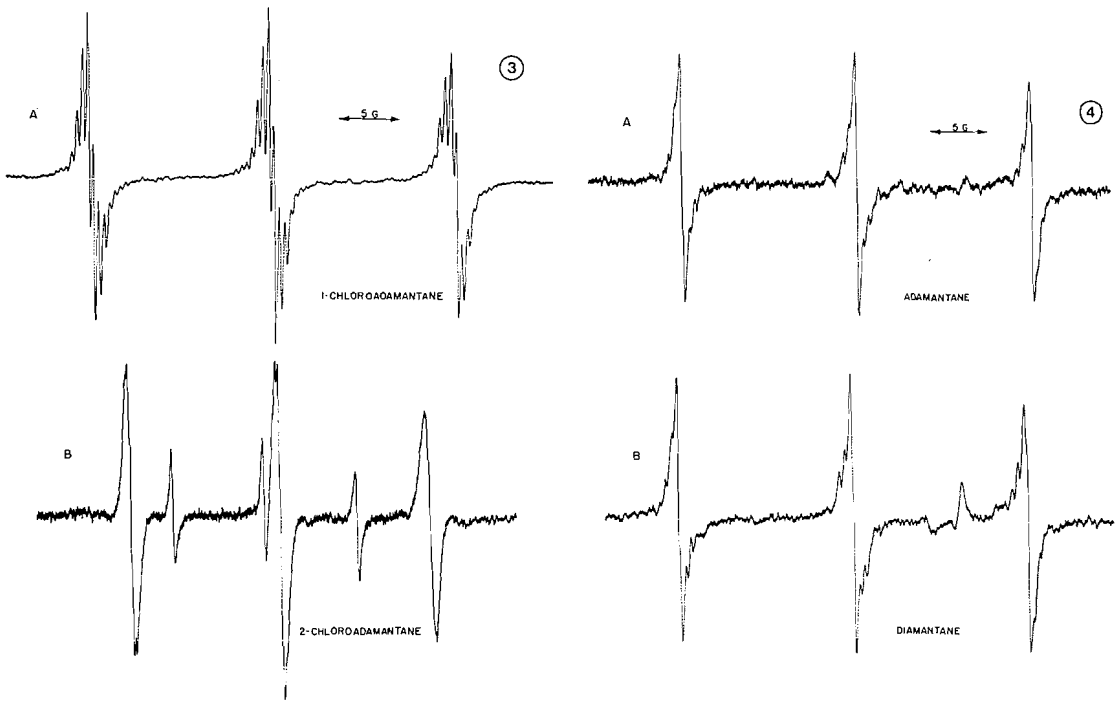

FIG. 3. First derivative e.s.r. spectra of radicals from adamantyl derivatives spin trapped by 2-methyl-2-nitrosopropane scavenger.

FIG. 4. First derivative e.s.r. spectra of radicals produced from adamantane and diamantane spin trapped by 2-methyl-2-nitrosopropane.

reported by Williams and co-worker (16) (14.5 G) and the fine structure due to the scavenged radical species is attributable to six equivalent nuclei with spin $\frac{1}{2}$ and coupling constant $a^H = 0.45 \pm 0.02$ G with a first-derivative peak-to-peak line width of *ca.* 0.3 G. This agrees well with the predicted spectrum for 1-adamantyl species, with little or no coupling being distinguishable from the γ-hydrogens of 1-adamantyl. No contribution from 2-adamantyl can be distinguished. Indeed, radiolysis and spin-scavenging experiments with 2-chloroadamantane do not show any spectra attributable to the 2-adamantyl radical at all (Fig. 3*b*). This is again a good indication of the instability of the 2-radical in solution (19) and the inability of this spin trap to scavenge these radicals prior to reaction. The fine structure exhibited in Fig. 3*b* appears to be interpretable in terms of radicals derived from the solvent (*n*-hexane) and could be due to hydrogen abstraction reactions, or other modes, by 2-adamantyl radicals on surrounding solvent molecules prior to scavenging.

In terms of experimental convenience, it was noted that best results (*i.e.* in terms of signal-to-noise ratio and radical populations produced) were obtained by direct radiolysis of degassed three-component systems under vacuum (adamantyl derivative at *ca.* 5–10 mol%, spin trap at 10^{-2} *M*, in a solvent such as *n*-hexane). Comparison with blank samples containing only spin trap in *n*-hexane showed that little or no spin scavenging of fragments from the solvent occurred, but that in the presence of either 1-chloroadamantane, or 2-chloroadamantane, intense (*ca.* 10–100 fold more intense) e.s.r. spectra resulted. The disadvantage of this method is that a possible mode of radical production from the adamantyl solute is via hydrogen abstraction initiated by solvent radicals. However, in view of the vastly different results from the 2-chloroadamantane relative to the 1-chloroadamantane, and the large increase in radical concentration over that observed for solvent alone, we feel that this reaction mode is, at best, a small contribution to the direct dissociative electron attachment mode believed to provide the major

Can. J. Chem. Downloaded from www.nrcresearchpress.com by 210.87.254.42 on 09/05/12
For personal use only.

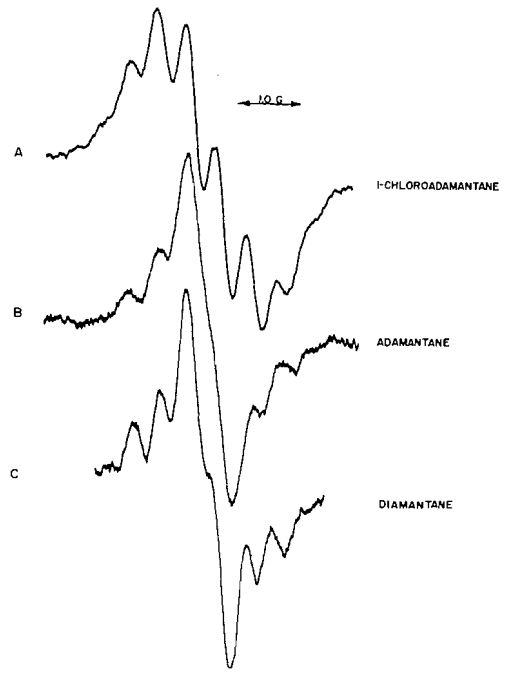

FIG. 5. The center line of the first derivative e.s.r. spectra from spin trapping by 2-methyl-2-nitrosopropane of radicals generated by radiolysis of (*a*) 1-chloroadamantane, (*b*) adamantane, and (*c*) diamantane.

source of radicals. Moreover, this form of secondary reaction is not possible for those cases where solid adamantyl derivatives were irradiated and then added to spin-trap solutions, an experimental technique that yielded qualitatively identical data. In view of the obvious analogies that this type of three-component system has with liquid scintillation counting techniques, it is possible that benzene would have made a better solvent system than *n*-hexane, reducing the possibility of solvent fragmentation, and increasing the energy transfer characteristics of the system as a whole.

In summary, due to long range coupling in the adamantane skeleton (9), a phenomenon apparently common to three-dimensional cage-type structures (26,27), it has not been possible to resolve adequately the hyperfine structure of e.s.r. signals from adamantane or adamantane derivatives, and thus to unequivocally identify the radical species produced by radiolysis in each molecule. However, fundamentally inferential evidence from a three-fold approach to this problem, involving Br_2 scavenging, spin scavenging, and comparative radiolyses of selected derivatives, has allowed us to make a reasonably consistent interpretation of the data. Even though resolution is so poor, computer simulations and direct comparison of envelopes to the e.s.r. spectra has proven to be a valuable adjunct in assigning structures, and has provided excellent supporting data in postulating formation of the 1-adamantyl radical at doses below *ca.* 3×10^{18} eV g^{-1}. Nevertheless, at least one anomaly seems to exist. Although spin trapping appears to deny the formation of 2-adamantyl species in solution, even from 2-adamantyl derivatives, Br_2 scavenging experiments show formation of both 1- and 2-adamantyl radicals on radiolysis of purified adamantane, albeit in a ratio of 3:1, respectively, but direct examination of e.s.r. spectra from radiolysis of adamantane itself discloses no discernible contribution. Nevertheless, prolonged radiolyses (*ca.* 5 h, 10^{19} eV g^{-1}) exhibit a typical spectrum from adamantane that in the light of the above data can only be explained by formation of the 2-adamantyl radical. We have no explanation of why the less stable species is enhanced at the expense of the more stable one on prolonged radiolysis.

Radiolyses of adamantyl derivatives has provided several interesting points. Firstly, although it is known that electron scavenging efficiency falls off as the molecular weight rises (28), both 1- and 2-adamantyl bromides and chlorides appear to undergo dissociative electron attachment quite readily (together with the 1-cyano derivative studied). Equally, 2-adamantanol and 2-adamantylamine appear to behave identically to simple aliphatic systems, with adamantanol resembling norborneol (27) directly, *i.e.* α-carbon radical formation. On the other hand, 1-adamantanol and 1-adamantylamine which lack the α-hydrogen, lead to vastly different behavior. By comparison of resulting envelopes, 1-adamantanol appears to produce a 2-adamantyl radical, which can be attributed to simple hydrogen loss at the β-position to the functional group (as is seen in radiolysis of *t*-butanol). On the other hand, 1-adamantylamine produces a spectral envelope quite unlike any from other derivatives. Attempts to explain this spectrum by loss of hydrogen from the $-NH_2$ group and consequent formation of an $-\dot{N}H$ radical have not been successful. Finally it is noted that direct radiolysis of purified diamantane (recrystallization), together with spin-trapping

Can. J. Chem. Downloaded from www.nrcresearchpress.com by 210.87.254.42 on 09/05/12
For personal use only.

evidence using 2-methyl-2-nitroso propane in solution, indicates that diamantane on radiolysis yields a similar radical to that from adamantane, the corresponding bridgehead radical (4-diamantyl).

We wish to thank The Research Corporation, The Dreyfus Foundation, and the American Cancer Society for partial support of this project and the Department of Chemical Engineering of W. Virginia University for use of their facilities. Material presented herein was taken from work submitted by GJH in partial fulfillment of the requirements for the M.S. degree at West Virginia University, 1973.

1. D. R. GEE, L. FABES, and J. K. S. WAN. Chem. Phys. Lett. **7**, 311 (1970).
2. L. BONNAZOLA and R. MARX. Chem. Phys. Lett. **8**, 413 (1971).
3. J. R. FERRELL, G. R. HOLDREN, R. V. LLOYD, and D. E. WOOD. Chem. Phys. Lett. **9**, 343 (1971).
4. W. G. FILBY and K. GÜNTHER. Chem. Phys. Lett. **14**, 440 (1972).
5. W. G. FILBY and K. GÜNTHER. Chem. Phys. Lett. **17**, 150 (1972).
6. W. G. FILBY and K. GÜNTHER. Z. Naturforsch. **27**, 1289 (1972).
7. R. MARX. Chem. Phys. Lett. **17**, 152 (1972).
8. R. V. LLOYD and M. T. ROGERS. Chem. Phys. Lett. **17**, 428 (1972).
9. P. J. KRUSIC, T. A. RETTIG, and P. v. R. SCHLEYER. J. Am. Chem. Soc. **94**, 995 (1972).
10. K. HATTENBACH and E. VOM BAUR. Atomkernenergie, **11**, 262 (1962).
11. G. J. HYFANTIS and A. C. LING. Chem. Phys. Lett. (1973). In press.
12. R. E. LINDER and A. C. LING. Can. J. Chem. **50**, 3982 (1972).
13. B. L. EMLING, R. J. HORVATH, A. J. SARACENO, E. F. ELLERMEYER, L. HAILE, and L. D. HUDAC. J. Org. Chem. **24**, 657 (1959).
14. W. D. EMMONS. J. Am. Chem. Soc. **79**, 5749 (1957).
15. W. D. EMMONS. J. Am. Chem. Soc. **79**, 6522 (1957).
16. J. A. WARGON and F. WILLIAMS. J. Am. Chem. Soc. **94**, 7917 (1972).
17. T. RICHERZHAGEN and D. H. VOLMAN. J. Am. Chem. Soc. **93**, 2062 (1971).
18. A. C. LING. J. Chem. Educ. In press.
19. I. TABUSHI, Y. AOYAMA, S. KOJO, J. HAMURO, and Z. YOSHIDA. J. Am. Chem. Soc. **94**, 1177 (1972).
20. P. v. R. SCHLEYER and R. D. NICHOLAS. J. Am. Chem. Soc. **83**, 2700 (1961).
21. T. RICHERZHAGEN, P. SVEJDA, and D. H. VOLMAN. J. Phys. Chem. **77**, 1819 (1973).
22. A. C. LING and J. E. WILLARD. J. Phys. Chem. **72**, 1918, 3349 (1968).
23. E. G. JANZEN. Acc. Chem. Res. **4**, 31 (1971).
24. C. L. HAMILTON and H. M. MCCONNELL. *In* Structural chemistry and molecular biology. *Edited by* Rich and Davison. Freeman and Co. 1968. pp. 115–148.
25. J. S. HUTZLER, R. J. COLTON, and A. C. LING. J. Chem. Eng. Data, **17**, 324 (1972).
26. L. BONNAZOLA and R. MARX. Mol. Phys. **19**, 405, 899 (1970).
27. J. GLOUX, M. GUGLIELMI, and H. LEMAIRE. Mol. Phys. **17**, 425 (1969).
28. J. E. WILLARD. Science, **180**, 553 (1973).

Can. J. Chem. Downloaded from www.nrcresearchpress.com by 210.87.254.42 on 09/05/12
For personal use only.

Can. J. Chem. Downloaded from www.nrcresearchpress.com by 210.87.254.42 on 09/05/12
For personal use only.

Canadian Journal of Chemistry

Published by
THE NATIONAL RESEARCH COUNCIL OF CANADA

Journal canadien de chimie

Publié par
LE CONSEIL NATIONAL DE RECHERCHES DU CANADA

Volume 52 Number 8(Part 1) April 15, 1974

Volume 52 numéro 8(partie 1) 15 avril 1974

The High Resolution Photoelectron Spectra of some Iodoalkanes, Iodocycloalkanes, Iodoalkenes, and Fluoroiodohydrocarbons

ROBERTO ANGELO ANTONIO BOSCHI
Sandoz AG, CH-4002, Basel, Switzerland
AND
DENNIS RUSSELL SALAHUB
Quantum Theory Group, Department of Applied Mathematics, University of Waterloo, Waterloo, Ontario N2L 3G1

Received October 17, 1973

The high resolution photoelectron spectra for the following iodine-containing molecules have been measured: iodomethane, iodoethane, 1-iodopropane, 1-iodobutane, 1-iodopentane, 1-iodohexane, 2-methyl-1-iodopropane, 3-methyl-1-iodobutane, 2-iodopropane, iodocyclopentane, iodocyclohexane, 2-methyl-2-iodopropane, trifluoroiodomethane, 2,2,2-trifluoro-1-iodoethane, pentafluoroiodoethane, 3,3,3,2,2,1,1-heptafluoro-1-iodopropane, iodobenzene, pentafluoroiodobenzene, vinyl iodide, allyl iodide. The spectra are discussed in terms of extended Hückel (EH) molecular orbital calculations and of the qualitative changes upon variation of the alkyl group.

On a mesuré les spectres de photoélectrons à haute résolution des iodures suivantes: iodométhane, iodoéthane, iodo-1 propane, iodo-1 butane, iodo-1 pentane, iodo-1 hexane, méthyl-2 iodo-1 propane, méthyl-3 iodo-1 butane, iodo-2 propane, iodocyclopentane, iodocyclohexane, méthyl-2 iodo-2 propane, trifluoroiodométhane, trifluoro-2,2,2 iodo-1 éthane, pentafluoroiodoéthane, heptafluoro-1,1,2,2,3,3,3 iodo-1 propane, iodobenzène, pentafluoroiodobenzène, iodure de vinyle et iodure d'allyle. On discute les spectres a l'aide des calculs d'orbitales moléculaires dans l'approximation de Hückel étendue et aussi en fonction des changements qualitatifs lors de la variation du groupe alkyle.
[Traduit par le journal]

Can. J. Chem., **52**, 1217 (1974)

Introduction

We have recently presented the far u.v. spectra of a large number of simple molecules containing a single iodine atom (1, 2). In these papers we found it useful to make comparisons with the photoelectron (p.e.) spectra and discussed some of the principle features of the latter. In the present paper we present the high resolution p.e. spectra in their own right. These are in almost all respects simpler than the u.v. spectra and give directly the ionization potentials (i.p.'s) of the molecule and (in the approximation of Koopmans' theorem (3)) the orbital energies, that is, the experimental quantities corresponding to the eigen values of the Hartree–Fock equations.

The molecules studied are (iodomethane), iodoethane, (1-iodopropane), (1-iodobutane), (1-iodopentane), 1-iodohexane, 2-methyl-1-iodopropane, (3-methyl-1-iodobutane), 2-iodopropane, iodocyclopentane, iodocyclohexane, (2-methyl-2-iodopropane), trifluoroiodomethane, 2,2,2-trifluoro-1-iodoethane, pentafluoroiodoethane, 3,3,3,2,2,1,1-heptafluoro-1-iodopropane, iodobenzene, pentafluoroiodobenzene, vinyl io-

Can. J. Chem. Downloaded from www.nrcresearchpress.com by 210.87.254.42 on 09/05/12
For personal use only.

dide, allyl iodide. Because of space restrictions the spectra of the molecules in parentheses are not presented here.[1]

Some of these molecules have been studied in part by previous workers. The p.e. spectrum of iodomethane is well known (4–8). It is included here for completeness and since correlations will be drawn with it in the discussion of the remaining spectra. The spectra of the 1-iodoalkanes ($C_nH_{2n+1}I$; n = 1–5) and a few branched molecules have been measured (9–11) and the first two i.p.'s discussed in terms of the competition between spin–orbit coupling and conjugation; however, the discussion so far has been limited to the two lowest bands. Baker *et al.* (10) presented the spectra of iodoethane, 1-iodopropane, 2-iodopropane, and 1-iodopentane and discussed them very briefly. Very recently Kimura *et al.* (11) studied the spectra of RX (R = ethyl, *n*-propyl, *n*-butyl; X = Cl, Br, I) and attempted to correlate the spectra with the Pauling electronegativity of the halogen atom and gave an interpretation in terms of equivalent orbitals. A correlation diagram for the vinyl halides including vinyl iodide has been given by Turner *et al.* (12) without presenting the spectra themselves. The iodobenzene spectrum is known (12). Below we give an interpretation of some of the higher bands which differs from that of ref. 12. The spectrum of 2,2,2-trifluoro-1-iodoethane has been presented by Turner (4) with, however, only a very brief discussion of the spin–orbit splitting of the first two bands.

The unifying feature of the present work is of course the presence of the iodine atom and the behavior of the various bands upon changing of the alkyl group. Below we attempt to give a consistent assignment for most of the bands out to about 18 eV. The assignment of the methyl iodide spectrum is quite straightforward. For the other molecules, with the exception of the work by Kimura *et al.* (11) on ethyl, propyl, and butyl iodide, virtually no attempt has been made to assign the bands at higher energy. Also since many of our spectra are better resolved than those available in the literature we feel that any repetition implied in the last paragraph is justified.

[1]The spectra are available at a nominal charge from the Depository of Unpublished Data, National Science Library, National Research Council of Canada, Ottawa, Canada K1A 0S2. The spectra are numbered D1 to D6 in the order in which they appear above.

To help in our interpretation of the spectra we have carried out molecular orbital (m.o.) calculations of the extended Hückel (EH) type (13) for all of the molecules.

Experimental and Computational Methods

The p.e. spectra were measured with a Perkin-Elmer PS 16 instrument using a HeI source and an electrostatic analyzer with a sector field of 127°. The resolution was approximately 20 mV. All chemicals were from Koch-Light or Fluka A.G. and were purified by gas-phase chromatography before use.

The EH program was based on a standard program (14) modified to calculate overlap integrals involving 5s and 5p orbitals (15, 16). The orbital exponents used were those proposed by Burns (17) which we have found usually give better overall agreement with observed p.e. spectra than the usual Slater values. A value of 1.5 for the constant k which enters the off-diagonal matrix elements was found to give the best results.

Calculations using a modified CNDO method (18) were also carried out; however, the agreement between these and the observed spectra was not nearly as good as that of the EH calculations. A re-evaluation of the parameters which enter the CNDO method or the inclusion of one-center exchange integrals to yield an INDO method could conceivably improve the agreement. Below we report only the EH results. For the fluorinated molecules the EH results failed to correlate with the observed spectra. This is a usual situation for EH calculations on molecules containing highly electronegative atoms. The EH results are not given in these cases but rather qualitative considerations are used to assign the bands.

Results and Discussion

Those spectra which we present are in Fig. 1 and the observed maxima (vertical i.p.'s) for all of the molecules, including those whose spectra are in the Depository of Unpublished Data, are gathered in Table 1 along with the results of the calculations. In all cases where the i.p.'s were also determined from Rydberg series in the far-u.v. spectrum (1) the two values agree within the experimental uncertainty. The molecules may be conveniently divided into four categories, *viz.*, normal iodoalkanes, branched and cyclic iodoalkanes, fluoroiodoalkanes, and iodoalkenes.

Normal Iodoalkanes

The prototype of this series is methyl iodide, the p.e. spectrum of which is well documented (4–8). We will give a brief description of this spectrum since the succeeding spectra may then be discussed with reference to it. The valence electronic configuration of ground-state methyl iodide (C_{3v} symmetry) is

$$(1a_1)^2(2a_1)^2(1e)^4(3a_1)^2(2e)^4$$

Can. J. Chem. Downloaded from www.nrcresearchpress.com by 210.87.254.42 on 09/05/12
For personal use only.

The lowest lying m.o.'s $1a_1$ and $2a_1$ are essentially the in-phase and out-of-phase combinations, respectively, of carbon 2s and iodine 5s atomic orbitals. The 1e m.o. may be regarded as a degenerate CH bonding orbital; the $3a_1$ m.o. corresponds to the CI bond and the 2e level to the 5p lone pairs of iodine which have π symmetry with respect to the CI bond.

The presence of the iodine atom leads to large interactions between electron spin and orbital angular momenta so that configurations involving unpaired electrons in degenerate m.o.'s with large coefficients on the iodine must be treated using double groups (19). Thus removal of an electron from 2e gives rise to $E_{3/2}$ and $E_{1/2}$ states which are observed at 9.54 and 10.14 eV, respectively. Ionization from $3a_1$ occurs at 12.5 while the two Jahn–Teller split components of 1e are observed at 14.7 and 15.5 (shoulder). A peak at 19.5 eV is assigned to $2a_1$. Ionization from $1a_1$ has not yet been observed. Price[2] predicts a value of about 21 to 21.5 eV for HI on the basis of an extrapolation in the series XH_n ($n = 0, 1, 2, 3, 4$) across a row in the periodic table. Since a carbon 2s electron is more tightly bound than a hydrogen 1s we would expect $1a_1$ to be a bit deeper than this in CH_3I, perhaps at around 22 or 23 eV. The HeII spectrum would locate this level. For CH_3Br, Åsbrink[3] in fact found the lowest band in the HeII spectrum just about 1 eV lower than the value which Price predicted for HBr.

Thus the whole of the p.e. spectrum of methyl iodide is qualitatively understood. The EH calculations mirror the observed spectrum very well, except of course for the splitting of the 2e and 1e levels due to spin–orbit coupling and Jahn–Teller distortion, respectively.

What happens when the symmetry of the molecule is lowered by substituting a longer alkyl group for the methyl group? Inasfar as the first two bands (corresponding to $E_{3/2}$ and $E_{1/2}$ of CH_3I^+) are concerned the question has been studied by Brogli and Heilbronner (9). If we assume C_s symmetry for the 1-iodoalkanes, then the 2e level is split into an a′ and an a″ level, both yielding $E_{1/2}$ states of the molecular cation, the a′ orbital being less tightly bound. For the case of zero spin–orbit coupling this is the only effect. The a′–a″ energy difference found in the EH results indicates that this split is rather small. The observed split is nearly the same as that of CH_3I (between 0.58 and 0.56 eV for all the 1-iodoalkanes) so it seems that the orbital is very much localized on the iodine atom and "sees" only the local cylindrical symmetry about the CI bond and that the orbital angular momentum is only slightly quenched by the alkyl group.

The observed and calculated i.p.'s for the five lowest states are shown in Fig. 2 as a function of the number of carbon atoms in the alkyl group. The gradual shift to lower i.p. and smaller spin–orbit splitting for the first two bands with increasing length of the alkyl chain can both be explained by a slight delocalization of the lone pair onto the alkyl group. This shift to lower i.p. is present but less accentuated in the EH results. The population on the iodine atom in the a′ orbital is 92, 91, 89, 87, 87, and 86% as the series is ascended. This slight delocalization is also consistent with the short vibrational progressions observed. Each of the bands shows a spacing near 1100 cm^{-1} which is assigned to a CH_2 wagging vibration (1, p. 289).

The third band in all of these spectra is in analogy with CH_3I and as supported by the EH results assigned to ionization of a CI $2p\sigma_C + 5p\sigma_I$ bonding electron. It too undergoes a shift to lower i.p. as the length of the alkyl group increases. This behavior is shown in Fig. 2, along with the EH results which reflect the shift satisfactorily. The shift is due to a gradual increase in the delocalization of the orbital over the molecule.

The following bands out to about 18 eV are due to ionizations from the CH and CC bonds. With the delocalized m.o.'s obtained from the EH calculations it is often not possible to identify orbitals corresponding to localized bonds so that when we speak of CC and CH bonds below it should be understood that we are referring to m.o.'s which are mainly bonding combinations of atomic orbitals between carbons or carbon and hydrogen.

For iodoethane and iodopropane there is a one-to-one correspondence between the calculated levels and the observed maxima while for the larger molecules fewer maxima are observed than calculated indicating an overlapping of close-lying bands. It would be interesting to know which of these peaks corresponds to mainly CC and which to CH orbitals. Calculations using the equivalent orbital method which is based on

[2]Professor W. C. Price. Personal communication.
[3]Dr. L. Åsbrink. Personal communication.

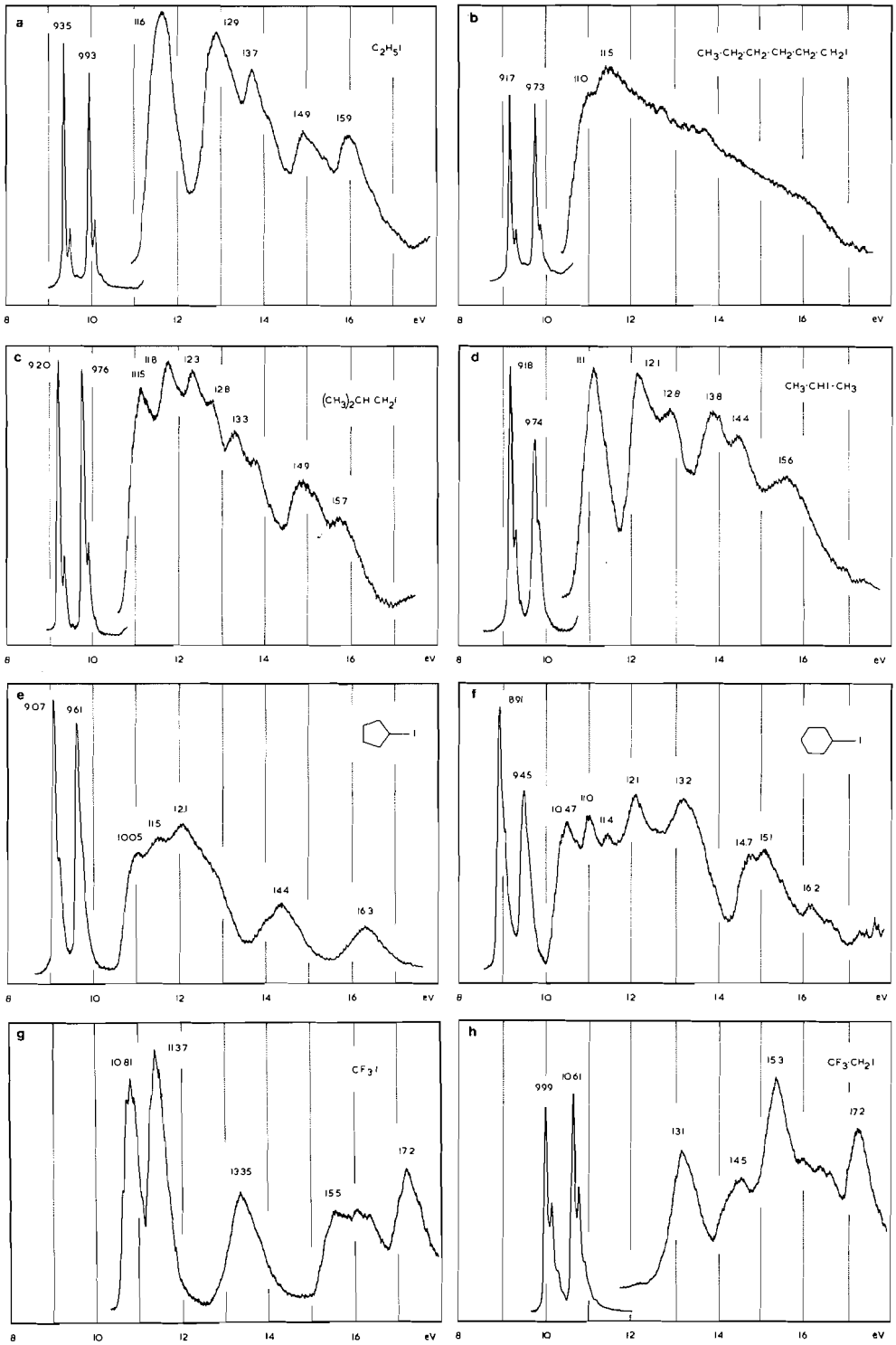

Can. J. Chem. Downloaded from www.nrcresearchpress.com by 210.87.254.42 on 09/05/12
For personal use only.

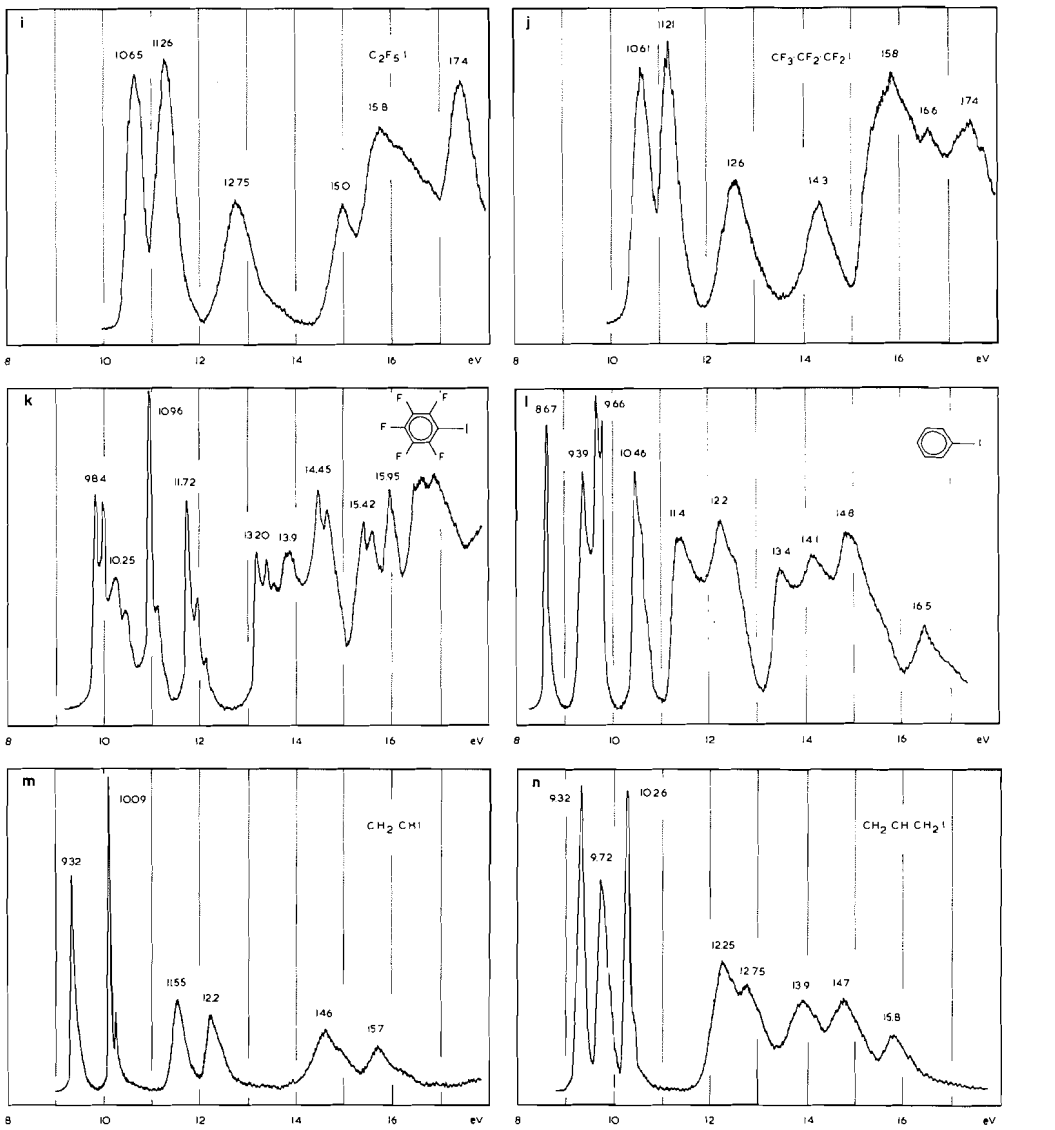

FIG. 1. The photoelectron spectra of (*a*) iodoethane, (*b*) 1-iodohexane, (*c*) 2-methyl-1-iodopropane, (*d*) 2-iodopropane, (*e*) iodocyclopentane, (*f*) iodocyclohexane, (*g*) trifluoroiodomethane, (*h*) 2,2,2-trifluoro-1-iodoethane, (*i*) pentafluoroiodoethane, (*j*) 3,3,3,2,2,1,1-heptafluoro-1-iodopropane, (*k*) iodobenzene, (*l*) pentafluoroiodobenzene, (*m*) vinyl iodide, (*n*) allyl iodide.

the concept of interacting bonds and is "calibrated" with observed spectra could be interesting in this respect. Kimura *et al.* (11) came to the conclusion, on the basis of a type of equivalent orbital calculation, that in ethyl iodide the ionization from the CC orbital precedes that from a CH orbital. They made several drastic simplifications, however, and we show below that in the case of ethyl iodide the substitution of fluorine for some or all of the hydrogens allows us to make this distinction assigning the bands at 12.9, 14.9, and 15.5 eV to CH orbitals, and that at 13.7 eV to the CC bonding electron. Similarly for propyl iodide the band at 12.9 eV is assigned to ionization from a CC orbital and that at 12.3 eV to a CH orbital. Throughout the series of 1-iodoalkanes the two bands which appear at 12.9 and 13.7 eV in iodoethane appear with nearly the same form only shifted slowly to lower i.p. This shift is well accounted for by the

Can. J. Chem. Downloaded from www.nrcresearchpress.com by 210.87.254.42 on 09/05/12
For personal use only.

TABLE 1. Observed and calculated (extended Hückel) ionization potentials (eV) and symmetry species for iodine containing molecules

Molecule	Ionization potential		Symmetry species
	Obs.	Calcd.	
CH_3I (C_{3v})	9.54	10.10	e
	10.16		
	12.5	11.82	a_1
	14.7	14.78	e
	15.5		
	19.5	19.70	a_1
		23.65	a_1
C_2H_5I (C_s)	9.35	10.04	a′
	9.93	10.17	a″
	11.6	11.77	a′
	12.9	13.49	a′
	13.7	14.15	a″
	14.9	14.74	a′
	15.9	15.15	a″
C_3H_7I (C_s)	9.26	10.02	a′
	9.83	10.16	a″
	11.4	11.53	a′
	12.3	13.20	a′
	12.9	13.55	a′
	13.5	13.89	a″
	13.8	14.53	a″
	14.4	14.77	a′
	15.9	15.40	a″
C_4H_9I (C_s)	9.23	9.99	a′
	9.79	10.17	a″
	11.27	11.48	a′
	11.8	12.98	a′
	12.3	13.36	a′
	13.5	13.75	a′
	14.1	13.90	a″
		14.17	a″
	14.8	14.78	a″
		14.87	a″
	16.0	15.48	a″
$C_5H_{11}I$ (C_s)	9.20	9.99	a′
	9.76	10.17	a″
	11.05	11.42	a′
	11.55	12.77	a′
	12.9	13.10	a′
		13.59	a′
		13.89	a′
	13.7	13.89	a″
		14.00	a″
	14.3	14.47	a″
		14.78	a′
		15.09	a″
	~15.5	15.54	a″
$C_6H_{13}I$ (C_s)	9.20	9.97	a′
	9.76	10.17	a″
	11.0	11.35	a′
$C_6H_{13}I$ (C_s) (*contd.*)	11.5	12.48	a′
		13.10	a′
		13.34	a′
		13.78	a′
		13.89	a′
		13.91	a″
		13.93	a″
		14.20	a″
		14.71	a″
		14.78	a′
		15.23	a″
		15.58	a″
i-C_4H_9I (C_s)	9.20	9.64	a′
	9.76	9.98	a″
	11.15	11.72	a′
	11.8	12.69	a″
	12.3	12.72	a′
	12.8	13.83	a′
	13.3	14.28	a″
		14.54	a″
	14.9	14.92	a′
		14.94	a″
	15.7	15.12	a′
i-$C_5H_{11}I$ (C_1)	9.20	9.92	a
	9.75	10.16	a
	11.05	11.40	a
	11.55	12.55	a
	11.95	12.91	a
	12.8	13.48	a
	13.4	13.69	a
		14.07	a
		14.44	a
		14.51	a
		14.89	a
		15.04	a
		15.34	a
i-C_3H_7I (C_s)	9.18	9.92	a″
	9.74	10.06	a′
	11.1	11.37	a′
	12.1	13.01	a″
	12.8	13.47	a′
	13.8	14.50	a″
	14.4	14.53	a″
		14.85	a′
	15.6	15.11	a′
c-$C_5H_{11}I$ (C_1)	9.07	8.89	a
	9.61	10.12	a
	10.05	10.81	a
	11.5	11.86	a
	12.1	12.51	a
		13.11	a

Can. J. Chem. Downloaded from www.nrcresearchpress.com by 210.87.254.42 on 09/05/12
For personal use only.

TABLE 1. (*Concluded*)

Molecule	Ionization potential Obs.	Ionization potential Calcd.	Symmetry species
c-$C_5H_{11}I$ (C_1) (*contd.*)		13.69	a
		14.15	a
		14.33	a
	14.40	14.40	a
		15.01	a
	16.3	15.40	a
c-$C_6H_{13}I$ (C_s)			
Equatorial	8.91	9.88	a″
	9.45	10.01	a′
	10.47	11.07	a′
	11.0	12.35	a″
	11.4	12.97	a′
	12.1	12.98	a″
		13.38	a″
	13.2	13.53	a′
		13.64	a′
	14.7	14.20	a″
		14.64	a′
		14.92	a″
	15.1	15.03	a′
	16.2	15.18	a′
Axial		9.58	a′
		9.81	a″
		11.45	a′
		12.34	a′
		12.36	a″
		12.93	a″
		13.37	a″
		13.51	a′
		13.97	a′
		14.20	a″
		14.61	a′
		14.95	a″
		15.12	a′
		15.19	a′

Molecule	Ionization potential Obs.	Ionization potential Calcd.	Symmetry species
t-C_4H_9I (C_{3v})	9.04, 9.59	9.87	e
	10.75	11.14	a_1
	11.9	12.72	e
	12.4	14.28	a_2
	13.0	14.53	e
	13.7	14.93	e
	15.2	14.98	a_1
Iodobenzene (C_{2v})	8.67	9.84	b_2
	9.39	10.19	b_1
	9.66	11.05	a_1
	10.46	12.46	a_2
	11.4	12.61	a_1
	12.2	12.62	b_1
		13.21	b_2
	13.4	13.25	a_1
		13.98	b_1
	14.1	14.01	b_2
	14.8	14.96	a_1
	16.5	15.97	a_1
Vinyl iodide (C_s)	9.32	10.01	a′
	10.09	10.31	a″
	11.55	11.74	a′
	12.2	13.07	a″
	14.6	13.81	a′
	15.7	14.93	a′
Allyl iodide (C_1)	9.32	10.02	a
	9.72	10.12	a
	10.26	11.70	a
	12.25	12.83	a
	12.75	13.16	a
	13.9	13.91	a
	14.7	14.70	a
	15.8	15.14	a

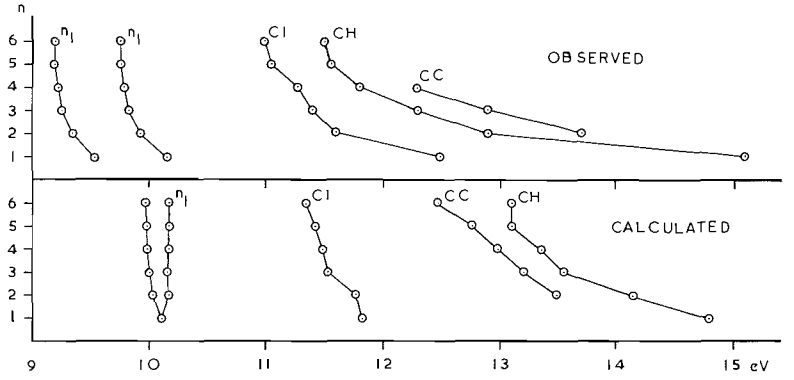

FIG. 2. Calculated and observed i.p.'s of 1-iodoalkanes as a function of the number of carbon atoms in the alkyl group.

Can. J. Chem. Downloaded from www.nrcresearchpress.com by 210.87.254.42 on 09/05/12
For personal use only.

Can. J. Chem. Downloaded from www.nrcresearchpress.com by 210.87.254.42 on 09/05/12
For personal use only.

EH calculations; however the order of the CH and CC levels is reversed from what we expect on the basis of the spectra of the fluorinated molecules, the uppermost calculated m.o. being primarily in the CC bonds. They are, however, reasonably close in energy and in view of the simple nature of the calculations it is not surprising to find inversion of some close-lying levels. We believe the qualitative arguments given below are in this instance more reliable than the calculations, so that we assign the first of these bands to ionization from a CH orbital and the second to a CC orbital. For the larger molecules this area of the spectrum degenerates into a single broad band because of the presence of a large number of close-lying levels (see Fig. 1*b*).

As was the case for methyl iodide there is then a large gap in the spectrum until the onset of ionization from levels involving carbon 2s and iodine 5s orbitals.

Branched and Cyclic Alkanes

As was the case for the u.v. spectra (1, p. 735) the p.e. spectra of the slightly branched molecules, 2-methyl-1-iodopropane and 3-methyl-1-iodobutane, are very similar to those of their straight-chain isomers so that the discussion above holds.

When the iodine is attached to a secondary or tertiary carbon (Fig. 1*d–f*) the mixing of the lone-pair orbitals with the alkyl group is presumably greater and results in a slight lowering of the first i.p. and a small decrease in the spin–orbit splitting. The appearance of the first component is essentially unaltered whereas the second has lost its discrete fine structure. A similar diffuseness was noted for the Rydberg bands leading to this i.p. (1, p. 735) and may be attributed to predissociation. The lowering of the i.p. for the first two bands is reflected in the EH results in a reasonable manner. The calculated first i.p. for cyclopentyl iodide is a bit too low compared with the other values.

The next band is once again assigned to ionization of a CI bonding electron. It too has undergone a shift to lower i.p. with respect to the 1-iodoalkanes and once again these shifts are closely paralleled by the EH results. The remaining peaks out to 18 eV are due to ionization of CC and CH bonding electrons although it is not easy to make definite assignments.

For isopropyl iodide there is nearly a one-to-one correspondence between the observed and calculated bands, only one calculated level being unaccounted for in the spectrum. This is predicted to occur in the 14–15 eV region where the spectrum consists of broad overlapping bands and is surely present although unresolved.

Fluoroiodoalkanes

Brundle and co-workers (20, 21) have examined the effect on p.e. spectra of substituting fluorine for all of the hydrogens of a molecule. Their main conclusion was that in planar molecules perfluorination causes the i.p.'s to shift upwards by 0–1 eV for π electrons and by 2–3 eV for σ electrons. In nonplanar molecules the above distinction cannot be made; however, it has been observed that all the levels are shifted to higher i.p. by varying amounts.

The spectra of CF_3I (**1**), CF_3CH_2I (**2**), C_2F_5I (**3**), and C_3F_7I (**4**) are shown in Fig. 1*g–j*. Below we discuss the effect of fluorination on the position of the lone-pair bands and their spin–orbit splitting and the effect on the CC and CH levels. The region above about 15.5 eV is complex owing to the presence of bands due to the ionization of fluorine lone pairs and electrons in CF bonds (see Fig. 1*g*). No attempt is made to analyze this region. As stated above, the EH calculations are not much help in this respect so that we prefer to use qualitative arguments.

The presence of two relatively sharp bands separated by nearly the same amount as the two lone-pair bands in the perhydrogeno compounds leaves the assignment of the first peaks of **1–4** to lone-pair ionizations beyond reasonable doubt. The center of gravity of these two bands has undergone a shift of 1.25–1.35 eV for the perfluoro compounds and of 0.65 eV for the partially fluorinated molecule **2**.

The most striking difference in these peaks is that they have become much broader and exhibit some poorly resolved fine structure. This broadening is of course least for **2** where the bands still resemble those of iodoethane, except that now the 1–0 transition has gained significantly in intensity. This fine structure indicates that the "lone pairs" are in fact somewhat delocalized over the molecule.

The splitting between the bands has, however, remained practically constant being 0.56, 0.62, 0.62, and 0.60 eV for **1–4** (taken between the most intense vibrational peak of each band) and 0.62,

Can. J. Chem. Downloaded from www.nrcresearchpress.com by 210.87.254.42 on 09/05/12
For personal use only.

0.58, and 0.57 eV for iodomethane, iodoethane, and iodopropane, respectively. A mechanism similar to that proposed by Brogli and Heilbronner (9) may be applicable. That is, we know that the orbital is delocalized because of the broadness of the band and the vibrational structure. We would therefore expect the spin–orbit splitting to be smaller. The inclusion of spatial effects, however, (by coincidence) nearly cancels this out. As the interaction with the rest of the molecule increases we would expect to see larger splittings dominated by the conjugative effects (see vinyl iodide below).

The following band in all the spectra is well separated both from the lone-pair bands and from the bands at higher i.p. and is assigned to ionization of a CI bonding electron. The shifts undergone with respect to the perhydrogeno molecules are 0.85, 1.5, 1.15, and 1.2 eV for **1**–**4**. It is not immediately apparent why the largest shift occurs for the partially fluorinated molecule. A plausible explanation in terms of equivalent orbitals proceeds as follows. The self-energy of the CI bond becomes more negative upon inclusion of fluorine. The presence of fluorines in the α position then leads to large interaction matrix elements with the fluorine lone pairs and the CF bonds causing a shift to lower i.p. for the perfluoro compounds but not for **2** since it only has fluorines in the β position. A study of further partially fluorinated iodides might throw some light on this.

The position of bands due to the CC and CH electrons is not obvious as these fall in the same region as the fluorine ionizations. However, a comparison of the spectra of C_2H_5I, **2**, and **3** is illuminating. Let us assume that in each molecule the CI and the CC bond undergo nearly the same shift upon fluorination. This is not unreasonable since they have the same symmetry and not too different energies. If we then shift the spectra so that the CI bands coincide (Fig. 3) we see that the 12.9 eV band of ethyl iodide becomes weaker for **2** and disappears altogether for **3** indicating that this band is due to ionization of a CH electron. This band is followed by a band which very nearly coincides in the three (shifted) spectra and is reasonably assigned to a CC electron. In a similar manner the band at 14.3 eV of **4**, which is now clearly separated from the fluorine bands is assigned to a CC orbital as is the 12.9 eV band of *n*-propyl iodide. The band at 12.3 eV in *n*-propyl iodide is absent in the (shifted) spectrum of **4** and is thus assigned to a CH orbital.

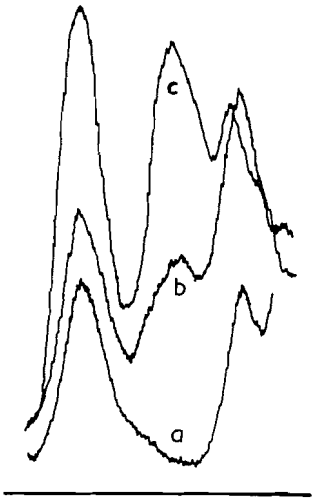

FIG. 3. Comparison of the spectra of iodoethane (*c*), 2,2,2-trifluoro-1-iodoethane (*b*), and pentafluoroiodoethane (*a*) shifted so that the bands due to ionization of the CI bonding electrons coincide.

Unsaturated Molecules

For most of the iodoalkanes discussed above it was rather easy to identify the bands due to the iodine lone-pair electrons. The lone pairs are reasonably well localized on the iodine atom and are influenced by a potential due to the alkyl group which has nearly C_{3v} symmetry so that a discussion in terms of spin–orbit coupling is meaningful and in fact the lone-pair bands are very similar to those in methyl iodide.

The situation in unsaturated iodides is somewhat more complicated since large conjugative effects may come into play, yielding rather delocalized lone pairs which give bands in the p.e. spectrum which have lost some of their characteristic sharpness.

We start our discussion of the unsaturated molecules with iodobenzene (Fig. 1*k*) since our discussion of vinyl iodide (Fig. 1*m*) will depend to some extent on this.

The p.e. spectrum of benzene is well known (22) and has bands at 9.6, 11.4, and 12.1 eV which are assigned to $e_{1g}(\pi)$, $e_{2g}(\sigma)$ and $a_{2u}(\pi)$ orbitals, respectively. If a halogen atom is now substituted for one of the hydrogens one of the lone pairs (out-of-plane) can conjugate with the π system of the ring. The other lone pair (in-plane) has σ symmetry and would interact with the ring σ

electrons. We would expect this interaction to be less and might expect an energy level diagram, such as that of Scheme 1, to result.

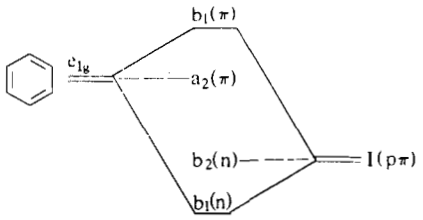

SCHEME 1

The e_{1g} level of benzene is split through mixing with the iodine π lone pair giving b_1 and a_2 levels. The a_2 orbital has a node running through the iodine atom so that this level should be quite close to the degenerate e_{1g} level of benzene. The b_1 orbitals are mixtures of ring and halogen orbitals, the relative weights depending on which halogen is considered.

It is instructive to consider the behavior of these levels throughout the series of halobenzenes (C_6H_5X; X = Cl, Br, I). In Table 2 we have gathered the i.p.'s for the $b_1(\pi)$, $a_2(\pi)$, $b_2(n)$, and $b_1(n)$ levels for all of the molecules. These are taken from Turner's book (12) or the present work. The difference between the $a_2(\pi)$ and $b_2(n)$ levels may be taken as the difference between the unperturbed orbitals. In Fig. 4 we have plotted the energy shift of the π lone-pair orbital *vs.* the distance between the unperturbed levels for the three halobenzenes. The variation is monotonic and we will use this figure later on in the discussion of vinyl iodide.

It might at first sight seem strange to have assigned the band at 9.39 eV to the $a_2(\pi)$ level since this level was much closer to 9.7 eV in the chloro and bromo compounds, and in fact there is a band at 9.66 in the iodobenzene spectrum. However in both chloro- and bromobenzene the lone-pair band is the strongest band in the spectrum and exhibits some vibrational structure so we must assign the 9.66 eV band of iodobenzene to the $b_2(n)$ orbital. In summary then we agree with the assignments of Turner *et al.* (12) for the first four bands as $b_1(\pi)$, $a_2(\pi)$, $b_2(n)$, $b_1(n)$.

TABLE 2. Ionization potentials of halobenzenes (eV)

	Ionization potential (eV)			
Molecule	$b_1(\pi)$	$a_2(\pi)$	$b_2(n)$	$b_1(n)$
C_6H_6	9.6	9.6		
C_6H_5Cl	9.06	9.69	11.32	11.69
C_6H_5Br	9.05	9.67	10.61	11.18
C_6H_5I	8.67	9.39	9.66	10.46

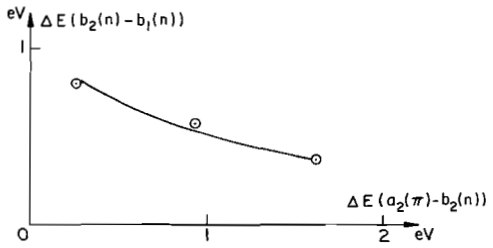

FIG. 4. Splitting of halogen lone-pair orbitals in halobenzenes *vs.* the separation of the unperturbed levels (eV).

Turner then assigned the following band at 11.4 eV to the third π level (a_{2u} in benzene). However it is now thought that the highest σ orbital precedes the lowest π (22) and the bands in benzene at 11.4 and 12.1 eV are assigned to ionization from the $3e_{2g}(\sigma)$ and $1a_{2u}(\pi)$ levels, respectively. We make the analogous assignment for the bands at 11.4 and 12.2 in iodobenzene. (It should be mentioned that agreement is not unanimous on this ordering (23).) The $3e_{2g}$ level should of course be split under the lower symmetry; however the magnitude of the splitting is liable to be small for σ electrons and is not resolved. Further confirmation of this assignment comes from the spectrum of pentafluoroiodobenzene (see below). Here the deepest π level occurs at 13.20 eV and the uppermost σ orbital at 13.9. The above assignment then gives shifts on perfluorination of 1.0 and 2.5 eV which are typical values for π and σ electrons, respectively (20, 21). The three other possible orderings of the lowest π and the highest σ orbitals in iodobenzene and pentafluoroiodobenzene would lead to shifts of the π level by 2.5, 1.8, and 1.7 eV and of the σ level by 1.0, 1.7, and 1.8 eV, respectively, which are not in keeping with previous experience.

We would expect ionization of a CI bonding electron to give rise to a band somewhere near 12.5 eV. There is a well pronounced shoulder on the high-energy side of the peak at 12.2 eV and we tentatively assign this to expulsion of an electron from the CI bond.

We have seen above the effect of fluorination on the spectra of ethyl and propyl iodide. As

Can. J. Chem. Downloaded from www.nrcresearchpress.com by 210.87.254.42 on 09/05/12
For personal use only.

TABLE 3. Predicted ionization potentials of vinyl halides (eV)

Molecule	Ionization potential (eV)					
	a*	b	c	d	e	f
C_2H_4	10.51					
C_2H_3Cl	10.51	11.32	0.81	0.47	11.79	11.80
C_2H_3Br	10.51	10.61	0.10	1.20	11.81	12.26
C_2H_3I	10.51	9.66	−0.85	0.45	9.21	9.32

*a, the unperturbed π level; b, the unperturbed lone-pair level (values taken from corresponding halobenzene); c, b − a; d, the predicted shift of the a'' lone pair (taken from Fig. 4); e, predicted value of a'' lone pair; f, observed values.

Brundle *et al.* (21) pointed out, in aromatic molecules perfluorination usually affects the π levels only slightly while shifting the σ levels to higher energy by about 2–4 eV. Thus in perfluorobenzene (12, 21) we find that the e_{1g} level occurs at 10.1 eV (a shift of 0.5 eV). This is followed by a gap of about 2.5 eV until a band at 12.8 eV which is due to the $e_{2u}(\pi)$ orbital (21). In iodobenzene the corresponding "gap" was about 3 eV and was filled with the two lone-pair bands separated by about 0.8 eV. We would expect to find these somewhat shifted in the fluorinated molecule.

In fact the first two π bands in pentafluoroiodobenzene occur at 9.84 and 10.25 eV and show some vibrational structure. These are shifted with respect to the corresponding bands in iodobenzene by 1.1 and 0.9 eV, respectively, which are reasonable values for π electrons. We then look for the third π band about 3 eV higher and assign the band at 13.20 accordingly.

This leaves two bands in the gap at 10.96 and 11.72 eV which are assigned to the in-plane and out-of-plane lone pairs, respectively. These are both shifted by about 1.3 eV. The band at 10.96 eV is sharp and the strongest in the spectra and must be assigned to the lone pair in the molecular plane. The shift of 1.3 eV is rather small for a σ electron so we presume this lone pair to be reasonably well localized and in fact the band is sharp and shows only a limited fine structure. The band at 11.72 on the other hand is considerably wider and shows three or four vibrational components indicating a larger degree of delocalization for this π lone pair. The following band at 13.9 is then assigned to the uppermost σ ring orbital as explained above.

As for the CI ionization, in the C_2H_5I–C_2H_5I case this band was shifted by 1.2 eV so we might look for it around 13.7 eV in the present case. This region is complicated; however, there is a small peak just at 13.7 eV.

We now turn to vinyl iodide (Fig. 1*m*). This is quite similar to the case of iodobenzene, one of the iodine lone pairs (a'' symmetry) mixing with the double bond and the other (a' symmetry) remaining relatively unaffected.

Let us also refer to the spectra of vinyl chloride (24) and vinyl bromide (25). The relevant data are gathered in Table 3. If we take the value for the unperturbed lone pair from the corresponding halobenzene and the unperturbed π level as the ethylene value 10.51 eV (12) and use Fig. 4 we can predict the location of the lone-pair bands. We see that the agreement (Table 3) is quite reasonable. Note that in vinyl iodide the unperturbed lone pair has a lower i.p. than ethylene so we would expect the uppermost orbital to be mostly on the iodine, in vinyl bromide the two are very close and highly mixed π and lone-pair orbitals would result, while in vinyl chloride the uppermost level will be mostly the C=C π orbital. The mixing can be seen in the shape of the bands in the vinyl iodide spectrum, the second band being very sharp and intense, a typical lone-pair band, while the first and especially the third are somewhat broader indicating a larger mixing. The first band is still, however, reasonably sharp and is surely predominately a lone-pair band.

The next band at 12.2 eV is assigned to expulsion of a CI bonding electron (12.5 eV in CH_3I, 11.6 eV in C_2H_5I). The remaining bands at 14.6 and 15.7 eV are due to ionization from σ levels in the CC and CH bonds. Both the EH and CNDO calculations indicate that the predominately CC orbital has a lower i.p. than the CH; however, this should be treated cautiously. A study of CF_2CFI might be illuminating in this respect.

Can. J. Chem. Downloaded from www.nrcresearchpress.com by 210.87.254.42 on 09/05/12
For personal use only.

In allyl iodide (C_1 symmetry) direct conjugation is not possible and because of the low symmetry we would expect a large amount of mixing of the orbitals. The structure of allyl iodide is (26)

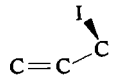

so that rather large "through space" interaction of the iodine with the double bond might be expected.

In fact the spectrum shows three reasonably sharp structureless close-lying bands at 9.32, 9.72, and 10.26 eV which should be due to mixtures of iodine lone pairs and the ethylenic link. The second band is somewhat broader and less intense than the first or third. Since lone-pair bands are normally the sharpest and most intense bands of a spectrum we assign the bands at 9.32 and 10.26 eV to ionizations from m.o.'s with appreciable populations on the iodine. The difference between these, 0.94 eV, when compared with the spin–orbit split in CH_3I (0.62 eV) indicates that the degree of delocalization is large.

There then follows a gap in the spectrum until a band at 12.25 eV which is likely due to expulsion of a CI bonding electron. This band is followed by at least four bands before 18 eV which are due to CC σ and CH electrons although definite assignments cannot be made.

To summarize our work, the high resolution photoelectron spectra of a large number of iodine containing molecules were presented. Extended Hückel molecular orbital calculations were used to help in the interpretation of these spectra and with some exceptions gave remarkably good agreement with the observed spectra in light of the severe approximations made in the method. These results coupled with some qualitative arguments led to reasonable interpretations of a large number of bands out to 18 eV. The utility of studying molecules in which some or all of the hydrogens are replaced by fluorines was further demonstrated.

This work was carried out in part at the University of Sussex and we would like to thank Professors M. F. Lappert and J. N. Murrell for their hospitality. Most of the spectra were measured on the PS-16 at the Perkin-Elmer Laboratories, Beaconsfield, and we would like to thank Dr. N. Ridyard for experimental assistance.

The award of post-doctorate fellowships from the U.S. Air Force (to R.A.B.) and the National Research Council of Canada (to D.R.S.) are gratefully acknowledged. We thank Messrs. G. King and B. Wilkins for measuring some of the spectra and Professor W. C. Price and Dr. L. Åsbrink for useful discussions.

1. R. A. Boschi and D. R. Salahub. Mol. Phys. **24**, 289, 735 (1972).
2. D. R. Salahub and R. A. Boschi. Chem. Phys. Lett. **16**, 320 (1972).
3. T. Koopmans. Physica, **1**, 104 (1933).
4. D. W. Turner. Phil. Trans. Roy. Soc. (London), A**268**, 7 (1970).
5. W. C. Price. Summer school in photoelectron spectroscopy. The Chemical Society, Lecture 9, 1972.
6. J. L. Ragle, I. A. Stenhouse, D. C. Frost, and C. A. McDowell. J. Chem. Phys. **53**, 178 (1970).
7. T. Baer, W. B. Peatman, and E. W. Schlag. Chem. Phys. Lett. **4**, 243 (1969).
8. T. Baer and B. P. Tsai. J. Electron Spectros. Relat. Phenom. **2**, 25 (1972).
9. F. Brogli and E. Heilbronner. Helvet. Chim. Acta, **54**, 1423 (1971).
10. A. D. Baker, D. Betteridge, N. R. Kemp, and R. E. Kirby. Anal. Chem. **43**, 375 (1971).
11. K. Kimura, S. Katsumata, Y. Aghiba, H. Matsumoto, and S. Nagakura. Bull. Chem. Soc. Japan, **46**, 373 (1973).
12. D. W. Turner, C. Baker, A. D. Baker, and C. R. Brundle. Molecular photoelectron spectroscopy. Wiley-Interscience, New York. 1970.
13. R. Hoffman. J. Chem. Phys. **39**, 1397 (1963).
14. R. Hoffman. QCPE No. 30, Quantum Chemistry Program Exchange, Indiana University, Bloomington, Indiana 47401.
15. K. Ruedenberg, C. C. J. Roothaan, and W. Jaunzemis. J. Chem. Phys. **24**, 201 (1956).
16. C. C. J. Roothaan. J. Chem. Phys. **24**, 947 (1956).
17. G. Burns. J. Chem. Phys. **41**, 1521 (1964).
18. R. Gleiter and T. Kobayashi. Helvet. Chim. Acta, **54**, 1081 (1971).
19. G. Herzberg. Molecular structure and molecular spectra III. Electronic spectra and electronic structure of polyatomic molecules. Van Nostrand, Princeton. 1966.
20. C. R. Brundle, M. B. Robin, N. A. Kuebler, and H. Basch. J. Am. Chem. Soc. **94**, 1451 (1972).
21. C. R. Brundle, M. B. Robin, and N. A. Kuebler. J. Am. Chem. Soc. **94**, 1466 (1972).
22. B. O. Johnson and E. Lindholm. Arkiv för Fysik, **39**, 65 (1969) and refs. therein.
23. A. W. Potts, W. C. Price, D. G. Streets, and T. A. Williams. Disc. Faraday Soc. **54**, 168 (1972).
24. R. F. Lake and Sir H. Thompson. Proc. Roy. Soc. (London), A**258**, 459 (1970).
25. D. Chadwick, D. C. Frost, A. Katrib, C. A. McDowell, and R. A. N. McLean. Can. J. Chem. **50**, 2647 (1972).
26. Tables of interatomic distances and configurations in molecules and ions. *Edited by* L. E. Sutton. Publication No. 11, The Chemical Society. 1958.

Can. J. Chem. Downloaded from www.nrcresearchpress.com by 210.87.254.42 on 09/05/12
For personal use only.

Synthesis of Substituted 9,10-Dihydroanthracenes by the Reduction of Anthraquinones in Hydriodic Acid[1]

ROGER N. RENAUD AND J. CAMPBELL STEPHENS

Division of Chemistry, National Research Council of Canada, Ottawa, Canada K1A 0R6

Received December 18, 1973

Substituted 9,10-dihydroanthracenes were synthesized by reducing the corresponding anthraquinone with a mixture of hydriodic acid, phosphorus, and iodine.

La synthèse de quelques dihydro-9,10 anthracènes par réduction de l'anthraquinone correspondante avec le système acide iodhydrique – phosphore – iode est exposée.

Can. J. Chem., **52**, 1229 (1974)

Can. J. Chem. Downloaded from www.nrcresearchpress.com by 210.87.254.40 on 09/05/12
For personal use only.

In connection with a spectroscopic investigation, we became interested in the synthesis of 1- and 2-substituted 9,10-dihydroanthracenes. Since many substituted anthraquinones are easily available, we decided to utilize these compounds as precursors for the 9,10-dihydro derivatives. Reducing agents such as lithium aluminum hydride (1, 2), sodium borohydride (3), aluminum alkoxides (4), diborane (5), zinc dust in basic medium (6), cyclohexyl-*p*-toluene sulfonate (7), diphenylsilane (8), sodium hydrosulfite (9), and nickel–aluminum alloy (10) give mainly 9,10-dihydroxy-9,10-dihydroanthracene, 9,10-dihydroxyanthracene, anthrone, anthrol, and/or anthracene. Organotin hydrides (11) do not reduce anthraquinone.

Sanchorawala and co-workers (12) have conducted an elaborate study of the reduction of 2-substituted anthraquinones by sodium borohydride in the absence and in the presence of aluminum chloride or boron fluoride. They obtained a very low yield of 9,10-dihydroanthracene when the substituent was hydrogen, and no dihydro compounds when the substituent was either chlorine, methyl, methoxy, or *t*-butyl.

The reduction of quinones in general under Wolff–Kishner conditions gives phenolic products resulting from the decomposition of the monosemicarbazone intermediate in presence of potassium hydroxide (13). Backer and coworkers (14) prepared polyaryl- and polymethyl-9,10-dihydroanthracenes by the Clemmensen reaction. Even though high yields of product can be obtained by this method, it requires long heating periods during which continuous addition of concentrated hydrochloric acid is required.

It is well known that a mixture of hydriodic acid and phosphorus reduces a variety of organic substrates including aryl olefins, arylcarbinols, aryl ketones, benzils, glycols, α-haloketones, and α,β-epoxyketones. In addition, a few quinones have also been reduced by this reagent to the corresponding hydrocarbons (15, 16). However, the reduction of substituted anthraquinones is reported to give anthrone (14) and/or anthracene (6), depending on the experimental conditions.

Our preliminary study with hydriodic acid and phosphorus at different temperatures and concentrations has revealed that anthraquinone can be reduced to 9,10-dihydroanthracene in good yields. The best result is obtained when a small amount of elemental iodine is present in the original mixture. However, the action of elemental iodine is not well understood. Under the best experimental conditions for anthraquinone (Table 1, run 1) many substituted anthraquinones were reduced to the 9,10-dihydro derivatives. The crude products obtained are usually better than 95% pure. Analytically pure compounds can be obtained by recrystallization or by direct sublimation. Only the product of reduction of 1-chloroanthraquinone, which was an oil containing some nonchlorinated compounds, was purified with difficulty. The purification was done by a fractional distillation under reduced pressure in a Späth bulb.

The only quinone of the series which could not be reduced to the dihydro derivative was 1-hydroxyanthraquinone. An unidentified product containing an equivalent of six methylene groups in addition to two keto groups was ob-

[1]NRCC No. 13800.

TABLE 1. Reduction of substituted anthraquinones to substituted 9,10-dihydroanthracenes

Run	Substituent	Yield*	Melting point† (°C)	Elemental analysis (%) C Found	C Calcd.	H Found	H Calcd.	Cl Found	Cl Calcd.
1	H	77	108–109 [108] (6)	92.98	93.33	6.65	6.67		
2	1-Cl	50	Oil	77.93	77.32	5.04	5.12	16.39	16.56
3	2-Cl	90	65–66	77.92	78.32	4.91	5.12	16.21	16.56
4	2-CH_3	92	53–54 [51] (17)	92.45	92.78	7.31	7.22		
5	2-COOH	15	182–183	80.11	80.35	5.26	5.35		
6	2-$C(CH_3)_3$	88	43–44	91.30	91.52	8.36	8.48		

*The yields are based on purified products.
†The numbers in square brackets correspond to the values reported in the literature.

tained. Pleus (18) claimed that he had prepared 9,10-dihydro-1-hydroxyanthracene from quinizarin in the presence of hydriodic acid and phosphorus at 0°. However, the reduction of 1-hydroxyanthraquinone, done under the same experimental conditions as Pleus, gave only the starting material.

Unfortunately, this method is not applicable to the reduction of deuterated anthraquinones, since rapid exchange occurs between the aromatic deuterium and the hydriodic acid proton. For instance, 1,4,5,8-tetradeuterioanthraquinone (96.8% d_4) (17) gave a product whose analysis was 3% d_2, 17% d_1, and 80% d_0. However, 1,4,5,8-tetradeuterio-9,10-dihydroanthracene can be prepared in 65% yield under the Clemmensen reduction conditions (14) from the corresponding quinone, without any deuterium scrambling.

Experimental

A stirred mixture of red phosphorus (4.2 g), iodine (1 g), 47% solution of hydriodic acid (30 ml), and quinone (15 mmol) was heated in an oil bath at 140 °C for 24 h. The mixture was allowed to cool down to room temperature and diluted with 200 ml of water. The resulting suspension was collected in a Buchner funnel and extracted with ether. The ethereal solution was washed with a solution of sodium thiosulfate, a solution of sodium bicarbonate and finally with water. (In the case of 9,10-dihydroanthracene-2-carboxylic acid, the washings with sodium thiosulfate and with sodium bicarbonate were omitted.) The solution was dried over sodium sulfate and evaporated to dryness. The product obtained was in general over 95% pure. Further purification was accomplished either by sublimation or by recrystallization from ethanol.

We are grateful to Dr. R. B. Layton (Postdoctorate Fellow) for helpful discussions.

1. E. BOYLAND and D. MANSON. J. Chem. Soc. 1937 (1951).
2. R. F. NYSTROM and W. G. BROWN. J. Am. Chem. Soc. **70**, 3738 (1948).
3. G. S. PANSON and C. E. WEILL. J. Org. Chem. **22**, 120 (1957).
4. S. COFFEY and V. BOYD. J. Chem. Soc. 2468 (1954).
5. D. S. BAPAT, B. C. SUBBA RAO, M. K. UNNI, and K. VENKATARAMAN. Tetrahedron Lett. 15 (1960).
6. V. VON RICHTER. The chemistry of carbon compounds. Vol. 3. Elsevier Publishing Co., Inc., New York, N.Y. 1946. p. 655–656; R. SCHOLL. Monatsh. **39**, 231 (1918).
7. W. KELLY and J. S. SHANNON. Aust. J. Chem. **13**, 103 (1960).
8. H. GILMAN and J. DIEHL. J. Org. Chem. **26**, 4817 (1961).
9. L. F. FIESER and M. FIESER. Reagents for organic synthesis. Vol. 1. John Wiley and Sons Inc., New York, N.Y. 1967. p. 1082.
10. J. H. P. TYMAN. J. Appl. Chem. **20**, 179 (1970).
11. H. G. KUIVILA and O. F. BEUMEL, JR. J. Am. Chem. Soc. **83**, 1246 (1961).
12. C. J. SANCHORAWALA, B. C. SUBBA RAO, M. K. UNNI, and K. VENKATARAMAN. Ind. J. Chem. **1**, 19 (1963).
13. D. TODD. Organic reactions. Vol. 4. John Wiley and Sons Inc., New York, N.Y. 1948. p. 378.
14. H. J. BACKER, J. STRATING, and L. H. H. HUISMAN. Rec. Trav. Chim. Pays-Bas, **58**, 761 (1939).
15. S. GABRIEL and E. LEUPOLD. Ber. **31**, 1272 (1898); R. SCHOLL and K. MEYER. Ber. **67**, 1232 (1934).
16. C. LIEBERMANN. Ann. **212**, 65 (1882).
17. O. FISCHER. J. Prakt. Chem. **92**, 49 (1915).
18. B. PLEUS. Ber. **35**, 2923 (1902).
19. J. L. CHARLTON and R. AGAGNIER. Can. J. Chem. **51**, 1852 (1973).

Can. J. Chem. Downloaded from www.nrcresearchpress.com by 210.87.254.40 on 09/05/12
For personal use only.

Formation of Adducts in the Nitration of 2,3- and 3,4-Dimethylbenzonitriles, and their Rearomatization. A 1,3-Nitro Shift[1]

ALFRED FISCHER AND COLIN CAMPBELL GREIG

Department of Chemistry, University of Victoria, Victoria, British Columbia

Received October 9, 1973

Nitration of 2,3-dimethylbenzonitrile in acetic anhydride gives the adduct 2-cyano-3,4-dimethyl-4-nitro-1,4-dihydrophenyl acetate as well as the expected nitro substitution products. Similarly 3,4-dimethylbenzonitrile affords 2-cyano-4,5-dimethyl-4-nitro-1,4-dihydrophenyl acetate as well as the 3,4-dimethylnitrobenzonitriles. Thermolysis or decomposition in acetic acid of the adducts gives the original dimethylbenzonitrile and its 5-nitro derivative as the major products, the latter apparently being formed by an intramolecular 1,3-shift of the nitro group. Decomposition of the adducts under more strongly acidic conditions results in the elimination of nitrous acid and the formation of 2-cyano-3,4-dimethylphenyl acetate and 2-cyano-4,5-dimethylphenyl acetate, respectively. In acidified methanol the adducts undergo transesterification at the acetate function and 2-cyano-3,4-dimethyl-4-nitro-1,4-dihydrophenol and 2-cyano-4,5-dimethyl-4-nitro-1,4-dihydrophenol are obtained.

La nitration du diméthyl-2,3 benzonitrile dans l'anhydride acétique conduit en plus des produits de substitution attendus au dérivé d'addition acétate de cyano-2 diméthyl-3,4 nitro-4 dihydro-1,4 phényle. De la même manière le diméthyl-3,4 benzonitrile fournit l'acétate de cyano-2 diméthyl-4,5 nitro-4 dihydro-1,4 de phényle de même que les diméthyl-3,4 nitrobenzonitrile. La thermolyse ou la décomposition en acide acétique des produits d'additions conduit au diméthylbenzonitrile original et à son dérivé substitué par un groupe nitro en position 5 comme produit majeur; ce dernier se formerait semble-t-il par un déplacement intramoléculaire 1-3 du groupe nitro. La décomposition des produits d'additions dans des conditions plus acides résultent dans l'élimination d'acide nitreux et la formation de l'acétate de cyano-2 diméthyl-3,4 phényle et de l'acétate cyano-2 diméthyl-4,5 phényle respectivement. Dans le méthanol acidifié les produits d'additions se transestérifient au niveau de la fonction acétate et l'on obtient les cyano-2 diméthyl-3,4 nitro-4 dihydro-1,4 phénol et cyano-2 diméthyl-4,5 nitro-4 dihydro-1,4 phénol. [Traduit par le journal]

Can. J. Chem., **52**, 1231 (1974)

Introduction

Aromatic hydrocarbons containing appropriately located methyl (or methylene) substituents when allowed to react with nitric acid in acetic anhydride give acetyl nitrate adducts containing the 4-nitro-1,4-dihydro-*p*-tolyl acetate moiety (1). Adducts in which the nitro group is attached to an unsubstituted nuclear position have not been observed and it is consistent with this that only those substrates in which the methyl (methylene) substituted position is not substantially less activated than an unsubstituted position form adducts. Thus *o*-xylene forms the diastereoisomeric adducts **1** in more than 50% yield but *m*-xylene gives over 99% of the nitro substitution products (2). In *o*-xylene the *ipso* 1-position is activated by the *ortho* 2-methyl group and is of comparable activation to the unsubstituted 3- and 4-positions. In *m*-xylene the *ipso* 1-position is weakly activated by the *meta* 3-methyl group whereas there is strong activation of the unsubstituted 2-position by two *ortho* methyl groups, and of the unsubstituted 4-position by *ortho* and *para* methyl groups.

The mechanism of adduct formation appears to involve the same initial step as nuclear substitution: addition of the nitronium or incipient nitronium ion but at a methyl (or methylene) substituted position. Since the methyl substituent, unlike hydrogen, is not readily lost as a positive species, the resulting phenonium ion adds acetate, presumably as acetic acid, to achieve the stable electrically-neutral state. If the reactivity of a substituted position relative to the unsubstituted positions is high then adducts should be formed even when the sub-

[1]For a preliminary communication, see ref. 1*g*.

Can. J. Chem. Downloaded from www.nrcresearchpress.com by 210.87.254.105 on 09/05/12
For personal use only.

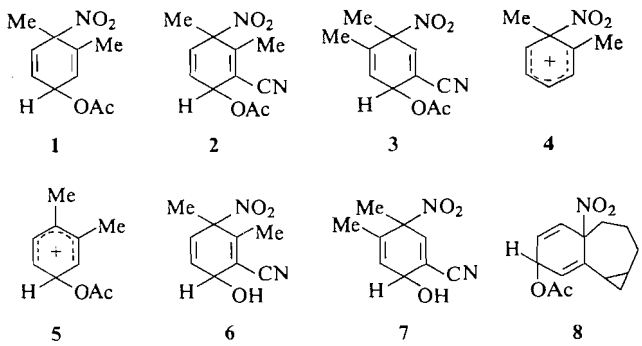

1 2 3 4

5 6 7 8

strate is only weakly activated or is even deactivated relative to benzene. The present work supports this hypothesis.

Decomposition of acetyl nitrate adducts of aromatic compounds results in rearomatization. A variety of rearomatization pathways has been observed. Thus the adducts of toluene, *o*-xylene, 1,2,3-trimethylbenzene, indane, and tetralin undergo 1,4-elimination of nitrous acid to give the appropriate aryl acetate (1). In strong acid the *o*-xylene adduct has been shown to lose acetic acid and undergo a 1,2-shift of the nitro group to give 3-nitro-*o*-xylene (3). The *p*-xylene adduct cannot rearomatize by simple loss of nitrous acid and in this case the elimination of nitrous acid is accompanied by migration of the acetate group to give 2,5-dimethylphenylacetate (1*b*). Loss of acetic acid and S_N2' substitution of nitro by external nucleophiles also occurs to form *p*-methylbenzyl derivatives (4). Adducts from 1,4-dimethylnaphthalene likewise undergo rearomatization by loss of nitrous acid and migration of the acetate group to form 1,4-dimethyl-2-naphthyl acetate and to a greater extent, by loss of acetic acid and intermolecular migration of the nitro group (through S_N2' substitution of the nitro group by nitrous acid) to form 4-nitromethyl-1-methylnaphthalene (1*e*, 4). Decomposition of the adducts obtained in the present work reveals a new pathway of aromatization: loss of acetic acid and apparent intramolecular 1,3-migration of the nitro group.

Results and Discussion

2,3-Dimethylbenzonitrile reacted slowly with nitric acid in acetic anhydride to give a mixture of adduct **2** (44%) and 2,3-dimethyl-4-(8%), -5-(32%), and -6-nitrobenzonitrile (16%). In *o*-xylene the *ipso* positions are more activated towards electrophilic attack by the nitronium ion than the unsubstituted positions.[2] Introduction of the 3-cyano group should reduce the reactivity at all positions but deactivation (relative to *o*-xylene) should be least and equivalent at positions *meta* to the cyano, *i.e.*, using the numbering appropriate to 2,3-dimethylbenzonitrile, at C-3 (*ipso* to methyl) and -5 (unsubstituted). Thus the 3-position should be most susceptible to electrophilic attack followed by the 5-, 2-(*ipso*), 6-, and 4-positions. The order in the case of the last three positions follows from the activating effects of the methyl groups ($2 > 6 > 4$, corresponding to $1 > 4 > 3$ in *o*-xylene (5)) and the greater *para* than *ortho* deactivation by cyano (6), *i.e.* C-4 more deactivated than C-2 and -6. No evidence for the formation of any adduct by attack of nitronium ion at C-2 was obtained but in the absence of knowledge of the precise n.m.r. spectrum of the product and of its ease of decomposition on work-up, it is not possible to say that it was not formed in small amount. The yields of the other products do indeed follow the predicted order.

3,4-Dimethylbenzonitrile when reacted with nitric acid in acetic anhydride gave adduct **3** (50%) and 3,4-dimethyl-2- (14%), -5- (28%), and -6-nitrobenzonitrile (9%). Nitration of 3,4-dimethylbenzonitrile would be predicted to occur preferentially at position 3 (*ipso*) followed by 5, 6, 2, and 4 (*ipso*). Aside from the ranking of positions 2 and 6 being reversed, this was the order observed. Ignoring steric and other proximity effects, attack at positions 2 and 6 should be in the ratio of the *ortho*:*para* methyl partial rate factors, *i.e.* 0.8:1 (2), whereas the 2-nitro substitution product constituted 14% and the

[2] 3,4-Dimethylphenylacetate, formed via the adduct **1**, is obtained in greater yield than the nitro substitution products (2, 5).

Can. J. Chem. Downloaded from www.nrcresearchpress.com by 210.87.254.105 on 09/05/12
For personal use only.

Can. J. Chem. Downloaded from www.nrcresearchpress.com by 210.87.254.105 on 09/05/12
For personal use only.

6-nitro 9% of the product mixture. No adduct resulting from *ipso* attack at the 4-position was detected but this is in accord with expectation as the 4-position, being *para* to the cyano group, is the least reactive.

The adducts **2** and **3**, which are secondary acetates, exhibit a much greater variety of reactions than the similar adducts of toluene (1*f*) and *o*-xylene (1*a*). Reactions involve acid-catalyzed loss of either the nitro or acetoxy groups. Loss of the acetate from the toluene or *o*-xylene adducts would be expected to occur by protonation at the ester function and unimolecular fission to generate the phenonium ion, **4**, in the case of the *o*-xylene adduct **1**. The predominant reaction of **1** is not this but rather the elimination of nitrous acid to form 3,4-dimethylphenylacetate and the analogous reaction occurs in the case of the toluene adduct. The loss of the nitro group probably occurs in a bimolecular (E2) process in which the 1-H is removed at the same time. Only weak bases (*e.g.* acetic acid) are available to remove the proton and thus the transition state would be expected to be E2 verging towards E1, and may be treated as a quasi-phenonium ion which would reflect the charge distribution of the classical phenonium ion **5**. The ester function is much more basic than a nitro group and thus protonation of the acetate and loss of acetic acid to form **4**, leading to 3-nitro-*o*-xylene (3), would be expected to be more facile than acid-catalyzed unimolecular fission (E1) of the nitro group to form the phenonium ion **5**, and, eventually, aryl acetate. It is presumably because of the assistance provided by the removal of the 1-H concurrently with the loss of the nitro group which makes the elimination to the aryl acetate preferred under most (weakly acidic) conditions. In sulfuric acid solution, the basicity of the medium is very low and this assistance is greatly attenuated. Consequently, loss of acetate is now the preferred pathway of rearomatization. Using the numbering appropriate to the adduct **1**, the positive charge in the phenonium ion **4** is concentrated on carbons 1, 3, and 5, whereas in **5** it is located mainly at carbons 2, 4, and 6.

Adducts **2** and **3** are much more stable and resistant to rearomatization than the adducts of toluene, *o*-xylene, and hemimellitene. Introduction of the electron-withdrawing cyano substituent would be expected to destabilize the transition state leading to **4** and also the E2 transition state which reflects the electron distribution in **5**. This effect is so marked that on treatment with acidified methanol $A_{AC}2$ transesterification of **2** to form **6** and of **3** to form **7** occurs in preference to the $A_{AL}1$ exchange of OAc for OMe via the cyano-substituted phenonium ions, which would otherwise be expected (4). It is evident that **2** and **3** undergo parallel methanolysis reactions. It is much more noteworthy that the rearomatization reactions of **2** and **3** (Scheme 1) parallel each other. Moreover, the presence of the cyano substituent has a striking influence on the course taken by these rearomatization reactions. Reference to the intermediates and products of the series of reactions undergone by **3** is made in parentheses in the following discussion. Thermolysis of **2** (**3**), or heating in inert solvent or in acetic acid, gives the original dimethylbenzonitrile **11** (**16**) and its 5-nitro derivative **13** (**18**) as the major products with, at most, only a small amount of the nitrous acid elimination product, the 2-cyano-dimethylphenyl acetate **9** (**14**). The elimination transition state with a charge distribution similar to that of **5** would have the cyano group attached to a carbon (C-2) on which positive charge is concentrated. In contrast, the phenonium ion **10** (**15**) (cyano-substituted **4**), formed by loss of acetate, would have the cyano substituent attached to a carbon which does not carry a formal positive charge. It would therefore be expected that the transition state leading to the phenonium ion would be of lower energy than that leading to the aryl acetate. The phenonium ion **10** (**15**), once formed, can either lose a nitronium ion in the reverse of the initial *ipso* nitration step to yield the original dimethylbenzonitrile **11** (**16**) or the nitro group may undergo a 1,3-shift to give a new phenonium ion **12** (**17**) which on loss of a proton gives the dimethylnitrobenzonitrile **13** (**18**). Loss of nitronium ion does not occur from phenonium ion **4** but *o*-xylene would be expected to be a poorer leaving group than the cyano-*o*-xylene, *i.e.* formation of the nitrophenonium ion **10** (**15**) from the corresponding dimethylbenzonitrile is more likely to be reversible than formation of **4** from *o*-xylene. It is reasonable that **10** (**15**) should undergo a 1,3-nitro shift to give **12** (**17**) rather than a 1,2-nitro shift as does **4**. A 1,2-shift of the nitro group in **10** (**15**) would result in the carbon atom to which the nitrile group is attached acquiring a formal positive charge. This would be an

Can. J. Chem. Downloaded from www.nrcresearchpress.com by 210.87.254.105 on 09/05/12
For personal use only.

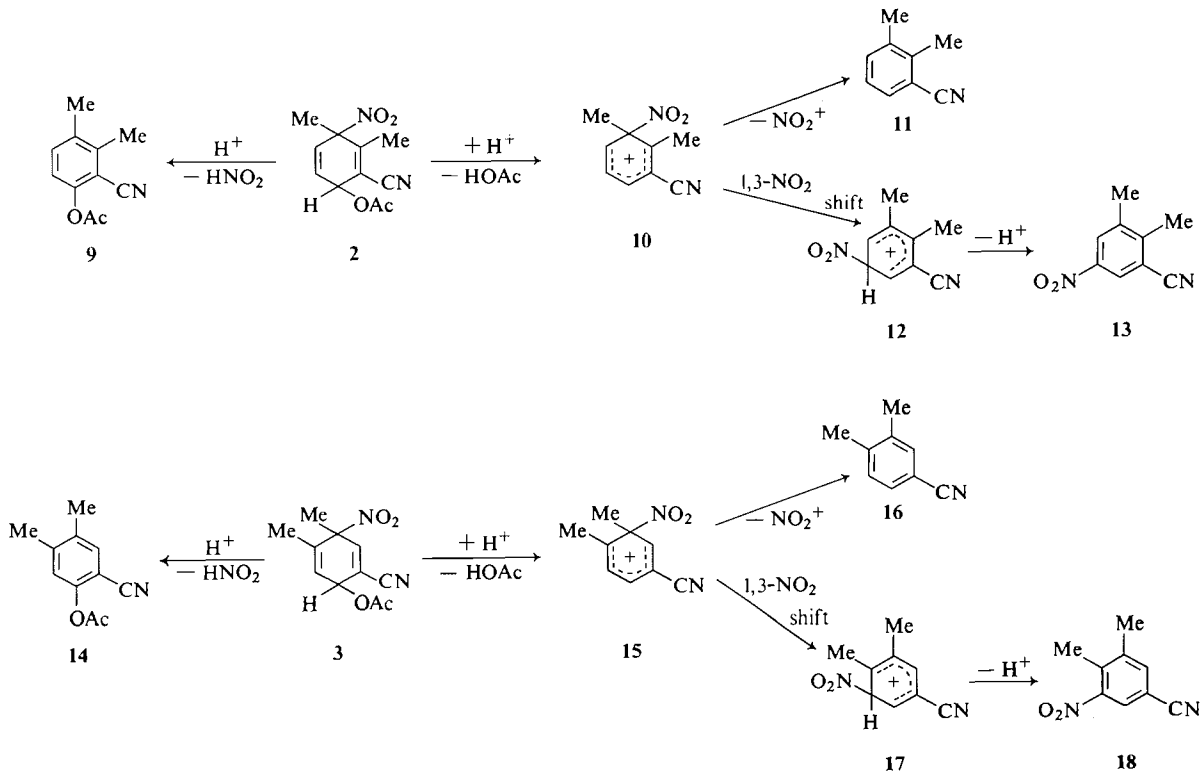

SCHEME 1

Can. J. Chem. Downloaded from www.nrcresearchpress.com by 210.87.254.105 on 09/05/12
For personal use only.

energetically unfavorable process compared to the 1,3-shift which preserves the formal zero charge on this carbon. The 1,3-nitro shift appears to be an intramolecular process since (*i*) there was no evidence for the formation of other nitro-substitution products expected if **13** (**18**) had been formed by a dissociation–renitration process and (*ii*) the formation of **13** (**18**) was not suppressed when the reaction was carried out in the presence of reactive arenes (toluene and mesitylene).

Hahn and Groen (7) have recently reported that the rearomatization in sulfuric acid of the adduct **8** gives the nitroarene resulting from a formal 1,3-nitro shift as well as the expected product from a 1,2-nitro shift. They argue that the formal 1,3-shift occurs by two successive 1,2-shifts. Direct evidence for nitro group migration in nitrohexamethylphenonium ion has been obtained by Olah and co-workers (8). Temperature dependent n.m.r. spectra show that the position of the nitro group is not fixed and it is claimed that the nitro group migrates around the ring by a series of 1,2-shifts. However, the 1,3-nitro shift in **10** to give **12** cannot occur by two consecutive 1,2-shifts since the initial 1,2-shift would give the phenonium ion precursor to 2,3-dimethyl-4-nitrobenzonitrile and the latter would then be obtained as a product of the rearomatization reaction, whereas only the 5-nitro derivative is formed. Similarly a 1,2-nitro shift in the opposite direction in **15** would give the phenonium ion precursor to 3,4-dimethyl-2-nitrobenzonitrile, yet the latter product is not formed. Clearly, the 1,3-nitro shift by which **10** (**15**) is converted into **12** (**17**) does not proceed through two consecutive 1,2-shifts.

When the adduct **2** (**3**) is decomposed under somewhat more acidic conditions, 5% sulfuric acid in acetic acid, or trifluoroacetic acid, elimination of nitrous acid to give the aryl acetate **9** (**14**) takes place in preference to the loss of acetate which leads via **10** (**15**) to **11** (**16**) and **13** (**18**). The explanation for this dramatic change in the reaction pathway with a relatively minor alternation in the reaction conditions is not obvious. We suggest that the acid-catalyzed loss of the nitro group, unlike the loss of acetate, does not occur via the conjugate acid form. Only a very small amount of this form would be present in these mixtures since nitro compounds, in contrast to acetates, are extremely weak bases. Rather, the acid catalysis is exhibited through a hydrogen-bonding solvation of the nitro group and such solvation is likely to be more sensitive to the acidity of the medium than is the equilibrium protonation of the acetate function. Thus as the acidity of the medium is increased, the possibility arises of a switchover from acid-catalyzed (via equilibrium protonation) loss of the acetate to acid-catalyzed (via hydrogen-bonding solvation) loss of the nitro function. The ability of trifluoroacetic acid, or of acetic acid in the presence of 5% sulfuric acid, to abstract a proton is probably not greatly reduced from that of acetic acid in pure acetic acid and the bimolecular requirements of the nitrous acid elimination can be fulfilled in these media. Formation of the aryl acetate **9** (**14**) in the sulfuric acid in acetic acid solution is complicated by further reaction to form the corresponding phenol, which is subsequently nitrated (or nitrosated and the product oxidized) to the 6-nitro derivative (Scheme 2). It appears that acetic acid is capable of cleaving the aryl acetate **9** (**14**) to form the corresponding phenol and acetic anhydride. Confirmation that the nitrophenol was formed by an intermolecular reaction was provided by the observation that addition of mesitylene to the reaction mixture from **3** reduced the amount of nitrophenol product relative to phenol and resulted in the formation of nitromesitylene.

Experimental

Ultraviolet spectra were determined on a Cary 17 spectrometer using cells of 1-mm path-length. Infrared spectra were obtained on a Beckman IR 20 spectrometer. Nuclear magnetic resonance spectra at 60 MHz were obtained on Perkin-Elmer R12A and Varian HA-60-IL spectrometers and at 220 MHz on the Varian HR 200 spectrometer at the Ontario Research Foundation, Sheridan Park, Ontario. Tetramethylsilane was used as an internal standard. Molecular weights were determined in methylene dibromide using an Hitachi Perkin-Elmer Model 115 molecular weight apparatus (vapor pressure osmometer). Mass spectra were obtained on Hitachi Perkin-Elmer RMU7 and AEI MS902 spectrometers. Dipole moments (p) were derived by use of Higasi's equation (9) from dielectric constant measurements (1*c*) of benzene solutions of the dienes. The dielectric constants were measured with a Sargent Chemical Oscillometer Model V with inductive cell compensator. Microanalyses were by Dr. A. D. Campbell, University of Otago, Dunedin, New Zealand and Microanalyses Laboratories Ltd., Toronto, Ontario. Vapor phase chromatography analyses were performed on a Micro Tek MT 220 gas chromatograph using QF1 and PEGA (5% w/w) on Varaport-30. Nitric acid was purified by distilling the fuming acid (300 cm^3) at 100 Pa (pascal)

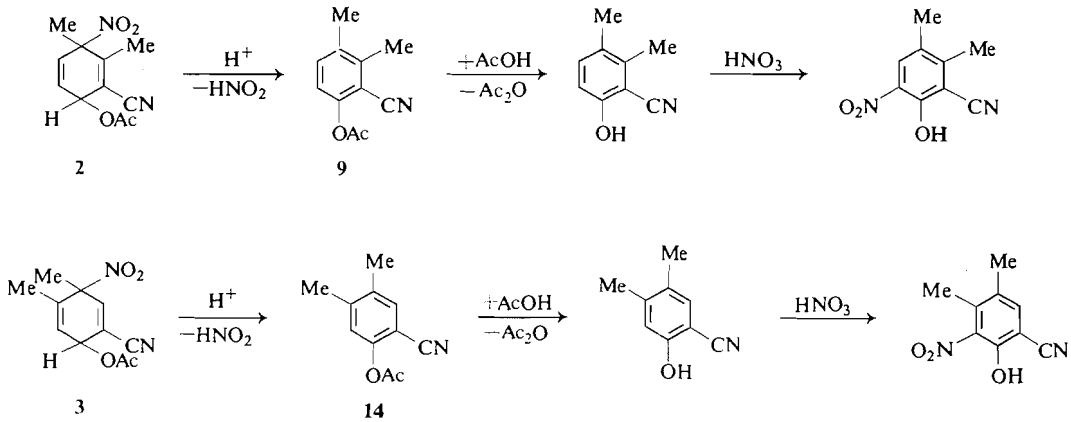

SCHEME 2

from urea (10 g) and sulfuric acid (500 cm^3). Alumina was deactivated with 3% of 10% acetic acid. Ether and pentane were dried by distillation from sodium and phosphorus pentoxide, respectively. The 2,3- and 3,4-dimethylbenzonitrile were from Aldrich Chemical Company, Inc. The 3,4-dimethylbenzonitrile (technical grade) was purified by chromatography on alumina and recrystallization from pentane, m.p. 65–66 °C (65.7 °C (10)).

Nitration of 2,3-Dimethylbenzonitrile in Acetic Anhydride

A solution of freshly distilled nitric acid (9.8 cm^3, 0.2 mol) in acetic anhydride (30 cm^3) was prepared at −10 °C and added to a stirred solution of 2,3-dimethylbenzonitrile (13 g, 0.1 mol) in acetic anhydride (30 cm^3) at 0 °C. The resulting mixture was allowed to stand at 12 °C for 24 h, at which time the n.m.r. spectrum indicated that approximately 25% of the material present was diene. The mixture was quenched with ammonia and worked up in the manner previously described (1*c*) to yield 17 g of a red oil whose n.m.r. spectrum indicated the following composition: 50% 2,3-dimethylbenzonitrile, 22% diene, 16% 5-, 8% 6-, and 4% 4-nitro-2,3-dimethylbenzonitrile. Chromatography on alumina at 0 °C and elution with ether–pentane mixtures gave unreacted 2,3-dimethylbenzonitrile in the 0–10% ether fractions, nitro compounds in the 20–40% ether fractions, and a diene in the 50–60% ether fractions.

Recrystallization from carbon tetrachloride of the residue obtained after removal of the solvent from the 50 and 60% ether fractions gave colorless cubes of 2-cyano-3,4-dimethyl-4-nitro-1,4-dihydrophenyl acetate (**2**), m.p. 98–99 °C; u.v. (CH_3OH) 208 nm (ε 1400 m^2 mol^{-1}); i.r. (Nujol) 2230 (CN), 1750 and 1230 ($OCOCH_3$), 1550 and 1385 cm^{-1} (NO_2); n.m.r. ($CDCl_3$) τ 3.58 (m, 1, 6-*H*), 3.67 (m, 1, 5-*H*), 3.88 (m, 1, 1-*H*), 7.81 (m, 6, 3-CH_3, and $OCOCH_3$), and 8.20 p.p.m. (s, 3, 4-CH_3); J_{15} = 0.12, J_{16} = 3.36, $J_{1,3\text{-}CH_3}$ = 1.42, J_{56} = 9.96 Hz; addition of the shift reagent tris-(1,1,1,2,2,3,3,-heptafluoro-7,7-[$^2H_6$]dimethyl-4,6-[$^2H_3$]octanedionato)europium(III) {Eu([$^2H_9$]fod)$_3$} shifted the 1-H to lowest field and moved the 6-H sufficiently far downfield from the 5-H to produce a 1st order spectrum. Decoupling of the 3-CH_3 from the 1-H allowed all of the couplings between the nuclear protons to be read from the spectrum and these coupling constants were then used to simulate the original spectrum, the simulation then being refined to give the parameters listed above; mass spectrum (70 eV) *m/e* (relative intensity) 190 (3, M − NO_2), 148 (100); ***p*** 10.1 × 10^{-30} C m (3.02 D).

Anal. Calcd. for $C_{11}H_{12}N_2O_4$ (M_r 236): C, 55.93; H, 5.12; N, 11.86. Found (238): C, 56.19; H, 5.19; N, 11.84.

The residue from the 20% ether fraction from the column was recrystallized from ethanol to yield 2,3-dimethyl-5-nitrobenzonitrile, m.p. 131–133 °C (131–132 °C (11)); i.r. (Nujol) 2230 (CN), 1525 and 1360 cm^{-1} (NO_2); n.m.r. ($CDCl_3$) τ 1.67 (nq, 1, *J* = 2.4 Hz, 6-*H*), 1.74 (nq, 1, *J* = 2.4 Hz, 4-*H*), 7.44 (s, 3, 2-CH_3), 7.56 p.p.m. (s, 3, 3-CH_3); mass spectrum (70 eV) *m/e* (relative intensity) 176 (97, M), 146 (34, M − NO), 130 (83, M − NO_2), 118 (29), 116 (22), 104 (49), 103 (100), 91 (39).

The residue from the 30% ether fraction was recrystallized from ethanol to give 2,3-dimethyl-6-nitrobenzonitrile, m.p. 109.5–110.5 °C (111 °C (11)); i.r. (Nujol) 2225 (CN), 1530 and 1350 cm^{-1} (NO_2); n.m.r. ($CDCl_3$) τ 1.96 (nq, 1, *J* = 8.6 Hz, 5-*H*), 2.46 (nq, 1, *J* = 8.6 Hz, 4-*H*), 7.40 (s, 3, CH_3), 7.55 p.p.m. (s, 3, CH_3); mass spectrum (70 eV) *m/e* (relative intensity) 176 (55, M) 146 (51, M − NO), 130 (19, M − NO_2), 118 (9), 116 (14), 104 (24), 103 (100), 91 (19), metastable peaks at 121.2 (176 → 146) and 82 (130 → 103, loss of HCN).

Also present in the 30% ether fraction was a small quantity of a compound whose n.m.r. spectrum showed a sharp resonance at τ 2.4. The identification of this compound as 2,3-dimethyl-4-nitrobenzonitrile was confirmed by synthesis (12) of an authentic specimen from 2,3-dimethyl-4-nitroaniline via the diazonium salt. The 2,3-dimethyl-4-nitrobenzonitrile had m.p. 87–89 °C (90–91 °C (12)); i.r. (Nujol) 2230 (CN), 1530 and 1375 cm^{-1} (NO_2); n.m.r. ($CDCl_3$) τ 2.42 (s, 2; 5-*H* and 6-*H*), 7.42 (s, 3, CH_3), and 7.61 p.p.m. (s, 3, CH_3); addition of Eu([$^2H_9$]fod)$_3$ caused the two coincident aromatic resonances to split into an AB quartet with *J* = 8.3 Hz; mass spectrum (70 eV) *m/e* (relative intensity) 176 (39, M), 159 (100, M − OH), 131 (57) 130 (16, M − NO_2), 115 (9), 104 (68), 103 (55), 91 (13).

The i.r., n.m.r., molecular weight and elemental analytical data confirm the presence of the substituents and functionalities depicted in **2**. That the adduct is a 1,4- rather than a 1,3-diene is demonstrated by the u.v.

Can. J. Chem. Downloaded from www.nrcresearchpress.com by 210.87.254.105 on 09/05/12
For personal use only.

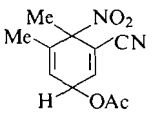

19

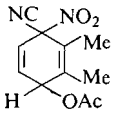

20

absorption maximum (208 nm). Conjugated cyclohexadienes absorb at 253 nm or greater (13). There are six structurally isomeric 1,4-cyclohexadienes which might be obtained by 1,4-addition of nitro and acetoxy groups from acetyl nitrate to 2,3-dimethylbenzonitrile. These may be sub-classified into three pairs of structural isomers, the members of each pair differing in that the locations of the acetoxy and nitro groups are interchanged. For convenience the members of a pair will be described as locational isomers. Coupling constants from the n.m.r. spectrum are consistent with structure **2** and its locational isomer but not with **19** nor **20** nor their locational isomers. Structures **2** and **20** have adjacent vinyl protons which would exhibit the observed 10 Hz coupling, and an allylic proton, which would exhibit three- (2.6–6.6 Hz) and four-bond (−2.6–3.9 Hz) couplings to the vinyl protons (14), as is also observed. On the other hand, structure **19** with non-adjacent vinyl protons should exhibit two three-bond vinyl–allylic couplings (2.6–6.6 Hz) and a smaller (1–2 Hz) coupling between the vinyl protons. The absence of coupling between the methyl groups (and between the allylic proton and *both* methyl groups) shows that those cannot be in a *cis*-2-butene relationship as in **20** and thus only **2** and its locational isomer are compatible with the full n.m.r. spectrum. Addition of the shift reagent Eu([$^2H_9$]fod)$_3$ caused the allylic proton to move downfield more rapidly than the vinyl protons. This shows that the allylic proton is closest to site of coordination of the europium atom, the acetoxy group. The shift reagent is known to coordinate at acetoxy in preference to nitro and cyano substituents (15) and confirmation that the coordination did in fact take place there with Eu([$^2H_9$]-fod)$_3$ was provided by the observation that the acetate methyl moved downfield much more rapidly than the other methyl groups on addition of the reagent. Thus the adduct has structure **2** rather than that of the locational isomer. The latter is unlikely on chemical grounds since the proton α to the nitro group should be readily removed by the ammonia during work-up, with concurrent loss of acetate, to form 6-nitro-2,3-dimethylbenzonitrile.

The nitro substitution products have established structures and these are confirmed by the spectral information. The 5-nitro isomer is unique in having *meta*-coupled protons (J = 2.4 Hz). The 4- and 6-nitro isomers both have *ortho*-coupled protons (J = 8.3 and 8.6 Hz, respectively) and are distinguished by their mass spectra which show the expected loss of OH for adjacent nitro and methyl groups (16) in the case of the 4-isomer, indeed this is the base peak, and no such peak in the case of the 6-isomer. The mass spectra of the 5- and 6-isomers are similar with both showing the loss of NO appropriate for nitrotoluene derivatives with non-adjacent nitro and methyl groups (16) and a base peak at 103 for loss of NO_2 plus HCN.

Nitration of 3,4-Dimethylbenzonitrile in Acetic Anhydride

A solution of freshly distilled nitric acid (23.0 cm^3, 0.36 mol) in acetic anhydride (50 cm^3) was prepared at −10 °C and added to a solution of 3,4-dimethylbenzonitrile (15 g, 0.11 mol) in acetic anhydride (60 cm^3) at 0 °C. The reaction mixture was allowed to react at 15 °C for 24 h at which time the n.m.r. spectrum showed that approximately 30% of the material present was diene. The mixture was worked up as previously described (1*c*) to give 23 g of a dark red oil, whose n.m.r. spectrum indicated the composition 41% 3,4-dimethylbenzonitrile, 29% diene, 16% 5-, 8% 2-, and 5% 6-nitro-3,4-dimethylbenzonitrile. Chromatography on alumina at 0 °C and elution with ether–pentane mixtures gave unreacted 3,4-dimethylbenzonitrile in the 10% ether fraction, nitro compounds in the 20–40% ether fractions and a diene in the 50% ether fraction.

Recrystallization from carbon tetrachloride of the residue obtained after removal of the solvent from the 50% ether fraction gave white cubes of 2-cyano-4,5-dimethyl-4-nitro-1,4-dihydrophenyl acetate (**3**), m.p. 87.5–88.5 °C, u.v. (CH_3OH) 207 nm (ε 1230 m^2 mol^{-1}); i.r. (Nujol) 2230 (CN), 1750 and 1230 ($OCOCH_3$), 1550 and 1380 cm^{-1} (NO_2); n.m.r. (220 MHz, $CDCl_3$) τ 3.20 (d, 1, 3-*H*), 4.08 (m, 1, 6-*H*), 4.17 (m, 1, 1-*H*) 7.83 (s, 3, $OCOCH_3$), 8.14 (m, 3, 5-CH_3), 8.18 p.p.m. (s, 3, 4-CH_3); J_{13} = 1.43, J_{16} = 3.24, $J_{1,5-CH_3}$ = 1.55, $J_{6,5-CH_3}$ = 1.48 Hz; irradiation at 8.14 collapsed the peak at 4.08 to a doublet and that at 4.17 to a quartet; p 11.4 × 10^{-30} C m (3.42 D).

Anal. Calcd. for $C_{11}H_{12}N_2O_4$ (M_r 236): C, 55.93; H, 5.12; N, 11.86. Found (M_r 238): C, 56.09; H, 5.22; N, 11.92.

The residue from the 20% ether fraction from the column was recrystallized from ethyl acetate to give 3,4-dimethyl-5-nitrobenzonitrile, m.p. 116–118 °C (118.5–121 °C (11)); i.r. (Nujol) 2240 (CN) 1530 and 1370 cm^{-1} (NO_2); n.m.r. ($CDCl_3$) τ 2.17 (d, 1, J = 1.8 Hz, 6-*H*), 2.40 (d, 1, J = 1.8 Hz, 2-*H*) 7.59 p.p.m. (s, 6, 3-CH_3 and 4-CH_3); irradiation at τ 7.59 sharpened the signals at 2.17 and 2.40 p.p.m. and allowed precise evaluation of the coupling constant; mass spectrum (70 eV) *m/e* (relative intensity) 176 (49, M) 159 (100, M − OH) 131 (47) 104 (71), metastable peak at 143.5 for 176 → 159 (loss of OH).

The residue from the 25% ether fraction on recrystallization from ethanol afforded 3,4-dimethyl-6-nitrobenzonitrile, m.p. 179–181 °C (170 °C (17)); i.r. (Nujol) 2235 (CN), 1525 and 1380 cm^{-1} (NO_2); n.m.r. ($CDCl_3$) τ 1.95 (s, 1, 5-*H*), 2.41 (s, 1, 2-*H*), 7.55 p.p.m. (s, 6, 3-CH_3 and 4-CH_3); mass spectrum (70 eV) *m/e* (relative intensity) 176 (35, M), 146 (35, M − NO), 130 (20), 118 (18), 116 (20), 104 (32), 103 (78), 91 (43), 77 (100).

The mother liquors from the recrystallizations of the foregoing two nitro compounds contained a third nitro compound, which was isolated after further chromatography of the residue of the combined mother liquors. Recrystallization from methylene chloride – pentane gave colorless crystals of 3,4-dimethyl-2-nitrobenzonitrile, m.p. 72–75 °C, unchanged by sublimation; i.r. (Nujol) 2230 (CN), 1525 and 1355 cm^{-1} (NO_2); n.m.r. ($CDCl_3$) τ 2.48 (*nq*, 1, J = 8 Hz, 6-*H*), 2.56 (*nq*, 1, J = 8 Hz, 5-*H*), 7.56 (s, 3, 3-CH_3), 7.72 p.p.m. (s, 3, 4-CH_3); mass spectrum (70 eV) *m/e* (relative intensity) 176 (18, M), 159.052 (56, M_r ($^{12}C_9{}^1H_7{}^{14}N_2{}^1O_{16}$) = 159.056, M − OH), 131 (63), 104 (100).

The i.r., n.m.r., molecular weight, and elemental analytical data confirm the presence of the substituents

Can. J. Chem. Downloaded from www.nrcresearchpress.com by 210.87.254.105 on 09/05/12
For personal use only.

and functionalities depicted in **3**, and the u.v. spectrum (λ_{max} 207 nm), the 1,4- rather than 1,3- arrangement of double bonds. Again, three pairs of structurally isomeric 1,4-adducts (**3**, **21**, **22**, and their locational isomers) can

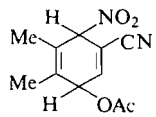

21

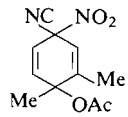

22

be conceived but only **3** and its locational isomer are consistent with the n.m.r. spectrum. Structure **22** has adjacent vinyl protons which would give a 10 Hz coupling, whereas the largest coupling observed is 3 Hz. Each of the three ring protons of structure **21** should be coupled to the other two, two of these should be coupled to both methyl groups and, moreover, the methyl groups should be coupled to each other. However, in the observed spectrum only one methyl group is split and only one ring proton is coupled to both other ring protons, consistent only with structure **3**. The locational isomer of **3** would be expected to undergo facile loss of acetic acid under the basic work-up conditions and thus only structure **3** itself conforms to the chemistry of the adduct. The three nitro substitution products have definitive n.m.r. spectra. 3,4-Dimethyl-2-nitrobenzonitrile has two *ortho* aromatic protons and accordingly exhibits an 8 Hz coupling. Its 5-nitro isomer has *meta* protons and a 1.8 Hz coupling and the 6-nitro isomer has *para* protons which appear as two singlets. The mass spectra of the 2-nitro and 5-nitro isomers each exhibit an intense 159 peak, a consequence of losing OH from the parent ion, as expected for compounds containing *ortho* nitro and methyl groups. A metastable peak for this transition is observed in the spectrum of the 5-nitro compound. The 159 peak is not present in the spectrum of the 6-nitro isomer. Instead, characteristic 146 (loss of NO) and 103 peaks (loss of NO_2 and HCN) are exhibited.

*Pyrolysis of 2-Cyano-3,4-dimethyl-4-nitro-1,4-dihydrophenyl Acetate (**2**)*

The diene was sufficiently thermally stable to be sublimed unchanged on heating. A sample (60 mg, 0.25 mmol) was decomposed by covering with sand and heating in a small scale sublimation apparatus at 200 °C for 10 min at a pressure of less than 10 Pa. After cooling the sand was extracted with ether and the ether evaporated. The n.m.r. spectrum of the residue showed that 2,3-dimethylbenzonitrile and 2,3-dimethyl-5-nitrobenzonitrile had been formed. Pyrolysis was also carried out by injecting a sample of the diene in acetone solution into the inlet, at 275 °C, of the vapor phase chromatograph. A small peak attributed to 6-acetoxy-2,3-dimethylbenzonitrile (trace) and major peaks from 2,3-dimethylbenzonitrile (75%) and its 5-nitro derivative (25%) were observed in the chromatogram. The identifications were confirmed by correspondence of retention times with authentic samples. Other nitro isomers were not present.

*Decomposition of 2-Cyano-3,4-dimethyl-4-nitro-1,4-dihydrophenyl Acetate (**2**) in Mesitylene and in Toluene*

The diene (60 mg, 0.25 mmol) was dissolved in mesitylene (3 cm^3) and heated under reflux at 165 °C for 1 h. Temperature-programmed vapor phase chromatography at 170–200 °C on PEGA showed peaks for mesitylene, 2,3-dimethylbenzonitrile, 6-acetoxy-2,3-dimethylbenzonitrile (trace), and 2,3-dimethyl-5-nitrobenzonitrile but none for 2-nitromesitylene. The mol ratio of dimethylbenzonitrile to nitro derivative was 3:2. Chromatography on alumina at −30 °C gave mesitylene in the pentane fraction, 2,3-dimethylbenzonitrile (15 mg, 0.11 mmol) in the 20% ether fraction and 2,3-dimethyl-5-nitrobenzonitrile (18 mg, 0.10 mmol) in the 40% ether fraction.

In a similar experiment in toluene 2,3-dimethylbenzonitrile and 2,3-dimethyl-5-nitrobenzonitrile were obtained but no nitrotoluenes were detected.

*Decomposition of **2** in Acetic Acid*

The diene (150 mg) was heated under reflux in acetic acid (2.5 cm^3) for 2 h. Ether was added and the solution washed with water and dilute ammonium hydroxide. The ethereal solution was dried and the ether evaporated. The residue contained 2,3-dimethylbenzonitrile and 2,3-dimethyl-5-nitrobenzonitrile in approximately equal amounts (by n.m.r.). The compounds were separated by chromatography on alumina and their identities confirmed by n.m.r. and, for the 5-nitro derivative, by m.p.

*Decomposition of **2** in Acetic Acid Containing Sulfuric Acid*

The diene (50 mg) was dissolved in a solution of 5% of sulfuric acid in acetic acid (0.4 cm^3) and kept at ambient temperature. After 6 h 30% of the diene had decomposed and absorptions at 1.96 (s, 9%) and at 2.64 and 3.03 p.p.m. (H_A and H_B of AB quartet, J = 8 Hz, 21%) had appeared. After 27 h 74% of the diene had decomposed. The peak at 1.96 p.p.m. had increased to 21%. A second AB quartet had appeared slightly upfield of the original and of approximately equal intensity (26%) to the remaining original quartet. The new quartet exhibited absorption at 2.89 and 3.31 p.p.m. (J = 8 Hz). After 93 h all of the diene had decomposed, the 1.96 absorption had increased to 29%, the original AB quartet had decreased to 13% and the higher field quartet had increased to 58%. When the experiment was repeated in CD_3CO_2D containing 20% acetic anhydride and 5% sulfuric acid neither the lower field quartet nor the characteristic pattern of three singlets in the methyl region expected for 2-cyano-3,4-dimethylphenyl acetate were observed. The reaction mixture was quenched with a solution of ammonia in methylene chloride at −78 °C and the excess ammonia pumped off at the same temperature. The mixture was filtered, the residue dissolved in water and the resulting solution extracted with ether. Evaporation of the filtrate gave a mixture of 94% of 2-cyano-3,4-dimethylphenol (see below); n.m.r. ($CDCl_3$) τ 2.86 (nq, 1, 5-*H*), 3.30 (nq, 1, 6-*H*), 7.61 (s, 3, 3-CH_3), 7.81 p.p.m. (s, 3, 4-CH_3), and 6% of the compound which exhibited a singlet at 1.96 p.p.m. and also had methyl absorption at 7.47 and 7.69 p.p.m. Evaporation of the ethereal extract gave a mixture of 46% of the 2-cyano-3,4-dimethylphenol and 54% of the second compound, identified as 2-cyano-3,4-dimethyl-6-nitrophenol; i.r. 3540 and 3420 (OH), 1545 cm^{-1} (NO_2); n.m.r. ($CDCl_3$) τ 1.96 (s, 1, 5-*H*), 7.47 (s, 3, 3-CH_3) 7.69 p.p.m. (s, 3, 4-CH_3); mass spectrum *m/e* 192.046 (M_r ($^{12}C_9{}^1H_8{}^{14}N_2{}^{16}O_3$) = 192.053), 162 (M − NO).

*Decomposition of **2** in Trifluoroacetic Acid*

The diene (300 mg) was dissolved in trifluoroacetic acid (2 cm^3). Decomposition was complete in 15 min, after which time the n.m.r. spectrum had no peaks in the diene

Can. J. Chem. Downloaded from www.nrcresearchpress.com by 210.87.254.105 on 09/05/12
For personal use only.

Can. J. Chem. Downloaded from www.nrcresearchpress.com by 210.87.254.105 on 09/05/12
For personal use only.

region and two sets of AB quartet resonances had appeared in the aromatic region. The trifluoroacetic acid was evaporated. The residue had i.r. (Nujol) 1780 and 1230 cm^{-1} ($OCOCH_3$); n.m.r. ($CDCl_3$) τ 2.68 (nq, 1, J = 8.4 Hz, 5-*H*), 3.04 (nq, 1, J = 8.4 Hz, 6-*H*), 7.56 (s, 3, 3-CH_3), 7.65 (s, 3, $OCOCH_3$), 7.72 (s, 3, 4-CH_3), and 2.83 (nq, 1, J = 2.5 Hz), 2.89 p.p.m. (nq, 1, J = 2.5 Hz), methyl region obscured. Vapor phase chromatography on PEGA at 200 °C showed the presence of two components in a 3:1 ratio, the same as that indicated by the integral of the two AB quartets in the aromatic region of the n.m.r. The major component was identified as 2-cyano-3,4-dimethylphenyl acetate (see below) by n.m.r. and v.p.c. The retention time on v.p.c., the n.m.r. spectrum and the absence of peaks for any other functionalities in the i.r. are consistent with the minor component being 3-cyano-4,5-dimethylphenyl acetate. Chromatography on alumina at −30 °C gave substantially pure 2-cyano-3,4-dimethylphenyl acetate.

Decomposition of ***2*** *in Acidified Methanol*

The diene (50 mg) was dissolved in a solution of methanol (1 cm^3) containing 1% sulfuric acid. This mixture was left at ambient temperature for 100 h, then cooled to −50 °C and neutralized by condensing gaseous ammonia into the solution. The solution was filtered to remove the precipitated ammonium sulfate and the filtrate evaporated. The residue was extracted with methylene chloride, the resulting solution dried ($MgSO_4$) and evaporated to give 2-cyano-3,4-dimethyl-4-nitro-1,4-dihydrophenol (**6**); i.r. (film) 3420 and 1050 (OH), 2230 (CN), 1555 and 1350 cm^{-1} (NO_2); n.m.r. ($CDCl_3$) τ 3.76 (q, 1, 6-*H*), 4.06 (q, 1, 5-*H*), 5.38 (m, 1, 1-*H*), 7.12 (b, 1, O*H*), 7.87 (d, 3, 3-CH_3), 8.22 p.p.m. (s, 3, 4-CH_3); J_{15} = 0.9, J_{16} = 3.1, $J_{1,1\text{-}OH}$ = 8.5, $J_{1,3\text{-}CH_3}$ = 1.5, J_{56} = 9.65 Hz; irradiation at 7.87 sharpened the multiplet at 5.38 and D_2O exchange caused the disappearance of the multiplet at 7.12 and sharpened the multiplet at 5.38, mass spectrum (70 eV) *m/e* (relative intensity) 176 (4), 148 (48), 147 (71), 133 (24), 132 (100), 116 (46).

When the decomposition of the diene in acidified methanol was carried out by heating under reflux for 24 h and the residue obtained on work-up chromatographed on silica, 2-cyano-3,4-dimethylphenol (6-hydroxy-2,3-dimethylbenzonitrile) was obtained, m.p. 135–137 °C; u.v. (CH_3OH) 307 (ε 310 m^2 mol^{-1}) at p*H* 2, 335 nm (ε 440 m^2 mol^{-1}) at p*H* 10; i.r. (Nujol) 3310 and 3220 (OH), 2225 cm^{-1} (CN); n.m.r. ($CDCl_3$) τ 2.84 (nq, 1, J = 8.5 Hz, 5-*H*), 3.27 (nq, 1, J = 8.5 Hz, 6-*H*), 3.6 (broad, 1, O*H*), 7.62 (s, 3, 3-CH_3), 7.82 p.p.m. (s, 3, 4-CH_3); the broad peak at 3.6 p.p.m. disappeared on addition of D_2O; mass spectrum (70 eV) *m/e* (relative intensity) 147.071 (69, M_r ($^{12}C_9{}^1H_9{}^{14}N{}^{16}O$) = 147.068), 132 (100, M − CH_3). The phenol was acetylated by heating under reflux in acetic anhydride for 1 h to give 2-cyano-3,4-dimethylphenyl acetate, m.p. 69–71.5 °C; i.r. (Nujol) 2225 (CN), 1780 and 1190 cm^{-1} ($OCOCH_3$); n.m.r. ($CDCl_3$) τ 2.73 (nq, 1, J = 8.5 Hz, 5-*H*), 3.08 (nq, 1, J = 8.5 Hz, 6-*H*), 7.58 (s, 3, 3-CH_3), 7.68 (s, 3, $OCOCH_3$), 7.75 p.p.m. (s, 3, 4-CH_3); mass spectrum (70 eV) *m/e* (relative intensity) 189 (10, M), 147.072 (100, M_r($^{12}C_9{}^1H_9{}^{14}N{}^{16}O$) = 147.068), 132 (51).

Pyrolysis of 2-Cyano-4,5-dimethyl-4-nitro-1,4-dihydrophenyl Acetate (3)

The diene (200 mg) was heated under sand at 150 °C for 15 min and worked up as described above for the 3,4-dimethyl isomer. The n.m.r. spectrum showed that 3,4-dimethylbenzonitrile (~50%) and 3,4-dimethyl-5-nitrobenzonitrile (~50%) had been formed together with a small amount of 2-cyano-4,5-dimethylphenyl acetate (~2%).

Pyrolysis in the inlet of the vapor phase chromatograph at 275 °C gave 3,4-dimethylbenzonitrile, 2-cyano-4,5-dimethylphenyl acetate, and 3,4-dimethyl-5-nitrobenzonitrile. 3,4-Dimethylbenzonitrile was the predominant product and the acetate was a minor constituent (~3%) but the actual proportions of products varied when pyrolyses were carried out at different times, presumably because the conditions of pyrolysis were not reproducible.

Decomposition of 2-Cyano-4,5-dimethyl-4-nitro-1,4-dihydrophenyl Acetate (3) in Mesitylene

The diene (60 mg) was dissolved in mesitylene (2 cm^3) and heated under reflux for 1 h. Vapor phase chromatography on QFI at 175 °C and on FFAP at 200 °C showed peaks for 3,4-dimethylbenzonitrile (70%) and 3,4-dimethyl-5-nitrobenzonitrile (30%). No 2-nitromesitylene was detected. Chromatography on alumina and elution with pentane and then ether gave only mesitylene in the pentane fraction and a mixture of 3,4-dimethylbenzonitrile and 3,4-dimethyl-5-nitrobenzonitrile in the ether, confirmed by n.m.r.

Decomposition of ***3*** *in Acetic Acid*

The diene (50 mg) was heated under reflux in acetic acid (5 cm^3) for 4 h. The mixture was worked up as described above for the 3,4-dimethyl isomer. The n.m.r spectrum showed that 3,4-dimethylbenzonitrile and 3,4-dimethyl-5-nitrobenzonitrile were formed in approximately equal amounts and v.p.c. analysis showed 3,4-dimethylbenzonitrile (~40%), 2-cyano-4,5-dimethylphenyl acetate (~10%), and 3,4-dimethyl-5-nitrobenzonitrile (~50%).

Decomposition of ***3*** *in Acetic Acid Containing Sulfuric Acid*

The diene (50 mg) was dissolved in a solution (0.4 cm^3) of 5% sulfuric acid in CD_3CO_2D and maintained at 37 °C. After 4 h a doublet at τ 3.15 p.p.m. had appeared and the diene peaks were reduced in intensity. After 96 h the doublet at 3.15 and the original vinyl resonances had disappeared and three new resonances at 2.45 (45% for 1 aromatic proton), 2.75 and 3.12 p.p.m. (55% for 2 aromatic protons) had appeared. On standing at ambient temperature colorless crystals of 2-cyano-4,5-dimethylphenol formed; n.m.r. (CD_3OD) τ 2.85 (s, 1, 3-*H*), 3.32 (s, 1, 6-*H*), 7.80 (s, 3, 5-CH_3), 7.86 p.p.m. (s, 3, 4-CH_3). The downfield singlet in the n.m.r. spectrum of the reaction mixture was assigned to 2-cyano-4,5-dimethyl-6-nitrophenol. The reaction mixture was quenched with a solution of liquid ammonia in methylene chloride at −78 °C and the excess ammonia pumped off at the same temperature. The residue was extracted with chloroform and passed through a short column of silica. Removal of the solvent gave a mixture of 2-cyano-4,5-dimethylphenol and 2-cyano-4,5-dimethyl-6-nitrophenol; mass spectrum *m/e* 192.050 (M_r ($^{12}C_9{}^1H_8{}^{14}N_2{}^{16}O_3$) = 192.053).

When this experiment was carried out with the addition of mesitylene (65 mg) the nitrocyanophenol (15%) and phenol (85%) were formed and 2-nitromesitylene was detected by v.p.c. of the product on QFI at 185 °C.

Decomposition of 3 in Trifluoroacetic Acid

The diene (100 mg) was dissolved in trifluoroacetic acid (2 cm^3). Decomposition was complete in 10 min, the n.m.r. spectrum exhibited no peaks in the diene region but showed that 2-cyano-4,5-dimethylphenyl acetate (τ 2.55, 2.94) had been formed. Vapor phase chromatography showed that a small amount of 3,4-dimethyl-5-nitrobenzonitrile was also present. Chromatography on alumina at -20 °C gave the acetate as a clear oil; i.r. (film) 2220 (CN), 1775 and 1180 cm^{-1} ($OCOCH_3$); n.m.r. ($CDCl_3$) τ 2.61 (s, 1, 3-*H*), 2.99 (s, 1, 6-*H*), 7.65 (s, 3, $OCOCH_3$), 7.70 (s, 3, 5-CH_3) and 7.73 p.p.m. (s, 3, 4-CH_3); the absence of coupling (> 1 Hz) between the aromatic protons confirms that they are *para* to each other; mass spectrum (70 eV) *m/e* (relative intensity) 189.0794 (18, M_r ($^{12}C_{11}{}^1H_{11}{}^{14}N^{16}O_4$) = 189.0790), 147 (100, M − $COCH_2$) 132 (51). Methanolysis of the acetate with 10% sulfuric acid in methanol gave after work-up and chromatography on silica, 2-cyano-4,5-dimethylphenol, m.p. 197.5–199 °C; i.r. (Nujol) 3260 (OH), 2225 cm^{-1} (CN); n.m.r. (CD_3OD—$CDCl_3$) τ 2.82 (s, 1, 3-*H*), 3.23 (s, 1, 6-*H*), 7.74 (s, 3, 5-CH_3), 7.83 p.p.m. (s, 3, 4-CH_3); mass spectrum (70 eV), *m/e* (relative intensity) 147.069 (100, M_r ($^{12}C_9{}^1H_9{}^{14}N^{16}O$) = 147.068), 146 (54, M − H), 132 (98, M − CH_3), 118 (22), 104 (13), 91 (21).

Decomposition of 3 in Acidified Methanol

The diene (250 mg) was dissolved in a solution of methanol (5 cm^3) containing 1% sulfuric acid. The resulting solution was allowed to stand at ambient temperature for 12 h and then worked up as described above for the 3,4-dimethyl isomer to give 2-cyano-4,5-dimethyl-4-nitro-1,4-dihydrophenol (7) (145 mg, 86%), m.p. 67–69 °C; i.r. (Nujol) 3440 (broad, OH), 2230 (CN), 1550 and 1355 cm^{-1} (NO_2); n.m.r. ($CDCl_3$) τ 3.35 (d, 1, 3-*H*), 4.04 (m, 1, 6-*H*), 5.45 (m, 1, 1-*H*), 6.9 (m, 1, O*H*), 8.20 (t, 3, 4-CH_3), 8.24 p.p.m. (s, 3, 5-CH_3); J_{13} = 1.1, J_{16} = 3.45, $J_{1,5-CH_3}$ = 1.5, $J_{1,1-OH}$ = 8, $J_{6,5-CH_3}$ = 1.5 Hz; D_2O exchange caused the disappearance of the resonance at 6.9 and sharpened the multiplet at 5.45 p.p.m., and irradiation at 8.20 collapsed the multiplet at 4.04 to a doublet; mass spectrum (70 eV) *m/e* (relative intensity) 147 (30, M − HNO_2), 132 (45), 131 (62), 116 (100).

We thank the National Research Council of Canada and the University of Victoria for financial support.

1. (*a*) D. J. Blackstock, A. Fischer, K. E. Richards, J. Vaughan, and G. J. Wright. Chem. Commun. 641 (1970); (*b*) D. J. Blackstock, J. Cretney, A. Fischer, M. P. Hartshorn, K. E. Richards, J. Vaughan, and G. J. Wright. Tetrahedron Lett. 2793 (1970); (*c*) A. Fischer, C. C. Greig, A. L. Wilkinson, and D. R. A. Leonard. Can. J. Chem. **50**, 2211 (1972); (*d*) A. Fischer and D. R. A. Leonard. Can. J. Chem. **50**, p. 3367; (*e*) A. Fischer and A. L. Wilkinson. Can. J. Chem. **50**, p. 3988; (*f*) A. Fischer and J. N. Ramsay. J. Chem. Soc. Perkin II, 237 (1973); (*g*) A. Fischer and C. C. Greig. J. Chem. Soc. Chem. Commun. 396 (1973).
2. A. Fischer, J. Vaughan, and G. J. Wright. J. Chem. Soc. (B), 368 (1967).
3. P. C. Myhre. J. Am. Chem. Soc. **94**, 7921 (1972).
4. J. N. Ramsay. Ph.D. Thesis, University of Victoria, Victoria, B.C. 1973.
5. A. Fischer and G. J. Wright. Aust. J. Chem. In press.
6. R. O. C. Norman and R. Taylor. Electrophilic substitution in benzenoid compounds. Elsevier, Amsterdam. 1965. p. 72.
7. R. C. Hahn and M. B. Groen. J. Am. Chem. Soc. **95**, 6128 (1973).
8. G. A. Olah, H. C. Lin, and Y. K. Mo. J. Am. Chem. Soc. **94**, 3667 (1972).
9. K. Higasi. Bull. Inst. Phys. Chem. Res. (Tokyo), **22**, 805 (1943).
10. S. F. Birch, R. A. Dean, F. A. Fidler, and R. A. Lowry. J. Am. Chem. Soc. **71**, 1362 (1949).
11. P. V. Divekar and L. C. Vining. Can. J. Chem. **42**, 63 (1964).
12. J. Vène, M. Kerfanto, and D. Raphalen. Bull. Soc. Chim. Fr. 1813 (1963).
13. A. I. Scott. Interpretation of the ultraviolet spectra of natural products. Pergamon Press, Oxford. 1964. Chap. 2.
14. E. W. Garbisch, Jr. J. Am. Chem. Soc. **86**, 5561 (1964).
15. J. K. M. Sanders and D. H. Williams. J. Am. Chem. Soc. **93**, 641 (1971).
16. H. Budzikiewicz, C. Djerassi, and D. H. Williams. Mass spectrometry of organic compounds. Holden-Day Inc., San Francisco. 1967. p. 516.
17. A. Brandstrom and S. A. I. Carlsson. Acta Chem. Scand. **21**, 983 (1967).

Can. J. Chem. Downloaded from www.nrcresearchpress.com by 210.87.254.105 on 09/05/12
For personal use only.

Interaction of Palladium(II) Acetate with Sodium and Lithium Acetate in Acetic Acid[1]

RAJ N. PANDEY[2] AND PATRICK M. HENRY

Department of Chemistry, University of Guelph, Guelph, Ontario N1G 2W1

Received October 22, 1973

Palladium(II) acetate in acetic acid in the absence of acetate ion exists as the trimeric species $Pd_3(OAc)_6$. The reaction of the trimer with NaOAc or LiOAc at 25° was not instantaneous. Spectral studies on fully equilibrated systems indicated the first equilibria involved transformation of trimer to dimer

$$2Pd_3(OAc)_6 + 6NaOAc \underset{}{\overset{K_{32}}{\rightleftharpoons}} 3Na_2Pd_2(OAc)_6$$

$$2Pd_3(OAc)_6 + 6LiOAc \overset{K'_{32}}{\rightleftharpoons} 3Li_2Pd_2(OAc)_6$$

with $K_{32} = 7.77 \times 10^4\ M^{-5}$ and $K'_{32} = 1.76 \times 10^2\ M^{-5}$. The kinetics of the slow transformation of trimer to dimer was studied. The reaction has the rate expression: rate = $[Pd_3(OAc)_6]$ $(k + k'[MOAc])$ (M = Li or Na). This rate expression is consistent with substitution processes suggesting the slow step of the reaction is the S_N2 attack of solvent or acetate on a Pd(II)–acetate bond to break one of the acetate bridges.

In the NaOAc system conversion of trimer to dimer was complete at 0.2 *M* NaOAc. Further addition of NaOAc caused the dimer to be converted to monomer.

$$Na_2Pd_2(OAc)_6 + 2NaOAc \overset{K_{21}}{\rightleftharpoons} 2Na_2Pd(OAc)_4$$

K_{21} is $7.6 \times 10^{-4}\ M^{-1}$ at 25°.

L'acétate de palladium(II) dans l'acide acétique, en l'absence d'ions acétate, existe sous la forme d'un trimère $Pd_3(OAc)_6$. La réaction du trimère avec NaOAc ou LiOAc à 25° n'était pas instantanée. Des études spectrales sur des systèmes complètement équilibrés indiquaient que le premier équilibre impliquait la transformation du trimère en dimère.

$$2Pd_3(OAc)_6 + 6NaOAc \overset{K_{32}}{\rightleftharpoons} 3Na_2Pd_2(OAc)_6$$

$$2Pd_3(OAc)_6 + 6LiOAc \overset{K'_{32}}{\rightleftharpoons} 3Li_2Pd_2(OAc)_6$$

avec $K_{32} = 7.77 \times 10^4\ M^{-5}$ et $K'_{32} = 1.76 \times 10^2\ M^{-5}$. La cinétique de la transformation lente du trimère en dimère a été étudiée. L'expression de la vitesse de réaction est: vitesse = $[Pd_3(OAc)_6]$ $(k + k'[MOAc])$ (M = Li ou Na). L'expression de vitesse est cohérente avec le processus de substitution qui suggère que l'étape lente de la réaction est l'attaque S_N2 du solvant ou de l'acétate sur une liaison Pd(II)–acétate pour briser un des ponts acétate.

Dans le cas du système NaOAc, la conversion du trimère en dimère était complète à 0.2 *M* NaOAc. Une nouvelle addition de NaOAc provoquait la conversion du dimère en monomère.

$$Na_2Pd_2(OAc)_6 + 2NaOAc \overset{K_{21}}{\rightleftharpoons} 2Na_2Pd(OAc)_4$$

K_{21} égale $7.6 \times 10^{-4}\ M^{-1}$ à 25 °C. [Traduit par le journal]

Can. J. Chem., **52**, 1241 (1974)

Introduction

In the past several years the field of Pd(II) catalysis has made considerable progress (for a recent review, see refs. 1 and 12) as witnessed by the discovery of many new organic syntheses. Many of the new Pd(II) catalyzed reactions are carried out in acetic acid solvent. In order to arrive at an understanding of the mechanism of these reactions it is necessary to know the various Pd(II) species present in this solvent. A previous study determined the interaction of

[1]Presented in part at the 164th National meeting of the American Chemical Society, New York, August, 1972, Abstract page INOR 29.

[2]Postdoctoral Fellow.

Can. J. Chem. Downloaded from www.nrcresearchpress.com by 210.87.254.5 on 09/05/12
For personal use only.

Pd(II) with LiCl in this solvent (2). This information was useful in interpreting the kinetics of exchange reactions (3). The present work is concerned with the interaction of palladium(II) acetate with lithium and sodium acetates in the chloride-free system. This system has also been used in studies of olefin oxidation (4, 5).

To the authors' knowledge the only previous work on this system was a brief study by McCaskie (6). His results suggested that the equilibrium involved conversion of a trimeric palladium(II) acetate species to a dimer by sodium acetate. Also the reaction of trimer to dimer was found to be a slow reaction. However his studies were too incomplete to conclusively define the equilibria over the whole range of acetate concentrations.

Experimental

Materials

Palladium acetate (purchased from Engelhard Chemicals and Catalysts, New Jersey) was purified by the method of Stephenson *et al.* (7). The acetic acid of high purity (Baker Chemical Co.) was dried by refluxing over triacetylborate, $B(OAc)_3$, and distilled (8). The Karl Fisher analysis of several preparations showed water contents of less than 0.01%. Lithium acetate (City Chemical Corporation, New York) and sodium acetate (Baker Chemical Co.) were all reagent grade. The reported amount of water in lithium acetate was 1%. Prior to making up solutions the salt was treated with calculated amounts of acetic anhydride and warmed. The Pd(II) stock solutions were analyzed by the dimethylglyoxime technique (9).

The molecular weights were measured using a Mechrolab vapor pressure osmometer, Model 301A as described previously (2).

Equilibrium Measurements

The majority of spectra were recorded on a Unicam S.P. 800 spectrophotometer using a 10 mm optical pathlength cell. A Cary 14 instrument was used when measurements requiring cells of 1, 5, and 100 mm pathlengths were made.

The addition of sodium or lithium acetate to solutions of palladium(II) acetate in acetic acid did not give an instantaneous change in spectra. In fact the solutions took periods of hours to come to equilibrium indicating the reaction of initial Pd(II) species with acetate was a slow reaction. For that reason equilibrium studies were carried out on solutions which were allowed to stand for a sufficient period of time to allow them to come to equilibrium. Spectra were measured in the 400 to 250 nm region. The acetic acid and metal acetates are transparent in this region.

The absorbance spectra of a series of completely equilibrated solutions of constant palladium(II) acetate concentration but varying [NaOAc] showed isosbestic points at 320 and 385 nm up to [NaOAc] = *ca.* 0.2 *M* at 25°. At this concentration the spectra showed little change with further increase in [NaOAc] to *ca.* 0.4 *M*. These results indicated one Pd(II) species was being completely converted to another species. At still higher [NaOAc] further changes in spectra occurred with new isosbestic points indicating the intermediate species was being converted to a third species.

Since molecular weight measurements indicated the Pd(II) species present in the absence of metal acetate is the trimer the first equilibrium must be represented by one of the following equilibria.

$$[1]\quad 2Pd_3(OAc)_6 + 6NaOAc \overset{K_{32}}{\rightleftharpoons} 3Na_2Pd_2(OAc)_6$$

$$[2]\quad Pd_3(OAc)_6 + 6NaOAc \overset{K_{31}}{\rightleftharpoons} 3Na_2Pd(OAc)_4$$

$$[3]\quad Pd_3(OAc)_6 + 4NaOAc \overset{K_{321}}{\rightleftharpoons} Na_2Pd_2(OAc)_6 + Na_2Pd(OAc)_4$$

$$[4]\quad Pd_3(OAc)_6 + 2NaOAc \overset{K_{33}}{\rightleftharpoons} Na_2Pd_3(OAc)_8$$

where

$$[5]\quad K_{32} = \frac{[Na_2Pd_2(OAc)_6]^3}{[Pd_3(OAc)_6]^2[NaOAc]^6}$$

$$[6]\quad K_{31} = \frac{[Na_2Pd(OAc)_4]^3}{[Pd_3(OAc)_6][NaOAc]^6}$$

$$[7]\quad K_{321} = \frac{[Na_2Pd_2(OAc)_6][Na_2Pd(OAc)_4]}{[Pd_3(OAc)_6][NaOAc]^4}$$

$$[8]\quad K_{33} = \frac{[Na_2Pd_3(OAc)_8]}{[Pd_3(OAc)_6][NaOAc]^2}$$

The extinction coefficient of the trimer, ε_{P_3}, at various wavelengths can be obtained from measurements in the absence of acetate while that of the other species, whether it be dimer or monomer, can be obtained from the region of [NaOAc] at which the intermediate species is the only Pd(II) species present. Then by the usual techniques values of K_{32}, K_{31}, K_{321}, and K_{33} can be calculated at various total palladium(II) and acetate concentrations. Sample calculations for the values of K_{32} and K_{31} are shown at one wavelength in Table 1. As can be seen K_{31} varies considerably while K_{32} remains constant. The average value for a number of measurements is $7.7 \times 10^4\ M^{-5}$. Similar data are shown for lithium acetate in Table 2.

The average value in this system is $1.76 \times 10^2\ M^{-5}$. The values of K_{321} and K_{33} (not shown in the tables) were calculated. The K_{321} values for sodium acetate varied from 56 to 139 M^{-3} whereas for lithium acetate, from 0.75 to 2.2 M^{-3}. Similarly the values for K_{33} for sodium and lithium acetates were 175 to 422 and 24 to 38, respectively. These results then indicated the conversion of trimer to dimer as the first step equilibria.

The second equilibrium was not as readily calculated because it did not go to completion even in saturated solutions of sodium or lithium acetate. Almost certainly this equilibrium consisted of the conversion of dimer to monomer where

Can. J. Chem. Downloaded from www.nrcresearchpress.com by 210.87.254.5 on 09/05/12
For personal use only.

TABLE 1. Calculated values of the equilibrium constants K_{32} and K_{31} at 25 °C, for the sodium acetate system at 360 nm*

			Dimer equilibria†		Monomer equilibria‡	
D_i $\lambda_{360\,nm}$	$[Pd_3(OAc)_6]_0 \times 10^3$ (M)	$[Pd_3(OAc)_6]_{eq} \times 10^3$ (M)	$[NaOAc]_{eq} \times 10^2$ (M)	$K_{32} \times 10^{-4}$ (M^{-5})	$[NaOAc]_{eq} \times 10^2$ (M)	$K_{31} \times 10^{-2}$ (M^{-4})
0.485	0.920	0.770	2.49	7.84	2.44	5.47
0.600	0.920	0.630	3.72	7.74	3.63	4.53
0.780	0.920	0.410	5.68	7.87	5.52	3.05
0.874	0.920	0.296	7.02	7.79	6.83	2.17
0.676	1.460	1.330	1.89	7.64	1.85	9.33
1.353	1.460	0.508	7.22	7.99	6.93	4.12
1.413	1.946	1.158	5.06	7.34	4.82	9.05
1.839	4.266	4.071	1.63	7.83	1.57	32.38
1.959	4.266	3.925	2.19	7.88	2.08	32.86

*ε_{trimer} at 360 mμ = 394 M^{-1} cm^{-1}.
†ε_{dimer} at 360 mμ = 809 M^{-1} cm^{-1}; $[Na_2Pd_2(OAc)_6] = 3/2([Pd_3(OAc)_6]_0 - [Pd_3(OAc)_6]_{eq})$.
‡$\varepsilon_{monomer}$ at 360 mμ = 404.5 M^{-1} cm^{-1}; $[Na_2Pd(OAc)_4] = 3([Pd_3(OAc)_6]_0 - [Pd_3(OAc)_6]_{eq})$.

TABLE 2. Calculated values of the equilibrium constants K_{32} and K_{31} at 25 °C for the lithium acetate system at 360 nm*

			Dimer equilibria†		Monomer equilibria‡	
D_i $\lambda_{360\,nm}$	$[Pd_3(OAc)_6]_0 \times 10^3$ (M)	$[Pd_3(OAc)]_{eq} \times 10^3$ (M)	$[LiOAc] \times 10^2$ (M)	$K_{32} \times 10^{-2}$ (M^{-5})	$[LiOAc]_{eq} \times 10^2$ (M)	K_{31} (M^{-4})
0.605	1.216	0.995	7.63	1.86	7.56	1.56
0.495	1.216	1.188	2.55	1.94	2.54	1.89
0.536	1.216	1.115	5.89	1.60	5.85	0.61
0.612	1.216	0.967	8.17	1.85	8.09	1.52
0.779	1.946	1.924	1.99	1.54	1.98	2.43
0.822	1.946	1.848	4.17	1.75	4.14	2.71
0.869	1.946	1.765	5.94	1.45	5.88	2.17
1.926	4.266	3.831	6.87	1.79	6.74	6.16

*ε_{trimer} = 394 M^{-1} cm^{-1}.
†ε_{dimer} = 641 M^{-1} cm^{-1}; $[Li_2Pd_2(OAc)_6] = 3/2([Pd_3(OAc)_6]_0 - [Pd_3(OAc)_6]_{eq})$.
‡$\varepsilon_{monomer}$ = 320.5 M^{-1} cm^{-1}; $[Li_2Pd(OAc)_4] = 3([Pd_3(OAc)_6]_0 - [Pd_3(OAc)_6]_{eq})$.

[9] $Na_2Pd_2(OAc)_6 + 2NaOAc \overset{K_{21}}{\rightleftharpoons} 2Na_2Pd(OAc)_4$

K_{21} is given by eq. 10.

$$[10] \quad K_{21} = \frac{[Na_2Pd(OAc)_4]^2}{[Na_2Pd_2(OAc)_6][NaOAc]^2}$$

The data were treated by the method of least-squares, estimation of non-linear parameters (10) was similar to that used previously (2). Defining the following quantities: T_m = the total molar concentration of trimer ($\frac{1}{3}[Pd(OAc)_2]_0$); L = the concentration of free acetate (as NaOAc or LiOAc); P_1 = the concentration of monomeric species $[Na_2Pd(OAc)_4]$; P_2 = the concentration of dimeric species $[Na_2Pd_2(OAc)_6]$; ε_{P_2} = the molar absorptivity of dimer; ε_{P_1} = the molar absorptivity of monomer eq. 10 can be rewritten.

$$[11] \quad K_{21} = P_1^2/P_2L^2$$

The following relationships can immediately be written:

$$[12] \quad D_i = \varepsilon_{P_1}P_1 + \varepsilon_{P_2}$$

$$[13] \quad T_m = \tfrac{2}{3}P_2 + \tfrac{1}{3}P_1$$

Equations 11 to 13 can be combined to give eq. 14.

$$[14] \quad D_i = (\varepsilon_{P_1} - \tfrac{1}{2}\varepsilon_{P_2})\frac{(L^2K_{21})}{4} + \sqrt{\frac{L^4K_{21}^2}{16} + 1.5L^2T_mK_{21} + 1.5\varepsilon_{P_2}T_m}$$

The non-linear least-squares treatment was applied to eq. 14. The program predicts the value, $\hat{D}_i$, of a dependent variable D_i by a suitable choice of parameters ε_{P_1}, ε_{P_2}, and K_{21} in eq. 14. The program computes the least-squares estimates of the parameters and adjusts these to minimize $\sum_{i=1}^{n}(D_i - \hat{D}_i)^2$. As an example a set of data at one wavelength the computed values of these parameters are given in Table 3. Absorbance data at five wavelengths (λ = 380, 365, 350, 340, 330 mμ), obtained at Pd(II) concentrations, 7.00×10^{-5}, 12.25×10^{-5}, 2.92×10^{-3}, 1.28×10^{-2} M, and [NaOAc] in the range 0.20 to 1.0 M

Can. J. Chem. Downloaded from www.nrcresearchpress.com by 210.87.254.5 on 09/05/12
For personal use only.

TABLE 3. Typical calculation of K_{21} from spectral data using the Marquardt non-linear least square technique*

[NaOAc] (M)	Absorbance at $\lambda_{365\ m\mu}$ Observed	Calculated†	$[Na_2Pd(OAc)_4] \times 10^5$ (M)	$[Na_2Pd_2(OAc)_6] \times 10^5$ (M)	% Dimer dissociated	$K_{21} \times 10^4$ (M^{-1})
0.20	0.610	0.608	3.58	4.34	29.19	
0.40	0.575	0.582	6.06	3.10	49.37	7.38
0.60	0.570	0.564	7.74	2.26	63.17	
0.80	0.555	0.552	8.90	1.68	72.62	
1.00	0.540	0.543	9.70	1.28	79.17	

*$[Pd(OAc)_2]_0 = 12.25 \times 10^{-5}$ M, optical pathlength = 100 mm, temperature = 25 °C.
†$\varepsilon_{dimer} = 1053\ M^{-1}\ cm^{-1}$; $\varepsilon_{monomer} = 422\ M^{-1}\ cm^{-1}$.

TABLE 4. Effect of trimer concentration on k_{obs} at fixed [NaOAc] and [LiOAc]

$[Pd_3(OAc)_6] \times 10^3$ (M)	[NaOAc] (M)	[LiOAc] (M)	$k_{obs} \times 10^4$ (s^{-1})
0.920	0.406		12.9
1.173	0.406		10.3
1.460	0.406		13.2
0.780	0.406		11.2
1.217		0.513	12.2
1.460		0.513	12.8
1.823		0.513	12.9
2.433		0.513	12.1

were treated in the above fashion. The groups of data characterized by a given value for T_m yielded K_{21} with relative variation of about ±10% from the average value of K_{21} which was $7.6 \times 10^{-4}\ M^{-1}$.

Kinetic Measurements

The interaction between trimeric palladium acetate and sodium or lithium acetate was followed spectrophotometrically by repetitive scans over a wavelength range 370–275 mμ. Reactants thermostatted at 25° were mixed and transferred rapidly (mixing time <0.5 min) to the cell for spectral measurements. This cell was also thermostatted at 25°.

Since the acetate salts were always in considerable excess the reaction was pseudo first order in trimer. The pseudo first order rate constant k_{obs}, was evaluated from the slope of the plot of $\log (D_\infty - D_t)$ *vs.* time at $\nu = 365$ nm. In order to avoid complications resulting from incomplete reaction acetate concentrations at which trimer was completely converted to dimer were used.

As shown in Table 4 the value of k_{obs} did not change with initial trimer concentration indicating the reaction is strictly first order in trimer.

Results

The molecular weight of palladium(II) acetate in dry acetic acid in the absence of acetate was found to be 667, which is very close to that expected for a trimeric species $Pd_3(OAc)_6$. Based on this result and the spectral studies carried out at 25°, the two equilibria in this system can be shown to be represented by eqs. 15 and 16 (M = Li or Na):

$$[15]\quad 2Pd_3(OAc)_6 + 6MOAc \overset{K_{32}}{\rightleftharpoons} 3M_2Pd_2(OAc)_6$$

$$[16]\quad M_2Pd_2(OAc)_6 + 2MOAc \overset{K_{21}}{\rightleftharpoons} M_2Pd(OAc)_4$$

with the value of K_{32} for M = Na ($7.77 \times 10^4\ M^{-5}$) being much higher than when M = Li ($1.76 \times 10^2\ M^{-5}$). The second equilibrium was studied only with NaOAc since K_{21} for LiOAc was too small for accurate determination. Even at the highest [LiOAc] the conversion to monomer was small. The K_{21} for NaOAc is $7.6 \times 10^{-4}\ M^{-1}$.

The values of the K_{32}'s are such that the dimer is practically the only species present in the NaOAc system at 0.2 M NaOAc while in the LiOAc system the corresponding value is 0.5 M LiOAc. At a total Pd(II) concentration of 0.0128 M and at 1.0 M NaOAc the dimer is only about 16% converted to monomer. However, because of the nature of the equilibrium the conversion is higher at lower Pd(II). Thus, as shown in Table 3, at $[Pd(II)] = 1.225 \times 10^{-4}$ the conversion at 1.0 M NaOAc is 79%.

The kinetics of the slow reaction of trimer with sodium or lithium acetate to form dimer (eq. 15)

Can. J. Chem. Downloaded from www.nrcresearchpress.com by 210.87.254.5 on 09/05/12
For personal use only.

Can. J. Chem. Downloaded from www.nrcresearchpress.com by 210.87.254.5 on 09/05/12
For personal use only.

was also studied. The reaction of sodium acetate with dimer to form monomer (eq. 16) was also slow but because of the complications arising from the fact this reaction did not go to completion, its kinetics were not studied.

The dependence of the pseudo first order rate constant, k_{obs}, on NaOAc or LiOAc concentration is shown in Figs. 1 and 2, respectively. The dependence is linear for both with a positive intercept. Since the first order rate constant, k_{obs}, did not change with initial $[Pd_3(OAc)_6]$ in either system the reaction is strictly first order in trimer. The complete rate expression is thus:

$$[17] \quad \frac{-d[Pd_3(OAc)_6]}{dt} = [Pd_3(OAc)_6] \times (k + k'[MOAc])$$

where the k for both LiOAc and NaOAc is about $1 \times 10^{-4}\ s^{-1}$ and k' for LiOAc is $2.7 \times 10^{-3}\ M^{-1}\ s^{-1}$ and $2.9 \times 10^{-3}\ M^{-1}\ s^{-1}$ for NaOAc.

To determine if association of lithium acetate is important its molecular weight was measured at two concentrations in the absence of Pd(II). At 0.05 M a value of 66 was obtained while at 0.1 M the value was 67.

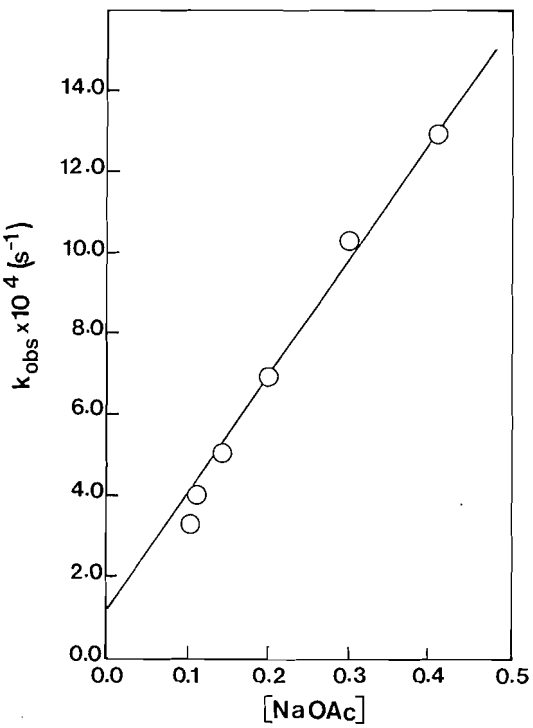

FIG. 1. Plot of k_{obs} *vs.* [NaOAc] at fixed $[Pd_3(OAc)_6]$ (=0.00092 M), temperature = 25 °C.

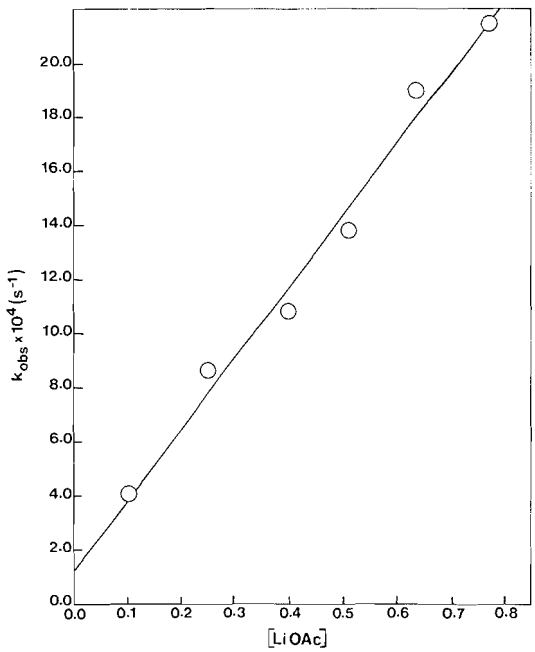

FIG. 2. Plot of k_{obs} *vs.* [LiOAc] at fixed $[Pd_3(OAc)_6]$ (=0.00122 M), temperature = 25 °C.

Discussion

The palladium(II) acetate system in acetic acid differs from the chloride system in two important aspects. First the equilibria are more complicated. Thus in the chloride-containing system only a dimeric and a monomeric palladium(II) chloride species need be considered (2) while in the acetate system trimeric, dimeric, and monomeric palladium(II) acetate species are found. Secondly, the conversion of dimer to monomer by chloride is rapid while the conversion of trimer to dimer and then to monomer by acetate is a slow reaction.

The reason for these differences must be related to the difference in the nature of chloride and acetate as bridging ligands. Thus palladium(II) acetate also exists as a trimer in benzene at 37° (7) and a crystal structure determination indicates the trimer molecule consists of a nearly equilateral triangle of palladium atoms (11). The Pd—Pd distance (*ca.* 3.15 Å) is such that the coordination at the metal atoms is approximately square planar. The geometry of the double acetate bridges apparently allows the palladium to achieve the favored coordination in the trimer while the chloride bridges do not permit this with the usual Pd—Cl—Pd bond angles of 90° (ref. 12, pp. 43 to 46).

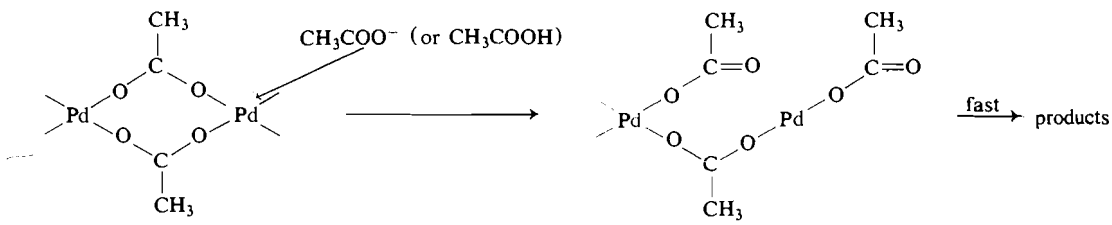

The rate expression for the reaction of acetate with the trimer (eq. 17) is of the form usually found for reaction of square planar complexes and indicates a solvent path as well as a reagent dependent path (13). The rate determining step almost certainly involves an S_N2 attack of acetate or acetic acid on one of the Pd(II)–oxygen bonds. This type of substitution is found for most square planar complexes (13).

The present results are in reasonable agreement with the preliminary studies of McCaskie (6). Thus his value of K_{32} for NaOAc is 5.4×10^5 M^{-5} while the value found in the present work is 7.7×10^4 M^{-5}. This difference is not too large considering the complicated equilibrium. The difference is due to the fact that he used a [NaOAc] of 0.797 M to determine the extinction coefficient of the dimer and at this concentration appreciable amounts of monomer are present. Also he found a rate expression of the form of eq. 17 for reaction of trimer with NaOAc. His constants are $k = 6.0 \times 10^{-5}$ s^{-1} and $k' = 1.8 \times 10^{-3}$ M^{-1} s^{-1} at 21° as compared with the present values of 1.0×10^{-4} s^{-1} and 3.2×10^{-3} M^{-1} s^{-1} at 25°.

One other difference between the acetate system and the chloride system is that in the latter the dimerization of LiCl must be taken into account. For that reason the molecular weight of LiOAc was measured. At 0.05 and 0.1 M the molecular weights found at 37.5° were 66 and 67, the same as the monomer (66) within experimental error. For comparison the measured molecular weight of LiCl at 0.1 M was about 15% higher than the monomeric species. Thus LiOAc is much less associated than LiCl and it was assumed that this as well as NaOAc is not appreciably associated in HOAc. On the other hand, in anhydrous acetic acid the salts are only slightly ionized with ionization constants of 2.63×10^{-7} M for NaOAc and 1.59×10^{-7} M for lithium acetate (14, 15). Thus the undissociated salts would be expected to be the reactive species. In the case of the reaction of acetate with trimer this must be the case; for if free acetate ion were the reactant the rate expression would show a $[MOAc]^{1/2}$ term, since free acetate would be proportional to the square root of the metal acetate concentration.

Finally the differences in equilibria between the chloride and acetate systems may well result in differences in the catalytic activity of Pd(II) in the two systems. The first requirement is that the metal acetate and palladium(II) acetate be allowed to come to equilibrium before organic reagent is added otherwise the reaction scheme will be very complicated. There is no assurance that this has always been done in the past. Even if equilibrium between Pd(II) and acetate has been achieved still further complications would arise if organic substrate was required to break the non-labile bridging acetates to form reactive intermediates.

The present study does not provide any information concerning the lability of the non-bridging acetates in the dimer and monomer. However they would be expected to react much more rapidly than bridging acetates.

The authors thank the National Research Council of Canada for financial support of this work and Dr. John E. McCaskie for communicating his unpublished results on $Pd(OAc)_2$–NaOAc catalysis. One of us (R.N.P.) would like to thank Mr. S. R. Singh for his help in computing.

1. P. M. MAITLIS. The organic chemistry of palladium. Vol. II. Academic Press, New York, N.Y. 1971.
2. P. M. HENRY. Inorg. Chem. **10**, 373 (1971).
3. P. M. HENRY. Acc. Chem. Res. **6**, 16 (1973).
4. W. KITCHING, Z. RAPPOPORT, S. WINSTEIN, and W. G. YOUNG. J. Am. Chem. Soc. **88**, 2054 (1966).
5. I. I. MOISEEV, M. N. VARGAFTIK, S. V. PESTRIKOV, O. G. LEVANDA, T. N. ROMANOVA, and YA. K. SIRKIN. Dokl. Akad. Nauk SSSR, 1365 (1969).
6. J. E. MCCASKIE. PH.D. Thesis. University of California, Los Angeles, Calif. 1971.
7. T. A. STEPHENSON, S. M. MOREHOUSE, A. R. POWELL, J. P. HEFFER, and G. WILKINSON. J. Chem. Soc. 3632 (1965).

Can. J. Chem. Downloaded from www.nrcresearchpress.com by 210.87.254.5 on 09/05/12
For personal use only.

8. W. C. EICHELBERGER and V. K. LA MER. J. Am. Chem. Soc. **55**, 3633 (1933).
9. W. W. SCOTT. Standard methods of chemical analysis. Vol. I. 6th ed. Van Nostrand, Princeton, N.J. 1962. p. 883.
10. D. W. MARQUARDT. J. Soc. Ind. Appl. Math. **11**, 431 (1963).
11. A. C. SKAPSKI and M. L. SMART. Chem. Commun. 658 (1970).
12. P. M. MAITLIS. The organic chemistry of palladium. Vol. 1. Academic Press, New York. N.Y. 1971.
13. F. BASOLO and R. G. PEARSON. Mechanisms of inorganic reactions. John Wiley and Sons, New York 1967. Chapt. 5.
14. S. BRUCKENSTEIN and I. M. KOLTHOFF. J. Am. Chem. Soc. **78**, 2974 (1956).
15. L. H. SUTCLIFFE and J. PROLL. Trans. Faraday Soc. **57**, 1078 (1961).

Can. J. Chem. Downloaded from www.nrcresearchpress.com by 210.87.254.5 on 09/05/12
For personal use only.

An Electron Spin Resonance Study of Radicals Formed by γ-Irradiation of 1-Substituted 5-Nitro-amino and 5-Nitroso-aminotetrazoles

RICHARD C. CATTON
Department of Chemistry, Malaspina College, Nanaimo, British Columbia
AND
RICHARD N. BUTLER
Department of Chemistry, University College, Galway, Ireland

Received October 2, 1973

γ-Irradiation of 1-methyl-5-methylnitro-aminotetrazole **1** and 1-methyl-5-nitro-aminotetrazole **2** resulted in cleavage of the exocyclic N—N bond giving only one detectable radical (NO_2·) in each case. The stability and motion of the NO_2· radicals formed in these systems was studied. The NO_2· radical obtained from compound **1** was immobile in the lattice while that obtained from compound **2** was rotating about the *y*-axis. Irradiation of 1-methyl-5-methyl-nitroso-aminotetrazole **3** and 1-phenyl-5-nitroso-aminotetrazole **4** did not give a simple N—N bond cleavage and radicals which could not be fully identified were encountered. The radical obtained from compound **3** appeared to be a nitroxide radical and that obtained from compound **4** appeared to arise from electron capture by the nitrosamino moiety.

L'irradiation γ méthyl-1 nitrométhyl-5 aminotétrazol **1** et du méthyl-1 nitro-5 aminotétrazol **2** conduit à la rupture de la liaison endocyclique N—N donnant seulement un radical détectable (NO_2·) dans chaque cas. La stabilité et le mouvement des radicaux NO_2· formés dans ces systèmes sont étudiés. Le radical NO_2· obtenu à partir du composé **1** est fixe dans le réseau alors que celui obtenu à partir du composé **2** tourne autour de l'axe *y*. L'irradiation du méthyl-1 nitrosométhyl-5 aminotétrazol **3** et du phényl-1 nitroso-5 aminotétrazol **4** n'a pas donné une simple rupture du lien N—N; des radicaux, qui n'ont pas pu être complètement identifiés, sont rencontrés. Le radical obtenu à partir du composé **3** semble être un radical d'oxyde d'azote et celui obtenu à partir du composé **4** semble provenir d'une fixation d'électrons par le fragment nitrosamine. [Traduit par le journal]

Can. J. Chem., **52**, 1248 (1974)

Although tetrazole derivatives are useful as photographic sensitizers (1) the photochemistry of these compounds was investigated only recently, mainly by Scheiner (2), who studied u.v. photolytic reactions in solution. We have previously reported on low temperature γ-irradiation of a series of alkyl substituted tetrazoles where the alkyl sites were the most reactive (3). With the single alkyl nitro-amino-tetrazole included in our previous study the exocyclic N—N bond was the reactive site. In this present work we intended to investigate the radicals formed by γ-irradiation of the primary and secondary nitro-amino and nitroso-amino-tetrazoles **1** to **4** in order to distinguish between the behavior of nitro-amino and nitroso-amino groups in lattices where hydrogen bonding is both present and absent.

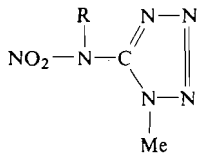

1 R = Me
2 R = H

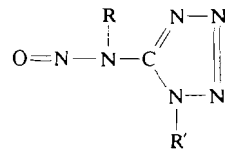

3 R = R′ = Me
4*a* R = H; R′ = Ph

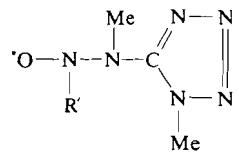

5

a R′ = Me
b R′ = H

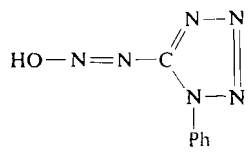

4*b*

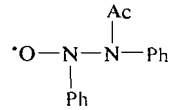

6

Experimental

The compounds **1** to **4** were prepared as previously described (4, 5). The samples were sealed in evacuated

Can. J. Chem. Downloaded from www.nrcresearchpress.com by 210.87.254.42 on 09/05/12
For personal use only.

TABLE 1. Electron spin resonance data for the NO_2· radical in various media

Compound/ matrix	Temperature (°K)	g_x	g_y	g_z	g_{ave}	A_x	A_y	A_z	A_{iso}
1	77[a,b]	2.0055	1.9916	2.0021	1.994	51.9	49.8	67.0	56.2
2	77[b]	2.0035	1.9920	2.0035	1.9997	56.6	48.7	56.6	54.0
	298[b]				2.0012				37.3
	77[b]	2.0051	1.9917	2.0026	1.9996	51.1	48.5	64.3	54.6
N_2O_4	293[c]					42.0	34.0	52.5	42.8
$NaNO_2$	298[d]	2.0055	2.0052	2.0059	2.0055	50.0	33.0	36.4	39.8
Argon	77[e]	2.0037	1.990	2.0037	1.9991	57.8	47.0	57.8	54.2
$NaNO_2$	77[f]	2.0057	1.9910	2.0015	1.9987	49.4	46.8	67.9	54.7

[a]Reference 3.
[b]This work.
[c]Reference 19.
[d]Reference 20.
[e]Reference 21.
[f]Reference 22.

quartz tubes and exposed to ^{60}Co γ-rays at 298 and 77 °K from a Vickrad source at a dose rate of *ca.* 4 Mrad h^{-1} for periods ranging from 1 to 8 h. The radiation time had no effect on the nature of the radicals formed. The e.s.r. signals described were detected only for irradiation at 77 °K. The e.s.r. spectra were measured at temperatures between 298 and 77 °K on a Varian E3 and a conventional X-band spectrometer, operating at approximately 9.3 GHz, using a Varian Variable Temperature Accessory. The *g*-values were determined with an accuracy of ±0.0002 using solid diphenyl-dipicrylhydrazyl (g = 2.0036) as a standard.

Results and Discussion

5-Nitro-aminotetrazoles

γ-Irradiation of compounds **1** and **2** resulted in cleavage of the exocyclic N—N bond yielding radicals which were identified as NO_2·. An interesting aspect of the study of these NO_2· radicals was the apparent role of the lattice in governing their stability and motion. In the case of compound **1** the NO_2· radical was rigid (immobile) in the lattice and was not bonded preferentially in any specific direction (3), as shown by the completely anisotropic *g*-tensor and the nitrogen hyperfine tensor. On warming the signal decayed and was completely annealed at 200 °K.

With compound **2**, on the other hand, the NO_2· radical was initially rotating in the lattice and was more stable since it was visible at room temperature and remained for some time before gradually decaying. The experimental parameters (Table 1) obtained from the e.s.r. spectrum (Fig. 1*a*) possessed axial symmetry due to the rapid rotation or reorientation of the molecule about the *y* axis, which we take to be parallel to the O---O direction. (We will also assign the *z* axis as the direction bisecting the O—N—O angle and the *x* axis as the direction perpendicular to the O—N—O plane of the radical.) Rotation of NO_2· about the *y* axis has been shown to occur in various media (6, 7). In the

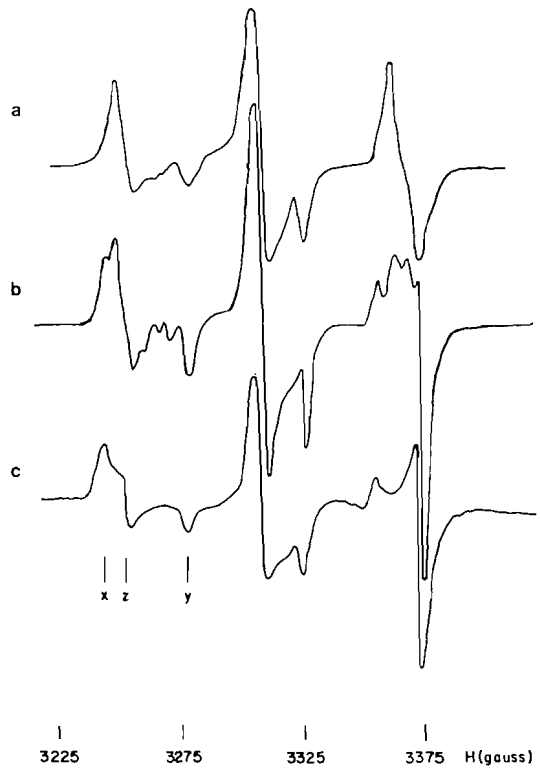

FIG. 1. First derivative X-band e.s.r. spectra of γ-irradiated nitraminotetrazoles (ν = 9267.6 Mc/s). (*a*) Compound **2** irradiated and measured at 77 °K. (*b*) Compound **2** irradiated at 77 °K, warmed to *ca.* 150 °K, and then measured at 77 °K. (*c*) Compound **1** irradiated and measured at 77 °K and compound **2** irradiated at 77 °K, warmed to 298 °K, and then measured at 77 °K.

Can. J. Chem. Downloaded from www.nrcresearchpress.com by 210.87.254.42 on 09/05/12
For personal use only.

present case it may arise from hydrogen bonding between the lattice and the radical as follows

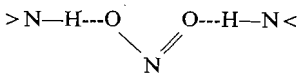

Spectra from samples of compound **2** which were heated to intermediate temperatures and remeasured at 77 °K indicated the presence of both NO_2· radicals rotating about the y axis and also stationary NO_2· radicals (Fig. 1*b*). When the sample was equilibrated at room temperature and the spectrum recorded at 77 °K only the stationary radicals comparable to those from compound **1** were detected. (Experimental g- and A- values for these NO_2· radicals are in Table 1.)

A comparison of the e.s.r. spectra (Fig. 1) of the NO_2· radical in compound **2** shows that the spectrum of the rotating radical can readily be derived from the experimental e.s.r. parameters of the immobile species using $g_\perp = \frac{1}{2}(g_x + g_z)$, $g_\parallel = g_y$ and $A_\perp = \frac{1}{2}(A_x + A_z)$, $A_\parallel = A_y$. In the axially symmetric case we obtained spectral lines from the assigned x and z directions (Fig. 1*c*) which coalesce into one line at the position halfway between the x and z peaks in Fig. 1*a*. The position of the lines associated with the axis of rotation however did not change. These formulas give calculated values of $A_\perp = 57.7$ G, $g_\perp = 2.0038$, and $g_\parallel = 1.9917$ which are in good agreement with the experimentally determined values of 56.6 G, 2.0035, and 1.9920, respectively.

The production of the two types of NO_2· radicals on heating may be due to changes in the lattice structure which include cleavage of the weak hydrogen bonds with the radicals. The existence of two inequivalent NO_2· radicals in a lattice has previously been explained (7) in terms of different types of sites where the radical may rotate freely and where such rotation is impossible. A similar phenomenon could also possibly occur with compound **2**.

The e.s.r. spectrum of compound **2**, when recorded at 298 °K, consisted of an isotropic triplet which may be due to a freely rotating NO_2· radical. The isotropic splitting ($A_{iso} = 37.2$ G) when compared to A_{iso} for the original NO_2· radicals from both compounds **1** and **2** at 77 °K (Table 1) is unusually low but such low values have been observed previously (8). The signal could also possibly arise from a different nitrogen containing radical and indeed it has been suggested that some previously assigned NO_2· radicals with low values of A_{iso} were in fact NO_3^{2-} radicals (9). However, we favor the former explanation since on recooling to 77 °K the sample re-exhibits a non-axially symmetric NO_2· radical. Hence both signals appear to be due to the same chemical species since they are readily interchangeable and one is not lost when converted to the other by a temperature change. The extra stability to thermal bleaching of the NO_2· radical in compound **2** may be due to the presence of hydrogen bonding in the lattice.

5-Nitroso-aminotetrazoles 3 and 4

In contrast to the 5-nitro-aminotetrazoles, exocyclic N—N bond cleavage was not the major interaction detected with compounds **3** and **4** and more complex radicals, which could not be fully identified, were encountered. When compound **3** was irradiated at 77 °K and the e.s.r. spectrum measured at the same temperature, signals due to two separate radicals (which we shall refer to as **A** and **B**) were observed (Fig. 2*a*). Heating the samples simplified the spectra and at 167 °K the species **A** was fully annealed leaving the second radical **B** (Fig. 2*b*) which decayed on warming to 298 °K. The spectrum of the radical **A** was typical of a nitroxide radical, being characterized by a large nitrogen triplet with A_{iso}, *ca.*, 12 G (Table 2) (10, 11). The possibility of g-anisotropy being involved was eliminated by using S-band spectrometry. Since only the nitrogen hyperfine splitting could be observed, the exact structure of the nitroxide radical could not be determined other than establishing its nitroxide nature. We tentatively suggest that a nitroxide radical such as **5***a* could possibly arise by nitroso trapping (10, 12) of a methyl radical. We have previously (3) detected methyl radicals in γ-irradiated alkyltetrazoles. The secondary splittings to be expected from a methyl group and a nitrogen atom bonded directly to the nitroxide function may be obscured in the linewidth of *ca.* 8 G. For example, the secondary splitting due to the nitrogen atom bonded directly to the nitroxide function of the radical **6** was found to be only 1.67 G and splitting from the ortho protons of the phenyl group bonded to the nitroxide function was not observable (13). A nitroxide radical of type **5***b* in which the absence of the proton splitting may be due to a rapid proton exchange is also a possibility (14), though less likely in our opinion, in view of our

Can. J. Chem. Downloaded from www.nrcresearchpress.com by 210.87.254.42 on 09/05/12
For personal use only.

TABLE 2. Electron spin resonance data for radicals found in γ-irradiated nitroso-aminotetrazoles

Compound	Radical	$g_\perp$	$g_\parallel$	g_{ave}	$A_\perp$ (G)	$A_\parallel$ (G)	A_{iso} (G)
3	**A**	2.0050	2.0023	2.0041	3[a]	30.8	12.3
	B			2.0061			H = 26.7
							N = 8.1
4	**C**	2.0100	2.0041	2.0080	—[b]	46.1	16–18
		Secondary splittings			—[b]	11.6(N)	
					—[b]	5.2(H)	

[a]The maximum value of $A_\perp$ which is determined by the linewidth of the ⊥ feature.
[b]Not resolved. The linewidth is *ca.* 13 G given $A_\perp$ a maximum value of *ca.* 4 G.

previous work (3). The e.s.r. spectrum of the radical **B** (Fig. 2*b*) appeared to be completely isotropic both at 77 and 298 °K. This suggests that the radical is either still rotating at 77 °K or that the ⊥ features only are visible, the ∥ features being too broad. The isotropic sextet, partially distorted by a broad unidentified peak, appears to arise from splittings due to nitrogen (8.1 G) and hydrogen (26.7 G) nuclei and is centered at $g = 2.0061$. Radical **B** therefore may be a species of the type HON^- which is isoelectronic with HOO· but a more precise assignment cannot be made. The formation of such a fragment would be of interest in view of the previously reported (15) loss of the fragment "[HON]" on u.v. photolysis of secondary nitrosamines of the type R—CH_2—N(NO)R in acidic media.

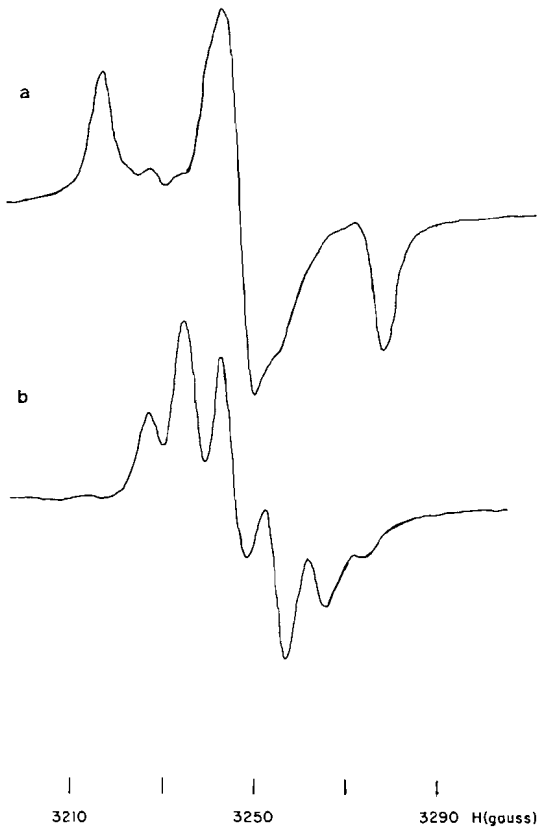

FIG. 2. X-band e.s.r. spectra of compound **3** γ-irradiated at 77 °K (ν = 9124.5 Mc/s). (*a*) Measured at 77 °K. (*b*) Warmed to *ca.* 180 °K and measured at 77 °K.

Compound **4**, although not directly analogous to **3** because of the replacement of the 1-*N*-methyl group by a phenyl group, is used here for comparison purposes. This compound is a primary nitrosamine and is exceptional insofar as such species are considered to be highly reactive intermediates in the diazotization process. We have recently prepared some such tetrazoles (5) and have established that the predominant structural contributions come from forms **4***a* and **4***b*. We (5), and others (16), were unable to prepare the comparable compound with the phenyl substituent replaced by a methyl group despite earlier claims of its isolation (17). γ-Irradiation of compound **4** yielded a radical characterized by a major nitrogen splitting accompanied by secondary splittings due to nitrogen and hydrogen which are visible on the ∥ features only. The ⊥ features of primary or secondary splittings could not be resolved (Fig. 3). This radical, **C**, appears to have a structure such as $^-O—N^·—NH—R$ and could arise by electron capture by the nitroso-amino moiety. The radical is similar to those observed in other secondary nitrosamines (18) and the magnitude of the nitrogen hyperfine splittings is in reasonable agreement. The radical decayed rapidly on heating.

The differences in the spectra due to the radicals **A** and **C** indicate that the species responsible for the spectra are not of the same type, the major difference being the presence of secondary nitrogen and hydrogen hyperfine structure from the radical **C**. The different

Can. J. Chem. Downloaded from www.nrcresearchpress.com by 210.87.254.42 on 09/05/12
For personal use only.

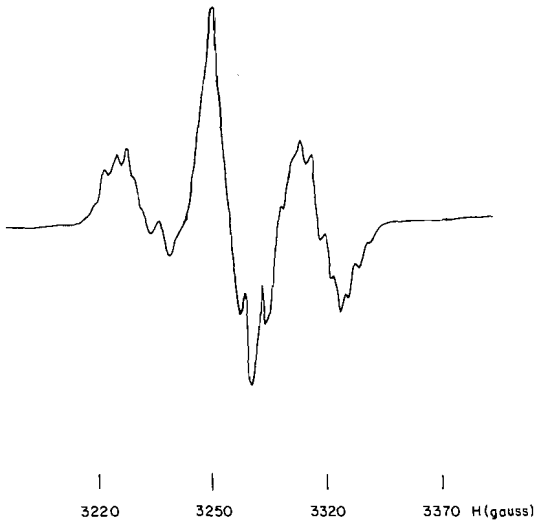

FIG. 3. Electron spin resonance spectrum of compound **4** γ-irradiated and measured at 77 °K (ν = 9200.3 Mc/s).

products may possibly be influenced by the nature of the lattices since hydrogen bonding is present with compound **4** but absent with compound **3**.

1. F. R. BENSON. Heterocyclic compounds. Vol. 8. *Edited by* R. C. Elderfield. Wiley, London. 1967. p. 1.
2. P. S. SCHEINER and W. M. RITCHMAN. J. Chem. Soc. Chem. Commun. 781 (1972); P. S. SCHEINER. Tetrahedron Lett. 4489 (1971); P. S. SCHEINER. J. Org. Chem. **34**, 199 (1969); P. SCHEINER and J. F. DINDA. Tetrahedron, **26**, 2619 (1970).
3. R. N. BUTLER, R. C. CATTON, and M. C. R. SYMONS. J. Chem. Soc. B, 378 (1970).
4. R. N. BUTLER and F. L. SCOTT. J. Org. Chem. **31**, 3182 (1966).
5. R. N. BUTLER, T. M. LAMBE, J. C. TOBIN, and F. L. SCOTT. J. Chem. Soc. Perkin I, 1357 (1973).
6. J. R. BRAILSFORD and J. R. MORTON. J. Magn. Reson. **1**, 575 (1969).
7. T. J. SCHAAFSMA and J. KOMMANDEUR. Mol. Phys. **14**, 517 (1968).
8. T. J. SCHAAFSMA and J. KOMMANDEUR. J. Chem. Phys. **42**, 438 (1965).
9. J. H. SHARP and M. C. R. SYMONS. J. Chem. Soc. A, 3075 (1970).
10. A. MACKOR, TH. A. J. W. WAJER, and TH. J. DE BOER. Tetrahedron, **24**, 1623 (1968).
11. N. EDELSTEIN, A. KWOK, and A. H. MAKI. J. Chem. Phys. **41**, 179 (1964); J. A. MCRAE and M. C. R. SYMONS. Nature, **210**, 1259 (1966).
12. C. LAGERCRANTZ. J. Phys. Chem. **75**, 3466 (1971); C. LAGERCRANTZ and K. TORSSELL. Acta Chem. Scand. **22**, 1935 (1968); A. R. FORRESTER and S. P. HEPBURN. J. Chem. Soc. C, 701 (1971).
13. G. R. CHALFONT, D. H. HEY, K. S. Y. LIANG, and M. J. PERKINS. Chem. Commun. 367 (1967).
14. J. C. BAIRD and J. R. THOMAS. J. Chem. Phys. **35**, 1507 (1961); J. PANNEL. Mol. Phys. **5**, 291 (1962).
15. Y. L. CHOW and A. C. H. LEE. Can. J. Chem. **45**, 311 (1967).
16. K. HATTORI, E. LIEBER, and J. P. HORWITZ. J. Am. Chem. Soc. **78**, 411 (1956).
17. R. STOLLE. J. Prakt. Chem. **134**, (2), 282 (1932).
18. G. R. STEVENSON, J. G. CONCEPCION, and J. CASTILLO. J. Phys. Chem. **77**, 611 (1973).
19. N. M. ATHERTON, R. H. DIXON, and G. H. KIRBY. Trans. Faraday Soc. **60**, 1688 (1964).
20. J. TATENO and K. GESI. J. Chem. Phys. **40**, 1317 (1964).
21. P. W. ATKINS, N. KEEN, and M. C. R. SYMONS. J. Chem. Soc. A, 2873 (1962).
22. H. ZELDES and R. LIVINGSTON. J. Chem. Phys. **35**, 563 (1961).

Can. J. Chem. Downloaded from www.nrcresearchpress.com by 210.87.254.42 on 09/05/12
For personal use only.

The γ-Radiolysis of Liquid Cyclohexane Containing Di-*n*-Propyl Disulfide

JOHN A. STONE AND JOSEPH ESSER

Chemistry Department, Queen's University, Kingston, Ontario

Received August 14, 1973

Di-*n*-propyl disulfide is an electron, positive ion, and free radical scavenger in γ-irradiated liquid cyclohexane. The efficiency of electron scavenging is comparable with that of sulfurhexafluoride and the efficiency of H atom scavenging is comparable with that of ethylene. The expected product of cyclohexyl radical scavenging, namely cyclohexylpropyl sulfide, accounts for only about one quarter of these radicals which disappear. No other sulfur-containing products are found. In cyclohexane solutions containing two different disulfides or a disulfide and a thiol a rapid equilibration of the thiyl groups leads to their statistical distribution between the sulfur-containing species.

Dans le cyclohexane liquide γ-irradié le disulfure de di-*n*-propyle agit comme piège pour les électrons, les ions positifs et les radicaux libres. Son efficacité comme piège pour les électrons est comparable à celle de l'hexafluorure de soufre alors que son efficacité à piéger les atomes d'hydrogènes est comparable à celle de l'éthylène. Le produit attendu lorsque le radical cyclohexyle est piégé à savoir le sulfure de cyclohexyle et de propyle correspond à seulement un quart de ces radicaux qui disparaissent. On ne trouve aucun autre produit contenant du soufre. Dans des solutions de cyclohexanes contenant deux disulfures différents ou un disulfure et un thiol un équilibre rapide des groupes thiyles conduit à leurs distributions statistiques parmi les différentes espèces contenant du soufre. [Traduit par le journal]

Can. J. Chem., **52**, 1253 (1974)

Introduction

Propanethiol in γ-irradiated liquid cyclohexane behaves mainly as a scavenger of cyclohexyl radicals, the major product being di-*n*-propyl disulfide which is formed by combination of thiyl radicals (1).

[1] $c\text{-}C_6H_{11}\cdot + C_3H_7SH \rightarrow c\text{-}C_6H_{12} + C_3H_7S\cdot$

[2] $C_3H_7S\cdot + C_3H_7S\cdot \rightarrow C_3H_7SSC_3H_7$

At low propanethiol concentrations the disulfide yields are nonlinear with dose signifying a competition with the thiol for radicals or their precursors.

Both thiols and disulfides are important protection agents in biological systems. Since the protective properties of disulfides in nonaqueous liquid systems have received little attention we have studied the behavior of di-*n*-propyl disulfide in γ-irradiated cyclohexane to complement our previous study with *n*-propanethiol.

Experimental

Di-*n*-propyl disulfide was prepared by the iodine oxidation of *n*-propanethiol. The results obtained with this material were indistinguishable from those obtained using Eastman Reagent Grade material. The disulfide was always fractionally distilled immediately prior to sample preparation. Two small impurity peaks were observed in the gas–liquid chromatogram of the disulfide, one before and one after the disulfide peak. Their total area was less than 1% that of the disulfide peak and they did not change in area measurably during radiolysis.

Cyclohexane (Phillips Pure Grade) was shaken with concentrated sulfuric acid, washed, dried, and distilled to reduce the cyclohexene content to an undetectable level ($< 10^{-5}$ *M*). Cyclohexylpropyl sulfide was prepared from cyclohexanethiol and propyl bromide in basic ethanol. After fractional distillation the purity was found by gas–liquid chromatography to be better than 98%.

Sample preparation and irradiation procedures have been described previously (1).

Results

The yields of all products are linear with dose from 0.5 to 2×10^{22} eV/l at 0.1 *M* di-*n*-propyl disulfide. The same is true at 2.62×10^{-3} *M* when, however, the propanethiol yield is very small and no dose dependence can be determined.

Figure 1 shows the effect of disulfide on the yields of products originating from cyclohexane alone, while Fig. 2 shows the corresponding yields of the new products, cyclohexylpropyl sulfide and *n*-propanethiol. No hydrogen sulfide or propane were detected ($G < 0.05$) and no other products were found. The disappearance of disulfide was measured at several of the lower concentrations, the results being shown in Table 1. The error limits quoted are the standard deviations for five or more measurements.

Can. J. Chem. Downloaded from www.nrcresearchpress.com by 210.87.254.42 on 09/05/12
For personal use only.

TABLE 1. The disappearance of di-*n*-propyl disulfide

Di-*n*-propyl disulfide (mol/l)	*G*(—di-*n*-propyl disulfide)	Dose × 10^{-22} (eV/l)
0.00056	0.67±0.04	1.0
0.0025	1.0 ±0.38	1.0
0.0026	0.84±0.19	2.0
0.0051	1.05±0.40	3.0

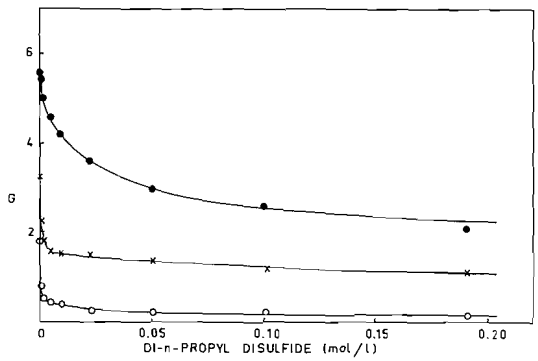

FIG. 1. The yields of hydrogen (●), cyclohexene (×), and bicyclohexyl (○) as functions of di-*n*-propyl disulfide concentration. The curve through the hydrogen points is calculated as described in the text. (Dose = 10^{19} eV g^{-1})

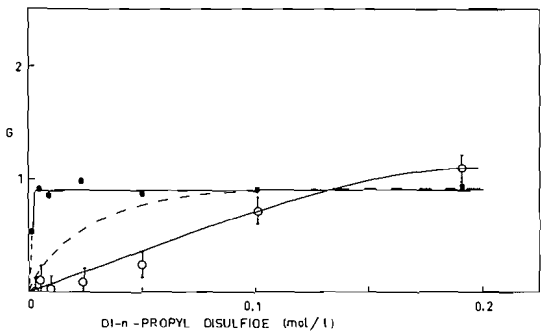

FIG. 2. The yields of cyclohexylpropyl sulfide (●) and *n*-propanethiol (Φ) as functions of di-*n*-propyl disulfide concentration. The broken line shows the yield of propanethiol expected from H atom scavenging. (Dose = 10^{19} eV g^{-1})

Di-*n*-propyl disulfide reduces $G(N_2)$ from a solution containing a fixed concentration of nitrous oxide (Fig. 3), while *G*(propane) is reduced in a solution containing a fixed concentration of cyclopropane (Fig. 4).

Radiolysis of cyclohexane containing both di-*n*-propyl disulfide and diethyl disulfide leads to the very rapid production of the mixed disulfide (Fig. 5). The same product is obtained from a solution initially containing ethanethiol and di-*n*-propyl disulfide (Fig. 6). There is no measurable change in the overall thiol concentration after this irradiation; the concentrations of the individual thiols were not determined.

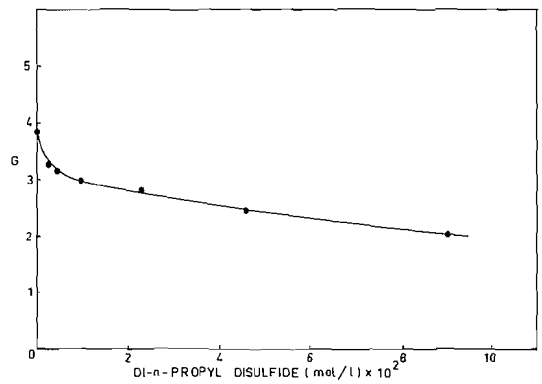

FIG. 3. The reduction in the N_2 yield by di-*n*-propyl disulfide from a solution 4.2×10^{-2} *M* in nitrous oxide. (Dose = 10^{19} eV g^{-1})

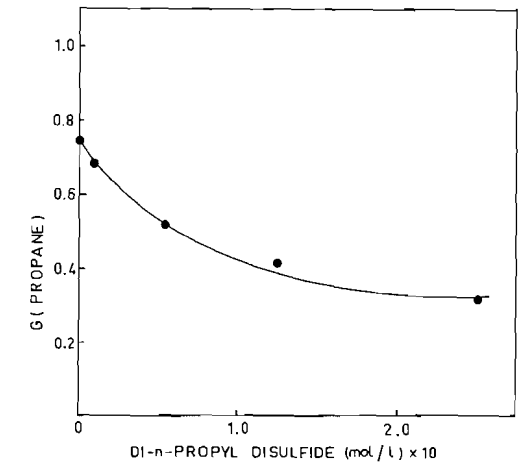

FIG. 4. The reduction in the propane yield by di-*n*-propyl disulfide from a solution 0.16 *M* in cyclopropane and 0.27 *M* in carbon tetrachloride. (Dose = 10^{19} eV g^{-1})

Discussion

Cyclopropane in irradiated liquid cyclohexane yields propane by H_2 transfer (2).

[3] $c\text{-}C_6H_{12}^+ + c\text{-}C_3H_6 \rightarrow c\text{-}C_6H_{10}^+ + C_3H_8$

Can. J. Chem. Downloaded from www.nrcresearchpress.com by 210.87.254.42 on 09/05/12
For personal use only.

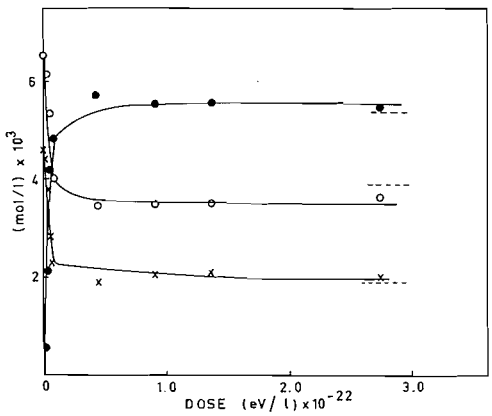

FIG. 5. The equilibration of thiyl groups in a solution initially 5.1×10^{-3} *M* in di-*n*-propyl disulfide and 5.4×10^{-3} *M* in ethanethiol. The broken lines show the calculated statistical distribution; (×) ethyl disulfide, (○) ethylpropyl disulfide, (●) di-*n*-propyl disulfide.

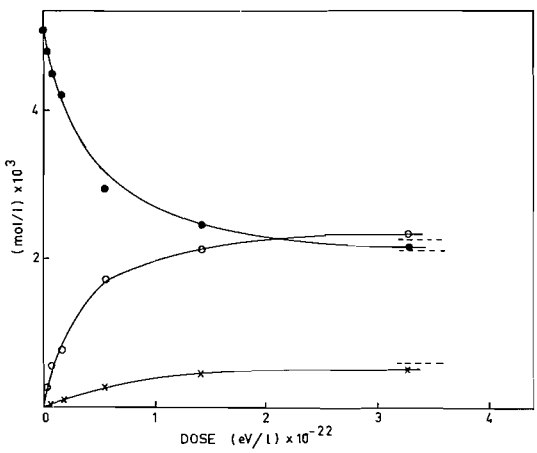

FIG. 6. The equilibration of thiyl groups in a solution initially 6.5×10^{-3} *M* in diethyl disulfide and 4.58×10^{-3} *M* in di-*n*-propyl disulfide. The broken lines show the calculated statistical distribution; (○) ethyl disulfide, (◉) ethylpropyl disulfide, (×) di-*n*-propyl disulfide.

Competition for $c\text{-}C_6H_{12}{}^+$ between cyclopropane and di-*n*-propyl disulfide is shown by the reduction of G(propane) from solutions containing a fixed concentration of cyclopropane (Fig. 4). Carbon tetrachloride is added to prevent electron scavenging by the disulfide. This latter property is shown by the reduction in nitrogen yield from a nitrous oxide solution (Fig. 3).

Di-*n*-propyl disulfide is, therefore, both an electron and a positive ion scavenger in liquid alkanes. Shida (3,4) has obtained spectroscopic evidence for the formation of alkyl disulfide cations and anions in γ-irradiated alkane glasses at 77 °K and has used the yield of anions to obtain a measure of the *W* value of solid alkanes. Electron scavenging by the disulfide group has also received much study in aqueous radiation chemistry (5).

Efficient electron scavengers such as methyl iodide, methyl bromide, and sulfurhexafluoride react at or near diffusion controlled rates in irradiated liquid cyclohexane (6). Di-*n*-propyl disulfide is even more effective at the same concentration than any of those solutes in reducing $G(H_2)$, *e.g.* $G(H_2) = 2.9$ for 0.19 *M* methyl bromide (6) whereas the value is 2.1 for the same concentration of di-*n*-propyl disulfide. We propose that the reduction in hydrogen yield is due to the scavenging of both electrons and H atoms. Although positive ion scavenging is also occurring this will not contribute significantly to the reduction in $G(H_2)$ since the resulting disulfide cations will be almost exclusively neutralized by disulfide anions. A detailed theoretical study of such scavenging has been made by Rzad (7).

G(H atoms) in γ-irradiated cyclohexane is 1.46, 61% of this yield having ionic precursors (1,6). When electron scavenging occurs the yield of H atoms will decrease. The experimental points for the hydrogen yield in Fig. 1 have been fitted by the empirical electron scavenging expression of Asmus *et al.* (6) together with a term for H atom scavenging. It is assumed that hydrogen is formed with unit efficiency upon electron–ion neutralization in the pure hydrocarbon and that none is formed when the disulfide

$$\Delta G(H_2) = G_{fi} + \frac{G_{gi}\sqrt{\alpha C}}{1 + \sqrt{\alpha C}} + \left[0.57 + \frac{0.89 G_{gi}}{G_{fi} + G_{gi}}\left(1 - \frac{\sqrt{\alpha C}}{1 + \sqrt{\alpha C}}\right)\right] \times \left[\frac{1}{1 + \dfrac{k_4[c\text{-}C_6H_{12}]}{k_5[C_3H_7SSC_3H_7]}}\right]$$

anion is involved. Where k_4 and k_5 are the rate constants for reactions 4 and 5, respectively;

[4] $\quad H\cdot + c\text{-}C_6H_{12} \rightarrow H_2 + c\text{-}C_6H_{11}\cdot$

[5] $\quad H\cdot + C_3H_7SSC_3H_7 \rightarrow \text{No } H_2$

α is an empirical parameter which describes the competition between electron capture by the disulfide and geminate ion – electron combination; and G_{fi} and G_{gi} are the free ion and geminate ion yields with values of 0.1 and 3.8, respectively (6). The best fit is obtained with $\alpha = 15$

Can. J. Chem. Downloaded from www.nrcresearchpress.com by 210.87.254.42 on 09/05/12
For personal use only.

Can. J. Chem. Downloaded from www.nrcresearchpress.com by 210.87.254.42 on 09/05/12
For personal use only.

M^{-1} and $k_4/k_5 = 0.003$. Di-*n*-propyl disulfide is therefore one of the most efficient electron scavengers in cyclohexane comparable with methyl bromide and sulfurhexafluoride for both of which $\alpha = 16\ M^{-1}$ (8). As an H atom scavenger the disulfide is comparable to ethylene for which the equivalent of k_4/k_5 has a value of 0.0048 (6).

The expected product of reaction (5) is *n*-propanethiol which is formed with increasing yield as the disulfide concentration is increased (Fig. 2). Except at the highest concentrations, however, the yield is lower than expected for the known yield of H atoms. This could be due to the disappearance of the thiol by reaction with cyclohexyl radicals when the disulfide concentration is low. We were not able to verify this hypothesis since the precision of the colorimetric thiol determination was not good. Gas–liquid chromatography could not be used since the thiol peaks were not reproducible and, in fact, for low concentrations ($5 \times 10^{-5}\ M$ or less) often failed to appear. It was ascertained that this behavior had no effect on any of the chromatographic determinations of the other products. The low thiol yield is discussed later.

The alkyl radical scavenging ability of the disulfide is illustrated by Fig. 1. At the lowest solute concentration, when $G(H_2)$ has been reduced to only a small extent, the yields of cyclohexene and bicyclohexyl are reduced considerably. ΔG(cyclohexene)/ΔG(bicyclohexyl) = 1 which is close to the value of 1.1 for the ratio of rate constants for disproportionation and combination of cyclohexyl radicals (9). The reduction in these yields at low disulfide concentrations may be ascribed with confidence to radical scavenging. The expected product of this reaction is cyclohexylpropyl sulfide. However the yield

$$[6]\quad c\text{-}C_6H_{11}\cdot + C_3H_7SSC_3H_7 \rightarrow c\text{-}C_6H_{11}SC_3H_7 + C_3H_7S\cdot$$

of this product is far lower than expected and never attains a G value greater than unity while from the decreases in cyclohexene and bicyclohexyl yields at the lowest disulfide concentration G(radicals scavenged) ≈ 4. A small fraction of the missing radicals may be scavenged by product thiol leading to regeneration of cyclohexane and disulfide (reactions 1 and 2). Such reactions can make only a minor contribution at low disulfide concentrations as shown by the expected thiol yield in Fig. 2. At higher disulfide concentrations scavenging by product thiol does not compete with that by disulfide since it is measured as a major product.

We considered the possibility that a contribution to the scavenging might be made by thiol either present initially as impurity in the disulfide or produced during sample preparation. No propanethiol was observable by gas–liquid chromatography in the freshly distilled disulfide. Propanethiol added at a concentration of 10^{-3} mol/l to the disulfide gave a chromatographic peak which was observable but was smaller than expected and was irreproducible in area. Thiol was not observable in a freshly prepared but unirradiated sample and the disulfide chromatographic peak area was the same as that of the stock solution which had been kept in the dark. We are, therefore, confident that reduction of the disulfide prior to irradiation did not occur and that the initial thiol concentration was negligibly small.

If allowance is made for radical scavenging by product thiol then it is expected that $G(\text{—}c\text{-}C_6H_{11}\cdot) \sim 1.8\ G(\text{—}C_3H_7SSC_3H_7)$ at low disulfide concentration. The experimental value for $G(\text{—}C_3H_7SSC_3H_7)$ is about a factor of two too low for the number of cyclohexyl radicals scavenged and only about one half of the disulfide that disappears is accounted for as the product cyclohexylpropyl sulfide. A possible explanation for some of the missing sulfur-containing products and the low yield of the expected product could be that radical attack occurs on hydrogen as well as on sulfur in the disulfide, the resulting radicals either disproportionating or combining.

$$[7]\quad c\text{-}C_6H_{11}\cdot + C_3H_7SSC_3H_7 \rightarrow c\text{-}C_6H_{12} + C_3H_7SS\underset{\cdot}{C}HCH_2CH_3$$

$$[8a]\quad 2C_3H_7SS\underset{\cdot}{C}HCH_2CH_3 \rightarrow C_3H_7SSCH_2CH_2CH_3 + C_3H_7SSCH{=}CHCH_3$$

$$[8b]\quad \rightarrow C_3H_7SSCHCH_2CH_3 \mid C_3H_7SSCHCH_2CH_3$$

$C_3H_7SS\underset{\cdot}{C}_3H_6$ would have a secondary structure and if k_{8a}/k_{8b} is taken as 1.63, the value suggested for the ratio of disproportionation to combination for *iso*-propyl radicals (10), 47% of the missing cyclohexyl radicals are accounted for.

Disulfides have seen much use as chain transfer agents in free radical polymerizations and although the rate constants for radical transfer are reasonably well known the site of radical attack

has seldom been determined. Pryor and Guard (11) have shown that attack by phenyl radicals is predominantly on sulfur for the lower alkyl disulfides but the attack shifts to hydrogen as the alkyl groups increase in size. For di-*n*-propyl disulfide 90% of the attack is on sulfur. We have found no information on the position of attack by alkyl radicals but expected that attack on sulfur should be favored.

The olefinic disulfide formed in [8*a*] would have chromatographic properties similar to the disulfide and might not be easily separable from it. We were not able to detect this possible product by using different chromatographic stationary phases with widely different polarities. The only clue to a so far unidentified product is an increase in the absorption band of the disulfide at 250 mμ. The concentration of disulfide actually decreases (Table 1). After correcting for this expected decrease the increase in absorption corresponds to a product with a G value of ~ 4, if its molar extinction coefficient is the same as that of the disulfide, which is of course highly unlikely. We have no evidence for the formation of polysulfides which are known to absorb in this region. Standard samples of tri- and tetrasulfides were observable by gas–liquid chromatography.

With increasing disulfide concentration the hydrogen yield decreases but the cyclohexylpropyl sulfide yield remains constant. This implies either that the yield of scavengeable cyclohexyl radicals remains constant as cationic and anionic reactions of the disulfide become increasingly important (as shown by the decreasing hydrogen yield) or that, fortuitously, the decrease in yield of this product from radical scavenging is exactly compensated for by a yield from a new source.

The well-known mobility of thiyl groups in disulfides and thiols is illustrated by Figs. 5 and 6. Such reactions have been initiated thermally (12) and photolytically (13) and are thought to be due to a chain reaction involving the thiyl radical. In the ethanethiol – di-*n*-propyl disulfide solution (Fig. 6) the first point for ethylpropyl sulfide at low dose gives a G value of 35. At the higher doses the system reaches an equilibrium situation when the thiyl groups are distributed, within experimental error, statistically between the thiols and disulfides. In the diethyl disulfide – di-*n*-propyl disulfide system (Fig. 5) equilibration is achieved even more rapidly. The initial G value for the mixed disulfide formation is 130 and again a statistical distribution of the three disulfides appears to be attained.

The authors thank the National Research Council of Canada and the Defence Research Board for financial support.

1. JOSEPH ESSER and JOHN A. STONE. Can. J. Chem. **51**, 192 (1973).
2. STEFAN J. RZAD, ROBERT H. SCHULER, and ANDRIES HUMMEL. J. Chem. Phys. **51**, 1369 (1969).
3. T. SHIDA. J. Phys. Chem. **72**, 2597 (1968).
4. T. SHIDA. J. Phys. Chem. **74**, 3055 (1970).
5. G. E. ADAMS, G. S. MCNAUGHTON, and B. D. MICHAEL. *In* The chemistry of ionization and excitation. *Edited by* G. R. A. Johnson and G. Scholes. Taylor and Francis Ltd., London. 1967. p. 281.
6. K.-D. ASMUS, JOHN M. WARMAN, and ROBERT H. SCHULER. J. Phys. Chem. **74**, 246 (1970).
7. S. J. RZAD. J. Phys. Chem. **76**, 3722 (1972).
8. G. W. KLEIN and R. H. SCHULER. J. Phys. Chem. **77**, 978 (1973).
9. W. A. KRAMER. J. Phys. Chem. **71**, 1171 (1967).
10. H. A. GILLIS. Can. J. Chem. **49**, 2861 (1971).
11. W. A. PRYOR and H. A. GUARD. J. Am. Chem. Soc. **86**, 1150 (1964).
12. E. N. GURYANOVA. Quart. Rep. Sulfur Chem. **5**, 113 (1970).
13. K. SAYAMOL and A. R. KNIGHT. Can. J. Chem. **46**, 999 (1968).

Can. J. Chem. Downloaded from www.nrcresearchpress.com by 210.87.254.42 on 09/05/12
For personal use only.

Elimination, Oxidation, and Transposition Reactions in Conformationally Biased Carbohydrates: Methyl 4,6-*O*-Benzylidene-α-D-altropyranosides Containing the Phenylthio Group[1]

STEPHEN HANESSIAN AND A. P. A. STAUB
Department of Chemistry, University of Montreal, Montreal, Quebec

Received September 7, 1973

The title compound containing a phenylthio group at C-3 and a methanesulfonate group at C-2 undergoes a quantitative transposition reaction in refluxing benzene to give the diequatorial isomer. In DMSO, a complex reaction takes place leading to elimination and oxidation at C-2. Oxidation of the title compound containing a phenylthio group at C-2, with acetic anhydride – DMSO gives the corresponding 3-uloside. With the isomeric 3-phenylthio derivative the enol acetate is formed. These results are rationalized based on mechanistic considerations.

Le composé ci-dessus nommé contenant les groupes phenylthio en C-3 et méthanesulfonate en C-2 subit une réaction de transposition quantitative par chauffage au reflux dans le benzène pour donner l'isomère diéquatorial. Dans le DMSO une réaction complexe a lieu conduisant aux composés résultant d'une élimination et d'une oxydation en position 2. L'oxydation du composé ci-dessus nommé contenant le groupe phenylthio en position 2 par le couple anhydride acétique – DMSO permet d'obtenir l'uloside-3 correspondant. Dans le cas du dérivé isomère phenlythio-3, on obtient l'acétate d'énol. L'étude du mécanisme de ces réactions permet d'interpréter les résultats obtenus.

Can. J. Chem., **52**, 1258 (1974)

Introduction

In a previous publication (1), we described the preparation of methyl 4,6-*O*-benzylidene-α-D-altropyranosides containing a phenylthio group at C-2 and -3, respectively, by the ring opening of appropriate epoxides with sodium thiophenoxide. The sulfonate esters of these compounds were found to undergo a variety of preparatively and mechanistically interesting reactions (2, 3) that seemed to depend on the location of the phenylthio and sulfonyloxy groups. Our rationale for investigating the chemistry of phenylthio ethers of polyfunctional compounds such as carbohydrates was based on the fact that the only proton α disposed to the sulfur atom was situated on the carbohydrate moiety. A primary objective was the exploration of reactions that might be triggered by the removal of a favorably disposed proton, the premise being that the sulfur atom in the phenylthio group would play an important role in stabilizing (4) incipient charged species in the transition state. Following our announced objective, we report the details of observations in the case of the conformationally and configurationally related methyl 4,6-*O*-benzylidene-2-*S*-phenyl-2-thio- and 3-*S*-phenyl-3-thio-α-D-altropyranoside sulfonates.

Results

When a solution of methyl 4,6-*O*-benzylidene-2-*O*-methanesulfonyl-3-*S*-phenyl-3-thio-α-D-altropyranoside (**1**) (1) was heated in dry benzene at reflux overnight, a new crystalline compound, isomeric with **1**, was isolated in quantitative yield. Nuclear magnetic resonance data revealed that the product was methyl 4,6-*O*-benzylidene-3-*O*-methanesulfonyl-2-*S*-phenyl-2-thio-α-D-glucopyranoside **2** (2). This assignment was corroborated by the transformation of **2** into the unsaturated derivative **8** in which the phenylthio group is situated at C-2 (*1*). The same type of transposition reaction was observed in the case of the 2-benzenesulfonate **3** and 2-*p*-toluenesulfonate **5** derivatives (Scheme 1). Under the same conditions, the configurationally related derivative **11** remained mostly unchanged.[2] In polar aprotic solvents such as dimethyl sulfoxide (DMSO) and *N*,*N*-dimethylformamide (DMF) a reverse but partial transposition was observed with **2**, giving approximately equal amounts of **1** and **2**. A notable difference in the reactions that

[1]Part of a series on preparative and exploratory carbohydrate chemistry.

[2]Traces of elimination products are formed (1, 2).

Can. J. Chem. Downloaded from www.nrcresearchpress.com by 210.87.254.6 on 09/05/12
For personal use only.

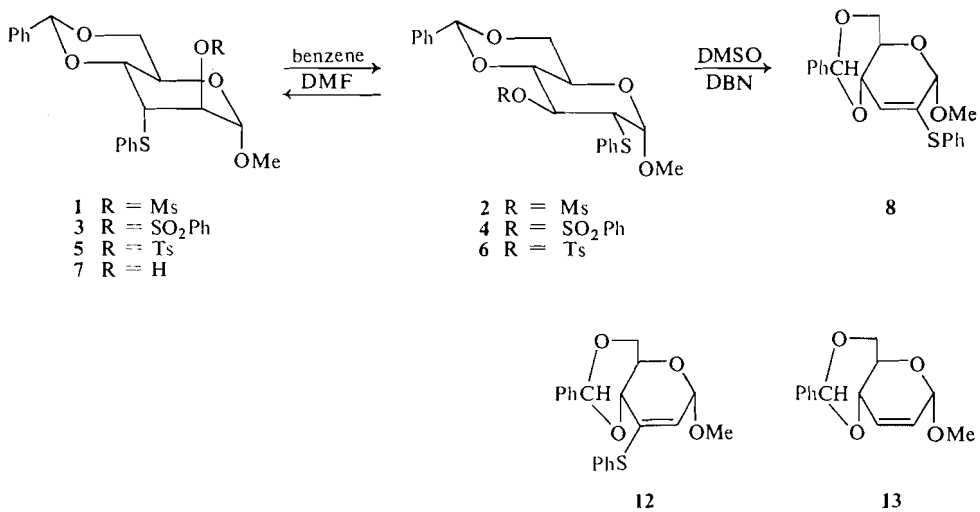

SCHEME 1

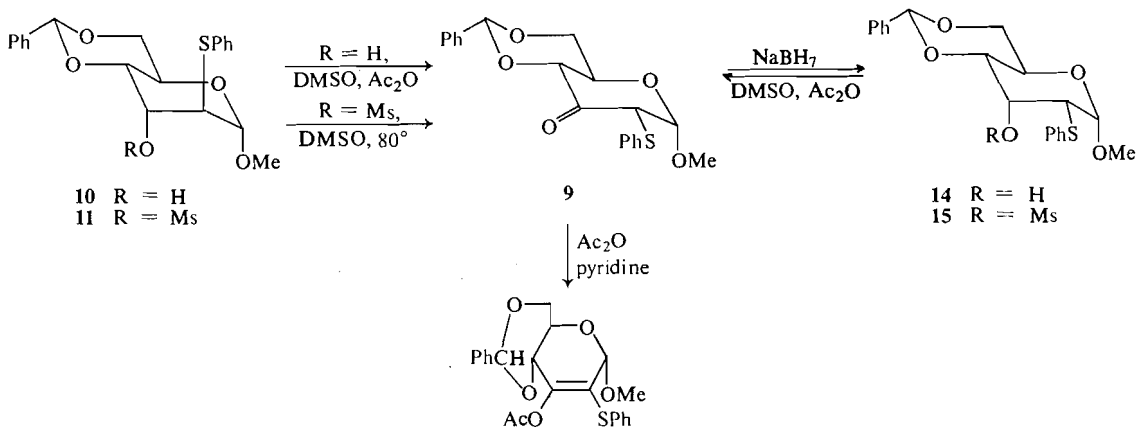

SCHEME 2

were conducted in DMSO, was the formation of a minor amount (~4%) of the 3-uloside **9**. The mechanistic significance of these results will be discussed in the following section. Heating a solution of **1** or **11** in DMSO alone (at 80°) gave the highly insoluble 3-uloside **9** in approximately 10–12% yield, in addition to the unsaturated products **8**, **12**, **13**, and a small amount of the transposed product **2** (Scheme 2). The uloside **9** was prepared independently by oxidation of methyl 4,6-*O*-benzylidene-2-*S*-phenyl-2-thio-α-D-altropyranoside **10** (1), in DMSO containing acetic anhydride. An excellent yield of the highly insoluble **9** was thus obtained. Reduction of **9** with sodium borohydride in a mixture of methanol and DMF gave the D-allo derivative **14**, as indicated by n.m.r. data. Oxidation of **14** with DMSO – acetic anhydride gave back the uloside **9**, thus confirming the epimerization at C-2 in the original oxidized product. Treatment of the uloside **9** with acetic anhydride in pyridine gave an 86% yield of the crystalline enol acetate derivative **16**.

When the 3-phenylthio derivative **7** was oxidized by the same procedure as described above, the major product was the enol acetate derivative **17**. A minor amount of the 2-methylthiomethyl ether was also formed. Oxidation of **7** to the

Can. J. Chem. Downloaded from www.nrcresearchpress.com by 210.87.254.6 on 09/05/12
For personal use only.

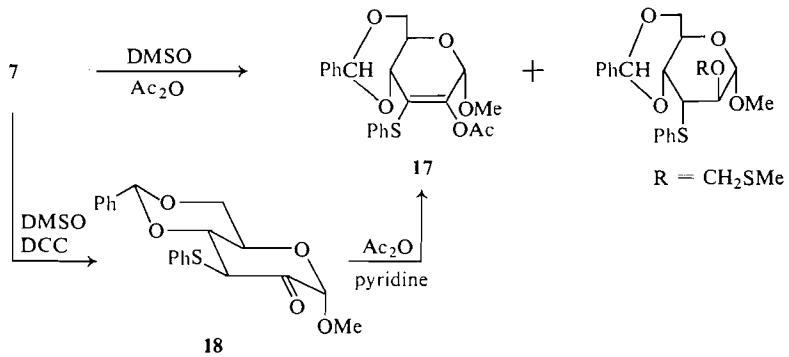

SCHEME 3

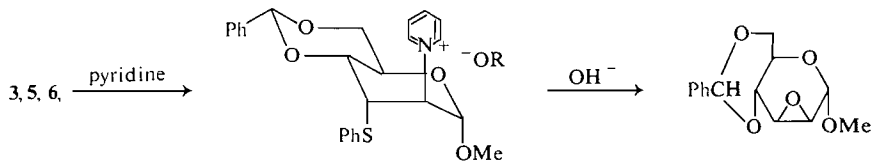

SCHEME 4

desired ketone was accomplished with the Pfitzner–Moffatt procedure (5) and a crude product corresponding to **18** was isolated in 71% yield. Treatment of the latter with acetic anhydride in pyridine effected a smooth transformation into the enol acetate **17**, in 87% yield (Scheme 3).

In an extension of our transposition studies, the tosylate and benzenesulfonates **5** and **3**, respectively, were heated in anhydrous pyridine. The products in both cases were the crystalline methyl 4,6-*O*-benzylidene-2-deoxy-2-*N*-pyridinium-3-*S*-phenyl-3-thio-α-D-altropyranoside sulfonates **19** and **20**, respectively (Scheme 4). Formation of **19** was also observed when the diequatorial phenylthio tosylate **6** was heated in pyridine. Treatment of **19** with aqueous sodium benzoate or with sodium azide in methylcellosolve, at room temperature or at 80° gave unchanged starting material. However, in aqueous sodium hydroxide, or in aqueous sodium azide at 70°, a crystalline product was obtained in 90% yield that was identified as methyl 2,3-anhydro-4,6-*O*-benzylidene-α-D-mannopyranoside **21** (6).

Discussion

The transformations of the sulfonate derivatives **1**, **3**, and **5** into their isomeric analogs **2**, **4**, and **6** involve double transposition of phenylthio and sulfonate groups with concomitant configurational inversion at the respective ring carbon atoms. While the intervention of 2,3-episulfonium ions is evident, the nature of the products seems to depend on the polarity of the solvent. In benzene, the reaction proceeds, in all probability, via a tight ion pair in which there is minimum separation of charged species and the product is the thermodynamically more stable diequatorial isomer. In such a diaxial–diequatorial rearrangement, steric decompression between the axial C-1 methoxyl and C-3 phenylthio group is an important driving force (Scheme 5). Although well known (7), the diaxial–diequatorial rearrangement has few precedents involving the phenylthio group (8, 9) and none, to our knowledge, in which the departing anionic species is a group of low nucleophilicity, such as alkyl and aryl sulfonates, and the assisting group is phenylthio. These results are of particular preparative significance since the rearrangement provides access to a selective and predetermined substitution pattern in the transposed products, which now comprise a vicinal diequatorial arrangement of substituents. Because of inherent structural and electronic properties, the participating ability of the sulfur atom in the phenylthio group is somewhat

Can. J. Chem. Downloaded from www.nrcresearchpress.com by 210.87.254.6 on 09/05/12
For personal use only.

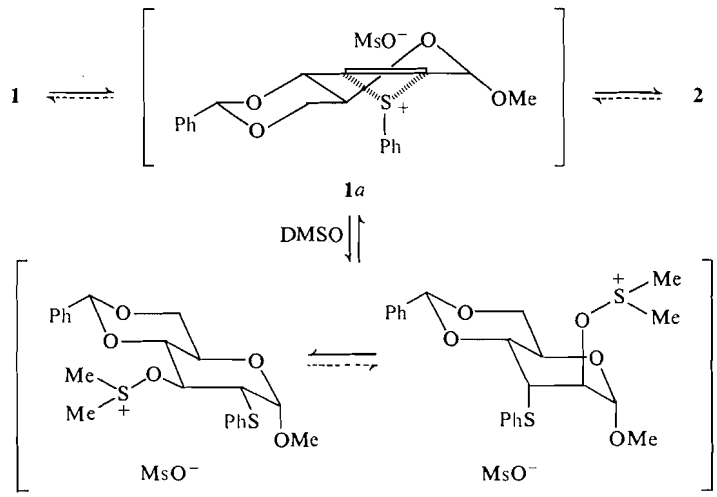

SCHEME 5

curtailed when compared to alkylthio and benzylthio analogs (10). The significance of this comparison can be appreciated if it is recalled that mesylation or tosylation of vicinally disposed alkylthio and alcohol groups frequently leads to the corresponding chlorides, rather than the sulfonates, as a result of the intervention of episulfonium ions and subsequent attack by chloride ion (11). The phenylthio group offers the advantage of having a sulfur atom that is of reduced nucleophilicity under normal conditions, allowing such reactions as sulfonylation to take place; yet, its participating ability can be called into play in polar solvents, or in nonpolar solvents, but at moderately elevated temperatures. The partial transposition of groups from the stable diequatorial, to the diaxial orientation in polar solvents such as DMSO and DMF denotes a certain separation of charges rendering the return to diequatorial orientation not as favored a pathway as in benzene. The intervention of DMSO as a competing nucleophile in these reactions seems evident in the formation of the uloside **9** from **1**, **2**, or **11**. The episulfonium ion, common to all three, can be attacked by the solvent to give two possible oxydimethylsulfonium ions (Scheme 5), that have the necessary structural features for oxidation to **9** by the generally accepted ylid pathway (5). The absence of the uloside **18** in these reactions demonstrates a certain preference for the equatorial oxydimethylsulfonium ion intermediate (Scheme 5). In view of the favorable dispositions of the phenylthio group for episulfonium ion formation in **1**, **2**, and **11**, a direct displacement of the 3-methanesulfonate group by DMSO can be excluded. In support of the above suggested intervention by the solvent as a reactant, it is of interest that no ulosides were formed when DMF was the solvent. The major product (~50%) was the diequatorial derivative **2**.

The formation of the unsaturated compounds **8** and **12** by the treatment of appropriate sulfonate esters with bases or by heating in aprotic solvents alone, represents an interesting example of *syn*-elimination (12–14). To the best of our knowledge, there are no precedents to this type of elimination reaction with *trans* vicinally-oriented phenylthio and sulfonate groups. Base-catalyzed eliminations are well known in the corresponding sulfones in the cyclohexane series (12, 15). Although the precise mechanism of *syn*-eliminations (concerted or carbanionic) is not known with certainty (13) it would appear that the acquisition of carbanionic character of the C-2 and -3 ring carbon atoms bearing the phenylthio group in the respective derivatives would be favored in the transition state of these elimination reactions. Attempts to incorporate a deuterium atom on the ring carbon atom α to the phenylthio group in the elimination of **11** were not successful. This is not surprising, since it is known that elimination in such cases can proceed at much faster rates than incorporation of deuterium (15, 16).

Alternatively, it is interesting to speculate that the unsaturated compounds arise, in part, from a common episulfonium ion intermediate such as **1***a* (Scheme 5). For example, the formation of **8**, among other products, in the DMSO-mediated elimination reaction of **1**, necessitates a pre-

Can. J. Chem. Downloaded from www.nrcresearchpress.com by 210.87.254.6 on 09/05/12
For personal use only.

Can. J. Chem. Downloaded from www.nrcresearchpress.com by 210.87.254.6 on 09/05/12
For personal use only.

liminary rearrangement to **2** followed by a *syn*-elimination, or an abstraction of a proton at the episulfonium ion stage. The unexpected formation of **13** from **11** during base treatment in DMSO, could be explained on the basis of a seemingly favored extrusion of the phenylthio group from an intermediate such as **1***a* or a concerted-type elimination of the mesyloxy and phenylthio groups. The latter possibility is reminiscent of the formation of olefins in the base-catalyzed eliminations of aliphatic phenylthio ethers (17*a*), and in the formation of unsaturated compounds from episulfonium ions (17*b*).

Irrespective of the actual mechanistic pathway (s), it appears that the underlying reasons for the different behavior of **1** relative to the configurationally related **11** in these and other reactions (1), are steric in nature. A projection along the C_2—C_3 bond in both derivatives reveals a severe interaction between the diaxial substituents at C-1 and -3 in **1**, which is presumably relieved in the transposed product **2** or the unsaturated products **12** and **13**. The same factors can be operative in the case of **11** insofar as some elimination reactions are concerned, steric relief being derived from loss of the axial mesyloxy group. The formation of unsaturated derivatives may also depend on the relative acidities of the protons situated on C-2 and -3 in **11** and **1**, respectively, in the presence of bases.

The regiospecific formation of the 2-pyridinium salts **19** and **20** follows other well-established patterns of ring-opening reactions in the analogous episulfonium ions (10). It was hoped that these salts would lend themselves to nucleophilic displacement reactions via 2,3-episulfonium ions, much the same way as they were formed, in the presence of pyridine as a nucleophile. The insolubility of these salts, even in aprotic solvents, precluded such a study. The unexpected formation of the epoxide **21** in the presence of aqueous sodium azide or aqueous base is reminiscent of the formation of **21** in the attempted methylation of **7** with methyl iodide and silver oxide (1). Although the two reactions are unrelated insofar as the reagents are concerned, it appears that the phenylthio group is somehow activated and is lost by intramolecular attack by an hydroxyl group at C-2. It is of interest that the displacement of an equatorially disposed pyridinium group in a compound related to **19**, but containing an oximino group at C-3 instead of the phenylthio group, could be effected with sodium benzoate in DMF at room temperature (18).

The transformations of **10** and **11** into **9** with DMSO–Ac_2O and DMSO, respectively, are accompanied by an epimerization at C-2. The same process takes place during the oxidation of **7** into **18** with DMSO–DCC. The corresponding enolic forms are therefore protonated from the least hindered β-side, so as to give the thermodynamically more stable equatorial epimers.

Epimerization has also been observed in the oxidation of other carbohydrate derivatives containing an axially-oriented azide or amide function, vicinal to an alcohol group (21, 22). The formation of an enol acetate in the oxidation of **7**, but not of **10**, with DMSO–Ac_2O can be rationalized on the basis of a more favorable stereoelectronic protonation (19, 20) of the enol **A** compared to that of enol **B**, in which the approach of the proton from the "α"- side is hindered (Scheme 6). The latter is consequently trapped as the enol acetate **17**. In the presence of acetic anhydride and pyridine, the enols derived from **9** and **18**, respectively, are much more susceptible to acetylation compared to the same process in DMSO as solvent, where the effective concentration of hydrogen ions is greater.

Experimental

General

Melting points are uncorrected. Nuclear magnetic resonance spectra were recorded for solutions in chloroform-*d* (unless otherwise stated) at 60 or 100 MHz, with tetramethylsilane as the internal standard. Infrared spectra were recorded with a Beckman IR-8 spectrometer. Optical rotation were measured with a Perkin-Elmer Model 141 automatic polarimeter. Thin-layer chromatography (t.l.c.) was performed with plates coated with silica gel GF_{254} and the spots were detected with a sulfuric acid spray and with the acidic ammonium molybdate spray (23). Conventional processing or processing in the usual manner signifies drying organic solutions with anhydrous sodium sulfate, filtration and evaporation of the filtrate under diminished pressure.

Methyl 4,6-O-Benzylidene-3-O-methylsulfonyl-2-S-phenyl-2-thio-α-D-glucopyranoside (2)

A solution of **1**, m.p. 101–102° (1.137 g, 2.5 mmol), in 25 ml of dry benzene was heated under reflux for 18 h. Removal of the solvent afforded 1.10 g (99%) of the title compound, which could be distinguished from **1** by t.l.c. ($CHCl_3$–2,2,4-trimethylpentane–MeOH, 10:5:0.6). Recrystallization from absolute ethanol gave an analytical sample, m.p. 142–143°; $[\alpha]_D^{25}$ −66.4° (*c*, 1.78 $CHCl_3$); n.m.r.: 5.51 (s, C*H*Ph), 5.07 (dd, $J_{3,2}$ = 10.6 Hz; $J_{3,4}$ = 9.4 Hz, H-3), 4.91 (d, $J_{1,2}$ = 3.1 Hz, H-1), 5.41 (s, OCH_3), 5.28 (q, $J_{2,3}$ = 10.6 Hz; $J_{2,1}$ = 3.1 Hz, H-2), 2.89 p.p.m. (s, OSO_2CH_3) etc.

Anal. Calcd. for $C_{21}H_{24}O_7S_2$: C, 55.73; H, 5.34; S, 14.17. Found: C, 55.40; H, 5.62; S, 13.87.

Treatment of **2** with 1,5-diazabicyclo[5.3.0]nonene (24) in DMSO at 80° gave the known crystalline **8** (m.p. and

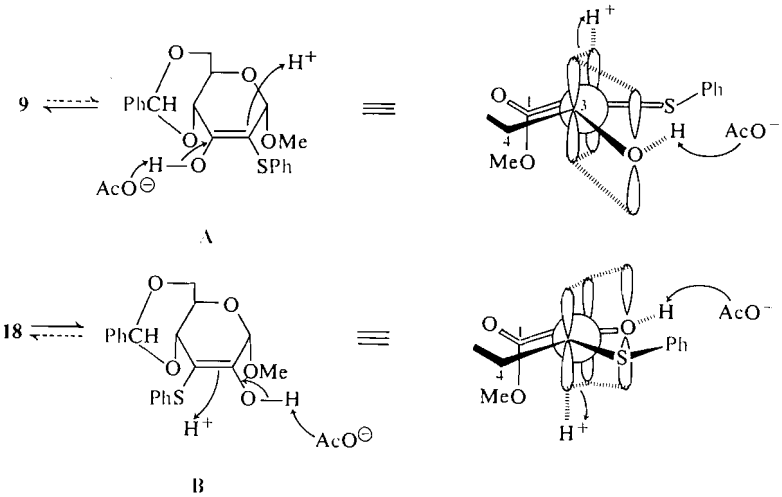

SCHEME 6

mixture m.p.) (1). When a solution of **2** (0.1 g, 0.21 mmol) was heated in 3 ml of DMSO at 80° during 24 h, a 1:1 mixture of **1** and **2** resulted. Separation by preparative t.l.c. gave 40 mg of **1** (m.p. and mixture m.p.). A small amount (4.1%) of the uloside **9**, as well as traces of the unsaturated derivatives **8**, **12**, and **13** were also formed. When the reaction was done in DMF, a 1:1 mixture of **1** and **2** (80%) was formed, as well as traces of **8**, **12**, and **13**, which were isolated and characterized. When **1** was heated in DMF (75°; 12 h), the major product was **2** (~50%).

Methyl 2-O-Benzenesulfonyl-4,6-O-benzylidene-3-S-phenyl-3-thio-α-D-altropyranoside (3)

To a solution of **7** (3.74 g, 10 mmol) in 15 ml of pyridine were added 3.6 ml (5.3 g, 30 mmol) of benzenesulfonyl chloride with cooling and stirring. After stirring at room temperature overnight, the solution was poured into ice water, the precipitate was filtered, washed and dried to give the title compound (4.2 g, 81%). Thin-layer chromatography ($CHCl_3$–2,2,4-trimethylpentane–MeOH, 10:5:1) indicated a slight contamination with the transposed product **4**. Recrystallization in ether–dichloromethane gave 3.9 g (75% of pure product, m.p. 114–115° (dec.); $[\alpha]_D^{25}$ +10.50 (*c*, 2.01 $CHCl_3$).

Anal. Calcd. for $C_{20}H_{26}O_7S_2$: S, 12.46. Found: 12.46.

Methyl 3-O-Benzenesulfonyl-4,6-O-benzylidene-2-S-phenyl-2-thio-α-D-glucopyranoside (4)

A solution containing 0.3 g (0.583 mmol) of **3**, m.p. 114–115°, in 5 ml of benzene was refluxed for 2 days. Evaporation of the solvent gave 0.298 g (99%) of the transposed product **4**, which was recrystallized from hot methanol, m.p. 120–121° (dec.); $[\alpha]_D^{25}$ −77.33° (*c*, 1.31 $CHCl_3$).

Anal. Calcd. for $C_{26}H_{26}O_7S_2$: C, 60.68; H, 5.09; S, 12.46. Found: C, 60.44; H, 5.13; S, 12.61.

Methyl 4,6-O-Benzylidene-2-S-phenyl-2-thio-α-D-ribo-hexopyranoside-3-ulose (9)

To a solution of **10** (1.55 g, 3.09 mmol) (1) in 4 ml of DMSO was slowly added 3 ml of acetic anhydride. After stirring at room temperature for 12 h, the thick slurry was poured into ice water (30 ml) and the pale-yellow solid was filtered, washed well with water, then with warm hexane. The highly insoluble colorless product (**9**) (1.06 g, 92%) was analytically pure, m.p. 204–205° (dec.); λ_{max}^{KBr} 1735 cm^{-1} (C=O).

Anal. Calcd. for $C_{20}H_{20}O_5S$: C, 64.50; H, 5.41; S, 8.61. Found: C, 64.30; H, 5.38; S, 8.60.

Methyl 3-Acetoxy-4,6-O-benzylidene-2-S-phenyl-2-thio-α-D-erythro-hex-2-enopyranoside (16)

Acetic anhydride (1.8 ml) was added to a cold suspension of **9** (0.575 g, 1.54 mmol) in 6 ml of pyridine. The suspension became homogeneous after 6 h and after stirring for a total of 24 h, the solution was poured into ice water, the crystalline product was filtered and washed with water to give the title compound (0.55 g, 86%). Recrystallization from hot ethanol gave an analytical sample, m.p. 113–114°; $[\alpha]_D^{25}$ −89.3° (*c*, 2.30 chloroform); λ_{max}^{KBr} 1760 cm^{-1} (enol acetate); n.m.r.: 5.55 (s, CHPh), 4.74 (s, H-1), 3.50 (s, OCH_3), 2.11 p.p.m. (s, $OCOCH_3$), etc.

Anal. Calcd. for $C_{22}H_{22}O_6S$: C, 63.75; H, 5.35; S, 7.73. Found: C, 63.59; H, 5.18; S, 7.73.

Methyl 4,6-O-Benzylidene-2-S-phenyl-2-thio-α-D-allopyranoside (14)

A suspension of **9** (2.232 g, 6 mmol) in 300 ml of methanol and 5 ml of DMF was treated with sodium borohydride (3 g) over a period of 15 min. After stirring for 1.5 h, the solution was evaporated to dryness, the solid residue was partitioned between 200 ml of chloroform and 200 ml of water, and the organic phase was processed in the usual manner to give the title compound as colorless crystals (2.01 g, 92%). Recrystallization from hot ethanol gave an analytical sample, m.p. 167–169°; $[\alpha]_D^{25}$ −47.9° (*c*, 2.17 chloroform); λ_{max}^{KBr} 3480 cm^{-1} (hydroxyl); n.m.r.: 5.51 (s, C*H*Ph), 4.85 (d, $J_{1,2}$ = 3.75 Hz, H-1), 3.50 p.p.m. (s, OCH_3), etc.

Anal. Calcd. for $C_{20}H_{22}O_5S$: C, 64.15; H, 5.92; S, 8.56. Found: C, 64.17; H, 5.74; S, 8.44.

Oxidation of **14** with acetic anhydride in DMSO gave the ulose derivative **9**, in 57% yield (m.p., mixture m.p., i.r.).

Can. J. Chem. Downloaded from www.nrcresearchpress.com by 210.87.254.6 on 09/05/12
For personal use only.

Can. J. Chem. Downloaded from www.nrcresearchpress.com by 210.87.254.6 on 09/05/12
For personal use only.

Methyl 4,6-O-Benzylidene-3-O-methylsulfonyl-2-S-phenyl-2-thio-α-D-allopyranoside (15)

To a stirred solution containing **14** (0.117 g, 0.31 mmol) in 2 ml of anhydrous pyridine, was slowly added 0.08 ml (1 mmol) of methanesulfonyl chloride with cooling. After standing 36 h at 5°, the solution was poured into ice water and the resulting crystalline product was recovered by filtration. The solid was washed with aqueous sodium bicarbonate, then with water and dried to give the title compound (0.115 g, 82%), m.p. 76–78°. Recrystallization from ethanol gave material having, m.p. 77–78°; $[\alpha]_D^{25}$ −79.1° (*c*, 0.32 chloroform); n.m.r.: 5.52 (s, C*H*Ph), 5.19 (t, $J_{3,2} = J_{3,4} = 3$ Hz; H-3), 4.91 (d, $J_{1,2} = 3.75$ Hz, H-1), 3.42 (s, OCH_3), 3.35 (dd, $J_{2,1} = 3.75$ Hz, $J_{2,3} = 3$ Hz, H-2), 3.03 p.p.m. (s, OSO_2CH_3), etc.

Anal. Calcd. for $C_{21}H_{24}O_7S_2$: C, 55.73; H, 5.34; S, 14.17. Found: C, 55.74; H, 5.30; S, 14.27.

Treatment of **15** with 1,5-diazabicyclo[5.3.0]nonene (DBN) in DMSO gave the known (1) crystalline **8** (m.p. and mixture m.p.).

Methyl 4,6-O-Benzylidene-3-S-phenyl-3-thio-α-D-arakinopyranoside-2-ulose (18)

A solution of 7 (0.374 g, 1 mmol) (1) in a mixture of DMSO (1.5 ml) and anhydrous benzene (1.5 ml) was treated sequentially with 0.08 ml (1 mmol) of trifluoroacetic acid and 0.62 g (3 mmol) of *N,N*-dicyclohexylcarbodiimide. After stirring at room temperature for 24 h, the solution was diluted with ether (25 ml), washed with aqueous sodium bicarbonate and the organic phase was processed as usual to give a syrup that crystallized after trituration with cold ether; yield (0.268 g, 71%) of crude **18**, homogeneous on t.l.c. (chloroform–2,2,4-trimethylpentane–methanol, 30:15:0:3).

Methyl 2-Acetoxy-4,6-O-benzylidene-3-S-phenyl-3-thio-α-D-erythro-hex-2-enopyranoside (17)

A. From (7).

A solution containing 0.5 g (1.33 mmol) of 7 in 3 ml of DMSO was treated with 2 ml of acetic anhydride. After stirring at room temperature for 24 h, the solution was poured into ice water, and processing was continued by extraction with ether. Evaporation of the organic phase gave the title compound (0.410 g) contaminated with a small amount of the 2-methylthiomethyl ether derivative of 7. The crystalline mixture was separated by preparative t.l.c. (benzene – ethyl acetate, 15:1) to give the pure product **17**, m.p. 121.5–122.5°; $[\alpha]_D^{25}$ +45.3° (*c*, 2.35 chloroform); λ_{max}^{KBr} 1755 cm^{-1} (enol acetate); n.m.r.: 5.52 (s, H-1), 5.38 (s, C*H*Ph), 3.38 (s, OCH_3), 2.05 p.p.m. (s, $OCOCH_3$), etc.

Anal. Calcd. for $C_{22}H_{22}O_6S$: C, 63.75; H, 5.35; S, 7.73. Found: C, 63.48; H, 5.68; S, 7.69.

B. From (**18**).

Treatment of a solution of **18** (0.134 g, 0.34 mmol) in pyridine with acetic anhydride and processing as for compound **16** gave 0.112 (87%) of crystalline **17** (m.p. and mixture m.p.).

Methyl 4,6-O-Benzylidene-2-deoxy-3-S-phenyl-2-N-pyridinium-3-thio-α-D-altropyranoside p-Toluenesulfonate (19)

A solution of methyl 4,6-*O*-benzylidene-3-*S*-phenyl-3-thio-2-*O*-*p*-toluenesulfonyl-α-D-altropyranoside **5** (0.2 g, 0.38 mmol) (25) in 5 ml of anhydrous pyridine was heated with stirring at 80–90° for 24 h, whereupon a crystalline product had separated out of solution. Filtration and recrystallization from boiling methanol gave the title compound in the form of needles (0.15 g), m.p. 225° (dec.); $[\alpha]_D^{25}$ −23.77° (*c*, 0.53 MeOH).

Anal. Calcd. for $C_{32}H_{33}O_7S_2N$: C, 63.24; H, 5.47; S, 10.55; N, 2.30. Found: C, 63.49; H, 5.36; S, 10.88; N, 2.13.

Similar treatment of the 3-toluenesulfonate **6** and the 2-benzenesulfonate **4** gave the respective 2-pyridinium salts **19** (92%) and **20** (87%), m.p. 240° (dec.); $[\alpha]_D^{25}$ −24.24 (*c*, 0.66 MeOH).

Anal. Calcd. for $C_{31}H_{31}O_7S_2N$: C, 62.82; H, 5.10; S, 10.82; H, 2.36. Found: 62.49; H, 5.36; S, 10.88; N, 2.13.

*Treatment of Methyl 4,6-O-Benzylidene-2-deoxy-3-S-phenyl-2-N-pyridinium-3-thio-α-D-altropyranoside p-Toluenesulfonate **19** with Aqueous Sodium Azide*

A solution containing the title compound (60 mg, 0.1 mmol) and sodium azide (33 mg, 0.5 mmol) in 2 ml of water was heated at 70° overnight. The crystalline precipitate that resulted was filtered, washed with water, and dried to give 25 mg (90%) of methyl 2,3-anhydro-4,6-*O*-benzylidene-α-D-mannopyranoside (**21**) m.p. and mixture m.p. 144°. The product was identical (i.r., n.m.r., t.l.c.) to an authentic sample.

The same results were obtained in 0.1 *N* sodium hydroxide (25°; 12 h).

Treatment of **19** with aqueous sodium benzoate, sodium azide in methanol or in methylcellosolve (80°) gave unchanged starting material.

*Treatment of Methyl 4,6-O-Benzylidene-2-O-methanesulfonyl-3-S-phenyl-3-thio-α-D-altropyranoside **1** and the Isomeric **11** with Dimethyl Sulfoxide*

A solution of **1** (0.18 g, 0.4 mmol) in 5 ml of DMSO was heated at 80° until the disappearance (t.l.c.) of starting material (*ca.* 3.5 h). The solution was poured into 30 ml of ice water and the solution was extracted with chloroform and processed in the usual manner to give a syrup. Trituration with 95% ethanol gave crystalline **9** (10 mg, 10%); m.p. and mixture m.p. 203–204°. The mother liquors consisted of a complex mixture of products containing four major products, (t.l.c.), **8, 2, 12, 13.**

Treatment of the isomeric **11** under the same conditions gave the uloside **9** in 12% yield. The mother liquors consisted of the same mixture of products as above.

Financial assistance from the National Research Council of Canada and a France–Quebec fellowship to A.P.A.S. is gratefully acknowledged.

1. S. Hanessian and A. P. A. Staub. Carbohydr. Res. **16**, 419 (1971); S. Hanessian and N. R. Plessas. Chem. Commun. 706 (1968).
2. S. Hanessian and A. P. A. Staub. Carbohydr. Res. **14**, 424 (1970).
3. S. Hanessian and A. P. A. Staub, Chem. Ind. 1436 (1970).
4. C. C. Price and S. Oae. Sulfur bonding. Ronald Press, New York. 1962.
5. J. G. Moffatt. *In* Oxidation. Vol. 2. *Edited by* R. L. Augustine and D. J. Trecker. Marcel Dekker. Inc., New York. 1971. p. 1.

6. L. F. WIGGINS. Meth. Carbohydr. chem. **2**, 188 (1963); G. J. ROBERTSON and C. E. GRIFFITH. J. Chem. Soc. 1195 (1935).
7. J. F. KING, K. ABIKAR, D. M. DEAKEN, and R. G. PEWS. Can. J. Chem. **46**, 1 (1968); D. H. R. BARTON and J. F. KING. J. Chem. Soc. 4398 (1958).
8. J. F. KING and K. ABIKAR. Can. J. Chem. **46**, 9 (1968).
9. N. LEBEL, R. F. CZAJA, and A. DEBOER. J. Org. Chem. **34**, 3112 (1969).
10. L. GOODMAN. Adv. Carbohydr. Chem. **22**, 109 (1967).
11. L. GOODMAN and J. E. CHRISTENSEN. J. Org. Chem. **29**, 1787 (1964).
12. N. LEBEL. Adv. Alicycl. Chem. **3**, 196 (1971).
13. F. BORDWELL. Acc. Chem. Res. **5**, 374 (1972); **3**, 281 (1970).
14. J. SICHER. Angew. Chem. Int. ed. **11**, 200 (1972).
15. See for example, W. M. JONES, T. G. SQUIRES, and M. LYNN. J. Am. Chem. Soc. **89**, 318 (1967) and references cited therein.
16. J. HINE and O. B. RAMSAY. J. Am. Chem. Soc. **84**, 973 (1962).
17. (*a*) R. A. BARTSCH and J. F. BUNNETT. J. Am. Chem. Soc. **91**, 1382 (1969). (*b*) D. C. OWSLEY, G. K. HELMKAMP, and S. N. SPURLOCK. J. Am. Chem. Soc. **91**, 3606 (1969).
18. W. A. SZAREK, B. T. LAWTON, and J. K. N. JONES. Tetrahedron Lett. 4867 (1969).
19. E. J. COREY and R. A. SNEEN. J. Am. Chem. Soc. **78**, 6269 (1956).
20. H. O. HOUSE. Modern synthetic reaction. 2nd ed. W. A. Benjamin Inc., 1972. p. 508, and references cited therein.
21. B. R. BAKER and D. H. BUSS. J. Org. Chem. **30**, 2308 (1965).
22. Y. ALI and A. C. RICHARDSON. Carbohydr. Res. **5**, 441 (1967).
23. W. MEYER zu RECKENDORF. Chem. Ber. **96**, 2019 (1963).
24. H. OEDIGER, H. J. KABBE, F. MOLLER, and K. EITER. Chem. Ber. **99**, 2012 (1966).
25. S. HANESSIAN and R. MASSE. Carbohydr. Res. In press.

Can. J. Chem. Downloaded from www.nrcresearchpress.com by 210.87.254.6 on 09/05/12
For personal use only.

Carbanions in Carbohydrate Chemistry: Synthesis of *C*-Glycosyl Malonates[1]

STEPHEN HANESSIAN AND ANDRE G. PERNET[2]

Department of Chemistry, University of Montreal, Montreal, Quebec

Received September 7, 1973

The condensation of 2,3,4,6-tetra-*O*-acetyl-α-D-glucopyranosyl bromide with sodio diethyl malonate led to crystalline diethyl 2-(2,3,4,6-tetra-*O*-acetyl-β-D-glucopyranosyl) malonate. The corresponding dibenzyl ester proved to be a versatile intermediate for the preparation of crystalline β-D-glucopyranosyl malonic acid and β-D-glucopyranosyl acetic acid derivatives. The anomeric configuration in these *C*-glycosides was determined by a chemical correlation. With 2,3,4,6-tetra-*O*-acetyl-β-D-glucopyranosyl chloride and sodio diethyl malonate, the major product was a 1,2-*O*-ketal derivative resulting from an attack of the carbanion on the 1,2-acetoxonium ion. The condensation of 2,3,4,6-tetra-*O*-benzyl-α-D-glucopyranosyl bromide with sodio diethyl malonate was conducted with, and without added bromide ion and the mechanistic implications of the results are discussed. *C*-Glycosides were also prepared in the D-mannofuranose series and their transformation into the D-lyxofuranose series (anomeric mixture) is described. The utility of n.m.r. shift reagents, and an apparent differential complexation by $Eu(DPM)_3$ and $Eu(FOD)_3$-d_{27} is demonstrated.

La condensation du bromure de 2,3,4,6-tétra-*O*-acétyl-α-D-glucopyrannosyle avec le malonate de diéthyle sodé a conduit au diéthyl 2-(2,3,4,6-tétra-*O*-acétyl-β-D-glucopyrannosyle) malonate cristallin. L'ester dibenzylique correspondant s'est révélé un intermédiaire général pour la préparation des dérivés des acides β-D-glucopyrannosyle malonique et β-D-glucopyrannosyle acétique cristallins. La configuration anomérique de ces *C*-glycosides fut déterminée par corrélation chimique. Avec le chlorure de 2,3,4,6-tétra-*O*-acétyl-β-D-glucopyrannosyle et le malonate de diéthyle sodé le produit prépondérant fut le dérivé *O*-acétal-1,2 résultant de l'attaque du carbanion sur l'ion acétoxonium-1,2. La condensation du bromure de 2,3,4,6-tétra-*O*-benzyle-α-D-glucopyrannosyle avec le malonate de diéthyle sodé fut effectuée à la fois en présence et en l'absence d'ion bromure externe et les applications mécanistiques sont discutées. Les *C*-glycosides furent également préparés dans la série D-mannofurannose et leur transformation en D-lyxofurannose (mélange anomérique) est décrite. On démontre l'utilité des réactifs qui induisent des déplacements en r.m.n. ainsi que la complexation différentielle apparente par $Eu(DPM)_3$ et $Eu(FOD)_3$-d_{27}.

Can. J. Chem., **52**, 1266 (1974)

As part of a program on the exploration of newer synthetic methods, we have been interested in functionalized *C*-glycosyl compounds (1) as intermediates in the synthesis of naturally-occurring *C*-nucleosides and their analogs (2). The few known members of this class of compounds possess diverse biological properties that are, in several instances, of medicinal significance.

The well-known *C*-alkyl and -aryl glycosyl compounds (3) are of limited synthetic utility, since these groups do not lend themselves to facile transformations into other more versatile functional groups such as ketonic, aldehydic, and carboxylic groups.[3] Such functionalized *C*-glycosyl compounds would be ideal precursors to *C*-nucleosides and related compounds (4). In a previous short communication (1), we had reported on a general method for the synthesis of functionalized *C*-glycosyl compounds by the condensation of sodio malonates with glycosyl halide derivatives. In this paper, we disclose details of this and subsequent work in the D-glucose and D-mannose series, and we discuss the relevant synthetic and mechanistic aspects of the reaction. The feasibility of such condensations with the relatively unstable acylglycosyl halides was initially explored with appropriately substituted D-glucopyranosyl halides. Inasmuch as the ultimately desired products were β-*C*-

[1]Part of a series on "Preparative and exploratory carbohydrate chemistry." Taken from the Ph.D. thesis of A.G.P., 1973.

[2]NRCC and France–Quebec fellow.

[3]See, however, ref. 4.

Can. J. Chem. Downloaded from www.nrcresearchpress.com by 210.87.254.6 on 09/05/12
For personal use only.

Can. J. Chem. Downloaded from www.nrcresearchpress.com by 210.87.254.6 on 09/05/12
For personal use only.

glycosyl compounds, the selection of D-glucopyranosyl halides with participating acyloxy groups at C-2 would permit the study of the stereochemistry of the reaction at the anomeric center (5). It was of interest to see whether the participating ability of the 2-acetoxy groups in α-acetobromoglucose **1** would lead to the same stereochemical result in *C*-glycosidation, as with related *O*- and *N*-glycosidations.

To the best of our knowledge, there are very few precedents for the reaction of cyclic α-haloethers with carbanions.[4] Thus, the reaction of 2-chlorotetrahydropyran with sodio diethyl malonate gave the 2-diethyl malonate derivative that could be further transformed into the corresponding acetic acid derivative by decarboxylation (6). In another report (7), α-acetobromoglucose was heated with sodio α-formamido diethyl malonate in ethanol and a product was isolated to which the structure of 2-(β-D-glucopyranosyl) glycine was assigned. In our hands, this reaction led to a complex mixture of products and subsequent condensations with acylglycosyl halides were done, with few exceptions, in non-hydroxylic solvents. No reaction was observed between α-acetobromoglucose and sodio diethyl malonate in benzene at room temperature. In tetrahydrofuran or dimethoxyethane, starting halide was recovered in high yield (~80%) but small amounts of 2,3,4,6-tetra-*O*-acetyl-D-glucal, formed by a base-catalyzed dehydrobromination, and the expected *C*-glycosyl malonate were formed. Another by-product, presumably formed by a transesterification reaction with the reagent, was also formed in some cases. This syrupy product had a higher content of diethyl malonyl residues with respect to acetate groups and was not further investigated. The distribution and nature of products in the condensation reaction (Scheme 1) were quite sensitive to the nature of the solvent and to the ratio of carbanion to halide. Optimum conditions were attained in 1,2-dimethoxyethane as solvent, in which the carbanion is soluble and not highly aggregated as it is in benzene (8). The maximal yield of crystalline product, designated as diethyl 2-(2,3,4,6-tetra-*O*-acetyl-β-D-glucopyranosyl) malonate (**2**), was 20%. Although this product could be crystallized directly from processed reaction mixtures after seeding, alternate methods of its isolation were also investigated. Since the product **2** was contaminated with the halide **1** (~20%) and the transesterification product and because of the similarities in chromatographic mobilities, the methods of separation were primarily concerned with selective transformations of **1** into products that had different polarities compared to **2**. Thus in one method, the remaining halide **1** in the mixture was converted into tetra-*O*-acetyl-D-glucopyranose and the resulting mixture was purified by chromatography. In another method, the halide **1** was transformed into 2,3,4,6-tetra-*O*-acetyl-D-glucal and the latter was removed from the mixture by ozonolysis. The desired *C*-glycoside **2** was obtained in approximately 20% yield by both methods.

Attempts to deacetylate the product **2** or to selectively hydrolyze the malonic ester groups, under mildly basic or acidic conditions, led to mixtures. These difficulties were attributed, in part, to the presence of the acidic malonic ester proton, which once removed in the basic medium, would afford a carbanionic species that would in turn undergo further reactions. This conclusion was supported by the observation that analogous compounds in another series (9), in which the malonate proton was absent, underwent smooth deacylation. Since our aim was to introduce functionalized substituents at the anomeric center capable of undergoing a variety of transformations that would eventually lead to *C*-nucleosides, we turned our attention to the dibenzyl ester analog of **2** as a more versatile source of *C*-glycosyl compounds. Condensation of **1** with sodio dibenzyl malonate in 1,2-dimethoxyethane gave a good yield of the *C*-glycosyl malonate **3** (Scheme 1). Some starting halide (~20%) was present in the crude product but no other-side-product was detected. Hydrogenation of the mixture over 20% palladium-on-charcoal gave crystalline 2-(2,3,4,6-tetra-*O*-acetyl-β-D-glucopyranosyl) malonic acid **4** in 51% overall yield (based on the halide **1**). The structural and anomeric configurational relationships between **2** and **3** were ascertained by esterification of the diacid **4** with triethyloxonium fluoroborate (10) and isolation of crystalline **2**. The diacid derivative **4** could also be decarboxylated quantitatively in refluxing acetic acid and the

[4]While this manuscript was in preparation, the synthesis of a *C*-glycosyl malonate based on our initial approach (1) was reported, see ref. 32.

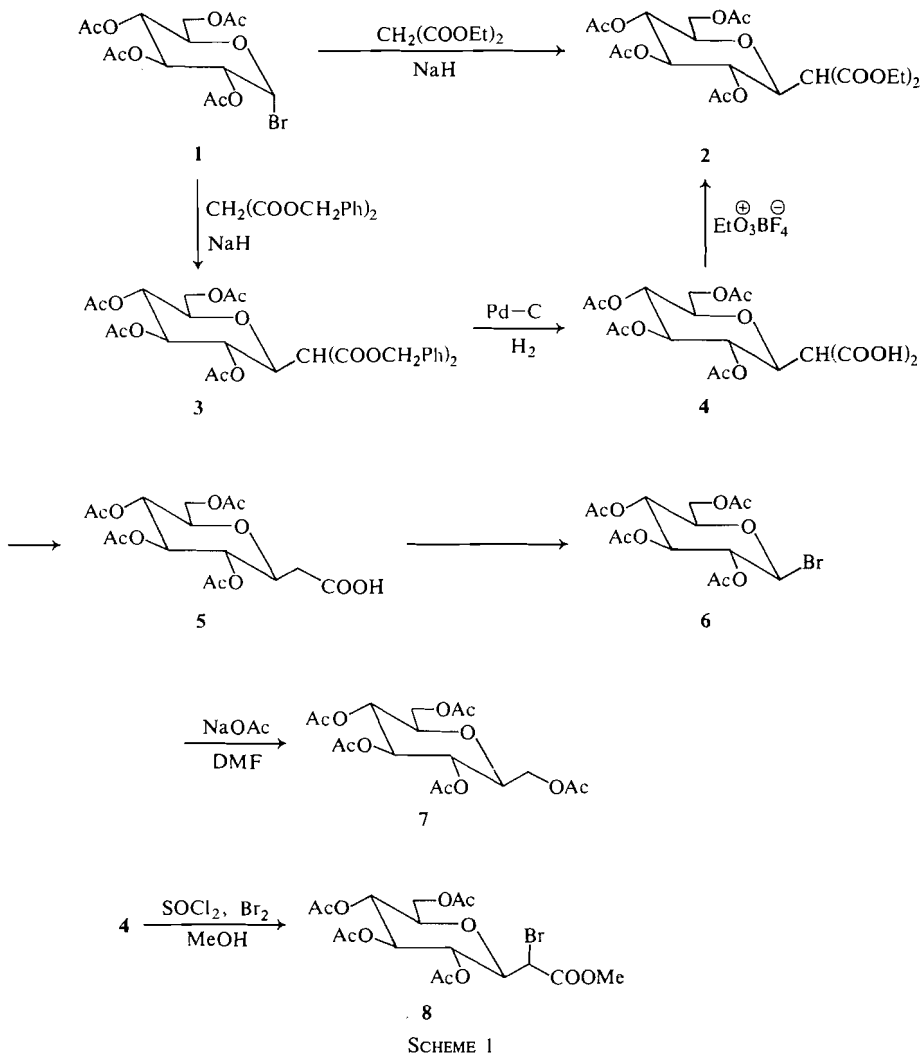

SCHEME 1

resulting monoacid **5** was isolated in crystalline form.

Although the preparative merit of the above reactions was demonstrated, there remained to assign the anomeric configuration to the *C*-glycosyl compounds **2** and **3**. Spectroscopic and polarimetric data, which can be reliably used for such assignments in *O*- and *N*-glucosyl derivatives, were not too informative in the case of **2** or **3**. Thus, even at 220 MHz the region of the anomeric and C-2 protons remained obscured by the H-6,6′ and the methylene protons of the malonic ester portion. In the presence of $Eu(DPM)_3$ and $Eu(FOD)_3$-d_{27}, however, characteristic paramagnetic shifts of some of the hydrogen atoms were observed, thus simplifying the otherwise complex spectrum of **2** (Fig. 1). At a finite concentration of shift reagent, attained by incremental additions, the patterns of H_m, H-1, and H-6,6′ were all resolved and allowed a first-order analysis. The H-6,6′ signals underwent a large downfield shift, relative to other signals. This behavior was in agreement with similar observations in the spectra of peracetylated carbohydrates in the presence of $Eu(DPM)_3$ (11). Although the H-1 and H_m signals could be adequately analyzed, a definitive anomeric assignment could not be made because the H-2 signal was still unresolved. The relatively large H-1,H-2 coupling constant could not be taken as an unambiguous indication of a 1,2-*trans* arrangement of protons, because of the lack of

Can. J. Chem. Downloaded from www.nrcresearchpress.com by 210.87.254.6 on 09/05/12
For personal use only.

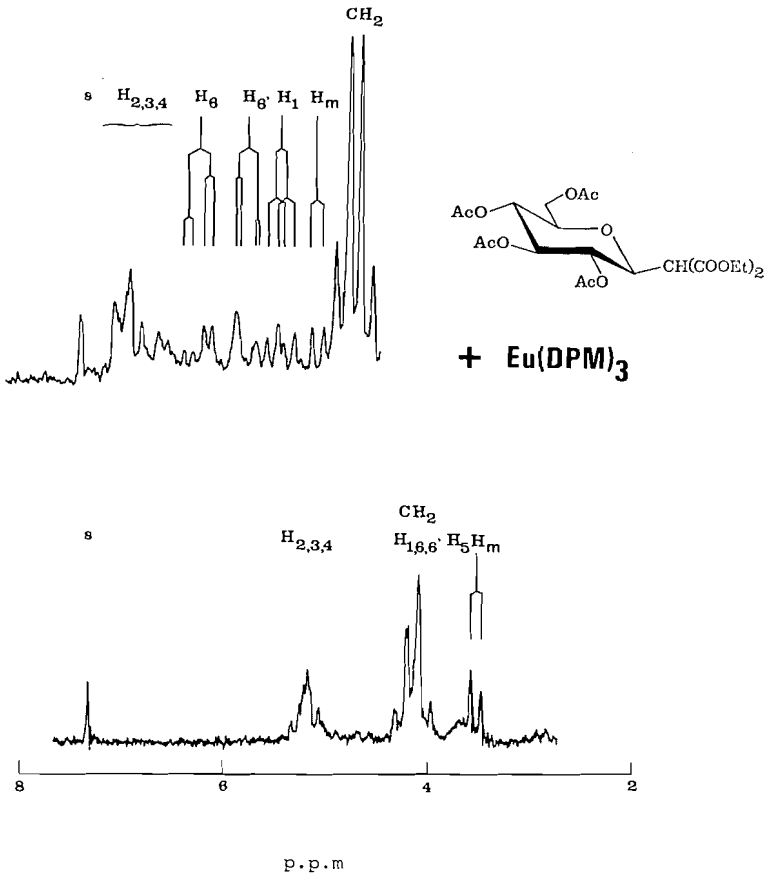

FIG. 1. Nuclear magnetic resonance spectrum of diethyl 2-(2,3,4,6-tetra-*O*-acetyl-β-D-glucopyranosyl) malonate **2** (lower spectrum) and in the presence of $Eu(DPM)_3$, in $CDCl_3$ at 60 MHz (upper spectrum). H_m refers to the malonic ester proton.

adequate models in the series. In the presence of $Eu(FOD)_3$-d_{27}, a different pattern of paramagnetic shifts was observed (Fig. 2). Incremental addition of the reagent caused a rapid shift of the H-2 triplet, from which a coupling constant could be calculated and correlated with that found in the H-1 pattern.

The two shift reagents were apparently interacting at different sites of the polyfunctional substrate **2**. From the above data, a β-configuration could be assigned to **2** with reasonable assurance. Chemical proof for the anomeric assignment was nevertheless obtained by a correlation with the reference compound **7** (12). Application of the modified Hundsdiecker reaction (13) to the acid **5** gave the crystalline bromide **6** in 87% yield. The latter was solvolyzed in the presence of anhydrous sodium acetate in *N*,*N*-dimethylformamide to give the known crystalline 1,3,4,5,7-penta-*O*-acetyl-2,6-anhydro-D-glucitol **7**, thus conclusively establishing the structure, as well as the β-anomeric configuration of **2** (and **3**).

The mass spectrum of **2** was in accord with its structure, and revealed a fragmentation pattern that was characteristic of its structure. Whereas a common fragmentation pathway of hexopyranose peracetates (14) involves cleavage of the glycosyloxy bond and the formation of a cyclic glycosyl oxonium ion at *m/e* 331, the corresponding *C*-glycosyl malonates do not give such an ion but fragment to give an ion that retains a portion of the C-1 substituent. Some of these fragments are shown in Scheme 2.

Having access to the anomerically substituted malonic and acetic acid derivatives (Scheme 1), experiments were attempted in order to introduce a versatile functional group such as a halogen

Can. J. Chem. Downloaded from www.nrcresearchpress.com by 210.87.254.6 on 09/05/12
For personal use only.

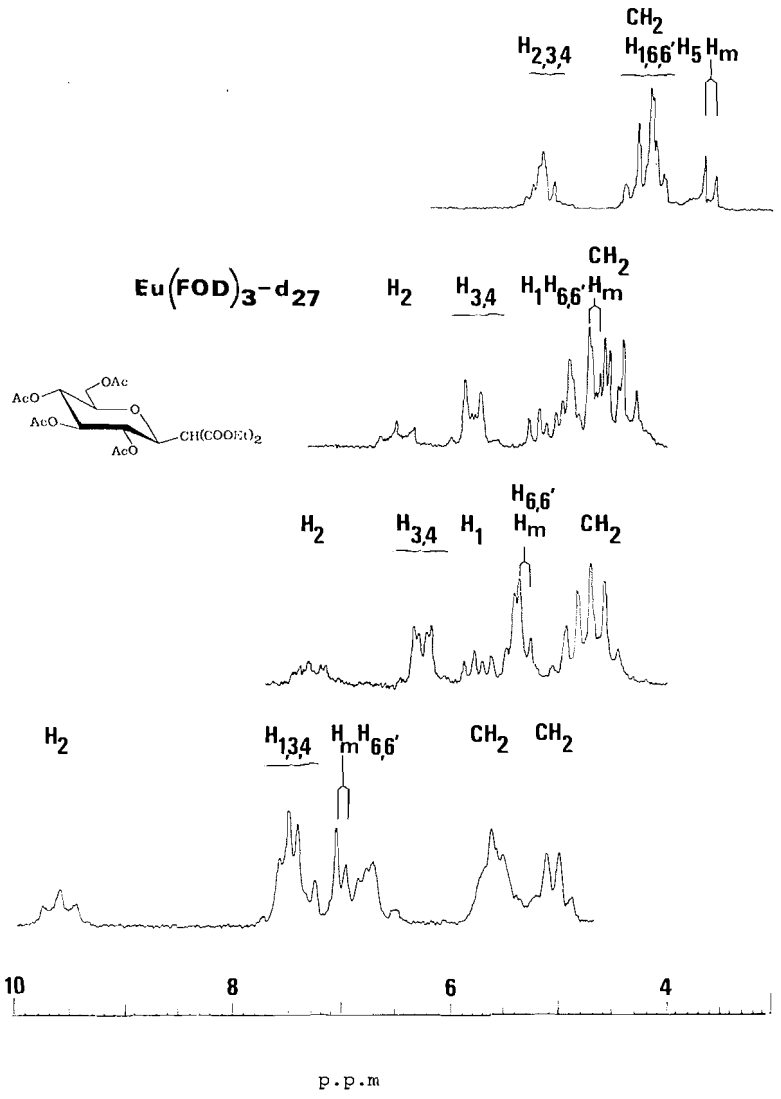

FIG. 2. Partial n.m.r. spectra of diethyl 2-(2,3,4,6-tetra-*O*-acetyl-β-D-glucopyranosyl) malonate **2** (upper spectrum) and in the presence of incremental amounts of $Eu(FOD)_3$-d_{27} (lower spectra), in $CDCl_3$ at 60 MHz. H_m refers to the malonic ester proton.

atom in the 2-position of the anomeric substituent. Treatment of the acid **5** with bromine in carbon tetrachloride (15), or with sulfuryl chloride and thionyl chloride (16), or with *N*-bromosuccinimide (17) were unsuccessful. However, when the malonic acid derivative **4** was treated with bromine in thionyl chloride (18) and the product was then treated with methanol, a 57% yield of the crystalline α-bromoester **8** was obtained. The above discussed reactions demonstrate not only the feasibility of C—C condensation reactions at the anomeric center but also illustrate the possibility of effecting various selective transformations in the *C*-aglycon portion. The functionalized anomeric substituents in these and related *C*-glycosyl compounds could then be used in the elaboration of various β-oriented heterocyclic systems, including those found in the medicinally important *C*-nucleosides.

The formation of β-*C*-glucosyl compounds can be explained by considering the following possibilities (Scheme 3): (*a*) a direct S_N2-type reaction on the anomeric carbon atom of the halide **1** or

Can. J. Chem. Downloaded from www.nrcresearchpress.com by 210.87.254.6 on 09/05/12
For personal use only.

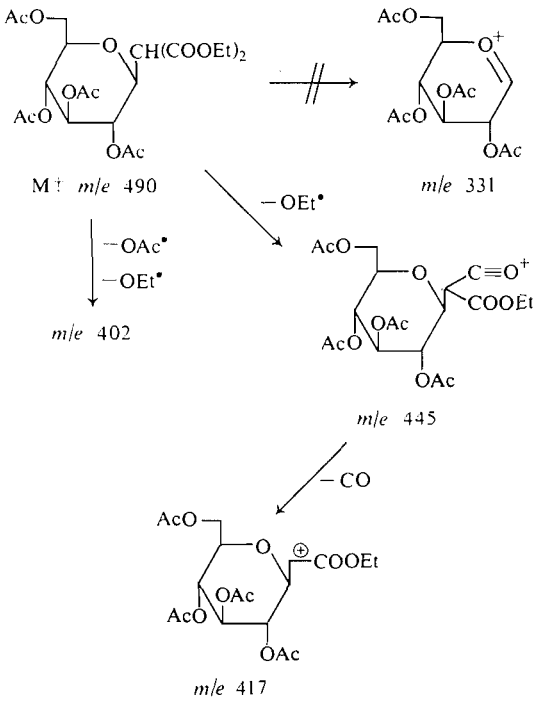

SCHEME 2

on an ion-pair in which the bromide ion has a specific α-orientation (**A**); (*b*) formation of an oxonium ion with possible stabilization by electronegative atoms in the solvent,[5] followed by β attack by the carbanion[6] (**B**); (*c*) formation of a 1,2-acetoxonium ion from the oxonium ion and subsequent attack of the carbanion on the anomeric carbon atom; (*d*) irreversible epimerization of an initially-formed α-*C*-glucosyl compound.[7] In order to gain further insight into some of these mechanistic possibilities, a model reaction was chosen, that would in all probability, proceed by way of 1,2-acetoxonium ions (5). When β-acetochloroglucose **9** was allowed to react with sodio diethyl malonate in 1,2-dimethoxethane or *N*,*N*-dimethylformamide, the sole product of the reaction was the ketal **10** (Scheme 4). The intervention of a 1,2-acetoxonium ion intermediate was therefore evident. In view of the absence of any ketal product in the reaction of **1** and the carbanion in 1,2-dimethoxyethane, it can be concluded that acetoxonium ions are not involved in the formation of the β-*C*-glucosyl compounds **2** and **3**. Most likely then, the mechanism involves attack on an ion-pair species in which the bromide has an α-orientation as in **A**. To test this hypothesis and to further study the role of the solvent, the condensation of **1** and sodio diethyl malonate was carried out in *N*,*N*-dimethylformamide, which would promote a better charge separation of paired ionic species and would allow a more effective participation of the C-2 acetoxy group. The product in this case consisted of a mixture of the *C*-glycoside **2** (~20%), the ketal **10** (~30%), and 2,3,4,6-tetra-*O*-acetyl-D-glucal (>50%). These results imply the initial formation, in part, of an acetoxonium ion and the products **2** and **10** could arise by way of a mixed pathway. A direct attack of the carbanion on the anomeric carbon atom of the acetoxonium ion **C** in this solvent cannot be excluded.

The structure of **10** was proved by spectroscopic and chemical means. Acetolysis gave α-D-glucose pentaacetate **14** (Scheme 4), as would be expected of a 1,2-ketal but not a *C*-glycoside.[8] Acetyl malonate was isolated and identified in this reaction. Conclusive proof of the 1,2-ketal structure was obtained by sequential methylation, hydrolysis (19), and oxidation to a lactone with bromine. The crystalline phenylhydrazide derivative **13**, obtained from the lactone, was identical with an authentic sample of 3,4,6-tri-*O*-methyl-D-gluconic acid phenylhydrazide (20).

A study of the reaction of sodio diethyl malonate with glycosyl halides containing non-participating substituents was next undertaken, primarily for mechanistic reasons. Condensation of 2,3,4,6-tetra-*O*-benzyl-α-D-glucopyranosyl bromide **15** (21) with sodio diethyl malonate in diethyl malonate afforded the anomeric *C*-glucosyl malonates **16** in high yield (Scheme 5). After hydrogenation and acetylation, a mixture was obtained that was richer in the β-anomer (approximately 3:1 β to α ratio). Two pathways could be envisaged to account for this result. A partial anomerization of the bromide **15** via ion-

[5]For a discussion of the formation of discrete oxonium intermediates with ether-type solvents in displacement reactions, see refs. 33 and 34; see also ref. 35.

[6]Anomerization, by return of bromide ion is considered somewhat unlikely because of the formation of the relatively insoluble sodium bromide during the reaction. The effective concentration of bromide ions in solution would be negligible.

[7]Epimerization of this type has been experimentally observed in the D-ribofuranose series, see ref. 9 and references cited therein.

[8]Acetolysis of **2** under the same conditions gave unchanged product.

Can. J. Chem. Downloaded from www.nrcresearchpress.com by 210.87.254.6 on 09/05/12
For personal use only.

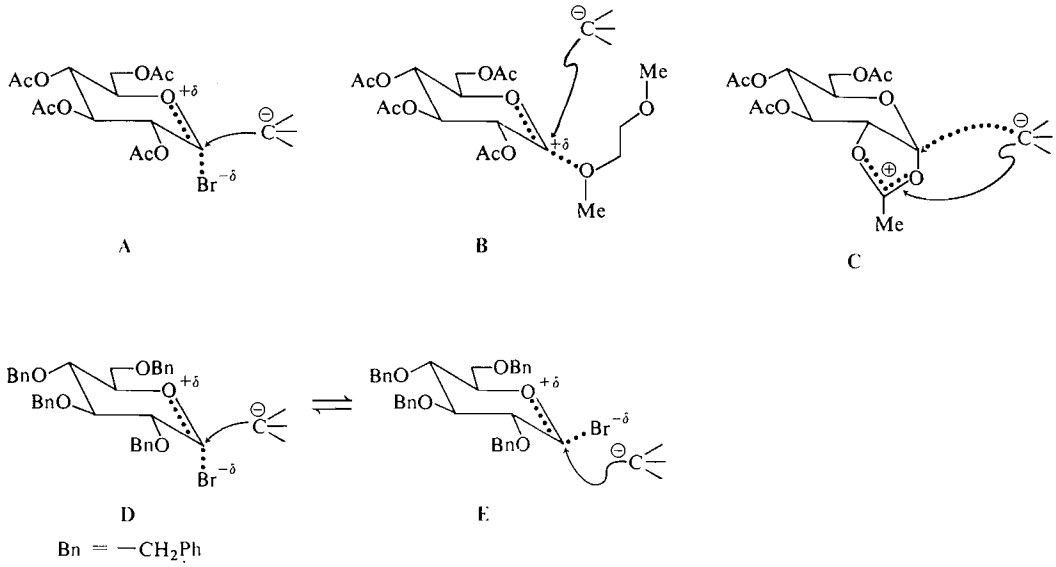

A B C

D E

SCHEME 3

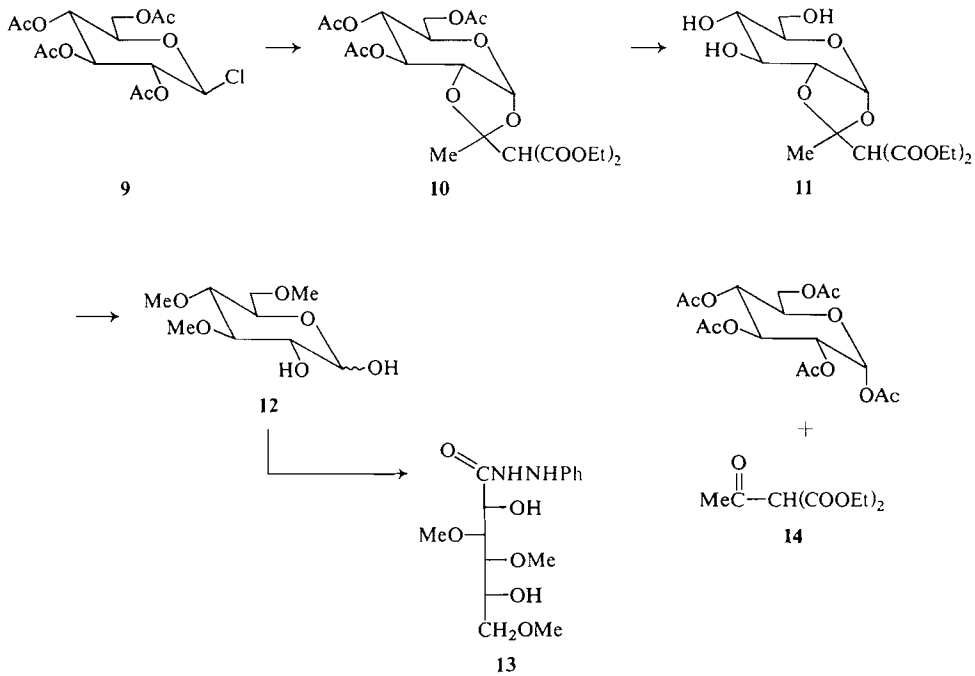

9 10 11

12

13 14

SCHEME 4

pair intermediates or oxonium-ion species, followed by attack of the carbanion on the anomeric carbon atom of two ion-paired species, in which the bromide ions were specifically α- and β-oriented (Scheme 3, **D** and **E**). Alternatively, the products could arise from attack of the carbanion on oxonium-ion species, possibly stabilized by solvent molecules (malonate). In view of the relative insolubility of the formed sodium bromide in the reaction mixture, appreciable anomerization by bromide ion return is somewhat unlikely and the alternative mech-

Can. J. Chem. Downloaded from www.nrcresearchpress.com by 210.87.254.6 on 09/05/12
For personal use only.

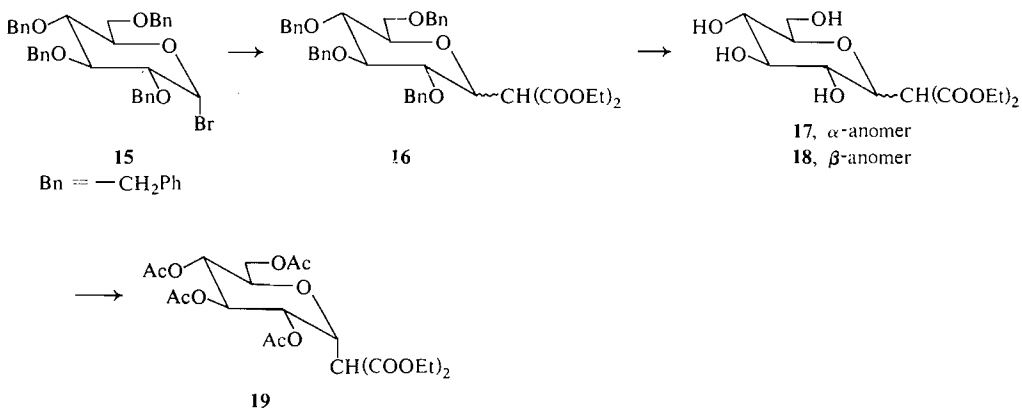

SCHEME 5

TABLE 1. Condensation of **15** with sodio diethyl malonate in the presence of added bromide ion[a]

Malonate (equiv.)	Salt added (equiv.)	$[\alpha]_D$ of mixture[b]	α to β ratio	Yield (%)
10	—	0.6°	23:77	81
10	NaBr (10)	+4.3°	27:73	92
10	*n*-Bu_4NBr (1)	+28.5°	56:44	92
10	*n*-Bu_4NBr (5)	+39.9°	69:31	72
10	*n*-Bu_4NBr (10)	+42.0°	72:28	85

[a]For reaction conditions see Experimental.
[b]Optical rotation of the mixture after hydrogenation and acetylation.

anism may be operative. In order to test the mechanistic consequence of an induced anomerization, the condensation was done in the presence of a soluble source of bromide ion, the premise being that the return of the bromide ion from the β-side would create a finite concentration of the more reactive β-bromide in the equilibrium **D** ⇄ **E** (Scheme 3). This assumption was based on published data that β-D-glucopyranosyl halides, containing non-participating substituents at C-2, underwent alcoholysis more rapidly than did the α-anomers (21*a*, 22). If this type of reactivity were to be operative in the present case, where the nucleophile is a carbanion, then a higher proportion of the α-*C*-glucopyranosyl malonate should form in the presence of added bromide ion. The addition of 10 equiv. of tetra-*n*-butylammonium bromide to the solution containing **15**, *prior to the addition of the carbanion*, led to a mixture in which the α-anomer was indeed predominant (Table 1).[9] Crystalline diethyl 2-(2,3,4,6-tetra-*O*-acetyl-α-D-glucopyranosyl) malonate **19** was isolated in 31% yield from such a condensation, after hydrogenolysis and acetylation. This result supports the contention that in the presence of added bromide ion, some β-bromide is formed either by direct anomerization or by attack of bromide ion on a solvated oxonium-ion intermediate. Since the equilibrium is in favor of the α-anomer because of the anomeric effect (23), the preponderance of the α-*C*-glucosyl compound must be the result of a faster reaction with the β-halide (Scheme 3, **E**). A crystalline by-product in the reactions where excess bromide ion was present was found to be tetraethyl 1,1,2,2,-ethanetetracarboxylate. The same compound was isolated from the reaction of 1,2-dibromocyclohexane with sodio diethyl malonate (24). Authentic product was obtained by treatment of a solution of sodio diethyl malonate with iodine.

The optical rotations of the crystalline *C*-glucosyl compounds **2** and **19** show that Hudson's rules (25) are obeyed in this class of compounds. Chemical evidence for the anomeric purity was obtained from periodate oxidation of the *C*-glycosyl malonates **17** and **18**, respectively,

[9]It is also evident from the data in Table 1, that the addition of sodium bromide is of negligible effect. This further supports the need for the presence of a soluble source of bromide ions.

Can. J. Chem. Downloaded from www.nrcresearchpress.com by 210.87.254.6 on 09/05/12
For personal use only.

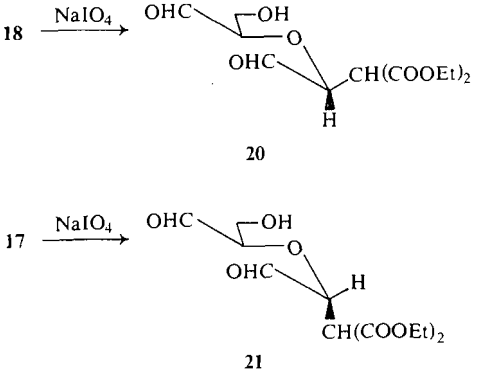

SCHEME 6

and the isolation of the epimeric dialdehydes **20** and **21** (Scheme 6).

The availability of 2,3:5,6-di-*O*-isopropylidene-D-mannofuranosyl halides (26, 27) prompted a study of their reactions with sodio diethyl malonate. Treatment of the bromide **22** (Scheme 7) with the carbanion in diethyl malonate as solvent gave the expected *C*-glycosyl malonates as an anomeric mixture in high yield. The preponderant anomer was the β-anomer. Both α- and β-anomers were isolated from the mixture by chromatography and their anomeric assignments were based on polarimetric and n.m.r. spectroscopic data. The β-anomer showed a higher negative rotation compared to the α-anomer. A larger H_1–H_2 coupling constant and a more deshielded malonic ester proton were found in the spectrum of the β-anomer. In the spectrum of the α-anomer however, H-4 was distinctly deshielded compared to the β-anomer.

The preponderant formation of the β-anomer **24** can again be explained by invoking a direct attack of the carbanion on the anomeric carbon atom in **22** or in a tightly-paired ionic species, in which the bromide ion has an α-orientation. Epimerization, if taking place at all, must be in favor of the minor α-anomer, because of the bulky isopropylidene groups. In a more polar solvent such as ethanol, the reaction gave **23** and **24** in addition to the corresponding anomeric *O*-ethyl glycosides in approximately equal amounts. Although the reaction is not particularly useful from the preparative standpoint, it demonstrates the role of the solvent and the relative nucleophilicities of the alkoxide and the carbanion. The higher proportion of α-*O*- and -*C*-glycosides can be explained by a more effective separation of charges in the transition state leading to a more favored (less hindered) α attack.

The D-mannofuranose structure can be used as a precursor to the D-lyxo series. The mixture of *C*-glycosyl compounds **23** and **24**, rich in the β-anomer, was treated with dilute acetic acid to give the diol **25**. The latter was oxidized with sodium periodate and the 5-aldehyde derivative was reduced with sodium borohydride to give a mixture of the anomeric diethyl 2-(2,3-*O*-isopropylidene-D-lyxofuranosyl) malonates **26**.

Experimental

General

Melting points are uncorrected. Infrared spectra were recorded on a Beckman IR-8 spectrometer. Nuclear magnetic resonance spectra were obtained in chloroform-*d*

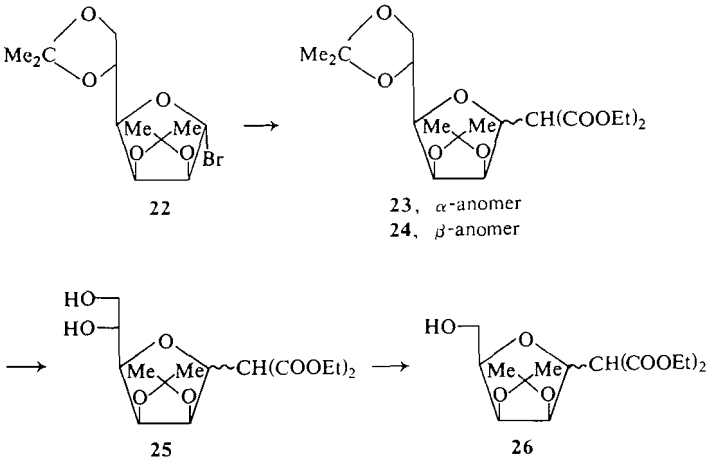

SCHEME 7

Can. J. Chem. Downloaded from www.nrcresearchpress.com by 210.87.254.6 on 09/05/12
For personal use only.

Can. J. Chem. Downloaded from www.nrcresearchpress.com by 210.87.254.6 on 09/05/12
For personal use only.

unless otherwise stated, at 60 and 220 MHz, with tetramethylsilane as internal reference (s, singlet; d, doublet; t, triplet; q, quartet; o, octet; m, multiplet; b, broad). Optical rotations were measured with a Perkin-Elmer model 141 automatic polarimeter. Mass spectra were done at low resolution on a Hitachi-Perkin-Elmer RMU-6D spectrometer with direct introduction of the sample in the ionizing chamber. Conventional processing, or processing in the usual manner, signifies drying of organic solution over anhydrous sodium sulfate, filtration, and evaporation under diminished pressure.

Chromatography

Thin-layer chromatography (t.l.c.) was done with plates coated with silica gel GF_{254} and with silica gel containing 2% boric acid (by weight). The following solvent systems were used: solvent A, chloroform–2,2,4-trimethylpentane–methanol (10:5:0.2); solvent B, chloroform–methanol (10:1); solvent C, toluene – ethyl acetate (10:1). The detection of *C*-glycosyl malonates was done with sulfuric acid in ethanol (20% by volume), followed by heating the plate at 100–110°.

The *C*-glycosyl malonates of the type described in this work appeared at first as orange-colored spots that eventually changed to dark brown on further heating. Glycosyl halides were detected by spraying the plates with a solution containing 20 g of silver nitrate and 20 ml of nitric acid in 100 ml of water. Black spots were produced within a few minutes at room temperature.

Column chromatography was performed with silica gel GF_{254} (with or without added 2% boric acid) by application of moderate suction. The conventional column was replaced by one fitted with a fritted disc (medium porosity) and a ground glass point that was connected to an appropriate suction flask. For the separation of components differing by 0.05 R_f units, a ratio of 1:20 of silica gel to substrate was found satisfactory.

Solvents and Handling of Carbanions

Due to the sensitivity of the glycosyl halides and the carbanions to moisture, all solvents used in the condensation reactions were dried rigorously prior to use. The preparation of the carbanions was done in a dry box and subsequent handling and transfers were performed with minimum exposure to air. These conditions are not mandatory for all condensations but they are advisable in the case of unstable glycosyl halides.

Diethyl 2-(2,3,4,6-Tetra-O-acetyl-β-D-glucopyranosyl) Malonate (2)

To a suspension of sodium hydride (10 g, 0.42 mol; previously washed with pentane) in 300 ml of 1,2-dimethoxyethane (DME) was added 65 ml of diethyl malonate, in portions and with stirring, until the evolution of hydrogen ceased, and the solution became clear. A solution of α-acetobromoglucose (56 g, 0.14 mol) in 50 ml of DME was slowly added, and after stirring overnight at room temperature, the solution was diluted with 2 l of ether and washed with water several times until the washings were neutral. The organic layer was then dried and processed as usual to give a mobile liquid, from which excess diethyl malonate was removed by distillation (30° at 10^{-3} Torr). A viscous yellowish syrup (32 g) was obtained that showed essentially three spots on t.l.c. (5 × 20 cm plate, solvent A), consisting of starting material **1** (~20%), and equal amounts of the title compound and a transesterified unknown product. Upon spraying the plate with sulfuric acid and heating, the spot corresponding to the title compound gave an orange color that turned to brown upon further heating.

A portion of the syrup (2 g) was dissolved in enough 95% ethanol to render it mobile, the solution was then seeded[10] and left at −20° for a few days, whereupon the title product **2** crystallized; yield 0.9 g, 20%; two recrystallizations from the minimum volume of 95% ethanol gave material having m.p. 88.5–89°; $[\alpha]_D^{25}$ −18.5° (*c*, 3.0 $CHCl_3$); n.m.r. (at 220 MHz): 1.27, 1.29 (t, J = 7 Hz, CH_3CH_2); 3.61 (d, $J_{m,1}$ = 6.2 Hz; H_m); 3.71 p.p.m. (o, $J_{5,4}$ = 9 Hz; $J_{5,6}$ = 5 Hz, $J_{5,6'}$ = 2.5 Hz; H-5). For spectra in the presence of n.m.r. shift reagents, see Figs. 1, 2. Eu(DPM)$_3$: H_m (d, $J_{m,1}$ = 6.2 Hz); H_1 (dd, $J_{1,m}$ = 6.2 Hz; $J_{1,2}$ = 9.75 Hz); Eu(FOD)$_3$-d_{27}: H_m (d, $J_{m,1}$ = 6.2 Hz); H_1 (dd, $J_{1,m}$ = 6.2 Hz; $J_{1,2}$ = 9.75 Hz); H_2 ($t_1H_{2,1}$ = $H_{2,3}$ = 9.75 Hz). Mass spectral data: *m/e* 445 (M^+ − EtO·); 417 (M^+ − EtO·—CO).

Anal. Calcd. for $C_{21}H_{30}O_{13}$: C, 51.43; H, 6.17. Found: C, 51.21; H, 6.18.

Alternate methods for obtaining **2** involve preliminary transformation of the residual acetobromoglucose into tetra-*O*-acetyl-D-glucose (method A) and tetra-*O*-acetyl-D-glucose (method B).

Method A

The syrup (32 g) resulting from a similar condensation to that described above was treated with NaI–Et_3N according to Ferrier and Sankey (28) and the conversion of residual **1** into tetra-*O*-acetyl-D-glucal was followed by t.l.c. The resulting dark brown syrup was dissolved in methanol (100 ml) and the solution was treated with ozone for 3 h. After diluting with 500 ml of dichloromethane, the colorless solution was washed with alkaline hydrogen peroxide (30 vol. in *N* NaOH), then with water. The organic phase was processed as usual to give a syrup (32 g) that contained the *C*-glycoside **2** and presumably a transesterification product in approximately equal amounts. A portion (1.02 g) of the syrup was separated by chromatography on silica gel (Grace Davidson G 950; substrate–adsorbent ratio ~1:300) with chloroform as the developing solvent. The title compound **2** was obtained from the appropriate fractions after evaporation to a syrup and keeping at 0° for a few days; yield 0.4 g (20%).

Method B

A portion (2 g) of the above syrup resulting from the condensation reaction was dissolved in a mixture of 1:3 water–acetone and the solution was treated with 0.3 g of silver nitrate and 0.106 g of silver carbonate. After stirring at room temperature for 2 h, the suspension was filtered and the combined filtrates and washings were evaporated to a small volume. The solution was extracted with chloroform and the extracts were processed in the usual manner to give a syrup that showed **2** (R_f ~0.8), the transesterified product (R_f ~0.85), and tetra-*O*-acetyl-D-glucose (R_f ~0.5) in solvent A (20 cm plate). The *C*-glycoside **2** was separated by column chromatography as described under B and was obtained in 20% yield.

[10]Seed crystals were obtained by preparative t.l.c. on 0.1 g of sample; the syrup so obtained crystallized at 0°.

Can. J. Chem. Downloaded from www.nrcresearchpress.com by 210.87.254.6 on 09/05/12
For personal use only.

The R_f 0.85 component was separated and isolated as a colorless syrup. Its n.m.r. spectrum showed a much larger ratio of ethyl hydrogens to acetyl methyl hydrogens. This product, assumed to arise by transesterification, was not investigated further.

2-(2,3,4,6-Tetra-O-acetyl-β-D-glucopyranosyl) Malonic Acid (4)

To a suspension of sodium hydride (3.5 g, 0.2 mol; previously washed with pentane) in 130 ml of 1,2-dimethoxyethane (DME) was added dibenzyl malonate (45 ml) until the evolution of hydrogen ceased. Acetobromoglucose (20 g, 49 mmol) dissolved in the minimum volume of DME was added to the clear solution and the whole was stirred at room temperature for 48 h. After the solution was concentrated (below 30°) to a small volume, ether (500 ml) was added and the solution was washed successively with *N* HCl (100 ml) and water. The organic phase was dried and evaporated to a syrup that was triturated with pentane several times to remove residual dibenzyl malonate. The remaining syrup (~80%) consisted essentially of *dibenzyl 2-(2,3,4,6-tetra-O-acetyl-β-D-glucopyranosyl) malonate* (**3**) as evidenced by t.l.c. (solvent A). The syrup was dissolved in ethanol and hydrogenated in the presence of 20% palladium-on-charcoal (29) (4.0 g). After 20 h, the catalyst was filtered and the filtrate was evaporated to a syrup that was dissolved in acetone, filtered, and the filtrate was evaporated. The title compound crystallized spontaneously and was recrystallized from ether to give **4** in several crops (10.5 g, 51%), m.p. 139–141°. After two recrystallizations, an analytical sample was obtained having m.p. 147° (with gas evolution); $[\alpha]_D^{25}$ −18° (*c*, 1.17 EtOH); n.m.r. (DMSO-d_6): 3.38 (d, $J_{m,1}$ = 7.5 Hz, H_m); 1.93, 2.02 p.p.m. (*s*, CH_3COO), etc.

Anal. Calcd. for $C_{17}H_{22}O_{13}$: C, 47.01; H, 5.11. Found: C, 46.89; H, 5.33.

2-(2,3,4,6-Tetra-O-acetyl-β-D-glucopyranosyl) Acetic Acid (5)

The above described product **4** (1.0 g, 2.3 mmol) was dissolved in 20 ml of glacial acetic acid and the solution was heated under reflux for 3 h. Evaporation of the solution to dryness gave the title compound in quantitative yield. Recrystallization from ether–pentane gave material having m.p. 104.5–105.5°. Three recrystallizations from the same solvent mixture gave pure material, m.p. 120–120.5°; $[\alpha]_D^{25}$ −4.3° (*c*, 1.95 $CHCl_3$); n.m.r.: 2.05, 2.10, 2.12 (s, CH_3COO); 2.62 (d, J = 6 Hz, CH_2COOH); 10.55 p.p.m. (*s*, $COOH$).

Anal. Calcd. for $C_{16}H_{22}O_{11}$: C, 49.23; H, 5.68. Found: C, 49.29; H, 5.96.

Esterification of 4 with Triethyloxonium Fluoroborate

An amount of **4** (30 mg) was dissolved in 2 ml of dichloromethane, the solution was cooled to 0° and treated with 0.2 g of triethyloxonium fluoroborate (10). After standing at 0° for 1 h, the solution was poured into aqueous sodium bicarbonate and chloroform was added. Processing the organic phase gave a syrup (20 mg, 59%) that had identical chromatographic and n.m.r. spectral properties to the diester **2**. Crystallization from the minimum volume of 95% ethanol gave **2**, m.p. and mixture m.p. 89–90°.

3,4,5,7-Tetra-O-acetyl-2,6-anhydro-1-bromo-1-deoxy-D-glycero-D-gulo-heptitol (6)

A solution of **5** (54 mg, 0.14 mmol) in 1 ml of carbon tetrachloride was treated with 30 mg of yellow mercuric oxide and 1 ml of carbon tetrachloride containing 40 mg of bromine and the mixture was heated under reflux in the dark for 3 h. The suspension was filtered through a bed (2 × 2 cm) of silica gel and the adsorbent was developed with chloroform. Evaporation of the chloroform solution gave the title compound which crystallized. The crystalline mass was triturated with cold ethanol and the crystals were filtered; yield 51 mg (87%). Two recrystallizations from 95% ethanol gave material having m.p. 119.5–120°; $[\alpha]_D^{25}$ −12.4° (*c*, 1.1 $CHCl_3$); n.m.r.: 2.05, 2.09, 2.11, 2.13 (*s*, CH_3COO), 3.45 p.p.m. (bs, CH_2Br), etc.

Anal. Calcd. for $C_{15}H_{21}O_9Br$: C, 42.37; H, 4.98. Found: C, 42.39; H, 5.05.

1,3,4,5,7-Penta-O-acetyl-2,6-anhydro-D-glycero-D-gulo-heptitol (7)

The above mentioned bromide 6 (30 mg, 0.07 mmol) was solvolyzed in 2 ml of DMF containing 30 mg (0.4 mmol) of anhydrous sodium acetate at 110° (36 h). The solvent was removed by azeotropic evaporation with 1-butanol, the resulting residue was dissolved in chloroform, and the solution was washed with water. Processing the organic phase in the usual way gave a syrup that crystallized; yield 20 mg (70%). Two recrystallizations from 2-propanol gave **7**, m.p. 94° (sublimes); $[\alpha]_D^{25}$ 0 ± 1° (*c*, 1.0 $CHCl_3$), (lit. (12), m.p. 89° $[\alpha]_D$ 0° ($CHCl_3$)).

Methyl 2-(2,3,4,6-Tetra-O-acetyl-β-D-glucopyranosyl) 2-Bromoacetate (8)

To a solution of the diacid **4** (0.25 g, 0.57 mmol) in 5 ml of dry thionyl chloride, were added 0.5 ml of bromine and 3 drops of a 1:1 acetic acid – hydrochloric mixture. The solution was heated at reflux for 3 h and then it was evaporated. After this process was repeated three times, the residue crystallized and the product was recrystallized from hot methanol to give the title compound (0.155 g, 57%); m.p. 145.5–146°; mass spectral data (AEI MS 902, at high resolution): M^+ 482.0419 and 484.0407 (Br isotope); calcd. for $C_{17}H_{22}O_{11}Br$: M^+ 482.0424 and 484.0404.

1,2-O-(2,2-Dicarbethoxy-1-methylethylidine)-3,4,6-tri-O-acetyl-α-D-glucopyranose (10) and its Acetolysis Product

To a solution containing sodium diethyl malonate (from 0.75 g of sodium and 6.0 ml of diethyl malonate) in 30 ml of *N*,*N*-dimethylformamide, were added 4 g (11 mmol) of β-acetochloroglucose **9** (30). After stirring at room temperature overnight, the solution was concentrated under vacuum, the residue was taken up in chloroform, and the solution was washed with water. Processing the organic layer in the usual manner gave the title compound as a chromatographically homogeneous syrup. The yield varied between 5 and 7 g (80–100%). Nuclear magnetic resonance: 1.30 (t, J = 7.5 Hz, CH_3CH_2); 1.89 (s, CH_3—C); 2.11, 2.13 (s, CH_3COO); 3.73 (s, H_m); 4.90 (q, $J_{4,5}$ = 8.25 Hz; $J_{4,3}$ = 3 Hz, H-4);

Can. J. Chem. Downloaded from www.nrcresearchpress.com by 210.87.254.6 on 09/05/12
For personal use only.

5.20 (t, $J_{3,4} = J_{3,2} = 3$ Hz, H-3); 5.75 p.p.m. (d, $J = 5.2$, H-1).

Acetolysis of **10** (50 mg in 1 ml of acetic anhydride, 1 ml of glacial acetic acid containing a micro drop of concentrated sulfuric acid, room temperature for 24 h, followed by conventional processing (aqueous sodium bicarbonate, extraction, etc.)) gave α-D-glucose pentaacetate (16 mg, 40%), m.p. 112–113° (from ethanol).

The mother liquors from the above described crystallization were concentrated to a syrup and the latter was extracted with pentane to give a mobile liquid that had an n.m.r. spectrum identical to acetyl diethylmalonate **14**; 2,4-dinitrophenylhydrazone derivative, m.p. and mixture m.p. 147° (lit. (31) m.p. 146–148°); n.m.r. for **14**: 1.28, 1.30 (t, CH_3CH_2); 2.04, 2.13, 2.21 (s, $CH_3C(=O)$— and $CH_3C(=O)$); 3.40 (s, H_m, integration corresponds to ~0.8 H due to presence of enolic forms); 4.25 p.p.m. (m, CH_3CH_2).

Acid hydrolysis (*N* HCl; reflux; 2 h) of **10** gave a single sugar that was identified as glucose by chromatography in common solvent systems.

1,2-O-(2,2-Dicarbethoxy-1-methylethylidene)-α-D-glucopyranose (11)

A solution containing 4.2 g of **10** in 30 ml of ethanol was treated dropwise with a 1 *N* solution of sodium ethylate until a p*H* of 7.5–9 was attained. The p*H* was checked periodically, and after 2 h the solution was neutralized with Dowex-50(H^+) and the filtrate was processed in the usual manner to give a colorless chromatographically homogeneous syrup in quantitative yield; n.m.r.: 1.80 (*s*, CH_3—C); 5.75 p.p.m. (d, $J_{1,2} = 5$ Hz, H-1 etc.

3,4,6-Tri-O-methyl-D-gluconic Acid Phenylhydrazide (13) from 11

The above obtained product **11** (0.74 g, 2 mmol) was methylated with 2 ml of methyl iodide and 1.5 g of silver oxide in 10 ml of *N*,*N*-dimethylformamide. After stirring at room temperature for 24 h, the suspension was filtered, the precipitate was washed with chloroform, and the filtrate and washings were evaporated to dryness to give the tri-*O*-methyl derivative of **11** as a chromatographically homogeneous syrup (0.7 g, 86%); n.m.r.: 5.92, 5.96, 6.0 (*s*, OCH_3); 5.70 p.p.m. (d, $J_{1,2} = 6$ Hz, H-1). A portion (0.5 g) of the above mentioned product was hydrolyzed according to a literature procedure (19) to give 3,4,6-tri-*O*-methyl-D-glucose (**12**) (0.2 g). The latter was oxidized in carbon tetrachloride (1 ml) containing 2 drops of bromine. After 24 h at room temperature, the solution was evaporated to dryness; the residue was treated with 0.3 ml of phenylhydrazine and the resulting solution was heated on a steam bath for 2–3 min. The phenylhydrazide derivative **13** crystallized on cooling and it was recrystallized from ether–chloroform to give the pure product, m.p. and mixture m.p. 126° (lit. (20), m.p. 126–127°).

2,3,4,6-Tetra-O-benzyl-α-D-glucopyranosyl Bromide (15)

Anhydrous hydrogen bromide was bubbled into a solution of 2,3,4,6-tetra-*O*-benzyl-1-*O*-*p*-nitrobenzoyl-α-D-glucopyranose (0.1 g) (21*a*) in 2 ml of anhydrous dichloromethane. After 4–5 min, the precipitated *p*-nitrobenzoic acid was removed by filtration on a sintered-glass funnel and the filtrate was evaporated to dryness. The title compound (21) was obtained as a colorless syrup in quantitative yield; n.m.r.: 3.50 p.p.m. (d, $J_{1,2} = 4.5$ Hz, H-1).

Condensation of 2,3,4,6-Tetra-O-benzyl-α-D-glucopyranosyl Bromide with Sodio Diethyl Malonate. Synthesis of Diethyl 2-(2,3,4,6-Tetra-O-acetyl-α-D-glucopyranosyl) Malonate (19)

A. Without Added Bromide Ion

Finely cut sodium (0.23 g, 10 mmol; previously washed with pentane) was added to diethyl malonate (30 ml) and the solution was heated at 50° for 1 h and then cooled. The mixture was added to a solution of the bromide **15** (prepared from 0.7 g, 1 mmol, of the corresponding 1-*p*-nitrobenzoate) in the minimum volume of diethyl malonate and the whole was stirred at room temperature for 40 h. The solution was diluted with 200 ml of ether, washed with water, and the organic phase was processed as usual to give a mobile liquid from which excess diethyl malonate was removed by distillation (30° at 50×10^{-3} Torr). The residual viscous colorless syrup consisted entirely of a mixture of anomeric *C*-glycosides, namely diethyl 2-(2,3,4,6-tetra-*O*-benzyl-α,β-D-glucopyranosyl) malonates, as evidenced by t.l.c. and n.m.r. data.

The syrup was dissolved in ethanol and hydrogenated in the presence of 20% palladium-on-charcoal during 24 h. After filtration of the catalyst and evaporation of the filtrate, a syrup (0.31 g, quantitative) was obtained that consisted of a 3:1 β to α ratio of *C*-glycosides (estimated from polarimetric data on an acetylated sample, see Table 1). The anomers could be readily distinguished by t.l.c. on silica gel containing 2% boric acid (solvent B); R_f 0.4 for the β-anomer and R_f 0.5 for the α-anomer. A portion (0.15 g) of the syrup was separated by preparative t.l.c. on the same support (20 × 20 cm plates) to give *diethyl 2-(α-D-glucopyranosyl) malonate* **17** and *diethyl 2-(β-D-glucopyranosyl) malonate* **18** as colorless syrups. These compounds were each converted into the crystalline acetates **19** and **2**, respectively, in essentially quantitative yield.

B. In the Presence of Added Bromide Ion

The previous experiment was repeated as described in A except that 10 equiv. of tetra-*n*-butylammonium bromide were added to a solution of the bromide **15** (from 0.33 g, 0.5 mmol, of the corresponding 1-*p*-nitrobenzoate) in diethyl malonate, approximately 10 min prior to the addition of the carbanion (from 0.115 g of sodium in 20 ml of diethyl malonate, 5 mmol). The same isolation procedure was followed as in A, except that the hydrogenated product was partitioned between ether and water. The ether phase afforded crystalline tetraethyl 1,1,2,2-ethanetetracarboxylate (approximately in a 1:5 ratio with respect to the sodio diethyl malonate used), m.p. and mixture m.p. 75–76° (lit. (24) m.p. 76°); n.m.r.: 1.27 (t, $J = 7.5$ Hz, CH_3CH_2); 4.25 (q, $J = 7.5$ Hz, CH_3CH_2); 4.12 p.p.m. (s, H_m).

The aqueous solution was evaporated to dryness and the residue was acetylated with acetic anhydride (1 ml) in pyridine (room temperature, 24 h). Conventional pro-

Can. J. Chem. Downloaded from www.nrcresearchpress.com by 210.87.254.6 on 09/05/12
For personal use only.

cessing gave a syrup[11] (0.25 g, 85%) that crystallized from a mixture of ether and pentane at 0° to give *diethyl 2-(2,3,4,6-tetra-O-acetyl-α-D-glucopyranosyl) malonate* **19** (0.16 g, 31%), m.p. 59–60° (resolidifies and melts at 72–73°); $[\alpha]_D^{25}$ 66.2° (*c*, 3.9 $CHCl_3$); n.m.r.: 1.27, 1.28 (t, CH_3CH_2); 2.0, 2.07 (s, CH_3COO); 3.87 p.p.m. (d, $J_{m,1}$ = 10.5 Hz, H_m) etc.

Anal. Calcd. for $C_{21}H_{30}O_{13}$: C, 51.43; H, 6.17. Found: C, 51.17; H, 6.17.

Tetraethyl 1,1,2,2-Ethanetetracarboxylate

Sodium (2.3 g, 0.1 mol) was dissolved in 10 equivalents of diethyl malonate and the solution was treated dropwise with iodine until the color persisted (~1 h). After standing at room temperature overnight, the solution was diluted with ether, washed with water, and the organic layer was processed as usual to give a mobile liquid from which excess diethyl malonate was removed by distillation. The crystalline residue consisted of the title compound; yield 32 g (quantitative, based on the amount of sodium used). Recrystallization from ether–pentane gave material with m.p. 75–76° (lit. (24), m.p. 76°).

*Periodate Oxidation and Anomeric Configurational Assignment of C-Glucosyl Malonates **17** and **18**. Isolation of Epimeric Dialdehydes*

*Dialdehyde **20***

An amount of **18** (80 mg) was dissolved in 2 ml of ethanol and the solution was treated with 3 equiv. of sodium metaperiodate in 2 ml of water. After 4 days in the dark, the solution was filtered, the precipitate was washed with ethanol, and the filtrate and washings were evaporated to dryness. The residue was extracted with chloroform, residual salts were removed by filtration, and the filtrate was evaporated to a syrup that was separated from traces of impurities by preparative t.l.c. (solvent B) to give the dialdehyde **20** (32 mg) as a syrup; R_f ~0.7 (silica gel – boric acid, solvent C); $[\alpha]_D^{25}$ −24° (*c*, 2.1 $CHCl_3$).

*Dialdehyde **21***

The same procedure was applied to **17**, to give the dialdehyde **21** as a syrup (R_f ~0.7); $[\alpha]_D^{25}$ 26° (*c*, 0.8 $CHCl_3$).

*Diethyl 2-(2,3:5,6-Di-O-isopropylidene-α- and β-D-mannofuranosyl Malonates (**23**, **24**)*

Finely cut sodium (1.67 g) was dissolved in 100 ml of diethyl malonate at 50–60°. The cooled solution was added to a solution of 2,3:5,6-di-*O*-isopropylidene-α-D-mannofuranosyl bromide **22** (6.7 g) (26, 27) in the minimum volume of diethyl malonate. The solution was stirred at room temperature overnight, diluted with a large excess of ether, and processed in the usual manner. Residual diethyl malonate was removed by distillation. The remaining colorless syrup (8.5 g, quantitative) consisted of an anomeric mixture of the title compounds in a ratio of 9:1 in favor of the β-anomer (n.m.r.). A portion of the syrup (0.2 g) was separated by preparative t.l.c. (solvent C) and the respective anomers were obtained as colorless syrups.

*Diethyl 2-(2,3:5,6-Di-O-isopropylidene-α-D-mannofuranosyl) Malonate (**23**)*; R_f ~0.7 (solvent C); $[\alpha]_D^{25}$ 17 ± 0.2° (*c*, 3.6 $CHCl_3$); n.m.r.: 1.50 (m, CH_3C, CH_3CH_2); 3.66 (d, $J_{m,1}$ = 9 Hz, H_m); 4.05 (dd, $J_{4,5}$ = 5 Hz; $J_{4,3}$ = 2.5 Hz, H-4); 4.73 (d, $J_{1,m}$ = 9 Hz, H-1); 4.93 (d, $J_{3,4}$ = 2.5 Hz, H-3); *m/e* 387 ($M^+ - CH_3$). *Diethyl 2-(2,3:5,6-Di-O-isopropylidene-β-D-mannofuranosyl) malonate (**24**)*; R_f ~0.75 (solvent C); $[\alpha]_D^{25}$ −45.5° (*c*, 7.2 $CHCl_3$); n.m.r.: 1.40 (m, CH_3C, CH_3CH_2); 3.62 (d, d, $J_{4,3}$ = 3 Hz; $J_{4,5}$ = 7, H-4); 3.87 (d, $J_{m,1}$ = 10.5, H-m); 4.3 (m, CH_3CH_2, H-1, H-5, H-6,6′); 4.85 (d, d, $J_{2,1}$ = 3 Hz, $J_{2,3}$ = 6 Hz, H-2); 5.05 p.p.m. (d.d, $J_{3,2}$ = 6 Hz; $J_{3,4}$ = 3 Hz, H-3); *m/e* 387 ($M^+ - CH_3$); *m/e* 329 ($M^+ - CH_3 - CH_3COCH_3$).

When the above described condensation was carried out in ethanol (6.6 mmol of sodium and 2.2 mmol of the bromide **22**), a syrup (0.8 g) was obtained that consisted of approximately equal amounts of four compounds as estimated from the relative intensities of the charred spots (t.l.c. solvent C). A portion of the product was separated by preparative t.l.c. to give **23** (90 mg); **24** (78 mg) and the syrupy anomeric ethyl 2,3:5,6-di-*O*-isopropylidene-D-mannofuranosides; α-anomer (35 mg; R_f ~0.8); β-anomer (60 mg, R_f ~0.65). The n.m.r. spectra of the *O*-glycosides were compatible with their structures.

*Diethyl 2-(2,3-O-Isopropylidene-α,β-D-lyxofuranosyl) Malonates (**26**)*

The syrupy mixture of **23** and **24** (1:9 ratio) (2.7 g, 6.2 mmol) was dissolved in 30 ml of 70% aqueous acetic acid and the solution was heated at 50–60° for 70 min. The solution was concentrated to dryness by azeotropic distillation with toluene to give the diol **25** as a colorless chromatographically homogeneous syrup (quantitative). The n.m.r. spectrum of this product was in agreement with its structure.

An amount of this syrup (2.03 g, 6.2 mmol) was dissolved in 40 ml of 50% aqueous methanol containing 1.8 (8.4 mmol) of sodium metaperiodate. After standing in the dark for 2 h the solution was filtered and the filtrate was evaporated to dryness. The residue was taken up in ether, the salts were filtered, and the filtrate was evaporated to a syrup (quantitative) that was homogeneous by t.l.c. (R_f ~0.5, solvent C). An n.m.r. spectrum of the product showed a singlet at 9.50 p.p.m., indicative of the aldehyde group at C-5.

A portion of the product (0.862 g, 2.6 mmol) was dissolved in 30 ml of methanol, 0.5 g (10 mmol) of sodium borohydride was added and the solution was stirred at room temperature for 40 min. The solution was neutralized with a few drops of glacial acetic acid and evaporated to dryness. The residue was taken up in ether and the solution was processed to give diethyl 2-(2,3-*O*-isopropylidene-α,β-D-lyxofuranosyl) malonate (**26**) as a colorless syrup (0.447 g, 57%), R_f 0.5 (solvent C). The corresponding 5-methanesulfonate, obtained as a colorless syrup in the usual way showed the expected n.m.r. spectral characteristics and correct integration.

Financial assistance from the National Research Council of Canada and a France-Quebec fellowship for A.G.P. are gratefully acknowledged. The 220 MHz spectra were recorded at the Ontario Research Foundation, Sheridan Park, Ontario.

[11]Polarimetric studies indicated an α to β ratio of approximately 3:1, see Table 1.

1. S. HANESSIAN and A. G. PERNET. Chem. Commun. 755 (1971).
2. R. J. SUHADOLNIK. Nucleoside antibiotics. Wiley-Interscience, New York. 1970; K. GERZON, D. C. DELONG, and J. C. KLINE. Pure Appl. Chem. **28**, 489 (1971); S. HANESSIAN and T. H. HASKELL. Antibiotics containing sugars. *In* The carbohydrates. Vol. 2. 2nd ed. *Edited by* W. Pigman and D. Horton. Academic Press, 1970. p. 139; J. J. FOX, K. A. WATANABE, and A. BLOCH. Prog. Nucl. Acid Mol. Biol. **5**, 251 (1966).
3. W. A. BONNER. Adv. Carbohydr. Chem. **6**, 251 (1951); T. G. BONNER, E. J. BOURNE, and S. MCNALLY. J. Chem. Soc. 761 (1962).
4. L. KALVODA, J. FARKAS, and F. SORM. Tetrahedron Lett. 2297 (1970); J. FARKAS, Z. FLEGELOVA, and F. SORM. Tetrahedron Lett. 2279 (1972); G. TRUMMLITZ and J. G. MOFFATT, J. Org. Chem. **38**, 1841 (1973).
5. B. CAPON. Chem. Rev. **69**, 407 (1969).
6. R. P. ZELINSKY, N. G. PETERSON, and H. R. WALLNER. J. Am. Chem. Soc. **74**, 1504 (1952); J. G. SCHUDEL and R. V. RICE. U. S. Pat. 2, 522, 966 (1950); Chem. Abstr. **45**, 62231 (1951).
7. J. V. KOSTIR and M. QUEISNEROVA. Chem. Listy, **43**, 277 (1949); Chem. Abstr. **45**, 553 (1951).
8. H. ZAUGG. J. Am. Chem. Soc. **83**, 837 (1961).
9. S. HANESSIAN and A. G. PERNET. Can. J. Chem. In press.
10. H. MEERWEIN. Org. Syn. **46**, 113 (1966).
11. R. F. BUTTERWORTH, A. G. PERNET, and S. HANESSIAN. Can. J. Chem. **49**, 981 (1971).
12. B. COXON and H. G. FLETCHER, JR. J. Am. Chem. Soc. **85**, 2637 (1963).
13. S. J. CRISTOL and W. C. FIRTH. J. Org. Chem. **26**, 280 (1960).
14. T. RADFORD and D. C. DEJONGH. Biomedical applications of mass spectrometry. *Edited by* G. R. Waller. J. Wiley & Sons, 1972. p. 313; S. HANESSIAN. Meth. Biochem. Anal. **19**, 105 (1971); N. K. KOCHETKOV and O. S. CHISOV. Adv. Carbohydr. Chem. **21**, 39 (1966).
15. J. R. DICE and J. N. BOWDEN. J. Am. Chem. Soc. **71**, 3107 (1949).
16. R. H. HORN, R. B. MILLER, and S. N. BLAKER. J. Chem. Soc. 2900 (1950); H. H. GUEST. J. Am. Chem. Soc. **69**, 300 (1947).
17. J. G. GLEASON and D. N. HARPP. Tetrahedron Lett. 3431 (1970).
18. E. SHWENK and D. PAPA. J. Am. Chem. Soc. **70**, 3626 (1948).
19. A. K. MITRA, D. H. BALL, and L. LONG. J. Org. Chem. **27**, 160 (1967).
20. W. N. HAWORTH, E. L. HIRST, and L. PANIZZON. J. Chem. Soc. 154 (1934).
21. (*a*) T. ISHIKAWA and H. G. FLETCHER, JR. J. Org. Chem. **34**, 563 (1969); (*b*) F. WEYGAND and H. ZIEMANN. Ann. **657**, 179 (1962).
22. R. U. LEMIEUX and A. R. MORGAN. J. Am. Chem. Soc. **86**, 1889 (1963).
23. R. U. LEMIEUX and N. J. CHU. Abstracts of papers, 133rd National Meeting of the American Chemical Society, 1958. p. 31 N; R. U. LEMIEUX. *In* Molecular rearrangements. Vol. II. Edited by P. de Mayo, Interscience, 1964. p. 709.
24. K. H. TAKEMURA, M. PUBLICKAL, and F. O. HOFF. J. Org. Chem. **36**, 3646 (1971).
25. C. S. HUDSON. J. Chem. Educ. **18**, 353 (1941).
26. J. B. LEE and T. J. NOLAN. Tetrahedron, **23**, 2792 (1967).
27. S. HANESSIAN, M. M. PONPIPOM, and P. LAVALLEE. Carbohydr. Res. **24**, 45 (1972).
28. R. J. FERRIER and G. H. SANKEY. J. Chem. Soc. 2339 (1966).
29. W. M. PEARLMAN. Tetrahedron Lett. 1663 (1967).
30. R. A. LEMIEUX. Meth. Carbohydr. Chem. **2**, 224 (1963).
31. H. LUND. Ber. **67B**, 935 (1934).
32. H. OHRUI and J. J. FOX. Tetrahedron Lett. 1951 (1973).
33. A. STREITWEISER, JR. and S. ANDREADES. J. Am. Chem. Soc. **80**, 6443 (1958).
34. H. WEINER and R. A. SNEEN. J. Am. Chem. Soc. **87**, 287 (1965).
35. D. NISHIMURA, A. HASEGAWA, and M. NAKAJIMA. Agr. Biol. Chem. (Tokyo), **36**, 1967 (1972).

Can. J. Chem. Downloaded from www.nrcresearchpress.com by 210.87.254.6 on 09/05/12
For personal use only.

Carbanions in Carbohydrate Chemistry: Approaches to Chemical Precursors of *C*-Nucleosides[1,2]

STEPHEN HANESSIAN AND ANDRE G. PERNET[3]

Department of Chemistry, University of Montreal, Montreal, Quebec

Received September 10, 1973

The condensation of D-ribofuranosyl halides containing participating (benzoate) and non-participating (benzyl) substituents, with sodio dialkyl malonates and sodio triethyl 1,1,2-ethanetricarboxylate is described. In the presence of participating groups at C-2, the major and sometimes exclusive products were the 1,2-ketal derivatives. Both α- and β-anomeric D-ribofuranosyl malonates were formed in the non-participating series. The possibility of epimerization (anomerization) was experimentally demonstrated.

Similar results were obtained with the more highly functionalized tricarbethoxy carbanion. For the participating series however, 20% of *C*-glycoside was obtained. Condensations with sodio diethyl malonate were also done in the D-*arabino* series (*O*-benzyl protecting group) and the anomeric *C*-glycosyl compounds were isolated and characterized. The mechanistic aspects of these condensations are discussed.

La condensation des halogénures de D-ribofurannosyle contenant des groupes participant (benzoate) et non-participant (benzyle) avec les sels de sodium des malonates de dialkyle et de l'éthane tricarboxylate-1,1,2 de triéthyle est décrite. En présence de groupes participants en position-2, les produits majoritaires et dans certains cas uniques furent les acétals-1,2. Les deux anomères α- et β-ribofurannosyle malonates furent formés lorsque l'on a utilisé les groupes non-participants. La possibilité d'une épimérisation (anomérisation) a été démontrée expérimentalement.

Des résultats semblables ont été obtenus avec les carbanions tricarbéthoxy les plus substituées; cependant, dans le cas de groupes participants on a obtenu 20% de *C*-glycoside. On décrit également les condensations du malonate de diéthyle sodé dans la série D-*arabino* (le substituant *O*-benzyle étant utilisé comme groupe protecteur) et les composés anomères *C*-glycosyles furent isolés et caractérisés. Les aspects mécanistiques de ces condensations sont discutés.

Can. J. Chem., **52**, 1280 (1974)

A new class of naturally occurring nucleosides, called *C*-nucleosides has emerged in recent years, in which the glycosyl portion is attached to the heterocyclic moiety by a C—C bond (2) (Scheme 1). The few members of this class of compounds, with the exception of pseudouridine, possess a variety of biological properties that are of medicinal importance. Thus, pyrazomycin (3) has significant antiviral activity, while formycin A and B (4, 5) and oxazinomycin (6) exhibit in addition, antitumor activity. Showdomycin (7) is reported to have antitumor as well as antibacterial activity. In addition, the varied chemotherapeutic activity of these *C*-nucleosides is the result of interesting modes of action at the molecular level.

The recently reported syntheses of formycin B (8), oxoformycin (a C-2 oxo analog of formycin B) (9), and a suggested route to pyrazomycin (10), utilized 1-cyano-β-D-ribofuranose tribenzoate as a key starting material (11). In a series of reactions, the latter was transformed into 1-amino-2,5-anhydro-1-deoxy-D-allonic acid tri-*O*-benzyl ether (12) which was ultimately used to construct the heterocyclic ring. In another synthesis of formycin B, the C-1 functionalized carbohydrate moiety was prepared by a multistep synthesis leading to 2,5-anhydro-3,5-di-*O*-benzyl-D-allose dimethyl acetal (13). A synthesis of a racemic precursor with the same general structure has also been reported (14). The synthetic approach to showdomycin (15) demonstrates an indirect, yet practical method, consisting of the ozonolysis of a *C*-aryl ribofuranose derivative, for the introduction of a four-

[1]Part of a series on "Preparative and exploratory carbohydrate chemistry", see also refs. 1 and 17. Taken from the Ph.D. Thesis of A. G. Pernet, 1973.

[2]Reported in part at the VI International Symposium on Carbohydrate Chemistry, at Madison, Wisconsin, U.S.A., August 1972.

[3]Holder of NRCC and France–Québec fellowships.

Can. J. Chem. Downloaded from www.nrcresearchpress.com by 210.87.254.42 on 09/05/12
For personal use only.

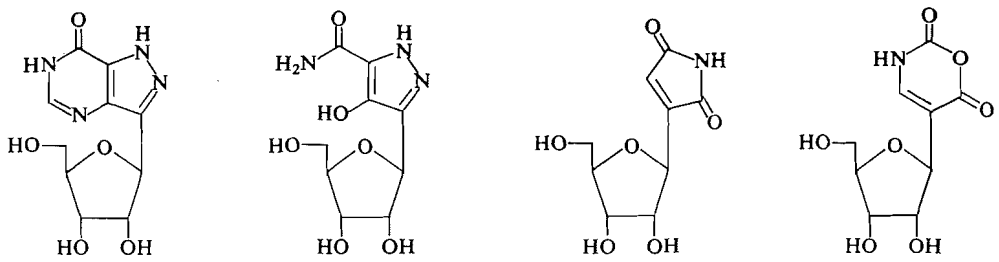

SCHEME 1

carbon functionalized *C*-substituent at the anomeric center. Another synthesis utilizes 1-cyano-β-D-ribofuranose tribenzoate as starting material to elaborate the heterocyclic ring (16).

A consideration of the presently available synthetic routes to *C*-nucleosides reveals that access to appropriately functionalized β-orientated *C*-substituents at the anomeric carbon atom is a crucial aspect. In this connection, it can be seen that in the showdomycin, oxazinomycin and pseudouridine types, the anomeric carbon atom is attached to a three-carbon unit as part of the heterocyclic ring, while in the formycins and pyrazomycin, the corresponding three contiguous atoms comprise two carbon atoms and one nitrogen atom. The design of versatile synthetic precursors to *C*-nucleosides must take these structural features into account and the C-1 substituents must lend themselves to transformations that would lead to the above-mentioned arrangement of atoms. With these considerations in mind, we investigated the reaction between carbanions and glycosyl halide derivatives, as general routes to C-1 functionalized *C*-glycosyl compounds. As indicated in the preceding paper (17), there were very few precedents (18) to the reaction of α-halo cyclic ethers with carbanions at the outset of this study in 1969 and none, to our knowledge, in the furanose series.[4]

It was shown in the preceding paper (17) that in addition to the nature of the C-2 substituent, the anomeric disposition of the starting halide derivative had an important bearing on the stereochemical outcome of the condensation reaction with carbanions. It was evident that in order to ensure a β-linkage in the product, a predominantly α-linked D-ribofuranosyl halide was required.

Results

The preparation of 2,3,5-tri-*O*-benzoyl-D-ribofuranosyl chloride or bromide by published procedures (20) gave products that were, at best, 1:1 anomeric mixtures (Table 1). The highest proportion of α-bromide (60%) was obtained by an adaptation of a procedure (12) in which 1-*O*-acetyl-2,3,5-tri-*O*-benzoyl-β-D-ribofuranose was treated with dry hydrogen bromide in benzene at 0°. Treatment of the β-chloride **1** or the bromide **2** (Scheme 2) with sodio diethyl malonate in 1,2-dimethoxyethane or *N*,*N*-dimethylformamide at room temperature, gave the ketal **3** in quantitative yield. The same product was obtained when the condensation was carried out in the presence of tetra-*n*-butylammonium chloride. The structure of **3** was deduced from n.m.r. spectroscopic data and from its conversion into **4** by acetolysis. Treatment of the bromide **2** (approximately 60% α-anomer, n.m.r.) with sodio diethyl malonate in diethyl malonate as solvent, gave the ketal **3** in 35% yield and a crystalline product (65% by n.m.r.; 43% isolated) that was assigned structure **5**. Its structure was derived from spectroscopic and microanalytical data, and by a chemical correlation that will be elaborated on in the Discussion section. Other malonic esters were also used. Isopropylidene malonate (21) was found to undergo hydrolysis during the condensation, while sodio benzylidene malonate did not have suitable solubility and dispersion properties in solvents of medium polarity. Condensation of the bromide **2** with mono- (22) and di-*t*-butyl malonates (23) gave in each case the ketal derivative corresponding to **3** and variable

[4]While this manuscript was in preparation a synthetic route to *C*-nucleosides based on our initial approach (1) was announced, see ref. 19.

Can. J. Chem. Downloaded from www.nrcresearchpress.com by 210.87.254.42 on 09/05/12
For personal use only.

TABLE 1. Anomeric 2,3,5-tri-*O*-benzoyl-D-ribofuranosyl halides

Anomeric substituent	Halide[a]	Solvent	Time	α:β ratio[b]
Acetate	Cl	Ether	4–11 days	0:100
Acetate	Cl	Benzene	1.5 h	20:80
Acetate	Br	$CHCl_3$	3 min	15:85
Acetate	Br	Benzene	30 min	60:40
p-Nitrobenzoate	Br	CH_2Cl_2	3.5 min	50:50

[a]Source of halide is HCl or HBr gas.
[b]Estimated by n.m.r.

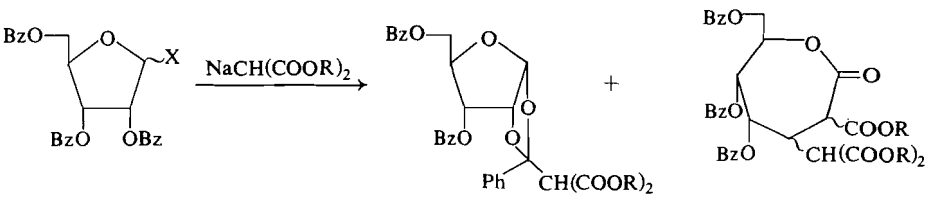

1 X = β-Chloride
2 X = α,β-Bromide
4 X = β-Acetate

3 R = Et
6 R = CH_2Ph

5 R = Et
7 R = CH_2Ph

SCHEME 2

amounts of the lactone-type structure. The ketals were easily transformed into **4** by acetolysis.

When the bromide **2** was treated with sodio dibenzyl malonate in benzene or in dibenzyl malonate as solvent, again the product was almost exclusively the ketal **6**. Hydrogenolysis of **6** and heating the resulting diacid in acetic acid gave **4**, as did an acetolysis reaction. Treatment of the bromide **2** with sodio dibenzyl malonate in 1,2-dimethoxyethane gave a mixture that contained predominantly the ketal **6**. A crystalline product was also isolated and assigned structure **7**. The structural relationship between **5** and **7** was established by chemical conversion.

It was apparent from these results that the participating ability of the C-2 benzoate group and the formation of the lactone by-product in these condensations imposed a severe limitation on the synthetic scope of the reaction. Attention was then focused on the reaction of 2,3,5-tri-*O*-benzyl-D-ribofuranosyl halides with sodio malonates (Scheme 3). The β-chloride **8** was used in the condensation, since the corresponding bromide was found to be unstable. Treatment of **8** with sodio diethyl malonate in diethyl malonate as solvent gave a syrup in high yield, containing the products **9** and **10**, that could not be separated by chromatography. After hydrogenolysis of the *O*-benzyl groups, and chromatographic examination on silica gel support containing 2% of boric acid, the two components **11** and **12** could be readily distinguished and they were separated by preparative t.l.c. or column chromatography (small scale). Diethyl 2-(β-D-ribofuranosyl)malonate (**11**) and the lactone **12** were isolated as colorless homogeneous syrups. The structure of **11** was confirmed by n.m.r. spectroscopic analysis of the tribenzoate **13** (Fig. 1), by mass spectrometric analysis at high resolution of the triacetate **14**, and by chemical transformations. The mass spectrum of **14** showed a molecular ion peak at *m/e* 418.1450 (calcd. 418.1475) corresponding to the expected molecular formula, $C_{18}H_{26}O_{11}$. Condensation of **8** with sodio diethyl malonate in 1,2-dimethoxyethane also gave a syrup in high yield. Chromatographic examination of the hydrogenolysis product revealed the formation of **11** and **12**, and a third product that was designated as the α-anomer **16**. These were separated by preparative t.l.c. to give **11** (~46%) and diethyl 2-(α-D-ribofuranosyl)malonate, **16** (~31%), as homogeneous syrups. The third minor component (~15%) was the lactone **12**. Alternatively, the three products could be separated by chromatography, as their benzoate derivatives **13**, **17**, and **5**, respectively. The n.m.r. spectra of **13** and **17** are shown in Fig. 1.

The proton assignments in both spectra were confirmed by spin decoupling experiments. Conclusive evidence for the anomeric identities of **11** and **16** was obtained from a comparison of the optical rotation of the periodate oxidized

Can. J. Chem. Downloaded from www.nrcresearchpress.com by 210.87.254.42 on 09/05/12
For personal use only.

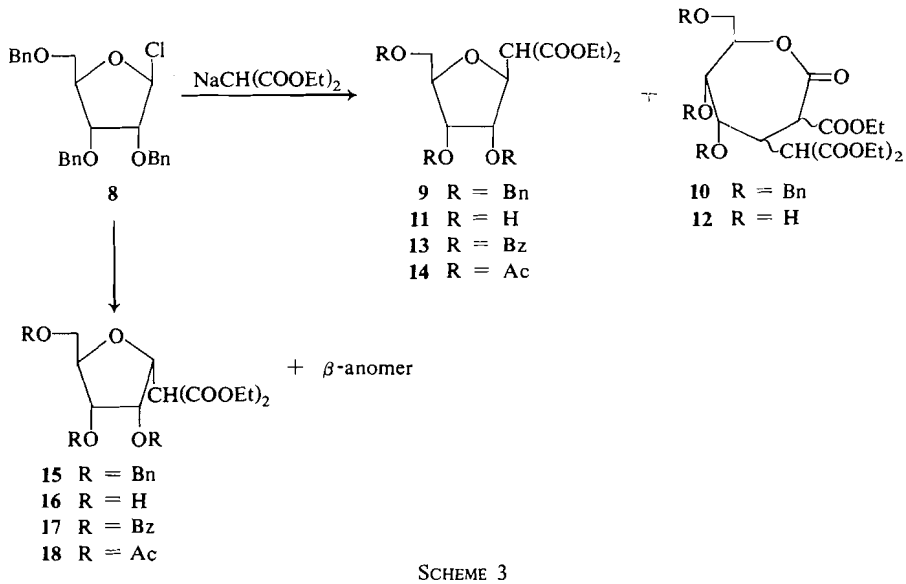

8

9 R = Bn
11 R = H
13 R = Bz
14 R = Ac

10 R = Bn
12 R = H

15 R = Bn
16 R = H
17 R = Bz
18 R = Ac

SCHEME 3

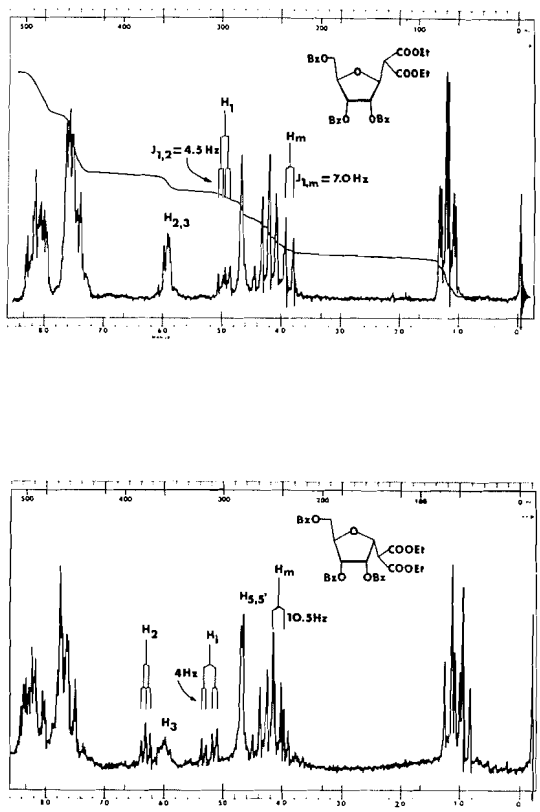

FIG. 1. Nuclear magnetic resonance spectra (at 60 MHz in $CDCl_3$) of diethyl 2-(2,3,5-tri-*O*-benzoyl-β-D-ribofuranosyl) malonate (**13**) (upper spectrum) and diethyl 2-(2,3,5-tri-*O*-benzoyl-α-D-ribofuranosyl) malonate (**17**) (lower spectrum).

product from **11**, with that of the known (17) dialdehyde **19** obtained from **20** (Scheme 4).

The instability of *O*-acylated *C*-ribofuranosyl malonates in protic basic media, coupled with the formation of mixtures in the condensation reactions in the *O*-benzylated series, prompted us to investigate the reaction of the halides **2** and **8** with sodio triethyl 1,1,2-ethanetricarboxylate. It was anticipated that the resulting *C*-glycosyl compounds would be stable towards ethanolysis conditions, because of the absence of a malonic ester type hydrogen atom. Furthermore, the product would have a potential four-carbon fragment at the anomeric center, with the desired state of oxidation for an eventual cyclization to the *C*-nucleoside showdomycin and its analogs. Condensation of the bromide **2** with sodio triethyl 1,1,2-ethanetricarboxylate in 1,2-dimethoxyethane gave a syrup that consisted of the *C*-glycosyl compound **21** and the ketal **22** (Scheme 5) in an approximate ratio of 1:2 (n.m.r.). Separation by column chromatography gave a 20% yield (non-optimized) of triethyl 1-(2,3,5-tri-*O*-benzoyl-β-D-ribofuranosyl)-1,1,2-ethanetricarboxylate (**21**), as a homogeneous syrup. The optical rotation of **21** was found to be of the same sign and relative magnitude as that of **13**. Their n.m.r. spectra (Fig. 2) were also similar with allowance made for the differences in the aglycone portion. Thus, in the spectrum of **21**, the anomeric proton was a doublet and the high field methylene singlet was characteristic of the

Can. J. Chem. Downloaded from www.nrcresearchpress.com by 210.87.254.42 on 09/05/12
For personal use only.

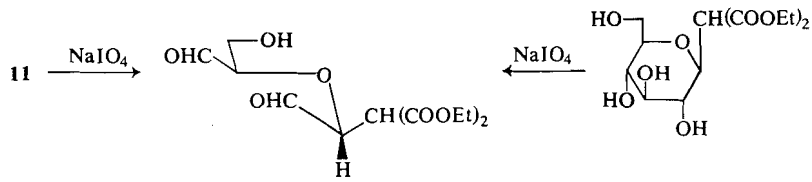

19 20

SCHEME 4

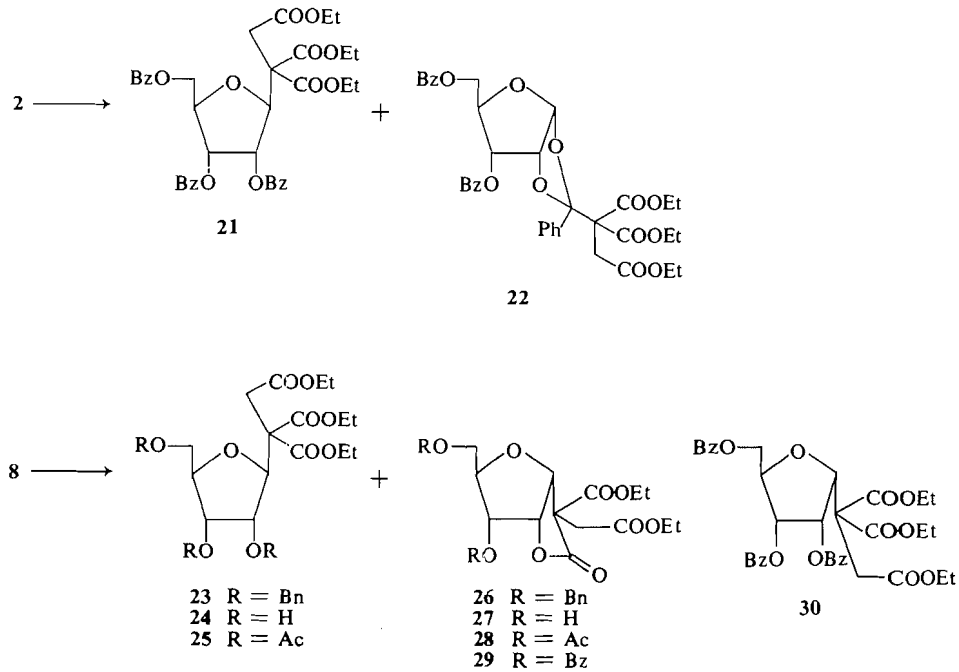

21 22

23 R = Bn
24 R = H
25 R = Ac

26 R = Bn
27 R = H
28 R = Ac
29 R = Bz

30

SCHEME 5

triester group and its point of attachment to the sugar. As could be anticipated, compound **21** was debenzoylated with sodium ethoxide without difficulty. The acetate derivative **25** gave a mass spectrum that was in accord with the structure (M^+ at *m/e* 504.1828; calcd. 504.1843). The ketal **22** was isolated as a syrup and characterized by n.m.r. spectral studies and by its transformation into **4** by acetolysis.

Treatment of **8** with sodio triethyl 1,1,2-ethanetricarboxylate in 1,2-dimethoxyethane and hydrogenation of the resulting product, gave a mixture of **24** (identified as its tribenzoate **21** and its triacetate **25**) and another product that was assigned the lactone structure **27**. The latter, formed in preponderance, was isolated as a homogeneous syrup. Its i.r. and n.m.r. spectral characteristics were in accord with the structure. The n.m.r. spectrum of the corresponding dibenzoate derivative **29** is shown in Fig. 2. Acetylation gave the diacetate **28**, analyzed by high resolution mass spectrometry (M^+ at *m/e* 416.1323; calcd. 416.1318). Treatment of the lactone **27** with a solution of sodium ethylate in ethanol afforded a syrup that was benzoylated to give the α-anomer **30**. The n.m.r. spectrum of this product was compatible with the structure, indicating that the opening of the lactone ring in **27** had proceeded in the manner anticipated.

The proven importance of D-arabinofuranosyl nucleosides (2, 25) such as 9-(β-D-arabinofuranosyl)adenine and 1-(β-D-arabinofuranosyl)cytosine as antiviral and antitumor agents, prompted us to extend our reactions to the D-*arabino* series with the aim of preparing *C*-arabinofuranosyl malonates as precursors to *C*-nucleosides. Al-

Can. J. Chem. Downloaded from www.nrcresearchpress.com by 210.87.254.42 on 09/05/12
For personal use only.

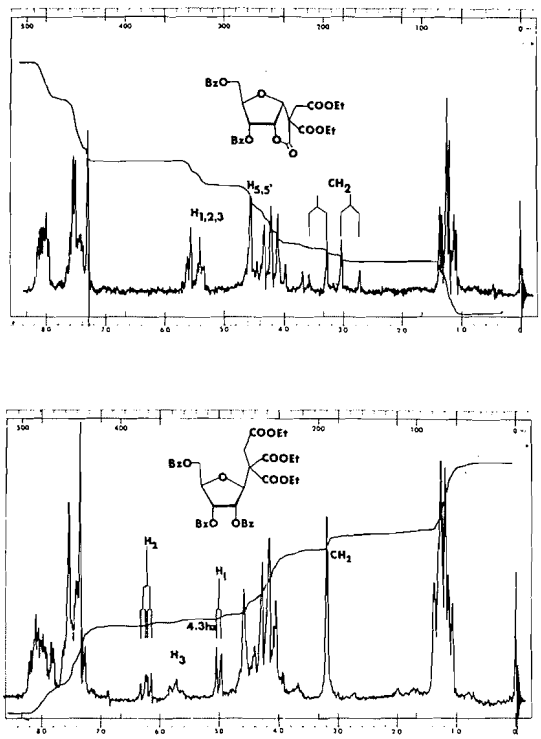

FIG. 2. Nuclear magnetic resonance spectra (at 60 MHz in $CDCl_3$) of diethyl 1-(α-D-ribofuranosyl)-1,1,2-ethanetricarboxylate, α-lactone dibenzoate (**29**) (upper spectrum) and triethyl 1-(β-D-ribofuranosyl) 1,1,2-ethanetricarboxylate tribenzoate (**21**) (lower spectrum).

though this class of compounds has not been encountered in nature as yet in this series, the synthesis of some analogs was deemed of interest in view of their potential biochemical properties. The synthesis of a *C*-D-arabinofuranosyl imidazole from the corresponding 1-cyano derivative has been recently reported (26). Treatment of 2,3,5-tri-*O*-benzyl-α-D-arabinosyl chloride **31** (27) with sodio diethyl malonate in diethyl malonate gave the expected *C*-glycoside **32** as a syrupy anomeric mixture, in quantitative yield. Hydrogenolysis of the benzyl groups gave a syrup that consisted of the respective anomers. These were separated by chromatography and obtained as homogeneous syrups. Again the similarity of the n.m.r. spectra of the respective acetates **35** and **36** precluded an anomeric assignment and recourse was made to a chemical correlation. Thus, periodate oxidation of the anomer whose acetate derivative had the more negative optical rotation value gave the same dialdehyde that was obtained from the known diethyl 2-(β-D-glucopyranosyl) malonate. Here too, Hudson's rules as formulated for *O*-glycosides, were obeyed (Scheme 6).

Discussion

Two general pathways could be envisaged in these condensation reactions (Scheme 7). Attack of the carbanion and/or internal participation could take place with α- and β-oriented ion-pair species (A–C). Alternatively, abstraction of halide ion by the cation[5] would lead to an oxonium-ion type D, with the carbanion as the tight counter-ion, and with possible stabilization by electronegative atoms in the solvent molecule[6] and by neighboring substituents (ethers or esters). The relative proportions of α- and β-ion pairs will depend on the anomeric composition of the original halide and the possibility of anomerization in solution. In view of the apparent insolubility of the formed sodium halide, it is difficult to assess the extent of anomerization, if any, in the presence of the reagent (17). The nature and composition of products in these condensation reactions will thus depend upon the relative reactivities of the various intermediates (Scheme 7) vis-à-vis the prevailing nucleophiles. Another noteworthy consideration is the state of aggregation and solvation (29) of the carbanions in solution and their effective sizes. It is known that in the presence of a solvent such as 1,2-dimethoxyethane, the rates of alkylation by carbanions are greatly increased, compared to those in inert solvents. This acceleration is due, in major part, to the ability of the solvent to solvate the cation by a bidentate donor mechanism (29), thus causing a dissociation of the aggregates and increasing the effectiveness of the carbanion as a nucleophile. The possibility of an "interconversion" between products, particularly in the case of *C*-glycosyl malonates (19), introduces yet another parameter and precludes the designation of a definitive and unified pathway for these reactions.

The formation of the ketal **3** in the reaction of the chloride **1** with sodio dialkyl malonates, under a variety of conditions, indicates that the formation of 1,2-benzoxonium ions of type C

[5]Insoluble sodium halide separates out in the reaction mixture.

[6]For a discussion of discrete oxonium intermediates with ether-type solvents in displacement reactions, see ref. 28.

Can. J. Chem. Downloaded from www.nrcresearchpress.com by 210.87.254.42 on 09/05/12
For personal use only.

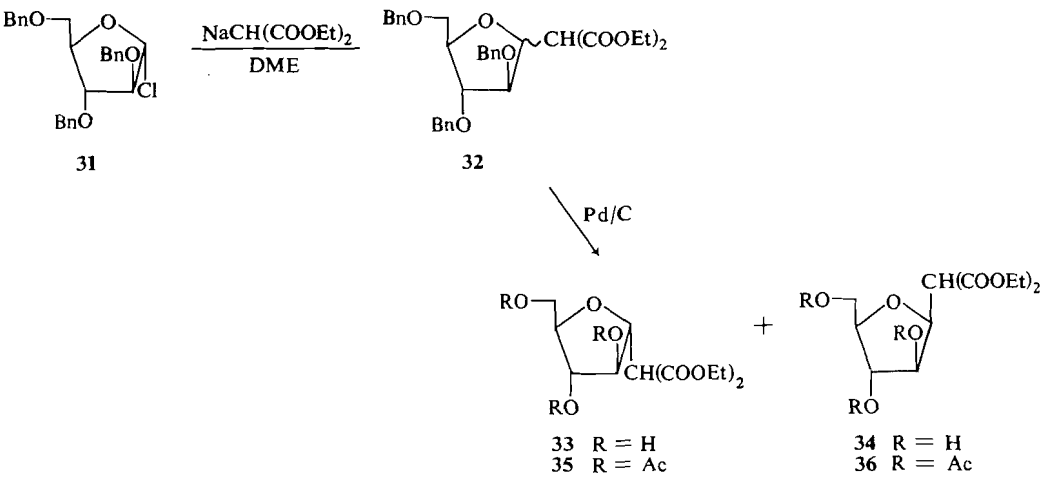

SCHEME 6

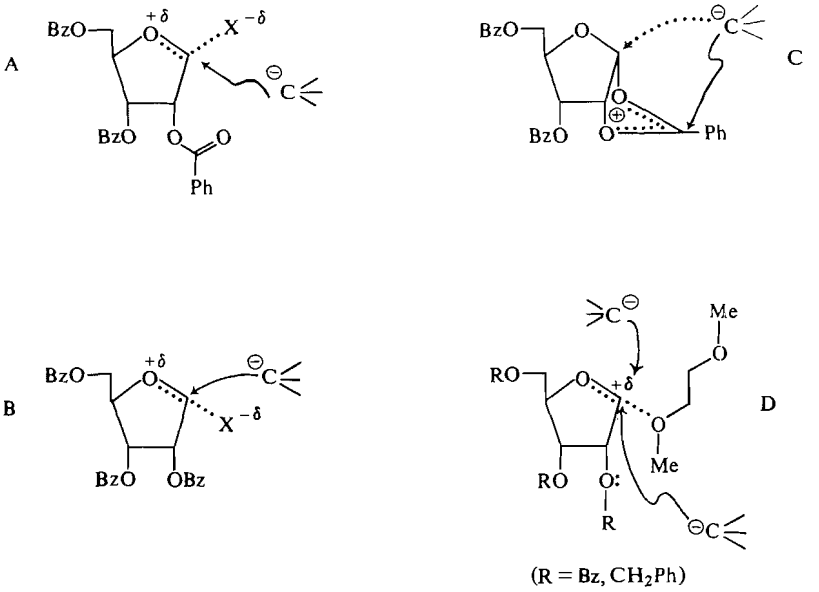

SCHEME 7

(Scheme 7) is heavily favored. Even in the presence of added chloride ion (to promote anomerization), intramolecular attack appears to be faster than that of the carbanion on the anomeric carbon atom. The lower proportion of ketal in the reaction of the bromide **2** with sodio diethyl malonate in diethyl malonate as solvent, compared to that of the β-chloride in the same solvent points to the importance of the nature and the stereochemical arrangement of halogen atoms on C-1 in determining the nature of the products. The role of the solvent and the state of aggregation of the carbanion can be appreciated when comparing the products from the reaction of **2** with sodio diethyl malonate in 1,2-dimethoxyethane and in diethyl malonate as solvent respectively. It seemed reasonable to assume that initially formed *C*-glycosyl malonates were the precursors of the lactones **5**, **7**, and **10**, in their respective reactions. This hypothesis was experimentally verified by treatment of a mixture of the benzoates **13** and **17** with sodio

Can. J. Chem. Downloaded from www.nrcresearchpress.com by 210.87.254.42 on 09/05/12
For personal use only.

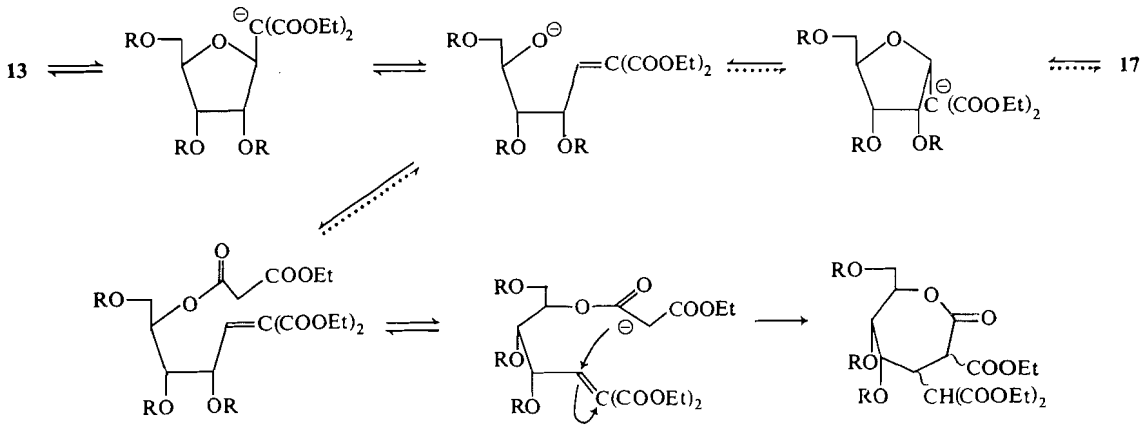

SCHEME 8

diethyl malonate, in a reaction simulating the actual reaction conditions. The sole product was indeed the lactone **5**, and it was isolated in crystalline form. It was therefore evident that *C*-glycoside formation was actually taking place in the condensation of **2** with sodio diethyl malonate in diethyl malonate, but that the products were undergoing further transformation in the reaction mixture. A plausible mechanism for the formation of the lactone is illustrated in Scheme 8. The base-catalyzed epimerization, triggered by the formation of the malonate anion takes place via the open-chain oxanion. The latter could react with excess diethyl malonate in a transesterification step and ultimately lead to the lactone **5**. Support in favor of the pathway suggested in Scheme 8 was gained by interrelating the lactones **5**, **7**, and **10**. Thus, hydrogenolysis of the tribenzyl ester **7** and esterification of the resulting diacid with triethyloxonium fluoroborate (30) gave the lactone **5**. Alternatively, hydrogenolysis of **10** followed by benzoylation of the triol **12** also gave crystalline **5**. The integrity of carbon atoms 2,3,4 bearing the *O*-substituents in the original halide **2** was therefore preserved in the respective lactones.[7] The lactone was extremely sensitive to basic conditions and attempts to effect selective hydrolysis with aqueous or alcoholic acid solutions failed. It was stable to acetolysis however, and it could be recovered unchanged. Microanalytical data were consistent with a molecular formula corresponding to $C_{38}H_{38}O_{14}$; however efforts to obtain mass spectral data on the corresponding acetate derivative were not successful due to the decomposition of the sample. Nuclear magnetic resonance spectra of **5** were not well resolved, even at 100 MHz and were informative only with respect to the ratio of benzoate to ethyl protons.

The formation of both α- and β-*C*-ribofuranosyl malonates in the reaction of **8** with sodio diethyl malonate in 1,2-dimethoxyethane was not unexpected in view of a similar experience in the D-glucopyranose series (17). The carbanion could attack one of several ion-paired species in solution (Scheme 7, *O*-benzyl analog), including solvent-stabilized oxonium ions of type D. The possibility of epimerization (anomerization) of an initially formed preponderant α-anomer cannot be excluded (Scheme 8, R = Bn). The lactone **5** was a minor product in these condensations. The formation of the β-*C*-glycoside **9** and the lactone **10** but not the α-*C*-glycoside, in the condensation of the β-halide **8** in diethyl malonate as solvent, can be attributed to a highly selective β-attack of the bulky carbanion aggregate on an α-oriented ion pair (Scheme 7) or to the irreversible epimerization of an initially formed α-anomer.[8] In a competing reaction, the oxanion (Scheme 8) could be diverted from the epimerization pathway to give the lactone **10** via a transesterification reaction with the solvent. Presumably, one or both of these pathways is favored when the condensation is carried out in diethyl malonate as solvent.

The acetate and benzoate derivatives **13** and

[7]The configurations of the carbon atoms bearing the branches are still unknown at this time.

[8]The formation of lactone types at the expense of the α-*C*-glycosides (Scheme 8) is an interesting possibility. These epimerization reactions are presently under study.

Can. J. Chem. Downloaded from www.nrcresearchpress.com by 210.87.254.42 on 09/05/12
For personal use only.

Can. J. Chem. Downloaded from www.nrcresearchpress.com by 210.87.254.42 on 09/05/12
For personal use only.

14, respectively, were particularly sensitive to bases in protic media, undoubtedly due to abstraction of the malonic ester proton and subsequent transformations. A similar observation was encountered in the attempted deacetylation of diethyl 2-(2,3,4,6-tetra-*O*-acetyl-β-D-glucopyranosyl) malonate (17) and in the debenzoylation of 1-cyano-2,3,5-tri-*O*-benzoyl-β-D-ribofuranose (12, 31).

Whereas the reaction of the bromide **2** with sodio diethyl malonates in 1,2-dimethoxyethane led to ketals almost exclusively, the analogous reaction with sodio triethyl 1,1,2-ethanetricarboxylate led to appreciable C—C condensation at the anomeric carbon atom. This could reflect, to some extent, the affinity of the carbanion for positive centers in the benzoxonium ion and oxonium ion intermediates (Scheme 7, **C**). The structural relationship between **14** and **25** was nicely demonstrated by mass spectrometry. Loss of ethyl radical and ketene from the molecular ion of **25**, situated at *m/e* 504.1828 (calcd. 504.1843) gave the ion at *m/e* 417.1336 (calcd. 417.1395) differing from the molecular ion of **14** (*m/e* 418.1475, calcd. 418.1450) by 1 a.m.u.

Although the *C*-glycoside **21** was obtained in a relatively modest yield (~20%), the simplicity of its preparation and isolation, coupled with the desirable structural features in the aglycone portion, make it a promising precursor to the *C*-nucleoside antibiotic showdomycin (Scheme 1) and its analogs. In the *O*-benzylated series, the preponderant formation of the α-*C*-glycoside **26** can be assumed from the amount of lactone **27**, formed after removal of the *O*-benzyl groups. The lactone is presumably formed by a spontaneous cyclization of the corresponding α-*C*-glycoside. Irrespective of the actual mechanistic pathway, (Scheme 7, *O*-benzyl analogs) the high preference for α-attack by the bulky carbanion is somewhat surprising.

The extensive studies of Fletcher and coworkers (32) on the solvolysis of D-arabinosyl halides containing non-participating substituents at C-2 have led to the general conclusion that β-D-arabinofuranosides are preponderant products, irrespective of the anomeric composition of the starting halide. The results have been rationalized on the basis of a higher stability of α-oriented ion pairs. The formation of approximately equal amounts of α- and β-D-arabinofuranosyl malonates **32** from the α-halide again calls for the intervention, at least in part, of oxonium-ion intermediates. Since the incorporation of chloride ion (as tetra-*n*-butylammonium chloride) did not change the proportion of products, it could be assumed that a β-oriented chloride (formed via anomerization), cannot be the direct precursor of the α-*C*-glycoside and the latter must arise by a different pathway. A α-oriented halide and/or specifically solvated oxonium intermediates could thus account for the two products. The possibility of epimerization of an initially formed β-anomer, to the less hindered α-anomer, cannot be excluded; however, no trace of lactone-type products were detected in the D-*arabino* series, even when the condensations were carried out in diethyl malonate as solvent.

To summarize, although the feasibility of C—C condensation reactions of carbanions with appropriately substituted pentofuranosyl halides was demonstrated, two drawbacks are apparent. Firstly, in the presence of participating groups at C-2, variable amounts of 1,2-ketal derivatives are formed that are synthetic impasses. Secondly, in the presence of non-participating groups, the *C*-glycosyl compounds that are formed are invariably mixtures of α- and β-anomers. Thus, the inherent structural features of the *O*-substituents in the two types of glycosyl halides, make the above discussed shortcomings somewhat unavoidable. Further, owing to the very similar chromatographic properties of some of the anomeric (epimeric) *C*-glycosyl malonates, their separation was effected on small scale in some cases for characterization purposes and yields are not optimized. The recorded spectroscopic and other physical characteristics should nevertheless serve as useful analytical criteria for related compounds.

Experimental

General

Melting points are uncorrected. Infrared spectra were recorded on a Beckman IR-8 spectrometer. Nuclear magnetic resonance spectra were obtained in chloroform-*d* unless otherwise stated, at 60 and 100 MHz with tetramethysilane as internal reference (s, singlet; d, doublet; t, triplet; q, quartet; m, multiplet; b, broad). Optical rotations were measured with a Perkin-Elmer Model 141 polarimeter. Mass spectra were done at low resolution on a Hitachi-Perkin Elmer RMU-6D spectrometer and at high resolution on an AEI MS-902 spectrometer, with direct introduction of the sample in the ionizing chamber. Conventional processing, or processing in the usual way signifies drying of organic solutions over anhydrous sodium sulfate, filtration, and evaporation under diminished pressure.

Can. J. Chem. Downloaded from www.nrcresearchpress.com by 210.87.254.42 on 09/05/12
For personal use only.

Chromatography

Pertinent details are given in the preceding paper (17). Solvent systems: solvent A, chloroform–2,2,4-trimethylpentane–methanol (10:5:0.2); solvent B, chloroform–methanol (10:1); solvent C, chloroform–acetone (10:1); solvent D, acetone – carbon tetrachloride (1:10). All *C*-glycosyl malonates described in this work gave orange-colored spots when the plates were sprayed with sulfuric acid and heated gradually. On further heating, the color changed to dark brown.

Solvents and Handling of Carbanions

Pertinent details are given in the previous publication (17). Pentofuranosyl halides (ester and *O*-benzyl ethers) are particularly prone to hydrolysis by traces of moisture and all condensation reactions were carried out with rigorously dried solvents. The use of a dry-box for handling the carbanion (manipulations with sodium, sodium hydride, etc.) is recommended.

Characterization of Syrupy Compounds

The syrupy *C*-glycosyl compounds could not be distilled and their purification for analytical purposes was done by chromatographic means. Microanalytical data in these cases were substituted by high resolution mass spectral data and these are included in appropriate sections.

Preparation and Anomeric Assignment of 2,3,5-Tri-O-benzoyl-D-ribofuranosyl Halides

Bromides

Anhydrous hydrogen bromide was bubbled through a solution of 1-*O*-acetyl-2,3,5-tri-*O*-benzoyl-β-D-ribofuranose (**4**), in chloroform. After 3 min the solution was rapidly evaporated to a syrup that consisted of the bromide **2** in an α/β anomeric ratio of 1:3 (±5%), as determined by n.m.r.; for the α-anomer; 5.40 (dd, $J_{2,1}$ = 4.5 Hz; $J_{2,3}$ = 6.75 Hz; H-2); 5.70 (dd, $J_{3,2}$ = 6.75 Hz; $J_{3,2}$ = 3 Hz; H-3); 6.75 p.p.m. (d, $J_{1,2}$ = 4.5 Hz; H-1); for the β-anomer: 6.10 (m, H-2, H-3); 6.45 p.p.m. (s, H-1). The ratio of anomers was determined from the area under the peaks corresponding to the anomeric hydrogens, and they were checked for correctness of integration, based on the area under the H-2 peak in the spectrum of the α-anomer.

When hydrogen bromide was bubbled through the solution as described above, but at 0° for 30 min according to a literature procedure (12), and the solution was left at room temperature for an additional 30 min, the ratio of anomeric bromides in the product was found to be 3:2 (±5%) in favor of the α-anomer. The condensations described in this work were done with the bromide prepared in this manner. When hydrogen bromide was passed into a solution containing the corresponding 1-*O*-*p*-nitrobenzoate derivative in dichloromethane (33) the anomeric ratio was 1:1 (±5%). Addition of small amounts of tetra-*n*-butylammonium bromide to the solutions caused partial equilibration to a mixture that was richer in the β-anomer (α/β ratio ~1:4).

Chlorides

Anhydrous hydrogen chloride was bubbled through a solution containing the 1-acetate **4** and the solution was kept at 0° for 4–11 days (34). Evaporation of the solution and analysis of the syrupy residue by n.m.r. spectroscopy showed the presence of the β-anomer exclusively; n.m.r. data (100 MHz); 5.98 (d, $J_{2,1}$ = <0.5; $J_{2,3}$ = 5 Hz; H-2); 6.15 (dd, $J_{3,2}$ = 5 Hz; $J_{3,4}$ = 7.5 Hz, H-3); 6.88 p.p.m. (s, H-1).

When anhydrous hydrogen chloride was passed through a solution of the 1-acetate **4** for 70–80 min at room temperature, the resulting product was richer in the β-anomer (α/β ratio, 1:4. ±5%). Addition of tetra-*n*-butylammonium chloride caused complete equilibration to the β-anomer within 10 min (n.m.r.).

Condensation of 2,3,5-Tri-O-benzoyl-D-ribofuranosyl Halides with Sodio Malonate Esters

1,2-O-(2,2'-Dicarbethoxy-1-methylethylidene)-α-D-ribofuranose Dibenzoate (3)

To a solution of 2,3,5-tri-*O*-benzoyl-β-D-ribofuranosyl chloride **1** (0.628 g, 1.48 mmol) in 2 ml of 1,2-dimethoxyethane was added a solution of sodio diethyl malonate (prepared from 0.1 g of sodium and 0.5 ml of diethyl malonate; 4.44 mmol). After stirring at room temperature overnight, the solution was diluted with a large excess of ether, and it was washed with water until the washings were neutral. Excess diethyl malonate was removed by distillation leaving **3** as a colorless syrup (0.79 g, quantitative) that was chromatographically homogeneous; n.m.r.: 1.20 (m, CH_3CH_2); 3.96 (s, H_m); 4.90 (dd, $J_{3,2}$ = 5.3 Hz; $J_{3,4}$ = 9 Hz, H-3); 5.29 (dd, $J_{2,1}$ = 4.5 Hz; $J_{2,3}$ = 5.3 Hz, H-2); 6.30 p.p.m. (dd, $J_{1,2}$ = 4.5 Hz, H-1) etc. The same product was obtained when the condensation was carried out in *N*,*N*-dimethylformamide.

Acetolysis of **3** (0.3 g) in 10 ml of a 1:1 acetic acid – acetic anhydride mixture containing 1 drop of sulfuric acid, followed by dilution with ether, neutralization ($NaHCO_3$), and processing in the usual way, gave a syrup (62%) that was chromatographically and spectroscopically (n.m.r.) identical to **4**. The syrup crystallized from a mixture of ether and pentane, m.p. and mixture m.p. with **4**, 130°.

3-Carbethoxy-5,6-dihydro-7-(hydroxymethyl)-2-oxo-4-oxepanediethyl Malonate, Tribenzoate (5)

A solution of the bromide **2** (α/β ratio, 3:2) prepared from 3 g of the corresponding 1-acetate **4**, in 5 ml of diethyl malonate, was treated with a solution of sodium diethyl malonate prepared from 0.72 g of sodium and 35 ml of diethyl malonate. The solution was stirred at room temperature overnight, a large excess of ether was added, and the solution was washed with water. Residual diethyl malonate was removed from the processed organic phase by distillation and the remaining syrup was found to consist of two products (t.l.c. and n.m.r.). The syrup was dissolved in ether, pentane was added and the solution was stored at −20° for 3 days. The crystalline product that separated (1.55 g) was assigned structure **5**. The mother liquors were chromatographed on silica gel and the fractions corresponding to **5** were collected, combined, and processed to give an additional 0.73 g of product (combined yield, 1.885 g, 43%); m.p. 98–98.5°; $[\alpha]_D^{25}$ 1.5 ± 0.2° (*c* 3.5, $CHCl_3$); n.m.r.: 1.13, 1.17, 1.25 (t, CH_3-CH_2); 4.2 (m, 9 protons); 4.85 (m, 3 protons, CH_2CH); 6.0 (m, 2 protons, C*H*—OBz); 7.5, 8.1 p.p.m. (15 protons, C_6H_5CO), etc. A mass spectrum of this product or its corresponding acetate could not be obtained due to decomposition.

Anal. Calcd. for $C_{38}H_{38}O_{14}$: C, 63.51; H, 5.33. Found: C, 63.32; H, 5.44.

Can. J. Chem. Downloaded from www.nrcresearchpress.com by 210.87.254.42 on 09/05/12
For personal use only.

From the remaining fractions of the chromatographic separation, a ~30% yield of **3** was obtained.

The product **5** could be revealed on t.l.c. plates (solvent A) with the sulfuric acid spray, but only after prolonged heating. It had an R_f that was very close to the ketal derivative **3**. Attempted debenzoylation with sodium ethylate in ethanol even under controlled conditions (p*H*, temperature) revealed the formation of a series of more polar products (t.l.c.) and eventually no product(s) could be isolated. The same lability was noticed towards bases in general. Under conditions of acetolysis however, it was recovered unchanged. Mild acid treatment was without effect but upon heating (2 *N* HCl), degradation took place and no products could be isolated.

1,2-O-(2,2'-Dicarboxy-1-methylethylidene)-3,5-di-O-benzoyl-α-D-ribofuranose Dibenzyl Ester (6)

Sodium (65 mg, 2.8 mmol) was dissolved in 1 ml of dibenzyl malonate and 10 ml of dry benzene. The homogeneous solution[9] was added to a solution of the bromide **2** (0.5 g, 1 mmol) in 3 ml of benzene. After stirring at room temperature overnight, the solution was diluted with excess ether, washed with water, and the organic phase was processed as usual to give a mobile syrup. Excess dibenzyl malonate was removed by trituration with petroleum ether (b.p. 30–60°) and the resulting syrup (>95%) was shown to consist almost exclusively of the title compound (t.l.c., n.m.r.).

Acetolysis of a sample led to **4**, m.p. and mixture m.p. 130°. Alternatively, 0.5 g of **6** were hydrogenated in ethanol (20% palladium-on-charcoal, 0.2 g) (35) overnight and the processed solution was refluxed in acetic acid for 2 h. Evaporation to dryness gave the acetate **4** (0.188 g, 53%); m.p. and mixture m.p. 130°.

3-Carboxy-5,6-dihydro-7-(hydroxymethyl)-2-oxo-4-oxepanemalonic Acid Tribenzyl Ester, Tribenzoate (7)

A solution containing **2** (5 g, 10 mmol) and sodium dibenzyl malonate (50 mmol, from 20 ml) in 20 ml of 1,2-dimethoxyethane was stirred at room temperature overnight and the solution was processed as described in the above preparation. Excess dibenzyl malonate was removed by passing the mobile syrup through a bed of silica gel, using first pentane as eluent, then chloroform. Evaporation of the chloroform eluates gave a syrup that showed the presence of **6** in addition to another compound that was difficult to reveal with the sulfuric acid spray (t.l.c., solvent A). The syrup was dissolved in a mixture of ether and pentane after storing at 0°, a crystalline product separated out to which structure **7** was assigned; yield 0.5 g (6%); m.p. 100.5–101° (from ether–pentane); n.m.r. (at 100 MHz): 3.87 (s, H_5; H-6); 4.12 p.p.m. (d, $J_{3,4}$ = 7 Hz, H-3), etc.

Anal. Calcd. for $C_{49}H_{52}O_{14}$: C, 70.21; H, 5.08. Found: C, 70.62; H, 4.83.

Hydrogenolysis of **7** (0.2 g) in ethanol in the presence of 20% Pd–C, in the usual way, gave a syrup in quantitative yield (0.15 g). A portion of this triacid (0.1 g) was dissolved in 2 ml of dichloromethane and treated at 0° with 0.1 g of triethyloxonium fluoroborate (30). The solution was stirred at room temperature for 1 h, it was neutralized with aqueous sodium bicarbonate and processed by extraction with chloroform. After drying and evaporation, the lactone **5** was obtained, first as a syrup (90 mg, 60%), then as a crystalline product, m.p. and mixture m.p. 91.92° (from ether–pentane).

Condensation of 2,3,5-Tri-O-benzoyl-D-ribofuranosyl Halides with Sodio Triethyl 1,1,2-Ethanetricarboxylate

Triethyl 1-(2,3,5-Tri-O-benzoyl-β-D-ribofuranosyl) 1,1,2-Ethanetricarboxylate (21)

To a solution of the bromide **2** (from 1 g, 2.4 mmol of the corresponding 1-acetate **4**) in the minimum volume of 1,2-dimethoxyethane was added a solution of sodio triethyl 1,1,2-ethanetricarboxylate (prepared from 0.17 g, 7.4 mmol of sodium and 1.8 g of the triester) in 5 ml of the same solvent. After stirring overnight at room temperature, excess ether was added, and the solution was processed by washing it with water, etc. Excess reagent was removed by distillation and the remaining syrup (quantitative) was examined by t.l.c. in solvent A. Two components, having R_f ~0.8 (title compound **21**) and R_f ~0.75 (ketal derivative) were present in an approximate ratio of 1:2 (estimated by n.m.r.). A portion of the syrup (0.8 g) was separated by chromatography on silica gel GF_{254} using chloroform as developer. Fractions containing **21** were combined and evaporated to a colorless syrup (0.17 g, 20%, based on **4**); $[\alpha]_D^{25}$ + 21.6° (*c* 6.9, $CHCl_3$); n.m.r. (Fig. 2): 1.20 (m, CH_3CH_2); 3.20 (s, CH_2COO); 5.0 (d, $J_{1,2}$ = 4.3 Hz, H-1); 5.73 (t, $J_{3,2}$ = 5.5 Hz, H-3); 6.22 p.p.m. (dd, $J_{2,3}$ = 5.5 Hz; $J_{2,1}$ = 4.3 Hz, H-2) etc; *m/e* 645.1959 (calcd. for $M^+ - EtO^\cdot$ 645.1972).

The triacetate **25**, obtained as a chromatographically homogeneous syrup, by debenzoylation (NaOEt, EtOH) of **21** and acetylation (acetic anhydride – pyridine, see later) gave a satisfactory mass spectrum at high resolution: M^+ 504.1828 (calcd. for $C_{22}H_{32}O_{13}$, M^+ 504.1843); *m/e* 459.1528 ($M^+ - EtO^\cdot$); *m/e* 417.1336 ($M^+ - EtO^\cdot - CH_2CO$), etc.

Fractions containing the ketal derivative **22** were collected, and processed to give a syrup; n.m.r.: 3.10 (s, CH_2COO), 5.13 (dd, $J_{3,4}$ = 10 Hz; $J_{3,2}$ = 4 Hz; H-3); 5.57 (t, $J_{2,1} = J_{2,3}$ = 4 Hz; H-2); 6.54 p.p.m. (d, $J_{1,2}$ = 4 Hz, H-1) etc. Acetolysis of a portion of **22** afforded the 1-acetate **4**, identical with an authentic sample.

Condensation of 2,3,5-Tri-O-benzyl-D-ribofuranosyl Chloride with Sodio Diethyl Malonate

Diethyl 2-(β-D-Ribofuranosyl) Malonate (11) and its Tribenzoate (13)

To a solution of 2,3,5-tri-*O*-benzyl-β-D-ribofuranosyl chloride **8** (36) (0.447 g, 0.79 mmol) in the minimum volume of diethyl malonate, was added a solution of sodio diethyl malonate (prepared from 70 mg, 3 mmol, of sodium and 5 ml of diethyl malonate) under rigorously anhydrous conditions (see general comments under Experimental). The solution was stirred at room temperature overnight, and a large excess of ether was added. The processing was continued by washing with water, etc. Excess diethyl malonate was removed from the final syrup by distillation. A thick colorless syrup was obtained (0.558 g) that showed a single spot on t.l.c. (solvent A). The syrup was dissolved in ethanol and the solution was hydrogenated in the presence of 20% Pd–C for 12 h. The catalyst was filtered, washed with ethanol

[9]Sodio dibenzyl malonate was soluble in benzene in contrast to the diethyl derivative.

Can. J. Chem. Downloaded from www.nrcresearchpress.com by 210.87.254.42 on 09/05/12
For personal use only.

and the filtrates were combined and evaporated to a syrup (quantitative). Chromatography on silica gel containing boric acid (solvent B) revealed two components, R_f ~0.5 and R_f ~0.3, in approximately equal amounts (estimated from zone intensities after charring and by n.m.r.). Separation (0.1 g) by preparative t.l.c. gave the R_f 0.5 component as a homogeneous syrup (30 mg) that was identified as the oxepane derivative **12**. Benzoylation of this product afforded the crystalline tribenzoate **5**. Acetylation of **12** and attempted investigation of the syrupy acetate by mass spectrometry was unsuccessful, due to decomposition, even at 50°.

The R_F ~0.3 component was likewise obtained as a syrup (25 mg) and proved to be the title compound **11**. Acetylation in the usual way (acetic anhydride, pyridine) gave the acetate **14** as the sole product (colorless syrup): mass spectral data: M^+ 418.1450 (calcd. for $C_{18}H_{26}O_{11}$, 418.1475); *m/e* 285.0973 (M − COOEt), etc.

Benzoylation of **11** in the usual way gave *diethyl 2-(2,3,5-tri-O-benzoyl-β-D-ribofuranosyl) malonate* (**13**), as a chromatographically homogeneous syrup; R_f ~0.8 (solvent A); $[\alpha]_D^{25}$ +21.8° (*c* 4.1, $CHCl_3$); n.m.r. (at 100 MHz): 3.84 (d, $J_{m,1}$ = 7.0 Hz, H_m); 4.92 (dd, $J_{1,2}$ = 4.5 Hz; $J_{1,m}$ = 7.5 Hz, H-1); 5.90 p.p.m. (m, H-2, H-3); etc. These assignments were confirmed by internuclear spin decoupling experiments (See also Fig. 1); $M^+ - CH_2OCOC_6$ *m/e* 469.1495 (calcd. for $M^+ - CH_2OCOC_6H_5$ 469.1498); *m/e* 482.1579 calcd. for $M^+ - C_6H_5COOH$ 482.1576).

*Diethyl 2-(α-D-Ribofuranosyl) Malonate (**16**) and its Tribenzoate (**17**)*

The same procedure as described for the preparation of **9** was repeated with the exception that 1,2-dimethoxyethane was used as solvent. Thus, from 2.23 g (4 mmol) of the halide **8** and 0.35 g (15 mmol) of sodium and 3.15 ml of diethyl malonate in 30 ml of 1,2-dimethoxyethane, a syrup was obtained in high yield. After hydrogenation as described above, the syrup obtained after work-up (0.985 g) showed the presence of three components when chromatographed on silica gel containing boric acid (solvent B). The R_f ~0.6 and R_f ~0.3 components were identified as compounds **12** and **11**, respectively. The third component, R_f ~0.55 was found to be the title compound **16**. A portion of the syrup (0.11 g) was separated by preparative t.l.c. on silica gel containing boric acid (solvent B), using eight 20 × 20 cm plates. *Diethyl 2-(α-D-ribofuranosyl) malonate* (**16**) was thus obtained as a clear syrup (44 mg, 31%, based on the reacted halide[10]). The β-*C*-glycoside **11** was isolated in the same way and it was obtained as a syrup (66 mg, 46%).

A portion of **16** was benzoylated in the usual manner (benzoyl chloride, pyridine) to give *diethyl 2-(2,3,5-tri-O-benzoyl-α-D-ribofuranosyl) malonate* (**17**), as a syrup; R_f ~0.82 (solvent A); $[\alpha]_D^{25}$ +71.6° (*c* 3.9, $CHCl_3$); n.m.r. (at 100 MHz): 4.08 (d, $J_{m,1}$ = 10.5 Hz, H_m); 5.12 (dd, $J_{1,2}$ = 4.0 Hz; $J_{1,m}$ = 10.5 Hz, H-1); 6.00 (t, $J_{3,2} = J_{3,4}$ = 4 Hz, H-3); 6.30 p.p.m. (t, $J_{2,1} = J_{2,3}$ = 4 Hz, H-2), etc. These assignments were confirmed by internuclear spin decoupling experiments (see also Fig. 1).

Alternatively, the hydrogenolysis product containing the compounds **12**, **11**, and **16** could be benzoylated and the resulting benzoates, **5**, **13**, and **17**, respectively, could be separated by a combination of column and t.l.c. (solvent A).

*Anomeric Configurational Assignment of the C-Glycosyl Malonate (**11**)*

A sample (35 mg) of diethyl 2-(β-D-ribofuranosyl) malonate **11** (purified by preparative t.l.c.) was dissolved in 2 ml of ethanol and the solution was treated with 4 equiv. of sodium metaperiodate in 2 ml of water. After standing at room temperature in the dark for 2 h, the solution was filtered, and the filtrate was evaporated to dryness. The solid residue was dissolved in chloroform, the solution was filtered through a sintered-glass funnel and the clear, colorless filtrate was evaporated to a syrup that showed essentially one spot on t.l.c. After preparative t.l.c. (solvent B), a syrup (23 mg) was obtained that showed $[\alpha]_D^{25}$ −21° (*c* 2.3, $CHCl_3$). Authentic dialdehyde **19** showed $[\alpha]_D^{25}$ −24° (*c* 2.1, $CHCl_3$) while the epimeric analog (17) showed $[\alpha]_D^{25}$ +26° ($CHCl_3$).

*Transformation of the C-Glycosyl Malonates **13** and **17** into the Oxepane Derivative **5***

Equal amounts (20 mg each) of **11** and **16** were dissolved in 2 ml of pyridine and benzoyl chloride was added. The mixture of benzoates **13** and **17** was isolated as a colorless syrup. The latter was dissolved in a solution of sodium diethyl malonate (from 10 mg of sodium and 2 ml of the ester). After storing at room temperature overnight the solution was diluted with ether, washed with water, and the organic layer was processed as usual to give a syrup (20 mg) that had the same chromatographic properties as the oxepane **5** (solvent A), as well as identical spectroscopic properties. Crystalline **5** was obtained from a mixture of ether and pentane at 0°; yield 10 mg; m.p. and mixture m.p. 93–95°. The mother liquors contained additional amounts of **5**, but further crystalline crops were not obtained.

Condensation of 2,3,5-tri-O-benzyl-β-D-ribofuranosyl Chloride with Sodio Triethyl 1,1,2-Ethanetricarboxylate

*Diethyl 1-(α-D-Ribofuranosyl)-1,1,2-ethanetricarboxylate α-Lactone (**27**), its Diacetate (**28**), and Dibenzoate (**29**)*

To a solution of the chloride **8** (prepared from 0.57 g, 1 mmol of the corresponding 1-*p*-nitrobenzoate) in the minimum volume of 1,2-dimethoxyethane, was added a solution of sodio triethyl 1,1,2-ethanetricarboxylate (prepared from 70 mg, 3 mmol of sodium and 0.944 g, 4 mmol of the ester) in 8 ml of the same solvent. After stirring at room temperature for 20 h, the solution was diluted with a large excess of ether, then it was washed with water, and the organic phase was processed to give a mobile liquid, from which excess ester was removed by distillation (80°, 10^{-5} Torr). The resulting colorless syrup (0.65 g) showed two components on t.l.c. (solvent A) of which the more polar was 2,3,5-tri-*O*-benzyl-D-ribofuranose (~30%). The syrup was subjected to hydro-

[10]In some experiments, hydrolysis of the halide prior to condensation led to variable amounts of 2,3,5-tri-*O*-benzyl-D-ribose. This could be minimized with proper precautions in handling.

Can. J. Chem. Downloaded from www.nrcresearchpress.com by 210.87.254.42 on 09/05/12
For personal use only.

genolysis in 80% aqueous ethanol in the presence of 20% Pd—C for 6 h. The catalyst was filtered and the filtrate was evaporated to a syrup that was dissolved in chloroform and the solution was extracted with water to remove D-ribose. Processing the organic phase gave a syrup (0.18 g, 50%) that consisted of two components, R_f ~0.6 and R_f ~0.57 (t.l.c. on silica gel containing boric acid, solvent B), corresponding to *triethyl 1-(β-D-ribofuranosyl)-1,1,2-ethanetricarboxylate* **24** and the title compound **27**, respectively.

Benzoylation (benzoyl chloride, pyridine) of an aliquot, and examination by n.m.r., showed a ratio of 4:1 for the benzoates **29** and **21**, respectively.

The original syrup (90 mg) was separated by preparative t.l.c. (silica gel containing boric acid, solvent C) to give **24** as a syrup, characterized as its tribenzoate **21** (n.m.r.) and triacetate **25** (mass spectrum). The title compound **27**, obtained as a colorless syrup (30 mg), was converted into its diacetate **28** (acetic anhydride, pyridine) and the latter was obtained as a clear syrup (quantitative); $[\alpha]_D^{25}$ +159° (*c* 0.9 $CHCl_3$); n.m.r.: 1.23 (t, CH_3CH_2); 2.02, 2.08 (*s*, CH_3COO); 3.0 p.p.m. (q, J_{gem} = 18 Hz CH_2COO); etc. Mass spectral data: M^+ 416.1323 (calcd. for $C_{18}H_{24}O_{11}$: 416.1318); *m/e* 371.0974 (M^+ − Eto·); *m/e* 343.1025 (M^+ − EtO·—CO·), etc.

Benzoylation (benzoyl chloride, pyridine) of the lactone **27** gave the corresponding dibenzoate **29** as a colorless syrup in high yield; $[\alpha]_D^{25}$ +144° (*c* 4.13, $CHCl_3$); λ_{max} 1790 (lactone), 1730 cm^{-1} (ester); n.m.r.: 1.20, 1.23 (t, CH_3CH_2); 3.17 (q, J_{gem} = 18 Hz, CH_2-COO); 5.50 p.p.m. (m, H-1, H-2, H-3), etc; see Fig. 2.

Triethyl 1-(α-D-Ribofuranosyl)1,1,2-Ethanetricarboxylate (25) and its Tribenzoate 30

A solution of the lactone **27** (10 mg) in 1 ml of ethanol containing a catalytic amount of sodium methylate was left standing at room temperature for 3 h. The solution was neutralized with Dowex-50 (H^+), filtered and the filtrate was evaporated to dryness to give crude **25**. The resulting syrup was benzoylated in the usual way, and the reaction mixture was processed to give **30** as a colorless syrup. Purification by preparative t.l.c. (solvent D) gave a syrup (15 mg, 90%) that was chromatographically different from the β-anomer **21** (compare R_f ~0.70, solvent D); n.m.r.: p.p.m. 3.10 (s, CH_2COO). The corresponding triacetate (syrup) showed M^+, 504.1823 (calcd. 504.1843).

Condensation in the D-Arabino Series

Diethyl 2-(α- and β-D-Arabinofuranosyl) Malonates 33 and 34, and their Acetates

Sodium (0.2 g, 9 mmol) was dissolved in 25 ml of diethyl malonate and the solution was added to a solution of freshly prepared 2,3,5-tri-*O*-benzyl-α-D-arabinofuranosyl chloride (**31**) (from 1 g, 1.75 mmol of the corresponding 1-*p*-nitrobenzoate derivative) in 1 ml of diethyl malonate. The solution was stirred at room temperature overnight, then it was diluted with excess ether, and processing was continued by washing with water, etc. The organic phase was evaporated to a mobile liquid from which diethyl malonate was removed by distillation. The syrup (1 g, quantitative) that remained consisted of the expected diethyl 2-(2,3,5-tri-*O*-benzyl-α,β-D-arabinofuranosyl) malonates (**32**), and showed a single spot on t.l.c. (solvent A). The syrup was dissolved in ethanol and hydrogenated in the presence of 20% Pd—C. After 10h, the catalyst was filtered and the filtrate was evaporated to a syrup (0.5 g, quantitative) that showed two spots on t.l.c. (solvent B) with R_f ~0.4 and R_f ~0.45, corresponding to the α- and β-anomeric title compounds respectively. Separation of 0.2 g by preparative t.l.c. (solvent B) gave equal amounts (30 mg) each of syrup *diethyl 2-(α-D-arabinofuranosyl) malonate* (**33**) and *diethyl 2-(β-D-arabinofuranosyl) malonate* (**34**). Acetylation of each product gave the corresponding acetates **35** and **36** as syrups, in high yield. *Diethyl 2-(2,3,5-tri-O-acetyl-α-D-arabinofuranosyl) malonate* (**35**) had $[\alpha]_D^{25}$ +28° ± 0.2° (*c* 5.9, $CHCl_3$); n.m.r.: 1.28 (t, CH_3CH_2); 2.10 (*s*, CH_3COO); 3.74 (d, $J_{m,1}$ = 9.7 Hz, H_m); 4.25 (m, H-4, H-5,5), 4.70 (dd, $J_{1,m}$ = 9.7 Hz; $J_{1,2}$ = 3 Hz, H-1); 5.12 (m, H-3); 5.38 p.p.m. (t, $J_{2,3}$ = $J_{2,1}$ = 3 Hz, H-2) etc; *m/e* 419 (M^+ +1); *m/e* 373 (M^+ − EtO·); *m/e* 345 (M^+ − CH_2OAc); *m/e* 358 (M^+ − CH_3COOH), etc.

Diethyl 2-(2,3,5-tri-O-acetyl-β-D-arabinofuranosyl) malonate (**36**), had $[\alpha]_D^{25}$ −2° ± 0.2° (*c* 6.4, $CHCl_3$); n.m.r.: 1.24, 1.28 (t, CH_3CH_2); 2.08 (*s*, CH_3COO); 3.71 (d, $J_{m,1}$ = 9.9 H, H_m); 4.20 (m, CH_3CH_2; H-5,5′; H-4); 4.71 (dd, $J_{1,2}$ = 3.8; $J_{1,m}$ = 9.9, H-1); 4.89 (dd, $J_{3,2}$ = 0.8; $J_{3,4}$ = 2.25 Hz, H-3); 5.40 p.p.m. (dd, $J_{2,1}$ = 3.8; $J_{2,3}$ = 0.8, H-2), etc. Mass spectral data were obtained as above.

Anomeric Configurational Assignment of the C-Glycosyl Malonate 33

A sample of **33** (40 mg) was dissolved in 2 ml of ethanol and two equivalents of sodium metaperiodate in 2 ml of water were added. After 20 h in the dark, the solution was filtered, the precipitate was washed with ethanol, and the filtrate and washings were evaporated to a syrup. The latter was redissolved in chloroform, the solution was filtered from a trace of inorganic salts, and evaporated to a syrup that was purified by preparative t.l.c. (solvent C). The dialdehyde **19** was obtained as a colorless syrup (36 mg); $[\alpha]_D^{25}$ +29.2° (*c* 3.6, $CHCl_3$). Authentic dialdehyde (17) obtained from the β-*C*-glucosyl malonate derivative **20** showed $[\alpha]_D^{25}$ −24° ($CHCl_3$) while the epimeric dialdehyde showed $[\alpha]_D^{25}$ +26° ($CHCl_3$).

Financial assistance from the National Research Council of Canada and a France-Quebec fellowship to A. G. Pernet are gratefully acknowledged. We thank Dr. T. Ogawa for mass spectral data on compounds **15**, **21**, and **30**.

1. S. Hanessian and A. G. Pernet. Chem. Commun. 755(1971). See also, T. Ogawa, A. G. Pernet, and S. Hanessian. Tetrahedron Lett. 3543 (1973).
2. R. J. Suhadolnik. Nucleoside antibiotics. Wiley-Interscience, New York. 1970; S. Hanessian and T. H. Haskell. *In* The carbohydrates. Vol. 2. Second ed. *Edited by* W. Pigman and D. Horton. Academic Press, 1970. p. 139; J. J. Fox, K. A. Watanabe, and A. Bloch. Prog. Nucl. Acad. Mol. Biol. **5**, 251 (1966).

3. K. GERZON, D. C. DELONG, and J. C. KLINE. Pure Appl. Chem. **28**, 489 (1971).
4. G. KOYAMA and H. UMEZAWA. J. Antibiot. (Jap.) **18**A, 175 (1965).
5. M. E. HORI, T. ITO, G. TAKIDA, G. KOYAMA. T. TAKEUCHI, and H. UMEZAWA. J. Antibiot. (Jap.) **17**A, 96 (1964).
6. K. SASAKI, Y. KASAKABE, and S. ESUMI. J. Antibiot. (Jap.) **25**, 151 (1972).
7. N. NISHIMURA, M. MAYMA, Y. KOMATSU, H. KATO, N. SHIMAOKA, and Y. TANAKA. J. Antibiot. (Jap.), **17**A, 148 (1964).
8. E. W. ACTON, R. J. RYAN, D. W. HENRY, and L. GOODMAN. Chem. Commun. 986 (1971).
9. M. BOBEK, J. FARKAS, and F. SORM. Tetrahedron Lett. 4611 (1970).
10. M. SPRINZL, J. FARKAS, and F. SORM. Tetrahedron Lett. 289 (1969).
11. M. BOBEK and J. FARKAS. Coll. Czech. Chem. Commun. **34**, 247 (1969).
12. M. BOBEK and J. FARKAS, Coll. Czech. Chem. Commun. **34**, 1684 (1969).
13. T. OGAWA, Y. KIKUCHI, M. MATSUI, H. OHRUI, H. KUGUHARA, and S. EMOTO. Agr. Biol. Chem. (Jap.) **36**, 1449, 1655 (1972).
14. G. JUST and A. MARTEL. Tetrahedron Lett. 1517 (1973).
15. L. KALVODA, J. FARKAS, and F. SORM. Tetrahedron Lett. 2297 (1970).
16. G. TRUMMLITZ and J. G. MOFFATT. J. Org. Chem. **38**, 1841 (1973).
17. S. HANESSIAN and A. G. PERNET. Can. J. Chem. **52**, 1266 (1974).
18. R. P. ZELINSKY, N. G. PETERSON, and H. R. WALLNER. J. Am. Chem. Soc. **74**, 1504 (1952); J. G. SCHEUDEL and R. V. RICE. U.S. Patent 2, 522, 966 (1950); Chem. Abstr. **45**, 6223 (1951); J. V. KOSTIR and M. QUEISNEROVA. Chem. Listy, **43**, 277 (1949); Chem. Abstr. **45**, 553 (1951).
19. H. OHRUI and J. J. FOX. Tetrahedron Lett. 1951 (1973).
20. R. K. NESS and H. G. FLETCHER, Jr. Carbohydr. Res. **19**, 423 (1972).
21. D. DAVIDSON and S. A. BERNARD. J. Am. Chem. Soc. **70**, 3426 (1948).
22. D. S. BRESLOW, E. BAUMGARTEN, and C. R. HAUSER. J. Am. Chem. Soc. **66**, 1286 (1944).
23. G. S. FONKEN and W. S. JOHNSON. J. Am. Chem. Soc. **74**, 831 (1952).
24. C. S. HUDSON. J. Chem. Ed. **18**, 353 (1941).
25. F. M. SCHABEL. Chemotherapy, **13**, 321 (1968).
26. C. BARNATHAN, T. H. DINH, A. KOLB, and J. IGOLEN. Compt. Rend. **294**, 2192 (1972).
27. C. P. J. GLAUDEMANS and H. G. FLETCHER, Jr. J. Org. Chem. **29**, 3284 (1964).
28. A. STREITWEISER, Jr. and S. ANDREADES. J. Am. Chem. Soc. **80**, 6553 (1958); H. WEINER and R. A. SNEEN. J. Am. Chem. Soc. **87**, 287 (1965).
29. H. E. ZAUGG. J. Am. Chem. Soc. **83**, 337 (1961); H. D. ZOOK and T. R. RUSSO. J. Am. Chem. Soc. **82**, 1258 (1960).
30. H. MEERWEIN. Org. Syn. **46**, 113 (1966).
31. J. A. MONTGOMERY and K. HEWSON. J. Heterocycl. Chem. **7**, 443 (1970).
32. C. P. J. GLAUDEMANS and H. G. FLETCHER, Jr. J. Am. Chem. Soc. **87**, 2456, 4636 (1965), and subsequent papers.
33. R. K. NESS and H. G. FLETCHER, Jr. Carbohydr. Res. **19**, 423 (1972).
34. J. J. FOX and J. WEMPEN. *In* Methods of carbohydrate chemistry. Vol. 2. *Edited by* R. L. Whistler and M. L. Wolfrom. Academic Press Inc., New York. 1963. p. 221.
35. W. M. PEARLMAN. Tetrahedron Lett. 1663 (1967).
36. J. D. STEVENS, R. K. NESS, and H. G. FLETCHER, Jr. J. Org. Chem. **33**, 1806 (1968).

Can. J. Chem. Downloaded from www.nrcresearchpress.com by 210.87.254.42 on 09/05/12
For personal use only.

The Wittig Synthesis and Photocyclodehydrogenation of 3-(2-Aryl)vinylindole Derivatives[1]

S. OSMUND DE SILVA AND VICTOR SNIECKUS

Department of Chemistry, University of Waterloo, Waterloo, Ontario

Received December 4, 1973

Wittig condensation of indole-1-(*p*-toluenesulfonyl)-3-methyltriphenylphosphonium iodide (**8**) with aromatic and heterocyclic aldehydes gives good yields of the 3-(2-aryl)-vinylindole derivatives **9***a–g* (Scheme 1). Compounds **11***a* and **11***b* are obtained similarly starting with the known indole-1-methyl-3-methyltriphenylphosphonium salt **10** and pyridine-3- and -4-aldehydes. An alternate Perkin-type condensation route provides the trisubstituted 3-vinylindoles **15***a* and **15***b* (Scheme 2) which cannot be synthesized by the Wittig route.

Compounds **9***a* and **9***b*; **9***e* and **11***b*; **13**, **15***a*, and **15***b*; as well as the previously known **12***a–c* undergo photocyclodehydrogenation to give benzo- and pyridocarbazole derivatives **16***a* and **16***b*; **18***a* and **19***a*, **18***b* and **19***b*; **17***a*, **17***b*, and **17***c*; and **16***c–e*, respectively in fair to good yields (Scheme 3). Compounds **9***d*, **9***f*, and **11***a* fail to photocyclize. The reasons for these failures are briefly explored and discussed.

La condensation de Wittig de l'iodure d'indole (*p*-toluènesulfonyl)-1 méthyltriphényl-phosphonium-3 (**8**) avec les aldéhydes aromatiques et hétérocycliques conduit avec de bons rendements aux (aryl-2)-3 vinylindoles **9***a–g* (schéma 1). Les composés **11***a* et **11***b* ont été obtenus d'une manière similaire en partant des sels connus de l'indole méthyl-1 méthyltriphénylphosphonium-3 (**10**) et des pyridinecarboxaldéhydes-3 et -4. L'utilisation de la condensation de Perkin fournit une méthode supplémentaire pour obtenir les vinyl-3 indoles trisubstitués **15***a* et **15***b* (schéma 2) qui n'ont pu être obtenus par la synthèse de Wittig.

Les composés **9***a* et **9***b*; **9***e* et **11***b*; **13**, **15***a* et **15***b*; de même que les composés déjà connus **12***a–c* subissent des photocyclodéshydrogénation pour donner les benzo et pyrido-carbazoles **16***a* et **16***b*; **18***a* et **19***a*, **18***b* et **19***b*; **17***a*, **17***b* et **17***c*; et **16***c–e*, respectivement avec des rendements variant entre acceptable et bon (schéma 3). Les composés **9***d*, **9***f* et **11***a* ne subissent pas la photocyclisation. On examine et discute les raisons de ces insuccès. [Traduit par le journal]

Can. J. Chem., **52**, 1294 (1974)

As a sequel to our investigations of the Wittig reaction for chain extension at the 2-position of the indole ring to yield 2-vinylindoles, *e.g.* **1** (1), we report on the analogous extension method at the indole 3-position. Aside from the desirable synthetic methodology, we were interested in the potential utility of the resulting 3-(2-aryl)vinylindoles (**2**, Ar = Ph, Pyridyl) for the development of an improved preparation of more highly condensed synthetic and naturally occurring heterocyclic systems by a photochemical route.[2]

Extensions of the classical aldol synthesis of 3-nitrovinylindoles (3, 4) and, to a lesser extent, alkenylation of indoles with ketones possessing at least one enolizable α-hydrogen have been used to prepare 3-vinylindole derivatives of the type **3** (X = CN, CO_2Et; R^1 = H or Me; R^2 = H, Me, or Ph (5)) and **4** (X = H or CN; Y = CN, CO_2Et, COAlkyl, $CONH_2$, Ph, and COAr; R^1 = H or Me; R^2 = Me or Ph; R^3 = H, Me, or Ph (6), respectively). The condensation of indole-3-aldehyde with α-picolinium salts has provided a number of 3-vinylindoles possessing basic structure **5** (7). The same reaction has been demonstrated for some corresponding γ-picolinium salts (7). Recently, the synthesis of 1-(3-indolyl)-2-phenylethylene (**2**, Ar = Ph) has been reported by two new routes: Wittig reaction of indole-3-aldehyde with $(Ph)_3P{=}CHPh$ (8) and a two-step sequence involving condensation of isatin with $LiC{\equiv}CPh$ followed by lithium aluminum hydride reduction

[1]Extracted in part from the Ph.D. Thesis of S. O. de S., University of Waterloo, 1973.

[2]We have previously reported on the photocyclodehydrogenation of the corresponding 2-(2-aryl)vinylindoles to benzo[*c*]carbazole and some pyridocarbazole derivatives (2).

Can. J. Chem. Downloaded from www.nrcresearchpress.com by 210.87.254.6 on 09/05/12
For personal use only.

Can. J. Chem. Downloaded from www.nrcresearchpress.com by 210.87.254.6 on 09/05/12
For personal use only.

(9). It is clear that there is a lack of general and direct methods for the preparation of 3-(2-aryl)vinylindoles which are disubstituted at the ring-interconnecting double bond, *i.e.* **2**. The 3-[2-(2-pyridyl)vinyl]indoles (and the corresponding 4-pyridyl isomers) can be obtained only as the quaternary salts (*e.g.* **5**).[3] The Wittig synthesis (8), in addition to suffering from low yields, has the formidable disadvantage in that the somewhat inaccessible and unexplored pyridine phosphonium methylides[4] would be required for its extension to the preparation of 3-(2-pyridyl)-vinylindoles (**2**, Ar = Pyridyl). Finally, it should be noted in passing that the chemistry of vinylindole derivatives remains largely an unexplored area (12, see also ref. 3, p. 125).

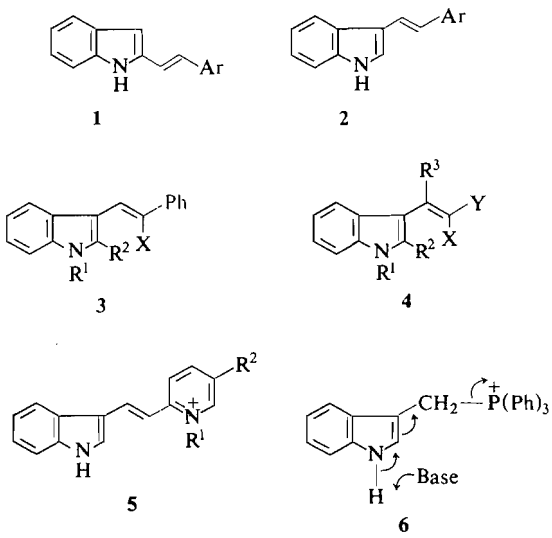

Wittig Synthesis of 3-(2-Aryl)vinylindole Derivatives 9a–g and 11a and b

The development of the Wittig synthesis in reverse to that used by Suvorov and co-workers (8) required that the expected gramine-type fragmentation (13) of the known (14) 3-methylindole phosphonium iodide under the basic conditions of the reaction be avoided (**6**, arrows). Indeed, when **6** was treated with pyridine-4-aldehyde in methanol in the presence of sodium methoxide, only a quantitative yield of triphenylphosphine was obtained.[5] This problem was overcome by taking advantage of the method recently described for indole *N*-protection by tosylation (16).[6] The *N*-tosyl salt **8**, prepared in three steps from gramine (**7**)[7] when subjected to the Wittig reaction with aromatic and heterocyclic aldehydes followed by treatment with base gave the 3-vinylindole derivatives **9***a–g* in good yield (Scheme 1). Since the intermediate *N*-tosyl compounds were usually noncrystalline and unstable substances and since it appeared that they were undergoing partial detosylation under the conditions of the reaction, their isolation was avoided and the adducts **9** were directly obtained by base treatment of the crude Wittig reaction product. The best yields of Wittig adducts were obtained by using sodium hydride in DMF; an alternate set of conditions, 1,5-diazabicyclo-[3.4.0]nonene-5 (DBN) in DMSO which was successful in our synthesis of 2-vinylindoles (1), led mainly to detosylation and thus triphenylphosphine formation. For example, under these conditions the reaction of **8** with pyridine-4-aldehyde gave only a 17% yield of adduct **9***f* and triphenylphosphine in 80%.

The *N*-methyl Wittig adducts **11***a* and *b* were also prepared using the known (14) phosphonium salt **10** and the requisite aldehydes. Compounds **9***a–g* and **11***a* and *b* were characterized by analytical and spectral data (Table 1). The complex overlap of the vinyl and aromatic proton region of the n.m.r. spectra precluded configurational assignment of the central double bond. However, *trans*-configuration is assumed for all adducts on the basis of their stability in

[3]Attempts to condense indole-3-aldehyde with 2- and 4-picoline under conditions used for the preparation of **5** failed although a 15% yield of the *N*-oxide of 3-[2-(4-pyridyl)vinyl]indole was prepared using γ-picoline *N*-oxide. This *N*-oxide was deoxygenated to **9***f*. Additionally, compound **5**, R^1 = Me; R^2 = H, was demethylated to **9***d*. The low yields make both methods synthetically undesirable (see Experimental section).

[4]For recent examples, see ref. 10; for a method by which they are conveniently generated *in situ*, see ref. 11.

[5]In contrast, this type of behavior was not observed in the Wittig reactions of 2-methylindole phosphonium iodide (1) in agreement with other experimental (13) and theoretical (15) comparisons of the gramine and isogramine systems.

[6]*N*-Acetyl- and *N*-benzoylindoles may also be useful *N*-protecting groups for some (17, 18) but not all (8*a*) base-catalyzed reactions.

[7]A product (i) which may have utility in indole chemistry was obtained when gramine (7) was treated with 2 equiv. of tosyl chloride (see Experimental section).

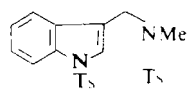

i

Can. J. Chem. Downloaded from www.nrcresearchpress.com by 210.87.254.6 on 09/05/12
For personal use only.

TABLE 1. Preparation and spectral data of 3-(2-aryl)vinylindole derivatives

Compound[a]	% yield	Melting point °C (solvent)	λ_{max}(EtOH) nm (ε)	τ values (DMSO-d_6) N—H[b]	Pyridine α-H	Other
9*a*	58	193–194[c] (MeOH)	[c]			[c]
9*b*	77	204–205 (EtOH)	231(3200) 287(sh, 10 500) 335(37 000)	−1.3		1.8–3.1 (m, 11H, aromatic and vinyl H) 6.2 (s, 3H, OCH_3)
9*c*[d]	72	206–207 (EtOH)	230(31 000) 273(25 000) 414(29 000)	−1.56		1.65–3.0 (m, 11H, aromatic and vinyl H) 1.82 (d, 2H, J = 9 Hz, o-NO_2-phenyl H) 2.25 (d, 2H, J = 9 Hz, m-NO_2-phenyl H)
9*d*[e]	47	190–191 (MeOH)	230(22 500) 278(8100) 346(31 000)	−1.4	1.4 (br d, 1H, J = 5 Hz)	1.8–3.0 (m, 10H, aromatic and vinyl H)
9*e*	51	195–196 (EtOH)	232(28 000) 255(10 100) 283(9000) 340(32 000)	−1.4	1.2 (br s, 1H, C_2—H) 1.6 (d, 1H, J = 5 Hz, C_6—H)	1.8–3.2 (m, 9H, aromatic and vinyl H)
9*f*	54	265–268 (EtOH)	233(23 000) 285(8200) 358(30 000)	−1.6	1.5 (d, 2H, J = 6 Hz)	1.97 (m, 2H, pyridine β-H) 2.0–3.33 (m, 7H, aromatic and vinyl H)
9*g*[f]	38	180–181 ($EtOH–H_2O$)	230(22 000) 285(13 000) 327(31 200)	−1.35		1.9–3.07 (m, 7H, aromatic and vinyl H) 3.4–3.7 (m, 3H, furyl H)
11*a*	42	145–146 (EtOH)	235(24 000) 277(9000) 285(sh, 9100) 360(31 000)		1.45 (d, 2H, J = 6 Hz)	1.85 (m, 2H, pyridine β-H) 2.0–3.1 (m, 7H, aromatic and vinyl H) 6.2 (s, 3H, NCH_3)
11*b*[g]	31.5	Gum	230(28 100) 253(9500) 280(9000) 343(31 000)		1.2 (br s, 1H, C_2—H), 1.63 (m, 1H, C_6—H)	1.8–3.3 (m, 9H, aromatic and vinyl H) 6.3 (s, 3H, NCH_3)
12*a*[d]	22	211–213[h] ($EtOH–H_2O$)	230(24 800) 253(sh, 10 750) 278(9200) 333(16 000)	−1.3		1.82 (s, 1H, vinyl H) 2.25–3.0 (m, 10H, aromatic H and CO_2H) 3.62 (s, 1H, vinyl H)
12*b*[d,i]	58	142–143 (EtOH)	241(13 370) 261(sh, 11 050) 285(sh, 7900) 340(12 950)			1.2–3.0 (m, 11H, aromatic and N—H) 3.6 (br s, 1H, vinyl H) 5.8 (q, 2H, J = 7 Hz, CH_2) 8.8 (t, 3H, J = 7 Hz, CH_3)

Can. J. Chem. Downloaded from www.nrcresearchpress.com by 210.87.254.6 on 09/05/12
For personal use only.

TABLE 1 (*Concluded*)

Compound[a]	% yield	Melting point °C (solvent)	λ_{max}(EtOH) nm (ε)	τ values (DMSO-d_6) N—H[b]	Pyridine α-H	Other
12*c*[d,j]	93	185 (EtOH)	239(15 250) 258(sh, 11 650) 283(sh, 8200) 340(13 750)	−2.15		1.4–2.8 (m, 11H, aromatic and vinyl H)
13[d]	42	183–185 (EtOH)	225(28 000) 267(9200) 335(13 000)	−1.55	1.35 (br d, 2H, J = 6 Hz)	2.12 (m, 2H, pyridine β-H) 2.2–3.15 (m, 5H, aromatic H) 3.32 (s, 1H, vinyl H) 5.57 (q, 2H, J = 7 Hz, CH_2) 8.76 (t, 3H, J = 7 Hz, CH_3)
14*a*[d]	68	139–140 (EtOH)	228(22 650) 264(17 600) 319(19 050)		1.3 (d, 2H, J = 7 Hz)	1.4–1.7, 1.9–2.8 (m, 8H, aromatic, vinyl and pyridine β-H) 7.28 (s, 3H, $COCH_3$), 7.62 (s, 3H, CH_3)
14*b*[d]	38–48	163–164 (EtOH)	228(22 650) 264(17 600) 320(19 050)		1.35 (d, 2H, J = 7 Hz)	1.5–2.87 (m, 8H, aromatic, vinyl, and pyridine β-H) 7.1 (q, 2H, J = 7 Hz, CH_2) 7.25 (s, 3H, $COCH_3$) 8.9 (t, 3H, J = 7 Hz, CH_3)
15*a*	81	214–215 (EtOH)	235(18 350) 288(8050) 342(12 100)	−1.6	0.6 (d, 2H, J = 7 Hz)	1.8–3.0 (m, 8H, aromatic, vinyl, and pyridine β-H) 7.63 (s, 3H, CH_3)
15[b]	91	231–232 (EtOH)	232(18 400) 285(8050) 346(12 100)	−1.6	1.4 (d, 2H, J = 7 Hz)	2.0–2.93 (m, 8H, aromatic, vinyl, and pyridine β-H) 7.16 (q, 2H, J = 7.5 Hz, CH_2) 8.9 (t, 3H, J = 7.5 Hz, CH_3)

[a]Analytical data: **9***b*: Anal. Calcd. for $C_{17}H_{15}NO$: C, 81.90; H, 6.06; N, 5.62. Found: C, 81.87; H, 6.01; N, 5.57.
9*c*: Anal. Calcd. for $C_{16}H_{12}N_2O_2$: C, 72.72; H, 4.58; N, 10.60. Found: C, 72.80; H, 4.51; N, 10.51.
9*e*: Anal. Calcd. for $C_{15}H_{12}N_2$: C, 81.79; H, 5.49; N, 12.72. Found: C, 81.62; H, 5.40; N, 12.69.
9*f*: Anal. Calcd. for $C_{15}H_{12}N_2$: C, 81.79; H, 5.49; N, 12.72. Found: C, 81.64; H, 5.63; N, 12.78.
9*g*: Anal. Calcd. for $C_{14}H_{11}NO$: C, 80.36; H, 5.30; N, 6.69. Found: C, 80.20; H, 5.28; N, 6.71.
11*a*: Anal. Calcd. for $C_{16}H_{14}N_2$: C, 82.02; H, 6.02; N, 11.96. Found: C, 82.10; H, 6.00; N, 11.87.
11*b*·CH_3I: Anal. Calcd. for $C_{17}H_{17}N_2I$: C, 54.25; H, 4.52; N, 7.46; I, 33.79. Found: C, 54.17; H, 4.54; N, 7.48; I, 33.80.
13: Anal. Calcd. for $C_{18}H_{16}N_2O_2$: C, 73.96; H, 5.52; N, 9.09. Found: C, 73.87; H, 5.48; N, 9.19.
14*a*: Anal. Calcd. for $C_{18}H_{16}N_2O$: C, 78.24; H, 5.84; N, 10.14. Found: C, 78.48; H, 5.93; N, 10.37.
15*a*: Anal. Calcd. for $C_{16}H_{14}N_2$: C, 82.02; H, 6.02; N, 11.96. Found: C, 81.88; H, 6.01; N, 12.11.
15*b*: Anal. Calcd. for $C_{17}H_{16}N_2$: C, 82.22; H, 6.49; N, 11.28. Found: C, 82.34; H, 6.75; N, 11.16.
[b]Broad singlet, 1H, exchangeable with D_2O.
[c]Literature (8, 9) m.p. 193–194 °C and u.v. and n.m.r. spectra.
[d]Infrared: ν_{max}(KBr) cm^{-1}: **9***c*: 1500, 1335 (NO_2); **12***a*: 1670 (CO); **12***b*: 3400 (NH), 1690 (CO); **12***c*: 2200 (CN); **13**: 3100 (NH), 1700 (CO); **14***a*: 1715 (CO); **14***b*: 1715 (CO).
[e]Characterized by formation of methiodide, m.p. 274 °C (dec.) lit. m.p. 273 °C, *cf.* ref. 36.
[f]Air sensitive compound.
[g]Methiodide, m.p. 233–235 °C.
[h]Literature (5*b*) m.p. 213 °C.
[i]Literature (5*c*) m.p. 142.5–143.5 °C and 53% yield.
[j]Literature (5*c*) m.p. 185 °C and 93% yield.

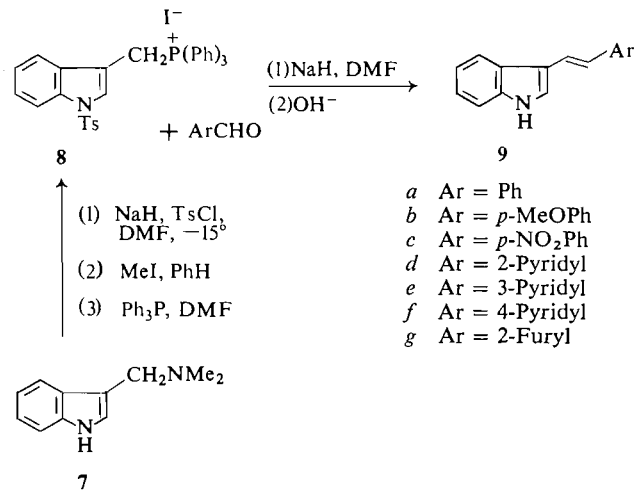

SCHEME 1

acidic solution and our previous results in the analogous preparation of 2-(2-aryl)vinylindole systems (**1**) (2).

Attempts to extend the Wittig synthesis to selected ketones (ethyl-4-pyridyl ketone, *N*-methyl-4-piperidone, and methyl vinyl ketone) failed. Finally, compound **8** with phthalic anhydride produced only small amounts of indole-3-aldehyde and triphenylphosphine, a reaction which may be of some mechanistic interest.

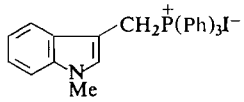

10

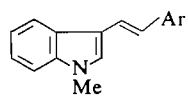

11

a Ar = 4-Pyridyl
b Ar = 3-Pyridyl

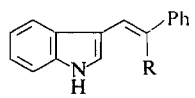

12

a R = CO_2H
b R = CO_2Et
c R = CN

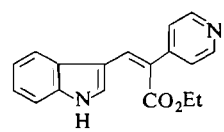

13

Preparation of Compounds 12a–c, 13, and 15a and b

In order to explore more extensively the photochemistry of the 3-(2-aryl)vinylindole derivatives (*vide infra*), compounds **12***a–c*, **13**, and **15***a* and *b* were also prepared by non-Wittig routes. Compounds **12***a–c* were known whereas **13** was obtained by a slight modification of the literature method (see Experimental section). On the other hand, **15***a* and *b* were synthesized by adaptation of a route (Scheme 2) which, although also previously described (19), deserves further exploitation.[8] However, since this Perkin-like condensation failed for the preparation of **15**, R = H ≡ **9***f*, the utility of the Wittig synthesis for this compound is maintained.

Physical and spectral data for compounds **12***a–c*, **13**, **14***a* and *b*, and **15***a* and *b* are included in Table 1. In all cases single isomers were obtained after crystallization (homogeneous by t.l.c. in several solvent systems) which are assumed to possess the stereochemistry shown in the structures (*Z*-isomers).

Photocyclization[9]

By analogy with the photochemical behavior of 2-(2-aryl)vinylindole derivatives (**1**) (2), irradiation of the corresponding 3-indolyl series (**2**) was expected to provide relatively short routes to benzo[*a*]- and a variety of pyridocarbazoles (**16–19**), compounds which were either unknown or prepared earlier by laborious methods (21–24). An additional incentive for the photochemical study was provided by the report of the isolation of an indole alkaloid, subincanine

[8]Compound **15***b* was first prepared in Dr. J. A. Joule's laboratories (Manchester). We are grateful to him for drawing our attention to this method and for experimental details.

[9]Few intramolecular photocyclization reactions of indoles are known, *cf.* ref. 20.

Can. J. Chem. Downloaded from www.nrcresearchpress.com by 210.87.254.6 on 09/05/12
For personal use only.

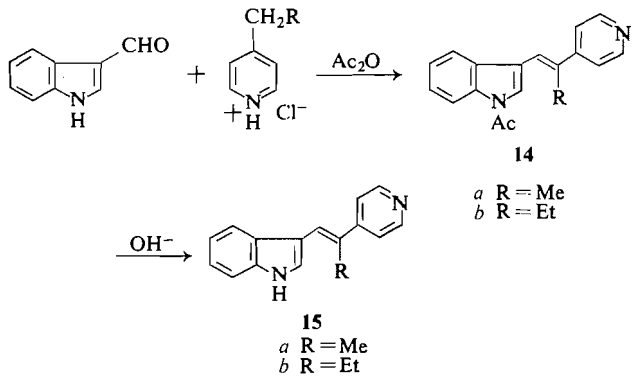

14

a R = Me
b R = Et

15

a R = Me
b R = Et

SCHEME 2

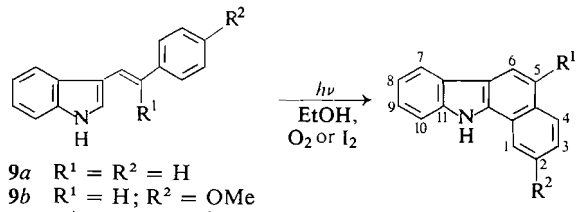

9*a* $R^1 = R^2 = H$
9*b* $R^1 = H; R^2 = OMe$
12*a* $R^1 = CO_2H; R^2 = H$
12*b* $R^1 = CO_2Et; R^2 = H$
12*c* $R^1 = CN; R^2 = H$

16

a $R^1 = R^2 = H$
b $R^1 = H; R^2 = OMe$
c $R^1 = CO_2H; R^2 = H$
d $R^1 = CO_2Et; R^2 = H$
e $R^1 = CN; R^2 = H$

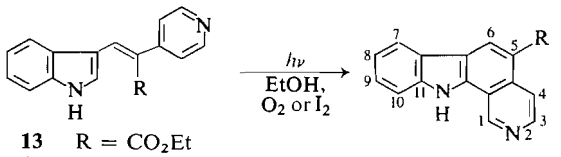

13 R = CO_2Et
15*a* R = Me
15*b* R = Et

17

a R = CO_2Et
b R = Me
c R = Et

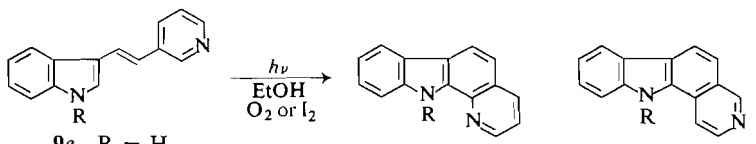

9*e* R = H
11*b* R = Me

18

19

a R = H
b R = Me

SCHEME 3

whose structure has a pyrido[3,2-*a*]carbazole (**17**) unit incorporated within it (25).

We first examined the series of compounds which do not possess a pyridine moiety. Photolysis of **9***a* and *b*, and **12***a–c* in the presence of iodine or oxygen produced the corresponding cyclodehydrogenated products **16***a* and *b*, and **16***c–e*, respectively (Scheme 3). Irradiation of **9***c* led to recovery of starting material. In the case of **9***g*, extensive decomposition was observed, a result which is probably due to the sensitivity of the furan ring to photooxidation (26). Results are summarized in Table 2.

Bizarre results were observed in the 3-(2-

Can. J. Chem. Downloaded from www.nrcresearchpress.com by 210.87.254.6 on 09/05/12
For personal use only.

Can. J. Chem. Downloaded from www.nrcresearchpress.com by 210.87.254.6 on 09/05/12
For personal use only.

TABLE 2. Photochemical preparation of benzo- and pyridocarbazoles

Compound[a]	% yield	Melting point °C (solvent)	λ_{max}(EtOH) nm (ε)	τ values (DMSO-d_6) N—H[b]	τ values (DMSO-d_6) Other
16*a*	36	227–229[c] (EtOH)	[c]	0.3	2.4–3.2 (m, 10H, aromatic H)
16*b*	24	221–223 (EtOH)	258(43 000) 283(34 000) 288(42 000) 304(32 000) 342(8000) 361(8200)	−1.7	0.46 (s, 1H, C_1—H) 0.93–2.8 (m, 8H, aromatic H)
16*c*[d,e]	56	222–223 (80% aqueous EtOH)	245(sh, 34 300) 255(36 300) 284(46 550) 304(19 900) 328(9700) 342(9400) 358(7750)	−2.67	0.9 (s, 1H, C_6—H) 0.5–2.8 (m, 8H, aromatic H) 3.9 (br, 1H, CO_2H, exchangeable with D_2O)
16*d*[d]	79	190 (EtOH)	240(41 000) 248(sh, 40 000) 267(24 000) 285(42 000) 303(28 000) 331(9000) 345(11 200)	−2.7	0.77 (m, 1H, C_1—H) 0.93 (s, 1H, C_6—H) 1.65 (d, 2H, J = 8 Hz, C_4—H) 2.1–2.8 (m, 6H, aromatic H) 5.52 (q, 2H, J = 7 Hz, CH_2) 8.56 (t, 3H, J = 7 Hz, CH_3)
16*e*[d]	79[f]	331 (EtOH)	235(47 000) 249(46 000) 265(38 000) 280(48 000) 288(51 000) 302(34 000) 334(10 000) 343(12 000) 358.5(9100)	−2.82	1.0 (s, 1H, C_6—H) 1.3–2.8 (m, 8H, aromatic H)
17*a*	79	237–238 (EtOH)	235(30 000) 249(32 000) 269(21 000) 290(42 000) 305(16 000) 373(12 000)	−0.02	0.56 (s, 1H, C_6—H) 0.72 (s, 1H, C_1—H) 1.0–2.7 (m, 6H, aromatic H) 5.55 (q, 2H, J = 7 Hz, CH_2) 8.65 (t, 3H, J = 7 Hz, CH_3)

Can. J. Chem. Downloaded from www.nrcresearchpress.com by 210.87.254.6 on 09/05/12
For personal use only.

TABLE 2 (*Concluded*)

Compound[a]	% yield	Melting point °C (solvent)	λ_{max}(EtOH) nm (ε)	τ values (DMSO-d_6) N—H[b]	τ values (DMSO-d_6) Other
17*b*	28	292–293 (EtOH)	238(40 150) 250(sh, 20 100) 255(sh, 28 700) 287(38 650) 307(sh, 16 700) 366(6600)	0.0	1.28 (br d, 1H, J = 6 Hz, C_1—H) 1.6 (br s, 1H, C_3—H) 1.65–2.8 (m, 6H, aromatic H) 7.28 (s, 3H, CH_3)
17*c*	48	251–252[g] (EtOH)			
18*a*	23	172–173[h] (EtOH)	[h]	−2.57	0.95 (br d, 1H, J = 7 Hz, C_2—H) 1.35–3.0 (m, 8H, aromatic H)
18*b*	20	128–130 (EtOH)	238(38 000) 256(34 000) 290(43 000) 333(13 000) 346(10 000) 363(9000)		[i]
19*a*	19	266–267[j] (EtOH)	[j]		1.0–2.8 (m, 10H, aromatic and indole N—H)
19*b*	17	195–197 (EtOH)	230(46 000) 242(42 000) 257(36 000) 282(48 000) 300(32 000) 353(9100) 371(8000)		1.4–2.9 (m, 9H, aromatic H) 6.6 (s, 3H, CH_3)

[a]Analytical data: **16***b*: Anal. Calcd. for $C_{17}H_{13}NO$: C, 82.57; H, 5.30; N, 5.66. Found: C, 82.61; H, 5.34; N, 5.60.
16*d*: Anal. Calcd. for $C_{19}H_{15}NO_2$: C, 78.87; H, 5.23; N, 4.84. Found: C, 78.91; H, 5.26; N, 4.79.
16*e*: Anal. Calcd. for $C_{17}H_{10}N_2$: C, 84.28; H, 4.16; N, 11.56. Found: C, 84.30; H, 4.21; N, 11.60.
17*a*: Anal. Calcd. for $C_{18}H_{14}N_2O_2$: C, 74.47; H, 4.86; N, 9.65. Found: C, 74.37; H, 4.90; N, 9.61.
17*b*: Anal. Calcd. for $C_{16}H_{12}N_2$: C, 82.73; H, 5.21; N, 12.06. Found: C, 82.62; H, 5.25; N, 12.12.
18*b*: Anal. Calcd. for $C_{16}H_{12}N_2$: C, 82.73; H, 5.21; N, 12.06. Found: C, 82.68; H, 5.27; N, 11.95.
19*b*: Anal. Calcd. for $C_{16}H_{12}N_2$: C, 82.73; H, 5.21; N, 12.06. Found: C, 82.81; H, 5.30; N, 12.18.
[b]Broad singlet, 1H, exchangeable with D_2O.
[c]Literature (23) m.p. 227–228 °C; u.v. spectrum identical to that reported (23).
[d]Infrared: ν_{max}(KBr) cm^{-1}: **16***c*: 3420 (NH), 1675 (CO); **16***d*: 3360 (NH), 1680 (CO); **16***e*: 3450 (NH), 2220 (CN); **17***a*: 1700 (CO).
[e]This compound was esterified under Fischer-Speier conditions to **16***d*, identical m.p. and mixture m.p.
[f]This compound precipitated as needles at the completion of the irradiation.
[g]Identical by m.p. and mixture m.p. with a sample provided by Dr. J. A. Joule, *cf.* footnote 10 in text.
[h]Literature (22) m.p. 172–173 °C; u.v. spectrum identical to that reported (23). Mixture m.p. undepressed with an authentic sample provided by Dr. R. H. F. Manske.
[i]Not determined due to insolubility.
[j]Literature (21) m.p. 265–266 °C; u.v. spectrum identical to that reported (23). Mixture m.p. undepressed with an authentic sample provided by Dr. R. H. F. Manske.

Can. J. Chem. Downloaded from www.nrcresearchpress.com by 210.87.254.6 on 09/05/12
For personal use only.

pyridyl)vinylindole series (**9***d–f*, **11***a* and *b*, **13**, and **15***a* and *b*). The photolysis of the 3-pyridyl derivatives **9***e* and **11***b* proceeded predictably to give mixtures of the expected pyridocarbazoles **18***a* and **19***a*, and **18***b* and **19***b*, respectively. Likewise the 4-pyridyl derivatives **13**, **15***a*, and **15***b* yielded compounds **17***a*, **17***b*, and **17***c*, respectively.[10] However, compound **9***d* showed no indication of pyridocarbazole (**18** or **19**) formation as evidenced by lack of development of typical aromatic fine structure absorption in the u.v. spectrum. Instead, strong absorption at 440 nm developed over an extended period of time which then partially diminished. Work-up of the reaction mixture gave a high recovery of starting material. An almost identical behavior was observed for compound **9***f*. A possible explanation for the failure of **9***d* and **9***f* to photocyclize may be the accumulation of a photostable intermediate (*e.g.* **20***a*) produced by a prototropic shift. It could then be argued that the success of the photocyclization of the 3-pyridyl case (**9***e*) is due to its inability to form an analogous intermediate. However, this analysis is not supported by the following observations: (*a*) the u.v. spectrum of the anhydro base **20***b* has been recorded (27) and shows no similarity to that developed during the photolysis of compound **9***d*; (*b*) the *N*-methyl derivative **11***a* which cannot form an analogous uncharged photointermediate also failed to photocyclize. Furthermore, the pyridinium salt **5**, R^1 = Me; R^2 = H, was stable to prolonged irradiation. The suggestion[11] that the lack of photocyclization is due to the inefficiency of the prior required *trans* → *cis* isomerization step (28) was pursued by a π–π^* sensitization experiment. Using compound (**9***f*) and biacetyl as the sensitizer, no evidence for photocyclization or *trans* → *cis* isomerization was obtained by u.v. spectral measurements. Finally, consideration was given to the possibility that the expected dihydro intermediate (*i.e.* **21**) is being produced but is stable to the normal oxidation conditions and thermally reverts to starting material. We tested this by following a literature precedent (29) in which exactly such a difficulty was overcome by using atomic iodine as the oxidant. Ultraviolet and t.l.c. evidence indicated that the pyridocarbazole (**17**, R = H) was slowly produced from **9***f* thus offering some support for the above hypothesis. However, since the conversion is so low as to preclude its isolation, no firm conclusion may be drawn regarding the potential intermediacy of **21**.

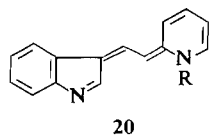

20

a R = H
b R = Me

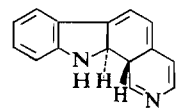

21

The contrasting photochemical behavior of compounds **9***d* and **9***f* when compared to **9***e* and especially **13** and **15***a* and *b* raise interesting mechanistic questions which require further exploration. In the present work, the synthetic utility of the photochemical route to benzo- and pyridocarbazoles **16–19** has been demonstrated.

Experimental

General experimental procedures may be found in a previous paper (1) except as follows. DMF and DMSO were dried by refluxing over calcium hydride followed by distillation. Anhydrous ethanol and methanol were prepared by refluxing the respective commercial absolute grade solvents over magnesium activated by iodine. Thin-layer chromatography was effected with Merck silica gel HF-254. Solvent systems routinely employed were dichloromethane–methanol, 10:1 and chloroform–methanol, 10:1. Preparative-layer chromatography (p.l.c.) was carried out with Merck silica gel GF-254. Column chromatography was carried out with Merck alumina (basic or neutral as specified) deactivated to activity III. The pyridine aldehydes were purchased from Aldrich Chemical Co. and were dried (Na_2SO_4) and distilled immediately before use.

Photochemical reactions were carried out in Pyrex vessels placed centrally in a Rayonet Photochemical Reactor equipped with 3500 Å lamps and internally cooled to 15–20° by a cold-finger condenser unless otherwise specified.

*Indole-1-(p-toluenesulfonyl)-3-methyltriphenylphosphonium Iodide (**8**)*

1-*p*-Toluenesulfonyl gramine was prepared by a modification of the procedure described by Suvorov and co-workers for the synthesis of 1-*p*-toluenesulfonyl indole (30). Sodium hydride (50% dispersion in mineral oil) (5.28 g, 110 mmol) placed in a flask under a slow stream of nitrogen was washed twice with dry petroleum ether (35–60°). The flask was immersed into a Dry Ice – carbon-tetrachloride bath (−15°) and 200 ml of DMF (freshly distilled) was added. To the stirred mixture was added dropwise a solution of 16.9 g (100 mmol) of gramine in 50 ml of dry DMF and stirring was continued for 1.5 h at

[10]The photochemical synthesis of **17***c* was also carried out in Dr. Joule's laboratories (35). We warmly thank him for a sample of **17***c*.

[11]We thank Professor D. G. Whitten for his interest in this problem.

Can. J. Chem. Downloaded from www.nrcresearchpress.com by 210.87.254.6 on 09/05/12
For personal use only.

−15°. A solution of vacuum-dried *p*-toluenesulfonyl chloride (19.1 g, 100 mmol) in 50 ml of dry DMF was added dropwise with stirring while maintaining the temperature at −15°. Stirring was continued at that temperature for 2 h, at 0 °C for a further period of 2 h, and at room temperature for 3 h. The solution was poured into 1.5 l of ice water and allowed to stand for 8 h. The aqueous layer was decanted and the remaining yellowish gum was extracted with methylene chloride (300 ml). The methylene chloride extract was washed with water (300 ml) and dried (Na_2SO_4). Chromatography on a short column (6 in. × 3/4 in.) of neutral alumina (grade III; methylene chloride) gave 1-*p*-toluenesulfonyl gramine as a yellow oil (30.1 g, 91%) which was homogeneous by t.l.c. in several solvent systems. A small sample of this oil when triturated with ice-cold cyclohexane deposited a white crystalline solid. Recrystallization from cyclohexane gave a sample, m.p. 71°; u.v. λ_{max} (EtOH), 252 (11 500), 284 (sh, 9100), 291 nm (sh, 8500); n.m.r. ($CDCl_3$) τ 1.9–3.0 (m, 9H, aromatic H), 6.5 (br s, 2H, CH_2), 7.75 (br s, 9H, CH_3).

The yellow oil (30 g, 91.4 mmol) obtained above was dissolved in dry benzene (400 ml) and treated with methyl iodide (17.0 g, 134 mmol). Stirring at room temperature for 6 h produced a bulky white solid. Filtration and vacuum-drying gave 1-*p*-toluenesulfonyl gramine methiodide as a white powder (40.2 g, 98%). Recrystallization of a sample from methanol–benzene (1:1) gave an analytical sample, m.p. 235° (sinter), 241° (dec.).

Anal. Calcd. for $C_{19}H_{23}N_2SO_2I$: C, 48.51; H, 4.89; N, 5.96; S, 6.81; I, 27.02. Found: C, 48.42; H, 4.80; N, 5.89; S, 6.76; I, 26.95.

A solution of 9.4 g (20 mmol) of 1-*p*-toluenesulfonyl gramine methiodide and 6.6 g (25 mmol) of triphenylphosphine in DMF (150 ml) was refluxed (oil bath at 150°) for 20 h under an atmosphere of nitrogen. The solvent was removed *in vacuo* and the brown gum-like residue was washed with benzene (2 × 100 ml). The gum was vigorously triturated with isopropanol (30 ml) to give compound **8** as a cream-colored solid (9.41 g, 70%). An analytical sample was prepared by repeated recrystallization from isopropanol, m.p. 134–135°; u.v. λ_{max} (EtOH) 238 (16 100), 258 (sh, 15 000), 263 (sh, 14 300), 271 (sh, 10 100), 288 (9700), 295 nm (9000); n.m.r. ($CDCl_3$) τ 2.0–3.2 (m, 24H, aromatic H), 4.67 (br d, 2H, J = 14 Hz, CH_2P), 7.75 (br s, 3H, CH_3).

Anal. Calcd. for $C_{34}H_{29}NO_2PSI$: C, 60.63; H, 4.31; N, 2.08; P, 4.60; S, 4.76; I, 18.87. Found: C, 60.60; H, 4.27; N, 2.01; P, 4.57; S, 4.78; I, 18.81.

1-p-Toluenesulfonyl-3-(N-methyl-N-p-toluenesulfonyl)-aminomethyl Indole (i)

Gramine (**7**) (1.69 g, 10 mmol) was treated with sodium hydride (0.72 g, 15 mmol) and *p*-toluenesulfonyl chloride (3.82 g, 20 mmol) in dry DMF according to the conditions described for the preparation of 1-*p*-toluenesulfonyl gramine above. The reaction mixture was poured into water (1.5 l) and the resulting precipitate was recrystallized from ethanol – methylene chloride (1:1) to give 1.0 g (21.5%) of the title compound, m.p. 238°; i.r. ν_{max} 1370, 1175 cm^{-1} (NSO_2R); u.v. λ_{max} (MeOH) 254 (11 600), 284 (9200), 291 nm (8700); n.m.r. ($CDCl_3$) τ 1.9 (br d, 4H, tosyl-*o*-H), 2.0–3.0 (m, 9H, aromatic H) 4.72 (br s, 2H, CH_2), 7.0 (br s, 3H, NCH_3), 7.76 (br s, 6H, tosyl CH_3).

Anal. Calcd. for $C_{24}H_{24}N_2O_4S_2$: C, 61.07; H, 5.17; N, 6.04; S, 13.79. Found: C, 61.01; H, 5.20; N, 6.14; S, 13.71.

Wittig Syntheses of 3-(2-Aryl)vinylindole Derivatives 9a–g and 11a and b

Compounds **9***a–g* and **11***a* and *b* were prepared according to the general directions described for **9***d* and **9***e* below, using 1–8 mmol of starting phosphonium salt (**8**) and a two-fold excess of aldehyde in approximately 100 ml of DMF. The reaction mixtures were invariably stirred at room temperature for 4–20 h and then at 80° for additional 4–20 h. The isolation of the intermediate *N*-*p*-toluenesulfonyl derivative of **9***d* is given; however, in all other cases direct hydrolysis to the 3-vinylindoles was effected as described for compound **9***e*. Compounds **9***c–g* and **11***a* were obtained as solids upon work-up; compound **11***b* was obtained as a gum and was purified by column chromatography over basic alumina (dichloromethane) to give a yellow homogeneous (t.l.c.) oil.

3-[2-(2-Pyridyl)vinyl]indole (9d)

To a stirred solution of 1-*p*-toluenesulfonyl-indole-3-methyltriphenylphosphonium iodide (**8**) (1.35 g, 2 mmol) in 110 ml of dry DMF under nitrogen there was added sodium hydride (50% dispersion in mineral oil) (0.096 g, 2 mmol) followed by a solution of pyridine-2-aldehyde (0.43 g, 4 mmol) in 15 ml of DMF. The mixture was stirred at room temperature for 10 h and then at 80° (oil bath temperature) for 14 h. The solvent was removed *in vacuo* and the residual gum was suspended in water (200 ml), and extracted with ether (200 ml). The organic extract was shaken vigorously with 2 *N* hydrochloric acid (100 ml) and the layers were separated. The acid layer was basified with solid sodium carbonate and extracted with ether (200 ml). The ether solution was dried (Na_2SO_4) and evaporated. The resulting residue was chromatographed over basic alumina (grade III; dichloromethane) to afford a gum (0.565 g) which was homogeneous by t.l.c. in several solvent systems; n.m.r. ($CDCl_3$) showed it to be 1-*p*-toluenesulfonyl-3-[2-(2-pyridyl)vinyl]indole: τ 1.9 (br d, 1H, pyridine α-H), 2–3.3 (m, 14H, vinyl and aromatic H), 7.84 (s, 3H, CH_3).

The gum (0.565 g) was dissolved in ethanol (50 ml) and 10% aqueous sodium hydroxide solution (100 ml) was added. The mixture was heated at 70° until it became homogeneous. Excess alkali was neutralized with dilute hydrochloric acid and the solution was rendered basic with solid sodium carbonate. Cooling in ice provided a yellow solid which was filtered and recrystallized from methanol to give 0.147 g (47%) of compound **9***d*.

3-[2-(3-Pyridyl)vinyl]indole (9e)

The reaction was carried out as described for the preparation of **9***d* using 2.69 g (4 mmol) of phosphonium salt **8**, 0.19 g (4 mmol) of sodium hydride (50% dispersion in mineral oil), 0.86 g (8 mmol) of pyridine-3-aldehyde, and 125 ml of dry DMF. After stirring at room temperature for 4 h and at 80° for 20 h, the solvent was removed *in vacuo*. The residual gum was suspended in 2 *N* sodium hydroxide solution (100 ml) and the mixture was refluxed for 1 h. The solution was acidified with 2 *N* hydrochloric acid (500 ml) and washed with ether (3 × 100 ml). The aqueous solution was basified with solid sodium carbonate and extracted with ether (400 ml). The ether extract

Can. J. Chem. Downloaded from www.nrcresearchpress.com by 210.87.254.6 on 09/05/12
For personal use only.

was dried (Na_2SO_4) and evaporated to dryness. The resulting yellow gum was triturated with ethanol to give 0.45 g (51%) of **9***e* as a crystalline solid.

Attempted Wittig Reaction between Phosphonium Salt **8** *and Phthalic Anhydride*

Compound **8** (1.35 g, 2 mmol), sodium hydride (0.092 g, 2 mmol), and phthalic anhydride (0.296 g, 4 mmol) in 100 ml of DMF were allowed to react as described for the preparation of **9***e*. After stirring at room temperature for 6 h and at 70–80° for 14 h, the solvent was removed *in vacuo* and the residue was dissolved in 100 ml of methanol. To this mixture was added 50 ml of a 6% aqueous solution of sodium hydroxide and the whole was stirred at 60–70° for 3 h. The bulk of the methanol was removed *in vacuo* and the remaining solution was diluted with 200 ml of water. Extraction of this basic solution with dichloromethane and subsequent chromatography over neutral alumina (dichloromethane) gave 0.024 g of triphenylphosphine identified by comparison with an authentic sample.

The above basic solution was acidified with 2 *N* hydrochloric acid. Extraction with dichloromethane followed by chromatography over neutral alumina (dichloromethane) yielded 0.028 g of indole-3-carboxaldehyde identical with authentic material as shown by spectral, m.p., and mixture m.p. comparison.

Non-Wittig Syntheses of Compounds **9***f*, **9***d*, **12***a–c*, **13**, *and* **15***a and b*

*3-[2-(4-Pyridyl)vinyl]indole (***9***f)*

The *N*-oxide of the title compound was prepared by adoption of a literature method (31). Indole-3-carboxaldehyde (1.45 g, 10 mmol), 4-picoline *N*-oxide (2.18 g, 20 mmol), piperidine (0.5 ml), and acetic acid (0.4 ml) were suspended in 25 ml of dry toluene and refluxed for 17 h under a Dean–Stark trap. The dark brown reaction mixture was cooled and the yellow solid was collected and washed with ice-cold ethanol. Recrystallization from ethanol gave 0.25 g (15%) of bright yellow crystals, m.p. 266° (dec.); u.v. λ_{max} (EtOH) 288 (38 000), 389 (26 000) nm; n.m.r. (DMSO-d_6) τ −1.65 (br s, 1H, exchanged with D_2O, NH), 1.87 (br d, 2H, J = 6 Hz, pyridine α-H), 2.2–3.1 (m, 9H, aromatic- and vinyl-H). This compound was subjected to deoxygenation according to the method described by Howard and Olszewski (32). An intimate mixture of the *N*-oxide (0.236 g, 1 mmol) and triphenylphosphine (0.288 g, 1.1 mmol) was heated at 250° for 45 min under an atmosphere of nitrogen. The reaction mixture was allowed to cool and was triturated with hot benzene (50 ml). The yellow solid was collected by filtration and crystallized from ethanol. There was obtained 0.076 g (35%) of **9***f*, shown to be identical to an authentic sample by m.p. and mixture m.p. determination.

*3-[2-(2-pyridyl)vinyl]indole (***9***d)*

According to the method of Ho (33) a mixture of the known (see footnote *e*, Table 1) salt **5**, R^1 = Me; R^2 = H, (0.362 g, 1 mmol) and 1,4-diazabicyclo[2.2.2]octane (DABCO) (0.224 g, 2 mmol) in dry DMF (5 ml) was refluxed for 3 h. The reaction mixture was allowed to cool and was poured into water (30 ml). The resulting solution was extracted with ether (50 ml). The ether solution was extracted with 2 *N* hydrochloric acid and the acid extract was basified and extracted with ether (50 ml). Evaporation of the solvent afforded a yellow gum which on trituration with methanol deposited compound **9***d* as a yellow crystalline solid, 0.022 g (10%), shown to be identical to an authentic sample prepared by the Wittig reaction.

*2-Phenyl-3-(3-indolyl)acrylic Acid (***12***a)*

A mixture of 2.72 g (20 mmol) of phenyl acetic acid, 1.45 g (10 mmol) of indole-3-aldehyde, 1.64 g (20 mmol) of sodium acetate, and 60 ml of acetic anhydride was gently refluxed under nitrogen in an oil bath for 12 h. The reaction mixture was poured into water (750 ml) and the resulting mixture was stirred vigorously for 3 h. The solid product was collected by filtration and then dissolved in ether (700 ml). The ether solution was extracted with 3 × 200 ml portions of 10% sodium bicarbonate solution. The combined basic extract was acidified with dilute hydrochloric acid solution and the resulting colorless solid was collected by filtration. Recrystallization from ethanol gave 0.82 g (26%) of *2-phenyl-3-[3-(1-acetyl)-indolyl]acrylic acid* (m.p. 265° (dec.); i.r. ν_{max} (KBr) 1705 (CO), 1680 cm^{-1} (CO_2H); u.v. λ_{max} (EtOH) 227 (sh, 23 370), 248 (sh, 17 840), 314 nm (14 080)) which was deacetylated as follows. A suspension of the acrylic acid derivative (0.540 g, 1.8 mmol) in 10% aqueous sodium hydroxide solution (70 ml) was heated on a steam bath for 40 min and the resulting yellow solution was cooled in ice and carefully acidified with dilute hydrochloric acid. The yellow solid was collected by filtration and recrystallized from ethanol–water (2:1) to give 0.355 g (83%) of compound **12***a*.

Compounds **12***b* and **12***c* were prepared by a literature method (5*c*).

*Ethyl 2-(4-Pyridyl)-3-(3-indolyl)acrylate (***13***)*

Ethyl 4-pyridylacetate. The method of Uskoković and co-workers (34) for the preparation of ethyl 3-ethyl-4-pyridylacetate was employed.[12] Into a 3-necked 2-l round-bottom flask flushed with nitrogen was added 70 ml (0.17 mol) of *n*-butyllithium in hexane. The solution was cooled to −60° and 18.2 g (0.18 mol) of freshly distilled (from NaH) diisopropylamine was added dropwise with stirring. After 10 min, 7.7 g (0.083 mol) of γ-picoline (freshly distilled from CaH_2) in THF (100 ml) was added dropwise. Stirring was continued for another period of 10 min and 30 g (0.26 mol) of diethyl carbonate in dry THF (100 ml) was added dropwise. The resulting dark-red solution was stirred at −60° for 30 min and then at room temperature for 2 h. Benzene (100 ml) was added followed by 10 ml of a saturated solution of sodium sulfate. The mixture was dried (Na_2SO_4) and filtered. The filtrate was evaporated *in vacuo* to yield a brown oil which was shaken with a mixture of 20 ml of ice water and 17 ml of concentrated hydrochloric acid. The acid extract was separated, cooled in ice, and basified with concentrated ammonium hydroxide. The mixture was extracted with dichloromethane (3 × 50 ml) and the extract was dried (sodium sulfate) and evaporated *in vacuo* to give a brown oil. High-vacuum distillation gave 8.2 g (60%) of *ethyl 4-pyridylacetate* as an oil, b.p. 98–101° (0.4 mm); i.r. ν_{max} 1700 cm^{-1}; n.m.r. ($CDCl_3$) τ 1.45 (br d, 2H, J = 6 Hz, pyridine α-H), 2.77 (br d, 2H, pyridine β-H), 5.8 (q, 2H,

[12]We are grateful to Dr. Uskoković for providing experimental details.

Can. J. Chem. Downloaded from www.nrcresearchpress.com by 210.87.254.6 on 09/05/12
For personal use only.

J = 7 Hz, CH_2CH_3), 6.4 (s, 2H, CH_2CO_2Et), 8.8 (t, 3H, J = 7 Hz, CH_3).

For the preparation of **13**, the procedure of Blume and Lindwall (5*c*) was adopted. A mixture of ethyl 4-pyridylacetate (4.95 g, 30 mmol), indole-3-aldehyde (4.35 g, 30 mmol), piperidine (10 ml), and pyridine (1 ml) was heated at 80° (oil bath temperature) for 12 h. The solution was evaporated to dryness *in vacuo* and the resulting brown gum was triturated with hot water (100 ml). The aqueous layer was decanted and the remaining gum was dissolved in ether (400 ml). The ether solution was extracted with 2 *N* hydrochloric acid (4 × 100 ml). The acidic extract was basified with solid sodium carbonate. The resulting solid was collected and recrystallized from ethanol to give 3.64 g (42%) of **13** as yellow needles.

*1-Acetyl-3[2-methyl-2-(4-pyridyl)vinyl]indole (**14***a*)

The procedure communicated to us by Joule[8] was modified as follows. A mixture of 1.45 g (10 mmol) of indole-3-aldehyde, 4.3 g (10 mmol) of 4-ethylpyridine hydrochloride, and 25 ml of acetic anhydride was refluxed gently in an oil bath under a blanket of nitrogen for 2.5 h. The reaction mixture was evaporated to dryness *in vacuo* and the residue was basified with a saturated sodium carbonate solution and extracted with ether (500 ml). An ether insoluble solid was collected by filtration. The ether solution was extracted with 2 × 500 ml of 2 *N* hydrochloric acid and the combined acid extract was basified with solid sodium carbonate. Extraction with ether gave, after evaporation, a solid which was combined with ether insoluble materials above and the whole was recrystallized from ethanol to give 1.89 g (68%) of compound **14***a*.

*3-[2-Methyl-2-(4-pyridyl)vinyl]indole (**15***a*)

A solution of 1.38 g (5 mmol) of **14***a* in 100 ml of ethanol was added to a solution of 0.68 g (10 mmol) of sodium ethoxide in 50 ml of ethanol and the mixture was refluxed with stirring for 30 min. The reaction mixture was cooled and acidified with 2 *N* aqueous hydrochloric acid. Most of the ethanol was removed *in vacuo* and the resulting solution was basified with a 10% aqueous sodium carbonate solution. Cooling in ice brought about precipitation of an off-white solid which was collected and recrystallized from ethanol to give 0.95 g (81%) of compound **15***a*.

Compounds **14***b* and **15***b* were prepared similarly.

*Photocyclization to Benzo- and Pyridocarbazoles **16**a–e, **17**a–c, **18**a and b, and **19**a and b*

Irradiations were carried out as previously described (2) on 100–500 mg scale. Ratios of 3-vinylindole–iodine–EtOH were typically 10:1:10 (w/w/v). All products were obtained as crystalline solids upon work-up with the exception of the mixtures **18***a* and **19***a*, and **18***b* and **19***b* which were separated by preparative-layer chromatography as described for one case below.

*11H-Pyrido[2,3-a]carbazole (**18***a*) *and 11H-Pyrido[4,3-a]carbazole (**19***a*)

A solution of 150 mg of 3-[2-(3-pyridyl)vinyl]indole (**9***e*) and 30 mg of iodine in 150 ml of ethanol was irradiated for 40 h. Enough sodium thiosulfate solution was added to destroy any remaining iodine and the solution was basified with solid sodium carbonate. Removal of solvent *in vacuo* followed by preparative layer chromatography (silica gel GF-254)(dichloromethane–methanol, 9:1) gave 35 mg (23%) of **18***a* and 28 mg (19%) of **19***a*.

*Photolysis of 3-[2-(2-Pyridyl)vinyl]indole (**9***d*)

A mixture of 100 mg of **9***d* and 20 mg of iodine in 100 ml of ethanol was irradiated. Ultraviolet examination of the reaction mixture after 2 h of irradiation showed a new peak at 440 nm. Further irradiation (9 h) showed no further change in the u.v. spectrum. On prolonged irradiation (24 h), the peak at 440 nm decreased in intensity. At no stage was there detected the characteristic u.v. absorption (λ_{max} (EtOH) 238 (40 100), 250 (sh, 28 720), 255 (sh, 20 020), 287 (38 600), 306 (sh, 16 670), 366 nm (6600)) of the expected product, 11*H*-pyrido[3,2-*a*]carbazole. Irradiation was discontinued and enough sodium thiosulfate solution was added to destroy the iodine. The mixture was basified with solid sodium carbonate and the solvent was removed *in vacuo*. The residue was extracted with dichloromethane and the extract was dried (Na_2SO_4) and evaporated. The resulting yellow residue was recrystallized from ethanol to give 91 mg of recovered **9***d*.

The same results were observed when a mixture of 10 mg of **9***d* and 0.5 mg of iodine in 40 ml of cyclohexane was irradiated at room temperature or at 0°.

Attempts to obtain isolable amounts of 11*H*-pyrido[3,4-*a*]carbazole by irradiation of **9***f* using (*a*) biacetyl as the sensitizer ($NiSO_4$ filter, I_2, 3500 Å, 24 h) (28) and (*b*) atomic iodine as the oxidant ($NiSO_4$ filter, I_2, 3500 Å and Hanovia C-H 3 (85 W), 108 h) (29) were unsuccessful.

We gratefully acknowledge the financial support of the National Research Council of Canada and Bristol Laboratories. We are indebted to Reilly Tar and Chemical Corp. and to M and T Products, Hamilton, for generous gifts of pyridine derivatives and triphenylphosphine, respectively. Thanks are due to Norman Reed, Morris Sabanski, Harvey Waterman, and Y.-C. Wong for assistance with preparations of intermediates. Drs. R. H. F. Manske and M. Kulka kindly provided several authentic samples of pyridocarbazoles.

1. J. A. EENKHOORN, S. O. DE SILVA, and V. SNIECKUS. Can. J. Chem. **51**, 792 (1973).
2. S. O. DE SILVA and V. SNIECKUS. Synthesis, 254 (1971).
3. R. J. SUNDBERG. The chemistry of indoles. Academic Press, Inc., New York. 1970. p. 222.
4. F. TROXLER. *In* Indoles. Part II. *Edited by* W. J. Houlihan. Wiley-Interscience, New York. 1972. p. 233.
5. (*a*) R. SEKA. Chem. Ber. **57**, 1868 (1924); (*b*) R. B. VAN ORDER and H. G. LINDWALL. J. Org. Chem. **10**, 128 (1945); (*c*) R. C. BLUME and H. G. LINDWALL. J. Org. Chem. **11**, 185 (1946); (*d*) A. F. AMES, D. E. AMES, C. R. COYNE, T. F. GRAY, I. M. LOCKHART, and R. S. RALPH. J. Chem. Soc. 3388 (1959).
6. W. E. NOLAND and D. N. ROBINSON. J. Org. Chem. **22**, 1134 (1957); J. BERGMAN. Acta Chem. Scand. **26**, 970 (1972); J. BERGMAN and R. CARLSSON. J. Heterocycl. Chem. **9**, 833 (1972).
7. F. TROXLER. *In* Indoles. Part II. *Edited by* W. J. Houlihan. Wiley-Interscience, New York. 1972. pp. 253 and 444 ff.
8. (*a*) N. N. SUVOROV, I. A. ORLOVA, and K. F. TURCHIN. Khim. Geterotsikl. Soedin. 250 (1969); (*b*) J. BERGMAN. Acta Chem. Scand. **26**, 970 (1972).
9. J. BERGMAN. Acta Chem. Scand. **25**, 1277 (1971).

10. G. FODOR, J.-P. FUMEAUX, and V. SANKARAN. Synthesis, 464 (1972); E. MARUSZEWSKA-WIECZORKOWSKA and J. MICHALSKI. Rocz. Chem. **38**, 625 (1964).
11. E. C. TAYLOR and S. F. MARTIN. J. Am. Chem. Soc. **94**, 2874 (1972).
12. L. R. SMITH. *In* Indoles. Part II. *Edited by* W. J. Houlihan. Wiley-Interscience, New York. 1972. p. 86.
13. R. J. SUNDBERG. The chemistry of indoles. Academic Press, Inc., New York. 1972. p. 93 ff.
14. H. HELLMANN and O. SCHUMACHER. Ann. **640**, 79 (1961).
15. R. P. RYAN, W. G. LOBECK, JR., C. M. COMBS, and Y.-H. WU. Tetrahedron, **27**, 2325 (1971).
16. R. E. BOWMAN, D. D. EVANS, and P. J. ISLIP. Chem. Ind. (London), 33 (1971); R. E. BOWMAN and D. D. EVANS. J. Chem. Soc. Perkin 1, 1926 (1972); R. E. BOWMAN, D. D. EVANS, J. GUYETT, H. NAGY, J. WEALE, and D. J. WEYELL. J. Chem. Soc. Perkin 1, 438 (1973).
17. H. PLIENINGER, C. WAGNER, and H. IMMEL. Ann. **743**, 95 (1971).
18. F. EIDEN and U. KUCKLAENDER. Arch. Pharm. (Weinheim), **304**, 523 (1971).
19. A. P. PHILLIPS. J. Am. Chem. Soc. **76**, 3986 (1954).
20. W. A. REMERS. *In* Indoles. Part I. *Edited by* W. J. Houlihan. Wiley-Interscience, New York. 1972. p. 182.
21. R. H. F. MANSKE and M. KULKA. Can. J. Res. [B], **27**, 291 (1949).
22. R. H. F. MANSKE and M. KULKA. Can. J. Chem. **30**, 712 (1952).
23. G. R. CLEMO and D. G. I. FELTON. J. Chem. Soc. 671 (1951).
24. G. R. CLEMO and D. G. I. FELTON. J. Chem. Soc. 1658 (1952).
25. A. J. GASKELL and J. A. JOULE. Tetrahedron Lett. 77 (1970).
26. A. SCHONBERG. Preparative organic photochemistry. Springer-Verlag, New York. 1968. p. 427 ff.
27. A. P. GRAY and W. L. ARCHER. J. Am. Chem. Soc. **79**, 3554 (1957); A. M. ACKERMAN and H. VELDSTRA. Rec. Trav. Chim. **73**, 629 (1954).
28. D. G. WHITTEN and Y. L. LEE. J. Am. Chem. Soc. **94**, 9142 (1972).
29. T. KNITTEL-WISMOSKY, G. FISCHER, and E. FISCHER. Tetrahedron Lett. 2853 (1972); Chem. Commun. 84 (1972).
30. A. D. NEKLYNDOV, L. A. SHCHUKINA, and N. N. SUVOROV. J. Gen. Chem. U.S.S.R. **37**, 747 (1967).
31. E. D. PARKER and A. FURST. J. Org. Chem. **23**, 201 (1958).
32. E. HOWARD, JR. and W. F. OLSZEWSKI. J. Am. Chem. Soc. **81**, 1483 (1959).
33. T.-L. Ho. Synthesis, 702 (1972).
34. M. USKOKOVIĆ, C. REESE, H. L. LEE, G. GRETHE, and J. GUTZWILLER. J. Am. Chem. Soc. **93**, 5904 (1971).
35. J. A. JOULE *et al.* To be submitted.
36. R. N. CASTLE and C. W. WHITTLE. J. Org. Chem. **24**, 1189 (1959).

Can. J. Chem. Downloaded from www.nrcresearchpress.com by 210.87.254.6 on 09/05/12
For personal use only.

The Synthesis of 1,7- and 1,8-Dimethylphenazines

ALFRED TAURINS AND ANDREW DAVENPORT LONG[1]

Department of Chemistry, McGill University, P.O. Box 6070, Station A, Montreal, Quebec H3C 3G1

Received November 6, 1973

The cyclization of 2',4- and 2',5-dimethyl-2-nitrodiphenylamine with sulfur in boiling diphenyl ether gave 1,7- (**1**) and 1,8-dimethylphenazine (**2**), respectively. A mixture of **1** and **2**, obtained by the condensation of 3,4-diaminotoluene with 3-methylcatechol, was separated into components by chromatography. The u.v. and i.r. spectra of **1** and **2** were recorded.

La cyclisation des diméthyl-2',4 et -2',5 nitro-2 diphénylamine avec le soufre dans de l'éther diphénylique bouillant conduit respectivement aux diméthyl-1,7 (**1**) et diméthyl-1,8 (**2**) phénazines. Le mélange de **1** et de **2** obtenu par condensation du diamino-3,4 toluène avec le méthyl-3 catéchol peut être séparé en ses constituants par chromatographie. On rapporte les spectres u.v. et i.r. des composés **1** et **2**.

[Traduit par le journal]

Can. J. Chem., **52**, 1307 (1974)

Introduction

In a framework of a major study of the reactivity of methyl groups attached to the phenazine nucleus in various positions, it was necessary to prepare several dimethylphenazines. In the group of 10 possible isomers, 6 dimethylphenazines have been mentioned in the literature, mainly as derivatives of various *o*-quinones, without studying their chemical and physical characteristics. Among the four unknown isomers (1,4-, 1,7-, 1,8-, and 1,9-dimethylphenazines) 1,7- (**1**) and 1,8-dimethylphenazine (**2**) have been prepared (1) only as a mixture by the Merz–Ris reaction (2, 3) from 3,4-diaminotoluene (**3**) and 3-methylcatechol (4), and the mixture has been tested (1) for their combined pesticide action without a separation of the isomers **1** and **2** beforehand.

In this work, 1,7- (**1**) and 1,8-dimethylphenazine (**2**) were prepared for the first time in pure state by two procedures. First, they were synthesized by unequivocal reactions involving the Waterman–Vivian (4) cyclization and secondly, a mixture of both isomers **1** and **2** was obtained by the Merz–Ris (2, 3) reaction and then the components were separated by extensive chromatography. The u.v. and i.r. spectra of **1** and **2** were recorded.

Discussion

(a) Synthesis of 1,7- (1) and 1,8-Dimethylphenazine (2) by Unequivocal Reactions

The key intermediate for the synthesis of 1,7-dimethylphenazine (**1**) was 2',4-dimethyl-2-nitrodiphenylamine (**5**) which was prepared by the condensation of 4-chloro-3-nitrotoluene (**7**) with *o*-toluidine (**8**) in the presence of anhydrous sodium acetate (4). Repeated experiments produced the compound **5** always in low yields. Two explanations may be offered to this effect. The reaction between **7** and **8** could be inhibited by the steric hindrance of the methyl group in *o*-toluidine (**8**) or by the destabilization of the carbanion-type intermediate (Meisenheimer complex (**10**)) by the methyl group in the ring originating from **7**.

1,8-Dimethylphenazine (**2**) was obtained from 2',5-dimethyl-2-nitrodiphenylamine (**6**) which was prepared by the condensation of *o*-toluidine (**8**) with 3,4-dinitrotoluene (**9**). The yields of **6** were only in a range of 20%, probably due to the low reactivity of *o*-dinitrobenzenes towards nucleophilic substitution by an aniline.

The cyclization of 2',4- (**5**) and 2',5-dimethyl-2-nitrodiphenylamine (**6**) into 1,7- (**1**) (Scheme 1) and 1,8-dimethylphenazine (**2**) (Scheme 2), respectively, was carried out by heating these substances with sulfur in refluxing diphenyl ether following the general scheme of the Waterman–Vivian reaction (4). The yields of **1** and **2** were 20 and 8%, respectively. The compounds were purified by chromatography and vacuum sublimation.

(b) Preparation of 1,7- (1) and 1,8-Dimethylphenazine (2) by Chromatographic Separation

The separation of the mixture of 1,7- (**1**) and

[1]Deceased.

Can. J. Chem. Downloaded from www.nrcresearchpress.com by 210.87.254.40 on 09/05/12
For personal use only.

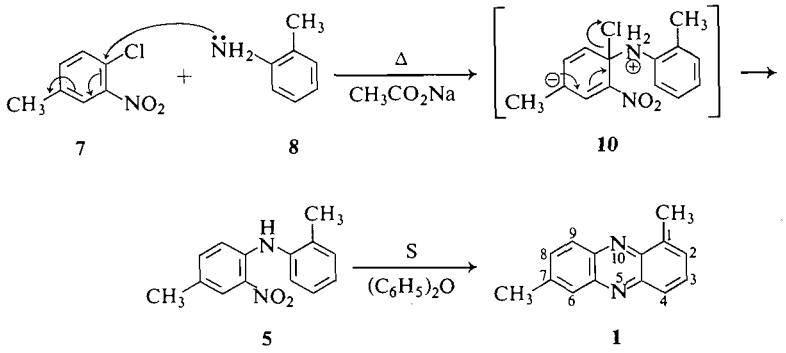

SCHEME 1

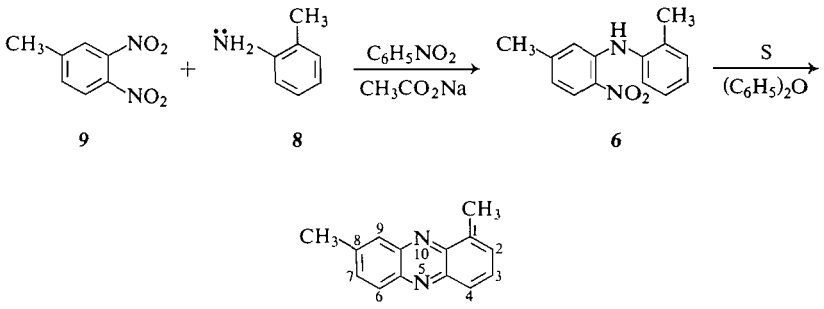

SCHEME 2

1,8-dimethylphenazines (**2**), obtained by the Merz–Ris reaction (2, 3), by a repeated extensive chromatography was possibly due to the fact that the high-melting isomer **2** was retained longer on an alumina column than the low-melting one (**1**) when ethyl ether – benzene (1:40) was used as an eluant.

Experimental

2′,4-Dimethyl-2-nitrodiphenylamine (5)

A mixture of 17.5 g (0.102 mol) of 4-chloro-3-nitrotoluene (**7**), 12.1 g (0.113 mol) of *o*-toluidine (**8**), and 17.0 g (0.207 mol) of anhydrous sodium acetate, in a 100-ml flask fitted for stirring and reflux, was heated in an oil-bath at 190–218° for 24 h and then at 218–228° for further 24 h. The dark red product was cooled to room temperature, mixed with 400 ml of ethyl ether and 200 ml of water, and the aqueous layer discarded. The ethyl ether layer then was extracted with water (3 × 200 ml), 5% hydrochloric acid (5 × 200 ml), and water (3 × 200 ml). Evaporation of the ether solution left a dark oily residue which was distilled with superheated steam. The first 1.5 l of the distillate contained only the starting materials. The next 10 l contained an orange-red solid material, which was extracted with ether. The solvent was evaporated to give 1.7 g (6.9%) of a red-orange compound, m.p. 85–89°. Recrystallization from methanol (30 ml) with Nuchar carbon gave 1.05 g (yield 4.3%) of bright orange-red crystals of 2′,4-dimethyl-2-nitrodiphenylamine (**5**), m.p. 92.5–93.5°. Vacuum sublimation raised the melting point of **5** to 93.0–95.0°.

Anal. Calcd. for $C_{14}H_{14}N_2O_2$: C, 69.4; H, 5.8; N, 11.6. Found: C, 69.7; H, 5.9; N, 11.7.

Infrared (KBr): 1640w, 1575m, 1520s, 1410m, 1345s, 1260vs, 1200w, 1150s, 1070w, 950m, 865w, 828m, 780m, 760m, 745vs.

1,7-Dimethylphenazine

A mixture of 3.26 g (0.0135 mol) of 2′,4-dimethyl-2-nitrodiphenylamine (**5**), 8.64 g (0.268 gram-atom) of sulfur, and 100 ml of diphenyl ether was stirred and refluxed for 5 h. The mixture was cooled, diluted to 300 ml with benzene, refrigerated overnight, and filtered. The red-brown filtrate was extracted with water (100 ml) and 20% hydrochloric acid (5 × 100 ml). The acid extract was treated with Norit and the deep-orange filtrate made basic with 160 ml of 50% sodium hydroxide solution. The precipitate was filtered off, washed with water, and dried at reduced pressure to obtain 1.04 g of a brown solid, melting in the range of 90–100°.

Vacuum sublimation of the material obtained (bath temperature 90°) gave 0.61 g of yellow crystals, melting range 100–110°. Chromatography of the sublimate on 100 g of alumina (Fisher A-540) using benzene as eluant gave 0.58 g of a yellow solid, m.p. 113–115°, which was sublimed to obtain 0.56 g (yield 20%) of 1,7-dimethylphenazine (**1**), m.p. 114–117°. A sample prepared by the catechol route melted at 117–118° and the mixture melting point of the two samples was 116.5–117.5°.

Can. J. Chem. Downloaded from www.nrcresearchpress.com by 210.87.254.40 on 09/05/12
For personal use only.

Can. J. Chem. Downloaded from www.nrcresearchpress.com by 210.87.254.40 on 09/05/12
For personal use only.

Anal. Calcd. for $C_{14}H_{12}N_2$: C, 80.7; H, 5.8; N, 13.5. Found: C, 81.0; H, 5.9; N, 13.5.

Mass spectrum: *m/e* 208, intense peaks at M − 1 and M − 2; i.r. (KBr): 3050m, 3020w, 2970s, 2950s, 2915vs, 1632m, 1650w, 1520m, 1482s, 1450m, 1433m, 1372m, 1348m, 1215w, 1128s, 1117m, 1067w, 1052m, 1032w, 1005w, 908w, 874w, 860s, 830m, 810vs, 770vs, 758s, 848s, 638m, 602s, 580m, 555w, 538w, 520m, 412w, 370w; u.v. (methanol): λ_{max} 210 (log ε 4.30), 254 (log ε 5.10), 364 nm (log ε 4.06).

2′,5-Dimethyl-2-nitrodiphenylamine (6)

Nitrobenzene (5 ml) was added to a mixture of 0.91 g (5 mmol) of 3,4-dinitrotoluene (**9**), 1.4 g (1.5 mmol) of *o*-toluidine (**8**), and 0.50 g of anhydrous sodium acetate and the mixture was heated at 152–158° for 48 h. The dark red mixture was then steam distilled to obtain two fractions: (*i*) 1800 ml, containing an orange red oil and (*ii*) 3700 ml, with an orange-red solid. The second fraction was extracted with ethyl ether (3 × 500 ml). The solution was dried over anhydrous sodium sulfate and the solvent was evaporated to give red crystals which, on recrystallization from 10 ml of methanol (Norit), gave 0.18 g (yield 14.8%) of orange-red crystals, m.p. 81–85°, of 2′,5-dimethyl-2-nitrodiphenylamine (**6**). Chromatography of the material on alumina, using benzene as the solvent and *n*-hexane as the eluent, raised the melting point of **6** to 82–88°. An analytically pure sample of **6**, m.p. 89–90°, was obtained by recrystallization from *n*-hexane.

Anal. Calcd. for $C_{14}H_{14}N_2O_2$: C, 69.4; H, 5.8; N, 11.6. Found: C, 69.6; H, 5.7; N, 11.7.

Infrared (KBr): 1620s, 1575m, 1520s, 1495s, 1435s, 1260vs, 1185w, 1100w, 1075w, 1035m, 955w, 925w, 755vs.

1,8-Dimethylphenazine (2)

A mixture of 2.42 g (0.01 mol) of 2′,5-dimethyl-2-nitrodiphenylamine (**6**), 6.40 g of sulfur, and 75 ml of diphenyl ether was heated in a flask equipped with a stirrer and condenser, and refluxed for 2.5 h. The dark orange reaction mixture was cooled, filtered (residue 1 on the filter) and the filtrate vacuum distilled (bath temperature 80–100°, pressure 3 mm/Hg) to give a yellow distillate containing diphenyl ether and some 1,8-dimethylphenazine (**2**), and a residue 2 in the distilling flask. The distillate was extracted with 20% hydrochloric acid (6 × 50 ml), the acid solution made alkaline with concentrated ammonia solution (150 ml), and extracted with chloroform (3 × 50 ml). The solvent was evaporated to give a yellow oil (residue 3). The residues 1, 2, and 3 were combined and subjected to distillation with superheated steam.

The middle fraction of the distillates containing 1,8-dimethylphenazine (**2**) was evaporated and the residue dissolved in 15 ml of 1:1 *n*-hexane–benzene and placed on a chromatography column of 100 g of alumina (Fisher No. A-540). The chromatogram as eluted with 1:1 *n*-hexane–benzene solution (1200 ml) to obtain 12 fractions. The fractions 4 to 11 from the second run were combined, evaporated, and the residue vacuum sublimed (bath temperature 120°, pressure 3 mm/Hg) to obtain 0.196 g (yield 9.4%) of yellow crystals, m.p. 141–144°. This material was rechromatographed on 50 g of alumina using 700 ml 1:1 *n*-hexane–benzene, followed by 100 ml benzene, as eluants. Ten fractions were obtained in this third run. The fractions 4 to 9 were combined, evaporated and the residue vacuum sublimed to produce 0.165 g (yield 7.9%) of 1,8-dimethylphenazine, m.p. 146.5–147.0°.

Anal. Calcd. for $C_{14}H_{12}N_2$: C, 80.7; H, 5.8; N, 13.5. Found: C, 81.0; H, 5.8; N, 13.5.

Mass spectrum: *m/e* 208; intense peaks M − 1 and M − 2; i.r. (KBr): 3045m, 2970s, 2950s, 2910vs, 1630m, 1518m, 1480w, 1428w, 1375m, 1362m, 1340m, 1195vw, 1065vw, 1052vw, 1032w, 1005w, 912w, 895w, 855s, 830s, 772s, 752m, 642m, 602w, 555w, 528w, 520m, 412w, 345w; u.v. (methanol): λ_{max} 210 (log ε 4.42), 254 (log ε 5.08), 364 nm (log ε 4.12).

Chromatographic Separation of 1,7- (1) and 1,8-Dimethylphenazine (2) Obtained by the Merz–Ris Reaction

A mixture of **1** and **2** was prepared from 3,4-diaminotoluene (**3**) (53.7 g, 0.44 mol) and 3-methylcatechol (**4**) (43.4 g, 0.35 mol).

It was established that the separation of 1,7- and 1,8-dimethylphenazine can best be achieved by using alumina as absorbent (Voelm Grade I or Fisher No. 540), in a ratio substance–alumina, 1:200–300. The eluant used consisted of diethyl ether – benzene 1:40. During the chromatography, the eluent was collected in small fractions, 2.5, 5, and 10 ml. The solvent was evaporated and the melting points of residues determined. The residual samples were combined according to their melting point ranges, and the combined fractions rechromatographed. The chromatography was repeated five times, until the two fractions, low melting (**1**) at 117–118° and high melting (**2**) at 147–148°, did not change on a further chromatography. At the later stages of the chromatography, the i.r. spectra were also used to follow the separation. The isomer **1** showed four characteristic strong bands at 810vs, 770vs, 758s, and 748s cm^{-1}, while the **2** isomer had only two bands in the same region, at 772vs and 752vs cm^{-1}.

We are grateful to the National Research Council of Canada for financial assistance.

1. Shell International Research. Maatschappij N.V. Neth. Appl. 6, 511, 395 (1966). Chem. Abstr. **65**, P2279e (1966).
2. V. Merz. Ber. **19**, 725 (1886).
3. C. Ris. Ber. **19**, 2206 (1886).
4. H. C. Waterman and D. L. Vivian. J. Org. Chem. **14**, 289 (1949).

The Electron Pair in Chemistry

R. DAUDEL
Centre de Mécanique Ondulatoire Appliquée de C.N.R.S., Paris, France
AND
R. F. W. BADER, M. E. STEPHENS, AND D. S. BORRETT
Department of Chemistry, McMaster University, Hamilton, Ontario
Received October 11, 1973

The reality of the electron pair as a fundamental unit in the electronic structure of molecular systems is evidenced by calculations which show that the most probable partitioning of a system is the one which localizes pairs of electrons in well-defined spatial regions or loges. The loges in turn, correspond to those regions of space generally associated with core, bonded, and nonbonded electrons. In terms of information theory, they yield the maximum amount of information concerning the localizability of the electrons. The most probable three-loge partitioning of the six-electron BH($X^1\Sigma^+$) system, for example, is dominated by the event which places two electrons in each of three loges, the location and shape of the loges being such as to justify the labelling of the electron pairs they localize as core, bonded and nonbonded. Since the loges are defined in real space and are totally nonoverlapping, one may define the volume of space occupied by pairs of electrons. In BH, for example, the volume of space required to contain 95% of the nonbonded pair of electrons is over two times larger than that required to contain 95% of the bonded pair. It is possible to define core loges which exhibit pair occupation probabilities ranging in value from 95% in LiH^+ to 85% in BH. Corresponding probabilities ranging in value from 75% to 90% are obtained for bonded and nonbonded loges. In the set of molecules studied here, the occurrence of events with such high probabilities is found only for loges which maximize the probability of a pair occupation.

Le fait que le doublet électronique est une unité fondamentale de la structure électronique de systèmes moléculaires est établi par des calculs qui montrent que la répartition la plus probable d'un système est celle qui localise les doublets électroniques dans des régions de l'espace bien définies ou loges. Les loges aux électrons liés ou non-liés, à leur tour correspondent à ces régions de l'espace généralement associées au noyau. Par rapport aux données de la théorie, on obtient le maximum de renseignements concernant la manière de localiser les électrons. La répartition la plus probable en trois loges des six électrons du système BH ($X^1\Sigma^+$) par exemple, est dominée par le cas qui place deux électrons dans chacune des trois loges; l'emplacement et la forme des loges sont tels qu'ils justifient la dénomination des doublets électroniques, liés ou non-liés, et qu'ils les localisent comme noyau. Puisque les loges sont définies dans un espace réel et sont entièrement sans recouvrement, on peut définir le volume de l'espace occupé par les doublets électroniques. Pour BH par exemple, le volume de l'espace nécessaire pour contenir 95% d'un doublet électronique non-lié dépasse en importance, deux fois celui qui est nécessaire pour contenir 95% d'un doublet électronique lié. Il est possible de définir des loges du noyau qui présentent des possibilités d'occupation d'un doublet de valeurs allant de 95% dans le LiH^+ à 85% dans le BH. Des probabilités similaires de valeurs allant de 75% à 90% sont obtenues pour des loges liées ou non-liées. Dans l'ensemble des molécules étudiées ici, la présence de cas avec de telles probabilités élevées est trouvée seulement pour des loges qui maximisent une probabilité d'occupation d'un doublet. [Traduit par le journal]

Can. J. Chem., **52**, 1310 (1974)

Introduction

Since the electron pair was first postulated to be of fundamental importance by Lewis (1) it has played a dominant role in the conceptual development of chemistry. The origins of the concepts bonded pair, unshared pair, and core of electrons are to be found in his paper, "The Atom and the Molecule" published in 1916. Nonetheless, the extent to which the distribution of electrons in a molecular system resembles pairs of electrons localized in specific spatial regions has not been determined.[1] Since the electronic wavefunction and charge distribution of a many-electron system

[1]A description of a system in terms of a localized set of molecular orbitals does not provide an answer to this question. Every orbital in a system extends over all space, and even within a localized set, there is a nontrivial overlap of *the charge distributions* arising from different orbitals. Furthermore, the occupation number of the orbital is fixed at two and thus a test of the importance of the pair concept is not possible.

Can. J. Chem. Downloaded from www.nrcresearchpress.com by 210.87.254.5 on 09/05/12
For personal use only.

Can. J. Chem. Downloaded from www.nrcresearchpress.com by 210.87.254.5 on 09/05/12
For personal use only.

are everywhere nonzero and pervade all space, there can be no partitioning of a system into completely localized groups of electrons. However, one can, within the framework of quantum mechanics, inquire as to *the probability* of an event which localizes fixed numbers of electrons in fixed spatial regions. If the electron pair concept is indeed fundamental, then one should find that of all possible events, the dominant one localizes pairs of electrons in some set of spatial regions. This probabilistic measure of the extent of localization within a system was proposed by Daudel (2).

Daudel and co-workers (2–4) have reasoned that there should be some "best" decomposition of the physical space of a system into a number of mutually exclusive spaces, called loges. The "best" loges were to represent the most probable (in a quantum mechanical sense) division of the physical space of the system into localized groups of electrons. This paper is concerned with determining the "best" loge decomposition of simple molecular systems and determining their properties. Does the dominant event indeed correspond to a partitioning into pairs? If so, to what extent, and are the loges containing these pairs spatially localized in such a way that they correspond to the usual concepts of core, bonded and unshared pairs of electrons?

Consider the partitioning of a total system containing N electrons into two mutually exclusive volumes (loges) Ω and Ω'. Then the probability of the *event* that n electrons will be found in the loge Ω when the remaining $(N - n)$ are confined to Ω' is

$$[1]\quad P_n(\Omega) = \frac{N!}{n!(N-n)!} \times \int_\Omega \mathrm{d}x_1 \ldots \int_\Omega \mathrm{d}x_n \int_{\Omega'} \mathrm{d}x_{n+1} \ldots \times \int_{\Omega'} \mathrm{d}x_N \Gamma^{(N)}(x_1, x_2, \ldots x_N)$$

where $\Gamma^{(N)}$ is a diagonal element of the spinless N-particle density matrix,

$$\Gamma^{(N)}(x_1, x_2, \ldots x_N) = \Sigma_{\text{spins}} \psi^*(x_1', x_2', \ldots x_N') \psi(x_1', x_2', \ldots x_N')$$

and the primes denote products of space and spin variables, $x_i' = x_i\sigma_i$. The binomial coefficient in eq. 1 accounts for the indistinguishability of the electrons, so that it matters not which n electrons are considered to be in Ω when the remaining $(N - n)$ are in Ω'. Since the wavefunction is assumed to be normalized, one has

$$[2]\quad \Sigma_n P_n(\Omega) = 1$$

The *average number* of particles in a given loge is

$$[3]\quad \bar{N}(\Omega) = \Sigma_n n P_n(\Omega) = \int_\Omega \rho(x)\mathrm{d}x$$

a result which, as indicated in eq. 3, must be equivalent to the integration of the charge density $\rho(x)$ over the same volume of space. If a single event has a dominant probability, it is referred to as the *leading event*. If $P_n(\Omega)$ is a leading event and the probability distribution of the other events is symmetrical about $P_n(\Omega)$, in particular if the probabilities of the *satellite events* $P_{n-1}(\Omega)$ and $P_{n+1}(\Omega)$ are equal to one another, then $\bar{N}(\Omega)$ will equal n. In other words, one must distinguish between the number of electrons localized in a given loge to yield a leading event and the average occupation number of the loge.

More recently, Aslangul (5) has proposed that the concepts of information theory be used to define the "best" division of a system into loges. According to this theory (6) our knowledge about a given system is a maximum when the "missing information function" $I(P_n,\Omega)$ is minimized, where

$$[4]\quad I(P_n,\Omega) = -\Sigma_n P_n(\Omega) \ln P_n(\Omega)$$

If the probability of one particular event (n particles in Ω) approaches a certainty, then

$$P_n(\Omega) \to 1 \text{ and } \Sigma_{m \neq n} P_m(\Omega) \to 0$$

In this instance our knowledge of the system would be maximal as we would know with certainty that n electrons are in Ω and $(N - n)$ in Ω'. Correspondingly, in this case $I(P,\Omega)$ approaches zero. At the other extreme, when all events are equally probable, our knowledge of the specific state of the system is minimal and the missing information function is maximized.

With this definition of the best set of loges one is still faced with the problem of finding that partitioning which does indeed minimize $I(P,\Omega)$. It is an additional aim of the present paper to find what properties of a system may be employed to yield loges minimizing the missing information function. In particular, we report on results which indicate that the boundaries of the "best" loges may in some cases be determined by the topographical features of the electronic charge distribution.

Bader and co-workers (7, 8) have proposed a

Can. J. Chem. Downloaded from www.nrcresearchpress.com by 210.87.254.5 on 09/05/12
For personal use only.

partitioning of a molecular system based on just such properties of the charge distribution. Specifically, the surface is defined by the gradient paths, traced out by the vectors $\nabla\rho(\boldsymbol{x})$, which pass through a null point $\nabla\rho(\boldsymbol{x}) = 0$ between a pair of adjacent nuclei. Thus, the surfaces are defined by the sets of paths of steepest descent through the charge distribution starting from the internuclear minima. Since the partitioning surfaces $S(\boldsymbol{x})$ are defined by $\nabla\rho(\boldsymbol{x})$, they have the property that

$$d\rho(\boldsymbol{x})/dn = 0 \quad \forall \boldsymbol{x} \in S(\boldsymbol{x})$$

where $\boldsymbol{n}$ is the unit vector normal to $S(\boldsymbol{x})$. Hence they are called surfaces of zero flux. This partitioning of a system into fragments enables one to partition any molecular property into fragment contributions. In particular, it yields values for the kinetic and potential energies of the fragments which are not only well-defined, but satisfy the quantum-mechanical virial theorem. These fragments represent spatially localized electron populations in the sense that the fragments are separated from one another by the minima in the electronic charge distribution. The question naturally arises as to whether or not such fragments correspond to the "best" loges for the system, *i.e.*, is $I(P,\Omega)$ minimized? This would require that an essential part of the information contained in the many-electron probabilities be retained in just the charge distribution $\rho(\boldsymbol{x})$, which is a one-electron probability function. ($\rho(\boldsymbol{x})$ is N times the probability density of one electron being at $\boldsymbol{x}$, with the other electrons anywhere in the total space of the system.)

The systems investigated here are $LiH^+(X^2\Sigma^+)$, $LiH(X^1\Sigma^+)$, $BeH^+(X^1\Sigma^+)$, $BeH(X^2\Sigma^+)$, $BH(X^1\Sigma^+)$ (ref. 9*a*), and $BeH_2(X^1\Sigma_g^+)$ (9*b*).[2] Their charge distributions are displayed in Fig. 1 and the principal features of these distributions are usefully summarized in terms of their virial fragment properties (10) which are given in Table 1.

The virial partitioning of LiH^+ and LiH yield average populations very close to two for the (Li) fragments and close to one and two for the (H) fragments, respectively. Thus the minima in $\rho(\boldsymbol{x})$ in LiH^+ and LiH partition the systems into a core distribution on Li with one and two bonding electrons, respectively, contained in the (H) fragment. The separation of the total charge into two fragment pairs is not as pronounced in BeH^+ as in the isoelectronic molecule LiH. Even so, the net charge on the (Be) fragment in BeH^+ is $+1.743$. The charge transfer from A → H is only slightly less in BeH and BH than in LiH. One would anticipate that the leading event for such a partitioning into fragments (loges) would be one which placed two electrons in (H) and three and four, respectively, in the (Be) and (B) fragments, these latter populations corresponding to a two-electron core (clearly discernible in Fig. 1) and one unshared valence electron in (Be) and an unshared pair in (B). The distinguishing feature of the charge distributions of BeH and BH is the extent to which the unshared valence density is confined to the nonbonded side of the

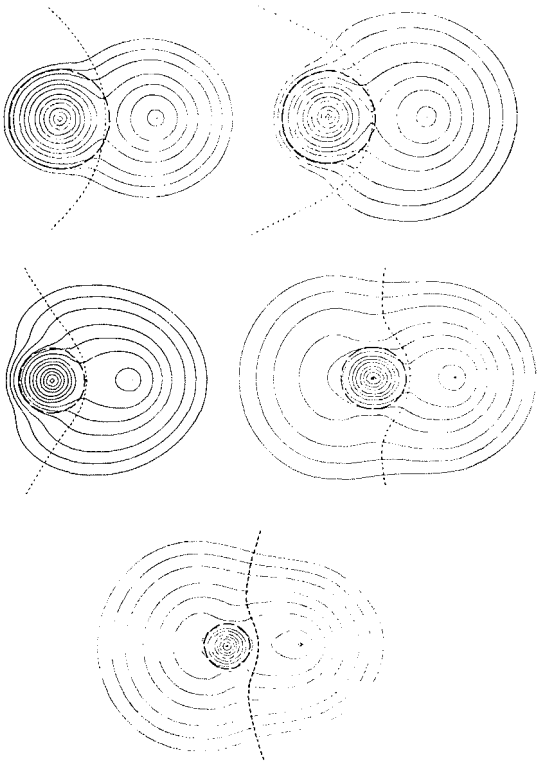

FIG. 1. Contour maps of the electronic charge distributions for (reading from left to right on succeeding rows) $LiH^+(X^2\Sigma^+)$, $LiH(X^1\Sigma^+)$, $BeH^+(X^1\Sigma^+)$, $BeH(X^2\Sigma^+)$, and $BH(X^1\Sigma^+)$. In each diagram the curve indicated by short dashes denotes the virial partitioning surface of zero-flux which defines the (A) and (H) fragments. The circle denoted by the longer dashes defines the boundary of the "best" spherical loge centered on the A nucleus. The contours in this figure and Fig. 3 (in a.u.) increase in value from the outermost contour inwards in steps of 2×10^n, 4×10^n, 8×10^n. The smallest contour is 0.002 with n increasing in steps of unity to yield a maximum contour value of 20.

[2]All functions are close to the Hartree–Fock limit.

TABLE 1. Characteristics of the charge distributions

AH	Bond lengths (a.u.)	$\bar{N}$(A)	$\bar{N}$(H)	Nonbonded charge on (A)
$LiH^+(X^2\Sigma^+)$	3.015	2.037	0.963	1.01
$LiH(X^1\Sigma^+)$	3.015	2.089	1.911	1.06
$BeH^+(X^1\Sigma^+)$	2.479	2.257	1.743	1.14
$BeH(X^2\Sigma^+)$	2.538	3.132	1.868	1.96
$BH(X^1\Sigma^+)$	2.336	4.246	1.754	2.75
$BeH_2(X^1\Sigma_g^+)$	2.540	2.278	1.861	—

Be and B nuclei and the very diffuse and extended nature of this region of the distribution (10). If we define the nonbonded charge on (A) as the total amount of charge contained in the volume on the nonbonded side of a plane through the A nucleus and perpendicular to the internuclear axis, we obtain the figures listed as such in Table 1. Such a plane almost halves a core density (yielding nonbonded populations of ~unity for (Li)) and indicates that 96% and 88% of the unshared valence density is localized in the nonbonded regions of the (Be) in BeH and the (B) in BH, respectively.

Core Loge

We illustrate a number of the principles involved in the loge partitioning method by detailing our search for core loges in diatomic molecules. The six electron $BH(X^1\Sigma^+)$ molecule is among the simplest systems which should exhibit all three kinds of electron pairs, core, bonded, and nonbonded.

Figure 2 illustrates results of a search for the best spherical loge in a two-loge partitioning of this system. Plotted in Fig. 2 are the values of the $P_n(\Omega)$ and $I(P,\Omega)$, where the volume Ω refers to a spherical loge centered on the boron nucleus of variable radius r. Also plotted, is the fluctuation in $\bar{N}(\Omega)$, $\Lambda(\bar{N},\Omega)$ where $\Lambda(\bar{N},\Omega) = \overline{N^2}(\Omega) - (\bar{N}(\Omega))^2$. Aside from the trivial peaks in $P_0(\Omega)$ for $r = 0$ and in $P_6(\Omega)$ for $r = \infty$, the single most probable event is obtained for a loge of radius 0.7 a.u. which simultaneously maximizes $P_2(\Omega)$ and minimizes $I(P,\Omega)$. The satellite events $P_1(\Omega)$ and $P_3(\Omega)$ have small and almost equal probabilities and thus $\bar{N}(\Omega)$, the average number of electrons in this most probable core loge, is two, as determined by the leading event $P_2(\Omega)$. In this two-loge partitioning there is an 85% probability of finding two electrons in a core loge of radius 0.70 a.u. and four electrons in the remainder of

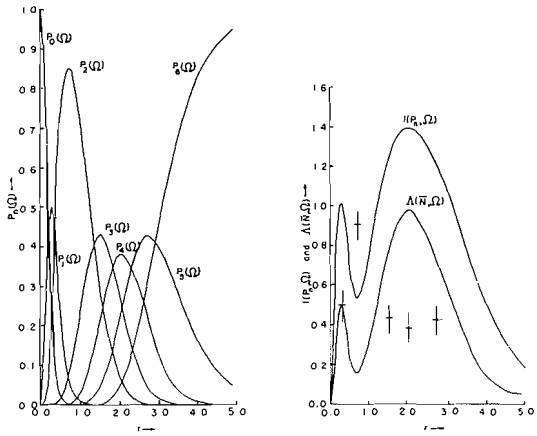

FIG. 2. The variation in the probabilities $P_n(\Omega)$, the missing information function $I(P,\Omega)$ and the fluctuation of $\bar{N}(\Omega)$, $\Lambda(\bar{N},\Omega)$ for a spherical loge of variable radius r (in a.u.) centered on the boron nucleus in $BH(X^1\Sigma^+)$. The positions of the maxima in the $P_n(\Omega)$ values for each value of n are indicated on the plot showing the variation in $I(P,\Omega)$ and $\Lambda(\bar{N},\Omega)$.

the system. Note that maximizing a single event, for example $P_1(\Omega)$, does not necessarily lead to a minimum in $I(P,\Omega)$. In the case of the maximum in $P_1(\Omega)$, the satellite events of zero and two electrons in Ω, have relatively high probabilities and $I(P,\Omega)$ attains a maximum value for this particular loge. The reality of the core electron pair concept as a dominant entity in electronic structure is evidenced in the maximum value of $P_2(\Omega)$ being so much in excess of the maxima observed for $P_1(\Omega)$, $P_3(\Omega)$, etc. Thus, while one can find a region of space which will localize a pair of electrons with an 85% probability, the maximum probability of localizing three or four electrons in a volume element of similar shape is only 43% or 38%, respectively.

Note that the variation in the missing information function $I(P,\Omega)$ parallels the fluctuation in $\bar{N}(\Omega)$, $\Lambda(\bar{N},\Omega)$. The use of the fluctuation in a loge population as a measure of the extent of the localization of the electrons has been proposed by Denis *et al.* (11).

Table 2 lists the properties of the best spherical core loges for the diatomic systems considered here. Only the probabilities for the leading event and the two satellite events are listed as these alone account for over 99% of the total probability. In each case, $I(P,\Omega)$ is minimized by a loge whose radius maximizes the probability of the pair occupation of the core loge. The probability of the satellite events $P_1(\Omega)$ and $P_3(\Omega)$ are nearly

Can. J. Chem. Downloaded from www.nrcresearchpress.com by 210.87.254.5 on 09/05/12
For personal use only.

TABLE 2. Properties of best spherical core loges in AH

AH	r_c	$P_1(\Omega)$	$P_2(\Omega)$	$P_3(\Omega)$	$\bar{N}(\Omega)$	$I(P,\Omega)$
LiH^+	1.55	0.0286	0.9427	0.0285	1.999	0.2604
LiH	1.42	0.0438	0.9123	0.0428	1.999	0.3635
BeH^+	1.00	0.0455	0.8969	0.0561	2.011	0.4103
BeH	0.95	0.0584	0.8804	0.0589	2.001	0.4602
BH	0.70	0.0714	0.8532	0.0716	2.002	0.5364

TABLE 3. Properties of virially defined (A) fragments

AH	Bonded radius of A (a.u.)	P_1(A)	P_2(A)	P_3(A)	$\bar{N}$(A)	$I(P,A)$
LiH^+	1.408	0.0054	0.9527	0.0418	2.036	0.2070
LiH	1.344	0.0069	0.8995	0.0912	2.089	0.3622
BeH^+	1.049	0.0034 P_2(A)	0.7536 P_3(A)	0.2261 P_4(A)	2.257	0.6379
BeH	1.072	0.0426 P_3(A)	0.7903 P_4(A)	0.1591 P_5(A)	3.132	0.6526
BH	1.001	0.0494	0.6757	0.2503	4.246	0.8549

equal to one another in all the cases and hence $\bar{N}(\Omega) = 2.00$. Note that the continuous decrease in $P_2(\Omega)$ from its value in LiH^+ to that in BH, parallels the extent to which the spherical loge encompasses the majority of the density in the (A) fragment. The greater degree of isolation of the core electrons from the remainder of the system found in LiH^+ as compared to BH is reflected in the $\Lambda(\bar{N},\Omega)$ values. In LiH^+, the fluctuation is only 0.05 compared to a value of 0.16 in BH.[3]

Table 3 lists the probabilities for a two-loge partitioning of the same molecules, using the surfaces of zero-flux to define the loges. For LiH^+ where the virial fragments possess near integer average populations, the missing information function $I(P,\Omega)$ attains a value significantly less than that obtained for the best spherical core loge. In LiH, the spherical core loge and the virial partitioning yield comparable results. In the remaining systems, the average populations of the virial fragments deviate more from integer values in the order BeH, BeH^+ and BH and P_2(H) (= P_2(Be) in BeH^+, P_3(Be) in BeH, and P_4(B) in BH) decreases in the same order. Clearly, in those cases where the virial partitioning method yields fragments which approximate a pair of core or bonded electrons, then the surfaces of zero-flux appear to yield the best decomposition of the system into loges, *e.g.*, LiH^+ and LiH. In general, however, the virial fragments contain both core and valence density with populations differing from integer values. In these cases, it is thus possible to define a *core* loge with a pair occupancy which surpasses in probability that for the virial fragment. Further discussion of the virial fragments is deferred until a consideration of the loge decomposition of the valence density.

The distance of the minimum in $\rho(x)$ along the internuclear axis from the A nucleus (the bonded radius of the (A) fragment) is listed in Table 3. The virial fragment partitioning gives the "best" loges in those two cases, LiH^+ and LiH, where the radius of the spherical loge required to maximize $P_2(\Omega)$, and hence minimize $I(P,\Omega)$, exceeds in value the bonded radius of (A). These examples suggest that the "minima in $\rho(x)$", the zero-flux surfaces, represent ultimate boundaries for the definition of the "best" loges.

The maximum values for $P_2(\Omega)$ and corresponding minimum values for $I(P,\Omega)$ reported in Tables 2 and 3 represent the best two-loge partitioning of these systems obtained from a large number of trials using surfaces which yielded

[3]Core loges and their corresponding probabilities have been previously determined by Daudel for Li_2 (12).

Can. J. Chem. Downloaded from www.nrcresearchpress.com by 210.87.254.5 on 09/05/12
For personal use only.

Can. J. Chem. Downloaded from www.nrcresearchpress.com by 210.87.254.5 on 09/05/12
For personal use only.

loges of various shapes and average numbers of electrons. The dominant requirement for the best loge appears to be one which maximizes $P_2(\Omega)$, the pair occupation probability.[4] For example, the charge distribution in the core region of B in BH is slightly ellipsoidal in shape, with the major axis directed along the internuclear axis. A loge was defined such that its surface coincided with a contour line of constant density. This yielded a core loge which reflected the quadrupolar distortion of the charge distribution. The missing information function was minimized when the boundary contour was such that $P_2(\Omega)$ was again maximized. The value of $P_2(\Omega)$ obtained for this more elaborate loge is slightly less than that obtained for the spherical core (0.8384 compared to 0.8532) and correspondingly, $I(P,\Omega)$ was increased slightly over the spherical core (0.5748 as compared to 0.5364).

In summary, the above results indicate that the most probable two-loge partitioning of a molecular system is one which isolates as one of the loges a core distribution, of shape and size such that $P_2(\Omega)$ is maximized. The *average* population of the loge need not necessarily be equal to 2.00 (*e.g.*, the (Li) fragment loges in LiH^+ and LiH). A doubly occupied core is a very probable entity in electronic structure. The charge distribution of LiH^+ may be partitioned by the surface of zero-flux into a doubly occupied core loge and a singly occupied bond loge with a probability in excess of 95%. Similarly, the distributions of LiH and BeH^+ may be partitioned to yield a doubly occupied core loge and a doubly occupied bond loge with probabilities of 91% and 90%, respectively. The pair concept is clearly dominant in these systems. In systems with an odd number of electrons, the pair occupancy requirement is greater for the core loge than it is for the bond loge (*e.g.*, LiH^+) and the same requirement for a bond loge exceeds that for a loge containing the nonbonded density (*e.g.*, see BeH below). This ordering is the one expected on energetic grounds.

[4]In only two cases did we obtain a loge which, while maximizing $P_2(\Omega)$, did not yield the lowest value obtained for $I(P,\Omega)$, *i.e.*, was not the "best" loge. In both cases the "best"loge and the one which maximized $P_2(\Omega)$ were very similar, and the differences in their $P_2(\Omega)$ and $I(P,\Omega)$ values very small. One example is the "best" core loge in LiH as defined by the surface of zero-flux, with $P_2(\Omega) = 0.90$ and $I(P,\Omega) = 0.3622$ and the best of the spherical core loges with $P_2(\Omega) = 0.91$ and $I(P,\Omega) = 0.3635$.

Partitioning of the Valence Charge Distribution

With the definition of the best spherical core loges in BH and BeH, we turn to the question of whether or not the valence electrons exhibit a correspondingly high probability of pairwise separation. If the pair concept is valid for the valence charge distribution, one would anticipate a two-loge partitioning of the remaining charge density to yield a bonded pair and an unshared pair in BH, and a bonded pair and a single nonbonded electron in BeH. The nonbonded populations of the (Be) and (B) fragments previously referred to, indicate that only a small increase in the volume of the nonbonded region defined by the planar surface will yield loges which, with the core loge excluded, will possess average populations of one and two electrons in BeH and BH, respectively. Accordingly, a radial partitioning surface was defined, centered on the Be or B nucleus, making an angle α with the internuclear axis and extending from the surface of the core loge to infinity (see Fig. 3). Thus, an intuitively probable three-loge partitioning of BeH and BH may be defined in terms of the core radius r_c and the angle α. Both r_c and α were varied independently to minimize the missing information function yielding the results listed in Table 4.

We shall denote a given event with the symbol (n_c,n_n,n_b) indicating that n_c electrons are in the core loge, n_n in the nonbonded loge, and n_b in the bond loge. Correspondingly, the probabilities of the events are indicated by a double subscript as $P_{n_c,n_n}(\Omega_c,\Omega_n)$ where necessarily $n_b = N - (n_c + n_n)$. The "best" core loge radius was found to be the same as that obtained for the two-loge partitioning of BH, the value maximizing $P_2(\Omega_c)$. The value of $I(P,\Omega_c,\Omega_n)$ was minimized when r_c and α were varied to maximize the probability of the event (2,2,2), a pair occupation of each loge. The probabilities of the most important events are given in Table 4. (Together they account for 99% of the total probability.) Note the dominant probability obtained for the event (2,2,2). Since the probabilities of all eight satellite events are close to being symmetrically paired with respect to (2,2,2), the average populations of all three loges equal 2.00.

Similar results were obtained for the five-electron system BeH. In this system the dominant event is (2,1,2), the unpaired electron being most likely found in the nonbonded loge. Thus, there is a 69% probability of spatially localizing the six electrons in BH into three pairs, the three loges

Can. J. Chem. Downloaded from www.nrcresearchpress.com by 210.87.254.5 on 09/05/12
For personal use only.

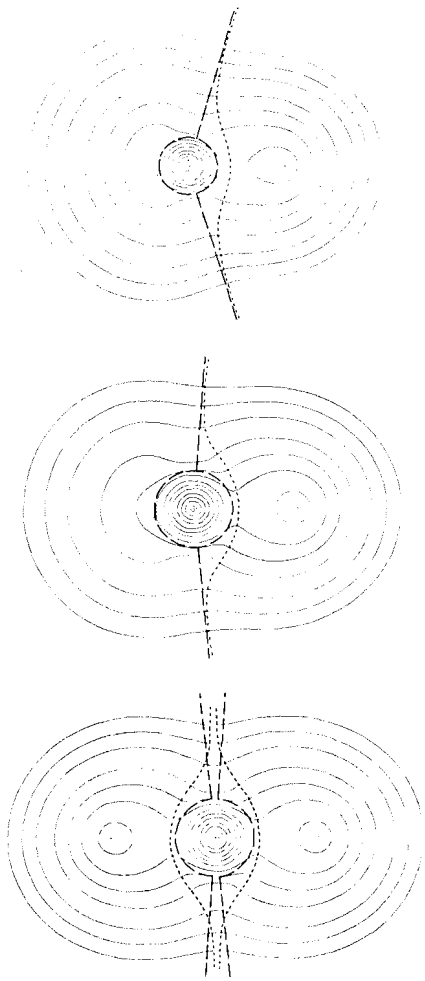

FIG. 3. Contour maps of the electronic charge distributions in BH($X^1\Sigma^+$), BeH($X^2\Sigma^+$), and $BeH_2(X^1\Sigma_g^+)$ showing the boundaries of the best three-loge partitioning of these systems (the long dashed lines) and, for comparison, the surfaces of zero-flux defining the (A) and (H) fragments (in short dashed lines). The angle α is measured (counterclockwise) from the internuclear axis up to the position of the radial line separating the bonded and nonbonded loges.

corresponding to core, nonbonded, and bonded regions of space. Similarly, in BeH there is a 77% probability of localizing two pairs of electrons in a core and bond loge while confining the remaining electron to a loge in the nonbonded region of space.

To illustrate that the important requirement for the minimization of $I(P,\Omega)$ is the maximization of $P_2(\Omega)$, rather than simply obtaining loges with average occupations of 2.00, we report another three-loge partitioning of BH. In this case the

TABLE 4. (*a*) Three-loge partitioning in BH

(*i*) Probabilities of events (n_c, n_n, n_b)*

n_c \ n_n	1	2	3
1	0.0026	0.0253	0.0391
2	0.0831	**0.6870**	0.0781
3	0.0377	0.0302	0.0016

(*ii*) Maximum two-loge probabilities and $I(P,\Omega)$ values

	Core	Nonbonded	Bonded
$P_2(\Omega)$	0.8532	0.7431	0.7649
$I(P,\Omega)$	0.5364	0.7981	0.7491

*r_c = 0.7 a.u., α = 73°, $\bar{N}(\Omega_c)$ = 2.001, $\bar{N}(\Omega_n)$ = 1.998, $\bar{N}(\Omega_b)$ = 1.999, $I(P,\Omega_c,\Omega_n)$ = 1.2328.

(*b*) Three-loge partitioning in BeH

(*i*) Probabilities of events (n_c,n_n,n_b)*

n_c \ n_n	0	1	2
1	0.0016	0.0250	0.0301
2	0.0541	**0.7744**	0.0511
3	0.0250	0.0329	0.0011

(*ii*) Maximum two-loge probabilities and $I(P,\Omega)$ values

	Core	Nonbonded	Bonded
$P_n(\Omega)$	0.8804(n = 2)	0.8328(n = 1)	0.8297(n = 2)
$I(P,\Omega)$	0.4602	0.5800	0.5931

*r = 0.95 a.u., α = 85°, $\bar{N}(\Omega_c)$ = 2.001, $\bar{N}(\Omega_n)$ = 1.007, $\bar{N}(\Omega_b)$ = 1.992, $I(P,\Omega_c,\Omega_n)$ = 0.9614.

system (with the exception of the core loge) was symmetrically halved by a σ_v symmetry plane. This yielded two identical valence loges, and average populations of 2.00 for all three loges. The value of $I(P,\Omega)$ increases from its "best" value of 1.2328 to 1.9408. In the case of the symmetrical valence loges, the events (2,1,3) and (2,3,1) are almost as probable as (2,2,2), their values being 0.213, 0.213, and 0.320, respectively. The average population of 2.00 obtained for the two valence electron pairs arises as an average over three events of comparable probability, rather than being the result of one leading event. Clearly, if one does not distinguish between bonded and nonbonded regions of space, one sacrifices possible information about the system.

In both BH and BeH, the radial surface partitioning the valence charge distribution into bonded and nonbonded loges, approximates closely a surface traversing the minimum in the

Can. J. Chem. Downloaded from www.nrcresearchpress.com by 210.87.254.5 on 09/05/12
For personal use only.

"trough" which occurs in this region of the charge distribution. This pinched effect in the contours of $\rho(x)$ provides a "natural" partitioning of the valence charge distribution into bonded and nonbonded loges.

The outer contour illustrated in the contour maps of the charge distribution has the value of 0.002 a.u. This particular contour is chosen since it defines a nonbonded size and shape for a molecule which agrees well with experimental estimates of these quantities (13). In general, it envelopes a region of space containing over 98% of the total charge present in the system. The 0.002 a.u. contour, together with the partitioning surfaces, define boundaries for the bonded and nonbonded loges, thereby enabling one to determine the volume of space occupied by the pairs of electrons in these two loges. With this physical definition of size, one finds that in BH, the nonbonded or "lone pair" electrons occupy a volume of space considerably larger than that required to contain the bonded pair, the ratio of the volumes of the nonbonded to bonded loges being 1.51. Even in BeH where there is but a single electron in the nonbonded loge as compared to the pair in the bonded loge, the ratio of loge volumes, nonbonded to bonded, is equal to 0.962. These volume ratios would clearly be enhanced if a contour of smaller value, say 0.001 a.u. was used to define the outer boundaries of the loges, since the charge density falls off more rapidly in the outer regions of the bonded loge than it does for the nonbonded loge.[5] This disparity in the volumes of space filled by nonbonded and bonded pairs of electrons is in accord with one of the basic postulates of Gillespie's theory of molecular geometry (that lone pairs of electrons occupy a larger volume of space than do bonded pairs (15)).

The probability of the leading event in a three-loge partitioning is generally less than that obtained in a two-loge partitioning because of the greater number of satellite events in the former case, all with finite probabilities. One may obtain the corresponding two-loge probabilities for any of the three loges by collapsing two of the loges into one and summing over all possible events for the combined loge. For example, the value of $P_2(\Omega)$ for the nonbonded loge in BH is given by

$$P_2(\Omega_n) = \sum_{n_c=0}^{4} P_{n_c,2}(\Omega_c,\Omega_n)$$

The probabilities of the leading events obtained for the core, nonbonded and bonded loge for a corresponding two-loge partitioning are listed in Table 4 together with their $I(P,\Omega)$ values. A meaningful comparison of probabilities is possible only if the number of loges is held constant and a comparison of $I(P,\Omega)$ values requires that the total number of events, *i.e.*, the number of loges and the total number of electrons, be the same in the systems compared. Probabilities obtained for a loge in a two-loge partitioning (*i.e.*, loge of interest plus the remainder of the system) will be referred to as "the probabilities" for that loge.

In both BeH and BH, the core loge exhibits a higher probability than either of the valence loges. This greater degree of localizability of the core electrons is also evident in the probabilities of the three-loge partitioning probabilities. In both BH and BeH, the principal satellite events are those which retain a pair of electrons in the core loge.

Reference to Fig. 3 indicates that in both BH and BeH the surfaces defining the "best" bond loges closely mimic in shape and lie adjacent to the zero-flux surfaces defining the (Be) and (H) fragments. Thus, the (H) fragments in these two molecules, as defined by the paths of steepest descent through $\rho(x)$, should be good approximations to the "best" bond loges. Reference to Tables 3 and 4 indicates that the probabilities of the leading events and $I(P,\Omega)$ values are comparable in the two cases. This is particularly true for BeH for which $P_2(H) \equiv P_3(Be) = 0.79$ with $I(P,H) = 0.6526$ compared to $P_2(\Omega_b) = 0.83$ and $I(P,\Omega_b) = 0.5931$.

We consider next the partitioning of the six-electron system, BeH_2. On the basis of the results previously obtained for BeH, one would anticipate the best three-loge partitioning to yield a core loge and two bond loges all with *average* populations of 2.00. If a core loge with $\bar{N}(\Omega_c) =$

[5]One could define a ratio of loge volumes by demanding that the boundary contours be chosen such that the same percentage of the total loge population be included in each volume. In BH, the 0.002 a.u. contour of the bonded loge defines a volume containing 95% of the bonded pair, while for the nonbonded loge, one must integrate out to the 0.001 a.u. contour to obtain the same fraction of its pair of electrons. This yields a ratio of nonbonded to bonded loge volumes equal to 2.11. Robb *et al.* (14) have proposed a definition of the size of nonbonded and bonded pairs of electrons based on the r.m.s. radii of localized molecular orbitals.

Can. J. Chem. Downloaded from www.nrcresearchpress.com by 210.87.254.5 on 09/05/12
For personal use only.

2.00 is to be retained, then the two identical bond loges are necessarily defined by a planar surface (originating at the surface of the core loge) perpendicular to the internuclear axis at the molecular mid-point. With α fixed at 90°, the only variable in this case is the radius of the core loge, and $I(P,\Omega)$ was minimized for $r_c = 0.93$ a.u., a value slightly less than that found for BeH. A summary of the results for this symmetrical partitioning is given in Table 5. The results are surprising. While the event (2,2,2) is the leading one, its probability is greatly reduced, to 33% compared to a value of 69% for (2,2,2) in BH and 77% for (2,1,2) in BeH. In BeH_2, the satellite events (2,1,3) and (2,3,1) have probabilities of 22% indicating an appreciable fluctuation in the populations of the bond loges. A comparison of the $P_2(\Omega)$ values for core and bond loges in BeH and BeH_2 in a two-loge partitioning, indicates that the localizability of the core loge is as well defined in BeH_2 as in BeH, but the bond loges in BeH_2 have $P_2(\Omega_b)$ values of only 37% (compared to 83% in BeH) and $P_1(\Omega_b)$ and $P_3(\Omega_b)$ values of 25%. The changes in the dimensions of the bond loge in passing from BeH to BeH_2 are very small, α is increased by 5° and r_c decreased by 0.02 a.u. Certainly, the disposition of the charge distribution in the bond loges is very similar in the two cases, a fact which is considered in more detail later. If α is set equal to 90° in BeH itself, the changes in the probability distribution and $I(P,\Omega)$ values are very small, the probability of the event (2,1,2) decreasing to 0.7682 and the value $I(P,\Omega_c,\Omega_b)$ increasing to 0.9694. The only significant difference between the two situations is that in one case the bond loge borders a singly occupied nonbonded loge, while in the other, it borders a doubly occupied bonded loge.

A rather remarkable increase in the probability of the bond loge is obtained if one sacrifices the concept of the traditional tight spherical core, the most probable single pair in the system. If one transfers directly the boundary of the best bond loge in BeH to BeH_2, that is, a surface defined by the radial arms ($\alpha = 85°$) and their intersection with the spherical core ($r_c = 0.95$ a.u.), then the "core" is extended to include an annular region of valence density (Fig. 3). This yields a three-loge partitioning of BeH_2 with a probability of 78% for its leading event (2,2,2), compared to 77% for the event (2,1,2) in BeH itself. The pair probability for this expanded core decreases to 83% from its "best" value of 88%, but this is more than

TABLE 5. Three-loge partitioning in $BeH_2(X^1\Sigma_g^+)$

(*a*) Symmetrical partitioning*

(*i*) Probability of events $(n_c,n_b,n_{b'})$

n_c \ n_b	1	2	3
1	0.0100	0.0201	0.0201
2	0.2179	0.3268	0.2179
3	0.0231	0.0231	0.0077

(*ii*) Leading events for two-loge partitioning and $I(P,\Omega)$ values

	Core	Bonded
$P_2(\Omega)$	0.8715	0.3706
$I(P,\Omega)$	0.4862	1.4276

*$r_c = 0.93$ a.u., $\alpha = 90°$, $\bar{N}(\Omega_c) = 1.998$, $\bar{N}(\Omega_b) = 2.001$, $\bar{N}(\Omega_{b'}) = 2.001$, $I(P,\Omega_c,\Omega_b) = 1.8914$.

(*b*) Extended core loge partitioning*

(*i*) Probability of events $(n_c,n_b,n_{b'})$

n_c \ n_b	1	2	3
1	0.0007	0.0242	0.0242
2	0.0235	0.7821	0.0235
3	0.0563	0.0563	0.0008

(*ii*) Maximum two-loge probabilities and $I(P,\Omega)$ values

	Core	Bonded
$P_2(\Omega)$	0.8294	0.8638
$I(P,\Omega)$	0.5884	0.5023

*$r_c = 0.95$ a.u., $\alpha = 85°$, $\bar{N}(\Omega_c) = 2.075$, $\bar{N}(\Omega_b) = 1.963$, $\bar{N}(\Omega_{b'}) = 1.963$, $I(P,\Omega_c,\Omega_b) = 0.9391$.

(*c*) Virial partitioning*

(*i*) Probability of events $(n_c,n_b,n_{b'})$

n_c \ n_b	1	2	3
1	0.0001	0.0032	0.0032
2	0.0189	0.7003	0.0189
3	0.1125	0.1125	0.0015

(*ii*) Maximum two-loge probabilities and $I(P,\Omega)$ values

	Core	Bonded
$P_2(\Omega)$	0.7384	0.8204
$I(P,\Omega)$	0.6972	0.5702

*$\bar{N}(c) = 2.277$, $\bar{N}(b) = 1.861$, $\bar{N}(b') = 1.861$, $I(P,\Omega_c,\Omega_b) = 1.0783$.

Can. J. Chem. Downloaded from www.nrcresearchpress.com by 210.87.254.5 on 09/05/12
For personal use only.

compensated for by a dramatic rise in the pair probability for the bond loge to 86%. The average loge populations are now necessarily different from 2.00, being 2.075 for the core and 1.963 for the bond loges with corresponding unsymmetrical distributions in the probabilities of the satellite events $P_1(\Omega)$ and $P_3(\Omega)$ for all three loges. The value of $P_3(\Omega_c)$ contributes 11% to the total probability of this extended core distribution. Since the spherical core has a high individual pair probability, one must assume that there is a significant probability that a single electron occupy the annular valence region between the two bond loges, and that this electron fluctuates between this region and the bond loges. Thus, the leading satellite event for the bond loges is $P_1(\Omega_b)$ (with a value of 8%) as opposed to $P_3(\Omega_c)$ for the core loge. Clearly, what is the "best" definable core loge for a system is not necessarily the best in a total partitioning of the system.

Any attempt to define a corresponding expanded core loge, to include a portion of the valence charge density, in the isoelectronic system BH, caused a dramatic decrease in the probability of the event (2,2,2) and a corresponding increase in $I(P,\Omega_c,\Omega_n)$. It would appear from these limited examples that an expanded core loge is only necessary as a buffer between two otherwise neighboring bond loges.

The final set of entries in Table 5 refer to the three-loge partitioning of BeH_2, using the surfaces of zero-flux to define (H) and (Be) fragment loges (Fig. 3). The general nature of these results is similar to those obtained in the "best" three-loge partitioning, but the probability of the leading event (2,2,2) is lower by 8% and the value of $I(P,\Omega_c,\Omega_b)$ is increased in value from 0.9391 to 1.0783. As in the "best" case, the leading satellite events are (3,1,2) and (3,2,1), corresponding to a fluctuation of an electron between a bond loge and the valence region of the expanded core.

In summary, we have been able to partition the space of a small molecular system into regions which provide the maximum possible information regarding the localizability of the electrons and exhibit a minimum in the fluctuation of the number of electrons which they contain. In some cases the boundaries of these "best" loges are determined by the surfaces of zero-flux in $\rho(\boldsymbol{x})$; in all cases the boundaries of the "best" bond loges lie near such surfaces (see Fig. 3). From the present examples, it would appear that the virially defined fragments provide good approximations to the "best" loges. Thus, in addition to exhibiting the maximum information regarding the localizability of the electrons in a system and a minimum fluctuation in $\bar{N}$, the "best" loges also exhibit or approximate the properties of the virial fragments, a satisfaction of the virial relationship and a maximum degree of transferability between different systems (7, 8), as evidenced here by the (H) fragment in BeH and BeH_2.

Calculations

$\Gamma^{(N)}(\boldsymbol{x}_1,\boldsymbol{x}_2,\ldots\boldsymbol{x}_N)$ was calculated using a Hartree–Fock wave function (9). In such a case, the calculation of the probability of an event, $P_n(\Omega)$, reduces to the evaluation of a sum of products of terms, each term representing the extent of overlap of a pair of orbitals over a loge. The overlap integrals between all possible pairs of orbitals over all the loges in a system were first evaluated by numerical integration using Gaussion quadrature techniques. These integrals were then grouped into products of terms as determined by the expression for a given $P_n(\Omega)$ or $P_{n,n'}(\Omega,\Omega')$. The number of such products in a diagonal element of the spinless N-electron density matrix is $N!N_\alpha!N_\beta!$, where N_α and N_β are the number of α and β electrons, respectively. Determining, ordering, and manipulating such a large number of products is the factor which at the moment limits the size of system which can be conveniently studied in the manner described here.

The accuracy of the numerical results was such that the sum of the $P_n(\Omega)$ or $P_{n,n'}(\Omega,\Omega')$ values never differed from unity by more than ± 0.00005 (eq. (2)) and the values of $\bar{N}(\Omega)$ as calculated in terms of the $P_n(\Omega)$ and by a direct numerical integration of $\rho(\boldsymbol{x})$ (eq. 3) in general agreed to within ± 0.0003. All computations were performed on a CDC 6400 computer.

One of us (R.F.W.B.) wishes to express his thanks to the Centre de Mécanique Ondulatoire Appliquée (Paris) for the hospitality afforded him during his visit and to the Centre National De La Recherche Scientifique (France) and the National Research Council of Canada for their support of the Canada–France Scientific Exchange Programme.

1. G. N. Lewis. J. Am. Chem. Soc. **33**, 762 (1916).
2. R. Daudel. C. R. Acad. Sci. **237**, 601 (1953); R. Daudel. The fundamentals of theoretical chemistry. Pergamon Press, Oxford. 1968.
3. R. Daudel, H. Brion, and S. Odiot. J. Chem. Phys. **23**, 2080 (1955); S. Odiot. Cahiers Phys. **81**, 1 (1957).

4. C. ASLANGUL, R. CONSTANCIEL, R. DAUDEL, and P. KOTTIS. Adv. Quantum Chem. **6**, 93 (1972).
5. C. ASLANGUL. C. R. Acad. Sci., Ser. B, **272**, 1 (1971).
6. E. SHANNON. Bell Syst. Tech. J. **27**, 379 (1948).
7. R. F. W. BADER and P. M. BEDDALL. J. Chem. Phys. **56**, 3320 (1972).
8. R. F. W. BADER, P. M. BEDDALL, and J. PESLAK, JR. J. Chem. Phys. **58**, 557 (1973).
9. (*a*) P. E. CADE and W. M. HUO. J. Chem. Phys. **47**, 614 (1967); (*b*) M. C. GOLDBERG and J. R. RITER, JR. J. Phys. Chem. **71**, 3111 (1967).
10. R. F. W. BADER and P. M. BEDDALL. J. Am. Chem. Soc. **95**, 305 (1973).
11. A. DENIS, J. LONGLET, AND J. P. MARLRIEU. Theoret. Chim. Acta, **29**, 117 (1973).
12. R. DAUDEL. J. Chim. Phys. **51**, 553 (1954).
13. R. F. W. BADER, W. H. HENNEKER, and P. E. CADE. J. Chem. Phys. **46**, 3341 (1967).
14. M. A. ROBB, M. J. HAINES, and I. G. CSIZMADIA. J. Am. Chem. Soc. **95**, 42 (1973).
15. R. J. GILLESPIE. Molecular geometry. Van Nostrand – Reinhold Co. Ltd., London. 1972.

Can. J. Chem. Downloaded from www.nrcresearchpress.com by 210.87.254.5 on 09/05/12
For personal use only.

Intramolecular Bromoamination. Part I

DONALD E. HORNING AND JOSEPH M. MUCHOWSKI[1]

Bristol Laboratories of Canada, Candiac, Quebec

Received October 10, 1973

The addition of bromine to 2,2-diphenyl-4-pentenylamine (**8***a*) resulted in the formation of 2-bromomethyl-4,4-diphenylpyrrolidine hydrobromide (**10***a*), the structure of which was established by its mass spectrum and other properties. Analogous products were obtained from the corresponding methyl secondary amine and two methyl-substituted primary amines.

The bromomethylpyrrolidines **10***a* and **10***c* gave the aziridines **11***a* and **11***b* on treatment with sodium hydride in DMF. Dry hydrogen bromide converted the unsubstituted aziridine **11***a* to 3,3-diphenyl-5-bromopiperidine hydrobromide (**12***a*). Liberation of the methyl substituted bromomethylpyrrolidine **10***b* from the hydrobromide salt resulted in the spontaneous transformation to a single 2-methyl-3-bromopiperidine (**12***b*) of unestablished stereochemistry.

L'addition du brome sur la diphényl-2,2 pentènyl-4 amine (**8***a*) conduit au bromhydrate de la bromométhyl-2 diphényl-4,4 pyrrolidine (**10***a*) dont la structure a été déterminée par spectrométrie de masse ainsi que par d'autres propriétés. Des produits analogues ont été obtenus à partir de la méthylamine secondaire correspondante ainsi que de deux amines primaires substituées par des groupes méthyles.

Les bromométhylpyrrolidines **10***a* et **10***c* par traitement avec de l'hydrure de sodium dans le DMF conduisent aux aziridines **11***a* et **11***b*. L'acide bromhydrique sec transforme l'aziridine non-substitué **11***a* en bromhydrate de diphényl-3,3 bromo-5 pipéridine (**12***a*). La neutralisation de l'acide bromhydrique libère la bromométhylpyrrolidine substitué par un groupe méthyle (**10***b*) qui se transforme spontanément en une seule méthyl-2 bromo-3 pipéridine (**12***b*) de stéréochimie non déterminée.

[Traduit par le journal]

Can. J. Chem., **52**, 1321 (1974)

The first intramolecular haloamination reactions were carried out almost a century ago by Ladenburg (1,2) and Merling (3) but the structures of the products were not assigned correctly until 1900. At that time Willstatter (4) demonstrated that the zinc and hydroiodic acid reduction of the products obtained from dimethylamino-4-pentene (**1**, $R^1 = R^2 = CH_3$) and bromine or iodine gave 1,1,2-trimethylpyrrolidinium iodide (**3**, $R^1 = R^2 = CH_3$). The five-membered

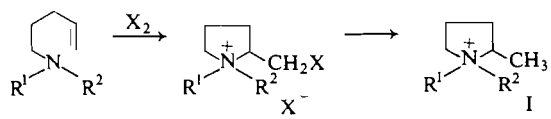

1 **2** **3**

cyclic structure **2** ($R^1 = R^2 = CH_3$; X = Br, I) was assigned to the adducts on the basis of this observation. The intramolecular haloamination reaction does not appear to have been examined further until 1962. In connection with their interest in the kinetics of the iodocyclization of various unsaturated systems, Shilov and coworkers (5) reported that primary as well as tertiary 4-pentenyl amines underwent the cyclization reaction. Subsequent publications (6–8) from that laboratory were devoted to a further elaboration of the mechanism and the generality of the reaction.[2] In all cases the products were assigned five-membered cyclic structures (**2**), presumably on the basis of Willstatter's observation and by mechanistic analogy to other halocyclization reactions (9).[3]

In relation to studies (14,15) concerning

[1]To whom enquiries should be addressed. Present address: Syntex, S.A., Division de Investigacion, Calle Carretera Mexico-Toluca No. 2822, Apartado Postal 10-820, Mexico 10, D. F.

[2]The existence of this reaction has evidently not been generally recognized in the chemical literature of the western world. Recent standard (!) reference texts (10–13) state only that, depending on the conditions untilized and the degree of *N*-substitution, amines undergo *N*-halogenation and/or oxidation to imines, nitriles, or carbonyl compounds in the presence of halogens. In point of fact, we too were unaware of the existence of this reaction until after[3] our studies were completed.

[3]We thank Dr. T. Conway of these laboratories for bringing ref. 9 to our attention.

Can. J. Chem. Downloaded from www.nrcresearchpress.com by 210.87.254.42 on 09/05/12
For personal use only.

Can. J. Chem. Downloaded from www.nrcresearchpress.com by 210.87.254.42 on 09/05/12
For personal use only.

various polycyclic antidepressants, it became necessary to prepare 4-aminomethylpyrrolidines of type **5**. Of several synthetic sequences which were expected to provide **5**, that proceeding via

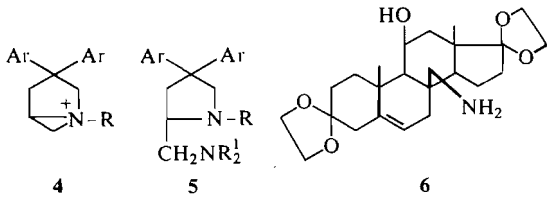

4 **5** **6**

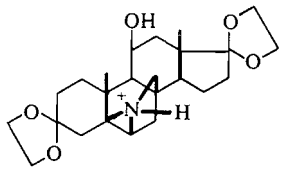

7

an aziridinium salt **4** (R = H, alkyl)[4] or a suitable precursor thereof (*e.g.* a β-haloamine), appeared to be especially attractive in view of the studies of Nagata *et al.* (17). These authors showed that certain δ,ε-unsaturated amines (*e.g.* **6**) gave aziridines, when treated with lead tetraacetate and potassium carbonate or aziridinium salts (*e.g.* **7**), when subjected to the action of *N*-chlorosuccinimide (NCS). Speculation concerning the mechanism[5] of the latter reaction led to the prediction that halogens alone ought to convert δ,ε-unsaturated amines to 2-halomethylpyrrolidinium salts,[2] which are well-known precursors of aziridines and/or aziridinium salts. It was indeed gratifying to find that the addition of bromine at room temperature to a dichloromethane solution of various 2,2-diphenyl-4-pentenylamines **8**[6] (Scheme 1) gave fair to excellent yields (see Table 1) of bromo hydrobromide salts to which the five-membered structures **10** were assigned on mechanistic grounds (see below, however).

Treatment of these salts with 2 mol of sodium hydride in dimethylformamide gave the aziridines **11***a* and **11***b* (Scheme 2), the structures of which were established by elemental analyses and spectroscopic techniques. The n.m.r. spectra, in particular, were uniquely consistent with a 1-azabicyclo[3.1.0]hexane system. For the parent compound (**11***a*), the two apparent doublets (Fig. 1) centered at δ 1.41 ($J \approx 2.8$ Hz) and δ 1.85 ($J \approx 5.5$ Hz)[7] were assigned to the C-6 *endo* and *exo* protons, respectively. As expected, replacement of the bridgehead proton by a methyl group as in **11***b* (Fig. 2) resulted in the collapse of the above multiplet to two apparent singlets (δ 1.57 and 1.62). The multiplets centered at δ 2.53 and 2.79 clearly were due to the C-5 and -4 protons since, for the 5-methyl compound, the former absorption was no longer present and the latter was replaced by an AB quartet ($J_{AB} = 13.8$) centered at δ 2.82. The low-field AB quartet ($J_{AB} = 12.2$ Hz) with doublets centered at δ 3.44 and 4.02 was necessarily assigned to the protons at C-2 since it remained essentially unaltered in the 5-methyl compound ($J_{AB} = 12.7$ Hz with doublets centered at δ 3.57 and 4.18). Finally, it should be noted that the absorption for the *endo* protons in both **11***a* (δ 1.85) and **11***b* (δ 1.62) were significantly broadened. This was probably due to long range coupling (20) with the equatorial proton at C-4, and on this basis the high (δ 2.47) and the low (δ 3.18) absorptions for **11***b* were assigned to the C-4 equatorial and axial protons, respectively.

If the parent aziridine was subjected to the

[4]For a recent paper on the synthesis of compounds of type **5** from aziridinium salts see ref. 16.

[5]We reasoned that one interpretation of the formation of the aziridinium salt **7** was that NCS had served as a source of Cl^+ to provide the chloronium ion **i**, which had then cyclized to the β-haloamine **ii** (the other product being succinimide). The intramolecular displacement of

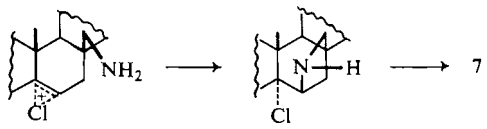

i **ii**

chloride ion from **ii** could then have produced the aziridinium salt **7**. It has recently been disclosed (18), however, that the *N*-chloroamine is the precursor of **7**. Therefore, in this case at least, intermediates such as **i** or **ii** cannot intervene, and, in fact, this reaction is now thought to be of the "nitrenoid" type.

[6]These amines were prepared (see Table 1) by standard techniques from the corresponding nitriles.

[7]These coupling constants were obtained by direct measurement and therefore they cannot be considered to be very accurate. The geminal coupling constant must be ≤0.5 Hz. This value and the other *J* values cited above were almost identical to those reported (19) for 2-phenylaziridine wherein J_{trans}, J_{cis}, and J_{gem} were 3.6, 6.0, and 0.6 Hz, respectively. Furthermore, the proton at C-2 resonated at δ 2.66, while the C-3 hydrogens *trans* and *cis* to this proton appeared at δ 1.48 and 1.86, respectively.

TABLE 1. Yields and physical constants of some substituted 4-pentenylamines

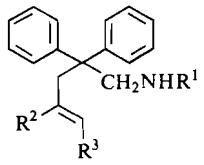

8

Compound No.	R^1	R^2	R^3	Yield (%)[a]	Melting point (°C) of hydrobromide	Analysis: Calcd. C	Calcd. H	Calcd. N	Found C	Found H	Found N
8*a*	H	H	H	88	223–225[b]	64.15	6.34	4.40	63.96	6.29	4.47
8*b*	H	H	CH_3	93	235–236[b]	65.07	6.67	4.21	65.08	6.78	4.39
8*c*	H	CH_3	H	89	225–226[b]	65.07	6.67	4.21	65.29	6.69	4.40
8*d*	CH_3	H	H	89	224–226[c]	65.07	6.67	4.21	65.03	6.54	4.35

[a]Yields of the crude undistilled bases.
[b]Crystallized from 2-propanol.
[c]Crystallized from acetonitrile.

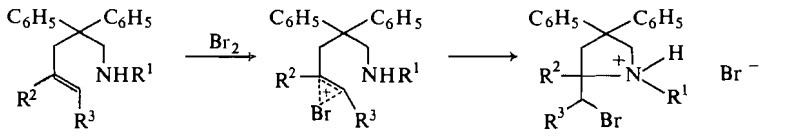

8 **9** **10**

a $R^1 = R^2 = R^3 = H$
b $R^1 = R^2 = H$; $R^3 = CH_3$
c $R^1 = R^3 = H$; $R^2 = CH_3$
d $R^2 = R^3 = H$; $R^1 = CH_3$

SCHEME 1

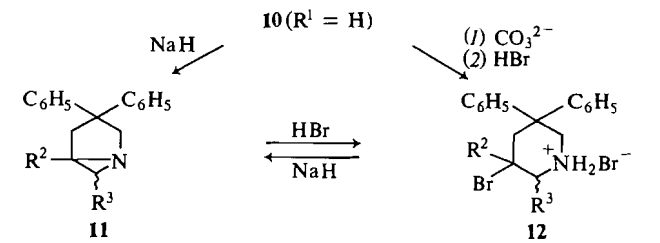

11
a $R^2 = R^3 = H$
b $R^2 = CH_3$, $R^3 = H$

12
a $R^2 = R^3 = H$
b $R^2 = H$, $R^3 = CH_3$

SCHEME 2

action of dry hydrogen bromide, a salt isomeric with **10***a* was produced (Scheme 2). The six-membered structure **12***a* was assigned to this compound on the expectation that the aziridinium salt would be opened in a manner such that the product derived from the thermodynamically more stable secondary carbonium ion would be obtained. Treatment of **12***a* with sodium hydride in DMF regenerated the aziridine **11***a*.

Although the structures assigned to **10***a* and **12***a* were reasonable on mechanistic grounds, more definitive evidence for the ring size in these compounds was desired. The n.m.r. spectra (free bases, see Figs. 3 and 4), though distinctly different and not inconsistent with structures **10***a* and **12***a*, were of a complexity[8] such that a clear

[8]This complexity persisted at 100 MHz; decoupling experiments did not lead to useful information.

Can. J. Chem. Downloaded from www.nrcresearchpress.com by 210.87.254.42 on 09/05/12
For personal use only.

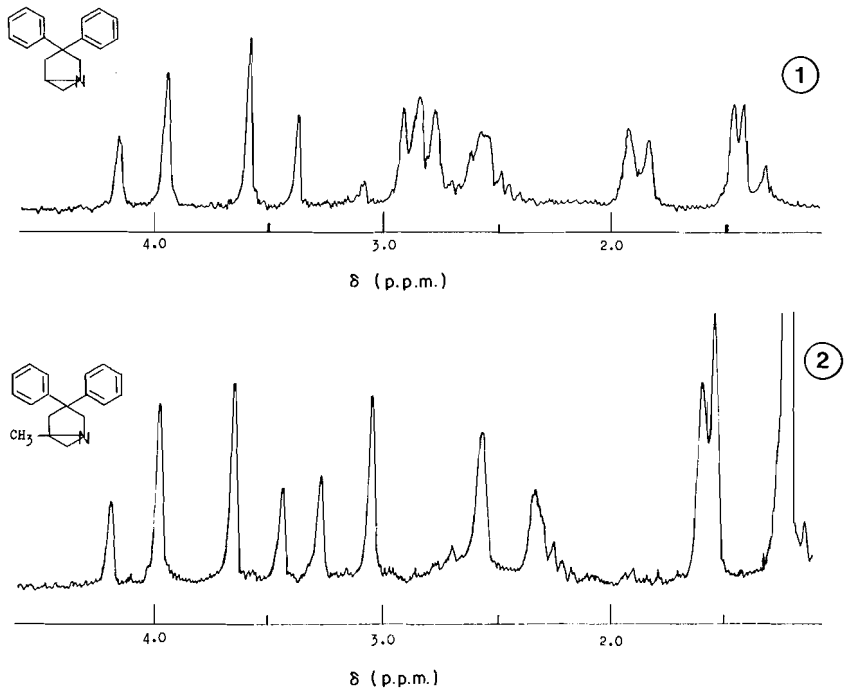

FIG. 1. The n.m.r. spectrum of the aliphatic protons of **11***a* in $CDCl_3$.
FIG. 2. The n.m.r. spectrum of the aliphatic protons of **11***b* in $CDCl_3$.

TABLE 2. Yields and physical constants of some 2-bromomethylpyrrolidinium bromides (**10**) and 3-bromopiperidinium bromides (**12**)

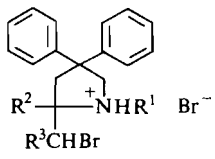

10

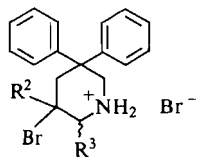

12

Compound No.	R^1	R^2	R^3	Yield (%)[a]	Melting point (°C)[b]	Analysis Calcd. C	Calcd. H	Calcd. N	Found C	Found H	Found N
10*a*	H	H	H	88–95	241–243[c]	51.40	4.82	3.53	51.31	4.76	3.47
10*b*	H	H	CH_3	69	194–196	52.59	5.14	3.40	52.51	5.20	3.45
10*c*	H	CH_3	H	68–71	162–164	52.59	5.14	3.40	52.58	5.04	3.41
10*d*	CH_3	H	H	33	211–213	52.59	5.14	3.40	52.48	5.10	3.58
12*a*	—	H	H	63	225–226	51.40	4.82	3.53	51.51	4.77	3.62
12*b*	—	H	CH_3	75	199–202	52.59	5.14	3.40	52.70	5.04	3.48

[a]Yields of once crystallized products.
[b]Melting point of analytical specimen.
[c]This salt was crystallized from 2-propanol; all the others were crystallized from acetonitrile.

cut decision concerning the annular size in the two isomers could not be reached. The mass spectrum of **10***a* was, however, consonant only with the bromomethylpyrrolidine structure (see Table 3). In addition to the weak molecular ion peaks at *m/e* 315 and 317, the spectrum showed an intense fragment due to the loss of the bromomethyl group at *m/e* 222 (32% of the base

Can. J. Chem. Downloaded from www.nrcresearchpress.com by 210.87.254.42 on 09/05/12
For personal use only.

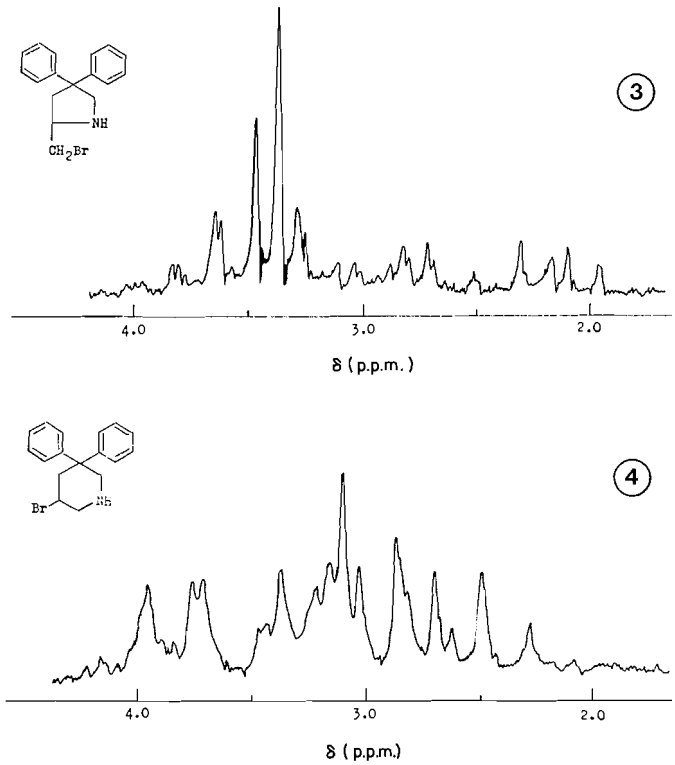

FIG. 3. The n.m.r. spectrum of the aliphatic protons of **10***a* in $CDCl_3$ (after D_2O exchange).
FIG. 4. The n.m.r. spectrum of the aliphatic protons of **12***a* in $CDCl_3$ (after D_2O exchange).

peak at *m/e* 56). This fragmentation mode is characteristic (ref. 21, p. 312) of α-substituted pyrrolidines. The above process was evidently of even greater importance for compounds **10***b* (*m/e* 222; 85% of base peak at *m/e* 70) and **10***c* (*m/e* 236; 54% of base peak at *m/e* 70), and for the latter compound, the loss of the bromomethyl group was immensely favored over the alternative loss of the methyl group (*m/e* 316, 314; 1%). The base peaks at *m/e* 56 and 70 shown by compounds **10***a*, and **10***b* and **10***c*, respectively, must have stemmed from a process which involved an initial β-cleavage to a stable diphenylmethyl radical ion. Finally, the spectra of each of the pyrrolidine derivatives had a strong peak at *m/e* 165 (fluorenyl cation) which is typical (ref. 21, p. 89) of compounds which contain a diphenylmethyl moiety.

Unfortunately, when the above spectra were measured, a specimen of **12***a* was no longer available. The mass spectrum of **12***b* was, however, fully consistent (see below) with the six-membered structure.

At one stage during this investigation, a chemical proof of the ring size in compounds **10** and **12** was contemplated. Since the majority of the methods which were considered required conversion of the salts to the free bases, it was necessary to establish the stability of the latter substances. As determined from an examination of the n.m.r. spectra, the free base corresponding to **12***a* was stable in deuteriochloroform at probe temperature (37°), while that of **10***a* underwent slight decomposition after several hours (peak broadening and appearance of weak new absorptions). In contrast to the parent system, liberation of the methyl derivative **10***b* from its salt (δ_{CH_3} = 1.80) resulted in the immediate appearance of two methyl doublets centered at δ 1.67 and 1.18. The latter absorption continued to grow at the expense of the former until, after 45 min the integral ratio was 85:15 in favor of the latter. If such a solution was treated with gaseous hydrogen bromide a salt (δ_{CH_3} = 1.50), isomeric[9] with the original one, could be isolated

[9]The n.m.r. spectrum of the crude bromination product of 2,2-diphenyl-4-hexenylamine showed that this isomer constituted about 9% of the product mixture.

Can. J. Chem. Downloaded from www.nrcresearchpress.com by 210.87.254.42 on 09/05/12
For personal use only.

TABLE 3. Mass spectra[a] of some 2-bromomethylpyrrolidinium bromides (**10**) and 2-methyl-3-bromo-5,5-diphenylpiperidinium bromide (**12***b*)

(**10***a*)		(**10***b*)		(**10***c*)		(**12***b*)	
m/e	(Relative intensity)[b]	*m/e*	(Relative intensity)	*m/e*	(Relative intensity)	*m/e*	(Relative intensity)
317	1	331	1	331	2	331	3
315	1	329	1	329	2	329	3
236	16	250	11	250	14	250	13
222	32	223	16	249	28	249	8
180	9	222	85	237	11	222	19
179	9	180	34	236	54	181	9
178	11	179	17	220	8	180	60
165	18	178	16	210	12	179	21
129	9	165	24	181	8	178	18
91	12	115	10	180	50	165	30
86	20	91	20	179	30	143	8
84	41	82	18	178	25	115	10
83	9	80	18	165	39	91	22
82	11	70	100	150	8	80	15
80	10	69	14	129	9	70	26
56	100	58	35	128	9	69	19
51	11			115	11	58	100
49	35			91	27	56	10
44	29			82	14		
				81	11		
				80	24		
				79	11		
				77	12		
				70	100		
				69	19		
				44	9		
				42	16		
				41	11		

[a]Measured with an Atlas CH-7 spectrometer using an ionization energy of 70 eV. The spectrum of (**10***a*) was measured at room temperature on the free base, whereas the spectra of the remaining compounds were determined on the salts using the heated inlet (120–140°) technique.
[b]Intensities rounded off to the nearest percent. With the exception of the molecular ions, peaks with a relative intensity of less than 8% were not tabulated.

in good yield. The enhanced rate of isomerization in this case, over that of the parent compound is consistent with the rate increase to be expected in the solvolysis of a secondary *vs.* a primary alkyl bromide (22). The six-membered structure **12***b* was assigned to this compund on mechanistic grounds, and was strongly supported by the mass spectrum. In addition to the expected fragment at 250 (13% of base peak at *m/e* 59) due to the loss of $Br^{\cdot}$, cleavage of the six-membered ring appears to have taken place so as to give two isomeric diphenylmethyl radical ions. The major cleavage occurred between C-5 and -6 and this ion then fragmented by two pathways. One of these (ref. 21, p. 314) led to the base peak at *m/e* 58, while the other (ref. 21, p. 313) gave rise to the intense (60%) fragment (diphenylethylene) at *m/e* 180. To account for the ion at *m/e* 222 (19%) it is necessary to postulate an initial cleavage between C-4 and -5. After the transfer of $H^{\cdot}$ from C-6 to C-4, cleavage α to the nitrogen occurred (loss of $(CH_3CHBr)^{\cdot}$ with the formation of the *m/e* 222 fragment ($(C_6H_5)_2C{=}CH\overset{+}{N}H{=}CHCH_3$)).

In a precisely executed study, Lattes and coworkers (23–27) showed that olefins reacted with primary or secondary amines in the presence of mercuric salts. Both the intermolecular (23, 24)[10] and intramolecular (25–28) variants of this reaction were shown to occur, the former giving rise to 2-aminoethyl mercuric salts. δ,ε-Unsaturated amines cyclized predominantly[11] or exclusively to 2-substituted pyrrolidines, while ε,δ-unsaturated amines gave piperidine derivatives as the sole products. These reactions were said to proceed via cleavage of an initially formed

[10]Hall *et al.* (33) have recently reported this reaction as well.
[11]The minor products were six-membered.

Can. J. Chem. Downloaded from www.nrcresearchpress.com by 210.87.254.42 on 09/05/12
For personal use only.

TABLE 4. Yields and properties of some levulinonitriles

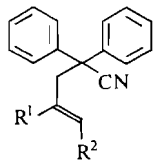

R^1	R^2	Yield (%)	Boiling point (°/mm) Observed	Boiling point (°/mm) Reported	Infrared (cm^{-1})[a]
H	H	90	116–119/0.01	129–131/1.5[b]	2238, 1645, 930
CH_3	H	85	118–120/0.03	126–127/0.03[c]	2240, 1654, 913
H	CH_3	88	127–128/0.01[d]	—	2236, 1674(w), 974

[a]Recorded as neat liquids.
[b]See ref. 29.
[c]See ref. 30.
[d]Anal. Calcd. for $C_{18}H_{17}N$: C, 87.41; H, 5.66. Found: C. 87.62; H, 5.64.

mercurinium ion **13** (X = HgCl, $HgOCOCH_3$) and, in the case of the δ,ε-unsaturated amines, the five-membered product **14** (X = HgCl, $HgOCOCH_3$) was formed by a stereospecific *trans* opening of this mercurinium ion.

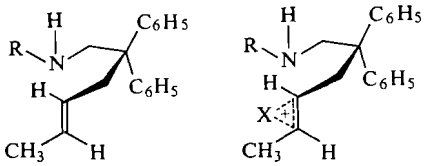

13

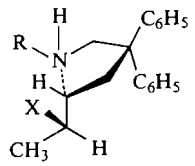

14

In view of the studies of Shilov *et al.* (5–7, 9) and Lattes and co-workers (23–28), it is highly probable that the intramolecular bromoamination reactions described in this work occurred via bromonium ion intermediates. On this basis, the bromination product **10***b* of **8***b*, would have structure **14** (R^1 = H; R^2 = C_6H_5; X = Br), but this assignment cannot be considered to be established in the absence of supporting evidence.

In closing, it is of value to point out that we are not unaware of the synthetic potential of the intramolecular[12] bromoamination reaction and future publications[13] will elaborate on this and other aspects of the reaction.

Experimental

The melting points were determined in a Gallenkamp melting point apparatus and are not corrected. The i.r. spectra were measured with a Unicam SP-200G i.r. spectrophotometer.

Preparation of the Nitriles

A 55% dispersion of sodium hydride in mineral oil (100 mmol) was washed free of the carrier with hexane, layered with anhydrous DMF (125 ml), and then cooled to 0°. Solid diphenylacetonitrile (100 mmol) was then added portionwise with stirring, and when gas evolution had ceased, the requisite allylic halide (100 mmol) dissolved in DMF (50 ml) was added in a dropwise manner. The cooling bath was removed, and after 2–3 h at room temperature the solution was poured into ice water and extracted with benzene. The extract was washed well with water, dried over sodium sulfate, and the solvent was then removed *in vacuo*. The residual oil was distilled *in vacuo*. For the yields and physical properties of these nitriles see Table 4.

Preparation of the Primary Amines 8a–8c

The nitrile (40 mmol) in dry ether (50 ml) was added dropwise at room temperature to a stirred suspension of lithium aluminum hydride (80 mmol) in dry ether (150 ml). After 2 h at room temperature, water was cautiously added at 0° to decompose the excess hydride, then 20% sodium hydroxide solution was added until a granular precipitate was obtained. The ether phase was decanted, combined with an ether washing of the solid residue, and then extracted with 10% hydrochloric acid. The acid phase was made basic with sodium hydroxide solution, and the product was extracted into dichloromethane. The

[12]The intermolecular variant of this reaction always gave 1,2-dibromoalkanes.

[13]Indeed, a recent publication (32) from these laboratories has described the application of the principles delineated herein as a central and vital portion of the total synthesis of several 14-hydroxymorphinans.

Can. J. Chem. Downloaded from www.nrcresearchpress.com by 210.87.254.42 on 09/05/12
For personal use only.

TABLE 5. N.m.r. spectra of some 2-bromomethylpyrrolidinium bromides (**10**) and 3-bromopiperidinium bromides (**12**)

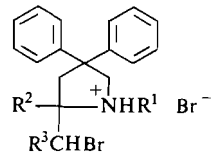

10

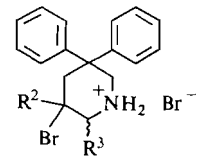

12

Compound No.	R^1	R^2	R^3	Solvent	Nuclear magnetic resonance (δ)[a]
10*a*	H	H	H	DMSO-d_6 – $CDCl_3$(1:1)	2.31–4.48(m,7H)[b], 7.06–7.42(m,10H), 9.78 (s,2H, W_H = 12)
10*b*	H	H	CH_3	Polysol-d_6	1.80 (d,3H,J = 6.5), 3.11–3.81 (m,4H), 4.44–4.71 (m,2H), 7.14–7.46 (m,10H), 9.66 (s,2H,W_H = 27)
10*c*	H	CH_3	H	Polysol-d_6	1.38 (s,3H), 3.02 (s,2H), 3.72 (s,2H), 4.23 (q,2H,$J \approx$ 13), 7.17–7.37 (m,10H), 9.44 (s,2H)
10*d*	CH_3	H	H	Polysol-d_6	2.48–5.00 (m,8H), 3.05 (s,3H), 7.17–7.56 (m,10H)
12*a*	H	H	H	DMSO-d_6	2.67–4.52 (m,7H), 7.17–7.54 (10H), 9.04 (s,1H,W_H = 25)
12*b*	H	H	CH_3	Polysol-d_6	1.50 (d,3H,J = 5.8), 2.67–4.54 (m,6H), 7.12–7.49 (m,10H), 8.84 (s,2H, W_H = 60)

[a]Recorded with a Varian A60-A spectrometer in solvents containing tetramethylsilane as an internal standard.
[b]d, doublet; m, multiplet; q, quartet; s, singlet. The J values and peak widths at half height are given in Hz.

extract was dried over sodium sulfate, and evaporated *in vacuo*. The residual oil was sufficiently pure to be used in the next step. The amines were characterized as hydrobromide salts which were prepared in ether and crystallized from an appropriate solvent (see Table 1). The i.r. spectra of the neat bases had bands at 3383 ± 15 and 3314 ± 4 cm^{-1}.

Preparation of the Secondary Amine **8***d*

The procedure of Johnstone *et al.* (31) was used.

The primary amine **8***a* (20 mmol) in dry dichloromethane was treated dropwise with trifluoroacetic anhydride (8 ml) at 15–25°. After 15 min, the solution was washed with dilute sodium bicarbonate solution and then with water. The dried solution was evaporated *in vacuo*, and the residue was taken up in dry acetone (80 ml) containing methyl iodide (80 mmol). The solution was warmed almost to reflux temperature, powdered potassium hydroxide (80 mmol) was then added, and the mixture was then heated at reflux temperature for 10 min. The solvent was removed *in vacuo*, water was added to the residue, and the product was then extracted into dichloromethane. Evaporation of the dried extract gave the oily alkylated trifluoroacetamide. This material was dissolved in methanol (120 ml), 1 *N* sodium hydroxide solution (60 ml) was added, and the resultant was maintained at reflux temperature for ½ h. The cooled solution was evaporated to a small volume *in vacuo* and the residue was diluted with water. The product was extracted into dichloromethane, the extract was dried over sodium sulfate and evaporated *in vacuo*. The residual oil was pure enough to be used in the next step. The i.r. spectrum (neat) had a band at 3330(w) cm^{-1}. The amine was characterized as the hydrobromide salt (see Table 1).

Bromination of the Unsaturated Amines

A solution of bromine (50 mmol) in dichloromethane (50 ml) was added dropwise at room temperature to a stirred solution of the amine (50 mmol) in dichloromethane (150 ml). The solvent was then removed *in vacuo* and the residue was crystallized from a suitable solvent. For the yields and properties of these salts see Table 2. The n.m.r. spectra of the salts are recorded in Table 5.

Preparation of the Aziridines

A 55% dispersion of sodium hydride in mineral oil (20 mmol) was freed of the carrier with hexane, layered with dry DMF (80 ml), and then cooled to 0° in a nitrogen atmosphere. The solid salt (**10***a*, **10***c*, or **12***a*; 10 mmol) was added portionwise at 0°, and then the mixture was stirred at room temperature for 1–1.5 h. The mixture was poured into a large volume of ice water, the product was extracted into benzene, the extract was washed well with water, and then dried. Evaporation of the solvent *in vacuo* gave oils which crystallized spontaneously. These aziridines were stable for prolonged periods at 0°. They could not be recrystallized; for analysis a small portion was sublimed under high vacuum. See Table 6 for the physical properties and yields of these compounds. The n.m.r. spectra of the aliphatic region of the aziridines are shown in Figs. 1 and 2.

Can. J. Chem. Downloaded from www.nrcresearchpress.com by 210.87.254.42 on 09/05/12
For personal use only.

TABLE 6. Yields and physical constants of some bicyclic aziridines

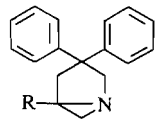

11

Compound No.	R	Yield (%)[a]	Melting point (°C)[b]	Analysis					
				Calcd.			Found		
				C	H	N	C	H	N
11*a*	H	95[c]	74–75[d]	86.77	7.28	5.95	86.62	7.24	5.93
11*b*	CH_3	97	65–66[d]	86.70	7.68	5.62	86.68	7.71	5.57

[a]Yield of the crude crystalline product.
[b]Melting point of the analytical specimen.
[c]The yield was 98% from the 6-membered bromo compound **12***a*.
[d]After sublimation at 60°/0.05 mm.

*3,3-Diphenyl-5-bromopiperidine Hydrobromide (**12a**)*

A solution of the aziridine **11***a* (930 mg, 3.95 mmol) in dry 1,2-dichloroethane (15 ml) was cooled to −20° and hydrogen bromide dissolved in the same solvent (17 mg/ml, 25 ml) was added at −10 to −20°. The cooling bath was removed, and after 2 h at room temperature the solvent was removed *in vacuo* and the residue was crystallized from acetonitrile. The yield and physical constants of this compound are recorded in Table 2. The n.m.r. spectrum is recorded in Table 5.

*2-Methyl-3-bromo-5,5-diphenylpiperidine Hydrobromide (**12b**)*

The pyrrolidinium salt **10***b* was dissolved in water and the solution was made basic with sodium carbonate solution. The base was extracted with chloroform, the solvent was dried over sodium sulfate, filtered, and then left at room temperature for 5 h. Dry hydrogen bromide was passed through the solution, the solvent was evaporated *in vacuo*, and the residue was crystallized from acetonitrile. The yield and physical constants of this compound are given in Table 2. The n.m.r. spectrum is recorded in Table 5.

We are indebted to Dr. M. Maddox and Dr. L. Tokes, Syntex Research, Palo Alto, California, for measuring the mass spectra, and for assisting in the interpretation thereof.

1. A. LADENBURG. Chem. Ber. **14**, 1344 (1881).
2. A. LADENBURG. Ann. Chem. **247**, 58 (1888).
3. G. MERLING. Chem. Ber. **17**, 2139 (1884); **19**, 2628 (1886).
4. R. WILLSTATTER. Chem. Ber. **33**, 365 (1900).
5. E. N. RENGEVICH, V. I. STANINETS, and E. A. SHILOV. Dokl. Akad. Nauk SSSR, **146**, 111 (1962).
6. V. I. STANINETS and E. A. SHILOV. Ukr. Khim. Zhur. **31**, 1286 (1965).
7. V. I. STANINETS and E. A. SHILOV. Ukr. Khim. Zhur. **34**, 1132 (1968).
8. YU. V. MELIKA, V. I. STANINETS, and T. A. DEGURKO. Dokl. Akad. Nauk Ukr. SSR, 531 (1969).
9. V. I. STANINETS and E. A. SHILOV. Russ. Chem. Rev. **40**, 272 (1971).
10. P. A. S. SMITH. The chemistry of open chain organic nitrogen compounds. Vol. 1. W. A. Benjamin Inc., New York. 1965. pp. 50–51.
11. B. C. CHALLIS and A. R. BUTLER. The chemistry of the amino group. *Edited by* S. Patai. Interscience Publishers, London. 1968. pp. 302–304.
12. C. A. BUEHLER and D. E. PEARSON. Survey of organic syntheses. Wiley Interscience, New York. 1970. pp. 642–643.
13. I. T. HARRISON and S. HARRISON. Compendium of organic synthetic methods. Wiley Interscience, New York. 1971. pp. 151, 405, 466, 472.
14. J. M. MUCHOWSKI and D. E. HORNING. U.S. Patent No. 3,484,457 (1969); Chem. Abstr. **72**, 90148t (1970).
15. B. BELLEAU and I. MONKOVIC. U.S. Patent No. 3,532,722 (1970); Chem. Abstr. **74**, 12987t (1971).
16. C. F. HAMMER, S. R. HELLER, and J. H. CRAIG. Tetrahedron, **28**, 239 (1972).
17. (*a*). W. NAGATA, S. HIRAI, K. KAWATO, and T. AOIKI. J. Am. Chem. Soc. **89**, 5045 (1967); (*b*) W. NAGATA, S. HIRAI, K. KAWATO, and T. OKUMURA. J. Am. Chem. Soc. **89**, 5046.
18. W. NAGATA. Lectures in heterocyclic chemistry. (*Supplement to* J. Heterocycl. Chem. Vol. 9.) **1**, 529 (1972).
19. S. J. BROIS. J. Org. Chem. **27**, 3532 (1962).
20. R. A. Y. JONES. Annual review of NMR spectroscopy. Vol. 1. *Edited by* E. F. Mooney. Academic Press, London. 1968. pp. 27–29.
21. H. BUDZIKIEWICZ, C. DJERASSI, and D. H. WILLIAMS. Mass spectrometry of organic compounds. Holden-Day, Inc., San Francisco. 1967.
22. A. STREITWIESER. Solvolytic displacement reactions. McGraw-Hill Book Company, Inc., New York. 1962. p. 35.
23. A. LATTES and J. J. PERIE. C.R. Acad. Sci. **262**, 1591 (1966); Tetrahedron Lett. 5165 (1967).

Can. J. Chem. Downloaded from www.nrcresearchpress.com by 210.87.254.42 on 09/05/12
For personal use only.

24. J. J. PERIE and A. LATTES. Bull. Soc. Chim. Fr. 583 (1970).
25. J. J. PERIE, J. P. LAVAL, and A. LATTES. C.R. Acad. Sci. **272**, 1141 (1971).
26. J. J. PERIE, J. P. LAVAL, J. ROUSSEL, and A. LATTES. Tetrahedron Lett. 4399 (1971).
27. J. J. PERIE, J. P. LAVAL, J. ROUSSEL, and A. LATTES. Tetrahedron, **28**, 675, 701 (1972).
28. H. HODJAT, A. LATTES, J. P. LAVAL, J. MOULINES, and J. J. PERIE. J. Heterocycl. Chem. **9**, 1081 (1972).
29. E. M. SCHULTZ, C. M. ROBB, and J. M. SPRAGUE. J. Am. Chem. Soc. **69**, 2454 (1947).
30. P. YATES, G. D. ABRAMS, M. J. BETTS, and S. GOLDSTEIN. Can. J. Chem. **49**, 2850 (1971).
31. R. A. W. JOHNSTONE, D. W. PAYLING, and C. THOMAS. J. Chem. Soc. C, 2223 (1969).
32. I. MONKOVIC, T. T. CONWAY, H. WONG, Y. G. PERRON, I. J. PACHTER, and B. BELLEAU. J. Am. Chem. Soc. **95**, 7910 (1973).
33. H. K. HALL, J. P. SCHAEFER, and R. J. SPANGGORD. J. Org. Chem. **37**, 3069 (1972).

Can. J. Chem. Downloaded from www.nrcresearchpress.com by 210.87.254.42 on 09/05/12
For personal use only.

Can. J. Chem. Downloaded from www.nrcresearchpress.com by 210.87.254.5 on 09/05/12
For personal use only.

Etude conformationnelle des alcényl phénylcétones par spectrographies infrarouge, ultraviolette et par l'utilisation de l'effet Overhauser nucléaire et de complexe de lanthanide Eu(dpm)$_3$ en résonance magnétique nucléaire

NGUYEN THOAI[1] ET TRINH-MINH-CHAU[2]

C.E.R.C.O.A.-C.N.R.S., 2 rue Henry Dunant, 94320 Thiais, France

Reçu le 10 août

Par les études spectrographiques (i.r., u.v., effet Overhauser nucléaire et l'utilisation des chélates d'europium en r.m.n.), nous avons montré que, du fait de l'encombrement stérique du noyau benzénique, les alcényl phénylcétones étudiées $R_1R_2C{=}CR_3{-}COC_6H_5$, existent de préférence sous la conformation privilégiée *s-cis*. Quand ces cétones possèdent un substituant alkyle (R_3 = Me, Et) sur le carbone en α du carbonyle, la molécule n'est plus plane. La torsion de la molécule se fait dans ce cas non pas autour de la liaison $CO{-}C_6H_5$, mais $CO{-}C{=}$. L'angle dièdre ainsi formé est voisin de 65°. Nous avons proposé en particulier un système d'abaques qui, avec l'emploi de Eu(dpm)$_3$, permet une détermination rapide de la conformation préférentielle de cétones α,β éthyléniques de structure non rigide et d'apprécier dans le cas d'une conformation non plane l'ordre de grandeur de l'angle dièdre entre les chromophores C=C et C=O.

By the use of i.r., u.v. and n.m.r. (n.O.e. and europium chelates) we have shown that a series of phenyl ketones ($R_1R_2C{=}CR_3{-}CO{-}C_6H_5$) exist within the *s-cis* conformation probably because of the steric bulk of the benzene ring. When these ketones have an alkyl substituent (R_3 = Me, Et) on the carbon atom α to the carbonyl group, the molecule is no longer planar. The molecular torsion in this case is not around the $CO{-}C_6H_5$ bond but rather at the $CO{-}C{=}$ bond. The resulting dihedral angle is about 65°. We propose a tabular method which together with the use of Eu(dpm)$_3$ allows rapid determination of the preferred conformation of non rigid α,β-unsaturated ketones and in the case of non-planar conformations allows the estimation of the dihedral angle between the C=C and C=O chromophores. [Journal translation]

Can. J. Chem., **52**, 1331 (1974)

Les études de structure et de conformation des cétones α,β éthyléniques ont été nombreuses tant par infrarouge (1),[3] ultraviolette (2) que par résonance magnétique nucléaire (3);[4] pourtant peu a été entrepris (1*e*, 3*b*) sur les alcényl phénylcétones à conjugaison croisée de type $R_1R_2C{=}CR_3{-}CO{-}C_6H_5$. Voir fig. 1. Ainsi il a été montré que la phényl-1 propène-2 one-1 (R_3 = H) est de conformation *s-cis* (1*e*), tandis que la méthyl-2 phényl-1 butène-2 one-1 (R_3 = Me) est, d'après Combaut et Giral (3*c*) de conformation préférentielle *s-trans*. Des deux exemples précités nous remarquons que le simple passage de R_3 = H à R_3 = Me entraine un changement structural important: d'une conformation *s-cis* on passe à une conformation *s-trans*. En l'absence d'études systématiques, il nous semble intéressant de préciser dans une étude plus générale, la conformation de cette série de cétones en fonction des substituants R_1, R_2, R_3 sur la liaison éthylénique (tableau 1).

L'étude par infrarouge et ultraviolette nous a permis de dégager deux cas bien distincts suivant que le carbone en α du carbonyle est porteur de l'hydrogène (R_3 = H) ou d'un substituant alkyle (R_3 = Me, Et). Dans le premier cas les molécules sont planes et de conformation prédominante *s-cis*, dans le second cas elles ne sont pas planes, et la torsion s'opère autour de la liaison $-\underset{\underset{O}{\|}}{C}{-}C{=}$. Ces résultats sont confirmés par les méthodes spectrales récentes:

[1]A qui toute correspondance devra être adressée.

[2]Adresse actuelle: Unité de Recherches de Pharmacologie Chimique de l'I.N.S.E.R.M., laboratoire rattaché à l'U.E.R. No 70 Broussais, Hôtel-Dieu de l'Université de Paris VI. 17 rue du fer à moulin, 75005 Paris, France.

[3]Pour une étude par spectrographie Raman, voir réf. 1*i*.

[4]En particulier par l'effet de solvant en r.m.n. (3*e*–3*h*).

TABLEAU 1. Caractéristiques infrarouges et ultraviolette des cétones **1–11**

N°	Composé	Infrarouge (cm^{-1})			Ultraviolette (nm)	
		$\nu_{C=O}$	$\nu_{C=C}$	$\nu_{CO} - \nu_{CC}$	λ_{max}^{EtOH}	ε
1	$CH_2:CH—CO—C_6H_5$	1677[a]	1611[a]	66	254[a]	11 300[a]
2	$CH_3—CH:CH—CO—C_6H_5$(E)	1677	1618	59	257	15 900
3	$CH_3—CH:CH—CO—C_6H_5$(Z)	1675	1620	55	256	15 800
4	$(CH_3)_2C:CH—CO—C_6H_5$	1675	1615	60	261	16 000
5	$CH_2:CCH_3—CO—C_6H_5$	1705	1650	45	245	9540
6	$CH_3—CH:CCH_3—CO—C_6H_5$(E)	1707	1655	52	244[b]	12 340[b]
7	$CH_2:CEt—CO—C_6H_5$	1710	1655	55	—	—
8	$CH_2:CCH_3—CH_2—CO—C_6H_5$	1690	1645	45	247	8500
9	$CH_3—CO—C_6H_5$	1700[c]	—	—	240[d]	13 000[d]
10	$CH_3—CH:CCH_3R$	—	1657[c]	—	—	—
11	$CH_2:CCH_3R$	—	1653[c]	—	—	—

[a]Valeurs données par (1*e*).
[b]Literature λ = 247 nm, ε = 13 000 (3*c*).
[c]Valeurs données par L. B. Bellamy (1*b*).
[d]Valeurs données par (15).

effet Overhauser (4) et complexes à l'europium (5)[5] en résonance magnétique nucléaire. Pour la dernière méthode nous avons proposé un système d'abaques qui permet une détermination rapide de la conformation préférentielle des cétones α,β éthyléniques de structure non rigide et d'apprécier dans le cas d'une conformation non plane l'ordre de grandeur de l'angle dièdre entre les chromophores C=C et C=O.

Etude par spectrographies infrarouge et ultraviolette

Dans le tableau 1, nous avons relevé les bandes de vibration de valence $\nu_{C=O}$ et $\nu_{C=C}$, prises en solution dans le tétrachlorure de carbone. On voit distinctement que ces cétones sont groupées en deux familles.

Famille 1, cétones sans substituant sur le carbone C_α. Les bandes de vibration de valence $\nu_{C=O}$ sont toutes voisines de 1675 cm^{-1} et les bandes de vibration de valence $\nu_{C=C}$ sont voisines de 1615 cm^{-1}. La tête de file de cette famille est la phényl-1 propène-2 one-1 dont la conformation *s-cis* préférentielle a été bien établie (1*e*), on peut déduire raisonnablement que les autres cétones de la famille ont aussi la conformation préférentielle *s-cis*. L'analogie se trouve également dans les spectres u.v. de ces cétones (tableau 1) où l'on remarque d'une part un coefficient d'extinction moléculaire de même ordre de grandeur (ε = 10 000) d'autre part un effet bathochrome régulier par substituant ainsi qu'un effet hyperchrome.

Famille 2, cétones porteuses d'un substituant alkyle sur le carbone C_α. Ces cétones ont des bandes de vibration $\nu_{C=O}$ et $\nu_{C=C}$ voisines de 1700 cm^{-1} et 1650 cm^{-1}, respectivement. Ces bandes sont plus élevées que les bandes correspondantes dans la famille 1 et elles sont proches de celles des cétones **8** et **9** où il n'y a pas de conjugaison entre les liaisons C=O et C=C. Cette absence de conjugaison est relevée également par spectrographie u.v. où l'on observe une diminution du coefficient d'extinction moléculaire et une bande d'absorption maximale plus faible que la valeur théorique obtenue par incrément. Ces observations, et compte tenu des comparaisons avec les cétones connues du tableau 1, nous conduisent à conclure que dans la famille 2, le système conjugué est limité au groupe $C_6H_5—CO—$ et que la déconjugaison entre les liaisons C=O et C=C est due à la non planéité entre ces chromophores. En comparant les coefficients d'extinction moléculaire des cétones **5** et **1** de structure équivalente, la relation de Braude (1*c*) donne un angle dièdre ψ entre les chromophores C=O et C=C de 73° environ. Cet angle est de 74° pour la cétone **6**.

Etude par résonance magnétique nucléaire

Effet Overhauser nucleaire (e.O.n.) (voir fig. 1).

Pour compléter les observations tirées des spectres infrarouges et ultraviolets, nous avons

[5]Nous n'avons pas utilisé l'effet de solvant en r.m.n. car s'il permet de distinguer une conformation *s-cis* d'une conformation *s-trans* (3*e*, 3*f*, 3*h*), il ne permet pas de préciser le cas d'une conformation non plane (3*g*), surtout quand le soluté comporte un noyau aromatique riche en électrons (3*i*).

Can. J. Chem. Downloaded from www.nrcresearchpress.com by 210.87.254.5 on 09/05/12
For personal use only.

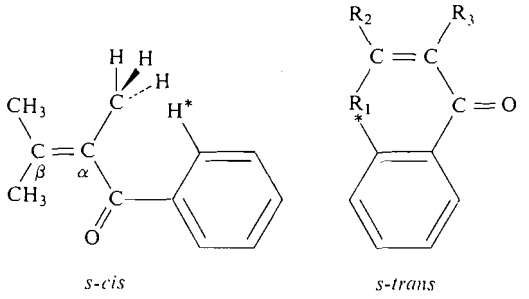

FIG. 1. Les modèles moléculaires.

étudié l'effet Overhauser que pouvait produire une irradiation successive des différents substituants R_1, R_2, R_3 sur la résonance du proton H_o *ortho* du phényle. Pour la cétone **4** de la famille 1[6] ($R_1 = R_2 = Me$; $R_3 = H$), on remarque que l'irradiation du proton ($R_3 = H$) sur le carbone C_α provoque sur H_o une exaltation d'intensité de 15%, ce qui signifie que la distance entre les protons en question est inférieure à 3 Å. Cette distance est compatible avec une conformation *s-cis* concordante avec les conclusions tirées des spectres infrarouges et ultraviolets. Par contre aucun e.O.n. n'est observé quand on irradie successivement les différents substituants R_1, R_2, R_3 des cétones **5** et **6**. Mises à part les autres causes d'absence de e.O.n., on peut, du point de vue des distances interatomiques, supposer qu'aucun des protons des groupes méthyles R_1 et R_3 ne se trouvait au voisinage des protons H_o *ortho* du phényle. Or sur modèles moléculaires[7] on trouve que cette situation n'est compatible ni avec une conformation *s-cis*, ni avec une conformation *s-trans*.[8] Toujours sur modèles moléculaires, une distance $d > 3$ Å n'est observable que sur une conformation où la liaison éthylénique est tordue d'un angle de 90° par rapport au système conjugué C_6H_5—C=O, nous sommes donc en droit de supposer que la structure vraie est proche de cette valeur de 90°.

Cétone	Proton éthylénique	Déplacement chimique (p.p.m.) par rapport au TMS	Solvant
5	$R_1 = H$	5.90	$CDCl_3$
6	$R_1 = H$	6.42	$CDCl_3$
7	$R_1 = H$	5.75	CCl_4

Etude par complexe à l'europium Eu(dpm)$_3$

L'emploi des chélates de terre rare en r.m.n. est un autre moyen pour apprécier les structures géométriques des molécules. Si l'on admet que le déplacement chimique induit par le complexe est essentiellement dû à une interaction de type pseudocontact (5*c*) et qu'il suit approximativement la relation de McConnell et Robertson (5*d*) chaque proton i d'une molécule peut être caractérisé par son terme géométrique

$$[1] \qquad G_i = \frac{3\cos^2\theta_i - 1}{r_i^3}$$

Le problème pratique est celui de l'appréciation des angles θ_i et des distances r_i qui ne seraient mesurables que sur un complexe défini. En l'absence de cette possibilité, plusieurs modèles approchés ont été envisagés (6), il semble que le modèle qui répondrait le mieux à la relation de McConnell pour une cétone est celui où l'atome paramagnétique de terre rare est placé sur l'axe du C=O à une distance voisine de 3 Å de l'atome d'oxygène. Nous avons essayé cette approche sur des cétones éthyléniques de structure bien connue, cétones **12**–**19**. Voir tableau 2 où sont figurés également les déplacements chimiques induits des protons situés en R_1, R_2, R_3 et leurs rapports deux à deux $F_{1,2}, F_{3,2}, F_{3,1}$.[9]

$$[2] \quad F_{1,2} = \frac{\Delta\delta(H)_{R_1}}{\Delta\delta(H)_{R_2}} = \frac{G_1}{G_2} = \frac{3\cos^2\theta_1 - 1}{r_1^3} \times \frac{r_2^3}{3\cos^2\theta_2 + 1}$$

$$[3] \quad F_{3,2} = \frac{\Delta\delta(H)_{R_3}}{\Delta\delta(H)_{R_2}} = \frac{G_3}{G_2} = \frac{3\cos^2\theta_3 - 1}{r_3^3} \times \frac{r_2^3}{3\cos^2\theta_2 - 1}$$

[6]Pour les cétones **2** et **3** de la même famille, la proximité des signaux des protons éthyléniques et benzéniques ne nous a pas permis de procéder à une irradiation sélective de ces protons.

[7]Pour les mesures sur modèles moléculaires, voir la partie expérimentale et la réf. 13.

[8]Les modèles moléculaires montrent que dans le cas d'une conformation *s-trans* avec un noyau aromatique non coplanaire, les protons du groupement R_1 se trouvent très proche de l'axe D_6 du benzène donc très déblindés (fig. 1). Cette éventualité n'étant pas observé, les protons éthyléniques dans le cas des cétones **5**, **6** et **7** ont des déplacements chimiques normaux.

[9]Ces rapports ne sont pas indépendants. Deux suffisent, nous donnons néanmoins ici les trois rapports car ils permettent dans la pratique une lecture rapide des résultats sur abaques.

Can. J. Chem. Downloaded from www.nrcresearchpress.com by 210.87.254.5 on 09/05/12
For personal use only.

TABLEAU 2. Les déplacements chimiques

No.	Composé	$F_{1,2}$	$F_{3,2}$	$F_{3,1}$	
2	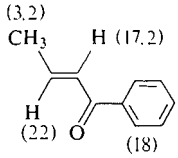	6.9	5.4	0.8	$F_{1,2} > F_{3,2} \gg F_{3,1}$
4	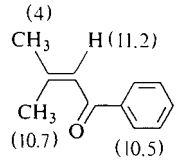	2.7	2.8	1.0	$F_{1,2} \simeq F_{3,2} \gg F_{3,1}$
5	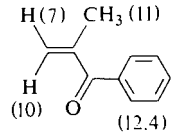	1.4	1.5	1.1	$F_{3,2} \simeq F_{1,2} > F_{3,1}$
6	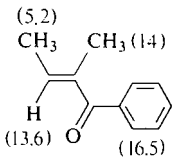	2.6	2.7	1.0	$F_{3,2} \simeq F_{1,2} > F_{3,1}$
12	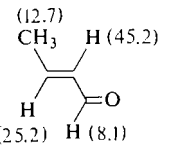	2.0	3.6	1.8	$F_{3,2} > F_{1,2} \gg F_{3,1}$
13	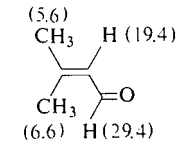	1.2	3.5	3.0	$F_{3,2} > F_{3,1} > F_{1,2}$
14	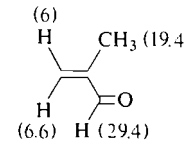	1.3	2.1	1.6	$F_{3,2} > F_{3,1} > F_{1,2}$
15	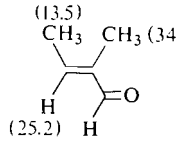	1.9	2.3	1.3	$F_{3,2} > F_{1,2} > F_{3,1}$
16	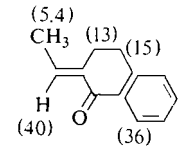	7.4	2.3	0.3	$F_{1,2} \gg F_{3,2} \gg F_{3,1}$

Can. J. Chem. Downloaded from www.nrcresearchpress.com by 210.87.254.5 on 09/05/12
For personal use only.

TABLEAU 2. (*conclu*)

No.	Composé	$F_{1,2}$	$F_{3,2}$	$F_{3,1}$	
17	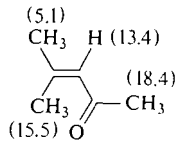	3.0	2.6	0.9	$F_{1,2} > F_{3,2} \gg F_{3,1}$
18	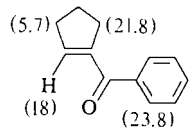	3.2	3.8	1.2	$F_{3,2} > F_{1,2} > F_{3,1}$
19	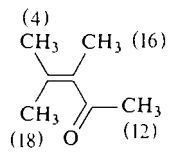	4.5	4.0	0.9	$F_{1,2} \simeq F_{3,2} \gg F_{3,1}$

$$[4]\quad F_{3,1} = \frac{\Delta\delta(H)_{R_3}}{\Delta\delta(H)_{R_1}} = \frac{G_3}{G_1} = \frac{3\cos^2\theta_3 - 1}{r_3^3} \times \frac{r_1^3}{3\cos^2\theta_1 - 1}$$

Pour chaque molécule, grâce aux modèles moléculaires (13), nous avons calculé les facteurs géométriques G_i correspondants aux conformations types: angle dièdre $\psi = 0, 45, 90, 135, 180°$ et nous portons les rapports F_{ij} en fonction de l'angle dièdre ψ sur des graphiques (fig. 2). Comme les variations des rapports $G_i/G_j = g(\psi)$ sont continues, on peut lier les points représentatifs par une courbe continue donnant les rapports $F_{i,j} = G_i/G_j$ en fonction de l'angle dièdre ψ. L'ensemble constitue les abaques de la fig. 2 *A–D*. Si on considère par exemple les abaques de fig. 2*B* correspondants à la cétone **15**, on observe trois zones:

zone (*a*) où $F_{3,2} > F_{1,2} \gg F_{3,1}$
ψ de 0 à 60° → *s-cis*

zone (*b*) où $F_{1,2} > F_{3,2} > F_{3,2}$
ψ de 60 à 150° → croisé

zone (*c*) où $F_{3,2} > F_{1,2} > F_{3,1}$
ψ de 150 à 180° → *s-trans*

Le produit **15** ayant $F_{3,2} = 2.3 > F_{1,2} = 1.9 > F_{3,1} = 1.3$, sa conformation correspondrait à la zone (*c*), angle ψ de 150 à 180°, c'est à dire à une conformation *s-trans*. De la même façon nous avons fait pour toutes les cétones de référence du tableau 2, cétones **12**, **16** (fig. 2*C*) **13**, **17**, **19** (fig. 2*D*), pour chacune d'elle les correspondances marquées sur les graphiques sont tout à fait satisfaisantes, que ces cétones soient de conformation *s-cis* ou *s-trans* prédominante. Compte tenu de ces résultats, ces abaques pouvaient servir d'outil pour remonter, des déplacements chimiques induits à la conformation privilégiée d'une cétone α,β éthylénique. Nous avons par conséquent appliqué cette technique aux cétones **2**, **4**, **5** et **6** (tableau 2) pour lesquelles nous avons également calculé les rapports $F_{i,j}$ des déplacements chimiques induits. Les correspondances entre l'ordre relatif des quantités $F_{i,j}$ calculées avec les zones des abaques pour chaque type de cétone considérée sont portées sur les zones hachurées. Ainsi la cétone **2** (fig. 2*C*) et la cétone **4** (fig. 2*D*) ont des angles dièdres ψ voisins de 0°. Elles ont la conformation *s-cis* prédominante. Pour la cétone **5** ($F_{3,2} \simeq F_{1,2} > F_{3,1}$) fig. 2*A* et la cétone **6** ($F_{3,2} \simeq F_{1,2} > F_{3,1}$) fig. 2*B*, l'ordre et l'amplitude de décroissance des $F_{i,j}$ ne permettent pas de les placer dans la zone des angles $\psi \simeq 0$ ou $\simeq 180°$, mais dans une zone où l'angle ψ est voisin de 60°. Compte tenu des erreurs et de l'imprécision des déterminations géométriques, ces

Can. J. Chem. Downloaded from www.nrcresearchpress.com by 210.87.254.5 on 09/05/12
For personal use only.

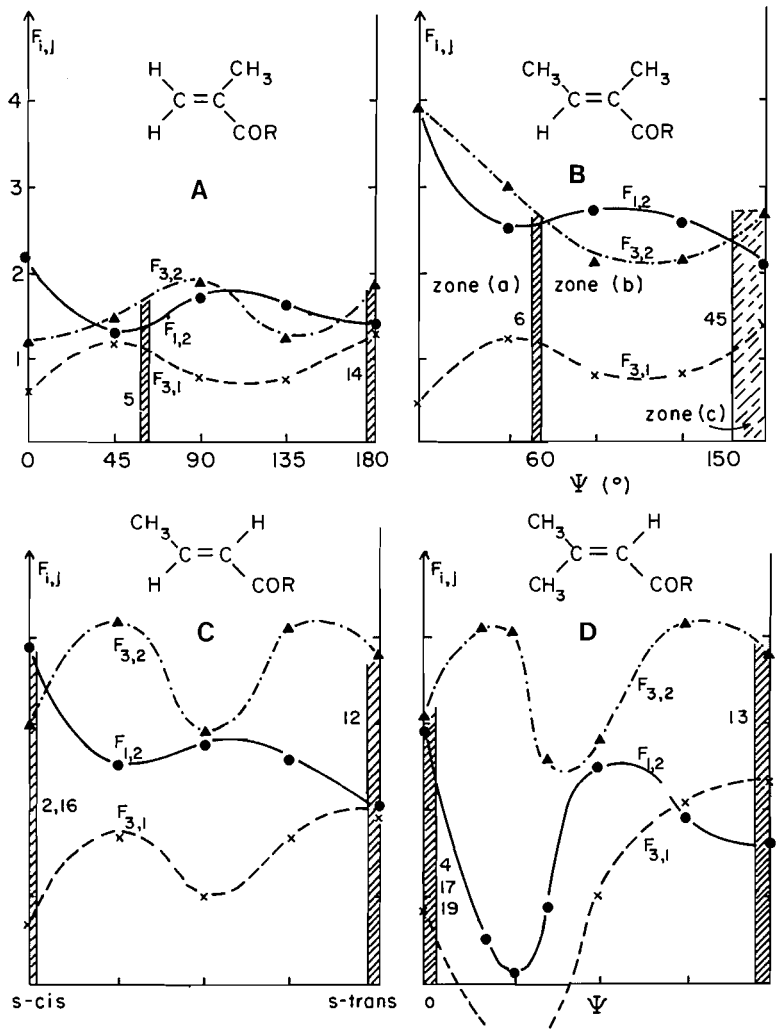

FIG. 2. Les rapports en fonction F_{ij} de l'angle dièdre ψ: $F_{1,2}$ (—·—), $F_{3,1}$ (---), $F_{3,2}$ (—trait plein). *A*, cétones **5** et **14**; *B*, cétones **6** et **15**; *C*, cétones **2**, **12** et **16**; *D*, cétones **4**, **13**, **17** et **19**.

résultats sont tout à fait concordants avec ceux des études par infrarouge, ultraviolet et par effet Overhauser.[10]

Conclusion

En conclusion, chacune des méthodes utilisées: i.r., u.v., r.m.n. apporte des renseignements sur la conformation des alcényl phénylcétones $R_1R_2C{=}CR_3{-}CO{-}C_6H_5$. Ces renseignements se confondent et se complètent comme en témoignent les résultats portés dans le tableau ci-dessous.

Cétone	Infrarouge	Ultraviolet	Effet Overhauser	Eu-(dpm)$_3$
2	*s-cis*	*s-cis*		0° → *s-cis*
4	*s-cis*	*s-cis*	positif	0° → *s-cis*
5	croisée	ψ ~ 73°	négatif ψ ~ 90°	ψ ~ 60°
6	croisée	ψ ~ 74°	négatif ψ ~ 90°	ψ ~ 60°

[10] *A priori*, rien n'indique que l'équilibre conformationnel des cétones libres et à l'état de complexe soit le même (14*a*,*b*), néanmoins pour chaque proton d'une molécule étudiée les courbes des déplacements chimiques induits par Eu(dpm)$_3$ en fonction des rapports croissant de S/L (substrat–ligand) dans les limites de 0.050 à 0.400 sont toutes des droites, ce qui laisserait supposer que l'équilibre conformationnel n'est pas perturbé par le complexant (14*c*).

Can. J. Chem. Downloaded from www.nrcresearchpress.com by 210.87.254.5 on 09/05/12
For personal use only.

Can. J. Chem. Downloaded from www.nrcresearchpress.com by 210.87.254.5 on 09/05/12
For personal use only.

La concordance des résultats obtenus par ces différentes méthodes montre en particulier l'intérêt de la méthode des abaques dans l'étude conformationnelle de cétones α,β éthyléniques. Pour ces cétones, la conformation *s-cis* est privilégiée quand il n'existe pas de substituant alkyle sur le carbone éthylénique en α du carbonyle. Quand la molécule possède en cet endroit un groupement alkyle (R_3 = Me, Et), elle n'est pas plane. La torsion s'effectue dans ce cas non pas autour de la liaison C_6H_5—CO, mais autour de la liaison CO—C═(3*g*). L'angle dièdre des deux plans ainsi formé est de l'ordre de 60–70°.[11]

Partie expérimentale

Mesures spectrales

Infrarouge

Les spectres infrarouges ont été enregistrés à l'aide des appareils Perkin–Elmer, modèle 21 à prisme de chlorure de sodium ou modèle 137G à réseau sur des échantillons en solution à 10% dans le tétrachlorure de carbone avec le polystyrène en référence.

Ultraviolette

Les spectres d'absorption ultraviolette ont été enregistrés sur un appareil Unicam SP 800 à double faisceau avec des cuves en quartz de transversée optique de 1 cm, avec des échantillons en solution dans l'alcool.

Résonance magnétique nucléaire

Effet Overhauser nucléaire (e.O.n.)

Les spectres ont été enregistrés sur un appareil Varian HA 100 avec le tétraméthyl silane comme référence interne. Les solvants utilisés sont soit le benzène-d_6, soit le deutérochloroforme pour commodité de lecture du spectre dans la région étudiée. Chaque solution est dégazée 15 mn par un courant d'azote avant chaque enregistrement.

Eu(dpm)$_3$

Les spectres ont été enregistrés sur un appareil Varian A 60 sur des échantillons en solution dans le tétrachlorure de carbone, avec le tétraméthylsilane comme référence interne. Le complexe $Eu(dpm)_3$ a été préparé suivant la méthode de Eisentraut-Sievers (7), sublimé et maintenu en atmosphère anhydre avant chaque mesure. Les valeurs des déplacements induits en ppm sont des valeurs extrapolées à une mole de concentration hypothétique en chélate, obtenues à partir de cinq à six mesures en concentration croissante (rapport substrat–ligand de l'ordre de 0.050 à 0.400) de chélate de lanthanide.

Synthèse

La pureté des produits a été vérifiée par un appareil Varian HiFi 1200 à détecteur à ionisation de flamme avec une colonne de 3 m à 15% de silicone sur Chromosorb W. Tous les composés étudiés ont fourni des résultats analytiques correspondant à la formule à ±0.2% au plus pour C et H.

Les alcényl phénylcétones de **2** à **8** ont été préparées selon la méthode classique E. P. Fuson *et al.* (8) à partir des chlorures d'acide correspondants (9). La cyclopentényl phénylcétone **18** a été préparée selon (10). Les aldéhydes de **12** à **15**, de même que la méthyl-4 pentène-3 one-1 (**17**) et la cétone **19** sont des produits commerciaux, purifiés soit par distillation soit par chromatographie en phase gazeuse.

Les configurations (*E*) et (*Z*) des cétones **2** et **3** ont été déterminées par synthèse diénique (11) avec le diphényl-1,3 isobenzofurane donnant, respectivement, le diphényl-1,4 benzoyl-2 méthyl-3 oxo-1,4 tétrahydro-1,2,3,4 naphtalène (*E*) et (*Z*) (12).

α-*Ethylidène tétralone* **16**

À 4 g de KOH dans 100 ml d'éthanol sont ajoutés 26 g de tétralone. Le mélange est refroidi par bain de glace vers 5 °C. On ajoute ensuite 100 ml d'acétaldéhyde. On laisse le mélange réactionnel sous agitation pendant 12 h. La solution obtenue est neutralisée par l'acide acétique, décantée, filtrée, séchée sur $MgSO_4$, puis distillée, Eb_{15} = 149–152 °C. Le mélange brut est composé de 30% d'isomère (*Z*) et de 70% d'isomère (*E*) qui ont été séparés par chromatographie en phase gazeuse (carbowax, 220 °C). Analyse: $C_{12}H_{12}O$; i.r. ν_{CO} = 1675 cm^{-1}, ν_{CC} = 1620 cm^{-1}; r.m.n. (CCl_4) (p.p.m.) (*a*) doublet, 3 protons, 1.9 (*E*), 2.1 (*Z*); (*b*) quadruplet, 1 proton, 6.9 (*E*), 6.1 (*Z*); (*c*) multiplet, 4 protons, 2.8 (*E*), 2.8 (*Z*); (*d*) multiplet, 3 protons, 7.4 (*E*), 7.4 (*Z*); (*e*) multiplet, 1 proton, 8.1 (*E*), 8.1 (*Z*); couplage, $^3J_{ab}$ = 7 Hz.

Modèle moléculaire

Les distances interatomiques et les angles dièdres ont été mesurés sur les modèles de Dreiding en nous inspirant de la méthode de ApSimon (13).

[11]Il est intéressant de noter que pour les alcényl alkylcétones, Faulk et Fry (3*d*) avaient signalé un angle dièdre de 90° entre les liaisons C═O et C═C, c'est à dire qu'il y a rupture totale de conjugaison entre les deux chromophores. Dans notre cas, l'extention de la conjugaison à un noyau aromatique semble avoir pour effet de ramener cette rupture totale vers une rupture partielle de conjugaison.

1. (*a*) R. L. Erskine et E. S. Waight. J. Chem. Soc. 3425 (1960). (*b*) L. J. Bellamy. The infrared spectra of complex molecules. John Wiley, N.Y. 1960. p. 132. (*c*) E. A. Braude et C. J. Timmons. J. Chem. Soc. 3766 (1955). (*d*) J. Lecomte. Bull. Soc. Chim. Fr. 717 (1955). (*e*) J. Kossany. Bull. Soc. Chim. Fr. 704 (1965) et les références citées. (*f*) F. H. Cottee, B. P. Straughan, C. J. Timmons, W. F. Forbes, et R. Shilton. J. Chem. Soc. (B), 1146 (1967). (*g*) A. J. Bowles, W. O. George, et W. F. Maddams. J. Chem. Soc. (B), 810 (1969). (*h*) K. Noack et R. N. Jones. Can. J. Chem. **39**, 2225 (1961). (*i*) K. Noack et R. N. Jones. Can. J. Chem. **39**, 2201 (1961).
2. (*a*) J. E. Baldwin. J. Org. Chem. **30**, 2423 (1965). (*b*) R. B. Turner et D. M. Woitle. J. Am. Chem. Soc. **73**, 1403 (1951). (*c*) L. K. Evans et A. E. Gillams. J. Chem. Soc. 815 (1941).
3. (*a*) L. M. Jackman et R. H. Wiley. J. Chem. Soc. 2886 (1960). (*b*) G. Combaut et L. Giral. Bull. Soc. Chim. Fr. 3258 (1969) et les références citées. (*c*) G. Combaut et L. Giral. Bull. Soc. Chim. Fr. 3717 (1970) et les références citées. (*d*) D. D. Faulk et A.

FRY. J. Org. Chem. **35**, 364 (1970). (*e*) D. H. WILLIAMS. Tetrahedron Lett. 2305 (1965). (*f*) C. J. TIMMONS. Chem. Commun. **22**. 576 (1965). (*g*) F. H. COTTEE et C. J. TIMMONS. J. Chem. Soc. (B), 326 (1968). (*h*) Y. FUJISE et S. ITÔ. Chem. Pharm. Bull. **14**, 797 (1966). (*i*) P. DIEHL, J. Chim. Phys. **61**, 199 (1964).

4. (*a*) G. MOREAU. Bull. Soc. Chim. Fr. 1770 (1969). (*b*) R. E. SCHIRMER, J. H. NOGGLE, J. P. DAVIS, et P. A. HART. J. Am. Chem. Soc. **92**, 3266 (1970). (*c*) R. A. BELL et J. K. SAUNDERS. Can. J. Chem. **48**, 1114 (1970).
5. (*a*) C. BEAUTE, Z. W. WOLKOWSKI, et N. THOAI. Tetrahedron Lett. 817 (1971); Chem. Commun. 700 (1971) (*b*) C. C. HINCKLEY. J. Org. Chem. **35**, 2834 (1970). (*c*) H. M. MCCONNELL et R. E. ROBERTSON. J. Chem. Phys. **29**, 1361 (1958). (*d*) J. BRIGGS, F. A. HART, G. P. MOSS et E. W. RANDALL. Chem. Commun. 364 (1971). (*e*) G. N. LA MAR. J. Chem. Phys. **41**, 2992 (1964); J. Chem. Phys. **43**, 235 (1965).
6. (*a*) G. E. HAWKES, D. L. LEIBFRITZ, D. W. ROBERTS, et J. D. ROBERTS. J. Am. Chem. Soc. **95**, 1659 (1970).
7. K. J. EISENTRAUT et R. E. SIEVERS. J. Am. Chem. Soc. **87**, 5254 (1965).
8. R. C. FUSON, R. E. CHRIST, et G. M. WHITMAN. J. Am. Chem. Soc. **58**, 2450 (1936).
9. E. P. KOHLER. Am. Chem. J. **42**, 395 (1909).
10. N. JONES et H. T. TAYLOR. J. Chem. Soc. 4017 (1959).
11. A. S. ONISCHENKO. Diene synthesis. *Edited by* S. Monson. 1964. p. 3.
12. TRINH-MINH-CHAU. Thèse de Doctorat d'Etat. Paris (1971) N^{c} d'enregistrement C.N.R.S. AO 7109.
13. J. W. APSIMON. Can. J. Chem. **46**, 808 (1968).
14. (*a*) W. G. BENTRUDE, HAN-WAN TAN, et K. C. YEE. J. Am. Chem. Soc. **94**, 3264 (1972). (*b*) J. F. CAPUTO et A. R. MARTIN. Tetrahedron Lett. 4547 (1971). (*c*) P. KRISTIANSEN et T. LEDAAL. Tetrahedron Lett. 2817 (1971).
15. A. R. GILLAM et E. S. STERN. An introduction to electronic absorption in organic chemistry. Edward Arnold Ltd., London. 1960. p. 141.

Can. J. Chem. Downloaded from www.nrcresearchpress.com by 210.87.254.5 on 09/05/12
For personal use only.

Etude de la formation d'exciplexes du 1,3,6,8-tetraphénylpyrène et du 1,2,3,4-tetraphénylnaphtalène

CLAUDE RULLIÈRE ET MARGUERITE-MARIE DENARIEZ-ROBERGE

Laboratoire de Recherche en Optique et Laser, Département de Physique, Université Laval, Québec 10

Reçu le 21 novembre 1973

Nous présentons ici l'étude de la formation de complexes fluorescents entre d'une part le 1,3,6,8-tetraphénylpyrène et le 1,2,3,4-tetraphénylnaphtalène et d'autre part le *N,N*-diméthylaniline. L'influence du substituant sur la formation des complexes est discutée ainsi que la possibilité d'obtenir l'effet laser à partir du niveau excité de ces complexes. Enfin on déduit de ces mesures l'affinité électronique de ces composés.

We wish to report the formation of fluorescent complexes of 1,3,6,8-tetraphenylpyrene and 1,2,3,4-tetraphenylnaphtalene with *N,N*-dimethylaniline. The effect of substitution on the formation of and the possibility of laser action from this complex is discussed. An indirect measurement of the electron affinity is deduced.

Can. J. Chem., **52**, 1339 (1974)

Introduction

Knibbe *et al.* (1) ont montré que l'introduction de *N,N*-diméthylaniline dans une solution de certains composés organiques, conduisait à l'apparition, dans le spectre de fluorescence de la solution, d'une nouvelle bande d'émission déplacée vers le rouge. Il expliqua cette nouvelle bande de fluorescence par la formation d'un complexe, stable seulement à l'état excité, appelé exciplexe. Ce complexe se formait pas transfert de charge et son existence était liée à des conditions sur l'affinité électronique et le potentiel d'ionisation des corps mis en présence. Plus tard Tavares (2) étudia les exciplexes de plusieurs composés aromatiques. Ce dernier expliquait l'échec obtenu dans la recherche des exciplexes du benzphénantrène par une perte de planéité de la molécule.

Pour notre étude nous avons sélectionné deux molécules (1,2,3,4-tetraphénylnaphtalène et 1,3,6,8-tetraphénylpyrène) pour deux raisons: d'une part, à cause de l'effet de substitution, la planéité de ces molécules est moindre que celle des composés non substitués et il était donc intéressant de voir si la formation d'exciplexes, connue pour le pyrène et le naphtalène (2, 3), serait affectée par des substituants; d'autre part, dans le cadre d'une étude sur les lasers à colorants, nous avons montré (4) qu'un bon effet laser était possible avec le 1,3,6,8-tetraphénylpyrène. Afin d'étendre l'effet laser de ce colorant dans le rouge, il était intéressant de connaître les caractéristiques cinétiques d'un éventuel exciplexe de ce corps, pour voir si un effet laser serait aussi possible à partir du niveau excité de cet exciplexe.

Conditions et dispositifs expérimentaux

Le 1,2,3,4-tetraphénylnaphtalène et 1,3,6,8-tetraphénylpyrène (obtenus de la compagnie K et K Inc.) ont été purifiés par chromatographie sur colonne d'alumine. Le *N,N*-diméthylaniline (obtenu de la compagnie Aldrich Chemical) était purifié par distillation après addition d'anhydride acétique. Le solvent utilisé était du cyclohexane de qualité spectroscopique. Le *N,N*-diméthylaniline était gardé à l'abri de la lumière sous atmosphère d'azote. Les solutions étaient préparées en lumière rouge et dégazées par barbotage d'azote. Les différents spectres d'absorption et de fluorescence ont été mesurés respectivement sur un appareil spectronic 505 et un fluorimètre Aminco type 768H. Les mesures de temps de vie ont été effectuées à l'aide du dispositif expérimental suivant: la seconde harmonique d'un laser à rubis déclenché, d'une durée de 20×10^{-9} s sert à exciter la solution à étudier. La fluorescence émise est recueillie sur un monochromateur Bausch and Lomb. Un photomultiplicateur RCA de type IP 28 et un oscilloscope Tektronix 7904 permet de mesurer l'évolution dans le temps de cette fluorescence avec une résolution temporelle de quelques nanosecondes. Pour les spectres de fluorescence, la longueur d'onde excitatrice était choisie de telle sorte que seul l'hydrocarbure aromatique soit excité. Ceci était aisé pour le 1,3,6,8-tetraphénylpyrène, car sa bande d'absorption est nettement distincte de celle du *N,N*-diméthylaniline. Par contre pour le 1,2,3,4-tetraphénylnaphtalène ceci était plus difficile et nous avons joué sur les rapports des coefficients d'extinction, en travaillant avec une forte concentration d'hydrocarbure (10^{-3} *M*/l).

Résultats

Spectres d'émission de l'exciplexe

Les figs. 1 et 2 montrent les changements obtenus dans les spectres de fluorescence des solutions pour des concentrations croissantes de *N,N*-diméthylaniline, la concentration de l'hydrocarbure aromatique restant constante. Ces

Can. J. Chem. Downloaded from www.nrcresearchpress.com by 210.87.254.105 on 09/05/12
For personal use only.

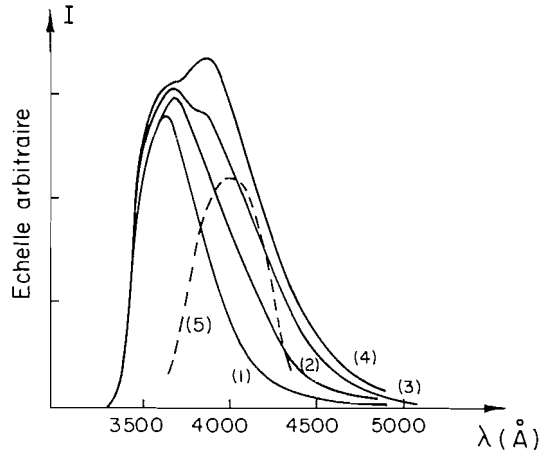

FIG. 1. Spectre de fluorescence d'une solution de 1,2,3,4-tetraphénylnaphtalène (10^{-3} *M*/l) dans le cyclohexane pour différentes concentrations de *N*,*N*-diméthylaniline. Courbes (1) [DMA] = 0; (2) [DMA] = 2.37×10^{-2} *M*/l; (3) [DMA] = 4.74×10^{-2} *M*/l; (4) [DMA] = 7.11×10^{-2} *M*/l; (5) spectre de l'exciplexe obtenu par différence entre 1 et 4.

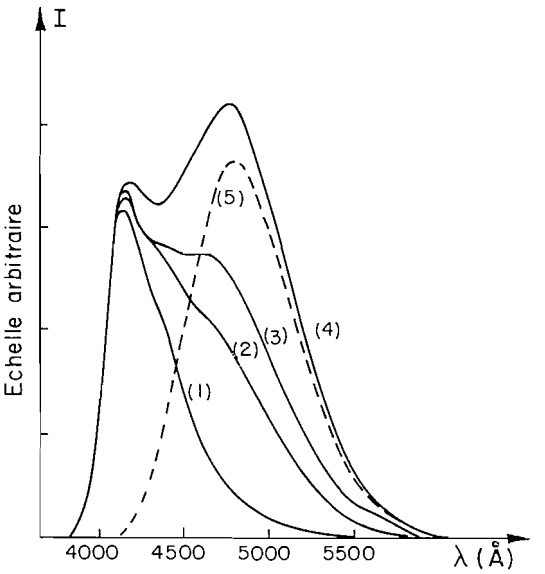

FIG. 2. Spectre de fluorescence d'une solution de 1,3,6,8-tetraphénylpyrène (2.5×10^{-5} *M*/l) dans le cyclohexane pour différentes concentrations de *N*,*N*-diméthylaniline. Courbes (1) [DMA] = 0; (2) [DMA] = 0.23 *M*/l; (3) [DMA] = 0.323 *M*/l; (4) [DMA] = 0.576 *M*/l; (5) spectre de l'exciplexe obtenu par différence entre 1 et 4.

spectres ne sont pas corrigés pour la sensibilité spectrale de l'appareil et sont normalisés à la bande de fluorescence de l'hydrocarbure aromatique pur. Nous avons vérifié que les spectres d'absorption des différentes solutions ne montrent pas de nouvelle bande lors de l'addition de *N*,*N*-diméthylaniline alors que les figs. 2 et 3 présentent la croissance d'une nouvelle bande d'émission. Désignons par A l'hydrocarbure aromatique et par DMA le *N*,*N*-diméthylaniline. Considérons le schéma cinétique classique de la formation d'un exciplexe en nous limitant aux réactions suivantes.

[1] $\mathrm{A} + h\nu \xrightarrow{k} \mathrm{A}^*$ excitation de A

[2] $\mathrm{A}^* \xrightarrow{k_f} \mathrm{A} + h\nu_f$ fluorescence de A*

[3] $\mathrm{A}^* \xrightarrow{k_i} \mathrm{A}$ désexcitation non radiative de A*

[4] $\mathrm{A}^* + \mathrm{DMA} \xrightarrow{k_q} (\mathrm{ADMA})^*$ formation de l'exciplexe

[5] $(\mathrm{ADMA})^* \xrightarrow{k_{fe}}$ ADMA $+ h\nu_e$ fluorescence de l'exciplexe

[6] $(\mathrm{ADMA})^* \xrightarrow{k_{ie}}$ ADMA désexcitation non radiative de l'exciplexe

Dans nos conditions expérimentales, étant en régime stationnaire nous pouvons écrire

$$[7] \quad \frac{\mathrm{d}[\mathrm{ADMA}]^*}{\mathrm{d}\nu} = k_q[\mathrm{A}^*][\mathrm{DMA}] - (k_{fe} + k_{ie})[\mathrm{ADMA}^*] = 0$$

D'autre part, dans le domaine des concentrations étudiées, l'intensité des bandes de fluorescence est proportionnelle à la concentration de la substance emissive. Nous pouvons donc écrire en désignant par I_E et I_A les intensités d'émission respectives du complexe et de l'hydrocarbure aromatique et par K_i des constantes de proportionnalité

$$[8] \quad \frac{I_E}{I_A} = \frac{K_E[\mathrm{ADMA}^*]}{K_A[\mathrm{A}^*]} = \frac{K_E k_q}{K_A(k_{fe} + k_{ie})}[\mathrm{DMA}] = K[\mathrm{DMA}]$$

soit donc pour le rapport I_E/I_A une loi linéaire en fonction de la concentration de *N*,*N*-diméthylaniline. C'est bien ce que nous montre les figs. 3*a* et *b*.

L'apparition d'une nouvelle bande de fluorescence, l'absence de nouvelle bande dans les spectres d'absorption et la croissance linéaire du rapport I_E/I_A nous montrent que nous sommes

Can. J. Chem. Downloaded from www.nrcresearchpress.com by 210.87.254.105 on 09/05/12
For personal use only.

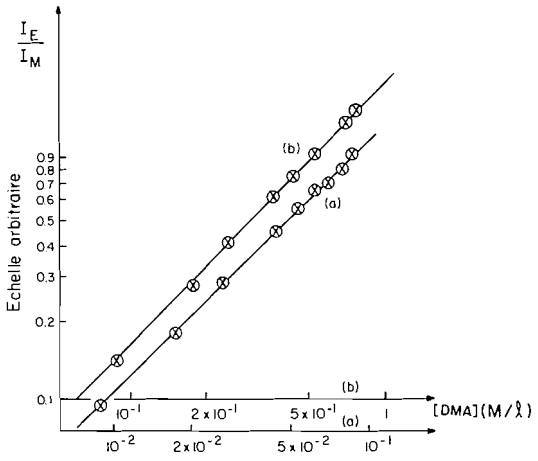

FIG. 3. Courbes I_E/I_A en fonction de [DMA]: (*a*) 1,2,3,4-tetraphénylnaphtalène; (*b*) 1,3,6,8-tetraphénylpyrène.

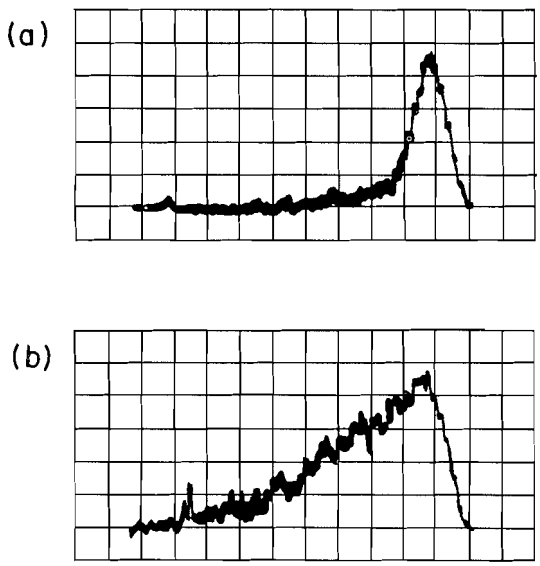

FIG. 4. (*a*) Profil du pulse excitateur; 20 ns/div; (*b*) profil de l'émission de l'exciplexe du 1,3,6,8-tetraphénylpyrène. λ = 4800 Å; [DMA] = 0.576 *M*/l; 20 ns/div.

bien en présence d'un exciplexe tel que décrit par Knibbe *et al.* (1) et Tavares (2).

Mesure des temps de vie

Les figs. 4*a* et *b* nous montrent respectivement le profil de l'impulsion excitatrice et la variation temporelle correspondante de l'émission de l'exciplexe du 1,3,6,8-tetraphénylpyrène. En prenant en considération seulement la partie de la courbe située après le passage de l'impulsion, nous avons mis en évidence pour nos deux composés une décroissance exponentielle de l'intensité en fonction du temps correspondant à des temps de vie de 38 ± 2 ns pour le 1,3,6,8-tetraphénylpyrène et 20 ± 2 ns pour le 1,2,3,4-tetraphénylnaphtalène (fig. 5).

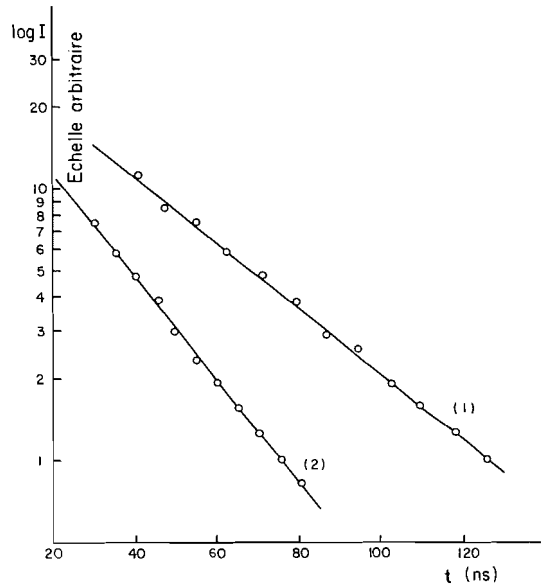

FIG. 5. Intensité de l'émission de l'exciplexe en fonction du temps. Courbes (1) tetraphénylpyrène; λ = 4800 Å; [DMA] = 0.576 *M*/l; (2) tetraphénylnaphtalène; λ = 4000 Å; [DMA] = 7.11×10^{-2} *M*/l.

Discussion

Influence du substituant

Il est à remarquer que, par exemple pour le 1,3,6,8-tetraphénylpyrène, la fluorescence de l'exciplexe commence à être importante pour des concentrations respectives en hydrocarbure aromatique et en *N*,*N*-diméthylaniline de 2.5×10^{-5} et 10^{-1} *M*/l, alors que Tavares (2) pour le pyrène travaille avec des concentrations respectives de 5×10^{-5} et 10^{-3} *M*/l. Nous travaillons donc à une concentration de *N*,*N*-diméthylaniline environ 100 fois plus grande. Ce fait semblerait indiquer, en supposant les mêmes sections efficaces d'émission dans les composés substitués et non substitués, que l'exciplexe a plus de difficultés à se former pour nos composés. En fait le nombre d'exciplexes formé dépend de la quantité k_q [DMA] [A*], soit du rapport k_q [DMA]/($k_f + k_i$). Pour le tetraphénylpyrène $(k_f + k_i)^{-1}$ = 2.28 ns (5) et pour le pyrène $(k_f + k_i)^{-1}$ = 200 ns (5) ce qui théoriquement nous oblige à travailler avec une concentration de *N*,*N*-diméthyl-

Can. J. Chem. Downloaded from www.nrcresearchpress.com by 210.87.254.105 on 09/05/12
For personal use only.

aniline 100 fois plus grande pour la même valeur de la constante k_q. En admettant que la diffusion intervient de la même manière dans les deux cas, il en résulte que la probabilité de formation de l'exciplexe n'est pas affectée par l'effet de substitution. On pourrait montrer que ceci est aussi vérifié pour le tetraphénylnaphtalène. On voit donc que la perte de planéité de la molécule ne semble pas réduire la formation d'exciplexe.

Possibilité d'effet laser

En ce qui concerne la possibilité d'effet laser sur l'exciplexe du 1,3,6,8-tetraphénylpyrène, nos résultats expérimentaux indiquent que ceci est improbable: d'une part, le temps de vie radiatif supérieur à 38 ns conduit à une section efficace d'émission trop faible pour obtenir un effet laser avec les énergies de pompage dont nous disposons actuellement; d'autre part, même en admettant qu'il soit possible d'obtenir un fort peuplement de l'exciplexe, on sait que dans le cas d'une densité d'exciplexes élevée, il existe une forte intéraction entre ces derniers qui conduit à une désexcitation non radiative (6). Pour obtenir le seuil de l'effet laser il faudrait donc pouvoir disperser les exciplexes sur une très grande longueur.

Mesure indirecte de l'affinité électronique

Tavares (2) a montré que la relation linéaire existante entre d'une part l'affinité électronique de l'accepteur et d'autre part la fréquence d'émission de l'exciplexe, était vérifiée dans son cas. Travaillant avec le même solvant et le même donneur, nous pouvons donc porter sur sa courbe $E_A = f(h\nu_c)$ nos valeurs de $h\nu_c$ et déduire ainsi l'affinité électronique de nos composés. Nous avons obtenu ainsi une valeur de 0.24 ± 0.02 eV pour le 1,2,3,4-tetraphénylnaphtalène et de 0.68 ± 0.02 eV pour le 1,3,6,8-tetraphénylpyrène. Ces valeurs nous semblent donner une bonne mesure de l'affinité électronique de ces corps. Il est à remarquer que ces valeurs sont plus élevées que les valeurs respectives de l'affinité électronique mesurée pour le naphtalène et pyrène non substitués. Mais l'affinité électronique d'un composé est d'autant plus grande que l'énergie du premier niveau non occupé de la molécule est faible (7). Or l'effet de substitution sur les molécules tend à abaisser l'énergie du premier niveau non occupé, comme le montre le déplacement vers le rouge du spectre d'absorption des dérivés substitués. Il s'en suit donc, comme nous le notons dans notre cas, une augmentation de l'affinité électronique.

Nous tenons à remercier M. Brunet pour le prêt du fluorimètre et le Dr. P. C. Roberge pour ses conseils lors de la préparation et la purification des produits et solutions.

1. H. KNIBBE, D. REHM et A. WELLER. Z. Physik. Chem. Neue Folge, **56**, 95 (1967).
2. A. M. TAVARES. Thèse, Victoria University, Manchester, England, 1968.
3. N. MATAGA, T. OKADA et K. EZUMI. Mol. Phys. **10**, 203 (1966).
4. C. RULLIÈRE et M. M. DENARIEZ-ROBERGE. Opt. Commun. **7**, 166 (1973).
5. I. B. BERLMANN. Handbook of fluorescence spectra of aromatic molecules. Academic Press, New York. 1971.
6. H. MASUHARA et N. MATAGA. Chem. Phys. Lett. **7**, 417 (1970).
7. F. A. MATSEN. J. Chem. Phys. **24**, 602 (1956).

Can. J. Chem. Downloaded from www.nrcresearchpress.com by 210.87.254.105 on 09/05/12
For personal use only.

The Acylation of β-Keto Ester Dianions

STUART NICHOLAS HUCKIN AND LARRY WEILER[1]

Department of Chemistry, University of British Columbia, Vancouver 8, British Columbia

Received October 31, 1973

A method for the successful acylation of the dianion of simple β-keto esters to yield β,δ-diketo esters has been developed. The dianion of methyl acetoacetate also reacts with the monoanion of methyl acetoacetate to give a triketo ester which cyclizes to methyl orsellinate. These dianions also add to nitriles to give 5-amino-3-keto-4-pentenoates which may in some cases cyclize to 4-hydroxypyridones.

On a mis au point une méthode qui permet l'acylation des dianions de β-céto esters simples afin d'obtenir des β,δ-dicéto esters. Le dianion de l'acétoacétate de méthyle réagit aussi avec le monoanion de l'acétoacétate de méthyle pour donner un ester tricétonique qui se cyclise pour fournir l'orsellinate de méthyle. Ces dianions s'additionne aussi aux nitriles pour fournir les amino-5 céto-3 penténoates qui dans certains cas se cyclisent en hydroxy-4 pyridones. [Traduit par le journal]

Can. J. Chem., **52**, 1343 (1974)

The acylation of the dianion of β-diketones has been the subject of several investigations in the past decade or so (1–9). This has been the most extensively investigated reaction of carbonyl multiple carbanions but it has also proved to be the most challenging and difficult to achieve in good yield. The interest in this reaction stems from the postulated intermediacy of β-polyketones in the biosynthesis of phenolic compounds (10, 11). The initial report which indicated the polycarbonyl origin of some phenolic compounds was the observation that heptane-2,4,6-trione (**1**) cyclizes to orcinol (**2**) (12), which was later confirmed by other workers (13, 14).

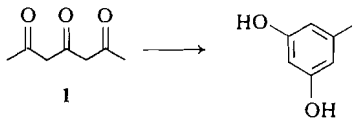

1 **2**

The laboratory synthesis of these postulated biosynthetic intermediates (**3**) has developed

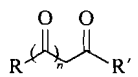

3

along two separate lines. One approach has involved the synthesis of polycarbonyl compounds in which the reactivity of the ketone groups is protected as a pyrone (15–18). The second approach has involved the direct synthesis of polycarbonyl compounds involving acylation of the multiple carbanions of smaller polycarbonyl precursors (7, 9). The results of both routes indicate that the conversion of either protected analogs of **3** or the acyclic compounds (**3**) to phenolic compounds is possible.

The major difficulty in the acylation of the dianion from a β-diketone, for example **4**, arises from the fact that the intial condensation product **5** possesses a more acidic proton than the

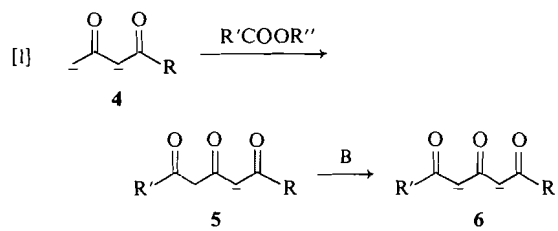

4 **5** **6**

monoanion of the starting material. Thus a proton will be transferred from the monoanion **5** to the dianion **4** to give the dianion **6**. Since the alkoxide that is formed during the condensation is not a sufficiently strong base to regenerate the dianion **4** from the corresponding monoanion, the maximum yield of product, based on the β-diketone, is 50%. In the initial acylations of β-keto dianions an excess of dianion was used (1); however, this approach would be unsatisfactory in a synthetic sequence in which the diketone is a valuable reagent. Addition of excess base, such as the metal amides, to these

[1]Author to whom correspondence should be addressed.

Can. J. Chem. Downloaded from www.nrcresearchpress.com by 210.87.254.42 on 09/05/12
For personal use only.

reactions often had deleterious effects (3) and occasionally improved the yield of triketone **6** (2). The yield of aroylation product (**6**, R″ = Aryl) can be very good using sodium hydride as the base in reaction 1 (5). However, this method is apparently limited to aroylations only. Similarly, acylation of the dianion of β-keto aldehydes is limited to aromatic esters (8).

Prior to our work (19) the only reported acylation of the dianion of a β-keto ester involved condensation of dianion **7** with methyl benzoate to give acid **8** or pyrone **9**, in 48 and 11% respectively, depending on the reaction conditions (20). Earlier we had developed a very

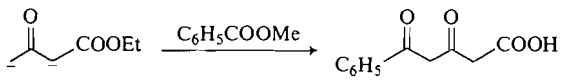

7 **8**

or

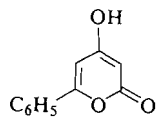

9

efficient method to generate the dianion of a range of β-keto esters (21). This involved treatment of the β-keto ester with 1 equiv. of sodium hydride followed by 1 equiv. of *n*-butyllithium or, alternately, with 2 equiv. of lithium diisopropylamide to produce the dianion of the β-keto ester. It was found that these intermediates undergo a variety of carbanion-type reactions to produce several novel and useful compounds (19, 21, 22).

In our initial studies it was found that the dianion **10** from methyl acetoacetate reacts violently with acyl halides even at −78 °C and

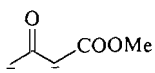

10

this reaction gave a complex mixture of products. Accordingly, less reactive acylating agents were investigated and it was found that dianion **10** reacts smoothly at 0 °C to give β,δ-diketo esters **11**. However, the yield in these condensations was not satisfactory (30–40%) in spite of their simplicity. No doubt one of the compli-

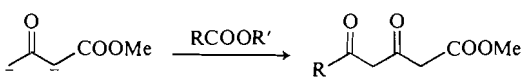

10 **11**

cations in this reaction was proton transfer from the monoanion of **11** to dianion **10** (*vide supra*).

Attempts to overcome this difficulty by employing an additional equivalent of base in the reaction were not successful, as any base strong enough to form the dianion was also sufficiently nucleophilic to attack the ester. For example lithium diisopropylamide and lithium *N*-isopropylcyclohexyl amide produced no reaction of dianion **10** with methyl acetate, whereas with methyl benzoate, good yields of the corresponding amides were obtained. The formation of these carboxamides was not unexpected (23). Hopefully the use of the recently reported H^+ arpoon bases would obviate this difficulty (24) but this has not been investigated to date.

It was then envisaged that the degree of conversion of dianion **10** to diketo ester **11** could be raised, if, after the addition of ½ equiv. of the ester, the quenched dianion was regenerated by addition of more base before adding further ester. Three equivalents of base are required for complete conversion of dianion **10** to **11**. But, after addition of ½ equiv. of ester, only ½ equiv. of base is needed to fully regenerate the dianion **10**. Such an addition would raise the maximum theoretical yield to 75%, whereupon addition of ¼ equiv. of base would regenerate the dianion **10** completely. While it is possible that alternate additions of ester and base in ever decreasing amounts would eventually give complete conversion of dianion to diketo ester **11**, such a procedure would be very time consuming and tedious. It was found that reaction of dianion **10** with ½ equiv. of ester, followed by addition of ½ equiv. of *n*-butyllithium and finally by a further ½ equiv. of ester, did give yields of **11** in excess of 50%.

Then it was adventitiously discovered that addition of 1 equiv. of base, after the addition of the first portion of ester, gave even higher yields of **11**. Thus the most convenient procedure involved reaction of dianion **10** with ½ equiv. of ester, addition of 1 equiv. more of base, and finally the remaining ½ equiv. of ester. In this manner, reaction of **10** with methyl acetate gave methyl 3,5-dioxohexanoate (**11**, R = Me) in 71% yield and with methyl butanoate gave methyl 3,5-dioxooctanoate (**11**, R = *n*-Pr) in 67% yield.

The product **11** (R = H), arising from the condensation of dianion **10** and methyl formate,

Can. J. Chem. Downloaded from www.nrcresearchpress.com by 210.87.254.42 on 09/05/12
For personal use only.

Can. J. Chem. Downloaded from www.nrcresearchpress.com by 210.87.254.42 on 09/05/12
For personal use only.

decomposed on all attempts to purify it and was consequently characterized by spectral data only. When the dianion **10** was reacted with ethyl butanoate a mixture of methyl and ethyl 3,5-dioxooctanoate was isolated, the latter product arising from transesterification during the reaction. To avoid this complication all subsequent reactions were performed with methyl esters.

It was also found that the yields of the diketo esters from the condensation of aromatic esters with dianion **10** were low. Reinvestigation of the crude product from these reactions revealed that the corresponding carboxylic acid **12** was formed

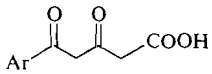

12

in significant amounts. We could only detect carboxylic acid products in the condensations with aromatic esters. Wolfe *et al.* were able to isolate only the carboxylic acid **12** (Ar = C_6H_5) from the aroylation of ethyl acetoacetate with methyl benzoate using sodium hydride in 1,2-dimethoxyethane (20). The mechanism of this hydrolysis, in both cases, remains obscure.

Recently it has been reported that very powerful nucleophiles, such as di- and trianions, react with the monoanions of β-keto esters to yield the acylated product (25). For example, it was possible to condense the dianion of 1-phenylbutane-1,3-dione with the monoanion of ethyl benzoylacetate and ethyl acetoacetate to produce tetraketones (eq. 2) (25). This could involve

[2] 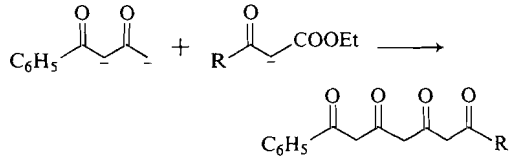

either a direct condensation of the dianion with a monoanion or elimination of ethoxide from the keto ester monoanion and condensation of the resulting acylketene with the dianion.

We have found that a similar acylation of methyl acetoacetate may be achieved. If, in generation of the dianion of methyl acetoacetate, only ½ equiv. of *n*-butyllithium is added and the reaction left at room temperature for a considerable time (5 days) before quenching, the methyl acetoacetate undergoes self-condensation and methyl orsellinate (**13**) is obtained (eq. 3). The

[3] 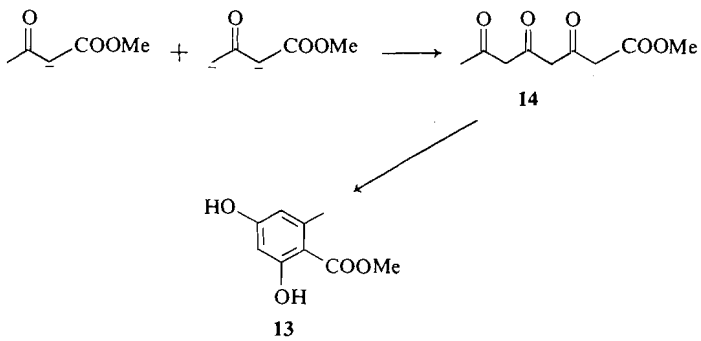

reaction time may be shortened considerably by raising the reaction temperature but as yet the maximum yield obtained is only 23%. It was also possible to isolate the intermediate triketo ester **14** by quenching the reaction carefully with a phosphate buffer (p*H* 6.5). The triketo ester **14** was characterized by its spectral properties but this compound was not sufficiently stable for elemental analysis. This material underwent spontaneous conversion to methyl orsellinate (**13**) on standing at 0 °C for 12 h. The triketo ester **14** has been synthesized via the carboxylation of the trianion of diacetylacetone and the cyclization of **14** to **13** was also reported in this work (26).

The n.m.r. spectra of all the acylated β-keto esters indicated that they existed, in solution at least, with the β-diketone mainly in the enol form. The n.m.r. spectra, or other spectroscopic data, did not permit a clear decision to be made as to which enol, or enols, are formed.

The reaction of dianion **10** with a nitrile also offers the possibility of adding an acyl group to the keto ester (eq. 4).

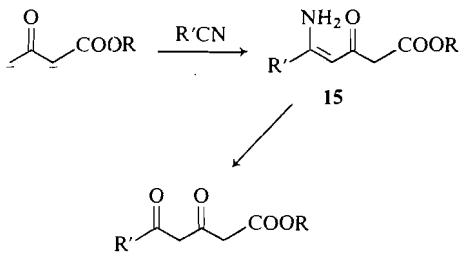

[4]

Recently it has been reported that ethyl acetoacetate may be condensed with benzonitrile using 2 equiv. of sodium amide to give the enamine **15** ($R' = C_6H_5$; R = Et) but the reaction is complicated by nucleophilic attack of the amide ion on the nitrile and subsequent condensation of the benzamidine with the keto ester to give the pyrimidone **16**.

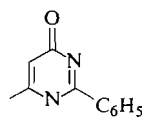

16

We found that the reaction between dianion **10** and benzonitrile was sluggish and extended reaction times were necessary to produce reasonable amounts of product. After 12 h at room temperature methyl 5-amino-3-oxo-5-phenyl-pent-4-enoate (**15**, $R' = C_6H_5$; R = Me) was isolated in good yield (66%) along with some (29%) hydroxypyridone **17**, which arises from cyclization of **15** ($R' = C_6H_5$; R = Me). In

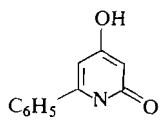

17

fact, this cyclization occurred in quantitative yield on attempted distillation of **15** ($R' = C_6H_5$; R = Me) and provides a ready route to **17**. Extension of this reaction to the condensation of acetonitrile with dianion **10** gave the enamine **15** (R′ = R = Me) in high yield and no evidence for the formation of the corresponding hydroxypyridone was observed. In fact this enamine (**15**, R′ = R = Me) appears to be quite stable to thermolysis and under a variety of conditions **15** (R′ = R = Me) sublimed unchanged.

The synthesis of the esters of 3,5-dioxohexanoic acid has been reported as early as 1906 (27*a*) and more recently in the photolysis of triacetic acid lactone (27*b*). However, the above acylation of the dianion of β-keto esters offers a new route to a wide range of β,δ-diketo esters which now can be prepared in reasonable yield. These intermediates may undergo further reactions and their chemistry awaits additional exploitation. The dianion of β-keto esters also undergoes condensation with nitriles to give the enamines **15** which may, in the case of $R' = C_6H_5$, be cyclized to the hydroxypyridone **17**.

Experimental

All melting points, which were recorded on a Kofler micro hot stage, and boiling points are uncorrected and are reported in °C. The i.r. spectra were recorded on a Perkin–Elmer Model 700 spectrometer and were calibrated with the 1601 cm^{-1} band of polystyrene. The u.v. spectra were recorded on a Unicam Model SP 800 or a Cary Model 14 spectrophotometer. The proton nuclear magnetic resonance spectra were recorded on either a Varian T-60 or HA-100 spectrometer and the chemical shifts are reported in δ units from internal tetramethylsilane. Low resolution mass spectra were recorded on an AEI MS-9 or an Atlas CH-4b mass spectrometer, and the high resolution spectra were recorded on the MS-9 spectrometer. Both instruments were operated at an ionizing potential of 70 eV. Vapor phase chromatograms were obtained on a Varian-Aerograph Model 90 P3 chromatograph using a 5 ft × ¼ in. column of 5% QF-1 on 60–80 mesh Chromosorb W.

The support used for all micro thin-layer and preparative thin-layer chromatography was silica gel PF_{254} (Merck). Merck silica <0.03 mm or finer than 200 mesh was used for column chromatography. Microanalyses were performed by Mr. Peter Borda, University of British Columbia, Vancouver.

All solvents were dried and distilled immediately before use. All reactions were run under an atmosphere of nitrogen or argon. Commerical sodium hydride (50–57% mineral oil) was used without prior washing to remove the mineral oil. Commercial solutions of *n*-butyllithium in hexane were used directly and were standardized by double titration (28) or direct titration (29).

Methyl 3,5-Dioxohexanoate (11, R = Me)

Sodium hydride (0.467 g, 11.0 mmol), as a 57% mineral oil dispersion, was weighed into a 50 ml oven-dried flask and tetrahydrofuran (*ca.* 25 ml) was distilled directly into this flask from lithium aluminum hydride. The flask was equipped with a magnetic stirrer, stoppered (septum cap), cooled in ice, and flushed with nitrogen. Methyl acetoacetate (1.160 g, 10.0 mmol) was added dropwise to the cooled slurry and the reaction allowed to stir for 10 min after the addition was complete. *n*-Butyllithium (5 ml, 10.5 mmol), as a 2.1 *M* solution in hexane, was added dropwise to the reaction and after 10 min the first portion of methyl acetate (0.372 g, 5.0 mmol) was added. After a further 15 min, additional *n*-butyllithium (5 ml, 10.5 mmol) was added very slowly. A further period of 15 min was allowed to elapse before the second portion of methyl acetate (0.371 g, 5.0 mmol) was added and the reaction stirred for a final 15 min

Can. J. Chem. Downloaded from www.nrcresearchpress.com by 210.87.254.42 on 09/05/12
For personal use only.

Can. J. Chem. Downloaded from www.nrcresearchpress.com by 210.87.254.42 on 09/05/12
For personal use only.

before being quenched with concentrated hydrochloric acid (3 ml). The reaction was worked up by the addition of ether (35 ml) and water (10 ml). The aqueous phase was separated and further extracted with ether (2 × 35 ml). The ethereal extracts were combined, washed with saturated sodium hydrogen carbonate solution (2 × 10 ml) and with saturated sodium chloride solution (4 × 15 ml), dried over anhydrous sodium sulfate and filtered. The solvents were removed under reduced pressure and the resulting yellow oil distilled under vacuum to give 1.120 g (71%) of **11** (R = Me); b.p. 44–46 °C (0.3 mm), (lit. (27*b*) b.p. 65°/11 mm); i.r. ($CHCl_3$) 3450, 1740, and 1600 cm^{-1}; n.m.r. ($CDCl_3$) δ 14.2 (broad s, exchangeable D_2O, 1H), 5.62 (s, 0.67H), 3.79 (s, 3H), 3.57 (s, 0.64H), 3.35 (s, 2H), 2.27 (s, 0.95 H), and 2.10 p.p.m. (s, 2.13H), 68% enol; mass spectrum, *m/e* (relative intensity) 158(6), 127(6), 126(8), 116(8), 107(8), 101(6), 98(9), 91(9), 85(43), 77(6), 69(21), 59(10) and 43(100).

Anal. Calcd. for $C_7H_{10}O_4$: C, 53.16; H, 6.37. Found: C, 53.14; H, 6.26.

*Methyl 3,5-Dioxooctanoate (**11**, R = n-Pr)*

This compound was prepared by the same procedure as that employed in the preparation of methyl 3,5-dioxohexanoate (**11**, R = Me). The reagents used in the preparation were sodium hydride (0.465 g, 11.0 mmol), as a 57% mineral oil dispersion, methyl acetoacetate (1.161 g, 10.0 mmol), two portions of *n*-butyllithium (4.6 ml, 10.6 mmol), as a 2.35 *M* solution in hexane, which gave 1.250 g (67%) of **11** (R = *n*-Pr), b.p. 83–85 °C (0.1 mm); i.r. (CCl_4) 3500, 1740, and 1595 cm^{-1}; n.m.r. (CCl_4) δ 14.3 (broad s, 0.97H), 5.52 (s, 0.98H), 3.66 (s, 3H), 3.20 (s, 1.96H), 2.26 (t, J = 7 Hz, 2.0H), 1.66 (m, 2.0H) and 0.96 p.p.m. (t, J = 7 Hz, 3.0H), 97% enol; mass spectrum, *m/e* (relative intensity) 186(41), 172(22), 158(68), 157(57), 143(81), 126(73), 115(62), 113(92), 101(100), 97(28), 85(73), 84(72), 71(90), 69(51), 59(81), and 43(17).

Anal. Calcd. for $C_9H_{14}O_4$: C, 58.05; H, 7.58. Found: C, 58.35; H, 7.47.

*Condensation of Ethyl Butanoate with Dianion **10***

This reaction was performed in a similar manner to that in which methyl 3,5-dioxohexanoate was prepared. The reagents used were sodium hydride (0.466 g, 11.0 mmol), as a 57% mineral oil dispersion, methyl acetoacetate (1.61 g, 10.0 mmol), two portions of *n*-butyllithium (4.5 ml, 10.6 mmol), as a 2.35 *M* solution in hexane, and two portions of ethyl butanoate (0.582 g, 5.0 mmol), which gave 1.441 g of a pale yellow oil. Vapor phase chromatographic analysis (140 °C) of this oil showed it to contain two components. Distillation through a short Vigreux column gave partial separation of these components and repeated distillation (three more times), although accompanied by considerable resinification of the oil, gave the pure components identified as methyl 3,5-dioxooctanoate (**11**, R = *n*-Pr) (0.619 g, 33%) by comparison of i.r. and n.m.r. spectra with those of **11** (R = *n*-Pr) prepared above, and ethyl 3,5-dioxooctanoate (0.223 g, 11%), b.p. 94–96 °C (0.1 mm); i.r. (CCl_4) 3500, 1740, and 1600 cm^{-1}; n.m.r. (CCl_4) δ 14.6 (broad s, exchangeable D_2O, 1H), 5.57 (s, 1H), 4.13 (q, J = 7 Hz, 2H), 3.08 (s, 2H), 2.27 (t, J = 7 Hz, 2H), 1.65 (m, 2H), 1.27 (t, J = 7 Hz, 2H) and 0.95 p.p.m. (t, J = 7 Hz, 3H); mass spectrum, *m/e* (relative intensity) 200(20), 156(47), 143(78), 126(70), 115(64), 113(80), 101(100), 97(30), 85(74), 84(70), 71(85), 69(15), 59(60), and 43(28).

Anal. Calcd. for $C_{10}H_{16}O_4$: C, 59.98; H, 8.05. Found: C, 59.98; H, 8.08.

*Methyl 3,5-Dioxopentanoate (**11**, R = H)*

This compound was prepared by the same procedure as that employed in the preparation of methyl 3,5-dioxohexanoate (**11**, R = Me). The reagents used in the preparation were sodium hydride (0.466 g, 11.0 mmol), as a 57% mineral oil dispersion, methyl acetoacetate (1.160 g, 10.0 mmol), two portions of *n*-butyllithium (4.5 ml, 10.6 mmol), as a 2.35 *M* solution in hexane, and two portions of methyl formate (0.300 g, 5.0 mmol), which gave 0.993 g (69%) of **11** (R = H) b.p. 55–56 °C (0.1 mm); i.r. (CCl_4) 3500, 1740, 1640, and 1590 cm^{-1}; n.m.r. (CCl_4) δ 13.5 (broad s, exchangeable D_2O, 1H), 7.72 (d, J = 5 Hz, 1H), 5.63 (d, J = 5 Hz, 1H), 3.72 (s, 3H), and 3.32 p.p.m. (s, 2H); mass spectrum, *m/e* (*a*) high resolution calcd. for $C_6H_8O_4$: 144.0422 a.m.u.; found: 144.0421 a.m.u.; (*b*) *m/e* (relative intensity) 144(5), 131(3), 127(2), 126(11), 113(15), 112(17), 101(100), 97(30), 85(67), 71(63), 59(43), and 43(28).

*Condensation of Methyl Benzoate with Dianion **10***

Sodium hydride (0.468 g, 11.0 mmol), as a 57% mineral oil dispersion, was weighed into a 50 ml oven dried flask and tetrahydrofuran (*ca.* 25 ml) was distilled directly into this flask from lithium aluminum hydride. The flask was equipped with a magnetic stirrer, stoppered (septum cap), cooled in ice, and flushed with nitrogen. Methyl acetoacetate (1.164 g, 10.0 mmol) was added dropwise to the cooled slurry and after the addition was complete the reaction was allowed to stir for 10 min. *n*-Butyllithium (5 ml, 10.5 mmol), as a 2.1 *M* solution in hexane, was added dropwise to the reaction and after 10 min the first portion of methyl benzoate (0.680 g, 5.0 mmol) was added. After a further 15 min additional *n*-butyllithium (5 ml, 10.5 mmol) was added very slowly. A further period of 15 min was allowed to elapse before the second portion of methyl benzoate (0.680 g, 5.0 mmol) was added and the reaction was stirred for a final 15 min before being quenched with concentrated hydrochloric acid (3 ml). The reaction was worked up by the addition of ether (35 ml) and water (10 ml). The aqueous phase was separated and further extracted with ether (2 × 35 ml). The ethereal extracts were combined, washed with saturated sodium hydrogen carbonate solution (4 × 15 ml) and with saturated sodium chloride solution (2 × 15 ml), dried over anhydrous sodium sulfate, and filtered. The solvents were removed under reduced pressure and the resulting red oil distilled under vacuum to give 0.817 g (37%) of methyl 3,5-dioxo-5-phenylpentanoate (**11**, R = C_6H_5), b.p. 127–129 °C (0.1 mm); i.r. (CCl_4) 3450, 1740, and 1600 cm^{-1}; u.v. (CH_3OH) 322 nm (1.3×10^3); n.m.r. (CCl_4) δ 14.3 (broad s, exchangeable D_2O, 1H), 7.87 (m, 2H), 7.37 (m, 3H), 6.26 (s, 1H), 3.70 (s, 3H), and 3.38 p.p.m. (s, 2H); mass spectrum, *m/e* (relative intensity) 220 (21), 205(11), 203(34), 189(26), 188(65), 174(16), 173(11), 163(57), 161(58), 147(74), 105(100), 85(15), 77(48), 69(51), 51(37), and 43(28).

Anal. Calcd. for $C_{12}H_{12}O_4$: C, 65.45; H, 5.49. Found: C, 65.42; H, 5.65.

The basic aqueous extract (saturated sodium hydrogen carbonate washings) was acidified to p*H* 2 by addition of

Can. J. Chem. Downloaded from www.nrcresearchpress.com by 210.87.254.42 on 09/05/12
For personal use only.

1 *M* hydrochloric acid and the resulting solution extracted with ether (3 × 35 ml); these ethereal extracts were combined, washed with saturated sodium chloride solution (3 × 15 ml), dried over sodium sulfate, and filtered. The solvents were removed under reduced pressure and the resulting solid recrystallized from a mixture of hexane and ether to give 0.684 g (30%) of 3,5-dioxo-5-phenylpentanoic acid (**12**, Ar = C_6H_5), m.p. 93–97 °C (lit. (20) m.p. 94–96 °C).

*Condensation of Methyl 4-Methoxybenzoate with Dianion **10***

This reaction was performed in a similar manner to the condensation of methyl benzoate with dianion **10** above. The reagents used were sodium hydride (0.467 g, 11.0 mmol), as a 57% mineral oil dispersion, methyl acetoacetate (1.161 g, 10.0 mmol), two portions of *n*-butyllithium (4.5 ml, 10.6 mmol), as a 2.35 *M* solution in hexane, and two portions of methyl 4-methoxybenzoate (0.831 g, 5.0 mmol), which gave 0.741 g (29%) of 5-(4-methoxyphenyl)-3,5-dioxopentanoic acid (**12**, Ar = *p*-MeO—C_6H_4) as colorless needles (from hexane–ether), m.p. 103–105 °C, and 1.051 g (42%) of methyl 5-(4-methoxyphenyl)-3,5-dioxopentanoate (**11**, R = *p*-MeO—C_6H_4), b.p. 142–143 °C (0.1 mm). These compounds were characterized as follows.

(*a*) 5-(4-Methoxyphenyl)-3,5-dioxopentanoic acid (**12**, Ar = *p*-MeO—C_6H_4); i.r. ($CHCl_3$) 3700, 3500, 1720, and 1600 cm^{-1}; u.v. (CH_3OH) 326 (7.1 × 10) and 287 nm (shoulder, 4.4 × 10^3); n.m.r. (CD_3COCD_3) δ 14.6 (broad s, exchangeable D_2O, 1H), 11.2 (broad s, exchangeable D_2O, 1H), 7.87 (m, 2H), 6.93 (m, 2H), 3.90 (s, 3H) and 3.37 p.p.m. (s, 2H); mass spectrum, *m/e* (relative intensity) 237(5), 236(43), 219(5), 218(42), 193(43), 192(96), 191(67), 178(50), 177(84), 161(68), 149(20), 136(57), 135(100), 121(21), 109(75), 108(57), 105(15), 92(32), 85(30), 77(37), 69(45), 51(35), 44(40), and 43(35).

Anal. Calcd. for $C_{12}H_{12}O_5$: C, 61.02; H, 5.12. Found: C, 61.08; H, 5.26.

(*b*) Methyl 5-(4-Methoxyphenyl)-3,5-dioxpentanoate (**11**, R = *p*-MeO—C_6H_4); i.r. (CCl_4) 3500, 1740, and 1600 cm^{-1}; u.v. (CH_3OH) 325 (5.4 × 10) and 285 nm (shoulder, 2.0 × 10^3); n.m.r. (CCl_4) δ 14.3 (broad s, exchangeable D_2O, 1H), 7.85 (m, 2H), 6.90 (m, 2H), 6.20 (s, 1H), 3.90 (s, 3H), 3.77 (s, 3H), and 3.47 p.p.m. (s, 2H); mass spectrum, *m/e* (relative intensity) 250(21), 217(57), 190(44), 177(65), 135(100), 109(23), 108(13), 107(15), 105(16), 104(32), 91(29), 77(29), 69(65), 59(23), and 43(55).

Anal. Calcd. for $C_{13}H_{14}O_5$: C, 62.39; H, 5.64. Found: C, 62.43; H, 5.72.

Base Dependency Study

(a) Lithium Diisopropylamide

(i) Attempted acylation with methyl acetate. Diisopropylamine (1.536 g, 15.0 mmol) was weighed into an oven-dried flask and tetrahydrofuran (*ca.* 25 ml) was distilled directly into this flask from lithium aluminum hydride. The flask was equipped with a magnetic stirrer, stoppered (septum cap), cooled in ice, and flushed with nitrogen. *n*-Butyllithium (7.5 ml, 15.8 mmol), as a 2.1 *M* solution in hexane, was added dropwise to the cooled solution and the reaction allowed to stand for 10 min after the addition was complete. Methyl acetoacetate (0.580 g, 5.0 mmol) was added to the reaction over a period of about 10 min and a further period of 10 min allowed to elapse before methyl acetate (0.370 g, 5.0 mmol) was added. After 10 min the reaction was quenched with concentrated hydrochloric acid (*ca.* 4 ml) and the reaction worked up by the addition of ether (35 ml) and water (10 ml). The aqueous phase was separated and further extracted with ether (2 × 35 ml). The ethereal extracts were combined, washed with water (3 × 20 ml) and with saturated sodium chloride solution (2 × 20 ml), dried over anhydrous sodium sulfate, and filtered. The solvents were removed at reduced pressure to give 0.601 g of pale yellow oil. Vapor phase chromatography analysis of this oil (120 °C) showed it to be methyl acetoacetate contaminated with minor amounts of diisopropylamine and methyl acetate. Both v.p.c. and t.l.c. analysis of this oil and the acidified crude reaction mixture failed to indicate any of the desired product, methyl 3,5-dioxohexanoate (**11**, R = Me). Distillation of the oil at reduced pressure gave 0.521 g (90%) of methyl acetoacetate, b.p. 51–52 °C (17 mm) identified by v.p.c. analysis and comparison of its i.r. and n.m.r. spectra with those of authentic material.

(ii) Attempted acylation with methyl benzoate. This reaction was run as above using 0.680 g (5.0 mmol) methyl benzoate to give 0.924 g (91%) of *N,N*-diisopropylbenzamide m.p. 68–69 °C (lit. (30) m.p. 69–71 °C); i.r. ($CHCl_3$) 1620 cm^{-1}; n.m.r. ($CDCl_3$) δ 7.30 (s, 5H), 3.67 (septuplet, J = 6 Hz, 2H) and 1.32 p.p.m. (d, J = 6 Hz, 12H); v.p.c. and t.l.c. analysis of the crude oil failed to show any of the desired products methyl 3,5-dioxo-5-phenylpentanoate (**11**, R = C_6H_5) or 3,5-dioxo-5-phenylpentanoic acid (**12**, Ar = C_6H_5).

(b) Lithium N-Cyclohexyl-N-isopropylamide

(i) Acylation with methyl acetate. *N*-Cyclohexyl-*N*-isopropylamine, which had been distilled from calcium hydride and stored over potassium hydroxide until used, was used in place of diisopropylamine above to give 0.537 g of a yellow oil. Vapor phase chromatography analysis of this oil (120 °C) showed it to contain methyl acetoacetate and methyl 3,5-dioxohexanoate (**11**, R = Me) in the ratio 93:7. Distillation of the oil at reduced pressure gave 0.486 g (88%) of methyl acetoacetate, b.p. 49–52 °C (17 mm), identified by comparison of i.r. and n.m.r. spectra with those of authentic material, and 40 mg of residue. The residue was distilled in a bulb-to-bulb distillation apparatus (bath temperature 50 °C) under vacuum (0.2 mm) to give 37 mg (4%) of methyl 3,5-dioxohexanoate (**11**, R = Me) which was identified by comparison with previously prepared material by v.p.c. (120 °C) and t.l.c.

(ii) Acylation with methyl benzoate. This reaction was run as above using methyl benzoate (5.0 mmol) to give a yellow semicrystalline material. Recrystallization from ether gave 1.080 g (88%) of *N*-cyclohexyl-*N*-isopropylbenzamide, m.p. 76–78 °C; i.r. ($CHCl_3$) 1620 cm^{-1}; n.m.r. (CCl_4) δ 7.30 (s, 5H), 3.87–3.00 (m, 2H), 2.20–1.00 (m, 10H), and 1.30 p.p.m. (d, J = 6 Hz, 6H); mass spectrum, *m/e* (relative intensity) 246(22), 245(37), 244(14), 230(22), 203(27), 202(46), 189(15), 188(39), 165(11), 164(37), 163(54), 162(62), 149(11), 148(41),

Can. J. Chem. Downloaded from www.nrcresearchpress.com by 210.87.254.42 on 09/05/12
For personal use only.

146(23), 145(32), 129(19), 128(19), 118(36), 117(41), 115(33), 105(72), 103(35), 85(33), 79(35), 78(44), 76(93), 56(83), and 54(100).

The mother liquors from the recrystallization were found by v.p.c. analysis (200 °C) to contain methyl 3,5-dioxo-5-phenylpentanoate and were subjected to chromatography on silica gel, using chloroform as eluent. The major component isolated from this chromatography was methyl 3,5-dioxo-5-phenylpentanoate (**11**, R = C_6H_5) (0.085 g, 8%), identified by comparison of its i.r. spectrum with that of previously prepared material.

Condensation of the Monoanion of Methyl Acetoacetate with Dianion ***10***

(a) At Room Temperature, Acid Quenching

Sodium hydride (0.466 g, 11.0 mmol), as a 57% mineral oil dispersion, was weighed into an oven-dried flask and freed from mineral oil by washing with hexane (*ca.* 15 ml) and decantation. The washing procedure was repeated twice with hexane and the residual hexane was removed by washing with tetrahydrofuran. After decantation of the tetrahydrofuran, fresh tetrahydrofuran was distilled directly into the flask from lithium aluminum hydride. The flask was equipped with a magnetic stirrer, stoppered (septum cap), cooled in ice, and flushed with nitrogen. Methyl acetoacetate (1.162 g, 10.0 mmol) was added dropwise to the cooled slurry and after the addition was complete the reaction was allowed to stand for a period of about 10 min. *n*-Butyllithium (2.2 ml, 5.1 mmol), as a 2.3 *M* solution in hexane, was added dropwise to the reaction which was then allowed to warm to room temperature. After a period of 24 h the reaction was quenched by addition of concentrated hydrochloric acid (*ca.* 1.5 ml) and worked up by addition of ether (35 ml) and water (5 ml). The aqueous phase, the p*H* of which was *ca.* 2, was separated and further extracted with ether (2 × 35 ml). The ethereal extracts were combined, washed with saturated sodium chloride solution (4 × 20 ml), dried over anhydrous sodium sulfate, and filtered. The solvents were removed under reduced pressure to give 0.983 g of brown oil. Distillation of this oil at reduced pressure gave 0.716 g (62%) of methyl acetoacetate, b.p. 45–47 °C (14 nm), identified by comparison of its i.r. and n.m.r. spectra with those of authentic material, and a brown solid residue which was crystallized from methanol to give 0.220 g (24%) of methyl orsellinate (**13**), m.p. 138–140 °C (lit. (31) m.p. 138–139 °C), mixture m.p. 138–140 °C.

(b) At Room Temperature, Buffered Quenching

This reaction was performed in the same manner as the preceding reaction. The reagents employed were sodium hydride (0.463 g, 11.0 mmol), as a 57% mineral oil dispersion, methyl acetoacetate (1.160 g, 10.0 mmol), and *n*-butyllithium (2.5 ml, 5.2 mmol), as a 2.1 *M* solution in hexane. After the 24 h reaction period, the reaction was quenched by adding it, via a stainless steel cannula, to a vigorously stirred mixture of ether (50 ml) and buffer solution (prepared by dissolving sodium dihydrogen orthophosphate (4 g) and disodium hydrogen orthophosphate (4 g) in water (20 ml)). The aqueous phase was separated, saturated with sodium chloride, and further extracted with ether (3 × 20 ml). The ethereal layers were combined, washed with saturated sodium chloride solution (20 ml), dried over anhydrous sodium sulfate, and filtered. The solvents were removed under reduced pressure and the resulting oil chromatographed on silica gel, using a mixture of benzene and ethyl acetate (1:1 v/v) as eluent. Three components were obtained from the chromatography, and these, in order of their elution, were methyl 3,5,7-trioxooctanoate (**14**) (83 mg, 8%), as a pale yellow, unstable oil, which on standing overnight at 0 °C was converted to methyl orsellinate in quantitative yield, methyl orsellinate (**13**) (155 mg, 17%) as cream colored needles, m.p. 138–140 °C; and methyl acetoacetate (0.679 g, 59%). Methyl 3,5,7-trioxooctanoate was characterized by; i.r. ($CHCl_3$) 3400, 1740, 1720, 1640, 1620 and 1600 cm^{-1}; n.m.r. (CCl_4) δ 14.60 (broad s, exchangeable D_2O, 1H), 6.20 (m, 1H), 3.96 (s, 3H), 3.70 (s, 2H), 3.67 (s, 2H) and 2.43 p.p.m. (s, 3H); mass spectrum, *m/e* (relative intensity) 184(9), 182(4), 151(4), 150(13), 143(7), 142(26), 127(40), 117(9), 113(27), 101(9), 100(24), 85(100), 73(21), 69(20), 61(34), and 43(100).

(c) At Reflux Temperature

Reaction mixture obtained similarly to *b* was allowed to warm to room temperature. The flask was then transferred to a glove bag where, under an atmosphere of nitrogen, the septum cap was removed and replaced with a reflux condenser, the top of which was stoppered with a fresh septum cap and heated under nitrogen until a moderate rate of reflux was obtained. After 2 h at reflux temperature,the heating was discontinued and the flask cooled in ice to 0 °C. The reaction was quenched with concentrated hydrochloric acid (*ca.* 1.5 ml) and worked up by the addition of ether (35 ml) and water (5 ml). The aqueous phase was separated and further extracted with ether (2 × 35 ml). The ethereal extracts were combined, washed with saturated sodium chloride solution (4 × 20 ml), dried over anhydrous sodium sulfate, and filtered. The solvents were removed under reduced pressure and distillation of the resulting oil at reduced pressure gave 0.821 g (71%) of methyl acetoacetate, b.p. 46–48 °C (14 mm), identified by comparison of its i.r. spectrum with that of authentic material, and a brown residue, which on titration with methanol gave 0.213 g (23%) of methyl orsellinate (**13**), as pale yellow needles, identified by comparison of its i.r. spectrum with that of authentic material.

Condensation of Benzonitrile with Dianion ***10***

Sodium hydride (0.467 g, 11.0 mmol), as a 57% mineral oil dispersion, was weighed into a 50 ml oven-dried flask and tetrahydrofuran (*ca.* 25 ml) was distilled directly into this flask from lithium aluminum hydride. The flask was equipped with a magnetic stirrer, stoppered (septum cap), cooled in ice, and flushed with nitrogen. Methyl acetoacetate (1.160 g, 10.0 mmol) was added dropwise to the cooled slurry and the reaction allowed to stir for 10 min after the addition was complete. *n*-Butyllithium (5 ml, 10.5 mmol), as a 2.1 *M* solution in hexane, was added dropwise to the reaction and after 10 min benzonitrile (1.031 g, 10.0 mmol) was added. The reaction mixture was allowed to warm to room temperature and stirred for 12 h before being quenched with concentrated hydrochloric acid (2 ml). The reaction was worked up by the addition of ether (35 ml) and water (10 ml) and the resulting precipitate filtered off. The precipitate was

Can. J. Chem. Downloaded from www.nrcresearchpress.com by 210.87.254.42 on 09/05/12
For personal use only.

washed with acetone (2 × 10 ml), air dried, and sublimed at 150 °C (0.2 mm) to give 0.547 g (29%) of 4-hydroxy-6-phenylpyridone (**17**) as colorless spars, m.p. 314–316 °C (lit. (32) m.p. 315–318 °C); i.r. (KBr disc) 1640, 1620, 1595, and 1560 cm^{-1}; u.v. (C_2H_5OH) 310 and 255 nm, (C_2H_5OH + NaOH) 240 nm; mass spectrum, *m/e* (relative intensity) 188(16), 187(100), 186(17), 160(6), 159(15), 158(10), 147(11), 146(6), 130(19), 104(33), 103(33), 91(14), 77(21), 69(9), and 51(15).

The aqueous phase of the filtrate was separated and further extracted with ether (2 × 35 ml). The ethereal extracts were combined, washed with saturated sodium chloride solution (6 × 15 ml), dried over anhydrous sodium sulfate, and filtered. The solvents were removed under reduced pressure and the resulting oil chromatographed on silica gel using ethyl acetate as eluent. The major fraction from this chromatography was collected, and freed from eluent by distillation at room temperature under reduced pressure to give 1.466 g (66%) of methyl 5-amino-3-oxo-5-phenyl-pent-4-enoate (**15**, R = Me; R′ = C_6H_5) as a pale yellow oil; i.r. ($CHCl_3$) 3550, 1740, 1615, and 1600 cm^{-1}; u.v. (C_2H_5OH) 325 nm; n.m.r. (CCl_4) δ 8.00 (broad s, exchangeable D_2O, 1H), 7.41 (m, 5H), 6.20 (broad s, exchangeable D_2O, 1H), 5.37 (s, 1H), 3.60 (s, 3H), and 3.27 p.p.m. (s, 2H); mass spectrum (*a*) high resolution calcd. for $C_{12}H_{13}NO_3$: 219.0895 a.m.u.; found: 219.0896 a.m.u.; (*b*) low resolution *m/e* (relative intensity) 219(26), 159(15), 146(47), 127(35), 121(32), 119(95), 118(95), 103(30), 84(52), 82(22), 59(46), and 43(100).

*Thermolysis of Methyl 5-Amino-3-oxo-5-phenylpent-4-enoate (**15**, R = Me; R′ = C_6H_5)*

Enamine **15** (R = Me; R′ = C_6H_5) (156 mg, 0.71 mmol) was placed in a bulb-to-bulb distillation apparatus and heated to 150 °C under reduced pressure (0.2 mm). After ½ h the starting material had completely disappeared and white spars had been deposited on the cooler parts of the apparatus. These crystals were collected and found to amount to 134 mg (100%) of 4-hydroxy-6-phenylpyridone (**17**), which exhibited identical m.p., and i.r. and u.v. spectra to that obtained previously.

*Methyl 5-Amino-3-oxohex-4-enoate (**15**, R = R′ = Me)*

Reaction was run as above using sodium hydride (0.467 g, 11.0 mmol), methyl acetoacetate (1.160 g, 10.0 mmol), *n*-butyllithium (5 ml of 2.1 *M*, 10.5 mmol), and acetonitrile (0.409 g, 10.0 mmol). The reaction mixture was allowed to warm to room temperature and stirred for 16 h before being quenched with concentrated hydrochloric acid (2 ml). The reaction was worked up by the addition of ether (35 ml) and water (10 ml). The aqueous phase was separated and further extracted with ether (2 × 35 ml). The ethereal extracts were combined, washed with saturated sodium chloride solution (4 × 15 ml), dried over anhydrous magnesium sulfate, and filtered. The solvents were removed under reduced pressure. The resulting semi-solid was crystallized from chloroform to give 1.490 g (86%) of **15** (R = R′ = Me) as long yellow needles, m.p. 103–104 °C. Sublimation at 175 °C (0.2 mm) gave colorless spars but did not raise the melting point; i.r. ($CHCl_3$) 3550, 1740, 1625, and 1610 cm^{-1}; u.v. (CH_3OH) 303 nm (16.8×10^3) and (CH_3OH + NaOH) 274 nm; n.m.r. ($CDCl_3$) δ 10.0 (broad s, exchangeable D_2O, 1H), 5.10 (s, 1H), 3.70 (s, 3H), 3.33 (s, 2H), and 1.97 p.p.m. (s, 3H); mass spectrum, *m/e* (relative intensity) 158(3), 157(26), 126(2), 125(3), 85(7), 84(100), 83(2), 70(2), 68(2), 54(2), 43(3), 42(5) and 41(4).

Anal. Calcd. for $C_7H_{11}O_3N$: C, 53.49; H, 7.05; N, 8.91. Found: C, 53.18; H, 6.99; N, 8.84.

We are grateful to the University of British Columbia and the National Research Council of Canada for support of this work.

1. C. R. Hauser and T. M. Harris. J. Am. Chem. Soc. **80**, 6360 (1958).
2. S. D. Work and C. R. Hauser. J. Org. Chem. **28**, 725 (1963).
3. R. J. Light and C. R. Hauser. J. Org. Chem. **25**, 538 (1960).
4. F. B. Kirby, T. M. Harris, and C. R. Hauser. J. Org. Chem. **28**, 2266 (1963).
5. M. L. Miles, T. M. Harris, and C. R. Hauser. J. Org. Chem. **30**, 1007 (1965).
6. T. M. Harris and R. L. Carney. J. Am. Chem. Soc. **89**, 6734 (1967).
7. K. G. Hampton, T. M. Harris, C. M. Harris, and C. R. Hauser. J. Org. Chem. **30**, 4263 (1965).
8. T. M. Harris, S. Boatman, and C. R. Hauser. J. Am. Chem. Soc. **87**, 3186 (1965).
9. T. M. Harris and G. P. Murphy. J. Am. Chem. Soc. **93**, 6708 (1971).
10. A. J. Birch and F. W. Donovan. Aust. J. Chem. **6**, 360 (1953).
11. (*a*) J. H. Richards and J. B. Hendrickson. The biosynthesis of steroids, terpenes, and acetogenins. W. A. Benjamin, New York, N.Y. 1964; (*b*) J. D. Bu'lock. The biosynthesis of natural products. McGraw-Hill, London. 1965.
12. J. N. Collie. J. Chem. Soc. **91**, 1806 (1907).
13. A. J. Birch, D. W. Cameron, and R. W. Richards. J. Chem. Soc. 4395 (1960).
14. J. R. Bethel and P. Maitland. J. Chem. Soc. 3751 (1960).
15. T. Money, F. W. Comer, G. R. Webster, I. G. Wright, and A. I. Scott. Tetrahedron, **23**, 3435 (1967).
16. J. L. Douglas and T. Money. Can. J. Chem. **45**, 1990 (1967).
17. J. L. Douglas and T. Money. Tetrahedron, **23**, 3545 (1967).
18. T. Money. Chem. Rev. **70**, 553 (1970).
19. S. N. Huckin and L. Weiler. Tetrahedron Lett. 2405 (1972).
20. J. F. Wolfe, T. M. Harris, and C. R. Hauser. J. Org. Chem. **29**, 3249 (1964).
21. (*a*) L. Weiler. J. Am. Chem. Soc. **92**, 6702 (1970); (*b*) S. N. Huckin and L. Weiler. J. Am. Chem. Soc. In press; (*c*) S. N. Huckin Ph.D. Thesis, University of British Columbia, Vancouver, British Columbia, 1973.
22. S. N. Huckin and L. Weiler. Tetrahedron Lett. 4835 (1971).
23. (*a*) K. W. Yang, J. G. Cannon, and J. G. Rose. Tetrahedron Lett. 1791 (1970); (*b*) B. Singh. Tetrahedron Lett. 321 (1971).

24. R. A. OLOFSON and C. M. DOUGHERTY. J. Am. Chem. Soc. **95**, 579, 582 (1973).
25. T. P. MURRAY and T. M. HARRIS. J. Am. Chem. Soc. **94**, 8253 (1972).
26. T. T. HOWARTH, G. P. MURPHY, and T. M. HARRIS. J. Am. Chem. Soc. **91**, 517 (1969).
27. (*a*) F. SPROXTON. J. Chem. Soc. **89**, 1186 (1906); (*b*) C. T. BEDFORD, J. M. FORRESTER, and T. MONEY. Can. J. Chem. **48**, 2645 (1970).
28. R. R. TURNER, A. G. ALTENEAU, and T. C. CHENG. Anal. Chem. **42**, 1835 (1970).
29. S. C. WATSON and J. F. EASTHAM. J. Organomet. Chem. **9**, 165 (1967).
30. B. PRAJSNAR and C. TROSZKIEWICZ. Rocz. Chem. **36**, 1029 (1968).
31. A. HESSE. J. Prakt. Chem. **57**, 268 (1852).
32. F. ARNDT, B. EISERT, H. SCHLOZ, and E. ARON. Chem. Ber. **69**, 2373 (1936).

Can. J. Chem. Downloaded from www.nrcresearchpress.com by 210.87.254.42 on 09/05/12
For personal use only.

The Transformation of Carvone into Racemic Grandisol

WILLIAM A. AYER AND LOIS M. BROWNE

Chemistry Department, University of Alberta, Edmonton, Alberta T6G 2E1

Received November 16, 1973

Grandisol (**1**) is one of the components of the pheromone complex emitted by the male boll weevil. We report the transformation of readily available eucarvone (**3**), via the photoisomer **4**, into grandisol in 20% overall yield. A key step in the synthesis is the Beckmann cleavage of oxime **15**, derived in three steps from **4**, to nitrile **16**. Hydrolysis of **16** followed by hydride reduction gives grandisol (**1**).

Le grandisol (**1**) est l'un des composants du complexe phéromone émis par l'antomone male. Nous rapportons la transformation de l'eucarvone (**3**) d'accès facile en grandisol; la synthèse se fait par l'intermédiaire du photoisomère **4** et le rendement global est de 20%. Dans l'étape clef de la synthèse, l'oxime **15**, obtenu en trois étapes à partir de **4**, subit un réarrangement de Beckmann pour conduire au nitrile **16**. L'hydrolyse de ce dernier suivit d'une réduction par l'hydrure de lithium aluminum conduit au grandisol (**1**).
[Traduit par le journal]

Can. J. Chem., **52**, 1352 (1974)

Grandisol (**1**) is one of the components of the sex pheromone of the boll weevil (1). We wish to report a facile stereoselective synthesis of grandisol starting from the monoterpene ketone carvone (**2**). We believe that this synthesis has some advantages over those previously reported (1, 2) in that the starting material is readily available and inexpensive, and the overall yield is reasonably high. Earlier syntheses (1, 2) all

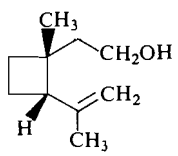

1

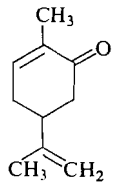

2

involve an *intermolecular* "2 + 2" cycloaddition in the construction of the cyclobutane ring. The synthesis reported herein differs from these in that it employs an efficient *intramolecular* cyclization for the formation of the 4-membered ring.

The initial steps utilize the well-known transformation of carvone into eucarvone (**3**) (3) and the equally well-studied photochemical transformation of eucarvone into the photoisomer **4** (4). The photoisomer **4** possesses not only the proper arrangement of carbon atoms but also has the required *cis*-relationship between the C-1 methyl and the C-5 hydrogen. The plan (Scheme 1) was to modify **4** by hydrogenation

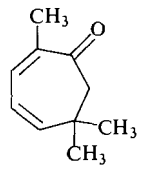

3

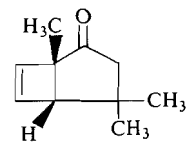

4

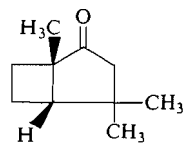

6

and ketone transposition to give **5**. Cleavage of the C_3—C_4 bond in **5** and adjustment of functionality would lead to grandisol (**1**). The method by which this has been accomplished is described below.

The first problem encountered was that of producing substantial amounts of the photoisomer **4** in a reasonably economical manner. In the original Buchi procedure (4*a*) the photoisomer **4** was produced in 36% yield after 22 days photolysis in ethanol. Later work (4*c*–*e*) has shown that the rate of formation of **4** is increased in more polar solvents. We have found that large scale photolysis in trifluoroethanol (4*e*) proceeds to completion (complete disappearance of eucarvone) in 3 days. However the photolysis product is a complex mixture and separation of **4** (in 48% yield) was tedious. This, coupled with

Can. J. Chem. Downloaded from www.nrcresearchpress.com by 210.87.254.5 on 09/05/12
For personal use only.

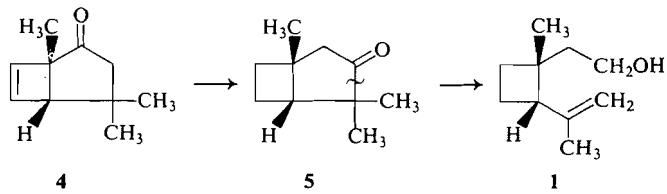

4 5 1

SCHEME 1

the relatively high cost of trifluoroethanol, led us to investigate other solvent systems. After some experimentation we have found that photolysis in ethylene glycol – trifluoroethanol (10:1) is virtually complete in 7 days and that the photoisomer is easily isolated from the photolysis mixture (see Experimental) in 52% yield. Hydrogenation of **4** over palladium-on-charcoal (4*a*) gave **6** in virtually quantitative yield.

Several methods (5) for effecting 1,2-ketone transposition were investigated. In one attempt the ketone **6** was first treated with lead tetraacetate (6) in refluxing acetic acid to give in 89% yield the α-acetoxyketone **7**. Attempted rearrangement of **7** to the isomeric α-acetoxyketone **7***a* under a variety of conditions (tetramethylammonium acetate (7), alumina (8), methanolic sulfuric acid followed by acetylation (9)) was unsuccessful. Compound **7** was recovered in each case which suggests that it is the thermodynamically more stable of the two possible positional isomers.

Another potential route (10) to the ketone **5** involves formation of the α-benzylidene ketone **8**. In the cases reported (10), reduction of the α-benzylidene ketone with lithium aluminum

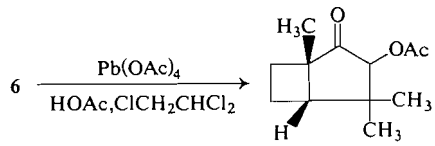

7

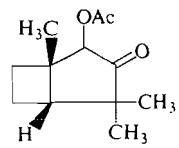

7*a*

hydride – aluminum chloride leads to the corresponding deoxy compound. In this case, however, the major reduction product was the α-benzyl ketone **9**, the product of 1,4-addition of hydride. Reduction of **8** by the Nagata modification (11) of the Wolff–Kishner reaction gave in 58% yield the desired benzylidene compound **10**. However, all attempts at oxidative cleavage (ozone, $KMnO_4$–$NaIO_4$ (12), $RuCl_3$–NaOCl (13)) were unsuccessful, unreacted **10** being recovered in each case. The highly hindered nature of the double bond in the benzylidene compound **10** is reflected in its u.v. spectrum (λ_{max} 249 nm, ε 2150). Normally (5*a*), this type

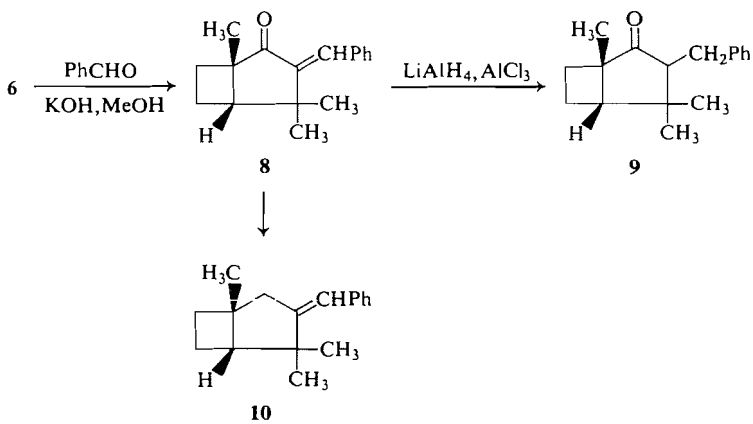

8 9 10

Can. J. Chem. Downloaded from www.nrcresearchpress.com by 210.87.254.5 on 09/05/12
For personal use only.

of compound absorbs at somewhat longer wavelength and with an extinction coefficient ten times as great. Presumably in this case steric crowding forces the chromophoric group to deviate from coplanarity.

The ketone transformation method which proved successful involved an intermediate oximinoketone. Initially formation of the oximinoketone presented problems. Treatment of ketone **6** with *n*-butyl nitrite under acid catalysis (14) for 12 h gave only starting ketone, whereas use of isoamyl nitrite with potassium *t*-butoxide in anhydrous *t*-butyl alcohol (15) led to formation of the oximinoketone **11**. When the reaction was carried out on a larger scale, however, very low yields of oximinoketone were obtained. The major compound isolated was the acid nitrile **12**, the product of Beckmann cleavage. When the reaction was carried out in dry benzene as solvent utilizing potassium *t*-amylate (16) as the base the oximinoketone **11** (as a mixture of *E* and *Z* isomers) was obtained consistently in yields of greater than 80%.

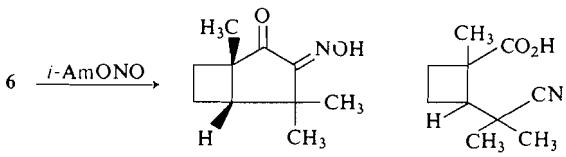

11 **12**

In an attempt to utilize Corey and Richman's ketone transposition method (17), the oximinoketone was reduced quantitatively with sodium borohydride to the oximinoalcohol **13***a*. Mild acetylation gave an acetoximino alcohol **13***b*. More vigorous acetylation gave a mixture of acetoximino acetate **13***c* and another compound which was tentatively identified as the cyanoaldehyde **14**. Attempted mesylation of the acetoximino alcohol gave a mixture of the acetoximino mesylate **13***d* and the cyanoaldehyde. Although this compound was not isolated in pure form, fragmentation to a cyanoaldehyde is well documented for α-hydroxyoximes (18). Since neither the acetoximino acetate nor the acetoximino mesylate could be prepared in good yield, reductive deoximation was attempted on the acetoximino alcohol. The product obtained after treatment with chromous acetate was shown by gas–liquid chromatography to be a mixture of at least eight components, the major of which was the cyanoaldehyde **14**.

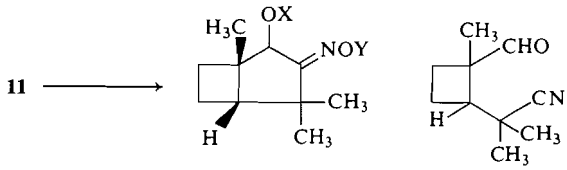

13 **14**

a X = Y = H
b X = H; Y = Ac
c X = Y = Ac
d X = Ms; Y = Ac

Utilization of the Wolff–Kishner reaction enabled us to remove the carbonyl group in the oximinoketone. Heating the oximinoketone with excess hydrazine (19) led to isolation of only a small quantity of oxime **15**; however, use of just 1½ equiv. of hydrazine hydrate and excess base (20) gave the crystalline oxime in 82% yield. Deoximation with titanium trichloride (21) gave the transposed ketone **5** in high yield.

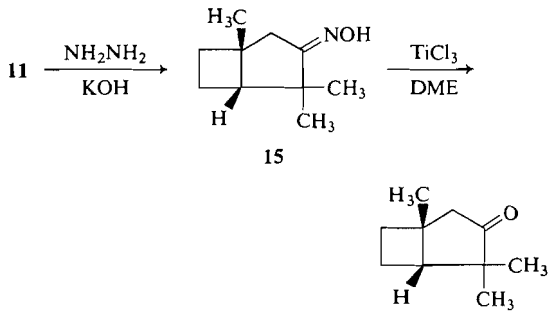

15 **5**

Although it is possible to envision methods for cleaving the C_3—C_4 bond in the ketone **5** itself, Beckmann cleavage of the oxime **15** should proceed in the desired direction (22) and this route was explored first.

When oxime **15** was treated with thionyl chloride in dimethylformamide at 0° for 2 h, the product was a mixture of two compounds. The components of the reaction product were separated by preparative gas–liquid chromatography and were identified as the isomeric nitriles **16** and **17** on the basis of the following spectral data. Compound **16**, which was the minor component, shows nitrile absorption at 2250 and exocyclic methylene at 1650 and 890 cm^{-1} in its i.r. The n.m.r. spectrum shows two vinyl protons as multiplets at τ 5.10 and 5.23, a vinyl methyl group at τ 8.33, and a methyl group at τ 8.64. Compound **17**, which was the major

Can. J. Chem. Downloaded from www.nrcresearchpress.com by 210.87.254.5 on 09/05/12
For personal use only.

Can. J. Chem. Downloaded from www.nrcresearchpress.com by 210.87.254.5 on 09/05/12
For personal use only.

component of the reaction mixture, shows nitrile absorption at 2220 cm^{-1} in the i.r. The n.m.r. spectrum displays a two proton singlet at τ 7.52 for the methylene adjacent to a cyano group, two three-proton multiplets for vinyl methyl groups at τ 8.50 and 8.55, and a methyl singlet at τ 8.62. When oxime **15** was treated with phosphorus pentachloride in dimethylformamide, with *p*-toluenesulfonyl chloride in refluxing pyridine, or with Beckmann's mixture the same mixture was obtained although the product distribution varied.

Use of phosphorus pentachloride in ether, ether–benzene, or alone gave, in addition to the two isomeric nitriles **16** and **17**, a third compound isolated in crystalline form. The crystalline compound was purified by chromatography and identified as lactam **18**. The i.r. spectrum of lactam **18** shows N—H absorption at 3510 and 3300 cm^{-1} as well as lactam carbonyl at 1660 cm^{-1}. The n.m.r. spectrum of compound **18** shows three methyl singlets (τ 8.72, 8.78, 8.90) and a two-proton singlet at τ 7.55 assigned to the C-1 methylene protons. Comparison of the chemical shift value of the C-1 methylene of lactam **18** with the C-5 methylene (τ 7.60) of ethyl 1-methyl-6-oxonepacotoate (**19**)[1] confirms that the methylene is α to the carbonyl rather than α to the nitrogen (C-2 methylene in **19** appears as two doublets at τ 6.42, 6.52). When the Beckmann cleavage was attempted using polyphosphoric acid or polyphosphoric ester as a catalyst, the same three compounds were obtained but again the product distribution varied.

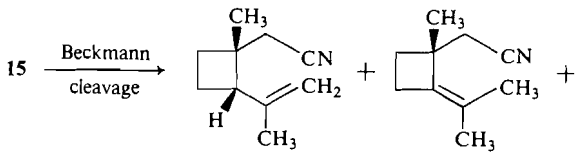

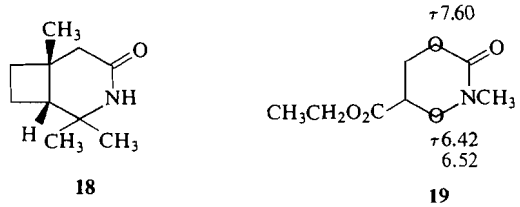

[1]R. Dawe, these laboratories, private communication

At this stage it seemed desirable to ascertain the stereochemistry (*E* or *Z*) of the oxime. Spectroscopic methods (23) do not give an unambiguous answer, especially if only one isomer is available. Attempted transoximation caused no change in oxime **15**. Direct oxime formation from ketone **5** furnished oxime **15**. These experiments suggest that the less hindered and presumably more stable (*E*)-oxime is in hand. In addition the cleavage reactions described above give products expected to arise from the (*E*)-oxime. We thus turned our attention to defining reaction conditions which would favor the formation of nitrile **16**. Reasoning that nitrile **17** may arise from proton-catalyzed rearrangement of **16** and that lactam **18** is formed when water is present, the Beckmann reaction was catalyzed by phosphorus pentachloride (1.1 equiv.) in anhydrous ether in the presence of 2,6-lutidine (2 equiv.). Work-up within 5 min (longer reaction times led to lower yields) gave nitrile **16** in *ca.* 85% yield. Since nitrile **16** is quite volatile, the reaction product was not purified at this stage but was directly hydrolyzed with potassium hydroxide in triglyme – ethylene glycol in a sealed tube. The carboxylic acid **20** was isolated as its cyclohexylamine salt in 62% overall yield from oxime **15**. The spectral data obtained for acid **20**, an intermediate in one of the previous syntheses, is in good agreement with that reported (*2a*).

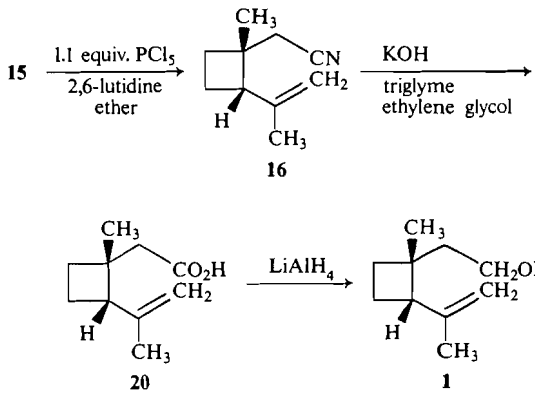

Finally, reduction of the cyclohexylamine salt of acid **20** with lithium aluminum hydride gave compound **1** in 92% yield. The i.r. and n.m.r. spectra of synthetic grandisol were identical with those published (1, 2) for grandisol and the mass spectra were very similar. The overall yield of grandisol (**1**) from eucarvone (**3**) was 20%.

Can. J. Chem. Downloaded from www.nrcresearchpress.com by 210.87.254.5 on 09/05/12
For personal use only.

Experimental

Solutions were dried over anhydrous magnesium sulfate unless otherwise specified. Melting points were determined on a Fisher-Johns or Leitz-Wetzlar hot-stage melting point apparatus and are uncorrected. Microanalyses were performed by the Microanalytical Laboratory of this department.

Infrared spectra were recorded on a Perkin-Elmer Model 337 grating i.r. spectrophotometer, a Unicam SP1000 grating i.r. spectrophotometer, or a Perkin-Elmer Model 421 dual grating i.r. spectrophotometer.

Nuclear magnetic resonance spectra were measured using a Varian Associates Model A-60 spectrometer or a Varian Model HR-100 spectrometer with tetramethylsilane as internal standard. Deuterium exchangeable protons are noted in text as D_2O.

Mass spectra were recorded on an A.E.I. Model MS-9 mass spectrometer or an A.E.I. Model GC/MS mass spectrometer with a WB separator and are reported as *m/e* (relative intensity).

The purity of all liquid products was monitored by gas chromatography utilizing a Varian Aerograph Gas Chromatograph Model A-90-P3 with helium as carrier gas on the following Chromsorb W (60–80 mesh) supported columns: 10 ft by $\frac{1}{4}$ in. polyester (10% PDEAS), 5 ft by $\frac{1}{8}$ in. polyethylene glycol (10% Carbowax 20M), 5 ft by $\frac{1}{8}$ in. silicone oil (10% SE-30), 5 ft by $\frac{1}{8}$ in. Zonyl E-7.

Preparation of Eucarvone (3) (3)

Carvone (100 g) was added dropwise to a stirred, cooled solution of hydrobromic acid in glacial acetic acid (500 g, 30% HBr in glacial HOAc). The rate of addition was adjusted such that the temperature of the solution was maintained between 8 and 12°. When addition was complete (approximately 0.5 h), the cooling bath was removed and stirring was continued a further 15 min. The solution was poured into water (800 ml). The lower organic layer was separated and the aqueous layer was extracted with ether. The organic fractions were combined, washed twice with water, neutralized ($NaHCO_3$), washed with water, dried (Na_2SO_4), then added dropwise to a stirred, cooled solution of potassium hydroxide (75 g) in methanol (300 ml). After addition was complete, the solution was concentrated on a steam bath, then poured onto a sulfuric acid (50 ml) – crushed ice (1:1) mixture. Water was added to dissolve the inorganic salts. The upper oily layer was separated and the aqueous layer extracted with ether. The organic fractions were combined, washed with saturated sodium bicarbonate solution, water, and dried (Na_2SO_4). The solution was concentrated and the residual oil fractionated using a spinning band apparatus to give 65 g (65%) eucarvone, **3**; b.p. 82° (7 mm); η_D^{24} 1.5050 (lit. (3) b.p. 82.5–84° (8 mm); η_D^{20} 1.5080).

1,4,4-Trimethylbicyclo[3.2.0]hept-6-en-2-one (4) (4)

A stirred solution of eucarvone (13.0 g) in ethylene glycol (500 ml) and trifluoroethanol (50 ml) was irradiated in a Pyrex vessel with an immersible mercury vapor lamp (250 W, Hanovia medium pressure) for 7 days. The photolysis mixture was diluted with water (500 ml), then continuously extracted with pentane for 48 h. The pentane solution was dried, concentrated *in vacuo* at room temperature, and the residual oil was fractionated through a 40 cm spinning band column to give 6.8 g (52%) unsaturated ketone, **4**; b.p. 90–91° (35 mm); η_D^{23} 1.4561 (lit. (4*a*) b.p. 110–111° (45 mm); η_D^{25} 1.4556); i.r. (neat): 1740 cm^{-1} (C=O); n.m.r. (CCl_4): τ 3.67 (d, 1, J = 2.5 Hz, *cis* C=C*H*), 3.90 (d, 1, J = 2.5 Hz, *cis* C=C*H*), 7.20 (d, 1, J = 17 Hz, *gem* CH_2), 7.44 (s, 1, C*H*), 8.26 (d, 1, J = 17 Hz, *gem* CH_2), 8.78 (s, 3, CH_3), 8.92 (s, 3, CH_3), 9.05 (s, 3, CH_3); 2,4-dinitrophenylhydrazone derivative, m.p. 162–163° (lit. (4*a*) m.p. 161.5–162.5°).

1,4,4-Trimethylbicyclo[3.2.0]heptan-2-one (6)

Unsaturated ketone **4** (5.8 g) was hydrogenated over 30% palladized charcoal (0.1 g) in methanol (100 ml) at room temperature and atmospheric pressure. After 1 equiv. of hydrogen had been consumed, the mixture was filtered and concentrated. The residual clear liquid (one compound by g.l.c. analysis (10% PDEAS, 10 ft × $\frac{1}{4}$ in., column temperature 150°, flow rate 60 ml/min)) was used in subsequent steps without further purification. Yield of saturated ketone **6** was 5.6 g (95%); η_D^{24} 1.4585 (lit. (4*a*) η_D^{25} 1.4556).

Anal. Calcd. for $C_{10}H_{16}O$: C, 78.90; H, 10.59. Found: C, 78.73; H, 10.35.

The i.r. (neat): 1735 cm^{-1} (C=O); n.m.r. (CCl_4): τ 8.78 (s, 3, CH_3), 8.97 (s, 3, CH_3), 9.10 (s, 3, CH_3); mass spectrum: *m/e* 152.1194 (67) (calcd. for $C_{10}H_{16}O$: 152.1201), 124(29), 109(89), 95(97), 82(100), 81(42), 69(57), 55(28), 41(97), 39(37); 2,4-dinitrophenylhydrazone derivative m.p. 148.5–150.5° (lit. (4*a*) m.p. 147.5–148°).

3-Acetoxy-1,4,4-trimethylbicyclo[3.2.0]heptan-2-one (7) (6)

A mixture of ketone **6** (3.95 g), lead tetraacetate (14.0 g), acetic acid (40 ml), and 1,2,2-trichloroethane (80 ml) was allowed to reflux for 4 days. The mixture was cooled and ethylene glycol (2 ml) was added to destroy excess lead tetraacetate. The mixture was then washed successively with water and sodium hydroxide solution (5%). The aqueous fraction was backwashed with ether. The organic fractions were combined, dried, concentrated, and distilled to give 4.85 g (89%) acetoxy ketone **7**; b.p. 65–71° (0.05 mm); η_D^{24} 1.4607.

Anal. Calcd. for $C_{12}H_{18}O_3$: C, 67.89; H, 9.50. Found: C, 68.16; H, 9.53.

The i.r. (neat): 1760 (C=O), 1750 (C=O), 1235 ($OCOCH_3$) cm^{-1}; n.m.r. (CCl_4): τ 4.36 (s, 1, C*H*OAc), 7.83 (s, 3, $OCOCH_3$), 8.77 (s, 3, CH_3), 8.84 (s, 3, CH_3), 9.20 (s, 3, CH_3); mass spectrum: *m/e* 210.1250 (5) (calcd. for $C_{12}H_{18}O_3$: 210.1256), 167(16), 139(10), 100(10), 72(50), 71(14), 43(100), 41(31).

3-Benzylidene-1,4,4-trimethylbicyclo[3.2.0]heptan-2-one (8)

A stirred solution of ketone **6** (1.4 g), benzaldehyde (3 ml), sodium hydroxide (0.9 g), methanol (45 ml), and water (25 ml) was heated on a steam bath for 48 h. The reaction mixture was cooled, diluted with water and extracted with methylene chloride. The organic fraction was dried and concentrated to an oil (0.6 g), which was purified by chromatography over alumina (BDH). Elution with petroleum ether (b.p. 65°) gave an oil which was a mixture of (*Z*)- and (*E*)- benzylidene ketones. Further elution with petroleum ether gave (*E*)-benzylidene

Can. J. Chem. Downloaded from www.nrcresearchpress.com by 210.87.254.5 on 09/05/12
For personal use only.

ketone as a crystalline compound (m.p. 57–59°); total yield 1.65 g (75%).

Anal. Calcd. for $C_{17}H_{20}O$: C, 84.96; H, 8.39. Found: C, 84.68; H, 8.18.

The u.v. (95% EtOH): 290 nm (ε 21 900), 226 nm (ε 11 650); i.r. ($CHCl_3$): 1710 (C=O), 1610 (C=C) cm^{-1}; n.m.r. ($CDCl_3$) *Z* isomer: τ 2.36 (s, 1, *cis* COC=C*H*), 2.70 (s, 5, Ar*H*), 8.12 (m, 5), 8.70 (s, 3, C*H*$_3$), 8.75 (s, 3, C*H*$_3$), 9.07 (s, 3, C*H*$_3$); *E* isomer: τ 3.43 (s, *trans* COC=C*H*), 8.72 (s, C*H*$_3$), 8.82 (s, C*H*$_3$), 8.95 (s, C*H*$_3$); mass spectrum: *m/e* 240.1516 (100) (calcd. for $C_{17}H_{20}O$: 240.1514), 225(35), 212(51), 197(46), 184(25), 170(29), 169(30), 155(32), 143(37), 129(80), 128(56), 115(33), 97(51), 95(83), 91(73), 77(40), 69(48), 41(88), 39(40).

*3-Benzyl-1,4,4-trimethylbicyclo[3.2.0]heptan-2-one (**9**)*

Benzylidene ketone **8** (0.5 g) in ether (20 ml) was added dropwise to a stirred suspension of lithium aluminum hydride (0.2 g) and aluminum chloride (0.98 g) in ether (70 ml). After addition was complete, the mixture was refluxed for 24 h, then cooled. Excess hydride was destroyed by cautious addition of 3 *N* sodium hydroxide, then water. The ether fraction was separated, dried, and concentrated. The crude product was chromatographed over alumina (BDH). Elution with petroleum ether (b.p. 65°) gave benzyl ketone **9**, as an oil (0.29 g, 56.5%); η_D^{24} 1.5230.

Anal. Calcd. for $C_{17}H_{22}O$: C, 84.25; H, 9.15. Found: C, 84.10; H, 9.07.

The i.r. (film): 1730 (C=O), 1600, 1500 cm^{-1}; n.m.r. ($CDCl_3$): τ 2.75 (s, 5, Ar*H*), 8.78 (s, 3, C*H*$_3$), 9.13 (s, 3, C*H*$_3$), 9.22 (s, 3, C*H*$_3$): mass spectrum: *m/e* 242.1678 (21) (calcd. for $C_{17}H_{22}O$: 242.1617), 173(100), 97(84), 91(43), 41(28).

*3-Benzylidene-1,4,4-trimethylbicyclo[3.2.0]heptane (**10**)*

Benzylidene ketone **8** (0.21 g), 85% hydrazine hydrate (29 ml), hydrazine dihydrochloride (0.73 g), and triethylene glycol (174 ml) were heated at 120° for 2 h. Potassium hydroxide pellets (1.1 g) were added and the temperature was slowly raised to 230°, allowing the low boiling material to distil. The reaction mixture was held at that temperature for 1.5 h then cooled, diluted with water, and extracted with petroleum ether. The petroleum ether fraction was washed with water, dried, concentrated, and the residual oil molecularly distilled (100°/0.5 mm). Yield 0.11 g (58%).

Anal. Calcd. for $C_{17}H_{22}$: C, 90.20; H, 9.80. Found: C, 89.87; H, 9.77.

The u.v. (methanol): 249 nm (ε 2150); i.r. (film): 1610 (conj. C=C), 1500 cm^{-1}; n.m.r. ($CDCl_3$): τ 2.83 (m, 6, Ar*H* and ArC*H*=C), 8.52 (s, 2), 8.73 (s, 6, C*H*$_3$), 8.95 (s, 3, C*H*$_3$); mass spectrum: *m/e* 226.1715 (6) (calcd. for $C_{17}H_{22}$: 226.1721), 198(9), 145(100), 129(11), 91(39).

*3-Oximino-1,4,4-trimethylbicyclo[3.2.0]heptan-2-one (**11**)*

In t-Butyl Alcohol

Isoamyl nitrite (1.2 g) was added dropwise to a stirred solution of ketone **6** (0.8 g) and potassium *t*-butoxide (1.2 g) in anhydrous *t*-butyl alcohol (15 ml) in a nitrogen atmosphere. The red solution was allowed to stir for 20 h, then was diluted with water, washed with ether, acidified (HCl), and extracted with ether. The ether fraction was dried and concentrated to an oil (0.63 g). Crystallization from ether gave oximinoketone **11**, (0.25 g, 26%). The mother liquor was concentrated and a portion (0.16 g) chromatographed over silica gel (6 g). Elution with chloroform gave a crystalline compound (0.085 g), 1-methyl-2(1-methyl-1-cyanoethyl)cyclobutyl carboxylic acid, **12**; m.p. 189–192°; i.r. ($CHCl_3$): 3400–2500 (CO-OH), 2220 (C≡N), 1710 (C=O) cm^{-1}; n.m.r. ($CDCl_3$): τ 8.86 (s, 3, C*H*$_3$), 8.72 (s, 3, C*H*$_3$), 8.57 (s, 3, C*H*$_3$), 7.83 (s, 4, C*H*$_2$), −1.95 (s, 1, COO*H*, D_2O); mass spectrum: *m/e* 181.1102 (5) (calcd. for $C_{10}H_{15}NO_2$: 181.1103), 155(9), 135(11), 126(14), 109(29), 95(30), 87(21), 69(100), 55(24), 41(86).

In Benzene

Ketone **6** (5.1 g) in anhydrous benzene (10 ml) was added dropwise to a stirred, cooled solution of potassium *t*-amylate (7.5 g, 75 ml of 0.85 *N* potassium *t*-amylate in benzene) (16) in anhydrous benzene, followed by dropwise addition of isoamyl nitrite (3.75 g, distilled and stored over molecular sieve 5A) in anhydrous benzene (10 ml). The purple solution was stirred at room temperature for 24 h. The solution was cooled and diluted with 5% aqueous HCl. The upper organic layer was separated and washed with saturated sodium bicarbonate solution. The aqueous fraction was neutralized ($NaHCO_3$) and extracted with methylene chloride. The organic fractions were combined, washed with brine, dried, and concentrated to an oil. The oil was chromatographed over silicic acid (200 g) using a quartz column and a u.v. light to monitor the separation. Elution with chloroform (400 ml) gave a crystalline mixture of (*E*)- and (*Z*)-oximinoketones (1.2 g). Further elution with chloroform gave crystalline (*E*)-oximinoketone (4.0 g); m.p. 128–131.5°. Total yield of oximinoketone was 5.2 g (88%).

Anal. Calcd. for $C_{10}H_{15}NO_2$: C, 66.27; H, 8.34; N, 7.73. Found: C, 65.92; H, 8.14; N, 7.55.

The i.r. ($CHCl_3$) *E* isomer: 3560, 3360 (NOH), 1740 (C=O), 1630 (C=N) cm^{-1}; *Z* isomer: 3200 (NOH), 1690 (C=O), 1580 (C=N) cm^{-1}; n.m.r. ($CDCl_3$) *E* isomer: τ 0.15 (br s, 1, NO*H*, D_2O), 8.59 (s, 3, C*H*$_3$), 8.75 (s, 6, C*H*$_3$); *Z* isomer: τ 8.65 (s, 3, C*H*$_3$), 8.79 (s, 3, C*H*$_3$), 8.82 (s, 3, C*H*$_3$): mass spectrum *E* isomer: *m/e* 181.1100 (21) (calcd. for $C_{10}H_{15}NO_2$: 181.1103), 164(22), 136(33), 109(45), 97(74), 95(25), 69(23), 55(100), 41(83), 39(36); *Z* isomer: *m/e* 181.1104 (19) (calcd. for $C_{10}H_{15}NO_2$: 181.1103) 164(9), 136(31), 109(26), 98(25), 97(100), 95(14), 69(28), 67(3), 55(63), 41(63), 39(30).

*3-Oximino-1,4,4-trimethylbicyclo[3.2.0]heptan-2-ol (**13a**)*

Sodium borohydride (0.050 g) in water (2 ml) was added dropwise to a stirred solution of oximinoketone **11** (0.226 g) in dimethoxyethane (8 ml). After addition was complete, stirring was continued for 30 min. The solution was diluted with water, carefully acidified (HCl), neutralized ($NaHCO_3$), and extracted with methylene chloride. The organic fraction was dried and concentrated to give 0.545 g (100%) of a crystalline oximino alcohol, **13***a*; m.p. 69–72.5°.

Anal. Calcd. for $C_{10}H_{17}NO_2$: C, 65.54; H, 9.35; N, 7.64. Found: C, 65.11; H, 9.25; N, 7.97.

The i.r. ($CHCl_3$): 3580, 3300, 1070 (NOH, OH), 1680 (w, C=N) cm^{-1}; n.m.r. ($CDCl_3$): τ 5.65 (s, 1, C*H*OH), 8.60 (s, 3, C*H*$_3$), 8.65 (s, 3, C*H*$_3$), 8.84 (s, 3, C*H*$_3$); a small quantity of another epimer was present as shown by a signal at τ 5.50 (C*H*OH); mass spectrum: *m/e* ($M^+ - OH$) 166.1235 (16) (calcd. for $C_{10}H_{16}NO$:

166.1231), 122(13), 114(12), 109(13), 97(45), 95(22), 87(43), 81(27), 69(100), 55(37), 53(21), 43(23).

*3-Acetoximino-1,4,4-trimethylbicyclo[3.2.0]heptan-2-ol (**13b**)*

Oximino alcohol **13***a* (0.1 g), benzene (1 ml), pyridine (1 drop), and acetic anhydride (0.14 g) were heated in an oil bath at 65° for 1 h. The mixture was concentrated by azeotropic distillation with benzene, dried *in vacuo* to give acetoximino alcohol **13***b*; m.p. 89.5–90.5°.

Anal. Calcd. for $C_{12}H_{19}NO_3$: C, 63.98; H, 8.50; N, 6.22. Found: C, 63.91; H, 8.52; N, 6.11.

The i.r. ($CHCl_3$): 3550, 3450, 1070 (OH), 1755 (C=O), 1660 (C=N) cm^{-1}; n.m.r. ($CDCl_3$): τ 5.45 (s, 1, C*H*OH), 6.20 (s, 1, O*H*, D_2O), 7.82 (s, 3, $OCOCH_3$), 8.63 (s, 6, CH_3), 8.80 (s, 3, CH_3); mass spectrum: *m/e* ($M^+ - OAc$) 182.1179 (2) (calcd. for $C_{10}H_{16}NO_2$: 182.1181), 136(24), 122(41), 109(39), 107(28), 97(60), 95(34), 82(30), 81(86), 69(100), 68(50), 67(27), 60(36), 55(46), 53(23), 45(32), 43(54), 41(59).

*Attempted Formation of Acetoximino Acetate (**13c**)*

Oximino alcohol **13***a* (0.125 g), acetic anhydride (0.2 g), pyridine (0.16 g), and benzene (2 ml) were heated in an oil bath (65°) for 0.5 h. Excess solvents were removed by azeotropic distillation with benzene and the residual oil (0.153 g) was dried *in vacuo*. This oil was a mixture of two compounds (t.l.c.: silica gel, chloroform–methanol). The i.r. and n.m.r. spectra were consistent with a mixture of acetoximino acetate **13***c* and cyanoaldehyde **14**.

The i.r. ($CHCl_3$): 2730 (CHO), 2230 (CN), 1720 (C=O); 1770, 1745 (C=O) cm^{-1}; n.m.r. ($CDCl_3$): τ −0.33 (s, C*H*O), 8.68 (s, CH_3), 8.70 (s, CH_3); 4.06 (s, C*H*OAc), 7.82 (s, $OCOCH_3$), 7.85 (s, $OCOCH_3$), 8.62 (s, CH_3), 8.77 (s, CH_3).

*Attempted Formation of Acetoximino Mesylate (**13d**)*

Acetoximino alcohol **13***b* (0.122 g), pyridine (2 drops), methanesulfonyl chloride (0.098 g), and benzene (1 ml) were allowed to stand at 0° overnight. Excess solvent was removed by azeotropic distillation with benzene and the residue (0.150 g) was dried *in vacuo*. The i.r. and n.m.r. spectra of the residue are consistent with a mixture of acetoximino mesylate **13***d*, cyanoaldehyde **14**, and acetoximino alcohol **13***b*.

*Attempted Reduction of Acetoximino Alcohol (**13b**) with Chromous Acetate (**17**)*

Acetoximino alcohol (0.4 g), tetrahydrofuran (6.4 ml), chromous acetate (1.6 g), and water (2 ml) were heated at 65° in a nitrogen atmosphere for 36 h. The mixture was allowed to cool, diluted with water, filtered, and extracted with methylene chloride. The methylene chloride fraction was washed with 10% hydrochloric acid, saturated sodium bicarbonate, water, then dried, and concentrated. Analysis of the residual oil by g.l.c. – mass spectrometry showed a mixture of eight compounds; three minor compounds had a molecular ion of 152. The i.r. and n.m.r. spectra are consistent with impure cyanoaldehyde, **14**; i.r. ($CHCl_3$): 2730, 2230, 1720 cm^{-1}; n.m.r. (CCl_4): τ −0.33 (s, C*H*O), 8.68 (s, CH_3), 8.70 (s, CH_3).

*3-Oximino-1,4,4-trimethylbicyclo[3.2.0]heptane (**15**)*

A mixture of oximinoketone **11** (0.760 g), hydrazine hydrate (85%, 0.238 ml), potassium hydroxide (0.3 g), and ethylene glycol (15 ml) was heated at 150° for 4 h. The reaction mixture was allowed to cool, diluted with water, acidified (HCl), neutralized ($NaHCO_3$), and extracted with pentane. The pentane fraction was washed with brine, dried, and concentrated to give 0.570 g (81.5%) crystalline oxime **15**; m.p. 118–119.5°.

Anal. Calcd. for $C_{10}H_{17}NO$: C, 71.81; H, 10.25; N, 8.37. Found: C, 71.53; H, 10.36; N, 8.56.

The i.r. ($CHCl_3$): 3580, 3290 (NOH), 1670 (C=N) cm^{-1}; n.m.r. (CCl_4): τ 0.80 (s, 1, NO*H*, D_2O), 7.07 (d, 1, J = 19 Hz, *gem* CH_2), 7.73 (d, 1, J = 19 Hz, *gem* CH_2), 8.70 (s, 3, CH_3), 8.93 (s, 6, CH_3); mass spectrum: *m/e* 167.1315 (7) (calcd. for $C_{10}H_{17}NO$: 167.1310), 152(38), 150(35), 138(15), 125(38), 124(57), 122(40), 109(24), 81(21), 79(23), 69(74), 68(20), 55(32), 53(24), 41(100).

*1,4,4-Trimethylbicyclo[3.2.0]heptan-3-one (**5**)*

Oxime **15** (0.430 g), dimethoxyethane (8 ml), water (4 ml), and titanium trichloride (1.5 equiv., 3.1 ml) were allowed to reflux 15 min. The cooled solution was diluted with water and extracted with methylene chloride. The methylene chloride fraction was washed with sodium bicarbonate solution, dried, and concentrated by distillation at atmospheric pressure; η_D^{22} 1.4590; i.r. (neat): 1735 (C=O) cm^{-1}; n.m.r. (CCl_4): τ 7.69 (q, 2, J = 19 Hz, CH_2CO), 8.67 (s, 3, CH_3), 9.05 (s, 3, CH_3), 9.10 (s, 3, CH_3); mass spectrum: *m/e* 152.1203 (2) (calcd. for $C_{10}H_{16}O$; 152.1201), 73(73), 67(100), 45(96), 41(20); 2,4-dinitrophenylhydrazone derivative: m.p. 169–171.5°.

Beckmann Cleavage Reaction

(a) Thionyl Chloride – DMF

Thionyl chloride (0.18 ml) was added to a cooled (0°), stirred solution of oxime **15** (0.5 g) in dimethylformamide (4 ml). The mixture was maintained at this temperature for 2 h, then diluted with water, neutralized ($NaHCO_3$), and extracted with pentane. The pentane extract was dried and excess solvent removed by distillation through a 12 ft column packed with glass helices. The mixture was separated by preparative gas–liquid chromatography on a Zonyl E-7 column (10 ft × $\frac{1}{8}$ in., column temperature 180°, 60 ml/min).

Compound **16** 0.057 g; retention time: 5.4 min; i.r. (CCl_4): 2250 (CN), 1650, 890 (C=CH_2) cm^{-1}; n.m.r. (CCl_4): τ 5.10 (m, 1, C=CH_2), 5.23 (m, 1, C=CH_2), 8.33 (br s, 3, C=C—CH_3), 8.64 (s, 3, CH_3); mass spectrum: *m/e* 149.1198 (1) (calcd. for $C_{10}H_{15}N$: 149.1204), 148(2), 134(3), 110(4), 94(5), 81(6), 79(12), 68(100), 67(80), 53(29).

Compound **17** 0.120 g; retention time: 6.6 min; i.r. (CCl_4): 2220 (CN), 1455, 1440 (C=C—CH_2) cm^{-1}; n.m.r. (CCl_4): τ 7.52 (s, 2, CH_2CN), 8.50 (m, 3, C=C—CH_3), 8.55 (m, 3, C=C—CH_3), 8.62 (s, 3, CH_3); mass spectrum: *m/e* 149.1200 (48) (calcd. for $C_{10}H_{15}N$: 149.1204), 134(22), 109(100), 107(28), 93(23), 81(42), 79(25), 69(30), 68(20), 67(67), 53(22), 41(32).

(b) Phosphorus Pentachloride – Ether

Oxime **15** (0.25 g) in ether (10 ml) was added dropwise to a stirred suspension of phosphorus pentachloride (0.34 g) in ether (10 ml). The reaction mixture was stirred overnight, then diluted with water, and the layers separated. The aqueous layer was washed with ether, the ether extracts combined, dried, and concentrated.

Can. J. Chem. Downloaded from www.nrcresearchpress.com by 210.87.254.5 on 09/05/12
For personal use only.

Can. J. Chem. Downloaded from www.nrcresearchpress.com by 210.87.254.5 on 09/05/12
For personal use only.

Chromatography of the residue over alumina (BDH) gave a crystalline lactam **18** (0.047 g); m.p. 110–111°.

Anal. Calcd. for $C_{10}H_{17}NO$: C, 71.81; H, 10.25; N, 8.37. Found: C, 72.14; H, 9.99; N, 8.23.

The i.r. ($CHCl_3$): 3510, 3300 (NH), 1660 (C=O) cm^{-1}; n.m.r. ($CDCl_3$): τ 7.55 (s, 2, CH_2CO), 8.72 (s, 3, CH_3), 8.78 (s, 3, CH_3), 8.90 (s, 3, CH_3); mass spectrum: *m/e* 167.1318 (3) (calcd. for $C_{10}H_{17}NO$: 167.1310), 152(100), 124(50), 70(76), 58(34), 41(14), 40(12).

*2-Isopropenyl-1-methylcyclobutane Acetic Acid (**20**)*

Oxime **15** (0.500 g) in anhydrous ether (10 ml) was added dropwise to a stirred suspension of phosphorus pentachloride (0.680 g) and 2,6-lutidine (0.690 ml) in ether (50 ml). The reaction mixture was stirred in an atmosphere of nitrogen for 5 min, then quenched with a saturated ammonium chloride solution. The aqueous and ethereal layers were separated and the aqueous layer was washed with ether. The ether extracts were combined, washed (saturated $NaHCO_3$ solution), dried, and concentrated by distillation through a 1 ft column packed with glass helices to give seconitrile **16**.

Crude seconitrile **16** was hydrolyzed with potassium hydroxide (2.5%) in ethylene glycol – triethylene glycol dimethyl ether (1:1) in a sealed tube at 200° for 24 h. The reaction mixture was cooled, diluted with water, and washed with ether. The ether washing was extracted with sodium bicarbonate solution and the aqueous fractions combined. The aqueous fractions were acidified to p*H* 5 with buffer solution and extracted with ether. The ether extract was washed (water) and dried. Cyclohexylamine (0.300 g) was added. The cyclohexylamine salt (0.491 g) of secocarboxylic acid **20** was collected (62% from oxime); m.p. 112.5–114.5°.

Anal. Calcd. for $C_{16}H_{29}NO_2$: C, 71.87; H, 10.93. Found: C, 71.68; H, 11.09.

The i.r. ($CHCl_3$): 3300–2400, 2000 ($\overset{+}{N}H_3$), 1570 (COO^-) cm^{-1}. In another experiment, salt formation was omitted and secocarboxylic acid **20** was isolated as an oil; b.p. 108–110° (0.5 cm); i.r. (CCl_4): 3300–2500 (COOH), 1710 (C=O), 1650, 890 (C=CH_2) cm^{-1}; n.m.r. (CCl_4): τ 0.4 (1, m, COO*H*, D_2O), 5.16 (m, 1, C=CH_2), 5.34 (m, 1, C=CH_2), 8.33 (br s, 3, C=C–CH_3), 8.67 (s, 3, CH_3); mass spectrum: *m/e* 168.1146 (5) (calcd. for $C_{10}H_{16}O_2$: 168.1150), 125(29), 109(16), 108(92), 93(23), 81(28), 69(26), 68(100), 67(62), 43(26), 41(28).

*cis-2-Isopropenyl-1-methylcyclobutane Ethanol (Grandisol) (**1**)*

A solution of lithium aluminum hydride in anhydrous ether (1 *M*, 2.5 ml) was added dropwise to a cooled (ice bath), stirred suspension of secocarboxylic acid **20** cyclohexylamine salt (0.350 g) in anhydrous ether (25 ml). The reaction mixture was stirred for 3 h then excess hydride destroyed by successive dropwise addition of water, 5% NaOH, and water. The precipitate was filtered and washed extensively with ether. The ether fractions were combined, washed successively with 5% HCl, brine, and dried. Excess solvent was removed by distillation through a 12 ft column packed with glass helices to give 0.189 g of an oil. Molecular distillation (1 mm/100°) gave racemic grandisol (0.186 g, 92%). The i.r. and n.m.r. are identical with the published spectra (1*b*); i.r. (CCl_4): 3620, 3500 (OH), 1640, 885 (C=C) cm^{-1}; n.m.r. (CCl_4): τ 5.18 (m, 1, C=CH_2), 5.37 (m, 1, C=CH_2), 6.43 (t, 2, J = 7.5 Hz, CH_2CH_2OH), 6.92 (br s, 1, O*H*, D_2O), 8.33 (br s, 3, C=CCH_3), 8.83 (s, 3, CH_3); mass spectrum: *m/e* 154.1354 (13) (calcd. for $C_{10}H_{18}O$: 154.1358), 139(11), 136(23), 121(25), 110(23), 109(53), 93(22), 81(26), 69(18), 68(100), 67(53), 56(21), 55(28), 53(27), 41(21), 39(26).

We gratefully acknowledge the financial support provided by the National Research Council of Canada.

1. (*a*) J. H. TUMLINSON, D. D. HARDEE, R. C. GUELDNER, A. C. THOMPSON, and P. A. HEDIN. Science, **166**, 1010 (1969); (*b*) J. H. TUMLINSON, R. C. GUELDNER, D. D. HARDEE, A. C. THOMPSON, P. A. HEDIN, and J. P. MINYARD. J. Org. Chem. **36**, 2616 (1971).
2. (*a*) R. ZURFLUH, L. L. DUNHAM, V. L. SPAIN, and J. B. SIDDALL. J. Am. Chem. Soc. **92**, 425 (1970); (*b*) R. C. GUELDNER, A. C. THOMPSON, and P. A. HEDIN. J. Org. Chem. **31**, 1855 (1972); (*c*) W. E. BILLUPS, J. H. CROSS, and C. V. SMITH. J. Am. Chem. Soc. **95**, 3438 (1973).
3. E. J. COREY and H. J. BURKE. J. Am. Chem. Soc. **78**, 174 (1965).
4. (*a*) G. BUCHI and E. M. BURGESS. J. Am. Chem. Soc. **82**, 4333 (1960); (*b*) J. J. HURST and G. H. WHITHAM. J. Chem. Soc. 710 (1963); (*c*) D. I. SCHUSTER, M. J. NASH, and M. L. KANTOR. Tetrahedron Lett. 1375 (1964); (*d*) D. I. SCHUSTER and D. H. SUSSMAN. Tetrahedron Lett. 1657 (1970); (*e*) H. HART and T. TAKINO. J. AMM. Chem. Soc. **93**, 720 (1971).
5. (*a*) J. E. BRIDGEMAN, C. E. BUTCHERS, E. R. H. JONES, A. KASAL, G. D. MEAKINS, and P. D. WOODGATE. J. Chem. Soc. (C), 244 (1970); (*b*) I. T. HARRISON and S. HARRISON. Compendium of organic synthetic methods. Wiley Interscience, Toronto. 1971. p. 429.
6. R. W. GUTHRIE, W. A. HENRY, H. IMMER, C. M. WONG, Z. VALENTA, and K. WIESNER. Coll. Czech. Chem. Commun. **31**, 602 (1966).
7. K. L. WILLIAMSON and W. S. JOHNSON. J. Org. Chem. **26**, 4563 (1961).
8. W. A. AYER and D. A. LAW. Can. J. Chem. **40**, 2088 (1962).
9. W. S. JOHNSON, B. GASTAMIDE, and R. PAPPO. J. Am. Chem. Soc. **79**, 1991 (1957).
10. J. E. BRIDGEMAN, E. R. H. JONES, G. D. MEAKINS, and J. WICHA. Chem. Commun. 898 (1967).
11. W. NAGATA and H. ITAZAKI. Chem. Ind. 1194 (1964).
12. R. U. LEMIEUX and E. VON RUDLOFF. Can. J. Chem. **33**, 1714 (1955).
13. S. WOLFE, S. HASAN, and J. CAMPBELL. Chem. Commun. 1420 (1970).
14. N. LEVIN and W. H. HARTUNG. Org. Synth. **3**, 191 (1955).
15. F. LITVAN and R. ROBINSON. J. Chem. Soc. 1997 (1938).
16. J. CONIA. Rec. Chem. Prog. **24**, 43 (1963).
17. E. J. COREY and J. E. RICHMAN. J. Am. Chem. Soc. **92**, 5276 (1970).
18. R. K. HILL. J. Org. Chem. **27**, 29 (1962).
19. D. ELAD and D. GINSBURG. J. Chem. Soc. 3052 (1954).

20. G. JUST and Y. LIN. Chem. Commun. 1350 (1968).
21. G. H. TIMMS and E. WILDSMITH. Tetrahedron Lett. 195 (1971).
22. (*a*) W. Z. HELDT and L. G. DONARUMA. Org. React. **11**, 1 (1960); (*b*) P. A. S. SMITH. *In* Molecular rearrangements. Vol. 1. *Edited by* P. de Mayo. Interscience Publishers, New York. 1963. p. 483; (*c*) P. A. S. SMITH (*Editor*). Open chain nitrogen compounds. Vol. 2. W. A. BENJAMIN, New York. 1966. p. 29; (*d*) R. T. CONLEY and S. GHOSH. *In* Mechanisms of molecular migrations. Vol. 4. *Edited by* B. S. THYAGARAJAN. Wiley Interscience, New York. 1971. p. 197.
23. (*a*) G. KARABATSOS, R. TALLER, and F. VANE. J. Am. Chem. Soc. **85**, 2326 (1963); (*b*) B. L. FOX. J. Org. Chem. **35**, 4234 (1970); (*c*) Z. W. WOLKOWSKI. Tetrahedron Lett. 825 (1971); (*d*) K. D. BERLIN and S. RENGARAJU. J. Org. Chem. **36**, 2912 (1971).

Can. J. Chem. Downloaded from www.nrcresearchpress.com by 210.87.254.5 on 09/05/12
For personal use only.

Mössbauer Spectra, Bonding, and Structure in Sn(IV) Acetylacetonates

G. M. BANCROFT[1] AND T. K. SHAM

Department of Chemistry, University of Western Ontario, London, Ontario N6A 3K7

Received October 11, 1973

^{119}Sn Mössbauer spectra have been recorded for sixteen acetylacetonates of the type $R_{2-x}Cl_xSnL_2$ (R = Me, Ph; L = anions of acetylacetone or substituted acetylacetone) and Cl_4SnHL. The quadrupole splittings have been used to assign stereochemistry for most of these compounds. The good correlation between quadrupole splitting and center shift for the dimethyl analogues shows that there is no appreciable Sn 5s character in the Sn—L bonds. The correlation between $^2J_{^{119}Sn-CH_3}$ and center shift for the dimethyl compounds is consistent with the above interpretation, and indicates that changes in $[\Psi(0)_{5s}]^2$ are dominant in determining both the center shift and J values for these compounds. The Mössbauer parameters for the compounds containing a neutral ligand show that the bonding properties of HL are very similar to those of L.

The dimethyl compounds all show a pronounced Goldanskii–Karyagin asymmetry in their spectra. The direction of this asymmetry is shown to be consistent with a positive quadrupole splitting for all the dimethyl compounds.

Les spectres de l'effet Mössbauer du ^{119}Sn ont été enregistrés pour seize acétylacétonates du type $R_{2-x}Cl_xSnL_2$ (R = Me, Ph; L = anions de l'acétylacétone ou de l'acétylacétone substituée) et Cl_4SnHL. Les multiplicités quadrupolaires ont été utilisées pour attribuer la stéréochimie de la plupart de ces composés. La bonne corrélation entre la multiplicité quadrupolaire et le déplacement du centre pour les analogues du diméthyle montre qu'il n'y a pas de caractère Sn 5s appréciable dans les liens Sn—L. La corrélation entre $^2J_{^{119}Sn-CH_3}$ et le déplacement du centre pour les composés diméthylés est compatible avec l'interprétation précédente; elle indique que les changements dans $[\psi(0)_{5s}]^2$ sont dominants pour la détermination du déplacement du centre et des valeurs de J de ces composés. Les paramètres de l'effet Mössbauer pour les composés contenant un ligand neutre montrent que les propriétés de liaison de HL sont très similaires à celles de L.

Les composés diméthylés montrent tous une asymétrie marquée de Goldanskii–Karyagin dans leur spectre. Il est montré que la direction de cette asymétrie est compatible avec une multiplicité d'un quadrupole positif pour tous les composés diméthylés.

[Traduit par le journal]

Can. J. Chem., **52**, 1361 (1974)

Introduction

A recent structural determination of $Me_2Sn(acac)_2$ (1) confirms the *trans*-structure proposed from Mössbauer quadrupole splittings (2). However, there is still controversy over the structures of related compounds. For example, McGrady and Tobias (3) assigned the *trans*-configuration to $Ph_2Sn(acac)_2$, whereas Mössbauer quadrupole splittings (2) strongly suggested the *cis*-structure. Also, the mixed Me, Cl and Ph, Cl complexes have been assigned the *trans*-structure in solution (4), whereas recent n.m.r. studies (5) strongly suggest that these compounds and $Ph_2Sn(acac)_2$ have the *cis*-configuration. A recent X-ray report also gives the *cis*-configuration for $Cl_2Sn(acac)_2$ (6).

[1]To whom all correspondence should be addressed.

As discussed in ref. 1, it is generally felt that in the *trans*-R_2Sn compounds, most of the Sn 5s character will be concentrated in the Sn—R bonds, and the SnL_2 bonds will involve only Sn 5p character. However, Parish and Platt (7) have pointed out that in *cis*-R_2Sn linkages the Sn 5s character in the Sn—R bonds should be substantially less and Mössbauer center shift values were consistent with this interpretation.

We have prepared and obtained Mössbauer spectra of sixteen substituted acetylacetonates of the type $R_{2-x}Cl_xSnL_2$ (R = Me, Ph, L = anions of acetylacetone (AcAc), trifluoroacetylacetone (TfAc), hexafluoroacetylacetone (HfAc), benzoylacetone (BzAc), and dibenzoylmethane (BzBz)) and Cl_4SnHL with two objectives in mind; first, to use Mössbauer quadrupole splittings to assign the stereochemistry of these

Can. J. Chem. Downloaded from www.nrcresearchpress.com by 210.87.254.42 on 09/05/12
For personal use only.

Can. J. Chem. Downloaded from www.nrcresearchpress.com by 210.87.254.42 on 09/05/12
For personal use only.

compounds; and second, to use the variations in center shift (c.s.), quadrupole splitting (q.s.), and $^2J_{^{119}Sn-CH_3}$ to examine the Sn—L and Sn—Me bond characteristics. In addition, we have been able to use the observed Goldanskii asymmetry in the spectra of the dimethyl compounds along with the recent X-ray data to determine the sign of the quadrupole splitting for the dimethyl compounds.

Experimental

The compounds were prepared using methods available in the literature (3, 4, 8–11), and the purity of the compounds was checked by m.p., infrared, n.m.r., chemical analyses, and Mössbauer spectra. The melting points and analyses (observed values in parentheses) for the new compounds are: $(CH_3)_2Sn(TfAc)_2$, m.p. 105–106, C 32.3 (32.0), H 3.14 (2.86); $(C_6H_5)_2Sn(TfAc)_2$, m.p. 66–68, C 45.6 (45.8), H 3.11 (2.95); and $Cl_2Sn(BzAc)_2$, m.p. 220–221, C 46.9 (47.7), H 3.51 (3.44).

The tin proton $^2J_{^{119}Sn-CH_3}$ coupling constants were obtained for the dimethyl acetylacetonates in deuterochloroform solution. They are in good agreement with those reported in the literature (3) (in parentheses). The $^2J_{^{119}Sn-CH_3}$ values (in Hz) for these compounds are $Me_2Sn(AcAc)_2$, 99.2 (99.3); $Me_2Sn(BzAc)_2$, 98.4; $Me_2Sn(BzBz)_2$, 97.2 (96.9); $Me_2Sn(TfAc)_2$, 101.0; $Me_2Sn(HfAc)_2$, (103.4). Errors are ± 0.2 Hz.

Mössbauer spectra were obtained using a 5mCi $BaSnO_3$ source at room temperature and an Austin Science Associates spectrometer. All absorbers were at 80 °K. Velocity calibration was carried out using a 1 mil 99.99% iron foil. Spectra were fitted to Lorentzian line shapes using the program written by A. J. Stone. A typical spectrum is shown in Fig. 1. All center shifts are reported with respect to the center of a room temperature $BaSnO_3$–$BaSnO_3$ spectrum.

Results and Discussion

Structure and Quadrupole Splittings

The Mössbauer parameters for all compounds are reported in Table 1 along with the previously reported values for $Me_2Sn(AcAc)_2$ (**1**), $Ph_2Sn(AcAc)_2$ (**6**), $Cl_2Sn(AcAc)_2$ (**11**), the $[Cl_4SnAcAc]^-$ compounds (**15**, **16**) and related phenyl tin oxinate compounds (**19**, **20**). Our parameters are in good agreement with these previously published values, but we have obtained a small quadrupole splitting for $Cl_2Sn(AcAc)_2$ which was previously not determined. The large decrease in χ^2 on going from a one peak to a two peak fit for $Cl_2Sn(BzAc)_2$, $Cl_2Sn(AcAc)_2$, $Cl_4Sn(HAcAc)$, and $Cl_4Sn(HBzAc)$ strongly supports the fitting of two peaks to these spectra. For example χ^2 decreased from 655 to 547 for a one and two peak fit respectively to $Cl_2Sn(AcAc)_2$. The error in these small quadrupole splittings is, of course, much larger than for the resolved splittings.

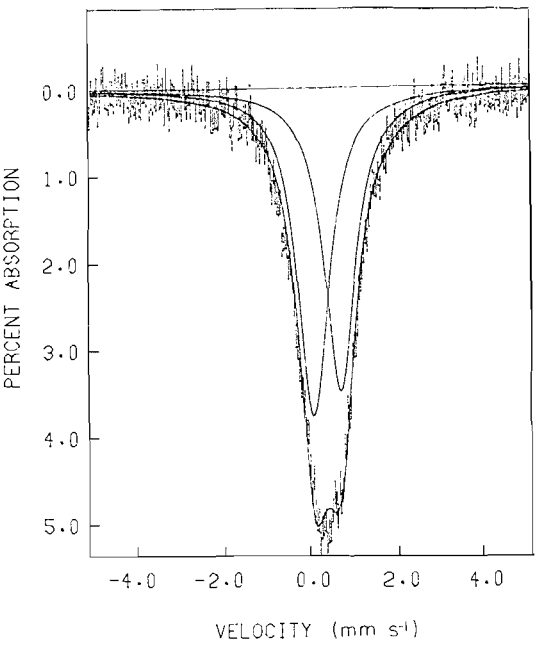

FIG. 1. Mössbauer spectrum of $Cl_4Sn(HBzAc)$ at 80 °K.

It is immediately apparent that the dimethyl compounds have quadrupole splittings in the 4 mm s^{-1} range, while the diphenyl compounds have quadrupole splittings in the 2 mm s^{-1} range. As discussed previously (2, 13), these splittings strongly indicate that the dimethyl compounds have *trans*-structures while the diphenyl compounds have *cis*-structures. The dichloro compounds have already been assigned the *cis*-structure (6), and the similarity of the quadrupole splittings for $Cl_2Sn(AcAc)_2$ and $Cl_4Sn(HAcAc)$ which must be *cis* is entirely consistent with this *cis*-structure (13).[2]

However, it is apparent that the *cis*-Ph_2SnL_2 isomers give substantially larger quadrupole splittings than that expected on an additivity model basis, and the discrepancy between observed (q.s.) and that predicted increases as we increase the electronegativity of L. Thus, if we use the previously derived partial quadrupole splittings (p.q.s.) for Me and Ph of -1.03 mm s^{-1} and -0.95 mm s^{-1} respectively (14), we can derive p.q.s. values for AcAc/2, BzBz/2, and

[2]Assuming the bonding properties of AcAc and HAcAc are identical. See next section.

TABLE 1. Mössbauer parameters for Sn(IV) acetylacetonates*

	Compound	Center shift	Quadrupole splitting
1	*trans*-$Me_2Sn(AcAc)_2$	1.16 (1.18)†	+4.02 (3.93)†
2	*trans*-$Me_2Sn(BzAc)_2$	1.06	+3.87
3	*trans*-$Me_2Sn(BzBz)_2$	1.18	+4.08
4	*trans*-$Me_2Sn(TfAc)_2$	1.32	+4.36
5	*trans*-$Me_2Sn(HfAc)_2$	1.43	+4.47
6	*cis*-$Ph_2Sn(AcAc)_2$	0.71 (0.74)†	2.07 (2.14)†
7	*cis*-$Ph_2Sn(AcBz)_2$	0.73	2.23
8	*cis*-$Ph_2Sn(BzBz)_2$	0.73	2.15
9	*cis*-$Ph_2Sn(TfAc)_2$	0.89	2.53
10	*cis*-$Ph_2Sn(HfAc)_2$	1.18	2.71
11	*cis*-$Cl_2Sn(AcAc)_2$	0.15 (0.25)‡	0.54 ± 0.10
12	*cis*-$Cl_2Sn(BzAc)_2$	0.08	0.54 ± 0.10
13	*cis*-$Cl_4Sn(HAcAc)$	0.41	0.70 ± 0.10
14	*cis*-$Cl_4Sn(HBzAc)$	0.47	0.65 ± 0.10
15	$[Cl_4SnAcAc][PyH]$	(0.47)§	(~0)
16	$[Cl_4SnAcAc][Et_3NH]$	(0.45)§	(~0)
17	*cis*-$ClSnMe(AcAc)_2$	0.61 ± 0.05	1.78 ± 0.05
18	*cis*-$ClSnPh(AcAc)_2$	0.61 ± 0.05	1.77 ± 0.05
19	*cis*-$Ph_2Sn(oxin)_2$	(0.73)‖	(1.65)‖
20	*cis*-$ClSnPh(oxin)_2$	(0.67)‖	(1.48)‖

*In mm s^{-1} at 80 °K. Errors are ± 0.02 mm s^{-1} except where specified. Line widths for all spectra are 1.10 ± 0.10 mm s^{-1}. χ^2 values for all spectra are 520 ± 50 for ~ 500 degrees of freedom. Values in parentheses have been reported previously.
†Reference 2.
‡Reference 29.
§Reference 11.
‖Reference 13, Table XXXV.

HfAc/2 of −0.03, −0.01, and +0.09 mm s^{-1}, respectively, from the *trans*-Me_2Sn compounds. Using these values, we can predict the quadrupole splittings for *cis*-$Ph_2Sn(AcAc)_2$, *cis*-$Ph_2Sn(BzBz)_2$, and *cis*-$Ph_2Sn(HfAc)_2$ of −1.84, −1.88, and −2.08 mm s^{-1}, compared to the observed quadrupole splittings of 2.07, 2.15, and 2.71 mm s^{-1}, respectively. The signs of these quadrupole splittings are quite likely positive since other *cis*-Ph_2Sn compounds have positive signs (15). The discrepancy in the magnitude of the quadrupole splittings (as is the proposed discrepancy in the signs (15)) may be due to increasing distortion from ideal geometry from L = AcAc to L = HfAc.

The structure of $ClSnMe(AcAc)_2$ and $ClSnPh(AcAc)_2$ cannot be obtained from the quadrupole splittings. The predicted quadrupole splittings for the *trans*-Me and Ph isomers are +1.94 and +1.78 mm s^{-1} respectively, while the predicted splittings for the *cis*-isomers are +2.03 and +1.87 mm s^{-1} respectively, compared to the observed values of 1.78 and 1.77 mm s^{-1}. Although the observed values are closer to those predicted for the *trans*-isomers, the *cis* and *trans* predicted quadrupole splittings are too similar to assign these structures with any confidence from quadrupole splittings. From other evidence, it seems likely that these two compounds have the *cis*-structure. First, recent n.m.r. studies suggest that these compounds are the *cis*-isomer in solution (5), and dipole moment data (16) suggest that the related compound $ClSnPh(oxin)_2$ (**20**, Table 1) has the *cis*-configuration.

Finally, it is interesting to notice that the predicted quadrupole splitting for the *cis*-ClSnR isomer is *larger* than, and of the same sign as, the predicted quadrupole splitting for the *trans*-isomer. It is apparent then that the *trans*-isomer need not always have the larger quadrupole splitting.

Bonding: Center Shifts and $^2J_{^{119}Sn-CH_3}$

It is now generally recognized (1) that bonding to the axial Me groups in *trans*-$Me_2Sn(AcAc)_2$ involves most of the Sn 5s character, while the bonds to the equatorial acetylacetonates involve mainly Sn 5p electrons. The center shift – quadrupole splitting correlation (Fig. 2) strongly supports the above argument and moreover suggests that Me—Sn—Me bonds contain virtually all the Sn 5s character for all these

Can. J. Chem. Downloaded from www.nrcresearchpress.com by 210.87.254.42 on 09/05/12
For personal use only.

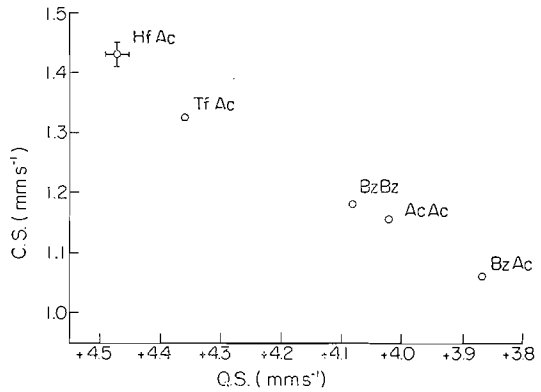

FIG. 2. Plot of c.s. *vs* q.s. for *trans*-Me_2SnL_2 compounds.

compounds, and that the Sn—L bonds only involve Sn 5p character. As the electronegativity of the equatorial ligands increases the p orbital imbalance $[-N_{p_z} + \frac{1}{2}(N_{p_x} + N_{p_y})]$ becomes more negative, the field gradient becomes more negative, and the quadrupole splitting becomes more positive (15). If the chelate ligands are only involved in bonding to Sn 5p electrons, a withdrawal of p electrons increases $[\Psi(0)_{5s}]^2$ by deshielding and the correlation between c.s. and q.s. with negative slope can be readily rationalized. This correlation is very similar to that for IX compounds (X = Na, K, Br, Cl, I) (17) in which the IX bond is thought to involve only I 5p orbitals.

If the Sn—L bond contained any appreciable 5s character, the c.s. would be expected to *decrease* with increase in electronegativity of L, because the c.s. is much more sensitive to changes in s orbital occupancy than p orbital occupancy (18). Thus, if there was any appreciable s character in the Sn—L bonds, we would expect a c.s.–q.s. correlation of positive slope, as for Fe compounds (17).

It is interesting that the c.s. and q.s. are much more sensitive to changes in L in these Sn compounds than in the substituted $Fe(AcAc)_3$ compounds studied earlier (19). This greater sensitivity is probably mainly accounted for by the lack of any s character in the Sn—L bonds, and the lower *local*[3] symmetry in the $Me_2Sn(AcAc)_2$ compounds than in the $Fe(AcAc)_3$ compounds.

[3]Considering just the nearest neighbor atoms to Sn and Fe. On this basis $Fe(AcAc)_3$ has local octahedral symmetry of oxygen about the iron.

The correlation between $^2J_{^{119}Sn-CH_3}$ and the center shift (Fig. 3) is entirely consistent with the lack of Sn 5s character in the Sn—L bonds in the dimethyl compounds. Assuming that the dominant term determining ^2J is the Fermi contact term, we assume with Pidcock *et al.* (20) that in a related series of compounds such as the dimethyl series, the factors affecting $^2J_{^{119}Sn-CH_3}$ are just $[\Psi(0)_{5s}]_{Sn}^2$, α^2 (the s character in the Sn—C bond), and the degree of covalency in the tin–carbon bond. It is also convenient to separate the ^{119}Sn center shift into similar terms:

$$\text{Center shift} \propto [\psi(0)_{5s}]_{Sn}^2 \sum_{bonds} \alpha^2 \times \text{covalency}$$

Pidcock has pointed out (21) that the n.m.r. $[\psi(0)_{5s}]^2$ refers to the square of the amplitude of the *atomic* wave function at the nucleus, and the α^2 and covalency expressions represent how much this orbital is populated by bonding. In contrast, the Mössbauer meaning of $[\Psi(0)_{5s}]^2$ has *included* these three terms, but when comparing ^2J and the c.s. it seems convenient to separate the c.s. as the J value. Since the c.s.–q.s. correlation indicates that virtually all the Sn 5s character is associated with the Sn—C bonds, α^2 and the covalency are constant. Changes in $[\psi(0)_{5s}]^2$ are thus dominant, and $[\psi(0)_{5s}]^2$ only varies due to shielding effects, *i.e.*, changes in 5p orbital populations. The positive correlation is consistent with this, *i.e.*, as the electronegativity of L increases, p electron density is delocalized onto the acetylacetonate ligands, $[\psi(0)_{5s}]^2$ increases, and both the c.s. and J values increase. The correlation is in contrast to the recent ones reported (12) in which the s character of the bonds and Bent's rule were dominant in determining the magnitude of ^2J.

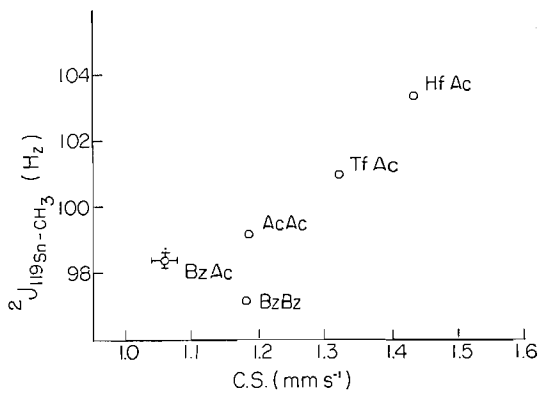

FIG. 3. Plot of $^2J_{^{119}Sn-CH_3}$ *vs* c.s. for Me_2SnL_2 compounds.

Can. J. Chem. Downloaded from www.nrcresearchpress.com by 210.87.254.42 on 09/05/12
For personal use only.

Can. J. Chem. Downloaded from www.nrcresearchpress.com by 210.87.254.42 on 09/05/12
For personal use only.

The diphenyl compounds all have a substantially lower c.s. than the dimethyl compounds, and this smaller c.s. has been rationalized in terms of a smaller 5s character in the Sn—Ph bond than in the Sn—Me bond (7). On this argument, there will be an appreciable s character in the Sn—L bonds in the diphenyl compounds, and as the electronegativity of L increases we would expect a much smaller increase in c.s. (or perhaps a decrease) than in the dimethyl compounds, and a poor or negative correlation between c.s. and q.s. The c.s.–q.s. correlation is not good, but there is still a substantial increase in c.s. as the electronegativity of L increases, indicating that any change in Sn—L 5s character between the dimethyl and diphenyl compounds is very much smaller than suggested by the simple group theory arguments presented previously (7).

Finally, it is interesting to note that the center shifts for the $Cl_4SnHAcAc$ and $[Cl_4SnAcAc]^-$ compounds are identical although the narrow line widths of 0.80 mm s^{-1} for the $[Cl_4SnAcAc]^-$ compounds indicate smaller quadrupole splitting than for the $Cl_4SnHAcAc$ compounds. These similar parameters indicate that the bonding properties of HAcAc and $AcAc^-$ are very similar in these tin compounds.

Goldanskii–Karyagin Asymmetry

All of the dimethyl compounds in this study gave pronounced asymmetry in their powder random spectra. To ensure that orientation effects were minimized, some of the spectra were taken on very finely ground powders which were dropped from a pipette into a plastic sample holder. The area ratio I_+/I_- (I_+ is the area of the line to positive velocities) was 0.85 ± 0.05 for all dimethyl compounds with the standard deviation in any one I_+/I_- being no larger than 0.05. The area ratio for $Me_2Sn(AcAc)_2$ (0.86 ± 0.05) is in reasonable agreement with that reported by Herber *et al.* (0.91) (22). Similar Goldanskii–Karyagin effects (23, 24) have been documented for organo-tin compounds (22, 25, 26) and iron compounds (27). Flinn *et al.* (28) showed that the ratio of the areas of the two lines ($R = I_{\frac{3}{2}}/I_{\frac{1}{2}}$) depends on the difference $\langle Z^2\rangle - \langle X^2\rangle$, where $\langle Z\rangle^2$ and $\langle X^2\rangle$ are the mean square vibrational amplitudes parallel and perpendicular, respectively, to the Z electric field gradient axis. In our *trans*-Me_2SnL_2 compounds, $\langle Z^2\rangle$ corresponds to the mean square vibrational amplitude of the tin along the CH_3—Sn—CH_3 bond axis (the Z *EFG* axis), while $\langle X^2\rangle$ corresponds to the mean square vibrational amplitude in the plane of the acetylacetonates. If $\langle Z^2\rangle > \langle X^2\rangle$, then $R < 1$; if $\langle Z^2\rangle < \langle X^2\rangle$, then $R > 1$ (28). This result can be used in two important ways, if $\langle Z^2\rangle - \langle X^2\rangle$ is known from crystallographic studies. First, if Mössbauer spectra can be obtained at room temperature, the crystallographic $\langle Z^2\rangle$ and $\langle X^2\rangle$ can be used to calculate R to compare with the measured R (22, 25). Spectra cannot be obtained at room temperature for our compounds, so such quantitative comparison is ruled out. More qualitatively, if the sign of $\langle Z^2\rangle - \langle X^2\rangle$ is known from crystallographic studies, R can be used to determine the sign of the quadrupole splitting (27). In our compounds, the X-ray study of $Me_2Sn(AcAc)_2$ shows that $\langle Z^2\rangle > \langle X^2\rangle$, and R must be less than 1. This identifies the positive velocity line as the $\pm\frac{3}{2}$ line, and immediately indicates that the sign of the q.s. for all the dimethyl compounds is positive.

A positive value of the q.s. has already been measured for *trans*-$Me_2Sn(AcAc)_2$ using the magnetic field technique (15). However, our results do indicate the considerable potential use of the Goldanskii–Karyagin asymmetry for obtaining the sign of the q.s. in high symmetry compounds if the sign of $\langle Z^2\rangle - \langle X^2\rangle$ is known from a crystallographic study.

We thank the National Research Council of Canada for an operating grant, and Dr. A. Pidcock for a helpful discussion.

1. G. A. Miller and E. O. Schlemper. Inorg. Chem. **12**, 677 (1973).
2. B. W. Fitzsimmons, N. T. Seeley, and A. W. J. Smith. Chem. Commun. 390 (1968); J. Chem. Soc. (A), 143 (1969).
3. M. M. McGrady and R. S. Tobias. J. Am. Chem. Soc. **87**, 1909 (1965).
4. Y. Kawasaki and T. Tanaka. J. Chem Phys. **43**, 3396 (1965); R. Ueeda, Y. Kawasaki, T. Tanaka, and R. Okawara. J. Organomet. Chem. **5**, 194 (1966).
5. K. A. Hersh and N. Serpone. Abstract to Canadian Institute of Chemistry annual meeting Montreal, June (1973).
6. G. A. Miller and E. O. Schlemper. Unpublished results.
7. R. V. Parish and R. H. Platt. Inorg. Chim. Acta, **4**, 589 (1970).
8. W. H. Nelson and D. F. Martin. J. Inorg. Nucl. Chem. **27**, 89 (1965).
9. C. Z. Moore and W. H. Nelson. Inorg. Chem. **8**, 138 (1969).
10. A. L. Allred and D. W. Thompson. Inorg. Chem. **7**, 1196 (1968).

11. D. W. THOMPSON, J. F. LEFELHOCZ, and K. S. WONG. Inorg. Chem. **11**, 1139 (1972).
12. G. M. BANCROFT and K. D. BUTLER. J. Chem. Soc. (Dalton), 1694 (1973) and references.
13. G. M. BANCROFT and R. H. PLATT. Adv. Inorg. Radiochem. **15**, 59 (1972).
14. M. G. CLARK, A. G. MADDOCK, and R. H. PLATT. J. Chem. Soc. (Dalton), 281 (1972).
15. R. V. PARISH and C. E. JOHNSON. J. Chem. Soc. (A), 1906 (1971).
16. F. P. MULLENS. Can. J. Chem. **48**, 1677 (1970).
17. G. M. BANCROFT. Mössbauer spectroscopy: an introduction for inorganic chemists and geochemists. McGraw-Hill, England. 1973.
18. J. K. LEES and P. A. FLINN. J. Chem. Phys. **48**, 882 (1968).
19. G. M. BANCROFT, A. G. MADDOCK, W. K. ONG, R. H. PRINCE, and A. J. STONE. J. Chem. Soc. (A), 1966 (1967).
20. A. PIDCOCK, R. E. RICHARDS, and L. M. VENANZI. J. Chem. Soc. (A), 1707 (1966).
21. A. PIDCOCK. Private communication.
22. R. H. HERBER, M. F. LEAHY, and Y. HAZONY. J. Chem. Phys. In press.
23. S. V. KARYAGIN, Dokl. Akad. Nauk. S.S.S.R. **140**, 1102 (1963).
24. V. I. GOLDANSKII, E. F. MAKAROV, and V. V. KHARPOV, Phys. Lett. **3**, 344 (1963).
25. R. H. HERBER and S. CHANDRA. J. Chem. Phys. **52**, 6045 (1970).
26. R. H. HERBER, S. CHANDRA, and Y. HAZONY. J. Chem. Phys. **53**, 3330 (1970).
27. G. M. BANCROFT, M. J. MAYS, and B. E. PRATER. J. Chem. Soc. (A), 956 (1970).
28. P. FLINN, S. L. RUBY, and W. L. KEHL. Science, **143**, 1434 (1964).
29. N. N. GREENWOOD and J. N. R. RUDDICK. J. Chem. Soc. (A), 1679 (1967).

Can. J. Chem. Downloaded from www.nrcresearchpress.com by 210.87.254.42 on 09/05/12
For personal use only.

The Crystal Structure of *cis*-Chlorobis(triethylphosphine)-1,10-phenanthrolineplatinum(II) fluoroborate, $(PtCl(PEt_3)_2(phen))BF_4$, a Complex Containing Monodentate 1,10-Phenanthroline

GORDON W. BUSHNELL, KEITH R. DIXON, AND MASOOD A. KHAN

Department of Chemistry, University of Victoria, Victoria, British Columbia

Received October 22, 1973

The crystal structure of *cis*-chlorobis(triethylphosphine)-1,10-phenanthrolineplatinum(II) fluoroborate has been determined and refined to an *R*-value of 0.051. The space group is $P2_1/c$ and the cell dimensions are $a = 0.9215(2)$, $b = 1.1991(3)$, $c = 2.6832(6)$ nm, $\beta = 99.38(3)°$, with 4 molecules per unit cell. The interatomic distances to Pt are: Pt—N(1), 213.7(19); Pt—N(2), 284.3(20); Pt—P(1), 223.9(7); Pt—P(2), 224.1(6); Pt—Cl, 236.1(6) pm.

The coordination number and geometry is discussed in terms of 5-coordinate tetragonal pyramidal and 4-coordinate square planar models, the latter being regarded as the more acceptable.

Monodentate *o*-phenanthroline is thus observed for the first time in the solid state. The structure of the complex in solution is discussed with the aid of conductance and nuclear magnetic resonance results which suggest the possibility of a novel fluxional system.

La structure cristalline du fluoroborate du *cis*-chlorobis(triéthylphosphine)-1,10 phénantroline de platine(II) a été déterminée et affinée á une valeur de $R = 0.051$. Le groupe d'espace est $P2_1/c$ et les dimensions de la maille sont $a = 0.9215(2)$, $b = 1.1991(3)$, $c = 2.6832(6)$ nm, $\beta = 99.38(3)°$, avec 4 molécules par maille élémentaire. Les distances interatomiques par rapport au Pt sont: Pt—N(1), 213.7(19); Pt—N(2), 284.3(20); Pt—P(1), 223.9(7); Pt—P(2), 224.1(6); Pt—Cl, 236.1(6) pm.

Le nombre de coordination et la géométrie sont traités en termes de modèles de pyramide tétragonale de coordonnée-5 et de plan carré de coordonée-4, le dernier est considéré le plus acceptable.

L'*o*-phénantroline monocoordonné est ainsi observé pour la première fois á l'état solide. La structure de complexe en solution est étudiée á l'aide de résultats de conductance et de résonnance magnétique nucléaire qui suggèrent la possibilité d'un nouveau système á flux.

[Traduit par le journal]

Can. J. Chem., **52**, 1367 (1974)

Introduction

The most common mode of coordination of platinum(II) is a four coordinate square planar arrangement (1). The existence of five coordinate complexes of platinum(II) has also been reported on the basis of spectroscopic (2–5) and X-ray diffraction (6–7) studies. In view of the rarity of five coordinate platinum complexes we considered it of interest to undertake a crystal structure study of $(PtCl(phen)(PEt_3)_2)(BF_4)$, since conductance and proton magnetic resonance studies had suggested a five-coordinate structure as the most likely for this complex in solution (8). However, the X-ray results for the solid show a very unusual structure with essentially monodentate phenanthroline. To our knowledge this is the first example of such a system.

Experimental

The preparation and characterization of the complex have already been described (8). ^1H nuclear magnetic resonance spectra were recorded at 60 MHz in acetone/dichloromethane solution using tetramethylsilane as internal reference on a Varian HA60 spectrometer with a variable low temperature accessory. ^{31}P nuclear magnetic resonance spectra were recorded at 40.5 MHz in dichloromethane solution using H_3PO_4 as external reference on a Varian XL-100 spectrometer with noise decoupling of protons.

A series of Weissenberg and Precession photographs were obtained using $CuK_{\bar{a}}$-radiation. The space group $P2_1/c$ was established unequivocally from the systematic absences. Cell parameters were measured using precession photographs. A crystal with dimensions (0.09 × 0.6 × 0.07 mm) was mounted along the *b* axis on a Picker 4-circle diffractometer. A set of 52 2θ measurements were obtained and the cell parameters were refined by the method of least squares using $\lambda = 71.069$ pm. The crystal data are listed in Table 1. The density was measured by floating the crystals in a solution of carbon tetrachloride and bromoform. Intensity measurements were made manually at room temperature on a Picker 4-circle diffractometer using MoK-radiation and a Zr filter. Reflections were scanned in the θ/2θ mode for 1 min at a rate of 2°/min in 2θ. The instrument was operated in the bisecting position with $\omega = 0$. Background measure-

Can. J. Chem. Downloaded from www.nrcresearchpress.com by 210.87.254.5 on 09/05/12
For personal use only.

TABLE 1. Crystal data for $[PtCl(pheu)(PEt_3)_2]BF_4$

System	Monoclinic
Space group	$P2_1/c$ (No. 14)
Molecular formula	$C_{24}H_{38}BClF_4N_2P_2Pt$
Molecular weight	733.84
Cell dimensions	$a = 0.9215$ (2) nm
	$b = 1.1991$ (3) nm
	$c = 2.6832$ (6) nm
	$\beta = 99.38$ (3) deg
Cell volume	2.9253 (11) nm^3
Density (calculated)	1.656 g cm^{-3}
Density (observed)	1.657 g cm^{-3}
No. of molecules per unit cell	4
Absorption coefficient ($MoK_{\bar{\alpha}}$)	52.6 cm^{-1}

ments were for 30 s at each end of the scan. The orientation of the crystal was checked twice a day using three reflections chosen for this purpose. One of the three reflections was used as an intensity standard and measured for every batch of 30 reflections. A total of 1859 independent reflections ($2\theta \leq 35°$) was measured, 1512 reflections were considered as "observed" using the criterion that the net count must be $> 1\sigma$, where σ is the standard deviation of the background count. The intensities were corrected for Lorentz and polarization effects but no absorption correction was applied.

Structure Determination

The structure was solved by the heavy atom method. A set of programs supplied by Penfold (9) was used for all the calculations. These programs are based upon ORFLS, FORDAP, ORTEP, and ORFFE. The full matrix was used in refinement and in the calculation of standard deviations. The atomic scattering factor curves for Pt, P, and Cl were those calculated by Cromer and Waber (10). Atomic scattering factors for F, N, C, and B were taken from the International Tables (11). All the atoms were assumed to be uncharged, and a correction was applied for the anomalous dispersion of Pt (12). A three-dimensional Patterson function was used to get the coordinates of the Pt atom. A subsequent Fourier synthesis showed the position of Cl, 2 P's, and 4 other non-hydrogen atoms. The coordinates of these 8 atoms and the scale factor were refined by minimization of $w(|F_o| - |F_c|)^2$. The weights were derived from the counting statistics and an experimentally determined instrument instability factor (0.04) using the formulae given by Stout and Jensen (13). No systematic variations of $w(|F_o| - |F_c|)^2$ were found during refinement. The "unobserved" reflections were included in the structure factor calculations but excluded from the least squares sums. The remaining light atoms were located using difference syntheses. The refinement was then continued with anisotropic temperature factors for the Pt, Cl, P, and F atoms and isotropic temperature factors for other non-hydrogen atoms. The final R-values were 0.051 ("unobserved" reflections excluded) and 0.073 (all reflections). Defining the weighted R value as $(\Sigma w\Delta^2/wF_o^2)^{1/2}$, the corresponding weighted R-values were 0.060 and 0.068. Shifts on the final cycle were less than 3% of the standard deviations. A final difference map gave no indication of any misplaced atom. The maximum electron density difference was 8.63×10^{-7} e pm^{-3} as compared to electron densities of 13.2×10^{-6} e pm^{-3} for the P atom and 5.91×10^{-6} e pm^{-3} for the N atom. The final positional and temperature factor parameters are listed in Tables 2 and 3. The structure factor table is in the Depository for Unpublished Data.[1]

Results

The crystal structure of $[PtCl(phen)(PEt_3)_2]BF_4$ consists of separate $[PtCl(phen)(PEt_3)_2]^+$ cations and $[BF_4]^-$ anions. The interatomic distances, bond angles, and least squares planes are given in Tables 4–7. A perspective view of the unit cell contents is shown in Fig. 1. The cell origin is at the lower left back and the axes are labelled. Some important crystal packing forces are provided by F . . . HC type contacts as listed in Table 8. The F . . . C contacts are shown as broken lines in Fig. 1. Assuming that the hydrogen atoms are placed on F . . . C lines, and a C—H bond distance of 109 pm, the F . . . H distances would vary between ~220–250 pm.

A stereoview of the $[PtCl(phen)(PEt_3)_2]^+$ cation is shown in Fig. 2. All the atoms are labelled and the covalent bonds are indicated as solid lines.

The interatomic distances between platinum and the five closest atoms are listed in Table 4(*a*). The first row gives the distances of the two phen nitrogen atoms from platinum. The two distances are unequal and indicate covalently bonded N(1) and almost uncoordinated N(2). The Pt—N(1) distance is consistent with the reported distances in $[Pt(PEt_3)_2(NO_2)_2]$ (210 pm) (14); $PtCl_2(C_5H_5N)(C_8H_{11}N)$ (210 pm) (15); $PtCl(C_5H_5N)(C_9H_{15}O)$[2] (220 pm) (16). The second row lists the two Pt—P distances, which are equal and in accord with the distances found in $[PtCl_3PEt_3]^-$ (222 pm) (17); $[Pt_2Cl_2(PEt_3)_4]^{2+}$ (225 pm) (17); *trans*-$[PtCl_2(PEt_3)_2]$ (230 pm) (18). A single entry in the third row gives the platinum to chlorine distance. This distance indicates that chlorine is bonded to platinum. The Pt—Cl distance in $[PtCl(phen)(PEt_3)_2]^+$ is consistent with the value of Pt—Cl bond lengths reported for $[PtCl_3PEt_3]^-$ (*cis* to P 230 pm, *trans* to P 238 pm) (17); $[Pt_2Cl_2(PEt_3)_4]^{2+}$ (240 pm) (17); *trans*-$[PtCl_2(PEt_3)_2]$ (229 pm) (18).

[1]Copies may be obtained at a nominal charge, upon request, from the Depository of Unpublished Data, National Science Library, National Research Council of Canada, Ottawa, Canada K1A 0S2.

[2]C_5H_5N = pyridine, $C_8H_{11}N$ = pyridinium propylide, $C_9H_{15}O$ = 2-methoxycyclo-octa-1,5-dienyl.

Can. J. Chem. Downloaded from www.nrcresearchpress.com by 210.87.254.5 on 09/05/12
For personal use only.

TABLE 2

(*a*) Positional parameters* for heavy and F_1–F_4 atoms

Atom	*X*	*Y*	*Z*
Pt	−0.2105(1)	0.2123(1)	0.11762(4)
Cl	−0.4653(6)	0.2162(6)	0.0865(2)
P(1)	−0.2253(7)	0.0297(6)	0.1000(2)
P(2)	0.0291(7)	0.2240(6)	0.1499(3)
F(1)	−0.4192(23)	0.2850(17)	0.2965(8)
F(2)	−0.1966(21)	0.3535(17)	0.3079(6)
F(3)	−0.3150(28)	0.3310(30)	0.3703(10)
F(4)	−0.2371(23)	0.1952(18)	0.3393(11)

*Estimated standard deviations in parenthesis.

(*b*) Anisotropic temperature parameters* for heavy and F_1–F_4 atoms

Atom	U_{11}	U_{22}	U_{33}	U_{12}	U_{13}	U_{23}
Pt	41(1)	57(1)	51(1)	−1(1)	13(1)	9(1)
Cl	44(4)	90(5)	90(5)	2(4)	11(4)	11(5)
P(1)	49(4)	59(5)	64(5)	−4(4)	10(4)	6(4)
P(2)	55(5)	58(5)	76(5)	−3(4)	12(4)	6(4)
F(1)	168(18)	148(17)	179(19)	−97(16)	−43(16)	52(15)
F(2)	156(16)	185(20)	108(14)	−79(15)	14(12)	39(13)
F(3)	216(27)	412(48)	175(24)	11(27)	88(20)	−104(26)
F(4)	148(18)	127(20)	302(31)	8(15)	28(18)	33(19)

*$T = \exp -2\pi^2(U_{11}h^2a^{*2} + U_{22}k^2b^{*2} + U_{33}l^2c^{*2} + 2U_{12}hka^*b^* + 2U_{13}hla^*c^* + 2U_{23}klb^*c^*)$. Tabulated values should be multiplied by 10 to obtain mean square amplitudes in pm^2.

TABLE 3. Positional and isotropic temperature parameters* N(1), N(2), C(1)—C(24) and B atoms

Atom	*X*	*Y*	*Z*	$U \times 10^{-1}$ $(pm)^2$
N(1)	−0.2583(18)	0.3759(15)	0.1420(7)	53(5)
N(2)	−0.1850(20)	0.3756(17)	0.0427(7)	73(6)
C(1)	−0.3243(25)	−0.0004(19)	0.0365(9)	63(8)
C(2)	−0.2536(29)	0.0656(23)	−0.0064(10)	94(9)
C(3)	−0.0538(25)	−0.0564(22)	0.1071(9)	70(8)
C(4)	−0.0906(29)	−0.1835(24)	0.0950(10)	95(10)
C(5)	−0.3511(28)	−0.0420(22)	0.1378(10)	80(9)
C(6)	−0.2934(36)	−0.0274(29)	0.1939(13)	134(13)
C(7)	0.0948(29)	0.1501(25)	0.2102(11)	95(9)
C(8)	0.0138(33)	0.1857(25)	0.2509(12)	105(10)
C(9)	0.0800(25)	0.3737(21)	0.1574(9)	70(8)
C(10)	0.2495(27)	0.3920(22)	0.1741(10)	82(9)
C(11)	0.1659(26)	0.1642(21)	0.1100(10)	75(8)
C(12)	0.1289(28)	0.2015(23)	0.0570(10)	89(9)
C(13)	−0.2675(23)	0.4609(19)	0.0576(8)	48(6)
C(14)	−0.2994(22)	0.4657(20)	0.1073(8)	49(6)
C(15)	−0.2859(23)	0.3849(19)	0.1876(9)	52(6)
C(16)	−0.3577(25)	0.4756(21)	0.2056(9)	65(8)
C(17)	−0.4047(23)	0.5639(19)	0.1715(9)	54(8)
C(18)	−0.3773(23)	0.5578(20)	0.1222(8)	53(6)
C(19)	−0.4288(25)	0.6455(22)	0.0863(9)	68(8)
C(20)	−0.4047(25)	0.6347(21)	0.0384(9)	67(8)
C(21)	−0.3221(24)	0.5461(20)	0.0216(9)	56(8)
C(22)	−0.2977(24)	0.5379(21)	−0.0284(9)	62(8)
C(23)	−0.2167(25)	0.4532(21)	−0.0429(9)	66(8)
C(24)	−0.1585(26)	0.3700(22)	−0.0053(10)	75(8)
B	−0.2972(50)	0.3017(41)	0.3282(19)	96(13)

*Estimated standard deviations are given in parentheses.

Can. J. Chem. Downloaded from www.nrcresearchpress.com by 210.87.254.5 on 09/05/12
For personal use only.

TABLE 4

(*a*) The platinum coordination

Bond	Length (pm)	Bond	Length (pm)
Pt—N(1)	213.7(19)	Pt—N(2)	284.3(20)
Pt—P(1)	223.9(7)	Pt—P(2)	224.1(6)
Pt—Cl	236.1(6)		

(*b*) The phenanthroline ligand bonds

Bond	Length (pm)	Bond	Length (pm)
N(1)—C(14)	143.3(26)	N(2)—C(13)	137.3(26)
N(1)—C(15)	129.4(26)	N(2)—C(24)	135.1(27)
C(15)—C(16)	139.8(28)	C(24)—C(23)	145.7(31)
C(16)—C(17)	142.0(28)	C(23)—C(22)	135.5(29)
C(17)—C(18)	138.9(26)	C(22)—C(21)	139.9(28)
C(18)—C(19)	145.2(29)	C(21)—C(20)	142.2(29)
C(18)—C(14)	141.1(27)	C(21)—C(13)	143.9(28)
C(13)—C(14)	141.2(26)	C(20)—C(19)	134.8(29)

(*c*) The triethylphosphine ligand bonds

Bond	Length (pm)	Bond	Length (pm)
P(1)—C(1)	183.2(24)	P(2)—C(7)	185.7(29)
P(1)—C(3)	187.1(24)	P(2)—C(9)	185.8(25)
P(1)—C(5)	187.1(26)	P(2)—C(11)	192.2(25)
C(1)—C(2)	162.1(32)	C(7)—C(8)	148.3(36)
C(3)—C(4)	158.4(33)	C(9)—C(10)	156.9(34)
C(5)—C(6)	152.3(36)	C(11)—C(12)	147.8(32)

(*d*) Tetrafluoroborate distances

Bond	Length (pm)	Bond	Length (pm)
B—F(1)	131.0(42)	B—F(2)	130.6(44)
B—F(3)	121.8(43)	B—F(4)	140.5(45)
F(1)—F(2)	218.4(25)	F(1)—F(3)	212.7(32)
F(1)—F(4)	216.0(29)	F(2)—F(3)	215.9(30)
F(2)—F(4)	213.4(28)	F(3)—F(4)	201.4(35)

*Estimated standard deviation in parentheses in tenths of a pm.

Since a five-coordinate (trigonal bipyramidal) structure was assigned previously (8) to the $[PtCl(phen)(PEt_3)_2]^+$ ion in solution we first consider the coordination number in the solid state. If the line Pt—N(2) were counted as a bond then the geometry around the Pt atom might be described as a distorted square pyramid with N(2) occupying the apical position. Elongation of the apical bond is quite common in square pyramidal complexes and several values are available for the ratio of the axial/equatorial bond lengths: $[Ni(CN)_5]^{2-}$, 1.17, (19); $[NiBr_2(triarsine)]$, 1.16, (20); $[PdBr_2(2\text{-}PIPI)_2]$,[3] 1.13, (21); $[PtCl(phen)(PEt_3)_2]^+$, 1.33, (this work). Since the ratio is considerably greater in our complex than in the other cases, and considering that the limited span of the phenanthroline ligand and the requirement of reasonable bond angles about N(1) set an upper limit on the Pt—N(2) length, we regard the platinum atom as four coordinate and approximately square planar.

Two other quantities, the non-bonded N(1) . . . N(2) bite and the N(1)—Pt—N(2) angle are consistent with this view. The N(1) . . . N(2) bite in the $[PtCl(phen)(PEt_3)_2]^+$ ion is (285 pm) which can be compared with the average value of (266 pm) in a series of phen complexes (22). No data are available for the phen molecule, so we

[3]PIPI = 2-phenylisophosphindoline.

Can. J. Chem. Downloaded from www.nrcresearchpress.com by 210.87.254.5 on 09/05/12
For personal use only.

TABLE 5. Bond angles in $[PtCl(phen)(PEt_3)_2]BF_4$*

(*a*) The platinum atom coordination

Bonds	Angle (deg)	Bonds	Angle (deg)
Cl—Pt—P(2)	174.8(3)	P(1)—Pt—N(1)	162.5(5)
Cl—Pt—P(1)	85.5(2)	Cl—Pt—N(1)	81.2(5)
P(1)—Pt—P(2)	99.5(2)	P(2)—Pt—N(1)	93.6(5)

(*b*) The phenanthroline ligand

Bonds	Angle (deg)	Bonds	Angle (deg)
N(1)—C(15)—C(16)	124.6(22)	N(2)—C(24)—C(23)	121.5(23)
N(1)—C(14)—C(18)	119.8(20)	N(2)—C(13)—C(21)	118.9(21)
C(15)—C(16)—C(17)	118.0(21)	C(24)—C(23)—C(22)	118.2(23)
C(16)—C(17)—C(18)	119.4(22)	C(23)—C(22)—C(21)	120.7(23)
C(17)—C(18)—C(14)	119.4(21)	C(22)—C(21)—C(13)	120.0(22)
C(18)—C(14)—C(13)	119.6(23)	C(21)—C(13)—C(14)	120.1(23)
C(18)—C(19)—C(20)	118.5(23)	C(21)—C(20)—C(19)	123.6(24)
C(19)—C(18)—C(14)	120.3(21)	C(20)—C(21)—C(13)	117.7(21)
C(14)—N(1)—C(15)	118.7(20)	C(13)—N(2)—C(24)	120.6(22)
Pt—N(1)—C(15)	116.6(16)		

(*c*) The triethylphosphine ligand

Bonds	Angle (deg)	Bonds	Angle (deg)
C(1)—P(1)—C(3)	105.7(11)	C(7)—P(2)—C(9)	109.1(12)
C(1)—P(1)—C(5)	98.9(11)	C(7)—P(2)—C(11)	99.0(12)
C(3)—P(1)—C(5)	106.2(11)	C(9)—P(2)—C(11)	104.1(11)
Pt—P(1)—C(1)	113.2(8)	Pt—P(2)—C(7)	117.9(9)
Pt—P(1)—C(3)	119.8(8)	Pt—P(2)—C(9)	108.5(8)
Pt—P(1)—C(5)	110.9(8)	Pt—P(2)—C(11)	117.1(8)
P(1)—C(1)—C(2)	111.6(16)	P(2)—C(7)—C(8)	111.8(21)
P(1)—C(3)—C(4)	111.2(17)	P(2)—C(9)—C(10)	112.8(17)
P(1)—C(5)—C(6)	109.7(20)	P(2)—C(11)—C(12)	110.7(18)

(*d*) The tetrafluoroborate ion

Bonds	Angle (deg)	Bonds	Angle (deg)
F(1)—B—F(2)	113.2(39)	F(2)—B—F(3)	117.5(44)
F(1)—B—F(3)	114.5(41)	F(2)—B—F(4)	103.8(34)
F(1)—B—F(4)	105.3(38)	F(3)—B—F(4)	100.1(39)

*Estimated standard deviations are given in parentheses in tenths of a degree.

calculated from the atomic coordinates (23, 24) the C . . . C and N . . . C bites in the structurally similar phenanthrene and 2,2′-bipyridine molecules to be 297 and 284 pm respectively. In the $[PtCl(phen)(PEt_3)_2]^+$ ion a low value of the N—M—N angle is also expected, owing to the more distant position of the uncoordinated end of the phen ligand. Thus the N—M—N angle is (68.2°) in the $[PtCl(phen)(PEt_3)_2]^+$ compared to the average value of (79.5°) in ten phen or dmp complexes of known structure (22). The line Pt . . . N(2) forms an angle of 79.9° with the least squares plane: N(1), Cl, P(1), P(2).

Table 5(*a*) lists the bond angles around platinum. The first row gives the bond angle values for the ligands *trans* to each other. The second and third rows list the bond angles for the ligands which are mutually *cis*. The deviations from the ideal values of 180° and 90° are quite significant.

Table 6(*a*) gives two least squares planes concerning the platinum coordination. The χ^2 values indicate a considerable departure from planarity.[4] Presumably the non-bonded ligand–ligand re-

[4] $\chi^2 = \Sigma_i |P_i^2/\sigma^2(P_i)|$; P_i = perpendicular distance of atom i from the plane. σ = estimated standard deviation.

Can. J. Chem. Downloaded from www.nrcresearchpress.com by 210.87.254.5 on 09/05/12
For personal use only.

TABLE 6. Least squares planes: $k_1x + k_2y + k_3z = k_4$*

(*a*) Platinum coordination†

No.	Plane	k_1	k_2	k_3	k_4	χ^2	P_{Pt} (pm)
1	Pt, Cl, N(1), P(1), P(2)	+0.351	+0.208	−0.913	−318	500	0.28
2	Cl, N(1), P(1), P(2)	+0.351	+0.224	−0.909	−318	329	5.69

*x, y, and z are the coordinates in pm along the orthogonal axis system, defined as x along a, y in the (a,b) plane, and z along c^*.
†Angle between plane 1,2 = 1.0°.

(*b*) The phenanthroline ligand†

No.	Plane	k_1	k_2	k_3	k_4	χ^2
1	N(1), N(2), C(13)—C(24)	−0.819	−0.498	−0.285	−93.1	81.9
2	N(1), C(14)—C(18)	−0.843	−0.456	−0.286	−61.0	2.7
3	N(2), C(13), C(21)—C(24)	−0.803	−0.539	−0.253	−119.5	1.7
4	C(13), C(14), C(18)—C(21)	−0.820	−0.507	−0.266	−95.4	3.9

†Angle between planes 2,3 = 5.6°; 2,4 = 3.4°; 3,4 = 2.2°.

TABLE 7. Distances of atoms from the phenanthroline least squares plane*

Atom	Distance (pm)	Atom	Distance (pm)
N(1)	+8	N(2)	−8
C(15)	+6	C(24)	−7
C(16)	−2	C(23)	+3
C(17)	−6	C(22)	+8
C(18)	−3	C(21)	+2
C(19)	−3	C(20)	+5
C(14)	−1	C(13)	−3

*Estimated standard deviation is about 2 pm.

pulsion is the main factor responsible for the distortion of the coordination square in the $[PtCl(phen)(PEt_3)_2]^+$ ion. Some important intra-ionic non-bonded distances are, N(1)—C(9) (307.6 pm); C(3)—C(11) (322.1 pm); C(1)—Cl (328.8 pm). There is little room for the ligands to move and form an ideal square configuration.

Table 4(*b*) lists the bond lengths within the phen ligand. Column 1 is for one half of the molecule and column 2 is for the corresponding features in the other half, except for the last pair of entries. A disparity of the corresponding bond lengths in the first four rows is noticeable. Recently a detailed tabulation of bond distances of coordinated phen and dmp has been presented by Frenz and Ibers (22).[5] Our values lie within the reported range.

The bond angles of the phen ligand are given in Table 5(*b*). The values of the two halves of the molecule are entered in columns 1 and 2, respectively. In general, the deviation from 120° is slight. The phen bond angles in the $[PtCl(phen)(PEt_3)_2]^+$ ion are comparable with the values found in $[Ni(phen)_2]^{2+}$ (22); $[ZnCl_2(phen)]$ (25); $[Ni\{S_2P(OC_2H_5)_2\}_2(phen)]$[6] (26), and in the analogous phenanthrene ($C_{14}H_{10}$) molecule (23).

Table 6(*b*) presents various least squares planes of the phen ligand. The phen ligand is non-planar but the three individual rings are planar. The non-planarity of the phen ligand is also reported in many other phen complexes (22, 25, 27, 28), and even the phenanthrene molecule was found (23) non-planar in the crystal phase. In Table 7 we present the distances of various atoms from the mean plane of the phen ligand. The entries in Table 7 indicate an approximate two-fold symmetry axis passing through C(13)—C(14) and C(19)—C(20). Such two-fold symmetry axis is also reported in $[Ni(phen)_3]^{2+}$ (22) and in the phenanthrene molecule (23).

The bond lengths and bond angles of the triethylphosphine ligands are listed in Tables 4(*c*) and 5(*c*), respectively. The entries in columns 1 and 2 correspond to the PEt_3 containing the P(1) and P(2) atoms respectively. These values are relatively inexact owing to the high thermal motion of the carbon atoms. The average P—C bond distance in $[PtCl(PEt_3)_2phen]^+$ is 187 pm as compared to the distances found in $[PtCl_3PEt_3]^-$ (184 pm) (17); $[Pt_2Cl_2(PEt_3)_4]^{2+}$ (184 pm) (17); $[\pi\text{-}C_5H_5CuPEt_3]$ (188 pm) (29). The average C—C distance is 154 pm and indicates a single bond. The C—C distances in [PtCl-

[5]dmp = 2,9-dimethyl phenanthroline.

[6]$S_2P(OC_2H_5)_2$ = *O,O'*-diethyldithiophosphate.

Can. J. Chem. Downloaded from www.nrcresearchpress.com by 210.87.254.5 on 09/05/12
For personal use only.

TABLE 8. F.....HC contacts*

Contact	Length (pm)	Contact	Length (pm)
F(2).....C^{I}(3)	315.8(29)	F(3).....C^{II}(2)	340.8(38)
F(2).....C(15)	322.8(29)	F(3).....C^{III}(5)	348.6(37)
F(2).....C(16)	324.9(30)	C(17).....F^{III}(1)	329.2(28)

*Estimated standard deviations are given in parentheses in tenths of a pm. Roman numerals as superscripts refer to the atoms with coordinates: I = $-x, \frac{1}{2}+y, \frac{1}{2}-z$; II = $x, \frac{1}{2}-y, \frac{1}{2}+z$; III = $-1-x, \frac{1}{2}+y, \frac{1}{2}-z$.

$(PEt_3)_2phen]^+$ are comparable with the data reported for $[PtCl_3PEt_3]^-$ (155 pm) (17); $[Pt_2Cl_2(PEt_3)_4]^{2+}$ (153 pm) (17); $[\pi\text{-}C_5H_5CuPEt_3]$ (154 pm) (29).

The values of bond angles given in Table 5(*c*) are in general close to 109° and show a tetrahedral arrangement around phosphorus and carbon atoms. These values are consistent with the values reported (17, 18, 29).

Table 4(*d*) and 5(*d*) contain the values for bond lengths and bond angles respectively for the tetrafluoroborate ion. The error of these values is generally high owing to the very high thermal motion of the fluorine atoms (a trend which is consistent with other crystal structures containing the BF_4^- ion). The bond angles (Table 5(*d*)) indicate the tetrahedral configuration of the tetrafluoroborate ion. The values of bond lengths and angles for the fluoroborate ion in our complex are in accord with the data reported for $[Cu(bipy)_2NH_3]BF_4$ (30), and $[Ni(FB(ONCHC_5H_3N)_3P)]BF_4$ (31).[7]

Discussion

The crystal structure results demonstrate for the first time that the ligand *o*-phenanthroline may be monodentate in the solid state. Unless the distinction between solids and solutions is clearly maintained any discussion becomes very complicated. For the solid state one can attempt to survey the literature to find out how common it is for a potentially bidentate ligand to be monodentate. The definition of a potentially bidentate ligand gives immediate difficulty. A solution is to restrict the field to molecules having chemically equivalent donor sites when uncoordinated. Then the survey shows that monodentate behavior is relatively rare in general and unknown for some ligands. *o*-Phenanthroline was apparently in the latter category. Since the orderly extension of coordination chemistry relies heavily on the characterization of definite crystalline compounds and *o*-phenanthroline is often used, the simple fact that it has now been observed to be monodentate in a crystalline compound is of some significance.

An alternative coordination scheme for the complex was:

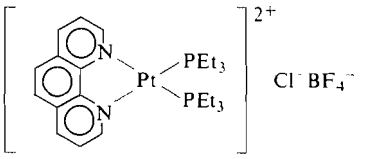

We know this to be electronically reasonable since the *cis*-$[Pt(pyridine)_2(PEt_3)_2]^{2+}$ ion has been prepared (32). With the phenanthroline ligand there are steric difficulties between the aromatic rings and the PEt_3 groups. A Courtaulds model could not be built and we would predict severe intra-ionic repulsion. When the title compound is refluxed in methanol there is a reaction, the first step of which is presumed to be phosphine dissociation, with the chlorine ligand remaining coordinated (8). Thus there appears to be no tendency toward the alternative scheme, and some support for our steric reasoning.

A fruitless attempt was made to recognize significant differences in the C—C and C—N bond lengths between the coordinated and uncoordinated ends of the *o*-phenanthroline ligand.

The previous spectroscopic results (8) which pertain to the solid state, namely the infrared evidence for coordinated chlorine and the *cis* arrangement of the PEt_3 groups, have been confirmed. However, the X-ray structure determination has raised an interesting question concerning the structure of this complex in solution. Here the evidence is that chlorine is coordinated (conductance), that the two PEt_3 groups are chemically inequivalent (^1H magnetic resonance) and most important that the phen ligand shows no difference between the two halves of the molecule (^1H magnetic resonance). There are three possible explanations for these results. (*a*) that in solution

[7] $FB(ONCHC_5H_3N)_3P$ = fluoroborotris(2-aldoximo-6-pyridyl)phosphine.

Can. J. Chem. Downloaded from www.nrcresearchpress.com by 210.87.254.5 on 09/05/12
For personal use only.

Can. J. Chem. Downloaded from www.nrcresearchpress.com by 210.87.254.5 on 09/05/12
For personal use only.

FIG. 1. The crystal packing in $[PtCl(phen)(PEt_3)_2]BF_4$. The Roman numeral superscripts on the Pt, B, and C(3) atoms refer to the ions with the following coordinates: I = 1 + x, y, z; II = 1 + x, $\frac{1}{2}$ + y, $\frac{1}{2}$ − z; III = −x, $\frac{1}{2}$ + y, $\frac{1}{2}$ − z; IV = 1 + x, $\frac{1}{2}$ − y, $\frac{1}{2}$ − z; V = −x, 1 − y, 1 − z.

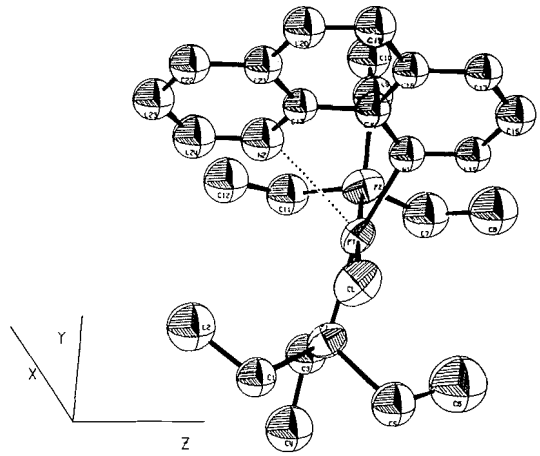

FIG. 2. A stereoview of the $[PtCl(phen)(PEt_3)_2]^+$ cation.

the complex is five-coordinate and trigonal bipyramidal, (*b*) that in solution the complex is four-coordinate with a monodentate phen rapidly exchanging its point of attachment between N(1) and N(2), (*c*) that the complex contains monodentate phenanthroline as in the solid state but the electronic difference between the coordinated and non-coordinated rings is too small to be detected by ^1H magnetic resonance spectroscopy. The last possibility may be rejected since we were previously able to distinguish easily between the two halves of a coordinated phenanthroline in which the nitrogen atoms were *trans* to phosphorus and chlorine respectively in the $[PtCl(phen)(PEt_3)]^+$ cation (8). The electronic asymmetry produced by different *trans* influences would be much smaller than that produced by coordination or non-coordination.

In attempts to distinguish between "*a*" and "*b*" we have carried out low temperature ^1H n.m.r. studies and find no evidence of asymmetry, even at $-85°$, the lowest temperature accessible before viscosity broadening of the spectrum and crystallization of the complex prevent further observation. Consequently, if exchange is occurring it is very fast on the n.m.r. time scale.

Information regarding the possibilities "*a*" and "*b*" is also potentially available from the magnitude of $^1J_{Pt-P}$. This coupling constant depends primarily on the s character of the Pt—P bond and is expected to decrease by $\sim 20\%$ on changing from $4(sp^2d)$ to $5(sp^3d)$ coordination provided that the ligand *trans* to the phosphorus under observation does not change, (33). The ^{31}P spectrum of the complex consists of a poorly resolved central doublet at 1.2 p.p.m. downfield from an external H_3PO_4 reference. The sidebands due to coupling with ^{195}Pt (34% abundant, $I = \frac{1}{2}$) have a quartet structure and analysis as an ABX system by standard procedures, (34), gives the parameters $^2J_{P_A-P_B} = 22$ Hz, $^1J_{P_A-Pt} = 3680$ Hz, $^1J_{P_B-Pt} = 3490$ Hz and $\nu_A - \nu_B = 14$ Hz.[8] These parameters were confirmed by showing that $^2J_{P_A-P_B}$ and $\nu_A - \nu_B$ correctly predict the shape of the central doublet. Typical values for $^1J_{Pt-P}$ for phosphorus *trans* to chlorine in a four-coordinate complex are in the range 3100–4200 Hz (33, 35). Our parameters for $[PtCl(PEt_3)_2(phen)][BF_4]$ lie in the center of this range and therefore suggest that we are dealing with a four-coordinate species but the width of the range makes a positive conclusion difficult.

In conclusion, we believe that the very unusual solid state structure of this complex may be attributed mainly to the known preference of platinum(II) for square planar geometry, together with the steric difficulty of forming a $[Pt(phen)(PEt_3)_2]^{2+}$ cation. In solution, the situation is not clear cut but the results suggest the possibility of a novel fluxional system in which the phenanthroline very rapidly exchanges its point of attachment to platinum.

We thank the University of Victoria and the National Research Council of Canada for research grants and Dr. E. J. Wells for access to his ^{31}P n.m.r. facilities.

1. F. A. COTTON and G. WILKINSON. Advanced inorganic chemistry. 3rd ed. Interscience Publisher, New York. 1972.
2. R. A. PLOWMAN and L. F. POWER. Aust. J. Chem. **24**, 303 (1971).
3. O. ST. C. HEADLEY, R. S. NYHOLM, C. A. MCAULIFFE, L. SINDELLARI, M. L. TOBE, and L. M. VENANZI. Inorg. Chem. Acta, **4**, 93 (1970).
4. B. CHISWELL and S. E. LIVINGSTONE. J. Chem. Soc. 1071 (1960).
5. T. D. DUBOIS and D. W. MEEK. Inorg. Chem. **8**, 146 (1969).
6. R. D. CRAMER, R. V. LINDSAY, C. T. PREWITT, and U. G. STOLBERG. J. Am. Chem. Soc. **87**, 658 (1965).
7. G. A. MAIR, H. M. POWELL, and L. M. VENANZI. Proc. Chem. Soc. 170 (1961).
8. K. R. DIXON and A. D. RATTRAY. Can. J. Chem. **51**, 618 (1973).

[8]Information on the signs of these parameters is not available from the spectrum except that the $^1J_{Pt-P}$ values have the same sign. It is not possible to identify which phosphorus atom in the complex is P_A and which is P_B.

Can. J. Chem. Downloaded from www.nrcresearchpress.com by 210.87.254.5 on 09/05/12
For personal use only.

9. B. R. PENFOLD. University of Canterbury crystallographic programs. Christchurch, New Zealand.
10. D. T. CROMER and J. T. WABER. Acta Cryst. **18**, 104 (1965).
11. J. A. IBERS. International tables for X-ray crystallography. Vol. III. I.U.Cr. Kynoch press, Birmingham. 1962. p. 201. Table 3.3.1A.
12. D. T. CROMER. Acta Cryst. **18**, 17 (1965).
13. G. H. STOUT and L. H. JENSEN. X-ray structure determination. Macmillan, New York. 1968. p. 456.
14. R. GRAZIANI. Inorg. Nucl. Chem. Lett. **8**, 701 (1972).
15. M. KEETON, R. MASON, and D. R. RUSSELL. J. Organomet. Chem. **33**, 259 (1971).
16. G. BOMBIERI, E. FORSELLINI, and R. GRAZIANI. J. Chem. Soc. (Dalton). 525 (1972).
17. G. W. BUSHNELL. Unpublished results.
18. G. G. MESSMER and E. L. AMMA. Inorg. Chem. **5**, 1775 (1966).
19. A. TERZIS, K. N. RAYMOND, and T. G. SPIRO. Inorg. Chem. **9**, 2415 (1970).
20. G. A. MAIR, H. M. POWELL, and D. E. HENN. Proc. Chem. Soc. 415 (1960).
21. J. W. COLLIER, F. G. MANN, D. G. WATSON, and H. R. WATSON. J. Chem. Soc. 1803 (1964).
22. B. A. FRENZ and J. A. IBERS. Inorg. Chem. **11**, 1109 (1972).
23. J. TROTTER. Acta Cryst. **16**, 605 (1963).
24. L. L. MERRITT and E. D. SCHROEDER. Acta Cryst. **9**, 801 (1956).
25. C. W. REIMANN, S. BLOCK, and A. PERLOFF. Inorg. Chem. **5**, 1185 (1966).
26. D. C. CRAIG, E. T. PALLISTER, and N. C. STEPHENSON. Acta Cryst. **B27**, 1163 (1971).
27. A. J. GRAHAM and R. H. FENN. J. Organomet. Chem. **25**, 173 (1970).
28. G. P. KHARE and R. EISENBERG. Inorg. Chem. **9**, 2211 (1970).
29. L. T. J. DELBAERE, D. W. MCBRIDE, and R. B. FERGUSON. Acta Cryst. **B26**, 515 (1970).
30. F. S. STEPHENS. J. Chem. Soc. (Dalton), 1350 (1972).
31. M. R. CHURCHILL and A. H. REIS, JR. Inorg. Chem. **11**, 1811 (1972).
32. K. R. DIXON and J. J. MCFARLAND. Unpublished results.
33. J. F. NIXON and A. PIDCOCK. Ann. rev. N.M.R. spectrosc. **2**, 345 (1969).
34. E. D. BECKER. High resolution n.m.r. Academic Press. New York and London. 1969.
35. G. G. MATHER, G. J. N. RAPSEY, and A. PIDCOCK. Inorg. Nucl. Chem. Lett. **9**, 567 (1973).

Can. J. Chem. Downloaded from www.nrcresearchpress.com by 210.87.254.5 on 09/05/12
For personal use only.

Can. J. Chem. Downloaded from www.nrcresearchpress.com by 210.87.254.105 on 09/05/12
For personal use only.

Product Studies of the Mutual Termination Reactions of *sec*-Alkylperoxy Radicals: Evidence for Non-cyclic Termination

JOHN E. BENNETT and RAYMOND SUMMERS

Shell Research Limited, Thornton Research Centre, P. O. Box 1, Chester CH1 3SH, England

Received October 15, 1973

The yields of alcohol and ketone from the mutual termination reaction of *sec*-butyl-, *sec*-hexyl-, cyclopentyl-, and cycloheptylperoxy radicals have been measured over the temperature range from −125 to +100 °C. The ratio of alcohol/ketone departs markedly from the value of unity predicted by the Russell mechanism, being greater (*ca.* 2.5) at +100 °C and considerably less (*ca.* 0.1) at −125 °C.

On a mesuré, à des températures entre −125 et +100 °C, les rendements en alcool et en cétone provenant des réactions d'arrêt mutuel des radicaux *sec*-butyl-, *sec*-hexyl-, cyclopentyl- et cycloheptylperoxy. Les rapports d'alcool sur cétone s'écartent d'une façon importante de la valeur de l'unité qui est prédite par le mécanisme de Russell; cette valeur est plus grande (~2.5) à +100 °C et considérablement plus faible (~0.1) à −125 °C. [Traduit par le journal]

Can. J. Chem., **52**, 1377 (1974)

The mutual termination reactions of primary or secondary alkylperoxy radicals are generally assumed to proceed through a cyclic transition state (*i.e.*, the Russell mechanism) (1–3)

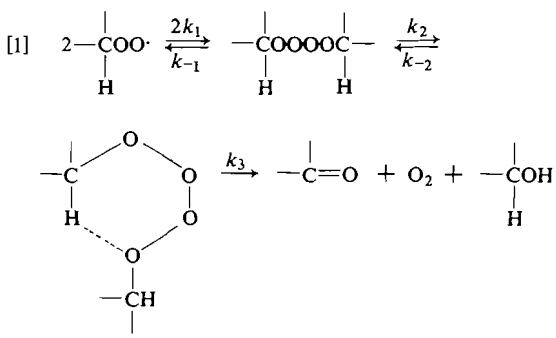

where the overall termination rate constant, $2k_t = 2k_1 k_2 k_3/k_{-1} k_{-2}$. On this basis it has been concluded from thermochemical calculations that the overall activation energy, E_t, should be negative (4). However, recent measurements (5) by electron spin resonance spectroscopy of $2k_t$ for several *sec*-alkylperoxy radicals have shown that E_t is positive (2–4 kcal mol^{-1}) and that the Arrhenius plots are not linear at low temperatures.

Product studies (6–8), mainly at ambient temperature, have shown that comparable yields of alcohol and ketone are formed as predicted by the Russell mechanism (eq. 1). However, detailed studies (9) have shown recently that at ambient temperatures considerable fractions of 1-ethoxyethylperoxy radicals and 1,2-diphenylethylperoxy radicals do not terminate by the Russell mechanism but form free alkoxy radicals by a route (eq. 2*a*) comparable to that postulated for the termination of *tert*-alkylperoxy radicals.

In view of the anomalous temperature dependence of the rate constants (5) we have now made product studies over a comparable temperature range (−125 to +100 °C) for the *sec*-alkylperoxy radicals from butane, hexane, cyclopentane, and cycloheptane. The peroxy radicals were formed by the photolysis of an oxygenated solution of di-*tert*-butyl peroxide (0.25 to 4%) in the appropriate hydrocarbon (5). This method formed specific *sec*-alkylperoxy radicals from butane, cyclopentane, and cycloheptane but gave a mixture of the 2- and 3-hexylperoxy radicals from hexane. The products were identified and their concentrations measured by gas–liquid chromatography.

Detailed product analyses were made for the cyclopentylperoxy radical and appropriate control experiments were carried out. The yields of

[2] 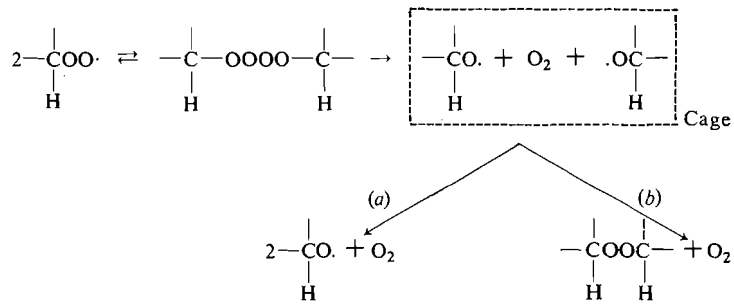

TABLE 1. Effect of temperature on the yields of alcohol and ketone from the mutual termination of cyclopentylperoxy radicals

Temperature (°C)	*tert*-Butanol (10^{-3} mol l^{-1})	Cyclopentanol (10^{-3} mol l^{-1})	Cyclopentanone (10^{-3} mol l^{-1})	Alcohol*/Ketone	Total yield† (%)
+40	14.8	5.4	4.1	1.32	64
+25	10.9	3.4	3.5	0.95	63
−10	5.7	1.5	2.5	0.60	71
−40	4.9	0.8	2.9	0.28	75
−65	3.3	0.5	2.3	0.22	86
−90	2.2	0.1	1.7	0.07	82

*Ratio of cyclopentanol/cyclopentanone.
†(Cyclopentanol + cyclopentanone)/*tert*-butanol.

the major products, cyclopentanol, cyclopentanone, and *tert*-butanol, are given in Table 1. The yield of *tert*-butanol was used to determine the extent of photolysis and thus to provide a product balance. In addition, small amounts of pentanal, dicyclopentyl, and dicyclopentyl peroxide (≈5% each) were observed at most temperatures.

In agreement with the published results (6–8) the yields of alcohol and ketone were approximately equal at room temperature. As the temperature was increased the yield of cyclopentanol relative to that of cyclopentanone increased slightly but below room temperature the ratio decreased rapidly with decreasing temperature (Table 1). A similar effect (10) has been observed previously in the radiolytic oxidation of solid cyclohexane, for which the ratio of alcohol/ketone was about 0.33 at −77 °C and 0.25 at −196 °C. The similar trend observed by both methods shows that the low alcohol/ketone ratio is not merely an artefact of the photolytic system.

Similar variations with temperature were found for the ratios of the yields of alcohol and ketone from the mutual termination of the *sec*-butyl-, *sec*-hexyl-, and cycloheptylperoxy radicals (Table 2).

The excess of alcohol at the higher temperatures can be accounted for by the occurrence of the non-terminating reaction 2*a* in addition to the Russell mechanism. At low temperatures the mutual termination reaction must proceed mainly via an alternative route which leads to the exclusive formation of ketone.

[3] 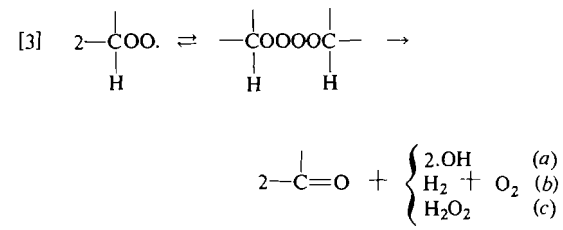

The formation of two hydroxyl radicals will not lead to termination. Although the elimination of molecular hydrogen has been observed in the decomposition of peroxides (9), the simultaneous formation of molecular hydrogen and oxygen from the tetroxide appears unlikely. The occurrence of the termination reaction 3*c* is supported by the detection by colorimetric analysis (11) of hydrogen peroxide in the samples. The yield increased as the temperature was decreased but was always less than the amount of ketone (2[H_2O_2]/

Can. J. Chem. Downloaded from www.nrcresearchpress.com by 210.87.254.105 on 09/05/12
For personal use only.

TABLE 2. Effect of temperature on the ratios of the yields of alcohol and ketone from the mutual termination of *sec*-alkylperoxy radicals

Temperature (°C)	Ratio of alcohol/ketone for			
	sec-Butyl	*sec*-Hexyl*	Cyclopentyl	Cycloheptyl
+100	—	—	—	2.5
+75	—	—	—	1.7
+50	—	1.0	1.4	1.0
+25	—	0.63	0.95	0.83
0	—	0.50	0.71	0.67
−25	0.48	0.34	0.40	—
−50	0.38	0.22	0.25	—
−75	0.20	0.16	0.14	—
−100	0.15	—	0.06	—
−125	0.11	—	—	—

*Ratio is (2-hexanol + 3-hexanol)/(2-hexanone + 3-hexanone) though all four products were determined separately.

[Ketone] = 0.35–0.55, instead of unity as required by reaction 3*c*).

The present results show that at low temperatures the mutual termination of *sec*-alkylperoxy radicals does not proceed through a cyclic transition state, as in the Russell mechanism, but through an alternative state, namely

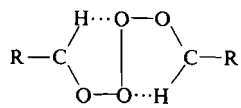

1. G. A. RUSSELL. J. Am. Chem. Soc. **79**, 3871 (1957).
2. J. A. HOWARD and K. U. INGOLD. J. Am. Chem. Soc. **90**, 1056 (1968); **90**, 1058 (1968).
3. R. E. KELLOGG. J. Am. Chem. Soc. **91**, 5433 (1969).
4. D. F. BOWMAN, T. GILLAN, and K. U. INGOLD. J. Am. Chem. Soc. **93**, 6555 (1971).
5. J. A. HOWARD and J. E. BENNETT. Can. J. Chem. **50**, 2374 (1972).
6. R. L. MCCARTHY and A. MACLACHLAN. J. Chem. Phys. **35**, 1625 (1961).
7. W. A. CRAMER. J. Phys. Chem. **71**, 1171 (1967).
8. A. MACLACHLAN. J. Am. Chem. Soc. **87**, 960 (1965).
9. D. LINDSAY, J. A. HOWARD, E. C. HORSWILL, L. ITON, and K. U. INGOLD. Can. J. Chem. **51**, 870 (1973).
10. R. BLACKBURN and A. CHARLESBY. Trans. Faraday. Soc. **62**, 1159 (1966).
11. G. DOBSON and G. HUGHES. J. Phys. Chem. **69**, 1814 (1965).

C-Acetylation of Ketones

STUART NICHOLAS HUCKIN AND LARRY WEILER[1]

Department of Chemistry, University of British Columbia, Vancouver, British Columbia V6T 1W5

Received January 11, 1974

The action of 2 equiv. of methyllithium on the monoanion of simple β-keto esters gives the β-diketone in good yield. This represents a facile and new method to achieve the *C*-acylation of a ketone.

La réaction de 2 équiv. de méthyllithium avec le monoanion de β-céto d'esters simples conduit avec de bons rendements aux β-dicétones. Cette approche représente une méthode nouvelle et facile pour provoquer une *C*-acylation d'une cétone. [Traduit par le journal]

Can. J. Chem., **52**, 1379 (1974)

Recently we have been interested in the generation of the dianions from β-keto esters (1–3) and in their chemistry (3–6). Usually we form these dianions by treating the corresponding β-keto esters with 1 equiv. of sodium hydride to give a monoanion which on subsequent treat-

[1]Author to whom correspondence should be addressed.

Can. J. Chem. Downloaded from www.nrcresearchpress.com by 210.87.254.105 on 09/05/12
For personal use only.

TABLE 2. Effect of temperature on the ratios of the yields of alcohol and ketone from the mutual termination of *sec*-alkylperoxy radicals

Temperature (°C)	Ratio of alcohol/ketone for			
	sec-Butyl	*sec*-Hexyl*	Cyclopentyl	Cycloheptyl
+100	—	—	—	2.5
+75	—	—	—	1.7
+50	—	1.0	1.4	1.0
+25	—	0.63	0.95	0.83
0	—	0.50	0.71	0.67
−25	0.48	0.34	0.40	—
−50	0.38	0.22	0.25	—
−75	0.20	0.16	0.14	—
−100	0.15	—	0.06	—
−125	0.11	—	—	—

*Ratio is (2-hexanol + 3-hexanol)/(2-hexanone + 3-hexanone) though all four products were determined separately.

[Ketone] = 0.35–0.55, instead of unity as required by reaction 3*c*).

The present results show that at low temperatures the mutual termination of *sec*-alkylperoxy radicals does not proceed through a cyclic transition state, as in the Russell mechanism, but through an alternative state, namely

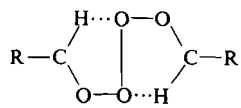

1. G. A. RUSSELL. J. Am. Chem. Soc. **79**, 3871 (1957).
2. J. A. HOWARD and K. U. INGOLD. J. Am. Chem. Soc. **90**, 1056 (1968); **90**, 1058 (1968).
3. R. E. KELLOGG. J. Am. Chem. Soc. **91**, 5433 (1969).
4. D. F. BOWMAN, T. GILLAN, and K. U. INGOLD. J. Am. Chem. Soc. **93**, 6555 (1971).
5. J. A. HOWARD and J. E. BENNETT. Can. J. Chem. **50**, 2374 (1972).
6. R. L. MCCARTHY and A. MACLACHLAN. J. Chem. Phys. **35**, 1625 (1961).
7. W. A. CRAMER. J. Phys. Chem. **71**, 1171 (1967).
8. A. MACLACHLAN. J. Am. Chem. Soc. **87**, 960 (1965).
9. D. LINDSAY, J. A. HOWARD, E. C. HORSWILL, L. ITON, and K. U. INGOLD. Can. J. Chem. **51**, 870 (1973).
10. R. BLACKBURN and A. CHARLESBY. Trans. Faraday. Soc. **62**, 1159 (1966).
11. G. DOBSON and G. HUGHES. J. Phys. Chem. **69**, 1814 (1965).

C-Acetylation of Ketones

STUART NICHOLAS HUCKIN AND LARRY WEILER[1]

Department of Chemistry, University of British Columbia, Vancouver, British Columbia V6T 1W5

Received January 11, 1974

The action of 2 equiv. of methyllithium on the monoanion of simple β-keto esters gives the β-diketone in good yield. This represents a facile and new method to achieve the *C*-acylation of a ketone.

La réaction de 2 équiv. de méthyllithium avec le monoanion de β-céto d'esters simples conduit avec de bons rendements aux β-dicétones. Cette approche représente une méthode nouvelle et facile pour provoquer une *C*-acylation d'une cétone. [Traduit par le journal]

Can. J. Chem., **52**, 1379 (1974)

Recently we have been interested in the generation of the dianions from β-keto esters (1–3) and in their chemistry (3–6). Usually we form these dianions by treating the corresponding β-keto esters with 1 equiv. of sodium hydride to give a monoanion which on subsequent treat-

[1]Author to whom correspondence should be addressed.

Can. J. Chem. Downloaded from www.nrcresearchpress.com by 210.87.254.105 on 09/05/12
For personal use only.

ment with 1 equiv. of *n*-butyllithium at 0° gives the dianion, for example, eq. 1 for methyl acetoacetate (**1**).

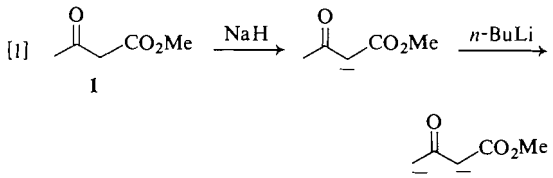

A slight excess of *n*-butyllithium at 0° does not react with these dianions. However, excess *n*-butyllithium at higher temperature does lead to a variety of carbonyl addition products (7).

Hence we were intrigued by the reports of the addition of excess methyllithium to the monoanions of fused 2-carboxymethylcyclohexanones which gave tertiary alcohols in a very clean reaction (eq. 2) (8,9). We have found that

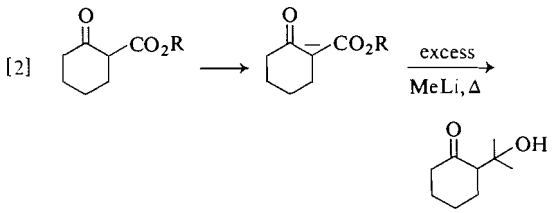

treatment of the monoanion of simple β-keto esters with only 1 equiv. of methyllithium leads to formation of the corresponding dianion in very good yield (2,3). Hence, it would appear that the β-keto ester dianion is an intermediate in the above reaction (eq. 2). This led us to study the reaction of the monoanion of a β-keto ester with exactly 2 equiv. of methyllithium.

The monoanions of two simple β-keto esters, methyl acetoacetate (**1**) and methyl 2-oxocyclohexanecarboxylate (**2**), were prepared by treating a solution of the β-keto ester in dry tetrahydrofuran with 1 equiv. of sodium hydride at 0 °C. These monoanions were then treated with 2 equiv. of methyllithium in hexane at 0 °C. After a ½-h period the reaction mixture was quenched with acid and worked up. A v.p.c. analysis of the crude oil indicated that a new product had been formed in greater than 90% in each case. From the reaction of methyl acetoacetate (**1**), pentane-2,4-dione was isolated in 80% yield as its 2,4-dinitrophenylhydrazone derivative (m.p. 207–209 °C). The analogous reaction with methyl 2-oxocyclohexanecarboxylate (**2**) gave 2-acetylcyclohexanone (b.p. 106–108°/15 mm) in 83% yield.

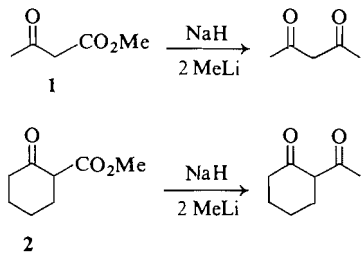

This represents a novel method to formally achieve the *C*-acetylation of a ketone and avoids any problems of self-condensation inherent in the Claisen reaction or difficulties with *O- vs. C*-acylation of the β-keto esters (10). Also it was found that treatment of the monoanions of **1** and **2** with 3 equiv. of methyllithium at 0° gave greater than 80% yields of the expected (8,9) tertiary alcohols **3** and **4**. In addition in these

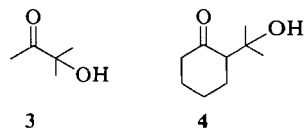

simple cases, it appears that excess methyllithium and higher reaction temperatures are deleterious to the yield of tertiary alcohol. The availability and different reactivities of organolithium compounds (7) represent a drawback to the overall generality of these reactions and hence we are studying the reactivity of the dianions of β-keto esters with other organometallic reagents.

We are grateful to the National Research Council of Canada and the University of British Columbia for support of this work.

1. L. WEILER. J. Am. Chem. Soc. **92**, 6702 (1970).
2. S. N. HUCKIN and L. WEILER. J. Am. Chem. Soc. In press.
3. S. N. HUCKIN. Ph.D. Thesis. University of British Columbia, Vancouver, British Columbia. 1973.
4. S. N. HUCKIN and L. WEILER. Tetrahedron Lett. 4835 (1971).
5. S. N. HUCKIN and L. WEILER. Tetrahedron Lett. 2405 (1972).
6. S. N. HUCKIN and L. WEILER. Can. J. Chem. This issue.
7. G. BRIEGER and D. C. SPENCER. Tetrahedron Lett. 4586 (1971).
8. R. M. COATES and J. E. SHAW. Chem. Commun. 515 (1968).
9. E. PIERS and R. D. SMILLIE. J. Org. Chem. **35**, 3997 (1970).
10. H. O. HOUSE. Modern synthetic reactions. 2nd edition. W. A. Benjamin, Inc. Menlo Park, California. 1972. Chapt. 11.

Can. J. Chem. Downloaded from www.nrcresearchpress.com by 210.87.254.105 on 09/05/12
For personal use only.

Can. J. Chem. Downloaded from www.nrcresearchpress.com by 210.87.254.40 on 09/05/12
For personal use only.

Canadian Journal of Chemistry | Journal canadien de chimie

Published by THE NATIONAL RESEARCH COUNCIL OF CANADA | *Publié par* LE CONSEIL NATIONAL DE RECHERCHES DU CANADA

Volume 52 Number 8(Part 2) April 15, 1974 | Volume 52 numéro 8(partie 2) 15 avril 1974

An Overview of Aeronomic Processes in the Stratosphere and Mesosphere

M. NICOLET

Institut d'Aéronomie Spatiale, 3 Avenue Circulaire, B-1180 Bruxelles, Belgique

Received October 1, 1973

The discrepancy noted between theoretical and observational concentrations of O_3 in the mesosphere and stratosphere can be explained by an effect of hydrogen compounds and of nitrogen oxides. Solar radiation dissociates water vapor and methane in the thermosphere and upper mesosphere. In the stratosphere the reaction of the excited oxygen atom $O(^1D)$ with methane and nitrous oxide leads to a destruction of these two molecules in the stratosphere which corresponds to a production of carbon monoxide with water vapor and of nitric oxide, respectively. Hydrogen and water vapor molecules also react with the electronically excited oxygen atom $O(^1D)$ leading to hydroxyl radicals. *In situ* sources of H_2 exist in the stratosphere and mesosphere: reaction of OH with CH_4, photodissociation of formaldehyde, and also reaction between hydroperoxyl radicals and hydrogen atoms. The vertical distribution of water vapor is not affected by its dissociation in the stratosphere and mesosphere since its reformation is rapid.

The ratio of the hydroxyl and hydroperoxyl radical concentrations cannot be determined with adequate precision and complicates the calculation of the destruction of ozone which occurs through reactions of OH and HO_2 not only with atomic oxygen at the stratopause but also directly in the middle stratosphere and with CO and NO in the lower stratosphere.

In addition to the various reactions involving nitric oxide and nitrogen dioxide, the reactions leading to the production and destruction of nitric acid and nitrous acid must be considered. Nitric acid molecules are involved in an eddy diffusion transport from the lower stratosphere into the troposphere and are, therefore, responsible for the removal of nitric oxide which is produced in the stratosphere. Atmospheric conditions must be known at the tropopause.

La différence que l'on note entre les concentrations théoriques et expérimentales du O_3 dans la mésosphère et la stratosphère peut être expliquée par une influence des composés d'hydrogène et des oxydes d'azote. La radiation solaire dissocie la vapeur d'eau et le méthane dans la thermosphère et dans la mésosphère supérieure. Dans la stratosphère, la réaction de l'atome excité d'oxygène $O(^1D)$ avec le méthane et l'oxyde nitreux mène à la destruction de ces deux molécules dans la stratosphère, ce qui correspond à la production respective du monoxyde de carbone avec de la vapeur d'eau et de l'oxyde nitrique. L'hydrogène et les molécules de vapeur d'eau réagissent aussi avec l'atome d'oxygène $O(^1D)$, excité électroniquement, produisant des radicaux hydroxyles. Des sources de H_2 existent *in situ* dans la stratosphère et la mésosphère; la réaction du OH avec du CH_4, la photodissociation du formaldéhyde et aussi la réaction entre les radicaux hydroperoxyles et les atomes d'hydrogène. La distribution verticale de la vapeur d'eau n'est pas modifée par sa dissociation dans la stratosphère et la mésosphère puisque sa reformation est rapide.

Le rapport des concentrations des radicaux hydroxyle et hydroperoxyle ne peut être

établi avec une précision convenable; il complique le calcul de la destruction de l'ozone qui se produit durant les réactions du OH et du H_2O, non seulement avec l'oxygène atomique à la stratopause, mais aussi directement dans la stratosphère moyenne et avec du CO et du NO dans la stratosphère inférieure.

En plus des diverses réactions concernant l'oxyde nitrique et le bioxyde d'azote, les réactions qui conduisent à la production et à la destruction de l'acide nitrique et de l'acide nitreux devraient être envisagées. Les molécules d'acide nitrique sont impliquées dans un transport de diffusion turbulent de la stratosphère inférieure à la troposphère, et sont, par conséquent, la cause de l'élimination de l'oxyde nitrique produit dans la stratosphère. Les conditions atmosphériques doivent être connues à la tropopause.

[Traduit par le journal]

Can. J. Chem. Downloaded from www.nrcresearchpress.com by 210.87.254.40 on 09/05/12
For personal use only.

Introduction

Even if much detailed work remains to be done, there is a general understanding of the various factors which are involved in the formation of the ozone layer and in the production of atomic oxygen. The researches of Chapman (1, 2) have led to a knowledge of the photochemistry of atmospheric oxygen in a pure oxygen atmosphere. Bates and Nicolet (3) in their general survey of the photochemistry of water vapor have investigated the extent to which atomic hydrogen and certain radicals catalyze the formation of molecular oxygen. Vibration–rotation bands of the hydroxyl radical OH, which appear in the airglow, aroused interest in the photochemistry of hydrogen–oxygen compounds (4, 5) and in particular of methane (6, 7) and of water vapor (3). Water vapor, which is quite abundant near ground level with a fractional volume concentration reaching 10^{-2}, decreases in mixing ratio with altitude. The water vapor content is very small in the stratosphere; $(4 \pm 1) \times 10^{-6}$ is not an unreasonable value to adopt for the order of magnitude of the fractional volume concentration of water vapor (8–11) in the stratosphere. Methane and molecular hydrogen, which have been found as permanent constituents of the troposphere, have continuous sources at ground level. Their total amounts by volume are, respectively, 1.5×10^{-6} (see ref. 12) and 0.5×10^{-6} (see refs. 12, 13). Unlike water vapor, however, their fractional concentrations are practically not affected through the troposphere. Consequently, above the tropopause, the combined H-atom content in CH_4 is more than 50% of the content in H_2O. Thus, the total amount of free hydrogen in the lower stratosphere cannot be far from 10^{-5}.

If the photodissociation of water vapor and methane occurs in the mesosphere and thermosphere, the reaction of H_2O with the electronically excited atomic oxygen in the ^1D state (14, 15) leads to the possibility of its dissociation in the stratosphere and troposphere. The concentrations of $O(^1D)$ produced by ozone photolysis in the stratosphere and troposphere are sufficiently large to lead to OH radicals not only from water vapor but also from methane and molecular hydrogen.

While the desirability of similar studies of the effect of nitrogen compounds has long been realized, comparatively few have been made because of lack of basic data. The importance of nitrogen oxides in controlling the ozone concentration was pointed out only in 1970 (16). Information on N_2O was given before by the calculation of its photodissociation rate (7, 17) and on NO, NO_2, and HNO_3 by the analysis of the principal reactions (18). Recently, new experimental and observational results have been obtained on nitrogen oxides, particularly by direct observation of the vertical distribution in the stratosphere of HNO_3 (19, 20), NO_2 (21), and NO (22, 23).

The importance of methane has been generally realized since McConnell *et al.* (24) showed that it was a major source of carbon monoxide in the troposphere through a reaction with hydroxyl radicals. Furthermore, these hydroxyl radicals are produced in sufficient concentration (25) to provide the destruction of carbon monoxide required by Weinstock (26). However, in moving through the latitudinal distribution of the tropopause, from high latitudes to the tropical zone, very different atmospheric conditions are detected; the difference in altitude of the polar and equatorial tropopauses is of the order of 10 km; a folded tropopause at mean latitudes may change the lower boundary conditions of the stratosphere. In other words, the nature of

Can. J. Chem. Downloaded from www.nrcresearchpress.com by 210.87.254.40 on 09/05/12
For personal use only.

the tropopause is an important factor which must be introduced in the study of the lower stratosphere.

Oxygen Photodissociation and Ozone Formation

Photodissociation of molecular oxygen is produced by the absorption of solar radiation in the weak Herzberg continuum beginning at 2424 Å,

[1] $$O_2 + h\nu(\lambda < 2424\ \text{Å}) \rightarrow 2O(^3P)$$

which occurs in the stratosphere. In the strong Schumann–Runge continuum

[2] $$O_2 + h\nu(\lambda < 1759\ \text{Å}) \rightarrow O(^3P) + O(^1D)$$

the dissociation occurs in the thermosphere. In the spectral range of the Schumann–Runge bands, where predissociation is observed, the absorption is extremely variable and the dissociation occurs in the mesosphere and upper stratosphere.

In the presence of a third body (N_2, O_2) the atoms liberated by photodissociation recombine

[3] $$(k_1);\quad O + O + M \rightarrow O_2 + M$$

or they unite with oxygen molecules

[4] $$(k_2);\quad O + O_2 + M \rightarrow O_3 + M$$

forming ozone. This molecule is destroyed by a two-body collision process

[5] $$(k_3);\quad O + O_3 \rightarrow 2O_2$$

and is also subject to photodissociation in the strong Hartley continuum

[6] $$O_3 + h\nu(\lambda < 3500\ \text{Å}) \rightarrow O_2 + O(^1D)$$

and in the weak Chappuis bands in the visible

[7] $$O_3 + h\nu(\lambda < 8000\ \text{Å}) \rightarrow O_2 + O(^3P)$$

An important aspect of the photodissociation of O_3 is the number of $O(^1D)$ atoms produced which react with H_2O, H_2, CH_4, and N_2O before they can be deactivated by atmospheric N_2 and O_2.

Considering the theoretical problem of oxygen dissociation and ozone formation, the equations governing the rates of change of the concentrations $n(O)$ and $n(O_3)$ are

[8] $$\frac{dn(O)}{dt} + 2k_1n(M)n^2(O) + k_2n(M)n(O_2)n(O) + k_3n(O_3)n(O) = 2n(O_2)J_2 + n(O_3)J_3$$

[9] $$\frac{dn(O_3)}{dt} + n(O_3)J_3 - k_2n(M)n(O_2)n(O) + k_3n(O)n(O_3) = 0$$

which lead to the general form

[10] $$\frac{dn(O)}{dt} + \frac{dn(O_3)}{dt} + 2k_1n(M)n^2(O) + 2k_3n(O_3)n(O) = 2n(O_2)J_2$$

where J_2 and J_3 are the photodissociation coefficients of O_2 and O_3, respectively.

It seems appropriate to discuss the photochemical behavior within the various atmospheric layers where various regimes can be distinguished. In the lower thermosphere, atomic oxygen becomes a major constituent. In the major part of the mesosphere, $n(O) > n(O_3)$ and there is a daytime photo-equilibrium for ozone with a photodissociation coefficient $10^{-3} \leq J_3 \leq 10^{-2}\ s^{-1}$. Thus, from [9]

[11] $$\frac{n(O_3)}{n(O)} = \frac{k_2n(M)n(O)}{J_3 + k_3n(O)} \simeq \frac{k_2n(M)n(O_2)}{J_3}$$

since $J_3 > k_3n(O)$, and from [10],

[12] $$\frac{dn(O)}{dt} + 2k_1n(M) \times \left\{1 + \frac{k_3k_2n(O_2)}{k_1J_3}\right\}n^2(O) = 2n(O_2)J_2$$

The time τ_O which is required in a sunlit atmosphere to reach about 50% of the photochemical equilibrium value (or to reach 80% from 50%) is given by

[13] $$\tau_O(50\%) = 0.275 \times \left\{\left[k_1n(M) + \frac{k_3k_2n(M)n(O_2)}{J_3}\right]n(O_2)J_2\right\}^{-1/2}$$

or

[14] $$\tau_O(50\%) = 0.275n_e(O)/n(O_2)J_2$$

if $n_e(O)$ is the photochemical equilibrium concentration. Application of [14] leads to the following times:

Altitude (km)	90	85	80	75	70
Time (h)	200	90	32	12	4

Thus, at the mesopause and above in the lower thermosphere, the vertical distribution of atomic oxygen concentration depends on the relative

Can. J. Chem. Downloaded from www.nrcresearchpress.com by 210.87.254.40 on 09/05/12
For personal use only.

importance of atmospheric transport conditions as compared with chemical conditions.

During the night J_2 and J_3 vanish; $n(O)$ slowly decays and $n(O_3)$ increases to attain the value $k_2n(M)n(O_2)/k_3$ but never exceeds the combined initial concentration $n(O) + n(O_3)$ of the odd oxygen atoms. Comparison of the observed and calculated ozone concentration in the mesosphere reveals that the calculated ozone concentration values are greater than those observed, particularly in the upper mesosphere. In an oxygen atmosphere, the steady state concentration of ozone molecules in the mesosphere is between 1×10^{10} cm^{-3} and 8×10^{10} cm^{-3}, which is more than the observed values (27). The reason for the difference is that hydrogen acts as a catalyst for the destruction of odd oxygen atoms. The catalytic action of hydrogen was first introduced by Bates and Nicolet (3), and various other studies (28–31) have shown how the ozone behavior in the mesosphere may be affected by hydrogen compounds.

Near the stratopause and in the whole stratosphere $n(O_3) > n(O)$ and another regime is established. The equation normally used in studies of the main part of the ozone layer in a pure oxygen atmosphere is

$$[15] \quad \frac{dn(O_3)}{dt} + \frac{2k_3J_3}{k_2n(M)n(O_2)}\,n^2(O_3) = 2n(O_2)J_2$$

with $n(O)$ in photochemical equilibrium. The differential eq. 15 indicates that the time τ_{O_3} required to attain equilibrium (in fact, to pass from zero concentration to 50% of the equilibrium value or from 50% to 80%) is

$$[16] \quad \tau_{O_3} = 0.275n_e(O_3)/n(O_2)J_2$$

where $n_e(O_3)$ is the photochemical equilibrium value

$$[17] \quad n_e^2(O_3) = \frac{k_2n(M)n^2(O_2)}{k_3}\frac{J_2}{J_3}$$

Figures 1*a* and 1*b* show the numerical results of eq. 16 for various solar conditions: overhead sun, 90°; 45° and 30°. It can be seen immediately that the time required to reach photochemical equilibrium conditions is less than 1 day at the stratopause and more than 10 years at 20 km. It is well known that the ozone concentration in the lower stratosphere does not reach equilibrium conditions and that its vertical and horizontal distribution depends on its transport conditions. Thus, there are important differences between the upper and lower stratosphere; below the stratopause photochemical equilibrium conditions can be considered and above the tropopause a complete departure from steady state conditions must be observed. The results of the calculation of the ozone concentration under photo-equilibrium conditions in an oxygen atmosphere are shown in Fig. 2. It is seen that it is difficult to obtain agreement between the calculated values and an average value (32) representing the observations. In the upper stratosphere, the limits of the observational and theoretical uncertainties are such that the effect of hydrogen and nitrogen compounds must be taken into account.

Reactions in a Hydrogen–Oxygen Atmosphere

Inspection of the rates of the reactions introduced by Bates and Nicolet (3) indicates

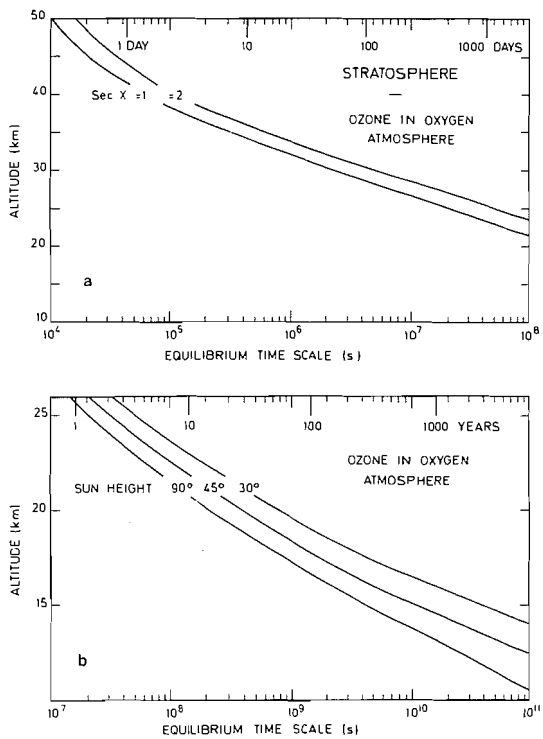

FIG. 1. (*a*) Equilibrium time scales for ozone in a pure oxygen atmosphere. Less than 1 day above 45 km, more than 1 year below 25 km (daytime). Overhead sun, sec $\chi = 1$, and 70°, sec $\chi = 2$. (*b*) Equilibrium time scales for ozone of a pure oxygen atmosphere in the lower stratosphere for various solar heights 90, 45, and 30°. With times greater than 1 year, there is always departure from photo-equilibrium conditions.

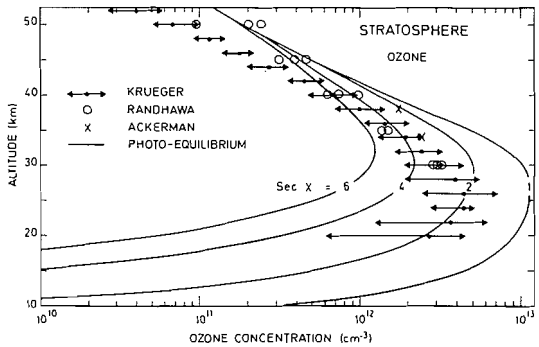

FIG. 2. Observed and calculated ozone profiles. Calculations for various solar zenith angles, sec χ = 1, 2, 4, and 6, photo-equilibrium conditions. Range in ozone concentrations observed by Krueger (32) of 24 rocket flights between 60° S and 64° N. Three observations by Randhawa (33) over White Sands and two observations by Ackerman (private communication, 1973) over Aire-sur-l'Adour, France.

that, in the mesosphere and stratosphere, a large number of them can be ignored.

In the stratosphere and mesosphere, a three-body reaction involving atomic hydrogen and molecular oxygen leads to hydroperoxyl radicals

[18] (a_1); $H + O_2 + M \rightarrow HO_2 + M + 46$ kcal

In the upper stratosphere and mesosphere the reaction of H with O_3 is also important

[19] (a_2); $H + O_3 \rightarrow O_2 + OH_{v \leq 9} + 77$ kcal

It may be concluded that hydrogen atoms are immediately transformed into hydroperoxyl radicals in the major part of the stratosphere since reaction 18 is rapid. However, in the neighborhood of the stratopause and in the mesosphere, reaction 19 which leads to OH has an important role.

An important reaction in the mesosphere and at the stratopause level which forms a chain leading to the reformation of oxygen molecules with the production of hydrogen atoms, in conjunction with reaction 19, is the bimolecular process

[20] (a_5); $OH + O \rightarrow H + O_2 + 16.6$ kcal

It is clear that if the effects of [20] are important in the mesosphere, they are relatively unimportant in the lower stratosphere where other processes involving ozone are more important. The chain reaction introduced by McGrath and Norrish (34)

[21] (a_6); $OH + O_3 \rightarrow HO_2 + O_2 + 39$ kcal

and

[22] (a_{6c}); $HO_2 + O_3 \rightarrow OH + 2O_2 + 31$ kcal

must be finally considered after having been rejected (35). Very recent measurements have been reported (36–38) with $a_6 = 1.3 \times 10^{-12} e^{-950/T}$ cm^3 s^{-1} which leads to $(5.5 \pm 1.5) \times 10^{-14}$ cm^3 s^{-1} at room temperature and to 1 to 2×10^{-14} cm^3 s^{-1} at temperatures of the lower stratosphere. Such values are less than those which were used in previous aeronomic studies. An upper limit $a_6 \leq 5 \times 10^{-13}$ cm^3 s^{-1} at room temperature (39) was adopted as the actual value in many studies of the stratosphere (28–31, 40, 41). According to Simonaitis and Heicklen (42) the reaction rate of [22] is $a_{6c} = 3.3 \times 10^{-14} e^{-1000/T}$ cm^3 s^{-1} which gives a value of 1.25×10^{-15} cm^3 s^{-1} at room temperature and low values of between 3 and 6×10^{-16} cm^3 s^{-1} in the lower stratosphere.

Instead of reaction 22 in the upper stratosphere and mesosphere the reaction leading to OH involves atomic oxygen (39)

[23] (a_7); $O + HO_2 \rightarrow O_2 + OH_{v \leq 6} + 55$ kcal

Kaufman (39) has suggested that $a_7 \geq 10^{-11}$ cm^3 s^{-1}. Reactions 20 and 23 must be compared since they represent, in the upper part of the stratosphere and in the mesosphere, the chain reaction which is involved in the ozone destroying mechanism through the direct attack of oxygen atoms and re-formation of oxygen molecules. Experimental data are needed in order to determine the ratio a_5/a_7 which must be known accurately for the calculation of the ratio $n(HO_2)/n(OH)$ in the upper stratosphere and mesosphere.

In the mesosphere, where $n(O) > n(O_3)$, the differential equation for atomic oxygen is written (43)

$$[24] \quad \frac{dn(O)}{dt} + 2n^2(O)\left[k_1 n(M) + \frac{k_3 k_2 n(M) n(O_2)}{J_{3a}}\right] + n(O)\left[a_2 n(H)\frac{k_2 n(M) n(O_2)}{J_{3a}} + a_5 n(OH) + a_7 n(HO_2)\right] = 2n(O_2) J_2$$

Can. J. Chem. Downloaded from www.nrcresearchpress.com by 210.87.254.40 on 09/05/12
For personal use only.

with

$$[25]\qquad \frac{n(O_3)}{n(O)} = \frac{k_2 n(M) n(O_2)}{J_3 + k_3 n(O) + a_2 n(H) + a_6 n(OH) + a_{6c} n(HO_2)} \simeq \frac{k_2 n(M) n(O_2)}{J_{3a}}$$

and

$$[26]\qquad J_{3a} \simeq J_3 + a_2 n(H)$$

Such an equation 25 corresponds to photochemical equilibrium conditions in the lower thermosphere and in the upper mesosphere. Numerical calculations near the mesopause level show that the rate coefficients are too small to lead to photochemical equilibrium conditions for atomic oxygen. Its vertical distribution in the lower thermosphere is subject to vertical transport conditions controlled by eddy diffusion.

The minimum which is observed near 75 km in the ozone concentration by Hays and Roble (27) is due to the action of atomic hydrogen; the net effect of the action of hydroxyl and hydroperoxyl radicals on atomic oxygen is to cause an important decrease of the ozone concentration.

In the region where atomic oxygen is in photochemical equilibrium, the conventional stratospheric equation 15 indicates that photochemical equilibrium values can be reached in the lower mesosphere and upper stratosphere. However, [15] must be replaced in a hydrogen–oxygen atmosphere (43, 44) by

$$[27]\qquad \frac{dn(O_3)}{dt} + 2n^2(O_3)\frac{J_3 k_3}{k_2 n(M) n(O_2)} + n(O_3) a_2 n(H) + n(O_3)\left[a_6 + \frac{a_5 J_3}{k_2 n(M) n(O_2)}\right] n(OH) + n(O_3)\left[a_{6c} + \frac{a_7 J_3}{k_2 n(M) n(O_2)}\right] n(HO_2) = 2n(O_2) J_2$$

If [27] is compared with [15], it is clear that the effect of hydrogen compounds is equivalent to an increase in the photodissociation coefficient J_3. In other words, the ozone dissociation is increased by additional processes involving H, OH, and HO_2 so that the equivalent O_3 photodissociation coefficient is written (43)

$$[28]\qquad J_{3A} = J_3[1 + A]$$

where A is given by

$$[29]\qquad 2J_3 k_3 n(O_3).A = a_2 n(H) k_2 n(M) n(O_2) + a_5 n(OH)\left[1 + \frac{a_6}{a_5}\frac{k_2 n(M) n(O_2)}{J_3}\right] + a_7 n(HO_2)\left[1 + \frac{a_{6c}}{a_5}\frac{k_2 n(M) n(O_2)}{J_3}\right]$$

By assuming reasonable numerical values, it is easy to see that $a_6 k_2 n(M) n(O_2)/a_5 J_3 < 1$ and $a_{6c} k_2 n(M) n(O_2)/a_7 J_3 < 1$ in the upper stratosphere and mesosphere and >1 in the lower stratosphere. Thus, at the stratopause, the conventional equation for equilibrium conditions is

$$[30]\qquad n(O_3) = \left[\frac{k_2}{k_3} n(M) n^2(O_2) \frac{J_2}{J_3(1 + A)}\right]^{1/2}$$

with the correction term $n(H)$ being negligible,

$$[31]\qquad [1 + A]^{1/2} = \left[1 + \frac{a_5 n(OH) + a_7 n(HO_2)}{2k_3 n(O_3)}\right]^{1/2}$$

By assuming that the values of $n(OH)$ and $n(HO_2)$ are known, it can be shown that the correction term can be applied in the mesosphere and at the stratopause where $2k_3 n(O_3) \simeq a_5 n(OH) + a_7 n(HO_2)$. Below the stratopause it is difficult to see how a correction term could be introduced except if the OH and HO_2 concentrations were increased by a factor of 5, at least. By assuming that the values of $n(OH)$ and $n(HO_2)$ are known, it is possible to see (Fig. 3) that the effect of hydroxyl and hydroperoxyl radicals can be considered in the lower stratosphere as loss processes for ozone. However, since the maximum value of the loss coefficient is, between 15 and 25 km, of the order of 10^{-8} s^{-1} for sec $\chi = 1$ and 10^{-9} s^{-1} for sec $\chi = 2$ the times which are required to reach chemical equilibrium are longer

Can. J. Chem. Downloaded from www.nrcresearchpress.com by 210.87.254.40 on 09/05/12
For personal use only.

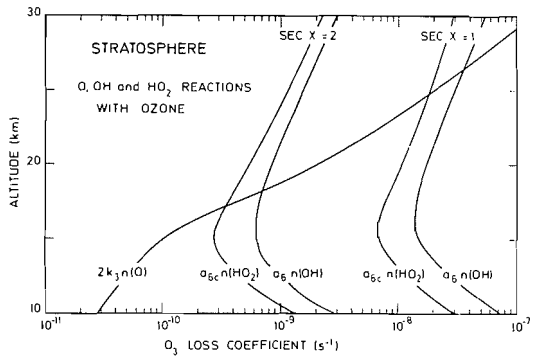

FIG. 3. Comparison between the various reactions (with O, OH, and HO_2) leading to the destruction of ozone molecules. Effect of OH and HO_2 is particularly important in the lower stratosphere for overhead sun conditions.

than 1 year. An increase of $n(OH)$ or $n(HO_2)$ would be necessary in order to reduce the time to less than 1 year.

Production of Hydroxyl and Hydroperoxyl Radicals

Water vapor can be dissociated by sunlight and its photodissociation coefficient for zero optical depth is 10^{-5} s^{-1}. The photodissociation occurs in the upper mesosphere due to the effect of Lyman-α and goes to the lower mesosphere by absorption in the spectral range of the Schumann–Runge bands. The photodissociation rate coefficient decreases in the mesosphere by a factor of the order of 1000 (43).

In the stratosphere, the photodissociation process is less important than the oxidation process. An effect caused by oxygen atoms, in their normal state ^3P, on H_2O has not been detected since the reaction is endothermic, but atoms in their first excited state ^1D lead to (45)

[32] $O(^1D) + H_2O \rightarrow OH + OH^*(v \leq 2) + 28.8$ kcal

The production of $O(^1D)$ atoms by photolysis of stratospheric ozone is important. A precise determination depends on the exact efficiency of $O(^1D)$ production in the processes

[33a] $O_3 + h\nu(\lambda < 3100\ \text{Å}) \rightarrow O_2(^1\Delta_g) + O(^1D)$

and

[33b] $O_3 + h\nu(\lambda < 4000\ \text{Å}) \rightarrow O_2(^3\Sigma_g^-) + O(^1D)$

According to DeMore and Raper (46), all oxygen atoms are $O(^1D)$ at $\lambda \leq 3100$ Å; for $\lambda > 3100$ Å there is a drop in the efficiency of production of $O(^1D)$ atoms (47). At 3130 Å and 25 °C the efficiency for $O(^1D)$ production was found to be 0.5 (48). However, at stratospheric temperatures it becomes very small (49). We may consider (50) the following working value for the quenching rate coefficient

[34] $k_Q(^1D) = 5 \times 10^{-11}$ cm^3 s^{-1}

due to N_2 and O_2. With this average value of k_Q, the production rate of $O(^1D)$ atoms leads to the photo-equilibrium concentration for various solar zenith angles illustrated in Fig. 4 for a conventional vertical distribution of O_3 (43). In the lower stratosphere, the concentration $n(O(^1D))$ is the order of 1 and a peak concentration of more than 100 cm^{-3} occurs near the stratopause. At the stratopause, the variation is small with solar zenith angle, but is very important in the lower stratosphere due to the sensitivity on the spectral efficiency of wavelengths near 3100 Å.

The reaction of $O(^1D)$ occurs not only with H_2O, but also with CH_4 and H_2. Thus, the presence of $O(^1D)$ atoms leads to the production of H atoms and OH radicals by H_2O, H_2, and CH_4 in the troposphere and stratosphere without a direct photodissociation process. Recent experimental analysis (51–55) leads to a rate coefficient

[35] $a^* = (3 \pm 1) \times 10^{-10}$ cm^3 s^{-1}

The production of HO radicals is illustrated in Fig. 5 where the minimum occurs at the tropopause, chosen here at 15 km.

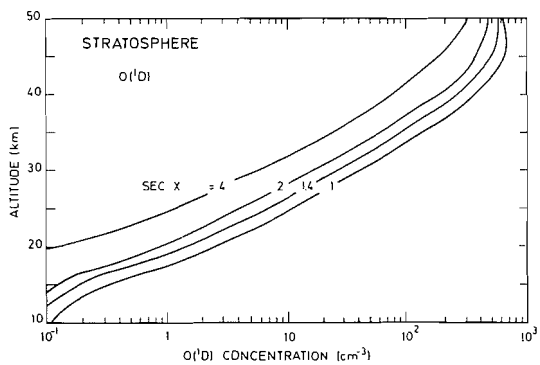

FIG. 4. Concentration of oxygen atoms in the excited state ^1D produced by ozone photodissociation. Variation with solar zenith angle for a constant ozone concentration.

Can. J. Chem. Downloaded from www.nrcresearchpress.com by 210.87.254.40 on 09/05/12
For personal use only.

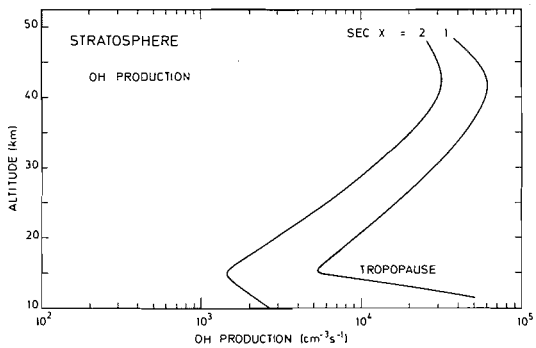

FIG. 5. Production of OH radicals in the stratosphere by reaction of $O(^1D)$ atoms with H_2O (4 p.p.m.v.), CH_4 (1.5 p.p.m.v.), and H_2 (0.5 p.p.m.v.) for two solar zenith angles, sec χ = 1 and 2.

Reactions in a Nitrogen–Oxygen Atmosphere

The theory of nitric oxide in the upper atmosphere is based on the ionospheric properties of the F and E regions (56–60). Ionic reactions lead to excited atoms $N(^2D)$ which react with O_2 to form nitric oxide molecules. In the stratosphere, the reaction of the electronically excited oxygen atom $O(^1D)$ with nitrous oxide (43, 62–65) is a natural source of nitric oxide. Cosmic rays (64, 66) must also be considered as a source particularly at high latitude since the production of nitrogen atoms is of the order of 1 atom per ion pair. Another source of nitric oxide at low levels (67, 68) is the reaction of OH radicals with NH_3; depending on its concentration in the stratosphere, ammonia may be an additional source of nitric oxide in the lower stratosphere.

If we consider the various reactions which are involved in the mesosphere and stratosphere (18, 62, 69–71), we write the differential equation for total odd nitrogen ($N + NO + NO_2 + NO_3 + 2N_2O_5 + HNO_2 + HNO_3$):

$$[36]\quad \frac{dn(N)}{dt} + \frac{dn(NO)}{dt} + \frac{dn(NO_2)}{dt} + \frac{dn(NO_3)}{dt} + 2\frac{dn(N_2O_5)}{dt} + \frac{dn(HNO_2)}{dt} + \frac{dn(HNO_3)}{dt} = P(N) + P(NO) - 2b_6 n(N)n(NO)$$

$P(N)$ is the direct production of nitrogen atoms and $P(NO)$ is the direct production of nitric oxide molecules and

$$[37]\quad (b_6);\ N + NO \rightarrow N_2 + O$$

Considering photo-equilibrium conditions, for each constituent we obtain

$$[38]\quad n(NO_2)[J_{NO_2} + b_3 n(O)] + n(NO_3)J_{NO-O_2} + n(HNO_2)J_{OH-NO} = n(NO)[b_2 n(M)n(O) + b_4 n(O_3) + b_{11} n(NO_3) + b_{21} n(M)n(OH) + b_{29} n(HO_2) + c_{5c} n(CH_3O_2)]$$

where

$$[39]\quad (b_2);\ O + NO + M \rightarrow M + NO_2$$

$$[40]\quad (b_3);\ O + NO_2 \rightarrow NO + O_2$$

$$[41]\quad (b_4);\ O_3 + NO \rightarrow NO_2 + O_2$$

$$[42]\quad (b_{11});\ NO + NO_3 \rightarrow 2NO_2$$

$$[43]\quad (b_{21});\ NO + OH + M \rightarrow HNO_2 + M$$

$$[44]\quad (b_{29});\ NO + HO_2 \rightarrow OH + NO_2$$

$$[45]\quad (c_5);\ CH_3O_2 + NO \rightarrow CH_3O + NO_2$$

$$[46]\quad (J_{NO-O_2});\ NO_3 + h\nu \rightarrow NO + O_2$$

$$[47]\quad J_{NO_2};\ NO_2 + h\nu \rightarrow NO + O$$

$$[48]\quad J_{OH-NO};\ HNO_2 + h\nu \rightarrow OH + NO$$

Making the usual approximations appropriate for the stratosphere (43) and assuming that

$$[49]\quad n(NO_2)J_{NO_2} < n(O_3)J_3$$

$$[50]\quad a_2 n(H) < a_6 n(OH)$$

Can. J. Chem. Downloaded from www.nrcresearchpress.com by 210.87.254.40 on 09/05/12
For personal use only.

the general equation for O_3 may be simplified to yield

$$[51]\quad \frac{dn(O_3)}{dt} + n(O_3)\{[a_6 n(OH) + a_{6c} n(HO_2) + b_9 n(NO_2)] + \frac{J_3}{k_2 n(M) n(O_2)}[2k_3 n(O_3) + a_5 n(OH) + a_7 n(HO_2) + a_{31} n(H_2O_2) + 2b_3 n(NO_2)]\} = 2n(O_2)J_2 + n(NO)[2J_{NO} + b_{11} n(NO_3) + b_{21} n(M) n(OH) + b_{29} n(HO_2) + c_{5c} n(CH_3O_2)] - n(HNO_2)J_{OH-NO} - n(NO_3)[J_{NO-O_2} - J_{NO_2-O}]$$

where

$$[52]\quad (b_9);\ O_3 + NO_2 \rightarrow NO_3 + O_2$$

$$[53]\quad (J_{NO});\ NO + h\nu \rightarrow N + O$$

$$[54]\quad (J_{NO_2-O});\ NO_3 + h\nu \rightarrow NO_2 + O$$

If we compare [51] with [27] without the introduction of nitrogen oxide effects, it is clear that we must compare the effect of $b_9 n(NO_2)$ (nighttime and daytime reaction) with $a_6 n(OH) + a_{6c} n(HO_2)$ (daytime reactions) and also $2b_3 n(NO_2)$ with $2k_3 n(O_3) + a_5 n(OH) + a_7 n(HO_2)$.

The reaction of NO_2 with O_3 has been studied in the laboratory (72, 73). Its rate coefficient is $b_9 = 1.23 \times 10^{-13}\, e^{-2470/T}$ cm^3 s^{-1} which leads to a rate of the order of 10^{-18} cm^3 s^{-1} in the lower stratosphere. Nevertheless, such a low value leads to an effect in the lower stratosphere which is of the same order of magnitude as $a_6 n(OH)$ (see Fig. 3) for $n(NO_2)/n(M) = 3 \times 10^{-9}$. Since reaction of NO_2 with O_3 plays its principal role for nighttime conditions, it seems that such a reaction cannot be neglected.

The rate coefficient of reaction 40 has been determined very accurately (74–76) to be $b_3 = 9.2 \times 10^{-12}$ cm^3 s^{-1}. In order to compare the effects of reactions 40 and 52, b_9 has been compared with $b_3 J_3/k_2 n(M) n(O_2) = b_3^e$, in Fig. 6. The reaction between atomic oxygen and nitrogen dioxide is generally more important than the reaction between ozone and nitrogen dioxide except near the tropopause even though the absolute value of the rate coefficient b_9 is only of the order of 10^{-18} cm^3 s^{-1}. However, this very small value leads to a more important effect than the action of the reaction between atomic oxygen and ozone. Using the observational values of $n(NO_2)$ by Ackerman and Muller (21) it is possible to make the comparison which is shown in Fig. 7. When the sun is overhead, it seems that the action of hydroxyl and hydroperoxyl is of the same order of magnitude as the action of nitrogen oxides. Concentrations of NO_2 greater than 10^8 cm^{-3} have a more important role in the NO_2 reaction with atomic oxygen than with ozone.

If we consider the production term in the general equation 51, there is in addition to the normal production by molecular oxygen $2n(O_2)J_2$ a general term depending on nitrogen oxides

$$[55]\quad n(NO)[2J_{NO} + b_{11} n(NO_3) + b_{21} n(M) n(OH) + b_{29} n(HO_2) + c_{5c} n(CH_3O_2)] - n(HNO_2)J_{OH-NO} - n(NO_3)[J_{NO-O_2} - J_{NO_2-O}]$$

Neglecting the effect of NO_3 and using photoequilibrium conditions for HNO_2, [55] is written

$$[56]\quad n(NO)[2J_{NO} + c_{5c} n(CH_3O_2)] + n(HO_2)[b_{29} n(NO) - b_{33} n(NO_2)]$$

where

$$[57]\quad (b_{33});\ HO_2 + NO_2 \rightarrow HNO_2 + O_2$$

The importance of [56] in the lower stratosphere depends on the values of $c_{5c} n(CH_3O_2)$ which is about 5×10^{-7} s^{-1} according to calculated values (71) at 15 km. Since $n(NO) < 10^9$ cm^3 in the lower stratosphere the effect of CH_3O_2 is negligible. However, it depends also on the difference $b_{29} n(NO) - b_{33} n(NO_2)$ which seems to be positive in a sunlit atmosphere. According to Simonaitis (private communication, 1973) the ratio $b_{29}/b_{33} = 7 \pm 2$ and, therefore, for $n(NO_2) < 7n(NO)$ a positive term must be added to the production term $2n(O_2)J_2$. In the lower stratosphere there is a large variation of the photodissociation of molecular oxygen with the solar zenith angle; if the production for overhead sun conditions is 1×10^5 and 1×10^6 oxygen atoms cm^{-3} s^{-1} at 15 and 20 km, respectively, the cor-

Can. J. Chem. Downloaded from www.nrcresearchpress.com by 210.87.254.40 on 09/05/12
For personal use only.

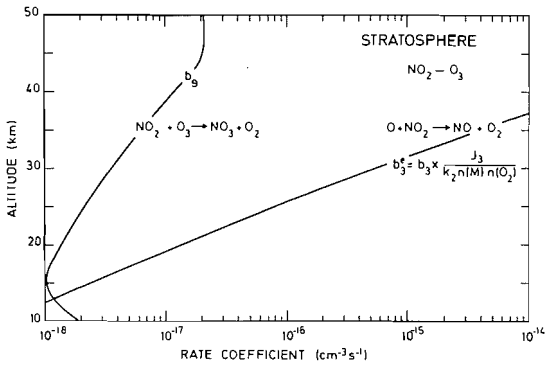

FIG. 6. Rate coefficients of nitrogen oxide with ozone and atomic oxygen. The equivalent rate coefficient b_3^e increases with height and is far greater than b_9 in the middle and upper stratosphere.

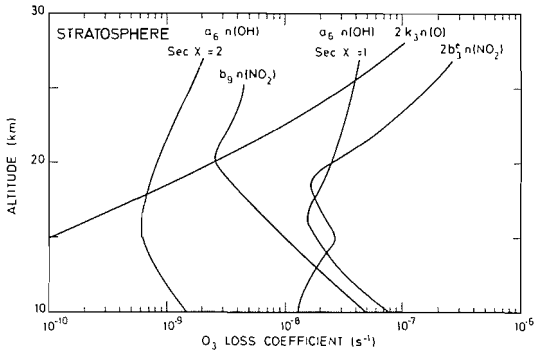

FIG. 7. Comparison of the various loss coefficients of ozone in the lower stratosphere when hydrogen and nitrogen compounds are involved; the NO_2 concentration is given by Ackerman and Muller (21).

responding values for a solar zenith angle of 60° are only 50 and 5×10^3 cm^{-3} s^{-1}. With NO concentrations of the order of 5×10^8 cm^{-3} and a rate coefficient which is perhaps not less than 2×10^{-12} cm^3 s^{-1}, the addition of 10^4 ozone molecules cm^{-3} s^{-1} is possible. Thus, the aeronomic behavior must be discussed in detail and special attention is required to consider the effect of the nitric oxide term of [56] compared with $2n(O_2)J_2$ when there is an artificial injection of nitrogen oxides in the stratosphere.

Production of Nitric Oxide

The reaction of the electronically excited atom $O(^1D)$ with nitrous oxide (43) is a natural source of nitric oxide in the stratosphere. It depends on the vertical distribution of N_2O molecules which is related to the photodissociation rate and to the variable flux of molecules from the troposphere. There is practically no stratospheric source of N_2O, and no transport of nitric oxide from the mesosphere is possible. A total production of the order $(1 \pm 0.5) \times 10^8$ NO molecules is possible. It is clear that the exact value is related to the vertical distribution of N_2O which depends strongly on the values of the eddy diffusion coefficient which are adopted (61, 64).

A second process which can produce nitric oxide is the reaction of nitrogen atoms with molecular oxygen. This leads, in less than 10 s in the lower stratosphere, to nitric oxide molecules. The production of nitrogen atoms is related to the normal ionization by cosmic rays (64, 66). One nitrogen atom, and consequently one nitric oxide molecule, is produced per ion pair due to the cosmic rays (77). The production of N atoms is shown in Fig. 8 for Thule in 1954 (solar activity minimum) and in 1958 (solar activity maximum) with a station of mean latitude Bismark in 1965 (solar activity minimum). It is clear that the production of nitrogen atoms (day and night process) is always more important in the polar (or high latitude) lower stratosphere than the production of nitric oxide which is shown in Fig. 8 for two solar zenith angles sec $\chi = 1$ and 2.

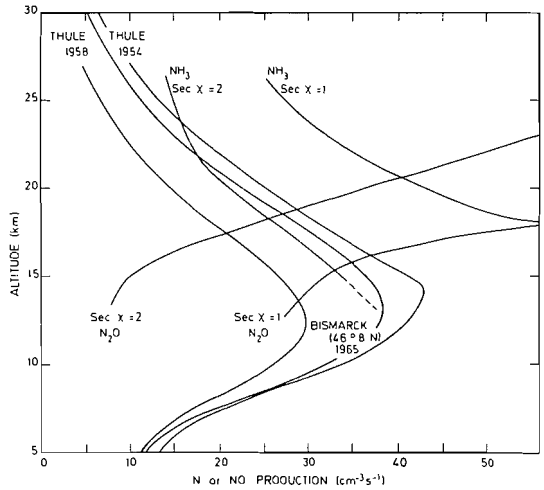

FIG. 8. Production of nitrogen atoms and nitric oxide molecules. The production of nitrogen atoms is given at Thule (Polar Cap) for maximum conditions (1954) and minimum conditions (1958) and at Bismark in 1965 (maximum conditions). The production of nitric oxide molecules from N_2O and NH_3 is given for sec $\chi = 1$ and 2, overhead sun conditions and height sun = 30°, respectively. Cosmic ray data from Neher (78, 79).

Can. J. Chem. Downloaded from www.nrcresearchpress.com by 210.87.254.40 on 09/05/12
For personal use only.

Can. J. Chem. Downloaded from www.nrcresearchpress.com by 210.87.254.40 on 09/05/12
For personal use only.

A third process for the production of nitric oxide in the stratosphere which can be considered is the oxidation of ammonia (67, 68, 80). The oxidation is initiated by the reaction

[58] $OH + NH_3 \rightarrow NH_2 + H_2O$

with a rate coefficient of $(1.5 \pm 0.4) \times 10^{-13}$ $cm^3\ s^{-1}$ at room temperature (68). According to Dove and Nip (81) its activation energy (measured between 1500 and 2000 °K) would be 1.1 kcal and the rate coefficient

[59] $k_{OH-NH_3} = 1.3 \times 10^{-14} T^{0.68}\, e^{-550/T}\ cm^3\ s^{-1}$

Such a formula leads to 1×10^{-13} $cm^3\ s^{-1}$ at 300 °K in good agreement with the value deduced by Stuhl.

The production of nitrogen oxide molecules may come directly from the following reaction

[60] $NH_2 + O_2 \rightarrow H_2O + NO + 109$ kcal

or

[61] $NH_2 + O_2 \rightarrow HNO + OH + 41$ kcal

with

[62*a*] $HNO + O_2 \rightarrow HO_2 + NO - 1$ kcal

[62*b*] $\rightarrow OH + NO_2 + 7$ kcal

The reactions should be studied in the laboratory in order to determine the exact oxidation paths of NH_2 and also the effect of O_3 and NO.

NH_3 concentrations at the ground have been presented by Junge (82) and mixing ratios of 1.2×10^{-9} have been observed above the trade wind inversion on Mauna Kea (3200 m) in Hawaii. Recent measurements by Georgii and Muller (83) lead to mixing ratios as low as 5×10^{-10} to 1×10^{-9} in the polar maritime air and to about 5×10^{-9} over the continent. Winter and summer values at 3 km are about 2×10^{-8} and 6×10^{-9}, respectively.

A knowledge of the flux of NH_3 into the stratosphere is required in order to determine the exact production of nitric oxide molecules. If we adopt as a working value a mixing ratio of the order of 10^{-9} in the lower stratosphere, we can determine the production of nitric oxide molecules if we know the concentration of OH radicals. Considering the OH concentration which will be determined later, we have represented in Fig. 8 the vertical distribution of the NO production in the lower stratosphere. With such conditions, it is clear that the production of nitric oxide due to the oxidation of NH_3 by OH occurs below 20 km.

Thus, it seems that the three sources which have been considered play a role in the production of nitric oxide in the stratosphere. However, there will be very important differences with latitude and season. A stratospheric observation of NH_3 is required.

Oxidation of Methane and Production of Carbon Monoxide

Methane is produced primarily by various bacterial decomposition processes leading to an average production (84) of 3.4×10^{11} CH_4 molecules $cm^{-2}\ s^{-1}$. Since the total number of CH_4 molecules is about 3.2×10^{19} cm^{-2} column, such a production corresponds to an estimated residence time of about 3 years (day and night).

The daytime destruction process of CH_4 leads to the production of CO (24, 85) with an average residence time of 0.4 year for CO if its volume fractional concentration is of the order of 0.1 p.p.m.v. The carbon monoxide molecules apparently could have a lifetime of the order of 0.1 year (71, 86–88). The sink of methane is a source for formaldehyde (25, 88) which leads to the production of H_2 and CO. There are different ways to reduce the differences between the various results. However, there are still difficulties in the interpretation according to a recent analysis made by Warneck (89) of the distribution of CO mixing ratios with latitude in the northern and southern hemisphere which were measured by Seiler (90).

Methane, which is mixed in the troposphere (12) is photodissociated in the mesosphere and is dissociated by oxidation processes in the stratosphere.

Atomic oxygen attacks methane through (64)

[63] (c_1); $O(^3P) + CH_4 \rightarrow CH_3 + OH - 2$ kcal

[64*a*] (c_{1a}^*); $O(^1D) + CH_4 \rightarrow CH_3 + OH +$ 43.5 kcal

and

[64*b*] (c_{1b}^*); $O(^1D) + CH_4 \rightarrow H_2 + CH_2O$

which occurs to the extent of 9% (91).

The other important reaction in the stratosphere is

[65] (c_2); $OH + CH_4 \rightarrow CH_3 + H_2O + 15$ kcal

In the lower stratosphere CO_2 is photodissociated at a very low rate and the production of CO

Can. J. Chem. Downloaded from www.nrcresearchpress.com by 210.87.254.40 on 09/05/12
For personal use only.

corresponds to the total oxidation process of CH_4 by reactions 64 and 65. The oxidation of carbon monoxide is attributed to

[66] (a_{36}); $OH + CO \rightarrow CO_2 + H + 24$ kcal

Methyl radicals, which are produced by oxidation processes of CH_4, react immediately with molecular oxygen to form methylperoxy radicals

[67] (c_{4a}); $CH_3 + O_2 + M \rightarrow CH_3O_2 + M + 26$ kcal

Methylperoxy radicals react with NO (92) leading to

[45*a*] (c_{5a}); $CH_3O_2 + NO \rightarrow CH_3O_2NO$

[45*b*] (c_{5b}); $\rightarrow H_2CO + HNO_2$

[45*c*] (c_{5c}); $\rightarrow CH_3O + NO_2$

According to Spicer *et al.* (92), there was no evidence for CH_3O radical production in their studies and they concluded that reaction 45*c* did not occur, contrary to expectation from atmospheric evidence. Levy (71) has considered that 45*c* is the reaction occurring with $c_{5c} \geq 5 \times 10^{-13}$ cm^3 s^{-1}. In the same way the reactions with NO_2 are

[68*a*] (c_{6a}); $CH_3O_2 + NO_2 \rightarrow CH_3O_2NO_2$

[68*b*] (c_{6b}); $\rightarrow H_2CO + HNO_3$

The photochemistry of formaldehyde (93, 94) indicates that two distinct primary processes occur

[69*a*] (c_{7a}); $H_2CO + h\nu \rightarrow HCO + H$; $J_{H-HCO} = 9.4 \times 10^{-5}$ s^{-1}

[69*b*] (c_{7b}); $\rightarrow CO + H_2$; $J_{CO-H_2} = 1.3 \times 10^{-4}$ s^{-1}

which leads to the production of formyl and carbon monoxide with atomic and molecular hydrogen, respectively. In addition, a rapid reaction such as

[70] (c_8); $OH + H_2CO \rightarrow HCO + H_2O + 36$ kcal

must also be introduced.

The formyl radical is photodissociated (95)

[71] (c_{11}); $HCO + h\nu \rightarrow CO + H$

or reacts with O_2 (96)

[72] (c_{12}); $HCO + O_2 \rightarrow CO + HO_2 + 40$ kcal

or reacts with OH

[73] (c_{13}); $HCO + OH \rightarrow H_2O + CO + 95$ kcal

Other reactions have been introduced (24, 71, 80, 85, 88):

[74] (c_{14}); $CH_3O_2 + CH_3O_2 \rightarrow 2CH_3O + O_2$

[75] (c_{15}); $CH_3O + O_2 \rightarrow HO_2 + H_2CO$

[76] (c_{16}); $CH_3O_2 + HO_2 \rightarrow CH_3O_2H + O_2$

[77] (c_{17}); $CH_3O_2H + OH \rightarrow H_2O + CH_3O_2$

[78] (c_{18}); $CH_3O_2H + h\nu \rightarrow CH_3O + OH$

The two following reactions are also considered

[79] (c_{19}); $CH_3O_2NO + h\nu \rightarrow CH_3O_2 + NO$

[80] (c_{20}); $CH_3O_2NO_2 + h\nu \rightarrow CH_3O_2 + NO_2$

Thus, with eqs. 63 to 80, it is possible to write for equilibrium conditions that

[81] $$n(H_2CO)[J_{H-HCO} + J_{H_2-CO} + c_8 n(OH)] = n(CH_4)[c_1 n(O) + c_1^* n(O^*) + c_2 n(OH)]$$
$$= n(HCO)[J_{H-CO} + c_{12} n(O_2) + c_{13} n(OH)] + n(H_2CO) J_{CO-H_2}$$

If we consider the various reactions involving the production and loss mechanisms of H, OH, and HO_2 and use [81] we obtain

[82] $$\frac{dn(H)}{dt} + \frac{dn(OH)}{dt} + \frac{dn(HO_2)}{dt} + n(OH) c_2 n(CH_4)[1 - X] + 2n(OH)[c_{13} n(HCO)$$
$$+ c_{17} n(CH_3O_2H)] = n(CH_4)[c_1 n(O) + c_1^* n(O^*)][1 + X] + n(CH_3O) c_{15} n(O_2)$$

with

[83] $$X = \frac{2J_{H-HCO} + c_9 n(O)}{J_{H-HCO} + J_{CO-H_2} + c_8 n(OH) + c_9 n(O) + c_{10} n(H)}$$

The ratio $X \simeq 2J_{H-HCO}/J_{CO-H_2}$ varies from 0.8 at 50 km to 0.7 near 15 km and is about 0.5 at ground level. Keeping only the important terms, the steady state conditions of eq. 82 lead to

[84] $$+ n(OH) c_2 n(CH_4)[1 - X] = n(CH_4)[c_1 n(O) + c_1^* n(O^*)][1 + X] + \ldots$$

which are the principal terms which must be introduced when methane is present. In the stratosphere, oxidation leads to a decrease in the mixing ratio of CH_4. However, the transport from the troposphere is such that its vertical profile has a weak gradient, as is shown from balloon samples and a rocket sample (12, 97).

Removal of Hydroxyl Radicals

The complexity of the chemical model requires an accurate determination of the profile of hydroxyl and hydroperoxyl radicals in the stratosphere and mesosphere.

In addition to the previous reactions discussed it is necessary to consider the following reactions leading to the re-formation of H_2O

[85] $$(a_{16});\quad OH + OH \rightarrow H_2O + O + 27\ \text{kcal}$$

and

[86] $$(a_{17});\quad OH + HO_2 \rightarrow H_2O + O_2$$

Reaction 86 is extremely important since recent measurements by Hochanadel *et al.* (98) indicate a rate coefficient $a_{17} = 2 \times 10^{-10}\ \text{cm}^3\ \text{s}^{-1}$.

In the discussion concerning the more important reactions of hydroxyl and hydroperoxyl radicals, the reactions involving HO_2 must be considered (43)

[87] $$(a_{27});\quad HO_2 + HO_2 \rightarrow H_2O_2 + O_2 + 42\ \text{kcal}$$

[88] $$(a_{30});\quad OH + H_2O_2 \rightarrow H_2O + HO_2 + 30\ \text{kcal}$$

[89] $$(a_{19});\quad OH + H_2 \rightarrow H_2O + H + 15\ \text{kcal}$$

Since photo-equilibrium conditions can be considered in the stratosphere where $n(H)$ is small, the equation for $n(OH)$ is written as

[90] $$n(OH)\left[a_{16}n(OH) + a_{17}n(HO_2) + a_{30}n(H_2O_2) + c_2\left(\frac{1-X}{2}\right)n(CH_4) + b_{27}n(HNO_3)\right]$$
$$= n(H_2O)[J_{H-OH} + a^*n(O^*)] + n(H_2)a_{24}{}^*n(O^*) + n(CH_4)\left[\frac{1+X}{2}\{c_1{}^*n(O^*) + c_1{}^*n(O^*)\}\right]$$

The ratio $n(OH)/n(HO_2)$ is

[91] $$n(HO_2)[a_{6c}n(O_3) + a_7n(O) + a_{17}n(OH) + 2a_{27}n(HO_2) + b_{29}n(NO) + b_{33}n(NO_2)]$$
$$= n(OH)[a_5n(O) + a_6n(O_3) + a_{19}n(H_2) + a_{30}n(H_2O_2) + a_{36}n(CO) + c_8n(H_2CO) + c_2Xn(CH_4)]$$

Equations 90 and 91 have been used to derive the ratio $n(OH)/n(HO_2)$ and $n(OH)$ using the values of the rate coefficients which were adopted here. With the aim of illustrating the day equilibrium in the stratosphere various figures have been prepared. In Fig. 9, the various percentages of the different coefficients affecting $n(OH)$ are given. In the upper troposphere and lower stratosphere the dominant path transforming OH to H + HO_2 is the reaction with CO. In the lower stratosphere when $n(CO)/n(M) \leq 5 \times 10^{-8}$ and in the middle stratosphere, the reaction of OH with O_3 plays the leading role (almost 100%). At the stratopause and in the upper stratosphere, the reaction with atomic oxygen transforming OH to H + HO_2 becomes the principal reaction. The effect of H_2, H_2CO, and CH_4 may be neglected in the first approximation although they can play a role in the lower troposphere. A remark must be made concerning the effect of CO in the lower stratosphere; the curve of Fig. 9 is deduced for a mixing ratio of 10^{-7} in the troposphere and 5×10^{-8} in the stratosphere. A decrease of these values leads to an increase of the effect of the reaction of OH with O_3 particularly in the lower stratosphere.

As far as HO_2 is concerned, it can be seen in Fig. 10 that, in the lower stratosphere, the reactions with nitric oxide cannot be neglected.

Can. J. Chem. Downloaded from www.nrcresearchpress.com by 210.87.254.40 on 09/05/12
For personal use only.

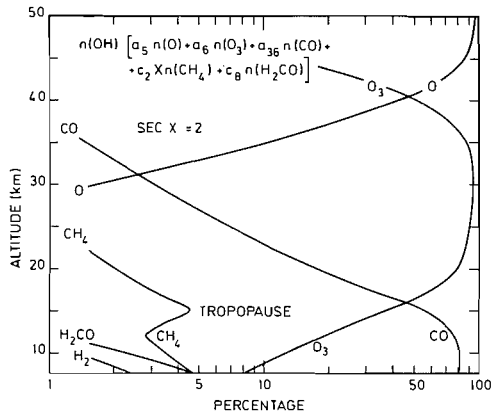

FIG. 9. Profiles (%) of the various terms affecting OH in the determination of the ratio $n(HO_2)/n(OH)$. CO effect due to its mixing ratio 5×10^{-8} in the stratosphere.

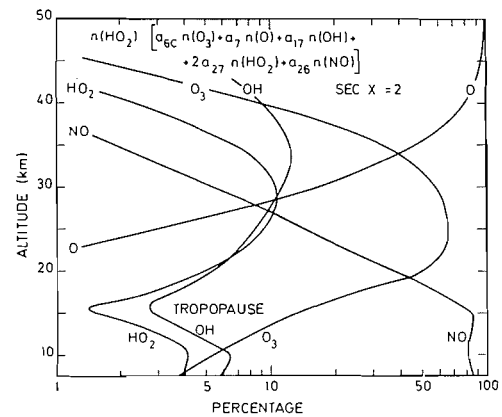

FIG. 10. Profiles (%) of the various terms affecting HO_2 in the determination of the ratio $n(HO_2)/n(OH)$. NO effect due to a mixing ratio 3×10^{-9} for NO_x.

Its exact role depends on the value of the rate coefficient and on the vertical distribution of its concentration which here is $n(NO_x)/n(M) = 3 \times 10^{-9}$. As for OH, the effects of the reaction of HO_2 with O_3 and O occur in the middle and upper stratosphere, respectively. However, it must be pointed out that the simultaneous effects of the reactions with OH, HO_2, and O at 30 km lead to a total of about 30% of the effect of all reactions. Another remark must be made concerning the effect of NO which depends strongly on the assumed value of the rate coefficient b_{29} (here 3×10^{-13}) (99) and on the vertical distribution of the nitric oxide concentration in the lower stratosphere. A value of the order of 10^{-12} cm^3 s^{-1} or more for the reaction between NO and HO_2 would increase its effect and the OH concentration.

Thus, the main features of Figs. 9 and 10 correspond to the effect on OH and HO_2 of atomic oxygen at the stratopause and in the upper stratosphere, of ozone in the middle stratosphere and lower stratosphere, and of carbon monoxide and nitric oxide in the lower stratosphere.

The essential features of the calculations appear very sensitive in the lower stratosphere to the adopted values for the concentration of CO and NO. In Fig. 11 the ratio $n(HO_2)/n(OH)$ is represented for the condition illustrated in Figs. 9 and 10. Another curve (NO = 0) shows that for a relative concentration of NO_x of 5×10^{-10}, the ratio $n(HO_2)/n(OH)$ increases from 15 to 60 at 15 km. When the reaction with CO is reduced (mixing ratio 10^{-8}), the ratio $n(HO_2)/n(OH)$ becomes less than 10 at 15 km. Thus, the behavior of OH and HO_2 in the lower stratosphere requires an exact knowledge of their rate coefficients with NO and NO_2.

With the ratio $n(HO_2)/n(OH)$ obtained from the numerical results illustrated in Fig. 11, it is easy to determine the vertical profile of OH. From the various effects occurring in the troposphere and mesosphere, we find that the reaction between OH and HO_2 is the dominant path for removal of hydroxyl and hydroperoxyl radicals in the stratosphere. However, in the lower stratosphere CH_4 and HNO_3 are also of the same importance (Fig. 12). If the value of 2×10^{-10} cm^3 s^{-1} reported by Hochanadel *et al.* (98) is reduced by a factor of 4, the impor-

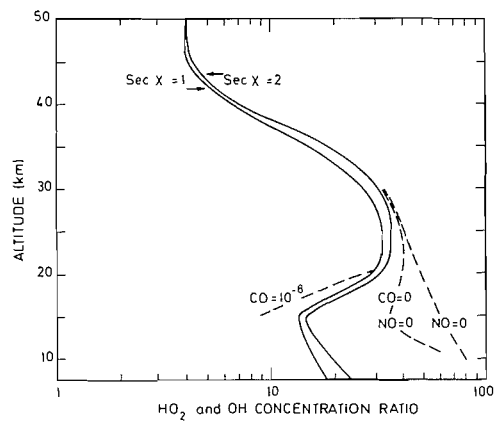

FIG. 11. Ratio $n(HO_2)/n(OH)$ in the stratosphere. Curve (NO—HO_2) using values given in Figs. 9 and 10. Curve NO = 0 when the mixing ratio of NO_x is reduced to 5×10^{-10}. Curve CO = 0, when CO is neglected. Curve CO = 0, NO = 0, neglecting the effect of CO and NO.

Can. J. Chem. Downloaded from www.nrcresearchpress.com by 210.87.254.40 on 09/05/12
For personal use only.

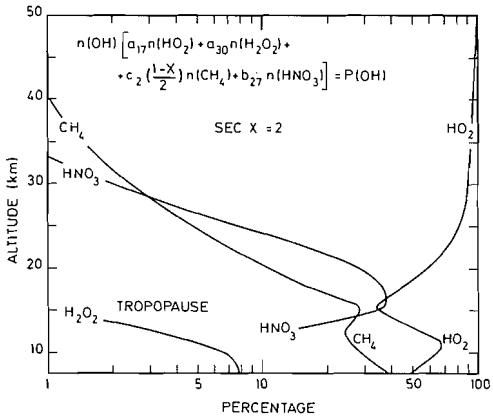

FIG. 12. Profiles (%) of the various terms determining the concentration of the hydroxyl radical, using values corresponding to profiles of Figs. 9 and 10. The HNO_3 concentrations correspond to an average value of observational results by Murcray *et al.* (20).

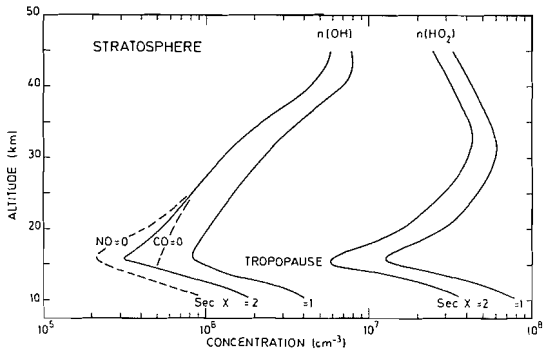

FIG. 13. OH and HO_2 concentrations in the stratosphere for conditions defined in Figs. 9 and 10. Changes when CO (curve CO = 0) is neglected, and when NO was a reduced mixing ratio to 5×10^{-10} (curve NO = 0).

tance of CH_4 and HNO_3 increases in the lower stratosphere. The effect of HNO_3 reaches more than 50% between 15 and 20 km. Calculated profiles for OH and HO_2 are presented in Fig. 13. As need scarcely be emphasized, the calculated values of the concentrations depend on the coefficients which are not yet well known for aeronomic purposes. It is clear that the OH concentration is now known in the stratosphere within a factor of 4. The OH and HO_2 profiles have to be provided to determine the wide range of reactions in which CO, CH_4, O_3, O, NO, NO_2, H_2O_2, HNO_3, HNO_2, and H_2O are involved in the stratosphere.

1. S. CHAPMAN. Mem. R. Met. Soc. **3**, 103 (1930).
2. S. CHAPMAN. Rep. Prog. Phys. **9**, 92 (1943).
3. D. R. BATES and M. NICOLET. J. Geophys. Res. **55**, 301 (1950).
4. D. R. BATES and M. NICOLET. C. R. Acad. Sci. Paris, **230**, 1943 (1950).
5. G. HERZBERG. J. R. Astron. Soc. Can. **45**, 100 (1951).
6. D. R. BATES and M. NICOLET. Publ. Astron. Soc. Pacific, **62**, 106 (1950).
7. D. R. BATES and A. E. WITHERSPOON. Mon. Not. R. Astron. Soc. **112**, 101 (1952).
8. E. J. WILLIAMSON and J. T. HOUGHTON. Q. J. R. Met. Soc. **91**, 330 (1965).
9. H. J. MASTENBROOK. J. Atm. Sci. **25**, 299 (1968).
10. H. J. MASTENBROOK. J. Atm. Sci. **28**, 1495 (1971).
11. N. SISSENWINE, D. D. GRANTHAM, and H. A. SANELA. J. Atm. Sci. **25**, 1129 (1968).
12. D. H. EHHALT and L. E. HEIDT. Pure Appl. Geophys. **106–108**, 1352 (1973).
13. U. SCHMIDT. Tellus (1974). In press.
14. D. R. CADLE. Disc. Faraday Soc. **37**, 66 (1964).
15. J. HAMPSON. Tech. Note 1627, Can. Arm. Res. Def. Establ. 1964.
16. P. J. CRUTZEN. Q. J. R. Met. Soc. **96**, 320 (1970).
17. D. R. BATES and P. B. HAYS. Planet. Space Sci. **15**, 189 (1967).
18. M. NICOLET. J. Geophys. Res. **70**, 679 (1965).
19. W. J. WILLIAMS, J. N. BROOKS, D. G. MURCRAY, F. H. MURCRAY, P. M. FRIED, and J. A. WEIMAN. J. Atm. Sci. **29**, 1375 (1972).
20. D. G. MURCRAY, A. GOLDMAN, A. CSOEKE-POECKH, F. H. MURCRAY, and W. J. WILLIAMS. J. Geophys. Res. **78**, 7033 (1973).
21. M. ACKERMAN and C. MULLER. Nature, **240**, 300 (1972).
22. M. ACKERMAN, J.-C. FONTANELLA, D. FRIMONT, A. GIRARD, N. LOUISNARD, C. MULLER, and D. NEVEJANS. Nature, **245**, 2057 (1973).
23. B. A. RIDLEY, H. I. SCHIFF, A. W. SHAW, L. R. MEGILL, L. BATES, C. HOWLETT, H. LEVAUX, and T. E. ASHENFELTER. Nature, **245**, 310 (1973).
24. J. C. MCCONNELL, M. B. MCELROY, and S. C. WOFSY. Nature, **233**, 187 (1971).
25. H. LEVY II. Science, **173**, 141 (1971).
26. B. WEINSTOCK. Science, **166**, 224 (1969).
27. P. B. HAYS and R. G. ROBLE. Planet. Space Sci. **21**, 273 (1973).
28. J. HAMPSON. Chemiluminescent emissions observed in the stratosphere and mesosphere. *In* Les problèmes météorologiques de la stratosphère et de la mésosphère. Presses Universitaires de France, Paris. 1966. pp. 393–440.
29. B. G. HUNT. J. Geophys. Res. **71**, 1385 (1966).
30. E. HESSTVEDT. Geofys. Publik, **27**, No 4 (1968).
31. H. U. DUTSCH. Q. J. R. Met. Soc. **94**, 483 (1968).
32. A. KRUEGER. Pure Appl. Geophys. **106–108**, 1272 (1973).
33. J. S. RANDHAWA. Pure Appl. Geophys. **106–108**, 1490 (1973).
34. W. D. MCGRATH and R. G. W. NORRISH. Nature, **182**, 235 (1958).
35. M. NICOLET. Ann. Geophys. **26**, 531 (1970).
36. J. C. ANDERSON and F. KAUFMAN. Chem. Phys. Lett. **19**, 483 (1973).
37. W. B. DEMORE. Science, **180**, 735 (1973).

Can. J. Chem. Downloaded from www.nrcresearchpress.com by 210.87.254.40 on 09/05/12
For personal use only.

38. R. SIMONAITIS and J. HEICKLEN. J. Photochem. **2**, 309 (1973).
39. F. KAUFMAN. Ann. Geophys. **20**, 106 (1964).
40. C. B. LEOVY. J. Geophys. Res. **74**, 417 (1969).
41. T. SHIMAZAKI and A. R. LAIRD. J. Geophys. Res. **75**, 3221 (1970).
42. R. SIMONAITIS and J. HEICKLEN. J. Phys. Chem. **77**, 1932 (1973).
43. M. NICOLET. Aeron. Acta, **A79**. 1970; Mesospheric models and related experiments. D. Reidel, Dordrecht. 1971. pp. 1–51.
44. M. NICOLET. Les constituants minoritaires dans la stratosphère et la mésosphère. *In* Les problèmes météorologiques dans la stratosphère et la mésosphère. Les Presses Universitaires, Paris. 1966. pp. 441–471.
45. R. ENGLEMAN. J. Am. Chem. Soc. **87**, 4193 (1965).
46. W. B. DEMORE and D. RAPER. J. Chem. Phys. **44**, 1780 (1966).
47. I. T. N. JONES and R. P. WAYNE. J. Chem. Phys. **51**, 3617 (1969).
48. R. SIMONAITIS, S. BRASLAVSKY, J. HEICKLEN, and M. NICOLET. Chem. Phys. Lett. **19**, 601 (1973).
49. C. L. LIN and W. B. DEMORE. J. Photochem. **2**, 161 (1973).
50. M. NICOLET. Planet. Space Sci. **20**, 1671 (1972).
51. G. PARASKEVOPOULOS and R. J. CVETANOVIĆ. Chem. Phys. Lett. **9**, 603 (1971).
52. R. SIMONAITIS and J. HEICKLEN. Int. J. Chem. Kinet. **5**, 231 (1973).
53. R. SIMONAITIS and J. HEICKLEN. J. Phys. Chem. **77**, 1090 (1973).
54. R. I. GREENBERG and J. HEICKLEN. Int. J. Chem. Kinet. **4**, 417 (1972).
55. R. F. HEIDNER and D. HUSAIN. Nature, **241**, 10 (1973).
56. R. B. NORTON and C. A. BARTH. J. Geophys. Res. **75**, 3903 (1970).
57. D. F. STROBEL. J. Geophys. Res. **76**, 2441 (1971).
58. D. F. STROBEL. J. Geophys. Res. **76**, 8384 (1971).
59. D. F. STROBEL, D. M. HUNTEN, and M. B. MCELROY. J. Geophys. Res. **75**, 4307 (1970).
60. M. NICOLET. Planet. Space Sci. **18**, 1111 (1970).
61. M. NICOLET and E. VERGISON. Aeron. Acta, **A91** (1971).
62. P. J. CRUTZEN. J. Geophys. Res. **76**, 7311 (1971).
63. M. B. MCELROY and J. C. MCCONNELL. J. Atmos. Sci. **28**, 1095 (1971).
64. M. NICOLET and W. PEETERMANS. Ann. Geophys. **28**, 751 (1972).
65. H. JOHNSTON. Proc. Nat. Acad. Sci. USA, **69**, 2369 (1972).
66. P. WARNECK. J. Geophys. Res. **77**, 6589 (1972).
67. M. B. MCELROY and J. C. MCCONNELL. Second conference of CIAP, November 1972, p. 164, 1973.
68. F. STUHL. J. Chem. Phys. **59**, 635 (1973).
69. H. S. JOHNSTON. Science, **173**, 517 (1971).
70. H. S. JOHNSTON. Lawrence Radiation Laboratory Report UCRL-20568. 1971.
71. H. LEVY II. Planet. Space Sci. **21**, 575 (1973).
72. H. S. JOHNSTON and D. M. YOST. J. Chem. Phys. **17**, 386 (1949).
73. R. GRAHAM. Unpublished.
74. D. D. DAVIS, J. T. HERRON, and R. H. HUIE. J. Chem. Phys. **58**, 530 (1973).
75. T. G. SLANGER, B. J. WOOD, and G. BLACK. Int. J. Chem. Kinet. **5**, 615 (1973).
76. A. B. HARKER and H. S. JOHNSTON. J. Phys. Chem. **77**, 1153 (1973).
77. G. BRASSEUR and M. NICOLET. Planet. Space Sci. **21**, 939 (1973).
78. H. V. NEHER. J. Geophys. Res. **72**, 1527 (1967).
79. H. V. NEHER. J. Geophys. Res. **76**, 1637 (1971).
80. P. CRUTZEN. *In* Physics and chemistry of upper atmosphere. *Edited by* B. McCormac. Reidel, Dordrecht. 1973.
81. J. E. DOVE and W. S. NIP. Third symposium on gas kinetics. Brussels, August 27–31, 1973.
82. C. JUNGE. Air chemistry and radioactivity. Academic Press, New York. 1963.
83. H. W. GEORGII and W. J. MULLER. Tellus (1974). In press.
84. E. ROBINSON and R. C. ROBBINS. *In* Emissions, concentrations and fate of gaseous atmospheric pollutants in air pollution control. Part II. *Edited by* Strauss. John Wiley and Sons, New York. 1971. pp. 1–93.
85. S. C. WOFSY, J. C. MCCONNELL, and M. B. MCELROY. J. Geophys. Res. **77**, 4477 (1972).
86. B. WEINSTOCK and T. Y. CHANG. Tellus (1974). In press.
87. B. WEINSTOCK and H. NIKI. Science, **176**, 290 (1972).
88. H. LEVY II. Planet. Space Sci. **20**, 919 (1972).
89. P. WARNECK. Tellus (1974). In press.
90. W. SEILER. Tellus (1974). In press.
91. C. L. LIN and W. B. DEMORE. J. Phys. Chem. **77**, 863 (1973).
92. C. W. SPICER, A. VILLA, H. A. WIEBE, and J. HEICKLEN. J. Am. Chem. Soc. **95**, 13 (1973).
93. R. D. MCQUIGG and J. G. CALVERT. J. Am. Chem. Soc. **91**, 1950 (1969).
94. J. G. CALVERT, J. A. KERR, K. L. DEMERJIAN, and R. D. MCQUIGG. Science, **175**, 751 (1972).
95. J. W. C. JOHNS, S. H. PRIDDLE, and D. A. RAMSAY. Disc. Faraday Soc. **35**, 90 (1963).
96. G. R. MCMILLAN and J. G. CALVERT. Oxid. Comb. Rev. **1**, 83 (1965).
97. C. CUMMING and R. P. LOWE. J. Geophys. Res. **78**, 5259 (1973).
98. C. J. HOCHANADEL, J. A. GHORMLEY, and P. J. OGREN. J. Chem. Phys. **56**, 4426 (1972).
99. D. D. DAVIS, W. A. PAYNE, and L. J. STIEF. Science, **179**, 280 (1973).

Can. J. Chem. Downloaded from www.nrcresearchpress.com by 210.87.254.40 on 09/05/12
For personal use only.

Reaction Kinetics Involving O and N Compounds

H. NIKI

Fuel Sciences Department, Scientific Research Staff, Ford Motor Company, Dearborn, Michigan 48121

Received September 1, 1973

Experimental work performed during the past 4 years is reviewed briefly for aeronomically interesting reactions involving ground electronic states of O and N compounds.

On décrit les travaux expérimentaux accomplis depuis 4 années sur des réactions intéressantes du point de vue aéronomique qui impliquent les états électroniques fondamentaux de composés O et N. [Traduit par le journal]

Can. J. Chem., 52, 1397 (1974)

Can. J. Chem. Downloaded from www.nrcresearchpress.com by 210.87.254.6 on 09/05/12
For personal use only.

Introduction

At the York IAGA symposium in 1968, Schiff (1) reviewed the status of laboratory work on neutral reactions involving oxygen and nitrogen. At that time it appeared that rate constants for many fast reactions involving simple N and O compounds were reasonably well-established for aeronomic purposes. However, with recent phenomenal progress in atmospheric measurements and modeling calculations, it has become apparent that highly accurate kinetic data are needed over the temperature range of 200–300 K for these fast reactions and also for slow reactions such as $NO + O_3 \rightarrow NO_2 + O_2$, and $NO_2 + O_3 \rightarrow NO_3 + O_2$. Accordingly, kinetic studies of reactions involving N and O compounds in ground electronic states have been actively pursued. This paper will attempt to discuss some of the recent significant developments in experimental methods and the ensuing kinetic data.

Nitrogen- and oxygen-containing species of aeronomic interest include O, OH, O_3, NO, NO_2, NO_3, N_2O_5, HNO_2, HNO_3, and NH_3 (2). Kinetic studies of reactions among these numerous species clearly require a wide variety of experimental methods of production and detection. Several experimental methods discussed by Schiff (1) and by Kaufman (3) at the last IAGA symposium have been employed with substantially improved accuracies. In particular, flow experiments have continued to enjoy wide popularity. Ground state atomic oxygen sufficiently free of other reactive species has been produced by thermally decomposing N_2O or O_3 on a Nernst glower. The method of producing "vibrationally cool" OH in a discharge-flow is by the titration reaction $H + NO_2 \rightarrow OH + NO$ (4). In addition to the now familiar detection methods such as electron spin resonance (e.s.r.), mass spectrometry, and O + NO chemiluminescence, the resonance fluorescence method is widely used with great success for monitoring $O(^3P)$ and $OH(^2\Pi)$ in flow experiments (5, 6). In this method, a small fraction of these species present in a reaction system is selectively excited by resonance radiation and the ensuing fluorescence emission is detected. Because of its excellent detection sensitivity, concentrations of the reactive species needed for kinetic studies are sufficiently low to largely eliminate otherwise complicating chemical conditions arising from side reactions of reactive impurities and reaction products. As an example, it is now possible to study reactions involving OH without interference from the bimolecular reaction $2OH \rightarrow H_2O + H$. With the likely availability of various resonance lamps and tunable lasers in the near future, the resonance fluorescence method promises to be a powerful general tool for the detection of atoms and simple radicals. Nevertheless, in spite of these improved methods of production and generation, one should keep in mind that "plug-flow" experiments are subject to uncertainties associated with flow measurements, flow characteristics, and uncontrolled wall reactions (3).

Among the most notable advances are the combined uses of (i) pulsed and modulated photolysis to generate reactive species selectively, (ii) emission and absorption spectroscopic techniques to monitor these species with high sensitivity and selectivity, and (iii) improved signal processing techniques such as photon counting, signal averaging, and phase sensitive detection. To illustrate, $O(^3P)$ can be produced by collisional deactivation of photochemically

Can. J. Chem. Downloaded from www.nrcresearchpress.com by 210.87.254.6 on 09/05/12
For personal use only.

generated $O(^1D)$, and similarly, OH ($^2\Pi$) either by the $O(^1D)$ reactions of H-containing compounds (*e.g.* $O(^1D) + H_2O = 2HO$) or by direct photodissociation of H_2O_2. Notably, the extent to which photolysis provides a clean source of O and OH depends greatly on the reaction under study. Hydrogenous impurities and excited species are often produced as photochemical side products, and thereby present a potential source of uncertainties in the kinetic data. Recently, a selective generation of $O(^3P)$ by dye-laser flash photolysis of O_3 in the Chappius band has been successfully used to study the reaction $O + O_3 \rightarrow 2O_2$ (7). Typical detection techniques used in flash photolysis work include resonance fluorescence for O and OH, chemiluminescence for O, and u.v. absorption for OH, O_3, and NO_2. These combined methods of production and detection often allow accurate measurements of chemical lifetimes of the reactive species under chemically and physically well-defined conditions. As a result, kinetic data on a large number of reactions involving O and OH are now available over a wide range of pressures and temperatures. However, extreme care in gas handling is frequently necessary to ensure a high degree of accuracy for these values. Impurities in the sample, absorption and decomposition of sample gases on the reactor walls, and resulting inaccuracies in pressure measurements are common nagging problems for handling most of the N and O compounds.

Direct kinetic studies are not readily feasible for reactions involving species such as NO_3, N_2O_5, and HNO_2, because of the difficulties associated with both generation and detection. As an example, N_2O_5 is present in equilibrium with NO_2 and NO_3, both of which pose potential interference to the reaction of N_2O_5 under study. In some fortuitous circumstances, sufficiently reliable rate data can be obtained from indirect studies. Rate constants for the reactions $O + NO_2 + M \rightarrow NO_3$ and $NO_3 + NO \rightarrow 2NO$ have been derived from detailed kinetic analysis of NO_2 photolysis in a high pressure of N_2 (8). It appears at least for the time being that kinetic knowledge of these elusive reactions can be gained by methodical studies of complex reaction systems.

Review of Recent Rate Data

Since extensive evaluations of kinetic data on aeronomically important reactions are available in the NBS Chemical Kinetic Data Survey Series (9) and CIAP Monograph (10), this review will attempt to summarize some of the kinetic data reported since 1969. Reactions will be discussed in the approximate order of the preceding introductory remarks on experimental methods beginning with O, OH, O_2, O_3, and NO_3. Rate constants are given in molecule cm^{-3} concentration units, and enthalpy of reaction at 298 K; ΔH^0_{298} is shown after each equation in kcal mol^{-1}. Temperature coefficients are given in the Arrhenius form with the activation energy in kcal mol^{-1}.

[1] $O + O_2 + M \rightarrow O_3 + M$; $\Delta H = -24.6$

This reaction provides a principal sink of O atoms and also the sole source of O_3 in the mesophere and stratosphere. Prior to 1969, kinetic data on this reaction were obtained mainly by discharge and thermal decomposition flow methods. The reported rate constants scatter over a factor of 2 at all temperatures in the range 200–300 K. In contrast, nearly all recent studies have been made using time-resolved vacuum u.v. photolysis and the results at 300 K agree within 20%. In all cases, concentrations of $O(^3P)$ atoms generated by photodissociation of O_2 were kept sufficiently low to ensure negligible effects of side reactions such as $O + O + M \rightarrow O_2 + M$, $O + O_3 \rightarrow 2O_2$, and $O_2(^1\Delta) + O_3 \rightarrow O + 2O_2$. High precision exhibited by these photochemical studies can also be attributed, in part, to the use of a much wider range of M concentrations than attainable in flow experiments.

Donovan *et al.* (11) observed O-atom decay via resonance absorption transitions ($2^3P_J - 3^3S_1$) in flash photolysis ($\lambda > 1750$ Å) and obtained $k_1 = 4.6 \pm 2.6$, 5.0 ± 1.2, and $4.9 \pm 2.1 \times 10^{-34}$ for M = He, Ar, and Kr, respectively, at 300 K (11). The indicated errors are 3 standard deviations.

Slanger and Black (12) monitored the O atom decay by resonance fluorescence in a premixed bulk flow system. In this work, O atoms generated by a Xe lamp ($\lambda = 1470$ Å) were built up to a stationary state concentration prior to kinetic measurements. They reported $k_1 = (4.4 \pm 0.6) \times 10^{-34}$ for M = Ar and $(7.0 \pm 1.0) \times 10^{-34}$ for M = N_2 at 300 K.

Stuhl and Niki (13) used the O + CO chemiluminescence detection method for O atoms in their pulsed photolysis studies ($\lambda > 1050$ Å). They obtained $k_1 = 5.4 \times 10^{-34}$ for M = N_2

Can. J. Chem. Downloaded from www.nrcresearchpress.com by 210.87.254.6 on 09/05/12
For personal use only.

and 6.4×10^{-34} for M = O_2 at 300 K with an overall uncertainty of 25%.

Huie *et al.* (14) carried out the most extensive measurements of k_1 utilizing pulsed O_2 photodissociation and resonance fluorescence detection. At 300 K the value of k_1 for M = Ar was 3.63×10^{-34} with the relative M efficiencies of Ar:He:N_2 = 1.0:0.92:1.6. At 218 K the relative efficiencies were Ar:N_2 = 1.0:1.7. They obtained an Arrhenius expression $k_1 = (6.57 \pm 0.59) \times 10^{-35} \exp[(1.014 \pm 0.046)/RT]$ for M = Ar over the temperature range 200–346 K.

These recent results agree well with those obtained earlier at 300 K by Kaufman and Kelso (15). However, the temperature coefficients determined by Huie *et al.* for M = Ar are substantially lower than those of Clyne *et al.* (16), $k_1 = 2.4 \times 10^{-35} \exp(1.80/RT)$, and Mulcahy and Williams (17), $k_1 = 4.7 \times 10^{-35} \exp(1.68/RT)$. This suggests that the production rate of O_3 in the stratosphere could be nearly a factor of 2 lower than that estimated from these previously reported values.

[2] $\quad O + O_3 \rightarrow 2O_2; \quad \Delta H = -93.6$

This is one of the major sinks for "odd" oxygen and is therefore important in determining the vertical profile of O and O_3 densities. Early attempts to measure k_2 directly by mixing O and O_3 in a flow system were largely unsuccessful because H atoms produced from hydrogenous impurities in discharge sources contributed to the removal of O atoms in the presence of O_3 by the fast chain reactions $H + O_3 \rightarrow OH + O_2$ and $OH + O \rightarrow H + O_2$, and also because metastable species such as $O_2(^1\Delta_g)$ were produced which reacted rapidly with O_3.

Lundell *et al.* (18) and McCrumb and Kaufman (19) avoided some of these difficulties by producing O by the thermal dissociation of N_2O or O_3 over a Nernst glower. By a calorimetric probe detection of O atoms, Lundell *et al.* (18) obtained $k_2 = (1.46 \pm 0.06) \times 10^{-14}$ at 296.2 K and $k_2 = 3.2 \times 10^{-11} \exp(-4.5/RT)$ over the temperature range 273–343 K. However, their results were subject to some uncertainties, because the O-atom decay due to wall effects was up to 50% of the overall rate and also other heat producing reactions could not be ruled out entirely. McCrumb and Kaufman (19) followed the O-atom decay by O + NO chemiluminescence under $[NO] \leq [O] < [O_3]$. Values for k_3 were derived by fitting the observed decay of [O] and using 9.2×10^{-12} for $O + NO_2 \rightarrow NO + O_2$ and $1.3 \times 10^{-12} \exp(-2.5/RT)$ for $O_3 + NO \rightarrow NO_2 + O_2$. The maximum possible error due to $O_2(^1\Delta_g) + O_3 \rightarrow 2O_2 + O$ was estimated to be about an 8% underestimation. They reported $k_2 = (7.5 \pm 0.6) \times 10^{-15}$ at 298 K and $k_2 = (1.05 \pm 0.18) \times 10^{-11} \exp[(-4.31 \pm 0.10)/RT]$ over the temperature 269–409 K, which is about half that of Lundell *et al.* (18).

Davis *et al.* (7) used the technique of flash photolysis–resonance fluorescence. They avoided the problems of electronically excited O and O_2 by generating $O(^3P)$ directly from dye-laser flash photolysis of O_3 in the Chappius band at 6000 Å. The measured value of k_2 was 1.06×10^{-14} at 300 K and $k_2 = (2.0 \pm 0.8) \times 10^{-11} \exp[-(4.52 \pm 0.15)/RT]$.

The agreement between McCrumb and Kaufman (19) and Davis *et al.* (7) is within about 25% at both 298 K and 220 K. It appears, therefore, that the value of k_2 is now known to a reasonably high degree of accuracy.

[3] $\quad O + NO + M \rightarrow NO_2 + M; \quad \Delta H = -73.2$

Baulch *et al.* (20) reviewed earlier discharge-flow data on this reaction and recommended $k_3 = 3.0 \times 10^{-33} \exp(1.87/RT)$ for M = Ar, and O_2 over the temperature range 200–500 K with an estimated uncertainty of 20%. Some of the relative M efficiencies determined by Kaufman and Kelso (15) are Ar:He:N_2:O_2:H_2O:N_2O = 1.0:0.8:1.5:1.0:6.3:2.2 at 300 K. Recent photochemical studies give support to these previous conclusions.

Slanger and Black (12) measured a rate constant of 13.5×10^{-32} for M = Ar at 300 K in their pulsed photolysis – resonance fluorescence experiments. This value is approximately twice that of the previous determinations. To account for this large value, they suggested very rapid reaction ($k \sim 10^{-11}$) of the vibrationally excited NO_2 product with a second O atom. On this basis, $k_3 = (6.8 \pm 0.5) \times 10^{-32}$ was reported by dividing the measured value by the stoichiometric factor of 2.

In a subsequent pulsed photolysis – chemiluminescence study by Stuhl and Niki (13), O-atom lifetime was kept sufficiently short so that the possible error due to the $NO_2(v > 0)$ product was less than a few percent. They give $k_3 = 6.65 \times 10^{-32}$ for M = He at 300 K with a claimed accuracy of 10%. Their value is in reasonable agreement with the previous measurements of 4.7 to 5.1×10^{-32} (21, 22).

Atkinson and Cvetanović (23) used a modu-

Can. J. Chem. Downloaded from www.nrcresearchpress.com by 210.87.254.6 on 09/05/12
For personal use only.

lated generation of $O(^3P)$ by $Hg(^3P_1) + N_2O \rightarrow Hg(^1S_0) + N_2 + O(^3P)$ and chemiluminescence phase-shift measurements of O-atom decay. For M = N_2O they give $k_3 = (14.2 \pm 1.1) \times 10^{-32}$ at 299 K and an Arrhenius expression $k_3 = 9.4 \times 10^{-33} \exp[(1.60 \pm 0.3)/RT]$ over 300–470 K. These results combined with Kaufman's relative M efficiencies of Ar:N_2O = 1.0:2.2 agree well with previous determinations.

[4] $O + NO_2 \rightarrow NO + O_2$; $\Delta H = -45.89$

This constitutes a crucial step for the "catalytic" removal of atmospheric O_3. Until 1973, no value was available for k_4 below 280 K. Numerous discharge-flow data at 300 K exhibit a factor of 3 variation in k_4.

Davis *et al.* (24) have carried out the most extensive measurements of k_4 by the flash photolysis – resonance fluorescence method over the temperature range 230–339 K. The rate constant was found to be $k_4 = (8.70 \pm 0.65) \exp[(0.024 \pm 0.041)/RT]$. A simple average of all of their data gives $k_5 = (9.12 \pm 0.44) \times 10^{-12}$, independent of temperature. They state that use of an all-glass reaction vessel is essential to avoid wall decomposition of NO_2 to NO. This may account, in part, for the lower value of $k_4 = 4.4 \times 10^{-12}$ obtained by Stuhl and Niki (25) in a large (17 l) stainless steel reactor. Subsequently, Slanger *et al.* (26) took precautions to avoid effects of wall reactions of NO_2 and of the NO_2–N_2O_4 equilibrium. They photolyzed a premixture of O_2–NO–NO_2 in a Pyrex flow system by repetitive pulses of 1470 Å radiation and detected $O(^3P)$ by its chemiluminescent reaction with NO. They measured $k_4 = 9.2$ and 10.5×10^{-12} with error limits of ±15% at 296 K and 240 K, respectively, in excellent agreement with those of Davis *et al.* (24). The only discharge-flow study made since 1969 is that of Clyne and Cruse (6), who report $k_4 = (6.1 \pm 0.6) \times 10^{-12}$ at 298 K. They used a clean Pyrex reactor and detected $O(^3P)$ by resonance fluorescence. The H-atom impurity in these experiments was less than 1% of O atoms.

Harker and Johnston (8) obtained from NO_2 photolysis $k_3(M)/k_4 = 0.18$ and 0.20 for 1 atm N_2 and Ar, respectively, at 297 K in a long-path infrared cell. These ratios were based on the molecular modulation spectrum of NO_2 in a steady flow experiment. The relative M efficiencies for k_3 are not consistent with those of Kaufman and Kelso (15), Ar:N_2 = 1.0:1.5. It appears that their value of k_4 would range from 9 to 13 $\times 10^{-12}$. The most recent data on steady state photolysis of NO_2 in N_2 by Wu and Niki (28) gives $k_3(M)/k_4 = 0.32$ for M = 1 atm N_2, which supports a value of about 9×10^{-12} for k_4. The NBS review (9) recommends $k_4 = 9.1 \times 10^{-12}$ for the temperature range 220–500 K with estimated error limits of ±20%. Certainly more work should be done to narrow this uncertainty.

[5] $O + NO_2 + M \rightarrow NO_3 + M$; $\Delta H = -49 \pm 5$

This reaction channel is presumably distinct from reaction 4, and is intimately related to the corresponding isotope exchange reactions (27). Several determinations of the rate ratio, $k_5(M)/k_4$, indicate that this reaction occurs to the extent of 20–30% of reaction 4 for M = 1 atm N_2 at 300 K.

Troe (29) measured the quantum yield of NO_2 at λ = 3660 Å as a function of N_2 pressure up to 200 atm. He observed third order kinetics up to 10 atm, and a limiting second order value of 2×10^{-11} above 100 atm. His value for $k_5(M)/k_4$ is (0.27 ± 0.03) at 1 atm N_2, in agreement with (0.33 ± 0.08) reported earlier by Schuck *et al.* (30).

Harker and Johnston (8) photolyzed NO_2 in 1 atm N_2 and measured the NO_2 decay and N_2O_5 formation by long-path i.r. spectroscopy. They found $k_5(M)/k_4$ to be (0.221 ± 0.005). Under similar experimental conditions, Wu and Niki (28) determined $k_5(M)/k_4 = 0.32$ with an estimated error limit of 25%. This value is based on the kinetic analysis of NO formation as monitored by O_3–NO chemiluminescence.

The simple average of these four measurements, $k_5(M)/k_4 = 0.28$, in combination with $k_4 = 9.2 \times 10^{-12}$ gives $k_5 = 1.0 \times 10^{-31}$ with a probably uncertainty of 30%.

[6] $O + HNO_3 \rightarrow OH + NO_3$; $\Delta H = -1 \pm 5$

$\rightarrow O_2 + HNO_2$; $\Delta H = -46.3$

There is a factor of 10^4 discrepancy for the values of k_6 between direct and indirect studies. Jaffe and Ford (60) inferred $k_6 \sim 10^{-11}$ from overall quantum yield measurements in a steady state photolysis of NO_2–HNO_3 mixtures at λ = 3660 Å. From a similar experiment at λ = 2650 Å, Berces and Forgeteg (31) derived $k_6 \sim 10^{-10}$. Morris and Niki (32) attempted a direct determination of k_4 by the discharge flow – mass spectrometry method. They were able to

Can. J. Chem. Downloaded from www.nrcresearchpress.com by 210.87.254.6 on 09/05/12
For personal use only.

assign only an upper limit $k_5 \leq 1.5 \times 10^{-14}$ at 300 K. Morley and Smith (33) flash-photolyzed NO_2 in the presence of HNO_3 to observe the OH product by resonance absorption. Based on their negative results, they also deduced $k_6 \leq 1.3 \times 10^{-14}$. Therefore, this reaction is less important than previously considered as a removal mechanism of HNO_3 in the stratosphere.

[7] $\quad O + NH_3 \rightarrow OH + NH_2; \quad \Delta H = 3.0$

Results of two recent discharge-flow studies are in reasonable agreement. Albers *et al.* (34) used both e.s.r. and mass spectrometry and determined $k_7 = 2.5 \times 10^{-12} \exp(-6.0/RT)$ over the temperature range 300–910 K. In this work reaction 7 could not be separated from subsequent reactions, and a correction factor of 2.9 based on the observed stoichiometry, $\Delta(O)/\Delta(NH_3)$, was used in the data analysis. Kurylo *et al.* (35) give $k_7 = (6.7 \pm 1.5) \times 10^{-12} \exp(-6.60 \pm 0.13/RT)$ over the temperature range 361–667 K. They derived k_7 from the O-atom decay as observed by e.s.r. and a stoichiometric factor of 3.5 taken as a simple average of 2.9 by Albers *et al.* (34) and 4.4 by Wong and Potter (36). Benson (37) comments that the reported values of the A factor is about a factor of 10 too low, judged either on empirical or on theoretical grounds. More information is necessary to establish k_7 firmly.

[8] $\quad O + N_2O_5 \rightarrow 2NO_2 + O_2; \quad \Delta H = -47$

Davis (38) recently reported $k \leq 2 \times 10^{-13}$ at 298 K. In these experiments, N_2O_5 was generated by reacting a known amount of NO_2 with excess O_3. Ground state atomic oxygen was produced by dye-laser flash photolysis of O_3 at $\lambda = 5900$ Å, and was detected by resonance fluorescence. This value for k should be regarded as an upper limit because of the possible removal of O by NO_2 and NO_3 present in equilibrium with N_2O_5 and O_3 in this system.

[9] $\quad OH + NO + M \rightarrow HNO_2 + M; \quad \Delta H = -50$

The hydroxyl radical is an important chain carrier in atmospheric oxidation reactions. This reaction may act as a chain termination step depending on the subsequent fate of the product HNO_2. Five independent determinations of k_9 have been made since 1972, and all agree within $\pm 50\%$.

Anderson and Kaufman (5) reported preliminary results obtained by the discharge flow – resonance fluorescence method. They give (4 ± 2) and $(2.5 \pm 1) \times 10^{-31}$ for $M = 5$ and 10 Torr Ar, respectively, at 297 K. Morley and Smith (33) used flash photolysis of NO_2–H_2–NO–He mixtures at 30 Torr total pressure, and u.v. absorption detection of OH. They found $k_9 = (4.1 \pm 0.6)$ and $(1.9 \pm 0.3) \times 10^{-31}$ for M = He at 300 K and 416 K, respectively, which corresponds to an activation energy of $-(1.6 \pm 0.5)$ kcal mol^{-1}. The relative M efficiencies of $He:H_2 = 1.0:(2.3 \pm 0.9)$ were also determined. Stuhl and Niki (39) studied this reaction over 5–82 Torr He at 300 K by the flash photolysis – resonance fluorescence method. The rate constant was found to be nonlinearly dependent on M = He in this pressure range. The values of k_{13} given as termolecular rate constant range from 5.2×10^{-31} at 5 Torr to 1.9×10^{-31} at 82 Torr. Westenberg and deHaas (40) determined by discharge flow – e.s.r. method $k_9 = 12$, 8.0, and 3.5×10^{-31} at 273, 298, and 395 K, respectively, over a range of 0.5–5 Torr He. They state that the rate constant with M = Ar was about a factor of 2 lower.

Temperature coefficients and M efficiencies of this reaction should be determined more extensively.

[10] $\quad OH + NO_2 + M \rightarrow HNO_3 + M; \quad \Delta H = -49.5$

This provides a major atmospheric source of HNO_3 and also acts as a chain-terminating step. Direct kinetic data on this reaction together with those of reaction 9 have been recently obtained by several groups. All these results agree within $\pm 50\%$ and suggest the transition from second to third order kinetics at relatively low diluent pressures.

Morley and Smith (33) obtained k_{10} at (300 ± 8) K and (416 ± 10) K for $M = 20$–300 Torr, and compared the experimental results with calculations based on the RRKM theory. Typically, the thermolecular rate constants at 300 K were 1.4, 0.8, and 0.4×10^{-30} for $M = 30$, 100, and 300 Torr He. They also determined the relative M efficiencies of $He:H_2:SF_6 = 1.0:(4.0 \pm 1.0):(4.8 \pm 0.8)$. Anderson and Kaufman (5) report k_{10} at 297 K for $M = 0.5$–8 Torr N_2. Their values for the termolecular rate constant are pressure independent up to about 4 Torr He, $k_{10} = (1.0 \pm 0.3) \times 10^{-31}$, and decrease with a further increase in Ar pressure. For $M = 8$ Torr N_2, k_{10} was $(2.0 \pm 0.5) \times 10^{-30}$. Westenberg and deHaas (40) obtained pressure independent

Can. J. Chem. Downloaded from www.nrcresearchpress.com by 210.87.254.6 on 09/05/12
For personal use only.

values of $k_{10} = 4.7$, 2.9, and 1.3×10^{-30} at 273, 298, and 395 K, respectively, for $M = 1$–5 Torr He. Data at 298 K for M = Ar were about a factor of 2 lower.

Simonaitis and Heicklen (41) measured the quantum yield of CO_2 in the photolysis of NO_2–H_2O–CO–He mixtures at 300 K and 423 K, and derived k_{10} relative to $OH + CO \rightarrow CO_2 + H$, $k = 7 \times 10^{-13} \exp(-1100/RT)$. They give a temperature independent value of $k_{10} = 1.1 \times 10^{-29}$ for M = H_2O in the low pressure limit. They found He to be about 1/8 as efficient as H_2O.

[11] $OH + NH_3 \rightarrow H_2O + NH_2$; $\Delta H = -13$

This reaction may be important as a removal mechanism of NH_3 and also as a source for oxides of nitrogen in the atmosphere. Stuhl (42) reports $k_{11} = (1.5 \pm 0.4) \times 10^{-13}$ at 298 K, as obtained by pulsed photolysis – resonance fluorescence. This value is in reasonable agreement with a theoretical value of 5×10^{-13} computed by Tunder *et al.* (43) using the Johnston–Parr method. Subsequent reactions of NH_2 with other atmospheric constituents are not known at the present time.

[12] $OH + HNO_3 \rightarrow H_2O + NO_3$; $\Delta H = -18 \pm 5$

Hampson *et al.* (9) reviewed all the kinetic data on this reaction available prior to 1970. They give a preferred value of $k_{12} = 5 \times 10^{-14}$ at 300 K with an estimated uncertainty of a factor of 3. More recent flash photolysis – resonance absorption work of Morley and Smith (33) reports $k_{12} = (1.3 \pm 0.5) \times 10^{-13}$ at 300 K, in good agreement with a previous value of 1.6×10^{-13} obtained by Hussain and Norrish (44) using a similar method. The steady-state photochemical study of HNO_3–NO_2 by Berces and Forgeteg(31) gives precisely a factor of 10 greater value, but appears to suffer from complications due to heterogenous reactions.

[13] $O_2 + 2NO \rightarrow 2NO_2$; $\Delta H = -27.3$

Thermal oxidation of NO by this reaction displays third order kinetic behavior under a wide range of experimental conditions. All the kinetic data available prior to 1970 has been reviewed by Baulch *et al.* (20). The only recent work on this system is that of Stedman *et al.* (45). By the NO–O_3 chemiluminescence detection method of NO, they measured the decay of NO ranging from 1 Torr to 1 mTorr as a function of O_2 pressure in a static reactor. The observed value of k_8 as defined by $d[NO]/dt = k_8/2[NO]^2[O_2]$ was $(2.0 \pm 0.1) \times 10^{-38}$, in agreement with previous measurements.

[14] $O_3 + NO \rightarrow NO_2 + O_2$; $\Delta H = -47.7$

This together with reaction 4 constitutes a key reaction in determining the atmospheric concentration of both O_3 and NO. The earliest study of this reaction was carried out by Johnston and Crosby (46) in 1954. They employed the stopped flow – u.v. absorption ($\lambda = 2537$ Å) method and made measurements, 65 in all, at 216 K and 322 K. The data points scatter by ±50%. An Arrhenius expression of $k_{14} = 1.3 \times 10^{-12} \exp[-(2.5 \pm 0.3)/RT]$ was given.

In 1964, Clyne *et al.* (47) reported $k_{14} = (1.6 \pm 0.1) \times 10^{-14}$ at 293 K and $k_{14} = 9.5 \times 10^{-13} \exp[-(2.46 \pm 0.15)/RT]$ over the range 216–322 K. These values are based on O_3 decay as measured by NO + O_3 chemiluminescence. A later work by Clough and Thrush (48) using the same technique differentiates between two competitive reaction channels, $k_{14a} = (7.2 \pm 1.7) \times 10^{-12} \exp[-(2.33 \pm 0.15)/RT]$ for the formation of the ground electronic state NO_2 (^2A) and $k_{14b} = (1.3 \pm 0.2) \times 10^{-12} \exp[-(4.18 \pm 0.3)/RT]$ for the excited NO_2 (^2B) formation.

Flow – mass spectrometry studies by Philips and Schiff (49) and by Sharma *et al.* (50) give $k_{14} = (2.1 \pm 0.5) \times 10^{-14}$ at 298 K and $(2.0 \pm 0.2) \times 10^{-14}$ at 296 K, respectively.

Stedman and Niki (51) produced NO and O_3 by steady-state photolysis of NO_2–O_2 mixtures in a static reactor and monitored the subsequent decay of both reactants in the dark by O_3–NO chemiluminescence. Their value for k_{14} is $(1.73 \pm 0.1) \times 10^{-14}$ at 300 K. This experiment has been repeated and verified by Wu and Niki (28), $k_{14} = (1.85 \pm 0.1) \times 10^{14}$. Ghormley *et al.* (54) produced NO *in situ* by the reaction of $O(^1D)$ with N_2O in flash photolysis of O_3–O_2–N_2O mixtures, and detected O_3 and the product NO_2 by u.v. absorption. They found $k_{14} = (1.4 \pm 0.1) \times 10^{-14}$ at 298 K.

Thus it appears that $k_{14} = 1.8 \times 10^{-14}$ at 300 K is reliable within ±20%. Temperature coefficients warrant further study.

[15] $O_3 + NO_2 \rightarrow NO_3 + O_2$; $\Delta H = -25 \pm 5$

The most extensive kinetic data available prior to 1969 are those of Johnston and Yost (52). They followed NO_2 by its absorption at 4400–

Can. J. Chem. Downloaded from www.nrcresearchpress.com by 210.87.254.6 on 09/05/12
For personal use only.

4800 Å in a stopped flow reactor. Ozone concentration during the reaction was determined assuming a stoichiometry $\Delta(NO_2)/\Delta(O_3) = 2$. From the decay of O_3, they obtained $k_{15} = 6.1 \times 10^{-17}$ at 294 K with a standard deviation of 10%. An activation energy of 7.0 ± 0.6 kcal mol^{-1} was reported over the temperature range of 286–302 K, giving $k = 9.8 \times 10^{-12} \exp(-7.0 \pm 6/RT)$.

Ford *et al.* (53) measured k_{15} in a 50 l stirred flow reactor using u.v. absorption of O_3 and wet chemical detection of NO_2. The stoichiometry varied from 0.9 to 4.8. Although the individual determinations scatter over a factor of 4, they derived an average value of $k_{15} = 3.3 \times 10^{-17}$. Ghormley *et al.* (54) observed O_3 and NO_2 by u.v. absorption in flash photolysis of O_3–O_2–N_2O mixtures. The average value of k_{15} at 298 K, based on three runs, was $(3.3 \pm 0.2) \times 10^{-17}$. Wu *et al.* (55) determined $k_{15} = (4.4 \pm 0.4) \times 10^{-17}$ at 299 ± 1 K in a static reactor from the decay of O_3 in excess NO_2, as monitored by the NO–O_3 chemiluminescence detector. Davis (38) found $k_{15} = (3.5 \pm 0.4) \times 10^{-17}$ at 298 K in his stop flow – mass spectrometry work. Most recently, Graham and Johnston (56) obtained preliminary results of $k_{15} = 1.23 \times 10^{-13} \exp(-2.47/RT)$ between 230–270 K in a long path i.r. cell. Their data suggest that NO_2 undergoes polymerization beyond N_2O_4 at these low temperatures.

In summary, it appears that both the A factor and activation energy for k_{15} are considerably lower than that originally reported by Johnston and Yost.

[16] $NO_3 + NO \rightarrow 2NO_2$; $\Delta H = -22.7$

There are only indirect values available for k_{16} at 300 K. Hisatsume *et al.* (57) examined the kinetics of the N_2O_5–NO system by i.r. spectroscopy. They obtained $k_{16}/K = (0.60 \pm 0.06)$ s^{-1} at 296 K, where $K = ([N_2O_5]/[NO_2][NO_3])_{eq}$. This ratio in combination with $K = 1.24 \times 10^{-11}$ cm^{-3} of Schott and Davidson (58) gives $k_{16} = (7.4 \pm 0.7) \times 10^{-12}$.

Recently, Harker and Johnston (8) studied the kinetic behavior of the product N_2O_5 in a steady-state photolysis of NO_2–N_2 by i.r. absorption. They found $k_{16}/K = 0.71 \pm 0.02$ s^{-1} at 296 K, and thus $k_{16} = (8.8 \pm 1.8) \times 10^{-12}$, in agreement with that of Hisatsume *et al.* (57).

[17] $NO_3 + NO_2 \rightarrow NO + NO_2 + O_2$; $\Delta H = 4.5$

No new information is available for this reaction. Baulch *et al.* (59) gives a preferred value of $k_{17} = 2.3 \times 10^{-13} \exp(-1600/RT)$ over the temperature range of 300–850 K.

[18] $NO_3 + NO_2 + M \rightarrow N_2O_5 + M$; $\Delta H = -22$

This occurs commonly in a NO_2–O_3 mixture as a secondary reaction following reaction (15), and also maintains equilibrium concentrations of NO_3 and NO_2 in the N_2O_5 system. However, no direct data is available on this reaction. Values of k_{18} can be calculated from the data on the reverse reaction and the equilibrium constant. Baulch *et al.* (59) recommend $k_{18} = 2.8 \times 10^{-30}$ and 3.8×10^{-12} as the limiting low and high pressure values, respectively, at 300 K.

[19] $N_2O_5 + M \rightarrow NO_2 + NO_3 + M$; $\Delta H = +22$

All the available kinetic data on this reaction date back to 1960. The review by Baulch *et al.* (59) gives $k_{19} = 2.2 \times 10^{-5} \exp(-19.3/RT)$ for M = N_2O_5 plus NO over the range 300–340 K. Clearly, more work should be done to establish the M efficiencies and temperature coefficients for this reaction.

Conclusion

For the past 4 years, significant progress has been made on the knowledge of aeronomically interesting reactions involving oxygen and nitrogen compounds. Many of the simple atom–molecule reactions have been studied over a wider range of experimental conditions with substantially improved accuracy, primarily as a result of recent developments of sensitive detection methods. Several slow, complex reactions have also been examined more extensively. However, adequate generation and production methods of reactive polyatomic species are still lacking and await future development. Computer-aided spectroscopic methods such as derivative, correlation, and Fourier transform spectroscopy, and also photoionization – mass spectrometry are some of the advanced techniques in sight.

1. H. I. SCHIFF. Can. J. Chem. **47**, 1903 (1969).
2. H. JOHNSTON and D. GARVIN. Natl. Bur. Stand. Rep. 10931 (Oct. 1972).
3. F. KAUFMAN. Can. J. Chem. **47**, 1917 (1969).
4. F. KAUFMAN and F. P. DELGRECO. 9th Int. Symp. Combust., Ithaca, N.Y. Combustion Institute, Pittsburgh, Penn. 1963. p. 659.
5. J. G. ANDERSON and F. KAUFMAN. Chem. Phys. Lett. **16**, 375 (1972).

Can. J. Chem. Downloaded from www.nrcresearchpress.com by 210.87.254.6 on 09/05/12
For personal use only.

6. M. A. A. CLYNE and H. W. CRUSE. J. Chem. Soc. Faraday Trans. II, **68**, 1281 (1927).
7. D. D. DAVIS, W. W. WONG, R. L. SCHIFF, J. O. LEPHARDT, J. E. PRUSACZYK. W. A. PAYNE, L. J. STIEF, R. E. HUIE, and J. T. HERRON. Proc. 2nd Conf. Climatic Impact Assessment Program, Cambridge, Mass. (U.S. Dept. of Transportation, Washington, D.C.). *Edited by* A. J. Broderick. Nov. 1972. p. 126.
8. A. B. HARKER and H. S. JOHNSTON. J. Phys. Chem. **77**, 1153 (1973).
9. R. F. HAMPSON. (Editor.) Natl. Bur. Stand. Rep. 10692 (1972); 10828 (1972). Chemical kinetics data survey series I–VI. NBSIR Reports (1972–1973).
10. Climatic impact assessment program monograph No. 1 (U.S. Dept. of Transportation, Washington, D.C.). *Edited by* A. J. Broderick. Nov. 1972.
11. R. J. DONOVAN, D. HUSSAIN, and L. J. KIRSCH. Trans. Faraday Soc. **66**, 2551 (1970).
12. T. G. SLANGER and G. BLACK. J. Chem. Phys. **53**, 3717 (1970).
13. F. STUHL and H. NIKI. J. Chem. Phys. **55**, 3943 (1971).
14. R. E. HUIE, J. T. HERRON, and D. D. DAVIS. J. Phys. Chem. **76**, 2653 (1972).
15. F. KAUFMAN and J. R. KELSO. J. Chem. Phys. **46**, 4541 (1967).
16. M. A. A. CLYNE, D. J. MCKENNEY, and B. A. THRUSH. Trans. Faraday Soc. **61**, 2701 (1965).
17. M. F. R. MULCAHY and D. J. WILLIAMS. Trans. Faraday Soc. **64**, 59 (1968).
18. O. R. LUNDELL, R. D. KETCHESON, and H. I. SCHIFF. 12th Int. Symp. Combust., Poitiers, France. Combustion Institute, Pittsburgh, Penn. 1969. p. 307.
19. J. L. MCCRUMB and F. KAUFMAN. J. Chem. Phys. **57**, 1270 (1972).
20. D. L. BAULCH, D. D. DRYSDALE, and D. G. HORNE. High temperature reaction rate data (The University, Leeds). No. 5. July 1970.
21. F. KAUFMAN. Ann. Rev. Phys. Chem. **20**, 45 (1969).
22. E. A. OGRYZLO and H. I. SCHIFF. Can. J. Chem. **37**, 1690 (1969).
23. R. ATKINSON and R. J. CVETANOVIĆ. J. Chem. Phys. **56**, 432 (1972).
24. D. D. DAVIS, J. T. HERRON, and R. E. HUIE. J. Chem. Phys. **58**, 530 (1973).
25. F. STUHL and H. NIKI. Chem. Phys. Lett. **1**, 197 (1970).
26. T. G. SLANGER, B. J. WOOD, and G. BLACK, Proc. 2nd Conf. Climatic Impact Assessment Program, Cambridge, Mass. (U.S. Dept. of Transportation, Washington, D.C.). *Edited by* A. J. Broderick. Nov. 1972. p. 144.
27. F. S. KLEIN and J. T. HERRON. J. Chem. Phys. **44**, 3645 (1966).
28. C. H. WU and H. NIKI. 166th American Chemical Society Meeting, Chicago, Ill. Aug. 1973. Paper No. 121.
29. J. TROE. Ber. Bun. Phys. Chem. **73**, 906 (1969).
30. E. A. SCHUCK, E. R. STEPHENS, and R. R. SCHROCK. J. Air Pollut. Control Assoc. **16**, 695 (1966).
31. T. BERCES and S. FORGETEG. Trans. Faraday Soc. **66**, 640 (1970).
32. E. D. MORRIS, JR. and H. NIKI. J. Phys. Chem. **75**, 3193 (1971).
33. C. MORLEY and I. W. M. SMITH. J. Chem. Soc. Faraday Trans. II, **68**, 1016 (1972).
34. E. A. ALBERS, K. HOYERMANN, H. G. WAGNER, and J. WOLFRUM. 12th Int. Symp. Combust. (Poitiers, France). Combustion Institute, Pittsburgh, Penn. 313 (1969).
35. M. J. KURYLO, G. A. HOLLINDEN, H. F. LEFEVRE, and R. B. TIMMONS. J. Chem. Phys. **51**, 4497 (1969).
36. E. L. WONG and A. E. POTTER. J. Chem. Phys. **43**, 3371 (1965).
37. S. W. BENSON. 12th Int. Symp. Combust. (Poitiers, France). Combustion Institute, Pittsburgh, Penn. 320 (1969).
38. D. D. DAVIS. American Institute of Aeronautics and Astronautics Meeting, Denver, Col. Paper No. 73–501 (June 1973).
39. F. STUHL and H. NIKI. J. Chem. Phys. **57**, 3677 (1972).
40. A. A. WESTENBERG and N. DEHAAS. J. Chem. Phys. **57**, 3677 (1972).
41. R. SIMONAITIS and J. HEICKLEN. Int. J. Chem. Kinet. **4**, 529 (1972).
42. F. STUHL. J. Chem. Phys. **59**, 635 (1973).
43. R. TUNDER, S. MAYER, E. COOK, and L. SCHIELER. *Cited in* D. D. Drysdale and A. C. Lloyd. Oxid. Combust. Rev. **4**, 157 (1970).
44. D. HUSSAIN and R. G. NORRISH. Proc. Roy. Soc. A, **273**, 165 (1963).
45. D. H. STEDMAN, E. E. DABY, F. STUHL, and H. NIKI. J. Air Pollut. Control Assoc. **22**, 260 (1972).
46. H. S. JOHNSTON and H. J. CROSBY. J. Chem. Phys. **22**, 689 (1954).
47. M. A. A. CLYNE, B. A. THRUSH, and R. P. WAYNE. Trans. Faraday Soc. **60**, 359 (1964).
48. P. N. CLOUGH and B. A. THRUSH. Trans. Faraday Soc. **63**, 915 (1964).
49. L. F. PHILIPS and H. I. SCHIFF. J. Chem. Phys. **36**, 1509 (1962).
50. H. D. SHARMA, R. E. JERVIS, and K. Y. WONG. J. Phys. Chem. **74**, 923 (1970).
51. D. H. STEDMAN and H. NIKI. Environ. Sci. Technol. **1**, 735 (1973).
52. H. S. JOHNSTON and D. M. YOST. J. Chem. Phys. **17**, 386 (1949).
53. H. W. FORD, J. J. DOYLE, and N. ENDOW. J. Chem. Phys. **26**, 1336 (1957).
54. J. A. GHORMLEY, R. L. ELLSWORTH, and C. J. HOCHANADEL. J. Phys. Chem. **77**, 1341 (1973).
55. C. H. WU, E. D. MORRIS, JR., and H. NIKI. J. Phys. Chem. In press.
56. R. GRAHAM and H. S. JOHNSTON. Private communication.
57. I. C. HISATSUNE, B. CRAWFORD, and R. A. OGG. J. Am. Chem. Soc. **79**, 4648 (1957).
58. J. SCHOTT and N. DAVIDSON. J. Am. Chem. Soc. **80**, 1841 (1958).
59. D. L. BAULCH, D. D. DRYSDALE, and D. G. HORNE. NBSIR 73–206. *Edited by* R. F. Hampson. National Bureau of Standards, Wash., D.C. 1973.
60. S. JAFFE and H. W. FORD. J. Phys. Chem. **71**, 1832 (1967).

A Kinetics Review of Atmospheric Reactions Involving H_xO_y Compounds

D. D. DAVIS

Chemistry Department, University of Maryland, College Park, Maryland

Received November 6, 1973

Some 49 reactions involving compounds of the type H_xO_y have been examined in terms of their possible significance to stratospheric and mesospheric chemistry. Of this set of 49, some 20 processes were evaluated to be of potential importance. Within this subset of 20, the rate constants for 8 of these reactions were indicated as either having undergone a significant reevaluation within the last 2 years or were due to be reevaluated based on new data. A discussion of new experimental data resulting in these reevaluations is presented. Finally, recommendations are made as to the need for new experimental work.

Quelques 49 réactions impliquant des composés de type H_xO_y ont été examinées en fonction de leur importance possible dans la chimie stratosphérique et mésosphérique. De ce nombre, 20 réactions se sont révélées d'un intérêt potentiel.

Dans ce sous-ensemble de 20, les constantes de vitesse de 8 de ces réactions sont reliées soit à une réévaluation significative pendant les 2 dernières années, soit étaient dues pour être réévaluées en se basant sur de nouvelles données. On discute des nouvelles données expérimentales résultant de ces réévaluations. Finalement des recommendations sont faites quant au besoin de nouveaux travaux expérimentaux. [Traduit par le journal]

Can. J. Chem., **52**, 1405 (1974)

Introduction

In an effort to systematically examine the stratospheric and mesospheric reaction kinetics of H_xO_y compounds, this author has elected to classify these reactions into five major groups:

[A] $H_xO_y + H_xO_y \rightarrow$ products $x, y = 0,1,2$

[B] $H_xO_y + H_uO_v \rightarrow$ products $x, y = 0,1,2$; $u, v = 0,1,2$

[C] $H_xO_y + SO_2 \rightarrow$ products $x, y = 0,1,2$

[D] $H_xO_y + CO \rightarrow$ products $x, y = 0,1,2$

[E] $H_xO_y + CH_4 \rightarrow$ products $x, y = 0,1,2$

The possible encounters of type A, B, C, D, and E have been summarized in the form of two reaction grids (see Table 1).

From grid I, it can be seen that some 28 independent reactions of type A and B must be considered. Grid II shows another 21 reactions of types C, D, and E. An immediate question, therefore, is whether or not all 49 processes are of atmospheric significance, and hence must be used in chemical modelling studies. Fortunately, the answer to this question is no. Many of those reactions listed can be ruled out on thermodynamic or kinetic grounds. For example, in the case of reaction 26, $O_2 + O_2 \rightarrow O_3 + O$, the endothermicity of this process is $\sim$93 kcal/mol. Thus, an activation energy of at least 93 kcal/mol is to be expected. At the temperatures of the stratosphere and mesosphere, 210–273 °K, reaction 26 would clearly be unimportant. In the preceding example, a quick inspection of the thermodynamics of the reaction was sufficient to reject the process as not being of atmospheric importance. For a large number of reactions, however, careful kinetic comparisons need to be made with other possible competing reactions. In other cases, a modelling sensitivity test can be performed in which the rate constant for the reaction of interest is allowed to take on a range of values. The atmospheric importance of a particular reaction is then ascertained by a careful examination of the effect that this variation has on the output data of the model.

In the case of the 49 reactions listed in grids I and II, this author has used simple thermodynamic and kinetic arguments in conjunction with the modelling results of Crutzen (1), Hesstvedt (2), Johnston (3), and Nicolet (4), to reduce this set to 20 key processes. These 20 reactions have been labelled in Table 1 by placing the reaction number in parentheses. The list includes processes 3, 6, 7, 9, 10, 11, 13, 14, 16, 18, 20, 23, 24, 25, 30, 31, 33, 37, 38, and 44.

In the following text, Table 2 is presented which gives the experimental status of each of the above reactions. In each case, there is first a qualitative statement given as to why the

Can. J. Chem. Downloaded from www.nrcresearchpress.com by 210.87.254.5 on 09/05/12
For personal use only.

TABLE 1. Reaction grid showing possible encounters of the type* A, B, C, D, E

	H	OH	HO_2	H_2O_2	$O(^3P)$	O_2	O_3
				Grid I			
H	1	2	(3)	4	5	(6)	(7)
OH		8	(9)	(10)	(11)	12	(13)
HO_2			(14)	15	(16)	17	(18)
H_2O_2				19	(20)	21	22
$O(^3P)$					(23)	(24)	(25)
O_2						26	27
O_3							28
				Grid II			
SO_2	29	(30)	(31)	32	(33)	34	35
CO	36	(37)	(38)	39	40	41	42
CH_4	43	(44)	45	46	47	48	49

*Parentheses indicate key reactions.

reaction is considered to be important. Next, a list of all recent rate constant evaluations is presented. And finally, if any new kinetic data has been reported since the most recent evaluation, this work is cited and its possible influence on previous evaluations discussed. In those cases where the recommended value for a rate constant has changed significantly from one evaluation to another, further discussion is given explaining the basis for this change.

Discussion

Of the 20 reactions listed in the previous text, the rate constants for 8 of these have either recently undergone a significant reevaluation or would now appear to be due for one based on new rate data. The reactions of interest are 6, 13, 18, 24, 33, 37, 38, and 44.

Reaction 6 was recently reevaluated by the CIAP Kinetics review group (5), and was assigned a somewhat lower temperature dependence and a higher pre-exponential factor than given in the review by Baulch *et al.* (6) (CIAP, $E = -680$ cal/mol, $A = 6.7 \times 10^{-33}$; Baulch *et al.*, $E = -1000$ cal/mol, $A = 4.1 \times 10^{-33}$, for M = Ar or He). The new evaluation is based on the 300 °K data reviewed by Baulch *et al.* and the more recent low temperature work by Davis and Wong (7) and Kurylo (8), using flash photolysis – resonance fluorescence techniques. A quick calculation shows that at stratospheric temperatures of 220 °K, the new rate constant would be nearly 1.5 times smaller than that given by the evaluation of Baulch *et al.* This is not the case, however, since the third body efficiency for N_2 reported by Davis and Wong (7) and Kurylo (8) is nearly 3 times larger than the old value quoted. The net effect, therefore, is a rate constant at stratospheric temperatures (for M = N_2) which is ~1.5 times larger than that calculated from the previous evaluation by Baulch *et al.*

Although the value of the rate constant for reaction 13 ($OH + O_3 \rightarrow HO_2 + O_2$) changed by nearly a factor of 20 from 1971 to 1973, its value is now considered to be reasonably well established. The new evaluation quoted is based on the work of DeMore (9) and Anderson and Kaufman (10). These results were recently corroborated at 300 °K from investigations by Kurylo (8) and Davis and Schiff (11). In all, three different experimental techniques have now been used to examine this system: low intensity steady-state photolysis; discharge-flow with resonance fluorescence detection; and flash photolysis – resonance fluorescence.

Reaction 18 ($HO_2 + O_3 \rightarrow OH + 2O_2$) was believed for many years to be far too slow to be of any significance in atmospheric chemistry. The value of the rate constant now recommended, however, would indicate that this reaction may be of some importance. The latest results of Simonaitis and Heicklen (12), involving a relative rate study of the competing system

$$HO_2 + O_3 \rightarrow OH + 2O_2$$

and

$$HO_2 + HO_2 \rightarrow H_2O_2 + O_2$$

give a rate constant of $\sim 3.5 \times 10^{-16}$ cm^3 molecule^{-1} s^{-1} at 220 °K. This can be compared with the calculated value from the CIAP evaluation of $\sim 2.0 \times 10^{-16}$ cm^3 molecule^{-1} s^{-1}.

Can. J. Chem. Downloaded from www.nrcresearchpress.com by 210.87.254.5 on 09/05/12
For personal use only.

TABLE 2. Table of kinetic rate data*

[3] $H + HO_2 \rightarrow H_2 + O_2$ (*a*)
$OH + OH$ (*b*)
$H_2O + O$ (*c*)

Atmospheric significance
i. Important source of H_2 in the middle and upper mesosphere
ii. Of some importance in the mesosphere and upper stratosphere as a loss reaction for odd hydrogen

Evaluations

Baulch *et al.* (6)	(*a*) $4.2 \times 10^{-11} \exp(-350/T)$	290–800 °K
	(*b*) $4.2 \times 10^{-11} \exp(-950/T)$	290–800 °K
	(*c*) No recommendation	
CIAP (5)	Same as above	

New rate data

Westenberg and deHaas (17)	(a):(b):(c) 0.62:0.27:0.11	e.s.r.–discharge-flow technique	300 °K

Will not significantly influence CIAP value

[6] $H + O_2 + M \rightarrow HO_2 + M$

Atmospheric significance
i. Major source of HO_2 in the mesosphere and stratosphere
ii. Major loss reaction for H atoms in the mesosphere and stratosphere

Evaluations

Baulch *et al.* (6)	$4.1 \times 10^{-33} \exp(500/T)$	300–2000 °K
	M = Ar; Ar(1.0), He(1.8), N_2(2.1), O_2(1.7), H_2O(70)	
CIAP (5)	$6.7 \times 10^{-33} \exp(290/T)$	203–404 °K
	M = Ar; Ar(1.0), He(1.0), N_2(3.1), O_2(3.1), H_2O(25)	

New rate data: none

[7] $H + O_3 \rightarrow OH + O_2$

Atmospheric significance
i. Important OH source in the mesosphere and the middle and upper stratosphere
ii. Moderately important loss reaction for H atoms in the mesosphere and upper stratosphere

Evaluations

NBS	2.6×10^{-11}	300 °K
CIAP (5)	Same as above	

New rate data: None

[9] $OH + HO_2 \rightarrow H_2O + O_2$

Atmospheric significance
i. Important source of H_2O in both the stratosphere and mesosphere
ii. Major loss reaction for odd hydrogen (OH, HO_2, H)

Evaluations

Kaufman (23) (estimate)	$k = 1 \times 10^{-11}$	300 °K
Lloyd (19) (estimate)	$1.7 \times 10^{-11} \exp(-500/T)$	300 °K
Hochanadel *et al.* (24)	2×10^{-10}	300 °K
CIAP (5)	$2 \times 10^{-11} < k < 2 \times 10^{-10}$	300 °K

New rate data: None

[10] $OH + H_2O_2 \rightarrow H_2O + HO_2$

Atmospheric significance
i. Important loss reaction for OH throughout the stratosphere
ii. Important loss reaction for H_2O_2 in the stratosphere

Evaluations

Baulch *et al.* (6)	$1.7 \times 10^{-11} \exp(-910/T)$	300–800 °K
NBS	Same as above	
CIAP (5)	Same as above	

New rate data: None

Can. J. Chem. Downloaded from www.nrcresearchpress.com by 210.87.254.5 on 09/05/12
For personal use only.

TABLE 2. (*Continued*)

[11] $OH + O(^3P) \rightarrow O_2 + H$

Atmospheric significance
i. Major source of H atoms in both the stratosphere and mesosphere
ii. Major loss reaction for OH in both the stratosphere and mesosphere
iii. Major loss reaction for $O(^3P)$ in the mesosphere

Evaluations

Baulch *et al.* (6)	3.8×10^{-11}	300 °K
Wilson (21)	4.2×10^{-11}	300–1000 °K
CIAP (5)	4.2×10^{-11}	300–1000 °K

New rate data: None

[13] $OH + O_3 \rightarrow HO_2 + O_2$

Atmospheric significance
i. Possible important loss reaction for O_3 in the middle and upper stratosphere

Evaluations

NBS	$1.6 \times 10^{-12} \exp(-1000/T)$	220–450 °K
CIAP (5)	Same as above	

New rate data

Kurylo (8)	5.0×10^{-14}	300 °K
Davis and Schiff (11)	7.5×10^{-14}	300 °K

[14] $HO_2 + HO_2 \rightarrow H_2O_2 + OH$

Atmospheric significance
i. Major source of H_2O_2 in both the stratosphere and mesosphere
ii. Moderately important loss reaction for odd hydrogen (H, HO_2, OH) in the lower and middle stratosphere

Evaluations

Baulch *et al.* (6)	3.3×10^{-12}	300 °K
NBS	$3 \times 10^{-11} \exp(-500/T)$	300–1000 °K
CIAP (5)	$3 \times 10^{-11} \exp(-500/T)$	300–1000 °K

New rate data: None

[16] $HO_2 + O(^3P) \rightarrow OH + O_2$

Atmospheric significance
i. One of the major loss reactions for HO_2 in the mesosphere and the upper and middle stratosphere
ii. One of the major OH sources in the mesosphere and the upper and middle stratosphere
iii. One of the major loss reactions for odd oxygen [$O(^3P)$; O_3] in the mesosphere and upper stratosphere

Evaluations

Lloyd (19)	$8 \times 10^{-11} \exp(-500/T)$ (estimated)
CIAP (5)	Same as above

New rate data: None

[18] $HO_2 + O_3 \rightarrow OH + 2O_2$

Atmospheric significance
i. A possible significant source of OH at mid-stratospheric altitudes (see discussion section)

Evaluations

CIAP (5)	$k = 1 \times 10^{-12} \exp(-1875/T)$	220–450 °K

New rate data

Simonaitis and Heicklen (12) $3.3 \times 10^{-14} \exp(-1000/T)$ 225–298 °K
Relative rate measurement, k/k_a, where k_a is $HO_2 + HO_2 \rightarrow H_2O_2 + O_2$
Assumed k_a had zero temperature dependence

[20] $H_2O_2 + O(^3P) \rightarrow OH + HO_2$ (*a*)
$\rightarrow H_2O + O_2$ (*b*)

Atmospheric significance
i. Moderately important loss reaction for H_2O_2 in the mesosphere and upper stratosphere

Evaluations

CIAP (5)	$k(a + b) = 3.6 \times 10^{-11} \exp(-2950/T)$	283–373 °K

New rate data: None

Can. J. Chem. Downloaded from www.nrcresearchpress.com by 210.87.254.5 on 09/05/12
For personal use only.

TABLE 2. (*Continued*)

[23] $O(^3P) + O(^3P) + M \rightarrow O_2 + M$

Atmospheric significance
i. Moderately important loss reaction for $O(^3P)$ in the mesosphere and upper stratosphere

Evaluations

Johnston (3)	$3.80 \times 10^{-30} T^{-1} \exp(-170/T)$	$1000 < T < 8000$; $M = O_2$
CIAP (5)	Same as above	

New rate data

Campbell and Gray (25)	4.8×10^{-33}	298 °K; $M = N_2$
	10.1×10^{-33}	196 °K; $M = N_2$

Should not alter evaluation by Johnston significantly

[24] $O(^3P) + O_2 + M \rightarrow O_3 + M$

Atmospheric significance
i. Major reaction of $O(^3P)$ in the stratosphere and mesosphere
ii. Only known source of O_3 in the stratosphere and mesosphere

Evaluations

Johnston (3)	$4.6 \times 10^{-35} \exp(1050/T)$	200–1000 °K; $M = O_3$
	$1.2 \times 10^{-35} \exp(1050/T)$; $M = Ar$	
CIAP (5)	$6.6 \times 10^{-35} \exp(510/T)$; $M = Ar$;	200–346 °K
	Relative M efficiencies: Ar (1.0) N_2 (1.6) O_2 (1.7) H_2O (15)	

New rate data: None

[25] $O(^3P) + O_3 \rightarrow 2O_2$

Atmospheric significance
i. An important loss reaction for O_3 in the upper and middle stratosphere

Evaluations

Johnston (3)	$2.0 \times 10^{-11} \exp(-2410/T)$	200–1000 °K
NBS	$2.0 \times 10^{-11} \exp(-2410/T)$	188–1000 °K
CIAP (5)	$1.9 \times 10^{-11} \exp(-2300/T)$	220–1000 °K

New rate data: None

[30] $OH + SO_2 + M \rightarrow HSO_3 + M$

Atmospheric significance
i. A possible important reaction in the conversion of SO_2 to sulfuric acid aerosol

Evaluations: None

New rate data

Davis *et al.* (20)	$\sim 3 \times 10^{-31}$; $M = H_2O$;	Relative rate measurement 300 °K (The reference reaction in this system was $OH + CO \rightarrow CO_2 + H$)
Davis and Schiff (11)	Reaction is in the high pressure fall region above ~10 Torr of He. At 500 Torr He, the effective bimolecular rate constant is 2.5×10^{-3}	Flash photolysis – resonance fluorescence 300 °K

[31] $HO_2 + SO_2 \rightarrow OH + SO_3$

Atmospheric significance
i. A possible important reaction in the conversion of SO_2 to sulfuric acid aerosol

Evaluations

CIAP (5)	8.7×10^{-16}	300 °K

New rate data: None

Can. J. Chem. Downloaded from www.nrcresearchpress.com by 210.87.254.5 on 09/05/12
For personal use only.

TABLE 2. (*Concluded*)

[33] $SO_2 + O(^3P) + M \rightarrow SO_3 + M$

Atmospheric significance
i. Considered to be of possible importance in the conversion of SO_2 to sulfuric acid aerosol

Evaluations

Schofield (15)	$1 \times 10^{-33} \exp(500/T)$ for M = Ar, O_2, N_2, He;	250–1000 °K
CIAP (5)	Same as above	

New rate data

Davis *et al.* (16)	$3.4 \times 10^{-32} \exp(-1120/T)$ for M = N_2	353–220 °K
		Flash photolysis – resonance fluorescence
	Relative efficiencies N_2:He:Ar:SO_2	1.0:0.45:0.87:60

New data will have a significant effect on previous evaluations

[37] $OH + CO \rightarrow CO_2 + H$

Atmospheric significance
i. Only important atmospheric process known to convert CO to CO_2 in the stratosphere and mesosphere
ii. Important loss reaction for OH in the lower stratosphere

Evaluations

Schofield (15)	$1.1 \times 10^{-12} \exp(-515/T)$	
Baulch, Drysdale, and Lloyd	$9.3 \times 10^{-13} \exp(-540/T)$	
Wilson (21)	$5.1 \times 10^{-13} \exp(-300/T)$	200–2000 °K
CIAP (5)	$5.1 \times 10^{-13} \exp(-300/T)$	200–2000 °K

New rate data

Westernberg and deHaas (17)	$1.33 \times 10^{-13} \exp(-0.0/T)$	450–300 °K
Zellner and Smith (18)	$2.1 \times 10^{-13} \exp(-50/T)$	470–215 °K
Davis *et al.* (16)	$2.05 \times 10^{-13} \exp(-70/T)$	373–220 °K

New rate data will have a moderate effect on previous evaluations

[38] $HO_2 + CO \rightarrow CO_2 + OH$

Atmospheric significance
i. Considered at one time to be of possible importance in the conversion of CO to CO_2 in the stratosphere

Evaluations

Lloyd (19)	$\sim 1 \times 10^{-24}$
CIAP (5)	$\leq 1 \times 10^{-19}$

New rate data: None

[44] $OH + CH_4 \rightarrow CH_3 + H_2O$

Atmospheric significance
i. Major initial step in the oxidation of CH_4 in the stratosphere

Evaluations

Wilson (21)	$4.77 \times 10^{-11} \exp(-2500/T)$	300–2000 °K
CIAP (5)	Same as above	

New rate data

Davis *et al.* (26)	$2.5 \times 10^{-12} \exp(-1700/T)$ 240–373 °K	Flash photolysis – resonance fluorescence

New data will have a significant effect on previous evaluation

*The units for all rate constants reported in this table are in cm^3 $molecule^{-1}$ s^{-1} and cm^6 $molecule^{-2}$ s^{-2}.

Although the disagreement is only a factor of 2 it must be pointed out that all reported studies on this system have involved indirect measurements, with complex chemistry. It is not unreasonable, therefore, that the value of this rate constant could change in future evaluations by as much as a factor of 3. A final point that should be made in regards to reaction 18 is the role it might play in defining the ozone profile in the stratosphere. Whereas, it might first appear that an increase in the value of k_{18} would necessarily cause a reduction in the predicted ozone profile, Crutzen (1) has recently carried out calculations which indicate something quite different. Crutzen's argument is that an increase in k_{18} would cause an increase in the stratospheric OH concentration and this in turn would reduce the level of NO_2 via the reaction

$$OH + NO_2 + M \rightarrow HNO_3 + M$$

The subsequent reduction in NO_2 could then cause a lowering of the efficiency of the NO–

Can. J. Chem. Downloaded from www.nrcresearchpress.com by 210.87.254.5 on 09/05/12
For personal use only.

Can. J. Chem. Downloaded from www.nrcresearchpress.com by 210.87.254.5 on 09/05/12
For personal use only.

NO_2 catalytic cycle and thereby preserve O_3. His calculations show, in fact, that the faster value of k_{18} now being used could cause a very slight increase in the predicted profile of O_3.

Reaction 24 is one of the key reactions in the stratosphere. It is believed to be the single important source of ozone, and hence, any variation in the value of k_{24} has nearly a linear effect on an atmospheric model of the stratosphere. From Table 2, it can be seen that a significant change in the rate expression for this process took place from the 1968 Johnston review to the 1973 CIAP evaluation. This reevaluation was based on the recent work of Huie, Herron, and Davis (14), who made direct measurements of the rate constant for this system using the technique of flash photolysis – resonance fluorescence. The temperature range covered was 200–346 °K. From Fig. 1, it can be seen that the agreement between Johnston's evaluation (derived from the equilibrium constant and the k value for the reverse reaction) and the results of Huie *et al.* is within 10% at 298 °K. At stratospheric temperatures of 220 °K, the difference in k values is a factor of 2, the newer value (5) being a factor of 2 lower.

Reaction 33 has received considerable attention the last few years due to its possible importance in the conversion of SO_2 to sulfuric acid aerosol in the now well-known Junge aerosol belt (16–22 km). Nearly all of the work reviewed by Schofield (15) was carried out at 300 °K and the experimental techniques employed were mainly either discharge flow systems with e.s.r. detection or indirect photochemical methods. Because the reaction was known to be third order, Schofield assigned a negative temperature dependence to the reaction of −1000 cal/mol. More recently, Davis, Schiff, and Fischer (16) using the flash photolysis – resonance fluorescence technique examined this reaction over a temperature range of 353–220 °K for M = N_2, He, Ar, and SO_2. In this study a static reaction cell configuration was employed in which pressures as high as 1500 Torr could be used. Their results indicated lower values for the third order rate constants at 300 °K for all M gases employed; most importantly, the results showed the reaction to have a positive temperature dependence of 2000 cal/mol. The explanation given for the observed positive temperature dependence was that the third order reaction proceeded via a two step mechanism. The first step would involve the formation of the spin allowed triplet SO_3 molecule. The second step, the intersystem crossing of the SO_3 triplet to the single ground state SO_3, could then give rise to the observed positive temperature dependence. A comparison of the rate constants at 220 °K shows the results of Davis *et al.* (16) nearly 2 orders of magnitude lower than that predicted from Schofield's equation (15). If the results from this new study are correct, the importance of reaction 33 to the SO_2 aerosol conversion mechanism would appear to be negligible. A possible exception to this conclusion, however, would be if the reaction of triplet SO_3 with H_2O was found to be much faster than for the same reaction involving ground state singlet SO_3. The latter species would be formed from reaction 31 ($HO_2 + SO_2 \rightarrow OH + SO_3$).

The rate expression for the reaction of OH with CO (process 37) has undergone several changes in the last 10 years. In 1963, for example, the activation energy was listed as 10 kcal/mol; in 1965, 7.7 kcal/mol; in 1967, 2.5 kcal/mol; again in 1967, 1.0 kcal/mol; in 1972, 0.6 kcal/mol; and finally in 1973, $E_{act} \simeq 0.06$ kcal/mol. The near zero activation energy now being suggested is the result of new studies in 1973 by

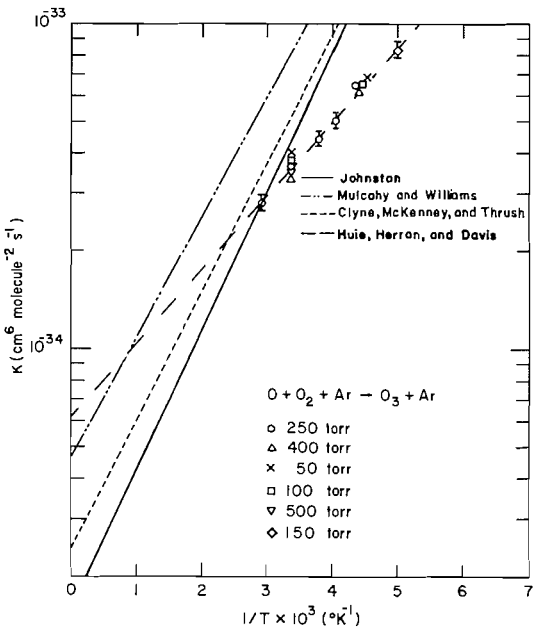

FIG. 1. Arrhenius plot for the reaction $O(^3P) + O_2 + M \rightarrow O_3 + M$; ——— Johnston (3), (—··—) Mulcahy and Williams (27), (-----) Clyne *et al.* (28), (— — —) Huie *et al.* (14).

Can. J. Chem. Downloaded from www.nrcresearchpress.com by 210.87.254.5 on 09/05/12
For personal use only.

Westenberg and deHaas (17), Zellner and Smith (18), and Davis, Schiff, and Fischer (16). The techniques employed in these three independent studies include discharge flow – e.s.r. detection, flash photolysis – absorption spectroscopy, and flash photolysis – resonance fluorescence. All three involved direct measurements of the OH radical concentration *vs.* reaction time. Below 373 °K, the data all lie within ~10% of each other. Since the temperature dependence for this reaction now appears to be very small it is quite possible that it does not, in fact, reflect a small threshold energy for the reaction but rather a small temperature dependence in the pre-exponential factor. The fact that the low temperature data do not extrapolate linearly into the high temperature results on this reaction could be due to two reasons: (*1*) the high temperature data are systematically in error because of the much more complex nature of the chemistry at these temperatures; or (*2*) the simple Arrhenius expression is inadequate for treating this system over an extended temperature range. The latter possibility has been considered by both Westenberg and deHaas and Zellner and Smith who applied transition state theory to this system. Both sets of calculations predicted strong curvature in the ln k *vs.* $1/T$ plot at temperatures above ~500 °K.

The rate constant for the reaction of HO_2 with CO (process 38) has also undergone some enormous fluctuations in the last 2 years. This reaction was listed in the set of 20 important atmospheric reactions because of the recently reported k value for this process of 10^{-12} cm^3 molecule^{-1} s^{-1}. This result, reported by Westenberg and deHaas, would have made this reaction the single most important atmospheric oxidation path for conversion of CO to CO_2. Previous to the Westenberg and deHaas measurement, Lloyd's 1971 evaluation (19) (based primarily on high temperature data) listed the value of the rate constant as 10^{-24} cm^3 molecule^{-1} s^{-1}. The 1973 CIAP evaluation is based on the newer results of Davis, Payne, and Stief (20) and Simonaitis and Heicklen (12). Both studies gave values in the range of 10^{-19} cm^3 molecule^{-1} s^{-1}, making reaction 38 of negligible importance to atmospheric modelling efforts. Two of the major differences between the experiments carried out by the latter two groups and those by Westenberg and deHaas were the total pressure and gas compositions. In Westenberg's experiments a low pressure discharge flow system with e.s.r. detection of H, O, and OH was employed, whereas Davis *et al.* (20) and Simonaitis and Heicklen (12) used high pressure photochemical methods containing large amounts of water vapor. It has been suggested by Davis *et al.* that a possible explanation for the 8 orders of magnitude difference might have been the presence of vibrationally and rotationally excited OH or HO_2 in Westenberg's experiments (17).

A final reaction whose rate expression would appear to be due for a reevaluation is process 44. The 1972 evaluation by Wilson (21) gives the activation energy as ~5 kcal/mol. This evaluation excluded (or minimized) the low temperature data of Greiner (22) and instead relied more upon the numerous high temperature results. However, the newer low temperature data (373–240 °K) of Davis, Schiff, and Fischer (16) corroborate the earlier results of Greiner, giving an activation energy of ~3.4 kcal/mol. In the latter study by Davis *et al.*, low flash energies which produced no more than 10^{10}–10^{11} OH radicals/cc were used in combination with resonance fluorescence detection. The probability of secondary reactions being important, therefore, appears to be quite small. As in the OH + CO system, the low temperature data for process 44 do not extrapolate linearly into the high temperature results. The explanation for this behavior is probably similar to that for the OH—CO reaction.

Recommendations for New Experimental Work

Thus far very little has been said about the reliability of the rate constants quoted in the text. However, since the recommending of new experimental work necessarily reflects the uncertainty in available rate data, an acceptable magnitude for this uncertainty must now be indicated. In this case, those reactions which this author feels are in need of additional work would typically have uncertainties of no smaller than ±50%, and in some cases the uncertainties might be as high as plus or minus a factor of 5.

It is this author's opinion that there are three general areas where additional experimental work would be desirable. These include: (1) ozone reactions, 7, 13, and 18; (2) SO_2 reactions, 30, and 31; and (3) radical–radical reactions, 3,

Can. J. Chem. Downloaded from www.nrcresearchpress.com by 210.87.254.5 on 09/05/12
For personal use only.

9, 11, 14, and 16. In the case of the first group mentioned, there have been no direct measurements of the temperature dependence of process 7 (presumably small) and only two measurements at 300 °K. The value of the rate constant for reaction 13 appears to be well established at 300 °K, but additional direct measurements of the temperature dependence of this process seem to be justified at this time. As pointed out earlier in the text, there have been no direct measurements of the reaction of HO_2 with O_3.

The two homogeneous gas phase reactions which now appear to provide a possible explanation for the presence and location of the Junge aerosol belt are processes 30 and 31. Only preliminary data at 300 °K are now available for reaction 30 and only relative rate measurements at 300 °K have been completed for reaction 31. Both must be studied as a function of temperature, and reaction 30 must be investigated also as a function of total pressure.

One of the most neglected areas of experimental kinetics has been that of radical–radical reactions. These measurements are necessarily difficult since absolute concentrations of transient species must be determined. In most cases, the rate constants quoted for these fast reactions have been estimated only. With the possible exception of reaction 14, very few direct measurements exist at 300 °K, and almost no temperature dependence studies have been carried out. Processes 3, 9, 11, 14, and 16 are of critical importance to present modelling efforts since in many regions of the atmosphere they control the important ratios HO_2:OH; O:OH; and H:OH.

The author would like to thank Professor Harold Schiff for extending to him an invitation to present this review paper on atmospheric kinetics. He would also like to express his appreciation to the CIAP office of the U.S. Department of Transportation and the IAGA Committee for providing financial support to allow this author to attend the IAGA meeting in Koyoto, Japan.

1. (*a*) P. J. CRUTZEN. J. Geophys. Res. **26**, 7311 (1971). (*b*) P. J. CRUTZEN. Q. J. R. Meteorol. Soc. **96**, 320 (1970). (*c*) P. J. CRUTZEN. Paper presented at the IAGA meeting, Kyoto, Japan. 1973.
2. (*a*) E. HESSTVEDT. Paper presented at CIAP workshop, Washington, D.C., Oct. 1972. (*b*) E. HESSTVEDT. Can. J. Chem. This issue.
3. H. S. JOHNSTON. Gas phase reaction kinetics of neutral oxygen species. NBS-NSRDS **20**, 1968 Supr. of Documents, U.S. Government Printing Office, Washington, D.C. 20402.
4. (*a*) M. NICOLET. Planet. Space Sci. **20**, 1671 (1972). (*b*) M. NICOLET and W. PEETERMAUS. Ann. Geophys. **4**, 751 (1972). (*c*) M. NICOLET and G. BRASSEUR. Planet. Space Sci. **21**, 939 (1973).
5. Climatic impact assessment program, second draft of monograph 1. The natural stratosphere. CIAP office, Department of Transportation, Washington, D.C.
6. D. L. BAULCH, D. D. DRYSDALE, D. G. HORNE, and A. C. LLOYD. Evaluated kinetic data for high temperature reactions. Vol 1. *In* Homogeneous gas phase reactions of the H_2O_2 system. Butterworth, London. 1972.
7. D. D. DAVIS and W. WONG. Int. J. Chem. Kinet. In press.
8. (*a*) M. F. KURYLO. Paper presented at the AIAA meeting, Denver, Colo. June 1973. (*b*) M. F. KURYLO. J. Phys. Chem. **76**, 3518 (1972).
9. W. D. DEMORE. Science, **180**, 735 (1973).
10. J. G. ANDERSON and F. KAUFMAN Chem. Phys. Lett. **19**, 483 (1973).
11. D. D. DAVIS and R. SCHIFF. Unpublished results.
12. (*a*) R. SIMONAITIS and J. HEICKLEN. J. Phys. Chem. **77**, 1096 (1973). (*b*) R. SIMONAITIS and J. HEICKLEN. J. Phys. Chem. **77**, 1932 (1973).
13. E. JOHNSTON. Catalytic reduction of stratospheric ozone by nitrogen oxides. AEC Report UCRL-20568.
14. R. HUIE, J. HERRON, and D. D. DAVIS. J. Phys. Chem. **76**, 2653 (1972).
15. K. SCHOFIELD. Planet. Space Sci. **15**, 643, 1336 (1967).
16. D. D. DAVIS, R. SCHIFF, and S. FISCHER. Unpublished results.
17. A. A. WESTENBERG and N. DEHAAS. J. Phys. Chem. **76**, 1586 (1972).
18. R. ZELLNER and I. W. M. SMITH. J. Chem. Soc. Faraday Trans. **11**, 1617 (1973).
19. A. C. LLOYD. Evaluation and estimated kinetic data for the gas phase reactions of the hydroperoxyl radical. NBS Report 10447. 1971.
20. D. D. DAVIS, W. PAYNE, and L. STIEF. Science, **179**, 280 (1973).
21. WM. E. WILSON, JR. J. Phys. Chem. Ref. Data, **1**, 535 (1972).
22. N. R. GREINER. J. Chem. Phys. **53**, 1070 (1970).
23. F. KAUFMAN. Ann. Geophys. **20**, 106 (1964).
24. C. J. HOCHANADEL, J. A. GHORMLEY, and P. J. OGREN. J. Chem. Phys. **56**, 4426 (1972).
25. I. M. CAMPBELL and C. N. GRAY. Chem. Phys. Lett. **18**, 607 (1973).
26. D. D. DAVIS, S. FISCHER, and R. SCHIFF. Unpublished results.
27. M. F. R. MULCAHY and D. J. WILLIAMS. Trans. Faraday Soc. **64**, 59 (1968).
28. M. A. A. CLYNE, D. J. MCKENNEY, and B. A. THRUSH. Trans. Faraday Soc. **61**, 2701 (1965).
29. L. I. AVRAMENKO and R. V. KOLESNIKOVA. Mechanisms and rate constants of elementary gas phase reactions involving hydroxyl. Interscience, New York. 1964. p. 25.
30. R. R. BALDWIN, A. C. NORRIS, and R. W. WALKER. 11th Symposium on Combustion. The Combustion Institute, 1965. p. 889.

31. R. V. BLUNDELL, W. G. A. COOK, D. E. HOARE, and G. S. MILNE. 10th Symposium on Combustion. The Combustion Institute, 1965. p. 445.
32. G. DIXON-LEWIS and A. WILLIAMS. 11th Symposium on Combustion. The Combustion Institute, 1967. p. 951.
33. D. D. DRYSDALE and A. LLOYD. Private communication.
34. C. P. FENIMORE and G. W. JONES. J. Chem. Phys. **65**, 2200 (1961).
35. R. M. FRISTROM. 9th Symposium on Combustion. Academic Press, N.Y. 1963. p. 560.
36. D. E. HOARE. Nature, **194**, 283 (1962); D. E. HOARE. Proc. R. Soc. A, **291**, 73 (1966); D. E. HOARE and G. B. PEACOCK. Proc. R. Soc. A, **291**, 85 (1966).
37. D. G. HORNE and R. G. W. NORRISH. Nature, **215**, 1373 (1967).
38. W. PAYNE, L. STIEF, and D. D. DAVIS. J. Am. Chem. Soc. In press.
39. WM. E. WILSON, JR., J. T. O'DONOVAN, and R. M. FRISTROM. 12th Symposium on Combustion. The Combustion Institute, 1969. p. 929.

Can. J. Chem. Downloaded from www.nrcresearchpress.com by 210.87.254.5 on 09/05/12
For personal use only.

Photochemistry of NO_x and HNO_x Compounds

HAROLD S. JOHNSTON AND RICHARD GRAHAM

Department of Chemistry, University of California and Inorganic Materials Research Division, Lawrence Berkeley Laboratory, Berkeley, California

Received November 20, 1973

Cross sections for absorption of radiation between 190 and 700 nm are given for N_2O, NO_2, NO_3, N_2O_4, N_2O_5, HNO_2, and HNO_3. The quantum yields and the primary products of photolysis of each of these substances are discussed. This article includes spectral data obtained in this laboratory for NO_2, NO_3, N_2O_5, HNO_2, and HNO_3 and it includes spectral data from the literature for N_2O and N_2O_4. The quantum yields are based both on results from this laboratory and from the literature.

Les sections droites d'absorption de radiation entre 190 et 700 nm sont données pour N_2O, NO_2, NO_3, N_2O_4, N_2O_5, HNO_2 et HNO_3. Les rendements quantiques et les produits initiaux de photolyse de chacune de ces substances sont discutés. Cet article comprend des données spectrales obtenues dans ce laboratoire pour NO_2, NO_3, N_2O_5, HNO_2 et HNO_3 et il inclut des données spectrales de la littérature pour N_2O et N_2O_4. Les rendements quantiques sont basés à la fois sur des résultats déduits de ce laboratoire et de la littérature. [Traduit par le journal]

Can. J. Chem., **52**, 1415 (1974)

Introduction

The photolysis of the oxides of nitrogen and of the oxyacids of nitrogen involves the absorption cross section σ and the primary quantum yield ϕ, each a function of wavelength. The cross section σ is defined at the average wavelength λ by

$$\ln I_0(\lambda)/I(\lambda) = \sigma(\lambda)[A]L$$

where [A] is the concentration of substance A in molecules cm^{-3}, L is the optical path length in cm, I_0 is the incident beam over the narrow wavelength band in units of photons $cm^{-2}\ s^{-1}$, and I is the transmitted intensity. The cross section σ is in units of cm^2, depends on wavelength λ, and for broad bands of radiation depends on the band width of radiation $\Delta\lambda$. The quantum yield for photolysis of A is the ratio of molecules of A destroyed per photon of radiation absorbed

$$\phi = \frac{\text{molecules of A destroyed}}{\text{photons of radiation absorbed}}$$

The quantum yield for forming a given product P is the ratio of the number of molecules of P formed per photon of radiation absorbed by A.

This article briefly reviews the literature for absorption cross sections of N_2O (190–315 nm), HNO_3 (190–325 nm), N_2O_4 (240–390 nm), N_2O_5 (285–380 nm); and it presents data from this laboratory for NO_2 (190–420 nm), N_2O_5 (210–290 nm), HNO_2 (300–400 nm), and NO_3 (450–680 nm). This article briefly reviews the literature for the quantum yields for photolysis of N_2O, NO_2, N_2O_4, and N_2O_5; and it presents data from this laboratory for the quantum yields of HNO_3 and HNO_2. The possible photolysis products of NO_3 are discussed. This article does not discuss nitric oxide (NO), which is a separate, full-sized research problem all in itself and which is being analyzed by others.

The purpose of this article is to collect in one place the values of cross section σ and quantum yield ϕ. The cross sections are given in Tables 1 to 3 and in Figs. 1 to 5. The quantum yields are indicated on some of the figures and are discussed separately for each case.

Experimental

The apparatus has been described previously (1). It consists of a silica cell 15 cm in diameter and 2 m long. It is equipped with nickel-coated stainless-steel end caps and with three mirrors to give multiple pass operation (White cell). Spectra were taken with optical paths between 8.6 and 34 m. Deuterium arc sources were used for radiation between 190 and 420 nm, and tungsten filament sources were used above 420 nm. Wavelengths were calibrated from a low-pressure mercury arc. A McPherson 1/3 m vacuum spectrometer was used for NO_2 and NO_3 and a McPherson 1 m monochromator was used for N_2O_5 and HNO_2.

Materials

Oxygen was purified by passing through a silica tube with copper turnings at 600 °C, through a column con-

Can. J. Chem. Downloaded from www.nrcresearchpress.com by 210.87.254.40 on 09/05/12
For personal use only.

taining pellets of 5% palladium on alumina at 350 °C, and then through columns of ascarite and phosphoric anhydride (P_2O_5). Ozone was prepared by electric discharge through purified oxygen with continuous input into a 1 atm flow system. Nitric oxide was purified by the method of Dinerman and Ewing (2). Nitrogen dioxide was purified as previously described (1). Dinitrogen pentoxide was prepared from nitrogen dioxide and ozone by the reaction

$$2NO_2 + O_3 \rightarrow N_2O_5 + O_2$$

The NO_3 radical was prepared in a low, steady state concentration by mixing N_2O_5 with an excess of ozone; in this system ozone undergoes a slow, catalytic decomposition. Nitrous acid vapor was prepared at a low equilibrium concentration in a system with excess NO, small amounts of H_2O, and very small amounts of NO_2

$$NO + NO_2 + H_2O = 2HNO_2$$

Discussion of Each Substance

Nitrous Oxide

The absorption cross sections for N_2O were read from a graph by Bates and Hayes (3). These cross sections are entered in Table 1 and on Figs. 1 and 2. The photolysis of nitrous oxide can give the following products as a function of wavelength

[1] $N_2O + h\nu \rightarrow N_2\ (X\ ^1\Sigma) + O(^1D) \quad \lambda < 337$ nm

[2] $\rightarrow N_2\ (X\ ^1\Sigma) + O(^1S) \quad \lambda < 210$ nm

[3] $\rightarrow NO\ (X\ ^2\Pi) + N(^4S) \quad \lambda < 250$ nm

Preston and Barr (4) state that the primary quantum yield for photolysis of nitrous oxide is 1.00 at all wavelengths below 337 nm, and the process forming atomic nitrogen (reaction 3) is 0.01 or less.

Nitrogen Dioxide

The photochemistry of NO_2 has been thoroughly reviewed by Hampson and Garvin (5). Here we present our data for the NO_2 spectrum and a summary of Hampson and Garvin's conclusions about quantum yields. The absorption spectrum of NO_2 with 8.6 m optical path, 1.3 nm resolution (full width at half maximum), averaged over 1 nm, with $(1–10) \times 10^{14}$ molecules cm^{-3}, and at 294 °K is given by Fig. 2, and values at each 5 nm between 190 and 420 nm are listed in Table 1. The concentration of N_2O_4 is less than 10^{10} molecules cm^{-3} for the points taken below 250 nm, and the contribution of N_2O_4 to the spectrum of NO_2 should be immeasurably small.

Hampson and Garvin (5) concluded that under atmospheric conditions the primary quantum yield for

[4] $NO_2 + h\nu \rightarrow NO\ (X\ ^2\Pi) + O(^3P)$

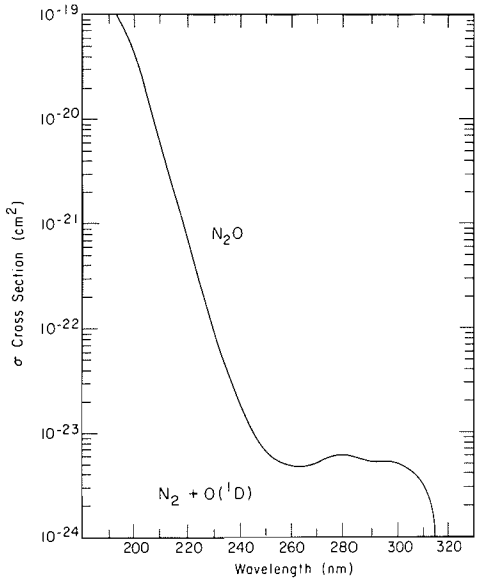

FIG. 1. Absorption cross sections, σ (cm²), as a function of wavelength with principal, energetically possible primary dissociation fragments. Nitrous oxide, N_2O.

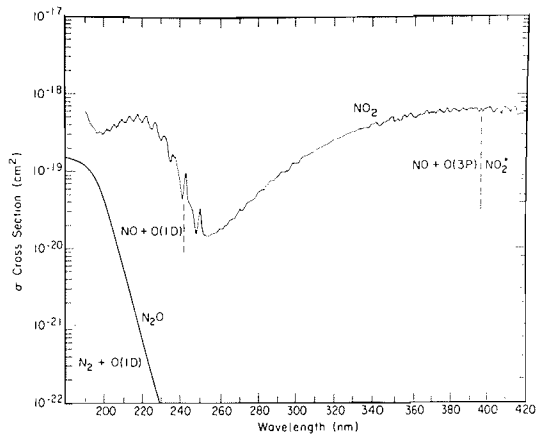

FIG. 2. Absorption cross sections, σ (cm²), as a function of wavelength with principal, energetically possible primary dissociation fragments. Nitrogen dioxide, NO_2, and portions of the N_2O spectrum.

is unity from 398 to 244 nm, and the primary quantum yield for

[5] $NO_2 + h\nu \rightarrow NO\ (X\ ^2\Pi) + O(^1D)$

is unity from 244 to 190 nm. There is some temperature and pressure dependent structure to the quantum yield above 398 nm. At 298 °K, above 398 nm, Hampson and Garvin recommend as primary quantum yield for formation of $O(^3P)$ the following values: 400, 0.70; 405, 0.29; 410,

Can. J. Chem. Downloaded from www.nrcresearchpress.com by 210.87.254.40 on 09/05/12
For personal use only.

Can. J. Chem. Downloaded from www.nrcresearchpress.com by 210.87.254.40 on 09/05/12
For personal use only.

TABLE 1. Absorption cross sections, σ (cm^2), for N_2O, NO_2, HNO_3, N_2O_4, and N_2O_5 at 5 nm intervals from 190 to 420 nm

λ (nm)	N_2O	NO_2 (10^{19} σ)	HNO_3	N_2O_4 (10^{19} σ)	N_2O_5
190	1.26(−19)	6.12	1.32(−17)		
195		3.64	9.10(−18)		
200	4.46(−20)	3.19	5.50(−18)		
205		4.27	2.55(−18)		
210	5.37(−21)	4.52	9.70(−19)		4.7(−18)
215		4.65	3.28(−19)		3.2(−18)
220	7.08(−22)	4.38	1.44(−19)		2.0(−18)
225		3.71	8.51(−20)		1.3(−18)
230	8.90(−23)	2.52	5.63(−20)		9.6(−19)
235		1.36	3.74(−20)		7.5(−19)
240	1.90(−23)	0.90	2.60(−20)	10.7	6.0(−19)
245		0.39	2.10(−20)		4.7(−19)
250	6.6(−24)	0.34	1.95(−20)	8.54	3.7(−19)
255		0.16	1.94(−20)		2.9(−19)
260	4.67(−24)	0.18	1.90(−20)	7.97	2.4(−19)
265		0.24	1.80(−20)		2.0(−19)
270	5.12(−24)	0.33	1.63(−20)	7.11	1.7(−19)
275		0.42	1.40(−20)		1.3(−19)
					8.9(−20)[a]
280	6.02(−24)	0.57	1.14(−20)	5.69	
					5.1(−20)[b]
285		0.72	8.77(−21)		
290	5.0(−24)	0.88	6.34(−21)	4.12	4.2(−20)
295		1.07	4.26(−21)		
300	5.0(−24)	1.33	2.76(−21)	3.02	2.45(−20)
305		1.65	1.68(−21)	2.85	
310	3.2(−24)	1.97	9.50(−22)	3.02	1.3(−20)
315	1(−24)	2.24	4.70(−22)		
320		2.61	1.80(−22)	4.27	7.5(−21)
325		2.94	2(−23)		
330		3.38		6.12	4.0(−21)
335		3.61			
340		4.17		6.90	2.7(−21)
345		4.30			
350		4.48		5.69	1.8(−21)
355		5.53			
360		4.96		3.20	1.0(−21)
365		5.84			
370		5.70		1.42	4.7(−22)
375		5.74			
380		6.52		0.57	1.3(−22)
385		6.45			
390		6.51		0.14	
395		6.08			
400		6.68			
405		6.52			
410		6.59			
415		6.03			
420		6.24			
425					
430					

[a]This work, 210–280 nm. This work gives 6.5(−20) for 285 and 3.9(−20) for 290 nm.
[b]Reference 10, 285–380 nm.

Can. J. Chem. Downloaded from www.nrcresearchpress.com by 210.87.254.40 on 09/05/12
For personal use only.

0.12; 415, 0.05; 420, 0.02; 425, 0.01; 435, 0.002; 440, 0.001; above 440, 0. Although the threshold to form $O(^1D)$ is 244 nm, the detailed pattern of quantum yield as a function of wavelength has not been reported.

Dinitrogen Tetroxide

The absorption spectrum of N_2O_4 was read from a graph by Hall and Blacet (6), and it is entered in Table 1 from 240 to 390 nm. Although 240 nm is the lowest wavelength given by Hall and Blacet, there is evidence that N_2O_4 has a strong absorption below 240 nm.

The photolysis of N_2O_4 can proceed by at least two paths

[6] $$N_2O_4 + h\nu \rightarrow NO_2 + NO_2$$

[7] $$N_2O_4 + h\nu \rightarrow N_2O_3 + O \rightarrow NO + NO_2 + O$$

Since NO_2 is in rapid equilibrium with N_2O_4, process 6 would be rapidly reversible, and would give an apparent quantum yield of zero. Reaction 7 would be rapidly followed by

[8] $$NO_2 + O \rightarrow NO + O_2$$

to give a quantum yield of 2 for formation of nitric oxide. Holmes and Daniels (7) found the overall quantum yield of NO was 0.4 ± 0.1 at 265 nm and 0.2 ± 0.1 at 280 nm. Presumably both processes 6 and 7 occur, and the resulting quantum yield is an average between 0 for one process and 2 for the other.

Dinitrogen Pentoxide

Dinitrogen pentoxide was prepared from nitrogen dioxide and ozone. Pure nitrogen pentoxide can be frozen out of a system containing excess ozone and sublimed from the white crystals formed. Pure nitrogen pentoxide undergoes a fairly rapid thermal decomposition (8) to give O_2 and NO_2, which overlaps the N_2O_5 spectrum. The NO_2 bands can be suppressed by excess ozone (9), but then the N_2O_5 spectrum has the O_3 and the NO_3 spectra superimposed. The flow rates of N_2, NO_2 in N_2, He, and O_3 were adjusted to give a slight excess of O_3 in the system. The absorption due to O_3 could then be corrected for by the structure found in its spectrum.

The absorption spectrum of 2.1×10^{14} molecules cm^{-3} of N_2O_5, between 210 and 290 nm, 17.2 m optical path, 0.87 resolution, and 298 °K, is listed in Table 1 and plotted on Fig. 3. Jones and Wulf (10) have reported N_2O_5 cross sections by means of photographic spectroscopy between

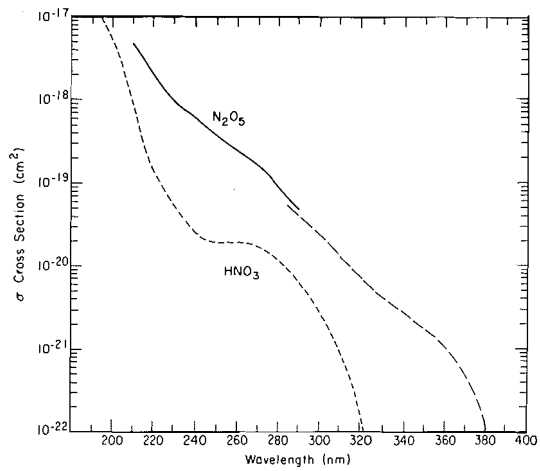

FIG. 3. Absorption cross sections, σ (cm^2), as a function of wavelength with principal, energetically possible primary dissociation fragments. Dinitrogen pentoxide, N_2O_5: (--), Jones and Wulf; (—), this study. Nitric acid, HNO_3.

285 and 380 nm. At 285 nm Jones and Wulf obtained a cross section of 5.1×10^{-20} cm^2, and we obtained 6.5×10^{-20} cm^2. The data of Jones and Wulf are included in Table 1 and Fig. 3, and they are in satisfactory agreement with our data. The uncertainty in our N_2O_5 spectrum, largely based on the uncertainty in correcting for O_3, is estimated to be $\pm 20\%$.

Studies of the photochemistry of N_2O_5 are greatly complicated by branching paths and by possible secondary chemical reactions. In pure N_2O_5 (almost unobtainable because of the thermal decomposition of N_2O_5 to NO_2) the reasonable primary processes are

[9] $$N_2O_5 + h\nu \rightarrow NO_2 + NO_3$$

[10] $$\rightarrow N_2O_4 + O \rightarrow 2NO_2 + O$$

Reaction 10 could be followed by either

[11] $$N_2O_5 + O \rightarrow 2NO_3$$

[12] $$N_2O_5 + O \rightarrow 2NO_2 + O_2$$

Reaction 9 is reversed by

[13] $$NO_2 + NO_3 \xrightarrow{M} N_2O_5$$

As NO_2 accumulates it may react with the oxygen atom

[8] $$NO_2 + O \rightarrow NO + O_2$$

N_2O_5 rapidly reacts with nitric oxide by way of

Can. J. Chem. Downloaded from www.nrcresearchpress.com by 210.87.254.40 on 09/05/12
For personal use only.

$$[14] \quad N_2O_5 \xrightarrow{M} NO_2 + NO_3$$

$$[15] \quad NO + NO_3 \rightarrow 2NO_2$$

The net quantum yield of destruction of N_2O_5 varies with mechanism; [9], [13], zero; [10], [11], [13], [13], zero; [10], [12], 2; [10], [8], [14], [15], 2. Holmes and Daniels (7) observed a quantum yield for loss of N_2O_5 at 280 nm in the absence of NO_2 of about 0.6. Murphy (11), as reported by Hampson (12), found inert-gas dependent quantum yields between 0.3 and 0.6 at 280 nm. Although these low, pressure-dependent quantum yields may be interpreted in terms of long-lived photo-excited N_2O_5, it is also possible (and, we think, more probable) that it is a matter of complex secondary thermal reactions such as [11] through [15].

The primary processes in the photolysis of N_2O_5 are not understood at this time, nor are the secondary reactions of oxygen atoms with N_2O_5 well understood.

The NO_3 Radical

The NO_3 radical was prepared in steady state relationship to N_2O_5 and excess O_3. The chemistry of NO_3 in this system has been reviewed in a textbook (13). There are four elementary chemical reactions

$$\left.\begin{aligned} [14] \quad & N_2O_5 \xrightarrow{M} NO_2 + NO_3 \\ [13] \quad & NO_2 + NO_3 \xrightarrow{M} N_2O_5 \end{aligned}\right\} K = \frac{[NO_2][NO_3]}{[N_2O_5]}$$

$$[16] \quad NO_2 + O_3 \xrightarrow{q} NO_3 + O_2$$

$$[17] \quad NO_3 + NO_3 \xrightarrow{r} NO_2 + NO_2 + O_2$$

The steady state concentration of NO_3 is

$$[NO_3] = (Kq/2r)^{1/3}[O_3]^{1/3}[N_2O_5]^{1/3}$$

At 300 °K, the equilibrium constant K is 1.2×10^{11} molecules cm^{-3}, and the ratio $q/2r$ is 1.7. Thus in units of molecules cm^{-3}, the concentration of NO_3 is

$$[NO_3] = \{1.9 \times 10^{11}[O_3][N_2O_5]\}^{1/3}$$

The absorption spectrum for NO_3 in the visible region (450 to 680 nm) was obtained in a flow system at 1 atm total pressure. The input gases were nitrogen containing 0.1% NO_2 (and a small amount of NO, which was separately measured and accounted for) and nitrogen plus ozone. Ozone was present in excess, so that NO and NO_2 were converted to N_2O_5. The amount of residual ozone was determined by its near ultraviolet absorption spectrum. For the spectrum presented in Table 2 and in Fig. 4, the cell concentrations at 22 °C were: O_3, 5.2×10^{16}; N_2O_5, 7.2×10^{14}; NO_3, 1.6×10^{14} molecules cm^{-3}. The NO_3 spectrum has been corrected for the absorption of visible light by ozone.

The absorption spectrum of NO_3 as presented in Table 2 and Fig. 4 is estimated to be uncertain by ±50%. This large uncertainty arises from the rate constants q and r entering the expression for the steady state concentration of NO_3 and from a 15% loss of N_2O_5 that reacted with water in the flowing gases to form nitric acid.

Schott and Davidson (14) measured the absorption coefficient at 652 nm of NO_3 at high temperatures in a shock-tube experiment. They extrapolated their results to 300 °K to obtain 8.4×10^{-19} cm^2 as the cross section at 652 nm. We find 2.1×10^{-19} at this wavelength.

To photolyze NO_3 to nitrogen dioxide and a ground state oxygen atom

$$NO_3 + h\nu \rightarrow NO_2 + O(^3P)$$

requires a wavelength of 578 nm or shorter, and the peaks of maximum absorption lie at longer wavelengths. The radical NO_3 has only slightly less energy (about 5 or 6 kcal mol^{-1}) than ground state O_2 and NO. The absorption spectrum in Fig. 4 has enough energy to proceed as

$$NO_3 + h\nu \rightarrow NO + O_2(^1\Sigma)$$

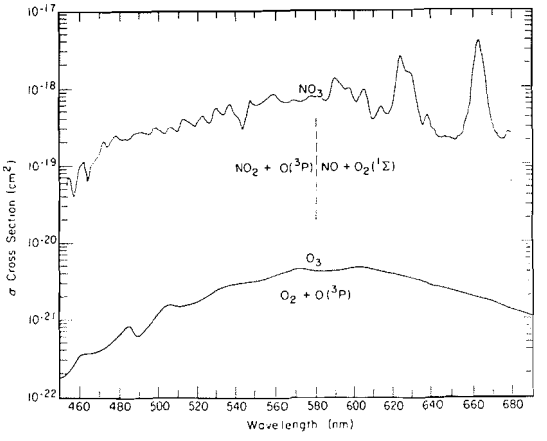

FIG. 4. Absorption cross sections, σ (cm^2), as a function of wavelength with principal, energetically possible primary dissociation fragments. NO_3 radical and the visible spectrum of ozone, O_3, for comparison (NO_3 is prepared from N_2O_5 plus excess O_3).

TABLE 2. Absorption cross section, σ (cm^2), for the NO_3 radical at 1 nm intervals from 450 to 680 nm

λ	$10^{19}\sigma$	λ	$10^{19}\sigma$	λ	$10^{19}\sigma$	λ	$10^{19}\sigma$
450		508	3.04	566	6.77	624	26.3
451	0.51	509	2.81	567	6.84	625	21.1
452	0.72	510	3.12	568	6.90	626	17.2
453	0.57	511	3.80	569	6.88	627	15.4
454	0.73	512	4.26	570	6.79	628	15.5
455	0.61	513	4.08	571	6.73	629	15.3
456	0.40	514	4.02	572	6.69	630	14.9
457	0.51	515	3.79	573	6.65	631	12.6
458	0.51	516	3.73	574	6.67	632	8.73
459	0.56	517	3.57	575	6.95	633	6.00
460	1.03	518	3.36	576	7.42	634	4.59
461	1.07	519	3.35	577	7.80	635	3.57
462	1.19	520	3.77	578	7.81	636	3.29
463	0.92	521	4.21	579	7.67	637	3.87
464	0.67	522	4.53	580	7.67	638	4.26
465	0.95	523	4.62	581	8.01	639	4.03
466	1.06	524	4.06	582	8.10	640	3.10
467	1.16	525	3.72	583	7.42	641	2.86
468	1.32	526	3.64	584	6.79	642	2.79
469	1.34	527	3.79	585	6.61	643	2.28
470	1.60	528	4.62	586	6.96	644	2.31
471	1.99	529	5.51	587	8.30	645	2.20
472	2.13	530	5.80	588	10.3	646	2.20
473	2.00	531	5.39	589	12.4	647	2.31
474	1.82	532	5.01	590	13.4	648	2.22
475	2.01	533	4.67	591	12.8	649	2.20
476	2.27	534	4.61	592	11.9	650	2.17
477	2.48	535	5.14	593	10.8	651	2.11
478	2.60	536	6.18	594	10.0	652	2.08
479	2.38	537	6.53	595	9.44	653	2.31
480	2.26	538	6.08	596	9.81	654	2.35
481	2.24	539	5.13	597	10.0	655	2.59
482	2.34	540	4.60	598	9.42	656	3.31
483	2.24	541	4.44	599	7.94	657	4.10
484	2.37	542	4.34	600	6.83	658	4.72
485	2.33	543	3.54	601	6.45	659	6.73
486	2.68	544	2.98	602	6.71	660	12.0
487	2.73	545	3.70	603	7.76	661	23.3
488	2.64	546	4.57	604	8.92	662	34.7
489	2.73	547	6.13	605	9.78	663	40.2
490	2.87	548	7.12	606	9.05	664	29.1
491	2.87	549	6.53	607	6.90	665	18.5
492	2.76	550	6.13	608	4.98	666	13.4
493	2.84	551	6.13	609	4.09	667	8.59
494	2.61	552	6.06	610	3.82	668	5.46
495	2.65	553	6.21	611	4.06	669	3.96
496	2.89	554	6.47	612	4.47	670	3.34
497	3.20	555	7.02	613	5.33	671	2.58
498	3.22	556	7.52	614	5.67	672	2.50
499	3.16	557	7.74	615	5.46	673	2.25
500	2.97	558	7.99	616	4.87	674	2.14
501	2.81	559	8.41	617	4.44	675	2.17
502	2.71	560	8.43	618	4.47	676	2.07
503	2.63	561	7.65	619	4.89	677	2.21
504	2.97	562	7.17	620	5.67	678	2.71
505	3.19	563	6.94	621	8.35	679	2.55
506	3.29	564	6.74	622	12.9	680	2.63
507	3.25	565	6.69	623	22.0		

Can. J. Chem. Downloaded from www.nrcresearchpress.com by 210.87.254.40 on 09/05/12
For personal use only.

TABLE 3. Absorption cross section, σ (cm^2), for nitrous acid vapor, HNO_2, at 1 nm intervals from 300 to 400 nm

λ	$10^{20}\sigma$	λ	$10^{20}\sigma$	λ	$10^{20}\sigma$	λ	$10^{20}\sigma$
300	0.79	325	2.00	350	3.89	375	1.72
301	0.80	326	1.45	351	5.58	376	1.51
302	0.69	327	2.05	352	4.95	377	1.62
303	0.76	328	3.33	353	6.98	378	1.77
304	0.81	329	2.48	354	11.3	379	2.10
305	0.96	330	3.14	355	12.3	380	2.52
306	1.04	331	4.86	356	5.99	381	3.18
307	0.85	332	3.35	357	3.85	382	4.11
308	0.96	333	2.51	358	3.78	383	5.57
309	1.11	334	2.99	359	3.50	384	6.78
310	1.07	335	3.02	360	3.02	385	6.40
311	1.10	336	2.45	361	2.65	386	4.72
312	1.31	337	1.93	362	2.54	387	3.12
313	1.24	338	2.80	363	2.82	388	2.07
314	1.46	339	4.99	364	3.86	389	1.42
315	1.32	340	3.69	365	4.69	390	1.01
316	0.88	341	4.51	366	5.24	391	0.72
317	0.97	342	9.22	367	7.31	392	0.57
318	1.57	343	5.82	368	12.3	393	0.54
319	1.51	344	3.35	369	12.8	394	0.42
320	1.79	345	3.34	370	7.44	395	0.35
321	2.54	346	3.57	371	4.33	396	0.32
322	2.11	347	3.35	372	3.24	397	0.28
323	2.02	348	2.73	373	2.74	398	0.20
324	2.39	349	2.75	374	2.16	399	0.21

although the state of the products has not been identified. By a molecular modulation technique, we found (work still in progress) that above 600 nm NO_3 dissociates to form NO, but the electronic state of the product O_2 was not determined. Ramsay (15) found the high resolution spectrum of NO_3 to show predissociation at all wavelengths. Thus above 578 nm, NO_3 is photodissociated to NO and to some form of O_2, probably (but not necessarily) with a large quantum yield; but below 578 nm it is not known whether the products are $NO_2 + O$ or $NO + O_2$.

Nitrous Acid

HNO_2 was prepared from mixtures of NO, NO_2, H_2O, and He. The concentration of HNO_2 present was calculated from thermochemical data (16) for the equilibrium

$$NO + NO_2 + H_2O = 2HNO_2$$

$$K = [HNO_2]^2/[NO]\,[NO_2]\,[H_2O]$$

The reactant gases NO and NO_2 were measured from their pressure in small glass pipettes, and they were added to the large (46 l) cell. Helium saturated with water vapor was added. There was a large excess of NO. The actual residual concentration of NO_2 was measured in terms of its known spectrum above 400 nm. The spectrum of N_2O_3 between 300 and 400 nm was obtained in separate experiments, and it was subtracted from the observed total spectrum. Thus the observed relatively weak spectrum of HNO_2 was corrected for the spectrum of NO_2 and the intense continuous spectrum of N_2O_3.

The absorption spectrum of HNO_2 is presented in Table 3 and Fig. 5. It was obtained with the following conditions: NO, 3.0×10^{19} molecules cm^{-3}; NO_2, 1.1×10^{15} molecules cm^{-3}; N_2O_3, 1.3×10^{15} molecules cm^{-3}; H_2O, 6.6×10^{16} molecules cm^{-3}; HNO_2 (calcd.), 1.22×10^{16} molecules cm^{-3}; 298 °K; 8.6 m optical path; 0.87 nm resolution. In other experiments several aliquots of He and H_2O were added to a similar mixture of gases. Beer's law was obeyed over the experimental range of HNO_2, (2–8) $\times 10^{15}$ molecules cm^{-3}. The position of the peaks in the spectrum agreed within 0.1 nm with those of King and Moule (17) whose high resolution study of the HNO_2 spectrum revealed no additional structure. The values of the cross sections in Table 3 and Fig. 5 are regarded as uncertain by $\pm 20\%$, on the basis of uncertainties in the corrections for N_2O_3.

A study of the quantum yield and primary photolysis products of nitrous acid is underway in this laboratory. Preliminary results are given

Can. J. Chem. Downloaded from www.nrcresearchpress.com by 210.87.254.40 on 09/05/12
For personal use only.

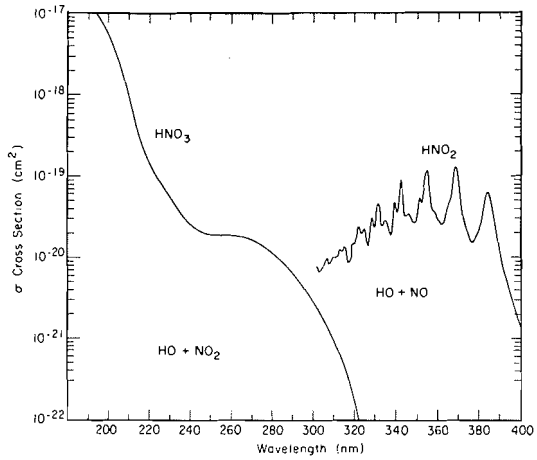

FIG. 5. Absorption cross sections, σ (cm^2), as a function of wavelength with principal, energetically possible primary dissociation fragments. Nitric acid, HNO_3, and nitrous acid, HNO_2.

here. Since HNO_2 is unstable in the gas phase, it is necessary to have excess of NO, H_2O, and NO_2 present in the system, with attendant small concentrations of N_2O_4 and N_2O_3 also present. The substances NO_2, N_2O_3, and N_2O_4 all absorb radiation in the same region as HNO_2. Thus it is desirable to minimize NO_2 as much as possible.

The possible primary products of HNO_2 photolysis include

[18] $$HNO_2 + h\nu \rightarrow HO + NO$$

[19] $$\rightarrow H + NO_2$$

[20] $$\rightarrow HNO + O$$

The third alternative would lead to nitrous oxide

$$2HNO \rightarrow H_2O + N_2O$$

The second alternative would probably be followed by $H + NO_2 \rightarrow HO + NO$, and thus be indistinguishable from the first. The reaction of HO with NO to reform nitrous acid is rapid

$$HO + NO \xrightarrow{M} HNO_2$$

so that no net change would be observed in a static system. By addition of excess carbon monoxide to the system, the presence of hydroxyl radicals can be identified

$$HO + CO \rightarrow CO_2 + H$$

A few experiments have been carried out in which HNO_2 has been photolyzed at 355 nm, and the products have been analyzed by a high resolution mass spectrometer which could differentiate between N_2O and CO_2. In the absence of added CO, no N_2O was observed. One run was made with the following composition: CO, 8.8×10^{18}; He, 1.0×10^{19}; NO, 4.4×10^{17}; H_2O, 4.4×10^{17}; NO_2, 3.2×10^{16}; and HNO_2, 7.0×10^{16} molecules cm^{-2}. Photolysis was carried out in a quartz cell 3.5 × 10 cm. No N_2O was observed but a large amount of CO_2 was found. The apparent quantum yield (no correction for the reaction

$$HO + NO \xrightarrow{M} HNO_2)$$

was 0.5. The indication is that either reaction 18 or reaction 19 occurs with a quantum yield of the order of magnitude of unity. Further work is being carried out.

Nitric Acid

The cross sections for absorption of ultraviolet radiation by nitric acid have been published by Johnston and Graham (1), and the values are entered in Table 1 and Figs. 3 and 5. Quantum yields for the process

$$HNO_3 + h\nu \rightarrow HO + NO_2$$

were determined by Johnston and Chang (18) in quartz cylinders with long exposure times to weak beams of monochromatic radiation and these results are reviewed here. Also, we photolyzed HNO_3 at 253.7 nm and observed the phase shift of NO_2 produced. The phase shift method (19) gave 1 molecule of NO_2 formed for 1 photon of 253.7 radiation absorbed by HNO_3, and the phase corresponded to a primary photochemical product. Thus at this one wavelength we have a direct determination of unit quantum yield for NO_2 production from photolysis of HNO_3.

In a small quartz cylinder with long-term exposure of pure HNO_3 to monochromatic radiation, the quantum yield of NO_2 production is very low, about 0.1. The reason for this low quantum yield is that the products of nitric acid photolysis reform nitric acid under these conditions; the sequence of reactions is

$$HNO_3 + h\nu \rightarrow HO + NO_2$$
$$HO + HNO_3 \rightarrow H_2O + NO_3$$
$$NO_2 + NO_3 \xrightarrow{M} N_2O_5$$
$$H_2O + N_2O_5 \xrightarrow{W} 2HNO_3$$

net: no change

where M refers to energy-transfer catalysts in the gas phase and W refers to the walls of the apparatus. The small degree of reaction that is observed is caused by thermal and photochemical

Can. J. Chem. Downloaded from www.nrcresearchpress.com by 210.87.254.40 on 09/05/12
For personal use only.

Can. J. Chem. Downloaded from www.nrcresearchpress.com by 210.87.254.40 on 09/05/12
For personal use only.

reactions involving N_2O_5 before it has a chance to react with water to reform HNO_3. Thus, long-term photolysis of pure nitric acid (20) vapor is an unsatisfactory method for studying the primary quantum yield for HNO_3 photolysis.

Upon addition of excess carbon monoxide to the nitric acid, the hydroxyl radical reacts with CO to produce CO_2

$$HNO_3 + h\nu \rightarrow HO + NO_2$$
$$HO + CO \rightarrow CO_2 + H$$
$$H + NO_2 \rightarrow NO + HO$$
$$HO + CO \rightarrow CO_2 + H$$
$$\text{net: } HNO_3 + 2CO \rightarrow NO + 2CO_2 + H$$

The interpretation of data in this system is somewhat ambiguous, since the fate of the final hydrogen atom is not known. If the second hydrogen atom does not react with nitric acid, the quantum yield to form carbon dioxide is 2, and the primary quantum yield for nitric acid destruction can be inferred. On the other hand, if the hydrogen atom attacks nitric acid, for example,

$$H + HNO_3 \rightarrow HO + HNO_2$$
$$HO + CO \rightarrow CO_2 + H$$
$$\text{net: } HNO_3 + CO \rightarrow HNO_2 + CO_2$$

then the secondary processes represent a chain reaction with an indeterminate relation between observed CO_2 and primary quantum yield.

Upon addition of excess carbon monoxide and excess oxygen, the hydrogen atom is converted to the HOO radical, any nitric oxide formed is converted to nitrogen dioxide, and the significant secondary processes are

$$HNO_3 + h\nu \rightarrow HO + NO_2$$
$$HO + CO \rightarrow CO_2 + H$$
$$H + O_2 + M \rightarrow HOO + M$$
$$NO_2 + HOO \rightarrow HNO_2 + O_2 \text{ (ref. 21)}$$
$$HNO_2 \xrightarrow[\text{time}]{HOO,\ O_2} NO_2 + \tfrac{1}{2}H_2O$$
$$\text{net: } HNO_3 + h\nu + CO + \tfrac{1}{4}O_2 \rightarrow CO_2 + NO_2 + \tfrac{1}{2}H_2O$$

For large degrees of reaction, secondary photolysis of NO_2 forms NO, which reacts heterogeneously with nitric acid

$$NO + 2HNO_3 \xrightarrow{W} H_2O + 3NO_2$$

Another role of added excess oxygen is to suppress this reaction. Extensive model calculations (18) with up to 40 elementary reactions confirmed that no known secondary reaction destroyed HNO_3 or NO_2. With added CO and O_2, the quantum yields of CO_2 and NO_2 were each 1.0 at 200 nm, and that for NO_2 was 1.0 at 255 and 300 nm. The quantum yield for the primary photolysis of HNO_3 to HO and NO_2 was 1.0 at all wavelengths.

The preliminary studies of the formation of CO_2 in the photolysis of HNO_2 were carried out by Dr. Shih-Ger Chang and Mr. Ed Quitevis. This work was supported by the Climatic Impact Assessment Program by means of an interagency agreement between the Department of Transportation and the Atomic Energy Commission through the Inorganic Materials Research Division, Lawrence Berkeley Laboratory.

1. H. S. JOHNSTON and R. GRAHAM. J. Phys. Chem. **77**, 62 (1973).
2. C. E. DINERMAN and G. E. EWING. J. Chem. Phys. **53**, 626 (1970).
3. D. R. BATES and P. B. HAYES. Planet. Space Sci. **15**, 189 (1967).
4. K. F. PRESTON and R. F. BARR. J. Chem. Phys. **54**, 3347 (1971).
5. R. F. HAMPSON (*Editor*). Chemical kinetics data survey VI. NBSIR 73-207. 1973. pp. 59–78.
6. T. C. HALL, JR. and F. E. BLACET. J. Chem. Phys. **20**, 1745 (1952).
7. H. H. HOLMES and F. DANIELS. J. Am. Chem. Soc. **56**, 630 (1934).
8. F. DANIELS and E. H. JOHNSTON. J. Am. Chem. Soc. **43**, 53 (1921).
9. H. J. SCHUMACHER and G. SPRENGER. Z. Phys. Chem. **B2**, 267 (1929).
10. E. J. JONES and O. R. WULF. J. Chem. Phys. **5**, 873 (1937).
11. R. F. MURPHY. The ultraviolet photolysis of the nitrogen oxides. Ph.D. Dissertation. University of California in Los Angeles. 1969.
12. R. F. HAMPSON (*Editor*). Chemical kinetics data survey VI. NBSIR 73-207. 1973. pp. 93–97.
13. H. S. JOHNSTON. Gas phase reaction rate theory. The Ronald Press Company, New York. 1966.
14. G. SCHOTT and N. DAVIDSON. J. Am. Chem. Soc. **80**, 1841 (1958).
15. D. A. RAMSAY. Proc. Colloq. Spectroscopy, Int., 10th, 583 (1962).
16. (*a*) A. P. ALTSHULLER. J. Phys. Chem. **61**, 251 (1957); (*b*) D. M. WALDORF and E. L. BALB. J. Chem. Phys. **39**, 432 (1963).
17. G. W. KING and D. MOULE. Can. J. Chem. **40**, 2057 (1962).
18. H. S. JOHNSTON, S. G. CHANG, and G. WHITTEN. J. Phys. Chem. **78**, 1 (1974).
19. H. S. JOHNSTON, G. E. MCGRAW, T. T. PAUKERT, L. W. RICHARDS, and J. VAN DEN BOGAERDE. Proc. Nat. Acad. Sci. **57**, 1146 (1967).
20. T. BERCES and S. FORGETEG. Trans. Faraday Soc. **66**, 633 (1970).
21. R. SIMONAITIS and J. HEICKLEN. Private communication.

Photolysis of O_x, HO_x, CO_x, and SO_x Compounds

K. H. WELGE[1]

Center of Research in Experimental Space Science and Chemistry Department, York University, Toronto, Ontario

Received November 3, 1973

This paper gives a review of the homogenous gas phase photolysis of inorganic oxide compounds of aeronomic interest. The review is concerned with results of laboratory investigations at wavelengths from the visible to the Schumann vacuum ultraviolet at about 1050 Å corresponding to the lithium fluoride transmission limit. The discussion is confined largely to the photolytic primary processes which are mostly photodissociation in the systems of interest. As kinetic processes are covered by other papers, secondary reactions of photolysis products are discussed here only in the context of the primary processes. The objective is to provide an overview of, and to critically assess, the state of knowledge as to the observations of dissociation processes and products, measurements of quantum yields, and studies of fragment energy distributions.

Cette publication présente une revue de la photolyse homogène en phase gazeuse d'oxydes inorganiques, composés à intérêt aéronomique. Cette revue concerne les résultats de recherches de laboratoire à des longueurs d'onde allant du visible à l'ultraviolet dans le vide de Schumann aux environs de 1050 Å qui correspond à la limite de transmission du fluorure de lithium. La discussion se limite essentiellement aux procédés photolytiques primaires qui sont avant tout une photodissociation dans les systèmes d'intérêt. Comme des procédés cinétiques sont étudiées dans d'autres publications, les réactions secondaires des produits de photolyse sont examinées ici dans le seul contexte des procédés primaires. Le but est de fournir un surplus de connaissances des mesures de rendements quantiques et des études sur les distributions énergitiques fragmentaires, et aussi de déterminer d'une façon critique l'état des connaissances concernant les observations des modes de dissociation et des produits. [Traduit par le journal]

Can. J. Chem., **52**, 1424 (1974)

Introduction

For the lower regions of the earth's atmosphere, the subject of this symposium, neutral photochemistry is of particular interest. This interest has grown during the last few years since the number of molecular constituents present or expected to be present in the lower atmosphere has dramatically increased. The photochemistry and the theoretical aeronomic models have become correspondingly complex and extensive. The models demand input data on elementary processes, such as absorption coefficients, quantum yields of the photochemical primary processes, and reaction rate constants, to an extent and accuracy that is in many cases not yet available. For example, in the stratosphere a total of 34 chemically different diatomic and polyatomic molecular species have been identified in a report by Garvin and Hampson (1) as known, or suspected, participants in the chemistry of this atmospheric region. However, as indicated in that report, for most of these species the quantum yields of the primary processes are not known, or not known sufficiently well, to permit modelling of the stratospheric chemistry. In the list of species for which quantum yield data are required are found not only radicals such as HO_2 and HCO but also simple and well-known molecules such as H_2O, SO_2 and others.

This paper is a brief review of laboratory photolysis work on a number of aeronomically important molecules in the u.v. and also vacuum ultraviolet at wavelengths >100 nm. Somewhat arbitrarily we have chosen O_2, O_3, H_2O, H_2O_2, HO_2, CO_2, SO_2, and SO_3. Other important molecules, listed for instance in the report by Garvin and Hampson (1) have been omitted because of the limited scope of the review. Diatomic radicals such as OH and SO have also been left out although their photolysis may be aeronomically important. Photolytic studies have not yet been performed on these species, as is true for radicals in general. The photolysis of a molecule is usually understood to include the primary photochemical processes as well as secondary reactions. This review, however, is essentially confined to the primary processes, *i.e.* their identifi-

[1]Present address: Fakultät für Physik, Universität Bielefeld, Bielefeld, W. Germany.

Can. J. Chem. Downloaded from www.nrcresearchpress.com by 210.87.254.105 on 09/05/12
For personal use only.

Can. J. Chem. Downloaded from www.nrcresearchpress.com by 210.87.254.105 on 09/05/12
For personal use only.

cation and quantum yields. Work on secondary reactions is included only as much as it is of direct interest for the primary process. Results are reported, rather than techniques and experimental details discussed.

In general, quantum yield measurements have been limited to relatively few wavelengths in extensive absorption regions, so that wavelength dependencies are largely unknown in detail. As to the reliability of existing data, it is difficult, if not impossible, in many cases to determine objectively and quantitatively the margin of error or generally the degree of confidence. Precision limits on quantum yield data, usually given by the scatter of repeated measurements in a work, are seldom less than $\pm 10\%$. More serious is the problem of absolute accuracy. In our opinion the only practical way to estimate objectively the reliability of quantum yield data is by comparison of measurements made by different workers using different techniques.

O_2

The O_2 absorption spectrum at wavelengths >100 nm consists of three regions: (*a*) the Schumann–Runge (S.-R.) bands (175–200 nm) superimposed on the Herzberg continuum (185–260 nm), (*b*) the S.-R. continuum (175–135 nm), and (*c*) the heavily structured region at $\lambda < 135$ nm. A recent comprehensive review of spectroscopic data and literature has been provided by Krupenie (2). The following dissociation processes[2] are energetically possible at $\lambda > 100$ nm:

[1]	$O_2 + h\nu \rightarrow O + O$	(242.4 nm)
[2]	$O + O(^1D)$	(175.0 nm)
[3]	$O(^1D) + O(^1D)$	(137.0 nm)
[4]	$O + O(^1S)$	(133.0 nm)
[5]	$O(^1D) + O(^1S)$	(109.8 nm)

At $\lambda > 175$ nm, spectroscopic work (see for instance Hudson (3)) indicates strong predissociation throughout the S.-R. bands, implying that process 1 has a quantum yield of practically unity. There has been a recent photochemical quantum yield study in the S.-R. band region at 184.9 and 193.1 nm by Washida *et al.* (4). At 184.9 nm they found a quantum yield for O_3 formation of $\Phi(O_3) = 2$ at O_2 pressures $\gtrsim 100$ Torr. This is consistent with a primary quantum yield of unity for the O_2 dissociation. However, at 193.1 nm $\Phi(O_3) = 0.3$ was found at O_2 pressures from 300 to 1200 Torr, indicating a quantum yield of less than unity at this wavelength. The apparent contradiction to the spectroscopic observation would need clarification by additional photochemical studies in the S.-R. bands.

It has been generally accepted that process 2 has unit quantum yield in the S.-R. continuum. Indeed there is plenty of evidence, though mostly from indirect experiments, for [2] being the dominant process. For references see the paper by Noxon (5), who identified the production of $O(^1D)$ by observation of the $^1D \rightarrow {}^3P$ emission at 630 nm. Systematic measurements of the $O(^1D)$ yield as a function of wavelength throughout the S.-R. continuum, in particular at the short and long wavelength wings, have not been reported. Also, the $O(^1D)$ production at wavelengths shorter than in the S.-R. continuum has not been studied.

Progress has been made with respect to $O(^1S)$ formation. The production of $O(^1S)$ has been qualitatively established by Filseth and Welge (6) who observed the $^1S \rightarrow {}^1D$ emission at 557.7 nm in pulsed photolysis experiments at wavelengths between ~ 105 and 135 nm. Relative and absolute quantum yield measurements of $O(^1S)$ formation have recently been made. Ridley *et al.* (7) have measured at 121.6 nm the $O(^1S)$ yield from O_2 relative to that from N_2O and obtained an upper limit of $\Phi(^1S, O_2, 121.6) \leq 0.03 \pm 0.01$. McEwan and Lawrence (8) have made first absolute quantum yield measurements at eight wavelengths between 120 and 88 nm. They found a maximum yield of about 10% at 109 and 104 nm. A relatively sudden increase of the yield with decreasing wavelength at 109 nm has been speculatively attributed to the occurrence of process 5, though this process would violate the spin conservation rule. The precision of these measurements was of the order of $\pm 30\%$.

O_3

Because of the central importance of ozone in atmospheric chemistry we discuss its laboratory photolysis in some detail, though a comprehensive treatment and coverage of the many studies on this subject is beyond the scope of the paper. A review on the ozone photochemistry has recently been given by Schiff (9). At wavelengths

[2]Ground state species are given without term symbols. The wavelengths given in parentheses correspond to the thermodynamic thresholds of the processes.

Can. J. Chem. Downloaded from www.nrcresearchpress.com by 210.87.254.105 on 09/05/12
For personal use only.

>200 nm, where most photolysis studies have been performed, the absorption spectrum exhibits the Chappuis (~800–450 nm), Huggins (~360–300 nm), and Hartley (~300–200 nm) regions. Absorption coefficient measurements at room temperature in these regions by different workers are in good agreement. We refer to the paper on this subject by Griggs (10). Measurements in the vacuum u.v. have been reported by Watanabe (11). The weak O—O_2 bond, together with the several metastable electronic states of O and O_2 at rather low energies, make a large number of dissociation processes and secondary reactions thermodynamically possible even in the near ultraviolet. The threshold wavelengths of some of the processes are shown in Table 1. Parentheses indicate spin forbidden fragment combinations.

TABLE 1. Threshold wavelengths (nm) of O_3 dissociation processes

O \ O_2	$X^3\Sigma_g^-$	$a^1\Delta_g$	$b^1\Sigma_g^+$
^3P	1180	(611)	(463)
^1D	(411)	310	266
^1S	(237)	199	

Photolysis in the Visible

In the Chappuis region

[1] $$O_3 + h\nu \rightarrow O + O_2$$

is the only spin allowed process. Since the work by Castellano and Schumacher (12) this process has been accepted to have a quantum yield of unity at wavelengths of "red-yellow light" used in those experiments. The quantum yield of O_3 consumption, $\Phi(-O_3)$, found to be 2, is explained by process 1 followed by

[I] $$O + O_3 \rightarrow O_2 + O_2$$

As $O_2(a^1\Delta_g)$ reacts with O_3 via

[II] $$O_2(a^1\Delta_g) + O_3 \rightarrow O + 2O_2$$

the result $\Phi(-O_3) = 2$ implies that

[2] $$O_3 + h\nu \rightarrow O + O_2(a^1\Delta_g)$$

does not occur to an appreciable extent in the Chappuis region.

The distribution of the excess energy in [1] (for instance, 1 eV at the peak absorption in the Chappuis region) has not been investigated in detail. Ellis *et al.* (13) have observed highly vibrationally excited oxygen, O_2^*, in the O_3 visible flash photolysis. This, however, has been attributed to the secondary reaction I. The yield $\Phi(-O_3) = 2$ together with the observation of O_2^* indicates that O_2^* does not sensitize O_3 decomposition, but is instead collisionally relaxed by O_3.

Photolysis in the Ultraviolet

Because of the strong continuum absorption in the Hartley region it is safe to assume that the photodissociation has a quantum yield of unity, and that dissociation occurs via spin allowed processes in this region. The allowed processes are

[1] $O_3 + h\nu \rightarrow O + O_2$ (1180 nm)

[3] $O(^1D) + O_2(a^1\Delta_g)$ (310 nm)

[4] $O(^1D) + O_2(b^1\Sigma_g^+)$ (266 nm)

with threshold wavelengths given in parentheses. In the Huggins region the spin forbidden processes

[5] $O_3 + h\nu \rightarrow O + O_2(a^1\Delta_g)$ (611 nm)

[6] $O + O_2(b^1\Sigma_g^+)$ (463 nm)

[7] $O(^1D) + O_2$ (411 nm)

must also be taken into account because of the weak absorption. It is generally assumed that [3] is the dominant dissociation in the Hartley band, although the basis for this evidence is not as conclusive and consistent as would be desirable for this very important process. The quantum yield of [3] has been quoted often to be "unity". However, the accuracy of previous work can only be interpreted, at best, to show that the yield is "close" to unity.

Production of $O_2(b^1\Sigma_g^+)$

The production of $O_2(b^1\Sigma_g^+)$ by process 4 had been previously suggested to be important at $\lambda \lesssim$ 266 nm. The $O_2(b^1\Sigma_g^+)$ yield, $\Phi(^1\Sigma)$, is, however, insignificant at wavelengths at least down to ~240 nm. Gauthier and Snelling (14) have performed experiments at 253.7 nm and concluded that $\Phi(^1\Sigma) \lesssim 0.05$ at this wavelength. Gilpin *et al.* (15) flash photolyzed O_3 in the region ~240–265 nm and measured the relative yield of $O_2(b^1\Sigma_g^+)$ and $O(^1D)$ by comparing the $^1D \rightarrow {}^3P$ emission with the $b^1\Sigma_g^+ \rightarrow X^3\Sigma_g^-$ emission. They obtained $\Phi(^1\Sigma)/\Phi(^1D) \lesssim 1/20$. Quantum yield measurements of $O_2(b^1\Sigma_g^+)$ production at other wavelengths are not known.

Production of $O(^1D)$

Usually, two studies by DeMore and Raper

Can. J. Chem. Downloaded from www.nrcresearchpress.com by 210.87.254.105 on 09/05/12
For personal use only.

(16, 17) have been used to show that $\Phi(^1D) = 1$ in the Hartley band at wavelengths up to ~300 nm. We therefore must discuss these studies in some detail. In the first work O_3 was photolyzed in liquid N_2 at 14 wavelengths from 248 to 334 nm and the production of N_2O was measured. Below 300 nm the N_2O yield was found to be constant within limits of error of about 25%. Between 300 and 302 nm the N_2O yield decreased by about a factor of 2, with a limit of error of 30%. At 334 nm the N_2O yield again dropped by another factor of about 2. This dependence shows that three different mechanisms occurred in the corresponding three wavelength intervals. The work suggests that $O(^1D)$ is a major fragment at $\lambda \leq 300$ nm. It does not however, provide an absolute $O(^1D)$ quantum yield measurement. That $\Phi(^1D)$ is unity at $\lambda \leq 300$ nm has rather been inferred from the constancy of the N_2O yield using the plausible argument that it is unlikely that two processes, producing $O(^1D)$ and $O(^3P)$, would have a constant relative yield over the range from 248 to 300 nm. Also, the drop of the N_2O yield at 300–302 nm by only 50% and not to zero, remains unexplained, leaving an essential uncertainty in the photolysis mechanism. In the second work DeMore and Raper photolyzed O_3 in liquid argon at 87 K. Two wavelengths, 253.7 and 313.3 nm, were used and the quantum yield of O_3 consumption, $\Phi(-O_3)$, was measured as a function of the O_3 concentration. The result was a linear dependence of the inverse yield, $1/\Phi(-O_3)$ on the O_3 concentration, $[O_3]$. The mechanism proposed for this was such that the primary quantum yield of $O(^1D)$ was given by the intercepts at $[O_3] = 0$. The relative $O(^1D)$ yields at the two wavelengths, $\Phi(^1D,313)/\Phi(^1D,254)$, were given by the ratio of the slopes. As has been pointed out previously by Schiff (9), the precision of the intercepts was practically insufficient to derive absolute yields. The slopes, however, were measured relatively precisely, indicating $\Phi(^1D,313)/\Phi(^1D,254) = 0.27$.

The gas phase photolysis of O_3 has been studied in several laboratories by measurement of the quantum yield, $\Phi(-O_3)$. In principle, such studies could be used to obtain the quantum yield of the primary products provided the mechanism of secondary reactions is established. The results of all these studies have been explained by assuming that in the Hartley band at $\lambda \lesssim 300$ nm the dissociation [3] is the only primary process involved. However, the problem is that the results of different groups show serious discrepancies. McGrath and Norrish (18) proposed the familiar chain mechanism:

[3′]	$O_3 + h\nu \rightarrow O(^1D) + O_2^{**}$
[II]	$O_2^{**} + O_3 \rightarrow O + 2O_2$
[I]	$O + O_3 \rightarrow 2O_2$
[III]	$O(^1D) + O_3 \rightarrow O_2^* + O_2$
[IV]	$O_2^* + O_3 \rightarrow O(^1D) + 2O_2$

where O_2^{**} was $O_2(a^1\Delta_g$ or $b^1\Sigma_g^+)$ and the chain carrier O_2^* an excited O_2 molecule in an unspecified state. O_2^{**} has since been identified as $O_2(a^1\Delta_g)$. The chain mechanism has been supported by Norrish and Wayne (19) in steady-state photolysis studies at 253.7 nm. At O_3 pressures 2 to 50 Torr they found with O_3 alone a linear increase of $\Phi(-O_3)$ up to 16.7 at 50 Torr. Extrapolation to low O_3 pressure yielded $\Phi(-O_3) \sim 4$. When N_2 or CO_2 was added the O_3 yield decreased further to $\Phi(-O_3) \sim 2$, an observation which does not agree with recent studies (see for instance the discussion by Lissi and Heicklen (20)). Jones and Wayne (21) essentially confirmed the chain mechanism at 253.7 nm. In a later study Jones and Wayne (22) performed experiments at 248, 253.7, 289/292, 297/302, 313.3, and 334.0 nm and again found $\Phi(-O_3) \sim 4$ at low O_3 pressure and chain decomposition with increasing pressure at all wavelengths ≤ 302 nm. Jones *et al.* (23) extended the $\Phi(-O_3)$ measurements at 253.7 nm to O_3 pressures between 2 and 0.05 Torr using photolysis in a flow system. They added O_2 at partial concentrations from 10 to 90% and again obtained $\Phi(-O_3) \sim 4$, independent of the O_2 concentration. The observation of a limiting value of $\Phi(-O_3) \sim 4$ at low O_3 pressure has been attributed in the above studies to the termination of the chain by the loss of the chain carrier species O_2^*.

Ellenrieder *et al.* (24) photolyzed O_3 at 253.7 nm using O_3 pressures from 10 to 100 Torr. They obtained $\Phi(-O_3) = 6$ at all pressures. With the addition of N_2 $\Phi(-O_3)$ decreased to an extrapolated limiting value given as 4. The result $\Phi(-O_3) = 6$ with O_3 alone contradicts the chain mechanism. Ellenrieder *et al.* (24) explain their observation by replacing the reaction IV in the chain mechanism by

[IV′]	$O_2^* + O_3 \rightarrow O + 2O_2$

where O_2^*, produced in the $O(^1D) + O_3$ reaction

Can. J. Chem. Downloaded from www.nrcresearchpress.com by 210.87.254.105 on 09/05/12
For personal use only.

is, however, as unspecified a species as in the chain mechanism. Lissi and Heicklen (20) have repeated O_3 photolysis experiments by O_3 quantum yield measurements at 228.8, 253.7, 280.0 nm using O_3 pressures from 0.1 to 2.7 Torr. With O_3 alone and with added He they obtained an average of $\Phi(-O_3) = 5.5$ at the three wavelengths with an error limit given in a later paper (25) as ± 0.5. In the presence of CO_2 and N_2 the O_3 yield decreased to an average value of $\Phi(-O_3) = 4.2 \pm 0.4$. These results agree with those of Ellenrieder *et al.* (24), though the different pressure regions of O_3 must be noted. They disagree with those of Wayne and co-workers. Lissi and Heicklen also have proposed reaction IV′ instead of IV. It must be noted, however, that yields of 6 and 4 could also be explained by a mechanism suggested by Bair and his co-workers. Webster and Bair (26) have made relative yield measurements at O_3 pressures of ~ 0.2 Torr using 253.7 nm radiation. The quantum yield found with O_3 alone and O_3–He mixtures exceeded that with O_3–N_2 mixtures by about a factor of 2. The authors have attributed the difference to the products of the reaction $O(^1D) + O_3$ and suggested that these products would change with the ozone pressure, if at high O_3 the chain mechanism were to occur. In a subsequent paper, Baiamonte *et al.* (27) indicated that the reaction between $O(^1D)$ and O_3 proceeds at low O_3 pressure via

$$[V] \qquad O(^1D) + O_3 \rightarrow O + O + O_2$$

$$[VI] \qquad O_2{}^* + O_2$$

where $O_2{}^*$ is vibrationally excited in levels $v'' \leq 30$. The branching ratio of the two channels was given as $k_V/k_{VI} \gtrsim 10$. Bair and co-workers have speculated that their results could be reconciled with the chain mechanism by an intermediate complex (O_4) resulting from $O(^1D) + O_3$. This complex would either decay at low O_3 pressure via [V] and [VI], or react at high O_3 pressure with O_3 to give $O(^1D)$,

$$O_4 + O_3 \rightarrow O(^1D) + 3O_2$$

a reaction that does not look very appealing.

The proposed gas phase mechanisms differ essentially in the products of the $O(^1D) + O_3$ reaction. In that respect O_3 photolysis studies have been concerned with the ground state O atom production at "fast" rates, that is, much faster than that of reaction I. Giarchardi and Wayne (28) and Davenport *et al.* (29) have measured the intermediate quantum yield, $\varphi(^3P)$, of $O(^3P)$ production, where $\varphi(^3P)$ is defined as the number of $O(^3P)$ produced in "fast" steps only. Giarchardi and Wayne reported $\varphi(^3P) \sim 0.7$ whereas Davenport *et al.* reported $\varphi(^3P) = 1$, and later (30) extended their measurements to obtain $\varphi(^3P) = 1.00 \pm 0.06$. Obviously, the gas phase photolysis of O_3 has not yet been sufficiently established to serve as a satisfactory basis for absolute or relative $O(^1D)$ quantum yield determinations.

A substantial progress has been achieved recently with respect to the relative quantum yield of $O(^1D)$ by Lin and DeMore (31) in experiments reported at this symposium. Using the insertion reaction technique they have made convincingly accurate measurements of the relative $O(^1D)$ yield as a function of the wavelength from 275 to 334 nm in the gas phase at a temperature of -40 °C. Within a scatter of a few percent the relative $O(^1D)$ yield was found to be constant at $\lambda \leq 305$ nm dropping by 50% at 308 nm and by 90% at 313 nm. At 334 nm the yield is virtually zero. The work is particularly interesting with respect to the dependence of the $O(^1D)$ yield in the threshold region of process 3.

Serious discrepancies exist between results of previous studies on this matter. Simonaitis *et al.* (25) have reported the yield at 313 nm to be $\Phi(^1D,313) = 0.50 \pm 0.05$. This result was obtained at 25 °C and the difference to Lin and DeMore's value could be attributed to the higher temperature. However, Jones and Wayne (21, 22) also working at room temperature obtained results indicating $\Phi(^1D,313)$ to be of the order of ~ 0.1, in agreement with Lin and DeMore. Furthermore, DeMore and Raper (16) found the $O(^1D)$ yield to drop already at ~ 300 nm, which could be attributed to the particular experimental conditions (liquid phase, low temperature). However, the work by DeMore and Raper (17) carried out also in the liquid phase and at low temperature indicates $\Phi(^1D,313) = 0.27$, making the common assumption that $\Phi(^1D)$ is unity at 253.7 nm. The difference between that result and the present one by Lin and DeMore has an interesting implication with respect to the absolute quantum yield: the difference is either due to the different experimental conditions of the two studies, or the $O(^1D)$ yield is lower at 253.7 nm than at 275–302 nm by a factor of 2.7. Finally, Castellano and Schumacher (32) have reported $\Phi(^1D) = 1$ at 313 nm. The discrepancies among the previous studies can hardly all be explained

Can. J. Chem. Downloaded from www.nrcresearchpress.com by 210.87.254.105 on 09/05/12
For personal use only.

by the different experimental conditions used. Further studies are obviously needed, for instance by Lin and DeMore's method, to find out how the $O(^1D)$ yield depends on the conditions such as pressure and temperature.

Production of $O_2(a^1\Delta_g)$

The production of $O_2(a^1\Delta_g)$ in the O_3 photolysis has been well established at 253.7 nm by direct observation through detection of the 1270 nm emission, by Gauthier and Snelling (14) and by Jones and Wayne (33). Since addition of N_2 and O_2 did not affect the emission, the production of $O_2(a^1\Delta_g)$ by reactions of $O(^1D)$ with O_3 has been excluded. The studies indicate that the $O_2(a^1\Delta_g)$ yield is close to unity. This observation together with the fact that the $O_2(b^1\Sigma_g^+)$ yield is practically negligible rather safely proves that the $O(^1D)$ is also unity at 253.7 nm, provided of course that spin allowed processes dominate, which is likely because of the strong absorption.

At other wavelengths, $O_2(a^1\Delta_g)$ has not been detected directly and much of the evidence for $O_2(a^1\Delta_g)$ is based on the same photolysis experiments concerned with the $O(^1D)$ production and carried out by O_3 quantum yield measurements. The studies are, however, in better agreement about the $O_2(a^1\Delta_g)$ production than about $O(^1D)$. At wavelengths $\lesssim 300$ nm the O_3 quantum yield has been observed to be reduced to $\Phi(-O_3) \sim 4$ in experiments by Lissi and Heicklen (20), Ellenrieder *et al.* (24), and also in recent experiments by Wayne and co-workers. The yield $\Phi(-O_3) \sim 4$ is explained by the high efficiency at which the added gases quench $O(^1D)$ to $O(^3P)$ whereas $O_2(a^1\Delta_g)$ is relatively unaffected, *i.e.* the $O(^1D) + O_3$ reaction is replaced by $O(^3P) + O_3$.

At wavelengths ≥ 310 nm $O_2(a^1\Delta_g)$ can be formed only by the spin forbidden dissociation [5]. The experiments by Jones and Wayne (22) and by Castellano and Schumacher (34) at 334 nm agree in the observation of $\Phi(-O_3) \sim 4$. This is explained by the production of electronically excited O_2 fragments by process 5 or 6. An electronically excited O_2 is required since vibrationally excited O_2 does not react with O_3. The branching ratio of the two possible processes has not yet been determined.

Photolysis in the Vacuum Ultraviolet

With one recent exception, photolysis experiments at wavelengths in the vacuum u.v. have not been reported. Ridley *et al.* (7) have measured the $O(^1S)$ quantum yield from O_3 relative to that from N_2O at the Lyman-α line (121.6 nm). The yield is negligibly small: $\Phi(^1S; O_3,121.6)/\Phi(^1S; N_2O,121.6) < 0.03$.

H_2O

A comprehensive and detailed review of the photolysis of water vapor has been given by Dixon (35). The absorption coefficient has been measured at wavelengths $\lesssim 185$ nm by Watanabe and Zelikoff (36). Above 185 nm the absorption coefficient drops steeply. It has been measured up to ~ 194 nm by Thompson *et al.* (37). The spectrum exhibits a first continuum ranging from the onset to ~ 143 nm. Another continuum with some structure follows from ~ 143 nm to ~ 125 nm. Below this wavelength the absorption spectrum shows a complex structure of strong predissociation. The dissociation processes with their threshold wavelengths are:

[1]	$H_2O + h\nu \rightarrow H_2 + O$	(247 nm)
[2]	$H + OH$	(242 nm)
[3]	$H_2 + O(^1D)$	(176 nm)
[4]	$H + OH(A^2\Sigma^+)$	(136 nm)
[5]	$H_2 + O(^1S)$	(132 nm)
[6]	$H + H + O$	(130 nm)

At wavelengths > 143 nm the dissociation [2] is apparently the dominant primary process. Rebbert *et al.* (38) have measured the quantum yield of molecular hydrogen production, $H_2O \rightarrow H_2 + O$, and have obtained a value of 0.025 ± 0.01 at 147 nm. Since one may assume that the overall quantum yield of dissociation is unity, the yield of process 2 would be correspondingly 0.975 ± 0.01 at this wavelength. Also, earlier work has indicated that [2] is the major process. From flash photolysis experiments in the region $\gtrsim 150$ nm Black and Porter (39) concluded that [2] has a yield of at least 90%. Ung and Back (40) performed photolysis experiments at 185 nm and did not observe H_2 production. Stief (41) photolyzed D_2O at 147 nm in the presence of C_2H_4 as deuterium atom scavenger and found a yield of 6% for $D_2 + O$. Studies by Cottin *et al.* (42) in which H_2O–D_2 and D_2O–H_2 mixtures were photolyzed at 147 nm and 185 nm did not show evidence for molecular hydrogen formation in the primary step. In summary, (*a*) the measurement by Rebbert *et al.* (38) at 147 nm appears to be the most accurate, and (*b*) although the wavelength dependence has not been measured in

Can. J. Chem. Downloaded from www.nrcresearchpress.com by 210.87.254.105 on 09/05/12
For personal use only.

detail, one may assume that the yield of process 2 is, within a couple of percent, close to unity at wavelengths >147 nm in the first absorption continuum. At shorter wavelengths, processes producing molecular hydrogen become increasingly significant as shown by the work of Rebbert *et al.* (38). At 123.6 nm and 104.8/106.7 nm the quantum yield of H_2 formation has been reported by these workers to be 0.13 ± 0.02 and 0.23 ± 0.03, respectively. The value at 123.6 nm is lower by about a factor of 2 than that obtained in a previous study by McNesby *et al.* (43). According to the spin selection rule, process 1 is not allowed and the O atom should be produced in the ^1D or ^1S state, depending on the wavelength. However, this has not yet been established.

The energy distribution in process 2 has been investigated by Welge and Stuhl (44) using vacuum u.v. flash photolysis and kinetic absorption spectroscopy. They found that the excess energy appears largely as translational energy of the fragments with little internal excitation. Photolysis experiments by Masanet and Vermeil (45) at 184.9, 147.0, and 123.6 nm are consistent with this observation. The production of $OH(A^2\Sigma^+)$ by process 4 has been well established by observation of the $A^2\Sigma^+ \rightarrow X^2\Pi$ fluorescence at photolyzing wavelengths of 130.6, 123.6, and 121.6 nm (46, 47). The yield of process 4 has not yet been well established, but appears to be of the order of 5–10% in this wavelength range. The $OH(A^2\Sigma^+)$ radicals are produced rotationally highly excited with a peculiar, strongly nonequilibrium rotational distribution.

A most interesting observation made by Clark and Noxon (48) on the H_2O photolysis must be mentioned. Irradiating H_2O vapor at 10^{-2} to 10 Torr in the wavelength region 150–170 nm, the formation of micrometer-sized particles was observed. The particles have a density of only ~ 0.2 g/cm^3, and thus do not consist of ordinary water liquid or solid phase, although they evidently are the result of H_2O photolysis. The process of formation is unknown; however, OH appears to be a necessary primary species. As to the rate of production, for instance at 10 Torr H_2O, the particle mass growth rate was equal to the rate of light absorption, indicating a quantum efficiency of unity. It is not obvious how this observation can be reconciled with the previous gas phase quantum yield measurements and further studies on this puzzling effect are warranted.

H_2O_2

The absorption coefficient of H_2O_2 has been measured by Holt *et al.* (49) at 253.7 nm and in the region 225–185 nm. Earlier measurements have been made by Urey *et al.* (50) at 275–325 nm. In the range 275–185 nm the absorption coefficient increases monotonically, with no observable structure. Schürgers and Welge (51) have made measurements in the region 200–120 nm. There is, however, a discrepancy of about a factor 2 between their and the previous measurements at ~ 200 nm. A reinvestigation of the H_2O_2 absorption at short wavelengths is suggested. The H_2O_2 molecule can undergo a number of dissociation processes. Some of these, with their threshold wavelengths, are:

[1]	$H_2O_2 + h\nu \rightarrow OH + OH$	(577 nm)
[2]	$H_2 + O_2(a^1\Delta_g)$	(533 nm)
[3]	$H_2O + O(^1D)$	(365 nm)
[4]	$H + HO_2$	(322 nm)
[5]	$2H + O_2$	(213 nm)
[6]	$OH(A^2\Sigma^+) + OH$	(200 nm)

Volman (52) has discussed the photolysis work prior to 1963, consisting mostly of gas phase photolysis studies at 253.7 nm with product analysis. As pointed out by Volman (52), the primary process at this wavelength can be assumed to be dissociation [1] since this and the proposed reaction mechanism explain the observed product distributions. Recent experiments by Gorse and Volman (53) are consistent with the earlier findings. The production of OH at wavelengths $\gtrsim 200$ nm has been established directly by ultraviolet flash photolysis and kinetic spectroscopy by Greiner (54), who observed the OH radical with a time resolution that permitted only a few collisions between production and detection. The radicals were found only in the $v'' = 0$ level, in rotational states $K \leq 7$, and at equal amounts in the electronic ground state doublet levels $^2\Pi_{1/2}$ and $^2\Pi_{3/2}$. Greiner also showed that the yield of process 3 is less than that of 1 by at least a factor of 5. Recently, HO_2 has been directly observed in the H_2O_2 photolysis at 253.7 nm by Pauckert and Johnston (55). This work implicitly excludes HO_2 as a primary product since its production is shown to be due to secondary reaction.

Can. J. Chem. Downloaded from www.nrcresearchpress.com by 210.87.254.105 on 09/05/12
For personal use only.

The vacuum u.v. photolysis has been investigated by Stief and DeCarlo (56) in steady-state experiments by product analysis. Experiments were performed at 253.7, 147.0, and 123.6 nm using C_2D_4 at H atom scavenger to discriminate between H and H_2 production in the primary steps. Attempts were made to determine whether $O(^1D)$ was produced, by adding N_2O and analyzing the products for N_2. At 253.7 and 147.0 nm the quantum yield of process 1 is found to be close to unity; at 123.6 nm the primary H_2 yield from all processes is given as 0.25, the yield of process 1 as ≤ 0.5, and that of process 4 as ≥ 0.25. These quantum yield data may have a considerable margin of uncertainty. They, however, suggest an increase of molecular hydrogen formation at short wavelengths. Electronically excited $OH(A^2\Sigma^+)$ is produced in the vacuum u.v. as qualitatively established by observation of the $A^2\Sigma^+ \rightarrow X^2\Pi$ fluorescence (47, 56). According to Kley (47) the $OH(A^2\Sigma^+)$ radicals are formed highly rotationally excited. Quantum yields for the $OH(A^2\Sigma^+)$ production have not been reported.

HO_2

The photolysis of the HO_2 radical has not yet been investigated. Bond dissociation energies for H—O_2 and HO—O of 47 and 64 kcal/mol respectively have been reported (see for instance Calvert and Pitts (57)). Photodissociation of the radical takes place in the ultraviolet, as shown by the continuum absorption observed at wavelengths ~280 to 185 nm. Troe (58) observed the HO_2 absorption between 280 and 220 nm, producing the radical by thermal decomposition of H_2O_2 in a shock tube at ~1000 °C. The absorption has been observed and coefficients measured at room temperature by Pauckert and Johnston (55) and by Hochanadel *et al.* (59) at wavelengths 195–245 nm and 185–260 nm, respectively. Pauckert and Johnston (55) produced the radical by H_2O_2 photolysis at 253.7 nm, using the modulated photolysis technique. Hochanadel *et al.* (59) flash photolyzed H_2O in the presence of O_2 and an excess of H_2, He, or Ar. According to both works the spectrum consists of a pure continuum with maximum absorption at 210 nm. The absorption spectra agree with respect to their shapes, but the absolute values of the measured absorption coefficients differ by about 30%.

CO_2

At wavelengths >100 nm it is energetically possible for the CO_2 molecule to dissociate into CO + O and C + O_2. The latter process has not been observed in photolysis and therefore will not be considered further. The dissociation processes yielding CO and O, with their threshold wavelengths, are:

[1]	$CO_2 + h\nu \rightarrow CO + O$	(227.5 nm)
[2]	$\rightarrow CO + O(^1D)$	(167.1 nm)
[3]	$\rightarrow CO + O(^1S)$	(128.6 nm)
[4]	$\rightarrow CO(a^3\Pi) + O$	(108.2 nm)

For the CO_2 absorption spectrum and coefficients we refer to the paper by Rabalais *et al.* (60) which also may serve for previous references. The CO_2 photolysis has been a subject of many laboratory investigations often with conflicting results, particularly as far as secondary reaction mechanisms are concerned. It is not possible to give a comprehensive account in this paper. We refer to publications, for instance, by Preston and Cvetanović (61), Slanger and Black (62), and Clark (63) that provide literature references and also discuss the controversial state of the CO_2 photolysis up to 1971.

Photolysis at Wavelengths >167 nm

Most studies made in this wavelength region indicate that the primary quantum yield, $\Phi_0(-CO_2)$, of the CO_2 decomposition is unity. DeMore and Mosesman (64) photolyzed CO_2 at 184.9 nm using high CO_2 pressures (65–800 p.s.i.) with added O_2. The production of O_3 via $O + O_2 + M \rightarrow O_3 + M$ served as a measure for the O atom yield of process 1 and thus for the CO_2 quantum yield. Inn and Heimerl (65) used a continuum light source and photolyzed CO_2 in the region 174–210 nm. They measured the CO yield by the resonance fluorescence of the 4th positive group excited with a CO lamp. Kreszenski *et al.* (66) performed steady-state photolysis experiments at 184.9 nm and measured product yields of O_2 and CO gas chromatographically. The CO yield was found to be $\Phi(CO) = (1.08 \pm 0.12)$ at 184.9 nm. As observed in numerous other CO_2 photolysis studies by product analysis, the ratio of the O_2 and CO yields was found to deviate from the theoretical value of 0.5 by a variable degree. More significantly, in this work evidence was presented that

Can. J. Chem. Downloaded from www.nrcresearchpress.com by 210.87.254.105 on 09/05/12
For personal use only.

indicates that the primary CO_2 quantum yield can be less than unity, as a value of 0.16 was found for the CO yield at 213.9 nm. Further investigations of this interesting deviation from unity quantum yield are warranted.

Photolysis at Wavelengths 167–140 nm

There have been a few recent studies that would indicate that the CO_2 primary quantum yield is also less than unity at wavelengths in this region. Inn and Heimerl (65) reported $\Phi(CO) = 0.5$ at wavelengths 150–167 nm which would suggest also $\Phi_0(-CO_2) = 0.5$. It must be noted that this result has been obtained in the same work in which $\Phi(CO) = 1$ was found at 174–210 nm. Inn (67) using the same technique as in the work by Inn and Heimerl (65) has reported $\Phi(CO) = 0.75$ at 147.0 nm. Most recent experiments by Filseth and Slanger (68) at 147.0, 149.2, and 156.0 nm, also using the CO resonance fluorescence technique, again seem to show that the CO yield is less than unity by variable amounts depending on the wavelength. On the other hand, most previous experiments have indicated that the CO_2 quantum yield is unity. In steady-state photolysis experiments with product analysis variable O_2 deficiencies usually occurred, and therefore $\Phi(CO)$ was used as the measure for $\Phi_0(-CO_2)$. Studies at 147.0 nm that indicate $\Phi_0(-CO_2) = 1$ have been carried out for instance by Warneck (69), Young *et al.* (70, 75), Yang and Serviedo (71), and Slanger and Black (62). Quick and Cvetanović (72) performed experiments at 157.5 and 163.3 nm that also indicated that the primary CO_2 quantum yield is unity. As mentioned above, in quantum yield experiments using end product analysis many inconsistencies are found in the material balance. A recent study on this intricate problem has been made by Loucks and Cvetanović (73) to whom we refer for a more detailed account. Their work shows that material balance of O_2 can indeed be obtained, though only under special experimental conditions. This would lend support to studies in which the quantitative production of CO has been used as a measure of the CO_2 primary yield. In summary, one must conclude that the CO_2 photolysis still needs further studies, with respect to the primary quantum yield as well as the reaction mechanism.

The production of $O(^1D)$ and the secondary reactions of this species in the CO_2 photolysis are of special interest and have been the subjects of many contradictory studies. Though the production of $O(^1D)$ has been indicated by indirect experiments, the species has so far escaped direct identification in the laboratory. Noxon (5) reported the observation of an emission at 630 nm in CO_2 photolysis experiments, but this was due to an experimental artifact, as found in later studies by Clark and Noxon (48, 74). A convincing and relatively unambiguous identification of $O(^1D)$ has been achieved by Quick and Cvetanović (72) at 157.5 and 163.3 nm by using the insertion reaction technique. Also in this work the $O(^1D)$ quantum yield has been investigated and found to be close to unity at these wavelengths. This agrees with the work by Slanger and Black (62) at 147.0 nm. Although $O(^1S)$ can be produced by photodissociation only at wavelengths < 128.6 nm, Young *et al.* (70, 75) and Noxon (5) have reported $O(^1S)$ emission at 557.7 nm in CO_2 photolysis experiments at longer wavelengths. Other experiments have not agreed with this observation (76), and recently Clark and Noxon (74) have found that the previous $O(^1S)$ emission had been caused by an experimental artifact.

Photolysis at Wavelengths < 140 nm

Neither process 1 nor 2 has been observed in this region. Process 3 has been established by the observation of $^1S \rightarrow {}^1D$ emission at 557.7 nm in numerous steady-state and flash photolysis experiments. Progress has also been made recently in the determination of the $O(^1S)$ quantum yield. Ridley *et al.* (7) have measured the yield at 121.6 nm relative to that from the photolysis of N_2O. They obtained $\Phi(^1S, CO_2)/\Phi(^1S, N_2O) = 0.31 \pm 0.06$. This is consistent with more extensive absolute measurements by Lawrence (77) at several wavelengths from 121.6 to 81.2 nm. At 121.6 nm the yield was found to be 0.1, within an order of magnitude. It rises to a maximum of about unity at wavelengths ~115–108 nm and decreases again with decreasing wavelength. Koyano *et al.* (78) have measured the relative wavelength dependence of the $O(^1S)$ yield in 0.2 nm steps through the heavily structured absorption band from 116 to 108 nm. The dependence agrees mostly with that of Lawrence (77).

The dissociation 4 has been identified and the absolute quantum yield of $CO(a^3\Pi)$ production has been measured in detail as a function of wavelength by Lawrence (96). The yield is a smooth function of the wavelength starting at the threshold and increasing continuously to a maximum of ~0.5 at 92 nm.

Can. J. Chem. Downloaded from www.nrcresearchpress.com by 210.87.254.105 on 09/05/12
For personal use only.

SO_2

The thermodynamic threshold energies for the dissociation processes of SO_2 into ground state fragments

[1] $SO_2 + h\nu \rightarrow SO + O$ (221 nm)

[2] $\rightarrow S + O_2$ (207 nm)

correspond to wavelengths at 221 and 207 nm, respectively. The SO_2 absorption beginning around 400 nm exhibits in the u.v. three characteristic regions: the forbidden triplet, and the first and second singlet regions, at wavelengths of ~400–340 nm, ~320–240 nm, and <240 nm, respectively. (For the absorption coefficients and spectra taken under low resolution at wavelengths ≥220 nm see, for instance, a recent paper by Sidebottom *et al.* (79).) Warneck *et al.* (80) have reported absorption coefficient measurements at wavelengths ≥185 nm. At shorter wavelengths in the vacuum u.v. measurements have been made by Golomb *et al.* (81).

The absorption of SO_2 in the triplet and particularly the first singlet region leads to a great variety of primary and secondary processes involving excited SO_2: fluorescence, non radiative intersystem crossing, intra- and intermolecular energy transfer, and reactive processes. The laboratory photochemistry of SO_2 in these non-dissociative states, of great interest for the photochemistry of sulfur compounds in the atmosphere, is a wide research area in itself, and a detailed survey is beyond the scope of this paper. We therefore indicate only a few recent investigations concerning the radiative lifetimes and collisional quenching of SO_2 in these states.

The radiative lifetime of the triplet state produced in the 400–340 nm absorption region has been found to be of the order of 1 ms. Collier *et al.* (82) and Sidebottom *et al.* (83) have reported lifetime values at zero pressure of $(7.9 \pm 1.7) \times 10^{-4}$ s and $(1.02 \pm 0.71) \times 10^{-3}$ s, respectively. Quenching coefficients for the triplet fluorescence have been measured for a number of added gases. (See for examples a paper by Mettee (84) and a number of papers by Calvert and co-workers (see Sidebottom *et al.* (79), and references therein).) For instance, the quenching rate constants of the main atmospheric gases, N_2 and O_2, are of the order of 1×10^8 l mol^{-1} s^{-1}.

Absorption in the first singlet region involves two excited states, as recently found by Brus and McDonald, according to a communication by Calvert (1973). The quenching of the singlet states has been the subject of a very large number of studies. It is a complex set of processes, involving internal radiationless transitions amongst the excited states as well as external energy transfer and reactions. The overall quenching efficiency of the singlet fluorescence for many gases is of the order of 1 to 0.1 per gas kinetic collision. Details may be found in recent papers by, for instance, Mettee (84), Rao *et al.* (85), Calvert (1973), Stockburger *et al.* (86), and Sidebottom *et al.* (79).

Photolytically, the region <240 nm is of interest because it contains the dissociation thresholds of processes 1 and 2. Previous studies at wavelengths down to 200 nm have been inconclusive and not specific as to the onset of photodissociation. SO radicals have been observed in flash photolysis experiments in the second singlet region (87, 88) but a distinction between their formation by photodissociation or by secondary reactions of excited SO_2 was not possible. Recently, Okabe (89) and Hui and Rice (90) have established the dissociation threshold of process 1 by investigating the wavelength dependence of the SO_2 fluorescence between 240 and 200 nm. Okabe observed the onset between 218.9 and 220.8 nm where the fluorescence yield dropped sharply. However, weak fluorescence still occurred at 200 nm indicating that the dissociation yield is not quite unity. Hui and Rice using higher resolution measured the fluorescence lifetime and yield. At $\lambda \geq 221$ nm the lifetime is ~40 ns dropping to ~5 ns at 215 nm. The fluorescence quantum yield is, for instance, close to unity at $\lambda \geq 225$ nm decreasing to ~0.1 at 215 nm.

At shorter wavelengths a large number of dissociation channels become energetically possible, with the fragments of processes 1 and 2 in different excited electronic states. It is not known which processes do occur, however. Only few photolysis experiments have been carried out at wavelengths <200 nm. Driscoll and Warneck (91) have photolyzed SO_2 at 184.9 nm and measured the SO_3 quantum yield. They obtained $\Phi(SO_3) = 0.50 \pm 0.07$ and deduced for process 2 an upper limit of ≤0.50. Lalo and Vermeil (92) have performed steady-state photolysis experiments at 147.0 and 123.6 nm and observed the production of SO_3 and of free sulfur, the latter being attributed speculatively to process 2 with the S atom in the ^1D state.

Can. J. Chem. Downloaded from www.nrcresearchpress.com by 210.87.254.105 on 09/05/12
For personal use only.

SO_3

The absorption of SO_3 has been observed by Fajans and Goodeve (93) consisting of weak diffuse bands superimposed on a continuum background. A measurement of the absorption coefficient from 230 to 150 nm at low resolution has been reported in the paper by Lalo and Vermeil (92). The SO_3 photolysis has been investigated very little. Kornfeld (94) performed experiments at wavelengths $\gtrsim$276 nm and found SO_2 formation. Norrish and Oldershaw (87) flash photolyzed SO_3 in the quartz ultraviolet and observed vibrationally excited SO radicals. A determination of the reaction mechanism and thus also of the primary processes was not possible. More recent work is not known, leaving the homogeneous SO_3 photolysis a virtually open problem.

I should like to thank Dr. R. F. Hampson and the group of authors of the National Bureau of Standards who are concerned with the "Chemical Kinetics Data Survey". They assisted me very much in preparing this paper by making preprint material of their forthcoming publications in that survey available to me. The help of Dr. S. V. Filseth in preparing the section on photolysis of CO_2 is greatly appreciated. I should also like to thank Dr. J. McConnell for his friendly and stimulating help.

1. D. Garvin and R. F. Hampson. Proceedings of the Second Conference on the Climatic Assessment Program. *Edited by* A. J. Broderick. 1972. p. 114.
2. P. Krupenie. J. Phys. Chem. Ref. Data, **1**, 423 (1972).
3. R. D. Hudson. Rev. Geophys. Space Phys. **9**, 305 (1971).
4. N. Washida, Y. Mori, and I. Tanaka. J. Chem. Phys. **54**, 1119 (1971).
5. J. F. Noxon. J. Chem. Phys. **52**, 1852 (1970).
6. S. V. Filseth and K. H. Welge. J. Chem. Phys. **51**, 839 (1969).
7. B. A. Ridley, R. Atkinson, and K. H. Welge. J. Chem. Phys. **58**, 3878 (1973).
8. M. J. McEwan and G. M. Lawrence. Preprint.
9. H. I. Schiff. Ann. Geophys. **28**, 67 (1972).
10. M. Griggs. J. Chem. Phys. **49**, 857 (1968).
11. K. Watanabe. Adv. Geophys. **5**, 153 (1958).
12. E. Castellano and H. J. Schumacher. J. Chem. Phys. **36**, 2238 (1962); Z. Phys. Chem. N.F. **34**, 198 (1962).
13. D. M. Ellis, J. J. McGarvey, and W. D. McGrath. Nature P.S. **229**, 153 (1971).
14. M. Gauthier and D. R. Snelling. Chem. Phys. Lett. **5**, 93 (1970); J. Chem. Phys. **54**, 4317 (1971).
15. R. Gilpin, H. I. Schiff, and K. H. Welge. J. Chem. Phys. **55**, 1087 (1971).
16. W. B. DeMore and O. F. Raper. J. Chem. Phys. **37**, 2048 (1962).
17. W. B. DeMore and O. F. Raper. J. Chem. Phys. **44**, 1780 (1966).
18. W. D. McGrath and R. G. W. Norrish. Nature, **182**, 235 (1958); Proc. R. Soc. Lond. A, **254**, 317 (1960).
19. R. G. W. Norrish and R. P. Wayne. Proc. R. Soc. Lond. A, **288**, 200 (1965).
20. E. Lissi and J. Heicklen. J. Photochem. **1**, 39 (1972).
21. I. T. N. Jones and R. P. Wayne. J. Chem. Phys. **51**, 3617 (1969).
22. I. T. N. Jones and R. P. Wayne. Proc. R. Soc. Lond. A, **319**, 273 (1970).
23. I. T. N. Jones, U. B. Kaczmar, and R. P. Wayne. Proc. R. Soc. Lond. A, **316**, 431 (1970).
24. G. v. Ellenrieder, E. Castellano, and H. J. Schumacher. Chem. Phys. Lett. **9**, 152 (1971).
25. R. Simonaitis, S. Braslavsky, J. Heicklen, and M. Nicolet. Chem. Phys. Lett. **19**, 601 (1973).
26. H. Webster III and E. J. Bair. J. Chem. Phys. **53**, 4532 (1970).
27. V. D. Baiamonte, L. G. Hartshorn, and E. J. Bair. J. Chem. Phys. **55**, 3617 (1971).
28. D. J. Giarchardi and R. P. Wayne. Chem. Soc. Faraday Disc. **53**, 172, 230 (1972).
29. J. Davenport, B. Ridley, H. I. Schiff, and K. H. Welge. Chem. Soc. Faraday Disc. **53**, 230 (1972).
30. J. Davenport, K. H. Welge, B. Ridley, and H. I. Schiff. Unpublished.
31. C. L. Lin and W. B. DeMore. I.A.G.A. Symposium, Kyoto, 1973.
32. E. Castellano and H. J. Schumacher. Z. Phys. Chem. N.F. **65**, 62 (1969).
33. I. T. N. Jones and R. P. Wayne. Proc. R. Soc. Lond. A, **321**, 409 (1971).
34. E. Castellano and H. J. Schumacher. Chem. Phys. Lett. **13**, 625 (1972).
35. R. S. Dixon. Radiation Res. Rev. **2**, 237 (1970).
36. K. Watanabe and M. Zelikoff. J. Opt. Soc. Am. **43**, 753 (1953).
37. B. A. Thompson, P. Harteck, and R. R. Reeves. J. Geophys. Res. **68**, 6431 (1963).
38. R. E. Rebbert, R. L. Lilly, and P. Ausloos. Abstract of paper given at ACS meeting, New York; private communication.
39. G. Black and G. Porter. Proc. R. Soc. Lond. A, **266**, 185 (1962).
40. A. Y. M. Ung and R. A. Back. Can. J. Chem. **42**, 753 (1964).
41. L. J. Stief. J. Chem. Phys. **44**, 277 (1966).
42. M. Cottin, C. Vermeil, and J. Masanet. C. R. **263**, 753 (1966); M. Cottin, J. Masanet, and C. Vermeil. J. Chim. Phys. **63**, 959 (1966).
43. J. R. McNesby, I. Tanaka, and H. Okabe. J. Chem. Phys. **36**, 605 (1962).
44. K. H. Welge and F. Stuhl. J. Chem. Phys. **46**, 2440 (1967).
45. J. Masanet and C. Vermeil. J. Chim. Phys. **66**, 1249 (1969).
46. T. Carrington. J. Chem. Phys. **41**, 2012 (1964).
47. D. Kley. Thesis, University of Bonn, Bonn, West Germany. 1967.
48. I. D. Clark and J. F. Noxon. Science, **174**, 841 (1971).
49. R. B. Holt, C. K. McLane, and O. Oldenberg, J. Chem. Phys. **16**, 225, 638 (1948).
50. H. C. Urey, L. H. Dawsey, and F. O. Rice. J. Am. Chem. Soc. **51**, 1371 (1929).
51. M. Schürgers and K. H. Welge. Z. Naturforsch. **23a**, 1508 (1968).

52. H. D. VOLMAN. Adv. Photochem. **1**, 43 (1963).
53. R. A. GORSE and H. D. VOLMAN. J. Photochem. **1**, 1 (1972).
54. N. R. GREINER. J. Chem. Phys. **45**, 99 (1966).
55. T. T. PAUKERT and H. S. JOHNSTON. J. Chem. Phys. **56**, 2824 (1972).
56. L. J. STIEF and V. J. DECARLO. J. Chem. Phys. **50**, 1234 (1969).
57. J. C. CALVERT and J. N. PITTS, JR. Photochemistry. John Wiley and Sons, Inc., N.Y. 1967. p. 825.
58. J. TROE. Ber. Bunsenges. Phys. Chem. **73**, 946 (1969); H. KIJEWSKY and J. TROE. Int. J. Chem. Kin. **3**, 223 (1971).
59. C. J. HOCHANADEL, J. A. GHORMLEY, and P. J. OGREN. J. Chem. Phys. **56**, 4426 (1972).
60. J. W. RABALAIS, J. M. MCDONALD, V. SCHERR, and S. P. MCGLYNN. Chem. Rev. **71**, 73 (1971).
61. K. F. PRESTON and R. J. CVETANOVIĆ. Comprehensive Chem. Kind. **4**, 47 (1972).
62. T. G. SLANGER and G. BLACK. J. Chem. Phys. **54**, 1889 (1971).
63. I. D. CLARK. J. Atmos. Sci. **28**, 847 (1971).
64. W. B. DEMORE and M. MOSESMAN. J. Atmos. Sci. **28**, 842 (1971).
65. E. C. Y. INN and J. HEIMERL. J. Atmos. Sci. **28**, 838 (1971).
66. D. C. KRESZENSKI, R. SIMONAITIS, and J. HEICKLEN. Planet. Space Sci. **1**, 170 (1971).
67. E. C. Y. INN. J. Geophys. Res. **77**, 1991 (1972).
68. S. V. FILSETH and R. T. SLANGER. Private communication.
69. P. WARNECK. J. Chem. Phys. **41**, 3435 (1964).
70. R. A. YOUNG, G. BLACK, and T. G. SLANGER. J. Chem. Phys. **48**, 2067 (1968).
71. J. Y. YANG and F. M. SERVIEDO. Can. J. Chem. **46**, 338 (1968).
72. L. M. QUICK and R. J. CVETANOVIĆ. Can. J. Chem. **49**, 2193 (1971).
73. L. F. LOUCKS and R. J. CVETANOVIĆ. J. Chem. Phys. **56**, 321 (1972).
74. I. D. CLARK and J. F. NOXON. J. Chem. Phys. **57**, 1033 (1972).
75. R. A. YOUNG, G. BLACK, and T. G. SLANGER. J. Chem. Phys. **49**, 4758 (1968).
76. F. STUHL and K. H. WELGE. Can. J. Chem. **47**, 1879 (1969).
77. G. M. LAWRENCE. J. Chem. Phys. **57**, 5616 (1972).
78. I. KOYANO, S. WAUCHOP, and K. H. WELGE. Unpublished.
79. H. W. SIDEBOTTOM, CH. C. BADCOCK, G. E. JACKSON, J. G. CALVERT, G. W. REINHARDT, and E. K. DAMON. Envir. Sci. Technol. **6**, 72 (1972).
80. P. WARNECK, F. F. MARMO, and J. O. SULLIVAN. J. Chem. Phys. **40**, 1132 (1964).
81. D. GOLOMB, K. WATANABE, and F. F. MARMO. J. Chem. Phys. **36**, 958 (1962).
82. S. S. COLLIER, A. MORIKAWA, D. H. SLATER, J. G. CALVERT, G. W. REINHARDT, and E. K. DAMON. J. Am. Chem. Soc. **92**, 217 (1970).
83. H. W. SIDEBOTTOM, C. C. BADCOCK, J. G. CALVERT, G. W. REINHARDT, B. R. RABE, and E. K. DAMON. J. Am. Chem. Soc. **93**, 2581 (1971).
84. H. D. METTEE. J. Phys. Chem. **73**, 1071 (1969).
85. S. N. RAO, S. S. COLLIER, and J. G. CALVERT. J. Am. Chem. Soc. **91**, 1616 (1969).
86. L. STOCKBURGER, S. BRASLAWSKY, and J. HEICKLEN. Preprint.
87. R. G. W. NORRISH and G. A. OLDERSHAW. Proc. R. Soc. Lond. A, **249**, 498 (1959).
88. N. BASCO and R. D. MORSE. Proc. R. Soc. Lond. A, **321**, 129 (1971).
89. H. OKABE. J. Am. Chem. Soc. **93**, 7095 (1971).
90. M.-H. HUI and S. A. RICE. Chem. Phys. Lett. **17**, 474 (1972).
91. J. N. DRISCOLL and P. WARNECK. J. Phys. Chem. **72**, 3736 (1968).
92. C. LALO and C. VERMEIL. J. Photochem. **1**, 321 (1972).
93. E. FAJANS and C. F. GOODEVE. Trans. Farad. Soc. **32**, 511 (1936).
94. G. KORNFELD. Trans. Farad. Soc. **33**, 614 (1937).
95. B. A. THOMPSON, R. R. REEVES, and P. HARTECK. J. Phys. Chem. **69**, 3964 (1965).
96. G. M. LAWRENCE. J. Chem. Phys. **56**, 3435 (1972).

Can. J. Chem. Downloaded from www.nrcresearchpress.com by 210.87.254.105 on 09/05/12
For personal use only.

Energy Transfer Processes in the Stratosphere

RAYMOND L. TAYLOR
Physical Sciences Incorporated, Wakefield, Mass. 01880

Received November 19, 1973

During the past decade or two considerable fundamental information has been acquired on the mechanisms and rates of molecular energy transfer among vibrational, rotational, and electronic states. It is a well-known fact that the rate and even the products of a chemical reaction can be markedly influenced by the degree of internal state excitation of the reactants. Also, it is clear that many of the chemical processes occurring in the upper atmosphere produce atoms or molecules in excited states. It will be the purpose of this paper to review the state of knowledge of energy transfer mechanisms and kinetic rates as it pertains to atmospheric constituents and to attempt to indicate possible important roles of energy transfer in the physics and chemistry of the stratosphere. Some specific examples will include vibrational relaxation of OH and O_3, the possible role of atomic species as quenchants, and electronic/vibrational energy transfer processes.

Au cours des deux dernières décennies, de l'information fondamentale considérable a été acquise sur les mécanismes et les vitesse de transfert d'énergie moléculaire entre les états vibrationnels, rotationnels et électroniques. C'est un fait bien connu que la vitesse et même les produits d'une réaction chimique peuvent être profondément influencés par le degré d'activation de l'état interne des réactifs. Aussi, est-il clair que plusieurs des processus chimiques survenant dans la haute atmosphère produisent des atomes ou des molécules aux états excités. Il sera du but de cette publication de donner un compte rendu sur les connaissances des mécanismes et des vitesses cinétiques de transfert d'énergie comme il appartient aux constituants atmosphériques et de tenter d'indiquer des rôles importants possibles de transfert d'énergie dans la physique et la chimie de la stratosphère. Quelques exemples précis comprendront une relaxation vibrationnelle de OH et O_3, le rôle possible d'espèces atomiques comme inhibiteurs et des processus de transfert d'énergie électronique/vibrationnelle. [Traduit par le journal]

Can. J. Chem., **52**, 1436 (1974)

I. Introduction

Stimulated by the possibility of environmental effects of high flying supersonic aircraft, there is considerable current interest in the detailed kinetic and transport processes in the stratosphere. An adequate description of the stratosphere will require detailed knowledge of many diverse phenomena such as radiation transport, photochemistry, chemical kinetic rates and mechanisms, molecular transport, turbulent diffusion coefficients, and the proper "boundary conditions" at the tropopause and mesopause. This paper concerns itself with one subset of this complex matrix of unknown quantities, the mechanisms and rate constants for molecular energy transfer processes.

It is recognized that energy transfer processes can play an important role in any detailed understanding of the chemistry of the stratosphere. Reactions which proceed in the stratosphere, such as

[1] $$N_2O + h\nu \rightarrow N_2 + O(^1D)$$

[2] $$H + O_3 \rightarrow OH^* + O_2$$

produce products in electronically excited states, *e.g.*, $O(^1D)$, or vibrationally excited states, *e.g.*, OH*. These excited species can engage in further reactions. Because the rate of these subsequent reactions is a function of the state of excitation of the reactants, it is important to know the kinetic history of this energy. It is the purpose of this paper to present the current state of knowledge of energy transfer, particularly vibrational energy processes, for the major atmospheric constituents. At the present time, the effect of reactant internal excitation on chemical rates in not well understood, although it is an active field of current research.

In the next section of this paper a brief review is presented of the various mechanisms, definitions, and terms useful in understanding molecular energy transfer. Section III reviews the present

Can. J. Chem. Downloaded from www.nrcresearchpress.com by 210.87.254.5 on 09/05/12
For personal use only.

Can. J. Chem. Downloaded from www.nrcresearchpress.com by 210.87.254.5 on 09/05/12
For personal use only.

state of knowledge of rate constants for molecular energy transfer concentrating on vibrational energy processes. In the last section future areas of investigation are outlined.

II. Mechanisms and Kinetics of Vibrational Energy Transfer

It is customary to express the course of a chemical reaction as

$$[3] \qquad A + B \underset{k_r}{\overset{k_f}{\rightleftarrows}} C + D$$

where k_f and k_r are the rate constants for the reaction in the forward and reverse directions, respectively. If A, B, C, and D are molecules with various internal states, then clearly k_f and k_r are sums over the individual rate constants k_i, for each internal state i, each rate constant weighted by its fractional population f_i, *e.g.*

$$[4] \qquad k_f = \sum_i k_i f_i$$

If the internal state distribution can be described by Boltzmann statistics, then

$$[5] \qquad f_i = \frac{g_i \exp(-E_i/kT)}{\sum_j g_j \exp(-E_j/kT)}$$

where E_i is the energy of the ith internal state, with degeneracy g_i.

The utility of the fundamental relations [3] to [5] obtains from the fact that, under many laboratory experimental conditions, the internal states of a molecule are in thermodynamic equilibrium, and the state of the system can be characterized by a unique temperature, T. In this situation a rate constant determination provides a unique value of k, but not, of course, for the individual k_i.

It has long been realized that many exothermic chemical reactions produce species in non-Boltzmann internal state distributions. The very large and active field of chemical laser reasearch is evidence of this fact. Long suspected theoretically but only recently conclusively demonstrated is the observation that an internal state rate constant k_i may differ considerably from k. For example, the rate constant for a vibrationally excited molecule may be orders of magnitude faster than for the ground state of that species (1–3). One might conclude that the vibrational excitation is providing some of the activation energy for the reaction.

It is clear that chemical reactions can produce internal state excitation and that such excitation can dramatically affect the rate and mechanisms of subsequent reactions. In any chemical kinetic system as varied and rich as the stratosphere, the possible importance of such effects should be recognized. At present, our understanding of the detailed effects of internal state excitation on the mechanism and rates of reactions is just beginning and provides speculation at best. However, the rates and mechanisms by which excited internal states of molecules, particularly vibrational states, come into local equilibrium with their surroundings is well understood for many species of aeronomic interest. In this paper such information will be reviewed in order that chemists might better be able to focus on the possible importance of energy transfer processes in the upper atmosphere, particularly the stratosphere.

We will emphasize in this review vibrational energy transfer. That is not because electronic and rotational energy are not important in chemcal reactions. Aeronomists have long studied the production and subsequent fate of excited electronic states of atoms and molecules, and these species are known to play a significant role in the understanding of many atmospheric phenomena. However, considerably less is known about the details of electronic energy transfer to the other internal states of molecules (4, 5). Rotational energy also plays a significant role in the mechanism and rate of a chemical reaction, particularly for species with a small moment of inertia. However, it is known that rotational energy is readily transferred to random thermal motion (translational energy) in a few collisions (6, 7); therefore except for very low pressure (high altitude) it will probably be an unimportant source of excitation.

Vibrational energy transfer is a kinetic process and is describable by most of the terms and language used by chemical kineticists. However, as with most fields of science, it has developed its own terminology. The following discussions attempt to explain and define some of this usage.

Let us consider a vibrationally excited molecule, A*. For example, the asterisk might denote one quantum of vibrational excitation. A* collides with a species M, and the vibrational energy is transferred into translational motion. This process may be expressed kinetically as

$$[6] \qquad A^* + M \underset{k_r}{\overset{k_f}{\rightleftarrows}} A + M$$

Can. J. Chem. Downloaded from www.nrcresearchpress.com by 210.87.254.5 on 09/05/12
For personal use only.

where A represents the molecule in its ground state. If we further assume that the concentration of A* is small so that $[A^*] \ll [A]$, or $[A] \approx$ constant $= [A]_\infty$ then the simple integration of [6] yields

$$[7] \quad [A^*] = \frac{k_r}{k_f}[A]_\infty(1 - \exp(-k_f[M]t)) + [A^*]_0 \exp(-k_f[M]t)$$

It can be seen that the system shows exponential temporal behavior with a "time constant"

$$[8] \quad \tau = 1/k_f\,[M]$$

τ is referred to as the relaxation time for the system. Since it contains a concentration, τ must always be referred to a specific pressure. Frequently, 1 atm is used for normalization, which leads to the common symbol $p\tau$ for the relaxation time of species A in 1 atm pressure of M at some specific temperature.

Another frequently employed description of the rate constant for vibrational energy transfer is the probability of energy transfer per collision, P. If a collision number Z_{AM} is defined as the number of gas kinetic collisions per second of molecule A at 1 atm pressure of molecule M, then

$$[9] \quad P(A,M) = (p\tau Z_{AM})^{-1}$$

Z_{AM} may be calculated from gas kinetic theory as

$$[10] \quad Z_{AM} = (8\pi kT/\mu_{AM})^{1/2}\,\sigma_{AM}{}^2\,N_M$$

where μ_{AM} is the reduced mass of the collision pair, σ_{AM} is the average gas kinetic collision diameter, and N_M is the density of M molecules at 1 atm pressure and temperature T.

Although some of the terminology may be different, vibrational energy transfer is a kinetic process, and a rate constant k, can easily be derived from the $p\tau$ or P's. For example,

$$[11] \quad k(A,M) = (p\tau N_M)^{-1} = P(A,M)\,Z_{AM}/N_M$$

More fundamental to the understanding of the kinetics of vibrational energy transfer is the fact that the transfer of energy between internal modes frequently involves many states of the molecules. For aeronomic interest most of the simple diatomic and polyatomic species have vibrational level spacing, ω, much greater than kT. Hence, at stratospheric temperatures only the ground and perhaps the first excited states are appreciably populated. For such systems, perturbed only slightly from equilibrium, a simple two level mechanism of vibrational relaxation (such as described by eqs. 6 to 8) suffices. However, for systems characterized by $\omega \approx kT$, many vibrational levels of the molecules may have to be included in describing the correct mechanism.

A complete description of the vibrational relaxation of a diatomic molecule must include the collisional and radiative rate processes into and out of each vibrational level. Under conditions where collisional processes dominate, this mechanism may be expressed kinetically as

$$[12] \quad \begin{aligned} &A_0 + M \underset{k_{10}}{\overset{k_{01}}{\rightleftarrows}} A_1 + M \\ &A_1 + M \underset{k_{21}}{\overset{k_{12}}{\rightleftarrows}} A_2 + M \\ &A_n + M \underset{k_{n+1,n}}{\overset{k_{n,n+1}}{\rightleftarrows}} A_{n+1} + M \end{aligned}$$

where each subscript represents a particular vibrational level of the molecule. In the mechanism represented by the set of eqs. 12, we have assumed that only nearest neighbor transitions take place, *i.e.*, $n \rightleftarrows n \pm 1$. This assumption appears reasonably valid for most species when $\omega > kT$. If it is further assumed that the relation between the individual rate constants is given by the harmonic oscillator selection rules (8), then a vibrational energy relaxation equation can be derived from the sum of eqs. 12

$$[13] \quad E_A(t) = E_A{}^\infty\,[1 - \exp(-t/\tau)]$$

where

$$[14] \quad \tau = \frac{1}{k_{10}[M](1 - \exp(-\omega_A/kT))}$$

$$[15] \quad E_A = \frac{\omega_A}{\exp(\omega_A/kT_V) - 1}$$

T_V is the vibrational temperature of A and $E_A{}^\infty$ is the vibrational energy of A at thermal equilibrium, *i.e.* when $T_V = T$.

It is evident that eqs. 13 and 14 are quite similar to eqs. 7 and 8, the major difference being the term $1 - \exp(-\omega_A/kT)$ which arises from consideration of the complete manifold of levels. For $\omega_A > kT$, this factor is essentially unity, and the similarity between eqs. 8 and 14 is clear.

There are several different types of vibrational energy transfer processes that are mechanistically

Can. J. Chem. Downloaded from www.nrcresearchpress.com by 210.87.254.5 on 09/05/12
For personal use only.

distinguishable. Process 6, in which the vibrational energy is exchanged with the translational mode, is called a vibration–translation or V → T process. Since it is not yet possible to decide whether the vibrational energy goes directly into translational motion or into rotation of one or more of the collision partners and then into translation, V → T processes are sometimes written V → R,T. Vibrational energy can also be exchanged between the vibrational modes of two molecules:

[16] $$A^* + B \rightleftarrows A + B^*$$

This is called a vibration–vibration (V → V) process. Process 16 can be energy resonant depending upon the level spacings. For $\omega_A \neq \omega_B$, the difference in energy, $\Delta E = \omega_A - \omega_B$, must be exchanged with the translational mode. For polyatomic molecules with many modes, vibrational energy may be collisionally transferred between modes, an intramolecular V → V process.

In recent years, it has become evident that there are at least two major types of molecular interactions operative in vibrational energy transfer. For V → T and non-resonant V → V ($\Delta E > \sim 200\ cm^{-1}$) processes, the important collisions are non-adiabatic or impulsive, and the short range, repulsive intermolecular forces dominate the interaction (8). For near-resonant V → V processes, the long range, multipolar forces are dominant (9). This difference in molecular interactions leads to large variations in the magnitudes of rate constants, the temperature dependences, and collision partner effects.

It is customary in the field of vibrational energy transfer to express all rate constants in the exothermic direction. The reverse rate constant is then simply related to the forward rate by the endothermicity of the process. Since the fundamental molecular interactions in energy transfer processes provide large variation in temperature dependence, there is no "universal" rate expression similar to the Arrhenius equation by which to correlate data. Instead one usually resorts to curve fits of data with complex expressions, the temperature form of which is believed to have some theoretical significance.

In general, the larger the quantum of vibrational energy that must be transferred to the translational mode, the slower will be the rate for that process. This is due to the poor coupling between the fast vibrational motion and the slower translational motion leading to an adiabatic collision with little or no energy transfer. Hence, it is only the high velocity tail of the Boltzmann distribution that is effective in most V → T transfer processes. Obviously, as one goes to higher gas temperatures (velocities) V → T transfer rates increase, in fact such processes generally show a very steep temperature dependence (8).

V → V processes generally have much larger rate constants than V → T reactions due to the fact that by exchanging a quantum of energy between different vibrational modes, less energy need be exchanged with translation. Energy resonant or near-resonant V → V processes are among the fastest of vibrational energy transfer reactions. Also, for V → V processes inverse or modest positive temperature dependence is usual (9).

As in most fields, there are always some exceptions to the above generalizations. For example, V → R → T exchange appears to be dominant in certain hydride-like molecules, such as HF, HCl, and possibly OH (10). For these cases, even though the vibrational quanta are large, the rate constants are also large, approaching gas kinetic. Also, other V → T interactions, *e.g.*, with atoms or radicals, may involve chemical forces, "sticky" collisions, or incipient hydrogen bonding. At the moment, all these latter terms are used merely to indicate our ignorance of the actual details of the molecular interactions that are responsible for the fast rates observed.

III. Status of Kinetic Rates for Atmospheric Constituents

A. Major Species

The mechanism for vibrational energy transfer within a gas mixture composed of N_2, O_2, CO_2, and H_2O is shown schematically in Fig. 1. Shown as an energy level diagram are the first or first few vibrational levels for the vibrational modes of CO_2(100), (010), and (001), the (010), (100), and (001) modes of H_2O, and the lower vibrational levels of N_2 and O_2. It must be recognized that the bending mode of CO_2(010) is doubly degenerate. The symmetric and asymmetric modes of H_2O(100) and (001) lie too high in energy ($\sim 3500\ cm^{-1}$) to be significantly populated under stratospheric conditions. The various paths for vibrational energy transfer within this molecular system are indicated by the numbered arrows. The justification for this particular mechanism is too lengthy to be discussed in this paper.

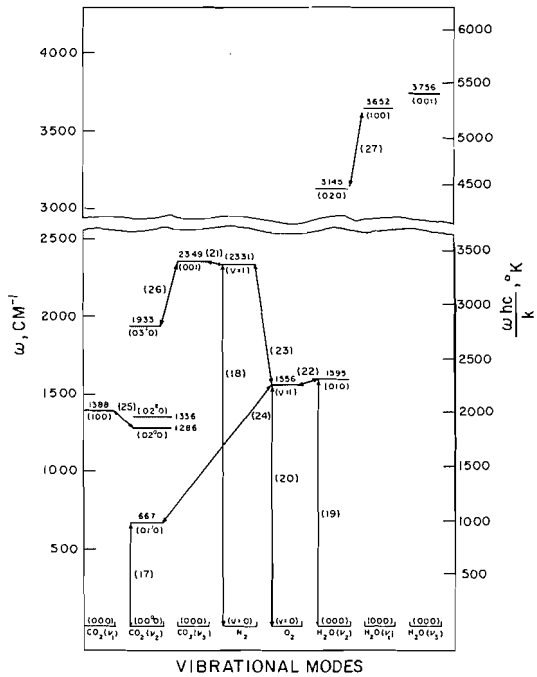

FIG. 1. Vibrational energy level diagram for the molecular system N_2, O_2, CO_2, and H_2O. Shown as arrows are the assumed vibrational energy transfer processes.

However, the mechanism is based on a combination of theory and experimental measurements which primarily developed over the past decade in response to the growth of laser technology.

The energy transfer paths shown on Fig. 1 can be grouped into various types of processes.

V → T processes

[17] $CO_2(010) + M \rightleftarrows CO_2(000) + M + 667\ cm^{-1}$

[18] $N_2(v = 1) + M \rightleftarrows N_2(v = 0) + M + 2331\ cm^{-1}$

[19] $H_2O(010) + M \rightleftarrows H_2O(000) + M + 1595\ cm^{-1}$

[20] $O_2(v = 1) + M \rightleftarrows O_2(v = 0) + M + 1556\ cm^{-1}$

V → V processes (intermolecular)

[21] $CO_2(001) + N_2(v = 0) \rightleftarrows CO_2(000) + N_2(v = 1) + 18\ cm^{-1}$

[22] $H_2O(010) + O_2(v = 0) \rightleftarrows H_2(000) + O_2(v = 1) + 39\ cm^{-1}$

[23] $N_2(v = 1) + O_2(v = 0) \rightleftarrows N_2(v = 0) + O_2(v = 1) + 775\ cm^{-1}$

[24] $O_2(v = 1) + CO_2(000) \rightleftarrows O_2(v = 0) + CO_2(010) + 889\ cm^{-1}$

V → V processes (intramolecular)

[25] $CO_2(100) + M \rightleftarrows CO_2(02^00) + M + 102\ cm^{-1}$

[26] $CO_2(001) + M \rightleftarrows CO_2(03^10) + M + 416\ cm^{-1}$

[27] $H_2O(100) + M \rightleftarrows H_2O(020) + 417\ cm^{-1}$

The numbers on the arrows of Fig. 1 correspond to the particular reactions 17 to 27, respectively. For processes 17 to 20 and 25 to 27 M may be any other collision partner in the gas. Obviously, many other V → T and V → V processes may be added to Fig. 1. However, the mechanism chosen is based on current experimental and theoretical understanding as summarized by Taylor and Bitterman (11).

The rate constants for reactions 17 to 27 are listed in Table 1 for a temperature $T = 300\ °K$. The rate constants are all listed for the exothermic process. Data for vibrational energy transfer are currently only available for temperatures greater than 300 °K.[1] Hence, extrapolation must be used to predict rate constants for the temperature regime of interest for stratospheric application, *i.e.*, $200 \leq T \leq 300\ °K$. For most of the listed processes the extrapolation below 300 °K will only change the rate constant by a factor of 2 or less.

Equations by which to calculate the rate constants for arbitrary temperatures are listed in Table 2. These expressions may be used to calculate the rate constants for specific temperatures of interest in the stratosphere. The form of the rate constants listed in Table 2 has been obtained by fitting to experimental data where available and using either a theoretical temperature dependence or the temperature dependence suggested by the general trend of the data.

One should not read too much physical significance into the mathematical form of the rate expressions listed in Table 2. For many V → T processes theory indicates an approximate temperature dependence such as $k \sim A \exp(-B/T^{1/3})$ where A and B are combinations of molecular parameters (8). This is the form that has been chosen to fit most of the data for the processes of Table 2. For V → V processes, particularly those in near energy resonance, theory indicates a much more complex temperature dependence. However, for computational convenience, the simpler $A \exp(\pm B/T^{1/3})$ form has been retained even for the V → V reactions. In two cases, reactions 22 and 26, data only exist at 300 °K,

[1]There are experiments presently underway in several laboratories to extend vibrational energy transfer rate data to temperatures as low as 100 °K. Some of these data will be relevant to reactions such as [21] and [25] above.

Can. J. Chem. Downloaded from www.nrcresearchpress.com by 210.87.254.5 on 09/05/12
For personal use only.

TABLE I. Vibrational transfer rates at 300 °K

Reaction number	Reaction		Rate constant (at 300 °K) (cm^3/molecule s)
17	$CO_2(010) + M \rightleftarrows CO_2(000) + M$	$M = CO_2$	4.8×10^{-15}
		$M = N_2, O_2$	2.3×10^{-15}
		$M = H_2O$	10^{-11}
18	$N_2(v = 1) + M \rightleftarrows N_2(v = 0) + M$	$M = N_2, O_2, CO_2$	$\ll 10^{-20}$
		$M = H_2O$	3.1×10^{-15}
19	$H_2O(010) + M \rightleftarrows H_2O(000) + M$	$M = H_2O$	$\sim 10^{-11}$
		$M = N_2, CO_2$	1.5×10^{-14}
20	$O_2(v = 1) + M \rightleftarrows O_2(v = 0) + M$	$M = N_2, O_2, CO_2$	4.5×10^{-19}
		$M = H_2O$	$\leq 4 \times 10^{-14}$
21	$CO_2(001) + N_2(v = 0) \rightleftarrows CO_2(000) + N_2(v = 1)$		6.0×10^{-13}
22	$H_2O(010) + O_2(v = 0) \rightleftarrows H_2O(000) + O_2(v = 1)$		$\sim 10^{-12}$
23	$N_2(v = 1) + O_2(v = 0) \rightleftarrows N_2(v = 0) + O_2(v = 1)$		6×10^{-18}
24	$O_2(v = 1) + CO_2(000) \rightleftarrows O_2(v = 0) + CO_2(010)$		6×10^{-15}
25	$CO_2(100) + M \rightleftarrows CO_2(02^00) + M$	$M = N_2, O_2$	$\geq 3 \times 10^{-11}$
26	$CO_2(001) + M \rightleftarrows CO_2(03^10) + M$	$M = N_2$	1.5×10^{-15}
		$M = O_2$	1.9×10^{-15}
		$M = CO_2$	4.8×10^{-15}
		$M = CO$	3.2×10^{-15}
		$M = H_2O$	4.0×10^{-13}
27	$H_2O(100) + M \rightleftarrows H_2O(020) + M$	$M = H_2O$	$\sim 4 \times 10^{-11}$ (see text)
		$M = N_2, O_2, CO_2$	$\sim 2 \times 10^{-13}$ (see text)
28	$CO(v = 1) + M \rightleftarrows CO(v = 0) + M$	$M = CO, N_2, O_2$	$< 10^{-20}$
		$M = H_2O$	2×10^{-14} (see text)
29	$N_2(v = 1) + CO(v = 0) \rightleftarrows N_2(v = 0) + CO(v = 1)$		1.5×10^{-14}
30	$CO(v = 1) + O_2(v = 0) \rightleftarrows CO(v = 0) + O_2(v = 1)$		3×10^{-18}
31	$CO_2(001) + CO(v = 0) \rightleftarrows CO_2(000) + CO(v = 1)$		1.7×10^{-13}
33	$NO(v = 1) + M \rightleftarrows NO(v = 0) + M$	$M = N_2, O_2$	9×10^{-19}
		$M = NO$	6.1×10^{-14}
		$M = CO_2$	4×10^{-14}
		$M = H_2O$	2×10^{-12}
		$M = CO$	6×10^{-15}
34	$N_2(v = 1) + NO(v = 0) \rightleftarrows N_2(v = 0) + NO(v = 1)$		1.0×10^{-15}
35	$CO(v = 1) + NO(v = 0) \rightleftarrows CO(v = 0) + NO(v = 1)$		2.1×10^{-14}
36	$N_2(v = 1) + N_2O(000) \rightleftarrows N_2(v = 0) + N_2O(001)$		2.5×10^{-13}
37	$OH(v = 1) + M \rightleftarrows OH(v = 0) + M$	$M = O_2$	1×10^{-15}
		$M = N_2$	3.6×10^{-16}
		$M = NO$	1.5×10^{-14}
		$M = N_2O$	4.8×10^{-15}
		$M = CO_2$	2.4×10^{-15}
		$M = H_2O$	2.0×10^{-14}
38	$N_2(v = 1) + O \rightleftarrows N_2(v = 0) + O$		3.1×10^{-15}
39	$O_2(v = 1) + O \rightleftarrows O_2(v = 0) + O$		7×10^{-14}
40	$CO(v = 1) + O \rightleftarrows CO(v = 0) + O$		2×10^{-15}
41	$CO_2(010) + O \rightleftarrows CO_2(000) + O$		5×10^{-18}
42	$O_3(100) + M \rightleftarrows O_3(001) + M$	$M = N_2, O_2, O_3, CO_2$	$\geq 4.9 \times 10^{-12}$
43	$O_3(100) + O_3(001) \rightleftarrows O_3(101) + O_3(000)$		See text
44	$O_3(100) + M \rightleftarrows O_3(000) + M$	$M = N_2$	2.4×10^{-14}
		$M = O_2$	2.9×10^{-14}
		$M = O_3$	1.1×10^{-13}
		$M = CO_2$	1.9×10^{-13}
45	$O_3(001) + M \rightleftarrows O_3(000) + M$		See text
50	$CO_2(001) + O_3(000) \rightleftarrows CO_2(100) + O_3(100)$		7.6 to 12×10^{-13}

Can. J. Chem. Downloaded from www.nrcresearchpress.com by 210.87.254.5 on 09/05/12
For personal use only.

Can. J. Chem. Downloaded from www.nrcresearchpress.com by 210.87.254.5 on 09/05/12
For personal use only.

TABLE 2. Rates of vibrational energy transfer processes

Reaction number	Reaction	References	Temperature range (°K)	Reaction rate constant (cm^{-3} $molecule^{-1}$ s^{-1})
17	$CO_2(010) + M \rightarrow CO_2(000) + M$	11, 23, 24, 58, 59	$200 < T < 2000$	$M = CO_2$; $k = 4.64 \times 10^{-10} \exp(-76.75/T^{1/3})$
				$M = N_2, O_2$; $k = 6.69 \times 10^{-10} \exp(-84.07/T^{1/3})$
		11, 23	$200 < T < 1200$	$M = H_2O$; $k = 3.22 \times 10^{-13} \exp(22.91/T^{1/3})$
18	$N_2(v = 1) + M \rightarrow N_2(v = 0) + M$	11, 13, 60	$1000 < T < 5000$	$M = N_2, O_2, CO_2$; $k = 8.53 \times 10^{-7} \exp(-273.10/T^{1/3})$
		11, 17, 61	$200 < T < 2000$	$M = H_2O$; $k = 1.07 \times 10^{-10} \exp(-69.90/T^{1/3})$
19	$H_2O(010) + M \rightarrow H_2O(000) + M$	11 (corrected by 0.1), 62–64	$200 < T < 600$	$M = H_2O$; $k = 1.0 \times 10^{-11} + 2.68 \times 10^{-8} \exp(-70.00/T^{1/3})$
		63	$200 < T < 400$	$M = N_2, CO_2$; $k = 5.37 \times 10^{-10} \exp(-70.00/T^{1/3})$
				$M = O_2$ (see process 22)
20	$O_2(v = 1) + M \rightarrow O_2(v = 0) + M$	11, 13, 60	$200 < T < 5000$	$M = N_2, O_2, CO_2$; $k = 4.81 \times 10^{-8} \exp(-169.60/T^{1/3})$
		11		$M = H_2O$; $k \leq 3.60 \times 10^{-10} \exp(-60.69/T^{1/3})$
21	$CO_2(001) + N_2(v = 0) \rightarrow CO_2(000) + N_2(v = 1)$	11, 24, 65, 66	$200 < T < 2000$	$k = 1.71 \times 10^{-6} \exp(-175.30/T^{1/3}) + 6.07 \times 10^{-14} \exp(15.27/T^{1/3})$
22	$H_2O(010) + O_2(v = 0) \rightarrow H_2O(000) + O_2(v = 1)$	11	$200 < T < 400$	$k = 1.00 \times 10^{-12}$
23	$N_2(v = 1) + O_2(v = 0) \rightarrow N_2(v = 0) + O_2(v = 1)$	11, 67	$200 < T < 5000$	$k = 1.74 \times 10^{-10} \exp(-124.00/T^{1/3})$
24	$O_2(v = 1) + CO_2(000) \rightarrow O_2(v = 0) + CO_2(010)$		$200 < T < 400$	$k = 1.78 \times 10^{-12} \exp(-37.94/T^{1/3})$
25	$CO_2(100) + M \rightarrow CO_2(020) + M$	11, 68, 69	$200 < T < 400$	$M = N_2, O_2$; $k \geq 3.0 \times 10^{-11}$
26	$CO_2(001) + M \rightarrow CO_2(030) + M$	11, 21, 24, 65	$200 < T < 2000$	$M = N_2$; $k = 1.00 \times 10^{-15} + 5.16 \times 10^{-11} \exp(-76.75/T^{1/3})$
		11, 21, 70		$M = O_2$; $k = 1.10 \times 10^{-15} + 7.31 \times 10^{-11} \exp(-76.75/T^{1/3})$
		11, 19, 24, 71		$M = CO_2$; $k = 3.0 \times 10^{-15} + 1.72 \times 10^{-10} \exp(-76.75/T^{1/3})$
		21, 24, 25		$M = CO$; $k = 2.20 \times 10^{-15} + 9.69 \times 10^{-11} \exp(-76.75/T^{1/3})$
		11, 70, 72	$200 < T < 1000$	$M = H_2O$; $k = 4.0 \times 10^{-13}$

Can. J. Chem. Downloaded from www.nrcresearchpress.com by 210.87.254.5 on 09/05/12
For personal use only.

TABLE 2. (*Continued*)

Reaction number	Reaction	References	Temperature range (°K)	Reaction rate constant (cm^{-3} $molecule^{-1}$ s^{-1})
27	$H_2O(100) + M \rightarrow H_2O(020) + M$	12, 73	$2000 < T < 4000$	$M = H_2O$; $k = 2.50 \times 10^{-12} T^{0.5}$
				$M = N_2, O_2, CO_2$; $k \approx 1.0 \times 10^{-14} T^{0.5}$
	Mechanism is author's preference			
28	$CO(v = 1) + M \rightarrow CO(v = 0) + M$	13, 14, 60	$200 < T < 5000$	$M = CO, N_2, O_2$; $k = 6.67 \times 10^{-8} \exp(-208.30/T^{1/3})$
		13, 14, 60	$1000 < T < 3000$	$M = H_2O$; $k = 3.12 \times 10^{-10} \exp(-64.99/T^{1/3})$
29	$N_2(v = 1) + CO \rightarrow N_2(v = 0) + CO(v = 1)$	15–18	$200 < T < 2000$	$k = 1.78 \times 10^{-6} \exp(-209.90/T^{1/3}) + 6.98 \times 10^{-13} \exp(-25.60/T^{1/3})$
30	$CO(v = 1) + O_2(v = 0) \rightarrow CO(v = 0) + O_2(v = 1)$	15, 74	$1000 < T < 3000$	$k = 3.50 \times 10^{-10} \exp(-124.00/T^{1/3})$
31	$CO_2(001) + CO(v = 0) \rightarrow CO_2(000) + CO(v = 1)$	19–24	$1000 < T < 3000$	$k = 1.56 \times 10^{-11} \exp(-30.12/T^{1/3})$
32	$CO(v = 1) + H_2O(000) \rightarrow CO(v = 0) + H_2O(010)$			Data can be interpreted as either a V → T or V → V process. See process 28 for V → T interpretation
33	$NO(v = 1) + M \rightarrow NO(v = 0) + M$	28, 75	$200 < T < 2000$	$M = N_2, O_2$; $k = 6.75 \times 10^{-7} \exp(-182.83/T^{1/3})$
		26–38		$M = NO$; $k = 2.49 \times 10^{-11} \exp(-40.19/T^{1/3})$
		28	$200 < T < 400$	$M = CO_2$; $k = 1.66 \times 10^{-11} \exp(-40.19/T^{1/3})$
		28		$M = H_2O$; $k = 7.47 \times 10^{-10} \exp(-40.19/T^{1/3})$
		28, 76		$M = CO$; $k = 2.49 \times 10^{-12} \exp(-40.19/T^{1/3})$
34	$N_2(v = 1) + NO(v = 0) \rightarrow N_2(v = 0) + NO(v = 1)$	28, 76, 77	$200 < T < 2000$	$k = 4.22 \times 10^{-10} \exp(-86.35/T^{1/3})$
35	$CO(v = 1) + NO(v = 0) \rightarrow CO(v = 0) + NO(v = 1)$	28, 76, 78	$200 < T < 2000$	$k = 3.58 \times 10^{-11} \exp(-49.93/T^{1/3}) + 1.26 \times 10^{-8} \exp(-115.13/T^{1/3})$
36	$N_2(v = 1) + N_2O(000) \rightarrow N_2(v = 0) + N_2O(001)$	21, 79–82	$200 < T < 2000$	$k = 5.4 \times 10^{-14} \exp(10.2/T^{1/3})$
37	$OH(v = 1) + M \rightarrow OH(v = 0) + M$	40, 41	$T = 300$	$M = O_2$; $k(1) = 1.0 \times 10^{-15}$ $= N_2$; $= 3.6 \times 10^{-16}$ $= NO$; $= 1.5 \times 10^{-14}$ $= N_2O$; $= 4.8 \times 10^{-15}$ $= CO_2$; $= 2.4 \times 10^{-15}$ $= H_2O$; $= 2.0 \times 10^{-14}$

Can. J. Chem. Downloaded from www.nrcresearchpress.com by 210.87.254.5 on 09/05/12
For personal use only.

TABLE 2. (*Concluded*)

Reaction number	Reaction	References	Temperature range (°K)	Reaction rate constant (cm^{-3} $molecule^{-1}$ s^{-1})
38	$N_2(v = 1) + O \rightarrow N_2(v = 0) + O$	52, 81–83	$200 < T < 3000$	$k = 1.07 \times 10^{-10} \exp(-69.90/T^{1/3})$
39	$O_2(v = 1) + O \rightarrow O_2(v = 0) + O$	84	$200 < T < 2000$	$k = 6.88 \times 10^{-9} \exp(-76.75/T^{1/3})$
40	$CO(v = 1) + O \rightarrow CO(v = 0) + O$	74, 83	$200 < T < 3000$	$k = 9.9 \times 10^{-8} \exp(-118.07/T^{1/3})$
41	$CO_2(010) + O \rightarrow CO_2(000) + O$	85	$200 < T < 3000$	$k = 2.32 \times 10^{-9} \exp(-76.75/T^{1/3})$
42	$O_3(100) + M \rightarrow O_3(001) + M$	46	300	$M = N_2, O_2, O_3, CO_2$; $k \geq 4.9 \times 10^{-12}$ Note: Data refer to $k_{42} + k_{43}$
43	$O_3(100) + O_3(001) \rightarrow O_3(101) + O_3(000)$	46	300	See above
44	$O_3(100) + M \rightarrow O_3(000) + M$	46	300	$M = N_2$; $k = 2.4 \times 10^{-14}$ Note: Data refer to $k_{44} + k_{45}$ $M = O_2$; $k = 2.9 \times 10^{-14}$ $M = O_3$; $k = 1.1 \times 10^{-13}$ $M = CO_2$; $k = 1.9 \times 10^{-13}$
45	$O_3(001) + M \rightarrow O_3(000) + M$		300	See above
46	$O_3(100) + M \rightarrow O_3(010) + M$			
47	$O_3(001) + M \rightarrow O_3(010) + M$		300	Possible alternate mechanism for [44] + [45]
48	$O_3(010) + M \rightarrow O_3(000) + M$			See text
49	$O_3(010) + CO_2(000) \rightarrow O_3(000) + CO_3(010)$			
50	$CO_2(001) + O_3(000) \rightarrow CO_2(100) + O_3(100)$	46, 49, 50	300	$k = 7.6$ to 12×10^{-13}

Can. J. Chem. Downloaded from www.nrcresearchpress.com by 210.87.254.5 on 09/05/12
For personal use only.

hence a temperature independent rate constant has been listed which should suffice for the temperature regime of 200–400 °K.

Of all the processes 17 to 27 shown on Fig. 1, those involving the relaxation of the H_2O molecule, processes 19 and 27, are presently least understood. The V → T relaxation of the bending mode of $H_2O(010)$ (which may actually proceed via a V → R → T mechanism) has been studied around room temperature, but the actual rate constant is unknown to an order of magnitude and the temperature dependence is uncertain. The mechanism and rate constant for the high lying modes $H_2O(100)$ and (001) are even less well understood. One would expect that the latter two modes would V → V couple strongly due to their close energy spacing and perhaps relax by an intramolecular V → V process to $H_2O(020)$, reaction 27. There are recent, unpublished shock-tube data (12) which indicate that at 2000–4000 °K, mode $H_2O(001)$ equilibrates in about 10–20 collisions with H_2O as a collision partner and in 500–1000 collisions with Ar. Whether this rate reflects a V → V coupling to $H_2O(020)$ or a direct V → T process has not yet been established.

From the entries in Tables 1 and 2 it can be seen that the magnitudes of the rate constants for vibrational energy transfer vary considerably. Therefore, any model for vibrational energy transfer among stratospheric species can be simplified and need not include all the processes 17 to 27. For example, from the rates listed in Table 1 for the stratospheric mixture of $N_2/O_2/CO_2/H_2O$, vibrational energy will flow from N_2 and (or) O_2 to CO_2 and H_2O via fast V → V processes 21 to 24. The CO_2 and H_2O will subsequently transfer this energy into the translational mode via V → T processes from the low lying modes $CO_2(010)$ or $H_2O(010)$, processes 17 and 19, respectively.

B. Minor Species

Except for CO there is considerably less experimental information about the vibrational relaxation of the minor stratospheric species; CO, O_3, NO_x, and OH. Therefore, it was decided to discuss each of these species separately rather than attempt an overall matrix such as Fig. 1. Furthermore, the minor species are present in the stratosphere in such small amounts that they will not affect the overall relaxation of the major components. However, since they may be formed vibrationally excited, it is of interest to determine how fast this excess energy may be lost to other species or to translational motion.

CO

In most respects, CO is quite similar to N_2 in its vibrational relaxation behavior. CO could replace N_2 in Fig. 1 and the major energy transfer processes and even rate constants would remain quite similar to those for N_2. There are substantial data on the rates of vibrational energy transfer for CO (13). In analogy to N_2, the important reaction paths are:

V → T processes

[28] $CO(v = 1) + M \rightleftarrows CO(v = 0) + M + 2143\ cm^{-1}$

V → V processes

[29] $N_2(v = 1) + CO(v = 0) \rightleftarrows N_2(v = 0) + CO(v = 1) + 188\ cm^{-1}$

[30] $CO(v = 1) + O_2(v = 0) \rightleftarrows CO(v = 0) + O_2(v = 1) + 587\ cm^{-1}$

[31] $CO_2(001) + CO(v = 0) \rightleftarrows CO_2(000) + CO(v = 1) + 605\ cm^{-1}$

[32] $CO(v = 1) + H_2O(000) \rightleftarrows CO(v = 0) + H_2O(010) + 548\ cm^{-1}$

There are good reliable data for process 28 with M = CO. Based on the Millikan and White (13) correlation scheme M = N_2, O_2, and CO_2 should have essentially the same rate as CO as indicated in Table 1, although there are no direct measurements for O_2 and CO_2. For M = H_2O, only the high temperature data of von Rosenberg *et al.* (14) exist. These data may be interpreted as either a V → T process 28 or V → V reaction 32. Following von Rosenberg we have selected the V → T interpretation. Extrapolation of the rate of this process to room temperature and below is not recommenedd since the mechanism has not been established.

The rate of the V → V reaction 29 has been measured by several workers (15–18). However, there is substantial scatter in the high temperature results making the determination of a temperature dependence difficult. We have chosen to use two separate expressions to cover the entire temperature range listed (Table 2). The room temperature rate measurement by Zittel and Moore (18) is considered reliable.

The CO_2/CO V → V process 31 has been the subject of many investigations (19–24), and its rate is quite well known over a large temperature range. It is to be noted that this rate, unlike the

analogous process 21 for CO_2/N_2, does not exhibit a negative temperature dependence. This has been explained theoretically by Rosser *et al.* (25).

Based on its kinetic similarity to N_2 and its small concentration, it is unlikely that CO plays a significant role in vibrational energy transfer in the atmosphere. However, for completeness the rates for processes 28 to 32 are listed in Tables 1 and 2.

NO_x

There are some data for vibrational energy transfer for certain nitrogen/oxygen compounds, in particular NO and N_2O. For NO the V → T process

[33] $NO(v = 1) + M \rightleftarrows NO(v = 0) + M + 1876\ cm^{-1}$

has been studied over a wide temperature range for M = Ar and NO (26–38). For M = H_2O, CO_2, N_2, and CO there are only measurements at 300 °K (28). Of particular significance is the fact that, in contrast to the other diatomics N_2, O_2, and CO, the NO V → T process for M = NO is very fast at room temperature with $k = 6 \times 10^{-14}$ cm^3/molecule s. Also, Billingsley and Callear (35, 36) have observed a very marked inverse temperature dependence around room temperature. However, recent work by Stephenson (38) using the well-established laser fluorescent technique casts doubt on some aspects of the Billingsley and Callear result. The explanation of these observations is not clear at present and has been ascribed to NO dimer formation (26, 36) or to spin–orbit coupling (39). In Table 2, a rate for M = N_2 is given based on some unpublished data of the author. This result may be considered tentative.

NO is known to V → V couple with N_2 and CO.

[34] $N_2(v = 1) + NO(v = 0) \rightleftarrows N_2(v = 0) + NO(v = 1) + 455\ cm^{-1}$

[35] $CO(v = 1) + NO(v = 0) \rightleftarrows CO(v = 0) + NO(v = 1) + 267\ cm^{-1}$

The rates for these processes are listed in Tables 1 and 2. For NO_2, there are no data on vibrational energy transfer processes. It might be expected that NO_2 would have a behavior between that of CO_2 and O_3, and hence would relax moderately quickly. There are many V → V reactions possible between the modes of NO_2 and the other atmospheric components.

There are data and theoretical calculations for the V → V process between N_2O and N_2.

[36] $N_2(v = 1) + N_2O(000) \rightleftarrows N_2(v = 0) + N_2O(001) + 106\ cm^{-1}$

This rate is listed in Tables 1 and 2.

To this author's knowledge, there are no measurements of vibrational relaxation on any of the nitrogen oxyacids, HNO, HNO_2, or HNO_3, nor similarly, for the compounds NO_3 and N_2O_5. One would expect that all these species would relax very quickly, perhaps as fast as H_2O.

OH

This is an interesting species because it is known that OH is formed vibrationally excited up to $v = 9$ via the reaction

$$H + O_3 \rightarrow OH^* + O_2$$

The subsequent fate of this vibrational excitation is important in understanding the ultimate kinetic role of OH radicals in the stratosphere. In analogy to other hydride-like molecules, such as H_2O, HF, HCl, etc., the V → T deexcitation of vibrationally excited OH might be expected to be fast and occur via a V → R → T process. However, Worley *et al.* (40, 41) have measured the rate of deactivation of $v = 9$ of OH by many molecular species including M = O_2, N_2, NO, N_2O, CO_2, and H_2O and find rate constants in the range of 0.36 to 20 $\times 10^{-14}$ cm^3/molecule s. Since the V → T deactivation of the $v = 9$ level should be approximately 9 times faster than for $v = 1$,[2] the rates for the process

[37] $OH(v = 1) + M \rightleftarrows OH(v = 0) + M + 3570\ cm^{-1}$

should be in the range of 0.3 to 20 $\times 10^{-15}$ cm^3/molecule s. This is surprisingly slow in view of the $H_2O(010)$ V → T process 19 which has a rate of $\sim 10^{-11}$ cm^3/molecule s at 300 °K.

Welge *et al.* (42) have measured the collisional deactivation of $v = 1$ in the first excited electronic state of OH ($A^2\Sigma^+$). They found that the near resonant process

$$OH(v = 0, K = 20) + M \rightleftarrows OH(v = 1, K = 15) + M + 27\ cm^{-1}$$

occurs with a rate of $\sim 10^{-11}$ cm^3/molecule s for M = Ar and N_2. Since there are other resonant

[2]The rate of V → T deexcitation for any vibrational level can be obtained from the relation $k(v = n) = nk(v = 1)$ which is most valid for harmonic oscillators (8).

Can. J. Chem. Downloaded from www.nrcresearchpress.com by 210.87.254.5 on 09/05/12
For personal use only.

Can. J. Chem. Downloaded from www.nrcresearchpress.com by 210.87.254.5 on 09/05/12
For personal use only.

$V \rightarrow R$ processes possible in the OH molecule, it is conceivable that the data of Worley *et al.* for $v = 9$ cannot be extrapolated to lower vibrational levels. However, until this question is resolved, we have chosen to use Worley's results in Tables 1 and 2.

$V \rightarrow V$ exchange between OH molecules, such as

$$OH(v = n) + OH(v = 0) \rightleftarrows OH(v = n - 1) + OH(v = 1)$$

should be very rapid and will also change the vibrational distribution of OH initially formed in a non-Boltzmann distribution. However, the concentration of OH radicals in the stratosphere is expected to be very small, and this intramode $V \rightarrow V$ process is probably unimportant.

Atoms

Although atoms themselves cannot have vibrational energy, then can act as very efficient collision partners for $V \rightarrow T$ processes. There are data which indicate that atomic O can be very efficient in $V \rightarrow T$ processes involving N_2, O_2, CO, and $CO_2(010)$.

[38] $N_2(v = 1) + O \rightleftarrows N_2(v = 0) + O + 2331\ cm^{-1}$

[39] $O_2(v = 1) + O \rightleftarrows O_2(v = 0) + O + 1556\ cm^{-1}$

[40] $CO(v = 1) + O \rightleftarrows CO(v = 0) + O + 2143\ cm^{-1}$

[41] $CO_2(010) + O \rightleftarrows CO_2(000) + O + 667\ cm^{-1}$

The rates for these processes are listed in Tables 1 and 2. Although most of the measurements to date are at high temperatures, using shock-tube techniques, the data have been extrapolated to room temperatures by using the functional forms given in Table 2. Until we understand the fundamental interactions producing these strong effects, such a large temperature extrapolation is to be considered tentative. Although processes 38 to 41 are probably not important in the stratosphere where the O-atom concentration is typically small, *i.e.*, 10^{-12} to 10^{-7} mole fraction, at higher altitudes where the molecular O_2 is primarily photodissociated, processes such as [38] may be very important in controlling the vibrational temperature of the molecular constituents.

O_3

Because of the obvious importance of O_3 chemistry in the stratosphere, it is of current interest to understand the mechanisms and rate constants for vibrational energy transfer of the O_3 molecule, particularly in collisions with the major atmospheric constituents, N_2, O_2, and CO_2. Recent experimental data (43) support earlier conclusions (44, 45) that vibrational excitation of O_3 occurs when O_3 is formed via three-body recombination. The subsequent fate of this vibrational energy could be of importance in understanding the chemistry of the O_3 molecule.

Until very recently, there were no data on the vibrational relaxation of O_3. However, recent exploitation of the coincidence between certain emission lines in the 9.4 μ CO_2 laser band and absorption lines in the asymmetric stretching (001) vibration/rotation band of O_3 has made it possible to use the well-developed laser fluorescence technique to study O_3 vibrational relaxaation (46). The results are very recent; the mechanism(s) are not definitive, but some initial features of the mechanism and rates of energy transfer for O_3 are now available.

A vibrational energy level diagram for the molecular system CO_2, N_2, O_2, and O_3 is shown in Fig. 2. This is similar to Fig. 1 except that O_3 has replaced H_2O, and all the arrows [17] to [27] indicating previous reaction paths have been omitted in Fig. 2 for clarity. It can be seen that vibrational levels of O_3 (47) generally lie low in energy compared to those for N_2, O_2, and CO_2. The only exception is the close energy resonance between the $CO_2(\nu_2)$ and $O_3(\nu_3)$ modes. Hence, one generalization can be made immediately: vibrational energy in low levels of O_3 will not

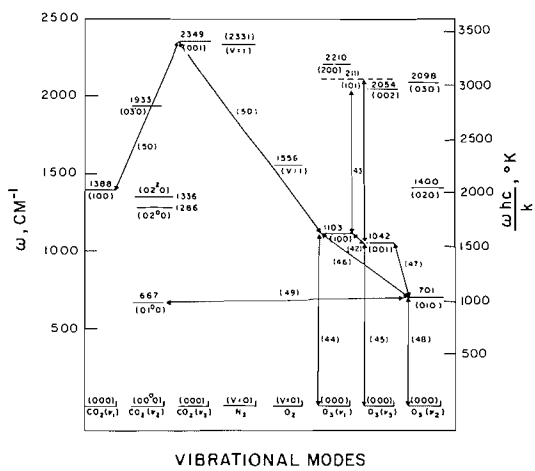

FIG. 2. Vibrational energy level diagram for the molecular system N_2, O_2, CO_2, and O_3. Shown as arrows are the various assumed vibrational energy transfer processes for the O_3 molecule.

Can. J. Chem. Downloaded from www.nrcresearchpress.com by 210.87.254.5 on 09/05/12
For personal use only.

readily V → V transfer to other atmospheric species at stratospheric temperatures.

The laser fluorescence experiment of Rosen and Cool (46) used a CO_2 laser to excite the $O_3(001)$ mode at room temperature. However, the temporal history of this non-equilibrium excitation was followed by emission from the (101) combination state of O_3 which exists at about 2111 cm^{-1} (see Fig. 2). The data of Rosen and Cool indicate that there is rapid V → V coupling between the (001) and (100) modes, most likely via process

[42] $O_3(100) + M \rightleftarrows O_3(001) + M + 61\ cm^{-1}$

as well as rapid coupling to form the (101) state

[43] $O_3(100) + O_3(001) \rightleftarrows O_3(101) + O_3 + 34\ cm^{-1}$

The sum of these processes occurs with a rate[3] $\geq 4.9 \times 10^{-12}$ cm^3/molecule s.

Following this excitation, the slower relaxation of O_3 could occur via two major paths.

(I) Direct V → T deactivation of modes (100) and/or (001):

[44] $O_3(100) + M \rightleftarrows O_3(000) + M + 1103\ cm^{-1}$

[45] $O_3(001) + M \rightarrow O_3(000) + M + 1042\ cm^{-1}$

(II) Intramolecular V → V transfer to mode (010) with subsequent V → T deactivation of this level:

[46] $O_3(100) + M \rightarrow O_3(010) + M + 402\ cm^{-1}$

[47] $O_3(001) + M \rightarrow O_3(010) + M + 341\ cm^{-1}$

[48] $O_3(010) + M \rightarrow O_3(000) + M + 701\ cm^{-1}$

The Rosen and Cool experiment does not distinguish between these alternate paths, but gives the overall rate of deactivation of the (100) and (001) states. For simplicity, mechanism I has been selected in listing the rate constants for M = N_2, O_2, O_3, and CO_2 in Tables 1 and 2.

CO_2 is seen to have a larger rate constant than the other collision partners in Tables 1 and 2. This could suggest the possible influence of the near resonant process

[49] $O_3(010) + CO_2(000) \rightleftarrows O_3(000) + CO_2(010) + 34\ cm^{-1}$

and indicate that reaction path II may be more important than path I at least for CO_2. However, this is speculation at present.

There are also data on the deactivation of $CO_2(001)$ by O_3 (46, 49, 50). The rate constant is fairly large, 7 to 12 $\times 10^{-13}$ cm^3/molecule s. There are various near resonant V → V processes that could be responsible for this rate. One shown on Fig. 2 is

[50] $CO_2(001) + O_3(000) \rightleftarrows CO_2(100) + O_3(100) + 21\ cm^{-1}$

Other possibilities exist, since there are many combinations of CO_2 and O_3 vibrational levels that match up to about 2300 cm^{-1}.

These data for O_3 vibrational energy transfer are listed in Tables 1 and 2. Since data presently only exist at 300 °K and the mechanism is uncertain, no temperature dependence has been suggested. The rate constants listed in Tables 1 and 2 are primarily from the data of Rosen and Cool (46). However, Stephenson (51) has reported to the author that he has recent data on O_3 relaxation which is consistent with that of Rosen and Cool.[4]

C. Electronic Energy Transfer

At present little can be definitely stated about the detailed mechanisms, rate constants, and temperature dependence of electronic → vibration energy transfer processes. For example, it is known that $O(^1D)$ atoms are quenched very rapidly by N_2.

[51] $O(^1D) + N_2 \rightleftarrows O(^3P) + N_2(v = ?)$

Conversly, $O_2(^1\Delta)$ is quenched by N_2 very slowly

[52] $O_2(^1\Delta) + N_2 \rightarrow O_2(^3\Sigma, v = ?) + N_2(v = ?)$

with $k < 1 \times 10^{-19}$ cm^3/molecule s. It is not known how this electronic energy is partitioned among the various degrees of freedom of the product species. It has long been conjectured that a significant amount of the $O(^1D)$ energy went into vibrational excitation of the N_2. If this were true, then $O(^1D)$ atoms could contribute a significant amount of energy for atmospheric species, and the subsequent relaxation of this vibrational energy would be of interest.

Fisher and Bauer (4) have developed a theory of electronic → vibration energy transfer which treats the process as a curve crossing mechanism. In cases where the intermediate state has largely ionic character, such as in the reaction

[3]The rapid rate for production of the $O_3(101)$ combination state is consistent with a similar process for the CO_2 molecule (48).

[4]The author wishes to thank Prof. Cool of Cornell University and Dr. Stephenson of NBS, Boulder, for permission to use their data prior to publication.

Can. J. Chem. Downloaded from www.nrcresearchpress.com by 210.87.254.5 on 09/05/12
For personal use only.

[53] $Na(3^2P) + N_2 \rightarrow Na(3^2S) + N_2^*$

their theory predicts strong coupling with a significant amount of the electronic energy going into vibrational excitation of the N_2. These predictions appear to be consistent with experimental data.

However, in the case of reaction 51, the intermediate state is mostly covalent in character and the Fisher and Bauer calculation indicates that less than 5% of the electronic excitation should be transferred into N_2 vibration. Initial experiments on the $O(^1D)/N_2$ system by Black and Eckstrom (52) were inconclusive (53). However, more recent, as yet unpublished, data indicated that about 35% of the $O(^1D)$ electronic energy may be transferred to the N_2 vibrational mode (54). Further, these same investigators claim that about 45% of the electronic energy is transferred to vibration in the analogous reaction

[54] $O(^1D) + CO \rightarrow O(^3P) + CO^*$

An experiment is presently underway on the above process by von Rosenberg and Trainor (55) but the results are as yet inconclusive. Clearly, these recent data are in conflict with the Fisher and Bauer theory. Delos (5) has recently criticized certain aspects of the Fisher and Bauer theory, and concludes that a simple curve crossing mechanism cannot readily explain the observed cross section for reaction 51.

The field of electronic energy transfer is once again very active. For example, experiments are currently underway on the processes

$$Hg(^3P_0) + CO \rightarrow Hg(^1S_0) + CO^* \text{ (ref. 56)}$$

and

$$Na(^2P) + CO \rightarrow Na(^2S) + CO^* \text{ (ref. 57)}$$

Although such processes are not directly relevant to aeronomic problems, their detailed investigations should allow further development of general understanding of electronic → vibration energy transfer processes.

D. Rotational Energy Transfer

It is not felt that rotational energy transfer is a significant kinetic problem in the stratosphere. In general, rotational thermalization times for species such as N_2, O_2, CO_2, and H_2O are only a few to a few tens of collisions at 300 °K (6, 7). Hence, these processes are very fast and should keep the rotational and translational temperatures equilibrated.

It should be kept in mind that a species like OH (and perhaps also H_2O) may vibrationally relax via a V → R process. This could lead to the preferential excitation of high rotational levels of molecules with rather large rotational level spacing. Under these conditions, rotational relaxation times could be significantly longer and chemical reactivity of rotationally hot molecules may have to be considered.

IV. Conclusions

In the previous section the status of energy transfer mechanisms and rate constants for stratospheric species was reviewed. It is clear that although some important gaps still exist in our understanding, there are substantial data by which to model energy transfer processes, particularly vibrational energy transfer. The most important missing information is the extent to which non-Boltzmann energy distributions can affect the kinetics of reactions, both mechanisms and rate constants. It will probably be a few years before theory and experiment will provide the necessary understanding of non-equilibrium kinetics to provide a definitive statement on this phenomenon. Meanwhile, there are recent experiments which suggest that vibrational excitation may increase the rate constant of a reaction by an order of magnitude or more. Therefore the effects of non-Boltzmann energy distributions on the kinetics of the stratosphere may well become significant as detailed knowledge of chemistry, energy transfer, and their interaction become more evident.

For the present practical problems of the possible stratospheric importance of aircraft effluents on stratospheric chemistry, the most important species are OH, H_2O, NO_x, and O_3. From the data of Table 1 it can be seen that these species (except for H_2O) will equilibrate their vibrational modes in about 10^3 to 10^4 collisions under stratospheric conditions. H_2O will relax more quickly, perhaps in as few as 10 collisions. Further, there are chemical processes for producing OH, NO, and O_3 with vibrational excitation in the stratosphere. If this vibrational energy is to affect the further chemistry of these species, then they must react in less than 10^4 collisions after their production in an excited state. Since these species are all minor constituents of the stratosphere (<p.p.m.), they will predominately collide with the major constituents, N_2 and O_2, before they can find a reactive partner. Hence, it

appears likely that these minor constituents will be collisionally deactivated before they engage in further chemical reactions.

The recent measurements of Black (54), that indicate that a large fraction of the electronic excitation of $O(^1D)$ may be transferred to N_2 vibration, offers another potential source of non-equilibrium phenomena. N_2 equilibrates its vibrational energy more slowly than any other atmospheric component. In particular, it probably relaxes by V → V transfer to other species, thereby providing a source of excitation to these latter molecules. Therefore, a possible energy path can be considered as solar flux → electronic excitation $O(^1D)$ → N_2 vibration → other stratospheric species. This mechanism might be significant at high altitudes in the stratosphere and in the mesosphere where significant photodissociation occurs producing $O(^1D)$.

At the present time it does not appear that vibrational energy transfer provides any first order effects on the chemistry of the stratosphere. However, as knowledge of the mechanisms and rate constants for stratospheric chemistry become more detailed, the influence of non-equilibrium distributions of energy can be assessed with more certainty. More research is currently needed on the processes of electronic → vibration energy transfer, the vibrational kinetics of important stratospheric species such as OH and O_3, and the kinetics of excited species including photochemical reactions.

1. T. J. Odiorne, P. R. Brooks, and J. V. V. Kasper. J. Chem. Phys. **55**, 1980 (1971).
2. L. J. Kirsch and J. C. Polanyi. J. Chem. Phys. **57**, 4498 (1972).
3. M. I. Buchwald, R. McFarlane, and S. H. Bauer. Laboratory of Plasma Studies, Report No. 104. Cornell University, Ithaca, N.Y. 1972.
4. E. R. Fisher and E. Bauer. J. Chem. Phys. **57**, 1966 (1972).
5. J. B. Delos. J. Chem. Phys. **59**, 2365 (1973).
6. K. Herzfeld and T. A. Litovitz. Absorption and dispersion of ultrasonic waves. Academic Press, Inc., New York. 1959.
7. R. G. Gordon, W. Klemperer, and J. I. Steinfeld. Ann. Rev. Phys. Chem. **19**, 215 (1968).
8. R. N. Schwartz, Z. I. Slawsky, and K. Herzfeld. J. Chem. Phys. **20**, 1591 (1952).
9. R. D. Sharma and C. A. Brau. J. Chem. Phys. **50**, 924 (1969).
10. C. B. Moore. J. Chem. Phys. **43**, 2979 (1965).
11. R. L. Taylor and S. A. Bitterman. Rev. Mod. Phys. **41**, 26 (1969).
12. R. Center and R. Kung. Private communication.
13. R. C. Millikan and D. R. White. J. Chem. Phys. **39**, 3209 (1963).
14. C. W. von Rosenberg, K. N. C. Bray, and N. H. Pratt. Proceedings of the Thirteenth Symposium (International) on Combustion, The Combustion Institute, Pittsburg, Pa. 1971. pp. 89–98.
15. Y. Sato, S. Tsuchiya, and K. Koratani. J. Chem. Phys. **50**, 1911 (1969).
16. T. I. McLaren and J. P. Appleton. Proceedings of the Eighth International Shock Tube Symposium. Chapman and Hall, London. 1971. p. 27.
17. C. W. von Rosenberg, K. N. C. Bray, and N. H. Pratt. J. Chem. Phys. **56**, 3230 (1972).
18. P. F. Zittel and C. B. Moore. Appl. Phys. Lett. **21**, 81 (1972).
19. W. A. Rosser, Jr. and E. T. Gerry. J. Chem. Phys. **54**, 4131 (1971).
20. D. J. Seery. J. Chem. Phys. **56**, 631 (1972).
21. J. C. Stephenson and C. B. Moore. J. Chem. Phys. **56**, 1295 (1972).
22. P. Borrell and G. E. Millward. J. Chem. Phys. **57**, 462 (1972).
23. M. I. Buchwald and S. H. Bauer. J. Phys. Chem. **76**, 3108 (1972).
24. Y. Sato and S. Tsuchiya. J. Phys. Soc. Jap. **33**, 1120 (1972).
25. W. A. Rosser, Jr, R. D. Sharma, and E. T. Gerry. J. Chem. Phys. **54**, 1196 (1971).
26. F. Robben. J. Chem. Phys. **31**, 420 (1959).
27. H. J. Bauer, H. O. Kneser, and E. Sittig. J. Chem. Phys. **30**, 1119 (1959).
28. N. Basco, A. B. Callear, and R. G. W. Norrish. Proc. R. Soc. Lond. A, **260**, 459 (1961).
29. K. L. Wray. J. Chem. Phys. **36**, 2597 (1962).
30. H. O. Kneser, H. J. Bauer, and H. Kosche. J. Acoust. Soc. Am. **41**, 1029 (1967).
31. W. D. Breshears and P. F. Bird. Nature, **224**, 268 (1969).
32. J. N. Bradley and D. Lewis. J. Chem. Phys. **50**, 544 (1969).
33. C. J. Hochanadel and J. A. Ghormley. J. Chem. Phys. **50**, 3075 (1969).
34. G. Kaminoto and H. Matsui. J. Chem. Phys. **53**, 3987 (1970).
35. J. Billingsley and A. B. Callear. Nature, **221**, 1136 (1969).
36. J. Billingsley and A. B. Callear. Trans. Faraday Soc. **67**, 257 (1971).
37. W. H. Green and J. K. Hancock. J. Quantum Electron. **9**, 50 (1973).
38. J. C. Stephenson. J. Chem. Phys. **59**, 1523 (1973).
39. E. E. Nikitin. Opt. Spectrosc. **9**, 8 (1960).
40. S. D. Worley, R. N. Coltharp, and A. E. Potter. J. Chem. Phys. **55**, 2608 (1971).
41. S. D. Worley, R. N. Coltharp, and A. E. Potter. J. Phys. Chem. **76**, 1511 (1972).
42. K. H. Welge, S. V. Filseth, and J. Davenport. J. Chem. Phys. **53**, 502 (1970).
43. C. W. von Rosenberg, Jr. and D. W. Trainor. J. Chem. Phys. **59**, 2142 (1973).
44. C. J. Hochanadel, J. A. Ghormley, and J. W. Boyle. J. Chem. Phys. **48**, 2416 (1968).
45. P. L. T. Beran and G. R. A. Johnson. J. Chem. Soc. Faraday I, **69**, 216 (1973).

Can. J. Chem. Downloaded from www.nrcresearchpress.com by 210.87.254.5 on 09/05/12
For personal use only.

46. D. I. ROSEN and T. A. COOL. J. Chem. Phys. **59**, 6097 (1973).
47. D. J. MCCAA and J. H. SHAW. J. Mol. Spectrosc. **25**, 374 (1968).
48. C. B. MOORE. Private communication.
49. T. A. COOL and J. R. AIREY. Chem. Phys. Lett. **20**, 67 (1973).
50. C. W. VON ROSENBERG, JR. and A. LOWENSTEIN. J. Chem. Phys. **59**, 2751 (1973).
51. J. C. STEPHENSON. Private communication.
52. G. BLACK and D. J. ECKSTROM. Excitation and deexcitation of vibration in gases by oxygen and nitrogen atoms. Final report, contract DAHC04-72-C-0015. Stanford Research Institute, Menlo Park, Calif. Feb. 16, 1973.
53. G. BLACK, R. L. SHARPLESS, and T. G. SLANGER. J. Chem. Phys. **58**, 4792 (1973).
54. G. BLACK. J. Chem. Phys. 1974. To be published.
55. C. W. VON ROSENBERG, JR. and D. W. TRAINOR. Private communication.
56. Y. FUSHIKI and S. TSUCHIYA. J. Chem. Phys. 1974. In press.
57. H-L. CHEN. Private communication.
58. C. J. S. M. SIMPSON, T. R. D. CHANDLER, and A. C. STRAWSON. J. Chem. Phys. **51**, 2214 (1969).
59. C. J. S. M. SIMPSON and T. R. D. CHANDLER. Proc. R. Soc. Lond. A, **317**, 265 (1970).
60. M. A. KOVACS and M. A. MACK. Appl. Phys. Lett. **20**, 487 (1972).
61. L. B. EVANS. J. Acoust. Soc. Am. **50**, 409 (1972).
62. H.-J. BAUER. J. Acoust. Soc. Am. **44**, 285 (1968).
63. R. G. MONK. J. Acoust. Soc. Am. **46**, 580 (1969).
64. M. C. HENDERSON, K. HERZFELD, J. BRY, R. COAKLEY, and G. CAVIERE. J. Acoust. Soc. Am. **45**, 109 (1969).
65. W. A. ROSSER, JR., A. D. WOOD, and E. T. GERRY. J. Chem. Phys. **50**, 4996 (1969).
66. M. MARGOTTIN-MACLOU, L. DOYENETTE, and L. HENRY. Appl. Opt. **10**, 1768 (1971).
67. W. D. BRESHEARS and P. F. BIRD. J. Chem. Phys. **48**, 4768 (1968).
68. R. D. SHARMA. J. Chem. Phys. **49**, 5195 (1968).
69. C. B. MOORE. Adv. Chem. Phys. **23**, 41 (1973).
70. W. A. ROSSER, JR. and E. T. GERRY. J. Chem. Phys. **51**, 2286 (1969).
71. D. J. SEERY. J. Chem. Phys. **56**, 4714 (1972).
72. D. F. HELLER and C. B. MOORE. J. Chem. Phys. **52**, 1005 (1970).
73. W. J. SARJEANT, Z. KUCEROVSKY, and E. BRANNEN. Appl. Opt. **11**, 735 (1972).
74. R. E. CENTER. J. Chem. Phys. **58**, 5230 (1973).
75. R. L. TAYLOR. Unpublished data.
76. R. L. TAYLOR, M. CAMAC, and R. M. FEINBERG. Proceedings of the Eleventh Symposium (International) on Combustion, The Combustion Institute, Pittsburg, Pa. 1967. pp. 49–65.
77. A. B. CALLEAR. Disc. Faraday Soc. **33**, 28 (1962).
78. A. B. CALLEAR. Appl. Opt. Suppl. **2**, 145 (1965).
79. J. F. ROACH and W. R. SMITH. J. Chem. Phys. **50**, 4114 (1969).
80. J. T. YARDLEY. J. Chem. Phys. **49**, 2816 (1968).
81. R. J. MCNEAL, M. E. WHITSON, JR., and G. R. COOK. Chem. Phys. Lett. **16**, 507 (1972).
82. R. J. MCNEAL, M. E. WHITSON, JR., and G. R. COOK. J. Chem. Phys. **57**, 4752 (1972).
83. D. J. ECKSTROM. J. Chem. Phys. **59**, 2787 (1973).
84. J. H. KIEFER and R. W. LUTZ. Proceedings of the Eleventh Symposium (International) on Combustion, The Combustion Institute, Pittsburg, Pa. 1967. p. 67.
85. R. E. CENTER. Proceedings of the Ninth International Shock Tube Symposium. Stanford University Press, Palo Alto, Calif. 1973. p. 383; also J. Chem. Phys. **59**, 3523 (1973).

Can. J. Chem. Downloaded from www.nrcresearchpress.com by 210.87.254.5 on 09/05/12
For personal use only.

Excited State Chemistry in the Stratosphere[1]

R. J. CVETANOVIĆ

Division of Chemistry, National Research Council of Canada, Ottawa, Canada

Received November 8, 1973

Potential involvement of excited states of molecules and molecular fragments in the chemistry of the stratosphere is discussed, with particular emphasis on the chemical behavior of electronically excited oxygen atoms.

On discute de l'impliquation possible des états excités de molécules et des fragments moléculaires dans la chimie de la stratosphère; on examine particulièrement la réactivité chimique des atomes d'oxygène excités électroniquement. [Traduit par le journal]

Can. J. Chem., **52**, 1452 (1974)

Introduction

As a result of the appreciable exothermicities of many chemical and photochemical reactions, the reaction products formed (molecules and molecular fragments) frequently acquire energies in substantial excess of the amounts corresponding to complete thermal equilibrium at the ambient temperature. Such *excited* species are equally well formed in the chemical and photochemical processes which occur in the stratosphere. For example, the basic stratospheric reactions of the Chapman mechanism may be written as

[1] $O_2 + h\nu \rightarrow O^* + O^*$

[2] $O_3 + h\nu\ (\lambda < 400\ nm) \rightarrow O_2^* + O^*$

[3] $O + O_2 + M \rightarrow O_3^* + M^*$

[4] $O + O_3 \rightarrow O_2^* + O_2^*$

[5] $O + O + M \rightarrow O_2^* + M^*$

The asterisks indicate potential presence of excess energy, but do not specify its form. Thus, all the products may possess excess translational and, subject to some restrictions, electronic energy. The diatomic (O_2^*) and triatomic products (O_3^*) may also be rotationally and vibrationally excited. Similarly, all other exothermic reactions in the stratosphere must form excited products. For example, OH with up to 2, 4, and 6 vibrational quanta respectively may be formed in the reactions

[6] $O(^1D_2) + H_2O \rightarrow OH^* + OH^* + 29$ kcal/mol

[6′] $O(^1D_2) + H_2(\text{or } CH_4) \rightarrow OH^* + H^*(\text{or } CH_3^*) + 44$ kcal/mol

[7] $O(^3P) + HO_2 \rightarrow OH^* + O_2^* + 55$ kcal/mol

Photochemical production of excited states is treated in detail in numerous photochemical and spectroscopic texts. *Chemical* production of excited states has been recently reviewed by Carrington and Garvin (1), with examples from the literature of experimental observations of chemically generated excited states, including the vibrationally excited OH from some of the reactions mentioned here.

The excitation energy indicated by asterisks in the above reactions may be translational, rotational, vibrational, electronic, or some combination of these. To specify it more precisely, the symbol $O^{*(t)}$, for example, may be used for a translationally excited oxygen atom in the ground electronic state, $O(^3P)$. $O_2^{*(t,r,v,e)}$ is then an O_2 molecule which is simultaneously translationally, rotationally, vibrationally, and electronically excited. Specifically, $O_2(^1\Delta_g)^{*(t,r,v)}$ would stand for an O_2 molecule in the $(^1\Delta_g)$ electronic state which is also translationally, rotationally, and vibrationally exicted. To be still more precise, it would be necessary in this case to state also the extent of the latter three types of excitation, if known. In principle, therefore, a very large number of different excited states may be generated in the stratosphere. The question naturally arises to what extent they can make distinctive contributions and whether it is necessary to consider explicitly and individually a very substantial number of

[1]NRCC No. 13718.

Can. J. Chem. Downloaded from www.nrcresearchpress.com by 210.87.254.105 on 09/05/12
For personal use only.

Can. J. Chem. Downloaded from www.nrcresearchpress.com by 210.87.254.105 on 09/05/12
For personal use only.

excited states in quantitative discussions of stratospheric chemistry.

An important role in the chemistry of the atmosphere is generally acknowledged for at least one excited species, the first electronically excited level of oxygen atoms, $O(2^1D_2)$. However, this excited species may be almost unique in this respect since apart from it and the two lowest singlets of $O_2(O_2(^1\Delta_g)$ and $O_2(^1\Sigma_g{}^+))$ it is uncertain whether any other excited species may contribute significantly to stratospheric chemistry. At the same time, potential chemical involvement of other excited species generated in the stratosphere cannot be definitely ruled out until adequate knowledge is obtained regarding the rates of their generation and loss (by radiation and collisional deexcitation) and particularly of their reaction rates at different levels of excitation. At present, it would be difficult and would probably serve little useful purpose to attempt a detailed and systematic discussion of all the excited species which may possibly be present in the stratosphere (and at still higher altitudes) although such a discussion may ultimately be necessary. In the present paper, only the progress made in recent years in the understanding of the chemical behavior of $O(2^1D_2)$ atoms will be briefly summarized and the potential implication of some other excited species in the chemistry of the stratosphere will be very briefly discussed.

Translational Excitation

Hot oxygen atoms in the ground electronic state are continuously generated in the atmosphere, for example by photolysis of O_2 at shorter wavelengths, by photolysis of ozone and of NO_2 in some spectral regions, and by quenching of $O(^1D_2)$ by O_2 and especially by N_2. Similarly, hot hydrogen atoms are perhaps generated to some extent in the reactions of $O(^1D_2)$ with H_2, the exothermicity of which is about 44 kcal/mol, and in the reaction of oxygen atoms with OH

[8] $$O + OH \rightarrow O_2 + H^{*(1)}$$

which is some 17 kcal/mol exothermic. It is therefore necessary to try to assess whether these and other translationally excited species are likely to play any role in the chemistry of the stratosphere. Their potential importance will have to depend on the rates of their production, the amount of the excess energy they possess, the rates of their cooling (moderation) by collisions with the chemically inert molecules present, and the rates of their chemical reactions with the chemically reactive constituents of the stratosphere. Unfortunately, most of this information is at present unavailable. Only a very tentative discussion may therefore be given here, in the hope that it may stimulate further thought and perhaps also some additional experimental work.

Considerable effort has been devoted in recent years to studies of chemical and physical behavior of kinetically excited atoms, in particular of hot hydrogen atoms (2–4). It has been clearly demonstrated that hot atoms are capable of entering into some reactions which occur at best only very slowly with the moderated ("thermalized") atoms. Thus, most chemical studies of the hot H, D, or T atoms have been based on their enhanced ability to react with different isotopic forms of molecular hydrogen, hydrocarbons, hydrogen halides, and halogens. The chemical reactions of hot hydrogen atoms with CO_2 and with N_2O have been studied recently (5). Theoretical studies of varying degrees of sophistication have been carried out in an attempt to characterize some of these reactions (6–11).

Although there is some disagreement in the literature about the exact mechanism of the cooling of hot atoms by some inert gases (12–14), the simple model of a completely elastic transfer of energy in collisions with the molecules of the moderator (the "billiard-ball" model) will be used here for illustration purposes. The average energy retained by the hot atom after n collisions, E_n, is (15)

[1] $$E_n = E_0 \exp(-\alpha n)$$

where E_0 is the initial energy of the hot atom and

$$\alpha = \{1 - (1 - \gamma)[1 - \ln(1 - \gamma)]\}/\gamma$$

with

$$\gamma = 4\,MM'/(M + M')^2$$

M and M' are the masses of the hot atom and the moderator.

For hot hydrogen atoms it is calculated from these expressions that E_n/E_0 is 0.93, 0.50, and 9×10^{-4} after 1, 10, and 100 collisions with

N_2. For hot oxygen atoms the corresponding values are 0.45, 3.7×10^{-4}, and 4.4×10^{-35}. In both cases O_2 is only a very slightly less efficient moderator than N_2. Efficient cooling of these hot atoms must evidently occur in the stratosphere in only a relatively small number of collisions with N_2 and O_2. (Should some inelastic energy transfer occur with these two moderators as well, their efficiency of moderation would be further enhanced.)

The combined concentrations of O_2 and N_2 in the stratosphere are some 5 to 6 orders of magnitude greater than the concentrations of the minor constituents which could possibly react chemically with hot atoms. Hot atoms generated in the stratosphere must therefore be rapidly thermalized by collisions with O_2 and N_2 and it may be tempting to predict that their reactions are unlikely to be of importance under any circumstances. However, although this may indeed turn out to be largely true, it is not possible to be certain that hot atoms can never contribute significantly to stratospheric chemistry, at least not until the rates of their reactions with different stratospheric constituents become known. A comparison with $O(^1D)$ may be instructive in this connection. $O(^1D)$ atoms are also destroyed in only a few collisions with N_2 and O_2 but, as a result of their extreme reactivity, are evidently able to play an important role by reacting with such substances as CH_4, H_2, and H_2O. If the rates of substantially translationally excited $O(^3P)$ atoms with these substances happen to be somewhat comparable to those of $O(^1D)$ atoms, although this may seem now not to be too probable, they could also make a significant contribution to stratospheric chemistry. These rates do not appear to be known at present and until they are determined it would not be safe to draw any firm conclusions.

An additional possibility which should be considered is that sufficiently translationally excited $O(^3P)$ atoms might conceivably react with N_2 under some atmospheric conditions to form N_2O. Such a reaction would require spin relaxation but it could be visualized in part as the reverse of the rapidly occurring collisional deexcitation of $O(^1D_2)$ by N_2, which apparently involves a rapid crossing between a repulsive triplet and the attractive singlet surface of the ground electronic state of N_2O. If such a reaction occurred even at a relatively low probability, its overall rate could be significant because of the very large concentration of N_2 in the atmosphere. However, Katakis and Taube (16) and Simonaitis *et al.* (17) could not detect any formation of N_2O in the photolysis of small amounts of O_3 in the presence of up to about 900 Torr of N_2, although under such conditions substantial $O^{*(1)}$ must have been formed. Gaedtke *et al.* (18), on the other hand, report measurable yields of N_2O even at 1 atm, presumed to be formed in the third order recombination of $O(^1D_2)$ with N_2.

The recombination of O_2 with hot $O(^3P)$ atoms in the ozone forming reaction

$$O^{*(1)} + O_2 + M \rightarrow O_3 + M$$

may be expected to be slower than with thermalized oxygen atoms because of the additional energy which has to be removed by the third body (M). However, this is not likely to have an appreciable effect on the overall rate of ozone production because the third order combination of O with O_2 is relatively slow under stratospheric conditions even with thermalized oxygen atoms so that numerous collisions of O with O_2 and N_2 precede a successful O_2 forming ternary collision.

Vibrational and Rotational Excitation

Vibrationally and rotationally excited species can be generated in the stratosphere both in chemical and photochemical reactions. Some of the excited species have been observed spectroscopically in analogous reactions in laboratory experiments (1), for example, as mentioned earlier, the vibrationally excited OH formed in the reactions of $O(^1D_2)$ with H_2, CH_4, and H_2O. Highly vibrationally excited O_2 has been observed in a number of photochemical and thermal reactions of aeronomic interest.

The potential importance of the vibrational and rotational excitation in the chemical reactions in the stratosphere depends on the relaxation times of the excited molecules and their reaction rates with the minor stratospheric constituents. The field of the collisional relaxation of vibrational and rotational excitation has been reviewed by Callear and Lambert (19) and is discussed in detail in another paper at this Symposium (20). The degradation occurs by stepwise transfer of the excess energy into translation, rotation, and vibration of the deactivating molecules. In the stratosphere the latter will be the molecules of O_2 and N_2.

Can. J. Chem. Downloaded from www.nrcresearchpress.com by 210.87.254.105 on 09/05/12
For personal use only.

Can. J. Chem. Downloaded from www.nrcresearchpress.com by 210.87.254.105 on 09/05/12
For personal use only.

Interconversion of vibrational energy into translational energy is generally slow, especially if the vibrational frequency is high. Millions of collisions may be required in some cases to deactivate a low (*e.g.* $v = 1$) vibrational level. Vibration–vibration energy transfer is generally much faster and near resonant vibration–vibration transfer tends to occur very efficiently. Molecules with a large vibrational amplitude, such as hydrides, are deactivated much more easily. Light molecules are generally more efficient deactivators than are heavy molecules. The theory of Schwartz, Slawsky, and Herzfeld (21) reproduces correctly the order of magnitude of many deactivation collision numbers and accounts approximately for all the main features of collisional relaxation of vibrational energy.

Very few (22–26) reaction rates have been measured for vibrationally excited species in the ground electronic state. Of particular aeronomic interest are the measurements of Worley, Coltharp, and Potter (22–25) of the rates of vibrationally excited OH radicals in the $v = 9$ state, formed by the reaction of H atoms with ozone. (This particular state was selected because of some experimental advantages.) The rate constants for collisional destruction of $OH^{*(v=9)}$ by, for example, N_2, O_2, CH_4, N_2O, H_2O, and O_3 are (22, 24, 25) (in units of 10^{-14} cm^3 $molecule^{-1}$ s^{-1}) 0.36, 1.0, 1.4, 4.8, 20, and 770. These values represent sums of vibrational deactivation and chemical reaction, but the relative extent of the two processes and the identity of reaction products when chemical reaction occurs are, unfortunately, not known. From these values some conclusions can be drawn, although it has to be remembered that they pertain to a particular vibrational level of OH. The effective value of the rate constant for $OH^{*(v=9)}$ destruction by air is 0.49×10^{-14} cm^3 $molecule^{-1}$ s^{-1}. Relative to this, the values for CH_4, N_2O, H_2O, and O_3 then become 2.9, 9.8, 41, and 1580. Thus, on the basis of these values, if $OH^{*(v=9)}$ radicals are formed in the stratosphere, about 0.05% of them would react with ozone at 15 km and about 2% at 40 km. This calculation has only an illustrative value and is based on the ozone concentration profile given by Nicolet (27) as an example. Nevertheless, it would seem to indicate that $OH^{*(v)}$ may play a role in the atmospheric chemistry of ozone although it should be mentioned that the above value of the rate constant of $OH^{*(v=9)}$ with O_3 is more than two orders of magnitude larger than the corresponding rate constant for $OH^{(v=0)}$ recently determined by Anderson and Kaufman (28) (5.5×10^{-14} cm^3 $molecule^{-1}$ s^{-1} at 297 °K). The difference between the rates of reaction of the two forms of OH with CH_4 is only very slight and any contribution of the $OH^{*(v)}$ to the overall reaction of OH with CH_4 in the stratosphere should therefore be negligible. Reaction with other minor constituents of the stratosphere may also be expected to be negligible.

Rotational excitation relaxes much more readily than vibrational excitation because rotational quanta are much smaller. It is therefore likely that under stratospheric conditions the rotationally excited species will be collisionally degraded before they have a chance to interact with molecules other than N_2 or O_2.

Electronic Excitation

A number of electronically excited species, such as for example $O(^1D_2)$, $O(^1S_0)$, $O_2(^1\Delta_g)$, $O_2(^1\Sigma_g^+)$, $O_3^{*(e)}$, $NO^{*(e)}$, $NO_2^{*(e)}$, and possibly other electronically excited molecules and molecular fragments, could conceivably be involved to a smaller or greater extent in some chemical reactions in the atmosphere. However, very few of these can be implicated at present with some certainty in the chemistry of the stratosphere. $O(^1D_2)$ atoms are generally believed to play an important role and the first two electronically excited states of O_2 ($O_2(^1\Delta_g)$ and $O_2(^1\Sigma_g^+)$) may make a significant contribution by reacting with ozone. A possible involvement of $O(^1S_0)$ atoms has been suggested, as will be mentioned later, although it is uncertain whether they are generated in the stratosphere to an appreciable extent.

$O_2(^1\Delta_g)$ and $O_2(^1\Sigma_g^+)$

The $O_2(^1\Delta_g)$ molecules are formed in the atmosphere mainly by the solar photolysis of ozone in the Hartley continuum while the $O_2(^1\Sigma_g^+)$ state is (29) probably formed in the stratosphere mainly in the reaction

$$O(^1D) + O_2 \rightarrow O(^3P) + O_2(^1\Sigma_g^+)$$

The radiative lifetime of $O_2(^1\Delta_g)$ is 60 min and that of $O_2(^1\Sigma_g^+)$ 12 s. (The two states are responsible for the intense day-glow emissions at 1.27 μ ($^3\Sigma_g^- \leftarrow {}^1\Delta_g$) and 762 nm ($^3\Sigma_g^- \leftarrow {}^1\Sigma_g^+$)).

Can. J. Chem. Downloaded from www.nrcresearchpress.com by 210.87.254.105 on 09/05/12
For personal use only.

The rate constants of the quenching of the $O_2(^1\Delta_g)$ state by O_2 (30), N_2 (31), and O_3 (31–34) are, respectively, 2×10^{-18}, 1.4×10^{-19}, and 4×10^{-15} cm^3 molecule^{-1} s^{-1}. If the last value is taken as the rate constant of the reaction

[9] $$O_2(^1\Delta_g) + O_3 \rightarrow 2O_2 + O$$

then the calculated fractions of the $O_2(^1\Delta_g)$ molecules which will react with stratospheric ozone at various altitudes (27) in reaction 9 rather than being quenched by O_2 and N_2 are approximately 0.2% at 15 km, 1.3% at 20 km, 5.9% at 30 km, 8.8% at 40 km, and 3.3% at 50 km. Any other chemical reactions of $O_2(^1\Delta_g)$ in the stratosphere would probably be very much slower.

The rate constants for reactions of $O_2(^1\Sigma_g^+)$ with O_2 and N_2 are (35) 4.5×10^{-16} and 1.8×10^{-15} cm^3 molecule^{-1} s^{-1}, respectively. The rates (35) of destruction of $O_2(^1\Sigma_g^+)$ by several minor stratospheric constituents, expressed relative to the total quenching of $O_2(^1\Sigma_g^+)$ by O_2 and N_2, are then: CO_2 288, CO 2.8, H_2O 2157, CH_4 72, N_2O 46, NO 27, and H_2 720. The corresponding value for ozone is 4580 or 15000 based respectively on the literature values of the rate constant for the $O_2(^1\Sigma_g^+)$ reaction with O_3 of 7×10^{-12} (36) or ca. 2.4×10^{-11} cc molecule^{-1} s^{-1} (60, 74). On the basis of these values, up to about 3% or even as much as 10% of the $O_2(^1\Sigma_g^+)$ molecules generated in the stratosphere could react with ozone. The products of the reaction with ozone are probably $2O_2 + O$.

Electronically Excited NO_2

Electronically excited NO_2 can at best be only a very minor constituent of the stratosphere. Since $NO_2^{*(e)}$ is rapidly quenched (37) by O_2 (at a specific rate of 2.0×10^{-11} cc molecule^{-1} s^{-1}), its fate in the stratosphere would be almost entirely collisional deexcitation, with only a small fraction of the collisions leading to transfer of electronic energy to excite O_2. Frankiewicz and Berry (38) have recently studied the interaction of $NO_2^{*(e)}$ (formed by irradiation with light of wavelengths between 405 and 700 nm) and have found that 7.5 and 0.14%, respectively, of the O_2 collisions which quench $NO_2^{*(e)}$ result in energy transfer with formation of $O_2(^1\Delta_g)$ and $O_2(^1\Sigma_g^+)$ molecules. Even at still shorter wavelengths, at which photodissociation into NO and $O(^3P)$ occurs, there appears (39) to be some formation of an electronically excited form of NO_2 which does not decompose rapidly but can transfer its electronic excitation energy to O_2.

$O(2^1D_2)$ Atoms

Oxygen atoms in their first electronically excited state, the lowest singlet $O(2^1D_2)$ (or $O(^1D)$, in short), are known to be present in the atmosphere and it is generally accepted that they play an important role in stratospheric chemistry. They possess about 45 kcal/mol more energy than the ground electronic state, $O(2^3P_2)$, and their radiative transition to this state, with emission at 630 nm, is strongly forbidden. Their radiative lifetime is therefore relatively very long. On the other hand, they readily undergo collisional deexcitation and are in general chemically extremely reactive. $O(^1D)$ atoms therefore generally decay in the stratosphere by collisional deactivation and to a much smaller extent by chemical reactions. The chemical reactions into which they enter, however, are aeronomically important.

Because of their importance for the chemistry of the upper atmosphere, the chemical and physical behavior of $O(^1D)$ atoms is of great current interest. Their direct observation and study, however, is made extremely difficult as a result of the great ease of their destruction in collisions with other molecules and the low probability of their forbidden emission at 630 nm. A variety of indirect methods has therefore been frequently used in their investigation. Proper understanding of the stratospheric role of $O(^1D)$ atoms requires adequate knowledge not only of the rates of their collisional destruction by various constituents of the stratosphere but also of the exact mechanisms of the chemical reactions into which they enter. This type of information was almost entirely lacking only a few years ago. However, the progress made in the past decade has been very gratifying and the general chemical and physical behavior of $O(^1D)$ atoms is now well understood.

$O(^1D)$ atoms are generated in the stratosphere mainly by photolysis of O_2 and O_3 and to a lesser extent by photolysis of N_2O and NO_2. The same processes have been used for their generation in laboratory experiments. The photolysis of N_2O has proved particularly convenient for this purpose because of its relatively

Can. J. Chem. Downloaded from www.nrcresearchpress.com by 210.87.254.105 on 09/05/12
For personal use only.

low chemical reactivity and the possibility to assess readily the rate of generation of $O(^1D)$ atoms by measuring the rate of production of nitrogen. The mechanism of photolysis of N_2O (at least between about 215 and 185 nm) is

[10] $$N_2O + h\nu \rightarrow N_2 + O(^1D)$$

with no more than 2–3% of the photolysis giving N_2 and $O(^3P)$ instead (40).

In the absence of other $O(^1D)$ consuming reactants, reaction 10 is rapidly followed by

[11*a*] $$O(^1D) + N_2O \rightarrow N_2 + O_2$$

[11*b*] $$O(^1D) + N_2O \rightarrow 2NO$$

where the ratio k_{11a}/k_{11b} is close to unity (41). The yield of N_2 per quantum of light absorbed (Φ_{N_2}) is therefore close to 1.5. However, in the presence of sufficient amounts of other substances (Q) capable of destroying $O(^1D)$ without producing N_2, reactions 11*a* and 11*b* do not occur and the quantum yield of N_2 is unity. The rate of N_2 formation provides then a direct measure (to within 2–3%) of the rate of generation of $O(^1D)$. By varying the $[Q]/[N_2O]$ ratio, this system can be used to determine (from the variation of Φ_{N_2} between the limiting values of 1 and 1.5) the efficiency of destruction of $O(^1D)$ by the added substance Q, *i.e.*

[12] $$O(^1D) + Q \rightarrow \text{destruction of } O(^1D)$$

N_2O photolysis was first used in this manner in 1963 by Yamazaki and Cvetanović (42), who found that $O(^1D)$ is very rapidly destroyed (at a rate comparable to its rate of attack on N_2O) by some substances (H_2, CO_2, Xe) but is affected extremely little or not at all by some other substances (SF_6, C_2F_6, Kr). The importance of this finding, although it was largely qualitative at first, was that it provided a convenient indirect probe for the presence of $O(^1D)$ atoms, which was badly needed at that time and which did indeed facilitate subsequent quantitative investigations. Yamazaki and Cvetanović (43) obtained the early quantitative data by photolyzing N_2O in the presence of carbon dioxide isotopically labelled with ^{18}O at wavelengths where CO_2 does not absorb light. In this system $O(^1D)$ atoms formed in reaction 10 rapidly exchange (16) with ^{18}O in $C^{18,18}O_2$, *i.e.* (refs. 43, 44)

[13] $$^{16}O(^1D) + C^{18,18}O_2 \rightarrow \tfrac{2}{3}\,^{18}O + \tfrac{1}{3}\,^{16}O + \tfrac{1}{3}\,C^{16,18}O_2 + \tfrac{2}{3}\,C^{18,18}O_2$$

The ground state oxygen atoms formed, ^{18}O and ^{16}O, do not exchange with $C^{18,18}O_2$ and are in this system recovered after the photolysis as molecular oxygen. The ratio (R) of $[^{16}O]/[^{18}O]$ in the recovered O_2 is greater the more $O(^1D)$ is removed in reaction with N_2O and an added gas (Q). In fact this ratio is given by an expression of the form

[2] $$R = [^{16}O]/[^{18}O] = A + B[N_2O]/[C^{18,18}O_2] + C[Q]/[C^{18,18}O_2]$$

A, B, and C are constants from which the ratios of the rate constants k_1, k_3, and k_4 can be evaluated. Experimentally, R is first plotted *vs.* $[N_2O]/[C^{18,18}O_2]$ at $[Q] = 0$, to obtain A and B, and then *vs.* $[Q]/[C^{18,18}O_2]$ at constant $[N_2O]/[C^{18,18}O_2]$ to evaluate C. Using this procedure, *relative* rate constants (given in the following in parentheses) were obtained for $O(^1D)$ reactions with CO_2 (1, taken as the basis for comparison), N_2O (1.6), Xe (0.82), and SF_6 (0).

The validity of these results had to be verified with alternative sources of $O(^1D)$ in order to establish whether the N_2O technique may be subject to some unknown systematic errors and complications, as questioned by some subsequent workers. This was done first in 1966 by Preston and Cvetanović (45), who used NO_2 photolysis at 214 nm as a source of $O(^1D)$ and its exchange with $C^{18,18}O_2$ in a manner basically similar to that described above. From the appropriate plots of $R = [^{16}O]/[^{18}O]$ they obtained the following relative rate constants: CO_2 (1), N_2O (1.1), Xe (0.78), N_2 (0.24), Kr (0.06), and SF_6 (0), which agreed satisfactorily with the results obtained by the N_2O technique (43, 46).

A third source of $O(^1D)$, the flash photolysis of O_3 in the Hartley band region, was used by Scott and Cvetanović (47) in 1971. The experiments were carried out in the presence of N_2O and an added substance (Q) competing with N_2O for $O(^1D)$ atoms. In these experiments N_2O was not photolyzed and N_2 was formed only by the attack of $O(^1D)$, generated by the photolysis of O_3, on N_2O. The relative rate constants were evaluated from the yields of N_2 at different $[Q]/[N_2O]$ ratios. The relative values obtained agreed again within the likely experimental uncertainties with the results obtained by the other two techniques, *i.e.* those with N_2O and NO_2 as sources of $O(^1D)$. In addition, the ozone photo-

Can. J. Chem. Downloaded from www.nrcresearchpress.com by 210.87.254.105 on 09/05/12
For personal use only.

TABLE 1. Rate constants of $O(^1D_2)$ reactions at 298 °K relative to CO_2 taken as unity[a]

Authors	Year	Ref.	O_2	O_3	CO	CO_2	N_2	N_2O	NO	NO_2	H_2	H_2O	CH_4	C_2H_6	C_3H_8	Neo-C_5H_{12}	Xe	SF_6
Yamazaki, Cvetanović	1964	43				1		1.6									0.82	0
Yamazaki, Cvetanović	1964	46					0.28								(1.89)		*0.89*	0
Preston, Cvetanović	1966	45				1	0.24	1.10		1.62					4.67		0.78	0
Snelling, Bair	1967	49		4.61			*0.30*										0.81	
Young *et al.*	1968	50	0.29			(1.72)	0.37	*1.31*	1.11									
Young *et al.*	1968	50	0.30			1	0.27		1.03		1.30		1.56					
Paraskevopoulos, Cvetanović	1969	40			0.59	1	0.31				2.0		2.5			7.9	1.00	0
DeMore	1970	53	0.23		0.41	1	0.23	1.14										
Donovan *et al.*	1970	54				1	0.37	1.6			3.2		3.7					
Yamazki	1970	55			0.79	1	0.29	1.06									1.00	
Loewenstein	1971	59	0.56			1	0.36											
Paraskevopoulos, Cvetanović	1971	63										2.64				*7.0*		
Paraskevopoulos *et al.*	1971	64	0.37			1		1.24		1.50							0.67	
Paraskevopoulos *et al.*	1971	64	0.25													*7.0*		
Scott, Cvetanović	1971	47	(0.66)			1		1.84				2.75				7.9	1.09	0
Slanger, Black	1971	65				1	0.26				1.28							
Clark, Noxon	1972	66	0.39		0.14	(0.71)	*0.30*											
Fortin *et al.*	1972	67					*0.30*					1.07						
Paraskevopoulos *et al.*	1972	70						1.02								*7.0*		
Simonaitis, Heicklen	1972	71						*1.31*				2.75						
Michaud *et al.*	1973	72												2.72	4.24	*7.0*		
Gauthier, Snelling	1973	73	0.37	2.96	0.35	1	0.27	1.22			1.5	1.85	1.9		4.0	5.2		
Snelling	1973	74	0.42				*0.30*											
Mean values[b]			0.35	3.79	0.46	1	0.30	1.31	1.07	1.56	1.86	2.21	2.42	2.72	4.30	7.00	0.89	0
Standard deviation			0.10	1.17	0.24	—	0.05	0.29	0.06	0.08	0.81	0.74	0.94	—	0.34	1.56	0.15	—

[a]Italicized values were used to reduce indirectly the relative rates to CO_2 basis.
[b]The values in parentheses and the italicized values are not used in the calculations of mean values.

TABLE 2. Summary of the mean relative rates and the absolute rate constants of reactions of $O(^1D_2)$ atoms at 298 °K

	Mean relative rates[a]			Absolute rate constants × 10^{10} (cc molecule^{-1} s^{-1})					
	Table 1[b]	Omnitab[c]		Noxon (ref. 56)	Gilpin *et al.* (ref. 60)	Heidner, Husain (refs.76–79)	Omnitab[c]		Recommended values
	A	B	C	D	E	F	G	H	I
O_2	0.35	0.42	0.41	0.6±0.3		0.70±0.05	0.88	0.60	0.74±0.15
O_3	3.79	4.21	2.94		2.5±1	2.7 ±0.2[d]	8.8	4.3	5.3 ±2.6
CO	0.46	0.42	0.43			0.73±0.07	0.87	0.62	0.77±0.15
CO_2	1	1	1			2.1 ±0.2	2.10	1.45	1.8 ±0.3
N_2	0.30	0.30	0.30			0.69±0.06	0.64	0.44	0.54±0.15
N_2O	1.31	1.23	1.21			2.2 ±0.2	2.57	1.76	2.2 ±0.4
NO	1.07	1.16	0.92			0.85±0.10	2.44	1.33	1.7 ±0.9
NO_2	1.56	1.55	1.56			2.3 ±0.2	3.26	2.26	2.8 ±0.5
NH_3									~4[e]
H_2	1.86	1.63	1.61			2.7 ±0.3	3.43	2.33	2.9 ±0.5
H_2O	2.21	1.94	1.95			3.0 ±0.3	4.09	2.83	3.5 ±0.6
H_2O_2									~5[e]
CH_4	2.42	2.26	2.21			3.1 ±0.4	4.74	3.20	4.0 ±0.9
C_2H_6	2.72	2.71	2.68				5.68	3.88	4.8 ±0.9
C_3H_8	4.30	4.47	4.43				9.38	6.42	8.0 ±1.5
neo-C_5H_{12}	7.0	6.94	6.86				14.6	9.94	12.3 ±2.3
Xe	0.89	0.83	0.77			1.0 ±0.1	1.74	1.12	1.4 ±0.4

[a]Expressed relative to the CO_2 rate taken as unity.
[b]Mean values from Table 1.
[c]Least squares computations of the mean relative and absolute rate constants carried out at the National Bureau of Standards by Dr. Robert F. Hampson. *Column B*: Omnitab computations for the sets of data used in Table 1 (omitting the values for SF_6 and the values in parentheses for O_2 and C_3H_8). *Columns C and H*: Omnitab computations of the mean relative and absolute rate constants, respectively, using the same data as in B plus all the absolute values in columns D, E, and F. *Column G*: The relative data of column B placed on an absolute scale by taking for CO_2 the value of 2.1 × 10^{-10} cc molecule^{-1} s^{-1}.
[d]Corrected value of Heidner, Husain, and Wiesenfeld (75).
[e]Roughly estimated by analogy, no measurements available.

lysis technique was used to obtain also the relative rates for O_2, H_2O, and neopentane.

Numerous relative rate constants of $O(^1D)$ reactions have been measured in the meantime by a number of investigators (40, 42, 43, 45–74). It would not be practical to describe these studies here even very briefly. The author has recently collected most of the relative rates of $O(^1D)$ reactions in the literature, in an attempt to evaluate for the forthcoming Climatic Impact Assessment Program Vol. I "The Natural Stratosphere, 1974", a consistent set of $O(^1D)$ rate constants, for the reactions of stratospheric interest. With a few omissions, these rate constants were reduced directly or indirectly to a common base by taking the rate for CO_2 to be unity and are summarized in Table 1. There is evidently a reasonable mutual consistency of the data from very diverse sources. Again with one or two omissions, as indicated, the mean values were evaluated for each compound and are listed in column A of Table 2. A more objective set of mean values from the same data (but before they were reduced to the common base) was computed by Dr. R. F. Hampson at the United States National Bureau of Standards using a least squares fitting computer program (termed Omnitab). The mean values obtained in this manner are listed in column B of Table 2.

In order to place the relative values on an absolute scale, at least some reliable absolute rate constants of $O(^1D)$ reactions are needed. Until very recently only two or three absolute values were available (56, 60) and their quoted experimental uncertainties were quite large. These values have now been supplemented by a number of recent determinations of Heidner, Husain, and Wiesenfeld (76–79), who have succeeded in monitoring directly the $O(^1D)$ atom concentrations by measuring their allowed $O(3^1D_2) \leftarrow O(2^1D_2)$ absorption at 115.2 nm. These and the earlier (56, 60) absolute determinations are listed in columns D, E, and F of Table 2. When these absolute values are used in addition to the relative values in Omnitab computations, a new set of mean values is obtained. These are listed as relative values (with CO_2 taken as unity) in column C and as

Can. J. Chem. Downloaded from www.nrcresearchpress.com by 210.87.254.105 on 09/05/12
For personal use only.

Can. J. Chem. Downloaded from www.nrcresearchpress.com by 210.87.254.105 on 09/05/12
For personal use only.

absolute values in column H of Table 2. The last column, I, in Table 2 gives a set of recommended absolute values with a somewhat arbitrary but hopefully conservative estimate of their likely total uncertainties.

An inspection of the data in Table 2 shows that most of the absolute values of the $O(^1D)$ rate constants of stratospheric interest appear to be now known with considerable accuracy. Some values seem to be subject to greater uncertainty, notably the values for ozone and NO, and some are altogether lacking (for example for H_2O_2 and NH_3) so that some further determinations would be highly desirable.

The rate constants listed in Table 2 are based on experimental measurements at room temperature. Since most of the $O(^1D)$ reactions of interest occur at close to each kinetic collision, it is likely that they do not require any activation energies. The values in Table 2 can then be used to a good approximation also for the lower temperatures in the stratosphere. Some support for this view comes from the observation that at least some of these reactions also occur rapidly even at liquid nitrogen temperature. It is possible, nevertheless, that some of the slower reactions do require small activation energies so that they may be slowed down even further at stratospheric temperatures. Thus, Simonaitis and Heicklen (71) have found an activation energy difference of about 1.2 kcal/mol for $O(^1D)$ reactions with CO and H_2O. However, this is an isolated result and further investigation is clearly necessary.

As already pointed out, $O(^1D)$ atoms when formed in the stratosphere may also be, to a smaller or greater extent, translationally excited. An effect of kinetically hot $O(^1D)$ atoms on their reaction rates has been suggested (61, 68, 80) although other recent attempts (81) to observe such effects have shown only minor differences, bordering on experimental uncertainties. Further experimental work is required to obtain additional information. In the meantime it would seem justifiable to assume that the reactions of $O(^1D)$ atoms in the stratosphere should not be appreciably influenced by their initial translational excitation.

Besides the need to know the rates at which $O(^1D)$ atoms react, it is equally important to know the exact mechanisms of their reactions in the stratosphere. Experimental rate determinations generally give only the overall rates of destruction of $O(^1D)$ atoms but do not specify whether they have been only deactivated to $O(^3P)$ or have been consumed in a chemical reaction or, if a chemical reaction takes place, what its products are. To obtain this information, special experiments are required to identify reaction products and determine their amounts. A number of experiments of this kind have been carried out. Only some of these will be mentioned here, for illustration purposes.

In 1964 Yamazaki and Cvetanović (46) studied the reaction of $O(^1D)$ with propane and discovered that $O(^1D)$ atoms, in contrast to $O(^3P)$ atoms, readily insert into the CH bonds of paraffins. However, because of the very high exothermicities of these reactions, of the order of 135–150 kcal/mol, the alcohols formed are highly vibrationally excited ("hot") and decompose if the total pressure of the gas is not sufficiently high to assure rapid collisional deactivation. In the case of propane, appreciable concentrations of the two alcohols, *n*- and *i*-propanol, formed in the statistical ratio of 3 primary to 1 secondary CH bond in propane, are observed only at pressures in excess of atmospheric. Their yields increase with the total pressure (of propane or of SF_6 added) but are far from reaching plateau values even at 2 to 3 atm. Paraskevopoulos and Cvetanović have subsequently found that, as anticipated, the hot alcohols obtained from higher alkanes are stabilized at lower pressure. Thus in the reaction of $O(^1D)$ with isobutane (82) the plateau values of iso- and tert-butanol, formed in the statistical ratio of 9 primary to 1 tertiary CH bond in isobutane, are already reached at pressures close to atmospheric. In the case of neopentane (83), the plateau value of neopentanol is attained at 150–200 Torr. The increasing ease of stabilization of the vibrationally excited alcohols with the number of atoms (and thus of degrees of freedom) in the molecule is in accord (84) with the theories of the unimolecular decomposition of the "chemically activated" (vibrationally hot) molecules.

In the case of CH_4, the $O(^1D)$–paraffin reaction of stratospheric interest, almost complete decomposition of the hot methanol, formed by $O(^1D)$ insertion, would be expected under atmospheric conditions. Lin and DeMore (85) have indeed recently observed a yield of methanol per $O(^1D)$ atom reacted of only 3% at a total pressure of 770 Torr (almost entirely CH_4). The

Can. J. Chem. Downloaded from www.nrcresearchpress.com by 210.87.254.105 on 09/05/12
For personal use only.

yield of methanol increased progressively with pressure to about 18% at 80 atm. At stratospheric pressures, the hot methanol would therefore be expected to decompose essentially entirely into CH_3 and OH.

Although an essentially indiscriminate insertion of $O(^1D)$ into the CH bonds is the major mode of reaction of $O(^1D)$ with paraffins, it is not the exclusive one. In the gas phase, the H-atom abstraction seems to be an important independent reaction path, persisting, for example, in the case of neopentane, well in excess of the pressure at which the alcohol appears to have attained its plateau value (83). (In the $O(^1D)$–methane reaction in the stratosphere the abstraction also gives CH_3 and OH, *i.e.*, the same products as formed from the decomposition of "hot" methanol, and it is therefore unimportant to know whether or not abstraction occurs as an independent process.) A third reaction path, first discovered by DeMore and Raper (86) in $O(^1D)$ reaction with methane in liquid argon solution, is the molecular elimination (to form H_2 and HCHO in this case). This reaction path is also observed in the gas phase. In the case of neopentane the products of molecular elimination are H_2 and pivalaldehyde, but their yields are very minor (83). On the other hand, Lin and DeMore (85) find for CH_4 in the gas phase a 9% molecular elimination (into H_2 and HCHO), which is roughly similar to the yield found by DeMore and Raper in liquid argon solution (86).

The reaction of $O(^1D)$ with neopentane has also proved very useful in experiments carried out by Paraskevopoulos and Cvetanović (40) to establish whether collisional deactivation of $O(^1D)$ to $O(^3P)$ or its chemical consumption take place in the reactions of different gases with $O(^1D)$. This is achieved by scavenging with excess neopentane essentially all the $O(^1D)$ atoms and with very small amounts of butene-1 essentially all the $O(^3P)$ atoms. This is possible because $O(^3P)$ atoms react much faster with butene-1 than with neopentane while $O(^1D)$ reacts with the two hydrocarbons at roughly comparable rates. When various amounts of another gas capable of competing for $O(^1D)$ (but not for $O(^3P)$) are added, the decrease in $O(^1D)$ will result in decreased yields of neopentanol. At the same time, if any $O(^3P)$ is formed in the reaction of the added gas with $O(^1D)$, typical products of $O(^3P)$ with butene-1 (87) (α-butene oxide, *n*-butanal, and a little methyl ethyl ketone) are observed. From the yields of the products the quantum yields $\Phi O(^1D)$ and $\Phi O(^3P)$ can be calculated and are summarized in Table 3. It is clear from the last two rows in Table 3 that SF_6 and He do not destroy $O(^1D)$ (nor induce any $O(^3P)$ formation), H_2 and CH_4 remove $O(^1D)$ chemically, *i.e.* without converting it to $O(^3P)$, and N_2, CO, CO_2, and Xe collisionally deactivate $O(^1D)$ to equivalent amounts of $O(^3P)$ without removing them chemically. These results were helpful, for example, in demonstrating the incorrectness of some early suggestions that CO removed $O(^1D)$ chemically, a process which would be intuitively unlikely in the gas phase at normal pressures. The data in Table 3 show clearly that CO does not remove $O(^1D)$ chemically but deactivates it quantitatively into equivalent amounts of $O(^3P)$. Results consistent with this finding were obtained in subsequent experiments of Slanger and Black (88), using a different technique. Similarly, Gaedtke and co-workers (18, 89) have found a very inefficient N_2O formation from $O(^1D)$ and N_2 at quite high pressures, although N_2O formation is appreciable in liquid nitrogen solutions. At stratospheric pressures N_2O formation should therefore be negligible.

The products of the reaction of $O(^1D)$ with O_2 appear to be (29, 35, 51, 56, 90–93) $O(^3P)$, $O_2(^1\Sigma_g^+)$, $O_2(^1\Sigma_g^+)^{*(v=1)}$, and $O_2^{*(v)}$ but the ratio of the last three is still uncertain. McCullough and McGrath (90) find large yields of $O_2^{*(v)}$ (with $v \leq 14$) while Snelling (74) finds a 75% yield of $O_2(^1\Sigma_g^+)$ and Gauthier and Snelling (73) find that approximately 25 to 50% of it is formed in the first vibrational level, *i.e.* $O_2(^1\Sigma_g^+)^{*(v=1)}$. In the reaction of $O(^1D)$ with ozone two reaction paths appear to be in competition, one leading to $O_2 + O_2$ and the other to $O_2 + O + O$. Baiamonte *et al.* (94) conclude that the rate of the latter is more than 10 times larger than the rate of the former reaction path while preliminary work of Davenport, Schiff, and Welge (95) indicates that the ratio of these two reaction channels is approximately unity.

$O(^1S_0)$ Atoms

The rate constants of some of the $O(^1S)$ reactions of interest are (96) (at 300 °K, in units of cm^3 $molecule^{-1}$ s^{-1}): O_2 3×10^{-13} ($7.4 \times$

TABLE 3. Discrimination between chemical removal and physical quenching of $O(^1D_2)$ atoms by different added gases (pressure of the added gas 615–630 Torr, N_2O 20.3–20.7 Torr, neopentane 61.2–61.8 Torr, butene-1 2.2–2.3 Torr; total pressure close to 700 Torr; temperature 25 ± 2 °C). Based on the data of Paraskevopoulos and Cvetanović (40)

Quantum yields[a]	SF_6	He	H_2	CH_4	N_2	Xe	CO	CO_2
$\Phi O(^1D)$	0.97	0.97	0.27	0.23	0.69	0.43	0.55	0.43
$\Phi O(^3P)$	0.03	0.02	0.03	0.03	0.29	0.55	0.45	0.58
$-\Delta\Phi O(^1D)$[b]	0	0	0.70	0.74	0.28	0.54	0.42	0.54
$\Delta\Phi O(^3P)$[b]	0	0	0	0	0.26	0.52	0.42	0.54

[a]Based on the $O(^1D)$ and $O(^3P)$ products formed in the presence of the added gas, as explained in the text. Mean values for each added gas are given.
[b]Differences of the quantum yields of the $O(^1D)$ and $O(^3P)$ products in the presence and absence of the added gas.

10^{-11}), $N_2 < 5 \times 10^{-17}$ (5.4×10^{-11}), O_3 5.8×10^{-10} (5×10^{-10}), $H_2O > 10^{-10}$ (3.5×10^{-10}), CH_4 2×10^{-14} (4×10^{-10}), N_2O 1.4×10^{-11} (2.2×10^{-10}), NO 5.5×10^{-10} (1.7×10^{-10}), NH_3 5×10^{-10} (probably about 4×10^{-10}), CO_2 3.8×10^{-13} (1.8×10^{-10}). The values in parentheses are the corresponding values for the $O(^1D)$ rate constants from Table 2. It is evident that $O(^1S)$ interacts much more slowly than $O(^1D)$ with O_2, N_2, CH_4, and CO_2 but at comparable or greater rates with O_3, NO, NH_3, and particularly H_2O. For this reason, it was pointed out by Schiff (97) that $O(^1S)$ may play a significant role in the stratosphere if its production rate is greater than 1% of $O(^1D)$. Unfortunately it is not known whether $O(^1S)$ is generated in the stratosphere and, if it is, at what rate, although it is energetically possible to produce $O(^1S)$ in a spin-allowed process from O_3 photolysis at $\lambda < 199.5$ nm. Of particular interest would be the reaction of $O(^1S)$ with H_2O. The reaction products are not known in any of these reactions, but it is probable that in the reaction with water the products are two OH radicals. Further investigation of the chemical behavior of $O(^1S)$ and of the potential rate of its generation in the stratosphere would evidently be very desirable.

Concluding Remarks

The object of this paper has been mainly to summarize briefly the progress made in recent years in the understanding of the chemical behavior of $O(^1D_2)$ atoms. Some general questions have also been raised, in the hope of stimulating further interest in the field of excited state chemistry in the stratosphere. It is clear that much remains to be done in this field. Potential involvement in stratospheric chemistry of some excited species not discussed here, such as for example of the low lying first triplet of ozone and of a low lying electronically excited state of HO_2 radical, has been occasionally suggested although such suggestions are of necessity still very tentative. Other excited molecules and molecular fragments may perhaps be involved as well and some are implicated in chemical processes at still higher altitudes in the atmosphere. Substantial further progress in this field may be expected through combined laboratory experiments, field observations, and theoretical work.

1. T. CARRINGTON and D. GARVIN. Comp. Chem. Kinet. **3**, 107 (1969).
2. R. WOLFGANG. Ann. Rev. Phys. Chem. **16**, 15 (1965).
3. R. WOLFGANG. Prog. React. Kinet. **3**, 97 (1965).
4. D. S. URCH. MTP International Review of Science, Series I. Vol. 8. Butterworths, London. 1972. p. 149.
5. R. E. TOMALESKY and J. E. STURM. J. Chem. Soc. Faraday Trans. II, **68**, 1241 (1972).
6. R. SUPLINSKAS. J. Chem. Phys. **49**, 5046 (1968).
7. M. KARPLUS, R. PORTER, and R. SHARMA. J. Chem. Phys. **40**, 2033 (1964); **43**, 3259 (1965); **45**, 3871 (1966).
8. R. PORTER and M. KARPLUS. J. Chem. Phys. **40**, 1105 (1964).
9. P. KUNTZ, E. NEMETH, J. POLANYI, and W. WONG. J. Chem. Phys. **52**, 4654 (1970).
10. D. L. BUNKER and M. D. PATTENGILL. J. Chem. Phys. **53**, 3041 (1970).
11. D. J. MALCOLME-LAWES. J. Chem. Phys. **57**, 5522 (1972).
12. R. D. PENZHORN and B. DE B. DARWENT. J. Phys. Chem. **72**, 1639 (1968).
13. R. A. FASS, J. W. HOOVER, and L. M. SIMPSON. J. Phys. Chem. **76**, 2801 (1972).
14. R. E. TOMALESKY and J. E. STURM. J. Chem. Soc. Faraday Trans. II, **68**, 1241 (1972).
15. W. F. LIBBY. J. Am. Chem. Soc. **69**, 2523 (1947).
16. D. KATAKIS and H. TAUBE. J. Chem. Phys. **36**, 416 (1962).
17. R. SIMONAITIS, E. LISSI, and J. HEICKLEN. J. Geophys. Res. **77**, 4248 (1972).
18. H. GAEDTKE, H. HIPPLER, and J. TROE. Ber. Bunsenges. Phys. Chem. **76**, 1101 (1972).
19. A. B. CALLEAR and J. D. LAMBERT. Comp. Chem. Kinet. **3**, 182 (1969).

Can. J. Chem. Downloaded from www.nrcresearchpress.com by 210.87.254.105 on 09/05/12
For personal use only.

Can. J. Chem. Downloaded from www.nrcresearchpress.com by 210.87.254.105 on 09/05/12
For personal use only.

20. R. L. TAYLOR. Can. J. Chem. This issue.
21. R. N. SCHWARTZ, Z. I. SLAWSKY, and K. F. HERZFELD. J. Chem. Phys. **20**, 159 (1952).
22. A. E. POTTER, JR., R. N. COLTHARP, and S. D. WORLEY. J. Chem. Phys. **54**, 992 (1971).
23. R. N. COLTHARP, S. D. WORLEY, and A. E. POTTER, JR. Appl. Opt. **10**, 1786 (1971).
24. S. D. WORLEY, R. N. COLTHARP, and A. E. POTTER. J. Chem. Phys. **55**, 2608 (1971).
25. S. D. WORLEY, R. N. COLTHARP, and A. E. POTTER, JR. J. Phys. Chem. **76**, 1511 (1972).
26. G. HANCOCK and I. W. M. SMITH. Chem. Phys. Lett. **8**, 41 (1971); Appl. Opt. **10**, 1827 (1971).
27. M. NICOLET. Planet. Space Sci. **20**, 1671 (1972).
28. J. G. ANDERSON and F. KAUFMAN. Chem. Phys. Lett. **19**, 483 (1973).
29. M. GAUTHIER and D. R. SNELLING. J. Chem. Phys. **54**, 4317 (1971).
30. R. P. STEER, R. A. ACKERMAN, and J. N. PITTS, JR. J. Chem. Phys. **51**, 843 (1969).
31. R. J. COLLINS, D. HUSAIN, and R. J. DONOVAN. J. Chem. Soc. Faraday Trans. II, **69**, 145 (1973).
32. K. H. BECKER, W. GROTH, and U. SCHURATH. Chem. Phys. Lett. **14**, 489 (1972).
33. F. D. FINDLAY and D. R. SNELLING. J. Chem. Phys. **54**, 2750 (1971).
34. I. D. CLARK, I. T. N. JONES, and R. P. WAYNE. Proc. R. Soc. A, **317**, 407 (1970).
35. S. V. FILSETH, A. ZIA, and K. H. WELGE. J. Chem. Phys. **52**, 5502 (1970).
36. T. P. J. IZOD and R. P. WAYNE. Proc. R. Soc. (Lond.), A, **308**, 81 (1968).
37. G. H. MEYERS, D. M. SILVER, and F. KAUFMAN. J. Chem. Phys. **44**, 718 (1966).
38. T. C. FRANKIEWICZ and R. S. BERRY. J. Chem. Phys. **58**, 1787 (1973).
39. K. D. BAYES. Fourteenth Symposium (Int.) Combustion, Pennsylvania State University, August 20–25, 1972. Combustion Institute, Pittsburgh, Penn. 1973. p. 303.
40. G. PARASKEVOPOULOS and R. J. CVETANOVIĆ. J. Am. Chem. Soc. **91**, 7572 (1969).
41. P. M. SCOTT, K. F. PRESTON, R. J. ANDERSEN, and L. M. QUICK. Can. J. Chem. **49**, 1808 (1971).
42. H. YAMAZAKI and R. J. CVETANOVIĆ. J. Chem. Phys. **39**, 1902 (1963).
43. H. YAMAZAKI and R. J. CVETANOVIĆ. J. Chem. Phys. **40**, 582 (1964).
44. D. L. BAULCH and W. H. BRECKENRIDGE. Trans. Faraday Soc. **62**, 2768 (1966).
45. K. F. PRESTON and R. J. CVETANOVIĆ. J. Chem. Phys. **45**, 2888 (1966).
46. H. YAMAZAKI and R. J. CVETANOVIĆ. J. Chem. Phys. **41**, 3703 (1964).
47. P. M. SCOTT and R. J. CVETANOVIĆ. J. Chem. Phys. **54**, 1440 (1971).
48. D. KATAKIS. J. Chem. Phys. **47**, 541 (1966).
49. D. R. SNELLING and E. J. BAIR. J. Chem. Phys. **47**, 228 (1967).
50. R. A. YOUNG, G. BLACK, and T. G. SLANGER. J. Chem. Phys. **49**, 4758 (1968).
51. D. BIEDENKAPP and E. J. BAIR. J. Chem. Phys. **52**, 6119 (1970).
52. D. BIEDENKAPP, L. G. HARTSHORN, and E. J. BAIR. Chem. Phys. Lett. **5**, 379 (1970).
53. W. B. DEMORE. J. Chem. Phys. **52**, 4309 (1970).
54. R. J. DONOVAN, D. HUSAIN, and L. J. KIRSCH. Chem. Phys. Lett. **6**, 488 (1970).
55. H. YAMAZAKI. Can. J. Chem. **48**, 3269 (1970).
56. J. F. NOXON. J. Chem. Phys. **52**, 1852 (1970).
57. G. ELLENRIEDER, E. CASTELLANO, and H. J. SCHUMACHER. Z. Phys. Chem. Neue Folge, **76**, 240 (1971).
58. E. CASTELLANO and H. J. SCHUMACHER. Z. Phys. Chem. Neue Folge, **76**, 258 (1971).
59. M. LOEWENSTEIN. J. Chem. Phys. **54**, 2282 (1971).
60. R. GILPIN, H. I. SCHIFF, and K. H. WELGE. J. Chem. Phys. **55**, 1087 (1971).
61. C. S. GOLDMAN, R. I. GREENBERG, and J. HEICKLEN. Int. J. Chem. Kinet. **3**, 501 (1971).
62. K. F. LANGLEY and W. D. MCGRATH. Planet. Space Sci. **19**, 413, 416 (1971).
63. G. PARASKEVOPOULOS and R. J. CVETANOVIĆ. Chem. Phys. Lett. **9**, 603 (1971).
64. G. PARASKEVOPOULOS, K. F. PRESTON, and R. J. CVETANOVIĆ. J. Chem. Phys. **54**, 3907 (1971).
65. T. G. SLANGER and G. BLACK. J. Chem. Phys. **54**, 1889 (1971).
66. I. D. CLARK and J. F. NOXON. J. Chem. Phys. **57**, 1033 (1972).
67. C. J. FORTIN, D. R. SNELLING, and A. TARDIF. Can. J. Chem. **50**, 2747 (1972).
68. R. I. GREENBERG and J. HEICKLEN. Int. J. Chem. Kinet. **4**, 417 (1972).
69. E. LISSI and J. HEICKLEN. Ionosphere Research Laboratory Scientific Report No. 387. The Pennsylvania State University. 1972.
70. G. PARASKEVOPOULOS, V. B. SYMONDS, and R. J. CVETANOVIĆ. Can. J. Chem. **50**, 1838 (1972).
71. R. SIMONAITIS and J. HEICKLEN. Int. J. Chem. Kinet. **4**, 529 (1972).
72. P. MICHAUD, G. PARASKEVOPOULOS, and R. J. CVETANOVIĆ. Unpublished results.
73. M. GAUTHIER and D. R. SNELLING. Unpublished results.
74. D. R. SNELLING. Can. J. Chem. **52**, 257 (1974).
75. R. F. HEIDNER III, D. HUSAIN, and J. R. WIESENFELD. Chem. Phys. Lett. **16**, 530 (1972).
76. R. F. HEIDNER III and D. HUSAIN. Nature, **241**, 10 (1973).
77. R. F. HEIDNER III and D. HUSAIN. Int. J. Chem. Kinet. **5**, 819 (1973).
78. R. F. HEIDNER III, D. HUSAIN, and J. R. WIESENFELD. J. Chem. Soc. Faraday Trans. II, **69**, 927 (1973).
79. R. F. HEIDNER III and D. HUSAIN. Unpublished results.
80. R. SIMONAITIS, R. I. GREENBERG, and J. HEICKLEN. Int. J. Chem. Kinet. **4**, 497 (1972).
81. G. PARASKEVOPOULOS *et al.* Private communication.
82. G. PARASKEVOPOULOS and R. J. CVETANOVIĆ. J. Chem. Phys. **50**, 590 (1969).
83. G. PARASKEVOPOULOS and R. J. CVETANOVIĆ. J. Chem. Phys. **52**, 5821 (1970).
84. K. J. MINTZ and R. J. CVETANOVIĆ. Can. J. Chem. **51**, 3386 (1973).
85. C. L. LIN and W. B. DEMORE. J. Phys. Chem. **77**, 863 (1973).
86. W. B. DEMORE and O. F. RAPER. J. Chem. Phys. **46**, 2500 (1967).
87. R. J. CVETANOVIĆ. Adv. Photochem. **1**, 115 (1963).
88. T. G. SLANGER and G. BLACK. J. Chem. Phys. **53**, 3722 (1970).

89. H. GAEDTKE, K. GLÄNZER, H. HIPPLER, K. LUTHER, and J. TROE. Fourteenth Symposium (Int.) Combustion, Pennsylvania State University, August 20–25, 1972. Combustion Institute, Pittsburgh, Penn. 1973. p. 295.
90. D. W. MCCULLOUGH and W. D. MCGRATH. Chem. Phys. Lett. **8**, 353 (1971).
91. T. P. J. IZOD and R. P. WAYNE. Chem. Phys. Lett. **4**, 208 (1969).
92. I. T. N. JONES, U. B. KACZMAR, and R. P. WAYNE. Proc. R. Soc. A, **316**, 431 (1970).
93. I. D. CLARK. Chem. Phys. Lett. **5**, 317 (1970).
94. V. D. BAIAMONTE, L. G. HARTSHORN, and E. J. BAIR. J. Chem. Phys. **55**, 3617 (1971).
95. J. E. DAVENPORT, H. I. SCHIFF, and K. H. WELGE. Private communication.
96. T. G. SLANGER and K. H. WELGE. Evaluation for C.I.A.P. Monographs. Vol. I. Natural stratosphere, 1974. To be published.
97. H. I. SCHIFF. *In* Natural stratosphere, 1974. C.I.A.P. Monographs. Vol. I. To be published.

Can. J. Chem. Downloaded from www.nrcresearchpress.com by 210.87.254.105 on 09/05/12
For personal use only.

Absorption Cross Sections of Stratospheric Molecules

R. D. HUDSON
NASA, L. B. Johnson Space Center, Houston, Texas
Received October 3, 1973

Can. J. Chem. Downloaded from www.nrcresearchpress.com by 210.87.254.42 on 09/05/12
For personal use only.

Photoabsorption cross sections necessary for calculations of the equilibrium conditions in the stratosphere fall into two distinct classes: cross sections for molecular oxygen and ozone, which control the transmission of solar radiation; cross sections for minor atmospheric species which are optically thin to solar radiation, and which are needed to calculate their rates of dissociation.

The principal absorption features of molecular oxygen are absorption bands of the Schumann–Runge system between 175 and 200 nm and a weak dissociation continuum which extends from 175 to 260 nm. The band structure consists of many sharp rotational lines, and it is necessary to calculate cross sections using measured band parameters. Two measurements of the line widths for these bands have obtained large line widths ($\sim$1 cm^{-1}) indicating predissociation. The agreement between the two sets of data is good for only a few lines. This has implications in the calculation of the transmission of solar radiation to the lower stratosphere. The continua have been measured by four groups. The results agree, within the respective experimental errors, near 220 nm, but disagree near 250 nm.

Ozone has a continuous absorption spectrum between 175 and 300 nm with band structure above 300 nm. Four sets of data are available which agree within $\pm$2%. The cross section above 300 nm is temperature dependent. The cross sections for the minor species are in general not as well known. In nitric oxide, carbon monoxide, ammonia, and sulfur dioxide, band structure dominates the absorption spectrum, and cross sections have been measured at insufficient spectral resolution. Other species, such as nitric acid, hydrogen peroxide, water vapor, carbon dioxide, nitrous oxide, and nitrogen dioxide, have continua over the entire spectra range from 175 to 300 nm. Cross sections for these species have been measured; however, cross sections for many molecules, *e.g.*, N_2O_5, NO_3, etc., have not been studied.

Les coupes de photoabsorption nécessaires pour les calculs des conditions d'équilibre dans la stratosphère se répartissent en deux classes distinctes: les coupes de l'oxygène et l'ozone moléculaires qui contrôlent la transmission des radiations solaires; les coupes d'espèces atmosphériques secondaires qui sont optiquement poreuses aux radiations solaires et qui sont nécessaires pour le calcul de leur vitesse de dissociation.

Les principales caractéristiques d'absorption de l'oxygène moléculaire sont des bandes d'absorption du système Schumann–Runge entre 175 et 200 nm et une faible dissociation continu qui s'étend de 175 à 260 nm. La structure de bandes consiste en plusieurs lignes fines de rotation et il est nécessaire de calculer les sections droites en utilisant les paramètres de bandes mesurés. Deux mesures de largeurs des lignes de ces bandes montrent d'importantes largeurs des lignes ($\sim$1 cm^{-1}) indiquant une prédissociation. L'accord entre les deux séries de données est bon pour quelques lignes seulement. Ceci comporte des implications dans le calcul de la transmission de radiation solaire à la stratosphère inférieure. La continuité a été mesurée par quatre groupes. Les résultats sont en accord, dans les limites des erreurs expérimentales respectives, près de 220 nm, mais sont en désaccord près de 250 nm.

L'ozone a un spectre d'absorption continue entre 175 et 300 nm avec une bande de structure au-dessus de 300 nm. Quatre séries de données sont connues et sont en accord à $\pm$2% près. Les sections droites au-dessus de 300 nm varient avec la température. Les sections droites d'espèces secondaires ne sont pas, en général, aussi bien connues. Dans l'oxyde nitrique, l'oxyde de carbone, l'ammoniaque et l'anhydride sulfureux, la bande de structure domine sur le spectre d'absorption et des sections droites ont été mesurées à une résolution spectrale insuffisante. D'autres espèces, telles que l'acide nitrique, le peroxyde d'hydrogène, la vapeur d'eau, l'anhydride carbonique, l'oxyde nitreux et le bioxyde d'azote, ont des spectres entiers continus dans l'intervalle de 175 à 300 nm. Des sections droites pour ces espèces ont été mesurées; cependant, elles n'ont pas été étudiées pour beaucoup de molécules, par exemple, N_2O_5, NO_3, etc.

[Traduit par le journal]

Can. J. Chem. Downloaded from www.nrcresearchpress.com by 210.87.254.42 on 09/05/12
For personal use only.

Introduction

This review is concerned with absolute total photo-absorption cross section measurements for molecules which are of importance in the stratosphere, the derivation of partial cross sections for photodissociation, etc., having been dealt with in preceding review papers (Johnston (1), Welge (2)). Details of the experimental procedures used in the measurement of photo-absorption cross sections and a discussion of the experimental errors have been given in a previous review article by Hudson (3) and will not be repeated here. Limiting the scope of the review to the stratosphere has automatically placed a lower limit on the wavelength range that needs to be considered because of the large absorption cross sections for molecular oxygen below 175 nm. Thus, this review is intended to supplement the earlier review of Hudson (3), by placing the emphasis on the wavelength range above 175 nm.

General Concepts

The cross sections needed for the calculation of photochemical rates in the stratosphere fall into two distinct classes. The first class consists of molecular oxygen and ozone, for these species are optically thick over most of the ultraviolet and hence determine the flux of solar radiation that reaches a particular altitude. The second class consists of the remainder of the minor constituents. These molecules are optically thin throughout the stratosphere and the total photo-absorption cross sections, in conjunction with quantum yields and transmitted solar fluxes, are needed in order to compute photochemical rates. The division into these two classes has another significance with regard to the accuracy to which the cross sections need to be measured. The Lambert–Beer law states:

$$[1] \qquad I(\lambda) = I_0(\lambda) \exp(-\Upsilon(\lambda))$$

where $\Upsilon(\lambda)$ is the optical depth, $I(\lambda)$ is the transmitted flux, and $I_0(\lambda)$ is the incident flux. $\Upsilon(\lambda)$ at an altitude, h, is given by

$$[2] \qquad \Upsilon(\lambda) = \int_h^\infty \sum_i n_i(h)\, \sigma_i(\lambda)\, \mathrm{d}h$$

where $n_i(h)$ is the number density and $\sigma_i(\lambda)$ is the total absorption cross section, respectively, of the ith component. For small errors in σ we may write

$$[3] \qquad \Delta I = -I_0 \exp(-\Upsilon(\lambda)) \cdot \Delta\Upsilon$$

or, dividing through by eq. 1,

$$[4] \qquad \frac{\Delta I}{I} = -\Delta\Upsilon = -\Upsilon \cdot \frac{\Delta\Upsilon}{\Upsilon}$$

It will be noted that the fractional error in the computation of the transmission at a given altitude is not given by the fractional error in the optical depth, but by the product of the optical depth and the fractional error in the optical depth. Hence, if accurate values of the transmitted fluxes are required at large optical depths, *i.e.* at the lower altitudes, then the cross sections for molecular oxygen and ozone must be known to within a few per cent at least. On the other hand, the photochemical rates for the minor species are given simply by the product of the transmitted flux and the relevant cross sections, and the errors in these quantities are directly proportional to the errors in the cross sections. Of course, errors in the optical depth also depend on the altitude profiles assumed for the absorbing species, which in turn places some fairly stiff limits on the errors in these quantities that can be tolerated.

Review of Published Cross Sections

In preparing this review I have performed a literature research up to March 1973, therefore this review should be current as of that date. Because of space limitations this review does not contain a complete set of cross section values for each molecule. The prepared figures and tables are used solely to compare the results of several determinations or to point out where difficulties in interpretation might arise. Table 1 lists those papers from which cross section data were taken for this review. This table lists the authors and the species measured, the experimental techniques, and the author's estimate of the experimental error. Wherever a blank occurs under one of the headings it may be assumed that no account of the measurement technique or error was given in the paper.

Most of the figures shown in this review were prepared by the Information Center at the Joint Institute for Laboratory Astrophysics, University of Colorado. Almost all of the data reproduced in these figures were presented in the original literature in graphical form. Blown up photographs of the figures were made and the

TABLE 1. Summary of experimental parameters for papers discussed in the review

Authors	Species	Experimental Techniques	Pressure Measurement	Bandwidth, A	Errors	Remarks
Hudson, et al. (1966)[6]	O_2	Photomultiplier; 158-195 nm; continuum source	McLeod gage	<1750 A $\Delta\lambda$=0.75 >1750 A $\Delta\lambda$=0.075	Random error, 10%; systematic error, 1%	Cross section measured at 300, 600, and 900°K
Ogawa[7]	O_2 CO_2	Photomultiplier; 170-235 nm; continuum light source	Mercury and oil manometer	.075 .057		
Ackerman, et al.[8]	O_2	Photomultiplier; 175-205 nm; line emission source	Mercury manometer and McLeod gage			Resolution defined by width of emission lines
Oitchburn and Young (1962)[11]	O_2	Photographic; 185-250 nm; continuum source			Constant error of 1.0×10^{-24} cm^2	
Blake, et al. (1966)[12]	O_2	Photomultiplier or ion chamber; 125-235 nm; continuum and line source	Oil and mercury manometers, McLeod gage	1-2	5%, 200-240 nm and 125-175 nm	Used double beam technique
Shardanand[13]	O_2	Photomultiplier; 200-280 nm; continuum light source	High pressure gage	2.5	±10%	Pressure gage reading appears in error by 1 atmosphere
Hasson and Nicholls[14]	O_2	Photomultiplier; 205-243 nm; continuum light source		2-14		
Inn and Tanaka (1953)[15]	O_3	Photomultiplier; 200-350 nm; continuum source	H_2SO_4 manometer		Cross section, 5%; wavelength error, ±.1 nm	
Griggs (1968)[16]	O_3	Photomultiplier; 200-360 nm; continuum source	H_2SO_4 manometer		Scatter of results less than ±1.5% between 200 and 300 nm; up to 6% outside this range	
DeMore and Raper (1964)[17]	O_3	Photomultiplier; 200-310 nm line emission source	Conversion of O_3 to O_2; O_2 pressure measured with gas buret calibrated against McLeod gage		4%	
Hearn (1961)[18]	O_3	Photomultiplier; 250-340 nm; line emission source	Pyrex spiral manometer calibrated against McLeod gage		Full discussion of errors given for each point	
Vigroux[19]	O_3	Photographic; 230-350 nm and 450-740 nm; continuum and line source	Titration with iodine solution			Measured temperature dependence
Tanaka, et al. (1953)[20]	O_3	Photomultiplier; 105-220 nm	H_2SO_4 manometer		10%	
Marmo (1953)[21]	NO	Photomultiplier; 110-230 nm line and continuum source	McLeod gage, mercury manometer, ion gage	0.85	Discusses effect of N_2O impurity on the results	
Thompson, et al. (1963)[22]	O_2, CO, CO_2, H_2O, N_2O, NH_3, NO, SO_2, CH_4	Photomultiplier; 185-400 nm; light source not discussed				Discussed purification of gases
Nakayama, et al. (1959)[26]	NO_2	Photomultiplier; 108-270 nm; line and continuum source	Micromanometer and silicone oil manometer	0.2	10-20% at wavelengths below 180 nm; higher at longer wavelengths	
Hall and Blacet (1952)[27]	NO_2, N_2O_4	Photomultiplier; 240-500 nm	Silicone manometer or mercury manometer	2-5	Errors discussed but no figures given	
Romand and Mayence (1949)[29]	N_2O	Photographic emulsion; 140-250 nm; line and continuum source	Manometers			
Holliday and Reuben[30]	N_2O	Photomultiplier; 190-280 nm; continuum source				Measured temperature dependence
Zelikoff, et al. (1953)[31]	N_2O	Photomultiplier; 108-210 nm; line and continuum source		0.85		NO_2 purity checked with mass spectrometer
Schmidt, et al.[33]	NHO_3	Photomultiplier; 160-440 nm; continuum source				
Tannenbaum, et al. (1953)[34]	NH_3	Photographic emulsion and photomultiplier; 160-300 nm; continuum light source			5-10%	
Watanabe and Zelikoff (1953)[35]	H_2O	Photomultiplier; 106-186 nm; line and continuum source	Alphatron gage calibrated against McLeod gage	1	Some possible sources discussed, but no numbers given	Purity of gas checked with mass spectrometer; pressure during a run observed to vary by 10%
Laufer and McNesby (1965)[36]	H_2O, CH_4	Photomultiplier; 110-180 nm; line and continuum source	Oil manometer	6.6		
Schurgers and Welge[37]	H_2O H_2O_2	Photomultiplier; 120-200 nm; line emission & continuum source	Capacitance manometer	2.5	±10%	
Holt, et al.[38]	H_2O_2	Photographic; 185-220 nm; continuum source	Titration with potassium permanganate		±10%	
Heimerl[39]	CO_2	Photomultiplier; 165.5-182.5 nm; continuum source	Mercury manometer	3.4	±20%	
Warneck, et al. (1964)[40]	SO_2	Photomultiplier; 184.9-315 nm; continuum and line source	Silicone oil manometer and dial gage	1		
Golomb, et al. (1962)[41]	SO_2	Photomultiplier; 105-217 nm; line and continuum source	Micromanometer	1	For wavelength above 135 nm, error is 10% where structure is displayed and less elsewhere	Purity of sample checked with mass spectrometer

Can. J. Chem. Downloaded from www.nrcresearchpress.com by 210.87.254.42 on 09/05/12
For personal use only.

Can. J. Chem. Downloaded from www.nrcresearchpress.com by 210.87.254.42 on 09/05/12
For personal use only.

data were digitalized by means of a Gerber data reduction system. Once the digitalized data had been obtained, they were permanently stored on magnetic tape. The review figures were then photocomposed from these tapes on a DD 280 cathode ray tube display.

Molecular Oxygen, O_2

The principal absorption features of molecular oxygen between 175 and 260 nm are the absorption bands of the Schumann–Runge system between 175 and 210 nm and the weak Herzberg dissociation continuum which extends from 175 to 260 nm. Two measurements of the band parameters are available, Ackerman and Biaumé (4) and Hudson and Mahle (5). Both measurements show large linewidths indicating predissociation, and a comparison of the linewidths obtained by these two groups is given in Table 2. It will be noted that the agreement for the broad lines, for example at $V' = 4$, are good, but for the narrow lines there are large discrepancies. As the absorption cross section in the wings of these lines will be directly proportional to the linewidths, it will be appreciated that these differences represent a large change in the absorption cross section and hence an even larger discrepancy in the transmission of solar radiation. The data of Hudson and Mahle (5) were obtained by fitting high resolution photoelectric band absorption profiles to a computer generated band model which included the triplet splitting of both the upper and lower states. The data of Ackerman and Biaumé (4) were obtained by measuring total linewidths from photographic spectra obtained at high resolution. Where the lines are unresolved, the triplet splitting of each rotational level is comparable to the predissociation broadening; therefore, one would expect the Ackerman and Biaumé (4) data, in general, to overestimate the widths. As the measurements of Hudson and Mahle (5) were obtained using band fitting procedures which take into account the triplet splitting, it is felt that their data are to be preferred.

TABLE 2. Predissociation line widths (full half-width) for the Schumann–Runge band system

	Full half-width (cm^{-1})	
V'	Hudson and Mahle (5)	Ackerman and Biaumé (4)
0	0.001*	1.00
1	0.002*	1.10
2	0.34±0.15	1.20
3	1.25±0.35	2.20
4	3.30±0.20	3.70
5	2.20±0.20	2.30
6	1.70±0.10	1.90
7	2.25±0.05	2.20
8	2.21±0.20	2.00
9	0.72±0.08	1.10
10	0.34±0.05	1.70
11	1.80±0.12	1.70
12	0.48±0.05	1.00
13	0.08±0.05	0.60
14	0.06±0.05	0.50
15	0.20±0.05	0.50
16	0.25±0.05	0.50
17	0.40*	0.50
18	0.40*	0.50
19	0.40*	0.50

*Calculated values.

Studies of the continua that underlie the Schumann–Runge bands between 175 and 210 nm have been made by Hudson *et al.*(6), Ogawa (7), and Ackerman *et al.* (8). Hudson and Mahle (5) have taken the data of Hudson *et al.* (6) and Ogawa (7) and corrected the measured cross sections for the contribution from the overlying band structure, using their measured linewidths for the rotational lines. The results of this calcu-

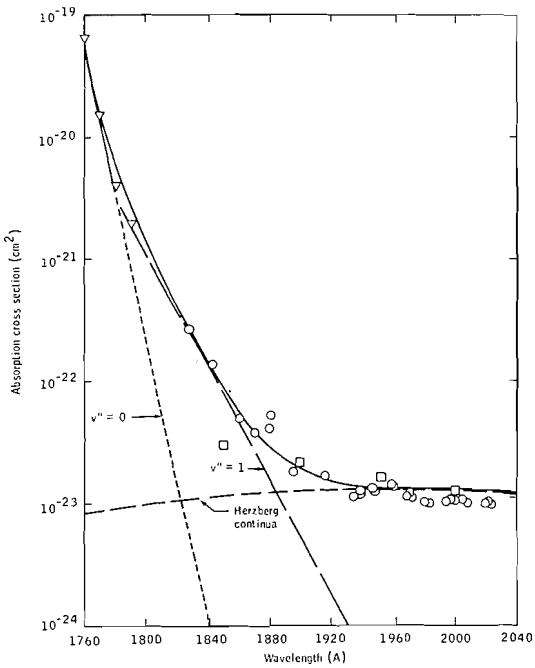

FIG. 1. Underlying continua between 176 and 204 nm; ○, data from column 4 of Table 3 from Hudson and Mahle (5); ▽, Hudson *et al.* (6); □, Ditchburn and Young (11).

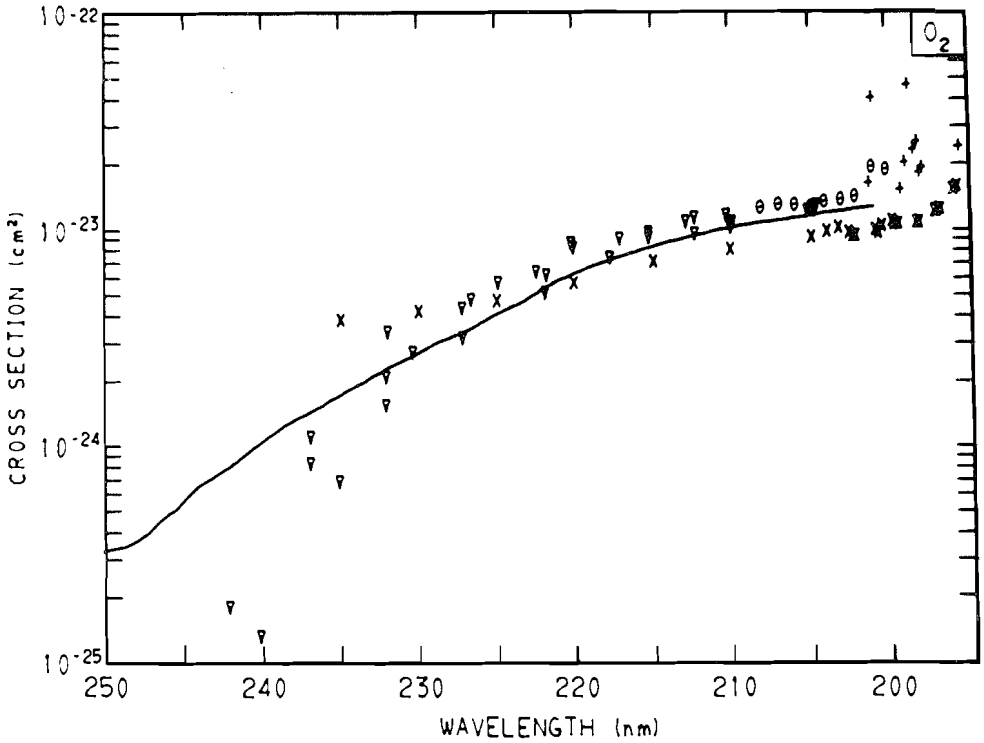

FIG. 2. Comparison of data for molecular oxygen, 210 to 260 nm; +, Ackerman *et al.* (8); —, Ditchburn and Young (11); ○, Blake *et al.* (12); ×, Ogawa (7); ▽, Hasson and Nicholls (14).

lation, taken from Hudson and Mahle (5), are shown in Fig. 1. Between 175 and 185 nm, the curve in Fig. 1 could be closely approximated by two exponential functions, ascribed by Hudson and Mahle (5) to transitions from the $V'' = 0$ and $V'' = 1$ rotational levels to the Schumann–Runge dissociation limit, and a reasonable extrapolation of the Herzberg continuum given by Jarmain and Nicholls (9). Hudson and Mahle (5) also found that if the cross sections at the $V'' = 0$ and $V'' = 1$ dissociation edges, obtained from Fig. 1, were used to predict the continuum cross section at 600 °K, excellent agreement was obtained with the experimental results obtained by Hudson *et al.* (6). These latter results are also consistent with the theoretical calculations of Allison *et al.* (10). Thus, it is felt that a self-consistent picture of the absorption in the region from 175 to 210 nm is obtained by using the band parameters and continuous absorption cross sections given by Hudson and Mahle (5).

The Herzberg continuum between 210 and 240 nm has been measured by Ditchburn and Young (11), Blake *et al.* (12), Ogawa (7), Shardanand (13), and Hasson and Nicholls (14). A comparison of the data from four of these groups is shown in Fig. 2. The data of Shardanand (13) are not shown as it is felt that an error in the pressure measurement was made during the experiment. The cross section in this wavelength interval is small, approaching values expected for Rayleigh scattering. Measured cross sections have all been found to increase linearly with pressure, an effect ascribed to the formation of O_4 molecules. A major problem in these measurements is the formation of ozone as a result of the dissociation of molecular oxygen in the absorption cell. Ozone has a cross section that increases to a maximum of 10^{-17} cm^2 at 250 nm, and thus small amounts can have a large effect on the measurements. The largest discrepancies in the data shown in Fig. 2 occur below 215 nm, where the Schumann–Runge bands become important, and above 230 nm, where the possibility of ozone contamination exists. It is felt that the later data of Hasson and Nicholls (14) is to be preferred.

Can. J. Chem. Downloaded from www.nrcresearchpress.com by 210.87.254.42 on 09/05/12
For personal use only.

Can. J. Chem. Downloaded from www.nrcresearchpress.com by 210.87.254.42 on 09/05/12
For personal use only.

TABLE 3. Comparison of ozone cross sections (in cm^2) at selected wavelengths

	Wavelength (nm)					
Authors	253.65	289.36	296.73	302.15	334.15	576.95
Inn and Tanaka (15)	1.14 (−17)	1.46 (−18)	5.75 (−19)	2.84 (−19)	5.74 (−21)	4.46 (−21)
Hearn (18)	1.15 (−17)	1.47 (−18)	5.96 (−19)	2.86 (−19)	4.76 (−21)	4.76 (−21)
DeMore and Raper (17)	1.15 (−17)	1.48 (−18)	5.86 (−19)			
Griggs (16)	1.13 (−17)	1.48 (−18)	5.98 (−19)	2.84 (−19)	5.57 (−21)	4.74 (−21)
Vigroux (19)	1.06 (−17)	1.56 (−18)	5.85 (−19)	2.82 (−19)	4.97 (−21)	4.74 (−21)

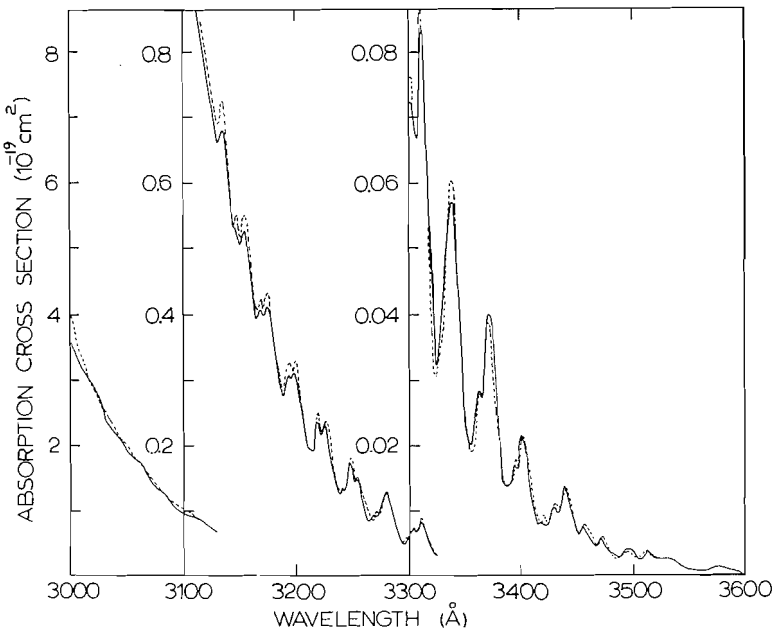

FIG. 3. Ozone cross sections, 300 to 360 nm; —, Griggs (16); ---, Inn and Tanaka (15).

Ozone, O_3

Measurements of the ozone cross section can be conveniently divided into three regions, 175 to 210 nm, 210 to 360 nm, and 450 to 850 nm. The region from 210 to 360 nm has been studied by Inn and Tanaka (15), Griggs (16), and DeMore and Raper (17), who all used a continuum light source, and by Hearn (18), who used a line emission source. These sets of data are in excellent agreement as is shown in Table 3. Vigroux (19) also studied ozone over this wavelength interval using photographic techniques. His data, also shown in Table 3, are consistently lower than those of the other authors. Vigroux (19), however, also studied the temperature dependence of the ozone cross section between 245 and 345 nm, that is, the region where an apparent continuum is overlaid by the Huggins bands, as illustrated in Fig. 3. The temperature effect that Vigroux (19) found as a function of wavelength is given in Table 4. It will be noted that the effect becomes much less at the shorter wavelengths, where indeed it is probably within the experimental error, indicating that the temperature dependence arises from the bands and not from the continuum. Further evidence for this conclusion is given by a comparison of the change in cross section at 331.2 and 239.9 nm, a maximum and minimum in the absorption curve. The minimum corresponds to absorption by high rotational levels and thus, as observed, it should be more temperature dependent than the maximum.

The region from 450 to 850 nm has been investigated by Inn and Tanaka (15), Griggs (16), and Vigroux (19). The data of Griggs (16) and of Vigroux (19) are in excellent agreement while that of Inn and Tanaka (15) is consistently lower by about 5–9%. Vigroux (19) also examined the temperature dependence of the cross section in this wavelength interval, but could detect none

TABLE 4. Temperature dependence of ozone cross section from Vigroux (19)

Wavelength (nm)	Cross section ratios $\frac{\sigma(181\ °K)}{\sigma(300\ °K)}$	$\frac{\sigma(214\ °K)}{\sigma(300\ °K)}$	$\frac{\sigma(243\ °K)}{\sigma(300\ °K)}$
340.1	0.89	0.86	0.89
331.2	0.90	0.86	0.90
329.9	0.50	0.57	0.69
320.0	0.91	0.86	0.90
319.0	0.67	0.73	0.81
310.0	0.88	0.88	0.92
300.4	0.90	0.91	0.95
290.6	0.92	0.94	0.96
279.9	0.96	0.96	0.98
269.7	0.97	0.97	0.98
260.6	0.96	0.98	0.98
250.0	0.96	0.98	0.98

Can. J. Chem. Downloaded from www.nrcresearchpress.com by 210.87.254.42 on 09/05/12
For personal use only.

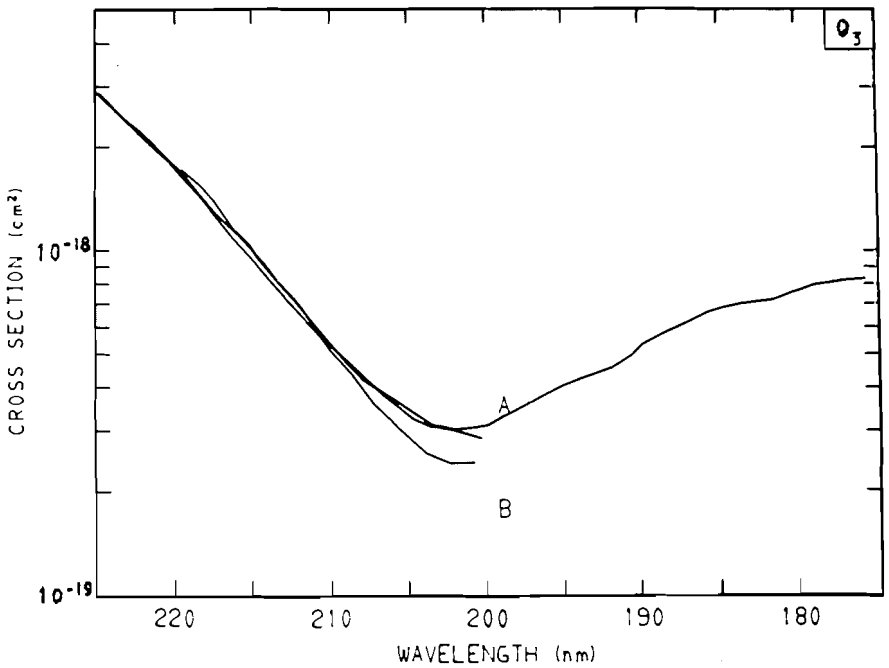

FIG. 4. Comparison of ozone cross section data, 175 to 225 nm; *A*, Inn and Tanaka (15); *B*, Griggs (16).

within his experimental error. In the wavelength range 175 to 210 nm, three sources of data are available. The data of Griggs (16), previously described, extends down to 200 nm, as does that of Inn and Tanaka (15). Tanaka *et al.* (20) obtained data from 106 to 220 nm. A comparison of these sets of data is given in Fig. 4. The data of Inn and Tanaka (15) and Tanaka *et al.* (20), not surprisingly, are consistent, while that of Griggs (16), although in agreement at 210 nm, is almost a factor of 2 lower at 200 nm. It is recommended that the data of Tanaka *et al.* (20) be used; however, as this wavelength region is an important "window" to solar radiation, further cross section measurements seem to be warranted.

Nitric Oxide, NO

Total absorption cross sections for nitric oxide have been measured between 175 and 235 nm by Marmo (21) and by Thompson *et al.* (22). The absorption spectrum in this spectral region is characterized by strong band structure which Marmo (21) observes to be strongly bandwidth dependent. In view of this fact, the published data are qualitative at best, and a set of best values cannot be compiled.

The aeronomic interest in this wavelength interval is centered on the predissociation of the nitric oxide gamma bands for $V' = 4$ and above. No measurements have been made of the predissociation linewidths; however, the line positions have been studied extensively (see Dressler and Meischer (23)) and the oscillator strengths have been measured by Bethke (24), and Hasson and Nicholls (25).

Nitrogen Dioxide, NO_2

Three measurements of the absorption cross section for nitrogen dioxide have been made. Nakayama *et al.* (26) have studied the region from 108 to 270 nm and Hall and Blacet (27) from 240 to 500 nm, and, more recently, Bass and Laufer (28) have measured the cross section between 300 and 360 nm. The experiment is not straightforward since nitrogen dioxide at room temperature consists of an equilibrium mixture of NO_2 and N_2O_4, the equilibrium being pressure dependent.

A comparison of the data of Hall and Blacet (27) and Bass and Laufer (28) shows differences of up to 25%, but these differences are not uniform, as, for example, at 300 nm the two sets agree within experimental error. The data of Hall and Blacet (27) and Nakayama *et al.* (26) overlap for only 30 nm and, except in the region near 250 nm,

Can. J. Chem. Downloaded from www.nrcresearchpress.com by 210.87.254.42 on 09/05/12
For personal use only.

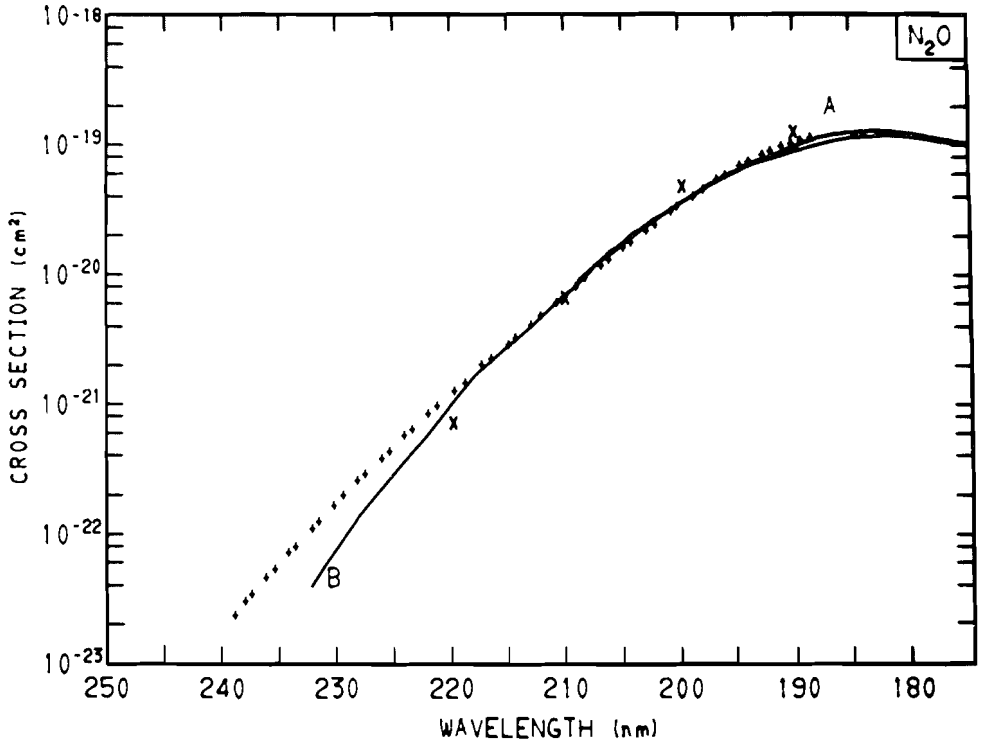

FIG. 5. Comparison of nitrous oxide cross section data, 175 to 250 nm; *A* and *B*, Romand and Mayence (29); +, Thompson *et al.* (22); ×, Holliday and Reuben (30).

where there is strong band structure, the agreement is within the respective experimental errors.

Nitrous Oxide, N_2O

This molecule has been studied by four groups in the region of interest. Romand and Mayence (29) performed measurements between 160 and 210 nm; Thompson *et al.* (22) between 185 and 240 nm; Holliday and Reuben (30) between 190 and 280 nm; and Zelikoff *et al.* (31) between 108 and 210 nm. A comparison of the data from these four groups obtained at room temperature is shown in Fig. 5. In general, the agreement is good, and within the experimental error of the respective groups. The data of Thompson *et al.* (22) does differ from the others above 220 nm, and it is felt that the data of Romand and Mayence (29) is to be preferred.

The cross section for nitrous oxide is also temperature dependent. This dependence has been measured by Romand and Mayence (29) and by Holliday and Reuben (30), and where the data can be compared the agreement is good. Curves illustrating the temperature dependence are given in Fig. 6.

Nitric Acid, HNO_3

Cross sections for nitric acid have been measured by Johnson and Graham (32), who covered the spectral range from 175 to 300 nm, and by Schmidt *et al.* (33), who covered the spectral range from 160 to 440 nm. The latter work, however, is labeled as preliminary, and could be subject to large errors due to corrections to the original data for NO_2 and N_2O_4 present in the nitric acid vapor. A comparison of the two sets of data between 180 and 320 nm is given in Fig. 7.

Ammonia, NH_3

The absorption cross section of ammonia has been measured between 160 and 230 nm by Tannenbaum *et al.* (34) and by Thompson *et al.* (22). In this wavelength region the absorption spectrum of ammonia consists of strong band structure overlying an apparent continuum,

Can. J. Chem. Downloaded from www.nrcresearchpress.com by 210.87.254.42 on 09/05/12
For personal use only.

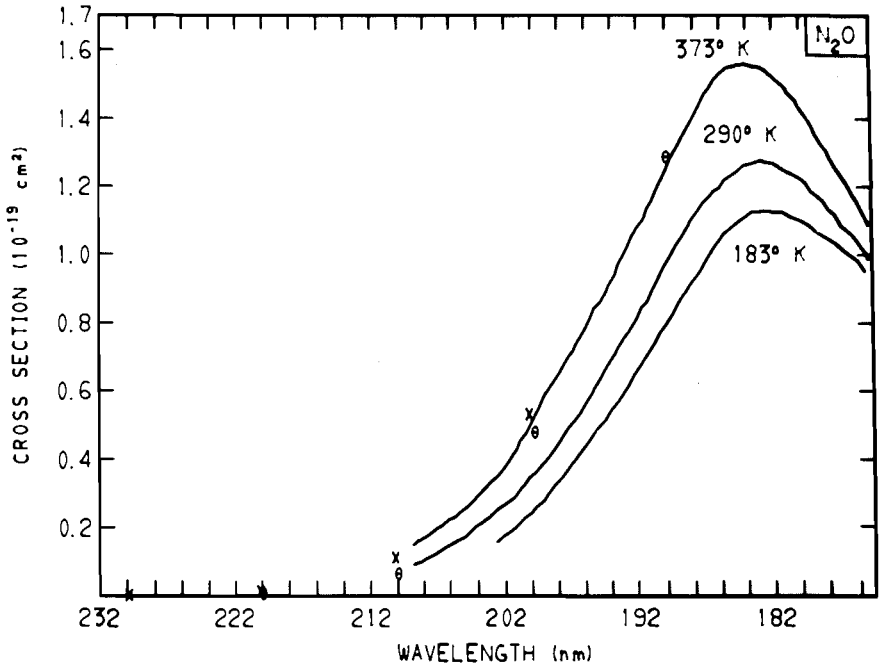

FIG. 6. Temperature dependence of nitrous oxide cross sections, 175 to 210 nm; —, Romand and Mayence (29); ○ and ×, Holliday and Reuben (30).

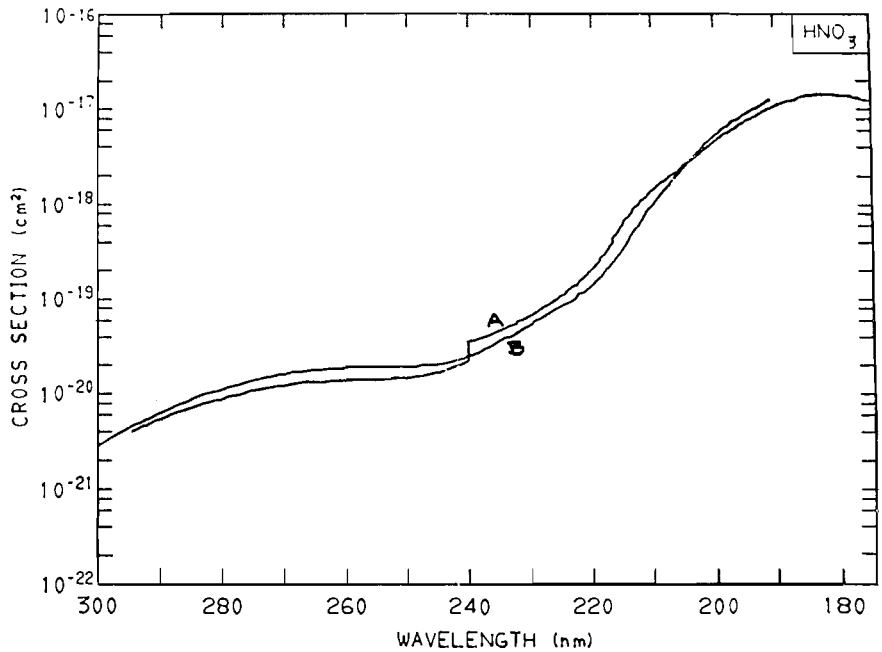

FIG. 7. Comparison of nitric acid cross section data, 180 to 300 nm; *A*, Schmidt *et al.* (33); *B*, Johnston and Graham (32).

Can. J. Chem. Downloaded from www.nrcresearchpress.com by 210.87.254.42 on 09/05/12
For personal use only.

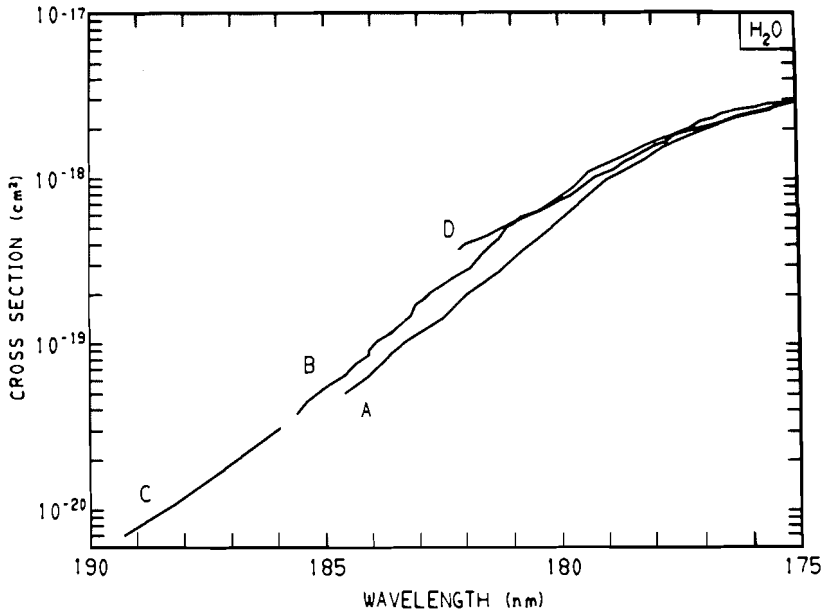

FIG. 8. Comparison of water vapor cross section data, 175 to 190 nm; *A*, Laufer and McNesby (36); *B*, Watanabe and Zelikoff (35); *C*, Thompson *et al.*(22); *D*, Schurgers and Welge (37).

although this continuum could be the result of band overlap. Both groups report the measured cross sections to be bandwidth dependent, and that the total cross sections have essentially fallen to zero by 230 nm. It is felt that the data should be considered qualitative at best.

Water Vapor, H_2O

Water vapor has a continuous spectrum between 175 and 190 nm, the cross section falling off rapidly toward longer wavelengths. Four measurements have been made in this wavelength region; Watanabe and Zelikoff (35), Laufer and McNesby (36), Thompson *et al.* (22), and Schurgers and Welge (37). A comparison of the results of these four measurements is given in Fig. 8. There is considerable scatter in the data, but it would appear that a smooth curve could be drawn through the data of Schurgers and Welge (37), Watanabe and Zelikoff (35), and Thompson *et al.* (22).

Hydrogen Peroxide, H_2O_2

Two measurements of the cross section for this molecule are available in the spectral range 175 to 230 nm; Holt *et al.* (38) and Schurgers and Welge (37). A comparison of the data from these two groups is given in Fig. 9. The region of overlap for these two sets of data is small, and within this region the argeement is not good. Holt *et al.* (38) did not use a vacuum monochromator; their instrument was equipped with the means for circulating nitrogen in the optical path. This equipment was designed to avoid the difficulty of absorption by molecular oxygen in the light path, and the sudden rise in the data near 200 nm could indicate that the system did not work adequately. For this reason it is felt that for wavelengths below 200 nm the data of Schurgers and Welge (37) is to be preferred.

Carbon Monoxide, CO

Only one measurement of the absorption cross section for carbon monoxide has been made at wavelengths above 175 nm, namely, that by Thompson *et al.* (22). This region of the spectrum is characterized by strong, sharp band structure and the data of Thompson *et al.* (22) is subject to considerable bandwidth dependence. The data should be considered qualitative at best.

Carbon Dioxide, CO_2

Above 175 nm the absorption spectrum of carbon dioxide consists of a continuum that falls off rapidly with increasing wavelength; superimposed on this is a weak band structure. Measurements have been made in this region by Thompson *et al.* (22), Heimerl (39), and Ogawa (7). A comparison of these sets of measurements is given in Figs. 10 and 11. As the data of Ogawa (7)

Can. J. Chem. Downloaded from www.nrcresearchpress.com by 210.87.254.42 on 09/05/12
For personal use only.

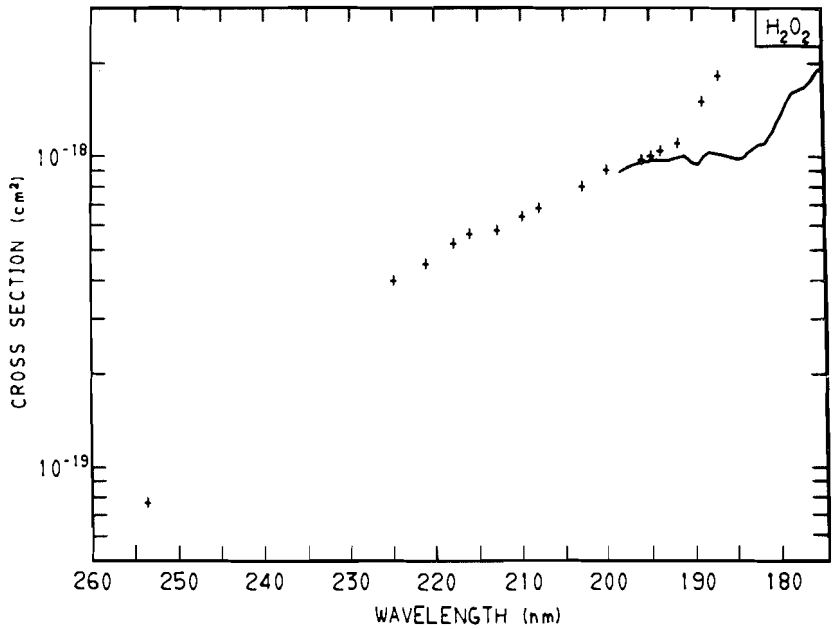

FIG. 9. Comparison of hydrogen peroxide cross section data, 175 to 260 nm; +, Holt *et al.* (38); —, Schurgers and Welge (37).

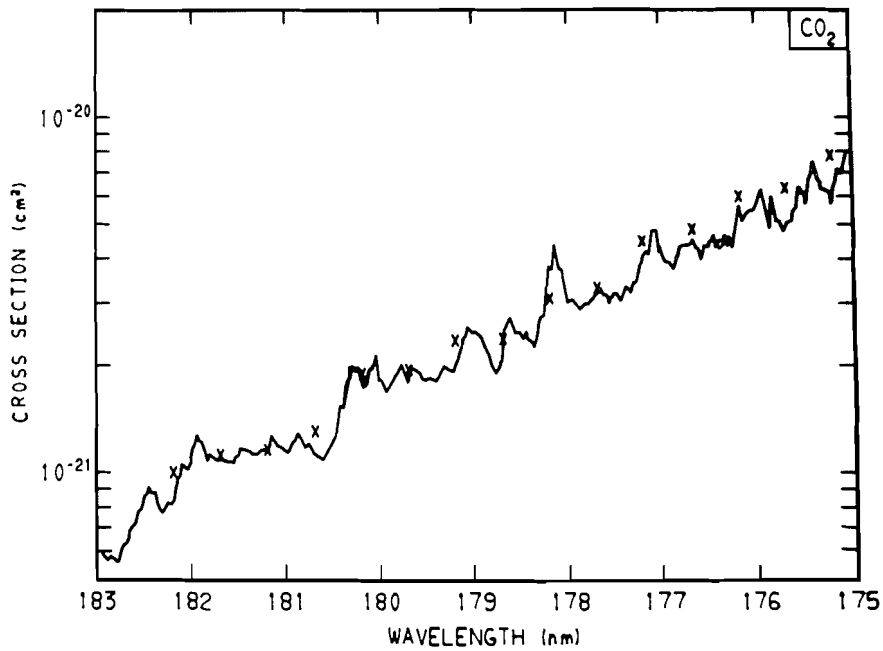

FIG. 10. Comparison of carbon dioxide cross section data, 175 to 183 nm; —, Ogawa (7); ×, Heimerl (38).

Can. J. Chem. Downloaded from www.nrcresearchpress.com by 210.87.254.42 on 09/05/12
For personal use only.

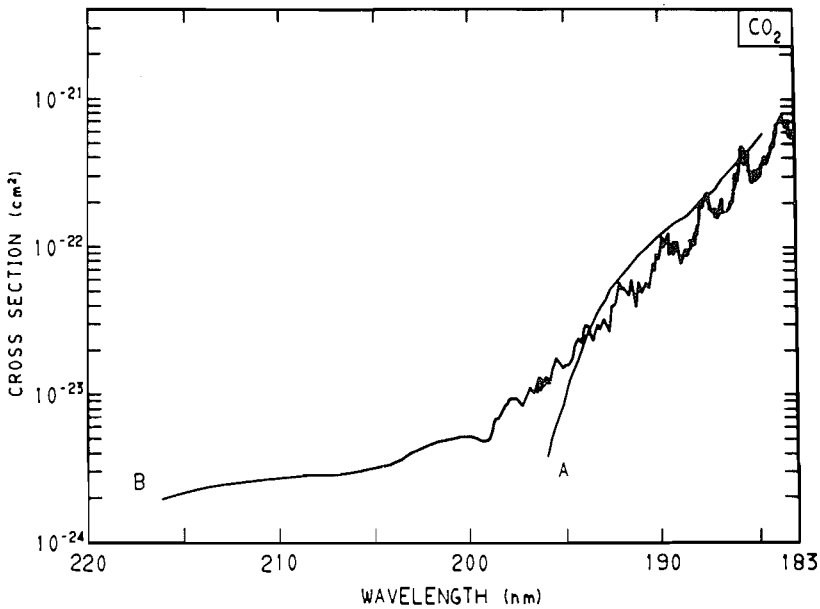

FIG. 11. Comparison of carbon dioxide cross section data, 183 to 215 nm; *A*, Thompson *et al.* (22); *B*, Ogawa(7).

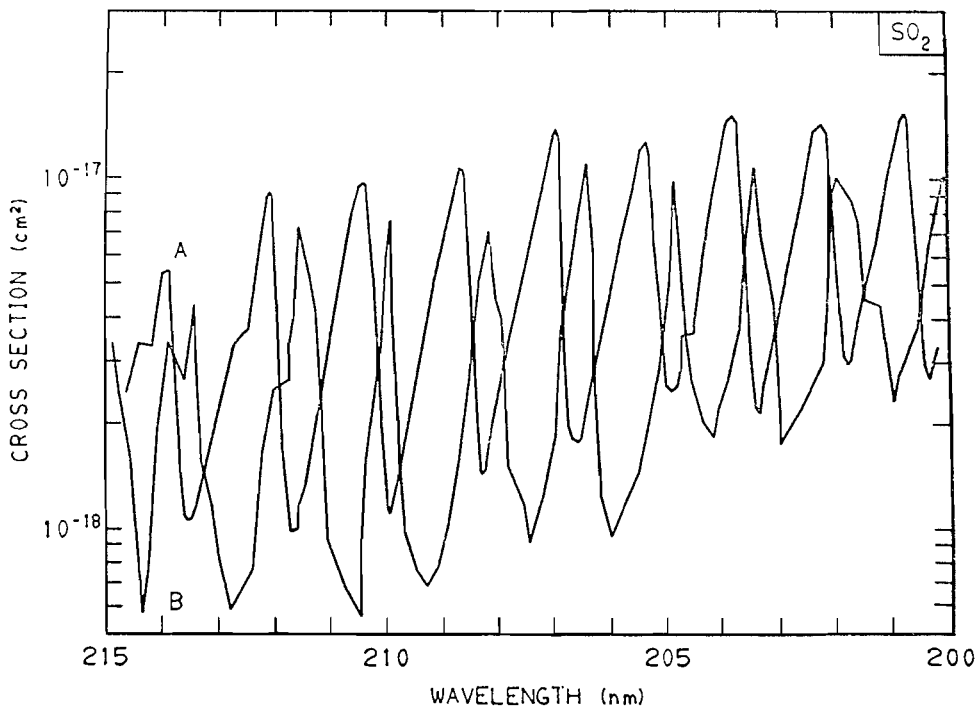

FIG. 12. Comparison of sulfur dioxide cross section data, 200 to 215 nm; *A*, Warnek *et al.* (40); *B*, Thompson *et al.* (22).

Can. J. Chem. Downloaded from www.nrcresearchpress.com by 210.87.254.42 on 09/05/12
For personal use only.

are continuous, and were obtained at high spectral resolution, they are to be preferred.

Sulfur Dioxide, SO_2

Measurements of the cross section of sulfur dioxide between 175 and 315 nm have been made by Warneck *et al.* (40), Golomb *et al.* (41), and by Thompson *et al.* (22). The data of Warneck *et al.* (40) and Golomb *et al.* (41) overlap over a narrow range and are self-consistent, coming from the same laboratory. The data of Thompson *et al.* (22), which covers the spectral range from 185 to 325 nm, differs markedly from the other two, both in the wavelength of the band structure that is observed and in the magnitude of the cross section. An example of this discrepancy is shown in Fig. 12. It is recommended that the data of Warneck *et al.* (40) and Golomb *et al.* (41) be used, with the proviso that the cross sections are probably bandwidth dependent.

1. H. S. JOHNSTON. Can. J. Chem. This issue.
2. K. H. WELGE. Can. J. Chem. This issue.
3. R. D. HUDSON. Rev. Geophys. Space Phys. **9**, 306 (1971).
4. M. ACKERMAN and F. BIAUMÉ. J. Mol. Spectrosc. **35**, 73 (1970).
5. R. D. HUDSON and S. H. MAHLE. J. Geophys. Res. **77**, 2902 (1972).
6. R. D. HUDSON, V. L. CARTER, and J. A. STEIN. J. Geophys. Res. **71**, 2295 (1966).
7. M. OGAWA. J. Chem. Phys. **54**, 2250 (1971).
8. M. ACKERMAN, F. BIAUMÉ, and G. KOCKARTS. Planet. Space Sci. **18**, 1639 (1970).
9. W. R. JARMAIN and R. W. NICHOLLS. Proc. Phys. Soc. Lond. **90**, 545 (1967).
10. A. C. ALLISON, A. DALGARNO, and N. W. PASACHOFF. Planet. Space Sci. **19**, 1463 (1971).
11. R. W. DITCHBURN and P. A. YOUNG. J. Atmos. Terr. Phys. **24**, 127 (1962).
12. A. J. BLAKE, J. H. CARVER, and G. N. HADDAD. J. Quart. Spectrosc. Radiat. Transfer, **6**, 451 (1966).
13. SHARDANAND. Phys. Rev. **186**, 5 (1969).
14. V. HASSON and R. W. NICHOLLS. J. Phys. B (At. Mol. Phys.), **4**, 1789 (1971).
15. E. C. Y. INN and Y. TANAKA. J. Opt. Soc. Am. **43**, 870 (1953).
16. M. GRIGGS. J. Chem. Phys. **49**, 857 (1968).
17. W. B. DEMORE and O. RAPER. J. Phys. Chem. **68**, 412 (1964).
18. A. G. HEARN. Proc. Phys. Soc. Lond. **78**, 932 (1961).
19. E. VIGROUX. Ann. Phys. **8**, 709 (1953).
20. Y. TANAKA, E. C. Y. INN, and K. WATANABE. J. Chem. Phys. **21**, 1651 (1953).
21. M. M. MARMO. J. Opt. Soc. Am. **43**, 1186 (1953).
22. B. A. THOMPSON, P. HARTECK, and R. R. REEVES. J. Geophys. Res. **68**, 6431 (1963).
23. K. DRESSLER and E. MEISCHER. Astrophys. J. **141**, 1266 (1965).
24. G. W. BETHKE. J. Chem. Phys. **31**, 662 (1959).
25. V. HASSON and R. W. NICHOLLS. J. Phys. B (At. Mol. Phys.), **4**, 1769 (1971).
26. T. NAKAYAMA, M. T. KITAMURA, and K. WATANABE. J. Chem. Phys. **30**, 1180 (1959).
27. T. C. HALL and F. E. BLACET. J. Chem. Phys. **20**, 1745 (1952).
28. A. M. BASS and A. H. LAUFER. Private communication.
29. J. ROMAND and J. MAYENCE. C. R. **228**, 998 (1949).
30. M. G. HOLLIDAY and B. G. REUBEN. Trans. Faraday Soc. **64**, 1735 (1968).
31. M. ZELIKOFF, K. WATANABE, and E. C. Y. INN. J. Chem. Phys. **21**, 1643 (1953).
32. H. JOHNSTON and R. GRAHAM. Private communication.
33. S. C. SCHMIDT, R. C. AMME, D. G. MURCRAY, and A. GOLDMAN. Nature Phys. Sci. **238**, 109 (1972).
34. E. TANNENBAUM, E. M. COFFIN, and A. J. HARRISON. J. Chem. Phys. **21**, 311 (1953).
35. K. WATANABE and M. ZELIKOFF. J. Opt. Soc. Am. **43**, 753 (1953).
36. A. H. LAUFER and J. R. MCNESBY. Can. J. Chem. **43**, 3487 (1965).
37. M. SCHURGERS and K. H. WELGE. Z. Naturforsch. **23**, 1508 (1968).
38. R. B. HOLT, C. K. MCLANE, and O. OLDENBERG. J. Chem. Phys. **16**, 225 (1948).
39. J. HEIMERL. J. Geophys. Res. **75**, 5574 (1970).
40. P. WARNECK, F. F. MARMO, and J. O. SULLIVAN. J. Chem. Phys. **40**, 1132 (1964).
41. D. GOLOMB, K. WATANABE, and F. F. MARMO. J. Chem. Phys. **36**, 958 (1962).

Can. J. Chem. Downloaded from www.nrcresearchpress.com by 210.87.254.42 on 09/05/12
For personal use only.

Stratospheric Aerosols Physicochemistry

J. BRICARD AND D. VIGLA

Laboratoire de Physique des Aerosols, Université de Paris VI, 11, Quai Saint-Bernard, Paris, France

Received October 3, 1973

The stratospheric aerosol layer, a few kilometers thick and centered a few kilometers above the tropopause, is currently believed to be composed of Aitken nuclei, composed principally of ammonium sulfate, and large particles greater than 1 μ; particles larger than 5 μ contain little sulfate and are believed to be of meteoritic origin.

With acceptance of the direct or indirect terrestrial origin of the stratospheric ammonium sulfate particles, three processes can be suggested for their occurrence in the stratosphere: (1) coagulation of stratospheric Aitken nuclei previously formed in the troposphere; (2) oxidation of SO_2 of terrestrial origin in the stratosphere to H_2SO_4 followed by nucleation and internal growth; and (3) reactions involving hydrous stratospheric ions such as $(H_3O)^+ . n(H_2O)$ which act as primary nuclei and facilitate reaction of gaseous constituents of terrestrial origin such as NH_3, O_2, and HCl.

La couche d'aérosol stratosphérique, épaisse de quelques kilomètres, centrée à quelques kilomètres au dessus de la tropopause, est couramment considérée comme étant composée de noyaux d'Aitken. Ceux-ci sont principalement composés de sulfate d'ammonium et de grosses particules plus grandes que 1 μ. Celles qui sont plus grandes que 5 μ contiennent un peu de sulfate et sont considérées comme étant d'origine météoritique.

En admettant l'origine terrestre directe ou indirecte des particules stratosphériques du sulfate d'ammonium, trois procédés peuvent être suggérés pour leur présence dans la stratosphère: (1) coagulation des noyaux stratosphériques d'Aitken préalablement formés dans la troposphère; (2) oxydation de SO_2, d'origine terrestre, dans la stratosphère, en H_2SO_4 suivie de production de germes et de croissance interne; (3) réactions faisant intervenir des ions stratosphériques hydratés tels que $(H_3O)^+ . n(H_2O)$ qui agissent comme noyaux initiaux et facilitent la réaction de constituants gazeux, d'origine terrestre, tels que NH_3, O_2 et HCl.

[Traduit par le journal]

Can. J. Chem., **52**, 1479 (1974)

I. Introduction

A few kilometers above the tropopause, there exists a highly structured layer of particles, several kilometers thick. Its existence has been established by studying from Earth the light scattered from the twilight sky, and verified by observing the light spread by search-lights or by alitude laser echo probing (lidar). These remote sensing techniques, reviewed by Rosen (1), allow detection of particles with diameters larger than 0.1 μ only, but do not allow the determination of the ambient particle size distribution. However, they are interesting for the discussion of the results of *in situ* samplings to be presented below.

Two recent remote sensing methods have supplied information on the stratospheric aerosol layer. Philipowsky *et al.* (2) determined the layer profile by a lidar ($\lambda = 0.694$ μ) and simultaneously measured in altitude the layer radiation in the i.r. spectrum ($3\ \mu < \lambda < 100\ \mu$). Calculations, employing the size distribution function of the particles of radius $R > 0.1$ μ in the layer obtained by direct measurements, showed that the radiated intensity values, between 3 and 100 μ, derived from both these data and the profile values supplied by the lidar, did not agree with the measurements unless a large population of particles <0.1 μ was assumed in the particle size distribution.

De Barry and Rössler (3), using rocket probing, measured the scattered radiation from the daytime sky simultaneously under two different angles and with two different wavelengths. The results of these measurements also imply an important concentration of particles less than 0.1 μ in diameter.

These important results will be examined later. We shall now discuss *in situ* sampling methods and examine the results.

Can. J. Chem. Downloaded from www.nrcresearchpress.com by 210.87.254.105 on 09/05/12
For personal use only.

Can. J. Chem. Downloaded from www.nrcresearchpress.com by 210.87.254.105 on 09/05/12
For personal use only.

II. Methods of *in situ* Sampling

1. Direct Determination of Aitken Nuclei Concentration

The air sample containing the particles to be studied is introduced into a chamber saturated with vapor (usually water) and the mixture is cooled by adiabatic expansion until supersaturation is sufficient for the particles to act as condensation nuclei. Each nucleus is thus carrying a water droplet and becomes visible, and a cloud is obtained in the expanding chamber with droplets with radii of several microns at atmospheric pressure. Using this method, all suspended particles with radii larger than 0.001 μ can be detected and counted in a known volume, but the particle sizes cannot be determined. The optical counting methods used in in stratospheric measurements by Junge *et al.* (4) will not be described here.

The difficulties met when using these techniques in the stratosphere are mainly losses of the droplets formed on the nuclei by later evaporation, and losses by diffusion of the droplets in pipes and taps. A decrease in the radii of the droplets formed on the nuclei at ambient (air) pressure, for a given supersaturation value (this effect remains unexplained so far (Schlarb effect)), entails a decrease of the scattered or absorbed light beam and therefore a noticeable counting loss. It should be noted that for stratospheric conditions, the particle diffusion coefficient is at least 10 times as large as it would be at normal pressure, and even at normal pressure losses by diffusion might be important in condensation nuclei counters. However, a correction coefficient allowing for all these errors can be determined.

Figure 1, taken from Junge *et al.* (4), is an example of the data obtained using this method. The main result is that there is a slow unsteady decrease to 100/cm^3 in the troposphere and a sharper decrease down to a value of a few particles/cm^3 at 5 km above the tropopause, the values being referred to ambient pressure. Only Junge *et al.* have carried out their measurements by this method; on the other hand, the remote sensing measurements by Philipowsky *et al.* (2) and De Barry and Rössler (3) suggested large concentrations of particles with radii below 0.1 μ. These results are inconsistent with Junge's direct measurements and further direct measurements should be carried out.

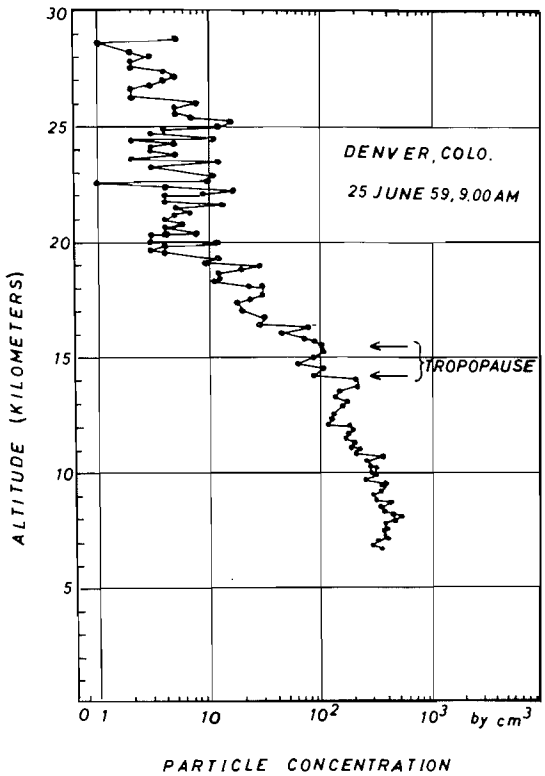

FIG. 1. Measured vertical profiles of Aitken nuclei (Published with the permission of Journal of Meterology.)

A new method for direct counting nuclei has been developed by Bricard *et al.* (5). A nuclei loaded air draught was sent through a methyl alcohol saturated chamber and chilled through a pipe maintained at the right temperature until supersaturation was enough for alcohol to condense on the condensation nuclei. Thanks to an optical device similar to Rosen's (18), the droplets formed on the nuclei contained in the air draught flowing out of the nozzle could be counted one by one. This device allows continuous counting and decreases diffusion losses, but has not yet been tried in the stratosphere.

2. Particles with Radii over 0.1 μ

The particles are collected on an adequate impaction surface and then observed with an electron microscope for size distribution. It is assumed that no particles with radii below 0.1 μ are collected. In fact, both the threshold, 0.1 μ, and the collection efficiencies were not clearly established in every case.

The following collecting techniques have been

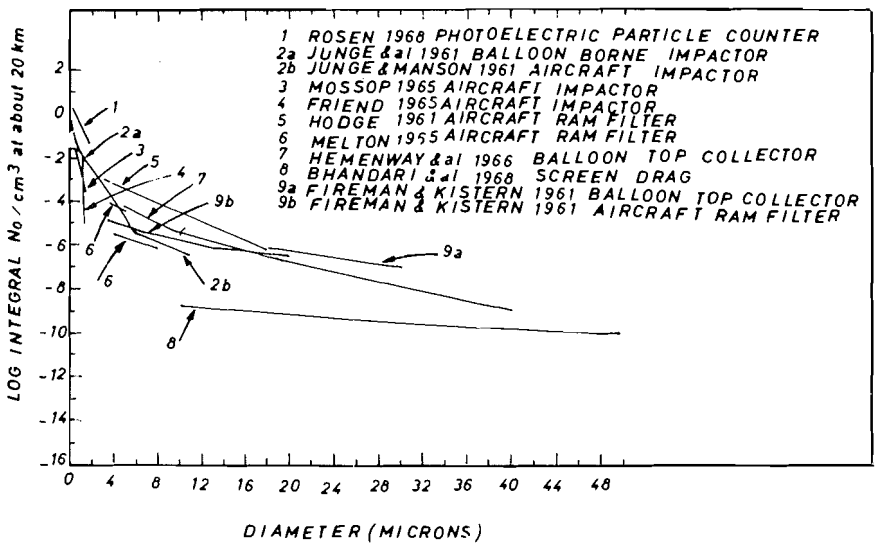

FIG. 2. Comparison of the results obtained by direct dust sampling methods. (Published with the permission of Space Science Reviews.)

used: (*i*) filtration, stratospheric air is sent through a filter flown on aircraft (7–9); (ii) impaction, using a collector on aircraft perpendicular to the air draught (10–12) or drawing the air through an appropriate impactor carried by balloons (13, 14); (*iii*) sedimentation on a horizontal plate exposed to the fall of the stratospheric aerosol (15, 16) or by hauling a balloon-borne plate (17); (*iv*) Rosen's photoelectric method (18) in which the particles with radii above 0.1 μ suspended in an air draught were counted and measured one by one in the light against a dark background.

(*a*) Figure 2, taken from Rosen, represents a comparison between the results thus obtained. All the samples had been taken in the stratosphere but not all at the same altitude. A slight correction was applied to the samples not taken at 20 km. In spite of the wide spread of the results due to uncertainty of accuracy in the measurements and mainly in collection, a discontinuity appears in the particle size distribution around $R = 5\ \mu$; this allows the particles to be divided into two size classes.

Using the average values given by these distributions, Rosen estimated the mass concentration of smaller particles at 10^{-13} g cm^{-3} of ambient air and that of larger particles at 3.10^{-14} g cm^{-3}.

For smaller particles ($R < 5\ \mu$) two different types of size distribution functions were found. According to Junge and Manson (10) concentration should be a continuously decreasing function of the particle radii, of the form

$$\frac{d\eta}{d \log R} = CR^{-2}$$

in the range $0.1\ \mu < R < 1\ \mu$.

These results are presented in Fig. 3, curve *A* (from Friend), the confidence limits resulting from uncertainty in the measurements being presented by curves *A'*. Friend's results are presented in the same figure (curves *B*); the confidence limits due to uncertainty are introduced in curves *B'*, corresponding to curves *A'*. It can be seen that Friend's curves emphasize a peak concentration around 0.3 μ; this does not appear in Junge's results, and that discrepancy between Friend and Junge is mainly manifest in the size range $R < 0.2\ \mu$. Friend's concentrations range between 0.012 and 0.069 particles/cm^3, the mass concentration varying between 5.0×10^{-2} and 2.6×10^{-3} pg/cm^3 using a particle density of 2 g/cm^3. It should be noted that the mass concentration peaks do not correspond to the largest radii.

Friend's measurements were in good agreement with Mossop's previous results (11) which report a peak for $R = 0.35\ \mu$ and particle concentrations between 0.017 and 0.042 cm^{-3}.

(*b*) Figure 4, from Junge *et al.* (4), shows an example of the variations of the concentration

Can. J. Chem. Downloaded from www.nrcresearchpress.com by 210.87.254.105 on 09/05/12
For personal use only.

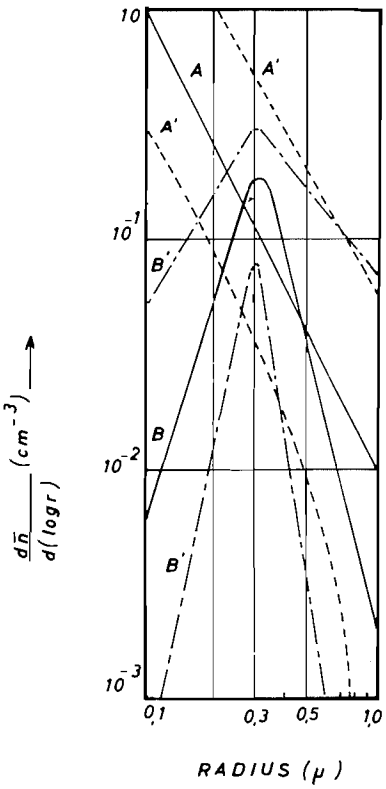

FIG. 3. Comparison of particle size concentration distributions of stratospheric sulfate particles. Curve *A*: Junge *et al.*; curve *B*: Friend. (Published with the permission of Tellus.) Curve *A'*: Curve *B'*: confidence limits of curve *A*, curve *B*.

of the particles with radii larger than about 0.1 μ, as a function of altitude, resulting in a peak at about 20 km. It is, however, difficult to distinguish these variations clearly since with impaction methods, especially, the collecting threshold (radius of the smallest particle collected) is not clearly established and varies with pressure, both concentration and size distribution remaining unchanged. An increase of apparent concentrations with increasing altitudes should result. The importance of the concentration peak can therefore be subject to uncertainty but the concentration decrease with altitude cannot.

Figure 5, from Rosen (1), represents the vertical concentration of aerosol with radii over 0.1 μ at three different latitudes. It showed a peak concentration a few kilometers above the tropopause, in agreement with Fig. 4. It is noteworthy that the variation of size distribution with altitude has not been investigated thoroughly, and this may explain the differences observed in the lower stratosphere – peak concentration (Junge, Friend, Mossop) and maximum diameter (19). In fact, Fig. 6 from Bigg shows the lack of a peak concentration of particles as a function of altitude, the low increase observed being at least partly due to variation in collection efficiencies as a function of pressure. Each flight is represented by a point. Rough limits of concentrations are indicated by the shaded region.

3. Physical Characteristics of the Particles

An important fact obtained from Friend's, Mossop's, and Bigg's investigations is that because of the moisture content of the particles when collected, the evaporation residues are smaller in size than the real particles. According to Mossop and Friend this should explain their disagreement with Junge concerning size distribution. Rosen also noticed a particle size decrease when the temperature of the air draught was raised before it entered the photoelectric counter. Another important fact noticed by Bigg, Friend, and Mossop was the existence in most particles of a solid nucleus; this will be discussed in Section III.2.

The recent observations of Bigg and Thompson (19), using an aircraft flying at altitudes between 20 and 37 km, illustrate the difficulty in interpreting the sample data. The collection method was based on that of the Rantz and Wong cascade impactor (20) the particles being fixed on an electron microscope grid, a method widely used by investigators since Junge; collection efficiency was deemed to be in the range of 50% for 0.05 μ particles at 20 km. The collected particles could be distributed into three classes: (*i*) central particle surrounded by a circular group of smaller discrete satellites; (*ii*) central particles surrounded by a nearly circular ring or stain without discrete satellites; (*iii*) simple particles without ring, stain, or satellites.

Owing to this diversified classification, uncertainty in the methods, and above all on collection efficiencies, particle size distribution is quite difficult to obtain.

III. Chemical Composition of the Particles

1. Method

Up to now the chemical composition of the stratospheric aerosol has been determined by analyzing the filter or impactor samples. Accord-

Can. J. Chem. Downloaded from www.nrcresearchpress.com by 210.87.254.105 on 09/05/12
For personal use only.

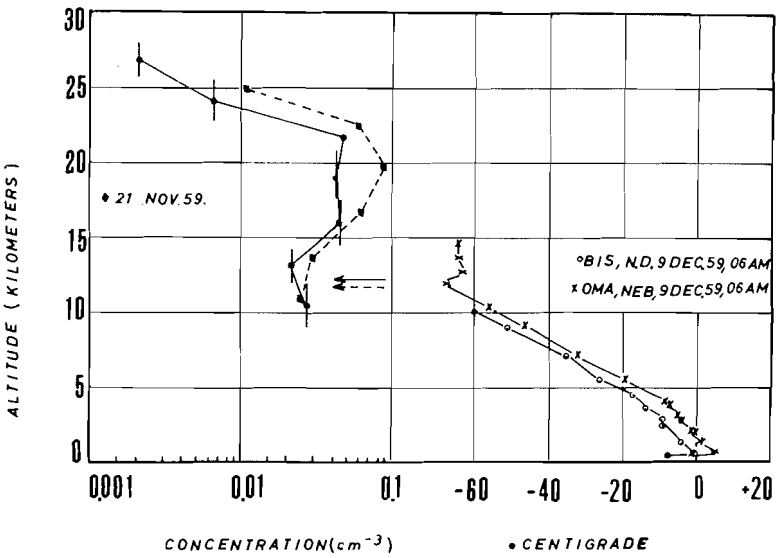

FIG. 4. Vertical profile of particles collected with impactor and the available temperature soundings closest in time and space. The vertical bars indicate the altitude interval over which the sample was collected. (Published with the permission of Journal of Meteorology.)

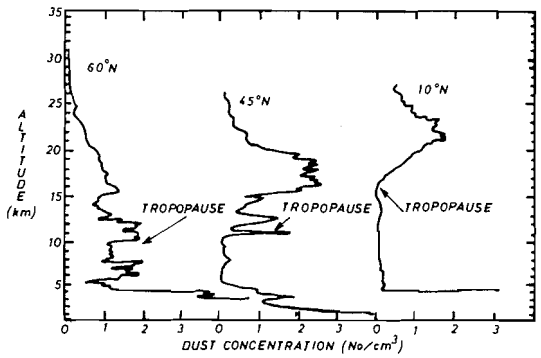

FIG. 5. Vertical distribution of dust at three latitudes determined by the photoelectric particle counter. (Published with the permission of Journal of Geophysical Research.)

ing to the investigators, several methods have been used: wet chemical analysis, electron microprobe analysis, neutron activation analysis, and electron microscope analysis (observation and diffraction).

It should be noted that since the amounts for analysis are very small, the filter and impactor surfaces must be free of any contaminants. As to the capacity of retention or absorption of minor constituents to be found in the stratosphere, Cadle (21) has shown the different behavior of polystyrene filters and impregnated cellulose fibers against NO_3^- and silicon; results showed that little or no nitrate was found on the polystyrene filters and impregnated filters lowered silicon concentrations.

2. *Results*

It has been generally observed (4, 10, 12, 21, 22) that sulfate was the main constituent of the aerosol; since its concentration varies widely with the samples, differences cannot be due to the use of different methods. There is no significant gradient in sulfate concentration between the tropical and temperate stratosphere along the slope of the layer (21). Yet a decrease in absolute concentration of several constituents was noticed by Cadle between 1969–1971, as shown by *in situ* results in Table 1, and verified by lidar measurements carried out during that period.

Nevertheless, the average concentration expressed in SO_4^{2-} equivalents can be considered to be in the range of 0.1 μg/m³ of ambient air. The values found by Junge were lower, but Cadle, by means of both impactors and filters, noticed that the former method supplied results lower by a factor of 5 than the latter method. The difference might be due to the fact that unlike filters, impactors are inefficient for collecting Aitken nuclei.

Sulfur was mainly found as SO_4^{2-}, the ammonium sulfate or the sulfuric acid being recognized by electron microscopy (11, 12, 19). It

Can. J. Chem. Downloaded from www.nrcresearchpress.com by 210.87.254.105 on 09/05/12
For personal use only.

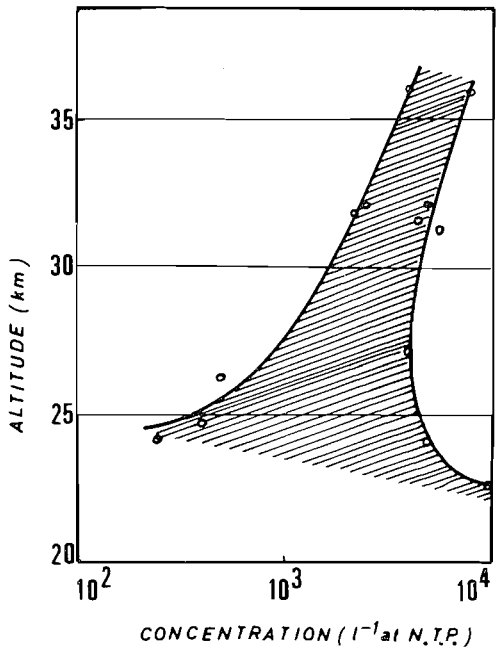

FIG. 6. Particle concentrations *vs.* altitude determined by particle collection. Each flight is represented by a point. (Published with the permission of Tellus.)

TABLE 1.

Date	SO_4^{2-} (μg^{-3})	NH^4 (μg^{-3})	NO^{3-} (μg^{-3})
5.11.70	0.20	0.0033	0.36
10.07.70	0.10	0.0025	0.12
2.03.71	0.10	0.0000	0.20
2.08.71	0.028	0.0027	0.027

should be noted that the H_2SO_4–H_2O mixture presents a eutectic point at $-72\,^{\circ}C$ for a 38% weight H_2SO_4 composition (44) (see the observation of liquid part in most particles, as noted in Section II.2*b*). Persulfate was also found by Friend. It must be noted that during laboratory experiments in tropospheric conditions, Bourbigot *et al.* (23) demonstrated the formation of nitrosyl hydrogen sulfate particles, which might also occur in stratospheric conditions.

According to Junge's studies the $[NH_4^+]/[SO_4^{2-}]$ concentration ratio was between 1 and 2, hence the assumption of ammonium sulfate as the main constituent of the stratospheric aerosol; recent sampling by Friend and by Cadle have shown that the ratio was lower. Besides the changes with time in the stratospheric aerosol composition (which can be compared to physical changes), the efficiency of the collecting method may play a great part. Thus, it should be possible to assume that the particles are different according to size distribution, the smaller being made of sulfuric acid, the bigger of ammonium sulfate.

Cadle (21) has also determined NO_3^- concentrations (Table 1), but the high concentrations obtained, $[NO_3^-]/[SO_4^{2-}]$ reaching a value of 6, might result from the nature of filters (impregnated filters) which should retain nitric acid vapors. As to the [Cl]/[Br] ratio, it was found by Cadle to be between 12 and 19, a value much lower than that found by Duce (55) (about 100 for aerosols collected near the sea surface).

By carrying out dialysis of aerosols deposited on a membrane, Mossop (11) has demonstrated that one or more insoluble nuclei exist in most collected particles. Several authors (1) have investigated which aerosols could be considered of cosmic origin. The highest content is 10% of the total mass of the stratospheric aerosol. Such a low proportion does not prevent these constituents from playing a large part in nucleation (see next Section).

IV. Mechanisms Resulting in a Condensed Phase

In the paragraph on the chemical composition of stratospheric aerosols, a number of constituents have been listed. We shall now give some schemes of chemical transformations likely to lead to the production of some of these constituents.

1. Metal Compounds

According to Gadsden (24) meteorites volatilized on their entry into the atmosphere may originate a layer containing metal ions at about 93 km altitude. According to the meteorite type, different proportions of ions, aluminum, nickel, and silicon compounds, are to be expected. Besides the part of metal vapor to be found as ions, the remaining part might react quickly to give stable oxides such as Fe_2O_3, FeO, Al_2O_3, according to the type of reaction

$$MX + \tfrac{1}{2}nO_2 \rightarrow MO_x(\text{gas}) + \ldots$$

where MX = metal compound.

If the oxides are formed quickly enough for the supersaturation reached to exceed critical supersaturation in spite of diffusion, then metal oxide aerosols will be formed. It should be

Can. J. Chem. Downloaded from www.nrcresearchpress.com by 210.87.254.105 on 09/05/12
For personal use only.

TABLE 2. Comparison of some SO_2 photochemical reaction rate studies

Reference	Initial $[SO_2]$	Relative humidity (%)	Rate of SO_2 consumption (% min^{-1})
Gerhard and Johnstone (28)	5–30 p.p.m.	32–91	$(1.7–3.3) \times 10^{-3}$
Renzetti and Doyle (57)	0.2–0.6 p.p.m.	50	0.11
Urone and Schroder (29)	10–20 p.p.m.	50	1.4×10^{-3}
Hall (56)	$[SO_2]$ = 56–230 mm Hg $[O_2]$ = 5–200 mm Hg	0	8×10^{-4}
Urone and Schroder (29)	1000 p.p.m.	0	3.9×10^{-4}
		50	4.6×10^{-4}
Bricard (35)	0.2 p.p.m.	0–90	10^{-4} to 7×10^{-4}*

*Values not adjusted to noonday sunlight.

noted that part of the metal ions thus created will neutralize to metal atoms which can then be oxidized by ozone (25).

2. Sulfur Dioxide Transformation

Sulfates are major constituents of both tropospheric and stratospheric aerosols and result mainly from the oxidation of SO_2 and perhaps H_2S, both of tropospheric origin. First oxidation of SO_2 into SO_3 occurs according to different mechanisms.

(a) Oxidation by Atomic Oxygen

Oxidation by atomic oxygen takes place according to the reaction

$$SO_2 + O + M \rightarrow SO_3 + M$$

M being the third body.

Mulcahy *et al.* (26) state a reaction rate constant of 7.4×10^{-33} $cm^6/molecule^2$ s.

*(b) Photochemical Transformation of SO_2 into SO_2**

Photochemical transformation of SO_2 into SO_2* (excited state) occurs by radiation absorption followed by oxidation by molecular oxygen. This mechanism first suggested by Blacet (27) has been further investigated by Gerhard and Johnstone (28), Urone and Schroder (29), Buffalini (30), Sidebottom *et al.* (31), and Allen *et al.* (32).

(c) SO_2 Reaction with Excited Oxygen

A proportion of oxygen molecules are to be found in an excited state either by energy transfer of other molecules or by radiation absorption. In this case the reaction

$$SO_2 + O_2*$$

may lead to the same kind of substances as the reaction in (*b*).

(d) Radical Oxidation

Investigations on stratospheric chemistry have also demonstrated the importance of radicals such as HO_2, and reactions such as

$$SO_2 + HO_2 \rightarrow SO_3 + OH$$

are likely to occur.

3. Results and Comparison of the Mechanism

The results of several investigators are listed in Table 2 (with respect to SO_2 conversion rate). The conditions of investigation explain the discrepancy of the results (which are often difficult to compare when the conditions are not well determined). Most quantitative studies have been made with large concentrations of SO_2, which makes extrapolation to the case of the atmosphere unreliable.

A comparison between mechanisms (*a*) and (*b*) has been made by Friend (33). If R_A and R_B be SO_3 production rates according to (*a*) and (*b*) respectively, then

$$R_A = \frac{d[SO_3]}{dt} = -\frac{d[SO_2]}{dt}$$

$$= k_A[SO_2][O][M]$$

In the stratosphere, the concentration of oxygen atoms is mainly determined by equilibrium between the two reactions

$$O_3 + h\nu \rightarrow O_2 + O$$

and

$$O_2 + O + M \rightarrow O_3$$

At the altitude we are interested in (20 km), Johnston's estimates are $[O] = 1.4 \times 10^5$, $[M] = 1.8 \times 10^{18}$ and hence $R_A \simeq 6.7 \times 10^{-10}[SO_2]$.

On the other hand

Can. J. Chem. Downloaded from www.nrcresearchpress.com by 210.87.254.105 on 09/05/12
For personal use only.

$$R_B = \frac{d[SO_4]}{dt} = \frac{d[SO_2]}{dt} = \Phi K_a[SO_2]$$

where Φ is the quantum yield and K_a the specific absorption rate equal to the product of irradiation by the absorption coefficient for the wavelength considered.

At 20 km, $K_A = 2.5 \times 10^{-3}$ (34). The value of Φ is estimated by Friend at 10^{-9}. Thus the ratio $R_A/R_B = 250$. Oxidation by atomic oxygen is therefore prevalent in sulfur dioxide photooxidation.

The value of Φ used in this estimate is considerably lower than values supplied by other investigators so far, hence the method leading to this result will now be discussed.

The number of condensation nuclei was compared during two experiments. In the former experiment, the irradiation spectrum was 2200–5000 Å, and in the latter one 2500–4000 Å. Because of this difference in irradiation, atomic oxygen was formed in much larger concentration in the former than in the latter. Now, in the latter experiment, there were no detectable condensation nuclei to verify the experimental results of Bricard *et al.* (35), whereas irradiation in the 2200–5000 Å range resulted in a large number of condensation nuclei. If one assumes that condensation nuclei are indicators of the transformation $SO_2 \rightarrow H_2SO_4$, then the value estimated for the sulfur dioxide change according to mechanism (*a*) is much higher than for (*b*).

4. Ionic Reactions Leading to Aggregate Formation

In the lower atmosphere small ions formed by irradiation are mainly found as oxonium ions. They grow larger with time and change according to the different gaseous impurities in the atmosphere. Because of the concentration of these ions *vs.* neutral particles in the lower troposphere they are quickly trapped and play a negligible part in the gas–aerosol conversion. Since the ionic concentration is rather high (47) in the stratosphere, the case might be quite different. With this assumption, fast ionic mechanisms might play an important part.

Coffey and Mohnen especially (37, 38) have demonstrated that oxonium ions reacted with ammonia traces according to

$$H_3O^+(H_2O)_n + NH_3 + M \rightarrow NH_4^+(H_2O)_{n+1} + M$$

Such ions can lead to "explosive" reactions, especially with nitric acid vapors

$$NH_4^+(H_2O)_m + 4NO_3 \rightarrow NH_3NO_3(H_2O)_n + H_3O^+(H_2O)_{m-n}$$

and with hydrogen chloride

$$NH_4^+(H_2O)_m + HCl \rightarrow NH_4Cl(H_2O)_n + H_3O^+(H_2O)_{m-n}$$

5. Addition Reactions

Some authors (37, 38) have noted that direct reactions are likely to occur between NH_3 and SO_2 and give a polymer of the form $(NH_3)_2$-$(SO_2)_n$. However, with their experimental conditions, Bricard *et al.* (39) and Friend (33) have found that ammonia did not lead to the formation of new particles; in Bricard's experiment aerosol concentrations which originated from photolysis of air enriched with sulfur dioxide were much larger.

After their formation $NH_4^+HSO_4^-$ embryos should fix NH_3 and form saline embryos according to the reactions

$$NH_3 + H_2SO_4.nH_2O \rightarrow NH_4^+HSO_4^-.nH_2O$$

$$NH_3 + NH_4HSO_4.nH_2O \rightarrow (NH_4)_2SO_4.nH_2O$$

$$2SO_2 + 2H_2O + O_2 \xrightarrow[NH_4^+]{\text{embryo}} 2H_2SO_4 \text{ (solution)}$$

The products of the first two reactions are saline embryos; they constitute a medium leading to catalytic oxidation of SO_2. Particle development is continuous as long as NH_3 is fixed and can neutralize the acid resulting from catalytic oxidation and SO_2 is fixed by the particle. This process should explain the origin of sulfate particles with radii larger than 0.1 μ by condensation either on Aitken nuclei of tropospheric origin or Mossop insoluble particles, or by homogeneous nucleation (33).

These fragmental results must be verified before being extended to the stratosphere.

V. Origin of the Stratospheric Aerosol

Since few experiments and samplings have been carried out up to now, the present investigations have only led to more or less reliable assumptions. However, it can be admitted that condensation nuclei (particles with radii smaller than 0.1 μ) have a tropospheric origin and particles with large radii (about 5 μ) have a meteoric origin. It remains to explain the kinetics of the middle-sized particles (from 0.1 to 5 μ). The kinetics, of course, will depend on the assump-

Can. J. Chem. Downloaded from www.nrcresearchpress.com by 210.87.254.105 on 09/05/12
For personal use only.

Can. J. Chem. Downloaded from www.nrcresearchpress.com by 210.87.254.105 on 09/05/12
For personal use only.

tion made about their origins, either stratospheric or tropospheric.

1. Stratospheric Origin

This is the assumption most generally made. It has been noted above that, in most cases, average-sized aerosols were made of sulfur, either as sulfates or sulfuric acid, which should result from *in situ* oxidation by atomic oxygen of SO_2 of tropospheric origin. Experiments we have conducted in tropospheric conditions (35) have shown that the other mechanisms in which direct SO_2 photooxidation occurred hardly contributed to aerosol formation. These results have been extended to the lower stratosphere by Friend (33).

One may assume homogeneous nucleation, *i.e.* direct formation of sulfuric acid particles from the vapor originated *in situ*. It can also be assumed that the sulfuric acid formed *in situ* is condensed on the condensation nuclei discovered by Junge or on the insoluble particles found by Mossop, Bigg, and Friend in sulfate particles. The latter assumption would be consistent with Rosen's results (6) and interpretation. Thus, according to Rosen, the mixing ratio (ratio of the total concentration of the stratospheric aerosols to the corresponding concentration of the air molecules) should be roughly constant as a function of altitude in the stratosphere, but this could occur only if the particle source was above and not below the stratosphere. This led him to ascribe an extra-terrestrial origin, *i.e.* above an altitude of 85 km, to the insoluble nuclei found in all the sulfate particles and thus to all stratospheric particles.

Theoretically, investigations of the kinetics of phase changes in one-body systems have led to satisfying results (53, 54). Nucleation rates can thus be evaluated as a function of ΔG, the reversible operation required in order to produce an embryo of such a size as to be in equilibrium with the mother phase. This would lead to important supersaturations (of several unities) in order to obtain noticeable nucleation rates. The nucleation theory has been taken up by Flood (48) and Reiss (49) in the case of several-body systems (heteromolecular condensation). It has been applied by Doyle (42) to the water – sulfuric acid mixture and his results have been lately developed by Kiang and Stauffer (43), who have specially studied the part played by relative moisture on nucleation rates.

The few data presently available on the composition of stratospheric aerosol have been listed above. In order to discuss the likely mechanism occurring in the *in situ* formation of sulfuric acid originating from sulfur dioxide and water vapor, the concentrations of both constituents in the stratosphere should be known. However, little data are available on the subject. Table 3 shows recent results and estimations (51, 52) of the different component concentrations. All the data needed to calculate the nucleation rates, nucleus size, and composition are supplied by these theoretical investigations. However, uncertainty about the macroscopic concept of liquid droplets applied to nuclei with radii in the range of 10 Å still remains, resulting in uncertainty in the value to be used for surface tension and the saturated vapor pressure of sulfuric acid.

Under normal temperature and pressure conditions, this nucleation mechanism was compared quantitatively with the condensation of sulfuric acid on a pre-existing aerosol (45, 46) and the experimental results showed that the latter mechanism had practically no effect at relative moisture values above 50%; this result is consistent with the above theories, taking account of their uncertainty.

These results also showed that for low relative moisture values, as in the stratosphere, heterogeneous nucleation should play a predominant part. This would explain the part played by condensation nuclei or insoluble particles. In stratospheric conditions (from 50 to 100 mb, −60 °C), however, most data required for calculation are poorly known (surface tension, sulfuric acid water vapor pressure, the ratio of water vapor concentration *vs.* sulfuric acid). So far, the use of calculations alone cannot determine whether heteromolecular or heterogeneous nucle-

TABLE 3.

Species	Average volume mixing ratio
H_2O	$(3.0\pm0.3)\times10^{-6}$
O_3	$(4.8\pm1.0)\times10^{-6}$
HNO_3	$(2.8\pm0.7)\times10^{-9}$
N_2O	$(210\pm50)\times10^{-9}$
	$(270\pm60)\times10^{-9}$
NO_2	$(22+8)\times10^{-9}$
	$-12)$
O	10^{-13}
SO_2	0.2×10^{-9}

Can. J. Chem. Downloaded from www.nrcresearchpress.com by 210.87.254.105 on 09/05/12
For personal use only.

ation during the *in situ* transformation of sulfur dioxide occurs.

Whichever the case, sulfuric acid particles are created which react with ammonia, according to a process described by Friend (33): the formation of ammonium sulfate is followed by fast oxidation of SO_2 because of NH_4^+ acting as a catalyst (decrease in the p*H*). Growth should be faster as indicated by the laboratory investigations in tropospheric conditions by Bricard *et al.* (39).

The occurrence of such a mechanism is dependent on the relative abundance of sulfur dioxide and ammonia as well as on the relative variations through time. From this process, it must be admitted that the formation of large nuclei is restricted by NH_3 concentration. It should then follow that larger particles be made of ammonium sulfate mainly, whereas smaller particles be made of sulfuric acid mainly, as apparently indicated by Cadle's results. Against this process, it is fairly difficult to think of ammonia arriving by "blasts" in the stratosphere, which would occur with SO_2 during volcanic eruptions.

It has also been noted that ions might take part in the formation of chemical species. On account of their rather high concentration (several thousands per cm^3) (50) they might be considered to affect nucleation. This is verified by a significant peak concentration of both ions and particles at an altitude of about 20 km.

2. Tropospheric Origin

From Martell's measurements (40) the radioactivity remaining in the stratosphere during times in the range of 1 year would be associated with particles smaller than 0.02 μ above 27 km in altitude and with particles in the range of 0.1 μ between 21 km and the tropopause. Martell also observed that Manson's measurements (41) showed that the specific radioactivity of particles originating from the sulfate layer quickly decreased with increasing particle radii.

It can be easily admitted that radioactive products are fixed directly on the natural particles when brought together, just as H_2SO_4 molecules formed by *in situ* oxidation can deposit progressively on the sulfate particles during their development, if Junge's assumption and the other ones developed above are accepted. The specific radioactivity should thus be independent of the particle size, which is not consistent with observation. Therefore, the assumption of the development of sulfate particles by progressive condensation of vapor is not consistent with the results of radioactive measurements.

It has been noted that the concentration of the middle-sized particles (radii in the range 0.1–1 μ) increased with altitude in the upper troposphere and the lower stratosphere with a significant peak between 3 and 9 km above the tropopause. On the other hand, the vertical profiles of Aitken nuclei showed a significant concentration decrease till about 20 km. All these middle-sized or small particles were sulfates.

These facts suggest that stratospheric aerosols could originate in the troposphere and enter the stratosphere by convective mixture. On the basis of this assumption, Aitken nuclei and stratospheric particles are found to include a wide distribution of sulfate particles and the increase of the middle-sized particle population above 10 km can be explained by coagulation of these Aitken nuclei. It should be noted, though they did not make this assumption, that Junge *et al.* (4) have shown by calculation the significance of the coagulation process for Aitken nuclei.

An application of Schmolukowsky's theory should allow calculation of the particle size distribution and residence time together at various altitudes. The number distribution of larger particles *vs.* altitude is shown in Fig. 7, using Martell's results; y is the average life of a particle at a given level and the curve n'/y represents the total number of middle-sized particles mixed and produced at every level or the total number of particles removed during a

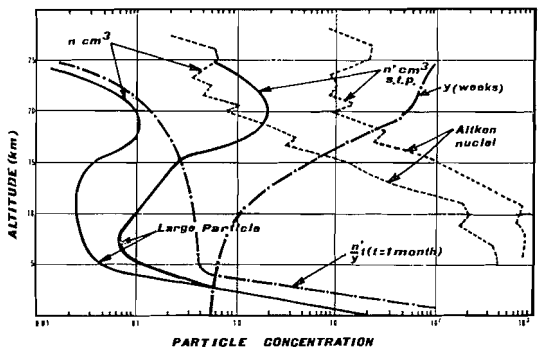

FIG. 7. The approximate number distribution and residence time of large particles. y is the average atmospheric life of a particle at each level. The curve $(n'/y)\,t$ represents the total number of large particles mixed into and produced at each level, on the total number removed, in the time interval t. (Published with the permission of Tellus.)

Can. J. Chem. Downloaded from www.nrcresearchpress.com by 210.87.254.105 on 09/05/12
For personal use only.

period of time. The distribution *vs.* altitude curve is thus somewhat similar to Fig. 1 which gives experimental results directly.

According to this approach, the nuclei found by Mossop, Friend, and Bigg in the large sulfate particles should not act as condensation nuclei but should be incorporated into the particles already developed. The same process should apply to radioactive products; this would explain the decrease of the specific activity of the sulfate particles as a function of increasing radii, whereas the assumption of continuous condensation and fixation on the pre-existent nuclei would result in a simlar fixation of radioactive products and vapor molecules.

The mechanism set forth by Martell has been rejected by several authors because concentration of condensation nuclei in the upper troposphere and lower stratosphere is not sufficient. We have seen that information on this point is not consistent, since the concentration range can vary noticeably according to different authors; more accurate data should allow the validity of Martell's assumption to be decided.

It can be noticed that little agreement has been reached so far on the origin of the stratospheric aerosol layer. No choice can be made between these assumptions as long as more accurate results on aerosol size distribution and the respective amounts of the various vapors found in the stratosphere are lacking.

1. J. M. ROSEN. Space Sci. Rev. **9**, 58 (1969).
2. S. PHILIPOWSKY, J. A. WEINMAN, D. R. CLEMSKA, G. S. KENT, and D. R. WRIGHT. J. Geophys. Res. **73**, 7553 (1968).
3. E. DE BARRY and F. RÖSSLER. J. Geophys. Res. **71**, 1011 (1966).
4. C. E. JUNGE, C. W. CHAGNON, and J. E. MANSON. J. Meteorol. **18**, 81 (1961).
5. J. BRICARD, G. MADELAINE, P. REISS, and P. Y. TURPIN. C.R. Acad. Sci. Paris, **275**, 837 (1972).
6. J. M. ROSEN. J. Geophys. Res. **69**, 4673 (1964).
7. P. W. HODGE. Smithson. Contrib. Astrophys. **4**, 145 (1961).
8. C. E. MELTON. Smithson. Contrib. Astrophys. **11**, 295 (1965).
9. E. L. FIREMAN and G. A. KASTNER. Geochim. Cosmochim. Acta, **24**, 10 (1961).
10. C. E. JUNGE and J. E. MANSON. J. Geophys. Res. **66**, 2163 (1961).
11. J. C. MOSSOP. Geochim. Cosmochim. Acta, **29**, 201 (1965).
12. J. P. FRIEND. Tellus, **18**, 465 (1966).
13. C. F. JUNGE. J. Meteorol. **18**, 501 (1961).
14. C. W. CHAGNON and C. E. JUNGE. J. Meteorol. **18**, 746 (1961).
15. C. L. HEMENWAY, D. W. HALLGREEN, and R. E. COON-LEVENTH. International Space Science Symposium, Vienna, 1966.
16. F. L. FIREMAN and G. A. KASTNER. Geochim. Cosmochim. Acta, **24**, 10 (1961).
17. N. BANDHARI, J. R. ARNOLD, and D. W. PARKIN. J. Geophys. Res. **73**, 1887 (1968).
18. J. M. ROSEN. J. Geophys. Res. **69**, 4673 (1964).
19. E. K. BIGG and W. J. THOMPSON. Tellus, **22**, 550 (1970).
20. W. E. RANZ and J. B. WONG. Ann. Ind. Hyg. Occup. Med. **5**, 464 (1952).
21. R. D. CADLE. Proceedings of the survey conference CIAP, February 15–16, 1972. p 130.
22. A. L. LAZRUS, B. GRANDRUD, and R. D. CADDLE. Geophys. Res. **76**, 8083 (1971).
23. Y. BOURBIGOT, J. BRICARD, G. MADELAINE, and D. VIGLA. C.R. Acad. Sci. Paris, t276, Ser. C, February, 1973. p. 547.
24. M. GADSDEN. J. Atmos. Terr. Phys. **3**, 151 (1968).
25. M. N. RUNDLE. The radiation atmosphere. *Edited by* McCormac. D. Rendel Publishing Company, Dordrecht, Holland. p. 90.
26. M. F. MULCAHY, J. R. STEVEN, and J. C. WARD. J. Phys. Chem. **71**, 2124 (1967).
27. F. E. BLACET. Ind. Eng. Chem. **44**, 1339 (1952).
28. E. R. GERHARD and H. F. JOHNSTONE. Ind. Eng. Chem. **47**, 972 (1955).
29. P. URONE and W. H. SCHRODER. Environ. Sci. Technol. **3**, 436 (1969).
30. M. BUFFALINI. Environ . Sci. Technol. **5**, 685 (1971).
31. H. W. SIDEBOTTOM, C. C. BABCOCK, G. E. JACKSON, J. G. CALVERT, G. REINHART, and E. P. DANCON. Environ. Sci. Technol. **6**, 72 (1972).
32. E. R. ALLEN, R. D. MCQUICY, and R. D. CADLE. Chemosphere, **1**, 25 (1972).
33. J. P. FRIEND. Atmos. Environ. To be published.
34. R. A. MCCLATCHEY, R. W. FENN, J. E. A. SELBY, F. E. VOLZ, and J. S. GARING. Optical properties of the atmosphere. Environmental Research Paper No. 354, A.F.C.R.L.71-0274. 1971.
35. J. BRICARD, M. CABANE, G. MADELAINE, and D. VIGLA. J. Coloid Interface Sci. **39**, 42 (1972).
36. J. F. CRONIN. Science, **172**, 847 (1971).
37. P. E. COFFEY and V. A. MOHNEN. Bull. Am. Phys. Sci. **17**, 392 (1972).
38. P. E. COFFEY. Thesis. State University of New York, Albany, New York. 1972.
39. J. BRICARD, G. MADELAINE, D. VIGLA, and M. DUPOUX. Proc. 7th Conf. Condensation Nuclei, Prague, Czechoslovakia. 1969.
40. E. A. MARTELL. Tellus, **18**, 486 (1966).
41. J. E. MANSON. Proc. A.E.C. Conf. TID-7632, February, 1962.
42. G. J. DOYLE. J. Chem. Phys. **35**, 795 (1961).
43. C. S. KIANG and D. STAUFFER. Preprint for the Faraday Division Symposium "Fogs and Smokes", March 28–30, 1973.
44. P. PASCAL. Traité de chimie minérale, Vol. XIII. p. 1349.
45. J. BRICARD, D. BOULAUD, G. MADELAINE, and D. VIGLA. Atmos. Environ. To be published.
46. D. BOULAUD. Thèse de Spécialité, Paris. 1973.
47. G. W. PALTRIDGE. J. Geophys. Res. **71**, 1945 (1966).

48. H. FLOOD. Z. Phys. Chem. A, **170**, 290 (1934).
49. H. REISS. J. Chem. Phys. **18**, 840 (1950).
50. R. D. HAKE, E. T. PIERCE, and W. VIEZE. Stratospheric Electricity, Stanford Res. Inst., Contract N 00014-72-C-0259.
51. J. E. HARRYS and N. W. B. STONE. Proceedings of the 2nd Conference on the Climatic Impact. November, 1972. p. 78.
52. J. P. FRIEND. Proceedings of the 1st Conference on the Climatic Impact. February 1972. p. 71.
53. R. BECKER and M. DOERING. Ann. Phys. **24**, 719 (1935).
54. M. VOLMER and A. WEBER. Z. Phys. Chem. **119**, 277 (1926).
55. DUCE. J. Geophys. Res. **70**, 1775 (1965).
56. T. C. HALL. Ph.D. Thesis. University of California, Los Angeles. 1953.
57. N. A. RENZETTI and G. T. DOYLE. Int. J. Air Pollut. **2**, 327 (1960).

Can. J. Chem. Downloaded from www.nrcresearchpress.com by 210.87.254.105 on 09/05/12
For personal use only.

The Ozone Distribution in the Atmosphere

H. U. DÜTSCH
Laboratory for Atmospheric Physics, ETH, Zürich, Switzerland
Received October 3, 1973

The world wide distribution of total ozone and its changes with season are discussed as well as the variability on different time scales. A climatology of the vertical ozone distribution is presented and an attempt is made to derive some inference on ozone transport by the general circulation and its interaction with photochemical processes. It is found that longer observational series in an improved network are needed for puttting such a derivation on a firmer basis. The observed year-to-year changes of world wide total ozone and of the vertical distribution indicate the importance of the quasi-biennial variation of the circulation in the tropical stratosphere for the poleward ozone flux. The suggested variation of ozone concentration in the upper stratosphere with the sunspot cycle must be further substantiated.

On traite de la distribution dans le monde entier de l'ozone total, de ses variations avec les saisons et de ses variations selon différentes échelles de temps.

On présente une climatologie de la distribution verticale d'ozone et l'on tente d'en tirer les conséquences sur le transport d'ozone, la circulation générale et l'interaction avec des processus photochimiques. On en conclut qu'un nombre plus élevé d'observations dans un réseau amélioré serait nécessaire afin d'établir sur une base plus solide de telles relations.

Les changements de la quantité totale d'ozone observés d'année en année dans le monde entier et de la distribution verticale montrent l'importance de la variation quasibiennale de la circulation dans la stratosphère tropicale pour le transport d'ozone vers les pôles. La relation suggerée pour la concentration d'ozone dans la couche supérieure de la stratosphère et le cycle des taches solaires doit être établie plus solidement

[Traduit par le journal]

Can. J. Chem., **52**, 1491 (1974)

Introduction

The emphasis in ozone research has, during the past few years, shifted towards the theoretical side in connection with the rapid new developments in photochemistry and also because of the prospects introduced by this of a possible anthropogenic influence on the ozone layer. Observational efforts have shifted towards measurements of other trace constituents which play a role in the new integrated photochemical system and which had hitherto not been directly observed at all at stratospheric levels. Although we already have a fairly broad knowledge of the ozone distribution in the atmosphere (which shall be reviewed in this paper) further and improved observations of the central substance of the new integrated photochemical system, namely the ozone, are still urgently needed. The intimate interaction between photochemical and transport processes demands comparison between a rather detailed observational material and the model studies.

Total Amount

Observational Techniques

The standard instrument for total ozone observations is the Dobson spectrophotometer with almost 100 units distributed over the world. Although the actual observation with this instrument is simple and rapid, good calibration and maintenance are rather difficult whereby the optical wedge is the most critical part. An accurate determination of the instrument constant is a lengthy procedure and requires good observing conditions. The possibility of a transfer of that constant from one instrument to others by easily transportable standard lamps is still debated and rather circumstantial. Direct comparison can not be avoided if strict uniformity of data is to be maintained.

Filter type instruments are also used routinely in part of the world network but their reliability is obviously less (1) and probably the falsification of results by bad observing conditions is greater than with the standard spectrophotometer. There

Can. J. Chem. Downloaded from www.nrcresearchpress.com by 210.87.254.105 on 09/05/12
For personal use only.

Can. J. Chem. Downloaded from www.nrcresearchpress.com by 210.87.254.105 on 09/05/12
For personal use only.

seems to be a tendency to overestimate extremes when filter instruments are used.

Recently a newly designed spectrophotometer used by Brewer and co-workers (2) avoids the optical wedge and is much smaller and thus more easily transportable than the Dobson instrument. It should also be better suited to give reliable measurements under cloudy sky conditions. The new spectrometer is adapted to continuous, fully automatic, monitoring of total ozone. Interesting observations on rapid short time total ozone fluctuations have already been obtained but this instrumentation is still under development.

Although the ground based network of total ozone stations has been growing until recently, it is still by no means adequate for synoptic representation of total ozone and monitoring of world wide or hemispheric ozone content of the atmosphere is still difficult. The solution to this problem will hopefully come from indirect satellite borne sensing, which has been successfully tested on Nimbus 3 and 4. Measurements in the i.r. 9.6 μ band (3) and of backscattered u.v. (b.u.v.) radiation (4) have been applied. Both methods cannot quite reach the accuracy of direct observations, but will nevertheless yield very important data especially, if ground based observations are used for checking and calibration. Obviously the b.u.v. method cannot be applied during the polar night and meteorological conditions are such that i.r. measurements also become unreliable in the same regions.

Variation of Total Ozone Content with Season and Latitude

The strong dependence of total ozone on season and latitude has been known since Dobson organized a small world network almost 50 years ago: a maximum in spring and in subpolar regions (where the peak-to-peak variation reaches almost 50% of the yearly average content) and a minimum near the equator all year round (Fig. 1). The extension of the network since the IGY has shown considerable asymmetry between the hemispheres. The ozone maximum lies in the south about 10° closer to the equator and the poleward decrease from there, which in the Northern hemisphere is almost nil, appears quite pronounced except at the turn from spring to summer. The seasonal increase in the Antarctic is delayed by 2–3 months compared to the north polar region; there is, however, no such phase difference in middle and lower

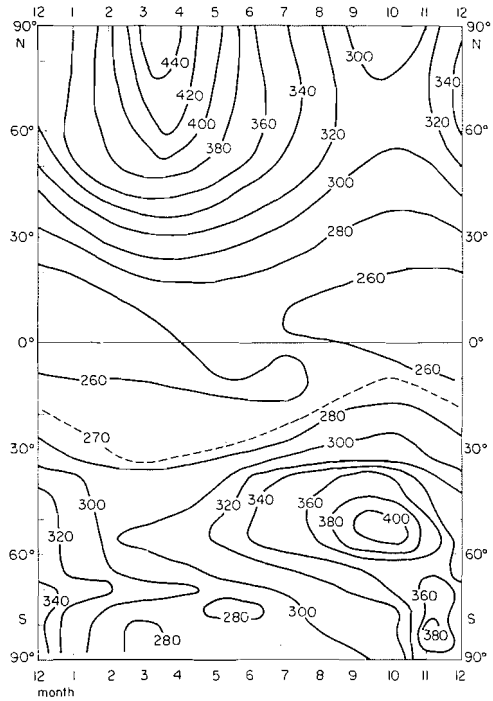

FIG. 1. Total ozone content as a function of season and latitude (isopleths labeled in Dobson ≡ 10^{-3} cm ozone, normal temperature and pressure). Although the main features are presumably correct there is still some uncertainty on details with respect to the Southern hemisphere, because many series are too short and the coverage is very poor between 50° and 60° S.

latitudes. While the rise of total ozone during winter comprises the Northern hemisphere, almost as a whole, this phenomenon, in the South does not extend over the polar circle. Only with the breakdown of the polar vortex in late spring, *i.e.* at a time when the poleward transport over lower latitudes has already ceased, does a strong ozone influx occur into the Antarctic. Also, with this delay the amplitude of the seasonal variation stays much smaller poleward of 55–60° than in the North, whereas there is not too much difference in middle latitudes.

Longitude Dependence

Although the latitude dependence of ozone content is, together with its seasonal variation, undoubtedly the dominant feature, there is also an influence of geographic longitude (5) (Fig. 2) which obviously reflects the quasi-stationary features of the upper air flow which are imposed on the atmosphere by the sea–land distribution. The main upper air troughs over eastern

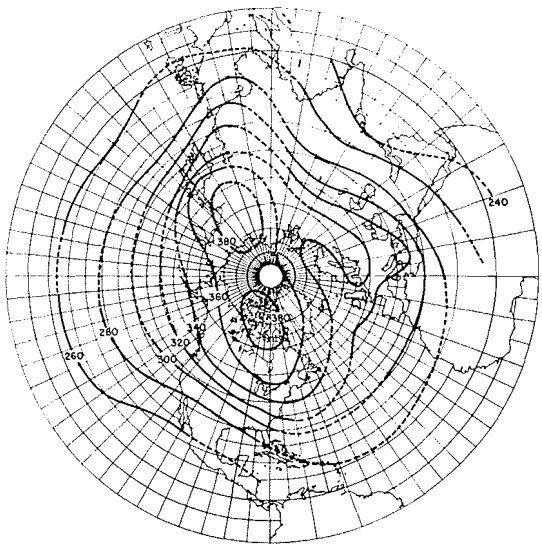

FIG. 2. Variation of total ozone content with longitude (annual mean). From London (5).

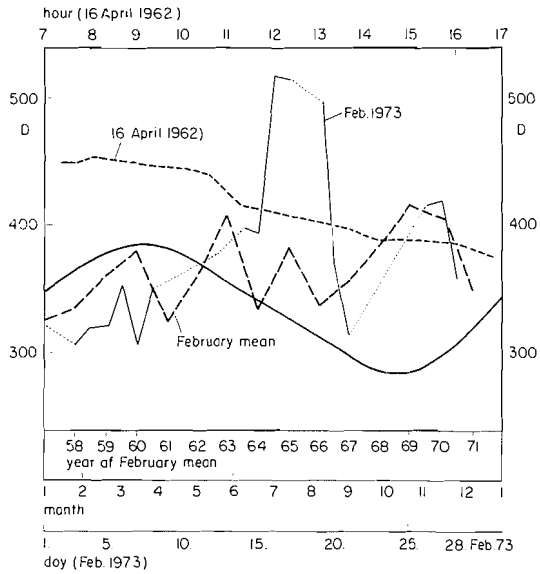

FIG. 3. Comparison between the seasonal variation (monthly mean values) (———), the day-to-day changes within 1 month (February 1973), given by daily mean values (———), possible variation within 1 day (16 April 1962, single readings) (- - - - -), and the differences between mean values of the same calendar month (February) from year-to-year (— —).

America, along the east Asiatic coast, and to a lesser extent over eastern Europe correspond with equatorward extensions of the high latitude, high ozone values. This feature has its strongest development at the time of the ozone maximum in late winter and early spring. It has been claimed that it is connected with the earth's magnetic field; however, this hypothesis does not explain the full complexity of the longitude dependence, and no suitable physical mechanism has been proposed to explain such a connection. There is, however, a very close relationship to the meteorological properties of the short time ozone fluctuations.

Day-to-day Variations of Total Ozone

In middle and high latitudes, in that part of the earth where the circulation is governed by moving pressure systems, *i.e.* by quasi-horizontal mass exchange between latitudes, a high variability of total ozone is observed (Table 1). Especially during the first half of the year, the variations of daily mean values within 1 month may exceed by far the seasonal variation (Fig. 3) and in extreme cases even the changes within 1 day can be of that magnitude. Normally high values are observed in upper air troughs above a cold troposphere and low amounts in warm anticyclones and over a flow of subtropical air. Although this points, in view of the latitudinal gradient, to the importance of advection, the fact

TABLE 1. Monthly mean values and standard deviation of total ozone from 45 years of observations at Arosa, Switzerland (47° N) in Dobson (10^{-3} cm normal temperature and pressure)

	Values	Standard deviation
I	347	43.7
II	370	50.5
III	381	42.8
IV	384	36.3
V	372	28.6
VI	352	22.9
VII	333	19.7
VIII	317	18.4
IX	298	20.4
X	285	23.1
XI	290	26.1
XII	315	33.3

that the differences between extremes are often much larger than differences in mean ozone content of the latitudes of origin proves the considerable contribution from the effect of vertical motion.

Due to the described connection between weather situation and ozone content, big dif-

Can. J. Chem. Downloaded from www.nrcresearchpress.com by 210.87.254.105 on 09/05/12
For personal use only.

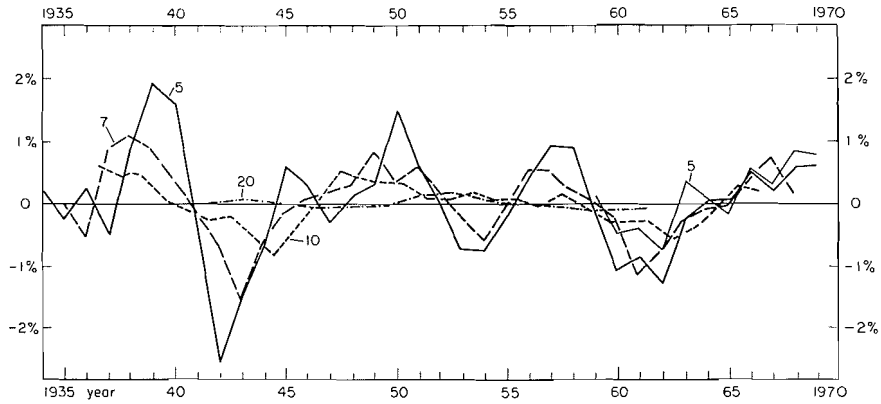

FIG. 4. The variability of "trends" in ozone content with time and the dependence of the trend intensity on the length of the chosen trend period (the center date of the period is shown) computed from the observational series at Arosa. C wavelength data were used; after 1959 trends (5 year period) for AD data are shown for comparison.

ferences between mean values for a given calendar month may occur from one year to the next. For February, where the variability is highest, these may be almost as large as the normal seasonal variation (Fig. 3). These deviations from normal are tied to circulation anomalies of *regional* extent and have a corresponding extension. Because of their occurrence a reasonably long series of observations is needed to establish a reliable ozone climatology at a given station. Although on a hemispheric scale positive and negative deviations will normally largely balance each other, the existence of year-to-year differences of the total hemispheric or even global ozone burden of the atmosphere is also indicated, apparently tied mainly to changes in the large scale stratospheric circulation from winter to winter. They will be discussed in the section Year-to-year Changes.

Long Term Trends of Atmospheric Ozone Content

All the "normal" variations in ozone distribution discussed in the previous section must be kept in mind when statistical studies on possible "trends" in atmospheric ozone content are made. Such trends are presently of special interest in connection with the problem of an anthropogenic influence on the ozone layer. As shown by studies on the 45 year series of ozone observations at Arosa, Switzerland, the magnitude of observational trends is rapidly decreasing with increasing length of the period for which the trend is computed (which has to be kept in mind if trends are compared) (Fig. 4).

It is seen that considerably larger trends (of both signs) than observed during the sixties occurred around 1940. Whether this was a world wide feature as has been claimed for the sixties cannot be tested because of lack of data; rather, it is felt that it is regional, namely connected to the strong circulation anomaly over Europe during three successive winters. Undoubtedly on the basis of the present network a beginning influence of a supersonic transport fleet on the ozone layer could only be significantly proved after a relatively long period of years!

Vertical Distribution

Experimental Techniques

Most of the experimental effort in ozone research during the past decade has gone into observations of the vertical distribution (which is obviously much more demanding than that of the total amount). After first attempts during the IGY, a number of regular observational programs have been carried out since 1963; some of these are still continuing.

While initially a rather broad spectrum of methods was used (direct and indirect ones), their number is now strongly reduced, namely to the Umkehr method as the only indirect procedure applied from the earth's surface and to the use of some, only slightly differing, types of electrochemical instruments for direct soundings. To obtain information on the upper part of the ozone layer (above about 10 mb) the satellite borne b.u.v. experiment (6) has been recently added and is promising for the future. None of the existing methods is perfect. Although in principle the electrochemical instruments are absolute, the most extensively used system, the

Can. J. Chem. Downloaded from www.nrcresearchpress.com by 210.87.254.105 on 09/05/12
For personal use only.

Can. J. Chem. Downloaded from www.nrcresearchpress.com by 210.87.254.105 on 09/05/12
For personal use only.

Brewer bubbler type, requires for a number of reasons simultaneously measured total amounts to which the results have to be adjusted by a single factor multiplication (7); a pump correction also has to be applied at lower pressures; it amounts to 20% at 10 mb and is not very accurate. The carbon–iodine type, on the other hand, requires a correction in the troposphere. Nevertheless the instrument intercomparison at Hohenpeissenberg (7) showed that after application of the mentioned corrections the different types agreed within about 2% and, between instruments of the same type, the agreement is even better. The biggest relative uncertainty in climatological values obtained from sounding programs must be expected at the flight top in the middle stratosphere (*i.e.* around 10 mb and above) where errors may be of the order of 10%.

Since 1965 all Umkehr measurements are evaluated centrally at the World Data Center in Toronto, Ontario, with the same objective procedure (8): this ensures comparability although such data inversion is not necessarily unique. Most of the older data have been reprocessed by the same program. Because the indirect method is much cheaper than soundings, by far the largest world wide data set stems from it (about 75%). However, the vertical resolution obtained is poor because the information content of an Umkehr curve (Fig. 5) is limited; even the main maximum, as comparison with simultaneous direct soundings shows, is diminished by the inherent smoothing effect. Vertical distribution derived from Umkehr observations may also be affected by sky conditions and there is a definite good weather bias in such data.

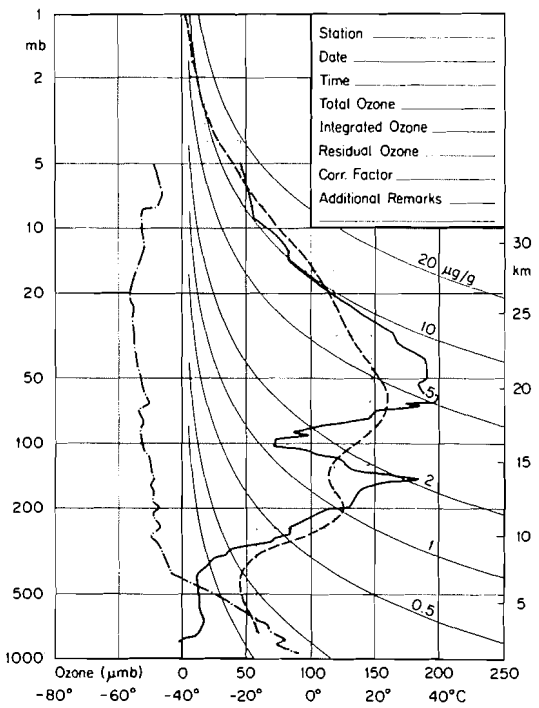

FIG. 5. Comparison between the vertical distribution obtained with a chemical ozone sonde (full line) and from simultaneous Umkehr observations (mean from morning and evening) over Switzerland: dotted line is the objectively derived block distribution which was then subjectively smoothed (dashed curve). (From ref. 9.)

For these reasons most of our present conceptions of the three dimensional ozone distribution and its variation in time is based on the less than 4000 soundings now available. Umkehr measurements are used to extend the distributions so obtained (which reach to about 10 mb) upwards into the upper stratosphere. For this purpose they could in the near future be supplemented by "Umkehr measurements from above," *i.e.* the world wide data from the b.u.v. satellite experiment. Ground based Umkehr would nevertheless not become obsolete. Careful Umkehr observations are important to detect long term ozone variations in the upper stratosphere (as will be shown in a later section).

Remarks on the Climatology of Vertical Ozone Distribution

The variability of ozone distribution in space and time, especially in the lower stratosphere, is rather high; an enormously dense network (again in space and time) would thus be needed to make direct use of ozone as a tracer (its mixing ratio below about 25 km is a very conservative property of an air parcel). Although such direct use is thus unrealistic (except maybe in some special experiments) ozone can (and must) nevertheless be used as a tracer in a more indirect way. From well-documented climatology, seasonal variation of vertical ozone distribution at different latitudes and longitudes of both hemispheres, including information on possible year-to-year differences, important inferences may be drawn on the properties of stratospheric circulation and especially on the interaction between photochemistry and transport (which can be clearly seen at certain levels). The present data are by no means adequate for this purpose because only a few stations provide

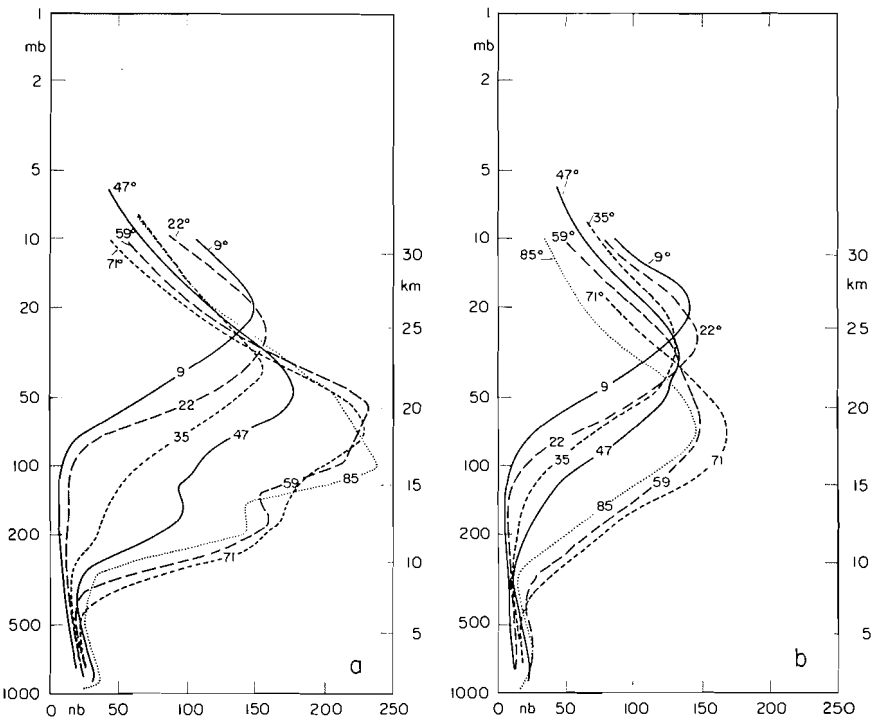

FIG. 6. Mean vertical ozone distribution at different latitudes in spring (March/April) (*a*) and fall (October/November) (*b*). (From ref. 9.)

an observational series which allows us to establish a really representative climatology.

Preliminary studies on the Swiss observational series indicate that 1 sounding per week continued over many years suffices to establish climatological mean values while at least 3 soundings per week are needed if year-to-year variations are to be studied.

Vertical Distribution at Different Latitudes

By comparing the vertical distribution at different latitudes (Fig. 6) it is easily seen that the observed distribution of total ozone, and especially its complete contrast to theoretical expectation (9), is produced by the strong poleward ozone increase in the lower stratosphere (at a level where photochemical relaxation times are so large that ozone redistribution by general circulation is the dominating factor). Above about 22 km, however, the meridional gradient is as predicted by theory (except in the inner Arctic in spring where circulation influences at still low sun apparently reach into the middle stratosphere). Also it can be seen that the seasonal variation is in the first approximation produced by the changes in the lower stratosphere.

The meridional cross section (Fig. 7) very clearly shows that the equatorial minimum in total ozone is mainly due to the high reaching tropical troposphere, which is still very poor in ozone at levels where the absolute maximum of the concentration is measured in polar regions. The level of the ozone peak which shows a minimum over midlatitudes of the fall hemisphere slopes strongly downward from low to high latitudes. For this reason the mixing ratio cross section (Fig. 8) looks very different. Top values are

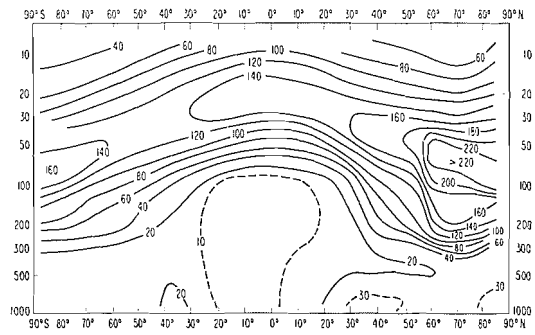

FIG. 7. Pole-to-pole cross section of vertical ozone distribution in March/April.

Can. J. Chem. Downloaded from www.nrcresearchpress.com by 210.87.254.105 on 09/05/12
For personal use only.

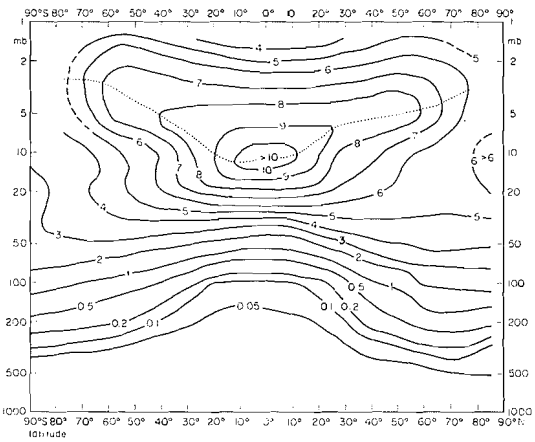

FIG. 8. Pole-to-pole cross section of ozone/air number mixing ratio for March/April. The upper part of this cross section is compiled from Umkehr data; there may be slight inconsistencies at the seam line.

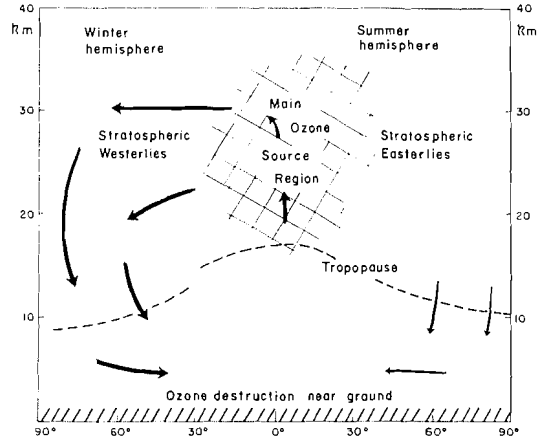

FIG. 9. Tentative model of ozone fluxes produced by the general circulation. (From ref. 13.)

found in the tropical middle stratosphere around (or slightly above) the 30 km level while the absolute concentration maxima in polar regions occur at so much higher total pressure that the mixing ratio belonging to them is comparatively insignificant. In considering transport processes by mixing, it is important to note that in the lower stratosphere (up to about 22 km) the mixing ratio isolines are sloping polewards, while above the horizontal gradient is reversed. It is interesting to note that the level of maximum mixing ratio ascends from low to high latitudes especially in fall; this agrees well with a 1 day cross section obtained from the satellite b.u.v. experiment.

Model of the Ozone Budget

Before the seasonal variation is discussed in more detail in the next sections, together with the implications on ozone transport which may be drawn from such data, a tentative general model of the ozone fluxes (Fig. 9) which, in their interaction with the photochemical processes, must explain the observations is given in the following.

From the main source region, namely the tropical stratosphere, below the mixing ratio maximum, a flux of ozone is directed into the winter hemisphere; this flux also has a downward component. This leads to the observed increase of the total amount; part of this ozone is transferred into the troposphere and destroyed (mainly) at the surface. The poleward flux ceases (after gradual decline) with the reversal of the stratospheric circulation in spring. However, the loss towards the troposphere continues, as shown by the further increase of ozone in that layer, going along with an even enhanced destruction at the ground; thus total ozone now falls off.

This general description does not say anything about the flux-producing mechanism. The easiest explanation would be a meridional cell and there is not much doubt any more that, especially at low latitudes, such processes give a major contribution. However, the single ascents in middle and high latitudes with their typical sandwich structure (Fig. 10, curve *b*) which is especially found in winter, at the time of maximum fluxes, and in spring show that large scale (quasi-) horizontal mixing must also be important especially in the lower part of the stratosphere over midlatitudes; there is much less indication of this at low latitudes (Fig. 11). Also the mentioned transfer of ozone into the troposphere can be directly substantiated by soundings. Figure 12, curve *b*, shows it in the initial stage: a strong increase in ozone concentration below the conventional tropopause while the temperature regime is presumably already adapted to the lower layer by strong vertical divergence. Figure 12, curve *a*, pictures an intrusion which has already reached lower levels; such observations are relatively rare because in the troposphere sharp peaks are rapidly destroyed by strong vertical mixing.

Seasonal Variation in Midlatitudes

The time cross section in Fig. 13 gives a useful survey of the seasonal variation at different levels: the height variation with season by 2 to

Can. J. Chem. Downloaded from www.nrcresearchpress.com by 210.87.254.105 on 09/05/12
For personal use only.

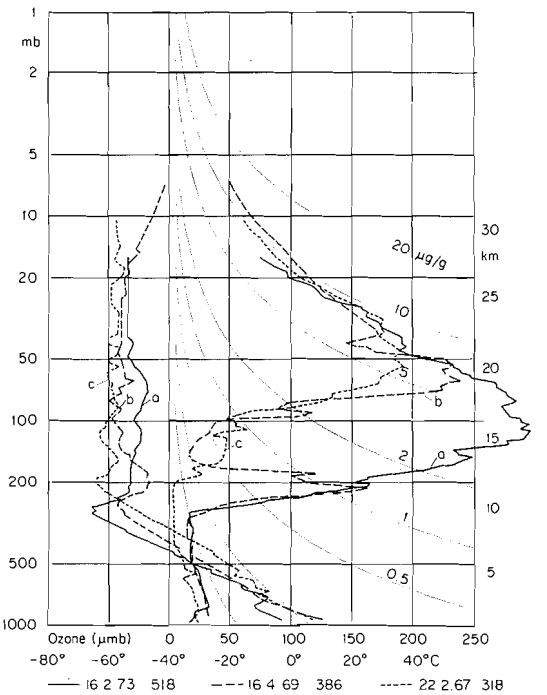

FIG. 10. Three types of vertical distributions over midlatitudes in winter and spring. (*a*) "Arctic" type, high single maximum at relatively low level. (*b*) Polar type, pronounced secondary maximum in the lower stratosphere. (*c*) Subtropical type, weak secondary maximum, small ozone content in the lower stratosphere.

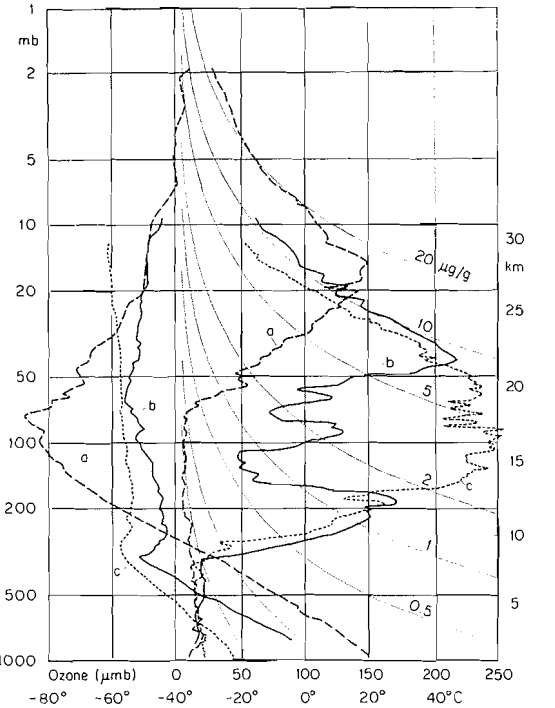

FIG. 11. Typical single soundings at different latitudes. (*a*) The equatorial distribution (Canal Zone, 9° N) is relatively smooth; (*b*) The greatest variability with height is found over midlatitudes; (*c*) Arctic soundings may show this single peak low level maximum as well as pronounced secondary maxima. (From ref. 9.)

3 km of the ozone maximum and the very rapid increase at that level in early winter and the downward propagation of this augmentation into the lower stratosphere and, with a larger delay, also into the troposphere are the most striking features; in addition we find a minimum concentration at the top of the strongly mixed troposphere with an altitude variation going with that of the tropopause.

Some of the details can be more easily seen when the seasonal changes at fixed levels are represented in Fig. 14. The transition between the late winter – spring maximum at lower levels and the summer peak in the middle stratosphere begins around 30 mb, *i.e.* close to the level where the latitudinal gradient changes sign. This means that at this height photochemical processes start to compete with the transport by the general circulation; at 10 mb photochemical influence dominates but there is still influence from ozone flux, as is shown by the clearly visible secondary maximum in January. In the upper stratosphere the seasonal maximum occurs around the equinoxes and is shifted further toward winter with increasing height; this is in agreement with the photochemical theory (temperature dependence of the ozone destroying reaction $O + O_3$).

In the three year series at Boulder, Colorado, at 40° N (*i.e.* 7° further south) the secondary winter maximum is, however, absent at 10 mb (Fig. 15) and already weak at 15 mb. It is tempting to assume that this difference is due to the fact that in winter photochemical processes are considerably faster at the lower latitude (*i.e.* at higher sun); however, as the two data sets do not overlap in time the influence of differences in stratospheric circulation which existed between the two periods (occurence or absence of midwinter stratospheric warmings) cannot be completely ruled out as a reason for the contrasting behavior.

The midwinter secondary maximum is also missing at 38° S at Aspendale where the observation is fully in phase with photochemical expectations. At 52° N at Berlin (Fig. 15) the winter increase at 10 mb is also observed but is only

Can. J. Chem. Downloaded from www.nrcresearchpress.com by 210.87.254.105 on 09/05/12
For personal use only.

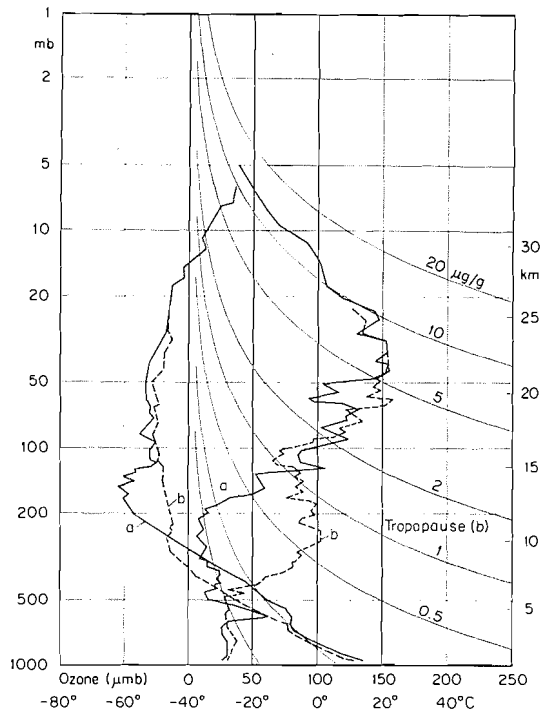

FIG. 12. Transfer of ozone into the troposphere. (*a*) Tongue of stratospheric ozone reaching into the lower troposphere on the equatorward side of the jet stream. (*b*) Early stage of the intrusion near the center of a cut-off low.

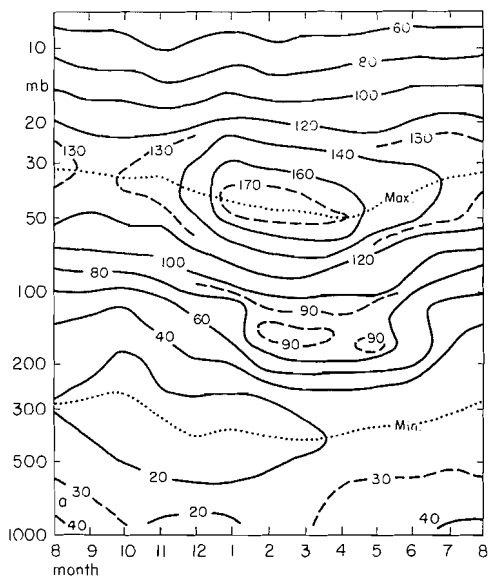

FIG. 13. Time cross section of vertical ozone distribution over Switzerland from 6 years of observations. (From ref. 14.)

weakly separated from a further rise to a spring maximum which is also indicated by the still incomplete series at Oslo (60° N). It can be suggested that this spring maximum at higher latitudes is not photochemically produced but arises in connection with the Arctic final warming in the stratosphere; this would explain why this effect is strongest over T3 at 83° N. More complete and uniform series from high latitudes than presently available are urgently needed to answer these questions.

In the lower part of the ozone layer (at and below the level of the maximum) the seasonal variation is clearly dominated by transport processes leading to the late winter – spring maximum (Fig. 14*b*). Direct transport from the main source region, the tropical stratosphere, seems to produce the rapid growth of the ozone peak, whereby the stratospheric extension of the winter hemispheric Hadley cell apparently plays an important role. The ozone transport and thus the increase is obviously strongest around the solstice when the meridional cell has its maximum development. The increase in the lower stratosphere seems to be produced by a different type of circulation; it is hardly due only to downward mixing from the maximum layer, although the strong upward increase of the mixing ratio could indicate this. The earlier start of the ozone rise at lower levels suggests that horizontal mixing from higher latitudes where concentrations are also higher at this time of the year at least contributes, whereby this mechanism becomes operative when the polar front disturbances intensify and extend further equatorward in fall.

The sharpest increase in the lower stratosphere comes in late winter when maximum values have already been reached in the peak layer but when the concentrations at these low levels in polar regions have also become very high. The decline of high ozone values accumulated by the winter time transport process starts first at the level of the primary advection (30 to 40 mb) with the diminishing intensity of the Hadley cell while loss processes continue. The beginning of the strongest decrease is gradually delayed towards lower levels and comes latest just above the tropopause. This indicates the importance of downward transport by vertical mixing.

One must, however, be careful with these arguments. Obviously the winter time transport has driven the ozone concentration far above the photochemical equilibrium level. With in-

Can. J. Chem. Downloaded from www.nrcresearchpress.com by 210.87.254.105 on 09/05/12
For personal use only.

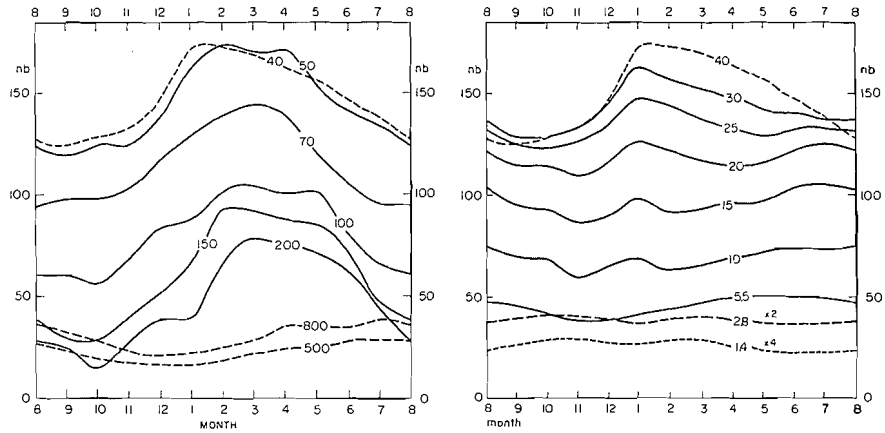

FIG. 14. Variation of ozone concentration at different levels over Switzerland, 47° N The curves for 5.5, 2.8, and 1.4 mb are from Umkehr observations; the values at the two top levels are multiplied by 2 and 4 respectively for better resolution.

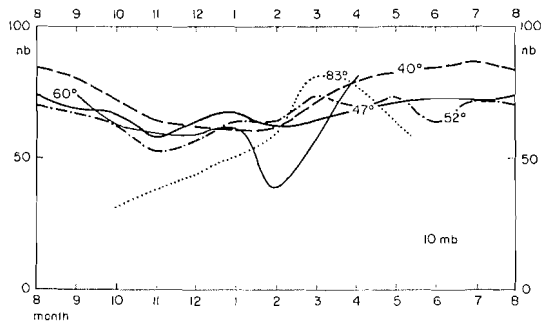

FIG. 15. Seasonal variation at 10 mb at different latitudes. (*a*) Boulder, Colorado, 40° N, (*b*) Switzerland, 47° N, (*c*) Berlin, 52° N, (*d*) Oslo, 60° N, (*e*) T3, 83° N The latter two series are very short (1 year or less).

creasing sun height the photochemical processes are accelerated and the question arises to what extent photochemical distribution of surplus ozone contributes to the observed loss, or down to what level such contribution is of any significance. In making conclusions about vertical transport this is of importance, especially with respect to the total transfer of ozone into the troposphere and its ultimate destruction at the ground, which are of main interest in the overall global ozone budget.

The Longitude Effect

Comparison between the seasonal variation over Switzerland (47° N) and over Sapporo, Japan (43° N) (Fig. 16), *i.e.* between a "normal" midlatitude station and one situated within the strong East-Asiatic upper air trough, shows that the "ridge" of total ozone connected with the trough is almost completely produced by much more pronounced accumulation of ozone in the lower stratosphere starting in early winter. Bedford in the vicinity of the East American trough shows intermediate values.

Interhemispheric Differences

As the total ozone regime differs considerably between the hemispheres it is of some interest to compare vertical distributions at the same latitude. The only Southern hemisphere station with

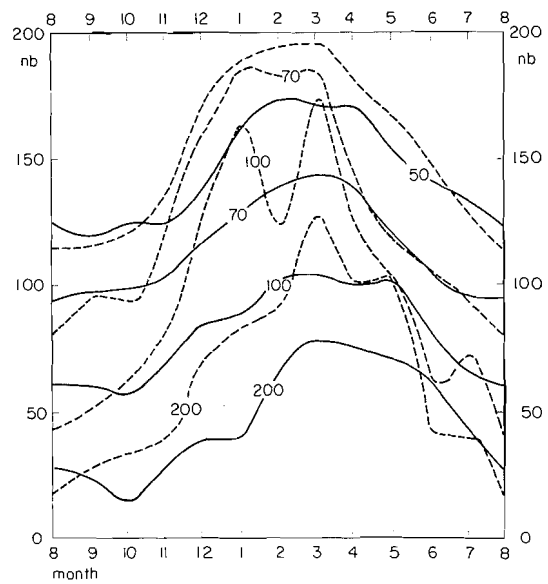

FIG. 16. Comparison of the seasonal variation at different levels between soundings made at different longitudes (Switzerland, full line; Japan, dashed line).

Can. J. Chem. Downloaded from www.nrcresearchpress.com by 210.87.254.105 on 09/05/12
For personal use only.

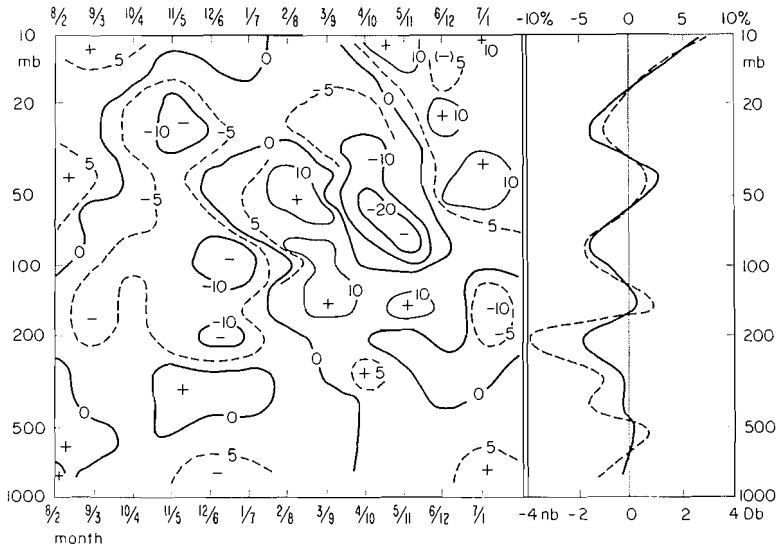

FIG. 17. Time cross section of the difference in ozone concentration between 38° N and 38° S (positive means higher values in the Northern hemisphere). At right: difference between yearly mean values (full line in nb, dashed line in %).

a record long enough to establish a representative climatology is Aspendale at 38° S. For comparison a weighted mean between Boulder, Colorado (40° N) and Albuquerque, New Mexico (35° N) is used.

Obviously the main late winter maximum around the 40 mb level is more pronounced in the Northern hemisphere (Fig. 17), but its buildup starts later and it is also more rapidly destroyed (whether the latter statement is representative is, however, still questionable; the effect may be due to the weather pattern during the relatively short American observational series). In the Southern hemisphere there seems to be less of a delay between the increase in the peak layer and in the lower stratosphere. This may be because in the South the poleward ozone flux ends in midlatitudes while in the North it continues in the inner Arctic and there is, as already mentioned, also some indication that at least part of the ozone flux into the lower stratosphere of midlatitudes has taken this detour. Representative climatologies at higher midlatitudes are needed in both hemispheres in order to follow up this problem.

Interestingly enough the largest difference (Fig. 17) between North and South (with higher values in the North) is found at 10 mb, *i.e.* at a level where at this latitude circulation influences seem to be minor and the distribution should be largely photochemically determined. The recent photochemistry could explain such differences by asymmetries in the distribution of other trace substances as NO_x. It must be mentioned, however, that the differences shown in Fig. 17 are hardly significant, considering the fact that the uncertainty of soundings is largest at this level. While there is not much difference in the amplitude of seasonal variation at stratospheric levels (with the exception possibly of the ozone peak layer) there is obviously much less variation in the Southern troposphere than in the North (while yearly means are very similar). Whether this indicates less transfer through the tropopause (10) has yet to be shown; such a theory would demand another explanation of the decrease of ozone content from spring to summer than was put forward above (namely loss toward the troposphere).

Seasonal Variation in Polar Regions

It is most interesting to compare vertical distribution between hemispheres for polar regions because of the big differences in the seasonal variation of the total amount found at high latitudes. Although considerable effort has been made to obtain data from these regions the number of soundings is still rather limited and the set of data is quite inhomogeneous with respect to instruments which were used as well as

Can. J. Chem. Downloaded from www.nrcresearchpress.com by 210.87.254.105 on 09/05/12
For personal use only.

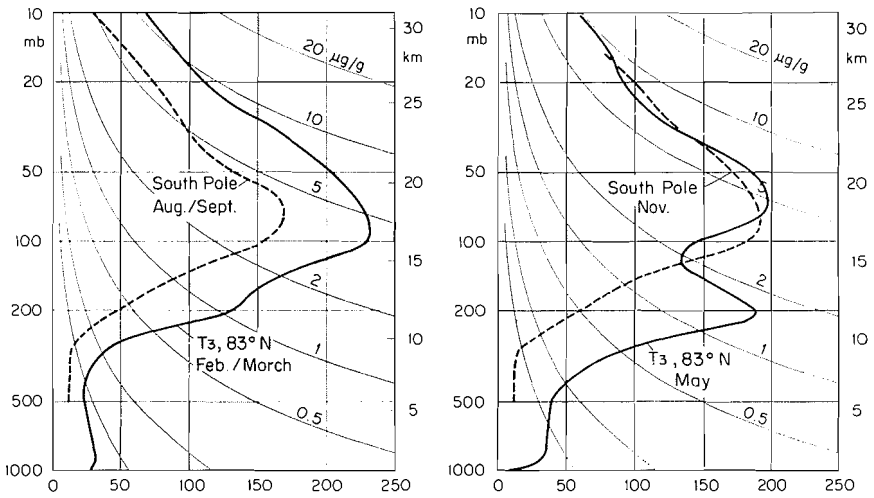

FIG. 18. Comparison between vertical distribution at T3 (83° N) and Amundsen–Scott (90° S). (*a*) February/March at T3 against August/September at the South Pole. (*b*) May against November.

the time of observations. In order to minimize effects possibly produced by these problems all observations poleward of 64° latitude for each hemisphere have been combined in the following discussion.

The level of the ozone maximum lies considerably below 20 km all year round and is situated somewhat lower in the Southern hemisphere than in the North. The seasonal variation at this level (and by this the attained maximum value) is considerably smaller in the South, where the phase difference already shown by the total amounts is very clear-cut. In the South the strong increase is delayed to late spring while in the North a first rise comes in early winter at the time of strongest northward ozone flux from low latitudes, showing that in this hemisphere such flux extends into the inner Arctic. Another strong rise is indicated at the turn from winter to spring, which might be in connection with the final stratospheric warming which occurs earlier in the North.

Also at higher levels a pronounced ozone increase is observed in the Arctic right at the beginning of winter while in the South it is delayed to spring. In both hemispheres a rapid decrease from spring to summer indicates that this maximum, up to the middle stratosphere, is produced by transport even if it occurs as late as in the Antarctic. The mean values at high levels seem much lower in the Antarctic; this is compatible with a domination of circulation effects up to these levels; however, in view of the mentioned strong inhomogenity of the material which has strongest influence at the top, not too much emphasis should be put on this statement. The discussed differences in ozone regime between Arctic and Antarctic are very drastically shown by comparing the vertical distribution obtained at T3 with that from the South Pole (Fig. 18).

Inadequacy of the Available Ozone Climatology

In summarizing we may say that we possess, at present, a reasonable conception of the three dimensional ozone distribution in the atmosphere and its variation in time; however, with few exceptions this knowledge is not accurate enough to allow us to draw definite conclusions about the ozone fluxes and thereby the flux producing mechanisms. What is still needed are continuous and extended enough sounding series to derive representative climatological means at about every 10° of latitude (even denser in midlatitudes) in both hemispheres. At least in midlatitudes of the Northern hemisphere observations at different longitudes are urgently needed.

Year-to-Year Changes

It is shown that the considerable variations of total ozone content from one year to the next, related to large scale weather patterns, are largely due to corresponding changes in the ozone concentration in the lower stratosphere

Can. J. Chem. Downloaded from www.nrcresearchpress.com by 210.87.254.105 on 09/05/12
For personal use only.

Can. J. Chem. Downloaded from www.nrcresearchpress.com by 210.87.254.105 on 09/05/12
For personal use only.

and thus have more regional significance. The 6 year series over Switzerland, however, also shows (Fig. 19) a biennial variation at the level of the ozone maximum (between about 60 and 30 mb) which is especially pronounced in the first half of the year and which is obviously independent of weather-related variations at lower levels. It is tempting to relate it to the quasi-biennial variation of the tropical stratospheric circulation. There is actually the phase relationship to be expected: high values are found in those years when according to Reed's (11) theory the 26 months cycle leads to descending motion over the subtropics. The intensity of the stratospheric winter time Hadley cell would thus be increased or decreased in a biennial rhythm and with it the poleward ozone flux from low latitudes. This is in agreement with the idea that the poleward flux goes more or less directly into the layer of the ozone peak in mid-latitudes. A continuation of the observational series is, however, needed in order to further confirm such a relation.

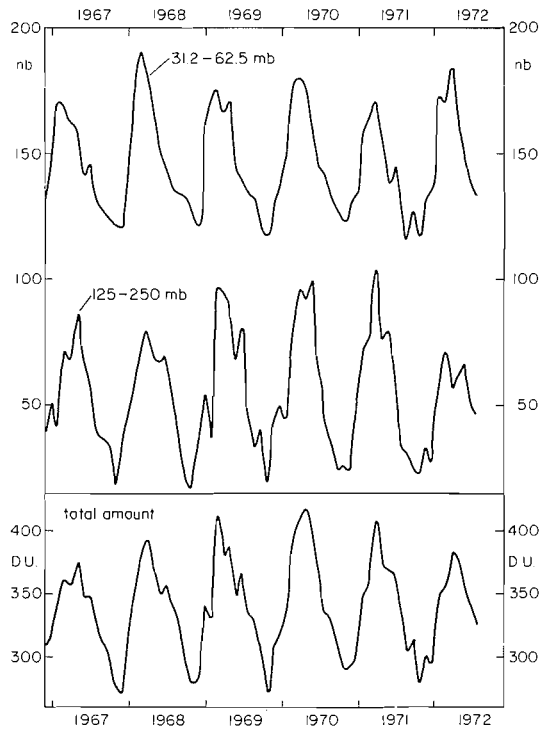

FIG. 19. Comparison between year-to-year variations in different layers and of the total amount over Switzerland 1967–1972. (From ref. 14.)

For the reasons given above single station observations of the total amount cannot be expected to show the biennial variation; however, it should appear in hemispheric means. A study of the winter time ozone content of the regions north of 40° (12) showed first of all a clear-cut connection between total ozone content and stratospheric temperature within this area (positive temperature deviation going with high ozone) but it also yielded certain deviations from this correlation showing a biennial rhythm, indicating that the intensity of the ozone flux, although it is clearly dependent also on other circulation features (as f.i. midwinter sudden stratospheric warmings), is connected with the 26 month cycle (Fig. 20). At present such studies are strongly hampered by the irregularity of total ozone observations in space and time and it is hoped that, in future, satellite monitoring of total ozone could provide a better basis for following the total ozone content of the atmosphere or of parts of it.

Variations in the Upper Stratosphere

The 15 year series of Umkehr observations at Arosa shows for the ozone concentration in the upper troposphere a variation which seems to be correlated with the sunspot number, whereby a certain time lag is indicated. The changes in ozone concentration were much stronger at the time of the very intense maximum during IGY than during that in the late sixties, which was

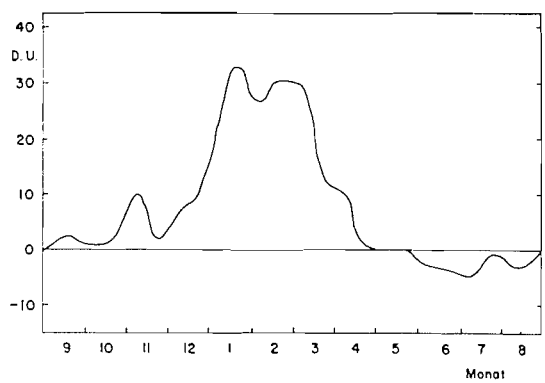

FIG. 20. Influence of the biennial variation on total ozone content of the atmosphere north of 40° N: Mean ozone content at the time of easterlies at 30 mb over Canton Island minus mean ozone content at the time of westerlies as a function of season (from 10 years of observations). A significant difference is found in winter with about a 1 month delay against the time of strongest poleward flux. (From ref. 12.)

much weaker than its predecessors. The correlation with this second maximum is, however, less well shown by the data obtained with a second instrument operated since 1967. Observations during another period are thus needed in order to confirm the reality of the correlation which could be produced by changes of u.v. radiation, by temperature variation, or also by alterations in the content of other trace substances.

Surface Ozone

Recently, sensors for continuously monitoring the ozone concentration at the surface have become available. As the ground is thought to be the main sink for stratosphere-borne ozone, it is hoped that the measurements of ozone at the surface could give additional useful information on the atmospheric ozone budget. This is, however, only the case if it is possible to obtain from such continuous registration inference on the ozone concentration of the lower troposphere above the planetary boundary layer. Very careful selection of sites free from any pollution and from influences of inversions is needed. Mountain stations would seem especially useful but even there disturbances by local circulation effects are indicated. Careful comparison with available sounding series may lead to useful concepts for finally evaluating destruction near the surface in connection with surface structure on one side and with stratospheric–tropospheric ozone transfer on the other side. It must be added that very careful maintenance and supervision are needed if reliable data are to be obtained with the instrumentation available at present.

Concluding Remarks

We have tried to obtain from this compilation of available ozone data some inference on the actual ozone fluxes and the flux producing circulation mechanisms. First of all such an attempt is, at the present stage, hampered by the incompleteness of most sounding series, the factual absence of such observations at many latitudes, and last but not least the inhomogeneity of the sounding material which is available. But also on the basis of an improved material which it is hoped will become available in the not too distant future, qualitative reasoning as it was applied here can only be a first step, but a good starting point from which numerical models must be developed. The final goal is certainly the inclusion of ozone and its photochemistry in modelling experiments of the general circulation. Good observational series leading to a proven climatology of the world wide ozone distribution will then be an important tool for checking the consistency of such models (with respect to dynamics and photochemistry) and for their further improvement.

1. R. D. Bojkov. Ann. Geophys. **25**, 293 (1969).
2. A. W. Brewer. Pure Appl. Geophys. **106**, 919 (1973).
3. C. Prabhakara, E. B. Rodgers, and V. V. Salomonson. Pure Appl. Geophys. **107**, 1226 (1973).
4. D. F. Heath, C. L. Mateer, and A. J. Krueger. Pure Appl. Geophys. **107**, 1238 (1973).
5. J. London. Beitr. Phys. Atmos. **36**, 254 (1963).
6. A. J. Krueger, D. F. Heath, and C. L. Mateer. Pure Appl. Geophys. **107**, 1254 (1973).
7. W. Attmannspacher and H. U. Dütsch. Ber. Deut. Wetterdienstes, No. 120 (1970).
8. C. L. Mateer and H. U. Dütsch. Uniform evaluation of "Umkehr" observations from the world network. I. Proposed standard Umkehr evaluation technique. NCAR, Boulder, Colorado. 1964.
9. H. U. Dütsch. Adv. Geophys. **15**, 219 (1971).
10. P. Fabian. Pure Appl. Geophys. **106**, 1044 (1973).
11. R. J. Reed. Bull. Am. Meteorol. Soc. **46**, 374 (1965).
12. W. Züllig. Beziehung zwischen der Intensität des stratosphärischen Polarnachtwirbels und dem Ozongehalt der Winterhemisphäre. LAPETH-7, ETH, Zürich. 1973.
13. H. U. Dütsch. World Surv. Climatol. **4**, 383 (1969).
14. H. U. Dütsch and Ch. C. Ling. Pure Appl. Geophys. **107**, 1139 (1973).

Can. J. Chem. Downloaded from www.nrcresearchpress.com by 210.87.254.105 on 09/05/12
For personal use only.

Solar Ultraviolet Flux below 50 Kilometers

M. ACKERMAN

Institut d'Aéronomie Spatiale de Belgique, B, 1180, Brussels, Belgium

Received August 22, 1973

The available values of the solar flux from 1700 Å to 4000 Å are presented. The penetration of this radiation in the stratosphere is discussed and the role of scattering on direct and global radiation in the troposphere is emphasized.

On présente les valeurs disponibles du flux solaire de 1700 Å à 4000 Å. On discute de la pénétration de cette radiation dans la stratosphère et on met en relief le rôle de la diffraction sur la radiation directe et globale au niveau de la troposphère.

[Traduit par le journal]

Can. J. Chem., **52**, 1505 (1974)

Can. J. Chem. Downloaded from www.nrcresearchpress.com by 210.87.254.40 on 09/05/12
For personal use only.

Introduction

The solar ultraviolet radiation penetrating into the atmosphere below 50 km has various actions. It dissociates molecular oxygen in the 2000 Å atmospheric window leading to the formation of ozone; it photodissociates minor constituents and has biological actions at ground level. The flux in the absence of absorption is a boundary condition of all the photochemical processes. Its stability as a function of time and solar conditions must also be known. Its penetration is controlled by various factors whose complexity increases with the atmospheric density. In the upper stratosphere the absorption is due to molecular processes related to the electronic spectra of oxygen and ozone. In the lower stratosphere and in the troposphere, Rayleigh scattering and interaction with aerosols also contribute to the filtering of the solar ultraviolet flux.

These various aspects will be summarized here. The choice between different sets of values will be discussed with emphasis on the practical aspects leading to the definition of input data for photochemical evaluations.

The Unabsorbed Flux

The ultraviolet solar radiation of wavelengths larger than 1800 Å is pertinent to the present subject. In the 2000 Å atmospheric window the solar u.v. can be observed without too much attenuation from stratospheric balloon altitude (1). Balloon measurements (1) have shown a different intensity distribution versus wavelength than previously deduced values (2) shortward of 2100 Å. The flux increases by a factor of 7 from 2000 to 2100 Å. In addition, recent rocket flights (3) have yielded fluxes at 1700 Å in agreement with the lowest values obtained between 1400 Å and 1900 Å (4). There should be an intensity change between 1950 Å and 1900 Å. Such a feature appears on high resolution rocket spectrograms obtained in 1957 (5). This feature is also supported by our balloon measurements below 1950 Å where, in spite of the low intensity and the already large absorption by oxygen, the data have been reduced taking into account the absorption in the Schumann–Runge bands (6). This latter spectral region is important for the photodissociation of nitric oxide in the δ bands (7), as shown in Figs. 1 and 2, where the δ bands of NO, the Schumann–Runge bands of O_2, and the solar flux are simultaneously shown. Most of the dissociation of O_2 of importance for the formation of O_3 takes place about 2000 Å (10) in the atmospheric optical window. Recent rocket data obtained by Broadfoot (8) are in agreement at wavelengths larger than 2100 Å with the data of Detwiler *et al.* (2)[1] even if these could have been based on underestimated carbon arc irradiance at short wavelengths (9).

It has been suggested by Brewer and Wilson (11) that the values published by Detwiler *et al.* (2) should be multiplied from 1800 Å to 2400 Å by 0.36. The mutual agreement shown in Table 1

[1]The data obtained by Broadfoot (8) is in agreement with the Detwiler *et al.* data (2), as published by Brinkman, Barth, and Green (Jet Propulsion Laboratory Tech. Rep. 32-951, 1966), not with the original report of the data (Table 1, ref. 2). There are substantial differences in the solar fluxes in the range $\lambda > 1700$–2100 Å as reported by Detwiler *et al.* (2) and Brinkman *et al.* for which no adequate reason has been given.

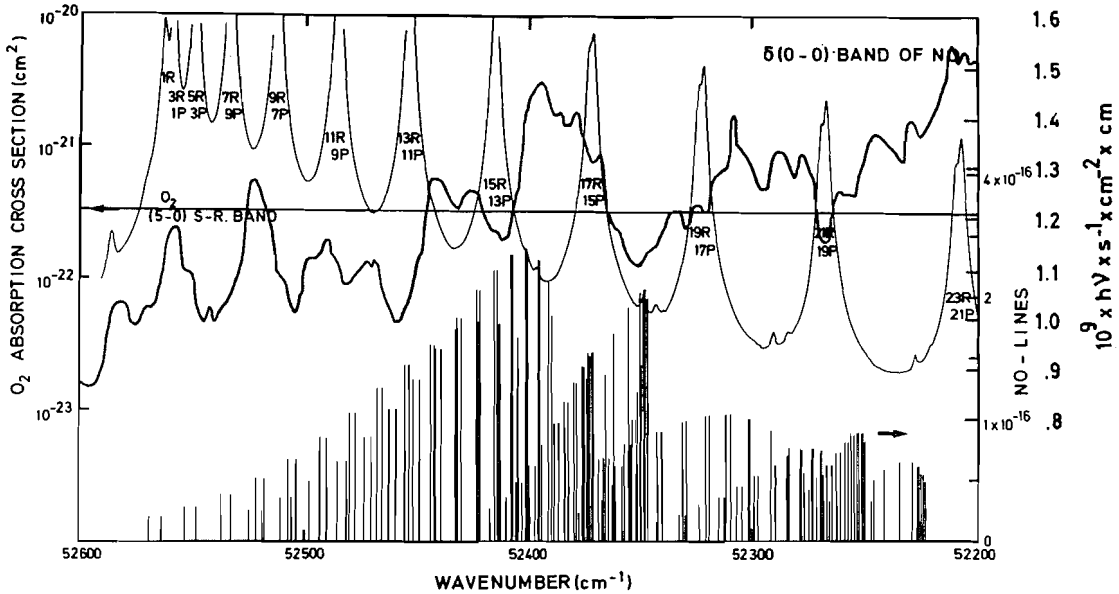

FIG. 1. Distribution of intensity of the NO lines in the δ(O–O) band and absorption cross section of O_2 *vs.* wavenumber after Cieslik and Nicolet (7). The solar flux taken from McAllister (5) and adapted for a solar black body temperature of 4660 °K is also shown. The choice of the average value of the flux represented by the horizontal line would in this case lead to an overestimate of the photodissociation of NO of which the dissociation limit is at 52 400 cm^{-1}.

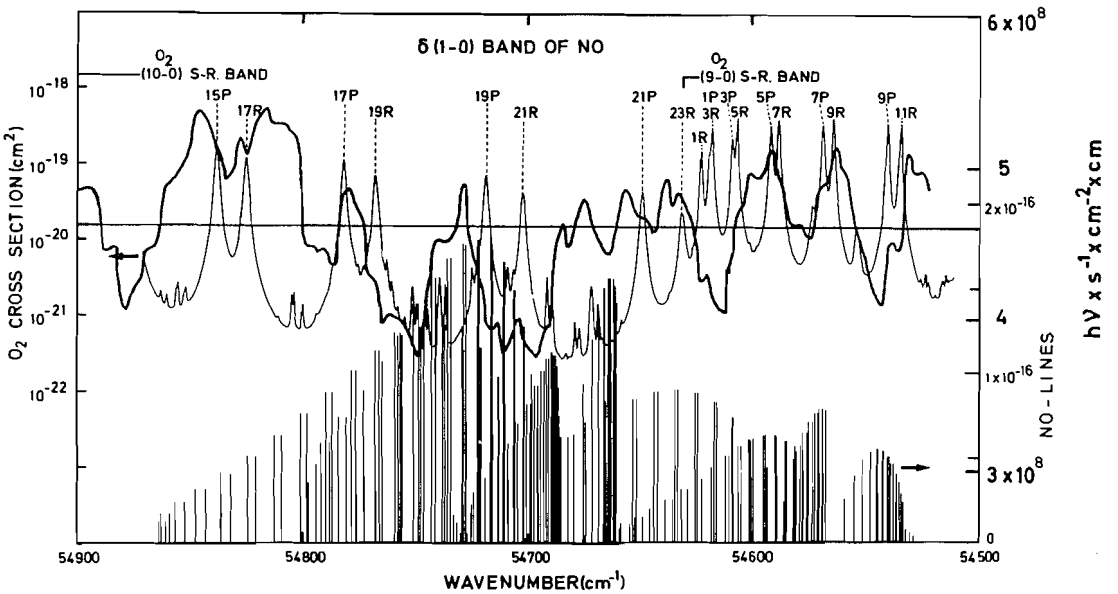

FIG. 2. Distribution of intensity of the NO lines in the δ(1–O) band and absorption cross section of O_2 *vs.* wavenumber after Cieslik and Nicolet (7). The solar flux taken from McAllister (5) and adapted for a solar black body temperature of 4580 °K is also shown. The choice of the average value represented by the horizontal line does not appear to introduce a large error in the photodissociation of NO even if an exact evaluation requires the use of the fine structure of the solar flux.

Can. J. Chem. Downloaded from www.nrcresearchpress.com by 210.87.254.40 on 09/05/12
For personal use only.

TABLE 1. Comparison between the most recent values of solar flux of interest to stratospheric ozone formation in the range of wavelength where they overlap

Wavelength interval (Å)	Flux (8) × 10^{-12} (hv cm^{-2} s^{-1})	Flux (12) × 10^{-12} (hv cm^{-2} s^{-1})	Ratio between values from ref. 8 and ref. 12
2105–2128	10.4	9.42	1.10
2128–2150	11.2	10.6	1.05
2150–2174	11.9	13.4	0.89
2174–2198	15.0	13.2	1.14
2198–2222	15.0	17.3	0.87
2222–2247	20.6	18.0	1.14
2247–2273	16.8	18.2	0.92

between more recent values (8, 12) where they overlap implies that the proposed reduction can hardly be accepted. Brewer and Wilson, using the equivalent of a broad band filter, have made the assumption that the change of sensitivity with wavelength of their detector had no influence on their measurements. They have used an intensity distribution of the solar radiation without taking into account the 2085 Å discontinuity and their ozone concentration above 30 km appears to be low. All these factors would have a tendency to bring their computed and observed integrated fluxes into better agreement.

At wavelengths larger than 2700 Å the ozone absorption decreases so much that the solar radiation reaches lower and lower altitudes in the stratosphere where the dissociation of ozone leads to significant (13) steady concentrations of excited oxygen atoms. These contribute to the transformation of molecules having their source at ground level, such as CH_4 and N_2O, into other species that have, in turn, their source in the stratosphere itself. Between 2700 Å and 3500 Å determinations of the solar flux with relatively high spectral resolution have been performed (8, 14); the quality of these determinations has been discussed by Broadfoot (8). These values are in close agreement with the low resolution data published by Tousey (15) in 1963 which are 10% higher on the average than those of Arvesen *et al.* (14).

The solar u.v. flux has been measured over long periods of time from 1150 Å to 3500 Å by means of broad band detectors from Nimbus 3 and 4 satellites. The data have been reported by Heath (16). It has been concluded that the variability of the flux appears particularly for the radiation originating from the solar chromosphere, while it reaches the limits of detectability in the case of the photospheric flux. Some effect, of the order of a few percent, can be expected in the transition region below 2100 Å relevant to the stratospheric photochemistry. It should affect the dissociation rate of O_2 and of NO, for example. The magnitude of the possible resulting change in ozone *vs.* time would be very small and most probably undetectable in the actual measurements.

The Atmospheric Attenuation

The attenuation of the solar u.v. in the 2000 Å atmospheric optical window can be represented by the molecular absorptions due to O_2 and O_3 (12, 17). This has an impact on the photodissociation of these latter constituents themselves and also on minor constituents. The rapidly changing absorption cross section of O_2 with wavelength and temperature in the Schumann–Runge bands is such that the photodissociation by the solar u.v. shortward of 2000 Å is specific to each set of aeronomic conditions, such as solar zenith angle, temperature vertical profile, ozone vertical distribution, and absorption spectrum of the species whose photodissociation is considered. Typical conditions have been evaluated (18, 19, 7, 20) for H_2O, NO, and HNO_3.

On the long wavelength side of the Hartley bands of ozone the attenuation of solar radiation in the stratosphere depends on ozone itself. The role of aerosols and air has to be added in the troposphere. As already pointed out by Larsen (21) the ozone effect can be separated from the other two since it mostly takes place well above the tropopause. Considerable work has been performed on scattering of solar radiation in the atmosphere with emphasis on polarization effects. Most of the considerations have been

Can. J. Chem. Downloaded from www.nrcresearchpress.com by 210.87.254.40 on 09/05/12
For personal use only.

given to the visible region of the spectrum and less work has been devoted to the ultraviolet with special concern about the influence of scattering on the operation of the Dobson spectrophotometer and on the topside ozone sounding from satellites. The solution of aeronomic problems of the troposphere requires the knowledge of the total number, by volume, of photons available for photochemical reactions. A theoretical evaluation requires taking into account the transparency of the atmosphere to evaluate the direct solar radiation and integration of the radiation scattered by the atmosphere over all directions. To evaluate the importance of this at ground level a simple model can be constructed where half of the radiation scattered is assumed to reach the surface. For this purpose an average attenuation due to aerosols can be taken from Elterman (22) and a scattering cross section for air can be used (23, 24). The various contributions are shown in Fig. 3, where the resulting transmission for the radiation coming directly from the sun and for the global radiation (sky added) are represented. The model is for a particular altitude, a zenith angle of 40°, and a total ozone amount of 0.250 cm, since experimental data are available for comparison. They have been obtained by Bener at the observatory of Davos.

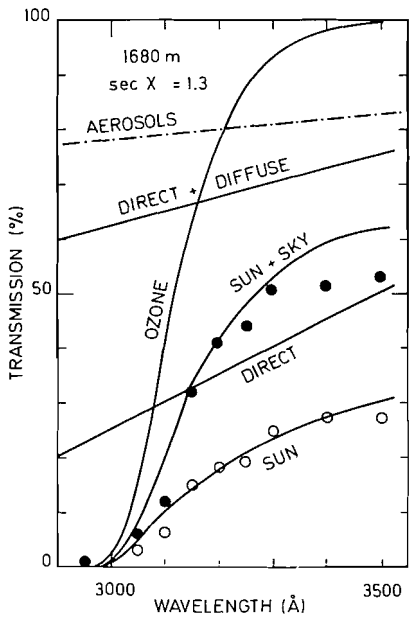

FIG. 3. Atmospheric optical transmission at an altitude of 1680 m, for a solar zenith angle of 40° and a total vertical ozone reduced thickness of 0.25 cm. The ozone contribution is represented by the line marked "ozone." The dot and dash line marked "aerosols" represents their contribution for an average amount (22), The transmission computed from the total air column and the scattering cross section (24) is represented by the line marked "direct," while an apparent transmission evaluated by assuming that one-half the scattered light reaches the ground is represented by the line marked "direct + diffuse." The curve "sun" indicates the resulting transmission for the direct solar radiation and can be compared to the values deduced from Bener's work (25) (●). The curve "sun + sky" shows the resulting transmission if the scattering component "direct + diffuse" is used and can be compared to the values deduced from Bener's work (25) (○).

The measured spectral distributions of global and sky u.v. fluxes received per unit area can be compared with the solar flux in absence of absorption (12) to compute the transmission of direct radiation and the apparent transmission of global radiation. The results are represented by the points in Fig. 3. They indicate that a very crude model gives a satisfactory representation of reality. In the 3000 Å region the flux received per unit surface from the sun is of the same order as the flux received from the sky so that computations neglecting the latter underestimate the photochemical action by a factor of about 2. In addition, the ozone layer high in the stratosphere is illuminated from below by the integrated scattered radiation coming from the troposphere.

Conclusions

Little attention has been paid to the influence of scattered radiation on the actinic effects of solar u.v. Even if a full treatment of the subject implying complex radiation transfer mechanisms is not required these phenomena should be kept in mind. The accuracy reached now in the determination of the absolute solar flux cannot be improved if the dimension of the efforts to measure it is not increased by a large factor. However, higher spectral resolution and higher accuracy of the measurements can still improve the actual situation.

1. M. ACKERMAN, D. FRIMOUT, and R. PASTIELS. *In* New techniques in space astronomy. *Edited by* Labuhin and Lüst. D. Reidel Publ. Co., Dordrecht, Holland. 1971.
2. C. R. DETWILER, D. L. GARRET, J. D. PURCELL, and R. TOUSEY. Ann. Geophys. **17**, 263 (1961).
3. M. ACKERMAN and P. SIMON. Sol. Phys. **30**, 345 (1973).

Can. J. Chem. Downloaded from www.nrcresearchpress.com by 210.87.254.40 on 09/05/12
For personal use only.

4. W. H. PARKINSON and E. M. REEVES. Sol. Phys. **10**, 342 (1969).
5. H. C. MCALLISTER. A preliminary photometric atlas of the solar ultraviolet spectrum from 1800 to 2965 Angstroms. University of Colorado Printing Services, Boulder, Colorado. 1960.
6. M. ACKERMAN, F. BIAUME, and G. KOCKARTS. Planet. Space Sci. **18**, 1639 (1970).
7. S. CIESLIK and M. NICOLET. Planet. Space Sci. **21**, 925 (1973).
8. A. L. BROADFOOT. Astrophys. J. **173**, 681 (1972).
9. E. PITZ. Appl. Opt. **10**, 813 (1971).
10. M. NICOLET. Planet. Space Sci. **20**, 1671 (1972).
11. A. W. BREWER and A. W. WILSON. Q. J. R. Meteorol. Soc. **91**, 452 (1965).
12. M. ACKERMAN. *In* Mesospheric models and related experiments. *Edited by* G. Fiocco. D. Reidel Publ. Co., Dordrecht, Holland. 1971.
13. R. D. CADDLE. Discuss. Faraday Soc. **37**, 66 (1964).
14. J. C. ARVESEN, R. N. GRIFFEN, and B. D. PEARSON. Appl. Opt. **8**, 2215 (1969).
15. R. TOUSEY. Space Sci. Rev. **2**, 3 (1963).
16. D. F. HEATH. J. Geophys. Res. **78**, 2779 (1973).
17. M. ACKERMAN. Ann. Geophys. **28**, 79 (1972).
18. M. NICOLET. *In* Mesospheric models and related experiments. *Edited by* G. Fiocco. D. Reidel Publ. Co., Dordrecht, Holland. 1971.
19. G. KOCKARTS. *In* Mesospheric models and related experiments. *Edited by* G. Fiocco. D. Reidel Publ. Co., Dordrecht, Holland. 1971.
20. F. BIAUME. J. Photochem. In press.
21. S. H. H. LARSEN. Geofys. Publ. **21**, No. 4 (1959–60).
22. L. ELTERMAN. Appl. Opt. **5**, 1769 (1966).
23. B. EDLÉN. J. Opt. Soc. Am. **43**, 339 (1953).
24. R. PENNDORF. Air Force Cambridge Research Center Tech. Note 55 – 206. 1955.
25. P. BENER. Technical Summary Report, contract AF 61 (052) – 54, Davos, Switzerland. 1960.

Can. J. Chem. Downloaded from www.nrcresearchpress.com by 210.87.254.40 on 09/05/12
For personal use only.

Sampling of Stratospheric Trace Constituents

D. H. EHHALT

National Center for Atmospheric Research,[1] Boulder, Colorado 80303

Received October 22, 1973

The measurement of stable atmospheric trace constituents is often separated into two steps: (*a*) the collection of a representative sample and (*b*) the analysis of the trace constituents in the laboratory. The main advantage of this approach is that the most sensitive detection methods can be used. The main disadvantage is that only a relatively limited number of data points can be taken along one sampling profile.

Basically two sampling techniques are used: (*a*) the collection of whole air samples or (*b*) the selective collection of one or more trace gases on a suitable trapping device. Whole air samples are taken either in the form of grab samples or by compression of air into pressure tanks or by condensing air in cryogenically cooled vessels. Stratospheric trace gases which have been measured by these methods include: CO_2, CH_4, CO, H_2O, H_2, N_2O, and the noble gases. Selective sampling is accomplished by passing air through molecular sieve beds, impregnated filters, or liquid nitrogen cooled traps. Trace gases retained and measured this way include CO_2, H_2O, N_2O, HNO_3.

Whole air samplers have been flown on high-flying aircraft, balloons, and rockets. The maximum altitude to which this technique can be usefully extended is 80 km. Selective trace gas samplers have been operated aboard aircraft and on balloons up to an altitude of about 35 km. Examples of the resulting trace gas profiles will be reported.

La mesure des constituants stables contenus en traces dans l'atmosphère est souvent divisée en deux étapes: (*a*) le prélèvement d'un échantillon représentatif, (*b*) l'analyse des constituants en traces dans le laboratoire. Le principal avantage de cette approche est, que des méthodes de détection plus sensibles peuvent être utilisées. Le principal désavantage c'est que seulement un nombre relativement limité de points donnés peuvent être retenus pour un échantillon en circluation.

En principe deux technique d'échantillonnage sont utilisées: (*a*) le prélèvement d'échantillons d'air entier ou (*b*) le prélèvement sélectif d'un ou plusieurs gaz en traces sur un dispositif approprié de captage. Les échantillons d'air entier sont pris soit en isolant tout simplement un volume définit d'air, soit par compression d'air dans des réservoirs sous pression ou soit par condensation d'air dans des vases refroidis de manière cryogène. Les gaz contenus en traces dans la strastosphère qui ont été mesurés par ces méthodes comprennent: CO_2, CH_4, CO, H_2O H_2, N_2O et les gaz rares. Un échantillonnage sélectif est réalisé en faisant passer de l'air à travers une couche de tamis moléculaire, de filtres imprégnés, ou de pièges refroidis au moyen d'azote liquide. Les gaz en traces tels CO_2, H_2O, N_2O, HNO_3 ont été retenus et mesurés de cette façon.

Les échantillonneurs d'air entier ont été fixés sur des avions, des ballons et des fusées volant à haute altitude. La hauteur maximum à laquelle cette technique peut être utilisée de façon rentable est de 80 km. Certains échantillonneurs de gaz en traces ont été utilisés à bord d'une avion et sur des ballons au dessus d'une altitude d'environ 35 km. Des exemples seront rapportés sur les profils qui résultent de l'étude de ces gaz.

[Traduit par le journal]

Can. J. Chem., **52**, 1510 (1974)

Introduction

A number of techniques have been devised to study atmospheric composition. One of the oldest is the direct sampling of air or selected atmospheric constituents. This method separates the determination into two steps: (*a*) the collection of a representative sample and (*b*) the analysis of the constituents in the laboratory. Sometimes analyses is also performed aboard the sampling platform. Most of the major atmospheric constituents have been measured in this manner but the method also is successful in measuring trace gases. The main advantage of this approach is that the collection devices used in the field can be kept simple and rugged and that the most sensitive laboratory detection methods can be utilized. The disadvantages are

[1]The National Center for Atmospheric Research is sponsored by the National Science Foundation.

Can. J. Chem. Downloaded from www.nrcresearchpress.com by 210.87.254.6 on 09/05/12
For personal use only.

Can. J. Chem. Downloaded from www.nrcresearchpress.com by 210.87.254.6 on 09/05/12
For personal use only.

that only a relatively limited set of data points can be taken along a given sampling mission, that its application is limited to those trace gases which are sufficiently stable to resist reaction during collection and storage, and that it is more sensitive to contamination than the remote techniques.

Of the many variants of this method most are of historical interest only, and I will limit this review to those which have yielded useful information on the trace gas distribution in the stratosphere. The collection techniques employed can be classified into two basic groups: (*a*) the collection of whole air samples and (*b*) the selective collection of one or more trace gases on a suitable trapping device. In the following sections, each collection technique is described briefly, its problems with respect to sample integrity (*i.e.*, fractionation and contamination) are identified, and the results obtained are shown.

Whole Air Sampling

As the term indicates, whole air sampling involves taking an air sample into a suitable container (ideally without fractionation of its constituents). This can be accomplished in several ways, the simplest being to expose a previously evacuated container to ambient air, and after pressure equilibration, to close it. In this way we obtain a so-called "grab sample" for which the sample pressure is that of ambient air at sampling altitude.

The Grab Sample

Because of its simplicity grab sampling can be carried out on any vehicle, aircraft, balloon, or rocket and the method has been used widely. For example, the atmospheric distribution of the noble gases was initially determined in this manner. In this case the only problem with sample integrity is that of fractionation due to mass discrimination during sample inhalation (*cf.* ref. 1). For other trace gases greater precautions are required to insure sample integrity. Reaction on the vessel walls have to be considered for the more reactive species and for this reason grab sampling so far has been limited to the measurement of the more stable trace gases like CH_4, CO, CO_2, N_2O, and H_2. But even for those the concentration might be altered by contamination. Contamination which is a problem in all sampling techniques can be caused by external and internal sources. External contamination is that released by the sampling vehicle due to outgassing of the skin and emissions from engine or other components. This problem can usually be eliminated by proper location of the air sample intake. Internal contamination is that due to the outgassing of the surfaces in contact with the sample during its collection, storage, and measurement. The latter presents a serious problem for some gases. For example, stainless steel which is widely used in the construction of sample containers releases H_2O, H_2, CO, CO_2, and CH_4 in significant amounts. Fortunately, electropolishing of the stainless steel surfaces and subsequent bake out at 400 °C serves to reduce outgassing rates for those gases by several orders of magnitude (2), and makes it possible to use stainless steel containers in stratospheric grab sampling (3). As an example I would like to discuss our measurements of molecular H_2 and CH_4 in the stratosphere. To obtain vertical profiles, eight evacuated stainless steel cans of 4 l volume were carried by balloon to an altitude of 30 km and opened at different altitudes during descent. The balloon sampling train is shown in Fig. 1. The payload is suspended about 150 m below the balloon to prevent H_2, which is present in the He used for balloon inflation to about 0.1%, from reaching the intake. To reduce contamination from the gondola itself, the sample intake is located about 6 m below and the inlet line is flushed about 20 times prior to sampling using a liquid N_2 cooled adsorption pump. (Most of the contamination from the gondola came from the battery pack which releases H_2, especially under load. It was therefore enclosed in a vacuum tight container.) As an additional precaution sampling was done during descent only. This virtually eliminated any external contamination (4). However, there were still internal sources of contamination. The amount of contamination was determined by simulating the sampling and measurement sequence with blank samples consisting of H_2 and CH_4-free N_2 and with samples of known composition. This was done in an environmental chamber simulating actual flight conditions (4). Such an evaluation of the contributions of the sampling system to the measured signal is an indispensable part of the calibration procedure for all sampling techniques.

The results for the balloon flights are summarized in Fig. 2. The balloons were launched

Can. J. Chem. Downloaded from www.nrcresearchpress.com by 210.87.254.6 on 09/05/12
For personal use only.

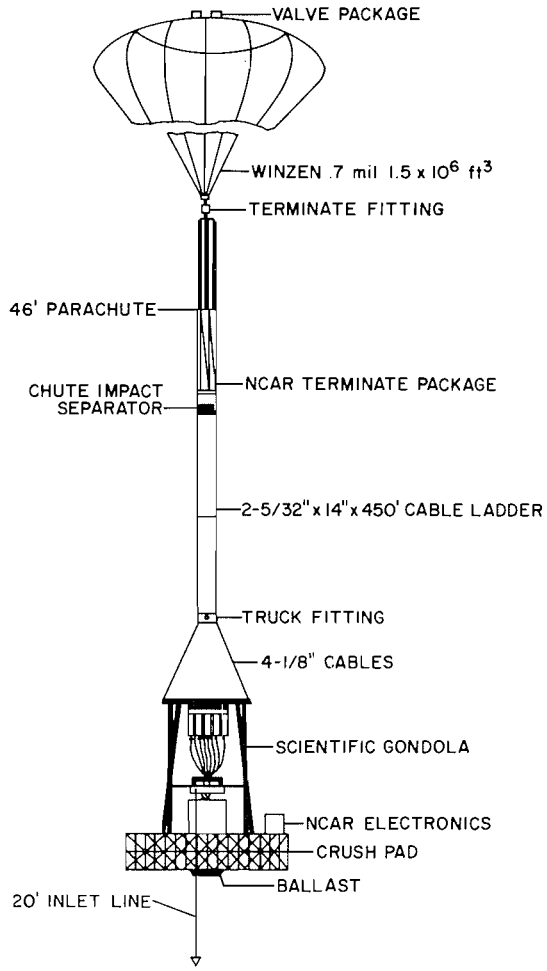

FIG. 1. Balloon sampling train. Note that the gondola is suspended about 150 m below the balloon and the intake is extended 6 m below the gondola.

from Palestine, Texas, at about 32° N. The CH_4 profiles, upper row, also include the data of Bainbridge and Heidt (5) after a small correction applied because their value for the CH_4 standard was somewhat high. In all cases the air samples collected below the tropopause have the same CH_4 mixing ratio as air samples obtained by aircraft flights in the upper troposphere over Texas. The data also agree well with the average tropospheric profile obtained over Scottsbluff, Nebraska, in 1966 which gave an average CH_4 mixing ratio of 1.32 p.p.m. The stratospheric portion of the CH_4 profiles shows a decrease in the mixing ratio *vs.* altitude starting at the tropopause. It appears that the gradient for the CH_4 mixing ratio is somewhat steeper directly above the tropopause and becomes weaker above 20 km. The standard error for the CH_4 stratospheric mixing ratio data is $\pm 5\%$.

The corresponding H_2 profiles are plotted in the lower row. Both the directly measured H_2 concentrations and the H_2 concentrations corrected for contamination are shown in order to indicate the magnitude of the corrections. The corrections are largest, approximately -1.3 p.p.m. for the highest altitudes, and decrease inversely with atmospheric density for the lower altitudes. The errors due to these corrections are indicated by the bars and they also decrease with altitude. Prior to the flight on 6 June 1972, the H_2 releasing parts had been identified and removed; thus the corrections are much smaller, approximately -0.16 p.p.m. at the maximum altitude. These measurements have a standard error of $\pm 5\%$. Again the results for the balloon samples collected below the tropopause agreed well with those for aircraft profiles over eastern Texas and with that of the average Scottsbluff profile in 1966 with an average H_2 mixing ratio of 0.49 p.p.m. The mixing ratio of H_2 appears to increase with altitude in the lower stratosphere. It reaches a maximum at about 25–27 km and decreases above. This also was true for the profile of 6 June 1972 which provides the most reliable set of data. For the latter, however, the H_2 maximum is much less pronounced, reaching only 0.75 p.p.m. compared to 1.4 p.p.m. and 1.3 p.p.m. in the previous two profiles. This could indicate that the H_2 contamination in the previous flights has been underestimated. To the best of our knowledge this was not the case. Furthermore the CH_4 profile on the same date also has an unusual shape, showing an increase between 25 and 29 km rather than the usual decrease. Both the low H_2 maximum and the unusual CH_4 profile may be related to the very high tropopause of 18 km reported by the Palestine, Texas, balloon station for that day. In any case, all the H_2 profiles show an increase with altitude in the lower stratosphere, a maximum at ~ 27 km and a decrease above.

The altitude range for grab sampling is limited. Because the sample pressure is that of ambient air, sample size decreases with altitude and the sensitivity of detection correspondingly decreases. On the other hand, internal contamination is practically independent of sample pressure and thus of altitude. Eventually the contribution of contamination to the signal be-

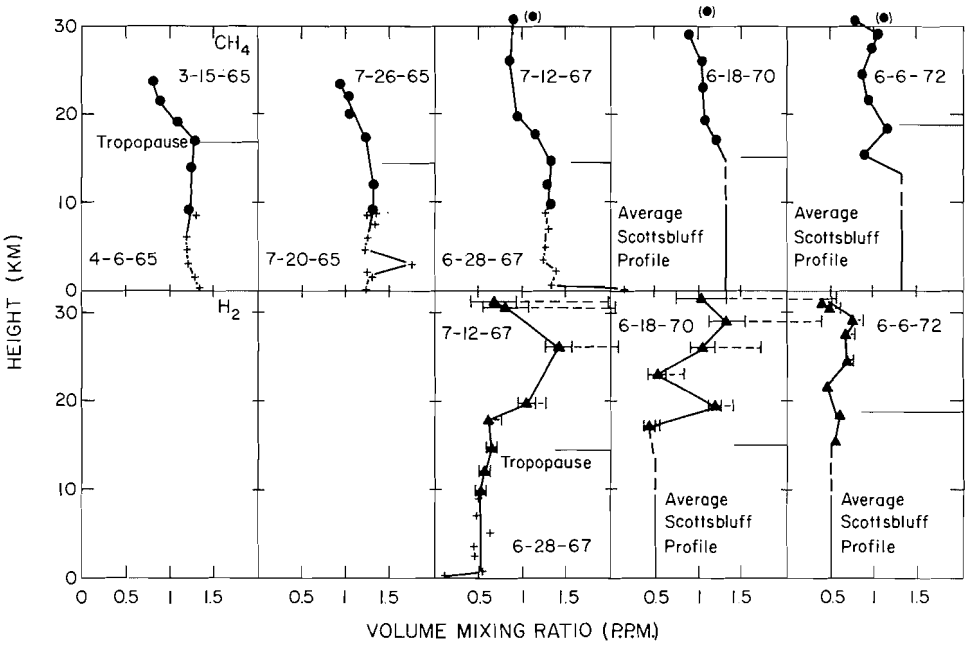

FIG. 2. Tropospheric and stratospheric profiles of molecular H_2 and CH_4 over eastern Texas, ~32° N. Crosses represent samples from aircraft flights collected on the lower dates; dots represent samples from balloon flights collected on the upper dates; triangles represent H_2 mixing ratios corrected for contamination; dashed lines connect them to the measured values; bars show errors for H_2 (no bars indicate an error $\leq 5\%$). The two earliest CH_4 profiles are those of Bainbridge and Heidt (5). The other CH_4 data are from Ehhalt and Heidt (4).

comes so large that the trace gas measurements are unreliable. Increasing the volume of the sample containers provides only a limited remedy because then surface area and total amount of contamination increase also. Finally there are trace gases like CO or N_2O which are present at lower concentration and thus more difficult to measure, thus requiring larger air samples. For all these reasons a number of attempts have been made to use some kind of compression to increase sample size.

Compressed Samples

One way of increasing the sample pressure is to use a compressor. Because of power requirements, this technique is limited to aircraft as the sampling platform. Other drawbacks include the danger of contamination, especially from lubricants used in the compressors, as well as the possibility of sample modification as the result of heating during compression. However, it is possible to use compressor systems of aircraft for sampling purposes. Junge and co-workers are running a program to obtain H_2, CO, and N_2O measurements aboard Boeing 707 commercial airliners and other aircraft (6–8). These investigators do not collect whole air samples for laboratory analysis but analyze the H_2 and CO concentration aboard the aircraft. N_2O is collected on a molecular sieve, a technique described below. In any case their success shows that the compression systems of these aircraft can be used for grab sampling. Seiler and Warneck's (8) results indicate a sharp decrease in the CO concentration above the tropopause, from a tropospheric value of 0.16 p.p.m. down to 0.04 p.p.m. at about 1 km above the tropopause. At higher altitudes the CO concentration remained constant up to about 3 km above the tropopause, their maximum level of measurement. The H_2 concentration changed very little across the tropopause in good agreement with our data.

Cryogenic Samples

Another way to increase the size of the whole air sample is condensation of air in liquid Ne, H_2, or He cooled samplers. This collection technique has some definite advantages: the compression ratio can be very large. Thus a large air sample is contained in a small volume of small surface area. The problems of sample modification and

Can. J. Chem. Downloaded from www.nrcresearchpress.com by 210.87.254.6 on 09/05/12
For personal use only.

Can. J. Chem. Downloaded from www.nrcresearchpress.com by 210.87.254.6 on 09/05/12
For personal use only.

contamination are minimized. In fact, most gas reaction rates are slowed down considerably at the low temperatures so that a number of the more reactive constituents are preserved, at least as long as the air sample is kept cold. Finally the sampler requires very little power and can be carried on a variety of sample platforms.

Several types of cryogenic samplers have been developed in the past and some of them have been flown (see ref. 9). But only two experiments, both flown on rockets, have returned useful data or show promise of returning useful data. I will first briefly describe the design and operation of a cryogenic rocket sampler, the ENCAR samplers, developed and flown by Martell and his associates (10).

The cryogenic rocket sampler is a device designed to collect a large uncontaminated sample, of a few hundred liters at standard temperature and pressure (STP), of high altitude air for subsequent analyses of trace gases and radioactive fallout aerosol particles in the laboratory. Essentially, it is a large cryopump cooled with liquid Ne, which freezes out all of the atmospheric gases except H_2, He, and Ne. The basic design is shown in Fig. 3. The sampler is carried aloft by an Aerobee rocket. Sampling intervals can be chosen between 40 and 80 km altitude. Air sampling is initiated by ejecting the split nose cone and pulling off the inlet cap at the threshold sampling altitude. The sampler is closed about 10 s later by rotating the "ball" closure valve clockwise and compressing the rounded surface into an O-ring sealed seat. Because radioactive fallout aerosol concentrations were too low, application of the sampler has been concentrated on the analysis of trace gases.

The cryogenic sampler has some additional problems. Partly because of the initial requirement that the air sample be collected quantitatively, it was decided to sample during rocket ascent while the rocket is spin stabilized in a well-defined upright position. At that time the rocket is travelling at about 4 Mach which has a number of consequences on sampler design and operation.

(*a*) A shock wave develops during sampling which heats the inhaled air to 1300 °K for about 10 ms. (The location of the shock wave is above the first coil but below the closure valve.) As a consequence the more reactive gases may experience changes in their concentration due to enhanced reaction rates.

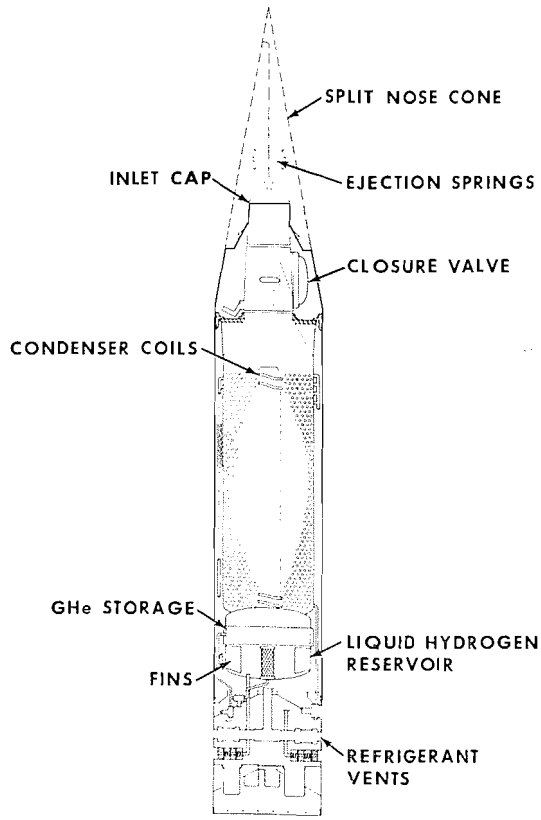

FIG. 3. Schematic drawing of "ENCAR" sampler flown on 4 September 1968 (ENCAR—*EN*closed *C*ryocondenser for *A*ir *R*ecovery; *cf.* Denton (9)).

(*b*) To accommodate the large heat load (~100 l of air STP have to be cooled from 1300 °K to 30 °K in 10 s) a large heat exchange surface area is required: about 10 m^2. Such a large surface is difficult to free from contaminants, especially from H_2O.

(*c*) The sampler has to be opened and closed very quickly, resulting in the particular opening and closing procedure mentioned above. As a consequence the poorly baked out exterior of the closure valve is open to the condenser part for an extended period prior to launch and results in some contamination of the sampler with H_2O.

Although most of the contamination problems can be corrected, these corrections require extensive auxiliary measurements; sampler preparation, bake out sample collection, and recovery procedures have to be simulated in the laboratory by running blank samples.

The data obtained on the rocket flight of 4 September 1968 are summarized in Table 1. The sampling altitude interval was between

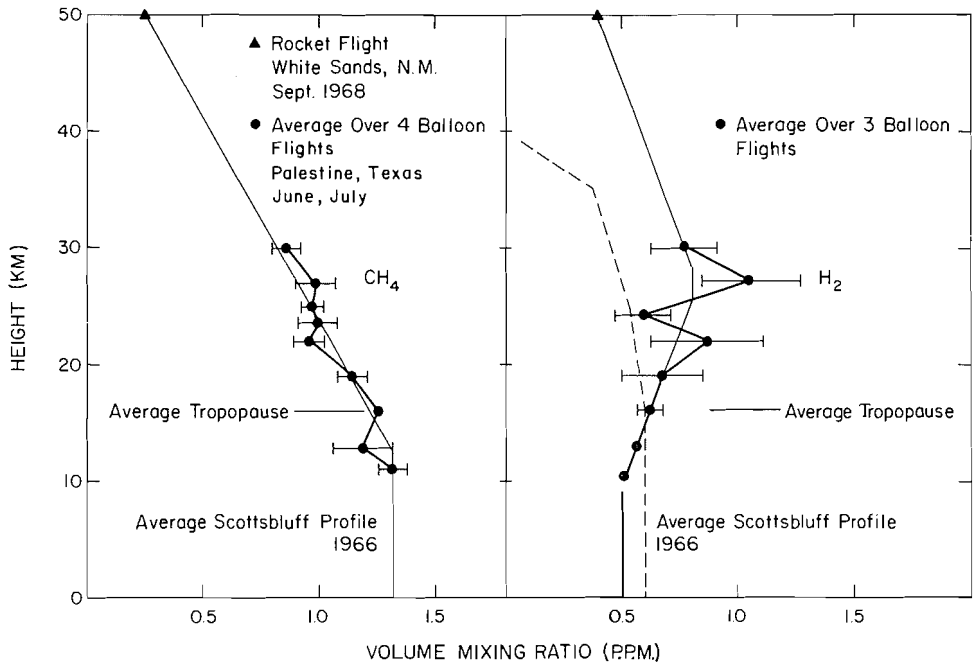

FIG. 4. Stratospheric H_2 and CH_4 profiles averaged over the individual profiles in Fig. 2 are compared with the results from the ENCAR rocket flight. Bars indicate mean standard deviation due to scatter in individual profiles. Dashed H_2 profile is from a model calculation by Hesstvedt (21). Heavy lines connect measured values. Thin lines represent curves adopted as average.

TABLE 1. Average trace gas concentration between 44 and 62 km altitude. Air sample was obtained on 4 September 1968 by a cryogenic sampler carried on an Aerobee rocket

Trace gas	Volume mixing ratio (p.p.m.)	Reference
H_2	$0.40 + 0.05$ $0.40 - 0.10$	19
H_2O	3–10*	19
CH_4	0.25 ± 0.02	11
CO_2	308 ± 3	20
N_2O	0.00 ± 0.005	Unpublished

*Measurement only allows setting of upper and lower limits.

44 km and 62 km. Thus the mean sampling altitude was ~50 km. Except for H_2O for which the contamination was large and only limits on the concentration can be given, the measured concentrations are rather accurate. In particular, estimates show that the brief heating in the shock wave does not alter the concentrations appreciably and the collected sample is indeed representative. At most 2.5% of the H_2 (4), 1.5% of the CH_4 (11), and less than that for N_2O could be oxidized in the shock wave. None of these gases should be produced. The H_2 and CH_4 measurement can be compared to the balloon profiles shown earlier. In Fig. 4, the data give the average for the four balloon flights in June and July. We see that the rocket results agree well with the relatively slow, linear decrease of CH_4 in the lower and middle stratosphere. For H_2, the combined measurements show an increase in the mixing ratio from 0.5 p.p.m. at the tropopause to 0.8 p.p.m. at 28 km with a decrease at higher altitudes. The latter decrease is not well defined, because data between 30 and 50 km altitude are lacking. In fact a very recent balloon experiment indicates that the increase continues to somewhat higher altitudes. In Fig. 4 the data points between 30 and 50 km are connected with a straight line.

Another successful rocket flight was made on May 23, 1973. The air sample is in the process of analysis and the results will be published soon.

A different type of rocket-borne liquid Ne cooled cryogenic air sampler has been developed by Ballard.[2] This is a much smaller unit, de-

[2]Information acquired by private communication with H. N. Ballard, Atmospheric Science Laboratory, USAECOM, White Sands Missile Range, N.M. in 1973.

Can. J. Chem. Downloaded from www.nrcresearchpress.com by 210.87.254.6 on 09/05/12
For personal use only.

Can. J. Chem. Downloaded from www.nrcresearchpress.com by 210.87.254.6 on 09/05/12
For personal use only.

signed to collect only 1 l STP of ambient air, and carried on a small Arcas rocket. The design is simple. The heat exchanger which serves also as the liquid Ne reservoir is held inside an evacuated, thermally insulated vessel. A single sampling valve is opened and closed below 60 km during descent on a parachute. A small sampler has some advantages: it is flown on a much cheaper rocket and its construction is cheaper. Since air sampling is accomplished during descent the problems associated with shock waves are eliminated. The sample is large enough to allow all of the trace gas measurements done on the ENCAR sample, but because of the small sample size, isotopic analysis cannot be performed. Thus, in principle, the method is promising. However, the samples obtained have only been analyzed for CO_2 and so far give excessively high concentrations: 450 p.p.m.v. and higher.[3] Obviously with the present sampler design fractionation must take place, possibly due to insufficient cooling capacity.

This concludes the list of whole air samplers used in the past. I might mention in passing that we have recently installed a cryosampler on a balloon, replacing the grab sample bottles with liquid Ne cooled pressure cylinders of stainless steel. A first, successful flight was made in September 1973, for which the data are not yet available. We plan to measure vertical profiles of N_2O, CO, and CO_2 in addition to profiles of H_2 and CH_4.

Selective Sampling

There are trace substances of interest for which even compression cannot provide a sufficiently large sample for analysis and one must resort to methods which provide an enrichment of the substance of interest during the course of sampling, *i.e.* selective sampling. A well-known example is the filtration of aerosols, in which only the particles are deposited and retained on the filter and the air is pumped away. Large volumes of air can be processed in this manner and the "enrichment" can be substantial. Selective sampling has been applied for trace gases, mainly for isotopic measurements which require large amounts of a given trace substance, but a few measurements of stratospheric trace gas concentrations using enrichment techniques do exist.

Enrichment by Freeze Out

When air is passed through a liquid N_2 cooled cold trap a number of trace gases are frozen out essentially quantitatively at their partial pressures in the atmosphere, including CO_2, H_2O, N_2O, NO_2, HNO_3, SO_2, H_2S, NH_3, and higher organic molecules. Enrichment factors of the order of 1000 can easily be obtained for these gases (such cold traps typically have a volume of 1 l and allow flow rates of about 100 l/min; thus in a 10 min period 1000 l of air can be processed). An enrichment factor of 1000 brings many of the above gases into a concentration range which allows their measurement. The method is most easily used on an aircraft where the ram pressure provides for the air flow. We have flown such traps aboard the NCAR Sabreliner up to 13 km altitude to collect H_2O and CO_2 for isotopic analysis. As it turned out, the concentration measurement of N_2O is readily obtained as a by-product of these measurements. N_2O follows CO_2 quantitatively during gas separation in the laboratory and the N_2O/CO_2 ratio can be determined in the mass spectrometer along with the measurement of $^{13}C/^{12}C$ and $^{18}O/^{16}O$ isotope ratios. Thus we have obtained a number of N_2O profiles in the upper troposphere and lower stratosphere; an example is shown in Fig. 5. In the upper troposphere the N_2O concentration varies around 0.24 p.p.m., in good agreement with the tropospheric measurements of Schütz *et al.* (7).

Enrichment on Molecular Sieves

Many trace gases are adsorbed on molecular sieves with reasonable retention volumes. Thus air passed through a sieve bed will be stripped of such trace gases as CO_2, H_2O, N_2O, SO_2, NO, and NO_2. These gases will be quantitatively retained until so much is accumulated on the sieve that breakthrough occurs. Proper dimensioning of the sieve bed allows collection of quite large samples at high flow rates without breakthrough.

The trace gases are extracted in the laboratory by passing carrier gas through the heated sieve bed. Another technique involves the displacement of the trace gases by adding a gas which is preferentially adsorbed, such as H_2O, to the

[3]Information acquired by private communication with H. N. Ballard, Atmospheric Science Laboratory, USAECOM, White Sands Missile Range, N.M. in 1973.

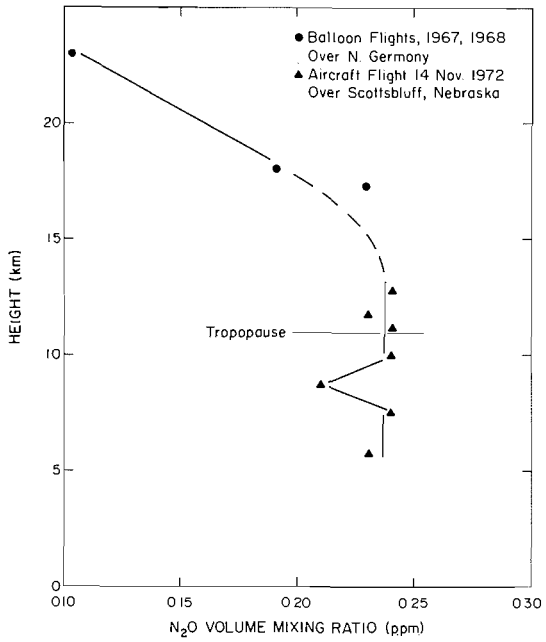

FIG. 5. Vertical profile of N_2O volume mixing ratio. The tropopause on all flights was near 11 km. The balloon data are from Schütz *et al.* (7). The aircraft data are our own unpublished results.

carrier gas stream. In this way excessive heating and destruction of trace gases can be avoided. The use of sieve beds for the collection of CO_2 aboard balloons for ^{14}C analysis has been described in detail by Ashenfelter *et al.* (12). The authors point out that their sampling device should also be useful for measuring SO_2, NO_x, water vapor, and hydrocarbons in the stratosphere up to 37 km. The method can also be used on aircraft.

So far the only work with molecular sieves has been carried out by Junge and co-workers on N_2O in the stratosphere. To adsorb N_2O, air was pumped through a tube filled with 5A molecular sieve after CO_2 and H_2O had been taken out by first passing the air through tubes filled with sodium hydroxide, asbestos, and P_2O_5. Suction was provided using an evacuated 87 l sphere carried aboard the balloon (7). For analysis, the N_2O tube is heated to 300 °C and the N_2O is pumped into a gas chromatograph. The results of these measurements also are shown in Fig. 5. The results show a marked decrease of the N_2O concentration in the lower stratosphere. This feature has been confirmed recently by Murcray *et al.*[4] using a balloon-borne infrared spectrometer.

Selective Sampling on Filters

In studies of the stratospheric sulfate aerosol Lazrus *et al.* (13) sometimes observed nitrate ion present in higher concentrations than sulfate ion. Only cellulose filter showed such results. Polystyrene filters always showed zero or very low NO_3^- concentrations. This excluded the possibility that the NO_3^- ion was associated with aerosols but indicated the presence of gaseous NO_3^-. Subsequent laboratory experiments confirmed that HNO_3 is adsorbed on cellulose but not on polystyrene filters. At that time, of course, Murcray *et al.* (14) had discovered the presence of HNO_3 in the upper atmosphere, which made the finding of Lazrus *et al.* (13) quite plausible. In fact the NO_3 measurements, although not yet calibrated absolutely, agree fairly well with Murcray's data. Most of the Lazrus *et al.* data have been collected aboard RB 57F aircraft and provide a good latitudinal profile around 20 km altitude. Some NO_3^- data have been obtained on balloons and these allow the construction of a vertical profile, shown in Fig. 6. It indicates a steep increase in the HNO_3 volume mixing ratio between 0.6 p.p.b. at 18 km and 5 p.p.b. at 20 km. Both the position of this increase, as well as the concentration, agree well with the more detailed profiles published by Murcray *et al.*[4]

It is conceivable that filter sampling which allows processing of very large air volumes can be used to collect other trace gases as well by impregnating filters with suitable reactants. Such techniques have been successfully used in tropospheric sampling. Natusch *et al.* (15) developed an $AgNO_3$ impregnated filter which allows collection of H_2S and measurement down to concentrations as low as 5 p.p.t. (5×10^{-12}). Forrest and Newman (16) collected SO_2 on Whatman 541 filters impregnated with a solution of KOH, and triethanolamine. Moore (17) adapted this method to NO_2 collection on filters (*cf.* also Levaggi *et al.* (18)) and also developed a technique to collect NH_3 on filters. So far these

[4]D. G. Murcray, A. Goldman, F. H. Murcray, W. J. Williams, J. N. Brooks, and D. B. Barker. Vertical distribution of minor atmospheric constituents as derived from airborne measurements of atmospheric emission and absorption infrared spectra. Preprint.

Can. J. Chem. Downloaded from www.nrcresearchpress.com by 210.87.254.6 on 09/05/12
For personal use only.

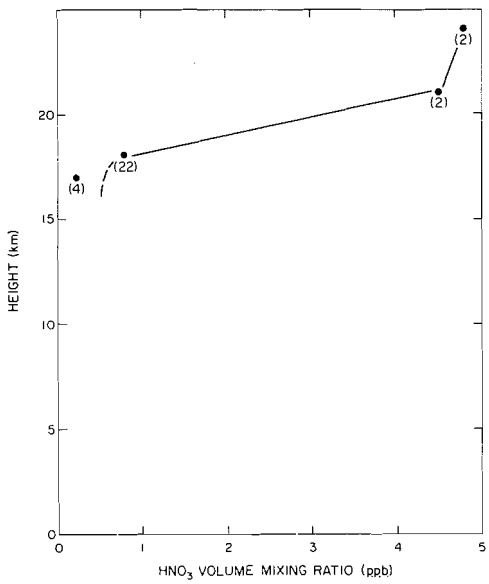

FIG. 6. Vertical profile of the HNO_3 volume mixing ratio obtained by NO_3 collections on cellulose filters. Data are from Lazrus *et al.* (13). Numbers indicate the number of samples included in the average. The samples were collected north of 30° N in different seasons and years.

techniques have only been used near the earth's surface. In fact they require an appreciable relative humidity (>20%) and not too low a temperature to operate at full efficiency. Thus the filter technique will require modification and testing before it can be applied to stratospheric sampling.

Conclusion

This completes the list of air sampling techniques which have provided information on stratospheric trace gas concentrations. There are, of course, other techniques adaptable to stratospheric sampling. One which is used widely in the troposphere involves the bubbling of air through absorber or chemically reactive solutions. However, such methods are cumbersome and do not lend themselves readily to routine aircraft or balloon sampling to obtain vertical and latitudinal distributions. These methods, however, could be useful in exploratory studies of various minor atmospheric constituents.

1. G. R. MARTIN. The composition of the atmosphere above 60 km. *In* Rocket exploration of the upper atmosphere. *Edited by* R. L. F. Boyd and N. J. Seaton. Pergamon, London. 1954. pp. 161–168.
2. E. STRAUSSER. Proc. 4th Int. Vacuum Congr. Institute of Physics and the Physical Society, London, England. 1968. p. 469.
3. L. E. HEIDT and D. H. EHHALT. J. Chromatogr. **69**, 103 (1972).
4. D. H. EHHALT and L. E. HEIDT. Pure Appl. Geophys. **106–108**, 1352 (1973).
5. A. E. BAINBRIDGE and L. E. HEIDT. Tellus, **18**, 221 (1966).
6. U. SCHMIDT. Large scale distribution of H_2 in the troposphere. lower stratosphere and in ocean surface waters. Presented at the Commission on Atmospheric Chemistry and Global Pollution International Symposium on Atmospheric Trace Gases, Mainz, Germany, 2–5 April 1973.
7. K. SCHÜTZ, C. JUNGE, R. BECK, and B. ALBRECHT. J. Geophys. Res. **75**, 2230 (1970).
8. W. SEILER and P. WARNECK. J. Geophys. Res. **77**, 3204 (1972).
9. E. H. DENTON. Sci. Prog. Oxf. **58**, 539 (1970).
10. E. A. MARTELL. J. Appl. Meteorol. **9**, 170 (1970).
11. D. H. EHHALT, L. E. HEIDT, and E. A. MARTELL. J. Geophys. Res. **77**, 2193 (1972).
12. T. E. ASHENFELTER, J. GRAY, JR., R. E. SOWL, M. SVENDSEN, and K. TELEGADAS. J. Geophys. Res. **77**, 412 (1972).
13. A. L. LAZRUS, B. GANDRUD, and R. D. CADLE. J. Appl. Meteorol. **11**, 389 (1972).
14. D. G. MURCRAY, T. G. KYLE, F. H. MURCRAY, and W. J. WILLIAMS. J. Opt. Soc. Am. **59**, 1131 (1969).
15. D. F. S. NATUSCH, H. B. KLONIS, H. D. AXELROD, R. J. TECK, and J. P. LODGE, JR. Anal. Chem. **44**, 2067 (1972).
16. J. FORREST and L. NEWMAN. Atmos. Environ. **7**, 1 (1973).
17. H. E. MOORE. Isotopic measurement of atmospheric nitrogen compounds. Presented at the Commission on Atmospheric Chemistry and Global Pollution International Symposium on Atmospheric Trace Gases. Mainz, Germany, 2–5 April 1973. Accepted for publication in Tellus.
18. D. A. LEVAGGI, W. SIU, M. FELDSTEIN, and E. L. KOTHNY. Environ. Sci. Techol. **6**, 250 (1972).
19. T. G. SCHOLZ, D. H. EHHALT, L. E. HEIDT, and E. A. MARTELL. J. Geophys. Res. **75**, 3049 (1970).
20. E. A. MARTELL. The distribution of minor constituents in the stratosphere and lower mesosphere. *In* Physics and chemistry of upper atmospheres. *Edited by* B. McCormac. D. Reidel Pub. Co., Dordrecht, Holland. 1973. In press.
21. E. HESSTVEDT. Geophys. Publ. Norway, **27**, 1 (1968).

Can. J. Chem. Downloaded from www.nrcresearchpress.com by 210.87.254.6 on 09/05/12
For personal use only.

Stratospheric Aerosol Determinations

D. J. HOFMANN
Department of Physics and Astronomy, University of Wyoming, Laramie, Wyoming
Received October 8, 1973

This review consists of a summary and comparison of the results of ongoing programs to study the stratospheric aerosol by a variety of techniques. In view of the considerable degree of disagreement among various experimental techniques in the past, the importance of comparative studies is emphasized. Many of the results are still in preliminary form, and only relatively new results are presented.

Both remote and *in situ* measurements are discussed; the former consist mainly of lidar observations while the latter comprise impactor sampling and light-scattering particle detectors. Discussion is divided along traditional lines, *i.e.*, by particle size, with "small" particles those of radii ≤ 0.1 μm and "large" particles those of radii ≥ 0.1 μm, with emphasis on the latter because of the considerably greater body of knowledge available for these particles.

Cette revue consiste en un résumé et une comparaison des résultats de programmes antérieurs qui étudient l'aérosol stratosphérique par une variété de techniques. En vue du degré considérable de désaccord parmi les techniques expérimentales variées dans le passé, l'importance des études comparatives est soulignée. Un grand nombre des résultats est encore sous une forme préliminaire mais, seuls les résultats relativement récents sont présentés.

Les mesures à distance et *in situ* sont toutes deux examinées; la première consiste principalement en observations lidar alors que la dernière comprend un échantillonnage à percussion et des détecteurs de particules à diffusion lumineuse. La discussion est répartie suivant les directives traditionnelles, c'est à dire par la grosseur de la particule, avec les "petites" particules dont le rayon ≤ 0.1 μm et les "grosses" dont le rayon ≥ 0.1 μm. On insiste sur ces dernières à cause d'un ensemble de connaissances considérablement plus grand disponible pour ces particules. [Traduit par le journal]

Can. J. Chem., **52**, 1519 (1974)

Introduction

To review available stratospheric aerosol measurements at this time is a difficult task. Not because very little is known; quite the contrary, a great deal is being learned about this important stratospheric constituent. Unfortunately, most of the significant results are very recent and thus of a preliminary nature at this writing and cannot all be included at this time. It thus behooves the author to discuss less recent results, while knowing full well that they do not contain the whole story.

Since its discovery by Junge *et al.* (1), the stratospheric "sulfate layer" has remained a strange but prominent feature of the upper atmosphere. This layer, the major portion of which occurs between about 10 and 25 km altitude, depending on latitude and season, generally begins just above the local tropopause. The major constituent of the particle layer is sulfur, generally thought to be in the form of sulfuric acid droplets. Its presence does not become noticeable to the untrained eye, without the aid of sensitive instrumentation, unless a cataclysmic event such as a major volcanic eruption injects into the stratosphere a substantial amount of material in excess of the so-call "natural background" aerosol. It is, however, this latter component that we are really interested in. Volcanic injections are transient events which, when averaged over time, are of a rather insignificant consequence; that is to say, uninteresting in a scientific sense except perhaps to serve as a tracer of stratospheric motions. At any rate, we can rest assured that the global climate will not be seriously and irreversibly altered by volcanism. The "natural background" aerosol or particulate content of the stratosphere, if indeed it exists (and most evidence now suggests that it does), is far more interesting since it involves a mechanism which is not well understood and is apparently related to a continuous natural process which is taking place. One must then be

Can. J. Chem. Downloaded from www.nrcresearchpress.com by 210.87.254.105 on 09/05/12
For personal use only.

Can. J. Chem. Downloaded from www.nrcresearchpress.com by 210.87.254.105 on 09/05/12
For personal use only.

TABLE 1. Climatic Impact Assessment Program aerosol research programs

Instrument	Agency	Platform	Aerosol property measured	Remarks
			>0.1 μm radius	
Dustsonde	University of Wyoming	Balloon	Particle concentration	Detects individual particles by light-scattering techniques during balloon ascent
Lidar	NASA–ARC/SRI	Ground level	Scattering ratio	Tunable dye laser and pulsed ruby laser for atmospheric sounding
Lidar	NCAR	Aircraft	Scattering ratio	Tunable dye laser for atmospheric sounding
Lidar	NASA–LRC	Ground level	Scattering ratio	Pulsed ruby laser and neobidium laser for atmospheric sounding
Sampler	LASL	Aircraft	Mass concentration and composition	Impact filters. Analysis by gamma irradiation, X-ray fluorescence, and electron microscopy
Sampler	NCAR	Aircraft	Mass concentration and composition	Impact filters. Analysis by neutron activation, X-ray fluorescence, and colorometric measurements
Sampler	CSIRO (Australia)	Balloon	Particle concentration, size, and composition	Impact electron microscope grids chemically treated
Solar extinction	University of Wyoming	Satellite	Extinction coefficient	Determines infrared extinction caused by aerosols at satellite sunrise and sunset
			<0.1 μm radius	
Condensation nuclei counter	University of Wyoming	Balloon	Particle concentration	Detects individual particles by light-scattering techniques following growth by condensation
GE Aitken nuclei detector	TSC/GE/NOAA	Aircraft	Particle concentration	Detects particles by measuring integrated light scattering following condensation
Gerdien tube	NOAA	Aircraft	Ion density	Modified for aircraft use
Gerdien tube	University of Wyoming	Balloon	Ion density	Uses balloon ascent for air flow
Gerdien tube	University of Minnesota (Duluth)	Balloon	Ion density	Uses pump for air flow

concerned else this natural balance be upset by some as yet unknown cause resulting from man's intrusion into this region of space.

Research Methods and Monitoring Programs

Table 1 summarizes current stratospheric aerosol research techniques and organizations engaged in utilizing these techniques under the CIAP program. Although some of these programs are still in the early developmental stages, a number of them are currently producing data and others have been for several years.

Some of these efforts will be more or less limited while others are extensive in spatial and temporal scope. For example, the aircraft filter sampling programs involve seasonal surveys (Project Airstream) over a latitude range from 75° N to 51° S and at six altitudes between 12 and 19 km.

The University of Wyoming's balloon program involves monthly soundings from Laramie, Wyoming, in addition to annual soundings from the ice island T-3 at 85° N and the South Pole and bimonthly soundings from five other stations in Alaska, Canada, the United States, Panama, and Australia. In addition to particulates, ozone and water vapor are also measured. The latter program will be referred to extensively in this report as it is the one best known to the author.

Aerosol Characteristics

Although there are at least three rather distinct groups of particles (Aitken or condensation nuclei ($r < 0.1$ μm), medium particles (0.1 μm $\leq r \leq 1$ μm), and large particles ($r > 1$ μm), the latter probably of meteoric origin (2) it is generally sufficient to divide them into two classes with a radius of 0.1 μm as the dividing size. While a wealth of measurements (though perhaps not knowledge) for the >0.1 μm particles exists, a corresponding lack of measurements and knowledge concerning the <0.1 μm, commonly called condensation nuclei (c.n.), is evident. For this reason a proportionally small amount of space will be devoted to the latter component.

Condensation Nuclei

Rosen (3) has reviewed the available stratospheric c.n. measurements and estimated the applicable concentrations for the indirect measurements. His results are given in Table 2. The

TABLE 2. Condensation nuclei measurements

Method	Estimated concentration (cm^{-3})	Reference
Ion density	60	Kroening (15) Rosen (2)
Condensation nuclei counter	~1	Junge (20)
Infrared emission	600	Pilipowskyj *et al.* (16)
Solar aureole	300	Newkirk and Eddy (17)
Sky brightness	80	DeBary and Rossler (18)

several orders of magnitude difference between the direct measurement (c.n. counter) and the others is an apparent discrepancy.

That c.n. may be present in relatively large numbers is one possible explanation of why simultaneous impactor and filter sulfate collection disagree by at least an order of magnitude (4). In comparison to impactors, filters are much more efficient for collecting particles in the c.n. size range. However, particle concentrations cannot be extracted from the filter analysis. Some of the indirect measurements could be significantly in error since they depend on the assumptions made concerning scattering due to larger particles. The average c.n. concentration probably lies between 10 and 100 per cm^3 at stratospheric heights.

Little is known about the composition of c.n. A major portion is probably made up of the same material as the larger particles (*i.e.*, sulfuric acid); however, inclusions in particles examined by electron microscopy by Bigg *et al.* (5) appeared electron dense and are probably micrometeoritic.

Although the very small particles scatter in a Rayleigh manner and are probably not numerous enough to be important in the overall radiation picture, they may play a role in the formation of larger particles. In addition, since very small particles may be an important product of jet engine exhaust in the stratosphere, the importance of the measurement of the current natural background of c.n. is manifest.

>0.1 μm Radius Aerosol

As mentioned earlier, a great deal of data by a

Can. J. Chem. Downloaded from www.nrcresearchpress.com by 210.87.254.105 on 09/05/12
For personal use only.

Can. J. Chem. Downloaded from www.nrcresearchpress.com by 210.87.254.105 on 09/05/12
For personal use only.

number of different techniques exists for these particles which constitute the conventional "sulfate layer". Only recent results will be discussed here, relying on the general improvement of technique with age.

Vertical Concentration Distribution

The most complete vertical aerosol distributions are obtained from balloon soundings and lidar soundings. Interpretation of the latter in terms of particle concentration, however, involves the use of an aerosol model; *i.e.*, a size distribution and composition. In addition, the lidar return is subject to normalization (a point in the atmosphere having zero aerosol concentration must be assumed to correct for Rayleigh scattering from air molecules). Also, the Rayleigh component varies from day-to-day so that a measure of atmospheric density or temperature is necessary. With the current low aerosol concentrations ($\sim 1/cm^3$), the lidar return due to aerosol is only about 10% of the Rayleigh return and small corrections such as those due to atmospheric density fluctuations and absorption of the signal as it passes through the aerosol itself must be considered. For these reasons, accurate absolute concentrations cannot at this time be extracted from the lidar data. On a relative basis, with accurate air density data, the instrument should be well suited for day-to-day monitoring since the aerosol characteristics do not appear to change excessively with time.

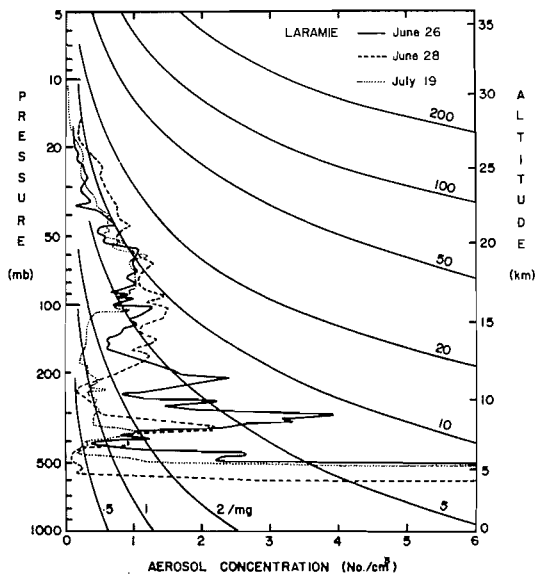

FIG. 1. A comparison of the vertical distribution of aerosol particles having diameters greater than 0.3 μm over Laramie, Wyoming, in 1972. The smooth curves are lines of constant mixing ratio in units of particles/mg of air.

Figure 1 shows a comparison of the vertical distribution of particles having diameters greater than 0.3 μm for three balloon soundings of the dustsonde over Laramie by the University of Wyoming group during the summer of 1972. The tropopause occurred at about 13 km in these soundings and, as is usually observed, delineates the lower boundary of the stratospheric "sulfate layer" occurring between about 15 and 22 km with a typical particle concentration of $1/cm^3$. The large variations in the troposphere are commonly observed. Figure 1, from Rosen *et al.* (6), was used to show the decay of an apparent low-level dust cloud just below 10 km possibly injected by a volcano which erupted on June 19.

Size Distribution

Although extensive efforts are currently being made to measure the aerosol size distribution in the 0.1–1 μm range, no definitive result exists as yet. The question of a maximum in the spectrum remains, and from the dustsonde results for particles with diameters greater than 0.3 μm and greater than 0.5 μm, one can conclude that the spectrum decreases monotonically above a diameter of 0.3 μm such that the concentration ratio of these two sizes is about 4 in the stratosphere.

Composition

Extensive composition measurements have been made possible by the filter sampling technique. Cadle (4) has reviewed these measurements and Table 3 is taken from his work. The high nitrate (NO_3^-) concentrations observed are thought to be due to nitric acid vapor absorbed

TABLE 3. Average chemical composition of IPC filter samples collected over the central United States at 17–18 km altitude*

Date	SO_4^{2-} (μg/m³)	NH_4^+ (μg/m³)	NO_3^- (μg/m³)
May 11, 1970	0.20	0.0033	0.36
October 17, 1970	0.10	0.0025	0.12
February 3, 1971	0.10	0.0000	0.20
February 28, 1971	0.028	0.0027	0.027

*Data of Lazrus *et al.* (8, 19).

Can. J. Chem. Downloaded from www.nrcresearchpress.com by 210.87.254.105 on 09/05/12
For personal use only.

by the IPC filters. The sulfate and ammonium ions are included since they are thought to be the important constituents of the stratospheric aerosol. The sulfate dominates all other trace elements but its form as sulfuric acid or ammonium sulfate appears to depend on altitude with sulfuric acid dominating at the lower levels of the stratosphere (5). It is generally believed that the sulfate aerosol is formed in the stratosphere through gas-phase reactions (7) with SO_2 as the principal agent for oxidation. The SO_2 source has not as yet been determined. It could be due to volcanic injection and/or natural injection of tropospheric SO_2.

Discussion of Aerosol Observations

Global Aerosol Distribution

Although extensive programs to measure global distribution of aerosol are underway, reportable results are few. While aircraft experiments are able to sample in an extensive latitude range, they are generally limited in vertical resolution. Balloon measurements suffer the reverse disadvantage, having excellent vertical resolution but requiring numerous soundings to gain any latitude range. Remote sensing from a satellite platform is the ultimate solution, but it is too far in the future to provide answers to some of the critical questions being posed now.

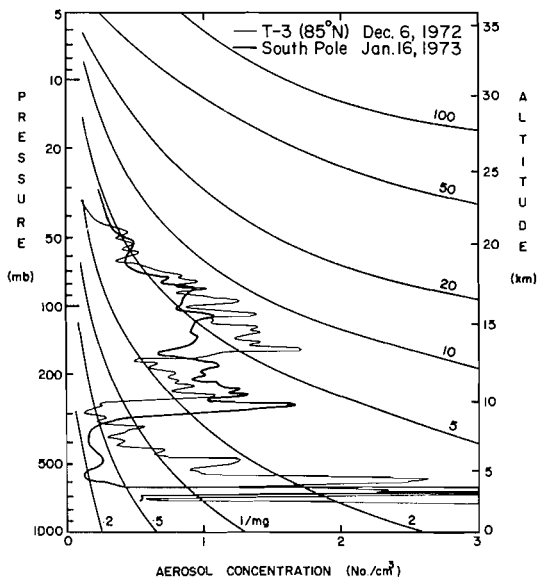

FIG. 2. The vertical distribution of aerosol particles having diameters greater than 0.3 μm over the ice island T-3 and the South Pole 6 weeks apart. Smooth curves are lines of constant mixing ratio in units of particles/mg of air.

Sulfate aerosol filter collections in the northern and southern hemispheres suggest no large differences in concentration (8). Furthermore, the vertical distributions of aerosol in the two polar regions were found to be very similar by the University of Wyoming group (9). A comparison of soundings made from the ice island T-3 at 85° N and the South Pole are shown in Fig. 2. Similar results were obtained a year earlier. The total particle loading at the poles is at least as great as that at midlatitudes, again suggesting the truly global nature of this phenomenon.

The global consistency of the sulfate layer makes explanation of the sulfur origin somewhat difficult. The northern hemisphere appears to be the dominant sulfur producer by at least a factor of 2 (10) with 93% of man-made SO_2 being produced in the northern hemisphere and a larger land mass in the northern hemisphere. Volcanic injection appears to be an improbable source of the particles observed in the polar regions since the vertical distribution at the South Pole did not change substantially when measured a year apart.

The role of the oceans in the sulfur cycle is not well understood. They are presumed to provide a sulfur return to the land mass in the form of H_2S. However, this component has not been measured. Dimethyl sulfide $[(CH_3)_2S]$ has recently been discovered in sea water by Lovelock *et al.* (11). This organosulfur compound may account for the missing ocean return and may also play a role as a stratospheric sulfur source. A source of such a global nature would be more readily reconcilable with the aerosol measurements.

Aerosol Time Variations

No presently utilized research techniques have been used extensively enough over the past 10 years to give a clear picture of the time variations of the aerosol concentration. What data there is suggests a definite decrease in stratospheric particulate loading since the late 1963 – early 1964, immediate post-Agung period. (Mt. Agung on Bali erupted in March 1963, apparently injecting a large amount of material into the stratosphere). Among this evidence are the twilight measurements of Volz (12), the lidar measurements of

Can. J. Chem. Downloaded from www.nrcresearchpress.com by 210.87.254.105 on 09/05/12
For personal use only.

Grams and Fiocco (13) during the post-Agung period compared to more recent lidar measurements by a number of groups, and the measurements with the light-scattering dustsonde of Rosen (14). The latter instrument is the same as that used on the University of Wyoming's program and measurements date back to 1963. The magnitude of the decrease in total aerosol loading (particles/cm^2 column) over a 10 year period with this instrument is of the order of a factor of 4–5 for particles having diameters greater than about 0.3 μm. However, there are considerable fluctuations (by factors of at least 3) and the number quoted above is an average.

Monthly soundings from Laramie by the University of Wyoming group have been conducted since late 1971 and these results are currently under study. Figure 3 is an example of three soundings, illustrating how the aerosol profile varies with time. The arrows in the figure signify the height of the tropopause in each sounding. Although the soundings in Fig. 3 suggest little variation in the aerosol concentration above about

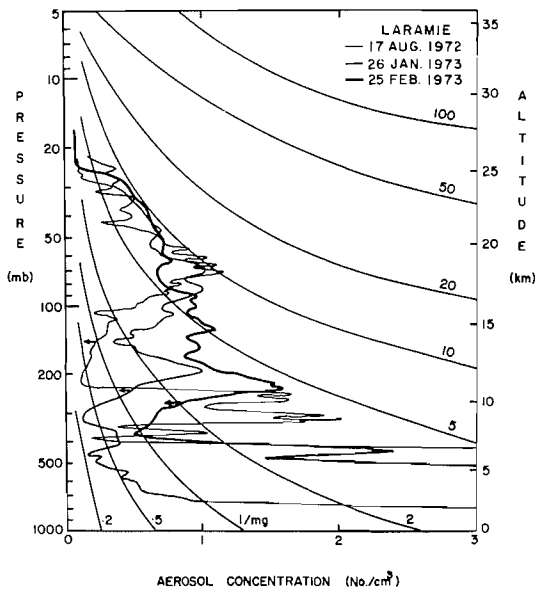

FIG. 3. A comparison of the vertical distribution of aerosol particles having diameters greater than 0.3 μm over Laramie, Wyoming, on three occasions. The arrows mark the observed position of the tropopause. The smooth curves are lines of constant mixing ratio in units of particles/mg of air.

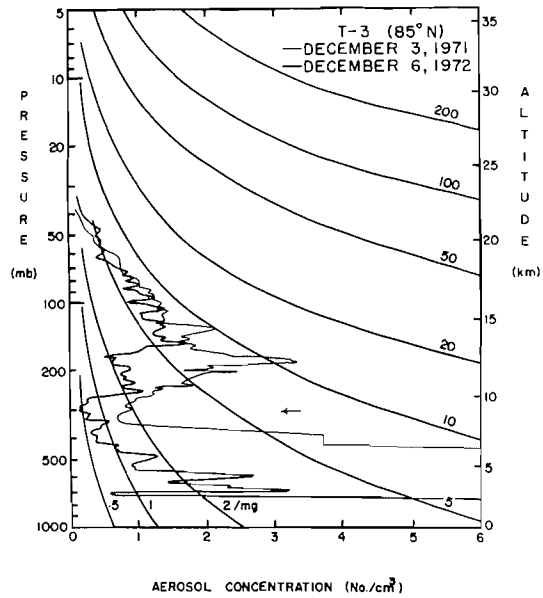

FIG. 4. The vertical distribution of aerosol particles having diameters greater than 0.3 μm over the ice island T-3 on two occasions a year apart. The arrow marks the observed tropopause position in 1971. Smooth curves are lines of constant mixing ratio in units of particles/mg of air.

20 km, the picture is somewhat more complicated with the degree of variation apparently depending on time; *i.e.*, some periods display more variability than others. Definite connections with volcanic activity, meteor showers, seasonal effects, etc. have not yet been established; however, the total aerosol loading at northern midlatitudes appears to be highest in winter and lowest in summer.

The stratospheric aerosol in the polar regions has been measured by the University of Wyoming group for the past two winters. The results from the ice island T-3 taken 1 year apart are shown in Fig. 4. Above an altitude of about 15 km, little change is evident. Below this altitude, the observed decrease is similar to that observed at Laramie during this period. High concentrations of particles in the lower atmosphere (below 9 km) were again observed in 1972, though not as extensive as those seen in 1971. The average particle size below 9 km altitude was observed to be smaller than in the stratosphere. The source of this high concentration of small particles in the Arctic troposphere is unknown.

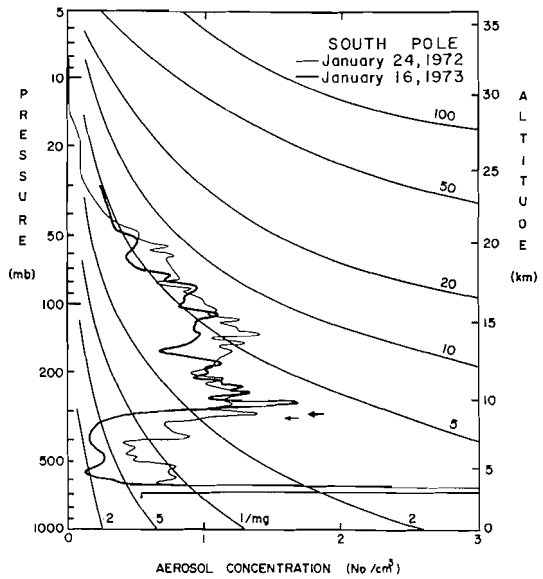

FIG. 5. The vertical distribution of aerosol particles having diameters greater than 0.3 μm over the South Pole on two occasions a year apart. The arrows mark the observed tropopause positions. Smooth curves are lines of constant mixing ratio in units of particles/mg of air.

Measurements by the University of Wyoming group of the stratospheric aerosol 1 year apart at the South Pole are shown in Fig. 5. Except for the sharp layer at about 3 km altitude in the 1973 sounding, which was due to a low-lying cloud over the 2.8 km polar icecap, little change is seen at any altitude. Since no significant volcanic activity occurred during this period, profiles such as those in Figs. 2 and 5 may be indicative of the "natural" (*i.e.*, non-volcanic) stratospheric aerosol background in the polar regions.

Comparative Studies

A number of comparative studies have recently been carried out to check the consistency of the various techniques of measuring the stratospheric aerosol. Among these comparisons were the following.

(*a*) Comparison of the University of Wyoming balloon-borne aerosol counter and the CSIRO balloon-borne impactor with the NASA/LRC and NCAR lidars and the NCAR and LASL filter samples on an RB57 aircraft. The studies were conducted at Laramie, Wyoming, in June and September, 1972.

(*b*) Comparison of the NCAR lidar with NCAR and LASL filter samples on an RB57 aircraft. This study was conducted in July 1972.

(*c*) Comparison of the University of Wyoming balloon-borne aerosol counter and the CSIRO balloon-borne impactor on a number of occasions between December 1971 and September 1972.

Although the analyses are not complete at this time, general agreement among the results has been obtained. As indicated earlier, comparison (*a*) showed the importance of using the correct air density profile in analyzing the lidar return signal. Comparison (*c*) has shown in a preliminary manner that the electron microscope grid impactor analysis technique presently used is essentially correct.

Complete agreement or explanation of disagreement among all techniques is an absolute necessity if a credible state of knowledge is to be reached.

The University of Wyoming program is sponsored by the Climatic Impact Assessment Program of the United States Department of Transportation, the National Science Foundation, and the Office of Naval Research. The author would like to acknowledge the contribution of his co-investigators J. M. Rosen and T. J. Pepin in this research project.

1. C. E. JUNGE, C. W. CHAGNON, and J. E. MANSON. J. Meteorol. **18**, 81 (1961).
2. J. M. ROSEN. Space Sci. Rev. **9**, 58 (1969).
3. J. M. ROSEN. Proceedings International Conference on Aerospace and Aeronautical Meteorology, American Meteorological Society, Boston, Mass. May 22–26, 1972. pp. 205–208.
4. R. D. CADLE. Trans. Am. Geophys. Union, **53**, 812 (1972).
5. E. K. BIGG, A. ONO, and W. J. THOMPSON. Tellus, **22**, 550 (1970).
6. J. M. ROSEN, D. J. HOFMANN, T. J. PEPIN, and J. KROENING. Nature, **240**, 347 (1972).
7. J. E. MANSON, C. E. JUNGE, and C. W. CHAGNON. The possible role of gas reactions in the formation of the stratospheric aerosol layer. *In* Chemical reactions in the lower and upper atmosphere. *Edited by* R. D. Cadle. Interscience, New York. 1961. p. 139.
8. A. L. LAZRUS, B. GANDRUD, and R. D. CADLE. J. Geophys. Res. **76**, 8083 (1971).
9. D. J. HOFMANN, J. M. ROSEN, T. J. PEPIN, and R. G. PINNICK. Nature, **245**, 369 (1973).
10. W. W. KELLOGG, R. D. CADLE, E. R. ALLEN, A. L. LAZRUS, and E. A. MARTELL. Science, **175**, 587 (1972).
11. J. E. LOVELOCK, R. J. MAGGS, and R. A. RASMUSSEN. Nature, **237**, 452 (1972).

Can. J. Chem. Downloaded from www.nrcresearchpress.com by 210.87.254.105 on 09/05/12
For personal use only.

12. F. E. VOLZ. Appl. Opt. **8**, 2505 (1969).
13. G. GRAMS and G. FIOCCO. J. Geophys. Res. **72**, 3523 (1967).
14. J. M. ROSEN. J. Geophys. Res. **73**, 479 (1968).
15. J. L. KROENING. J. Geophys. Res. **65**, 145 (1960).
16. S. PILIPOWSKYJ, J. A. WEINMAN, B. R. CLEMESHA, G. S. KENT, and R. W. WRIGHT. J. Geophys. Res. **73**, 7553 (1968).
17. G. NEWKIRK, JR. and J. A. EDDY. J. Atmos. Sci. **21**, 35 (1964).
18. E. DEBARY and F. ROSSLER. J. Geophys. Res. **71**, 1011 (1966).
19. A. L. LAZRUS, B. W. GANDRUD, and R. D. CADLE. J. Appl. Meteorol. **11**, 389 (1972).
20. C. E. JUNGE. J. Meteorol. **18**, 501 (1961).

Can. J. Chem. Downloaded from www.nrcresearchpress.com by 210.87.254.105 on 09/05/12
For personal use only.

Water-vapor Measurements in the Lower Stratosphere

H. J. MASTENBROOK
Naval Research Laboratory, Washington, D.C. 20375

Received October 19, 1973

Nearly 10 years of water-vapor measurements to heights of 30 km provide a basis for assessing the natural concentration of stratospheric water vapor and its variability. The measurements which began in 1964 have been made at monthly intervals from the mid-latitude location of Washington, D.C., using a balloon-borne frost-point hygrometer. The observations show the mixing ratio of water-vapor mass to air mass in the stratosphere to be in the general range of 1 to 4 p.p.m. with a modal concentration between 2 and 3 p.p.m. An annual cycle of mixing ratio is evident for the low stratosphere. A trend of water-vapor increase observed during the first 6 years does not persist beyond 1969 or 1970. The 6 year increase was followed by a marked decrease in 1971, with mixing ratios remaining generally below 3 p.p.m. thereafter. The measurements of recent years suggest that the series of observations may have begun during a period of low water-vapor concentration in the stratosphere.

Presque 10 années de mesures de la vapeur d'eau jusqu'à des hauteurs de 30 km ont permis d'obtenir une base solide afin d'évaluer la concentration naturelle de la vapeur d'eau dans la stratosphère et ses changements. Les mesures qui ont commencées en 1964 ont été relevées à chaque mois à partir de l'emplacement à mi-latitude de Washington, D.C., à l'aide d'un ballon-sonde équipé d'un hygromètre (point de gelée). Les observations montrent que le rapport de mélange entre la masse de vapeur d'eau et la masse d'air se situe dans la stratosphère généralement aux environs de 1 à 4 p.p.m. avec une concentration modale de 2 à 3 p.p.m. Un cycle annuel du rapport de mélange a été enregistré pour la basse stratosphère. La tendance observée vers une augmentation de la vapeur d'eau lors des 6 première années n'a pas continuée après 1969 ou 1970. L'augmentation observée durant 6 années a été suivie de façon marquée par une diminution en 1971 entraînant des rapports de mélange qui se situent généralement en-dessous de 3 p.p.m. Les mesures enregistrées durant ces dernières années suggèrent que la série d'observations a peut être commencée durant une période de basses concentrations en vapeur d'eau dans la stratosphère. [Traduit par le journal]

Can. J. Chem., **52**, 1527 (1974)

Introduction

Water vapor plays a significant role in the radiation budget and chemistry of the stratosphere and it is therefore important to determine its stratospheric distribution and variability. Systematic observations of the vertical distribution of water vapor over Washington, D.C., have been conducted by personnel of the Naval Research Laboratory since January 1964. The observations are made at approximately 1 month intervals and extend to altitudes of about 30 km.

The instrumentation is a balloon-borne frost-point hygrometer, configured to measure ambient frost-point temperature during a balloon descent. The descent sounding provides the means of avoiding extraneous water vapor which evolves from the balloon and instrument train.

The resulting information from this program of observations was reported after the accumulation of 2 years of data (1) and 6 years of data (2). With nearly a decade of data on hand, it is appropriate to update the earlier findings.

Vertical Distribution

All the data accumulated by NRL appear in Fig. 1 as frequency distributions of the mixing ratios for selected pressure levels. The class interval is 0.5 p.p.m. mixing ratio. Ninety percent or more of the observations at stratospheric levels fall within a narrow distribution range with a mode between 2 and 3 p.p.m. The distribution broadens at the 20 mb and 15 mb levels, but the mode remains essentially constant with height.

For many applications it is necessary to select a single curve to represent the vertical distribution. The average is frequently selected for this purpose, but averages of the level distributions do not give typical values for the 20 mb and

Can. J. Chem. Downloaded from www.nrcresearchpress.com by 210.87.254.42 on 09/05/12
For personal use only.

15 mb levels, due to a few cases of anomalously high mixing ratios at these levels. The anomalous cases are in the first 2 years of data and may be attributed to problems which were encountered with the aspirating blowers early in the operation. The median of the distributions corresponds closely to the mode at all levels and is therefore a preferred measure of the vertical distribution. The vertical distribution of mixing ratio expressed in terms of both the median and the average appears in Table 1.

TABLE 1. Mixing ratio profile 1964–1973*

Level (mb)	Mixing ratio (p.p.m.) Median	Average
15	2.73	4.07 (76)
20	2.67	3.29 (89)
40	2.73	2.77 (95)
60	2.61	2.68 (98)
80	2.63	2.66 (97)
100	2.68	2.77 (98)

*Vertical profile of mixing ratio over Washington, for the data period 1964–73, expressed in terms of the median and the average. The number of observations appears in parentheses after the averages.

Time Variation

Data for the nearly 10 years of observations appear as a time series in Fig. 2 for the 90 mb and 60 mb levels. The data symbols distinguish between the first 6 years of data and a time series analysis of that data, and data collected subsequent to the analysis. The first 6 years of data were examined through a regression analysis for the best fit of a linear trend and a sinusoidal cycle with a period of 1 year. A significant annual cycle was found to have a maximum amplitude near the base of the stratosphere. The cycle decreases in amplitude and the phase progresses in time with increase in altitude. The most interesting feature of the times series is the trend of mixing ratio increase of 1 p.p.m. which is significant at the 1% level.

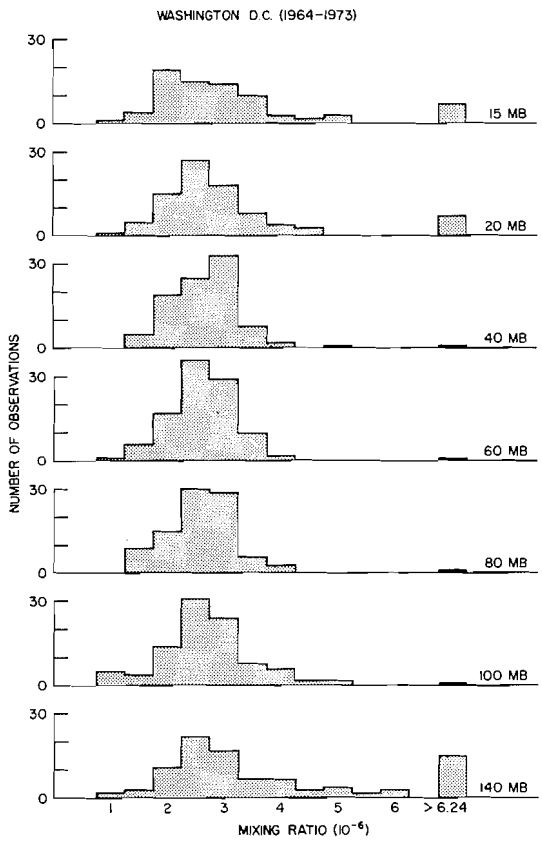

FIG. 1. Frequency distribution of mixing ratio for selected pressure levels for the period 1964–73 at Washington, D.C.

The data accumulated subsequent to the analysis show that the trend of increase does not continue beyond 1969 or 1970. The mixing ratio decreases in 1971 and remains generally below 3 p.p.m. thereafter. The presence of trends of several years' duration in only 10 years of data suggests that more years of data are needed to assess the normality of water-vapor distribution and variability.

Tropopause Control

Dobson *et al.* (3) first proposed that the upward movement of air through the cold region of the tropical tropopause accounted for the dryness of the stratosphere since the saturation mixing ratios at the tropical tropopause agree well with the observed water-vapor mixing ratio in the stratosphere. If the tropical tropopause is indeed the principal determinant of stratospheric water-vapor concentration, then a correspondence should exist between trends of saturation mixing ratio in the tropical tropopause region and the observed trends of stratospheric water-vapor concentration. The meteorological data for several tropical stations over the same 6 year period were examined for evidence of this correspondence.

Figure 3 shows the 3 month running averages of minimum saturation mixing ratios derived

Can. J. Chem. Downloaded from www.nrcresearchpress.com by 210.87.254.42 on 09/05/12
For personal use only.

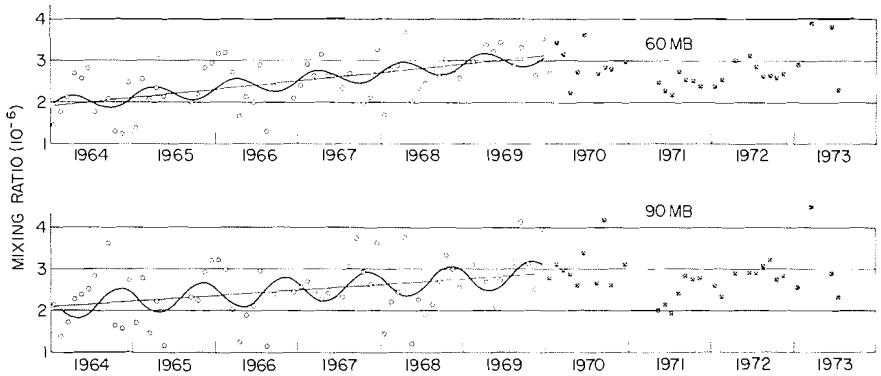

FIG. 2. Mixing ratio data for two selected pressure levels over Washington, D.C. Each circle represents one observation. The curves represent the best fit of a linear trend and annual cycle to the first 6 years of data. Cross-marked circles are data collected after the time-series analysis.

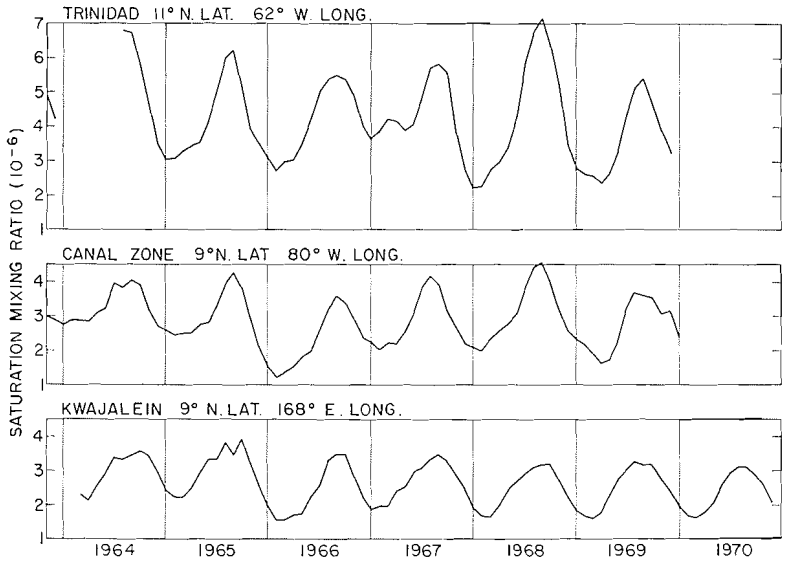

FIG. 3. Three month running averages of minimum saturation mixing ratios for tropical stations Trinidad, Canal Zone, and Kwajalein as determined from temperature and pressure data from the daily meteorological soundings.

from temperature and pressure data for three tropical stations. An annual cycle of 1 to 2 p.p.m. amplitude is quite apparent for all stations. A quasi-biennial cycle is evident, and accounts for the low minimum at Kwajalein and the Canal Zone in the winter of 1965–66, as well as the higher minimum for the winter 1964–65. What is not observed is a long-term trend of increase in saturation mixing ratios corresponding to the increase in water vapor; in fact, the trends at all three stations show a small decrease in this ratio.

Data records which begin in January 1960 are available for Singapore (1° N). Figure 4 shows the 3 month running averages of saturation mixing ratio for the tropopause level as derived from tropopause temperatures and pressures. The curves for tropopause temperature and pressure are also shown to illustrate the strong correlation that exists between tropopause temperature, pressure, and saturation mixing ratio, which allows for the inference of saturation mixing ratio trends from trends in either the tropopause temperature or pressure.

During the 5 year period of record subsequent to 1 January 1964, when the trend of water-vapor

Can. J. Chem. Downloaded from www.nrcresearchpress.com by 210.87.254.42 on 09/05/12
For personal use only.

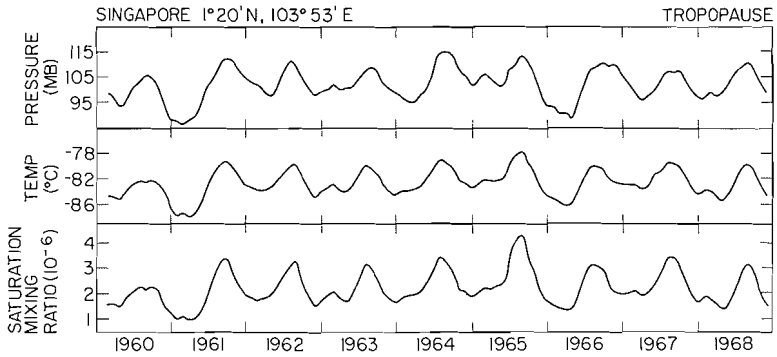

FIG. 4. Three month running averages of pressure, temperature, and saturation mixing ratio at the tropopause for Singapore.

TABLE 2. Six year linear regression values*

Six year period	Singapore, tropopause saturation mixing ratio (p.p.m.)			Washington, D.C., 90 mb observed mixing ratio (p.p.m.)		
	b	ΔMR	*r*	*b*	ΔMR	*r*
1960–65	1.74	1.05	0.37			
1961–66	2.06	0.51	0.18			
1962–67	2.25	0.26	0.90			
1963–68	2.45	−0.17	−0.06			
1964–69				2.04	0.91	0.38
1965–70				2.06	1.12	0.46
1966–71				2.38	0.58	0.25
1967–72				2.63	0.58	0.15

*Six year trends of saturation mixing ratio (MR) at the tropopause level for Singapore, and 6-year trends in the observed stratospheric mixing ratio at the mid-latitude location of Washington, D.C. The table gives the mixing ratio at the beginning of the trend period (*b*), the 6 year change in mixing ratio (ΔMR), and the correlation coefficient (*r*). A 6 year increase of 1 p.p.m. in the tropopause saturation mixing at Singapore is followed by a similar increase in the stratospheric mixing ratio at mid-latitude with a lag of 4 or 5 years.

increase at mid-latitude was observed, the trend of tropopause saturation mixing ratio at Singapore has a slightly negative slope, in general agreement with the other tropical stations for this period. However, the linear trend for the 6 year period starting with 1960 shows an increase of 1 p.p.m. in saturation mixing ratio for the tropical tropopause, just equal to the increase in observed water-vapor mixing ratio for the 1964–69 period.

The trend is largely influenced by the low saturation mixing ratio in 1960 and 1961. Angell and Korshover (4) examined the trends of tropical tropopause pressure and found a trend of tropopause pressure increase with time for Canton Island (3° S) which began at least as early as 1957. An increase over the period of a decade was found for all the tropical stations which they examined.

In examining the record of tropopause temperature and saturation mixing ratio for Singapore, it is also of interest to note that there is no evidence of a pronounced increase in the months following the Mt. Agung eruption in March 1963 similar to the increase of stratospheric temperatures reported by Newell (5). If the increase in stratospheric temperature had extended downward to the tropical tropopause level, an increase in stratospheric water vapor might have occurred as suggested by Newell.

The trends of saturation mixing ratio at Singapore, and the observed trend of water-vapor mixing ratio for the mid-latitude stratosphere, are shown in Table 2 for running 6 year

Can. J. Chem. Downloaded from www.nrcresearchpress.com by 210.87.254.42 on 09/05/12
For personal use only.

intervals. The 6 year increase in saturation mixing ratio at Singapore is greatest for the period 1960–65. The 6 year change decreases in successive 6 year intervals, becoming negative for the last interval. The observed stratospheric mixing ratio increase is greatest for the 1965–70 interval with the change decreasing in successive intervals. A correspondence appears between the observed stratospheric mixing ratio in the mid-latitude stratosphere and the saturation mixing ratio at the tropical tropopause 4 or 5 years earlier.

Conclusion

Water-vapor measurements in the stratosphere over nearly a decade show the vertical distribution of the mixing ratio to an altitude of 28 km to be essentially constant with a median value in the range of 2.6 to 2.7 p.p.m. The temporal variation shows a significant annual cycle and a trend of increase during the first 6 years. This trend of increase comes to an end in 1969 or 1970, and is followed by a nearly level trend in the succeeding years. The trend of water-vapor increase at mid-latitudes was preceded by a corresponding increase in saturation mixing ratio at the tropical tropopause.

1. H. J. MASTENBROOK. J. Atmos. Sci. **25**, 299 (1968).
2. H. J. MASTENBROOK. J. Atmos. Sci. **28**, 1495 (1971).
3. G. M. B. DOBSON, A. W. BREWER, and B. M. CWILONG. Proc. Roy. Meteorol. Soc. A, **185**, 144 (1946).
4. J. K. ANGELL and J. KORSHOVER. 1974: Quasi-biennial and long-term fluctuations in tropopause pressure and temperature. Mon. Weather Rev. (1974). To be published.
5. R. E. NEWELL. J. Atmos. Sci. **27**, 977 (1970).

Can. J. Chem. Downloaded from www.nrcresearchpress.com by 210.87.254.42 on 09/05/12
For personal use only.

Recent Stratospheric Spectra of NO and NO_2

M. Ackerman, D. Frimout, C. Muller, D. Nevejans

Institut d'Aéronomie Spatiale de Belgique, 3, Avenue Circulaire, B – 1180, Bruxelles

AND

J. C. Fontanella, A. Girard, L. Gramont, and N. Louisnard

Office National d'Etudes et de Recherches Aérospatiales, 29, Avenue de la Division Leclerc, Chatillon, France

Received August 22, 1973

NO and NO_2 spectra obtained by means of a grid spectrometer from a balloon gondola and from a Concorde are presented. The corresponding stratospheric abundance of these species is deduced.

On présente les spectres de NO et NO_2 obtenus au moyen d'un spectromètre à grille placé dans une nacelle de ballon et un Concorde. On en déduit l'importance de chacune de ces espèces dans la stratosphère. [Traduit par le journal]

Can. J. Chem., 52, 1532 (1974)

Introduction

Interest in stratospheric chemistry has grown during the past few years. The lowest stratosphere had been particularly neglected from this point of view and was considered to be a region where photochemistry was unimportant. This conclusion was based on the fact that ozone has a long lifetime in the low stratosphere even if most of the ozone molecules have a relatively short lifetime in the whole atmosphere. It is now recognized that active chemical processes take place throughout the stratosphere. They involve species for which the mixing ratios by volume are lower than 1 p.p.m. The analytical methods necessary to measure these constituents are not numerous and have to be selected by taking into account both the properties of the molecules to be measured and of the atmosphere itself.

Infrared spectroscopy appears to be particularly well suited to satisfy both aspects by presenting a high specificity and by being well adapted to the atmospheric dimensions. These qualities have been recognized for a long time by many authors, and have been exploited by means of ground based instruments. Infrared spectrometers acquire even more versatility when operated from space platforms.

Determinations of NO and NO_2 are necessary to define their possible role in the stratospheric photochemistry. Absorption spectra of nitrogen oxides obtained from a balloon gondola and from an aircraft (Concorde 001) will be discussed here.

Instrumentation and Experiments

The spectra discussed have been obtained in absorption using the setting sun as a source. The method has advantages that have already been pointed out (1). A complete description of the spectrometers will be given elsewhere for the balloon-borne as well as for the aircraft-borne (2) equipment. In the case of the balloon experiment it can be summarized as follows. Since the postulated amount of absorber on the optical path is small and a relatively fast wavelength scanning is necessary, the spectrometer used had to have the double advantage of large light input combined with high resolving power. Girard (3) developed this type of grid spectrometer. The instrument of 60 cm focal length was equipped with a 6 cm × 6 cm "Yvon et Jobin" grating ruled at 60 grooves/mm and used in the sixth order. The foreoptics was a 4.2 m focal length modified Cassegrain telescope of 32 cm diameter. The detector was a liquid nitrogen cooled "SAT" InSb photo element. An instrumental profile of 0.1 cm^{-1} half width was achieved with a square grid of 18 × 18 mm having a step of 0.2 mm. The instrument was mounted on a sun-seeker equipped with the electronics used for the synchronous detection of the detector output, with the voltage controlled oscillators, and with the transmitter used in the telemetry radio link. The 320 kg gondola was launched from Aire sur l'Adour in the afternoon of May 14, 1973, with an 11.6×10^6 ft^3 "Winzen" balloon.

The instrument used on Concorde 001 was similar. Due to the limited dimension of the CaF_2 window (10 cm diameter) adapted to the skin of the aircraft the light input was smaller, giving a somewhat smaller signal-to-noise ratio. While the body of the balloon spectrometer was open to the ambient air, the aircraft

Can. J. Chem. Downloaded from www.nrcresearchpress.com by 210.87.254.42 on 09/05/12
For personal use only.

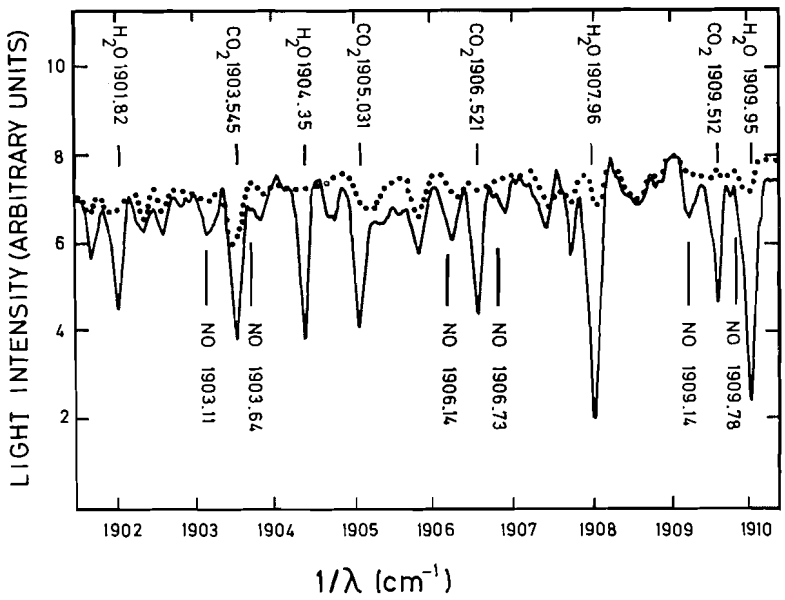

FIG. 1. Intensity of solar radiation recorded at 40 km altitude *vs.* wavenumber in cm^{-1}. The dotted line represents the spectrum at a solar zenith angle of 86°. The continuous line represents the spectrum at a zenith angle of 94°. The absorption lines due to stratospheric NO, CO_2, and H_2O are indicated.

instrument was flushed with dry nitrogen. A sun seeker was mounted to bend the solar radiation at a right angle and to track the sun over amplitudes of azimuth and elevation angles of about 10°. The spectra discussed here were obtained on constant heading trajectories travelled over at Mach 2 between the northwest of Spain and the west of Cornwall.

Results

Nitric Oxide

Recording of the solar spectrum from the balloon gondola at an altitude of 40 km started when the solar zenith angle was 86°. The spectra showed then little structure partly attributed to solar CO absorption lines (4). As shown in Fig. 1 telluric absorptions become more and more pronounced for solar zenith angles larger than 90° due to the increase of optical path reaching lower and lower altitudes in the stratosphere. Absorption lines of NO, CO_2, and H_2O were mostly present. CO_2 and H_2O lines were identified on the basis of the AFCRL infrared compilation (5). For NO other laboratory data were used (6). The amount of NO on the optical path was deduced from the integrated line absorption cross sections for 220 °K listed in Table 1 (7). The number density of NO *vs.* altitude was inferred from the total amounts measured and represented in Fig. 2 by division

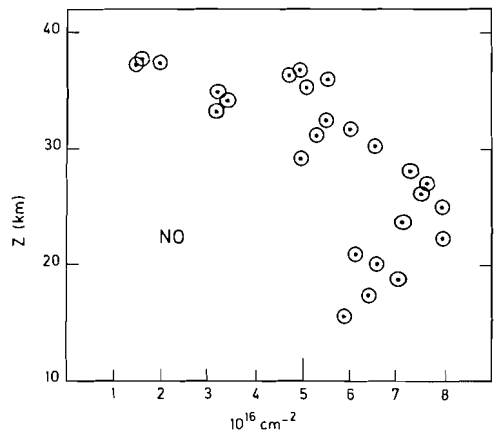

FIG. 2. Total number of NO molecules observed from the balloon gondola on the optical path *vs.* grazing altitude of solar rays.

of the atmosphere in successive layers of 3 km thickness. The deduced values are given in Table 2 with the corresponding mixing ratios. The limits of error indicated correspond to the maximum scattering of the original data points taken for grazing ray altitudes from 38 to 15 km. The results are represented in Fig. 3 with other experimental data. On June 6, 1973, the aircraft spectrometer previously flown on board a Cara-

Can. J. Chem. Downloaded from www.nrcresearchpress.com by 210.87.254.42 on 09/05/12
For personal use only.

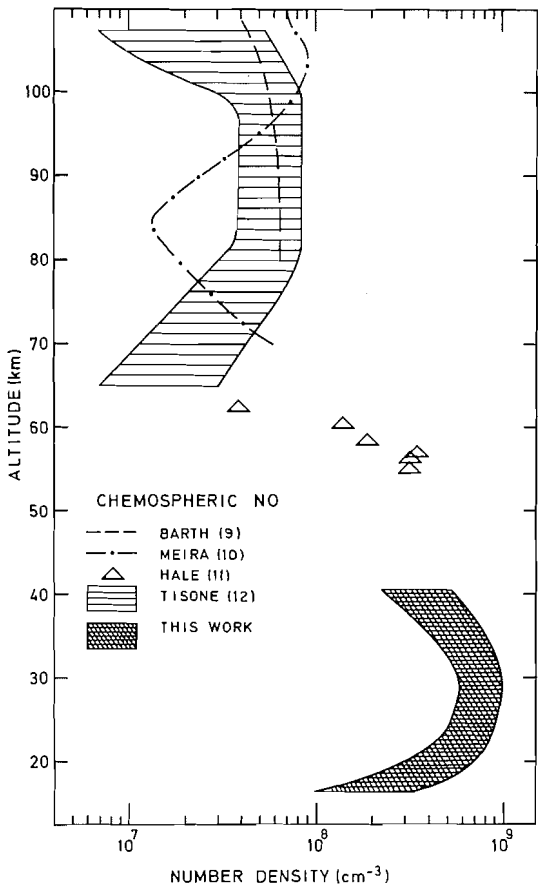

FIG. 3. Experimental values of the number density of nitric oxide *vs.* altitude in the chemosphere. The results published by Barth (9), Meira (10), Hale (11), and Tisone (12) are shown with those presented here for the stratosphere.

velle airplane (8) was used on board the Concorde prototype 001, in the same spectral region and with the same resolving power. The integrated amounts of NO measured in this latter case along the optical path from 15.2 km are respectively at solar zenith angles of 88 and 90°, equal to $(3 \pm 1) \times 10^{16}$ and $(5.5 \pm 1) \times 10^{16}$ molecules/cm^2. The results are within experimental uncertainties in agreement with the data presented in Fig. 2.

Nitrogen Dioxide

Spectra of NO_2 in the 1617 cm^{-1} band have been obtained from Concorde at an altitude of 16 km on July 6, 1973. The zenith angle changed during the flight from 88 to 91°. The spectrum for this latter case is shown in Fig. 4. The NO_2 lines have been identified according to recent data (13) based on molecular constants that are

TABLE 1. Wavenumbers and integrated absorption cross sections (220 °K) of the observed NO lines

$1/\lambda$ (cm^{-1})	s ($cm^2\ cm^{-1}$)
1903.112	14.8×10^{-20}
1903.643	6.45
1906.142	13.7
1906.729	5.99
1909.139	12.3
1909.79	5.37
1912.076	10.7
1912.787	4.66

TABLE 2. Nitric oxide results

Altitude (km)	NO number density (cm^{-3})	NO mixing ratio (by volume)
37.5	$(5 \pm 2) \times 10^8$	$(4.4 \pm 1.8) \times 10^{-9}$
34.5	$(6 \pm 2) \times 10^8$	$(3.4 \pm 1.2) \times 10^{-9}$
31.5	$(8 \pm 2) \times 10^8$	$(2.8 \pm 0.7) \times 10^{-9}$
28.5	$(8 \pm 2) \times 10^8$	$(1.8 \pm 0.5) \times 10^{-9}$
25.5	$(7.4 \pm 2) \times 10^8$	$(9.7 \pm 2.2) \times 10^{-10}$
22.5	$(6.5 \pm 2) \times 10^8$	$(5.7 \pm 1.8) \times 10^{-10}$
19.5	$(4.6 \pm 2) \times 10^8$	$(2.5 \pm 1.1) \times 10^{-10}$
16.5	$(2 \pm 1) \times 10^8$	$(6.7 \pm 3.5) \times 10^{-11}$

in close agreement with those used by Ackerman and Muller (1, 14) to determine a vertical distribution of NO_2 from stratospheric spectra. The computed total number of molecules in the optical path has been obtained by using the line strengths applied previously (1, 14) that agree within 20% with the more recent values (13). The total number of molecules observed from 16 km at zenith angles of 88 and 90° are respectively $(3.2 \pm 1) \times 10^{16}$ cm^{-2} and $(4.2 \pm 1.5) \times 10^{16}$ cm^{-2}. These numbers are within experimental uncertainties in agreement with the lowest values of the verticle profile published previously by Ackerman and Muller.

Conclusion

The results presented here indicate without ambiguity the presence of NO and NO_2 in the stratosphere. The measurements from balloon and aircraft are complementary, since in this particular case the molecules are photochemically linked. The comparison of the aircraft data obtained at low altitude and solar zenith angle smaller than 90° with the vertical profiles deduced from balloon measurements taken at solar zenith angle larger than 90° is particularly useful. It indicates that the transformation of NO into NO_2 in sunset conditions probably cannot

Can. J. Chem. Downloaded from www.nrcresearchpress.com by 210.87.254.42 on 09/05/12
For personal use only.

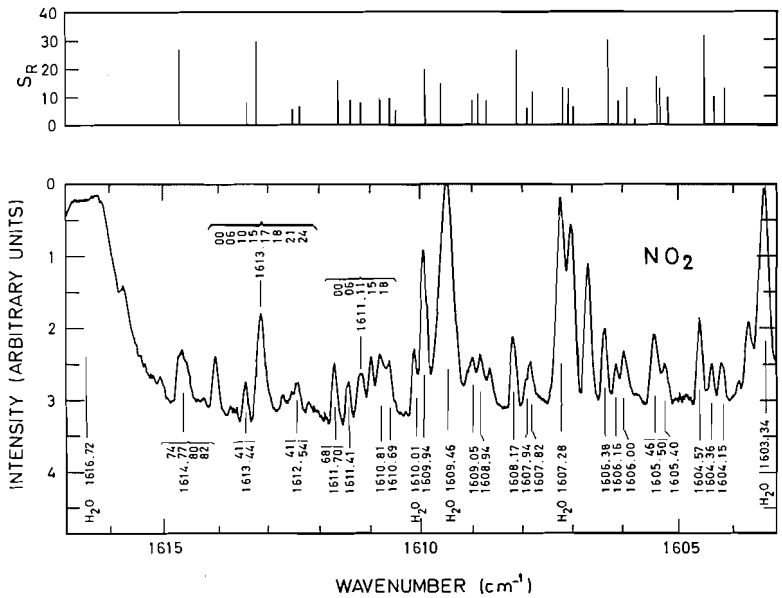

FIG. 4. Solar spectrum recorded from Concorde 001 at an altitude of 16 km and a zenith angle of 91° between 1603 and 1617 cm^{-1}. Telluric water vapor (5) and nitrogen dioxide (13) lines are indicated. The computed relative intensities (1, 14) are represented for NO_2 in the upper part of the figure.

be neglected and that simultaneous measurements of both species have to be performed, especially because changes of NO_x with time cannot be excluded. Such measurements present some technical difficulties that will soon be overcome in future flights. The limited number of measurements performed separately leaves at present a relatively large range of uncertainty. The method of Limb measurement that one is forced to use to observe constituents in very small concentrations also presents inherent uncertainty factors. Values of concentrations of H_2O and CO_2 deduced from the spectra obtained by means of the balloon-borne spectrometer, however, give confidence in the results that can be obtained. Using the Jansson and Korb tables (15) the analysis of the H_2O absorption at 1904.35 cm^{-1} and at 1909.95 cm^{-1} and of CO_2 at 1906.521 cm^{-1} yields respective mixing ratios by volume of these two constituents between 25 and 35 km equal to $(3.4 \pm 0.7) \times 10^{-6}$ and $(2.6 \pm 0.7) \times 10^{-4}$, in agreement with the generally accepted values.

Thanks are due to the flight test crews of Concorde 001 for their help and for the accuracy achieved in performing the trajectories required for the observations. This work has been sponsored in part by the Climatic Impact Assessment Program office of the U.S. Department of Transportation through the Office of Naval Research under contract N00014-73-C-0076, by the "Centre National d'Etudes Spatiales", and by the "Comité sur les Conséquences des Vols Stratosphériques".

1. M. ACKERMAN and C. MULLER. Pure Appl. Geophys. **106–108**, 1325 (1973).
2. N. LOUISNARD, L. GRAMONT, A. GIRARD, M. ACKERMAN, and D. FRIMOUT. Air borne and balloon borne spectroscopy for the study of atmospheric gas pollutants. 2nd AIAA/NOAA Conference on the Sensing of Environmental Pollutants Proceedings. 1973. To be published.
3. A. GIRARD. Appl. Opt. **2**, 79 (1963).
4. M. MIGEOTTE, L. NEVEN, and J. SWENSON. Mem. Soc. R. Sci. Liège, Special Vol. **2** (1957).
5. R. A. MCCLATCHEY, W. S. BENEDICT, S. A. CLOUGH, D. E. BURCH, R. F. CALFEE, K. FOX, L. S. ROTHMAN, and J. S. GARING. Air Force Cambridge Research Laboratories infrared compilation. 1973.
6. T. C. MICHELS. J. Quant. Spectrosc. Radiat. Transfer, **11**, 1735 (1971).
7. S. CIESLIK and C. MULLER. Aeronomica Acta A nr 114 (1973).
8. A. GIRARD, J. C. FONTANELLA, and L. GRAMONT. C. R. Acad. Sci. Paris, **276B**, 845 (1973).
9. C. A. BARTH. J. Geophys. Res. **69**, 3301 (1964).
10. L. G. MEIRA, JR. J. Geophys. Res. **76**, 202 (1971).
11. L. C. HALE. *In* McElroy, Proceedings of the survey conference. TSC-OST-72-13 U.S. Department of Transportation, (1972).
12. G. C. TISONE. J. Geophys. Res. **78**, 746 (1973).
13. R. TOTH. Private communication.
14. M. ACKERMAN and C. MULLER. Nature, **240**, 300 (1972).
15. P. A. JANSSON and C. L. KORB. J. Quant. Spectrosc. Radiat. Transfer, **8**, 1399 (1968).

Can. J. Chem. Downloaded from www.nrcresearchpress.com by 210.87.254.42 on 09/05/12
For personal use only.

Measurements of NO, NO_2, and HNO_3 in the Stratosphere

H. I. SCHIFF
York University, Downsview, Ontario

Received December 6, 1973

Atmospheric models designed to predict the effect on the ozone budget of the injection of nitric oxide into the stratosphere by high-flying aircraft require a knowledge of the NO concentration in the unperturbed atmosphere. Moreover, a monitoring program will require a base line against which to measure the magnitude of any future stratospheric pollution. A number of measurements have recently been reported, not only on NO, but also on NO_2, and HNO_3 which are interconverted by stratospheric photochemistry. All the methods but two employ "remote-sensing" optical absorption or emission techniques. Infrared solar absorption using long optical paths at twilight has proven to be very sensitive in detecting trace atmospheric constituents but quantitative interpretation appears to be very difficult. Chemiluminescence and direct "particle" sampling have provided *in situ* measurements.

The spread in the reported values of mixing ratios is very large for NO_2, appreciable, but smaller for NO, and smallest for HNO_3. Insufficient data are available to assess how much of this spread is due to measurement errors and how much is due to natural variability in the mixing ratios. Intercomparisons of the measurements for different nitrogen compounds are made by consideration of the principal chemical reactions governing their relative concentrations. Discrepancies exist which should diminish as more accurate chemical rate data and synoptic stratospheric measurements become available.

Des modèles atmosphériques conçus pour prévoir l'influence sur la quantité de l'ozone, d'éjections d'oxydes nitriques dans la stratosphère par des avions à haute altitude nécessite une connaissance de la concentration de NO dans l'atmosphère non perturbée. De plus, un programme contrôle nécessitera une ligne de base en fonction de laquelle on mesurera l'importance de n'importe quelle pollution stratosphérique ultérieure. Un nombre de mesures a été récemment donné, non seulement pour NO, mais aussi pour NO_2 et HNO_3 qui sont convertis l'un dans l'autre par la photochimie stratosphérique. Toutes les méthodes à l'exception de deux, emploient les techniques de "télé-réception" d'absorption ou d'émission optique. L'absorption infra-rouge solaire empruntant de longs chemins optiques en demi-obscurité s'est montré très sensible à la détection de traces de constituants atmosphériques mais une interprétation quantitative se révèle très difficile. La chimiluminescence et l'échantillonnage direct de "particule" ont fourni des mesures *in situ*.

L'étalement des valeurs indiquées des rapports de mélanges est très important pour NO_2, appréciable mais plus petit pour NO, et le plus faible pour HNO_3. Il est difficile d'estimer, en raison d'un manque de données, la dépendance de cet étalement en fonction des erreurs de mesures et de sa variabilité naturelle. Des inter-relations des mesures des différents composés azotés sont faites en considérant les réactions chimiques principales qui régissent leurs concentrations relatives. Les différences existantes doivent diminuer pour que plus de données cinétiques chimiques et plus de mesures stratosphériques sommaires deviennent disponibles. [Traduit par le journal]

Can. J. Chem., **52**, 1536 (1974)

World attention has recently been drawn (*1*, *2*) to the possibility of a serious depletion of the ozone shield in the stratosphere by the injection of nitric oxide by a fleet of supersonic aircraft. The determination of the natural abundance of NO in the stratosphere was soon recognized to be of paramount importance for a number of reasons. Obviously, the magnitude of the effect will depend on the percentage increase of NO from anthropogenic sources over those from natural sources. Secondly, a reliable base line of natural NO abundances must be provided in order to monitor any future increases. Finally, the most stringent test for theoretical models designed to predict the effect of artificial NO injection into the stratosphere is their ability to account for the ozone balance in an unperturbed atmosphere.

A great deal of effort has been expended in devising instrumentation to measure the very small NO concentrations anticipated in the stratosphere. Results are just becoming available,

Can. J. Chem. Downloaded from www.nrcresearchpress.com by 210.87.254.40 on 09/05/12
For personal use only.

Can. J. Chem. Downloaded from www.nrcresearchpress.com by 210.87.254.40 on 09/05/12
For personal use only.

not only for the concentration of NO, but also for the related compounds, NO_2 and HNO_3.

These compounds, each containing one nitrogen atom, are frequently referred to collectively as "NO_x" since they are interconverted by the photochemistry occurring in the stratosphere. The principal reactions believed to govern the relative abundance of NO and NO_2 are

[1] $$NO + O_3 \rightarrow NO_2 + O_2$$

[2] $$NO_2 + O \rightarrow NO + O_2$$

[3] $$NO_2 + h\nu \rightarrow NO + O$$

For steady state conditions

[A] $$\frac{[NO]}{[NO_2]} = \frac{J_1 + k_2[O]}{k_1[O_3]}$$

where J_1, the rate constant for reaction 3, is the product of the solar flux intensity, the NO_2 absorption coefficient, and the quantum yield of the reaction, all integrated over wavelength. The half-time to attain steady state is of the order of 100 s in the daytime stratosphere. Since the lifetime for eddy diffusion and other transport processes at these altitudes is approximately 1 month, steady state should be a good approximation.

The principal reactions believed to govern the ratio of NO_2 to HNO_3 are

[4] $$HO + NO_2 + M \rightarrow HNO_3 + M$$

[5] $$HNO_3 + h\nu \rightarrow HO + NO_2$$

[6] $$HO + HNO_3 \rightarrow H_2O + NO_3$$

For steady state conditions

[B] $$\frac{[NO_2]}{[HNO_3]} = \frac{J_5 + k_6[HO]}{k_4[HO][M]}$$

However, in this case the half-time to attain steady state is of the order of 1 month, approximately the same as for atmospheric transport processes. Thus, the steady state approximation must be considered to have only marginal validity.

With two exceptions all measurements of stratospheric NO_x have been made by infrared spectroscopic techniques. These techniques are fully discussed by Farmer (3) in this issue and only a brief summary of the principal advantages and difficulties will be given here.

Absorption of solar infrared radiation from balloons and aircraft at sunrise and sunset, when the solar zenith angle is greater than 90°, provides long, nearly horizontal, optical paths which not only increase sensitivity but also minimize complications due to changes in temperature and pressure. Although with this technique spectral features of very minor constituents can be observed, quantitative analysis of the data is very difficult. It is necessary to know many spectroscopic properties of the absorber including detailed spectral assignments, line strengths, and shapes. The line shape will not be constant throughout the column because of differences in temperature and pressure, both of which will change with solar zenith angle. It is difficult to find "clean" spectral regions which are not also overlapped within the resolution of the instrument by absorption features of other atmospheric constituents. The unfolding of the geometry factor to provide height profiles is difficult and care must be taken to account for refraction of the ray by the air mass. Height profile information is virtually unattainable from measurements with solar zenith angles at the height of the instruments smaller than 90°. For this reason balloon measurements which reach higher altitudes and look down are to be preferred over aircraft measurements, which look horizontally or upwards.

Although infrared emission spectra are even more difficult to interpret spectroscopically, the advent of more sensitive detectors may make emission more sensitive than absorption. It may then become possible to make differential measurements at higher elevation angles and thereby obviate some of the problems associated with long path-length absorption.

In summary then, infrared absorption techniques are now capable of detecting NO_x compounds in the stratosphere, but quantitative measurements appear to be extremely difficult.

Absorption in the visible region has recently been used by Brewer *et al.* (4) to measure stratospheric NO_2. By taking ratios of intensities at three wavelengths, 437.7, 444.8, and 450.0 nm, which correspond to maxima and minima in the NO_2 absorption curves, the authors believe they have effectively discriminated against absorption by other molecules and against Rayleigh scattering. Measurements were taken from an aircraft during ascent and descent at twilight and at noon using absorption from the clear zenith sky as well as from direct solar absorption. The method is analogous to that used on a routine basis for

ozone measurements from the ground and is described by Brewer (5).

The methods described so far are all "remote sensing" methods. The only *in situ* measurement reported to date in the lower and middle stratosphere are those of Lazrus *et al.* (10) using direct particle sampling for HNO_3 and those of Ridley *et al.* (6) using chemiluminescence detection of NO. Since the chemiluminescence method is not described elsewhere in this symposium, it will now be described in some detail.

The method is based on the sequence of reactions

$$[7a] \quad NO + O_3 \rightarrow NO_2^* + O_2$$

$$[7b] \quad \rightarrow NO_2 + O_2$$

$$[8] \quad NO_2^* \rightarrow NO_2 + h\nu$$

$$[9] \quad NO_2^* + M \rightarrow NO_2 + M$$

The radiation emitted by the electronically excited NO_2^* molecule in reaction 8 is a continuum extending from about 590 to 3000 nm. If the air to be analyzed is passed through a reaction vessel to which sufficient O_3 is added so that reactions 7–9 are virtually complete within the volume viewed by a photomultiplier, the signal intensity, I, will be given by the expression

$$I = AFX_{NO}/P$$

where F is the mass flow rate of the air, P is the pressure, X_{NO} is the mixing ratio of NO in the sampled air, and A is a constant involving geometry factors of the instrument, the response of the photometric detection system, and the rate constants of the reactions.

Instruments based on this principle were constructed for flights on balloons and on high-flying aircraft. A schematic diagram is shown in Fig. 1 for the balloon configuration. Ambient air is drawn through a 2.4 m length of 7.6 cm i.d. black, anodized aluminum tube, a light baffle, and a heated annular space, into a gold-coated, Pyrex reaction vessel. After reaction with O_3, added to the reaction vessel, the gas flows through additional light baffles into an analyzer region where its flow rate, pressure, temperature, and O_3 content are monitored, and is exhausted through a 2.4 m length of tubing attached upward to the payload support lines. A mixture of approximately 7% O_3 in Freon-13 is added either directly to the reaction region for measurements or upstream of the inlet light baffle to remove all NO from the sampled air in order to provide a true background photomultiplier reading. Provision is made for "on-board" calibration by addition of small, known amounts of NO to the sampled air.

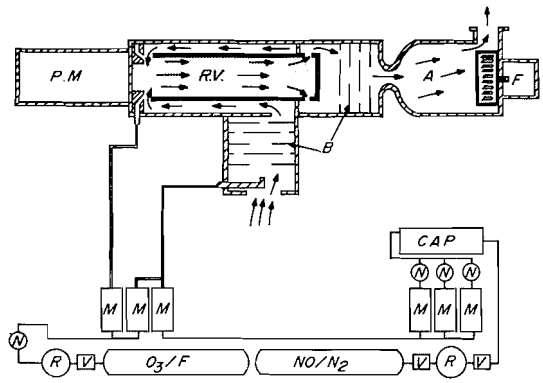

FIG. 1. Schematic diagram of the chemiluminescence instrument used for the *in situ* NO measurement. O_3/F, cylinder containing approximately 10% O_3 in Freon; NO/N_2, cylinder containing 1 p.p.m. NO in N_2 for calibration; V, on–off valves; R, diaphragm gas regulators; M, magnalatch valves; N, needle valves; CAP, ballast volume and capillary flow meters; P.M., photomultiplier; R.V., reaction vessel; B, light baffles; A, analyzer section; F, exhaust fan.

The instrument is turned on and off by ground command. Once on, its operation is completely automatic through a programmed sequence of background measurements, and successive ambient air and calibration measurements. The chemiluminescence is detected by a cooled photomultiplier–filter combination. Photon counting is used, with the count rate recorded by an on-board tape recorder as well as being telemetered to the ground.

The detection limit of the instrument is 0.02 p.p.b.v. The total error produced by uncertainties in count rates, flow calibrations, and calibrating gas concentrations is estimated to be 60% for the low NO concentrations encountered.

Three possible sources of error related to air sampling from the balloon configuration were considered. The first involves contamination by the balloon itself and the flight packages. To test this, measurements were taken from a single balloon flight during three cycles of ascent, float, and descent. The worst conditions for this type of contamination should be during the ascent mode when the sampler is moving through the balloon wake, and the best conditions should be during descent. Within the uncertainty of the measurements no differences were detected

Can. J. Chem. Downloaded from www.nrcresearchpress.com by 210.87.254.40 on 09/05/12
For personal use only.

Can. J. Chem. Downloaded from www.nrcresearchpress.com by 210.87.254.40 on 09/05/12
For personal use only.

among the results obtained during these three flight modes of the balloon. This strongly suggests negligible contamination from the balloon.

The second possibility is self-contamination by the NO used for calibration and by the relatively large amounts of O_3 used to produce the chemiluminescence. Again such contamination should be greater during ascent than during descent. An additional test was made in a subsequent flight which also carried an ozone-sonde located near the sampler inlet tube. The NO sampler was turned on and off for 10 min intervals during the flight. The O_3 content of the ambient air was found to be the same whether or not NO and O_3 were being passed through the NO sampler. This provided strong evidence against self-contamination.

Finally, consideration was given to the possibility that the NO content of the sampled air was reduced by passage through the 2.4 m inlet tube, either by adsorption or by surface reaction with the stratospheric O_3. (Gas phase consumption of NO by reaction 7 during passage through the inlet tube amounts to about 10% and was included in the data reduction.) Laboratory experiments were performed under similar conditions of flow, pressure, temperature, NO and O_3 concentrations as those encountered in the stratosphere. These experiments showed differences of less than 10% when 0.2 p.p.b. of NO was introduced at the front and at the back of the inlet tube. Therefore, no evidence has been found to date to suggest serious sampling errors in these "*in situ*" NO measurements.

Results of Stratospheric NO_x Measurements

(a) HNO_3 Measurements

By far the most extensive NO_x measurements to date are those of HNO_3 by Murcray and coworkers (7). Several of the infrared bands are relatively free from interference by other stratospheric constituents. The band at 11.17 μ has been observed both in emission and in absorption. Figure 2 shows the envelope of results obtained by this group at mid-latitudes (*ca.* 30° N) using either a grating spectrometer or a filter radiometer carried by balloons. On occasions when they have been flown together these instruments have shown differences as large as 30%, attributable to difficulties inherent in making absolute radiance measurements. The authors believe their results to have an accuracy of ±30%. The larger spread in the data in Fig. 2 must, therefore, represent real fluctuations in HNO_3 mixing ratios with time at the same location. Moreover, for a given flight, structure has been seen in the altitude profile, reminiscent of the layers observed routinely in the ozone height distribution. Murcray (8) has also made recent measurements in Fairbanks, Alaska, which gave somewhat higher mixing ratios and, in some cases, showed a layer at 14 km. The results of Harries (9) from emission in the submillimeter range and Lazrus *et al.* (10) from particle samples are consistent with those of Fig. 2.

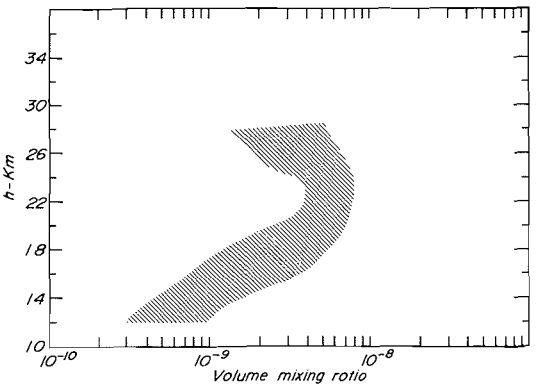

FIG. 2. Envelope of HNO_3 volume mixing ratios obtained by Murcray and co-workers from balloon measurements at mid-latitudes. It should be noted that this group usually report their results as mass mixing ratios (p.p.b.m.).

(b) NO_2 Measurements

Goldman *et al.* (11) observed NO_2 in the stratosphere by observation of the ν_3 band at 6.25 μ. Although this band is strong and relatively free from interference, the authors did not feel that the laboratory data was sufficiently well established to warrant quantitative analysis of their NO_2 observations. Ackerman and Muller (12, 13), however, did analyze the data of Goldman *et al.* (11) along with their own balloon measurements of the $\nu_1 + \nu_3$ band at 3.4 μ. This band is much weaker than the ν_3 band and is also seriously overlapped by CH_4 bands. The results of the Ackerman and Muller's analysis is shown in Fig. 3.

Farmer *et al.* (3) used an interferometer aboard Concorde to measure the 3.4 μ absorption. They believe the resolution to be sufficient to permit them to differentiate between NO_2 and CH_4 absorptions. A tentative value for mixing ratio

Can. J. Chem. Downloaded from www.nrcresearchpress.com by 210.87.254.40 on 09/05/12
For personal use only.

of 1.8 ± 0.5 p.p.b. over the 15–20 km range is reported.

Ackerman *et al.* (14) measured the 6.25 μ absorption from Concorde. They applied the same analytical procedure they used previously (12) and derived a total column density. Such measurements, looking horizontally, are incapable of yielding height profiles. However, an average mixing ratio can be obtained for the altitude at, or above, the measurement height. From their total column density an average mixing ratio of 5×10^{-10} can be obtained above 15 km.

Murcray (8) has recently obtained new laboratory data on the ν_3 band of NO_2 which he has used to interpret the observations of Ackerman *et al.* (14) to give an average mixing ratio of $2–3 \times 10^{-10}$ above 16 km. He also used this new laboratory data to analyze the earlier ν_3 balloon measurements of Goldman *et al.* (11), and gives an average mixing ratio at or above 30 km of 5×10^{-9}. Taken together these calculations imply a layer of NO_2 at, or above, 30 km with a much lower mixing ratio below this altitude.

Harries (9) interpretation of the emission spectrum in the submillimeter range, taken from Concorde, led to an initial value for NO_2 of 20 p.p.b.v. with considerable uncertainty. More recently this group (15) have used the more intense Q branch during Concorde flights over South Africa, and into the Arctic Circle. Exact figures with errors are not yet available but their present estimate for the mixing ratio is below 5 p.p.b.v.

Brewer *et al.* (4) have recently reported results using absorption in the visible and the intensity ratio technique. Measurements were taken from the ground and from aircraft. The ground-based measurements are subject to interference by tropospheric NO_2 and Fig. 3 shows only the aircraft results. The authors believe the twilight results to be very reliable but give no error estimates. Their noontime curve shows two measurements in which they express confidence. Although they have less confidence in the noontime height profile, because of the greater difficulty in these measurements, they believe that the total vertical column density above the aircraft is correct. These results are very much higher than those of other observers. Their daytime measurements would be very difficult to reconcile with measured O_3 densities, since at 40 km such high values of NO_2 would lead to an O_3 destruction rate some 20 times the production rate. Moreover, the higher value at noon compared with twilight is contrary to the behavior predicted by present photochemical knowledge. Photodissociation of HNO_3 during the daytime cannot account for such diurnal variations because the photodissociation half-life is many weeks at the lower altitudes. For similar reasons the authors' suggestion that NO_2 is converted to NO_3 by reaction with O_3 in the evening and reconverted to NO_2 by photodissociation of NO_3 in the morning is difficult to accept since the half-life of the $NO–O_3$ reaction in the stratosphere is more than 1 week. Until a satisfactory explanation can be offered these results must be treated with some caution.

(c) NO Measurements

Toth *et al.* (16) identified weak absorption features in the 5.3 μ region as being due to NO. The observations were made on March 11, 1973, with an interferometer from an aircraft flying at 35° N latitude and an altitude of 12 km. The NO mixing ratio was reported to have a constant value of 1.0 ± 0.2 p.p.b.v. from 11 to 26 km. This figure was later revised to 0.8 ± 0.2 p.p.b.v. The same group also made two additional observations (3) from Concorde in June 13, 1973, at 16 km and 45.50° N. They report mixing ratios of 0.2 and 0.4 p.p.b.v. at 12.8 and 15.2 km respectively.

Ackerman *et al.* (17) also observed these same absorption features with their grille spectrophotometer from Concorde at 16 km and from a balloon at altitudes up to 40 km. The balloon flight was made in May, 1973, in France at 43° N latitude. The height profiles they deduce are shown in Fig. 4.

Murcray *et al.* (18) have drawn attention to the fact that the NO lines used in the above estimates are coincident, within the resolution of the instruments, with the CO_2 satellite bands and with solar CO emission lines. Thus, the estimates are likely to represent upper limits. Murcray *et al.* (18) failed in their attempt to observe NO absorption up to 30 km and place an upper limit of 1.0 p.p.b.v. in the mixing ratio up to this altitude.

Figure 4 also shows the results of the *in situ* NO measurements (6) made by the chemiluminescent technique. They represent measurements taken from three balloon flights in New Mexico at 33° N, two over the altitude range 17–24 km in

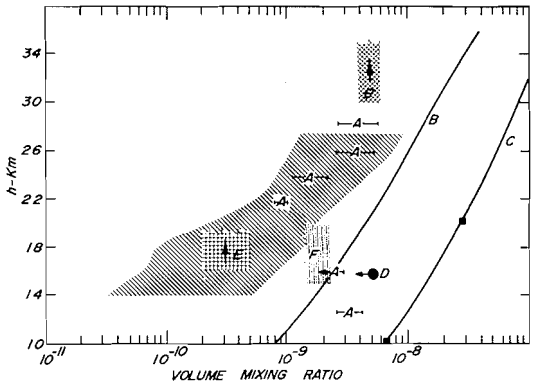

FIG. 3. Volume mixing ratios of NO_2. A, ref. 13; B, Brewer *et al.* (4), twilight aircraft measurement; C, Brewer *et al.* (4), mid-day aircraft measurement; D, Harries (15), upper limit from Concorde measurement; E, Ackerman *et al.* (14), from Concorde, twilight measurement calculated from total column density, assuming constant mixing ratio above 15 km; F, Farmer *et al.* (3), from Concorde, twilight measurements; G, Murcray (8) interpretation of balloon data assuming constant mixing ratio above 30 km; unlabelled shaded area "equivalent" NO_2 ratios calculated from the HNO_3 data of Fig. 2, from eq. B, as explained in text.

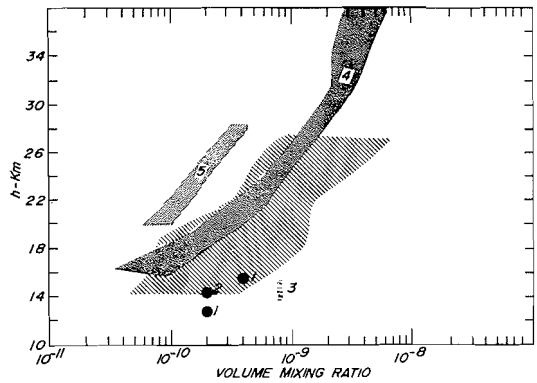

FIG. 4. Volume mixing ratios of NO. 1, Farmer (3), from Concorde, twilight measurement; 2, Ackerman *et al.* (17), from Concorde, twilight measurement; 3, Toth *et al.* (16), from aircraft, reported as constant mixing ratio over altitude range 11 to 26 km; 4, Ackerman *et al.* (17), from balloon, twilight; 5, Ridley *et al.* (6), *in situ* chemiluminescence measurement, mid-day; unlabelled shaded area "equivalent" NO ratios calculated from HNO_3 data of Fig. 2 from eqs. A and B as explained in text.

December 1972 and March 1973, and the other over the altitude range 23–27 km on June 20, 1973. The results were obtained during ascent, float, and descent over these altitude ranges.

Intercomparison of Results

There appears to be a wide spread in the results of the NO_2 measurements, an appreciable, but smaller spread in NO results, and the smallest spread for HNO_3, although it must be remembered that in the case of HNO_3 most of the measurements were taken by the same group. In the case of NO it should be pointed out that the *in situ* chemiluminescence measurements were made during mid-day while all the infrared absorption measurements were made at twilight. It will be seen from expression A that this would have the effect of increasing the difference between these results. The magnitude of the difference due to changes in solar zenith angle is not known precisely. It is difficult to believe that it would be as large as that shown in Fig. 6 of the paper by Hesstvedt (19) since this would result in unreasonably high values for mid-day NO concentrations derived from the twilight absorption measurements.

No simultaneous NO_x measurements taken from the same location by different groups using

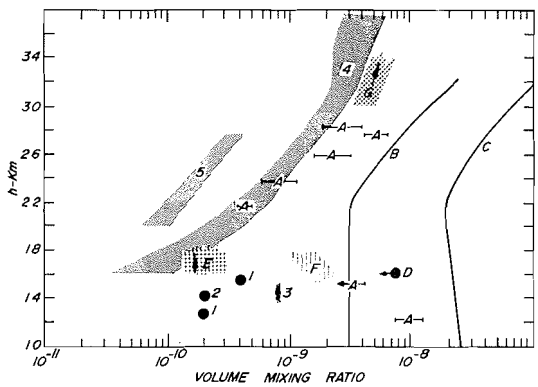

FIG. 5. Intercomparison of NO and NO_2 data. NO data as in Fig. 4, NO_2 data of Fig. 3 recalculated as "equivalent" NO from expression A in text. Numbers and letters are for the references given in Figs. 3 and 4.

different techniques have yet been reported. Thus, it is not possible to decide how much of the spread shown in Figs. 2–4 is due to real variability of NO_x mixing ratios.

Figure 5 shows a comparison of the NO observations of Fig. 4 with the NO_2 measurements recalculated as "equivalent" NO from expression A. The NO_2 results appear to be consistently higher than those for NO. As mentioned earlier, the photochemical steady state approximation used to derive expression A should be a good one. The values of J and k_2 seem to be known with accuracies greater than the differences between

Can. J. Chem. Downloaded from www.nrcresearchpress.com by 210.87.254.40 on 09/05/12
For personal use only.

Can. J. Chem. Downloaded from www.nrcresearchpress.com by 210.87.254.40 on 09/05/12
For personal use only.

average values of the NO_2 and NO measurements, although only one study (20) has been made of k_2 at stratospheric temperatures. The remaining uncertainty in the use of expression A is the value of O_3. In Fig. 5 the average height profile given by Dütsch (21) for Spring, 35° N has been used. In this issue Dütsch (22) has pointed out that O_3 densities may vary by more than 50% from one location to another at the same time and at one location from day to day. Therefore, all NO_x measurements should be accompanied by simultaneous O_3 measurements taken at the same altitude.

In Figs. 3 and 4, the HNO_3 mixing ratios are shown as equivalent NO_2 and NO respectively, as calculated from expression B. The upper bounds are calculated using the maximum HNO_3 measurements and the lowest reasonable limits for the HO density. The converse limits were used to obtain the lower bounds of the "equivalent" NO_x. We have pointed out that in the case of expression B, the use of the steady state approximation is of marginal validity. A value of unity has been adopted in these calculations for the quantum yield of HNO_3 dissociation involved in J_5. Johnston (23) believes this to be the correct value for the quantum yield in the wavelength region 255–315 nm but there is less certainty in the shorter wavelength region 200–255 nm. There are also some uncertainties in the values of k_4 and k_6. Finally, no measurements are available for the HO concentrations at these altitudes and recourse must be made to values calculated from atmospheric models. The rate constants used to determine HO densities in the models are still not well defined. The HO estimates are, however, not highly sensitive to the choice of these rate constants since self-regulation effects are operative in the HO chemistry. For example, if one tries to maximize the HO density by adopting the lowest reported value for its main termination reaction

$$HO + HO_2 \rightarrow H_2O + O_2$$

then one finds that the HO_2 concentration will build up and, consequently, so will H_2O_2 by the process

$$HO_2 + HO_2 \rightarrow H_2O_2 + O_2$$

resulting in a decrease in HO by

$$HO + H_2O_2 \rightarrow H_2O + HO_2$$

Finally, there is always the possibility that chemical reactions not yet included in the current models play important, if not dominant, roles. For example, NH_3 chemistry is not well understood (24). Oxidation may produce NO_x, but may also provide a sink by reactions such as

$$NH_2 + NO \rightarrow N_2 + H_2O$$

Observations of NO_x mixing ratios in the stratosphere are currently too sparse and disparate to provide good tests for models aimed at explaining the O_3 budget in the unperturbed statosphere or to provide predictions of the effects of additional amounts of NO introduced by man. If present NO_x levels as low as those reported by Ridley *et al.* (6) are confirmed then HO_x chemistry plays an important role throughout the unperturbed lower stratosphere in determining the O_3 budget. If the higher values of NO_x are correct then NO_x destruction of O_3 is more important in this region. It is hoped that results of simultaneous measurements using different techniques on all NO_x compounds and on O_3 will soon become available. Synoptic measurements of the altitude, temporal, and geographic dependencies of NO_x will, of course, be required before true understanding of the unperturbed stratosphere and predictions of anthropogenic perturbations can be achieved.

The author would like to thank Prof. J. C. McConnell for helpful discussions and for providing many of the calculations used in the intercomparison of the measurements.

1. P. J. Crutzen. J. Geophys. Res. **76**, 7311 (1971).
2. H. S. Johnston. Science, **173**, 517 (1971).
3. C. B. Farmer. Can. J. Chem. This issue.
4. A. W. Brewer, C. T. McElroy, and J. B. Kerr. Nature, **246**, 129 (1973).
5. A. W. Brewer. Pure Appl. Geophys. **106**, 919 (1973).
6. B. A. Ridley, H. I. Schiff, A. W. Shaw, L. Bates, C. Howlett, H. LeVaux, L. R. Megill, and T. E. Ashenfelter. Nature, **245**, 310 (1973); Planetary Space Sci. In press.
7. A. Goldman, D. G. Murcray, F. H. Murcray, W. J. Williams, J. N. Brooks, and C. M. Bradford. J. Geophys. Res. **78**, 5273 (1973).
8. D. G. Murcray. Private communication.
9. J. E. Harries. Nature, **241**, 515 (1973).
10. A. L. Lazrus, B. Gandrad, and R. D. Cadle. J. App. Meteorol. **11**, 389 (1972).
11. A. Goldman, D. G. Murcray, F. H. Murcray, W. J. Williams, and F. S. Bonomo. Nature, **225**, 443 (1970).
12. M. Ackerman and C. Muller. Nature, **240**, 300 (1972).
13. M. Ackerman and D. Frimont. Bull. Acad. R. Belg. Cl. Sci. **55**, 948 (1969).

14. M. ACKERMAN, J. C. FONTANELLA, D. FRIMONT, A. GIRARD, L. GRAMONT, N. LOUISNARD, C. MULLER, and D. NEVEJANS. Can. J. Chem. This issue.
15. J. E. HARRIES. Private communication.
16. R. A. TOTH, C. B. FARMER, R. A. SCHINDLER, O. F. RAPER, and P. W. SCHAPER. Nature, **244**, 7 (1973).
17. M. ACKERMAN, J. C. FONTANELLO, D. FRIMONT, A. GIRARD, N. LOUISNARD, C. MULLER, and D. NEVEJANS. Nature. In press.
18. D. G. MURCRAY, A. GOLDMAN, W. J. WILLIAMS, F. H. MURCRAY, J. VAN ALLEN, and S. C. SCHMIDT. J. Appl. Opt. In press.
19. E. HESSTVEDT. Can. J. Chem. This issue.
20. M. A. A. CLYNE, B. A. THRUSH, and R. P. WAYNE. Trans. Faraday Soc. **60**, 359 (1964).
21. H. U. DUTSCH. Adv. Geophys. **15**, 219 (1971).
22. H. U. DUTSCH. Can. J. Chem. This issue.
23. H. S. JOHNSTON. Can. J. Chem. This issue.
24. J. C. MCCONNELL. J. Geophys. Res. **78**, 7812 (1973).

Can. J. Chem. Downloaded from www.nrcresearchpress.com by 210.87.254.40 on 09/05/12
For personal use only.

Infrared Measurements of Stratospheric Composition

C. B. FARMER

Jet Propulsion Laboratory, California Institute of Technology, Pasadena, California 91103

Received December 7, 1973

The observational techniques and results of i.r. measurements of the minor and trace molecular composition of the lower stratosphere are reviewed. Emphasis is given to those theoretical aspects of the formation of emission and absorption spectra which affect the quantitative interpretation of observational data in terms of the vertical distribution of observed molecular species.

The principal experimental techniques currently being used are briefly reviewed, followed by a detailed summary of current knowledge of the abundances and spatial variability of the known minor constituents. The question of the determination of the minimum detectable concentration of a constituent molecule and its relationship to the instrumental parameters, the molecular transition intensities, and observation geometry is discussed; upper limit concentrations are given for some additional species of importance in current stratospheric studies.

Les techniques et les résultats expérimentaux des mesures infra-rouge de la composition moléculaire mineure et de trace de la plus basse stratosphère sont analysés. On insiste sur ces aspects théoriques de formation de spectres d'émission et d'absorption qui influencent l'interprétation quantitative de données expérimentales en termes de distribution verticale d'espèces moléculaires observées.

Les principales techniques expérimentales couramment utilisées sont brièvement analysées, suivies d'un résumé détaillé de connaissances courantes des abondances et de variabilité spatiale des constituants mineurs connus. La question de la détermination de la concentration minimum décelable d'une molécule constituante et son rapport avec les paramètres des appareils, les intensités de transition moléculaires et la géométrie d'observation sont discutés; les concentrations de limite supérieure sont donnée pour des espèces additionnelles importantes en rapport avec les études stratosphériques courantes.

[Traduit par le journal]

Can. J. Chem., **52**, 1544 (1974)

Introduction

Remote sensing measurements of the stratosphere, by emission or absorption techniques at i.r. wavelengths, have provided the source of much of our present knowledge of the compositional structure of this atmospheric region. This is of course a direct consequence of the fact that the characteristic frequencies of molecular rotational and vibrational transitions lie in the i.r. range. Until quite recently there has been relatively little attention paid to the detailed composition of the stratosphere and most of the high resolution spectral observations of the atmosphere have been made from the surface of the Earth, under which condition the spectral features arising from stratospheric molecules are masked by the intense absorptions of the tropospheric gases. Notable exceptions to this generalization, however, are the long established series of balloon observations of Murcray and his co-workers (1), the studies of stratospheric water vapor by Houghton's group at Oxford (see for example refs. 2 and 3), and the satellite observations of the ozone layer by Prabakhara *et al.* (4).

The stimulus provided by the need to understand the detailed background composition of the lower stratosphere in the context of present day concerns over the possible climatic and physiological impact of introducing reactive species into the region, has occasioned a marked increase in recent years in the application of radiometric and high resolution spectroscopic techniques to the problem. Observations have been made from balloon and high altitude aircraft platforms although, as yet, there have been no satellite based studies of stratospheric composition other than for ozone and water vapor.

An important aspect of the current studies of stratospheric aeronomy is the emphasis placed on the quantitative accuracy of the interpretation of the observational data. Consequently, in this review we shall give some attention to the theoretical

Can. J. Chem. Downloaded from www.nrcresearchpress.com by 210.87.254.6 on 09/05/12
For personal use only.

Can. J. Chem. Downloaded from www.nrcresearchpress.com by 210.87.254.6 on 09/05/12
For personal use only.

basis of the relationships between the total molecular cross section and its distribution and the corresponding observed atmospheric absorption or emission. In this way the relative advantages of the different observation modes and analysis techniques can be better understood. Following this we shall describe the experimental methods presently being used and summarize the present status of the compositional knowledge derived from them.

Formation of Spectra

In both spectroscopic and radiometric measurements, the problem can be stated generally as the interpretation of an observed variation of radiance with frequency, caused by the absorption or emission of radiation by a particular molecule (and identified by its precise frequency location), in terms of the distribution of the number density along the optical path of the observation. We shall consider radiation arriving at a point in the atmosphere from successive layers below or above the altitude of observation.

Let $q(h)$ and $k(\nu,h)$ be the molecular number density and the monochromatic extinction coefficient at frequency ν, at height h where the pressure and temperature are $p(h)$ and $T(h)$ respectively. If more than one molecular species contributes to the absorption or emission of radiation at ν, then

$$k(\nu, h)q(h) = \sum_i k_i(\nu, h)q_i(h)$$

the summation being taken over all species q_i active at ν.

We define $\sigma(\nu,\theta,H,h)$ as the *optical depth* of the atmospheric path between h and the observer at height H, at a zenith distance θ. The optical depth is given by

$$[1] \quad \sigma(\nu, \theta, H, h) = \int_H^h q(h')g(\theta, h')k(\nu, h')\mathrm{d}h$$

where $g(\theta,h')$ is the geometric factor relating the observation path to the radial path. The monochromatic transmittance of the atmospheric column between H and h is then simply

$$[1a] \qquad t(\nu,\theta,H,h) = \mathrm{e}^{-\sigma(\nu,\theta,H,h)}$$

The spectral intensity at the observer viewing the atmosphere in *emission* is

$$[2] \quad I_e(\nu, \theta, H) = \int_H^\infty B[\nu, T(h)] \times \frac{\partial t}{\partial h}(\nu, \theta, H, h)\mathrm{d}h$$

where $B[\nu,T,(h)]$ is the Planck function at frequency ν and temperature T. The corresponding expression for the intensity at the observer viewing the *absorption* of solar radiation is

$$[3] \quad I_a(\nu,\theta,H) = I^{\odot}(\nu)\, t(\nu,\theta,H,\infty) + I_e(\nu,\theta,H)$$

where $I^{\odot}(\nu)$ is the intensity of solar radiation at the top of the atmosphere. The contribution from the second term, the atmospheric emission, can be neglected in comparison to the transmitted solar energy, except at the largest i.r. wavelengths in regions of very strong absorption. By combining eq. 1 with eq. 2 or eq. 3 to obtain the full expression for emission or absorption, it is seen that the unknown, $q(h)$, appears under one sign of integration with respect to h for the absorption case whereas it appears under a double sign of integration over height in the emission case.

In practice, the intensity is measured over a finite spectral interval, $\Delta\nu$, defined by the instrumental slit function in the spectroscopic case (the spectral resolution) or by the transmission characteristics of the optical filters used in the radiometric case. For simplicity we shall assume that the instrumental function can be represented as a square passband of width $\Delta\nu$. The observed intensity, denoted by $\bar{I}$, is

$$[4] \quad \bar{I}(\nu, \theta, H) = \frac{1}{\Delta\nu} \int_{\nu-(\Delta\nu/2)}^{\nu+(\Delta\nu/2)} I(\nu', \theta, H)\, \mathrm{d}\nu'$$

The observations can be made by recording the variation of $\bar{I}$ with respect to ν for different zenith angles, θ, and base altitudes, H. In the following section we shall descuss briefly the way in which these three observation variables can be used to aid in the recovery of the total column abundance,

$$\int_H^\infty q(h)\mathrm{d}h$$

and its vertical distribution, $q(h)$, from the measured values of $\bar{I}$. Prior to this it will be useful to note a few of the characteristic properties of the intensity distribution in the two cases.

Examination of eqs. 1 and 2 shows that a quantitative interpretation of observations made in *emission* requires that the measurements be made in absolute radiance terms, and the observational procedure must therefore include the appropriate intensity calibration. It is also necessary that the variation of T with h be known in order to make an objective determination of $q(h)$. The accuracy to which $T(h)$ must be known depends on the

Can. J. Chem. Downloaded from www.nrcresearchpress.com by 210.87.254.6 on 09/05/12
For personal use only.

values of the effective emission temperatures through the range of frequencies covered by the particular spectral emission feature of interest. For example, if the line is isolated from adjacent lines of other atmospheric molecules, the determination of σ will be relatively insensitive to errors in the assumed $T(h)$ whereas, in the analysis of lines which are closely blended with others, small errors in $T(h)$ can lead to very large errors in the determination of $t(h)$ and hence $q(h)$.

In the *absorption* case, $I^{\odot}(\nu)$ can be eliminated by normalizing the observed intensities at all frequencies with respect to the measurements in the local continuum, where $k(\nu) \rightarrow 0$. Thus in absorption we can obtain $\bar{\imath}(\nu)$ directly from the measurements, but here again the level of the true continuum must be verified by determination of the contribution to the extinction by nearby features or by examination of the variation of $\bar{I}(\nu)$ with θ, in order to avoid errors in the derived value of σ.

Observation Modes: Properties of $k(\nu,h)$, θ, and H

We shall consider now the general description of the modes of observation of the stratosphere which have been employed in recent investigations using i.r. methods, and outline the properties of the observation variables, ν, θ, and H, in terms of their value in the derivation of the compositional profile, $q(h)$.

To date, three different measurement techniques have been used: medium and high resolution emission spectroscopy, high resolution absorption spectroscopy, using the Sun as the radiation source, and radiometry in emission. By radiometry, we refer to the use of a relatively broad band-pass optical filter to isolate a specific molecular band, or portion of a band, the emission intensity measurements being made both in the total filter bandwidth and in the adjacent (transparent) regions. Details of the experimental techniques involved in each of these are given in the following sections, together with some comments on more sophisticated methods, optimized for specific chosen molecules, which have evolved from the basic observational modes mentioned above; these are used in absorption and emission and include selective chopping radiometers, and optical and gas correlation filters.

In general, for observations made within a finite spectral interval, it is not possible to derive from a single observation of the emission or absorption spectrum ($\bar{I}(\nu,H,\theta)$ *vs.* ν for fixed θ and H) a unique description of the variation of the molecular density with height, $q(h)$, unless some *a priori* knowledge of the scale height or altitude location of the absorber q is available. Likewise, as we shall see, it is possible in the absorption case to determine from a single spectrum a close approximation to the *total column abundance* of the absorbing molecule, but any description of the distribution of this abundance with altitude requires that an assumption be made regarding the form of the distribution. It is thus necessary to make use of the other observational variables, zenith distance, θ, and the observation base height, H, to obtain independent information from which the full description of $q(h)$ can be determined. The manner in which ν, θ, and H, contribute to the derivation of $q(h)$ can be seen from the properties of the functions of which they are variables, namely $k(\nu,h)$, $g_H(\theta,h)$, and $\sigma(\nu,\theta,H)$, respectively.

Extinction Coefficient

In the stratosphere the width of spectral lines in the i.r. varies from the collision-broadened width at the lowest altitudes to the Doppler width at near i.r. wavelengths for the higher altitudes. The shapes of individual lines are described in terms of the variation of $k(\nu)$ with frequency from the line center, ν_0, and the pressure and Doppler-broadened half widths, γ_L and γ_D. The line shapes are related to the extinction coefficient through the line intensity S^0, *viz.*

$$[5] \qquad k(\nu) = S^0 f(\nu-\nu_0)$$

For Doppler-broadened lines,

$$[6] \quad f(\nu-\nu_0) = \frac{1}{\gamma_D\sqrt{\pi}} \exp - \left(\frac{\nu-\nu_0}{\gamma_D}\right)^2$$

the Doppler half width (in cm^{-1}) being given by

$$[7] \qquad \gamma_D = \frac{\nu_0}{c}\left(\frac{2kT}{m}\right)^{1/2}$$

k being the Boltzmann constant and m the molecular weight. For collision-broadened lines, the full expression for the line shape (for all line center frequencies) is

$$[8] \quad f(\nu-\nu_0) = \frac{1}{\pi}\left(\frac{\nu}{\nu_0}\right)^2\left[\frac{\gamma_L}{(\nu-\nu_0)^2+\gamma_L^2} + \frac{\gamma_L}{(\nu+\nu_0)^2+\gamma_L^2}\right]$$

For most purposes the terms correcting for the asymmetry at long wavelengths and the induced emission can be neglected, and the simple Lorentz expression is used, *viz.*

Can. J. Chem. Downloaded from www.nrcresearchpress.com by 210.87.254.6 on 09/05/12
For personal use only.

$$[9] \quad f(\nu - \nu_0) = \frac{1}{\pi}\left[\frac{\gamma_L}{(\nu - \nu_0)^2 + {\gamma_L}^2}\right]$$

However, for a large part of the range of conditions encountered in the stratosphere ($p \approx 10^{-1}$ to 10^{-3} atm; $T \approx 220$ to 270 °K) and over the range of frequencies covered by i.r. observations ($\nu \approx 10^4\,cm^{-1}$ ($\sim 1\,\mu m$) to $10\,cm^{-1}$ (~ 1 mm)), the actual line shape is described by a convolution of the Doppler- and collision-broadened shapes. The properties of this combined line shape, the Voigt profile, have been tabulated both in terms of the variation of $k(\nu)$ with ν, and the dependence of the total integrated absorption or emission over the line on the physical properties of the absorbing column of gas (5, 6).

As an example of the range of overlap of the line-width regimes at i.r. wavelengths in the stratosphere, a molecule of average molecular weight, CO, has line half-widths from pressure broadening varying from $\sim 10^{-2}\,cm^{-1}$ at 10 km to $\sim 10^{-4}\,cm^{-1}$ at 50 km altitude, while its Doppler widths cover the range from 10^{-2} to $10^{-6}\,cm^{-1}$ over the range of wavelengths of interest.

The intrinsic line strengths and half-widths are dependent on the local temperature conditions, also, and this must therefore be taken into account in the interpretation of the observed absorption or emission in terms of molecular concentration. In terms of the manner in which the dependence of $k(\nu)$ on the local atmospheric conditions can be used as a discriminator in the determination of $q(h)$, however, the predominant factor is the dependence of line half-width on pressure. The collision-broadened width is linearly related to pressure, *viz.*

$$[10] \quad \gamma_L = {\gamma_L}^0 p$$

and we may consider, for the purposes of illustration, a pure Lorentz-shaped line and examine the range of dependence of the extinction coefficient on pressure between the line center and its extreme wing. From eqs. 5, 9, and 10

$$[11] \quad k(\nu) = \frac{S^0 p}{\pi}\left[\left(\frac{\nu - \nu_0}{{\gamma_L}^0}\right)^2 + p^2\right]^{-1}$$

so that $k(\nu)$ is proportional to p in the wing of the line ($\nu - \nu_0 \gg {\gamma_L}^0 p$) and proportional to $1/p$ at the line center ($\nu = \nu_0$). Consequently, in the formation of an isolated spectral line, at different values of ν the extinction coefficient $k(\nu)$ reaches a maximum value at different altitudes (p). We should note, however, that in the presence of other lines this discrimination will become very much less pronounced; nevertheless, in principle, for a single isolated line and with *monochromatic* observation conditions, it is possible to use the dependence of $k(\nu)$ on p in the pressure-broadened regime as a weighting function to determine $q(h)$. Such conditions are approached in the case of laser transmission or optical heterodyne radiometer measurements. In practice, when observations are made over a finite spectral interval, as has been the case to date, the integration over $\Delta\nu$ shown in eq. 4 has the effect of masking the intrinsic shape of the line. Thus as $\Delta\nu$ becomes large compared to the line width, measurements of $I(\nu)$ over intervals of ν within $\Delta\nu$ tend to be redundant. Consequently the use of $k(\nu)$ as a weighting function for $q(h)$ is strongly dependent on the value of $\Delta\nu$.

Observation Geometry and Base Altitude

Much of the emphasis in current remote sensing of the stratosphere is directed towards the detection and measurement of candidate molecular species whose relative abundances are small and the intensity variations, by which they may be studied, very weak. For this purpose the enhancement of the total column abundance along the line of sight when the observations are made at large zenith distances can be exploited. Under these conditions, if the field of view covers the region close to the Earth's limb, an observation at a single zenith distance can provide a direct indication of the probable altitude location of the absorber, in addition to an approximate value for the integrated column density. To derive an *unambigous* solution for the total abundance and its vertical distribution, however, the observations must be made over several values of the zenith angle θ. The strong dependence of the geometrical factor, $g(\theta,h)$ on zenith distance, for angular distances close to 90°, renders it the most powerful of the weighting factors available for the determination of $q(h)$.

The well-known expression for the variation of the optical path length L with zenith angle, for large values of θ in a spherical atmosphere, is

$$[12] \quad L = \sqrt{\frac{\pi r \mathscr{H}}{2}}\exp\left[\frac{r}{2\mathscr{H}}\cos^2\theta\right] \times \left[1 - \operatorname{erf}\sqrt{\frac{r}{2\mathscr{H}}\cos^2\theta}\right]$$

where r is the Earth's radius and $\mathscr{H}$ the scale

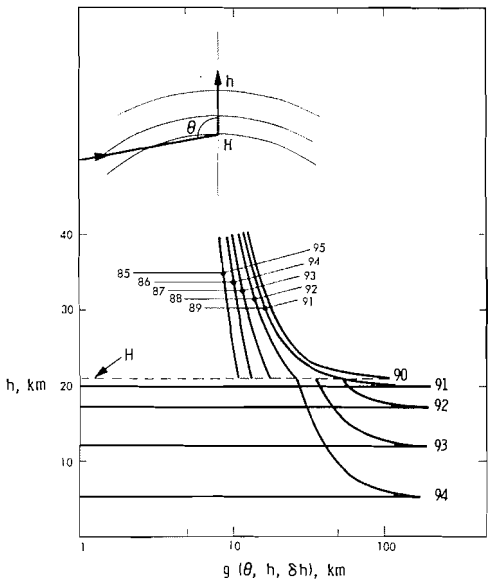

FIG. 1. Contribution to the optical path by the geometric factor $g(\theta,h,\delta h)$ for atmospheric layers above and below the observation altitude H, for $85° < \theta < 94°$. The figure is drawn for $H = 21$ km and an elemental layer thickness $\delta h = 1$ km.

height. Figure 1 shows the variation of the ratio of the geometric path to the radial path at height h, for different values of the zenith angle of observation. It should be noted that the figure represents only the geometric factor, *i.e.* it does not contain the variation of density with height; $q(h)$ is defined here (eq. 1) as the absolute number density of species q and not the relative mixing ratio. From observations at a given H and v, for different values of θ when $\theta > 90°$, it is possible to recover the structure of q as a function of h. The geometric factor should also include any contribution to the optical path resulting from refraction along the path. In practice this is negligible for observations in the stratosphere where the grazing altitude (altitude of closest approach) exceeds 15 km, *i.e.* the effect of refraction is negligible for virtually all stratospheric geometries.

For observations made at varying H, *i. e.*with v and θ held constant, the weighting functions are similar to those shown in Fig. 1 for the appropriate value of θ, but with the added advantage that, to obtain discrimination with respect to height h, the viewing angle θ need not be restricted to angles larger than 90°.

In practice, a combination of the variation of v, θ, and H is used to obtain the necessary independence between the sets of observational data from which the corresponding values for $q(h)$ can be extracted. The methods of analysis of the observational data are described briefly in the following section, but it is appropriate in the discussion of the influence of observational geometry to illustrate the general characteristics of the variation of $\bar{I}(v)$ with θ for representative types of vertical mixing profile.

Figure 2 shows the variation with zenith angle of the intensity of a weak spectral feature observed in absorption, for four different vertical distributions of a fixed total column abundance. Case (*a*) assumes the species to have a scale height $\mathscr{H}$ equal to that of the bulk atmosphere, *i.e.* uniform mixing. Case (*b*) represents the situation where the gas is restricted to a layer 5 km thick, the base of the layer being above the observation point. In cases (*c*) and (*d*) the bulk of the gas is in a 5 km thick layer, with the observational level at the top of the layer (*c*) and 5 km above the layer (*d*). Thus, for observations made *below* the level of a layered species, for zenith angles less than 90° there is clearly very little discrimination from which to determine its scale height, but the observation of a maximum at 90° is a unique indication that the gas is not uniformly mixed and that its effective lower altitude limit is above the observation point. The greatest discrimination occurs of course where the observations are continued through 90°; the general shape of the change of intensity distinguishes uniform from non-uniform

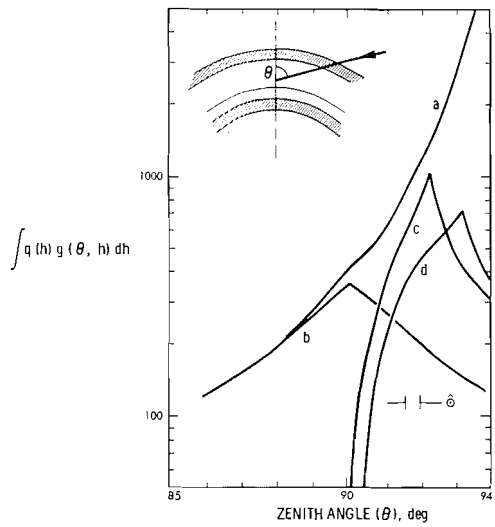

FIG. 2. Variation of total column density as a function of zenith angle, for four different vertical distributions of the (fixed) total abundance. (For details of the distributions see text.)

Can. J. Chem. Downloaded from www.nrcresearchpress.com by 210.87.254.6 on 09/05/12
For personal use only.

Can. J. Chem. Downloaded from www.nrcresearchpress.com by 210.87.254.6 on 09/05/12
For personal use only.

mixing, and the angular positions of the onset and maximum of the observed absorption give directly the altitude range of the constituent if it is layered below the observer.

In practice the discrimination provided by these characteristics is degraded by the finite angular size of the radiation source; the angular diameter of the Sun is shown in Fig. 2 to illustrate this effect, although it is usually possible to minimize this loss of vertical resolution by tracking a fixed portion of the Sun's disk during the period of each observation.

Similar characteristics for the emission case with a modeled atmospheric temperature structure have been examined by Harries (7), who shows that under certain circumstances the angular range close to, but less than, 90° can provide height discrimination. This fact is of particular importance in the emission case, where the observational data might be severely affected by the inclusion of the (hot) planetary limb in the instrument field of view.

Analysis of Observational Data

The full expressions for the observed emitted intensity $\bar{I}_e$ or absorption $\bar{a}$ from eqs. 1–4, for a non-scattering optical path, are

$$[13]\quad \bar{I}_e(\nu, \theta, H) = \frac{1}{\Delta\nu}\int_{\nu-(\Delta\nu/2)}^{\nu+(\Delta\nu/2)}\int_H^\infty B[\nu, T(h')]\frac{\partial}{\partial t}\exp\left[-\int_H^{h'} q(h)g(\theta, h)k(\nu, h)dh\right]dh'd\nu$$

and

$$[14]\quad \bar{a}(\nu, \theta, H) = 1 - \frac{\bar{I}_a(\nu, \theta, H)}{\bar{I}^\odot(\nu)} = 1 - \frac{1}{\Delta\nu}\int_{\nu-(\Delta\nu/2)}^{\nu+(\Delta\nu/2)}\exp\left[-\int_H^\infty q(h)g(\theta, h)k(\nu, h)dh\right]d\nu$$

While eqs. 13 and 14 are characteristically different, they are both nonlinear in $q(h)$ and must be solved numerically by iterative methods, the solution being the profile, $q(h)$ for which the computed intensity or absorption agrees with all the corresponding observations. We shall not attempt to give an account of the computational details involved in the analysis of the observational data, but will describe briefly the approaches which are most frequently adopted.

General Method

The procedure in most cases is to divide a model atmosphere into a number of layers, assigning a mean temperature to each at the mean (Curtis–Godson) pressure of the layer. By means of "line-by-line" calculations, for each absorber q_i active at frequency ν, the optical extinction is computed at suitable small intervals, δν, across the frequency range of interest, using the (known) values for the intrinsic transition strengths, their half-widths, and ground-state energies. Taking some starting assumption for the variation of mixing ratio with height, a theoretical mean value for the emitted intensity or the absorption is computed from [13] and [14] by summation over all layers and over the frequency range of the instrument function. These computed values are compared with the observed values at each frequency, and the values of $q(h)$ assigned to each layer adjusted in an iterative process until the mean value of the differences between the observed and calculated values is minimized. In this procedure the difference remaining in the dominant layer for each observation, indicated by the geometric factor $g(\theta,h)$, is given the greatest weight in driving the iteration to a solution. Good examples of the application of this method can be seen in the work of Murcray *et al.* (8) in the determination of vertical mixing profiles for CO and N_2O.

Equivalent Width Method

It is not always necessary to reproduce the variation of $\bar{I}_e(\nu)$ or $\bar{a}(\nu)$ *vs.* ν in detail: the integrated emission or absorption over the frequency extent of a feature is independent of the instrument function, and this property provides a convenient parameter for comparison of the observed and calculated spectra. The use of $\int\bar{a}(\nu)d\nu$, the "equivalent width" of a line or feature, must be treated with caution, however, since its independence of Δν is valid only if the integration is taken between limits where $\bar{a}(\nu) \to 0$ (eq. 14).

The equivalent width method is particularly useful in the analysis of isolated or very weak features in absorption spectra which are close to the detection limit. The relationship between the integrated absorption of a line and its Doppler- and pressure-broadened half-widths, intrinsic intensity, and the molecular cross section, can be

Can. J. Chem. Downloaded from www.nrcresearchpress.com by 210.87.254.6 on 09/05/12
For personal use only.

used directly to determine an approximate value for the molecular abundance from the observed spectrum. This relationship (the "curve of growth") has been tabulated for lines of mixed Doppler and Lorentz profile by Jansson and Korb (6). For most transitions at near i.r. frequencies, the dependence of $k(\nu)$ on temperature is small, over the range of temperatures encountered in the stratosphere ($\sim$220 to 270 °K). Thus, if a mean value for the effective pressure p_{eff} over the observation path is assumed, and if the line strength and pressure-broadened half-width are known, the observed equivalent width can be directly converted to a value for the total molecular abundance along the path. For an assumed constant mixing profile, and for small θ, $p_{eff} = p_H/2$; for large values of θ, p_{eff} must be determined as a function of the geometric factor. The calculation can be repeated for $p_{eff} = p_H$ and $p_{eff} = 0.01p_H$, say, to assess the error incurred by the assumption of the scale height or location of the absorber. By this procedure it is found that the uncertainty in the derived total vertical abundance is typically not greater than $\pm 30\%$. Nevertheless, for weak spectral lines it is not possible to gain any information regarding the *vertical distribution* of the total abundance without making *independent* measurements at two or more values of the zenith angle or base altitude.

Band Model Method

An alternative method which has been used to reduce the computational complexity is the so-called "band model" method, where the distribution of line strengths and spacings is represented by an appropriate function. A review of band models and their ranges of validity has been given by Goody (9). This procedure is particularly suited to molecular bands where the individual lines are closely packed or overlapping and where an empirical treatment of the variation of extinction coefficient with frequency can be substituted for (often unavailable) detailed quantum assignments. The method has been used in the past for radiometric measurements of stratospheric water vapor (2) and, more recently, the interpretation of observations of the nitric acid layer by Murcray *et al.* (8) (see later).

Minimum Detectable Abundance

The concept of the "minimum detectable abundance" of a particular molecule is of importance both in the design of observations and in setting an upper limit for its abundance if it is not detected in the spectrum. The minimum detectable abundance is that amount of absorber which will produce a change in the observed intensity or absorption which is just discernable (by some stated statistical margin, n) against the random variations (noise) in the observational data. For absorption spectra this can be estimated in terms of the "noise equivalent width" of the instrument under given observation conditions; if N is the fractional noise level superimposed on the observed signal level, the noise equivalent width is $nN\Delta\nu$. When the noise level is very small, the equivalent widths of lines which produce a maximum change in the continuum level comparable to the noise fluctuations follow a linear relationship with the total absorber amount, *i.e.*

$$[15] \quad \int_0^\infty \bar{a}(\nu)\, d\nu = S(T) \int_H^\infty q(h) g(\theta, h)\, dh$$

where $S(T)$ is the line strength at some mean stratospheric temperature. If U is the total *vertical* column abundance then, assuming uniform mixing, the minimum detectable abundance U_{min} is given by

$$[16] \quad U_{min} = \frac{nN\Delta\nu}{S(T)} \left[\int_H^\infty g(\theta, h)\, dh \right]^{-1}$$

A similar estimate can be made for measurements in emission, but here the noise equivalent width must be given in terms of a specified emission temperature contrast between the line center and the adjacent continuum. For features of interest that are closely blended with stronger lines of other constituents, the noise equivalent width at the nominal frequency of the line may not be on the linear part of the curve of growth. Under these conditions upper limit concentrations from emission spectra can only be safely estimated by a full calculation of the theoretical spectrum, for progressively smaller total absorber amounts, until the noise equivalent intensity fluctuations are reached.

Instrumentation and Experimental Methods

In discussing the experimental techniques which have been employed for i.r. studies of stratospheric composition, it is perhaps useful to distinguish between two quite distinct measurement objectives. These might be termed "specific" and "survey" measurements. In the first of these, the investigation is concerned with a detailed study of the distribution and temporal variability of a particular molecule, whose pres-

TABLE 1. Principal stratospheric infrared experimental groups

Experimental group	Instrument	Platform	Region	Principal molecules
Ackerman	Grating	Balloon	Near i.r. 3–4 μm	CH_2, NO_2, NO
Farmer	Michelson	Aircraft	Near i.r. 1–7 μm	CH_4, NO, NO_2, N_2O, H_2O, CO, O_3
Girard	Grille spectrometer	Aircraft, balloon	Near i.r. 4–10 μm	NO
Houghton	Radiometer	Balloon	Mid i.r.	H_2O
Harries	Michelson	Aircraft	Far i.r. 10–30 cm^{-1}	H_2O, HNO_3, O_3, N_2O, NO_2
Kuhn	Radiometer	Aircraft	Far i.r.	H_2O
Lowe	Grating	Aircraft	Near i.r.	CH_4, CO_2
Marten	Michelson	Aircraft, balloon	Far i.r. 30–200 cm^{-1}	H_2O, O_2, O_3
Murcray	Grating, radiometer	Balloon	Near/mid i.r. 3–30 μm	HNO_3, H_2O, CO, CH_4, N_2O, NO_2, O_3

ence as a minor constituent is already known together with its approximate abundance. For such measurements an experimental technique can be used which is more economic in its use of observational data to be acquired than is possible in the case of "survey" observations, where the spectrum must be recorded over a relatively large frequency range in order to search for evidence of suspected but previously undetected constituents. An example of this difference in approach can be seen in the detection of nitric acid (see next section) in absorption and emission spectra, and the subsequent study of its distribution by means of radiometers having optical pass-bands chosen to provide the maximum discrimination between the nitric acid features and the background. In this section we shall describe briefly the methods which are currently being used in i.r. measurements of the stratosphere; the principal groups of investigators and the salient features of their experimental techniques are summarized in Table 1.

Radiometry

As far as composition studies of the stratosphere are concerned (as opposed to remote sounding of the physical structure) the emission radiometry technique has been applied only to the more abundant species, water vapor and ozone (with the recent exception of nitric acid cited above). The reason for this will become apparent from consideration of the resolution requirements for the detection and measurement of the rarer species. It should be pointed out, however, that the techniques of selective filtering using Fabry–Perôt, gas correlation, and pressure-modulated filter radiometers, which are currently in use to provide improved height discrimination for temperature sounding, will undoubtedly find direct application to the measurement of the less abundant trace gases in the future. In addition to their selectivity such methods are able to achieve an effective spectral resolution comparable to the width of the lines of the gas of interest under stratospheric conditions, while having sufficient energy grasp to allow the measurements to be made rapidly and with the required accuracy. Selective radiometers of this type have not as yet been used for atmospheric composition measurements, but they are prime candidates for use in future remote monitoring of the upper atmosphere from spacecraft. A detailed description of these techniques can be found in the review of remote sensing methods by Houghton and Taylor (10).

The main application of broad band radiometry to detailed compositional studies of the stratosphere to date has been the balloon-borne meaments of downward radiation from water vapor by Houghton and his co-workers. The instrument used a gold-doped detector and filter, both cooled to liquid air temperature, the combination isolating the whole of the 6.3 μ band (*i.e.* between 1300 and 1800 cm^{-1}). The radiometer provided a relatively inexpensive means of monitoring the stratospheric water vapor profile up to altitudes of

Can. J. Chem. Downloaded from www.nrcresearchpress.com by 210.87.254.6 on 09/05/12
For personal use only.

Can. J. Chem. Downloaded from www.nrcresearchpress.com by 210.87.254.6 on 09/05/12
For personal use only.

about 25 km. A detailed description of the radiometer is given by Williamson and Houghton (2) and the results of the measurements are considered in the next section together with those derived from other i.r. measurements. Kuhn has also studied stratospheric water vapor by emission radiometry, in this case using a pyroelectric (TGS) detector and filter to cover a portion of the rotational band between 18 and 23 μ. A special emphasis of this work has been to investigate the injection of tropospheric water vapor into the stratosphere from the penetration of thunder clouds. The instrument, which was mounted in an aircraft, and the general measurement technique are described by Barrett *et al.* (11).

Spectroscopic Methods

Apart from water vapor, ozone, nitrous oxide, and methane, which are present in the lower stratosphere at volume mixing ratios of the order of 1 in 10^6, the trace constituents of importance to current aeronomic studies are at much lower concentrations, typically <1 in 10^9. As a result of this they appear in absorption or emission spectra as very weak features, which are often obscured by the interference from bands of the more abundant species. The search for them must therefore be made at high spectral resolutions and an estimate of the resolution required can be made using the minimum detectable criterion given in the previous section.

Consider an i.r. transition having a (typical) line strength of 10^{-19} cm^{-1} (mol cm^{-2})$^{-1}$. Under conditions of observation where a geometric path advantage of 100 can be gained ($\theta \sim 90°$), the minimum detectable cross section for an instrument having a 3σ (random fluctuation) uncertainty level of 10^{-2} is

$$U_{\min} = \frac{10^{-2}\Delta\nu}{10^{-19}10^{2}} = 10^{15}\Delta\nu \text{ mol cm}^{-2}$$

If we assume the gas to be uniformly mixed, with a scale height of ~ 6 km ($p_H = 0.1$ atm), the molecular concentration at the base altitude is $10^{15}\ \Delta\nu/(6 \times 10^5) = 1.6 \times 10^9\ \Delta\nu$ mol cm^{-3}, giving an equivalent minimum detectable mixing ratio of 10^{-9} for an instrumental width of 0.6 cm^{-1}. This order of magnitude estimate illustrates the need for spectral resolutions of ~ 0.1 cm^{-1} for the detection and measurement of trace constituents which may be present in the lower stratosphere at volume concentrations of less than a few parts per billion.

In their work covering more than a decade of successful balloon observations, Murcray and his group at the University of Denver have used a conventional grating spectrometer covering the wavelength range from 3 to 30 μ, viewing the atmosphere both in emission and absorption. The spectral resolution in their more recent observations is ~ 0.3 cm^{-1} and the r.m.s. noise level in their spectra is $<2\%$. Examples of the results of this painstaking work can be seen in the published solar spectra covering the 700 to 2100 cm^{-1} range (1). This work has provided a wealth of information on several molecules, including CO, N_2O, NO_2, H_2O, and CH_4, but in retrospect perhaps the most important outcome of these observations was the discovery in 1968 of stratospheric nitric acid, which was largely responsible for initiating the present interest in its precursors, NO and NO_2. Reference to these results will be found in the description of individual molecules in the next section.

In an endeavor to achieve higher spectral resolution while keeping the observation time to a minimum, many groups have exploited techniques which provide the advantages of multiplexing the spectral information together with increasing the energy throughput of the instrument. In most cases this has involved the use of a suitably adapted version of the Michelson interferometer, the interferogram being recorded in the emission or the solar transmission modes, and subsequently transformed by fast Fourier techniques to the required spectrum.

Harries and the group at the National Physical Laboratory have used a modular Michelson interferometer of the type developed by Gebbie for atmospheric emission measurements, with a helium cooled Rollin bolometer to cover the submillimeter range from 3 to 30 cm^{-1}. The unapodized spectral resolution achieved is 0.06 cm^{-1} and the observations have been made principally from aircraft, a number of these having been from the Anglo–French SST Concorde prototype. These observations have yielded significant new data on the latitude variations of several species, notably HNO_3, NO_2, and H_2O. A description of the instrumentation in the form used for these measurements has been given by Harries *et al.* (12) and details of the results of the observations can be found in the relevant references cited in the following sections.

The author and the group at the Jet Propulsion Laboratory have developed a fast scanning

Can. J. Chem. Downloaded from www.nrcresearchpress.com by 210.87.254.6 on 09/05/12
For personal use only.

stepped interferometer covering the near i.r. region from ~ 1 to 8 μm (a range of some 8000 cm^{-1}). The instrument, based initially on a modification of the Connes interferometer by Beer (13), has been described by Schindler (14). The resolution achieved is ~ 0.2 cm^{-1} (unapodized) and spectra covering the full frequency range at maximum resolution can be recorded in 2 to 3 min. Measurements have been made from high altitude aircraft, viewing a portion of the Sun's disk with a tracking optical system. Some of these observations have been made from the SST Concorde, the high speed of which has enabled the relative motion of the Sun to be reduced almost to zero over the period of recording each interferogram, thereby minimizing the uncertainty in defining the precise optical path of each measurement. The noise level in solar spectra recorded with the instrument is typically between 10^{-2} and 10^{-3} of the background intensity and the observations to date have yielded information on the altitude and latitude variations of a number of stratospheric molecules, including N_2O, NO, NO_2, H_2O, CO, CH_4, together with revised upper limits for several others. An account of the use of the instrument in aircraft observations, and a discussion of the minimum concentrations which can be detected, has been given by Farmer *et al.* (15).

Girard, at the Office National d'Etudes et de Recherches Aerospatiales has used a version of his grille spectrometer (16) to obtain the luminosity and resolution required for stratospheric observations at high detectivity. The instrument has been used with a solar tracker to record the spectrum in absorption from a balloon platform and from aircraft (Caravelle and Concorde). The overall spectral range, using nitrogen cooled InSb and HgCdTe detectors, is 4000 to 700 cm^{-1}, although the window used for the Concorde observation limits this range to ~ 1250 cm^{-1}. For a given observation, the selection of the entrance grille (which replaces the slit of a conventional grating spectrometer) restricts the frequency range to a few tens of cm^{-1}, but against this the spectral resolution is very high (~ 0.08 cm^{-1}) and the spectral scans can be made rapidly *i.e.* 0.2 cm^{-1} per second. For the stratospheric observations to date, made in collaboration with Ackerman's group at the Institut d'Aeronomie, the instrument has been used in the 1900 cm^{-1} region and has provided the most precise of the i.r. measurements of NO, from the many lines of the 1–0 band which it was able to resolve. The Girard instrument has the advantage of great flexibility in its application to the current spectroscopic investigation of the stratosphere; once a spectral region of potential interest has been identified from broader range spectral surveys, the grille spectrometer can readily be centered on the region and a more detailed high resolution study made, with corresponding economy in the use of the observational data.

Discussion of the Results of Infrared Observations

Nitrous Oxide

Stratospheric nitrous oxide has been measured using *in situ* methods by Schutz *et al.* (17), by Harries (18) in the far i.r., and by Goldman *et al.* (19, 20), who observed the ν_3 fundamental at 2224 cm^{-1} in the near i.r. region. The data of Schütz *et al.* and Harries are in reasonable agreement, and indicate an N_2O mixing ratio of about 0.250 p.p.m.v. at the tropopause, decreasing gradually to about 0.220 p.p.m.v. at 15 km. Harries' data cover a latitude range from 5° S to 48° N and show no significant latitude variation.

The results of Goldman *et al.* are derived from two separate sets of observations. The more recent (1972) set, covering the greater range of stratospheric altitudes, shows a variation of from 0.33 p.p.m.v. at the tropopause falling to about 0.15 p.p.m.v. at 18 km. This is in comparison with a value of 0.11 p.p.m.v. at 13 km from the 1968 observations. The large difference at the lower altitude between the two observation periods may perhaps be the result of temporal or seasonal variations.

Our results were obtained from both the ν_3 and $2\nu_1$ (2560 cm^{-1}) bands for data obtained at 12 km and, in addition, the $\nu_1 + \nu_2$ (1880 cm^{-1}) band for observations at 16 km. From these we derive a value of 0.20 ± 0.02 p.p.m.v. for the N_2O mixing ratio, with no discernable variation between altitudes of 12 and 20 km in the latitude range from 33° N to 68° N. This result refers only to the period of the year between March and June. It should be pointed out, however, that these observations have so far been limited to two fixed altitudes so that, taking into account the variation of tropopause height with altitude, the results could hide any small systematic increase in the mixing ratio with latitude at the tropopause height, if there were a compensating fall-off in the mixing ratio with height above the tropopause. In general the results are in good agreement with those of Schütz *et al.* and Harries. In view of its

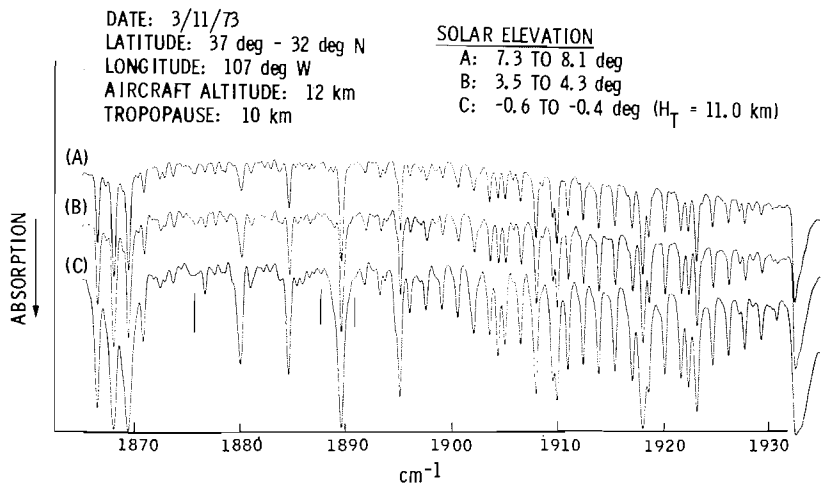

FIG. 3. Stratospheric solar spectra in the region of the 1–0 band at 1876 cm^{-1}. Three of the weak NO features are indicated by vertical bars.

probable role as the principal source of NO in the lower stratosphere (see, for example, Nicolet and Peetermans (21)) it is of fundamental importance that the detailed seasonal and spatial variations of N_2O be determined to a greater degree of refinement than is possible from the observations made to date.

Nitric Oxide

Among the expected trace molecular constituents of the lower stratosphere, nitric oxide is of particular importance because of the role it is thought to play in the net depletion of ozone in this region. A number of recent papers have been devoted to this question, but at the time when concern over the possible perturbation of this catalytic balance was first expressed no measurements of the abundance of NO in the lower stratosphere had been made. It therefore became a prime molecular species for which to search in the continued high resolution spectroscopic investigation of the stratosphere.

Nitric oxide was first detected from sunrise spectra taken during a flight on March 11, 1973, over Albuquerque, New Mexico; the result has been reported by Toth *et al.* (22). The observed NO features, in the *R* and *Q* branches of the 1–0 fundamental at 1876 cm^{-1}, were very weak and close to the detection limit. Furthermore, the initial spectra were taken over a restricted range of observation conditions so that it was not possible to extract with any accuracy the variation of NO mixing ratio with altitude. The derived total molecular cross section gave, on the assumption of constant mixing, a mean apparent mixing ratio of 1.0 ± 0.2 p.p.b.v.[1] The NO features as they appear in the stratospheric spectrum are shown in Fig. 3; the region illustrated is dominated by the ν_2 band of H_2O vapor and $3\nu_2$ band of CO_2.

On March 16, 1973, Ridley *et al.* (23) obtained *in situ* data from a balloon-borne chemiluminescense instrument at a latitude of 33°, which yielded an NO mixing ratio of 0.1 p.p.b.v. with an estimated accuracy of $\pm 60\%$. This result referred to the altitude range from 17.4 to 23 km. Subsequently, on May 14, 1973, Ackerman *et al.* (24) observed the 1–0 NO band with a balloon-borne grille spectrometer over Southern France (latitude $\sim 43°$ N). The Girard instrument was capable of a higher spectral resolution than that used by Toth *et al.* and this factor, together with the advantage gained from the balloon altitudes, enabled these observers to determine for the first time with precision the NO mixing ratio and its vertical profile. Ackerman *et al.* report values which vary from 0.07 p.p.b.v. at 16.5 km to 4.4 p.p.b.v. at 37.5 km. For these balloon observations Girard chose to examine the region of the 1–0 band between 1900 and 1910 cm^{-1} and an example of the spectra obtained from these flights is shown in Fig. 4.

Farmer *et al.* (25) made two additional observations of NO on the evening of June 13th with the instrument mounted in the French Concorde

[1]This preliminary value was subsequently corrected by more extensive analysis to a revised value of 0.8 ± 0.2 p.p.b.v.

Can. J. Chem. Downloaded from www.nrcresearchpress.com by 210.87.254.6 on 09/05/12
For personal use only.

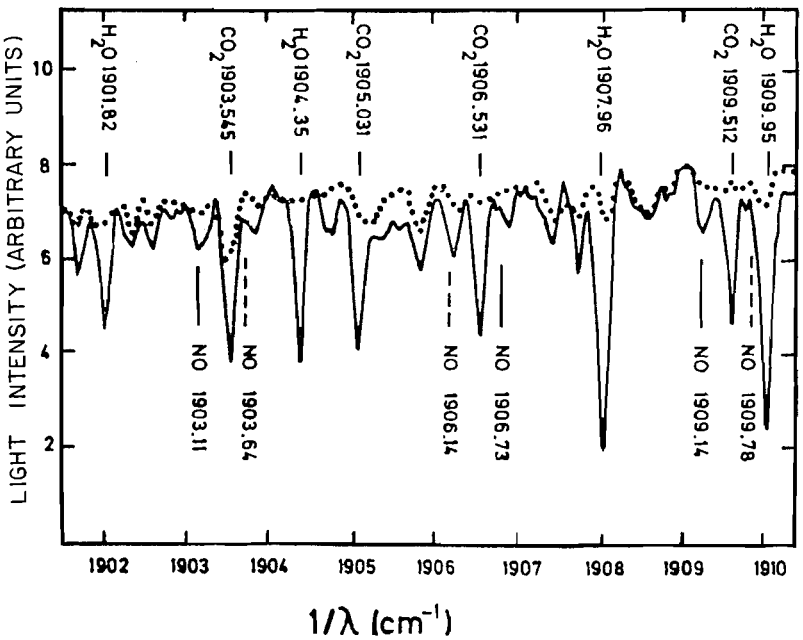

FIG. 4. Observation of stratospheric NO in the 1–0 band (after Ackerman *et al.* (24); published with the permission of the Editor, Aeronomica Acta).

prototype 001, flying at an altitude 16 km between 45 to 50° N latitude. At solar zenith distances of 91.6° and 90.5°, which correspond to tangential ray altitudes of 12.8 and 15.2 km, mixing ratios of 0.2 and 0.4 p.p.b.v., respectively, were obtained.

The results summarized here show marked differences among the individual observations, which were made under widely differing conditions of location, season, and time of day. It is clear that more extensive observations of NO are required before any firm description of its spatial and temporal variations can be given.

Nitrogen Dioxide

Nitrogen dioxide was first observed in the grating spectra of Goldman and co-workers (1, 26) covering the ν_3 band (at 1617 cm^{-1}). A quantitative analysis of these data, and additional lower resolution spectra covering the much weaker $\nu_1 + \nu_3$ band (2906 cm^{-1}), was carried out by Ackerman and Muller (27) who derived mixing ratios ranging from an upper limit of 2.3 p.p.b.v. at 16.1 km to a (observed) value of 4.0 $\pm$ 1.5 p.p.b.v. at 28.3 km. Harries (18), from emission spectra covering the rotational lines in the 20 to 30 cm^{-1} region, reported an average mixing ratio of 20 p.p.b.v. for NO_2, but pointed out that the accuracy of his measurement was severely limited by spectral assignment uncertainties. Harries has subsequently revised his value for the average mixing ratio to 5 p.p.b.v. (28).

In the rotational region the NO_2 lines observed and reported to date are severely blended with the very much stronger lines of more abundant species such as H_2O, N_2O, O_3, O_2 and the spectrum in this region is consequently difficult to analyze. The ν_3 band at 1617 cm^{-1} is strong and, at stratospheric altitudes, is relatively free from interference from the overlying 6.3 μm water vapor bands. The third band which can be used for i.r. observations of NO_2 ($\nu_1 + \nu_3$ at 2906 cm^{-1}) is some 30 times weaker than the ν_3 band and is severely blended with lines of the CH_4 bands in the 3 μ region. Thus it would appear that the most favorable band for the investigation of NO_2 is ν_3 although, until recently, the analysis of spectra obtained in this region (see, for example, Murcray *et al.* (1)) has not been attempted, perhaps as a result of difficulties associated with rotational quantum assignments for the band.

From spectra obtained from the Concorde observations, which covered the region of the $\nu_1 + \nu_3$ band, Farmer *et al.* (25) were able to detect two features due to NO_2 which, after a thorough comparison with high resolution CH_4 spectra, were

Can. J. Chem. Downloaded from www.nrcresearchpress.com by 210.87.254.6 on 09/05/12
For personal use only.

Can. J. Chem. Downloaded from www.nrcresearchpress.com by 210.87.254.6 on 09/05/12
For personal use only.

found to be sufficiently isolated to be amenable to unambiguous analysis. From these a tentative mixing ratio was derived for NO_2 of 1.8 ± 0.5 p.p.b.v. over the 15 to 20 km altitude range. The importance of this result lies in the fact that it was obtained simultaneously with the observations of NO (see previous section). The combination of these results yields a value for the ratio of NO_2 to NO (at 16 km), for sunset conditions, of $(NO_2/NO) = 4.5$.

Nitric Acid

One of the most interesting, and at the time unexpected, discoveries in spectroscopic studies of the stratosphere was the observation of nitric acid by Murcray *et al.* (29) during a series of balloon flights in 1967–1968. The molecule was seen in absorption spectra (at a resolution of ~ 0.3 cm^{-1}) in three separate bands, *i.e.* in the 7.5, 5.8, and 11.3 μ regions. The band at 11.3 μ was subsequently measured in emission, using both wide and narrow band radiometers ($\Delta\nu = 70$ and 6 cm^{-1}). Nitric acid was later observed by Lazrus *et al.* (30) and by Harries (18) from submillimeter emission spectra taken with an aircraft mounted instrument having a resolution of ~ 0.07 cm^{-1}. The original results of Murcray *et al.* were interpreted with the aid of laboratory spectra of Rhine *et al.* (31) as being equivalent to an average mixing ratio of about 3.2 ± 1.0 p.p.b.v., with a distribution similar to ozone. Lazrus *et al.* at 20 km obtained HNO_3 mixing ratios between 2 and 4 p.p.b.v. Harries' values, from the tropopause to about 16 km, were also scattered between 2 and 4 p.p.b.v., averaging to a constant mixing ratio of 3 p.p.b.v. and showing no dependence on latitude. The later results reported by Murcray *et al.*, as shown in their plot of mixing ratio *vs.* altitude, show a mixing ratio of about 1 p.p.b.v. beginning at 12 km which gradually increases to a maximum of about 4.6 p.p.b.v. in the range of 20–24 km. There appears to be, however, some discrepancy between the range of concentrations given in their text and those shown in their plotted data.

Water Vapor

Stratospheric water vapor has been measured by Goldman *et al.* (32) from a region of the pure rotational band between 24 and 29 μ, and by Harries (18) in the far i.r. between 300 and 1000 μ (10 to 30 cm^{-1}). The results of Goldman *et al.* indicate a change in the mixing ratio with altitude, with a broad minimum at 15 km and a maximum around 25 km; at the maximum, the values range from 6.9 to 9.7 p.p.m.v. Harries, however, found a constant mixing ratio for water vapor of 3 p.p.m.v. in the stratosphere up to altitudes of 60 km. These results can be compared with the earlier values of Houghton (see, for example, Pick and Houghton (33)) and Mastenbrook (34) who give mixing ratios of 5 p.p.m.v. and 3–4 p.p.m.v., respectively.

Our results using principally the ν_2 band of H_2O centered at 1594.73 cm^{-1} indicate an approximately constant mixing ratio of 2.4 ± 0.30 p.p.m.v. over the altitude range from 14 to 20 km. No significant variation with latitude was observed, apart from some indication of a trend towards an increase in the mixing ratio at the lowest latitudes of observation (*i.e.* $\sim 30°$ N lat.) (see Fig. 5). The relatively small uncertainty quoted with these values is a result of the wide range of line intensities observed in the spectra, which permit close fitting of the observed and calculated absorption. The values derived from the ν_2 band were verified by additional analyses carried out for many other regions where the spectrum is characterized by water vapor features, *viz.* the $2\nu_2$, ν_1, and ν_3 bands.

Carbon Monoxide

Carbon monoxide has been measured over the altitude range from 8 to 12.5 km by Seiler and Warneck (35) using *in situ* methods, and by remote sensing of the near i.r. (1–0) band from 12 to 15 km by Murcray *et al.* (8). Seiler and Warneck's data show a sharp decline in the CO mixing ratio at the tropopause, leveling off in the stratosphere to a constant value of 0.04 p.p.m.v. From their data Murcray *et al.* obtained a similar value for the mixing ratio and extended the measurements to 15 km.

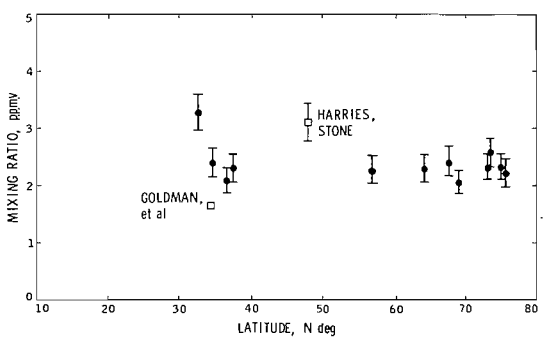

FIG. 5. Stratospheric latitude variation of H_2O at 16 km altitude.

Can. J. Chem. Downloaded from www.nrcresearchpress.com by 210.87.254.6 on 09/05/12
For personal use only.

Our observations, again for the 1–0 (2143 cm^{-1}) band, confirm the constant vertical mixing profile above the tropopause, but show a marked decrease in mixing ratio with latitude, from 0.068 p.p.m.v. at 33° N to 0.021 p.p.m.v. at 76° N. These results, with the associated measurement uncertainties, are summarized in Fig. 6, from which it would appear that the Seiler and Warneck values, obtained at 50° N latitude, are consistent with this latitude variation, whereas the Murcray *et al.* value (30° N) is considerably lower.

Carbon Dioxide

In recent years carbon dioxide has been measured by numerous investigators, using a variety of experimental techniques and with remarkably concordant results. These measurements have shown in general that CO_2 is uniformly mixed vertically from the surface to as high as 62 km, with reported values for the mixing ratio ranging from 310 to 340 p.p.m.v. Our value of 325 $\pm$ 20 p.p.m.v., obtained from analysis of the $3\nu_2$ band at 1932.5 cm^{-1}, is in good agreement with these previous measurements, and no variation with latitude could be discerned.

The important problem with respect to CO_2 is not so much further refinement of the absolute value of its concentration as the determination of any long term variation or increase. This has been estimated as being of the order of 1 p.p.m. per year, the significance of the magnitude of such a change being the concomitant change to the radiation balance which it might ultimately cause. At present none of the remote observational techniques discussed here is capable of achieving the absolute accuracy required for such a measurement, although it may perhaps be possible to extract long term variations by statistical methods from data taken over a period of some months.

Methane

Stratospheric methane has been measured by Ackerman and Muller (36) and Lowe and McKinnon (37), by analysis of the near i.r. (ν_3) band at 3018 cm^{-1}, and by Kyle *et al.* (38) using the ν_4 band in the region of 1300 cm^{-1}. Kyle *et al.* presented their data in terms of the "quantity of methane per air mass" above different levels in the stratosphere, and reported a decrease by a factor of 2 to 5 in this quantity at 30 km over that at sea level. Ackerman and Muller's values indicated a nearly constant mixing ratio (of about 2 p.p.m.v.) to 25 km, decreasing to 0.75 $\pm$ 0.4 p.p.m.v. at 33.6 km. Lowe and McKinnon also reported constant mixing to 25 km, but their mean value of 0.94 $\pm$ 0.16 p.p.m.v. for the mixing ratio was lower by a factor of 2 than that of Ackerman and Muller in the same altitude range. Although Lowe and McKinnon's data were collected over a considerable range of latitudes, they saw no evidence for any latitude variation in the methane mixing ratio.

Our data also indicate constant vertical mixing for methane between 11 and 20 km, but with some latitude dependence. The results are summarized in Fig. 7. From the ν_3 band we obtained mixing ratios varying from 1.2 $\pm$ 0.05 p.p.m.v. at 17° N to 0.60 $\pm$ 0.04 p.p.m.v. at 76° N. This result is seemingly in disagreement with the latitude independence reported by Lowe and McKinnon; the difference may not be of any significance, however, in view of the limited data available to date, although it should be noted that a latitude and seasonal variation of stratospheric CH_4 is not unexpected considering its biogenic origin.

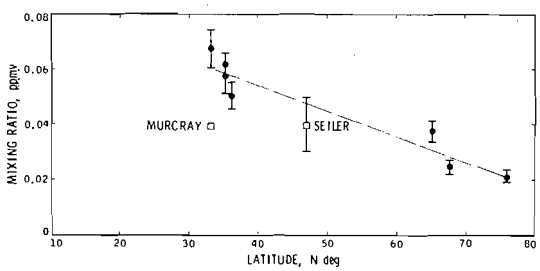

FIG. 6. Latitude variation of CO at 16 km altitude.

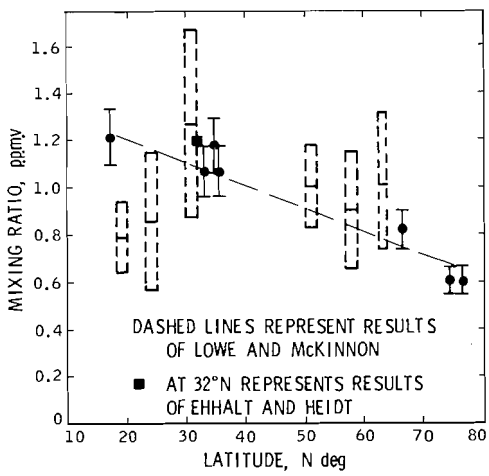

FIG. 7. Latitude variation of CH_4 at 16 km altitude.

Can. J. Chem. Downloaded from www.nrcresearchpress.com by 210.87.254.6 on 09/05/12
For personal use only.

Other Molecules

A number of other species, such as H_2O_2, H_2CO, HCl, SO_2, N_2O_5, and NO_3, have been postulated as important trace constituents in the stratosphere, but have not yet been detected in i.r. spectra. For several of these species, little or no laboratory data on the spectral assignments and line strengths exist, due either to the transitory nature of the species or the complexity of their spectral features, and as a consequence information concerning them cannot be extracted from the observational data. For others however, the required spectral information does exist and the reason that no detection has been made in these cases is that their abundances (if present at all) are below the current limits of detectability of the instrumentation. In this latter case, it is important for atmospheric modeling purposes that upper limits be reported which specify the minimum detectable amounts of the applicable species which could have been detected under the existing experimental conditions, and hence that the amounts actually present are below these limits.

We have recently undertaken the laboratory spectroscopic investigation of the ν_1 and ν_5 H_2CO bands in the 2800 cm^{-1} region and have made several spectral quantum assignments for lines in this region. Analysis of stratospheric spectra is complicated in this region as a result of severe blending with several weak bands of methane, and this has entailed further work on these bands in order to determine which H_2CO lines are best suited to analysis. Although this work is not complete, by applying the results so far obtained to the analysis of our stratospheric spectra we can report that to date no positive detection has been made, and can place an upper limit on H_2CO of 2 p.p.b.v. Similarly, the spectra have been searched for evidence of the presence of HCl (in the region of the 1–0 band at 2886 cm^{-1}). In this case the line intensities are well known and an upper limit to the HCl concentration in the lower stratosphere is placed at 0.18 p.p.b.v.

The author gratefully acknowledges the considerable help given by his colleagues, Drs. M. T. Chahine and O. F. Raper, in the preparation of this review.

The work at the Jet Propulsion Laboratory, California Institute of Technology, included here was carried out under the auspices of the Climatic Impact Assessment Program, Department of Transportation by agreement with the National Aeronautics and Space Administration (Contract NAS 7-100).

1. D. G. MURCRAY, F. H. MURCRAY, W. J. WILLIAMS, T. G. KYLE, and A. GOLDMAN. Appl. Opt. **8**, 2519 (1969).
2. E. J. WILLIAMSON and J. T. HOUGHTON. Q. J. R. Meteorol. Soc. **91**, 330 (1965).
3. H. J. BOLLE. Z. Geophys. **36**, 1 (1970).
4. C. PRABHAKARA, B. J. CONRATH, R. A. HANEL, and E. J. WILLIAMSON. J. Atmos. Sci. **27**, 689 (1970).
5. D. G. HUMMER. Mem. R. Astrol. Soc. **70**, 1 (1965).
6. P. A. JANSSON and C. L. KORB. J. Quant. Spectrosc. Radiat. Transfer, **8**, 1399 (1968).
7. J. E. HARRIES. Private communication.
8. D. G. MURCRAY, A. GOLDMAN, F. H. MURCRAY, W. J. WILLIAMS, J. N. BROOKS, and D. B. BARKER. Proceedings of the second conference on the climatic impact assessment program. U.S. Department of Transportation, November 14–17, 1972. p. 86. Available through National Information Technical Service, Springfield, Va. 22151. DOT-TSC-OST-73-4.
9. R. M. GOODY. Atmospheric radiation. Vol. I. Theoretical basis. Oxford University Press, New York. 1964.
10. J. T. HOUGHTON and F. W. TAYLOR. Rep. Prog. Phys. **36**, 827 (1973).
11. E. W. BARRETT, P. M. KUHN, and A. SHLANTA. Proceedings of the second conference on the climatic impact assessment program. U.S. Department of Transportation, November 14–17, 1972. p. 34. Available through National Information Technical Service, Springfield, Va. 22151. DOT-TSC-OST-73-4.
12. J. E. HARRIES, N. R. SWANN, J. E. BECKMAN, and P. A. R. ADE. Nature, **236**, 159 (1972).
13. R. BEER. Appl. Opt. **9**, 301 (1970).
14. R. A. SCHINDLER. Appl. Opt. **9**, 301 (1970).
15. C. B. FARMER, R. A. TOTH, R. A. SCHINDLER, and O. F. RAPER. Proceedings of the second conference on the climatic impact assessment program. U.S. Department of Transportation, November 14–17, 1972. p. 65. Available through National Information Technical Service, Springfield, Va. 22151. DOT-TSC-OST-73-4.
16. A. GIRARD. Appl. Opt. **2**, 83 (1963).
17. K. SCHÜTZ, C. JUNGE, R. BECK, and B. ALBRECHT. J. Geophys. Res. **75**, 2230 (1970).
18. J. E. HARRIES. Nature, **241**, 515 (1973).
19. A. GOLDMAN, D. G. MURCRAY, F. H. MURCRAY, W. J. WILLIAMS, T. G. KYLE, and J. N. BROOKS. J. Opt. Soc. **60**, 1466 (1970).
20. A. GOLDMAN, D. G. MURCRAY, F. H. MURCRAY, and W. J. WILLIAMS. J. Opt. Soc. **63**, 843 (1973).
21. M. NICOLET and W. PEETERMANS. Ann. Geophys. **28**, 4, 751 (1972).
22. R. A. TOTH, C. B. FARMER, R. A. SCHINDLER, O. F. RAPER, and P. W. SCHAPER. Nature, **244**, 7 (1973).
23. B. A. RIDLEY, H. I. SCHIFF, A. W. SHAW, L. BATES, C. HOWLETT, H. LEVAUX, L. R. MEGILL, and T. E. ASHENFELTER. Nature, **245**, 5424, 310 (1973).
24. M. ACKERMAN, J. C. FONTANELLA, D. FRIMOUT, A. GIRARD, L. GRAMONT, N. LOUISNARD, C. MULLER, and D. NEVEJANS. Aeron. Acta, A, **120** (1973).
25. C. B. FARMER, R. A. TOTH, R. A. SCHINDLER, O. F. RAPER, and P. W. SCHAPER. Unpublished results.
26. A. GOLDMAN, D. G. MURCRAY, F. H. MURCRAY, and W. J. WILLIAMS. Nature, **225**, 443 (1970).

27. M. ACKERMAN and C. MULLER. Nature, **240**, 300 (1972).
28. J. E. HARRIES. Private communication.
29. D. G. MURCRAY, T. G. KYLE, F. H. MURCRAY, and W. J. WILLIAMS. J. Opt. Soc. **59**, 1131 (1969).
30. A. L. LAZRUS, B. GANDRUD, and R. D. CADLE. J. Appl. Meteorol. **11**, 389 (1972).
31. P. E. RHINE, L. D. TUBBS, and D. WILLIAMS. Appl. Opt. **8**, 1500 (1969).
32. A. GOLDMAN, D. G. MURCRAY, F. H. MURCRAY, W. J. WILLIAMS, and J. N. BROOKS. Appl. Opt. **12**, 1045 (1973).
33. D. R. PICK and J. T. HOUGHTON. Q. J. R. Meteorol. Soc. **95**, 535 (1970).
34. H. J. MASTENBROOK. J. Atmos. Sci. **28**, 1495 (1971).
35. W. SEILER and P. WARNECK. J. Geophys. Res. **77**, 3204 (1972).
36. M. ACKERMAN and C. MULLER. Proceedings of the Joint Meeting of the Am. Geophys. Union and the Am. Meteorol. Soc. Aug. 15–17, 1972. p. 12-1.
37. R. P. LOWE and D. MCKINNON. Can. J. Phys. **50**, 668 (1972).
38. T. G. KYLE, D. G. MURCRAY, F. H. MURCRAY, and W. J. WILLIAMS. J. Geophys. Res. **74**, 3421 (1969).

Can. J. Chem. Downloaded from www.nrcresearchpress.com by 210.87.254.6 on 09/05/12
For personal use only.

Observations of Stratospheric Aerosol Layers by Optical Radar

M. HIRONO, M. FUJIWARA, O. UCHINO, AND T. ITABE
Department of Physics, Kyushu University, Fukuoka, Japan

Received October 10, 1973

A ruby laser radar has been constructed at Fukuoka (33° N), south-west Japan, for the purpose of probing the upper atmosphere. Observations of stratospheric aerosol layers have been carried out since October 1972. Data obtained show that the layers of enhanced optical backscattering due to aerosols in the height range of 16–30 km were found throughout the period of observation. One of the layers always appeared at about 20 km height and varied to some extent in its height, structure, and peak value of scattering, day-to-day and month-to-month. Other layers appeared in the region above 25 km and seemed more variable. Height profiles of non-Rayleigh backscattering cross section β_M are calculated for each night and each month of the observation and compared with the temperature, wind velocity, and ozone concentration in the stratosphere. The individual scattering profile is most likely controlled by the large scale structure of the temperature profile of the night. The mean value of β_M in the region around 20 km has its minimum in January and increases from winter to summer. Comparison is also made with the geometrical cross section of the aerosols deduced from the small ion density data and the results show that a large fraction of the aerosol mass is in the range of Aitken particles.

Un radar laser de rubis a été construit à Fukuoka (33° N) au sud-ouest du Japon, en vue d'explorer la haute atmosphère. Des observations des couches d'aérosol stratosphérique ont été effectuées depuis octobre 1972. Les données obtenues montrent que des couches de dispersion optique en retour dues aux aérosols dans l'intervalle de hauteur de 16–30 km ont été observées. Une des couches apparaissait toujours autour de 20 km de hauteur et, dans une certaine mesure, sa hauteur sa structure et la valeur de son pic de diffusion variaient de jour en jour, de mois en mois. D'autres couches apparaissaient dans la région au-dessus de 25 km et paraissaient plus variables. Des profils de hauteur de sections droites β_M de diffusion en retour de non-Rayleigh sont calculés pour chaque nuit et chaque mois de l'observation et comparés avec la température, la vitesse du vent et la concentration de l'ozone dans la stratosphère. Le profil de diffusion individuel est, très probablement, contrôlé par la grande échelle de structure de la courbe de la température de la nuit. La valeur moyenne de β_M dans la région autour de 20 km est minimum en janvier et augmente de l'hiver à l'été. Une comparaison est aussi faite avec la coupe géométrique des aérosols déduite de données de densité de petit ion et les résultats montrent qu'une grande fraction de la masse de l'aréosol se situe dans le domaine des particules d'Aitken.
[Traduit par le journal]

Can. J. Chem., **52**, 1560 (1974)

Introduction

Laser radar has made possible the remote measurement of the aerosol layers in the upper atmosphere with the advantage of the ability to observe easily an atmospheric region of a large vertical extent without disturbing the state of the region.

The existence of an aerosol layer in the lower stratosphere, called the 20 km sulfate layer, is well established. Investigations of this layer have been made by various methods including direct sampling (1, 2), *in situ* optical technique (3), twilight sky measurement (4), and searchlight technique (5). Laser radar was used for the observation of this layer first by Fiocco and Grams (6) and then systematic routine studies by laser radar were made by several research groups such as those in Jamaica (7), Boulder (8), Adelaide (9), Fukuoka (10), and Menlo Park (11).

The main constituent of aerosols in the lower stratosphere has been shown to be sulfate or ammonium sulfate. However, the number density, size distribution, and their variabilities in time and space are not yet known exactly. The mechanism of formation of the layer is also not fully understood. Many more observations are necessary to increase our knowledge about the layer.

Increasing the knowledge about the stratospheric aerosols is of significant importance since it is believed that the aerosols are not only good tracers of the atmospheric circulation but also catalytic for the variation of ozone concentration. Fiocco and Grams (6) found a negative correla-

Can. J. Chem. Downloaded from www.nrcresearchpress.com by 210.87.254.6 on 09/05/12
For personal use only.

Can. J. Chem. Downloaded from www.nrcresearchpress.com by 210.87.254.6 on 09/05/12
For personal use only.

tion between ozone concentration and the amount of aerosols in the stratosphere. Ozone in the stratosphere plays an important role in preventing harmful u.v. solar radiation from penetrating into the ground level atmosphere. Decreasing the ozone concentration therefore would possibly have some influence on human beings.

In this paper, we report the results of observations of the stratospheric aerosols by laser radar, carried out in Fukuoka (33° N, south-west Japan) since October 1972. The height profiles of the scattering ratio $R(h)$ and non-Rayleigh backscattering cross section $\beta_M(h)$ of each night are calculated and compared with the profiles of temperature and wind velocity measured by the Fukuoka Meteorological Observatory. The peak values of β_M are 1 to 2 $\times$ 10^{-9}/cm with variability from day-to-day and month-to-month. The heights of the layer peak are around 20 km and these also vary to some extent. Frequently, other layers appear even in the region above 25 km. The nightly profile of β_M has a close relation with the large scale structure of the temperature profile of the night. Monthly mean values of β_M of three height regions, 19.5–22.5 km, 22.5–25. 5km, and 25.5–28.5 km, are calculated and compared with the zonal wind, ozone concentration, and geometric cross section of the aerosols deduced from the small ion density. The data of the ozone concentration and small ion density observed by radiosonde over Kagoshima located at a distance of about 200 km south of Fukuoka are supplied by courtesy of the Meteorological Agency. In the lowest region, β_M has its minimum value in January and seems to have a tendency to increase from winter to summer. In the upper regions, the variations of β_M are less systematic. The ozone concentration shows a marked enhancement in January and reversal of zonal wind from westerly to easterly occurred in December and January in the upper regions. The size distribution of the aerosols is discussed, and the results of small ion data analysis are compared with the results of laser radar observations. It is shown that a large fraction of the aerosol mass involved is in the range of Aitken particles.

Equipment, Method of Observation, and Analysis

Characteristics of the laser radar system are summarized in Table 1. The transmitter consists of a ruby laser, a rotating shutter used to cut off the fluorescent emission from the ruby, and a refractive telescope of 10 cmϕ. The receiver consists of a reflective telescope of 30 cmϕ, an interference filter, and a photomultiplier. The laser is fired at a rate of 1 pulse every 20–30 s and the energy output is about 0.5 J/pulse. Additional details on the instrumentation were given in a previous paper (10).

TABLE 1. Characteristics of laser radar

Transmitter	
*Laser	Q-switched ruby laser
Wavelength	6943 Å
Output energy	1 J/pulse (single pulse)
Pulse duration	50 ns
Maximum pulse repetition rate	0.2/s
*Telescope	10 cmϕ
Beam divergence	1 mrad
*Rotating shutter	24 000 r.p.m.
Receiver	
*Telescope	30 cmϕ (Cassegrain)
Field of view	1 mrad
*Filter bandwidth	7 Å
*Photomultiplier	EMI 9558QB (S-20)

Return signals (output of the photomultiplier) are displayed on the synchroscope and its traces photographed. Photon counting in each 1.5 km height interval is available for a return from above 12 km. The photon count $C(h)$ originating at a small height interval Δh at a height h for the vertical sounding is given by

$$[1] \qquad C(h) = k\Delta h \frac{B_R(h) + B_M(h)}{h^2}$$

where k is a constant for the particular laser radar including the transmission coefficient of the atmosphere, $B_R(h)$ the Rayleigh backscattering coefficient for the atmospheric molecules, and $B_M(h)$ the Mie backscattering coefficient for the aerosols. The height interval Δh can be absorbed in the constant $K = k\Delta h$ for the case of observation over an equidistant range, which in our case is 1.5 km.

The first step in the analysis of the data is to match the vertical profile of the observed photon count $C(h)$ with that of the computed Rayleigh backscattering which is expected from the atmospheric molecules. Molecular densities were obtained using the local scale height of the U.S. Standard Atmosphere 1962 starting from the base level density determined from the pressure and temperature measurements obtained by radiosonde in Fukuoka at each night the laser

observation was made. A typical result of the total photon count *vs.* altitude is shown in Fig. 1*a* along with the theoretical curve of the amount of Rayleigh backscattering. In most cases, the vertical gradients of the observational $C(h)$ curve fit those of the theoretical curves almost completely between the height of 13 and 16 km. So this region appears to be a region of minimum aerosol content and we choose a height 15.75 or 15 km as the height of the normalization, which involves negligible aerosol content.

The second step is to calculate the vertical profiles of the scattering ratio $R(h)$ which shows the ratio of the total backscattering coefficient to the Rayleigh backscattering coefficient and is given by

$$[2] \qquad R(h) = \frac{B_R(h) + B_M(h)}{B_R(h)}$$

The $R(h)$ profile deduced from the curves in Fig. 1*a* is shown in Fig. 1*b*.

Finally, the non-Rayleigh backscattering cross section $\beta_M(h)$ is given by

$$[3] \qquad \beta_M(h) = 4\pi N(h)\sigma_R B_M(h)/B_R(h) = 4\pi N(h)\sigma_R(R(h) - 1)$$

where $N(h)$ is the number density of the atmosphere and σ_R the backscattering cross section per unit solid angle of a molecule. Figure 1*c* shows the $\beta_M(h)$ calculated with the use of the values shown in Figs. 1*a* and *b*.

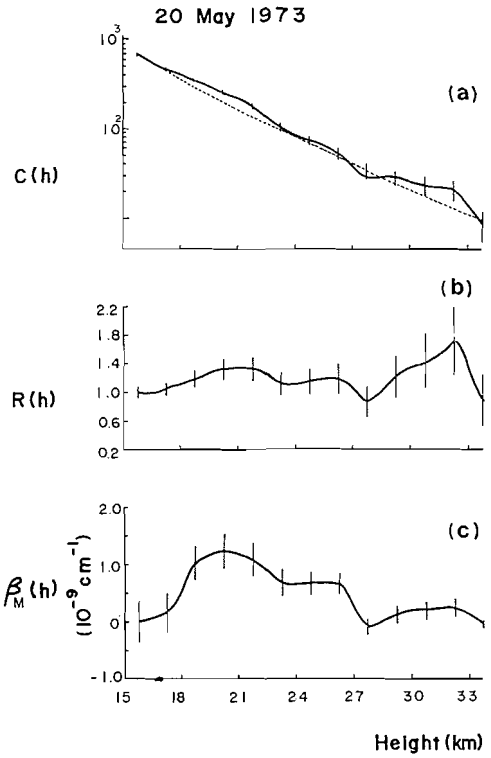

FIG. 1. Three steps of data analysis: (*a*) photon count *vs.* height compared with theoretical curve (dashed line) of Rayleigh backscattering, (*b*) scattering ratio, and (*c*) non-Rayleigh backscattering cross section per unit volume *vs.* height.

Observational Results and Discussions

Excessive scattering occurred in the region of 16–30 km every night observation was made; this showed the existence of aerosols. Figure 2 shows the vertical profiles of the non-Rayleigh backscattering cross section of several nights in March and May and mean profiles for each month of observation are shown in Fig. 3. The existence of an aerosol layer near 20 km is clearly shown though the height of the peaks varies to some extent from day-to-day and from month-to-month. Peak values of β_M are 1 to 2 × 10^{-9}/cm, comparable to those observed in Menlo Park, California, during the same period of our observation (11) and those observed in Adelaide during the period April 1969 to April 1970 (9) but much smaller than those observed before

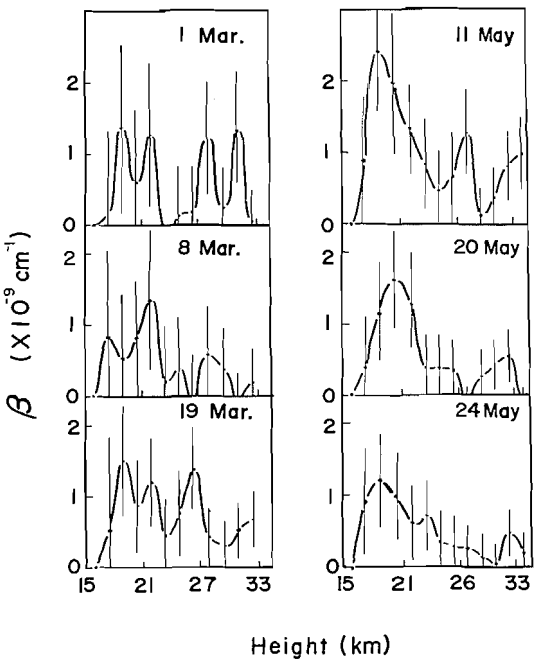

FIG. 2. Non-Rayleigh backscattering cross section observed in March 1973 and May 1973.

Can. J. Chem. Downloaded from www.nrcresearchpress.com by 210.87.254.6 on 09/05/12
For personal use only.

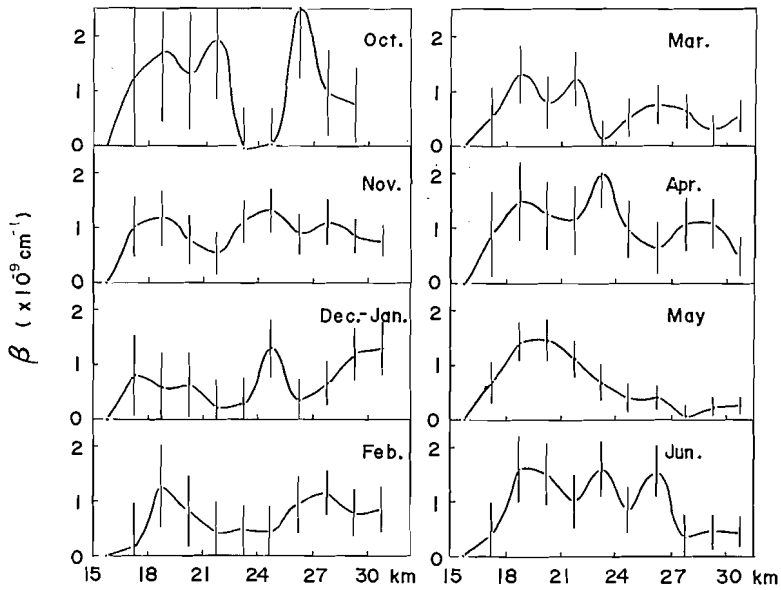

FIG. 3. Monthly mean profiles of non-Rayleigh backscattering cross section observed during the period October 1972 to June 1973.

1965 (12). It can also be seen from the figures that even in the region above 25 km aerosol layers exist which seem to be more variable in time.

Comparison with the Meteorological Elements

In Fig. 4 individual $\beta_M(h)$ profiles are compared with the corresponding temperature and wind velocity profiles obtained from local radiosonde flights carried out by the Fukuoka Meteorological Observatory. The peak of the lower layer (20 km layer) is always observed to appear at the height of the temperature minimum or a few kilometers above this height. The height of the peak has a positive correlation with the height of the temperature minimum; the coefficient of the correlation is calculated to be 0.42 ± 0.20.

The heights of the tropopause are also marked in Fig. 4. In winter and spring there appeared to be two tropopauses, one showing the extension of the equatorial tropopause and the other the polar tropopause. The height of the upper tropopause (and also the lower tropopause) does not seem to have significant correlation with the height of the layer peak. However, if we choose a tropopause above which there is no region of a few kilometers of mean temperature gradient less than -2 °C/km, then the height of the tropopause has a positive correlation which is estimated to be 0.39 ± 0.19. We can conclude from

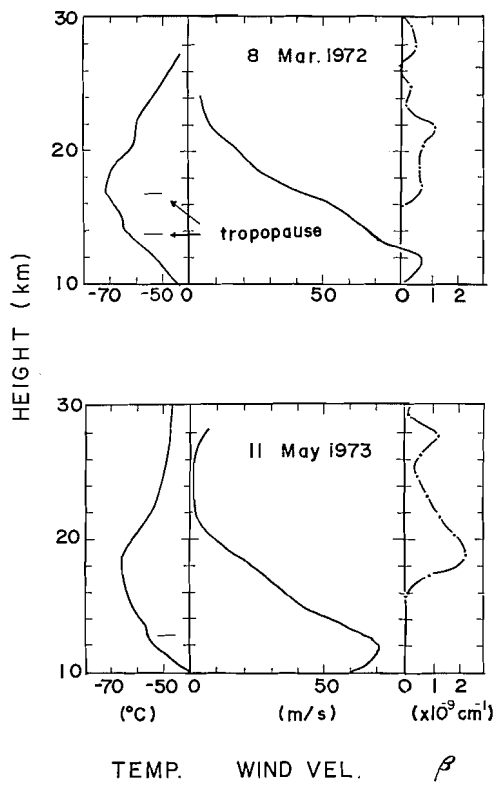

FIG. 4. Examples of height profile of non-Rayleigh backscattering cross section, temperature, and wind velocity.

Can. J. Chem. Downloaded from www.nrcresearchpress.com by 210.87.254.6 on 09/05/12
For personal use only.

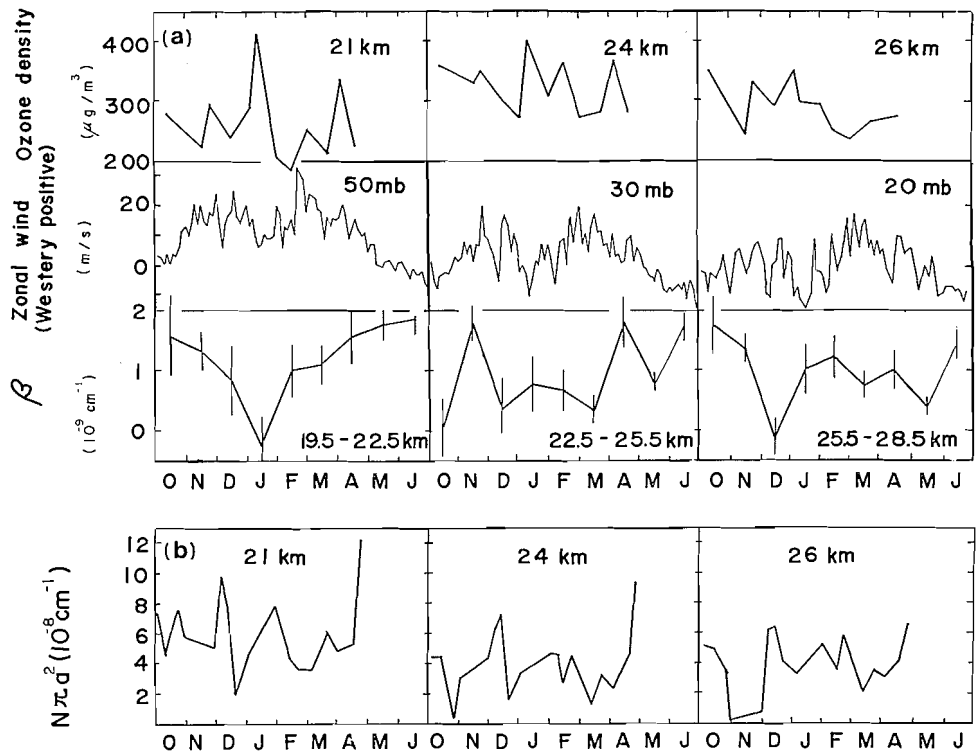

FIG. 5. Time variability of (*a*) mean values of non-Rayleigh backscattering cross section in contrast to zonal winds, ozone concentrations and (*b*) geometrical cross section of aerosols deduced from small ion density.

these facts that the large scale structure of the temperature profile has an important influence on the behavior of the 20 km layer.

Sometimes the upper layers appeared at the height of the temperature inversion and sometimes they did not. The relation between the height of these layers and the change of temperature gradient is not yet clear. An appreciable relation between the height of the layer peak and the wind velocity profile is not found.

Time Variability of β_M, Wind Field, and Ozone Concentration in the Stratosphere

To see the time variability of the non-Rayleigh backscattering cross section β_M, we selected three height regions, 19.5–22.5 km, 22.5–25.5 km, and 25.5–28.5 km, and calculated the mean values of them in every region for each month. The β_M of a month is calculated from the total photon count $C(h)$ of 3 or 4 nights of observation of the month. The height of the normalization was chosen, in this case, at 15 km. The results are summarized in Fig. 5. The zonal wind velocity at altitudes of 50, 30, and 20 mb measured at Fukuoka and the ozone concentrations at heights 21, 23, and 26 km measured at Kagoshima are plotted in Fig. 5*a*.

In the region 19.5–22.5 km, β_M shows minimum aerosol content in January and seems to have a tendency to increase from winter to summer. The result is very similar to that obtained at Menlo Park (11). Ozone concentration shows a marked enhancement in January. Whether there is real causal relation of this enhancement to the minimum β_M in January or not should be looked upon with some caution, until it is confirmed by fuller examination.

The aerosol layers seem to be more variable in winter than in summer. This may be due to the transmission of the planetary waves through the stratosphere. In May and June, an easterly wind prevails and the layers seem to be more stable. An easterly wind prevents the transmission of the planetary waves from the troposphere (13).

In the upper regions, the variation of β_M is less systematic. In the uppermost region, the zonal wind reverses its direction from westerly to easterly in December and January; the decrease of β_M seems to accompany this reversal. Many more observations are necessary to make sure

Can. J. Chem. Downloaded from www.nrcresearchpress.com by 210.87.254.6 on 09/05/12
For personal use only.

Can. J. Chem. Downloaded from www.nrcresearchpress.com by 210.87.254.6 on 09/05/12
For personal use only.

whether the decrease of β_M is related with the reversal of zonal wind and enhancement of ozone concentration or not. It seems from the original data that the ratio of the photomultiplier noises to the return signals from the atmospheric molecules exceeds 1.0 at a height 33 km or higher. The S/N ratio around 27 km is estimated at about 3.

Large values of β_M in October and November in the upper regions have been inferred in our previous paper to depend at least in part on the dust of the comet Giacobini–Zinner.

Comparison with the Small Ion Density Distribution in the Stratosphere

The small ions, with molecular weight about 100, are produced by cosmic rays in the stratosphere (14). The flux of cosmic rays is a function of geomagnetic field at the place of observation and the interplanetary magnetic field distribution modulated mainly by the solar wind, which is considerably variable depending on the solar activity. The ion pair production per unit volume per second is denoted by q which takes the maximum value in the lower stratosphere. Let the small ion number density be n_i, then the continuity equation is written as

$$[4] \qquad dn_i/dt = q - \alpha n_i^2 - \eta N n_i$$

where N denotes number density of particulates and α and η are the recombination coefficient of the ions and the attachment coefficient respectively. According to Kroening (15) and Rosen (3) the term containing η is important in determining the ion density n_i from eq. 4 after the eruption of Mt. Agung of Bali in 1963. The presence of particulates tends to decrease the ion density considerably.

If the root mean square value of the radius of the existing particulates a is so small that

$$[5] \qquad 0.025\ \mu < a < 0.1\ \mu$$

then we have approximately in the stratosphere

$$[6] \qquad \eta = \pi a^2 G_i$$

where G_i denotes the most probable thermal velocity of the small ions, and πa^2 is taken as the mean cross section of the particulates. At an altitude 14 km just below the tropopause over our station, the aerosol density should take minimum value according to Rosen (3). The quasi steady state may be supposed in eq. 4 to let $d/dt = 0$, and we may take $N = 0$ on the right side of the equation at 14 km. It follows that

$$[7] \qquad q = \alpha n_i^2$$

We calculated n_i from the radiosonde electrical conductivity data at Kagoshima, about 200 km south of Fukuoka, assuming the ion mobility 1.3 $cm^2/V\ s$ at standard temperature and pressure (16). As shown in Fig. 6, n_i at 14 km and sun spot numbers vary in the opposite sense, the correlation coefficient being -0.50 ± 0.18. This tendency is in accord with the variation of cosmic ray intensity with sun spot number for a longer period, for example 11 years (17). In the same figure the variation of $\Sigma K_p\ day^{-1}$ is also shown. The correlation coefficient between n_i (14 km) and $\Sigma K_p\ day^{-1}$ is -0.23 ± 0.25 for the whole period, but 0.41 ± 0.23 if we eliminate the data on November 1 and December 6. Thus the sense of their variations are nearly the same except on a few days. The ion production seems to be modulated by the variation in the magnetosphere or the solar wind near the earth to about the same extent as by solar activity. According to Neher and co-worker (18) the altitude distributions of q are shown at the geomagnetic latitudes 17° and 25° in the years 1939 and 1940. From these data we deduced an average distribution of q in 1972 and 1973 at 21° taking into account the solar activity as shown in Fig. 7. The q value, however,

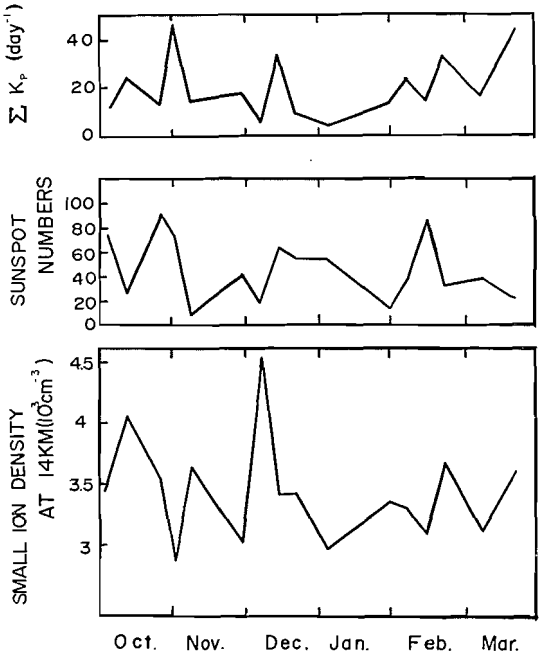

FIG. 6. Comparison of the small ion density at 14 km with sunspot numbers and $\Sigma K_p\ day^{-1}$ (J.G.R., Provisional).

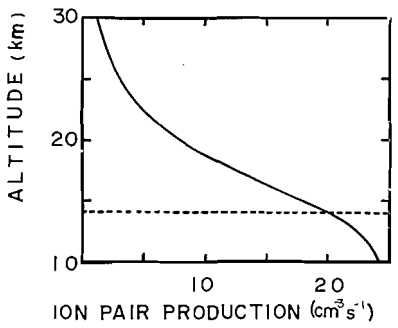

FIG. 7. Ion pair production *vs.* altitude at geomagnetic latitude 21°.

may change to some extent according to sun spot numbers during half a year of the present observation. We take, therefore

$$[8] \qquad q(14\text{ km}) = \alpha n_i(14\text{ km})^2$$

as a first approximation of q value at 14 km using observed values of n_i and theoretical values of α (19) as shown in Fig. 8. The mean value of q(14 km) for the period from October 1972 to April 1973 is 19.1 $\pm$ 5.2 $cm^{-3}\ s^{-1}$, which agrees fairly well with the value 19.8 $cm^{-3}\ s^{-1}$ at 14 km shown in Fig. 7. It should be noted that the standard deviation reaches 27% which is somewhat greater than the estimation on the basis of data of Neher and co-worker (17).

The value of q at any altitude is calculated in proportion to q(14 km) assuming the similar shape of vertical distribution as Fig. 7. Using the q and n_i values and molecular weight 100 for the ions, from eq. 4 we obtain

$$[9] \qquad N\pi a^2 = \frac{q - \alpha n_i^2}{G_i n_i}$$

at any altitude, as shown in Fig. 5*b*.

The obtained $N\pi a^2$ is only an approximate value, but of significant importance to show the order of magnitude of the aerosol content inferred from a different viewpoint. The mean values of $N\pi a^2$ and the corresponding laser radar backscattering cross sections for the whole period at three altitudes are shown in Table 2. It may be seen that the laser radar cross sections per unit volume is about 2% of $N\pi a^2$. The ratio $Q = \beta_M/N\pi a^2 = \sigma_b/\pi a^2$ is usually called scattering efficiency and the numerical values were obtained by van de Hulst (20) and Deirmendjian (21) for many cases, including the case of non-absorbing spherical particles; the latter results for the refractive indices m = 1.55, 1.315 (ice), and 1.29 (water) are shown in Fig. 9 with $x = 2\pi a/\lambda$, where λ denotes wavelength. If the curves m = 1.315 or 1.55 and Q = 0.02 are adopted, we have x = 0.47 or 0.63, which means a = 0.05 μ or 0.07 μ. The values are smaller than the lower limit of the size distribution obtained by Junge (22), *i.e.* $dN(r)/dr = cr^{-(\delta+1)}$ confined within the range 0.1 $\mu < r <$ 2 μ, with δ = 3.5, where $N(r)$ denotes number of particles with radius smaller than r and c is a constant. His sampling with impactors in 1959 yielded a mass concentration of 0.003 to 0.012 $\mu g/m^3$ sulfate at 20 km; the Aitken counter yielded very few particulates smaller than 0.1 μ.

Recently Lazrus *et al.* (2) have found much higher aerosol concentrations in 1970 and 1971

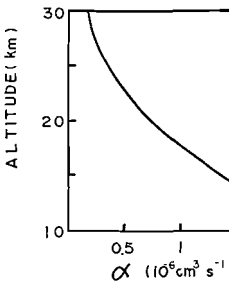

FIG. 8. Calculated recombination coefficient *vs.* altitude.

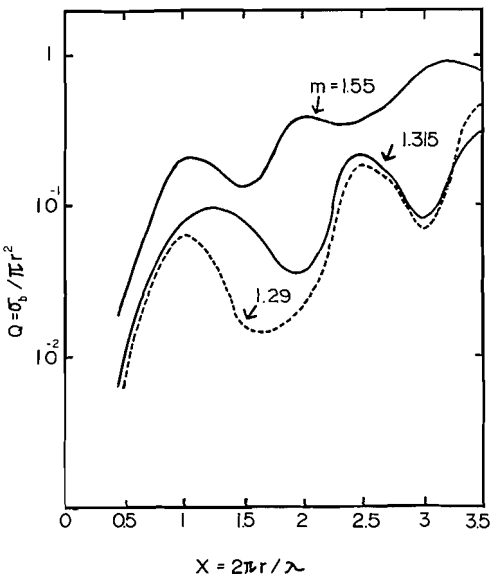

FIG. 9. Calculated backscattering efficiency against $x = 2\pi r/\lambda$ (after Deirmendjian (21)). Note that $r = a$ in the text.

Can. J. Chem. Downloaded from www.nrcresearchpress.com by 210.87.254.6 on 09/05/12
For personal use only.

TABLE 2. Mean values for the whole period

Altitude (km)	$N\pi a^2$ (cm^{-1})	β_M (cm^{-1})	Q
21	5.97×10^{-8}	9.77×10^{-10}	1.64×10^{-2}
24	3.98×10^{-8}	7.37×10^{-10}	1.85×10^{-2}
26	4.06×10^{-8}	9.20×10^{-10}	2.27×10^{-2}

at 17–19 km by filter sampling, namely 0.1–0.2 $\mu g/m^3$ of SO_4^{2-} and other compositions. They suggest that a large fraction of the aerosol seems to be Aitken nuclei with radius smaller than 0.1 μ to escape collection by impactors and that the old Aitken counter results are estimated to be incorrect for volatile particulates. This hypothesis is strongly supported by the recent study of Friend *et al.* (23).

Let $S_A = N\pi a^2$, then the mass density of aerosols per unit volume is given by

$$M = S_A (4/3)\rho a \quad [10]$$

where ρ denotes the density of the internal structure of the particulates. If we take $\rho \sim 1$ g/cm^3, $S_A = 6 \times 10^{-8}$/cm, and $a = 5 \times 10^{-6}$ cm, then it follows that $M = 4 \times 10^{-13}$ g/cm^3 = 0.4 $\mu g/m^3$, which is about twice the value obtained by Lazrus *et al.* at 18 km in May 1970 when laser radar echoes from the 20 km sulfate layer disappeared. According to van de Hulst (20), it follows approximately that $Q \propto a^2$ for $x \ll 1$. The non-Rayleigh echoes would decrease to about one-tenth if a decreases to about one-third of the above estimate even without change of S_A; then the echoes would be hardly detectable. Thus our estimate that the effective mean radius a is roughly equal to one-half the Junge lower limit not only satisfies the requirement of the scattering efficiency but also meets the expectation of mass density measurements of filter sampling by Lazrus *et al.* At present we have no means to estimate the size distribution function, but it seems that most particulates are concentrated near the region $0.05\ \mu < r < 0.07\ \mu$. This finding agrees well with the above-mentioned hypothesis of Lazrus *et al.* (2). Of course a much smaller number of particulates may be in the region of the old Junge distribution, but they would almost escape detection by laser radar.

Conclusion

Laser radar soundings have been conducted at Fukuoka for the purpose of investigating the stratospheric aerosols since October 1972. Conclusions are summarized as follows.

1. Layers of excess scattering due to aerosols appeared every night the observation was made in the lower stratosphere of up to 30 km. One of the layers always appeared at an altitude of about 20 km and in most cases had the largest value of non-Rayleigh backscattering cross sections, in the range 1 to 2×10^{-9}/cm. This layer varied in its height and peak value day-to-day and month-to-month to some extent. In the region above 25 km, there frequently appeared other layers which seemed to be more variable in time.

2. The vertical profiles of β_M of every night were compared with the profiles of temperature and wind velocity of the night. The large scale structure of the temperature profile of a night seemed to have an important influence on the 20 km layer of the night. The height of temperature minimum and the tropopause had positive correlation with the height of the layer peak. Coefficients of the correlation were estimated to be 0.42 ± 0.20 and 0.39 ± 0.19, respectively. (When there was more than one tropopause, we chose the one above which there was no region of a few kilometers of mean temperature gradient less than -2 °C/km.) The relation between the small scale structure of the temperature profile and the height of the upper layers was not clear.

3. Monthly mean values of β_M of three height regions were calculated and compared with the zonal wind field and ozone concentration in the regions. In the 19.5–22.5 km region, the monthly mean value of β_M had its minimum value in January and increased from winter to summer, contrary to the results of winter maximum observed in Adelaide (9). In the upper regions, the variation of β_M is less systematic. The enhancement of ozone content in January and the reversal of the zonal wind in the upper regions in December and January were noticeable. Much more observation is necessary to make sure of the relation between these phenomena. In our previous paper large values of β_M in October and

Can. J. Chem. Downloaded from www.nrcresearchpress.com by 210.87.254.6 on 09/05/12
For personal use only.

November were inferred to be accompanied with the influx of the meteoric dust particles.

4. The aerosol concentrations were also estimated from the small ion density distributions deduced by radiosonde in the stratosphere. From these data and backscattering cross sections by laser radar, we obtained the mean radius of the particulates and mass density of the aerosols which were about 0.05 μ and 0.4 $\mu g/m^3$, respectively. These values, which show a rough order of magnitude, are consistent not only with the requirements of the theoretical scattering efficiency but also the expected values by filter sampling of Lazrus *et al.* (2).

The authors are indebted to many members of the Meteorological Agency. The stratospheric wind and temperature data were supplied through courtesy of Fukuoka Meteorological Observatory and ozone and electrical conductivity data were supplied through courtesy of the Agency in Tokyo.

1. C. E. JUNGE, C. W. CHAGNON, and J. E. MANSON. J. Meteorol. **18**, 81 (1961).
2. A. L. LAZRUS, B. GANDRUD, and R. D. CADLE. J. Geophys. Res. **75**, 8083 (1971).
3. J. M. ROSEN. Space Sci. Rev. **9**, 58 (1969).
4. F. E. VOLTZ and R. M. GOODY. J. Atmos. Sci. **19**, 385 (1962).
5. L. ELTERMAN. Appl. Opt. **5**, 1769 (1966).
6. G. FIOCCO and G. GRAMS. J. Atmos. Sci. **21**, 323 (1964).
7. G. S. KENT, B. R. CLEMESHA, and W. G. WRIGHT. J. Atmos. Terr. Phys. **29**, 169 (1967).
8. B. G. SCHUSTER. J. Geophys. Res. **75**, 3123 (1970).
9. D. J. GAMBLING, K. BARTUSEK, and W. G. ELFORD. J. Atmos. Terr. Phys. **33**, 1403 (1971).
10. M. HIRONO, M. FUJIWARA, O. UCHINO, and M. MATSUO. Mem. Fac. Sci. Kyushu Univ. Ser. **4**, 111 (1972); M. HIRONO, M. FUJIWARA, O. UCHINO, and T. ITABE. Rep. Ionos. Space Res. Jap. **26**, 237 (1972).
11. P. B. RUSSEL, W. VIEZEE, and R. D. HAKE. Semiannual Rep. Contract NAS 2-7261 Stanford Research Institute. July 1973.
12. G. GRAMS and G. FIOCCO. J. GEOPHYS. Res. **72**, 3523 (1967).
13. J. D. CHARNEY and P. G. DRAZIN. J. Geophys. Res. **66**, 83 (1961).
14. C. DUBS, R. FILZ, L. KATZ, D. SMART, A. WEINBERG, and K. YATES. Handbook of geophysical and space environment. *Edited by* S. L. Valley *et al.* 1965.
15. J. L. KROENING. J. Geophys. Res. **65**, 145 (1962).
16. Y. MORITA, H. ISHIKAWA, and M. KANADA. J. Geophys. Res. **76**, 3431 (1971).
17. H. V. NEHER and H. R. ANDERSON. J. Geophys. Res. **67**, 1309 (1962).
18. H. V. NEHER and W. H. PICKERING. Phys. Rev. **61**, 407 (1942).
19. B. L. LOEB. Basic processes of gaseous electronics. University of California Press. 1955.
20. H. C. VAN DE HULT. Light scattering by small particles. John Wiley and Sons, New York. 1957.
21. D. DEIRMENDJIAN. Tables of Mie scattering cross sections and amplitudes. R-407-PR. The Rand Corporation. 1963.
22. C. E. JUNGE. J. Geophys. Res. **68**, 3975 (1963).
23. J. P. FRIEND, R. LEIFER, and M. TRICHON. J. Atmos. Sci. **30**, 465 (1973).
24. R. D. CADLE. EOS. **53**, 812 (1972).
25. G. FIOCCO and L. D. SMULLIN. Nature, Lond. **199**, 1275 (1963).

Can. J. Chem. Downloaded from www.nrcresearchpress.com by 210.87.254.6 on 09/05/12
For personal use only.

A Review of Upper Atmospheric Photochemistry

PAUL CRUTZEN[1]

National Center for Atmospheric Research,[2] Boulder, Colorado 80302 and University of Colorado, Boulder, Colorado 80302

Received November 30, 1973

A review is given of the photochemical processes which determine the distribution of important minor constituents in the stratosphere and mesosphere. Although it is necessary to consider many reactions, it seems that for the first time satisfactory rate data are available for most of these processes. There is, however, a lack of knowledge about the detailed steps of the gas-phase oxidation of methane which affects theoretical results in the lower stratosphere. It is shown that rather fair agreement exists between the calculated and measured concentrations of several of the constituents. However, deviations exist concerning CH_4, H_2, and the NO profile which was obtained with the chemiluminescent technique.

Nitrogen oxides catalyze destruction of ozone and reduce total ozone in the atmosphere considerably. The reduction of ozone by other reactions is also discussed. Some estimates are presented of the ozone reductions which could result from the operation of large fleets of supersonic aircraft due to exhaust injections of nitrogen oxides into the stratosphere.

It is indicated that total ozone is rather insensitive to variations in the stratospheric water vapor content (there is a slight increase in total ozone, when the H_2O content is increased). Total ozone is, however, much more sensitive to changes in the stratospheric NO_x content. Variations in the stratospheric NO_x content over long periods may explain those variations which have taken place in total ozone. It is essential to monitor variations in the solar output in the wavelength region 1750–2400 Å, as these may change the stratospheric NO_x content and ozone production rates.

The reintroduction of the ozone-destroying reaction $HO_2 + O_3 \rightarrow OH + 2O_2$ leads to an *increase* in calculated total ozone. The reason for this surprising result is given.

A discussion is given of the possible role of vibrationally excited H_2 and electronically excited O_3 in the photochemistry of the mesosphere and thermosphere.

Nous passons en revue les processus photochimiques qui déterminent la distribution des constituants mineurs importants de la stratosphère et de la mésosphère. Bien qu'il faille tenir compte de nombreuses réactions, il semble que, pour la première fois, des données cinétiques satisfaisantes soient accessibles pour la plupart de ces processus. On n'a, cependant, qu'une connaissance insuffisante du progrès détaillé de l'oxydation en phase gazeuse, du méthane qui influe sur les résultats théoriques de la basse stratosphère. Il apparait que les concentrations calculées et mesurées de plusieurs constituants concordent assez bien. Cependant, on constate des différences en ce qui concerne CH_4 et H_2, et la coupe verticale de NO qui est obtenue par la technique de chimiluminescence.

Les oxydes d'azote catalysent la destruction de l'ozone et réduisent considérablement l'ozone total de l'atmosphère. Nous examinons également la réduction de l'ozone par d'autres réactions. Nous présentons quelques calculs concernant des réductions d'ozone qui pourraient résulter de l'usage de groupes considérables d'avions supersoniques à la suite de l'injection d'oxydes d'azote dans la stratosphère.

Il apparait que l'ozone total ne réagit pas sensiblement aux variations de la teneur atmosphérique en vapeur d'eau (il y a une légère augmentation de l'ozone total quand la teneur en H_2O augmente).

L'ozone total est cependant beaucoup plus sensible aux changements stratosphériques de la teneur en NO_x. Les variations de la teneur en NO_x dans la stratosphère sur de longues périodes peuvent expliquer celles qui se sont produites dans l'ozone total. Il est indispensable de contrôler les variations des radiations solaires entre les longueurs d'onde 1750–2400 Å, car elles peuvent changer la valeur en NO_x stratosphérique, et les vitesses de formation de l'ozone.

Can. J. Chem., **52**, 1569 (1974)

[1]Present address: Institute of Meteorology, Arrhenius Laboratory, University of Stockholm, Bergiusvägen 65, Frescati, Stockholm, Sweden.

[2]The National Center for Atmospheric Research is sponsored by the National Science Foundation.

Can. J. Chem. Downloaded from www.nrcresearchpress.com by 210.87.254.40 on 09/05/12
For personal use only.

Si l'on réintroduit la réaction $HO_2 + O_3 \rightarrow OH + 2O_2$ qui détruit l'ozone on calcule une augmentation de l'ozone total. Nous donnons la raison de ce résultat surprenant.

Nous examinons le rôle possible de H_2 excité par des vibrations et de O_3 excité électroniquement dans la photochimie de la mésosphère et de la thermosphère.

Introduction

Ozone is one of the most remarkable minor gases in the earth's atmosphere. Ozone is important for several reasons. (*a*) It provides a shield against lethal ultraviolet radiation below about 310 nm (1). The question whether exhaust gases from high-flying aircraft can destroy ozone (2, 3) has, therefore, developed into a major concern. (*b*) In absorbing ultraviolet radiation at wavelengths shorter than 3100 Å ozone constitutes the main energy source of the stratosphere and mesosphere. Ozone is therefore important for the climate of the upper atmosphere. (*c*) Its presence in the troposphere seems to be of importance for reactions occurring within the nitrogen and carbon cycles of the troposphere (4–6).

The first quantitative theory of upper atmospheric odd oxygen (atomic oxygen and ozone) was developed by Chapman (7). This theory explains the distribution of atomic oxygen and ozone in terms of reactions 1 to 5 (see Table 1). For almost 30 years, Chapman's theory, complemented with considerations of transport, was very successful in describing the gross temporal and spatial behavior of atmospheric ozone (see *e.g.* ref. 8). However, especially after careful determinations of the rate coefficients k_2 and k_4 (9), it became clear that, in order to explain the characteristics of upper atmospheric ozone, it is necessary to consider additional reactions to reduce atmospheric ozone.

It is the main aim of this paper to give a review of the present status of our knowledge of the photochemistry of the upper atmosphere. The standard set of reactions now thought to be of importance for describing the ozone chemistry of the stratosphere and mesosphere is presented in Table 1. Except for a few reactions, the rate coefficients were all chosen to be equal to those recommended in NBS reports (10, 48). Rate coefficients are listed (in cm molecule s units) only whenever rate coefficients were not recommended in the NBS reports or whenever coefficients based on very recent laboratory work became available.

Catalytic Chains of Ozone Destruction

There is now general agreement that odd oxygen is mainly destroyed by catalytic reactions. The catalysis by hydroxy particles was first postulated by Bates and Nicolet (11). In the mesosphere hydroxy particles are produced by reaction 6*a*, mainly under the action of Ly-α radiation near 1216 Å. It was pointed out (12) that hydroxy particles could also be produced by reactions 19, 20*a*, and 21, especially below 60 km. Following a suggestion by McGrath and Norrish (13), Hampson (14) proposed an additional catalytic chain of reactions 11 and 12 for the stratosphere. This idea was first taken up by Hunt (15) to compute the distribution of ozone in the stratosphere. To obtain reasonable agreement between observed and theoretical total ozone, Hunt adopted a rate coefficient $k_{12} = 10^{-14}$ for reaction 12, which was expected to be the slowest and therefore most critical reaction of the chain [11] and [12]. For several years to come, modelers adopted Hunt's rate coefficient to explain features of the observed ozone distributions in the atmosphere. However, only very recently have measurements been made of the rate constant for reaction 12. Laboratory experiments (16, 17) now indicate a stratospheric value of k_{12} of between 10^{-16} and 10^{-15}. Such low values for k_{12} cannot explain the ozone observations. However, as will be discussed later, this does not mean that reaction 12 is unimportant.

Finally, it was proposed by Crutzen (18) that oxides of nitrogen were of crucial importance for the ozone budget of the atmosphere, mainly due to the reaction chain [24] and [25]. From measurements of nitric acid by Murcray and coworkers (19, 20) it may be deduced that NO and NO_2 are present in the stratosphere in large enough quantities to affect critically the global abundance of ozone. Adopting recommended rate coefficients (20), it may now be concluded that mixing ratios for NO_x (NO and NO_2 together) of 1–10 p.p.b. between 10 and 40 km are very important for the ozone budget of the atmosphere below 40 km. Recent determinations of prevailing mixing ratios of NO_2 (21) and of NO (22) have shown that NO and NO_2 are present in the stratosphere with the required concentrations. Probably the most important source for stratospheric NO is provided by the oxidation of N_2O by $O(^1D)$ atoms via reactions 3*a* and 22*b* (2, 23,

Can. J. Chem. Downloaded from www.nrcresearchpress.com by 210.87.254.40 on 09/05/12
For personal use only.

Can. J. Chem. Downloaded from www.nrcresearchpress.com by 210.87.254.40 on 09/05/12
For personal use only.

24). Additional stratospheric NO may be produced under the action of cosmic rays, mainly at high latitudes (25, 26). The oxidation of NH_3 has been proposed as a significant source of NO_x in the stratosphere (27). However, NH_3 is probably very efficiently removed by heterogeneous processes from the atmosphere, at least judging from the upper limit of 0.08 p.p.b. of its abundance above 1650 m reported by Kaplan (28). Its oxidation is therefore not a significant source for NO in the stratosphere, which contains sulfuric acid droplets. Large quantities of NO are produced in the thermosphere by ionospheric reactions (29). It has been argued (26, 30) that little of this thermospheric NO_x can penetrate down into the stratosphere, due to the pair of reactions 27 and 28, despite the action of the NO-restoring reactions 29 to 32. Nevertheless, the possibility of significant downward transport of NO in the winter season at middle and high latitudes should not be entirely disregarded.

It seems most likely that the question of the ozone balance of the upper atmosphere must be solved in terms of the chemical species introduced before. A catalytic role of SO_2 and other sulfur compounds may be ruled out, because of the endothermicity of the reaction $SO_2 + O \rightarrow SO + O_2$, the slow rate of the reaction $SO_2 + O_3 \rightarrow SO_3 + O_2$ (10), and the low mixing ratios (<3.5 p.p.b.) of SO_2 in the stratosphere (32).

Although it is known that oxides of Na, Br, and Cl catalyze destruction of odd oxygen in the laboratory (33), this is unlikely to be important in the stratosphere. Chlorine compounds are occasionally injected into the stratosphere by volcanic eruptions. Their role in the ozone balance will, therefore, be discussed further in a later section.

Description of the Adopted Model

To test the reliability of our present knowledge of the photochemical processes taking place in the stratosphere and mesosphere, it is appropriate to calculate the distributions of chemical constituents and to compare them with observations. The model used for this purpose is one dimensional, so that the exchange of matter is simulated by the eddy diffusion concept which describes the steady-state concentration of any chemical constituent X by the equation

$$[\mathrm{I}] \qquad P_X - D_X + \frac{\partial}{\partial z}\left\{K_z[\mathrm{M}]\frac{\partial \mu_X}{\partial z}\right\} = 0$$

where P_X, D_X = photochemical production, destruction rates of the chemical species X (molecule cm^{-3} s^{-1}), z = altitude, [M] = concentration of air molecules, and $\mu_X = [X]/[M]$ (particle mixing ratio of the species X).

$$[\mathrm{II}] \quad K_z = \begin{cases} 10^4 \text{ cm}^2 \text{ s}^{-1} & z \leqslant 50 \text{ km} \\ 10^4 \exp\{0.13(z - 50)\} & z > 50 \text{ km} \end{cases}$$

Calculations were performed for the odd oxygen, odd hydrogen, and odd nitrogen compounds, and for H_2, H_2O, CH_4, CO_2, and CO. Applying eq. I, the total odd hydrogen (H, OH, HO_2, H_2O_2), odd oxygen (O, O_3), and odd nitrogen contents (N, NO, NO_2, HNO_3) were calculated at each level. Subsequently a subdivision took place by calculating each of the individual components, as described in an earlier paper (34). A constant solar zenith angle θ, such that $\sec\theta = 1.4$, was applied. It is believed that the calculated profiles are most characteristic for the low latitudes. The adopted boundary conditions were as follows.

(*a*) Lower boundary (tropopause)

$\mu_{N_2O} = 2.5 \times 10^{-7}$ (35); $\mu_{NODD} = 2 \times 10^{-10}$ (assumed)

$[O_3] = 5 \times 10^{11}$ (36); $\mu_{H_2} = 5 \times 10^{-7}$ (37)

$\mu_{H_2O} = 3 \times 10^{-6}$ (38); $\mu_{CH_4} = 1.5 \times 10^{-6}$ (39)

$\mu_{CO_2} = 3.2 \times 10^{-4}$ (40); $\mu_{CO} = 10^{-7}$ (41)

(*b*) Upper boundary (95 km)

$\mu_{NODD} = 2.5 \times 10^{-7}$ (42); $\mu_{CH_4} = \mu_{N_2O} = 0$

For H_2, H_2O, CO_2, and O_2, flux boundary conditions were applied according to the formula

$$[\mathrm{III}] \qquad F = K[\mathrm{M}]\frac{\partial}{\partial z}\mu_X = D_X H_X$$

where D_X = photochemical destruction rate of X at top level and H_X = scale height of X (assumed to be equal to 5 km). The odd hydrogen, odd oxygen, and carbon monoxide concentrations were calculated with the mass-conservation relationships:

$$\mu_{HODD} = 2(6.5 \times 10^{-6} - \mu_{H_2} - \mu_{H_2O})$$

$$\mu_{OODD} = 0.419 - 2\mu_{O_2}$$

$$\mu_{CO} = 3.2 \times 10^{-4} - \mu_{CO_2}$$

TABLE 1. List of reactions to be considered in the chemistry of the upper atmosphere

Reaction number	Reaction	
1	$O_2 + h\nu \rightarrow 2O$	$\lambda < 2424$ Å
2	$O + O_2 + M \rightarrow O_3 + M$	
3*a*	$O_3 + h\nu \rightarrow O(^1D) + O_2$	$\lambda < 3100$ Å
3*b*	$O_3 + h\nu \rightarrow O + O_2$	3100 Å $< \lambda <$ 11 400 Å
4	$O + O_3 \rightarrow 2O_2$	
5	$O + O + M \rightarrow O_2 + M$	
6*a*	$H_2O + h\nu \rightarrow H + OH$	$\lambda < 2400$ Å
6*b*	$H_2O + h\nu \rightarrow H_2 + O(^1D)$	$\lambda = 1216$ Å (64)
7	$O + OH \rightarrow H + O_2$	
8	$H + O_2 + M \rightarrow HO_2 + M$	
9	$HO_2 + O \rightarrow OH + O_2$	$k_9 = 2 \times 10^{-11}$ (assumed)
10	$H + O_3 \rightarrow OH^* + O_2$	
11	$OH + O_3 \rightarrow HO_2 + O_2$	
12	$HO_2 + O_3 \rightarrow OH + 2O_2$	
13	$HO_2 + HO_2 \rightarrow H_2O_2 + O_2$	
14	$H_2O_2 + h\nu \rightarrow 2OH$	
15	$HO_2 + OH \rightarrow H_2O + O_2$	$k_{15} = 2 \times 10^{-10}$ (56)
16*a*	$H + HO_2 \rightarrow H_2O + O$	$k_{16a} = 10^{-11}$ (64)
16*b*	$H + HO_2 \rightarrow H_2 + O_2$	$k_{16b} = 10^{-11}$ (64)
17	$H_2O_2 + OH \rightarrow HO_2 + H_2O$	
18	$O(^1D) + M \rightarrow O + M$	
19	$O(^1D) + H_2O \rightarrow 2OH$	
20*a*	$O(^1D) + CH_4 \rightarrow CH_3 + OH$	
20*b*	$O(^1D) + CH_4 \rightarrow CH_2O + H_2$	
21	$O(^1D) + H_2 \rightarrow H + OH$	
22*a*	$O(^1D) + N_2O \rightarrow N_2 + O_2$	
22*b*	$O(^1D) + N_2O \rightarrow 2NO$	
23	$N_2O + h\nu \rightarrow N_2 + O(^1D)$	$\lambda < 3370$ Å
24	$NO + O_3 \rightarrow NO_2 + O_2$	
25	$NO_2 + O \rightarrow NO + O_2$	
26	$NO_2 + h\nu \rightarrow NO + O$	$\lambda \lesssim 3975$ Å
27	$NO + h\nu \rightarrow N + O$	$\lambda \lesssim 1910$ Å
28	$NO + N \rightarrow N_2 + O$	
29	$N + O \rightarrow NO + h\nu$	$k_{28} = 1.5 \times 10^{-17}$ (77)
30	$N + O_2 \rightarrow NO + O$	
31	$N + O_3 \rightarrow NO + O_2$	
32*a*	$N + OH \rightarrow NO + H$	
32*b*	$N + HO_2 \rightarrow NO + OH$	$k_{32} = 2 \times 10^{-10}$ (assumed)
33	$NO_2 + O_3 \rightarrow NO_3 + O_2$	$k_{33} = 1.23 \times 10^{-13} \exp(-2470/T)$ (78)
34*a*	$NO_3 + h\nu \rightarrow NO + O_2$	$J_{34a} = 6.6 \times 10^{-2}$ (79)
34*b*	$NO_3 + h\nu \rightarrow NO_2 + O$	
35	$NO_3 + NO_2 (+ M) \rightarrow N_2O_5 (+ M)$	
36	$N_2O_5 + h\nu \rightarrow NO_2 + NO_3$ $\rightarrow NO + NO_2 + O_2$ $\rightarrow 2NO_2 + O$	
37	$NO_3 + NO \rightarrow 2NO_2$	
38	$OH + NO_2 (+ M) \rightarrow HNO_3 (+ M)$	
39*a*	$HNO_3 + h\nu \rightarrow OH + NO_2$	
39*b*	$OH + HNO_3 \rightarrow H_2O + NO_3$	
40	$CH_4 + OH \rightarrow CH_3 + H_2O$	$k_{40} = 2.5 \times 10^{-12} \exp(-1650/T)$ (80)
41	$CH_3 + O_2 (+ M) \rightarrow CH_3O_2 (+ M)$	
42	$CH_3O_2 + NO \rightarrow CH_3O + NO_2$	
43	$CH_3O_2 + HO_2 \rightarrow CH_3O_2H + O_2$	
44	$CH_3O_2H + h\nu \rightarrow CH_3O + OH$	
45	$CH_3O + O_2 \rightarrow CH_2O + HO_2$	
46*a*	$CH_2O + h\nu \rightarrow CO + H_2$	$\lambda \lesssim 3500$ Å
46*b*	$CH_2O + h\nu \rightarrow H + HCO$	$\lambda \lesssim 3500$ Å
47	$CH_2O + OH \rightarrow CHO + H_2O$	$k_{47} = 1.4 \times 10^{-11}$ (81)

Can. J. Chem. Downloaded from www.nrcresearchpress.com by 210.87.254.40 on 09/05/12
For personal use only.

TABLE 1. (*Concluded*)

Reaction number	Reaction	
48	$CHO + O_2 \rightarrow CO + HO_2$	
49	$CO + OH \rightarrow CO_2 + H$	$k_{49} = 2.1 \times 10^{-13} \exp(-75/T)$ (80)
50	$CO_2 + h\nu \rightarrow CO + O$	$\lambda < 2000$ Å
51	$CH_3O_2 + NO_x (+ M) \rightarrow CH_3O_2NO_x (+ M)$	$x = 1, 2$
52	$CH_3O_2 + NO_x \rightarrow CH_2O + HNO_{x+1}$	$x = 1, 2$
53	$CH_3O + NO_x (+ M) \rightarrow CH_3ONO_x (+ M)$	$x = 1, 2$
54	$CH_3O + NO_x \rightarrow CH_2O + HNO_x$	$x = 1, 2$
55	$CH_3O + HO_2 \rightarrow CH_3OH + O_2$	
56	$H + H + M \rightarrow H_2 + M$	
57	$H_2 + O \rightarrow H + OH$	
58	$H_2 + OH \rightarrow H_2O + H$	
59	$CH_3OH + h\nu \rightarrow CH_2O + H_2$	$\lambda \lesssim 2000$ Å
60*a*	$CH_3OH + OH \rightarrow CH_3O + H_2O$	
60*b*	$CH_3OH + O \rightarrow CH_2OH + OH$	$k_{60b} = 2.8 \times 10^{-12} \exp(-1140/T)$ (82)

For the numerical computations the atmosphere was divided into layers of 1 km thickness.

The solar irradiance data and absorption cross sections for O_2 and O_3 were taken from Ackerman (43) and the penetration of solar radiation through the Schumann–Runge bands of O_2 was simulated following Kockarts (44). The photodissociation coefficients for NO were interpolated from the tables published by Cieslik and Nicolet (31). Included in this study were recent data on the quantum yield of $O(^1D)$ production by reaction 3*a* near 3100 Å (45, 46). Both data sets agree well with previous work (47). Absorption cross sections for remaining species were taken from NBS reports (48). The albedo of the lower atmosphere of about 30% was taken into account for all wavelengths larger than 3300 Å.

Comparison of Theoretical and Observed Distributions of Important Chemical Species

Ozone (Fig. 1)

A comparison shows very reasonable agreement between the theoretical and observed distributions from Krueger *et al.* (49), the measured values being on the low side by about 10 to 20% above 25 km, in which region the distribution of ozone is dominated by photochemistry. These calculations were performed adopting presently recommended measured values for rate coefficients. This may, therefore, indicate that the present photochemical theory for stratospheric ozone is satisfactory. But many more measurements, especially of the distribution of NO_x particles in the stratosphere, are necessary to test this.

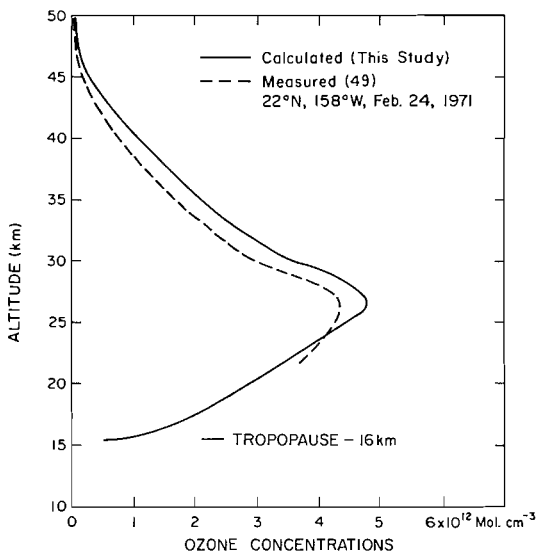

FIG. 1. Calculated and measured vertical profiles of ozone concentrations.

Odd Nitrogen Compounds (Fig. 2)

A theoretical distribution and some examples of observed distributions of NO (22, 50), NO_2 (21), and HNO_3 (83) are presented in Fig. 2. The HNO_3 data represent an average of several HNO_3 measurements obtained with the filter-collection technique. The agreement between the two HNO_3 profiles is fair, with the measured values somewhat on the low side. It should be added that there is still a question whether HNO_3 vapor is collected with unit efficiency on the filter. In fact, HNO_3 profiles, obtained by solar infrared absorption technique (20), indicated somewhat

Can. J. Chem. Downloaded from www.nrcresearchpress.com by 210.87.254.40 on 09/05/12
For personal use only.

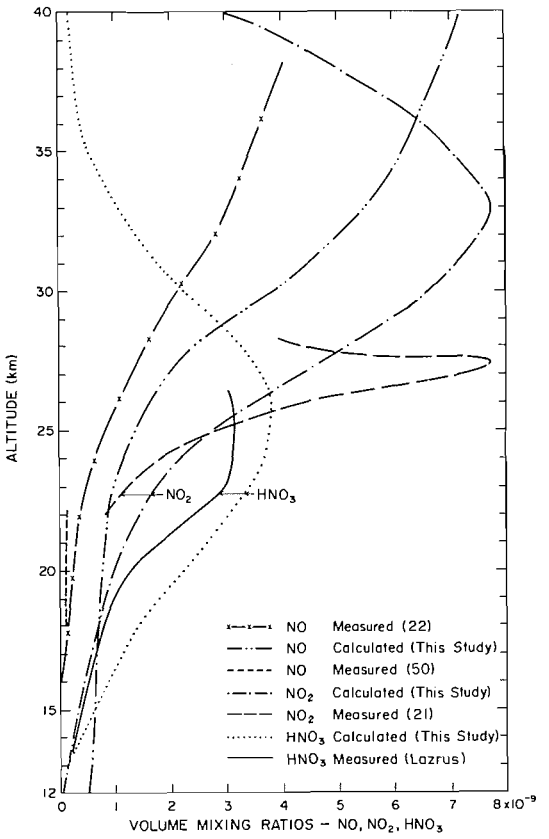

FIG. 2. Calculated and observed profiles of mixing ratios of NO, NO_2, and HNO_3.

higher HNO_3 mixing ratios than those calculated. The height of maximum concentrations of nitric acid agree well in all these cases, being between 24 and 26 km.

The curve of measured NO_2 by Ackerman and Muller (21) in Fig. 2 is drawn through the points at which those workers report NO_2 concentrations. Although altitude-averaged mixing ratios between 20 and 30 km of calculated and reported NO_2 are similar, there is a rather large disagreement between the general shapes of the altitude profiles. The reason for this deviation is not clear, but it may be expected that the average of many NO_2 profiles, when these become available, will be much smoother and possibly more in line with the calculated profile.

The NO concentrations reported by Schiff *et al.* (50) agree badly with theoretical estimates. Provided that the NO measurements are indeed correct, this seems to indicate a severe lack of knowledge of the chemistry taking place in the lower stratosphere. The agreement between the theoretical estimates and Ackerman's measured NO profile (22) is better, especially if we take into consideration that Ackerman's measurements were done at sunset, under which condition NO is partly converted to NO_2.

Methane (Fig. 3)

The calculated and measured CH_4 profiles (37, 51) are in very good agreement below about 30 km, if all curves are shifted to assume the same mixing ratio at the tropopause level. The profile by Kyle *et al.* (52), not shown in Fig. 3, indicates a much faster decrease of mixing ratio with altitude. Above about 30 km Ehhalt and Heidt's measurements (37) indicate much larger concentrations of CH_4 than those calculated, which may indicate that vertical mixing or mean motions above 30 km are much faster than adopted in this model (53). It is not possible to explain this feature with a revised chemical chain or revised rate coefficients. This problem will be discussed in a later section of this paper.

Molecular Hydrogen (Fig. 4)

The two profiles of H_2 show a similar general behavior with an increase of mixing ratio with altitude above the tropopause up to about 28 km; this can be explained by H_2 production as an intermediate in the methane oxidation cycle, mainly via reaction 46*a* (6). However, the experi-

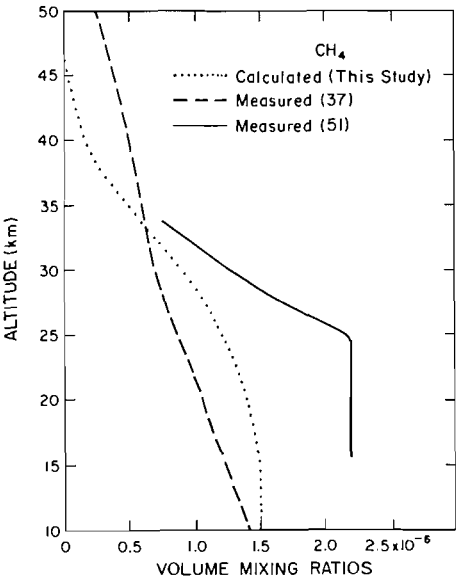

FIG. 3. Calculated and measured profiles of mixing ratios of CH_4.

Can. J. Chem. Downloaded from www.nrcresearchpress.com by 210.87.254.40 on 09/05/12
For personal use only.

Can. J. Chem. Downloaded from www.nrcresearchpress.com by 210.87.254.40 on 09/05/12
For personal use only.

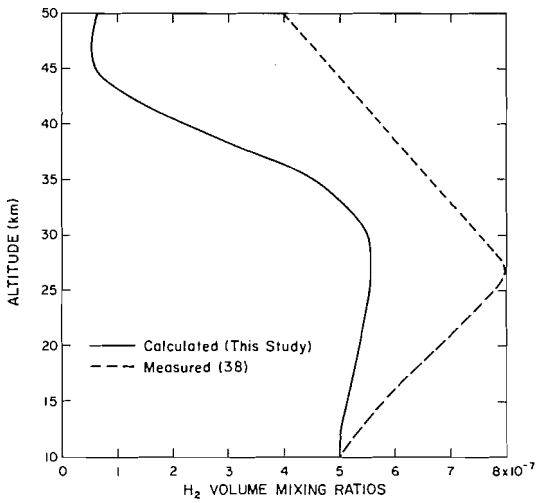

FIG. 4. Calculated and measured vertical profiles of mixing ratios of H_2.

mental profile shows a much larger increase with altitude than the theoretical one, indicating a larger production of H_2 than that following from the adopted photochemical chain and reaction coefficients. As a possible explanation of this feature it may be interesting to consider the formation of methanol in the cold, lower stratosphere by the (probably very fast) reaction

[55] $$CH_3O + HO_2 \rightarrow CH_3OH + O_2$$

and dissociation of methanol according to

[59] $CH_3OH + h\nu \rightarrow CH_2O + H_2 \quad \lambda < 200$ nm (54)

Additional reactions which must be considered are reactions 60*a* and 60*b*. If these reactions are fast, then no appreciable production of H_2 may occur. The rate constant derived for reaction 60*b* is based on indirect information.

OH Concentrations (Table 2)

Anderson (55) has measured OH concentrations in the altitude region from 45 to 70 km near 5×10^6 molecules/cm^2 (with error bars: 2 to 9×10^6). As can be seen from Table 2 (columns 8 and 9), the calculated OH concentrations fall within the limits of the experimental results. The calculated values were obtained by adopting a rate coefficient $k_{15} = 2 \times 10^{-10}$ for the reaction

[15] $$HO_2 + OH \rightarrow H_2O + O_2$$

In the NBS report of recommended rate coefficients for modeling work (10) it is proposed that $2 \times 10^{-11} \leqslant k_{15} \leqslant 2 \times 10^{-10}$. Reaction 15 being the most important reaction removing odd hydrogen particles, a lower value for k_{15} would result in larger computed concentrations of H, OH, and HO_2. Calculations show that $k_{15} = 2 \times 10^{-11}$ leads to much larger computed OH concentrations (2×10^7 cm^{-3}) than those measured. They also result in too small concentrations of ozone near 50 km (4.1×10^{10} cm^{-3}) compared to the measurements (49); this is due to the increased catalytic reduction of ozone by increased quantities of H, OH, and HO_2. The conclusion is therefore that k_{15} has a value close to 2×10^{-10}, as measured by Hochanadel *et al.* (56).

The calculated and measured N_2O and CO profiles are shown in Figs. 5 and 6. They will not be discussed here (see refs. 35 and 76).

On the Relative Role of HO_x and NO_x Particles in Reducing Odd Oxygen and the SST Problem

As discussed previously destruction of ozone and atomic oxygen takes place by catalytic processes involving either H, OH, and HO_2 or NO and NO_2. A comparison of the relative importances of these processes has been carried out before (2, 18) and it was shown that catalytic destruction of ozone by NO_x molecules below 40 km, in which region almost all atmospheric ozone is located, was much more important than by HO_x particles. Furthermore, it was shown that

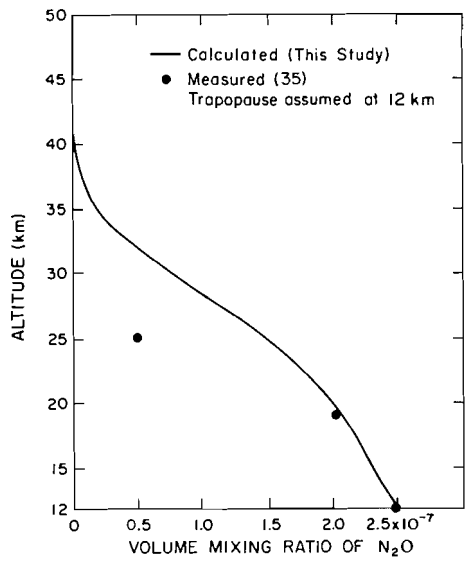

FIG. 5. Calculated and observed vertical mixing ratios of N_2O.

TABLE 2. Calculated concentrations of O_3, OH, and NO_x and ozone destruction rates (molecule cm^{-3} s^{-1}) by catalytic action of oxides of nitrogen (D_n) and oxides of hydrogen (D_h)*

Height (km)	$(O_3)_1$	$(O_3)_2$	$(OH)_1$	$(OH)_2$	$(NO_x)_1$	$(NO_x)_2$	D_{n1}	D_{n2}	D_{h1}	D_{h2}
50	6.7(10)	6.7(10)	7.4(6)	7.4(6)	4.3(7)	4.3(7)	5.9(4)	5.9(4)	5.6(6)	5.6(6)
45	3.0(11)	3.0(11)	1.1(7)	1.1(7)	1.9(8)	1.9(8)	9.1(5)	9.1(5)	4.9(6)	4.9(6)
40	1.1(12)	1.1(12)	8.0(6)	7.9(6)	8.5(8)	8.5(8)	6.4(6)	6.4(6)	1.5(6)	1.5(6)
35	2.1(12)	2.1(12)	3.5(6)	3.2(6)	2.4(9)	2.4(9)	7.5(6)	7.5(6)	4.8(5)	4.4(5)
30	3.5(12)	3.3(12)	1.5(6)	1.1(6)	3.8(9)	4.0(9)	3.5(6)	3.6(6)	2.2(5)	1.6(5)
25	4.4(12)	4.1(12)	7.6(5)	3.7(5)	3.3(9)	4.3(9)	5.9(5)	7.3(5)	1.2(5)	4.6(4)
20	2.9(12)	2.7(12)	3.7(5)	1.8(5)	2.5(9)	3.4(9)	4.1(4)	5.6(4)	3.8(4)	9.6(3)
17	1.2(12)	1.2(12)	1.7(5)	1.1(5)	2.1(9)	2.3(9)	2.8(3)	3.0(3)	9.6(3)	1.9(3)
Total ozone (molecule cm^{-2})	7.1(18)	6.8(18) -4%								

*Subscript 1, calculated using the recommended value of rate coefficient k_{12}; subscript 2, calculated neglecting this reaction.

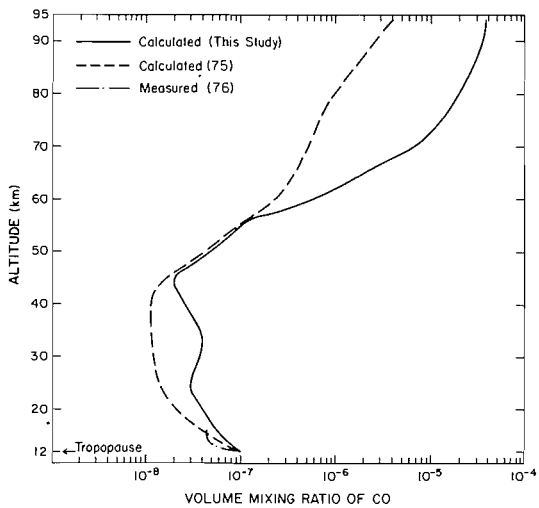

FIG. 6. Calculated and measured vertical profiles of mixing ratios of CO.

HO_x particles are important above 40 km and that the Chapman reaction 4 is important between 40 and 60 km. However, in these studies the important reaction

[12] $$HO_2 + O_3 \rightarrow OH + 2O_2$$

in the HO_x catalytic cycle was completely removed as it was believed that the reaction was very slow. Recent measurements (16, 17) indicate a non-negligible rate for reaction 12. This reaction was therefore again included in the reaction scheme. The rates of ozone destruction (in molecule cm^{-3} s^{-1}) by NO_x and HO_x molecules, as calculated with the present model, are shown in Table 2 (column 8, D_{n1}, and column 10, D_{h1}, respectively). Again, it is shown that from 20 to 40 km ozone destruction by NO and NO_2 is much more important than by the HO_x particles.

Through the formation of nitric acid in reaction 38 there is a conversion of catalytic NO_x into nitric acid molecules which do not react with atomic oxygen or ozone. Therefore, it follows that the catalytic HO_x molecules in fact protect ozone from more destruction by converting NO_x into HNO_3, mainly below about 35 km. It also means that an increase in the stratospheric water vapor content may result in an increase of total atmospheric ozone (2,6). Computations performed with the present model indeed indicated an increase in total ozone but only by about 1.5% when the stratospheric content of water vapor was as much as doubled. This low number seems to indicate that stratospheric ozone is surprisingly insensitive to changes in the stratospheric water vapor content. Therefore, it now seems very unlikely that the increase in stratospheric water vapor by about 50% from 1964–1969 as measured by Mastenbrook (57) can explain the increase in total ozone during the last decade by about 6% (58, 59). Instead, an increase in ozone by this amount may be caused by variations in solar activity, for instance by changing the stratospheric NO content (2), or by changes in the circulation of the lower stratosphere.

DeMore (16) has claimed, concluding from laboratory studies of an H_2O–O_3 system, that reaction 12 should be very important in removing ozone from the atmosphere. Such an extrapolation should, however, be done with great caution. To show this, calculations were performed in which reaction 12 was neglected. The results of these calculations are shown in Table 2. The computations show that the deletion of the ozone-removing reaction 12 leads to *less* ozone. The explanation for this result is not difficult to find.

Can. J. Chem. Downloaded from www.nrcresearchpress.com by 210.87.254.40 on 09/05/12
For personal use only.

Can. J. Chem. Downloaded from www.nrcresearchpress.com by 210.87.254.40 on 09/05/12
For personal use only.

Although reaction 12 indeed removes some ozone, it is also, in the lower stratosphere below 30 km, the main reaction producing OH. With more OH present, more NO_2 is converted to nitric acid and the catalytic destruction of ozone is reduced (compare the results in Table 2).

Stratospheric ozone is sensitive to the stratospheric NO content. This is clearly shown by the result of a computation in which the flux of N_2O into the stratosphere was increased by only about 20% (this was done by increasing the lower boundary mixing ratio of N_2O from 2.5×10^{-7} to 3.0×10^{-7}). It was found that total ozone decreased by 3%. Possible changes of N_2O production in the soil may therefore feed back through changing the atmospheric ozone content and the penetration of solar ultraviolet radiation to ground levels (34).

A problem of considerable concern is whether injections of exhaust gases from high-flying aircraft into the stratosphere may change the total atmospheric ozone content and thereby alter protection at ground level from dangerous solar ultraviolet radiation (2, 3). Computations to estimate the effect of NO injections were first performed by Johnston (3), adopting a pure photochemical model in which the influence of atmospheric motions were neglected, and by Crutzen (34, 60). These models did not consider the loss of NO_x into HNO_3, which should reduce the effects of injected NO_x on the ozone. With the present model new estimates of the effect of NO_x injections on the ozone content were calculated, taking into account the conversion of NO_x into HNO_3. Adopted were the results obtained by Mahlman (61) from a three-dimensional point-source tracer experiment and calculations were performed for a latitude close to 30–40° N, where most of the injections from the point source accumulated. This case tends to simulate conditions in the mid-latitude regions, where air transport is most intensive. The following results were obtained. For a fleet of 500 U.S. SST's as projected in the 1960's, flying about 7 h per day at 20 km, a decrease in total ozone by 8.5% was calculated. Assuming a similar dispersion pattern for Concorde effluents, it was calculated that a fleet of 200 Concordes flying at 18 km (the altitude of the injections is a significant factor (60)) for 7 h per day would cause a decrease in total ozone in the same latitude belt by about 1%. From purely chemical considerations these estimates are underestimations of a real effect as the steady-state model adopted in this study assumes that an immediate equilibrium is established between the concentrations of NO, NO_2, and HNO_3, while in reality it will take a year, thus allowing for more NO_x and more catalytic ozone destruction.

Additional Topics

Possible Long-term Variations in Solar Ultraviolet Radiation

According to measurements by Heath (62) there are variations in the solar ultraviolet output between 1200 and 3000 Å with larger variations at shorter wavelengths. In order to estimate the effects of possible variations in the solar ultraviolet irradiance, model computations were performed in which the ultraviolet irradiances were increased in the wavelength regions 1750–2000 Å (by 50%) and 2000–2400 Å (by 20%). In the first case total ozone increased by 2.8%, in the second case by 3.2%. A combination of both events would thus lead to an increase by 6%, as observed in the Northern hemisphere (58, 59, 63), but uncertain in the Southern hemisphere (63). The largest effects showed up above 30 km. The calculated increases in ozone brought about by increased irradiances from 1750–2000 Å were mainly due to reductions in the NO content of the upper stratosphere where NO is dissociated under the action of ultraviolet radiation at about 1910 Å (reactions 27 and 28). It is therefore very important to monitor the ultraviolet region from 1750–2400 Å for possible long-term variations in the solar output.

Lack of Knowledge about Processes Leading to the Oxidation of Methane

The oxidation of methane leads to important production of CO and H_2 (5, 60). There also is a question to what degree the methane oxidation forms a chain reaction with regard to OH formation or whether OH is lost via reaction 40 (60). To find out the importance of this problem, it was decided to compare the results from two computations: one in which it was assumed that there was a net gain of OH molecules resulting from the methane oxidation (this is the standard assumption, used in all but one computation of this study) and one in which it was assumed that OH was lost in the methane oxidation cycle. The results of the computation showed that OH concentrations were reduced in the latter case by a factor of about 2 at 17 km, 1.4 at 20 km, 1.15 at 25 km, and less above. The largest effects showed up, therefore,

Can. J. Chem. Downloaded from www.nrcresearchpress.com by 210.87.254.40 on 09/05/12
For personal use only.

at SST flight levels. Good knowledge of the way in which methane is oxidized in the stratosphere may therefore be of some importance when estimating the environmental effect of high-flying aircraft.

The Possible Role of Vibrationally Excited H_2 in the Mesosphere and Thermosphere

Molecular hydrogen in the mesosphere and lower thermosphere is formed by reactions 6*b*, 16*b*, and 56 and destroyed by reactions 21, 57, and 58. Reaction 57

$$[57]\quad H_2 + O \rightarrow H + OH, \qquad k_{57} = 2.9 \times 10^{-11} \exp(-4275/T)$$

is very slow in this region of the atmosphere due to low ambient temperatures and a large activation energy (8.5 kcal/mol). Reaction 16*b* being fast according to recent measurements (64), there is a large production of H_2 in the upper mesosphere, so that H_2 becomes the dominant hydrogen species above 70 km (see Fig. 7, full line curves). In this model water vapor falls off rather rapidly with altitude, starting from about 50 km and reaching a mixing ratio of 10^{-6} at 80 km. These results were obtained neglecting reaction 6*b*, which probably yields H_2 with an efficiency of 13% (65), and production of H_2 in the photolysis of CH_4 in the mesosphere (66). Thus, H_2 may be a very important constituent above 50 km. There are, however, some reasons why the altitude profiles of H_2O and H_2 may differ from those shown in Fig. 7 by full lines. It is namely conceivable that the H_2 formed in reactions 6*b*, 16*b*, and 56 is vibrationally excited, thus containing an energy of at least 10.2 kcal/mol for $v = 1$, possibly sufficient to make the reaction

$$[57]^* \quad H_2{}^* + O(^3P) \rightarrow H + OH, \qquad k_{57}{}^* = 2.9 \times 10^{-11} \text{ (assumed)}$$

temperature independent. Calculations performed, making these assumptions, produced the results of the dashed curves in Fig. 7, which show the buildup of H_2 appreciably reduced and much more H_2O near the mesopause. It was assumed in the calculations that deactivation of vibrationally excited H_2 by N_2 or O_2 takes place with an efficiency of 10^{-5} per collision. It is also possible that atomic oxygen, instead of reacting according to reaction 57, relaxes vibrationally excited H_2 to its ground state.

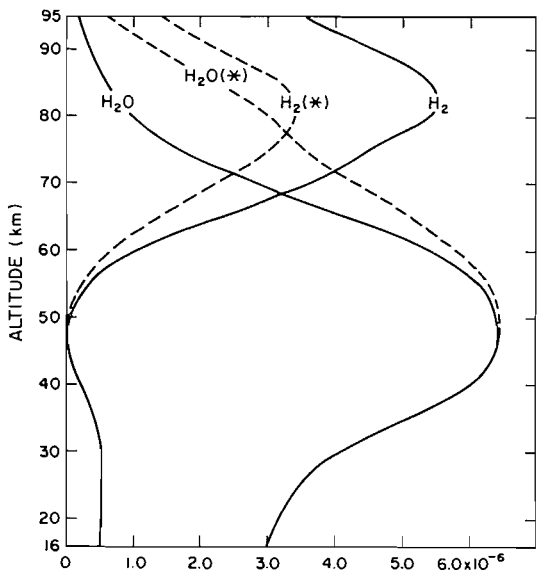

FIG. 7. Vertical distribution of mixing ratios of H_2 and H_2O. The profiles indicated by asterisks were calculated taking into account the possible formation of vibrationally excited H_2 and its reaction with $O(^3P)$.

Excited Ozone

Theoretical calculations performed by Wahl and Wilson (67) indicate that in reaction 2 ozone molecules are formed initially in the ground state $O_3(^1A_1)$ and in the electronically excited state $O_3(^3B_2)$ with comparable probabilities.

$$[2]\qquad O + O_2 + M \rightarrow \begin{cases} O_3(^1A_1) + M \\ O_3(^3B_2) + M \end{cases}$$

The internal energy of the excited state is equal to about 0.6 eV ($\simeq$ 14 kcal/mol). Radiation from the excited state is highly forbidden and deactivation by collisions with O_2 and N_2 may occur with probabilities between 10^{-4} and 10^{-5} per collision (67). Consequently, electronically excited O_3 may be sufficiently long-lived near and above the mesopause to be of aeronomic interest. Possible reactions of $O_3(^3B_2)$ include, for example,

$$O(^3P) + O_3(^3B_2) \rightarrow O_2(?) + O_2(?)$$

$$O_3(^3B_2) + h\nu \rightarrow O(?) + O_2(?)$$

The first reaction may explain the $O_2(^1\Delta_g)$ nightglow emissions from the thermosphere between 80 and 100 km (68).

Different Choice of Eddy Diffusion Coefficients

Wofsy and McElroy (53) propose that measured high methane concentrations (37, 39) in the upper stratosphere should be explained in terms of larger vertical mixing than hitherto believed.

Can. J. Chem. Downloaded from www.nrcresearchpress.com by 210.87.254.40 on 09/05/12
For personal use only.

In order to test their hypothesis a computation was performed adopting their high eddy diffusion coefficients. The calculated CH_4 and also H_2 altitude distribution indeed came into much better agreement with the observations, thereby not affecting the calculated distributions of NO, NO_2, HNO_3, and O_3 considerably. This model now allows for more flux of NO downwards from the ionosphere to reach the stratosphere with an effect on total ozone. This could contribute to variations in total ozone with periods related to the solar cycle periods (18, 2). However, it is clearly necessary to study the distribution of minor constituents at least in a two-dimensional model, thereby taking into account both the effect of horizontal and vertical eddy motions and of mean meridional motions.

Chlorine Reactions

As already stated it seems unlikely that chlorine oxides are present in the stratosphere in large enough concentrations to play a major role in the global ozone balance. Nevertheless, it has been proposed that they may affect the atmospheric total ozone content (69). Therefore, it seems appropriate to discuss this matter briefly. Some of the important reactions that should be considered are:

[61] $Cl + O_3 \rightarrow ClO + O_2$
$k_{61} \geq 6.7 \times 10^{-13}$ at $T = 295$ °K (70)

[62] $ClO + O_3 \rightarrow OClO + O_2$
$k_{62} \leq 5 \times 10^{-15}$ at $T = 295$ °K (71)

[63] $ClO + O \rightarrow Cl + O_2$
$k_{63} = 5.3 \times 10^{-11}$ (70)

[64] $O + OClO \rightarrow ClO + O_2$
$k_{64} = 5 \times 10^{-13}$ at $T = 295$ °K (71)

[65] $Cl + HO_2 \rightarrow HCl + O_2$
very fast, $k_{65} \approx 4 \times 10^{-10}$?

[66] $Cl + CH_4 \rightarrow HCl + CH_3$
$k_{66} = 8 \times 10^{-11} \exp(-1910/T)$ (72)

[67] $OH + HCl \rightarrow H_2O + Cl$
$k_{67} = 1.5 \times 10^{-11} \exp(-1000/T)$

The rate coefficient for reaction 67 was estimated from that for the reaction $OH + HBr \rightarrow H_2O + Br$ (73), a comparison of this rate constant with that for reaction 67 at $T \simeq 1900$ °K (74), and consideration of the fact that the reaction of OH with HCl is less exothermic than that with HBr. Assuming that ozone is indeed mainly limited by the catalytic action of chlorine oxides it is possible to estimate the concentrations of Cl and ClO which are required to balance the ozone production due to reactions 1 and 2 close to the center of main ozone production near 30 km. We find

$$[Cl]_{req} = 2J_1[O_2]/2k_{61}[O_3] \simeq 10^5 \text{ cm}^{-3}$$

assuming a fast rate constant $k_{63} = 10^{-11}$ cm^3 s^{-1}.

$$[ClO]_{req} = 2J_1[O_2]/2k_{63}[O] = 5 \times 10^8 \text{ cm}^{-3}$$

corresponding to a volume mixing ratio of about 10^{-9} at 30 km.

Atoms of Cl are reactive to CH_4 and probably even more important to HO_2 and it is necessary to investigate if these reactions are an efficient sink for Cl and ClO particles. It seems that the important reaction which can reform Cl from HCl is reaction 67, so that, neglecting reaction 65,

$$[HCl]_{req} > k_{66}[Cl][CH_4]/k_{67}[OH] \simeq 2 \times 10^9 \text{ cm}^{-3}$$

corresponding to a volume mixing ratio of 5×10^{-9}. Farmer (84) determined the mixing ratio of HCl in the low stratosphere to be less than 10^{-10}. It seems, therefore, unlikely that Cl and ClO can affect the global ozone distribution critically. Furthermore, a negative correlation between volcanic activity and total ozone (63) is not very clear. One would expect rather strong variations in total ozone in a stratosphere in which ozone would be reduced to a large degree by the catalytic action of oxides of chlorine which derive their main source from sporadic volcanic injection of HCl and Cl_2. Nevertheless, in regions close to volcanic activity and in the upper stratosphere and mesosphere, there may be an effect.

Summary

The results and discussions of this paper have indicated that our knowledge of the chemistry of the upper atmosphere has improved considerably over the last years. For the first time it is now possible to calculate ozone profiles from a chemical scheme containing few guesses of rate coefficients. It is shown that the calculated ozone profile agrees remarkably well with the observed profile at low latitudes. Also for some other species as HNO_3, CH_4, and N_2O the agreement is rather satisfactory. There exist, however, some

severe discrepancies for NO_2 and especially NO, gases which are so important for the ozone budget of the upper atmosphere. However, with only a few measured vertical profiles of these and other constituents available, we may still not expect any close agreement. Only the average profile of a large set of measured ones should be compared with these theoretically estimated profiles. Anyhow, it seems unlikely that it is possible to construct a one-dimensional eddy diffusion model which yields satisfactory agreement between theoretical and observed profiles simultaneously for all important minor constituents. As stated before, it seems most likely that oxides of nitrogen are most important in reducing the atmospheric ozone content. Total ozone is sensitive to changes in the flux of N_2O into the stratosphere. Calculations indicate that total ozone may decrease by almost 1% due to the catalytic action of NO_x injected by 200 Concorde-type aircraft flying at an altitude of 18 km for 7 h per day. Computations indicated that an increase in stratospheric H_2O may lead to a minor increase in total ozone. The reintroduction of the reaction $HO_2 + O_3 \rightarrow OH + 2O_2$ into the chemical chain leads to a slight increase in ozone, contrary to what could be expected from laboratory experience. Variation in the solar irradiance between 1750 and 2400 Å may have important effects on total ozone and may explain the increase in total ozone which took place over the last decade. A good knowledge of the way in which methane is oxidized in the atmosphere seems to be important also for environmental predictions connected with future SST flights.

In the upper mesosphere and lower thermosphere the effects of excited H_2 and O_3 may be important. It has been indicated that H_2 may be by far the most important hydrogen species between 70 and 120 km and that the mixing ratio of H_2O may already start to fall off at an altitude of 50 km.

This study was partly supported by the Atmospheric Sciences Section, National Science Foundation, and the Department of Transportation through NST Grant No. GA-28688X2.

1. K. Smith, P. Bener, M. Caldwell, F. Daniels, Jr., A. Giese, T. Goldsmith, W. Klein, J. Lee, F. Urbach, A. Zucker, and D. Holtz. Biological Impacts of Increased Intensities of Solar Ultraviolet Radiation. National Academy of Sciences, Washington, D.C. 1973.
2. P. J. Crutzen. J. Geophys. Res. **76**, 7311 (1971).
3. H. S. Johnston. Science, **173**, 517 (1971).
4. H. Levy. Science, **173**, 141 (1971).
5. J. C. McConnell, M. B. McElroy, and S. C. Wofsy. Nature, **233**, 187 (1971).
6. P. Crutzen. Pure Appl. Geophys. **106–108**, 1385 (1973).
7. S. Chapman. Q. J. R. Meteorol. Soc. **3**, 103 (1930).
8. R. A. Craig. The upper atmosphere. Academic Press, N.Y. 1965.
9. S. W. Benson and A. E. Axworthy. J. Chem. Phys. **26**, 1718 (1957).
10. D. Garvin (*Editor*). Chemical kinetics data survey. IV. Preliminary table of chemical data for modelling of the stratosphere. National Bureau of Standards, Washington, D.C. 1973.
11. D. R. Bates and M. Nicolet. J. Geophys. Res. **55**, 301 (1950).
12. R. D. Cadle. Disc. Faraday Soc. **37**, 66 (1964).
13. W. D. McGrath and R. G. W. Norrish. Proc. R. Soc. A, **254**, 317 (1960).
14. J. Hampson. Chemiluminescent emission observed in the stratosphere and mesosphere. Les problèmes météorologiques de la stratosphère et de la mésosphère. Presses Universitaires de France, Paris. 1965. p. 393.
15. B. G. Hunt. J. Geophys. Res. **71**, 1385 (1966).
16. W. B. DeMore. Science, **180**, 735 (1973).
17. R. Simonaitis and J. Heicklen. J. Phys. Chem. **77**, 1932 (1973).
18. P. J. Crutzen. Q. J. R. Meteorol. Soc. **96**, 320 (1970).
19. D. G. Murcray, T. G. Kyle, F. H. Murcray, and W. J. Williams. Nature, **218**, 78 (1968).
20. D. G. Murcray, A. Goldman, A. Csoeke-Poeckh, F. H. Murcray, W. J. Williams, and R. N. Stocker. J. Geophys. Res. **78**, 7033 (1973).
21. M. Ackerman and C. Muller. Nature, **240**, 300 (1972).
22. M. Ackerman, D. Frimout, C. Muller, D. Nevejans, J. C. Fontanella, A. Girard, and N. Louisnard. Nature, **245**, 205 (1973).
23. M. G. McElroy and J. C. McConnell. J. Atmos. Sci. **28**, 1095 (1971).
24. M. Nicolet and W. Peetermans. Ann. Geophys. **28**, 751 (1972).
25. P. Warneck. J. Geophys. Res. **77**, 6589 (1972).
26. G. Brasseur and M. Nicolet. Planet. Space Sci. **21**, 939 (1973).
27. J. C. McConnell. J. Geophys. Res. **78**, 7812 (1973).
28. L. D. Kaplan. Pure Appl. Geophys. **106–108**, 1341 (1973).
29. R. B. Norton and C. A. Barth. J. Geophys. Res. Space Phys. **75**, 3903 (1970).
30. D. F. Strobel. J. Geophys. Res. **76**, 8384 (1973).
31. S. Cieslik and M. Nicolet. In press.
32. J. E. Harries. Nature, **241**, 515 (1973).
33. F. Kaufman. Ann. Rev. Phys. Chem. **20**, 45 (1969).
34. P. J. Crutzen. Ambio, **1**, 41 (1972).
35. K. Schütz, C. Junge, R. Beck, and B. Albrecht. J. Geophys. Res. **75**, 2230 (1970).
36. H. U. Dütsch. Arch. Meteorol. Geophys. Bioklimatol. **A13**, 167 (1962).
37. D. H. Ehhalt and L. E. Heidt. Pure Appl. Geophys. **106–108**, 1352 (1973).

Can. J. Chem. Downloaded from www.nrcresearchpress.com by 210.87.254.40 on 09/05/12
For personal use only.

38. E. J. WILLIAMSON and J. T. HOUGHTON. Q. J. R. Meteorol Soc. **91**, 330 (1965).
39. A. E. BAINBRIDGE and L. E. HEIDT. Tellus, **18**, 221 (1966).
40. W. BISCHOF and B. BOLIN. Tellus, **22**, 431 (1970).
41. W. SEILER and C. E. JUNGE. J. Geophys. Res. **75**, 2217 (1970).
42. G. WITT, J. E. DYE, and N. WILHELM. Report AP-8, Institute of Meteorology, University of Stockholm, Stockholm, Sweden. 1973.
43. M. ACKERMAN. Ultraviolet absorption related to mesospheric processes, mesospheric models and related experiments. *Edited by* G. Fiocco. Reidel Publ. Co. Dordrecht, Holland. 1971. pp. 149–159.
44. G. KOCKARTS. Penetration of solar radiation in the Schumann–Runge bands of molecular oxygen, mesospheric models and related experiments. *Edited by* G. Fiocco. Reidel Publ. Co. Dordrecht, Holland. 1971. pp. 160–176.
45. C. L. LIN and W. B. DEMORE. O(^{1}D) production in ozone photolysis near 3100 Å. Jet Propulsion Laboratory. Caltech. Pasadena, California. 1973. Preprint.
46. H. JOHNSTON, D. MARTIN, and J. GIRMAN. The quantum yield from O(^{1}D) in the photolysis of ozone. 1973. Preprint. Dept. of Chemistry, University of Berkeley.
47. I. T. N. JONES and R. P. WAYNE. Proc. R. Soc. Lond. A, **319**, 273 (1970).
48. R. F. HAMPSON (*Editor*). J. Phys. Chem. Ref. Data, **2**, 267 (1973).
49. A. J. KRUEGER, D. F. HEATH, and C. L. MATEER. Pure Appl. Geophys. **106–108**, 1254 (1973).
50. B. A. RIDLEY, H. I. SCHIFF, A. W. SHAW, L. MEGILL, L. BATES, C. HOWLETT, H. LEVAUX, and T. ASHENFELTER. Planet. Space Sci. **22**, 19 (1974).
51. M. ACKERMAN and C. MULLER. Pure Appl. Geophys. **106–108**, 1325 (1973).
52. T. G. KYLE, D. G. MURCRAY, F. H. MURCRAY, and W. J. WILLIAMS. J. Geophys. Res. **74**, 3421 (1969).
53. S. C. WOFSY and M. B. MCELROY. J. Geophys. Res. **78**, 2619 (1973).
54. J. G. CALVERT and J. N. PITTS, JR. Photochemistry. John Wiley and Sons, New York. 1966. p. 442.
55. J. G. ANDERSON. J. Geophys. Res. **76**, 7820 (1971).
56. C. J. HOCHANADEL, J. A. GHORMLEY, and P. J. OGREN. J. Chem. Phys. **56**, 4426 (1972).
57. H. J. MASTENBROOK. Can. J. Chem. This issue.
58. W. D. KOMHYR, E. W. BARRETT, G. SLOCUM, and H. K. WEICKMANN. Nature, **232**, 390 (1971).
59. H. JOHNSTON, G. WHITTEN, and J. BIRKS. J. Geophys. Res. **78**, 6107 (1973).
60. P. J. CRUTZEN. Proceedings of the Survey Conference on the Climatic Impact Assessment Program. U.S. Dept. of Transportation. Cambridge, Mass. 1972. pp. 80–89.
61. J. D. MAHLMAN. AIAA Paper No. 73-528. American Institute for Aeronautics and Astronautics/American Meteorological Society International Conference on the Environmental Impact of Aerospace Operations in the High Atmosphere. Denver, Colorado. June 1973.
62. D. F. HEATH. J. Geophys. Res. **78**, 2779 (1973).
63. J. K. ANGELL and J. KORSHOVER. Mon. Weather Rev. **101**, 426 (1973).
64. E. ALLEN and G. MOORTGAT. To be published.
65. J. R. MCNESBY and H. OKABE. Adv. Photochem. **3**, 157 (1963).
66. B. G. HUNT. J. Atmos. Phys. **33**, 1869 (1971).
67. A. C. WAHL and C. W. WILSON. Private communication.
68. W. F. J. EVANS, E. J. LLEWELLYN, and A. VALLANCE JONES. J. Geophys. Res. **77**, 4899 (1972).
69. R. S. STOLARSKI and R. J. CICERONE. Can. J. Chem. This issue.
70. M. A. A. CLYNE and J. A. COXON. Proc. R. Soc. A, **303**, 207 (1968).
71. M. A. A. CLYNE and H. W. CRUSE. Trans. Faraday Soc. **67**, 2869 (1971).
72. D. D. DAVIS, W. BRAUN, and A. M. BASS. Int. J. Chem. Kinet. **2**, 101 (1970).
73. G. A. TAKACS and G. P. GLASS. J. Phys. Chem. **77**, 1182 (1973).
74. W. E. WILSON, JR., J. T. O'DONOVAN, and R. M. FRISTROM. 12th Symp. Combust. (The Combustion Institute, Pittsburgh, Penn.). 1969. p. 929.
75. S. C. WOFSY, J. C. MCCONNELL, and M. B. MCELROY. J. Geophys. Res. **77**, 4477 (1972).
76. W. SEILER and P. WARNECK. J. Geophys. Res. **77**, 3204 (1972).
77. M. MANDELMAN, T. CARRINGTON, and R. A. YOUNG. J. Chem. Phys. **58**, 84 (1973).
78. H. JOHNSTON and R. GRAHAM. Unpublished results.
79. H. S. JOHNSTON. Private communication.
80. D. D. DAVIS. Private communication.
81. E. D. MORRIS and H. NIKI. J. Chem. Phys. **55**, 1991 (1971).
82. H. F. LEFEVRE, J. F. MEAGHAN, and R. B. TIMMONS. Int. J. Chem. Kinet. **IV**, 103 (1972).
83. A. LAZRUS. Private communication.
84. C. B. FARMER. Can. J. Chem. This issue.

Can. J. Chem. Downloaded from www.nrcresearchpress.com by 210.87.254.40 on 09/05/12
For personal use only.

HO_x, NO_x, and ClO_x: Their Role in Atmospheric Photochemistry

STEVEN C. WOFSY AND MICHAEL B. MCELROY
Center for Earth and Planetary Physics, Harvard University, Cambridge, Massachusetts

Received November 26, 1973

Sources of atmospheric odd nitrogen and hydrogen are reviewed and their role in ozone photochemistry is discussed. A model, containing few adjustable parameters, gives good agreement with observed distributions of stratospheric and mesospheric ozone. Nitric oxide emitted by supersonic aircraft would lead to a significant reduction in the concentration of atmospheric ozone if the globally averaged source of NO should exceed 2×10^7 molecules cm^{-2} s^{-1}. A traffic model projected by Broderick *et al.* for 1990 could lead to a reduction of about 2% in the column density of O_3.

Sources of atmospheric chlorine are discussed. It is argued that HCl should be the dominant form of atmospheric chlorine and that it is produced mainly from aerosols of marine origin. The atmospheric source strength is about 2×10^8 tons per year according to Chesselet *et al.* and HCl may be removed by gas phase reaction with NH_3. The role of chlorine compounds as a catalyst for recombination of odd oxygen is discussed and shown to play no major role in the normal atmosphere. Reactions of OH and HO_2 with O_3 may provide an important sink for tropospheric odd oxygen such that O_3 may not be a passive tracer for tropospheric motions.

Les sources de quelque azote et hydrogène atmosphériques sont revues et leur rôle dans la photochimie de l'ozone est étudié. Un modèle, contenant deux paramètres adjustables, est en bon accord avec les distributions d'azone stratosphérique et mésosphérique observées. L'oxyde nitrique émis par des avions supersoniques amènera une réduction significative de la concentration de l'ozone atmosphérique si la moyenne globale de la source de NO doit dépasser 2×10^7 molécules cm^{-2} s^{-1}. Un modèle de traffic, projet de Broderick *et al.*, pour 1990 pourra mener à une réduction de près de 2% dans la densité de la colonne d'O_3.

Les sources du chlore atmosphérique sont étudiées. On démontre que HCl est la forme dominante du chlore atmosphérique et qu'il est produit essentiellement d'aérosols d'origine marine. D'après Chesselet *et al.*, la force de la source atmosphérique est de près de 2×10^8 tonnes par an, et le HCl peut être éliminé par une réaction en phase gazeuse avec NH_3. Le rôle des composés du chlore comme catalyseur pour la recombinaison de quelque oxygène est étudié et démontre jouer aucun rôle majeur dans l'atmosphère normale. Les réactions du OH et du H_2O avec du O_3 peuvent fournir un important affaiblissement pour quelque oxygène troposphérique tel que O_3 ne pourra être un traceur passif pour les déplacements troposphériques. [Traduit par le journal]

Can. J. Chem., **52**, 1582 (1974)

Introduction

The intent here is to provide a brief summary of recent work on the transport and chemistry of trace stratospheric gases which are now believed to play a role in determining the equilibrium concentration of atmospheric ozone. The summary is in no sense complete, neither in content nor in reference to original material. More general reviews are given elsewhere in this volume by Crutzen (1) and Nicolet (2). We shall emphasize simple one-dimensional model studies carried out in this laboratory and particularly highlight models which relate to the possible perturbation of the stratosphere by future fleets of supersonic aircraft. We shall offer a brief discussion of chemical processes as they affect the distribution of chlorine compounds in the atmosphere. The work on chlorine had as its impetus the possible modification of the stratosphere by the space shuttle. The shuttle, now under development and scheduled for operation in the 1980's, will emit HCl as an exhaust product. A systematic study of its consequences is now in progress under the auspices of the National Aeronautics and Space Administration. This paper offers an initial attempt to define the problem and an attempt to focus on some of the major uncertainties and targets for future research.

Ozone in the Normal Stratosphere

Odd oxygen atoms are produced in the atmosphere mainly by dissociation of O_2 in the

Can. J. Chem. Downloaded from www.nrcresearchpress.com by 210.87.254.6 on 09/05/12
For personal use only.

Can. J. Chem. Downloaded from www.nrcresearchpress.com by 210.87.254.6 on 09/05/12
For personal use only.

Herzberg continuum:

[1] $h\nu + O_2 \rightarrow O + O$

They are removed in the statosphere by the simple reaction

[2] $O + O_3 \rightarrow O_2 + O_2$

first discussed by Chapman (3), and by more complex reaction schemes terminating in

[3] $O + HO_2 \rightarrow OH + O_2$

[4] $O + OH \rightarrow O_2 + H$

and

[5] $O + NO_2 \rightarrow NO + O_2$

The importance of HO_x, in the context of the ozone problem, was first recognized by Bates and Nicolet (4). The importance of NO_x was identified by Crutzen (5). For present purposes we define HO_x as $H + OH + HO_2$, NO_x as $N + NO + NO_2 + NO_3 + 2{\cdot}N_2O_5 + HNO_2 + HNO_3$.

The major source of stratospheric HO_x is the reaction

[6] $O(^1D) + H_2O \rightarrow OH + OH$

with a small contribution from

[7] $O(^1D) + H_2 \rightarrow OH + H$

and a similar reaction with methane.

NO_x is formed by oxidation of N_2O and NH_3, and by dissociation of N_2 following absorption of cosmic rays.

The primary oxidation process for N_2O is

[8] $O(^1D) + N_2O \rightarrow NO + NO$

and this source of stratospheric NO_x has been relatively well characterized in the recent literature (6–8). The contribution from NH_3 remains somewhat uncertain. Stratospheric ammonia is believed to be removed mainly by reactions such as

[9] $OH + NH_3 \rightarrow N_2O + NH_2$

and

[10] $h\nu + NH_3 \rightarrow NH_2 + H$

The subsequent details of the reaction scheme are uncertain. It is reasonable to expect NO and NO_2 as major products. One cannot, however, rule out the possibility that [9] and [10] might lead to a net sink for stratospheric NO_x, through reactions such as

[11] $NH_2 + NO \rightarrow N_2 + H_2O$

[12] $NH + NO \rightarrow N_2 + OH$

as discussed by McConnell (9) and McConnell and McElroy (10). Further laboratory data are required to clarify the situation. In addition, there is an urgent need for atmospheric measurements of NH_3 and its possible products. Later in this paper we shall argue that formation of aerosols would provide a major sink for atmospheric NH_3. Aerosol formation could be initiated by a gas phase reaction of NH_3 with HCl

[13] $NH_3 + HCl + M \rightarrow NH_4Cl + M$

or a similar reaction with HNO_3. If further work confirms this possibility, it may be necessary to extend present chemical models for the stratosphere to include reactions involving chlorine compounds, notably HCl, ClO, Cl_2, Cl, and NH_4Cl. In the meantime, the contribution of NH_3 chemistry to the stratospheric NO_x budget remains uncertain.

Absorption of cosmic rays initiates a complex chemistry (11) in which NO_x is formed by reactions such as

[14] $N_2^+ + e \rightarrow N + N$

[15] $NO^+ + e \rightarrow N + O$

[16] $N_2 + e \rightarrow N + N$

The product atoms may be released in excited states and it is especially important to define the relative yields of $N(^4S)$ and $N(^2D)$. Excess production of the former can lead to net destruction of NO_x by reactions such as

[17] $N(^4S) + NO \rightarrow N_2 + O$

[18] $N(^4S) + NO_2 \rightarrow N_2O + O$

[19] $\rightarrow N_2 + O_2$

[20] $\rightarrow N_2 + O + O$

The latter will be efficiently quenched in the stratosphere with production of NO by the reaction

[21] $N(^2D) + O_2 \rightarrow NO + O$

Reaction 21 is the major source of NO in the atmosphere above 100 km, while [17] is the dominant sink for mesospheric and thermospheric odd nitrogen.

The potential importance of the cosmic ray related source of stratospheric NO_x has been emphasized in a recent paper by Ruderman and

Can. J. Chem. Downloaded from www.nrcresearchpress.com by 210.87.254.6 on 09/05/12
For personal use only.

Chamberlain (12). They pointed out that the cosmic ray flux reaching the atmosphere is largest at times of low solar activity and that its effects are confined mostly to high geomagnetic latitudes. NO_x produced at high latitudes must be transported to low latitudes before it can have any significant effect on O_3. Subsequent modification of O_3 should be phase shifted with respect to the cosmic ray source, and Ruderman and Chamberlain (12) made some preliminary estimates of the magnitude of the phase shift. Their estimates are in satisfactory agreement with phase shifts observed by Angell and Korshover (13) in an analysis of ozone data taken at Tromso and Arosa (see also ref. 14). The importance of Ruderman and Chamberlain's contribution is twofold. First, it provides a reasonable mechanism to account for the much discussed correlation not heretofore widely accepted by the meteorological community. Second, the work implies that absorption of cosmic rays in the stratosphere may indeed lead to significant production of NO_x which should be included in detailed attempts to model stratospheric chemistry and dynamics. A major uncertainty is the estimation of the rate of NO_x production by cosmic rays, for which experimental data are lacking.

Estimates for the concentration of major forms of NO_x and HO_x are given in Figs. 1 and 2. The results shown here were taken from the study by McElroy *et al.* (15) and are intended to represent mean (24 h average) conditions at a latitude of 30° N, for a solar declination of +12°. The tropopause is at 16 km. In the context of O_3 photochemistry we are particularly concerned with concentrations of NO and NO_2 for the height

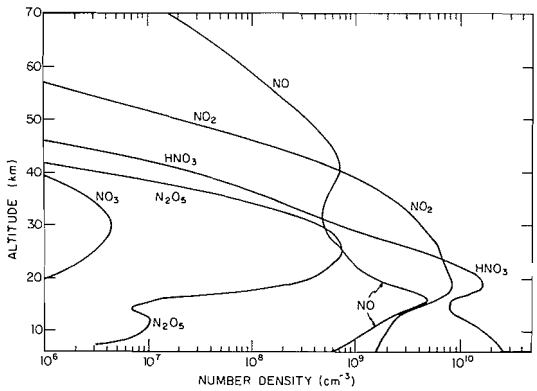

FIG. 1. Calculated vertical distributions of individual NO_x constituents in the normal atmosphere, 30° N latitude, solar declination +12°. From McElroy *et al.* (15).

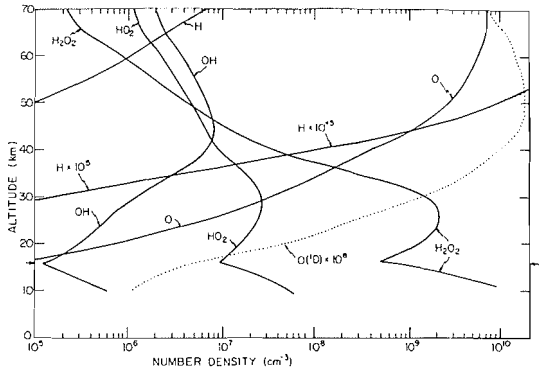

FIG. 2. Calculated number densities (24 h average) for hydrogenous radicals, H_2O_2, $O(^3P)$, and $O(^1D)$ for the normal atmosphere, 30° N latitude, solar declination +12°. The tropopause is at 16 km. From McElroy *et al.* (15).

range 30 to 50 km, and with concentrations of H and OH above 50 km. The concentration of O_3 below 30 km is controlled mainly by dynamics. Reaction 5 is the major loss process for odd oxygen below 45 km. The Chapman reaction 2 is important between 45 and 55 km, whereas reactions 3 and 4 dominate above 55 km.

The concentration of NO_x in the important height range 30 to 50 km is determined by a balance of input associated with oxidation of N_2O, reaction 8, and removal by vertical transport. Analyses of the various uncertainties are given by McConnell and McElroy (10) and by McElroy *et al.* (15). They concluded that the concentration of NO_x should be relatively well determined for this height range, although major uncertainties may remain at lower elevations. Vertical motion was treated using the expedient concept of eddy diffusion, with diffusivities chosen to reproduce observed concentrations of CH_4 and N_2O (16).

McElroy *et al.* (15) used the concentrations of NO_x and HO_x given in Figs. 1 and 2 to compute concentrations of O_3. The calculation is relatively straightforward for the atmosphere above 30 km where photochemical processes dominate for odd oxygen. Results are shown in Fig. 3, which includes also a comparison with observational data obtained by Johnson *et al.* (17), Hering and Borden (18), Hilsenrath *et al.* (19), and Krueger *et al.* (20). Theory agrees with experiment within permissible observational error limits. The agreement is taken as a measure of the overall validity of the techniques employed to calculate NO_x and

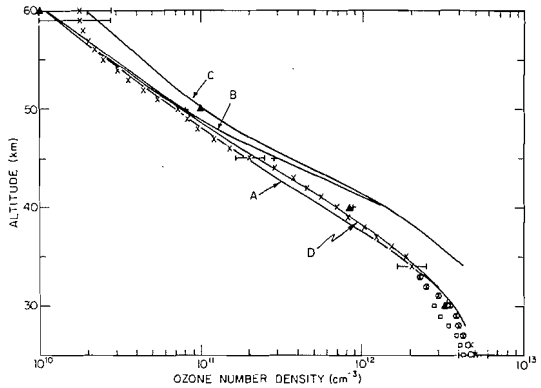

FIG. 3. Calculated ozone profiles are shown for the normal atmosphere, 30° N latitude, +12° solar declination. Curve A was calculated with the complete chemical model and computed NO_x profiles; reactions involving NO_x were omitted in curve B; reactions involving NO_x and HO_x were omitted in curve C. Curve D was the same model as A, but with a slower value for the reaction rate of NO with O_3 (*cf.* ref. 15). Observations shown are as follows: Hilsenrath *et al.* (19), X, (with error bars) chemiluminescent rocketsonde, and ○, Mast–Brewer electrochemical balloonsonde, at Wallops Is. (38° N), Sept. 16, 1968; △, Johnson *et al.* (17), as corrected by Evans *et al.*, rocketsonde solar u.v. absorption from White Sands (32° N), June 14, 1949; +, Krueger *et al.* (20), rocketsonde solar u.v. absorption from Pt. Magu, Calif. (34° N), June 18, 1970; □, Hering and Borden, Mast–Brewer balloonsondes from Tallahassee, Fla. (30.4° N), 1966 summer average. Figure taken from McElroy *et al.* (15).

HO_x and lends support to the general reliability of the theoretical model.

Modification of Ozone by Supersonic Aircraft

We shall model possible effects of NO_x introduced into the stratosphere by high flying aircraft. We consider aircraft at cruise altitudes of 17, 20, and 25 km. The lowest altitude is appropriate for the Concorde. The intermediate value is adopted for an advanced version of the American supersonic transport (SST), and the highest value could apply for a conceptual future hypersonic transport (HST). We shall model the vertical distribution of NO_x input for a given aircraft with a triangular shape function centered on the appropriate altitude. The triangular function is taken to give a vertical extent of 2 km at the half-intensity point for the Concorde and HST. A somewhat broader width of 4 km is adopted for the SST.

Emission rates of NO_x are of course largely unknown for SST and HST. We adopted data given by Broderick *et al.* (21) for the Concorde. From their emission rates we estimate that Concorde, carrying 100 passengers at a cruise speed of 2.1×10^3 km h^{-1} for approximately 7 h per day, would emit a globally averaged quantity of NO_x equivalent to 7.74×10^4 molecules cm^{-2} s^{-1}. Similarly, the corresponding NO_x emission rate for SST would be 5.73×10^5 molecules cm^{-2} s^{-1}, with an assumption that the advanced SST should carry 600 passengers at a cruise speed of 3.2×10^3 km h^{-1}, for 7 h a day.

A summary of the various computations for O_3 in the perturbed atmosphere is given in Fig. 4. An effort was made in these computations to include all of the possible feedback mechanisms which occur in the perturbed atmosphere. For example, a perturbation of ozone leads to a change in the transmission of the atmosphere at ultraviolet wavelengths, with a resulting alteration in the source of odd oxygen. A change in atmospheric transmission also affects the natural source of NO_x associated with reactions 8 through 10. Reduction in the concentration of O_3 leads to a decrease in computed values for stratospheric temperature with consequent effect on the rates of various chemical reactions. These feedback mechanisms were properly included in all computations for the perturbed environment. The consequence of thermal adjustment is shown explicitly in the figure.

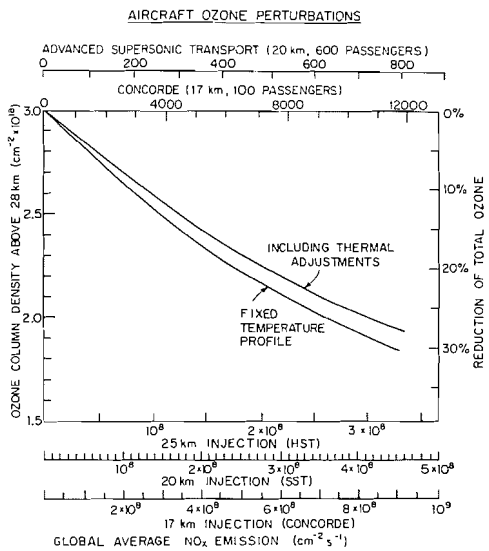

FIG. 4. Perturbations in ozone induced by artificial injections of NO_x. A detailed discussion of the various scales is given in the text. Figure taken from McElroy *et al.* (15).

Can. J. Chem. Downloaded from www.nrcresearchpress.com by 210.87.254.6 on 09/05/12
For personal use only.

Can. J. Chem. Downloaded from www.nrcresearchpress.com by 210.87.254.6 on 09/05/12
For personal use only.

The left vertical axis in Fig. 4 gives the column density computed for O_3 in the atmosphere above 28 km, at a latitude of 30° N for a solar declination of 12°. Results are shown for a variety of NO_x inputs as given by the separate scales for the bottom horizontal axis. We note that the perturbation in ozone expected for a given input of NO_x is a moderately sensitive function of the height at which injection occurs. For example, an input of NO_x equivalent to 2×10^8 molecules cm^{-2} s^{-1} at 25 km leads to a reduction by approximately 25% in the computed column density of O_3 above 28 km. The inputs required at 20 and 17 km in order to provide a similar reduction in O_3 are 2.75×10^8 and 5.5×10^8 cm^{-2} s^{-1} respectively. A fleet of 775 Concordes flying for 7 h a day at 17 km would reduce O_3 above 28 km by 3%. A traffic model projected by Broderick *et al.* (21) for 1990 would provide for a corresponding reduction of 2.4% for O_3 above 28 km.[1]

The right vertical axis in Fig. 4 shows an attempt to define the approximate change in total O_3 column due to aircraft operations. For present purposes we assume that the atmosphere consists of two distinct regions. In one zone chemical time constants for O_3 are short compared with time constants for dynamics, and the concentration of O_3 should be accurately modeled by a photochemical equilibrium theory. In the second zone, dynamical time constants are short compared with chemical values, and the distribution of O_3 is set by the details of the atmospheric motion field. The boundary between these two zones describes a surface whose height should be an increasing function of increasing latitude. Ozone is released into the dynamical zone primarily at lower latitudes. A reduction in O_3 at the boundary between the chemical and dynamical zones would lead to a reduction in O_3 at all locations within the dynamical zone. The reduction factor will be approximately equal to the reduction which applies in the low latitude region of the boundary surface. Somewhat arbitrarily, we identify the boundary surface with the level at which the chemical time constant for O_3 is 15 days. Concentrations of O_3 along the boundary can then be derived with the photochemical model and concentrations below the boundary may be scaled accordingly. The reduction factors indicated on the right hand vertical scale reflect this procedure. We believe that the procedures followed here are unlikely to lead to major error. In particular, our conclusions are relatively insensitive to the precise criterion used to define the boundary between the chemical and dynamical zones.[2]

Origin and Chemistry of Atmospheric Chlorine

There is little doubt that the atmosphere, at least in marine environments, contains significant quantities of gaseous chlorine. The gas was first identified by Junge (22) and was subsequently observed by Duce (23), Buat-Menard and Chesselet (24), and Chesselet *et al.* (25). In all cases, combinations of molecular sieves and filters were used to eliminate particles with radii greater than 0.1 μ. In addition, Junge measured the concentration of Aitken nuclei and showed that at most 2% of the transmitted chlorine could be present in these particles. The mixing ratio (v/v) of total gaseous chlorine,[3] at least for the marine atmosphere near ground level, is apparently in the range $1\text{–}6 \times 10^{-9}$. Junge (22) measured gaseous chlorine just above the trade-wind inversion at Hawaii and found concentrations which were approximately a factor of 2 less than values measured in the near surface area. Chesselet *et al.* (25) observed a decrease in the concentration of gaseous chlorine carried by an air mass of marine origin as the air mass passed over land in rural France. The French data may be interpreted to yield a lifetime for gaseous chlorine in the near surface atmosphere of about 0.4 days, but probably reflects dilution of marine air by chlorine-poor air from aloft.

The studies by Chesselet and associates (24–26) strongly support the hypothesis of a marine ori-

[1]The projected 1990 fleet would support an annual traffic volume of 5.9×10^{12} passenger km if aircraft were assumed to fly at all times with a full complement of passengers. This figure may be compared with the present traffic of 4.4×10^{11} passenger km per year. It is assumed that the bulk of air transport in 1990 will be carried by current or improved versions of existing aircraft such as B747 and DC 10. The estimated NO_x emission rate adopted here for the 1990 fleet is 4.3×10^7 molecules cm^{-2} s^{-1} and it is distributed over the height range 16–21 km.

[2]The analysis given here is not sufficiently precise to allow a quantitative estimate for O_3 reduction at any particular latitude. The estimates in Fig. 4 should be useful at all latitudes. The reduction factor at high latitudes may be somewhat smaller than given here. The reduction at equatorial latitudes could be a little larger than the mean estimates derived in the present analysis.

[3]We assume here, as justified below, that HCl is the major form of gaseous atmospheric chlorine.

Can. J. Chem. Downloaded from www.nrcresearchpress.com by 210.87.254.6 on 09/05/12
For personal use only.

gin for gaseous atmospheric chlorine. Under quiet wind conditions the mixing ratio of gaseous chlorine in marine air is relatively constant with a value between 1.2 and 2.4 $\times 10^{-9}$. Strong variations in the gaseous mixing ratio were observed as the surface wind speed increased above about 20 knots. The increase in gas phase chlorine was accompanied by a slight decrease in the Cl:Na observed in the particulate phase, and Chesselet *et al.* (25) estimated that approximately 3% of the chlorine initially present in the particulate phase was eventually released as gas. This figure implies a net global production of gaseous chlorine equal to about 2×10^8 tons per year when combined with the estimate (25) of 6×10^9 tons per year for the total quantity of particulate chlorine injected into the atmosphere, mainly by bubbling at the sea surface (27). This production may be compared with the source from volcanoes estimated to be approximately 9×10^6 tons per year (28). Gaseous chlorine production associated with industrial activity, mainly HCl, can be estimated in various ways to give approximately 10^7 tons per year, a source strength comparable to the volcanic mechanism but small compared with marine aerosols.

Earlier objections by Valach (29) to the hypothesis of marine origin were effectively answered by Duce (23). Valach argued that the observed deficit of chlorine in the particulate form was not sufficient to account for the rather large concentrations of gaseous chlorine observed. The apparent contradiction is readily resolved. The lifetime for the gaseous component is much longer than that for the particulate form. Thus even a small efficiency, 3%, for the conversion from particle to gas is sufficient to account for comparable abundances of chlorine in the separate phases of the atmosphere. This matter is discussed further by Buat-Menard (26), Buat-Menard and Chesselet (24), and Chesselet *et al.* (25).

Mechanisms for production of gaseous chlorine from marine particles are discussed by Robbins *et al.* (30) and by Eriksson (28). Robbins *et al.* believed that atmospheric NO_2 could be hydrolyzed in the vapor phase to form HNO_3, with the latter dissolving in sea salt particles, lowering the pH of the particles, and subsequently releasing HCl. Eriksson also favored HCl as the gaseous product but thought that SO_3 was a more likely candidate than HNO_3 as the absorbed species responsible for the necessary reduction in the pH of the particles. The precise mechanism remains unclear. Laboratory studies by Buat-Menard (26) leave little doubt, however, that gaseous chlorine is indeed produced when marine particles are exposed to common atmospheric air. Gaseous chlorine was not observed if procedures were implemented to eliminate gases such as SO_3 and H_2SO_4 in the air stream to which the particle sample was exposed.

If we adopt a mean value of 1.2×10^{-9} for the mixing ratio of gaseous atmospheric HCl, consistent with the preceding discussion, we can readily compute a mean value for the corresponding atmospheric lifetime. If we consider a net global HCl source of 2.2×10^8 tons per year, we estimate a mean lifetime of 9.5 days,[4] which may be compared with the empirical lifetime of 0.4 day derived by Chesselet *et al.* (25) over rural France. The two results can be reconciled if we assume that the major sink for HCl occurs over land and if we assume that only 15% of the land mass is effective as a sink for HCl. This figure might be reasonable if the sink involved a spatially variable minor component of the atmosphere. Ammonia could be a suitable candidate and reaction 13 might provide a plausible mechanism. Measurements by Junge (22), Georgii (31), and Breeding *et al.* (32) indicate that the concentration of NH_3 is indeed variable and suggest that the concentration over land may be significantly higher than marine values. Establishment by Kaplan (33) of a low upper limit (<0.08 p.p.b.) for NH_3 above Mont-Louis is consistent with the similar upper limit on HCl (<0.1 p.p.b.) near the tropopause determined by Farmer (34). Both constituents must have quite short lifetimes (~ 1 day) if the concentrations are to fall off so dramatically away from the near surface environment. Further work is required in order to elucidate the chlorine removal process. In particular we need data on the global distribution of HCl and NH_3, as well as measurements to define the efficiency of various soils as sinks for HCl. We may note, however, that the effective rate constant for reaction 13 need not be very large, 10^{-35} cm^6 s^{-1} would suffice, to account for the observed HCl loss; Mohnen has suggested that NH_4Cl aerosol formation is catalyzed by small ions and has ap-

[4]This lifetime presumes a scale height of 7 km for gaseous atmospheric chlorine. Junge's (22) Hawaiian data suggest that the actual scale height may be somewhat less, perhaps 3 km, and the derived lifetime should be lowered accordingly.

TABLE 1. Chlorine reactions[a]

Reaction No.	Rate expression	References and remarks	Reaction
1	$2.1 \times 10^{-11} \exp(-1037/T)$	Takas and Glass (63)	$OH + HCl \rightarrow H_2O + Cl$
2	$2 \times 10^{-11} \exp(-2164/T)$	Galante and Gislason (53) Westenberg and deHaas (64)	$Cl + H_2 \rightarrow HCl + H$
3	$1 \times 10^{-11} \exp(-1605/T)$	Benson *et al.* (47)	$H + HCl \rightarrow H_2 + Cl$
4	$1.88 \times 10^{-11} \exp(-3573/T)$	Wong and Belles (66)	$O + HCl \rightarrow OH + Cl$
5	1.84×10^{-11}	Clyne and Watson[c]	$Cl + O_3 \rightarrow ClO + O_2$
6	$1.6 \times 10^{-33} \exp(800/T)$	Widman and DeGraff (65) Hippler and Troe (55)	$Cl + Cl + M \rightarrow Cl_2 + M$
7	1.7×10^{-33}	Johnston *et al.* (37) Nicholas and Norrish (58)	$Cl + O_2 + M \rightarrow ClOO + M$
8	$1.3 \times 10^{-11} \exp(-1000/T)$	Clyne and White (49) Johnston *et al.* (37)	$ClOO + M \rightarrow Cl + O_2 + M$
9	$1.3 \times 10^{-12} \exp(-1150/T)$	Johnston *et al.* (37) Clyne and White (49) Clyne and Coxon (41)	$ClO + ClO \rightarrow ClOO + Cl$
10	1.44×10^{-12}	Johnston *et al.* (37)	$Cl + ClOO \rightarrow ClO + ClO$
11	1.5×10^{-10}	Johnston *et al.* (37)	$Cl + ClOO \rightarrow Cl_2 + O_2$
12	1.7×10^{-11}	Clyne and Watson[c]	$ClO + NO \rightarrow Cl + NO_2$
14[b]	2.2×10^{-3} 6.0×10^{-5} 2.4×10^{-6} 1.5×10^{-6}	Durie and Ramsay (39) Pannetier and Gaydon (38) Porter (40) Johnston *et al.* (37) Clyne and Coxon (41)	$ClO + h\nu \rightarrow Cl + O$
15[b]	2.0×10^{-7}, 1.9×10^{-8}, 0., 0.	Romand and Vodar (60) Myer and Samson (57)	$HCl + h\nu \rightarrow H + Cl$
16	5.3×10^{-11}	Bemand, Clyne, and Watson (42)	$O + ClO \rightarrow Cl + O_2$
17[b]	1.6×10^{-3}, 1.4×10^{-3} 1.3×10^{-3}, 1.3×10^{-3}	Gibson and Bayliss (54) Seery and Britton (61)	$Cl_2 + h\nu \rightarrow Cl + Cl$
22	5×10^{-32}	Johnston *et al.* (37) Net reaction	$ClO + ClO + M \rightarrow Cl_2 + O_2 + M$
23[b]	1.9×10^{-3}, 9.8×10^{-8}, 0., 0.	Johnston *et al.* (37)	$ClOO + h\nu \rightarrow Cl + O_2$
27	3.5×10^{-11}	Stedman *et al.* (62)	$H + Cl_2 \rightarrow HCl + Cl$
28	$1.36 \times 10^{-11} \exp(-1560/T)$	Niki and Weinstock (59) Clyne and Coxon (48)	$O + Cl_2 \rightarrow ClO + Cl$
30	0.	Assumed	$ClO + O_3 \rightarrow ClOO + O_2$
32	1×10^{-11}	Estimate	$H + ClO \rightarrow HCl + O$
34	1×10^{-11}	Estimate	$Cl + HO_2 \rightarrow HCl + O_2$
35	0.	Assumed	$ClOO + O_3 \rightarrow ClO + 2O_2$
37	$5 \times 10^{-11} \exp(-1791/T)$	Clyne and Walker (50) Davis, Braun, and Bass (52)	$Cl + CH_4 \rightarrow HCl + CH_3$

[a]All concentrations are assumed in units of cm^{-3}.
[b]Photolysis rates are 24 h means and are given at 50, 30, 15, and 0 km altitudes.
[c]Preliminary results communicated by R. T. Watson.

parently observed particle formation (see ref. 35). The NH_4Cl mechanism is consistent with Junge's (22) Hawaiian observations carried out at an elevation of 3 km. He found that the gaseous precursors of NH_4^+, NO_3^-, Cl^-, and SO_4^{2-} at 3 km were all reduced relative to their ground level values in proportions consistent with removal of NH_4Cl, NH_4NO_3, and $(NH_4)_2SO_4$.

It has been well known since the early work of Norrish and Neville (36) that gaseous chlorine can photosensitize recombination of O_3. A variety of reactions has been studied more recently and many of the important rate constants have been measured (see for example ref. 37). Chlorine compounds are also known to react with other important minor constituents of the atmosphere, such as CH_4, H_2, NO, and possibly N_2O. A summary of the various important reactions and rate constants is given in Table 1. In order to investigate their possible effect on atmospheric O_3, we consider a situation in which the mixing ratio of total chlorine has the value 10^{-9}, at all

Can. J. Chem. Downloaded from www.nrcresearchpress.com by 210.87.254.6 on 09/05/12
For personal use only.

Can. J. Chem. Downloaded from www.nrcresearchpress.com by 210.87.254.6 on 09/05/12
For personal use only.

altitudes. The consequent distribution of major chlorine compounds is shown in Fig. 5.

The major components are HCl and ClO, at least with the particular reaction scheme adopted here. The important source reactions for HCl are

[22] $$Cl + H_2 \rightarrow HCl + H$$

and

[23] $$Cl + CH_4 \rightarrow HCl + CH_3$$

The gas is removed by

[24] $$OH + HCl \rightarrow H_2O + Cl$$

Reaction of Cl with O_3 provides the dominant source of ClO:

[25] $$Cl + O_3 \rightarrow ClO + O_2$$

The major sinks are

[26] $$ClO + NO \rightarrow Cl + NO_2$$

[27] $$ClO + O \rightarrow Cl + O_2$$

and

[28] $$ClO + h\nu \rightarrow Cl + O$$

with [26] playing a major role in the troposphere and lower stratosphere. The rate for photolysis of ClO is not well known. The weak near u.v. absorption bands (4,0), (3,0), .., (0,0) were not included in the present analysis since the upper levels were apparently observed in emission by Pannetier and Gaydon (38) and there is no evidence for predissociation (see also ref. 39). We extrapolated data by Johnston *et al.* (37) and Porter (40) in order to estimate the contribution of longer wavelengths to the net photolysis rate. Despite these uncertainties, the results shown in Fig. 5 should be reasonably reliable. Photolysis of ClO makes only a minor contribution (< 10%) to the major chemical paths in the present model.

We omitted possible formation of OClO by the reaction

[29] $$ClO + O_3 \rightarrow OClO + O_2$$

The reaction is surely slow (*cf.* ref. 41) and would be followed by photolysis

[30] $$h\nu + OClO \rightarrow O + ClO$$

although there might be some net loss of odd oxygen by the relatively slow reaction (42)

[31] $$O + OClO \rightarrow O_2 + ClO$$

The dominant chlorine removal of odd oxygen, however, is provided by [27], and reactions involving ClOO and OClO most likely make no more than a small contribution to the total O removal rate. The radical ClOO is removed mainly by

[32] $$ClOO + M \rightarrow Cl + O_2 + M$$

with a small contribution due to photolysis

[33] $$ClOO + h\nu \rightarrow Cl + O_2$$

The possible effects of chlorine catalysis on atmospheric O_3 are summarized in Fig. 6. The results given here were obtained following the procedures described by McElroy *et al.* (15), modified to include the chlorine reactions in Table 1. Strengths of various loss processes for odd oxygen are shown in Fig. 7 for an assumed mixing ratio of 10^{-9}. Although effects of chlorine catalysis extend over a wide height range, their

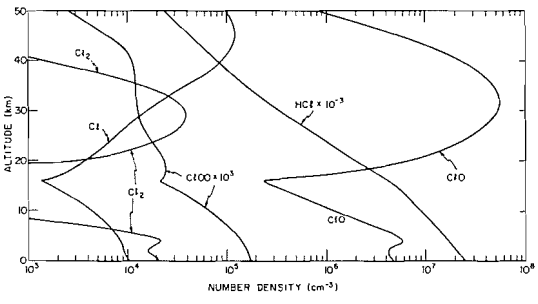

FIG. 5. The distribution of gaseous chlorine constituents is shown as a function of altitude in the troposphere and stratosphere. The total mixing ratio of all gaseous chlorine compounds has been arbitrarily set at $f = 1 \times 10^{-9}$ (v/v).

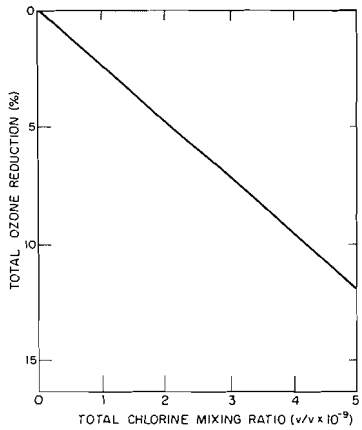

FIG. 6. Catalytic reduction of ozone is shown as a function of the mixing ratio for all forms of gaseous chlorine. The ozone reduction was calculated by the method of McElroy *et al.* (15).

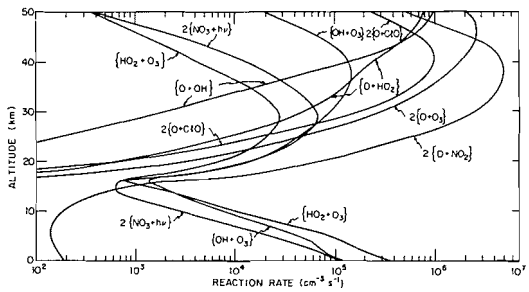

FIG. 7. Recombination of O and O_3 is shown in terms of the elementary reaction rates. The mixing ratio of total gaseous chlorine has been arbitrarily chosen as $f = 1 \times 10^{-9}$ (v/v).

influence is generally small compared with reactions 3 through 5. If one accepts Farmer's (34) upper limit for the mixing ratio of stratospheric HCl, 10^{-10}, and the results in Fig. 5 which indicate that HCl is the major chlorine compound, it would seem to follow that chlorine catalysis can at most play a minor role in the normal atmosphere. It should be emphasized, however, that the various sinks for HCl discussed here (reaction with NH_3, rain out, wash out, heterogeneous absorption) are effective only at low altitudes, below about 18 km. The space shuttle would provide a source of HCl which would extend to high altitudes, ~50 km, where natural sources of HCl are either very small or totally absent. The effects of such high altitude sources merit further study but cannot be reliably assessed until such time as the natural chlorine cycle is better established. We may note that the space shuttle could affect the stratospheric NO_x budget by increasing the effective loss rate of NH_3 through [13]. Reactions involving N_2O, for example

[34] $$Cl + N_2O \rightarrow ClO + N_2$$

are also possible though not established. Finally we note that chlorine from the shuttle could have an indirect influence if reactions such as 22 and 23 could provide a source of HO_x comparable to reactions 6 and 7 which control HO_x production in the normal atmosphere.

We may note in Fig. 7 the apparent importance of reactions

[35] $$HO_2 + O_3 \rightarrow OH + O_2 + O_2$$

and

[36] $$OH + O_3 \rightarrow HO_2 + O_2$$

as sinks for tropospheric odd oxygen. Elsewhere, Chameides and Walker (43) discussed a possible source of tropospheric odd oxygen through the reaction sequence

[37] $$HO_2 + NO \rightarrow OH + NO_2$$

[38] $$NO_2 + h\nu \rightarrow NO + O$$

followed by

[39] $$O + O_2 + M \rightarrow O_3 + M$$

The relative importance of the sources and sinks represented by [35] through [39] depends on the branching of HO_2 between reactions 35 and 37. Reactions 35 and 36 could provide a height integrated sink for tropospheric O_3 of about 2×10^{11} molecules cm^{-2} s^{-1}, comparable to the total flux of O_3 believed to emanate from the stratosphere (44, 45). As a consequence of the large rates for [35] and [36], the distribution of tropospheric O_3 may be directly affected by local chemistry. This conclusion, drawn earlier by Chameides and Walker (43) from a consideration of tropospheric source strengths, is in disagreement with conventional views which regard O_3 as a passive tracer, both in the lower stratosphere and troposphere.

NOTE ADDED IN PROOF: After completion of this work, we learned of a discussion of atmospheric chlorine by Stolarski and Cicerone which was in part presented at the IUGG meeting in Kyoto. Their article also appears in this issue of the Canadian Journal of Chemistry.

Nien Dak Sze made valuable contributions to the discussion of chlorine chemistry in this paper. We are indebted also to James Friend for a useful discussion and to Max Havlick for service beyond the call of duty in the preparation of this manuscript. The work was supported jointly by the Atmospheric Sciences Division of the National Science Foundation and the National Aeronautics and Space Administration under grant numbers GA 33990X and NGR 22-007-067 respectively to Harvard University.

Permission to reprint Figs. 1, 2, 3, and 4, which originally appeared in The Journal of the Atmospheric Sciences (ref. 15) is gratefully acknowledged.

1. P. J. CRUTZEN. Can. J. Chem. This issue.
2. M. NICOLET. Can. J. Chem. This issue.
3. S. CHAPMAN. Mem. R. Met. Soc. **3**, 103 (1930).
4. D. R. BATES and M. NICOLET. J. Geophys. Res. **55**, 301 (1950).
5. P. J. CRUTZEN. Q. J. R. Met. Soc. **96**, 320 (1970).
6. P. BATES and P. B. HAYS. Planetary Space Sci. **15**, 189 (1967).
7. M. B. MCELROY and J. C. MCCONNELL. J. Atmos. Sci. **28**, 1095 (1971).

Can. J. Chem. Downloaded from www.nrcresearchpress.com by 210.87.254.6 on 09/05/12
For personal use only.

8. M. NICOLET. Aeronomic reactions of hydrogen and ozone. *In* Mesospheric models and related experiments. Reidel, Dordrecht, Holland. 1971. pp. 1–51.
9. J. C. McCONNELL. J. Geophys. Res. **78**, 7812 (1973).
10. J. C. McCONNELL and M. B. McELROY. J. Atmos. Sci. **30**, 1465 (1973).
11. P. WARNECK. J. Geophys. Res. **77**, 6589 (1972).
12. M. A. RUDERMAN and J. W. CHAMBERLAIN. Origin of the sunspot modulation of ozone: its implication for stratospheric NO injection. Institute for Defense Analysis, JSS-73-18-3. 1973.
13. J. K. ANGELL. and J. KORSHOVER. Mon. Weather Rev. (1973). In press.
14. H. S. JOHNSTON. Astronaut. Acta (1973). In press.
15. M. B. McELROY, S. C. WOFSY, J. E. PENNER, and J. C. McCONNELL. J. Atmos. Sci. **31**, 287 (1974).
16. S. C. WOFSY and M. B. McELROY. J. Geophys. Res. **78**, 2619 (1973).
17. F. S. JOHNSON, J. D. PURCELL, R. TOUSEY, and K. WATANABE. J. Geophys. Res. **57**, 157 (1952).
18. W. S. HERING and T. R. BORDEN. Ozonesonde observations over North America, Vol. 4. Air Force Cambridge Res. Labs. Environ. Res. Papers. 1967.
19. E. HILSENRATH, L. SEIDEN, and P. GOODMAN, J. Geophys. Res. **74**, 6873 (1969).
20. A. J. KRUEGER, D. F. HEATH, and C. L. MATEER. Variations in the stratospheric ozone field inferred from Nimbus satellite observations. NASA preprint TM-X-66108. (NTIS-N73-12379). 1972.
21. A. J. BRODERICK, J. MORELEY ENGLISH, and A. K. FORNEY. American Institute of Aeronautics and Astronautics paper 73–508. 1973.
22. C. E. JUNGE. Tellus, **9**, 528 (1957).
23. R. A. DUCE. J. Geophys. Res. **74**, 4597 (1969).
24. P. BUAT-MENARD and R. CHESSELET. C.R. Acad. Sci. Paris, **272**, 1330 (1971).
25. R. CHESSELET, J. MORELLI, and P. BUAT-MENARD. Some aspects of the geochemistry of marine aerosols. *In* The changing chemistry of the oceans. Wiley Interscience, New York. 1972. pp. 93–114.
26. P. BUAT-MENARD. Thesis, University of Paris, Paris, France. 1970.
27. D. C. BLANCHARD. The electrification of the atmosphere by particles from bubbles in the sea. *In* Oceanography. *Edited by* M. Sears. Pergamon Press, Oxford. 1963.
28. E. ERIKSSON. Tellus, **11**, 63 (1960).
29. R. VALACH. Tellus, **19**, 509 (1967).
30. R. C. ROBBINS, R. D. CADLE, and D. L. ECKHARDT. J. Meterol. **16**, 53 (1959).
31. H. W. GEORGII. J. Geophys. Res. **68**, 3963 (1963).
32. R. J. BREEDING, J. P. LODGE, J. B. PATE, D. C. SHEESLEY, H. B. KLONIS, B. FOGLE, J. A. ANDERSON, T. R. ENGLERT, P. L. HAAGENSON, R. B. McBETH, A. L. MORRIS, R. POGUE, and A. F. WARTBURG. J. Geophys. Res. **78**, 7057 (1973).
33. L. D. KAPLAN. Pure Appl. Geophys. **106–108**, 1341 (1973).
34. C. B. FARMER. Can. J. Chem. This issue.
35. C. S. KIANG, D. STAUFFER, and V. A. MOHNEN. Nat. Phys. Sci. **244**, 53 (1973).
36. R. G. W. NORRISH and G. H. J. NEVILLE. J. Chem. Soc. 1864 (1934).
37. H. S. JOHNSTON, E. D. MORRIS, and J. VAN DER BOGAERDE. J. Am. Chem. Soc. **91**, 7712 (1969).
38. G. PANNETIER and A. G. GAYDON. Nature, **161**, 242 (1948).
39. R. A. DURIE and P. A. RAMSEY. Can. J. Phys. **36**, 35 (1958).
40. G. PORTER. Disc. Farad. Soc. **9**, 63 (1950).
41. M. A. A. CLYNE and J. A. COXON. Proc. R. Soc. A, **303**, 207 (1968).
42. P. P. BEMAND, M. A. CLYNE, and R. T. WATSON. J. Chem. Soc. Farad. Trans. I, **69**, 1356 (1973).
43. W. CHAMEIDES and J. C. G. WALKER. J. Geophys. Res. (1973). In press.
44. H. U. DÜTSCH. Doctoral thesis, Zürich. 1946.
45. P. FABIAN and C. E. JUNGE. Arch. Met. Geoph. Biokl. Ser. A, **19**, 161 (1970).
46. N. BASCO and S. K. DOGRA. Proc. R. Soc. A, **323**, 29, 401, 417 (1971).
47. S. W. BENSON, F. R. CRUICKSHANK, and R. SHAW. Int. J. Chem. Kin. **1**, 29 (1969).
48. M. A. A. CLYNE and J. A. COXON. Trans. Farad. Soc. **62**, 2175 (1966).
49. M. A. A. CLYNE and I. F. WHITE. Trans. Farad. Soc. **67**, 2068 (1971).
50. M. A. A. CLYNE and R. F. WALKER. J. Chem. Soc. Farad. Trans. I, **69**, 1547 (1973).
51. J. A. COXON. Trans. Farad. Soc. **64**, 2118 (1968).
52. D. D. DAVIS, W. BRAUN, and A. M. BASS. Int. J. Chem. Kin. **2**, 101 (1970).
53. T. J. GALANTE and E. A. GISLASON. Chem. Phys. Lett. **18**, 231 (1973).
54. G. E. GIBSON and N. S. BAYLISS. Phys. Rev. **44**, 188, 193 (1933).
55. H. HIPPLER and J. TROE. Chem. Phys. Lett. **19**, 607 (1973).
56. C. E. JUNGE. Tellus, **8**, 127 (1956).
57. J. A. MYER and J. A. R. SAMSON. J. Chem. Phys. **52**, 266 (1970).
58. J. E. NICHOLAS and R. G. W. NORRISH. Proc. R. Soc. A, **307**, 391 (1968).
59. H. NIKI and B. WEINSTOCK. J. Chem. Phys. **47**, 3249 (1967).
60. J. ROMAND and B. VODAR. C. R. Acad. Sci. **226**, 238 (1948).
61. D. J. SEERY and D. BRITTON. J. Phys. Chem. **68**, 2263 (1964).
62. D. STEDMAN, H. D. STEFFENSON, and H. NIKI. Chem. Phys. Lett. **7**, 173 (1970).
63. G. A. TAKAS and G. P. GLASS. J. Phys. Chem. **77**, 1948 (1973).
64. A. A. WESTENBERG and N. DE HAAS. J. Chem. Phys. **48**, 4405 (1968).
65. R. P. WIDMAN and B. A. DEGRAFF. J. Phys. Chem. **77**, 1325 (1973).
66. E. L. WONG and F. E. BELLES. Rate measurements for the reaction of hydrogen chloride and deuterium chloride with atomic oxygen. NASA Technical Note TN D-6495. 1971.
67. C.-H. WU and H. S. JOHNSTON. Bull. Soc. Chim. Belg. **81**, 135 (1972).

Can. J. Chem. Downloaded from www.nrcresearchpress.com by 210.87.254.6 on 09/05/12
For personal use only.

Reduction of Stratospheric Ozone from High-flying Aircraft, Studied in a Two-dimensional Photochemical Model with Transport

EIGIL HESSTVEDT

Institute of Geophysics, University of Oslo, Blindern, Oslo 3, Norway

Received October 3, 1973

A steady state two-dimensional model of the stratospheric ozone layer is presented. Chemical reactions involving oxygen, hydrogen, and nitrogen are considered along with the effect of a parameterized, two-dimensional transport, by mean motion and by eddies. The model is in reasonable agreement with observed ozone data. The reduction of ozone from emission of NO_x from high flying aircraft is studied, assuming a fleet of 500 supersonic aircraft in transatlantic operation, flying at given altitudes. The effect is found to depend critically upon flight level. For mid-latitude, summer, the ozone column density is reduced by 0.3% for a flight level of 18 km. For flight levels of 23 and 28 km the reduction is 2 and 5%, respectively. Accordingly, the increase in u.v. radiation amounts to approximately 0.6, 4, and 10% for the same flight levels.

Un modèle bidimensionnel d'une couche d'ozone stratosphérique est présenté à l'état stationnaire. Des réactions chimiques impliquant l'oxygène, l'hydrogène et l'azote sont examinées en même temps que l'influence d'un transport bidimensionnel à paramètres, par mouvement moyen et par turbulences. Le modèle est en accord acceptable avec les données observées de l'ozone. Considérant une flotte de 500 avions supersoniques en opération transatlantique, volant à une altitude donnée, la réduction de l'ozone à partir d'émission de NO_x émanant d'avions à haute altitude est examinée. L'influence dépend essentiellement du niveau du vol. Pour la mi-latitude, en été, la densité de la colonne d'ozone diminue de 0.3% pour un niveau de vol de 18 km. Pour des niveaux de vol de 23 et 28 km la diminution est respectivement de 2 et 5%. En conséquence, l'augmentation des radiations u.v. s'élève approximativement à 0.6, 4 et 10% pour les mêmes niveaux de vol. [Traduit par le journal]

Can. J. Chem., **52**, 1592 (1974)

Introduction

The magnitude of the effect of future supersonic flights upon the ozone layer has been vigorously debated over the last 2 or 3 years. The opinions cover a wide spectrum from "a negligible effect" to "catastrophe". The present study indicates that the effect lies between these two extremes and depends very strongly upon the flight level. For aircraft of the same category as the "Concorde", with a cruising altitude of 18 km or lower, the ozone reduction is likely to be only a few tenths of a per cent. However, the effect increases very rapidly with increasing flight level. Although no immediate danger seems to exist, the long term effect of increased u.v. radiation may be considerable if bigger aircraft fly at higher altitudes than say 20 km.

One way to approach the problem is to use photochemical models. Since the lifetime of ozone is comparable to or longer than the characteristic time for atmospheric transport, such models must also include transport processes to give realistic results for the lower part of the ozone layer, *i.e.* below about 25 km. The model presented here is an extension of a more simplified model presented earlier this year (1). In that model odd nitrogen (NO_y) profiles were computed from one-dimensional models. Horizontal transport of NO_y was disregarded; this made the model less suitable for studies of the effect of NO_x emissions from aircraft. Only one case, and certainly an unrealistic one, could be studied, namely a uniform distribution over the globe of all supersonic routes. In the present model nitrogen compounds, as well as ozone, are allowed to move vertically and horizontally with the prescribed, parameterized transport. This makes it possible to study a variety of cases; only one is reported here, 500 aircraft are assumed to fly zonally at 50° latitude, at heights of 18, 23, and 28 km, respectively.

Two-dimensional Transport Model

The stratospheric model presented here is a two-dimensional steady state model with transport. Four versions of the model are computed:

Can. J. Chem. Downloaded from www.nrcresearchpress.com by 210.87.254.5 on 09/05/12
For personal use only.

Can. J. Chem. Downloaded from www.nrcresearchpress.com by 210.87.254.5 on 09/05/12
For personal use only.

two sets of transport data are used, and for each set models are computed for summer and winter conditions. The models range from the Equator to the Pole and from the tropopause up to 35 km. The differentials in the analytical expressions for the transport are replaced by finite differences. The distance between the grid points in the model is 1 km vertically and 5° latitude horizontally. A relaxation method is applied to compute steady state solutions.

Standard profiles are used for temperature and density (2). The parameterized transport in the model is based upon data given by Gudiksen *et al.* (3). Their data for the vertical eddy diffusion coefficient K_{zz} have been modified, mainly in the upper part (4, 5). The K_{zz} profiles used in the present model are given in Fig. 1.

Gudiksen's data, with the modified K_{zz}, have been used below to compute the meridional ozone distribution for winter and summer. The results are shown in Fig. 2. It is readily seen that this model (model B) suffers from a serious deficiency, since it fails to reproduce an ozone layer in high latitudes. A closer agreement with observed ozone distribution requires a faster transport than given by Gudiksen *et al.* This is true, in particular, for horizontal transport. In order to reproduce a realistic ozone distribution it was decided to use a modification of Gudiksen's data: all data for K_{yy} and K_{yz} were multiplied by 8, while w was multiplied by 2. This brings the transport data into better agreement with earlier data (6). The ozone distributions obtained from these modified data will be referred to below as model A. The resulting ozone distribution is shown in Fig. 3. Although the ozone values are on the whole on the high side, the theoretical distribution is now in much better agreement with the observed data.

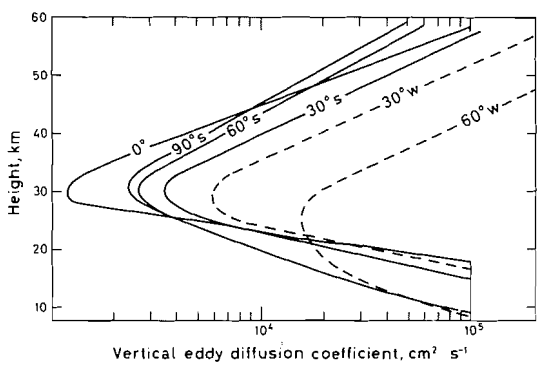

FIG. 1. Profiles of vertical eddy diffusion coefficient.

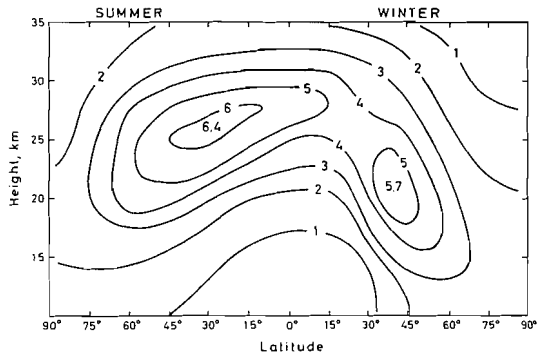

FIG. 2. Theoretical ozone distribution (units: 10^{12} cm^{-3}), model B, based on transport data from Gudiksen *et al.*

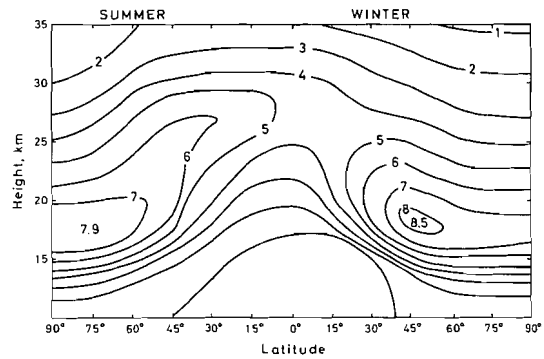

FIG. 3. Theoretical ozone distribution (units: 10^{12} cm^{-3}), model A, based on a modification of the data used in model B.

Ozone Photochemistry

The boundary conditions for ozone are as follows. At 35 km photochemical equilibrium is assumed. Data for the column density of ozone above 35 km are taken from time dependent photochemical models for the region 35–70 km recently computed by the author (unpublished). The data are given in Table 1. At the tropopause a constant value of 10^{12} cm^{-3} is taken for the ozone number density. The models are extended 5° into the opposite hemisphere, and values computed for 5° latitude, winter, are used at the boundary in the summer model, and vice versa for the winter model. Over the Pole the horizontal flux of ozone is taken to be zero.

The photochemical reactions included in our model are specified in Table 2. Other reactions were also considered, but were found to be of little importance for the present model. Recent data for reaction rates are used; most of them are taken from Chemical kinetics data

TABLE 1. Number densities of ozone ($\times 10^{-12}$ cm^{-3}) at 35 km and column density of ozone above 35 km ($\times 10^{-18}$ cm^{-2})

	Summer					Winter		
	90°	60°	45°	30°	0°	30°	45°	60°
$[O_3]$ ($\times 10^{-12}$)	1.60	1.96	2.34	2.44	2.22	1.59	1.38	0.67
Column density ($\times 10^{-18}$)	1.03	1.08	1.14	1.21	1.15	0.86	0.75	0.48

TABLE 2. Reactions and reaction rate coefficients

Reaction No.	Reaction	Rate constant
1	$O(^3P) + O_2 + M \rightarrow O_3 + M$	$k_1 = 1.07 \times 10^{-34} \exp(510/T)$
2	$O(^3P) + O_3 \rightarrow 2O_2$	$k_2 = 1.9 \times 10^{-11} \exp(-2300/T)$
3	$O_2 + h\nu \rightarrow O(^3P) + O(^3P)$	$175 \text{ nm} < \lambda < 242.4 \text{ nm}$
4	$O_2 + h\nu \rightarrow O(^3P) + O(^1D)$	$\lambda < 175$ nm
5	$O_3 + h\nu \rightarrow O(^3P) + O_2$	$\lambda > 310$ nm
6	$O_3 + h\nu \rightarrow O(^1D) + O_2$	$\lambda < 310$ nm
7	$OH + O(^3P) \rightarrow H + O_2$	$k_7 = 4.2 \times 10^{-11}$
8	$HO_2 + O(^3P) \rightarrow OH + O_2$	$k_8 = 7 \times 10^{-11}$
9	$H + O_2 + M \rightarrow HO_2 + M$	$k_9 = 2.08 \times 10^{-32} \exp(290/T)$
10	$H + O_3 \rightarrow OH + O_2$	$k_{10} = 2.6 \times 10^{-11}$
11	$OH + HO_2 \rightarrow H_2O + O_2$	$k_{11} = 2 \times 10^{-10}$
12	$H_2O_2 + h\nu \rightarrow 2OH$	$187.5 \text{ nm} < \lambda < 382.5 \text{ nm}$
13	$HO_2 + HO_2 \rightarrow H_2O_2 + O_2$	$k_{13} = 3 \times 10^{-11} \exp(-500/T)$
14	$OH + H_2O_2 \rightarrow H_2O + HO_2$	$k_{14} = 1.7 \times 10^{-11} \exp(-910/T)$
15	$H_2O + h\nu \rightarrow OH + H$	$135 \text{ nm} < \lambda < 237.5 \text{ nm}$
16	$O(^1D) + M \rightarrow O(^3P) + M$	$k_{16} = 5.9 \times 10^{-11}$
17	$O(^1D) + H_2 \rightarrow OH + H$	$k_{17} = 2.9 \times 10^{-10}$
18	$HO_2 + O_3 \rightarrow OH + 2O_2$	$k_{18} = 10^{-13} \exp(-1250/T)$
19	$OH + O_3 \rightarrow HO_2 + O_2$	$k_{19} = 1.6 \times 10^{-12} \exp(-1000/T)$
20	$O(^1D) + H_2O \rightarrow 2OH$	$k_{20} = 3.5 \times 10^{-10}$
21	$H_2 + OH \rightarrow H_2O + H$	$k_{21} = 10^{-10} \exp(-2950/T)$
22	$O(^1D) + O_3 \rightarrow 2O_2$	$k_{22} = 5 \times 10^{-10}$
23	$HO_2 + h\nu \rightarrow OH + O(^3P)$	
24	$CO + OH \rightarrow H + CO_2$	$k_{24} = 2.1 \times 10^{-13} \exp(-115/T)$
25	$NO + HO_2 \rightarrow OH + NO_2$	$k_{25} = 2 \times 10^{-13}$
26	$NO + O_3 \rightarrow NO_2 + O_2$	$k_{26} = 9 \times 10^{-13} \exp(-1200/T)$
27	$NO_2 + h\nu \rightarrow NO + O$	$J_{NO_2} = 6.5 \times 10^{-3}$
28	$NO_2 + O \rightarrow NO + O_2$	$k_{28} = 9.12 \times 10^{-12}$
29	$HNO_3 + h\nu \rightarrow HO_2 + NO$	$\lambda < 370$ nm
30	$HNO_3 + h\nu \rightarrow OH + NO_2$	$370 \text{ nm} < \lambda < 546 \text{ nm}$
31	$OH + HNO_3 \rightarrow H_2O + NO_3$	$k_{31} = 1.7 \times 10^{-11} \exp(-1650/T)$
32	$N_2O + h\nu \rightarrow N_2 + O$	$\lambda < 390$ nm
33	$N_2O + O(^1D) \rightarrow NO + NO$	$k_{33} = 9 \times 10^{-11}$
34	$OH + NO_2 + M \rightarrow HNO_3 + M$	$k_{34} = 1.05 \times 10^{-11} \exp(-170/T) \cdot f$ where $f = 4 \times 10^{-11}/(4 \times 10^{-11} \cdot [M] + 10^{13}/(1 + 5000/T)^4)$

survey IV (7). Computations of dissociation rates are based upon Ackerman's data for the solar flux and absorption cross sections for O_2 and O_3 (8).

It is now well established that the net destruction of ozone below 40 km is mainly due to reactions between nitrogen oxides and odd oxygen (9)

$$NO + O_3 \rightarrow NO_2 + O_2$$

$$NO_2 + O \rightarrow NO + O_2$$

Together with photodissociation of NO_2, whereby NO and O are reformed, these reactions form a cycle within which the internal equilibrium between NO and NO_2 is quickly established (characteristic time ~ 100 s). If their sum, often

Can. J. Chem. Downloaded from www.nrcresearchpress.com by 210.87.254.5 on 09/05/12
For personal use only.

Can. J. Chem. Downloaded from www.nrcresearchpress.com by 210.87.254.5 on 09/05/12
For personal use only.

denoted by NO_x, is known, the number densities of these two components are approximately given by

$$[3.1]\quad [NO_2] = k_{26}[O_3][NO_x]/(k_{26}[O_3] + k_{28}[O] + J_{NO_2}$$

$$[3.2]\quad [NO] = [NO_x] - [NO_2]$$

The net destruction of odd oxygen from reactions 26 to 28 is

$$[3.3]\quad 2k_{28}[NO_2][O]$$

To a first approximation, the net rate of change of ozone (or, to be exact, of odd oxygen) is given by

$$[3.4]\quad \frac{\partial[O_3]}{\partial t} \approx 2J_2[O_2] - 2k_{28}[NO_2][O]$$

where $[NO_2]$ is expressed above as a function of $[NO_x]$, and [O] is given by

$$[3.5]\quad [O] = J_3[O_3]/k_1[M][O_2]$$

This gives for the photochemical equilibrium value of ozone

$$[3.6]\quad [O_3]_e \approx \frac{J_2[O_2]\cdot k_1[M][O_2]}{k_{28}[NO_2]J_3}$$

In combination with [3.1], the expression [3.6], although simplified, demonstrates how theoretical values of ozone are influenced by uncertainties in the reaction rate coefficients k_1, k_{26}, k_{28}, J_2, and J_3. But perhaps the most uncertain parameter is $[NO_x]$. Since $[O_3]$ is inversely proportional to this quantity, accurate knowledge of its distribution in space is essential.

The main source of NO_x in the stratosphere is destruction of N_2O through the reaction

$$N_2O + O(^1D) \rightarrow NO + NO$$

N_2O is of terrestrial origin. It has a relatively long lifetime and the rapid mixing in the troposphere ensures a constant mixing ratio in this part of the atmosphere. In our model the tropospheric value, assumed to be 2.5×10^{-7}, is taken for the N_2O mixing ratio at the lower boundary (the tropopause). Upward diffusion of N_2O also takes place in the stratosphere, but here the mixing is much slower and competes with photodissociation and with the reaction with $O(^1D)$ mentioned above. The odd nitrogen, NO_y ($NO + NO_2 + HNO_3$), which is initially produced by the latter reaction by the formation of NO, is distributed on the components HNO_3 (~70%), NO_2 (~20%), and NO (~10%).

Vertical profiles of the NO_y mixing ratio are given in Fig. 4 for different latitudes, summer and winter. In the part of the stratosphere which is of immediate interest to us here, the latitudinal variations are small, but by no means negligible (within about 25% from the mean for each level).

As we go to greater heights, HNO_3 is destroyed, mainly through photodissociation and reaction with OH. At the upper boundary of our model there is only little HNO_3 left. The distribution of NO_y upon the three components HNO_3, NO_2, and NO, is shown in Fig. 5, for 60° and 30°, summer.

From the profiles of NO_y shown in Fig. 4, one may compute vertical distributions of NO_x, NO_2, and NO. A most useful check on the validity of the nitrogen chemistry in stratospheric models could be made if measurements of NO_2 and NO and their distributions in space were

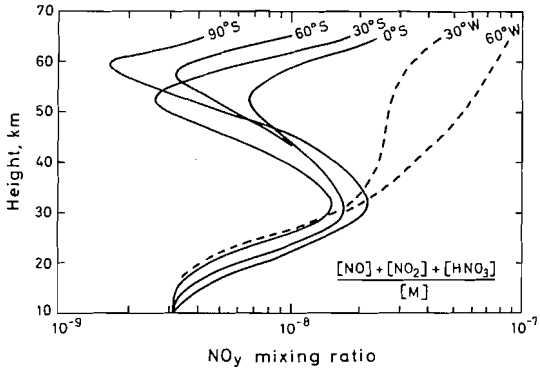

FIG. 4. Vertical profiles of the NO_y mixing ratio.

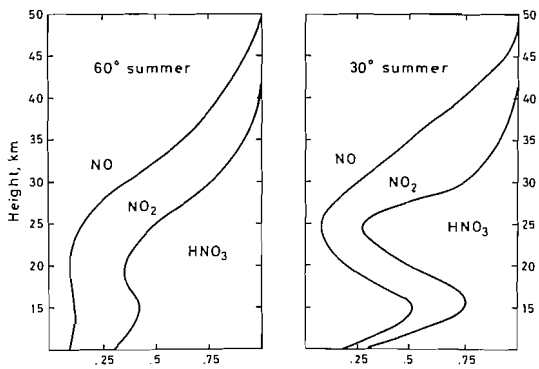

FIG. 5. Distribution of NO, NO_2, and HNO_3 in total NO_y normalized to unity.

Can. J. Chem. Downloaded from www.nrcresearchpress.com by 210.87.254.5 on 09/05/12
For personal use only.

available. Ackerman and Muller (10) have interpreted the NO_2 measurements of Ackerman and Frimont (11) and Goldman *et al.* (12). Our computations are in reasonable agreement with their results, the only difference being that our maximum is found 2 km higher (the peak value is very close to the observed one, 8×10^{-9} for the NO_2 mixing ratio) and that our minimum at about 20 km is less pronounced. It should, however, be remembered that the observation was made for solar zenith angles larger than 91°. It is therefore not unlikely that the observed distribution of NO_2 is indicative of the daytime distribution of NO_x, rather than NO_2. As already mentioned, the characteristic time for conversion of NO to NO_2 is short (≤ 110 s). This is demonstrated in Fig. 6, where the lifetime of NO and the abundance of NO (given as $[NO]/[NO_x]$) is plotted against solar zenith angle. Just before sunset the equilibrium number density of NO drops to very low values, and in view of the short lifetime, the time lag must be of secondary importance. Hence one can hardly use observations of NO, performed at low sun, as an indication of daytime NO.

We shall now return to the ozone modeling. It is of great interest to consider the lifetimes of the components in the model. It has been found that $O(^1D)$, $O(^3P)$, H, and OH have very short lifetimes in the ozone layer: for $O(^1D)$ it is less than 2×10^{-7} s, for $O(^3P)$ less than 0.2 s, for H less than 2×10^{-3} s, and for OH less than 20 s, all for daytime conditions. Photochemical equilibrium is thus a good approximation for these components, which, like NO, all vanish at night.

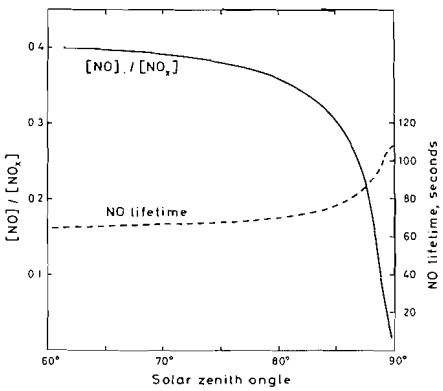

FIG. 6. Lifetime and decay of NO as a function of solar zenith angle.

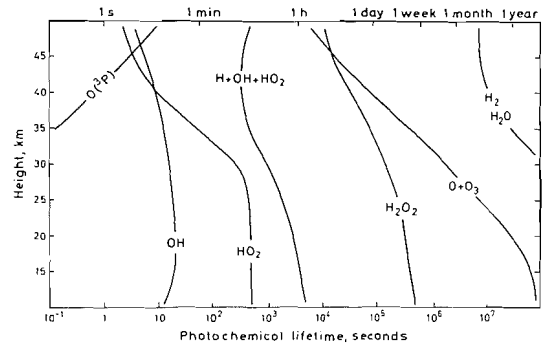

FIG. 7. Lifetimes of oxygen and hydrogen components, daytime conditions, 45°, summer.

The lifetimes of O_2, H_2, and H_2O are many years in the lower stratosphere (see Fig. 7). We may therefore assume that these components are mixed and take 0.2095, 5×10^{-7}, and 5.5×10^{-6}, respectively, for their mixing ratios.

HO_2 is in rapid exchange with H and OH. In the computations it is convenient to consider the sum (odd hydrogen) of these three components, which has a lifetime of 1 hour or less. The assumption of photochemical equilibrium for daytime conditions is accordingly a fair approximation. The lifetime of H_2O_2 is less than 4 days in the region 10–35 km. The photochemistry is therefore faster than the transport, and photochemical equilibrium gives sufficient accuracy for our problem.

In the computations, of course, complete expressions for loss and production are applied. Equation 3.4 represents a simplification of the ozone photochemistry. The complete loss terms contain a long series of reactions, most of which are of little importance. Beside reaction 28 only three of them, reactions 2, 18, and 19 in Table 2, contribute significantly. At levels where the photochemistry of ozone is not dominated by the transport, *i.e.* above about 25 km, approximately 20% of the total loss is through these three reactions.

The nighttime chemistry of ozone is very slow in the ozone layer and may be neglected in comparison to the daytime photochemistry. This simplifies the computations considerably.

Theoretical Ozone Distribution

The computed steady state distributions of ozone, for summer and winter, are shown in Figs. 2 and 3. A comparison of theoretical and

TABLE 3. Reduction (in %) of total ozone above 10 km, resulting from a fleet of 500 SST in transatlantic traffic

Model	Flight level (km)	Latitude, summer					Latitude, winter			
		75°	60°	45°	30°	15°	15°	30°	45°	60°
A	18	0.3	0.3	0.3	0.2	0.1	←	≪0.1	→	
	23	2.5	2.2	1.7	1.2	0.6	←	0.1	→	
	28	6.0	5.7	4.3	2.8	1.6	0.4	0.55	0.55	0.55
B	18	1.0	0.8	0.6	0.3	0.1				
	23	5.9	5.7	4.4	1.8	0.6				

observed ozone distribution seems to support the conclusion that our model is a plausible simulation of the processes which determine the mean ozone distribution in the real stratosphere.

As already mentioned, model B, which is based upon the data of Gudiksen *et al.*, gives too little ozone in high latitudes. A stronger poleward transport seems to be needed to produce a high-latitude ozone layer with a peak at 18 km. In model A all data for K_{yy} and K_{yz} are multiplied by 8, while w is multiplied by 2. This brings the theoretical distribution into much better agreement with observations, in particular in the summer hemisphere. However, the model gives, in general, too high ozone values. A third model has been computed, where Gudiksen's data for K_{yy} and K_{yz} were multiplied by 8, while w was kept unchanged. This lowered the high-latitude peak values from 7.9×10^{12} to 6.6×10^{12} cm^{-3} for the summer, and from 8.5×10^{12} to 6.5×10^{12} cm^{-3} for the winter. As far as ozone is concerned, this gives an even more realistic distribution than model A.

The photochemical lifetime of ozone increases rapidly with decreasing height. For 45°, summer, it is 4 days at 35 km, $2\frac{1}{2}$ weeks at 30 km, $2\frac{1}{2}$ months at 25 km, 10 months at 20 km, and 2 years at 10–15 km. Atmospheric transport therefore becomes increasingly important as we descend through the stratosphere. In the upper part of the model (30–35 km), ozone is nearly in photochemical equilibrium, while below about 22 km the chemistry is dominated by transport. Arguments about the influence of SST upon the ozone layer have very often been based upon purely photochemical models without the consideration of transport. From what is said above, such models are quite unrealistic. Conclusions drawn from such models should be appraised with scepticism.

Effect of Supersonic Transport upon the Ozone Layer

The model described above may be used to estimate the effect of emission of NO_x from high-flying aircraft upon the ozone layer. Since values for the NO_x emission per unit weight of fuel are now available, a realistic prognosis for future traffic density and routing would make it possible to compute the perturbations in the NO_x distribution and, as a consequence, the decrease in ozone column density as a function of latitude and season. A computation along this line is presented here.

The basis for our computation is: A reference fleet of 500 four-engine aircraft of the Concorde type is considered, each performing 3 flights of $2\frac{1}{2}$ h per day. The fuel flow is assumed to be 5.000 kg/h per engine. The emission of NO_x (converted to NO_2) is assumed to be 18.6 g/kg fuel. We shall further assume that all these aircraft operate on transatlantic routes. This is simulated in our model by the introduction of a "point" source (width 5° latitude and height 1 km) at 50° latitude. Computations are made for three different flight levels, 18, 23, and 28 km, respectively. The ozone distributions thus obtained differ very little from the unperturbed distribution (shown in Fig. 3), the difference being of the order of a few per cent or less. The results are given in Table 3. It will be seen that the effect of supersonic traffic upon stratospheric ozone is small in the winter. The meridional transport is very fast and the excess NO_x is transported polewards before it can diffuse up to the "sensitive zone" above about 22 km. In the summer the poleward transport is much slower, and the emitted NO_x has time to diffuse to heights where it can affect the ozone. In this connection, it is very important to remember that the influence of NO_x may be small at the

Can. J. Chem. Downloaded from www.nrcresearchpress.com by 210.87.254.5 on 09/05/12
For personal use only.

level where it is emitted, since the ozone chemistry here is very slow. A significant effect will occur when NO_x has time to diffuse to greater heights. The ozone reduction at these heights will then, in turn, affect the ozone distribution at lower levels through transport.

Even in summer the effect of stratospheric flights is found to be small for flight levels up to 18 km. Most of the emitted NO_x will then be transported downwards and lost to the troposphere. It should, however, be remembered that our result depends to some extent on the data used for the vertical mixing (see Fig. 1). As we go to higher flight levels, the situation rapidly becomes more serious. For a flight level of 23 km, ozone is reduced by about 2% (5% for model B), and for a flight level of 28 km the reduction is 5% for model A. Thus our computations indicate that the choice of flight level for possible future supersonic transport is of the greatest importance.

The figures given for ozone reduction may be converted to increase in erythemogenic u.v. radiation (13) by multiplying by 2: accordingly, for model A the increase in u.v. radiation is found to be 0.6, 4, and 10% for flight levels of 18, 23, and 28 km respectively. It appears from our computations that the emitted NO_x to a certain extent is accumulated in the stratosphere during the summer, but is transported away during the winter. The time available for building up a significant NO_x perturbation is therefore long, but not infinitely long. The values given in Table 3 may thus be overestimates. The effect of the cutoff in NO_x accumulation during the winter is now being studied in a time-dependent model. The results of these computations will be available later this year.

The author thanks Dr. Ivar S. A. Isaksen for valuable discussions. Part of the work reported here is supported by NASA under contract: NGR 52–155–002.

1. E. HESSTVEDT. Proceedings of the AGARD Conference on Atmospheric Pollution by Aircraft Engines, London, April 9–13, 1973. AGARD-CP-125.
2. A. E. COLE, A. COURT, and A. J. KANTOR. Handbook of geophysics and space environments. *Edited by* S-L. Valley. Air Force Cambridge Research Laboratories, Bedford, Mass. 1965.
3. P. H. GUDIKSEN, A. W. FAIRHALL, and R. J. REED. J. Geophys. Res. **73**, 4461 (1968).
4. I. S. A. ISAKSEN. Geofys. Publ. **30**, 2 (1973).
5. I. S. A. ISAKSEN and E. HESSTVEDT. NASA Contract Report (NASA CR-2314, August 1973).
6. R. J. REED and K. E. GERMAN. Mon. Weather Rev. **93**, 313 (1965).
7. D. GARVIN. (*Editor*). Chemical kinetics data survey IV, NBSIR-203. National Bureau of Standards, Washington, D.C. May 1973.
8. M. ACKERMAN. Mesospheric models and related experiments. *Edited by* G. Fiocco. D. Reidel Publ. Co., Dordrecht, Holland. 1971.
9. E. HESSTVEDT. Proceedings of the Second Conference on CIAP. November 14–17, 1972. *Edited by* A. J. Broderick. U.S. Dept. of Transportation. DOT-TSC-OST-73-4.
10. M. ACKERMAN and C. MULLER. Aeron. Acta, A, No. 106, 1972.
11. M. ACKERMAN and D. FRIMONT. Acad. R. Belg. Bull. Classe Sci. (Bruxelles), **55**, 948 (1969).
12. A. GOLDMAN, D. G. MURCRAY, F. H. MURCRAY, W. T. WILLIAMS, and F. S. BONONOMO. Nature, **229**, 434 (1970).
13. E. HESSTVEDT. Water, Air Soil Pollut. **2**, 49 (1973).

Can. J. Chem. Downloaded from www.nrcresearchpress.com by 210.87.254.5 on 09/05/12
For personal use only.

The Interaction of Ozone Photochemistry and Dynamics in the Stratosphere. A Three-dimensional Atmospheric Model

JULIUS LONDON AND JAE H. PARK

Department of Astro-Geophysics, University of Colorado, Boulder, Colorado 80302

Received October 31, 1973

In the stratosphere the relaxation times for transport and ozone photochemistry in an oxygen–hydrogen–nitrogen system are approximately comparable. Therefore, realistic models used to calculate ozone variations need to be based on the interaction of the photochemistry and dynamics in this region.

The model used in the present study is the three-dimensional global circulation model developed at the National Center for Atmospheric Research. The photochemical calculations for ozone are carried out as time dependent in a three-dimensional O–H–N system.

The dynamic model is started from an atmosphere initially at rest and then spun up to a steady state circulation corresponding to mid-January. An initial observed ozone distribution is added and the model is then run through 30 simulated days. Analysis of the time variation of the ozone distribution shows that photochemistry dominates the ozone changes in the sub-solar middle stratosphere, and transport processes redistribute the ozone poleward and downward into the troposphere. Although the general pattern of ozone changes seem to be correct, the model produces too much ozone in the Southern hemisphere subtropical stratosphere and transports too much ozone into the Northern subtropical troposphere. The computed lower boundary flux of about 5×10^{10} cm^{-2} s^{-1} corresponds quite well to estimates given in the literature.

Dans la stratosphère, les temps de relaxation de transport et la photochimie de l'ozone dans un système oxygène–hydrogène–azote sont approximativement comparables. Par conséquent, des modèles réalistes utilisés pour calculer les variations de l'ozone se doivent d'être basés sur l'interaction de la photochimie et de la dynamique dans cette région.

Le modèle utilisé dans l'étude actuelle est le modèle tridimensionnel de circulation globale, développé au Centre National de Recherches Atmosphériques. Les calculs photochimiques pour l'ozone sont effectués comme dépendant du temps dans le système tridimensionnel O–H–N.

Le modèle dynamique est parti d'une atmosphère initiallement au repos et puis est tourné à une circulation en régime constant correspondant à la mi-janvier. Une distribution initiale d'ozone observée est ajoutée et le modèle est alors fait passer à travers 30 jours simulés. L'analyse de la variation du temps de distribution de l'ozone révèle que la photochimie domine les transformations de l'ozone dans la stratosphère sub-solaire moyenne, et le processus de transport redistribue l'ozone vers le haut et vers le bas dans la troposphère. Bien que le type général des transformations de l'ozone semble être correct, le modèle produit trop d'ozone dans l'hémisphère du sud de la stratosphère subtropicale et transport trop d'ozone à la troposphère subtropicale du nord. Le flux de limite inférieure estimée à environ 5×10^{10} cm^{-2} s^{-1} correspond bien aux estimations données dans la littérature. [Traduit par le journal]

Can. J. Chem., **52**, 1599 (1974)

Introduction

Early routine observations of atmospheric ozone showed that the total amount of ozone in a vertical column varies systematically with weather patterns (1, 2) and with season and latitude (3, 4). As a result of the development of a global network of total ozone observing stations, sufficient data became available to show that there is also a significant geographic variation in total ozone (5). The fact that the bulk of the ozone must be located in the upper atmosphere had already been established by the careful measurements made in 1917 by Strutt (6). However, the photochemical explanation of its origin and approximate vertical distribution did not come until 1930 (7). Subsequent observations from the ground (8) and by use of balloons (9), verified the approximate height distribution predicted by Chapman and placed the ozone maximum at about 25 km.

Although the approximate amount and vertical distribution of atmospheric ozone could be ex-

Can. J. Chem. Downloaded from www.nrcresearchpress.com by 210.87.254.42 on 09/05/12
For personal use only.

Can. J. Chem. Downloaded from www.nrcresearchpress.com by 210.87.254.42 on 09/05/12
For personal use only.

plained by the photochemical theory, it was soon recognized that the theory could not, by itself, explain the maximum found during the spring and at high latitudes, and the large day-to-day variations in total ozone. In an effort to remove this difficulty Chapman incorrectly attributed the observed latitudinal and seasonal variation in total ozone to seasonal changes in upper atmospheric temperature (10).

The first direct attempt at combining photochemical processes with atmospheric transport to reproduce the observed ozone distribution was made by Prabhakara (11), who assumed equilibrium "pure oxygen" photochemistry in a two-dimensional time dependent model with parameterized mean and eddy motions. Subsequent two-dimensional studies by Gebhart (12, 13) involved non-equilibrium "oxygen" and "oxygen–hydrogen" photochemistry. Three-dimensional models were presented by Bryon-Scott (14) for an "oxygen only" atmosphere and by Hunt (15) for an oxygen–hydrogen photochemical system, the latter making use of the 18 vertical level general circulation hemispheric model developed at the Geophysical Fluid Dynamics Laboratory (now of NOAA).

It is presently recognized that ozone photochemistry in the stratosphere is far more complicated than given by the reaction scheme first suggested by Chapman (see, for instance, ref. 16). Some attempts have been made to couple the photochemistry of an oxygen–hydrogen–nitrogen system with atmospheric motions in a two-dimensional model (see, for instance, ref. 17). The present study discussed below is concerned with the evaluation of the ozone distribution involving a three-dimensional model with interacting O–H–N photochemistry and atmospheric motions.

Ozone Prediction Equation

The continuity equation for ozone for a unit volume is given by

$$[1] \qquad \frac{\partial \chi_3}{\partial t} = \left(\frac{\partial \chi_3}{\partial t}\right)_{tr} + \left(\frac{\partial \chi_3}{\partial t}\right)_{ph}$$

where χ_3 is the particle mixing ratio of ozone. The subscript "tr" and "ph" represent the contributions of transport and photochemical processes, *i.e.*,

$$[2] \qquad \left(\frac{\partial \chi_3}{\partial t}\right)_{tr} = -\frac{1}{M}\nabla \cdot (M\chi_3 V) + D_{sub}$$

and

$$[3] \qquad M\left(\frac{\partial \chi_3}{\partial t}\right)_{ph} = \text{photochemical production minus destruction of } O_3$$

where M is the air particle density, V is the three-dimensional wind vector, and D_{sub} represents the diffusion on a scale smaller than the scale of the observed or computed wind velocities. The relative importance of [2] and [3] can be determined from the time scales associated with each of the processes: that is, the exchange time for atmospheric transport τ_{tr} and the photochemical relaxation time τ_{ph}. In the troposphere, the photochemical relaxation time for ozone is long compared to the exchange time for atmospheric transport; this implies that the ozone distribution is primarily controlled by transport processes. In the upper stratosphere (above about 35 km) τ_{ph} is shorter than τ_{tr}.

At heights of about 15–35 km the relaxation times for transport and ozone photochemistry are comparable, at least as to order of magnitude. Thus, realistic computations of stratospheric ozone must involve the interaction of the photochemistry and dynamics of that region.

The Transport Model

The atmospheric transport model used for the present study is the three-dimensional global circulation model (GCM) developed at NCAR (see refs. 18 and 19). The NCAR GCM is a 12 layer spherical global model (0–36 km) with a grid spacing of 3 km in the vertical and 5° of latitude and longitude except near the poles.

The basic equations used in the GCM are the equations of motion for horizontal motions, u and v; the Richardson's equation for the vertical wind, w (derived from the hydrostatic, mass continuity, and thermodynamic equations); the pressure tendency equation for pressure, p (derived from the hydrostatic and mass continuity equations); the continuity equation for moisture, q; the hydrostatic equation for air density, ρ; and the equation of state for temperature, T.

The model incorporates radiational heating and cooling due to clouds, water vapor, carbon dioxide, and ozone, the latter based on a prescribed ozone distribution (from observations) in the troposphere and stratosphere. Also included in the model is a hydrological cycle involving evaporation, condensation, cloud formation, and precipitation. The sub-grid scale horizontal and vertical transports of momentum, sensible heat,

Can. J. Chem. Downloaded from www.nrcresearchpress.com by 210.87.254.42 on 09/05/12
For personal use only.

and moisture are dealt with in the model using the same kinematic eddy diffusivity coefficients for each of the three properties mentioned (see ref. 20). The model is started from an atmosphere at rest and allowed to come to equilibrium (after 60 simulated days corresponding to January 15). The sun is then allowed to progress through the course of each day with varying declination from day-to-day. The model predicts atmospheric parameters every 6 min during each 24 h period. The wind fields, neutral density, and temperature thus predicted in the GCM are used for calculating the ozone transport in the present study.

The upper boundary is rigid at 36 km so that there is no upward flux at 36 km. The lower boundary is at the earth's surface with orography corresponding to an approximation of the topography of the earth's surface. Use is made of the condition of continuity between the Prandtl and Ekman layers in the lower boundary condition.

The lower boundary condition for ozone (at $z = 10$ m) is slightly different from that used in the GCM. The sub-grid diffusion term D_{sub} in eq. 2 is given by

$$[4] \qquad D_{sub} = -\frac{1}{M}\frac{\partial F}{\partial Z} + D_{sub\text{-}H}$$

where F is the vertical flux in the Ekman layer and D_{sub-H} is the horizontal diffusion of ozone.

The Ekman layer vertical flux of ozone is expressed as

$$[5] \qquad F = -MK_v\frac{\partial \chi_3}{\partial Z}$$

and is set equal to the Prandtl layer flux, *i.e.*,

$$[6] \qquad F = -MK_v\frac{\partial \chi_3}{\partial Z} = -C_D M_S(\chi_{3S} - \chi_{3G})V_S$$

where χ_{3S} is the value of χ_3 at the boundary (10 m), χ_{3G} is the value of χ_3 at the ground, C_D is the drag coefficient, M_S and V_S the air density and horizontal wind in the boundary layer.

The ozone mixing ratio at the ground (χ_{3G}) is assumed to be 2/3 of the amount at anemometer height (10 m) over the ocean and 1/3 over the land (see ref. 21). It is further assumed that the drag coefficient used for the Prandtl layer is 10^{-3} over the ocean and 2×10^{-3} over the land (22).

The Photochemical Model for Ozone

In the earth's atmosphere, ozone is formed by the photodissociation of molecular oxygen and the subsequent recombination of atomic and diatomic oxygen in the presence of a third body. The ozone is then destroyed by photodissociation and by recombination with atomic oxygen, hydrogen, and nitrogen products. The principal reactions involved in the chain of photochemical production and destruction of stratospheric ozone are listed in Table 1 and a schematic diagram showing the interactions of these oxygen, hydrogen, and nitrogen reactions is shown in Fig. 1. Reactions in the big circles (equilibrium cycles I, II, and III) are so fast that the particles in each cycle are in mutual equilibrium and therefore the ratios among them can be determined photochemically. Instead of considering individual reactive particles, it is more appropriate and convenient to group several particle species which are in mutual equilibrium among themselves as shown in the diagram; that is, odd oxygen particles ($[O_x] = [O(^1D)] + [O(^3P)] + [O_3]$), odd hydrogen particles ($[HO_x] = [H] + [OH] + [HO_2] + [HNO_3]$), and odd nitrogen particles ($[NO_x] = [N] + [NO] + [NO_2] + [HNO_3] + [NO_3]$). Nitric acid will be treated not only as an odd nitrogen particle but also as an odd hydrogen particle. In a pure photochemical model, the time changes of $[O_x]$, $[HO_x]$, and $[NO_x]$ are given by (the chemical species are given in units of particle density)

$$[7] \quad \left(\frac{\partial[O_x]}{\partial t}\right)_{ph} = [2(J_1 + J_2)[O_2] + J_8[NO_2]] - [2k_2[O(^3P)]\cdot[O_3] + k_3[OH]\cdot[O(^3P)] + k_4[HO_2]\cdot[O(^3P)] + 2k_8[O(^1D)]\cdot[O_3] + k_9[H]\cdot[O_3] + k_{10}[OH]\cdot[O_3] + k_{11}[HO_2]\cdot[O_3] + k_{19}[NO]\cdot M\cdot[O(^3P)] + k_{20}[NO_2]\cdot[O(^3P)] + k_{21}[NO]\cdot[O_3] + k_{25}[NO_2]\cdot[O_3]]$$

$$[8] \quad \left(\frac{\partial[HO_x]}{\partial t}\right)_{ph} = [2(J_6[H_2O] + J_7[H_2O_2] + k_7[O(^1D)]\cdot[H_2O])] - [2(k_{12}[OH]\cdot[OH] + k_{13}[OH]\cdot[HO_2] + k_{16}[H]\cdot[HO_2] + k_{17}[HO_2]\cdot[HO_2] + k_{23}[HNO_3]\cdot[OH])]$$

TABLE 1. Principal reactions in the chain of photochemical production and destruction of stratospheric ozone

No.	Reaction	
	Chemical reactions and rate coefficients	
1	$O(^3P) + O_2 + M = O_3 + M$	$k_1 = 1.10 \times 10^{-34} e^{510/T}$ (c)
2	$O(^3P) + O_3 = O_2 + O_2$	$k_2 = 1.90 \times 10^{-11} e^{-2300/T}$ (c)
3	$O(^3P) + OH = H + O_2$	$k_3 = 4.2 (\pm 1.7) \times 10^{-11}$ (c)
4	$O(^3P) + HO_2 = OH + O_2$	$*k_4 \geq 1.00 \times 10^{-11}$ (k)
5	$O(^1D) + N_2 = O(^3P) + N_2$	$k_5 = 2.90 \times 10^{-11}$ (c)
6	$O(^1D) + O_2 = O(^3P) + O_2$	$k_6 = 4.50 \times 10^{-11}$ (c)
7	$O(^1D) + H_2O = OH + OH$	$k_7 = 2.80 \times 10^{-10}$ (c)
8	$O(^1D) + O_3 = O_2 + O_2$	$k_8 = 2.50 \times 10^{-10}$ (f)
9	$O_3 + H = OH + O_2$	$k_9 = 2.60 \times 10^{-11}$ (c)
10	$O_3 + OH = HO_2 + O_2$	$k_{10} = 1.30 \times 10^{-12} e^{-956/T}$ (a)
11	$O_3 + HO_2 = OH + 2O_2$	$k_{11} = 1.00 \times 10^{-13} e^{-1250/T}$ (m)
12	$OH + OH = H_2O + O(^3P)$	$k_{12} = 1.00 \times 10^{-11} e^{-550/T}$ (c)
13	$OH + HO_2 = H_2O + O_2$	$k_{13} \geq 1.00 \times 10^{-11}$ (k)
14	$OH + H_2O_2 = HO_2 + H_2O$	$k_{14} = 1.70 \times 10^{-11} e^{-910/T}$ (c)
15	$H + O_2 + M = HO_2 + M$	$k_{15} = 2.08 \times 10^{-32} e^{290/T}$ (c)
16	$H + HO_2 = H_2 + O_2$	$k_{16} = 4.20 \times 10^{-11} e^{-350/T}$ (c)
17	$HO_2 + HO_2 = H_2O_2 + O_2$	$k_{17} = 3.00 \times 10^{-11} e^{-500/T}$ (c)
18	$N_2O + O(^1D) = NO + NO$	$k_{18} = 6.60 \times 10^{-11}$ (c)
19	$O(^3P) + NO + M = NO_2 + M$	$k_{19} = 6.90 \times 10^{-32}$ (c)
20	$O(^3P) + NO_2 = NO + O_2$	$k_{20} = 9.10 \times 10^{-12}$ (c)
21	$O_3 + NO = NO_2 + O_2$	$k_{21} = 9.00 \times 10^{-13} e^{-1200/T}$ (c)
22	$OH + NO_2 + M = HNO_3 + M$	k_{22} = function of height (c)
23	$HNO_3 + OH = H_2O + NO_3$	$k_{23} \simeq 1.30 \times 10^{-13}$ (c)
24	$HNO_3 + O(^3P) = OH + NO_3$	$k_{24} < 1.50 \times 10^{-14}$ (c)
25	$O_3 + NO_2 = NO_3 + O_2$	$k_{25} = 1.23 \times 10^{-13} e^{-2470/T}$ (h)
26	$NO_3 + NO = NO_2 + NO_2$	$k_{26} = 8.70 \times 10^{-12}$ (c)
27	$N + O_2 = O + NO$	$k_{27} = 1.02 \times 10^{-14} T e^{-3130/T}$ (c)
28	$N + NO = O + N_2$	$k_{28} = 5.10 \times 10^{-11} e^{-170/T}$ (c)
29	$NO_3 + NO_2(+M) = N_2O_5(+M)$	k_{29} = function of height (c)
30	$NO + HO_2 = NO_2 + OH$	$k_{30} = 2.00 \times 10^{-13}$ (c)

[9] $$\left(\frac{\partial[NO_x]}{\partial t}\right)_{ph} = [2k_{18}[O(^1D)] \cdot [N_2O] + J_{10}[N_2O]] - [2k_{28}[N] \cdot [NO]]$$

In eqs. 7, 8, and 9 the first bracket on the right is the net source and the second bracket is the net sink for each system.

In the troposphere and stratosphere, $O(^1D)$, $O(^3P)$, H, OH, HO_2, and H_2O_2 are in photochemical equilibrium (see ref. 23). Their number densities are therefore given by

[10] $$[O(^1D)] = \frac{(J_3 + J_4)[O_3]}{k_5[N_2] + k_6[O_2]}$$

[11] $$[O(^3P)] = \frac{2(J_1 + J_2)[O_2] + (J_3 + J_4 + J_5)[O_3] + J_8[NO_2]}{k_1[O_2] \cdot M + k_2[O_3] + k_3[OH] + k_4[HO_2] + k_{20}[NO_2]}$$

[12] $$[H] = \frac{k_3[O(^3P)] \cdot [OH] + J_6[H_2O]}{k_9[O_3] + k_{15}[O_2] \cdot M + k_{16}[HO_2]}$$

[13] $$[HO_2] = \frac{k_{10}[O_3] \cdot [OH] + k_{14}[H_2O_2] \cdot [OH] + k_{15}[H] \cdot [O_2] \cdot M}{k_4[O(^3P)] + k_{11}[O_3] + k_{13}[OH] + k_{16}[H] + 2k_{17}[HO_2] + k_{30}[NO]}$$

[14] $$[OH] = \left\{\frac{J_6[H_2O] + J_7[H_2O_2] + k_7[O(^1D)] \cdot [H_2O]}{k_{12} + k_{13}[HO_2]/[OH] + k_{16}[H] \cdot [HO_2]/[OH]^2 + k_{17}[HO_2]^2/[OH]^2 + k_{23}[HNO_3]/[OH]}\right\}^{1/2}$$

Can. J. Chem. Downloaded from www.nrcresearchpress.com by 210.87.254.42 on 09/05/12
For personal use only.

TABLE 1. (*Concluded*)

No.	Reaction	
	Photodissociations and rates	
1	$O_2 + h\nu = O(^3P) + O(^3P)$	$1750 < \lambda < 2000$ Å; $J_1 = 1.30 \times 10^{-7}$; see ref. n
2	$O_2 + h\nu = O(^3P) + O(^3P)$	$2000 < \lambda < 2424$ Å; $J_2 = 1.21 \times 10^{-9}$ (e)
3	$O_3 + h\nu = O(^1D) + O_2$	$\lambda < 2600$ Å; $J_3 = 7.00 \times 10^{-4}$ (t)
4	$O_3 + h\nu = O(^1D) + O_2$	$2600 < \lambda < 3100$ Å; $J_4 = 8.98 \times 10^{-3}$ (g)
5	$O_3 + h\nu = O(^3P) + O_2$	$3100 < \lambda < 7600$ Å; $J_5 = 4.44 \times 10^{-4}$ (r)
6	$H_2O + h\nu = OH + H$	$1750 < \lambda < 1950$ Å; $J_6 = 1.72 \times 10^{-6}$ (q, n)
7	$H_2O_2 + h\nu = OH + OH$	$1875 < \lambda < 3000$ Å; $J_7 = 1.63 \times 10^{-4}$; see ref. s
8	$NO_2 + h\nu = NO + O(^3P)$	$2900 < \lambda < 4000$ Å; $J_8 = 8.78 \times 10^{-3}$ (l)
9	$HNO_3 + h\nu = OH + NO_2$	$1900 < \lambda < 3150$ Å; $J_9 = 1.37 \times 10^{-4}$ (j, i)
10	$N_2O + h\nu = NO + N(^4S)$	$2100 < \lambda < 2500$ Å; $J_{10} = 1.18 \times 10^{-7}$ (u, see ref. b)
11	$N_2O + h\nu = N_2 + O(^1D)$	$2900 < \lambda < 3370$ Å; $J_{11} = 1.62 \times 10^{-8}$ (u)
12	$NO_3 + h\nu = NO + O_2$	Visible; $J_{12} = 1.00 \times 10^{-2}$ (c)
13	$NO + h\nu = N + O$	$\lambda < 1908$ Å (δ band); $J_{13} = 1.00 \times 10^{-5}$ (p, d)

NOTES: *Estimate; k_i units: $cm^{3(6)}$ molecule $^{-1(2)}$ s^{-1}; J_i (top of atm) unit: s^{-1}.

REFERENCES USED IN TABLE 1:

a. J. G. Anderson and F. Kaufman. Unpublished results.
b. D. R. Bates and P. B. Hays. Planet. Space Sci. 15, 189 (1967).
c. Climatic Impact Assessment Program, monograph 1. The natural stratosphere. U.S. Department of Transportation, 1972.
d. S. Cieslik and M. Nicolet. The aeronomic dissociation of nitric oxide, Aeronomica Acta A-N112-1973, Institut D'aeronomie Spatiale de Belgique. 1973.
e. R. W. Ditchburn and P. A. Young. J. Atmos. Terrest. Phys. 24, 127 (1962).
f. R. H. Gilpin, H. I. Schiff, and K. H. Welge. Unpublished results.
g. E. C. Y. Inn and Y. Tanaka. J. Opt. Soc. Am. 43, 870 (1953).
h. H. S. Johnston. Quarterly Progress Report, Climatic Impact Assessment Program, University of California, Berkley, California. 1973.
i. H. S. Johnston and S. G. Chang. Photolysis of nitric acid vapor. Lawrence Berkley Laboratory, Report LBL-1865. 1973.
j. H. S. Johnston and R. Graham. J. Phys. Chem. 77, 62 (1973).
k. F. Kaufman. Ann. Geophys. 20, 106 (1964).
l. P. A. Leighton. Photochemistry of air pollution, Academic Press, New York. 1961.
m. D. Garvin (Editor). Chemical kinetics data survey IV. Preliminary tables of chemical data for modeling of the stratosphere, NBSIR-203. 1973.
n. J. H. Park. Ozone photochemistry and energy budget in the middle atmosphere, Ph.D. Thesis, University of Colorado. 1972.
p. J. H. Park. Unpublished results.
q. B. A. Thompson, P. Harteck, and R. R. Reeves, Jr. J. Geophys. Res. 68, 6431 (1963).
r. E. Vigroux. Ann. Geophys. 9, 709 (1953).
s. D. H. Volman. Adv. Photochem. 1, 43 (1963).
t. K. Watanabe, E. C. Y. Inn, and M. Ze'likoff. J. Chem. Phys. 21, 1026 (1953).
u. P. Young. Doctoral Thesis, University of Reading, Reading, England. 1961.

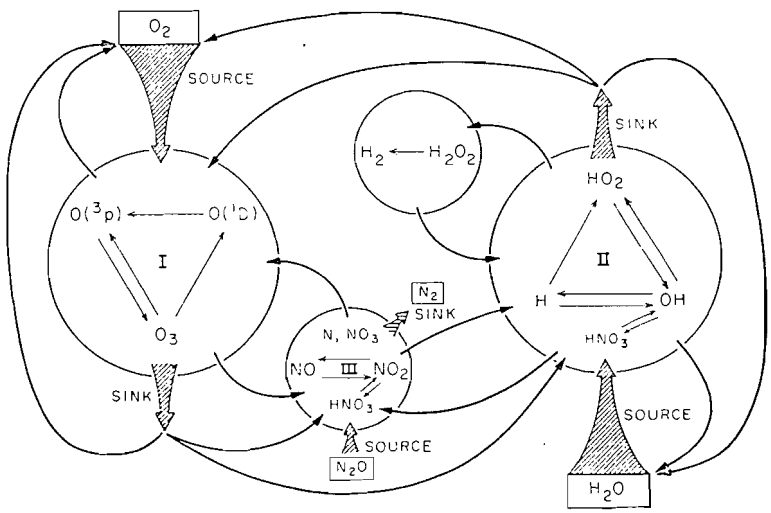

FIG. 1. Schematic diagram of the major oxygen–hydrogen–nitrogen reactions for ozone photochemistry in the stratosphere.

Can. J. Chem. Downloaded from www.nrcresearchpress.com by 210.87.254.42 on 09/05/12
For personal use only.

$$[15] \qquad [H_2O_2] = \frac{k_{17}[HO_2] \cdot [HO_2]}{k_{14}[OH] + J_7}$$

The concentration of NO_x is not in photochemical equilibrium. However, the ratios between [NO] and $[NO_2]$, between $[NO_3]$ and $[NO_2]$, and between [N] and $[NO_2]$ are assumed to be independent of atmospheric transport (see refs. 24 and 25); therefore, we can write

$$[16] \qquad \frac{[NO]}{[NO_2]} = \frac{k_{20}[O(^3P)] + k_{25}[O_3] + J_8}{k_{19}[O(^3P)] \cdot M + k_{21}[O_3] + 2 \cdot k_{26}[NO_3] + k_{30}[HO_2]} \equiv R_1$$

$$[17] \qquad \frac{[NO_3]}{[NO_2]} = \frac{k_{23}[HNO_3] \cdot [OH]/[NO_2] + k_{24}[HNO_3] \cdot [O(^3P)]/[NO_2] + k_{25}[O_3]}{k_{26}[NO] + k_{29}[NO_2] \cdot M + J_{12}} \equiv R_2$$

$$[18] \qquad \frac{[N]}{[NO]} = \left(\frac{J_{13}}{k_{27}[O_2]}\right) \cdot R_1 \equiv R_3$$

The ratio between $[HNO_3]$ and $[NO_2]$ in the stratosphere is given by (24)

$$[19] \qquad \frac{[HNO_3]}{[NO_2]} = \frac{k_{22}[OH] \cdot M}{k_{23}[OH] + k_{24}[O(^3P)] + J_9} \equiv R_4$$

However, because of its longer photochemical lifetime in the troposphere as compared to transport processes, an additional condition is used for the ratio ($[HNO_3]/[NO_2]$); that is, the ratio given by eq. 19 is modified so that the lowest four layers in the model (10.5, 7.5, 4.5, and 1.5 km) are always 1/2, 1/5, 1/15, and 1/100 of the value of the fifth layer (13.5 km). This condition is equivalent to rain washout of HNO_3, although the numbers used are somewhat arbitrary.

The species $[NO_2]$, [NO], $[NO_3]$, [N], and $[HNO_3]$ are then computed by

$$[20] \qquad [NO_2] = [NO_x]/(1 + R_1 + R_2 + R_3 + R_4)$$

$$[21] \qquad [NO] = [NO_2] \cdot R_1$$

$$[22] \qquad [NO_3] = [NO_2] \cdot R_2$$

$$[23] \qquad [N] = [NO_2] \cdot R_3$$

$$[24] \qquad [HNO_3] = [NO_2] \cdot R_4$$

By using eq. 16, the change of $[O_x]$ (eq. 7) is further simplified to

$$[25] \quad \left(\frac{\partial[O_3]}{\partial t}\right)_{ph} = \{2(J_1 + J_2)[O_2] - [2k_2[O(^3P)] \cdot [O_3] + k_3[OH] \cdot [O(^3P)] + k_4[HO_2] \cdot [O(^3P)] + 2k_8[O(^1D)] \cdot [O_3] + k_9[H] \cdot [O_3] + k_{10}[OH] \cdot [O_3] + k_{11}[HO_2] \cdot [O_3] + 2k_{20}[NO_2] \cdot [O(^3P)] + 2k_{25}[NO_2] \cdot [O_3] - 2k_{26}[NO] \cdot [NO_3] - k_{30}[HO_2] \cdot [NO]]\} \Big/ \left(1 + \frac{[O(^3P)]}{[O_3]}\right)$$

Therefore, by knowing (or assuming) the initial total amounts of O_2, H_2O, O_3, and NO_x, eqs. 10 to 24 can be solved by iterations for $[O(^1D)]$, $[O(^3P)]$, [H], $[HO_2]$, [OH], $[H_2O_2]$, [NO], $[NO_2]$, $[NO_3]$, [N], and $[HNO_3]$. When the equilibrium values are substituted into eq. 25, $(\partial O_3/\partial t)_{ph}$ can be computed for the rate of photochemical change of O_3.

An average of 10 iterations were performed for eqs. 10 to 24 to converge for each point using the conditions

$$[26] \qquad \left|1 - \frac{[OH]_1}{[OH]_2}\right| < 10^{-3}$$

and

$$[27] \qquad \left|1 - \frac{[NO_2]_1}{[NO_2]_2}\right| < 10^{-3}$$

where subscripts 1 and 2 denote the values com-

Can. J. Chem. Downloaded from www.nrcresearchpress.com by 210.87.254.42 on 09/05/12
For personal use only.

Can. J. Chem. Downloaded from www.nrcresearchpress.com by 210.87.254.42 on 09/05/12
For personal use only.

puted at two subsequent iterations. With these convergence criteria $(\partial O_3/\partial t)_{ph}$ can be computed with an error, arising from the numerical procedure, of less than 0.1%.

Computations

Three sets of time dependent computations were carried out starting from an initial ozone distribution corresponding to a zonally averaged cross section of observed ozone (see Fig. 2) as given for December–January by Dütsch (26). These were: (*a*) photochemistry only—60 simulated days; (*b*) transport only—60 simulated days; (*c*) combined photochemistry and transport—30 simulated days.

The photochemical computations were made for every 30 min and for zenith angles (Z) < 90°. For $Z \geqslant 90°$ no photochemical computations were made, and the initial values at sunrise were taken as the previous sunset concentrations. Thus, no nighttime destruction of ozone (or other species) were included in the present photochemical scheme. The implications of this procedure will be discussed below. The neutral density and temperature as computed at each time step in the GCM was used for the photochemical computations. For the computations of ozone transport, u, v, w, ρ, and T and the ozone flux terms were computed for every grid point at 6 min intervals during the entire day.

In the case of the combined photochemical and transport computation, every 5th time step contained a photochemical term. As above, the photochemical terms were included only for the sunlight hours, but the transports were carried for each 24 h period.

The assumed water vapor distribution (held constant with time) is shown in Fig. 3 and is based on observations and summaries of Mastenbrook (27, 28), McKinnon and Morewood (29), Scholtz *et al.* (30), and London and Sasamori (31). The NO_x volume mixing ratio was assumed to be 10^{-8} from 50 km to 30 km, decreasing to 2×10^{-9} at 15 km, and then increasing to 7×10^{-9} at the surface (32–37). This vertical profile represents an approximate average of the varied observed values.

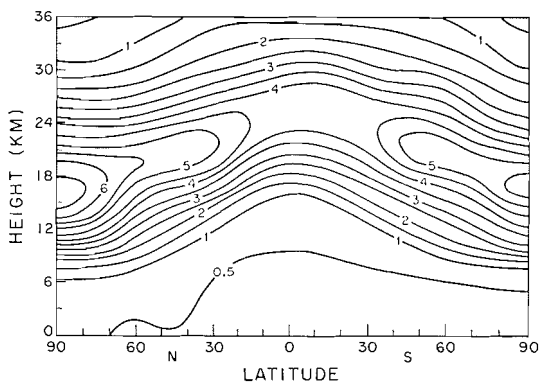

FIG. 2. Initial ozone distribution (10^{12} cm^{-3}) (after Dütsch (26)).

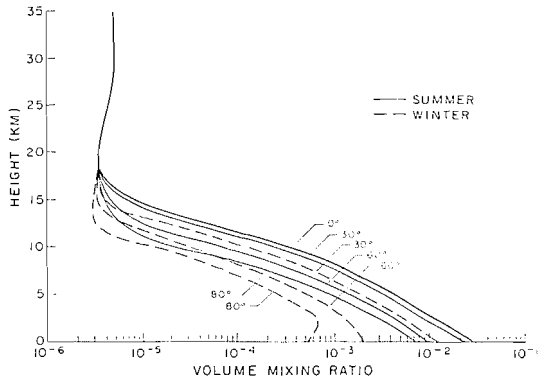

FIG. 3. The assumed water vapor distribution (see text for references).

Results

Photochemistry

The net production of ozone in the real atmosphere (containing hydrogen and nitrogen products) is always less than for an atmosphere assuming oxygen as the only photochemically active gas. In the upper stratosphere and mesosphere (above about 40 km) the hydrogen cycle is very effective in the reduction of the photochemically produced ozone. NO_x interactions become more important in the region from 20 to 40 km. When both the hydrogen and nitrogen products are introduced into the ozone photochemical scheme, however, the reaction of OH with NO_2 to form HNO_3 (at levels below 35 km) somewhat diminished the effectiveness of each system in destroying ozone. Thus, oxygen–hydrogen–nitrogen photochemistry is required for a realistic time dependent photochemical calculation for stratospheric ozone.

The computed distribution of the net photochemical ozone source for January 15 and for the condition described above is given in Fig. 4. The maximum net production is in the summer polar regions above 35 km. From about 30° N to the South Pole there is relatively little net production

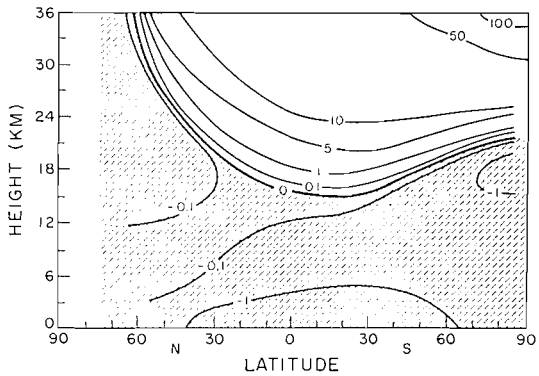

FIG. 4. The net photochemical production of ozone (Jan. 15) (10^5 cm^{-3} s^{-1}).

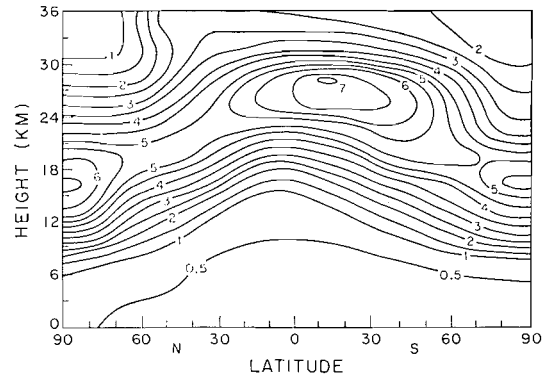

FIG. 5. The computed average ozone distribution (Feb. 5–14), photochemistry only (10^{12} cm^{-3}).

of ozone in the region of about 16–22 km. In the winter polar stratosphere and in the troposphere there is a net destruction, albeit small. The computed integrated net production over the globe for the prescribed initial condition and including estimated nighttime destruction (1×10^{12} cm^{-2} s^{-1}) is 5×10^{12} cm^{-2} s^{-1}. This is about 100 times the estimated value of the global destruction of ozone at the ground (21).

The net production rate decreases as the ozone concentration builds up and after 30 days the computed value is reduced to less than 10^{12} cm^{-2} s^{-1}. The computed net production rate is also quite sensitive to the assumed initial amount of NO_x. For instance, a fivefold increase of NO_x at all levels would result in a net global ozone production rate of about -2.5×10^{12} cm^{-2} (*i.e.*, *net destruction*). Of course, this destruction rate would decrease as the ozone concentration decreased. The photochemical distribution tends to a steady state value which, in each case, depends on the assumed concentrations of the photochemically active gases.

The calculated ozone distribution after 30 days is shown in vertical cross section on Fig. 5. The major change from the initial distribution is the development of a strong maximum at sub-solar latitudes at a height of about 28 km. Comparison between the initial distribution given in Fig. 2 with the computed values in Fig. 5 shows that in general there is a net increase of the ozone concentration in the stratosphere centered around sub-solar latitudes. The ozone concentration is increased in the model down to about 24 km in the South Pole regions, and to 15 km in equatorial regions.

As the ozone concentration at about 30 km and 25° S builds up, however, the net production decreases somewhat. This is indicated by the increased vertical gradient found at this height in the Southern hemisphere subtropics. Photochemical computations extended to 60 days (not shown here) show that the photochemical distribution changes rather slowly. The initial distribution, assumed from observations, was equivalent to an average ozone amount of about 0.32 cm (STP) (standard temperature and pressure). This value increased to about 0.38 cm (STP) in 30 days and 0.40 cm (STP) in 60 days.

Comparison of Figs. 2 and 5 also show that there is a very slight ozone destruction in the polar stratosphere and everywhere in the troposphere. The photochemical destruction is increased somewhat at lower levels, particularly in equatorial regions. At these latitudes solar u.v. radiation at wavelengths below 3100 Å can penetrate down to the lower troposphere (because of smaller optical depths). Then, because there is a relatively large amount of water vapor in this region, sufficient OH will be formed to have a noticeable effect on the ozone destruction rate.

In the present photochemical model, nighttime ozone chemistry was not considered. After sunset, most of the species ($O(^1D)$, $O(^3P)$, H, OH, HO_2, N, and NO) disappear quickly (almost within an hour). The species H_2O_2 and HNO_3 remain almost constant during the night and do not affect the ozone directly. Only the NO_2 particles will react with ozone (reaction 25) to produce NO_3 and O_2. Then NO_3 and NO_2 recombine in the presence of a third body (reaction 29) to lead to N_2O_5. For the chemical scheme (Table 1) adopted in this model, N_2O_5 is considered as the sink reservoir for NO_x particles during the night.

Can. J. Chem. Downloaded from www.nrcresearchpress.com by 210.87.254.42 on 09/05/12
For personal use only.

Can. J. Chem. Downloaded from www.nrcresearchpress.com by 210.87.254.42 on 09/05/12
For personal use only.

The global nighttime average destruction rate of ozone by the mechanism discussed above is of the order of 10^{12} cm^{-2} s^{-1} for January conditions and for an NO_2 mixing ratio of 5×10^{-9}. This is the same order of magnitude as the average daytime net production rate as discussed above. Sample calculations show that the global amount of O_3 can be overestimated by about 30% over a period of 100 days by neglecting nighttime ozone destruction.

Transport

The mean meridional and vertical circulation derived from the general circulation model for mean January conditions has been discussed by Kasahara *et al.* (20). Their results show a three-cell pattern in the troposphere with a weaker two-cell structure in the stratosphere. The circulation pattern is stronger in the Northern than Southern hemisphere, particularly with regard to the Hadley cell. Comparison with observations (*e.g.*, ref. 38) indicate that the downward branch of the Hadley circulation in the Northern hemisphere as computed by the GCM is probably too large. This will tend to distort the vertical transport of ozone in the sub-tropics as will be discussed below. There are also some differences between the computed and observed distributions in the north and south polar regions.

The calculated ozone distribution resulting from transport terms in eq. 2 along with lower boundary condition (eq. 6) is shown in Fig. 6 for the 10 day average, February 5–14. Comparison of the initial distribution shown in Fig. 2 with the derived distribution after 30 days of transport indicates what would happen to the ozone if there were no photochemistry and the ozone were sloshed back and forth by atmospheric motions.

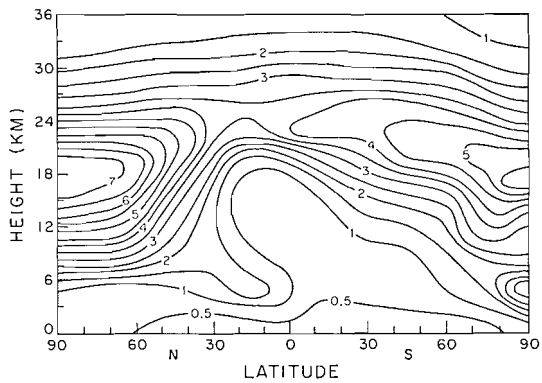

FIG. 6. The computed average ozone distribution (Feb. 5–14), transport only (10^{12} cm^{-3}).

Ozone transport results in a divergence (depletion) in the equatorial stratosphere at the top of the Hadley cell and accumulation in polar regions. The strong influence of the Hadley circulation in the Northern hemisphere is clearly shown in the ozone intrusion through the sub-tropical tropopause region. However, the large amounts of ozone brought down into the sub-tropical troposphere do not correspond to observed values. These are the result of too strong a return (downward) flow computed by the GCM as mentioned earlier.

Comparison of Figs. 2 and 6 also reveals a peculiar buildup of ozone in the south polar troposphere at about 4–6 km. This is undoubtedly fictitious and is probably the consequence of an incorrect temperature and wind field prediction in that region. Also, sample experiments indicate that the numerical procedures used in the GCM could lead to incorrect vertical fluxes in the vicinity of the Antarctic Plateau (and the Himalayas).

It is obvious from the strong ozone buildup in the north polar regions that atmospheric transport plays the major role in maintaining the observed distribution. When the transport terms are separated into mean and eddy fluxes it is seen that the poleward transport is accomplished by the mean flux from equatorial to sub-tropical latitudes and large scale eddy flux in mid-latitudes. The manner in which the mean and eddy horizontal and vertical ozone fluxes contribute to the total transport has been discussed by Hunt (15) and by London and Park (39).

The small decrease of ozone in the lower levels corresponds to the downward flux of ozone through the lower boundary.

Photochemistry and Transport

Combined effects of photochemistry in an oxygen–hydrogen–nitrogen system and atmospheric motions as derived from the general circulation model described above were computed for a period of 30 days. The resulting average distribution for the 10 day interval (corresponding to February 5–14) is shown on Fig. 7.

Comparison with the initial distribution (Fig. 2) shows that changes in the ozone concentration above about 24 km are largely produced by photochemical interactions whereas changes below that level are mostly associated with various

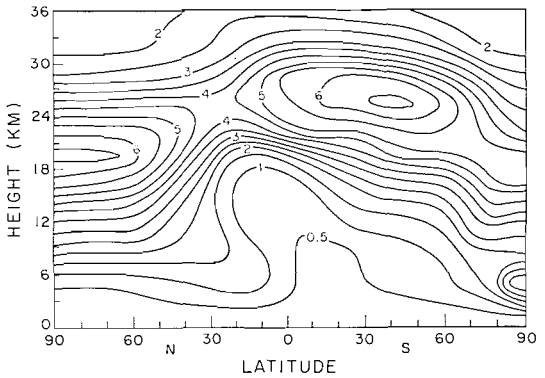

FIG. 7. The computed average ozone distribution (Feb. 5–14), photochemistry and transport (10^{12} cm^{-3}).

stratospheric transport mechanisms. The ozone concentration has increased in the layer above 22 km at latitudes from the equator to about 60° S. This is apparently in response to the excessive net photochemical production in this region as discussed above. It is also probable that the south poleward transport out of the southern sub-tropical stratosphere has been somewhat underestimated. There has been a strong ozone decrease centered at about 20 km and 30° N and an increase at about 10 km at the same latitude. These changes are consistent with the observed circulation pattern in the sub-tropics. However, as already pointed out, the Hadley cell as derived in the GCM is somewhat stronger than the observed circulation. As a result, the decrease of ozone at the top of the Hadley cell and the strong intrusion in the sub-tropical troposphere have been exaggerated in the model. Ozone observations in the sub-tropics (see, for instance, ref. 40) do not show the tropospheric distribution as indicated in Fig. 7. Numerical experiments performed with the model have indicated that ozone is not exactly conserved in the model in this region. Thus, part of the fictitious buildup might be due to the differencing scheme (and the mesh size) used in the model. Additional experiments are now underway to correct this problem.

The model is able to predict correctly the general buildup of ozone in the polar regions, although the strong increase immediately above the Antarctic Plateau as shown in Fig. 7 is certainly incorrect as discussed above.

Lower Boundary Flux

As pointed out earlier, there is a net photochemical ozone production in the sub-solar stratosphere, and a transport of the ozone poleward and downward into the troposphere where it is eventually destroyed in contact with the ground. In steady state conditions, the sink at the surface must balance the source due to photochemical production.

The lower boundary flux was computed by use of eq. 6 where M_s, χ_{3s}, and V_s are computed at each time step by the GCM. The smoothed latitudinal distribution of the (downward) surface flux corresponding to January 15 is shown in Fig. 8.

The computed flux is a maximum of 7.0×10^{10} cm^{-2} s^{-1} at latitude 60° N decreasing to 3.5×10^{10} cm^{-2} s^{-1} at the equator, then increasing to a maximum of about 6.0×10^{10} cm^{-2} s^{-1} at about 30° S, and decreasing to a minimum of 2.0×10^{10} cm^{-2} s^{-1} at about 60° S. The average surface flux is about 5×10^{10} cm^{-2} s^{-1} for the globe with slightly higher values computed for the Northern as compared to the Southern hemisphere. This value is the same as the estimate given by Fabian and Junge (21) as the annual global ozone sink at the surface. They also estimate a larger sink in the Northern hemisphere, although their hemispheric difference is bigger than ours.

A global ozone sink of the order of 5×10^{10} cm^{-2} s^{-1} represents an annual destruction rate of the order of 20%. Large scale variations in the surface wind patterns could, therefore, noticeably affect the long-term storage of ozone, which in turn could appear as periodic and/or aperiodic trends in total ozone. Since the global ozone sink is quite well established, at least as to order of

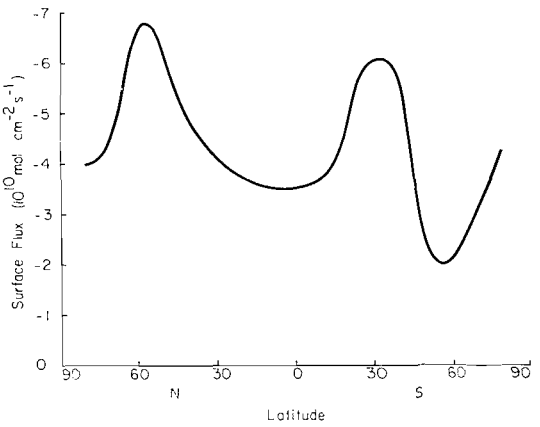

FIG. 8. The computed latitudinal variation of the downward ozone flux at the surface.

Can. J. Chem. Downloaded from www.nrcresearchpress.com by 210.87.254.42 on 09/05/12
For personal use only.

magnitude, we conclude that the net photochemical ozone production as computed in the present model from the observed ozone distribution is at least 1 order of magnitude too high.

Efforts are presently underway to refine the photochemistry by including nighttime destruction and a realistic latitudinal variation of NO_x. In addition, some improvements are being made in the finite differencing scheme in order to better conserve ozone mass in the transport calculations.

Support for the research discussed above came from the Atmospheric Sciences Section, National Science Foundation, and the Department of Transportation through NSF Grant GA-28688X2 and the Computing Facility of the National Center for Atmospheric Research. We would like to thank Julianna Chow, Gloria Williamson, and Jean Kelley for programming and technical assistance. In addition, we have benefited from many discussions with our colleagues involved in the GCM program at NCAR, especially Robert Dickinson, Takashi Sasamori, and Warren Washington.

1. D. N. HARRISON and G. M. B. DOBSON. Q. J. R. Meteorol. Soc. **51**, 363 (1925).
2. G. M. B. DOBSON and D. N. HARRISON. Proc. R. Soc. Lond. A, 660 (1926).
3. G. M. B. DOBSON, D. C. HARRISON, and J. LAWRENCE. Proc. R. Soc. Lond. A, **114**, 521 (1927).
4. G. M. B. DOBSON, D. C. HARRISON, and J. LAWRENCE. Proc. R. Soc. Lond. A, **122**, 456 (1929).
5. J. LONDON. Beit. Phys. Atmos. **36**, 253 (1963).
6. R. J. STRUTT. Proc. R. Soc. **94**, 260 (1918).
7. S. CHAPMAN. Mem. R. Meteorol. Soc. III, 103 (1930).
8. F. W. GÖTZ, A. R. MEETHAM, and G. M. DOBSON. Proc. R. Soc. **145**, A416 (1934).
9. E. REGENER and V. REGENER. Phys. Z. **35**, 788 (1934).
10. S. CHAPMAN. Phil. Mag. X, 345 (1930).
11. C. PRABHAKARA. Mon. Weather Rev. **91**, 411 (1963).
12. R. GEBHART. Arch. Met. Geoph. Biokl. Ser. A, **17**, 301 (1968).
13. R. GEBHART. Arch. Met. Geoph. Biokl. Ser. A, **20**, 247 (1971).
14. R. BYRON-SCOTT. Publ. Meteorol. **87**, 386 (1967).
15. B. G. HUNT. Mon. Weather Rev. **97**, 287 (1969).
16. P. CRUTZEN. J. Geophys. Res. **76**, 7311 (1971).
17. E. HESSTVEDT. Proc. Int. Assoc. Geomag. Aeronom. Symp. Jap. IUGG Publications House, 39 tec, Rue Gay-Lussac, Paris V. 1973. p. 11.
18. A. KASAHARA and W. M. WASHINGTON. J. Atmos. Sci. **28**, 657 (1971).
19. W. M. WASHINGTON. Climatic Impact Assessment Program Proc. Sec. Conf. Nov., Cambridge, Mass. National Technical Information Service, Springfield, Va. 1972. p. 358.
20. A. KASAHARA, T. SASAMORI, and W. M. WASHINGTON. National Center for Atmospheric Research, manuscript 2120-73-C (1973).
21. P. FABIAN and C. E. JUNGE. Arch. Met. Geoph. Biokl. Ser. A, **19**, 161 (1970).
22. W. C. SWINBANK. Private communication.
23. J. H. PARK. Ph.D. Thesis. University of Colorado, Boulder, Colorado. 1972.
24. M. NICOLET. Planet. Space Sci. **20**, 1671 (1972).
25. J. H. PARK and J. LONDON. Unpublished results.
26. H. U. DÜTSCH. Private communication.
27. H. J. MASTENBROOK. J. Atmos. Sci. **26**, 299 (1968).
28. H. J. MASTENBROOK. J. Atmos. Sci. **28**, 1495 (1971).
29. D. MCKINNON and H. W. MOREWOOD. J. Atmos. Sci. **27**, 483 (1970).
30. T. G. SCHOLTZ, D. H. EHHALT, L. E. HEIDT, and E. A. MARTELL. J. Geophys. Res. **75**, 3049 (1970).
31. J. LON ON and T. SASAMORI. Unpublished results.
32. H. W GEORGII and D. JOST. Pure Appl. Geophys. **59**, 217 (1964).
33. D. G. MURCRAY, A. GOLDMAN, F. H. MURCRAY, W. J. WILLIAMS, J. N. BROOKS, and D. B. BARKER. Proc. American Institute of Aeronautics and Astronautics, 11th Aero. Sci. Meeting, Washington, 10 (1973).
34. R. A. TOTH, C. B. FARMER, R. A. SCHINDLER, O. F. RAPER, and P. W. SCHAPER. Nat. Phys. Sci. **244**, 7 (1973).
35. J. E. HARRIES. Nature, **241**, 515 (1973).
36. H. I. SCHIFF. Unpublished results.
37. M. ACKERMAN, J. C. FONTANELLA, D. FRIMOUT, A. GIRARD, N. LOUISNARD, C. MULLER, and D. NEVEJANS. Submitted to Nature.
38. D. G. VINCENT. Q. J. R. Meteorol. Soc. **94**, 333 (1968).
39. J. LONDON and J. H. PARK. Pure Appl. Geophys. **106–108**, 1611 (1973).
40. W. S. HERING and T. R. BORDEN, JR. Environ. Res. Papers, Air Force Cambridge Res. Lab. Rep. No. 162, 1965.

Can. J. Chem. Downloaded from www.nrcresearchpress.com by 210.87.254.42 on 09/05/12
For personal use only.

Stratospheric Chlorine: a Possible Sink for Ozone

R. S. STOLARSKI AND R. J. CICERONE

Space Physics Research Laboratory, The University of Michigan, Ann Arbor, Michigan 48105

Received January 18, 1974

This study proposes that the oxides of chlorine, ClO_x, may constitute an important sink for stratospheric ozone. A photochemical scheme is devised which includes two catalytic cycles through which ClO_x destroys odd oxygen. The individual ClX constituents (HCl, Cl, ClO, and OClO) perform analogously to the respective constituents (HNO_3, NO, NO_2, and NO_3) in the NO_x catalytic cycles, but the ozone destruction efficiency is higher for ClO_x. Our photochemical scheme predicts that ClO is the dominant chlorine constituent in the lower and middle stratosphere and HCl dominates in the upper stratosphere. Sample calculations are performed for several ClX altitude profiles: an assumed 1 p.p.b. volume mixing ratio, a ground level source, and direct injection by volcanic explosions. Finally we discuss certain limitations of the present model: uncertainty in stratospheric OH concentrations, the possibility that ClOO exists, the need to couple ClO_x cycles with NO_x and HO_x cycles, and possible heterogeneous reactions.

Cette étude suggère que les oxydes de chlore, ClO_x, peuvent être une raison importante de la diminution de l'ozone stratosphérique. Un schéma photochimique est élaboré, lequel inclut deux cycles catalytiques par l'intermédiaire desquels ClO_x détruit l'oxygène impair. Les constituants individuels ClX (HCl, Cl, ClO et OClO) agissent de façon analogue aux constituants respectifs (HNO_3, NO, NO_2 et NO_3) dans les cycles catalytiques des NO_x, mais la destruction de l'ozone est plus efficace pour ClO_x. Notre schéma photochimique laisse prévoir que ClO est le constituant chlore dominant dans la basse et moyenne stratosphère et que HCl domine dans la haute stratosphère. Des calculs types sont effectués pour plusieurs profiles d'altitude des ClX: un rapport de mélange en volume de 1 p.p.b. est considéré, une source au niveau du terrain et des injections directes par des explosions volcaniques. Finalement nous discutons certaines limitations du modèle présent: incertitude des concentrations en OH dans la stratosphère, la possibilité de l'existence de ClOO, le besoin de réunir les cycles de ClO_x avec ceux des NO_x et HO_x et des réactions hétérogènes possibles. [Traduit par le journal]

Can. J. Chem., **52**, 1610 (1974)

Introduction

Recent studies have pointed out the crucial effect of catalytic cycles in stratospheric ozone chemistry (*e.g.*, refs. 1–3). Extensive work has been done on the cycles of the nitrogen oxides, NO_x, and the hydrogen oxides, HO_x. Both are potential ozone destroyers through their cyclic reactions with ozone and atomic oxygen. It is likely that there are numerous other catalytic cycles potentially capable of influencing stratospheric chemistry. Here we focus attention on one possibility, previously neglected, involving the oxides of chlorine, ClO_x, and propose a chemical reaction scheme for gas-phase chlorine in the stratosphere which is analogous to the NO_x catalytic cycle, but even more efficient for ozone destruction.

Chlorine from ground level sources can diffuse upward through the troposphere into the stratosphere. Likely sources are industry, sea salt spray, and fumaroles. Also explosive volcanic eruptions and solid fuel rockets may directly inject chlorine into the stratosphere.

We will show from source estimates that reasonable ClO_x levels can yield ozone destruction rates comparable to those for NO_x. In reality, ozone destruction by ClO_x depends on all the complexities of stratospheric chemistry, e.g., interaction with NO_x and HO_x cycles.

Gas-phase Chlorine Reactions

Gas-phase chlorine injected or transported into the stratosphere forms a number of different molecules the most important of which are HCl, Cl, ClO, OClO, ClOO, and Cl_2. We shall define the sum of all of these as ClX. Reaction rates for transfer amongst the various ClX species are rapid and local steady-state chemistry may be used to calculate the ratio of each chlorine species to ClX independent of transport. Figure

Can. J. Chem. Downloaded from www.nrcresearchpress.com by 210.87.254.5 on 09/05/12
For personal use only.

TABLE 1. Chlorine reactions in the stratosphere

	Reaction	Rate (cm^3 $molecule^{-1}$ s^{-1})*
[1]	$h\nu + HCl \rightarrow H + Cl$	Slow, see text
[2]	$h\nu + Cl_2 \rightarrow Cl + Cl$	Fast, see text
[3]	$Cl + O_3 \rightarrow ClO + O_2$	$4.3 \times 10^{-11} \exp(-500/RT)$
[4]	$ClO + O \rightarrow Cl + O_2$	$1.2 \times 10^{-10} \exp(-500/RT)$
[5]	$ClO + O_3 \rightarrow OClO + O_2$	$\leq 5 \times 10^{-15}$
[6]	$Cl + ClO \rightarrow Cl_2 + O$	5×10^{-11}
[7]	$OClO + O \rightarrow ClO + O_2$	5×10^{-13}
[8]	$h\nu + ClO \rightarrow Cl + O$	Slow, see text
[9]	$h\nu + OClO \rightarrow O + ClO$	See text
[10]	$Cl + CH_4 \rightarrow HCl + CH_3$	$8.8 \times 10^{-11} \exp(-3800/RT)$
[11]	$OH + HCl \rightarrow H_2O + Cl$	$1.8 \times 10^{-11} \exp(-2000/RT)$
[12]	$Cl + O_2 + M \rightarrow ClOO + M$	$K = (k_{12}/k_{13}) = 3.6 \times 10^{-21}$ cm^3
[13]	$ClOO + M \rightarrow Cl + O_2 + M$	
[14]	$HCl + O \rightarrow OH + Cl$	$6.8 \times 10^{-12} \exp(-5100/RT)$
[15]	$ClO + NO \rightarrow Cl + NO_2$	1.7×10^{-11}
[16]	$Cl + NH_3 \rightarrow HCl + NH_2$	1×10^{-12}

*See text for rate references.

1 shows our proposed ClX reaction scheme and Table 1 lists the reactions and their rates. The major ozone destroying catalytic cycle is the set of reactions

[3] $Cl + O_3 \rightarrow ClO + O_2$

[4] $ClO + O \rightarrow Cl + O_2$

net $O_3 + O \rightarrow 2O_2$

The rate of [3] has been measured recently at room temperature by Watson[1] to be 1.85×10^{-11} cm^3 $molecule^{-1}$ s^{-1}. Its maximum activation energy is 1 kcal mol^{-1} and we have assumed 0.5 kcal mol^{-1}. Rate [4] has been measured by Bemand *et al.* (4) as 5.3×10^{-11} cm^3 $molecule^{-1}$ s^{-1} at room temperature and again we have assumed an activation energy of 0.5 kcal mol^{-1}. ClO is photodissociated in the ultraviolet by [8]. We used the cross section of Johnston *et al.* (5) and the solar intensities of Brinkmann *et al.* (6) to determine that [8] is 10 times slower than [4] at all altitudes. It has therefore been neglected.

A second catalytic cycle is initiated by [5]

[5] $ClO + O_3 \rightarrow OClO + O_2$

[7] $OClO + O \rightarrow ClO + O_2$

net $O + O_3 \rightarrow 2O_2$

Reaction 5 forms OClO, chlorine dioxide, distinct from the peroxy radical ClOO discussed later. The effect of this cycle is to lower the net ozone destruction because a fraction of the total available ClX is diverted to OClO and [7] is

[1]R. T. Watson, personal communication, 1973.

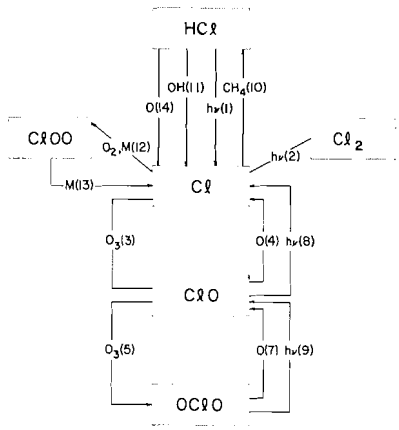

FIG. 1. Chemical reaction scheme for gas-phase chlorine.

two orders of magnitude slower than [4]. Even if 90% of the total ClX were OClO the odd oxygen destruction rate of the Cl–ClO cycle would be larger than that of the ClO–OClO cycle. Reaction 5 is slow with an upper limit rate (7) of 5×10^{-15} cm^3 $molecule^{-1}$ s^{-1}. Photodissociation of OClO [9] is probably faster than [7] and provides a return to ClO which gives no net destruction of ozone. Although we have performed some calculations including the ClO–OClO cycle we show here only calculations for which $k_5 = 0$.

Cl may also react with CH_4 and NH_3 to form HCl

[10] $Cl + CH_4 \rightarrow HCl + CH_3$

[16] $Cl + NH_3 \rightarrow HCl + NH_2$

Can. J. Chem. Downloaded from www.nrcresearchpress.com by 210.87.254.5 on 09/05/12
For personal use only.

TABLE 2. Input data*

Altitude	T (°K)	[O]	[O_3]	[CH_4]	High [OH]	Low [OH]
5	270	3(3)	3.3(11)	2(13)	8(5)	8(5)
10	238	6.5(3)	4.3(11)	1(13)	6(5)	4(5)
15	218	2.2(4)	6.5(11)	5(12)	3(5)	5(4)
20	212	3.0(5)	1.8(12)	2.5(12)	1(6)	1.7(5)
25	220	6.0(6)	4.3(12)	1.2(12)	2(6)	9(5)
30	232	2.7(7)	3.5(12)	5(11)	5(6)	2.5(6)
35	243	1.2(8)	1.7(12)	1.5(11)	1(7)	3.5(6)
40	255	3.8(6)	5.0(11)	4(10)	1.2(7)	3(6)
45	265	1.2(9)	1.5(11)	1(10)	1.3(7)	4(6)
50	272	2.5(9)	5.0(10)	2(9)	1(7)	4(6)
55	269	4.4(9)	1.8(10)	1(9)	8(6)	3(6)
60	255	7.0(9)	6.3(9)	4(8)	6(6)	2(6)

*Concentrations are per cm^3. Numbers in parentheses are powers of 10.

Reaction 10 has been measured at room temperature by Davis *et al.* (8) to have a rate of 1.7×10^{-13} cm^3 $molecule^{-1}$ s^{-1}. Its activation energy is 3.8 kcal mol^{-1} (9). Kondratiev (10) gives an estimated rate for [16] of $\sim 10^{-12}$ cm^3 $molecule^{-1}$ s^{-1}. Since ammonia concentrations in the stratosphere are small (11) we have chosen to neglect [16] in our calculation. HCl is returned to Cl by reaction with O and OH

[11] $$HCl + OH \rightarrow Cl + H_2O$$

[14] $$HCl + O \rightarrow OH + Cl$$

Reaction 11 measured by Takacs and Glass (12) is by far more important than [14] which has been measured by Balakhnin *et al.* (13). At altitudes of 50–60 km the rates of [11] and [14] become comparable. HCl acts as a temporary storage tank for ClO_x analogous to HNO_3 for NO_x.

The three-body reaction 12, has been studied by Johnston *et al.* (5). They give an equilibrium constant of 3.64×10^{-21} cm^3. This implies a [ClOO]/[Cl] ratio of $<10^{-3}$ at stratospheric pressures and indicates that [12] is unimportant. When one uses more recent values of thermodynamic constants one finds $K_{12} \sim 4 \times 10^{-19}$ at 300 K and 8×10^{-21} at 220 K.[2] This indicates that ClOO could possibly be important if it is as reactive as Cl, but this is not likely.

The only ClX compound not yet mentioned is Cl_2 which is rapidly photodissociated via [2] to 2Cl in the visible and near ultraviolet. Seery and Britton's (14) cross section implies a lifetime for Cl_2 of ~400 s. Thus, concentrations will be low.

Under all of the above assumptions, ratios of individual constituents to total ClX can be calculated for local, steady-state chemistry. They are

[17] $$\frac{[ClO]}{[ClX]} = \frac{1}{1 + \frac{k_4}{k_3}\frac{[O]}{[O_3]}\left(1 + \frac{k_{10}[CH_4]}{k_{11}[OH] + k_{14}[O]}\right) + \frac{k_5[O_3]}{J_9 + k_7[O]}}$$

[18] $$\frac{[HCl]}{[ClX]} = \frac{k_4}{k_3}\frac{[O]}{[O_3]}\left(\frac{k_{10}[CH_4]}{k_{11}[OH] + k_{14}[O]}\right)\frac{[ClO]}{[ClX]}$$

[19] $$\frac{[Cl]}{[ClX]} = \frac{k_4[O]}{k_3[O_3]}\frac{[ClO]}{[ClX]}$$

[20] $$\frac{[OClO]}{[ClX]} = \frac{k_5[O_3]}{J_9 + k_7[O]}\frac{[ClO]}{[ClX]}$$

[2]D. Garvin, personal communication, 1973.

Can. J. Chem. Downloaded from www.nrcresearchpress.com by 210.87.254.5 on 09/05/12
For personal use only.

TABLE 3. Ratios of chlorine compounds to ClX

Altitude	High OH ratios			Low OH ratios		
	[ClO]/[ClX]	[HCl]/[ClX]	[Cl]/[ClX]	[ClO]/[ClX]	[HCl]/[ClX]	[Cl]/[ClX]
5	0.90	0.10	2.3(−8)	0.90	0.10	2.6(−7)
10	0.93	0.075	4.0(−8)	0.98	0.11	5.0(−7)
15	0.89	0.11	8.6(−8)	0.57	0.43	9.8(−7)
20	0.92	0.078	4.4(−7)	0.67	0.33	1.5(−5)
25	0.84	0.16	3.4(−6)	0.70	0.30	3.3(−4)
30	0.82	0.18	1.8(−5)	0.69	0.31	1.6(−3)
35	0.73	0.27	1.5(−4)	0.50	0.50	5.2(−3)
40	0.50	0.50	1.1(−3)	0.21	0.79	7.4(−3)
45	0.27	0.72	6.3(−3)	0.12	0.87	0.014
50	0.20	0.77	0.028	0.12	0.86	0.030
55	0.093	0.84	0.065	0.061	0.90	0.026
60	0.052	0.78	0.17	0.037	0.84	0.024

Reactions 3 and 4 control the ratio of Cl to ClO at altitudes greater than ~35 km. At lower altitudes reaction 15 meshes the ClO_x cycle with the NO_x cycle[3]

[3] $$Cl + O_3 \rightarrow ClO + O_2$$

[15] $$ClO + NO \rightarrow Cl + NO_2$$

$$NO_2 + O \rightarrow NO + O_2$$

net $$O + O_3 \rightarrow 2O_2$$

Since [15] ties chlorine to the complex, incompletely understood NO_x cycle it will be neglected in this paper. Reaction 15 is fast[4] and will tend to convert ClO to Cl leading back to HCl. Thus the ratios in Table 3 would show higher fractions of HCl at low altitudes. The last section of the paper will discuss the implications of neglect of interactions with NO_x, HO_x, CO_x, etc.

Table 2 lists the input data used in the ratio calculation and Table 3 shows the ratios for two cases, high OH and low OH, corresponding to the extremes of the OH model calculations of Wofsy *et al.* (15). The OH concentration is very important because of its role in returning chlorine from its storage tank, HCl, to the catalytic cycle of Cl–ClO. Another important factor governing the amount of chlorine in the HCl tank is [14] which is unusually slow for an O atom reaction. If this rate were significantly increased HCl would be rapidly converted to Cl. Reaction 15 below 30 km will convert ClO to Cl more rapidly and tends to make more Cl available for forming HCl by [10].

[3]D. Garvin, personal communication, 1973.
[4]D. Garvin, personal communication, 1973.

Ozone Destruction Rates

Figure 2 shows calculated odd oxygen destruction rates *vs.* altitude for an assumed constant ClX mixing ratio of 1 p.p.b. Destruction rates for any other value of ClX can be linearly scaled. Also shown in Fig. 2 are the destruction rates for the Chapman mechanism reaction

[21] $$O + O_3 \rightarrow 2O_2$$

and the two catalytic cycles of NO_x; the NO–NO_2 cycle and the NO_2–NO_3 cycle. All of these were calculated using the rates and NO_x profiles of McConnell and McElroy (3). The chlorine cycle, according to the present calculations, is not the dominant loss mechanism for odd oxygen but it is significant if ClX concentrations are near the 1 p.p.b. range. It should be noted that the NO_x profiles used here represented mixing

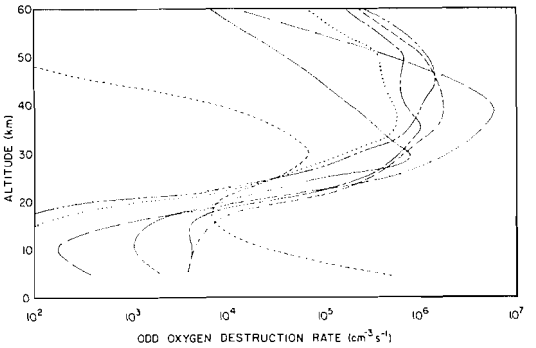

FIG. 2. Odd oxygen destruction rates *vs.* altitude. (-·-) NO–NO_2 cycle; (---) NO_2–NO_3 cycle; (—·—) Chapman mechanism; (. . .) ClO_x volcanic source; (—··—) ClO_x 1 p.p.b. high OH; (—·—·—) ClO_x 1 p.p.b. low OH; (——) ClO_x ground level source.

Can. J. Chem. Downloaded from www.nrcresearchpress.com by 210.87.254.5 on 09/05/12
For personal use only.

Can. J. Chem. Downloaded from www.nrcresearchpress.com by 210.87.254.5 on 09/05/12
For personal use only.

ratios of more than 10 p.p.b. in the altitude region (>20 km) most important for ozone destruction. Thus Fig. 2 illustrates the fact that ClO_x is more efficient for ozone destruction than NO_x. In Table 4 we show the column-integrated odd oxygen destruction rates for each of the seven mechanisms graphed in Fig. 2. The calculations for stratospheric ozone destruction due to direct injection by volcanic explosions are described in the next section.

Sources of Chlorine and Model Calculations

A number of ground level chlorine sources exist. Fumaroles emit gaseous Cl_2 and HCl (16). Sea salt spray contributes chlorine-containing particles (17), some of which lead to gaseous chlorine. Industrial processes emit chlorine in many forms, particularly HCl (18). All of these contribute directly to the tropospheric chlorine budget and indirectly to the stratosphere via transport upward through the troposphere. Junge (19) has measured the gaseous chlorine content at sea level to be ~1 p.p.b. This concentration will vary with altitude in the troposphere because of loss through rainout of HCl but indicates that the assumed value for Fig. 3 is reasonable.

Other potential sources of stratospheric chlorine are direct injections by volcanic explosions (20, 21) and solid fuel rockets. Data on gaseous contents of eruptions are very sparse. Those explosive events which penetrate the tropopause are likely to involve large amounts of chlorine because they are often associated with intrusions of sea water (16). It is not known whether the chlorine will be in the gas phase or associated with ash cloud particles. Odd oxygen destruction rates were calculated for a volcanic injection source estimated in the following way. The data of Eaton (20) and Cronin (21) were

TABLE 4. Column-integrated odd oxygen destruction rates (molecules cm^{-2} s^{-1})

Chapman mechanism	3×10^{12}
NO–NO_2 cycle	7.5×10^{12}
NO_2–NO_3 cycle	3.1×10^{11}
ClO_x cycle, 1 p.p.b.	
High OH	3.9×10^{12}
Low OH	2.3×10^{12}
ClO_x cycle	
Ground level source	4.4×10^{11}
Volcanic source	1.2×10^{12}

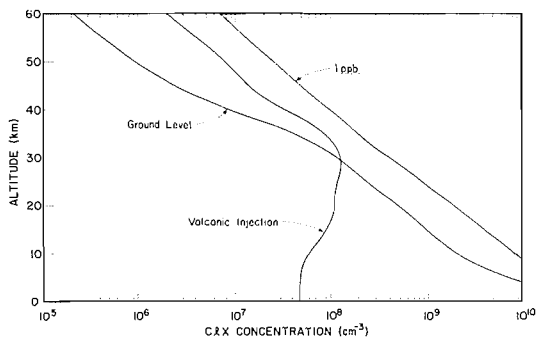

FIG. 3. Total gaseous chlorine (ClX) *vs.* altitude. The profiles due to ground level sources and direct injection into the stratosphere by volcanoes were computed as described in the text. A profile corresponding to an assumed 1 p.p.b. mixing ratio is also shown.

used to estimate a global and time averaged volcanic injection source strength of $\sim 10^{11}$ g/year. The injection rate certainly falls off rapidly with altitude and we guessed an exponential falloff with an e-folding height of 7 km. This is not unlike an observed ash cloud-top height distribution (20). Although the source strength is not very large and the statistics are very uncertian, the potential importance of this source is the direct injection of chlorine to stratospheric altitudes where ozone destruction occurs. Large volcanic eruptions which penetrate to the middle or upper stratosphere where most of the ozone destruction occurs could leave a noticeable local ozone hole.

In order to evaluate the destruction rate for this volcanic injection profile we used steady-state results from a one-dimensional eddy diffusion model for ClX. The diffusion equation was solved by an implicit technique with 2 km altitude steps and 5 day time steps. Tests were run with 12 h time steps with no change in results. The eddy diffusion coefficient was the seasonal average of Hays and Olivero (22). The density was taken as zero at 120 km and the flux to the ground was proportional to the density at the ground. The proportionality constant is the diffusion velocity near the ground which we took as 0.007 cm/s (23). Loss due to rainout with a 30 day period was included in the troposphere (24). This model was also used to evaluate a ground level source. These results were scaled to Junge's (19) measurement at the ground and the resulting ozone destruction rates are shown in Fig. 2. The ClX profile is given in Fig. 3 along with the ClX profile for the volcanic source described above

and a 1 p.p.b. constant mixing ratio. Figure 2 shows the corresponding odd oxygen destruction rates.

Summary

We have proposed a chemical scheme for gas-phase chlorine reactions in the stratosphere. We have shown that total ClX concentrations of ~ 1 p.p.b. give significant ozone destruction rates. A ClX concentration of 1 p.p.b. at 16 km implies about 0.1 p.p.b. of HCl. This is equal to the upper limit set by Farmer's (25) measurement. Indications are, therefore, that Fig. 2 gives an upper limit to the ClO_x ozone destruction. More precise statements cannot be made until the details of the interaction of chlorine chemistry with nitrogen, hydrogen, and carbon chemistry are investigated. Reaction 15 tying the ClO_x and NO_x cycles together tends to diminish the ozone destruction capacity of ClO_x. However, it converts NO to NO_2, thereby increasing the destruction of ozone by NO_x. Cl reactions with carbon compounds have been discussed by Prinn (26) in relation to the CO_2 stability problem on Venus and should be considered in a more detailed evaluation of stratospheric Cl chemistry. Finally, the next stage of stratospheric chlorine calculations should include a careful reevaluation of all possible chlorine sources and possible sinks such as adsorption on aerosols.

NOTE ADDED IN PROOF: The role of chlorine oxides in the stratosphere has also been discussed by M. J. Molina and F. S. Rowland in a paper submitted to Nature and is further elaborated by P. Crutzen and by S. Wofsy and M. McElroy in this issue.

We thank Donald Stedman (University of Michigan), Robert D. Hudson (NASA), David Garvin (National Bureau of Standards), Douglas Davis (University of Maryland), Harold Johnston (University of California, Berkeley), and Andrew Nagy (University of Michigan) for helpful discussions.

1. P. CRUTZEN. Q. J. R. Meteorol. Soc. **96**, 320 (1970).
2. H. JOHNSTON. Science, **173**, 517 (1971).
3. J. C. MCCONNELL and M. B. MCELROY. J. Atmos. Sci. **30**, 1465 (1973).
4. P. BEMAND, M. CLYNE, and R. WATSON. J. Chem. Soc. Faraday I, **8**, 1356 (1973).
5. H. JOHNSTON, E. MORRIS, JR., and J. VAN DEN BOGAERDE. J. Am. Chem. Soc. **91**, 7712 (1969).
6. R. BRINKMANN, A. GREEN, and C. BARTH. Jet. Prop. Lab. Tech. Report No. 32-951. 1966.
7. M. CLYNE and J. COXON. Proc. R. Soc. A, **303**, 207 (1968).
8. D. DAVIS, W. BRAUN, and A. BASS. Int. J. Chem. Kinet. **2**, 101 (1970).
9. J. KNOX and R. NELSON. Trans. Faraday Soc. **55**, 937 (1959).
10. V. KONDRATIEV. COM-72-10014, National Tech. Information Service, Springfield, Virginia. 1972.
11. J. MCCONNELL. J. Geophys. Res. **78**, 7812 (1973).
12. G. TAKACS and G. GLASS. J. Phys. Chem. **77**, 1948 (1973).
13. V. BALAKHNIN, V. EGOROV, and E. INTEZAROVA. Kinet. Catal. **12**, 258 (1971).
14. D. SEERY and D. BRITTON. J. Phys. Chem. **68**, 226 (1964).
15. S. WOFSY, J. MCCONNELL, and M. MCELROY. J. Geophys. Res. **77**, 4477 (1972).
16. G. MACDONALD. Volcanoes. Prentice-Hall, Englewood Cliffs, N.J. 1972.
17. R. DUCE. J. GEOPHYS. Res. **74**, 4597 (1969).
18. Q. R. STAHL. Litton Systems Report PB 188 067. 1969.
19. C. JUNGE. Tellus, **9**, 528 (1957).
20. G. EATON. J. Geophys. Res. **68**, 521 (1963).
21. J. CRONIN. Science, **172**, 847 (1971).
22. P. HAYS and J. OLIVERO. Planet. Space Sci. **18**, 1729 (1970).
23. B. BOLIN and C. KEELING. J. Geophys. Res. **68**, 3899 (1963).
24. W. JACOBI and K. ANDRE. J. Geophys. Res. **68**, 3799 (1963).
25. C. B. FARMER. Can. J. Chem. This issue.
26. R. PRINN. J. Atmos. Sci. **28**, 1058 (1971).

Can. J. Chem. Downloaded from www.nrcresearchpress.com by 210.87.254.5 on 09/05/12
For personal use only.

Climatic Effects of Stratospheric Chemistry

ROBERT E. DICKINSON

National Center for Atmospheric Research,[1] Boulder, Colorado

Received October 15, 1973

The paper reviews the present understanding of the climatic effects of stratospheric chemical composition within the general framework of climate modeling. The modulation of radiative fluxes by carbon dioxide, ozone, and aerosols provides an input to climate models. It is difficult observationally to distinguish between climate variation forced by changes in these or other external parameters and internal noise of the system. Indeed, ozone concentration is so coupled to atmospheric dynamics that it should be regarded as one of the internal variables. One-dimensional vertical and latitudinal climate models are described, and their conclusions as to tropospheric and stratospheric climate change discussed.

Les revisions des publications présentent une compréhension des influences climatiques de composition chimique stratosphérique, au sens général du terme, de type de climat. La modulation de flux de rayonnement par l'anhydride carbonique, l'ozone et des aérosols procure un apport aux types de climat. Il est difficile de distinguer expérimentalement entre la variation de climat contrainte par les changements de tels ou tels autres paramètres externes et de bruit interne du système. En effet, la concentration de l'ozone est tellement associée à la dynamique de l'atmosphère qu'elle devrait être considérée comme une des variables internes. Des types de climat à une dimension verticale et de latitude sont décrits, et leurs conclusions quant au changement de climat troposphérique et stratosphérique sont examinées. [Traduit par le journal]

Can. J. Chem., **52**, 1616 (1974)

Introduction

This paper will be primarily concerned with the climatic effects of stratospheric chemical composition and be interested in chemical processes only insofar as they determine the composition. The subject will be approached through consideration of the following four questions: (*a*) What is climate? (*b*) What are the present and future efforts toward modeling climate? (*c*) How does the stratospheric composition affect tropospheric and stratospheric climate (role of O_3, CO_2, aerosols, etc.)? (*d*) How does climate affect stratospheric chemistry?

The third question is the main theme of this paper. The need for considering the others is perhaps not so obvious. The first question is treated briefly because of a need nowadays in making quantitative calculations to be somewhat more precise in definition than is done with the usual loose usage of the term climate. The modeling of climate as treated in the second question is the means by which quantitative answers as to climatic effects must be derived and refined. Changes in climate (due to changes in composition or otherwise) will in turn change certain aspects of stratospheric chemistry and hence should be regarded as internal climatic variables rather than external influences and accordingly should be calculated jointly with other variables of a climate model. Thus we cannot adequately consider climatic effects of chemistry without also addressing the fourth question as to climatic effects on chemistry, that is the feedback of climate on chemistry.

Definition of Climate

Climate, of course, is concerned with the average behavior of the atmosphere rather than the day-to-day fluctuations referred to as weather. The weather is now known to be fundamentally unpredictable after about a 2 week interval. However, atmospheric behavior averaged over 2 weeks or even considerably longer contains a large noise factor given by the essentially random weather component. Leith (1) has suggested that to make the definition of climate precise, we partition all physical variables into either an internal system characterized by relatively rapid fluctuations or an external system within which the internal system is embedded and through which the internal system is provided relatively slowly changing

[1]The National Center for Atmospheric Research is sponsored by The National Science Foundation.

Can. J. Chem. Downloaded from www.nrcresearchpress.com by 210.87.254.5 on 09/05/12
For personal use only.

Can. J. Chem. Downloaded from www.nrcresearchpress.com by 210.87.254.5 on 09/05/12
For personal use only.

influences. The distinction then between internal system and external system is in general somewhat arbitrary but becomes quite definite for a particular mathematical model where there is a clear distinction between the variables to be computed by the model and those that are externally prescribed.

Figure 1 is used to indicate this partitioning between internal and external variables in current and future general circulation models (GCM's). The present paper will be largely concerned with the relationship of ozone, carbon dioxide, and stratospheric aerosols to climate. The distribution of carbon dioxide provides an obvious example of an external variable in that all present and future projected GCM's specify it as fully mixed with a given mixing ratio. However, even the carbon dioxide does have sources and sinks and varies with time, albeit slowly, so that simple residence time box models of the atmosphere and oceans intended to predict CO_2 as an internal variable have been devised (*e.g.*, ref. 2). Stratospheric aerosols presumably depend on the global circulation for providing their gaseous precursors, as well as their redistribution within and removal from the stratosphere, but the mechanics of their formation is now sufficiently uncertain as to preclude immediate coupling to large-scale circulation models.

Climate has been formally defined by Leith in terms of an ensemble of initial states such that all the climatic properties of the states are determined by the probability distribution of the climatic ensemble. Practically, if we make the fundamental assumption that different initial conditions will not lead to a different climatic regime, we can regard as climate the values of variables averaged over a fixed time interval after the noise component has been removed. For longer time intervals the noise component should be smaller. Lorenz (3) has discussed the possibility that many long time-scale fluctuations may be due only to the internal dynamics of the atmosphere–ocean–land–ice system without the need for any significant external changes. Such fluctuations in view of the above definition would be noise not removed by taking a long time average. The question as to what is noise is obviously very crucial to our understanding of climate and may be very difficult to answer. Figure 2 from Mitchell (4) shows long-term trends of mean surface temperatures, indicating an increase of 0.6 °C between the 1880's and the 1940's and a decrease of about 0.3 °C from then to 1970. The increase has sometimes been interpreted as due to the observed trend of increasing CO_2 and the decrease due to the trend of increasing tropospheric aerosol loading, both resulting from man's activities. This explanation cannot be ruled out and conceivably could be established quantitatively in a model which included various possible positive feedbacks on surface temperature by ice–albedo, water vapor mixing ratio, and cloudiness that I shall discuss later. However, our present knowledge of climatic effects of CO_2 and aerosol changes is yet too inadequate to even evaluate to within a factor of 2 the expected global mean temperature trend. Indeed, we cannot say whether the observed temperature variations must have been due to any external influence. They may well be long period noise rather than variations in climate as defined here.

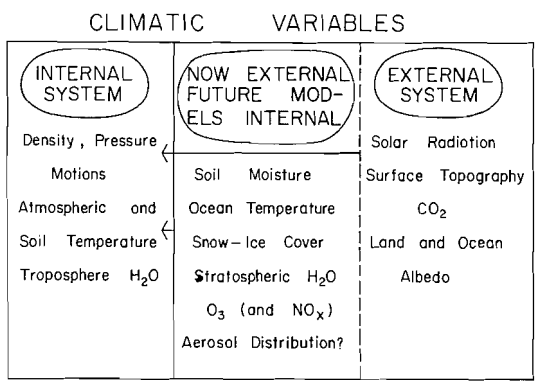

FIG. 1. The present and future partitioning of GCM variables into internal and external climatic variables.

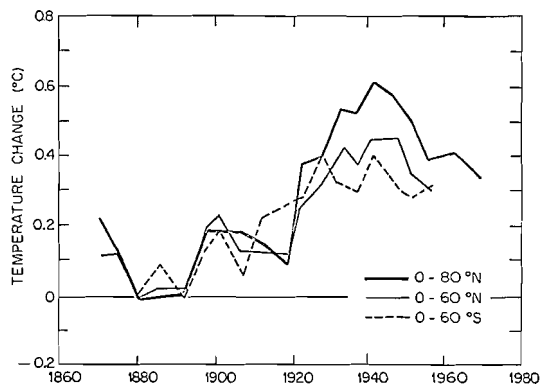

FIG. 2. Mean annual temperature for various latitude bands from Mitchell (4).

Can. J. Chem. Downloaded from www.nrcresearchpress.com by 210.87.254.5 on 09/05/12
For personal use only.

Climatic Models

The chemical composition of the stratosphere directly affects the absorption of solar and infrared radiation. The next section shall go into further detail as to how CO_2, O_3, and aerosols modulate radiative fluxes. The convergence of these fluxes provides sources of heating of the atmosphere and surface, and it is by this heating that climate is affected. To make use of these fluxes, we must consider two distinct problems: first, how the present day values of these fluxes determine in part the current climate and second, and perhaps more importantly, how changes in these fluxes lead to climate change. The effect of changes of these fluxes on climate is not easily evaluated but requires application of sophisticated mathematical models of climate. The development of such models is far from complete and the inadequacy of present models limits the accuracy by which climatic effects can be determined. Thus, it is important to recognize what has been done in the development of climate models, what is currently available, and what models we can expect to be operational in the near future. A thorough review of the topic of climate modeling is now in preparation (5). It is possible to give only a brief overview here. I will distinguish between models that determine stratospheric climate and those that are primarily useful for tropospheric climate.

It is useful to categorize climate models according to the geometric degrees of freedom. The simplest models of climate are essentially one dimensional with dependence on other dimensions being parameterized or simply neglected. One type of model, to be discussed further, is analogous to the one-dimensional chemical models in that it neglects horizontal dependence or at best assumes horizontal global averaging, but includes with fine resolution the vertical radiative and convective heat transfer processes. Other types of models completely parameterize the vertical dependence and determine variations with horizontal coordinates. Of the horizontal models, perhaps most important in the present context are those developed to describe statistics of the surface thermal balance. These could be used to study the role of stratospheric heat inputs on tropospheric climate.

For considering stratospheric climate in more than one dimension we may use certain types of dynamic models which treat only the stratosphere and ignore coupling to the troposphere. However, an entirely adequate model, even for considering only the stratosphere, should begin at the earth's surface and not only provide considerable vertical resolution for dynamic and radiative processes from there on into the stratosphere but also be appropriately coupled to the surface energy budget. Current GCM's partly satisfy these requirements but are not satisfactory climate models because sea surface temperatures and ice cover are prescribed rather than calculated and with existing computers it is only practical to solve the models for a year or two of simulated time. The computing time limitations of these models result from the fact that GCM's describe climate through first generating all the details of day-to-day weather. More useful models for study of climate changes would treat this climatic noise statistically rather than in detail so that integrations of hundreds of years could be carried out with the ocean temperatures and ice cover included as internal variables of the system. These models are especially necessary for evaluating the effect of possible changes of stratospheric composition on tropospheric climate. Any such changes would probably have an immediate effect on tropospheric climate which would be rather small compared to natural noise, but which would become much more significant if they persisted on the time scale over which ocean temperatures and ice cover would adjust.

Models capable of providing realistic descriptions of the change of climate in response to changing external conditions are not now available and will require some time to develop. It is, however, possible to combine existing models to determine at least whether climate is sensitive to possible changes in external conditions.

The global averaged radiative convective models (*e.g.*, ref. 6) provide one simple approach to this question of sensitivity by determining as a function of the vertical coordinate the radiative fluxes and the mean temperature profile that allows balance between these fluxes and other vertical energy transfer processes. These models include the vertical distribution of absorbers and scatterers and so can be used to compare the changes of heating rates and surface temperature implied by possible changes in these parameters with those due to changes in solar constant and surface albedo. The distribution of water vapor and the heat transfer by convection have been treated with simple and probably inadequate empirical parameterizations. For example, the

Can. J. Chem. Downloaded from www.nrcresearchpress.com by 210.87.254.5 on 09/05/12
For personal use only.

water vapor distribution has been assumed to conserve relative humidity, and convection, to keep the lapse rate from exceeding 6.5 °K/km. Much of our present knowledge of climate change due to variation in chemical composition has been derived from these or yet simpler models (7) so we shall discuss some of their conclusions in following sections. To answer whether a temperature change predicted by such a model is observable, it is necessary to know the noise level of natural temperature fluctuations. Empirical studies of GCM noise levels (8) together with theoretical expressions for the rate of decrease of noise with increased averaging time (9) may be used for this purpose, but for longer intervals this procedure will give a lower limit to the noise level since it does not allow for the increased long period noise due to coupling of atmosphere to oceans and ice.

Surface heat balance models (10, 11) depending only on latitude may be used to calculate changes in surface temperature with changes in incident solar radiation. These models have parameterized ice cover in terms of surface temperature thus providing a strong positive feedback on surface temperature, and increasing its sensitivity to changes in solar radiation. In other words decreased incident radiation leads to more ice, hence higher albedo and further reduction in the net radiation absorbed by the atmosphere–earth system. The absence of this and other feedbacks in one-dimensional vertical models certainly increases the unreliability of their conclusions. On the other hand, existing surface heat balance models are too crude in their parameterization of vertical processes to yield information concerning the climatic effect of changes localized to the stratosphere with the possible exception of changed tropospheric solar heating due to changed aerosol content.

The large GCM's, while not directly useful for studies of climatic change over many years, are now able to simulate much of the climatic detail of the *present* lower stratosphere and hence to provide considerable information as to what physical factors are most important in determining the observed climate. Besides modeling the radiative role of CO_2 and O_3 as discussed in the next section, these studies, *e.g.*, refs. 12, 13, have confirmed the strong dynamic coupling between troposphere and stratosphere that has been suggested by many earlier theoretical and observational studies. For example, much of the zonal asymmetry in the winter hemisphere and consequent large quasi-horizontal eddy transports derive from planetary waves propagating upward from the troposphere. Indeed the irregular topography of continental areas plays a large role in generating stratospheric eddies (12). The magnitude of this effect is illustrated in Fig. 3 which shows the northward eddy heat transport obtained at different levels in model simulation at NCAR with and without mountains.

Effect of Composition and its Variation on Climate

We now turn to the question of the determination of mean climate by its stratospheric chemical constituents and of climatic changes occurring in response to chemical changes. The global mean temperature structure of the stratosphere depends primarily on the balance between incoming solar u.v. radiation and outgoing thermal radiation, the latter largely emitted by 15 μ bands of CO_2 and to a lesser extent by 9.6 μ bands of O_3. Figure 4 from Dickinson (14) shows the net infrared cooling occurring between 30 and 80 km as calculated for the 9.6 μ bands alone and for the sum of the 9.6 μ bands and 15 μ bands. The temperature profile assumed for the calculation was a 1962 US standard atmosphere, but below 70 km very similar results are obtained for a global mean profile. The profile for u.v. heating (at least up to 70 km) must be essentially similar since the temperature and hence infrared cooling adjust to balance this heating. The increase of the cooling with altitude in the stratosphere results largely from the vertical increase of temperature and reflects the increase of solar energy absorption by ozone with decreasing u.v. optical depth. The upward decrease of cooling above 50 km (*i.e.*, in the mesosphere) and corresponding decrease of temperature reflect the vertical decrease of ozone mixing ratios in conjunction with optically thin u.v. absorption.

For temperature changes which are relatively small in amplitude and which have a vertical scale of one-scale height or greater, the infrared cooling is essentially linear in the local temperature change and so given by the product of the temperature change and a ("Newtonian") cooling coefficient, shown in Fig. 5 from Dickinson (14). Hence we can simply evaluate temperature change due to change in heating rates. Temperature relaxes back to its equilibrium value with an e-folding

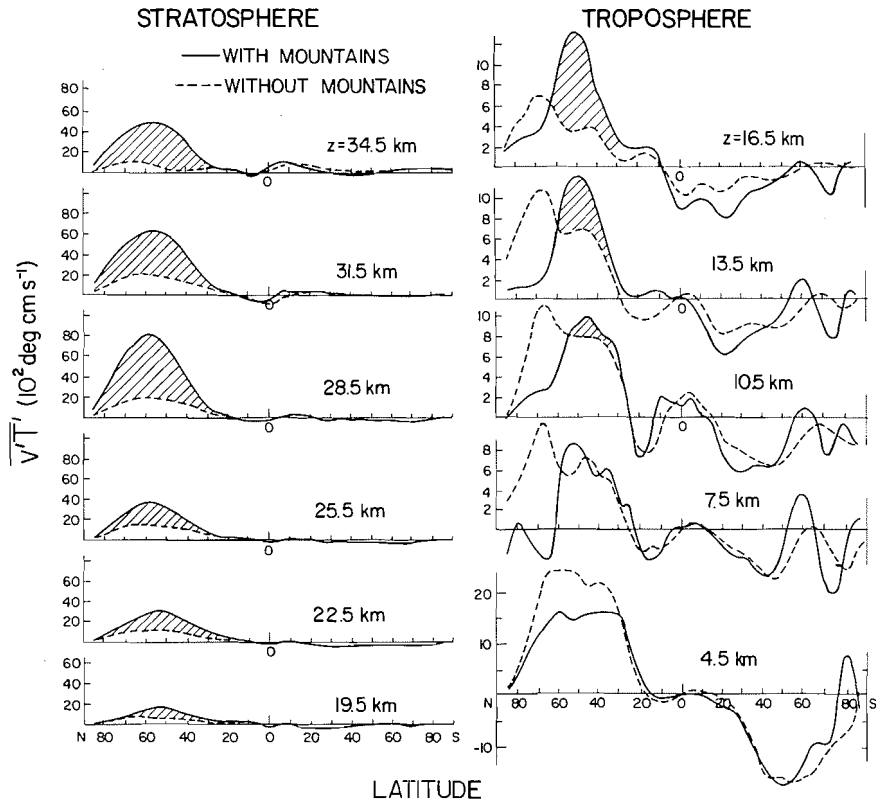

FIG. 3. Eddy heat transport at different levels of the NCAR GCM (from ref. 12) showing difference with and without mountains.

time of from 5 days at the stratopause to 15–20 days or more in the lower stratosphere.

Conventionally the global mean tropopause is regarded as the interface between a stratospheric temperature profile given by radiative equilibrium as described above and a tropospheric profile determined primarily by moist convection. Stone (15) on the other hand has argued, on the basis of a simple climate model involving horizontal and vertical eddy heat fluxes and ignoring moist convection, that the vertical heat transfer by large-scale eddies may be largely responsible for maintaining the tropospheric lapse rate. This issue as to whether vertical heat transfer by moist convection or by large-scale eddies is most influential is very important for understanding such climatic features as cloudiness–albedo and can only be resolved by considering models that contain both. As a result of the strong negative feedback of vertical eddy heat fluxes Stone's model predicts that the mean static stability (*i.e.*, difference between adiabatic temperature lapse rate and actual rate) should only change by a few percent with a factor of 2 change in solar radiation, even though the ground temperature changes by as much as 50–100 °C. On the other hand, if a moist convective lapse rate were to be preserved, the static stability would be extremely sensitive to surface temperature, a change of surface temperature being amplified by a threefold factor in the upper troposphere according to Kraus (16). Numerical experiments currently being carried out with the GCM at NCAR by Washington and Schneider show relative humidity at 3 km, and hence cloudiness and cloud albedo to be negatively correlated with mean ocean temperature. Thus in the model there is *such* a large sensitivity of tropospheric static stability to variations in surface temperature through control of lapse rate by moist convection that cloudiness gives a positive feedback effect on surface temperature.

Manabe and Wetherald (6), assuming surface albedo, cloudiness, and the tropospheric lapse rate to be fixed, have derived vertical temperature

Can. J. Chem. Downloaded from www.nrcresearchpress.com by 210.87.254.5 on 09/05/12
For personal use only.

Can. J. Chem. Downloaded from www.nrcresearchpress.com by 210.87.254.5 on 09/05/12
For personal use only.

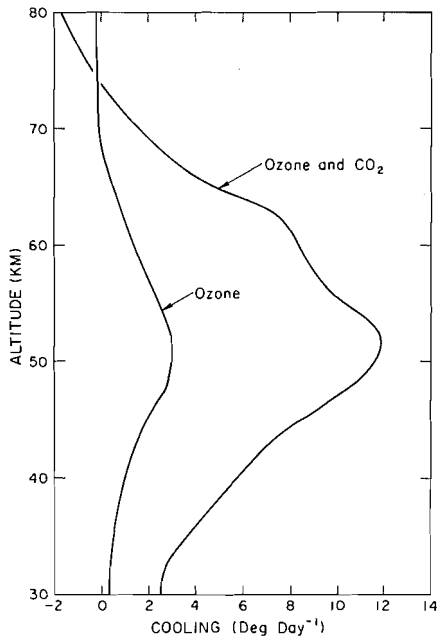

FIG. 4. Infrared cooling between 30 and 80 km calculated by Dickinson (14) for 15 μ CO_2 and 9.6 μ O_3 bands and 1962 US standard atmosphere.

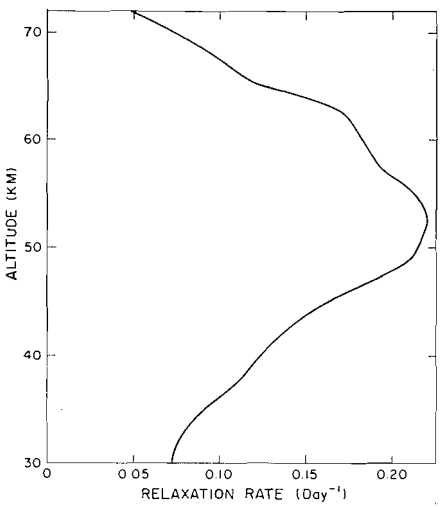

FIG. 5. Perturbation infrared cooling rate per 1 degree temperature perturbation according to Dickinson (14).

profiles between 0 and 40 km for a standard CO_2 distribution, half and double its value as shown in Fig. 6. Doubling CO_2 increases the infrared cooling and hence decreases temperature by as much as 10–20 °C above 30 km whereas the lower troposphere is increased 2° by the increased "greenhouse" trapping of surface emission and to a

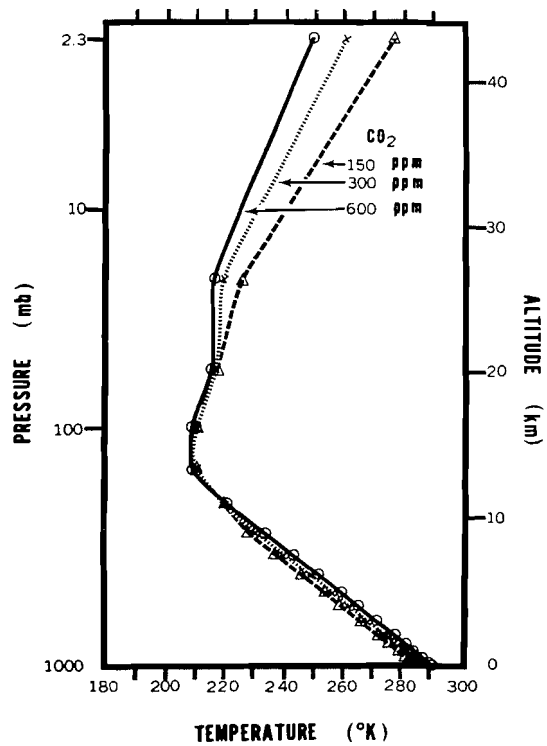

FIG. 6. Temperature profiles for 150, 300, and 600 p.p.m. CO_2 concentration calculated by Manabe and Wetherald (6) using radiative equilibrium and moist convective adjustment.

lesser extent by exchange with the colder stratosphere. The surface temperature likewise increases by ~2 °C. The increased thermal trapping as given by the increase of water vapor concentration implied by the assumption of constant relative humidity doubles the surface temperature increase compared to that derived with constant absolute humidity. In the stratosphere, the 15 μ cooling above 30 km is dominated by the emission from nonoverlapping Lorentz lines so that on the basis of analytic expressions for cooling from such lines we expect the cooling and hence variation of temperature to scale like the square root of CO_2 concentration.

To study the effect of large variations in ozone distributions Manabe and Wetherald (6) have used profiles of ozone observed for different latitudes in April (Fig. 7). The temperature profiles they computed for these different ozone profiles are shown in Fig. 8. The high equatorial profile gives a somewhat warmer stratosphere above 22 km and a sharper and colder tropopause at 100 mb. The equatorial profile reduces surface

Can. J. Chem. Downloaded from www.nrcresearchpress.com by 210.87.254.5 on 09/05/12
For personal use only.

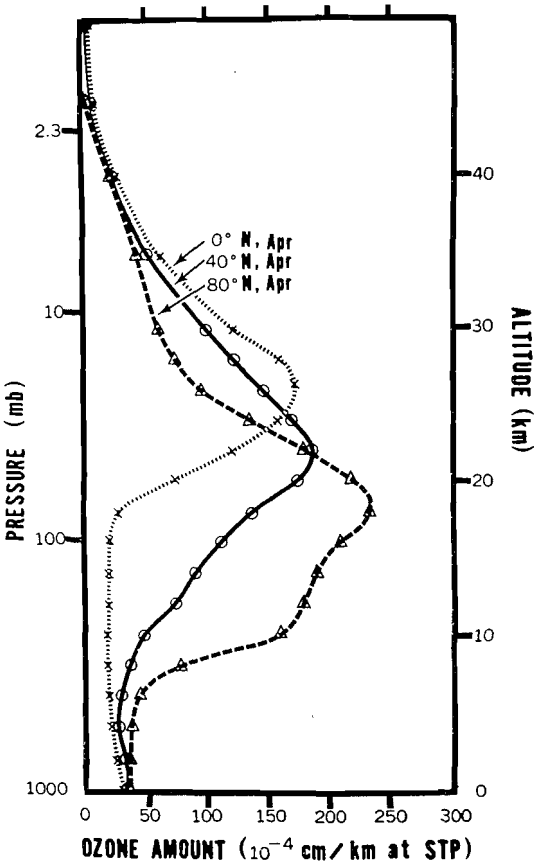

FIG. 7. Three different ozone profiles used by Manabe and Wetherald (6).

temperature by 1° and the polar profile increases it by 1° relative to the mid-latitude profile.

Carbon dioxide has been increasing from 290 p.p.m. in the mid 19th century to present values of 325 p.p.m. and to extrapolated values of 400 p.p.m. by the 21st century, suggesting a net cooling of the upper stratosphere from the pre-industrial value of 1–2 °C and 3–5 °C respectively, based on scaling from the calculations discussed above. The total ozone in the Northern Hemisphere has increased over the last decade at a rate of approximately 1% per year (*cf.* ref. 19). There is no reason to expect changes in the total ozone measurements to reflect changes in ozone above 30 km, but if a 10% increase of ozone were to occur at the stratopause it would increase the global mean temperature at this level by nearly 5 °C.

The impact of industrial activity on aerosol concentrations appears largely localized to Northern Hemisphere continents and to the immediately downwind ocean areas. Thus variations in stratospheric aerosol seem essentially controlled by volcanic activity, as indicated in Fig. 9, showing year-to-year variations in transmittance of solar radiation at Mauna Loa and, in particular, a discontinuous 2% drop after the Mt. Agung eruption. Unfortunately the radiative properties of global stratospheric aerosol such as size distribution, number concentrations, and complex index of refraction are still too poorly known to allow derivation of stratospheric heating rates. However, the effect on tropospheric climate involves largely the diminution by these particles of total solar radiation reaching the troposphere which can be estimated from measured variations in the attenuation of direct radiation. A 2% change in direct radiation corresponds to at least the 0.3% change in total radiation suggested by Budyko (10) depending on the aerosol size distribution and hence ratio of forward scattering to absorption and backscattering. A 1% reduction in solar radiation reaching the lower troposphere would produce essentially a 1 °C drop in global mean temperature if surface

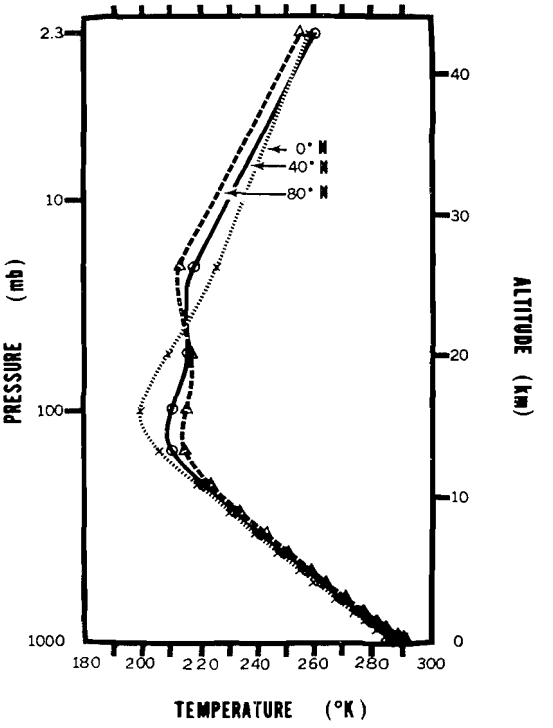

FIG. 8. Temperature profiles calculated as in Fig. 6 except with 300 p.p.m. CO_2 and the ozone profiles of 7.

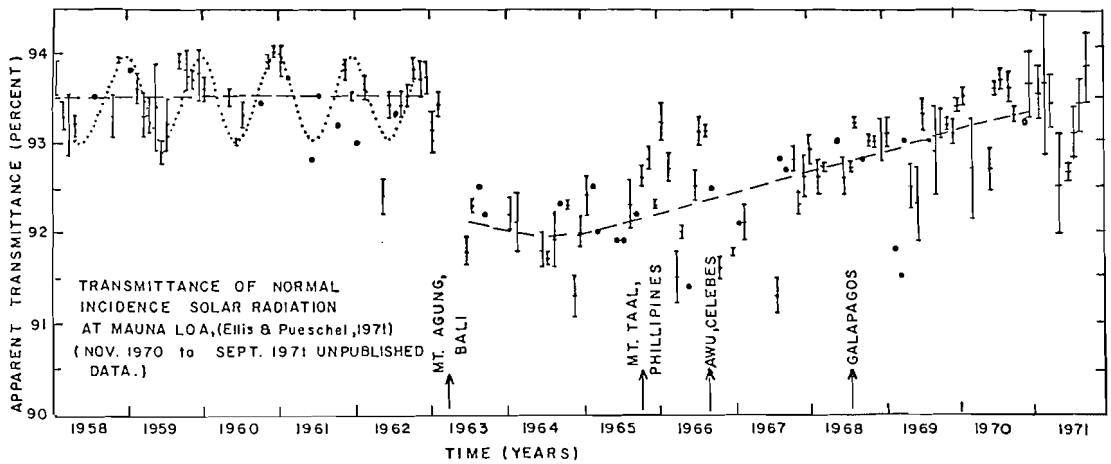

FIG. 9. Transmittance of solar radiation at Mauna Loa, from Mitchell (4).

albedo, water vapor distribution, and cloudiness were to remain fixed. However, the latitudinal models with temperature – ice albedo coupling indicate the positive feedback by ice cover generates a threefold or greater enhancement of the temperature decrease, whereas conservation of relative humidity gives another factor of 2. Even without coupling of surface temperature to cloudiness there is consequently the possibility of an ice age with as little as 1% reduction in solar radiation if it were to persist long enough for ocean surface temperatures to come into equilibrium.

I have not considered here stratospheric water vapor. Newell (17) has discussed the possible increase in mother-of-pearl clouds over Norway accompanying an increase of stratospheric humidity. The consequent change in global albedo and trapping of infrared radiation would be small but perhaps not negligible.

The paper up to this point has concentrated primarily on the radiative effects of stratospheric change on tropospheric climate. It seems likely, however, that stratospheric changes could also have a significant impact on the troposphere through modification of dynamic coupling mechanisms. Changes of stratospheric static stability, for example, would change the reflection and transmission coefficients of the stratosphere to planetary waves. The resulting phase shifts of these waves in the troposphere could significantly alter such climatic features as longitudinal variations of rainfall. The frequency of mid-winter stratospheric warmings could also be sensitive to such changes. Quantitative dynamic models with longitudinal resolution need to be worked out to study such effects but are not presently available.

Impact of Climate on Stratospheric Chemistry

In considering the effect of climate on stratospheric chemistry I shall consider only the effect on ozone distribution, since the coupling between meteorology and other stratospheric chemicals of climatic importance is still too poorly known to say much about it. The climatic parameters most significant for the ozone distribution are temperature in the upper stratosphere and ozone transport in the lower stratosphere.

Ozone depends on temperature through the temperature dependence of the chemical relations which determine its net chemical production and loss. The direct and catalytic loss processes for odd oxygen are accelerated by increased temperature with consequent reduction in ozone concentrations. Less ozone absorbs less u.v. radiation tending to again reduce stratospheric temperature. Quantitative models of this negative feedback have been constructed by Blake and Lindzen (18) which indicate that between the levels of 30 and 50 km the temperature dependence of ozone is essentially as important as the temperature dependence of infrared cooling in minimizing temperature excursions.

The bulk of total ozone resides in the lower stratosphere as a rather unreactive species having been carried downward from the region of net ozone production between altitudes of 25 and 30 km. Most of this transport is carried out in the

Can. J. Chem. Downloaded from www.nrcresearchpress.com by 210.87.254.5 on 09/05/12
For personal use only.

winter hemisphere by disturbances generated in the troposphere which penetrate upward into the stratosphere. Climate trends in the statistics of these disturbances due to modification of their tropospheric sources or transmission into stratosphere could possibly account for the observed trends of total ozone, but we need much more reliable climatic models of the average interaction between ozone chemistry and the general circulation before this speculation could be subjected to quantitative examination.

Conclusion

In conclusion, the details of the global aerosol distribution and its radiative properties are still too poorly known for long-term changes to be related to climate change. Ozone and CO_2 distributions are less of a problem. However, the most serious obstacle preventing determination of the possible climatic change due to changing stratospheric composition is the absence of reliable quantitative models of climate.

The permission of Authors and Publishers to reproduce Fig. 3 (from ref. 12), Figs. 6, 7, 8 (from ref. 6), and Figs. 2, 9 (from ref. 4) is gratefully acknowledged.

1. C. E. LEITH. Unpublished.
2. C. D. KEELING. The carbon dioxide cycle: reservoir models to depict the exchange of atmospheric carbon dioxide with the oceans and land plants. *In* Chemistry of the lower atmosphere. *Edited by* S. I. Rasool. 1973. pp. 251–329.
3. E. N. LORENZ. Meteorol. Monogr. **5**, 1 (1968).
4. J. M. MITCHELL. A reassessment of atmospheric pollution as a cause of long-term changes of a global temperature. *In* Global effects of environmental pollution. 1973. In press.
5. S. H. SCHNEIDER and R. E. DICKINSON. To be published.
6. S. MANABE and R. J. WETHERALD. J. Atmos. Sci. **24**, 241 (1967).
7. S. H. SCHNEIDER. J. Atmos. Sci. **29**, 1413 (1972).
8. R. CHERVIN and S. H. SCHNEIDER. Unpublished.
9. C. E. LEITH. J. Appl. Meteorol. **12**, 1066 (1973).
10. M. I. BUDYKO. Tellus, **21**, 611 (1969).
11. W. D. SELLERS. J. Appl Meteorol. **8**, 392 (1969).
12. A. KASAHARA, T. SASAMORI, and W. WASHINGTON. J. Atmos. Sci. **30**, 1229 (1973).
13. J. D. MAHLMAN and S. MANABE. Proc. Survey Conf., Climatic Impact Assessment Program, U.S. Dept. Transportation, DOT-TSC-OST-72-13. 1972. pp. 186–193.
14. R. E. DICKINSON. J. Geophys. Res. **78**, 4451 (1973).
15. P. H. STONE. J. Atmos. Sci. **30**, 521 (1973).
16. E. B. KRAUS. Nature, **245**, 129 (1973).
17. R. E. NEWELL. Proc. Survey Conf., Climatic Impact Assessment Program, U.S. Dept. Transportation, DOT-TSC-OST-72-13. 1972. pp. 165–185.
18. D. BLAKE and R. S. LINDZEN. Mon. Weather Rev. In press.
19. H. U. DÜTSCH. Can. J. Chem. This issue.

Can. J. Chem. Downloaded from www.nrcresearchpress.com by 210.87.254.5 on 09/05/12
For personal use only.

Uncertainties in Stratospheric–Mesospheric Modeling

J. C. McCONNELL
Department of Physics, York University, Toronto, Ontario

Received January 14, 1974

Some of the problems and uncertainties of stratospheric–mesospheric modeling are discussed in terms of the variables which constitute the continuity equation. The status of one- and two-dimensional eddy coefficients, required in the evaluation of the flux equation, are briefly reviewed. The production and loss terms are discussed both generally and with respect to the particular uncertainties in the CH_4, H_2O–HO_x, NO_x, and O_3 chemistries.

Certains problèmes et incertitudes de la représentation stratosphérique–mésosphérique par modèle sont examinés en fonction de variables qui constituent l'équation de continuité. Les conditions des coefficients de turbulence à une et deux dimensions, nécessaires pour l'évaluation de l'équation du flux sont brièvement revisées. Les termes de production et de perte sont étudiés d'une manière générale et aussi par rapport aux incertitudes particulières dans la chimie de CH_4, H_2O–HO_x, NO_x et O_3.

[Traduit par le journal]

Can. J. Chem., **52**, 1625 (1974)

Can. J. Chem. Downloaded from www.nrcresearchpress.com by 210.87.254.42 on 09/05/12
For personal use only.

Introduction

In the past few years there has appeared a plethora of atmospheric models, each using different assumptions concerning chemistry and dynamics such that the situation is sometimes confusing for those not in the mainstream of atmospheric modeling. Following the suggestion from the convener of the symposium, H. I. Schiff, I will attempt to outline some of the problems and limitations of the various approaches used in modeling the stratosphere and mesosphere. Also I will discuss the uncertainties in the various parameters used which are crucial, such as eddy diffusion coefficients, chemical rate coefficients, and solar fluxes. Part of what I shall cover has been mentioned by the previous reviewers. However, the following is an attempt to highlight the problems in such a fashion that it will be useful to those not involved in atmospheric modeling.

The determination of the properties of a fluid requires five equations, *viz.* the three equations of motion, the continuity equation, and the thermodynamic equation. Few studies attempt to solve all five equations simultaneously due to their great complexity. Most aeronomic models use from one to three equations. The discussion following is centered on the equation of continuity for k interacting constituents

$$[1] \quad \frac{\partial n_i}{\partial t} + \nabla \cdot \Phi_i = P_i - L_i n_i \quad i = 1, \ldots, k$$

where P_i is the production rate of n_i, L_i (n_1,.., n_i,...n_k) is the loss frequency of n_i, and Φ_i is the flux of the ith constituent. The next few sections discuss the general problems involved in evaluating Φ_i, P_i, and L_i, while the later sections discuss problems specific to CH_4, HO_x, NO_x, and O_3 chemistries.

Flux Equations and Transport Data

Experiments indicate that molecular diffusion is not adequate to describe the transport of mass below about 90–100 km and one must invoke transport by mean motions – circulation, and by variation of atmospheric velocities about this temporal or average circulation – eddy transport.

In the stratosphere and mesosphere one normally assumes that eddy diffusion predominates over molecular diffusion. The usual one-dimensional mixing length approximation to the vertical flux of a minor constituent is

$$[2] \quad \Phi_i = -K_z M \, \mathrm{d}f_i/\mathrm{d}z = -K_z \left\{ \frac{\mathrm{d}n_i}{\mathrm{d}z} + \frac{n_i}{H_{AV}} \right\}$$

where f_i is the mixing ratio (by number), M is the atmospheric number density, and K_z is the vertical diffusion coefficient. H_{AV} is the atmospheric scale height. The atmosphere is assumed to be at rest. Many dynamicists shudder at the thought of using one-dimensional eddy coefficients in a three-dimensional problem. Nevertheless, properly used they are inexpensive, and can assist in

Can. J. Chem. Downloaded from www.nrcresearchpress.com by 210.87.254.42 on 09/05/12
For personal use only.

determining the important processes occurring in the atmosphere.

In two space dimensions (*i.e.* meridional and vertical) one no longer makes the assumption of a static background atmosphere. Allowing for mean motions and variations about the mean, Reed and German (1) suggested that the meridional flux be given by

$$[3] \quad \Phi_{mi} = n_i v - K_{yy}\frac{\partial n_i}{\partial z} - K_{yz}\left\{\frac{\partial n_i}{\partial z} + \frac{n_i}{H_{AV}}\right\}$$

and the vertical flux be given by

$$[4] \quad \Phi_{vi} = n_i w - K_{zz}\left\{\frac{\partial n_i}{\partial z} + \frac{n_i}{H_{AV}}\right\} - K_{yz}\frac{dn_i}{dz}$$

where K_{yy} and K_{zz} are the horizontal and vertical eddy diffusion coefficients respectively. The vertical and horizontal components of the mean motion are w and v respectively. K_{yz} is the term due to correlation between vertical and horizontal velocity fluctuations about the mean motion. Reed and German (1) show that $K_{yz} \simeq \bar{\alpha}K_{yy}$, where $\bar{\alpha}$ is the preferred or mean mixing slope. This means that if the mean mixing slope is greater than the mean mixing ratio slope (isoline) then contragradient transport can occur which is contrary to the simple Fickian diffusion model.

The problem is in knowing how reliable the transport data are. With this in mind the various methods of obtaining transport data are discussed along with the results obtained from some recent studies.

Eddy transport coefficients are derived from many sources. One method that has been employed is the analysis of heat transport in the thermosphere and mesosphere (2). The main uncertainty is in the calculation of the heat sources. Vertical eddy coefficients have also been derived from analysis of gravity waves in the stratosphere and mesosphere (3, 4). The method used by Justus (4) is based on the relation between K_z and the offset condition for dissipation of internal gravity waves obtained by Hines (5, 6). The values obtained by Justus (4) probably represent upper limits to K_z. Another method uses the result that the vertical distribution of some constituents depends sensitively on the interaction of chemistry and transport. By modeling the chemistry and varying K_z one may compare the calculations with the measured vertical distribution of gas. Depending on the chemical lifetime of the gas one can probe different regions of the atmosphere. This has been done using N_2O (7), CH_4 (8), O, and O_2 (9). The reliability of this method depends very much on our knowledge of the chemical processes involved. Figure 1 shows some values of K_z now in use in atmospheric models. The consensus of the most recent studies seems to indicate fairly rapid transport in the upper stratosphere and mesosphere contrary to some older studies (11). This means that many of the older aeronomic models may be inaccurate due to erroneous transport data.

Heat transport data in the stratosphere have been utilized to deduce two-dimensional K's (1, 12). Evaluation of these coefficients, however, is very susceptible to the availability of a large amount of reliable data. A comparison of some eddy coefficients from two independent studies (1, 12), shown in Fig. 2, shows just how sensitive the K's are to different data sets. To date the data compiled by Luther (12) seem to be the best available. Analysis of radioactive debris deposited in the stratosphere has also yielded information on eddy coefficients. In this case the K's are varied to obtain agreement between the measured and calculated distributions of radioactive debris. Some of the data from the study of Gudiksen *et al.* (10) are compared with the heat transport data in Fig. 2. Considering the complete set of data for 50 and 100 mb throughout the year, one finds that generally the largest values of K_{yy} and K_{yz} are obtained by Reed and German (1) and the smallest values by Gudiksen *et al.* (10). For K_{zz} there is much less dispersion in the three sets of

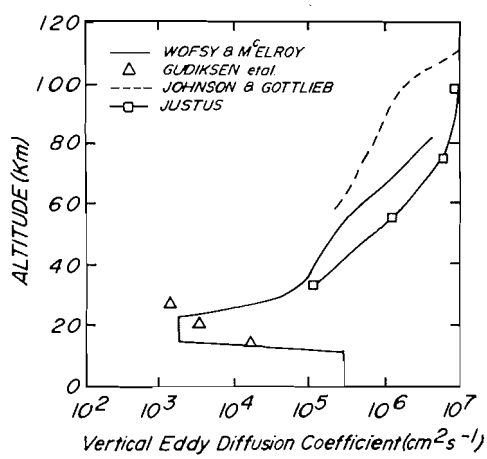

FIG. 1. Vertical eddy diffusion coefficients *vs.* altitude: Johnston and Gottlieb (2), Justus (4), Wofsy and McElroy (8), and Gudiksen *et al.* (10) (after Justus (4)).

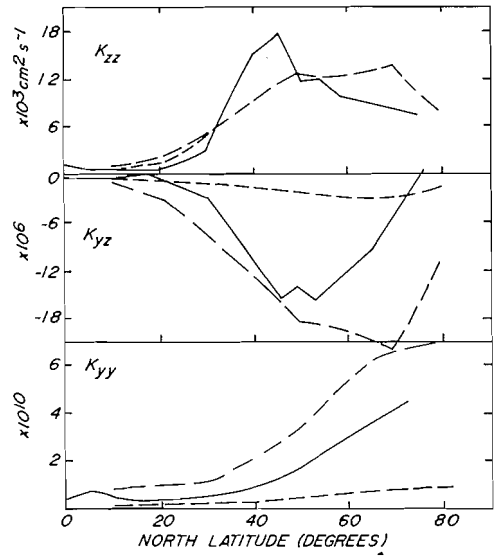

FIG. 2. Profiles of two-dimensional eddy coefficients K_{zz}, K_{yz}, K_{yy} *vs.* latitude for the period January to March for a pressure of 50 mb. (— —) Reed and German (1); (——) Luther (12); (---) Gudiksen *et al.* (10).

data. The reliability of the data is such that for modeling it would seem appropriate to investigate the effect of using all three data sets.

Mean vertical and meridional velocity fields in the stratosphere and mesosphere have been deduced by Murgatroyd and Goody (13) and Murgatroyd and Singleton (14) on the basis of heat budget calculations, no allowance being made for eddy motions. More recent data has been analyzed by Vincent (15). He calculated the mean meridional circulations from zonally averaged sources and sinks of momentum and heat.

A few points are worth noting with regard to using K's in models. The observed mean wind fields and eddy coefficients are not independent since K_{yy} is deduced on the basis of the mean deviation of the winds about the mean circulation. Thus it is not wholly consistent to take a velocity field from one set of results and K's from another. Also transport data are a function of the space and time scales used to deduce them and so K's obtained by studying large scale motions will be inappropriate for use in problems with a smaller scale, *e.g.* initial dispersal of a contaminant from an aircraft flying in the stratosphere. Lastly, we have implicitly assumed that the K's obtained by the different methods should be the same. This may not be so, since the effective mixing length of an air parcel (and so K) will depend on the property of interest. For example the heat content of a parcel of air may equilibrate more or less rapidly with its surroundings than density. In addition to different K's for different properties, there may be different K's for different chemical species. This could occur due to different species undergoing differing amounts of depletion inside the same air parcel because of different chemical lifetimes. A comparison of the various relaxation times associated with mixing, chemistry, etc. would be illuminating (*cf.* ref. 16). So far this has not been done.

A major problem with transport data is that there is as yet no simple and inexpensive way of obtaining estimates of K, especially of the K_{ij}. If this were so it would enable the models to much more readily incorporate feedback from the chemistry into the dynamics.

Chemical Production and Loss

The evaluation of P_i and L_i in [1] frequently requires knowledge of solar fluxes and molecular absorption cross sections. Thus the uncertainty in these parameters will propagate nonlinearly into the solution for n_i. The status of solar fluxes and cross sections has been reviewed in detail at this conference (17, 18) and all I wish to do is to pick out the most important points.

Solar flux measurements are fairly well established in the spectral region $\lambda > 2100$ Å and for L_α (17, 19, 20). For $\lambda < 2100$ Å there still remains a problem particularly in the region $\lambda \sim 1600$ Å, the region of the solar temperature minimum. This region, however, is not of direct interest to stratospheric and mesospheric chemistry. Rather it is the region 1800–2100 Å that is very important, since it is at these wavelengths that NO and H_2O are dissociated in the mesosphere and that O_2 is dissociated in the stratosphere.

It has recently been suggested that O_3 densities have been increasing in the past decade (21), and that the increase is due to the gradual recovery of the stratosphere from NO_X input by bomb tests in the period 1952–1962 (21, 22). In order to distinguish such variations of O_3 (or any other species) due to man's activity from natural long term variability, it is important to know how solar radiation varies with time. According to Heath (23), there is perhaps a 3% variation of solar radiation at about 3000 Å, and about 6% variation at about 1750 Å with about a 22 month periodicity. Any longer term variations could have

Can. J. Chem. Downloaded from www.nrcresearchpress.com by 210.87.254.42 on 09/05/12
For personal use only.

Can. J. Chem. Downloaded from www.nrcresearchpress.com by 210.87.254.42 on 09/05/12
For personal use only.

been masked by the degradation of the instruments sensitivity. Obviously more work is required in order to obtain information on long term solar radiation variability.

The attenuation of solar radiation in the stratosphere and mesosphere is dependent mainly on absorption by O_2 and O_3. The main uncertainty is evaluation of the absorption of radiation by the Schuuman–Runge bands of O_2 due to lack of accurate knowledge on the width of the lines in the bands (18). This appears to be an area which requires further experimental work. Absorption by CO_2 is also important in the upper mesosphere where CO_2 shields $O_2(^1\Delta)$ from ionization (24). Absorption of L_α by CH_4 and H_2O is important in the mesosphere. Until the recent work of Ausloos *et al.* (*cf.* ref. 25) the dissociation products had not been uniquely identified. Most of the cross section data for the more important reactions are reasonably well known. The most uncertain data is for the long wavelength tail of the H_2O cross section.

In addition to solar fluxes and cross sections, the solution of [1] requires a fairly detailed knowledge of the reactions involved in the chemistry of n_i. In the past few years there has been an explosion of work on reactions which are of interest to atmospheric chemistry. Most of this has been collected in National Bureau of Standard Reports (26, 27) and has been carefully evaluated. One should caution, however, that the evaluators have sometimes been too intent on fitting rate data acquired over a large temperature range to a single Arrhenius' expression. This frequently results in expressions which are erroneous at stratospheric temperatures (*e.g.* CO, CH_4).

A point to note is that in the past many modelers have quoted other modelers' rate data without inquiring carefully into the pedigree of that data. This trait appears to have slowed down but I would still recommend checking carefully the information available for an important rate constant.

There are still a good many reactions whose rate constants are not well determined. The reactions of importance are briefly discussed in a later section. In addition, there may be a good many reactions of which we are not aware, yet which are important to some aspect of stratospheric and mesospheric aeronomy.

Approximations to the Continuity Equation

There are various approximations used to solve the equation of continuity. The method frequently used in simplifying [1] is to compare time constants associated with each term in the continuity equation and retain those terms with the shortest time constants. Thus the time constant τ_c associated with chemistry is $1/L_i$ (or n_i/P_i). The diffusion time constant τ_K is approximately l^2/K where l is a length representative of the scale of the diffusion. Frequently the $\partial n/\partial t$ term is driven by changes in solar insolation and so has a time constant $\simeq 1/2$ day except at sunset when it can become much shorter.

The simplest approximation used is one of photochemical steady state which ignores motions and any time dependence. This seems reasonable if $\tau_c \ll 1$ day $\ll \tau_K$ for vertical motion. One chooses a solar zenith angle and solves the equation. However, this approximation is also used if $\tau_c > 1$ day but with $\tau_K > \tau_c$, *i.e.* one averages chemical production and loss over many days. A fixed solar zenith angle is assumed or else photodissociation rates are averaged over the day. This method seems quite reasonable in practice but has certain limitations. Choosing a fixed solar zenith or Joshua angle (Joshua 10.V13) can sometimes lead to severe problems when the dissociation rate is in the optically thick regime, *e.g.* the reason that the peak of the O_3 distribution calculated by many authors is much higher than that observed, is that an average solar zenith angle of say 45–60° has been used when really most of the dissociation at a given altitude is occurring at much smaller angles. Another limitation is that the averaging process itself may not be appropriate. However, this turns out to be important only in the more complex systems (see later).

In general in the stratosphere and mesosphere the time constants associated with diffusion are of the order of days or longer. Thus when flow is included in the continuity equation for calculation of n_i, *i.e.* $\nabla \cdot \Phi_i \neq 0$, the common approximation is to adopt average insolation conditions in order to avoid solving the complete time dependent problem. This again usually appears adequate but the previous caveats remain. Quite frequently in this type of calculation P_i and L_i involve species n_j, whose chemical time constants are much shorter than a day. In this case the photochemical steady state approximation is used to calculate the n_j using conditions of averaged insolation and the n_j are then used in P_i and L_i. This type of averaging is more open to question. However, in many of the applications to date the calculations of the distribution of constituents n_i with long time constants should

Can. J. Chem. Downloaded from www.nrcresearchpress.com by 210.87.254.42 on 09/05/12
For personal use only.

not differ by more than say 50% than those obtained from full (much more expensive) day–night time dependent models which are not normally run to steady state. For the constituents n_j (with $\tau_c \ll 1$ day) the above calculations appear to yield reasonable *average* n_j. Obviously the daily variation of n_j will not be simulated.

At first sight in the case with $\partial n_i/\partial t \neq 0$ one is limited in time stepping by the shortest time constant τ_c. However, this is not so, as reasonable (at least qualitatively) solutions may be obtained by taking large time steps if implicit-finite difference schemes are used to integrate. However, to my knowledge there does not appear to be, in the aeronomic literature, adequate documentation of the dependence of either n_i or the conservation properties of the solution on the values of the time step chosen (28, 29).

In solving the continuity and flux equations for each constituent one requires two boundary conditions. The lower boundaries of many of the longer lived constituents are chosen to be fixed, equal to the observed value if such is available. Other conditions chosen are photochemical steady state, *i.e.* a boundary is chosen at a location where diffusion is not a controlling process. This is adequate for upper boundaries of constituents such as O_3, and radicals such as OH, H, etc., in the stratosphere and mesosphere. Flux upper boundary conditions are also imposed on constituents such as CH_4, N_2O, etc. or NO_X when one can better estimate the flux than a mixing ratio.

For many of the modeling problems boundary conditions do not pose a major problem, but for constituents such as NO_X, NH_3, SO_X tropospheric values of mixing ratios are not well determined. Thus, picking a tropospheric value as representative of the base of the stratosphere is, at best, guessing. Since the errors in the boundary conditions can be expected to propagate into the region of interest this adds additional uncertainty to the calculations over and above that inherent in Φ_i, P_i, and L_i. However, some of the potential uncertainties in n_i due to boundary conditions are somewhat ameliorated by the presence of stratospheric sources which tend to overwhelm the effects due to boundary conditions.

In the past, many modelers have chosen boundary conditions out of computational simplicity rather than with regard to the physics of the situation (*cf.* ref. 28). Consequently the results have been rather odd!

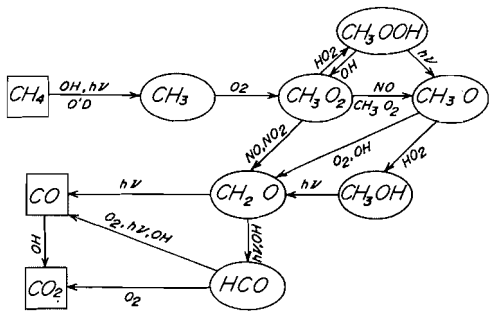

FIG. 3. CH_4–CO chemistry.

Individual Systems

The following section is a brief discussion of the present status of our knowledge of the stratospheric and mesospheric cycles of relatively long lived constituents such as CH_4 and H_2O and the reactions that occur as a result of their destruction by sunlight or radicals.

CH_4

CH_4 is produced at the surface of the earth and is destroyed in the atmosphere. The reactions for the initial breaking of the CH_3—H bond,

$$[5a] \quad CH_4 + OH \rightarrow CH_3 + H_2O$$

$$[5b] \quad + O(^1D) \rightarrow CH_3 + OH$$

$$[5c] \quad + h\nu(L_\alpha) \rightarrow CH_2 + H_2$$
$$\rightarrow CH + H_2 + H$$
$$\rightarrow CH_3 + H$$

seem reasonably well identified (30, 31). In addition, on the basis of laboratory chemistry, the eventual production of CH_2O seems certain. Destruction of CH_2O leads to CO and CO is, in turn, oxidized to CO_2 via

$$[6] \quad CO + OH \rightarrow CO_2 + H$$

This much seems reasonable since the calculated CH_2O and CO densities tie in with measurements of these species in the air and in rainwater (*cf.* refs. 30, 32). Much less certain are the intermediate paths from CH_3O_2 to CH_2O. The suggestions to date are shown in Fig. 3, which schematically outlines CH_4 oxidation. The schemes to convert CH_3O_2 to CH_2O involve HO_X and NO_X radicals (31, 33) and thus CH_4 chemistry is linked to both HO_X and NO_X chemistry in a nonlinear fashion. Because of the lack of definitive rates this coupling has not been explored in detail although it could be of more importance than has been generally realized. CH_4 destruction also leads to production of H_2

Can. J. Chem. Downloaded from www.nrcresearchpress.com by 210.87.254.42 on 09/05/12
For personal use only.

and H_2O (31) and thus to further coupling between H_2O and CH_4 cycles in the stratosphere and mesosphere.

CH_4, and CO in the lower stratosphere, have time constants long enough that transport process are very important in determining their distribution. A comparison of measured CH_4 and CO profiles with theory should lead to a better understanding of atmospheric dynamics.

As pointed out by Burke (34) CH_4 may also be a source of ionization in the D region via photolysis by L_α

[7] $$CH_4 + L_\alpha \rightarrow CH + H_2 + H$$

(*cf.* ref. 25) followed by the chemionizing reaction

[8] $$CH + O \rightarrow CHO^+ + e$$

H_2O and HO_X

It was the classic work of Bates and Nicolet in 1950 (35) that laid the cornerstone for aeronomy of H_2O. In spite of the large amount of work devoted to study of H_2O chemistry in the intervening years the most substantive theoretical development was the suggestion by Hampson (36) that $O(^1D)$ (formed by photolysis of O_3) reacting with H_2O was a source of HO_X radicals in the stratosphere. The present chemical scheme is shown in Fig. 4. The main features are that there is a net transport of H_2O to the troposphere and that the stratosphere probably acts as a source for H_2. In addition both H_2O and H_2 act as sources of the radicals H, OH, HO_2. Some H_2O flows upwards and is converted to H_2 and finally to H and escapes out the top of the atmosphere by Jeans escape (37). The basic flow pattern is shown in Fig. 5. This is based on the work of Hunten and Strobel (37). It does not include the H_2 source from CH_4 via CH_2O which should modify the altitude of the flow reversals somewhat. Nevertheless the basic pattern should remain unchanged.

The time constants involved for H_2O and H_2 in the stratosphere and mesosphere range from a few thousand years in the lower stratosphere to a few days in the upper mesosphere and so the mixing ratios of H_2 and H_2O must be determined using dynamics. However, the time constants involved in the production and loss of hydrogenous radicals HO_X is usually much shorter and photochemical steady state calculations should be adequate for average daytime densities. A time dependent calculation is required, of course, to trace the radical densities throughout the night.

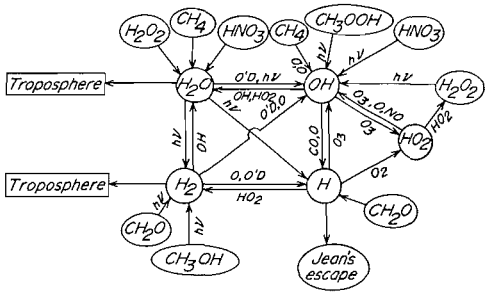

FIG. 4. H_2O–HO_X chemistry.

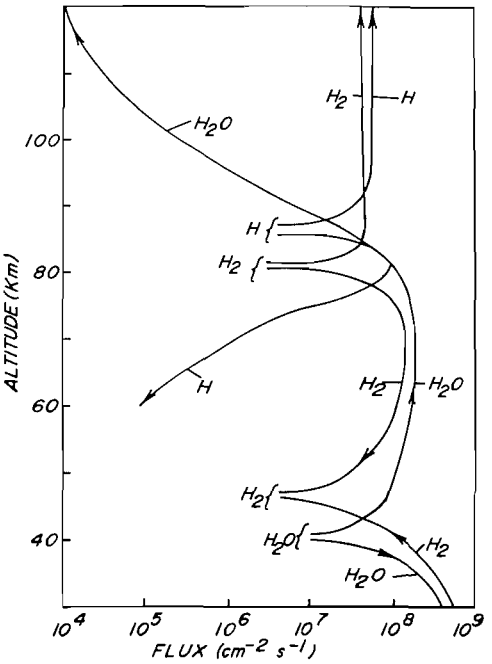

FIG. 5. Flows of H_2O, H_2, and H *vs.* altitude (after Hunten and Strobel (37)).

Knowledge of the OH to HO_2 ratio is important in the stratosphere (38). The main reactions involved in determining this ratio in the mesosphere are

[9] $$H + O_2 \xrightarrow{M} HO_2$$

[10] $$HO_2 + O \rightarrow OH + O_2$$

[11] $$OH + O \rightarrow H + O_2$$

and in the stratosphere

[12] $$OH + O_3 \rightarrow HO_2 + O_2$$

[13] $$HO_2 + O_3 \rightarrow OH + 2O_2$$

Of the rate coefficients required for these schemes perhaps the most uncertain are [10] and [11]

Can. J. Chem. Downloaded from www.nrcresearchpress.com by 210.87.254.42 on 09/05/12
For personal use only.

which are known only to within a factor of 3 (26, 27). Also, although of late the data on [13] is reasonably well determined at room temperature the activation energy is still not well known (39, 40) so that the OH/HO_2 rates cannot yet be well determined (by calculation) in the stratosphere. Other important reactions with poorly determined rates are the radical scavenging reactions

[14] $$OH + HO_2 \rightarrow H_2O + O_2$$

[15] $$H + HO_2 \rightarrow H_2 + O_2$$

Knowledge of these rates is important in determining the absolute OH, HO_2 densities and also production rates of H_2O and H_2. The latter quantities, however, are much less sensitive to changes in the rates of [14] and [15], since the production rates are to a large extent determined by the rate of destruction of H_2O and H_2, *i.e.* the $\nabla \cdot \Phi_i$ term does not dominate the continuity equation (*cf.* ref. 37).

An important process in the H_2O cycle is the dissociation of H_2O which occurs primarily in the Schuuman–Runge (S.R.) and L_α wavelength regions. Calculation of the dissociation rate in the S.R. region is hindered through lack of accurate knowledge of O_2 attenuation in the S.R. bands (18). In the L_α region H_2 is produced (*cf.* ref. 25), although many models have not included this effect.

NO_X

Nitrogen oxides, NO_X ($\simeq NO + NO_2 + HNO_3$) have only recently been recognized as playing an important role in stratospheric O_3 chemistry (41, 42). In solving the problem of the distribution of the oxides of nitrogen one finds that there is a mixture of time constants involved. The time constant for chemical distribution of NO_X is much longer than a day while the time constants associated with conversion of one form of NO_X to another are short, usually much less than a day. Hence it is usual to assume steady state to calculate the internal distribution of NO_X while including transport in the calculation of the vertical distribution of NO_X (43, 44).

The main sources of NO_X are oxidation of N_2O (7, 45, 46) and NH_3 (44, 47) and air fixation by cosmic rays (48). There is also the possibility of an NO source from ionospheric reactions (49). However, since the photolysis of NO in the mesosphere leads to odd nitrogen destruction (50),

[16] $$NO + h\nu \rightarrow N + O$$

[17] $$N + NO \rightarrow N_2 + O$$

stratospheric NO from this source must be transported from the ionosphere primarily during the polar nights. There is also much uncertainty concerning the NH_3 source since evaluation of this source requires knowledge of NH_3 mixing ratios in the upper troposphere and this information is not available (however, see ref. 51). In addition NH_3 low temperature oxidation chemistry is not well known and one cannot preclude the possibility that destruction of NH_3 leads to NO_X destruction (44, 47, 52).

Our knowledge of boundary conditions of NO_X leaves a lot to be desired. Knowledge of NO_X densities in unpolluted environments in the troposphere is very sparse, and in the past few years we seem to have better height information on NO_X in the stratosphere than in the troposphere (*cf.* ref. 53). The upper boundary condition is very important in determining mesospheric NO densities (50). Normally either assumed flux or measured mixing ratios are applied (44). However, unless the model assumptions are wildly inaccurate, the uncertainty in the upper boundary conditions does not propagate into the middle stratosphere (44). This is also the case for the tropopause boundary, *i.e.* for reasonable values of the tropopause mixing ratio the error does not propagate more than some 5–6 km into the stratosphere. This is because stratospheric sources of N_2O dominated the effect of the boundary conditions (44, 54).

The chemistry of NO_X appropriate to the lower stratosphere is shown in Fig. 6. Many of the important rates are reasonably well determined including the quantum yield for dissociation of

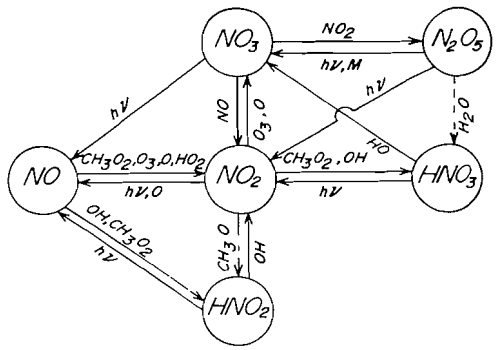

FIG. 6. NO_X chemistry.

Can. J. Chem. Downloaded from www.nrcresearchpress.com by 210.87.254.42 on 09/05/12
For personal use only.

HNO_3 (Johnston, private communication, 1973). One parameter of importance not yet well determined is the dissociation rate of NO in the $\delta(0, 0)$ band (50, 55). As mentioned earlier there are still problems in calculating the attenuation by the O_2 S.R. bands. Uncertainty in this parameter will lead to deficiencies in attempting to model accurately NO_X densities in the upper mesosphere.

Below 30 km the time constant for photodissociation of HNO_3 is greater than 1 day. Thus below this height, HNO_3 should not, on average, change much due to daily variations in insolation, and day–night averaged dissociation rates should be appropriate for calculating HNO_3 densities. Such is not the case for NO_2 which has a dissociation rate ~ 100 s. Many calculations of NO_X profiles have used average insolation conditions below 30 km to calculate NO, NO_2, and HNO_3 densities. This leads to problems when comparing calculated NO_X densities with measurements, particularly NO and NO_2. Converting the average NO_2 densities to equivalent daytime densities NO_2^{D1} and comparing them with NO_2 densities calculated using insolation conditions more appropriate to a time dependent calculation, *i.e.* NO_2^{D2}, yields for the ratio of $[NO_2^{D2}]$ to $[NO_2^{D1}]$

$$[18] \qquad w = \frac{[NO_2^{D2}]}{[NO_2^{D1}]} \simeq \frac{(1 + 2X)(1 + R + X)}{\left(1 + \frac{\alpha}{2}R + 2X\right)(1 + X)}$$

X is the $[NO]/[NO_2]$ ratio, R is the $[HNO_3]/[NO_2]$ ratio, both calculated for average insolation conditions, and α is the ratio of daytime OH densities to 'average' densities. For altitudes 30, 24, and 18 km, $w = 1.1, 1.3, 1.5$ respectively. This also leads to inaccuracies in calculating odd oxygen loss rates.

O_3

The chemical time constants involved in the O_3 or odd oxygen problem vary from a few hours at the mesospause to the order of a year at the O_3 peak. Most models, because of this mixture of time constants, usually use average insolation conditions and ignore transport. As mentioned earlier a single average angle is usually not appropriate due to the large O_2 and O_3 optical thicknesses and generally leads to O_3 peak heights which are not in agreement with observations.

Photochemical steady state is appropriate down to about 30 km, since $\tau_K \gg \tau_{chem} \geq 1$ h. Below 30 km, models with dynamics are required. There have been some simple one-dimensional models (*cf.* ref. 33). However, the two-dimensional models of Prabhakara (56), Rao and Christie (57), and Hesstvedt (58) are more appropriate dynamically. The problems are uncertainty in the dynamical data and the inclusion of complex chemistry. From the point of view of examining key reactions and complex feedback mechanisms the one-dimensional models have not outlived their usefulness, but due regard should be given to their limitations.

As has been discussed earlier O_3, H_2O, CH_4, and NO_X chemistries are all ultimately related. The largest chemical uncertainties at present pertain to reactions [10], [11] in the mesosphere and the [12], [13] cycle in the stratosphere. This latter cycle itself is important not so much because it destroys O_3, but because OH determines the amount of NO_X tied up as HNO_3 and HNO_3 does not directly affect O_3 (44, 59).

Recently Stolarski and Cicerone (60) and Wofsy and McElroy (61) have noted that chlorine containing compounds in the stratosphere could lead to a depletion of O_3. Much of the uncertainty in the conclusions is based on lack of knowledge of mixing ratios of Cl compounds in the upper troposphere. However, the agreement of the present models of O_3 without Cl destruction and O_3 measurements above 30 km would seem to imply that Cl destruction of O_3 is not a major loss for O_3. The main HO_X, NO_X, and ClO_X catalytic destruction cycles for O_3 are shown in Fig. 7.

Coupling

The distribution of each of the species mentioned previously is directly or indirectly dependent on transport, and in turn each species is dependent on the interacting chemistries. Thus one cannot deal with the problem of determining the distribution of a stratospheric constituent in isolation. An example is the case of O_3–H_2O chemistry where increasing H_2O leads to a decrease in O_3, but if the calculations are repeated including NO_X in the scheme, O_3 is increased. This is due to the OH increase tying up more NO_X as HNO_3, resulting in less O_3 destruction by NO_2 (33, 62). Another example is the N_2O source of stratospheric NO which is sensitive to O_3 via optical thickness and O^1D effects (44). However,

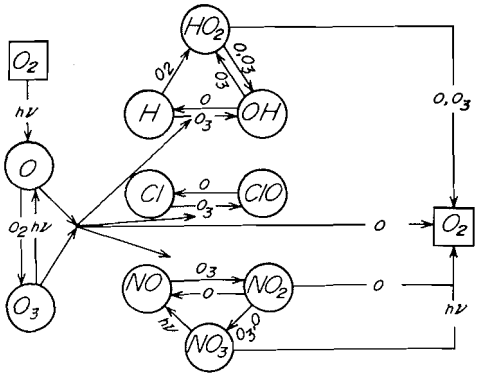

FIG. 7. O_3 chemistry.

the change in NO production concomitant with O_3 change is not as large as might have first been supposed (62).

Another coupling mechanism is that due to temperature effects. Solar ultraviolet absorption by O_3 is a major heat source in the stratosphere and several of the reactions in the O_3 cycle are temperature sensitive. However, in this case the feedback is negative and a runaway effect is avoided when O_3 is changed (57, 62). Thus a decrease in O_3, for example, leads to a decrease in heating and so temperature. A decrease in temperature leads to a decrease in O_3 destruction compensating the original change. The dynamics of the stratosphere is a function of the O_3 heating rate. Thus changing O_3 will affect stratospheric motions which play a major role in the O_3 budget in the lower stratosphere. The major chemical couplings between the various constituents themselves and between them and temperature and dynamics are shown schematically in Fig. 8.

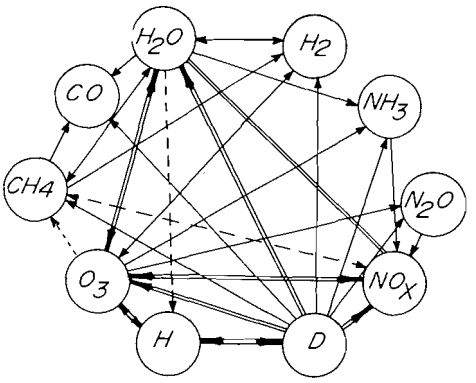

FIG. 8. Coupling in stratospheric–mesospheric chemistry and dynamics. H and D represent heating and dynamics respectively. The double arrows indicate the more important couplings.

The stratosphere–mesosphere region is not a closed box and so one must also be concerned with the relations between this region and the thermosphere and troposphere. The thermosphere is a source of NO_X which may affect O_3 chemistry. The biosphere is the source of many of the stratospheric species such as N_2O(NO), CH_4, H_2, and H_2O. Thus changes in sources or sinks of species such as these could lead to changes in O_3 in the stratosphere in a time which would reflect the time constant of the species causing the change. In fact, it could be such changes that cause long term variations in O_3 rather than solar insolation changes.

Perturbations

Underlying the current explosion of effort to explain the natural stratosphere is the question 'how will the stratosphere respond to a major influx of pollutants from anthropogenic sources such as high-flying aircraft or space shuttles?' The main constituents which cause concern (at present) are H_2O, NO_X, and Cl compounds. At present, no one has yet contradicted the conclusion of Johnston (42) that introduction of NO_X into the stratosphere in amounts comparable to natural sources will lead to a reduction in O_3. Rather, it is the amount of the reduction which appears to be the main cause for disagreement and even this appears to be coming to a consensus (perhaps prematurely considering our knowledge of stratospheric dynamics). H_2O from aircraft appears to be a much less serious hazard (33). The situation with regard to Cl from a shuttle could be serious. As for NO_X, the seriousness depends on the number of flights per year (60, 61).

What is at least a little confusing in this highly political and controversial area is the lack of a standard in dealing with the effects of NO_X (and Cl) on stratospheric O_3. At present it would seem reasonable to use the data of Broderick *et al.* (63) on NO_X emission projections for 1990 as a standard against which other models could be judged; thus statements on the effects of SST fleets could be put in a much more reasonable perspective than they are at present.

This work was supported by a grant from the National Research Council of Canada.

1. R. J. REED and K. E. GERMAN. Mon. Weather Rev. **93**, 313 (1965).
2. F. S. JOHNSON and B. GOTTLEIB. Planet. Space Sci. **18**, 1707 (1970).

Can. J. Chem. Downloaded from www.nrcresearchpress.com by 210.87.254.42 on 09/05/12
For personal use only.

3. R. S. LINDZEN. Tides and gravity waves in the upper atmosphere. *In* Mesospheric models and related experiments. *Edited by* C. G. Fiocco. D. Reidel, Dortrecht, Holland. 1971. pp. 122–130.
4. C. G. JUSTUS. A.I.A.A. paper No. 73-495 (1973).
5. C. O. HINES. J. Geophys. Res. **75**, 3937 (1970).
6. C. O. HINES. J. Geophys. Res. **78**, 335 (1973).
7. D. R. BATES and P. B. HAYS. Planet. Space Sci. **15**, 189 (1967).
8. S. C. WOFSY and M. B. MCELROY. J. Geophys. Res. **78**, 2619 (1973).
9. F. D. COLEGROVE, N. B. HANSON, and F. S. JOHNSON. J. Geophys. Res. **70**, 493 (1965).
10. P. H. GUDIKSEN, A. W. FAIRHALL, and R. J. REED. J. Geophys. Res. **73**, 4461 (1968).
11. H. LETTAU. Diffusion in the upper atmosphere. *In* Compendium of meteorology. *Edited by* T. F. Malone. Waverly Press, Baltimore. 1951. pp. 320–333.
12. F. M. LUTHER. A.I.A.A. paper No. 73-498 (1973).
13. R. J. MURGATROYD and R. M. GOODY. Q. J. R. Meteorol. Soc. **84**, 225 (1958).
14. R. J. MURGATROYD and F. SINGLETON. Q. J. R. Meteorol. Soc. **87**, 125 (1961).
15. D. G. VINCENT. Q. J. R. Meteorol. Soc. **94**, 333 (1968).
16. M. B. MCELROY. Astrophys. J. **150**, 1125 (1967).
17. M. ACKERMAN. Can. J. Chem. This issue.
18. R. D. HUDSON. Can. J. Chem. This issue.
19. A. L. BROADFOOT. Astrophys. J. **173**, 681 (1972).
20. A. F. TIMOTHY and J. G. TIMOTHY. J. Geophys. Res. **75**, 6950 (1970).
21. H. S. JOHNSTON, G. WHITTEN, and J. BIRKS. J. Geophys. Res. **78**, 6107 (1973).
22. H. M. FOLEY and M. A. RUDERMAN. J. Geophys. Res. **78**, 4441 (1973).
23. D. F. HEATH. J. Geophys. Res. **78**, 2779 (1973).
24. R. E. HUFFMAN, D. E. PAULSEN, J. C. LARRABEE, and R. B. CAIRNS. J. Geophys. Res. **76**, 1028 (1971).
25. K. H. WELGE. Can. J. Chem. This issue.
26. D. GARVIN (*Editor*). Chemical kinetics data survey V. NBS1 R73-206, Washington. 1973.
27. R. F. HAMPSON (*Editor*). Chemical kinetics data survey VI. NBS1 R73-207, Washington. 1973.
28. D. F. STROBEL. Radio Sci. **7**, 1 (1972).
29. T. SHIMAZAKI. Radio Sci. **7**, 695 (1972).
30. J. C. MCCONNELL, M. B. McElroy, and S. C. WOFSY. Nature, **233**, 187 (1971).
31. S. C. WOFSY, J. C. MCCONNELL, and M. B. MCELROY. J. Geophys. Res. **77**, 4477 (1972).
32. I. E. GALBALLY. J. Geophys. Res. **77**, 7129 (1972).
33. P. J. CRUTZEN. Can. J. Chem. This issue.
34. R. B. BURKE. J. Geophys. Res. **77**, 1998 (1972).
35. D. R. BATES and M. NICOLET. J. Geophys. Res. **55**, 301 (1950).
36. J. HAMPSON. Rep. TN 1627/64, Can. Armament. Res. Develop. Establ., Toronto, Ontario. 1964.
37. D. M. HUNTEN and D. F. STROBEL. Unpublished.
38. M. NICOLET. Can. J. Chem. This issue.
39. R. SIMONAITIS and J. HEICKLEN. J. Phys. Chem. **77**, 1932 (1973).
40. W. B. DEMORE and E. TSCHUIKOW-ROUX. Unpublished.
41. P. J. CRUTZEN. Q. J. R. Meteorol. Soc. **96**, 320 (1970).
42. H. S. JOHNSTON. Science, **173**, 517 (1971).
43. P. J. CRUTZEN. J. Geophys. Res. **76**, 7311 (1971).
44. J. C. MCCONNELL and M. B. MCELROY. J. Atmos. Sci. **30**, 1465 (1973).
45. M. NICOLET. *In* Aeronomic reactions of hydrogen and ozone in mesospheric models and related experiments. *Edited by* G. Fiocco. Reidel, Dordrecht, Holland. 1971. pp. 1–51.
46. M. B. MCELROY and J. C. MCCONNELL. J. Atmos. Sci. **28**, 1095 (1971).
47. J. C. MCCONNELL. J. Geophys. Res. **78**, 7812 (1973).
48. P. WARNECK. J. Geophys. Res. **77**, 6589 (1972).
49. D. F. STROBEL, D. M. HUNTEN, and M. B. MCELROY. J. Geophys. Res. **75**, 4307 (1970).
50. D. F. STROBEL. J. Geophys. Res. **76**, 8384 (1971).
51. C. B. FARMER. Can. J. Chem. This issue.
52. F. STUHL. J. Chem. Phys. **59**, 635 (1973).
53. H. I. SCHIFF. Can. J. Chem. This issue.
54. G. BRASSEUR and M. NICOLET. Planet. Space Sci. **21**, 939 (1973).
55. S. CIESLIK and M. NICOLET. Planet. Space Sci. **21**, 925 (1973).
56. C. PRABHAKARA. Mon. Weather Rev. **91**, 411 (1963).
57. V. R. K. RAO and A. D. CHRISTIE. J. Atmos. Sci. **30**, 667 (1973).
58. E. HESSTVEDT. Can. J. Chem. This issue.
59. H. I. SCHIFF and J. C. MCCONNELL. Unpublished.
60. R. S. STOLARSKI and R. J. CICERONE. Unpublished.
61. S. C. WOFSY and M. B. MCELROY. Can. J. Chem. This issue.
62. M. B. MCELROY, S. C. WOFSY, J. E. PENNER, and J. C. MCCONNELL. Unpublished.
63. A. J. BRODERICK, J. M. ENGLISH, and A. K. FORNEY. A.I.A.A. paper No. 73-508 (1973).

Can. J. Chem. Downloaded from www.nrcresearchpress.com by 210.87.254.42 on 09/05/12
For personal use only.

Canadian Journal of Chemistry

Published by
THE NATIONAL RESEARCH COUNCIL OF CANADA

Journal canadien de chimie

Publié par
LE CONSEIL NATIONAL DE RECHERCHES DU CANADA

Volume 52 Number 9 May 1, 1974

Volume 52 numéro 9 1 mai 1974

Kinetics of Dehydration of Aromatic Aldehydes Determined by the Rotating Disc Electrode Technique

R. G. BARRADAS, O. KUTOWY, AND D. W. SHOESMITH[1]

Department of Chemistry, Carleton University, Ottawa, Canada, K1S 5B6

Received July 23, 1973

The rate constant for the irreversible dehydration of a number of aromatic aldehyde hydrates has been measured. The hydrates were generated by constant potential electrolysis of the respective aromatic acid at a rotating disc electrode. The aldehydes are then further reduced to the alcohol. The rate constant can be calculated from the ratio of the concentration of intermediate aldehyde to the total concentration of products.

The theory was further extended to include the reverse hydration of the aldehyde to the hydrate and applied in the case of *m*-chlorobenzaldehyde. A value for the equilibrium constant of $K = 1.30 \pm 0.25$ was obtained for this reaction.

On a mesuré les constantes de vitesse pour la déshydratation irréversible d'un certain nombre d'hydrates d'aldéhydes aromatiques. Les hydrates étaient formés par électrolyse à potentiel constant des acides aromatiques correspondants utilisant une électrode à disque rotatif. Les aldéhydes peuvent être réduits jusqu'au niveau de l'alcool. Les constantes de vitesse peuvent être calculées à partir des rapports de concentration de l'aldéhyde intermédiaire sur la concentration totale des produits.

On a élargi la théorie de façon à inclure l'hydratation de l'aldéhyde pour reformer l'hydrate et cette théorie a été appliquée au cas du *m*-chlorobenzaldéhyde. On a obtenu une valeur de $K = 1.30 \pm 0.25$ pour la constante d'équilibre de cette réaction.

[Traduit par le journal]

Can. J. Chem., **52**, 1635 (1974)

Introduction

A method for determining the rate constant, k_2, for a chemical reaction coupled to an electrochemical reaction using the technique of constant potential electrolysis at a rotating disc electrode has been published (1). The method was applied to the electroreduction of aromatic carboxylic acids (2), an example of the common ECE mechanism:

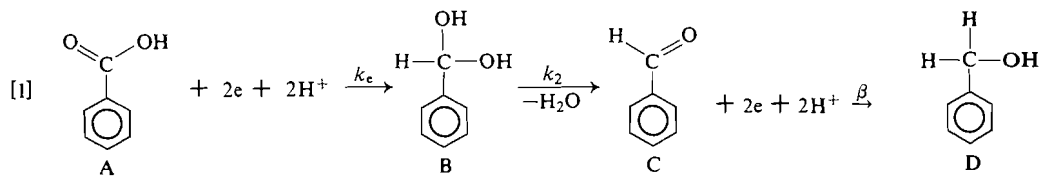

Where k_e, k_2, and β represent the rate constants for the respective steps. The constant, k_e, is the heterogeneous rate constant for the first electron transfer, and β is the rate constant for the mass transfer controlled conversion of C to D.

The theory developed (2), was, however,

[1]Present address: Research Chemistry Branch, Atomic Energy of Canada Limited, Whiteshell Nuclear Research Establishment, Pinawa, Manitoba R0E 1L0.

erroneously applied, and the data used were suspect due to the low buffer capacity employed. In the present communication the previously derived theory was reapplied to results obtained under more controlled conditions.

Since such dehydration reactions have been shown to be reversible (2) an attempt to include this reversibility has been made. However only in the case of *m*-chlorobenzaldehyde was such an extension found to be feasible.

Theory

The advantage of using the rotating disc electrode is that the rate of convective diffusion of species to and from the electrode surface can be accurately controlled. Diffusion of species can be confined to a narrow layer of solution of thickness δ close to the electrode surface, where δ is given by (3)

$$[2] \qquad \delta = 1.80D^{1/3}\nu^{1/6}\omega^{-1/2}$$

where D is the diffusion coefficient ($cm^2\ s^{-1}$) of the diffusing species, ν the solution kinematic viscosity in ($kg\ m^{-1}\ s^{-1}$) $\times\ 10^{-1}$ and ω the angular rotation speed of the electrode in radians s^{-1}.

The rate constant for mass transfer is given by (4)

$$[3] \qquad \beta = DA/V\delta\ s^{-1}$$

where A is the electrode area (cm^2) and V the solution volume (cm^3).

The first electron transfer can be controlled by the rate of diffusion or the rate of electron transfer depending on the electrode potential. The second electron transfer is assumed to be always diffusion controlled at the potentials necessary to initiate step 1. The volume of solution is assumed large compared to that of the diffusion layer and the chemical step only takes place outside the diffusion layer.

A number of different experimental conditions are possible; each necessitating a slightly different theoretical model.

1. Chemical Step - Irreversible

The theory for this situation has been published (1). Two sets of experimental conditions are possible.

(*a*) The potential is cathodic enough to make the first electron transfer step diffusion controlled.

(*b*) The reactant concentration is high and the electrode potential low so that the first electron transfer step is controlled by the heterogeneous electrochemical rate. If the degree of conversion of reactant to products is maintained below $\simeq 5\%$ then the reactant concentration can be taken as constant throughout the experiment.

Condition (*b*) was applied in the present paper and values of k_2 were calculated using the derived expression for the ratio of concentrations, R, defined by (2)

$$[4] \quad R = \frac{C_B^{\,b} + C_c^{\,b}}{C_B^{\,b} + C_c^{\,b} + C_D^{\,b}} = \frac{\beta^2 - k_2^{\,2} - 2k_2\beta\exp(-\beta t) + k_2^{\,2}\exp(-\beta t)}{2\beta^2 + tk_2\beta^2 - t\beta k_2^{\,2} - 2k_2\beta}$$

where $C_x^{\,b}$ are the bulk solution concentrations of the respective species.

Previously (2) the expression

$$[5] \qquad k_2 \propto (R - \exp(-\beta t))$$

was used to estimate the value of k_2. The proportionality constant for eq. 5 was calculated using a value of k_2 for benzaldehyde estimated from the data presented in Figs. 2 and 5 of ref. 2. k_2 for the other aldehydes was then calculated from eq. 5 by comparing the ratio R of that aldehyde at a number of values of βt, to the value of R for benzaldehyde at the same value of βt.

Equation 5 was obtained from eq. 4 by neglecting all the squared constant terms and limiting the analysis to times such that the linear terms in t can also be neglected.

The terms in $k_2^{\,2}$ and β^2 cannot, however, be eliminated since they are of the same order of magnitude as the exponential terms.

Values of k_2 calculated using relationship [5] indicate that the rates of dehydration are in the following order for a series of ring-substituted aromatic acids:

$$m\text{-Cl} > o\text{-Cl} > \text{benzoic} > o\text{-CH}_3 > o\text{-OH}$$

This is contrary to the order expected on the basis of substituent effects. Also relationship [5] implies that the largest instantaneous concentration of intermediate will be attained with the fastest rate of dehydration. This is opposite to the predictions of the theory presented (2).

2. Chemical Step - Reversible

The theory for the reversible case will only be solved for the experimental conditions actually

applied. These correspond to the assumptions of 1(*b*) above. The theory could be simply extended to include case 1(*a*) if necessary.

The scheme for the present situation can be written as follows

$$[6] \qquad \frac{dC_A^b}{dt} = 0$$

$$[7] \qquad \frac{dC_B^b}{dt} = k_e(C_A^b)_i - k_f C_B^b + k_b C_c^b$$

$$[8] \qquad \frac{dC_c^b}{dt} = k_f C_B^b - k_b C_c^b - \beta C_c^b$$

$$[9] \qquad \frac{dC_D^b}{dt} = \beta C_c^b$$

Equations 6 to 9 are subject to the following conditions

$$[10] \qquad \text{At } t = 0; \quad C_A^b = (C_A^b)_i$$

$$[11] \qquad (C_B^b)_i = (C_c^b)_i = (C_D^b)_i = 0$$

At $t > 0$, $x = \delta$, all concentrations are equal to their bulk solution concentrations.

$(C_x)_i$ refers to the initial concentration of species X.

The above scheme can be solved by simple integration and by Laplace Transform to yield:

$$[12] \qquad C_B^b = k_e(C_A^b)_i\left[\frac{k_b + \beta}{\alpha\gamma} + \frac{(k_b + \beta - \alpha)}{\alpha(\alpha - \gamma)}\exp(-\alpha t) + \frac{(k_b + \beta - \gamma)}{\gamma(\gamma - \alpha)}\exp(-\gamma t)\right]$$

$$[13] \qquad C_c^b = k_f k_e(C_A^b)_i\left[\frac{1}{\alpha\gamma} + \frac{\exp(-\alpha t)}{\alpha(\alpha - \gamma)} + \frac{\exp(-\gamma t)}{\gamma(\gamma - \alpha)}\right]$$

$$[14] \qquad C_D^b = \beta k_f k_e(C_A^b)_i\left[\frac{t}{\alpha\gamma} + \frac{(1 - \exp(-\alpha t))}{\alpha^2(\alpha - \gamma)} + \frac{(1 - \exp(-\gamma t))}{\gamma^2(\gamma - \alpha)}\right]$$

where

$$[15] \qquad \alpha = 0.5[\theta + (\theta^2 - 4\beta k_f)^{1/2}]$$

$$[16] \qquad \gamma = 0.5[\theta - (\theta^2 - 4\beta k_f)^{1/2}]$$

and

$$[17] \qquad \theta = (k_f + k_b + \beta)$$

The ratio, R, defined by the first equality in eq. 4 will be independent of both k_e and $(C_A^b)_i$.

Computation of eqs. 12 and 13 shows that the individual values of C_B^b and C_c^b become constant for larger values of βt. Under these conditions dC_B^b/dt and dC_c^b/dt (eqs. 7 and 8) are both equal to zero; hence

$$[18] \qquad \frac{dC_c^b}{dt} = 0 = k_f C_B^b - k_b C_c^b - \beta C_c^b$$

which leads to the relationship

$$[19] \qquad \frac{C_c^b}{C_B^b} = \frac{k_f}{(k_b + \beta)}$$

For $k_b \gg \beta$, eq. 19 reduces to

$$[20] \qquad \frac{C_c^b}{C_B^b} = \frac{k_f}{k_b}$$

Under these conditions the ratio of hydrate to aldehyde should be independent of electrode rotation speed.

For $k_b \ll \beta$, eq. 19 becomes

$$[21] \qquad \frac{C_c^b}{C_B^b} = \frac{k_f}{\beta}$$

which is equivalent to the irreversible case.

Equation 19 offers a simple means of separating k_f and k_b. For large enough values of βt the slope of the plot of alcohol concentration (C_D^b) against t should be linear yielding an estimate of C_c^b. C_B^b can then be obtained from the analyzed yield of aldehyde, $C_B^b + C_c^b$. If the analysis is repeated for a number of β values, k_f and k_b can be calculated.

The consistency of the values obtained could be checked in the following manner. Using the values of k_f and k_b as calculated by the above method a value of the equilibrium constant, K, can be used to compute the theoretical product ratio, R, as a function of βt for a series of k_f values. Comparison with the experimental ratio would then enable k_f and k_b to be calculated.

Previously (2) the separation of k_2 into k_f and k_b was affected using the equation

$$[22] \qquad k_2 C_B^b = k_f C_B^b - k_b C_c^b$$

For short times

$$[23] \qquad k_2 \simeq k_f$$

Equation 23 can be shown to apply, under the present conditions, only in the time interval

$t \lesssim 1$ h; a range which is experimentally difficult to investigate.

The method employed in this paper however uses the data obtained over the whole time range of the electrolysis.

Experimental

The experimental method previously applied (2) was again used to follow the concentrations of products. Since the theory is based on the conversion of less than 5% of reactant to product the use of an "*in situ*" technique such as i.r. spectroscopy is subject to the disadvantage that the signals from the products are swamped by that of the reactant. Since concentrations of products rarely exceed 10^{-3} *M* in solution, quantitative analysis using n.m.r. was not considered.

Because both aldehyde and alcohol concentrations must be known as a function of time, any method of data acquisition not involving an interruption of the electrolysis current necessitates a sampling technique.

G.l.c. was deemed the most useful technique to quantitatively separate the products from reactant since in this case treatment of the sample to remove excess unreacted acid was not necessary.

I.r. spectroscopy was found to be useful only in the case of salicylic acid, where the aldehyde and alcohol absorbances are sufficiently distinct to be used for analysis. Even in this case error is introduced by the necessity to remove unreacted salicylic acid.

The experimental set-up and electrode design have been previously described (2). A number of modifications were incorporated into the experimental procedure and these are explained below.

Working Electrode

In the present work the electrode, once prepared by electroplating mercury on copper from acidic $Hg(NO_3)_2$, was stored under mercury between runs, replating being unnecessary. On storing, copper amalgam separated out on the surface of the electrode but could be removed by excess mercury. This method of electrode maintenance led to better reproducibility than if the surface was replated between each run.

The condition of the electrode surface changed slightly over the period of a long (9 h) electrolysis. This can be seen by the change in Tafel slope and the lowering of the overvoltage in 1 *N* HCl, Fig. 1. The slightly lower overvoltage on the plated electrode can be accounted for by the catalytic action of copper dissolved in the mercury (8). Figure 1, plots 3 and 4, indicate that the electrode deteriorates somewhat throughout the electrolysis.

Apparatus

Constant potential electrolyses were performed using a potentiostat (Wenking Model 70 HP 10 or Chemical Electronics Type TR 70-2A) and a Beckmann Rotating Disc electrode unit. Chemical analyses were performed on an F and M 402 Gas Chromatograph using a silicone gum rubber SE52 column, and on a Unicam SP 800 u.v. spectrophotometer.

Analysis

The main analytical method was g.l.c. as previously reported (2). The products from the electrolysis of

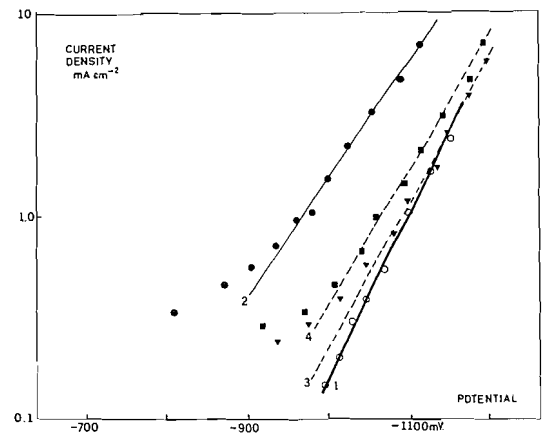

FIG. 1. Steady-state current Voltage plots recorded in 1 *N* HCl for various electrode conditions; (*1*) pure Hg pool electrode, Tafel slope = 120 mV; (*2*) Cu electrode, 170 mV; (*3*) mercury-plated copper electrode prior to electrolysis; 140 mV; (*4*) plated electrode after a 3 h electrolysis, 150 mV.

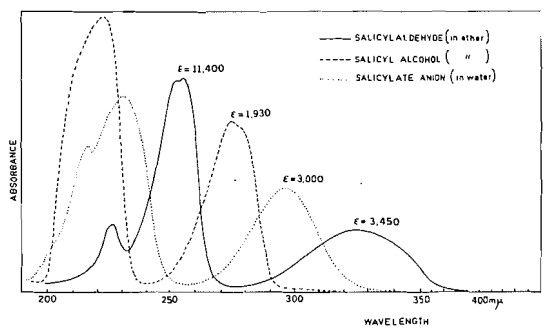

FIG. 2. U.v. characteristics of peaks used for analysis of electrolyzed salicylic acid solutions.

salicylic acid were analyzed by u.v. spectrophotometry. Figure 2 shows the absorbance characteristics.

The products were extracted into ether, and analyzed directly. In the case of salicylic acid the extract was neutralized with sodium carbonate to remove the acid. The acid was then estimated from the salicylate anion absorbance in aqueous solution. In all other cases the acid was estimated using g.l.c. as the methyl ester formed by reaction with diazomethane (5).

Product identification has been previously described (2). However identification of the alcohols by re-oxidation to the acid was inconclusive. A more positive identification was achieved by constant potential electrolysis of a standard aldehyde sample at the rotating disc electrode, at potentials on the plateau of the waves attributed to the reduction of aldehyde to alcohol (6, 7). Coulometric analysis showed that in all cases reported the number of electrons transferred $n = 2 \pm 0.2$. The g.l.c. peaks obtained from the products coincided with those attributed to alcohol in the reduction of the acid at higher potentials. Further evidence was obtained by a second electrolysis of the sample (already electrolyzed) at lower

potentials where only Step 3 could occur (*i.e.* aldehyde $\xrightarrow{2e+2H^+}$ alcohol). Subsequent g.l.c. analysis showed the aldehyde peak to have disappeared and the alcohol peak to have increased.

Chemicals

The aromatic acids were from Eastman Kodak (Highest Purity) and were used without further purification. The phosphate buffers were BDH (Analar grade) as was the HCl and boric acid.

Solutions

The composition of the solutions was as follows; 0.6 *M* KCl; 0.8 *M* phosphate buffers to p*H* 6.2; 0.1 *M* aromatic acid. Where necessary the p*H* was adjusted to 6.2 using 1 *N* HCl or 1 *N* NaOH. In the electrolysis of salicylic acid KCl was 0.35 *M* and H_3BO_3 0.25 *M*. The conditions for salicylic acid were identical to those used previously. During experiments at high buffer capacity the p*H* was maintained by manual addition of HCl at regular intervals. This was necessary because of the simultaneous hydrogen evolution.

Choice of Experimental Conditions

In order to obtain reasonably high concentrations of products a sufficiently cathodic potential was necessary. However, increasing the potential cathodically led to a large increase in the hydrogen evolution current. This had two effects. First the condition of the electrode deteriorated. This could be observed by a test similar to that demonstrated in Fig. 2. Secondly if the evolution of gas bubbles was too copious the results obtained became erratic.

Results and Discussion

Figures 3 and 4 show the aldehyde and alcohol yields as a function of time for a number of aromatic carboxylic acids studied. Unlike the aldehyde yields obtained previously (2), the present plots, Fig. 3, attain a plateau value as predicted by the theory.

Figure 5 shows the product ratio analyzed according to the irreversible scheme with the conditions stated in section 1(*b*) of the theory. The values of k_2 taken from this figure are tabulated in Table 1.

The values of k_2 for benzoic acid and *p*-CH_3 benzoic acid can only be considered as order of magnitude estimates since they are close to the limits of applicability of the theory. The plot for salicylic acid was outside the range of the theory, and no value for k_2 can hence be estimated.

Similar plots to those of Fig. 5 for data obtained in solutions of low buffer capacity (2) fall below the plots obtained in the present work. For benzaldehyde and *p*-methylbenzaldehyde they fall outside the range of the theory. The

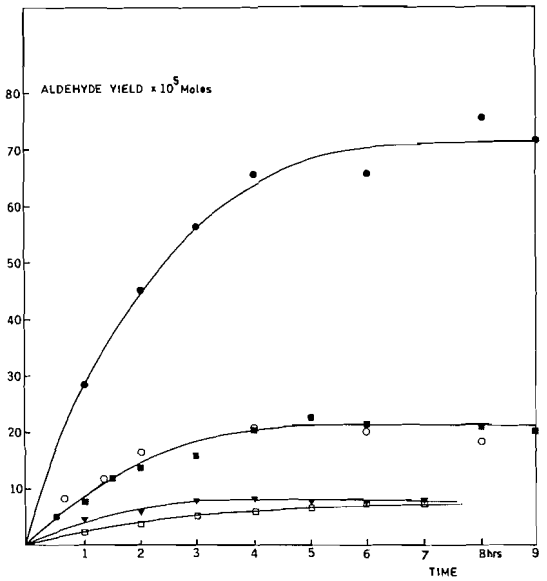

FIG. 3. Aldehyde yields as a function of time for various aromatic carboxylic acids $\beta = 10^{-4}$ s^{-1} (ω = 2300 r.p.m.). ●, *m*-chlorobenzoic acid electrolyzed at $E = -1.95$ V; ■, benzoic acid, $E = -1.95$ V; ○, salicylic acid, $E = -1.95$ V; ▼, *p*-methylbenzoic acid, $E = -2.01$ V; □, *o*-chlorobenzoic acid, $E = -2.01$ V.

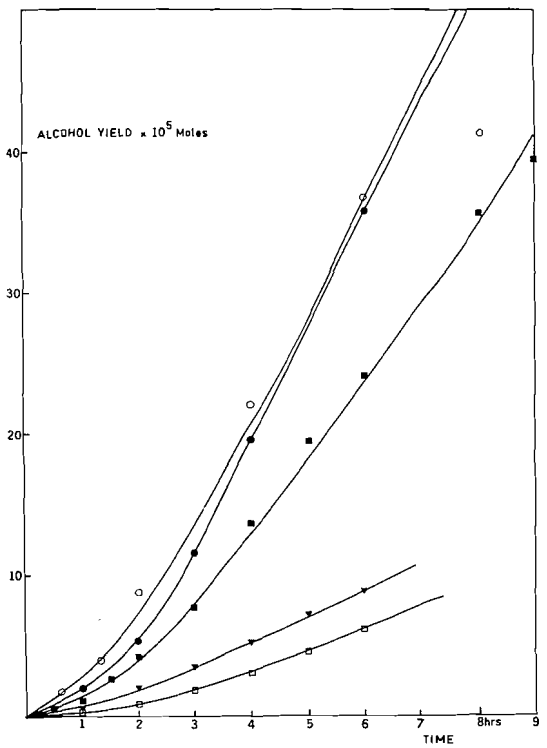

FIG. 4. Alcohol yields as a function of time. Legend same as Fig. 3.

TABLE 1. Values of the rate constant k_2

Compound	k_2
Benzoic acid	$\sim 10^{-2}$ s^{-1}
p-CH_3 benzoic	$\sim 10^{-2}$ s^{-1}
o-Cl benzoic	6×10^{-4} s^{-1}
m-Cl benzoic	$(1.5 \text{ to } 2.0) \times 10^{-4}$ s^{-1}

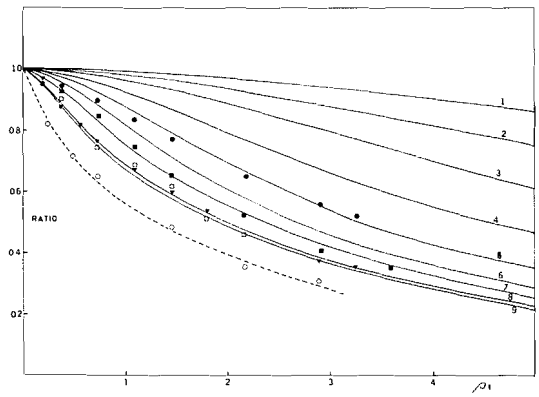

FIG. 5. Data of Fig. 3 and Fig. 4 plotted according to eq. 3 for the irreversible case. ●, *m*-chlorobenzoic acid; ■, *o*-chlorobenzoic acid; ▼, benzoic acid; □, *p*-methyl benzoic acid; ○, salicylic acid. Plots are theoretical curves for varying values of k_2; (*1*) 10^{-5} s^{-1}; (*2*) 2×10^{-5}; (*3*) 4×10^{-5}; (*4*) 8×10^{-5}; (*5*) 1.6×10^{-4}; (*6*) 3.2×10^{-4}; (*7*) 6.4×10^{-4}; (*8*) 1.024×10^{-2}; (*9*) 1.024.

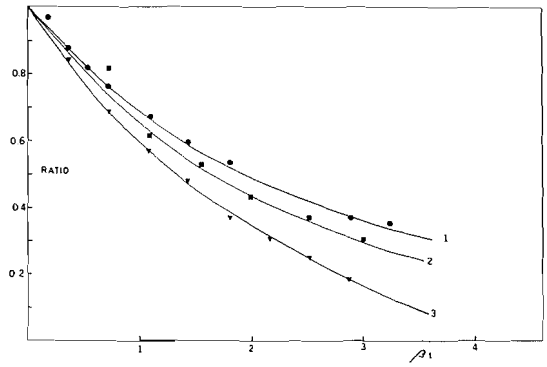

FIG. 6. Product Ratio, *R*, for electrolysis of benzoic acid at $E = -1.95$ V in phosphate buffers (p*H* 6.2) for varying total buffer concentrations. (*1*) 0.8 *M* total buffer concentration + manual p*H* adjustment with 1 *N* HCl. (*2*) 0.15 *M* total buffer concentration + manual p*H* adjustment. (*3*) 0.074 *M* total buffer concentration + *no* adjustment.

effect of the buffer capacity on the product ratio for benzaldehyde is shown in Fig. 6.

For the values of k_2, tabulated above, to be meaningful the product ratio must be independent of the buffer capacity. Unfortunately attempts to obtain data at higher buffer capacities were frustrated for the reasons stated in the experimental section.

However, confidence can be placed in the present results for the following reasons.

1. The concentration of intermediates attains a plateau when plotted as a function of βt.

2. Chemical analysis indicated yields in the range 85% to 90%, except in the case of salicylic acid. No dimeric or polymeric products were detected. Such an analysis, however, can only be considered approximate since it involved a calculation made on a very small conversion of reactant to products. Percentage yields based on synthetic scale experiments (9) were in the range 70 to 80%, indicating a substantial loss of reactant via side reactions. However the last experiments were performed with much smaller buffer capacities than those employed in the present work, in order to obtain high current efficiencies.

3. The coulometric experiments performed on the aldehydes yielded values for $n = 2.0 \pm 0.2$. This indicates that the conversion of aldehyde to alcohol proceeds efficiently with very little loss of material in side reactions. Hence any significant loss of material in the overall reduction of acid to alcohol must occur in the first electron transfer step. However the calculation of k_2 is independent of the rate of this step and only requires that it be constant. Hence loss of material in side reactions at this stage of the process will not affect the calculation of the chemical rate constant, providing the rate of production of intermediates is constant. That this is in fact the case can be seen by plotting the total product yield, $C_B^b + C_c^b + C_D^b$, as a function of time. Straight lines passing through the origin were obtained in all cases except that of salicylic acid. The slope of such a plot would in fact yield a value for k_c. Deviations from linearity were observed for previously obtained, Figs. 1 and 16 of ref. 2.

For the solutions of low buffer capacity, Fig. 6 plots 2 and 3, the aldehyde yields showed a peak when plotted against the electrolysis time. This could be accounted for by a decrease in the electrochemical rate for the first electron transfer step. This was also indicated by a corresponding decrease in the rate of production of alcohol and a fall in the percentage yield. The amount of acid converted to products,

TABLE 2. Data for *m*-chlorobenzoic acid at −1.95 V

ω(r.p.m.)	δ cm	β s^{-1}	C_c^b/C_B^b	k_f and k_b ($s^{-1} \times 10^4$)
(*a*) 500	2.25×10^{-3}	4.64×10^{-5}	1.10	(k_f; 4.82; 10.78; 2.65)
(*b*) 1285	1.40×10^{-3}	7.5×10^{-5}	1.07	(k_b; 3.92; 10; 1.70)
(*c*) 2300	1.05×10^{-3}	10^{-4}	0.98	(K; 1.23; 1.08; 1.56)

however, did not fall substantially, as demonstrated by the analysis of unreduced acid.

Hence the main effect of low buffer capacity would appear to be to cause a local pH increase close to the electrode surface, leading to possible dimerization or polymerization products, rather than a decrease in the electrochemical rate.

A similar decrease in the aldehyde to alcohol ratio was noted at low pH values. In this case the ratio was not only dependent on the buffer capacity but was reduced even in well buffered solutions. This can be attributed to acid catalysis, leading to a large proportion of the chemical reaction taking place within the diffusion layer:

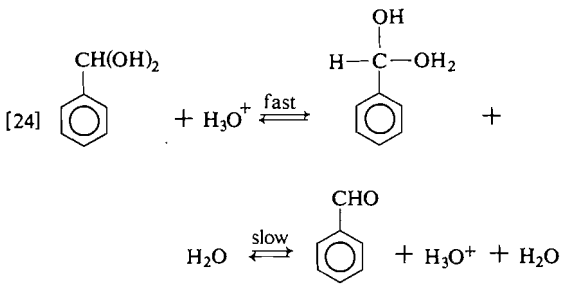

The data obtained for salicylic acid did not permit the calculation of a value for k_2. Possible explanations for this are:

1. k_2 is very fast and a substantial degree of conversion of hydrate to aldehyde occurs within the diffusion layer. This would lead to an increase in the rate of diffusion of the aldehyde back to the electrode and hence a smaller proportion of aldehyde in the total analysed product.

2. The estimated yield of product in the case of salicylic acid was around 70% under the conditions employed, indicating a possible loss of products to dimers and polymers.

3. In the u.v. analysis for salicyl alcohol, unreduced acid was removed by treating the other extracts with dilute aqueous alkali. Loss of salicylaldehyde, which is soluble in alkali, could be observed by the decrease in its u.v. absorbance on successive treatments. The alcohol absorbance was unaffected.

Reversible Analysis

Equation 19 offers a means of examining the reversibility of the dehydration reaction. Variation of the angular velocity of the electrode, and hence β, should yield data from which k_f and k_b can be calculated. However only in the case of *m*-chlorobenzaldehyde were the product yields sufficiently high to give reproducible changes in product ratio with changes in β.

In the case of benzoic acid the experimental product ratio was insensitive to changes in β. This is equivalent to the condition expressed by eq. 20. Hence

$$[25] \qquad k_{b(\text{benzoic})} \gg \beta$$

This is not a surprising result considering that when treated as irreversible the dehydration rate constant, k_2, is at the upper limit of measurement for the theory.

For *o*-chloro- and *p*-methylbenzoic acids the product yields were too small to yield meaningful changes in product ratio on changing β. This could be improved by an increase in cathodic potential. However this leads to scattered data for the reasons stated in the experimental section.

The results for *m*-chlorobenzaldehyde are listed in Table 2, yielding the k_f and k_b values shown.

The values of k_f, k_b show a large spread when determined by this method. However, the equilibrium constants calculated on the basis of these values are quite accurate and can be used to calculate more accurate value for k_f and k_b.

The data of Table 2 lead to the value

$$K = 1.30 \pm 0.25$$

Using a value of $K = 1.3$ a series of product ratio calibration plots were constructed. Fig. 7 shows the experimental data and the closest fitting theoretical curve, yielding

$$k_f = (6.5 \pm 1.5) \times 10^{-4}\ s^{-1}$$

$$k_b = (4.2 \pm 1.0) \times 10^{-4}\ s^{-1}$$

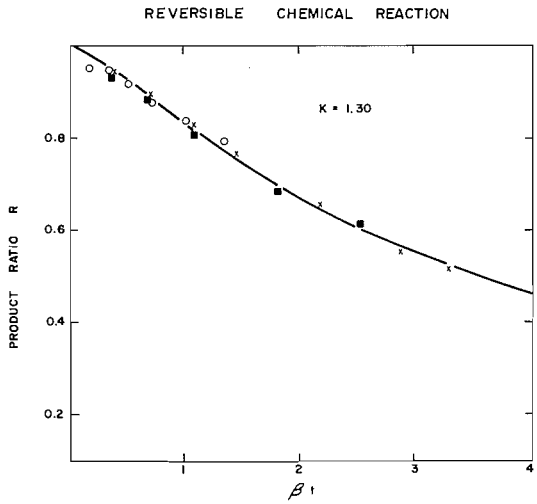

FIG. 7. Product ratio as a function of βt for the three runs listed in Table 2; ×, ω = 2300 r.p.m.; ■, ω = 1285 r.p.m.; ○, ω = 500 r.p.m. The plot represents the theoretical curve for $K = 1.30$, $k_f = 6.5 \times 10^{-4}$, s^{-1} for the reversible case (*b*) (see Theory section).

The error limits were estimated by constructing calibration curves for $K = 1.05$ and 1.55 and computing maximum and minimum values of k_f and k_b. This, taken together with the spread of data around the theoretical product ratio, leads to the estimated errors quoted above.

Financial support for this work is gratefully acknowledged from grants awarded by N.R.C.C. and Environment Canada (NACWRR).

1. J. A. HARRISON and D. W. SHOESMITH. J. Electroanal. Chem. **28**, 301 (1970).
2. J. A. HARRISON and D. W. SHOESMITH. J. Electroanal. Chem. **32**, 125 (1971).
3. V. G. LEVICH. Physicochemical hydrodynamics. Prentice-Hall, New York. 1962.
4. A. J. BARD and K. S. V. SANTHANAM. *In* Electroanalytical chemistry. Vol. 4. *Edited by* A. J. Bard. Dekker. 1970.
5. H. SCHLENK and J. L. GELLERMAN. Anal. Chem. **32**, 1412 (1960).
6. L. HOLLECK and H. MARSEN. Z. Elektrochem. **57**, 944 (1953).
7. R. M. POWERS and R. A. DAY. J. Am. Chem. Soc. **80**, 808 (1958).
8. A. N. FRUMKIN. Hydrogen overvoltage and adsorption phenomena. Part II, p. 287. *In* Advances in Electrochemistry and Electrochemical Engineering. Vol. 3. *Edited by* P. Delahay and C. W. Tobias. Interscience, New York. 1963. Part II. p. 287.
9. D. W. SHOESMITH. Ph.D. Thesis. University of Newcastle-upon-Tyne, England, 1970.

The Interaction of Electrochemically Produced Radical Cations with Substituted Styrenes

B. LIONEL FUNT AND VICTOR VERIGIN

Department of Chemistry, Simon Fraser University, Burnaby 2, British Columbia

Received September 14, 1973

Relatively stable radical cations of 9,10-diphenylanthracene (DPA) were formed by controlled potential electrolysis of solutions in acetonitrile. The rates of decay of the ions were measured in the absence and presence of substituted styrenes, including α-methylstyrene, *trans*-β-methylstyrene, *p*-methylstyrene, and styrene. In rigorously dried solvent the radical cation was relatively stable, and its rate of decay was independent of its initial concentration. In the presence of monomers the rates of decay were increased greatly and were related to the position of the methyl substituent in the styrene structure.

The rate was proportional to $[DPA^{\ddagger}][M]^2$. A mechanism is suggested and interpreted to show that the rates of cation decay are indicative of the rates of propagation in the polymerization process.

L'électrolyse à potentiels contrôlés de solutions dans l'acétonitrile du diphényl-9,10 anthracène (DPA) permet d'en obtenir les radicaux cations qui sont relativement stables. Les taux de décomposition des ions ont été mesurés en l'absence et en présence de styrènes substitués incluant l'α-méthylstyrène, le β-méthylstyrène-*trans*, le *p*-méthylstyrène et le styrène. Dans des solvants parfaitement anhydres le radical cation est relativement stable et son taux de décomposition est indépendant de sa concentration initiale. En présence de monomères les taux de décomposition augmentent considérablement et sont reliés à la position du substituant méthyle dans la structure du styrène.

Le taux est proportionnel à $[DPA^{\ddagger}][M]^2$. On suggère un mécanisme qui est interprété pour montrer que les taux de décomposition du cation représentent les taux de propagation du processus de polymérisation. [Traduit par le journal]

Can. J. Chem., **52**, 1643 (1974)

Can. J. Chem. Downloaded from www.nrcresearchpress.com by 210.87.254.6 on 09/05/12
For personal use only.

In electrochemically initiated polymerizations the electron transfer may take place directly to the monomer (1) or indirectly through the formation of an intermediate generated at the electrode (2, 3). If the intermediate is sufficiently stable diffusion from the electrode can be ignored as a rate-determining step. Under these conditions the interaction of the intermediate with the monomer can be studied under homogeneous conditions and the kinetics investigated in terms of elementary process steps.

Although long-lived anions are well known (4), have been generated electrochemically (5, 6), and their subsequent interaction studied (7), corresponding studies on radical cations are relatively few.

Mengoli and Vidotto (8, 9) have shown that long-lived cations can also be generated electrochemically. In view of the fundamental importance and generality of such studies we began an investigation to confirm some of Mengoli and Vidotto's results and to expand the study of stable radical cation interactions to other monomers and systems. Our aim was to apply the methods of competitive kinetics in a manner analogous to that employed in kinetic spectroscopy. The decay of the radical cations can be measured in the presence and absence of monomer. A comparison of the total decay rates is therefore obtained, which, for low concentration of monomer, should yield the rate constant for the initial step in the polymerization process.

Experimental

The electrolyses were performed at constant electrode potential in the cell shown in Fig. 1. During the electrolysis a characteristic deep blue color of the diphenylanthracene ($DPA^{\ddagger}$) radical cation was observed.

The decay kinetics were measured at a rotating disc electrode sealed into the same cell. For the kinetic studies various amounts of monomer were injected into the cell and the rate of radical cation decay was measured as before. A Model 170 Electrochemistry System (Princeton Applied Research Corporation) was used both for the generation of the radical cation and for the electroanalytical determination of the rate of decay.

The reference electrode was a $Ag–AgClO_4$ couple in CH_3CN saturated with $LiClO_4$. The cations were generated at a controlled potential of 1.3 V relative to this couple. Electrolysis for a period of 5–10 min produced a concentration of radical cations of $2–3 \times 10^{-4}$ *M*

Can. J. Chem. Downloaded from www.nrcresearchpress.com by 210.87.254.6 on 09/05/12
For personal use only.

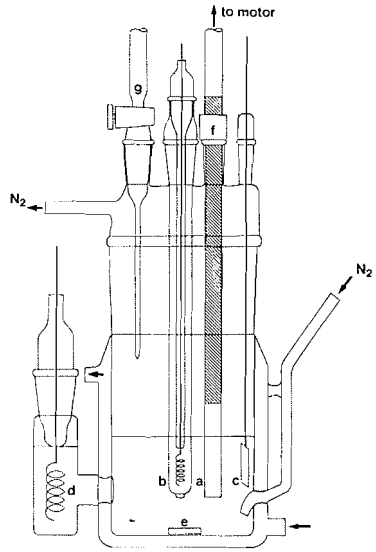

FIG. 1. Electrolytic cell with: (*a*) rotating disc electrode; (*b*) Ag–$AgClO_4$ reference electrode; (*c*) analytical counter electrode; electrolytic working electrode; (*d*) electrolytic counter electrode; (*e*) magnetic stirrer, (*f*) carbon brush contact; (*g*) burette.

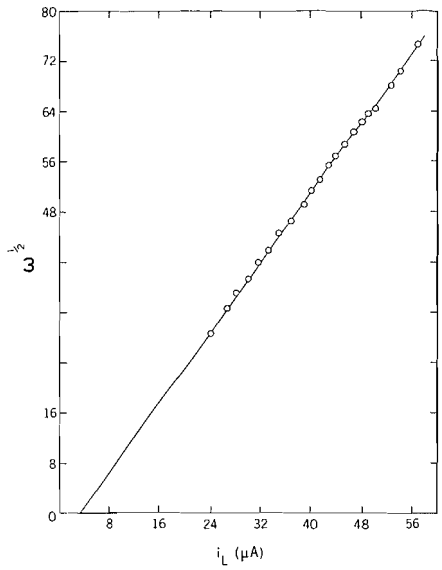

FIG. 2. Variation of limiting current with $\omega^{1/2}$ for the oxidation of 10^{-3} *M* DPA at the RDE; [TBAP] = 5×10^{-2} *M* in CH_3CN; $T = 0$ °C.

in a solution volume of 30 ml. The temperature was maintained at 0 °C by circulation of thermostatically controlled coolant through the outer jacket of the reaction cell.

For the analytical determinations of [$DPA^{\ddagger}$] a Pt rotating disc electrode, 2-mm diameter, was polarized at 0.8 V and the limiting current was measured.

Materials

Monomers, substituted styrenes, were dried over CaH_2, then passed through an alumina column, and finally fractionally distilled at reduced pressure. Acetonitrile was dried over $CaSO_4$, fractionally distilled, and stored over a molecular sieve. Methylene chloride was dried over P_2O_5 prior to fractionation and storage. Tetrabutylammonium perchlorate (TBAP) was dried in vacuo at 90 °C. 9,10-Diphenylanthracene (DPA) was obtained in high purity (Aldrich) and crystallized from alcohol before use.

Results

It was essential to confirm that the rotating disc electrode was providing reliable analytical data, and that these data were comparable to those obtained with diffusion limited electroanalytical techniques. The crucial experimental test is the check of the predicted linearity of the square root of the rotation rate versus the limiting current (11). This test is shown in Fig. 2. Furthermore, an independent check by means of a stationary electrode, with periodic renewal of the diffusion layer, provided results which were in agreement with those obtained at the rotating disc electrode. It was therefore concluded that the analytical technique was reliable.

The rate of decay of $DPA^{\ddagger}$ in CH_3CN (in the absence of monomer) was found to be independent of its initial concentration and to proceed at a constant rate, in keeping with zero order kinetics. The data in Table 1 show a rate of decay which is essentially constant over a 250% change in initial concentration.

TABLE 1. Decay of $DPA^{\ddagger}$ in absence of monomer

$[DPA^{\ddagger}]_0 \times 10^4$ (mol l^{-1})	Rate of decay $\times 10^6$ (mol l^{-1} min^{-1})
2.70	5.23
3.70	5.23
6.80	5.10

This result was unexpected and quite surprising. Mengoli and Vidotto (9) and Sioda (10) have both recorded first-order decay. However, on re-examination of their experimental conditions it was noted that such behavior was obtained only on addition of water to the reacting system. The equation given by Sioda is

$$-d[DPA^{\ddagger}]/dt = (0.083[H_2O] - 0.056)\,[DPA^{\ddagger}]$$

The second term becomes negligible only at concentrations of water > 1 *M*.

TABLE 2. Rate of $DPA^{\ddagger}$ reaction in presence of monomers

p-Methylstyrene		*trans*-β-Methylstyrene	
$[M]_0$ (mol l^{-1})	Apparent rate constant (min^{-1})	$[M]_0$ (mol l^{-1})	Apparent rate constant (min^{-1})
0.010	0.047	0.020	0.123
0.020	0.192	0.040	0.261
0.030	0.345	0.060	0.749
0.048	0.648	0.079	1.060
0.071	1.438	0.099	1.643
0.100	2.99		

In the presence of monomer however, the rate of $DPA^{\ddagger}$ decay becomes of first order. The data at 0 °C for a number of initial concentrations of monomer are shown in Figs. 3 and 4 for styrene and α-methylstyrene. The relevant pseudo first-order constants (from the slopes of such curves) are listed in Table 2. A number of points are immediately evident from the data. The rates of disappearance of the radical cations show a first-order dependence on $[DPA^{\ddagger}]$, are sensitive to the concentration of monomer, and depend on the structure of the monomer. Each of these points deserves further elucidation and comment.

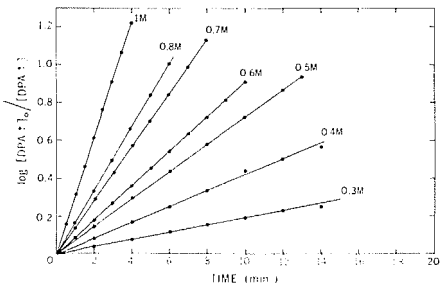

FIG. 3. Decay kinetics of $DPA^{\ddagger}$ at 0 °C in the presence of variable concentrations of styrene; [TBAP] = 5×10^{-2} *M* in CH_3CN.

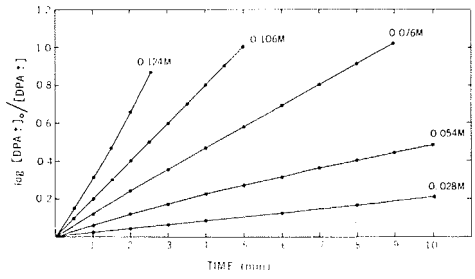

FIG. 4. Decay kinetics of $DPA^{\ddagger}$ at 0 °C in the presence of variable concentrations of α-methylstyrene; [TBAP] = 5×10^{-2} *M* in CH_3CN.

The dependence of the rate on the first power of the $[DPA^{\ddagger}]$ is in keeping with results of other studies (12) but should be contrasted with the results obtained in the absence of monomer. Results with three different initial concentrations of $DPA^{\ddagger}$ fall accurately on the same linear semi-log plot shown in Fig. 5, and differ markedly from the concentration independent, zero-order data found in the absence of monomer.

An inspection of the data in Table 2 and of Figs. 3 and 4 further shows that the rate dependence on monomer concentration is not linear or first order. Indeed the initial rate of disappearance of the radical cation depends on $[M]_0^2$. This is shown quite conclusively in Fig. 6. Thus the overall kinetics were of the form $-d[DPA^{\ddagger}]/dt = k[DPA^{\ddagger}][M]^2$. Inasmuch as the monomer was in considerable excess relative to the concentration of $DPA^{\ddagger}$ the concentration of monomer was essentially at its initial value $[M]_0$ during the experiment.

It was also important to determine that the

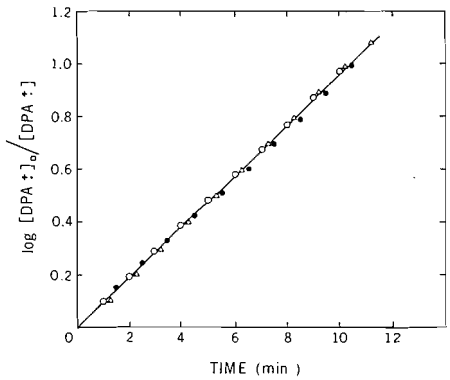

FIG. 5. Decay kinetics at various initial concentrations of $DPA^{\ddagger}$ at 0 °C with 0.47 *M* styrene and 5×10^{-2} *M* TBAP in CH_3CN: ○, $[DPA^{\ddagger}]_0 = 2.5 \times 10^{-4}$ *M*; ●, $[DPA^{\ddagger}]_0 = 5.0 \times 10^{-4}$ *M*; △, $[DPA^{\ddagger}]_0 = 7.5 \times 10^{-4}$ *M*.

Can. J. Chem. Downloaded from www.nrcresearchpress.com by 210.87.254.6 on 09/05/12
For personal use only.

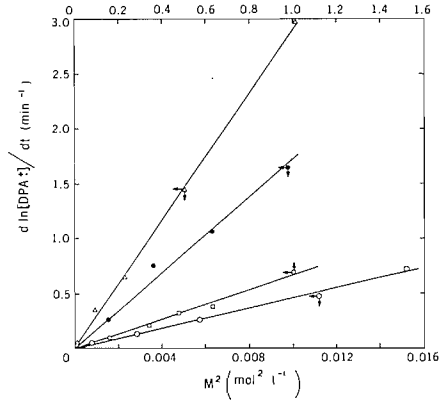

FIG. 6. Second-order dependence on monomer concentration at 0 °C of: △, *p*-methylstyrene; ●, *trans*-β-methylstyrene; □, styrene (top axis); ○, α-methylstyrene; [TBAP] = 5×10^{-2} *M* in CH_3CN.

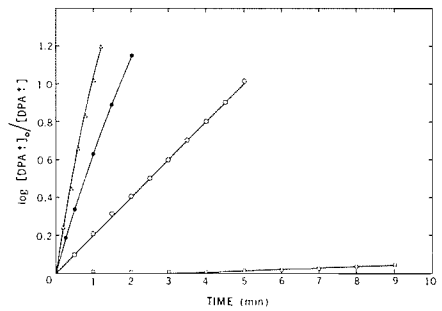

FIG. 7. Decay kinetics of $DPA^{+\cdot}$ at 0 °C in the presence of a fixed concentration (0.1 *M*) of several monomers: △, *p*-methylstyrene; ●, *trans*-β-methylstyrene; ○, α-methylstyrene; □, styrene; [TBAP] = 5×10^{-2} *M* in CH_3CN.

supporting electrolyte was not interfering with the rate of $DPA^{+\cdot}$ decay or otherwise influencing the interaction with the monomer. Experiments were performed at several concentrations of TBAP and no measurable change in rate of ion decay was observed.

The effect of monomer structure on the rate of interaction with $DPA^{+\cdot}$ is shown in Fig. 7. The rate decreases with decrease in the electron withdrawing power of the substituent group.

A comparison of α-methylstyrene and *trans*-β-methylstyrene is particularly interesting. From the structures, it appears that the smaller steric hindrance of the *trans*-β-monomer accounts for its greater reactivity.

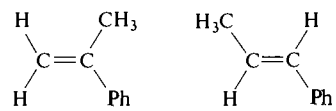

α-Methylstyrene *trans*-β-Methylstyrene

Discussion

In order to provide a rational interpretation of the kinetic results, one must consider mechanisms which are compatible with zero-order decay of $DPA^{+\cdot}$ in the absence of monomer and first-order decay when monomer is present. Furthermore the mechanism must show second-order dependence on the monomer concentration.

The zero-order decay of $DPA^{+\cdot}$ is indicative of a surface or diffusion limited process and may be due to a low concentration of reactant interacting with the $DPA^{+\cdot}$. Spontaneous change in the $DPA^{+\cdot}$ radical cation cannot occur as this would similarly introduce a concentration dependence. In the presence of traces of water or added nucleophiles the rate of radical cation decay is greatly accelerated and the rate becomes dependent on the $DPA^{+\cdot}$ concentration. It is noteworthy that the concentration independent decay is observed only in systems where the $DPA^{+\cdot}$ shows the longest life-time and where the impurity levels have been reduced to very low levels.

The second-order dependence on monomer concentration is consistent with the following mechanism.

$$[1] \qquad A^{+\cdot} + M \underset{k_{-1}}{\overset{k_1}{\rightleftarrows}} AM^{+\cdot}$$

$$[2] \qquad AM^{+\cdot} + M \xrightarrow{k_2} AM_2^{+\cdot}$$

On the stationary state assumption this leads to a rate

$$-\frac{d[A^{+\cdot}]}{dt} = \frac{k_2 k_1 [A^{+\cdot}][M]^2}{k_{-1} + k_2[M]}$$

The limiting rate when $k_{-1} \gg k_2[M]$ indicates that the rate constant is k_2K_1 (where K_1 is the equilibrium constant k_1/k_{-1}). An alternative interpretation based on a fast pre-equilibrium followed by a slow reaction leads directly to the same formulation. The rate constant k_2 is identified with the rate constant for propagation of the polymer chain.

Dietz and Larcombe (12) consider that the equilibrium constant K_1 must be small. They note that with a nucleophile, Nu, the equilibrium is displaced to the left. They argue that when **2**

Can. J. Chem. Downloaded from www.nrcresearchpress.com by 210.87.254.6 on 09/05/12
For personal use only.

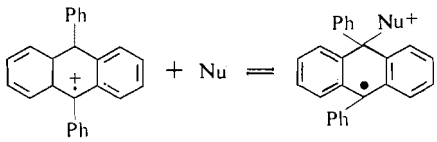

1 2

is formed by electrochemical reduction of a dication, the nucleophile should be lost and the radical cation produced. Their cyclic voltammograms support this interpretation.

At the inception of this work the intention was to compare the rates in the presence and absence of monomer according to the rate scheme

$$[3] \qquad A^{\ddagger} \xrightarrow{k_d} X \quad \text{Rate 1}$$

$$[4] \qquad A^{\ddagger} + M \xrightarrow{k_i} M^{\ddagger} + A \quad \text{Rate 2}$$

$$[5] \qquad M^{\ddagger}_n = M \xrightarrow{k_p} M^{\ddagger}_{n+1} \quad \text{Rate 2}$$

At low concentrations of M the rate constant k_i was to be evaluated by extrapolation to zero concentration of monomer.

The observed kinetics forced us to abandon this approach as the rate dependence was not that expected from previous studies. The rate constant can be interpreted as reflecting the propagation constant for the polymerization, k_p, which is k_2 of reaction 2.

No fully satisfactory explanation is evident for the differences in kinetics found from those reported by Mengoli and Vidotto (9) and Sioda (10). Although Sioda reports that first-order decay is observed for $DPA^{\ddagger}$ even in the absence of water, he limits his consideration to a minimum water content of $<0.03\%$ and his data are based on higher water contents. It is possible that the residual water leads to the kinetic differences observed.

Preliminary studies with methylene chloride as solvent have shown that the choice of solvent will affect the rate of radical ion decay and of polymer formation. This is probably a manifestation of the effect of dielectric constant on an ionic reaction. The role of ion pairs has not been considered in our kinetic treatment, but the rate constant for addition of monomer may reflect the ionic environment of the reacting entity. These effects will be investigated in further studies. They may account for the different kinetic behavior observed by Mengoli and Vidotto in some systems (9).

In any polymerizing system the rate constant k_2 is directly related to the rate constant for propagation. The addition steps in the polymerization should occur in the same manner in electrochemically initiated polymerization as in other cationic polymerizations initiated by relatively stable radical cations.

The authors thank the National Research Council of Canada for financial support.

1. N. YAMAZAKI, J. TANAKA, and S. NAKAHAMA. J. Macromol. Sci. (Chem.), **6**, 1121 (1968).
2. G. PARRAVANO. J. Am. Chem. Soc. **73**, 628 (1951).
3. W. B. SMITH and H. G. GILDE. J. Am. Chem. Soc. **82**, 659 (1960).
4. M. SZWARC. Carbanions, living polymers and electron transfer processes. Interscience, New York. 1968.
5. B. L. FUNT, S. N. BHADANI, and D. RICHARDSON. J. Polym. Sci. **4**, 2871 (1966).
6. B. L. FUNT and V. HORNOF. J. Polym. Sci. **9**, 2171 (1971).
7. G. MENGOLI and G. VIDOTTO. Makromol. Chem. **129**, 73 (1969).
8. G. MENGOLI and G. VIDOTTO. IUPAC Symposium on macromolecules, Helsinki, **1**, 285 (1972).
9. G. MENGOLI and G. VIDOTTO. Die Makromol. Chimie, **150**, 277 (1971).
10. R. E. SIODA. J. Phys. Chem. **72**, 2322 (1968).
11. R. N. ADAMS. Electrochemistry at solid electrodes. Dekker, New York. 1969. p. 83.
12. R. DIETZ and B. E. LARCOMBE. J. Chem. Soc. (B), 1369 (1970).

Can. J. Chem. Downloaded from www.nrcresearchpress.com by 210.87.254.6 on 09/05/12
For personal use only.

Spectrométrie de masse d'imines aliphatiques

GILLES LEDUC ET YVES ROUSSEAU

Département de chimie, Université de Montréal, C.P. 6128, Montréal, Québec

Reçu le 3 juillet 1973[1]

Les principaux mécanismes de fragmentation de quatre imines aliphatiques soumises à l'impact électronique sont rapportés. Ces mécanismes sont supportés par les spectres enregistrés pour les imines deutériées et par la détermination des transitions métastables importantes. Pour l'ion $(R_1)_2\ C{=}\overset{+\cdot}{N}\ (R_2)_3$, l'élimination du radical $R_2^{\cdot}$ est préférentielle si $R_1^{\cdot}$ et $R_2^{\cdot}$ sont des radicaux méthyles ou éthyles. On rapporte les potentiels d'ionisation des produits étudiés.

The electron impact induced fragmentation pattern of four aliphatic imines are reported. These are derived from studies involving deuteriated imines and from the observed metastable transitions. The elimination of the $R_1^{\cdot}$ radical from $(R_1)_2\ C{=}\overset{+\cdot}{N}\ (R_2)_3$ appears to be preferred provided $R_1^{\cdot}$ and $R_2^{\cdot}$ are methyl or ethyl radicals. The ionization potentials of the compounds studied have been determined.

Can. J. Chem., **52**, 1648 (1974)

Introduction

Bien que la structure moléculaire des imines ($R'R''C{=}N{-}R'''$) ressemble à celle des composés carbonylés, ces derniers ont été beaucoup plus étudiés en spectrométrie de masse. De fait, il y a peu d'études rapportées sur les modes de décomposition des imines par impact électronique; ceci est sans doute dû à leur instabilité. Toutefois il est possible d'établir un parallélisme entre les processus de fragmentation de ces deux classes de composés; lorsque le radical $R'''\cdot$ est un méthyle, la fragmentation des imines se fait d'une façon similaire à celle des composés carbonylés (1, 2). Ainsi la liaison en α du groupement C=N se brise facilement pour donner un radical $R'\cdot$ et un ion contenant l'atome d'azote. Egalement si les radicaux $R'\cdot$ ou $R''\cdot$ sont suffisament grands pour permettre une transposition de McLafferty un ion correspondant à ce réarrangement sera présent dans le spectre. Par contre la présence d'un radical $R'''\cdot$ plus grand favorise également d'autres modes de clivage de ce côté de la molécule. Ainsi il peut se produire un bris de la liaison en β de l'azote, ou si $R''''\cdot$ est suffisamment long, une transposition de McLafferty.

La présente étude a donc pour but de mettre en évidence les principaux types de clivage de ces molécules, de mesurer le potentiel d'ionisation des composés étudiées et de démontrer que la présence d'un ion $(M + 1)^+$ s'explique par une réaction ion–molécule.

Partie expérimentale

On donne au tableau 1 la liste des imines qui ont été préparées en utilisant un système à vide afin d'éviter tout contact de ces composés avec l'air et pour permettre des distillations à froid. La synthèse se fait par condensation directe de l'amine avec l'acétone ou la propionaldéhyde (3). On introduit les deux réactifs dans le système à vide en prenant bien soin de pomper l'air emprisonné dans les liquides. Les deux composés sont ensuite mis en présence dans un piège commun. Quinze minutes plus tard le mélange réactionnel est transféré dans un ballon contenant du tamis moléculaire pour permettre la déshydratation. Ce mélange est enfin distillé; on laisse évaporer le liquide à la température de la pièce et l'imine est condensée dans un piège (plongeant dans un bain liquide–solide au chloroforme, $T = -63\,^{\circ}C$). Les réactifs de départ sont ainsi éliminés par pompage à cause de leur plus grande volatilité. Une dizaine de distillations sont nécessaires à la purification du produit. Les composés étudiés ont une masse moléculaire de 99 et une détermination de la masse exacte à *m/e* 99 (à l'aide d'un spectromètre de masse MS-902 de la compagnie A.E.I., en utilisant la méthode de recouvrement de pics) permet de vérifier la composition atomique comme étant $C_6H_{13}N$. La détermination de la masse exacte des autres ions est faite également à l'aide de cet appareil qui est aussi utilisé pour déterminer des transitions métastables en utilisant un dispositif à défocalisation commercial fourni par la compagnie A.E.I. Pour la détermination des spectres à basse résolution, l'évaluation des potentiels d'ionisation et la mise en évidence des réactions ions–molécules un spectromètre CEC-21-104 est utilisé. Dans tous les cas le système d'injection des gaz s'est avéré adéquat et l'énergie des électrons ionisant était de 70 eV, Les potentiels d'ionisation ont été évalués par la méthode

[1]Révision reçue le 17 janvier 1974.

Can. J. Chem. Downloaded from www.nrcresearchpress.com by 210.87.254.40 on 09/05/12
For personal use only.

TABLEAU 1. Structure, potentiel d'ionisation, point d'ébullition des imines étudiées

Numéro du composé	Structure	Potentiel d'ionisation	Point d'ébullition (e)	
			Trouvé	Litt. (3)
1*a*	$(CH_3)_2C{=}NC_3H_7$	8.31	106–107	107
1*b*	$(CH_3)_2C{=}NC_3D_7$	—	—	
2*a*	$(CH_3)_2C{=}NC_3H_7$—*i*	8.36	91–92	
2*b*	$(CH_3)_2C{=}NC_3D_7$—*i*	—	—	
3*a*	$C_2H_5CH{=}NC_3H_7$	8.55	100–101	101
3*b*	$C_2H_5CH{=}NC_3D_7$	—	—	
4	$C_2H_5CH{=}NC_3H_7$—*i*	8.50	85–86	

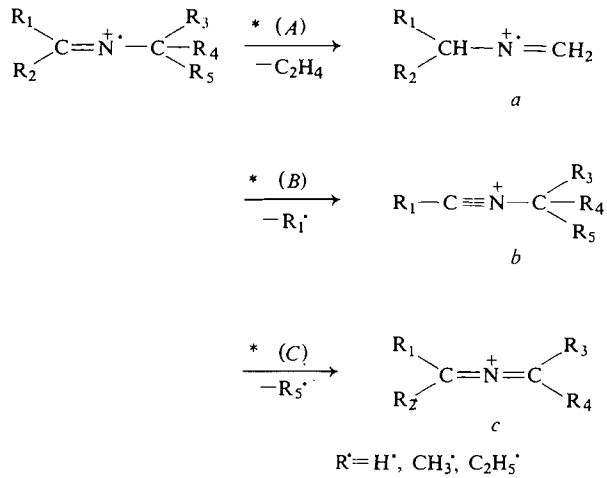

SCHÉMA 1

de Warren (4), le standard interne étant le toluène (potentiel d'ionisation 8.82 eV (5)).

Résultats et discussions

Mécanismes de fragmentation

Les principaux mécanismes de fragmentation de l'ion moléculaire sont indiqués au schéma 1 et les intensités relatives des ions sont données au Tableau 2; les ions résultant de ces fragmentations se retrouvent à *m/e* 98 ($M^{\cdot+} - H^{\cdot}$), 84 ($M^{\cdot+} - CH_3^{\cdot}$), 70 ($M^{\cdot+} - C_2H_5^{\cdot}$) et 71 ($M^{\cdot+} - C_2H_4$) pour les imines non deutériées. Il existe donc une compétition entre trois modes de clivages primaires, le premier, *A*, est une transposition de type McLafferty (*m/e* 71) qui, bien qu'elle se semble pas être prépondérante, est une caractéristique de la structure moléculaire des composés. Les deux autres types de fragmentation sont des clivages simples donnant soit les ions **b** comme pour les composés carbonylés ou encore les ions **c**. Si on considère, pour les composés **1***a*, **1***b*, **2***b*, **3***b*, **4**, la perte des radicaux méthyles ou éthyles, les ions résultant du clivage de type *B* ont des intensités relatives plus faibles que ceux issus d'un clivage de type *C*.

Ceci s'explique par la plus grande stabilité des ions résultant puisque les ions de type **b**, qui semblent moins intenses, sont cependant ceux qui donnent par un clivage ou réarrangement subséquent les ions les plus intenses du spectre (*m/e* 42 et 43). D'ailleurs les ions de type **c** sont probablement plus stables en raison de leur structure ionique permettant de répartir la charge sur trois atomes alors que pour les ions de types **b** la charge ne peut se répartir que sur deux atomes.

Au schéma 2 on indique comment les ions **b** peuvent subir un clivage conduisant à la formation des ions *m/e* 56 (C_3NH_6), 43 (C_3H_7), 42 (C_2NH_4), 28 (CNH_2). D'ailleurs l'étude des spectres des homologues deutériés ainsi que celle des transitions métastables observées confirment le mécanisme tel que décrit. En comparant les spectres on se rend compte que dans les cas où

Can. J. Chem. Downloaded from www.nrcresearchpress.com by 210.87.254.40 on 09/05/12
For personal use only.

TABLEAU 2. Intensités relatives des principaux ions dans les spectres de masse des imines

m/e	**1***a*	**1***b*	**2***a*	**2***b*	**3***a*	**3***b*	**4**
28	9.85	11.7	5.97	7.86	27.0	14.1	37.7
29		7.33		5.14	8.25	14.1	7.03
30	10.4	17.7		13.1	8.25	26.8	
32		17.5		7.36		7.00	
42	100	13.7	100	11.8	23.7	9.00	18.9
43	23.7	100	16.1	100	100	7.23	100
50		18.7		16.1		100	
56					12.6		24.1
57						12.0	
70	59.4				87.8		17.2
71	13.0				7.64		
72		50.8				71.5	
74		6.0				3.0	
77						21.7	
84	16.1		45.2				55.5
88		4.75		40.7			
91		9.17		8.21			
98	1.94		3.21		1.15		1.77
99	6.27		10.5		5.07		6.89
104		1.00		2.21		0.77	
105		0.58		0.86		1.46	
106		6.41		12.0		11.8	

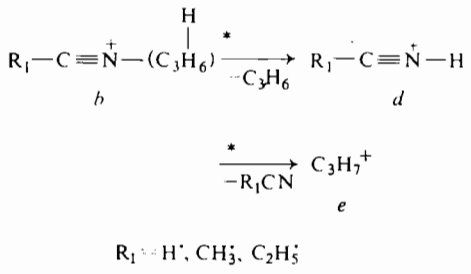

SCHÉMA 2

$R_1\cdot$ est un groupe méthyle (**1***a* et **2***a*) l'intensité enregistrée à *m/e* 42 est plus grande que dans les cas où $R_1\cdot$ est un atome d'hydrogène ou un éthyle (**3***a* et **4**). Pour ces derniers composés les ions à *m/e* 56 et 28 sont plus intenses que pour les composés **1***a* et **2***a*. Le processus permettant aux ions de type **b** de se fragmenter pour donner un ion de type **d** est bien démontré par les résultats obtenus (spectres de masse et transitions métastables).

Les ions à *m/e* 42 et 43 sont les plus importants; pour les composés **1***a* et **2***a* l'ion à *m/e* 42 (C_2H_4N) est le plus intense du spectre tandis que pour les composés **3***a* et **4** l'ion à *m/e* 43 (C_3H_7) est le plus intense. Afin d'expliquer la formation prépondérante soit de l'ion propylium pour les composés **3***a* et **4** soit de l'ion de réarrangement **d** pour les composés **1***a* et **2***a* on peut faire appel aux différentes formes de résonnance de l'ion **b**

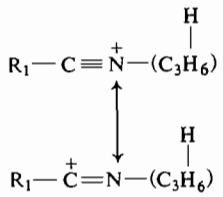

Dans le cas des composés **1***a* et **2***a*, $R_1\cdot$ est un radical méthyle qui peut aider à stabiliser la charge positive alors que pour les composés **3***a* et **4**, $R_1\cdot$ est un atome d'hydrogène.

Pour les composés **1***a* et **2***a* la charge étant mieux répartie elle restera de préférence sur la partie azotée de la molécule lors du clivage, tandis que dans le cas des deux autres composés elle se retrouvera préférentiellement sur le radical propyle. Il s'agit d'une compétition entre les deux fragments qui se forment et la charge se retrouvera sur le fragment qui peut mieux la stabiliser.

La transition $70 \xrightarrow{*} 30$ pour les composés **1***a* et **3***a* peut s'expliquer comme suit.

Par un mécanisme semblable la présence d'ions à *m/e* 44 dans le cas des composés **2***a* et **4** s'expliquerait à partir d'un ion à *m/e* 84. Cepen-

Can. J. Chem. Downloaded from www.nrcresearchpress.com by 210.87.254.40 on 09/05/12
For personal use only.

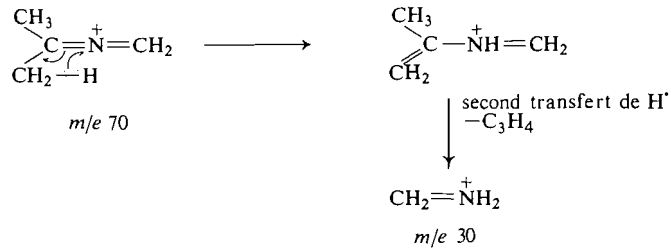

dant ces ions sont beaucoup moins intenses et leur spectre de transitions métastables n'a pas été déterminé.

Il ne fait aucun doute que d'autres mécanismes de fragmentation sont possibles, mais ceux décrits semblent les plus importants pour la caractérisation de ces composés. Ils ont été déterminés à l'aide des spectres des composés deutériés et de l'étude des transitions métastables. Ils indiquent, d'une façon générale, que ces modes de fragmentation sont assez bien définis.

Réactions ions–molécules

Une étude de la variation du rapport de l'intensité des ions à *m/e* 100 sur l'intensité des ions à *m/e* 99 montre que ce rapport varie avec la pression et l'extrapolation de la droite obtenue à pression nulle donne une valeur de 7.3% ce qui correspond au rapport isotopique calculé pour ces molécules. De plus, si on augmente le potentiel des électrodes qui poussent les ions hors de la chambre d'ionisation, le rapport *I* (*m/e* 100)/*I* (*m/e* 99) diminue. Ces deux faits mettent donc en évidence que les ions à *m/e* 100 sont en partie dus à des réactions entre ions et molécules et des études présentement en cours devraient permettre d'établir la nature exacte de ces réactions.

Potentiels d'ionisation

La reproductibilité des mesures des potentiels d'ionisation se situe aux environs de ± 0.1 eV et la différence de potentiel entre le standard interne (toluène) et l'imine étant de 0.3 et 0.5 eV, selon le composé étudié, l'erreur sur la mesure du potentiel d'ionisation peut difficilement être plus grande que 0.2 eV. Les potentiels mesurés sont inférieurs à celui du toluène alors que ceux d'autres imines aliphatiques rapportés par Turner et son collaborateur en 1964 (6) sont supérieurs à celui du toluène.

Conclusion

L'étude de la fragmentation des imines induite par impact électronique a permis de démontrer l'importance du clivage primaire de type *B* qui est caractéristique des imines étudiées. Ensuite, les ions de type **b** se fragmentent également pour donner les ions les plus intenses du spectre à *m/e* 42 our 43 selon le cas. Ces clivages caractéristiques qui se traduisent par un spectre de masse bien défini apportent des indications précises sur la structure du composé. Pour ce qui est des potentiels d'ionisation on constate que les imines "cétoniques" ont des potentiels d'ionisation plus bas que les imines "aldéhydiques". Au chapitre des réactions ions–molécules il est évident que les ions à *m/e* 100 sont, en partie, des ions provenant de telles réactions qui sont favorisées par la présence de l'atome d'azote qui est un site basique important sur la molécule.

Les auteurs tiennent à remercier particulièrement le Conseil National de Recherches du Canada pour l'aide financière apportée sous forme de bourses et d'octrois. Ils remercient également Monsieur A.S. Blair pour son assistance technique.

1. N. FISHER et C. DJERASSI. Chem. Ber. **99**, 1541 (1966).
2. W. CARPENTER, A. M. DUFFIELD et C. DJERASSI. J. Am. Chem. Soc. **89**, 6167 (1967).
3. W. LAYER. Chem. Rev. **63**, 489 (1963).
4. R. W. KISER. Introduction to mass spectrometry and its applications. Prentice-Hall Inc., Englewood Cliffs, N.J. 1965.
5. D. W. TURNER. Adv. Phys. Org. Chem. **4**, 31 (1966).
6. M. I. AL. JOBOURY et D. W. TURNER. J. Chem. Soc. 4434 (1964).

Can. J. Chem. Downloaded from www.nrcresearchpress.com by 210.87.254.40 on 09/05/12
For personal use only.

Synthetic Cardenolides and Related Products. III.[1] Isocardenolides[2]

J. M. FERLAND

Ayerst Research Laboratories, Montréal, Québec

Received November 1, 1973

The synthesis of novel cardenolides, closely related to naturally-occurring cardiotonic agents, is described. They were obtained from 17β-[3-furyl]androstanes derived from digitoxigenin, gitoxigenin, digoxigenin, and strophanthidin by hypohalous acid or organic peracid oxidation. The preparation of β-D- and α-L-glycosidic derivatives is also reported.

On a synthétisé de nouveaux agents cardiotoniques, isomères des cardénolides naturels. Ils ont été obtenus par l'oxidation à l'aide de l'acide hypohaleux ou des peracides organiques de [3-furyl]-17β androstanes, dérivés de la digitoxigénine, la digoxigénine, la gitoxigénine et la strophanthidine. Des dérivés β-D- et α-L-glycosidiques sont aussi décrits.

Can. J. Chem., **52**, 1652 (1974)

As part of a program aimed to improve the therapeutic ratio of cardiotonic agents, we prepared novel isocardenolides,[3] which possessed all the characteristics of the natural cardenolides except for the location of the oxo group of the 5-membered lactone (3). In addition, 21-hydroxydigitoxigenin was also synthesized.

When 17β-[3-furyl]-5β-androstane-3β,14β-diol 3-acetate (**2***b*) was treated with a hypohalous acid in aqueous dioxane, lactones **3***a* and **4** were isolated. The major product was **3***a* when 1 equiv. of the oxidant was used, while a larger excess of the reagent (2 equiv.) afforded mainly lactone **4**. The structures were ascertained by spectral analyses (see Experimental). Furthermore, the aldehyde **4** was converted to the acid **5** and to the corresponding saturated lactone-aldehyde **6** by reducing the ene-dione system with zinc and acetic acid. Finally, **3***a* and **4** were both oxidized with potassium permanganate to the well-known (5) α-ketolactone **7**. This constitutes an unambiguous proof of the 17β-stereochemistry of lactone **3***a* (Scheme 1).

Scheme 2 illustrates a likely mechanism for the formation of **3***a* and **4**. Initially an electrophilic attack of X^+ of the hypohalous acid on the less-hindered side of the furan ring, concerted with a nucleophilic addition of OH^-, affords **9**. Elimination of HX, followed by rearrangement of the resulting hydroxyfuran **10**, yields **3***a*. In a competitive pathway further oxidation of **9** gives the bromolactone[4] **11**, which is converted into **4** by an internal attack of the 14-hydroxyl on the carboxyl group with concomitant elimination of HX.

The furyl derivatives (**2**) were in general obtained by diisobutylaluminum hydride reduction of the natural cardenolides (**1**) (6). An alternative process for the preparation of **2***a* was also used. Reduction of digitoxigenin **1***a* with an excess diisobutylaluminum hydride afforded the diol **8**, which was oxidized to **2***a* with 1 equiv. triethylamine – sulfur trioxide complex (7) (Scheme 1). In this last process the key step involves the formation of an unstable lactol **13**, which upon elimination of water affords the furan ring. This lactol originates from the cyclization of the hydroxyaldehyde **12** resulting from the oxidation of the diol **8** (Scheme 3).

In Scheme 4 are outlined the furan derivatives (**2**) and the isomeric cardenolides (**3**) that were prepared from digitoxigenin (**1***a*), digoxin (**1***b*), digoxigenin (**1***c*), and gitoxigenin (**1***d*). During the hypohalous acid oxidation of the furan, the 3-alcohols had to be protected as esters. In order to be able to regenerate the 3-hydroxy derivatives **3***c*, it was preferable to use chloroacetates rather than acetates. The latter could not be hydrolyzed under conditions (Na_2CO_3 or NaOH) which would prevent the opening of the lactone. On the other hand the chloroacetates were readily removed with potassium bicarbonate.

Since it is a well-established fact that cardiac

[1]For Parts I and II see refs. 1*a* and *b*.

[2]This work was presented in part at the 6th International Symposium on the Chemistry of Natural Products, Mexico, April 22, 1969 (2*a*).

[3]Other types of isocardenolides and modified butenolides have been reported in the literature (4).

[4]Oxidation of 17β-[3-furyl] steroids in C/D *trans* series has yielded similar halolactones (2*b*).

Can. J. Chem. Downloaded from www.nrcresearchpress.com by 210.87.254.40 on 09/05/12
For personal use only.

Can. J. Chem. Downloaded from www.nrcresearchpress.com by 210.87.254.40 on 09/05/12
For personal use only.

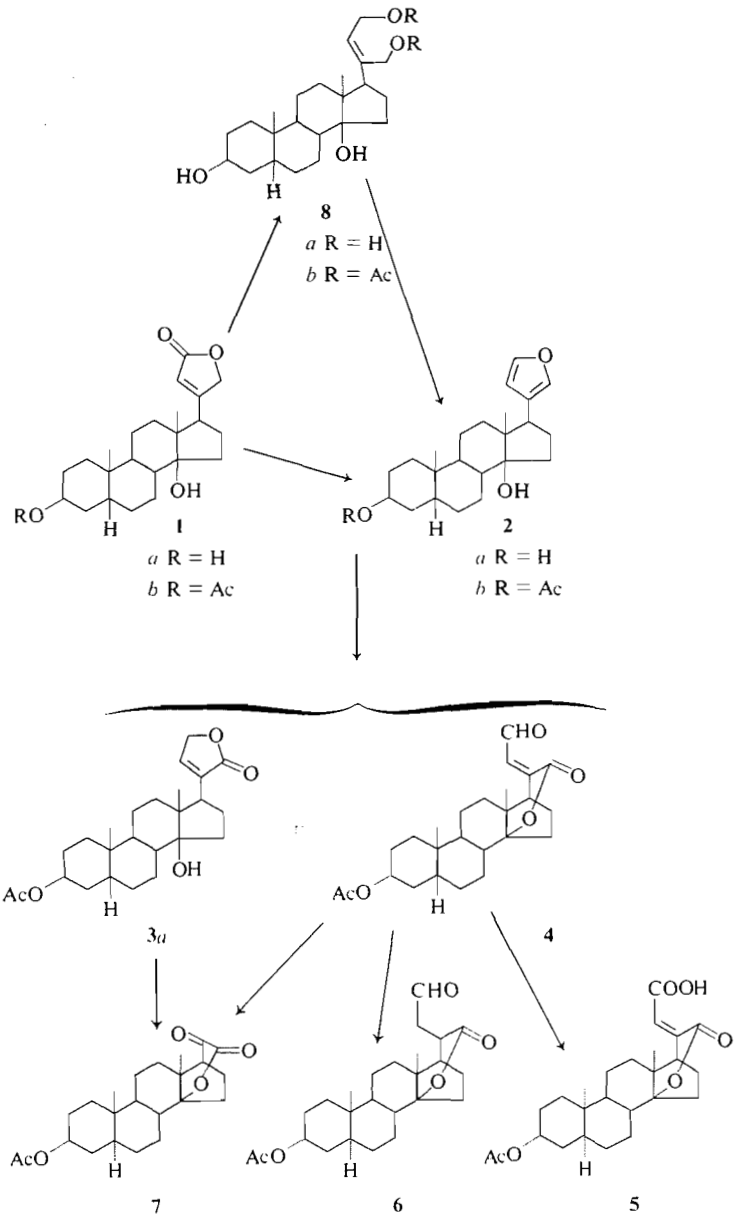

SCHEME 1

glycosides have greater therapeutic applications than the cardiac aglycones (9), it was obvious that our modified cardenolides should be converted into β-D- and α-L-pyranyloxy derivatives by a modified Koenigs–Knorr synthesis. Accordingly **3***c* and **3***m* were condensed with 2,3,4,6-tetraacetyl-α-D-glucopyranosyl bromide (12) to give as expected (10, 11) the acetylated β-D-glucopyranosyl derivatives **3***d* and **3***n*, and the orthoester **3***f* (characterized only in this case). Alcohol **3***c* was also condensed with 2,3,4-tribenzoyl-α-L-rhamnosyl bromide (13) to give, with net retention of configuration (10, 14), the α-L-rhamnopyranosyloxy analog **3***g*. The protecting esters were hydrolyzed as described by Zorbach *et al.* (15).

In a similar sequence of reactions digitoxin **1***b* was reduced by diisobutylaluminum hydride to afford **2***d*. Prior to the hypohalous acid oxidation

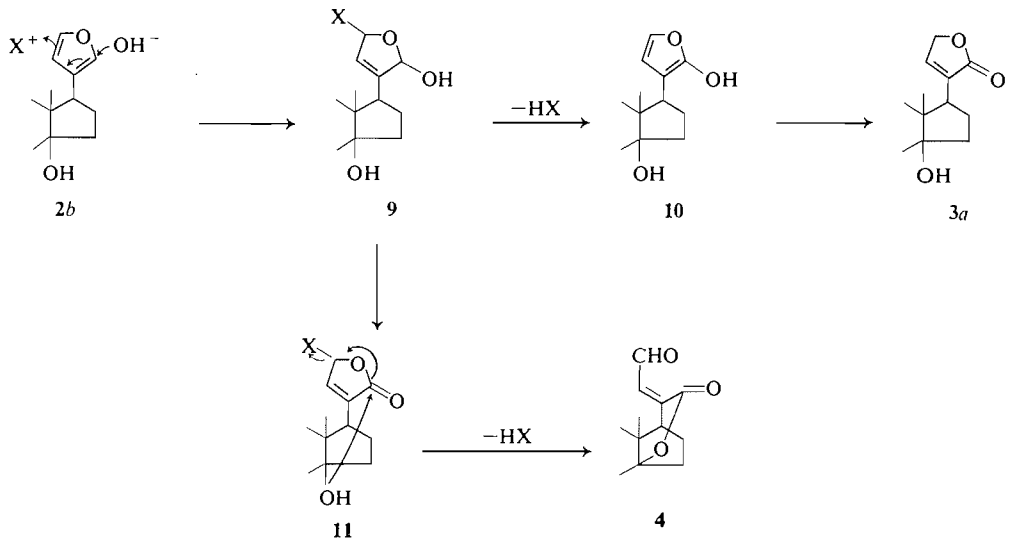

SCHEME 2

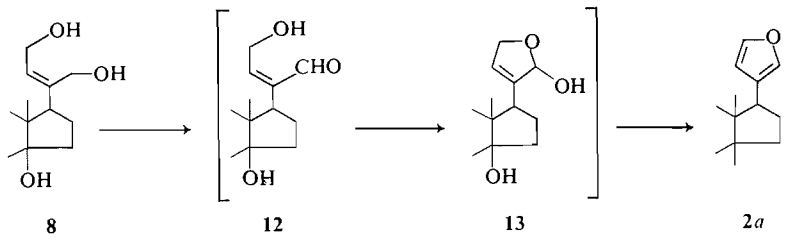

SCHEME 3

the hydroxyl groups of the sugar portion were protected as acetates. Regeneration of the alcohols was effected by mild hydrolysis with potassium bicarbonate at 37° for 15 days (17).

Finally a slightly different process had to be used to obtain the isocardenolide analog **19***b* of strophanthidin **14**. The 3-tetrahydropyranyl ether **15** (18) was reduced with diisobutylaluminum hydride to give the 17β-[3-furyl]-19-alcohol (**16***a*) (identified as the 3,19-diacetate, **16***b*), which was oxidized with manganese dioxide (8) to the aldehyde **17**. Removal of the pyranyl ether and chloroacetylation afforded **18** which was converted in the usual manner to the isocardenolide **19***a*. The 3-alcohol **19***b* as well as the pyranosyl derivatives **19***c* and **19***d* were obtained as previously described (Scheme 5).

The anomeric configurations of the pyranosyloxy isocardenolides **3***e*, **3***h*, **3***o*, and **19***d* were confirmed by application of the Klyne rule of molecular rotational additivity (16).

In order to obtain other modified lactones, **2***b* was oxidized with organic peracides to yield lactones **20** and **21**. The proportion of each was dependant on the experimental conditions. For example, lactone **20** was the major component when the solvent was acetone while in acetic acid **21** was predominant. The structures were again ascertained by spectral analysis. Furthermore potassium permanganate oxidation of both lactones afforded the known ketolactone **7**. Finally, reduction of **20** with sodium borohydride followed by acid treatment yielded digitoxigenin **1***b*. This constitutes an unequivocal proof of the 17β-stereochemistry of **20** and a novel synthesis of natural cardenolides (Scheme 6).

Can. J. Chem. Downloaded from www.nrcresearchpress.com by 210.87.254.40 on 09/05/12
For personal use only.

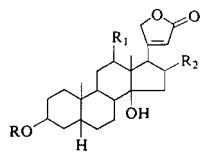

1

a R = R_1 = R_2 = H (digitoxigenin)

b R = Tridigitoxosyloxy; R_1 = R_2 = H (digitoxin)

c R = R_2 = H; R_1 = OH (digoxigenin)

d R = R_1 = H; R_2 = OH (gitoxigenin)

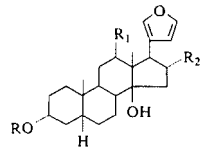

2

a R = R_1 = R_2 = H

b R = CCH_3; R_1 = R_2 = H

c R = CCH_2Cl; R_1 = R_2 = H

d R = Tridigitoxosyloxy; R_1 = R_2 = H

e R = Tridigitoxosyloxy tetraacetate; R_1 = R_2 = H

f R = R_2 = H; R_1 = OH

g R = CCH_3; R_1 = $OCCH_3$; R_2 = H

h R = CCH_2Cl; R_1 = $OCCH_2Cl$; R_2 = H

i R = R_1 = H; R_2 = OH

j R = CCH_3; R_2 = $OCCH_3$; R_1 = H

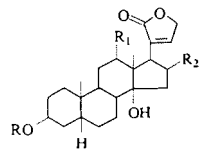

3

a R = CCH_3; R_1 = R_2 = H

b R = CCH_2Cl; R_1 = R_2 = H

c R = R_1 = R_2 = H

d R = β-D-Tetraacetylglucopyranosyloxy; R_1 = R_2 = H

e R = 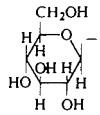 R_1 = R_2 = H

f R = 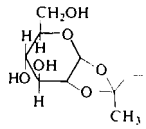 R_1 = R_2 = H

g R = α-L-Tribenzoylrhamnopyranosyloxy; R_1 = R_2 = H

h R = R_1 = R_2 = H

i R = Tridigitoxosyloxy tetraacetate; R_1 = R_2 = H

j R = 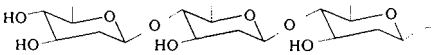

k R = CCH_3; R_1 = $OCCH_3$; R_2 = H

l R = CCH_2Cl; R_1 = $OCCH_2Cl$; R_2 = H

m R = R_2 = H; R_1 = OH

n R = β-D-Tetraacetylglucopyranosyloxy; R_2 = H; R_1 = OH

o R = 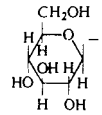 R_1 = OH; R_2 = H

p R = CCH_3; R_2 = $OCCH_3$; R_1 = H

SCHEME 4

Can. J. Chem. Downloaded from www.nrcresearchpress.com by 210.87.254.40 on 09/05/12
For personal use only.

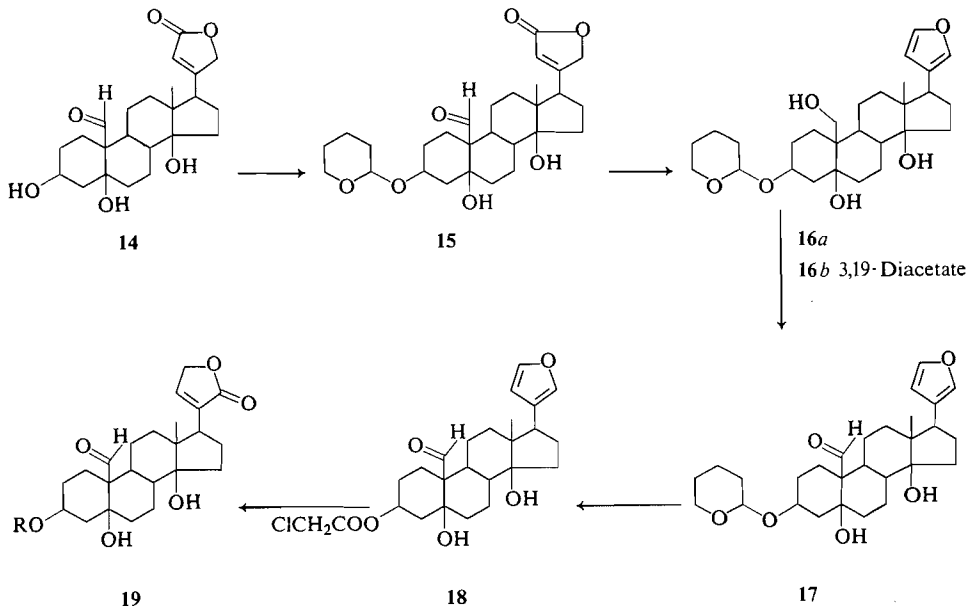

a R = $ClCH_2CO$
b R = H
c R = Tetraacetyl-β-D-glucopyranosyloxy
d R = β-D-Glucopyranosyloxy

SCHEME 5

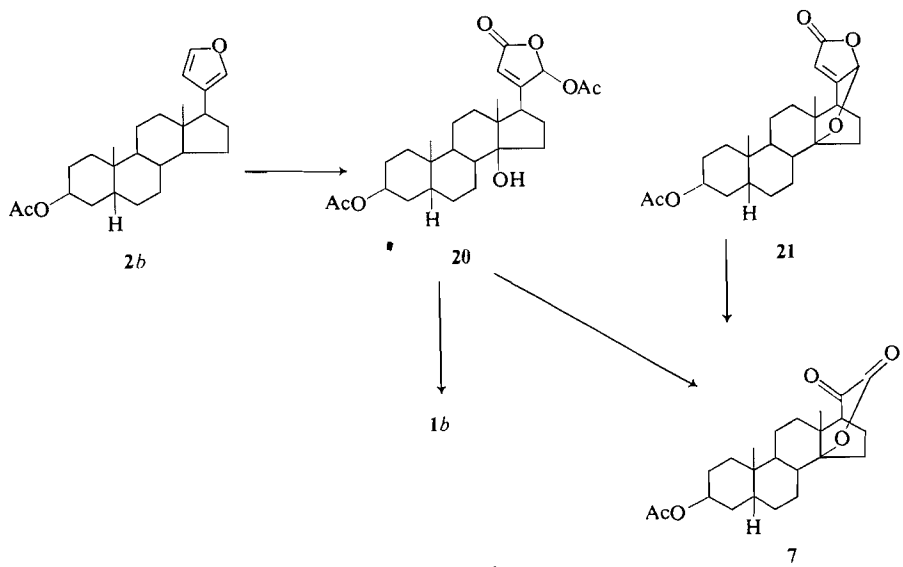

SCHEME 6

Can. J. Chem. Downloaded from www.nrcresearchpress.com by 210.87.254.40 on 09/05/12
For personal use only.

Can. J. Chem. Downloaded from www.nrcresearchpress.com by 210.87.254.40 on 09/05/12
For personal use only.

Although two isomers of lactone **21** may exist (**22** and **23**), we assign structure **22** to the isolated compound on conformational grounds.

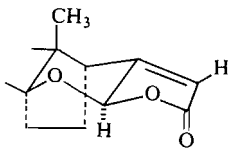

22

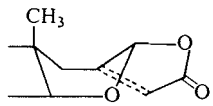

23

Some of the results of the biological evaluation of our modified cardenolides have already been published (19) and will be described completely elsewhere.

Experimental

Melting points are uncorrected. The i.r. spectra were taken on a Perkin-Elmer 225 i.r. spectrophotometer and n.m.r. were recorded on a Varian-A-60A spectrometer operating at 60 MHz; TMS was used as internal standard. Merck silica gel 60 (60–230 mesh) was used. The $[\alpha]_D$ were taken at 20–23° in 1% chloroform solutions. Otherwise, the solvent is mentioned.

17β-[3-Furyl] Derivatives

Diisobutylaluminum Hydride Reduction

The reduction of the cardenolides was carried out by the slightly modified method of Minata and Nagasaki (6). The following example will illustrate the procedure.

17β-[3-Furyl]-3β-tetrahydropyranyloxy-5β,14β-androstane-5,14,19-triol (16a)

A 27% solution of diisobutylaluminum hydride in hexane (20 ml) diluted with dry THF (20 ml) was added dropwise, over a period of 5 min, under nitrogen, to a stirred solution at −20° of strophanthidin THP ether (**20**) (3.15 g) in dry THF (130 ml). The reaction mixture was stirred at the same temperature for 30 more min and allowed to warm up to 0° while a saturated solution of sodium potassium tartrate was added dropwise. After stirring for 15 min at room temperature, the mixture was filtered and the salts washed with ethyl acetate. The filtrate was washed to neutrality (salt saturated water), dried, and evaporated. The crude product was chromatographed on silica gel to give the title product (1.9 g).

In a similar way reduction of digitoxin, digitoxigenin, digoxigenin, and gitoxigenin gave **2***d*, **2***a*, **2***f*, and **2***i*, respectively.

Esters

17β-[3-Furyl]-5β,14β-androstane-3β,5,14,19-tetrol 3,19-Diacetate (16b)

A solution of the 3-THP ether **16***a* (0.100 g) in ethanol (3 ml) and 0.1 *N* hydrochloric acid (0.1 ml) was stirred at 45–50° for 4 h. The mixture was then concentrated under reduced pressure to half its original volume and poured into ice cold water. It was extracted with ethyl acetate and the organic solution washed with salt saturated water, dried, and evaporated (0.080 g).

The crude alcohol was acetylated in pyridine (1 ml) and acetic anhydride (0.5 ml) at room temperature overnight. The solution was poured into ice cold water and extracted with ethyl acetate. The organic solution was washed to neutrality, dried, and evaporated to give the title product. It was crystallized twice from methylene chloride – ether (0.057 g), m.p. 178–180°, $[\alpha]_D$ +41.6°.

Anal. Calcd. for $C_{27}H_{38}O_7$: C, 68.33; H, 8.07. Found: C, 68.44; H, 8.09.

The i.r. ν_{max}($CHCl_3$): 3570, 1720, and 865 cm^{-1}; n.m.r. ($CDCl_3$): 0.73 (C-18, CH_3), 2.06 and 2.11 (3- and 19-OAc), 3.20 (OH), 4.45 (C-19,—CH_2—O), 6.50 (C-4, H-furyl) 7.27 (C-5, H-furyl), and 7.36 p.p.m. (C-2, H-furyl).

In a similar way acetylation of **2***a*, **2***f*, **2***i*, and **2***d* gave, respectively, after chromatography:

2*b*. Yield 60% from **1***a*, methanol–water, m.p. 155–157°, $[\alpha]_D$ +17.5°.

Anal. Calcd. for $C_{25}H_{36}O_4$: C, 74.96; H, 9.06. Found: C, 74.61; H, 8.65.

2*g*. Yield 35% from **1***c*, methanol–water, m.p. 158–161°, $[\alpha]_D$ +35.2°.

Anal. Calcd. for $C_{27}H_{38}O_6$: C, 70.71; H, 8.35. Found: C, 70.42; H, 8.07.

2*j*. Yield 35% from **1***d*, methylene chloride – ether, m.p. 170–172°, $[\alpha]_D$ −14.9°.

Anal. Calcd. for $C_{27}H_{38}O_6$: C, 70.72; H, 8.35. Found: C, 70.49; H, 8.56.

2*e*. The crude 17β-furyl derivative **2***d* was acetylated for 4 days at room temperature; yield 55% from **1***b*, ethyl acetate – hexane, m.p. 169–171°, $[\alpha]_D$ +51.0°.

Anal. Calcd. for $C_{49}H_{72}O_{16}$: C, 64.18; H, 7.91. Found: C, 63.89; H, 7.89.

17β-[3-Furyl]-3β-tetrahydropyranyloxy-5,14-dihydroxy-5β,14β-androstan-19-al (17)

A mixture of the 19-alcohol (**16***a*) (3.4 g) in acetonitrile (680 ml) and activated neutral MnO_2 (68 g) was stirred overnight at room temperature. It was then filtrated and the filtrate evaporated. The residue obtained was used as such for the following reaction.

The n.m.r. ($CDCl_3$): 0.85 (C-18, CH_3), 4.71 (3-H, M), 6.4 (C-4, H-furyl) 7.17 (C-5, H-furyl), 7.24 (C-2, H-furyl), and 10.2 p.p.m. (CHO, S).

17β-[3-Furyl]-3β,5,14-trihydroxy-5β,14β-androstan-19-al 3-Chloracetate (18)

A solution of the 3-THP ether (**17**) (2.8 g) in ethanol (90 ml) and 0.1 *N* hydrochloric acid (30 ml) was stirred for 4 h at 45–50°. The mixture was then concentrated *in vacuo* to half its original volume and poured into ice cold water. The mixture was extracted with ethyl acetate and the organic solution washed with salt saturated water, dried, and evaporated to give the 3-alcohol (2.3 g).

That alcohol (1.8 g) in pyridine (1.3 ml) and dioxane (13 ml) at 10° was reacted with chloroacetyl chloride (1 ml) in dioxane (3 ml). The addition of the acid chloride was done over a period of 5 min. The mixture was then stirred at the same temperature for 1 h and neutralized with 10% ammonium hydroxide. It was diluted with water and extracted with ethyl acetate. The organic solution was washed with salt saturated water, dried, and evaporated. The crude product (2.0 g) was chromatographed on silica gel (benzene – ethyl acetate 3:1) to afford the title product (1.5 g).

Can. J. Chem. Downloaded from www.nrcresearchpress.com by 210.87.254.40 on 09/05/12
For personal use only.

The analytical sample crystallized twice from ethyl acetate – hexane, m.p. 211–213°, $[\alpha]_D$ +8.8°.

Anal. Calcd. for $C_{25}H_{33}ClO_6$: C, 64.59; H, 7.15. Found: C, 64.85; H, 7.16.

The i.r. $\nu_{max}(CHCl_3)$: 3580, 1730, 1705, 1015, and 865 cm^{-1}; n.m.r. ($CDCl_3$): 0.8 (C-18, CH_3), 4.06 (O, $ClCH_2C$—O, 2H), 6.4 (C-4, H-furyl), 7.17 (C-5, H-furyl), 7.24 (C-2, H-furyl), and 10.2 p.p.m. (CHO, S).

In a similar way chloroacetylation of **2***a* and **2***f* gave, respectively:

2*c*. Yield 70% (from **1***a*), ether–hexane, m.p. 166–168°. The n.m.r. ($CDCl_3$): 4.04 p.p.m. ($ClCH_2C$—). After hydrolysis with sodium bicarbonate and acetylation, the product obtained was identical with **2***b*.

2*h*. Yield 70% (from **1***c*), benzene–ether–hexane, m.p. 162–164°, $[\alpha]_D$ +24.7°.

Anal. Calcd. for $C_{27}H_{36}Cl_2O_6$: C, 61.47; H, 6.87; Cl, 13.44. Found: C, 61.34; H, 6.92; Cl, 13.45.

21,23-Dinor-5β,14β-chol-20-ene-3β,14,20,24-tetrol (8a)

To a stirred solution at −20°, of digitoxigenin (500 mg) in dry THF (10 ml) was added dropwise, under nitrogen, a solution of diisobutylaluminum hydride (30% in hexane, 8.6 ml, diluted with dry THF (8.6 ml)). The solution was then stirred at room temperature for 1½ h. A saturated solution of Rochelle salt was then added and the solid obtained removed by filtration and washed carefully with chloroform–EtOH, 95:5. The filtrate was washed with salt saturated water, dried, and evaporated to give the crude title product **8***a*. It was identified as the corresponding triacetate **8***b*. That product was crystallized from CH_2Cl_2–ether, m.p. 120–122°.

Anal. Calcd. for $C_{29}H_{44}O_7$: C, 69.02; H, 8.75. Found: C, 69.11, H, 9.10.

The i.r. $\nu_{max}(CHCl_3)$: 3600, 1732, 1220, and 1018 cm^{-1}; n.m.r. ($CDCl_3$): 0.8 (C-18, CH_3), 0.95 (C-19, CH_3), 2.05 (acetates), 4.70 (C-24, CH_2, J = 6 Hz, doublet), 4.75 (C-20, CH_2), and 5.75 p.p.m. (C-22 H, J = 6 Hz, triplet).

17β-[3-Furyl]-5β,14β-androstane-3β,14-diol 3-Acetate (2b)

To a stirred solution at 15° of the crude tetrol (**8***a*) (5.0 g) in DMSO (14 ml) and triethylamine (16 ml) was added dropwise a solution of triethylamine – sulfur trioxide complex (5.0 g) in DMSO (15 ml). After 15 min, the reaction was poured into water (200 ml) and the amine neutralized with 10% sulfuric acid. The mixture was extracted with $CHCl_3$ and the organic layer washed with water, dried, and evaporated. The crude product obtained was acetylated and worked out the usual way. It was then crystallized from methanol to give the title product (3.5 g) as proven by mixture melting point and i.r. analysis.

17β-Isomeric Lactones (3, 19)

3β,14,23-Trihydroxy-24-nor-5β,14β-chol-20-en-21-oic Acid γ-Lactone 3-Acetate (3a)

Procedure A. To a solution of the furyl derivative **2***b* (2.00 g) in dioxane (100 ml) and water (8 ml) was added portionwise *N*-bromosuccinimide (0.90 g) over a period of 5 min. The solution was then stirred for 30 min and diluted with ether. The ethereal fraction was washed with salt saturated water, dried, and evaporated. The oil obtained was dissolved in acetic acid (100 ml) and stirred in the presence of zinc dust (10 g) for ½ h. The zinc was removed by filtration and the filtrate diluted with chloroform. The organic solution was washed with water until neutral, dried, and evaporated. The product obtained was chromatographed on silica gel; the title product was crystallized from methylene chloride – ether, m.p. 172–173°, $[\alpha]_D$ −5.6°.

Anal. Calcd. for $C_{25}H_{36}O_5$: C, 72.08; H, 8.71. Found: C, 71.71; H, 8.46.

The i.r. $\nu_{max}(CHCl_3)$: 3620, 3440, 1753, 1737 (inflexion), and 1725 cm^{-1}; n.m.r. ($CDCl_3$): 0.80 (C-18, CH_3), 1.0 (C-19, CH_3), 2.07 (C-3, OAc), 4.83 (C-23, CH_2), and 7.37 p.p.m. (C-22, CH).

Procedure B. A solution of *N,N*-dimethyldichlorohydantoin (181 mg) in dioxane (6 ml) was added dropwise, over a period of 10 min, to a stirred solution at 50° of **2***b* (0.750 g) in dioxane (14 ml), acetic acid (2 ml), and water (2 ml). The solution was stirred at the mentioned temperature for 5 more min and diluted with ether. The product was isolated, treated with zinc in acetic acid, and purified as in procedure A. The pure product was identical with **3***a* as shown by mixture melting point and i.r. analysis, yield, 30%.

The following products were made according to procedure A. **3***k*. Yield 25%, methylene chloride – ether, m.p. 224–228°, $[\alpha]_D$ +25.7°.

Anal. Calcd. for $C_{27}H_{38}O_7$: C, 68.33; H, 8.07. Found: C, 67.97; H, 7.82.

3*p*. Yield 25%, methylene chloride – ether, m.p. 228–230°, $[\alpha]_D$ +6.3°.

Anal. Calcd. for $C_{27}H_{38}O_7$: C, 68.33; H, 8.07. Found: C, 68.03, H, 8.06.

The following products were made according to procedure B. **3***i*. Yield 45%, ether–hexane, m.p. 139–142°, $[\alpha]_D$ +45.7°. In this case 1.7 equiv. of *N,N*-dimethylhydantoin had to be used for optimum yield.

Anal. Calcd. for $C_{49}H_{72}O_{17}$: C, 63.07; H, 7.78. Found: C, 62.77; H, 7.91.

3*b*. Yield 55%, methylene chloride – ether–hexane, m.p. 199–201°. The n.m.r. ($CDCl_3$): 4.07 p.p.m. ($ClCH_2C$—). **3***l*. Yield 50%, benzene–ether–hexane, m.p. 129–131°. The n.m.r. ($CDCl_3$): 4.07 and 4.18 p.p.m. ($ClCH_2C$—). **19***a*. Yield 30%. That product, after chromatography, could not be crystallized and was used as such to get **19***b*.

Hydrolysis of Esters

14,23-Dihydroxy-3β-tridigitoxosyloxy-24-nor-5β,14β-chol-20-en-21-oic Acid γ-Lactone (3j)

A solution of the lactone **2***i* (3.0 g) and sodium bicarbonate (3.14 g) in methanol (350 ml) and water (90 ml) was kept at 37° for 14 days. The methanol was then evaporated and the aqueous solution extracted three times with $CHCl_3$–EtOH, 2:1. The organic solution was washed with salt saturated water, dried, and evaporated. The crude product was chromatographed (ethyl acetate – acetone, 75:25) to yield the title compound. Crystallization from $CHCl_3$–ether – petroleum ether (30–65°) gave the analytical sample (0.735 g), m.p. 185–190°, $[\alpha]_D$ −8.5°.

Can. J. Chem. Downloaded from www.nrcresearchpress.com by 210.87.254.40 on 09/05/12
For personal use only.

Anal. Calcd. for $C_{41}H_{64}O_3$: C, 63.47; H, 8.43. Found: C, 63.59; H, 8.60.

The n.m.r. ($CDCl_3$): 0.7 (C-18, CH_3), 0.87 (C-19, CH_3), 4.82 (CH_2—O—, lactone), and 7.47 p.p.m. (=CH, lactone).

In a similar way was obtained **3***m*. Yield 55%, acetone – ethyl acetate – hexane, m.p. 234–236°, $[\alpha]_D$ +2.5°.

Anal. Calcd. for $C_{23}H_{34}O_5$: C, 70.74; H, 8.78. Found: C, 70.67; H, 8.75.

3β,14,23-Trihydroxy-24-nor-5β,14β-chol-20-en-21-oic Acid γ-Lactone (3c)

A solution of the 3-chloroacetate **3***b* (14.6 g) and potassium bicarbonate (4.6 g) in methanol (1300 ml) and water (160 ml) was refluxed for 3 h. Most of the methanol was removed under reduced pressure, the mixture diluted with water, and extracted with ether. The ethereal solution was washed with salt-saturated water, dried, and evaporated. The product obtained was chromatographed on silica gel (ethyl acetate – benzene, 1:1) to afford the title product.

After acetylation, that compound was identical with **3***a* as shown by mixture melting point and i.r. analysis.

In a similar fashion was obtained **19***b*. Yield 70%, methanol, m.p. 201–204°, $[\alpha]_D$ +17.9°.

Anal. Calcd. for $C_{23}H_{32}O_6$: C, 68.29; H, 7.97. Found: C, 68.48; H, 8.01.

The n.m.r. ($CDCl_3$): 0.8 (C-18, CH_3), 3.45, 4.15 (OH), 4.8 (CH_2-O, lactone), 7.25 (=CH, lactone), and 10.02 p.p.m. (CHO, S).

Pyranosyloxy Derivatives

3β-(β-D-Tetraacetylglucopyranosyloxy)-14,23-dihydroxy-24-nor-5β,14β-chol-20-en-21-oic Acid γ-Lactone (3d)

A mixture of alcohol **3***c* (9.0 g), dried magnesium sulfate (27 g), acetobromoglucose (20 g) was stirred at room temperature, under nitrogen, protected from light, in dry dichloroethane (150 ml) (free from alcohols). After 15 min, dry freshly prepared silver carbonate (15 g) was added and the mixture stirred for 1 h more.

The silver and magnesium salts were removed by filtration and the filtrate evaporated under vacuum. The crude product was dissolved in a minimum amount of methylene chloride, at room temperature, and precipitated with ether. Crystallization from CH_2Cl_2–ether gave the title product (4.0 g, 1st crop; 2.0 g, 2nd crop).

The analytical sample was crystallized from methylene chloride – ethanol, m.p. 206–209°, $[\alpha]_D^{EtOH}$ −57.4°.

Anal. Calcd. for $C_{37}H_{52}O_{13}$: C, 63.05; H, 7.44. Found: C, 62.87; H, 7.14.

The n.m.r. ($CDCl_3$): 0.8 (C-18, CH_3), 0.9 (C-19, CH_3), 2.0 and 2.08 (O$\overset{O}{\overset{\|}{C}}$—$CH_3$, 12 protons), 2.9 (C-14, OH), 4.8 (CH_2-O, lactone), and 7.28 p.p.m. (=CH, lactone).

Mother liquors were chromatographed on silica gel to afford the orthoester (**3***f*). Crystallization from pentane gave the analytical sample (1.0 g), m.p. 105–107°, $[\alpha]_D$ +24.4°.

Anal. Calcd. for $C_{27}H_{52}O_{13}$: C, 63.05; H, 7.44. Found: C, 63.19; H, 7.42.

The n.m.r. ($CDCl_3$): 0.8 (C-18, CH_3), 0.92 (C-19, CH_3), 1.73 (orthoacetate, CH_3), 2.78 (C-14, OH), 4.82 (CH_2—O, lactone, triplet J = 2.5 Hz), and 7.3 p.p.m. (=CH, lactone, doublet J = 5.5 Hz).

This product in acetone containing a trace of hydrochloric acid gave **3***c*.

3β-(β-D-Glucopyranosyloxy)-14,23-dihydroxy-24-nor-5β,14β-chol-20-en-21-oic Acid γ-Lactone (3e)

A solution of the acetylated glucosyl derivative **3***d* (1.0 g) and potassium bicarbonate (470 mg) in methanol (180 ml) and water (20 ml) was stirred at room temperature for 10 days. Methanol was then evaporated at reduced pressure (bath temperature < 30°) until a precipitate appeared. The mixture was diluted with water and extracted with ether, chloroform, chloroform–ethanol (9:1 3 × 100 ml fractions, 9:2 3 × 100 ml fractions). The last three fractions were evaporated (0.600 g) and the product crystallized from methanol–water (450 mg), m.p. 237–240°, $[\alpha]_D^{EtOH}$ −39.4°.

[M] Calcd. for **3***b* + methyl β-D-glucopyranoside: (−2300°) + (−6600°) = −8900°. [M] Calcd. for **3***b* + methyl α-D-glucopyranoside: −2300° + 30 800° = + 28 500°. Found for **3***e*: −21 000°. The glycosidic linkage in **3***e* has the β configuration.

Anal. Calcd. for $C_{29}H_{44}O_9$: C, 64.90; H, 8.23. Found: C, 64.97; H, 8.25.

The n.m.r. ($CDCl_3$): 0.7 (C-18, CH_3), 0.88 (C-19, CH_3), 3.27, 3.78, 4.71 (OH), 4.78 (CH_2—O, lactone), and 7.45 p.p.m. (=CH, lactone).

14,23-Dihydroxy-3β-(α-L-rhamnopyranosyloxy)-24-nor-5β,14β-chol-20-en-21-oic Acid γ-Lactone (3h)

The coupling of **3***c* (4.0 g) with tribenzoyl-α-L-rhamnopyranosyl bromide was done as for **3***d*. The product isolated was chromatographed on silica gel to give *14,23-dihydroxy-3β-(tribenzoyl-α-L-rhamnopyranosyloxy)-24-nor-5β,14β-chol-20-en-21-oic acid γ-lactone* (**3***g*) (4.0 g).

3*g* was hydrolyzed as for **3***e*. The mixture obtained after evaporation of methanol and dilution with water was extracted with ether, chloroform, chloroform–isopropanol, 4:1 (3 × 200 ml fractions). The last three fractions were dried, evaporated, and crystallized from ethanol–hexane (2.5 g), m.p. 225–228°. The analytical sample, m.p. 228–230° was obtained from the same solvent mixture, $[\alpha]_D^{EtOH}$ −55.4°.

[M] Calcd. for **3***b* + methyl α-L-rhamnoside: (−2300°) + (−11 100°) = −13 400°. [M] Calcd. for **3***b* + methyl β-L-rhamoside: −2300° + 14 600° = +12 300°. Found for **3***h*: −29 000°. The glycosidic linkage in **3***h* has the α configuration.

Anal. Calcd. for $C_{29}H_{44}O_8$: C, 66.90; H, 8.52. Found: C, 66.82; H, 8.47.

The n.m.r. ($CDCl_3$): 0.7 (C-18, CH_3), 0.88 (C-19, CH_3), 1.10 (C-6, rhamosyl CH_3), 3.23, 3.90, 4.37, 4.53 (OH), 4.65 (CH_2—O, lactone), and 7.45 p.p.m. (=CH, lactone).

3β-(β-D-Glucopyranosyloxy)-12β,23-dihydroxy-24-nor-5β,14β-chol-20-en-21-oic Acid γ-Lactone (3o)

A mixture of **3***m* (1.7 g) anhydrous magnesium sulfate (4.3 g), and acetobromoglucose (4.0 g) was stirred under nitrogen at 45–50° in dry dichloroethane (100 ml). The flask was protected from light and dry freshly prepared silver carbonate (2.8 g) was added and the whole stirred for 2 h. The product isolated as for **3***d* was chromatographed to give **3***n* (1.7 g).

3*n* was hydrolyzed as for **3***e*. The mixture was extracted

Can. J. Chem. Downloaded from www.nrcresearchpress.com by 210.87.254.40 on 09/05/12
For personal use only.

with ether, chloroform, benzene–isopropanol, 9:1, 9:2, and 9:3. The last three fractions were dried, evaporated, and crystallized twice from methanol, (350 mg), m.p. 236–238°, $[\alpha]_D^{EtOH}$ −14.8.

[M] Calcd. for **3***m* + methyl β-D-glucopyranoside: 980–6600° = −5620°. [M] Calcd. for **3***m* + methyl α-D-glucopyranoside: 980 + 30 800° = +31 780°. Found for **3***e*: −8100. The glycosidic linkage in **3***o* has the β-configuration.

Anal. Calcd. for $C_{29}H_{44}O_{10}$: C, 63.03; H, 8.02. Found: C, 63.07; H, 8.03.

The n.m.r. ($CDCl_3$): 0.66 (C-18, CH_3), 0.93 (C-19, CH_3), 4.93 (CH_2—O—, lactone), and 7.60 p.p.m. (=CH, lactone).

*3β-(β-D-Glycopyranosyloxy)-5,14-dihydroxy-19-oxo-24-nor-5β,14β-chol-20-en-21-oic Acid γ-Lactone (**19***d*)

The coupling of **19***b* (0.550 g) with acetobromoglucose was done as for **3***o*. The product obtained was chromatographed on silica gel to give the *tetraacetylated* β-D-*glucopyranosyloxy derivative* **19***c* (320 mg). **19***c* was hydrolyzed as for **3***e*. The mixture was extracted with ether, chloroform, chloroform–isopropanol (9:1, 9:2 (3 × 50 ml fractions), 9:3 (3 × 50 ml fractions)). The last six fractions were dried, evaporated and crystallized from methanol–ether (180 mg), m.p. 233–235°. $[\alpha]_D^{EtOH}$ −11.6°.

[M] Calcd. for **19***b* + methyl β-D-glucopyranoside: 7200 − 6600° = +600°. [M] Calcd. for **19***b* + methyl α-D-glucopyranoside: 7200 + 30 800° = +38 000°. Found for **19***d*: −6200°. The glycoside linkage in **19***d* has the β-configuration.

Anal. Calcd. for $C_{29}H_{42}O_{11}$: C, 61.46; H, 7.46. Found: C, 61.30; H, 7.55.

The n.m.r. (DMSO-*d*): 0.67 (C-18, CH_3), 4.66 (CH_2—O—, lactone), 7.47 (=CH—, lactone), and 10.2 p.p.m. (CHO, S).

*3β,14-Dihydroxy-23-oxo-24-nor-5β,14β-chol-20-en-21-oic Acid δ-Lactone 3-Acetate (**4**)*

To a solution of **3***a* (1.0 g) in dioxane (50 ml) and water (4 ml) was added *N*-bromosuccinimide (0.90 g) and the mixture stirred at room temperature for 5 min. The solution was then diluted with ether and the ethereal solution washed with sodium bicarbonate, salt saturated water, dried, and evaporated. The crude product was crystallized several times from ether (0.350 g), m.p. 220° (dec.). That compound could not be analyzed but was identified from the two products **5** and **6**.

The i.r. ν_{max}(KBr): 1721, 1705, 1675, 1623, and 760 cm^{-1}; n.m.r. ($CDCl_3$): 1.0 (C-18 and 19, $2CH_3$), 6.87 (=CH, 1 proton, J = 7 Hz doublet), and 10.3 p.p.m. (CHO, J = 7 Hz doublet).

*3β,14-Dihydroxy-23-oxo-24-nor-5β,14β-cholan-21-oic Acid δ-Lactone 3-Acetate (**6**)*

A solution of **4** (2.3 g) in acetic acid (230 ml) was stirred with zinc dust (23 g) at room temperature for ½ h. The zinc was removed by filtration and the filtrate diluted with chloroform. The organic solution was washed with water until neutral, dried, and evaporated. The residue was crystallized twice from acetone–hexane, m.p. 179–181°, $[\alpha]_D$ −43.9°.

Anal. Calcd. for $C_{25}H_{36}O_5$: C, 72.08; H, 8.71. Found: C, 72.14; H, 8.50.

The i.r.: ν_{max}($CHCl_3$): 2840, 2730, and 1720 cm^{-1}; n.m.r. ($CDCl_3$): 9.80 p.p.m. (CHO).

*3β,14-Dihydroxy-24-nor-5β,14β-chol-20-ene-21,23-dioic Acid δ-Lactone 3-Acetate (**5**)*

To a solution of **4** (0.330 g) in ethanol (50 ml) was added silver nitrate (0.217 g) in water (7 ml). While the solution was vigorously stirred, a solution of sodium hydroxide (0.217 g) in water (7 ml) was added dropwise and the mixture stirred at room temperature for 3 h. The silver oxide was then removed, the ethanol evaporated, and the solution poured into ice cold 20% sulfuric acid. The solid obtained was filtered, washed with water, and taken into chloroform. The organic solution was extracted with a 10% sodium carbonate solution and the latter acidified. It was then extracted with chloroform which was washed with water, dried, and evaporated. The residue (0.220 g) was crystallized twice from methylene chloride – ether, m.p. 263–264°, $[\alpha]_D$ −17.5°.

Anal. Calcd. for $C_{25}H_{34}O_6$: C, 69.74; H, 7.96. Found: C, 70.04; H, 8.07.

The i.r. ν_{max}(Nujol): 3450, 1700, and 1640 cm^{-1}; the u.v. (EtOH): λ_{max} 232 nm, ε 13 760.

*3β,14,21ξ-Trihydroxy-5β-card-20(22)-enolide 3,21-Diacetate (**20**)*

(*A*) A mixture of **2***b* (1.0 g), sodium acetate (1.0 g), and peracetic acid (40% solution, 1.0 ml) was stirred at room temperature for 30 min in chloroform. It was then diluted with more chloroform and washed with water until free from peracid, dried, and evaporated. The solid obtained was acetylated overnight. The solution was poured into ice cold water and the mixture extracted with ether. The ethereal solution was washed with diluted sulfuric acid, salt saturated water, dried, and evaporated. The crude product was crystallized twice from ether (0.180 g), m.p. 180–183°, $[\alpha]_D$ −25.9°.

Anal. Calcd. for $C_{27}H_{38}O_7$: C, 68.33; H, 8.07. Found: C, 68.22; H, 7.95.

The n.m.r. ($CDCl_3$): 6.18 (=CH, lactone), and 6.66 p.p.m. (C-21, H).

(*B*) A mixture of **2***b* (0.100 g), sodium acetate (0.1 g), acetic acid (1.0 ml), and *m*-chloroperbenzoic acid (0.125 g) in acetone (10 ml) was stirred at room temperature for 5 h. The solvent was then evaporated to one third its initial volume, poured into water, and the solid obtained filtered, and taken in chloroform. The organic solution was washed with sodium bicarbonate solution, water, dried, and evaporated. The solid obtained was crystallized twice from methylene chloride – ether to give **20** as proven by mixture melting point and i.r. analysis, yield 50%.

*3β,21-Dihydroxy-14,21-oxido-24-nor-5β,14β-chol-20-en-23-oic Acid γ-Lactone 3-Acetate (**21**)*

(*A*) The mother liquors obtained from crystallization of **20** (method *A*) were chromatographed on silica gel to give the title product after crystallization from methylene chloride – ether (0.150 g), m.p. 217–219°, $[\alpha]_D$ +42.9°.

Anal. Calcd. for $C_{25}H_{34}O_5$: C, 72.44; H, 8.27. Found: C, 72.82; H, 8.04.

The n.m.r. ($CDCl_3$): 0.85 (C-18, CH_3), 1.0 (C-19, CH_3), 2.03 (C-3, OAc), 5.66 (=CH, lactone), and 5.73 p.p.m. (C-21, H).

(*B*) A mixture of **2***b* (2.0 g) sodium acetate (2.0 g) and *m*-chloroperbenzoic acid (2.50 g) in acetic acid (100 ml)

Can. J. Chem. Downloaded from www.nrcresearchpress.com by 210.87.254.40 on 09/05/12
For personal use only.

was stirred at room temperature for 4 h. It was then diluted with chloroform and washed with sodium bicarbonate and water, dried, and evaporated. The oil obtained was crystallized from methylene chloride – ether (0.685 g), and proven to be identical with **21** by mixture melting point and i.r. analysis.

3β,14-Dihydroxy-5β-card-20-enolide 3-Acetate (Digitoxigenin Acetate) (1b)

A solution of **20** (0.150 g) in methanol (7 ml) and water (1 ml) containing sodium hydroxide (0.014 g) was stirred at 0° in the presence of sodium borohydride (0.150 g), for 1 h. It was then poured into 5% ice cold sulfuric acid. The solid obtained was filtered, washed with water, dried, and crystallized from acetone–ether (0.120 g), m.p. 222–224°, identical with digitoxigenin acetate as proven by mixture melting point and i.r. analysis.

3β,14-Dihydroxy-20-oxo-5β,14β-pregnan-21-oic Acid γ-Lactone 3-Acetate (7)

To a stirred solution of **20** (200 mg) in acetone (10 ml) was added powdered potassium permanganate (200 mg). More permanganate was added (100 and 50 mg) after 10 and 50 min. The mixture was then stirred for 1½ h.

The acetone was evaporated and the solid acidified to p*H* 4 with 5% sulfuric acid and extracted with methylene chloride. The organic solvent was evaporated to a volume of 10 ml and diluted with ether. The mixture was washed with sodium bicarbonate, salt saturated water, dried, and evaporated. The residue was crystallized several times from acetone–hexane, (40 mg), m.p. 235–237°, $[\alpha]_D$ −67.3°; (lit. (7), m.p. 235–238°, $[\alpha]_D$ −66.8°).

Anal. Calcd. for $C_{23}H_{32}O_5$: C, 71.10; H, 8.30. Found: C, 70.73; H, 8.01.

The same product was obtained under identical conditions from **3***a*, **4**, and **21**.

The author wishes to thank Dr. G. Schilling and his associates for analytical data, Mr. R. Dinoi for invaluable technical assistance, Dr. Y. Lefebvre for stimulating discussions, and Dr. R. Deghenghi for encouragement and support.

1. (*a*) J. M. Ferland, Y. Lefebvre, R. Dinoi, and R. Deghenghi. Can. J. Chem. **49**, 2676 (1971); (*b*) J. M. Ferland, Y. Lefebvre, R. Deghenghi, and K. Wiesner. Tetrahedron Lett. 3617 (1966).
2. R. Deghenghi. Pure Appl. Chem. **21**, 153 (1970).
3. Y. Lefebvre and J. M. Ferland. U.S. Patents 3,398,138 and 3,431,258.
4. (*a*) G. R. Pettit, B. Green, and G. L. Dunn. J. Org. Chem. **35**, 1377 (1970); (*b*) G. R. Pettit, B. Green, A. K. Das Gupta, P. A. Whitehouse, and J. P. Yardley. J. Org. Chem. **35**, 1381 (1970); (*c*) K. Heusler, J. Kebrle, C. Meystre, H. Ueberwasser, P. Wieland, G. Anner, and A. G. Wettstein. Helv. Chim. Acta, **42**, 2043 (1959); (*d*) R. D. Hoffsommer, H. L. Slater, D. Taub, and N. L. Wendler. J. Org. Chem. **27**, 353 (1962); (*e*) B. Camerino and U. Valcavi. U.S. Patent, 3,068,229 (1962). Chem. Abstr. **58**, 9183 (1963); (*f*) J. E. Baldwin. Tetrahedron, **20**, 2933 (1964).
5. K. Meyer. Helv. Chim. Acta, **33**, 1238 (1949).
6. H. Minata and T. Nagasaki. J. Chem. Soc. 377 (1966).
7. J. R. Parikh and W. van E. Doering. J. Am. Chem. Soc. **89**, 5505 (1967).
8. I. T. Harrison. Proc. Chem. Soc. 110 (1964).
9. Fieser and Fieser. Steroids. Reinhold Publishing Corp., New York. 1959. p. 799.
10. W. W. Zorback and K. Ventrakamana. Adv. Carbohydr. Chem. **21**, 273 (1966).
11. C. D. Hurd and R. P. Holysz. J. Am. Chem. Soc. **72**, 2005 (1950).
12. C. E. Red emann and C. Niemann. Org. Synth. Coll. **3**, 11.
13. R. K. Ness, H. G. Fletcher Jr., and C. S. Hudson. J. Am. Chem. Soc. **73**, 296 (1951).
14. A. Thompson and M. L. Wolfron. The carbohydrates. *Edited by* W. Pigman. Academic Press Inc., New York. N.Y. 1957. p. 156.
15. W. W. Zorback, S. Saeki, and W. Bühler. J. Med. Chem. **6**, 298 (1963).
16. W. Klyne. Proc. Biochem. Soc. 288th Meeting, Biochem. J. **47**, xli (1950).
17. L. Sawlewicz, H. H. A. Linde, and K. Mewer. Helv. Chim. Acta, **51**, 1353 (1968).
18. Von K. Lingner, K. Irmscher, W. Küssner, R. Hotovy, and J. Gillissen. Arzneim. Forsch. **13**, 142 (1963).
19. G. Pastelin and R. Mandez. Eur. J. Pharmacol. **19**, 291 (1972).

Kinetics of the Abstraction of H from Group IV Methyls by CF_3 and CD_3 Radicals

T. N. Bell, P. Slade, and A. G. Sherwood

Department of Chemistry, Simon Fraser University, Burnaby 2, British Columbia

Received August 13, 1973

CD_3 radicals from the photolysis of hexadeuteroacetone abstract H atoms from group IV methyls

$$CD_3 + (CH_3)_4M \rightarrow CD_3H + CH_2M(CH_3)_3$$

Through additional work on the Sn and Ge systems, a comparison of the data for CF_3 or CD_3 + $(CH_3)_4M$ (where M = C, Si, Ge, Sn) leads to the reactivity ratio $R_{CF_3}/R_{CD_3} \sim 58$ at 373 K. Arrhenius parameters for the abstraction processes are reported.

Les radicaux CD_3 obtenus par photolyse de l'hexadeuteroacétone enlèvent les atomes d'hydrogène des groupes méthyles des méthyles métaux du groupe IV

$$CD_3 + (CH_3)_4M \rightarrow CD_3H + CH_2M(CH_3)_3$$

Grâce à des travaux additionnels dans des systèmes contenant de l'étain et du germanium une comparaison a pu être faite pour les données concernant les réactions du CF_3 ou du CD_3 avec les $(CH_3)_4M$ (dans lesquels M = C, Si, Ge et Sn); on peut tirer de ces données que le rapport de réactivité $R_{CF_3}/R_{CD_3} \approx 58$ à 373 K. On rapporte les paramètres d'Arrhenius pour les processus d'abstraction. [Traduit par le journal]

Can. J. Chem., **52**, 1662 (1974)

Introduction

The reactivity of CF_3 relative to the CH_3 radical in H abstraction varies according to the nature of the substrate and appears to depend on the protonic or hydridic nature of the hydrogen atom, *e.g.* refs. 1, 2. We have previously measured the Arrhenius parameters for CF_3 attack on the group IV methyls (3), and the present work completes measurements of the reactivity of CD_3 with these compounds.

Of particular concern is whether changes in the central atom, from carbon through silicon, germanium, and tin, has a marked effect on the H abstraction reaction. Further we wish to re-examine the results of the methyl reactions obtained by Chaudrhy and Gowenlock (4).

Experimental

Materials

Hexadeuteroacetone was obtained from Stohler Isotope Chemicals. Mass spectrometric analysis showed that the main impurity was CD_2HCOCD_3 present to about 5%.

Hexadeuteroazomethane was obtained from Merck, Sharp and Dohme Ltd., and was purified by two distillations, with that fraction collected at $-131°$ being retained for use and stored in a blackened bulb.

Tetramethylstannane and tetramethylgermane were obtained from Alpha Inorganics Ltd. and subjected to distillation three times. The fraction collected at $-98°$ was thoroughly degassed and stored for use in a blackened bulb.

Apparatus and Procedure

A greaseless vacuum system was employed, and reactions were carried out in an Ultrasil cell of 125.4 ml illuminated volume. The cell was enclosed in a furnace whose temperature was controlled to $\pm 0.2°$. The photolytic light source was a P.E.K. 200 W high pressure mercury arc. The 3130 Å line was isolated through the filter combination, Corning CS754 with solution filters of nickel sulfate, potassium chromate, and potassium hydrogen phthalate (5). The 3660 Å spectral region was isolated using a combination of filters (Corning CS760 and 052) (6).

In a typical experiment the radical source and substrate were admitted separately into the reaction vessel, and allowed to mix. Photolyses were carried out in the temperature range 25–150°, after which the products were separated and analyzed by gas chromatography and mass spectrometry.

Results

The photolysis of hexadeuteroacetone is generally represented by

$$[1a] \qquad HDA \xrightarrow{h\nu} 2CD_3 + CO$$

At temperatures less than 100° the stability of the acetyl radical is such that the production of methyl radicals is best represented by two steps, [1*b*] and [2],

Can. J. Chem. Downloaded from www.nrcresearchpress.com by 210.87.254.40 on 09/05/12
For personal use only.

Can. J. Chem. Downloaded from www.nrcresearchpress.com by 210.87.254.40 on 09/05/12
For personal use only.

[1b] $HDA \rightarrow CD_3 + CD_3CO$

[2] $CD_3CO \rightarrow CD_3 + CO$

Due to isotopic impurity (5%), the additional species CD_2H and CD_2HCO will be formed.

When the rate of the acetyl decomposition, reaction 2, is high, the interpretation of the kinetics of methane formation is straightforward. This involves methyl radical attack on the parent molecule. The Arrhenius plot relevant to this process has extensive curvature below 100°, indicating an additional source of methane, of lower activation energy. This has been observed in both the case of acetone and hexadeuterocetone photolyses (7, 8). Several mechanistic interpretations for the additional methane have been proposed, including abstraction from absorbed acetone on the walls, diffusion of radicals, and abstraction from acetyl by methyl radicals. An excellent summary is to be found in the monograph by Steacie (9).

We feel H abstraction from acetyl is likely to be the greatest contributing factor in producing the additional methane under our experimental conditions, and with a desire to maintain simplicity have chosen to regard the methyl + acetyl abstraction reaction as the only complicating factor. Our kinetic analysis on this basis is compatible with the experimental results.

Thus the following reactions are proposed for methane production, where $Ac = Acd_6 + Acd_5$.

[3] $CD_3 + Ac \rightarrow CD_4$

[4] $CD_2H + Ac \rightarrow CD_3H$

[5] $CD_3 + Acd_5 \rightarrow CD_3H$

[6a] $CD_3 + CD_3CO \rightarrow CD_4$

[6b] $CD_2H + CD_3CO \rightarrow CD_3H$

[6c] $CD_3 + CD_2HCO \rightarrow CD_3H$

[6d] $CD_3 + CD_2HCO \rightarrow CD_4$

In the presence of substrate CD_3H arises from

[7] $CD_3 + M(CH_3)_4 \rightarrow CD_3H$

Analysis of the ethane produced shows that the only important ethane producing reaction is

[8] $CD_3 + CD_3 \rightarrow C_2D_6$

At higher temperatures where acetone photolysis is represented by [1a], and the acetyl concentration is negligible, we have, R_a = rate formation of a product from the photolysis of acetone alone, R_t = rate formation of a product from the photolysis of acetone plus substrate

$$[9] \quad \frac{R_t(CD_3H)}{R_t(CD_4)} - \frac{R_a(CD_3H)}{R_a(CD_4)} = \frac{R(CD_3H)}{R(CD_4)} = \frac{k_7[M(CH_3)_4]}{k_3[Ac]} = R_{diff}$$

In experiments with acetone alone

$$[10] \quad R_a(CD_4)/R_a^{1/2}(C_2D_6) = k_3[Ac]/k_8^{1/2}$$

then

$$[11] \quad \frac{R(CD_3H)}{R(CD_4)} \times \frac{R_a(CD_4)}{R_a^{1/2}(C_2D_6)} = \frac{k_7[M(CH_3)_4]}{k_8^{1/2}}$$

The left hand side of eq. 11 is experimentally measurable to yield $k_7/k_8^{1/2}$. A test of the validity of eq. 9 was made at 100° for a constant concentration of acetone (30 Torr), with varying amounts of tetramethyl germane. A good straight line was obtained, Fig. 1, which also includes results at 73° (see below).

At temperatures where the acetyl radical concentration is important (<100°) the kinetic analysis is complicated through methane formation from reactions 6a, 6b, 6c, 6d. Attempts to use hexadeuteroazomethane as a better low temperature radical source proved fruitless, in that the experimental data did not follow simple kinetics, presumably due to reaction between the azomethane and group IV alkyl.

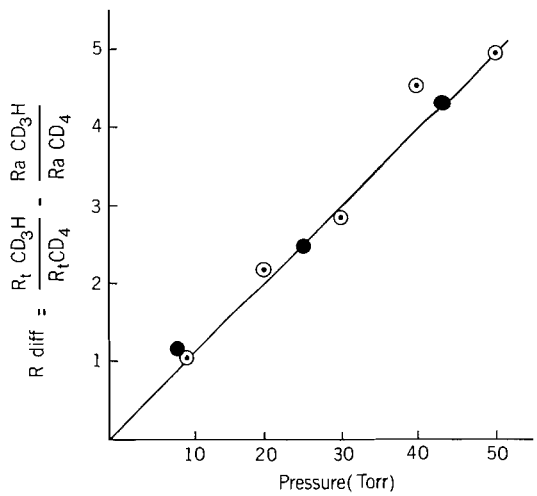

FIG. 1. Plot showing first order dependence of R_{diff} on pressure of tetramethylgermane. ● represent experiments at 73 °C normalized to the results at 100 °C (represented by ⊙) from the slopes of the two separate first order plots.

Can. J. Chem. Downloaded from www.nrcresearchpress.com by 210.87.254.40 on 09/05/12
For personal use only.

The complexities of the kinetic analysis in the case of acetone may be simplified, however, by reasonable approximation, from which the rate constant of interest k_7 may be extracted.

Taking into account the full reaction mechanism proposed which involves the acetyl radical in its isotopic forms, expressions may be derived for $R_a(CD_3H)/R_a(CD_4)$ and $R_t(CD_3H)/R_t(CD_4)$.

These expressions may be simplified by substitution, thus, for 95% isotopically pure HDA, $[Acd_5] \sim [0.05\ Ac]$ and $[CD_2H]/[CD_3] = [CD_2HCO]/[CD_3CO] \sim 0.025$. From statistical consideration A_5/A_4 should be 1/6 and assuming additionally a kinetic isotope effect of K

$$k_5/k_4 = A_5K/A_4$$

i.e.

$$k_5 = 0.17Kk_4$$

Similar arguments can be applied to reactions 6*a* to 6*d*. The assumption of the same kinetic isotope effect of K should not lead to a large error in the magnitude of the values relating to the derived expressions.

$$k_{6b} = k_{6a} \qquad k_{6c} = 0.33Kk_{6a} \qquad k_{6d} = 0.67k_{6a}$$

This leads to a new expression for R_{diff} given by eq. 12, which differs from eq. 9, in the additional term containing the acetyl radical.

$$[12] \quad \frac{R_t(CD_3H)}{R_t(CD_4)} - \frac{R_a(CD_3H)}{R_a(CD_4)} = \frac{k_7[M(CH_3)_4]}{(k_3[Ac] + 1.02k_6[CD_3CO])_t} = R_{diff}$$

From results on the acetone photolysis referred to above, the complication which we ascribe to the acetyl radical should be present at $T < 100°$ where eq. 12 should apply. This raises the question whether the concentration $[CD_3CO]$ occurring in the denominator of eq. 12 is affected by substrate concentration. As a test R_{diff} was measured as a function of substrate concentration $[Ge(CH_3)_4]$ at 73° as well as 100°. The results are included in Fig. 1 on a comparative basis, and show a good linear relationship within the same limits in both cases. We are confident therefore that the denominator in [12] is not sensitive to substrate within our experimental concentrations where $[Ac] \sim [substrate] \sim 30$ mm. In order to extract a value for k_7 from the experimental data, an equation similar to [11] is required. When acetyl radicals are present

$$[13] \quad \frac{R_a(CD_4)}{R_a^{1/2}(C_2D_6)} = \frac{(k_3[Ac] + 1.02k_{6a}[CD_3CO])_a}{k_8^{1/2}}$$

(substrate absent)

Multiplying [12] by [13] and rearranging terms leads to [14]

$$[14] \quad R = R_{diff} \times \frac{R_a(CD_4)}{R_a^{1/2}(C_2D_6)} = \frac{k_7[M(CH_3)_4]}{k_8^{1/2}} \left\{ \frac{(k_3[Ac] + 1.02k_{6a}[CD_3CO])_a}{(k_3[Ac] + 1.02k_{6a}[CD_3CO])_t} \right\}$$

Thus

$$[15] \quad \log\left(\frac{R}{[(MCH_3)_4]}\right) = \log\left(\frac{k_7}{k_8^{1/2}}\right) + \log\left\{\frac{(k_3[Ac] + 1.02k_{6a}[CD_3CO])_a}{(k_3[Ac] + 1.02k_{6a}[CD_3CO])_t}\right\}$$

We have shown that the term $(k_3[Ac] + 1.02\ k_{6a}[CD_3CO])_t$ is not sensitive to substrate concentration, and the temperature dependance of the numerator and denominator of this second term should be identical. Thus the second log term within which the low temperature complexities are collected should be unity. Hence the kinetic analysis should allow for a treatment of the data leading to a value of $k_7/k_8^{1/2}$ from which k_7 may be extracted at the lower temperature.

The results for a series of experiments in which HDA (30 mm) and either tetramethyl stannane 30 mm or tetramethylgermane 30 mm, were photolyzed for periods 2–5 min, and the resultant products analyzed, are given in Table 1. An Arrhenius plot of $\log k_7/k_8^{1/2}$ *vs.* $1/T$ is shown in Fig. 2.

The Arrhenius plot yields the following kinetic parameters, taking $k_{recombination}$ for CD_3 radicals $= 10^{13.35}$ (10).

$Sn(CH_3)_4$

$$\log A\ (\text{ml mol}^{-1}\ \text{s}^{-1}) = 12.16 \pm 0.10$$
$$E = 11.29 \pm 0.27\ \text{kcal mol}^{-1}$$

$Ge(CH_3)_4$

$$\log A\ (\text{ml mol}^{-1}\ \text{s}^{-1}) = 11.4 \pm 0.17$$
$$E = 10.13 \pm 0.28\ \text{kcal mol}^{-1}$$

The reactivity of these two compounds for H abstraction by methyl radicals is very little different.

TABLE 1. Rate data of H abstraction by CD_3*

Temperature (°C)	$R_{diff} = \frac{R_t(CD_3H)}{R_t(CD_4)} - \frac{R_aCD_3H}{R_aCD_4}$		$\frac{R_aCD_4}{R_a^{1/2}C_2D_6}$ ($mol^{1/2}\ ml^{-1/2}\ s^{-1/2} \times 10^6$)	$k_7/k_8^{1/2}$ from eq. 11 ($ml^{1/2}\ mol^{-1/2}\ s^{-1/2}$)	
	$Ge(CH_3)_4$	$Sn(CH_3)_4$	Acetone alone	$Ge(Me)_4$	$Sn(CH_3)_4$
150	2.872	3.677	0.143	0.361	0.462
	2.670	4.217		0.335	0.530
137.5	2.734	4.176	0.084	0.196	0.299
	2.847	4.816		0.204	0.345
125	3.510	4.317	0.055	0.159	0.196
	3.970	4.137		0.180	0.188
	3.537	4.037		0.161	0.183
100	2.910	3.399	0.0235	0.0530	0.0619
	2.785	3.669		0.0507	0.0669
	2.802	3.269		0.0511	0.0596
75	1.891		0.014	0.0193	0.0270
	2.790			0.0285	
	3.230	2.650		0.0330	
	3.138			0.0320	
50	1.409	1.641	0.0069	0.0065	0.0076
	1.521	1.311		0.0070	0.0061
25	0.639	0.517	0.0050	0.0020	0.0016
	0.732	0.544		0.0023	0.0017

*Pressure of substrate 30 Torr, acetone ($d_5 + d_6$) 30 Torr in each case.

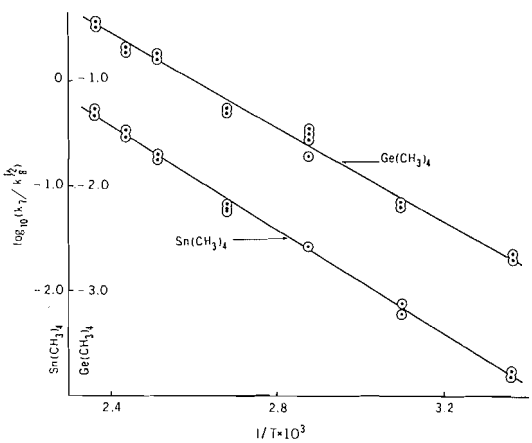

FIG. 2. Arrhenius plot of $\log_{10}$ ($k_7/k_8^{1/2}$ ($ml^{1/2}\ mol^{-1/2}\ s^{-1/2}$)) *vs.* $1/T$.

It is of interest to compare the reactivities of other group IV methyls, and data are available for $Si(CH_3)_4$ (2), and also $C(CH_3)_4$ (11).

We have previously measured (3) Arrhenius parameters for H abstraction by CF_3 radicals for the group IV methyls, and these can now be compared with the CD_3 radical reactions.

The data is collected in Table 2 where it can be seen that $E_{CD_3} - E_{CF_3}$ varies between 2.6 and 4.0 kcal, and that the reactivity of CF_3 radicals is considerably greater than that for CD_3 in H abstraction, on average $R_{CF_3}/R_{CD_3} = 58$.

For a particular radical the reactivity, relative to $Si(CH_3)_4 = 1.0$ for H abstraction, is as follows. (Temperature = 400 K.)

M	Reactivity	
	CD_3	CF_3
Si	1.0	1.0
Sn	0.77	0.67
Ge	0.57	0.57
C	0.43	0.32

The reactivity toward each radical shows the same trend.

Discussion

The summary of the rate data contained in Table 2 for Group IV methyls involving H abstraction by both CF_3 and CD_3 radicals suggests that A factors are normal, and that overall, the results correlate well with one another.

Can. J. Chem. Downloaded from www.nrcresearchpress.com by 210.87.254.40 on 09/05/12
For personal use only.

TABLE 2. Summary of rate data for H abstraction from group IV methyls CF_3 and CD_3 radicals*

Compound	CD_3 radicals†		CF_3 radicals†		$\Delta E = E_{CD_3} - E_{CF_3}$	Relative reactivity R_{CF_3}/R_{CD_3}
	log A	E	log A	E		
$C(CH_3)_4$	12.3	12.0 (ref. 8)	12.0	8.4 (ref. 3)	3.6	48
$Si(CH_3)_4$	12.0	10.8 (ref. 2)	11.9	7.3 (ref. 3)	3.5	64
$Ge(CH_3)_4$	11.4	10.1	11.7	7.4 (ref. 3)	2.7	64
$Sn(CH_3)_4$	12.2	11.3	11.7	7.3 (ref. 3)	4.0	56

*Units of A ml mol^{-1} s^{-1}. Units of E kcal mol^{-1}.
†Experimental values.

Chaudhry and Gowenlock in their observations (4) suggested that A factors decreased along the series Si–Ge–Sn–Pb accompanied by corresponding significant changes in E. They then correlated the change of activation energy with the $J(^{13}C—H)$ coupling constants, obtaining a smooth trend from Si–Ge–Sn–Pb. When the present results in Table 2 were plotted in a similar manner no smooth correlation was obtained.

Unfortunately no experimental data or Arrhenius plots were included in the reported work of Chaudhry and Gowenlock, and it is therefore impossible to comment critically on this difference in the observations. We might point out one difference in the two sets of experiments, Gowenlock used azomethane as a radical source, assumed a literature value for the Arrhenius parameters for H abstraction for methyl radicals from azomethane, and assumed simple kinetics.

We have pointed out above that our attempts to use hexadeuterozomethane as a radical source were discarded because the data was inconsistent with the simple kinetic order expected for the H transfer process, despite a good Arrhenius plot.

Thus while azomethane is a well known radical source which certainly behaves normally with $Si(Me)_4$ (12), it is possible that the higher members of the group IV alkyls engage in some additional complicating molecular reaction, which occurs at a sufficiently fast rate that this interferes with the kinetic analysis applied to the formation of methane. In this context it should be noted that trimethylamine and trimethylphosphine often undergo molecular reactions at vastly differing rates with identical reagents.

One of the purposes of the present work was to determine whether changes in the central atom of the metal alkyl gives rise to significant changes in the reactivity of each compound toward CF_3 and CD_3 radical attack. Previously it has been shown (2, 13) that in this type of reaction polar effects can be significant in affecting the activation energy in the case of CF_3 radical attack, leading to marked differences in the relative reactivities R_{CF_3}/R_{CD_3}. In hydrocarbon systems $E_{CF_3} < E_{CH_3}$ by some 3 kcal (14). From Table 2 it is seen that a similar activation energy difference applies to the present work; indeed if it is assumed that the A factors are constant along the series, and these are normalized to $10^{12.0}$ (ml mol^{-1} s^{-1}) the differences $E_{CD_3} - E_{CF_3}$ are essentially constant ~3.2 kcal mol^{-1}.

The Arrhenius data are similar (8) to those for CF_3 and CD_3 attack on boron trimethyl where $E_{CD_3} - E_{CF_3} \sim 3.4$ kcal and the relative reactivity $R_{CF_3}/R_{CD_3} \sim 45$.

If polar effects are assumed to be negligible in the case of H abstraction by CD_3, the Polanyi equation (15),

$$E = 0.49(D_{C—H} - 74.3)$$

may be used to give a reasonable estimate of the bond strength $D_{C—H}$.

In the case of neopentane this yields $D_{C—H} \sim$ 98 kcal (11), and for the other group IV methyls a value ~96–97 kcal may be estimated.

This leads to an exothermicity ~9 kcal for H abstraction with an enthalpy difference for abstraction ($\Delta H_{CF_3} - \Delta H_{CD_3}$) for a given compound ~3 kcal.

We have suggested previously (2) that $E_{CD_3} - E_{CF_3}$ of the order of 3 kcal is a little high for such enthalpy differences, and that some enhancement of the CF_3 reactivity results from a lowering of E_{CF_3} due to an attractive polar effect.

$$F_3C^{\delta+} \text{----} {}^{\delta-}H—R$$

Can. J. Chem. Downloaded from www.nrcresearchpress.com by 210.87.254.40 on 09/05/12
For personal use only.

We propose that this is the case in the present systems with the magnitude of the effect essentially constant. This is in contrast to systems containing hydrogen atoms more protonic in nature which leads to a much smaller activation energy difference due to a repulsive polar effect.

The differences in reactivity of the metal alkyls towards H abstraction by both CF_3 and CD_3 varies but little along the series for each radical. Such differences as exist show a reactivity sequence Si > Sn > Ge > C with Si having approximately twice the reactivity of carbon. The above sequence follows the Allred Rochow electronegativity values (16) for the central atom Si 1.74, Sn 1.72, Ge 2.02, C 2.5.

Previously (2, 3) we have noted, qualitatively, some correlation between reactivity and proton chemical shift, for hydrogen transfer purposes involving CF_3 and CD_3 radicals. These correlations are summarized in Fig. 3.

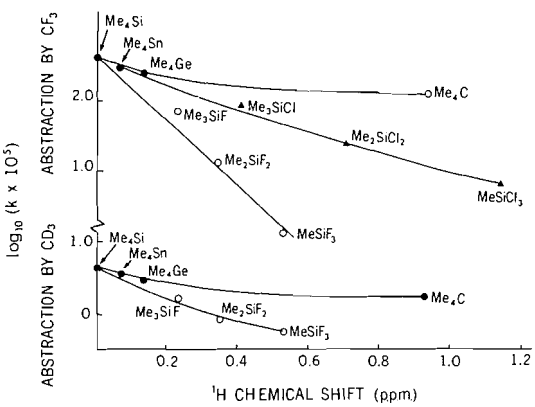

FIG. 3. Plot of $\log_{10}$ ($k_{\text{abstraction}}$ ml mol^{-1} s^{-1}) *vs.* proton chemical shift at 373 K.

In summary, interpretation of the relative reactivities of CF_3 and CD_3 in H abstraction has been based on an enthalpy effect which includes D_{C-H} of the substrate and the products of reaction, together with an attractive or repulsive polar effect in the case of CF_3. Reference to Fig. 3 would indicate that in some way the chemical shift correlates with these parameters.

We are grateful to the National Research Council of Canada for financial support.

1. J. C. AMPHLETT and E. WHITTLE. Trans. Faraday Soc. **62**, 1662 (1966).
2. T. N. BELL and A. E. PLATT. J. Phys. Chem. **75**, 603 (1971).
3. T. N. BELL and A. E. PLATT. Int. J. Chem. Kinet. **2**, 299 (1970).
4. A. U. CHAUDRHY and B. G. GOWENLOCK. J. Organometal. Chem. **16**, 221 (1969).
5. J. G. CALVERT and J. N. PITTS. Photochemistry. John Wiley and Sons, Inc., New York, N.Y. 1966. p. 732.
6. W. J. CHENG, J. NIMOY, and S. TOBY. J. Phys. Chem. **71**, 3075 (1967).
7. R. D. GILES and E. WHITTLE. Trans. Faraday Soc. **61**, 1425 (1965).
8. T. N. BELL and A. E. PLATT. Int. J. Chem. Kinet. **3**, 307 (1971).
9. E. W. R. STEACIE. Atomic and free radical reactions. Vol. 1. Reinhold, New York. 1954. p. 318 seq.
10. A. SHEPP. J. Chem. Phys. **24**, 939 (1956).
11. J. A. KERR and D. TIMLIN. J. Chem. Soc. A, 1241 (1969).
12. J. A. KERR, A. STEPHENS, and J. C. YOUNG. Int. J. Chem. Kinet. **1**, 339 (1969).
13. T. N. BELL and U. F. ZUCKER. J. Phys. Chem. **74**, 979 (1970).
14. A. F. TROTMAN-DICKENSON and G. S. MILNE. Tables of bimolecular gas reactions. National Standard Reference Data Series, National Bureau of Standards, 9 (1967).
15. A. F. TROTMAN-DICKENSON. Chem. Ind. 379 (1965).
16. F. A. COTTON and G. WILKINSON. Advanced inorganic chemistry. 3rd ed. Interscience, New York, N.Y. 1972. p. 114.

Can. J. Chem. Downloaded from www.nrcresearchpress.com by 210.87.254.40 on 09/05/12
For personal use only.

The Determination and Statistical Mechanical Interpretation of the Solubility of Water in Benzene, Carbon Tetrachloride, and Cyclohexane

SAUL GOLDMAN

Department of Chemistry, University of Guelph, Guelph, Ontario

Received October 4, 1973

The solubility of water in each of benzene, carbon tetrachloride, and cyclohexane, was determined at 5° intervals over the range 10 to 40 °C. The solubilities were converted to Henry's law constants and these constants were interpreted by means of a statistical mechanical theory based on Zwanzig's perturbation theory of fluids. A fitting-parameter in the form of a correction factor to the water–solvent pairwise potential function was required. The values of this parameter for the benzene–water and cyclohexane–water systems could be rationalized on the basis of anisotropy of solvent polarizability. The values of the parameter for the carbon tetrachloride – water system were consistent with a hydrogen-bonding interaction between water and carbon tetrachloride.

La solubilité de l'eau dans le benzène, le tétrachlorure de carbone, et le cyclohexane, a été déterminée à tous les 5° dans l'intervalle de 10 à 40 °C. Les solubilités ont été converties en constantes de la loi d'Henry et ces constantes ont été interprétées à l'aide d'une théorie de mécanique statistique basée sur la théorie de perturbation de Zwanzig des fluides. Un paramètre pouvant s'adapter, de la forme d'un facteur de correction, à la fonction de potentiel du couple eau-solvant, a été nécessaire. Les valeurs de ce paramètre pour les systèmes benzène–eau et cyclohexane–eau pourraient être rationnalisées en s'appuyant sur l'anisotropie de la polarisabilité du solvant. Les valeurs du paramètre pour le système tétrachlorure de carbone-eau étaient cohérente avec une interaction par des ponts hydrogène entre l'eau et le tétrachlorure de carbone.

[Traduit par le journal]

Can. J. Chem., **52**, 1668 (1974)

Can. J. Chem. Downloaded from www.nrcresearchpress.com by 210.87.254.42 on 09/05/12
For personal use only.

Introduction

Recent advances in the statistical mechanical theory of hard-sphere fluids have facilitated the prediction, from molecular properties, of solubilities and related thermodynamic functions with an accuracy that was hitherto not possible. Scaled-particle theory (1–3) provides the equations required for the calculation of the thermodynamic functions associated with cavity formation in a hard-sphere fluid. A number of workers (4–6) have used the results of this theory to obtain the hard-sphere properties of real systems. However any reasonably accurate theoretical correction of a hard-sphere system to one that obeys a more realistic potential requires knowledge of the two-body radial distribution function. Lebowitz' (7) exact solution of the generalized Percus–Yevick equation provides analytic expressions for the Laplace transform of the radial distribution function for a binary hard-sphere mixture. There is some evidence (8) that the structure of real liquids is closely approximated by that of a hard-sphere fluid, so that a hard-sphere radial distribution function should serve as a reasonable approximation when applied to a real system.

Zwanzig (9) first provided the formalism, in the form of a perturbation theory of fluids, that is required to correct a hard-sphere reference fluid to one that obeys a more realistic potential. Zwanzig's formulation shows how the system Helmholtz free energy, in excess of that of the hard-sphere reference system, can be expressed as an infinite series in $(1/T)$, where T is temperature.

Recently several refinements to Zwanzig's theory have appeared. One approach, proposed almost simultaneously by Mansoori and coworkers (10–12), and by Rasaiah and Stell (13), involves the application of the variational method to a truncated form of Zwanzig's equation. A second approach, which was introduced first by McQuarrie and Katz (14) and which was later refined by Leonard, Henderson, and Barker (15–17) involves expansion of the system configuration integral as a double Taylor series in two parameters. As with Zwanzig's method, one parameter varies the depth of a modified

Can. J. Chem. Downloaded from www.nrcresearchpress.com by 210.87.254.42 on 09/05/12
For personal use only.

potential in the attractive region. The second parameter varies the steepness of the modified potential in the repulsive region. Still another perturbation theory that incorporates Zwanzig's idea was recently proposed by Weeks, Chandler, and Andersen (18). These authors, whose theory pertains to a simple Lennard–Jones fluid, separate their intermolecular pair potential into two parts. One part (the reference part) includes all the repulsive forces in the Lennard–Jones potential, and the other part (the perturbation potential) contains all the attractive forces. Starting with this separation, Weeks, Chandler, and Andersen developed a relatively accurate and simple method for calculating the radial distribution function. Subsequently Verlet (19), and Verlet and Weis (20) tested the Weeks–Chandler–Andersen (W.C.A.) theory by comparison with computer results. It was thereby shown that the basic assumptions of the W.C.A. model were justified. Verlet and Weis (20) also reexpressed the W.C.A. theory in an analytical form.

The above extensions of the original Zwanzig idea have been shown to give good results when applied to simple systems. Recently Neff and McQuarrie applied the Leonard–Henderson–Barker theory to the system neon in argon and found that most of the predicted values of the solubility and related thermodynamic functions were good (21).

Therefore it seemed worthwhile to apply Zwanzig's theory, in some appropriate form, to more complex liquid solutions. Since the above theories are strictly applicable only to systems of spherical monatomic particles, it is unrealistic to expect *ab initio* predictions of thermodynamic functions for polyatomic anisotropic systems to be accurate. However, some information that reflects the dominant factors operative in such systems can be obtained by fitting the experimental results to a molecular theory that contains a physically interpretable parameter. This approach will be taken here.

The systems chosen for study were water in each of benzene, carbon tetrachloride, and cyclohexane. Lennard–Jones (6–12) parameters are available for each of these solvents and Stockmayer parameters are available for water. These molecules are not spherical but neither are they markedly elongated, so that a hard-sphere reference system should be roughly applicable. Solubility was chosen as the experimentally measured quantity both because it strongly reflects solute–solvent interactions and because it is now possible to measure the solubility of water in each of the chosen solvents with the requisite accuracy. Lastly, these specific systems were considered to be worthwhile because of their general chemical interest.

Experimental

Materials

The solvents used were all certified grade, further purified as described below. Benzene was washed successively with concentrated sulfuric acid, water, 1 *N* sodium hydroxide solution, and finally with water. The product was dried with silica gel, and then distilled. Carbon tetrachloride was dried with calcium chloride and then distilled in the absence of light under an atmosphere of dry nitrogen. Cyclohexane was washed with water, dried with silica gel, and then distilled. A 4 ft silvered, vacuum-jacketed distilling column packed with Raschig rings was used for each distillation, and in each case the central fraction was retained for use. The densities of the purified solvents at 25.00 ± 0.02 °C were found to be: benzene, 0.87365 ± 0.00002 (lit. (22*a*, 23*a*) 0.87368, 0.87370); carbon tetrachloride, 1.58416 ± 0.00002 (lit. (22*b*, 23*a*) 1.5842, 1.58426); cyclohexane, 0.77390 ± 0.00002 (lit. (23*b*) 0.7739). Distilled water was used for all the equilibrations.

Apparatus and Procedure

The organic solvents were equilibrated with an excess of water in 175 ml milk-dilution bottles fitted with Bakelite screw caps having Teflon inserts. The bottles were clamped lengthwise on a Plexiglass rotor immersed in a water thermostat the temperature of which was maintained to within 0.02 °C of the required value. The bottles were given end-over-end rotation at 20 r.p.m. Through the use of different equilibration times and by approaching equilibrium from both supersaturation and undersaturation (achieved by using pre-heated and pre-cooled saturated solutions respectively) it was found that equilibrium was achieved, for all systems, within 1 h. After equilibration the bottle was removed from the rotor, and was suspended vertically in the water bath, with only the cap and neck of the bottle above the water surface; the upper level of the lighter phase was well under the surface of the bath water. Aliquots (at least 5 ml) of the water-saturated organic solvent were taken for analysis with calibrated Hamilton syringes fitted with Chaney adaptors. These syringes were found to deliver the solvents used here with an accuracy of ±0.2%.

All the analyses for water were performed with an Aquatest II automatic Karl Fischer Titrator (model 702, Photovolt). The aliquot to be analyzed was injected directly into the titration vessel provided with the instrument. During the analyses the coulometer-current generated by the instrument was checked with an accurate milliameter to ensure that it had the proper value.

Although it has been known for some time, it is apparently not widely realized that at room temperature, in the presence of light, a very slow reaction occurs between H_2O and CCl_4 to produce HCl and other pro-

Can. J. Chem. Downloaded from www.nrcresearchpress.com by 210.87.254.42 on 09/05/12
For personal use only.

TABLE 1. Solubilities of water in the organic solvents

	Benzene				Carbon tetrachloride				Cyclohexane			
Temperature (°C)	Sol* $\times 10^4$ (mol/l)	S.d.† $\times 10^4$ (mol/l)	Literature value $\times 10^4$ (mol/l)	Ref.	Sol* $\times 10^4$ (mol/l)	S.d.† $\times 10^4$ (mol/l)	Literature value $\times 10^4$ (mol/l)	Ref.	Sol* $\times 10^4$ (mol/l)	S.d.† $\times 10^4$ (mol/l)	Literature value $\times 10^4$ (mol/l)	Ref.
10	217.1	3.0			52.3	0.9			14.7	2.0		
15	256.1	2.5	265 ± 5‡	40	60.5	1.9			18.5	3.1		
20	301.7	1.9			74.7	2.4			25.5	2.2		
25	351.8	5.3	349 ± 5	27	88.7	2.0	87 ± 3	27	30.1	2.6	24 ± 3	27
			347 ± 15	28								
30	395.0	7.0			103.5	1.3			41.0	2.3		
35	464.9	3.2	465 ± 5‡	40	123.8	2.9			48.5	2.0		
40	524.3	4.5			143.3	1.2			55.2	2.8		
		$\overline{\text{s.d.}} \times 10^4 = 3.9$				$\overline{\text{s.d.}} \times 10^4 = 1.8$				$\overline{\text{s.d.}} \times 10^4 = 2.4$		

*Sol means solubility.
†S.d. means sample standard deviation.
‡Uncertainty estimated from uncertainty in ref. 27.

ducts (24). However it was found by careful testing that this problem was effectively avoided by purifying the CCl_4 in a darkened dry environment (see above) and by using darkened equilibration bottles and fresh reagents for the CCl_4 experiments.

Results

The solubilities of water in each of the solvents at the indicated temperatures are entered, on a molar basis, in columns 2, 6, and 10, of Table 1. Each of these entries represents the average of at least six independent solubility experiments. Thus a total of 137 separate equilibrations and analyses were carried out. The entries in columns 3, 7, and 11, of Table 1 represent the respective sample standard deviations. For each solvent the variances of the solubilities were found, by a Hartley F_{max} test (25), to be homogeneous (not a function of temperature) at both the 5% and 1% levels of significance. Therefore the standard deviations for each solvent were pooled, and the means of the standard deviations (s.d.) are given under columns 3, 7, and 11.

Whereas a variety of values for the solubility of water in the solvents studied here have previously been reported (26), most of these values are based on methods that lack the accuracy which is now possible. In the past decade however, good values for several of the solubilities here sought have appeared, and these values are given in columns 4, 8, and 12, of Table 1. A comparison of these solubilities with the corresponding values found here, shows that the agreement is satisfactory; in no case are the means (for the same solvent and temperature) significantly different. The relatively high percent error found with cyclohexane (both in the present work and in ref. 27) is a consequence of the combined effects of the very low solubility of water in this solvent, and the general problem associated with accurate water analysis.

Treatment of the Data

It has previously been shown (at 25 °C) that in a variety of solvents in which the solubility of water is low, the partial pressure of water dissolved in these solvents is proportional to its molarity at all water concentrations up to and including saturation (27, 28). In particular, water has been found to exhibit this proportionality in each of benzene, carbon tetrachloride, and cyclohexane (27). Further, since the solubility of water is sufficiently low in each of these solvents so that its molarity is proportional to its mole fraction (within the experimental error of both this work and that of ref. 27), the above pressure–molarity proportionality is in fact a manifestation of Henry's law behavior. That is, water obeys Henry's law at all concentrations up to saturation in each of these solvents. If it is assumed that this behavior found at 25 °C (the middle of the present temperature range) occurs also at the other temperatures studied here, then for each of our water-saturated solutions we may write:

$$[1] \qquad P = K_H X$$

where P = partial pressure of water over the water-saturated solution = vapor pressure of pure water, K_H = Henry's law constant for water, X = solubility of water (mole fraction units). From their definitions it is clear that K_H and X depend on both solvent and temperature, whereas P is a function only of temperature. The use of the vapor pressure of pure water for P in eq. 1 is an approximation since one should use the vapor pressure of water saturated with the organic solvent. Clearly however the solubilities of our solvents in water are so low, that the approximation is adequate. For example, the solubility of benzene in water at 25 °C is 0.023 mol/l (29). Therefore the partial pressure of water over this benzene-saturated aqueous solution is less than the partial pressure of pure water at 25 °C by a factor of 0.9996. It is assumed in this calculation that the water in this water-rich benzene-saturated solution obeys Raoult's law. This correction (less than 0.1%) is negligible with respect to the present experimental error (at best 1%) and is therefore omitted.

From the known vapor pressure (30) and second virial coefficient (31*a*) of water, the compressibility factor for water vapor over the range 10–40 °C may be shown to be ~0.999–0.997. Therefore water vapor is sufficiently ideal under these conditions to justify the omission of virial corrections.

The values of the Henry's law constants for water, calculated by eq. 1, are given in Table 2. The solubilities (molar basis) from Table 1 were converted to mole fraction units with the solvent density used for the appropriate solution density. Again, this approximation is permissible because of the low water solubilities. The values for both

Can. J. Chem. Downloaded from www.nrcresearchpress.com by 210.87.254.42 on 09/05/12
For personal use only.

TABLE 2. Henry's law constants for water

	ln K_H					
	Benzene		Carbon tetrachloride		Cyclohexane	
t (°C)	Observed*	Calculated†	Observed*	Calculated‡	Observed*	Calculated§
10	1.850	1.847	3.191	3.210	4.345	4.333
15	2.008	2.006	3.368	3.342	4.439	4.404
20	2.154	2.160	3.466	3.470	4.429	4.472
25	2.298	2.308	3.593	3.594	4.560	4.538
30	2.469	2.452	3.725	3.714	4.538	4.602
35	2.582	2.591	3.821	3.830	4.645	4.664
40	2.728	2.725	3.940	3.942	4.780	4.723

*Derived from the experimental data; K_H has units atm.
†ln K_H (calcd) = 11.017 − 2596.7/T.
‡ln K_H (calcd) = 10.856 − 2165.1/T.
§ln K_H (calcd) = 8.4035 − 1152.5/T.

the solvent density and the vapor pressure of water at the required temperatures were taken from published tabulations (30, 32).

It was found that the dependence of the Henry's law constant on temperature could be represented, for each solvent, by the familiar 2-parameter equation:

$$[2] \qquad \ln K_H = E + \frac{F}{T}$$

where T is temperature in °K. Least-squares estimates of E and F for each solvent are given in Table 2 and the fit is demonstrated in Fig. 1. From the least-squares estimates of E and F, the standard state enthalpy and entropy of transfer for water have been calculated by eq. 3 and eq. 4:

$$[3] \qquad \Delta H_{tr}^0 = -RF$$

$$[4] \qquad \Delta S_{tr}^0 = RE$$

where R = 1.9872 cal/deg. mol and these values are given in Table 3. The entries in this table represent averages over the temperature range 10–40 °C. The thermodynamic transfer functions ΔH_{tr}^0 and ΔS_{tr}^0 represent the change in enthalpy and entropy respectively that occur when 1 mol of water initially present in a hypothetical unit mole fraction solution of water in a solvent at temperature T is transferred to the state of an ideal gas at 1 atm and temperature T. The standard deviations given with ΔH_{tr}^0 and ΔS_{tr}^0 were calculated from the least-squares estimates of the standard deviations of F and E respectively. These latter estimates were obtained by the application of the law of accumulation of errors (33) to eq. 2.

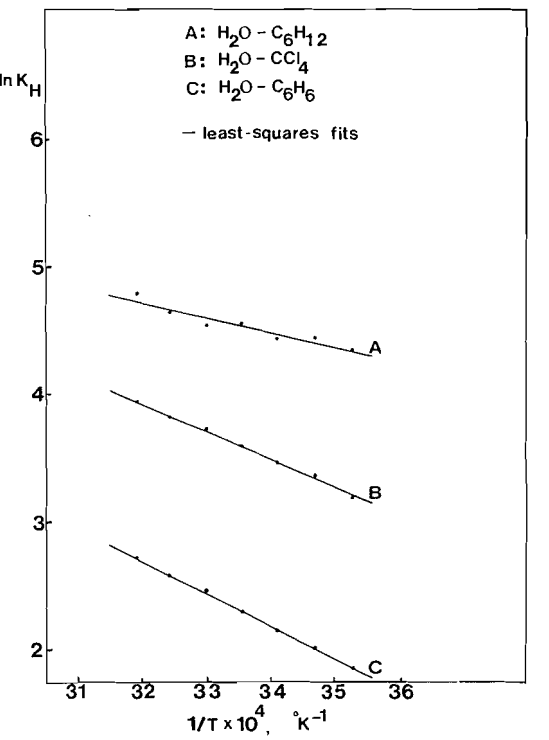

FIG. 1. Variation of the Henry's law constant with temperature.

TABLE 3. Thermodynamic transfer functions for water

Solvent	ΔH_{tr}^0 (kcal/mol)	ΔS_{tr}^0 (cal/mol deg)
Benzene	5.16±0.07	21.89±0.23
Carbon Tetrachloride	4.30±0.10	21.57±0.35
Cyclohexane	2.29±0.32	16.70±1.06

Can. J. Chem. Downloaded from www.nrcresearchpress.com by 210.87.254.42 on 09/05/12
For personal use only.

Can. J. Chem. Downloaded from www.nrcresearchpress.com by 210.87.254.42 on 09/05/12
For personal use only.

Statistical Mechanical Analysis

Background

The Zwanzig equation for the system Helmholtz free energy of a multicomponent mixture can be expressed in the form:

$$[5] \quad A = A^{HS} + 2\pi \sum_{i,j} \rho_i N_j \times \int_{d_{ij}}^{\infty} r^2 u_{ij}(r) g_{ij}{}^{HS}(r)\, dr + ...$$

where A is the Helmholtz free energy of the real system, A^{HS} and $g_{ij}{}^{HS}(r)$ are respectively the Helmholtz free energy and two-body radial distribution function for the hard-sphere reference mixture, d_{ij} is the hard-sphere diameter between particles i and j, $u_{ij}(r)$ is the potential energy of interaction between particles i and j, and ρ and N are the particle number density and number of particles respectively. In eq. 5 $u_{ij}(r)$ and $g_{ij}(r)$ are taken to be spherically symmetric. The higher order terms in eq. 5 involve higher order distribution functions which are presently unknown, and therefore the series, when applied to liquid solutions, is generally truncated after the first correction term.

Whereas it may in principle be possible to apply one or more of the previously mentioned extensions of Zwanzig's theory (see Introduction) to the present problem, this is presently not feasible and therefore will not be done. For example, a rigorous extension of any of the refined theories to the present systems would have to take into account the angle-dependence of each of the radial distribution function, the dipole field of water, and the polarizability of benzene and cyclohexane. Such a task, given our present state of knowledge, is virtually impossible. Moreover, even if the calculation were possible, it still would not eliminate the additional uncertainties engendered by the application of a hard-sphere reference system to nonspherical polyatomic particles.

In view of the foregoing considerations it is clear that a more modest, semi-empirical approach is indicated. Thus eq. 5 truncated to the first order will be accepted as correct, and the required values of d_{ij} will be obtained by setting them equal to the corresponding Lennard–Jones (6–12) parameters σ_{ij}. We will return to this point later (see Selection of Data). A fitting-parameter is introduced in the form of a factor that modifies the value of the water–solvent interaction energy. The values of this parameter will be adjusted in order to fit the theoretically calculated solubilities to those found experimentally. Therefore this parameter will absorb the effects of all the approximations in the theoretical development. Despite this, it will be shown that the values this parameter assumes can in fact be rationalized in terms of molecular properties.

Derivation

The solute will be denoted by the subscript "2" and the solvent by "1". The Zwanzig result, truncated to the first order, is used for the system Helmholtz free energy. Thus:

$$[6] \quad A = A^{HS} + A^{corr}$$

$$[7] \quad A^{corr} = 2\pi \sum_{i,j} \rho_i N_j \int_{d_{ij}}^{\infty} r^2 u_{ij}(r) g_{ij}{}^{HS}(r)\, dr$$

From eq. 6 and the definition of the chemical potential in a binary system

$$[8] \quad \mu_2 = \left(\frac{\partial A}{\partial N_2}\right)_{V,T,N_1}$$

it follows that

$$[9] \quad \mu_2 = \mu_2{}^{HS} + \mu_2{}^{corr}$$

where

$$\mu_2{}^{HS} = \left(\frac{\partial A^{HS}}{\partial N_2}\right)_{V,T,N_1}$$

$$\mu_2{}^{corr} = \left(\frac{\partial A^{corr}}{\partial N_2}\right)_{V,T,N_1}$$

From thermodynamics

$$[10] \quad \ln K_H = \frac{\mu_2{}^0 - (\mu_2{}^0)_g}{kT}$$

where k is the Boltzmann constant. The superscript 0 denotes standard state, the outer subscript g denotes gas, and the absence of such a subscript denotes solution. The standard state for water in the gas is the ideal gas at 1 atm and temperature T, and its standard state in solution is the extrapolated hypothetical unit mole fraction solution at T. It will be assumed that the internal and rotational partition functions for water are the same in solution as in the gas. Under this assumption these degrees of freedom don't contribute to K_H and are therefore not included below. Hence:

$$[11] \quad (\mu_2{}^0)_g = -kT \ln \left[\left(\frac{2\pi m_2 kT}{h^2}\right)^{3/2} kT \right]$$

where h is Planck's constant and m_2 is the mass of a water molecule.

From thermodynamics

$$[12] \qquad \mu_2^0 = \lim_{X_2 \to 0} [\mu_2 - kT \ln X_2]$$

where X denotes mole fraction.

Combining eqs. 9–12, and using the superscript $^\bullet$ to denote the limit as $X_2 \to 0$:

$$[13] \qquad \ln K_H = \left(\frac{\mu_2^{HS}}{kT} - \ln X_2\right)^\bullet + \ln\left[\left(\frac{2\pi m_2 kT}{h^2}\right)^{3/2} kT\right] + \left(\frac{\mu_2^{corr}}{kT}\right)^\bullet$$

Scaled-particle theory is used to calculate the properties of the hard-sphere reference system. To facilitate a comparison with other work, the following definitions are made:

$$R^* \equiv \frac{d_{22}}{d_{11}} \qquad y \equiv \frac{\pi}{6}\rho_1 d_{11}^3 \qquad \chi(y) \equiv \frac{1 + y + y^2}{(1 - y)^3}$$

If μ_2^{HS} is expressed in terms of equations 2.7, 5.1, and 5.3 of ref. 3, and eq. 8 is applied to eqs. 6 and 7, the result is

$$[14] \qquad \ln K_H = \ln (RT/\bar{V}_1) + \left(\frac{\mu_2^{HS}}{kT}\right)^\blacksquare + \left(\frac{\mu_2^{corr}}{kT}\right)^\bullet$$

where

$$\left(\frac{\mu_2^{HS}}{kT}\right)^\blacksquare = -\ln(1 - y) + R^*\left(\frac{3y}{1 - y}\right) + R^{*2}\left(\frac{3y}{1 - y} + \frac{9y^2/2}{(1 - y)^2}\right) + R^{*3} y\chi(y)$$

$$\left(\frac{\mu_2^{corr}}{kT}\right)^\bullet = I_{11} + I_{12}$$

$$I_{11} = \frac{2\pi\rho_1 N_1}{kT} \int_{d_{11}}^{\infty} r^2 u_{11}(r) \left\{\frac{\partial g_{11}^{HS}(r)}{\partial N_2}\right\}^\bullet_{N_1,T,V} dr$$

$$I_{12} = \frac{4\pi\rho_1}{kT} \int_{d_{12}}^{\infty} r^2 u_{12}(r)\{g_{12}^{HS}(r)\}^\bullet \, dr$$

In eq. 14 $\bar{V}_1$ is the molar volume of the pure solvent. It is seen from a comparison of eq. 14 with eq. 23 of ref. 21 that our standard state and hard-sphere terms (first two terms on the right-hand side of eq. 14) are identical with those of ref. 21 but our correction term is different.

In the derivation of eq. 14 it was assumed that the pairwise potential functions were all spherically symmetric. Whereas the solvent–solvent and water–solvent interaction potentials can be approximated by spherically symmetric functions (see below), the water–water term cannot. However it is seen from eq. 14 that the water–water term doesn't enter into the expression for $\ln K_H$. Therefore this complication need not be considered.

Calculations

Explicit analytic expressions for $g_{ij}^{HS}(r)$ are not in general available. However Lebowitz' solution of the Percus–Yevick equation for a hard-sphere mixture (7) provides accurate explicit expressions for the Laplace transform of $rg_{ij}^{HS}(r)$. Therefore the integrals required for the calculation of $(\mu_2^{corr}/kT)^\bullet$ were recast as follows (34):

$$[15] \qquad I_{12} = \frac{4\pi\rho_1}{kT} \int_{d_{12}}^{\infty} r^2 u_{12}(r)\{g_{12}^{HS}(r)\}^\bullet \, dr = \frac{4\pi\rho_1}{kT} \int_0^{\infty} U_{12}(s) G_{12}^\bullet(s) \, ds$$

$$[16] \qquad I_{11} = \frac{2\pi\rho_1 N_1}{kT} \int_{d_{11}}^{\infty} r^2 u_{11}(r) \left\{\frac{\partial g_{11}^{HS}(r)}{\partial N_2}\right\}^\bullet_{N_1,T,V} dr$$

$$= \frac{2\pi\rho_1}{kT} \int_0^{\infty} U_{11}(s) N_1 \left\{\frac{\partial G_{11}(s)}{\partial N_2}\right\}^\bullet_{N_1,T,V} ds$$

Can. J. Chem. Downloaded from www.nrcresearchpress.com by 210.87.254.42 on 09/05/12
For personal use only.

where

$$G_{ij}(s) = \int_{d_{ij}}^{\infty} e^{-sr} r g_{ij}^{HS}(r)\, dr$$

$$ru_{ij}(r) = \int_{0}^{\infty} e^{-sr} U_{ij}(s)\, ds$$

Radial Distribution Function

Explicit expressions for $G_{11}(s)$ and $G_{12}(s)$ for a binary hard-sphere mixture of any composition have been given elsewhere (7, 21) and these expressions are not repeated here.[1] From these expressions it may be shown that

$$[17] \quad G_{12}^{\bullet}(s) = \frac{s^2 e^{sd_{12}}\{[0.75(-\eta_1 d_{11}^3)(d_{22} - d_{11}) - d_{12}(1 + (\xi^{\bullet}/2))]s - (1 + 2\xi^{\bullet})\}}{D^{\bullet}(s)}$$

$$[18] \quad N_1\left\{\frac{\partial G_{11}(s)}{\partial N_2}\right\}^{\bullet}_{N_1,T,V} = \frac{s}{12\eta_1 D^{\bullet}(s)}\left\{a + b(s) + \frac{L_2^{\bullet}(s)\, e^{sd_{22}}\gamma^{\bullet}(s)}{D^{\bullet}(s)}\right\}$$

with

$$\xi^{\bullet} = \frac{\pi\rho_1 d_{11}^3}{6} = \eta_1 d_{11}^3$$

$$D^{\bullet}(s) = S^{\bullet}(s)\, e^{2sd_{12}} - L_2^{\bullet}(s)\, e^{sd_{22}}$$

$$L_2^{\bullet}(s) = 12\eta_1[(1 + (\xi^{\bullet}/2))]d_{11}s^2 + 12\eta_1(1 + 2\xi^{\bullet})s$$

$$S^{\bullet}(s) = [12\eta_1(1 + 2\xi^{\bullet})]s - 18(\eta_1 d_{11}^2)^2 s^2 - 6(\eta_1 d_{11}^2)(1 - \xi^{\bullet})s^3 - (1 - \xi^{\bullet})^2 s^4$$

$$\gamma^{\bullet}(s) = a + b(s) - e^{sd_{11}}X(s) + e^{2sd_{12}}Y(s)$$

$$Y(s) = a + s[2\pi\rho_1(1 + 2\xi^{\bullet}) + 4\pi\rho_1 d_{22}^3\eta_1 - (d_{11} + d_{22})a] - 6\pi s^2\rho_1 d_{22}^3(\eta_1 d_{11}^2) + \pi\rho_1 d_{22}^3 s^3(\eta_1 d_{11}^2) - d_{22}^2\rho_1\pi s^3(1 - \xi^{\bullet}) + \frac{\pi}{3}\rho_1 d_{22}^3(1 - \xi^{\bullet})s^4$$

$$X(s) = 2\pi d_{22}s^2\rho_1\left[\left(1 + \frac{\xi^{\bullet}}{2}\right) + \frac{3}{2}\eta_1 d_{11}^2(d_{22} - d_{11})\right] + a + s[2\pi\rho_1(1 + 2\xi^{\bullet}) - d_{11}a]$$

$$b(s) = -e^{sd_{22}}\{12\eta_1 d_{11}s^2\left[\frac{\pi}{12}d_{22}^3\rho_1 + \frac{\pi}{4}d_{22}^2(d_{11} - d_{22})\rho_1\right] + s[4\pi\eta_1 d_{22}^3\rho_1 - 6\pi\eta_1 d_{22}(d_{22} - d_{11})^2\rho_1] + a\}$$

$$a = 6\pi\eta_1\rho_1(d_{22} - d_{11})^2$$

Intermolecular Potential Energy

A Lennard–Jones (6–12) potential is used for $u_{11}(r)$. Thus

$$u_{11}(r) = 4\varepsilon_{11}\left[\left(\frac{\sigma_{11}}{r}\right)^{12} - \left(\frac{\sigma_{11}}{r}\right)^{6}\right] \qquad r > d_{11}$$

where ε_{11} represents the depth of the potential well, and σ_{11} is the value of r at which $u_{11}(r)$ is zero. From Laplace transform tables it may readily be shown that

$$[19] \quad U_{11}(s) \equiv L^{-1}\{ru_{11}(r)\} = 4\varepsilon_{11}\left[\sigma_{11}^{12}\left(\frac{s^{10}}{10!}\right) - \sigma_{11}^{6}\left(\frac{s^4}{4!}\right)\right]$$

where $L^{-1}\{f(r)\}$ represents the inverse Laplace transform of $f(r)$.

[1]In the present work, as in ref. 21, $G_{ij}(s)$ represents the Laplace transform of $rg_{ij}(r)$. In ref. 7 the Laplace transform of $rg_{ij}(r)$ is represented by $[G_{ij}(s)/12(\eta_i\eta_j)^{1/2}]$. Equation 41 of ref. 7 for $G_{12}(s)$ is missing a factor of 12 in the numerator.

Can. J. Chem. Downloaded from www.nrcresearchpress.com by 210.87.254.42 on 09/05/12
For personal use only.

For the water–solvent intermolecular potential energy it is assumed that the valence and dispersion contributions are given by a Lennard–Jones (6–12) potential, and the dipole-induced dipole contribution is given by

$$[20] \qquad u_{\text{dip}}(r) = -\left(\frac{u_2^{*2}\bar{\alpha}_1}{r^6}\right)$$

$$[21] \qquad u_2^* = u_g^*\left[\frac{2D+1}{2D+n_d^2}\cdot\frac{n_d^2+2}{3}\right]$$

In eqs. 20 and 21, D is the dielectric constant of the solvent, n_d is the refractive index of water for sodium light, u_2^* is the dipole moment of water in solution, u_g^* is the dipole moment of water in the gas phase, and $\bar{\alpha}_1$ is the mean polarisability of the solvent. The expression for $u_{\text{dip}}(r)$ (eq. 20) represents the angle-averaged potential energy of interaction of a non-polarizable point-dipole with a particle of polarizability $\bar{\alpha}_1$. The angle-averaged potential used here is consistent with the present model wherein the water molecule in solution is assumed free to rotate. Due to the reaction field of the solvent acting on the polarizability of the water molecule, u_2^* is different from u_g^*. Equation 21, taken from classical electrostatic theory (35), gives an estimate of u_2^*. A dimensionless fitting-parameter f_{12} is introduced at this stage. This parameter is introduced to facilitate fitting the theoretically derived expression for the Henry's law constant to the experimentally determined values of this constant. Hence

$$[22] \qquad u_{12}(r) = f_{12}\left\{4\varepsilon_{12}\left[\left(\frac{\sigma_{12}}{r}\right)^{12} - \left(\frac{\sigma_{12}}{r}\right)^{6}\right] - \frac{u_2^{*2}\bar{\alpha}_1}{r^6}\right\} \qquad r > d_{12}$$

and

$$[23] \qquad U_{12}(s) \equiv L^{-1}\{ru_{12}(r)\} = f_{12}\left\{4\varepsilon_{12}\left[\sigma_{12}^{12}\left(\frac{s^{10}}{10!}\right) - \sigma_{12}^{6}\left(\frac{s^4}{4!}\right)\right] - u_2^{*2}\bar{\alpha}_1\left(\frac{s^4}{4!}\right)\right\}$$

Method of Calculation

Gauss Quadrature was used to evaluate the integrals I_{11} and I_{12}. In each case the interval of integration (0 to ∞) was subdivided into seven smaller intervals. Each of these intervals was integrated separately using successively 10, 20, and 40 Gaussian points. The Gaussian points used were of 15-figure accuracy and double-precision arithmetic was used throughout. In this way it was proven that the required integrals were known to at least 10-figure accuracy, an accuracy that is much higher than what is actually required. The accuracy of the programs used was further verified by applying them, *mutatis mutandis*, to previously published work (ref. 21).

Selection of Data

The values of D and n_d required with eq. 21 were taken from the literature (36), u_g^* was 1.85 Debyes (31*b*), and the values for $\bar{\alpha}_1$ were taken to be (37): 103.2×10^{-25} cc, 105.0×10^{-25} cc, and 108.7×10^{-25} cc for benzene, carbon tetrachloride, and cyclohexane, respectively.

The values of the solvent parameters ε_{11} and σ_{11} were taken from published tabulations (31*c*) and are given in Table 4. These parameters derive from gas-phase viscosity data. The values selected from the available data were both consistent with the present work and were self-consistent. They were self-consistent in the sense that by using the values of σ_{11} in Table 4, the ratio $\sigma_{C_6H_6}^3 : \sigma_{CCl_4}^3 : \sigma_{C_6H_{12}}^3$ is quite close (within 5%) to the ratio of the molar volumes $\bar{V}_{C_6H_6} : \bar{V}_{CCl_4} : \bar{V}_{C_6H_{12}}$. At least a rough correspondence between these ratios is expected for liquids composed of near-spherical particles. Such a correspondence was not found with other values of σ_{11}.

The values given for water in Table 4 (H_2O–H_2O) are Stockmayer parameters, also derived from viscosity data (31*b*). These values are

TABLE 4. Lennard–Jones (6–12) parameters

Pair	$\left(\frac{\varepsilon}{k}\right)$ (°K)	$\sigma(=d)$ (Å)
C_6H_6–C_6H_6	335.	5.628
CCl_4–CCl_4	327.	5.881
C_6H_{12}–C_6H_{12}	324.	6.093
H_2O–H_2O	775.	2.520
C_6H_6–H_2O	509.5	4.0740
CCl_4–H_2O	503.4	4.2005
C_6H_{12}–H_2O	501.1	4.3065

Can. J. Chem. Downloaded from www.nrcresearchpress.com by 210.87.254.42 on 09/05/12
For personal use only.

Can. J. Chem. Downloaded from www.nrcresearchpress.com by 210.87.254.42 on 09/05/12
For personal use only.

consistent with the present work, whereas parameters derived from the second virial coefficient of steam are not. The reason for this is unclear, but it may be a consequence of the smaller values of σ obtained from viscosity data, and the present identification of σ with d.

The values of ε_{12} and σ_{12} were calculated by the approximate Lorentz–Berthelot combining rules:

$$\sigma_{12} = (1/2)(\sigma_{11} + \sigma_{22})$$

$$\varepsilon_{12} = (\varepsilon_{11}\varepsilon_{22})^{1/2}$$

The values of d_{ij} were obtained by setting d_{ij} equal to σ_{ij}. Thus the reference system is hard-sphere-additive, and this is consistent with the Percus–Yevick equation for $g_{ij}^{HS}(r)$ (7).

Summary of Calculations

The parameters in Table 4 together with eqs. 14–23 give rise to the quantities entered in Table 5. The values of f_{12} given in Table 5 are those values which, by modifying the values of I_{12} (see eqs. 15 and 23), cause the theoretically derived Henry's law constants to equal the appropriate smoothed Henry's law constants (Table 2 columns 3, 5, 7). Thus eq. 14 together with the values in Table 5 reproduce the least-squares lines in Fig. 1. Statistical mechanical expressions for ΔH_{tr}^0 and ΔS_{tr}^0 were not derived because of the unknown theoretical temperature-dependence of f_{12}. However inasmuch as the entries in Table 5 reproduce both the solubilities and the temperature-dependence of the solubilities, these quantities are implicitly accounted for.

Discussion

The variation of f_{12} with temperature is demonstrated in Fig. 2. It is seen that with each solvent f_{12} decreases with temperature. The curves are all slightly concave upward. If the model and the accompanying assumptions were perfect, f_{12} would be unity for all systems (dashed line). The value of f_{12} is nowhere grossly different from unity; the spread including all solvents and temperatures is 0.938 to 1.174. However the calculated solubilities are very sensitive to f_{12} and therefore these values require comment.

The behavior of f_{12} may be due to the present application of scaled-particle theory and a hard-sphere radial distribution function to systems comprised of non-spherical particles. Unfortunately this possibility is very difficult to explore quantitatively, since appropriate non-spherical analogues of scaled-particle theory and the hard-sphere radial distribution function are not available. Therefore this approach will not be pursued. Instead, as is implied by eq. 22, f_{12} will be interpreted as a correction factor to $u_{12}(r)$. It is shown below that this approach, for the benzene–water and cyclohexane–water systems, is subject to a numerical check.

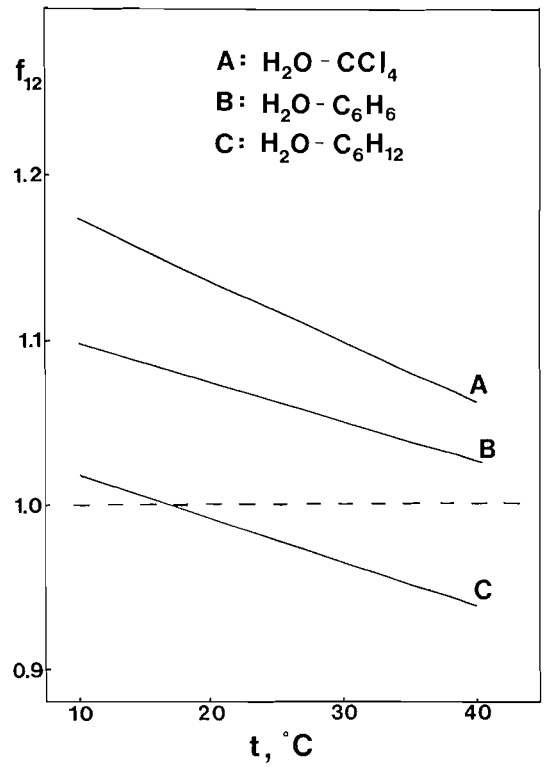

FIG. 2. The variation of f_{12} with temperature.

The benzene–water and cyclohexane–water systems are considered first. Equation 22 can be written in the form

$$u_{12}(r) = 4(\varepsilon_{12}f_{12})\left[\left(\frac{\sigma_{12}}{r}\right)^{12} - \left(\frac{\sigma_{12}}{r}\right)^{6}\right] - \frac{u_2^{*2}(\bar{\alpha}_1 f_{12})}{r^6} \qquad r > d_{12}$$

Thus f_{12} can be considered to be a correction factor common to both $\bar{\alpha}_1$ and ε_{12}. This in turn suggests that when f_{12} is different from unity, the values used for $\bar{\alpha}_1$ and ε_{12} in the calculation of I_{12} are incorrect by the same proportion. A

Can. J. Chem. Downloaded from www.nrcresearchpress.com by 210.87.254.42 on 09/05/12
For personal use only.

TABLE 5. Calculated values of the various contributions to ln K_H*

Temperature (°C)	Benzene					Carbon Tetrachloride					Cyclohexane				
	$\ln\left(\frac{RT}{\bar{V}_1}\right)\left(\frac{\mu_2^{HS}}{kT}\right)^2$		I_{11}	$-I_{12}$	f_{12}	$\ln\left(\frac{RT}{\bar{V}_1}\right)\left(\frac{\mu_2^{HS}}{kT}\right)^2$		I_{11}	$-I_{12}$	f_{12}	$\ln\left(\frac{RT}{\bar{V}_1}\right)\left(\frac{\mu_2^{HS}}{kT}\right)^2$		I_{11}	$-I_{12}$	f_{12}
10	5.578	9.858	1.172	14.761	1.098	5.496	11.595	1.308	15.189	1.174	5.383	10.473	1.126	12.649	1.018
15	5.590	9.593	1.116	14.293	1.086	5.507	11.240	1.245	14.650	1.154	5.394	10.175	1.074	12.239	1.004
20	5.601	9.338	1.063	13.842	1.073	5.519	10.903	1.187	14.138	1.135	5.406	9.886	1.025	11.844	0.991
25	5.611	9.091	1.012	13.407	1.061	5.529	10.575	1.130	13.640	1.116	5.416	9.606	0.977	11.461	0.977
30	5.622	8.853	0.964	12.987	1.049	5.540	10.263	1.077	13.165	1.098	5.427	9.334	0.932	11.091	0.964
35	5.632	8.623	0.919	12.582	1.038	5.550	9.960	1.026	12.706	1.080	5.437	9.071	0.888	10.733	0.951
40	5.642	8.400	0.875	12.192	1.026	5.560	9.670	0.977	12.265	1.062	5.447	8.816	0.846	10.387	0.938

*$\ln K_H = \ln\left(\frac{RT}{\bar{V}_1}\right) + \left(\frac{\mu_2^{HS}}{kT}\right)^2 + I_{11} + I_{12}$.

TABLE 6. Comparison of range of f_{12} with solvent polarizability ratios

Solvent	$\frac{(\alpha_1)_{min}}{\bar{\alpha}_1}$	$\frac{(\alpha_1)_{max}}{\bar{\alpha}_1}$	Range of f_{12}
Benzene	0.615	1.193	1.026–1.098
Cyclohexane	0.815	1.075	0.938–1.018

physical origin of this common correction factor to $\bar{\alpha}_1$ and ε_{12} can be understood by the reference to the London formula for the dispersion energy. By equating the coefficient of the Lennard–Jones dispersion term (the coefficient of $-1/r^6$) to the coefficient predicted by the London formula (31*d*):

$$4\varepsilon_{12}\sigma_{12}^{\,6} = k'\alpha_1\alpha_2$$

where

$$k' = \frac{3}{2}\left(\frac{E_{I_1}E_{I_2}}{E_{I_1} + E_{I_2}}\right)$$

and E_{I_1}, E_{I_2} are constants, approximately equal to the ionization energies of the molecules. Thus if α_2 (see below) and σ_{12} (here identified with d_{12}) can be considered as constants:

[24] $$\varepsilon_{12} = k''\alpha_1$$

Equation 24 states that, other factors being constant, ε_{12} and α_1 are proportional. Thus if as was done here, α_1 is taken to be the mean of the three principal components of polarizability of the solvent, then ε_{12} must correspond to the depth of the Lennard–Jones potential well reckoned with all solvent orientations equally likely. This situation was here approximated by using values of ε_{12} derived from gas phase viscosities in conjunction with the mean solvent polarizability. However eq. 24 also implies that if the effective solvent polarizability α_1' is different from $\bar{\alpha}_1$ such that

[25] $$\alpha_1' = f_{12}\bar{\alpha}_1$$

then both the values of ε_{12} and α_1 used in the calculation of $u_{12}(r)$ must be corrected by the same factor f_{12}. In view of eq. 25 it is seen that f_{12} represents the ratio of the effective solvent polarizability to the mean solvent polarizability.

In the derivation the water molecule in solution was assumed free to rotate and therefore $\bar{\alpha}_2$ was used for α_2. This assumption has some justification since water is small relative to benzene or cyclohexane, it is nearly spherical in shape, and it is completely surrounded by solvent molecules. On the other hand, a solvent molecule (C_6H_6 or C_6H_{12}) next to a water molecule in solution is larger and less spherical than water and is surrounded both by other solvent molecules and a water molecule. Under such circumstances the solvent molecule is unlikely to be free to rotate and therefore its effective or manifest polarizability α_1' is unlikely to equal $\bar{\alpha}_1$.

Since f_{12} is defined by eq. 25, limiting values of f_{12} for each solvent can be calculated from the known components of polarizability of each solvent. Subsequently the values obtained for f_{12} for the benzene–water and cyclohexane–water systems (Table 5) can be compared with these limits. Both cyclohexane and benzene are markedly anisotropic with respect to polarizability. The principal components of polarizability (in cc) are: (63.5×10^{-25}, 123.1×10^{-25}, 123.1×10^{-25}) and (92.5×10^{-25}, 116.8×10^{-25}, 116.8×10^{-25}) for benzene and cyclohexane respectively (37). The limits entered in columns 2 and 3 of Table 6 are based on these values. The ranges of values of f_{12} entered in column 4 Table 6 are taken from Table 5.

It is clear from Table 6 that the range of f_{12} for both the benzene–water and cyclohexane–water systems is well within the limits set by the maximum and minimum possible values of $(\alpha_1/\bar{\alpha}_1)$. Therefore only a slight off-average polarizability manifested by a solvent molecule next to a water molecule in solution can account for the calculated values of f_{12}. The decrease in f_{12} (or α_1') with increasing temperature is also consistent with this explanation. At lower temperatures the central water molecule is more able to favorably turn a neighboring solvent molecule than at higher temperatures since increasing kT reduces the influence of angle-dependent potentials. The specific geometries of the water and solvent molecules probably exert an increasingly important influence on the value of α_1' as the temperature increases.

The foregoing argument cannot be used for

Can. J. Chem. Downloaded from www.nrcresearchpress.com by 210.87.254.42 on 09/05/12
For personal use only.

the carbon tetrachloride–water systems, since carbon tetrachloride is isotropic with respect to polarizability. However the behavior of f_{12} for this system is similar to its behavior in the benzene–water and cyclohexane–water systems so that an analogous situation is likely to exist. It has been reported (38, 39) that aliphatic chlorine atoms can form weak hydrogen bonds in solution. Such specific interactions between molecules are only roughly taken into account by the combining rule used to obtain ε_{12}. Therefore if such an interaction occurs to an extent beyond that predicted by the square root combining rule, the calculated values of $u_{12}(r)$ would be too small (insufficiently negative) and therefore the resultant values of f_{12} would be positive, as was in fact the case. Furthermore since hydrogen bonds are strongly direction-dependent, this effect should diminish with increasing temperature and therefore f_{12} should decrease with increasing temperature. This also was found to occur.

The author is grateful to the National Research Council of Canada and the Chemistry Department of the University of Guelph for financial assistance.

1. H. REISS, H. L. FRISCH, and J. L. LEBOWITZ. J. Chem. Phys. **31**, 369 (1959).
2. H. REISS, H. L. FRISCH, E. HELFAND, and J. L. LEBOWITZ. J. Chem. Phys. **32**, 119 (1960).
3. J. L. LEBOWITZ, E. HELFAND, and E. PRAESTGAARD. J. Chem. Phys. **43**, 774 (1965).
4. R. A. PIEROTTI. J. Phys. Chem. **67**, 1840 (1963).
5. E. WILHELM. J. Chem. Phys. **58**, 3558 (1973).
6. N. S. SNIDER and T. M. HERRINGTON. J. Chem. Phys. **47**, 2248 (1967).
7. J. L. LEBOWITZ. Phys. Rev. **133**, A895 (1964).
8. L. VERLET. Phys. Rev. **165**, 201 (1968).
9. R. W. ZWANZIG. J. Chem. Phys. **22**, 1420 (1954).
10. G. A. MANSOORI and F. B. CANFIELD. J. Chem. Phys. **51**, 4958 (1969).
11. G. A. MANSOORI and F. B. CANFIELD. J. Chem. Phys. **51**, 4967 (1969).
12. G. A. MANSOORI and T. W. LELAND, JR. J. Chem. Phys. **53**, 1931 (1970).
13. J. RASAIAH and G. STELL. Mol. Phys. **18**, 249 (1970).
14. D. A. MCQUARRIE and J. L. KATZ. J. Chem. Phys. **44**, 2393 (1966).
15. J. A. BARKER and D. HENDERSON. J. Chem. Phys. **47**, 4714 (1967).
16. P. J. LEONARD, D. HENDERSON, and J. A. BARKER. Trans. Faraday Soc. **66**, 2439 (1970).
17. D. HENDERSON and P. J. LEONARD. *In* Physical chemistry, an advanced treatise. Vol. VIII B. *Edited by* H. Eyring, D. Henderson, and W. Jost. Academic Press, Inc., New York. 1971. pp. 413–510.
18. J. D. WEEKS, D. CHANDLER, and H. C. ANDERSEN. J. Chem. Phys. **54**, 5237 (1971).
19. L. VERLET. *In* Proceedings of the sixth IUPAP conference on statistical mechanics. *Edited by* S. A. Rice, K. F. Freed, and J. C. Light. The University of Chicago Press, Chicago. 1972. p. 379.
20. L. VERLET and J. J. WEIS. Phys. Rev. A, **5**, 939 (1972).
21. R. O. NEFF and D. A. MCQUARRIE. J. Phys. Chem. **77**, 413 (1973).
22. A. WEISSBERGER and E. S. PROSKAUER. Organic solvents. 2nd ed. Vol. VII. Interscience Publishers, Inc., New York. 1955: (*a*) p. 72; (*b*) p. 194.
23. J. TIMMERMANS. The Physico-chemical constants of binary systems. Vol. I. Interscience Publishers, Inc., New York. 1959: (*a*) p. 240; (*b*) p. 604.
24. M. E. MITTEN, K. S. DRESS, and W. G. KROCHTA. *In* Encyclopedia of industrial chemical analysis. Vol. 8. *Edited by* F. D. Snell and L. S. Ettre. Interscience Publishers, Inc., New York. 1969. p. 320.
25. Biometrika tables for statisticians. 2nd ed. Vol. I. *Edited by* E. S. Pearson and H. O. Hartley. Cambridge University Press, New York. 1958. Table 31, p. 179.
26. A. SEIDELL. Solubilities of inorganic and metal organic compounds. 4th ed. Vol. I. American Chemical Society, Washington, D.C. 1958. pp. 1134–1135.
27. J. R. JOHNSON, S. D. CHRISTIAN, and H. E. AFFSPRUNG. J. Chem. Soc. A. 77 (1966).
28. S. GOLDMAN. PH.D. Thesis. McGill University, Montreal, Quebec, 1969.
29. J. E. DESNOYERS, G. E. PELLETIER, and C. JOLICOEUR. Can. J. Chem. **43**, 3232 (1965).
30. R. A. ROBINSON and R. H. STOKES. Electrolyte solutions. 2nd rev. ed. Butterworths, London. 1959. p. 457.
31. J. O. HIRSCHFELDER, C. F. CURTISS, and W. R. BIRD. Molecular theory of gases and liquids. John Wiley and Sons, New York. 1954: (*a*) pp. 214, 1148; (*b*) p. 1200; (*c*) pp. 1111, 1112, 1213; (*d*) p. 963.
32. R. F. BRUMEL and K. V. BIBBER. *In* International critical tables. Vol. III. McGraw-Hill Book Company, Inc., New York. 1929. pp. 28, 29.
33. V. V. NALIMOV. The application of mathematical statistics to chemical analysis. Pergamon Press, London. 1963. p. 167.
34. H. L. FRISCH, J. L. KATZ, E. PRAESTGAARD, and J. L. LEBOWITZ. J. Phys. Chem. **70**, 2016 (1966).
35. C. J. F. BÖTTCHER. Theory of electric polarization. Elsevier Publishing Company, Houston, Texas. 1952. p. 70.
36. Handbook of Chemistry and Physics. 41st ed. The Chemical Rubber Company, Cleveland, Ohio. 1959–1960. pp. 2513, 2936.
37. LANDOLT–BÖRNSTEIN. Zahlenwerte und Functionen. Vol. I. Part 3. Springer, 1951. p. 511.
38. T. D. EPLEY and R. S. DRAGO. J. Am. Chem. Soc. **89**, 5770 (1967).
39. B. B. HOWARD, C. F. JUMPER, and M. T. EMERSON. J. Mol. Spectrosc. **10**, 117 (1963).
40. S. D. CHRISTIAN, H. E. AFFSPRUNG, and S. A. TAYLOR. J. Phys. Chem. **67**, 187 (1963).

Can. J. Chem. Downloaded from www.nrcresearchpress.com by 210.87.254.42 on 09/05/12
For personal use only.

The Photochemical Reactivity of Some Benzoylthiophenes. II. Photocycloaddition[1]

D. R. ARNOLD[2], R. J. BIRTWELL, AND B. M. CLARKE, JR.

Photochemistry Unit, Department of Chemistry, University of Western Ontario, London, Ontario N6A 3K7

Received November 14, 1973

The photochemical reactivity of 2- and 3-benzoylthiophene and their *para*-cyano and *para*-methoxy derivatives, upon irradiation in the presence of isobutylene, has been studied. All six ketones undergo photocycloaddition at the carbonyl group under these conditions. The resulting oxetanes are thermally unstable; they eliminate formaldehyde and yield the 1-aryl-1-thienyl-2-methylpropene. The existing generalizations, potentially useful for predicting this photochemical reactivity, are reviewed.

On a étudié la réactivité photochimique des benzoyl-2 et -3 thiophènes et de leurs dérivés *para*-cyano et *para*-méthoxy lors de leur irradiation en présence d'isobutylène. Dans ces conditions les six cétones subissent une photocycloaddition impliquant le groupement carbonyle. Les oxétanes qui en résultent sont thermiquement instables; ils expulsent de la formaldéhyde et fournissent les aryl-1 thiényl-1 méthyl-2 propènes. On passe en revue les généralisations déjà proposées et qui sont potentionnellement utiles pour prédire cette réactivité photochimique. [Traduit par le journal]

Can. J. Chem., **52**, 1681 (1974)

Introduction

A goal of the organic photochemist is to be able to predict the photochemical reactivity of a molecule based, preferably, upon the structure of the ground state and reasoning by analogy with related compounds. The knowledge of the nature of the accessible electronic excited states, gleaned from spectroscopic studies, may also be useful. Extensive efforts have, in fact, resulted in several generalizations with regard to the photochemical reactivity of carbonyl compounds. In this paper we review these generalizations and compare the predictions with the observed reactivity of 2- and 3-benzoylthiophene and their *para*-cyano and *para*-methoxy derivatives upon irradiation in the presence of isobutylene. In addition, the few previous reports concerning the photochemical reactivity of these and similar thiophene ketones will be reviewed in perspective.

Part I of this series reported results of the study of the u.v. absorption and phosphoresence emission spectra of these ketones which made possible the assignment of electronic configuration and energy for several of the electronic excited states (1). The lowest excited singlet in all cases in non-polar solvents, is an n,π* state of the carbonyl chromaphore. The lowest triplet of the 2-benzoylthiophene derivatives (**1***a–c*) has π,π* character and is assigned to the 2-thienoyl moiety. The 3-benzoylthiophene derivatives (**2***a–c*) have an n,π* triplet, associated with the carbonyl group, of lowest energy. These results are summarized in the partial state diagrams for these molecules which are shown in Fig. 1.

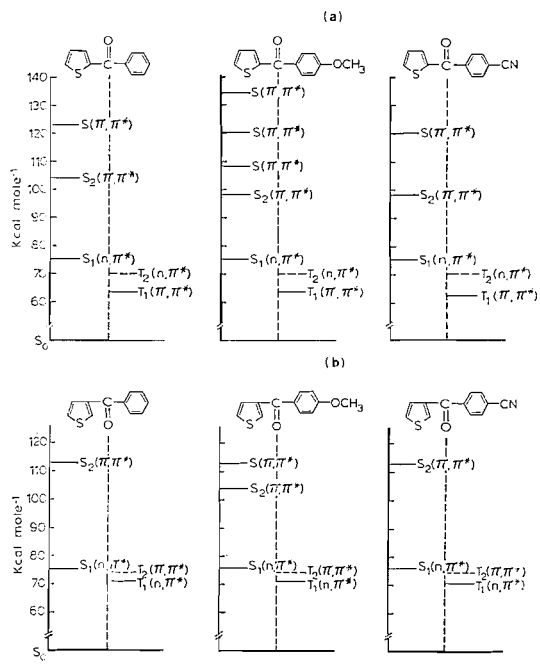

FIG. 1. Partial energy diagrams (*a*) for the 2-benzoylthiophenes, (*b*) for the 3-benzoylthiophenes.

[1]Contribution No. 94 from the Photochemistry Unit.
[2]Alfred P. Sloan Fellow 1972–1974.

Can. J. Chem. Downloaded from www.nrcresearchpress.com by 210.87.254.5 on 09/05/12
For personal use only.

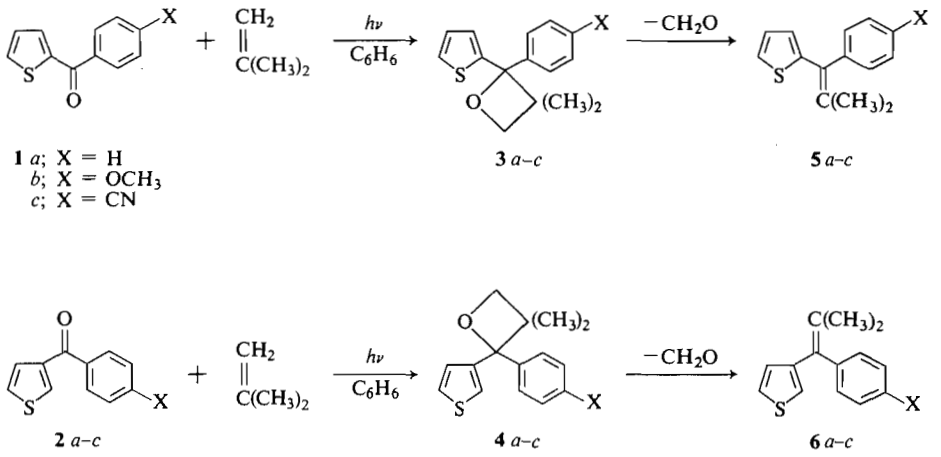

1 *a*; X = H
b; X = OCH_3
c; X = CN

3 *a–c* **5** *a–c*

2 *a–c* **4** *a–c* **6** *a–c*

SCHEME 1

Results

Irradiation of the 2- and 3-benzoylthiophenes studied (**1***a–c* and **2***a–c*) in the presence of isobutylene, results in photocycloaddition at the carbonyl group. The oxetanes (**3***a–c* and **4***a–c*), formed initially, are thermally unstable; they eliminate formaldehyde and give the olefins (**5***a–c* and **6***a–c*). We were unable to isolate any of the oxetanes but could detect and characterize, by n.m.r., all but two (**3***a* and *b*).

The structures assigned to the olefins **5***a–c* and **6***a–c* are consistent with the n.m.r. spectra. In the case of **5***a*, *b* and **6***a*, *b*, the structures have been firmly established by comparison with authentic samples synthesized by dehydration of alcohols made by the Grignard reaction of isopropyl magnesium bromide with the ketones **1***a*, *b* and **2***a*, *b*.

We found no evidence of photoisomerization of the thiophene ring in the product olefin or in recovered starting ketone. No cyclobutane products which might have arisen from photocycloaddition of the olefin to the thiophene ring were detected. However, the material balance was not always good and the n.m.r. spectrum of the crude reaction mixture indicated that in some cases products, which were not characterized, were formed in small amounts.

Discussion

The possible photochemical reactions of the benzoylthiophenes (**1***a–c*, **2***a–c*) which must be considered include (*1*) photocycloaddition to the carbonyl group to give the oxetane; (*2*) photocycloaddition to the thiophene ring to give the cyclobutane, and; (*3*) photoisomerization of the thiophene ring. Obviously the possibility also exists that no photochemical reaction will occur. Of these possibilities photocycloaddition to the carbonyl group is the reaction observed. Armed with the considerable experience obtained from studies of related carbonyl compounds, would this photochemical reactivity have been predictable?

On the basis of structural considerations alone, and in view of the similarity of the ground state reactivity of thiophene and benzene, one might predict photochemical reactivity parallel to that observed for the analogous benzophenone derivatives. Benzophenone and 4,4′-dimethoxybenzophenone are known to form the oxetanes upon irradiation in the presence of isobutylene (2). The photocycloaddition of 4,4′-dicyanobenzophenone had not been previously studied; it also forms the oxetane under these conditions.[3] Thus, this first approximation, while correct in this instance, is certainly fortuitous in view of the difference in the nature of the lowest triplets for the 2- and 3-benzoylthiophene derivatives assigned on the basis of the spectroscopic study (1).

One generalization of photochemical reactivity of carbonyl compounds that is widely accepted is that carbonyl singlet and triplet n,π* states are much more reactive toward photocycloaddition

[3]The phosphoresence emission from 4,4′-dicyanobenzophenone (MCIP at 77 °K) has the vibrational structure (0-0 − 0-1 separation = 1640 cm^{-1}) and is typical of an n,π* triplet. The triplet energy (E_T = 63.4 kcal mol^{-1}) is low compared with that of benzophenone (68.6 kcal mol^{-1}) and 4-cyanobenzophenone (66.4 kcal mol^{-1}) (3) and reflects the strong electron withdrawing nature of the cyano group.

Can. J. Chem. Downloaded from www.nrcresearchpress.com by 210.87.254.5 on 09/05/12
For personal use only.

Can. J. Chem. Downloaded from www.nrcresearchpress.com by 210.87.254.5 on 09/05/12
For personal use only.

with olefins to give the oxetane than are states of other electronic configuration. Since the n,π* singlet is usually short lived, due to rapid intersystem crossing, the n,π* triplet is usually the reactive state in these reactions. A corollary therefore is, carbonyl compounds which emit from an n,π* triplet are generally reactive in this reaction. It should be made clear that "reactivity" in this context refers to the rate controlling steps leading to cycloaddition products and should not be interpreted to mean high quantum yield or even good yield of product, since many complicating factors (*eg.* reversible formation of an intermediate, lifetime of the excited state, competing reactions with comparable rates, etc.) are not taken into account. Nevertheless, this corollary has been used and the products obtained from a large number of carbonyl compounds can be correlated with triplet emission (2, 4). However, the products obtained upon irradiation of ketones **1***a–c* belie this generalization since the phosphorescence emission from these ketones is clearly π,π* in nature.

With some carbonyl compounds, aliphatic ketones for example, the intersystem crossing rate is known to be slow; bimolecular reactions of the n,π* singlet are then observed (5). The n,π* singlet could be responsible for the reactivity of **1***a–c* if intersystem crossing is slow enough. While we have no evidence on this point, the positioning of the excited states summarized in the energy level diagram (Fig. 1*a*), with the π,π* triplet rather close in energy and below the n,π* singlet ($E_{n,\pi^{*1}} - E_{\pi,\pi^{*3}} = 4300\ cm^{-1}$), should lead to a rapid intersystem crossing process so that a bimolecular reaction would be precluded (6). This need not be the case; the energy level diagram for 2-naphthaldehyde is similar to that for **1***a–c*, (the separation of the π,π* triplet and n,π* singlet is, however, significantly larger ($E_{n,\pi^{*1}} - E_{\pi,\pi^{*3}} = 7000\ cm^{-1}$)), and photocycloaddition has recently been shown to occur at the carbonyl group and via an n,π* singlet reaction (7).

Ketones **1***a–c* join a growing list of carbonyl compounds, the photochemical reactivity of which is not predictable by attributing characteristic reactivity to the accessible excited states. Furthermore, advances made in understanding the mechanism(s) of the photocycloaddition reaction force a reevaluation of this generalization, particularly when attempting to predict synthetic utility.

It seems *a priori* reasonable that the most rigorous, and perhaps least useful (in view of the amount of information required), generalizations of photochemical reactivity will be those based upon extrapolation of characteristic reactivity in different types of reactions. For example, carbonyl compounds that are efficiently reduced, by hydrogen abstraction by the carbonyl oxygen atom, upon irradiation in the presence of hydrogen donors should be expected to undergo photocycloaddition to olefins to form oxetanes. Furthermore, intramolecular hydrogen abstraction, leading to Norrish type II cleavage or photoenolization of β-alkyl-α, β-unsaturated carbonyl compounds should compete with oxetane formation. This generalization assumes an "alkoxy radical-like" state, regardless of electronic configuration, is responsible for these reactions. There is little fundamental basis for this generalization since it is now known that several different types of intermediates can precede any radical intermediate that may be involved. Still, the products obtained from a large number of carbonyl compounds can be predicted on this basis.

There have been very few reports concerning the photochemical reactivity of thiophene carbonyl compounds. For alkyl thiophene ketones, enough is known so that a consistent reactivity pattern seems established. Both 2- and 3-acetylthiophene are known to be stable to irradiation in isopropanol (8). Neckers and co-workers have recently found that *n*-propyl-2-thiophene ketone and *n*-propyl-3-(2,5-dimethylthiophene) ketone[4] do not undergo the Norrish type II reaction (9). Thus, these ketones are unreactive toward hydrogen abstraction and are not to be expected to give the oxetanes upon irradiation in the presence of olefins.

The photocycloaddition of 2-acetyl thiophene to tetramethylethylene and isobutylene, shown in Scheme 2, has recently been studied (10). The products were reported to be the cyclobutanes which result from cycloaddition of the olefin to the 2,3-position of the thiophene; no oxetanes were detected.[5]

[4]A cautionary note should be made with regard to the expected similarity between the excited states of 3-thiophene ketones and 3-(2,5-dimethylthiophene) ketones. While 3-benzoylthiophene emits from the carbonyl n,π* triplet, the emission from 3-benzoyl-2,5-dimethylthiophene is very different and is π,π* in nature.

[5]In a private communication, Dr. Cantrell has expressed doubt concerning the structure assignment of some of the adducts reported in this preliminary communication (10).

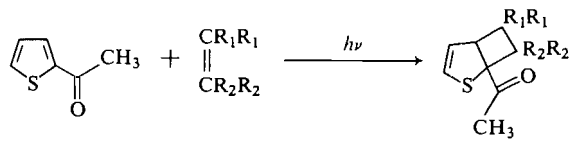

7 **8** *a*; $R_1 = R_2 = CH_3$ **9** *a*; $R_1 = R_2 = CH_3$
b; $R_1 = CH_3$, $R_2 = H$ *b*; $R_1 = CH_3$, $R_2 = H$
c; $R_1 = H$, $R_2 = CH_3$

SCHEME 2

The only alkylthiophene ketone for which an emission spectrum is reported is 2-acetylthiophene. In this case the lowest triplet has been assigned the π,π^* configuration (10). There is good reason to expect the triplet of *n*-propyl-2-thiophene to be similar to that of 2-acetylthiophene. It seems likely, in view of the small separation of the n,π^* and π,π^* triplets in 3-benzoylthiophene that the lowest triplet of 3-alkylthiophene ketones will also have the π,π^* configuration. Thus, the lack of hydrogen abstraction by the carbonyl oxygen and the lack of photocycloaddition to the carbonyl group are consistent with predictions based on characteristic reactivity and on the electronic configuration of the excited state.

The reactivity of 2- and 3-benzoylthiophene upon irradiation in hydrogen donating solvents is far from clear. Predictions based on the photocycloadditions reported here would be for hydrogen abstraction by the carbonyl oxygen to occur. Traynard and Blanchi have studied the reactivity of 2- and 3-benzoylthiophene upon irradiation in isopropanol (11). They report quantum yields for the disappearance of the ketone of 0.17 for 2-benzoylthiophene, and 0.25 for 3-benzoylthiophene compared to 1.23 for benzophenone. However, the products of these reactions, which they presumed to be the pinacols, were not isolated and were characterized only by u.v. spectra. Neckers, on the other hand, has been unable to detect photoreduction products from 2-benzoylthiophene under comparable conditions (9). Further work is required to define the reactivity of these ketones toward hydrogen abstraction; it seems clear, however, that the reaction will not be useful for synthesis of the reduction products and, that if hydrogen abstraction does occur, the reaction is much less efficient than with benzophenone.

There was one previous report of a photocycloaddition reaction between 2-benzoylthiophene and an olefin, isobutylene. Cantrell reported photocycloaddition to give the cyclobutane analogous to those obtained with 2-acetylthiophene; however, the product was not isolated and characterized[5] (10). If the product is in fact the cyclobutane, the difference in conditions which lead to cyclobutane *vs.* oxetane are not yet clear.

There are several reported examples of positional isomerization of substituted thiophenes. This reaction has been extensively studied by Wynberg and Kellogg and their co-workers and has recently been reviewed (12). The interchange of the thiophene carbons 2 and 3 of alkyl- and aryl-substituted thiophenes occurs via the intermediate cyclopropenyl thioketone or thioaldehyde and is a fairly general reaction which appears to involve the lowest singlet (π,π^*) state. This reaction is apparently inhibited by carbonyl substitution; thiophene aldehyde and acetylthiophene do not photorearrange (13). This correlation is strengthened by the lack of photoisomerization of **1***a–c* and **2***a–c*.

The qualitative differences in stability of the oxetanes **3***a–c*, **4***a–c*, toward loss of formaldehyde, encountered during attempted isolation indicates a decomposition mechanism in which positive charge develops on the benzylic, thienylic carbon. The two oxetanes which we are unable to detect, **3***a* and *b*, are those which potentially form the most stable carbonium ion while the relative stability of **4***c* is a reflection of the electron withdrawing capability of the *para*-cyano group. This behavior has precedence since 2,2-di(4-methoxyphenyl)-3,3-dimethyloxetane is difficult to isolate; the olefin is obtained in high yield (2). The σ^+ values for 2- and 3-thienyl (-0.85 and -0.49, compared with σ^+ for methoxy -0.78), gleaned from solvolysis studies, indicate an ability of the thiophene ring to stabilize an adjacent carbonium ion (14).

Conclusions

The state diagrams for the 2- and 3-benzoylthiophenes indicate significant differences in the

Can. J. Chem. Downloaded from www.nrcresearchpress.com by 210.87.254.5 on 09/05/12
For personal use only.

Can. J. Chem. Downloaded from www.nrcresearchpress.com by 210.87.254.5 on 09/05/12
For personal use only.

relative positions of analogous electronic excited states; in particular **1***a–c* have a lowest triplet of π,π^* character while **2***a–c* have an n,π^* triplet of lowest energy. Nevertheless, the qualitative behavior of both series upon irradiation in the presence of isobutylene is the same, photocycloaddition at the carbonyl group. Therefore, for synthetic purposes, the generalization of photochemical reactivity based upon the spectroscopic identification of accessible excited states is not yet useful.

A question is raised concerning the adequacy of predictions based upon reactivity in different types of reactions. Part III of this series reports the extension of this study to 2-benzoyl-3-methylthiophene and 2-(2-methylphenyl)thiophene ketone where photoenolization would be predicted to compete with photocycloaddition. In fact, while photoenolization cannot be observed, photocycloaddition of olefins to these ketones does occur.

Experimental

General

The synthesis of the ketones **1***a–c* and **2***a–c* and the description of the general experimental approach were reported in Part I (1). Irradiations were carried out using a Hanovia 450-W medium-pressure mercury vapor lamp (679A36) in a quartz cooling jacket which was immersed in a constant temperature bath at 10°. The samples, contained in sealed quartz tubes (20 mm diameter) having a volume of 40 ml, were arranged around the lamp at a distance of 25 mm; they were not degassed.

*Irradiation of 2-Benzoylthiophene (**1***a) with Isobutylene*

2-Benzoylthiophene (0.16 g) was dissolved in benzene (30 ml) in a quartz irradiation tube and cooled in an ice bath. Isobutylene was bubbled through the solution until a gain in weight of 4 g was observed and the tube was sealed with a rubber cap. The sample was irradiated at 10° for 16 h, an aliquot was withdrawn, and after removal of the benzene and isobutylene the n.m.r. spectrum of the mixture was taken. This spectrum showed complex absorption in the aromatic region (7.94–6.65 p.p.m.) and aliphatic region (2.3–0.7 p.p.m.) with two sharp singlets at 1.98 and 1.68 p.p.m. Irradiation for longer periods caused little further change.

Chromatography of the total reaction mixture after removal of the benzene and isobutylene, gave a fraction eluted with 10% benzene–hexane which had the two singlets at 1.98 and 1.68 p.p.m. in the n.m.r. Bulb-to-bulb distillation of this sample gave 40 mg of 1-phenyl-1-(2-thienyl)-2-methylpropene (**5***a*). The i.r. and n.m.r. spectra of this material were identical to those of an authentic sample prepared by the Grignard method: i.r. ν_{max}^{neat}, 1600, 1440, 1220, 1020, 830, 760, 700 cm^{-1}; n.m.r., 1.98 (s), 1.68 (s), (allylic protons), 7.40–6.60 p.p.m. (complex), (thienyl and phenyl protons).

Anal. Calcd. for $C_{14}H_{14}S$: C, 78.48; H, 6.59. Found: C, 78.31; H, 6.65.

*Irradiation of 2-(4-Methoxybenzoyl)thiophene (**1***b) with Isobutylene*

2-(4-Methoxybenzoyl)thiophene (1 g) was dissolved in a solution of 25% isobutylene in benzene (40 ml) and irradiated in a quartz tube at 10° for 20 h. An aliquot was withdrawn and after evaporation of the solvent and excess isobutylene the n.m.r. spectrum was taken. This spectrum had complex absorption in the aromatic and aliphatic regions with two sharp singlets at 1.98 and 1.74 p.p.m.

Chromatography of the crude reaction mixture, after evaporation of the solvent and excess isobutylene, on Shawinigans base washed alumina, gave a fraction eluting with 25% benzene–hexane, which retained the singlets at 1.98 and 1.74 p.p.m. Bulb-to-bulb distillation of this sample gave 50 mg of 1-(4-methoxyphenyl)-1-(2-thienyl)-2-methylpropene. The i.r. and n.m.r. spectra were identical with those of an authentic sample prepared by the, Grignard route: i.r. $\nu_{max}^{CHCl_3}$, 1610, 1510, 1470, 1450 1300, 1290, 1180, 1115, 1035 cm^{-1}; n.m.r., 3.71 (s), (methoxyl); 1.98 (s), 1.74 (s), (allylic protons); 7.20–6.70 p.p.m. (complex), (thienyl and phenyl protons).

*Irradiation of 2-(4-Cyanobenzoyl)thiophene (**1***c) with Isobutylene*

2-(4-Cyanobenzoyl)thiophene (2.5 g) was dissolved in 25% isobutylene in benzene (300 ml) and irradiated through quartz in an immersion well reactor (Ace Glass 6515-25-03; 450 Hanovia W medium-pressure mercury vapor lamp) for 20 h. An aliquot was withdrawn and after removal of the benzene and excess isobutylene the n.m.r. spectrum was determined. This spectrum was in accord with formation of the oxetane in about 90% yield. Oxetane formation was consistent with the i.r. spectrum which showed the carbonyl band had essentially disappeared while strong absorption developed a 980 cm^{-1} typical of oxetanes. i.r. $\nu_{max}^{CHCl_3}$, 2240, 1715, 1645, 1610, 1500, 1465, 1415, 1370, 980 cm^{-1}; n.m.r., 4.52, 4.15 (quartet, $J = 5$ Hz), (methylene protons); 1.12 (s), 1.01 p.p.m. (s), (methyls on the oxetane).

An attempt was made to purify the oxetane by crystallization from methanol, chromatography on Shawinigans basic alumina, and sublimation; however, all attempts led to decomposition of the oxetane to 1-(4-cyanophenyl)-1-(2-thienyl)-2-methylpropene. This product was therefore sublimed (180°, 0.01 mm) giving lemon yellow crystals. Recrystallization from methanol yielded 1.92 g (77%) of the olefin as colorless leaflets, m.p. 96–97°. i.r. ν_{max}^{KBr}, 2240, 1600, 1440, 1220, 870, 818, 710, 700 cm^{-1}; n.m.r., 2.00 (s), 1.78 (s), (allylic protons), 7.75–6.75 p.p.m. (complex), (thienyl and phenyl protons).

Anal. Calcd. for $C_{15}H_{13}NS$: C, 75.30; H, 5.48 Found: C, 75.10; H, 5.33.

*Irradiation of 3-Benzoylthiophene (**2***a) with Isobutylene*

3-Benzoylthiophene (0.5 g) was dissolved in a 25% solution (by volume) of isobutylene in benzene (40 ml) and irradiated in a quartz tube for 20 h. A sample was withdrawn and after removal of the solvent the n.m.r. spectrum was determined. This spectrum showed a complex aliphatic and aromatic region; however, there was a quartet at 4.40, 4.15 p.p.m. ($J = 5$ Hz) and a singlet at 1.05 p.p.m. characteristic of the oxetane, and two singlets at 1.90 and 1.74 p.p.m. indicative of the olefin.

Chromatography of the reaction mixture on Shawini-

Can. J. Chem. Downloaded from www.nrcresearchpress.com by 210.87.254.5 on 09/05/12
For personal use only.

gans base washed alumina gave a fraction eluting with 20% benzene–hexane which showed the two singlets at 1.90 and 1.74 p.p.m. No oxetane was obtained from the column. Bulb-to-bulb distillation of this fraction yielded 60 mg of 1-phenyl-1-(3-thienyl)-2-methylpropene. The i.r. and n.m.r. spectra of this material were identical to those of an authentic sample prepared by the Grignard route: i.r. $\nu_{max}^{CDCl_3}$, 1605, 1490, 1450, 1285, and 1035 cm^{-1}; n.m.r., 1.90 (s), 1.74 (s), (allylic protons); 7.45–6.64 p.p.m. (complex), (phenyl and thienyl protons).

Irradiation of 3-(4-Methoxybenzoyl)thiophene (2b) with Isobutylene

3-(4-Methoxybenzoyl)thiophene (1 g) was dissolved in a 25% solution (by volume) of isobutylene in benzene (40 ml) and irradiated in a quartz tube at 10° for 20 h. A sample was withdrawn and after evaporation of the solvent the n.m.r. spectrum was determined. A quartet at 4.20, 3.93 p.p.m. (J = 7 Hz) characteristic of oxetane formation, and two singlets in the aliphatic region at 1.88 and 1.76 p.p.m. for the olefin were observed.

Chromatography on Shawinigans basic alumina gave a fraction eluted with 25% benzene–hexane which retained the two singlets at 1.88 and 1.76 p.p.m. in the n.m.r. Bulb-to-bulb distillation of this fraction gave 46 mg of 1-(4-methoxyphenyl)-1-(3-thienyl)-2-methylpropene. The i.r. and n.m.r. spectra of this sample were identical to those of a sample prepared by the Grignard route: i.r. $\nu_{max}^{CDCl_3}$, 1610, 1515, 1250, 1180, and 1040 cm^{-1}; n.m.r., 1.88 (s), 1.76 (s), (allylic protons); 3.76 (s), (methoxyl); 7.16–6.71 p.p.m. (complex), (thienyl and phenyl protons).

Irradiation of 3-(4-Cyanobenzoyl)thiophene (2c) with Isobutylene

3-(4-Cyanobenzoyl)thiophene (0.1 g) was dissolved in a 25% solution of isobutylene in benzene (20 ml) and irradiated in a quartz tube at 10° for 20 h. Removal of the solvent gave a dark oil, the n.m.r. spectra of which indicated the formation of the oxetane in about 90% yield with no concomitant olefin formation: n.m.r., 4.39, 4.15 (quartet, J = 5 Hz), (methylene protons), 1.07 and 1.00 p.p.m (s), (methyl groups on oxetane).

Attempted bulb-to-bulb distillation of the oxetane gave 1-(4-cyanophenyl)-1-(3-thienyl)-2-methylpropene. i.r. $\nu_{max}^{CDCl_3}$, 2250, 1715, 1660, 1610, 1515, 1295, 1275, 1175 cm^{-1}; n.m.r., 1.90 (s), 1.73 (s), (allylic protons); 8.20–6.70 p.p.m. (complex), (phenyl and thienyl protons).

Anal. Calcd. for $C_{15}H_{13}NS$: C, 75.30; H, 5.48. Found: C, 75.13; H, 5.49.

Preparation of 1-Phenyl-1-thienyl-1,2-methylpropenes

The procedure developed by Garbisch was used (15).

Magnesium (0.24 g), 2-bromopropane (1.24 g), and dry ether (15 ml) were placed in a dry flask fitted with a reflux condenser and drying tube. A crystal of iodine was added and the reaction started, the ether boiled gently until nearly all the magnesium had dissolved and then the reaction was heated under reflux for 10 min. The reaction mixture was cooled and the benzoylthiophene (0.15 g) in dry ether (5 ml) was added with stirring. After 10 min the reaction mixture was poured into 10% aqueous ammonium chloride (50 ml), the ether layer was separated and the aqueous layer extracted with two portions of ether (50 ml). The combined ether extracts were washed with water and dried over anhydrous sodium sulfate. Removal of the ether left the alcohol as a yellow oil.

The alcohol was not purified but was immediately dehydrated to the olefin by shaking with 25% sulfuric acid in acetic acid (5 ml) for 30 s. This mixture was poured into a mixture of ether (50 ml) and water (150 ml). The ether layer was separated and the aqueous layer extracted twice with ether (50 ml). The combined ether extracts were washed twice with 10% sodium bicarbonate (150 ml), followed by water (100 ml), and then dried over anhydrous calcium chloride. Removal of the ether gave a red oil which was chromatographed on Shawinigans base washed alumina and in all cases gave the olefin upon elution with 25% benzene–hexane. After removal of the solvent the samples were bulb-to-bulb distilled giving clear oils.

1-Phenyl-1-(2-thienyl)-2-methylpropene

The yield by the above procedure was 45 mg (26%). The i.r. and n.m.r. spectra of this sample were essentially the same as those observed for the olefin obtained from the irradiation of **1***a* with isobutylene.

1-(4-Methoxyphenyl)-1-(2-thienyl)-2-methylpropene

The yield of olefin by the above procedure was 62 mg (37%). The i.r. and n.m.r. spectra of this olefin were essentially the same as those observed for the olefin obtained from the irradiation of **1***b* with isobutylene.

Anal. Calcd. for $C_{15}H_{16}OS$: C, 73.75; H, 6.60. Found: C, 73.61; H, 6.72.

1-Phenyl-1-(3-thienyl)-2-methylpropene

The yield of olefin by the above procedure was 53 mg (31%). The i.r. and n.m.r. spectra of this olefin were essentially the same as those observed for the olefin obtained from the irradiation of **2***a* with isobutylene.

Anal. Calcd. for $C_{14}H_{14}S$: C, 78.48; H, 6.59. Found: C, 78.55; H, 6.59.

1-(4-Methoxyphenyl)-1-(3-thienyl)-2-methylpropene

The yield of olefin by the above procedure was 65 mg (39%). The i.r. and n.m.r. spectra of this olefin were essentially the same as those observed for the olefin obtained from the irradiation of **2***b* with isobutylene.

Anal. Calcd. for $C_{15}H_{16}OS$: C, 73.75; H, 6.60. Found: C, 73.57; H, 6.84.

This work was supported by a grant from the National Research Council of Canada.

1. D. R. Arnold and R. J. Birtwell. J. Am. Chem. Soc. **95**, 4599 (1973).
2. (*a*) D. R. Arnold, R. L. Hinman, and A. H. Glick. Tetrahedron Lett. 1425 (1964); (*b*) D. R. Arnold. Adv. Photochem. **6**, 301 (1968).
3. W. G. Herkstroeter, A. A. Lamola, and G. S. Hammond. J. Am. Chem. Soc. **86**, 4537 (1964).
4. (*a*) J. P. Wagner and G. S. Hammond. Adv. Photochem. **5**, 21 (1968); (*b*) J. P. Wagner. Acc. Chem. Res. **4**, 168 (1971).
5. J. C. Dalton and N. J. Turro. Annu. Rev. Phy. Chem. **21**, 499 (1970).

6. A. A. LAMOLA. J. Chem. Phys. **47**, 4810 (1967); R. M. HOCKSTROSSER. Acc. Chem. Res. **1**, 266 (1968); M. A. EL-SAYED. Acc. Chem. Res. **1**, 8 (1968).
7. N. C. YANG, M. KIMURA, and W. EISENHARDT. J. Am. Chem. Soc. **95**, 5058 (1973).
8. N. D. HEINDEL. J. Heterocycl. Chem. **3**, 379 (1966).
9. D. C. NECKERS. Private communication.
10. T. S. CANTRELL. Chem. Commun. 155 (1972).
11. P. TRAYNARD and J. P. BLANCHI. J. Chim. Phys. **69**, 284 (1972).
12. H. WYNBERG. Acc. Chem. Res. **4**, 65 (1971).
13. A. COUTURE and A. L. COMBIER. Tetrahedron, **27**, 1059 (1971); Chem. Commun. 891 (1971).
14. E. A. HILL, M. L. GROSS, M. STASIEWICZ, and M. MANION. J. Am. Chem. Soc. **91**, 7381 (1969).
15. E. W. GARBISCH. J. Org. Chem. **26**, 4165 (1961).

Can. J. Chem. Downloaded from www.nrcresearchpress.com by 210.87.254.5 on 09/05/12
For personal use only.

Electronic Chemiluminescence in M + X_2 Reactions: Dissociation Energies of the Alkaline Earth Monohalides MX (M = Ca, Sr, Ba; X = F, Cl, Br)

MICHAEL MENZINGER

Department of Chemistry, University of Toronto, Toronto, Ontario M5S 1A1

Received October 23, 1973

Electronic chemiluminescence has been observed for nine reactions of Group II*a* metal atoms (M = Ca, Sr, Ba) with dihalogen molecules (X_2 = F_2, Cl_2, Br_2).

In all cases one or more electronically excited states of the monohalide MX* were observed. Continuum emission, presumably due to dihalides MX_2*, was seen in all systems, and the emission intensity increased in the order $F_2 < Cl_2 < Br_2$. Recombination to form MX_2* appears thus to be a fairly general process in these systems.

From the highest vibrational levels of MX populated in the upper electronic state(s) we have calculated the following lower limits to the ground state dissociation energies D_0^0 (MX) (in kcal/mol):

	Br	Cl	F
Ca	97.4±1.5	115.0±1.5	128.4±2
Sr	93.5±2	123.9±3	127.3±1.5
Ba	104.6±2	119.7±1.5	141.4±5

Information on the vibrational state distributions of the excited MX* is discussed from a qualitative point of view. Accordingly, the fluorides are formed with inverted vibrational distributions, which bear clear evidence of the direct nature of the interaction dynamics. The electronically excited chlorides and bromides, however, tend to be formed with monotonically decreasing, near-statistical distributions. This is consistent with the formation of long lived collision complexes. Reasons for these trends are discussed in terms of the energetics of the complete decomposition.

La chimiluminescence électronique a été observée pour neuf réactions d'atomes métalliques du groupe II*a* (M = Ca, Sr, Ba) avec des molécules dihalogénées (X_2 = F_2, Cl_2, Br_2).

En tous cas, un ou plusieurs états excités électroniquement du monohalogénure MX* sont observés. Une émission continue, due probablement aux dihalogénures MX_2*, est observée dans tous les systèmes et l'intensité d'émission augmente selon l'ordre: $F_2 < Cl_2 < Br_2$. Une recombinaison pour former le MX_2* paraît être ainsi un procédé assez général dans ces systèmes.

Des plus hauts niveaux vibrationnels du MX peuplés dans l'état (ou les états) électroniques supérieur, nous avons calculé les limites inférieures des énergies de dissociation à l'état fondamental D_0^0 (MX) (en kcal/mol):

	Br	Cl	F
Ca	97.4±1.5	115.0±1.5	128.4±2
Sr	93.5±2	123.9±3	127.3±1.5
Ba	104.6±2	119.7±1.5	141.4±5

Des données sur les distributions de l'état vibrationnel du MX* excité sont traitées d'un point de vue qualitatif. Ainsi les fluorures sont formés avec des distributions vibrationnelles renversées, faisant clairement preuve de la nature directe de l'interaction dynamique. Pourtant, les chlorures et les bromures, excités électroniquement, ont tendance à se former avec des distributions quasi-statistiques diminuant régulièrement. Ceci est conforme à la formation de complexes à collision, de longue vie. Des raisons pour ces tendances sont traitées en fonction d'énergitique du procédé de désintégration.

[Traduit par le journal]

Can. J. Chem. Downloaded from www.nrcresearchpress.com by 210.87.254.6 on 09/05/12
For personal use only.

Can. J. Chem. Downloaded from www.nrcresearchpress.com by 210.87.254.6 on 09/05/12
For personal use only.

Introduction

The determination of dissociation energies D^0 for simple diatomic molecules is frequently fraught with difficulties, as can be seen from the wide discrepancies in some literature data. The alkaline earth halides form no exception: some values differ by as much as 50 kcal, and the experimental data for CaCl, CaBr, SrCl, SrBr, and BaBr are so inadequate, that Gaydon (1 and references therein), refrains from recommending D_0^0-values. The study of chemiluminescence spectra offers a relatively little explored (2–5) pathway for obtaining lower limit estimates of D_0^0, and we report here a systematic study of dissociation energies for 9 alkaline earth halides.

The reactions of the Group II*a* metal atoms Ca, Sr, Ba with dihalogen molecules F_2, Cl_2, Br_2 are sufficiently exothermic for a fraction of the metal halide products to be formed in electronically excited states (2). We have recorded the ensuing electronic chemiluminescence spectra (CL) for the matrix of 9 reactions (M = Ca, Sr, Ba; X = F, Cl, Br). From an analysis of the CL spectra, the highest populated vibrational level of the emitter was determined by direct level count, or else if vibrational structure was not resolved up to the highest level indirectly by calculating v_{max} from the envelope of a vibrational sequence. Lower bounds of the metal monohalide dissociation energies $D_0^0(MX)$ were then deduced from energy conservation:

$$[1] \qquad E + W + \Delta D_0^0 = E' + W'$$

where ΔD_0^0 is the difference in energies of the newly formed MX bond and the old X_2 bond, E and W are translational and internal energies of reactants. The primed quantities refer to products. Neglecting product translation (and rotation),[1] eq. 1 reduces to the inequality

$$[2] \qquad D_0^0(MX) \geqslant \varepsilon_{el}' + \varepsilon'(v') + D_0^0(X_2) - (E + W)$$

which becomes an equality only in the limit where all the available energy is found as electronic–vibrational excitation in a detectable fraction of the products, and where v' is replaced by v_{max}', the highest vibrational level populated. Whether this condition is actually fulfilled in our particular reactions, *i.e.* whether the energy partitioning favors the accumulation of essentially all the available energy in internal excitation of a detectable fraction of products, depends solely on the (*a priori* unknown) reaction dynamics.

Information on partitioning of product energy

$$[3] \qquad W' = \varepsilon_{el}' + \varepsilon'(v') + \varepsilon'(J')$$

can in principle be obtained from an analysis of the CL spectra. From a qualitative point of view we discuss this in the last section but a quantitative analysis is in progress, and results will be published elsewhere. The determination of dissociation energies is presented in the Results section and these are discussed in the Discussion section.

[1]For the present purposes, rotational energy is assumed to be negligible compared to vibration.

Experimental

The experimental arrangement (4) consists of a 1 in. diameter quartz tube inside a resistance heated oven, which is evacuated by an oil-diffusion pump. On the upstream end of the oven halogen gas was admitted through a needle valve while a pea size lump of alkaline earth (Ca, Sr, Ba; Alpha Inorganics, purity better than 99.0%) metal was evaporated at ~1000 °K. The resulting flame was viewed through an upstream quartz window by a Spex 3/4 m Monochromator (grating 1200 grooves/mm, blazed at 5000 Å). Detection was by a cooled (−40 °C) Photomultiplier (EMI 9558B (S20 response) for spectra extending into the i.r., particularly Sr and Ca halides, EMI 6256A (S13 response) for Ba halides), followed by an electrometer–stripchart recorder combination. The spectral slitwidth in all experiments was 0.2–1 Å, as noted in the figure captions. The oven temperature, which was monitored by an Iron Constantan thermocouple located between the heating coils and the quartz-tube, could be kept constant within ± 5° over a period of 30 min without special regulation. Typical oven temperatures, ranging from 920–1030 °K, were chosen to give a reasonably intense flame without raising the metal vapor pressure beyond practicable limits. The pressure was monitored by a capacitance manometer immediately downstream of the oven. Base pressures were less than 2 mTorr, and reagent gas pressures were less than 1 mTorr. At these pressures vibrational and electronic quenching of MX* are negligible (see below), while there is a certain degree (6) of quenching of continuous emission ascribed to dihalides MX_2*. Although the equilibrium vapor pressure of metal (7) at these temperatures lies in the 10–50 mTorr range, under flow conditions the steady state vapor pressure is appreciably lower, particularly as a salt film on the surface of the metal curtails the evaporation rate. This is also the reason why the flame intensity decreases slowly, limiting the running time to ~90 min.

Results

All nine reactions gave clearly visible chemiluminescence. The total light intensity increases

Can. J. Chem. Downloaded from www.nrcresearchpress.com by 210.87.254.6 on 09/05/12
For personal use only.

in the sequence Br ≃ Cl → F and Ca ≃ Sr → Ba, paralleling the trend of the total reaction cross sections as predicted by the harpooning model. MX* emission bands from one or more of the first electronically excited states (A, B, C, D depending on the system) are superimposed on a broad and more or less intense quasi-continuum (2, 32), which has been ascribed to MX_2* formed in two body radiative recombination (2) and which spans the entire visible region. The fluorine reactions differ from the rest in that Ca/F_2 and Sr/F_2 show only weak MF_2* continuum emission, while in Ba/F_2 it is weak in the blue and green part of the spectrum but a strong continuum appears in the 5000–8000 Å region.

We describe here only the clearly identifiable alkaline earth monohalide bands. Sections of the spectra which are relevant here are reproduced in Figs. 1 through 8. The full spectra, in particular the continua ascribed (2) to electronically excited dihalides MX_2* will be discussed elsewhere. The qualitative features of the spectra from the first few excited states (A, B, C) of alkaline earth halides are as follows: The strongly ionic ground state MX ($X^2\Sigma^+$) molecules have an unpaired nonbonding electron belonging to the metal atom. Its excitation is responsible for the lowest electronic states. Due to the essentially nonbonding nature of the electron, the bond parameters (ω_e, $\omega_e x_e$, r_e) change only little in these transitions, a fact that strongly favors vibrational overlap in $v' = v''$ transitions. The prominent features of all MX spectra are therefore intense $\Delta v = 0$ sequences flanked by the much weaker $\Delta v = \pm 1$ sequences (except for the relatively high lying $C(^2\Pi)$ states in the Ca and Sr-halides). The A and C states are $^2\Pi$ whose 1/2 and 3/2 components are well separated by spin–orbit interaction (Hund's case *a*), while the B state is $^2\Sigma^+$ showing a small degree of spin-splitting (case *b*) (5). The highest vibrational levels v_{max}' were identified by direct count, and confirmed by comparison with calculated term values (8). In a number of cases, however, the sequences became dense (quasi-continuous) beyond the last clearly resolved vibrational band, as in the cases of CaCl(A), CaBr(A), SrCl(A), BaF(C), mainly due to a tightening of the sequences and the piling up of bands at a turning point (head of heads). In all these cases, the outline of the head of heads was clearly visible and the calculated quantum number of the turning point v_t' was chosen as a lower limit estimate of v_{max}'. The approximate nature of this procedure is obvious, as we were unable to ascertain how far the sequence folds back upon itself beyond the turning point.

The spectroscopic constants (T_e, ω_e, $\omega_e x_e$) are taken from Rosen (8) and the data relevant to the analysis are collected in Table 1. Reactant energies ($E + W$) were evaluated at 1000 °K by assuming equipartition for translation[2] and rotation, and by using harmonic oscillator partition functions for vibration. The halogen dissociation energies used are $D_0^0(Br_2) = 45.44$ kcal/mol (10), $D_0^0(Cl_2) = 57.08$ kcal/mol (10, 11) and $D_0^0(F_2) = 37.1$ kcal/mol (12). While the former two are highly accurate, there is still some discussion (1, 8, 12) about the F_2 value, and a readjustment of $D_0^0(F_2)$ would reflect itself in the D_0^0(MF) values.

Once v_{max}' was known either by direct count or by the method just described, $\varepsilon(v_{max}')$, the vibrational energy was evaluated from the ω_e', $\omega_e' x_e'$ data. Calculation of D_0^0(MX) using eq. 3 was straightforward, and the results are presented in Table 1.

A question of crucial importance in the present work is whether the MX* emitters are in their primary energy distribution, or whether the initial distribution has been relaxed by collisional energy transfer. To test this point, Ba/Cl_2 and Ca/Cl_2 spectra were recorded (6) with ~0.05 Torr He or N_2 added as quenching gases. The MX* spectra were identical to the ones obtained without buffer gas and we conclude that a degradation of the primary vibrational distribution did not take place even at these high pressures. This is corroborated by the recent (13) lifetime measurements of the barium halides using a pulsed dye laser. The radiative lifetimes of BaX (X = F, Cl, Br, I) are about 15 ns. This is *ca.* 2–3 orders of magnitude shorter than the time between successive gasphase collisions, assuming realistic energy transfer cross sections.

[2]The average energy of reaction is given (9) by

$$\int_0^\infty f(E,T)E^2\sigma(E)dE / \int_0^\infty f(E,T)E\sigma(E)dE$$

where $f(E,T)$ is the distribution function of relative kinetic energy and $\sigma(E)$ is the reaction cross section. Preliminary experiments with variable energy molecular beams have shown that $\sigma(E)$ varies sufficiently slowly with collision energy to justify taking $\sigma(E)$ outside the integral sign and replacing the expression by $\frac{1}{2}RT$. The thermal spread introduced by $(W + E)$ may contribute to population of the highest v' states. This is accounted for by the D_0^0-error limits.

Can. J. Chem. Downloaded from www.nrcresearchpress.com by 210.87.254.6 on 09/05/12
For personal use only.

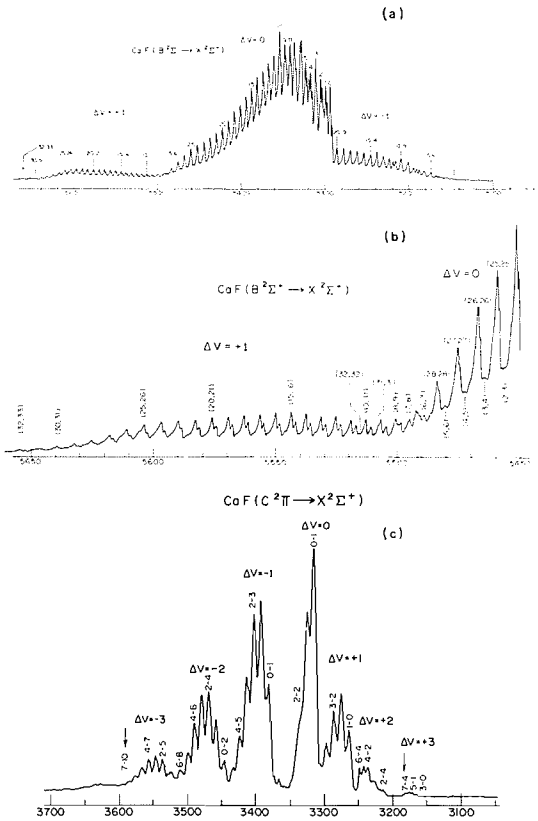

FIG. 1. (*a*) Tracing of CaF($B \rightarrow X$) system. Spectral slitwidth: 0.8 Å. (*b*) Detail of the CaF($B \rightarrow X$) $\Delta v = -1$ sequence. The spin splitting of the vibrational bands is clearly seen. The highest level identifiable in the $\Delta v = 0$ sequence is $v_{max}' = 32$. Spectral slitwidth: 0.25 Å. (*c*) The CaF($C \rightarrow X$) system. The bond parameters (ω_e', r_e') change substantially in the transition, thus the appreciable intensity of the $\Delta v = 0$ sequences. Spectral slitwidth: 1.5 Å.

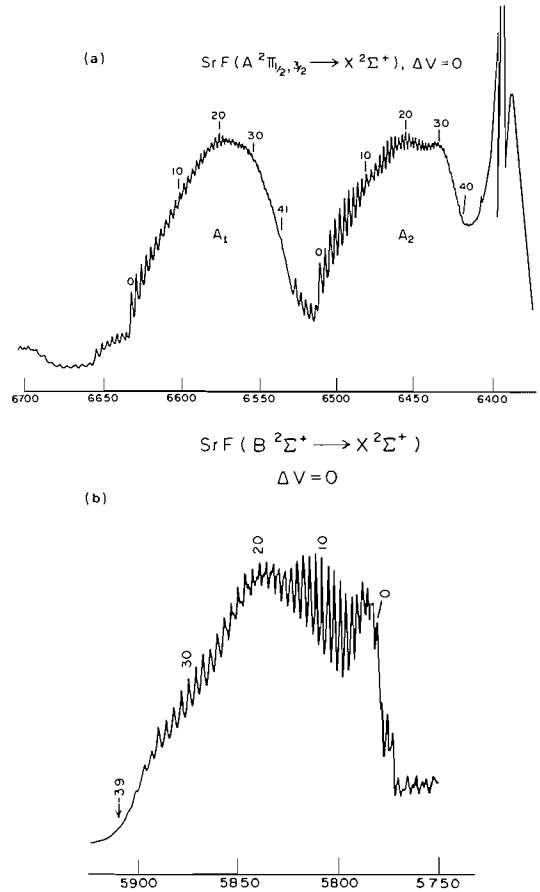

FIG. 2. (*a*) SrF($A \rightarrow X$) system, $\Delta v = 0$ sequence. Spectral slitwidth: 0.7 Å. (*b*) SrF($B \rightarrow X$) system, $\Delta v = 0$ sequence. Spectral slitwidth: 0.75 Å.

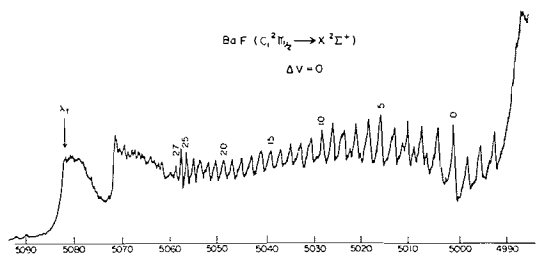

FIG. 3. BaF($C_1 \rightarrow X$) system. Spectral slitwidth: 0.2 Å.

CaF

Three distinct band systems were observed in this reaction: the relatively dense $A(^2\Pi) \rightarrow X$ in the 5800–6300 Å region, the distinctly banded $B(^2\Sigma) \rightarrow X$ between 5600–5800 Å and the strongly banded $C(^2\Pi) \rightarrow X$ at 3600–3800 Å. A weak continuum is found at the blue side of the CaF bands. The Ca resonance line at 4226.7 Å ($^1P_1$) is observed.

We have here the advantage of comparing two transitions with well resolved vibrational structure, allowing a double check of the D_0^0 value. The $\Delta v = 0$ sequence of the R branch ($J = K + 1/2$ component) of the $B(^2\Sigma^+)$–$X(^2\Sigma^+)$ system at 5291 Å is flanked by the much weaker $\Delta v = +1$, -1 sequences. Although there exists overlap between $\Delta v = 0, \pm 1$, the $v' = v'' = 32$ band is seen superimposed on the $\Delta v = -1$ sequence (Fig. 1*b*). The dissociation energy corresponding to $v_{max}' = 32$ is D_0^0(CaF) $\geqslant$ 129.1 kcal.

In the C → X system (3150–3650 Å), $\Delta v \neq 0$ transitions are quite prominent besides $\Delta v = 0$ and the sequences overlap somewhat (Fig. 1*c*)

Can. J. Chem. Downloaded from www.nrcresearchpress.com by 210.87.254.6 on 09/05/12
For personal use only.

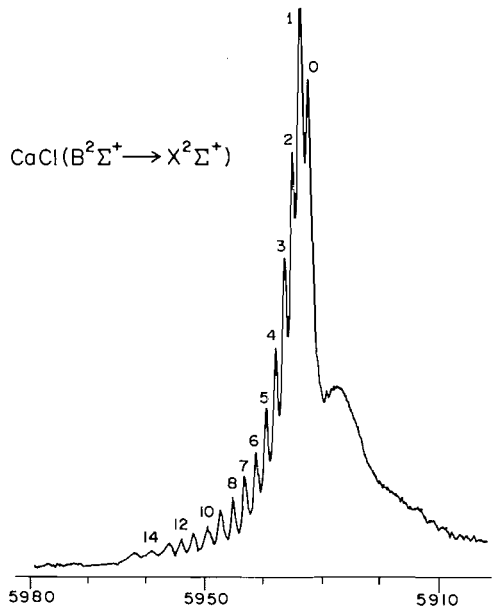

FIG. 4. CaCl($B \rightarrow X$) system. Spectral slitwidth: 0.2 Å.

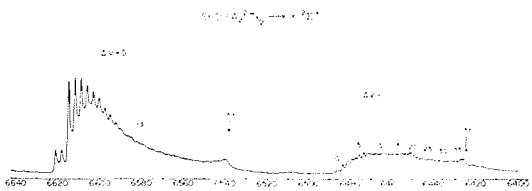

FIG. 5. SrCl($A \rightarrow X$) system. Spectral slitwidth: 0.2 Å.

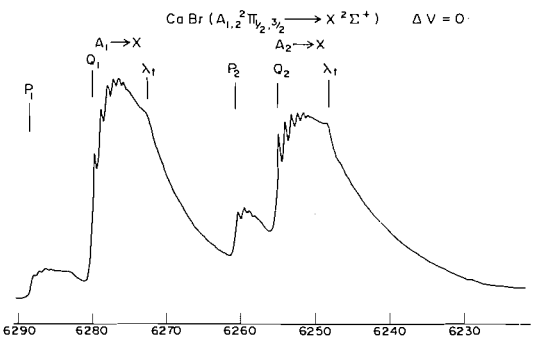

FIG. 6. CaBr($A \rightarrow X$) system. Spectral slitwidth: 0.4 Å.

making identification of v_{max}' difficult. The highest level discernible is the $(7 \rightarrow 4)$ band of the $\Delta v = +3$ sequence. With $v_{max}' = 7$ we obtain $D_0^0 \geqslant 127.6$ kcal.

The two values derived above differ by one

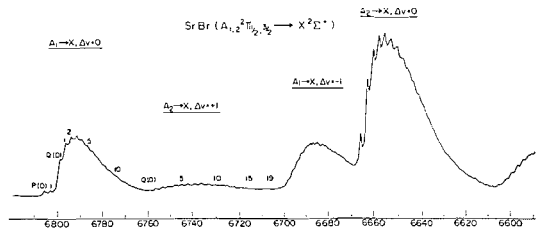

FIG. 7. SrBr($A \rightarrow X$) system. Spectral slitwidth: 0.35 Å.

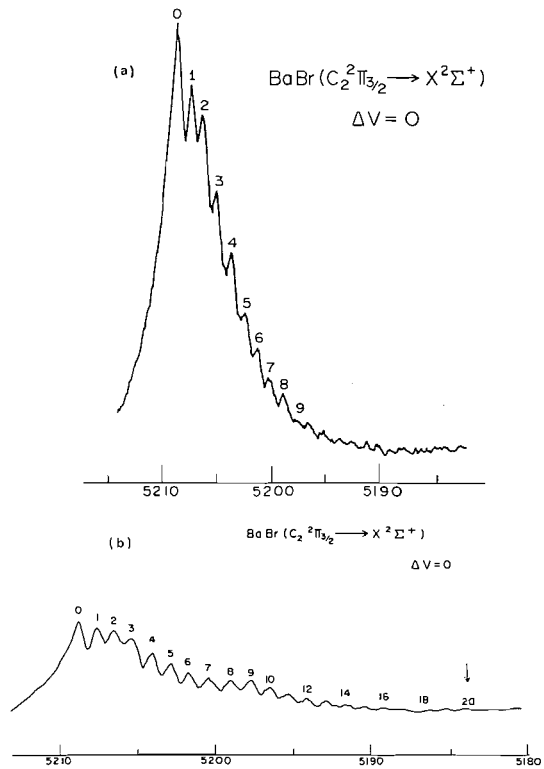

FIG. 8. (*a*) BaBr($C_2 \rightarrow X$), $\Delta v = 0$ sequence. Spectral slitwidth: 0.6 Å. This low intensity spectrum gives the general shape of the distribution. (*b*) BaBr($C \rightarrow X$), $\Delta v = 0$. Higher v' are resolved in this tracing.

vibrational quantum, and we recommend their mean value D_0^0(CaF) $\geqslant 128.4 \pm 2$ kcal.

SrF

Similar to CaF, the $A(^2\Pi)$, $B(^2\Sigma^+)$, $C(^2\Pi)$ states are populated here, giving rise to banded emission in the ranges 6300–6900 Å, 5600–5950 Å, and 3600–3800 Å, respectively. We also observe a very weak continuum and the Sr resonance lines at 4607 Å ($^1P_1$), and 6892 Å ($^3P_1$).

The $(A_1, A_2 \rightarrow X)$, $\Delta v = 0$ sequences (Fig. 2*a*) show resolved vibrational structure up to $v' = 41$

TABLE 1

(*a*) Analysis of observed MF* bands

Molecule	State populated	Intensity	v_{max}'	$\varepsilon'(v_{max}')$	$E + W$	D_0^0	Comment
CaF	$C^2\Pi$	Weak	7	10.0	6.0	127.6	Continuum very weak
	$B^2\Sigma^+$	Medium	32	44.1		129.1	
	$A_2{}^2\Pi_{3/2}$	Strong					
	$A_1{}^2\Pi_{1/2}$	Strong					
	$X^2\Sigma^+$						
SrF	$C^2\Pi$	Medium	13	16.4	6.0	127.1	Continuum very weak
	$B^2\Sigma^+$	Medium	39	46.9		127.44	
	$A_2{}^2\Pi_{3/2}$	Strong	40	47.8		122.76	
	$A_1{}^2\Pi_{1/2}$	Strong	41	48.7		122.86	
	$X^2\Sigma^+$						
BaF	$D'^2\Sigma^+$	Very weak			6.0		Strong BaF_2* continuum at 6000–7500 Å
	$D^2\Sigma^+$	Very weak					
	$C_2{}^2\Pi_{3/2}$	Strong					
	$C_1{}^2\Pi_{1/2}$	Strong	48 ± 5	53.2 ± 4.2		141.4 ± 5	
	$X^2\Sigma^+$						

(*b*) Analysis of observed MCl* bands

Molecule	State populated	Intensity	v_{max}'	$\varepsilon'(v_{max}')$	$E + W$	D_0^0	Comment
CaCl	$B^2\Sigma^+$	Medium	16	16.3	6.3	115.22	Medium continuum
	$A_2{}^2\Pi_{3/2}$	Strong	>6	6.78		103.74	
	$A_1{}^2\Pi_{1/2}$	Strong					
	$X^2\Sigma^+$						
SrCl	$C^2\Pi$	Weak					Strong continuum
	$B^2\Sigma^+$	Strong					
	$A_2{}^2\Pi_{3/2}$	Strong	38 ± 2	29.9	6.3	123.4	
	$A_1{}^2\Pi_{1/2}$	Strong					
	$X^2\Sigma^+$						
BaCl	$C_2{}^2\Pi_{3/2}$	Strong	17	13.6	6.3	119.95	Strong continuum
	$C_1{}^2\Pi_{1/2}$	Strong					
	$X_1{}^2\Sigma^+$						

(*c*) Analysis of observed MBr* bands

Molecule	State populated	Intensity	v_{max}'	$\varepsilon'(v_{max}')$	$E + W$	D_0^0	Comment
CaBr	$B^2\Sigma^+$	Medium			6.6		Strong continuum
	$A_2{}^2\Pi_{3/2}$	Strong	16	12.9		97.4	
	$A_1{}^2\Pi_{1/2}$	Strong	16	12.9			
	$X^2\Sigma^+$						
SrBr	$B^2\Sigma^+$	Strong			6.6		Strong continuum
	$A_2{}^2\Pi_{3/2}$	Strong	19	11.8		93.5	
	$A_1{}^2\Pi_{1/2}$	Strong					
	$X^2\Sigma^+$						
BaBr	$C_2{}^2\Pi_{3/2}$	Strong	20		6.6	104.6	Strong continuum
	$C_1{}^2\Pi_{1/2}$	Strong		10.9			
	$X^2\Sigma^+$						

Can. J. Chem. Downloaded from www.nrcresearchpress.com by 210.87.254.6 on 09/05/12
For personal use only.

Can. J. Chem. Downloaded from www.nrcresearchpress.com by 210.87.254.6 on 09/05/12
For personal use only.

and 40 for A_1 and A_2, respectively. The corresponding dissociation energies are $D_0^0(\mathrm{SrCl}) \geqslant 122.8$ and 122.9 kcal, respectively.

The $B(^2\Sigma) \rightarrow X$, $R_{K-1/2}$, $\Delta v = 0$ sequence is well resolved, giving a $v_{max}' = 39$ by direct level count (Fig. 2*a*). The resulting dissociation energy is $D_0^0(\mathrm{SrF}) = 127.4 \pm 1.5$ kcal/mol.

In the $C(^2\Pi) \rightarrow X$ band (14), the most prominent sequences are $\Delta v = 0, +1$ with $v' = 14$ as the highest level. The corresponding dissociation energy becomes $D_0^0(\mathrm{SrF}) = 127.1 \pm 1.5$ kcal/mol, in almost exact agreement with the value obtained from the B-state (Fig. 2*b*).

The average $D_0^0(\mathrm{SrF}) \geqslant 127.3 \pm 1.5$ kcal/mol of these latter values is recommended over that derived from the A state. The reason for this apparent underpopulation of the $A_{1,2}$ states may be dynamical in nature, or may be simply due to our inability to resolve states of higher than $v' = 40$ and 41 in A_2 and A_1.

BaF

The strongest BaF emission is due to the banded $C(^2\Pi) \rightarrow X(^2\Sigma)$ system at 4850–4130 Å, while there exists a series of weak overlapping sequences in the 3600–4000 Å region, due to the $D(^2\Sigma^+) \rightarrow X(^2\Sigma^+)$ transitions. No evidence could be found for *A* and *B* state emission (expected in the 7860–8740 Å and 6720–7730 Å regions, respectively (8)) although the EMI 9558 Photomultiplier response extends beyond 8500 Å. A weak continuum, possibly due to BaF_2*, extends from 3200–6000 Å, while intense continuum emission occurs over the 6000–8000 Å region. A distinguishing feature of the BaF spectrum is its extreme richness in atomic lines from highly excited Ba (compared to the much sparser Ba excitation in the Ba/Cl_2 system (6)).

The $\Delta v = 0$ sequences of both fine structure components $C_1(^2\Pi_{1/2})$ and $C_2(^2\Pi_{3/2})$ form heads of heads, but the former (Fig. 3*a*) is spread out wider and better suited than the latter and we base our analysis on it. Vibrational levels up to $v' = 28$ are well resolved, but the spectrum becomes noisy and dense thereafter, and bands pile up towards two successive heads of heads (turning points), one at 5072 Å and the second one at 5083 Å. The former belongs to the $\Delta v = +1$ sequence of the $C_2(^2\Pi_{3/2}) \rightarrow X$ fine structure component, and the latter to the $C_1(^2\Pi_{1/2}) \rightarrow X$, $\Delta v = 0$ sequence. Formation of the sharp turning points demonstrates that vibrational levels are populated, at least up to the turning point with $v_{max}' > v_t'$ and that $v' = 28$ is not to be identified with v_{max}. The positions of the turning points were calculated from published spectroscopic data (5, 8, 13, 15, 16), and the computed values agree approximately with observation. The wavelengths of the turning points and the vibrational quantum numbers (in brackets) are: Jenkins and Harvey (15): 5086.98 Å (51); Rosen (8): 5088.7 Å (53); Kushawaha *et al.* (16): 5049.9 Å (24), and Cruse *et al.* (13): 5068.7 Å (43). The observed turning point lies between Rosen's and Cruse's values, and we chose the average $v_t' > 48 \pm 5$ for the turning point quantum number.

Setting $v_{max}' \sim v_t'$ is a conservative estimate, since it is very likely that the sequence folds back upon itself beyond v_t'. The corresponding dissociation energy is $D_0^0(\mathrm{BaF}) \geqslant 141.4 \pm 5$ kcal/mol.

CaCl

The prominent features are the $A(^2\Pi) \rightarrow X$ and $B(^2\Sigma^+) \rightarrow X$ systems superimposed on a strong $CaCl_2$* continuum extending from ~3100 Å into the red. Also observed are the 4227 Å ($^1P_1$) and 6537 Å ($^3P_1$) Ca resonance lines. The $B \rightarrow X$ system is reproduced in Fig. 4. Vibrational structure in the $A_1, A_2 \rightarrow X$ systems is only partially resolved due to the convergence of bands towards turning points (heads of heads) with $v_t' = 11$ (17). Since the corresponding D_0^0 is much smaller than that obtainable from the $B \rightarrow X$ system, we base our analysis on the latter.

In the $B \rightarrow X$, $\Delta v = 0$ sequence, the P-branch is head forming and vibrational structure is clearly resolved. Direct count gives $v_{max}' = 16$, and $D_0^0(\mathrm{CaCl}) \geqslant 115.0 \pm 1.5$ kcal/mol.

SrCl

Emission from the $A(^2\Pi)$ states is superimposed on a broad $SrCl_2$ continuum together with the Sr resonance lines at 4607 Å (^1P) and 6893 Å ($^3P_1$). Figure 5 shows the $A \rightarrow X$ band. The $B \rightarrow X$ system was not used for the present analysis because the sequences are much "tighter" due to small $\Delta\omega_e$, $\Delta\omega_e x_e$, and the formation of turning points. The $A \rightarrow X$ main sequences show clear vibrational structure in the P and Q branches, up to $v' = 11$ and 13 for A_1 and A_2, respectively. Thereafter the sequences become dense and decay into long, exponentially decreasing tails. It is obvious that higher vibrational levels than 11 and 13 are populated and the occurrence of turning points (heads of heads) in the $A_2 \rightarrow X$ sequences allows a better estimate of v_{max}: the $\Delta v = 0$ sequence has a turning point at $\lambda_t = 6538$ Å. The

Can. J. Chem. Downloaded from www.nrcresearchpress.com by 210.87.254.6 on 09/05/12
For personal use only.

turning points calculated from literature data (8, 17–19) lie at considerably shorter wavelengths. This is not surprising, since the data were evaluated from lower vibrational levels, and extrapolation to higher v' is bound to lead to errors. As a conservative compromise for $v_{max}' \geqslant v_t'$ we use the quantum number corresponding to the experimental λ_t, as calculated from Harrington's, Singh's and Novikov's data. The average of these values is $v_t = 35 \pm 3$.

The $A_2 \rightarrow X$ ($\Delta v = -1$) sequence exhibits vibrational structure up till $v' \sim 38$ as well as a turning point, $\lambda_t = 6425$ Å. Again, the calculated turning points (8, 17–19) deviate from the observed one, although less than in the main sequence. Singh's (19) and Rosen's (8) data yield the lowest quantum numbers $v'(\lambda_t) = 40$ and 35. Again, we adopt the average, $v_{max} > v_t > v(\lambda_t) = 38 \pm 2$ as a conservative estimate of v_{max}, and in good agreement with the direct count. The corresponding dissociation energy is $D_0^0(\text{SrCl}) \geqslant 123.9 \pm 3$ kcal/mol.

The faintly visible $C(^2\Pi) \rightarrow X$ system in the 3800–4100 Å region consists of a series of overlapping sequences without resolved structure. Determination of v_{max}' if difficult here, but even if $v_{max}' = 0$, the resulting dissociation energy would be $D_0^0(\text{SrCl}) \geqslant 123.4$ kcal, in good agreement with the above value. This is considerably higher than previous values by Hildenbrand (20) $D_0^0 = 95.9$ kcal/mol, Jonah and Zare (2) $D_0^0 \geqslant 99$ kcal/mol, Krasov and Karaseva (21) $D_0^0 = 108 \pm 10$ kcal/mol, Ryabova and Gurvich (22) $D_0^0 = 95.1 \pm 5.7$ kcal/mol. In particular, it is surprising that D_0^0(SrCl) exceeds the value for BaCl, contrary to the expected homologous order. Whether this is due to specific bonding effects or to the lower limit nature of the D_0^0 values, remains to be seen.

BaCl

This molecule has been studied previously (2, 4) but for completeness' sake we repeat the relevant information. The spectrum is dominated by the two C_1, $C_2 \rightarrow X$ sequences $\Delta v = 0$. The $C_2 \rightarrow X$ band at 5140 Å is clearly resolved and is reproduced in Fig. 1 of ref. 4. The highest vibrational level is $v_{max}' = 17$ by direct count. The dissociation energy becomes $D_0^0(\text{BaCl}) \geqslant 119.7 \pm 1.5$ kcal/mol.[3]

[3]In the previous analysis (4) we reported $D_0^0(\text{BaCl}) = 121$ kcal/mol. The difference stems from the previous neglect of the vibrational energy in W.

CaBr

Emission from the $A_1(^2\Pi_{1/2})$, $A_2(^2\Pi_{3/2})$, and $B(^2\Sigma^+)$ states is superimposed on a broad structureless $CaBr_2$*-continuum, apart from the 4227 Å ($^1P_1$) Ca resonance line. The $B \rightarrow X$ system is too dense for a meaningful analysis. The main sequences of the $A \rightarrow X$ system are reproduced in Fig. 6.

The lowest levels are clearly resolved in P and Q branches of both fine structure components. Heads of heads (turning points) are apparent in both Q_1 and Q_2 branches at $\lambda_t(Q_1) = 6272$ Å and $\lambda_t(Q_2) = 6248$ Å. These are in excellent agreement with Harrington's data (17), yielding $v_{max}' \geqslant v_t' = 16$ for both components. The dissociation energy corresponding to the A_2 state is $D_0^0(\text{CaBr}) \geqslant 97.4 \pm 1.5$ kcal/mol.

SrBr

We observe the $A_{1,2}(^2\Pi_{1/2,3/2}) \rightarrow X(^2\Sigma^+)$ and $B(^2\Sigma^+) \rightarrow X(^2\Sigma^+)$ band systems superimposed on an intense continuum that spans the entire visible region, as well as the Sr resonance lines 4607 Å (^1P) and 6892 Å ($^3P_1$). Part of the $A \rightarrow X$ system is reproduced in Fig. 7.

In both the $B \rightarrow X$ and $A_{1,2} \rightarrow X$ main sequences, vibrational structure is resolved up to a certain point ($v' = 15$, 13, 10 in the above order) beyond which bands merge into a long, exponentially decreasing, structureless tail. The $\Delta v = +1$ sequence of the $A_2 \rightarrow X$ system, however, is clearly resolved up to $v_{max}' = 19$. With this value, we obtain $D_0^0(\text{SrBr}) \geqslant 93.5 \pm 2$ kcal/mol.

BaBr

Only the $C_{1,2}(^2\Pi_{1/2,3/2}) \rightarrow X$ system and the Ba resonance lines at 5535 Å ($^1P_1$) and 7906 Å ($^3P_1$) appear relatively weakly on the very prominent $BaBr_2$* continuum which spans the entire visible region (~3200–~7000 Å).

A part of the $C \rightarrow X$ system is presented in Fig. 8. The $C_2 \rightarrow X$, $\Delta v = 0$ sequence is clearly resolved, while the $C_1 \rightarrow X$, $\Delta v = 0$ sequence is much tighter. This difference arises, as in the other MX ($^2\Pi \rightarrow {}^2\Sigma$) transitions, from the vibrational dependence of the spin–orbit coupling constant A_v and the difference between effective B_v values in the two fine structure components.

The highest resolved level in the C_2 system is $v_{max}' = 20$ and the corresponding dissociation energy $D_0^0(\text{BaBr}) \geqslant 104.6 \pm 2$ kcal/mol.

Discussion

The ground state dissociation energies for alkaline earth halides have been determined by various

TABLE 2. Comparison of D_0 (MX) data (in kcal/mol)

	This work	Ionic bonding	Mass spectra	Flame equilibria	LBS	
					Corrected	Uncorrected
CaF	128.4±2	125±2[b]	126.4±1.6[c]	135±7[d]	125[c]	89.9[a]
SrF	127.3±1.5	127[c]	129.5±1.6[c]	132±7[d]	124[c]	73.8[a]
BaF	141.4±5	137[c]	140.3±1.6[c]	145±6[d]	157[c]	87.6[a]
						87±17[g]
CaCl	115.0±1.5	105±10[a]	95.7±3[h]		95[f]	69±14[g]
		94[e]	94.2±3[f]			63.6[a]
SrCl	123.9±3	108±10[e]	95.9±3[f]	100±10[d]	96.7[f]	64.5[a]
BaCl	119.7±1.5	110±10[e]	105±3[f]	117.6±5[d]	102.6[f]	73.8[a]
			104.2±3[h]			62±12[g]
CaBr	97.4±1.5	90±15[a]				66±13[g]
SrBr	93.5±2	90±15[e]				64.5[a]
BaBr	104.6±2	100±15[ae]				64.5±13[g]

[a]Reference 1.
[b]Reference 34.
[c]Reference 24.
[d]Reference 22.
[e]Reference 21.
[f]Reference 20.
[g]Reference 23.
[h]Reference 26.

methods over the past 40 years. A representative compilation of the most important determinations is given in Table 2. More data can be found in refs. 1, 8, 23 and references listed therein. For the fluorides and chlorides there exist a sizeable body of data, while published work on bromides is scant and of doubtful accuracy.

The earliest determinations were spectroscopic in nature, based on predissociation data and on linear Birge–Sponer extrapolations (LBS) of band head data. Gaydon (1) summarized these attempts by pointing out that LBS strongly underestimate the true values in the predominantly ionic MX molecules. Nonlinear polynomial extrapolations of the Birge–Sponer variety also give higher and more realistic values (14, 25, 26). Hildenbrand (20, 24) has shown that an ionicity correction applied to the LBS for the fluorides (24) and chlorides (20) brings the thus corrected values (Table 2 Column 5) into remarkable agreement with the more trustworthy mass spectrometric determinations (Table 2 Column 3). The latter (1, 8, 20, 24, 26) rely on the rapid establishment of chemical and thermal equilibrium in a Knudsen effusion cell, a condition that should not be taken for granted. A further avenue to D_0^0(MX) is the study of flame equilibria (1, 22, 23) (Table 2 Column 4). Departure from equilibrium as well as presence of interfering species in the flame may give rise to considerable errors.

The dissociation energies recommended by Gaydon (1) and Rosen (8) are invariably based on either or both of these two equilibrium methods. The mass spectrometric and flame photometric values usually agree reasonably well with each other, although the latter are generally somewhat higher. In the case of the fluorides, the agreement of the present data $D_0^0(\text{CaF}) \geqslant 128.4 \pm 2$ kcal/mol, $D_0^0(\text{SrF}) \geqslant 127.3 \pm 1.5$ kcal/mol and $D_0^0(\text{BaF}) \geqslant 141.4 \pm 5$ kcal with Gaydon's (1), Rosen's (8) and Hildenbrand's (14, 15) recommended values is surprisingly good.

For the chlorides, the situation is already less homogenous: Rosen's values are all based on mass spectrometric studies, while Gaydon recommends only a value for BaCl, which is presumably heavily weighted by Ryabova and Gurvich's (22) flame study. The agreement with our (4, 26) $D_0^0(\text{BaCl}) \geqslant 119.7 \pm 1.5$ kcal is gratifying. For both CaCl and SrCl, however, our dissociation energies $D_0^0(\text{CaCl}) \geqslant 115.0 \pm 1.5$ kcal/mol and $D_0^0(\text{SrCl}) \geqslant 123.9 \pm 3$ kcal/mol lie considerably above Rosen's (8) values, and for that matter above any literature values reported previously. In the CaCl system there is little doubt about the validity of the present value since v_{max} was determined by direct level count. We recommend it over the previous values. Somewhat surprising is the high value for SrCl, which exceeds both CaCl and BaCl, although for a homologous series of molecules, D_0^0 is expected (21, 27) to increase in the order Ca < Sr < Ba. We have therefore re-

Can. J. Chem. Downloaded from www.nrcresearchpress.com by 210.87.254.6 on 09/05/12
For personal use only.

Can. J. Chem. Downloaded from www.nrcresearchpress.com by 210.87.254.6 on 09/05/12
For personal use only.

peated the experiments several times under different conditions to ascertain whether the C state could be populated by a transfer process (*e.g.* $SrCl_2^* + SrCl \rightarrow SrCl^*(C') + SrCl_2$). Even at the lowest oven temperatures (*i.e.* Sr-pressures) and Cl_2 pressures, the $C \rightarrow X$ system could be observed with the same relative intensity as in the standard runs. From this we conclude that $SrCl(C^2\Pi)$ is indeed formed in a bimolecular primary process, and that the suggested $D_0^0(SrCl) \geqslant 123.9 \pm 3$ kcal/mol is correct.

The literature on the bromide dissociation energies is scant: we are aware of only two sets of data: (*a*) linear Birge–Sponer extrapolations (23) which are known to strongly underestimate the D_0^0 of ionic molecules, and (*b*) theoretical estimates (21) based on the Rittner electrostatic model. With an appropriate choice of metal ion polarizabilities, this method works very well for the fluorides, but less so for chlorides and bromides. This is to be expected since covalent contributions may make the electrostatic model decreasingly applicable in the order F → Cl → Br and Ba → Sr → Ca. The predictions for the bromides (Table 2 Column 2) must therefore be taken with caution. Our values lie well within the wide error limits of the model calculations, in all cases close to the upper limit. Their order Sr < Ca < Ba is somewhat surprising, particularly since here the apparent anomaly of SrBr is opposite that in the chlorides.

An examination of the entire 3 × 3 matrix of D_0^0 values reveals the trends and irregularities: For each metal M, the dissociation energy increases as expected with increasing electronegativity of the halogen (Br < Cl < F), and the increase in bond energy varies between 30 and 37 kcal in these sequences. The vertical sequences (same halogen, varying metal) show a less pronounced, and more erratic trend: Binding energies increase by 5–13 kcal only in going from CaX → BaX, and the strontium halides, in all cases, interrupt the expected (27) monotonic increase of D_0^0 with decreasing metal ionization potential. Sr possesses a d^{10} shell, and the well known decreased shielding of d-orbitals may be partly responsible for the observed trends.[4] The fact, however, that SrBr < CaBr and SrF < CaF while SrCl > SrF shows that the effect of the electronic structure of M is quite subtle, and not well understood.

A further point of caution is the fact that our D^0 values are lower limit estimates only, depending on how closely eq. 2 approaches an equality. This is the case when all the available energy is released as excitation of the product molecules in a detectable fraction of MX*. As will be discussed below in more detail, the chlorides and bromides show a tendency to form MX* via longlived statistically equilibrated collision complexes. This entails an (approximately) exponentially decreasing vibrational distribution which makes the higher quantum states more difficult to identify and suggests that our chloride and bromide values particularly may be appreciably below the true D_0^0.

Energy Partitioning in Products

The original goal of the present investigation was the study of energy partitioning between product states. A full report on this aspect will be published elsewhere, and we discuss here only preliminary conclusions and qualitative trends.

In a previous communication (4) concerned with the Ba/Cl_2 system we concluded that BaCl $(C^2\Pi)$ was formed vibrationally equilibrated, *i.e.* the vibrational distribution drops monotonically and near exponentially from $v' = 0$. This is indicative of reaction via a longlived collision complex. The curiously hermaphroditic aspect of that system lies in the fact that the electronic ground-state $BaCl(X)$, however, is formed via a direct mechanism. This demonstrates the dependence of the interaction dynamics on the shape and energetics of the relevant potential energy surfaces.

To interpret spectral intensities in terms of emitter state population in an unambiguous way, one first has to know (calculate) the transition probabilities (*i.e.* Franck–Condon Factors $q_{v'v''}$ and for precise work the rarely accessible electronic transition moment matrix element $\bar{R}_e^2$). Secondly, to account for the overlapping of bands and particularly for the piling up towards heads of heads (or merely the tightening or loosening of sequences), a spectral simulation is necessary. For qualitative purposes, however, it suffices to realize that we can obtain a measure of the population $N(v')$, (without actually calculating FCF's) by summing the intensities of bands originating from v' over all final states v'': $N(v') \sim \sum I(v',v'')$.

[4]See for instance the oscillatory trends in ionization potentials of group IIIA atoms, which is customarily explained (27) by similar shielding effects.

Can. J. Chem. Downloaded from www.nrcresearchpress.com by 210.87.254.6 on 09/05/12
For personal use only.

In the majority of molecules considered here, the Franck–Condon parabolas are very narrow (except for the cases noted above) particularly for not too high v', and only one term ($v'' = v'$) needs to be considered in the summation. In this simplest approximation, the population is taken proportional to the area under a vibrational band in most intense $\Delta v = 0$ sequence.

The overlapping of bands poses a more serious problem, particularly where the sequences converge towards a turning point. A computer program for the synthesis of electronic spectra has been written by A. E. Redpath (to whom the author expresses his thanks). For a few systems, the synthesized spectra agree fairly well with experiments, while for the majority only preliminary and qualitative results are available at the time of writing. In the absence of reliable spectroscopic constants (particularly rotational constants) the iterative improvement of synthesized spectra becomes very time consuming. For this reason we discuss here only qualitative conclusions, while quantitative results will be published as they become available.

The *CaF*($B \rightarrow X$), $\Delta v = 0$, *SrF*($B \rightarrow X$), $\Delta v = 0$, *and BaF*($C \rightarrow X$), $\Delta v = 0$, sequences (Figs. 1*a*, 2*b*, 3) show strongly non-exponential envelopes. The calculations indicate non-Boltzmann vibrational distributions that are, however, not as strongly inverted as the band envelopes would suggest. The population inversions are quite clear, however, indicating a strong contribution from a direct interaction mechanism, and a lifetime of the collision complexes that is short on the time scale of intramolecular relaxation.

For *CaCl*($A \rightarrow X$), $\Delta v = 0$, the occurrence of and convergence towards turning points aggravate the interpretation, but if one takes the piling up of bands into account, a monotonically decreasing energy distribution is obtained, and a Boltzmann distribution is highly likely. In the *CaCl*($B \rightarrow X$), $\Delta v = 0$ system (Fig. 4), the exponential nature of the energy distributions is apparent from the band envelope (except for the apparent inversion of $v' = 0,1$). The *SrCl*($A \rightarrow X$) sequences (Fig. 5), and *eo ipso* the $N(v')$ show near exponential fall off, unaffected by the turning point in the $A_2 \rightarrow X$ subband. The $B \rightarrow X$ and $C \rightarrow X$ systems are too little resolved for reaching a conclusion. The statistical (exponential) nature of the *BaCl*(*C*) distribution has been the subject of a previous communication (4),[4] and recent computer results indicate that it can be characterized by a single vibrational temperature $T_v \sim 2000 \pm 100$ °K.

The *CaBr*($A \rightarrow X$) system (Fig. 6) shows a tightening of the sequences and convergence towards a head of heads (λ_t), which partly accounts for the non-exponential appearance of the bands. Preliminary computer simulations with estimated rotational constants strongly suggest an exponential $N(v')$ distribution. The same holds for the *SrBr*($A,B \rightarrow X$) sequences (Fig. 7). For the *BaBr*($C \rightarrow X$), $\Delta v = 0$, sequence a near statistical distribution is immediately apparent (Fig. 8), and the spectral simulation using reasonable, estimated rotational constants gives a vibrational temperature of $T_v \simeq 1100 \pm 100$ °K.

We conclude that the fluorides (CaF(*B*), SrF(*B*), BaF(*C*)) are formed with non-equilibrated, inverted $N(v')$ distributions, while the chlorides (CaCl(*A*,*B*), SrCl(*A*), BaCl(*C*)) and bromides (CaBr(*A*), SrBr(*A*), BaBr(*C*)), are formed vibrationally equilibrated. Molecular beam scattering experiments (28–30) in the M + (Cl_2, Br_2) systems have shown strongly asymmetric angular distributions for MX (forward scattering), indicating essentially direct interaction dynamics. Since most of the MX are formed in their electronic groundstate ($X^2\Sigma^+$), this means that in the groundstate channels reaction occurs by direct dynamics. Although no beam experiments on M + F_2 reactions have been reported to date, there is no reason why they should not follow the same general pattern.

The internal equilibration and non-equilibration respectively of collision complexes in different systems is connected to their lifetime (33). Simple energetic considerations (4, 33) shed light on the lifetime of collision complexes: According to classical R.R.K. theory (31) the lifetime of a molecule with internal excitation E that lies $E - E_0$ above the dissociation threshold E_0 is proportional to

$$[4] \qquad \tau_D \sim \left(\frac{E}{E - E_0}\right)^{s-1}$$

where s is the effective number of oscillators. In the series of triatomic MX_2* complexes we take $s = 3$ as constant. The lifetime problem then reduces to a balance of the binding energy of the complex ($\sim E$) and the excess energy above dissociation threshold ($E - E_0$). The binding energies are not known, particularly for the excited MX_2* states involved. The contrast between MF* and MCl* vibrational distributions can be

understood on the basis of a simple bond-energy argument: F_2 has the lowest and all fluorides MF the highest dissociation energy, making the M + $F_2 \rightarrow$ MF, MF* reactions more exothermic than the corresponding Cl_2 counterparts. $E - E_0$ increases and τ_D is correspondingly shortened, even if we assume E to be similar in both cases. The bromides behave similarly to the chlorides in this respect.

The author is indebted to Miss G. Theodorakopoulos for assistance with the experiments, and to Mr. A. E. Redpath for writing the spectral simulation computer program. This work has been supported by the National Research Council of Canada and by the Research Corporation.

1. A. G. GAYDON. Dissociation energies and spectra of diatomic molecules. 3rd ed. Chapman and Hall, London. 1968.
2. C. D. JONAH and R. N. ZARE. Chem. Phys. Lett. **9**, 65 (1971).
3. (*a*) CH. OTTINGER and R. N. ZARE. Chem. Phys. Lett. **5**, 243 (1970). (*b*) C. D. JONAH, R. N. ZARE, and CH. OTTINGER. J. Chem. Phys. **56**, 263 (1972). (*c*) J. L. GOLE and R. N. ZARE. J. Chem. Phys. **57**, 5331 (1972).
4. M. MENZINGER and D. WREN. Chem. Phys. Lett. **18**, 431 (1973).
5. G. HERZBERG. Spectra of diatomic molecules. Van Norstrand, Princeton, N.J. 1967.
6. D. WREN and M. MENZINGER. Chem. Phys. Lett. **20**, 471 (1973).
7. R. E. HONIG and D. A. KRAMER. RCA Rev. **30**, 285 (1969).
8. B. ROSEN, *Editor*. Données spectroscopiques concernant les molécules diatomiques. Pergamon Press, Oxford. 1970.
9. M. MENZINGER and R. WOLFGANG. Angew. Chem. **8**, 438 (1969).
10. R. J. LE ROY and R. B. BERNSTEIN. J. Chem. Phys. **52**, 3869 (1970).
11. R. J. LE ROY and B. R. BERNSTEIN. Chem. Phys. Lett. **5**, 42 (1970).
12. J. BLAUER and W. SOLOMON. J. Chem. Phys. **57**, 3587 (1972).
13. H. W. CRUSE, P. J. DAGDIGIAN, and R. N. ZARE. Discuss. Faraday Soc. In press.
14. M. M. NOVIKOV and L. V. GURVICH. Opt. Spectrosc. **22**, 395 (1967).
15. F. A. JENKINS and A. HARVEY. Phys. Rev. **39**, 922 (1932).
16. V. S. KUSHAWAHA, B. P. ASTHANA, R. SHANKER, and C. M. PATHAK. Spectrosc. Lett. **5**, 407 (1972).
17. R. E. HARRINGTON. Ph.D. Thesis. University of California, Berkeley, 1942.
18. M. M. NOVIKOV and L. V. GURVICH. Opt. Spectrosc. **19**, 76 (1965).
19. J. SINGH, K. P. R. NAIR, K. N. UPADHYA, and D. K. RAI. Opt. Pura. Apl. (Spain), **3**, 76 (1970).
20. D. C. HILDENBRAND. J. Chem. Phys. **52**, 5751 (1970).
21. L. S. KRASOV and N. V. KARASEVA. Opt. and Spectrosc. **19**, 14 (1965).
22. V. G. RYABOVA and L. V. GURVICH. High Temp. **2**, 749 (1964).
23. V. I. VEDENEEV, L. V. GURVICH, V. N. KONDRATIEV, V. A. MEDVEDEV, and YE. L. FRANKEVICH. Bond energies, ionization potentials and electron affinities. St. Martin's Press, New York. 1966.
24. D. C. HILDENBRAND. J. Chem. Phys. **48**, 3657 (1968).
25. R. J. LE ROY. Energy levels of a diatomic near dissociation: Specialist periodical report of the chemical society (Lond.); *Edited by* R. F. Barrow. 1973.
6. K. F. ZMBOV. Chem. Phys. Lett. **4**, 191 (1969).
27. F. A. COTTON and G. WILKINSON. Advanced inorganic chemistry. Interscience, New York. 1972.
28. (*a*) C. A. MIMS. Ph.D. Thesis. Berkeley, California, 1972. (*b*) S. M. LIN. Ph.D. Thesis. Berkeley, California, 1972. (*c*) S. M. LIN, C. A. MIMS, and R. R. HERM. J. Chem. Phys. **58**, 327 (1973).
29. J. A. HABERMANN, K. G. ANLAUF, R. B. BERNSTEIN, and J. VAN ITALLIE. Chem. Phys. Lett. **16**, 442 (1972).
30. H. J. LOESCH and D. R. HERSHBACH. Private communication.
31. K. LAIDLER. Theories of chemical kinetics. McGraw–Hill, Toronto. 1965.
32. M. MENZINGER. Disc. Faraday Soc. In press.
33. R. WOLFGANG. Acc. Chem. Res. **3**, 48 (1969).
34. G. BLUE, J. GREEN, R. BAUTISTA, and J. MARGRAVE. Bull. Am. Phys. Soc. **8**, 112 (1963).

Can. J. Chem. Downloaded from www.nrcresearchpress.com by 210.87.254.6 on 09/05/12
For personal use only.

The Formation of Dibenzoyl Peroxide in the Autoxidation of Benzaldehyde in the Presence of Lithium Chloride[1]

K. BÜHLER, W. DIESCH, AND A. K. GHOSH

Institut für Organische Chemie, Biochemie und Isotopenforschung der Universität Stuttgart, Stuttgart, W. Germany

Received June 18, 1973[2]

During the autoxidation of benzaldehyde catalyzed by lithium chloride, 26% (by weight) dibenzoyl peroxide is formed. The lithium chloride is responsible for the acceleration of the oxygen uptake and the formation of dibenzoyl peroxide.

Au cours de l'autoxydation du benzaldéhyde, catalysée par le chlorure de lithium, on forme 26% (en poid) de peroxyde de benzoyle. Le chlorure de lithium est responsable de l'accélération de la consommation de l'oxygène et de la formation du peroxyde de benzoyle. [Traduit par le journal]

Can. J. Chem., 52, 1700 (1974)

Can. J. Chem. Downloaded from www.nrcresearchpress.com by 210.87.254.105 on 09/05/12
For personal use only.

During the investigation of the effect of halides on the autoxidation of organic compounds (1, 2), it was observed that lithium chloride accelerates the autoxidation of benzaldehyde if the aldehyde is mixed with a small amount of dibenzoyl peroxide.

From curves 0 and 1 of Fig. 1, it is evident that dibenzoyl peroxide affects the autoxidation rate of benzaldehyde only to a small extent. The addition of 1% lithium chloride, however, catalyzes the autoxidation (*cf.* curve 2 of Fig. 1). After 5 h, the amount of oxygen consumed was almost twice as much as when lithium chloride was absent. Furthermore, analysis showed that the reaction product contained 22% dibenzoyl peroxide. When the product was allowed to stand in contact with air, the concentration of dibenzoyl peroxide rose to 26%.

Dibenzoyl peroxide is also formed if a suspension of lithium chloride in pure benzaldehyde is autoxidized. The addition of dibenzoyl peroxide to the suspension, however, makes the rate of oxygen consumption more reproducible. Table 1 shows the yields of dibenzoyl peroxide obtained under different conditions.

Some patents (3–5) mentioned that dibenzoyl peroxide is prepared by the autoxidation of benzaldehyde – benzoic acid anhydride mixtures (according to Nef's (6) reaction) in the presence of lithium, magnesium, or other salts; hence, the effect of lithium benzoate on the autoxidation of a 3% solution of dibenzoyl peroxide in benzaldehyde was investigated.

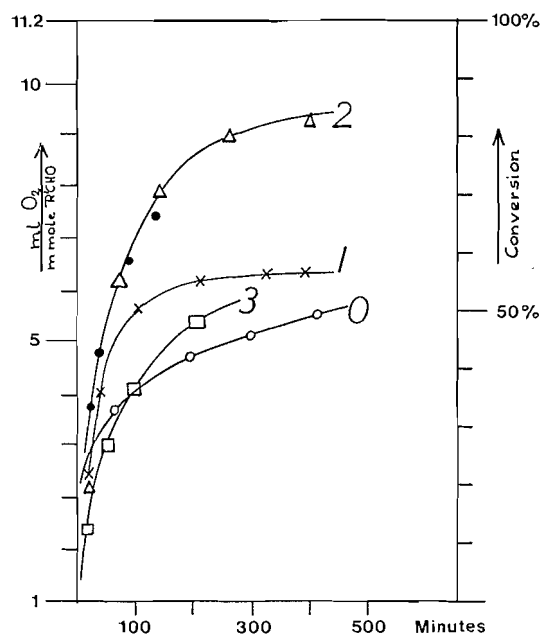

FIG. 1. Autoxidation of benzaldehyde at 50°; curve 0 (○), 10 ml pure benzaldehyde; curve 1 (×), 2 ml benzaldehyde, 3% (0.13 mol/l) dibenzoyl peroxide; curve 2 (△), 2 ml benzaldehyde, 3% (0.13 mol/l) dibenzoyl peroxide, 1% (0.24 mol/l) lithium chloride; curve 3 (□), 2 ml benzaldehyde, 3% (0.13 mol/l) dibenzoyl peroxide, and 3% (0.24 mol/l) lithium benzoate; curve 4 (●), 2 ml benzaldehyde, 3% (0.13 mol/l) dibenzoyl peroxide, and 2.6% (0.24 mol/l) $[N(CH_3)_4]Cl$.

If a 3% solution of dibenzoyl peroxide in benzaldehyde is autoxidized in the presence of lithium benzoate (*cf.* curve 3 of Fig. 1), the reaction product contains only 2% dibenzoyl peroxide; therefore, it is assumed that no additional peroxide is formed. Its formation

[1]Dedicated to Prof. Dr. Hellmut Bredereck on his 70th birthday.

[2]Revision received January 22, 1974.

TABLE 1. Yield of peroxide

Reactants	Temperature (°)	O_2 uptake (ml)	Concentration of peroxide (%)
Benzaldehyde (10 ml) containing			
3% dibenzoyl peroxide 1% lithium chloride	50	834	22
3% dibenzoyl peroxide 1% lithium chloride	40	789	13
3% dibenzoyl peroxide 1% lithium chloride	50	900	22
1% lithium chloride 4% lithium benzoate	50	987	20
3% dibenzoyl peroxide 3% lithium benzoate 1% lithium chloride	50	795	16

during the autoxidation (*cf.* curve 2 of Fig. 1) must have been due only to lithium chloride.

The yield of dibenzoyl peroxide is dependent on the cation. Like LiCl, $[N(CH_3)_4]Cl$ accelerates the autoxidation of benzaldehyde (*cf.* curve 4 of Fig. 1) but the yield of dibenzoyl peroxide under comparable experimental conditions is only 3.6% (LiCl, 26%). The effect of KCl is small and lies within experimental errors. Therefore, we postulate that the solubility of LiCl in the reaction medium is optimum for the formation of dibenzoyl peroxide.

The acceleration of the rate of autoxidation of benzaldehyde by lithium chloride and dibenzoyl peroxide is explained by the fact that the decomposition of dibenzoyl peroxide is catalyzed by chloride ions (7–9). The radicals (R·) which are formed in the decomposition of dibenzoyl peroxide produce, by reaction with benzaldehyde, benzoyl radicals, as shown in eq. 1.

[1] $$R\cdot + R'-C(=O)H \rightarrow RH + R'-\dot{C}=O$$

These benzoyl radicals react with oxygen, starting the chain reaction shown in eqs. 2 and 3.

As Kirmse and Horner (10) observed that dibenzoyl peroxide is formed if sodium peroxybenzoate reacts with benzenesulfochloride, it is possible that a certain part of the dibenzoyl peroxide, which is produced in the autoxidation, arises from the decomposition of peroxybenzoic acid, catalyzed by lithium chloride.

If the autoxidation was interrupted after an O_2 uptake of 34% of the theoretical value, the reaction mixture contained 10% (by weight) benzoic acid anhydride and 1.9% (by weight) dibenzoyl peroxide. Therefore, the main part of dibenzoyl peroxide is formed via benzoic acid anhydride. (A detailed mechanism for the formation of benzoic acid anhydride will be given in a later publication.)

This benzoic acid anhydride acylates the peroxy-benzoic acid to dibenzoyl peroxide (11), as shown in eq. 4.

If the reaction mixtures, which were autoxidized at 50° in the presence of dibenzoyl peroxide and lithium chloride, were examined by t.l.c., no phenol could be detected. During the autoxidation of pure benzaldehyde, phenol is formed in such an amount that it can easily be detected by t.l.c. of the reaction mixture. A quantitative determination of phenol in one sample after extraction with 2 *N* KOH showed that in the presence of dibenzoyl peroxide and lithium chloride about ten times less phenol is formed than in the autoxidation of pure benzaldehyde. Further investigations will show whether this

[2] $$R'-\dot{C}=O + O_2 \rightarrow R'-C(=O)-O-O\cdot$$

[3] $$R'-C(=O)-O-O\cdot + R'-C(=O)H \rightarrow R'-\dot{C}=O + R'-C(=O)-O-OH$$

Can. J. Chem. Downloaded from www.nrcresearchpress.com by 210.87.254.105 on 09/05/12
For personal use only.

[4] 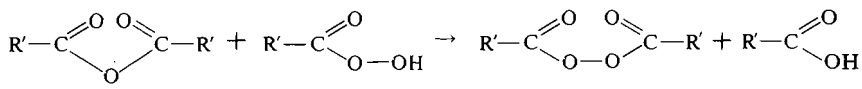

low phenol content is responsible for the higher conversion of benzaldehyde to benzoic acid.

Experimental

Materials

Benzaldehyde was twice distilled at 10 Torr under highly purified nitrogen. Lithium chloride (D.A.B.6 quality) was dried over KOH at 150° and 10^{-2} Torr. Benzoyl peroxide was a gift of Elektrochemische Werke München. It was recrystallized from a chloroform–methanol mixture (12). The O_2 uptake was measured with the apparatus developed by Bredereck and co-workers (1, 13). The concentration of dibenzoyl peroxide in the reaction mixtures was determined iodometrically (13).

Autoxidation of a Solution of 3% Dibenzoyl Peroxide in Benzaldehyde in the Presence of Lithium Chloride

A suspension of 1.05 g (0.025 mol) lithium chloride in 100 ml (0.99 mol) benzaldehyde containing 3.15 g (0.013 mol) dibenzoyl peroxide was autoxidized at 50° for 5 h. The reaction vessel was a three-necked flask with a gas inlet tube, a condenser, and an efficient stirrer. The oxygen was dried over KOH pellets. The reaction product was cooled overnight; then the concentration of dibenzoyl peroxide was determined iodometrically and was found to be 23.0% (by weight) dibenzoyl peroxide. The reaction product was poured into an open porcelain dish and allowed to stand in contact with air for 24 h. During this time, the concentration of dibenzoyl peroxide rose to 26.8% (determined iodometrically).

The reaction product was stirred with a solution of 100 g sodium carbonate in 400 ml water and the residue was filtered off. The residue (32.6 g) was crystallized from a chloroform–methanol mixture (1:1); yield, 25.0 g dibenzoyl peroxide, m.p. 104–105°, mixture melting point with an authentic sample 104° (lit. (14) 103°).

The filtrate contained an oil (8 g) which was extracted from the water by ether. After evaporation of the ether, the residue was separated by fractionating distillation in high vacuum into benzaldehyde (about 30%), benzoic acid anhydride (about 30%), and benzoic acid (about 13%). By t.l.c. dibenzoyl peroxide (about 10%) was detected. A further ingredient was not identified.

In a second experiment, a suspension of 10.0 g (0.24 mol)lithium chloride in 1000 g (9.44 mol)benzaldehyde (Cl^- concentration, 0.25 mol/l) was autoxidized at 50°. After an O_2 uptake of about 51 g (1.6 mol or 34% of the theoretical value) the autoxidation was interrupted and the peroxide concentration determined iodometrically: 1.9% dibenzoyl peroxide.

Excess benzaldehyde was removed by distillation at 33–34°/10^{-3} Torr. The residue was dissolved in ether and benzoic acid was extracted with a KOH solution. After evaporation of the ether, 120 g of a yellow oil remained. This oil was recrystallized from light petroleum; yield, 90 g benzoic acid anhydride, m.p. 44°, mixture melting point with an authentic sample 39° (lit. (15) 42°). By several fractional crystallizations of the filtrate, 10 g benzoic acid anhydride were isolated and dibenzoyl peroxide was enriched.

The residue was separated by column chromatography (Pharmacia SR 25/45 column, filled with 100 g silica gel, benzene as eluent). From the first fractions 6 mg dibenzoyl peroxide was isolated and was identified by a mixture melting point with an authentic sample. The other fractions were analyzed by t.l.c.; they proved to be mixtures of dibenzoyl peroxide and benzoic acid anhydride.

The t.l.c. was made on sheets according to Stahl (16, 17). All compounds were identified by u.v.-absorption. Dibenzoyl peroxide was further identified on sheets, which contained sodium fluorescein (17) as the spot of the peroxide turned gradually from reddish to colorless within a few days.

Determination of Phenol

In a third experiment the ether extract of 20 g reaction product was shaken with 20 ml of a 2 *N* KOH solution. The alkaline solution was washed with ether, acidified with perchloric acid and extracted with 20 ml ether. The ether was evaporated *in vacuo* and the residue acidified with 1 drop of perchloric acid. The phenol was then titrated according to Siggia (18): the titration showed 4 mg phenol. The reaction product, therefore, contained 0.02% phenol.

Pure benzaldehyde (10 ml) was autoxidized at 50° for 3 h. Then the phenol concentration in 1 g of reaction product was determined according to the procedure of Siggia (18). The titration showed 0.2% phenol.

We thank Prof. Dr. Hellmut Bredereck for the generous support of the investigations.

1. H. Bredereck, A. Wagner, R. Blaschke, G. Demetriades, and K. G. Kottenhahn. Chem. Ber. **92**, 2628 (1959).
2. H. Bredereck, K. Bühler, K. Posselt, Th. Haug, and H. W. Sonneborn. Chem. Ber. **102**, 2190 (1969).
3. U.S. Patent 3,438,882 of Pfizer, Chas., and Co., Inc.; J. J. Beereboom and J. S. Buckley. Chem. Abstr. **71**, 12843f (1969).
4. U.S. Patent 3,397,245 of Koppers Company Inc.; H. R. Appell. Chem. Abstr. **69**, 76954j (1968).
5. USSR Patent 170,952; Yu. A. Ol'dekop and G. S. Bylina. Chem. Abstr. **63**, 9880a (1965).
6. J. U. Nef. Justus Liebigs Ann. Chem. **298**, 284 (1897).
7. H. Bredereck, A. Wagner, R. Blaschke, and G. Demetriades. Angew. Chem. **71**, 340 (1959).
8. C. H. Bamford and E. F. T. White. J. Chem. Soc. 4490 (1960).
9. J. K. Kochi, B. M. Graybill, and M. Kurz. J. Am. Chem. Soc. **86**, 5257 (1964).
10. W. Kirmse and L. Horner. Chem. Ber. **89**, 836 (1956).

Can. J. Chem. Downloaded from www.nrcresearchpress.com by 210.87.254.105 on 09/05/12
For personal use only.

11. W. P. JORISSEN and W. E. RINGER. J. Prakt. Chem. (2) **72**, 176 (1905).
12. D. TAUB. Chem. Eng. News, **27**, 46 (1949).
13. W. DIESCH. Dissertation. Universität Stuttgart, Stuttgart, W. Germany, 1968.
14. C. BRODIE. J. Chem. Soc. **17**, 270 (1864).
15. CH. GERHARDT. Justus Liebigs Ann. Chem. **87**, 76 (1853).
16. E. STAHL. Dünnschichtchromatographie, Springer Verlag, Berlin. 1962. p. 508 (No. 90d).
17. E. STAHL. Dünnschichtchromatographie, Springer Verlag, Berlin. 1962. p. 509 (No. 101A).
18. S. SIGGIA. Quantitative organic analysis via functional groups, J. Wiley and Sons, Inc., London. 1949. p. 111.

Can. J. Chem. Downloaded from www.nrcresearchpress.com by 210.87.254.105 on 09/05/12
For personal use only.

Studies of β-Diketone Complexes of Rhenium. VI. The Crystal and Molecular Structure of *cis*-Dichloropentane-2,4-dionato-*trans*-bis(triphenylphosphine)rhenium(III)

I. D. BROWN, C. J. L. LOCK,[1] AND CHE'NG WAN

Institute for Materials Research, McMaster University, Hamilton, Ontario

Received November 8, 1973

A compound, obtained in large yields from the reaction of acetylacetone and oxodichloroethoxobis(triphenylphosphine)rhenium(V) in benzene, has been shown by single crystal X-ray diffraction to be *cis*-dichloropentane-2,4-dionato-*trans*-bis(triphenylphosphine)rhenium(III). The crystals are monoclinic with $a = 13.06(1)$, $b = 18.30(1)$, $c = 16.55(1)$ Å, and $\beta = 112.7(2)°$. The space group is $P2_1/c$ and there are four molecules per unit cell. A total of 3841 independent reflections, of which 2686 were observed, were examined by film methods, the intensities being measured with a microdensitometer. The structure was refined by full matrix least-squares analysis to an R_2 value of 0.068. The ligands are arranged around the rhenium atom in the manner described by the compound name to give a rough octahedron of nearest neighbours and the Re—Cl (2.369 Å av.), Re—O (2.02 Å av.), and Re—P (2.474 Å av.) distances are as expected.

Un composé, obtenu avec un bon rendement par la réaction de l'acétylacétone et de l'oxodichloroéthoxobis(triphénylphosphine) du rhénium(V) dans du benzène, a été établi par diffraction de rayons-X d'un cristal comme étant du *cis*-dichloropentane dionato-2,-4 *trans*-bis(triphénylphosphine) du rhénium(III). Les cristaux sont monocliniques avec $a = 13.06(1)$, $b = 18.30(1)$, $c = 16.55(1)$ Å et $\beta = 112.7(2)$. Le groupe d'espace est $P2_1/c$ et on a quatre molécules par maille. Un total de 3841 réflections indépendantes, dont 2686 observées, sont examinées par les méthodes de film, les intensités sont mesurées à l'aide d'un microdensitomètre. La structure est raffinée par analyse de moindres carrés d'une matrice entière à une valeur de $R_2 = 0.068$. Les liaisons sont disposées autour de l'atome de rhénium de la manière décrite par le composé cité pour donner un octaèdre approximatif formé par les voisins les plus proches et, tel que prévu, les distances moyennes sont Re—Cl (2.369 Å), Re—O (2.02 Å) et Re—P (2.474 Å). [Traduit par le journal]

Can. J. Chem., **52**, 1704 (1974)

Introduction

Several types of β-ketoenenolate complexes of rhenium have been synthesized (1, 2). Many of the complexes synthesized by Grove *et al.* (2) by the direct interaction of oxodichloroethoxobis(triphenylphosphine)rhenium(V) and β-diketones can exist in different isomeric forms. In order to understand the mechanism of the unusual reaction which gives rise to so many different products, it is necessary to know the detailed molecular structure of the products. To this end we have examined the crystal structures of the reaction products by single crystal X-ray methods.

The reaction of oxodichloroethoxobis(triphenylphosphine)rhenium(V) with acetylacetone in benzene gave two products after short reaction times (2). Oxodichloropentane-2,4-dionato(triphenylphosphine)rhenium(V), the expected product, was obtained in rather low yields; the main product of the reaction was dichloropentane-2,4-dionatobis(triphenylphosphine)rhenium(III). This product was unexpected, particularly since the reduction has involved the removal of two *trans* groups and their replacement by a pentane-2,4-dionate group which, if bidentate, must occupy two *cis* positions at the rhenium atom. Since there are three possible geometric isomers which could result from the reaction, we have examined the product by single crystal X-ray diffraction and our results are presented in this paper.

Experiments

$ReCl_2(acac)[P(C_6H_5)_3]_2$ was prepared by the method of Grove *et al.* (2).[2] A solution of purple $ReOCl_2(OEt)[P(C_6H_5)_3]_2$ (3) (2 g) and pentane-2,4-dione (2 ml) in benzene (30 ml) was boiled under reflux for 6 hours, con-

[1]Author to whom correspondence should be addressed.

[2]acac is the anion of the β-ketoenol form of acetylacetone, $C_5H_7O_2^-$; Et is the ethyl radical, C_2H_5.

Can. J. Chem. Downloaded from www.nrcresearchpress.com by 210.87.254.6 on 09/05/12
For personal use only.

Can. J. Chem. Downloaded from www.nrcresearchpress.com by 210.87.254.6 on 09/05/12
For personal use only.

centrated to 15 ml, and allowed to cool. The product was obtained as microcrystals and was separated by filtration. The crystals were washed with a little benzene and diethyl ether.

Anal. Calcd. for $C_{41}H_{37}Cl_2O_2P_2Re$: C, 55.9; H, 4.2; Cl, 8.1; P, 7.0. Found: C, 55.8; H, 4.4; Cl, 8.0; P, 6.9.

Single crystals were obtained by dissolving the microcrystals in a dichloromethane and benzene mixture (2:1 volume ratio) and evaporating the solution slowly at room temperature. Crystals obtained by this method were orange plates.

X-Ray Crystallography

A crystal of $ReCl_2(acac)[P(C_6H_5)_3]_2$, showing sharp extinctions when viewed with polarized light, was cut into a rough cyclinder with dimensions 0.07, 0.09, 0.13 mm. The specimen was mounted so that the longest dimension of the crystal, which was parallel to c^*, was the rotation axis. Precession photographs showed the crystal was monoclinic, $P2_1/c$; the systematic absences were, $h0l$, $l = 2n + 1$ and $0k0$, $k = 2n + 1$. Cell parameters were obtained by calibrating precession photographs of the $(0kl)$ and $(h0l)$ zones with TiO_2 (rutile: a = 4.5929(5) and c = 2.9591(3) Å) (4). The density of a few crystals was determined by flotation in a carbon tetrachloride – bromoform mixture. The crystal data for $ReCl_2(acac)[P(C_6H_5)_3]_2$ are

$C_{41}H_{37}Cl_2O_2P_2Re$ f.w. 880.75

Monoclinic, a = 13.06(1), b = 18.30(1), c = 16.55(1) Å, β = 112.7(2)°, V = 3649 Å^3, $P2_1/c$ (C_{2h}^5, No. 14), ρ_o = 1.61(8), Z = 4, ρ_c = 1.60(1) (22 °C, MoKα, λ = 0.71069Å), μ = 37.9 cm^{-1}.

Reflection intensities for layers nkl, n = 0–4 and hml, m = 0–6, were obtained from films recorded on an integrating precession camera using zirconium filtered MoKα radiation. All intensities were measured using a Joyce–Loebl microdensitometer and then corrected for Lorentz and polarization effects. Absorption corrections were not applied and this could introduce a maximum error in F_o of 11%; the average error would be considerably less. Standard errors, σ, were assigned to each reflection according to the methods of Ibers (5) and Hughes (6) and weights, $w = 1/\sigma^2$, were used throughout the refinement.

Solution of the Structure

The coordinates of the rhenium atoms were obtained from Patterson syntheses projected on (100) and (010). Six more atoms, which formed a rough octahedron around rhenium, were found from a three-dimensional difference synthesis. The two smaller peaks were assigned as the oxygen atoms of the chelated β-ketoenolate group because they were *cis*. Successive projection Fourier and electron density different syntheses did not reveal further atoms but all non-hydrogen atoms were detected in a three-dimensional synthesis using structure factors satisfying $F_o/F_c \leq 1.5$ (about 2500 in all). It was also possible to distinguish the phosphorus atoms from the chlorine atoms at this point, since the atoms identified as chlorine were more than 3.0 Å away from any phenyl carbon atom. From this point, the phenyl rings were refined as rigid groups rather than as individual carbon atoms, using the rigid body approach of Scheringer (7), and Ibers and La Placa (8).[3] Three cycles of refinement dropped R_1 and R_2 to 0.083.[4] At this stage common reflections were averaged and unobserved reflections for which $F_c < F_{min}$ were given zero weight. In addition, temperature factors, which previously were isotropic for all atoms, were made anisotropic for all atoms except carbon. No attempt was made to locate hydrogen atoms in the crystal. Subsequent refinement was teminated when R_1 = 0.0771 and R_2 = 0.0680.[5] For the last cycle of refinement no parameter shifted by more than 0.1σ.

A three-dimensional difference showed the largest residual peak at 0.015, 0.15, 0.35 (~0.15 e/Å^3) and the largest valley at 0.15, 0.15, 0.25 (~0.1 e/Å^3), both between the rhenium atom, Pl and Cl2. 3841 independent reflections were measured and represent about 39% of the reflections theoretically accessible with a precession angle of 30°. Of these reflections, 2686 were observed. 2789 reflections were given non zero weight in the final refinement and included the observed reflections, except three which were of doubtful accuracy because they were near the back-stop shadow, and 116 unobserved reflections for which $F_c > F_{min}$ (F_{min} was the minimum observed intensity in that region of reciprocal space). For these unobserved reflections the value of Δ, used in calculating the least-squares matrix, was defined as $F_c - 0.6F_{min}$.

Throughout the refinement, the scattering curves for C, Cl, O, and P were those tabulated in the International Tables (10), while that for Re was taken from Cromer and Waber (11). Anomalous dispersion corrections for rhenium, chlorine, and phosphorus were taken from Cromer (12).

The final atom parameters are shown in Table 1 and the values of F_o and F_c are given in Table 2.[6]

Results and Discussion

Figure 1[7] shows one complete molecule and the principal intramolecular distance and angles are given in Table 3. The ligands which surround the rhenium atom are at the apices of a distorted

[3]Each phenyl group was treated as an atomic unit of D_{6h} symmetry, with each carbon atom 1.392 Å (9) from the center of the ring. Six variable parameters were used to define the ring (three positional and three angular) and each carbon atom was assigned an individual variable isotropic temperature factor. The program used was GROUPLS, written by Dr. J. S. Stephens for the CDC-6400 computer.

[4]$R_1 = \frac{\Sigma||F_o| - |F_c||}{\Sigma|F_o|}$; $R_2 = \left(\frac{\Sigma w(|F_o| - |F_c|)^2}{\Sigma w F_o^2}\right)^{\frac{1}{2}}$

[5]Another refinement was carried out omitting the 116 unobserved reflections for which $F_c > F_{min}$ giving a total of 2683 reflections used in the refinement. For the final cycle R_1 = 0.0697 and R_2 = 0.0655 and the atom parameters, bond lengths and bond angles did not differ significantly from those given herein.

[6]Table 2 is available, at nominal charge, from the Depository of Unpublished Data, National Science Library, National Research Council of Canada, Ottawa, Canada K1A 0S2.

[7]Figures 1 and 2 were prepared with the aid of the program ORTEP written by Johnson (21).

Can. J. Chem. Downloaded from www.nrcresearchpress.com by 210.87.254.6 on 09/05/12
For personal use only.

TABLE 1. (*a*) Atom parameters for $ReCl_2(acac)(P(C_6H_5)_3)_2$ ($\times 10^3$)*

Atom	*x*	*y*	*z*	*U*
Re	282.13(5)	146.54(3)	216.33(4)	
Cl1	243.5(3)	28.4(2)	256.4(3)	
Cl2	357.5(3)	197.0(2)	359.1(3)	
P1	92.4(3)	186.5(2)	197.3(3)	
P2	471.8(3)	106.6(2)	238.8(3)	
O1	312.6(9)	242.6(5)	171.9(7)	
O2	218.3(8)	113.5(5)	88.4(6)	
C1	300(1)	261(1)	92(1)	43(4)
C2	262(1)	216(1)	22(1)	43(4)
C3	219(1)	148(1)	19(1)	36(4)
C4	334(2)	340(1)	83(1)	65(6)
C5	168(2)	102(1)	−62(1)	56(5)
C11	−141(1)	125(1)	−84(1)	51(5)
C12	−117(1)	198(1)	−62(1)	54(5)
C13	−49(1)	218(1)	22(1)	49(5)
C14	−5(1)	164(1)	86(1)	44(4)
C15	−29(1)	91(1)	64(1)	49(5)
C16	−97(1)	71(1)	−21(1)	57(5)
C21	−59(1)	96(1)	388(1)	60(6)
C22	55(1)	109(1)	415(1)	49(5)
C23	98(1)	133(1)	356(1)	53(5)
C24	28(1)	146(1)	269(1)	38(4)
C25	−85(1)	134(1)	242(1)	47(5)
C26	−129(1)	109(1)	301(1)	60(5)
C31	5(1)	431(1)	205(1)	57(5)
C32	−60(1)	377(1)	221(1)	53(5)
C33	−33(1)	304(1)	222(1)	59(5)
C34	61(1)	284(1)	206(1)	48(5)
C35	127(1)	338(1)	190(1)	65(6)
C36	99(1)	411(1)	190(1)	58(5)
C41	704(1)	47(1)	521(1)	54(5)
C42	729(1)	108(1)	482(1)	46(5)
C43	660(1)	128(1)	397(1)	44(4)
C44	567(1)	87(1)	351(1)	29(4)
C45	540(1)	26(1)	390(1)	40(4)
C46	609(1)	6(1)	475(1)	54(5)
C51	512(1)	−106(1)	103(1)	65(6)
C52	602(1)	−76(1)	171(1)	82(7)
C53	590(1)	−11(1)	211(1)	59(5)
C54	488(1)	24(1)	182(1)	49(5)
C55	397(1)	−6(1)	113(1)	54(5)
C56	409(1)	−70(1)	73(1)	75(7)
C61	654(1)	290(1)	152(1)	69(6)
C62	616(1)	303(1)	219(1)	65(6)
C63	562(1)	248(1)	244(1)	41(4)
C64	545(1)	180(1)	204(1)	42(4)
C65	583(1)	167(1)	137(1)	45(4)
C66	637(1)	222(1)	111(1)	64(6)

(*b*) Anisotropic temperature factors U_{ij} ($\times 10^3$)†

Atom	U_{11}	U_{22}	U_{33}	U_{12}	U_{13}	U_{23}
Re	30.5(4)	28.5(4)	29.7(3)	−2.2(5)	12.9(2)	−0.8(4)
Cl1	41(2)	29(2)	49(2)	2(3)	16(2)	3(2)
Cl2	37(2)	47(3)	36(2)	−6(3)	14(2)	−12(2)
P1	26(2)	22(2)	29(2)	4(2)	11(2)	0(2)
P2	37(3)	28(2)	34(2)	−5(3)	18(2)	−9(2)
O1	47(7)	24(6)	47(6)	5(7)	29(6)	−2(5)
O2	30(6)	24(5)	36(6)	−6(6)	15(5)	−10(5)

*Estimated standard deviations from the least squares programs are given in brackets. The atoms C11, C12, ...C16; C21, C22, ...C26; etc., were refined as six groups and the estimated standard deviations given are derived from the group refinement.

†The temperature factor parameters U_{ij} were obtained from $\beta_{ij} = 2\pi^2 b_i b_j U_{ij}$ where β_{ij}'s appear as a temperature effect through $\exp[-(\beta_{11}h^2 + ... + 2\beta_{12}hk + ...)]$ in the structure factor expression and b_i are the reciprocal lattice vectors.

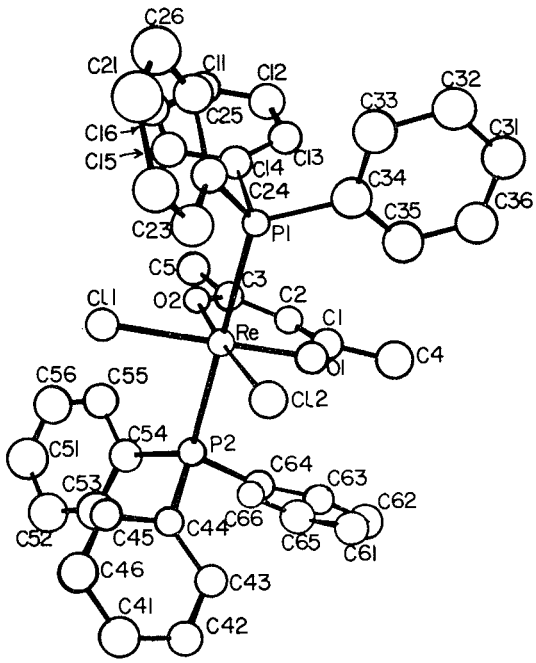

FIG. 1. The molecular structure of $ReCl_2(C_5H_7O_2)(P(_6H_5)_3)_2$. The numbering of the atoms is as in Table 1.

octahedron and the bulky triphenylphosphine groups are *trans* as expected. The Re—Cl (2.37 Å av.) and Re—O (2.03 Å av.) distances found here are close to those observed in $Re(acac)_2Cl_2$ (Re—Cl 2.33 Å and Re—O, 1.99 Å av.) (13). The Re—P lengths of 2.485(4) and 2.469(5) Å are longer than the M—P distance for most second and third row transition metals (14) but agree well with those found in other rhenium compounds containing triphenylphosphine or diethylphenylphosphine groups (14–18). Similar Re—P distances have been noted previously by Bright and Ibers (19) who postulated the apparent lengthening was caused by steric hindrance. However, all the Re—(bonded atom) distances are consistent with a rhenium covalent radius of 1.37 ± .01 Å and thus the Re—P distances may not be unduly long.

Bond distances and angles in the acetylacetonate group are normal (20) and bond distances of the equivalent sets within the acetylacetonate group do not differ by more than 1.5σ in the extreme case. The atoms O1C1C2C3O2 are coplanar and the dihedral angle between this plane and the O1ReO2 plane is 6°, such that the rhenium atom is 0.16 Å out of the first plane. The two methyl carbon atoms are also apparently displaced from the same plane in the opposite direction to the rhenium atom, C4 by 0.13 Å and C5 by 0.08 Å. The P—C bond lengths and C—P—C angles for the two triphenylphosphine groups are within the range that has been observed in a number of complexes of triphenylphosphine (16).

The packing of the molecules within the unit cell is shown in Figure 2. In the *a* direction, molecules with identical rhenium *y*, *z* values form chains, the intermolecular contact being made between the phenyl rings. Considering a single molecule, the arrangement of the phenyl groups on each phosphine appears random but

TABLE 3. Interatomic distances and bond angles in $Re(acac)Cl_2(P(C_6H_5)_3)_2$*

(*a*) *Interatomic distances*

Atom pair	Distance (Å)	Atom pair	Distance (Å)
Bonded			
Re—O1	2.00(1)	C2—C3	1.35(3)
Re—O2	2.05(1)	C1—C4	1.55(3)
Re—Cl1	2.371(4)	C3—C5	1.51(2)
Re—Cl2	2.367(4)	P1—C14	1.84(1)
Re—P1	2.485(4)	P1—C24	1.85(1)
Re—P2	2.469(4)	P1—C34	1.85(1)
O1—C1	1.30(2)	P2—C44	1.83(1)
O2—C3	1.32(2)	P2—C54	1.84(1)
C1—C2	1.35(2)	P2—C64	1.87(1)
Non-bonded distances			
Cl1—O2	3.09(1)	P1—Cl1	3.425(5)
Cl2—O1	3.04(1)	P1—Cl2	3.470(5)
Cl1—Cl2	3.559(6)	P2—O1	3.16(1)
O1—O2	2.77(1)	P2—O2	3.29(1)
P1—O1	3.23(1)	P2—Cl1	3.418(7)
P1—O2	3.17(1)	P2—Cl2	3.348(7)

(*b*) *Bond angles*

Bonds	Angle(°)	Bonds	Angle(°)
P1—Re—Cl1	89.7(2)	Re—P2—C64	110.4(3)
P1—Re—Cl2	91.3(2)	Re—O1—C1	129(1)
P1—Re—O1	91.4(3)	Re—O2—C3	128(1)
P1—Re—O2	88.2(3)	O1—C1—C2	125(2)
P2—Re—Cl1	89.8(2)	O2—C3—C2	124(2)
P2—Re—Cl2	87.6(1)	Cl—C2—C3	127(2)
P2—Re—O1	89.2(4)	O1—C1—C4	114(2)
P2—Re—O2	93.0(3)	O2—C3—C5	111(2)
O1—Re—O2	86.5(4)	C2—C1—C4	121(2)
Cl1—Re—Cl2	97.4(2)	C2—C3—C5	125(2)
O1—Re—Cl2	87.7(3)	C14—P1—C24	104.2(3)
O2—Re—Cl1	88.5(3)	C24—P1—C34	99.7(3)
Re—P1—C14	109.2(3)	C34—P1—C14	102.1(2)
Re—P1—C24	118.4(2)	C44—P2—C54	101.3(3)
Re—P1—C34	120.9(3)	C54—P2—C64	104.8(3)
Re—P2—C44	117.5(3)	C64—P2—C44	103.0(3)
Re—P2—C54	118.1(2)		

*Estimated standard deviations are given in brackets and are in parts of the last place of the value given.

Can. J. Chem. Downloaded from www.nrcresearchpress.com by 210.87.254.6 on 09/05/12
For personal use only.

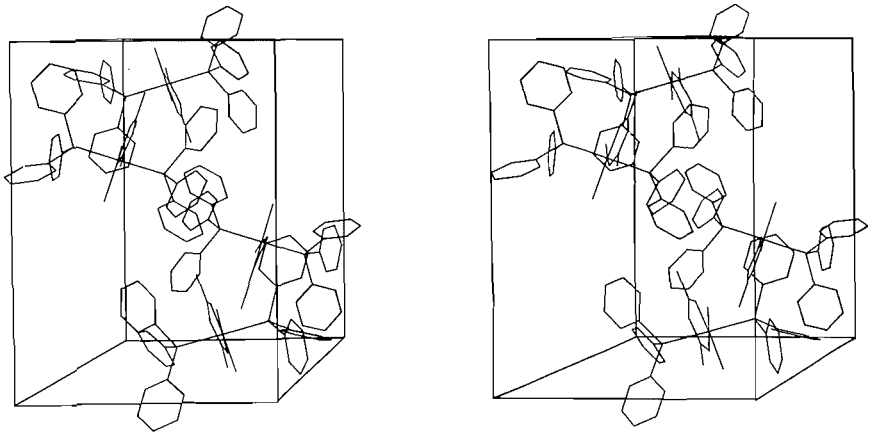

FIG. 2. Stereogram (stereoscopic pair of perspective projections) of four molecules of $Re(acac)Cl_2(P(C_6H_5)_3)_2$ in the unit cell viewed down the c^* axis. The a and b axes run parallel to the horizontal and vertical edges of the paper, respectively.

the packing diagram shows clearly that the orientation is such that rings on neighbouring molecules lie parallel and in contact.

Packing in the b direction is quite similar to that in the c^* direction. In the b direction molecules with roughly the same rhenium z values are arranged such that the phenyl rings of one molecule fit into the "equatorial" belt (defined by the β-ketoenolate ring and the chlorine atoms) of the next molecule. In the c^* direction a similar effect is observed for molecules in a given half of the cell (defined by $1/2b$), although at $b = 0$ and $1/2$ packing in the c^* direction is primarily determined by the phenyl ring contacts. The principal difference in the packing in the b and c^* directions is that the molecules are arranged such that the molecular dipoles lie very roughly in the c^* direction, thus maximizing the dipole–dipole interactions.

We thank the National Research Council of Canada for financial support.

1. R. COLTON, R. LEVITUS, and G. WILKINSON. J. Chem. Soc. 4121 (1960).
2. D. E. GROVE, N. P. JOHNSON, C. J. L. LOCK, and G. WILKINSON. J. Chem. Soc. 490 (1965).
3. N. P. JOHNSON, C. J. L. LOCK, and G. WILKINSON. Inorg. Synth. **9**, 147 (1967).
4. D. T. CROMER and K. HERRINGTON. J. Am. Chem. Soc. 77, 4708 (1955).
5. J. A. IBERS. Acta Cryst. **9**, 652 (1956).
6. E. W. HUGHES. J. Am. Chem. Soc. **63**, 1737 (1941).
7. C. SCHERINGER. Acta Cryst. **16**, 546 (1963).
8. S. J. LA PLACA and J. A. IBERS. Acta Cryst. **18**, 511 (1965).
9. J. A. IBERS, J. Chem. Phys. **40**, 3129 (1964).
10. J. A. IBERS. International tables for X-ray crystallography. Vol. III. Kynoch Press, Birmingham (1962).
11. D. T. CROMER and J. T. WABER. Acta Cryst. **18**, 104 (1965).
12. D. T. CROMER. Acta Cryst. **18**, 17 (1965).
13. I. D. BROWN, C. J. L. LOCK, and C. WAN. Can. J. Chem. **51**, 2073 (1973).
14. P. W. R. CORFIELD, R. J. DOEDENS, and J. A. IBERS. Inorg. Chem. **6**, 197 (1967).
15. H. W. W. EHRLICH and P. G. OWSTON. J. Chem. Soc. 4368 (1963).
16. R. J. DOEDENS and J. A. IBERS. Inorg. Chem. **5**, 204 (1967).
17. D. BRIGHT and J. A. IBERS. Inorg. Chem. 7, 1099 (1968).
18. D. BRIGHT and J. A. IBERS. Inorg. Chem. **8**, 703 (1969).
19. D. BRIGHT and J. A. IBERS. Inorg. Chem. **8**, 709 (1969).
20. E. C. LINGAFELTER and R. L. BRAUN. J. Am. Chem. Soc. **88**, 2951 (1966).
21. C. K. JOHNSON. U.S. Atomic Energy Commission Report, ORNL-3794. Revised June, 1965.

Can. J. Chem. Downloaded from www.nrcresearchpress.com by 210.87.254.6 on 09/05/12
For personal use only.

Apparent Molal Volumes and Heat Capacities of Urea and Methyl-Substituted Ureas in H_2O and D_2O at 25 °C

PATRICK R. PHILIP, GÉRALD PERRON, AND JACQUES E. DESNOYERS[1]

Department of Chemistry, Université de Sherbrooke, Sherbrooke, Québec J1K 2R1

Received October 22, 1973

The apparent molal volumes and heat capacities of urea, 1,1- and 1,3-dimethylurea, and tetramethylurea were measured in H_2O and D_2O at 25 °C. From these data, urea–water interactions seem to cause an overall structure-breaking effect and the substituted ureas, an overall structure-making effect. The effect of the hydrogen-bonding interactions to the volume and heat capacity seems to be small compared with the intrinsic and hydrophobic contributions of a methylene group, as reflected by the isotope effect. Furthermore, transfer values seem to show a significant specificity to the degree and position of methyl substitution.

Les volumes molaires apparents et les capacités calorifiques de l'urée, de la diméthyl-1,1 et -1,3 urée et de la tétraméthylurée ont été mesurés dans H_2O et D_2O à 25 °C. A partir de ces données, les interactions urée-eau semblent causer un effet global de déformation de structure et les urées substituées, un effet global de formation de structure. L'influence des interactions des ponts hydrogènes sur le volume et la capacité calorifique semble être faible comparée avec les contributions intrinsèque et hydrophobe d'un groupe méthylène, tel que réflété par l'effet isotopique. En outre les valeurs de transfert semblent montrer une spécificité significative au degré et à la position de la substitution par un groupe méthyle.

Can. J. Chem., **52**, 1709 (1974)

Introduction

An understanding of amide–water interactions is important in many fields of chemistry and biochemistry as, for instance, in the problems related to the conformational stability of polypeptides (1). As a result, numerous studies of aqueous solutions of amides, urea, and alkyl-substituted ureas have been undertaken by spectroscopic (2–4), thermodynamic (5–12), transport (13–18), and n.m.r. (19, 20) techniques.

These solutes interact with water through hydrogen bonds with N—H and C=O groups. These interactions are probably short ranged and short lived, as indicated by the temperature dependence of the chemical shift and the concentration dependence of the ^{14}N rotational correlation time (20). The great solubility (21) of urea in water and the similarity between the enthalpy of solution of urea in water (5–11) and the enthalpies of fusion of water (22) and urea (23) suggest that urea–water interactions are similar to water–water interactions. From osmotic and activity coefficients (12) and enthalpies of dilution (11), excess thermodynamic functions (24) may be evaluated; below 3.3 *m* in urea, the excess entropies are negative indicating significant urea–water interactions. *Ab initio* molecular orbital calculations (25) on amide–water and water–water dimers show similar stability of NH.....OH_2, CO.....HOH, and H_2O.....HOH hydrogen bonds.

It is well known and generally observed that the energy of a hydrogen bond is decreased by the deuterium isotope substitution and consequently that hydrogen bonding interactions are strengthened, at least at low temperatures; typical cases where this has been inferred are studies of hydrophobic hydration (26–28), alcohol–water (29) or tetrahydrofuran–water mixtures (30), helix – random coil transformation (31, 32), and self-association of *N*-methylacematide in CCl_4 (33). It was therefore felt that a comparative thermodynamic study of urea and alkyl-substituted ureas in H_2O and D_2O could yield useful information on the N—H and C=O bonds with water.

The chosen properties were apparent molal volumes and heat capacities. These properties can now be measured precisely (8–35) and have proven to be useful for the study of solute–solvent and solute–solute interactions (9–28).

[1]To whom correspondence should be addressed.

Can. J. Chem. Downloaded from www.nrcresearchpress.com by 210.87.254.105 on 09/05/12
For personal use only.

TABLE 1. Apparent molal volumes and heat capacities of methyl-substituted ureas in water at 25 °C

Molality	$10^3 (d - d_0)$* (g cm^3)	$10^3 \left(\frac{\sigma - \sigma_0}{\sigma_0}\right)$*	ϕ_V (cm^3 mol^{-1})	ϕ_C (J K^{-1} mol^{-1})
		1,1-Dimethylurea		
0.050629	0.484	$-\ 0.95_5$	78.72	248.9
0.089075	0.829	$-\ 1.76_5$	78.94	245.6
0.49593	4.587	$-\ 9.50_5$	78.70	244.7
1.00846	9.271	− 18.97	78.39	241.9
2.02284	17.884	− 36.25	78.08	238.7
2.57817	22.199	− 44.84	77.97	237.7
		1,3-Dimethylurea		
0.050056	0.423	$-\ 0.73_8$	79.84	270.8
0.10382	0.850	$-\ 1.50_3$	80.07	272.7
0.47193	3.805	$-\ 6.11_2$	79.96	277.0
1.05754	8.536	− 13.53	79.57	273.6
2.04944	16.127	− 26.39	79.17	267.4
2.99589	22.733	− 38.51	78.94	262.5
4.96960	34.350	− 65.44	78.71	251.5
6.35092	40.917	− 82.64	78.66	246.3
		Tetramethylurea		
0.054745	0.070	$-\ 0.63_2$	115.21	431.5
0.10450	0.109	$-\ 1.16_8$	115.45	433.8
0.50439	0.731	$-\ 6.00_6$	114.97	426.4
1.00294	1.912	− 13.51	114.37	413.9
2.07826	4.399	− 32.41	113.88	394.0
3.02284	5.664	− 49.58	113.98	382.8
5.00053	10.690	− 87.78	113.14	356.7
7.00948	12.654	−123.92	113.25	339.6

d_0 0.997047 g cm^{-3}
c_{p0} 4.1793 J K^{-1} g^{-1}

*The subscript 0 refers to the pure solvent.

Experimental and Results

Densities (d) were measured to $\pm 3 \times 10^{-6}$ g cm^{-3} with two digital densimeters (34, 35) and differences in volumetric specific heats (σ) to $\pm 7 \times 10^{-5}$ J K^{-1} cm^{-3} with a flow microcalorimeter (8). The chemicals, urea (Fisher certified) and substituted ureas (Eastman Kodak), were purified as follows: urea was dried under vacuum at 60 °C for 48 h; 1,1- and 1,3-dimethylurea, respectively, were recrystallized from a 50–50 methanol–water mixture and from pure methanol and dried in the same way as urea; tetramethylurea was used as such. The deuterated samples (urea and dimethylureas) were prepared by dissolving the protonated forms in an excess of D_2O twice, followed each time by evaporation and drying under vacuum. The protons on the nitrogen atom were 96 ± 2 % exchanged as checked by n.m.r. analysis. Light water was redistilled from an alkaline permanganate solution and D_2O (Stohler Isotope Chemicals, 99.8 %) was used as such. All solutions were prepared by weight.

The ranges of measurements in H_2O were, respectively, 0.05–2.58, 0.05–6.35, and 0.05–7 m for 1,1-dimethylurea, 1,3-dimethylurea, and tetramethylurea. In D_2O only two measurements on deuterated samples were made at 0.1 and 0.5 aquamolal (number of mol of solute per 55.51 mol of solvent) and the infinite dilution values obtained by linear extrapolation. This was justified since in H_2O the concentration dependence of the apparent molal volumes (ϕ_V) and apparent molal heat capacities (ϕ_C) of the protonated solutes is very nearly linear below 0.5 m. The experimental data in H_2O and D_2O are given in Tables 1 and 2. The derived ϕ_V and ϕ_C are given in a quadratic function, along with the data for urea in H_2O (8, 10), in Table 3. The excess volumes and heat capacities in H_2O and D_2O were estimated from the concentration dependence, assuming a linear behavior with both solvents below 0.5 m. The derived standard and excess transfer functions are summarized in Table 4. In H_2O, the expected uncertainties are 0.05 cm^3 mol^{-1} and 0.5 J K^{-1} mol^{-1} for ϕ_V and ϕ_C; in D_2O, they are probably somewhat larger. The transfer functions are reliable to about 0.1 cm^3 mol^{-1} and 1.0 J K^{-1} mol^{-1} in the best conditions.

Discussion

Nonpolar solutes or large tetraalkylammonium cations, which are usually considered hydrophobic, exhibit anomalous large positive standard partial molal capacities $\bar{C}_p^0$ ($\equiv \phi_C^0$) (26, 36), positive $\Delta C_{p\mathrm{tr}}^0$ ($H_2O \rightarrow D_2O$) (28) and ΔV_{tr}^0 ($H_2O \rightarrow D_2O$) (37), and negative $\bar{V}^{\mathrm{ex}}$

Can. J. Chem. Downloaded from www.nrcresearchpress.com by 210.87.254.105 on 09/05/12
For personal use only.

TABLE 2. Apparent molal volumes and heat capacities of methyl-substituted ureas in D_2O at 25 °C

Aquamolality	$10^3 (d - d_0)$	$10^3 \left(\frac{\sigma - \sigma_0}{\sigma_0}\right)$	ϕ_V	ϕ_C
		Deuterated urea		
0.10850	1.674	− 2.76	43.89	84.5
0.52260	7.808	−12.57	44.09	89.8
		Deuterated 1,1-dimethylurea		
0.11276	0.363	− 2.68	78.63	253.5
0.53283	1.783	−12.40	78.42	251.3
		Deuterated 1,3-dimethylurea		
0.10234	0.179	− 1.75	79.99	291.5
0.52319	1.008	− 8.84	79.77	288.7
		Tetramethylurea		
0.11346	−1.262	− 2.00	115.44	453.5
0.52723	−5.137	−10.02	114.58	438.7

d_0 1.10452 g cm^{-3}
c_{p0} 4.2116 J K^{-1} g^{-1}

TABLE 3. Apparent molal volumes and heat capacities of urea and substituted ureas in H_2O at 25 °C; polynomial coefficients of $\phi_Y = \phi_Y^0 + A_Y m + B_Y m^2$

	Volumes			Heat capacities			
	ϕ_V^0 (cm^3 mol^{-1})	A_V	B_V	ϕ_C^0 (J K^{-1} mol^{-1})	A_C	B_C	m_{max}
Urea (10, 8)	44.24	0.1159	−0.0032	87.45	5.566	−0.3283	10
1,1-Dimethylurea	78.88	−0.506	+0.058	247.77	− 6.991	+1.200	2.5
1,3-Dimethylurea	80.04	−0.489	+0.043	274.40	− 2.784	−0.290	6.4
Tetramethylurea	115.30	−0.733	+0.063	434.57	−20.708	+1.024	7.0

TABLE 4. Standard and excess volumes and heat capacities of transfer from H_2O to D_2O of urea and methyl-substituted ureas at 25 °C

	ΔV_{tr}^0 (cm^3 mol^{-1})	ΔC_{ptr}^0 (J K^{-1} mol^{-1})	ΔV_{tr}^{ex}†	ΔC_{ptr}^{ex}†
Urea	-0.3_6	(− 4.4)*	$+0.3_8$	+ 7.6
1,1-Dimethylurea	-0.2_2	(+ 6.2)	-0.0_2	− 1.0
1,3-Dimethylurea	-0.0_2	(+17.8)	-0.0_4	− 6.2
Tetramethylurea	$+0.2_8$	+22.9	-1.3_8	−15.7

*Values between parentheses are not corrected for the small difference between intrinsic values of the protonated and deuterated molecules.
†The excess transfer functions are defined by $\Delta Y_{tr}^{ex} = A_Y(D_2O) - A_Y(H_2O)$ in the concentration range 0–0.5 m.

(38), ΔV_{tr}^{ex} ($H_2O \rightarrow D_2O$) (28), and ΔC_{ptr}^{ex} ($H_2O \rightarrow D_2O$) (28). Information on solute–solvent interactions in aqueous solutions can be deduced from these thermodynamic properties and from H_2O to D_2O transfer functions.

Partial molal heat capacities are usually compared with the intrinsic heat capacities $\bar{C}_p$(in) of the solutes. In the case of the present solutes, exact $\bar{C}_p$(in) are unknown but can be reasonably approximated by the molar heat capacity of the pure substances: urea 93 (39), dimethylureas 140,[2] and tetramethylurea 253[3] J K^{-1} mol^{-1}. For deuterated molecules we can estimate them from the isotopic mass differences. Then we must add 6 and 3 J K^{-1} mol^{-1},

[2]Estimated from the variation of the heat of solution with temperature (5) and the present $\bar{C}_p^0$.

[3]Measured to ±0.5 % with the flow calorimeter.

Can. J. Chem. Downloaded from www.nrcresearchpress.com by 210.87.254.105 on 09/05/12
For personal use only.

TABLE 5. Average effects of substituting a —H atom by a —CH_3 group on methyl-substituted ureas

	$\delta\overline{V}^0(H_2O)$ ($cm^3\ mol^{-1}$)	δV_{tr}^0 ($cm^3\ mol^{-1}$)	$\delta\overline{C}_p^0(H_2O)$ ($J\ K^{-1}\ mol^{-1}$)	δC_{ptr}^0 ($J\ K^{-1}\ mol^{-1}$)
1/2 (1,1-Dimethylurea–urea)	17.3	0.0_7	$80._2$	$5._3$
1/2 (1,3-Dimethylurea–urea)	17.9	0.1_7	$93._5$	$11._1$
1/4 (Tetramethylurea–urea)	17.8	0.1_6	$86._8$	$6._8$

respectively, to obtain the intrinsic values of deuterated urea and dimethylureas; the ΔC_{ptr}^0 values in Table 4 corrected for this isotope effect should be $-10._4$, $+3._2$ and $+14._8$ $J\ K^{-1}\ mol^{-1}$ for urea, and 1,1-and 1,3-dimethylurea, respectively. The intrinsic volumes $\overline{V}$(in) can be considered, in first approximation, equal for the deuterated and protonated molecules and thus the ΔV_{tr}^0 need not be corrected.

The positive $\overline{C}_p^0 - \overline{C}_p$(in) and ΔC_{ptr}^0, and negative $\overline{V}^{ex}$, ΔV_{tr}^{ex}, and ΔC_{ptr}^{ex} of alkyl-substituted ureas are analogous to those of n-Bu_4NBr (28) which is usually considered an overall hydrophobic solute;[4] the only anomaly is the ΔV_{tr}^0 which is negative with dimethylureas. With urea, $\overline{C}_p^0 - \overline{C}_p$(in) is negative ($\simeq -5\ JK^{-1}\ mol^{-1}$) in H_2O; all the other transfer and excess functions of urea have also an opposite sign with respect to substituted ureas. By analogy with the behavior of structure-breaking ions, urea would be called an overall structure breaker; there is obviously an increase in ordering of water molecules from the new urea–water interactions but the overall number of hydrogen-bonding interactions has decreased.

Supporting evidence for this overall structure-breaking effect of urea comes from the B_η viscosity coefficient (42–44); the deviation from Einstein's law is negative in H_2O (-0.076 (18)) and even more so in D_2O (-0.086 (44)). Similarly, B_η increases with temperature in both H_2O and D_2O ($dB_\eta/dT\ (H_2O) = +0.0010$ (17); $dB_\eta/dT\ (D_2O) = +0.0012$ (44)).

It has been observed that the addition of hydrogen-bonding groups such as —OH (45, 46) and —COONa (46) on a hydrophobic solute reduces $\overline{C}_p^0$ significantly and makes $\overline{C}_p^{ex}$ positive at 25 °C (46, 47). Similarly the addition of a —NH_2 group on an alkyl chain (6) reduces $\overline{C}_p^0$ by 187 $J\ K^{-1}\ mol^{-1}$.

[4]Like the substituted ureas, n-Bu_4NBr shows a negative $\overline{C}_p^{ex}$ (negative deviation from the Debye–Hückel limiting law) at 25 °C. However, at 5 °C, n-Bu_4NBr now shows a slightly positive $\overline{C}_p^{ex}$ (40), as in the case of linear-chain alcohols (41). We must therefore be careful at this stage in drawing conclusions from the sign of $\overline{C}_p^{ex}$.

However, in the case of urea, the small values of $\overline{C}_p^0 - \overline{C}_p$(in) and ΔC_{ptr}^0 suggest that the hydrogen-bonding group contributes a relatively small amount to the decrease in heat capacity and that the large changes in $\overline{C}_p^0$ and $\overline{C}_p^{ex}$ accompanying the addition of an hydrogen-bonding group on alkyl chain is probably due to some kind of interference or competition between water in the hydrophobic hydration layer and that hydrogen bonded to the polar group.

A closer examination of the alkyl-substitution effect may throw some light on the value and relative importance of these hydrogen-bonding interactions. Methyl substitution on amino groups has three effects: (*i*) a contribution from the methyl group itself (intrinsic and hydrophobic), (*ii*) a hindrance of hydrogen-bonding ability of the substituted amino group, (*iii*) a decrease of hydrogen-bonding ability of the carbonyl group as indicated by the dipole moments (48) and the nuclear quadrupole resonance (49).

The average methylene contributions (—CH_3 minus —H) to volumes and heat capacities for the different alkyl-substituted ureas are shown in Table 5.

The addition of a methylene group on an alkyl chain increases $\overline{V}^0$ and $\overline{C}_p^0$ by 15.9 $cm^3\ mol^{-1}$ (50) and 90 $J\ K^{-1}\ mol^{-1}$ (6, 26, 28, 45, 51) in H_2O. For transfer functions the only valuable data based on tetraalkylammonium cations (28, 37) are: $\delta V_{tr}^0 = 0.1\ cm^3\ mol^{-1}$ and $\delta C_{ptr}^0 = 5\ J\ K^{-1}\ mol^{-1}$ (in agreement with the values of Kresheck *et al.* (26) for alkanes). From the values in Table 5, it is obvious that the main contributions to the addition of a methylene group are the intrinsic value and the hydrophobic hydration. There are, however, significant differences between the alkyl-substituted ureas, especially with heat capacities. If the hydrogen-bonding interactions had no effect or no specificity among the various homologs, the methylene group contribution would be the same for all ureas. Except for 1,1-dimethylurea, δV_{tr}^0 and δC_{ptr}^0 (Table 5) are greater than the expected

Can. J. Chem. Downloaded from www.nrcresearchpress.com by 210.87.254.105 on 09/05/12
For personal use only.

values, probably due to interactions between water and N—H and C=O groups which exist with the unsubstituted molecule and are hindered or decreased with 1,3-dimethylurea and tetramethylurea. Furthermore, with respect to heat capacities, the difference is larger with 1,3-dimethylurea than tetramethylurea. Concerning these two molecules, the hydrogen-bonding ability of amino groups is hindered and only the carbonyl–water interactions can be considered. A possible explanation is that the C=O–water interactions are the most important and that they are maximal when the dipole moment is the greatest (1,3-dimethylurea larger than tetramethylurea (48, 49)).

We are grateful to the National Research Council of Canada and Environment Canada for financial support of this project. We would also like to thank Dr. A. Hade of the Université du Québec à Montréal for the loan of an Anton Paar digital densimeter Model DMA 02C.

1. J. S. Franzen and R. E. Stephens. Biochemistry, **2**, 1321 (1963).
2. I. M. Klotz and J. S. Franzen. J. Am. Chem. Soc. **84**, 3461 (1962).
3. G. Barone, E. Rizzo, and V. Vitagliano. J. Phys. Chem. **74**, 2230 (1970).
4. C. de Loze, P. Combelas, P. Bacelon, and C. Garrigou-Lagrange. J. Chim. Phys. **69**, 397 (1972).
5. S. Subramanian, T. S. Sarma, D. Balasubramanian, and J. C. Ahluwalia. J. Phys. Chem. **75**, 815 (1971).
6. J. Konicek and I. Wadso. Acta Chem. Scand. **25**, 1541 (1971).
7. K. R. Lindfors, S. H. Opperman, M. E. Glover, and J. O. Seese. J. Phys. Chem. **75**, 3313 (1971).
8. P. Picker, P. A. Leduc, P. R. Philip, and J. E. Desnoyers. J. Chem. Thermodyn. **3**, 631 (1971).
9. P. R. Philip, J. E. Desnoyers, and A. Hade. Can. J. Chem. **51**, 187 (1973).
10. F. T. Gucker, F. W. Gage, and C. E. Moser. J. Am. Chem. Soc. **60**, 2582 (1938).
11. E. P. Egan and B. B. Luff. J. Chem. Eng. Data, **11**, 192 (1966).
12. V. E. Bower and R. A. Robinson. J. Phys. Chem. **67**, 1524 (1963).
13. J. G. Albright and R. Mills. J. Phys. Chem. **69**, 3120 (1965).
14. G. C. Hammes and P. R. Schimmel. J. Am. Chem. Soc. **89**, 442 (1967).
15. J. C. Macdonald and J. J. Guerrera. J. Chem. Eng. Data, **15**, 546 (1970).
16. J. C. MacDonald, J. Serphillips, and J. J. Guerrera. J. Phys. Chem. **77**, 370 (1973).
17. H. M. Chadwell and B. Asnes. J. Am. Chem. Soc. **52**, 3507 (1930).
18. T. T. Herskovits and T. M. Kelly. J. Phys. Chem. **77**, 381 (1973).
19. R. L. Vold, E. S. Daniel, and S. O. Chan. J. Am. Chem. Soc. **92**, 6771 (1970).
20. E. G. Finer, F. Franks, and M. J. Tait. J. Am. Chem. Soc. **94**, 4424 (1972).
21. F. W. Miller and H. R. Dittmar. J. Am. Chem. Soc. **56**, 848 (1934).
22. Handbook of chemistry and physics. 50th Ed. The Chemical Rubber Co. Cleveland, Ohio. 1969–1970.
23. T. A. Zordan, D. G. Hurkot, M. Peterson, and L. G. Hepler. Thermochim. Acta, **5**, 21 (1972).
24. H. L. Friedman. J. Chem. Phys. **32**, 1351 (1960).
25. A. Johansson and P. A. Kollman. J. Am. Chem. Soc. **94**, 6196 (1972).
26. G. C. Kresheck, H. Schneider, and H. A. Scheraga. J. Phys. Chem. **69**, 3132 (1965).
27. J. E. Desnoyers, R. Francescon, P. Picker, and C. Jolicoeur. Can. J. Chem. **49**, 3460 (1971).
28. P. R. Philip and J. E. Desnoyers. J. Sol. Chem. **1**, 353 (1972).
29. L. Benjamin and G. C. Benson. J. Phys. Chem. **67**, 858 (1963).
30. D. N. Glew and H. Watts. Can. J. Chem. **51**, 1933 (1973).
31. M. Calvin, J. Hermans Jr., and H. A. Scheraga. J. Am. Chem. Soc. **81**, 5048 (1959).
32. H. A. Scheraga. Ann. N.Y. Acad. Sci. **84**, 608 (1960).
33. G. C. Kresheck, D. Kierleber, and R. J. Albers. J. Am. Chem. Soc. **94**, 8889 (1972).
34. O. Kratky, H. Leopold, and H. Stabinger. Z. Angew. Phys. **27**, 273 (1969).
35. P. Picker, E. Tremblay, and C. Jolicoeur. J. Sol. Chem. (In press.)
36. H. S. Frank and W. Y. Wen. Disc. Faraday Soc. **24**, 133 (1957).
37. B. E. Conway and L. H. Laliberté. Trans. Faraday Soc. **66**, 3032 (1970).
38. J. E. Desnoyers, M. Arel, G. Perron, and C. Jolicoeur. J. Phys. Chem. **73**, 3346 (1969).
39. Selected values of chemical thermodynamic properties. Circular of the National Bureau of Standards 500. Washington D.C. 1952.
40. G. Perron and J. E. Desnoyers. (In preparation.)
41. C. Jolicoeur. Private communication.
42. R. L. Kay. Adv. Chem. Series, **73**, 1 (1968).
43. J. E. Desnoyers and G. Perron. J. Sol. Chem. **1**, 199 (1972).
44. G. A. Vidulich. Private communication.
45. E. M. Arnett, W. B. Kover, and J. V. Carter. J. Am. Chem. Soc. **91**, 4028 (1969).
46. J. E. Desnoyers, R. Pagé, G. Perron, J. L. Fortier, P. A. Leduc, and R. F. Platford. Can. J. Chem. **51**, 2129 (1973).
47. P. A. Leduc and J. E. Desnoyers. Can. J. Chem. **51**, 2993 (1973).
48. W. D. Kumler and G. M. Fohlen. J. Am. Chem. Soc. **64**, 1944 (1942).
49. D. and M. Rogers. J. Chem. Phys. **57**, 3726 (1972).
50. J. E. Desnoyers and M. Arel. Can. J. Chem. **45**, 359 (1967).
51. P. A. Leduc, J.-L. Fortier, and J. E. Desnoyers. J. Phys. Chem. In press.

Can. J. Chem. Downloaded from www.nrcresearchpress.com by 210.87.254.105 on 09/05/12
For personal use only.

Preparation and Nuclear Magnetic Resonance Study of Phosphorus Compounds Containing Alkenyl Functional Groups[1]

PETER W. CLARK, JOHN L. S. CURTIS, PHILIP E. GARROU, AND GEORGE E. HARTWELL[2]

Department of Chemistry, Indiana University, Bloomington, Indiana 47401

Received October 3, 1973

The phosphines $PPh_n(CH_2CH_2CH{=}CH_2)_{3-n}$, n = 2–0, $PPh_n(CH_2CH_2CH_2CH{=}CH_2)_{3-n}$, n = 1 or 2, and $PPh_2CH_2CH{=}CH_2$ have been synthesized and studied by ^1H and ^{31}P magnetic resonance. The n.m.r. spectra of $PPh_2(OCH_2CH{=}CH_2)$, its oxide, $O{=}PPh_2(OCH_2CH{=}CH_2)$, and its Arbuzov rearrangement product, $O{=}PPh_2(CH_2CH{=}CH_2)$, have been investigated by ^{31}P decoupling of the proton spectrum, selective proton decoupling of the ^{31}P spectrum, and comparison with computer-simulated spectra to determine the spin–spin coupling constants. The n.m.r. spectra of the related oxides $O{=}PPh_2CH_2CH_2CH{=}CH_2$, $O{=}P(CH_2CH_2CH{=}CH_2)_3$, and $O{=}P(OCH_2CH{=}CH_2)_3$ are also assigned. The data indicate that $^3J_{PH} > {}^2J_{PH}$ for alkenylphosphines, $^2J_{PH}$ is larger for phosphine oxides than for phosphines, and $^3J_{PH}$ is little changed in comparing phosphorus(III) with phosphorus(V) compounds.

On a synthétisé les phosphines $PPh_n(CH_2CH_2CH{=}CH_2)_{3-n}$, n = 2–0, $PPh_n(CH_2CH_2CH_2CH{=}CH_2)_{3-n}$, n = 1 ou 2 et $PPh_2CH_2CH{=}CH_2$ et étudié leurs spectres de résonance magnétique du proton et du ^{31}P. Les spectres r.m.n. du $PPh_2(OCH_2CH{=}CH_2)$, de son oxyde $O{=}PPh_2(OCH_2CH{=}CH_2)$ et de son produit de réarrangement d'Arbuzov $O{=}PPh_2(CH_2CH{=}CH_2)$, ont été examiné en découplant le phosphore du spectre du proton, en découplant d'une façon sélective des protons du spectre du ^{31}P et par comparaison avec des spectres simulés par ordinateur pour déterminer les constantes de couplage spin–spin. Les spectres r.m.n. des oxydes $O{=}PPh_2CH_2CH_2CH{=}CH_2$, $O{=}P(CH_2CH_2CH{=}CH_2)_3$ et $O{=}P(OCH_2CH{=}CH_2)_3$ ont aussi été attribués. Les données indiquent que $^3J_{PH} > {}^2J_{PH}$ pour les alkénylphosphines que $^2J_{PH}$ est plus grand pour les oxydes de phosphine que pour les phosphines et que le $^3J_{PH}$ ne subit que peu de changement lorsque l'on compare les composés du phosphore(III) avec les composés du phosphore(V). [Traduit par le journal]

Can. J. Chem., **52**, 1714 (1974)

Introduction

The use of phosphine and phosphite compounds as ligands in low-valent transition metal complexes has increased steadily during the last decade (1). Tertiary phosphorus compounds are able to stabilize electron rich metal atoms since phosphorus participates in σ donation to the metal and may also accept electron density from the metal into energetically favorable d orbitals. In spite of the widespread use of phosphorus compounds as ligands, little n.m.r. data on phosphines containing alkenyl groups is available even though they have been shown to function as chelates with a large number of transition metals (2–8). The determination of the structure of metal–phosphorus complexes is frequently based on the assignment of their ^1H and ^{31}P spectra. In general, a corresponding amount of data concerning the uncomplexed phosphorus ligands has not appeared. We wish to report the ^1H and ^{31}P magnetic resonance spectra of a representative series of phosphine, phosphinite, and phosphite complexes and to present generalizations concerning the chemical shift and coupling data (Fig. 1) for these potential ligands.

Experimental

All reactions were run under an atmosphere of argon using freshly distilled reactants and solvents. Due to the air sensitivity of the phosphorus(III) compounds, all manipulations were carried out under an inert atmosphere. All phosphines were stored under argon and were removed by syringe while under an argon flow.

$PClPh_2$, PCl_2Ph, and PCl_3 were purchased from Aldrich Chemical Co. 4-Bromo-1-butene and 5-bromo-1-butene were purchased from Pierce Chemical Co. The phosphites $P(OCH_2CH{=}CH_2)_3$ and $O{=}P(OCH_2CH{=}CH_2)_3$ were a gift from the Weston Chemical Co.

^{31}P spectra were recorded on a Varian XL-100 spectrometer using 50% by volume solutions in $CHCl_3$. ^1H spectra were obtained on a Varian HR 220 spectrometer using 50% solutions in $CDCl_3$. Phosphorus decoupling power was generated using standard components: an HP-5100B frequency synthesizer, an HP-10515A fre-

[1]Contribution No. 2352. Department of Chemistry, Indiana University.

[2]To whom inquiries should be addressed.

Can. J. Chem. Downloaded from www.nrcresearchpress.com by 210.87.254.6 on 09/05/12
For personal use only.

TABLE 1. Preparation of phosphorus(III) compounds

Compound	Alkene	Chlorophosphine	Boiling point (°C)	Yield (%)
$PPh_2(OCH_2CH{=}CH_2)$	$HOCH_2CH{=}CH_2$	$PClPh_2$		92
$PPh_2{-}CH_2CH{=}CH_2$	$ClCH_2CH{=}CH_2$	$PClPh_2$	118–128(0.2 Torr)	80
$PPh_2((CH_2)_2CH{=}CH_2)$	$Br(CH_2)_2CH{=}CH_2$	$PClPh_2$	115 (0.1 Torr)	85
$PPh_2((CH_2)_3CH{=}CH_2)$	$Br(CH_2)_3CH{=}CH_2$	$PClPh_2$	152–154(0.8 Torr)	67
$PPh((CH_2)_2CH{=}CH_2)_2$	$Br(CH_2)_2CH{=}CH_2$	PCl_2Ph	120–122(0.2 Torr)	79
$PPh((CH_2)_3CH{=}CH_2)_2$	$Br(CH_2)_3CH{=}CH_2$	PCl_2Ph	131–133(1.0 Torr)	84
$P((CH_2)_2CH{=}CH_2)_3$	$Br(CH_2)_2CH{=}CH_2$	PCl_3	65– 75(1.0 Torr)	54

quency doubler, an HP-230B tuned amplifier, and an ENI 10 W broad band power amplifier. The additional equipment necessary, a probe matching network, attenuator, and a through-line power SWR meter allowed generation of up to 10 W decoupling power at 89 MHz for the HR 220 probe while observing proton decoupling in the frequency sweep mode.

Theoretical spectra were obtained using a Nicolet n.m.r. spectrum calculation program (NMRCAL) NIC-80/S-7117-D.

Preparation of $P(CH_2CH_2CH{=}CH_2)_3$

All of the PR_3 ligands were prepared by the general method outlined here for $P(CH_2CH_2CH{=}CH_2)_3$. The specific alkene and phosphine chloride used are tabulated in Table 1 along with boiling points and yields.

A Grignard reagent was prepared under argon in a predried reaction vessel by the slow addition of 4-bromo-1-butene (66.0 g, 0.489 mol) in 150 ml of predried ether to magnesium turnings (13.2 g, 0.544 mol) in 300 ml of refluxing ethyl ether. When the formation of the Grignard reagent was complete, phosphorus trichloride (18.7 g, 0.136 mol) in 250 ml of ethyl ether was added dropwise to the solution while maintaining the temperature at 0 °C. Upon completion of the addition, the excess Grignard reagent was hydrolyzed with 50 g of NH_4Cl in 250 ml of water. The organic layer was siphoned into a second flask, dried over Na_2SO_4, and distilled under reduced pressure. All manipulations were carried out under a flow of argon since the phosphine is air sensitive.

All reported oxides were prepared by air oxidation. They were then washed with hexane, dried, and checked for purity by examination of their ^1H and ^{31}P n.m.r. spectra. $O{=}PPh_2(CH_2CH{=}CH_2)$ was also prepared by Arbuzov rearrangement of $PPh_2(OCH_2CH{=}CH_2)$ as described below.

Preparation of $PPh_2(OCH_2CH{=}CH_2)$

This reaction was carried out in a manner similar to that previously reported (9) under a flow of argon in a predried reaction vessel using freshly distilled allyl alcohol and $PClPh_2$. Allyl alcohol (2.8 ml, 0.041 mol), pyridine (3.2 ml, 0.041 mol), and 40 ml of dry ethyl ether were chilled to 0° in an ice bath. $PClPh_2$ (7.1 ml, 0.040 mol) in ether (4 ml) was added over a period of 30 min. The solution was allowed to stir for 20 min and the pyridine hydrochloride, which had precipitated, was then separated by filtration using standard Schlenk technique. The excess reagents and ethyl ether were removed under vacuum. The liquid product cannot be distilled due to extensive Arbuzov rearrangement to $O{=}P(CH_2CH{=}CH_2)$ when heated (10). Purity was checked by ^1H n.m.r. integration and by the absence, in the ^{31}P n.m.r. spectra, of resonances due to species produced by rearrangement or oxidation.

Allowing $PPh_2(OCH_2CH{=}CH_2)$ to come into contact with air for 12 h resulted in its oxidation to $O{=}PPh_2(OCH_2CH{=}CH_2)$ which may also be synthesized by reacting diphenylphosphinic chloride with allyl alcohol in the presence of triethylamine in ether (11).

Results and Discussion

Nuclear Magnetic Resonance Chemical Shifts

A considerable effort has been spent in the interpretation of ^{31}P chemical shifts (12, 13). Changes in the number of substituents and their electronegativities, the degree of π-bonding, and the resultant bond angles about the phosphorus have all been considered. The interrelationships among these parameters and the importance of each have, however, not been established for even the symmetrically substituted phosphines, PR_3. For unsymmetrically substituted compounds the problem is more difficult.

The phosphorus chemical shift values listed in Table 2 can, however, be separated into three groups: PR_3, $\delta = +16$ to $+30.7$ p.p.m.; $O{=}PR_3$, $O{=}P(OR)R_2$, and $O{=}P(OR)_3$, $\delta = -45.9$ to $+1.9$ p.p.m.; and $P(OR)R_2$ and $P(OR)_3$, $\delta = -113$ to -138.8 p.p.m. The large chemical shift difference between groupings is of value for qualitative (12) and semi-quantitative determination of sample purity for these compounds.

Examination of the ^1H n.m.r. spectra of the 13 phosphorus compounds shows three olefinic protons in the region 4.11 to 5.14 τ; methylene protons are observed in the region 7.65 to 8.56 τ for butenyl and pentenyl, *ca.* 7 τ for allyldiphenylphosphine and allyldiphenylphosphine oxide, and *ca.* 5.5–5.7 τ for phosphinites, phosphites, and their oxides.

The phenyl resonance consists of two multiplets, ratio 2:3, consistent with the usual assign-

Can. J. Chem. Downloaded from www.nrcresearchpress.com by 210.87.254.6 on 09/05/12
For personal use only.

Can. J. Chem. Downloaded from www.nrcresearchpress.com by 210.87.254.6 on 09/05/12
For personal use only.

TABLE 2. Nuclear magnetic resonance data

Compound[a]	^{31}P	H_1	H_2	H_3	H_4	H_5	H_6	H_7	H_8	^3J (H_1–H_3)	^3J (H_2–H_3)	^3J (H_3–H_4)	$^2J_{PH}$	$^3J_{PH}$
$PPh_2OCH_2CH{=}CH_2$[b] (map)	−113.0	4.81	4.99	4.21	5.74			2.53	2.72	17.0	10.3	5.2		9.6
$O{=}PPh_2OCH_2CH{=}CH_2$ (mapo)	−30.9	4.73	4.83	4.13	5.53			2.20	2.63	17.0	10.4	5.6		8.6
$P[OCH_2CH{=}CH_2]_3$[c] (tap)	−138.8	4.76	4.90	4.15	5.72					17.0	10.4	5.2		8.0
$O{=}P[OCH_2CH{=}CH_2]_3$ (tapo)	+1.9	4.69	4.81	4.11	5.50					17.0	10.4	5.6		8.8
$PPh_2CH_2CH{=}CH_2$ (app)	+17.1	5.10	5.14	4.31	7.23			2.60	2.74	17.0	10.3	7.0	≤0.8	6.0
$O{=}PPh_2CH_2CH{=}CH_2$ (appo)	−28.2	4.85	4.85	4.23	6.87			2.20	2.48			7.4	14.4	6.0
$PPh_2(CH_2)_2CH{=}CH_2$ (mbp)	+16.5	5.06	5.11	4.19	7.9	7.9		2.60	2.70	17.0	10.3	5.9		7.5
$O{=}PPh_2(CH_2)_2CH{=}CH_2$ (mbpo)	−30.8	5.03	5.11	4.25	7.65	7.65		2.27	2.61	17.0	10.3	5.4		
$PPh_2(CH_2)_3CH{=}CH_2$ (mpp)	+17.6	5.06	5.13	4.28	7.91	8.51	8.02	2.66	2.86	17.2	10.3	6.6	≤0.8	8.0
$PPh[(CH_2)_2CH{=}CH_2]_2$[d] (dbp)	+25.4	5.00	5.08	4.17	7.92	8.20		2.52	2.68	17.2	10.2	6.6	≤0.8	
$PPh[(CH_2)_3CH{=}CH_2]_2$[e] (dpp)	+26.3	5.10	5.12	4.32	7.95	8.56	8.36	2.58	2.75	17.0	10.4	6.6	≤0.8	8.5
$P[(CH_2)_2CH{=}CH_2]_3$[f] (tbp)	+30.2	4.98	5.06	4.18	7.86	8.53				17.1	10.2	6.0	≤0.8	7.8
$O{=}P[(CH_2)_2CH{=}CH_2]_3$[g] (tbpo)	−45.9	4.90	4.98	4.24	7.57	8.25				17.1	10.3		10.6	

[a]The ^1H n.m.r. spectra of all compounds were analyzed at 16 °C at 220 MHz in 50% (vol.) $CDCl_3$ with TMS as reference at τ 10.0. ^{31}P chemical shifts (±0.3 p.p.m.) are relative to 85% H_3PO_4. Chemical shifts are for the center of the multiplet. All peak intensities were checked by integration.

[b]Additional coupling constants are: $^4J(P{-}H_3) \leq 0.8$ Hz, $^5J(P{-}H_1)$ and $^5J(P{-}H_2) \leq 1$ Hz.

[c]Additional coupling constants are: $^4J(P{-}H_3) \leq 0.8$ Hz, $^5J(P{-}H_1)$ and $^5J(P{-}H_2) \leq 1$ Hz.

[d]Additional coupling constants are: $^3J(H_4{-}H_5') = {}^3J(H_4'{-}H_5) = 7.0$ Hz, $^3J(H_4'{-}H_5') = J(H_4{-}H_5) = 8.0$ Hz, $^2J(P{-}H_5) = {}^2J(P{-}H_5') \leq 0.8$.

[e]Additional coupling constants are: $^3J(H_5{-}H_6') = {}^3J(H_5'{-}H_6) = 7.0$ Hz, $^3J(H_5'{-}H_6') = {}^3J(H_5{-}H_6) = 8.0$ Hz, $^2J(P{-}H_6) = {}^2J(P{-}H_6') \leq 0.8$.

[f]Additional coupling constants are: $^3J(H_4{-}H_5') = {}^3J(H_4'{-}H_5) = 6.0$ Hz, $^3J(H_4'{-}H_5') = {}^3J(H_4{-}H_5) = 10.5$ Hz, $^2J(H_4{-}H_4') = {}^2J(H_5{-}H_5') = 10$ Hz, $^2J(P{-}H_5) = {}^2J(P{-}H_5') \leq 0.8$ Hz.

[g]Additional coupling constants are: $^3J(H_4{-}H_5') = {}^3J(H_4'{-}H_5) = 6.0$ Hz, $^3J(H_4'{-}H_5') = {}^3J(H_4{-}H_5) = 10.5$ Hz, $^2J(H_4{-}H_4') = {}^2J(H_5{-}H_5') = 10$ Hz, $^2J(P{-}H_5) = {}^2J(P{-}H_5') = 10.6$ Hz.

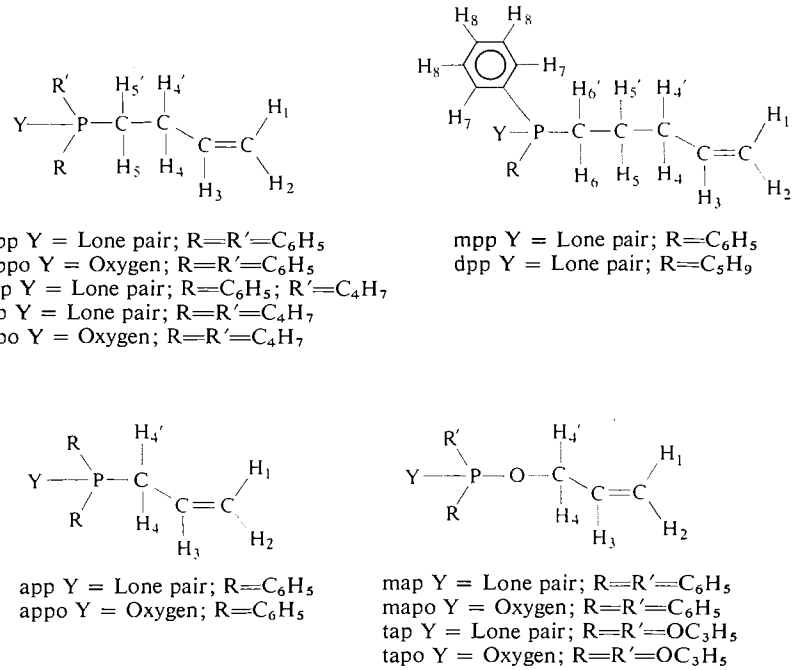

FIG. 1. Numbering system for the protons of the compounds studied.

ment of two lower field *ortho* protons and three higher field *meta–para* protons. The *ortho* protons in the oxides are shifted to lower fields, 2.20–2.27 τ, than the corresponding phosphorus(III) compounds, 2.52–2.66 τ. This difference in chemical shifts for the *ortho* protons is helpful in the determination of sample purity.

Nuclear Magnetic Resonance Spin–Spin Coupling Constants

The reported variations in the magnitude of P–H couplings are large. In phosphine compounds, PR_3, the observed vicinal coupling constant is larger than the geminal coupling constant $^3J_{PH} > {}^2J_{PH}$; *e.g.* in $P(CH_2CH_3)_3$, $^3J_{PH} = +13.65$ and $^2J_{PH} = +0.5$ (12); and in $P[CH(CH_3)_2]_3$, $^3J_{PH} = +11.73$ and $^2J_{PH} = -2.27$ Hz (14).

The magnitudes of both the geminal and vicinal phosphorus–hydrogen coupling constants have been shown to have angular dependence. The geminal coupling constants in a rigid structure like that for 1-phenyl-3,4-dimethylphosphocyclo-3-pentene vary between +25 Hz for $^2J_{PH}$ at a dihedral angle of 9° from the phosphine lone pair to the geminal hydrogen to −6 Hz for $^2J_{PH}$ where the hydrogen is at a dihedral angle of 111° (15). In compounds where free rotation about the P—C bond is possible $^2J_{PH}$ represents the weighted average of the coupling constants, depending upon the populations of the various conformers. Vicinal coupling constants in cyclic compounds containing the P—O—C linkage have been related to the P—O—C—H dihedral angle with $^3J_{PH}$ reaching a maximum when phosphorus is *trans* to hydrogen and a minimum in the *gauche* position (16). Another study (17) on such cyclic compounds has shown vicinal coupling constants can also be related to the stereochemistry of the phosphorus lone pair. Values as large as 33 Hz have been observed (18). In systems with fast rotation about the O—C bond axis, average $^3J_{PH}$ coupling constants were observed (12), *e.g.* $O{=}P(OCH_2CH_3)_3$, 8.7 Hz and $P(Ph)(OCH_2CH_3)_2$, 6.9 Hz.

The presence of only one methylene group in allyldiphenylphosphinite (map) and tris(allyl)-phosphite (tap) permitted the interpretation and assignment of all phosphorus–hydrogen couplings (Table 2). The assignment of the larger coupling in the methylene resonance (Fig. 2) to $^3J_{PH}$ for map was confirmed by ^{31}P partial decoupling of the ^1H n.m.r. spectrum resulting in

Can. J. Chem. Downloaded from www.nrcresearchpress.com by 210.87.254.6 on 09/05/12
For personal use only.

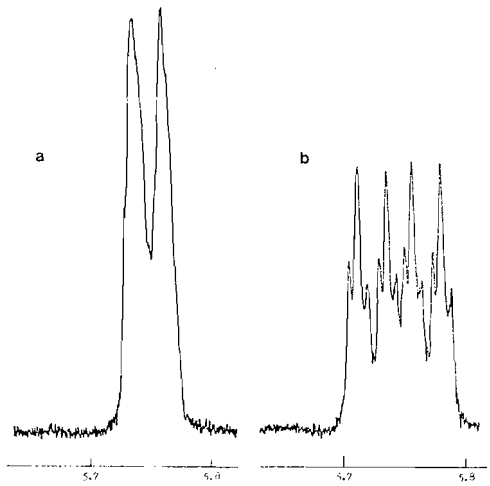

FIG. 2. The 220 MHz ^{1}H n.m.r. spectrum of the methylene region of allyldiphenylphosphinite (map): (*a*) phosphorus decoupled, (*b*) normal.

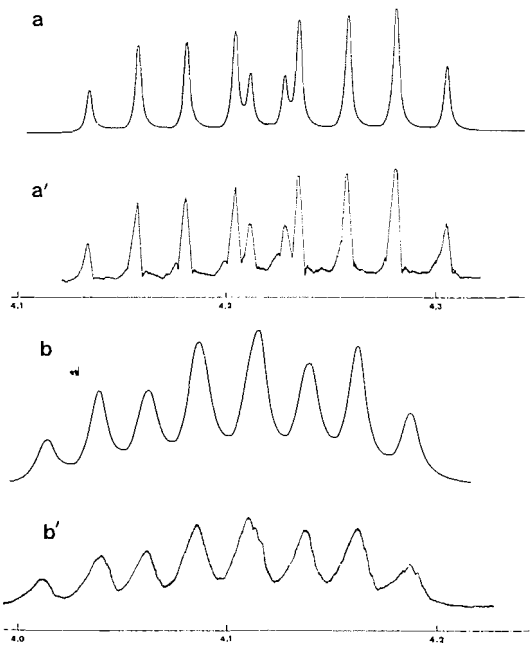

FIG. 3. The 220 MHz ^{1}H n.m.r. spectra of the H_3 olefinic proton in: (*a*) allyldiphenylphosphinite (map), computer simulated, (*a'*) observed; (*b*) triallylphosphate (tapo), computer simulated, (*b'*) observed.

collapse of the quartet of triplets to a pseudo doublet of triplets. The larger remaining coupling in this methylene resonance (Fig. 2*a*) was assigned as vicinal coupling to the olefinic proton, H_3, $^3J(H_3–H_4) = 5.2$ Hz, confirmed by comparison with the computer simulated spectrum (Fig. 3*a*). The vicinal phosphorus–hydrogen coupling for tap was confirmed by observation of the hydrogen coupled ^{31}P resonance at $\delta = -138.8$ in which a septet (single peak $w_{1/2} = 2.2$ Hz) is observed due to coupling to six equivalent methylene protons with $^3J_{PH} = 8.0$ Hz. Additional coupling, $^3J(H_3–H_4) = 5.3$ Hz, was assigned by comparison of the ^{1}H n.m.r. spectrum to the synthesized spectrum (Fig. 3*b*); broadening of the multiplet may be due to additional H–H coupling across phosphorus. The long range phosphorus–hydrogen coupling in map and tap is $^4J(P–H_3) \leqslant 0.8$ Hz, $^5J(P–H_1)$ and $^5J(P–H_2) \leqslant 1$ Hz. Surprisingly, for the oxides of map and tap, $^3J_{PH} = 8.6$ and 8.8 Hz, respectively, varying less than 1 Hz from the corresponding coupling in map and tap.

The assignment of the coupling in the phosphine compounds reported in Table 2 resulted in values of $^2J_{PH} \leqslant 0.8$ Hz and $^3J_{PH} = 6.0$–8.5 Hz. No effort was made to determine the signs of the geminal coupling constants since the values are quite small. The vicinal coupling constants were assumed to be positive. The interpretation of the multiplets for the methylene protons becomes increasingly complicated with increasing numbers of methylene groups due to overlap of the resonances. The assignment of $^2J_{PH} \leqslant 0.8$ and $^3J_{PH} = 6.0$ Hz for the methylene protons in allyldiphenylphosphine (app) is based upon analysis of the ^{1}H n.m.r. spectrum as an A_2BCDX system ($A_2 = H_4$, H_4'; $B = H_2$; $C = H_1$; $D = H_3$; $X = P$) and is confirmed, with assignment of $^3J(H_3,H_4) = 7.0$ Hz, by comparison of the H_3 resonance to the computed spectrum. In the butenyl- and pentenylphosphines the vicinal coupling between H_3 and the adjacent methylene protons, H_4, was obtained from analysis of the H_3 resonance. Phosphorus–hydrogen coupling of similar magnitude to that in app occurs in the other phosphines, for example in tbp $^2J_{PH} \leqslant 0.8$ and $^3J_{PH} = 7.8$ Hz. However, in the oxides of these phosphines the magnitude of the geminal coupling $^2J_{PH}$ is much greater. In allyldiphenylphosphine oxide (appo) $^2J_{PH} = 14.4$ and $^3J_{PH} = 6.0$, and in tributenylphosphine oxide (tbpo) $^2J_{PH} = 10.6$ Hz. This behavior has been previously observed upon complexation of phosphorus(III) compounds to transition metals (19). Thus the large change in $^2J_{PH}$ (from *ca.* 0 to *ca.* 10–14) is valuable in indicating an increase in oxidation state or coordination number of the phosphorus.

The ^{1}H n.m.r. spectra of tributenylphosphine

Can. J. Chem. Downloaded from www.nrcresearchpress.com by 210.87.254.6 on 09/05/12
For personal use only.

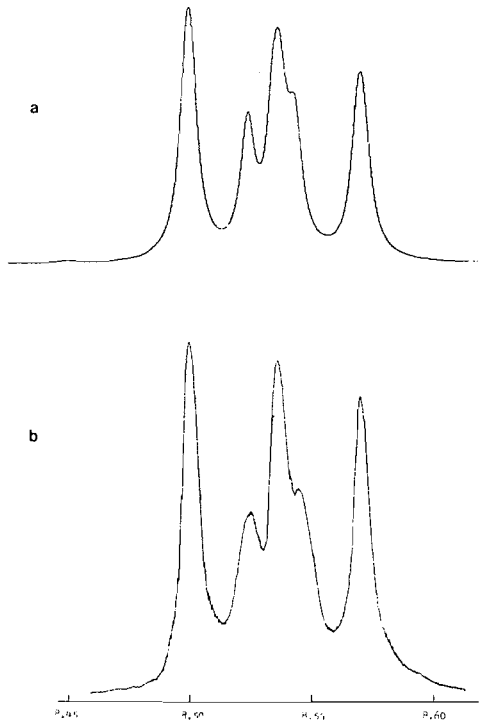

FIG. 4. The 220 MHz ^1H n.m.r. spectra of the methylene protons, H_5, for tributenylphosphine (tbp): (*a*) computer simulated, (*b*) observed.

(tbp) and tributenylphosphine oxide (tbpo) revealed the expected nonequivalence of the methylene protons. These protons appear as part of a pseudo AA'BB'MX pattern (A,A' = H_5,H_5'; B,B' = H_4,H_4'; M = H_3; X = P) since the coupling through the phosphorus and that to H_1 and H_2 is relatively small. For tbp, the spectrum of these methylene protons was computer simulated as a six-spin system using the data in Table 2. Figure 4 compares the calculated and observed spectra of the H_5 protons at 8.53 τ. The H_4 resonance at 7.86 τ was also synthesized with the phosphorus coupling determined by ^{31}P decoupling of the ^1H n.m.r. and by observation of the methylene proton coupling in the ^{31}P n.m.r. spectrum. The ^1H n.m.r. spectrum of tbp did not change between −50 and 50°. The spectrum of tbpo was similar except for the effect of the change of $^2J_{PH}$, from $\leqslant 0.5$ for tbp, to 10.6 Hz for tbpo. The vicinal methylene coupling is 6.0 and 10.5 Hz for both compounds. This data is consistent with rapid rotation about the carbon–carbon bond with a preference for conformer (I), Fig. 5.

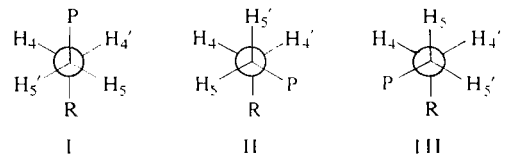

FIG. 5. Possible conformers of $PCH_2—CH_2R$.

In contrast, the calculated spectra for the H_5 resonances of dibutenylphenylphosphine (dbp) and dipentenylphenylphosphine (dpp) require average vicinal methylene coupling constants of 7 and 8 Hz. These values are also consistent with a rapid rotation about the axis of the two methylene groups but with a nearly equal population of the three conformers.

Vicinal methylene coupling constants could not be determined for butenyldiphenylphosphine (mbp) or pentenyldiphenylphosphine (mpp) due to overlap of resonances.

Practically no variation was observed in the magnitude of the *trans* or *cis* coupling constants for the olefinic protons. The geminal coupling was less than 1.5 Hz.

To conclude, the previously reported behavior showing $^3J_{PH} > {}^2J_{PH}$ for non-cyclized phosphines also occurs in the alkenyl phosphines reported in this work. For the two phosphine oxides in which $^2J_{PH}$ could be determined, appo and tbpo, the magnitude is much larger than in the corresponding phosphine. In the three compounds for which it was possible to obtain $^3J_{PH}$ for *both* the phosphorus(III) and the phosphorus(V) compounds, the change was minimal. Thus, $^2J_{PH}$ in the phosphine oxides studied is greater than $^3J_{PH}$. For all of the compounds only minimal changes in the olefinic coupling constants were observed.

1. G. M. KOSOLAPOFF and L. MAIER. Organic phosphorus compounds. Vols. 1 and 2. Wiley-Interscience Publishers, Inc., New York. 1972.
2. R. S. NYHOLM. Soumen Kemistelenti, 165 (1969).
3. P. W. CLARK and G. E. HARTWELL. Inorg. Chem. **9**, 1948 (1970).
4. G. E. HARTWELL and P. W. CLARK. Chem. Commun. 1115 (1970).
5. P. E. GARROU and G. E. HARTWELL. J. Organometal. Chem. **53**, 331 (1973).
6. W. HEWERTSON and I. C. TAYLOR. Chem. Commun. 428 (1970).
7. K. ISSLEIB and M. HAFTENDORN. Z. Anorg. Allg. Chem. **351**, 9 (1967).
8. R. N. HASZELDINE, R. J. LUNT, and R. V. PARISH. J. Chem. Soc. A, 3705 (1971).

Can. J. Chem. Downloaded from www.nrcresearchpress.com by 210.87.254.6 on 09/05/12
For personal use only.

9. A. E. ARBUZOV and K. V. NIKONOROV. Zh. Obshch. Khim. **18**, 2008 (1948).
10. A. W. HEIRIOTT and K. MISLOW. Tetrahedron Lett. **25**, 3013 (1968).
11. K. D. BERLIN, T. H. AUSTIN, and M. NAGABHUSHANAM. J. Org. Chem. **30**, 1267 (1965).
12. J. R. VANWAZER and J. M. LETCHER. *In* Topics in phosphorus chemistry. *Edited by* M. Grayson and E. J. Griffith. Interscience Publishers, Inc., New York. 1967.
13. D. PURDELA. J. Magn. Res. **5**, 23 (1971).
14. R. B. JOHANNESEN, J. A. FERRETTI, and R. K. HARRIS. J. Magn. Res. **3**, 84 (1970).
15. J. P. ALBRAND, D. GAGNAIRE, J. MARTIN, and J. B. ROBERT. Bull. Soc. Chim. Fr. 40 (1969).
16. D. W. WHITE and J. G. VERKADE. J. Magn. Res. **3**, 11 (1970).
17. W. G. BENTRUDE and H. W. TAN. J. Am. Chem. Soc. **94**, 8222 (1972).
18. M. KAINOSHO, A. NAKAMURA, and M. TSUBOI. Bull. Chem. Soc. Jap. **42**, 1713 (1969).
19. J. A. CONNOR, J. P. DAY, and G. K. MCEWEN. J. Chem. Soc. Dalton, 347 (1973).

Can. J. Chem. Downloaded from www.nrcresearchpress.com by 210.87.254.6 on 09/05/12
For personal use only.

Nuclear Magnetic Resonance Studies of Solvation of Halides: ^{19}F Studies of Solvent and Counterion Effects on Chemical Shift[1]

JAMES P. K. TONG AND COOPER H. LANGFORD
Department of Chemistry, Carleton University, Ottawa, Canada K1S 5B6
AND
THOMAS R. STENGLE
Department of Chemistry, University of Massachusetts, Amherst, Mass. 01002

Received July 25, 1973

We report new measurements adding to the literature on solvent and counter ion dependence of $^{19}F^-$ chemical shift. These are compared to earlier results for $^{35}Cl^-$, $^{79}Br^-$, and $^{127}I^-$. The observations support the following points: (1) there are few systematic differences between behavior of anion shifts in dilute and moderately concentrated aqueous solution, (2) anion shifts commonly show larger sensitivity to solvent than counter ion over convenient ranges of variation so that "solvent shift" may be easily measured. Using the concept of collision effects on shifts developed by Richards and his collaborators, it is possible to separate, in many cases, the large effects arising from contact, or primary solvation sphere, collisions from the smaller effects of outer sphere interactions.

We find no preferential solvation of F^- by H_2O in mixtures with CH_3OH; at most, small preference over C_2H_5OH and formamide, and a small opposite preference in favor of diols. However, water appears strongly preferred in the primary solvation shell over acetone, acetonitrile, dioxane, and (in contrast to other halides), dimethylsulfoxide. Solvation by amines involving both outer and inner sphere site occupation is considered.

The inter-anion effects on fluoride ion chemical shifts tend to undermine the concept of additivity of ionic effects on shifts.

On rapporte de nouvelles mesures qui s'ajoutent à la littérature qui traite de la dépendance du déplacement chimique de $^{19}F^-$ par rapport au solvant et à l'ion complémentaire. Elles sont comparées avec des résultats antérieurs pour $^{35}Cl^-$, $^{79}Br^-$ et $^{127}I^-$. Les observations soutiennent les points suivants: (1) il y a peu de différences systématiques entre le comportement des déplacements des anions en solution aqueuse diluée et peu concentrée, (2) dans des intervalles convenables de variation les déplacements des anions montrent fréquemment une plus grande sensibilité au solvant que ceux des ions complémentaires pour ces intervalles; le déplacement dû au solvant peut être facilement mesuré. Utilisant le concept des effets de collision sur les déplacements, développé par Richards et ses collaborateurs, il est possible de séparer, dans plusieurs cas, les effets importants provenant d'un contact, ou de solvation primaire de sphères et de collisions provenant des effets plus petits d'interactions de l'extérieur des sphères.

On ne trouve pas de solvatation préférentielle de F^- par H_2O dans des mélanges avec CH_3OH; au plus, il y a une petite préférence sur C_2H_5OH et la formamide, et une petite préférence en faveur des diols. Cependant, dans la solvatation primaire de l'enveloppe, l'eau apparait fortement favorisée à l'acétone, l'acétonitrile, le dioxanne, et (à l'opposé des autres halogénures) le diméthylsulfoxyde. La solvatation par les amines impliquant l'occupation d'un site à l'extérieur et à l'intérieur de la sphère est considérée.

Les effets entre anions sur les déplacements chimiques de l'ion fluorure tendent à soulever le concept d'additivité des effets ioniques sur les déplacements.

[Traduit par le journal]

Can. J. Chem., **52**, 1721 (1974)

Introduction

Since the 1965 paper of Frankel, Stengle, and Langford (1), which showed by cross reference to an n.m.r. line width method that the chemical shift of the central atom of a symmetrical complex could be used to probe the intimate solvation environment of a solute species, several authors have extended the application of the ideas to the study of the solvation of simple ions of alkali metals (2–4) and halides (4–6). Espe-

[1]Financial support from the National Research Council of Canada and the U.S. Air Force Office of Scientific Research is acknowledged.

Can. J. Chem. Downloaded from www.nrcresearchpress.com by 210.87.254.105 on 09/05/12
For personal use only.

Can. J. Chem. Downloaded from www.nrcresearchpress.com by 210.87.254.105 on 09/05/12
For personal use only.

cially in the case of the halides of chlorine, bromine, and iodine, the idea has been fruitful, because it has (happily) been the case that the chemical shift of these ions is much more sensitive to solvent than to counter ions (5, 6) which simplifies the necessary separation of effects that must precede an analysis of solvation. On the other side of the ledger, the chemical shifts of these three halides are not easily measured with precision, which renders weaker interactions (such as those involving outer solvation spheres) unmeasurable and thus limit the precision of discussion. For example, we have[2] carried out a quantitative comparison of the "preferential" solvation of chloride by water *versus* acetonitrile with the gas phase mass spectrometer solvent to ion association data of Kebarle and his colleagues (7). A simplest model, which assumes that the occupation of any one site in contact with an ion is independent of the occupant of any other, yields close agreement between observed n.m.r. preferential solvation curves and those calculated using Kebarle's gas phase interaction energies in conjunction with experimental data on the bulk activity of the solvents derived from measurements on liquid mixtures in the absence of solute. The difference between the simple model and the experiments suggests only that there is a small complementarity in which a solvating water molecule in the inner shell favors another. But, it is not clear whether this is a real deviation from the simple model or is a reflection of the limitation of the approximation that only the solvent molecules in the immediate neighborhood of the ion contribute to its chemical shift. Thus, we are motivated to examine fluoride chemical shifts further. It is possible to do fluoride work at high field so that an easily measurable number of hertz represents a very small value in terms of p.p.m. Sensitivity to all factors is available.

One must admit, at once, that sensitivity has a price. When all relevant factors become easily measurable, confusion is a likely result. In the case of fluorine n.m.r., papers exist (8) which have examined medium effects on fluorine nuclei in molecules. These are at least an order of magnitude smaller than the effects we intend to discuss here, once it is understood that our subject is the symmetrical ^1S species, $^{19}F^-$. We must also note that previous data on fluoride chemical shifts (9) have led to suggestions which must be considered suspect unless fluoride is a radically different case from related simple closed shell ions. Since there is strong evidence to believe that fluoride chemical shifts are dominated by the paramagnetic term (like those of other halides and alkali metal ions), we should develop a theory of fluoride shifts in a fashion consistent with the work of Richards and his colleagues (10–12) on the other ions. This is a theory which emphasizes the importance of "collisional" interaction on the dynamic electron distribution about the nucleus under observation. It is a theory of short range effects. One mainstay of the support of this view is the frequent observation that counterion effects on the chemical shift of a given ion remain nearly linear to concentrations approaching the "wet solid" (10, 11), and in some cases are extrapolated from dilute solution to the crystal (13). This rules out a large role for factors such as long range bulk solvent ordering *because effects remain comparable up to a concentration in which bulk is simply nonexistent.* In this regard, we have a circumstance in which experiment is supporting pure theory in that the most reasonable theory of shifts is dominated by the paramagnetic term and requires attention to short range interactions.

There remains only one question: how shall we understand more complex behavior of chemical shift dependence on concentration in cases where sensitivity is high and subtle effects are accessible? The aim of this paper is to show (for $^{19}F^-$) that the smaller effects can be accommodated within accepted theory of "collisional" effects by recognizing that *the molecules in collision with a particular observed nucleus (as that of $^{19}F^-$) are subjected to perturbations by neighbors (in the outer solvation sphere of fluoride).* That is, first sphere neighbors perturb F^- but second sphere molecules perturb the first sphere molecules and thus have a second order effect on F^-. The success of our attempt to bring small effects into the theory depends on the existence of a rational sequence of increasing effects from cross ion (other anion on anion), to secondary solvating molecules, to cations and to primary solvating molecules. We are convinced that the data below are consistently (although possibly not uniquely) interpretable under such a scheme. We present them in such a context (as opposed to others) because of the strong emphasis on short range

[2]Unpublished work.

Can. J. Chem. Downloaded from www.nrcresearchpress.com by 210.87.254.105 on 09/05/12
For personal use only.

factors imposed by the original work of Richards and collaborators (10–12) and supported by many others (2, 14, 15).

The development of this interpretation will begin with the analysis of solvent effects in which we attempt to distinguish smaller effects from larger ones, and then interpret them in comparison with the large effects that have been reported for the remaining halide ions. Following this, we turn to an extension of earlier discussions of the effects of other ions on fluoride shifts. With an overall interpretation, it is finally possible to make some remarks on the factors affecting solvent distribution around the fluoride ion. We call such distribution "preferential solvation"; zero preference is simply a special case.

Results and Discussion

(I) Fluoride Shifts in Mixed Aqueous Organic Solvents

The fluoride chemical shifts (referred to the 100% aqueous solution of the same molarity) were obtained in binary aqueous organic mixed solvent systems of various compositions (expressed in mole percent of the organic solvent) when solubility of the fluoride salt, KF in most of our studies, and the miscibility of the binary solvent system in the presence of the fluoride permitted. The solvent composition shifts are plotted in Figs. 1, 2 and 3. Special attention is drawn to the difference of the scales of the chemical shifts. Positive values of fluoride chemical shifts, σ, are at higher fields relative to the reference while negative ones are at lower fields.

In the case of the aqueous dipolar aprotic and amine mixed solvent systems (and including *t*-butanol), phase separation or precipitation (in the case of *N*,*N*-dimethylformamide) occurs at below 45 mol% of the organic component for fluoride concentrations kept as low as 0.08 *M*. The fluoride shifts are plotted as a function of solvent compositions in Figs. 1 and 2. The lack of knowledge of the shift in pure organic solvent, σ(ORG), limits a study of preferential solvation.[3] Despite such difficulties, the nature of solvation of the fluoride ion in these solvent systems may be accommodated consistently in the framework outlined above.

There are two noteworthy points: (*i*) there is a striking similarity of the magnitudes of fluoride ion shifts on the addition of acetonitrile, 1,4-dioxane, *N*,*N*-dimethylformamide, and acetone to water; and (*ii*) the magnitude (regardless of the sign) of these shifts is small (Fig. 1). In order to

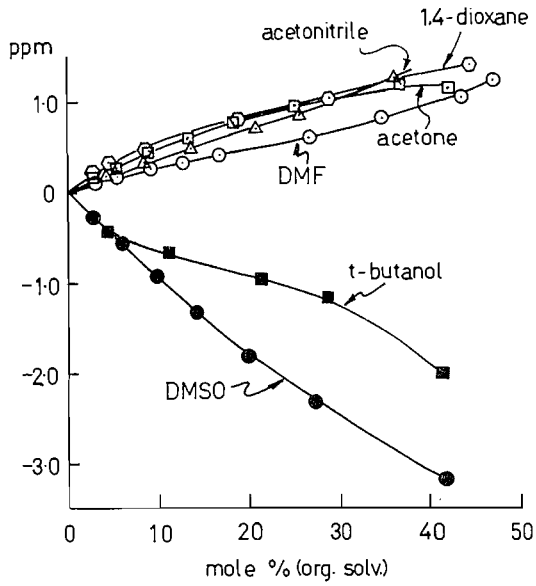

FIG. 1. $^{19}F^-$ n.m.r. chemical shifts of 0.08 *M* KF in mixed aqueous organic solutions at 32.5°. ⊙, *N*,*N*-dimethylformamide; ⊡, acetone; △, acetonitrile; ⊙, 1,4-dioxane; ■, *t*-butanol; ●, dimethylsulfoxide.

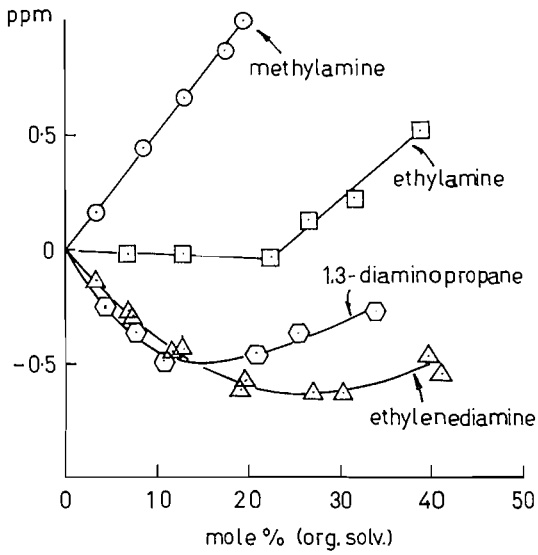

FIG. 2. $^{19}F^-$ n.m.r. chemical shifts of 0.08 *M* KF in aqueous organic amine solutions at 32.5°. ⊙, methylamine; ⊡, ethylamine; △, ethylenediamine; ⊙, 1,3-diaminopropane.

[3]This point will be obvious later where the usual equation for preferential solvation appears.

Can. J. Chem. Downloaded from www.nrcresearchpress.com by 210.87.254.105 on 09/05/12
For personal use only.

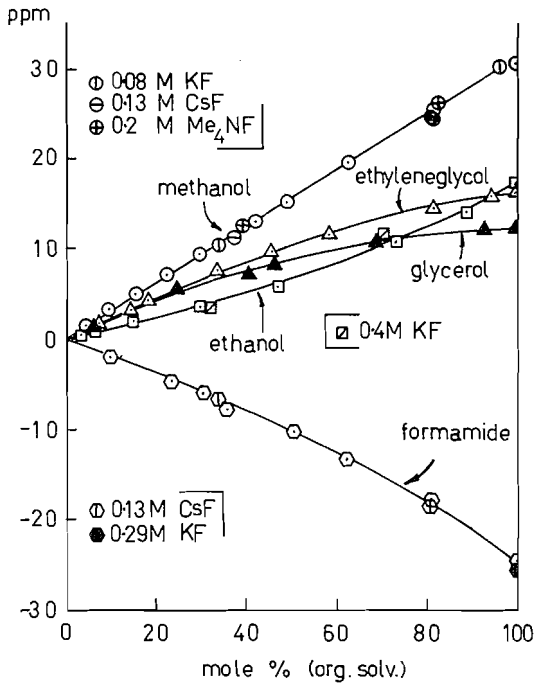

FIG. 3. $^{19}F^-$ n.m.r. chemical shifts of KF in mixed aqueous protic organic solvent solutions at 32.5°. ⊙, 0.2 *M* KF (methanol); □, 0.08 *M* (ethanol); △, 0.08 *M* KF (ethyleneglycol); ▲, 0.08 *M* KF (glycerol); ⊙, 0.4 *M* KF (formamide).

demonstrate the smallness of the magnitudes, a table of *averaged initial shift gradients* with respect to mole percent of organic solvents is prepared as in Table 1. These averages are taken from the data points for each mixed solvent system (for consistency) in the region of the curves between pure water and a point where a change of slope (if any) becomes significant. The averaged initial shift gradients of these solvents are similar, varying between 0.023 to 0.033 p.p.m. per mole percent organic component. Such values are approximately an order of magnitude smaller than those for alcohols and formamide, regardless of the sign. There are two possibilities, either: (*i*) the action of all these organic solvents on the ion is extremely similar to water, as, for example, would be expected for D_2O, or (*ii*) the *perturbation of the fluoride ion by the organic solvent is indirect* (an outer sphere perturbation).

The fluoride ion is similar to the rest of the halide ions: chloride, bromide, and iodide, in the sense of being a mononegative ion having a ^1S ground state electronic configuration. If the solvent is interacting with the halide ions in similar ways, the magnitude of the solvent shifts, due to the ion–solvent interaction, would increase as $F^- < Cl^- < Br^- < I^-$, following the decrease in the ΔE terms in the paramagnetic term in the Ramsey equation for chemical shift (16). Such a trend appears for solvents: D_2O, methanol, dimethylsulfoxide, acetonitrile, and *N*,*N*-dimethylformamide, as far as literature is available (6, 17, 18). From Table 2, the trend is obvious, with the exception of the iodide ion in methanol. In fact, the correlation of the solvent shifts of the halide ions in a particular solvent to their corresponding shifts in D_2O is reasonably linear in all cases but that of iodide in methanol (Fig. 4). If such a correlation is general, *one would expect the fluoride ion shift in acetonitrile, N,N-dimethylformamide, and dimethylsulfoxide to be between −20 to −30 p.p.m., or −0.2 to −0.3 p.p.m. per mol% for zero preferential solvation.* Experience does not suggest similarity of the four organic solvents:

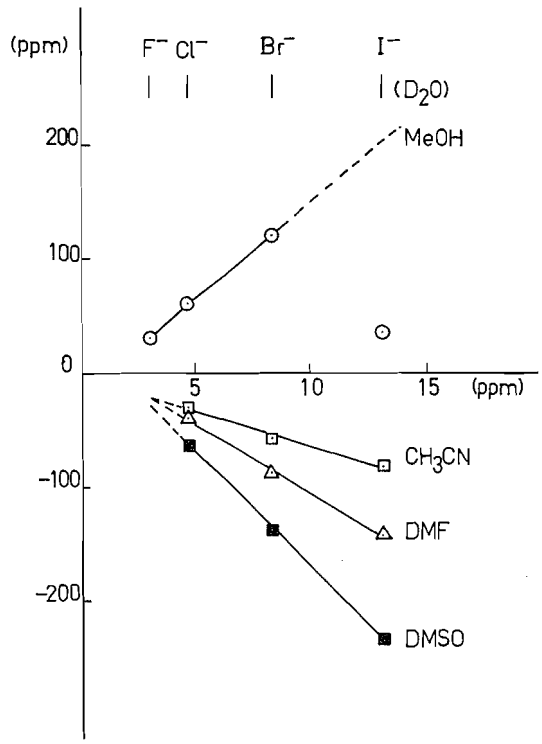

FIG. 4. Correlation of halide ion chemical shifts in solvents to D_2O referring to their corresponding aqueous solutions of the same concentration. ⊙, methanol; □, acetonitrile; △, *N*,*N*-dimethylformamide; ⊡, dimethylsulfoxide.

TABLE 1. Averaged solvent composition shift gradient of fluoride ion in binary aqueous organic mixed solvent systems

Organic solvent	Limit of solvent composition range	Shift gradient (p.p.m./mol%)	Correlation coefficient (%)
CH_3OH	100%	0.308	99.98
C_2H_5OH	50%	0.123	99.93
t-Butanol	50%	−0.043	−98.22
Ethyleneglycol	50%	0.210	99.81
Glycerol	50%	0.172	99.08
CH_3NH_2	20%	0.05	99.97
$C_2H_5NH_2$	23%	−0.0017	−96.15
Ethylenediamine	12%	−0.039	−99.73
1,3-Diaminopropane	12%	−0.045	−99.29
Formamide	50%	−0.207	−99.77
DMF	50%	0.023	99.79
Acetone	50%	0.028	97.03
DMSO	50%	−0.078	99.49
Acetonitrile	50%	0.033	99.85
Dioxane	50%	0.030	98.58
D_2O*	100%	0.030	—

*References 14 and 17.

TABLE 2. Halide ion chemical shifts in various solvents (ref. aqueous solutions of same salts and same concentrations)

Solvent	F^-	Cl^-	Br^-	I^-
D_2O*	2.96[14]	4.7[17]	8.3[17]	13.2[17]
MeOH	30.6†	60[18]	120[18]	35[6]
DMSO‡	—	−63[6]	−137[6]	−233[6]
CH_3CN‡	—	−31[6]	−57[6]	−81[6]
DMF‡	—	−40[6]	−88[6]	−142[6]

*Results are from sodium or potassium halides.
†This work, with KF.
‡Results are from 0.2 *M* or 0.25 *M* tetraethylammonium halides.

N,*N*-dimethylformamide, acetonitrile, acetone, and 1,4-dioxane, to water. We find that expected fluoride shifts (Fig. 4) in two of these solvents are large negative, while those observed are all small positive and similar.

To understand the observed contradiction, we propose the secondary solvent effect on the fluoride ion chemical shifts, an outer sphere effect, or perturbation. The organic solvent molecules in the outer sphere are perturbing the water molecules in contact with the fluoride ion, and thereby the fluoride ion. Such an outer sphere interaction may give rise to an upfield or downfield shift, but in any case, one of a magnitude smaller than a typical primary sphere interaction. (Note that this means that water is strongly preferred in the primary sphere of the fluoride ion in any of these dipolar aprotic solvents, at least up to 50 mol% of the organic component.)

In the previous examples, further addition of an organic solvent never results in a change of sign of the chemical shift. Such a change of sign would indicate a different character of interaction and a change of solvent shift mechanism.[4] With this additional idea, the results for aqueous amines may be understood in a similar fashion. Methylamine looks similar to methanol (*vide infra*), but other amines have a downfield shift region first, followed by a region of upfield shifts. An entirely plausible reason for the initial downfield region of these curves is that at low mole fractions of the amines, they fail to compete effectively for primary solvation sites. Comparing the dipolar aprotic solvents just discussed, that hydrogen bond donor amines produce outer sphere shifts the opposite of outer sphere shifts produced by hydrogen bond

[4]This point will be elaborated below.

Can. J. Chem. Downloaded from www.nrcresearchpress.com by 210.87.254.105 on 09/05/12
For personal use only.

Can. J. Chem. Downloaded from www.nrcresearchpress.com by 210.87.254.105 on 09/05/12
For personal use only.

acceptor dipolar aprotics is quite reasonable. The change of sign of shift in the aqueous ethylamine system is an example clearly indicating the change of solvent shift mechanism at some stage of solvent composition, most plausibly from outer sphere interaction to primary.

The fluoride ion shifts in aqueous *t*-butanol are shown in Fig. 1. The earlier part of this curve, below 10 mol%, has been obtained before in detail (19) and is consistent with our extrapolation. Examining the curve and Table 1, it would appear to contrast to the other alcohols studied in having a small and downfield shift. This could be similar to the outer sphere shift shown by the amines. Water is probably the preferred solvent adjacent to the fluoride ion in this mixed solvent system.

The extrapolated fluoride shift in pure dimethylsulfoxide is about −25 p.p.m. (Fig. 4). From the intermediate magnitude of the observed shifts (Fig. 1 and Table 1), we cannot assign the cause of the observed fluoride shifts with any confidence. If σ(ORG) is taken as −25 p.p.m., it seems that, up to 40 mol% of dimethylsulfoxide, water is still the preferred solvent at the fluoride ion.

Within our category of organic solvents, methanol, ethanol, ethyleneglycol, glycerol, and formamide allowed a full range solvent composition study; and the results are summarized in Fig. 3. From Fig. 3 and Table 1, it is recognized that the effect of these solvents on the fluoride chemical shift is of an order of magnitude greater than those we previously attributed to outer sphere interactions. It is then logical to assign these shifts as the consequence of primary solvation sphere interactions of the fluoride ion with the organic solvents.

Now, outer sphere interactions do also occur in the aqueous alcohols and formamide systems, and affect the fluoride ion shifts, but the much larger shifts due to inner sphere interactions may render them nearly unnoticeable. *The discussion below is based on this assumption.* According to the model adopted to a greater or lesser degree by many workers (1–4, 6), which intrinsically assumed a unique mechanism of shift and solvation, the average composition (mole fraction) of the organic component in the solvation sphere, $X_S(\mathrm{ORG})$, of the probe solute, the fluoride ion in this paper, is taken to be given by the following relationship:

$$[1] \qquad X_S(\mathrm{ORG}) = \frac{\sigma - \sigma(H_2O)}{\sigma(\mathrm{ORG}) - \sigma(H_2O)}$$

where σ is the observed chemical shift of the probe solute in the binary solvent, and $\sigma(H_2O)$ and σ(ORG) are the shifts in pure water and pure organic solvent respectively. Taking the chemical shift in water as reference, and hence setting $\sigma(H_2O)$ equal to zero, we simply have the solvation sphere solvent composition directly proportional to the chemical shift, σ; but the knowledge of σ(ORG) is required in order to derive some understanding of the preferential solvation phenomenon. When σ(ORG) is known, the preferential solvation of the probe solute in the mixed solvents can be understood from the variation of σ with respect to the bulk solvent composition, again is the mole fraction of the organic component. It must be noted that the quantity $X_S(\mathrm{ORG})$ should vary between 0 and 1, and so is the quantity σ/σ(ORG); therefore, σ should bear the same sign as σ(ORG) throughout (*i.e.* no change of sign of shift) unless there is a change of "mechanism" of shift.

Assuming outer sphere contribution to fluoride chemical shift is negligible as compared to those of primary solvation sphere, we can comment on the preference of the fluoride ion for these solvents as compared to water in the mixtures with reference to Fig. 3. In aqueous methanol, the chemical shifts are definitely linear with the bulk solvent composition, which is an indication of no preference of the fluoride ion for either solvent. Slight preference for water over the organic component is indicated in both aqueous ethanol and aqueous formamide solvent systems. In both aqueous ethyleneglycol and aqueous glycerol solvent systems, there is an indication of some preference of the organic components to water. Such an effect has been understood as resulting from the chelating power of the glycols (9).

The lack of preferential solvation in the aqueous methanol system does not, however, imply equality of energetics of interaction of the two solvent molecules with fluoride. Simple models have been developed by Frankel, Langford, and Stengle (20) and Covington, Lilley, Newman, and Porthouse (4), where identifiable thermodynamic parameters were obtained. Both give similar results. We have (in the notation of ref. 4):

Can. J. Chem. Downloaded from www.nrcresearchpress.com by 210.87.254.105 on 09/05/12
For personal use only.

[2] $$\frac{\sigma}{\sigma(\mathrm{ORG})} = \frac{K^{1/n}(Y)}{1 + K^{1/n}(Y)}$$

where K is defined as the equilibrium constant for the following solvation process, assuming n solvation sites at the fluoride ion for both water and the organic solvent,

$$F^-(H_2O)_n + n(\mathrm{ORG}) \overset{K}{\rightleftharpoons} F^-(\mathrm{ORG})_n + nH_2O$$

and Y is the bulk activity ratio of the organic component to water in their mixture, $[a(\mathrm{ORG})/a(H_2O)]$. Equation 2 may be rearranged to be expressed in terms of mole fraction of the organic component, $X(\mathrm{ORG})$, and bulk activity coefficients, $f(\mathrm{ORG})$ and $f(H_2O)$, of both solvents for a direct comparison to experimental observations.

[3] $$\frac{\sigma}{\sigma(\mathrm{ORG})} = \frac{K^{1/n}[f(\mathrm{ORG})/f(H_2O)]X(\mathrm{ORG})}{1 - \{1 - K^{1/n}[f(\mathrm{ORG})/f(H_2O)]X(\mathrm{ORG})\}}$$

For no preferential solvation cases, according to eq. 3, the term $K^{1/n}[f(\mathrm{ORG})/f(H_2O)]$ must equal unity. The activity coefficient ratio of methanol to water in their binary mixtures, at 39.9°, may be calculated from literature data (21). It is not equal to unity, nor is it constant with varying bulk solvent composition; this implies that $K^{1/n}$ is not independent of the composition. Thus, the lack of preferential solvation by methanol should not be taken to imply equivalence of interaction energies between the fluoride ion and water molecules or methanol molecules. The population of the primary solvation sphere is determined not only by energetics of ion solvent interaction but also by other factors.

In order to confirm that the observed fluoride ion shifts in the above mixed solvents is mainly a consequence of ion–solvent interactions, the fluoride salt (KF) concentration and the cation of the fluorides (K^+, Cs^+, and CH_4N^+) were varied. It must be emphasized that such points are not expected to lie on the original curves, because fluoride shifts have been demonstrated to be dependent on salt concentrations as well as the nature of the counterions, in water (in this paper and ref. 22) as well as in mixed solvents (9). In addition, the preference of the preferential solvation behavior may change somewhat when the solute concentration varies, especially at concentrations where overlap of co-spheres of the solute takes place (23). It is found, however, that the data points so obtained (Fig. 3) *differ little enough from the ones discussed to suggest no modification of interpretations.*

As a final point to compare primary sphere solvent shifts to outer sphere solvent shifts, it is interesting to note that the *t*-butanol and those parts of amine curves assigned to outer sphere effects produce small negative shifts (Table 1), which is to be contrasted to the positive values associated with placing alcohols or amines into the primary solvation sphere. The simplest interpretation which is plausible is that alcohols or amines in the secondary sphere render the F...H hydrogen bond in the primary sphere stronger. If this is so, the opposite is probably correct for the dipolar aprotic solvents, namely: *N*,*N*-dimethylformamide, acetonitrile, acetone, and 1,4-dioxane. These appear to render the F...H hydrogen bond to solvating water molecules less strong.

Finally, it is probably worth noting that attempts to correlate the shifts to bulk solvent parameters, like dielectric constant and dipole moment (24), acidity (pK_a) (25), Gutman's donar number (26), CTTS to iodide (27), solvent polarity parameter (Z-value) (28), and even heat of vaporization (29), failed. If hydrogen bonding is the chief fluoride solvent interaction, which is plausible just from the solubility point of view, one might correlate the fluoride ion shifts to the hydrogen bond donicity of the solvents; but we have failed to find an independent measure of that parameter.

(II) Effects of Ions on $^{19}F^-$ Chemical Shifts in Aqueous Solutions

Figures 5 through 9 summarize our measurements on counter-ion dependence of $^{19}F^-$ chemical shifts (compare ref. 11) and add new observations on anion effects as well. The fluoride chemical shifts reported in these studies were referred to the infinite dilution shift of fluoride ion in water as established by NaF, for the sharpness of the resonance signal even in dilute solutions and the good linearity of shift with molarity at several other temperatures studied (between 35° to 83°).

Figure 5 illustrates again the monotonic dependence of shift on the salt concentration

Can. J. Chem. Downloaded from www.nrcresearchpress.com by 210.87.254.105 on 09/05/12
For personal use only.

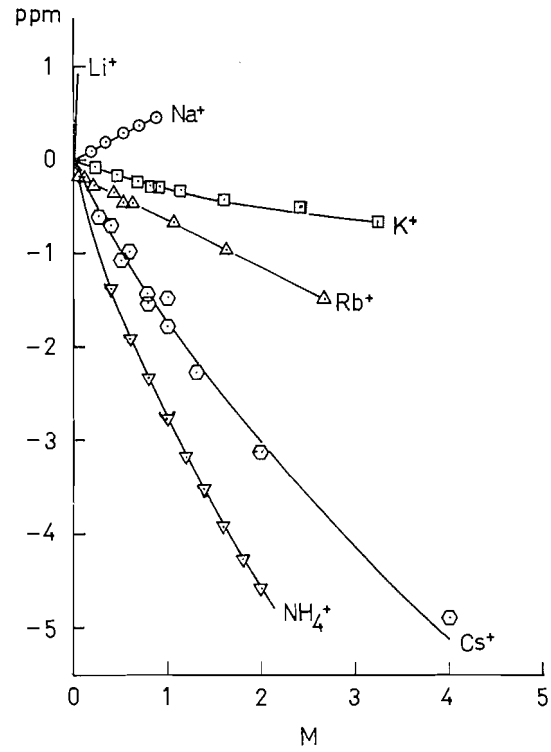

FIG. 5. Concentration dependence of $^{19}F^-$ n.m.r. chemical shifts of various aqueous fluoride salts solutions at 32.5°.

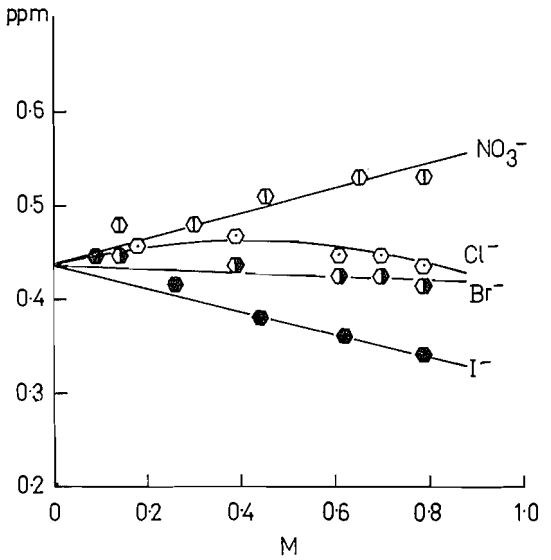

FIG. 6. $^{19}F^-$ n.m.r. chemical shifts in aqueous NaF solutions at 32.5° as a function of added sodium salts with other anions keeping total Na^+ concentration at 0.88 *M*. (The point at 0 *M* is a real data point, corresponding to 0.88 *M* NaF solution.)

(compare ref. 11). The effect on $^{19}F^-$ shift appears to be increasingly paramagnetic in the order $Li^+ \ll Na^+ < (H_2O) < K^+ < Rb^+ < Cs^+ < NH_4^+$, and is in some minor contrast to previous observations with other halide ions (11). It is consistent with the trend of solid state fluoride ion shifts (13), *with the exception of LiF.*

Fluoride ion is nearly as strong a base as ammonium ion is an acid in water; but according to our observations, the fluoride shifts in aqueous NH_4F solutions are due largely, if not completely, to ion–ion interactions. Should hydrolysis be important, it would cause an upfield shift, because the products of hydrolysis, HF and HF_2^- are at very high fields (44 to 55 p.p.m. for the former and 32 p.p.m. for the latter) relative to the aqueous fluoride ion (13, 30, 31). Simple equilibrium calculations confirm that HF and HF_2^- are unimportant.

The most important results of Fig. 5 are the implications of a simple dependence of fluoride shifts on ionic concentrations from very dilute to quite concentrated solutions. This is not consistent with bulk water structure affecting shifts. It is more easily understood in terms of short range cation–anion interactions, which, according to the collisional repulsive overlap model (10–12), would in fact predict the above order of fluoride shifts. However, we must mention that at very high concentrations of aqueous KF solutions, Connick and Poulson (22) observed the shift of fluoride resonance to higher field after a minimum at *ca.* 5 *M*. This turnover was interpreted in terms of outer sphere collisions at lower concentrations and inner sphere (contact) collisions at higher concentrations. (Note that K^+ has small effects at lower concentrations.) Deverell and Richards observed similar behavior with aqueous LiCl solutions, where $^{35}Cl^-$ was the probe ion (11).

The extraordinary high field shifting effect of lithium ion suggests the possibility of local hydrolysis of the fluoride ion by the highly polar lithium ion (32, 33), where the process may be represented as:

$$Li^+ + H_2O + F^- \rightleftharpoons Li^+ \ldots OH^- \ldots H^+ \ldots F^-$$

These observations indicate that simple ionic collision is not enough to account for all the concentration dependence of ionic shifts. Our observations do not give us a parallel to the classes of solvent effects that would permit detailed classification. The observed order, how-

Can. J. Chem. Downloaded from www.nrcresearchpress.com by 210.87.254.105 on 09/05/12
For personal use only.

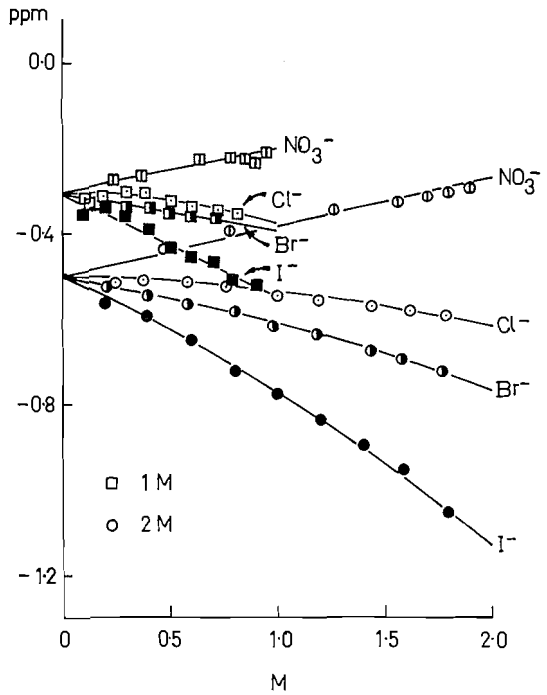

FIG. 7. $^{19}F^-$ n.m.r. chemical shifts in aqueous KF solutions at 32.5° as a function of added potassium salts with other anions keeping total K^+ concentrations at 1 *M* and 2 *M* respectively. (The points at 0 *M* are real data points, corresponding to 1 *M* and 2 *M* KF solutions respectively.)

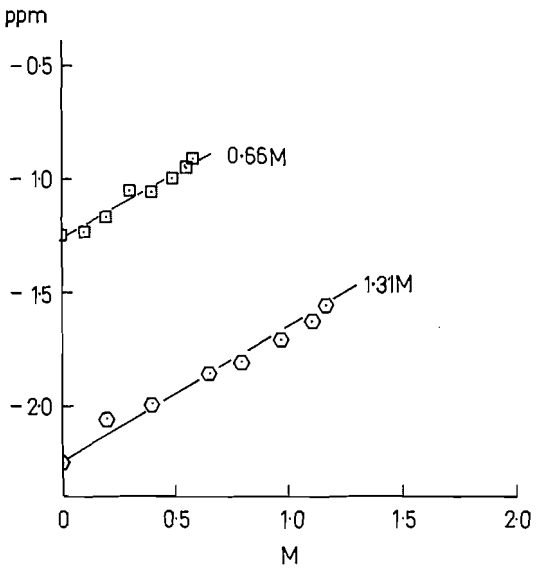

FIG. 8. $^{19}F^-$ n.m.r. chemical shifts in aqueous CsF solutions at 32.5° as a function of added CsI keeping total Cs^+ concentrations at 0.66 *M* and 1.31 *M* respectively.

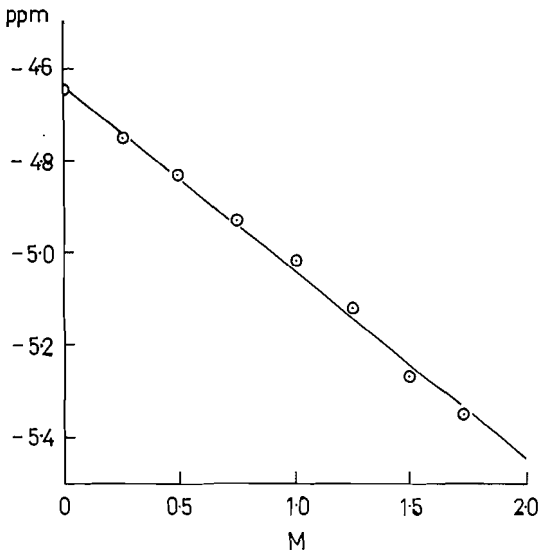

FIG. 9. $^{19}F^-$ n.m.r. chemical shifts in aqueous NH_4F solution at 32.5° as a function of added NH_4Cl keeping total NH_4^+ concentration at 2 *M*.

ever, suggests most effects are from contact, which is especially reasonable for the larger ions, Rb^+, Cs^+, and NH_4^+, since they are only weakly hydrated.

The remaining Figs. 6 to 9 show that anion effects on $^{19}F^-$ are smaller than cation effects (as expected) but readily observable. Figures 6 and 7 suggest an anion order toward increasing paramagnetic shift of $NO_3^- < (F^-) < Cl^- < Br^- < I^-$, which is as expected (11). Such an order *could* reflect effects of direct anion–anion collisions, but closer inspection reveals that anion effects are *cation dependent*.

To provide a clear indication, numerical results are presented in Table 3 to supplement the Figs. 6 through 9. In Table 3, the values in the fourth column are extrapolated fluoride ion shifts at infinite dilution in the given concentration of the added electrolyte. (Of course, this does not apply to the fluoride salt.) The fifth column is the net fluoride ion shift due to the added anion, which is the difference between the fluoride shift in the pure fluoride salt solution, $\sigma(F^-)$, and the extrapolated fluoride shift in the pure added electrolyte, σ, of the same cation and same concentration. The last column is the anion effect normalized to 1.0 *M* of the electrolyte solutions, merely for the sake of comparison; linear variation is not claimed nor implied.

Examining the normalized anion induced

TABLE 3. Anion effects on $^{19}F^-$ chemical shifts in aqueous solutions at 32.5°

Cation	Anion	Concentration (M)	Shift(σ) (p.p.m.)	Anion effect σ − σ(F^-) (p.p.m.)	Normalized anion effect to 1.0 M
Na^+	F^-	0.88	σ(F^-) = 0.44	0.00	0.00
	NO_3^-		0.55	0.11	0.12_5
	Cl^-		0.43	−0.01	-0.01_1
	Br^-		0.42	−0.02	-0.02_3
	I^-		0.33	−0.11	-0.12_5
K^+	F^-	1.0	σ(F^-) = −0.31	0.00	0.00
	NO_3^-		−0.20	0.11	0.11
	Cl^-		−0.38	−0.07	−0.07
	Br^-		−0.40	−0.09	−0.09
	I^-		−0.55	−0.24	−0.24
	F^-	2.0	σ(F^-) = −0.50	0.00	0.00
	NO_3^-		−0.27	0.23	0.11_5
	Cl^-		−0.61	−0.11	-0.05_5
	Br^-		−0.76	−0.26	−0.13
	I^-		−1.13	−0.63	-0.31_5
Cs^+	F^-	0.66	σ(F^-) = −1.25	0.00	0.00
	I^-		−0.90	0.35	0.53
	F^-	1.31	σ(F^-) = −2.25	0.00	0.00
	I^-		−1.47	0.78	0.59_5
NH_4^+	F^-	2.0	σ(F^-) = −4.64	0.00	0.00
	Cl^-		−5.45	−0.81	-0.40_5

TABLE 4. Sources and quality of solvents

Solvent	Manufacturer	Grade	Remarks
CH_3OH	Fisher	Spectral	No further purification
C_2H_5OH	Gooderham & Worts	Absolute	No further purification
t-Butanol	Fisher	Cert. reagent	No further purification
Ethyleneglycol	Eastman Organic		Dried with CaO and BaO, vacuum distilled
Glycerol	Fisher	Cert. reagent	Claimed 99.9% mol purity
CH_3NH_2	Fisher	Reagent	Claimed to be 30–35% in water. Estimated by p.m.r. signal integration as to contain 69.8% of water by weight
$C_2H_5NH_2$	Eastman Organic		Claimed to be 70% in water. p.m.r. signal integration estimated 37.1% of water by weight
Ethylenediamine	Fisher	Certified anhydrous	Dried with Type 5A molecular sieve, then CaO and BaO; distillated
1,3-Diaminopropane	Aldrich	I.r. analyzed	No further purification
Formamide	Fisher	Cert. reagent	Dried with CaO and BaO. Vacuum distilled
N,*N*-Dimethylformamide (DMF)	Aldrich		Dried with Type 4A molecular sieve, and vacuum distilled
Acetone	Aldrich	Spectral	Claimed maximum water content as 0.05%
Dimethylsulfoxide (DMSO)	Fisher	Spectral	Assumed zero water content
Acetonitrile	Fisher	Cert. reagent	Assumed zero water content
1,4-Dioxane	Fisher	Cert. reagent	Claimed 99% mol purity
Water			Doubly distilled

Can. J. Chem. Downloaded from www.nrcresearchpress.com by 210.87.254.105 on 09/05/12
For personal use only.

Can. J. Chem. Downloaded from www.nrcresearchpress.com by 210.87.254.105 on 09/05/12
For personal use only.

shifts in Table 3, one may notice that the effect of the same anions on the fluoride shifts are similar (though differing) in magnitude and direction with sodium and potassium as the cations. However, the effect of iodide in CsI solutions is a few times larger in magnitude than, and opposite in direction to, those in NaI and KI solutions. In addition, the chloride effect in NH_4Cl solutions is very much larger than that in both NaCl and KCl solutions.

This has two consequences: first, it undermines the commonly assumed "additivity" principle (9, 11) for cation and anion contributions to shift; and second, it suggests that an important aspect of anion effect is not from anion–anion collision but from effects of anions on the collisions of cations with the probe anion.

Experimental

The sources of fluoride ions in the mixed aqueous solvent studies were KF (Fisher $KF.2H_2O$), CsF (Alfa, 99.8% purity), and $(CH_3)_4NF$ (Eastman Organic, $(CH_3)_4NF.3H_2O$). In the study of aqueous fluoride salt solutions and the effects of added electrolytes, the sources of fluoride ion, in addition, were reagent grade LiF, NaF (Fisher), RbF (Alfa), NH_4F (Fisher $NH_4F.2H_2O$, but found to be NH_4F); and the other electrolytes were NaCl (Fisher), NaBr (Anachemia), NaI, $NaNO_3$ (Fisher); KCl (Fisher), KBr (Merck), KI (Analar), KNO_3 (Fisher); CsI (Alfa) and NH_4Cl (Fisher). The salts were used without further purification. The fluoride stock solutions were standardized by conductometric titration with $Ca(NO_3)_2$ solution previously standardized by anhydrous NaF. These determinations were accurate to ± 1 to 3%. The stock solutions were stored in polyethylene bottles. It was found that there was no significant change in chemical shift of the solution after four months storage. Sample solutions were prepared in glass volumetric flasks, and used when freshly prepared, but no significant change in chemical shift occurred in 3 days time at room temperature. The solvents used were of known water content if purification happened to be undesirable. Their sources are tabulated in Table 4.

In mixed solvent studies, samples were prepared to known concentrations by volume in terms of molarity, then weighed for calculation of solvent compositions in mole percents. Diamagnetic susceptibility corrections relative to the fluoride shift in the pure aqueous solution of the same concentrations of fluoride in terms of molarity have been estimated. The corrections were all small.

The fluoride chemical shifts were observed on a Varian XL-100 n.m.r. spectrometer at 32.5° and referred to an arbitrary external reference sample of 7.39 *m* aqueous KF solution. Positive values of fluoride chemical shifts, σ, are higher field shifts, and negative ones are lower field shifts, with respect to a chosen reference.

1. L. S. Frankel, T. R. Stengle, and C. H. Langford. Chem. Commun. 393 (1965).
2. E. G. Bloor and R. G. Kidd. Can. J. Chem. **46**, 3425 (1968).
3. E. H. Erlich, M. S. Greenberg, and A. I. Popov. Spectrochim. Acta, Part A, **29**, 543 (1973).
4. A. K. Covington, T. H. Lilley, K. E. Newman, and G. A. Porthouse. Faraday Trans. I, **69**, 963 (1973).
5. C. H. Langford and T. R. Stengle. J. Am. Chem. Soc. **91**, 4014 (1969).
6. T. R. Stengle, Y. E. Pan, and C. H. Langford. J. Am. Chem. Soc. **94**, 9037 (1972).
7. R. Yamdagni and P. Kebarle. J. Am. Chem. Soc. **94**, 2940 (1972).
8. W. T. Raynes and M. A. Raza. Mol. Phys. **20**, 555 (1971).
9. A. Carrington, F. Dravnicks, and M. C. R. Symons. Mol. Phys. **3**, 174 (1960).
10. C. Deverell and R. E. Richards. Mol. Phys. **10**, 551 (1966).
11. C. Deverell and R. E. Richards. Mol. Phys. **16**, 421 (1969).
12. J. D. Halliday, R. E. Richards, and R. R. Sharp. Proc. R. Soc. (Lond.), A**133**, 45 (1969).
13. I. C. Wang. Acta Phys. Sinica, **20**, 41 (1964).
14. C. Deverell, K. Schaumburg, and H. J. Bernstein. J. Chem. Phys. **49**, 1276 (1968).
15. E. G. Bloor and R. G. Kidd. Can. J. Chem. **50**, 3926 (1972).
16. J. A. Pople, W. G. Schneider, and H. J. Bernstein. High resolution nmr. McGraw-Hill Book Co., Inc., New York. 1959.
17. A. Loewenstein and M. Shporer. Chem. Commun. 214 (1968).
18. C. Hall. Q. Rev. **25**, 87 (1971).
19. M. C. R. Symons and M. J. Blandamer. *In* Hydrogen-bonded solvent systems. *Edited by* A. K. Covington and P. Jones. Taylor and Francis Ltd., London. 1968. p. 211.
20. L. S. Frankel, C. H. Langford, and T. R. Stengle. J. Phys. Chem. **74**, 1376 (1970).
21. International critical tables. Vol. III. McGraw–Hill Book Co., Inc. 1928. p. 290.
22. R. E. Connick and R. E. Poulson. J. Phys. Chem. **62**, 1002 (1958).
23. Y. E. Pan. M.Sc. Thesis. University of Massachusetts, Amherst, Mass. 01002, U.S.A., 1971.
24. A. J. Gordon and R. A. Ford. The chemist's companion. Wiley–Interscience. 1972.
25. R. H. Boyd. *In* Solute–solvent interactions. *Edited by* J. F. Coetzee and C. D. Ritchie. Marcel Dekker, New York. 1969. p. 97.
26. V. Gutmann. Non-aqueous chemistry. *In* Topics in current chemistry. Vol. 27. 1972.
27. M. J. Blandamer and M. F. Fox. Chem. Rev. **70**, 59 (1970).
28. E. M. Kosower. An introduction to physical organic chemistry. John-Wiley and Sons, Inc., 1968.
29. CRC Handbook of chemistry and physics. 53rd ed. 1972.
30. R. Hague and L. W. Reeves. J. Am. Chem. Soc. **89**, 250 (1967).
31. K. Schaumburg and C. Deverell. J. Am. Chem. Soc. **90**, 2495 (1968).
32. R. A. Robinson and H. S. Harned. Chem. Rev. **28**, 419 (1941).
33. T. C. Huang. Hua Hsueh T'ung Pao. Acta Chim. Sinica, 513 (1964).

A Sequence of Attaching the Unit $CH_2CH_2COCH_3$ to 2,2,6-Trimethylcyclohexanone

CIRILL SCHMIDT, KEIR LEIGH ADAMS, AND UWE FECHNER

Department of Chemistry, University of Prince Edward Island, Charlottetown, Prince Edward Island

Received November 19, 1973

A method is described of joining the 2-oxo-butyl group to a ketone. The sequence is illustrated by the synthesis of dihydro-β-ionone (**2**) from 2,2,6-trimethylcyclohexanone (**1**).

On décrit une méthode permettant d'ajouter un groupe oxo-2 butyle à une cétone. Les étapes sont illustrées grâce à la synthèse de la dihydro β-ionone (**2**) à partir de la triméthyl-2,2,6 cyclohexanone (**1**). [Traduit par le journal]

Can. J. Chem., **52**, 1732 (1974)

Can. J. Chem. Downloaded from www.nrcresearchpress.com by 210.87.254.5 on 09/05/12
For personal use only.

In the course of our synthetic studies in the terpene field we required a method which would allow the attachment of a four carbon atom unit to a ketone in such a manner as exemplified by the conversion of 2,2,6-trimethylcyclohexanone (**1**) to dihydro-β-ionone (**2**). Similar synthetic goals were undertaken for the synthesis of xanthatin but the successful methods reported joined only one or two carbon atom fragments in several steps (1). Our intention was to add four carbon atoms in one step with a minimum amount of subsequent change in functionality.

It was obvious that the vast experience concerning the chemistry of ionone should be of great help in this work. Consequently we selected our synthetic path via the well-known β-ionone **13**. The latter compound is manufactured on a multi-ton scale by the acid cyclization of pseudoionone (2*a*). Other very efficient methods starting with β-cyclocitral are also known (2*b*). However, the synthesis of β-ionone starting from 2,2,6-trimethylcyclohexanone has not been reported yet, although it was attempted by Miki and Hara (3).

The present communication reports on the synthesis of β-ionone **13** and dihydro-β-ionone **2** and correlates our data with the previous investigations concerning some pertinent β-ionone derivatives.

In a Nef reaction we reacted the recently reported acetylene ketal **3** (4) with ketone **1** leading to a single, crystalline adduct **4** in a good yield. The stereochemistry of the latter compound is assigned as drawn assuming an axial attack on the most stable conformation of 2,2,6-trimethylcyclohexanone (**1**).

The readily obtainable acetylenic ketone **5**[1] was then hydrogenated catalytically in the hope of obtaining hydroxyketone **6** which could have been dehydrated to the unsaturated ketone **2**. According to our spectral data, however, the product was present almost exclusively in the form of spiroketal **7**. The stereochemistry of the latter compound was not investigated.

It became obvious that the two oxygen functions in compound **5** could not be handled simultaneously if both of them were unprotected. Therefore we attempted to hydrogenate dioxolane **4** in the presence of Raney nickel and also with palladium-on-charcoal. Unfortunately only 1 mol of hydrogen was consumed by **4**, apparently due to steric hindrance.

Since our plan to retain the keto group in the free or protected form proved to be incompatible with the subsequent steps, we reduced ketone **5** to acetylene diol **8***a* with $LiAlH_4$ at room temperature. It was assumed that in refluxing tetrahydrofuran with the same reagent the corresponding ethylenic diol could have been formed. The acetylenic diol **8***a*, however, was recovered unchanged even after 24 h of refluxing in tetrahydrofuran with $LiAlH_4$. Since propargylic alcohols can readily be reduced by $LiAlH_4$ to allyl alcohols (5), the inertness of **8***a* towards further reduction is attributed to electrostatic repulsion by an alcoholate ion at C-1.

The acetylene diol **8***a* was also prepared by

[1]The same ketone **5** was reported by Attenburrow *et al.* (10), prepared by a different sequence. However, the quoted u.v. maxima (219 mμ and 298 mμ) are different from ours. Since we carried our sequence to conclusive identification, we do not doubt our results.

Can. J. Chem. Downloaded from www.nrcresearchpress.com by 210.87.254.5 on 09/05/12
For personal use only.

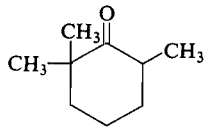

1

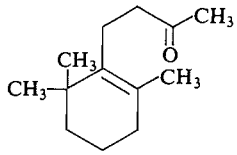

2

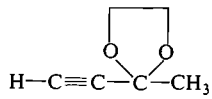

3

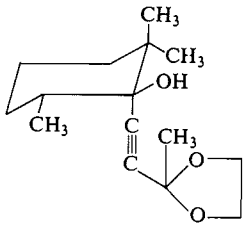

4

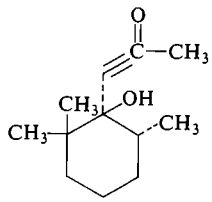

5

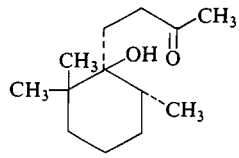

6

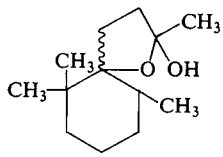

7

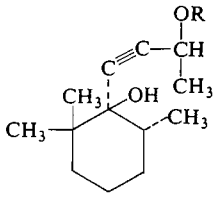

8

a R = H
b R = $COCH_3$
c R = $CH(CH_3)O$ Butyl

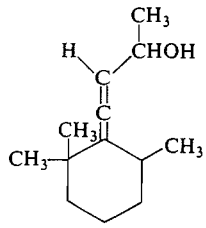

9

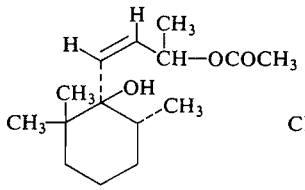

10

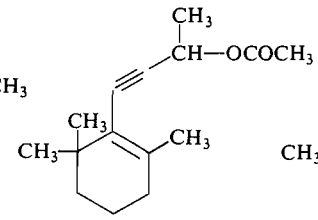

11

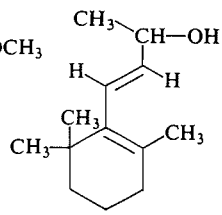

12

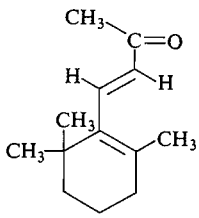

13

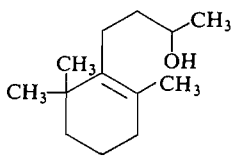

14

Can. J. Chem. Downloaded from www.nrcresearchpress.com by 210.87.254.5 on 09/05/12
For personal use only.

Miki and Hara by the Grignard reagent of 1-butyne-3-ol on ketone **1** (3). We found that the Nef reaction of the butoxy-ethyl ether of the same acetylene alcohol on ketone **1** followed by hydrolysis was more convenient for the preparation of the same compound (**8***c* → **8***a*).

While we have been unable to reduce acetylenediol **8***a* in refluxing tetrahydrofuran, Miki and Hara (3) claimed to have reduced the same compound to allene **9** in ether. In our hands a treatment of **8***a* with a large excess of $LiAlH_4$ in ether as well as in tetrahydrofuran led to the recovery of the starting material only. The discrepancy might be attributable to some contaminants in the $LiAlH_4$ supply of the earlier experimenters.[2]

It was advisable to prepare acetate **8***b* since it is known that during the catalytic reduction of acetylenic 1,4-diols even the two hydroxyl groups interact to form inert furan derivatives (6). The hydrogenation of **8***b* however, stopped at the olefinic stage furnishing compound **10**, similar to the behavior of dioxolane **4** which also consumed only 1 mol of hydrogen.

A literature survey revealed that *cis*-β-ionone has so far been noticed only as an intermediate in the photochemical isomerization of *trans*-β-ionone (7*a* and *b*) to the corresponding pyrane or as a valence isomer being in equilibrium with the same pyrane in temperature-dependent n.m.r. studies (7*c*). We attempted, therefore, to convert acetate **10** to *cis*-β-ionone. Unfortunately our results failed at the dehydration of **10**.

When the acetylenic acetate **8***b* was heated in pyridine with $POCl_3$, olefin **11** was formed in a good yield. The reduction of **11** with $LiAlH_4$ led to β-ionol **12** adducing evidence for the contention that diol **8***a* could not be reduced to compound **9** because of electrostatic repulsion. Compound **12** was identified by comparison with an authentic sample of β-ionol (8). A sequence similar to **8***b* → **11** → **12** was used in the synthesis of zeaxanthin (9).

Oxidation of allylic alcohol **12** with active MnO_2 (10) in acetone led to β-ionone identified with an authentic sample.

The reduction of β-ionone **13** to dihydro-β-ionol **14** was previously carried out by reduction with sodium in refluxing ethanol (11). We repeated the same experiment but with the more modern analytical methods found that the yield did not exceed 40%. After considerable experimentation it was found that the reduction could be carried out in a yield of 80% in a mixture of $(CH_3)_3COH$ and tetrahydrofuran. The choice of our experimental conditions was aided by some recent data obtained by House and co-workers (12) on the reduction of α,β-unsaturated ketones.

Recently in a preliminary communication it was claimed without any experimental details that β-ionone **13** could be reduced to dihydro-β-ionol with $NaBH_4$ (13). However, it was not mentioned what solvent was used. Therefore, we used methyl alcohol but the product isolated proved to be the expected β-ionol **12** only.

The virtually quantitative oxidation of alcohol **14** to dihydro-β-ionone (**2**) with Jones reagent completed the sequence. An authentic sample of dihydro-β-ionone was prepared by the catalytic hydrogenation of β-ionone with which our compound **2** was identical (14).

The application of catalytic hydrogentation to achieve the conversion of β-ionone **13** to dihydro-β-ionone **2** is obviously less advantageous than the route outlined here since a certain amount of tetrahydroionone always contaminates the desired product.

The preferential reduction of an α,β-double bond compared to a γ,δ-double bond in a conjugated α,β,γ,δ-dienone is probably unique to β-ionone **13** and related systems since in 3-keto steroids the γ,δ-double bond is reduced (15). Presently we are in the process of establishing the scope and limitations of the sequence by applying it to other ketones.

Experimental

All melting points were taken on a Fisher-Johns melting point apparatus and are uncorrected. The elemental analyses were carried out by Pascher Mikroanalytical Laboratorium, Bonn, West Germany and Schwarzhopf Mikroanalytical Laboratory, Woodside, N.Y. The i.r. spectra were recorded on a Perkin-Elmer Model 137B infracord spectrophotometer. The u.v. spectrograms were taken on a Coleman Hitachi Model 124 double-beam grating spectrophotometer. The n.m.r. spectra were recorded on a Varian Associates 56.4 MHz spectrophotometer. The mass spectra were obtained with a Hitachi Perkin-Elmer Model RMS-4 spectrometer.

*2,2-Ethylenedioxy-4-(1-hydroxy-2,2,6-trimethylcyclohex-1-yl)-3-butyne (**4**)*

A solution of 13 g of 2,2-ethylenedioxy-3-butyne (4) in anhydrous tetrahydrofuran (30 ml) was added to liquid ammonia (600 ml) containing 4.88 g of sodium amide (17).

To the latter solution 9.5 g of 2,2,6-trimethylcyclohexanone dissolved in anhydrous tetrahydrofuran (20 ml) was added dropwise in 20 min. The solution was stirred magnetically and allowed to react for 7 h. Then NH_4Cl

[2]The question is currently being investigated in our laboratory.

Can. J. Chem. Downloaded from www.nrcresearchpress.com by 210.87.254.5 on 09/05/12
For personal use only.

(70 g) was added and the ammonia was evaporated. The residue was dissolved in water (200 ml) and ether (100 ml) and the water layer was extracted with ether (4 × 200 ml). The ether extracts were washed with saline and dried ($MgSO_4$). After evaporation a t.l.c. homogeneous oil was obtained which crystallized in 3 days (yield: 16.50 g, 98%; m.p. 42°). An analytical sample was prepared by recrystallizing from benzene–pentane, m.p. 47°; mass spectrum (70 eV) *m/e* (relative intensity) 252 (30, parent), 237 (45), 219 (35), 209 (20), 191 (20), 137 (100); i.r. ($CHCl_3$) 3500, 2950, 2200, 1450, 1360, 1320, 1220, 1170, 1100, 1020, 970, 940, 850, cm^{-1}; u.v., end absorption; n.m.r. at 60 MHz ($CDCl_3$) 9.03 (s, 3, 2-methyl), 9.00 (s, 3, 2-methyl), 8.9 (d, 3, J = 3 Hz, 6-methyl), 8.3 (s, 3, dioxolane–methyl), 6.00 (s, 4, O—CH_2—CH_2—O).

Anal. Calcd. for $C_{15}H_{24}O_3$: C, 71.39; H, 9.59. Found: C, 71.21; H, 9.53.

Hydrogenation of Dioxolane 4

A solution of 0.5 g of dioxolane **4** dissolved in ethanol (100 ml) was hydrogenated in the presence of Raney nickel (100 mg) at 30 p.s.i. room temperature for 18 h. Only 1 equiv. of hydrogen was consumed and the n.m.r. of the product revealed the presence of olefinic protons. The same observation was made in the presence of palladium 10% – charcoal.

4-(1-Hydroxy-2,2,6-trimethylcyclohex-1-yl)-3-butyne-2-one (5)

A solution of 1.75 g of dioxolane **4** in methanol (30 ml) and water (5 ml) was stirred magnetically at room temperature for 18 h in the presence of *p*-toluenesulfonic acid (200 mg). The solution was then diluted to 100 ml with water and extracted with chloroform (4 × 100 ml). The combined extracts were washed with 5% $NaHCO_3$ solution, then with saline. After drying ($MgSO_4$) and evaporation a t.l.c. homogeneous oil was obtained, (yield: 1.42 g, 97%); mass spectrum (70 eV) *m/e* (relative intensity) 208 (15, parent), 193 (30), 175 (22), 165 (30), 110 (100); i.r. ($CHCl_3$) 3500, 2950, 2200, 1680, 1460, 1350, 1220, 1040, 970, 780 cm^{-1}; u.v.$_{max}$ (96% C_2H_5OH) 230 nm (ε 5050); n.m.r. at 60 MHz ($CDCl_3$) τ 9.00 (d, 3, J = 3 Hz, 6-methyl), 8.9 (s, 6, 1,1-dimethyl), 7.67 (s, 3, $COCH_3$).

This compound was already prepared by a different route (10) but our u.v. data disagree with those reported previously. Its composition is characterized in terms of acetylenic diol **8***a*.

4-(1-Hydroxy-2,2,6-trimethylcyclohex-1-yl)-3-butyn-2-ol (8a)

(A) Reduction of Ketone 5

To a solution of 3.33 g of ketone **5** in dry tetrahydrofuran (30 ml) 10.93 of LiAl(O-*tert*-butyl)$_3$H or 3.2 g of $LiAlH_4$ was added. The mixture was stirred magnetically at room temperature for 20 h. Then the reaction mixture was poured on ice, filtered through celite, and extracted with ether (4 × 150 ml). The combined extracts were washed with water, dried ($MgSO_4$), and evaporated to dryness. The t.l.c. homogeneous product crystallized on standing (yield: 3.02 g, 90%; m.p. 95°). An analytical sample was obtained by recrystallizing from benzene–pentane; m.p. 105–106°; mass spectrum (70 eV) *m/e* (relative intensity) 210 (30, parent), 193 (30), 177 (100), 149 (100); i.r. ($CHCl_3$) 3400, 2930, 1450, 1370, 1325, 1240, 1115, 1075, 970, 950, 900, 820 cm^{-1}; u.v., end absorption; n.m.r. at 50 MHz ($CDCl_3$) τ 9.05 (s, 6, 2,2-dimethyl), 8.95 (d, 3, J = 3 Hz, 6-methyl), 8.6 (d, 3, J = 6 Hz, CHOH-CH_3), 5.60 (m, 1, CHOH).

Anal. Calcd. for $C_{13}H_{22}O_2$: C, 74.24; H, 10.54. Found: C, 73.92; H, 10.54.

(B) Nef Reaction on 2,2,6-Trimethylcyclohexanone (1)

To a solution of sodium amide (17) prepared from sodium (290 mg) in liquid ammonia (300 ml) 3-(1-butoxy-β-ethoxy)-but-1-yne (6) (2.18 g dissolved in 10 ml of dry THF) was added. After stirring magnetically for ½ h ketone **1** (500 mg dissolved in 5 ml of dry THF) was dripped into the acetylide solution in 20 min. The reaction mixture was stirred for 4 h then decomposed with NH_4Cl (3 g). After the ammonia had been evaporated the product was dissolved in water (100 ml) and extracted with ether (4 × 60 ml). After evaporation and drying ($MgSO_4$) a yellow oil (3 g) was obtained which was devoid of carbonyl (i.r.) and consisted of the adduct and the excess acetylene only (t.l.c.). The mixture was hydrolyzed without isolation in methanol (100 ml) and water (10 ml) in the presence of *p*-toluensulfonic acid (100 mg) by stirring magnetically at room temperature for 18 h.

The reaction mixture was diluted with water (100 ml) and extracted with chloroform (4 × 70 ml). The combined extracts were dried ($MgSO_4$) and all volatile components were removed by evacuation at 0.5–0.2 mm Hg for 1 h, leaving a crystalline residue. This was recrystallized from benzene–pentane yielding 0.565 g of acetylene diol **8***a* (70%, m.p. 105°). Spectroscopic properties were identical to those described in the preceding paragraph.

Attempted Reduction of 8a

Acetylenediol **8***a* (0.5 g) was refluxed with $LiAlH_4$ (1 g) in tetrahydrofuran (30 ml) for 24 h, and worked up as described for the preparation of **8***a*, only the starting material was recovered. The same result was obtained with anhydrous ether as the solvent.

4-(1-Hydroxy-2,2,6-trimethylcyclohex-1-yl)-3-butyn-2-yl Acetate (8b)

A solution of 3.09 g of acetylenediol **8***a* in pyridine (25 ml) and acetic anhydride (25 ml) was allowed to stand at room temperature overnight. The reaction mixture was then poured on ice and extracted with ether (4 × 75 ml). The combined ether extracts were washed in the presence of ice with 10% H_2SO_4, then in succession with 5% $NaCHO_3$ solution and water. After drying ($MgSO_4$) and evaporating the ether, a t.l.c. homogeneous oil was obtained (yield: 3.56 g, 96%); mass spectrum (70 eV) *m/e* (relative intensity) 252 (30, parent), 237 (40), 234 (100); i.r. ($CHCl_3$) 3580, 2950, 1740, 1450, 1365, 1330, 1240, 1140, 1100, 1030, 970, 950 cm^{-1}; u.v., end absorption; n.m.r. at 60 MHz ($CDCl_3$) τ 9.06 (d, 3, J = 3 Hz, 6-methyl), 8.99 (s, 3, 2-methyl), 8.93 (s, 3, 2-methyl), 8.50 (d, 3, J = 8 Hz, C≡C—CH—CH_3), 8.00 (s, 3, $OOCCH_3$), 4.50 (g, 1, CH—$OCOCH_3$).

The acetylenic acetate **8***b* was characterized in terms of crystalline dihydro derivative **10**.

4-(2,6,6-Trimethylcyclohex-1-en-1-yl)-3-butyn-2-yl Acetate (11)

To a solution of 3.2 g of acetate alcohol **8***b* in pyridine (20 ml) 3.8 ml of $POCl_3$ was added in 10 min. The reaction mixture was heated at 90° for 18 h under dry nitrogen and stirred magnetically. Then the solution was cooled and poured on ice. The product was extracted with chloroform

(4 × 100 ml). The combined extracts were washed with 10% sulfuric acid in the presence of ice. After washing with 5% $NaHCO_3$ and then with water, the chloroform solution was dried ($MgSO_4$) and concentrated *in vacuo*, furnishing a t.l.c. homogeneous oily product (yield: 2.48 g, 80%); mass spectrum (70 eV) *m/e* (relative intensity) 234 (25, parent) 177 (83), 159 (100), 131 (40), 91 (86); i.r. ($CHCl_3$) 2910, 2210, 1730, 1440, 1360, 1330, 1240, 1075, 1020, 950 cm^{-1}; u.v.$_{max}$ (96% C_2H_5OH) 234 nm (ε 7300); n.m.r. at 60 MHz ($CDCl_3$) τ 8.9 (s, 6; 6,6-dimethyl), 8.5 (d, 3, J = 8 Hz, $CHCH_3$), 8.17 (s, 3, 2-methyl), 7.90 (s, 3, $COCH_3$), 4.5 (m, 1, $CHOCOCH_3$). This product was characterized in terms of β-ionone **13**.

trans-β-Ionol (12)

To a solution of 0.6 g of acetate **11** in dry tetrahydrofuran (30 ml) 1.2 g of $LiAlH_4$ was added while cooling with ice and stirring magnetically. The reaction mixture was then stirred and refluxed for 18 h. After cooling with ice the excess reagent was destroyed by the addition of water. Then the reaction mixture was filtered with celite and washed with chloroform. The water phase was extracted with chloroform (4 × 70 ml). The combined extracts were washed with water, dried ($MgSO_4$), and concentrated. A t.l.c. homogeneous oil was obtained (yield: 0.425 g, 85%) which was distilled at 105°/2 mm Hg; mass spectrum (70 eV) *m/e* (relative intensity) 194 (15, parent), 176 (100), 161 (80), 146 (70); i.r. ($CDCl_3$) 3450, 2920, 1450, 1350, 1240, 1130, 1040, 970, 940, 910, 860; u.v.$_{max}$ (96% C_2H_5OH) 237 nm (ε 4200); n.m.r. at 60 MHz ($CDCl_3$) τ 9.03 (s, 6, 2,2-dimethyl), 8.73 (d, 3, J = 6 Hz, CH—CH_3), 8.37 (s, 3, 1-methyl), 5.70 (m, 1, $CHOH$), 4.57 (d of d, 1, olefinic), 3.95 (d, 1, J = 14 Hz, olefinic). The product was identical in every respect with β-ionol prepared by the $NaBH_4$ reduction of authentic β-ionone (8).

cis-4-(1-Hydroxy-2,2,6-trimethylcyclohex-1-yl)-but-3-en-2-yl Acetate (10)

A solution of 0.3 g of acetylene acetate **8***b* in ethyl acetate (70 ml) was hydrogenated at room temperature for 18 h at 30 p.s.i. in the presence of 5% Pd–C (30 mg). After filtration and evaporation the t.l.c. homogeneous product crystallized on standing (yield: 0.285 g, 95%; m.p. 68°). An analytical sample was obtained by recrystallizing from benzene–pentane, m.p. 77°; mass spectrum (70 eV) *m/e* (relative intensity) 254 (20, parent), 194 (100), 179 (15); i.r. ($CHCl_3$) 3450, 2950, 1725, 1460, 1370, 1260, 960 cm^{-1}; u.v. end absorption; n.m.r. at 60 MHz ($CDCl_3$) τ 9.11 (s, 3, 2-methyl), 8.94 (s, 3, 2-methyl), 8.7 (d, 3, J = 7 Hz, CH-CH_3), 7.95 (s, 3, $COCH_3$), 4.5 (m, 1, $CHOCHOCH_3$), 3.80 (m, 2, olefinic).

Anal. Calcd. for $C_{15}H_{26}O_3$: C, 70.83; H, 10.30. Found: C, 71.02; H, 10.25.

trans-β-Ionone (13)

A solution of 0.211 g of alcohol **12** dissolved in acetone (25 ml) was stirred magnetically at room temperature for 8 h with active MnO_2 (10). After filtration and evaporation an oil was obtained, which was purified on silica gel thick layer preparatory plates furnishing 0.180 g of pure product (yield: 0.18 g, 85%), mass spectrum (70 eV) *m/e* (relative intensity) 192 (80, parent), 177 (100), 162 (70); i.r. ($CHCl_3$) 2900, 1650, 1600, 1450, 1350, 1250, 1160, 1120, 950, 900 cm^{-1}; u.v.$_{max}$ (96% C_2H_5OH) 295 nm (ε 1050), 228 (6450); n.m.r. at 60 MHz ($CDCl_3$) τ 8.9 (s, 6, 2,2-dimethyl), 8.23 (s, 3, 6-methyl), 7.73 (s, 3, $COCH_3$), 3.86 (d, 1, J = 17 Hz, olefinic), 2.66 (d, 1, J = 17 Hz, olefinic). The product was identical in terms of all spectral data with an authentic sample of β-ionone purchased from Aldrich Chemical Co., Milwaukee, U.S.A.

Dihydro-β-ionol (14)

A solution of 1.42 g of β-ionone **13** dissolved in $(CH_3)_3COH$ (45 ml) and tetrahydrofuran (100 ml) was stirred magnetically under dry nitrogen for 18 h with cut pieces of Na (2 g) at room temperature. The remaining pieces of Na were destroyed by the addition of methanol (20 ml). The yellow reaction mixture was diluted with water (200 ml) and extracted with ether (3 × 150 ml). The combined ether extracts were washed with water, dried ($MgSO_4$) and concentrated *in vacuo* leading to 1.15 g of t.l.c. homogeneous dihydro-β-ionol (yield: 80%), mass spectrum (70 eV) *m/e* (relative intensity) 196 (40, parent), 181 (20), 166 (100); i.r. ($CHCl_3$) 3500, 1600, 1450, 1350, 1250, 1100, 940 cm^{-1}; u.v., end absorption; n.m.r. at 60 MHz ($CDCl_3$) τ 9.00 (s, 6, 2,2-dimethyl), 8.77 (d, 3, J = 6 Hz, $HOCHCH_3$), 8.37 (s, 3, 6-methyl), 6.20 (m, 1, $CHOH$). The product was characterized in terms of dihydro-β-ionone **2** whose composition was based on *trans*-β-ionone **13**.

Dihydro-β-ionone (2)

A solution of 0.3 g of dihydro-β-ionol (**14**) dissolved in acetone (30 ml) was titrated at room temperature, while stirring magnetically, with Jones reagent (16) until a permanently brown solution resulted. After dilution with water (100 ml) the solution was extracted with chloroform (4 × 50 ml). The combined chloroform extracts were washed with 5% $NaHCO_3$ solution, dried ($MgSO_4$), and concentrated *in vacuo* to a t.l.c. homogeneous oil (yield: 0.27 g, 89%); mass spectrum (70 eV) *m/e* (relative intensity) 194 (30, parent), 179 (40), 164 (100); i.r. ($CHCl_3$) 2950, 1710, 1450, 1350, 1250, 1150 cm^{-1}; u.v., end absorption; n.m.r. at 60 MHz ($CDCl_3$) τ 9.05 (s, 6, 2,2-dimethyl), 8.43 (s, 3, 2-methyl), 7.85 (s, 3, $COCH_3$). The product was found identical in terms of all spectroscopic data with an authentic sample of dihydroionone prepared from β-ionone by partial hydrogenation (14).

2-Hydroxy-2,6,6,10-tetramethyl-1-oxa-spiro[4,5]-decane (7)

A solution of acetylene ketone **5** (0.24 g) in methanol (70 ml) was hydrogenated in the presence of 5% Pd–C (50 mg) at room temperature and at a pressure of 30 p.s.i. After filtration and evaporation the oily residue was dissolved in chloroform, dried ($MgSO_4$), and concentrated *in vacuo* again (yield: 220 mg, 90%); mass spectrum (70 eV) *m/e* (relative intensity) 212 (0, no parent peak), 194 (100), 179 (30), 161 (30); i.r. ($CHCl_3$) 3350, 2950, 1705 (weak), 1440, 1360, 1100, 1050, 970, 860 cm^{-1}; u.v., end absorption; n.m.r. at 60 MHz ($CDCl_3$) τ 9.20 (s, 3, 2-methyl), 9.00 (d, 3, J = 6 Hz, 6-methyl), 8.66 (s, 3, 2-methyl), 8.50 (s, 3, $HOCCH_3$). An analytical sample was prepared by distilling the sample at approximately 100°/0.5 mm Hg.

Anal. Calcd. for $C_{13}H_{24}O_2$: C, 73.54; H, 11.39. Found: C, 73.24; H, 11.51.

We want to thank Mr. A. Mak for technical help. The financial assistance of the National Research Council of Canada and the Senate Research Committee of the University of Prince Edward Island is greatly appreciated.

Can. J. Chem. Downloaded from www.nrcresearchpress.com by 210.87.254.5 on 09/05/12
For personal use only.

We thank Drs. R. Duffy and J. Rigney for encouraging this work.

1. O. S. BHANOT and P. C. DUTTA. J. Chem. Soc. (C), 2583 (1968).
2. (*a*) H. MAYER and O. ISLER. *In* Carotenoids. *Edited by* O. Isler. Birkhauser Verlag, Basle. 1971; (*b*) Beilstein's Handbuch der Organischen Chemie, VII, third supplemental volume. Springer-Verlag, New York. 1968. p. 634.
3. T. MIKI and Y. HARA. Chem. Pharm. Bull. (Jap.) **4**, 85, 89 (1956).
4. G. GIUSTI. Bull. Soc. Chim. Fr. 753, (1972).
5. H. H. INHOFFEN, F. BOHLMANN, and G. RUMMERT. Leib. Ann. Chem. **569**, 226 (1950).
6. H. H. GUTMANN and H. LINDLAR. *In* H. G. Viehe's Chemistry of acetylenes. M. Dekker, New York. 1969. p. 360.
7. (*a*) G. BUCHI and N. C. YANG. J. Am. Chem. Soc. **79**, 2318, (1957); (*b*) V. RAMAMURTHY, Y. BUTT, C. YANG, P. YANG, and R. S. H. LIU. J. Org. Chem. **38**, 1247 (1973). (*c*) E. N. MARVELL, G. CAPLE, T. A. GOSNIK, and G. ZIMMER. J. Am. Chem. Soc. **88**, 619 (1966).
8. E. INHOFFEN, F. BOHLMANN, and M. BOHLMANN. Ann. Chem. **565**, 35 (1949).
9. D. E. LOEBER, S. W. RUSSEL, T. P. TOUBE, B. C. L. WEEDON, and J. DIMENT. J. Chem. Soc. (C), 404 (1971).
10. J. ATTENBURROW, A. F. B. CAMERON, J. H. CHAPMAN, R. M. EVANS, B. H. HEMS, A. B. A. JANSEN, and T. WALKER. J. Chem. Soc. 1904 (1952).
11. Y. R. NAVES and P. BACHMANN. Helv. Chim. Acta, **26**, 2151 (1943).
12. K. W. BOWERS, R. W. GIESE, J. GRIMSHAW, H. O. HOUSE, N. H. KOLODNY, K. KRONBERGER, and D. K. ROE. J. Am. Chem. Soc. **92**, 2783 (1970).
13. Y. NAKATINI and T. YAMANISHI. Tetrahedron Lett. **24**, 1995 (1969).
14. Y. R. NAVES and P. ARDIZIO. Helv. Chim. Acta, **32**, 206 (1949).
15. J. A. CAMPBELL and J. C. BABCOCK. J. Am. Chem. Soc. **81**, 4069 (1959).
16. L. F. FIESER and M. FIESER. Reagents for organic synthesis. J. Wiley and Sons, Inc., New York. 1967. p. 142.
17. T. H. VAUGHN, R. R. VOGT, and J. A. NIEUWLAND. J. Am. Chem. Soc. **56**, 2120, (1934).

Can. J. Chem. Downloaded from www.nrcresearchpress.com by 210.87.254.5 on 09/05/12
For personal use only.

Some Reactions of Isothiazoline-3- and -5-thiones

MOHINDER S. CHAUHAN, MOHAMED E. HASSAN, AND DAVID M. MCKINNON

Department of Chemistry, University of Manitoba, Winnipeg, Manitoba R3T 2N2

Received November 13, 1973

Reactions of certain 3-bromothio-1,2-dithiolium bromides with primary amines produce isothiazoline-5-thiones. These compounds form adducts of varying stability with acetylenic reagents. Comparison of their reactivity with the isomeric isothiazoline-3-thiones indicates that while the former react rapidly to form only monoadducts, the latter react more slowly to form monoadducts which react more rapidly to form diadducts.

La réaction de certains bromures de bromothio-3 dithiolium-1,2 avec des amines primaires conduit aux isothiazolinethiones-5. Ces composés forment des produits d'addition de stabilité variable avec des réactifs acétyléniques. La comparaison de leurs réactivités avec celles de leurs isomères isothiazolinethiones-3 montre que les premières réagissent rapidement pour conduire à des produits de monoaddition alors que les dernières réagissent plus lentement pour former des produits de monoaddition qui réagissent plus rapidement pour former des produits de diaddition.

[Traduit par le journal]

Can. J. Chem., **52**, 1738 (1974)

Although cycloaddition reactions of 1,2-dithiole-3-thiones with various acetylenic and other reagents have been widely studied (1–4), much less has been reported on these reactions applied to the isoelectronic and structurally related isothiazoline-3- (**1**) and -5-thiones (**2**).

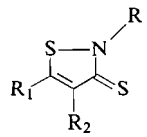

1

a R = Me; R_1 = Ph; R_2 = H
b R = R_1 = Ph; R_2 = H
c R = Me; R_1 = R_2 = Ph

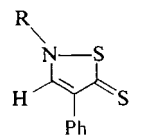

2

a R = Ph
b R = Me
c R = $PhCH_2$
d R = $(CH_3)_2CH$
e R = $\overline{CH_2—(CH_2)_4—CH}$—
f R = $C_6H_4oCH_3$
g R = $C_6H_4mCH_3$
h R = $C_6H_4pCH_3$
i R = $C_6H_4pOCH_3$

Reactions of two *N*-alkylisothiazoline-5-thiones and one 5-iminoisothiazoline with dimethyl acetylenedicarboxylate are reported (5) to give 1,3-dithioles and thiazole derivatives, respectively, and 2,4-diphenylisothiazoline-5-thione (**2***a*) reacted similarly with dimethyl acetylenedicarboxylate (6). Only one such reaction is reported for the isomeric isothiazoline-3-thiones. The 2-methyl-5-phenyl compound (**1***a*) reacted with benzonitrile oxide to form an unstable adduct which decomposed to form 2-methyl-5-phenylisothiazoline-3-one and phenylisothiocyanate (7).

Within recent years certain isothiazoline-3- and -5-thiones have become available through a variety of syntheses. *N*-Alkyl-3-thiones are prepared (8) by reaction of 3-alkylthio-1,2-dithiolium salts with aliphatic amines or by sulfurization of *N*-alkylisothiazolium salts (6) but these methods are inapplicable to the synthesis of *N*-arylisothiazoline-3-thiones, as 1,2-dithiole-3-imines are obtained instead (6, 9). Recently (10) however, a synthesis of a 2,5-diphenyl-3-methylthioisothiazolium salt by oxidation of a β-aminothione was reported and we have found that dealkylation of this in pyridine gave the desired isothiazoline-3-thione **1***b*.

N-Alkylisothiazoline-5-thiones are available by treatment of certain imines with carbon disulfide (11) but this method is inapplicable to the *N*-aryl compounds. These may be prepared by

Can. J. Chem. Downloaded from www.nrcresearchpress.com by 210.87.254.105 on 09/05/12
For personal use only.

Can. J. Chem. Downloaded from www.nrcresearchpress.com by 210.87.254.105 on 09/05/12
For personal use only.

dealkylation of the corresponding 5-alkylthioisothiazolium salts (6) or in one case by treatment of 3-bromothio-4-phenyl-1,2-dithiolium bromide with aniline. We have found that this reaction is also applicable to other aromatic amines and to aliphatic amines. The bromide salt reacts vigorously with alcoholic solutions of primary amines to form the new thiones **2***b–i* conveniently and in good yield. Since the preparation of a wide variety of isothiazolinethiones is now feasible, it seemed desirable to study in more detail their cycloaddition reactions to determine to what extent these paralleled those of the 1,2-dithiole-3-thiones, in particular with respect to the effect of the ring nitrogen, and the effect, if any, of substituents on reactivity and products.

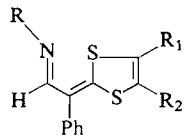

3

a R = Ph; $R_1 = R_2$ = COPh
b R = R_1 = Ph; R_2 = H
c R = Ph; R_1 = H; R_2 = Ph
d R = Me; $R_1 = R_2 = CO_2Me$
e RN = O; $R_1 = R_2 = CO_2Me$
f R = Ph; $R_1 = R_2 = CO_2Me$

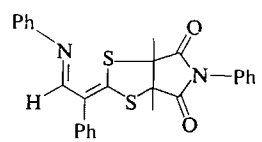

4

2,4-Diphenylisothiazoline-5-thione (**2***a*) reacted rapidly with dibenzoylacetylene to give a dibenzoyl-1,3-dithiole derivative (**3***a*), similarly to known (12) reactions of dithiolethiones. It also reacted with phenylacetylene but we were unable to crystallize the adduct formed. In this case reaction of the thione with the unsymmetrically substituted acetylene could give two geometrically isomeric products (13) **3***b* and *c*. These probably mutually interfere with crystallization. The adduct also appears to be unstable and reverts to starting material, for although a satisfactory mass spectrum indicating the parent ion was obtained, starting thione was always detectable on chromatography, even after repeated attempts of purification. Reaction with diphenylacetylene was similar. Chromatography indicated the formation of a red compound but attempted crystallization gave only starting material. Reaction of the thione with *N*-phenylmaleimide gave an adduct which appears to be the 1,3-dithiolanedicarboximide **4** but reaction with diethyl azodicarboxylate gave only decomposition products.

Reaction of *N*-alkylisothiazoline-5-thiones with dimethyl acetylenedicarboxylate also proceeded rapidly. The thione **2***b* gave a crystalline aldimine adduct **3***d* in good yield but from the reaction of the *N*-benzyl compound **2***c* an oil was obtained. Trituration of this with ethanol gave only the aldehyde **3***e*, presumably by hydrolysis of the initially formed aldimine. This aldehyde had been previously reported as a product from the reaction of 4-phenyl-1,2-dithiole-3-thione with dimethyl acetylenedicarboxylate (14).

In contrast to the above rapid reactions of the 5-thiones, the 3-thiones (**1**) reacted much more slowly with dimethyl acetylenedicarboxylate. Treatment of 2-methyl-5-phenylisothiazoline-3-thione (**1***a*) with the ester in boiling benzene for 24 h gave a mixture of products from which were obtained starting thione and an orange oil, formed by combination of thione with 2 mol of ester. This is probably the spiran diadduct **5***a*. Initial reaction of the thione **1***a* with ester would have given a monoadduct **6***a* and further reaction with more ester would provide **5***a*. No monoadduct **6***a* was obtained, suggesting that the rate of the second reaction is greater than that of the first. These reactions correspond to reactions in the dithiole series (13) and it is interesting that reactions of 3-phenylimino-1,2-dithioles with dimethyl acetylenedicarboxylate give only diadducts of type **5**. None of the intermediate monoadducts of type **6** was obtained there either. One possibility is that the 2-methyl-5-phenylisothiazoline-3-thione could undergo thermal rearrangement to 2-methylimino-5-phenyl-1,2-dithiole, as has been found for the benzo-compound (14) and that the iminodithiole underwent the subsequent reactions. However, the isothiazolinethione was unchanged in boiling benzene indicating that it is a direct precursor of the mono- and diadducts.

The marked difference in reactivity of the two isoelectronic thione systems **1** and **2** with dimethyl acetylenedicarboxylate is interesting. For reactions of the thiones **2**, structures such as **8**, involving sulfur d-orbital participation are possible, corresponding to contributing structures of 2-

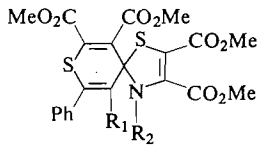

5

a $R_1 = H; R_2 = Me$
b $R_1 = Ph; R_2 = Me$
c $R_1 = H; R_2 = Ph$

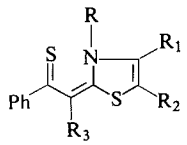

6

a $R_1 = R_2 = CO_2Me; R = Me; R_3 = H$
b $R_1 = R_2 = CO_2Me; R = Me; R_3 = Ph$
c $R_1 = R_2 = CO_2Me; R = R_3 = Ph$
d $R_1 = H; R_2 = Ph; R_3 = H, R = Me$
e $R_1 = H; R_2 = p\text{Tol}; R_3 = H; R = Me$

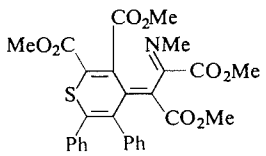

7

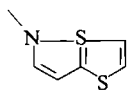

8

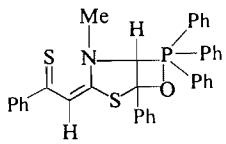

9

thioacylmethylene-1,3-dithioles, or intermediates in their formation from 1,2-dithiole-3-thiones (15). Since no such intermediates are possible in the reactions of compounds **1** the reaction may proceed with greater difficulty.

2-Methyl-4,5-diphenylisothiazoline-3-thione (**1***c*) also reacted with the ester. A crystalline diadduct **5***b* was obtained, along with a small amount of deep red material. The mass spectrum and analysis indicated that it contains one sulfur atom less than the spiran diadduct. On this basis and because of its deep color we tentatively assign to it the conjugated thiopyran structive **7**, which could have arisen from the diadduct by extrusion of sulfur by a mechanism analogous to a step in the sulfur catalyzed rearrangements of 2-thiophenacylidene-1,3-dithioles to 3-thiophenacylidene-1,2-dithioles (thiathiophthenes) (16).

2,5-Diphenylisothiazoline-3-thione (**1***b*) also reacted with dimethyl acetylenedicarboxylate. The product here was the known (13) diadduct **5***c*. Once more no monoadduct was obtained.

Attempts to synthesize diadducts from the imine adducts (**3**) formed from the isothiazoline-5-thiones were unsuccessful. Thus **3***f* was recovered from further treatment with dimethyl acetylenedicarboxylate, **3***d* gave the aldehyde **3***e* by hydrolysis during the work-up. These results are comparable to those of Behringer *et al.* (5) and may reflect the different electronic effects of the nitrogen and sulfur containing side chains in the isomeric systems **3** and **6**.

To enable synthesis of thioacylmethylene-thiazoles **6** from the thiones **1**, a reagent is required which does not undergo further reaction with the thiazole. Accordingly, treatment of **1***a* with phenacylidenetriphenylphosphorane or *p*-methylphenacylidenetriphenylphosphorane gave the thiazoles **6***d* and *e*, respectively, and triphenylphosphine oxide. Similar reactions of phosphoranes with azides are known (17). The reaction probably proceeds via the adduct **9**, with subsequent extrusion of triphenylphosphine oxide to form the thiazole.

Experimental

Thin-layer chromatography was performed on "Camag" silica gel type D.S.F. 5, supplied by Mondray Ltd. Development of plates was performed in benzene. The i.r. spectra were performed on a Perkin-Elmer model 337 spectrophotometer and n.m.r. spectra were obtained on a Varian model 56/60A spectrometer in deuteriochloroform using tetramethylsilane as an internal standard.

Preparation of 2-Alkyl-4-phenylisothiazoline-5-thiones (2b–i)

4-Phenyl-1,2-dithiole-3-thione (2.1 g, 0.01 mol) (18) dissolved in carbon tetrachloride (50 ml) was slowly treated with a solution of bromine (1.76 g, 0.011 mol) in carbon tetrachloride (20 ml) with stirring. The yellow solid formed was collected, washed with carbon tetrachloride, and briefly dried to remove excess carbon tetrachloride. The solid was added portionwise to solutions of the desired amines (~0.05 mol) in ethanol (50 ml). A vigorous reaction ensued. After 5 min the mixture was diluted with water and the product stirred with 10% hydrochloric acid. The products crystallized immediately or on trituration with ethanol and were recrystallized from ethanol or benzene – petroleum ether 1:1 mixture. The results are summarized in Table 1.

Reaction of 2,4-Diphenylisothiazoline-5-thione with Dibenzoylacetylene

The thione (26.9 mg, 0.1 mmol) in benzene (2 ml) was

Can. J. Chem. Downloaded from www.nrcresearchpress.com by 210.87.254.105 on 09/05/12
For personal use only.

Can. J. Chem. Downloaded from www.nrcresearchpress.com by 210.87.254.105 on 09/05/12
For personal use only.

added to a solution of dibenzoylacetylene (23.4 mg, 0.1 mmol) in hot benzene (2 ml). The solution turned red immediately. The solution was boiled briefly, then evaporated. A red oil was obtained which crystallized on standing. The product was recrystallized from toluene–ethanol, 1:1 mixture as red prisms, m.p. 162–163° (95%).

Anal. Calcd. for $C_{31}H_{21}O_2S_2N$: C, 73.96; H, 4.16; S, 12.70; N, 2.77. Found: C, 73.85; H, 4.30; S, 12.63; N, 2.91.

The mass spectrum: M^+ 503, calcd. 503.

Reaction of 2,4-Diphenylisothiazoline-5-thione with Phenylacetylene

To the thione (269 mg, 1 mmol) in benzene (10 ml) was added phenylacetylene (102 mg, 1 mmol) and the mixture was refluxed 24 h. Chromatography gave initially an orange band which was purified by rechromatography to give a red oil (20 mg). This could not be crystallized and appears on chromatography to revert partially to starting material.

The mass spectrum: M^+ 371, calcd. 371; the n.m.r. spectrum: τ 3.48, 3.21 (1 H singlets, the vinyl protons), 2.95–2.45 (30H bands, the aromatic protons), 1.95 (two superimposed 1H singlets, the aldimine protons).

Reaction of 2,4-Diphenylisothiazoline-5-thione with Diphenylacetylene

The thione (269 mg, 1 mmol) and the acetylene (178 mg, 1 mmol) in benzene were refluxed 26 h. Chromatography indicated the formation of a red product but attempted isolation gave only starting materials.

Reaction of 2,4-Diphenylisothiazoline-5-thione with N-Phyenylmaleimide to Form Adduct 4

The thione (269 mg, 1 mmol) and *N*-phenylmaleimide (173 mg, 1 mmol) in benzene were refluxed 3 h. Evaporation gave a yellow solid which was recrystallized from toluene as fine yellow crystals, m.p. 180–182° (76%).

Anal. Calcd. for $C_{25}H_{18}O_2N_2S_2$: C, 67.87; H, 4.07; N, 6.33; S, 14.49. Found: C, 67.69; H, 4.11; N, 6.45; S, 14.67.

The n.m.r. spectrum: τ 5.30 and 5.03 (2H doublets, the dithiolane ring protons, J = 7.5 Hz), 2.82–2.40 (15 H bands, the aromatic protons), 1.82 (1H singlet, the aldimine proton); the i.r. spectrum: 1710 cm^{-1} (C=O str). The mass spectrum: M^+ 442, calcd. 442.

Reaction of 2,4-Diphenylisothiazoline-5-thione with Diethyl Azodicarboxylate

The thione (269 mg, 1 mmol) and the ester (174 mg, 1 mmol) in benzene (10 ml) were refluxed together 10 h. Chromatography gave only starting material and dark decomposition products.

Reaction of 2-Methyl-4-phenylisothiazoline-5-thione with Dimethyl Acetylenedicarboxylate to form 3d

The thione (207 mg, 1 mmol) in benzene (10 ml) was mixed with a solution of the ester (142 mg, 1 mmol) in benzene (10 ml) and warmed briefly. The red solution was evaporated to yield an orange oil which crystallized on trituration under ethanol. The product was crystallized from ethanol as red needles, m.p. 111° (82%).

Anal. Calcd. for $C_{16}H_{15}O_4NS_2$: C, 54.95; H, 4.29; N, 4.02; S, 18.05. Found: C, 55.05; H, 4.30; N, 3.90; S, 18.21.

The n.m.r. spectrum: τ 6.46 (3H doublet, the nitrogen methyl, J = 2.0 Hz), 6.25 and 6.16 (two 3H singlets, the ester methyls), 2.68 (5H singlet, the aromatic protons), 2.07 (1 H doublet, the aldimine proton, J = 2.0 Hz); the i.r. spectrum: 1705 cm^{-1} (C=O); the mass spectrum: M^+ 349, calcd. 349.

Reaction of Dimethyl 2-(1-Phenyl-2-methyliminoethylidene)-1,3-dithiole-4,5-dicarboxylate with Dimethyl Acetylenedicarboxylate

The dithiole (359 mg, 1 mmol) and the ester (142 mg, 1 mmol) in benzene (20 ml) were refluxed 48 h. Examination by t.l.c. indicated that some decomposition had occurred but the product was mainly the aldehyde **3***e* (56%).

Reaction of Dimethyl 2-(1-Phenyl-2-phenyliminoethylidene)-1,3-dithiole-4,5-dicarboxylate with Dimethyl Acetylenedicarboxylate

Treatment of equimolar quantities in boiling benzene for 48 h gave only starting material.

Reaction of 2-Benzyl-4-phenylisothiazoline-5-thione with Dimethyl Acetylenedicarboxylate to Form Dimethyl α-Phenylformylmethylene-1,3-dithiole-4,5-dicarboxylate (3e)

The thione (283 mg, 1 mmol) in benzene (10 ml) was treated with dimethyl acetylenedicarboxylate (142 mg, 1 mmol). The solution turned red immediately and was evaporated to give a red oil. This could not be crystallized, even after t.l.c., but trituration under ethanol gave the aldehyde **3***e* as orange prisms, m.p. 127–129°, from benzene (61%). The product was identical (mixture m.p., i.r., and n.m.r.) to an authentic sample (14).

Reaction of 2-Methyl-5-phenylisothiazoline-3-thione with Dimethyl Acetylenedicarboxylate

The thione (207 mg, 1 mmol) and the ester (142 mg, 1 mmol) in benzene (10 ml) were refluxed 24 h. The mixture gradually turned dark. Chromatography using chloroform as an eluent yielded three main fractions. The first eluted gave starting material (30%) and a second orange band which was purified by further chromatography. Evaporation yielded **5***a* as an orange oil which could not be crystallized (37%).

The n.m.r. spectrum: τ 7.16 (3H singlet, the *N*-methyl), 6.32–6.08 (four 3H singlets, the ester protons, not properly resolved), 3.56 (1H singlet, the methine proton), 2.60–2.51 (5H bands, the aromatic protons; the mass spectrum: M^+ 491, calcd. 491.

A third dark fraction appears to consist of polymeric material and was not further investigated.

Reaction of 2-Methyl-4,5-diphenylisothiazoline-3-thione with Dimethyl Acetylenedicarboxylate

The thione (283 mg, 1 mmol) was treated with the ester (142 mg, 1 mmol) as above. Chromatography using chloroform as an eluent gave a number of bands. The first eluted was starting thione (50%). An orange band next eluted gave on evaporation a red oil, which crystallized from methanol as red prisms, m.p. 159–160° (21%). Use of a two-fold excess of ester increased the yield to 68%.

Anal. Calcd. for $C_{28}H_{25}NO_8S_2$: C, 59.26; H, 4.40; N, 2.46; S, 11.28. Found: C, 59.36; H, 4.28; N, 2.51, S, 11.18.

The n.m.r. spectrum: τ 7.26 (3H singlet, the *N*-methyl),

Can. J. Chem. Downloaded from www.nrcresearchpress.com by 210.87.254.105 on 09/05/12
For personal use only.

TABLE 1. Preparation of isothiazoline-5-thiones

Compound	Melting point	Yield (%)	Formula	Analysis (%) Calculated C	H	N	S	Found C	H	N	S
2*b*	150–152	73	$C_{10}H_9NS_2$	57.97	4.35	6.76	30.91	57.78	4.17	6.59	31.15
2*c*	120–122	61	$C_{16}H_{15}NS_2$	67.84	4.59	4.95	22.64	67.67	4.68	5.05	22.64
2*d*	120–121	55	$C_{12}H_{13}NS_2$	61.28	5.52	5.94	27.23	61.09	5.44	5.76	27.21
2*e*	146–147	50	$C_{15}H_{17}NS_2$	65.31	6.18	5.09	23.25	65.43	6.25	5.15	23.12
2*f*	142–143	56	$C_{16}H_{15}NS_2$	67.84	4.59	4.95	22.64	67.68	4.48	4.98	22.40
2*g*	151–153	54	$C_{16}H_{15}NS_2$	67.84	4.59	4.95	22.64	67.71	4.68	4.94	22.69
2*h*	178–179	52	$C_{16}H_{15}NS_2$	67.84	4.59	4.95	22.64	67.71	4.76	4.79	22.54
2*i*	145–146	55	$C_{16}H_{15}ONS_2$	64.21	4.34	4.68	21.40	63.98	4.43	4.72	21.54

6.30 and 6.24 (two 6H singlets, the ester methyls, not properly resolved), 2.70 (10H singlet, the aromatic protons): the mass spectrum: M^+ 567, calcd. 567.

Examination of another more strongly adsorbed band gave a dark red solid which crystallized as dark red needles, m.p. 255°, from methanol (7 mg). The mass spectrum: M^+ 535, calcd. for $C_{22}H_{19}NO_4S$ 535. The compound was not further investigated.

Preparation of 2,5-Diphenylisothiazoline-3-thione

2,5-Diphenyl-3-methylthioisothiazolium perchlorate (10) (383.5 mg, 1 mmol) in pyridine (10 ml) was refluxed for 5 min. The mixture was poured into water and ether extracted. The ether layer was washed with dilute hydrochloric acid, dried, and evaporated to give yellow crystals. The product was recrystallized from acetic acid as yellow flakes, m.p. 160° (30%).

Anal. Calcd. for $C_{15}H_{11}NS_2$: C, 66.91; H, 4.09; N, 5.20; S, 23.79. Found: C, 66.74; H, 4.17; N, 5.29; S, 23.68.

The mass spectrum: M^+ 269, calcd. 269.

Reaction of 2,5-Diphenylisothiazoline-3-thione with Dimethyl Acetylenedicarboxylate

2,5-Diphenylisothiazoline-3-thione (26.9 mg, 0.1 mmol) and the ester (14.2 mg, 0.1 mmol) in benzene (15 ml) were refluxed 24 h. The solvent on evaporation gave a yellow oil, which on chromatography yielded the spiran diadduct **5***c* (51%), identical (mixture m.p. and mass spectrum) to an authentic specimen (13).

Reaction of 2-Methyl-5-phenylisothiazoline-3-thione with Phenacylidene Triphenylphosphorane

The thione (207 mg, 1 mmol) and the phosphorane (380 mg, 1 mmol) were melted together and heated under nitrogen for 1 h at 180°. The red mixture was dissolved in benzene and chromatographed. A number of bands were obtained but the first red band eluted gave a red oil which crystallized on standing and was recrystallized from benzene as orange prisms, m.p. 144–145° (36%).

Anal. Calcd. for $C_{18}H_{15}NS_2$: C, 69.85; H, 4.85; N, 4.53; S, 20.62. Found: C, 70.04; H, 4.71; N, 4.54; S, 20.84.

The n.m.r. spectrum: τ 6.44 (3H singlet, the methyl protons), 3.57 (1 H doublet, the exocyclic methine proton, split by the thiazoline proton, J = 1 Hz), 2.90–2.06 (11H bands, the aromatic protons and the thiazoline proton); the mass spectrum: M^+ 309, calcd. 309.

Other bands from the chromatogram gave starting thione and triphenylphosphine oxide.

Reaction of 2-Methyl-5-phenylisothiazoline-3-thione with p-Methylphenacylidenetriphenylphosphorane

The reaction carried out as above gave the thioacyldenethiazole as red prisms, m.p. 185°, from toluene (41%).

Anal. Calcd. for $C_{19}H_{17}NS_2$: C, 70.59; H, 5.26; N, 4.33; S, 19.81; Found: C, 70.41; H, 5.28; N, 4.36; S, 19.66.

The n.m.r. spectrum: τ 7.55 (3H singlet, the aromatic methyl), 6.39 (3H singlet, the *N*-methyl), 3.50 (1H doublet, J = 1.0 Hz), 2.79–2.05 (10H bands, the aromatic and thiazoline protons); the mass spectrum: M^+ 323, calcd. 323.

We wish to thank Mr. M. Arneson for the preparation of mass spectra and Mr. R. Dickinson for n.m.r. spectra. Financial support by the National Research Council of Canada is also gratefully acknowledged.

1. D. M. McKinnon and J. M. Buchshriber. Can. J. Chem. **49**, 3299 (1971) and references therein.
2. P. Rioult and J. Vialle. Bull. Soc. Chim. Fr. 2883 (1967).
3. F. Boberg and J. Knoop. Ann. **708**, 148 (1967).
4. M. Maguet, Y. Poirier, and J. Teste. Bull. Soc. Chim. Fr. 1503 (1970).
5. H. Behringer, J. Kilger, and R. Wiedenmann. Tetrahedron Lett. 1185 (1968).
6. G. E. Bachers, J. M. Buchshriber, and D. M. McKinnon. Can. J. Chem. **50**, 2568 (1972).
7. G. Le Coustumer and Y. Mollier. C. R. Acad. Sci. Paris, Ser. C, **270**, 433 (1970).
8. G. Le Coustumer and Y. Mollier. Bull. Soc. Chim. Fr. 3076 (1970).
9. U. Schmidt, A. Luttringhaus, and F. Hubinger. Ann. **631**, 138 (1960).
10. F. Boberg and W. von Gentzkow. Ann. 256 (1973).
11. R. Mayer, H. J. Hartmann, and J. Jentzsch. J. Prakt. Chem. **31**, 312 (1966).
12. M. Ahmed, J. M. Buchshriber, and D. M. McKinnon. Can. J. Chem. **48**, 1991 (1970).
13. J. M. Buchshriber, D. M. McKinnon, and M. Ahmed. Can. J. Chem. **47**, 2039 (1969) and references therein.
14. H. Boshagen, H. Feltkamp, and W. Geiger. Ber. **100**, 2435 (1967).
15. N. Losach. Adv. Heterocycl. Chem. **13**, 161 (1971).
16. S. Davidson and D. Leaver. Chem. Commun. 540 (1972).
17. P. Ykman, G. l'Abbé, and G. Smets. Tetrahedron, **27**, 5623 (1971).
18. E. K. Fields. J. Am. Chem. Soc. **77**, 4255 (1955).

Can. J. Chem. Downloaded from www.nrcresearchpress.com by 210.87.254.105 on 09/05/12
For personal use only.

Selective Hydrolysis and Oxidation of the Bismethylenedioxy Protective Group During Angular Methyl Migration in Corticosteroid Analogs

L. P. MAKHUBU, Z. G. HAJOS, AND G. R. DUNCAN[1]

Faculty of Pharmacy, University of Toronto, Toronto, Ontario M5S 1A1

Received October 23, 1973

An attempt to achieve a 10β → 9β methyl migration in a 9,11α-epoxy-4,4-dimethylated derivative of cortisol (**3**) using BF_3, failed to result in a clean reaction product. In contrast a 9α-amino-11-oxo derivative (**9**) rearranged smoothly to 20(*R*)-3β-acetoxy-9β-methyl-17α,20-methylenedioxy-19-norpregn-5(10)-en-20-ol-11-one-21-oic acid (**10**) with sodium nitrite and acetic acid. During the migration, the protecting bismethylenedioxy group underwent selective hydrolysis and oxidation. The structure of the product has been established by i.r., n.m.r., and mass spectra analyses and a mechanism has been proposed for its formation. The product is an intermediate in the synthesis of 4,4-dimethylcucurbitacin and cortisol analogs, the goal of this chemical and biological investigation.

Au cours de nos essais en vue de faire migrer le méthyle de la position 10β vers 9β en faisant réagir du BF_3 sur l'époxy-9,11α diméthyl-4,4 cortisol (**3**) aucun produit prépondérant n'est formé. Par opposition à cette réaction le dérivé amino-9α oxo-11 (**9**) se réarrange facilement sous l'influence du nitrite de sodium et de l'acide acétique pour donner l'acide acétoxy-3β méthyl-9β méthylenedioxy-17α,20 nor-19 pregnèn-5(10) ol-20(*R*) one-11 oique-21 (**10**). Au cours de cette migration le groupe protecteur bisméthylenedioxy a subi une hydrolyse sélective et une oxydation. On a établi la structure du produit par infrarouge, r.m.n. et par des analyses de spectrométrie de masse et on propose un mécanisme pour sa formation. Le produit est un intermédiaire dans la synthèse d'analogues du diméthyl-4,4 cucurbitacine et cortisol qui est le but de cette étude chimique et biologique. [Traduit par le journal]

Can. J. Chem., **52**, 1744 (1974)

Can. J. Chem. Downloaded from www.nrcresearchpress.com by 210.87.254.42 on 09/05/12
For personal use only.

In view of the structural and biological similarities between glucocorticoids and cucurbitacins we have recently synthesized steroids which possess a blend of certain cortisol and cucurbitacin functionalities. En route to one of these (**1**), a selective hydrolysis and oxidation of the bismethylenedioxy (BMD) protective group during a $C_{10} \rightarrow C_9$ methyl migration was encountered and is reported herein.

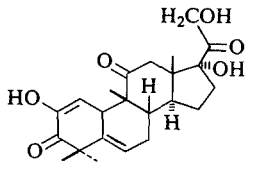

1

Initially (Scheme 1) it was planned to arrive at the desired 4,4,9β-trimethyl derivative (**4**) by a rearrangement of the epoxide **3**. Such a rearrangement had been previously described by ApSimon and Rosenfeld (1) on an androst-5-en-3,17-dione derivative. We converted therefore the known (2) BMD derivative of cortisol (**2**) in a three-step synthesis to 17α,20:20,21-bismethylenedioxy-9,11α-epoxy-4-pregnen-3-one (**3**). The three steps involved introduction of the 9(11)-double bond, epoxidation of the latter, and C-4 dimethylation of the 4(5)-unsaturated 3-one as shown in Scheme 1 (for details see Experimental section). The n.m.r. spectrum of **3** had a well-resolved doublet at δ 3.17 p.p.m. ($J = 5$ Hz) which was assigned to the C-11β proton, which couples with the C-12β proton only. The C-11β and C-12α protons are roughly at right angles and do not couple. An unresolved multiplet due to the C-6 proton occurred at 5.7 p.p.m., while the BMD group appeared at δ 3.98 (s, 2, 21-H), 5.02 (s, 2, 17-O—CH_2—O—), 5.07 (s, 1, 21-O—C—O—), and 5.19 (s, 1, 21-O—C—O—) in

agreement with previous observations (3). Dimethylation caused an upfield shift of the n.m.r. signal of the C-10 methyl group from 1.50 to 1.26 p.p.m., which is most likely due to steric interaction with the 4β axial methyl group in the molecule. The two C-4 methyl groups appeared as a singlet at 1.20 p.p.m. in the $CDCl_3$ solvent system.

[1]To whom all correspondence should be directed.

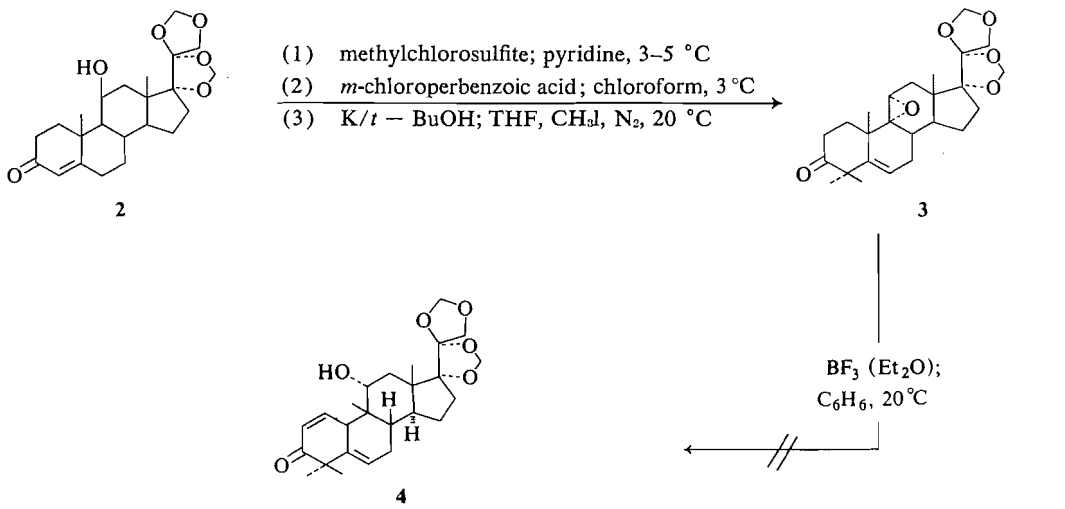

2 3 4

SCHEME 1

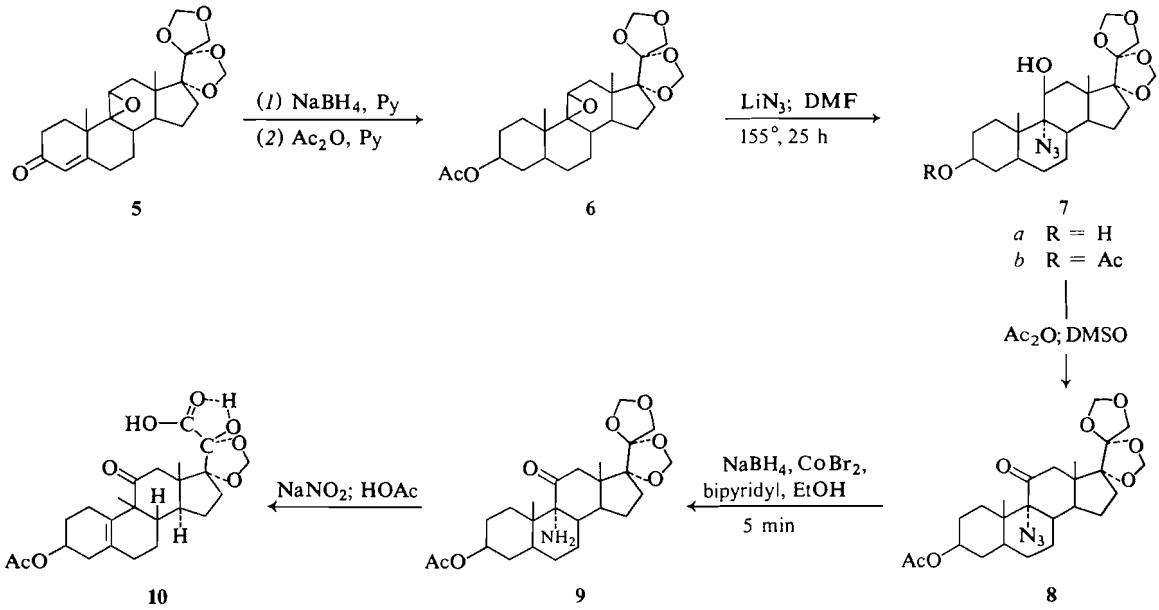

5 6 7 a R = H b R = Ac 8 9 10

SCHEME 2

We attempted rearrangement of the epoxy compound **3** using a small amount of BF_3 gas and also with BF_3 etherate in benzene as previously described (1, 4). It was expected that the opening of the α-epoxide would be accompanied by the migration of the C-10β methyl group to the C-9 position and thus result in the formation of the B/C-*cis* fused derivative **4**, an analog of the cucurbitacins. However, only inseparable mixtures were obtained. We assume that our negative results may be due to the rather complex C-17 side chain system. Similar negative results have been reported in the attempted rearrangement of several lanostane derivatives, whereas simple 17-oxo compounds have been found to undergo smooth rearrangement.

At this point we decided to try to construct the desired molecular skeleton via rearrangement of a 9α-amino-10β-methyl compound (5). The starting material of our synthesis was the known (6) 9β,11β-epoxide **5** (Scheme 2). In contrast to the above described n.m.r. spectrum

Can. J. Chem. Downloaded from www.nrcresearchpress.com by 210.87.254.42 on 09/05/12
For personal use only.

Can. J. Chem. Downloaded from www.nrcresearchpress.com by 210.87.254.42 on 09/05/12
For personal use only.

of the isomeric 9α,11α-epoxy derivative **3**, the signal of the C-11α proton appeared as a distorted quartet at δ 3.42 p.p.m. in the n.m.r. spectrum of **5**, indicating coupling with both protons at C-12. The stereochemistry of the epoxide was important, since it determined the direction of addition of the azido group to the C-9α position.

From the known 9β,11β-epoxide **5**, sodium borohydride reduction in pyridine (7) followed by acetylation gave the 3β-acetoxy compound **6**. Nuclear magnetic resonance spectroscopy established the A/B-*trans* configuration of the compound (**6**) by the appearance of the C-10 methyl signal at δ 0.99 p.p.m. The C-3α axial proton appeared at 4.68 p.p.m. as a broad multiplet in agreement with two large a,a-couplings with the C-2 and C-4β axial protons in the molecule.

Epoxide ring opening of **6** with lithium azide followed by oxidation of the 11β axial hydroxyl group of **7***b* using acetic anhydride and dimethyl sulfoxide (8) gave the 9α-azido-11-keto-BMD derivative **8**. Reduction of the keto azide with sodium borohydride, cobaltous bromide, and bipyridyl (9) gave the desired 9α-amino-10β-methyl-BMD derivative **9** in 48% yield. This procedure gave in our hands a cleaner reduction product than by using catalytic hydrogenation (5). The pattern of the proton signals of the BMD group in the n.m.r. spectrum of **9** was essentially identical with that of the above discussed BMD derivative **3** (Scheme 1). This fact deserves special mention since the change in this pattern helped in the elucidation of the structure of the rearrangement product **10**.

We attempted rearrangement of the C-10β methyl group of **9** to the desired C-9β methyl position under the reaction conditions previously reported in the literature (5), *i.e.* with sodium nitrite and acetic acid. The most striking feature in the n.m.r. spectrum of the rearrangement product **10** was the complete absence of the aforementioned complex pattern of the BMD protons. Only the sharp singlet representing the methylene protons between the C-17 and C-20 oxygen atoms was still present in the spectrum but even this was shifted downfield from 5.02 to 5.30 p.p.m. due to the rearrangement in the remainder of the BMD group. Infrared spectroscopy showed a broad band between 3400–3600 cm^{-1} due to carboxylic acid absorption. A broad band at 1650 cm^{-1} of the i.r. spectrum suggested an H-bonded hydroxy acid, a feature possible with the proposed structure (**10**). The aforementioned downfield shift of the 17,20-methylene protons in the n.m.r. spectrum of **10** also supports the suggested structural change from a methylenedioxy to a hydroxy acid function. A singlet of six protons at δ 1.22 p.p.m. was assigned to the C-13 and to the C-9β methyl groups. The downfield shift of the C-13 methyl signal from 1.09 to 1.22 p.p.m. is also in agreement with the postulated structure (**10**). The fact that the position of the 9β methyl signal coincided with that of the C-10β methyl signal of compound **9** is in agreement with similar findings of the literature (10). The β-orientation of the C-9 methyl is in accord with the topside migration of the C-10β methyl group and expulsion of the α-oriented 9-amino substituent. The absence of a signal in the olefinic region indicated that it was not the C-1 but rather the C-5 proton which participated in the rearrangement, thereby placing the double bond in the indicated 5(10) position. A singlet of three protons at δ 2.10 p.p.m. was due to the 3β-acetate methyl protons.

Mass spectral analysis of the hydroxy acid **10** was also in agreement with the suggested formula. It revealed the parent ion at 448 *m/e* and the fragmentation pattern is shown in Fig. 1.

As to the mechanism of the observed rearrangement we would like to propose initial protonation at the most exposed (least hindered) C-21 oxygen atom of the BMD ring system as shown in Scheme 3. Ring opening under the acidic reaction conditions should lead to the alcohol **B**, with the simultaneous expulsion of formaldehyde, and the introduction of the C-20 hydroxyl group from the less hindered outer (α) side of the molecule by an S_N2-type of attack. The selective opening of the C-20,21-dioxolane ring is quite likely due to relief of steric interaction with the β-axial C-13 methyl group. In agreement with data of the literature (11) we indicate compound **9** (partial structure **A**) in its 20(*R*) absolute configuration.

The resulting primary alcohol **B** undergoes dehydrogenation to the corresponding aldehyde **C**. Oxidation of the latter in the presence of sodium nitrite then gives the rearrangement product **10** (partial structure **D**). The oxidation sequence may be promoted by anchimeric assistance provided by the C-20 hydroxyl group.

We believe that the above described selective hydrolysis and oxidation of the bismethylenedioxy (BMD) protective group is without

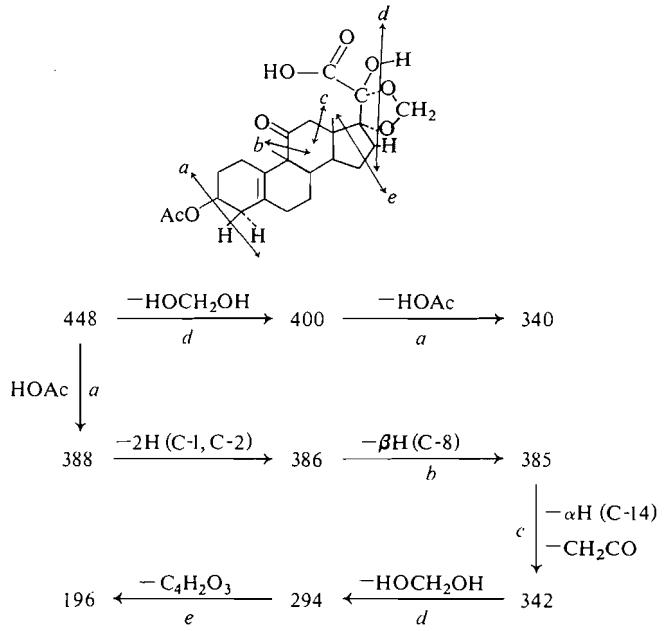

FIG. 1. Mass spectral fragmentation pathway of compound **10**.

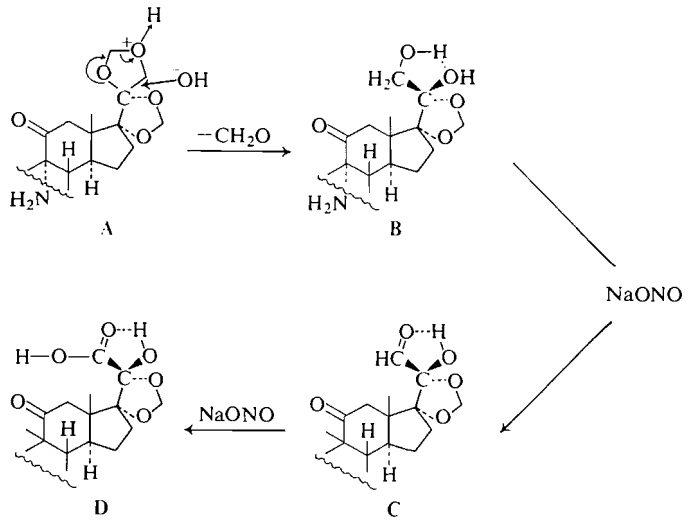

SCHEME 3

precedent. It enabled us to secure the rearrangement of the 10β methyl group to the 9β position with the concomitant formation of the C-20 carboxylic acid derivative of the 17,20-protected corticoid side chain. Since the 4,4-dialkylation of 19-norsteroids has already been reported (12*a*,*b*), compound **10** (20(*R*)-3β-acetoxy-9β-methyl-17α,20-methylenedioxy-19-norpregn-5(10)-en-20-ol-11-on-21-oic acid) may be considered an intermediate towards the synthesis of the 4,4-dimethylcucurbitacin and cortisol analogs, the object of our synthetic and physiological investigation.

Experimental

All melting points were determined using a Kofler block and are corrected. Absorption spectra were determined in methanol using a Zeiss PMQ II u.v. spectro-

Can. J. Chem. Downloaded from www.nrcresearchpress.com by 210.87.254.42 on 09/05/12
For personal use only.

Can. J. Chem. Downloaded from www.nrcresearchpress.com by 210.87.254.42 on 09/05/12
For personal use only.

photometer, in methylene chloride using a Beckman IR-8 i.r. spectrophotometer, and in $CDCl_3$ with TMS as internal standard using a Varian HA-100 n.m.r. spectrophotometer. Optical rotations were determined using a Bellingham & Stanley Pepol 60 spectropolarimeter with chloroform as the solvent unless otherwise stated. Elemental analyses were performed by A. B. Gygli, Microanalysis Laboratory, Toronto or by H. Thommen, University of Basel, Basel, Switzerland.

"Worked up as usual" will mean a solution of the material in a water immiscible organic solvent is washed in turn with 1 *N* hydrochloric acid, 5% sodium carbonate and water (two or three times), dried over anhydrous sodium sulfate, and evaporated to dryness *in vacuo*.

Acetylation "as usual" was performed as follows: x mg of substance was dissolved in $10x$ ml of dry pyridine and $8x$ ml of acetic anhydride was added. The mixture was allowed to stand at room temperature for 16 h in the dark after which $100x$ ml of methanol was added with cooling. The mixture was then "worked up as usual".

17α,20:20,21-Bismethylenedioxy-4,4-dimethyl-9,11α-epoxy-5-pregnen-3-one (3)

(a) Dehydration

17α,20:20,21-Bismethylenedioxy-11β-hydroxy-4-pregnen-3-one (**2**) (2) (1.0 g) and pyridine (30 ml) in tetrahydrofuran (75 ml) were cooled to 3–5°. Methyl chlorosulfite (3 ml) was added (13) dropwise and the mixture was stirred for 30 min. It was then allowed to come to room temperature and poured into water. After the usual work-up, recrystallization from methylene chloride methanol gave large crystalline prisms (900 mg, 88%); m.p. 218–220°; ν_{max} 1658 cm^{-1} (Δ^4-3-keto group); $[\alpha]_D^{23}$ −24° (*c* 1); λ_{max} 240 nm (ε 16 210); n.m.r. signals at δ 0.80 (s, 3, 18-H), 1.33 (s, 3, 19-H), 3.98 (s, 2, 21-H), 5.03 (s, 2, 17-O—CH_2—O), 5.07 and 5.19 (s, 2, 21-O—CH_2—O—), 5.40 (m, 1, 11-H), and 5.72 (d, 1, 4-H).

Anal. Calcd. for $C_{23}H_{30}O_5$: C, 71.46; H, 7.71. Found: C, 71.71; H, 7.62.

(b) Epoxidation

17α,20:20,21-Bismethylenedioxy-4,9(11)-pregnadien-3-one (1.12 g) and *m*-chloroperbenzoic acid (4) (560 mg) in chloroform (75 ml) were stirred at 5° for 48 h. After the usual work-up and recrystallization from methylene chloride – acetone, rhombic crystals were obtained (550 mg, 52%), m.p. 257–260°; ν_{max} 1667 cm^{-1} (Δ^4-3-CO); n.m.r. signals at δ 0.94 (s, 3, 18-H), 1.50 (s, 3, 19-H), 3.20 (d, 1, 11-H), 4.01 (s, 2, 21-H), 5.02 (s, 2, 17-OCH_2O—), 5.07 and 5.18 (s, 2, 21-OCH_2O—), and 5.86 (d, 1, 4-H).

Anal. Calcd. for $C_{23}H_{30}O_6$: C, 68.67; H, 7.45. Found: C, 68.61; H, 7.44.

(c) 4,4-Dimethylation

17α,20:20,21-Bismethylenedioxy-9α,11α-epoxy-4-pregnen-3-one (550 mg) in tetrahydrofuran (50 ml) was methylated (14) using potassium metal (1.0 g) in *tert*-butyl alcohol (50 ml) followed by methyl iodide (2.0 ml). The product was recrystallized from methylene chloride – methanol to give **3** as crystalline plates (345 mg, 70%); m.p. 273–275°; ν_{max} 1698 cm^{-1} (3-CO); $[\alpha]_D^{23}$ −12° (*c* 1.0). For n.m.r. spectrum *cf.* theoretical part.

Anal. Calcd. for $C_{25}H_{36}O_6$: C, 69.42; H, 8.40. Found: C, 69.69; H, 8.07.

Methyl Migration Attempt on Compound 3

17α,20:20,21-Bismethylenedioxy-9α,11α-epoxy-4,4-dimethyl-5-pregnen-3-one (100 mg) in anhydrous benzene (30 ml) was treated with boron trifluoride etherate (6 ml). The mixture was stirred at room temperature for 10 min. Upon evaporation of the benzene, a tarry material was obtained. No major product was observed on thin-layer chromatography (silica gel, benzene–acetone 9:1).

The above reaction was repeated. Instead of the etherate, BF_3 gas was bubbled through the solution of the steroid for 5 min. On evaporating the solvent a tarry material was again obtained.

17α,20:20,21-Bismethylenedioxy-9,11β-epoxy-5α-pregnan-3β-ol Acetate (6)

17α,20:20,21-Bismethylenedioxy-9β,11β-epoxy-4-pregnen-3-one (**5**) (6) (1.3 g) and sodium borohydride (400 mg) in dry pyridine (15 ml) were stirred at room temperature for 4.5 h (7). The mixture was poured into water and worked up as usual. The viscous oil obtained lacked the carbonyl absorption in the i.r. This material was acetylated as usual. Chromatography on a silica gel column using benzene–acetone as eluent (0, 3, and 5% acetone, respectively) gave **6** (220 mg, 15%); m.p. 198–201° (MeOH); ν_{max} 1730, 1247 (acetate), 1114, 1089, 1059, 1029, 1007 cm^{-1} (BMD group); n.m.r. signals at δ 0.99 (s, 3, 18-H), 1.02 (s, 3, 19-H), 1.99 (s, 3, $COCH_3$), 3.45 (q, 1, 11α-H), 3.96 (s, 2, 21-H), 4.68 (m, 1, 3α-H), 5.04 and 5.20 (s, 2, 21-OCH_2O—), and 5.02 (s, 2, 17-OCH_2O—).

Anal. Calcd. for $C_{25}H_{36}O_7$: C, 66.93; H, 8.10. Found: C, 66.49; H, 8.34.

17α,20:20,21-Bismethylenedioxy-9α-azido-5α-pregnan-3β,11β-diol (7a)

Acetate **6** (800 mg) was reacted with lithium azide in *N*,*N*-dimethylformamide at 155 °C for 25 h. The azido alcohol *7a* was isolated in 30% yield (120 mg); m.p. 240–241°; ν_{max} 3636, 3509 (OH), 2105 cm^{-1} (—N_3); $[\alpha]_D^{23}$ −62.40, (*c* 1.0).

Anal. Calcd. for $C_{23}H_{35}N_3O_6$: C, 61.02; H, 7.71; N, 9.35. Found: C, 61.13; H, 8.01; N, 9.08.

Also isolated was the azido acetate 17α,20:20,21-bismethylenedioxy-11β-hydroxy-9α-azido-5α-pregnan-3β-ol acetate (*7b*), in 42% yield (168 mg); m.p. 235–238°.

Anal. Calcd. for $C_{25}H_{37}N_3O_7$: C, 61.06; H, 7.52; N, 8.53. Found: C, 61.20; H, 7.41; N, 8.57.

17α,20:20,21-Bismethylenedioxy-3β-acetoxy-9α-azido-5α-pregnan-11-one (8)

Compound *7b* (300 mg) was oxidized in acetic anhydride and dimethyl sulfoxide to give **8** in 66% yield; m.p. 210–215°; ν_{max} 2123 (N_3), 1739 (acetate), 1727 cm^{-1} (11-CO).

Anal. Calcd. for $C_{25}H_{35}N_3O_7$: C, 61.32; H, 7.23; N, 8.58. Found: C, 61.37; H, 7.23; N, 8.60.

17α,20:20,21-Bismethylenedioxy-3β-acetoxy-9α-amino-5α-pregnan-11-one (9)

Cobaltous bromide (14 mg) and bipyridyl (26 mg) were added successively into 2 ml of 95% ethanol. The azide **8** (70 mg) was then added followed by the cautious addition of sodium borohydride (21 mg) (9). (The solution turned from pink to dark blue, with evolution of gas.) After 5 min, excess sodium borohydride was destroyed and the

solution was poured into water and extracted with chloroform. The chloroform extract was washed with water, dried over anhydrous sodium sulfate, and evaporated *in vacuo*. Recrystallization of the residue from methanol gave the amine **9** (30 mg, 48%); m.p. 264–266°; ν_{max} (KBr) 3610, 3546 (NH_2), 1727 (acetate), 1698 cm^{-1} (11-CO); n.m.r. signals at δ 1.09 (s, 3, 18-H), 1.18 (s, 2, NH_2), 1.22 (s, 3, 19-H), 2.01 (s, 3, $COCH_3$), 3.98 (s, 2, 21-H), 4.70 (m, 1, 3α-H), 5.04 (s, 2, 17-OCH_2O—), 5.22 and 5.30 (s, 2, 21-OCH_2O—). The signal at δ 1.18 disappeared upon addition of D_2O.

Anal. Calcd. for $C_{25}H_{37}NO_7$: C, 64.76; H, 8.06; N, 3.03. Found: C, 64.35; H, 7.87; N, 3.10.

*20(R)-3β-Acetoxy-9β-methyl-17α,20-methylenedioxy-19-norpregn-5(10)-en-20-ol-11-on-21-oic Acid (**10**)*

The amine **9** (18 mg) was dissolved in glacial acetic acid (1 ml) and water (1 ml). The mixture was cooled to 0 °C. To this was added a solution of sodium nitrite (110 mg) in water (1 ml), also at 0 °C. The solution was stirred at this temperature for 3 h. After the usual work-up, column chromatography on silica gel (benzene–acetone, 0, 2, and 3% acetone) gave 10 mg of the major product as an amorphous solid. Thin-layer chromatography on silica gel in benzene–acetone 4:1, and benzene – ethyl acetate 5:2 showed the product to be homogeneous. The i.r., n.m.r., and mass spectral data of the compound are described in detail above (*cf.* theoretical part). In addition the relative intensity of the M + 1 and M + 2 peaks with respect to the parent ion M^+ in the mass spectrum was 25.80 and 5.02%, respectively, in good agreement with expected (15) values of 26.76 and 5.04% (however, see footnote 2).

[2]Reference 15, p. VIII line 3 should read wz instead of wx and p. IX line 5 should be 2.0048×10^{-3} instead of 2.0048×10^{-2}.

The authors wish to express their thanks to the Medical Research Council of Canada for supporting this research and to Merck-Frosst Laboratories, Montreal, Canada, for their generous gift of steroids.

1. J. W. ApSimon and J. M. Rosenfeld. Chem. Commun. 1271 (1970).
2. J. A. Edwards, M. C. Calzada, and A. Bowers. J. Med. Chem. **7**, 528 (1964).
3. T. A. Crabb and R. C. Cookson. Tetrahedron Lett. 679 (1964).
4. J. W. ApSimon, R. R. King, and J. M. Rosenfeld. Can. J. Chem. **47**, 1989 (1969).
5. O. E. Edwards and T. Sano. Can. J. Chem. **47**, 3489 (1969).
6. R. E. Beyler, F. Hoffman, L. H. Hoffman, L. H. Sarett, and M. Tishler. J. Org. Chem. **26**, 2426 (1961).
7. K. Kupfer. Tetrahedron, **15**, 193 (1961).
8. D. J. Albright and L. Goldman. J. Am. Chem. Soc. **89**, 2416 (1967).
9. K. Ponsold. J. Prakt. Chem. **36**, 148 (1967).
10. J. R. Bull and A. Tuinman. Tetrahedron, **29**, 1101 (1973).
11. W. T. Moreland, D. P. Cameron, R. G. Berg, and C. E. Maxwell. J. Am. Chem. Soc. **84**, 2966 (1962).
12. (*a*) V. Permutti and Y. Mazur. J. Org. Chem. **31**, 705 (1966); (*b*) L. Nedelec. *In* Organic reactions in steroid chemistry. Vol. II. *Edited by* J. Fried and J. A. Edwards. Van Nostrand Reinhold Co., New York. 1972. p. 92, lines 5–7.
13. E. M. Chamberlin, E. W. Tristam, T. Utne, and J. M. Chemerda. J. Org. Chem. **25**, 295 (1960).
14. H. Mori, J. Yamada, Y. Takahashi, K. Yasuda, K. Tsuneda, K. Shibata, S. Wada, and O. Takatani. Chem. Pharm. Bull. **16**, 1795 (1968).
15. J. H. Beynon and A. E. Williams. Mass and Abundance Tables. Elsevier, New York. 1963. pp. viii–ix.

Can. J. Chem. Downloaded from www.nrcresearchpress.com by 210.87.254.42 on 09/05/12
For personal use only.

The Reaction of 2,4,6-Trinitrotoluene and 2,4,6-Trinitrotoluene-d_3 with Sodium Isopropoxide in Isopropyl Alcohol[1]

E. BUNCEL,[2] A. R. NORRIS, K. E. RUSSELL, P. SHERIDAN, AND H. WILSON

Department of Chemistry, Queen's University, Kingston, Ontario K7L 3N6

Received August 30, 1973

The reaction of sodium isopropoxide with 2,4,6-trinitrotoluene (TNT) and TNT-d_3 (deuterated methyl group) in isopropanol has been investigated using stopped-flow techniques. Two absorbing species, identified as a σ-complex and the TNT anion (TNT^-) are formed in this reaction. The formation of TNT^- involves a rate determining proton transfer as shown by the observation of an isotope effect ($k_{TNT}/k_{TNT\text{-}d_3} = 8.4 \pm 1.4$ at 30 °C). A spectrum of the σ-complex was calculated from initial rate data and was observed experimentally at low temperatures (λ_{max} = 435, 495 nm). The effects of added salts on rates and equilibria of σ-complex and TNT^- formation have been determined.

In this study the possible involvement of free alkoxide ions and ion-pairs in the reactions has been evaluated. The free alkoxide ion is the more reactive species in deuteron transfer whilst in σ-complex formation the free ions and ion-pairs have comparable reactivity. A rationale of this behavior is presented.

The kinetic parameters are, for deuteron transfer: $k_i^D = 850 \pm 100\ M^{-1}\ s^{-1}$ at 30 °C, $\Delta H^{\ddagger} = 14.9 \pm 1.1$ kcal mol^{-1}, $\Delta S^{\ddagger} = 5.1 \pm 2.9$ cal $deg^{-1}\ mol^{-1}$; for σ-complex formation: $k' = 1870 \pm 150\ M^{-1}\ s^{-1}$ at 30 °C, $\Delta H_{\sigma}^{\ddagger} = 10.2 \pm 0.3$ kcal mol^{-1}, $\Delta S_{\sigma}^{\ddagger} = -9.8 \pm 1.1$ cal $deg^{-1}\ mol^{-1}$.

On a étudié la réaction de l'isopropylate de sodium avec la trinitro-2,4,6 toluène (TNT) et le TNT-d_3 (le groupe méthyl est deutéré) dans l'alcool isopropylique utilisant les techniques de "flux stoppé". Deux espèces qui absorbent se forment au cours de cette réaction; elles ont été identifiées comme étant le complexe σ et l'anion du TNT (TNT^-). La formation de l'ion TNT^- implique un transfert de proton dans l'étape déterminante de la réaction telle que démontré par l'observation d'un effet isotopique ($k_{TNT}/k_{TNT\text{-}d_3} = 8.4 \pm 1.4$ à 30 °C). On a calculé un spectre du complexe σ à partir des données impliquant les vitesses initiales et ce spectre fut observé expérimentalement à basse température (λ_{max} = 435 et 495 nm). On a déterminé les effets d'addition de sels sur les vitesses et sur l'équilibre du complexe σ et de la formation de l'ion TNT^-.

Au cours de cette étude on a évalué l'implication possible d'ions alcoolates libres et de paires d'ions dans les réactions. L'ion alcoolate libre est l'espèce la plus réactive pour le transfert du deutérium alors que pour la formation du complexe σ les ions libres et les paires d'ions ont une réactivité comparable. On présente une rationalisation de ce comportement.

Les paramètres cinétiques sont, pour le transfert du deutérium: $k_i^D = 850 \pm 100\ M^{-1}\ s^{-1}$ à 30 °C, $\Delta H^{\ddagger} = 14.9 \pm 1.1$ kcal mol^{-1}; $\Delta S^{\ddagger} = 5.1 \pm 2.9$ cal $deg^{-1}\ mol^{-1}$; et pour la formation du complexe: $k' = 1870 \pm 150\ M^{-1}\ s^{-1}$ à 30 °C, $\Delta H_{\sigma}^{\ddagger} = 10.2 \pm 0.3$ kcal mol^{-1}, $\Delta S_{\sigma}^{\ddagger} = -9.8 \pm 1.1$ cal $deg^{-1}\ mol^{-1}$. [Traduit par le journal]

Can. J. Chem., **52**, 1750 (1974)

Introduction

Alkoxide ions in alcoholic solution can participate in proton abstraction, σ-complex formation, and radical anion production in their reactions with nitroaromatic compounds (2). Such reactions with 2,4,6-trinitrotoluene (TNT) would produce the species **1**, **2**, and **3**, respectively. The anion **1** could react further with TNT to give a Janovsky (3) complex **4**.

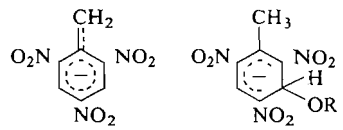

1

2a

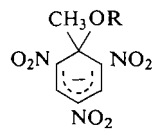

2b

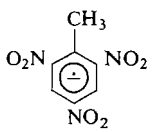

3

It has proven difficult to correlate the different colors produced in these reactions with the above

[1]For previous paper in this series see ref. 1.

[2]Author to whom correspondence should be addressed.

Can. J. Chem. Downloaded from www.nrcresearchpress.com by 210.87.254.40 on 09/05/12
For personal use only.

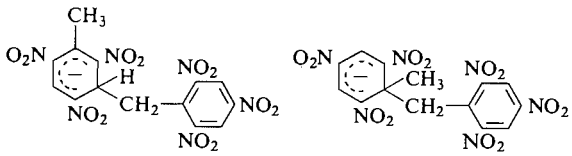

4*a* 4*b*

species (1,2). Direct observation of the species **1**–**4** by n.m.r. has thus far not proven possible.

Bernasconi (4) observed the formation of a Janovsky complex when an excess of TNT was reacted with sodium ethoxide in ethanol. The complex was identified by its characteristic spectrum but it was not possible to decide whether substitution occurred in the 1- or 3-position. The ability of **1** to act as a nucleophile was recently demonstrated in some synthetic work (5*a*); TNT^- is also involved in H/D exchange (5*b*).

At low concentrations of TNT ($\sim 10^{-5}$ *M*) and alkoxide ($\sim 10^{-3}$ *M*) a purple species is produced. Past reviewers (2) concluded that the anion **1** was responsible for the purple coloration. This conclusion has been substantiated in a recent study (1) which showed purple formation to be associated with a large primary isotope effect.

In addition to the purple, a brown coloration often forms in these reactions and has been variously attributed to a radical anion **3**, a charge transfer complex, or a σ-complex **2** (2). Identification with a σ-complex seems possible, especially since cyanide and sulfite ions have been shown to form σ-complexes with TNT (6). The formation of the σ-complex was postulated in our earlier investigation of the TNT–ethoxide system (1) ([TNT] = 5×10^{-5} to 10^{-4} *M*, [NaOEt] = 4×10^{-3} to 4×10^{-2} *M*), even though it was not directly observed, in order to explain the kinetic behavior. Bernasconi (4) using T-jump techniques observed a rapid pre-equilibrium in this system and tentatively associated it with σ-complex formation. Kinetic data for this process could not be derived accurately and no spectral characteristics of the proposed σ-complex were obtained.

The kinetics of the reaction of sodium isopropoxide in isopropanol with TNT and TNT-d_3 have been investigated at various wavelengths and a variety of temperatures using stopped-flow techniques. The effects of added salts have also been determined. As in our previous study, we attempted to rationalize the data in terms of simultaneous formation of σ-complex **2** and anion **1**.

$$[1] \qquad TNT + RO^- \underset{k_b'}{\overset{k'}{\rightleftharpoons}} TNT{\cdot}OR^- \text{ (brown)}$$

$$[2] \qquad TNT + RO^- \underset{k_b}{\overset{k}{\rightleftharpoons}} ROH + TNT^- \text{ (purple)}$$

However the results indicate this scheme to be inadequate. It has been found necessary to consider the individual roles of free ions and ion-pairs in both σ-complex formation and the proton transfer.

Results

When a solution of sodium isopropoxide in isopropanol (4×10^{-3} *M*) is added to a solution of TNT (2×10^{-5} *M*) in isopropanol, one observes during the first instant a hint of a transient brownish coloration. Almost immediately this brown color disappears and one is left with a deep purple solution. If the experiment is performed with TNT-d_3, the brown color persists for several seconds but is thereafter replaced by the permanent purple. When TNT-d_3 is reacted with sodium isopropoxide in isopropanol at low temperatures (*ca.* −60°) it is possible to obtain a spectrum of the brown species (Fig. 1). The wavelengths of the absorption maxima, as well as the extinction coefficients, are fully characteristic of σ-complexes in the trinitrobenzene series, where such complexes could be unambiguously identified by n.m.r. (2). Identification of the brown species as a σ-complex is made on this basis.

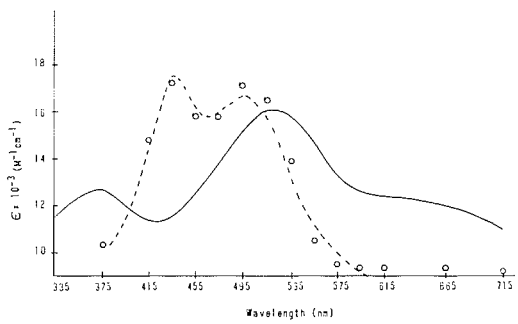

FIG. 1. Spectral characteristics of products of interaction of 2,4,6-trinitrotoluene with sodium isopropoxide in isopropanol: measured spectrum of TNT^- at 30° (—); measured low-temperature spectrum of σ-complex (---); calculated values (eq. 17) of extinction coefficients of σ-complex (○).

Can. J. Chem. Downloaded from www.nrcresearchpress.com by 210.87.254.40 on 09/05/12
For personal use only.

Can. J. Chem. Downloaded from www.nrcresearchpress.com by 210.87.254.40 on 09/05/12
For personal use only.

A study of the kinetics of the formation of the brown species was initiated using stopped-flow techniques. In order to optimize conditions for detection of the brown species, TNT-d_3 was used and the reaction was followed at 435 nm. With an excess of added base ([NaOR]:[TNT-d_3] $\geq$ 20:1) the reactions were found to follow first-order kinetics. Values of k_{obs}^{σ}, obtained from linear plots of ($\log A_{\infty}^{435} - \log A_t^{435}$) *vs.* time are given in Table 1. The observed rate constants were found to be linearly related to the stoichiometric base concentration, *i.e.*,

$$[3] \qquad k_{obs}^{\sigma} = k'[NaOR]_0 + k_b'$$

These experiments were repeated at various temperatures and k',k_b', and K' ($= k'/k_b'$) were calculated from plots of k_{obs}^{σ} *vs.* $[NaOR]_0$ (Table 2). Activation parameters were obtained in the normal manner. For the forward reaction, $\Delta H_{\sigma}^{\ddagger} = 10.2 \pm 0.3$ kcal mol^{-1}, $\Delta S_{\sigma}^{\ddagger} = -9.8 \pm 1.1$ cal deg^{-1} mol^{-1}, and for the reverse reaction $\Delta H_{\sigma}^{\ddagger} = 9.3 \pm 1.0$ kcal mol^{-1}, $\Delta S_{\sigma}^{\ddagger} = -24.6 \pm 3.5$ cal deg^{-1} mol^{-1}.

Inspection of the oscilloscope traces obtained at different wavelengths and on different time scales (Fig. 2) revealed that two reactions were occurring: a rapid formation of the brown species accompanied by a much slower formation of purple. It was desirable to obtain rate data for the slow stage, *i.e.*, the proton (deuteron) transfer process. However, with TNT as substrate, non-first-order kinetics resulted; on the other hand the reaction of TNT-d_3 gave satisfactory first-order kinetics when followed at 665 nm. At this wavelength interference from the brown species is negligible. Plots of $\log (A_{\infty}^{665} - A_t^{665})$ *vs.* time were linear after the initial 5% of reaction and values of k_{obs}^{TNT-} were calculated from the linear portions of the graphs. The data are given in Table 3.

TABLE 1. Observed first-order rate constants (k_{obs}) for σ-complex formation at 30 °C and 435 nm

$[NaOR]_0 \times 10^3$ (M)	k_{obs} (s^{-1})[a]
1.37	7.01
2.72	9.01
2.74	9.01
4.08	13.13
6.85	16.84
8.16	20.04
10.88	24.41
13.60	28.67
13.70	28.82

[a]Linear least-squares analysis gave errors of ± 1% in slopes from which k_{obs} values were calculated.

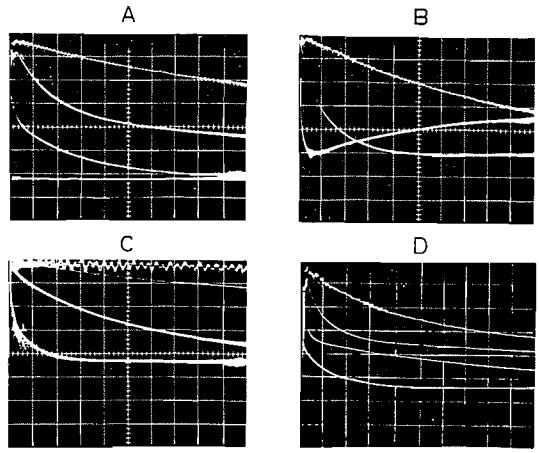

FIG. 2. Representative oscilloscope traces for reaction of TNT-d_3 with sodium isopropoxide in isopropanol at 30 °C. Vertical scale 0–100% transmission: (*A*) $[NaOR]_0 = 1.37 \times 10^{-3}$ *M*, $[TNT\text{-}d_3]_0 = 2.48 \times 10^{-5}$ *M*, 535 nm, horizontal scales 0.01, 0.1, and 1.0 s/division. (*B*) $[NaOR]_0 = 1.37 \times 10^{-3}$ *M*, $[TNT\text{-}d_3]_0 = 2.48 \times 10^{-5}$ *M*, 435 nm, horizontal scales 0.01, 0.1, and 1.0 s/division. (*C*) $[NaOR]_0 = 1.37 \times 10^{-3}$ *M*, $[TNT\text{-}d_3]_0 = 2.48 \times 10^{-5}$ *M*, 665 nm, horizontal scales 0.005, 0.05, 0.5, and 5.0 s/division. (*D*) $[NaOR]_0 = 1.17 \times 10^{-3}$ *M*, $[NaClO_4] = 13.5 \times 10^{-3}$ *M*, $[TNT\text{-}d_3]_0 = 5.69 \times 10^{-5}$ *M*, horizontal scales 0.02, 0.1, 1.0, and 5.0 s/division.

As stated previously, when TNT was used as the substrate non-first-order kinetics were observed both in σ-complex formation (at 435 nm) and in anion formation (at 665 nm). However it was possible to derive kinetic parameters using initial rate methods (see Experimental). The initial rate data, obtained at various wavelengths, are presented in Table 4 as values of $(IR)_H$, defined by eq. 4. Corresponding values of

$$[4] \qquad (IR)_H = \frac{\left(\frac{dA}{dt}\right)_{t=0}}{[TNT]_0[NaOR]_0}$$

$(IR)_D$, obtained using TNT-d_3, are also presented in Table 4. Determination of $(IR)_H$ as a function of initial base concentration showed that the value of $(IR)_H$ decreased with increasing $[NaOR]_0$. For example, using absorbance data recorded at 535 nm, $(IR)_H$ decreased from a value of 9.0×10^7 at 1.37×10^{-3} *M* base concentration to a value of 7.3×10^7 at 6.85×10^{-3} *M* base.

TABLE 2. Determination of rate and equilibrium constants for σ-complex formation as a function of temperature

Temperature (°C)	k' (M^{-1} s^{-1})[a]	k_b' (s^{-1})[a]	K'(M^{-1})[a]
8.4	570 ± 14	1.35 ± 0.08	420 ± 30
12.7	770 ± 30	1.66 ± 0.18	470 ± 70
15.9	900 ± 50	2.10	440 ± 40
25.4	1580 ± 70	3.64	440 ± 40
30.0	1870 ± 150[b]	4.75 ± 0.37	400 ± 60
35.6	2815 ± 90	6.35	440 ± 40
40.4	4030 ± 380	8.17	490 ± 60

[a]Errors from least-squares analysis.
[b]Error estimated from reproducibility of runs.

TABLE 3. Observed and calculated first-order rate constants for reaction of TNT-d_3 with sodium isopropoxide followed at 665 nm and 30 °C

	$k_{obs}^{TNT-d_3}$ (s^{-1})			
		Calculated[b]		
$[NaOR]_0 \times 10^3$ (M)	Measured[a]	I	II	III
1.286	0.261 ± .007	0.255	0.271	0.250
1.370	0.279 ± .005	0.265	0.278	0.262
2.572	0.352 ± .007	0.374	0.355	0.385
2.740	0.358 ± .006	0.385	0.360	0.397
3.858	0.417 ± .007	0.443	0.417	0.467
5.144	0.443 ± .006	0.489	0.470	0.522
6.430	0.518 ± .007	0.520	0.506	0.561
6.850	0.526 ± .014	0.529	0.516	0.571
7.716	0.532 ± .024	0.544	0.542	0.590
10.29	0.594 ± .011	0.577	0.603	0.630
13.70	0.635 ± .010	0.604	0.667	0.666
19.32	0.73 ± .02	0.631	0.747	0.701
25.72	0.80 ± .02	0.648	0.820	0.724
32.10	0.82 ± .02	0.658	0.870	0.738

[a]Errors from least-squares analysis of data.
[b]I, assumes no ion-pairing, $k_1^D = 310\ M^{-1}\ s^{-1}$ and $K' = 440\ M^{-1}$; II, assumes all reactivity due to free ion, $K_3 = 2.78 \times 10^4\ M^{-1}$, $K' = 440\ M^{-1}$, and $k_1^D = 848\ M^{-1}\ s^{-1}$; III, assumes all reactivity due to ion-pair, $K_3 = 2.78 \times 10^4\ M^{-1}$, $K' = 440\ M^{-1}$, and $k_{ip}^D = 360\ M^{-1}\ s^{-1}$.

Since isopropanol has a reasonably low dielectric constant, 19.4 (7), it was deemed necessary to study the effects of added salts ($NaClO_4$ and $NaBPh_4$) upon reaction rates in order to examine the role of ion-pairing effects. Reactions using TNT-d_3 were followed at 665 nm, the total electrolyte being kept constant (*i.e.*, $[NaOR]_0 + [Salt]_0 = constant$), and $k_{obs}^{TNT^-}$ values were calculated as described previously (Table 5). Similar measurements at 435 nm revealed that the effect of added salt upon σ-complex formation was more pronounced than at 665 nm; thus the equilibrium absorbance was much lower than expected. Figure 2 illustrates an oscilloscope trace obtained at low base ($1.17 \times 10^{-3}\ M$) and high salt ($1.35 \times 10^{-2}\ M$) concentration.

Approximate values of the equilibrium constant for formation of the brown species were obtained from the equilibrium absorbance readings at 435 nm (suitably corrected for contribution from the anion as given in the Experimental). The data indicate (Table 6) that the added salts have the more pronounced effect on the back reaction. The relative amount of brown species formed in the initial fast part of the reaction is much less than in the salt-free system but it still proved possible to analyse this

Can. J. Chem. Downloaded from www.nrcresearchpress.com by 210.87.254.40 on 09/05/12
For personal use only.

Can. J. Chem. Downloaded from www.nrcresearchpress.com by 210.87.254.40 on 09/05/12
For personal use only.

TABLE 4. Initial rate measurements on TNT[a] and TNT-d_3[b] (30 °C)

λ (nm)	$(IR)_H \times 10^{-7}$ (M^{-2} s^{-1})	$(IR)_D \times 10^{-7}$ (M^{-2} s^{-1})
375	3.60	1.13
395	3.98	2.35
415	5.67	4.28
435	7.69	6.00
455	7.10	5.05
475	8.41	5.05
495	9.85	6.12
515	10.44	5.69
535	8.80	3.80
555	5.05	1.33
575	3.16	0.55
595	2.94	0.43
615	3.08	0.44
665	2.40	0.36
715	1.39	0.22

[a]$[TNT]_0 = 4.601 \times 10^{-5}$ M; $[NaOR]_0 = 1.61 \times 10^{-3}$ M.
[b]$[TNT\text{-}d_3]_0 = 3.635 \times 10^{-5}$ M; $[NaOR]_0 = 6.43 \times 10^{-3}$ M.

reaction kinetically. For ease of comparison with the salt-free system both sets of data are plotted in Fig. 3.

Discussion

The reaction scheme proposed for the TNT–ethoxide system (eqs. 1 and 2) to account for σ-complex and TNT^- formation, is found to be inadequate for the TNT–isopropoxide system. Thus, (*i*) the variation of $k_{obs}^{TNT^-}$ with $[NaOR]_0$ is not of the expected form; (*ii*) the slight decrease in $(IR)_H$ with increasing $[NaOR]_0$ is unexpected, and (*iii*) the effects of added salts upon rates and equilibria are not predicted. However a modified scheme may be presented which is in accord with all the current observations. This scheme will be discussed in two sections, one referring to σ-complex formation and the other to the deuteron transfer.

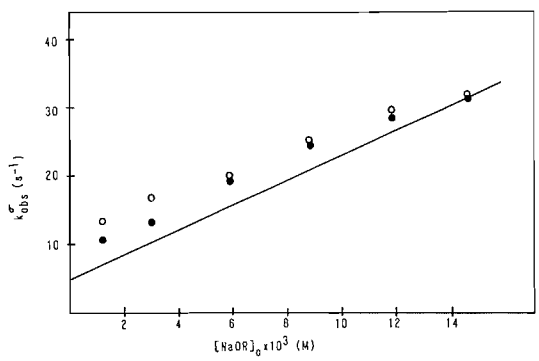

FIG. 3. Variation of k^{σ}_{obs} with base concentration for reaction of TNT-d_3 with sodium isopropoxide followed at 435 nm at 30°: with no added salt (—); with added $NaClO_4$ (●); with added $NaBPh_4$ (○).

σ-Complex Formation

Scheme 1 is proposed for σ-complex formation. This considers the possibility that sodium isopropoxide, in its reaction with TNT, can have different reactivities in its associated and dissociated states. It is a more generalized scheme than that advanced by Crampton and Khan (8) for the reaction of alkali metal methoxides with nitroanisoles in methanol. It is assumed, in both cases, that the σ-complex and its ion-pair, ($TNT \cdot OR^-$, Na^+), have identical visible spectra.

$$\begin{array}{ccc} TNT + RO^- + Na^+ & \underset{k_{bi}'}{\overset{k_i'}{\rightleftharpoons}} & TNT\cdot OR^- + Na^+ \\ K_3 \uparrow\downarrow & & K_2 \uparrow\downarrow \\ TNT + (RO^-, Na^+) & \underset{k'_{b,ip}}{\overset{k_{ip}'}{\rightleftharpoons}} & (TNT\cdot OR^-, Na^+) \end{array}$$

SCHEME 1

The observed equilibrium constant for σ-complex formation is given by eqs. 5 and 6;

$$[5]\quad K_{obs} = \frac{[TNT\cdot OR^-] + [(TNT\cdot OR^-, Na^+)]}{[TNT]([RO^-] + [(RO^-, Na^+)])}$$

$$[6]\quad K_{obs} = \frac{K_i'(1 + K_2[Na^+])}{(1 + K_3[Na^+])} = \frac{K_{ip}'(1 + K_2[Na^+])K_3}{(1 + K_3[Na^+])K_2}$$

where $K_i' = k_i'/k_{b,i}'$ and $K'_{ip} = k_{ip}'/k'_{b,ip}$. Experimentally it was observed that the equilibrium constant for σ-complex formation decreased as salts were added (see Figs. 2 and 3). This could indicate that $K_3 > K_2$, *i.e.*, that in isopropanol the formation of the base ion-pair (RO^-, M^+) is favored over formation of ion-pairs of the σ-complex.

Scheme 1 is also consistent with the observed first-order kinetics for σ-complex formation. If f is the fraction of base existing in the dissociated state then k^{σ}_{obs} is given by eq. 7 (*cf.* eq. 3). The

$$[7]\quad k^{\sigma}_{obs} = k_i'f[NaOR]_0 + k_{ip}'(1 - f)[NaOR]_0 + \frac{k'_{b,ip}K_2[Na^+] + k'_{b,i}}{1 + K_2[Na^+]}$$

TABLE 5. Effects of added salts on observed rate constants for reaction of TNT-d_3 with sodium isopropoxide at 30 °C

$[NaOR]_0 \times 10^3$ (M)	[Salt] $\times 10^3$ (M)	$k_{obs}^{NaClO_4}$ (s^{-1})	$k_{obs}^{NaBPh_4}$ (s^{-1})	$k_{obs}^{No\ salt}$ (s^{-1})
1.17	13.47	0.14	0.12	0.24
2.93	11.71	0.34	0.31	0.36
5.86	8.78	0.55	0.55	0.49
8.78	5.86	0.65	0.68	0.57
11.71	2.93	0.71	0.77	0.63
14.64	—	0.67	0.67	0.67

TABLE 6. Variation of equilibrium constant (K_{obs}) for σ-complex formation with added $NaBPh_4$

$[NaOR]_0 \times 10^3$ (M)	$[NaBPh_4] \times 10^3$ (M)	k_{obs}^{σ} (s^{-1})	K_{obs} (M^{-1})[a]	k' ($M^{-1}\ s^{-1}$)[b]	k_b' (s^{-1})[b]
1.17	13.7	13.3	152	1710	11.3
2.93	11.7	16.7	156	1880	11.4
5.86	8.78	20.0	180	1750	9.7
8.78	5.86	24.7	266	1970	7.4
11.7	2.93	29.1	514	2110	4.1

[a]See Experimental for details of calculation; assumes $\varepsilon_\sigma = 1.6 \times 10^4\ M^{-1}\ cm^{-1}$.
[b]Assumes that $k_{obs} = k'[NaOR]_0 + k_b'$ and $K_{obs} = k'/k_b'$.

base is known to have a high association constant ($K_3 = 1.91 \times 10^4\ M^{-1}$ at 25 °C) (9) and if K_2 and f have relatively small values then the contribution of the free alkoxide ion to the overall rate will be small so that k^{σ}_{obs} will be given by eq. 8.

$$[8] \qquad k^{\sigma}_{obs} = k_{ip}'[NaOR]_0 + k'_{b,i}$$

Plots of k_{obs} *vs.* $[NaOR]_0$ are in fact linear (see *e.g.*, Fig. 3). Such linearity however is also consistent with the assumption that the reactivity of the (RO^-, Na^+) species is comparable to that of the free base in σ-complex formation, *i.e.*, $k_i' = k_{ip}'$. The possibility that the free alkoxide ion has high reactivity and is responsible for the major part of the reaction can be discounted since that would require a linear relationship between k^{σ}_{obs} and $[NaOR]_0^{1/2}$.

It is found that addition of salts ($NaClO_4$, $NaBPh_4$), at a given base concentration, leads to an increase in k^{σ}_{obs}. It was shown earlier (see Table 6) that the increase in k^{σ}_{obs} is due to an increased rate of the back reaction. This could simply be due to increased activity of the σ-complex, although a similar result was explained by Crampton in terms of specific interactions involving the cation (8). One might also have ascribed the increased rate to larger reactivity of the ion-pairs, as compared to the free alkoxide ions, but since even at the lowest base concentrations used ion-pairs already constitute 85% of the base present, the maximum expected increase in rate would be only about 18%. In practice the rate almost doubled at high salt concentrations. Although the possibility that the sodium alkoxide ion-pair is the more reactive species cannot be rigorously excluded, the present results are entirely consistent with equal reactivity of ion-pairs and free ions.

Deuteron Transfer

As in the case of σ-complex formation, one must take into account the possible involvements of ion-pairs and free ions in proposing a kinetic scheme for deuteron transfer. This is done in Scheme 2.

$$\begin{array}{ccc} \text{TNT-}d_3 + RO^- + Na^+ & \underset{k^D_{b,i}}{\overset{k_i^D}{\rightleftharpoons}} & \text{TNT-}d_2^- + Na^+ + ROH \\ K_3 \uparrow\downarrow & & \uparrow\downarrow K_4 \\ \text{TNT-}d_3 + (RO^-, Na^+) & \underset{k^D_{b,ip}}{\overset{k_{ip}^D}{\rightleftharpoons}} & (\text{TNT-}d_2^-, Na^+) + ROH \end{array}$$

SCHEME 2

We consider three possible situations in which the species responsible for the proton transfer process have different reactivities, a treatment somewhat analogous to that used above for σ-complex formation. Firstly we shall consider the possibility that the free alkoxide ion is entirely responsible for TNT^- formation; then the ion pair is assumed to carry out this role and, finally, the two species are considered to have comparable reactivities.

For the case that the free alkoxide ion is the

Can. J. Chem. Downloaded from www.nrcresearchpress.com by 210.87.254.40 on 09/05/12
For personal use only.

Can. J. Chem. Downloaded from www.nrcresearchpress.com by 210.87.254.40 on 09/05/12
For personal use only.

only species responsible for TNT^- formation one can derive eq. 13. This requires several algebraic transpositions, starting with eq. 9.

$$[9] \qquad k_{obs}^{TNT^-} = \frac{k_i^D[RO^-]}{1 + K_{obs}[RONa]_0}$$

The latter assumes that one may ignore the back reactions. This is probably valid, since under all experimental conditions investigated virtually complete conversion of the TNT to anion occurred. The pre-equilibrium formation of σ-complex is also assumed, with an equilibrium constant K_{obs} defined by eq. 5. Equation 9 may be transformed into [10] directly.

$$[10] \quad (k_{obs}^{TNT^-})^{-1} = \frac{1}{k_i^D[RO^-]} + \frac{K_{obs}([RO^-] + [(RO^-, Na^+)])}{k_i^D[RO^-]}$$

From the definition of the association constant for the alkoxide ion-pair, K_3, it follows that

$$[11] \quad (k_{obs}^{TNT^-})^{-1} = \frac{1}{k_i^D[RO^-]} + \frac{K_{obs}(1 + K_3[Na^+])}{k_i^D}$$

Furthermore it is apparent from eq. 6 that $K_{obs}(1 + K_3[Na^+]) = K_i'(1 + K_2[Na^+])$ and therefore,

$$[12] \quad (k_{obs}^{TNT^-})^{-1} = \frac{1}{k_i^D[RO^-]} + \frac{K_i'(1 + K_2[Na^+])}{k_i^D}$$

If, as assumed earlier, $K_2[Na^+] \ll 1$, then

$$[13] \quad (k_{obs}^{TNT^-})^{-1} = \frac{1}{k_i^D[RO^-]} + \frac{K_i'}{k_i^D}$$

One can calculate the values of $[RO^-]$ from the known value of the association constant, K_3, and the plot of $(k_{obs}^{TNT^-})^{-1}$ *vs.* $[RO^-]^{-1}$ can be constructed and exhibits the linearity predicted for this mechanistic scheme.

We now proceed to the case where the ion pair is taken to be the sole reactive form of the base. Using a procedure similar to that outlined above it can readily be shown that eq. 14 must hold.

$$[14] \quad \frac{[(RO^-, Na^+)]}{k_{obs}^{TNT^-}} = \frac{1}{k_{ip}^D} + \frac{K_i'[RONa]_0}{k_{ip}^D(1 + K_3[Na^+])}$$

This predicts that the plots of $[(RO^-, Na^+)]/k_{obs}^{TNT^-}$ *vs.* $[RONa]_0/(1 + K_3[Na^+])$ should be linear. The concentrations of the various species were calculated from the known value of K_3. The resulting plot is non-linear which appears to discount this possibility.

For the situation in which the free ions and ion pairs have equal reactivity the rate expression 9 becomes

$$[15] \quad k_{obs}^{TNT^-} = k^D[RONa]_0/(1 + K'[RONa]_0)$$

This predicts that the plot of $1/k_{obs}^{TNT^-}$ *vs.* $1/[RONa]_0$ should be linear. The plots were constructed for data at several temperatures and showed marked deviations from linearity in all cases.

A tentative conclusion may be drawn on the basis of these kinetic treatments. It is seen that only in the case where the free alkoxide ions are considered as the reactive species can the experimental data be correlated over the whole range of base concentration investigated. The superiority of this mechanism is further illustrated by comparison of the observed and calculated rate constants for TNT^- formation shown in Table 3. In the following discussion we assume the free alkoxide to be the reactive species and proceed to analyze the data accordingly.

It is possible to calculate the variation of the association constant, K_3, with temperature under conditions where the isopropoxide exists predominantly as ion pairs. For such a situation, $[RO^-] \simeq [RONa]^{1/2}/K_3^{1/2}$ and hence[3]

$$[16] \qquad (k_{obs}^{TNT^-})^{-1} = \frac{K_3^{1/2}}{k_i^D[RONa]^{1/2}} + \frac{K_i'}{k_i^D}$$

Plots of $1/k_{obs}^{TNT^-}$ *vs.* $[RONa]^{-1/2}$ exhibit satisfactory linearity at all temperatures studied (Fig. 4). From the intercepts values of K_i/k_i^D at different temperatures are obtained. One can then calculate the variation of k_i^D with temperature, provided that K_i' is given by k'/k_b', which is the ratio of slope to intercept in the k_{obs} *vs.* $[RONa]_0$ plot for σ-complex formation. These data are given in Table 7 and yield the following values of the activation parameters for the deuteron transfer: $\Delta H^{\ddagger} = 14.9 \pm 1.1$ kcal

[3]This is a very good approximation at the higher base concentrations when the degree of dissociation is low. It is realized however that this approximation breaks down at the lower base concentrations and consequently these points are given less emphasis in the plots in Fig. 4.

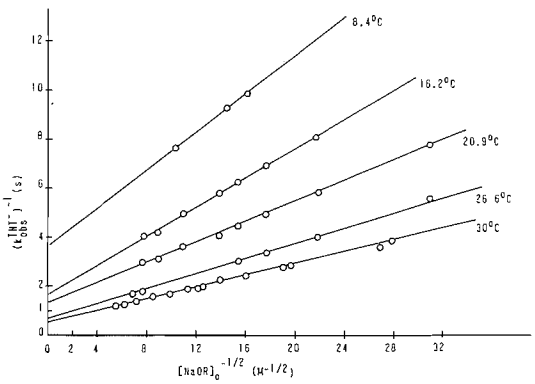

FIG. 4. Plot of $(k_{obs}^{TNT^-})^{-1}$ *vs.* $[NaOR]_0^{-1/2}$ for reaction of TNT-d_3 with sodium isopropoxide (665 nm) at various temperatures.

mol^{-1}, $\Delta S^{\ddagger} = 5.1 \pm 2.9$ cal deg^{-1} mol^{-1}. Similar values were obtained by Ainscough and Caldin (2) for the TNT–ethoxide system. Also from the slopes of these plots K_3 can be evaluated since k_i^D is now known. It is thus found that K_3 increases with increasing temperature, as expected for ion-pair formation (10). The values of K_3 which are so derived (Table 7) are comparable to those obtained conductimetrically (9). The thermodynamic parameters for the association are: $\Delta H^0 = 12.4 \pm 0.6$ kcal mol^{-1}, $\Delta S^0 = 59 \pm 2$ cal deg^{-1} mol^{-1}. The ΔH^0 value appears reasonable for ion-pair formation (10).

The effect of added $NaBPh_4$ and $NaClO_4$ on TNT^- formation remains to be explained. According to eq. 13, which is applicable to the preferred mechanism,[4] one would predict two opposing effects on $k_{obs}^{TNT^-}$. Thus addition of the salts reduces the concentration of free alkoxide ion but, simultaneously, K_{obs} also decreases. The experimental observations (see Results, Table 5) are in qualitative agreement with this analysis. Since the dissociation constants of the salts in isopropanol are unknown it is not feasible to attempt a quantitative treatment without making undue assumptions.

Initial Rate Studies

From the initial rate studies (see Results) one can obtain further evidence of the involvement of free ions in proton transfer, and also evaluate the primary kinetic isotope effect for this process. In addition, the results can be used to derive a spectrum of the σ-complex.

[4]Considering the alternative mechanism in which ion-pairs are responsible for the proton transfer, eq. 14 may be rewritten as

$$k_{obs}^{TNT^-} = k_{ip}^{D}[(Na^+, OR^-)]/(1 + K_{obs}[NaOR]_0)$$

so that addition of salt should always lead to an increase in the rate constant.

TABLE 7. Variation of rate constant for deuteron transfer (k_i^D) and the ion-pair association constant (K_3) with temperature

Temperature (°C)	$k_i^D(M^{-1}\ s^{-1})$	$K_3 \times 10^{-3}(M^{-1})$
8.4	121	2.08
12.7	167	3.08
16.2	262	6.37
20.9	344	4.74
21.5	400	5.66
25.1	550	7.04
26.6	630	8.94
30.0	848	10.00

The evidence for the involvement of dissociated alkoxide in proton transfer lies in the variation of $(IR)_H$ with base concentration. It was found that $(IR)_H$ decreased with increasing concentration of base. Such behavior is to be expected if alkoxide ion is the reactive species since $(IR)_H$ is given by eq. 17, where l is the cell

$$[17]\quad (IR)_H = \frac{l\varepsilon_T k_i^H}{[NaOR]_0^{1/2} K_3^{1/2}} + l\varepsilon_\sigma k'$$

path length and ε_T, ε_σ are the molar extinction coefficients of TNT^- and σ-complex, respectively.

Initial rate measurements offer a method for derivation of the kinetic isotope effect in the proton transfer process. If it is assumed that σ-complex formation is associated with a negligible isotope effect (11), then

$$[18]\quad (IR)_H - (IR)_D = \frac{l\varepsilon_T}{K_3^{1/2}} \times \left[\frac{k_i^H}{([NaOR]_0^H)^{1/2}} - \frac{k_i^D}{([NaOR]_0^D)^{1/2}}\right]$$

This equation reduces rather conveniently under the conditions of measurement ($[NaOR]_0^D = 4[NaOR]_0^H$) to eq. 19 using the experimental value 10^4 for K_3. A plot of $(IR)_H - (IR)_D$ *vs.* $l\varepsilon_T$ should be linear with slope $= (2k_i^H - k_i^D)/8$.

$$[19]\quad (IR)_H - (IR)_D = l\varepsilon_T (2k_i^H - k_i^D)/8$$

The resulting plot exhibits some scatter, though not outside the limits of accuracy expected for a method based on initial rates. Using the value of k_i^D obtained earlier, k_i^H can be calculated and hence the isotope effect: $k_i^H/k_i^D = 8.4 \pm 1.4$ at 30 °C.

It is possible to derive a theoretical spectrum

Can. J. Chem. Downloaded from www.nrcresearchpress.com by 210.87.254.40 on 09/05/12
For personal use only.

Can. J. Chem. Downloaded from www.nrcresearchpress.com by 210.87.254.40 on 09/05/12
For personal use only.

of the brown species which is ascribed to the σ-complex from the known $(IR)_D$ values. With TNT-d_3 as the substrate the initial reaction leads almost exclusively to σ-complex formation since the rate of the proton transfer process is depressed as a result of the kinetic isotope effect. The expression for $(IR)_D$, analogous to eq. 17, contains ε_σ as the only unknown term. Values of ε_σ were calculated at different wavelengths and the spectrum so obtained is shown in Fig. 1. The general shape of this calculated curve is in satisfactory agreement with that obtained experimentally and is characteristic of a σ-complex (2).

Mechanistic Conclusions

The above discussion shows that all the experimental data can be rationalized in terms of a mechanism in which free alkoxide ion is largely responsible for the proton transfer. It remains to be explained why the free ion should be the more reactive species in proton transfer when it has comparable reactivity to the ion-pair in σ-complex formation.

Both the proton transfer and σ-complex formation involve development of negative charge in the aromatic system. Hence one can envisage the cation being involved in transition state stabilization (12). One would expect that the free metal cation would be equally capable of stabilizing developing negative charge, in both processes. The ion-pair, however, can fulfil the role in σ-complex formation (13) but not nearly as adequately in proton transfer. This is seen by referring to structures **5** and **6**, for σ-complex formation and proton transfer, respectively. In the former we have a six-membered cyclic transition state which should be much more favorable than the eight-membered structure in the latter case (14).

The ion-pairing effects described in this system were not detected in the ethoxide ion reaction largely as a result of the considerably lower ion-pair association constants in the ethanolic medium (9). However the inductive argument given in that study, concerning the pre-equilibrium formation of a σ-complex, has been fully substantiated in the present work. Moreover, even though rigorous identification of the purple species has thus far not proven possible, the observation of the large isotope effect may be taken as strong evidence that the purple species is in fact the 2,4,6-trinitrobenzyl anion formed by rate-determining proton transfer.

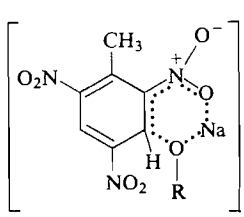

5

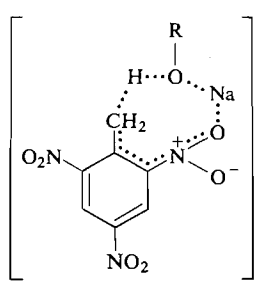

6

Experimental

Materials

The preparation and purification of TNT and TNT-d_3 were as previously described (1). The melting points were rechecked and found to be as previously listed and n.m.r. analysis of TNT-d_3 revealed an extent of deuteration of ~99%. Spectroquality isopropanol was dried over 4A molecular sieves and fractionally distilled (82.4 °C) from anhydrous barium oxide. The solvent was stored under dry nitrogen. Stock solutions of sodium isopropoxide were prepared from freshly cut sodium and isopropanol and stored under an atmosphere of dry nitrogen; they were standardized immediately before use. All solutions were used within a few days of preparation. The sodium perchlorate and tetraphenylboron were dried under vacuum before use.

Procedure

Kinetic measurements were made with a Durrum-Gibson stopped-flow spectrophotometer. The temperature in the cell compartment and drive syringe chamber was thermostatically controlled to ±0.1 °C. Reactions were monitored by photographing traces of % transmission *vs.* time on the oscilloscope at various wavelengths. A calibration curve, correlating the reading on the photograph to the absorbance obtained on a Cary 14 spectrophotometer for the same solution, was used to obtain true values of the absorbance. Pseudo first-order rate constants were obtained in the normal way. The concentrations of base and substrate were in the same range as employed in the ethoxide studies (1).

Initial rate measurements were made using three methods, as given below. (*i*) Values of absorbance for the first 20% of reaction were plotted *vs.* time. The best smooth curve through the experimental points was drawn and the tangent at the origin estimated by sight. The slope of this tangent gave the initial rate. (*ii*) Procedure (*i*) was repeated but the slope of the tangent was checked using the straight edge – mirror technique (15). (*iii*) Data for the first 20% of reaction were subjected to a curve fitting procedure and the initial rates were obtained by applying the Differentiated Gregory-Newton Method (16) to the resulting smooth curve. The initial rates used in calculating values of (IR) are the mean of the values obtained by each of the above methods. At low base concentrations ($< 5 \times 10^{-3}$ *M*) the initial rates are

reproducible within 3–5%, while at higher base concentrations, and particularly in the TNT case, the error involved is as high as ±10%.

The low temperature spectrum was obtained by placing 0.1 ml of a solution of TNT-d_3 in isopropanol into a cell which was surrounded by a chloroform slush. A similar slush was used to cool the base solution before adding it to the cell. Concentrations were chosen so as to reproduce conditions of the kinetic runs. Whilst mixing the two reagents, nitrogen was bubbled through the cell to facilitate dispersion of the colored species throughout the viscous medium. The brown color of the solution persisted for several minutes. In this type of experiment the actual concentration of σ-complex is not known accurately and hence extinction coefficients could not be evaluated.

The spectrum of the purple anion was obtained by reacting a known concentration of TNT in isopropanol with a 100-fold excess of sodium isopropoxide. Under these conditions the TNT is quantitatively converted to the purple anion. The reactions were followed at various wavelengths on the stopped-flow spectrophotometer and the extinction coefficients were calculated from the respective A_∞ values.

An approximate value of K_{obs}, the equilibrium constant for σ-complex formation, was calculated from traces at 435 nm and 665 nm with TNT-d_3 as substrate. From the trace at 435 nm an estimate of A_{eq} and the time required to reach the equilibrium position was made. The absorbance at 665 nm (mostly due to TNT^-) was estimated at this given time and thus the apparent equilibrium absorbance at 435 nm could be corrected for the contribution from the purple species. Thus the equilibrium concentration of σ-complex and K_{obs} are given by

$$[\sigma]_{eq} = \frac{A_{eq}^{435} - A_{eq}^{665}(\varepsilon_T^{435}/\varepsilon_T^{665})}{\varepsilon_\sigma^{435}}$$

$$K_{obs} = \frac{[\sigma]_{eq}}{([TNT_0] - [\sigma]_{eq})[NaOR]_0}$$

1. E. BUNCEL, A. R. NORRIS, K. E. RUSSELL, and R. TUCKER. J. Am. Chem. Soc. **94**, 1646 (1972).
2. J. B. AINSCOUGH and E. F. CALDIN. J. Chem. Soc. 2546 (1956); M. R. CRAMPTON. Adv. Phys. Org. Chem. **7**, 211 (1969); M. J. STRAUSS. Chem. Rev. **70**, 667 (1970); E. BUNCEL, A. R. NORRIS, and K. E. RUSSELL. Q. Rev. London, **22**, 123 (1968).
3. J. V. JANOVSKY and L. ERB. Ber. **19**, 2155 (1866).
4. C. F. BERNASCONI. J. Org. Chem. **36**, 1671 (1971).
5. (*a*) K. G. SHIPP, L. A. KAPLAN, and M. E. SITZMANN. J. Org. Chem. **37**, 1966 (1972). (*b*) E. BUNCEL, K. E. RUSSELL, and J. WOOD. Chem. Commun. 252 (1968).
6. (*a*) E. BUNCEL, A. R. NORRIS, and W. PROUDLOCK. Can. J. Chem. **46**, 2759 (1968). (*b*) A. R. NORRIS. Can. J. Chem. **45**, 175 (1967). (*c*) L. H. GAN and A. R. NORRIS. Can. J. Chem. **52**, 8 (1964).
7. W. DANNHAUSER and L. W. BAHE. J. Chem. Phys. **40**, 3058 (1964).
8. M. R. CRAMPTON and H. A. KHAN. J. Chem. Soc. Perkin II, 1173 (1972).
9. J. BARTHEL, R. WACHTER, and M. KNERR. Electrochim. Acta, **16**, 723 (1971).
10. M. SZWARC. Carbanions, living polymers and electron transfer processes. Chapt. V. Interscience, New York, N.Y. 1968.
11. L. H. GAN and A. R. NORRIS. Can. J. Chem. **49**, 2490 (1971).
12. J. D. REINHEIMER, J. T. GREIG, and T. C. COCHRAN. J. Am. Chem. Soc. **83**, 2873 (1961).
13. F. DEL CIMA, G. BIGGI, and F. PIETRA, J. Chem. Soc. Perkin II, 55 (1973).
14. R. P. BELL and M. A. D. FLUENDY. Trans. Faraday Soc. **59**, 1623 (1963); H. WILSON and E. S. LEWIS. J. Am. Chem. Soc. **94**, 2283 (1972).
15. R. LIVINGSTONE. *In* Technique of organic chemistry. Vol. VIII. P. 1. Interscience, New York, N.Y. 1953. p. 182.
16. E. S. SWINBOURNE. *In* Analysis of kinetic data. Nelson, London. 1971.

Can. J. Chem. Downloaded from www.nrcresearchpress.com by 210.87.254.40 on 09/05/12
For personal use only.

Nitrosation with Lithium Nitrite[1]

M. F. CHEN[2] AND S. F. MACDONALD

Division of Biological Sciences, National Research Council of Canada, Ottawa, Ontario K1A 0R6

Received December 14, 1973

Alcoholic lithium nitrite and 1 mol of HCl may be used to nitrosate ketones. The yields are comparable to those obtained when alkyl nitrites are used with catalytic amounts of HCl.

On peut utiliser le nitrite de lithium alcoolique avec 1 mol de HCl pour effectuer la nitrosation des cétones. Les rendements se comparent avantageusement avec ceux obtenus lorsque cette réaction est effectuée avec des nitrites d'alkyles en présence d'une quantité catalytique de HCl. [Traduit par le journal]

Can. J. Chem., **52**, 1760 (1974)

Can. J. Chem. Downloaded from www.nrcresearchpress.com by 210.87.254.5 on 09/05/12
For personal use only.

There are disadvantages attending the use of alkyl nitrites and HCl in nitrosating reactive methylene groups (1, 2), Alkyl nitrites are toxic and unstable, the lower members are gases, and the higher ones leave an alcohol in the product. The solubility of lithium nitrite in dimethylformamide makes it the reagent of choice for converting alkyl halides to nitro compounds (3). We find that its solubility in alcohols can be exploited similarly to generate *in situ* the alkyl nitrites required for nitrosations. Lithium nitrite is ridiculously expensive but it is easily obtained from barium nitrite and lithium sulfate. The examples below show that typical nitrosations, usually carried out with an alkyl nitrite and HCl, are conveniently done with alcoholic solutions of lithium nitrite and molar amounts of HCl.

2-Butanone and 3-pentanone were nitrosated in this way. We also attempted to nitrosate *n*-butyraldehyde because aldehydes, in contrast to ketones, do not appear to have been nitrosated directly (*cf.* ref. 4). The nature of the product suggests an explanation. Whether lithium nitrite and ethanolic HCl were used or the latter alone, the n.m.r. spectrum of the product showed that it was the polymeric aldehyde, presumably *m*- or *p*-butyraldehyde (*cf.* ref. 5).

Levulinic acid and its ethyl ester give their 5-chloro-5-oximino derivatives (5%) with nitrosyl chloride (6) but the 3- and 5-oximino derivatives are obtained indirectly by nitrosating acetylsuccinic acid (40%) (7) and β-ketoadipic acid (8), respectively. The lithium nitrite method converted ethyl levulinate into ethyl 3-oximino-4-oxo-pentanoate (60%), the structure of which was confirmed by its conversion to 2,4-dimethyl-3-carbethoxy-5-carbethoxymethylpyrrole.

We were particularly interested in the pyrroles **1** and **2** obtained by nitrosating diethyl 3-oxoglutarate and diethyl β-ketoadipate, respectively, then reducing the crude products and benzyl acetoacetate with zinc dust and acetic acid (Knorr synthesis) (9). When lithium nitrite was used instead of amyl nitrite, the yields of **1** were somewhat lower but those of **2** were higher. The use of sodium nitrite and acetic acid resulted, as expected, in definitely lower yields, 25 and 46%, respectively. We took this occasion to confirm our suspicion that the ritual addition of ammonium acetate has no effect on these Knorr syntheses.

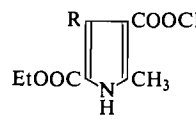

1 R=CH_2COOEt

2 R=CH_2CH_2COOEt

Experimental

Lithium Nitrite (10, 11)

A solution of lithium nitrite, free of barium and sulfate ions, was obtained by mixing equivalent amounts of saturated aqueous barium nitrite (City Chemical Corp.) and lithium sulfate. After removing the barium sulfate (centrifuge), the solution was evaporated (rotary), and the residue was dried over KOH (20°, 0.2 mm). Titration with permanganate (12) revealed the nitrite content and thus the degree of hydration ($LiNO_2 \cdot ca.\ 1H_2O$). The solubilities of the monohydrate and of the anhydrous salt in absolute ethanol are about 0.6 and 0.4 mol per 100 ml, respectively; both are more soluble in methanol.

2-Oxo-3-oximinobutane

Lithium nitrite monohydrate (7.2 g, 0.1 mol) in 15 ml of ethanol and HCl (4 g, 1.1 mol) in 10 ml of ethanol

[1]Issued as NRCC No. 13863.

Can. J. Chem. Downloaded from www.nrcresearchpress.com by 210.87.254.5 on 09/05/12
For personal use only.

were added in alternate portions to 2-butanone (7.2 g, 0.1 mol), stirring at 15–20°. The solution was then stirred 1 h longer, ethanol was removed (rotary), and the residue was sublimed (65°, 12 mm) as colorless crystals, 65% (lit. (1) 50–74% using alkyl nitrites), m.p. 75–76° (lit. (13) m.p. 76.5°).

2-Oximino-3-oxo-pentane

3-Pentanone (0.1 mol) was nitrosated as above but at 30–35° and with methanol (2 × 10 ml) as the solvent. The residue left after removing the methanol was shaken with ether and water. The dried ($MgSO_4$) ether layer was concentrated and the crystalline product was filtered off. Yield 55% (lit. (1) 30–70% using amyl nitrite), m.p. 60–61° (lit. (4) m.p. 59–62°, (14) m.p. 69–72°).

Ethyl 3-Oximino-4-oxo-pentanoate

Solutions of lithium nitrite (0.05 mol) and of HCl (0.055 mol) in ethanol were gradually added to ethyl levulinate (0.05 mol) at 25–35°. The temperature was then allowed to rise while stirring continued until the KI–starch test was negative. The ethanol was removed (rotary, 35°), the residue was shaken with ether and water, and the dried (Na_2SO_4) ether layer was evaporated. The solution of the residue in ether–hexane (1:10) was filtered through a column of activated silica gel, the solvent was removed, and the residue distilled at 1×10^{-4} mm. Ethyl levulinate (1.4 g, b.p. 63°) was followed by the product (5.4 g, 60%, b.p. 97°). It was a pale yellow oil which darkened on standing; n.m.r. ($CDCl_3$) CH_3 at δ 2.35, no CH_2CH_2 at 2.7.

Anal. Calcd. for $C_7H_{11}NO_4$: C, 48.55; H, 6.40; N, 8.09. Found: C, 48.52; H, 6.55; N, 8.03.

2,4-Dimethyl-3-carbethoxy-5-carbethoxymethylpyrrole

(*a*) A Knorr synthesis (*cf.* below) was carried out with ethyl-3-oximino-4-oxo-pentanoate (1.73 g), ethyl acetoacetate (1.43 g), acetic acid (10 ml), and zinc dust (2.5 g) at 65°. The crude product was recrystallized as colorless needles (43%), m.p. 86–87°, Ehrlich's reaction positive.

Anal. Calcd. for $C_{13}H_{19}NO_4$: C, 61.64; H, 7.56; N, 5.53. Found: C, 61.47; H, 7.66; N, 5.68.

(*b*) (By reductive alkylation (*cf.* 15).) 2,4-Dimethyl-3-carbethoxypyrrole (1 g) was dissolved in a stirred solution made up from acetic anhydride (5 ml), hydriodic acid (66%, 5 ml), and hypophosphorous acid (50%, 1.5 ml). Glyoxylic acid (1 g) was then added in portions at 20°, after which stirring was continued for 1 h. The solution was poured into water to precipitate 2,4-dimethyl-3-carbethoxy-5-carboxymethylpyrrole (60%), m.p. 157–159° (lit. (16) m.p. 152–153°). This was left overnight in 10% ethanolic HCl at 20°. The ethanol was evaporated and the residue was stirred with water, separated, dried, and recrystallized from hexane (thimble) The product formed colorless needles (79%), m.p. 86–87°.

The products of *a* and *b* had identical n.m.r. spectra and the mixture m.p. was unchanged.

Benzyl 2-Methyl-4-carbethoxymethyl-5-carbethoxypyrrole-3-carboxylate (*1*)

Diethyl β-ketoglutarate (202 g, 1 mol) (17) was stirred and cooled in an ice bath while solutions of lithium nitrite (71 g, 1 mol) in 200 ml of ethanol and HCl (40 g) in 100 ml of ethanol were dropped in at a rate which maintained the temperature at 20°. The reaction was completed (KI–starch test) by stirring for a further 2 h at 20°.

Acetic acid (1 l) and benzyl acetoacetate (200 g) were stirred in a bath of ice water while the above solution and zinc dust (250 g) were added at a rate which kept the temperature at 65°. The bath was then removed and more zinc was added until there was no further temperature rise. The mixture was then maintained 2 h at 95° and the supernatant was added to 5 l of ice water, the zinc being washed with hot acetic acid. When the oil solidified it was separated and recrystallized from 300 ml of ethanol. Yield 49–51%, m.p. 119–120°, remelt 125° (lit. (9) 55%, m.p. 120–125°).

Benzyl 2-Methyl-4-(2-carbethoxyethyl)-5-carbethoxypyrrole-3-carboxylate (*2*)

As in the preceding preparation, diethyl β-ketoadipate (0.7 mol) (obtained by method *ii* in ref. 18) was nitrosated with lithium nitrite (0.7 mol) in 105 ml of ethanol and HCl (0.77 mol) in 70 ml of ethanol. This product was converted into the pyrrole using 700 ml of acetic acid, 140 g of benzyl acetoacetate, 150 g of zinc dust, and 3.5 l of ice water. The pyrrole was separated, dried, and recrystallized from 1.1 l of ethanol. Yield 75%, m.p. 143–146° (lit. (9) 68%, m.p. 140–142°). Using amyl nitrite and adding ammonium acetate we regularly get 60–65%, m.p. 145–146°, in 2.5 *M* runs.

1. O. TOUSTER. Org. React. **7**, 327 (1953).
2. H. METZGER. *In* Methoden der organischen Chemie. *Edited by* E. Muller. Georg Thieme Verlag. Stuttgart. 1968. Vol. X, part 1, p. 897; Vol. X, part 4, p. 7.
3. N. KORNBLUM, H. O. LARSON, R. K. BLACKWOOD, D. D. MOOBERRY, E. P. OLIVETO, and G. E. GRAHAM. J. Am. Chem. Soc. **78**, 1497 (1956).
4. L. CLAISEN and O. MANASSE. Chem. Ber. **22**, 526 (1889).
5. A. FRANKE and H. WOZELKA. Monatsh. Chem. **33**, 349 (1912).
6. H. RHEINBOLDT and O. SCHMITZ-DUMONT. Ann. Chem. **444**, 113 (1925).
7. O. DIELS and K. SCHLEICH. Chem. Ber. **49**, 284 (1916).
8. D. SHEMIN, C. S. RUSSELL, and T. ABRAMSKY. J. Biol. Chem. **215**, 613 (1955).
9. S. F. MacDONALD. J. Chem. Soc. 4176 (1952).
10. W. C. BALL and H. H. ABRAM. J. Chem. Soc. **103**, 2130 (1913).
11. J. BUREAU. Ann. Chim. (Paris), [11], **8**, 5 (1937).
12. W. W. SCOTT. Standard methods of chemical analysis. 2nd ed. Van Nostrand, New York. 1920. p. 521.
13. Org. Syn. Col. Vol. **2**, p. 204.
14. E. JÄNECKE. Chem. Ber. **32**, 1095 (1899).
15. M. W. ROOMI and S. F. MacDONALD. Can. J. Chem. **48**, 139 (1970).
16. H. FISCHER and E. BARTHOLOMÄUS. Chem. Ber. **45**, 1919 (1912).
17. D. M. MacDONALD and S. F. MacDONALD. Can. J. Chem. **33**, 573 (1955).
18. S. F. MacDONALD and R. J. STEDMAN. Can. J. Chem. **33**, 466 (1955).

Preparation and Characterization of Nitrogen Bonded Nitrile and Amide Complexes of Pentaamminecobalt(III)-Linkage Isomers of Cyanopyridines

ROBERT J. BALAHURA
The Department of Chemistry, University of Guelph, Guelph, Ontario

Received September 6, 1973

The preparation, characterization, and properties of pentaamminecobalt(III) complexes with 1,2-dicyanobenzene, 1,3-dicyanobenzene, 1,4-dicyanobenzene; 3- and 4-cyanobenzaldehyde; 4-acetylbenzonitrile; and 2-, 3-, and 4-cyanopyridine are described. The ligands are all bonded to cobalt via the nitrile nitrogen and undergo facile hydrolysis to the corresponding carboxamides according to the equation:

$$(NH_3)_5CoN{\equiv}C{-}R^{3+} + OH^- \rightarrow (NH_3)_5CoNHCOR^{2+}$$

Production of a carboxamido complex provides a chemical proof for bonding via the nitrile nitrogen. For the ambidentate cyanopyridines this has been used to assign nitrile bonding. For the 4-cyanopyridine ligand the linkage isomer bonded through the pyridine nitrogen has also been prepared and characterized.

On décrit la préparation, la caractérisation et les propriétés des complexes du pentaaminocobalt(III) avec le dicyano-1,2 benzène, le dicyano-1,3 benzène, le dicyano-1,4 benzène, les cyano-3 et -4 benzaldéhydes, l'acétyl-4 benzonitrile et les cyano-2, -3 et -4 pyridines. Tous les ligands sont attachés au cobalt par l'intermédiaire de l'azote du groupe nitrile et chacun subit facilement l'hydrolyse pour fournir la carboxamide correspondante d'après l'équation:

$$(NH_3)_5CoN{\equiv}C{-}R^{3+} + OH^- \rightarrow (NH_3)_5CoNHCOR^{2+}$$

La formation des complexes carboxamido fournit une preuve chimique que la liaison se fait par l'intermédiaire de l'azote du groupe nitrile. Dans le cas des cyanopyridines ambidentates cette propriété a été utilisée pour déterminer le fait que la liaison se fait par le groupe nitrile. [Traduit par le journal]

Can. J. Chem., **52**, 1762 (1974)

Introduction

Previous studies involving transition-metal complexes of organic nitriles have primarily been concerned with establishing the nature of the nitrile–metal bond (1–6). Clarke and Ford (7) have prepared a series of ruthenium(II) and ruthenium(III) complexes with organic nitriles as possible models for molecular nitrogen compounds. These authors (8), as well as many others (9–13), have also investigated various metal complexes containing cyanopyridines. Since a cyanopyridine is an ambidentate ligand the latter work was primarily concerned with establishing unambiguously the coordinating atom. Such assignments have relied predominantly on infrared evidence involving comparison of the complexed and uncomplexed ligand stretching frequencies. However, the shifts observed depend upon inductive, resonance, and steric effects (9) as well as upon the particular metal and its oxidation state (7, 8). Therefore, the conclusions as to the isomer involved can sometimes be ambiguous.

Our studies on nitrile complexes were initiated in order to investigate their oxidation–reduction properties (14). However, during the purification procedure it was found that the nitrile coordinated complexes were easily hydrolyzed (15) in dilute basic solution to form a new class of carboxamido compounds. We now wish to report the characterization and properties of these nitrile and carboxamido complexes.

In addition, the hydrolysis reaction referred to above provides an unambiguous chemical means of distinguishing between the linkage isomers of the cyanopyridine complexes.

Experimental

Reagents

Organic nitriles were purchased from the Aldrich Chemical Co. and were used without further purification. Nitrosyl tetrafluoroborate was obtained from the Research Inorganic Organic Chemical Corporation. Rexyn 102(H) cation exchange resin was obtained from Fisher Scientific and the Sephadex resins from Pharmacia Chemicals, Montreal. Elemental analyses were performed by M–H–W Laboratories, Garden City, Michigan.

Can. J. Chem. Downloaded from www.nrcresearchpress.com by 210.87.254.5 on 09/05/12
For personal use only.

Can. J. Chem. Downloaded from www.nrcresearchpress.com by 210.87.254.5 on 09/05/12
For personal use only.

Syntheses

Azidopentaamminecobalt(III) chloride was prepared by a modification of the method of Linhard and Flygare (16). The perchlorate salt was obtained by adding a slight excess of a saturated solution of silver perchlorate to a slurry of the chloride salt, filtering off the precipitated silver chloride, then adding sodium perchlorate to the filtrate and cooling to 0 °C.

I. Substituted Benzonitriles

$[(NH_3)_5Co(1,3\text{-dicyanobenzene})](ClO_4)_3$

Four grams of nitrosyl tetrafluoroborate was added to 75 ml of triethylphosphate (TEP) containing 4A molecular sieves and the solution was allowed to stir for 1 h. Traces of water in the TEP will cause the initially colorless solution to turn light blue to green (depending on the amount of water present) due to reaction with the nitrosyl tetrafluoroborate. To this solution 8.0 g of $[Co(NH_3)_5N_3](ClO_4)_2$ was added slowly with stirring over a period of 20 min. The solution was stirred for a further 2 h and then 20 g of 1,3-dicyanobenzene was added. The resulting solution was heated on a steam bath for 2 h. The solution was filtered while hot, allowed to cool and filtered again to remove any unreacted ligand. The filtrate was then added to a stirred solution of 500 ml of 2-butanol and 500 ml of diethyl ether. The resulting precipitate was filtered and recrystallized by dissolving in warm water to which a few drops of concentrated HCl had been added, filtering, and adding concentrated $HClO_4$. The addition of $HClO_4$ precipitated a yellow product composed primarily of the desired nitrile. Addition of solid $NaClO_4$ to the filtrate from above resulted in a second fraction (orange) containing at least three different complexes. Recrystallization of the first fraction from dilute $HClO_4$ yielded the pure nitrile.

Anal. Calcd. for $[Co(NH_3)_5(C_8H_4N_2)](ClO_4)_3$: C, 16.8; H, 3.33; N, 17.2. Found: C, 17.0; H, 3.58; N, 17.7.

The second fraction was subjected to cation exchange chromatography on Rexyn 102(H) in the sodium ion form. Elution was carried out with increasing concentration of sodium chloride up to 1.0 *M*. Three bands were obtained: an orange band that moved down the column with the characteristics of a 2+ ion, a yellow band characteristic of a 3+, and a higher charged orange species which did not move down the column. These bands were separated physically and the complexes recovered as described previously (17). On the weakly acid column the yellow nitrile complex band is slowly depleted to form the orange band of the 2+ ion. This particular compound was found to be the pentaamminecobalt(III) complex of the conjugate base of 3-carboxamidobenzonitrile. It was recrystallized from dilute $NaClO_4$ solution at a p*H* of 7.0.

Anal. Calcd. for $[Co(NH_3)_5(NHCOC_6H_4CN)](ClO_4)_2$: C, 19.7; H, 4.10; N, 20.1. Found: C, 19.6; H, 3.97; N, 19.8.

$[(NH_3)_5Co(1,4\text{-dicyanobenzene})](ClO_4)_3$

This complex was prepared and purified as described earlier (14), as well as being prepared by the same procedure as described for the 1,3-dicyanobenzene compound. Since difficulty had been encountered in obtaining a pure sample of the nitrile complex by purification on the weakly acidic resin, Rexyn 102(H), in the sodium ion form, the complex was chromatographed on a SP-Sephadex C-25 cation exchange resin. The latter resin is strongly acidic and prevents hydrolysis of the nitrile on the column. Elution was carried out with aqueous NaCl starting with a 0.05 *M* solution and gradually increasing the concentration to 0.2 *M*. This gave a partial separation of orange and yellow fractions with apparent 3+ charges. These two bands were well separated from a yellow band of a higher charged species. The bands were separated physically and the overlap portion of the two 3+ bands discarded. The complexes were then removed from the resin using a solution 2.0 *M* in NaCl and 0.1 *M* in HCl. The yellow (3+) complex was precipitated from solution by the addition of concentrated $HClO_4$ and recrystallized from dilute $HClO_4$. This fraction yielded the desired nitrile complex.

Anal. Calcd. for $[Co(NH_3)_5(NCC_6H_4CN)](ClO_4)_3$: C, 16.8; H, 3.33; N, 17.2. Found: C, 16.9; H, 3.87; N, 17.9.

The orange (3+) complex was also isolated as above but was recrystallized from dilute $NaClO_4$ at p*H* 7.0. This gave the conjugate base of the carboxamido complex. Apparently, the latter complex is protonated while on the resin and thus behaves as a 3+ ion.

Anal. Calcd. for $[Co(NH_3)_5(NHCOC_6H_4CN)](ClO_4)_2$: C, 19.7; H, 4.10; N, 20.1. Found: C, 19.6; H, 3.95; N, 19.9.

$[(NH_3)_5Co(1,2\text{-dicyanobenzene})](ClO_4)_3$

This compound was prepared using the same procedure as outlined for the 1,3-dicyanobenzene complex. Selective recrystallization with $NaClO_4$–$HClO_4$ gave two fractions, a first yellow fraction of the nitrile and a second orange-yellow fraction containing at least three other components. The first fraction was recrystallized twice from dilute perchloric acid and gave the required nitrile.

Anal. Calcd. for $[Co(NH_3)_5(NCC_6H_4CN)](ClO_4)_3$: C, 16.8; H, 3.33; N, 17.2. Found: C, 16.3; H, 3.78; N, 17.0.

Cation exchange chromatography did not yield any carboxamido complex as in the previous cases and the products in the second fraction were not fully characterized.

$[(NH_3)_5Co(4\text{-cyanobenzaldehyde})](ClO_4)_3$

Five grams of $NOBF_4$ were added to 50 ml of TEP containing 4A molecular sieves. The solution was allowed to stir for 0.5 h. Eight grams of $[(NH_3)_5CoN_3](ClO_4)_2$ was added slowly and the mixture allowed to stir for 2 h. At this point 15 g of 4-cyanobenzaldehyde was added and the solution heated to 60–70 °C for 1.5 h. The solution was then cooled, filtered, and added to 1000 ml of a 1:1 mixture of 2-butanol and diethyl ether. The resulting precipitate was filtered and washed with 95% ethanol, ether, and air dried. The crude complex was recrystallized once by dissolving it in warm water acidified with HCl, filtering, and adding concentrated perchloric acid to effect precipitation. This complex was then subjected to cation exchange chromatography on both Rexyn 102(H) in the sodium ion form and on SP-Sephadex C-25. On Rexyn, a separation into two bands was observed; the faster moving band was orange in color and was eluted as a 2+ ion and was followed by a slower moving (3+) yellow band. On Sephadex, similar behavior was observed as for the 1,4-dicyanobenzene complex. A third band (< 5%) was obtained on Rexyn which did not move down the column. No attempt was made to isolate the band. The 2+ and 3+ bands were separated as before and the 3+ recrystallized from dilute $HClO_4$.

Anal. Calcd. for $[Co(NH_3)_5(NCC_6H_4CHO)](ClO_4)_3$: C, 16.7; H, 3.49; N, 14.7. Found: C, 16.8; H, 3.50; N, 14.5.

The 2+ band was recrystallized from dilute $NaClO_4$ at p*H* 7.0. However, continued recrystallization and ele-

Can. J. Chem. Downloaded from www.nrcresearchpress.com by 210.87.254.5 on 09/05/12
For personal use only.

mental analyses showed that the solid obtained was a mixture of $[Co(NH_3)_5(NH_2COC_6H_4CHO)](ClO_4)_3$ and $[Co(NH_3)_5(NHCOC_6H_4CHO)](ClO_4)_2$ (15).

Recrystallization from a neutral solution containing NaI gave a satisfactory analysis for the iodide salt of the conjugate base.

Anal. Calcd. for $[Co(NH_3)_5(NHCOC_6H_4CHO)]I_2 \cdot H_2O$: C, 17.0; H, 3.73; N, 14.9. Found: C, 16.9; H, 3.84; N, 14.9.

[Co(NH$_3$)$_5$(3-cyanobenzaldehyde)](ClO$_4$)$_3$

This complex was prepared and purified exactly as the 4-cyanobenzaldehyde compound, except that the reaction time was 2.5 h at 65–70 °C. The yellow nitrile band was recrystallized from dilute perchloric acid.

Anal. Calcd. for $[Co(NH_3)_5(NCC_6H_4CHO)](ClO_4)_3$: C, 16.7; H, 3.49; N, 14.7. Found: C, 16.7; H, 3.56; N, 14.5.

The orange 2+ band was isolated as the perchlorate salt and was shown to precipitate as a mixture of acid and base forms of the carboxamido complex. The iodide salt gave a satisfactory analysis (15).

[Co(NH$_3$)$_5$(4-acetylbenzonitrile)](ClO$_4$)$_3$

The 4-acetylbenzonitrile complex was prepared using the same procedure as described above except that the reaction mixture was heated on a steam bath for 1.5 h. Recrystallization from dilute $HClO_4$ yielded two fractions; the less soluble yellow fraction contained the desired nitrile complex and the remaining fraction contained a mixture of complexes. The first fraction was recrystallized twice from dilute $HClO_4$.

Anal. Calcd. for $[Co(NH_3)_5(NCC_6H_4COCH_3)](ClO_4)_3$: C, 18.4; H, 3.75; N, 14.3. Found: C, 18.7; H, 3.85; N, 14.2.

Chromatography of the second fraction gave more nitrile complex and the corresponding carboxamido complex. The latter complex was converted to the iodide salt as before.

Anal. Calcd. for $[Co(NH_3)_5(NHCOC_6H_4COCH_3)]I_2$: C, 19.3; H, 4.11; N, 15.0. Found: C, 19.1; H, 4.06; N, 14.7.

II. Cyanopyridines

4-Cyanopyridine

The initial part of the preparation was as described previously in I. The crude product was recrystallized from water acidified with a few drops of concentrated HCl by adding solid $NaClO_4$. The first addition of $NaClO_4$ precipitates a yellow solid sparingly soluble in perchlorate media. This fraction was filtered and recrystallized twice from dilute $NaClO_4$ and finally subjected to cation exchange chromatography on the weakly acidic resin CM-Sephadex C-25-120. Elution with 0.2 *M* NaCl gave a separation into two components: an orange band which eluted with the characteristics of a 2+ ion and a yellow band which moved as a 3+ ion. The complexes were isolated as described in Section I. The yellow 3+ ion was recrystallized from H_2O by addition of solid $NaClO_4$. This fraction was the required nitrile coordinated complex (referred to as complex **1** in the following sections).

Anal. Calcd. for $[Co(NH_3)_5(C_6H_4N_2)](ClO_4)_3$: C, 13.2; H, 3.48; N, 17.9. Found: C, 13.1; H, 3.60; N, 17.7.

The 2+ ion was recrystallized from $NaClO_4$–$HClO_4$ and was shown to be the carboxamido complex $[(NH_3)_5CoNHC(O)-C_6H_4NH](ClO_4)_3$. On the column this complex was deprotonated and eluted as a 2+ ion.

Anal. Calcd. for $[Co(NH_3)_5(C_6H_6N_2O)](ClO_4)_3$: C, 12.8; H, 3.72; N, 17.4. Found: C, 12.6; H, 3.64; N, 17.1.

After proceeding with the first fraction as outlined above, more solid $NaClO_4$ was added to the filtrate until an orange precipitate was obtained. This fraction was subjected to cation exchange chromatography on Rexyn 102(H) in the sodium ion form. Elution with NaCl increasing in concentration from 0.1 to 0.6 *M* separated three bands. The first band moved down the column as a 2+ ion and was shown to be the carboxamido complex isolated above. The second band eluted with the characteristics of a 3+ ion and separated from more highly charged species which remained at the top of the column. This complex was the pyridine bonded isomer and will be referred to as complex **2**.

Anal. Calcd. for $[Co(NH_3)_5(C_6H_4N_2)](ClO_4)_3 \cdot H_2O$: C, 12.8; H, 3.72; N, 17.4. Found: C, 12.6; H, 3.91; N, 17.4.

No attempt was made to isolate the higher charged species which could have been the 6+ dimer expected if both nitrile and pyridine nitrogens were coordinated to $(NH_3)_5Co^{3+}$.

If the reaction mixture was heated to 65 °C for 15 min approximately 50% more of complex **1** was isolated. At best, the preparation described yields approximately 500 mg of complex **1**, 2 g of complex **2**, and 4 g of carboxamido complex.

3-Cyanopyridine

The same initial procedure was carried out here as for 4-cyanopyridine. Initial recrystallization yielded two main fractions. The first yellow fraction was further recrystallized by dissolving the complex in dilute HCl and precipitating the compound with concentrated $HClO_4$. This procedure was repeated twice to yield the desired nitrile complex.

Anal. Calcd. for $[Co(NH_3)_5(C_6H_4N_2)](ClO_4)_3$: C, 13.2; H, 3.48; N, 17.9. Found: C, 12.9; H, 3.51; N, 17.7.

In a second preparation this fraction was chromatographed on SP-Sephadex C-25 resin and an identical product obtained.

Found: C, 13.4; H, 3.72; N, 17.6.

The second fraction was submitted to cation exchange chromatography on Rexyn 102(H) as described for the 4-cyanopyridine complexes. This yielded the corresponding carboxamido complex.

Anal. Calcd. for $[Co(NH_3)_5(C_6H_6N_2O)](ClO_4)_3 \cdot H_2O$: C, 12.4; H, 3.61; N, 16.9. Found: C, 12.0; H, 3.60; N, 16.4.

A small amount of yellow nitrile complex was also isolated which was identical to the recrystallized fraction collected earlier.

2-Cyanopyridine

The same procedure was used here as for the 4-cyanopyridine complex. The first yellow fraction was recrystallized twice from dilute $HClO_4$ to yield the required nitrile.

Anal. Calcd. for $[Co(NH_3)_5(C_6H_2H_4)](ClO_4)_3 \cdot H_2O$: C, 12.8; H, 3.72; N, 17.4. Found: C, 12.8; H, 3.34; N, 17.3.

Repeated attempts to chromatograph this material produced only carboxamido complex due to hydrolysis of the nitrile on the ion exchange resin.

The second orange fraction was submitted to cation exchange chromatography on Rexyn 102(H) in the sodium

Can. J. Chem. Downloaded from www.nrcresearchpress.com by 210.87.254.5 on 09/05/12
For personal use only.

ion form. This procedure allowed isolation of the carboxamido complex.

Anal. Calcd. for $[Co(NH_3)_5(C_6H_6N_2O)](ClO_4)_3$: C, 12.8; H, 3.72; N, 17.4. Found: C, 12.7; H, 3.76; N, 17.4.

Physical Measurements

Electronic spectra were recorded with a Beckman Acta CIII spectrophotometer. The infrared spectra were obtained with a Beckman IR12.

Proton magnetic resonance spectra were recorded with a Varian A-60A spectrometer.

Potentiometric titrations were carried out using a Radiometer model 26 p*H* meter.

Results

Rexyn 102(H) and CM-Sephadex C-25 are weakly acidic cation exchange resins and in the sodium ion form exist at a p*H* of approximate 7–8. Chromatography on these resins gave two well separated complexes: an orange complex with characteristics of a 2+ ion and a yellow complex which moved down the column as a 3+ ion. Furthermore, if the separation procedure was prolonged, the 3+ ion was depleted and produced the 2+ ion. Chromatography of this mixture of complexes on the strongly acidic resin, SP-Sephadex C-25, produced only a partial separation of the orange and yellow bands noted above and also indicated that the two bands could be associated with 3+ ions. These observations indicated that the yellow 3+ band is consistent with the characteristics of the expected nitrile complex **1** and that the 2+ orange band (3+ on SP-Sephadex) is consistent with its formulation as the conjugate base of the corresponding coordinated carboxamido complex **2** (*vide infra*). Furthermore, the nitrile complex **1** reacts under neutral or slightly basic conditions to

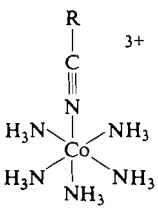

1

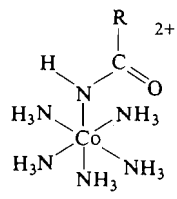

2

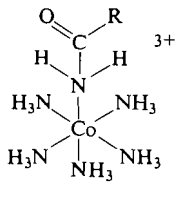

3

yield complex **2**. The observations on SP-Sephadex also indicate that complex **2** can be protonated to form the acidic complex **3**. The charges on the complexes have been determined by comparison with the elution properties of complexes of known charge and are consistent with the microanalytical data. It should be pointed out that for the carboxamido complexes derived from the cyanopyridines two sites for protonation are available: the coordinated nitrogen and the remote pyridine nitrogen. Evidence to be presented in the following sections indicates protonation at the latter site.

Infrared Spectra

The C≡N stretching frequency can provide a good indication of the mode of coordination to the metal. Table 1 gives the ν(C≡N) for the complexes and the ligands. For the aromatic nitrile complexes an increase (18) in ν(C≡N) of 55–70 cm^{-1} is observed with respect to the free ligand. For the disubstituted nitriles two bands were observed for the complexes. One band may be attributed to the coordinated nitrile and the other to the free nitrile. The free nitrile stretching frequency was very close to that observed in the uncomplexed ligand and was assigned on this basis. The carbonyl stretching frequencies due to the remote substituents in 3- and 4-cyanobenzaldehyde and 4-acetylbenzonitrile appear at 1684, 1700(doublet); 1686, 1700(sh); and 1676 cm^{-1} respectively.

For the corresponding carboxamido complexes no coordinated nitrile band was observed in the infrared spectrum as expected. For the 3- and 4-cyanobenzene carboxamido complexes, $(NH_3)_5CoNHCOC_6H_4CN^{2+}$, a nitrile band was observed at 2236 and 2234 cm^{-1} respectively and assigned to the remote cyano group. This fact confirms that only the coordinated nitrile group has been hydrolyzed. Also, in the case of the 4-acetyl, 3- and 4-formylbenzene carboxamido complexes, no nitrile stretching frequency was

TABLE 1. Stretching frequencies for nitrile complexes of $(NH_3)_5Co^{3+}$ [a]

Ligand	ν(C≡N), cm^{-1} Complex	Free ligand
1,2-Dicyanobenzene	2290(s) 2240(m)[b]	2235(m)
1,3-Dicyanobenzene	2295(s) 2245(m)[b]	2235(m)
1,4-Dicyanobenzene	2295(s) 2235(m)[b]	2230(m)
4-Cyanobenzaldehyde	2290(s)	2220(m)
3-Cyanobenzaldehyde	2295(s)	2230(m)
4-Acetylbenzonitrile	2290(s)	2230(m)
2-Cyanopyridine	2295(m)	2240(m)
3-Cyanopyridine	2310(m)	2230(w)
4-Cyanopyridine	**1** 2305(m) **2** 2250(w)	2235(w)

[a]Spectra were obtained using Nujol mulls.
[b]This is assigned to the uncoordinated C≡N from comparison to the free ligand.

TABLE 2. Wavelengths and extinction coefficients of maxima in the visible spectra of $(NH_3)_5Co^{3+}$ nitrile complexes[a]

Ligand	Wavelength, nm (extinction coefficient, M^{-1} cm^{-1})
Benzonitrile[b]	469(79); 330 (82)
1,2-Dicyanobenzene	466(66); ~328 (shoulder)
1,3-Dicyanobenzene	466(75); 330 (74)
1,4-Dicyanobenzene[c]	469(79); 329 (87)
4-Cyanobenzaldehyde	472(78); ~340 (shoulder)
3-Cyanobenzaldehyde	472(76); ~330 (shoulder)
4-Acetylbenzonitrile	468(79)
2-Cyanopyridine	471(73); ~335 (shoulder)
3-Cyanopyridine	472(66); ~340 (shoulder)
4-Cyanopyridine **1**[d]	469(66)

[a]All spectra in aqueous solution.
[b]See ref. 17.
[c]See ref. 14.
[d]Wang and Gould (29) report $\lambda_{max}(\varepsilon_{max})$ at 468 nm (78 M^{-1} cm^{-1}) for a 4-cyanopyridine complex of $(NH_3)_5Co^{3+}$.

observed. For these particular compounds the carbonyl stretching frequencies of the remote group were observed at 1685, 1700, and 1690 cm^{-1} respectively. The ν(C=O) for the carboxamido carbonyl (adjacent to the cobalt) occurred at about 1600 cm^{-1} and was obscured by the NH_3 bending modes of the ammine ligands.

Substantial increases in ν(C≡N) were observed for coordinated 2- and 3-cyanopyridine and for complex **1** with 4-cyanopyridine indicating that the ligands are bonded through the nitrile nitrogen. Complex **2** with 4-cyanopyridine shows only a small increase in ν(C≡N) and its bonding atom cannot be assigned.

The pyridine bands in the 1400–1600 cm^{-1} region due to symmetric and anti-symmetric in-plane ring deformations of the C—C and C—N stretching vibrations are also expected to be sensitive to the bonding atom. Coordination through the pyridine nitrogen causes these bands to shift to higher energy whereas coordination through the nitrile group should not affect the bands. In this region of the spectrum complex **2** had bands at 1624, 1550, 1505, and 1426 cm^{-1} whereas for complex **1** only three bands could be definitely observed at 1600, 1550, and 1417 cm^{-1}. Comparison to the free ligand bands which occur at 1591, 1545, 1495, and 1415 cm^{-1} implies that complex **2** is coordinated through the pyridine nitrogen while complex **1** is nitrile bonded. In view of the small shifts involved further evidence is required to differentiate between the isomers.

Electronic Spectra

The wavelengths and extinction coefficients for the peak maxima of the nitriles in the visible region are summarized in Table 2. The maxima for the $^1A_{1g} \rightarrow {}^1T_{1g}$ band all lie at wavelengths less than that observed for $Co(NH_3)_6^{3+}$ as expected for coordinated nitrile ligands. The spectra of the substituted benzonitrile complexes are identical in both H_2O and 1 *M* $HClO_4$. However, the spectral changes upon addition of base indicate the "fast"[1] formation of a new complex. Figure 1 shows the visible region of the spectrum of the 1,3-dicyanobenzene complex of $Co(NH_3)_5^{3+}$ and also the spectrum obtained upon addition of base. The change from neutral to basic medium produced a completely new spectrum shifting the low energy band from 466 nm

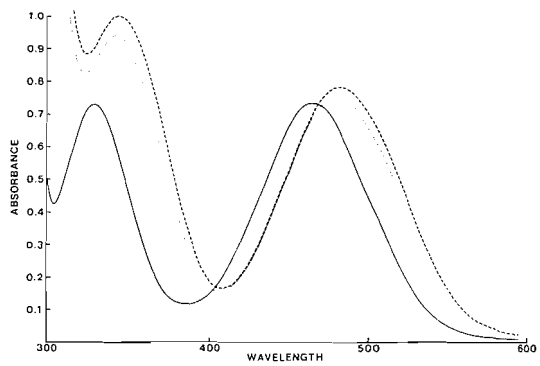

FIG. 1. Visible spectrum of $[(NH_3)_5CoNC-C_6H_4-CN](ClO_4)_3$ in H_2O (—); in base, p*H* 9 (---); and spectrum produced by addition of acid to the basic solution to p*H* 1 (...). [Co(III)] = 1.97 × 10^{-3}, 5 cm cells.

[1]The formation of the complex can be followed with a stopped-flow spectrometer.

Can. J. Chem. Downloaded from www.nrcresearchpress.com by 210.87.254.5 on 09/05/12
For personal use only.

Can. J. Chem. Downloaded from www.nrcresearchpress.com by 210.87.254.5 on 09/05/12
For personal use only.

to 483 nm and the $^1A_{1g} \rightarrow {}^1T_{1g}$ band from 330 nm to 345 nm. Figure 1 also shows the spectrum obtained by making this basic solution acidic (~p*H* 1). If this acidic solution was then in turn made basic, the previous spectrum was regenerated indicating a reversible reaction. These observations can be explained in terms of the reactions summarized below:

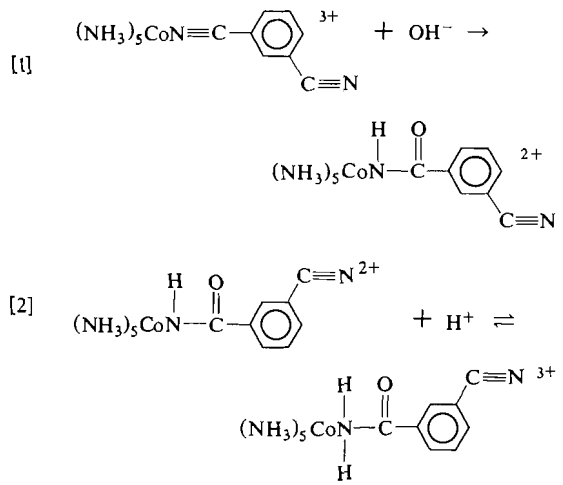

The carboxamido complexes, isolated chromatographically had identical spectra to those obtained from hydrolysis of the nitrile complexes as described above. The visible spectral data for the carboxamido complexes are summarized in Table 3.

The cyanopyridine complexes show similar behavior to that above. However, small changes in the extinction coefficients (< 1%) were observed for identical samples recorded at p*H* 7 and p*H* 1. The pK_a's for 2-, 3-, and 4-cyanopyridine are −0.26, 1.35, and 1.90 respectively (19). For the complexes the pK_a's might be expected to be about 1–1.5 pK_a units less[2] than those for the free ligands. Therefore, a small amount of the protonated 4+ complex could be responsible for the observed changes in ε.

Figure 2*a*, *b*, *c* shows the visible spectra of the nitrile-bonded cyanopyridine complexes in H_2O and in basic solution (p*H* 10). The spectra in basic solution are identical to the spectra of the carboxamido complexes obtained by cation exchange chromatography of the crude products.

[2]p*K*a's were enhanced by approximately 1–1.5 units for cyanophenol complexes of $(NH_3)_5Co^{3+}$ and similar changes might be expected for the cyanopyridines. See ref. 15.

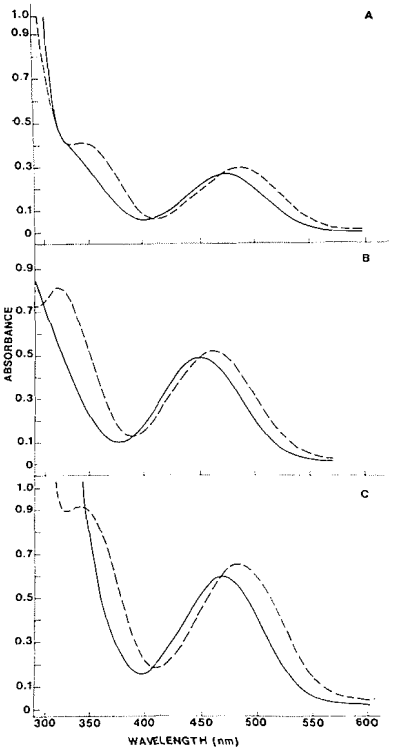

FIG. 2. Visible spectrum of

(*A*) 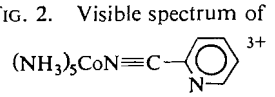

(*B*) 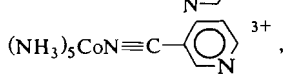

,

(*C*) 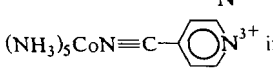

in H_2O

— and dilute base ---, respectively.

The change in the spectra is due to hydrolysis of the coordinated nitrile in analogy with the substituted benzonitrile complexes. This hydrolysis provides the best evidence for assigning nitrile bonded structures to the 2- and 3-cyanopyridine complexes as well as complex **1** with 4-cyanopyridine.

Complex **2** with 4-cyanopyridine has two clearly defined peak maxima at 474 and 335 nm with extinction coefficients of 63 and 66 M^{-1} cm^{-1} respectively. Addition of base to an aqueous solution of this complex does not produce an instantaneous change as described above. Thus we assign the pyridine bonded structure to complex **2** with 4-cyanopyridine. However, addition of base to the pyridine bonded isomer does cause a slow reaction to occur over a period of 20 min.

TABLE 3. Wavelengths and extinction coefficients of maxima in the visible spectra of carboxamido complexes of $(NH_3)_5Co^{3+}$ [a]

Complex	Wavelength, nm (extinction coefficient, M^{-1} cm^{-1})
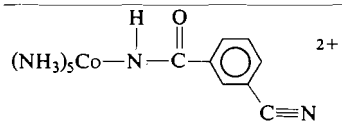	486(81); 347 (105)
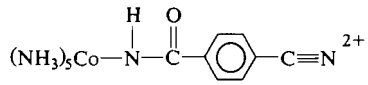	484(89); 343 (125)
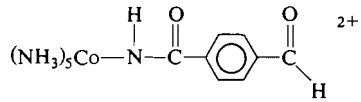	488(83)
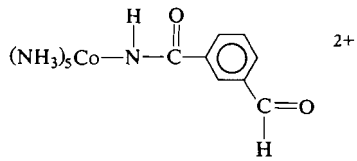	487(79); ~340 (shoulder)
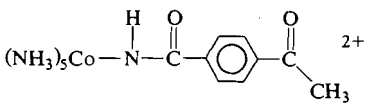	486(87)
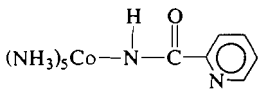	485(76); 345(96) 482(74)[b]
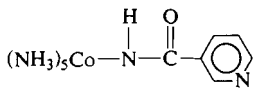	485(72); 347 (91) 484(72)[b]
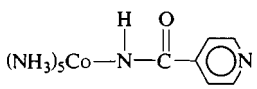	484(74); 344 (94) 482(72)[b]

[a] All spectra run in H_2O.
[b] In 0.1 M $HClO_4$. The peak at approximately 345 nm is completely masked by a charge transfer band.

For the first 15 min good isosbestic points are obtained and the spectrum produced has λ_{max} (ε_{max}) at 480 (60) and 337 nm (61 M^{-1} cm^{-1}). Addition of acid at this point produces a spectrum with peak maxima at 476 and 338 nm with extinction coefficients of 57 and 59 M^{-1} cm^{-1} respectively. This could possibly be the pyridine bonded isonicotinic acid complex formed by slow hydrolysis of the free nitrile group. Ion exchange of reaction mixtures indicated the presence of at least two complexes and some uncoordinated organic ligand. The following scheme is consis-

Can. J. Chem. Downloaded from www.nrcresearchpress.com by 210.87.254.5 on 09/05/12
For personal use only.

TABLE 4. Equilibrium constants for some carboxamidopentaammine-cobalt(III) complexes[a]

Complex	pK_a (25 °C)	Free amide pK_a (20 °C)
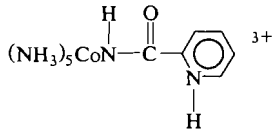	2.33	2.10[b]
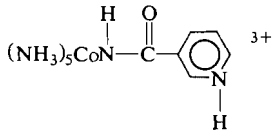	3.57	3.35[b]
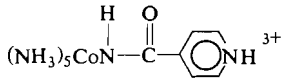	3.67	3.61[b]
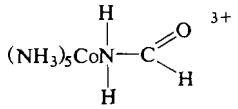	1.59[c]	>14
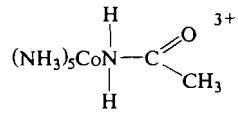	2.16	~14

[a] pK_a's determined potentiometrically at $\mu = 0.01$ *M* according to ref. 30.
[b] See ref. 19, p. 146.
[c] $\mu = 0.02$ *M*.

tent with the observations:

[3] 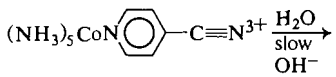

Complex **2**

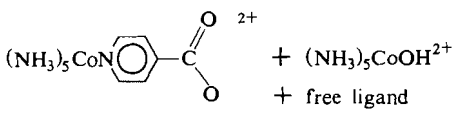

1

It should be emphasized that addition of base to complex **1** instantaneously produced a quantitative yield of carboxamido complex.

The visible spectra of the carboxamidopyridino complexes are also p*H* sensitive but in this case the following equilibrium is postulated

[4] 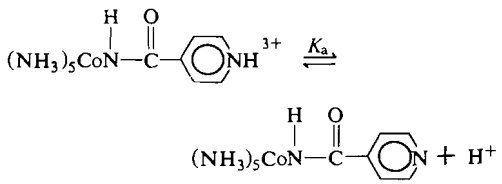

where protonation is now at the remote pyridine N rather than as shown in **2**. The equilibrium constants were obtained by potentiometric titration of the acid form of the complexes with standard potassium hydroxide. These results are given in Table 4 along with the corresponding values for picolinamide, nicotinamide, and isonicotinamide. Also included in Table 4 are values for complexes where protonation occurs at the coordinated nitrogen as opposed to a remote site.

Can. J. Chem. Downloaded from www.nrcresearchpress.com by 210.87.254.5 on 09/05/12
For personal use only.

TABLE 5. Proton magnetic resonance spectra of $(NH_3)_5Co(nitrile)^{3+}$ in d_6-DMSO[a]

Ligand	Chemical shift *cis*-NH_3	Chemical shift *trans*-NH_3	Others	
1,2-Dicyanobenzene	6.18	6.56	C_6H_4	1.90 (center of multiplet)
1,3-Dicyanobenzene	6.12	6.52	C_6H_4	1.65 (center of multiplet)
1,4-Dicyanobenzene	6.14	6.53	C_6H_4	1.83
4-Cyanobenzaldehyde	6.12	6.54	C_6H_4	1.77
			C—*H*	−0.17
3-Cyanobenzaldehyde	6.12	6.56	C_6H_4	1.68 (center of multiplet)
			C—*H*	−0.13
4-Acetylbenzonitrile	6.10	6.52	C_6H_4	1.78 (center of multiplet)
			CH_3	7.37
2-Cyanopyridine	6.10	6.58	C_5H_4N	1.65 (center of multiplet)
3-Cyanopyridine	6.12	6.59	C_5H_4N	1.36 (center of multiplet)
4-Cyanopyridine				
complex **1**	6.12	6.61	C_5H_4N	2.10, 2.01; 0.99, 0.90.
complex **2**	6.28	6.48	C_5H_4N	1.79, 1.73; 1.35, 1.29.

[a]All chemical shifts are relative to the solvent peak at τ 7.48.

Although comparison of the equilibrium constants obtained for the complexes to those of the free amides is not strictly applicable it does suggest that protonation occurs at the pyridine nitrogen rather than at the coordinated nitrogen.

Proton Magnetic Resonance Spectra

The chemical shifts of the various protons of the nitrile complexes are shown in Table 5. These serve primarily to confirm the presence of the groups derived from the organic ligand. The spectra are typical of those observed for other nitrile bonded complexes (14).

The spectra of the carboxamido complexes are summarized in Table 6. A peak due to the N—H proton appears while the remaining ligand peaks are little changed from the corresponding nitrile n.m.r. spectra. This indicates that the —N≡C— linkage has been replaced by the —NHCO— grouping.

For the 4-carboxamido complex the conjugate base $(NH_3)_5CoNHC(O)$ 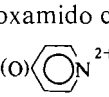 $^{2+}$ gave a rather broad peak at 1.30 τ and a doublet at 2.23, 2.33 τ due to the pyridine protons. However, in the acid form of the complex the peaks were shifted downfield and the expected AA′XX′ pattern was obtained. This provides more direct evidence for protonation occurring at the pyridine nitrogen.

It should also be noted that the difference between the *cis*- and *trans*-NH_3 resonances follows the empirical rule proposed earlier (20) for nitrogen bonded complexes. Also, qualitatively, the *cis–trans* difference in the carboxamido complexes seems to be always much less than for the corresponding nitrile complexes and this may be useful in the characterization of these complexes.

Discussion

The visible spectra of the nitrile complexes are consistent with their formulation as nitrile bonded as discussed in the results section. The most significant observation is the dramatic change that occurs in the visible spectrum upon addition of base to a solution of a nitrile complex. The peaks are shifted irreversibly to lower wavelengths by as much as 15 nm. The observations are consistent with hydrolysis of the coordinated nitrile to the coordinated conjugate base of the corresponding amide. The reaction may be visualized as a nucleophilic attack of hydroxide ion on the nitrile carbon as shown below:

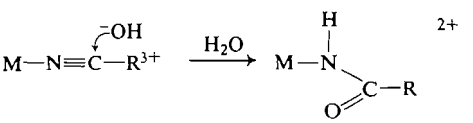

Evidently this process is made facile by polarization of the N≡C bond by the $(NH_3)_5Co^{3+}$ group thus making the nitrile carbon quite electrophilic and susceptible to attack by nucleophiles. This reaction appears to be instantaneous when taking routine spectra and a stopped-flow study of the kinetics of the hydrolysis was undertaken. The second order rate constants for hydrolysis at 25 °C are approximately 100–300 $M^{-1}\,s^{-1}$ (21). The reaction is analogous to base hydrolysis of

Can. J. Chem. Downloaded from www.nrcresearchpress.com by 210.87.254.5 on 09/05/12
For personal use only.

TABLE 6. Proton magnetic resonance spectra of carboxamido complexes of $(NH_3)_5Co^{3+}$ in d_6-DMSO[a]

Complex	Chemical shift *cis*-NH_3	Chemical shift *trans*-NH_3	Others	
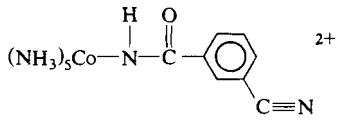	6.65	6.77	N*H* C_6H_4	5.19 2.08 (center of multiplet)
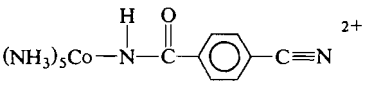	6.63	6.78	N*H* C_6H_4	5.14 2.02
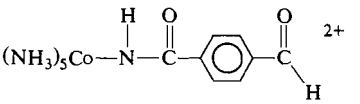	6.66	6.77	N*H* C*H* C_6H_4	5.13 −0.11 1.99
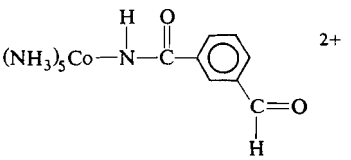	6.66	6.76	N*H* C*H* C_6H_4	5.16 −0.11 2.01 (center of multiplet)
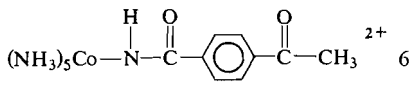	6.64	6.78	N*H* CH_3 C_6H_4	5.18 7.43 2.04
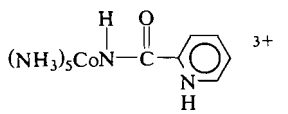	6.58	6.72	N—H py NH C_5H_4N	5.90 4.60 1.65 (center of multiplet)
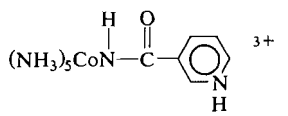	6.60	6.72	N—H py NH C_5H_4N	5.88 4.67 0.83, 1.83 (multiplet)
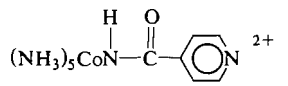	6.66	6.77	N—H C_5H_4N	5.11 1.30, 2.23, 2.33
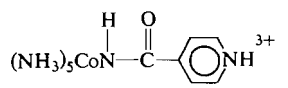	6.59	6.70	N—H py NH C_5H_4N	6.12 4.63 0.83, 0.93, 1.68, 1.78

[a]All chemical shifts are relative to the solvent peak at τ 7.48.

the free ligands but can be carried out under much milder conditions. In fact, a rate enhancement of about 10^6 to 10^{10} is observed with respect to hydrolysis of the free ligands (15, 22).

The fact that the nitrile-coordinated complexes, $(NH_3)_5Co(nitrile)^{3+}$, readily undergo hydrolysis to the analogous carboxamido compounds provides an unequivocal chemical proof that co-

Can. J. Chem. Downloaded from www.nrcresearchpress.com by 210.87.254.5 on 09/05/12
For personal use only.

Can. J. Chem. Downloaded from www.nrcresearchpress.com by 210.87.254.5 on 09/05/12
For personal use only.

ordination takes place through the nitrile nitrogen. This has been clearly demonstrated for the substituted aromatic nitrile complexes. For multisubstituted nitriles in which more than one donor group is available this fact can be used to differentiate between the possible isomers. For example, the cyanopyridines can coordinate either through the nitrile or pyridine nitrogens and many studies have concerned themselves with the problem of determining which nitrogen atom is coordinated to the metal. For coordination through the nitrile nitrogen, hydrolysis to form the coordinated carboxamide should be observed. Using this criterion we have been able to assign unambiguously the bonding atom for the $(NH_3)_5Co^{3+}$ complexes of the cyanopyridines. We find the 2- and 3-cyanopyridine complexes are coordinated via the nitrile nitrogen. The main product isolated with the 4-cyanopyridine does not undergo fast base hydrolysis to form the carboxamido analog and is thus coordinated through the pyridine nitrogen (complex **2**). The remaining 3+ ion isolated is the linkage isomer coordinated through the nitrile nitrogen (complex **1**). Considering the basicities of 3- and 4-cyanopyridine, we should also expect to obtain the linkage isomer (bonded through the pyridine nitrogen) with 3-cyanopyridine. This was not observed. Also, one would expect 2-cyanopyridine to coordinate via the nitrile nitrogen because steric factors make the lone pair on the pyridine nitrogen inaccessible.

The visible spectra of the amide complexes, isolated from the preparative procedure via ion exchange chromatography are identical with the spectra obtained by adding dilute base to solutions of the nitrile complexes. Addition of acid to either of the above solutions also causes further shifts in the spectra. These observations are readily explained if protonation occurs at the coordinated nitrogen as shown in eq. 2. The protonated forms of the complexes are all very strong acids, and as has been discussed previously (17)[3], this fact provides support for the coordinated nitrogen being the site of protonation. Similar changes have been observed for the $(NH_3)_5Co^{3+}$ complexes of formamide (17), acetamide (23),[3] and sulfamate (24). The acidity of the NH_2 protons in these latter complexed ligands has been increased by 10^{14} with respect to the free amides. Spectrophotometric data indicate that the pK_a's of the carboxamido complexes reported herein are all around 2. This is consistent with the value of 1.65 determined for the $(NH_3)_5CoNH_2COC_6H_5^{3+}$ complex (15).

The carboxamidopyridine complexes also have pK_a's $\sim$2–4 but in this case protonation occurs at the uncoordinated pyridine nitrogen as indicated in eq. 4. Apparently the coordinated nitrogen is much too acidic to be protonated. However, small differences in the ultraviolet spectra of solutions with $[H^+] = 0.1$ and $[H^+] = 1.0\ M$ at constant ionic strength indicate that protonation does take place at the coordinated nitrogen to a small extent in these acidic solutions.

The results obtained for the 1,2-dicyanobenzene complex do not seem to conform to the general reactions outlined previously. In this case, hydrolysis of the nitrile in dilute NaOH and subsequent ion exchange gave a product which did not have a nitrile stretching frequency in the infrared. Presumably both nitriles are rapidly hydrolyzed. Also, other hydrolysis products were isolated from this preparation and these will be discussed elsewhere.

The nitrile complexes synthesized in this study provide a new synthetic route to carboxamido complexes of $(NH_3)_5Co^{3+}$ via base hydrolysis. In addition, the hydrolysis reaction allows an unequivocal assignment of nitrile coordination where more than one coordination site is available. As evidenced by the facility of the hydrolysis (even on the cation-exchange column) care must be taken in order to obtain pure nitrile complexes. In view of the many examples of hydrolysis of nitriles involving metal complexes (25–27) this reaction may be of more general synthetic value.

The author wishes to acknowledge the financial support of this research from the National Research Council of Canada.

1. R. A. WALTON. Spectrochim. Acta, **21**, 1795 (1965).
2. R. A. WALTON. Q. Rev. (Lond.), **19**, 126 (1965).
3. A. P. ZUUR, A. H. REINTJES, and W. L. GROENEVELD. Rec. Trav. Chim. **89**, 385 (1970), and references therein.
4. B. J. HATHAWAY and D. G. HOLAH. J. Chem. Soc. 2400 (1964).
5. M. F. FARONA and N. J. BREMER. J. Am. Chem. Soc. **88**, 3735 (1966).
6. B. L. ROSS, J. G. GRASSELLI, W. M. RITCHEY, and H. D. KAESZ. Inorg. Chem. **2**, 1023 (1963).
7. R. E. CLARKE and P. C. FORD. Inorg. Chem. **9**, 277 (1970).

[3]However, for the $(NH_3)_5Co^{3+}$ complex with acetamide, evidence has been presented in favor of protonation at the carbonyl oxygen. See ref. 28.

8. R. E. CLARKE and P. C. FORD. Inorg. Chem. **9**, 495 (1970).
9. F. FARHA, JR. and R. T. IWAMOTO. Inorg. Chem. **4**, 844 (1965).
10. I. PILJAC and R. T. IWAMOTO. Inorg. Chim. Acta, **3**, 49 (1969).
11. R. A. WALTON. J. Inorg. Nucl. Chem. **28**, 2229 (1966).
12. D. K. KEPERT, D. TAYLOR, and A. H. WHITE, Inorg. Chem. **11**, 1639 (1972).
13. P. T. WONG and D. G. BREWER. Can. J. Chem. **47**, 4589 (1969).
14. R. J. BALAHURA, G. B. WRIGHT, and R. B. JORDAN. J. Am. Chem. Soc. **95**, 1137 (1973).
15. D. PINNELL, G. B. WRIGHT, and R. B. JORDAN. J. Am. Chem. Soc. **94**, 6104 (1972).
16. M. LINHARD and H. FLYGARE. Z. Anorg. Chem. **262**, 328 (1950).
17. R. J. BALAHURA and R. B. JORDAN. J. Am. Chem. Soc. **92**, 1533 (1970).
18. H. J. COERVER and C. CURRAN. J. Am. Chem. Soc. **80**, 3522 (1958).
19. K. SCHOFIELD. Hetero-aromatic nitrogen compounds. Butterworths, London. 1967. p. 148.
20. R. J. BALAHURA and R. B. JORDAN. Inorg. Chem. **9**, 1567 (1970).
21. R. J. BALAHURA, P. COCK, and W. L. PURCELL. J. Am. Chem. Soc. In press.
22. E. LAVIRON. C. R. **250**, 3671 (1960).
23. R. J. BALAHURA and L. HUTLEY. Can. J. Chem. **51**, 3712 (1973).
24. L. L. PO and R. B. JORDAN. Inorg. Chem. **7**, 526 (1968).
25. D. A. BUCKINGHAM, A. M. SARGESON, and A. ZANELLA. J. Am. Chem. Soc. **94**, 8246 (1972).
26. M. A. BENNETT and T. YOSHIDA. J. Am. Chem. Soc. **95**, 3030 (1973).
27. J. L. SILVER, M. Y. AL-JANABI, R. M. JOHNSON, and J. L. BURMEISTER. Inorg. Chem. **10**, 994 (1971).
28. D. A. BUCKINGHAM, F. R. KEENE, and A. M. SARGESON. J. Am. Chem. Soc. **95**, 5649 (1973).
29. Y. WANG and E. GOULD. J. Am. Chem. Soc. **91**, 4998 (1969).
30. A. ALBERT and E. SERJEANT. The determination of ionization constants. Chapman and Hall, Ltd., London. 1971.

Can. J. Chem. Downloaded from www.nrcresearchpress.com by 210.87.254.5 on 09/05/12
For personal use only.

Autoprotolysis Constants of Water–*N*-Methylacetamide Mixtures. A New Application of the Hammett Relationship to Acidity Constants

JEAN-CLAUDE HALLE, RAYMOND HARIVEL, AND RENE GABORIAUD

Laboratoire de Physicochimie des Solutions (Pr. R. Schaal) E.N.S.C.P., 11 rue Pierre et Marie Curie 75231 Paris cedex 05

Received September 24, 1973

The hydrogen electrode can be used to measure proton activities of both acid and basic solutions in water–*N*-methylacetamide (NMA) mixtures, and hence to calculate autoprotolysis constants for the different mixtures. The intermediate acidities between the acid and basic regions are established by the use of buffer solutions of variously substituted phenols, whose acidities in the different water–NMA mixtures have been established. The diminution of the acidity constants with increasing concentrations of *N*-methylacetamide cannot be explained by the increased dielectric constants of the solution. Instead, we propose a new adaptation of the Hammett relationship ($pK_H - pK_X = \rho\sigma_X$), which places *N*-methylacetamide between water and DMSO, and close to alcohols, which have a dielectric constant 5-fold smaller. Because of its precision, this method of analysis allows one to classify into one or more homogeneous families compounds having the same chemical function which would be classified together by the classical treatment of Hammett.

En plus de la mesure du produit ionique apparent, le bon fonctionnement de l'électrode d'hydrogène nous a permis la construction, dans chacun des mélanges eau–NMA, d'une échelle d'acidité reliant les milieux acides aux milieux basiques. Pour cela, nous avons calibré des solutions tamponnées préparées à partir de phénols diversement substitués. Comme il s'avère que l'augmentation de la constante diélectrique du milieu ne rend pas compte de la diminution de la plupart des constantes d'acidité lorsque le mélange s'enrichit en NMA, nous proposons une nouvelle adaptation de la relation de Hammett ($pK_H - pK_X = \rho\sigma_X$) qui conduit à placer le NMA entre l'eau et le DMSO, très près des alcools dont la constante diélectrique est pourtant 5 fois plus faible. De par sa précision, la méthode permet par ailleurs l'amélioration du classement, en une ou plusieurs familles homogènes, des composés de même fonction chimique, classement provenant du traitement plus classique de l'équation de Hammett.

Can. J. Chem., **52**, 1774 (1974)

Because of the failure of different electrostatic theories to take account of the effect of changes in solvent, the overall dielectric constant of a mixed solvent is no longer considered the principal variable in explaining the dissociation of acids (1–3). A new solvent parameter $g(S)$ based on solubility measurements, has been developed which characterizes each solvent mixture S. This has been found to give an excellent linear correlation with ΔpK_a^S for a large number of compounds, referred to the pK_a^S of a reference compound; the intercept and slope of the lines depends only on the nature of the solute (3, 4). However, because the dielectric constant of the mixed organic–water solvents tested up until now has been less than that of water, it was desirable to verify the theory with solvent mixtures having a dielectric constant greater than 80. Then, we have chosen mixtures of water with *N*-methylacetamide, which has a dielectric constant of 178.9 at 30° (5, 6). Such solvent mixtures are also of interest for comparison with water – dimethyl sulfoxide mixtures (7, 8). The greater basicity of *N*-methylacetamide (9–11) and its capability of forming hydrogen bonds, would be expected to make the acid–base properties of water–NMA mixtures quite different from those of water – dimethyl sulfoxide mixtures.

In order to determine pK_a^S values of an acid HA in a mixed solvent S, it is necessary to have an acidity scale pS^+ ($\equiv -\log a_{S^+}$, where a_{S^+} represents the activity of the solvated protons), and this in turn requires the determination of the ionic product K_s ($\equiv a_{S^+} \cdot a_{S^-}$, where a_{S^-} represents all the possible anionic forms of the solvent molecules) of each solvent mixture.

Determination of Autoprotolysis Constant of Water–NMA Mixtures

In pure NMA, the hydrogen electrode can be used to indicate the activity of the solvated proton (12), so that we have made use of a method which has already proved adequate for many solvent mixtures (7, 13, 14). In the cell utilized:

Can. J. Chem. Downloaded from www.nrcresearchpress.com by 210.87.254.40 on 09/05/12
For personal use only.

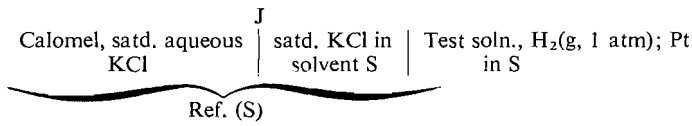

the potential of the hydrogen electrode is measured in relation to an internal reference in the solvent S[Ref.(S)]. This is justified by the perfect stability and reproducibility of the junction J. The measurement of the electromotive force of the cells A and B shown below:

$$\text{Ref.(S)} \mid^{J'} \text{HCl } (a)^1 \text{ in S, } H_2\text{(g, 1 atm); Pt} \qquad \text{A}$$

$$\text{Ref.(S)} \mid^{J''} \text{NaOH } (b) \text{ in S, } H_2 \text{ (g, 1 atm); Pt} \qquad \text{B}$$

leads immediately, in the special case when the concentrations of acid and base are equal ($a = b = c$), to the ionic product K_s of the solvent mixture, by extrapolating to zero ionic strength the expression

$$[1] \quad Y = \frac{1}{u}(E_A - E_B) - 2 \log c = \frac{1}{u}(E_{J'} - E_{J''}) + pK_s + 2 \log f_{\pm}$$

where $u = 2.3\ RT/F = 0.0582$ V at 20 °C.
The linearity of the graphs of Y plotted against $\sqrt{c}$ (Fig. 1) justifies the approximation of the mean activity coefficient $f_{\pm}$ by the simplified Debye–Hückel expression: $\log f_{\pm} \simeq -B\sqrt{I}$. On the other hand, the measurement acidity of the buffer solutions shows that under our operating conditions (same ionic strength I in the compartments containing the hydrogen electrode) the junction potentials $E_{J'}$ and $E_{J''}$ are identical.[2]

Table 1 gives the extrapolated pK_s values.[2] The ionic product of the water–NMA mixtures diminishes with increasing content of organic solvent, and the variations observed, though less than those which characterize water–DMSO mixtures, are comparable to those observed for water–alcohol mixtures (13, 15) (Fig. 2). On the other hand, with about 10% of NMA by weight, the pK_s values pass through a shallow minimum, which is due to the fact that the proton exchange reaction between water and NMA (H_2O + NMA $\leftrightarrows$ OH^- + NMA,H^+) competes with the autoprotolysis constant of water in the value of the ionic product of the mixture. This situation is similar to one previously encountered in the methanol–DMSO mixtures (14), but different to that observed in the case of water–DMSO mixtures because of the weaker basicity of DMSO (9–11).

Table 1 also contains the numerical values of the coefficient B in the simplified Debye–Hückel expression. These values, which are given by the half-slope of the curves $Y = f(\sqrt{c})$, are (though not very precise) sufficient for calculating activity coefficients. While the mixtures rich in water are characterized by insignificant variation in B, beyond 70% NMA by weight, a rapid decrease of this coefficient occurs, so that it approaches zero in a mixture containing 94.8% of NMA by weight. These results point out the impossibility of calculating the B coefficient

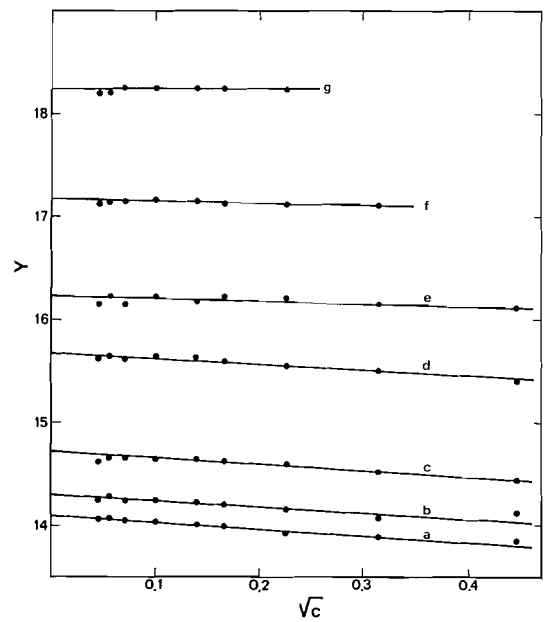

FIG. 1. Determination of autoprotolysis constant in water–NMA mixtures at 20 °C by extrapolation to zero ionic strength of $Y = (1/u)(E_A - E_B) - 2 \log c$. Curves a to g correspond to mixtures containing 9.15, 27.2, 45.1, 66.2, 75.6, 85.1, and 94.8% (w/w), respectively, of NMA.

[1]The use of hydrochloric acid to obtain acid solutions is justified by its complete dissociation in NMA (12).

[2]The details of the experimental technique used for the determination of pS^+ values of buffer solutions and the e.m.f. of cells A and B are available, at a nominal charge, from the Depository of Unpublished Data, National Science Library, National Research Council of Canada, Ottawa, Canada K1A 0S2.

Can. J. Chem. Downloaded from www.nrcresearchpress.com by 210.87.254.40 on 09/05/12
For personal use only.

TABLE 1. pK_s and B values for water–NMA mixtures at 20 °C

% NMA (w/w)	pK_s	B
9.15	14.08	0.3_1
27.2	14.30	0.3_0
45.1	14.70	0.3_0
66.2	15.68	0.2_8
75.6	16.23	0.1_3
85.1	17.17	0.1_0
94.8	18.24	0.0

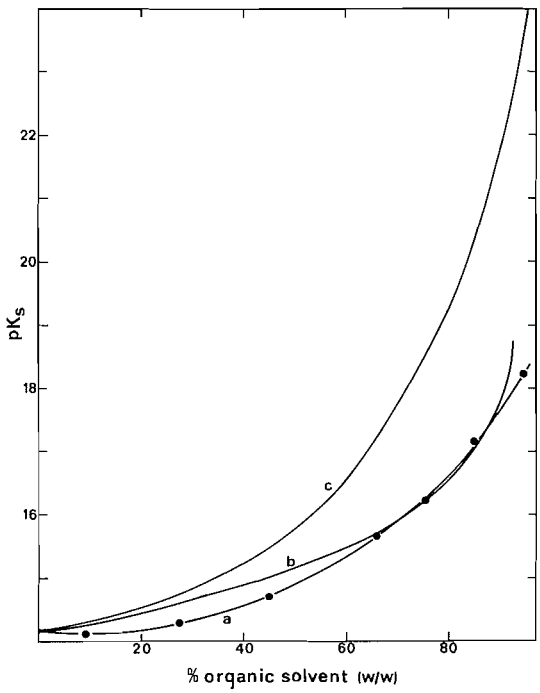

FIG. 2. Comparison of autoprotolysis constants of mixtures of water with (*a*) *N*-methylacetamide; (*b*) isopropanol; (*c*) dimethyl sulfoxide.

a priori making use of the measured overall dielectric constant of the mixture (5), probably because this calculation does not take into account the preferential solvation of ions.

Determination of Acidity in Water–NMA Mixtures

In water–NMA mixtures the measurement of acidity constants by u.v. or visible spectrophotometry is limited to narrow domains of pS^+ from 1 to 3 obtained with strong acids and $pS^+ = pK_s - 3$ to $pK_s - 1$ obtained with strong bases. In order to bridge these regions of acidity and basicity, we have measured a large number of acidities in intermediate region by potentiometry, using a hydrogen electrode or, when the compounds are easily reducible by hydrogen (nitro compounds), a glass electrode.

The selection of acids to be used for preparing buffer solutions is conditioned by the wish to obtain in each mixed solvent an acidity scale as extended as possible, with the differences between the pS^+ values of successive buffers not greater than 0.5 pK unit. On the other hand, in order to establish Hammett-type correlations between the acidity constants determined in water–NMA mixtures with those in water, we have restricted ourselves to compounds of the same chemical functionality. For this reason we have chosen mono- and poly-substituted phenols which offer a very extended range of acidities.

Since the pS^+ values of the buffers depend on the acidity constants of the buffer acids[2], only the numerical values of the pK_a^S are given (Table 2). Besides phenols, we have also studied benzoic acid, in order to relate our determinations to those carried out by Reynaud at 25 °C (5). The two series of measurements agree very well (as would be expected since in this temperature region, variation of pK_a with temperature is negligible).

Influence of the Content of NMA on Acidities

It is usual to represent the effect of a substitutent X on the ionization of a chemical function in a medium S by means of the empirical relationship of Hammett (21):

$$[2] \qquad pK_H^S - pK_X^S = \rho^S\sigma_X$$

The influence of the solvent is included in the reaction constant ρ^S (which depends also on the functional group ionizing and on the temperature). The elimination of the substituent constant σ_X between two solvents S_1 and S_2 allows us to group compounds belonging to the same chemical type into one or more homogeneous families. The relation:

$$[3] \quad pK_X^{S_2} = \frac{\rho^{S_2}}{\rho^{S_1}} pK_X^{S_1} + pK_H^{S_2} - \frac{\rho^{S_2}}{\rho^{S_1}} pK_H^{S_1}$$

requires graphs of the relationship: $pK_X^{S_2} = f(pK_X^{S_1})$, to be linear with slope and intercept depending only on the solvents. We have already examined from this point of view the influence of change of solvent on the ionization of various compounds, particularly in the case

Can. J. Chem. Downloaded from www.nrcresearchpress.com by 210.87.254.40 on 09/05/12
For personal use only.

TABLE 2. pK_a^S values of benzoic acid and substituted phenols in water–NMA mixtures at 20 °C

Number	Compound	pK_a^S at % NMA (w/w) = 0[a]	9.15	27.2	45.1	66.2	75.6	85.1
1	Benzoic acid	4.20[f]	4.18	4.31	4.47	4.92	5.18	5.60
2	*p*-Methoxyphenol	10.21[b]	10.26	10.46	10.73	11.32	11.67	12.08
3	Phenol	10.00[b]	10.04	10.28	10.46	11.00	11.29	11.69
4	*p*-Chlorophenol	9.42[b]	9.46	9.64	9.78	10.25	10.51	10.88
5	*o*-Bromophenol	8.44[b]	8.42	8.65	8.88	9.21	9.39	9.66
6	*p*-Cyanophenol	7.97[c]	7.93	7.93	7.96	8.33	8.55	8.91
7	*o*-Cyanophenol	7.18	7.08	7.18	7.29	7.58	7.76	8.02
8	2,4-Dichlorophenol	7.89[d]	7.90	8.01	8.09	8.36	8.56	8.81
9	2,6-Dichlorophenol	6.79[d]	6.87	6.98	6.98	7.14	7.21	7.35
10	2,4,6-Trichlorophenol	6.4[e]	6.25	6.19	6.18	6.23	6.29	6.39
11	*m*-Nitrophenol	8.38[b]	8.30	8.32	8.40	8.72	9.04	9.35
12	*p*-Nitrophenol	7.15[b]	7.02	6.95	6.96	7.22	7.43	7.68
13	2,5-Dinitrophenol	5.22[f]	5.10	4.82	4.71	4.73	4.86	5.03
14	2,4-Dinitrophenol	4.09[f]	3.87	3.57	3.32	3.26	3.38	3.42
15	2,6-Dichloro-4-nitrophenol	3.55[g]	—[h]	—[h]	2.93	2.70	2.85	2.95

[a]At 25 °C
[b]Reference 16.
[c]Reference 17.
[d]Reference 18.
[e]Reference 2.
[f]Reference 19.
[g]Reference 20.
[h]Insoluble.

when the solvent is progressively changed from water to DMSO (22–24). If, for each water–NMA mixture, we plot the pK_a^S of phenols against their pK_a in water (pK_a^W), we obtained a good linear correlation (Fig. 3). As expected from the eq. 3, the values of the ratio ρ^S/ρ^W deduced directly from the slope of the various straight lines observed are consistent with those calculated from the intercepts by substituting into $pK_H^S - (\rho^S/\rho^W)pK_H^W$ with the appropriate pK_H values. The situation is then identical to that found for water–DMSO mixtures, where the *ortho*-substituted phenols seem to belong to the same homogeneous family, but where the variations of the reaction constant ρ^S become smaller when the mixture contains more than 50% of the organic solvent (Fig. 4).[3] However, because phenols whose aqueous acidities are very close (*p*-nitro and *o*-cyano, *m*-nitro and *o*-bromo) show in water–NMA mixtures differences in acidity too big to be compatible with variations of ρ^S (*cf.* Table 2 and Fig. 3), we questioned the precision of the proposed relationship (which might be due to the fact that ΔpK_a^S values were small), and sought a more rigourous one. We therefore reconsidered the problem by eliminating this time the reaction constant ρ^S. In each solvent S the fact that the substituted compounds X and Y belong to the same family as the non-substituted compound H, taken as the reference, implies the equality:

$$[4] \quad pK_H^S - pK_Y^S = (pK_H^S - pK_X^S)\,\sigma_Y/\sigma_X$$

The graphs of $pK_H^S - pK_Y^S$ plotted as a function of $pK_H^S - pK_X^S$ are of interest for two reasons: if the compounds belong to the same family of Hammett indicators, the experimental points should fit on straight lines passing through the origin;[4] and furthermore the correlations thus established should be capable of good precision because the slopes ($\equiv \sigma_Y/\sigma_X$) can be of reasonable magnitude.

We have applied this treatment to acidities determined in water–NMA mixtures by choosing *p*-nitrophenol as the base compound (X ≡

[3]It should be pointed out that the increase in ρ^S as the solvent mixtures become richer in NMA excludes the possibility of the existence of an acidity function in the tertiary mixtures water–NMA–OH^- governing phenol indicators, because the equidistance between curves of pK_a as a function of percentage NMA is not observed over any part of the range of mixtures. A similar situation characterizes most aqueous solvents, notably water–DMSO mixtures, where the invariance of the reaction constant with medium has never been observed, in spite of the diversity of acids studied (phenols, substituted acetic and benzoic acids, indoles, polynitroanilines (NH ⇄ N^-), and anilinium ions) (8, 22–25). Such observations must rob any acidity functions constructed in these solvent mixtures of fundamental thermodynamic significance.

[4]The origin of the axes represents a hypothetical medium where the reaction constant would be zero.

Can. J. Chem. Downloaded from www.nrcresearchpress.com by 210.87.254.40 on 09/05/12
For personal use only.

Can. J. Chem. Downloaded from www.nrcresearchpress.com by 210.87.254.40 on 09/05/12
For personal use only.

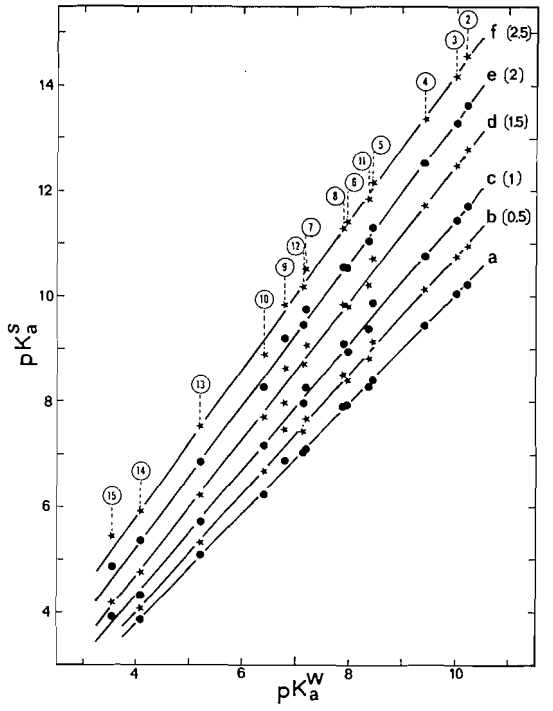

FIG. 3. Correlation of pK_a^S with pK_a^W for variously substituted phenols (numbered as in Table 2) in aqueous mixtures containing (*a*) 9.15%, (*b*) 27.2%, (*c*) 45.1%, (*d*) 66.2%, (*e*) 75.6%, and (*f*) 85.1% NMA (w/w). For clarity curves *b* to *f* have been shifted vertically to extents indicated on the graph.

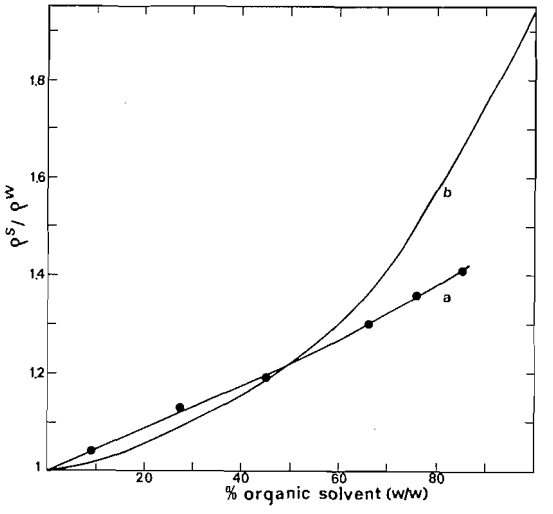

FIG. 4. Variation of ratio ρ^S/ρ^W for phenols with content of organic solvent in (*a*) water–NMA and (*b*) water–DMSO mixtures.

p–NO_2). The fact that the graphs for the *meta*- and *para*-substituted phenols (compounds **2**, **4**, **6**, **11**) and the 2,4- and 2,5-dintirophenols (**13**, **14**) gave straight lines passing through the origin allows us to conclude that these compounds constitute with phenol (**3**) and *p*-nitrophenol (**12**) a perfectly homogeneous family (Fig. 5).

On the other hand, to the extent that the points representing *o*-bromo and *o*-cyanophenol (**5**, **7**) and the dichloro- and trichloro-substituted phenols (**8**, **9**, **10**, **15**) fit on curved lines, we must exclude these indicators from the preceding family. This new method of analyzing the data leads to a classification more precise than correlations of $pK^S = f(pK^W)$. It is our opinion that the existence of these curved lines of Fig. 5 is not fortuitous and that we are not observing statistical scatter of experimental error (estimated at 0.1 logarithmic unit). Furthermore, the application of this analysis to p*K* values of benzoic acids measured in water–DMSO mixtures (where the correlation $pK^S = f(pK^W)$ has already permitted the differentiation of *ortho* isomers (24) shows again much curvature (26). On the other hand, in those cases when correlations are linear, the curves obtained are independent of the composition and of the nature of the mixed

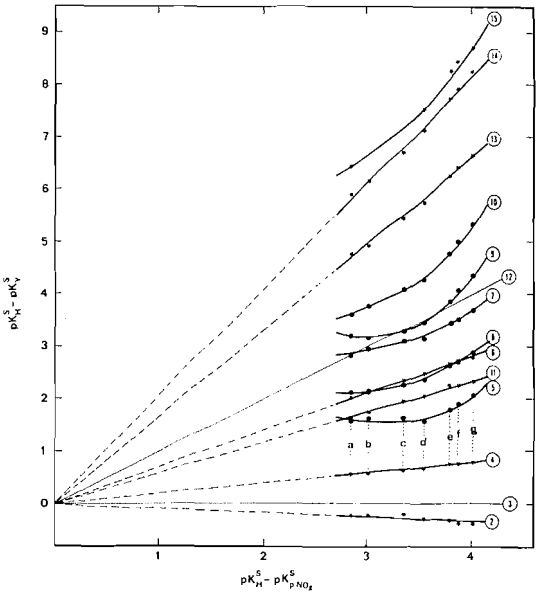

FIG. 5. Influence of substituent *Y* on the acidity of phenol (numbered as in Table 2), *p*-nitrophenol being taken as standard. Composition of water–NMA mixtures: (*a*) 0%, (*b*) 9.15%, (*c*) 27.2%, (*d*) 45.1%, (*e*) 66.2%, (*f*) 75.6%, (*g*) 85.1% NMA (w/w).

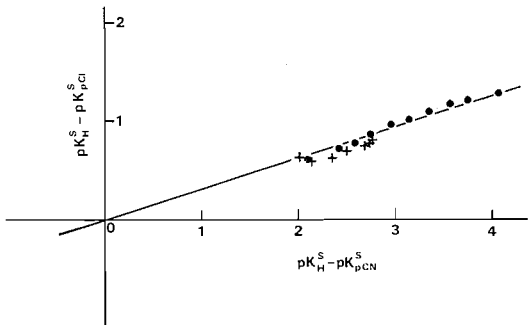

FIG. 6. Influence of *p*-chloro and *p*-cyano substituents on acidity of phenol in water–NMA (+) and water–DMSO (●).

solvent used; an example is given in Fig. 6. This feature, a consequence of eq. 4 is related to the nature of the solvent variable $g(S)$, since the effects of substituents are directly proportional to $g(S)$, which can be used to fix their numerical values (3). The comparison of the effects of substituents in different families in several mixed solvents will be covered in a later article. However for the present we may note that water–NMA mixtures have properties incompatible with the electrostatic theories, since the acidities of acids of type AH decrease very rapidly while the dielectric constant of a medium increases, but accommodated by the $g(S)$ treatment, which relates the differentiating power of the solvent (exaltation of effects of substituents) to its solubilizing power. From this point of view, *N*-methylacetamide appears as a moderately differentiating solvent, having properties intermediate between those of methanol and of dimethyl sulfoxide, in spite of its very high dielectric constant.

Experimental

N-Methylacetamide (Schuchardt) was purified by the procedure of Pucci *et al.* (27); the criterion of purity was that of Reynaud (5). Because of the melting point of NMA (29.5 °C) (6, 12), water–NMA solutions were prepared using a stock solution made up of 5% water and 95% NMA by volume. Mixtures containing less than 50% NMA by weight were obtained by adding an accurately known volume of carbon dioxide-free water to a known volume of the stock solution. With the exception of the mixture containing 94.8% NMA by weight, prepared by weighing pure NMA, the other solutions were prepared by the inverse procedure.

The phenols were commercial products, recrystallized to constant melting point and absorption spectrum. Buffered solutions were prepared by ten-fold dilution of stock solutions ($I = 0.1\ M$), introducing the quantity of NMA necessary to obtain the desired percentage. These stock solutions, often made up with mixed media for reasons of solubility, were obtained by weighing the phenol and half-neutralizing it with sodium hydroxide. They were sufficiently stable to be used for up to one week after their preparation.

TABLE 3. Influence of dimethyl sulfoxide and of *N*-methylacetamide content on the normal potential E_{og}^S (in mV) of the glass electrode (Radiometer G 202 B), with reference to its value E_{og}^W in water

Organic solvent	$E_{og}^W - E_{og}^S$ at % w/w =					
	20	40	60	70	80	90
DMSO	15	30	45	52	60	68
NMA	23	47	64	70	94	106

The electrochemical vessel used has already been described by us (7, 13). In the pS^+ regions studied, the glass electrode used (Radiometer G 202 B with an aqueous filling) has a good reversibility. Previous study (28) indicated little or no variations for the normal potential E_{og} of the glass electrode in aqueous–organic media, and particularly in aqueous alcoholic solvents. This led Morel (29) to postulate the invariance of this potential in different mixtures. Our results (Table 3) show that this proposition is not verified in aprotic dipolar solvents, and that the variations of E_{og}^S, already noticeable in the presence of DMSO, become considerable in the presence of *N*-methylacetamide which implied a standardization of the glass electrode in each mixed solvent.[2]

We are grateful to Professor J. T. Edward (McGill University) for fruitful discussion and for help in writing this article.

1. M. BORN. Z. Phys. **1**, 45 (1920); F. BRYCMAN-HAUPSTEIN and B. TREMILLON. Bull. Soc. Chim. Fr. 1837 (1965); R. ALEXANDER and A. J. PARKER. J. Am. Chem. Soc. **89**, 5549 (1967); R. A. ROBINSON and R. G. BATES. J. Res. NBS **70A**, 553 (1966); R. REYNAUD. Ph.D. thesis, Paris, 1966; M. POSTEL and J. VEDEL. J. Electroanal. Chem. **38**, 223 (1972); E. BOULANGER and J. VEDEL. J. Electroanal. Chem. **40**, 133 (1972).
2. G. CHARLOT and B. TREMILLON. Les réactions chimiques dans les solvants et les sels fondus. Gauthier-Villars, Paris. 1963.
3. P. LETELLIER and R. GABORIAUD. J. Chim. Phys. **70**, 941 (1973).
4. P. LETELLIER, R. GABORIAUD, and R. SCHAAL. Bull. Soc. Chim. Fr. 973 (1972); P. LETELLIER. Bull. Soc. Chim. Fr. 1569 (1973).
5. R. REYNAUD. Bull. Soc. Chim. Fr. 3945 (1968).
6. R. DAWSON, P. G. SEARS, and R. H. GRAVES. J. Am. Chem. Soc. **77**, 1986 (1955).
7. J.-C. HALLE, R. GABORIAUD, and R. SCHAAL. Bull. Soc. Chim. Fr. 1851 (1969).
8. J.-C. HALLE, R. GABORIAUD, and R. SCHAAL. Bull. Soc. Chim. Fr. 2041 (1970).
9. D. LANDINI, G. MODENA, G. SCORRANO, and F. TADDEI. J. Am. Chem. Soc. **91**, 6703 (1969).

Can. J. Chem. Downloaded from www.nrcresearchpress.com by 210.87.254.40 on 09/05/12
For personal use only.

10. W. L. REYNOLDS and K. A. LAMPE. J. Inorg. Nucl. Chem. **30**, 2860 (1968).
11. J. T. EDWARD and I. C. WANG. Can. J. Chem. **40**, 966 (1962).
12. D. S. REID and C. A. VINCENT. J. Electroanal. Chem. **18**, 427 (1968).
13. R. GABORIAUD and R. SCHAAL. J. Chim. Phys. **66**, 730 (1969).
14. J.-C. HALLE, F. TERRIER, and R. GABORIAUD. Bull. Soc. Chim. Fr. 37 (1973).
15. J. KILPI and H. VARSILA. Z. Phys. Chem. A**177**, 427 (1936).
16. A. I. BIGGS and R. A. ROBINSON. J. Chem. Soc. 388 (1961).
17. M. M. FICKLING, A. FISHER, B. R. MANN, J. PACKER, and J. VAUGHAN. J. Am. Chem. Soc. **81**, 4226 (1959).
18. R. A. ROBINSON. J. Res. NBS, **68**A, 159 (1964).
19. G. KORTUM, W. VOGEL, and K. ANDRUSSOW. Dissociation constants of organic acids in aqueous solution. Butterworths, London. 1961.
20. R. A. ROBINSON. J. Res. NBS, **71**A, Phys. and Chem. 385 (1967).
21. L. P. HAMMETT. Physical organic chemistry. McGraw-Hill Book Co., New York. 1940. Chapt. VII.
22. J.-C. HALLE. C. R. Acad. Sc. **271**C, 1109 (1970).
23. J.-C. HALLE. Ph.D. thesis, Paris, C.N.R.S. A.O. 5780. 1971.
24. J.-C. HALLE and R. SCHAAL. Anal. Chim. Acta, **60**, 197 (1972).
25. J.-C. HALLE, F. TERRIER, and R. SCHAAL. Bull. Soc. Chim. Fr. 1225 (1973).
26. J.-C. HALLE and R. GABORIAUD. Unpublished results.
27. A. E. PUCCI, J. VEDEL, and B. TREMILLON. J. Electroanal. Chem. 253 (1969).
28. J. JUILLARD. Bull. Soc. Chim. Fr. 2040 (1970).
29. J. P. MOREL. Ph.D. thesis, Clermont-Ferrand, C.N.R.S. A.O. 3249. 1969.

Can. J. Chem. Downloaded from www.nrcresearchpress.com by 210.87.254.40 on 09/05/12
For personal use only.

Evidence for Restricted Rotation in the ^1H and ^{19}F Nuclear Magnetic Resonance Spectra of Cyclopentadienylperfluoroalkyliron and Nickel Complexes

K. STANLEY, R. A. ZELONKA, J. THOMSON, P. FIESS, AND M. C. BAIRD

Department of Chemistry, Queen's University, Kingston, Ontario K7L 3N6

Received November 13, 1973

Several series of compounds $CpFeCOLR_F$, $CpNiPPh_3R_F$, and mer-$Fe(CO)_3LR_FI$ (R_F = CF_3, CF_2CF_3, $CF(CF_3)_2$; L = PPh_3, $PMePh_2$, PMe_2Ph), some of them new compounds, have been prepared and characterized. Evidence for restricted rotation about both metal–alkyl and phosphorus–aryl bonds is deduced from the variable temperature ^1H and ^{19}F n.m.r. spectra of the complexes. The presence of two ν_{CO} in the i.r. spectra of the pseudotetrahedral iron complexes suggests that these compounds exist as diastereomers, the coordinated phosphine and the nickel constituting chiral centers.

On a préparé et caractérisé plusieurs séries de composés du type $CpFeCOLR_F$, $CpNiPPh_3R_F$ et mer-$Fe(CO)_3LR_FI$ (R_F = CF_3, CF_2CF_3, $CF(CF_3)_2$; et L = PPh_3, $PMePh_2$, et PMe_2Ph), dont quelques uns sont des nouveaux produits. En se basant sur les spectres r.m.n. du proton et du fluor des complexes déterminés à diverses températures, on déduit que la rotation est empêchée autour des liens métals-alkyle et phosphore alkyle. La présence de deux fréquences ν_{CO} dans le spectre infrarouge des complexes pseudotétraédriques du fer indique que ces composés existent sous forme de diastéréoisomères dans lesquels la phosphine coordonnée et le nickel constituent les centres chiro. [Traduit par le journal]

Can. J. Chem., **52**, 1781 (1974)

Introduction

We have previously utilized n.m.r. data to demonstrate hindered rotation and preferred conformations in a number of cyclopentadienyliron, cobalt, nickel, and rhodium complexes containing tertiary phosphines and either alkyl or perfluoroalkyl groups (1, 2). Arguments were based largely on temperature dependences of line widths and vicinal coupling constants between phosphorus and the α-hydrogen(s) or α-fluorine(s) of the alkyl group, and suggested that bulky phosphines can force a coordinated alkyl group to favor a particular conformation, although rotation about a metal–carbon σ-bond is apparently relatively unhindered in complexes containing smaller ligands.

We now present data for series of perfluoroalkyl nickel and iron complexes of the general formulae $CpNiLR_F$, $CpFe(CO)LR_F$, and $Fe(CO)_3R_FIL$ (L = tertiary phosphine; R_F = CF_3, CF_2CF_3, $CF(CF_3)_2$). The first two series complement work done on a nickel alkyl series (1) and the isoelectronic cobalt series, $CpCoILR_F$ (2), while the last represents an initial attempt, albeit largely unsuccessful, to extend our work to octahedral systems.

Experimental

Infrared spectra were run on Perkin–Elmer 180 and Beckman IR-10 spectrometers, n.m.r. spectra on a Bruker HX60 instrument with internal lock. Fluorine spectra were generally run on methylene chloride solutions locked on $CFCl_3$ or C_6F_6; chemical shifts are reported relative to the former, upfield shifts being positive. Melting points were done on a Gallenkamp Melting Point Apparatus, while chemical analyses were done by Schwarzkopf Microanalytical Laboratory, Woodside, New York.

The compounds $CpFeCOPPh_3CF_3$ (3), $CpFeCOPPh_3CF_2CF_3$ (3), $CpFeCOPPh_3CF(CF_3)_2$ (3), $Fe(CO)_3IPPh_3CF(CF_3)_2$ (4), $CpNiPPh_3CF_3$ (5), and $CpNiPPh_3CF_2CF_3$ (6) were prepared as described in the literature. The new compound $CpFeCOPMePh_2CF(CF_3)_2$ was prepared by irradiation of a solution of $CpFe(CO)_2CF(CF_3)_2$ with the phosphine (3), while the new compounds $Fe(CO)_3ILCF(CF_3)_2$ (L = $PMePh_2$, PMe_2Ph) were prepared by treating benzene solutions of $Fe(CO)_4ICF(CF_3)_2$ with the appropriate phosphine (4). The compound $CpNiPPh_3CF(CF_3)_2$ was prepared by the same method as the perfluoromethyl and ethyl analogs (5, 6), while attempts to prepare $CpFeCOPMePh_2CF_2CF_3$, $CpFeCOPMe_2PhCF_2CF_3$, and $CpFeCOPMe_2PhCF(CF_3)_2$ were unsuccessful. Analytical data and physical properties are listed in Table 1.

Results

Proton n.m.r. data are listed in Table 2. In all cases, the cyclopentadienyl resonances of the nickel compounds were singlets, while those of the iron compounds were doublets because of coupling to phosphorus. The chemical shifts of the methyl resonances of the compounds were generally as expected with the exception of that of the compound $CpFeCOPMePh_2CF(CF_3)_2$,

Can. J. Chem. Downloaded from www.nrcresearchpress.com by 210.87.254.6 on 09/05/12
For personal use only.

TABLE 1. Analytical data and physical properties of the new compounds

Compound	Color	Melting point (°C)	Found (%)		Calculated (%)	
			C	H	C	H
$CpFeCOPMePh_2CF(CF_3)_2$	Orange-brown	100–108	50.95	3.52	51.00	3.51
$Fe(CO)_3IPMePh_2CF(CF_3)_2$	Brown	128–130(d)	36.02	2.16	35.88	2.06
$Fe(CO)_3IPMe_2PhCF(CF_3)_2$	Black	106–107(d)	29.47	1.93	29.29	1.94
$CpNiPPh_3CF(CF_3)_2$	Golden-brown	132–134	56.00	3.66	56.24	3.64

TABLE 2. Proton n.m.r. data at 300 °K in $CDCl_3$

Compound	$\tau_{C_5H_5}$	τ_{CH_3}(J in Hz)*	Other resonances (τ)
$CpFeCOPPh_3CF_3$	5.50(d, J = 1.5)	—	~2.5(m)
$CpFeCOPPh_3CF_2CF_3$	5.51(d, J = 1.4)	—	~2.5(m)
$CpFeCOPPh_3CF(CF_3)_2$	5.52(d, J = 1.8)	—	~2.5(m)
$CpFeCOPMePh_2CF(CF_3)_2$	5.50(d, J = 1.6)	8.07(dd, J_{HF} = 2.3, J_{HP} = 9.2)	~2.6(m)
$Fe(CO)_3IPPh_3CF(CF_3)_2$†	—		~2.7(m)
$Fe(CO)_3IPMePh_2CF(CF_3)_2$†	—	8.12(d, J_{PH} = 9.5)	~2.8(m)
$Fe(CO)_3IPMe_2PhCF(CF_3)_2$†	—	8.65(d, J_{HP} = 10)	~3.0(m)
$CpNiPPh_3CF_3$	5.08	—	~2.6(m)
$CpNiPPh_3CF_2CF_3$	5.08	—	~2.6(m)
$CpNiPPh_3CF(CF_3)_2$	5.08	—	~2.6(m)

*d = doublet, dd = double doublet, m = multiplet.
†In C_6D_6.

for which long range coupling to the α-fluorine was also observed. Similar couplings have been noted previously in the n.m.r. spectra of the compounds $CpCoIPMePh_2CF_2CF_3$, $CpCoIPMePh_2CF(CF_3)_2$, and $CpCoIPMe_2PhCF(CF_3)_2$ (2), although they are obviously not a general feature of the spectra of most of the compounds discussed here and in ref. 2.

The phenyl resonances of the compounds at room temperature were, as expected, complex multiplets. In the case of $CpFeCOPPh_3CF(CF_3)_2$, which contains the bulkiest phosphine and perfluoroalkyl groups studied, the phenyl resonances broadened and coalesced into two broad bands in the temperature range 290–300 °K. Similar observations have been made previously for the compounds $CpCoIPPh_3R_F$ (R_F = CF_3, CF_2CF_3, $CF(CF_3)_2$) (2), coalescence occurring at about 220, 240, and 300 °K respectively (2). In the cases of the nickel compounds, coalescence of the phenyl resonances occurred at about 220 ($CF(CF_3)_2$), 210 (CF_2CF_3) and <210 °K (CF_3).

The ^{19}F n.m.r. data are listed in Table 3. The ^{19}F spectrum of $CpFeCOPPh_3CF_3$ has been discussed previously (1). It contains a doublet at −13.5 p.p.m. (J_{PF} = 2.9 Hz at room temperatures), which broadens and coalesces at low temperatures. Presumably at lower temperatures, the CF_3 resonance would have been resolved into an ABC system, as is observed in some fluorinated halocarbons (7); the data certainly suggested temperature and solvent dependence of vicinal phosphorus–fluorine couplings.

The ^{19}F n.m.r. spectrum of $CpFeCOPPh_3CF_2CF_3$ consists of an ABX_3M (X_3 = CF_3, M = ^{31}P) system, the two α-fluorine atoms being diastereotopic because of the chiral iron atom. The CF_3-decoupled spectrum was very similar to that illustrated in ref. 2. As before (2), the chemical shifts and coupling constants were calculated using the appropriate equations (ref. 8, p. 69), identification of the correct solution being made using INDOR techniques based on population transfer (ref. 8, p. 45).

The ^{19}F spectral parameters changed very little in the temperature range 300–193 °K, as is shown in Table 3. In particular, the temperature dependences of the chemical shifts of the α-fluorine atoms and their vicinal coupling constants to the phosphorus varied somewhat less than was observed for the isoelectronic complex, $CpCoIPPh_3CF_2CF_3$(2).

The two trifluoromethyl groups of the per-

Can. J. Chem. Downloaded from www.nrcresearchpress.com by 210.87.254.6 on 09/05/12
For personal use only.

TABLE 3. ^{19}F n.m.r. data at room temperature

Compound	δ(α-CF, CF_2, CF_3; J in Hz)*	δ(β-CF_3; J in Hz)*
$CpFeCOPPh_3CF_3$	−13.5(d, J_{PF} = 2.9)	—
$CpFeCOPPh_3CF_2CF_3$	63.3(m, J_{PF} = 43.6)(δ65.3, J_{PF} = 41.8 at 193 °K) 59.9(m, J_{PF} = 1.4)(δ60.2, J_{PF} = 0.04 at 193 °K)	81.7(t, $J_{CF_2-CF_3}$ = 2.1)
$CpFeCOPPh_3CF(CF_3)_2$	173.2(m, J_{PF} = 37.9)	66.3, 66.9(m, J_{CF-CF_3} = 11, $J_{CF_3-CF_3}$ = 9)
$CpFeCOPMePh_2CF(CF_3)_2$	175.6(m, J_{PF} = 26.4)	66.1, 67.4(m, J_{CF-CF_3} = 10, $J_{CF_3-CF_3}$ = 10)
$CpNiPPh_3CF_3$	−3.1(d, J_{PF} = 14.0)	—
$CpNiPPh_3CF_2CF_3$	80.2(dq, J_{PF} = 38.0)	82.0(t, $J_{CF_2-CF_3}$ = 2.0)
$CpNiPPh_3CF(CF_3)_2$	188.0(m, J_{PF} = 85.5)	67.7(d, J_{CF-CF_3} = 11)
$Fe(CO)_3PPh_3CF(CF_3)_2I$	155.8(m, J_{PF} = 10)	66.5(dd, J_{PF} = 1.9, $J_{CF_3-CF_3}$ = 10.5)
$Fe(CO)_3PMePh_2CF(CF_3)_2I$	156.8(m, J_{PF} = 11)	67.0(dd, J_{PF} = 2.0, $J_{CF_3-CF_3}$ = 10.4)
$Fe(CO)_3PMe_2PhCF(CF_3)_2I$	157.1(m, J_{PF} = 11)	67.1(dd, J_{PF} = 1.9, $J_{CF_3-CF_3}$ = 10.4)

*d = doublet, t = triplet, dd = double doublet, dq = double quartet, m = multiplet.

fluoroisopropyl complexes are diastereotopic because of the chiral iron atoms, and thus the fluorine atoms of these complexes comprise $AM_3M_3'X$-type systems. In contrast to the isoelectronic cobalt complexes (2), selective decoupling of the CF_3 resonances permitted accurate measurement of the vicinal coupling between the α fluorine atom and the phosphorus in each. In the case of the triphenylphosphine complex, $^3J_{PF}$ changed negligibly (< 1 Hz) in the range 200–300 °K; in the case of the methyldiphenylphosphine complex, $^3J_{PF}$ decreased regularly from 30.0 Hz at 350 °K (in toluene) to 18.3 Hz at 210 °K in methylene chloride. Solvent effects were relatively small.

The ^{19}F n.m.r. spectra of the pseudotrigonal nickel compounds were all less complex than their pseudotetrahedral iron and cobalt analogs because the nickel atoms are not chiral. In the case of the trifluoromethyl complex, the chemical shift of the CF_3 resonance changed from −3.14 to −2.80 p.p.m. in the temperature range 293 to 183 °K; the value of $^3J_{PF}$ remained constant.

The CF_3 chemical shift of the perfluoroethyl complex was also constant in the temperature range 293–173 °K, although the CF_2 resonance shifted from 80.2 to 81.9 p.p.m. Again $^3J_{PF}$ remained constant. Although the CF_3 chemical shift, J_{CF-CF_3} and $^3J_{PF}$ of the perfluoroisopropyl complex remained unchanged in the range 293 to 185 °K, the CF resonance shifted from 188.0 to 191.2 p.p.m.

The ^{19}F n.m.r. spectra of the octahedral complexes, $Fe(CO)_3LCF(CF_3)_2I$, were noteworthy only for their close similarity. Virtually no change in $^3J_{PF}$ was observed, in contrast to the pseudotetrahedral cyclopentadienyliron and cobalt compounds.

The i.r. spectra of all the complexes were generally consistent with the formulations and, except for the carbonyl stretching region, are of little interest in the present context. Carbonyl stretching frequencies for the carbonyl compounds are presented in Table 4.

Discussion

The small temperature-dependence for both values of $^3J_{PF}$ of the compound $CpFeCOPPh_3CF_2CF_3$ is in accord with previous suggestions (1, 2) that primary alkyl compounds of this type exist predominantly in conformation **1**, although other rotamers may populate.

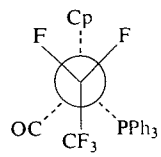

1

Although analogous iron compounds with smaller phosphines could not be isolated, the large variations with temperature of $^3J_{PF}$ of the compounds $CpFeCOPMePh_2CF(CF_3)_2$ (see below) and $CpCoIPMePh_2CF_2CF_3$ (2) show quite clearly that major changes in the relative populations of rotamers can cause quite large changes in the vicinal coupling constants.

The large difference in the two values of $^3J_{PF}$ for the compound $CpFeCOPPh_3CF_2CF_3$ are

Can. J. Chem. Downloaded from www.nrcresearchpress.com by 210.87.254.6 on 09/05/12
For personal use only.

TABLE 4. Infrared data for the carbonyl complexes

Compound	ν_{CO}(cm^{-1}, in cyclohexane)*
$CpFeCOPPh_3CF_3$	1944 ($\Delta\nu_{1/2} \approx 12\ cm^{-1}$)
$CpFeCOPPh_3CF_2CF_3$	1959, ~1956 (asymmetric: $\Delta\nu_{1/2} \approx 14\ cm^{-1}$)
$CpFeCOPPh_3CF(CF_3)_2$	1972, 1956 ($\Delta\nu_{1/2} \approx 8\ cm^{-1}$)
$CpFeCOPMePh_2CF(CF_3)_2$	1965(br), 1952(br) ($\Delta\nu_{1/2} \approx 15\ cm^{-1}$)
$Fe(CO)_3IPPh_3CF(CF_3)_2$	2130(w), 2070(s), 2055(m)
$Fe(CO)_3IPMePh_2CF(CF_3)_2$	2115(m), 2060(s), 2045(s,sh)
$Fe(CO)_3IPMe_2PhCF(CF_3)_2$	2120(m), 2060(s), ~2050(m,sh)

*sh = shoulder, br = broad, m = medium, s = strong.

also consistent with rotamer **1**, as *trans* and *gauche* coupling constants would probably be quite different. Distinction between the two cannot be made at present.

The constant value of $^3J_{PF}$ of the compound $CpFeCOPPh_3CF(CF_3)_2$ suggests that it also exists predominantly in a single conformation, an expected conclusion as this compound should be even more crowded then the perfluoroethyl analog. If, as previously suggested (1), the order of decreasing steric requirements of the other ligands on the iron is Cp > PPh_3 > CO, then the preferred rotamer would be

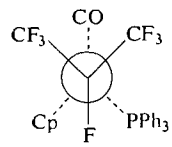

2

The observed value of $^3J_{PF}$, 37.9 Hz, would then correspond to a *gauche* coupling constant, and it is tempting to assign the larger value of $^3J_{PF}$ of the perfluoroethyl compound (43.6 Hz) also to a *gauche* coupling constant. The large difference in $^3J_{FF}$ of the perfluorethyl (2.1 Hz) and isopropyl complexes (11 Hz) indicate, however, that substituent effects can have quite large effects on vicinal coupling constants. Furthermore, in the cobalt series, no correlation of *gauche* or *trans* coupling constants was apparent in the CF_3, CF_2CF_3, and $CF(CF_3)_2$ compounds and certainly the time-averaged value of $^3J_{PF}$ of $CpFeCOPPh_3CF_3$ (2.9 Hz) cannot be an average of the *gauche* and *trans* vicinal coupling constants of the perfluoroethyl compound.

The large change with temperature of $^3J_{PF}$ of $CpFeCOPMePh_2CF(CF_3)_2$ suggests that this compound does exist as an equilibrium mixture of rotamers, the relative populations of which are strongly temperature dependent. We have previously suggested that the major factors affecting the relative rotamer stabilities are steric interactions between the ligands. Thus it is not surprising that rotation about the iron–carbon bond becomes more hindered on going from the methyldiphenylphosphine to the triphenylphosphine complex. Similar effects were noted in the series $CpCoILCF_2CF_3$ (L = PPh_3, $PMePh_2$, PMe_2Ph) (2).

Results with the nickel series were mildly disappointing. An extensive series of similar, non-fluorinated compounds has been thoroughly studied (1), and it was hoped that the two series would correlate with each other. Indeed, the lack of temperature dependence of $^3J_{PF}$ in the spectrum of $CpNiPPh_3CF(CF_3)_2$ is in accord with previous conclusions (1) that secondary alkyl compounds in this series exist predominantly in configuration **3**.

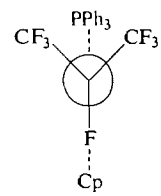

3

However, by analogy with the ^1H n.m.r. spectrum of $CpNiPPh_3CH_2SiMe_3$ (1), it was anticipated that the value of $^3J_{PF}$ for $CpNiPPh_3CF_2CF_3$ would be temperature dependent, indicating some steric hindrance to rotation and population of more than one rotamer. The lack of temperature dependence of $^3J_{PF}$ might thus suggest virtually free rotation about the nickel carbon bond, perhaps not a surprising conclusion, as the CF_3 group is undoubtedly significantly smaller than a trimethylsilyl group.

The ^1H n.m.r. and i.r. spectra of the triphenyl-

Can. J. Chem. Downloaded from www.nrcresearchpress.com by 210.87.254.6 on 09/05/12
For personal use only.

Can. J. Chem. Downloaded from www.nrcresearchpress.com by 210.87.254.6 on 09/05/12
For personal use only.

phosphine complexes provided evidence for hindered rotation about the phosphorus–carbon bonds also. As was observed for the series $CpCoIPPh_3R_F$ ($R_F = CF_3, CF_2CF_3, CF(CF_3)_2$) (2), the phenyl resonances are complex, well-resolved time-averaged multiplets at ambient temperatures, but broaden and coalesce into broad, featureless bands at lower temperatures. Approximate coalescence temperatures decrease in the order $CpFeCOPPh_3CF(CF_3)_2 \sim CpCoIPPh_3CF(CF_3)_2 > CpCoIPPh_3CF_2CF_3 > CpCoIPPh_3CF_3 \sim CpNiPPh_3CF(CF_3)_2 > CpNiPPh_3CF_2CF_3 > CpNiPPh_3CF_3$. This is the expected order of decreasing crowding about the metal atoms, and it seems that the data are best explained in terms of restricted rotation about the phosphorus–aryl bonds. Similar observations have been made for triphenylphosphonium salts (9) and complexes of benzylphenylphosphines (10).

The presence of two carbonyl stretching bands of similar intensities in the i.r. spectra of the iron monocarbonyl complexes is noteworthy; the broadness of the band in the spectrum of the trifluoromethyl derivative probably also indicates the presence of two unresolved bands. Similar doubling of carbonyl bands in similar compounds has been attributed to the presence of more than one staggered rotamer (11–13), a conclusion which, in the case of $CpFeCOPMePh_2CF(CF_3)_2$, is in accord with the ^{19}F n.m.r. evidence. The trifluoromethyl compound, however, can exist only in one staggered conformation, and the ^{19}F n.m.r. data are in accord with the perfluoroethyl and triphenylphosphine-isopropyl derivatives also existing predominantly in only one staggered conformation. As suggested previously (2), however, a coordinated triphenylphosphine is chiral because of the two possible twists about the phosphorus–aryl bonds, and thus the compounds should all exist as diastereomers on the i.r. time scale.[1] Ample precedents exist for this phenomenon (14–17), which explains the i.r. spectra and which might also contribute to the unusual broadness of the carbonyl bands in the i.r. spectrum of $CpFeCOPMePh_2CF(CF_3)_2$.

As pointed out previously (1), conformational effects on vicinal phosphorus–fluorine and –hydrogen coupling constants may be expected to occur in planar and octahedral complexes when an alkyl group is *cis* to the phosphine(s) but not *trans*. Although the stereochemistry of tertiary phosphine derivatives of the compounds $Fe(CO)_4R_FI$ ($R_F = CF_3, CF_2CF_3, CF(CF_3)_2$) was not known, it was hoped that they would be suitable for studies of the type discussed above. Perfluoroisopropyl derivatives of three phosphines of quite different steric requirements were chosen for initial studies.

The parent tetracarbonyl derivatives are all known compounds (4, 18, 19). Their i.r. spectra in the carbonyl stretching region are very similar (Table 5), consisting of one strong and several weak bands. Although the multiplicity of bands has been taken as evidence that the compounds are probably the *cis* isomers, (18, 19), the pattern is much more like that of *trans*- than of *cis*-$Fe(CO)_4I_2$ (20) (Table 5). The presence of only one strong band certainly seems inconsistent with a *cis* structure, for which four bands of approximately equal intensity would be expected, while one strong and one weak band would be expected for *trans* isomers, with local C_{4v} symmetry. The presence of a perfluoroalkyl ligand, which does not have four-fold symmetry, might well lower the overall symmetry sufficiently that other modes could become weakly allowed as well.

Assuming a *trans* structure, the most obvious structure for the monophosphine complexes is **4**.

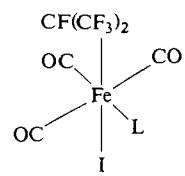

4

The i.r. spectra are consistent with this structure, in which the perfluoroisopropyl group is *cis* to the phosphine, although other isomers cannot be ruled out. The similarity of the i.r. spectra of the three compounds prepared certainly suggests that they have the same structure. The lack of variation in $^3J_{PF}$ among the three compounds studied suggests that all exist in the same conformation, *i.e.* either all exist predominantly in one conformation, or all experience essentially unhindered rotation about the iron–carbon bonds. Space-filling molecular models suggest that the latter possibility is much more likely; a single *cis* phosphine does little to hinder rotation

[1]Although not on the n.m.r. time scale, as rotation about the phosphorus–aryl bonds is rapid on the n.m.r. time scale (see above).

TABLE 5. Infrared data for octahedral tetracarbonyliron(II) complexes

Compound	ν_{CO} (cm^{-1})	Reference
cis-$Fe(CO)_4I_2$	2131(s), 2087(vs), 2085(sh), 2062(s)	20
trans-$Fe(CO)_4I_2$	2102(vw), 2081(vs), 2047(vw)	20
$Fe(CO)_4CF_3I$	2147(w), 2107(vw), 2087(vs), 2054(w)	19
$Fe(CO)_4CF_2CF_3I$	2146(w), 2140(w), 2112(vw), 2087(vs), 2056(w)	19
$Fe(CO)_4CF(CF_3)_2I$	2146(w), 2118(w), 2086(vs), 2052(w)	18

TABLE 6. Rotational barriers

Compound	Barrier (kcal mol^{-1})	Bond	Reference
Cp_3UCHMe_2	10.5 ± 0.5	U—$CHMe_2$	21
$MeMn(CO)_5$	2.7 ± 0.5	Mn—CH_3	22
$[CpMo(CO)_3]_2$	15.3 ± 1	Mo—Mo	23
$[CpFe(CO)_2]_2$ (unbridged isomer)	~7	Fe—Fe	23
$CF_3CX_2CF_3$ (X = Cl, Br, I)	5.1–7.1	C—C	7

of the alkyl group, as most possible conformations can be achieved without a CF_3 group eclipsing the phosphine.

In summary, the n.m.r. data are consistent with hindered rotation about both metal–carbon and phosphorus–carbon bonds in phosphine-substituted perfluoroalkyl compounds. In addition, certain rotamers appear to be more highly populated than others, although separate rotamers could not be detected at low temperatures. Although the results of our investigations so far have been somewhat frustrating in that we have been unable to estimate either barriers to rotation or relative rotamer populations, we list in Table 6 a few rotational barriers which have been reported in the literature for similar compounds, and note that the 5–10 kcal/mol barriers which our conclusions would require are not as unlikely as has been suggested (9). In addition, we note that for the compounds $CpFe(CO)_2SiCl_2Me$ (12) and $CpFe(CO)_2GeX_2R$ (X = Cl, Br, I; R = Me, Et, *n*-Pr, *i*-Pr) (13), the enthalpy differences between rotamers vary between 0.7 and 2.3 kcal/mol, the *trans* form (**5**) being favoured in all cases in non-polar solvents.

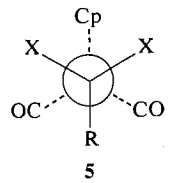

5

1. J. THOMSON, W. KEENEY, W. F. REYNOLDS, and M. C. BAIRD. J. Organomet. Chem. **40**, 205 (1972).
2. R. J. BURNS, P. B. BULKOWSKI, S. C. V. STEVENS, and M. C. BAIRD. J. Chem. Soc. Dalton Trans. In press.
3. R. B. KING, R. N. KAPOOR, and K. H. PANNELL. J. Organomet. Chem. **20**, 187 (1969).
4. R. B. KING, R. N. KAPOOR, and L. W. HOUK. J. Inorg. Nucl. Chem. **31**, 2179 (1969).
5. M. D. RAUSCH, Y. F. CHANG, and H. B. GORDON. Inorg. Chem. **8**, 1355 (1969).
6. D. W. MCBRIDE, E. DUDEK, and F. G. A. STONE. J. Chem. Soc. 1752 (1964).
7. F. J. WEIGERT and W. MAHLER. J. Am. Chem. Soc. **94**, 5314 (1972).
8. R. A. HOFFMANN, S. FORSÉN, and B. GESTBLUM. N.M.R., Basic Principles Prog. Vol. 5. 1971.
9. J. M. BROWN and K. MERTIS. J. Organomet. Chem. **47**, C5 (1973).
10. J. H. NELSON and D. A. REDFIELD. Inorg. Nucl. Chem. Lett. **9**, 807 (1973).
11. W. JETZ and W. A. G. GRAHAM. J. Am. Chem. Soc. **89**, 2773 (1967).
12. J. DALTON. Inorg. Chem. **11**, 915 (1972).
13. B. V. LOKSHIN, F. S. DENISOV, B. Z. GEVORKYAN, N. E. KOLOBOVA, and K. N. ANISIMOV. Bull. Acad. Sci. U.S.S.R. **20**, 1831 (1971).
14. D. GUST and K. MISLOW. J. Am. Chem. Soc. **95**, 1535 (1973).
15. V. G. ALBANO, P. L. BELLOW, and M. SANSONI. Chem. Commun. 899 (1969).
16. V. G. ALBANO, P. L. BELLON, and M. SANSONI. J. Chem. Soc. A, 2420 (1971).
17. I. S. BUTLER and A. E. FENSTER. Inorg. Chim. Acta, **7**, 79 (1973).
18. R. B. KING, S. L. STAFFORD, P. M. TREICHEL, and F. G. A. STONE. J. Am. Chem. Soc. **83**, 3604 (1961).
19. E. PITCHER and F. G. A. STONE. Spectrochim. Acta, **18**, 585 (1962).
20. M. PANKOWSKI and M. BIGORGNE, J. Organomet. Chem. **19**, 393 (1969).
21. T. J. MARKS, A. M. SEYAM, and J. R. KOLB. J. Am. Chem. Soc. **95**, 5529 (1973).
22. A. B. DEMPSTER, D. B. POWELL, and N. SHEPPARD. J. Chem. Soc. A, 1129 (1970).
23. R. D. ADAMS and F. A. COTTON. Inorg. Chim. Acta, **7**, 153 (1973).

Can. J. Chem. Downloaded from www.nrcresearchpress.com by 210.87.254.6 on 09/05/12
For personal use only.

Synthesis of Nucleotides from O^2,2′-Cyclouridine[1]

KELVIN K. OGILVIE AND DONALD J. IWACHA[2]

Department of Chemistry, University of Manitoba, Winnipeg, Manitoba R3M 2N2

Received November 28, 1973

Procedures for the synthesis of protected O^2,2′-cyclouridines and their incorporation into dinucleoside monophosphates have been developed. The properties of these molecules with snake venom and spleen phosphodiesterases have been investigated. The cyclonucleotides are easily converted into arabinouridine nucleotides and thus provide a convenient route to these compounds.

On a développé des méthodes pour synthèse de cyclouridines-O^2,2′ protégés et pour leur incorporation dans des monophosphates de dinucléoside. On a examiné les propriétés de ces molécules vis à vis le venin de serpent et les phosphodiestérases de la rate. Les cyclonucléotides sont facilement transformés en nucléotides d'arabinouridine et fournissent ainsi une méthode simple d'arrivée à ces composés.

[Traduit par le journal]

Can. J. Chem., **52**, 1787 (1974)

Introduction

A great deal of interest has developed in arabinonucleotides. The activity of arabinonucleotides toward enzymes (1–4), their antitumor and antiviral activities (5, 6), and the role of the arabino 2′-hydroxyl group in nucleotide structure and activity (7, 8) have generated a need for the rapid synthesis of oligoarabinonucleotides. While there have been several reports on the synthesis of nucleotides containing arabinonucleoside units (1, 9, 10), there has been much less attention paid to the stepwise synthesis of oligoarabinonucleotides of predetermined sequence.

It had occurred to us that the cyclopyrimidine nucleosides as intermediates might provide an attractive route to the synthesis of oligoarabinonucleotides. For example O^2,2′-cyclouridine (1), which is readily available in high yield from uridine (11), closely resembles a deoxynucleoside in the carbohydrate portion of the molecule. Further it is known that mild acid (12) or base (13) treatment readily converts **1** into arabinouridine (**2**). Thus it would seem that the versatile methods which are available for the synthesis of oligodeoxynucleotides (14, 15), should be directly applicable to the synthesis of oligocyclopyrimidines which should be easily converted by mild acid or base into the corresponding oligoarabinonucleotides. Further, the cyclonucleotides themselves are of interest due to the modification of the pyrimidine ring.

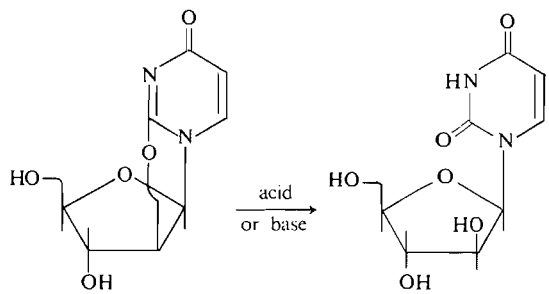

1 **2**

In this manuscript we describe the synthesis of dinucleoside monophosphates containing cyclouridine units, their interaction with spleen and snake venom phosphodiesterases, and, their conversion to arabinouridine nucleotides. A preliminary account of one of these reactions has previously been reported (16).

Except for our initial report (16) O^2,2′-cyclopyrimidines have not been used in a stepwise synthesis of nucleotides. Nagyvary and Provenzale (10, 17) have converted existing pyrimidine nucleotides into arabinonucleotides via the cyclopyrimidine intermediate. Schramm and Ulmer-Schurnbrand (18) have converted uridylic acid into polyarabinouridylic acids via the O^2,2′-cyclouridylate intermediates. Ikehara and Tezuka (19) have described the synthesis of O^6,2′-cyclouridylyl-(3′–5′)-O^6,2′-cyclouridine (**3**).

[1]Part XII in a series on anhydronucleosides. Part XI is ref. 20.

[2]NRCC Scholarship Holder 1968–1972.

Can. J. Chem. Downloaded from www.nrcresearchpress.com by 210.87.254.6 on 09/05/12
For personal use only.

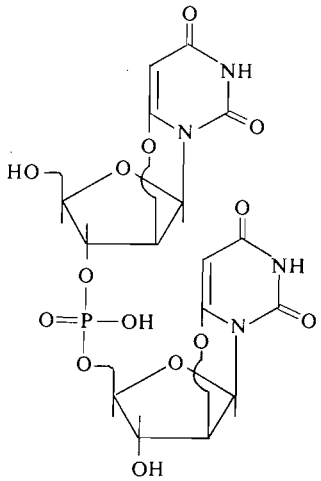

3

The properties of this latter nucleotide toward phosphodiesterases are of interest when compared to the corresponding nucleotide of O^2,2′-cyclouridine (**15**, see below). There have also been two major reports on the incorporation of 8,2′-thioanhydropurine nucleosides into dinucleoside monophosphate units (20, 21).

Results and Discussion

Synthesis of O^2,2′-Cyclouridine Nucleotides

The same general approach as used in the synthesis of deoxynucleotides (14, 15) was considered for the cyclouridines: the phosphorylation of a suitable 5′-protected cyclonucleoside (**4**) followed by condensation with a 3′-protected cyclonucleoside (**6**).

The triphenylmethyl protecting groups have been generally used (22, 23) for selectively protecting the 5′-hydroxyl groups in nucleosides. When **1** was treated with triphenylmethyl chloride (Scheme 1) in hot pyridine **4***a* was not obtained. Rather the cyclolinkage had been destroyed and after removal of the trityl group 2′-chloro-2′-deoxyuridine was obtained. This compound could also be obtained by treating **1** with pyridinium hydrochloride. Compound **4***a* was obtained by treating 5′-*O*-trityluridine (**7***a*) with diphenyl carbonate in DMF (11). The trityl group itself turned out to be too resistant to acid hydrolysis to be generally useful since hydrolysis of the cyclolinkage occurred simultaneously with hydrolysis of the trityl group.

Compound **4***b* was obtained from **7***b* as above or by treating **1** with monomethoxytrityl chloride at room temperature in pyridine. Conditions for removal of the monomethoxytrityl group (80% HOAc, 1½ h at room temperature (23)) did not affect the cyclouridine linkage.

Two base labile protecting groups which have been used in nucleotide synthesis are the acetyl (24) and the β-benzoylpropionyl (25) groups. Both of these groups can be removed with mild base while the β-benzoylpropionyl group can be selectively removed with hydrazine. Thus **4***b* was converted into **5***a* and *b* which yielded **6***a* and *b* on treatment with 80% acetic acid at room temperature.

With the protected cyclouridines **4** and **6** being readily available, the phosphorylation of these compounds was investigated. In the first sequence (Scheme 2), **4***b* and β-cyanoethyl phosphate (βCEP) were condensed using dicyclohexylcarbodiimide (DCC) and the resulting intermediate was condensed directly with isopropylidineuridine (U-ISP) using triisopropylbenzenesulfonyl chloride (TPS). The cyanoethyl derivative of 5′-*O*-monomethoxytrityl-O^2,2′-cyclouridylyl-(3′–5′)-isopropylidineuridine (**8***a*) was obtained in 27% isolated yield. On treatment with 80% acetic acid at room temperature followed by pyridine – ammonium hydroxide (5:2) **8***a* was converted into **9***a*. The treatment of the nucleotides containing cyclouridine units with phosphodiesterases will be discussed together below. Compound **9***a* was converted to **10***a* or *b* on treatment with sodium hydroxide and/or hot acetic acid. Both **10***a* and *b* were completely degraded by phosphodiesterases to the expected products. These results confirm the identity of compound **9**.

The β,β,β-trichloroethyl group has also been used as a phosphate protecting group (26). As a result compound **8***b* was synthesized from **4***b* using a procedure (Scheme 2) very similar to the one used by Neilson and Werstiuk in the ribonucleotide area (27). Removal of the monomethoxytrityl group with acetic acid produced **9***b*. Treatment of **8***b* with hot acetic acid followed by treatment with zinc and acetic acid gave **10***b*.

Compound **9***a* was obtained in an overall yield of 40% from **4***b* by (*1*) phosphorylating **4***b* with trichloroethyl phosphate using TPS, (*2*) removing the trichloroethyl group at this point with copper zinc in DMF, and (*3*) condensing the product with U-ISP and triphenyl phosphine-2,2′-dithiodipyridine (TPP-PDS (28)). Removal of the monomethoxytrityl group gave **9***a*. It is interest-

Can. J. Chem. Downloaded from www.nrcresearchpress.com by 210.87.254.6 on 09/05/12
For personal use only.

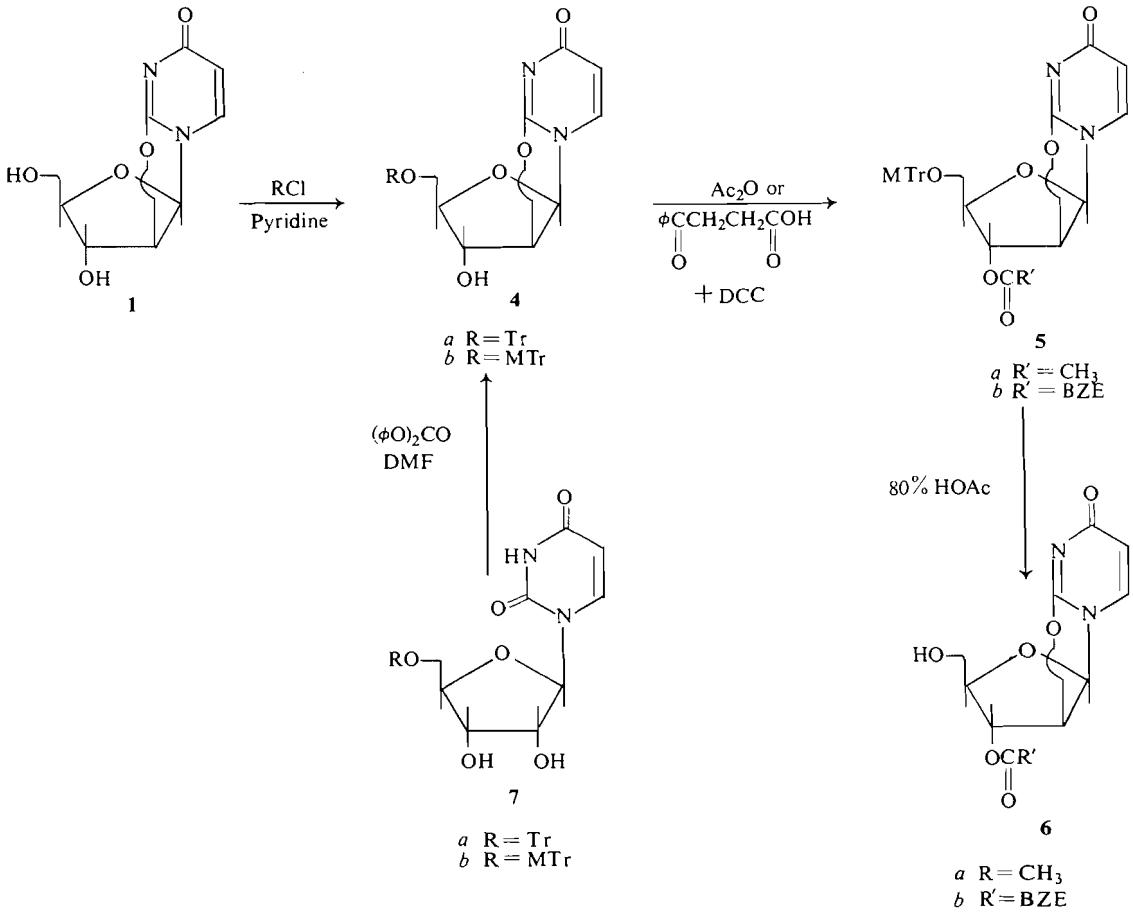

Tr = Triphenylmethyl
MTr = *p*-Methoxyphenyldiphenylmethyl
BZE = β-Benzoylethyl
DCC = Dicyclohexylcarbodiimide

SCHEME 1

ing to note that in these syntheses only small amounts of cyclonucleoside 3′-phosphates were detected in the final products. This might indicate that condensation yields were quite high but poor recovery of products was experienced. Most losses probably occur at extraction stages in the procedures. However, we have not been able to significantly improve isolated yields.

To determine whether the cyclonucleoside unit could be added to the 3′-end of a nucleotide chain, compound **12** was synthesized. The condensation of **11** with **6***a* using TPP-DPS followed by removal of protecting groups gave **12** in 23% yield. Compound **12** was treated with hot acetic acid to produce thymidylyl-(3′–5′)-arabinouridine (TpaU) which gave complete degration to thymidine 3′-phosphate and arabinouridine with spleen enzyme. With snake venom enzyme TpaU was degraded to the extent of 72% after 24 h. The undegraded material was completely degraded with either spleen enzyme or on prolonged treatment with snake venom. Previous reports have indicated (1) that dinucleoside monophosphates containing arabinonucleosides required more enzyme and longer incubation times than the corresponding ribonucleotides in order to achieve complete degradation.

The route to the dicyclouridine monophosphate (**15**) is outlined in Scheme 3. The important intermediate in the reaction is compound **14** which is readily obtained from **13** using copper–

Can. J. Chem. Downloaded from www.nrcresearchpress.com by 210.87.254.6 on 09/05/12
For personal use only.

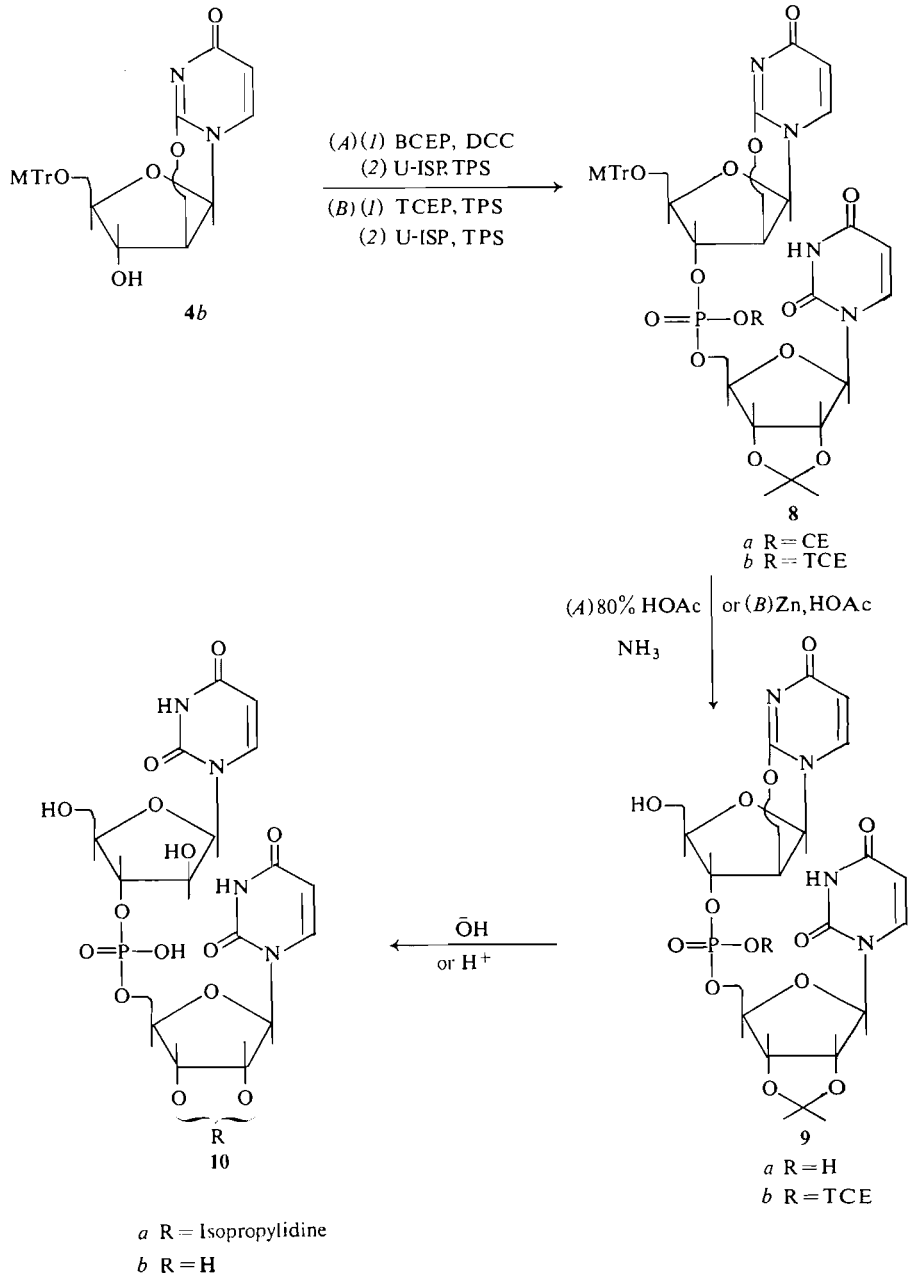

SCHEME 2

zinc in DMF. Compound **13** was prepared by condensing the cyclohexylammonium salt (**26**) of β,β,β-trichloroethyl phosphate with **4***b* using TPS. We were unable to obtain any **13** using either DCC or TPP-DPS as condensing agents. Apparently cyclohexylamine is too strong a base to be displaced using these latter reagents. All three condensing agents gave quantitative phosphorylation of **4***b* by the pyridinium salt of βCEP. However, the conditions required to remove the cyanoethyl group (7 *M* NH_4OH (29) or 1 *N* NaOH (23)) also cause hydrolysis of the cyclonucleoside. Methanol–pyrrolidine (9:1) has been used (30) to remove the cyanoethyl group from phosphodiesters but this reagent also caused degradation of **1**.

Can. J. Chem. Downloaded from www.nrcresearchpress.com by 210.87.254.6 on 09/05/12
For personal use only.

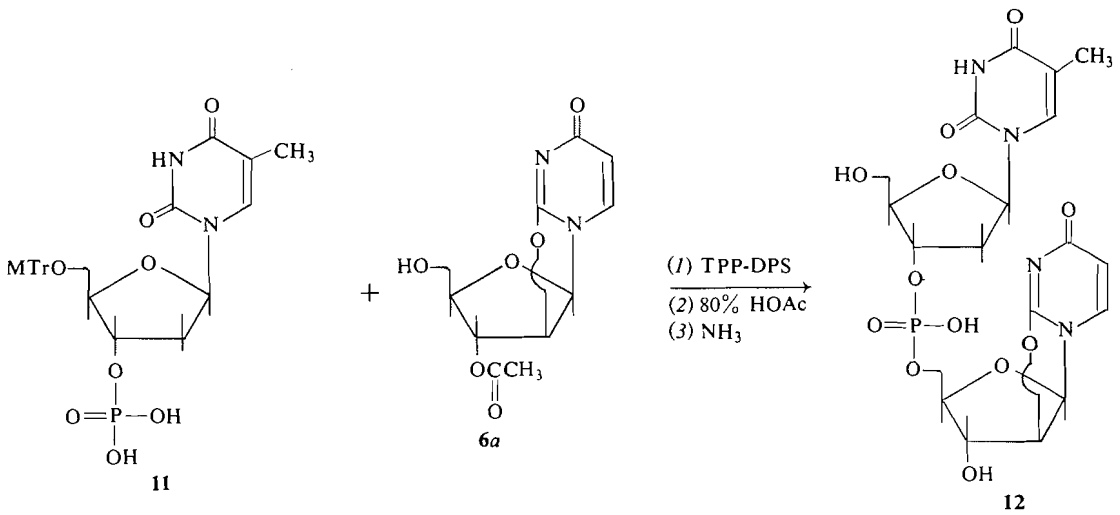

Condensation between **14** and **6***a* followed by removal of protecting groups gave 39 and 46% isolated yields of **15** using DCC or TPP-DPS as condensing agents. Again no cyclouridine 3′-phosphate was observed in the products of the reaction. Compound **15** was converted to arabinouridylyl-(3′–5′)-arabinouridine (**16**) by sodium hydroxide. Compound **16** was completely degraded to arabinouridine 3′-phosphate and arabinouridine by spleen enzyme and was slowly degraded by snake venom enzyme to arabinouridine 5′-phosphate and arabinouridine.

Enzyme Studies on Nucleotides Containing Cyclouridine

cUpU-ISP (**9***a*) was completely degraded by snake venom enzyme to cU and pU-ISP. However, spleen enzyme which operates from the 5′-end of a nucleotide did not degrade the molecule at all. TpcU (**12**) on the other hand was completely degraded by spleen enzyme but was not degraded by snake venom. However after 7 h (at 37 °C and p*H* 9.2) with snake venom 7% of **12** had been converted to the arabinonucleotide which is degraded by the enzyme to thymidine and arabinouridine 5′-phosphate. After 24 h 35% of the cyclouridine nucleotide had been hydrolyzed by the basic medium to the arabinonucleotide which was degraded by the enzyme. The nucleotide cUpcU (**15**) was not degraded by either spleen or snake venom. Clearly the presence of a cU moiety in the chain blocks the recognition ability of the enzymes and prevents degradation. These results make an interesting contrast to those obtained by Ikehara and Tezuka (19) for compound **3**; they reported that this molecule was degraded by snake venom phosphodiesterase.

The difference in reactivities of **3** and **15** might imply that snake venom phosphodiesterase requires the anti conformation of the base for recognition. In **3** the base is nearly *anti* while in **15** it is close to the *syn* conformation. Of course there is a significant change in electronic and H-bonding characteristics of **15** as compared to **3**. Further it has been observed that the cyclopurine nucleotides are not substrates for either snake venom or spleen phosphodiesterases (20). In the cyclopurines the base is constrained in a near *anti* conformation.

We have found (35) that **12**, **1**, and **9***a* are weak competitive inhibitors of snake venom phosphodiesterase with their effectiveness as inhibitors being in the ratio of 1:2:25. They are also weak competitive inhibitors of spleen phosphodiesterase in the ratio 10:1.2:1.

In summary, methods have been developed which incorporate cyclouridine into dinucleoside monophosphate units. These compounds are of interest as analogues of natural nucleotides and provide a convenient route to arabinouridine nucleotides.

Experimental

A complete description of all our general methods, reagents and chemicals, enzyme assays, and general procedures has been given in ref. 20 with the following exceptions.

General Methods

Column chromatography was carried out on silica gel

Can. J. Chem. Downloaded from www.nrcresearchpress.com by 210.87.254.6 on 09/05/12
For personal use only.

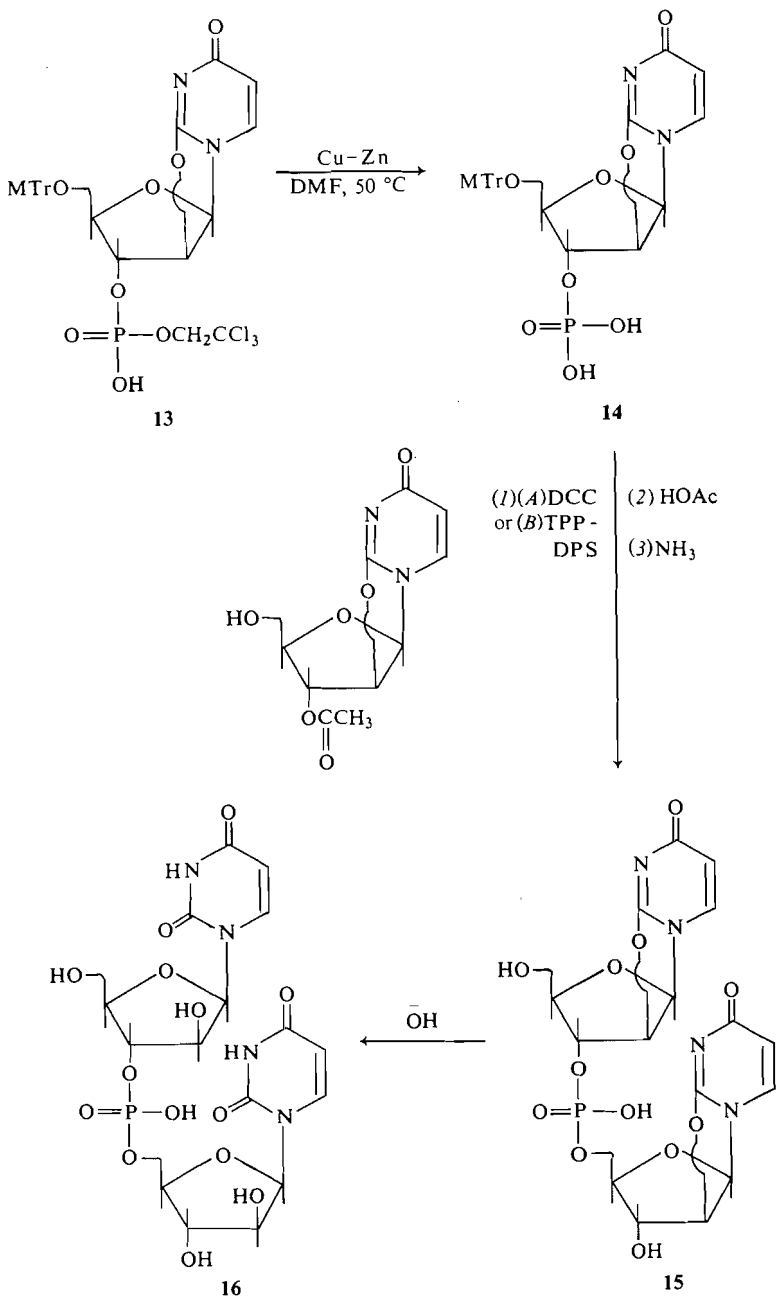

SCHEME 3

(60–200 mesh) from Fisher Scientific. A slurry of silica gel was allowed to settle under its own weight at the desired flow rate. The eluant was monitored by thin-layer chromatography.

For aqueous solutions containing nucleosides, the absorption maxima and corresponding extinction coefficients used were: O^2,2′-cyclouridine (250 nm, 7820 (13)); uridine (262 nm, 10 100 (30)); arabinouridine (263 nm, 10 500 (12)); and thymidine (267 nm, 9650 (30)). The term O.D. unit refers to the extinction of a nucleotide solution at neutral p*H* in 1 ml of solution using a 1-cm light path quartz cell. A number in subscript refers to the wavelength used in determination of the O.D. unit. Mass spectra were obtained on a Finnigan 1015 mass spectrometer.

Reagents and Chemicals

The dicyclohexylammonium salt of β,β,β-trichloroethyl

Can. J. Chem. Downloaded from www.nrcresearchpress.com by 210.87.254.6 on 09/05/12
For personal use only.

Can. J. Chem. Downloaded from www.nrcresearchpress.com by 210.87.254.6 on 09/05/12
For personal use only.

phosphate was prepared by dropping the phosphorodichloridate into a cooled solution of water–dioxane (1:1). After removal of the solvents, the residue was dissolved in ethanol–dioxane (1:1) and cyclohexylamine was added. The precipitated product was recrystallized from ethanol–dioxane (m.p. 194–198 °C (26)).

O^2,2′-Cyclouridine (m.p. 244–248 °C, 83% (11)), 5′-*O*-trityluridine (m.p. 114.5–116 °C, 89%, (22)), 5′-*O*-monomethoxytrityluridine (m.p. 98–102 °C, 76%, (31)), 2′,3′-*O*-isopropylidineuridine (m.p. 161–162.5 °C, 69%, (32)), and 5′-*O*-monomethoxytritylthymidine (m.p. 103–105 °C, 85%, (23)) were prepared by established procedures.

2′-Chloro-2′-deoxyuridine (dU-Cl)

(*A*) O^2,2′-Cyclouridine (3.4 g, 15 mmol) and trityl chloride (4.6 g, 16.1 mmol) were dissolved in pyridine (50 ml) and the solution was refluxed for 2 h. The solution was poured into ice water (500 ml) with stirring. The precipitate was collected by filtration and washed with petroleum ether (40 ml). The precipitate was dissolved in chloroform and dried over anhydrous sodium sulfate The solvents were removed under reduced pressure and the residue was crystallized from ethyl alcohol to yield 3.9 g (52%) of material (m.p. 164–166.5 °C, R_f 0.70 (ethylacetate)) assumed to be 5′-*O*-trityl-2′-chloro-2′-deoxyuridine ($\lambda_{max}^{(EtOH)}$, 259 nm (10 700)). A sample of this material (200 mg) was dissolved in 80% acetic acid and the solution heated on a steam bath for 20 min. The solvents were removed at reduced pressure and the last traces of acetic acid were removed by evaporation of ethanol. The residue was crystallized from ethanol (EtOH) to yield 69 mg (66%) of 2′-chloro-2′-deoxyuridine (m.p. 202–206 °C, lit. (33) m.p. 205–206 °C; R_f 0.21 (ethylacetate); $\lambda_{max}^{(EtOH)}$ 260 nm).

(*B*) O^2,2′-Cyclouridine (50 mg) was dissolved in pyridine (4 ml), 1 drop of concentrated hydrochloric acid was added, and the solution was heated on a steam bath for 2 h. The solvents were removed at reduced pressure and the residue was crystallized from ethyl acetate to give 25 mg of dU-Cl (mixture m.p. 200–205 °C).

As further proof of the identity of dU-Cl, 25 mg of the material and methanol (0.3 ml) containing sodium methoxide (8.1 mg) were dissolved in dimethylformamide and the solution was heated at 70–75 °C for 2 h. The solution was cooled and triturated with ether – petroleum ether (2:3, 50 ml). The solvent was decanted and the residue crystallized from ethanol to give O^2,2′-cyclouridine (5.2 mg, 24%).

5′-O-Trityl-O^2,2′-cyclouridine (4a)

5′-*O*-Trityluridine (670 mg, 1.36 mmol) was dissolved in dimethylformamide (1.5 ml) and treated with diphenyl carbonate (390 mg, 1.8 mmol) and sodium bicarbonate (10 mg). The mixture was heated at 150° for 30 min and then was poured into ether. The precipitated gum was crystallized from ethanol to yield 400 mg (62.5%) of **4***a* (m.p. 2.5-218°, lit. (13) m.p. 217–219 °C).

Stability of the Cyclolinkage to Acid

10% Acetic Acid

Compound **4***a* (10 mg) was dissolved in 10% acetic acid (1 ml) and the solution was heated on a steam bath for 10 min. In addition to unreacted **4***a*, two non-trityl containing nucleosides were present and identified as **1** and **2** in the ratio of 2:1.

80% Acetic Acid

Compound **4***a* (10 mg) was dissolved in 80% acetic acid (1 ml) and the solution was stirred at room temperature for 21 h. In addition to **4***a*, compounds **1** and **2** were present in a ratio of 7:1.

5′-O-Monomethoxytrityl-O^2,2′-cyclouridine (4b)

(*A*) O^2,2′-Cyclouridine (4.35 g, 19.2 mmol) and monomethoxytrityl chloride (6.0 g, 19.5 mmol) were stirred in pyridine (100 ml) for 4 days. The solvent was removed at reduced pressure and the residue was dissolved in a mixture of chloroform–water (600 ml, 1:1). The chloroform layer was separated and washed with water (2 × 50 ml). The organic solution was dried over anhydrous sodium sulfate and then concentrated. Crystallization occurred to yield 5.70 g (60%) of **4***b*; m.p. 155–158 °C; $\lambda_{max}^{(EtOH)}$ 229 nm (16 800); R_f 0.26 (tetrahydrofuran); principal bands in the i.r. spectrum (KBr disk) occurred at 6.06, 6.13, and 14.2 μ.

Anal. Calcd. for $C_{29}H_{26}H_2O_6$: C, 69.87; H, 5.26; N, 5.62. Found: C, 70.23; H, 5.28; N, 5.53.

(*B*) 5′-*O*-Monomethoxytrityluridine (730 mg, 1.41 mmol) was dissolved in dimethylformamide (0.7 ml) and was treated with diphenyl carbonate (392 mg, 1.82 mmol) and sodium bicarbonate (7 mg). The mixture was heated at 150° for 30 min. After cooling, the mixture was poured into ether. The precipitated gum was crystallized from ethanol to yield 91 mg of **4***b*.

5′-O-Monomethoxytrityl-3′-O-acetyl-O^2,2′-cyclouridine (5a)

Compound **4***b* (2.5 g, 5.0 mmol) and acetic anhydride (0.8 ml, 8.5 mmol) were dissolved in pyridine (15 ml) and the solution was stirred for 18 h and poured into ice water (500 ml) with stirring. The precipitated product was collected by filtration and dissolved in chloroform. Concentration of the solution to a small volume followed by the addition of hexane yielded 2.57 g (95%) of **5***a*; m.p. 104–107 °C; $\lambda_{max}^{(EtOH)}$ 230 nm (19 000); R_f 0.36 (THF); principal bands in the i.r. spectrum (KBr disk) occurred at 5.70, 6.08, and 14.2 μ.

Anal. Calcd. for $C_{31}H_{28}N_2O_7$: C, 68.88; H, 5.22; N, 5.18. Found: C, 68.78; H, 5.14; N, 5.08.

3′-O-Acetyl-O^2,2′-cyclouridine (6a)

Compound **4***b* (21.7 g, 40 mmol) was dissolved in 80% acetic acid and the solution was stirred for 4 h. The solvent was removed at reduced pressure and the last trace of acetic acid was removed by evaporation of ethanol. The residue was dissolved in ethanol–chloroform and the solution was poured into ether. The precipitate was filtered to yield 8.35 g (83%) of **6***a*; m.p. 205–208 °C; $\lambda_{max}^{(EtOH)}$ 249 (8220) and 224 nm (9600); R_f 0.13 (THF); principal band in the i.r. spectrum (KBr disk) occurred at 5.73 and 6.10 μ.

Anal. Calcd. for $C_{11}H_{12}N_2O_6$: C, 49.25; H, 4.51; N, 10.44. Found: C, 49.10; H, 4.50; N, 10.26.

5′-O-Monomethoxytrityl-3′-O-(β-benzoylpropionyl)-O^2,2′-cyclouridine (5b)

Compound **4***b* (4.0 g, 9.0 mmol), 3-benzoylpropionic acid (4.28 g, 24.0 mmol), and dicyclohexylcarbodiimide (6.6 g, 32.0 mmol) were dissolved in pyridine (80 ml) and the solution was stirred for 13 h. Cold water (24 ml) was added and the mixture was stirred for 6 h. The insoluble dicyclohexylurea was removed by filtration and was

Can. J. Chem. Downloaded from www.nrcresearchpress.com by 210.87.254.6 on 09/05/12
For personal use only.

washed with pyridine–water (1:1, 50 ml). The filtrate and washings were extracted with chloroform (3 × 200 ml) and the aqueous layer discarded. The chloroform layer was extracted with saturated sodium bicarbonate solution (2 × 150 ml), washed once with water, concentrated to a small volume, and applied to a silica gel column (3.5 × 46 cm) in ether. The column was eluted first with ether (4.5 l) followed by tetrahydrofuran (3.5 l). Pure **5***b* was obtained in the tetrahydrofuran fractions. Concentration of the solution followed by precipitation of the product with hexane yielded 4.3 g (82.5%) of **5***b*; m.p. 94.97 °C; $\lambda_{max}^{(EtOH)}$ 236 nm (29 000); R_f 0.42 (THF); principal bands in the i.r. spectrum occurred at 5.71, 5.93, 6.06, and 14.2 μ.

Anal. Calcd. for $C_{39}H_{34}N_2O_8$: C, 71.11; H, 5.20; N, 4.25. Found: C, 70.68; H, 5.27; N, 4.42.

3′-O-(β-Benzoylpropionyl)-O²,2′-cyclouridine (6b)

Compound **5***b* (4.02 g, 6.1 mmol) was dissolved in 80% acetic acid and the solution was stirred for 4.5 h. The solvent was removed at reduced pressure and the last trace of acetic acid was removed by evaporation of ethanol. The residue was dissolved in ethanol and applied to 15 thick-layer plates. The plates were developed in ethyl acetate and in tetrahydrofuran. The nucleoside band at R_f 0.15 was eluted from the plates with tetrahydrofuran. Concentration of the solution followed by addition of hexane to precipitate the product yielded **6***b* (2 g, 85%); m.p. 178–180 °C; $\lambda_{max}^{(EtOH)}$ 244 and 18 700); R_f 0.16 (THF); principal bands in the i.r. spectrum occurred at 5.72, 5.92, 6.17, and 13.3 μ.

Anal. Calcd. for $C_{19}H_{18}N_2O_7 \cdot \frac{1}{2}H_2O$: C, 57.72; H, 4.84; N, 7.08. Found: C, 57.61; H, 4.70; N, 7.03.

The β-Cyanoethyl Derivative of 5′-O-Monomethoxytrityl-O²,2′-cyclouridylyl-(3′–5′)-2′,3′-O-isopropylideneuridine (8a)

β-Cyanoethyl phosphate (9.0 mmol) was dried by evaporation of pyridine (2 × 10 ml). 5′-*O*-Monomethoxytrityl-*O*²,2′-cyclouridine (1.0 g, 2.0 mmol), dicyclohexylcarbodiimide (6.6 g, 32 mmol), and pyridine (10 ml) were added and the mixture was stirred for 3 days. After the addition of cold water (14 ml), stirring was continued for 16 h. The mixture was filtered to remove dicyclohexylurea and the residue was washed with pyridine–water (1:1, 35 ml). The combined filtrates were extracted with chloroform–ethanol (5:1, 400 ml). After separation of the layers, the organic layer was concentrated to a volume of ~75 ml. The organic layer was extracted with saturated aqueous sodium chloride (10 ml) and then concentrated at reduced pressure. Pyridine (10 ml) was added to dissolve the MTr-cUp(CE). The mixture was filtered to remove undissolved salts and dicyclohexylurea and the filtrate was concentrated to a gum at reduced pressure.

The gum was dried by evaporation of pyridine (2 × 10 ml). 2′,3′-*O*-Isopropylideneuridine (900 mg, 3.16 mmol) was added and the mixture was dried by evaporation of pyridine (2 × 10 ml). Triisopropylbenzenesulfonyl chloride (1.2 g, 4.0 mmol) and pyridine (10 ml) were added and the solution was concentrated to a volume of ~5 ml. The solution was stirred for 18 h. Pyridine (7 ml) was added to increase the volume of the solution. After the addition of cold water (8 ml), stirring was continued for 1 h. The solution was extracted with chloroform and the layers were separated. The organic layer was concentrated to a small volume and the solution was poured into ether with stirring. The residue was dissolved in tetrahydrofuran and applied to 20 thick-layer, plates. The plates were developed in ethyl acetate and tetrahydrofuran. The nucleotide band with R_f 0.23 was eluted with tetrahydrofuran and ethanol followed by concentration and addition of hexane to yield 480 mg (27%) of **8***a*; m.p. 140–150 °C with softening at 134 °C (34); $\lambda_{max}^{(EtOH)}$ 232 (25 500), 250 nm (sh); R_f^A 0.94; principal bands in the i.r. spectrum (KBr disk) occurred at 4.42, 5.89, 6.05, and 14.1 μ.

Anal. Calcd. for $C_{44}H_{44}N_5O_{14}P$: C, 58.86; H, 4.94; N, 7.80. Found: C, 58.63; H, 5.03; N, 7.75.

O²,2′-Cyclouridylyl-(3′–5′)-2′,3′-O-isopropylideneuridine (9a)

Compound **8***a* (30 mg) was dissolved in 80% acetic acid (0.5 ml) and the solution was stirred for 2 h. The solvent was removed at reduced pressure. The residue was dissolved in pyridine ammonium hydroxide (5:2) and the solution was stirred for 30 min. The solution was applied to Whatman papers and developed in Solvent B. The product **9***a* (R_f 0.69) was eluted with water and applied to Whatman electrophoretic paper. The product (R_m^{Tp} 0.33) was eluted with water and identified through its paper chromatographic and electrophoretic properties and its u.v. spectrum (Table 1). Snake venom enzyme degraded **9***a* to cU (R_f^B 0.71; 2.80 O.D.$_{250}$ units) and isopropylidineuridine 5′-phosphate (pU-ISP) (R_f^B 0.60; 3.65 O.D.$_{260}$ units) with pU-ISP/cU = 1.01. Spleen enzyme did not degrade **9***a* at all. The structure of **9***a* was further confirmed by its conversion to the arabinonucleotides **10***a* and **10***b* below.

Arabinouridylyl-(3′–5′)-2′,3′-O-isopropylideneuridine (10a)

Compound **9***a* (4.80 O.D.$_{255}$ units) was dissolved in 1 *N* sodium hydroxide and the solution was stirred for 1 h. The solution was neutralized with Dowex 50W-X8 resin, filtered, and applied to Whatman paper developed in solvent A. The product (R_f^A 0.28) was eluted with water and characterized by its paper chromatographic and electrophoretic properties (Table 1) and its hydrolysis by

TABLE 1. Physical properties of cyclouridine nucleotides

Compound	R_f Values on paper chromatography* Solvent A	Solvent B	R_m†	$\lambda_{max}^{(H_2O)}$ (nm)
9*a*	0.30	0.66	0.35	255
10*a*	0.28	0.66	0.38	262
10*b*	0.15	0.60	0.38	262
12	0.17	0.61	0.35	260
TpaU	0.14	0.60	0.36	264
15	—	—	0.37	250, 223
16	0.16	—	0.36	263

*Whatman 3 MM paper. Solvent A, isopropyl alcohol – concentrated ammonium hydroxide – water (7:1:2, v/v/v); solvent B, ethanol–water (7:3, v/v).

†Electrophoretic mobility relative to thymidine 3′-phosphate (Tp) in triethylammonium bicarbonate buffer (p*H* 7.5).

Can. J. Chem. Downloaded from www.nrcresearchpress.com by 210.87.254.6 on 09/05/12
For personal use only.

spleen phosphodiesterase. Spleen enzyme degraded **10***a* to arabinouridine 3′-phosphate (aUp) (2.45 O.D.$_{263}$ units; R_f^A 0.03) and isopropylidineuridine (U-ISP) (2.17 O.D.$_{262}$ units; R_f^A 0.72) with aUp/U-ISP = 1.1.

*Arabinouridylyl-(3′–5′)-uridine (**10***b*)

(*A*) Compound **8***a* (16 mg) was dissolved in 80% acetic acid (5 ml) and the solution was refluxed for 2 h. The solvent was removed at reduced pressure, the residue was dissolved in pyridine – ammonium hydroxide (5:2, 2 ml), applied to Whatman paper, and developed in solvent A. The product **10***b* was eluted from the paper with water and characterized by its chromatographic and electrophoretic properties and by its u.v. spectrum (Table 1). Snake venom degraded **10***b* to arabinouridine (**2**) (5.24 O.D.$_{263}$ units; R_f^A 0.49) and uridine 5′-phosphate (pU) (5.79 O.D.$_{262}$ units; R_f^A 0.04) with pU/**2** = 1.1.

(*B*) Compound **9***a* was heated with 80% acetic acid on a steam bath for 2.5 h. The product, **10***b*, was identical with the material produced by method A above.

The β,β,β-*Trichloroethyl Ester of 5′-O-Monomethoxytrityl-O*^{2}*,2′-cyclouridylyl-(3′–5′)-2′,3′-O-isopropylideneuridine (**8***b*)

β,β,β-Trichloroethyl phosphate (420 mg, 1.0 mmol cyclohexylammonium salt) was dissolved in dry pyridine (25 ml) and converted to the pyridinium salt by evaporation of pyridine (2 × 25 ml). Triisopropylbenzenesulfonyl chloride (450 mg, 1.5 mmol) and pyridine (25 ml) were added and the solution was stirred for 30 min. 5′-*O*-Monomethoxytrityl-*O*^{2},2′-cyclouridine (250 mg, 0.5 mmol) was added and the solution was stirred for 4 h. After the addition of more TPS (225 mg, 0.75 mmol), the solution was stirred for 17 h. The solution was cooled, cold water (5 ml) was added, and the resulting solution was stirred for 30 min and then poured into ice water (50 ml). The solution was extracted with methylene chloride (4 × 25 ml) and the combined methylene chloride extracts were washed with water (4 × 25 ml) and concentrated to a gum at reduced pressure.

The gum was dried by evaporation of pyridine at reduced pressure (2 × 25 ml). TPS (225 mg, 0.75 mmol) and pyridine (25 ml) were added and the solution was stirred for 30 min. 2′,3′-*O*-Isopropylideneuridine (280 mg, 1.0 mmol) was added and the solution was stirred for 6 h. After the addition of more TPS (100 mg, 0.30 mmol), stirring was continued for 19 h. Cold water (5 ml) was added and after stirring for 30 min the solution was poured into ice water (50 ml). After extraction with methylene chloride (4 × 25 ml), the combined methylene chloride extracts were washed with water (4 × 25 ml) and concentrated at reduced pressure to a small volume. The solution was applied to 10 thick-layer plates and developed in ethyl acetate and tetrahydrofuran. The band with R_f 0.43 was eluted with tetrahydrofuran which was concentrated and upon the addition of hexane a white precipitate formed, identified as **8***b* (111 mg, 23%, m.p. 140–150 °C). Physical properties are listed in Table 1.

Anal. Calcd. for $C_{43}H_{42}Cl_3N_4O_{14}P$: C, 52.91; H, 4.34; N, 5.74. Found: C, 53.06; H, 4.46; N, 5.61.

The β,β,β-*Trichloroethyl Derivative of O*^{2}*,2′-Cyclouridylyl-(3′–5′)-2′,3′-O-isopropylidineuridine (**9***b*)

Compound **8***b* (48 mg) was dissolved in 80% acetic acid and the solution was stirred for 4.5 h. After removal of the solvent at reduced pressure the residue was dissolved in a small volume of ethanol and applied to Whatman paper which was developed in solvent C. The nucleotide band appeared at R_f^C 0.62 and was eluted with water which on lyophilization gave **9***b* (30 mg, 86%); R_f 0.20 (THF); $\lambda_{max}^{(H_2O)}$ 255 nm. The structure was further confirmed by conversion of **9***b* to **9***a* below.

O^2*,2′-Cyclouridylyl-(3′–5′)-2′,3′-O-isopropylideneuridine (**9***a*)

Compound **9***b* (4.6 mg) was dissolved in 80% acetic acid (0.5 ml). Zinc (5 mg) was added and the mixture was stirred for 1 h. After filtration, the solvent was evaporated at reduced pressure. The residue was dissolved in ethanol–water and applied to Whatman electrophoresis paper. A nucleotide band occurred at R_m^{Tp} 0.28 and was eluted with water to yield **9***a*. Spleen enzyme did not affect this nucleotide but snake venom degraded a sample to **1** (3.5 O.D.$_{250}$ units) and pU-ISP (4.5 O.D.$_{262}$ units) with pU-ISP/**1** = 0.99.

One-half of the above product was hydrolyzed with base to **10***a* which was completely degraded by both snake and spleen enzymes in the correct manner and ratios.

*Direct Synthesis of **9***a *from **4***b

Compound **4***b* (50 mg) was phosphorylated with β,β,β-trichloroethyl phosphate (cyclohexylammonium salt) using TPS (150 mg) in pyridine (5 ml) as described above. After quenching the reaction in the normal way the product was extracted into methylene chloride. Thin-layer chromatography showed no **4***b* remaining. After removal of solvents, the residue was treated with Cu–Zn in DMF at 50 °C for 30 min. The solution was filtered, the residue washed with 50% aqueous pyridine (100 ml), and the combined washings and filtrate were passed through a Dowex 50W-X8 (pyridinium form) column. The eluant was concentrated to a small volume and added dropwise to ether (250 ml). The precipitate was collected by filtration and dried overnight over P_2O_5.

This residue was further dried by evaporation of pyridine (3 × 2 ml) and condensed with isopropylidineuridine (0.11 mmol) using triphenylphosphine (130 mg) and 2,2′-dithiodipyridine (110 mg) in pyridine (1 ml) at room temperature. After 18 h, water (2 ml) was added and stirring continued for 2 h. The reaction mixture was then poured into ether, the solvents decanted, and the residue treated with 80% HOAc for 4 h at room temperature. The solution was applied to Whatman paper which was developed in solvent C. The nucleotide band at R_f^C 0.12 was eluted and identified as **9***a* (0.04 mmol determined spectroscopically). Very little (< 10%) cUp was detected. Presumably most of the loss of material occurs at the extraction steps.

Thymidylyl-(3′–5′)-O^2*,2′-cyclouridine (TpcU, **12**)*

5′-*O*-Monomethoxytritylthymidine (80 mg, 0.15 mmol) was phosphorylated with β-cyanoethyl phosphate (0.3 mmol) and mesitylenesulfonyl chloride (MS) (130 mg, 0.6 mmol) in the usual way. The cyanoethyl group was removed with 7 *M* ammonium hydroxide at 70 °C for 1.5 h. The product was dried by evaporation of pyridine and condensed with **6***a* (20 mg, 0.3 mmol) in pyridine (0.7 ml). The solution was stirred for 6.5 h. After the addition of

Can. J. Chem. Downloaded from www.nrcresearchpress.com by 210.87.254.6 on 09/05/12
For personal use only.

cold water (0.7 ml), stirring was continued for 16 h whereupon the solvents were removed at reduced pressure and the residue was dissolved in chloroform (4 ml). The chloroform solution was washed with water (3 × 1 ml) and then evaporated. The residue was treated with 80% HOAc at room temperature for 2.5 h to remove the trityl group and the products were isolated by chromatography on Whatman paper in solvent B. The product appeared at R_f^B 0.52 and was separated from a trace of Tp by preparative paper electrophoresis at p*H* 7.5. To remove the acetyl group, this product was treated with 15% ammonium hydroxide in ethanol for 90 min. Removal of solvents gave TpcU (**12**, 23%, see Table 1).

Compound **12** was completely degraded by spleen enzyme to Tp (R_f^B 0.58; 7.75 O.D.$_{267}$ units) and cU (R_f^B 0.69; 6.28 O.D.$_{250}$ units) with Tp/cU = 1.01. Incubation of TpcU with snake venom enzyme partially hydrolyzed the TpcU to TpaU and yielded TpcU (R_f^B 0.61; 8.2 O.D.$_{260}$ units; 93%), and paU (R_f^B 0.44; 0.4 O.D.$_{263}$ units) and T (R_f^B 0.75; 0.3 O.D.$_{267}$ units) with paU/T = 1.23. Incubation of **12** with snake venom for 24 h caused a 35% hydrolysis to TpaU which was degraded to T and paU with paU/T = 0.86.

Thymidylyl-(3′–5′)-arabinouridine (TpaU)

Compound **12** was treated with 80% HOAc on a steam bath for 2 h. and the product, TpaU, was isolated by paper chromatography in solvent A. The product was completely degraded by spleen enzyme to Tp (R_f^A 0.05; 4.87 O.D.$_{267}$ units) and arabinouridine (aU) (R_f^A 0.52; 4.80 O.D.$_{263}$ units) with Tp/aU = 1.1. TpaU was slowly hydrolyzed to arabinouridine 5′-phosphate (paU) (R_f^A 0.02; $\lambda_{max}^{(H_2O)}$ 263 nm) and T (R_f^A 0.63) with paU/T = 0.99. For example after 24 h, TpaU was 72% hydrolyzed by snake venom. The remaining material could be completely degraded either by further treatment with snake venom or by treatment with spleen enzyme and to the expected products.

Studies on the Phosphorylation of 4b

(*A*) Compound **4***a* (100 mg, 0.2 mmol) and β,β,β-trichloroethyl phosphate (cyclohexylammonium salt, 0.4 mmol) were condensed using TPS (0.8 mmol) in pyridine (10 ml) as described previously. The product was treated with Cu–Zn in DMF at 50 °C for 30 min. Paper electrophoresis showed complete conversion of the initial product **13** (R_m^{Tp} 0.13) to compound **14** (R_m^{Tp} 0.55). No other nucleoside material was present. Compound **14** was converted to cyclouridine 3′-phosphate (R_m^{Tp} 1.0; $\lambda_{max}^{(H_2O)}$ 250 nm) on treatment with 80% HOAc at room temperature for 3 h.

(*B*) Compound **4***b* could not be phosphorylated with β,β,β-trichloroethyl phosphate (cyclohexylammonium salt) using either DCC or TPP-DPS as condensing agents in the standard procedures.

(*C*) All three condensing agents (TPS, DCC, and TPP-DPS) quantitatively phosphorylated **4***b* using the pyridinium salt of β-cyanoethyl phosphate in the standard procedures.

Treatment of Cyclouridine with Methanol–Pyrrolidine

Cyclouridine (5 mg) was treated with methanol–pyrrolidine (9:1) under gentle reflux (80–85 °C) for 4 h. After 4 h the products were isolated by chromatography on Whatman paper in solvent C. None of the products contained the cyclouridine structure since the $\lambda_{max}^{(H_2O)}$ of all products was near 260 and not 250 nm.

*Synthesis of O^2,2′-Cyclouridylyl-(3′–5′)-O^2,2′-cyclouridine (**15**, cUpcU)*

(*A*) 5′-*O*-Monomethoxytrityl-O^2,2′-cyclouridine (250 mg, 0.5 mmol) was phosphorylated with β,β,β-trichloroethyl phosphate (cyclohexylammonium salt) (1.0 mmol) using triisopropylbenzenesulfonyl chloride (2.0 mmol) in pyridine (25 ml) in the usual manner. After the addition of cold water (5 ml), the solution was poured into ice water (50 ml), and the product extracted into methylene chloride (4 × 25 ml) which was washed with water (4 × 25 ml). The solvents were removed by evaporation at reduced pressure and the residue was dissolved in dimethylformamide (10 ml); Cu–Zn was added and the mixture was heated, with stirring, at 50° for 30 min. After filtration, the residue was washed with 50% aqueous pyridine (25 ml). The combined filtrates were applied to a Dowex 50W-X8 (pyridinium form) column and the product, MMTr-cUp, was eluted with 50% aqueous pyridine (200 ml). The solution was concentrated to a small volume and slowly dropped into ether (500 ml) with stirring. The ether was decanted and the residue was dissolved in pyridine (10 ml).

The solvent was removed by evaporation at reduced pressure and the gum was dried by evaporation of pyridine (3 × 10 ml), 3′-*O*-Acetyl-O^2,2′-cyclouridine (125 mg, 0.46 mmol) was added and the compounds were dried by evaporation of pyridine (1 × 10 ml). Dicyclohexylcarbodiimide (10 mmol) and pyridine (10 ml) were added and the mixture was stirred for 11 days. Cold water (10 ml) was added and stirring was continued for 12 h. After filtration, the residue was washed with 50% aqueous pyridine (10 ml) and the combined filtrates were evaporated at reduced pressure. The residue was dissolved in 80% acetic acid and the solution was stirred for 4 h. The solvent was removed by evaporation at reduced pressure and the residue was dissolved in ammonium hydroxide – ethanol (1:3). After stirring for 1 h, the solution was applied to Whatman papers and developed in solvent C for 3 days. The nucleotide band with R_f^C 0.16 was eluted with water and lyophilized to yield 93 mg (39%) of cUpcU ($\lambda_{max}^{(H_2O)}$ 250 and 223 nm, and λ_{min} 240 and 213 nm). The product was not degraded by spleen or snake venom phosphodiesterase.

(*B*) 5′-*O*-Monomethoxytrityl-O^2,2′-cyclouridine 3′-phosphate (MTr-cUp) was synthesized by phosphorylation of 5′-*O*-monomethoxytrityl-O^2,2′-cyclouridine (250 nm, 0.5 mmol) with trichloroethyl phosphate (cyclohexylammonium salt, 1 mmol) followed by treatment with Cu–Zn in dimethylformamide at 50° in the manner described in method *A*.

MMTr-cUp was dried by evaporation of pyridine (3 × 10 ml), 3′-*O*-acetyl-O^2,2′-cyclouridine (270 mg, 1.0 mmol) was added, and the mixture was dried by evaporation of pyridine (1 × 10 ml). Triphenylphosphine and 2,2′-dithiodipyridine (2.5 mmol each) were added with pyridine (5 ml) and the solution was stirred for 12 h. Cold water (2 ml) was added to the cooled solution and stirring was continued for 2 h. The solution was dropped into ether with stirring and the precipitate was dissolved in 80% acetic acid. The solution was stirred for 4 h, the solvent was removed by evaporation at reduced pressure,

and the residue was dissolved in ammonium hydroxide – ethanol (1:3). After stirring for 1 h, the solution was chromatographed on Whatman paper in solvent C for 3 days. The nucleotide band with R_f^C 0.12 was eluted with water and lyophilized to yield 118 mg (46%) of cUpcU ($\lambda_{max}^{(H_2O)}$ 250 and 223 nm, and λ_{min} 240 and 214 nm). The product was not degraded by snake venom or spleen phosphodiesterase.

*Arabinouridylyl-(3′–5′)-arabinouridine (aUpaU, **16**)*

cUpcU (15.8 mg) was dissolved in 2 *N* sodium hydroxide (1 ml) and the solution was stirred for 20 min. After neutralization with Dowex 50W-X8 resin (pyridinium form) and filtration, the solution was applied to Whatman papers and developed in solvent A. The band with R_f^A 0.15 was eluted with water to yield aUpaU ($\lambda_{max}^{(H_2O)}$ 260 nm). Incubation of aUpaU (10 O.D. units) with spleen enzyme gave complete degradation to aUp (R_f^A 0.09; 5.01 O.D. units) and aU (R_f^A 0.59; 4.84 O.D. units) with aUp/aU = 1.03. Incubation with snake venom enzyme (for 7 h) gave paU (R_f^A 0.07; 1.63 O.D. units), aU (R_f^A 0.55; 1.71 O.D. units), and aUpaU (R_f^A 0.16; 6.76 O.D. units; 68%) with paU/aU = 0.95. The undegraded aUpaU could be completely degraded either by prolonged treatment with snake venom enzyme or by spleen enzyme to give the expected products.

Effect of Cyclouridines on Snake Venom Enzymes (35)

Snake Venom

The *p*-nitrophenyl ester of thymidine 5′-phosphate was used as reference compound for snake venom hydrolyses ($K_m = 4.78 \times 10^{-4}$ *M* with $V_{max} = 7.25$ μmol/min, mg). Lineweaver–Burke plots and regression line analysis showed that **12**, **1**, and **9***a* were all weak, competitive inhibitors of snake venom phosphodiesterase with **12** < **1** < **9***a* (1:2:25).

Spleen Enzyme

A simlar analysis of spleen phosphodiesterase using the *p*-nitrophenyl ester of thymidine 3′-phosphate as reference ($K_m = 4.55 \times 10^{-3}$ *M*, with $V_{max} = 0.33$ μmol/min) showed that **12**, **1**, and **9***a* were weak competitive inhibitors of the enzyme with **12** > **1** > **9***a* (10:1.2:1). Full details of these studies will be reported elsewhere.

We wish to acknowledge financial assistance from the National Research Council of Canada.

1. W. J. Wechter. J. Med. Chem. **10**, 762 (1967).
2. W. J. Wechter, A. J. Mikulski, and M. Laskowski. Biochem. Biophys. Res. Commun. **30**, 318 (1968).
3. M. Staub, N. R. Warner, and P. Reichard. Biochem. Biophys. Res. Commun. **46**, 1824 (1972).
4. D. R. Pollard and J. Nagyvary. Biochemistry, **12**, 1063 (1973).
5. G. A. LePage and E. M. Hersh. Biochem. Biophys. Res. Commun. **46**, 1918 (1972).
6. R. A. Long, G. L. Szekeres, T. A. Khwaja, R. W. Sidwell, L. N. Simon, and R. K. Robins. J. Med. Chem., **15**, 1215 (1972).
7. J. C. Maurizot, W. J. Wechter, J. Brahms, and C. Sadron. Nature, **219**, 377 (1968).
8. J. Brahms, J. C. Maurizot, and J. Pilet. Biochem. Biophys. Acta, **186**, 110 (1969).
9. J. Smrt and F. Sorm. Coll. Czech. Chem. Commun. **32**, 3169 (1967).
10. J. Nagyvary and R. G. Provenzale. Biochemistry, **8**, 4769 (1969).
11. A. Hampton and A. W. Nichol. Biochemistry, **5**, 2076 (1966).
12. D. M. Brown, A. R. Todd, and S. Varadarajan. J. Chem. Soc. 2388 (1956).
13. J. J. Fox and I. Wempen. Tetrahedron Lett. 643, (1965).
14. T. M. Jacob and H. G. Khorana. J. Am. Chem. Soc. **86**, 1630, (1965).
15. R. L. Letsinger and K. K. Ogilvie. J. Am. Chem. Soc. **91**, 3350 (1969).
16. K. K. Ogilvie and D. Iwacha. Can. J. Chem. **48**, 862 (1969).
17. R. G. Provenzale and J. Nagyvary. Biochemistry, **9**, 1744 (1970).
18. G. Schramm and I. Ulmer-Schurnbrand. Biochem. Biophys. Acta, **145**, 7 (1967).
19. M. Ikehara and T. Tezuka. J. Am. Chem. Soc. **95**, 4054 (1973).
20. K. K. Ogilvie and L. A. Slotin. Can. J. Chem. **51**, 2397 (1973).
21. S. Uesugi, M. Yasumoto, M. Ikehara, K. N. Fang, and P.O.P.Ts'O. J. Am. Chem. Soc. **94**, 5480 (1972).
22. R. Lohrmann and H. G. Khorana. J. Am. Chem. Soc. **86**, 4188 (1964).
23. H. Schaller, G. Weimann, B. Lerch, and H. G. Khorana. J. Am. Chem. Soc. **85**, 3821 (1965).
24. P. T. Gilham and H. G. Khorana. J. Am. Chem. Soc. **80**, 6212 (1958).
25. R. L. Letsinger, K. K. Ogilvie, and P. S. Miller. J. Am. Chem. Soc. **91**, 3360 (1969).
26. F. Eckstein. Chem. Ber. **100**, 2228 (1967).
27. T. Neilson and E. S. Werstiuk. Can. J. Chem. **49**, 3004 (1971).
28. T. Mukaiyama and M. Hashimoto. J. Am. Chem. Soc. **94**, 8528 (1972).
29. J. L. Darlix, H. P. M. Fromageot, and P. Fromageot. Biochem. Biophys. Acta, **145**, 517 (1967).
30. Handbook of Biochemistry. 2nd Ed. *Edited by* H. A. Sober. Chemical Rubber Co., Cleveland, Ohio. 1968. pp. 041 and 658.
31. M. Smith, D. H. Rammler, I. H. Goldberg, and H. G. Khorana. J. Am. Chem. Soc. **84**, 430 (1962).
32. Y. F. Shealy and J. D. Clayton. J. Am. Chem. Soc. **91**, 3082 (1969).
33. J. P. H. Verheyden and J. G. Moffatt. J. Org. Chem. **37**, 2289 (1972).
34. R. L. Letsinger and K. K. Ogilvie. J. Am. Chem. Soc. **89**, 4801 (1967).
35. P. A. Rheault. M.Sc. Thesis, University of Manitoba, Winnipeg, Manitoba, 1972.

Can. J. Chem. Downloaded from www.nrcresearchpress.com by 210.87.254.6 on 09/05/12
For personal use only.

Bimolecular Reactions of Trapped Ions. VIII. Reactions in Propane and Propane–Methane Mixtures[1]

BRUCE H. SOLKA, ANDREW Y.-K. LAU, AND ALEX. G. HARRISON

Department of Chemistry, University of Toronto, Toronto, Ontario M5S 1A1

Received November 13, 1973

The ion-molecule reactions in propane and in methane–propane mixtures have been studied using an ion-trapping technique and rate coefficients have been measured for the reactions occurring. In pure propane the $C_2H_5^+$ primary ions react by H^- transfer to form $C_3H_7^+$ whereas $C_2H_4^+$ reacts to form $C_3H_6^+$ (25%) and $C_3H_7^+$ (75%). Using isotopically labelled propanes it was found that both *n*-propyl and *i*-propyl ions were formed with the *n*-propyl ions reacting slowly to produce *i*-propyl ions. In various deuterium labelled methane–propane mixtures $C(H,D)_5^+$ reacts with the propane with a rate constant of $\sim 1.5 \times 10^{-9}$ cm^3 molecule^{-1} s^{-1} in agreement with the calculated collision rate. It is shown that no hydrogens from the CH_5^+ ion are incorporated in the product ions which are found to be $C_2H_5^+$ (70%), $(CH_3)_2CH^+$ (25%), and $CH_3CH_2CH_2^+$ (5%).

Les réactions ion–molécule dans le propane et les mélanges méthane–propane ont été étudiées en utilisant une technique qui consiste à piéger les ions. Les coefficients de vitesse pour les réactions qui ont lieu ont été mesurés. Dans le propane pur les ions primaires $C_2H_5^+$ réagissent par un transfert de H^- pour former $C_3H_7^+$ pendant que $C_2H_4^+$ réagit pour former $C_3H_6^+$ (25%) et $C_3H_7^+$ (75%). Utilisant des propanes marqués par des isotopes, on trouve que les ions *n*-propyles et *i*-propyles sont formés avec les ions *n*-propyles qui réagissent lentement pour produire les ions *i*-propyles. Dans divers mélanges méthane–propane marqués par le deutérium $C(H,D)_5^+$ réagit avec le propane avec une constante de vitesse de $\sim 1.5 \times 10^{-9}$ cm^3 molécule^{-1} s^{1-} en accord avec la vitesse calculée de collision. Les hydrogènes de l'ion CH_5^+ ne sont pas incorporés dans les ions produits, lesquels sont $C_2H_5^+$ (70%), $(CH_3)_2CH^+$ (25%) et $CH_3CH_2CH_2^+$ (5%).
[Traduit par le journal]

Can. J. Chem., **52**, 1798 (1974)

Introduction

Recent work in this laboratory (1) has shown that CD_5^+ reacts with ethane by D^+ transfer to form initially $C_2H_6D^+$, the rate of reaction being only slightly lower than the collision rate estimated from the ion – induced dipole model of ion–molecule reactions (2). At the low pressures used a significant fraction of the $C_2H_6D^+$ ions decomposed to form $C_2H_5^+$ and $C_2H_4D^+$, the relative abundances indicating essentially complete H/D scrambling in $C_2H_6D^+$ prior to decomposition.

The reactions of CH_5^+ with higher hydrocarbons have been studied in less detail. Ausloos *et al.* (3) have studied the radiolysis of mixtures of methane with small amounts of propane, *n*-butane, *i*-butane, or *n*-pentane. From end-product analysis they concluded that the CH_5^+ ion produced in methane reacted with the added alkane to produce alkyl ions of lower carbon content (*i.e.*, $C_2H_5^+$ in propane, $C_2H_5^+$ and $C_3H_7^+$ in *n*-butane, etc.). From isotopic labelling experiments they concluded that the hydrogen from CH_5^+ was not incorporated in the ionic product, the reaction with propane-d_8, for example, being given by

$$[1] \quad CH_5^+ + C_3D_8 \rightarrow CH_4 + CD_3H + C_2D_5^+$$

The reaction can thus be described nominally as an alkide ion abstraction reaction. Ausloos *et al.* (3) made no measurements of the rate of reaction, nor did they report products resulting nominally from H^- abstraction from the alkane. Such products have been observed in the reaction of H_3^+ with propane and the butanes (4, 5). Haynes and Kebarle (6) have observed formation of both $C_2D_5^+$ and $C_3D_7^+$ in that α-particle radiolysis of methane (5 mm pressure) containing small amounts (~ 100 p.p.m.) of propane-d_6. However both CH_5^+ and $C_2H_5^+$ were present as reactant ions and the product distribution from reaction of CH_5^+ cannot be established.

Products resulting from nominal H^- abstraction as well as from nominal alkide ion ab-

[1]Presented in part at the 56th Canadian Chemical Conference of the Chemical Institute of Canada, Montreal, Quebec, June, 1973. For part VII see ref. 22.

Can. J. Chem. Downloaded from www.nrcresearchpress.com by 210.87.254.105 on 09/05/12
For personal use only.

Can. J. Chem. Downloaded from www.nrcresearchpress.com by 210.87.254.105 on 09/05/12
For personal use only.

straction have been observed in chemical ionization studies (7–9) of the reaction of CH_5^+ with C_6 and higher alkanes. No rate constants have been reported from these studies. In the case of *n*-decane it has been shown (9) by using CD_5^+ as the reactant that there is no incorporation of hydrogens from the reactant ions in the products.

The present work reports a detailed study, using an ion-trapping technique (10), of the ion–molecule reactions in methane–propane mixtures. The rate coefficients of the reactions occurring have been determined and, using appropriate isotopic labelling, the relative yields of the products $C_2H_5^+$, *n*-$C_3H_7^+$, and *i*-$C_3H_7^+$ from reaction of propane have been determined. A brief study of the reactions occurring in pure propane is also reported.

Experimental

The ion-trapping technique has been described in detail (10) and only a brief summary need be given here. Primary reactant ions are produced by a short pulse of electrons of suitable energy and are trapped in the negative space charge of a continuous electron beam of ~5 eV energy (insufficient to cause ionization) and ~8 μA trap current. A known and variable time after the primary ion production a voltage pulse applied to the repeller electrode removes the ions for mass analysis using a conventional magnetic deflection mass spectrometer. Delay times between the ionizing and withdrawal pulses (and, hence, reaction times) of up to 4 ms have been employed.

Source concentrations, usually approximately 1×10^{13} molecules cm^{-3}, were not measured directly but were related to the sample inlet pressure through observations of the rate of decay of CH_4^+ with reaction time in pure CH_4. All rate constants are therefore relative to the value (11) 1.20×10^{-9} cm^3 $molecule^{-1}$ s^{-1} for the $CH_4^+ + CH_4$ reaction. At the inlet and source pressures used gas flow both into and out of the ion source is molecular with the result that the gas composition in the ion source is the same as that in the inlet system. For experiments with gas mixtures two different approaches were used. In the first, a gas mixture was prepared accurately by volume and admitted through a single inlet system calibrated against methane. In the second, each component was admitted through a separate inlet system. Both inlet systems exhibited molecular flow and were calibrated with methane. Comparable results were obtained by the two methods.

The results are presented in the accompanying figures as a fraction of the total ionization where the total ionization represents the sum of the collected ion currents at each time delay setting. The errors quoted for the rate coefficients represent the standard deviations of three or more determinations.

The propane and methane were research grade gases. Methane-d_4, propane-2,2-d_2, propane-1,1,1,3,3,3-d_6, and propane-d_8 were obtained from Merck, Sharp, and Dohme, Montreal. All materials were carefully degassed before use.

Results and Discussion

Reactions in Pure Propane

Figure 1 shows typical results obtained in pure propane at ionizing electron energies such that $C_3H_8^+$, $C_3H_7^+$, $C_3H_6^+$, $C_2H_5^+$, and $C_2H_4^+$ are the only primary ions. The $C_3H_8^+$ ion is essentially unreactive ($k < 0.03 \times 10^{-9}$ cm^3 $molecule^{-1}$ s^{-1}) whereas both $C_3H_6^+$ and $C_3H_7^+$ are produced by ion–molecule reactions but are themselves unreactive. These results are in agreement with the high-pressure studies of Munson *et al.* (12).

In agreement with this pressure study we conclude that $C_2H_5^+$ reacts by H^- abstraction to form $C_3H_7^+$ whereas $C_2H_4^+$ reacts both by H^- abstraction and by H_2^- abstraction to form $C_3H_7^+$ and $C_3H_6^+$, respectively. The plot of $I_{C_3H_6^+}$ *vs.* $\Delta I_{C_2H_4^+}$, the $C_2H_4^+$ which had reacted[2] (Fig. 2) shows that 25 ± 1% (average of three determinations) of the $C_2H_4^+$ ions yield $C_3H_6^+$

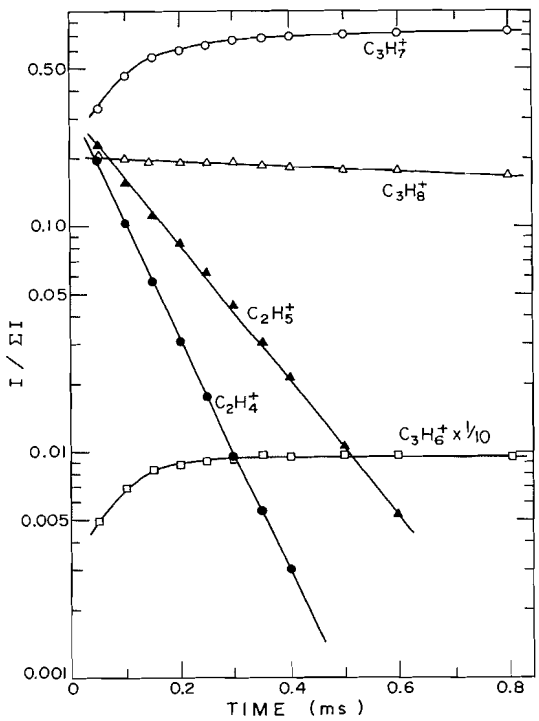

FIG. 1. Propane system: $[C_3H_8] = 12.6 \times 10^{12}$ molecules cm^{-3}.

[2]This plot is most readily achieved by reversing the abscissa scale as shown in Fig. 2.

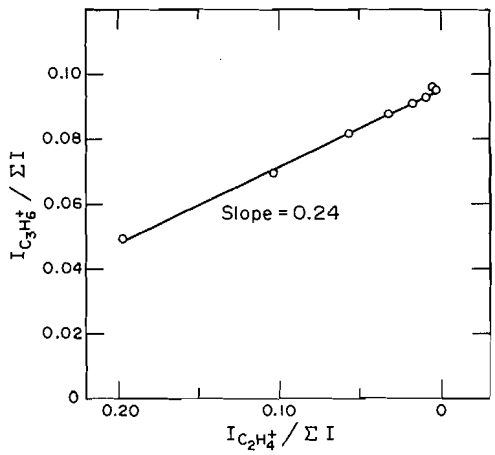

FIG. 2. $I_{C_3H_6^+}$ *vs.* $- I_{C_2H_4^+}$, conditions as for Fig. 1.

as a product, the remainder yielding $C_3H_7^+$. Bone and Futrell (13), using a tandem mass spectrometer, found that the reaction of $C_2H_4^+$ with propane gave $C_3H_7^+$ and $C_3H_6^+$ in the ratio 0.7:0.3 at ~0.3 eV ion kinetic energy, with the ratio increasing dramatically with increasing ion kinetic energy. The ratio 0.75:0.25 found in the present work provides still further evidence (10, 14) that the primary ion kinetic energy is approximately 0.4 eV in the trapped-ion technique.

Typical results for the $CH_3CD_2CH_3$ and $CD_3CH_2CD_3$ systems are shown in Figs. 3 and 4, respectively. Several points are of interest. First, the major $C_3(H,D)_6^+$ product is $C_3D_5H^+$ in the d_6 compound and $C_3DH_5^+$ in the d_2 compound, indicating that the H_2^- abstraction specifically removes a methyl and methylene hydrogen. (This result is also in agreement with the results of Bone and Futrell (13).) In contrast the H^- abstraction reactions are much less specific with both $M - H^+$ and $M - D^+$ being observed in both cases. A further interesting observation is that in both the d_2 and the d_6 propane the ions formed by $H^-(D^-)$ abstraction from a terminal methyl (*i.e.*, $C_3H_5D_2^+$ in propane-d_2 and $C_3D_5H_2^+$ in propane-d_6) are themselves reactive as shown by the decrease at longer delay times. The reactions can be described by

[2] $CH_3CD_2CH_2^+ + CH_3CD_2CH_3 \rightarrow CH_3\overset{+}{C}DCH_3 + CH_3CD_2CH_2D$

[3] $CD_3CH_2CD_2^+ + CD_3CH_2CD_3 \rightarrow CD_3\overset{+}{C}HCD_3 + CD_3CH_2CD_2H$

corresponding to conversion of the *n*-propyl ion to the *s*-propyl ion. Since Bone and Futrell (13) have shown from their tandem experiments that the (presumably) *s*-propyl ion formed by dissociative ionization of propane is unreactive with propane the present observations provide strong circumstantial evidence that the *n*-propyl cation formed by H^- abstraction does not rearrange to the *s*-propyl structure but is converted to the *s*-propyl structure by hydride abstraction ion–molecule reactions exemplified by [2] and [3].

The rate constants determined for the reactions in the various propanes studied are summarized in Table 1. The total rate coefficients for disappearance of the various isotopic $C_2(H,D)_4^+$ and $C_2(H,D)_5^+$ ions are in good agreement with each other. The rate coefficient of $0.85 \pm 0.05 \times 10^{-9}$ cm^3 molecule^{-1} s^{-1} for reaction of $C_2H_4^+$ is somewhat higher than the value of $0.63 \pm 0.10 \times 10^{-9}$ cm^3 molecule^{-1} s^{-1} reported by Munson *et al.* (12); however the value of $0.56 \pm 0.06 \times 10^{-9}$ cm^3 molecule^{-1} s^{-1} for reaction of $C_2H_5^+$ is in good agreement with the value of $0.62 \pm 0.13 \times 10^{-9}$ cm^3 molecule^{-1} s^{-1} obtained in the pressure studies by Munson *et al.* (13). The reaction of the *n*-propyl ions (reactions 2 and 3) are quite slow, the rate coefficients being $\sim 3 \times 10^{-11}$ cm^3 molecule^{-1} s^{-1}.

Reactions in Methane–Propane Mixtures

Two types of runs were carried out with methane–propane mixtures (including isotopic variants). The first type were on mixtures containing 10–20% propane and were designed to measure the rate coefficients for the reactions occurring. The second type involved the use of mixtures containing < 1% of the propane and were carried out at electron energies such that

TABLE 1. Rate coefficients for ion molecule reactions in propanes

Reactant ion	Neutral	$k \times 10^9$ (cm^3 molecule^{-1} s^{-1})
$C_2H_4^+$	C_3H_8	0.85 ± 0.05
$C_2H_5^+$	C_3H_8	0.56 ± 0.06
$C_2H_2D_2^+$	$CH_3CD_2CH_3$	0.85 ± 0.1
$C_2H_3D^+$	$CH_3CD_2CH_3$	0.79 ± 0.05
$C_2H_3D_2^+$	$CH_3CD_2CH_3$	0.50 ± 0.05
$CH_3CD_2CH_2^+$	$CH_3CD_2CH_3$	0.03 ± 0.005
$C_2D_2H_2^+$	$CD_3CH_2CD_3$	0.89 ± 0.03
$C_2D_3H^+$	$CD_3CH_2CD_3$	0.84 ± 0.02
$C_2D_3H_2^+$	$CD_3CH_2CD_3$	0.50 ± 0.05
$C_2D_4H^+$	$CD_3CH_2CD_3$	0.47 ± 0.05
$CD_3CH_2CD_2^+$	$CD_3CH_2CD_3$	0.03 ± 0.01

Can. J. Chem. Downloaded from www.nrcresearchpress.com by 210.87.254.105 on 09/05/12
For personal use only.

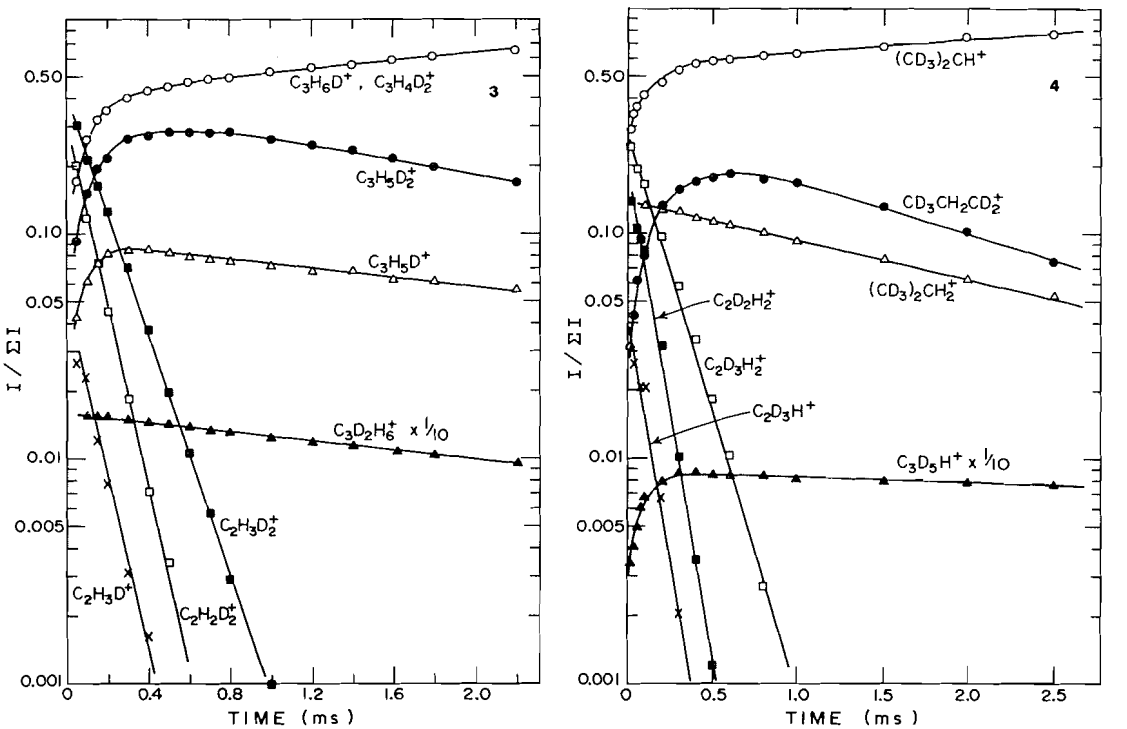

FIG. 3. Propane-2,2-d_2 system: $[CH_3CD_2CH_3] = 12.4 \times 10^{12}$ molecules cm^{-3}.
FIG. 4. Propane-1,1,1,3,3,3-d_6 system: $[CD_3CH_2CD_3] = 12.0 \times 10^{12}$ molecules cm^{-3}.

$C(H,D)_4^+$ was the only significant primary ion produced from methane. These runs were designed to determine the product distribution from reaction of $C(H,D)_5^+$ with the propane.

Figures 5 and 6 show typical results obtained in a mixture containing 24.3% propane and 75.7% methane-d_4. As shown in Fig. 5 the CD_3^+ and CD_4^+ primary ions produced from CD_4 react rapidly, primarily with CD_4 to produce $C_2D_5^+$ and CD_5^+, respectively. It is well known (10, 15–17) that in pure methane (or methane-d_4) neither the $C_2(H,D)_5^+$ nor the $C(H,D)_5^+$ ion undergoes further reaction and the decrease observed beyond 0.3 to 0.4 ms must be because of reaction with propane. From the linear portion of the semilogarithmic plots at longer delay times the rate coefficients for reaction of $C(H,D)_5^+$ and $C_2(H,D)_5^+$ with the propane present can be evaluated. Figure 6 shows the plot of the propane based ions for the CD_4–C_3H_8 mixture described. It can be seen that the major product ions are $C_3H_7^+$, which increases in intensity throughout the time range studied, and $C_2H_5^+$, which shows an initial increase before decreasing at longer times due to reaction with propane. (The increase in $C_3H_6^+$ is the result of the reaction of the $C_2H_4^+$ primary ion produced from propane.)

The rate coefficients measured for reaction of $C(H,D)_5^+$ with the various propanes studied are summarized in Table 2. The experimental rate coefficients are all in reasonable agreement and, in addition, are in reasonable agreement with the collision rate calculated from the ion – induced dipole model (2). This model yields calculated collision rates varying from 1.56×10^{-9} cm^3 $molecule^{-1}$ s^{-1} ($CD_5^+ + C_3H_8$) to 1.66×10^{-9} cm^3 $molecule^{-1}$ s^{-1} ($CH_5^+ + C_3H_6D_2$). The results show that essentially every collision between $C(H,D)_5^+$ and $C_3(H,D)_8$ leads to reaction; a similar result was found (1) for reaction of CD_5^+ with ethane.

Table 3 summarizes the results obtained for reaction of $C_2(H,D)_5^+$ with $C_3(H,D)_8$. There are two entries for each mixture in Table 3, one is that for reaction of the $C_2(H,D)_5^+$ secondary ion derived from reaction of $C(H,D)_3^+$ with the methane while the other is that for reaction of the $C_2(H,D)_5^+$ primary ion produced largely by electron impact ionization of the propane. The

Can. J. Chem. Downloaded from www.nrcresearchpress.com by 210.87.254.105 on 09/05/12
For personal use only.

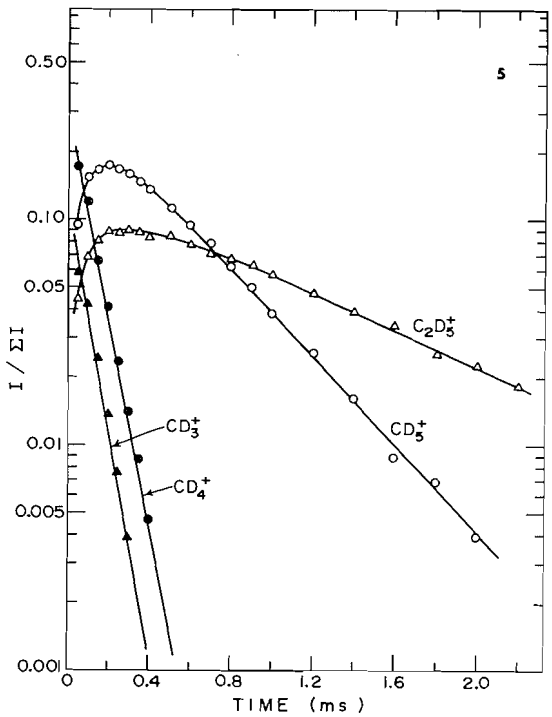

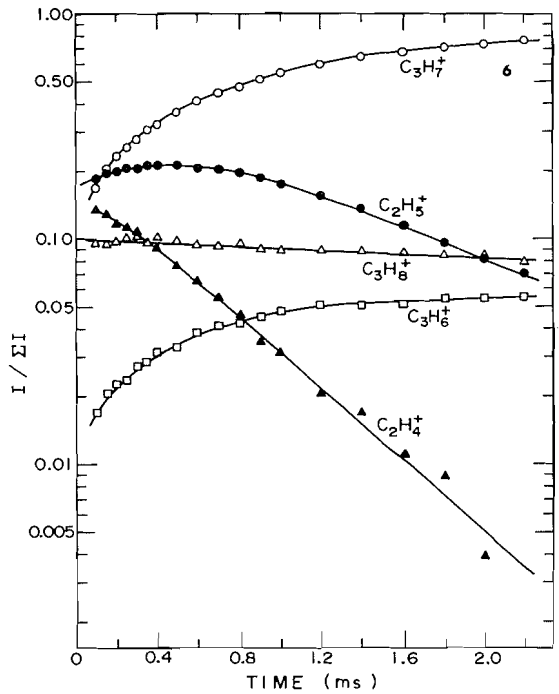

FIG. 5. Methane-d_4–propane system: $[CD_4] = 9.53 \times 10^{12}$ molecules cm^{-3}; $[C_3H_8] = 3.06 \times 10^{12}$ molecules cm^{-3}.

FIG. 6. Methane-d_4–propane system: conditions as for Fig. 5.

TABLE 2. Rate coefficients for reaction $C(H,D)_5^+ + C_3(H,D)_8 \rightarrow$ Products

System	Reactant ion	$k \times 10^9$ (cm^3 molecule^{-1} s^{-1})
CD_4–C_3H_8	CD_5^+	1.53 ± 0.2
CH_4–C_3D_8	CH_5^+	1.54 ± 0.15
CH_4–$(CH_3)_2CD_2$	CH_5^+	1.71 ± 0.1
CH_4–$(CD_3)_2CH_2$	CH_5^+	1.51 ± 0.01

rate coefficient for reaction of the latter ion was derived from the linear semilogarithmic plot at long reaction times since as shown in Fig. 6 there is some production of the ion at shorter reaction times.

The rate coefficients measured for reactions of the primary and secondary ions are in reasonable agreement with each other and with the values obtained in the pure propanes (Table 1). This latter agreement provides reassurance that the mixture compositions were accurately determined. The rate coefficients are all in the range 0.5 to 0.6 $\times 10^{-9}$ cm^3 molecule^{-1} s^{-1}, approximately 40% of the collision rate coefficient of 1.31 $\times 10^{-9}$ to 1.42 $\times 10^{-9}$ cm^3 molecule^{-1} s^{-1} (depending on reduced mass of colliding pair) calculated from the ion-induced dipole model (2).

Table 4 summarizes the rate data for reaction of $C_2H_5^+$ with the *n*-alkanes. The thermoneutral reaction with ethane is relatively inefficient (~ 20% of collisions lead to reaction), however, as the size of the alkane increases the reaction efficiency rapidly approaches unity. The reaction of $C_2H_5^+$ with propane to form $(CH_3)_2CH^+$ is ~22 kcal mol^{-1} exothermic and this reaction exothermicity increases slightly for higher alkanes. Similarly H^- abstraction to form a primary alkyl ion is ~10 kcal mol^{-1} exothermic for propane and the higher *n*-alkanes. The lower reaction efficiency for propane and butane is not entirely explained by the reaction energetics but appears to be related to the size of the neutral reactant.

Product Distribution from Reaction of CH_5^+

Figure 7 shows the plot of ion intensities *vs.* reaction time, covering the range from 0.1 to 1.0 ms for a 150:1 $[CH_4]:[CH_3CD_2CH_3]$ mix-

Can. J. Chem. Downloaded from www.nrcresearchpress.com by 210.87.254.105 on 09/05/12
For personal use only.

Can. J. Chem. Downloaded from www.nrcresearchpress.com by 210.87.254.105 on 09/05/12
For personal use only.

TABLE 3. Rate coefficients for reaction $C_2(H,D)_5^+ + C_3(H,D)_8 \rightarrow$ Products

System	$k \times 10^9$ (cm^3 molecule^{-1} s^{-1})	Reactant ion
C_3H_8	0.56 ± 0.06	$C_2H_5^+$ (primary)
CD_4–C_3H_8	0.62 ± 0.05	$C_2H_5^+$ (primary)
	0.63 ± 0.05	$C_2D_5^+$ (secondary)
CH_4–C_3D_8	0.47 ± 0.05	$C_2D_5^+$ (primary)
	0.53 ± 0.06	$C_2H_5^+$ (secondary)
CH_4–$(CD_3)_2CH_2$	0.56 ± 0.05	$C_2D_3H_2^+$ (primary)
	0.54 ± 0.05	$C_2H_5^+$ (secondary)
CH_4–$(CH_3)_2CD_2$	0.58 ± 0.07	$C_2D_2H_3^+$ (primary)
	0.64 ± 0.03	$C_2H_5^+$ (secondary)

TABLE 4. Rate coefficients for reaction of $C_2H_5^+$ with *n*-alkanes

Reactant pair	$k \times 10^9$ (cm^3 molecule^{-1} s^{-1}) Exp. (ref.)	Calcd.	k_{exp}/k_{calcd}
$C_2H_5^+ + C_2H_6$	0.28 (1)	1.25	0.22
$C_2H_5^+ + C_3H_8$	0.56*	1.35	0.40
$C_2H_5^+ + n$-C_4H_{10}	0.75 (23)	1.45	0.52
$C_2H_5^+ + n$-C_5H_{12}	1.4_0 (24)	1.60	0.88
$C_2H_5^+ + n$-C_6H_{14}	2.3_0 (24)	2.20	~1.0

*This work.

ture at $\sim 4 \times 10^{13}$ molecule cm^{-3} total ion source concentration. The ionizing electron energy was adjusted so that only CH_4^+ was produced by electron impact ionization of methane. At the source concentrations used CH_4^+ had reacted completely with methane by 0.1 ms with the result that CH_5^+ accounted for ~90% of the total ionization at 0.1 ms. Beyond 0.1 ms the decrease in CH_5^+ results from reaction with the propane-d_2. The only product ions observed were $C_2H_3D_2^+$ (*m/e* 31), $C_3H_6D^+$ (*m/e* 44), and $C_3H_5D_2^+$ (*m/e* 45). Particularly noteworthy is the observation that the *m/e* 30 ion which could be $C_2H_4D^+$ shows no increase but rather decreases with reaction time. It is probable that *m/e* 30 is predominantly $C_2H_2D_2^+$ which reacts slowly with $C_3H_6D_2$ to produce in part $C_3H_5D^+$ (*m/e* 42) which shows a slow and quite small increase with reaction time.

Figure 8 shows a similar plot for a 150:1 $[CH_4]:[CD_3CH_2CD_3]$ mixture at $\sim 4 \times 10^{13}$ molecule cm^{-3} total ion source concentration. The product ions which increase significantly with reaction time due to reaction with CH_5^+ are $C_2D_3H_2^+$ (*m/e* 32), $C_3D_6H^+$ (*m/e* 49), and $C_3D_5H_2^+$ (*m/e* 48), in order of decreasing importance. There was no $C_2D_4H^+$ (*m/e* 33) formed nor is there any increase in *m/e* 31 corresponding to formation of $C_2H_3D_2^+$. The decrease in *m/e* 31 probably results from reaction of $C_2D_3H^+$ which produces in part $C_3D_5H^+$ according for some of the small increase at *m/e* 47. (The *m/e* 47 will also be produced as $C_3D_4H_3^+$ from the d_5 impurity (~3%) present in the propane.)

The products formed were confirmed by runs in CD_4–C_3H_8 mixtures where only $C_2H_5^+$ and $C_3H_7^+$ were observed as products and in CH_4–C_3D_8 mixtures where only $C_2D_5^+$ and $C_3D_7^+$ were observed as products. In summary there was no evidence that the H/D from $C(H,D)_5^+$ was incorporated in any of the products nor was there any evidence for H/D interchange in the partially labelled propane after reaction with CH_5^+ but prior to fragmentation. In particular no $C_3(H,D)_9^+$ was observed in methane–propane systems analogous to the significant yield of $C_2(H,D)_7^+$ in methane–ethane systems.

The fractional yields of products from reaction of CH_5^+ with the propanes may be determined by plotting the product ion intensities *vs.* the CH_5^+ which has reacted. Such plots for the data of Figs. 7 and 8 are shown in Figs. 9 and 10 where $I(\text{product})/\Sigma I$ is plotted against $I(CH_5^+)/\Sigma I$.[3] As anticipated the plots give straight lines in the initial regions. The downward curvature of the $C_2(H,D)_5^+$ plot at greater extent of reaction results from reaction of this ion with the

[3]In Figs. 9 and 10 the abscissa scale is reversed. This achieves the same result as plotting the product ion intensities *vs.* $\Delta I_{CH_5^+}$, the CH_5^+ which has reacted.

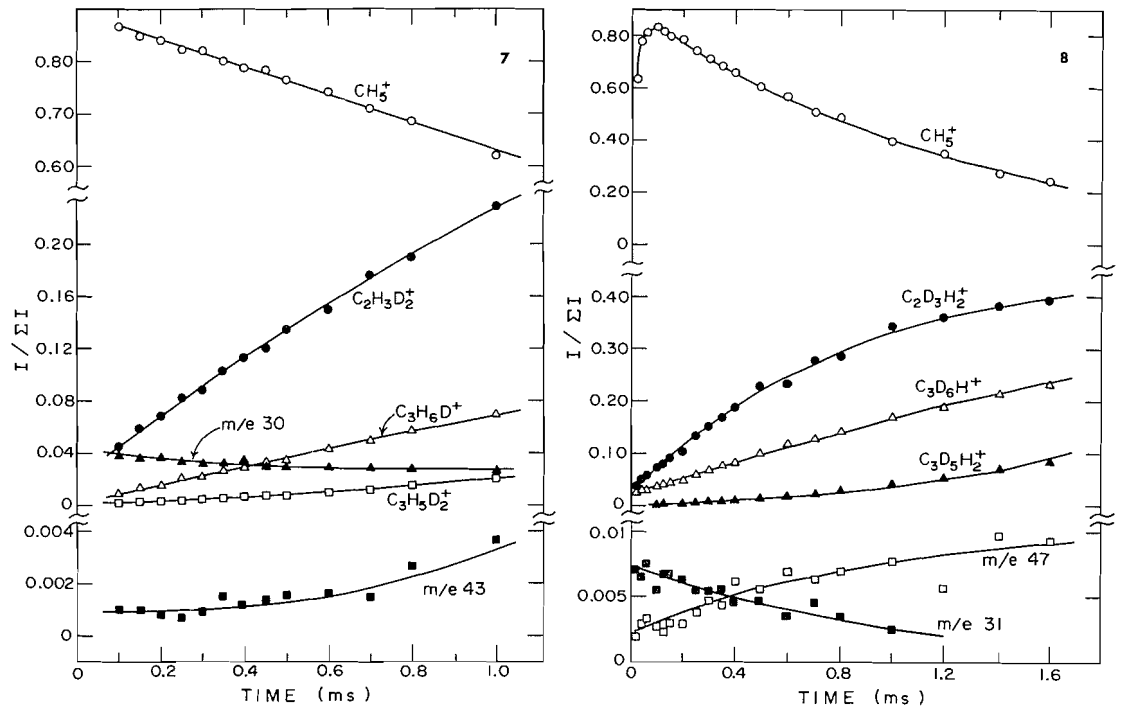

FIG. 7. Methane–propane-2,2-d_2 system: $[CH_4]$: $[CH_3CD_2CH_3]$ = 150:1; total ion source concentration $\approx 3\,5 \times 10^{13}$ molecules cm^{-3}.

FIG. 8. Methane–propane-1,1,1,3,3,3-d_6 system: $[CH_4]$:$[CD_3CH_2CD_3]$ = 150:1; total ion source concentration $\approx 3.5 \times 10^{13}$ molecules cm^{-3}.

propane to give the two propyl ions which show an upward curvature over the same region. The fractional yields determined from such plots (average of three separate determinations for each propane) are recorded in Table 5.

In the methane–propane system, as mentioned previously, there is no evidence for formation of $C_3(H,D)_9^+$ (protonated propane) analogous to $C_2(H,D)_7^+$ observed in the methane–ethane system (1). In this latter system the $C_2(H,D)_5^+$ alkyl ion was shown to be formed by loss of $(H,D)_2$ from the protonated ethane with essentially complete scrambling of the H/D in the protonated ethane. A similar mechanism is not operative in the propane system. Statistical loss of $(H,D)_2$ from $C_3(H,D)_9^+$ would lead in the propane-d_2 case to $[C_3H_5D_2^+]$:$[C_3H_6D^+]$:$[C_3H_7^+]$ = 3:2:0.4 while the observed ratio is 1:5:0. In the propane-d_6 case statistical loss of $(H,D)_2$ would lead to $[C_3HD_6^+]$:$[C_3H_2D_5^+]$:$[C_3H_3D_4^+]$ = 1:6:5 compared to the experimental result of 6:1:0.

The formation of $C_3(H,D)_7^+$ by reaction of CH_5^+ with the partially labelled propanes is consistent only with specific loss of a secondary or a primary hydrogen (or deuterium) in combination with the hydrogen from CH_5^+. This is in agreement with the results obtained by Volpi and co-workers (5) from reaction of H_3^+ with labelled propanes. However both these results differ from the conclusions reached by Pettersson and Lindholm (18) from a study of the reaction of CDO^+ with propane (C_3H_8) using a tandem mass spectrometer. They observed an increase in the *m/e* 44 signal over that observed when CHO^+ was reacted with C_3H_8. They attributed this increase to formation of $C_3H_6D^+$ produced by loss of H_2 from a $C_3H_8D^+$ intermediate. They concluded that in this intermediate all H/D had become equivalent. However, they did no confirmatory experiments reacting CHO^+ with C_3D_8 which would have been more conclusive and in light of the present results and those of Volpi and co-workers (5) their conclusions must be considered suspect.

The $C_2(H,D)_5^+$ product ion is the major product accounting for ~70% of the total reaction. Again this is a very specific reaction

Can. J. Chem. Downloaded from www.nrcresearchpress.com by 210.87.254.105 on 09/05/12
For personal use only.

Can. J. Chem. Downloaded from www.nrcresearchpress.com by 210.87.254.105 on 09/05/12
For personal use only.

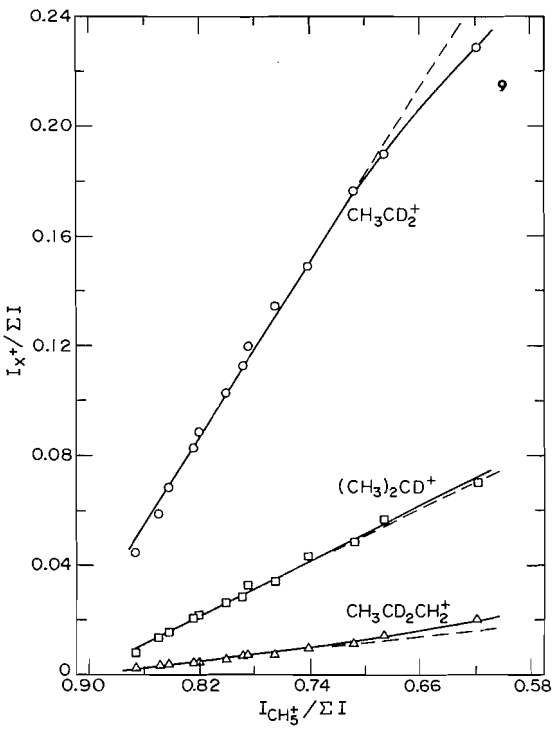

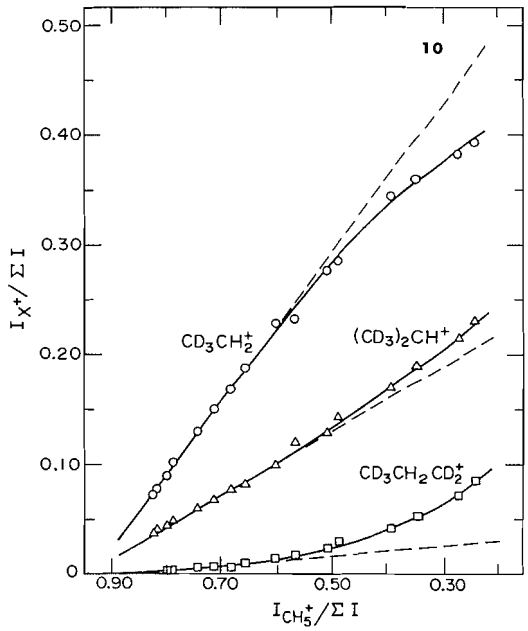

FIG. 9. Methane–propane-d_2 system: $I_{X^+}/\Sigma I$ *vs.* $-I_{CH_4^+}/\Sigma I$; data from Fig. 7.
FIG. 10. Methane–propane-d_6 system: $I_{X^+}/\Sigma I$ *vs.* $-I_{CH_5^+}/\Sigma I$, data from Fig. 8.

TABLE 5. The fractional yields of products from reaction of CH_5^+ and H_3^+ with propane

	Fractional yield			ΔH (reaction)	
Product ion	$CH_5^+ + (CH_3)_2CD_2$	$CH_5^+ + (CD_3)_2CH_2$	$H_3^+ + (CH_3)_2CD_2$*	CH_5^+	H_3^+
Ethyl	0.75 ± 0.09	0.71 ± 0.01	0.68	−13	−38
n-Propyl	0.05 ± 0.02	0.04 ± 0.01	0.17	−6	−31
i-Propyl	0.25 ± 0.03	0.25 ± 0.03	0.15	−22	−47

*From ref. 5.

forming only $C_2H_3D_2^+$ from $CH_3CD_2CH_3$ and only $C_2D_3H_2^+$ from $CD_3CH_2CD_3$. Scrambling of the H/D in a $C_3(H,D)_9^+$ intermediate would lead to a large yield of $C_2DH_4^+$ in the d_2 case and to a large yield of $C_2HD_4^+$ in the d_6 case. Similarly scrambling of the H/D in the propane preceding loss of a methyl with the hydrogen from CH_5^+ would also produce high yields of $C_2DH_4^+$ and $C_2D_4H^+$, respectively. We conclude that formation of the ethyl cation involves the specific loss of one of the terminal methyl groups which, for the reaction to be thermochemically allowed, must combine with the H from CH_5^+ to form methane. This conclusion is in agreement with that reached by Ausloos *et al.* (3) from studies of the radiolysis of methane–propane mixtures and also with the results of Volpi and co-workers (5) for reaction of H_3^+ (or D_3^+) with propane.

In the fourth column of Table 5 we present the fractional yields obtained by Volpi and co-workers (5) for reaction of H_3^+ with propane-2,2-d_2 from high pressure chemical ionization studies. The fractional yield of ethyl ions is practically identical for reaction of both H_3^+ and CH_5^+. The major difference is that CH_5^+ is much more specific in abstracting a secondary hydrogen to yield *s*-propyl$^+$ while H_3^+ shows little specificity and exhibits a much greater yield of *n*-propyl cation.

Can. J. Chem. Downloaded from www.nrcresearchpress.com by 210.87.254.105 on 09/05/12
For personal use only.

The explanation of the similarities and differences in the reactions of CH_5^+ and H_3^+ are not clear. In the final two columns of Table 5 we summarize the exothermicity of the overall reaction of H_3^+ and CH_5^+ to form the observed products. The formation of the ethyl cation is not the most exothermic reaction and the observation of this species as the most abundant product with the same yield in both systems argues against formation of a $C_3(H,D)_9^+$ complex in which the excess energy becomes randomized since in this case the most exothermic reaction should show the highest yield.[4] This conclusion is in agreement with the isotopic labelling experiments. The specific formation of *i*-propyl$^+$ in the reaction of CH_5^+ however may be related to the energetics of the reaction. The formation of *n*-propyl$^+$ is only 6 kcal mol^{-1} exothermic compared to 22 kcal mol^{-1} exothermic for formation of *i*-propyl$^+$ and the specific formation of *i*-propyl$^+$ may be related to the reaction exothermicity. By contrast in the reaction of H_3^+ formation of both the propyl cations is strongly exothermic and little specificity is observed.

The overall independence of the fractional yields of the products, particularly $C_2H_5^+$, on the reaction exothermicities suggests that the product yields are determined primarily by the site of attack of the reactant ion. Csizmadia and Tomasi (19) recently have calculated the interaction energy resulting from the approach of a proton towards propane using the electrostatic potential model of Tomasi and co-workers (20) which has been shown (20, 21) to give the correct order of protonation energies as well as providing reliable representations of the approach paths in the case of simple cyclic molecules. These calculations show that the energetically most favored path of approach of the proton is towards a terminal carbon leading, presumably, to displacement of an ethyl cation and formation of methane. Approaches from directions leading to attack on a methyl hydrogen or methylene hydrogen were less favorable and provide little evidence favoring one over the other. In all cases the interaction energies were much less than for the cyclic molecules containing heteroatoms (20, 21) as would be expected. These calculations are in agreement with the experimental results for reaction of both CH_5^+ and H_3^+ suggesting that indeed the interaction between the neutral propane and the approaching positive charge determines the direction of attack and the products resulting therefrom.

The authors are indebted to the National Research Council of Canada for continued financial support and to Professor I. G. Csizmadia for useful discussions and for communication of results prior to publication.

[4]This conclusion only applies rigorously if the frequency factors for the various fragmentation reactions are very similar or if the excess energy is low compared to the threshold for one of the processes. It is possible that in the fragmentation of a $C_3(H,D)_9^+$ species the cleavage to form $C_2(H,D)_5^+$ would have a higher frequency factor than the reactions forming $C_3(H,D)_7^+$. However, should such a situation prevail it is unlikely that the much less exothermic CH_5^+ reaction would give the same $C_2(H,D)_5^+$ yield as the strongly exothermic H_3^+ reaction.

1. A. S. Blair, E. J. Heslin, and A. G. Harrison. J. Am. Chem. Soc. **94**, 2935 (1972).
2. G. Gioumousis and D. P. Stevenson. J. Chem. Phys. **29**, 294 (1958).
3. P. Ausloos, S. G. Lias, and R. Gorden, Jr. J. Chem. Phys. **39**, 3341 (1963).
4. V. Aquilanti and G. G. Volpi. J. Chem. Phys. **44**, 2307 (1966).
5. V. Aquilanti, A. Galli, A. Giardini-Guidoni, and G. G. Volpi. J. Chem. Phys. **48**, 4310 (1968).
6. R. M. Haynes and P. Kebarle. J. Chem. Phys. **45**, 3899 (1966).
7. F. H. Field and M. S. B. Munson. Adv. Chem. Series, **58**, 167 (1966).
8. R. P. Clow and J. H. Futrell. J. Am. Chem. Soc. **94**, 3748 (1972).
9. D. F. Hunt and C. N. McEwen. Org. Mass. Spectrom. **7**, 441 (1973).
10. A. A. Herod and A. G. Harrison. Int. J. Mass Spectrom. Ion Phys. **4**, 415 (1970).
11. S. K. Gupta, E. G. Jones, A. G. Harrison, and J. J. Myher. Can. J. Chem. **45**, 3107 (1967).
12. M. S. B. Munson, J. L. Franklin, and F. H. Field. J. Phys. Chem. **68**, 3098 (1964).
13. L. I. Bone and J. H. Futrell. J. Chem. Phys. **46**, 4084 (1967).
14. A. A. Herod, A. G. Harrison, and N. A. McAskill. Can. J. Chem. **49**, 2217 (1971).
15. F. H. Field and M. S. B. Munson. J. Am. Chem. Soc. **87**, 3289 (1965).
16. S. Wexler, A. Liftshitz, and A. Quattrochi. Adv. Chem. Series, **58**, 193 (1966).
17. A. S. Blair and A. G. Harrison. Can. J. Chem. **51**, 1645 (1973).
18. E. Pettersson and E. Lindholm. Arkiv. Fysik, **24**, 49 (1963).
19. I. G. Csizmadia and J. Tomasi. Private communication.
20. R. Bonaccorsi, E. Scrocco, and J. Tomasi. J. Chem. Phys. **52**, 5270 (1970).
21. C. Ghio and J. Tomasi. Theoret. Chem. Acta, **30**, 151 (1973).
22. A. G. Harrison and A. S. Blair. Int. J. Mass Spectrom. Ion Phys. **12**, 175 (1973).
23. M. S. B. Munson. J. Phys. Chem. **71**, 3966 (1967).
24. L. W. Sieck, S. K. Searles, and P. Ausloos. J. Res. Natl. Bur. Stds. **75A**, 147 (1971).

The Rates and Products of Addition of 4-Chlorobenzenesulfenyl Chloride to a Series of Side Chain Methyl Substituted Styrenes[1]

GEORGE H. SCHMID AND DENNIS G. GARRATT

Department of Chemistry, University of Toronto, Toronto, Ontario

Received December 20, 1973

The rates of addition and the product compositions have been determined for the addition of 4-chlorobenzenesulfenyl chloride to a series of seven side chain methyl substituted styrenes in 1,1,2,2-tetrachloroethane at 25°. Unlike the addition to the corresponding series of methylated ethylenes, the effect of the methyl groups is not cumulative. The effect of the methyl groups depends upon whether or not the β-methyl group is *cis* to the phenyl. When it is *cis*, the rate of addition is decreased compared to styrene and substitution of additional methyl groups has only a small effect on the rate of addition. In compounds lacking a *cis*-β-methyl group the rate of addition more closely resembles that for addition to the methylated ethylenes. Steric hindrance between the *cis*-methyl and phenyl groups is believed to be the cause of this difference in behavior between the ethylene and styrene series.

On a déterminé, à 25° dans des solutions de tétrachloro-1,1,2,2 éthane les vitesses d'addition et la composition des produits formés par l'addition du chlorure de chloro-4 benzènesulfényle sur une série de sept styrènes substitués par des groupes méthyles sur la chaine latérale. Contrairement à ce qui a été observé lors d'additions sur des séries correspondantes d'éthylènes méthylés, l'effet des groupes méthyles n'est pas cumulatif. L'effet des groupes méthyles dépend de la position *cis* ou *trans* du groupe méthyle en β par rapport au phényle. Quand il est *cis* la vitesse d'addition est diminuée par comparaison à la vitesse d'addition au styrène et la substitution de groupes méthyles additionnels n'a alors que peu d'effet sur la vitesse d'addition. Dans les composés où il n'y a pas de groupe méthyle *cis* par rapport au groupe phényle la vitesse d'addition ressemble plus à celle observée pour des additions à des éthylènes méthylés. On croit que les interférences stériques entre des groupes méthyles *cis* et les groupes phényles sont la cause de la différence dans la réactivité entre les dérivés de l'éthylène et du styrène.

[Traduit par le journal]

Can. J. Chem., **52**, 1807 (1974)

Can. J. Chem. Downloaded from www.nrcresearchpress.com by 210.87.254.5 on 09/05/12
For personal use only.

It has recently been shown (2) that progressively substituting the hydrogens on ethylene by methyl groups causes a cumulative increase in the rate of addition of 4-chlorobenzenesulfenyl chloride. As part of an investigation of the effect of alkene structure on the rates and products of addition of arenesulfenyl chloride, we have examined the effect of progressively increasing the number of methyl groups on the side chain of styrene. This paper reports the results of that study.

Results

We have measured the rate of addition of 4-chlorobenzenesulfenyl chloride to styrene (**1**) and all its methylated derivatives (**2** and **3**) in 1,1,2,2-tetrachloroethane (TCE) at 25° by means of the stopped flow technique using a Durrum-Gibson stopped-flow spectrophotometer. The rate of disappearance of 4-chlorobenzenesulfenyl chloride was followed by measuring the decrease in its absorption at 392.5 nm. The addition was found to exhibit normal second-order kinetics, first order in olefin and first order in sulfenyl chloride, to 80% completion of the reaction. The rate data are presented in Table 1.

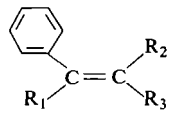

	R_1	R_2	R_3
1	H	H	H
2	CH_3	H	H
3	H	CH_3	H
4	H	H	CH_3
5	CH_3	CH_3	H
6	CH_3	H	CH_3
7	H	CH_3	CH_3
8	CH_3	CH_3	CH_3

The product composition was determined by means of p.m.r. spectroscopy. The assignment of chemical shift positions to the protons in the products is based upon the fact that protons α

[1]Reactions of sulfenyl chlorides and their derivatives Part X. For Part IX see ref. 1.

TABLE 1. The specific rate constants for the addition of 4-chlorobenzenesulfenyl chloride to a series of side chain methyl substituted styrenes at 25° in 1,1,2,2-tetrachloroethane

Alkene	No. of methyl groups	k_2 (M^{-1} s^{-1})	k_{rel}	No. of runs
Styrene (**1**)	0	62.0±0.2	1.0	6
2-Phenylpropene (**2**)	1	265 ±3	4.3	4
cis-1-Phenylpropene (**3**)	1	43.0±0.2	0.69	17
trans-1-Phenylpropene (**4**)	1	118.3±0.7	1.9	12
(*Z*)-2-Phenylbutene-2 (**5**)	2	42.0±0.3	0.68	3
(*E*)-2-Phenylbutene-2 (**6**)	2	422 ±5	6.8	3
1-Phenyl-2-methylpropene (**7**)	2	26.0±0.1	0.42	7
2-Phenyl-3-methylbutene-2 (**8**)	3	9.05±0.01	0.15	4

or β to chlorine are considerably deshielded relative to those α or β to sulfur (3, 4). This method has been extensively used by a number of workers (5, 6) and has been found to be applicable to the products of addition of arenesulfenyl chlorides to *cis*- and *trans*-1-phenylpropene (7) and styrene (6). The p.m.r. data are given in Table 2 for all the adducts.

The data in Table 2 as well as previously reported results for the addition of 4-chlorobenzenesulfenyl chloride to *cis*- and *trans*-1-phenylpropene (7) are in accord with the nonregiospecific (8) but *anti*-stereospecific addition. For example, the p.m.r. spectrum of the initial product of addition to 2-phenylpropene (**2**) shows four single peaks. The two peaks at δ 1.96 and 3.85 disappear with time while the other two increase. Such a result is consistent with the isomerization of a pair of isomeric Markownikoff[2] and anti-Markownikoff adducts. Such isomerizations are well documented (9). Consequently we assign the singlets at δ 1.96 and 3.85 to the methyl and methine protons of the anti-Markownikoff isomer while the singlets at δ 2.13 and 3.63 are assigned to the corresponding protons of the Markownikoff isomer. Similar assignments are made for the adducts to the other substituted styrenes.

The kinetic controlled product composition was determined by immediate p.m.r. analysis of the reaction mixture. This *in situ* determination of the adduct isomer ratio is necessary because of the known tendency of many β-chlorosulfides to isomerize. The thermodynamic controlled product composition was determined by allowing the p.m.r. sample tubes to stand at 25° until the product composition, as determined by p.m.r., remained constant. The kinetic and thermodynamic controlled product compositions are given in Table 3.

[2]In this series the compound with the chlorine attached to the benzylic carbon is defined as the Markownikoff adduct.

Discussion

On the basis of the kinetic results obtained for the addition of 4-chlorobenzenesulfenyl chloride to a series of methylated ethylenes, a similar cumulative effect might be expected for the methylated styrenes. Examination of the data in Table 1 reveals that this expectation is not realized. In fact the effect of the methyl groups is varied. Sometimes substitution increases the rate; sometimes the rate is decreased. A similar difference between the effect of substituting methyl groups on ethylene and styrene has been found in bromination (10).

Another difference between the ethylene and styrene series is the relative rate of addition to *cis–trans* isomers. In the ethylene series and for alkyl substituted ethylenes in general the ratio $k_c/k_t > 1$ while for the two styrene cases reported in Table 1 $k_c/k_t < 1$. It has recently been claimed that a ratio $k_c/k_t > 1$ is diagnostic of a bridged transition state in the rate determining step of electrophilic additions to alkenes (11). All available evidence indicates that the rate determining transition states for all the additions of 4-chlorobenzenesulfenyl chloride to the substituted styrenes in Table 1 are bridged yet $k_c/k_t < 1$. Thus the magnitude of the k_c/k_t ratio appears to be a poor criterion of bridging.

An understanding of the data can be obtained by dividing the compounds into two series as shown in Table 3. The two series differ in the location of the methyl substituent on the β-car-

Can. J. Chem. Downloaded from www.nrcresearchpress.com by 210.87.254.5 on 09/05/12
For personal use only.

TABLE 2. Observed p.m.r. chemical shifts for adducts of 4-chlorobenzenesulfenyl chloride with methyl-substituted styrenes (δ)

Adduct	Configuration	H_α	H_β	H_γ	$J_{\alpha\beta}$	$J_{\beta\gamma}$
ϕ—CHCl(CH₂SAr)		4.83,t(1H)	3.44,m(2H)			
ϕ—CHCl(CH₂Cl)		4.65,t(1H)	3.80,d(2H)			
ϕ—C(CH₃)Cl(CH₂SAr)			2.13,s(3H) 3.63,s(2H)			
ϕ—C(CH₃)SAr(CH₂Cl)			1.96,s(3H) 3.85,s(2H)			
ϕ—CHCl—CHSAr—CH₃	*threo*	4.97,d(1H)	3.66,g(1H)	1.23,d(3H)	5.5	7.0
	erythro	4.82,d(1H)	3.49,m(1H)	1.38,d(3H)	7.0	7.0
ϕ—CHSAr—CHCl—CH₃	*threo*	4.34,m(1H)	4.34,m(1H)	1.44,d(3H)		6.5
	erythro	4.14,d(1H)	4.32,g(1H)	1.54,d(3H)	7.0	6.5
ϕ—C(CH₃)Cl—CHCH₃	*threo*	2.12,s(3H)	3.72,g(1H)	1.48,d(3H)		7.0
	erythro	2.17,s(3H)	3.67,g(1H)	1.33,d(3H)		6.5
ϕ—C(CH₃)SAr—CHCH₃	*threo*	2.02,s(3H)	3.97,g(1H)	1.32,d(3H)		6.8
	erythro	2.09,s(3H)	3.84,g(1H)	1.61,d(3H)		7.0
ϕ—CHCl—C(CH₃)₂SAr		4.78,s(1H)		1.21,s(3H) 1.40,s(3H)		
ϕ—CHSAr—C(CH₃)₂Cl		4.16,s(1H)		1.63,s(3H) 1.76,s(3H)		
ϕ—C(CH₃)Cl—C(CH₃)₂SAr			2.03,s(3H)	1.25,s(3H) 1.21,s(3H)		
ϕ—C(CH₃)SAr—C(CH₃)₂Cl			1.75,s(3H)	1.48,s(3H) 1.33,s(3H)		

bon. In series 2 each compound contains a methyl group *cis* to the phenyl while in series 1, all the compounds lack this *cis*-methyl group. The presence of this *cis*-methyl group has a major effect upon the rate of addition. In series 1, the rate generally increases with increased methyl substitution. The effect of the methyl groups is about what is found for the addition to the methylated ethylenes. Thus substitution of one methyl group produces a threefold increase for the ethylenes while an increase of 1.9 or 4.3 is found for the monosubstituted styrene depending upon its position.

In series 2 substitution of methyl groups leads to a general *decrease* in the rate. The effect of the methyl groups in this series is opposite to their effect on the rate of addition in the ethylene series. Thus the increase in rate of addition between ethylene and 2-methylbutene-2 is a factor of 46 while the rate decrease between styrene and 2-phenyl-3-methylbutene-2 is a factor of 7.

The mechanism of addition of arene and alkane sulfenyl chlorides to alkenes has been proposed to involve the rate determining formation of an episulfonium ion which upon attack

Can. J. Chem. Downloaded from www.nrcresearchpress.com by 210.87.254.5 on 09/05/12
For personal use only.

Can. J. Chem. Downloaded from www.nrcresearchpress.com by 210.87.254.5 on 09/05/12
For personal use only.

TABLE 3. The kinetic and thermodynamic controlled products of the addition of 4-chlorobenzenesulfenyl chloride to a series of side chain methyl substituted styrenes at 25° in 1,1,2,2-tetrachloroethane

Series 1							Series 2						
			Product composition						Product composition				
			KCP*		TCP*				KCP*		TCP*		
Alkene	$k_2(M^{-1}\,s^{-1})$	k_{rel}	M†	aM†	M†	aM†	Alkene	$k_2(M^{-1}\,s^{-1})$	k_{rel}	M†	aM†	M†	aM†
$C_6H_5CH{=}CH_2$	62.0±0.2	1	83	17	100	0	$C_6H_5CH{=}CH_2$	62.0±0.2	1	83	17	100	0
$C_6H_5C(CH_3){=}CH_2$	265 ±3	4.3	87	13	100	0	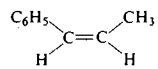	43.0±0.2	0.69	66	34	30	70
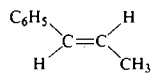	118.3	1.9	100	0	62	38	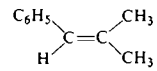	26.0±0.8	0.42	37	63	65	35
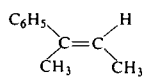	442 ±5	7.1	88	12	94	6	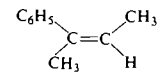	42.0±0.3	0.68	36	64	87	13
							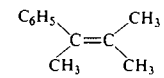	9.05±0.01	0.15	55	45	‡	‡

*KCP = kinetic controlled product; TCP = thermodynamic controlled product.
†M = Markownikoff; aM = anti-Markownikoff.
‡Decomposition and rearrangement.

TABLE 4. Analytical data for the adducts of 4-chlorobenzenesulfenyl chloride and side chain methylated styrenes

Alkene	C (%)		H (%)		S (%)	
	Calcd.	Found	Calcd.	Found	Calcd.	Found
Styrene	59.58	59.62	4.29	4.33	11.36	10.99
2-Phenylpropene	60.61	60.64	4.75	4.75	10.79	10.62
cis-1-Phenylpropene	60.61	60.67	4.75	4.68	10.79	10.76
trans-1-Phenylpropene	60.61	60.59	4.75	4.65	10.79	10.69
(*Z*)-2-Phenylbutene-2	61.74	61.94	5.18	5.21	10.30	10.70
(*E*)-2-Phenylbutene-2	61.74	62.04	5.18	4.94	10.30	10.45
1-Phenyl-2-methylpropene	61.74	62.21	5.18	5.22	10.30	10.64
2-Phenyl-3-methylbutene-2	62.77	62.70	5.27	5.76	9.86	9.99

by chloride ion forms the adduct in the product determining second step. The effect of methyl

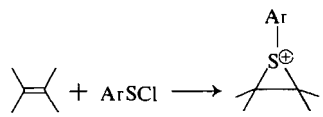

Rate determining step

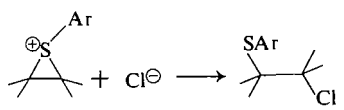

Product determining step

groups on the rate of addition to compounds **1**–**8** can be understood by examining their effect on the structure of the rate determining transition state.

The effect of the β-methyl group in *cis*-1-phenylpropene is known to force the phenyl out of the plane of the ethylenic double bond. This effect is evident in the difference between the u.v. spectra of the *cis–trans* isomers (12). This effect should also be important in the addition reaction. Consequently in the rate determining transition state for compounds in series 1, the phenyl group can exert its normal resonance effect, while in the rate determining transition state for compounds in series 2 it cannot. As a result the two transition states differ in their electronic structure. In series 1, the transition state is more unsymmetrical because of the ability of the phenyl group to delocalize the charge on the benzylic carbon and as a result it requires less bridging by the sulfur. This view is supported by the kinetic data in series 1. The effect of the methyl group depends upon its position, an α-methyl having a more pronounced effect than one in the β-position. In fact, the effect of adding an α-methyl group to styrene and *trans*-1-phenylpropene is quite similar: an increase in the rate of 4.3 and 3.7, respectively.

Further evidence for this structure of the transition state is provided by examining the kinetic controlled product composition for the compounds in series 1. The structure of the episulfonium ion intermediate should be similar to the structure of the transition state leading to it. Thus for series 1, the structures of the episulfonium ions should also be unsymmetrical. Thus kinetic controlled attack by chloride ion should occur at the benzylic carbon. According to the results in Table 3, this is exactly what is observed.

The effect of methyl groups on the rate determining transition state for the compounds in series 2 is not as clear cut. It can be argued that the phenyl group exerts only an inductive effect in series 2 and that this causes a decrease in the rate of addition which results in the ratio $k_c/k_t < 1$. However, it is not clear why the substitution of additional methyl groups does not increase the rate. The results of series 2 imply that the carbon atoms of the episulfonium-ion-like rate determining transition state, must bear little positive charge and consequently the methyl groups exert little polar effect. This implies a symmetrical transition state with strong bridging between sulfur and both carbons. Again the kinetic controlled product composition is in accord with such a structure for the rate determining transition state and intermediate episulfonium ion. Chloride ion attacks at both carbon atoms of the episulfonium ion which implies that the ions in series 2 are symmetrical and more strongly bridged than those in series 1.

It is instructive to compare our results with those obtained for the addition of bromine to this same series of side chain methyl substituted

Can. J. Chem. Downloaded from www.nrcresearchpress.com by 210.87.254.5 on 09/05/12
For personal use only.

styrenes (13). Again it was found that there is no simple relationship between the number of methyl groups and the rate of bromine addition. The additions are nonstereospecific although *anti* addition is favored. Styrenes with α-methyl groups were found to be substantially more reactive than those with only β-methyl groups. These results are taken as evidence that the intermediates formed in the bromine addition to styrenes resemble open α-phenylcarbonium ions more than bromonium ions. These results are in contrast with ours and provide further evidence that bridged intermediates as well as bridged rate determining transition states are involved in the addition of arenesulfenyl chlorides to styrenes.

The results of progressively substituting methyl groups for hydrogen on the rate and products of addition of 4-chlorobenzenesulfenyl chloride to styrene are entirely different from those observed for ethylene. In the case of ethylene the polar effect of the methyl groups is the dominant factor, steric effects are minimal. In the case of the styrene derivatives the steric effect of a *cis*-β-methyl group has a pronounced effect on both the rate of addition and the product composition.

Experimental

All melting and boiling points are uncorrected. Microanalyses were carried out by A. B. Gygli Microanalysis Laboratory, Toronto, Ontario.

4-Chlorobenzenesulfonyl Chloride and 1,1,2,2-Tetrachloroethane

These were prepared and purified as previously described (2).

Kinetics and Product Compositions

These were carried out as previously described (2).

cis- and trans-2-Phenyl-2-butenes

These compounds were prepared by the method of Yates and Rolston (13) and isolated by preparative g.l.c. on an SE-30 column at 160°.

All other olefins were obtained commercially and their purity was verified by g.l.c.

Analytical samples were prepared as previously described (2). Chemical analysis of the adducts is given in Table 4. In the case of the adducts of *cis*- and *trans*-1-phenylpropene and (*E*)- and (*Z*)-2-phenylbutene-2 the analytical samples were a mixture of the Markownikoff and anti-Markownikoff isomers.

Continued financial support from the National Research Council of Canada is gratefully acknowledged.

1. G. H. Schmid and V. M. Csizmadia. Int. J. Sulfur Chem. In press.
2. G. H. Schmid and D. G. Garratt. Can. J. Chem. **51**, 2463 (1973).
3. J. R. Cavanaugh and B. P. Dailey. J. Chem. Phys. **34**, 1093 (1961).
4. B. P. Dailey and J. N. Schoolery. J. Am. Chem. Soc. **77**, 3977 (1955).
5. G. M. Beverly and D. R. Hogg. Chem. Commun. 138 (1966).
6. W. H. Mueller and P. E. Butler. J. Am. Chem. Soc. **90**, 2075 (1968).
7. G. H. Schmid, V. M. Csizmadia, V. J. Nowlan, and D. G. Garratt. Can. J. Chem. **50**, 2457 (1972).
8. A. Hassner. J. Org. Chem. **33**, 2684 (1968).
9. G. H. Schmid and V. M. Csizmadia. Can. J. Chem. **50**, 2465 (1972).
10. K. Yates and J. Rolston. J. Am. Chem. Soc. **91**, 1483 (1969).
11. G. Collin, U. Jahnke, G. Just, G. Lorenz, W. Pritzkow, M. Rollig, and L. Winguth. J. Pract. Chemie, **311**, 238 (1969).
12. H. Suzuki. Electronic absorption spectra and geometry of organic molecules. Academic Press, New York. 1967. p. 293.
13. K. Yates and J. Rolston. J. Am. Chem. Soc. **91**, 1469 (1969).

Can. J. Chem. Downloaded from www.nrcresearchpress.com by 210.87.254.5 on 09/05/12
For personal use only.

Rearrangement Reactions in the Electron Impact Fragmentation of Isobutene[1]

MARGARET S.-H. LIN AND ALEX. G. HARRISON

Department of Chemistry, University of Toronto, Toronto, Ontario M5S 1A1

Received November 19, 1973

The detailed mass spectrum of isobutene has been examined using both D and ^{13}C labelling. It is shown that at low average internal energies of the molecular ion complete randomization of hydrogens and of carbons occurs prior to fragmentation to form $C_3H_5^+$. As the average internal energy of the molecular ion increases (by increasing the ionizing electron energy) the extent of both carbon and hydrogen randomization decreases. Carbon scrambling is complete in the molecular ion prior to fragmentation to form C_2 ions under all conditions studied. The results are consistent with a skeletal isomerization of the isobutene molecular ion by a mechanism involving a series of 1,3 ring closures to form methylcyclopropane type ions.

On a examiné en détail le spectre de masse de l'isobutylène utilisant les techniques de marquage au deutérium et au ^{13}C. On a montré qu'à des niveaux d'énergies internes relativement basse pour l'ion moléculaire il y a distribution au hasard des hydrogènes et des atomes de carbone avant la fragmentation conduisant à l'ion $C_3H_5^+$. A mesure que l'énergie interne moyenne de l'ion moléculaire augmente (en augmentant l'énergie d'ionisation) le taux de distribution au hasard du carbone et de l'hydrogène diminue. La redistribution des carbones est complète dans l'ion moléculaire avant la fragmentation pour conduire à des ions contenant deux atomes de carbone dans toutes les conditions étudiées. Les résultats obtenus sont en accord avec l'hypothèse qu'il y a une isomérisation au nivau du squelette de l'ion moléculaire de l'isobutylène par un mécanisme impliquant une série de fermetures de cycles 1,3 pour donner des ions du type méthylcyclopropane. [Traduit par le journal]

Can. J. Chem., **52**, 1813 (1974)

Introduction

It is well known (1–4), from deuterium labelling studies, that considerable hydrogen rearrangement occurs in unsaturated hydrocarbon molecular ions prior to fragmentation. The deuterium retention in the $C_3(H,D)_5^+$ ion formed from 1-butene-4-d_3 near the appearance potential threshold (1, 4) can be explained only on the basis of randomization of all H/D and is not consistent with a mechanism involving 1,3 hydrogen shifts only. Similar results have been obtained (3) in a study of labelled pentenes and it has been suggested (3) that the hydrogen rearrangements occur predominantly by 1,2 shifts. However, Meisels *et al.* (4) have shown that the ^{13}C retention in the $C_3H_5^+$ ion produced near the appearance potential threshold from 1-butene-4-^{13}C is 75% demonstrating loss of carbon identity and rearrangement of the carbon skeleton.[2] Such skeletal rearrangements will also result in hydrogen rearrangement and implicate a mechanism(s) other than simple 1,2 or 1,3 hydrogen shifts. Meisels *et al.* (4) have proposed a sequence of 1,3 ring closures to methylcyclopropane ions to explain the skeletal isomerization in the 1-butene molecular ion. Both the deuterium labelling studies (1, 4) and the ^{13}C labelling study (4) present some evidence that the amount of hydrogen rearrangement and skeletal rearrangement decrease with increasing internal energy indicating that fragmentation becomes competitive with isomerization at higher internal energies.

In connection with other studies we had available deuterium and ^{13}C labelled isobutenes and we have carried out a detailed study of the electron impact fragmentation of isobutene. The results show that for low energy $C_4H_8^+$ ions fragmenting to form $C_3H_5^+$ both carbon and hydrogen randomization are complete, whereas the extent of hydrogen and skeletal rearrangement clearly decreases for ions of higher excitation energy. In contrast carbon skeletal rearrangement is complete prior to fragmentation to $C_2H_4^+$ at all internal energies. The results are not consistent with hydrogen rearrangement by simple 1,2 or 1,3 shifts only but, in agreement

[1]The work reported here will constitute part of the Ph.D. Thesis to be submitted by M. S.-H. Lin to the University of Toronto.

[2]By contrast, in the 75 eV mass spectrum of propene-3-^{13}C (5) the $C_2H_3^+$ and CH_3^+ fragment ions show ~50% ^{13}C retention. This is not consistent with loss of carbon identity but has been rationalized in terms of 1,3 hydrogen shifts.

Can. J. Chem. Downloaded from www.nrcresearchpress.com by 210.87.254.5 on 09/05/12
For personal use only.

Can. J. Chem. Downloaded from www.nrcresearchpress.com by 210.87.254.5 on 09/05/12
For personal use only.

with the results for 1-butene (4), are consistent with a sequence of 1,3 ring closures to form methylcyclopropane ions.

Experimental

Low resolution spectra were obtained using a 90° 6 in. radius-of-curvature magnetic deflection mass spectrometer described previously (6). Samples were introduced through a room temperature inlet system to the source at ~100 °C. The ionizing electron current was ~10 μA with a repeller voltage of 3 V (1.1 eV ion exit energy) and the electron energy variable between 11 eV (nominal) and 75 eV. For the ^{13}C labelling studies mass spectra were obtained using an AEI MS-902 double focussing mass spectrometer at a resolution (~ 14 000) sufficient to resolve ^{13}C—CH doublets in the mass region of interest. The ratios $^{13}CC_yH_x/C_{y+1}H_x^+$ were obtained from repeated measurements of the intensities of the relevant peaks. Samples were introduced through a room temperature inlet system with a source temperature of ~150 °C. The ionizing electron current was 100 μA with the electron energy being varied between 20 eV (nominal) and 70 eV. Metastable peak intensities corresponding to fragmentation reactions occurring in the first drift region of the MS-902 were measured by the defocussing technique described earlier (7).

Unlabelled isobutene (Matheson research grade) was used without further purification. Isobutene-d_2 (2-methylpropene-1,1-d_2) and isobutene-d_6 (2-methyl-d_3-propene-3,3,3-d_3) were obtained from Merck, Sharp and Dohme, Montreal and were used without further purification. Low energy analysis in the molecular ion region showed the isobutene-d_2 to be 96.8% d_2, 0.9% d_1, and 2.3% d_0, while the isobutene-d_6 was 93.1% d_6, 6.5% d_5, 0.3% d_4, and 0.1% d_0. Corrections for these isotopic impurities have been made only in the molecular ion region. Isobutene-^{13}C (2-methylpropene-2-^{13}C) was obtained from Merck, Sharp, and Dohme, Montreal. Repeated measurements at low electron energy and low resolution yielded the ratio $^{13}CC_3H_8^+/C_4H_8^+ = 0.480 \pm 0.003$; this ratio was confirmed by high resolution measurements at 70 eV. Assuming normal ^{13}C isotopic abundance in the methyl and methylene positions this ratio yields the following % abundances.

$(CH_3)_2C = {}^{13}CH_2$	0.74%
$CH_3({}^{13}CH_3)C = CH_2$	1.49 ± 0.01%
$(CH_3)_2{}^{13}C = CH_2$	30.20 ± 0.14%
$(CH_3)_2C = CH_2$	67.57 ± 0.14%

Results

The mass spectrum (75 eV) of isobutene is shown in Fig. 1*a*. The major fragment ions are $C_3H_5^+$ (*m/e* 41), $C_3H_3^+$ (*m/e* 39), and $C_2H_4^+$ (*m/e* 28) with other significant fragment ions being $C_4H_7^+$ (*m/e* 55), $C_3H_4^+$ (*m/e* 40), $C_2H_5^+$ (*m/e* 29), and $C_2H_3^+$ (*m/e* 27). Metastable peaks (first drift region) were observed for formation of $C_3H_5^+$ and $C_3H_4^+$ from the molecular ion. No metastable peaks were observed for formation of $C_2H_4^+$ and it is probable that this ion also originates by direct fragmentation of the molecular ion. Consequently the major emphasis in the present work was directed toward a study of the label distribution in the $C_3H_5^+$ and $C_2H_4^+$ ions since this gives the clearest indication of the extent of rearrangement in the molecular ion prior to fragmentation. The results concerning formation of the $C_4H_7^+$ ion were inconclusive because of the isotopic impurities present and the possibility of significant primary hydrogen–deuterium isotope effects.

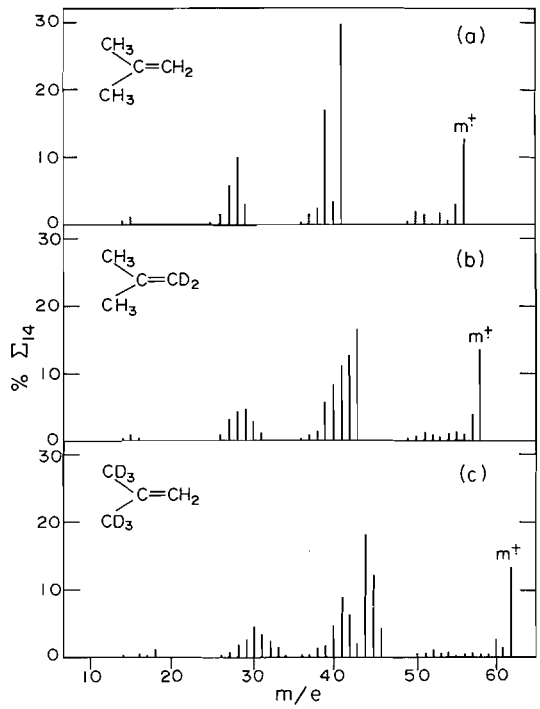

FIG. 1. Mass Spectra of (*a*) $(CH_3)C{=}CH_2$, (*b*) $(CH_3)_2C{=}CD_2$, and (*c*) $(CD_3)_2C{=}CH_2$.

Mass Spectra of Isobutene-d_2 and Isobutene-d_6

The 75 eV mass spectra of the two deuterium labelled isobutenes are shown in Figs. 1*b* and *c*.[3] The mass spectra of isobutene and the labelled isobutenes in the C_3 region are presented in Table 1 as a function of electron energy. The spectra at each electron energy for the three compounds were determined immediately fol-

[3]The complete spectra, in tabular form, are available, at a nominal charge from the Depository of Unpublished Data, National Science Library, National Research Council of Canada, Ottawa, Canada K1A 0S2.

Can. J. Chem. Downloaded from www.nrcresearchpress.com by 210.87.254.5 on 09/05/12
For personal use only.

lowing each other without alteration of any of the instrumental parameters. Also shown in Table 1 are the spectra observed for fragmentation reactions occurring in the first drift region of the MS-902.

The experimental results for the labelled isobutenes are compared in Table 1 with the ion intensities calculated assuming complete H/D randomization in the $C_4(H,D)_8^+$ molecular ion prior to fragmentation. To carry out these calculations it was assumed that the total intensity for each $C_3(H,D)_n^+$ species was the same as the intensity of $C_3H_n^+$ in the spectrum of the unlabelled isobutene at the same electron energy.

As can be seen the metastable peak intensity data and the electron impact mass spectral data at 11.0 and 11.5 eV (nominal) for the labelled isobutenes are in good agreement with the distribution calculated assuming complete H/D scrambling in the molecular ion prior to fragmentation to form $C_3(H,D)_5^+$ and $C_3(H,D)_4^+$.[4] As the electron energy is increased the experimental distribution begins to deviate considerably from the distribution calculated assuming complete scrambling. This is particularly noticeable for formation of the $C_3(H,D)_5^+$ ion where for isobutene-d_2 the $C_3H_3D_2^+$ (*m/e* 43) and $C_3H_5^+$ (*m/e* 41) intensities are considerably greater than the calculated intensities whereas the $C_3H_4D^+$ (*m/e* 42) intensity is considerably less. Although part of the *m/e* 41 increase could be due to an abnormally high intensity for $C_3HD_2^+$ (*i.e.*, nonrandom distribution in forming $C_3(H,D)_3^+$) the *m/e* 43 signal can only be $C_3H_3D_2^+$. The low intensity of $C_3H_4^+$ (and thus $C_3(H,D)_4^+$) indicates that the decreased intensity at *m/e* 42 relative to the calculated intensity cannot be entirely accounted for by nonrandom distribution in $C_3(H,D)_4^+$ (*i.e.* abnormally low intensity of $C_3H_2D_2^+$). The results indicate that, compared to the complete randomization observed at low electron energies, isobutene-d_2 preferentially loses CH_3 or CHD_2 (to form $C_3H_3D_2^+$ and $C_3H_5^+$, respectively) at higher electron energies (14 eV and higher).

This conclusion is confirmed by the results for the d_6 isobutene. Of the $C_3(H,D)_5^+$ ions only $C_3H_2D_3^+$ (*m/e* 44) suffers from interference ($C_3D_4^+$) and since the total $C_3(H,D)_4^+$ intensity is relatively small this interference is minor. Comparing the experimental distributions in the region *m/e* 44 to *m/e* 46 at 14 eV or higher with those calculated assuming randomization we observe that the $C_3H_2D_3^+$ (*m/e* 44) and $C_3D_5^+$ (*m/e* 46) intensities are higher than the calculated intensities while the $C_3HD_4^+$ intensity is lower. Thus loss of CD_3 or CH_2D is favored over loss of CDH_2. Thus for both compounds the preferred fragmentation at 14 eV or higher involves loss of the three methyl hydrogens or of the two ethylenic hydrogens along with one methyl hydrogen. Loss of two methyl hydrogens with one methylene hydrogen is of considerably lower probability. The latter loss can originate only by considerable isotopic exchange between the two positions. This aspect will be discussed further below in light of the ^{13}C labelling results.

Table 2 summarizes the mass spectral data for the C_2 ions as a function of electron energy for the unlabelled and deuterium labelled isobutenes. The intensities are expressed as a % of the total C_2 ion intensity. For each of the labelled compounds the experimental results are compared with the relative intensities calculated assuming complete H/D scrambling prior to formation of the $C_2(H,D)_x^+$ ($x = 2$ to 5) ions. For these calculations the total intensities for each $C_2(H,D)_x^+$ species were assumed to be identical to that observed for the corresponding $C_2H_x^+$ ion at the same electron energy.

At the lowest electron energies only $C_2(H,D)_4^+$ is observed and for the labelled compounds it is observed that the experimental intensities are close to those calculated assuming complete H/D scrambling. As the electron energy is increased and more C_2 ions are observed the experimental distribution begins to differ from that calculated assuming complete scrambling. In light of the observation (see below) that at 70 eV the carbon retention is ~50% for all C_2 ions ($C_2H_3^+$ to $C_2H_5^+$) indicating complete scrambling of the carbons the significance of the deviations from scrambling in the deuterium labelling results is not clear. Of the C_2 ions only $C_2H_4^+$ appears to originate directly from the molecular ion with $C_2H_3^+$ and $C_2H_5^+$ originating by further fragmentation of the $(M - 1)^+$ species. It is possible that the deviations from scrambling reflect isotope effects in formation of the $(M - H)^+$ and $(M - D)^+$

[4]The fragmentation to form $C_3(H,D)_5^+$ could not be examined in the absence of $C_3(H,D)_4^+$ ions because the appearance potentials of the two species were found to be practically identical.

Can. J. Chem. Downloaded from www.nrcresearchpress.com by 210.87.254.5 on 09/05/12
For personal use only.

TABLE 1. Mass spectra of isobutenes in C_3 region as function of energy (intensities % total C_3 ions)

Metastable spectra			11.0 eV		11.5 eV		14.0 eV		18.0 eV		30.0 eV		75.0 eV	
m/e	Exp.	Calcd.	Exp.	Calcd.	Exp.	Calcd.	Exp.	Calcd.	Exp.	Calcd.	Exp.	Calcd.	Exp.	Calcd.
							Isobutene							
36													0.2	
37											0.2		2.6	
38									0.1		1.0		4.5	
39							0.7		11.4		30.8		31.2	
40	7.4		7.5		7.0		12.7		10.6		7.7		5.9	
41	92.6		92.5		93.0		86.6		77.9		60.3		54.9	
							Isobutene-d_2							
36													0.2	0.2
37											0.1	0.2	1.4	2.0
38											0.4	0.6	2.5	3.1
39							0.4	0.3	3.1	4.1	8.5	11.4	10.0	13.1
40		1.6	1.9	1.6	1.8	1.5	3.3	3.1	6.9	8.4	15.8	18.2	14.7	18.1
41	14.9	14.1	14.0	14.2	14.4	14.0	16.8	16.6	18.8	15.6	21.3	14.2	19.7	12.6
42	50.0	51.2	51.1	51.2	50.0	51.3	42.8	49.1	33.4	44.0	24.0	34.0	22.2	30.6
43	35.0	33.0	33.0	33.0	33.8	33.2	36.7	31.0	37.9	27.8	30.0	21.5	29.1	19.8
							Isobutene-d_6							
36													0.2	0.2
37													0.7	0.7
38											0.2	0.1	2.2	2.2
39											1.0	0.2	2.7	2.0
40							0.1	0.1	1.7	1.2	6.3	3.8	7.9	5.8
41							0.6	0.4	5.1	6.1	15.2	16.5	15.1	16.7
42	0.9	1.6	1.6	1.6	2.1	1.5	3.8	3.0	5.9	6.4	10.6	12.7	10.5	12.4
43	2.9	4.2	4.6	4.3	4.3	4.0	5.7	7.3	5.0	6.1	3.9	4.4	3.2	3.4
44	31.8	34.6	35.5	34.6	36.1	34.7	38.7	33.6	40.5	30.1	32.9	23.2	30.2	22.2
45	52.6	49.6	48.1	49.6	47.5	49.8	41.0	46.4	32.1	41.7	21.8	32.3	20.5	29.4
46	11.6	9.9	10.2	9.9	10.0	10.0	10.1	9.3	9.8	8.4	8.1	6.5	7.0	5.9

TABLE 2. Mass spectra of isobutenes in C_2 region (intensities % C_2 total ions)

	14.0 eV		18.0 eV		25.0 eV		75.0 eV	
m/e	Exp.	Calcd.	Exp.	Calcd.	Exp.	Calcd.	Exp.	Calcd.
				Isobutene				
25							0.7	
26					1.2		7.2	
27					17.1		28.6	
28	100.0		92.6		60.9		49.1	
29			7.4		20.8		14.3	
				Isobutene-d_2				
25							0.6	0.5
26					0.8	0.6	4.9	4.1
27					8.9	6.6	17.5	13.3
28	23.1	21.4	22.6	19.9	22.8	22.3	25.7	26.1
29	54.7	57.2	50.1	53.9	34.0	38.9	27.5	32.7
30	22.2	21.4	24.4	23.9	24.1	24.2	16.9	18.2
31			2.8	2.6	9.4	7.4	6.9	5.1
				Isobutene-d_6				
25							0.2	0.2
26							1.7	0.8
27					1.3	0.5	3.9	3.1
28					3.7	2.5	10.2	7.0
29					8.6	9.2	15.2	15.3
30	24.0	21.4	23.4	19.9	22.6	19.2	25.8	20.8
31	55.3	57.2	51.0	53.1	30.9	34.8	19.8	28.1
32	20.6	21.4	21.9	22.5	20.0	20.4	13.7	15.6
33			2.9	3.0	10.7	11.2	7.7	7.7
34			0.8	0.8	2.4	2.2	1.9	1.5

ions in the labelled isobutenes. Such isotope effects will correspondingly influence the intensity distributions in fragment ions originating by further decomposition of $(M - H)^+$ and $(M - D)^+$.

Isobutene-^{13}C (2-Methyl Propene-2-^{13}C)

Table 3 presents the intensity ratios ($^{13}CC_{n-1}H_x^+/C_nH_x^+$) measured for various ions at 70 eV using the MS-902 at a resolution sufficient to resolve ^{13}C—CH doublets. The sample contained 30.2% ^{13}C in the 2-position. From the intensity ratios measured the % C2 retention in each fragment ion has been calculated and is shown in the final column of Table 3. The details of the method of calculation are given in the Appendix.

Assuming loss of only a methyl or methylene carbon in formation of the C_3 ions one would expect 100% C2 retention, whereas assumption of complete scrambling of the carbons would lead to a prediction of 75% C2 retention. The $C_3H_5^+$ and $C_3H_4^+$ ions both show ~86% C2 retention indicating extensive skeletal rearrangement but not sufficient to result in complete carbon equivalence. On the other hand the C_2 ions all show ~50% retention of C2, which is the value predicted assuming complete carbon scrambling. Surprisingly the $C_3H_3^+$ ion shows almost complete retention of C_2 (96%). Metastable peaks were observed for the following reactions forming $C_3H_3^+$.

[1] $C_4H_7^+ \rightarrow C_3H_3^+ + CH_4$

[2] $C_3H_5^+ \rightarrow C_3H_3^+ + H_2$

[3] $C_3H_4^+ \rightarrow C_3H_3^+ + H$

Since there are so many routes leading to formation of $C_3H_3^+$ the mechanistic conclusions to be drawn from the high retention result are not clear.

Table 4 presents the ^{13}C retention data for the $C_3H_5^+$ ion as a function of electron energy. The $^{13}CC_2H_5^+/C_3H_5^+$ ratios from 70 to 20 eV (nominal) electron energy were obtained from the mass-resolved peaks. The ratio in the energy range 11.5 to 13.5 eV (nominal) was obtained from the low resolution spectra after correction of the *m/e* 41 intensity $C_3H_5^+$ for $^{13}CC_2H_4^+$. This correction amounted as a maximum to

Can. J. Chem. Downloaded from www.nrcresearchpress.com by 210.87.254.5 on 09/05/12
For personal use only.

Can. J. Chem. Downloaded from www.nrcresearchpress.com by 210.87.254.5 on 09/05/12
For personal use only.

TABLE 3. ^{13}C retention data for ions in isobutene-^{13}C

Ion species	Intensity ratio	% C2 retention
$\frac{^{13}CC_3H_8^+}{C_4H_8^+}$	0.480±0.003	—
$\frac{^{13}CC_2H_5^+}{C_3H_5^+}$	0.390±0.001	86.5
$\frac{^{13}CC_2H_4^+}{C_3H_4^+}$	0.388±0.002	86.1
$\frac{^{13}CC_2H_3^+}{C_3H_3^+}$	0.445±0.002	96.0
$\frac{^{13}CCH_5^+}{C_2H_5^+}$	0.198±0.002	49.6
$\frac{^{13}CCH_4^+}{C_2H_4^+}$	0.196±0.003	49.2
$\frac{^{13}CCH_3^+}{C_2H_3^+}$	0.195±0.003	48.9

TABLE 4. ^{13}C retention in $C_3H_5^+$ as function of electron energy

Electron energy (eV, nominal)	$\frac{^{13}CC_2H_5^+}{C_3H_5^+}$	% C2 retention
70	0.390±0.001	86.5
40	0.389±0.001	86.3
30	0.387±0.003	85.9
24	0.375±0.003	83.8
22	0.357±0.003	80.4
21	0.352±0.003	79.5
20	0.352±0.003	79.5
11.5–13.5	0.344±0.005	78.0

0.5% of the total *m/e* 41 intensity and was calculated from the measured $C_3H_4^+$ intensity assuming complete scrambling of the carbons in formation of $C_3H_4^+$.[5] Over the electron energy range 11.5 to 13.5 eV the observed ratio remained constant within experimental error.

The % C2 retention in $C_3H_5^+$ decreases from ~86% at 75 eV to ~78% at low electron energy. For the two fragmentation reactions

[4] $$^{13}CC_3H_8^+ \rightarrow {}^{13}CC_2H_5^+ + CH_3$$

[5] $$C_4H_8^+ \rightarrow C_3H_5^+ + CH_3$$

the metastable peak intensity ratio m_4^*/m_5^* was found to be 0.358 ± 0.020 for fragmentation reactions occurring in the first drift region of the double focussing mass spectrometer. This leads to a calculated C2 retention of 74.2 ± 5% in agreement with the 75% retention calculated assuming complete carbon equivalence in $C_4H_8^+$ prior to fragmentation. The results clearly show that the % retention of C2 decreases as the electron energy, and hence, the average excitation energy of $C_4H_8^+$, decreases.

Over the nominal electron energy range 10–13 eV the $C_2H_4^+$ ion is the only significant fragment ion in the C_2 region. The ratio $^{13}CCH_4^+/C_2H_4^+$ was found to be 0.198 ± 0.005 from which one obtains 51.4 ± 1% C2 retention. This compares favorably with the result at 75 eV and both are in good agreement with the 50% retention calculated assuming complete carbon randomization.

Discussion

The ^{13}C labelling results clearly show that for the lowest energy $C_4H_8^+$ ions fragmenting to form $C_3H_5^+$ carbon skeletal isomerization has proceeded sufficiently prior to fragmentation to make all carbon atoms equivalent. Hence the % retention of C2 is that predicted assuming complete randomization of the carbons. As the average internal energy of the $C_4H_8^+$ ions is increased by increasing the electron energy the extent of skeletal rearrangement prior to fragmentation decreases as shown by the increased C2 retention in the $C_3H_5^+$ fragment ion. In contrast, over the entire electron energy range studied, skeletal rearrangement has led to complete randomization of carbons prior to fragmentation to form $C_2H_4^+$. The deuterium labelling results parallel the ^{13}C labelling results. At the lowest average internal energies resulting in fragmentation to form $C_3(H,D)_5^+$ complete H/D randomization has occurred prior to fragmentation. As the average internal energy of the fragmenting ion increases the extent of H/D randomization decreases.

The results clearly show that the hydrogen and carbon randomization reactions are rate processes and that fragmentation of the molecular ion becomes kinetically competitive with the randomization reactions as the internal energy

[5]The alternative of assuming 100% retention of C2 in the $C_3H_4^+$ ion changes the measured $^{13}CC_2H_5^+/C_3H_5^+$ ratio to 0.350 ± 0.005 from the reported value of 0.344 ± 0.005. Since the retention in $C_3H_4^+$ is ~86% at 70 eV and appears to decrease with decreasing electron energy the assumption of complete scrambling appears more reasonable.

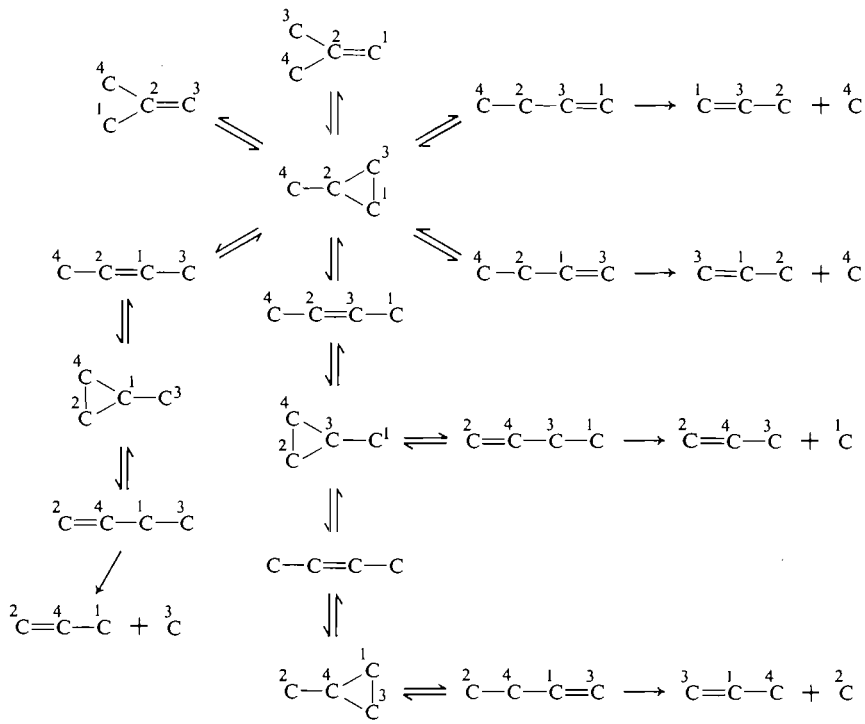

SCHEME 1

of the $C_4H_8^+$ ions is increased. Although the hydrogen randomization can be rationalized in terms of a series of 1,2 or 1,3 hydrogen shifts, this cannot be the only isomerization reaction occurring since such hydrogen shifts will not lead to carbon randomization. In addition, appearance potential measurements (8) indicate that at the threshold the $C_3H_5^+$ ion formed from isobutene has the allyl structure; such a structure cannot be achieved by simple 1,2 or 1,3 hydrogen shifts. A plausible mechanism for skeletal isomerization leading to carbon randomization and to formation of allyl ions on fragmentation involves a sequence of 1,3 ring closures to form methylcyclopropane ions as illustrated schematically in Scheme 1.[6] This mechanism has been suggested by Wagner (9) to explain the radiation-induced rearrangement of solid pentenes and hexenes at 77 °K and by Meisels *et al.* (4) to explain the carbon skeletal rearrangement in the 1-butene molecular ion at low ionizing energies. It is obvious that a number of ring closures and openings are necessary before complete randomization of the carbons is attained with formation of allyl ion. Consequently it is not surprising that $C_4H_8^+$ ions of high internal energy, with a consequent short lifetime with respect to fragmentation, do not achieve complete randomization. The sequence of ring closures and openings proposed in Scheme 1 also leads to hydrogen randomization and it is not necessary to postulate 1,2 or 1,3 hydrogen shifts to explain the results, although such shifts are not precluded.

The authors are indebted to the National Research Council of Canada for financial support.

Appendix

To calculate the ratio of $^{13}CC_2H_x^+/C_3H_x^+$ we consider the fragmentation of the unlabelled species $(CH_3)_2C{=}CH_2$ (67.57%) and the singly labelled species $CH_3(^{13}CH_3)C{=}CH_2$ (1.49%), $(CH_3)_2C{=}{}^{13}CH_2$ (0.74%), and $(CH_3)_2{}^{13}C{=}CH_2$ (30.20%). In addition molecular ions containing two ^{13}C labels also can contribute to formation of $^{13}CC_2H_x^+$. The only significant $^{13}C_2C_2H_8$ species will contain a label at C2 and may be represented as $^{13}CH_3(CH_3)^{13}C{=}CH_2$ with an

[6]For simplicity only the carbon skeleton is shown in Scheme 1 and the positive charge is omitted.

Can. J. Chem. Downloaded from www.nrcresearchpress.com by 210.87.254.5 on 09/05/12
For personal use only.

abundance of ~3.3% of the $(CH_3)_2{}^{13}C{=}CH_2$ species. In the following derivation α represents the fraction of $C_3H_x{}^+$ ions containing C2. We further assume that for those C_3 ions containing C2 the remaining two carbons are selected at random from the remaining three carbons. The relation between the measured intensity ratio and α may be derived as follows:

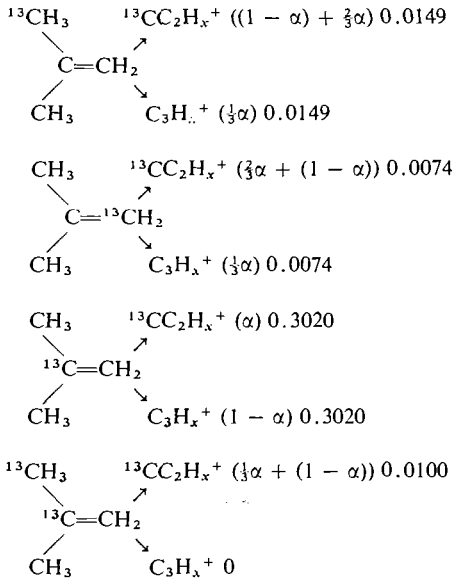

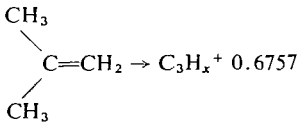

From these relative amounts one calculates the relation

$$\frac{{}^{13}CC_2H_x{}^+}{C_3H_x{}^+} = \frac{0.0323 + 0.2846\alpha}{0.9777 - 0.2945\alpha}$$

Similar reasoning leads for the C_2 ions to the expression

$$\frac{{}^{13}CCH_x{}^+}{C_2H_x{}^+} = \frac{0.0222 + 0.2945\alpha}{0.9984 - 0.2978\alpha}$$

1. W. A. BRYCE and P. KEBARLE. Can. J. Chem. **34**, 1249 (1956).
2. W. H. MCFADDEN. J. Phys. Chem. **67**, 1074 (1963).
3. B. J. MILLARD and D. F. SHAW. J. Chem. Soc. (B), 664 (1965).
4. G. G. MEISELS, J. Y. PARK, and B. G. GIESSNER. J. Am. Chem. Soc. **91**, 1555 (1969).
5. H. H. VOGE, C. D. WAGNER, and D. P. STEVENSON. J. Catal. **2**, 58 (1963).
6. B. G. KEYES and A. G. HARRISON. J. Am. Chem. Soc. **90**, 5671 (1968).
7. C. W. TSANG and A. G. HARRISON. Org. Mass Spectrom. **3**, 647 (1970).
8. G. G. MEISELS, J. Y. PARK, and B. G. GIESSNER. J. Am. Chem. Soc. **92**, 254 (1970).
9. C. D. WAGNER. J. Phys. Chem. **71**, 3445 (1967).

Can. J. Chem. Downloaded from www.nrcresearchpress.com by 210.87.254.5 on 09/05/12
For personal use only.

Can. J. Chem. Downloaded from www.nrcresearchpress.com by 210.87.254.6 on 09/05/12
For personal use only.

Canadian Journal of Chemistry | Journal canadien de chimie

Published by THE NATIONAL RESEARCH COUNCIL OF CANADA
Publié par LE CONSEIL NATIONAL DE RECHERCHES DU CANADA

Volume 52 Number 10 May 15, 1974 | Volume 52 numéro 10 15 mai 1974

The Stability of Some Metal Complexes in Mixed Solvents

KWAN-KIT MUI AND W. A. E. MCBRYDE
Department of Chemistry, University of Waterloo, Waterloo, Ontario N2L 3G1
AND
EVERT NIEBOER
Department of Chemistry, Laurentian University, Sudbury, Ontario P3E 2C6

Received November 14, 1973

Acidity constants and stability constants of certain metal complexes (nickel(II), zinc(II), and manganese(II)) with ethylenediamine and glycine were determined at 25 °C and in 0.1 *M* ionic strength in mixed aqueous solutions of methanol (MeOH), dioxane (DOX), acetonitrile (MeCN), and dimethylformamide (DMF). In general, the stability constants of the metal complexes and the first protonation constant of glycine increase with increasing composition of the co-solvent in the order

$$H_2O < MeOH < MeCN \sim DMF < DOX$$

The protonation constants of ethylenediamine pass through a minimum at some particular solvent composition, while the second protonation constant of glycine exhibits behavior characteristic of the particular solvent employed.

These results are discussed in terms of medium and solvent effects and properties of the solvent that might affect these, but find more satisfactory explanation in terms of solvent displacement during the association reactions. The observations can be accounted for in terms of a complete equilibrium constant incorporating the concentration (activity) of each solvent substance.

Les constantes d'acidité et les constantes de stabilité de complexes de certains métaux (nickel(II), zinc (II) et manganèse(II)) avec l'éthylènediamine et la glycine sont déterminées à 25 °C et à une concentration de 0.1 *M* dans des solutions aqueuses de méthanol (MeOH), de dioxanne (DOX), d'acétonitrile (MeCN) et de diméthylformamide (DMF). En générale, les constantes de stabilité des complexes de métaux et la constante de la première protonation de la glycine sont croissantes quand la composition de leur solvant augmente selon l'ordre

$$H_2O < MeOH < MeCN \sim DMF < DOX$$

Les constantes de protonation de l'éthylènediamine passe par un minimum à une certaine composition particulière du solvant, alors que la constante de la seconde protonation de la glycine manifeste un comportement caractéristique du solvant particulier utilisé.

Ces résultats sont discutés en termes du milieu, des effets du solvant et des propriétés du solvant qui pourraient influencer ces derniers; mais ils sont expliqués, de façon plus satisfaisantes, en termes de déplacement de solvant durant les réactions d'association. Les observations peuvent être interprétées en termes de constante d'équilibre complet incluant la concentration (activité) de chaque substance de solvant.

[Traduit par le journal]

Can. J. Chem. Downloaded from www.nrcresearchpress.com by 210.87.254.6 on 09/05/12
For personal use only.

Introduction

The possibility of utilizing mixed solvents to improve analytical methods involving complex formation have been noted elsewhere (1). Furthermore, studies of equilibrium and kinetics in mixed solvents may be of assistance in interpreting the role of solvent in inorganic reactions. Previous studies of the solvent effect on complex equilibria have been concerned mainly with simple organic acids and metal chelates in selected solvents such as dioxane and alcohols of low molecular weight. Of the few metal ions and ligands studied, the metal complexes increased in stability as the concentration of non-aqueous solvent (co-solvent) increased. This trend also held good for protonation constants of ligands with a carboxylate group, but those with amine groups behaved differently. So far no systematic studies in different solvents with a wide range of solvent compositions have been made.

As part of a larger study of free-energy correlations in coordination chemistry we have undertaken the measurement of complex equilibria for three metal ions (Ni^{2+}, Zn^{2+}, and Mn^{2+}) and the hydrogen ion with the ligands ethylenediamine and glycine in mixed aqueous solutions of four organic solvents, with composition of the latter ranging from 0 to 80% by volume. The solvents were chosen to examine how such of their properties as basicity, dielectric constant, and tendency to solvation might influence complex stability. The possible effects of hydrolysis of these solvents was also considered.

Experimental

Acidity and stability constants were determined by means of acid–base titration of the ligand with ethylenediamine or potassium hydroxide (sodium hydroxide in the case of aqueous dioxane solution) as the titrant. In each titration 0.1 *M* potassium nitrate (or sodium perchlorate in aqueous dioxane solution) was employed as background electrolyte.

Reagents

Standard 1 *M* solutions of KOH and NaOH were prepared from ampoules of British Drug Houses concentrated volumetric solutions, and standardized by titration. All chemicals were of analytical reagent grade unless otherwise indicated. Glycine was recrystallized (2), and ethylenediamine redistilled from sodium. Nickel(II) perchlorate was prepared by displacement from nickel(II) nitrate by heating a solution of the latter to fumes in perchloric acid. Zinc perchlorate was prepared direct from zinc metal (Fisher certified) by dissolution in perchloric acid. Manganese(II) perchlorate was obtained from the G.F. Smith Chemical Co. Sodium perchlorate solution (1.0 *M*) was prepared by neutralization of sodium carbonate with perchloric acid. The concentrations of Zn^{2+} and Mn^{2+} were determined by direct complexometric titration with EDTA (3), while Ni^{2+} was determined according to Schwarzenbach's procedure (4).

Methanol was purified by redistillation and DMF by vacuum distillation (2). Dioxane was purified by the method of Kraus and Vingee (5). Baker's A.R. grade acetonitrile was used without further purification.

Apparatus

A Radiometer Model PHM4d p*H* meter, equipped with a G202B glass electrode and a K401 saturated calomel electrode was used for the p*H* titrations. The meter and electrodes were calibrated to read p*H* with two suitable buffers with any necessary correction to match the Nernst slope being made with the temperature compensation control. All titrations were conducted in a water-jacketed cell compartment (6) thermostatted at 25 ± 0.1 °C. A stream of nitrogen gas, after passing through granules of Ascarite, was bubbled into the solution and formed an inert atmosphere over the solutions titrated. The p*H* values were measured to ±0.005 unit. Titrants were added by an Agla microsyringe of total volume 0.5 cc (Burroughs and Wellcome Co. Ltd., London, England).

The calomel electrode was cleaned and refilled frequently after working in the mixed solvents. For titrations in dioxane solutions when sodium perchlorate was the background electrolyte a sleeved electrode was used. This consisted of a glass tube of slightly greater diameter fitted over the calomel electrode and terminating in a small fritted disc. The sleeve was charged with 3.5 *M* ammonium chloride solution. Following each titration the glass and calomel electrodes were conditioned in 0.1 *M* hydrochloric acid before re-use.

Dielectric constants of the mixed solvents were measured by a dipolmeter (Wissenschaftlich-Technische Werkstüllen, Germany) with the cells appropriate to the range of values measured.

Solutions for Measurement

Stock solutions of the metal nitrates and perchlorates (0.1 *M*) were prepared in slightly acidic media (p*H* 3–4). Solutions for potentiometric titrations were prepared by adding 10 cc of the supporting electrolyte (1.0 *M* solutions of KNO_3 or $NaClO_4$) and a measured volume of the co-solvent to a 100 cc volumetric flask which contained known amounts of the metal ion (C_M), ligand (C_L), and added acid (C_H). The solution was made up to the mark with doubly distilled water. The mole fraction of co-solvent (n_s) was calculated from the volume composition.

Acidity Measurements

The "activity" of hydrogen ion was measured by the p*H* meter, but converted to concentration by an empirical factor Γ (7), which was determined for each solvent composition and background electrolyte used by measurements of p*H* of solutions of known hydrogen-ion concentration

$$[1] \qquad \Gamma = 10^{-pH}/[H]$$

(Compare Van Uitert and Haas factor U_H (8).) All acidity and other equilibrium constants were calculated as concentration quotients.

TABLE 1. Dissociation constants of protonated ligands at 25 °C supporting electrolyte = 0.1 *M* KNO_3 (0.1 *M* $NaClO_4$ in DOX)

System (v/v%)		n_2	ε^{25}	Γ	Glycine		Ethylenediamine	
					pK_{a1}*	pK_{a2}*	pK_{a1}*	pK_{a2}*
Aqueous		0.00	78.54	[0.851]	2.34	9.65	7.18	10.05
MeOH	55	0.352	57.3	0.572	2.87	9.43	6.67	9.48
	60	0.400	55.3	0.546	3.04	9.42	6.62	9.43
	65	0.452	53.0	0.528	3.12	9.41	6.58	9.39
	70	0.509	50.7	0.518	3.23	9.40	6.55	9.37
	75	0.571	48.0	0.527	3.38	9.41	6.53	9.36
	80	0.640	45.5	0.564	3.51	9.46	6.54	9.35
DOX	0	0.000	78.54	0.890	2.33	9.60	7.12	10.00
	20	0.050	61.4	0.869	2.60	9.64	6.98	9.89
	40	0.123	44.3	0.827	2.94	9.70	6.79	9.77
	50	0.173	35.7	0.868	3.17	9.76	6.73	9.73
	60	0.240	27.5	1.03	3.45	9.84	6.70	9.75
	70	0.329	19.3	1.41	3.81	9.98	6.78	9.85
	75	0.386	16.4	1.89	4.05	10.07	6.86	9.94
	80	0.457	13.5	2.76	4.33	10.23	7.03	10.10
MeCN	20	0.0787	72.5	0.94	2.59	9.68	7.11	9.96
	40	0.186	63.7	1.07	2.90	9.79	7.12	9.96
	50	0.255	59.4	1.22	3.08	9.84	7.14	9.98
	60	0.339	54.3	1.48	3.29	9.95	7.19	10.04
	70	0.444	49.5	2.02	3.63	10.11	7.30	10.15
	75	0.506	47.4	2.42	3.82	10.20	7.37	10.23
	80	0.577	45.0	3.12	4.11	10.35	7.48	10.34
DMF	20	0.0551	74.0	0.554	2.50	9.52	7.03	9.81
	40	0.135	69.0	0.330	2.78	9.46	6.89	9.62
	50	0.189	65.0	0.253	2.97	9.46	6.80	9.54
	60	0.259	60.8	0.196	3.26	9.51	6.75	9.45
	70	0.352	56.2	0.170	3.65	9.65	6.77	9.46
	75	0.412	53.5	0.174	3.96	9.78	6.84	9.52
	80	0.483	50.9	0.197	4.28	9.98	7.08	9.58

It seems appropriate to furnish the following additional practical information concerning measurements of p*H* in mixed solvents. It was repeatedly observed that in order to obtain steady, reproducible results, each measurement must be carried out with glass electrodes that had undergone preconditioning as follows. Each electrode was immersed in a well-stirred mixed solvent for several days before use. At intervals the electrode was washed with distilled water and conditioned overnight in 0.1 *M* hydrochloric acid. The electrode was then tested with aqueous buffers. The procedure was repeated until reproducible results were obtained. Before each titration in mixed solvent the electrodes were pre-conditioned for at least an hour in solvent of identical composition to that about to be titrated. Presumably this practice results in a reasonably consistent and appropriate hydrogen-ion activity in the outer layer of hydrated (solvated) gel in the glass membrane.

Determination of Equilibrium Constants

From the p*H* titrations sets of corresponding values of $\bar{n}_H$, p*H* for the ligands alone, or $\bar{n}_L$, p*L* for the metal complexes could be obtained by methods that have been fully described elsewhere, *e.g.*, ref. 9. From this information acidity constants or stability constants respectively could be derived either by Bjerrum's method of successive approximations, or by computerized calculations (10).

Results

In Table 1 are given values of the factor Γ, measured dielectric constants ε, and the acidity constants for the two ligands at a number of compositions for each solvent. The variation of pK_a, for each ligand is shown as a function of solvent composition in Fig. 1*a* and *b*. Values of all stability constants determined at the indicated solvent compositions are presented in Table 2. Each value reported is the mean of at least two independent determinations. The variation of log K_1 values with solvent composition is shown in Fig. 2.

Discussion

Activity Measurements and Medium Effects

Part of the information required to determine complex stability constants are the acidity con-

Can. J. Chem. Downloaded from www.nrcresearchpress.com by 210.87.254.6 on 09/05/12
For personal use only.

Can. J. Chem. Downloaded from www.nrcresearchpress.com by 210.87.254.6 on 09/05/12
For personal use only.

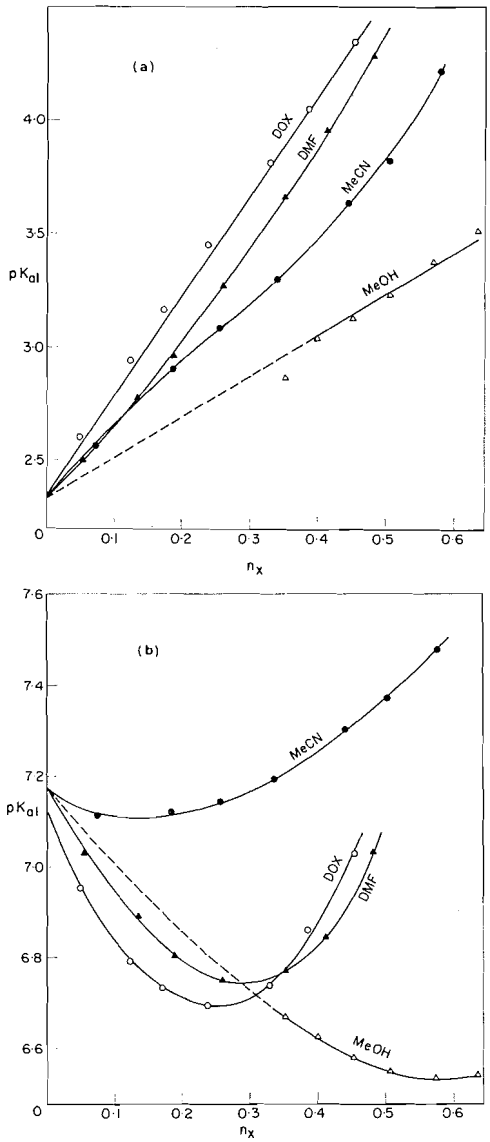

FIG. 1. Variation of first acid dissociation constants of ligands with composition of mixed solvents at 25 °C: (*a*) glycine; (*b*) ethylenediamine.

stants of the ligands. A considerable body of the literature of reactions in non-aqueous or mixed solvents has been taken up with defining a scale or scales of acidity that may be applied in such varied media. The so-called "universal scale of acidity", which is based on the standard state for hydrogen-ion activity in water, has been discussed by a number of authors, and a good contemporary summary given by Bates (11). In order to relate our results to this theoretical approach we briefly review the significance of p*H* measurements in solvents other than pure water.

When the potential of an electrode reversible to an ion i is measured in a mixed solvent the indicated activity of the ion may be related to a standard state either in that solvent or in strictly

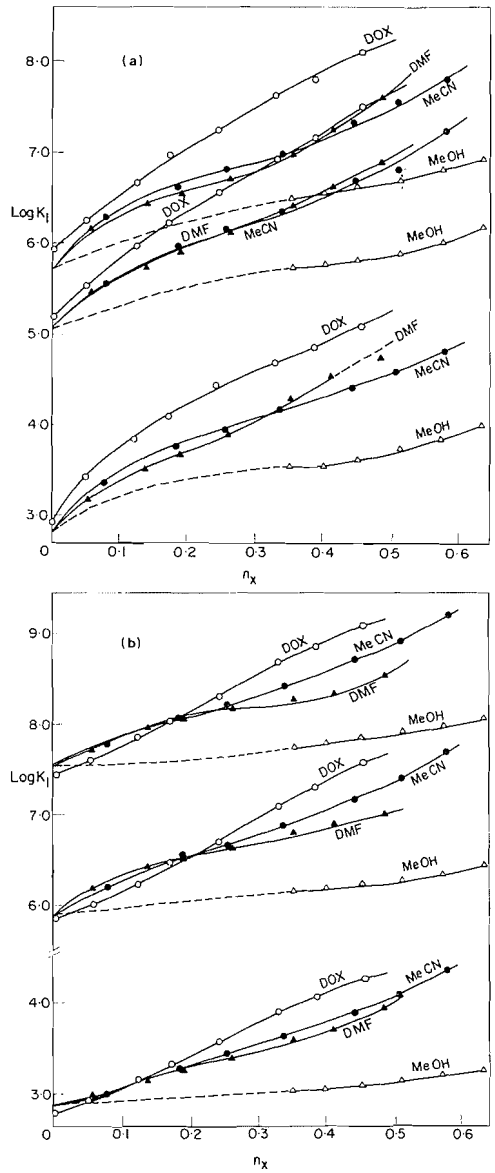

FIG. 2. Variation of first metal complex stability constants with composition of mixed solvents at 25 °C: (*a*) glycine complexes; (*b*) ethylenediamine complexes. The uppermost set of curves applies to nickel complexes, the middle set to zinc complexes, and the lowest set to manganese(II) complexes.

TABLE 2. Stability constants of metal complexes in mixed aqueous organic solvents at 25 °C*

(*a*) Aqueous methanol: (in 0.1 *M* KNO_3)

Volume (%)	Stability constants					
	Ethylenediamine			Glycine		
	Ni(II)	Zn(II)	Mn(II)	Ni(II)	Zn(II)	Mn(II)
0	7.56	5.91	2.85	5.83	5.08	2.83
	6.29	4.81	(1.9)	4.70	4.06	(2.0)
	4.30	2.10	—	3.30	2.39	—
55	7.74	6.15	3.03	6.52	5.74	3.55
	6.32	4.93	2.08	5.29	4.65	2.53
	4.27	1.89	—	3.65	2.60	—
60	7.78	6.19	3.07	6.58	5.77	3.57
	6.35	4.97	2.10	5.35	4.68	2.61
	4.28	1.92	—	3.71	2.57	—
65	7.84	6.23	3.11	6.65	5.83	3.65
	6.40	5.01	2.15	5.41	4.73	2.68
	4.30	1.96	—	3.77	2.58	—
70	7.92	6.28	3.15	6.72	5.92	3.76
	6.50	5.06	2.18	5.49	4.81	2.77
	4.41	1.98	—	3.84	2.68	—
75	7.98	6.34	3.23	6.83	6.04	3.87
	6.56	5.12	2.28	5.58	4.93	2.87
	4.48	2.07	—	3.93	2.81	—
80	8.07	6.43	3.26	6.96	6.21	4.01
	6.66	5.20	2.31	5.70	5.08	3.00
	4.57	2.16	—	4.05	2.98	—

*Values are in the order of log K_1, log K_2, log K_3; values in parentheses are of fair accuracy only: $\sigma \sim 0.1$–0.2; values in square brackets are only approximate: $\sigma > 0.2$.

(*b*) Aqueous dioxane (in 0.1 *M* $NaClO_4$)

Volume (%)	Stability Constants					
	Ethylenediamine			Glycine		
	Ni(II)	Zn(II)	Mn(II)	Ni(II)	Zn(II)	Mn(II)
0	7.44	5.85	2.79	5.96	5.19	2.94
	6.05	4.69	[1.9]	4.76	4.14	—
	4.07	1.94	—	3.29	2.73	—
20	7.58	5.99	2.93	6.25	5.53	3.43
	6.21	4.78	2.01	5.00	4.46	(2.6)
	4.17	1.86	—	3.49	2.86	—
40	7.86	6.22	3.16	6.66	5.97	(3.8)
	6.44	5.00	(2.2)	5.38	4.88	[3.0]
	4.33	1.98	—	(3.8)	3.08	—
50	8.03	6.47	3.33	6.99	(6.2)	(4.1)
	6.62	5.25	(2.4)	(5.7)	5.19	—
	4.49	2.13	—	4.05	(3.2)	—
60	8.29	6.70	3.57	7.27	6.54	(4.4)
	6.82	5.40	2.61	5.99	5.47	—
	4.64	2.32	—	4.32	3.36	—
70	8.68	7.08	3.90	7.66	6.93	(4.7)
	7.26	5.91	2.95	6.33	5.75	—
	5.05	2.68	[1.7]	4.63	3.65	—
75	8.84	7.29	4.06	7.83	7.18	[4.9]
	7.44	6.10	3.13	(6.5)	5.90	—
	5.20	2.81	[1.8]	4.80	3.77	—
80	9.09	7.56	4.27	8.13	7.51	[5.1]
	7.71	6.39	3.29	6.64	6.10	—
	5.47	3.00	[2.1]	5.03	3.98	—

Can. J. Chem. Downloaded from www.nrcresearchpress.com by 210.87.254.6 on 09/05/12
For personal use only.

TABLE 2. (*Concluded*)

(*c*) Aqueous acetonitrile (in 0.1 *M* KNO_3)

Volume (%)	Stability constants					
	Ethylenediamine			Glycine		
	Ni(II)	Zn(II)	Mn(II)	Ni(II)	Zn(II)	Mn(II)
20	7.74	6.19	2.98	6.30	5.54	3.36
	6.34	5.08	—	5.08	4.50	2.43
	4.21	2.29	—	3.57	2.80	—
40	8.04	6.51	3.29	6.61	5.96	3.74
	6.60	5.40	[2.3]	5.42	4.89	2.76
	4.35	2.32	—	3.86	3.00	—
50	8.20	6.65	3.44	6.84	6.16	(3.9)
	6.77	5.48	(2.5)	5.57	5.06	(2.9)
	4.43	2.23	—	4.00	3.12	—
60	8.42	6.88	3.65	6.98	6.26	(4.2)
	6.97	5.78	(2.7)	5.79	5.29	(3.2)
	4.61	2.51	—	4.16	3.31	(2.3)
70	8.71	7.17	3.90	7.35	6.71	(4.4)
	7.21	5.99	(2.9)	6.07	5.67	(3.6)
	4.83	2.57	—	4.49	3.70	(2.4)
75	8.91	7.40	(4.1)	7.58	6.85	(4.6)
	7.41	6.21	(3.1)	6.31	5.79	(3.6)
	4.99	2.78	—	4.71	3.76	(2.5)
80	9.20	7.68	(4.4)	7.84	7.26	[4.8]
	7.71	6.48	(3.8)	6.48	6.04	[3.8]
	5.30	2.98	—	4.94	4.03	[2.8]

(*d*) Aqueous DMF (0.1 *M* KNO_3)

Volume (%)	Stability constants					
	Ethylenediamine			Glycine		
	Ni(II)	Zn(II)	Mn(II)	Ni(II)	Zn(II)	Mn(II)
20	7.71	6.18	2.98	6.17	5.46	3.18
	6.40	5.04	—	5.02	4.36	(—)
	4.45	2.28	—	3.52	2.68	—
40	7.94	6.42	3.14	6.44	5.74	3.52
	6.60	5.29	2.26	5.36	4.69	2.58
	4.65	2.45	—	3.86	2.96	(—)
50	8.06	6.53	3.26	6.56	5.92	3.67
	6.74	5.38	2.34	5.52	4.92	2.72
	4.82	2.51	(1.6)	4.03	3.11	(—)
60	8.16	6.63	3.40	6.70	(6.1)	(3.9)
	6.90	5.52	2.47	5.75	(5.2)	(3.0)
	5.00	2.60	1.85	4.26	(3.3)	(2.4)
70	8.26	6.78	3.59	7.02	6.44	4.30
	7.10	5.69	2.66	6.06	5.57	3.41
	5.27	2.86	1.96	4.68	3.68	(2.7)
75	8.33	6.88	3.71	7.26	6.65	[4.6]
	7.24	5.83	2.76	6.24	5.79	[3.6]
	5.48	3.10	2.03	4.91	3.89	[2.9]
80	8.52	7.00	3.95	7.64	6.92	[4.7]
	7.45	6.02	2.89	6.56	5.98	[3.8]
	5.83	3.30	2.17	5.24	4.18	[3.1]

Can. J. Chem. Downloaded from www.nrcresearchpress.com by 210.87.254.6 on 09/05/12
For personal use only.

Can. J. Chem. Downloaded from www.nrcresearchpress.com by 210.87.254.6 on 09/05/12
For personal use only.

aqueous solution. In the latter event, the activity of the ion ${}_wa_i^*$ is related to the medium effect coefficient ${}_wY_i^*$ as follows:

$$[2] \qquad {}_wa_i^* = C_i \cdot {}_wY_i^*$$

where C_i is the stoichiometric concentration of the ion and ${}_wY_i^*$ is Harned and Owen's medium effect (12) given by the following relation

$$[3] \quad \log ({}_wY_i^*/{}_wY_i) = \log {}_mY_i + \log ({}_sY_i^*/{}_wY_i)$$

where ${}_mY_i$ is the primary medium effect and ${}_sY_i^*$ the secondary medium (salt) effect. Thus

$$[4] \qquad {}_wY_i^* = {}_mY_i \cdot {}_sY_i^*$$

A pH measurement, $pH_{(x)}^*$, is a measure of the hydrogen-ion activity ${}_wa_H^*$ in the mixed solvent with reference to the aqueous standard state, given as follows

$$[5] \qquad pH_{(x)}^* = \hat{E}_j - \log {}_wa_H^*$$

when $\hat{E}_j$ is a term incorporating the liquid junction potential, which depends on the solvent composition. For a cell based on glass and calomel electrodes

$$[6] \quad \hat{E}_j = \{E_{gl}^0 - E_{gl}^{0*} - (E_j - E_j^*)\}/2.3RT/F$$

in which the asterisk indicates a value in the mixed solvent (13). The quantity δ is defined (11) as follows

$$[7] \quad pH_{(x)}^* - p_sa_H^* = \hat{E}_j - \log {}_mY_H = \delta$$

where ${}_sa_H^*$ is the activity of hydrogen ion in the mixed solvent referred to the standard state in that solvent. When δ is known for a particular solvent composition ${}_sa_H^*$ can be determined from a pH-meter reading.

This δ is related to our log Γ by the following equation

$$[8] \qquad -\log \Gamma = \delta - \log {}_sY_H^*$$

Van Uitert and Haas (8) determined log Γ in mixed solvents containing electrolyte at several ionic strengths, and by extrapolation of their values to zero ionic strength when ${}_sY_H^* \rightarrow 1$, a value of δ was determined. From our results δ can only be estimated through an estimate of ${}_sY_H^*$; to make this we have employed the Davies' equation (14), recognizing that this has no established validity in solvents other than water. In Table 3 are given our estimates of δ for various compositions of three solvents. Those in methanol are comparatively small, suggesting that $\hat{E}_j$ and log ${}_mY_H$ must compensate to a considerable degree in this region of solvent composition.

TABLE 3. δ values in mixed solvent systems

		δ for solvent =	
V (%)	MeOH	DOX	MeCN
0		−0.0614	−0.042
20		−0.110	−0.0982
40		−0.186	−0.178
50		−0.311	−0.248
55	0.0713		
60	0.0834	−0.565	−0.353
65	0.0873		
70	0.0838	−1.088	−0.512
75	0.0609	−1.474	−0.603
80	0.0145	−2.043	−0.729

Solvent Effect on the Acidity Constants of Ligands

As shown by the data of Table 1 and in Fig. 1, our results confirm those of other workers respecting the difference in behavior of the carboxyl-group ionization compared to that of the ammonium group (1, 15), and also show that these differences are roughly found to apply in all four solvents examined. Thus for the dissociation of —COOH in glycine, pK_{a1} increases more or less linearly with increasing concentration of co-solvent. The trend of dissociation of the substituted ammonium hydrogen is non-linear, and in most cases passes through a maximum (minimum pK_a) at some solvent composition.

The variation in pK_{a1} for glycine with solvent composition, like that for carboxylic acids in general, can be interpreted by an electrostatic model with the aid of the Born equation (16). The failure of the cationic acids of ethylenediamine (H_2en^{2+}, Hen^+) to conform to the Born model has been discussed in terms of the relative importance of the solvent effect and dielectric effect, and the former is assumed to be greater in acids involving $\equiv NH^+$ dissociation (17). Recently the non-electrostatic contribution to the change in pK_a has been regarded as representing the sum of medium effects for individual ions (1). Evidence given later in this paper strongly links what has been regarded as the exceptional behavior of the amine group on protonation to an appreciable amount of interaction with the co-solvent.

Solvent Effect on the Stabilities of Metal Complexes

Figure 2 shows a parallelism in the variation of the complex stability constants from one metal

Can. J. Chem. Downloaded from www.nrcresearchpress.com by 210.87.254.6 on 09/05/12
For personal use only.

to the next for a given solvent. Similar trends are observed for log K_2 and log K_3. The relative solvent effect in increasing the stability constants of the metal complexes at a particular n_x of solvent follows the order

$$\text{DOX} > \text{MeCN} > \text{MeOH} > \text{H}_2\text{O}$$

From this ranking DMF has been omitted because observations in this solvent appear less regular and depend somewhat on the ligand.

There is an apparent relative increase in stability in DMF solutions in passing from $ML \rightarrow ML_2 \rightarrow ML_3$. This anomaly may possibly be the result of hydrolysis of DMF in aqueous solution. It is known that this substance is appreciably hydrolyzed in alkaline aqueous solution, though less so in neutral and acidic solution. However, in most of our experiments with slightly buffered solutions in which pK_a or log K_n was being measured, no serious unsteadiness or drift in pH readings was observed so that at the time hydrolysis was not suspected as a problem. The result of this occurring would be to lower the pH of solutions, which would in turn lead to an overestimate in log K_n. The effect would be more serious as the pH became higher, as would be the case for measurement of log K_3.

An equation of the form

$$[9] \qquad \log K_{ML}^* - \log K_{ML} = an_x + b$$

in which a and b are constants that may be characteristic of the metal ion, ligand, or solvent (15), was of comparatively little value in correlating the present results. Evidently specific solvent–solute interactions necessitate that a and b must be functions of n_x. In the next section the authors will discuss these results from the viewpoint of displacement of solvent molecules accompanying the complex-forming reaction.

The order of dielectric constants of the solvents

$$\varepsilon_{H_2O}\,(78.0) > \varepsilon_{MeCN}\,(37.5) > \varepsilon_{MeOH}\,(32.6) > \varepsilon_{DOX}\,(2.0)$$

does not exactly follow the order of relative solvent effects as noted above. Thus a continuum model of solvent based on coulomb interactions is of only limited value in interpreting the present results (18). According to recent summaries (19, 20) empirical solvent parameters from physical and chemical measurements on pure nonaqueous solvents have made it possible to establish the following polarity order

$$\text{H}_2\text{O} > \text{MeOH} > \text{MeCN} > \text{DMF} > \text{DOX}$$

which is very similar to the order of the solvent effect previously given. Kreshkov (21) found that the autoprotolysis constant (K_s) of the solvent provides a measure of the "absolute scale" of acidity of solvents. The greater the value of pK_s the less is the solvent ionized, the smaller the solvating capacity, and so forth. The magnitudes of K_s (22) again follow closely the polarity order, differing only in the interchange of positions of MeCN and DMF. The foregoing evidence is all suggestive of the probable importance of interactions with solvent in the overall reactions of complex formation.

Displacement of Solvent Molecules

A recent communication (23) has stressed the importance of taking into account the elimination of coordinated water molecules as a cause contributing to the medium effect. Thus a reaction of complex formation may be described by the equation

$$[10] \qquad \text{M(aq)} + \text{L(aq)} = \text{ML(aq)} + w\text{H}_2\text{O}$$

The increase in apparent stability of ML in an aqueous mixed solvent compared to that in water alone derives in some part from the lower activity (or concentration) of water in the mixed solvent compared to this value in pure water. A complete equilibrium constant (24) $K^{*\prime}$ will therefore include a term in the concentration of water, and will relate to the apparent formation constant K^* as $K^{*\prime} = K^*[\text{H}_2\text{O}]_s^n$, where $[\text{H}_2\text{O}]_s$ is the concentration of water in the mixed solvent. This explanation incorporates the assumption that solvation of the reacting species is almost exclusively by water molecules.

Alternatively the possibility might be considered that both water and co-solvent molecules could be involved in solvation. Thus in a mixed solvent molecules of both kinds may be regarded as ligands that are coordinated to or associated with each central ion or molecule. In general, formation of a complex BA_n may be written as

$$[11] \qquad \text{BA}_{n-1}(x\text{H}_2\text{O}, b\text{S}) + \text{A}(y\text{H}_2\text{O}, a\text{S}) = \text{BA}_n(z\text{H}_2\text{O}, t\text{S}) + w\text{H}_2\text{O} + d\text{S}$$

A complete equilibrium constant is given by

$$[12] \qquad K^{*\prime} = \frac{[\text{BA}_n][\text{H}_2\text{O}]_s^w[\text{S}]^d}{[\text{BA}_{n-1}][\text{A}]} = K^*[\text{H}_2\text{O}]_s^w[\text{S}]^d$$

In aqueous solution b, a, t, and d are all zero, and w will be represented in this case by a different symbol j.

Can. J. Chem. Downloaded from www.nrcresearchpress.com by 210.87.254.6 on 09/05/12
For personal use only.

Now if we set aside the secondary medium effect for the several species involved in formation of BA_n by working throughout in a constant and relatively high concentration of background electrolyte, the stoichiometric equilibrium constants (concentration quotients) $K^{*\prime}$ and K' in mixed solvent and water respectively can be related to the standard free energy of transfer and to the apparent equilibrium constants as follows:

$$[13] \quad \log K^{*\prime} - \log K' = -\Delta G_R^t/2.3RT$$

$$[14] \quad \log K^{*\prime} - \log K' = \log K^* - \log K + \log \frac{[H_2O]_s^w[S]^d}{[H_2O]^j}$$

where

$$\Delta G_R^t = \Delta G_{BA_n}^t + w\Delta G_{H_2O}^t + d\Delta G_s^t - \Delta G_{BA_{n-1}}^t - \Delta G_A^t$$

$$= 2.3RT \log \frac{{}_mY_{BA_n} \cdot {}_mY_{H_2O}^w \cdot {}_mY_s^d}{{}_mY_{BA_{n-1}} \cdot {}_mY_A}$$

Here ΔG_i^t is the standard molar free energy of transfer of the species i from water to the mixed solvent, and ${}_mY_i$ is the corresponding primary medium effect coefficient.

It is commonly held that water molecules are preferentially, if not almost exclusively, solvated in mixed solvents (23, 25), although there is certainly evidence (26) that methanol molecules are capable of appreciable solvation from aqueous methanol solutions. If the co-solvent is essentially inactive with respect to solvation in reaction 11, $d \sim 0$. In that case, from eqs. 13 and 14

$$[15] \quad \log K^* - \log K = -\Delta G_R^t/2.3RT - w \log [H_2O]_s + j \log [H_2O]$$

and if we assume in this case that $w = j$ this becomes

$$[15a] \quad \log K^* - \log K = -\Delta G_R^t/2.3RT - w \log ([H_2O]_s/[H_2O])$$

Equation 15*a* should describe the variation of K^* with solvent composition; if the medium effect is assignable strictly to variation in solvent composition according to a mass law relationship, that is, if $K^{*\prime}$ is a proper equilibrium constant independent of the composition of the solvent, then ΔG_R^t must be a constant. Accordingly, a plot of $\log K^*$ *vs.* $\log [H_2O]_s$ should be linear with a slope equal to w. This correlation was tested for all sets of data; it yielded approximately linear plots for all metal complexes in dioxane or acetonitrile, but poorer linear relationships in methanol. For the metal glycinates and for pK_{a1} for glycine the values of the slopes of the best-fit lines for the solvents dioxane, acetonitrile, and dimethylformamide were about 2.5, while the average slopes for aqueous methanol solutions had lower values, around 1.0 to 1.7. For the metal ethylenediamine complexes the average slopes in dioxane and acetonitrile were again around 2.5, but smaller in DMF and methanol, and no linear correlations were found for protonation of this ligand.

The recurrence of a value about 2.5 (maximum 3.0) for the slopes in the foregoing correlations with the solvents of lowest polarity, but of distinctly lower values for the correlations in methanol prompted the testing of a second hypothesis. Suppose that j represents a solvent transfer number characteristic of the particular reaction being examined, but that part of this number could be attributed to the transfer of co-solvent, *i.e.*, to d in reaction 11. Thus

$$[16] \quad j = w + d$$

with $d \neq 0$ in the case of a more polar solvent such as methanol. From eqs. 13, 14, and 16 can be derived

$$[17] \quad (j \log [S] + \log K^*) - \log K = -\Delta G_R^t/2.3RT - w \log ([H_2O]_s/[S]) + j \log [H_2O]$$

Equation 17 contains two unknown parameters, j and w. It could be used, as eq. 15*a* was, to find a value of w, provided a value of j could be assigned beforehand. There is no theoretical basis for doing this, but the previous correlations had suggested a value of $w_{max} = 3$, and on this account a trial value of $j = 3$ was put into eq. 17. Plots of $(j \log [S] + \log K^*) = Y$ *vs.* $\log([H_2O]_s/[S]) = X$ were then drawn, and disclosed remarkably good straight lines, of which examples are given in Fig. 3. Accordingly, it seemed reasonable to assign values of w to the gradients of Y on X. Values obtained in this way are shown in Table 4. With only two small exceptions these values of w are equal to or less than three.

It is obvious that the values of w (and by inference also of d) suggested in Table 4 cannot have any precise significance in view of the arbitrary choice of j in eq. 17. Nevertheless it is remarkable that the values of w approach 3 in those co-solvents, except as subsequently noted, in which on the basis of polarity one would expect minimum solvation, and that the values are uniformly

Can. J. Chem. Downloaded from www.nrcresearchpress.com by 210.87.254.6 on 09/05/12
For personal use only.

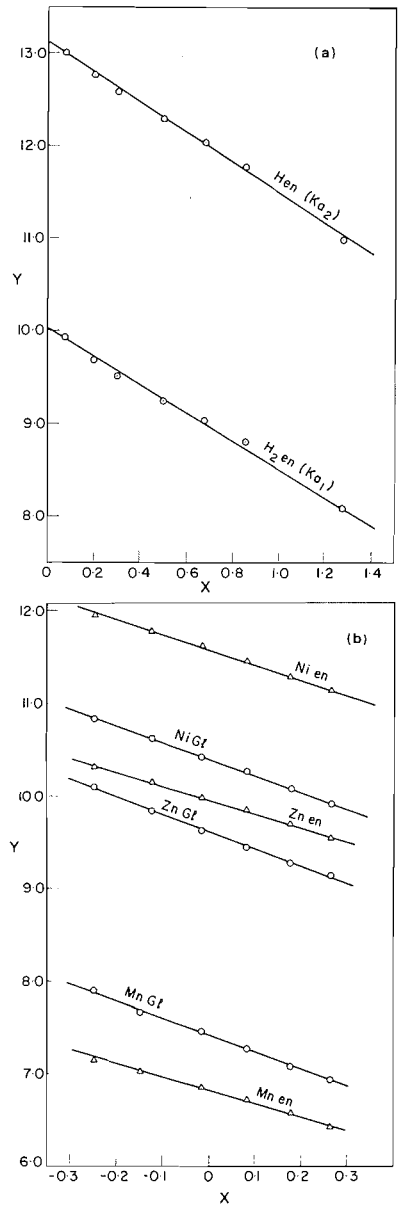

FIG. 3. Correlations based on eq. 17. (*a*) Acidity constants of ethylenediamine; (*b*) stability constants of 1:1 complexes.

smallest in methanolic solutions where, in spite of some opinions to the contrary, solvation could be significant. It is also remarkable that linear correlations based on eq. 17 were found for all K_1 and K_2 values for the metal and proton complexes of both ligands in all four mixed solvents examined. In particular, the correlations for pK_{a2} for glycine and for pK_{a1} and pK_{a2} for ethylenediamine contrast with the non-linear relationships observed for n_x (Fig. 1*b*), and the poor correlations found by the application of eq. 15*a*. With respect to these protonation reactions, the analysis in this paper assigns an appreciable amount of the medium effect to solvation of the bases by the co-solvent, or at least to an appreciable value of d in eq. 11.

Values of $\Delta G_R{}^t$ are also found from this correlation; according to the values of j used and of w found, individual values of $\Delta G_R{}^t$ can be calculated for each solvent composition, and measures of dispersion about a mean value assigned. Results consonant with the values in Table 4 are given in Table 5. As previously mentioned, the significance of the apparent constancy of $\Delta G_R{}^t$ is that $K^{*\prime}$ is independent of solvent composition for any given system. Thus eq. 12 defines the complete equilibrium constant in the mixed solvent, and contains terms that compensate for changes in solvent composition. It is also worth noting that when w approaches j, solvation by the co-solvent is unimportant. In this event, the standard free energy of transfer to that solvent is very small. This follows from eq. 12 which shows that $K^{*\prime}$ and $K^{\prime}$ become equivalent as $d \rightarrow 0$.

Recognizing the arbitrariness with which a value of j was selected in order to determine the values of w given in Table 4, the authors have considered the choice of j values by other criteria. A computer-assisted analysis showed that correlations obtained with eq. 17 were not particularly sensitive to the value of j assigned; reasonable linear regressions were obtained with values of j increasing in steps from 2 to 4, and corresponding values of w obtained. An objective basis for the choice of a value for j was that which gave a minimum variance in the value of w for each system. It is questionable, however, whether the experimental data are of sufficient accuracy to permit such a procedure, for in the event it produced considerable variations in the individual values of j and w, including some negative values of d (which might be significant), but these values were much more difficult to rationalize with the character of the solvents and reactions concerned than those given in Table 4.

The final question to be considered is what, if any, physical significance should be attributed to the values of w and d found in this way. They certainly do not imply that the relative solvation of individual species is independent of solvent composition. The notion that a characteristic

TABLE 4. Values of w and Δw in solvent systems ($j = 3.0$)

Solute	Equilibrium constant	DOX		MeCN		DMF		MeOH	
		w	Δw	w	Δw	w	Δw	w	Δw
Metal ethylenediamine									
Ni	K_1	2.77±0.02	0.01	2.68±0.02	0.09	2.11±0.10	−0.24	1.60±0.04	−0.03
	K_2	2.76±0.04		2.59±0.03		2.35±0.05		1.63±0.04	
Zn	K_1	2.82±0.02	−0.04	2.70±0.03	0.07	2.15±0.09	−0.12	1.48±0.03	−0.02
	K_2	2.86±0.03		2.63±0.04		2.27±0.07		1.50±0.03	
Mn	K_1	2.63±0.02	0.02	2.62±0.04	−0.22	2.26±0.04	0.28	1.41±0.06	−0.02
	K_2	2.61±0.03		2.84±0.23		1.98±0.03		1.43±0.05	
Metal glycine									
Ni	K_1	3.07±0.04	0.15	2.76±0.03	0.10	2.64±0.07	−0.09	1.80±0.02	0.06
	K_2	2.92±0.08		2.66±0.04		2.73±0.03		1.74±0.02	
Zn	K_1	3.13±0.01	0.25	2.85±0.06	0.08	2.69±0.02	−0.19	1.87±0.03	0.08
	K_2	2.88±0.09		2.77±0.05		2.88±0.03		1.79±0.03	
Mn	K_1	2.91±0.07		2.71±0.06	0.02	2.83±0.03	−0.02	1.88±0.03	0.03
	K_2			2.69±0.07		2.85±0.05		1.85±0.03	
Acid ligands									
$H_n$en	K_{a1}	1.48±0.04	−0.15	1.78±0.06	−0.01	1.43±0.07	0.17	0.69±0.01	−0.01
	K_{a2}	1.63±0.03		1.79±0.06		1.26±0.06		0.70±0.01	
H_nG1	K_{a1}	2.94±0.01	0.98	2.74±0.02	0.71	2.99±0.06	1.15	2.16±0.09	1.18
	K_{a2}	1.96±0.05		2.03±0.05		1.84±0.03		0.98±0.02	

TABLE 5. $\Delta G_R{}^t$ in complex equilibria (kcal/mol)

Solute	Equilibrium constant	$\Delta G_R{}^t$ for solvent =			
		DOX	MeCN	DMF	MeOH
Metal ethylenediamine					
Ni	K_1	0.61±0.01	0.59±0.01	1.49±0.06	1.66±0.004
	K_2	0.65±0.02	0.89±0.01	1.27±0.03	1.87±0.004
Zn	K_1	0.56±0.01	0.42±0.01	1.27±0.05	1.63±0.003
	K_2	0.59±0.02	0.53±0.02	1.18±0.04	1.86±0.003
Mn	K_1	0.84±0.01	0.72±0.01	1.38±0.02	1.72±0.01
	K_2	0.89±0.02	0.66±0.05	1.58±0.01	1.80±0.01
Metal glycine					
Ni	K_1	−0.15±0.02	0.87±0.01	0.56±0.04	0.91±0.002
	K_2	0.12±0.05	0.30±0.01	0.37±0.02	1.06±0.002
Zn	K_1	−0.29±0.01	−0.07±0.02	0.38±0.01	0.96±0.003
	K_2	0.04±0.05	0.06±0.02	0.17±0.02	1.08±0.003
Mn	K_1	−0.19±0.04	−0.004±0.02	0.21±0.02	0.87±0.003
	K_2		0.26±0.02	0.38±0.02	1.16±0.003
Acid ligands					
$H_n$en	K_{a1}	3.20±0.02	2.16±0.02	3.17±0.04	2.96±0.001
	K_{a2}	2.90±0.02	2.17±0.02	3.54±0.03	3.03±0.001
H_nG1	K_{a1}	0.15±0.003	0.42±0.01	0.32±0.03	0.94±0.01
	K_{a2}	2.04±0.03	1.66±0.02	2.52±0.02	2.45±0.002

number of molecules of each solvent is eliminated during each association reaction appears to satisfy the thermodynamic requirements of the data. This inference cannot, however, tell much about the nature of the association between solute species and solvent molecules, for instance, whether the value of j is due only to molecules in the primary solvation or coordination zone, or includes molecules external to but closely associated with these. Some of the different opinions concerning, for

Can. J. Chem. Downloaded from www.nrcresearchpress.com by 210.87.254.6 on 09/05/12
For personal use only.

example, the solvation of ions by methanol in aqueous methanol solutions depend on altogether different experimental evidence (25, 26).

Relationships Among Equilibrium Constants

Rossotti and co-workers (23) have shown that for systems like those considered here certain ratios of equilibrium constants are essentially independent of the solvent composition. This comes about because these ratios are themselves equilibrium constants of reactions, and their constancy in value results from the fact that these net reactions do not involve the release of any water molecules. We have adopted and extended these ideas to the data in this paper.

Consider the reactions

$$[\mathrm{I}] \qquad d_{\mathrm{I}}\mathrm{S} + w_{\mathrm{I}}\mathrm{H_2O} + \mathrm{BA_2} = \mathrm{BA} + \mathrm{A}$$

$$[\mathrm{II}] \qquad \mathrm{B} + \mathrm{A} = \mathrm{BA} + w_{\mathrm{II}}\mathrm{H_2O} + d_{\mathrm{II}}\mathrm{S}$$

$$[18] \qquad \mathrm{BA_2} + \mathrm{B} = 2\mathrm{BA} + \Delta w\mathrm{H_2O} - \Delta w\mathrm{S}$$

We put $\Delta w = w_{\mathrm{II}} - w_{\mathrm{I}}$, and note that $\Delta d = -\Delta w$ from eq. 16. Calling k the equilibrium constant for eq. 18 we have

$$[19] \quad \log k = \log (K_{\mathrm{I}}/K_{\mathrm{II}}) + \Delta w \log ([\mathrm{H_2O}]_s/[\mathrm{S}])$$

Values of Δw have been worked out in Table 4.

It is of interest to observe that for the reaction

$$[18a] \qquad \mathrm{ML_2} + \mathrm{M} = 2\mathrm{ML}$$

where Δw values are small for the metal complex formation the values of $K_1/K_2 = k$ are almost constant, independent of solvent, although they depend on the nature of the metal ion. These are quickly accessible from the data of Table 2. For the dissociation constants of the acids, the equilibrium constants for the reaction

$$[18b] \qquad \mathrm{H_2L} + \mathrm{L} = 2\mathrm{HL}$$

are given by the values of K_{a2}/K_{a1}. From the data of Table 1 it is seen that for ethylenediamine $pK_{a2} - pK_{a1}$ is roughly constant, independent of solvent composition, whereas for glycine the same quantity decreases with increasing concentration of co-solvent. This striking result is in complete accord with the change of Δw values in the two sets of protonation reactions. In the former case Δw values are small, so that the effect of change in solvent composition on K_{a2}/K_{a1} predicted by eq. 19 will be small. In the second case the value of $\Delta w \sim 1$ will lead to an appreciable modification of the ratio as the solvent composition changes.

The equilibrium constants for the reactions of glycine

$$\mathrm{M} + \mathrm{HL} = \mathrm{ML} + \mathrm{H} \qquad k_1$$

$$\mathrm{ML} + \mathrm{HL} = \mathrm{ML_2} + \mathrm{H} \qquad k_2$$

when expressed to include the contribution of solvent appear as

$$[19a] \quad \log k_{\mathrm{i}} = \log (K_{\mathrm{i}}/K_{a1}) + \Delta w \log ([\mathrm{H_2O}]_s/[\mathrm{S}])$$

Upon examination it is found that values of $\log k_{\mathrm{i}}$ are independent of solvent composition in the whole concentration range investigated, though they vary with the nature of the metal complexes. A corresponding relationship cannot be found among the other stability and acidity constants given in Tables 1 and 2. The explanation again seems inherent in the w values which for K_{a1} of glycine are of comparable magnitudes to those of the metal complexes in the same solvents.

In all of the foregoing discussion there has been the assumption that all these association reactions include the elimination of a fixed number of molecules of solvent; and that when the co-solvent is relatively non-polar these will be water molecules eliminated, but that when polar co-solvents are considered some of the molecules eliminated may be of these instead of water molecules. The evidence for these inferences is mainly the goodness of fit and wide applicability of the correlations suggested by eq. 17. The relationship in eq. 16 is an assumption also, but it finds some added credibility from the fact that where Δw is small in the combination of two equilibria the resultant $k_{\mathrm{I}}/k_{\mathrm{II}}$ is essentially constant irrespective of solvent composition. Now if on some grounds it can be deduced that Δw is small in this case, it is still necessary that Δd be small also for the ratio $k_{\mathrm{I}}/k_{\mathrm{II}}$ to remain constant. That so many instances of the constancy of this ratio were found among the data in this paper, even among cases where involvement of the co-solvent is quite plausible (*e.g.*, in methanolic solutions), supports the assumption that $|\Delta d| \sim |\Delta w|$, and that eq. 16 is reasonable.

Representation of complex equilibria in mixed solvents by a complete equilibrium constant in which allowance is made for variation in composition of both solvent partners appears to furnish a suitable explanation for a large share of the primary medium effect. This hypothesis will require considerable further testing before it can be adopted as a general principle. As a matter of

Can. J. Chem. Downloaded from www.nrcresearchpress.com by 210.87.254.6 on 09/05/12
For personal use only.

record it should be mentioned that Bjerrum and Jørgensen (27) proposed a somewhat similar explanation of shifts in equilibrium constants with changes in composition of mixed solvents, but their ideas were not thought to be upheld by spectrophotometric evidence (28).

The authors are grateful for financial support from the National Research Council of Canada.

1. D. B. RORABACHER, W. J. MACKELLAR, F. R. SHU, and SISTER M. BONAVITA. Anal. Chem. **43**, 561 (1971).
2. D. D. PERRIN, W. L. F. ARMAREGO, and D. R. PERRIN. Purification of laboratory chemicals. Pergamon Press, Oxford. 1966.
3. A. I. VOGEL. Textbook of quantitative inorganic analysis, 3rd ed. Longmans Green and Co., London. 1961.
4. G. SCHWARZENBACH and H. FLASCHKA. Complexometric titrations, 5th German edition. *Translated by* H. M. Irving. Methuen and Co., London. 1969.
5. C. A. KRAUS and R. A. VINGEE. J. Am. Chem. Soc. **56**, 511 (1934).
6. D. D. PERRIN and I. G. SAYCE. Chem. Ind. 661 (1966).
7. W. A. E. MCBRYDE. Analyst, **94**, 337 (1969); **96**, 739 (1971).
8. L. G. VAN UITERT and C. G. HAAS. J. Am. Chem. Soc. **75**, 451 (1952).
9. M. T. BECK. The chemistry of complex equilibria. Van Nostrand–Reinhold Co., London. 1970.
10. J. K. ROMARY, D. L. DONNELLY, and A. C. ANDREWS. J. Inorg. Nucl. Chem. **29**, 1805 (1967).
11. R. G. BATES. Determination of pH. 2nd ed. John Wiley and Sons, New York. 1973.
12. H. S. HARNED and B. B. OWEN. Physical chemistry of electrolyte solutions, 3rd ed. Reinhold Publishing Corp., New York. 1958.
13. W. J. GELSEMA, C. L. DELIGNY, A. G. REMIJNSE, and H. A. BLIJLEVEN. Rec. Trav. Chim. **85**, 647 (1966).
14. C. W. DAVIES. J. Chem. Soc. 2093 (1938).
15. H. IRVING and H. ROSSOTTI. Acta Chem. Scand. **10**, 72 (1956).
16. M. BORN. Z. Phys. **1**, 45 (1920).
17. R. G. BATES, M. PAABO, and R. A. ROBINSON. J. Phys. Chem. **67**, 1883 (1963); **70**, 247 (1966).
18. L. G. HEPLER. Aust. J. Chem. **17**, 587 (1964).
19. C. REICHARDT. Angew. Chem. Int. Ed. **4**, 29 (1965).
20. F. W. FOWLER, A. R. KATRITZKY, and R. J. D. RUTHERFORD. J. Chem. Soc. B, 460 (1971).
21. A. P. KRESHKOV. Talanta, **17**, 1029 (1970).
22. R. G. BATES. *In* Solute-solvent interaction. *Edited by* J. F. Coetzee and C. D. Ritchie. Marcel Dekker, New York. 1969.
23. G. FARAGLIA, F. J. C. ROSSOTTI, and H. S. ROSSOTTI. Inorg. Chim. Acta, **4**, 488 (1970).
24. W. M. MARSHALL. J. Phys. Chem. **76**, 720 (1972).
25. W. J. MACKELLAR and D. B. RORABACHER. J. Am. Chem. Soc. **93**, 4379 (1971).
26. Z. LUZ and S. MEIBOOM. J. Chem. Phys. **40**, 1058 (1964).
27. J. BJERRUM and C. K. JØRGENSON. Acta Chem. Scand. **7**, 951 (1953).
28. L. I. KATZIN and E. GEBERT. Nature, **175**, 425 (1955).

Can. J. Chem. Downloaded from www.nrcresearchpress.com by 210.87.254.6 on 09/05/12
For personal use only.

Enthalpy–Entropy Compensation for Micellization and Other Hydrophobic Interactions in Aqueous Solutions

CARMEL JOLICOEUR AND PATRICK R. PHILIP
Département de Chimie, Université de Sherbrooke, Sherbrooke, Québec
Received November 16, 1973

The temperature dependence of the critical micelle concentration for 26 ionic and 48 non-ionic surfactants in aqueous solutions has been reexamined and used to calculate ΔH_m^0 and ΔS_m^0, the heats and entropies of micellization, at 25 and 50 °C. ΔH_m^0 and ΔS_m^0 values exhibit a significant correlation with compensation temperatures (T_c) of 319 and 222 °K at 25 °C for the groups of ionic and non-ionic surfactants respectively. These results are compared with T_c values which are expected to be characteristic of pairwise interactions between hydrophobic solutes.

La dépendance, vis-à-vis de la température, de la concentration critique de micellisation de 26 détergents ioniques et de 48 détergents non ioniques, en solution aqueuse, a été réexaminée et utilisée pour calculer les enthalpies et entropies de micellisation, ΔH_m^0 et ΔS_m^0 à 25 et 50 °C. Ces valeurs de ΔH_m^0 et ΔS_m^0 présentent une corrélation significative avec des températures respectives de compensation (T_c) de 319 et 222 °K pour les composés ioniques et non ioniques à 25 °C. Ces résultats sont comparés avec des valeurs de T_c considérées comme caractéristiques des interactions par paires entre solutés hydrophobes.

Can. J. Chem., **52**, 1834 (1974)

Introduction

Linear correlations between enthalpy and entropy changes have often been observed in studies of isothermal solution processes where, typically, the size of homologous solutes, or the composition of the solvent, is varied in a systematic way (1–5). Such behavior has proven to be rather common for processes or reactions occurring in aqueous media, involving a variety of solute species ranging from rare gases to biological macromolecules.

In a recent survey of the enthalpy–entropy (H/S) compensation phenomenon in aqueous solutions of small molecules and in biological systems, Lumry and Rajender (6) pointed to a large number of thermodynamic and kinetic (activation) measurements which exhibit linear H/S correlation. The slopes of the correlation lines (correlation temperature, T_c) lie in a narrow range between 250 and 315 °K; for most systems in which the solvent is highly aqueous, T_c falls between 270 and 290 °K. This remarkable constancy is suggested to originate in a common process occurring in the solvent, and perturbation of the two-state equilibrium in liquid water provides an elegant means of explaining H/S compensation in aqueous media (7).

Fitting in this general scheme, the solvation thermodynamics of hydrophobic solutes exhibit H/S compensation as illustrated by the standard entropies and enthalpies of hydration of various compounds containing alkyl groups of varying length (7). The recent suggestion by Friedman and co-worker (8) that some H/S compensation is also effective in the pairwise interaction between hydrophobic solutes has prompted us to look for H/S correlation in the process of micelle formation. Since hydrophobic interactions contribute largely to the stability of micelles (9, 10), a general H/S correlation, if it exists, might yield a T_c value characteristic of such interactions.

Treatment of Data and Calculations

Each of the available sets of data on the temperature dependence of the c.m.c. (critical micelle concentration) for 48 non-ionic (11–14) and 26 ionic (11, 15) surfactants were fitted by least-square analyses to a third degree polynomial

$$[1] \quad \ln [\text{c.m.c.}] = A + BT + CT^2 + DT^3$$

where [c.m.c.] is the c.m.c. on the mole fraction scale. In the association equilibrium model, the standard free energy change for the micellization of one mole of surfactant monomers is given by (16)

$$[2] \qquad \Delta G_m^0 = RT \ln [\text{c.m.c.}]$$

Application of the Gibbs–Helmholtz equation to eq. 1 yields the standard heat of micellization

Can. J. Chem. Downloaded from www.nrcresearchpress.com by 210.87.254.105 on 09/05/12
For personal use only.

Can. J. Chem. Downloaded from www.nrcresearchpress.com by 210.87.254.105 on 09/05/12
For personal use only.

$$[3] \quad \Delta H_m^0 = -RT^2 \frac{d \ln [c.m.c.]}{dT} = -RT^2(B + 2CT + 3DT^2)$$

The molar entropy of micellization was obtained in the usual way, from

$$[4] \quad \Delta S_m^0 = \frac{\Delta H_m^0 - \Delta G_m^0}{T}$$

Values of ΔH_m^0 and ΔS_m^0 are reported in Table 1 along with other pertinent information on the temperature range and the number of c.m.c. measurements in the original investigation.

In this study, all the available data were included, except those showing excessive scattering or discontinuity in $d(\ln [c.m.c.])/dT$. Also, in a few cases where different data sets of similar precision were available for a given compound, we chose the results of experiments covering the largest temperature range.

The relations used in calculating the thermodynamic quantities ΔH_m^0 and ΔS_m^0 are derived from the monomer–polymer equilibrium model of micellization (16). Since the model has been shown accurate only for systems in which the number of monomers per micellar aggregate is large, *i.e.* >20, and not strongly temperature-dependent (17, 18), the results obtained with short chain surfactants ($R \leqslant C_8H_{17}$) must be regarded with caution. For the lower homologs the c.m.c. is high and not as sharply defined as with the higher homologs (19, 20); thus, solutions of the former are likely to contain a wide distribution of micelle sizes.

Finally, because of the large change in the molar heat capacity of the surfactant upon micellization, the accuracy of the Gibbs–Helmholtz ΔH_m^0 depends on the temperature interval between c.m.c. measurements. Any error introduced in the evaluation of ΔH_m^0 will of course be carried over to ΔS_m^0, shifting both values on the axes of the H/S correlation plots given below.

Results and Discussion

The standard enthalpies and entropies of micellization listed in Table 1 are divided into two groups, ionic and non-ionic. For each category of solute, we plot ΔH_m^0 against ΔS_m^0 as shown in Figs. 1 and 2. The least-square slopes of these correlation plots are given in Table 2, for experimental temperatures of 25 and 50 °C, along with the relevant standard deviations on ΔH_m^0 and T_c (σ_H and σ_T) and the intercept on the ΔH_m^0 axis, ΔH_m^*. A reasonably accurate H/S correlation is found in each case, and the T_c values for ionic and non-ionic surfactants differ by $\simeq 100$ °K.

The group of non-ionic surfactants, which are expected to show the typical behavior of hydrophobic solutes, exhibit a T_c value significantly lower than "Lumry's law", *i.e.* $T_c = 285$ °K. This is a more general statement of a well known fact that, for these solutes, entropy effects dominate the micelle formation process near room temperature, much more so than in the many aqueous systems surveyed by Lumry and Rajender (6). For the group of ionic surfactants examined here, the T_c found is not significantly different from 285 °K in view of the magnitude of σ_T in this series. It is intriguing that the electrostatic effects, which are known to contribute to ΔG_m^0 (19, 21, 22) of ionic surfactants, apparently bring these systems in the more general type of H/S compensation.

To examine these results in the working scheme of Lumry and Rajender (6), we can picture the micellization process as made up of two parts: (*a*) the "solvent" part (dehydration of the hydrocarbon chains) and (*b*) the "chemical" part (aggregation of the hydrocarbon chains to form the micellar unit). This amounts to an oversimplification of the three contributions to ΔG_m^0 considered by Poland and Scheraga (10). If the desolvation of the inert hydrocarbon solutes involves only a shift of the equilibrium populations of the two types of water species (*c.f.* the relaxational contribution in Ben-Naim's treatment (23)), then it will show exact H/S compensation at all experimental temperatures. Instead, the observation of an H/S relationship of the form

$$\Delta H_m^0 = \Delta H_m^* + T_c \Delta S_m^0$$

with both T_c and ΔH_m^* temperature dependent (Table 2), shows that the chemical part (5) and probably other contributions in the solvent part, have a more complicated behavior.

As is the purpose of this report, we want to compare the T_c values characteristic of hydrophobic interactions which lead to clustering of the solute species ("bulk hydrophobic interactions" (24)) with those which can be related to pairwise interactions of hydrophobic solutes. We quote below several data on dilute aqueous

Can. J. Chem. Downloaded from www.nrcresearchpress.com by 210.87.254.105 on 09/05/12
For personal use only.

TABLE 1. Enthalpies and entropies of micellization of various surfactants in water at 25 °C

Compound	Range of temperature (°C)	Number of experimental points	ΔH_m^o (kcal mol^{-1})	ΔS_m^o (cal K^{-1} mol^{-1})	Reference
Non ionic					
Dimethyl dodecyl amine oxide	1–50	7	1.74	26.2	11
Octyl/oxyethylene/6 alcohol	15–45	8	3.49	29.0	11
Octyl/oxyethylene/9 alcohol	15–35	3	3.31	27.7	11
Decyl/oxyethylene/3 alcohol	15–35	3	2.38	30.7	11
Decyl/oxyethylene/6 alcohol	15–45	6	4.86	38.3	11
Decyl/oxyethylene/9 alcohol	15–35	3	2.15	28.5	11
Dodecyl/oxyethylene/6 alcohol	15–55	7	6.89	49.8	11
Dodecyl/oxyethylene/7 alcohol	1–25	4	6.08	48.1	11
Dodecyl/oxyethylene/30 alcohol	1–55	7	3.43	38.4	11
Hexadecyl/oxyethylene/30 alcohol	1–55	7	6.93	54.0	11
Decyl/oxyethylene/10–0 alcohol	25–75	4	5.41	38.0	11
Decyl/oxyethylene/14–9 alcohol	25–75	3	6.10	39.7	11
Decyl/oxyethylene/20–0 alcohol	25–75	3	6.01	38.4	11
Decyl/oxyethylene/29–4 alcohol	25–75	3	5.28	36.0	11
Tridecyl/oxyethylene/5–2 alcohol	25–75	3	2.25	33.3	11
Tridecyl/oxyethylene/10–1 alcohol	25–75	3	1.59	30.9	11
Tridecyl/oxyethylene/15–2 alcohol	25–75	3	3.04	34.6	11
Tridecyl/oxyethylene/20–0 alcohol	25–75	3	4.37	38.9	11
Tridecyl/oxyethylene/30–6 alcohol	25–75	3	3.72	35.5	11
Hexyl/oxyethylene/6 alcohol	20–45	5	3.26	24.0	11
Dodecyl/oxyethylene/4 alcohol	5–45	4	5.58	46.8	11
Dodecyl/oxyethylene/23 alcohol	5–45	4	4.40	42.1	11
Ethyl butyl/oxyethylene/6 alcohol	20–40	3	1.25	16.9	11
Butyl hexyl/oxyethylene/6 alcohol	15–25	3	3.02	30.0	11
Butyl hexyl/oxyethylene/9 alcohol	20–40	3	2.21	27.0	11
Nonyl benzene/oxyethylene/5–0 alcohol	25–75	3	10.57	64.2	11
Nonyl benzene/oxyethylene/15–4 alcohol	25–75	3	0.80	29.5	11
Nonyl benzene/oxyethylene/30–2 alcohol	25–75	3	1.67	31.0	11
Dodecyl benzene/oxyethylene/5–0 alcohol	25–75	3	4.03	43.5	11
Dodecyl benzene/oxyethylene/10–2 alcohol	25–75	3	6.92	53.4	11
Dodecyl benzene/oxyethylene/15–1 alcohol	25–75	3	4.03	43.4	11
Dodecyl benzene/oxyethylene/20–1 alcohol	25–75	3	6.85	52.7	11
Dodecyl benzene/oxyethylene/30–6 alcohol	25–75	3	13.23	73.5	11
p,tert-octyl benzene/oxyethylene/6 alcohol	15–85	8	1.59	29.8	11
p,tert-octyl benzene/oxyethylene/7 alcohol	15–85	8	1.37	29.0	11
p,tert-octyl benzene/oxyethylene/8 alcohol	15–85	8	1.37	29.0	11
p,tert-octyl benzene/oxyethylene/9 alcohol	15–85	8	1.35	29.0	11
p,tert-octyl benzene/oxyethylene/10 alcohol	15–85	8	1.09	27.7	11

Can. J. Chem. Downloaded from www.nrcresearchpress.com by 210.87.254.105 on 09/05/12
For personal use only.

TABLE 1 (*Concluded*)

	Range of temperature (°C)	Number of experimental points	ΔH_m^0 (kcal mol^{-1})	ΔS_m^0 (cal K^{-1} mol^{-1})	Reference
Nonyl benzene/oxyethylene/15 alcohol	21–45	6	2.36	36.7	11
Decyl/oxyethylene/12 oxymethyl	10–75	8	3.51	32.5	11
Dodecyl/oxyethylene/12 oxymethyl	20–76	5	7.35	48.0	11
Polyoxyethylene/12 lauryl alcohol	25–65	5	1.46	30.5	12
Polyoxyethylene/23 lauryl alcohol	25–65	4	2.00	33.0	12
p,*tert*-octyl phenoxy/polyethoxy/9–10 ethanol	25–45	3	2.1	32.0	13
p,*tert*-octyl phenoxy/polyethoxy/12–13 ethanol	25–45	3	2.1	32.0	13
p,*tert*-octyl phenoxy/polyethoxy/30 ethanol	25–45	3	4.3	37.0	13
p,*tert*-nonyl phenoxy/polyethoxy/30 ethanol	25–45	3	4.0	38.0	13
Polyoxyethylene/28 *n*-dodecanol	15–55	4	7.78	52.9	14
Anionic					
Sodium dodecylsulfate	10–70	13	−0.05	17.3	11
Sodium octylsulfate	10–55	10	0.15	12.5	11
Sodium decylsulfate	0–65	14	0.35	16.0	11
Sodium tetradecylsulfate	25–75	11	−0.68	18.0	11
Sodium hexadecylsulfate	25–90	8	−8.31	−3.6	11
Potassium decanoate	25–45	3	0.06	12.7	11
Potassium dodecanoate	15–60	5	0.26	16.3	11
Sodium dodecanoate	20–50	7	1.63	20.7	11
Potassium tetradecanoate	25–65	6	−0.27	17.1	11
Sodium *p*, octyl benzene sulfonate	25–60	4	−2.07	9.9	11
Sodium dodecyl benzene sulfonate	25–75	5	5.42	37.0	11
Octyl-1-benzene sulfonate	23–50	4	0.03	11.8	11
Decyl-1-benzene sulfonate	22.5–80	11	−4.86	−2.2	11
Cationic					
Decylammonium chloride	20–60	4	−1.66	8.9	11
Dodecylammonium chloride	15–60	7	0.38	17.7	11
Tetradecylammonium chloride	25–60	4	−0.09	19.1	11
Octyl trimethylammonium bromide	20–60	4	6.37	32.7	11
Decyl trimethylammonium bromide	25–60	4	−0.93	10.3	11
Dodecyltrimethylammonium bromide	1–70	8	−0.16	15.8	11
Tetradecyltrimethylammonium bromide	30–70	3	−2.61	10.6	11
Hexadecyltrimethylammonium bromide	25–70	5	−2.21	14.5	11
Hexadecylpyridium chloride	13–80	4	−1.29	17.6	11
Hexadecylpyridium bromide	25–55	6	−5.77	3.7	11
Dodecylpyridium chloride	25–50	3	−5.12	−0.8	11
Dodecylpyridium bromide	5–70	14	−0.73	14.4	11
Dodecylpyridium iodide	20–40	6	−2.97	9.4	15

Can. J. Chem. Downloaded from www.nrcresearchpress.com by 210.87.254.105 on 09/05/12
For personal use only.

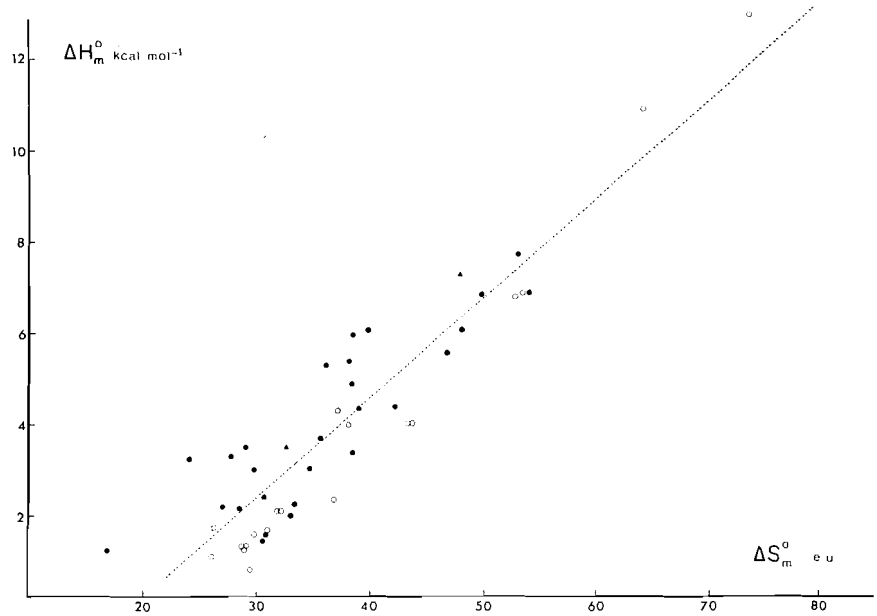

FIG. 1. Enthalpies and entropies of micellization for non-ionic aqueous surfactants at 25 °C: □, dimethyl dodecylamine oxide; ●, alkyl oxyethylene/alcohols; ○, aryl oxyethylene/alcohols; ▲, alkyl oxyethylene/oxymethyl.

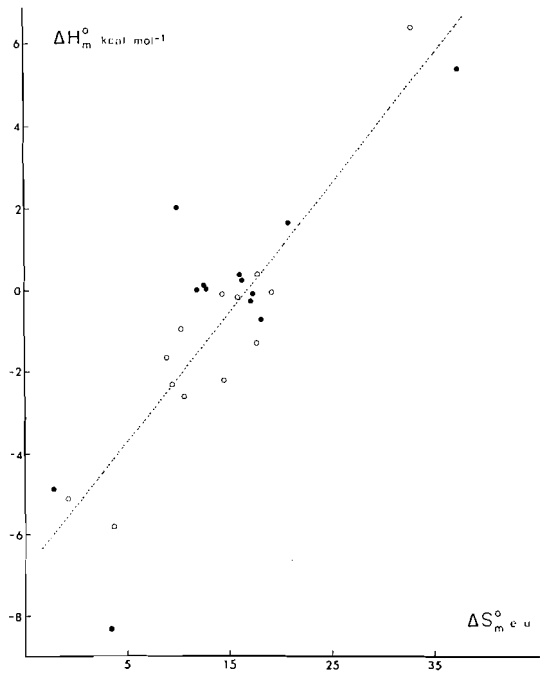

FIG. 2. Enthalpies and entropies of micellization for ionic aqueous surfactants at 25 °C: ●, anionic; ○, cationic.

mixtures containing inert or hydrophobic solutes and in which the heat and entropy effects can be assumed to originate mainly from pairwise solute–solute interactions.

The standard heats and entropies of transfer of argon, from water to aqueous ethanol solutions of increasing concentration, show linear H/S correlation with $T_c \simeq 275$ °K (6). Likewise, for the transfer of argon from water to aqueous solutions of the lower aliphatic alcohols (MeOH → *n*BuOH, mole fraction 0.015), the data of Ben-Naim (25) exhibit H/S correlation with $T_c \simeq 300$ °K. Similar results are found in the

TABLE 2. Results of enthalpy–entropy correlations in micellization of ionic (I) and non-ionic (NI) surfactants

	Temperature			
	25°		50°	
Correlation[a]	I	NI	I	NI
T_c (°K)	319	222	311	242
ΔH^* (kcal mol^{-1})	−5.35	−4.32	−5.21	−5.28
σ_T (°K)	23	13	58	16
σ_H (kcal mol^{-1})	1.05	0.99	1.06	1.19

[a] T_c, slope of ΔH_m^o *vs.* ΔS_m^o plot; ΔH^*, intercept of ΔH_m^o *vs.* ΔS_m^o plot; σ_T, standard deviation on T_c; σ_H, standard deviation on ΔH_m^o.

Can. J. Chem. Downloaded from www.nrcresearchpress.com by 210.87.254.105 on 09/05/12
For personal use only.

transfer of hydrocarbons (Methane → *n*Butane) from water to aqueous solutions of R_4NBr (R = Me → *n*Bu) (26). There, the T_c value correlating the data for either the series of salts or the series of hydrocarbons is 285 °K (6). To the extent that the above data reflect dominantly the consequences of pairwise solute–solute interactions, it appears that the latter exhibit the more general type of H/S correlation, *i.e.* ~285 °K, rather than the one found for the clustering of non-ionic micellar solutes. This may be thought of as a distinction criteria between the two types of interactions (pairwise *vs.* cluster), but other results on the excess functions of alcohol–water mixtures do not fit in this simple classification.

In the total excess functions of aqueous alcohol mixtures, the net predominance of the TS^{EX} term had been pointed out (27), indicating that, if there exists a T_c value correlating a series of data for different alcohols, it would be well below 298 °K. In accordance with this, recent model calculations on the excess enthalpies and free energies of dilute solutions of aliphatic alcohols have shown that the solvent contribution to the ROH–ROH interaction exhibits H/S correlation with $T_c < 285$ °K. The calculated energy and entropy Gurney coefficients, which account for the effect of solvent displacement from the solvation co-spheres of the solute as they interact, yield a T_c value of $\simeq 240$ °K (8) (neglecting the data for MeOH). It is interesting to note that the latter value is less than T_c in "Lumry's law", while the results of model calculations pertain most directly to solvent effects in solute–solute interactions. Further data and model calculations on excess enthalpies and entropies of dilute solutions of hydrophobic solutes will most certainly help to attain a more accurate definition of the frequently invoked "solvent structural effects" in solute–solute interactions.

Financial support from the Ministère de l'Education du Québec is gratefully acknowledged.

1. I. M. Barclay and J. A. V. Butler. Trans. Faraday Soc. **34**, 1445 (1938); J. A. V. Butler. Trans. Faraday Soc. **33**, 235 (1937).
2. H. S. Frank. J. Chem. Phys. **13**, 493 (1945).
3. F. Vaslow and D. Doherty. J. Am. Chem. Soc. **75**, 928 (1953); D. Doherty and F. Vaslow. J. Am. Chem. Soc. **74**, 931 (1952).
4. J. Leffler and E. Grunwald. Rates and equilibria of organic reactions. John Wiley, New York. 1963.
5. L. G. Hepler and W. F. O'Hara. J. Phys. Chem. **65**, 811 (1961).
6. R. Lumry and S. Rajender. Biopolymers, **9**, 1125 (1970).
7. C. V. Krishnan and H. L. Friedman. J. Solution Chem. **2**, 37 (1973).
8. C. V. Krishnan and H. L. Friedman. J. Solution Chem. **2**, 119 (1973).
9. W. Kauzmann. Adv. Protein Chem. **14**, 1 (1959).
10. D. C. Poland and H. A. Scheraga. J. Phys. Chem. **69**, 2431 (1965).
11. P. Mukerjee and K. J. Mysels. Critical micelle concentrations of aqueous surfactant systems. Natl. Stand. Ref. Data. Ser., Natl. Bur. Stand. Washington D.C. 36, 1971.
12. P. Becher and H. Arai. J. Colloid Interface Sci. **27**, 634 (1968).
13. A. Ray and G. Nemethy. J. Phys. Chem. **75**, 809 (1971).
14. H. Schott, J. Pharm. Sci. **58**, 1521 (1969).
15. M. N. Jones, G. Agg, and G. Pilcher. J. Chem. Thermodyn. **3**, 801 (1971).
16. M. F. Emerson and A. Holtzer. J. Phys. Chem. **69**, 3718 (1965).
17. J. M. Corkill, J. F. Goodman, and S. P. Harrold. Trans. Faraday Soc. **60**, 202 (1964).
18. D. G. Hall and B. A. Pethica. Non ionic surfactants. *Edited by* M. J. Schick. M. Dekker Inc., New York. 1967. Chapt. 16.
19. K. Shinoda. Colloidal surfactants. *Edited by* E. Hutchinson and P. Van Rysselberghe. Academic Press, New York. 1963. Chapt. 1, p. 20.
20. J. E. Desnoyers, M. Arel, and P. A. Leduc. Can. J. Chem. **47**, 547 (1969).
21. R. D. Geer, E. H. Eylat, and E. W. Anacker. J. Phys. Chem. **75**, 369 (1971).
22. M. F. Emerson and A. Holtzer. J. Phys. Chem. **71**, 3320 (1967).
23. A. Ben-Naim. Trans. Faraday Soc. **66**, 2749 (1970).
24. J. J. Kozak, W. S. Knight, and W. Kauzmann. J. Chem. Phys. **48**, 675 (1968).
25. A. Ben-Naim. J. Phys. Chem. **69**, 3245 (1965).
26. W. Y. Wen and J. H. Hung. J. Phys. Chem. **74**, 170 (1970).
27. F. Franks and D. J. G. Ives. Q. Rev. Lond. **20**, 1 (1966).

A Proton Spin–Lattice Relaxation Study of Molecular Motion in Several Addition Complexes of Trimethylamine and Trimethylphosphine

T. T. ANG[1] AND B. A. DUNELL

Chemistry Department, University of British Columbia, Vancouver, British Columbia V6T 1W5

Received November 13, 1973

The spin–lattice relaxation times of the solid complexes of trimethylamine with I_2, ICl, Br_2, BCl_3, and BBr_3 and the relaxation null times of trimethylphosphine – boron trichloride and – boron tribromide have been measured over a range of temperature by pulsed proton magnetic resonance. A minimum in T_1 corresponding to reorientation of the methyl groups about the C—N bonds is observed in each complex, although in the case of Me_3NBr_2 the minimum corresponds to a combination of methyl group reorientation and reorientation of the whole Me_3N moiety. The complexes with the boron trihalides show a second minimum in T_1. These minima have been analyzed in terms of either of two possible motions, reorientation of NMe_3 about its threefold axis, or that same motion combined with isotropic molecular tumbling. We favor the interpretation involving the simpler motion. Activation energies have been measured for all the motions. The barriers to reorientation of methyl groups about the C—N bond in the moiety Me_3N appear to increase as the thermal stability of the complex decreases.

Les temps de relaxation spin–réseau des complexes solides de la triméthylamine avec I_2, ICl, Br_2, BCl_3, et BBr_3 et les temps zéro de relaxation du triméthylphosphine – trichlorure de bore et tribromure de bore ont été mesurés dans un intervalle de température par la "résonance magnétique du proton par pulsation". Un minimum de T_1 qui correspond à la réorientation des groupes méthyles autour des liaisons C—N est observé dans chacun des complexes bien que dans le cas de Me_3NBr_2 le minimum correspond à la combinaison de la réorientation du groupe méthyl et de la réorientation de tout l'ensemble de Me_3N. Les complexes avec les trihalogénures de bore montrent un second minimum de T_1. Ces minima ont été analysés en fonction de l'un des deux mouvements possibles, réorientation de NMe_3 autour de son axe ternaire, ou encore le même mouvement associé à l'agitation moléculaire isotrope. Nous préférons l'interprétation impliquant le mouvement le plus simple. Les énergies d'activation ont été mesurées pour tous les mouvements. Les barrières à la réorientation des groupes méthyles autour de la liaison C—N dans la partie Me_3N tentent à augmenter lorsque la stabilité thermique du complexe diminue. [Traduit par le journal]

Can. J. Chem., **52**, 1840 (1974)

Nuclear magnetic resonance studies of methyl group reorientation and other molecular motions in solid addition complexes involving methyl compounds of elements from main groups III and V have been made in several laboratories (1–5). As a further contribution to these studies, we have measured activation energies for the molecular motions in the complexes of trimethylamine with I_2, ICl, Br_2, BCl_3, and BBr_3 and of trimethylphosphine with BCl_3 and BBr_3.

An analysis of the nature of the motions in the solid addition complexes with the halogens was made by Fyfe and Ripmeester (3) by broad-line n.m.r. techniques, and of the motions in $Me_3N.BCl_3$ and $Me_3N.BBr_3$ by Yim and Gilson (2), also by the wide-line method. These two groups also estimated activation energies from their line width data, but as they point out, there are approximations and uncertainties inherent in this method of obtaining activation energies so that the derived results must be regarded with some reservation.

Experimental

The halogen addition complexes were prepared by mixing anhydrous Me_3N (Eastman Kodak) with reagent grade I_2, Br_2 (Alfa Inorganics), or ICl (BDH) and purifying according to the method of Strømme (6) and Hassel and Hope (7). Analyses for C, H, N agreed well with theoretical values.

Anal. Calcd. for $C_3H_9I_2N$: C, 11.52; H, 2.90; N, 4.48. Found: C, 11.20; H, 2.76; N, 4.32.

Anal. Calcd. for C_3H_9ClIN: C, 16.27; H, 4.10; N, 6.32. Found: C, 16.16; H, 4.17; N, 6.29.

Anal. Calcd. for $C_3H_9Br_2N$: C, 16.45; H, 4.15; N, 6.45. Found: C, 16.32; H, 4.13; N, 6.60.

[1]Present address: School of Chemical Sciences, Universiti Sains Malaysia, Penang, Malaysia.

Can. J. Chem. Downloaded from www.nrcresearchpress.com by 210.87.254.6 on 09/05/12
For personal use only.

Can. J. Chem. Downloaded from www.nrcresearchpress.com by 210.87.254.6 on 09/05/12
For personal use only.

The boron halide – amine complexes were prepared from Me_3N (as above) and BCl_3 (Matheson) or BBr_3 (Alfa) according to literature methods (8, 9). The trichloride complex was recrystallized three times from absolute ethanol and the tribromide complex from benzene. Analyses for C, H, N again agreed well with theoretical values.

Anal. Calcd. for $C_3H_9BCl_3N$: C, 20.44; H, 5.15; N, 7.94. Found: C, 20.48; H, 5.09; N, 8.07.

Anal. Calcd. for $C_3H_9BBr_3N$: C, 11.62; H, 2.90; N, 4.52. Found: C, 11.46; H, 3.11; N, 4.63.

The boron halide trimethylphosphine complexes were formed from Me_3P (Pfaltz and Bauer) and boron trihalides (as above) by a literature method (10) and purified by vacuum sublimation onto a cold finger which was at room temperature.

Anal. Calcd. for $C_3H_9BCl_3P$: C, 18.62; H, 4.69. Found: C, 18.57; H, 4.70.

Proton spin–lattice relaxation times at a Larmor frequency of 30 MHz were measured, as described previously (4), using a π–t–$\pi/2$ series of pulses on a Bruker pulse spectrometer. The broad-line, c.w. spectra of the Me_3P complexes were obtained at 16 MHz on a Varian spectrometer (4). Plots of log $[(M_0 - M_t)/2M_0]$ against t for the Me_3P complexes were distinctly non-linear between about 80 and 200 K. Below 80 K and above 200 K the non-linearity was less marked, and at and above 210 K the decay of magnetization appeared to be a simple exponential. The parameter which has been analyzed for these complexes is t_0, the null-time, at which $M_t = 0$. The correction to t_0 for the inhomogeneity of H_1 (11) was small. For all the other complexes reported here the decay of magnetization was apparently exponential and the standard deviation for the slope of the straight line on the semilogarithmic plot was, from the least squares fit, less than 5% in all the samples studied.

Results and Discussion

The theoretical extension by Dunn and McDowell (5) of earlier developments (12–15) of Bloembergen, Purcell, and Pound (B.P.P.) theory (16) is particularly useful in considering systems in which there may be methyl group rotation (C_3 motion), reorientation of a moiety XMe_3 about its threefold axis (C_3' motion), and isotropic tumbling of the whole molecule. For a tetrahedral configuration at the nitrogen atom in each of our compounds, eq. 1 of Dunn and McDowell becomes (their angle $\delta = 70°32'$)

$$[1]\quad \frac{1}{T_1} = \frac{9\gamma^4\hbar^2}{80\omega_0 r^6}\left[\frac{4}{27}f(\omega_0\tau_{C1}) + \frac{32}{27}f(\omega_0\tau_{C3}) + \frac{32}{27}f(\omega_0\tau_{C4}) + \frac{76}{27}f(\omega_0\tau_{C5})\right]$$

where τ_{C1} is the correlation time for isotropic rotations; $\tau_{C3}^{-1} = \tau_{C1}^{-1} + \tau_C^{-1}$, τ_C being the correlation time for C_3 rotation of a methyl group; $\tau_{C4}^{-1} = \tau_{C1}^{-1} + \tau_{C2}^{-1}$, τ_{C2} being the correlation time for C_3' rotation of the NMe_3 moiety; $\tau_{C5}^{-1} = \tau_{C1}^{-1} + \tau_C^{-1} + \tau_{C2}^{-1}$ and r is the interproton distance in the methyl group.

$$f(\omega_0\tau) = \omega_0\tau/(1 + \omega_0^2\tau^2) + 4\omega_0\tau/(1 + 4\omega_0^2\tau^2)$$

The correlation times τ_C, τ_{C1}, and τ_{C2} will be assumed to have an Arrhenius dependence on the temperature with activation energies E, E_1, and E_2, respectively. Thus,

$$[2]\quad \tau_C = \tau_C^0 \exp(E/RT)$$

The Halogen Complexes

The temperature dependence of the spin–lattice relaxation times of the three halogen complexes of trimethylamine is shown in Fig. 1. The second moment studies of Fyfe and Ripmeester (3) lead us to suggest that the relaxation mechanism between 150 and 300 °K for the

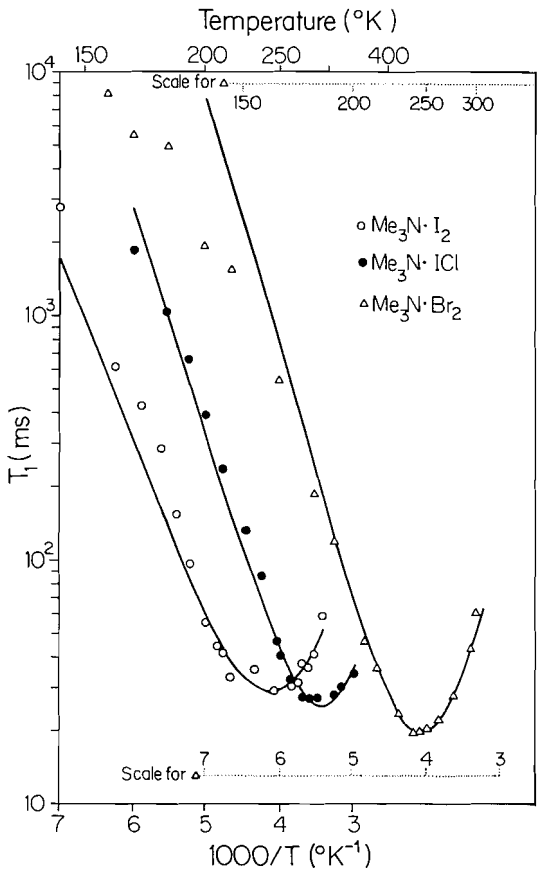

FIG. 1. Spin–lattice relaxation time as a function of reciprocal temperature for trimethylamine–halogen complexes. ○, Me_3NI_2; ●, Me_3NICl; △, Me_3NBr_2. Lines through the points are the best-fit lines described by the parameters in Table 1.

TABLE 1. Activation parameters for addition complexes of trimethylamine and trimethylphosphine

Compound	Motion causing relaxation	E_a from c.w. studies* (kcal/mol)	This work			
			E_a (kcal/mol)	τ_C^0 (s)	T_1 minimum (ms)	
					Observed	Theoretical
Me_3NI_2	C_3	6.9±0.4	3.39±0.20	(2.9 ±1.2) $\times 10^{-12}$	29.0± 1.0	17.4
Me_3NICl	C_3	6.2±0.5	4.31±0.20	(1.9 ±0.7) $\times 10^{-12}$	25.4± 0.6	17.4
Me_3NBr_2	C_3+C_3'	6.8±0.5	4.71±0.10	(3.0 ±0.6) $\times 10^{-13}$	20.0± 0.5	14.1
Me_3NBCl_3	C_3	1.6–1.9	2.71±0.06	(1.7 ±0.3) $\times 10^{-12}$	28.0± 0.4	17.4
	C_3'	9.3	13.6 ±0.9	(1.2 ±1.5) $\times 10^{-17}$	53.4± 2.4	40.5‡
	C_3+iso†					35.9‡
Me_3NBBr_3	C_3	1.7–2.0	(*a*)2.89±0.19	(4.4 ±3.2) $\times 10^{-13}$	50.5± 6.2	34.8
			(*b*)3.17±0.25	(1.1 ±0.5) $\times 10^{-12}$	62.5±10.0	34.8
	C_3'	9.1	14.5 ±0.5	(6.1 ±4.0) $\times 10^{-17}$	53.2± 1.2	40.5‡
	C_3'+iso					35.9‡
Me_3PBCl_3	C_3		1.69±0.03		22.2± 0.3§	17.4
	C_3'		12.8 ±0.3	(3.9 ±1.3) $\times 10^{-16}$	56.0± 0.7‖	51.0‡
	C_3'+iso					53.5‡
Me_3PBBr_3	C_3		1.25±0.03		25.6± 0.4§	17.4
	C_3'		13.7 ±0.3	(7.0 ±2.8) $\times 10^{-16}$	61.5± 1.0‖	51.0‡
	C_3'+iso					53.5‡

*See refs. 2 and 3.
†iso signifies isotropic molecular tumbling.
‡Includes an intermethyl contribution.
§Value shown is t_0/ln 2: Since the decay in M_2 is non-exponential, the significance of this value is doubtful.
‖Value shown is t_0/ln 2: Since the decay in M_2 is exponential here, the value is considered to be meaningful.

iodine and iodine monochloride complexes is probably C_3 motion of the methyl groups and for the bromine complex is probably a combined C_3 and C_3' motion. For relaxation by the C_3 motion, the theoretical value of T_1 is found by putting $\tau_{C1} = \tau_{C2} = \infty$ in eq. 1. At the T_1 minimum, where $\omega_0\tau_C = 0.616$, the theoretical value of the relaxation time, neglecting intermethyl interactions and the effects of cross correlations (17, 18), is $T_1 = 17.4$ ms for $r = 1.79$ Å and a Larmor frequency of 30 MHz. The solid lines for the I_2 and ICl complexes in Fig. 1 are the best fits of the experimental points to a B.P.P. relaxation mechanism involving a single motion, the coefficient of $f(\omega_0\tau_C)$ being chosen for each case to produce the best fit. For the case of the Br_2 complex, the theoretical value of T_1 is assumed to be that obtained by putting $\tau_C = \tau_{C2}$ and $\tau_{C1} = \infty$ in eq. 1. For this case, a minimum in T_1 requires $\omega_0\tau_C = 0.910$, and if $r = 1.79$ Å and $\nu_0 = 30$ MHz, the theoretical value of the minimum is 14.1 ms, again considering only interactions within a single methyl group. The solid line corresponds to

$$T_1^{-1} = K[f(\omega_0\tau_C) + (19/16)\, f(\omega_0\tau_C/2)]$$

with K chosen to give the best fit to the experimental points, and τ_C given by [2]. The parameters of best fit are listed in Table 1 together with activation energies obtained from line shape studies (3) for comparison. Our values of the activation energies, which are shown with the standard deviations computed from the least squares fits, are uniformly smaller than the barrier heights obtained from c.w. spectra. One assumes that the disagreement is largest in the case of the iodine complex because here the line shape on the high temperature side of the transition which is due to C_3 motion is considerably influenced by the C_3' motion, whose transition is very close to that of the C_3 reorientation.

Support of the assignments of C_3 motion to the relaxation mechanism for the I_2 and ICl complexes and of $C_3 + C_3'$ motion to the mechanism for the Br_2 complex can be inferred from the following considerations. The correlation time at the mid-point of the second moment transition for a particular motion should be approximately

$$[3] \qquad \tau_C = (\gamma\sqrt{M_2})^{-1}$$

where M_2 is the second moment at the mid-point. The mid-transition second moments and tem-

Can. J. Chem. Downloaded from www.nrcresearchpress.com by 210.87.254.6 on 09/05/12
For personal use only.

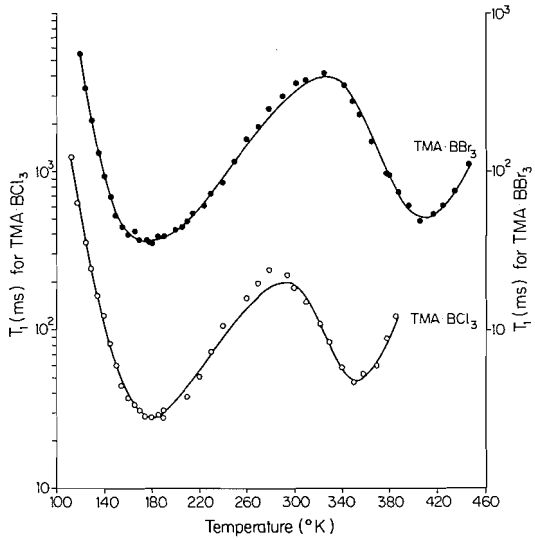

FIG. 2. Spin–lattice relaxation time as a function of temperature for trimethylamine–borontrichloride and bromide. ○, Me_3NBCl_3, ●, Me_3NBBr_3. Lines through the points are the best-fit lines described by the parameters in Table 1.

peratures for the three complexes are 17 G^2 at 130 °K for C_3 motion in $Me_3N.I_2$; 18 G^2 at 154 °K for C_3 motion in $Me_3N.ICl$; and 15 G^2 at 140 °K for $C_3 + C_3'$ motion in $Me_3N.Br_2$ (3). Using eqs. 2 and 3 and appropriate values of τ_C^0 and E_a from Table 1, we predict the second moment mid-transition temperatures to be 118, 138, and 129 °K, respectively. These agree adequately well with the observed values.

The theoretical values of 17.4 ms for the T_1 minimum in the I_2 and ICl complex and of 14.1 ms in the Br_2 complex do not agree very well with the experimental values of 30, 27, and 20 ms. Gutowsky and his co-workers (19), however, have attributed a disagreement of a similar kind in hexamethyldisilane to quantum mechanical effects in the torsional states of the methyl group modifying classical reorientation.

Trimethylamine – Boron Trihalide Complexes

Spin–lattice relaxation times for Me_3NBCl_3 and Me_3NBBr_3 are plotted in Fig. 2 as functions of temperature. In the BCl_3 complex, the low temperature minimum can be described by a B.P.P. relaxation involving a single motion. Because the two minima are well separated in temperature, it can be assumed that the relaxation mechanisms responsible for them are independent and that the rates of relaxation by each mechanism add in a simple manner. A resolution into relaxation times characteristic of each of two mechanisms can be obtained on this assumption. Although Yim and Gilson conclude that the higher temperature motion which they observe in their line shape studies (2) is probably C_3' reorientation of the trimethylamine group, their evidence leaves open the possibility that isotropic tumbling of the whole molecule may be involved. If we assume that C_3' motion and isotropic rotation occur with equal correlation times in the region of the high temperature minimum, and that C_3 motion is very rapid, we may put $\tau_C = 0$ and $\tau_{C1} = \tau_{C2}$ in [1] and obtain

$$[4]\quad \left(\frac{1}{T_1}\right)_{\text{intra } CH_3} = \frac{\gamma^4\hbar^2}{60\omega_0 r^6} \times [f(\omega_0\tau_{C1}) + 8f(\omega_0\tau_{C1}/2)]$$

for the case in which only intramethyl interactions are considered. The contribution of intermethyl interactions to the relaxation rate may here be estimated (20) by assuming that when $\tau_C \ll \tau_{C1}$ and τ_{C2} the average position of each proton of a methyl group is on the C_3 rotation axis and that the three methyl groups interact as three superimposed 3-spin systems whose motion is rotation about one threefold axis combined with isotropic rotation. By appropriate manipulation of [1] (we could let a series of correlation times τ' apply to the motion of the "collapsed" methyl spins and put $\tau_C' = \tau_{C2}$, $\tau_{C1}' = \tau_{C1}$, and $\tau_{C2}' = \infty$) we get

$$[5]\quad \left(\frac{1}{T_1}\right)_{\text{inter } CH_3} = 3 \times \frac{3\gamma^4\hbar^2}{20\omega_0 r_*^6} \times [f(\omega_0\tau_{C1}) + 3f(\omega_0\tau_{C1}/2)]$$

where r_* is the distance between the collapsed methyl spins. Addition of [4] and [5] gives

$$[6]\quad \frac{1}{T_1} = \frac{\gamma^4\hbar^2}{60\omega_0 r^6}\left[\left\{1 + 27\left(\frac{r}{r_*}\right)^6\right\} f(\omega_0\tau_{C1}) + \left\{8 + 81\left(\frac{r}{r_*}\right)^6\right\} f(\omega_0\tau_{C1}/2)\right]$$

For simple C_3' motion combined with very fast C_3 rotation of each methyl group the rate of spin–lattice relaxation, including a contribution from intermethyl interactions, is

$$[7]\quad \frac{1}{T_1} = \frac{\gamma^4\hbar^2}{\omega_0}\left[\frac{2}{15r^6} + \frac{27}{20r_*^6}\right] f(\omega_0\tau_{C2})$$

Can. J. Chem. Downloaded from www.nrcresearchpress.com by 210.87.254.6 on 09/05/12
For personal use only.

Can. J. Chem. Downloaded from www.nrcresearchpress.com by 210.87.254.6 on 09/05/12
For personal use only.

The high temperature T_1 minimum in Me_3NBCl_3 can be fitted by the functional form of either [6] or [7]. The parameters of best fit for both the low and high temperature minima are shown in Table 1. The choice of which motion best describes the high temperature relaxation process must be made on the basis of the agreement between the observed (best fit) and theoretical values of the T_1 minimum. T_1 is a minimum when $\omega_0\tau_{C2} = 0.616$ in [7], or, for the case of the NMe_3 moiety with $r_* = 3.02$ Å, when $\omega_0\tau_{C1} = 1.125$ in [6]. The appropriate theoretical T_1 minima in Table 1 were calculated from [6] and [7]. For the BCl_3 complex, a C_3' motion without isotropic tumbling agrees with the observed depth of minimum better than C_3' motion plus isotropic tumbling with the same correlation time, but in either case the theoretical minimum is significantly smaller than the experimental value. Isotropic tumbling (with $\omega_0\tau_{C1} \sim 1$) plus very fast C_3 and C_3' motions would give, including intermethyl interactions, a T_1 minimum of 213 ms. This value, four times the observed value, seems to exclude that combination of motions. Isotropic tumbling ($\omega_0\tau_{C1} \sim 1$) plus very fast C_3 motion and no C_3' motion gives a T_1 minimum of 44 ms, which is better than any of the other values that have been considered. Studies of motions in XMe_3 moieties in other compounds (19, 21, 22) suggest, however, that it is improbable that isotropic tumbling is much more rapid than C_3' reorientation at a given temperature.

The analysis for the BBr_3 complex is similar but is complicated by the fact that the low temperature minimum in T_1 is too broad to be fitted by a single B.P.P. function with one relaxation time. An attempt was made to fit the results to a Cole–Davidson distribution function (23, 24) whose width was given by $\delta = 2.86/3.23$, *i.e.*, the ratio of the slopes of the straight lines on the low and high temperature sides of the minimum. This distribution gave, however, a T_1 minimum which was much lower and less broad than that observed. Satisfactory fits for the low temperature minimum can be found by assuming that it is the sum of two or more B.P.P. functions with slightly differing activation energies, τ_C° values, and minima. Appropriate values of these parameters to give fits to the experimental points can be obtained by application of a non-linear least squares computer program to all the data points (25). An X-ray crystal structure determination (26) shows a slight deviation from C_{3v} symmetry and suggests that the most suitable fit may be given by two B.P.P. functions weighted in the ratio of 1:2 for C_3 reorientation involving one unique and two equal methyl groups plus a third B.P.P. function for the high temperature motion. The best fit parameters for such a scheme give the unique methyl group an activation energy of 3.58 ± 0.18 kcal/mol and the other two an activation energy of 2.70 ± 0.07 kcal/mol. In the X-ray structure it is the unique methyl group which has the longer C—N bond and it might be expected to have the lower activation energy. Internuclear distances calculated from theoretically generated proton positions show the same number of intermethyl proton–proton distances less than 2.5 Å and also the same number of proton–bromine distances less than 3.0 Å for each methyl group. The proton to bromine contacts are 2.84 Å for the unique methyl group and 2.70 Å for the other methyl groups. An equally good fit is given by two quite independent B.P.P. functions for the lower temperature minimum plus a third B.P.P. function for the high temperature process. One could rationalize such a scheme if there were two inequivalent molecules in the unit cell. The positions of the light atoms in the BBr_3 complex are more uncertain than those in the BCl_3 complex according to the X-ray results (26), and we suggest that this uncertainty may mask small differences in environment in the tribromide complex. We list in Table 1 the parameters for the best fit of the whole curve to three unrestricted B.P.P. functions.

The crystal structure allows one to check the approximate second moments calculated by Yim and Gilson (2) for Me_3NBCl_3 and Me_3NBBr_3 from the then known structure of the trifluoride complex. Proton positions were generated by a computer program from an assumed C—H bond length of 1.097 Å and these coordinates were used in a second program to give interproton distances from which a rigid lattice second moment was calculated. The values for the BCl_3 and BBr_3 complexes were 27.1 and 26.8 G^2, respectively, which are slightly smaller than Yim and Gilson's 30.2 G^2. If their theoretical, high temperature value for $C_3 + C_3'$ motion is reduced proportionally, it becomes 1.6 G^2, which agrees a little better with their observed 1.25 G^2, but still leaves open the question of the extent to which isotropic tumbling might be significant.

As in the case of the halogen complexes, the

TABLE 2. Theoretical second moments (in G^2) for Me_3NBX_3 and Me_3PBX_3

	Theoretical second moment contribution						
		Intramolecular but intermethyl		Intermolecular		Total	
Motion	Intra-CH_3	Me_3N	Me_3P	Me_3NBX_3	Me_3PBX_3	Me_3NBX_3	Me_3PBX_3
Rigid	21.5	3.3* 3.5†	1.4*‡	2.2§ 2.0§	2.2	27.0 27.0	25.1
C_3	5.4	2.8*	1.2‡	0.7	0.7	8.9	7.3
C_3+C_3'	0.6	0.7	0.3	0.3	0.3	1.6	1.2

*Calculated by the method of ref. 27.
†Calculated from assumed rigid lattice proton coordinates.
‡Includes a contribution of 0.2 G^2 for H–P interactions.
§Value which makes the total second moment equal to 27.0 G^2, which is a mean value calculated from proton coordinates generated from the X-ray structures of Me_3NBCl_3 and Me_3NBBr_3 (ref. 26).

correspondence between the spin–lattice relaxation mechanisms and the motions which produce the second moment transitions can be checked by the aid of eq. 3 and the activation parameters obtained from the T_1 results. The experimental mid-points of the second moment transitions (2) are 97 and 235 °K for Me_3NBCl_3 and 100 and 272 °K for Me_3NBBr_3. The values predicted from relaxation studies are 90 and 246 °K for the chloride and 86 °K (with the (*a*) parameters) or 101 °K (with the (*b*) parameters) and 264 °K for the bromide. The agreement is satisfactory.

Trimethylphosphine – Boron Trihalide Complexes

The experimental second moments of Me_3PBCl_3 and Me_3PBBr_3 are shown as functions of temperature in Fig. 3. Theoretical second moments have been estimated for these complexes for various kinds of rotational motion and summarized in Table 2. The intramethyl contribution is based on tetrahedral bond angles and a C—H bond length of 1.097 Å; a C—P bond length of 1.84 Å was used in estimating the intramolecular, intermethyl contribution by Smith's method (27); and the intermolecular contribution is assumed to be the same as that estimated for trimethylamine complexes. A contribution from nuclei outside a sphere of radius 6 Å has been included, and so has the contribution from H–P interactions. The experimental second moments at 80 °K agree well with the theoretical value for C_3 motion of all the methyl groups, and the experimental values at high temperature are a little lower than the theoretical values for $C_3 + C_3'$ motion.

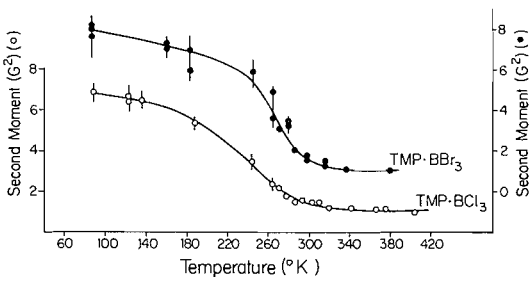

FIG. 3. Second moment as a function of temperature for trimethylphosphine–borontrichloride and bromide. ○, Me_3PBCl_3; ●, Me_3PBBr_3.

The null times, t_0, obtained for the triphenylphosphine complexes from spin–lattice relaxation studies are plotted against temperature in Fig. 4. In both complexes the low temperature minimum in t_0 is believed to correspond to C_3 rotation of methyl groups. The high temperature minima lie within the range of temperature for which the *Z*-component of magnetization decays exponentially and T_1 and t_0 are simply related by $t_0 = T_1 \ln 2$. The theoretical depths for a T_1 minimum due to C_3' motion and for a minimum due to equally fast C_3' motion and isotropic rotation are very nearly the same and are in moderately good agreement with the observed depths, so that the relaxation results do not distinguish whether the high temperature motion involves isotropic rotation. The activation parameters and experimental and theoretical depths of minima are listed in Table 1. Calculation of the theoretical depths for the high temperature minimum follows eqs. 6 and 7 in which r_* is taken to be 3.60 Å in the Me_3P group. Albert and Ripmeester have noted (28) that non-exponential behavior is modified or even eliminated if an overall molecular tumbling motion is superimposed on a system in which the principal relaxation mechanism is methyl group

Can. J. Chem. Downloaded from www.nrcresearchpress.com by 210.87.254.6 on 09/05/12
For personal use only.

TABLE 3. Comparison of thermal stability of trimethylamine complexes and the barriers to methyl group reorientation in their Me_3N moieties

Substance	Activation energy of C_3 motion of N-methyl groups (kcal/mol)	Thermal stability of complex	Reference
$Me_3N.BCl_3$	2.71 ± 0.06	Stable on heating to 250 °C for 1 hour	8
$Me_3N.BBr_3$	2.89 ± 0.19 3.17 ± 0.25	Melts at 238 °C with some decomposition	9
$Me_3N.GaMe_3$	3.10 ± 0.08 (ref. 29)	Begins to show perceptible dissociation only above 110 °C	31
$Me_3N.AlMe_3$	3.18 ± 0.04 (ref. 29)	Not perceptibly dissociated in the gas phase up to 148 °C	32
$Me_3N.I_2$	3.39 ± 0.20	Decomposes at 66 °C	6, 33
$Me_3N.BMe_3$	3.63 ± 0.03 (ref. 4)	$K_p = 0.472$ for gas phase dissociation at 100 °C	34
$Me_3N.ICl$	4.31 ± 0.20	Not very stable even at room temperature	7
$Me_3N.Br_2$	4.71 ± 0.10	Decomposes slowly at room temperature	33
Me_3N (solid)	5.75 ± 0.14 (ref. 30)		

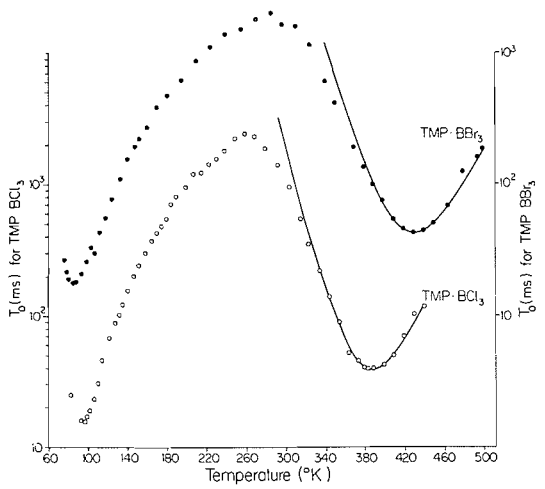

FIG. 4. Spin-lattice relaxation "null-time" as a function of temperature for trimethylphosphine–borontrichloride and bromide. ○, Me_3PBCl_3; ●, Me_3PBBr_3. The solid lines have been calculated from the parameters of best fit given in Table 1 for the high temperature relaxation process, for which $T_1 = t_0/\ln 2$.

reorientation. They found that a correlation time as large as 0.4 s for the molecular tumbling motion was still effective in reducing the non-exponential character of the relaxations. We may comment that in Me_3PBCl_3 the correlation time for the high temperature relaxation mechanism is 0.1 s at 194 °K according to the parameters given for that complex in Table 1. This is the temperature range in which the non-exponential relaxation disappears in Me_3PBCl_3. It is unclear as to whether we should interpret this as indicating that the high temperature motion involves molecular tumbling or that superimposing a C_3' motion on methyl group reorientation also removes non-exponential relaxation behavior. We favor the latter view. In summary, then, the spin–lattice relaxation results are not definitive in determining whether molecular tumbling is involved in the motion that has been observed in the higher temperature range of any of the BX_3 complexes studied here. On the whole, we favor Yim and Gilson's interpretation for all four complexes.

The possibility of quantum mechanical tunnelling by the methyl group (35–37) should probably not be ignored in these systems where the energy barriers to C_3 motion are small. Our measurements at relatively high temperatures (above 70 K) do not give, however, any clear indication of how important the tunnelling mechanism may be in these systems.

The Barrier to Methyl Group Reorientation in the Me_3N Moiety

Increase in the activation energy for the C_3 reorientation of the methyl groups in the moiety Me_3N in the complexes studied here and elsewhere is paralleled by a decrease in the thermal stability of the complexes. This trend is summarized in Table 3, in which we report the stability of each complex as best we can from the available references. We would suggest first that Table 3 indicates that the barriers to methyl group reorientation in the Me_3N moiety are mainly of intramolecular origin. Our views on why the activation energy for methyl group rotation decreases with increasing stability of complex are entirely speculative. Valence shell electron pair repulsion theory (38) suggests that

Can. J. Chem. Downloaded from www.nrcresearchpress.com by 210.87.254.6 on 09/05/12
For personal use only.

Can. J. Chem. Downloaded from www.nrcresearchpress.com by 210.87.254.6 on 09/05/12
For personal use only.

the C—N—C bond angles will increase as the lone pair on nitrogen in trimethylamine becomes progressively more strongly involved in a donor–acceptor bond. One might postulate a slight shift in the hybridization pattern on nitrogen as the complexes became more thermally stable. If we consider a hybridization involving 3 orbitals of a type $s^{\frac{1}{4}+\delta}\ p^{\frac{3}{4}-\delta}$ contributing to N—C bonds and 1 orbital of a type $s^{\frac{1}{4}-3\delta}\ p^{\frac{3}{4}+3\delta}$ contributing to the N-acceptor bond, we can allow δ to increase from zero to small but finite values as the stability of the complex increases. This would increase the C—N—C angles and the intermethyl distances in the Me_3N moiety. Unfortunately, the scanty evidence provided by measurements that have been made of atomic coordinates is at best equivocal. Lide and Mann (39) find that the parameters C—N = 1.472 ± 0.008 Å and C—N—C = 108.7 ± 1.0° are consistent with their microwave results from the gas phase of trimethylamine. At the other end of the scale of barrier heights, the X-ray diffraction study of $Me_3N.BCl_3$ (26) gives $C_{(1)}$—N = 1.523 ± 0.006 Å, $C_{(2)}$—N = 1.500 ± 0.004 Å, $C_{(1)}$—N—$C_{(2)}$ = 107.2 ± 0.2°, and $C_{(2)}$—N—$C_{(2')}$ = 109.9 ± 0.4°. The parameters for $Me_3N.BBr_3$ (26) are $C_{(1)}$—N—$C_{(2)}$ = 107.3 ± 0.8° and $C_{(2)}$—N—$C_{(2')}$ = 108.0 ± 1.2°. The X-ray results of Strømme (6) and Hassel and Hope (7) do not fix the coordinates of the lighter atoms sufficiently definitely to be useful in this context. The lengthening of the C—N bonds as a complex is formed, which is indicated in the atomic parameters, can be understood as a shift of electron density from the C—N bonds to the N-acceptor bond, and serves to lower the barrier to methyl group reorientation.

The financial support of the National Research Council of Canada in the form of a Grant-in-Aid of this research is gratefully acknowledged. We are also grateful to the X-ray diffraction group in the Chemistry Department for their kindness in letting us use their programs for generating proton positions and calculating interatomic distances.

1. B. A. Dunell, C. A. Fyfe, C. A. McDowell, and J. Ripmeester. Trans. Faraday Soc. **65**, 1153 (1969).
2. C. T. Yim and D. F. R. Gilson. Can. J. Chem. **48**, 515 (1970).
3. C. A. Fyfe and J. Ripmeester. Can. J. Chem. **48**, 2283 (1970).
4. T. T. Ang and B. A. Dunell. J. Chem. Soc. Faraday II, **68**, 1331 (1972).
5. M. B. Dunn and C. A. McDowell. Mol. Phys. **24**, 969 (1972).
6. K. O. Strømme. Acta Chem. Scand. **13**, 268 (1959).
7. O. Hassel and H. Hope. Acta Chem. Scand. **14**, 391 (1960).
8. E. Wiberg and W. Sutterlin. Z. anorg. allg. Chem. **202**, 31 (1931).
9. R. C. Osthoff, C. A. Brown, and H. Clark. J. Am. Chem. Soc. **73**, 4045 (1951).
10. E. Sirtl and A. Adler. Z. Naturforsch. **16b**, 403 (1961).
11. K. van Putte. J. Magn. Reson. **2**, 174 (1970).
12. R. Kubo and K. Tomita. J. Phys. Soc. Jap. **9**, 888 (1954).
13. T. Yukitoshi, H. Suga, S. Seki, and J. Itoh. J. Phys. Soc. Jap. **12**, 506 (1957).
14. E. O. Stejskal and H. S. Gutowsky. J. Chem. Phys. **28**, 388 (1958).
15. D. E. Woessner. J. Chem. Phys. **36**, 1 (1962).
16. N. Bloembergen, E. M. Purcell, and R. V. Pound. Phys. Rev. **73**, 679 (1948).
17. R. L. Hilt and P. S. Hubbard. Phys. Rev. A **134**, 392 (1964).
18. M. F. Baud and P. S. Hubbard. Phys. Rev. **170**, 384 (1968).
19. S. Albert, H. S. Gutowsky, and J. A. Ripmeester. J. Chem. Phys. **56**, 1332 (1972).
20. S. Albert, H. S. Gutowsky, and J. A. Ripmeester. J. Chem. Phys. **56**, 3672 (1972).
21. J. M. Chezeau, J. Dufourcq, and J. H. Strange. Mol. Phys. **20**, 305 (1971).
22. G. W. Smith. J. Chem. Phys. **51**, 3569 (1969).
23. D. W. Davidson and R. H. Cole. J. Chem. Phys. **19**, 1484 (1951).
24. T. M. Connor. Trans. Faraday Soc. **60**, 1574 (1964).
25. B. A. Dunell, M. D. Pachal, and S. E. Ulrich. Can. J. Chem. **51**, 1107 (1973).
26. P. H. Clippard, J. C. Hanson, and R. C. Taylor. J. Cryst. Mol. Struct. **1**, 363 (1971).
27. G. W. Smith. J. Chem. Phys. **42**, 4229 (1965).
28. S. Albert and J. A. Ripmeester. J. Chem. Phys. **57**, 2641 (1972).
29. T. T. Ang and B. A. Dunell. J. Chem. Soc. Faraday II. **70**, 17 (1974).
30. A. W. K. Khanzada and C. A. McDowell. To be published.
31. G. E. Coates. J. Chem. Soc. 2003 (1951).
32. N. Davidson and H. C. Brown. J. Am. Chem. Soc. **64**, 316 (1942).
33. H. Böhme and W. Krause. Chem. Ber. **84**, 170 (1951).
34. H. C. Brown, J. Chem. Soc. 1248 (1956); D. P. N. Satchell and R. S. Satchell. Chem. Rev. **69**, 251 (1969); F. G. A. Stone. Chem. Rev. **58**, 101 (1958).
35. P. S. Allen and S. Clough. Phys. Rev. Lett. **22**, 1351 (1969).
36. F. Apaydin and S. Clough. J. Phys. C, **1**, 932 (1968).
37. S. Clough. J. Phys. C, **4**, 2180 (1971).
38. R. J. Gillespie and R. S. Nyholm. Q. Rev. **11**, 273 (1967).
39. D. R. Lide, Jr. and D. E. Mann. J. Chem. Phys. **28**, 572 (1958).

Isomérisation photochimique de l'azobenzène en solution. I

JACQUES RONAYETTE, RENÉ ARNAUD, PHILIPPE LEBOURGEOIS ET JACQUES LEMAIRE

Laboratoire de Photochimie, U.E.R. de Sciences Exactes et Naturelles et Ecole Nationale Supérieure de Chimie, Université de Clermont, Ensemble Scientifique des Cézeaux, 63170, Aubière, France

Reçu le 24 juillet, 1973

L'isomérisation photochimique de l'azobenzène en solution peut être sensibilisée par des composés aromatiques (chrysène, phénanthrène, naphtalène) ou carbonylés (benzile, biacétyle). La comparaison des régimes photostationnaires et des rendements quantiques initiaux d'isomérisation permet de proposer un mécanisme de cette sensibilisation. Par transferts d'énergie triplet-triplet, contrôlés par la diffusion, on peuple les niveaux triplets $T_\beta{}^t$ et $T_\beta{}^c$ des formes *trans* et *cis*. Ces niveaux se désactivent non radiativement sans donner lieu à une isomérisation; il intervient, dans la forme *cis*, une conversion interne quantitative vers un niveau triplet $T_\alpha{}^c$, alors que dans la forme *trans* le niveau $T_\beta{}^t$ subit une transition non radiative vers l'état fondamental. La conversion interne $T_\beta{}^t \rightarrow T_\alpha{}^t$, dans cette forme *trans*, a lieu avec une faible probabilité (0.04 à 0.06). Les niveaux $T_\alpha{}^t$ et $T_\alpha{}^c$ sont responsables de l'isomérisation; ils se désactivent vers les deux formes isomères de l'azobenzène avec une égale probabilité.

The photochemical isomerization of azobenzene can be sensitized by aromatic compounds (chrysene, phenanthrene, naphthalene) or by carbonyls (benzil, biacetyl). Comparison of the photostationary states and the initial quantum yields of isomerization leads to the deduction of a mechanism for this sensitization. The triplet levels $T_\beta{}^t$ and $T_\beta{}^c$ of the *trans* and *cis* forms are populated by diffusion-controlled, triplet-triplet energy transfer. These levels are deactivated nonradiatively without giving rise to isomerization. The $T_\beta{}^c$ level of the *cis* form undergoes a quantitative internal conversion to another triplet level $T_\alpha{}^c$, while the $T_\beta{}^t$ level of the *trans* form undergoes a nonradiative transition to the ground state. The internal conversion $T_\beta{}^t \rightarrow T_\alpha{}^t$ in the *trans* isomer occurs with low probability (0.04 to 0.06). The levels $T_\alpha{}^t$ and $T_\alpha{}^c$ are the intermediates in the isomerization; they are deactivated to the two isomeric forms of azobenzene with equal probability. [Journal translation]

Can. J. Chem., **52**, 1848 (1974)

Introduction

Le groupement azo (—N=N—) intervient dans de nombreux colorants et dans certaines substances photochromes. On peut envisager l'étude de la réactivité photochimique de ce groupement soit dans la série des dérivés azoïques aliphatiques (azoalcanes) soit dans celle des dérivés aromatiques.

Les azoalcanes sont essentiellement le siège de processus d'isomérisation en phase liquide et de processus photolytiques en phase gazeuse (1, 2). La structure électronique de l'état fondamental et des états singulets S_1 et S_2 est relativement simple, mais le deuxième état singulet n'est accessible qu'à très courtes longueurs d'onde (inférieures à 200 nm). Nous avons choisi d'étudier l'azobenzène *cis* et *trans* (Ph—N=N—Ph) car on peut facilement exciter cette molécule dans ses deux plus bas niveaux singulets S_1 et S_2 sans qu'il y ait de processus photolytiques. En outre, l'azobenzène *trans* est une substance qui se prête bien à une ultrapurification par zone fondue alors que les azoalcanes ne sont pas des produits commerciaux courants. Il convient de dire, néanmoins, que l'azobenzène n'est pas une molécule facile à aborder sur le plan théorique.

L'azobenzène a déjà été l'objet de quelques études détaillées. Zimmerman et ses collaborateurs (3) ont mesuré les rendements quantiques d'isomérisation directe à 25 °C, en solution dans l'isooctane et ont examiné les régimes photostationnaires obtenus. Les mêmes mesures ont été effectuées ultérieurement par Yamashita *et al.* (18) puis par Fischer et ses collaborateurs (19). Les resultats de Yamashita diffèrent notablement de ceux obtenus par Zimmerman *et al.* (3) et Fischer et ses collaborateurs (19).

Rau a pu observer une fluorescence de la forme *trans* de l'azobenzène en solutions très acides; à température ambiante, le rendement quantique de fluorescence est inférieur à 0.001. Ce rendement quantique augmenterait sensiblement à basse température (4, 5). Les réactions photochimiques de l'azobenzène dissous dans des solutions très acides ont été récemment décrites par Mauser *et al.* (6). Par ailleurs, dans

Can. J. Chem. Downloaded from www.nrcresearchpress.com by 210.87.254.6 on 09/05/12
For personal use only.

Can. J. Chem. Downloaded from www.nrcresearchpress.com by 210.87.254.6 on 09/05/12
For personal use only.

un solvant à hydrogène mobile comme l'isopropanol, l'azobenzène peut être le siège de processus de photoréduction; Hashimoto et Kano ont récemment étudié cette photoréduction directe et sensibilisée (7).

L'isomérisation photosensibilisée des azobenzènes susceptible d'apporter des éléments de compréhension nouveaux conduit à des résultats expérimentaux et des conclusions contradictoires. Le tableau suivant rassemble les résultats obtenus par Jones et Hammond (8) en employant des sensibilisateurs non fluorescents et dont les états excités sont de nature $\pi\pi^*$.

Sensibilisateur (S)	Energie du triplet (kcal mol^{-1})	Régimes photostationnaires (% *cis*)
3-Acétylpyrène	45	1.8
β-Acétonaphtone	59.3	1.5
Triphénylène	66.6	1.6

Ces auteurs proposent le mécanisme suivant, où A_T^* est un état excité triplet qui n'a plus de caractère "*cis*" ou "*trans*".

$$S^* + \textit{trans}\ A \xrightarrow{k_1} S + A_T^*$$

$$S^* + \textit{cis}\ A \xrightarrow{k_2} S + A_T^*$$

$$A_T^* \xrightarrow{k_3} \textit{trans}\ A$$

$$A_T^* \xrightarrow{k_4} \textit{cis}\ A$$

Soient t_∞ et c_∞ les concentrations de *trans* et de *cis* à l'état photostationnaire. Dans des conditions de sensibilisation totale où tous les photons sont absorbés par le donneur, on peut écrire

$$t_\infty/c_\infty = k_2k_3/k_1k_4.$$

Comme Hammond et son collaborateur (8) estiment que les transferts d'énergie sont contrôlés par la diffusion, les constantes k_1 et k_2 sont égales; cette expression se réduit à

$$k_3/k_4 = t_\infty/c_\infty.$$

La valeur de k_3/k_4 ainsi mesurée est égale à 60. Si le peuplement du niveau triplet responsable de l'isomérisation est quantitatif lors de l'excitation directe, on peut écrire

$$k_3/k_4 = t_\infty/c_\infty\ \varepsilon_t/\varepsilon_c$$

ε_t et ε_c étant les coefficients d'extinction moléculaire des formes *trans* et *cis* de l'azobenzène. Dans ce cas, selon les mesures de Zimmerman *et al.* (3), le rapport k_3/k_4 est égal à 4 pour une excitation dans la bande ($\pi\pi^*$) et à 2 pour une excitation dans la bande ($n\pi^*$). Pour interpréter les valeurs différentes du rapport k_3/k_4 obtenues en sensibilisation totale et en excitation directe, Hammond et ses collaborateurs admettent que l'isomérisation est en partie issue directement des états singulets lors de l'excitation directe.

Fischer (9) a examiné l'isomérisation de l'azobenzène sensibilisé par le triphénylène et le naphtalène; ils obtiennent à 313 nm des états stationnaires beaucoup plus riches en *cis* (de 20 à 40%). Pour que la part d'intensité lumineuse absorbée par l'azobenzène soit réduite, les sensibilisateurs ont été utilisés à fortes concentrations; dans ces conditions, la densité optique à la longueur d'onde d'irradiation est très supérieure à 1 (70 par exemple). Le rapport des constantes de désactivation du triplet a été trouvé voisin de 4. Fischer conclue que le peuplement des triplets à partir des singulets est quantitatif et que l'isomérisation directe ou sensibilisée implique seulement les niveaux triplets.

La revue des travaux publiés sur la réactivité photochimique de l'azobenzène montre que le mécanisme de la photoisomérisation n'est pas élucidé; le nombre des niveaux triplets impliqués et leur disposition n'avaient pu être précisés. Dans un article récent consacré à la photochimie de l'azobenzène et de ses dérivés substitués, Griffiths (10) souligne également l'importance qu'il convient d'attribuer à l'étude du mécanisme d'isomérisation. Le travail présent a été entrepris dans le but de préciser, autant que faire se peut, les propriétés des niveaux triplets.

Notons qu'en 1970 est parue une étude théorique de la forme *trans* de l'azobenzène dans l'état fondamental et excité de nature $\pi\pi^*$ par une méthode de configuration d'interaction en champ autocohérent. Les énergies du niveau singulet $S(\pi\pi^*)$ et du niveau triplet correspondant $T(\pi\pi^*)$ ont été estimées respectivement égales à 93.6 et 46.5 kcal mol^{-1} (11).

Il reste à signaler que pour interpréter les spectres d'absorption de l'azobenzène *trans* et *cis*, Suzuki (12) a étudié par traitement monoélectronique les orbitales moléculaires de ces deux formes. L'azobenzène *trans* est une molécule plane où l'on prévoit l'existence d'une transition interdite $n\pi^*$ et d'une transition permise $\pi\pi^*$. L'azobenzène *cis* est une molécule où

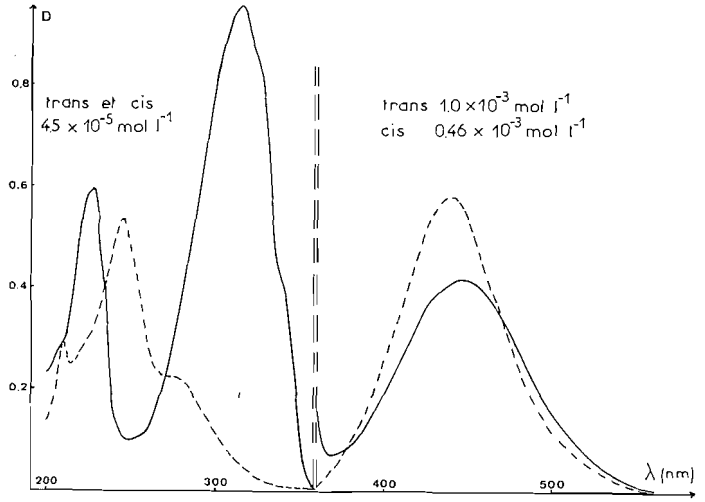

FIG. 1. Spectres d'absorption de l'azobenzène *trans* (—) et *cis* (---) en solution dans le cyclohexane.

l'angle formé par le plan des noyaux benzéniques est évalué à 56°. Cette non-planéité permet une interaction entre orbitales n et π et les niveaux singulets n'ont plus de caractère nπ* et ππ* aussi précis que ceux de la forme *trans*.

Techniques expérimentales

L'azobenzène *trans* utilisé est une substance Aldrich ultra purifiée par zone fondue. L'azobenzène *cis* a été préparé par photoisomérisation de l'azobenzène *trans* et purifié par chromatographie en phase liquide sur colonne de gel de silice. L'azobenzène *cis* contenait initialement environ 2% d'azobenzène *trans*. Les spectres d'absorption de la forme *trans* et de la forme *cis* ainsi préparés (déduction faite de l'absorption due au *trans*) sont représentés sur la fig. 1, et le tableau 1 rassemble les valeurs des coefficients d'extinction molaire (en mol^{-1} l cm^{-1}) mesurées dans les différents solvants.

Les solutions d'azobenzène soigneusement dégazées ont été irradiées à l'aide d'un monochromateur Bausch et Lomb équipé d'une lampe à vapeur de mercure "haute pression" Osram HBO 200 W. Nous avons mesuré les rendements quantiques d'isomérisation par dosages spectrophotométriques associés à une actinométrie basée soit sur la photolyse de l'acide oxalique sensibilisée par le nitrate d'uranyle, soit sur la photoréduction de ferrioxalate de potassium.

A titre de vérifications de nos techniques expérimentales, nous avons mesuré à nouveau les rendements quantiques initiaux d'isomérisation directe de l'azobenzène dissous dans du cyclohexane, $\Phi^0_{t\to c}$ et $\Phi^0_{c\to t}$. Le tableau 2 rassemble nos résultats, résultats sensiblement identiques à ceux obtenus par Zimmerman *et al.*, dans l'isooctane. Dans les conditions d'excitation *nπ** nos résultats ne sont pas en accord avec ceux de Yamashita *et al.*

En outre, nous avons mesuré les rendements quantiques d'isomérisation directe dans différents solvants et vérifié que ces rendements ne dépendaient pas de la concentration d'azobenzène (*cf.* tableaux 3 et 4).

TABLEAU 1. Coefficients d'extinction molaire (mol^{-1} l cm^{-1} $\log_{10}$) d'azobenzène *cis* et *trans* dans les différents solvants

λ (nm)	Cyclohexane		Méthanol		Isopropanol	
	ε_t	ε_c	ε_t	ε_c	ε_t	ε_c
254	2200	8300	2240	7260	2520	7320
313	21100	1160	20500	—	25200	1650
334	17000	135	16600	—	20600	258
345	9000	40	9260	—	11500	—
365	120	39	—	—	400	—
436	390	1260	475	—	570	1580

TABLEAU 2. Variation des rendements quantiques initiaux d'isomérisation directe d'azobenzène dans du cyclohexane en fonction de la longueur d'onde d'excitation

λ (nm)	Mesures de Zimmerman (3)		Nos mesures	
	$\Phi^0_{t\to c}$	$\Phi^0_{c\to t}$	$\Phi^0_{t\to c}$	$\Phi^0_{c\to t}$
313	0.10	0.41	0.10	0.42
365	0.12		0.14	
436	0.27	0.55	0.28	0.55

Nous avons également vérifié par dosages spectrophotométriques, dans de plus larges limites de concentration (2×10^{-3} à 4×10^{-5} mol l^{-1}), que le régime photostationnaire ne dépendait pas de la concentration initiale d'azobenzène et qu'il était compatible avec les rendements quantiques initiaux déterminés.

Les résultats précédents concernant l'isomérisation de la forme *cis* ont été acquis sur des échantillons d'azobenzène *cis* purifié par chromatographie. Mais la conservation de cette forme s'est avérée difficile, et nous avons préféré préparer cet isomère par irradiation de la forme

Can. J. Chem. Downloaded from www.nrcresearchpress.com by 210.87.254.6 on 09/05/12
For personal use only.

TABLEAU 3. Rendements quantiques initiaux d'isomérisation directe d'azobenzène dans trois solvants

λ (nm)	Cyclohexane		Isopropanol		Méthanol	
	$\Phi^0_{t\to c}$	$\Phi^0_{c\to t}$	$\Phi^0_{t\to c}$	$\Phi^0_{c\to t}$	$\Phi^0_{t\to c}$	$\Phi^0_{c\to t}$
313	0.10±0.02	0.42±0.02	0.10±0.02	0.50±0.03	0.14±0.02	—
436	0.28±0.02	0.55±0.02	0.26±0.02	0.42±0.02	0.28±0.02	—

TABLEAU 4. Variation du rendement quantique d'isomérisation directe d'azobenzène *trans* dans du cyclohexane en fonction de la concentration

[Azobenzène *trans*] (mol l^{-1})	$\Phi_{t\to c}$ (313 nm)
6.4×10^{-6}	0.11
2.0×10^{-5}	0.09
6.0×10^{-5}	0.10
1.0×10^{-4}	0.09
2.0×10^{-4}	0.08

trans à 345 nm. Nous avons également vérifié que le rendement quantique $\Phi_{c\to t}$ restait constant avec le degré d'avancement de la réaction; il s'avérait donc inutile de séparer la forme *cis* du mélange irradié. Cette remarque reste valable pour les expériences de sensibilisation.

Toutes les tentatives d'inhibition de la photoisomérisation de l'azobenzène par des substances à bas niveau triplet se sont avérées négatives. Il n'est donc pas étonnant que la présence d'une forme ne modifie pas la cinétique d'isomérisation de l'autre forme.

Résultats expérimentaux

Isomérisation photosensibilisée par les hydrocarbures aromatiques

En photosensibilisation, il est difficile de limiter l'azobenzène à la seule fonction d'accepteur car dans le domaine de longueur d'onde utilisable, les coefficients d'extinction molaire des formes *cis* et *trans* sont élevés. En employant des sensibilisateurs aromatiques à des densités optiques convenables ($D_s < 1.5$), on doit accepter qu'un certain nombre de photons soit absorbé par l'azobenzène.

Nous avons vérifié que les formes *cis* et *trans* de l'azobenzène aux concentrations employées (voisines de 10^{-5} mol l^{-1}) ne modifient pas la fluorescence des donneurs aromatiques utilisés. Il convient, dès à présent, de noter qu'aucun niveau singulet des sensibilisateurs employés ne peut être désactivé par les deux formes de l'azobenzène dans le domaine de concentrations exploré, quelque soit le mécanisme de désactivation employé (transfert singulet–singulet ou formation d'exciplexe). Les niveaux singulets des azobenzènes *cis* et *trans* ne peuvent donc pas être produits en employant un sensibilisateur et ils ne sont pas impliqués dans les isomérisations sensibilisées.

L'intervention d'exciplexes triplets dans le mécanisme d'isomérisation sensibilisée ne peut être écartée *a priori*. Quelques rares désactivations d'états triplets sont interprétées dans la littérature, en termes d'excimères ou exciplexes triplets (13). Il est raisonnable de faire intervenir un exciplexe quand les transferts triplet–triplet possibles sont endothermiques ou quand un processus spécifique de l'exciplexe apparait. Dans notre étude, il apparait raisonnable de supposer que les transferts d'énergies sont exothermiques, une formation d'exciplexe n'a donc pas de conséquences cinétiques particulières. En outre, l'isomérisation *cis–trans* qui a lieu en excitation directe ne peut être en sensibilisation un processus spécifique d'un exciplexe intermédiaire. Nous acceptons donc un schéma cinétique classique impliquant uniquement des transferts d'énergie triplet–triplet. Dans le cas le plus général, ce schéma cinétique serait donc

$$\text{Sensibilisateur}(S_0) + h\nu \xrightarrow{\Phi_S(I_a)_S} \text{Sensibilisateur}(T_1^S)$$

$$\text{Sensibilisateur}(T_1) \xrightarrow{k_d} \text{Sensibilisateur}(S_0)$$

$$\text{Sensibilisateur}(T_1) + \text{azo } \textit{trans}(S_0) \xrightarrow{k_t^S} \text{Sensibilisateur}(S_0) + \text{azo } \textit{trans}(T_\alpha^t)$$

$$\text{Sensibilisateur}(T_1) + \text{azo } \textit{cis}(S_0) \xrightarrow{k_c^S} \text{Sensibilisateur}(S_0) + \text{azo } \textit{cis}(T_\alpha^c)$$

$$\text{Azo } \textit{trans}(S_0) + h\nu \xrightarrow{\Phi_t(I_a)_{trans}} \text{Azo } \textit{trans}(T_\alpha^t)$$

$$\text{Azo } \textit{trans}(S_0) + h\nu \xrightarrow{\Phi_c(I_a)_{cis}} \text{Azo } \textit{cis}(T_\alpha^c)$$

$$\text{Azo } \textit{trans}(T_\alpha^t) \xrightarrow{k_{tc}} \text{Azo } \textit{cis}(S_0)$$

$$\text{Azo } \textit{trans}(T_\alpha^t) \xrightarrow{k_{tt}} \text{Azo } \textit{trans}(S_0)$$

Can. J. Chem. Downloaded from www.nrcresearchpress.com by 210.87.254.6 on 09/05/12
For personal use only.

$$\text{Azo } cis\ (T_\alpha^c) \xrightarrow{k_{ct}} \text{Azo } trans\ (S_0)$$

$$\text{Azo } cis\ (T_\alpha^c) \xrightarrow{k_{cc}} \text{Azo } cis\ (S_0)$$

où ϕ_S, ϕ_t, ϕ_c sont respectivement les rendements quantiques de formation des triplets du sensibilisateur, de la forme *trans* et de la forme *cis*, T_1^S, T_α^t, T_α^c; k_t^S, k_c^S sont les constantes des transferts d'énergie qui produisent les niveaux triplets T_α^t, T_α^c responsables de l'isomérisation. Si ε_S, ε_t, ε_c sont, respectivement, les coefficients d'extinction molaire du sensibilisateur, de la forme *trans* et de la forme *cis* à la longueur d'onde d'irradiation, τ est la durée de vie réelle du sensibilisateur, c_∞ et t_∞ les concentrations des formes *cis* et *trans* en régime photostationnaire, on obtient

$$[1]\quad \frac{t_\infty}{c_\infty} = \frac{\phi_t \Phi^0_{c\to t}}{\phi_c \Phi^0_{t\to c}} \cdot \frac{\varepsilon_c\phi_c + \dfrac{\varepsilon_S\phi_S(S)}{\dfrac{1}{\tau k_c^S} + \dfrac{k_t^S}{k_c^S} t_\infty + c_\infty}}{\varepsilon_t\phi_t + \dfrac{\varepsilon_S\phi_S(S)}{\dfrac{1}{\tau k_t^S} + \dfrac{k_c^S}{k_t^S} c_\infty + t_\infty}}$$

Nous avons utilisé comme sensibilisateur le naphtalène, le phénanthrène et le chrysène dont les coefficients d'extinction molaire dans le cyclohexane, à la longueur d'onde d'excitation, 313 nm, sont respectivement 136, 197 et 7230 mol^{-1} l cm^{-1}. Les énergies, les durées de vie et les rendements quantiques de population des plus bas niveaux triplets de ces donneurs sont indiqués dans le tableau 5.

Le chrysène et le phénanthrène sont les seuls hydro carbures aromatiques condensés non substitués qui ne forment pas d'excimères à partir de leur niveau singulet; ils ne présentent pas d'auto-désactivation de cet état excité et la population de leur niveau triplet ne dépend pas de leur concentration. L'état singulet du naphtalène par contre, est autodésactivé par formation d'excimère, la population de son niveau triplet est alors fonction de la concentration de l'état fondamental.

TABLEAU 5. Propriétés physiques des sensibilisateurs

	E_T (kcal mol^{-1})	τ (s)	Φ_s
Naphtalène	60.9	3.6×10^{-3}	0.80 (14)
Phénanthrène	62.2	2×10^{-3}	0.80 (15)
Chrysène	57.2	—	0.82 (15)

La figure 2 illustre les résultats concernant les régimes photostationnaires obtenus avec les trois sensibilisateurs aromatiques dans des solutions dégazées ou aérées. Sur le plan expérimental nos mesures les plus correctes sont obtenues quand la densité optique à 313 nm est inférieure à 1.5. Néanmoins, nous avons pu, avec le chrysène, faire des mesures jusqu'à une densité optique calculée égale à 6. Dans de telles conditions, un "effet de peau" est à redouter (absorption des photons dans les premières couches de solution et annihilation des espèces excitées). Il ne semble pas intervenir dans nos conditions expérimentales. Dans les conditions de sensibilisation totale ($D_S \to \infty$), un calcul analogue au précédent conduit à l'expression

$$\frac{t_\infty}{c_\infty} = \frac{\phi_t}{\phi_c} \frac{\Phi^0_{c\to t}}{\Phi^0_{t\to c}} \frac{k_c^S}{k_t^S}$$

Les valeurs maximales des rendements quantiques d'isomérisation directe (voisines de 0.5) nous suggèrent d'admettre que les niveaux triplets, T_α^t et T_α^c, responsables de l'isomérisation, se désactivent vers les deux formes de l'azobenzène avec la même probabilité ($k_{tt} \simeq k_{tc}$; $k_{cc} \simeq k_{ct}$). Comme nous le verrons plus loin, cette hypothèse *fondamentale* est compatible avec tous nos résultats expérimentaux. Dans ce cas

$$t_\infty/c_\infty = k_c^S/k_t^S$$

Pour atteindre le rapport des constantes de transfert k_c^S et k_t^S, on peut donc effectuer l'extrapolation des courbes expérimentales qui représentent les variations de c_∞/t_∞ en fonction de $1/D_S$ et qui apparaissent être linéaires pour le chrysène et le phénanthrène (fig. 3). On obtient ainsi $k_t^S/k_c^S = 0.04$. Avec le naphtalène, les variations de c_∞/t_∞ en fonction de $1/D_S$ dans le domaine des grandes densités optiques ne sont plus linéaires. Il n'est pas possible, par extrapolation, d'obtenir une valeur correcte du rapport des constantes de transfert (*cf.* fig. 3).

Nous avons vérifié que l'oxygène dissous dans le cyclohexane à des concentrations voisines de 10^{-3} mol l^{-1} n'a pas d'influence sur la vitesse d'isomérisation directe. Comme le montre la fig. 3, l'oxygène dissous inhibe l'isomérisation sensibilisée sans la supprimer totalement. Une telle inhibition s'interprète par une désactivation des niveaux triplets des aromatiques par l'oxygène avec une vitesse vraisemblablement proche de celle d'un processus contrôlé par la diffusion.

Can. J. Chem. Downloaded from www.nrcresearchpress.com by 210.87.254.6 on 09/05/12
For personal use only.

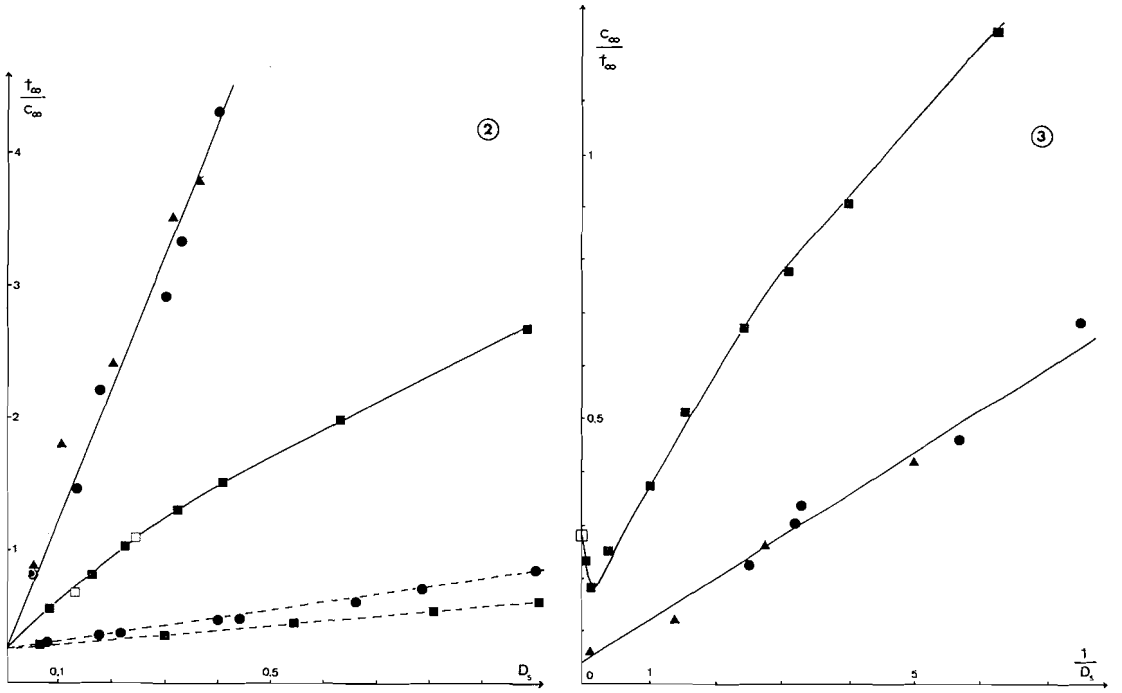

FIG. 2. Etude des régimes photostationnaires; t_∞ et c_∞, concentrations d'azobenzène *trans* et *cis*; D_S, densité optique du sensibilisateur; —, solution dégazée; - - -, solution aérée; ●, phénanthrène; ▲, chrysène; □, naphtalène (azobenzène initialement sous forme *cis*); ■, naphtalène (azobenzène initialement sous forme *trans*).

FIG. 3. Etude des régimes photostationnaires. Variations de c_∞/t_∞ en fonction de $1/D_S$ (solution dégazée); ●, phénanthrène; ▲, chrysène; ■, naphtalène; □, point déterminé par Fischer dans le cas du naphtalène.

Comme il subsiste en présence d'oxygène une sensibilisation pour des concentrations d'azobenzène proches de 10^{-5} mol l^{-1}, la plus grande des constantes k_c^S doit être voisine de 10^{10} $mol^{-1}\,l\,s^{-1}$.

En présence d'oxygène t_∞/c_∞ est fonction linéaire de D_S. L'expression 1 est compatible avec une telle linéarité car dans nos conditions expérimentales, nous pouvons faire les approximations suivantes.

$$\frac{1}{\tau_{O_2} k_c^S} + \frac{k_t^S}{k_c^S} t_\infty + c_\infty \simeq \frac{1}{\tau_{O_2} k_c^S} \simeq 10^{-3}$$

$$\frac{1}{\tau_{O_2} k_t^S} + \frac{k_c^S}{k_t^S} c_\infty + t_\infty \gg \frac{\varepsilon_S \phi_S(S)}{\varepsilon_t \phi_t} \simeq 0.5 \times 10^{-4}$$

où τ_{O_2} voisin de 10^{-7} s est la durée de vie des niveaux triplets des hydrocarbures aromatiques en présence d'oxygène. Donc

$$\frac{t_\infty}{c_\infty} = \frac{\phi_t \Phi^0_{c\to t}}{\phi_c \Phi^0_{t\to c}} \left(\frac{\varepsilon_c \phi_c}{\varepsilon_t \phi_t} + \frac{\phi_S \tau_{O_2} k_c^S}{\varepsilon_t \phi_t} D_S \right)$$

La pente de la droite nous permet de vérifier que k_c^S est voisin de 10^{10} $mol^{-1}\,l\,s^{-1}$, ce qui justifie notre approximation.

Sensibilisation par des composés carbonyles

Le benzile

Le benzile Ph—CO—CO—Ph présente en solution dans le cyclohexane deux bandes d'absorption dont les maximums sont à 260 et 490 nm. L'énergie de son plus bas niveau triplet est voisine de 54 kcal/mol (16). Le benzile est excité dans son premier état singulet S($n\pi^*$) à 365 nm en présence d'azobenzène. L'azobenzène doit être utilisé à une concentration suffisamment faible pour que les conditions d'une sensibilisation totale soient réalisées, et suffisamment forte pour que le dosage spectrophotométrique soit possible et que le transfert d'énergie ait une vitesse notable.

En sensibilisation, nous obtenons plus rapidement l'état stationnaire qu'en excitation directe à 365 nm mais cet état est plus pauvre en azobenzène *cis* (5% de *cis* contre 60% en excitation directe). La tangente à l'origine de la courbe de

Can. J. Chem. Downloaded from www.nrcresearchpress.com by 210.87.254.6 on 09/05/12
For personal use only.

TABLEAU 6. Rendements quantiques d'isomérisation sensibilisée par du benzile

[Benzile] (mol l^{-1})	[Azobenzène *trans*] (mol l^{-1})	[Azobenzène *cis*] (mol l^{-1})	$(\Phi^S_{t\to c})^0$	$(\Phi^S_{c\to t})$
6.55×10^{-3}	3.0×10^{-5}	0	0.027	—
5.90×10^{-3}	3.3×10^{-5}	0	0.026	—
4.55×10^{-3}	3.8×10^{-5}	0	0.032	—
5.30×10^{-3}	8.0×10^{-5}	0	0.024	—
3.30×10^{-3}	1.0×10^{-5}	2.0×10^{-5}	—	0.49
3.20×10^{-3}	0.7×10^{-5}	1.9×10^{-5}	—	0.45
3.52×10^{-3}	1.0×10^{-5}	4.25×10^{-5}	—	0.52
3.62×10^{-3}	2.5×10^{-5}	4.85×10^{-5}	—	0.51

disparition ou d'apparition du *trans* nous permet d'obtenir le rendement quantique initial d'isomérisation sensibilisée de la forme *trans* $(\Phi^S_{t\to c})^0$ et le rendement quantique d'isomérisation de la forme *cis* $\Phi^S_{c\to t}$ à partir de mélanges de composition variable. Ces rendements $\Phi^S_{c\to t}$ ne dépendent pas de la concentration initiale de forme *trans* et ils ont la même signification cinétique que les rendements initiaux $(\phi^S_{c\to t})^0$.

Dans nos conditions expérimentales, le transfert d'énergie vers l'azobenzène *cis* et *trans* est quantitatif, les rendements quantiques étant indépendants de la concentration en azobenzène. Dans ces conditions de sensibilisation totale, nos mesures sur l'état photostationnaire nous permettent d'accéder directement au rapport des constantes de transfert du benzile vers les états excités responsables de l'isomérisation. Dans ce cas

$$(c_\infty)/(t_\infty) = k_t^S/k_c^S = 0.05.$$

En solution dans le cyclohexane, le benzile excité à 390 nm émet une phosphorescence dont le maximum est à 560 nm, l'énergie du niveau triplet correspondant étant voisine de 54 kcal/mol. L'addition d'azobenzène *trans* ou *cis* provoque l'extinction de cette phosphorescence. On interprète cette désactivation du niveau triplet du benzile par des transferts d'énergie triplet–triplet exothermiques. En effet, l'énergie du niveau triplet du benzile est voisine de l'énergie du plus bas niveau singulet de l'azobenzène (54 kcal/mol); il existe donc dans les azobenzènes *trans* et *cis* un niveau triplet d'énergie inférieure à celle du triplet du benzile. Nous appellerons χ_t^S et χ_c^S, les constantes de vitesse des transferts d'énergie triplet–triplet entre le benzile et les formes *trans* et *cis* de l'azobenzène.

Les mesures des variations de l'intensité de phosphorescence du benzile avec la concentration d'azobenzène *trans* ajouté, permettent de déterminer la constante de transfert. La droite de Stern-Volmer correspondante a pour équation

TABLEAU 7. Variation de l'intensité de phosphorescence du benzile en fonction de la concentration d'azobenzène *trans*

[Azobenzène *trans*] (mol l^{-1})	I_p^0	I_p	I_p^0/I_p
0.6×10^{-6}	68	39	1.7
4.5×10^{-6}	66	22	3.0
5.1×10^{-6}	66	17	3.9
8.1×10^{-6}	69	11.5	6.0
1.0×10^{-5}	68	10	6.8
2.06×10^{-5}	69	6	11.5

$$I_p^0/I_p = 1 + \chi_t^S \tau t$$

où I_p^0 est l'intensité de phosphorescence du benzile en l'absence d'azobenzène *trans*, I_p est l'intensité de phosphorescence du benzile en présence d'azobenzène *trans*, τ est la durée de vie réelle du triplet du benzile et t est la concentration de l'azobenzène *trans*.

Le tableau 7 rassemble nos résultats.

La pente de la droite donne $\chi_t^S\tau = 5.9 \times 10^5$. L'ordre de grandeur du produit $\chi_t^S\tau$ montre que l'extinction de phosphorescence n'implique pas un transfert singulet–singulet. En effet, la désactivation du niveau singulet du benzile de durée de vie voisine de 10^{-9} s exigerait que la constante de transfert soit égale à 10^{14} mol^{-1} l s^{-1} ce qui est impossible même dans un transfert de résonance. La durée de vie du niveau triplet du benzile à 25 °C en solution dans le cyclohexane est proche de 10^{-4} s.[1] La constante χ_t^S du transfert triplet–triplet est donc voisine de celle d'une processus contrôlé par la diffusion.

[1]J. F. Madet. Communication personnelle.

Can. J. Chem. Downloaded from www.nrcresearchpress.com by 210.87.254.6 on 09/05/12
For personal use only.

Can. J. Chem. Downloaded from www.nrcresearchpress.com by 210.87.254.6 on 09/05/12
For personal use only.

Pour examiner l'extinction de la phosphorescence du benzile par l'azobenzène *cis*, il est nécessaire de préparer ce composé par irradiation préalable de l'azobenzène *trans* à 345 nm. Après addition de benzile au mélange ainsi obtenu, on mesure la phosphorescence du benzile partiellement éteinte et on irradie ensuite le mélange à 365 nm pour provoquer le retour de la forme *cis* vers la forme *trans*. On mesure au cours de cette irradiation la phosphorescence du benzile et on constate que l'intensité de cette phosphorescence ne varie pas (*cf.* tableau 8 relatif à deux expériences indépendantes). Cette expérience permet de conclure que $\chi_c^S = \chi_t^S$.

Il convient de remarquer dès à présent que le rapport des constantes χ_t^S et χ_c^S déduites de l'extinction de phosphorescence est égal à 1 alors que le rapport des constantes k_t^S et k_c^S déduites de l'isomérisation sensibilisée est égal à 0.05. Nous donnerons plus loin une interprétation de ce résultat. Notons également qu'après une isomérisation sensibilisée de la forme *trans*, il est toujours possible de provoquer un retour quantitatif de l'azobenzène *cis* vers la forme *trans* par simple chauffage thermique. Il n'apparait donc pas de processus entrainant la disparition irréversible de l'azobenzène *trans* compétitif avec l'isomérisation (s'il existait, un tel processus serait facilement observable lors d'étude de longue durée du régime photostationnaire).

Le biacétyle

On peut espérer sensibiliser l'isomérisation de l'azobenzène par le biacétyle CH_3—CO—CO—CH_3, un donneur carbonylé dont le niveau triplet est proche de celui du benzile (E = 55 à 57 kcal/mol). D'ailleurs, la phosphorescence du biacétyle est éteinte en présence d'azobenzène *trans* et *cis*. L'excitation du biacétyle se fait à 465 nm et l'analyse de l'émission à 520 nm. En faisant varier la concentration de l'azobenzène *trans*, nous obtenons une droite de Stern-Volmer dont la pente est $\chi_t^S\tau = 8.25 \times 10^5$ mol^{-1} l. Avec une durée de vie du triplet du biacétyle $\tau = 2 \times 10^{-4}$ s, nous avons $\chi_t^S = 4.1 \times 10^9$ mol^{-1} l s^{-1}.

TABLEAU 8 Invariance de la phosphorescence du benzile en présence de concentrations variables d'azobenzène *cis* et *trans*

[Azobenzène] (mol l^{-1})	% *trans*	I_p
1.55×10^{-5}	26	7.5
	87	7.5
	97	7.5
1.11×10^{-5}	36	11
	74	11
	96	11

On peut suivre la disparition de *trans* azobenzène dans l'irradiation à 365 nm d'un mélange de biacétyle en concentration 0.113 mol l^{-1} et de *trans* azobenzène en concentration égale à 10^{-5} mol l^{-1}. En fait, à la photoisomérisation sensibilisée se superpose un processus photochimique de disparition irréversible de l'azobenzène (il s'agit très vraisemblablement d'une photoréduction de l'azobenzène *cis* par les radicaux issus de la réaction du niveau triplet du biacétyle avec le solvant). Cette réaction parasite rend le biacétyle impropre à toute étude quantitative de l'isomérisation sensibilisée.

Interprétation des résultats expérimentaux

Le benzile permet d'étudier l'isomérisation sensibilisée sans être gêné par les processus impliqués dans l'excitation directe. L'extinction de la phosphorescence du benzile par les deux formes *cis* et *trans* de l'azobenzène est interprétée en termes de transfert d'énergie triplet–triplet. Les constantes χ_c^S et χ_t^S de ce transfert du benzile vers les deux formes de l'azobenzène sont égales et voisines de celles d'un processus contrôlé par la diffusion.

Les rendements quantiques d'isomérisation sensibilisée $(\Phi^S_{t\to c})^0$ et $(\Phi^S_{c\to t})$ sont indépendants de la concentration en azobenzène. Le transfert triplet–triplet dans les deux cas est donc quantitatif. En outre, si l'on tient compte de notre hypothèse fondamentale concernant l'égale probabilité de désactivation des niveaux triplets responsable de l'isomérisation en chacune des formes *cis* et *trans*, les valeurs très différentes de ces rendements d'isomérisation (0.03 et 0.50, respectivement) montrent que le transfert d'énergie produit primairement un niveau triplet de configuration différente dans chaque forme de l'azobenzène. Le rendement $(\Phi^S_{t\to c})^0$ est voisin de 0.03. Comme le rendement de population du triplet du benzile est proche de 1 (0.92) (17), et que le transfert est quantitatif, nous admettrons que ce transfert d'énergie produit un état triplet T_β^t différent de l'état excité triplet T_α^t responsable de l'isomérisation. La conversion interne $T_\beta^t \to T_\alpha^t$ a alors lieu avec une probabilité voisine

Can. J. Chem. Downloaded from www.nrcresearchpress.com by 210.87.254.6 on 09/05/12
For personal use only.

de 0.06 (égale probabilité de désactivation de $T_\alpha{}^t$ vers les deux formes *cis* et *trans* de l'azobenzène).

Dans le cas du *cis*, le rendement ($\Phi^S{}_{c\to t}$) est voisin de 0.50. Le transfert d'énergie étant quantitatif, nous admettrons que l'on peuple soit directement l'état triplet $T_\alpha{}^c$ responsable de l'isomérisation, soit un état triplet intermédiaire $T_\beta{}^c$ qui se désactiverait *quantitativement* par conversion interne rapide vers le niveau triplet $T_\alpha{}^c$. Ces deux triplets de l'azobenzène *cis* ne peuvent être différenciés.

Les constantes de population $k_c{}^S$ et $k_t{}^S$ des états excités responsables de l'isomérisation, apparaissent donc être des produits de constantes de vitesse de processus contrôlés par la diffusion $\chi_t{}^S$ et $\chi_c{}^S$ par des probabilités de conversion interne entre les niveaux triplets des azobenzènes. On obtient alors

$$k_t{}^S/k_c{}^S = \chi_t{}^S \times 0.06/\chi_c{}^S \times 1 = 0.06$$

Cette valeur du rapport $k_t{}^S/k_c{}^S$ est bien en accord avec la valeur déterminée à partir de l'état photostationnaire (0.05) obtenu avec le benzile.

L'étude expérimentale des régimes photostationnaires obtenus en sensibilisant l'isomérisation par des carbures aromatiques met en évidence le comportement différent du chrysène et du phénanthrène d'une part, et du naphtalène d'autre part. Avec le chrysène et le phénanthrène la mesure du rapport des constantes de vitesse des processus produisant les niveaux triplets responsables de l'isomérisation conduit à $k_t{}^S/k_c{}^S = 0.04$ soit un rapport très voisin de ceux obtenus avec le benzile à partir du régime photostationnaire (0.05) ou à partir des vitesses initiales d'isomérisation (0.06). En outre, l'étude de la photoisomérisation sensibilisée en milieu aéré permet de vérifier que la plus grande des constantes $k_c{}^S$ est voisine de 10^{10} mol^{-1} l s^{-1}. Ces deux sensibilisateurs se comportent donc comme le benzile bien que l'énergie de leur niveau triplet soit différente de celle du plus bas niveau triplet du benzile. Avec l'azobenzène *trans*, nous admettrons à nouveau un transfert vers le niveau triplet $T_\beta{}^t$ qui se désactive avec un probabilité de 0.04 vers le niveau triplet $T_\alpha{}^t$ responsable de l'isomérisation. Le triplet de la forme *cis* est, pour sa part peuplé soit directement soit par conversion rapide $T_\beta{}^c \to T_\alpha{}^c$ déjà proposé.

Certains de ces résultats expérimentaux concernant les régimes photostationnaires sont assez comparables à ceux de Hammond et son collaborateur (8), obtenus avec d'autres sensibilisateurs aromatiques. Hammond et son collaborateur ont, en effet, obtenu des états photostationnaires dont la teneur en forme *cis* est proche de 2%, ce qui conduit à un rapport de la constante $k_t{}^S$ à la constante $k_c{}^S$ égal à 0.02. Mais contrairement à ces auteurs, nous n'avons nul besoin de faire intervenir les niveaux singulets dans le mécanisme d'isomérisation directe. Par ailleurs, comme nous l'avons précisé en présentant les résultats expérimentaux, l'emploi de naphtalène ne peut conduire par extrapolation à une valeur correcte du rapport des constantes de vitesse $k_c{}^S$ et $k_t{}^S$. En effet, à des concentrations moyennes de naphtalène, le régime photostationnaire obtenu est notablement plus pauvre en forme *cis* que celui obtenu en excitation directe. Mais quand on augmente la concentration de naphtalène pour se rapprocher des conditions de sensibilisation totale, le mélange en régime photostationnaire s'enrichit en forme *cis*, alors qu'il devrait s'appauvrir. A forte concentration, le naphtalène devient un sensibilisateur inefficace car il y a autodésactivation de son niveau singulet excité (avec une formation d'excimère). La population du plus bas niveau triplet diminue et comme l'azobenzène *trans* absorbe toujours une part des photons, l'importance de l'isomérisation directe croit par rapport à celle de l'isomérisation sensibilisée. On obtient alors des régimes photostationnaires intermédiaires qui se rapprochent d'autant plus de ceux obtenus en excitation directe que la concentration de naphtalène est grande. Nos résultats ne sont d'ailleurs compatibles qu'avec la mesure de Fischer (9) réalisée avec la plus forte concentration de naphtalène, 0.5 *M*; dans ces conditions, l'isomérisation ne peut être étudiée qu'en sensibilisation partielle et le désaccord apparent entre Hammond et Fischer s'explique aisément. A des concentrations plus faibles en naphtalène, les résultats de Fischer apparaissent compatibles avec les mesures que nous avons effectuées en milieu non dégazé, conditions dans lesquelles le naphtalène est également un sensibilisateur inefficace.

En conclusion, dans cette première partie de l'étude du comportement photochimique de l'azobenzène en solution, nous avons pu expliquer les divergences qui apparaissaient entre les travaux de Hammond et son collaborateur (8) et ceux de Fischer, tant sur le plan des résultats expérimentaux que sur celui des interprétations. Le mécanisme de l'isomérisation sensibilisée de

Can. J. Chem. Downloaded from www.nrcresearchpress.com by 210.87.254.6 on 09/05/12
For personal use only.

l'azobenzène, que nous proposons, implique deux niveaux triplets de chacune des formes *trans* et *cis:*

(*i*) Les niveaux triplets $T_\beta{}^t$ et $T_\beta{}^c$, respectivement des formes *trans* et *cis*, obtenus directement par transfert d'énergie à partie de composés aromatiques ou carbonylés; ces niveaux se désactivent non radiativement sans donner lieu à une isomérisation *cis–trans*.

(*ii*) Les niveaux $T_\alpha{}^t$ et $T_\alpha{}^c$ des formes *trans* et *cis* que nous n'avons pas peuplés, dans cette première partie, par transfert d'énergie mais qui résultent de conversions internes des triplets $T_\beta{}^t$ $T_\beta{}^c$, respectivement; ces niveaux sont responsables de l'isomérisation.

La conversion interne $T_\beta{}^t \rightarrow T_\alpha{}^t$ a lieu avec une faible probabilité (0.04 à 0.06) alors que la conversion interne $T_\beta{}^c \rightarrow T_\alpha{}^c$ est quantitative. Les niveaux triplets de la forme *cis* n'apparaissent pas discernables sur le plan expérimental. Si l'on se réfère au traitement monoélectronique des niveaux singulets proposé par Suzuki (12), on pourrait penser que les niveaux triplets de l'azobenzène *trans* ont un caractère $n_+\pi^*$ et $\pi\pi^*$ bien défini et que toute conversion interne entre ces états est interdite. Les niveaux triplets de l'azobenzène *cis* n'auraient plus de caractère $n_-\pi^*$ et $\pi\pi^*$ marqué et les transitions entre ces états seraient permises.

Dans une deuxième partie, dont nous rapportons les résultats dans l'article suivant, nous avons examiné la photoisomérisation de l'azobenzène sensibilisée par des colorants et sa photoréduction. Nous pourrons préciser ainsi quelques propriétés des niveaux triplets de l'azobenzène *trans* et *cis*. Il apparaitra alors possible de différencier expérimentalement les niveaux triplets de la forme *trans* alors que les niveaux triplets de la forme *cis* resteront indiscernables. Il apparaitra également nécessaire de considérer, comme nous l'avons fait dès cet article, des niveaux triplets propres à chaque forme *trans* ou *cis* de l'azobenzène.

1. I. I. Abram, G. S. Milne, B. S. Solomon et C. Steel. J. Am. Chem. Soc. **91**, 1220 (1969).
2. L. Arin et C. Steel. J. Phys. Chem. **76**, 1885 (1972).
3. G. Zimmerman, Lue Yung Chow et Un Jin Paik. J. Am. Chem. Soc. **80**, 3528 (1958).
4. H. Rau. Ber. Bunsenges, **71**, 48 (1967).
5. H. Rau. Ber. Bunsenges, **72**, 408 (1968).
6. H. Mauser, D. J. Francis et H. J. Niemann Z. Phys. Chem. (Frankfurt), **82**, 318 (1972).
7. S. Hashimoto et K. Kano. Bull. Chem. Soc. Jap. **45**, 852 (1972).
8. L. B. Jones et G. S. Hammond. J. Am. Chem. Soc. **87**, 4219 (1965).
9. E. Fischer. J. Am. Chem. Soc. **90**, 796 (1968).
10. J. Griffiths. Chem. Soc. Rev. Vol. 1. **4**, 481, (1972).
11. D. Bontschev et E. Rastchin. Monatsh. Chem. **101**, 1454 (1970).
12. H. Suzuki. Electronic absorption spectra and geometry of organic molecules. Academic Press Inc. 1967. p. 499 à 512.
13. G. Castro et R. M. Hochstrasser. J. Chem. Phys. **45**, 4252 (1966).
14. A. R. Horrocks et F. Wilkinson. Proc. Roy. Soc. A, **306**, 257 (1968).
15. C. A. Parker et T. A. Joyes. Trans. Faraday Soc. **62**, 2785 (1966).
16. H. H. Richtol et A. Belorit. J. Chem. Phys. **45**, 35 (1966).
17. J. G. Calvert et J. N. Pitts, Jr. Photochemistry. John Wiley and Sons, Inc. 1966. p. 309.
18. S. Yamashita, H. Ono et O. Toyama. Bull. Chem. Soc. Jap. **35**, 1849 (1962).
19. D. Gegiou, K. A. Muszkat et E. Fischer. J. Am. Chem. Soc. **90**, 3907 (1968).

Isomérisation photosensibilisée par des colorants et photoréduction de l'azobenzène en solution. II

JACQUES RONAYETTE, RENÉ ARNAUD ET JACQUES LEMAIRE

Laboratoire de Photochimie, U.E.R. de Sciences Exactes et Naturelles et Ecole Nationale Supérieure de Chimie, Université de Clermont, Ensemble Scientifique des Cézeaux, 63170 Aubière, France

Reçu le 24 juillet, 1973

L'isomérisation photochimique de l'azobenzène en solution peut être sensibilisée par des colorants à bas niveau triplet (rose de Bengale, éosine Y, fluorescéine, bleu de methylène) mais ne peut être inhibée par de telles substances. Les niveaux triplets $T_\beta{}^c$ et $T_\alpha{}^c$ de la forme *cis* sont expérimentalement indiscernables. Par contre, les résultats expérimentaux obtenus permettent de vérifier, dans la forme *trans*, l'existence de deux niveaux triplets $T_\beta{}^t$ et $T_\alpha{}^t$ à propriétés différentes; une population, par transfert d'énergie, du triplet d'énergie inférieure $T_\alpha{}^t$ conduit à une isomérisation de rendement quantique voisin de 0.5 alors que la population du triplet $T_\beta{}^t$ ne provoque qu'une isomérisation difficile (rendement quantique voisin de 0.03). La photoréduction de l'azobenzène dans l'isopropanol a été également examinée; seule la forme *cis* est photoréductible et il apparait expérimentalement très difficile de savoir si l'on peut sensibiliser cette photoréduction. Un diagramme de Jablonski de l'azobenzène sous ses deux formes est présenté, en guise de conclusions.

The photochemical isomerization of azobenzene in solution can be sensitized by dyes which have low-lying triplet states (rose Bengal, eosin Y, fluoroscein, methylene blue) but cannot be inhibited by such compounds. The two triplet levels, $T_\beta{}^c$ and $T_\alpha{}^c$, of the *cis* form are indistinguishable experimentally. On the other hand, the experimental results verify the existence of two triplet levels, $T_\beta{}^t$ and $T_\alpha{}^t$, with different properties, in the *trans* form. Population, by energy transfer, of the lower triplet, $T_\alpha{}^t$, leads to isomerization with a quantum yield near 0.5, whereas population of the triplet $T_\beta{}^t$ only rarely leads to isomerization (quantum yield about 0.03).

The photoreduction of azobenzene in isopropanol also has been studied. Only the *cis* form is photoreducible and it is very difficult experimentally to determine whether this photoreduction can be sensitized.

A Jablonski diagram of the two forms of azobenzene is presented to correlate these observations. [Journal translation]

Can. J. Chem., **52**, 1858 (1974)

Introduction

Dans l'article précédent, nous avons proposé un mécanisme d'isomérisation de l'azobenzène en solution, sensibilisée par des composés aromatiques ou carbonylés. Pour la forme *trans*, ce mécanisme impliquerait deux niveaux triplets à propriétés différentes, $T_\alpha{}^t$ et $T_\beta{}^t$; la conversion interne entre ces états interviendrait avec une faible probabilité. Pour la forme *cis*, les deux niveaux triplets $T_\alpha{}^c$ et $T_\beta{}^c$ ne seraient plus expérimentalement discernables. Pour, d'une part, confirmer ce mécanisme et pour, d'autre part, préciser autant que faire se peut les propriétés de ces niveaux triplets, nous avons entrepris l'étude de l'isomérisation de l'azobenzène, sensibilisée ou inhibée par des colorants.

En milieu désoxygéné, la photoréduction de l'azobenzène dans des solvants à hydrogène mobile est, avec l'isomérisation la seule manifestation des états excités. S. Hashimoto et K. Kano (1) ont récemment étudié cette photoréduction directe et sensibilisée; elle est décelable une fois le régime photostationnaire atteint et n'a lieu que pour des longueurs d'onde d'irradiation inférieures à 420 nm. Le produit de la photoréduction est l'hydrazobenzène Φ—NH—NH—Φ. Selon ces auteurs, la photoréduction de l'azobenzène serait sensibilisée par le fluorène et des composés aromatiques carbonylés, et inhibée par le thiophène, le benzonitrile et l'acide benzoïque. Il convient de noter qu'Hashimoto et Kano ayant utilisé une lumière non monochromatique, ne peuvent préciser l'importance de l'excitation directe devant les processus de sensibilisation. Cette étude reste d'ailleurs très qualitative, aucun rendement

Can. J. Chem. Downloaded from www.nrcresearchpress.com by 210.87.254.105 on 09/05/12
For personal use only.

Can. J. Chem. Downloaded from www.nrcresearchpress.com by 210.87.254.105 on 09/05/12
For personal use only.

quantique n'ayant été déterminé. Nous avons donc réexaminé cette photoréduction en nous attachant à l'aspect quantitatif des phénomènes.

Résultats expérimentaux

Nous avons choisi d'utiliser des colorants dont le niveau triplet est à basse énergie. Les colorants xanthéniques employés et le bleu de méthylène ne sont pas tous des "sensibilisateurs" classiques car l'efficacité de population de leur plus bas niveau triplet varie dans de grandes limites; ce paramètre nous a d'ailleurs semblé interessant pour l'étude de notre mécanisme.

Ces colorants ne sont solubles que dans des solvants polaires. Il faut donc être conscient d'une possible modification de la disposition énergétique des niveaux triplets de l'azobenzène dans ces solvants. Néanmoins, les mesures en excitations directes qui montrent que les rendements $\Phi^0_{t\to c}$ et $\Phi^0_{c\to t}$ sont indépendants du solvant laissent supposer que les mécanismes de conversion interne des triplets, donc leur disposition énergétique, ne sont pas sensiblement modifiés par le changement de solvant.

Les colorants xanthéniques utilisés dans cette étude sont les sels disodiques de la fluorescéine et de l'éosine Y et le rose de Bengale B.

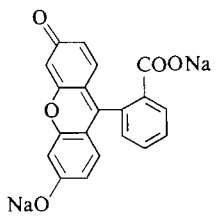

Sel disodique de la fluorescéine

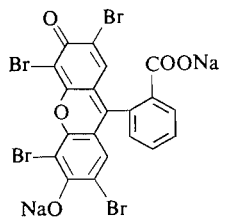

Sel disodique de l'éosine Y

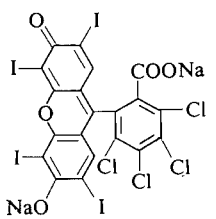

Rose de Bengale

Les énergies des niveaux triplets des formes ioniques correspondant à la fluorescéine, à l'éosine Y et au rose de Bengale B sont, respectivement, de 47.2, 45.5 et 43 kcal/mol; elles ont été déterminées par Kearns et Chambers (2, 3) à partir de l'étude du spectre de phosphorescence de ces colorants à 77 °K en solution dans un mélange d'éthanol et de méthanol. Nous avons également employé le bleu de méthylène (chlorure de 3.9 diméthylaminophénazothionium) de formule

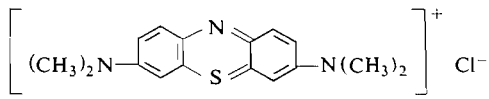

dont le plus bas niveau triplet est situé vers 33 kcal (2).

Les spectres d'absorption de ces quatre sensibilisateurs sont présentés sur les figs. 1 et 2.

Dans nos essais de sensibilisation, en solution dans le méthanol, ces colorants ont été employés à des concentrations suffisamment faibles (10^{-5} à 10^{-4} M) pour que l'on puisse négliger la forme dimère (l'énergie du niveau triplet d'une forme dimère serait d'ailleurs proche de celle du niveau correspondant du monomère, l'écart étant voisin de 1.2 kcal/mol (3)). En outre, la fluorescence du rose de Bengale B, de l'éosine Y et de la fluorescéine en présence d'azobenzène aux concentrations employées dans les conditions de sensibilisation n'est pratiquement pas modifiée.

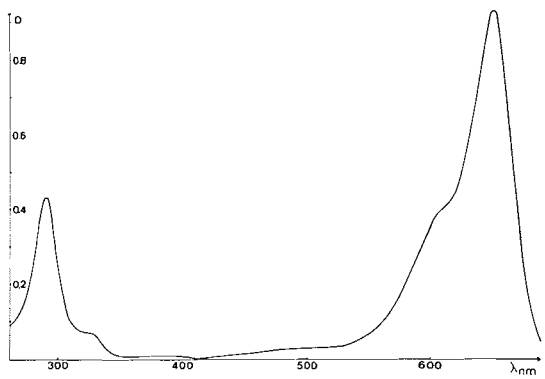

FIG. 1. Spectre d'absorption du bleu de méthylène (5.7×10^{-6} M) en solution dans le méthanol.

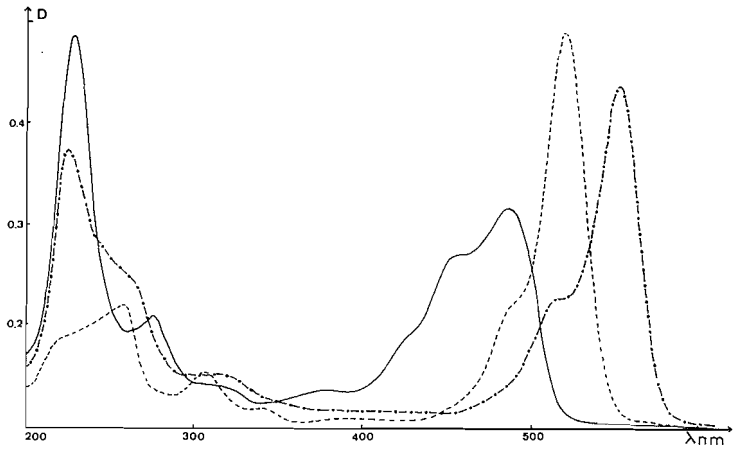

FIG. 2. Spectre d'absorption des sels disodiques de la fluorescéine (—), de l'éosine Y (-----) et du rose de Bengale (-.-.-) en solution dans le méthanol; fluorescéine = 4.8×10^{-5} *M*; eosine Y = 0.85×10^{-5} *M*; rose de Bengale = 1.2×10^{-5} *M*.

TABLEAU 1. Isomérisation d'azobenzène *trans* sensibilisée par le rose de Bengale dans du méthanol; $\lambda_{excit} = 546$ nm

[Rose de Bengale] (mol l^{-1})	[Azobenzène *trans*] (mol l^{-1})	$(\Phi^S_{t\to c})^0$
2.36×10^{-5}	4.5×10^{-5}	0.0019
2.27×10^{-5}	6.1×10^{-5}	0.0056
1.93×10^{-5}	6.95×10^{-5}	0.0066
2.14×10^{-5}	1.96×10^{-4}	0.018
2.87×10^{-5}	5.03×10^{-4}	0.019
3.14×10^{-5}	1.06×10^{-3}	0.016

Isomérisation photosensibilisée par le rose de Bengale

Aux concentrations d'azobenzène employées, une irradiation du mélange à 546 nm permet de réaliser des conditions de sensibilisation totale, les photons étant uniquement absorbés par le rose de Bengale (le coefficient d'extinction molaire de cette substante à 546 nm est 45 150 $mol^{-1}\,l\,cm^{-1}$).

Nos essais de photosensibilisation de l'isomérisation sur la forme *trans* ont permis de mesurer le rendement quantique $(\Phi^S_{t\to c})$ pour différentes concentrations initiales d'azobenzène. Pour des concentrations relativement élevées (supérieures ou égales à 5.10^{-4} mol/l), nous avons mesuré l'apparition de *cis* par dosage spectrophotométrique à 436 nm. Aux concentrations de forme *trans* plus faibles, nous avons mesuré la vitesse de disparition de cette forme.

Nos résultats sont rassemblés dans le tableau 1. Lorsque l'azobenzène *trans* est en concentration suffisante, le rendement $(\Phi^S_{t\to c})^0$ reste constant.

Dans le domaine de concentrations de l'azobenzène *trans* où le transfert d'énergie reste fonction de la concentration d'azobenzène, le rendement $(\Phi^S_{t\to c})^0$ dépend aussi de la concentration du sensibilisateur. Pour des concentrations d'azobenzène *trans* voisines de 6.10^{-5} mol l^{-1}, nous avons obtenu les rendements suivants (tableau 2). Le rendement quantique

TABLEAU 2. Variation de $\Phi^S_{c\to t}$ en fonction de la concentration de rose de Bengale

[Rose de Bengale] (mol l^{-1})	$(\Phi^S_{t\to c})^0$
2.27×10^{-5}	0.0056
1.03×10^{-5}	0.0090
5.33×10^{-6}	0.0122
2.27×10^{-6}	0.0216

Can. J. Chem. Downloaded from www.nrcresearchpress.com by 210.87.254.105 on 09/05/12
For personal use only.

TABLEAU 3. Variation de $\Phi^S_{c\to t}$ en fonction de la concentration d'azobenzène *cis*

[Rose de Bengale] (mol l^{-1})	[Azobenzène *trans*] (mol l^{-1})	[Azobenzène *cis*] (mol l^{-1})	($\Phi^S_{c\to t}$)
2.39×10^{-5}	0.77×10^{-5}	1.82×10^{-5}	0.14
2.28×10^{-5}	1.51×10^{-5}	5.75×10^{-5}	0.18
2.54×10^{-5}	1.87×10^{-5}	1.07×10^{-4}	0.20
2.41×10^{-5}	2.54×10^{-5}	1.36×10^{-4}	0.29
2.39×10^{-5}	2.76×10^{-5}	1.74×10^{-4}	0.42
2.41×10^{-5}	3.35×10^{-5}	2.47×10^{-4}	0.30
2.69×10^{-5}	4.10×10^{-5}	3.78×10^{-4}	0.35

d'isomérisation sensibilisée augmente sensiblement quand la concentration du donneur décroit. Ceci s'interprète aisément par une autodésactivation du rose de Bengale, qui pourrait conduire à la formation du dimère. Cette autodésactivation produit un déficit de la population du niveau triplet sensibilisateur.

Les mesures faites à partir de la forme *cis* correspondent au tableau 3. Nous considérons que le rendement ($\Phi^S_{c\to t}$) devient indépendant de la concentration d'azobenzène. Les déterminations actinométriques à 546 nm sont difficiles et introduisent des erreurs expérimentales importantes.

Nous avons également constaté que le régime photostationnaire obtenu dans l'isomérisation sensibilisée est pauvre en azobenzène *cis* (95% de *trans* contre 5% de *cis*). Le rapport des constantes de transfert déjà définies k_t^S et k_c^S est alors voisin de 0.05.

Isomérisation sensibilisée par l'éosine Y

Nous irradions à 436 nm l'éosine en concentration voisine de 2.10^{-4} mol l^{-1} en présence d'azobenzène. Le coefficient d'extinction molaire de l'éosine à 436 nm est 1780 $mol^{-1}\,l\,cm^{-1}$. Nous ne sommes alors pas dans des conditions de sensibilisation totale; aussi pour déterminer les rendements $(\Phi^S_{t\to c})^0$ et ($\Phi^S_{c\to t}$), il faudra tenir compte de l'intensité absorbée directement par l'azobenzène. La vitesse initiale mesurée est la somme d'une vitesse d'isomérisation sensibilisée et d'une vitesse d'isomérisation directe.

Les mesures de vitesses initiales d'isomérisation sensibilisée de la forme *trans* mettent en évidence l'existence d'un maximum dans la variation de $(\Phi^S_{t\to c})^0$ en fonction de la concentration d'azobenzène (tableau 4). Par contre le rendement ($\Phi^S_{c\to t}$) reste constant.

Le régime photostationnaire atteint lors de la sensibilisation de la forme *trans* correspond à un mélange de 14% de *cis* et 86% de *trans*. Il est différent de celui obtenu avec le benzile et rose de Bengale car nous n'opérons pas dans des conditions de sensibilisation totale. Ce régime photostationnaire ne nous permet pas de calculer une valeur correcte du rapport k_t^S/k_c^S.

Isomérisation sensibilisée par la fluorescéine

La fluorescéine permet également de réaliser une isomérisation sensibilisée de la forme *trans* de l'azobenzène par irradiation à 436 nm. En solution 10^{-4} *M*, la sensibilisation est partielle, aussi tenons-nous compte de la vitesse d'isomérisation directe pour déterminer le rendement sensibilisé $(\Phi^S_{t\to c})^0$.

Comme pour l'éosine Y, le rendement $(\Phi^S_{t\to c})^0$ varie avec la concentration d'azobenzène et passe par un maximum (tableau 5).

Nous n'avons pu déterminer les valeurs du rendement ($\Phi^S_{c\to t}$) car il s'avère impossible de mesurer par dosage spectrophotométrique simultanément la fluorescéine et l'azobenzène *cis*; ces deux molécules dans l'état fondamental forment un complexe qui se traduit par une non additivité des densités optiques dans le domaine visible.

Isomérisation sensibilisée ou inhibée par le bleu de méthylène

A 578 nm, le bleu de méthylène en concentration voisine de 10^{-5} mol l^{-1} peut photosensibiliser l'isomérisation de la forme *cis* de l'azobenzène. Le coefficient d'extinction molaire du bleu de méthylène à 578 nm est 31 600 $mol^{-1}\,l\,cm^{-1}$.

Nous avons rassemblé nos résultats dans le tableau 6. Bien que les conditions d'une sensibilisation totale soient pratiquement remplies, il a été tenu compte de la faible vitesse d'isomérisation directe.

Avec la forme *trans*, pour des concentrations

Can. J. Chem. Downloaded from www.nrcresearchpress.com by 210.87.254.105 on 09/05/12
For personal use only.

TABLEAU 4. Isomérisation d'azobenzène *trans* et *cis* sensibilisée par l'éosine Y dans du méthanol; $\lambda_{excit} = 436$ nm

[Eosine Y] (mol l^{-1})	[Azobenzène *trans*] (mol l^{-1})	[Azobenzène *cis*] (mol l^{-1})	$(\Phi^S_{t\to c})^0$	$(\Phi^S_{c\to t})$
1.2×10^{-4}	2.0×10^{-5}	—	0.043	—
2.6×10^{-4}	3.2×10^{-5}	—	0.049	—
2.5×10^{-4}	5.6×10^{-5}	—	0.115	—
2.5×10^{-4}	8.2×10^{-5}	—	0.081	—
2.1×10^{-4}	9.6×10^{-5}	—	0.025	—
3.2×10^{-4}	2.2×10^{-4}	—	0.013	—
2.11×10^{-4}	1.8×10^{-5}	3.4×10^{-5}	—	0.36
2.51×10^{-4}	3.1×10^{-5}	4.3×10^{-5}	—	0.35
1.95×10^{-4}	3.4×10^{-5}	7.3×10^{-5}	—	0.35

TABLEAU 5. Isomérisation d'azobenzène *trans* sensibilisée par la fluorescéine dans du méthanol; $\lambda_{excit} = 436$ nm

[Fluorescéine] (mol l^{-1})	[Azobenzène *trans*] (mol l^{-1})	$(\Phi^S_{t\to c})^0$
1.15×10^{-4}	2.1×10^{-5}	0.0037
1.10×10^{-4}	6.4×10^{-5}	0.013
1.68×10^{-4}	1.2×10^{-4}	0.03
1.36×10^{-4}	1.8×10^{-4}	0.017
1.13×10^{-4}	2.0×10^{-4}	0.016
1.20×10^{-4}	3.7×10^{-4}	0.003

TABLEAU 6. Sensibilisation d'isomérisation d'azobenzène par le bleu de méthylène dans du méthanol; $\lambda_{excit} = 578$ nm

[Bleu de méthylène] (mol l^{-1})	[Azobenzène *trans*] (mol l^{-1})	[Azobenzène *cis*] (mol l^{-1})	$(\Phi^S_{c\to t})$
1.05×10^{-5}	0.8×10^{-5}	3.1×10^{-5}	0.003
1.85×10^{-5}	3.3×10^{-5}	1.53×10^{-4}	0.015
2.20×10^{-5}	2.0×10^{-5}	5.75×10^{-4}	0.035

variant de 3.10^{-5} à 10^{-3} mol l^{-1}, les différentes irradiations à 578, 546 et 436 nm n'ont révélé aucune photosensibilisation.

Nous avons également procédé à des essais d'inhibition de l'isomérisation en irradiant de l'azobenzène à 436 nm en présence de bleu de méthylène. Nous n'avons pas excité sélectivement l'azobenzène *trans*, aussi dans ces conditions expérimentales, l'azobenzène *trans* absorbait 43% de la lumière. Ces essais n'ont pu mettre en évidence une inhibition de l'isomérisation.

Etude de la photoreduction

D'après S. Hashimoto et K. Kano (1), l'azobenzène en solution dans l'isopropanol peut se photoréduire en donnant l'hydrazobenzène.

$$\Phi\text{—N=N—}\Phi \xrightarrow[\text{isopropanol}]{h\nu} \Phi\text{—NH—NH—}\Phi$$

L'hydrazobenzène est dosé par technique spectrophotométrique à 242 nm, le coefficient d'extinction molaire correspondant étant voisin de 20 000 mol^{-1} l cm^{-1}. A cette longueur d'onde, la forme *cis* de l'azobenzène présente également un coefficient d'extinction élevé (11 000 mol^{-1} l cm^{-1}). Nous avons irradié l'azobenzène *trans* à 313 nm (fig. 3, courbe 1) en suivant parallèlement la disparition d'azobenzène *trans* et l'apparition d'hydrazobenzène. L'augmentation de la densité optique à 242 nm au début de l'irradiation est due à l'apparition de la forme *cis*, puis à la photoréduction lorsque le régime photostation-

Can. J. Chem. Downloaded from www.nrcresearchpress.com by 210.87.254.105 on 09/05/12
For personal use only.

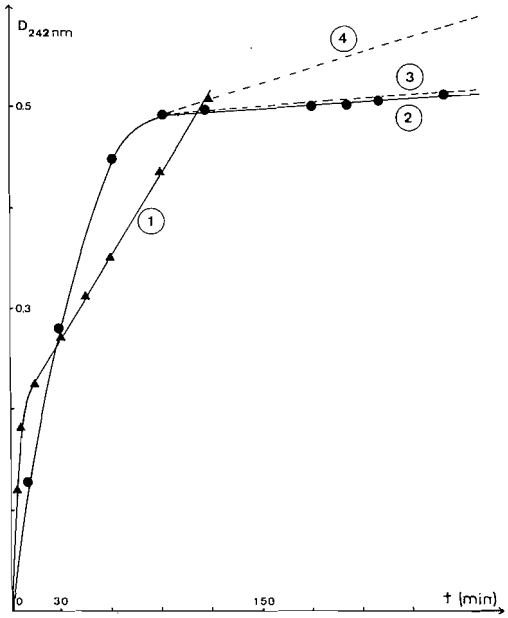

FIG. 3. Photoréduction de l'azobenzène dans l'isopropanol; *1*, courbe expérimentale à 313 nm; *2*, courbe expérimentale à 345 nm; *3*, courbe calculée en supposant la forme *cis* photoréductible à 345 nm; *4*, courbe calculée en supposant la forme *trans* photoréductible à 345 nm.

naire d'isomérisation est atteint. En fait, on atteint un régime "pseudo stationnaire" puisque la formation du produit de photoréduction entraine la consommation irréversible d'azobenzène. Pour des irradiations suffisamment longues (au delà de 2 h dans nos conditions expérimentales), nous avons constaté une diminution de la densité optique à 242 nm; cette diminution est probablement due à une photolyse de l'hydrazobenzène.

L'étude de la photoréduction à cette unique longueur d'onde ne permet pas de préciser la forme de l'azobenzène qui est photoréductible. Nous avons alors irradié l'azobenzène en solution dans l'isopropanol à 345 nm. A cette longueur d'onde, l'absorption de la forme *cis* est négligeable devant celle de la forme *trans*. La fig. 3 montre qu'il n'y a pratiquement aucune photoréduction; ce phénomène intervient donc à partir d'un état excité de la forme *cis*.

Nous pouvons confirmer ce fait en analysant quantitativement les courbes de photoréduction à 313 et 345 nm. Si la photoréduction à 313 nm impliquait un état excité de la forme *trans*, le rendement quantique de photoréduction serait voisin de 0.0029. Si, au contraire, la photoréduction impliquait un état excité de la forme *cis*, le rendement quantique serait de 0.018. En admettant que les rendements quantiques de photoréduction ne varient pas pour un même état excité, on peut alors calculer la vitesse de photoréduction à 345 nm des deux formes de l'azobenzène. La fig. 3 montre alors que la courbe expérimentale 2 coincide avec la courbe calculée 3 en admettant que *la forme cis se photoréduit seule avec un rendement de* 0.018. La courbe 4 a été calculée en admettant que la forme *trans* se photoréduirait seule avec un rendement de 0.0029.

Par ailleurs, nous avons irradié l'azobenzène en solution dans l'isopropanol, en excitant dans la bande d'absorption visible à 436 et 405 nm. Bien qu'à cette longueur d'onde, l'absorption de la forme *cis* soit prépondérante, nous n'avons décelé aucune photoréduction. Une étude quantitative de la sensibilisation de la photoréduction par le fluorène et le chrysène n'a pu être effectuée en utilisant une technique spectrophotométrique comme unique moyen de dosage de l'hydrazobenzène.

Interprétation des résultats expérimentaux

Isomérisation photosensibilisée

Si l'on ne tient compte que des résultats acquis avec les hydrocarbures aromatiques et le benzile, on peut assurer que les deux formes *cis* et *trans* de l'azobenzène ont des niveaux triplets T_β^c et T_β^t différents. Ces deux niveaux se distinguent par la facilité de leur conversion interne vers les niveaux triplets T_α^c et T_α^t responsables de l'isomérisation mais aucun argument expérimental ne permet jusqu'ici de penser que ces niveaux triplets T_α^c et T_α^t sont réellement distincts. Par emploi de colorants qui sont des sensibilisateurs dont les niveaux triplets sont à basse énergie, on peut alors espérer peupler par transfert d'énergie ces niveaux T_α et tenter de les différencier. Il convient néanmoins de dire qu'il n'existe que peu de données quantitatives sur les niveaux triplets des colorants xanthéniques employés (état de protonation, durée de vie, énergie ...). Aussi devons-nous exploiter avec prudence les résultats acquis avec ces colorants.

Dans nos conditions expérimentales de sensibilisation, la fluorescence des colorants xanthéniques n'étant pas modifiée, nous pouvons accepter un schéma cinétique classique impliquant uniquement un transfert triplet–triplet.

Can. J. Chem. Downloaded from www.nrcresearchpress.com by 210.87.254.105 on 09/05/12
For personal use only.

Can. J. Chem. Downloaded from www.nrcresearchpress.com by 210.87.254.105 on 09/05/12
For personal use only.

On pourrait cependant penser que l'interaction du niveau triplet des colorants et de l'azobenzène dans l'état fondamental met en jeu un transfert d'électrons dont le mécanisme serait le suivant:

$$^3C^* + A \rightleftarrows C^- + A^+ \rightarrow {}^1C + A_{cis} + A_{trans}$$

où C représente le colorant et A l'azobenzène. Un tel mécanisme intervient par exemple entre ces colorants xanthéniques et des donneurs classiques comme les amines aliphatiques (4). Un processus de transfert d'électrons est sensible à la polarité du solvant. Nous n'avons pu utiliser ce critère expérimental car les colorants xanthéniques utilisés se dissolvent très mal dans des solvants apolaires. Si un tel mécanisme d'isomérisation sensibilisée intervenait, on ne devrait plus utiliser les critères énergétiques réglant les transferts triplet–triplet et aucun renseignement sur les énergies des niveaux triplets des deux formes de l'azobenzène ne pourrait être obtenu. Mais dans ce cas, l'éosine Y qui présente des sites halogénés devrait manifester, dans son niveau triplet, de meilleures propriétés acceptrices que la fluorescéine. Or, comme nous le verrons plus loin, si l'on tient compte de la population du plus bas niveau triplet de ces deux colorants, la fluorescéine est un sensibilisateur plus efficace que l'éosine Y pour la photo isomérisation de la forme *trans*. Le rose de Bengale dont le rendement de population du plus bas niveau triplet est voisin de 1[1] est un sensibilisateur peu efficace de l'isomérisation *trans* → *cis*. Or, là encore, ses bonnes propriétés d'accepteur devraient le faire participer à un transfert d'électrons facile. Nous écartons donc l'intervention de ces transferts dans nos mécanismes d'isomérisation.

Si l'on analyse de façon détaillée les variations des rendements $(\Phi^S_{t\rightarrow c})^0$ en fonction de la concentration d'azobenzène *trans*, on remarque que la fluorescéine et l'éosine Y se comportent très différemment du rose de Bengale. Il apparait dans les trois cas, tout d'abord une augmentation de la vitesse du transfert d'énergie triplet–triplet avec la concentration initiale d'azobenzène *trans*. Le rendement quantique d'isomérisation sensibilisée pour le rose de Bengale devient ensuite indépendant de la concentration en azobenzène alors que les rendements quantiques d'isomérisation sensibilisée pour la fluorescéine et l'éosine passent par des maximums.

Pour l'éosine Y et la fluorescéine, quelques mesures des rendements de population des niveaux triplets ϕ_{ST} ont été effectuées. Si pour la fluorescéine les résultats sont concordants, il n'en est pas de même pour l'éosine.

Fluorescéine

$\phi_{S_1T_1} = 0.05 \pm 0.02$ (5) en solution dans l'eau

$\phi_{S_1T_1} = 0.04 \pm 0.005$ (6) en solution dans 30% d'eau et 70% d'éthanol

Eosine Y

$\phi_{S_1T_1} = 0.71 \pm 0.10$ (5) en solution dans l'eau

$\phi_{S_1T_1} = 0.43 \pm 0.04$ (6) en solution dans l'éthanol

Si la fluorescéine et l'éosine Y étaient susceptibles de produire par transfert triplet–triplet le niveau $T_\beta{}^t$ obtenu avec le benzile, les rendements quantiques d'isomérisation sensibilisée devraient être, au maximum,

Fluorescéine

$$(\Phi^S_{t\rightarrow c})^0 = 0.05 \times 0.05^2 \times 0.50^3 = 0.0012$$

Eosine

$$(\Phi^S_{t\rightarrow c})^0 = 0.43 \times 0.05 \times 0.50 = 0.011$$

ou $$= 0.71 \times 0.05 \times 0.50 = 0.018$$

Ces valeurs sont très inférieures à celles mesurées. Il faut donc admettre que le niveau atteint après transfert d'énergie est le niveau triplet $T_\alpha{}^t$ responsable de l'isomérisation, le niveau $T_\beta{}^t$ n'étant pas alors peuplé pour de simples raisons énergétiques. Ceci nous permet de situer le niveau $T_\beta{}^t$ à une énergie comprise entre celle du niveau triplet de la fluorescéine (47 kcal mol^{-1}) et celle du niveau triplet du benzile (54 kcal mol^{-1}). Dans le cas de la fluorescéine, la valeur maximum du rendement $(\Phi^S_{t\rightarrow c})^0$, 0.03 correspond certainement à un transfert quantitatif puisqu'elle nous conduit à admettre comme rendement de transition inter-systèmes dans ce donneur:

$$\phi_{S_1T_1} = \frac{(\Phi^S_{t\rightarrow c})^0}{0.50} = \frac{0.03}{0.50} = 0.06$$

[1]Nous n'avons pas trouvé dans la littérature la valeur du rendement de population du plus bas niveau triplet du rose de Bengale. Mais les valeurs admises pour la fluorescéine (0.05), l'éosine (0.77 ou 0.43) et l'érythrosine (1.07) nous font penser que la population du triplet du rose de Bengale est quantitative.

[2]Valeur moyenne mesurant la probabilité de la conversion interne $T_\beta{}^t \rightarrow T_\alpha{}^t$.

[3]Valeur admise comme probabilité de désactivation du $T_\alpha{}^t$ vers les deux formes.

valeur proche de celles publiées dans la littérature.

Le transfert triplet–triplet qui intervient entre l'éosine Y et la forme *cis* de l'azobenzène est quantitatif car le rendement[4] ($\Phi^S_{c\to t}$) devient indépendant de la concentration en azobenzène *cis*. On peut déduire de cette mesure une valeur du rendement de transition inter-systèmes dans l'éosine Y en admettant que, comme dans le cas de benzile on peuple quantitativement le triplet $T_\alpha{}^c$ de la forme *cis*:

$$\phi_{S_1T_1} = \frac{(\Phi^S_{c\to t})^0}{0.50} = \frac{0.355}{0.50} = 0.71$$

valeur égale à celle mesurée par Porter (5) et que nous adopterons dorénavant. Les valeurs de $\phi_{S_1T_1}$ adoptées nous permettent de construire les courbes représentant les variations de:

$$2\frac{(\Phi^S_{t\to c})^0}{\phi_{S_1T_1}}$$

en fonction de la concentration d'azobenzène, c'est-à-dire la probabilité de population du niveau $T_\alpha{}^t$ par transfert d'énergie à partir de ces colorants (fig. 4). Les valeurs du maximum de la courbe relative à l'éosine Y montrent que la population du niveau $T_\alpha{}^t$ n'est pas quantitative. Ce fait est encore plus évident à forte concentration d'azobenzène *trans*, tant pour l'éosine Y que pour la fluorescéine. Pour expliquer la partie décroissante de ces courbes de variations du rendement $(\Phi^S_{t\to c})^0$ en fonction de la concentration d'azobenzène *trans*, il est nécessaire d'admettre que l'azobenzène peut désactiver un niveau précurseur du plus bas niveau triplet T_1 du colorant sans que ce processus conduise à une isomérisation sensibilisée efficace. Ce précurseur ne peut pas être le niveau singulet S_1 du colorant car celui-ci n'est pas désactivé par l'azobenzène aux concentrations employées. Ce précurseur pourrait être un "deuxième triplet" T_2 du colorant, de durée de vie plus courte que celle du plus bas niveau triplet T_1 (le rapport des deux durées de vie ne devrait pas excéder 10). Ce deuxième triplet serait alors désactivé par l'azobenzène par un transfert d'énergie qui produirait le niveau $T_\beta{}^t$ conduisant à une isomérisation

[4]Comme nous l'avons déjà précisé, le rendement $\Phi^S_{c\to t}$ déterminé avec des mélanges contenant initialement des concentrations variables de forme *trans* est indépendant de la composition du mélange et il a la même signification cinétique qu'un rendement initial.

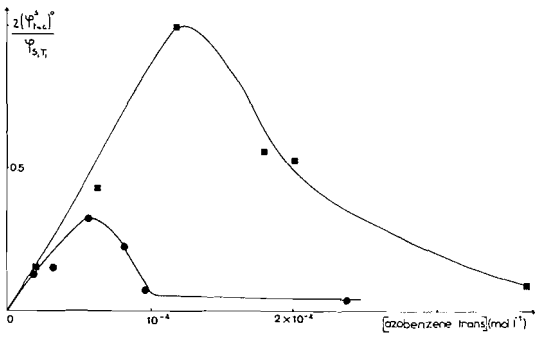

FIG. 4. Variation du rendement de population du niveau triplet $T_\alpha{}^t$ en fonction de la concentration d'azobenzène *trans*; ■ fluorescéine; ● eosine Y.

inefficace. Ce transfert d'énergie inhibe, bien entendu, la population du plus bas niveau triplet du colorant et donc l'isomérisation rapide par transfert produisant le niveau $T_\alpha{}^t$. On ne peut obtenir une telle courbe avec la forme *cis* car quelque soit le niveau triplet peuplé on parvient toujours quantitativement au niveau $T_\alpha{}^c$. Il faut noter au passage qu'un tel effet inhibiteur de la concentration en azobenzène ne peut s'interpréter par un mécanisme impliquant un transfert d'électrons. (Les deux triplets du colorant ainsi mis en jeu pourraient correspondre aux différents états de protonation du colorant. Une étude ultérieure de l'isomérisation sensibilisée des azobenzènes dans des milieux d'acidités différentes pourrait nous fournir quelques indications sur une telle possibilité).

Le fait expérimental qui nous parait important concerne la possibilité de peupler directement le triplet de la forme *trans* $T_\alpha{}^t$ responsable de l'isomérisation, avec la fluorescéine et l'éosine Y. Il apparait au contraire impossible de provoquer une telle population avec le rose de Bengale qui ne conduit qu'à des isomérisations très inefficaces. L'interprétation des phénomènes observés avec le rose de Bengale est beaucoup plus délicate. Les résultats indiqués dans les tableaux 1 et 3 montrent que les transferts d'énergie vers ces formes *cis* et *trans* deviennent quantitatifs dès que la concentration en azobenzène est supérieure à 2×10^{-4} mol l^{-1}.

Dans le cas de l'azobenzène *cis* ($\Phi^S_{c\to t} = 0.35$) on peuple quantitativement le niveau $T_\alpha{}^c$. Nous n'obtenons pas un rendement égal à 0.50 car il y a une certaine autodésactivation du rose de Bengale à la concentration employée (2×10^{-5} mol l^{-1}), autodésactivation qui provoque un déficit dans la population du niveau triplet du

Can. J. Chem. Downloaded from www.nrcresearchpress.com by 210.87.254.105 on 09/05/12
For personal use only.

sensibilisateur. Dans le cas de l'azobenzène *trans* ($(\Phi^S_{t\to c})^0 = 0.018$) on peuple quantitativement le niveau $T_\beta{}^t$ et non le niveau $T_\alpha{}^t$. Là encore, on n'obtient pas un rendement égal à 0.03 comme avec les sensibilisateurs "haute énergie" à cause de l'autodésactivation du rose de Bengale. L'étude du régime photostationnaire nous fournit un rapport des constantes $k_t{}^S/k_c{}^S$ égal à 0.05. Une telle valeur est bien caractéristique d'une sensibilisation produisant le niveau $T_\beta{}^t$ de l'azobenzène *trans*. La population du niveau $T_\beta{}^t$ dont l'énergie est supérieure à 47 kcal mol^{-1}, par un transfert issu du rose de Bengale, ne peut impliquer le plus bas niveau T_1 du rose de Bengale (43 kcal mol^{-1}) mais un deuxième triplet d'énergie supérieure, précurseur du niveau T_1. Il est à remarquer que même aux faibles concentrations d'azobenzène, le niveau $T_\alpha{}^t$ n'est pas peuplé à partir du niveau T_1 du rose de Bengale. Un tel transfert d'énergie peut être interdit pour des raisons géométriques ou énergétiques. L'énergie du niveau triplet $T_\alpha{}^t$ ayant été calculée égale à 46.5 kcal mol^{-1} (8), ce transfert d'énergie est plutôt interdit pour des raisons énergétiques. La comparaison avec la fluorescéine et l'éosine Y de structures moléculaires voisines nous induit à penser que les facteurs géométriques ne sont pas prépondérants.

L'expérience montre enfin que le bleu de méthylène dont l'énergie du niveau triplet inférieur de durée de vie 6.10^{-5} s (7) est très base, 33 kcal mol^{-1} (2), ne peut sensibiliser que l'isomérisation de l'azobenzène *cis*. Aux concentrations d'azobenzène employées, le transfert d'énergie n'est pas quantitatif et les faibles valeurs du rendement sensibilisé $(\Phi^S_{c\to t})^0$ pourraient traduire un transfert d'énergie légèrement endothermique. Il est à remarquer que le transfert inverse, c'est-à-dire issu du niveau triplet $T_\alpha{}^t$ de l'azobenzène, énergétiquement possible, ne se manifeste pas sur le plan expérimental.

Le diagramme énergétique suivant (schéma 1) résume ces considérations énergétiques. Nous avons placé à titre très indicatif le deuxième niveau triplet des colorants xanthéniques. Pour interpréter les courbes de l'isomérisation sensibilisée, nous avons fait intervenir un deuxième triplet T_2 dont le peuplement devrait se faire à partir du premier niveau singulet des colorants, toutes les irradiations ayant été faites dans leur bande d'absorption visible. Or, l'énergie de la transition 0–0 correspondant au premier niveau singulet se situe vers 55 et 52 kcal mol^{-1} respectivement pour la fluorescéine et l'éosine Y (3); dans le cas du rose de Bengale, elle serait située vers 50 kcal mol^{-1}. Le niveau $T_\beta{}^t$ de l'azobenzène *trans* doit donc être situé en dessous de 50 kcal mol^{-1}.

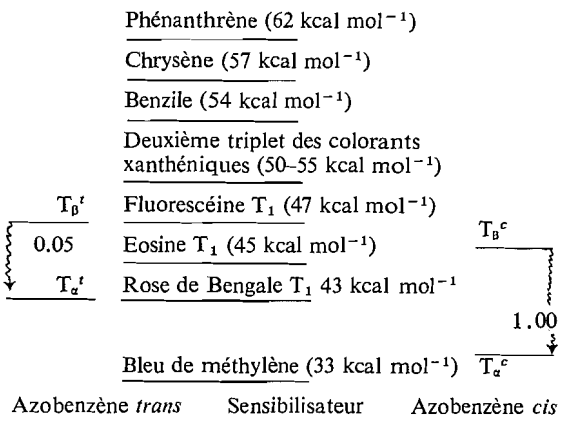

SCHÉMA 1

Photoreduction

L'étude expérimentale nous a montré que la photoréduction était un mécanisme propre à la forme *cis* de l'azobenzène. Elle n'a lieu que lorsque l'azobenzène *cis* est excité dans la bande d'absorption $S_2(\pi\pi^*)$. Le rendement quantique de la réduction photochimique est toujours faible ($\Phi_r = 0.018$), on ne peut rendre ce processus compétitif avec la photoisomérisation et il devient très difficile à étudier quantitativement. Il apparait en outre expérimentalement très difficile d'étudier la sensibilisation de la photoréduction et les travaux précédents ne peuvent être pris en considération.

La photoréduction peut être issue soit directement du deuxième singulet $S_2(\pi\pi^*)$, soit du triplet $T_\beta{}^c$ qui serait alors peuplé directement à partir du singulet $S_2(\pi\pi^*)$ et non à partir du singulet $S_1(n\pi^*)$. La photoréduction ne peut être issue du triplet $T_\alpha{}^c$ car les études d'isomérisation montrent qu'un tel triplet est peuplé quantitativement à partir de l'un quelconque des deux niveaux singulets $S_1(n\pi^*)$ ou $S_2(\pi\pi^*)$.

Conclusions

L'étude de l'isomérisation sensibilisée et de la photoréduction nous a permis de préciser dans une certaine mesure les propriétés des niveaux triplets des deux formes de l'azobenzène. En guise de conclusion, nous pouvons maintenant représenter le mécanisme d'isomérisation directe

Can. J. Chem. Downloaded from www.nrcresearchpress.com by 210.87.254.105 on 09/05/12
For personal use only.

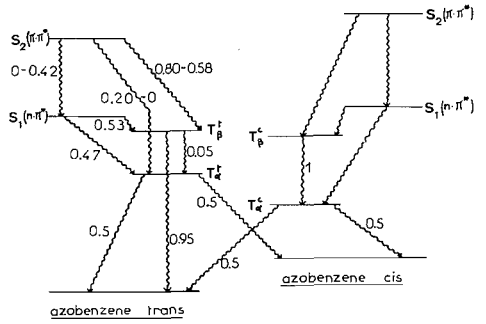

SCHÉMA 2. Diagramme de Jablonski de l'azobenzène en solution.

à l'aide du schéma 2. Comme nous allons le voir, les rendements quantiques de transition intersystèmes indiqués sur ce diagramme sont donnés seulement à titre indicatif.

Si l'on considère la forme *trans*, la conversion interne $S_2(\pi\pi^*) \rightarrow S_1(n\pi^*)$ n'est certainement pas quantitative puisqu'il y a effet de longueur d'onde sur le rendement quantique d'isomérisation directe. On ne peut accéder directement à la probabilité de cette transition car on ne peut observer ni fluorescence, ni processus issu spécifiquement du niveau singulet $S_1(n\pi^*)$ dans les solvants utilisés. On doit se contenter d'assurer que la probabilité de la conversion interne $S_2 \rightarrow S_1$ est comprise entre 0 et 0.42.

Nous avons estimé que la probabilité de la conversion interne $T_\beta{}^t \rightarrow T_\alpha{}^t$ est voisine de 0.05; compte tenu des résultats obtenus en isomérisation directe, on peut en déduire les rendements de transition intersystèmes suivants:

$$\phi_{S_1 \rightarrow T_\beta{}^t} = 0.53$$

$$\phi_{S_1 \rightarrow T_\alpha{}^t} = 0.47$$

si l'on admet une population quantitative des niveaux triplets et une désactivation non radiative du triplet $T_\beta{}^t$ vers l'état fondamental de l'azobenzène *trans* (avec une probabilité de 0.95). En fait, on ne sait distinguer expérimentalement une désactivation non radiative directe du singulet $S_1(n\pi^*)$ d'une désactivation impliquant le niveau $T_\beta{}^t$ comme intermédiaire. Le rendement $\phi_{S_1 \rightarrow T_\alpha{}^t}$ ne saurait être très différent de 0.50. Avec les mêmes hypothèses que précédemment, et en tenant compte des limites du rendement quantique de la conversion interne $S_2 \rightarrow S_1$, on peut déterminer les limites de rendement de population des triplets $T_\beta{}^t$ et $T_\alpha{}^t$ à partir du niveau $S_2(\pi\pi^*)$.

$$0.58 \leq \phi_{S_2 \rightarrow T_\beta{}^t} \leq 0.80$$

$$0 \leq \phi_{S_2 \rightarrow T_\alpha{}^t} \leq 0.20$$

Si l'on considère la forme *cis*, il n'y a pas d'effet de longueur d'onde significatif sur les rendements quantiques d'isomérisation directe et tous nos résultats concernant les sensibilisations s'interprètent en admettant une conversion interne $T_\beta{}^c \rightarrow T_\alpha{}^c$ quantitative. Il apparait expérimentalement impossible de préciser les rendements des diverses transitions inter-systèmes. La seule conclusion interessante est que dans le cas d'une excitation directe ou d'une sensibilisation, le triplet $T_\alpha{}^t$ responsable de l'isomérisation est peuplé quantitativement (abstraction faite du faible pourcentage de molécules qui disparaissent par photoréduction dans les solvants appropriés).

Il convient de revenir sur notre hypothèse fondamentale d'une désactivation des deux niveaux triplets $T_\alpha{}^c$ et $T_\alpha{}^t$ avec une égale probabilité vers les deux formes *cis* et *trans* dans l'état fondamental. Dans la plupart des cas où nous estimons que la population des niveaux T_α est quantitative, le rendement quantique d'isomérisation est effectivement voisin de 0.50. Cette circonstance s'est présentée dans les cas suivants: (*i*) excitation de la forme *cis* dans les niveaux $S_1(n\pi^*)$ et $S_2(\pi\pi^*)$; (*ii*) sensibilisation de l'isomérisation de la forme *cis* par le benzile; (*iii*) sensibilisation de l'isomérisation de la forme *trans* par la fluorescéine.

Il convient de dire que le travail rapporté dans les deux articles présents n'est qu'une approche du problème du comportement photochimique de l'azobenzène. Des expériences complémentaires sur le mécanisme de photoréduction et sur l'isomérisation sensibilisée par des colorants sont actuellement en cours au laboratoire.

1. S. HASHIMOTO et K. KANO. Bull. Chem. Soc. Jap. **45**, 852 (1972).
2. D. R. KEARNS et R. W. CHAMBERS. J. Am. Chem. Soc. **89**, 5455 (1967).
3. D. R. KEARNS et R. W. CHAMBERS. Photochem. Photobiol. **10**, 215 (1969).
4. R. S. DAVIDSON et R. F. BARTHOLOMEW. J. Chem. Soc. C, 2347 (1971).
5. P. G. BOWERS et G. PORTER. Proc. Roy. Soc. **A299**, 348 (1967). B. SOEP, A. KELLMANN, M. MARTIN et L. LINDQVIST. Chem. Phys. Lett. Vol. 13, n° 3, 241 (1972).
6. M. MEMOTO, H. KOKUBUN et M. KIOZUMI. Bull. Chem. Soc. Jap. **42**, 1223 (1969).
7. R. NILSSON, P. B. MERKEL et D. R. KEARNS. Photochem. Photobiol. **16**, 109 (1972).
8. D. BONTSCHEY et E. RASTCHIN. Monatsh. Chem. **101**, 1454 (1970).

Can. J. Chem. Downloaded from www.nrcresearchpress.com by 210.87.254.105 on 09/05/12
For personal use only.

Isomérisation *cis–trans* de l'azobenzène catalysée par l'iode. III

RENÉ ARNAUD ET JACQUES LEMAIRE

Laboratoire de Photochimie, U.E.R. de Sciences Exactes et Naturelles et Ecole Nationale Supérieure de Chimie, Université de Clermont, Ensemble Scientifique des Cézeaux, 63170, Aubière, France

Reçu le 24 juillet 1973

L'isomérisation *cis–trans* de l'azobenzène peut être catalysée par l'iode. La constante de vitesse du processus de réaction de l'azobenzène *cis* avec les atomes d'iode a été évaluée à $2 \pm 1 \times 10^9$ mol^{-1} l s^{-1} soit une valeur très supérieure à celle de la constante de vitesse correspondante d'autres systèmes isomérisables. Cette très grande réactivité de l'azobenzène *cis* permet de mettre en évidence des effets de parois inattendus en phase liquide. Une méthode de microdosage des atomes d'iode peut être basée sur cette isomérisation catalysée.

The *cis–trans* isomerization of azobenzene can be catalyzed by iodine. The rate constant for the reaction of *cis*-azobenzene with iodine atoms was determined as $2 \pm 1 \times 10^9$ mol^{-1} l s^{-1}, *i.e.* a much larger value than that pertaining to other isomerizable systems. This very high reactivity of *cis*-azobenzene allowed the demonstration of surface effects which were unexpected in the liquid phase. A method for estimating low concentrations of iodine atoms can be based on this catalyzed isomerization. [Journal translation]

Can. J. Chem., **52**, 1868 (1974)

Dans le cadre plus général de nos études du comportement photochimique de l'azobenzène en solution, il apparaissait intéressant de déterminer la durée de vie des niveaux triplets responsables de l'isomérisation (1, 2). Une technique possible consistait à étudier l'inhibition de l'isomérisation *trans–cis* de l'azobenzène par l'iode moléculaire. L'énergie du triplet responsable de l'isomérisation dans la molécule *trans* a été évaluée à environ 44 kcal mol^{-1} (2); l'énergie du triplet $^3\Pi_{1u}$ de l'iode est voisine de 38 kcal mol^{-1} (3). Le transfert est donc énergétiquement possible. Une telle inhibition a lieu effectivement lorsque l'on excite sélectivement de l'azobenzène *trans* en présence d'iode; elle persiste pour des concentrations d'iode voisines de 10^{-4} *M* et elle disparait si la solution est aérée. Ces deux aspects expérimentaux laissent penser que l'inhibition observée ne résulte pas d'un transfert d'énergie triplet–triplet entre l'azobenzène et l'iode; en effet (*i*) l'oxygène ne serait pas susceptible d'éliminer ce transfert sans désactiver l'azobenzène; or nous avons montré que l'oxygène en concentration voisine de 10^{-3} *M* ne désactivait pas le triplet de l'azobenzène *trans* (1); (*ii*) pour que le triplet de l'azobenzène soit totalement désactivé par 10^{-4} *M* d'iode, il faudrait que sa durée de vie soit supérieure à 10^{-5} s, durée de vie incompatible avec de précédents essais d'inhibition (2).

Nous avons donc été induits à interpréter le phénomène d'inhibition comme résultant d'une catalyse par l'iode moléculaire de l'isomérisation *cis* → *trans* de l'azobenzène. De telles catalyses sont bien connues, en particulier pour les molécules éthyléniques (4–6); elles font intervenir des atomes d'iode et se déroulent selon les processus suivants.

$$cis + I \rightleftarrows (cis\text{–}I) \rightarrow (trans\text{–}I) \rightleftarrows trans + I$$

Résultats expérimentaux

Mise en évidence des effets de parois

Au cours des études préliminaires d'inhibition de l'isomérisation *trans–cis* de l'azobenzène par l'iode, nous avons remarqué une très grande irreproductibilité des phénomènes expérimentaux. La fig. 1 illustre cette irreproductibilité dans quelques expériences d'inhibition, réalisées en milieu dégazé, lors de l'irradiation avec une lumière monochromatique ($\lambda = 334$ nm) d'un mélange d'azobenzène 8.2×10^{-5} *M* et d'iode 4×10^{-4} *M*. Sur cette figure, nous avons porté, en ordonnée, la densité optique de la solution à 345 nm, longueur d'onde où nous pouvons doser sélectivement l'azobenzène *trans*, et en abcisse le temps exprimé en min. Dans tous les cas, le temps d'irradiation est 12 min; après la fin de l'excitation nous suivons l'évolution de la densité optique en fonction du temps. La courbe 1 représente l'isomérisation normale de l'azobenzène en l'absence d'iode; les courbes 2, 3, et 4 montrent que, dans certaines conditions, une

Can. J. Chem. Downloaded from www.nrcresearchpress.com by 210.87.254.105 on 09/05/12
For personal use only.

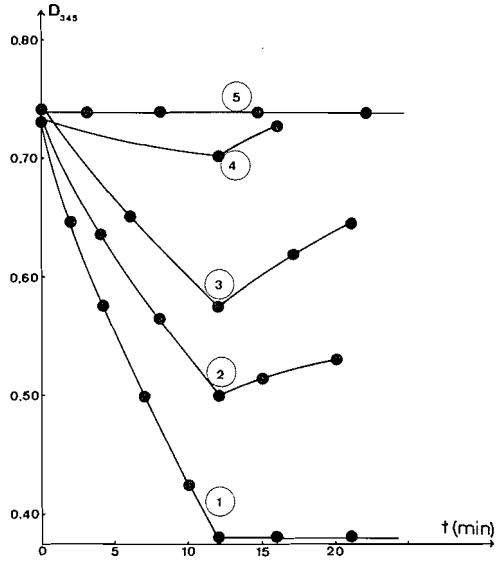

FIG. 1. Irreproductibilité de l'inhibition de l'isomérisation *trans–cis* de l'azobenzène par l'iode.

inhibition partielle de l'isomérisation se manifeste et la courbe 5 présente le cas d'une inhibition totale de l'isomérisation. Il faut remarquer que la courbe 4, qui correspond à une concentration d'iode de 2.12×10^{-4} *M*, traduit une inhibition plus importante que celles représentées par les courbes 2 et 3 pour lesquelles la concentration d'iode est voisine de 10^{-4} *M*.

Nous avons attribué ces irreproductibilités importantes à des effets de surface, les parois de la cellule étant susceptibles de provoquer la disparition des atomes d'iode qui catalysent l'isomérisation *cis* → *trans* de l'azobenzène. Ce n'est qu'après traitement de la cellule de mesure avec du mélange sulfo–chromique que nous avons pu obtenir des inhibitions reproductibles (en prenant en outre la précaution de ne réaliser qu'une expérience par cellule traitée). Entre deux manipulations, nous avons conservé la cellule remplie du mélange sulfo–chromique. Avant utilisation, nous l'avons rincée 30 à 40 fois à l'eau distillée et nous l'avons longuement séchée par mise sous vide de pompe à diffusion de mercure. Dans la suite de nos expériences, nous avons utilisé la technique d'irradiation à 334 nm du mélange azobenzène *trans* – iode comme test de contrôle de propreté de la cellule; lorsque l'inhibition de l'isomérisation *trans* → *cis* est totale (fig. 1, courbe 5), nous considérons que l'état des parois de la cellule permet de réaliser des mesures cinétiques correctes. Nous obtenons effectivement dans ces conditions, des mesures reproductibles des vitesses de photocatalyse. Des effets de parois semblables avaient été remarqués, en phase gazeuse, lors de l'étude de l'isomérisation *cis* → *trans* du 2-butène (7) et du dichloroéthylène (13).

Isomérisation cis → trans du stilbène photocatalysée par l'iode

Il convenait alors de savoir si, en éliminant ces effets de parois inattendus en phase liquide, nous obtiendrions des valeurs de constantes de vitesse sensiblement voisines de celles publiées. Dans ce but, nous avons choisi d'examiner l'isomérisation du stilbène. Selon Mazzucato et ses collaborateurs (8) le processus

$$\text{Stilbène } cis + \text{I} \xrightarrow{k_i} \text{Stilbène } trans + \text{I}$$

aurait une constante de vitesse k_i égale à 7.2×10^4 mol^{-1} l s^{-1}.

L'isomérisation *cis* → *trans* thermique du stilbène, en l'absence d'iode, est une réaction lente. A 20 °C les données de la littérature (9) nous permettent de calculer la constante de vitesse qui est égale à 10^{-13} s^{-1}. Ainsi la forme *cis* du stilbène a une durée de vie suffisamment grande pour que l'on puisse mesurer quantitativement des effets catalytiques d'isomérisation *cis* → *trans*.

Nous avons utilisé un dispositif comprenant une cellule en quartz de 1 cm d'épaisseur contenant une solution 5×10^{-5} *M* de stilbène *trans* en solution dans le cyclohexane et un réservoir adjacent contenant une solution 4×10^{-4} *M* d'iode moléculaire. On élimine l'oxygène dissous dans les solutions par congélation à −20 °C suivie de pompage sous vide d'environ 10^{-5} mm de mercure et d'un réchauffement à la température ambiante; on scelle la cellule après trois ou quatre cycles d'opérations. On irradie alors la solution de stilbène *trans* à 313 nm de manière à fabriquer du stilbène *cis* et l'on suit la réaction d'isomérisation *trans* → *cis* par mesure de la densité optique à 320 nm. A cette longueur d'onde les coefficients d'extinction molaire sont respectivement 15900 et 1170 mol^{-1} l cm^{-1} pour les stilbènes *trans* et *cis*. Lorsque l'état photostationnaire est atteint, on mélange les solutions d'iode et de stilbène; on irradie la solution ainsi obtenue à 545 nm, longueur d'onde à laquelle seule l'iode absorbe avec un coefficient d'extinction molaire égal à 800 mol^{-1} l cm^{-1}. On suit la

Can. J. Chem. Downloaded from www.nrcresearchpress.com by 210.87.254.105 on 09/05/12
For personal use only.

TABLEAU 1. Isomérisation *cis–trans* de l'azobenzène catalysée par l'iode

$[cis] \times 10^5$ (mol l^{-1})	$[I_2] \times 10^5$ (mol l^{-1})	$I_a \times 10^6$ (Einstein l^{-1} s^{-1})	$(V_{ph})_0 \times 10^7$ (mol l^{-1} s^{-1})	$[I] \times 10^9$ (atome-g l^{-1})	$k_i \times 10^{-6}$ (mol^{-1} l s^{-1})	Φ
2.5	18	1.3	5.3	6.7	3.2	0.41
2.7	22	1.5	6.6	7.2	3.4	0.44
3.04	5.6	0.4	4.3	3.8	3.7	1.1
3.7	8.7	0.6	4.6	4.6	2.7	0.77
3.9	11	0.8	5.0	5.3	2.4	0.62
4	12	0.85	5.1	5.5	2.3	0.6

cinétique, en maintenant la solution à 20 °C, par mesure de la densité optique à 320 nm; on détermine ainsi la vitesse initiale d'isomérisation catalysée v_i^0.

Le schéma cinétique de l'isomérisation photocatalysée est bien connu et identique à celui écrit plus loin pour l'azobenzène. La vitesse d'isomérisation s'écrit

$$(v_i)_0 = k_i[cis]_0[I] = \frac{k_i(\phi I_a)^{1/2}}{(k_r(M))^{1/2}}[cis]_0$$

où I_a est l'intensité lumineuse absorbée par l'iode; ϕ est le rendement quantique de photodissociation de l'iode moléculaire; k_i est la constante de vitesse du processus I + stilbène *cis* → I + stilbène *trans*; k_r est la constante de recombinaison des atomes d'iode; M est le partenaire d'un triple choc.

On détermine expérimentalement $(v_i)_0$ et en utilisant les données de la littérature $\phi = 0.46 \pm 0.07$ (10, 11) et $k_r(M) = (1.30 \pm 0.16) \times 10^{10}$ mol^{-1} l s^{-1} (12), on peut ainsi calculer les valeurs de k_i.

Nos expériences relatives au stilbène nous ont conduits à la valeur $k_i = 6.6 \times 10^4$ mol^{-1} l s^{-1}, proche de celle mesurée par Mazzucato et ses collaborateurs ($k_i = 7.2 \times 10^4$ mol^{-1} l s^{-1}).

Isomérisation cis → trans de l'azobenzène photocatalysée par l'iode

La constante de vitesse d'isomérisation thermique *cis* → *trans* de l'azobenzène, en l'absence d'iode, est voisine de 10^{-6} s^{-1} (calculée d'après les données de la littérature (9)). Cette réaction est suffisamment lente pour ne pas perturber les études de photocatalyse.

Le même dispositif et la même technique que dans le cas du stilbène ont été utilisés. Toutes nos mesures ont été effectuées à 20 °C. L'iode est excitée à 546 nm et on suit l'évolution de la réaction d'isomérisation *cis* → *trans* par analyse spectrophotométrique à 345 nm. A cette longueur d'onde les coefficients d'extinction molaire de la forme *trans* et de la forme *cis* sont, respectivement, 9000 et 40 mol^{-1} l cm^{-1}. On peut donc mesurer les variations de concentration de l'azobenzène *trans* et donc celles de l'azobenzène *cis* (on sait que l'isomérisation est le seul processus photochimique de l'azobenzène en solution dans le cyclohexane (1)).

Après mélange des solutions d'iode et d'azobenzène *cis*, la densité optique croit avant que ne débute l'irradiation à 546 nm, même si le mélange est conservé à l'obscurité totale; il s'agit soit d'une isomérisation catalysée thermiquement par l'iode, soit d'une isomérisation induite par les atomes d'iode provenant de la photolyse de l'iode moléculaire provoquée par le faisceau de mesure du spectrophotomètre. Durant la période très courte d'excitation de l'iode à 546 nm (Δt de 10 à 60 s), l'isomérisation est rapide et elle se poursuit longtemps après la fin de l'irradiation. Les mesures de densité optique exigeant le déplacement de la cellule d'irradiation, il convient de tenir compte des variations de la densité optique avant et après l'excitation pour déterminer correctement la vitesse de la photocatalyse. Les mesures de cette vitesse sont, de ce fait, délicates. Notons que dans nos conditions expérimentales, au bout d'environ 10^{-2} s, l'iode atteint 90% de sa concentration quasi-stationnaire. On peut donc assurer q'un état quasi stationnaire est atteint même dans les photolyses les plus brèves.

Le schéma cinétique de l'isomérisation *cis* → *trans* de l'azobenzène photocatalysée par l'iode est le suivant.

Amorçage photochimique

$$I_2 + h\nu \xrightarrow{\phi I_a} 2I$$

Isomérisation

$$I + \text{Azobenzène } cis \xrightarrow{k_1} I + \text{Azobenzène } trans$$

Can. J. Chem. Downloaded from www.nrcresearchpress.com by 210.87.254.105 on 09/05/12
For personal use only.

Rupture

$$2\mathrm{I} + M \xrightarrow{k_r} \mathrm{I}_2 + M$$

On calcule aisément les vitesses photochimiques d'isomérisation à l'instant initial

$$(V_{ph})_0 = k_i\left(\frac{\phi I_a}{k_r(M)}\right)^{1/2}[cis]_0$$

L'analyse numérique de nos courbes expérimentales obtenues à 20 °C conduit aux valeurs rassemblées en tableau 1.

La constante de vitesse k_i est nettement plus grande que celle correspondant à d'autres systèmes isomérisables (9). L'azobenzène *cis* présente une réactivité toute particulière vis à vis de l'iode.

En conclusion, l'iode catalyse avec une remarquable facilité l'isomérisation *cis* → *trans* de l'azobenzène. Etant donnée la rapidité des processus impliqués, les effets de parois deviennent perceptibles: il convient donc de travailler dans des cellules traitées avec le plus grand soin. On peut donc mettre au point une méthode de microdosage des atomes libres d'iode d'une extrême sensibilité.

1. J. RONAYETTE, R. ARNAUD, P. LEBOURGEOIS et J. LEMAIRE. Can. J. Chem. This issue.
2. J. RONAYETTE, R. ARNAUD et J. LEMAIRE. Can. J. Chem. This issue.
3. L. MATHIESON et A. L. G. REES. J. Chem. Phys. **25**, 753 (1956).
4. W. J. MUIZEBELT et R. J. F. NIVARD. Chem. Commun. 148 (1965).
5. S. YAMASHITA. Bull. Chem. Soc. Jap. **34**, 972 (1961).
6. G. ALOISI, G. CAUZZO et U. MAZZUCATO. Trans. Faraday Soc. **65**, 816 (1969).
7. R. B. CUNDALL et T. F. PALMER. Trans. Faraday Soc. **57**, 1936 (1961).
8. G. CAUZZO, U. MAZZUCATO et G. ALOISI. Gazz. Chim. Ital. **96**, 721 (1966).
9. R. B. CUNDALL. Progress in reaction kinetics. Vol. 2. 1964. p. 172.
10. D. BOOTH et R. M. NOYES. J. Am. Chem. Soc. **82**, 1868 (1960).
11. L. F. MEADOWS et R. M. NOYES. J. Am. Chem. Soc. **82**, 1872 (1960).
12. H. ROSMAN et R. M. NOYES. J. Am. Chem. Soc. **80**, 2410 (1958).
13. C. STEEL. J. Phys. Chem. **64**, 1588 (1960).

Can. J. Chem. Downloaded from www.nrcresearchpress.com by 210.87.254.105 on 09/05/12
For personal use only.

Structural Studies of Histamine H1 Effector Molecules: The Crystal Structure of the Antihistaminic Drug (+)-Chlorpheniramine Maleate; [(+)-*S*-1-(*p*-Chlorophenyl)-1-(2-pyridyl)-3-*N*,*N*-dimethylpropylamine maleate]

M. N. G. James[1] and G. J. B. Williams[2]

Department of Biochemistry, University of Alberta, Edmonton, Alberta T6G 2E1

Received November 16, 1973

Dextrorotatory chlorpheniramine maleate crystallizes from warm ethyl acetate in a $P2_1$ cell containing two formula units of the salt, with unit cell dimensions; $a = 5.7669(4)$ Å, $b = 20.338(2)$ Å, $c = 9.1347(8)$ Å, $\beta = 103.73(2)°$. Diffractometer data were collected with CuK_α radiation to $2\theta = 128°$. The structure was solved and refined to $R = 0.050$ and $wR = 0.066$. The absolute configuration is confirmed as being *S*. The alkylamine chain is asymmetrically disposed to the two aryl rings, the *p*-chlorophenyl ring being more exposed and the 2-pyridyl ring partially occluded. The molecule has an open side to which both hydrogen bond and π orbital overlap linkages can occur. The maleate mono-anion is hydrogen bonded to the dimethylamino group via a normal N—H···O linkage. The intramolecular hydrogen bond of the maleate ion is 2.444(5) Å long and is asymmetric.

Le maléate chlorprophénpyridamine dextrogyre cristallise dans l'acétate d'éthyle chaud; le groupe d'espace est $P2_1$; la maille contient deux molécules du sel et a pour dimensions: $a = 5.7669(4)$ Å, $b = 20.338(2)$ Å, $c = 9.1347(8)$ Å, $\beta = 103.73(2)°$. Les données du diffractomètre sont recueillies avec la radiation CuK_α à $2\theta = 128°$. La structure est déterminée et raffinée aux valeurs $R = 0.050$ et $wR = 0.066$. La configuration absolue est confirmée comme étant *S*. La chaine alcoyl-amine est asymétrique aux deux cycles aryles; le cycle du *p*-chlorophényle est plus ouvert et le cycle du pyridyl-2 est partiellement fermé. La molécule est sans encombrement sur un coté où on peut avoir une liaison hydrogène et des liaisons de recouvrement d'orbitales π. Le mono-anion maléate est lié par l'hydrogène au groupe diméthylamine par une liaison normale N—H···O. La liaison intramoléculaire et asymétrique de l'hydrogène et de l'ion maléate a une longueur de 2.444(5) Å. [Traduit par le journal]

Can. J. Chem., **52**, 1872 (1974)

Introduction

Numerous studies using various methods ranging from pharmacological screening (1, 2) through proton magnetic resonance (p.m.r.) (1, 3, 4) to quantum mechanics (5, 6) have been made in the past in an attempt to define both the pharmacodynamic moieties of histamine antagonists and their stereochemical relationships. These approaches have been fruitful in that generalized antihistamine formulations have been proposed (2, 7) and speculative receptor sites have been published (8, 9). Reliable proposals on active conformations and topology of receptor sites must, however, be based not only on a knowledge of the necessary chemical characteristics of an active drug but also on a firmly established knowledge of its permitted conformations. In an attempt to supply data relevant to this last point the X-ray crystallographic technique has recently been applied to the problem.

To date two structural descriptions of conformationally mobile drugs have appeared in the literature (10, 11). Because histadyl crystallizes with two molecules per asymmetric unit the X-ray investigation afforded two determinations of the molecular geometry (11). This circumstance is not general, however, and to obtain corroborating evidence for the conformation found in one crystallographic analysis another must be performed on a similar substance.

Dextrorotatory chlorpheniramine maleate (**1***a*)

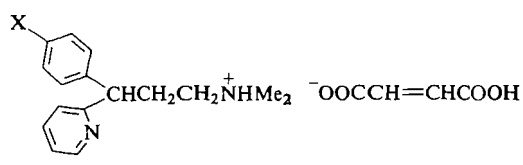

1

a X = Cl Chlorpheniramine maleate
b X = Br Brompheniramine maleate

[1]Author to whom correspondence should be addressed.
[2]Present address: Department of Chemistry, Brookhaven National Laboratory, Upton, Long Island, New York 11973.

Can. J. Chem. Downloaded from www.nrcresearchpress.com by 210.87.254.42 on 09/05/12
For personal use only.

Can. J. Chem. Downloaded from www.nrcresearchpress.com by 210.87.254.42 on 09/05/12
For personal use only.

was chosen as the next compound for study in our investigation into the structural characteristics of antihistaminic drugs for two reasons. The first was to allow comparison with the, already determined, structure of *dl*-brompheniramine maleate (**1***b*) (10), and the second was our intention to re-establish the absolute configuration of (+)-chlorpheniramine maleate using anomalous dispersion of the chlorine atom.

It has been shown that the histamine H1-receptor site exhibits stereoselectivity with respect to the chirality of the pheniramines (12), and a chemical argument has been presented to show that the more active (+)-pheniramines have the *S* absolute configuration (13) according to the convention of Cahn *et al.* (14). No fault could be found with this chemical argument but the stereochemistry of the previously designated (15) reference compound had not been established in a completely unambiguous way.

Experimental

Well shaped needles of the complex were grown by slowly cooling a solution in ethyl acetate. A columnar fragment was mounted along its length and photographed in the usual way. The diffraction symmetry, $2/m$, and systematic absences, $0k0$ with $k = 2n + 1$, together with the known optical activity of the compound defined the space group $P2_1$. The unit-cell dimensions were determined from the accurately centered 2θ values of twelve reflections in the range $90 < 2\theta < 120°$ by a least-squares procedure which also provided the orientation matrix of the crystal on a Picker FACS-1 diffractometer. These dimensions and some other data pertaining to this analysis are given in Table 1.

Intensity data were collected at room temperature (20 ± 2 °C) from a single crystal of dimensions $0.26 \times 0.21 \times 0.50$ mm. The incident radiation was CuK_α-monochromated from a highly oriented graphite crystal. The reflections were scanned in the θ-2θ mode with a scan speed of 2° per min over a peak width of $1.5 + 0.285 \tan\theta$ degrees; two stationary crystal – stationary counter background counts of 10 s each were measured at either end of the scan. Reflections were considered unobserved if $\sigma(I)/I > 0.35$, where $\sigma(I)$ is given by $(T + B + (kI)^2)^{1/2}$ and T is the total peak count, B the total background count, I the net intensity of the peak, and k is a small constant (0.04 in this case) included to allow for minor experimental errors. The unique part of reciprocal space limited by $4 < 2\theta < 128°$ was explored and of the 1784 reflections obtained, 1679 were found to have intensities significantly above background. Lorentz and polarization corrections (16) were applied and observational weights were calculated according to the expression $\sqrt{w} = 2F_o/[T + (kI)^2 + B]^{1/2}$ where T, I, B, and k are defined above.

A three dimensional Patterson synthesis was computed using coefficients sharpened by the $1/Lp$ function for a zero level of reciprocal space. Poor resolution was observed in this map; however, by comparison with an unsharpened synthesis it was possible to arrive at two probable atomic locations, and a symmetry minimum superposition (17) map obtained from these two positions revealed the chlorobenzene fragment and the maleate ion. This initial model was expanded by the difference Fourier method and refined through two cycles of unit-weighted block-diagonal least-squares to yield a conventional R factor ($R = \Sigma||F_o| - |F_c||/\Sigma|F_o|$) of 0.25. Throughout the refinement the y/b coordinate of the chlorine atom was fixed at 0.50. The scattering factors used were derived from the analytical coefficients of Cromer and Mann (18) except for the hydrogen curve which was that of Stewart *et al.* (19). The real part of anomalous dispersion ($\Delta f'$) for the non-hydrogen atoms were applied here and subsequently. These quantities for CuK_α radiation are Cl = 0.375, O = 0.055, N = 0.036, C = 0.021 electrons (20). The imaginary terms ($\Delta f''$) for chlorine and oxygen, 0.685 and 0.034 electrons respectively (20), were applied later.

Continued least-squares and difference Fourier refinement allowed: (*1*) sensible locations to be found for all hydrogen atoms except the second base dissociable proton of the maleate ion, and (*2*) the pyridyl ring nitrogen atom to be discerned from the six atoms which had hitherto all been treated as carbons. The conventional residual R was thereby decreased to 0.068.

In order to determine the absolute configuration, a Friedel pair analysis was performed. The original crystal was remounted on the diffractometer as it had been previously and 106 $hkl/h\bar{k}\bar{l}$ Friedel pairs of reflections collected. These data were processed in the normal way and structure factors were calculated for them using the original parameter set and the enantiomorphous set derived by reflection of the original through the plane $y = 0.5$. The agreement summary for these calculations is given below.

Model	$R = \frac{\Sigma\|\|F_o\| - \|F_c\|\|}{\Sigma\|F_o\|}$	$R' = \left\{\frac{\Sigma w(\Delta F)^2}{\Sigma w F_o^2}\right\}^{1/2}$
R	0.067	0.091
S	0.059	0.081

TABLE 1. Crystallographic data for (+)-chlorpheniramine maleate

Parameter	Value
Molecular formula	$C_{20}H_{23}N_2O_4Cl$
Molecular weight	380.97 daltons
Crystalline habit	Needles along *a* axis
Space group	$P2_1$ (C_2^2)
a	5.7669(4) Å
b	20.338(2) Å
c	9.1347(8) Å
β	103.73(2)°
V	1040.7 Å^3
ρ_{calc} (2 formula units/cell)	1.248 g/cm^3
ρ_{obs} (density gradient column)	1.248(2) g/cm^3
$\mu(CuK_\alpha)$	18.5 cm^{-1}
$\lambda(CuK_\alpha)$	1.54051 Å

These figures and the fact that three contradictions and 103 confirmations of the *S* model were found in the tabulation of structure factors from these calculations clearly imply that the correct hand of the (+)-chlorpheniramine molecule is *S* (21).

Five reflections with small Bragg angle and large intensities were deemed to be suffering from secondary extinction and so were coded unobserved at this point. A ΔF map computed on the basis of the parameter set of the *S* configuration revealed a peak of height 0.25 $e/Å^3$ in a chemically sensible location for the remaining hydrogen atom. Final convergence of the model was forced after 4 more block-diagonal cycles, using relaxation factors of 0.7 (22), by calculating 2 further cycles in which parameter shifts were damped down by using shift multipliers of 0.5 and 0.4. The final weighted and unweighted *R* factors over the included data are 0.064 and 0.050 respectively. The above mentioned Friedel pair tabulation and a listing of the observed structure amplitudes and final calculated structure factors were compiled.[3]

Results and Discussion

The positional and thermal vibration parameters used to describe the final model are given in Tables 2 and 3. Bond distances and interbond angles for the non-hydrogen atoms are contained in Fig. 1 which also presents the numbering scheme and atomic coding adopted here. The comparable molecular parameters involving the hydrogen atoms are given in Table 4. Using X to denote a carbon, nitrogen, or oxygen atom, then the e.s.d.'s in the distances Cl—X, X—X, and H—X average 0.005, 0.005, and 0.03 Å respectively. Error estimates for the angles Cl—X—X, X—X—X, X—X—H, H—X—H, and X—H—X average 0.3, 0.4, 3.0, 3.6, and 3.7° respectively. These e.s.d.'s were obtained from the atomic positional e.s.d.'s by the independent atom method of Ahmed *et al.* (23). Because interatomic correlations were neglected both in the least-squares refinement process and in the derivation of the above e.s.d.'s these quantities are underestimated and should be treated with caution.

Other authors have shown that the chlorine – aromatic carbon bond distance has a preferred magnitude of 1.737(16) Å in cases where the halogen atom is univalent (24–26). The value of 1.748(5) Å obtained for the present compound is insignificantly different from this expected value and supports the conclusions of the above

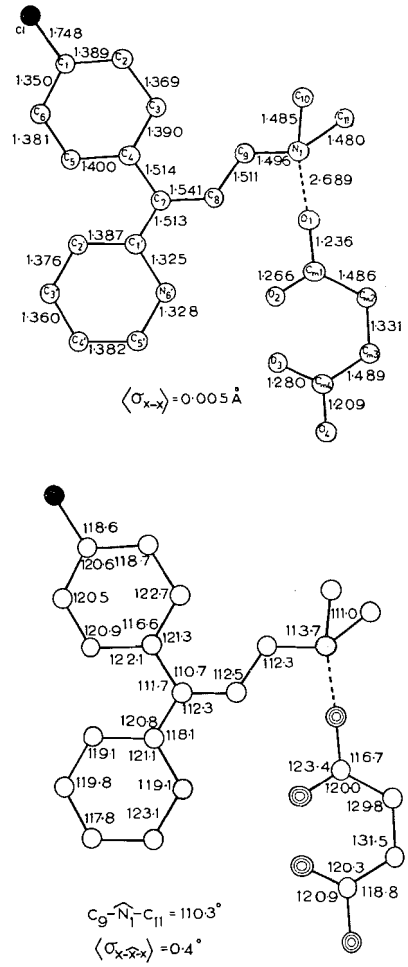

FIG. 1. Bond distances and angles for the non-hydrogen atoms of (+)-chlorpheniramine maleate.

citations that Sutton's (27) 1.70(1) Å is an underestimate of this distance.

The phenyl ring of this compound is planar with no member of this grouping displaced more than 0.01 Å from the plane with equation $-0.4624x + 0.6535y - 0.5992z = 5.1817$.[4] The ring, however, does exhibit several distortions from ideality; of the six intra-ring C···C bonds three are within 0.005 Å of 1.394 Å and a fourth is within 3σ of this accepted value (27). However the C(1)—C(6) and C(2)—C(3) bonds are both abnormally short being 1.350(5) and 1.369(5) Å respectively.

[3]These data are available, at a nominal charge, from the Depository of Unpublished Data, National Science Library, National Research Council of Canada, Ottawa, Canada K1A 0S2.

[4]This and similar equations in this paper are in the cosine form with reference to an orthogonal axial system (a,b,c^*) measured in Ångstroms.

Can. J. Chem. Downloaded from www.nrcresearchpress.com by 210.87.254.42 on 09/05/12
For personal use only.

TABLE 2. Atomic positional and anisotropic thermal vibration parameters ($\times 10^4$) for the non-hydrogen atoms of (+)-chlorpheniramine maleate

Atom	x/a	y/b	z/c	U_{11}*	U_{22}	U_{33}	U_{12}	U_{23}	U_{13}
Cl	855(3)†	5000(0)	2772(2)	641(5)	564(5)	496(5)	−81(4)	−131(4)	−24(4)
C(1)	2561(9)	5639(3)	3765(5)	430(11)	394(11)	316(8)	47(10)	−4(8)	−28(8)
C(2)	4515(9)	5867(3)	3269(4)	411(11)	548(16)	278(8)	59(11)	−56(9)	90(8)
C(3)	5829(7)	6374(2)	4031(4)	307(8)	488(13)	293(8)	53(9)	40(9)	104(6)
C(4)	5286(6)	6672(2)	5278(3)	242(6)	360(9)	278(7)	41(6)	57(6)	75(6)
C(5)	3301(6)	6427(2)	5735(4)	278(7)	424(11)	302(7)	−7(8)	−9(8)	97(6)
C(6)	1991(7)	5908(3)	4985(5)	296(9)	496(14)	344(9)	−15(9)	10(9)	60(7)
C(7)	6818(5)	7220(2)	6120(4)	235(6)	349(9)	313(7)	26(6)	71(6)	101(6)
C(8)	7665(5)	7053(2)	7808(3)	228(6)	269(7)	316(7)	9(5)	67(6)	68(5)
C(9)	9432(6)	7549(2)	8661(4)	237(6)	236(7)	379(8)	1(5)	67(6)	97(6)
N(1)	10838(4)	7284(1)	10133(3)	187(4)	197(5)	357(6)	11(4)	−11(4)	68(4)
C(10)	9339(6)	7063(2)	11156(4)	250(6)	276(7)	303(7)	10(6)	24(6)	66(5)
C(11)	12632(6)	7772(2)	10887(5)	235(7)	251(7)	493(11)	−21(6)	−47(8)	30(7)
C(1′)	5559(6)	7878(2)	5858(4)	249(6)	322(8)	329(8)	−23(6)	102(7)	55(6)
C(2′)	6025(10)	8315(2)	4798(5)	541(15)	345(11)	313(8)	−76(10)	59(8)	119(9)
C(3′)	4802(15)	8901(3)	4565(6)	863(28)	329(11)	401(13)	−42(16)	152(11)	88(15)
C(4′)	3171(11)	9044(3)	5376(7)	496(16)	349(12)	589(17)	58(11)	157(12)	104(13)
C(5′)	2843(11)	8591(3)	6436(10)	438(14)	356(12)	923(29)	126(11)	224(16)	288(17)
N(6′)	4003(8)	8022(2)	6669(6)	408(10)	396(11)	732(16)	138(9)	261(11)	324(11)
O(1)	13788(4)	6330(1)	9640(3)	277(5)	206(4)	385(6)	5(4)	−14(4)	130(4)
O(2)	10807(4)	5632(1)	8940(4)	208(4)	258(5)	753(12)	33(4)	−15(7)	99(6)
O(3)	10289(4)	4441(1)	8735(5)	218(5)	267(6)	817(13)	−36(5)	−84(7)	136(6)
O(4)	12565(6)	3591(1)	8769(6)	356(8)	229(5)	972(18)	−14(6)	−17(8)	236(10)
Cm(1)	13011(5)	5770(1)	9293(3)	224(6)	215(6)	332(7)	5(5)	3(5)	107(5)
Cm(2)	14808(5)	5247(1)	9294(4)	181(5)	229(6)	431(9)	−5(5)	−33(6)	103(6)
Cm(3)	14525(5)	4599(2)	9148(5)	203(6)	247(7)	470(10)	26(5)	−29(7)	116(6)
Cm(4)	12348(6)	4180(2)	8866(5)	262(7)	211(6)	478(11)	−9(5)	−19(7)	137(7)

*These U_{ij} values are coefficients in the expression exp $[-2\pi^2(a^{*2}U_{11}h^2 + b^{*2}U_{22}k^2 + c^{*2}U_{33}l^2 + 2a^*b^*U_{12}hk + 2b^*c^*U_{23}kl + 2a^*c^*U_{13}hl)]$.
†The estimated standard deviations in the atomic parameters are given in parentheses and refer to the least significant digit in the parameter.

TABLE 3. Atomic parameters ($\times 10^3$) for the hydrogen atoms of (+)-chlorpheniramine maleate

Atom	x/a	y/b	z/c	U_{iso}
H(1)	1127(5)	706(2)	1000(3)	43
H(2)	469(8)	559(2)	263(5)	82
H(3)	700(7)	652(2)	370(4)	73
H(5)	309(6)	657(2)	659(4)	60
H(6)	90(7)	581(2)	532(4)	74
H(7)	821(6)	728(2)	558(4)	58
H(81)	643(5)	700(2)	823(3)	48
H(82)	794(5)	668(1)	795(3)	48
H(91)	1053(6)	762(2)	790(3)	56
H(92)	864(6)	795(2)	890(3)	56
H(111)	1338(6)	792(2)	1001(4)	64
H(112)	1334(7)	766(2)	1180(4)	64
H(113)	1174(6)	819(2)	1115(4)	64
H(101)	840(6)	667(2)	1062(4)	59
H(102)	866(6)	741(2)	1167(4)	59
H(103)	1042(6)	698(2)	1197(4)	59
H(2′)	692(7)	812(2)	413(4)	75
H(3′)	532(6)	926(2)	387(4)	64
H(4′)	248(6)	948(2)	528(4)	64
H(5′)	146(6)	873(2)	712(4)	64
Hm(1)	1034(6)	486(2)	857(3)	57
Hm(2)	1640(6)	538(2)	966(3)	54
Hm(3)	1582(7)	429(2)	916(4)	74

Can. J. Chem. Downloaded from www.nrcresearchpress.com by 210.87.254.42 on 09/05/12
For personal use only.

Can. J. Chem. Downloaded from www.nrcresearchpress.com by 210.87.254.42 on 09/05/12
For personal use only.

TABLE 4*

(*a*) Bond distances involving the hydrogen atoms of (+)-chlorpheniramine maleate

Bond	Distance (Å)	Bond	Distance (Å)
C(2)—H(2)	0.83	C(9)—H(92)	0.99
C(3)—H(3)	0.86	N(1)—H(1)	0.55
C(5)—H(5)	0.87	C(10)—H(101)	1.02
C(6)—H(6)	0.79	C(10)—H(102)	0.98
C(2′)—H(2′)	0.98	C(10)—H(103)	0.87
C(3′)—H(3′)	1.06	C(11)—H(111)	1.04
C(4′)—H(4′)	0.97	C(11)—H(112)	0.86
C(5′)—H(5′)	1.16	C(11)—H(113)	1.05
C(7)—H(7)	1.05	Cm(2)—Hm(2)	0.94
C(8)—H(81)	0.90	Cm(3)—Hm(3)	0.97
C(8)—H(82)	0.78	O(3)—Hm(1)	0.87
C(9)—H(91)	1.06		

(*b*) Interbond angles involving the hydrogen atoms of (+)-chlorpheniramine maleate

Bonds	Angle (deg)	Bonds	Angle (deg)
The *p*-chlorophenyl system			
C(1)—C(2)—H(2)	104	C(4)—C(5)—H(5)	117
C(3)—C(2)—H(2)	136	C(6)—C(5)—H(5)	122
C(2)—C(3)—H(3)	118	C(5)—C(6)—H(6)	114
C(4)—C(3)—H(3)	119	C(1)—C(6)—H(6)	126
The pyridyl system			
C(1′)—C(2′)—H(2′)	114	C(3′)—C(4′)—H(4′)	118
C(3′)—C(2′)—H(2′)	126	C(5′)—C(4′)—H(4′)	124
C(2′)—C(3′)—H(3′)	119	C(4′)—C(5′)—H(5′)	116
C(4′)—C(3′)—H(3′)	121	N(6′)—C(5′)—H(5′)	121
The aliphatic portion			
C(4)—C(7)—H(7)	106	C(10)—N(1)—H(1)	104
C(1′)—C(7)—H(7)	103	C(11)—N(1)—H(1)	111
C(8)—C(7)—H(7)	114	N(1)—C(10)—H(101)	105
C(7)—C(8)—H(81)	112	N(1)—C(10)—H(102)	116
C(7)—C(8)—H(82)	113	N(1)—C(10)—H(103)	101
C(9)—C(8)—H(81)	114	H(101)—C(10)—H(102)	124
C(9)—C(8)—H(82)	118	H(101)—C(10)—H(103)	117
H(81)—C(8)—H(82)	85	H(102)—C(10)—H(103)	91
C(8)—C(9)—H(91)	100	N(1)—C(11)—H(111)	102
C(8)—C(9)—H(92)	112	N(1)—C(11)—H(112)	113
N(1)—C(9)—H(91)	111	N(1)—C(11)—H(113)	109
N(1)—C(9)—H(92)	106	H(111)—C(11)—H(112)	129
H(91)—C(9)—H(92)	115	H(111)—C(11)—H(113)	105
C(9)—N(1)—H(1)	106	H(112)—C(11)—H(113)	105
The maleate ion			
O(2)—Hm(1)—O(3)	159		
Cm(1)—Cm(2)—Hm(2)	115		
Cm(3)—Cm(2)—Hm(2)	114		
Cm(2)—Cm(3)—Hm(3)	124		
Cm(4)—Cm(3)—Hm(3)	104		

*Standard deviations average 0.03 Å for these distances and 3.0° for the angles.

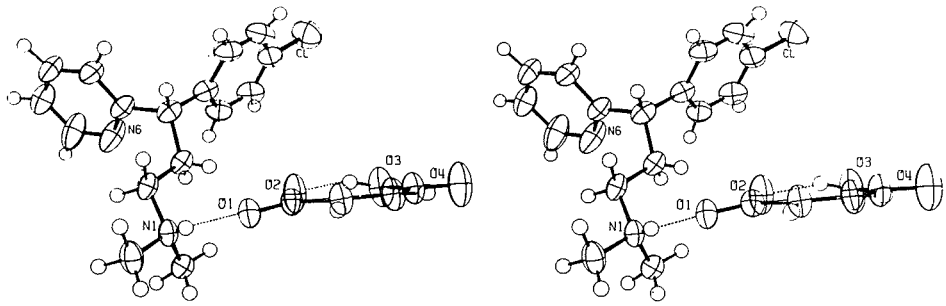

FIG. 2. A stereo pair of the (+)-chlorpheniramine maleate complex. The correct S absolute configuration is shown. The two upper carbon atoms of the benzene ring are C(2) and C(3).

The pyridyl ring is planar with a maximum exoplanar displacement of 0.01 Å from the plane, defined by the six atoms of this grouping, with equation $-0.5736x - 0.4311y - 0.6955z = -11.6439$. Although the interbond angles for this system fall close to expected values (28) some of the bond distances do not; C(3′)—C(4′) being shorter than 1.394 Å by 0.034 Å ($\sim 7\sigma$).

In both of these two rings the distortions from ideality may not be as large as are indicated because of the underestimated e.s.d.'s. It is possible however that uncorrected errors arising from absorption are partially responsible for these discrepancies. Another phenomenon which could be important in this regard is that of "inverse overlap" (29). Srinivasan has shown that centrosymmetric atomic groupings can lead to problems in least-squares refinement and it is thought that this effect may be partially responsible for these deviations from ideality. Serious effects on atomic positions, and thus bond distances, have been reported before (30).

The bond distances and interbond angles for the alkylamine chain of (+)-chlorpheniramine are not significantly different from those obtained for *dl*-brompheniramine (10). In both cases the X—X—X angles at C(8) and C(9) are greater than the tetrahedral value of 109.5° and the C(8)—C(9) bonds are shorter than the 1.54 expected here. That steric effects are not responsible for this is inferred from the fact that the angular distortions would tend to lengthen the chain whereas the bond distance distortion would shorten it. This observation must have its genesis in some electronic effect which imparts some measure of double bond character to the C(8)—C(9) linkage.

One view of the ionic complex which indicates that the phenyl and pyridyl rings and the alkylamine chain adopt a similar arrangement to those in *dl*-brompheniramine maleate is given in the computer-drawn Fig. 2 (31). The dihedral angle between the two planar aryl systems is 113.6°. The dihedral angles which define the relationship of the aryl systems to the alkyl portion are given by C(5)—C(4)—C(7)—C(8) = 53.7° and N(6′)—C(1′)—C(7)—C(8) = −43.4.[5] The alkylamine chain is again oriented unsymmetrically with respect to the two aromatic rings (Figs. 2 and 3). In this case, it is the 2-pyridyl ring which is partially obstructed by the dissymmetry and the *p*-chlorophenyl ring is exposed. In the previous structure (10) nitrogen atom N(1) was found to be 6.212 Å from the centroid of the exposed pyridyl ring and 5.568 Å

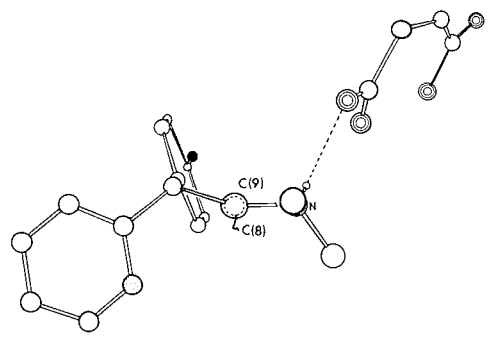

FIG. 3. A drawing of the (+)-chlorpheniramine maleate structure viewed down the C(9)—C(8) bond direction.

[5]These torsion angles are defined as follows: A—B—C—D is a set of atoms connected as shown, then the torsion angle A—B—C—D is the dihedral angle between the two planes defined by the positions of atoms ABC and BCD. A positive angle is one that requires a clockwise rotation of atom A to achieve superposition of the B—A and C—D bond vectors when viewed in the direction B—C.

Can. J. Chem. Downloaded from www.nrcresearchpress.com by 210.87.254.42 on 09/05/12
For personal use only.

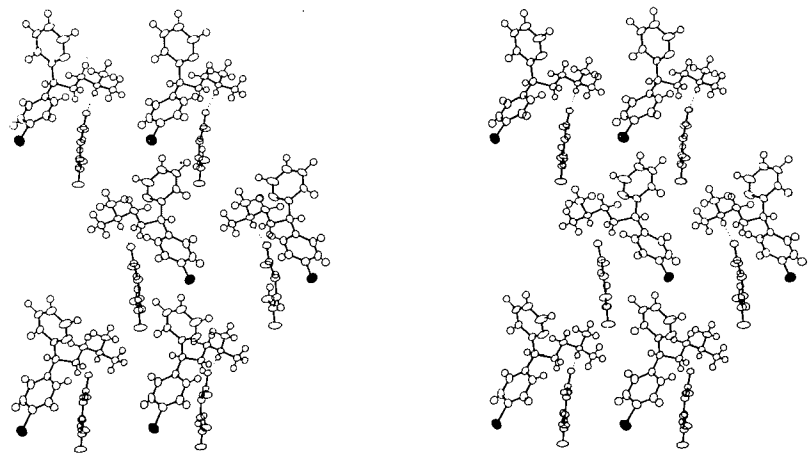

FIG. 4. A stereoscopic packing diagram of the crystal structure viewed parallel to a^*.

from the centroid of the phenyl system. In the present case the alkylamine basic center (N(1)) is 6.154 Å from the centroid of the exposed ring (*p*-chlorophenyl) and 5.402 Å from the occluded 2-pyridyl moiety. The similarity of these pairs of numbers is striking and, if the identity of the aryl systems is ignored Figs. 2 and 3 reveal that these two compounds adopt very similar solid state conformations and it is worthwhile noting here that in both species the drug molecule has an open side to which both a hydrogen bond acceptor and an aromatic system could interact.

Apart from the $\overset{+}{N}$–H---$\bar{O}$ hydrogen bond between the dimethylamino function and the maleate ion there are no specific intermolecular forces which can be singled out for mention. The stereoscopic packing diagram, Fig. 4, shows the structure viewed parallel to a^* and although this diagram gives the illusion of an interaction between the chlorine atom and the π electron density of a pyridyl ring, the 4.2 Å separation of these features implies that no such interaction occurs.

Two interesting aspects of the maleate ion are worthy of note: (*i*) the intra-ion hydrogen bond is of length 2.444 Å and is asymmetric; a finding which is in accord with our work on *dl*-brompheniramine maleate but at variance with that on other structures (32, 33); (*ii*) the two ends of the maleate ion have environments of quite different character. The hydrogen bond of length 2.689 Å between N(1) and O(1) represents a predominantly polar interaction between the protonated nitrogen atom and an ionized carboxyl group. Oxygen atom O(4), on the other hand, is approximately equidistant from three apolar carbon atoms which define the basal plane of the nitrogen pyramid in another molecule. This chain of alternating polar and non-polar bonding interactions which runs parallel to the crystallographic *b* axis is illustrated in Fig. 5.

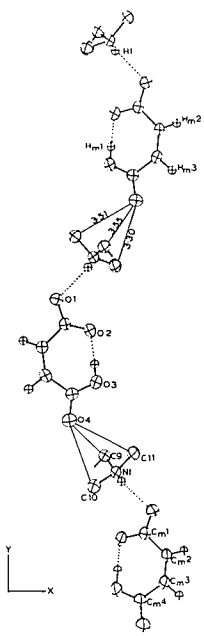

FIG. 5. The chain of polar and non-polar bonding interactions involving the maleate ion. This chain is not illustrated in Fig. 4.

Can. J. Chem. Downloaded from www.nrcresearchpress.com by 210.87.254.42 on 09/05/12
For personal use only.

The (+)-chlorpheniramine maleate sample used in this work was kindly supplied by Dr. J. G. Topliss of the Schering Corporation. One of us (G.J.B.W.) thanks the University of Alberta for financial support in the form of Teaching Assistantships and Intersession Bursaries throughout his Ph.D. studies, of which this work forms a part. Mr. L. Goulden's photographic expertise is gratefully acknowledged. The Medical Research Council of Canada has supported this research by a grant (#MA3406) to M.N.G.J. Grateful appreciation is also expressed to Dr. F. R. Ahmed, National Research Council of Canada, Ottawa for his set of crystallographic computer programs.

1. A. F. CASY and A. P. PARULKAR. Can. J. Chem. **47**, 423 (1969).
2. A. F. CASY and R. R. ISON. J. Pharm. Pharmacol. **22**, 270 (1970).
3. N. S. HAM. J. Pharm. Sci. **60**, 1764 (1971).
4. A. F. CASY, R. R. ISON, and N. S. HAM. Chem. Commun. 1343 (1970).
5. L. B. KIER. J. Med. Chem. **11**, 441 (1968).
6. J.-L. COUBEILS, P. COURRIERE, and B. PULLMAN. C. R. ACAD. PÆæIŒ, **272**, 1813 (1971).
7. D. T. WITIAK. *In* Medicinal chemistry. Vol. 2, 3rd ed. *Edited by* A. Burger. Wiley, New York. 1970. Chapt. 65.
8. M. ROCHE E SILVA. Chemotherapia, **3**, 544 (1961).
9. W. TH NAUTA, R. F. REKKER, and A. F. HARMS. *In* "Physico-chemical aspects of drug action. Vol. 7. *Edited by* E. J. Ariens. Pergammon Press, U.K. 1968.
10. M. N. G. JAMES and G. J. B. WILLIAMS. J. Med. Chem. **14**, 670 (1971).
11. G. R. CLARK and G. J. PALENIK. J. Am. Chem. Soc. **94**, 4005 (1972).
12. R. T. BRITTAIN, P. F. D'ARCY, and J. H. HUNT. Nature, **183**, 734 (1959).
13. A. SHAFIEE and G. HITE. J. Med. Chem. **12**, 266 (1969).
14. R. S. CAHN, C. K. INGOLD, and V. PRELOG. Angew. Chem. Int. Ed. **5**, 385 (1960).
15. I. WEISZ and A. DUDÁS. Monatsh. **91**, 840 (1960).
16. U. W. ARNDT and B. T. M. WILLIS. Single crystal diffractometry. Cambridge University Press, New York, N.Y. 1966. p. 277.
17. P. G. SIMPSON, R. D. DOBROTT, and W. N. LIPSCOMB. Acta Cryst. **16**, 169 (1965).
18. D. T. CROMER and J. B. MANN. Acta Cryst. A**24**, 321 (1968).
19. R. F. STEWART, E. R. DAVIDSON, and W. T. SIMPSON. J. Chem. Phys. **42**, 3175 (1965).
20. D. T. CROMER and D. LIBERMAN. J. Chem. Phys. **53**, 1891 (1970).
21. W. C. HAMILTON. Acta Cryst. **18**, 502 (1965).
22. L. I. HODGSON and J. S. ROLLET. Acta Cryst. **16**, 329 (1963).
23. F. R. AHMED, M. E. PIPPY, S. R. HALL, and C. P. HUBER. N.R.C. crystallographic programs for the IBM/360 system, world list of crystallographic computer programs; 2nd ed. Appendix p. 52.
24. R. RUDMAN. Acta Cryst. B**27**, 262 (1971).
25. J. J. H. MCDOWELL. Acta Cryst. B**25**, 2175 (1969).
26. G. J. PALENIK, J. DONOHUE, and K. N. TRUEBLOOD, Acta Cryst. B**24**, 1139 (1968).
27. L. E. SUTTON. (*Editor*). Tables of interatomic distances and configuration in molecules and ions, Supplement 1956–1959. Special Publication No. 18, The Chemical Society, London. 1965.
28. B. BAK, L. HANSEN-NYGAARD, and J. RASTRUP-ANDERSON. J. Mol. Spectrosc. **2**, 361 (1958).
29. R. SRINIVASAN. Acta Cryst. **14**, 1163 (1961).
30. R. PARTHASARATHY, J. G. SIME, and R. C. SPEAKMAN. Acta Cryst. B**25**, 1201 (1969).
31. C. K. JOHNSON. ORTEP, Report ORNL-3794, Oak Ridge National Laboratory, Oak Ridge, Tennessee. 1965.
32. R. D. ELLISON and H. A. LEVY. Acta Cryst. **19**, 260 (1965).
33. J. P. GLUSKER, W. OREHOWSKY, C. A. CASCIATO, and H. L. CARRELL. Acta Cryst. B**28**, 419 (1972).

Can. J. Chem. Downloaded from www.nrcresearchpress.com by 210.87.254.42 on 09/05/12
For personal use only.

The Crystal and Molecular Structure of the Antihistaminic Drug Triprolidine Hydrochloride Monohydrate [*trans*-1-(*p*-Tolyl)-1-(2-pyridyl)-3-(1-pyrrolidino)-prop-1-ene]

M. N. G. JAMES[1] AND G. J. B. WILLIAMS[2]

Department of Biochemistry, University of Alberta, Edmonton, Alberta T6G 2E1

Received November 16, 1973

The title compound crystallizes from anisole with 4 molecules per unit cell. The space group of this cell is $P2_1/c$ and the cell parameters are a = 14.777(2) Å, b = 9.5785(8) Å, c = 13.099(1) Å, and β = 90.48(2)°. Diffractometer data with CuK_α radiation to 2θ = 129° were collected and the structure solved and refined to weighted and unweighted R factors of 0.077 and 0.051 respectively. The 2-pyridyl ring and the *p*-tolyl system make dihedral angles of 29.7 and 55.3° respectively with the plane of the double bond. The inter-aryl dihedral angle is 106.5°. The protonated tertiary nitrogen atom is hydrogen bonded to the chloride ion and two chloride ions are connected via hydrogen bonds in a distorted square planar arrangement by two water molecules. The pyridyl ring is involved in a π orbital overlap linkage with another pyridyl ring on the same side of the molecule as is the hydrogen bond from the nitrogen function. Brief characteristics of a flexible receptor protein which will bind antihistamine drugs are given.

Le composé du titre cristallise dans l'anisole avec quatre molécules par maille. Le groupe d'espace de cette maille est $P2_1/c$ et ses paramètres sont: a = 14.777(2) Å, b = 9.5785(8) Å, c = 13.099(1) Å et β = 90.48(2)°. Les données du diffractomètre avec la radiation CuK_α à 2θ = 129° sont recueillies et la structure est déterminée et raffinée aux facteurs pondérés et non pondérés respectifs de R de 0.077 et 0.051. Le cycle pyridyle-2 et le système *p*-tolyle font, avec le plan de la double liaison, des angles dièdres respectifs de 29.7 et 55.3°. L'angle dièdre entre les aryles est de 106.5°. L'atome d'azote tertiaire protoné est lié par l'hydrogène à l'ion chlorure et deux ions chlorures sont reliés par liaisons d'hydrogène dans un arrangement plan carré déformé par deux molécules d'eau. Le cycle pyridyle est impliqué dans une liaison de recouvrement d'orbitales π ainsi qu'un autre cycle pyridyle du même côté de la molécule comme l'est la liaison hydrogène de la fonction azote. De brèves caractéristiques d'une protéine réceptrice flexible qui reliera les composés antihistaminiques sont présentées.

[Traduit par le journal]

Can. J. Chem., **52**, 1880 (1974)

Introduction

The introduction of a double bond into the flexible alkylamine chain of antihistaminic drugs is one way of introducing some stereochemical rigidity into these compounds without grossly changing their character. By suitable pharmacological screening of the geometric isomers of these unsaturated drugs some progress has been made towards defining the active conformations of their saturated analogs (1–3).

Triprolidine (**1**) was first synthesized as the *p*-chlorophenyl analog and as a mixture of geometric isomers (4). One of these isomers was shown to be a much more potent antihistamine than the other (4) and a two-dimensional X-ray crystallographic study of the less active β isomer of the *p*-bromophenyl hydrobromide compound revealed that the 2-pyridyl and alkylamine substituents of the double bond were *cis* (5). No detailed examination of the more active α isomer was performed but Adamson *et al.* (4) had gathered evidence to show that these compounds were *cis*/*trans* isomers and so it was inferred that the greater antihistaminic potency was derived from the *trans* arrangement of nitrogen containing substituents of the double bond.

Adamson and co-workers used comparative ultraviolet spectroscopy as a means of examining the conformation of their α and β isomers (4). By this means they were able to show that the more active α isomer probably adopted a conformation similar to that of a vinyl pyridine and that the form of the *cis* Py/CH_2N isomer most likely resembled a styrene derivative. The inference drawn from these results was that the 2-pyridyl function of the active *trans* (α) compound was probably nearly coplanar with the double

[1]Author to whom correspondence should be addressed.

[2]Present address: Department of Chemistry, Brookhaven National Laboratory, Upton, Long Island, New York 11973.

Can. J. Chem. Downloaded from www.nrcresearchpress.com by 210.87.254.6 on 09/05/12
For personal use only.

Can. J. Chem. Downloaded from www.nrcresearchpress.com by 210.87.254.6 on 09/05/12
For personal use only.

bond and that the phenyl ring was significantly twisted out of this common plane.

Kier (6) used this information in conjunction with that he had obtained from a molecular-orbital study of histamine to infer that the most probable active conformation of the agonist had a fully extended alkylamine chain. In this form an internitrogen separation of 4.55 Å was realized by Kier (6) and by arranging a model of triprolidine so that the closest reasonable approach of nitrogen atoms was obtained he was able to estimate the N—N distance as 4.8 ± 0.2 Å. It was felt that these distances were sufficiently similar to allow analogous binding of these two molecules to the same site. Because of the apparent importance placed on the above argument it was decided to choose the crystalline drug triprolidine hydrochloride monohydrate as the next compound for study in our program of structural investigations of this functional class of molecules.

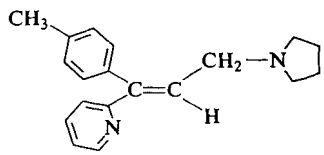

1

Experimental

Crystals of good quality were obtained by slowly cooling a warm solution of the compound in anisole. Diffraction symmetry ($2/m$) and systematic absences ($h0l$, $l = 2n + 1$; $0k0$, $k = 2n + 1$) were observed photographically and the space group thereby deduced as $P2_1/c$. Refined unit cell constants were obtained as part of the alignment process on a Picker FACS-1 diffractometer; these and some other pertinent data are contained in Table 1.

During the preliminary photography it was observed that the tendency of these crystals to become rose-colored on standing in air was greatly enhanced by X-irradiation. To minimize the effects of any attendant decomposition due to the X-rays, the total exposure time during the data collection was minimized by: (*i*) choosing the fastest $\theta/2\theta$ scan speed available, *i.e.* 2°/min in 2θ; (*ii*) decreasing the basic scan width to just accommodate the reflections. This width was 1.3° in 2θ and was modified as a function of θ to cope with the dispersion of the CuK_α doublet (ref. 7, pp. 173 174); (*iii*) taking fixed position background counts on either side of the Bragg reflection for only 4 s. each; (*iv*) first measuring those reflections with $2\theta < 100°$ and then examining the region of reciprocal space with $100° < 2\theta \leqslant 129°$.

As well as these stratagems the amount of short wavelength radiation falling on the crystal was diminished by using an incident beam graphite monochromator.

Despite the coloration of the crystal, which became progressively more severe as the intensity collection proceeded, the monitor reflections had shown only insignificant intensity changes at the end of the low θ data set and were still 98% of their original value at the end of the entire data collection. Of the 1911 reflections measured in the first part 1716 (89%) had net intensities greater than 3 times the standard error in the net intensity. In a similar manner 2516 (80%) of the 3123 reciprocal lattice points comprising the full set were considered observed.

TABLE 1. Some crystallographic constants for triprolidine hydrochloride monohydrate

Formula	$C_{19}H_{23}N_2{}^+Cl^-\cdot H_2O$
Molecular weight	332.88 daltons
Space group	$P2_1/c$
a	14.777(2) Å
b	9.5785(8) Å
c	13.099(1) Å
β	90.48(2)°
Z	4
ρ_{obs} (dioxane/benzene)	1.202(4) g/cm^3
ρ_{calcd}	1.192 g/cm^3
μ (CuK_α)	16.68 cm^{-1}

Data reduction procedures incorporated Lorentz and polarization corrections as appropriate to the normal-beam equatorial geometry of the FACS-1 system with partially polarized incident radiation (ref. 7, p. 277) and calculation of observational weights from the expression $\sqrt{w} = 2F_o/[T + (kI)^2 + B]^{1/2}$ (8). In this expression F_o is the derived structure amplitude, T, I, and B are the total, net, and background counts respectively, and k is a small constant (0.04 in this case) included to allow for minor experimental errors.

Structure solution was achieved without difficulty by means of a Patterson synthesis and a program (9) written to apply the symmetry minimum technique of Simpson *et al.* (10). Refinement of the initial model by difference Fourier and block-diagonal least-squares methods has resulted in weighted (observational weights) and unweighted R factors of 0.077 and 0.051 respectively for the 2516 observed data of the complete set. During the least-squares part of this refinement the temperature parameters of the hydrogen atoms were held constant at the final isotropic value of the atom to which they were bonded. Scattering factor tables for the non-hydrogen atoms were derived from the analytical coefficients of Cromer and Mann (11) and were corrected for the effects of anomalous dispersion by the terms $\Delta f_O' = 0.055$, $\Delta f_N' = 0.036$, $\Delta f_C' = 0.021$, $\Delta f_{Cl}' = 0.375$, and $\Delta f_{Cl}'' = 0.685$ electrons (12). The hydrogen atom curve used was that of Stewart *et al.* (13).

Tables 2 and 3 contain those atomic parameters used to describe the final model and were based on least-squares refinement using all the observed data. The observed structure amplitudes and the structure factors calculated from the final model were tabulated.[3]

Results and Discussion

Bond distances and interbond angles were calculated by the independent atom method (14)

[3]These data are available, at a nominal charge, from the Depository of Unpublished Data, National Science Library, National Research Council of Canada, Ottawa, Canada K1A 0S2.

Can. J. Chem. Downloaded from www.nrcresearchpress.com by 210.87.254.6 on 09/05/12
For personal use only.

TABLE 2. Positional and anisotropic vibration* parameters ($\times 10^4$) for the non-hydrogen atoms of triprolidine hydrochloride monohydrate†

Atom	x/a	y/b	z/c	U_{11}*	U_{22}	U_{33}	U_{12}	U_{23}	U_{13}
Cl(1)	8588(1)	921(1)	−702(1)	351(3)	619(4)	241(2)	6(2)	−44(2)	−21(2)
O(1)	9295(2)	−1451(3)	910(2)	446(9)	477(9)	527(10)	−63(7)	45(8)	55(7)
N(10)	8699(1)	2169(2)	1476(2)	188(5)	247(6)	187(5)	−6(4)	16(4)	9(4)
C(7)	6549(2)	559(3)	2359(2)	196(6)	178(6)	194(7)	22(5)	−1(5)	11(5)
C(8)	7222(2)	1069(3)	1799(2)	206(7)	256(7)	192(7)	0(6)	35(6)	0(5)
C(9)	8186(2)	1201(3)	2140(2)	207(7)	313(8)	212(8)	−27(6)	53(6)	10(6)
C(11)	8350(2)	3630(3)	1447(3)	258(8)	275(8)	377(10)	15(7)	41(7)	−27(7)
C(12)	9128(3)	4461(4)	1181(4)	332(11)	338(12)	932(24)	−67(9)	244(13)	−36(13)
C(13)	9953(2)	3675(4)	1315(3)	236(8)	377(11)	501(13)	−86(8)	54(10)	0(8)
C(14)	9682(2)	2287(3)	1749(2)	189(7)	310(9)	268(8)	−8(6)	0(7)	−7(6)
C(1′)	5623(2)	480(3)	1923(2)	190(6)	181(6)	192(7)	23(5)	−13(5)	17(5)
N(2′)	5397(1)	1443(2)	1217(2)	215(6)	248(6)	227(6)	29(5)	14(5)	−10(5)
C(3′)	4581(2)	1343(3)	794(2)	236(7)	285(8)	271(8)	56(6)	25(7)	−25(6)
C(4′)	3957(2)	344(3)	1014(2)	219(7)	336(10)	293(9)	39(6)	−71(7)	−22(6)
C(5′)	4190(2)	−641(3)	1742(3)	227(8)	266(8)	344(10)	−35(6)	−64(7)	38(7)
C(6′)	5024(2)	−572(3)	2201(2)	215(7)	240(7)	247(8)	−9(6)	6(6)	15(6)
C(1)	6703(2)	7(3)	3412(2)	178(6)	197(6)	194(7)	−10(5)	7(5)	5(5)
C(2)	7330(2)	−1030(3)	3610(2)	204(7)	213(7)	223(7)	2(5)	−4(6)	16(6)
C(3)	7438(2)	−1580(3)	4580(2)	226(7)	217(7)	237(7)	−3(6)	37(6)	−38(6)
C(4)	6930(2)	−1119(3)	5382(2)	266(8)	246(8)	192(7)	−67(6)	33(6)	−16(6)
C(5)	6305(2)	−48(3)	5198(2)	244(7)	279(8)	207(7)	−38(6)	−12(6)	35(6)
C(6)	6197(2)	480(3)	4233(2)	212(7)	234(7)	232(7)	24(6)	8(6)	16(6)
C(15)	7016(2)	−1778(4)	6415(3)	363(10)	393(10)	278(9)	−92(8)	73(8)	−45(8)

*These coefficients are defined by the expression: $\exp[-2\pi^2(U_{11}a^{*2}h^2 + U_{22}b^{*2}k^2 + U_{33}c^{*2}l^2 + 2U_{12}a^*b^*hk + 2U_{13}a^*c^*hl + 2U_{23}b^*c^*kl)]$.
†The estimated standard deviations of the atomic parameters are given in parentheses and refer to the least significant digit in the parameter.

Can. J. Chem. Downloaded from www.nrcresearchpress.com by 210.87.254.6 on 09/05/12
For personal use only.

TABLE 3. Positional and isotropic vibration parameters ($\times 10^3$) for the hydrogen atoms of triprolidine hydrochloride monohydrate

Atom	x/a	y/b	z/c	U_{iso}
H(10)	868(2)	185(3)	91(2)	48
H(8)	706(2)	144(2)	109(2)	46
H(3′)	448(2)	198(3)	33(2)	64
H(4′)	334(2)	34(3)	66(2)	64
H(5′)	377(2)	−137(3)	189(2)	59
H(6′)	521(2)	−123(3)	266(2)	57
H(2)	767(2)	−133(3)	315(2)	61
H(3)	787(2)	−234(3)	463(2)	61
H(5)	587(2)	30(3)	568(2)	66
H(6)	580(2)	108(2)	416(2)	42
H(91)	848(2)	31(3)	205(2)	66
H(92)	819(2)	163(3)	278(2)	49
H(111)	818(2)	382(3)	218(2)	84
H(112)	787(2)	367(3)	99(2)	67
H(121)	908(2)	536(3)	128(2)	91
H(122)	905(2)	478(4)	61(3)	102
H(131)	1043(2)	363(4)	81(3)	114
H(132)	1043(2)	402(3)	167(2)	81
H(141)	974(2)	229(3)	246(2)	72
H(142)	997(2)	146(3)	149(2)	66
H(151)	714(2)	−110(3)	688(2)	80
H(152)	754(2)	−186(3)	656(2)	62
H(153)	650(2)	−218(3)	662(2)	90
WH(1)	903(2)	−95(3)	38(2)	75
WH(2)	−1(2)	−129(4)	80(3)	106

and those involving the non-hydrogen atoms are displayed, together with the numbering scheme and atomic coding adopted, in Fig. 1. Molecular parameters involving the hydrogen atoms are given in Table 4. Using X to denote a carbon, nitrogen, or oxygen atom, the e.s.d.'s in the distances Cl—X, X—X, and X—H average 0.003, 0.003, and 0.03 Å respectively. The angles X—X—X, H—X—X, Cl—H—X, and H—X—H have average error estimates of 0.2, 1.6, 2.3, and 2.5° respectively.

Bond distances within the benzene ring average 1.384 Å and the four —C⋯C— bonds of the pyridyl ring average 1.378 Å, the associated error estimate being 0.004 Å in each case. These σ's were derived from the formula $\sigma_{\bar{x}}^2 = \sum(\bar{x} - x_i)^2/n(n-1)$. Benzenoid rings typically exhibit —C⋯C— bond distances of 1.394 Å, a value which is 2.5σ greater than our average value. This marginally significant discrepancy may be due to systematic thermal motion effects which have not been corrected for in our model.

The phenyl and pyridyl rings are individually planar. The maximum deviation of a defining atom from the phenyl plane, equation (in cosine form relative to a,b,c^* orthogonal axes measured in Å) $-0.6958x - 0.6892y - 0.2024z = -7.7804$, is 0.008 Å. In the case of the pyridyl ring the largest displacement is 0.003 Å and the plane is defined by the equation $0.3797x - 0.5862y - 0.7157z = 1.0727$. These two planes have an interplanar dihedral angle of 106.5°. Despite the similarity of this quantity with the interaryl angles in *dl*-brompheniramine maleate (15) (103.6°) and (+)-chlorpheniramine maleate (16) (113.6°) Fig. 2, which is a projection of the structure down the C(9)—C(8) bond, shows that only the 2-pyridyl ring is similarly arranged with respect to the alkylamine chain. Torsion angles about the ring to double bond linkages are given by N(2′)—C(1′)—C(7)—C(8) = 29.7° and C(2)—C(1)—C(7)—C(8) = 55.3°[4]. In this case it will be

[4]These torsion angles are defined as follows: if A—B—C—D is a set of atoms connected as shown then the torsion angle about the B—C bond is the dihedral angle between the two planes defined by the positions of ABC and BCD. A positive angle is one that requires a clockwise rotation of atom A to achieve superposition of the BA and CD bond vectors when viewed in the direction B → C.

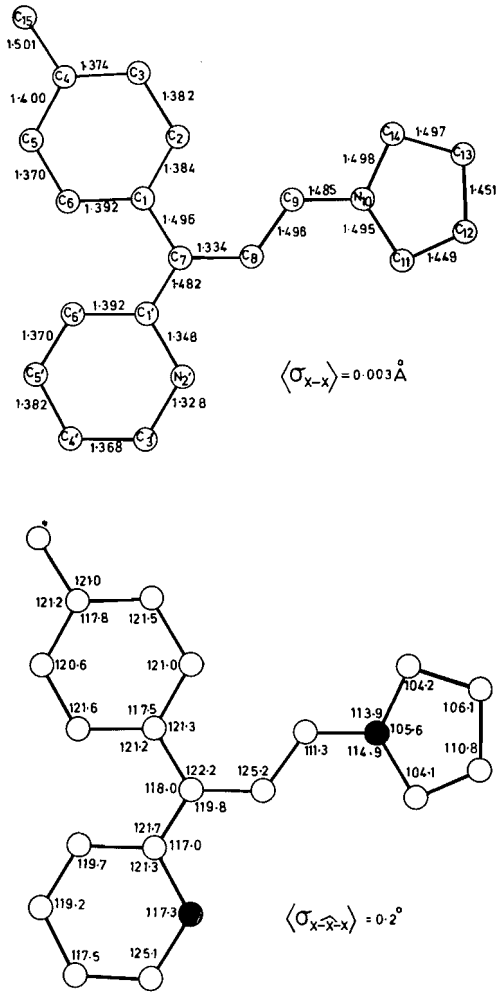

FIG. 1. Bond distances and interbond angles for the non-hydrogen atoms of triprolidine.

noticed that these two angles both have the same sign and the "butterfly wing" arrangement of aromatic rings observed for the pheniramines is not evident here.

The presence of a double bond between C(7) and C(8) forces coplanarity of the six atoms C(1), C(1′), C(7), C(8), C(9), and H(8). A least-squares plane defined by the positions of these six atoms was determined to have the equation $0.1913x - 0.9107y - 0.3661z = 0.2405$ and a maximum displacement from the plane for a defining atom of 0.04(4) Å for H(8).

Of the two aromatic systems, the pyridyl ring is more nearly coplanar with the ethylenic system than is the *p*-tolyl function, the dihedral angles between the appropriate planes being 29.7 and

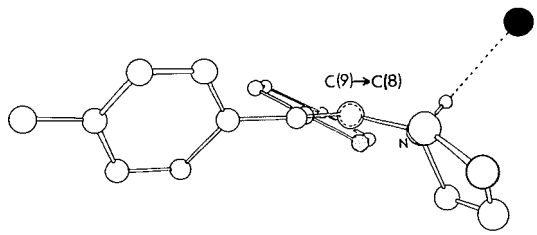

FIG. 2. A view of the triprolidine hydrochloride structure seen in the C(9)—C(8) bond direction. The two upper atoms of the *p*-tolyl ring are C(2) and C(3).

55.3°, respectively. This finding is in agreement with those results obtained by Adamson *et al.* (4) and could have been predicted on steric grounds. The serious overcrowding involved in the close approaches of hydrogen atoms is evident when attempt is made to build a coplanar *cis* Ph/CH_2 ethylene system from space filling models. The lack of an *ortho* hydrogen substituent on the 2-pyridyl moiety and the fact that the *cis* substituent to the aromatic base is hydrogen, permits this greater approach to coplanarity of the pyridyl and ethylenic systems. The fact that the coplanarity is not perfect is probably a result of steric interference between H(8) and the unshared electron pair on the heterocyclic nitrogen, evidence for this comment being derived from the 2.47(3) Å distance between N(2′) and H(8) and the fact that the closest approach expected on a van der Waal's radii basis is ~2.7 Å (17). It is possible that intermolecular base stacking interactions (see below) may be partially responsible for the 29.7° departure from coplanarity, but it is felt that the above mentioned close approach is probably more important in this regard.

The two bonds from the aryl systems to the ethylenic bond differ by 0.014(3) Å, the linkage to the more nearly coplanar pyridyl ring being the shorter. That the 29.7° torsion angle about the C(1′)—C(7) bond precludes extensive π electron delocalization over these two systems is indicated by this small difference and the fact that the 1.334(3) Å bonding distance between C(7) and C(8) is just that expected for an isolated C=C bond (18). That significant shortening of the bond joining an aromatic system to a coplanar exocyclic double bond is expected is to be inferred from the 0.06 Å difference in linkages of a similar nature observed by Fritchie and Wells (19). In their compound the torsion angle about the shorter bond was 6° and for the longer bond

Can. J. Chem. Downloaded from www.nrcresearchpress.com by 210.87.254.6 on 09/05/12
For personal use only.

Can. J. Chem. Downloaded from www.nrcresearchpress.com by 210.87.254.6 on 09/05/12
For personal use only.

TABLE 4. (*a*) Bond distances involving the hydrogen atoms of triprolidine hydrochloride monohydrate*

Bond	Distance (Å)	Bond	Distance (Å)
O(1)—WH(1)	0.89	C(8)—H(8)	1.00
O(1)—WH(2)	1.04	C(9)—H(91)	0.99
C(2)—H(2)	0.84	C(9)—H(92)	0.95
C(3)—H(3)	0.95	N(10)—H(10)	0.82
C(5)—H(5)	0.95	C(11)—H(111)	0.96
C(6)—H(6)	0.86	C(11)—H(112)	0.93
C(3′)—H(3′)	0.84	C(12)—H(121)	0.91
C(4′)—H(4′)	0.98	C(12)—H(122)	0.70
C(5′)—H(5′)	0.96	C(13)—H(131)	0.97
C(6′)—H(6′)	0.88	C(13)—H(132)	0.93
C(15)—H(151)	0.91	C(14)—H(141)	0.86
C(15)—H(152)	0.82	C(14)—H(142)	0.94
C(15)—H(153)	0.92		

(*b*) Angles involving the hydrogen atoms of triprolidine hydrochloride monohydrate*

Bonds	Angle (deg)	Bonds	Angle (deg)
The *p*-tolyl system			
C(1)—C(2)—H(2)	119.6	C(1)—C(6)—H(6)	116.6
C(3)—C(2)—H(2)	119.4	C(4)—C(15)—H(151)	108.4
C(2)—C(3)—H(3)	112.6	C(4)—C(15)—H(152)	111.5
C(4)—C(3)—H(3)	125.7	C(4)—C(15)—H(153)	114.8
C(4)—C(5)—H(5)	125.4	H(151)—C(15)—H(152)	76.8
C(6)—C(5)—H(5)	113.5	H(153)—C(15)—H(152)	129.9
C(5)—C(6)—H(6)	121.7	H(151)—C(15)—H(153)	105.2
The pyridyl system			
N(2′)—C(3′)—H(3′)	125.1	C(4′)—C(5′)—H(5′)	118.5
C(4′)—C(3′)—H(3′)	113.9	C(6′)—C(5′)—H(5′)	122.3
C(3′)—C(4′)—H(4′)	122.5	C(5′)—C(6′)—H(6′)	120.6
C(5′)—C(4′)—H(4′)	120.1	C(1′)—C(6′)—H(6′)	119.5
The aliphatic portion			
C(7)—C(8)—H(8)	117.2	C(13)—C(12)—H(121)	124.3
C(9)—C(8)—H(8)	117.5	C(11)—C(12)—H(122)	111.7
C(8)—C(9)—H(91)	108.8	C(13)—C(12)—H(122)	117.7
N(10)—C(9)—H(91)	104.1	H(121)—C(12)—H(122)	67.4
C(8)—C(9)—H(92)	107.3	C(12)—C(13)—H(131)	117.8
N(10)—C(9)—H(92)	105.2	C(14)—C(13)—H(131)	114.6
C(9)—N(10)—H(10)	105.5	C(12)—C(13)—H(132)	117.8
C(11)—N(10)—H(10)	108.5	C(14)—C(13)—H(132)	114.1
C(14)—N(10)—H(10)	109.6	H(131)—C(13)—H(132)	78.8
N(10)—C(11)—H(111)	104.6	N(10)—C(14)—H(141)	107.8
C(12)—C(11)—H(111)	109.6	C(13)—C(14)—H(141)	112.2
N(10)—C(11)—H(112)	108.5	N(10)—C(14)—H(142)	106.1
C(12)—C(11)—H(112)	112.5	C(13)—C(14)—H(142)	116.6
H(111)—C(11)—H(112)	116.4	H(141)—C(14)—H(142)	109.3
C(11)—C(12)—H(121)	117.8		
The water molecule			
WH(1)—O(1)—WH(2)	105		

*Estimated standard deviations average 0.03 Å for the distances and, except for H—X—H, 1.6° for the angles. For H—X—H the error estimates average 2.5°.

the aromatic plane was 89.5° from the plane of the double bond.

As with the other antihistaminic drugs studied by the X-ray crystallographic method the conformation about the C(8)—C(9) bond is *trans*. In the present case the N(10)—C(9)—C(8)—C(7) torsion angle is 162.5° (refer to Fig. 2).

The pyrrolidino group as a whole is not planar, although the four carbon atoms do define a good plane with equation $-0.0575x - 0.3633y - 0.9299z = -3.7422$. The largest displacement of a defining atom is 0.02 Å from this plane but N(10) is 0.46 Å out of the plane. The conformation of this ring could therefore be designated "E" (envelope) (20). An alternative description, although one that tends to obscure the essence of the conformation, may be given in terms of the torsion angles about the five bonds of this system. These torsion angles are: N(10)—C(11)—C(12)—C(13) = 16.1°, C(11)—C(12)—C(13)—C(14) = 2.5°, C(12)—C(13)—C(14)—N(10) = −20.1°, C(13)—C(14)—N(10)—C(11) = 30.0°, and C(14)—N(10)—C(11)—C(12) = 28.6°.

The centers of symmetry of this space group ($P2_1/c$) fall into two non-equivalent classes and these are the loci of important intermolecular bonding interactions. Figure 3 portrays the immediate environment of centers equivalent to that at the origin. The water molecule is involved in two hydrogen bonds to chloride ions and each chloride ion is hydrogen bonded to two waters as well as the protonated nitrogen atom of the pyrrole ring. This cluster of polar bonding forces is instrumental in linking together the various molecules of this structure and may be seen in the stereoscopic Fig. 4. The N^+—H···Cl^- bond is 3.094(3) Å in length and has an angular deviation from linearity of 1.1° at the hydrogen atom.

The arrangement of pyridyl rings around those inversion centers equivalent to that at the center of the cell represents another intermolecular bonding interaction which contributes to the stability of the crystals. The stacking of these aromatic systems is clearly seen near the viewer and slightly above the middle of Fig. 4. These planes are parallel and are separated by 3.466(3) Å, the displacement of their centroids is 4.004(3) Å and the closest approach of non-hydrogen atoms is the 3.533(3) Å between C(3′) and its inverted equivalent.

Inspection of Fig. 4 reveals another interesting point; the hydrogen bond and the π orbital overlap linkages are both from the same side of the

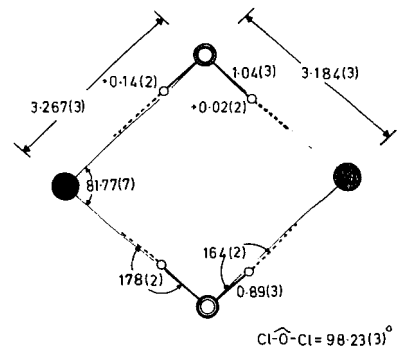

FIG. 3. A drawing showing the immediate environment of one class of inversion centers in the crystals of triprolidine hydrochloride monohydrate.

molecule. Because the antihistamine receptor site is presumed to bind the antagonist via the pyridyl ring and the tertiary nitrogen atom this observation is probably important. The observed geometries of four diaryl antihistamines in five different crystallographic environments are shown in Fig. 5. In each of these one side of the molecule is exposed and bears chemical entities to which both hydrogen bond and π orbital overlap linkages may be formed. Although the identity of the π electron binding group varies, it is thought to be the thenyl group in histadyl, the distance between the saturated nitrogen atom and the centroid of the exposed aromatic ring remains reasonably constant over the five structures. For the molecules of Fig. 5 these distances are 6.212, 6.154, 6.013, 6.47, and 5.93 Å for parts *a*,*b*,*c*,*d*, and *e* respectively. Because these drugs bind to the same site (22) they must have some similar structural features and it is thought that the above similarities probably reflect this common chemotherapeutic denominator.

At least three spatially distinct drug/receptor interactions are necessary to explain the stereoselectivity exhibited by the histamine H1 receptor (23, 24) and the only reasonable candidate through which the third interaction may occur is the remaining aromatic ring. Because of the paucity of antihistaminically active drugs with nonaromatic substituents in positions equivalent to that of the tolyl group in triprolidine another π overlap linkage is implicated here.

A fully extended histamine molecule ion has the centroid of its aromatic system separated by 4.94 Å from its alkylamine nitrogen atom (calculated from data given in ref. 25), and so cannot be expected to bind to the H1 site in the same

Can. J. Chem. Downloaded from www.nrcresearchpress.com by 210.87.254.6 on 09/05/12
For personal use only.

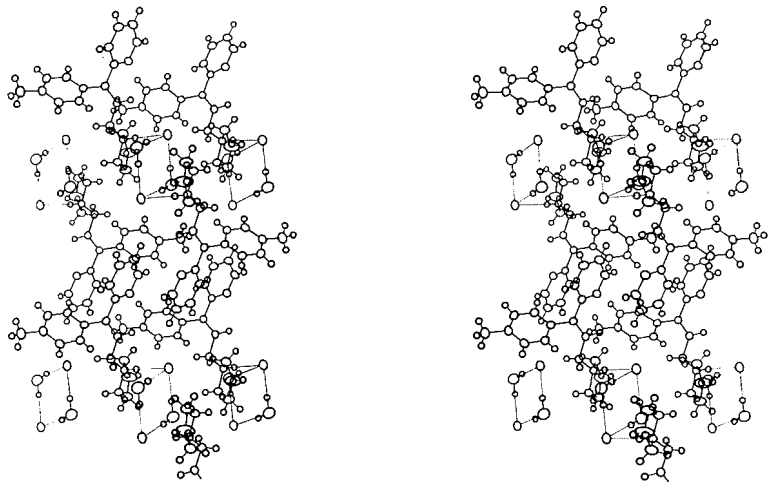

FIG. 4. A stereoscopic pair packing diagram for triprolidine hydrochloride monohydrate. This is a computer produced diagram (21) and the viewer's line of sight is parallel to the *b* axis.

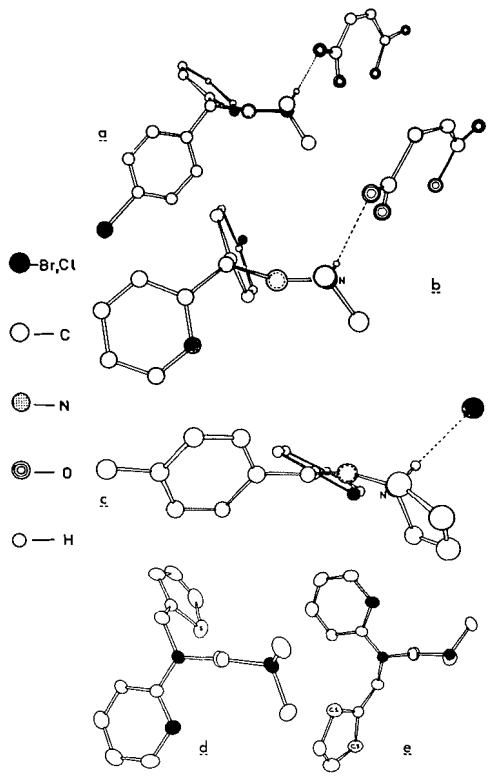

FIG. 5. A composite diagram showing five antihistaminic molecules viewed in the C(9)—C(8) (C_α—C_β) bond direction. The structures labeled *a*, *b*, and *c* are brompheniramine maleate (15), chlorpheniramine maleate (16), and triprolidine, respectively. The two independent molecules of histadyl (27) are denoted *d* and *e*. The thenyl ring of the histadyl molecule in *e* is disordered in the crystal and so the two atoms denoted C, S refer to carbon and sulfur atoms in these positions (27).

manner as an antihistamine molecule. Because of this fact, and also because of the greatly different physiological responses induced by the two classes of drugs, a flexible receptor protein is proposed which adopts different conformations when histamine and an antihistamine are bound (26).

We thank Drs. A. F. Casy and R. R. Ison for the sample used in this study and for their continued interest in this work. Mr. L. Goulden's photographic work is gratefully acknowledged. The crystallographic computer programs of Dr. F. R. Ahmed, National Research Council of Canada, Ottawa have been invaluable in this work. One of us (G.J.B.W.) thanks the University of Alberta for the award of Teaching Assistantships and Intersession bursaries during the course of his Ph.D. studies, of which this work forms a part. This research was supported from grant (#MA-3406) to M.N.G.J. from the Medical Research Council of Canada.

1. A. F. CASY and A. P. PARULKAR. Can. J. Chem. **47**, 423 (1969).
2. R. R. ISON. Ph.D. Thesis. University of Alberta, Edmonton, Alberta. 1970.
3. A. F. CASY and R. R. ISON. J. Pharm. Pharmacol. **22**, 270 (1970).
4. D. W. ADAMSON, P. A. BARRETT, J. W. BILLINGHURST, and T. S. G. JONES, J. Chem. Soc. 2315 (1957).
5. R. PEPINSKY, J. RATHLEV, and J. W. TURLEY. Acta Cryst. **11**, 295 (1958).
6. L. B. KIER. J. Med. Chem. **11**, 441 (1968).
7. U. W. ARNDT and B. T. M. WILLIS. Single crystal diffractometry. Cambridge University Press, Cambridge, U.K. 1966. pp. 173–174.
8. S. W. PETERSON and H. A. LEVY. Acta Cryst. **10**, 70 (1957).
9. P. D. CRADWICK. Ph.D. Thesis, University of Alberta, Edmonton, Alberta. 1969.

Can. J. Chem. Downloaded from www.nrcresearchpress.com by 210.87.254.6 on 09/05/12
For personal use only.

10. P. G. SIMPSON, R. D. DOBROTT, and W. N. LIPSCOMB. Acta Cryst. **18**, 169 (1965).
11. D. T. CROMER and J. B. MANN. Acta Cryst. A**24**, 321 (1968).
12. D. T. CROMER and D. LIBERMAN. J. Chem. Phys. **53**, 1891 (1970).
13. R. F. STEWART, E. R. DAVIDSON, and W. T. SIMPSON. J. Chem. Phys. **42**, 3175 (1965).
14. F. R. AHMED, M. E. PIPPY, S. R. HALL, and C. P. HUBER. N.R.C. crystallographic programs for the IBM/360 system, world list of crystallographic computer programs. 2nd ed. Appendix p. 52, program NRC12. Bronder-Offset, Rotterdam, Holland. 1966.
15. M. N. G. JAMES and G. J. B. WILLIAMS. J. Med. Chem. **14**, 670 (1971).
16. M. N. G. JAMES and G. J. B. WILLIAMS. Can. J. Chem. This issue.
17. L. PAULING. The nature of the chemical bond. 3rd ed. Cornell University Press, Ithaca, N.Y. 1960.
18. L. E. SUTTON, (*Editor*). Tables of interatomic distances and configuration in molecules and ions. The Chemical Society, London, U.K. Special Publication No. 18. 1965.
19. C. J. FRITCHIE and A. F. WELLS. Chem. Commun. 917 (1968).
20. British Carbohydrate Nomenclature Committee, Rules for conformation nomenclature for five- and six-membered rings in carbohydrates and their derivatives. J. Chem. Soc. D, 505 (1973).
21. C. K. JOHNSON. ORTEP, report ORNL-3794. Oak Ridge National Laboratory, Oak Ridge, Tennessee. 1965.
22. (*a*). P. B. MARSHALL. Brèt. J. Pharmacol. **10**, 270 (1955). (*b*) C. BOTRÉ, M. MARCHETTI, C. DEL VECCHIO, G. LIONETTI, and A. MEMOLI. J. Med. Chem. **12**, 832 (1969).
23. F. E. ROTH and N. M. GOVIER. J. Pharmacol. Exp. Ther. **124**. 347 (1958).
24. D. T. WITIAK, Z. MUHI-ELDEAN, N. MAHISHI, O. P. SETHI, and M. C. GERALD. J. Med. Chem. **14**, 24 (1971).
25. M. V. VEIDIS, G. J. PALENIK, R. SCHAFFRIN, and J. TROTTER. J. Chem. Soc. B, 2659 (1969).
26. G. J. B. WILLIAMS. Ph.D. Thesis. The University of Alberta, Edmonton, Alberta. 1972.
27. G. R. CLARK and G. J. PALENIK. J. Am. Chem. Soc. **94**, 4005 (1972).

Can. J. Chem. Downloaded from www.nrcresearchpress.com by 210.87.254.6 on 09/05/12
For personal use only.

Secondary Isotope Effects on the Ionization of 2-Nitropropane[1]

A. J. KRESGE, D. A. DRAKE, AND Y. CHIANG

Department of Chemistry, Illinois Institute of Technology, Chicago, Illinois 60616

Received October 11, 1973

The equilibrium isotope effect on the acid dissociation of 2-nitropropane in wholly aqueous solution at 25° was found to be $K_H/K_D = 1.23 \pm 0.03$ for complete deuteration of both methyl groups; the kinetic isotope effect for reaction of the same substrate with hydroxide ion, $k_H/k_D = 1.09 \pm 0.01$; and the kinetic isotope effect for reaction with tris-(hydroxymethyl)-methylamine, $k_H/k_D = 1.10 \pm 0.01$; both of the latter also refer to wholly aqueous solution at 25° and are for complete deuteration of both methyl groups. It is shown that the equilibrium isotope effect is largely, and the kinetic isotope effects probably partly, hyperconjugative in origin, thus supporting a hyperconjugative explanation of the anomalous effect of methyl groups on nitroalkane ionization.

Il a été prouvé que l'effet de l'équilibre de l'isotope sur la dissociation acide du nitro-2 propane dans une solution entièrement aqueuse à 25° est $k_H/k_D = 1.23 \pm 0.03$ pour une deutériation complète des deux groupes méthyles; l'effet cinétique de l'isotope pour une réaction du même substrat avec l'ion hydroxyde est $k_H/k_D = 1.09 \pm 0.01$; et l'effet cinétique de l'isotope pour une réaction suivie avec le tris-(hydroxyméthyl)-méthylamine est $k_H/k_D = 1.10 \pm 0.01$; les deux derniers se rapportent aussi à une solution entièrement aqueuse à 25° et sont pour une deutériation complète des deux groupes méthyles. On a prouvé que l'effet de l'équilibre de l'isotope est essentiellement d'hyperconjugaison à l'origine, tandis que les effets cinétiques de l'isotope le sont en partie probablement; ainsi on est favorable à une explication par voie d'hyperconjugaison de l'effet anormal des groupes méthyles sur l'ionisation des nitroalcanes. [Traduit par le journal]

Can. J. Chem., **52**, 1889 (1974)

Methyl groups are usually electron-donating relative to hydrogen when introduced into molecules in solution, and their consequent acid-weakening properties are well known. Methyl substitution at the α position of nitroparaffins, however, has quite the opposite effect; for example, in the simple series nitromethane, $pK_a = 10.22$ (1), nitroethane, $pK_a = 8.60$ (1), and 2-nitropropane, $pK_a = 7.74$ (2), a marked increase in acidity accompanies methyl substitution.

This unusual behavior was attributed some time ago to hyperconjugative stabilization of the C—N double bond in nitronate ions (eq. 1); this

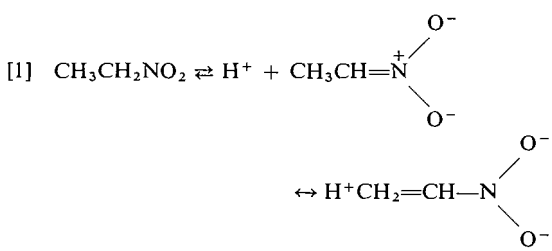

[1] $CH_3CH_2NO_2 \rightleftarrows H^+ + CH_3CH{=}N^+(O^-)(O^-) \leftrightarrow H^+CH_2{=}CH{-}N(O^-)(O^-)$

effect might be especially important here because the nitrogen end of the double bond is positively charged and therefore electron deficient (3). This explanation is supported by the fact that methyl substitution has a normal, *i.e.* acid-weakening, effect on the ionization of the *aci*-nitro tautomers of these substances (eq. 2): in this case, the double bond and positive charge exist in the acids as well as in the nitronate ions, and the effect of hyperconjugation on this equilibrium should thus cancel (4).

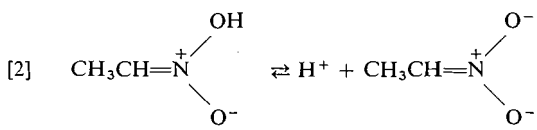

[2] $CH_3CH{=}N^+(OH)(O^-) \rightleftarrows H^+ + CH_3CH{=}N^+(O^-)(O^-)$

Hyperconjugation generally leads to sizeable secondary hydrogen isotope effects (5). In order to test this explanation, we have therefore measured the secondary isotope effect on nitroalkane ionization. We used 2-nitropropane and its 1,1,1,3,3,3-hexadeutero analog for this purpose, and determined the isotope effect on the rate of proton loss as well as on the acidity constant. Both kinetic and equilibrium isotope effects proved to be quite small, but they do support the

[1]This research was supported by grants from the National Science Foundation (GP-23578) and the Petroleum Research Fund of the American Chemical Society (5215-AC4).

Can. J. Chem. Downloaded from www.nrcresearchpress.com by 210.87.254.42 on 09/05/12
For personal use only.

hyperconjugative explanation. Their magnitude, moreover, is consistent with the results of a correlation of literature data on nitroalkane ionization which shows the hyperconjugative interaction to be rather weak.

Experimental

Materials

2-Nitropropane-1,1,1,3,3,3-d_6 was prepared by treating deuterated isopropyl bromide, obtained from hexadeuteroacetone (Stohler, 99.5 atom % D) via isopropyl alcohol (6), with sodium nitrite (7). In a typical synthesis, 33 g of sodium nitrite, 33 g of phloroglucinol, and 37 g of urea, all dried at 105° for 24 h, were added to a solution of 36 g of isopropyl-d_6 bromide in 230 ml reagent-grade dimethyl formamide. This mixture was stirred magnetically in a closed flask at room temperature for 72 h, during which time it changed from pale yellow to deep red-brown in color. The reaction mixture was then poured into 1.2 l of water, and the resulting solution was extracted with four 150 ml portions of ether. Ether was removed from the combined extracts and the residue was distilled rapidly at 15 mm pressure into a receiver cooled by a Dry Ice – acetone slurry. The distillate, about 5 ml, was washed first with 25 ml saturated aqueous sodium chloride solution and then with 0.5 ml concentrated sulfuric acid; it was then redistilled under reduced pressure. This gave 3.5 g of 2-nitropropane-d_6 (13% yield) containing no impurities detectable by n.m.r. or v.p.c.; the isotopic purity as shown by n.m.r. was 99.2%.

Ordinary 2-nitropropane was prepared in the same way from commercial isopropyl bromide, and samples of this were used for the kinetic and equilibrium measurements. All other substances were best available commercial grades. Solutions were prepared using deionized water which had been purified further by distillation from alkaline permanganate in glass apparatus.

Equilibrium Measurements

The position of equilibrium between 2-nitropropane and its acid dissociation products was measured by making use of the fact that the absorption band of the nitro compound at $\lambda_{max} = 202$ nm, $\varepsilon = 4.7 \times 10^3\ M^{-1}\ cm^{-1}$, is changed to $\lambda_{max} = 222$ nm, $\varepsilon = 11.8 \times 10^3\ M^{-1}\ cm^{-1}$, in the nitronate anion. The long-wavelength shoulder of the nitronate-ion band from 230 to 240 nm, where the nitro compound has negligible absorption, was used to estimate the concentration of the ionized form, and the concentration of unionized nitro compound was then obtained by difference. Total concentrations were determined for this purpose by measuring the absorbance of stock aqueous solutions of nitro compound at 200–205 nm where only the unionized form absorbs; the extent of dissociation of 2-nitropropane was negligible in these solutions at the concentrations employed (*ca.* $10^{-4}\ M$).

Measurements were made in tris-(hydroxymethyl)-methylamine buffers at an ionic strength of 0.10 *M* and buffer ratios ([BH^+]/[B]) of 1.0 and 2.0 The half-life of the ionization reaction in these solutions is of the order of 5 h; reaction mixtures were therefore allowed to equilibrate for 3 days in a constant temperature bath operating at 25.0 ± 0.02°. At the end of this time, aliquots were withdrawn and absorbance readings were taken (Cary 15 spectrometer) at 1 nm intervals over the region 230 to 240 nm. Each of these absorbances was then converted into a concentration, and the average of those was used to calculate the ratio of ionized to unionized forms of the nitro compound.

Absorbance readings were converted into concentrations with the aid of extinction coefficients determined for the normal and deuterated nitro compounds dissolved in water and for their nitronate ions in 0.10 *M* aqueous sodium hydroxide. No significant difference in extinction coefficient was found for the two unionized species over the region investigated, 200 to 210 nm. The two nitronate ions likewise had identical extinction coefficients in the vicinity of λ_{max}; at 222 nm, for example, $\varepsilon_H/\varepsilon_D = 1.0025 \pm 0.0085$ (average of six determinations). Beyond this region, however, the extinction coefficient of the deuterated ion was found to drop with increasing wavelength more rapidly than the extinction coefficient of the normal species: at 230 nm, $\varepsilon_H/\varepsilon_D = 1.058 \pm 0.006$ and at 240 nm, $\varepsilon_H/\varepsilon_D = 1.134 \pm 0.012$.

Kinetic Measurements

Rates of ionization of 2-nitropropane were determined spectroscopically by following the increase of absorbance due to nitronate ion. Experiments were done in sodium hydroxide solutions and in tris buffers; in both cases, the base concentration was varied but the ionic strength of the solutions was kept constant through the addition of sodium chloride.

For the runs in sodium hydroxide, aqueous base contained in a 1 cm quartz cuvette was first brought to thermal equilibrium with the thermostatted (25.0 ± 0.1°) cell compartment of the spectrometer (Cary 15). Enough of a 5% alcoholic solution of nitro compound to make the reaction mixture *ca.* $10^{-4}\ M$ in substrate was then added, and the absorbance at 225 nm was recorded for 3–4 half-lives (5–10 min). Infinity readings were taken after 8–10 half-lives, and rate constants were evaluated visually as slopes of plots of log $(A_\infty - A)$ *vs.* time.

The reactions in tris buffers, on the other hand, were much slower ($t_{1/2}$ = *ca.* 1 day), and an initial rate method was therefore used here. Appropriate volumes of substrate and buffer solutions, previously brought to 25.0°, were combined, and an aliquot of the resulting mixture was transferred to a cuvette and placed in the thermostatted cell compartment of the spectrometer. The absorbance at 235 nm was then recorded for *ca.* 10 min, which corresponded to about 1% reaction, and zero-order rate constants were calculated from the slopes of these linear traces. These zero-order constants were then transformed into first-order rate constants by dividing by the initial concentration of the nitro compound in the reaction mixture (*ca* $5 \times 10^{-3}\ M$).

Results

The equilibrium measurements are summarized in Table 1. The p*K* values listed there refer to the concentration quotients $[H^+][A^-]/[HA]$, with HA = 2-nitropropane and A^- = the corresponding nitronate anion, in tris-(hydroxymethyl)-methylamine buffers at an ionic

Can. J. Chem. Downloaded from www.nrcresearchpress.com by 210.87.254.42 on 09/05/12
For personal use only.

Can. J. Chem. Downloaded from www.nrcresearchpress.com by 210.87.254.42 on 09/05/12
For personal use only.

TABLE 1. Secondary isotope effect on the acid dissociation of 2-nitropropane[a]

Buffer ratio[b]	pK^c	
	$(CH_3)_2CHNO_2$	$(CD_3)_2CHNO_2$
1.0	7.449, 7.464	7.560, 7.561
	7.471, 7.495	7 605, 7.611
2.0	7.465, 7.471	7.535, 7.538
	7.489, 7.495	7.555, 7.561
	Av: 7.475 ± 0.006[d]	7.566 ± 0.010[d]
	$K_H/K_D = 1.233 \pm 0.033$[d]	

[a]Measured in tris-(hydroxymethyl)-methylamine buffers at 25°; ionic strength = $[BH^+Cl^-] = 0.10$ *M*.
[b]Buffer ratio = $[BH^+]/[B]$.
[c]At $\mu = 0.10$ *M*.
[d]Error limits are standard deviations of mean values.

strength of 0.10 *M*. The concentrations [HA] and $[A^-]$ were measured as described above, and $[H^+]$ was calculated using 8.069 as the pK_a of tris-(hydroxymethyl)-methylammonium ion (8) making no activity coefficient corrections; *i.e.* the activity coefficients of the tris-(hydroxymethyl)-methylammonium and hydrogen ions were assumed to be equal and that of the unprotonated amine was taken as unity. These assumptions are not unreasonable at the ionic strength employed (0.10 *M*), and they are supported by the fact that the result obtained for the normal substrate, when combined with activity coefficients calculated using the formula $\log \gamma_\pm = -0.5\mu^{1/2}/(1 + \mu^{1/2}) + 0.1\mu$, gives 7.70 as the zero-ionic strength pK_a of 2-nitropropane, in good agreement with the published value 7.74 (2).

These assumptions, of course, have little effect on the isotope effect, for measurements on the normal and the deuterated substrate were always made in identical buffers of the same p*H*; any uncertainty in $[H^+]$ would therefore cancel in the ratio of equilibrium constants K_H/K_D. The activity coefficients of 2-nitropropane and its nitronate ion, moreover, are likely to be unaffected by isotopic substitution, and the activity coefficients of these species will therefore also cancel in the ratio K_H/K_D. Thus, although the present measurements were made at $\mu = 0.10$ *M*, the result obtained, $K_H/K_D = 1.23 \pm 0.03$, is likely to be a very good approximation to the zero-ionic strength value of this isotope effect.

The results of the kinetic measurements are given in Tables 2 and 3. In the experiments using hydroxide ion to remove a proton from 2-nitropropane, the hydroxide ion concentration was always at least two orders of magnitude greater than the concentration of nitro compound, and the second-order rate constants of Table 2 were therefore obtained simply by dividing observed first-order specific rates by hydroxide ion concentrations. These data show no sensible variation in second-order rate constant with hydroxide ion concentration for either substrate. Linear least-squares fitting of first-order specific rates to hydroxide ion concentrations likewise gave good correlations with zero intercepts in both cases. The bimolecular rate constants obtained as slopes in the latter analysis were not significantly different from the simple averages given in Table 2, as was also the isotope effect: $k_H/k_D = 1.086 \pm 0.007$ (linear least squares) *vs.* 1.088 ± 0.005 (averages). The present value of k_H, $0.355 \pm 0.002\ M^{-1}\ s^{-1}$, is somewhat higher than $0.316 \pm 0.014\ M^{-1}\ s^{-1}$ obtained in a recent previous measurement at an ionic strength of 0.20 *M* (9), but agrees well with the result of another recent study at an unspecified ionic strength, $0.34 \pm 0.01\ M^{-1}\ s^{-1}$ (10).

In the experiments using tris-(hydroxymethyl)-methylamine buffers, the concentration of buffer base was again at least an order of magnitude greater than the substrate concentration. These reactions, moreover, were followed only to about 1% completion, and here again it is therefore permissible to consider the base concentration constant during a kinetic run. Second-order rate constants were evaluated by least-squares analysis as slopes of plots of observed first-order rate constants *vs.* tris-(hydroxymethyl)-methylamine concentration. The results for the two buffer ratios are in good agreement; they lead to $k_H/k_D = 1.092 \pm 0.008$ as the best value of the isotope effect for proton transfer from 2-nitropropane to tris-(hydroxymethyl)-methylamine.

The intercepts obtained in these least squares analyses of the buffer data represent the small amount of reaction which occurs through hydroxide ion in these solutions. The hydroxide ion concentrations of the buffers were therefore estimated and hydroxide ion rate constants were evaluated. It was again assumed that there is no ionic strength effect on the dissociation of tris-(hydroxymethyl)-methylammonium ion and that the effect on the ionization of water can be estimated with activity coefficients obtained from the formula $\log \gamma_\pm = -0.5\ \mu^{1/2}/(1 + \mu^{1/2}) + 0.1\mu$. The results are in reasonable agreement

TABLE 2. Secondary isotope effect on the rate of reaction of 2-nitropropane with hydroxide ion[a]

	k, M^{-1} s^{-1}	
[NaOH], M	$(CH_3)_2CHNO_2$	$(CD_3)_2CHNO_2$
0.0258	0.353, 0.353, 0.360	0.325, 0.326, 0.328
0.0418	0.358, 0.360, 0.367	0.327, 0.327, 0.328
0.0628	0.346, 0.346	0.325, 0.326, 0.328
0.0837	0.353, 0.354, 0.355	0.321, 0.323
0.1046	0.351, 0.354, 0.355	0.325
	Av.: 0.3546±0.0015	0.3258±0.0006
	k_H/k_D = 1.088±0.005	

[a]At 25°; ionic strength maintained at 0.10 M with NaCl; error limits are standard deviations of mean values.

TABLE 3. Secondary isotope effect on the reaction of 2-nitropropane with tris-(hydroxymethyl)-methylamine[a]

	10^5 k, s^{-1}	
[TRIS], M	$(CH_3)_2CHNO_2$	$(CD_3)_2CHNO_2$
[BH$^+$]/[B] = 0.20		
0.0100	0.700, 0.702, 0.704	0.645, 0.648, 0.652
0.0200	1.03, 1.04, 1.05	0.972, 0.972, 0.977
0.0300	1.39, 1.40, 1.40	1.28, 1.28, 1.29
0.0400	1.71, 1.71, 1.72	1.57, 1.58, 1.58
	10^5 k_H(s^{-1}) = (0.363±0.007) + (34.0±0.3)[B]	
	10^5 k_D(s^{-1}) = (0.347±0.006) + (30.9±0.2)[B]	
	k_H/k_D = 1.087±0.010	
[BH$^+$]/[B] = 0.10		
0.0100	0.99, 1.01, 1.01	0.93, 0.94, 0.95
0.0200	1.34, 1.34, 1.35	1.26, 1.26, 1.26
0.0300	1.69, 1.70, 1.72	1.58, 1.58, 1.59
0.0400	2.04, 2.04, 2.04	1.91, 1.91, 1.91
	10^5 k_H(s^{-1}) = (0.649±0.007) + (34.9±0.3)[B]	
	10^5 k_D(s^{-1}) = (0.618±0.004) + (32.1±0.1)[B]	
	k_H/k_D = 1.100±0.012	
	k_H/k_D (weighted average) = 1.092±0.008	

[a]At 25°; ionic strength maintained at 0.10 M with NaCl; error limits are standard deviations of mean values.

with the values measured directly in sodium hydroxide solutions: for the normal substrate, k_{HO} = 0.331 (B.R. = 0.1) and 0.370 (B.R. = 0.2) as compared to 0.355 (NaOH), and for the deuterated species, k_{HO} = 0.315 (B.R. = 0.1) and 0.354 (B.R. = 0.2) as compared to 0.326 (NaOH).

Discussion

Isotope effects

Secondary isotope effects of the magnitude observed here are known to be vibrational in origin, *i.e.* to be the result of changes in the force constants, and therefore the strength, of the isotopically substituted bonds. There is less certainty about the mechanisms which produce the necessary differences in bond strength, but four effects seem to have been fairly well identified; these involve changes in (1) hyperconjugative interaction, (2) polar effect,[2] (3) steric crowding, and (4) hybridization (itself perhaps a steric effect).

Bond hybridization in the methyl groups of 2-nitropropane does not change during the ionization reaction, and differences in hybridiza-

[2]This is better known as inductive effect. That name, however, has been rendered rather inaccurate by recent work which indicates that polar effects in molecules are transmitted by field and not inductive mechanisms (11). We suggest, therefore, that the more general term "polar effect" be used for this source of secondary hydrogen isotope effects.

Can. J. Chem. Downloaded from www.nrcresearchpress.com by 210.87.254.42 on 09/05/12
For personal use only.

Can. J. Chem. Downloaded from www.nrcresearchpress.com by 210.87.254.42 on 09/05/12
For personal use only.

tion can therefore be ruled out as a possible cause of the isotope effects observed here. It is also unlikely that these isotope effects are steric in origin, even though it may be argued that the methyl groups move apart and thus relieve back strain as the carbon atom to which they are bound changes from tetrahedral to trigonal during the ionization process. An isopropyl group, such as that in the system here, is certainly less crowded than a *t*-butyl group, and a strong case has been made out against any steric contribution to the secondary isotope effect on *t*-butyl chloride solvolysis (12). Even the solvolysis of neopentyldimethylcarbinyl chloride, a process quite definitely aided by strong steric acceleration, shows no steric isotope effect (13).

It is quite likely, on the other hand, that polar effects do make a significant contribution to the present isotope effects. The generation of charge and its subsequent redistribution which accompany nitroalkane ionization are not unlike those occurring in the ionization of carboxylic acids, where small but significant secondary isotope effects of polar origin have been found. For example, $K_H/K_D = 1.035$ for the pair CH_3CO_2H and CD_3CO_2H (14), and $K_H/K_D = 1.04$ for $(CH_3)_3CCO_2H$ and $(CD_3)_3CCO_2H$ (15).

It is possible to estimate the magnitude of the polar contribution in the present case by using the results of a recent critical survey of the relatively small number of authentic examples of this kind of isotope effect (16). This study, following an idea proposed earlier (15), correlated these isotope effects with the Taft equation and showed that the CD_3 group has an effective sigma constant of -0.011,[3] *i.e.* $\log K_D/K_H = -0.011\rho$. Values of ρ for the equilibrium ionization of nitroalkanes containing substituents capable only of polar interaction with the reaction center are available from the correlations described below. These vary from 0.12 to 0.40 and provide isotope effect estimates in the range $K_H/K_D = 1.006$ to 1.021 for two CD_3 groups. Somewhat larger values of ρ have been obtained in correlations of acidity constants of α-aryl nitroalkanes (18): for *meta* and *para* substituted phenylnitromethanes, $\rho = 0.83$ which leads to $K_H/K_D = 1.043$, whereas for similarily substituted 1-phenylnitroethanes, $\rho = 1.03$ and K_H/K_D becomes 1.054.

These estimates differ considerably among themselves, but they are nevertheless consistent in showing that changing polar effects can account for only a minor portion of the equilibrium isotope effect observed here, $K_H/K_D = 1.23 \pm 0.03$. This leaves changes in hyperconjugative interaction as the sole major cause of this effect.

The origin of the kinetic isotope effect is less clear. Not enough rate data are available for a Taft correlation of substrates with substituents capable only of polar interaction with the reaction center, but values of ρ for kinetic correlations of the two α-aryl nitroalkane series mentioned above have been made (18). For arylnitromethanes reacting with hydroxide ion, $\rho = 1.28$ which leads to $k_H/k_D = 1.067$ for two CD_3 groups; and for the same reaction of 1-arylnitroethanes, $\rho = 1.18$ which gives $k_H/k_D = 1.062$. Correlations for these substrates reacting with various amine bases have also been made (18); the ρ's range from 0.93 to 1.08 and the isotope effects, from 1.048 to 1.056.

These estimates approach the experimental values, $k_H/k_D = 1.09 \pm 0.01$ and 1.10 ± 0.01 (Tables 2 and 3), and that leaves little room for hyperconjugative contributions to these isotope effects. It is possible, however, that these estimates of the polar contribution may be too large, for they use ρ's based upon correlations of substrates which contain substituents capable of resonance as well as polar interaction with the reaction center; in the acidity constant correlations, these substrates gave ρ's consistently greater than those in which resonance interactions were not possible. A proportionate reduction in ρ for the kinetic situation would lower these polar isotope effect estimates to the point where hyperconjugative contributions became important. Any such reduction, however, still leaves the polar effect with a greater share of the isotope effect on the rate than on the equilibrium, which is in good agreement with the hypothesis that negative charge builds up on the α-carbon atom while the proton is being transferred but is largely delocalized onto the nitro group once the nitronate ion is fully formed (19).

This analysis leads to the conclusion that much of the equilibrium isotope effect found here

[3]This value should not be interpreted in the usual polar effect way, *i.e.* it should not be taken to mean that CD_3 is electron donating relative to CH_3, for that would imply different potential energy surfaces for the CH_3 and CD_3 groups in violation of the Born–Oppenheimer approximation. A better explanation is that polar effects in the rest of the molecule operate upon the methyl group in such a way as to cause an increase in negative charge to lower the force constants of the carbon–hydrogen bonds, and that makes $K(CH_3) > K(CD_3)$ (17).

TABLE 4. Correlations of nitroalkane acid dissociation constants

Substrate	$\Sigma\sigma^*$	n	N	$-\log K_a/p^a$ Obsd.	Calcd. Eq. 3[b]	Calcd. Eq. 4[c]
1. $(CH_3)_2CHNO_2$	0.000	6	−0.59	7.74[d,e]	7.87	8.45
2. $CH_3CH_2CH(CH_3)NO_2$	−0.100	5	−0.59	8.38[f]	8.26	8.46
3. $CH_3CH_2NO_2$	0.490	3	0	8.90[g]	8.76	8.95
4. $CH_3CH_2CH_2NO_2$	0.390	2	0	9.28[e]	9.15	8.96
5. $CH_3CH_2CH_2CH_2NO_2$	0.375	2	0	9.16[f]	9.15	8.96
6. $(CH_3)_2CHCH_2NO_2$	0.300	1	0	9.51[h]	9.53	8.97
7. $(CH_3)_2CHCH_2CH_2NO_2$	0.365	2	0	8.86[h]	9.16	8.96
8. $C_6H_5CH_2CH_2NO_2$	0.705	2	0	9.08[i]	9.04	8.92
9. $CNCH_2CH_2NO_2$	1.790	2	0	8.61[j]	8.66	8.79
10. $NO_2CH_2CH_2CH_2NO_2$	0.990	2	0	9.00[j]	8.94	8.89

[a]The K_a values are for wholly aqueous solution at 25°; p is a statistical factor equal to the number of equivalent dissociable protons in the nitroalkane.
[b]Calculated using $K_a/p = -7.87 + 0.35\Sigma\sigma^* + 0.35\ (n - 6)$; this correlation does not include CH_3NO_2.
[c]Calculated using $K_a/p = -9.00 + 0.12\Sigma\sigma^* - 0.94\ (N)$; this correlation does include CH_3NO_2.
[d]Reference 2(*a*).
[e]Reference 2(*b*).
[f]Reference 26.
[g]Reference 1.
[h]Reference 27.
[i]Reference 28.
[j]Reference 29.

is hyperconjugative in origin, and perhaps significant portions of the kinetic effects are as well. The present effects, however, are much weaker than isotope effects generally attributed to hyperconjugation tend to be. For example, the limiting solvolysis of isopropyl tosylate gives $k_H/k_D = 2.1$ for two CD_3 groups (20). But methyl groups stabilize carbonium ions much more strongly than they do carbon–nitrogen double bonds: the change in pK_a along the series nitromethane, nitroethane, 2-nitropropane (1, 2), shows the effect on C—N double bonds to be about 2 kcal/mol, whereas methyl group stabilization of carbonium ions, though difficult to evaluate precisely for these species in solution, is certainly an order of magnitude greater (21). It seems likely that this greater stabilization is the result of stronger hyperconjugative interaction as well as an increased polar effect, and a greater hyperconjugative isotope effect is therefore to be expected. In support of this explanation is the fact that secondary isotope effects on the hydrolysis of diethyl ketals, which have been attributed to hyperconjugation, are quite small: k_H/k_D ranges from 1.10 to 1.25 for four to six deuterium atoms (22); the carbonium ion produced in the rate-determining step here is stabilized by first-order conjugation with an ethoxy group, and the demand for hyperconjugative interaction is consequently diminished.

Multiple Correlations

Direct evidence for the weakness of the hyperconjugative interaction in nitronate ions, and additional support for its existence, may be obtained by analyzing literature data on nitroalkane dissociation constants. The values collected in Table 4 are limited to substrates which cannot interact with the reaction center by first-order conjugation. These data show no sensible relationship of the form $\log K_a/p = a + \rho^*\Sigma\sigma^*$: least squares analysis gives a correlation coefficient of only 0.174. However, when an additional term designed to allow for differences in hyperconjugation is added (eq. 3) (23), a relationship

$$[3] \qquad \log K_a/p = a + \rho^*\Sigma\sigma^* + (n - 6)h$$

with a correlation coefficient of 0.990 is obtained which reproduces the data with a standard deviation in K_a of 40%. In this treatment, n is the number of hydrogens in hyperconjugable position, *i.e.* attached to carbons β to the nitro group, and h is the magnitude of the hyperconjugative interaction. The value of h obtained, 0.35 ± 0.04, corresponds to 0.48 ± 0.05 kcal/mol per C—H bond or about 1.5 kcal/mol per methyl group. This is a rather weak interaction. It is in fact similar to the value obtained from an analogous treatment of heats of hydrogenation of *trans* disubstituted ethylenes: 0.44 ± 0.05 kcal/mol per C—H bond (23), which suggests

Can. J. Chem. Downloaded from www.nrcresearchpress.com by 210.87.254.42 on 09/05/12
For personal use only.

Can. J. Chem. Downloaded from www.nrcresearchpress.com by 210.87.254.42 on 09/05/12
For personal use only.

that the interaction in nitronate ions is with an effectively neutral center, *i.e.* the formal positive charge on nitrogen does not increase the amount of hyperconjugative electron release. The value of ρ^*, which measures the polar part of the interaction, is also small: 0.35 ± 0.11; this reinforces the idea that the $-NO_2^-$ group presents an essentially uncharged aspect to substituents attached to the α carbon atom of nitronate ions.

It is interesting that the acidity constant of nitromethane does not fit this three-parameter correlation very well. The experimental value exceeds that calculated from the relationship based upon the ten substrates of Table 4 by an entire pK unit: pK_a(obsd) = 10.22 (1) and pK_a(calcd) = 9.17. Inclusion of nitromethane in the correlation increases the standard deviation in K_a to 120% (from 40%) and also raises the uncertainties in the ρ^* and h parameters (without, however, changing their values significantly): $\rho^* = 0.36 \pm 0.24$ *vs.* 0.35 ± 0.11 and $h = 0.44 \pm 0.08$ *vs.* 0.35 ± 0.04. The calculated pK_a of nitromethane, 9.48, now agrees with the experimental value somewhat better, but the difference is still by far the largest deviation of the entire correlation. This suggests that the published acidity constant of nitromethane may be in error.

Dewar has lately questioned the importance of hyperconjugation, and has advanced alternative explanations for the phenomena generally taken as evidence in its support (24). In particular, he has successfully accounted for differences in the heats of hydrogenation of unsaturated hydrocarbons on the assumption that the energies of C—H and C—C bonds depend upon the state of hybridization of the carbon atoms involved and, in the case of C—H bonds, also on whether the bond is primary or secondary or tertiary (25). This analysis, when extended to the nitroalkane – nitronate ion equilibrium, places the substrates of Table 4 into two categories: those with one α hydrogen atom (entries 1 and 2) and those with two α hydrogens (entries 3 through 10), and it makes the prediction that the ionization reactions of the nitroalkanes in the first category will be less endothermic than those of the substrates in the second by 0.81 kcal/mol. Normal polar effects will, of course, introduce further differences among the members of each category, but these should be proportional to the sum of sigma constants for the substituent groups. We have therefore tested this model by fitting the data of Table 4 to eq. 4 with $N = -0.81/2.3RT$ for the first category defined above and $N = 0$ for the second. The

$$[4] \qquad \log K_a/p = a + \rho^*\Sigma\sigma^* + b(N)$$

result is a relationship with a correlation coefficient of 0.972 which reproduces the data with a standard deviation in K_a of 80%. The value of ρ^* is 0.40 ± 0.19 and $b = 2.17 \pm 0.41$. The latter puts the free energy of ionization of substrates in the first category 1.75 ± 0.32 kcal/mol below that of those in the second, which is in the right direction and in reasonable, if not good, quantitative agreement with the 0.81 kcal/mol predicted by the recommended bond energy changes.

It is interesting that nitromethane fits into this treatment much better than it did the correlation based upon eq. 3. Bond energy changes put this substrate into a separate category with $N = 2.94/2.3RT$. Use of this datum along with the values listed in Table 4 now gives a relationship with a slightly improved correlation coefficient, 0.975 *vs.* 0.972, although the standard deviation in K_a is somewhat larger, 130% *vs.* 80%. The uncertainty in ρ^* has gone up, 0.12 ± 0.24 *vs.* 0.40 ± 0.19, while that in b is down, 0.94 ± 0.18 *vs.* 2.17 ± 0.41, and the calculated pK_a of nitromethane, 10.44, now agrees well with the experimental value, 10.22. What is perhaps most significant of all, however, is the fact that the value of b is now not significantly different from unity, 0.94 ± 0.18, which means that the calculated energy separations of the three categories are in excellent agreement with predicted values.

It would appear, therefore, that the acidity constants of nitroalkanes fit Dewar's bond energy model just as well as a hyperconjugative scheme. It is difficult to see, however, how the bond energy model, at least without modification, can lead to secondary isotope effects. Dewar, in his critique (24), did consider the evidence for hyperconjugation from secondary isotope effects and found it wanting in several respects. In particular, he pointed out that isotopic substitution in a position from which hyperconjugation is not possible, *i.e.* α to the leaving group in the substrate of a carbonium ion forming reaction, also produces isotope effects, and he noted that steric and polar (inductive) explanations of secondary isotope effects had been proposed. In the decade following Dewar's analysis, it has become clear that α-hydrogen isotope effects are the result of

changes in hybridization, and the scope of steric and polar isotope effects has been defined. As a result, secondary isotope effects now occupy the position of providing some of the strongest evidence in support of hyperconjugation. Since the isotope effects observed here cannot be fully understood in other than hyperconjugative terms, they would seem to indicate that hyperconjugation does play a role in nitroalkane ionization, and that the hyperconjugative correlation is therefore to be preferred over the Dewar model.

1. R. G. PEARSON and R. L. DILLON. J. Am. Chem. Soc. **75**, 2439 (xo5).
2. (*a*) D. TURNBULL and S. H. MARON. J. Am. Chem. Soc. **65**, 212 (1943). (*b*) G. W. WHELAND and J. FARR. J. Am. Chem. Soc. **65**, 1433 (1943).
3. C. K. INGOLD. Structure and mechanism in organic chemistry. Cornell University Press, Ithaca, New York. 1st ed. 1953. p. 559; 2nd ed. 1969. p. 821.
4. A. STREITWIESER, JR. and J. H. HAMMONS. Prog. Phys. Org. Chem. **3**, 43 (1965).
5. Isotope effects in chemical reactions. *Edited by* C. J. Collins and N. S. Bowman. Van Nostrand Reinhold Co., New York, N.Y. 1970.
6. A. MURRAY and D. L. WILLIAMS. Organic synthesis with isotopes. Part II. Interscience Publishers, New York, N.Y. 1958. p. 1482.
7. N. KORNBLUM. Org. React. **12**, 101 (1962).
8. S. P. DATTA, A. K. GRYBOWSKI, and B. A. WESTON. J. Chem. Soc. 792 (1963).
9. R. P. BELL and D. M. GOODALL. Proc. R. Soc. Ser. A, **294**, 273 (1966).
10. A. T. KUHN. Part II Thesis. Oxford University, 1960. Quoted in ref. 9.
11. R. GOLDEN and L. M. STOCK. J. Am. Chem. Soc. **94**, 3080 (1972); C. L. LIOTTA, W. F. FISHER, G. H. GREEN, JR., and B. L. JOYNER. J. Am. Chem. Soc. **94**, 4891 (1972); L. M. STOCK. J. Chem. Educ. **49**, 400 (1972).
12. E. K. THORNTON and E. R. THORNTON. *In* Isotope effects in chemical reactions. *Edited by* C. J. Collins and N. S. Bowman. Van Nostrand Reinhold Co., New York, N.Y. 1970. p. 263 ff.
13. J. G. JEWETT and R. P. DUNLAP. J. Am. Chem. Soc. **90**, 809 (1968).
14. M. PAABO, R. G. BATES, and H. S. KLEIN. J. Phys. Chem. **70**, 540 (1966).
15. A. STREITWIESER, JR. and H. S. KLEIN. J. Am. Chem. Soc. **85**, 2759 (1964).
16. D. J. BARNES and J. M. W. SCOTT. Can. J. Chem. **51**, 411 (1973).
17. E. R. THORNTON. Ann. Rev. Phys. Chem. **17**, 349 (1966).
18. F. G. BORDWELL and W. J. BOYLE, JR. J. Am. Chem. Soc. **94**, 3907 (1972).
19. A. J. KRESGE. Can. J. Chem. This issue.
20. A. STREITWIESER, JR. and G. A. DAFFORN. Tetrahedron Lett. 1263 (1969).
21. D. BETHELL and V. GOLD. Carbonium ions, an introduction. Academic Press, New York, N.Y. 1967. Chapts. 4 and 5.
22. V. J. SHINER, JR. and S. CROSS. J. Am. Chem. Soc. **79**, 3599 (1957).
23. R. W. TAFT, JR. and M. M. KREEVOY. J. Am. Chem. Soc. **79**, 4011 (1957).
24. M. J. S. DEWAR. Hyperconjugation. Ronald Press, New York, N.Y. 1962.
25. M. J. S. DEWAR and H. N. SCHMEISING. Tetrahedron, **5**, 166 (1959); **11**, 96 (1960).
26. A. TALVIK, V. TIMOTHEUS, and H. TIMOTHEUS. Org. React. **4**, 478 (1967).
27. V. PIHL, V. TIMOTHEUS, A. PIHL, and A. TALVIK. Org. React. **2**, No. 2, 16 (1965).
28. S. HIIDMAA, A. PIHL, and A. TALVIK. Org. React. **3**, No. 2, 62 (1966).
29. A. TALVIK, H. TIMOTHEUS, E. LOODMAA, and V. TIMOTHEUS. Org. React. **8**, 409 (1971).

Can. J. Chem. Downloaded from www.nrcresearchpress.com by 210.87.254.42 on 09/05/12
For personal use only.

The Nitroalkane Anomaly[1]

A. J. KRESGE

The Department of Chemistry, Illinois Institute of Technology, Chicago, Illinois 60616

Received October 11, 1973

The effect of substituents on the reaction of nitroalkanes with base is analyzed in terms of two interactions which influence both rate and equilibrium constants and two others which affect the rates alone. The results of these calculations serve to explain the Brønsted relation with negative exponent given by data for the series nitromethane, nitroethane, and 2-nitropropane reacting with hydroxide ion, and also the Brønsted exponents greater than unity recently observed for the reactions of aryl-substituted nitroalkanes with hydroxide ion and other bases.

L'effet des substituants sur la réaction de nitroalcanes avec des bases est analysé en termes de deux interactions qui influencent et la constante de vitesse et la constante d'équilibre et deux autres qui affectent les vitesses seulement. Les résultats de ces calculs permettent d'expliquer la relation de Brønsted avec l'exposant négatif donné par les résultats obtenus pour la série nitrométhane, nitroéthane et nitro-2 propane qui réagissent avec l'ion hydroxide et aussi les exposants de Brønsted plus grand que l'unité qui ont été observés récemment pour les réactions de nitroalcanes substitués par des groupes aryles avec l'ion hydroxide et d'autres bases.

[Traduit par le journal]

Can. J. Chem., **52**, 1897 (1974)

Can. J. Chem. Downloaded from www.nrcresearchpress.com by 210.87.254.105 on 09/05/12
For personal use only.

Substituents usually have parallel effects on the rate and equilibrium constants of the same reaction. This is not true, however, of the neutralization of simple nitroalkanes by hydroxide ion (eq. 1).

[1] $R_2CHNO_2 + HO^- \rightleftarrows R_2CNO_2^- + H_2O$

For example, methyl substitution along the series nitromethane, nitroethane, and 2-nitropropane slows the rate of this reaction by nearly two orders of magnitude while changing its equilibrium constant in the opposite direction by a somewhat greater factor.

The data upon which this particular example of the nitroalkane anomaly is based have been in the literature for some time (1). Quite recently, however, they received renewed interest when it was pointed out that they lead to a Brønsted relation with a negative exponent (2), and when other more extensive series of nitroalkanes were discovered which gave Brønsted relations with exponents greater than unity (2, 3).

Brønsted exponents outside the limits zero to one present certain difficulties. They lead, for example, to the situation where a proton transfer reaction is acid-catalyzed (or base-catalyzed) in both directions. This follows from the fact that the sum of Brønsted exponents for a proton transfer and its reverse (eq. 2) must be unity: $\alpha + \beta = 1$. With α greater than one, $k_A = G_A(K_A)^\alpha$, and the rate of the forward reaction increases with increasing acidic properties (K_A)

$$[2] \qquad S + HA \underset{k_B}{\overset{k_A}{\rightleftarrows}} SH + B$$

$$k_A = G_A(K_A)^\alpha;\ k_B = G_B(K_B)^\beta = G_B'(K_A)^{-\beta}$$

of the proton donor, *i.e.* the forward reaction is acid-catalyzed. But now, since $\alpha + \beta = 1$, β must be negative, and $k_B = G_B(K_B)^{-\beta} = G_B'(K_A)^\beta$; this has k_B also increasing with the acidic, and not the basic, properties of the proton acceptor, and the reverse reaction is acid-catalyzed as well. With α negative, similar arguments lead to base-catalyzed proton transfer in both directions.

Before the discovery of values less than zero and greater than one, it was widely believed that Brønsted exponents measured transition state structure, and in particular that they were numerically equal to the fractional extent of proton transfer at the transition state of the reaction being correlated. Exponents outside the range zero to one are clearly incompatible with this idea.

Brønsted exponents less than zero and greater

[1]This research was supported by grants from the National Science Foundation (GP-23578) and the Petroleum Research Fund of the American Chemical Society (5215-AC4).

TABLE 1. Kinetic and equilibrium data for the reaction of nitroalkanes with hydroxide ion at 25°

Substrate	pK_a	k_{HO^-} (ref. 8) $M^{-1}\,s^{-1}$	ΔF^{0a} kcal/mol	$\Delta F^{\ddagger a}$ kcal/mol
CH_3NO_2	10.22 (ref. 6)	27.6	−4.51	16.14
$CH_3CH_2NO_2$	8.60 (ref. 6)	5.19	−6.96	16.89
$(CH_3)_2CHNO_2$	7.74 (ref. 1*b*, *c*)	0.316	−8.54	18.13
	$\delta_R\Delta F^{\ddagger} = +1.00\pm0.25^b$		$\delta_R\Delta F^0 = -2.02\pm0.43^b$	

[a]For substrate + HO^- corrected for symmetry using factors of 3 for CH_3NO_2, 2 for $CH_3CH_2NO_2$, and 1 for $(CH_3)_2CHNO_2$.
[b]Error limits are average deviations.

than one also run into trouble with regard to expected relationships among substituent effects on initial, final, and transition states. Brønsted relations are usually generated by making substituent changes in one of the reaction partners (the catalyst), and it is easy to show that the Brønsted exponent is then equal to the substituent effect on the free energy of activation, $\delta_R\Delta F^{\ddagger}$, divided by the substituent effect on the standard free energy of reaction, $\delta_R\Delta F^0$ (eq. 3) (4, 5). Since the structural changes which

$$[3] \qquad \alpha = \frac{\delta_R\Delta F^{\ddagger}}{\delta_R\Delta F^0}$$

accompany a chemical reaction occur smoothly and continuously as the system moves from initial state through transition state to final state, the structure of the transition state must be intermediate between the structures of the initial and final states. The interaction of a substituent with the system in the transition state will therefore also be intermediate between its interactions in the initial and final states, and the change which the substituent makes in the free energy of the transition state must thus lie between the changes it makes in the free energies of the initial and final states. It follows from this that $\delta_R\Delta F^{\ddagger}$ will be of the same sign as and less in absolute magnitude than $\delta_R\Delta F^0$, which requires α to be greater than zero and less than one.

This argument, however, assumes that the substituent interacts with the rest of the system in just one way. If there are two or more different kinds of interaction, and if these differ in sign and some lead or lag behind others, then they can easily combine to make $\alpha < 0$ ($\delta_R\Delta F^{\ddagger}$ and $\delta_R\Delta F^0$ of different sign) or $\alpha > 1$ ($\delta_R\Delta F^{\ddagger}$ and $\delta_R\Delta F^0$ similar in sign but $|\delta_R\Delta F^{\ddagger}| > |\delta_R\Delta F^0|$). Moreover, interactions can sometimes occur in the transition state without having initial state or final state counterparts; these contribute to $\delta_R\Delta F^{\ddagger}$ but not to $\delta_R\Delta F^0$ and thus help put α outside the range zero to one.

In this paper, we shall analyze the methyl group substituent effect on the nitroalkane-hydroxide ion reaction and show that four different interactions probably take place. Two of these occur only in the transition state. The net result is to make $\delta_R\Delta F^{\ddagger}$ positive and $\delta_R\Delta F^0$ negative, which makes α less than zero, in agreement with the observed value. One of these interactions, moreover, cannot contribute to the substituent effect in the newly discovered examples of the nitroalkane anomaly, and its omission makes α positive and greater than unity; this again is consistent with experiment.

Results

Experimental data defining the effect of α-methyl substitution along the series nitromethane, nitroethane, and 2-nitropropane are collected in Table 1. Only one of the acid dissociation constants, that for 2-nitropropane, seems to have been redetermined since the early work of Turnbull and Maron (1*b*) and Wheland and Farr (1*c*), whose results are summarized in the compilation by Pearson and Dillon (6). Although the recent value, $pK_a = 7.70$ (7), is in good agreement with the earlier result, $pK_a = 7.74$, it was measured at a much higher ionic strength (0.10 *vs.* 0.004 to 0.007 *M*) and thus includes a less certain activity coefficient correction. The early value is therefore used here. The rates of reaction of these nitroalkanes with hydroxide ion, on the other hand, have been determined several times, the most recent results and those used here being due to Bell and Goodall (8).

The acid dissociation constants were converted into equilibrium constants for the reaction of nitroalkane with hydroxide ion by dividing by the ion product of water, 10^{-14}, and the latter as well as the rate constants were corrected for symmetry using statistical factors (number of ionizable protons) of 3, 2, and 1, respectively, for CH_3NO_2, $CH_3CH_2NO_2$, and $(CH_3)_2CHNO_2$.

Can. J. Chem. Downloaded from www.nrcresearchpress.com by 210.87.254.105 on 09/05/12
For personal use only.

Can. J. Chem. Downloaded from www.nrcresearchpress.com by 210.87.254.105 on 09/05/12
For personal use only.

The results give $\delta_R\Delta F^{\ddagger} = +1.0$ kcal/mol and $\delta_R\Delta F^0 = -2.0$ kcal/mol as the average experimentally observed effects of substitution of one methyl group; this leads to $\alpha = -0.5 \pm 0.1$.

Initial and Final State Interactions

It is well known that the methyl group has an electron-donating and therefore acid-weakening polar effect in solution. Methyl substitution along the series of nitroalkanes of Table 1, however, raises the acidity of these substances, and that implies that some other property of this group must also be operating. It was in fact suggested some time ago that the acid strength of simple nitroparaffins is controlled by hyperconjugative stabilization of the C—N double bond in nitronate ions (**1**) (9), an explanation

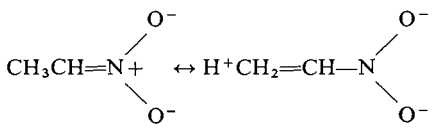

1

supported by the fact that the acidities of the *aci*-nitro tautomers of these substances fall in the normal polar-effect order: here the acids as well as their nitronate-ion conjugate bases contain the C—N double bond and hyperconjugative effects therefore cancel (10). Additional evidence for such a hyperconjugative interaction comes from the recently determined secondary hydrogen isotope effect on the ionization of 2-nitropropane, and a correlation of acid dissociation constants for a number of nitroalkanes is also consistent with this interpretation (7).

This hyperconjugative interaction was evaluated as the difference between the observed substituent effect, $\delta_R\Delta F^0 = -2.0$ kcal/mol, and the polar effect of the methyl group. The latter was estimated by treating the group as a simple linear dipole 1.10 Å in length, *i.e.* as the vector sum of three C—H bonds in a tetrahedral arrangement. Its effective magnitude was calculated from the increase in dipole moment brought about by methyl substitution in nitromethane, *i.e.* from the dipole moments of nitromethane and nitroethane, which are 3.50 and 3.68 *D* in the gas phase and 3.1 and 3.3 *D* in solution (11). The gas phase values give 0.46 *D* and the solution values, 0.50 *D* as the moment of the methyl group; the average of the two results was used.

Since recent investigations favor a field over an inductive mechanism for the transmission of polar effects (12), the polar effect of the methyl group was evaluated as the field (Coulomb) interaction between its dipole and the charges on the atoms of the nitro group. These were taken to be one unit positive charge on nitrogen in both the nitro compound and the nitronate ion and one-half unit negative charge on each oxygen in the nitro compound increasing to a full unit charge in the ion. This corresponds to complete delocalization of charge onto the nitro group in the ion. No direct information seems to be available on this point, but the simplifying assumption used here is consistent with the great acid-strengthening effect of the nitro group, much of which appears to be conjugative in nature (13), and also with the fact that the anion of dipotassium nitroacetate, the only nitronate ion examined by X-ray crystallography, is strictly planar (14). The methyl group dipole was also represented by its point charges, and eq. 4 was used to calculate the energy of interaction, U_{el}, between all pairs of charges, q_i and q_j, separated by distances r_{ij}; the effective dielectric constant, D, was taken to be 2.0 (15).

$$[4] \qquad U_{el} = \sum_{ij} q_i q_j / D r_{ij}$$

Distances were based upon a structure for the nitro compound which was patterned after the known geometry of nitromethane (16*a*): $r_{CN} = 1.475$ Å (16*b*), $r_{NO} = 1.22$ Å (16*a*), $\angle_{ONO} = 127°$ (16*a*), and $\angle_{HCH} = \angle_{HCC} = 109.5°$. The length of the C—N double bond of the nitronate ion was estimated using Pauling's relationship between bond length and bond order (17); the result, $r_{CN} = 1.295$ Å, is consistent with the lengths of the C—N double bonds in dimethylglyoxime, 1.27 Å (16*c*), formamidoxime, 1.301 Å (18*a*), and diazomethane, 1.32 Å (18*b*). The length of the N—O bond was assumed to remain unchanged during the ionization reaction, and bond angles about the α-carbon atom in the nitronate ion were taken to be 120°. The O—N—O angle in the ion was set at 134° on the assumption that the +7° deviation from a regular trigonal value in nitromethane (16*a*) is the result of electrostatic repulsion between the half-unit negative charges on the oxygen atoms: since these charges double in the ion, the angle deviation was doubled also.

The results of this analysis are a stabilizing initial-state interaction between methyl and nitro groups of −0.66 kcal/mol and a destabilizing final-state interaction of +0.54 kcal/mol.

Can. J. Chem. Downloaded from www.nrcresearchpress.com by 210.87.254.105 on 09/05/12
For personal use only.

The net polar contribution to $\delta_R\Delta F^0$ is therefore +1.19 kcal/mol. On the assumption that this and hyperconjugation make up all of the methyl group effect on the equilibrium reaction, the hyperconjugative effect then comes to −3.21 kcal/mol (Table 2).

Transition State Interactions

These polar and hyperconjugative effects will also operate in the transition state of the nitroalkane-hydroxide ion reaction and thus contribute to $\delta_R\Delta F^{\ddagger}$. At the transition state, however, neither interaction will be as great as in the final state, for the C—N double bond will be only partly formed and the negative charge will be only partly transferred from the hydroxide ion to the nitro group. Before the transition state effects can be evaluated, the extent of these partial changes must be determined, *i.e.* the structure of the transition state must be fixed.

Isotope effects are frequently useful in assessing transition state structure, and the fact that the primary hydrogen isotope effect on the present reaction is large (8) indicates that the proton is approximately half transferred. A more quantitative estimate may be obtained from the solvent isotope effect $(k_{HO^-})_{H_2O}/(k_{DO^-})_{D_2O}$; this effect is believed to decrease from unity to a minimum value of *ca.* 1/2.4 in a way (eq. 5) controlled by the fractional extent of proton transfer, x (19). This isotope effect is reported as 1/1.39 (1*a*) and 1/1.40 (20) for nitromethane and 1/1.36 (1*a*) and 1/1.35 (19*b*) for 2-nitropropane; use of the rounded value 1/1.4 in eq. 5 leads to $x = 0.38$.

$$[5] \qquad (k_{HO^-})_{H_2O}/(k_{DO^-})_{D_2O} = (1/2.4)^x$$

A closely similar result may be obtained by simply identifying x with $\Delta F^{\ddagger}/(2\Delta F^{\ddagger} + \Delta F^0)$, *i.e.* with the fraction of the total energy change which the system undergoes in passing from reactants through transition state to products that is complete at the transition state. The data of Table 1 give $x = 0.44$ for nitromethane, $x = 0.42$ for nitroethane, and $x = 0.41$ for 2-nitropropane.

The rounded average of all of these estimates, $x = 0.4$, was used in the present calculations. Accordingly, the order of the forming O—H bond was taken to be 0.4 and that of the breaking C—H bond, 0.6. Pauling's relationship (17) then gave 1.196 Å as the length of the bond being formed and 1.223 Å as that of the bond being broken, for an overall distance of 2.419 Å between the α-carbon atom and the oxygen of the former hydroxide ion. The proton being transferred was assumed to be moving in a plane perpendicular to the plane of the nitro group, at an angle of 101.7° to that plane, which is 40% of the way between regular tetrahedral (initial state) and trigonal (final state) angle values. The remaining bond angles about the α-carbon atom were also taken to be 40% of the way between tetrahedral and trigonal, and the C—N bond order was set at 1.4, which gave it a length, via the Pauling relation, of 1.223 Å.

Forty percent proton transfer implies that 40% of the negative charge formerly on the hydroxide ion has now been shifted onto the nitro compound. The hydroxide ion oxygen atom was therefore given 0.60 unit electronic charge and the rest, 0.4, was distributed over the forming nitronate ion. In the equilibrium calculations, it was assumed that all of the negative charge on the nitronate ion in the final state is delocalized onto the nitro group. It seems unlikely that this will be so in the transition state, for the partial double bond here will be less efficient at delocalizing charge than the fully formed double bond of the final state, and electrostatic attraction between the departing proton and the electron pair of the breaking bond should further inhibit the flow of negative charge away from the α-carbon atom. The charge developing on the nitronate ion in the transition state was therefore taken to be only partly delocalized onto the nitro group.

It is difficult to say just what the actual charge distribution is likely to be. Perhaps the simplest assumption is to equate the extent of delocalization with the π-order of the C—N bond, and

TABLE 2. The effect of an α-methyl group on the reaction of nitroalkanes with hydroxide ion

	Interaction energy, kcal/mol		
		$\delta_R\Delta F^{\ddagger}$	
Interaction	$\delta_R\Delta F^0$	TS-I	TS-II
Field, $CH_3 + NO_2$	+1.194	+0.188	+0.082
Hyperconjugation	−3.214	−1.286	−0.514
Field, $CH_3 + \alpha\text{-}C^-$	—	+0.970	+1.358
Field, $CH_3 + HO^-$	—	+0.591	+0.591
	−2.020	+0.463	+1.516
		$\alpha = -0.23$	−0.75

Can. J. Chem. Downloaded from www.nrcresearchpress.com by 210.87.254.105 on 09/05/12
For personal use only.

calculations were therefore done using such a model (TS-I), *i.e.* with 0.40 of 0.40 = 0.16 excess negative charge on the nitro group and the rest, 0.40 − 0.16 = 0.24, on the α-carbon atom. Delocalization, however, may well be a stronger function of π-bond order, and another set of calculations was therefore carried out with delocalization proportional to the π-order squared (TS-II); this put $(0.40)^2$ of 0.40 = 0.064 unit electronic charge on the nitro group and 0.336 on the α-carbon. The field interactions between these charges and the methyl group dipole were evaluated using eq. 4, and the contributions they make to $\delta_R\Delta F^{\ddagger}$ are listed in Table 2.

It seems reasonable that the hyperconjugative interaction of the methyl group with the C—N bond should also be a function of the π-order of that bond. Here again, however, no information on the exact nature of the relationship seems to exist, and the assumptions made in dealing with charge delocalization were therefore used again: in TS-I the hyperconjugative interaction was taken to be 0.40 of its final state value, and in TS-II, it was set at $(0.40)^2 = 0.16$ of the final state value.

In addition to these two effects, hyperconjugation and the field interaction between methyl and nitro groups, there will be yet two other interactions in the transition state. One of these is the field interaction between the methyl group and the undelocalized charge on the α-carbon atom, and the other is the field interaction between the methyl group and the charge still remaining on the oxygen atom of the former hydroxide ion. Neither of these effects is present in the initial or final state: the first is absent because no charge is assumed to reside on the α-carbon atom in the final state, and the second is absent because the hydroxide ion and nitroalkane have not yet come together in the initial state and because the hydroxide ion has been converted into an uncharged water molecule in the final state. These interactions were also evaluated using eq. 4, and their contributions to $\delta_R\Delta F^{\ddagger}$ are listed in Table 2.

Discussion

These calculations give Brønsted exponents which, like the observed value, are negative: α = −0.23 for TS-I and α = −0.75 for TS-II. The calculated results, moreover, bracket the experimental value, α = −0.5 ± 0.1, and their average is in fact equal to it.

This agreement, however, must be regarded as fortuitous, for the calculations contain a number of arbitrary features. Their significance lies not so much in their ability to reproduce experimental fact, but rather in the insight they provide into Brønsted relations, especially the demonstration that Brønsted exponents outside the range zero to one can be the natural result of reasonable combinations of quite ordinary substituent effects.

The data of Table 2 show that the negative Brønsted exponents which result from these calculations are produced by an interplay of polar and hyperconjugative effects. Only one polar interaction, a destabilizing effect, operates on the equilibrium process; it is weaker than the stabilizing hyperconjugative interaction, and the methyl group effect here consequently is dominated by hyperconjugation. In the transition state, two additional polar interactions come into play; both are destabilizing, and they combine with the other polar interaction to give a total polar effect which is now stronger than hyperconjugation. This makes the sign of the substituent effect on the rate process different from that on the equilibrium, and that in turn requires α to be negative.

It is interesting that omitting hyperconjugation from both $\delta_R\Delta F^{\ddagger}$ and $\delta_R\Delta F^0$ not only raises α above zero but also makes it greater than unity: α = 1.46 for TS-I and α = 1.70 for TS-II, for these values are similar to the Brønsted exponents obtained in the newly discovered examples of the nitroalkane anomaly (2, 3). In that work, substituent changes were made by introducing groups into the meta or para positions of benzene rings situated α or β to the nitro group, as, for example, in $ZC_6H_4CH_2NO_2$ or $ZC_6H_4CH_2CH(CH_3)NO_2$. Since the alkyl chains were not altered, hyperconjugation did not change along a given series, and it consequently made no contribution to $\delta_R\Delta F^{\ddagger}$ or $\delta_R\Delta F^0$. Resonance effects were also either weak or absent, and steric effects were constant. Thus, only polar interactions could contribute significantly to the substituent effects on both the rates and the equilibria. Since charge builds up on the α carbon atom in the transition state of this reaction before being delocalized away from the substituent onto the nitro group in the final state, and since the substituent sees the charge

Can. J. Chem. Downloaded from www.nrcresearchpress.com by 210.87.254.105 on 09/05/12
For personal use only.

on the base only in the transition state, it is reasonable that the polar interactions would be stronger in the transition state than in either the initial state or the final state; this, as the data of Table 2 show, makes α greater than unity.

This explanation is consistent with the fact that α becomes less anomalous in these systems, *i.e.* it decreases from 1.5 to 1.3 in the $ZC_6H_4CH_2NO_2$ series and from 1.1–1.2 to 0.9–1.0 in the $ZC_6H_4CH(CH_3)NO_2$ series (*3a*), when the hydroxide ion proton acceptor is replaced by weaker, amine, bases. These weaker acceptors will make the reaction less exothermic, and the transition state will therefore move to a later position along the reaction coordinate. The result will be a more fully developed C—N double bond, which will allow more charge delocalization, reducing the negative charge density on the α carbon atom and lowering the corresponding polar interaction. The polar contribution to $\delta_R\Delta F^{\ddagger}$ will also be reduced in these amine systems because the charge type of these bases is different from that of the hydroxide ion: this part of the transition state is now positively rather than negatively charged, and the polar interaction between the substituent and this charge will therefore oppose rather than reinforce the rest of the polar effect.

Two of the polar interactions listed in Table 2 operate only in the transition state and consequently play an important role in making α anomalous. Leaving them out gives α completely unremarkable values: $\alpha = 0.54$ for TS-I and $\alpha = 0.21$ for TS-II. The experimental equivalent of this situation may be approached by putting the substituent to be changed in the base rather than in the nitro compound. This converts the former intermolecular interaction between the substituent and the base into an intramolecular effect, and that gives it an initial or final state counterpart, *i.e.* the substituent can now interact with charge on the base in either the initial state or final state as well as in the transition state. The other interaction, that involving charge on the α carbon atom, will in this case still be without an initial or final state counterpart, but it should be much weaker than before because the substituent, being now in the base, is likely to be at a greater distance from the charge. The third polar interaction, that between the substituent and the charges on the nitro group, formerly intramolecular but now intermolecular, can also occur only in the transition state. However, it too will be weak because of the greater distances involved. The overall result will be a transition state effect dominated by the interaction of charge on the base with a substituent also in the base. In such a situation, $\delta_R\Delta F^{\ddagger}$ is unlikely to exceed $\delta_R\Delta F^0$, and α will be non-anomalous, *i.e.* between zero and one. It is significant in this connection that Brønsted relations for proton transfer from nitro compounds to a variety of amine, carboxylate ion, and phenoxide ion bases, constructed keeping the nitro compound constant but changing the base, have exponents which lie in the range 0.50 to 0.65 (*3b*, 21).

Even though these Brønsted exponents are non-anomalous, they are not necessarily equal to the extent of proton transfer at the transition states of these reactions, x, identified here with the order of the forming bond. For α to be equal to x, intermolecular interactions must make a negligible contribution to $\delta_R\Delta F^{\ddagger}$, and the charge distribution in the base must follow the bonding changes closely; the charge with which the substituent interacts must in fact be a linear function of x. It seems unlikely that these conditions will be met exactly. Intermolecular interactions, especially energy-lowering effects in flexible systems, are likely to be significant if small (4), and the redistribution of charge within the base will almost certainly be non-linear in x if charge delocalization takes place. Should the substituent undergo resonance as well as polar interactions with the rest of the system, further differences between α and x are likely to result. It would seem therefore that α will not in general be an accurate measure of x.

Anomalous Brønsted relations have also been discussed by Marcus in terms of his rate theory (22). He came to the conclusion that α would be normal and a good measure of x as long as the structural changes made along a reaction series did not alter its intrinsic barrier, *i.e.* did not produce changes in the free energy of activation without effecting corresponding changes in the standard free energy of reaction. This is equivalent to barring interactions which contribute to $\delta_R\Delta F^{\ddagger}$ without affecting $\delta_R\Delta F^0$, and is thus consistent with the conclusions reached here. Marcus states further, however, that, in systems involving proton transfer between pseudo acids, such as nitro or carbonyl compounds, and normal oxygen or nitrogen bases, structural variations in the base are unlikely to change the intrinsic barrier; Brønsted exponents obtained

from correlations constructed keeping the pseudo acid constant but changing the base should therefore be good measures of x. The present analysis, however, suggests that even in situations such as this, α may not reflect x very accurately.

1. (*a*) S. H. MARON and V. K. LA MER. J. Am. Chem. Soc. **60**, 2588 (1938); (*b*) D. TURNBULL and S. H. MARON. J. Am. Chem. Soc. **65**, 212 (1943); (*c*) G. W. WHELAND and J. FARR. J. Am. Chem. Soc. **65**, 1433 (1943).
2. F. G. BORDWELL, W. J. BOYLE, JR., J. A. HAUTALA, and K. C. YEE, J. Am. Chem. Soc. **91**, 4002 (1969); F. G. BORDWELL, W. J. BOYLE, JR., and K. C. YEE. J. Am. Chem. Soc. **92**, 5926 (1970); M. FUKYAMA, P. W. K. FLANAGAN, F. T. WILLIAMS, JR., L. FRAINIER, S. A. MILLER, and H. SHECHTER. J. Am. Chem. Soc. **92**, 4689 (1970).
3. (*a*) F. G. BORDWELL and W. J. BOYLE, JR. J. Am. Chem. Soc. **93**, 512 (1971); (*b*) **94**, 3907 (1972).
4. A. J. KRESGE, H. L. CHEN, Y. CHIANG, E. MURRILL, M. A. PAYNE, and D. S. SAGATYS. J. Am. Chem. Soc. **93**, 413 (1971).
5. A. J. KRESGE. J. Am. Chem. Soc. **92**, 3210 (1970); J. E. LEFFLER and E. GRUNWALD. Rates and equilibria of organic reactions. John Wiley and Sons, New York. 1963. p. 156.
6. R. G. PEARSON and R. L. DILLON. J. Am. Chem. Soc. **75**, 2439 (1953).
7. A. J. KRESGE, D. A. DRAKE, and Y. CHIANG. Can. J. Chem. This issue.
8. R. P. BELL and D. M. GOODALL. Proc. Roy. Soc. A, **294**, 273 (1966).
9. C. K. INGOLD. Structure and mechanism in organic chemistry. Cornell Univ. Press, Ithaca, N.Y. 1953. p. 559.
10. A. STREITWIESER, JR. and J. H. HAMMONS. Prog. Phys. Org. Chem. **3**, 43 (1965).
11. C. P. SMYTH. Dielectric behavior and structure. McGraw-Hill, New York, N.Y. 1955. p. 253.
12. R. GOLDEN and L. M. STOCK. J. Am. Chem. Soc. **94**, 3080 (1972); C. L. LIOTTA, W. F. FISHER, G. H. GREEN, JR., and B. L. JOYNER. J. Am. Chem. Soc. **94**, 4891 (1972); L. M. STOCK. J. Chem. Ed. **49**, 400 (1972).
13. D. J. CRAM. Fundamentals of carbanion chemistry. Academic Press, New York, N.Y. 1965. pp. 52, 58.
14. D. S. SUTOR, F. J. LLEWELLYN, and H. S. MASLEN. Acta Cryst. **7**, 145 (1954).
15. H. A. SCHERAGA. Adv. Phys. Org. Chem. **6**, 130 (1968).
16. Tables of atomic distances and configurations in molecules and ions. Special publication No. 11. The Chemical Society, London. 1958. (*a*) p. M 113. (*b*) p. S 16. (*c*) p. M 170.
17. L. PAULING. J. Am. Chem. Soc. **69**, 542 (1947); H. S. JOHNSTON. Gas phase reaction rate theory. Ronald Press, New York, N.Y. 1966. p. 81.
18. Tables of atomic distances and configurations in molecules and ions. Supplement. 1956–1959. Special publication No. 18. The Chemical Society, London. 1965. (*a*) p. M 65s. (*b*) p. M 61s.
19. (*a*) R. L. SCHOWEN. Prog. Phys. Org. Chem. **9**, 275 (1972); (*b*) V. GOLD and S. GRIST. J. Chem. Soc. Perkin II, 89 (1972).
20. P. JONES, J. L. LONGRIDGE, and W. F. K. WYNNE-JONES. J. Chem. Soc. 3606 (1965).
21. R. G. PEARSON and F. V. WILLIAMS. J. Am. Chem. Soc. **76**, 258 (1954); M. J. GREGORY and T. C. BRUICE. J. Am. Chem. Soc. **89**, 2327 (1967); J. E. DIXON and T. C. BRUICE. J. Am. Chem. Soc. **92**, 905 (1970); D. J. BARNES and R. P. BELL. Proc. Roy. Soc. Ser. A, **318**, 421 (1970).
22. R. A. MARCUS. J. Am. Chem. Soc. **91**, 7224 (1969).

Can. J. Chem. Downloaded from www.nrcresearchpress.com by 210.87.254.105 on 09/05/12
For personal use only.

Redetermination of the Mössbauer ^{119}Sn Chemical Shifts in K, Cs, and Cu Hexafluostannates

FRANK W. D. WOODHAMS AND R. ALAN HOWIE

Departments of Natural Philosophy and Chemistry, University of Aberdeen, Aberdeen AB9 2UE, Scotland

AND

OSVALD KNOP

Department of Chemistry, Dalhousie University, Halifax, Nova Scotia B3H 3J5

Received June 6, 1973[1]

The Mössbauer ^{119}Sn chemical shifts in $K_2SnF_6.H_2O$, Cs_2SnF_6, and $CuSnF_6.4H_2O$ have been redetermined. All three values, and the value for SnP_2O_7, are close, lying within 0.1 mm/s, and they define the lowest points on the ^{119}Sn chemical shift scale known to-date. The small differences in the shifts reflect the degree of hydration of the hexafluostannates.

Les déplacements isomériques de ^{119}Sn dans les spectres Mössbauer de $K_2SnF_6.H_2O$, Cs_2SnF_6 et $CuSnF_6.4H_2O$ ont été redéterminés. Leurs valeurs, ainsi que celle trouvée pour SnP_2O_7, diffèrent au maximum de 0.1 mm/s et constituent les plus bas déplacements chimiques de ^{119}Sn connus à ce jour. Les faibles différences dans les déplacements sont le reflet du degré d'hydratation des hexafluostannates.

Can. J. Chem., **52**, 1904 (1974)

In a recent Mössbauer study of SnP_2O_7 (1) some doubt arose about the reliability of the chemical-shift (δ) values reported in the literature for the hexafluostannates. A selection of these δ-values, for compounds closest to the hexafluostannates that we have studied, are given in Table 1; the shifts of other hexafluostannates (see ref. 2) lay in the range of values given in Table 1. In order to compare δ-values reported by different authors it is necessary to express chemical shifts relative to a well-defined standard compound at a specified temperature. Since originally β-Sn was favored as the standard, we have first quoted in Table 1 the shifts relative to this compound. The δ-values from refs. 2 and 3 were already relative to β-Sn; those from refs. 4 and 5 were converted using the authors' own value for $\delta(\beta\text{-Sn})$ relative to their chosen standard. The Lees and Flinn (4) shift for K_2SnF_6 is markedly higher (less negative) than the other δ-values reported, and slightly greater than that observed in SnP_2O_7 (1). The other shifts all agree within their experimental errors, which are, however, relatively large. Consequently it is impossible to determine the position, on the chemical shift scale, of SnP_2O_7 relative to the hexafluostannates with any degree of precision. This was particularly frustrating because the hexafluostannates have the largest negative chemical shifts yet observed in Sn compounds and $\delta(SnP_2O_7)$ was within the range for the hexafluostannates. We therefore decided to redetermine δ in the K, Cs, and Cu compounds using the same apparatus and technique as in ref. 1, thus minimizing the effect of uncertainties in calibration, conversion factors, and the identity of the materials investigated by previous authors.

$K_2SnF_6.H_2O$ was prepared as in ref. 6. It gave an X-ray powder pattern identical with that described there. Cs_2SnF_6, which was prepared as described in ref. 7, was analyzed for Cs and Sn; its powder pattern was similar to those of K_2PtCl_6 and Cs_2SnCl_6. The sample of $CuSnF_6.4H_2O$ was prepared as in ref. 8 and was analyzed for Cu and Sn. The analytical results and the appearance of the crystals agreed well with those reported by Sanchez.

The Mössbauer spectrometer has been described in ref. 9. The spectra were accumulated as mirror images in the first and second 200 channels of the analyzer; each spectrum was analyzed separately. The sources used were ^{119m}Sn in $BaSnO_3$ at room temperature. Their initial intensities were about 5 mCi. Velocity calibration was carried out using ^{57}Fe and the

[1]Revision received January 14, 1974.

Can. J. Chem. Downloaded from www.nrcresearchpress.com by 210.87.254.42 on 09/05/12
For personal use only.

TABLE 1. Mössbauer ^{119}Sn parameters of the hexafluostannates of K, Cs, and Cu*

Compound	Temperature (°K)	δ (mm/s) β-Sn	δ (mm/s) SnO_2 or $BaSnO_3$	Γ (mm/s)	χ^2	Reference
K_2SnF_6	78	−3.20(8)	−0.50(8)			3
	r.t.	−3.15(5)	−0.45(5)			2
		−2.91(3)	−0.43(2)			4
$K_2SnF_6.H_2O$	r.t.		−0.413(8)	0.85(3)	153, 195	This work
	77		−0.390(6)	1.01(2)	164, 181	This work
Cs_2SnF_6	80	−3.2(1)	−0.4(1)			5
		−3.14(8)	−0.44(8)			3
	r.t.		−0.374(8)	0.96(3)	139, 160	This work
	77		−0.281(10)	1.32(4)	201, 209	This work
$CuSnF_6$		−3.05(5)	−0.35(5)			2
$CuSnF_6.4H_2O$	r.t.		−0.456(10)	0.95(2)	225, 289	This work
	77		−0.415(10)	1.08(3)	154, 158	This work

*δ, chemical shift; Γ, line width. The results reported by other authors are given relative to both β-Sn and SnO_2 using the authors' figures for conversion. The results of the present work are given relative to $BaSnO_3$, which has a chemical shift identical to that of SnO_2; the δ values are the averages of the two mirror-image spectra. The standard deviations are in units of the last decimal place and are given with 95% confidence limits. The two χ^2 values refer to the spectra accumulated in channels 0–199 and 200–399 respectively.

data of ref. 10. We have quoted our chemical shifts with respect to $BaSnO_3$ at room temperature to comply with recommendations of the IUPAC (11); values relative to β-Sn are obtained by subtracting 2.570 mm/s, and to α-Sn, by subtracting 1.92 mm/s (4). Absorbers were prepared by dispersing the sample powder in acrylic disks. Each disk contained about 3 mg/cm^2 of natural Sn, so no appreciable thickness effects are expected. X-Ray powder patterns taken of sample powders mounted on the surface of similar acrylic disks were identical to those of the freshly prepared materials, and so were those of sample which had been stored for several months. The spectra showed no quadrupole splitting and were adequately fitted by a single Lorentzian line (for details of fitting procedure see ref. 9). The χ^2 of an acceptable fit was required to lie between the 1 and 99% limits of the χ^2 distribution, *i.e.* between about 150 and 242 spectra with 194 degrees of freedom.

To compare the Mössbauer parameters obtained in this work (Table 1) with the literature δ-values it was necessary to convert the latter from β-Sn to $BaSnO_3$ as reference. We first did this by using our measured value for the β-Sn–$BaSnO_3$ separation of 2.570(8) mm/s. The spread of the literature values remains, of course, unchanged and the Lees and Flinn shift for K_2SnF_6 is still high. However, since the shift for SnO_2, which is known to be identical with that for $BaSnO_3$ within an experimental uncertainty of ±0.02 mm/s, is given by all the authors quoted, we subsequently adjusted the literature values to SnO_2 using the authors' own $\delta(SnO_2)$ values. The results are shown in the fourth column of Table 1. The Lees and Flinn value for $\delta(K_2SnF_6)$ is now in much better agreement with those of the other workers. The improvement is due to the fact that the β-Sn–SnO_2 separation quoted by Lees and Flinn is only 2.48 mm/s compared with the 2.70 mm/s of ref. 3. Fenton and Zuckerman (12) have already previously drawn attention to the wide range of values quoted in the literature for the β-Sn–SnO_2 separation. Our value of 2.570(8) mm/s agrees well with the recent value of Williams and Kocher (13), 2.57(2) mm/s, which is based on a standard N.B.S. sodium nitroprusside dihydrate absorber, and that quoted by Greenwood and Gibb (14), 2.56 mm/s. We are unable to explain the wide range of values reported by other authors. Presumably they represent poor velocity calibration or non-linearity of the velocity scale.

The δ-values for the three hexafluostannates through the series $CuSnF_6.4H_2O$, $K_2SnF_6.H_2O$, Cs_2SnF_6, all lie within a range of less than 0.1 mm/s. This would suggest that the Sn atoms in these compounds occupy sites of the same coordination and similar symmetry, which are well known to be approximately octahedral (15). The change in the δ-value on cooling to 77 °K

Can. J. Chem. Downloaded from www.nrcresearchpress.com by 210.87.254.42 on 09/05/12
For personal use only.

approaches the high temperature limit of the second-order Doppler effect, about 0.07 mm/s over a 200 °K temperature range.

Although the state of hydration of the hexafluostannate samples used by previous authors is uncertain, and in any event not reported, it does not have a major effect on the δ-values. This might be expected, as the water molecule affects the electron density at the Sn nucleus only through F...H—O hydrogen bonds to some of the F atoms in the SnF_6 octahedra. However, the observed small decrease in δ with increasing hydration is consistent with this effect: increasing hydration reduces the donation of electrons from the F atom to which the water molecule is attached, so decreasing the s-electron density at the Sn atom.

The hexafluostannates define the lowest points on the δ scale known to-date. The chemical shift of SnP_2O_7 lies between those of Cs_2SnF_6 and $K_2SnF_6.H_2O$. The degree of covalency in the hexafluostannates and the pyrophosphate must thus be very similar, but considerably less than that of Sn in SnO_2 and $BaSnO_3$ (*cf.* ref. 1 for a more detailed discussion).

1. C.-H. Huang, O. Knop, D. A. Othen, F. W. D. Woodhams, and R. A. Howie. Can. J. Chem. In press.
2. V. F. Sukhoverkhov and B. Z. Dzevitskii. Dokl. Akad. Nauk SSSR, **177**, 611 (1967); (Engl. transl.) **177**, 1089 (1967).
3. V. I. Gol'danskii, E. F. Makarov, R. A. Stukan, T. N. Sumarokova, V. V. Khrapov, and V. A. Trukhtanov. Dokl. Akad. Nauk SSSR, **156**, 400 (1964); (Engl. transl.) **156**, 474 (1964).
4. J. K. Lees and P. A. Flinn. J. Chem. Phys. **48**, 882 (1968).
5. M. Cordey-Hayes. J. Inorg. Nucl. Chem. **26**, 915 (1964).
6. H. Kriegsmann and G. Kessler. Z. Anorg. Allg. Chem. **318**, 266 (1962).
7. R. J. Schmitt, E. L. Grove, and R. D. Brown. J. Am. Chem. Soc. **82**, 5292 (1960).
8. M. M. Sanchez. Acta Salmanticensia, ser. chim. **6**(2), 67 (1963); Chem. Abstr. **60**, 101746 (1964).
9. O. Knop, C.-H. Huang, and F. W. D. Woodhams. Am. Miner. **55**, 1115 (1970).
10. R. S. Preston, S. S. Hanna, and J. Heberle. Phys. Rev. **128**, 2207 (1962).
11. International Union of Pure and Applied Chemistry: Bull. No. 33 (1973), Nomenclature and Conventions for Reporting Mössbauer Spectroscopy.
12. D. E. Fenton and J. J. Zuckerman. Inorg. Chem. **8**, 1771 (1969).
13. D. E. Williams and C. W. Kocher. J. Chem. Phys. **52**, 1480 (1970).
14. N. N. Greenwood and T. C. Gibb. Mössbauer spectroscopy. Chapman and Hall, London, 1971. Table 14.5, p. 391.
15. C. Hebecker, H. G. von Schnering, and R. Hoppe. Naturwiss. **53**, 154 (1966).

Can. J. Chem. Downloaded from www.nrcresearchpress.com by 210.87.254.42 on 09/05/12
For personal use only.

The Relationship Between Ormocastrine and Podopetaline

STEWART MCLEAN AND RENUKA MISRA

Department of Chemistry, University of Toronto, Toronto, Ontario M5S 1A1

Received December 20, 1973

The difficulties that arose when an X-ray crystal structure analysis showed that podopetaline has the structure and stereochemistry previously assigned to ormocastrine have been resolved by showing that ormocastrine is in fact podopetaline hydrochloride. It has also been demonstrated that, of the other three constituents that had been isolated from *O. semicastrata*, 18-epiormosanine was obtained as its hydrochloride but ormosanine and piptanthine were free bases. The pK_a values of the alkaloids have been determined.

Les difficultés qui sont apparues lorsque l'analyse par rayon-X a montré que la podopétaline possède la structure et la stéréochimie qui avaient été antérieurement assignées à l'ormocastrine ont été résolues en prouvant que l'ormocastrine est en fait le chlorhydrate de podopétaline. On a aussi démontré que des trois autres constituants qui ont été extraits de *O. semicastrata*, seul l'épi-18 ormosanine a été obtenu sous forme de chlorhydrate alors que l'ormosanine et la piptanthine étaient obtenus sous forme de bases libres. On a déterminé les valeurs de pK_a des alkaloides. [Traduit par le journal]

Can. J. Chem., **52**, 1907 (1974)

We assigned the structure and relative configuration shown in **1** to a constituent, m.p. 263° (dec.), that we isolated from the seeds of *Ormosia semicastrata* and named ormocastrine (1, 2). Soon afterwards, Hart *et al.* (3) assigned the same structure **1**, now with the absolute configuration shown, to podopetaline on the basis of an X-ray crystal structure analysis of its hydrobromide. Podopetaline, m.p. 77.5–79°, is an alkaloid of *Podopetalum ormondii*, which has also afforded a material identical with ormocastrine. Since our assignments had been based on chemical transformations carried out on the small amount of ormocastrine we had isolated, it seemed that at some point we must have drawn a false conclusion from our results. We were concerned to find the source of this error, particularly since a critical part of our evidence rested on the fate of ormocastrine on hydrogenation and, since the stereochemical conclusions seemed soundly based, ormocastrine served as a link in the extensive network interconnecting stereochemical and structural variants of ormosanine, of which some have already been isolated from natural sources, some have also been synthesized, and some have, so far, been obtained only by synthesis (2, 4).

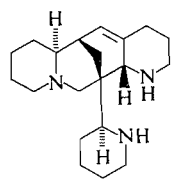

1

As a consequence we have reinvestigated ormocastrine and, on the basis of some of its physical characteristics, we were led to suspect that it was not, after all, a free base but a salt. Neutron activation analysis provided evidence that it contained chlorine in an amount compatible with its being a hydrochloride. It seemed probable, therefore, that we had isolated podopetaline hydrochloride and confirmation of this was obtained by carefully converting a sample of podopetaline to its monohydrochloride by titration in an automatic titrator. Repeated crystallizations of the material available from the two sources provided crystals, m.p. 270–272° (dec.) either separately or on admixture. Titration of ormocastrine with potassium hydroxide solution by the same method converted it to the free base, m.p. 78–80°, which did not depress the melting point of an authentic sample of podopetaline. Ormocastrine is consequently podopetaline hydrochloride and the name podopetaline should therefore be used for the alkaloid. However, since the X-ray analysis securely establishes the structure and stereochemistry of podopetaline, these features are also secure for 'ormocastrine' and assignments based on its relationship to transformation products and congeners are strengthened. These links are now, in fact, more securely forged and the confusion that resulted when it appeared that at least

Can. J. Chem. Downloaded from www.nrcresearchpress.com by 210.87.254.6 on 09/05/12
For personal use only.

Can. J. Chem. Downloaded from www.nrcresearchpress.com by 210.87.254.6 on 09/05/12
For personal use only.

one stereochemical feature in 'ormocastrine' had been misassigned has been removed.

In our isolation of 'ormocastrine' we had extracted it into chloroform from an aqueous solution (hydrochloric acid extract), adjusted to p*H* 10, approximately, (p*H* paper) by addition of base, and we had expected it to be a free base. The amount of material available did not permit a combustion analysis to be carried out, so we resorted to mass spectrometry to determine its formula and there was no sign of any peaks indicative of a molecular weight higher than that of $C_{20}H_{33}N_3$ which appeared to be the parent ion. It is clear now that more caution is required in identifying the nature of materials isolated in small amounts and subjected to structural studies. Our structural assignments to the free base were not in error; 'ormocastrine' is simply not the free base. These results immediately caused us to reexamine the other substances that we isolated from *O. semicastrata*. It is clear now that the ormosanine and piptanthine (m.p. 220°) that we obtained contained no chlorine and were, indeed, free bases. Since our piptanthine melted about 80° above the temperature previously recorded for this alkaloid and we had consequently proposed that we had isolated natural *racemic* piptanthine for the first time, we took particular care to confirm that this was not a salt. On the other hand, the material we described as 18-epiormosanine is a hydrochloride and careful basification of this on the automatic titrator allowed the free base, m.p. 121–122°, to be isolated.

The extraction into an organic phase of two free bases and two closely related hydrochlorides from a basic aqueous phase is unusual. This led us to examine the pK_a values of these alkaloids and, because material was in short supply, we carried the determinations out on a Radiometer automatic titrator and the results are displayed in Table 1. Because of the limitations of the technique used, the values reported are not considered to be uniformly precise but it is believed that they provide a satisfactory picture for purposes of comparison. Podopetaline and 18-epiormosanine exist largely as their salts at p*H* 10 and it is clear that the hydrochlorides of these alkaloids are appreciably soluble in chloroform. The variation in the pK_a values of the alkaloids is undoubtedly related to the stereochemical relationships of the three nitrogens in the molecules; this feature may prove to be of value in making or supporting stereochemical assignments made to alkaloids of this class but the selection of data available is too small at present to lead to useful generalizations.

TABLE 1. pK_a values for alkaloids of *O. semicastrata*

Alkaloid	pK_{a_1}	pK_{a_2}	pK_{a_3}
Ormosanine	5.1	8.0	10.3
Piptanthine	4.5	7.8	9.1
Podopetaline	4.3	8.2	10.6
18-Epiormosanine	4.7	8.0	11.1

Experimental

Melting points were determined on a Thomas-Kofler micro hot stage. Titrations and pK_a determinations were carried out on a Radiometer automatic titrator. The sample (~5 mg) was placed in about 1 ml of water and 0.1 *N* hydrochloric acid was added to bring the solution to p*H* 2. (The hydrochlorides dissolved immediately but the free bases remained in suspension until acidified.) The titrator was then set to carry out the titration with 0.1 *N* aqueous potassium hydroxide and the pK_a values shown in Table 1 correspond to half-neutralization p*H* values calculated from the curves obtained after the correction derived from a blank titration had been applied; at high p*H* values the titration curves showed discontinuities when the free base separated from solution but it is anticipated that the pK_a values are dependable to ± 0.2 units. Interconversion of free bases and monohydrochlorides (see below) was accomplished in a similar manner by using the titrator to bring the p*H* to the required value and then removing the water under high vacuum at low temperature. The residue was triturated with warm chloroform and the product was isolated by evaporation of the solution obtained.

The isolation of four constituents of *O. semicastrata* has been described previously (1). The ormosanine was recrystallized from ether–hexane and a sample, m.p. 175–177°, was analyzed.

Anal. Calcd. for $C_{20}H_{35}N_3$: C, 75.65; H, 11.11. Found: C, 75.60; H, 10.94; (Cl, 0.0).

A sample of the racemic piptanthine, m.p. 220–221° was recrystallized from ethyl acetate.

Anal. Calcd. for $C_{20}H_{35}N_3$: C, 75.65; H, 11.11. Found: C, 75.54; H, 11.00; (Cl, 0.0).

The 18-epiormosanine hydrochloride was recrystallized from methanol–ether; m.p. 275° (this does not appear to be a true m.p. since the sample decomposes at or near this temperature and its appearance depends on the rate of heating).

Anal. Calcd. for $C_{20}H_{36}N_3Cl$: C, 67.86; H, 10.25; Cl, 10.02. Found: C, 67.79; H, 10.09; Cl, 10.13.

A sample of the hydrochloride was converted to the free base (see above) which was recrystallized from acetone–hexane at $-10°$ and obtained as crystals, m.p. 121–122°. Mass spectrum *m/e* (relative intensity): 318 (11), 317 (42), 316 (9), 259 (7), 245 (6), 235 (8), 234 (38), 233 (15), 220 (12), 219 (52), 191 (11), 151 (38), 150 (9), 98 (40), 96 (14), 84 (100), 43 (47), and 32 (82).

The 'ormocastrine' (podopetaline hydrochloride) was recrystallized to constant m.p. from methanol–ether at

−20°. Authentic podopetaline was converted to its monohydrochloride (see above) which was also recrystallized to constant m.p. Both samples separately had m.p. 270–272° (value somewhat dependent on rate of heating since sample decomposes) and this was not depressed for a mixture of the two. The 'ormocastrine' was converted to its free base, which was recrystallized from ether–hexane. This sample had a m.p. 78–80° and did not depress the m.p. of an authentic sample of podopetaline.

We thank Dr. J. A. Lamberton, CSIRO, Melbourne, Australia, for a sample of podopetaline and for information about the progress of this work in his laboratory.

The neutron activation analyses were carried out at the University of Toronto's SLOWPOKE nuclear reactor and we thank Dr. R. G. V. Hancock for his assistance in this area.

Professor T. Hofmann, Department of Biochemistry, University of Toronto, provided us with the use of the Radiometer automatic titrator and valuable assistance in obtaining and interpreting the data.

The financial support of the National Research Council of Canada is gratefully acknowledged.

1. S. McLEAN, P. K. LAU, S. K. CHENG, and D. G. MURRAY. Can. J. Chen. **49**, 1976 (1971).
2. S. McLEAN, M. L. ROY, H.-J. LIU, and D. T. CHU. Can. J. Chem. **50**, 1639 (1972).
3. N. K. HART, S. R. JOHNS, J. A. LAMBERTON, M. F. MACKAY, A. McL. MATHIESON, and L. SATZKE. Tetrahedron Lett. 5333 (1972).
4. Z. VALENTA. Unpublished results.

Can. J. Chem. Downloaded from www.nrcresearchpress.com by 210.87.254.6 on 09/05/12
For personal use only.

Thermodynamics of Ionization of Nitroethane in Water–Ethanol Solvent Mixtures

TAKEKI MATSUI AND LOREN G. HEPLER
Department of Chemistry, The University of Lethbridge, Lethbridge, Alberta
AND
EARL M. WOOLLEY
Department of Chemistry, Brigham Young University, Provo, Utah

Received December 5, 1973

We have made glass electrode measurements that lead to values for the equilibrium constant for acid ionization of nitroethane in water and in aqueous ethanol mixed solvent systems. Calorimetric measurements have led to ΔH^0 values for the acid ionization of nitroethane in water and in aqueous ethanol. These results have been combined to yield $T\Delta S^\circ$ values for the ionization reactions in water and in aqueous ethanol. Our results have also been combined with previously reported equilibrium constants for ionization of water in aqueous ethanol to obtain thermodynamic data for the neutralization of nitroethane in the various solvent systems.

Nous avons effectué des mesures avec des électrodes de verre qui permettent d'établir les valeurs pour la constante d'équilibre de l'ionisation du nitroéthane dans l'eau et dans des systèmes contenant de l'éthanol aqueux. Des mesures calorimétriques ont permis d'établir les valeurs pour le ΔH^0 pour l'ionisation acide du nitroéthane dans l'eau et dans des solutions aqueuses d'éthanol. Ces résultats ont été combinés afin d'en tirer les valeurs $T\Delta S^0$ pour les réactions d'ionisation dans l'eau et dans l'éthanol aqueux. Nos résultats ont aussi été combinés avec des constantes d'équilibre rapportées antérieurement pour l'ionisation de l'eau dans l'éthanol aqueux afin d'en tirer les données thermodynamiques pour la neutralisation du nitroéthane dans divers systèmes de solvant. [Traduit par le journal]

Can. J. Chem., **52**, 1910 (1974)

Introduction

The nitroalkanes are interesting acids for several reasons. First, they are "carbon acids" rather than the more usual —O—H and —N—H acids that have been extensively investigated. The nitroalkanes also exhibit a variety of unusual acid–base properties as already reviewed (1*a*)[1] in connection with a previous investigation of the ionization of several such compounds in pure water as solvent.

Most of the recent investigations of nitroalkanes in solution have been concerned with the related problems of equilibrium constants and rate constants for proton transfer reactions and with acid–base catalysis, in part because of Bronsted coefficients that are outside the "normal" range. Little attention has been paid to the fact that the pK values for ionization of the aqueous nitroalkanes show unusual (1*a*) trends.

Many investigations (2) have shown that enthalpies and entropies can provide useful additions to the understanding gained from free energies in the form of equilibrium constants or rate constants. Various other investigations (3) have demonstrated the utility of similar studies that involve aqueous organic mixed solvent systems. We have therefore extended our earlier work (1*a*) to include electrochemical measurements leading to pK values and calorimetric measurements leading to ΔH^0 values for ionization of nitroethane in various water–ethanol solvent mixtures.

Experimental

All calorimetric measurements were made with an LKB 8700 Precision Calorimetry System used as an ampoule calorimeter. Results are reported in terms of the defined calorie (1 cal = 4.1840 J) and refer to 25.00 ± 0.05 °C.

Electrochemical measurements were made with the Metrohm E436 potentiometric titrator in combination with three different glass electrodes (Beckman 39301, Coleman 3-472, and Fisher 13-639-1) that all led to similar results. All results refer to 25.0 ± 0.1 °C.

Practical grade nitroethane from Baker Chemical

[1]Note that 2-nitropropane and 1-nitropropane have been transposed in Table 3, with the correct arrangment given in ref. 1*b*.

Can. J. Chem. Downloaded from www.nrcresearchpress.com by 210.87.254.105 on 09/05/12
For personal use only.

Can. J. Chem. Downloaded from www.nrcresearchpress.com by 210.87.254.105 on 09/05/12
For personal use only.

Company was purified as described previously (1). Other chemicals were prepared by standard methods.

Methods and Results

Our method for the electrochemical determination of the equilibrium constant for ionization of nitroethane in aqueous ethanol is similar to methods used in earlier determinations (4–6) of the ionization constants of water in aqueous organic mixtures and for determination of ionization constants for very weak acids and bases in water.

Initial measurements were made on two cells that we represent as follows: glass electrode| acidic chloride solution A|AgCl, Ag; glass electrode|alkaline chloride solution B|AgCl, Ag. A general expression for the potentials of these cells is

$$[1] \qquad E = k_1 + k_2 \ln (a_H a_{Cl^-})$$

The system was "standardized" by making initial measurements with solution A consisting of 0.0496 *M* HCl and 0.0496 *M* KNO_3 and with solution B consisting of 0.0496 *M* KOH and 0.0496 *M* KCl. The difference in the two measured potentials can be expressed as

$$[2] \quad E_A - E_B = k_2 \log (a_{H^+ \text{ in A}})(a_{OH^- \text{ in B}})/K_w = k_2 \log [(0.0496)^2 \gamma_\pm^2 / (1.00 \times 10^{-14})]$$

from which we evaluate k_2.

Further measurements were made on a similar cell with a solution consisting of 0.0496 *M* KOH, 0.0496 *M* KCl, and 0.1071 *M* nitroethane (HX). This solution can also be described as being a buffered solution in which $(X^-)/(HX) = 0.863$. We express the difference between the potential of this cell (E_{buffer}) and E_A as

$$[3] \quad E_A - E_{buffer} = k_2 \log (a_{H^+ \text{ in A}})/(a_{H^+ \text{ in buffer}})$$

The ratio of H^+ activities evaluated by way of eq. 3 in combination with $(X^-)/(HX)$ permits calculation of the equilibrium constant K for the acid ionization of aqueous nitroethane.

Extension to aqueous ethanol solutions is based on "titration" of acid solution A with anhydrous ethanol, with the potential E_A' being measured after each addition of ethanol. Similarly, titration of the nitroethane buffer solution with anhydrous ethanol leads to E'_{buffer} values. Then $(E'_A - E'_{buffer})$ at the same solvent composition leads by way of eq. 3 to the desired equilibrium constant for ionization of nitroethane in each particular solvent mixture. Results of these measurements are given in Table 1. Maximum spread between pK values determined at the same solvent composition with different electrodes or at different times was 0.06. All pK values are based on molarities of solute species $CH_3CH_2NO_2$, $CH_3CHNO_2^-$, and H^+. Our standard free energies of ionization are therefore appropriate to the hypothetical 1 *M* standard state for solutes. We were unable to make satisfactory measurements with solvent mixtures with the mol fraction of ethanol greater than about 0.55.

We have measured enthalpies of solution of liquid nitroethane in various water–ethanol mixtures, with results summarized in Table 2. All reported values are averages of at least two separate determinations, with final concentrations of nitroethane ranging from 0.01 to 0.03 *M*. An equation to represent the calorimetric process is the following:

$$[4] \qquad CH_3CH_2NO_2(liq) = CH_3CH_2NO_2(S) \qquad \Delta H_s^0$$

Here we use (S) to indicate that the preceding substance is dissolved in some solution S. Our unweighted averaging procedure to obtain ΔH_s^0 values implies that the enthalpy of dilution of $CH_3CH_2NO_2(S)$ is negligible in these dilute solutions, which is in accord with our calorim-

TABLE 1. Ionization constants of nitroethane in aqueous ethanol

X_e	pK_a	X_e	pK_a
0.0	8.57	0.2355	9.73
0.0250	8.68	0.2912	9.99
0.0488	8.79	0.3393	10.19
0.0715	8.90	0.3813	10.38
0.0931	9.01	0.4183	10.53
0.1335	9.23	0.4510	10.68
0.1704	9.41	0.5067	10.92

TABLE 2. Enthalpies of solution (ΔH_s^0) of nitroethane in aqueous ethanol

X_e	ΔH_s^0 (kcal mol^{-1})	X_e	ΔH_s^0 (kcal mol^{-1})
0.0	0.17	0.219	3.35
0.0388	1.16	0.290	2.95
0.0847	2.42	0.400	2.58
0.111	3.01	0.496	2.33
0.139	3.41_5	0.654	2.02
0.171	3.49	0.834	1.73

Can. J. Chem. Downloaded from www.nrcresearchpress.com by 210.87.254.105 on 09/05/12
For personal use only.

etric results. Total uncertainties in ΔH_s^0 values are estimated to be less than ± 0.05 kcal mol^{-1}.

We have also measured enthalpies of neutralization of nitroethane, with results summarized in Table 3. Again, each reported value is the average of at least two determinations. All experiments were done with final $CH_3CHNO_2^-$(S) concentrations ranging from 0.01 to 0.02 *M* and with NaOH concentrations ranging from 0.047 to 0.053 *M*. The calorimetric process is represented by

[5] $CH_3CH_2NO_2(liq) + OH^-(S) = CH_3CHNO_2^-(S) + H_2O(S) \quad \Delta H_n^0$

Because of the symmetry of this reaction, we have taken the average measured ΔH_n at each solvent composition to be the standard enthalpy change represented by ΔH_n^0, which is consistent with the absence of any general trend in measured molar enthalpies with solute concentrations. Total uncertainties in ΔH_n^0 values range from about ± 0.05 kcal mol^{-1} in pure water to about ± 0.10 kcal mol^{-1} in the solutions with highest alcohol contents.

Combination of our ΔH_s^0 and ΔH_n^0 values with enthalpies of ionization of water in aqueous ethanol as represented by

[6] $H_2O(S) = H^+(S) + OH^-(S) \quad \Delta H_w^0$

from the results of an earlier calorimetric investigation (7) permits calculation of the standard enthalpy of ionization of nitroethane:

[7] $CH_3CH_2NO_2(S) = H^+(S) + CH_3CHNO_2^-(S) \quad \Delta H_i^0$

[8] $$\Delta H_i^0 = \Delta H_n^0 - \Delta H_s^0 + \Delta H_w^0$$

The ΔH_w^0 values used in eq. 8 for calculation of ΔH_i^0 values are taken from earlier calorimetric results of Bertrand *et al.* (7). These ΔH_w^0 values are in satisfactory agreement with those reported by Avedikian and Dollet (8) for solutions containing less than about 30 mol % ethanol. Because there are large unexplained discrepancies between the reported (7, 8) ΔH_w^0 values for solutions with the mol fraction of ethanol (X_e) greater than about 0.3, we do not tabulate ΔH_i^0 values for solutions with $X_e > 0.30$.

We shall also want to consider the enthalpy of neutralization of dissolved nitroethane, as represented by

[9] $CH_3CH_2NO_2(S) + OH^-(S) = CH_3CHNO_2^-(S) + H_2O(S) \quad \Delta H_{ns}^0$

This enthalpy of neutralization is calculated from

[10] $$\Delta H_{ns}^0 = \Delta H_n^0 - \Delta H_s^0$$

and is seen to be independent of ΔH_w^0.

We have constructed graphs of ΔH_n^0, ΔH_s^0, and ΔH_w^0 against X_e and have then taken various ΔH^0 values at selected values of X_e to use in eqs. 8 and 10. Results of these calculations of ΔH_i^0 and ΔH_{ns}^0 are given in Table 4.

Our ΔH_n^0 values (Table 3) become steadily less exothermic as X_e increases. Our ΔH_i^0 values (Table 4) become less endothermic as X_e increases, with a small (very little larger than experimental uncertainties) irregularity in the range $X_e \cong 0.1$ to $X_e \cong 0.25$. In contrast to these ΔH_n^0 and ΔH_i^0 values that vary smoothly with X_e, our ΔH_s^0 values (Table 2) exhibit a substantial maximum at $X_e \cong 0.175$ while our ΔH_{ns}^0 values (Table 4) exhibit a minimum at $X_e \cong 0.125$. The maximum in ΔH_s^0 and the minimum in ΔH_{ns}^0 are both indicative of effects of solvent "structure" on solute–solvent interactions as previously discussed by Arnett, Franks, Ives, and others (3*b–e*).

Our results (Table 1) show that the acid ionization constant for nitroethane decreases

TABLE 3. Enthalpies of neutralization (ΔH_n^0) of nitroethane in aqueous ethanol

X_e	ΔH_n^0 (kcal mol^{-1})	X_e	ΔH_n^0 (kcal mol^{-1})
0.0	−10.75	0.219	−7.50
0.0386	−9.97	0.290	−7.05
0.0847	−9.09	0.399	−6.41
0.111	−8.65	0.495	−5.84
0.139	−8.26	0.655	−4.89
0.171	−7.91	0.834	−3.75

TABLE 4. Enthalpies of ionization (ΔH_i^0) and neutralization (ΔH_{ns}^0) of nitroethane in aqueous ethanol

X_e	ΔH_i^0 (kcal mol^{-1})	ΔH_{ns}^0 (kcal mol^{-1})
0.0	2.42	−10.92
0.05	2.4	−11.1
0.10	2.1_5	−11.5
0.125	1.85	−11.65
0.15	1.75	−11.55
0.175	1.65	−11.35
0.20	1.55	−11.05
0.30	1.45	−9.9

TABLE 5. Free energies (ΔG_i^0) and entropies ($-T\Delta S_i^0$) of ionization of nitroethane in aqueous ethanol

X_e	ΔG_i^0 (kcal mol^{-1})	$-T\Delta S_i^0$ (kcal mol^{-1})
0.0	11.69	9.27
0.05	12.00	9.60
0.10	12.34	10.19
0.125	12.52	10.67
0.15	12.69	10.94
0.175	12.82	11.17
0.20	12.99	11.44
0.30	13.68	12.23

TABLE 6. Free energies (ΔG_{ns}^0) and entropies ($-T\Delta S_{ns}^0$) of neutralization of nitroethane in aqueous ethanol

X_e	ΔG_{ns}^0 (kcal mol^{-1})	$-T\Delta S_{ns}^0$ (kcal mol^{-1})
0.0	−7.42	3.50
0.05	−7.43	3.67
0.10	−7.29	4.21
0.125	−7.20	4.45
0.15	−7.10	4.45
0.175	−7.05	4.30
0.20	−6.95	4.10
0.30	−6.49	3.41

steadily (increasing ΔG_i^0) with increasing X_e. From a graph of pK against X_e, we have selected pK values at certain X_e values and calculated the corresponding standard free energies of ionization (ΔG_i^0, molar scale) that are listed in Table 5. These ΔG_i^0 values have been combined with the corresponding ΔH_i^0 values (Table 4) to obtain the $-T\Delta S_i^0$ values that are also listed in Table 5. We see that the large increase in $-\Delta TS_i^0$ with increasing X_e causes ΔG_i^0 to increase (K to decrease) with increasing X_e, in spite of the fact that it requires less energy (decreasing ΔH_i^0) to remove a proton from $CH_3CH_2NO_2$(S) as X_e increases.

To obtain ΔG_{ns}^0 values (for the reaction represented by eq. 9) we combine our pK values (Table 1) with pK_w values (reported as $K_{a/a}$) from an earlier e.m.f. investigation (4), as summarized in Table 6. Combination of these ΔG_{ns}^0 values with corresponding ΔH_{ns}^0 values (Table 4) leads to the $-T\Delta S_{ns}^0$ values also listed in Table 6. The values in Tables 4 and 6 show that "compensation" of ΔH_{ns}^0 and $T\Delta S_{ns}^0$ values causes ΔG_{ns}^0 to increase smoothly with increasing X_e, in spite of extrema in ΔH_{ns}^0 and $T\Delta S_{ns}^0$ values at $X_e \cong 0.13$.

We are grateful to the National Research Council of Canada for support of this research.

1. T. MATSUI and L. G. HEPLER. Can. J. Chem. (*a*) **51**, 1941 (1973). (*b*) **51**, 3789 (1973).
2. J. W. LARSON and L. G. HEPLER. *In* Solute–solvent interactions. *Edited by* J. F. Coetzee and C. D. Ritchie. Marcel Dekker, Inc., New York, N.Y. 1969.
3. (*a*) F. J. MILLERO, C. H. WU, and L. G. HEPLER. J. Phys. Chem. **73**, 2453 (1969). (*b*) E. M. ARNETT and D. R. MCKELVEY. Rec. Chem. Progr. **26**, 185 (1965). (*c*) E. M. ARNETT, W. G. BENTRUDE, J. J. BURKE, and P. MCC. DUGGLEBY. J. Am. Chem. Soc. **87**, 1541 (1965). (*d*) E. M. ARNETT and D. R. MCKELVEY. J. Am. Chem. Soc. **87**, 1393 (1965). (*e*) F. FRANKS and D. J. G. IVES. Quart. Rev. (London) **20**, 1 (1966). (*f*) R. M. IZATT, D. EATOUGH, and J. CHRISTENSEN. J. Phys. Chem. **72**, 2720 (1968).
4. E. M. WOOLLEY, D. G. HURKOT, and L. G. HEPLER. J. Phys. Chem. **74**, 3908 (1970).
5. E. M. WOOLLEY, J. TOMKINS, and L. G. HEPLER. J. Solution Chem. **1**, 341 (1972).
6. E. M. WOOLLEY and L. G. HEPLER. Anal. Chem. **44**, 1520 (1972).
7. G. L. BERTRAND, F. J. MILLERO, C. H. WU, and L. G. HEPLER. J. Phys. Chem. **70**, 699 (1969).
8. L. AVEDIKIAN and N. DOLLET. Bull. Soc. Chim. Fr. 4551 (1967).

Can. J. Chem. Downloaded from www.nrcresearchpress.com by 210.87.254.105 on 09/05/12
For personal use only.

Ligand Abstraction in the Reaction of Aryldiazonium Ions with some Iron Complexes Containing Coordinated Cysteine, Maleonitriledithiol, or Triarylphosphine

JAMES A. CARROLL, DAVID R. FISHER, GEOFFREY W. RAYNER CANHAM, AND DEREK SUTTON[1]

Department of Chemistry, Simon Fraser University, Burnaby 2, British Columbia

Received November 23, 1973

The reactions of selected aryldiazonium tetrafluoroborates with $Fe(CO)_3(PR_3)_2$, $[Fe(mnt)_2]^-$, $[Fe(cystH)_2]^{2+}$, and $[Fe(CO)_2(cyst)_2]$ (mnt = $S_2C_2(CN)_2$, cyst = $SCH_2CH(NH_2)CO_2H$) result in abstraction of the ligand to yield arenediazophosphonium ions, *S*-(arenediazo)cysteine or the dinitrogen extrusion product ArS(CN)C=C(CN)SAr. Arylazo complexes of iron were not obtained. The products have been characterized and compounds related to *S*-(arenediazo)-cysteine, namely *S*-(arenediazo)triphenylmethyl mercaptan and *S*-(arenediazo)sulfones, have been synthesized for a detailed comparison of their Raman spectra. Assignments of ν(N=N) are made on the basis of ^{15}N- and ^2H-substitution experiments. The possible involvement of nucleophilic sulfur as a site for the activation and/or reduction of complexed dinitrogen in biological nitrogen fixation is proposed.

Les réactions de divers tétrafluoroborates d'aryldiazonium avec $Fe(CO)_3(PR_3)_2$, $[Fe(mnt)_2]^-$, $[Fe(cystH)_2]^{2+}$ et $[Fe(CO)_2(cyst)_2]$ (mnt = $S_2C_2(CN)_2$, cyst = $SCH_2CH(NH_2)CO_2H$) conduisent à l'enlèvement d'un ligand pour fournir les ions arènediazophosphonium, la *S*-arènediazocystéine ou les produits d'élimination d'azote moléculaire ArS(CN)C=C(CN)SAr. Les complexes arylazo du fer n'ont pas été obtenus. On a caractérisé les produits et l'on a synthétisé les composés reliés à la *S*-arènediazocystéine soit le *S*-arènediazotriphénylméthyl mercaptan et les *S*-arènediazosulphones dont on a examiné les spectres raman en détail. Les positions des bandes ν(N=N) ont été attribuées sur la base d'expériences dans lesquelles les azotes et les hydrogènes ont été remplacés par ^{15}N et ^2H. On propose un mécanisme possible impliquant du soufre nucléophile comme site d'activation ou de réduction pour la fixation d'azote par des processus biologique impliquant de l'azote moléculaire. [Traduit par le journal]

Can. J. Chem., **52**, 1914 (1974)

Introduction

Recently, there has been some interest in the reactions of aryldiazonium ions with a variety of transition metal complexes, with a view to synthesizing stable transition metal–arylazo complexes L_nMN_2Ar. Whilst in some instances the reactions appear to be straightforward additions or substitutions (1–10) there are examples in which the reactions are considerably more complex and products of insertion (11–14) and metallation (15) have been obtained. The mechanisms of these processes and of the formation of tetrazene complexes (16) are not yet known with certainty.

In the course of our studies of such reactions we have found that a further complication may quite frequently arise, which is the reaction of the diazonium ion with a nucleophilic center in the ligand itself. To cite an example, whereas the majority of aryldiazonium ions reacted smoothly with $Fe(CO)_3(PPh_3)_2$ to yield $[Fe(CO)_2(PPh_3)_2(N_2Ar)]^+$, *p*-diethylaminophenyldiazonium tetrafluoroborate reacted rapidly with ligated (or possibly with equilibrium-dissociated) triphenylphosphine to yield near quantitative amounts of $[Et_2N{\cdot}C_6H_4{\cdot}N_2PPh_3]BF_4$ (4). Further instances of apparent ligand abstraction[2] were found in the reaction of iron–cysteine and iron–maleonitriledithiol complexes with a range of aryldiazonium salts. Whilst we have been concerned solely with iron complexes, the effect is no doubt more general than this. Compounds similar to the products of these reactions, such as phosphodiazonium ions and arylazothiolates,

[1]To whom correspondence should be addressed.

[2]The sequence of events in these reactions is not known, and the term "ligand abstraction" is used here in the sense that the products are ligand–arylazo combinations (or related to them) rather than metal–arylazo complexes. A referee has correctly pointed out that metal–arylazo complexes may be formed initially and undergo rapid decomposition to species which recombine to give observed products. This possibility, as yet, lacks experimental verification.

Can. J. Chem. Downloaded from www.nrcresearchpress.com by 210.87.254.42 on 09/05/12
For personal use only.

TABLE 1. Analytical data

Compound	Calculated (%)				Found (%)				Melting point (°C)
	C	H	N	Other	C	H	N	Other	
1*a*	64.01	5.56	8.00	P 5.90	63.97	5.56	7.98	P 5.94	164 dec.
1*b*	62.03	4.54	5.79		62.31	4.83	5.25		92 dec.
1*c*	60.49	5.69	6.84		60.60	5.74	6.95		170 dec.
7*a*	58.17	2.44	8.48		56.90	2.33	8.47		145
7*b*	66.01	6.46	12.83		64.78	6.36	12.44		137
7*c*	61.19	3.97	7.86		61.04	4.00	8.01		156
8*a*	48.00	4.89	18.66		48.22	4.82	18.58		171 dec.
8*b*	47.04	5.13	16.46		46.89	5.14	16.31		172 dec.
8*c*	50.18	5.57	17.78		50.45	5.48	17.56		168 dec.
8*d*	44.43	4.15	17.26		44.52	4.07	17.38		174 dec.
8*e*	40.95	3.44	14.32		41.16	3.39	14.12		174 dec.
8*f*	40.03	3.74	20.71		39.85	3.60	20.64		157 dec.
8*g*	33.44	4.06	13.00		34.01	4.09	13.07		212 dec.
8*h**	35.55	3.32	13.81	Br 26.27	35.78	3.27	14.06	Br 26.28	186 dec.
8*j*†	36.60	3.08	14.22		36.61	3.14	14.13		180 dec.
9*a*	58.54	4.09	11.37		58.93	4.26	11.39		77
9*c*	49.49	3.11	14.42		49.74	3.21	14.47		136
9*d*	56.52	4.38	10.14		56.90	4.45	10.30		75

*Monohydrate.
†**8***j* is *S*-(2,6-dichlorobenzenediazo)cysteine.

have been reported in the literature previously but in most cases have been inadequately characterized. We have synthesized compounds from the iron complexes and from the ligands themselves. In this paper we report the characterization of these compounds, especially in regard to their spectroscopic properties. Structurally similar compounds have been synthesized and investigated for comparison.

Results and Discussion

Abstraction of Triarylphosphine from $Fe(CO)_3(PR_3)_2$

The addition of an acetone solution of $[p\text{-}Et_2NC_6H_4N_2]BF_4$ to an equimolar benzene solution of $Fe(CO)_3(PPh_3)_2$, in the manner utilized in the synthesis of $[Fe(CO)_2(PPh_3)_2N_2Ar]BF_4$ (4), caused an immediate intense red coloration, followed by deposition of red crystals of **1***a*. Approximately half the original $Fe(CO)_3(PPh_3)_2$ was recovered from the mother liquor, whereas all diazonium salt was expended. The fate of the remaining iron was not investigated, but no arylazo–iron complex was identified.

$$[XC_6H_4\text{—}N{=}N\text{—}PR_3]^{\oplus}\ BF_4^{\ominus}$$

1

a X = *p*-NEt_2; R = Ph
b X = *p*-OCH_3; R = Ph
c X = *p*-NEt_2; R = *p*-$C_6H_4OCH_3$

The identity of **1***a* was established by synthesizing it quantitatively from equimolar amounts of triphenylphosphine and the diazonium salt, by analysis (Table 1), and by its spectroscopic properties, described in detail below. Abstraction of PPh_3 from the iron complex was observed only with $[p\text{-}Et_2NC_6H_4N_2]BF_4$ (4). However, a wide variety of substituted diazonium salts all appeared to react with free triphenylphosphine in similar fashion. The products from all except *p*-OCH_3 and *p*-NEt_2 derivatives decomposed in solution. Those with electron-withdrawing mesomeric substituents were transient species under these conditions, decomposing totally within seconds; those with only inductive substituents or *m*-substituted mesomeric substituents decomposed a little more slowly, lasting in solution about a minute. Electron-donating mesomeric substituents rendered the compounds isolable as solids, though the *p*-OCH_3 derivative decomposed above 0 °C. Decomposition leads to extrusion of nitrogen and the formation of tetraarylphosphonium tetrafluoroborates. Changes in the nature of the phosphine also markedly affect the stability of the products. With tri(*p*-methoxyphenyl)phosphine, considerably enhanced stability to decomposition was observed as a general feature; conversely, the products from methyldiphenylphosphine were more unstable, with even Et_2NC_6-

Can. J. Chem. Downloaded from www.nrcresearchpress.com by 210.87.254.42 on 09/05/12
For personal use only.

Can. J. Chem. Downloaded from www.nrcresearchpress.com by 210.87.254.42 on 09/05/12
For personal use only.

$H_4N_2^+$ yielding a product decomposing at room temperature under dry nitrogen.

Compound **1***a* is a red needle crystalline solid, stable to air, and soluble in polar organic solvents such as acetone, ethanol, chloroform, and nitromethane. The solutions are not very stable, however, especially chloroform solutions which decompose in a few days with loss of nitrogen to a brown oil. It is insoluble in water, benzene, toluene, carbon tetrachloride, and diethyl-ether. The molar electrical conductivity of **1***a* in acetone (1.37×10^{-4} *M*) was 184 ohm^{-1} cm^2, a little higher than the range (120–175 ohm^{-1} cm^2) previously observed for typical 1:1 electrolytes (17) but considerably below the 2:1 electrolyte values of 230–290 ohm^{-1} cm^2. An osmometric molecular weight determination (4.25×10^{-3} *M* in acetone) gave an apparent molecular weight of 320 indicating **1***a* (mol. wt. 525) to be 67% dissociated at this concentration.

The structural formula presented for **1** is consistent with all available physical evidence; alternative possibilities illustrated as **2**–**5** can be eliminated as inconsistent with the physical (principally spectroscopic) and chemical evidence.

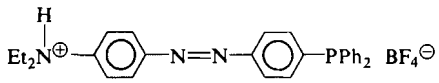

2

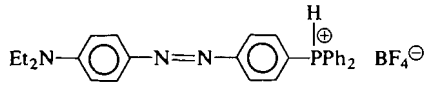

3

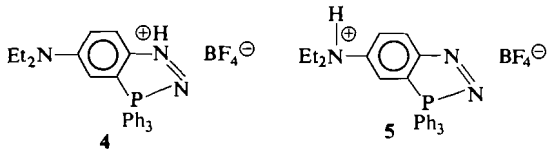

4 **5**

For example, N—H and P—H bonds (required by all these alternative formulations) are deduced to be absent by the lack of any bands in the i.r. or Raman spectra assignable as ν(N—H) or ν(P—H) and from the absence of the expected resonances in the n.m.r. spectra. The compounds cannot be deprotonated by base. Structures **2** and **3** are analogous to the well-known product of reaction of an aryldiazonium salt with triphenyl*amine*, *viz.*, Ar—N=N—$C_6H_4NHPh_2^{\oplus}$-$BF_4^{\ominus}$, and in our view required additional contrary evidence before definite exclusion. This was afforded by repeating the synthesis using tri(*p*-methoxyphenyl)phosphine, whereupon a similar product was obtained whose properties were consistent only with the formulation **1***c*. With this phosphine, coupling at the *para* position is clearly prevented. Furthermore, the n.m.r. spectrum of the product shows all CH_3O groups to be equivalent, eliminating the possibility of coupling through an *ortho* position.

The vibrational spectra of **1** showed, in addition to bands assignable to the phosphine, substituted-aryl and BF_4^- moieties, two bands due to vibrations of the —N=N—P group. These occurred for **1***a* at 1222 and 888 cm^{-1} in the i.r. spectrum and 1212 and 883 cm^{-1} in the Raman. Substitution of ^{15}N adjacent to phosphorus, using $[Et_2NC_6H_4{}^{14}N{\equiv}{}^{15}N]BF_4$, shifted these bands to 1210 (i.r.) (1200 Raman) and 878 (i.r.) (877 Raman) cm^{-1}, respectively.

Neither frequency is at all similar to typical values for ν(N=N) which lie in the range 1440–1650, although the lower frequency is in the range of values for ν(P—N), 860–910 cm^{-1}. Notably, however, values for ν(P=N) range from 1000 to 1350 cm^{-1} and those for ν(N—N) range from 850 to 1050 cm^{-1} (18, 19). The measured values for **1***a* are therefore probably indicative of a considerable contribution of the valence-bond formalism **1***a*′ to the electronic structure of the molecule, invalidating attempts to distinguish which of these two bands is to be assigned as ν(PN) and which is ν(NN). The

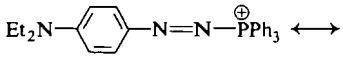

1*a*

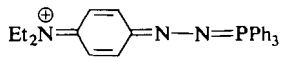

1*a*′

extensive delocalization clearly accounts for the intense color of the compounds, resulting primarily from an absorption band at about 500 nm having an extinction coefficient *ca.* 2×10^4 cm^{-1} M^{-1}. It is also apparent that the extent to which these compounds are stable towards decomposition is very much a function of the degree of electron, and consequently charge, delocalization. Substituents in *para* positions with electron donating mesomeric effects promote the **1***a*′ type of electron distribution and

Can. J. Chem. Downloaded from www.nrcresearchpress.com by 210.87.254.42 on 09/05/12
For personal use only.

confer increased stability, whether present on the aromatic rings attached to nitrogen as in **1***a*, *b* or phosphorus as in **1***c*. The enhanced stability of the whole range of tri(*p*-methoxy)phosphine derivatives is undoubtedly due to contributions from valence-bond structures such as **6**, whilst

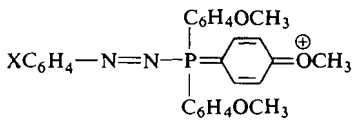

6

the reduced stability observed when PPh_3 is replaced by PPh_2Me may be a result of the inductive effect of methyl reducing the electronegativity of phosphorus and therefore lessening the ability of phosphorus d-orbitals to accept π-electrons from nitrogen. The inability of NPh_3 to form analogous compounds is a result of nitrogen's lack of low-lying vacant orbitals of correct symmetry. $AsPh_3$ reacted with $[p\text{-}Et_2NC_6H_4N_2]BF_4$ to give only an unstable oil which could not be characterized and no reaction occurred with $SbPh_3$. These differences from PPh_3 undoubtedly result from changes in nucleophilicity and from the reduced π-bonding capabilities of 4d and 5d orbitals with nitrogen. Other attempts were conducted with SPh_2, with which an unstable oil resulted, and $(EtO)_3P$, $(PhO)_3P$, and Ph_3PO, none of which appeared to react with $[p\text{-}Et_2NC_6H_4N_2]BF_4$.

Abstraction of Maleonitriledithiolate Dianion from $[Fe(mnt)_2]^{\ominus}$

Addition of solid $[p\text{-}FC_6H_4N_2]BF_4$ in small portions to an absolute methanol solution of $Na[Fe(mnt)_2]$ (mnt = maleonitriledithiolate, $S_2C_2(CN)_2$) at room temperature was accompanied by rapid gas evolution and a change in color from deep red to orange. Evaporation followed by recrystallization yielded a yellow solid identified as **7***a*. The same compound can

$$XC_6H_4SC(CN) = C(CN)SC_6H_4X$$

7

a X = *p*-F
b X = *p*-NEt_2
c X = *p*-OMe

be obtained similarly from $Na[Fe(NO)(mnt)_2]$ or directly by reacting the diazonium salt with $Na_2C_2S_2(CN)_2$. Unlike the above $Fe(CO)_3(PPh_3)_2$ reactions, similar behavior is obtained for all the diazonium salts used, leading for example to **6***b* and *c*. In no instance were we able to obtain any evidence for the formation of iron arylazo species, as might arise from coordination of $ArN_2^{\oplus}$ to $[Fe(mnt)_2]^{\ominus}$ or by substitution of $NO^{\oplus}$ by $ArN_2^{\oplus}$ in $[Fe(NO)(mnt)_2]^{\ominus}$. Neither were we able to prevent the loss of nitrogen to a sufficient extent to obtain the pure arylazothiolate intermediate expected to arise from the ligand abstraction reaction by comparison with the behavior of the iron–cysteine compounds described below.

Analyses (Table 1) and spectroscopic properties are in accord with the postulated structure **7**. As far as we are aware, these particular compounds do not appear to have been reported previously. Compounds RSC(CN)=C(CN)SR are known where R is aliphatic (20).

Abstraction of Cysteinyl from $Fe(CO)_2(cyst)_2$ and $[Fe(cystH)_2]^{2+}$

These experiments arose out of an effort to approach more closely the biologically important sulfur (especially cysteinyl) environment of iron in regard to our study of the interaction of transition metals with molecules related to dinitrogen. In no case investigated, for a wide range of diazonium salts, was there any evidence for the coordination of an arylazo group to iron. Instead, rapid abstraction of cysteinyl from either $Fe(CO)_2(cyst)_2$ (21) or $[Fe(cystH)_2]^{2+}$ (22) (cyst = $SCH_2CH(NH_2)CO_2H$; cystH = $HSCH_2CH(NH_2)CO_2H$) occurred to yield the iron-free, pale yellow *S*-(arenediazo)cysteines (**8**). These compounds were also synthesized

$$XC_6H_4N_2SCH_2CH(\overset{\oplus}{N}H_3)CO_2^{\ominus}$$

8

a X = H
b X = *p*-OCH_3
c X = *p*-CH_3
d X = *p*-F
e X = *p*-CF_3
f X = *p*-NO_2
g X = *p*-SO_3H
h X = *p*-Br
i X = *p*-Et_2N

from the diazonium salts and L-cysteine hydrochloride directly.

Reactions of diazonium salts with amino acids (23), and specifically with L-cysteine (24–26), have been documented in earlier literature but the products from L-cysteine have not been well established. Matsumoto (24) postulated the formation of an *S*-(arenediazo)cysteine intermediate in the reaction with diazobenzenesulfonic acid and the toxicity of this acid has been attributed to its reaction with thiol groups of

TABLE 2. ^{15}N-sensitive bands in the Raman spectra of p-$XC_6H_4N{=}N^*SCH_2CH(NH_3^{\oplus})CO_2^{\ominus}$ substituted at N*

Compound (X)	Raman bands (^{15}N values in parentheses)			
8*a* (H)	1433vs(1416vs)	1424vs(1406vs)	884w(879w)	768m(764m)
8*b* (OCH_3)	1435s(1428s)	1406vs(1393s)	889w(884w)	798w(794w)
8*c* (CH_3)	1438vs	1405s	889w,br	798s
8*d* (F)	1448vs(1433vs)	1410s(1399s)	892w(887w)	817m(814m)
8*g* (SO_3H)	1444vs	1404w	896w	777w

glutathione and L-cysteine (25). Zahn *et al.* (26) found *S*-(5-chloro-2-methylbenzenediazo)cysteine to be stable to 170°. We have not been able to find any reports detailing more exactly the characterization or properties of *S*-(arenediazo)-cysteines, so further examination as part of this study seemed appropriate.

The *S*-(arenediazo)cysteines prepared in this work are all pale yellow and are for the most part remarkably stable in the solid state. Satisfactory analyses (Table 1) were obtained for all but **8***i* which decomposed. All, except **8***g*, are quite insoluble in all the common solvents; solutions in dilute mineral acids slowly evolve gas. The sulfonic acid **8***g* is insoluble in dilute acid but soluble in water and most polar organic solvents. *S*-(Arenediazo) derivatives from thiols have not been notable for thermal stability and few examples of stable, well-characterized compounds exist (27–29). Interest in these compounds has centered around their photochemical *cis–trans* isomerism and utility in photographic applications (29, 30). The present cysteine derivatives appear to exhibit generally fair thermal and light stability.

Sulfur and nitrogen are each possible sites for the binding of the diazo group but vibrational spectroscopy shows unambiguously that binding is actually to sulfur. Cysteine exhibits a strongly active ν(S—H) at 2567 cm^{-1} (ν(S—D) 1864 cm^{-1}) in the Raman spectrum but no band assignable to ν(S—H) or ν(S—D) occurs in the spectra of **8**. On the other hand, the Raman active ν(C—S) shifts from 684 cm^{-1} in cysteine to about 640 cm^{-1} in the products. The i.r. spectra of the products show absorptions in the region 1400–1600 cm^{-1}, including bands closely similar to those characteristic of the $NH_3^{\oplus}$ and $CO_2^{\ominus}$ groups of the zwitterionic form of cysteine itself (31).

Isotopic substitution studies were conducted in an attempt to assign vibrations due to the Ar—N=N—S— group in the Raman and i.r. spectra. Only **8***a–d* and **8***g* were found to be undecomposed on exposure to the He—Ne laser exciting radiation (6328 Å) of the Raman spectrometer whilst the remainder exhibited varying degrees of decomposition and their spectra will not be discussed. Their instability is probably a result of localized thermal (rather than photochemical) decomposition. ^{15}N-substituted derivatives were synthesized for **8***a*, *b*, and *d* and bands which shifted are listed in Table 2. Of these, only the bands in the 1400 cm^{-1} region show considerable shifts. Bands which were observed in similar positions for the other compounds are also listed in Table 2, but care should be exercised in their interpretation; for example, we have not collected evidence as to whether or not the weak band at 1404 cm^{-1} in the Raman spectrum of **8***g* is ^{15}N sensitive. In each of these regions the corresponding i.r. bands are relatively weak and ^{15}N shifts are difficult to discern due to overlap with more intense absorption bands.

The presence of two strong ^{15}N-sensitive Raman bands may be interpreted in a number of ways, including (*i*) the presence of *cis*- and *trans*-isomers, (*ii*) strong coupling of ν(N=N) with other vibrational modes in the 1400 cm^{-1} region, especially ν(C—C) modes of the aromatic ring, (*iii*) coupling of ν(N=N) with ν(N—S) in the event that the N—S bond has considerable multiple-bond character, (*iv*) solid-state site-splitting effects. In an attempt to eliminate some of these possibilities, it seemed worthwhile to study the hitherto unpublished vibrational spectra of a number of related *S*-(arenediazo) compounds and compare their behavior with that of the *S*-(arenediazo)cysteines.

S-(Benzenediazo)triphenylmercaptan (28) was obtained spectrally pure in each of the *cis*- and *trans*-isomeric forms. Each isomer exhibits the expected single, ^{15}N-sensitive band due to

Can. J. Chem. Downloaded from www.nrcresearchpress.com by 210.87.254.42 on 09/05/12
For personal use only.

TABLE 3. Observed Raman bands in the ν(N=N) region (1350–1500 cm^{-1}) for the compounds listed (values for —N=^{15}N—S derivatives in parentheses)

Compound	Raman bands (cm^{-1})
cis-$C_6H_5N{=}NSCPh_3$	1492m (1473m)
trans-$C_6H_5N{=}NSCPh_3$	1424vs (1406vs)
trans-$C_6H_5N{=}NSO_2Ph$ (*9a*)	1488s(–) 1472vs(1466s) 1450vs(1438vs)
trans-$C_6D_5N{=}NSO_2Ph$ (*9b*)	1470vs (1452vs)
trans-*p*$NO_2C_6H_4N{=}NSO_2Ph$ (*9c*)	1496vs(1476m) 1470s(1461vs)
trans-*p*$CH_3OC_6H_4N{=}NSO_2Ph$ (*9d*)	1462vs 1423vs

ν(N=N), coincident in both the Raman and i.r. spectra (Table 3). It occurs at ~1490 cm^{-1} for the *cis*-isomer and at ~1420 cm^{-1} for the *trans*-isomer. As expected by symmetry, the Raman intensity of ν(N=N) in the *trans*-isomer is considerably greater and it is the most intense band in the spectrum. The separation of ~70 cm^{-1} is considerably greater than the separation (~10–40 cm^{-1}) of the bands in the *S*-(benzenediazo)-cysteines; the isotopic shifts (~20 cm^{-1}) are also much larger (except **8***a*). These observations, together with the fact that no changes in the relative intensities of the bands in the *S*-(benzenediazo)cysteines could be induced by repeated recrystallization or chromatography of the soluble member **8***g* or were observed in different syntheses of the remainder, do not seem to support the hypothesis that *cis*- and *trans*-isomers are present. The high intensity (Table 2) suggests the expected *trans*-isomer. Reactivity towards β-naphthol was also indicative of *trans*-isomers; no red color developed in dark but appeared slowly in diffuse light (28).

We next turned our attention to some benzenediazosulfones **9** which have been found to be isolable uniquely as *trans*-isomers (32). The presence of the —SO_2— moiety might be expected to enhance the N—S bond order by a $p\pi$–$d\pi$ mechanism. Some evidence of this capability on the part of —SO_2— is afforded by the somewhat short S—C (alkene) bond in $CH_3CH{:}CHSO_2C_6H_4CH_3$ (33). Despite the presence of the single *trans*-isomer, the spectrum of **9***a* exhibits two very intense bands in the 1400–1500 cm^{-1} region together with a band at ~1480 (in the position normally expected for ν(C=C) of an aromatic ring) whose intensity is unusually large. All three bands are sensitive to ^{15}N substitution (Fig. 1) and the situation appears, to a degree, to be reminiscent of the *S*-(benzenediazo)cysteines. Closer inspection reveals that this is not the case. The deuterated compound **9***b* exhibits a single, extremely intense Raman band in the ν(N=N) region at 1470 cm^{-1} which shifts (to 1452 cm^{-1}) by the expected ~20 cm^{-1} on ^{15}N substitution. The spectral differences between **9***a* and *b* result simply from changes in position of the ν(C—C) vibrations of the aromatic substituent R in the

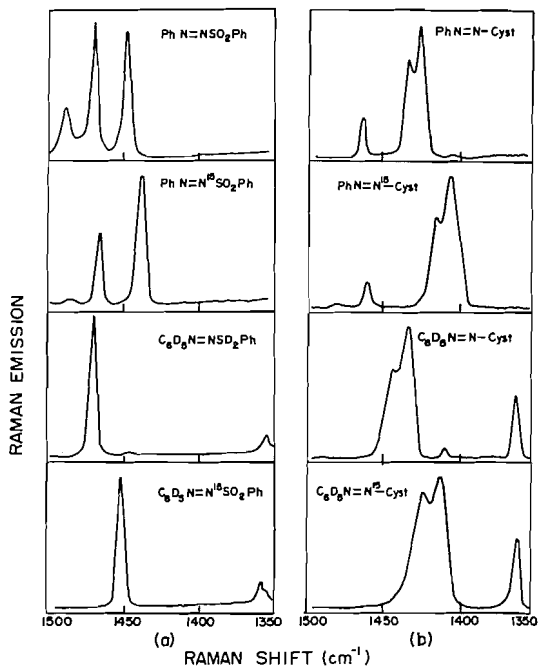

FIG. 1. Comparison of the effect of deuteration and ^{15}N substitution on the Raman spectra of (*a*) benzenediazophenylsulfone **9***a* and (*b*) *S*-(benzenediazo)cysteine **8***a*.

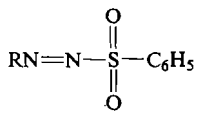

9

a R = C_6H_5 *c* R = *p*-$NO_2{\cdot}C_6H_4$
b R = C_6D_5 *d* R = *p*-$CH_3O{\cdot}C_6H_4$

Can. J. Chem. Downloaded from www.nrcresearchpress.com by 210.87.254.42 on 09/05/12
For personal use only.

Can. J. Chem. Downloaded from www.nrcresearchpress.com by 210.87.254.42 on 09/05/12
For personal use only.

deuterated and protonated forms and their interaction with ν(N=N). It is well known that deuteration shifts the A_1 and B_1 ν(C—C) modes in chlorobenzene from ~1480 and ~1440 cm^{-1}, respectively, to ~1350 and ~1320 cm^{-1} and that these positions in C_6H_5X and C_6D_5X are not very sensitive to the mass of X (34, 35). In **9***a*, the presence of ν(N=N) in the 1470 cm^{-1} region results in strong coupling with both ν(C—C) modes and the observation of three intense bands. ^{15}N substitution moves ν(N=N) to lower frequency and some coupling with ν(C—C) is still observed, in that the lower two bands shift down by only ~10 cm^{-1} each. The source of enhancement of ν(C—C) at ~1480 cm^{-1} has now been removed, and this mode is hardly visible in the spectrum at normal amplification. In **9***b* the ν(C—C) modes are too far removed from ν(N=N) for coupling to occur, so that ν(N=N) appears as a single band at 1470 cm^{-1} (with the expected ^{15}N shift of *ca.* 20 cm^{-1}) and the ν(C—C) modes (*cf.* A_1, at 1362 cm^{-1}) do not shift with ^{15}N substitution.

If a similar explanation holds for the *S*-(benzenediazo)cysteines we should expect deuteration to give rise to simplification of their spectra also. This does not occur, at least in the example we have studied, namely **8***a*. The bands in question appear with almost identical profiles in the original deuterated and ^{15}N-substituted compounds (Fig. 1); we infer that strong coupling of ν(N=N) with ν(C—C) is not occurring in these compounds.

Para-substituted benzenediazosulfones such as the *p*-nitro (**9***c*) and *p*-methoxy (**9***d*) compounds also show two bands in the ν(N=N) region. ^{15}N substitution of **9***c* results in not only an apparent shift but an inversion of intensity distribution in these bands (Table 3). Replacement of the electron-attracting *p*-NO_2 substituent by the electron-releasing *p*-OCH_3 appears to result in a considerable shift in the ν(N=N) region bands to lower energy, a result compatible, on a valence bond model, with increased contribution of structures such as

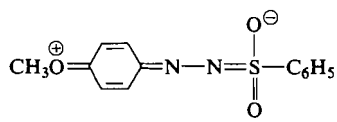

As a concluding comment, it seems to us worthwhile to point out the possible implications of these ligand abstraction reactions of the diazonium ion in regard to the mechanism of biological nitrogen fixation. If, as first suggested by Parshall (36) the formal analogy between the diazonium ion $Ar—\overset{\oplus}{N}\equiv N$ and a metal–dinitrogen complex $\sim\overset{\ominus}{M}—\overset{\oplus}{N}\equiv N$ is accepted,[3] then the observed preference of the diazonium ion for a nucleophilic sulfur atom over a neighboring iron atom raises the possibility, not previously considered, that the activation of dinitrogen by nitrogenase could involve coordination to iron or molybdenum followed by binding of the free end to sulfur:

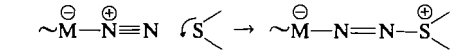

Nitrogenase possesses the requisite nucleophilic sulfur in cysteinyl residues and in "labile" sulfide; in addition, a ferredoxin is believed to be responsible for reduction to the NH_3 level, and this is likely to have a cube-like iron–sulfur framework (37). Recent model studies by van Tamelen *et al.* using a stable molybdenum–dinitrogen complex and synthetic, cube-like $(Fe—S)_4$ cluster agents of the ferredoxin structural type resulted in nitrogen fixation, postulated to be via an interaction of the (bound) dinitrogen with the cluster at an iron atom (38). The sulfur atoms of the cluster are, however, more accessible and must be considered as plausible alternative interactive sites, especially in view of the anticipated flow of electrons from the cluster to the dinitrogen in the reductive step.

Experimental

Reaction of $Fe(CO)_3(PPh_3)_2$ with $[p\text{-}Et_2NC_6H_4N_2]BF_4$

$Fe(CO)_3(PPh_3)_2$ (0.975 g) was dissolved in benzene (30 ml) and a solution of $[p\text{-}Et_2NC_6H_4N_2]BF_4$ (0.375 g) in acetone (10 ml) added dropwise. The solution turned red immediately and red crystals were later deposited. Analysis and spectroscopic properties showed the red crystals to be impure **1***a*.

Anal. Calcd.: C, 64.01; H, 5.56; N, 8.00; P, 5.90; F, 14.50. Found: C, 64.27; H, 5.52; N, 9.18; P, 4.36; F, 13.55.

Reaction of PPh_3 with Aryldiazonium Salts

Triphenylphosphine (1 mmol) was dissolved in acetone

[3]A number of different proposals for the mechanism of action of nitrogenase have been made in recent years. A view currently receiving some attention focusses on the possibility of an electron rearrangement in the $\sim\overset{\ominus}{M}—\overset{\oplus}{N}\equiv N$ moiety to yield "reduced ligand" structures such as $\sim M=\overset{\oplus}{N}=N^{\ominus}$ or $M^{\oplus}—N\!=\!N^{\ominus}$ which would be susceptible to facile protonation at nitrogen (see ref. 39).

Can. J. Chem. Downloaded from www.nrcresearchpress.com by 210.87.254.42 on 09/05/12
For personal use only.

(10 ml) and 1 mmol of the corresponding diazonium salt as a concentrated solution in acetone was added, with stirring, at 0 °C. In all cases the combined solutions immediately turned deep red. In all cases except the p-NEt_2 and p-OCH_3 derivatives, gas evolution commenced almost immediately, accompanied by loss of color. In each case a solid was obtained by the addition of ether. In the p-NEt_2 and p-OCH_3 cases the solids were **1***a* and *b*, respectively, (Table 1) but in all other cases only the quaternary phosphonium salts $[Ph_3PC_6H_4X]BF_4$ were recovered. Compound **1***a* is stable indefinitely as a solid at room temperature and melts with decomposition at 164 °C. Compound **1***b* decomposes at room temperature but was stored successfully at 0 °C for periods of time, m.p. 92 °C (dec.). Spectra for **1***a*: electronic (in EtOH) 224 nm(sh) (ε 14 × 10^3), 277 (6.3 × 10^3), 384 (4.1 × 10^3), 506 (23 × 10^3); n.m.r. (τ) 2.37 (m, 19 H, aromatics), 6.39 (q, 4H, CH_2CH_3), 8.76 (t, 6H, CH_2CH_3).

Reaction of $(p\text{-}CH_3OC_6H_4)_3P$ with $[p\text{-}Et_2NC_6H_4N_2]BF_4$

Equimolar acetone solutions of the phosphine and diazonium salt were mixed at room temperature. The red coloration formed immediately. The solution was reduced in volume *in vacuo*, and the residue recrystallized from acetone–ether to yield compound **1***c*. Nuclear magnetic resonance spectrum (τ) 2.0–3.5 (m, 16H, aromatics), 6.1 (s, 9H, OCH_3), 6.7 (q, 4H, CH_2CH_3) 8.8 (t, 6H, CH_2CH_3).

Reaction of $Na[Fe(mnt)_2]$ with $[p\text{-}FC_6H_4N_2]BF_4$

Solid $[p\text{-}FC_6H_4N_2]BF_4$ (0.845 g, 4.03 mmol) was added in small portions to a solution of $Na[Fe(mnt)_2]$ (0.382 g, 1.06 mmol) in absolute methanol (15 ml). Each addition produced gas evolution which decreased in the final stages. Volatiles were removed *in vacuo* and the residue extracted with benzene. The solvent was stripped and the product recrystallized from CH_2Cl_2 and then from CCl_4 to give yellow crystals of **7***a*, m.p. 145°.

Compounds **7***b* (m.p. 137°) and **7***c* (m.p. 156°) were obtained similarly, using methanol and dimethyl sulfoxide as solvents, respectively. Analyses are listed in Table 1. Infrared spectra (4000–400 cm^{-1}): **7***a* 3100, 3080 (w, vCH); 2230, 2220 (m, vCN); 1590, 1400 (m, arom.); 1490 (s, arom. and vC:C); 1295 w; 1225 (s, vCF); 1180 s, 1160s, 1095 m, 1015 m; 840 s, 815 msh (δ CH of 1,4 disubst. arom.); 635, 610 (w, vCS); 545 m; 515, 500 (m, δ CCN); 430 m, 420 m: **7***b*, **7***c* generally similar, allowing for differing substituents. Electronic spectra (λ_{max} (nm) $\log_{10}$ ε in parentheses): **7***a* (in CH_3OH) 334 (4.18), 248 (3.94) *ca.* 221 (4.28); **7***b* in CH_3CN, 402 (3.9), 325–300 (broad plateau of unresolved peaks, $\log_{10}$ ε 4.5 at 315 nm); **7***c* (in CH_3OH) 339 (4.4), 288 (4.2) 241 (4.6).

Mass spectra showed base peaks corresponding to parent ions at *m/e* values 330 (**7***a*), 436 (**7***b*), and 354 (**7***c*).

Reaction of $Na_2C_2S_2(CN)_2$ with $[p\text{-}FC_6H_4N_2]BF_4$

Dropwise addition of a methanol solution of $Na_2C_2S_2(CN)_2$ (0.091 g, 0.49 mmol) to a solution of $[p\text{-}FC_6H_4N_2]BF_4$ (0.203 g, 0.966 mmol) in 10 ml absolute methanol produced a red solution with little effervescence. After stirring 15 min the solvent was removed and the organic product separated from $NaBF_4$ as a benzene solution. The benzene was stripped off, and addition of CCl_4 to the remaining solid produced an uncharacterized dark red oil and a yellow solution. Crystals of **7***a* were obtained from the CCl_4-soluble fraction after evaporation, by recrystallization from methanol–water.

Anal. Calcd.: C, 58.17; H, 2.44; N, 8.48. Found: C, 57.84; H, 2.48; N, 8.59.

*S-(Benzenediazo)cysteines (**8**)*

(a) From $[Fe(cystH)_2]^{2+}$ or $[Fe(cyst)_2(CO)_2]$

The iron–cysteine complexes were obtained by literature methods (21, 22). An ice-cold aqueous solution of the aryldiazonium tetrafluoroborate was added to an equimolar aqueous solution of the iron complex. Immediate precipitation of the pale-yellow product occurred, which was filtered off, washed with cold water, ethanol, and diethyl ether. The compounds were found to be identical to samples prepared from L-cysteine directly (method *b* below) by elemental analysis and spectroscopy.

(b) From L-Cysteine

Stoichiometric quantities of L-cysteine hydrochloride monohydrate and corresponding diazonium tetrafluoroborate were mixed together in ice-cold aqueous solution, followed by the addition of the required amount of solid $NaHCO_3$ for neutralization. The flocculent pale-yellow precipitate was filtered off and washed with ice-cold water, ethanol, and diethyl ether. Analytical data and melting points are given in Table 1.

S-(Benzenediazo)triphenylmethylmercaptans

These were synthesized either by the method of Van Zwet and Kooyman (28) or from the diazonium tetrafluoroborate directly; thus benzenediazonium tetrafluoroborate (0.2 g) in water was added to a stirred solution of recrystallized (from aqueous acetone) triphenylmethylmercaptan (0.27 g) in acetone (5 ml) at 5 °C. The solution was neutralized with 10% NaOH and the yellow microcrystalline *cis*-isomer filtered off, washed well with ice-cold water followed by ice-cold methanol, dried *in vacuo*, and stored at −8°.

Anal. Calcd.: C, 78.92; H, 5.30; N, 7.36. Found: C, 78.82; H, 5.42; N, 7.25.

The *trans*-isomers were obtained from *cis*-isomers by boiling in benzene (29) and were stored in the dark. The isomers are easily distinguished by their Raman spectra (400–1600 cm^{-1}) (% relative intensities in parenthesis) *cis*: 404(9), 430(25), 482(8), 510(12), 528(10), 564(11), 619(23), 629(10), 671(15), 685(10), 711(11), 762(6), 848(19), 899(6), 930(4), 1001(100), 1035(29), 1150(38), 1190(23), 1320(5), 1445(4), 1485(11), 1492(29), 1580(16), 1592(25); *trans*: 618(8), 677(8), 758(4), 778(4), 846(6), 872(7), 1002(36), 1034(7), 1151(51), 1195(31), 1310(4), 1424(100), 1461(17), 1585(9), 1595(20).

The i.r. spectra of the isomers are differentiated by the following definitive absorptions; *cis*: 824s, 475m; *trans*: 1421s, 867w, 572m, 465m.

*trans-S-(Benzenediazo)phenylsulfones (**9**)*

Sodium benzenesulfinate in water and the appropriate diazonium salt in acetone were mixed in 1:1 mol ratio at 5 °C. The yellow crystalline precipitate was filtered off, washed with water and dried *in vacuo*. Further purification was not normally necessary, but some samples were obtained very pure by chromatography on silica gel with benzene as eluent. Analytical data are given in Table 1. Since the i.r. and Raman spectra of these compounds do not seem to have been recorded previously, the principal bands are given here for *trans*-$C_6H_5N_2SO_2Ph$; i.r. (250–1600 cm^{-1}): 315 w, 444 w, 485 m, 511 m, 536 m, 568 s,

617 s, 680 s, 721 m, 749 s, 767 s, 880 w, 997 w, 1070 m, 1086 s, 1148 s, 1158 s, 1169 vs, 1180 s, 1190 m, 1287 w, 1312 s, 1343 vs, 1351 vs, 1450 s, 1470 m, 1487 m, 1582 m; *Raman* (400–1600 cm^{-1}, % relative intensity in parenthesis): 615(24), 726(7), 750(9), 762(17), 884(9), 1001(64), 1022(8), 1150(100), 1165(20), 1194(31), 1450(61), 1472(67), 1488(29), 1585(23), 1594(18).

Isotopically substituted compounds were obtained by using isotopically labelled diazonium salts synthesized by diazotizations involving $Na^{15}NO_2$ (96%) or $C_6D_5ND_2$ purchased from Stohler Isotope Chemicals, California, U.S.A. Infrared spectra were recorded on Beckman IR 12 or Perkin-Elmer 457 instruments using samples pressed in KBr. Raman spectra are for solid samples using a Cary model 81 spectrometer and 6328 Å He–Ne excitation (Spectra-Physics 125 laser) delivering 20 mW at the sample. Where necessary the focussing lens was removed to eliminate or minimize sample decomposition. The relative intensities were not corrected for phototube response. Microanalyses were performed by the SFU microanalytical laboratory, Chemalytics Inc., Tempe, Arizona and Alfred Bernhardt, Germany. Proton n.m.r. spectra were run on a Varian A-60 at 60 MHz or a Varian HA-100 at 100 MHz.

We thank M. K. Yang for microanalytical results and the National Research Council of Canada for support of this work through operating grants.

1. R. B. KING and M. B. BISNETTE. J. Am. Chem. Soc. **86**, 5694 (1964); Inorg. Chem. **5**, 300 (1966).
2. S. TROFIMENKO. Inorg. Chem. **8**, 2675 (1969).
3. D. CASHMAN and F. J. LALOR. J. Organomet. Chem. **24**, C29 (1970).
4. D. R. FISHER and D. SUTTON. Can. J. Chem. **51**, 1697 (1973).
5. W. E. CARROLL and F. J. LALOR. J. Organomet. Chem. **54**, C37 (1973).
6. B. L. HAYMORE and J. A. IBERS. J. Am. Chem. Soc. **95**, 3052 (1973).
7. K. R. LAING, S. D. ROBINSON, and M. F. UTTLEY. Chem. Commun. 176 (1973).
8. A. J. DEEMING and B. L. SHAW. J. Chem. Soc. A, 1128 (1969).
9. T. E. NAPPIER and D. W. MEEK. J. Am. Chem. Soc. **94**, 306 (1972); A. P. GAUGHAN, B. L. HAYMORE, J. A. IBERS, W. H. MYERS, T. E. NAPPIER, and D. W. MEEK. J. Am. Chem. Soc. **95**, 6859 (1973).
10. S. CENINI, R. UGO, and G. LAMONICA. J. Chem. Soc. A, 3441 (1971).
11. G. PARSHALL. J. Am. Chem. Soc. **87**, 2133 (1965).
12. L. TONIOLO and R. EISENBERG. Chem. Commun. 455 (1971).
13. G. CAGLIO and M. ANGOLETTA. Gazz. Chim. Ital. **102**, 462 (1972).
14. D. F. GILL, B. E. MANN, and B. L. SHAW. J. Chem. Soc. Dalton, 311 (1973).
15. F. W. B. EINSTEIN and D. SUTTON. J. Chem. Soc. Dalton, 434 (1973); F. W. B. EINSTEIN, A. B. GILCHRIST, G. W. RAYNER CANHAM, and D. SUTTON. J. Am. Chem. Soc. **94**, 645 (1972).
16. F. W. B. EINSTEIN and D. SUTTON. Inorg. Chem. **11**, 2827 (1972); F. W. B. EINSTEIN, A. B. GILCHRIST, G. W. RAYNER CANHAM, and D. SUTTON. J. Am. Chem. Soc. **93**, 1826 (1971).
17. W. J. GEARY. Coord. Chem. Rev. **7**, 81 (1971).
18. H. BOCK, M. SCHNOLLER, and H. TOMDIECK. Chem. Ber. **102**, 1363 (1969).
19. W. WIEGRABE and H. BOCK. Chem. Ber **101**, 1414 (1968).
20. G. BAHR and G. SCHLEITZER. Chem. Ber. **90**, 438 (1957).
21. A. TOMITA, H. HIRAI, and S. MAKISHIMA. Inorg. Chem. **6**, 1746 (1967).
22. A. TOMITA, H. HIRAI, and S. MAKISHIMA. Inorg. Nucl. Chem. Lett. **4**, 715 (1968); M. P. SCHUBERT. J. Am. Chem. Soc. **55**, 4563 (1933).
23. A. N. HOWARD and F. WILD. Biochem. J. **65**, 651 (1957).
24. S. MATSUMOTO. J. Agr. Chem. Soc. Jap. **27**, 284 (1952).
25. R. NEDELJKOVIC and G. BARAC. Arch. Int. Pharm. **96**, 309 (1954).
26. H. ZAHN, B. WOLLEMANN, and O. WASCHKA. Z. Physiol. Chem. **294**, 100 (1954).
27. J. T. DUNN and W. A. FLETCHER. Trans. Kansas Acad. Sci. **37**, 123 (1934); A. HANTZSCH and H. FREESE. Chem. Ber. **28**, 3237 (1895).
28. H. VAN ZWET and E. C. KOOYMAN. Rec. Trav. Chim. Pays-Bas, **86**, 993 (1967).
29. L. K. H. VAN BEEK, J. R. G. C. M. VAN BEEK, J. BOVEN, and C. J. SCHOOT. J. Org. Chem. **36**, 2194 (1971).
30. H. JONKER, L. K. H. VAN BEEK, H. J. HOUTMAN, F. T. KLOSTERMANN, and E. J. SPIERTZ. J. Photogr. Sci. **20**, 53 (1972).
31. H. SHINDO and T. H. BROWN. J. Am. Chem. Soc. **87**, 1904 (1965); J. F. PEARSON and M. A. SLIFKIN. Spectrochim. Acta, **28A**, 2403 (1973).
32. H. C. FREEMAN, R. J. W. LEFEVRE, J. NORTHCOTT, and I. YOUHOTSKY. J. Chem. Soc. 3381 (1952).
33. A. H. KLAZINGA and A. VOS. Rec. Trav. Chim. Pays-Bas, **92**, 360 (1973).
34. S. PINCHAS and I. LAULICHT. Infrared spectra of labelled compounds. Academic Press, N.Y. 1971.
35. D. H. WHIFFEN. J. Chem. Soc. 1350 (1956).
36. G. W. PARSHALL. J. Am. Chem. Soc. **89**, 1822 (1967).
37. L. C. SIEKER, E. ADMAN, and L. H. JENSEN. Nature, **235**, 40 (1972).
38. E. E. VAN TAMELEN, J. A. GLADYSZ, and J. S. MILLER. J. Am. Chem. Soc. **95**, 1347 (1973); Chem. Eng. News, **51**(39), p. 15 (1973).
39. G. A. HEATH, R. MASON, and K. M. THOMAS. J. Am. Chem. Soc. **96**, 259 (1974).

Can. J. Chem. Downloaded from www.nrcresearchpress.com by 210.87.254.42 on 09/05/12
For personal use only.

A Synthesis of Muscalure, the Housefly Sex Attractant

TSE-LOK HO[1] AND CHIU MING WONG

Department of Chemistry, University of Manitoba, Winnipeg, Manitoba R3T 2N2

Received December 17, 1973

A convenient synthesis of muscalure starting from oleic acid or oleonitrile by reaction with C_5 organometallic reagents followed by Huang–Minlon reduction is reported.

On rapporte une synthèse facile de la muscalure utilisant comme produit de départ l'acide oléique ou oléonitrile sur lesquels on fait réagir un organométallique en C_5; la réduction de cet intermédiaire selon Huang–Minlon conduit au produit désiré.

[Traduit par le journal]

Can. J. Chem., **52**, 1923 (1974)

Can. J. Chem. Downloaded from www.nrcresearchpress.com by 210.87.254.40 on 09/05/12
For personal use only.

Muscalure ((*Z*)-9-tricosene) (**1**) is a sex pheromone isolated from the cuticle and feces of female housefly, *Musca domestica*. The structure (1) of this active ingredient was confirmed by a synthesis using the Wittig reaction. Three more reports of its synthesis have since appeared: (*a*) Eiter (2) employed the acetylide alkylation followed by semi-hydrogenation; (*b*) Cargill and Rosenblum (3) coupled erucic acid with methyl lithium and removed the carbonyl group by the Huang–Minlon method; (*c*) Gribble *et al.* (4) utilized the Kolbe electrolysis of mixed carboxylic acids. In short, construction of the carbon chain was based on $C_{14} + C_9$, $C_{15} + C_8$, $C_{22} + C_1$, and $C_{17} + C_6$ strategy, respectively.

Owing to the potential importance of muscalure in the study of pest control, an adequate supply from an economical synthesis is desirable. We wish to outline an alternative route to muscalure which is similar to Cargill's but involves instead a $C_{18} + C_5$ scheme. The even more readily available and inexpensive starting materials render our approach viable and competitive.

Oleic acid (**2**), having a *cis* double bond in the correct position, serves nicely as the C_{18} component. Thus reaction of **2** with *n*-pentyl lithium or condensation of oleonitrile (**3**) with *n*-pentylmagnesium bromide produced (*Z*)-trico-14-en-6-one (**4**) in 86 and 75% yields, respectively. This ketone is isomeric with Cargill's intermediate. Huang–Minlon reduction of **4** furnished muscalure in 89% yield. The method, outlined in Scheme 1, should obviously be adaptable to large scale preparation.

[1]To whom inquiries should be addressed.

The most recent synthesis (4) of muscalure also used oleic acid as a starting material. However, it was electrolytically degraded *in situ* to a C_{17} radical prior to a C—C bond formation with a C_6 counterpart which was similarly and concurrently derived from a C_7 carboxylic acid.

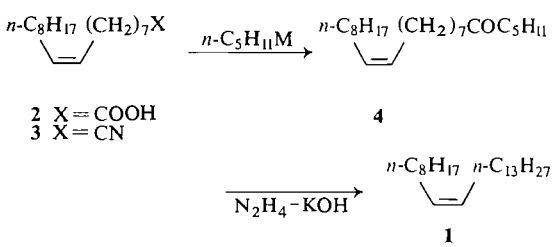

Experimental

(Z)-Trico-14-en-6-one

(*a*) A solution of *n*-pentyl lithium (34 ml, 1.2 *M* in hexane) prepared by the halogen exchange method from lithium metal and 1-bromopentane was added dropwise to oleic acid (5.64 g, 20 mmol) in dry ether (75 ml). The mixture was stirred for 1 h at room temperature, then quenched with aqueous NH_4Cl. The layers were separated and the aqueous phase was extracted with ether (3 × 50 ml). The combined organic solutions were dried ($MgSO_4$), concentrated, and distilled to give ketone **4** (5.78 g, 86%), b.p. 170–174° (~0.6 Torr); i.r. (neat) ν_{max} 3010, 1720 cm^{-1}; p.m.r. (CCl_4) δ 0.90 (6H, t, J = 4.5 Hz, CH_3), 1.1–2.2 (32H, m, CH_2), 2.30 (4H, t, J = 6 Hz, $COCH_2$), 5.28 (2H, t, J = 4.5 Hz, CH=CH); *m/e* 336 (M^+).

Anal. Calcd. for $C_{23}H_{44}O$: C, 82.07; H, 13.18. Found: C, 82.30; H, 13.25.

(*b*) Oleonitrile (6.60 g, 25 mmol) was added to the Grignard reagent generated from magnesium (1.44 g) and 1-bromopentane (9.06 g, 60 mmol) in dry ether (100 ml). After stirring at room temperature for 5 h, the reaction mixture was poured into ice water containing hydrochloric acid. The layers were separated and the aqueous solution was extracted with ether (2 × 50 ml). The ethereal solutions were dried ($MgSO_4$), evaporated to

dryness, and distilled to give ketone **4** (6.29 g, 75%), identical to the compound obtained above.

(Z)-9-Tricosene

A mixture of the ketone 4 (3.84 g, 11.4 mmol), 85% hydrazine hydrate (2.0 g, 40 mmol), potassium hydroxide (2.6 g), and diethylene glycol (25 ml) was heated to 140°. After most of the water had evaporated, the temperature was raised to 195–200° and maintained for 4 h. The cooled mixture was poured into water, and extracted with ether (2 × 40 ml). The extracts were dried, evaporated, and distilled to furnish the olefin **1** (3.30 g, 89%), b.p. 168–170° (~0.6 Torr); i.r. (neat) ν_{max} 3010, 1640 cm^{-1}; p.m.r. (CCl_4) δ 0.89 (6H, t, J = 5 Hz, CH_3), 1.43 (34 H, br s, CH_2), 2.05 (4H, pseudo-*t*, allylic CH_2), 5.27 (2H, t, J = 4.5 Hz CH=CH).

Anal. Calcd. for $C_{23}H_{46}$: C, 85.63; H, 14.37. Found: C, 85.50; H, 14.48.

This work was supported in part by a grant from the National Research Council of Canada.

1. D. A. Carlson, M. S. Mayer, D. L. Silhacek, J. D. James, M. Beroza, and B. A. Bierl. Science, **174**, 76 (1971).
2. K. Eiter. Naturwissenschaften, **59**, 468 (1972).
3. R. L. Cargill and M. G. Rosenblum. J. Org. Chem. **37**, 3971 (1972).
4. G. W. Gribble, J. K. Sanstead, and J. W. Sullivan. Chem. Commun. 735 (1973).

Can. J. Chem. Downloaded from www.nrcresearchpress.com by 210.87.254.40 on 09/05/12
For personal use only.

A Kinetic Study of High Pressure Aqueous Oxidations of Organic Compounds Using Elemental Oxygen

JAY E. TAYLOR AND JOHN C. WEYGANDT[1]

Department of Chemistry, Kent State University, Kent, Ohio 44242

Received August 27, 1973

The high pressure (< 136 atm) and high temperature (< 250°) reactions of elemental oxygen with aqueous solutions of selected soluble alcohols, ketones, and acids have been examined in detail for the first time. Saturated acids and methyl alcohol are not oxidized under the imposed conditions. The end product for the oxidation of ketones and primary alcohols is mainly carbon dioxide at 200 °C; however, appreciable yields of acids are obtained at 250 °C. *tert*-Butyl alcohol and secondary alcohols form the corresponding ketones which are then further oxidized. Those alcohols and ketones which were studied quantitatively all exhibited second-order kinetics, first order in organic compound and first order in oxygen. The compounds are listed below in the order of decreasing rate at 200°, ΔH^* in kcal/mol and ΔS^* in entropy units are noted in parentheses: 2-butanone (16.0, −25) > *tert*-butyl alcohol (24.2, −9) > cyclopentanone (12.4, −36) > isobutyl alcohol (21.5, −17) > *sec*-butyl alcohol (23.9, −15) > *n*-butyl alcohol > (21.3, −22) > acetone (15.1, −37). The alcohols have both higher entropies and enthalpies of activation than the ketones. Two non-chain mechanisms are proposed. (I) A ketone equilibrates with its enol which oxidizes to a metastable oxygenated intermediate. At 250° the intermediate decomposes to an acid or at 200° it is further oxidized to carbon dioxide. (II) Alcohols oxidize by an initial bimolecular mechanism to the corresponding ketone or aldehyde which may then be oxidized further.

On a examiné en détail pour la première fois les réactions de l'oxygène élémentaire à haute pression (< 136 atm) et à haute température (< 250°) sur des solutions aqueuses de divers alcools, cétones et acides solubles. Dans les conditions utilisées, les acides saturés et l'alcool méthylique ne sont pas oxydés. Le produit final de l'oxydation des cétones et des alcools primaires est principalement le dioxyde de carbone à 200 °C; toutefois des quantités appréciables d'acides sont obtenues à 250 °C. L'alcool *tert*-butylique et les alcools secondaires forment les cétones correspondantes qui sont oxydées d'une manière subséquente. Les alcools et les cétones qui ont été étudiés quantitativement montrent tous des cinétiques du deuxième ordre; premier ordre en composé organique et premier ordre en oxygène. On rapporte plus loin par ordre décroissant de vitesse à 200° une liste des composés examinés. On rapporte entre parenthèses les ΔH^* en kcal et les ΔS^* en unités entropiques. Butanone-2 (16.0, −25) > alcool *tert*-butylique (24.2, −9) > cyclopentanone (12.4, −36) > alcool isobutylique (21.5, −17) > alcool *sec*-butylique (23.9, −15) > alcool butylique (21.3, −22) > acétone (15.1, −37). Les alcools ont des entropies et des enthalpies d'activation qui sont plus grandes que celles des cétones correspondantes. On propose deux mécanismes qui ne sont pas en chaine. (I) La cétone s'équilibre avec son énol qui est oxydé en un intermédiaire métastable oxygéné. A 250° l'intermédiaire se décompose en acide ou à 200 °C il est alors oxydé plus loin en dioxyde de carbone. (II) Les alcools sont oxydés par un mécanisme bimoléculaire initial vers la cétone correspondante ou l'aldéhyde qui est alors oxydé plus loin.

[Traduit par le journal]

Can. J. Chem., **52**, 1925 (1974)

The high pressure oxidation of organic compounds by molecular oxygen in either aqueous or nonaqueous solution has received little attention. No mechanistic studies have been reported and the existing literature is generally utilitarian in nature. The topics discussed include the disposal of organic wastes (1–4), the oxidation of benzene to phenol (5), the oxidation of cyclohexane to cyclohexanol and cyclohexanone (6–8), and the oxidations of alkyl aromatic hydrocarbons, primary alcohols, and aldehydes to their corresponding acids (9, 10).

In contrast, liquid phase oxidations of organic compounds at subexplosion level pressures and moderate temperatures have received much attention with the fairly general conclusion that the reactions are of a free radical chain type. Since it appears that the mechanism of oxidation

[1]Present address: Department of Chemistry, Ashland College, Ashland, Ohio 44805. Oxidation Fellow, 1964–1965. Goodyear Fellow, 1965–1966.

Can. J. Chem. Downloaded from www.nrcresearchpress.com by 210.87.254.6 on 09/05/12
For personal use only.

Can. J. Chem. Downloaded from www.nrcresearchpress.com by 210.87.254.6 on 09/05/12
For personal use only.

under high pressure–temperature aqueous conditions varies significantly from the low pressure–temperature work, the present study is of some interest.

This work encompasses both qualitative and quantitative studies of water solutions of organic compounds at 68 and 136 atm (1000 and 2000 p.s.i.) total pressure and 160 to 250 °C.

Experimental

Qualitative Reactor

This reactor (not shown) consists of a stainless steel vessel, 10 ml capacity, with a screw cap, oxygen inlet, and a narrow mouth glass liner which fits snugly inside the steel vessel. A Teflon O-ring with an aluminum retainer was employed as a seal. The cap was fitted with a high pressure tube of sufficient length so that the reactor may be shaken by an oscillating shaft. The tube is connected to an oxygen reservoir (to prevent contamination of the oxygen supply in case of an explosion), a blow out plate, a high pressure gauge, and an oxygen tank which serves as the source of high pressure oxygen.

Quantitative Reactor for Kinetic Studies

This reactor consists of stainless steel inner and outer jackets with various attachments and an inner vessel fabricated of either glass or Teflon.

The inner stainless steel jacket A as shown in Fig. 1 has a cavity $1\frac{5}{8}$ in. in diameter and $1\frac{1}{2}$ in. deep. The openings C and D are for the sampling tube and oxygen inlet, respectively.

The sampling system (not shown) consists of a 3-way, 2-stem Aminco valve connected at C with a 3 ft length of high pressure tubing, 1/4 in. × 1/16 in. The upper half of this tube is encased in a condenser jacket to maintain room temperature. The center inlet of the Aminco valve is blocked and there are two outer connections, one to the reactor and one to an open tube. This pressure tube is lined with a 1/16 in. × 1/32 in. Teflon tube which extends through C to the bottom of the reactor as seen at M.

The outer jacket B supports the sealing plate E which in assembly is forced against a 2 in. × 1/16 in. Teflon O-ring G by seven bolts F to effect a gas-tight pressure seal. The O-ring is positioned by a 1/64 in. raised edge each in A and G.

Either Teflon or glass may be used for the inner vessel H–J whose sole purpose is to prevent contamination of the reactant solutions by the stainless steel or its corrosion products formed with high pressure oxygen and water. The 25 ml volume Teflon vessel H is fitted with a 13 mm diameter Teflon tube J which extends 15 mm below the center of the lid I so that a glass bulb K containing the reactant may be kept totally immersed in water. Direct contact of the organic material with high pressure oxygen is thereby prevented upon cracking the bulb K.

The oxygen outlet is connected to an oxygen reservoir, a blow out plate, high pressure gauge, and oxygen tank as with the qualitative apparatus.

The reactors were fabricated at Kent State University. The valves, tubing, and connectors were purchased from American Instrument Co.

The reactors, both qualitative and quantitative, are

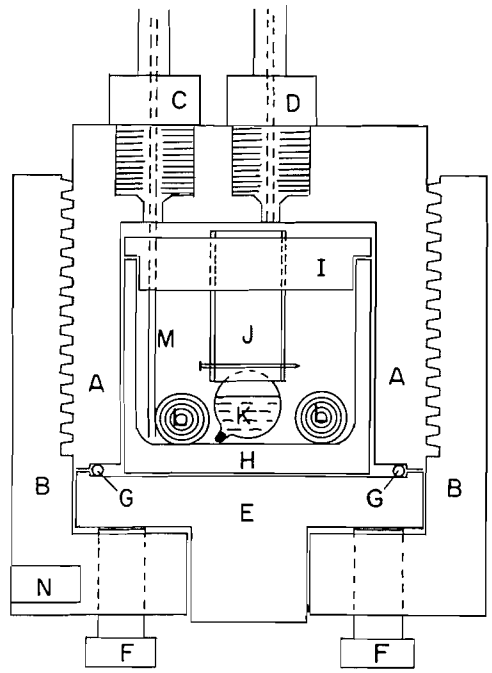

FIG. 1. Diagram of the quantitative reactor. A, externally threaded inner stainless steel jacket; B, internally threaded, chrome plated, outer steel jacket; C, pressure connection to sampling valve; D, pressure connection for oxygen inlet; E, stainless steel sealing plate; F, seven bolts for tightening sealing plate; G, 2 in. × 1/16 in. Teflon O-ring; H, Teflon liner; I, Teflon cap for the liner; J, Teflon tube to maintain immersion of bulb K; K, pressure sensitive glass bulb containing reactant; L, 1 cm glass balls; M, sample tube; N, hole for pry bar to disassemble reactor.

agitated by an external mechanical shaker to insure dissolution of oxygen and to effect rapid mixing of the organic compound for the quantitative studies. Two 1-cm glass balls shown at L abet the mixing. Temperature control is maintained by an air bath which can be raised or lowered about the reactor. The samples are analyzed by gas chromatography using either Carbowax or Polypak columns.

The reactors are sufficiently overdesigned so that when an explosion occurs, it is contained within the apparatus and offers no danger to the operator or the equipment. Those explosions which did occur generally resulted in clogging of the oxygen inlet tube by carbon and were probably due to direct contact of the organic compound with oxygen. The Teflon liner has survived several explosions with minimal damage. The most devasting conflagration resulted from the attempted use of perfluorotoluene as a solvent in a qualitative reactor. The liner, tubing, and blow out plate with its holder were damaged beyond repair with the latter being partially fused by the exiting gases.

Qualitative Procedures

Three milliliters of approximately 0.5 *M* solution of the organic compound are placed in the glass liner of the

Can. J. Chem. Downloaded from www.nrcresearchpress.com by 210.87.254.6 on 09/05/12
For personal use only.

small reactor, which is then assembled, pressurized, and heated to the desired temperature. After 4 h, including the heating time, the reactor is cooled, the pressure released, and the products are determined by gas chromatography.

Quantitative Rate Determinations

To initiate the reaction at a precise time under known conditions of temperature and pressure, the organic compound is placed in a tared 12 mm diameter bulb K. This bulb is blown from the end of a 3 in. long, 4 mm Pyrex tube using a 6 mm length of the tubing. The bulb containing the organic compound is immersed in a Dry Ice – trichlorethylene mixture. It is then evacuated and sealed under reduced pressure with elimination of the stem. The severed tube and bulb are reweighed, and the weight of the reactant is then determined after correction for air displacement. The bulb is of such thickness that it withstands 20 atm pressure but shatters between 50 and 80 atm. Some practice is needed to blow a satisfactory bulb. As previously mentioned, a tube extending from the liner cap holds the bulb below the surface of the water to insure that the organic compound does not come in direct contact with gaseous oxygen when the bulb breaks.

To begin the reaction, 12.5 ml of water, the two 1-cm glass mixing balls L, and the sealed bulb with the reactant are placed in the liner of the kinetic reactor. After assembly and pressurization to 20 atm, the reaction temperature is attained by heating 20° above that temperature for about 2 h followed by 1 h at the desired temperature in the air bath. To attain the final pressure, additional oxygen is then introduced causing the bulb to break inside the reactor. Stirring is started immediately initiating the reaction. Periodically, samples of the solution are collected using the dual valve collection system. The % reactant remaining and the detectable products are determined in the collected samples.

The first-order rate constant, k', is evaluated at a constant oxygen pressure using a standard graphical procedure based on the disappearance of the original compound. Typical first-order rate plots are shown in Figs. 2 and 3. The second-order rate constant, k_{obs}, is determined by dividing k' by mol/l of dissolved oxygen calculated from known solubilities (11) of oxygen in water at the indicated temperatures. It is necessary to extrapolate from 500 p.s.i., the maximum pressure recorded in that paper, to the indicated pressure using Henry's law. Correction is also made for the partial pressure of water vapor. $\Delta H^{\ddagger}$ is obtained from the Arrhenius activation energy since $E_a = \Delta H^{\ddagger} + RT$.

Results

A summary of the total collection of aqueous oxidation data follows. Carbon dioxide is the presumed product unless other products are indicated.

(*1*) Short chain saturated carboxylic acids are inert under the described conditions (see Table 1).

(*2*) Ketones are oxidized at the α carbon. At 250° 2-butanone yields a nearly equimolar quantity of acetic acid with a trace of propionic acid. Acetone forms lesser amounts of acetic acid. In both cases the acetic acid yields greatly decrease at 200° (see Table 1).

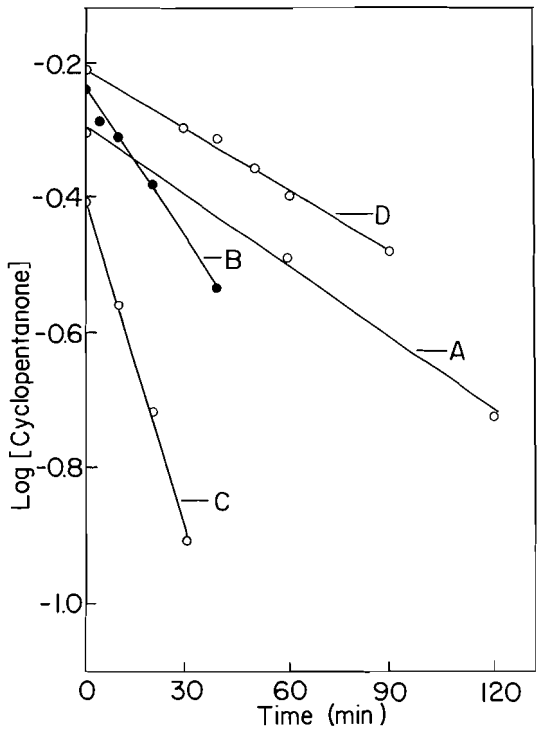

FIG. 2. First-order rate curves for cyclopentanone (*A*) 160° and 136 atm total pressure, (*B*) 180° and 136 atm, (*C*) 200° and 136 atm, (*D*) 180° and 68 atm total pressure.

(*3*) The bulk of formaldehyde is completely oxidized to carbon dioxide but the Cannizzaro reaction is also in evidence since methyl formate, methyl alcohol, and formic acid were detected (see Table 1).

(*4*) The products of oxidation of primary alcohols vary both with the specific alcohol and with temperature. Methyl alcohol is unaffected at 250° after 6 h. Ethyl alcohol is nearly completely oxidized at 250° with formation of 50% yields of acetic acid. At 200° the amount of acetic acid is decreased as both % of product and total yield. At 200° *n*-butyl alcohol forms traces of butyric acid. No detectable organic products at 200° are obtained from isobutyl alcohol (see Table 1).

(*5*) Secondary and tertiary alcohols form the corresponding ketones as isolatable intermediates. These ketones are further oxidized in accordance with their relative reactivity. For example, *sec*-butyl alcohol gives low yields of acetic acid at 200° and small amounts of 2-butanone whereas *tert*-butyl alcohol gives nearly

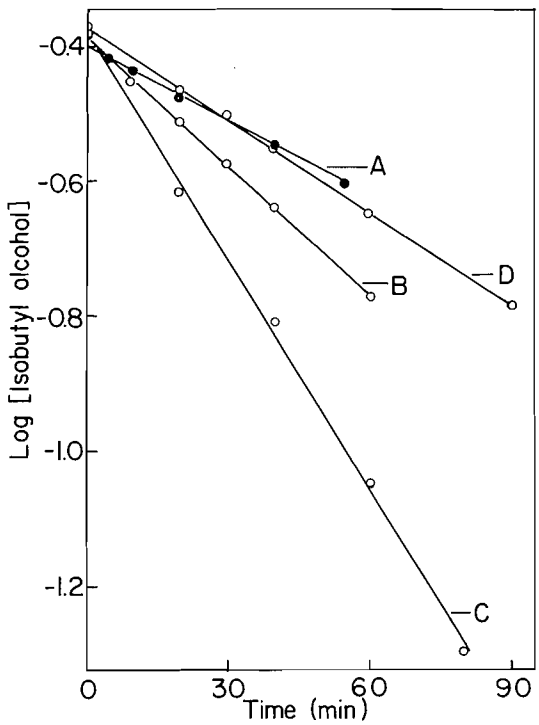

FIG. 3. First-order rate curves for isobutyl alcohol (*A*) 180° and 136 atm total pressure, (*B*) 190° and 136 atm, (*C*) 200° and 136 atm, (*D*) 200° and 68 atm total pressure.

equimolar yields of acetone. Formaldehyde was isolated in trace amounts. It appears, therefore, to be an intermediate formed by oxidation of the severed CH_3 group. Isopropyl alcohol forms acetone in excellent yields at 200° (see Table 1).

(*6*) Ethylene glycol and its derivatives undergo carbon–carbon bond scission with partial formation of formic acid (see Table 1).

(*7*) A demonstration of typical dependence of the rate of oxidation on the concentration of organic compound and on oxygen is seen in Figs. 2 and 3 where the rate plots for cyclopentanone and isobutyl alcohol at three temperatures and second oxygen concentrations are shown. The first-order dependence of the rate on both the organic molecule and oxygen concentrations indicates an overall second-order reaction. The second-order rate constants k_{obs} are calculated as previously described. The first- and second-order rate constants for all compounds studied are listed in Table 2.

(*8*) Quantitative comparison of the rates of oxidation shows that the decreasing order of reactivity for the ketones is 2-butanone, cyclohexanone, cyclopentanone, and acetone. With alcohols the order is *tert*-, iso-, *sec*-, and *n*-butyl alcohols. Erratic results were obtained with 2,2-dimethyl-1-propanol (neopentyl alcohol) which oxidizes at a rate similar to *sec*-butyl alcohol. Considering all the compounds, 2-butanone is the most rapidly oxidized at 200°. This is followed by *tert*-butyl alcohol, cyclopentanone, isobutyl alcohol, *sec*-butyl alcohol, *n*-butyl alcohol, and acetone (see Table 2).

(*9*) The alcohols exhibit higher values for both the enthalpy and entropies of activation, $\Delta H^{\ddagger}$ and $\Delta S^{\ddagger}$, as compared to the ketones. Among the ketones, 2-butanone has the highest values of both $\Delta H^{\ddagger}$ and $\Delta S^{\ddagger}$; acetone is intermediate in $\Delta H^{\ddagger}$ but has the lowest $\Delta S^{\ddagger}$. For the alcohols *tert*-butyl alcohol has both the highest $\Delta S^{\ddagger}$ and $\Delta H^{\ddagger}$, and *n*-butyl alcohol has the lowest of these values (Table 3).

Discussion

Elemental oxygen is characterized by the diversity of its reactions which include hydrocarbon autoxidations, gas phase radical oxidations, enzymatic oxidations, singlet oxygen reactions, and catalyzed oxidations of ascorbic acid, cysteine, etc.

The high pressure oxidations, herein described, present yet another aspect of the reactions of elemental oxygen. They are kinetically of second order; first order each in oxygen and the organic substance. The products are the apparent result of an oxidative scission of either a carbon–carbon or a carbon–hydrogen bond. Since these features differ considerably from those of a characteristic chain reaction, it is concluded at this time that these high pressure aqueous oxidations are not of that type.

The effect of the solvent water upon the reaction is threefold. First, it acts as a diluent for the high pressure oxygen and a dispersant of the heat of reaction, thereby preventing localized temperature increases and excessive rates of reaction. Second, the reactant is modified by hydration by adding the heat and entropy of hydration to the ground state properties of the reactant. Third, it appears to have a damping effect on the radical–chain mechanism.

Little is known concerning the state of the oxygen molecule under pressure in water. The solubility of oxygen in water varies with temperature and at 150° a minimum in solubility is

Can. J. Chem. Downloaded from www.nrcresearchpress.com by 210.87.254.6 on 09/05/12
For personal use only.

TABLE 1. Qualitative aqueous oxidations

Reactant	Temperature (°C)	% oxidized	Product	Mol ratio % product / % oxidized
Acetic acid	250	0		
Propionic acid	250	0		
Acrylic acid	250	100		
Formaldehyde	200	80	Methyl formate	
			Formic acid	
			Methyl alcohol	
Acetone	200	10	Acetic acid	Trace
	250	80	Acetic acid	0.25
2-Butanone	200	~100	Acetic acid	0.2–0.3
	250	100	Acetic acid	~1.0
			Propionic acid	Trace
Cyclopentanone	250	100	Succinic acid*	
Cyclohexanone	250	100	Succinic acid*	
			Glutaric acid*	
Methyl alcohol†	250	0		
Ethyl alcohol	200	15–20	Acetic acid	Trace
	250	95	Acetic acid	0.5
Isopropyl alcohol	200	40–50	Acetone	0.8–1.0
			Acetic acid	Trace
	250	95	Acetone	0.2
			Acetic acid	<0.1
n-Butyl alcohol‡	200	~15	Butyric acid	Trace
sec-Butyl alcohol‡	200	~20	2-Butanone	Trace
			Acetic acid	0.1
Isobutyl alcohol‡	200	~80		
tert-Butyl alcohol‡	200	~100	Acetone	~1.0
			Acetic acid	Trace
			Formaldehyde	Trace
Neopentyl alcohol‡	200	24		
Ethylene glycol	250	40	Formic acid	
Diethylene glycol	250	90	Ethylene glycol, etc.	0.3
Triethylene glycol	250	95	Ethylene glycol, etc.	0.25
Phenol	25	10–20	Brown polymer(?)	
Phenol	200	100	Brown polymer(?)	

NOTE: Total pressure, 136 atm; partial pressure of oxygen 121 atm at 200° and 97 atm at 250 °C. Reaction time, 4 h including 1–1.5 h warm-up. Unless otherwise indicated the products are carbon dioxide and water.
*Detected as the anhydride in the residue after distillation of the solvent water.
†Six hour reaction time.
‡One hour reaction time.

noted. Above this temperature there is a continuous increase in solubility with increasing temperature (11). This increase is undoubtedly due in part to the decreased hydrogen bonding of water which permits a more efficient accommodation of the oxygen molecules into the water structure.

Is there concordant change in the oxygen molecule? The possibility of a singlet–triplet equilibrium with a hyperreactive singlet species is considered. Since the singlet–triplet conversion requires 22 kcal/mol (12) and the observed activation energies vary between 12 and 24 kcal/mol, this proposal is presently rejected. The considerations of other possible reactive forms, *e.g.*, the O_4 molecule, are not eliminated but are not further discussed in this paper.

Since there are several kinds of reactions with differing products, a single mechanism does not appear to be adequate for the high pressure oxidations.

Mechanism I concerns ketones. The rate of enolization is slow at room temperature but may be assumed to be rapid at elevated temperatures. Accordingly, the keto–enol exchange may be treated as a simple equilibrium at 200°.

Can. J. Chem. Downloaded from www.nrcresearchpress.com by 210.87.254.6 on 09/05/12
For personal use only.

TABLE 2. Summary of experimental rate data

Compound	Temperature (°C)	Partial pressure O_2* (Atm)	Exp. $k' \times 10^2$* (min^{-1})	Calcd. k_{obs}† ($l\ mol^{-1}\ min^{-1}$)
Acetone	200	121	0.105‡	0.0080
	220	113	0.242	0.0156
	220	45	0.119	0.0193
	240	103	0.567	0.0305
2-Butanone	160	130	2.24	0.199
	180	126	5.35	0.455
	200	121	13.75	1.05
	200	53	7.15	1.25
Cyclopentanone	160	130	0.834	0.0742
	180	126	1.733	0.148
	180	58	0.788	0.145
	200	121	3.60	0.274
Cyclohexanone	180	126	1.92	0.164
n-Butyl alcohol	180	126	0.0737	0.00625
	190	124	0.136	0.0110
	200	121	0.230	0.0175
	200	53	0.115	0.0200
sec-Butyl alcohol	180	126	0.193	0.0164
	190	124	0.361	0.0289
	200	121	0.690	0.0526
	200	53	0.322	0.0563
Isobutyl alcohol	180	126	0.830	0.0704
	190	124	1.50	0.120
	200	121	2.63	0.201
	200	53	1.08	0.189
tert-Butyl alcohol	180	126	2.28	0.193
	190	124	4.37	0.351
	200	121	8.22	0.627
	200	53	4.03	0.704
Neopentyl alcohol	200	121	0.47	0.035

*The total pressure in all cases is either 136 or 68 atm.
†Based on the calculated concentration of dissolved oxygen in mol l^{-1}.
‡The average reliability of the rate constants is estimated at ± 5%.

TABLE 3. Kinetic parameters

Compound	E_a (kcal/mol)	$\Delta H^{\ddagger}$ (kcal/mol)	$\Delta F^{\ddagger}$ (kcal/mol)	$\Delta S^{\ddagger}$ (cal/deg mol)
Acetone	16.1	15.1	32.6	−37
2-Butanone	16.9	16.0	28.0	−25
Cyclopentanone	13.3	12.4	29.3	−36
n-Butyl alcohol	22.2	21.3	31.9	−22
sec-Butyl alcohol	24.8	23.9	30.9	−15
Isobutyl alcohol	22.4	21.5	29.6	−17
tert-Butyl alcohol	25.1	24.2	28.5	−9

[1] $$K = [\text{Enol}]/(\text{Ketone})$$

where [Enol] and [Ketone] represent the existing concentrations of these entities, and [A] = sum of Enol + Ketone.

[2] $$[\text{Enol}] = [\text{A}]K/(K + 1)$$

Noting that both the simple double bond (*e.g.*, acrylic acid) and the enol structure (phenol) are readily attacked by oxygen, Table 1, it is pro-

Can. J. Chem. Downloaded from www.nrcresearchpress.com by 210.87.254.6 on 09/05/12
For personal use only.

TABLE 4. Estimated values* for the keto-enol equilibria

	Temperature (°C)	K	ΔH_K (kcal/mol)	k_1	E_1 (kcal/mol)
Acetone	200	0.0026		3.1	
	220	0.0043	11.9†	3.6	4.1
	240	0.0070		4.3	
2-Butanone	160	0.15		1.5	
	180	0.23	9.1†	2.4	9.7
	200	0.36		4.0	
Cyclopentanone	160	0.108		0.76	
	180	0.17	9.1†	1.0	5.5
	200	0.27		1.3	

*The last digit for each number listed is not significant. The overall reliability of these data is not known.
†In the calculation (15) of ΔH_{enol} the value of O—(C_d)(H) was determined from O—(C_2), O—(C)(H), and O—(C_d)(C). Also C_p for the enol was assumed equal to C_p for the ketone.

posed that oxidation of ketones occurs via enol intermediates. Thus

$$[3] \qquad -\frac{dA}{dt} = k_1[\text{Enol}][O_2] = (k_1K)/(K + 1)[A][O_2]$$

$$[4] \qquad k_{obs} = k_1K/(k + 1)$$

where k_{obs} is from Table 2 and k_1 is the rate constant for the reaction of oxygen with the enol. If K is close to unity, the observed values of $\Delta H^{\ddagger}_{obs}$ will change with temperature due to the factor $K/(K + 1)$. See ref. 13 for a clearly defined example of such a change. Since $\Delta H^{\ddagger}_{obs}$ is constant over the imposed temperature range, the values of K are assumed not to be closely equal to unity for each ketone.

Since neither the enolization constants K at the desired temperatures nor the corresponding enthalpies had been determined, estimation of these values was attempted. The available data are equilibrium constants at room temperature determined from the data of Gero given for pure liquids (14): acetone, 1.5×10^{-6}; cyclopentanone, 8.8×10^{-4}; and 2-butanone, 1.2×10^{-3}.

The values for ΔH_K, the enthalpy of enolization, were estimated by the method of Benson (15) where the estimated ΔH_{enol} is subtracted from ΔH_{ketone}. The C_p values for enol and ketone were assumed to be roughly equal. The equilibrium constants K were then estimated from the van't Hoff equation using the above data.

Using the enolization constants K, estimation of the rate constants k_1 for the reaction of oxygen with the enol can be made from eq. 4. Finally the Arrhenius activation energies were estimated from the k_1 values. E_1 and k_1, it should be noted, are secondary extrapolations and the original experimental errors may be magnified in these calculations. However, certain correlations can be made (see Table 4).

From Tables 2 and 3 it is seen that acetone widely differs in rate from the other two ketones. In Table 4 the rate constants k_1 for the three ketone enolates are roughly equivalent. This is reasonable since the structural differences among three compounds are minor.

Acetone and cyclopentanone enolates have the lowest activation energies, E_1. This is consistent with their structures. Acetone enolate is the simplest of the three compounds. Cyclopentanone enolate has the most open double bond structure; this is due to the internal bond angles which average 108° and effect spreading of the exterior bond angles. Thus, the normal 120° bond angles associated with a double bond are exceeded in cyclopentanone enolate.

With both acetone and 2-butanone it is noted (Table 1) that the yields of acetic acid are much higher at 250 than at 200°; that is, a slower but more complete oxidation occurs at the lower temperature. Since acetic acid is not detectably oxidized at either temperature, the formation of a semistable intermediate is clearly indicated. At 200° the intermediate is of such stability that the rate of oxidation is faster than the rate of thermal decomposition. At 250° the thermal decomposition exceeds oxidation in rate, and acetic acid is formed along with another intermediate which is further oxidized.

A mechanism has been developed which takes into account the second-order reaction, the formation of the enol, and the transitory oxygenated

Can. J. Chem. Downloaded from www.nrcresearchpress.com by 210.87.254.6 on 09/05/12
For personal use only.

intermediate. This mechanism with 2-butanone as an example is shown below.

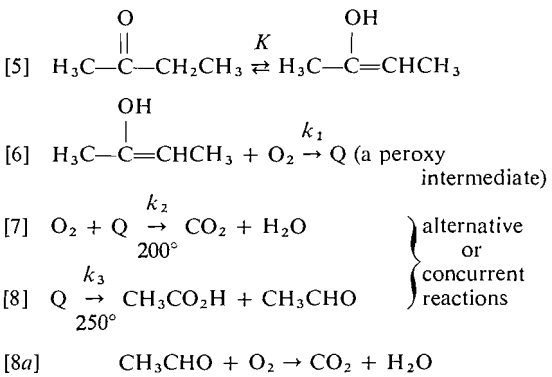

Following the equilibrium formation of the enol in [5], the rate-determining step is [6] which identifies the overall second-order nature of the oxidation. Equations 7 and 8 are alternatives which follow [6]. Reaction 8 is a unimolecular decomposition, possibly resulting from electron pair transfers within a transitory four-membered peroxy ring (not shown). Reaction 7 is an undefined oxidation of greater complexity having both a lower enthalpy and entropy of activation than [8]. With these conditions reaction 7 predominates at the lower temperatures and [8] at the higher temperatures; both [7] and [8] are, as indicated, faster than [6]. The oxidation of acetaldehyde [8*a*] follows [8] in rapid succession.

Since the evidence for the above mechanism is based solely on product analysis and rate and reaction order correlations, the proof is not absolute. A radical–chain mechanism, similar to that proposed for acetone (16) in the presence of di(*tert*-butyl) peroxide or as proposed for the liquid phase oxidation of 2-butanone (17) and other ketones (18), cannot be totally eliminated. After formation of the enolate a radical–chain mechanism could effect the consummation of the oxidation. In view of the present data and by arguments similar to those to be presented against such a mechanism for the alcohols, the radical–chain mechanism is not indicated at this time for any part of the reaction.

The correlative evidence for the enol intermediate does, however, give strong support for the presently described mechanism in aqueous solutions. Conceivably, the radical–chain mechanism may be in effect for pure compounds or nonaqueous solutions, and the molecular mechanism may hold for aqueous solutions.

Mechanism II concerns the alcohols. It is clear from the formation of formaldehyde and the excellent yields of acetone resulting from the oxidation of *tert*-butyl alcohol that oxidative severage of a carbon–carbon bond occurs. Attack of the oxygen is then, by implication, on the methyl groups of the *tert*-butyl alcohol. The singular unreactivity of methanol to oxidation gives further credence to this idea since, if oxidation occurred only on the carbinol group, methanol should be readily oxidized. Thus, it appears that the alcohols are all oxidized on the carbon(s) adjacent to the carbinol group by an approach of the oxygen molecule backside to the hydroxyl. Further, in view of the second-order kinetics and the negative entropies of activation, a transitory intermediate which decomposes to products is proposed. A mechanism is outlined below for *tert*-butyl alcohol.

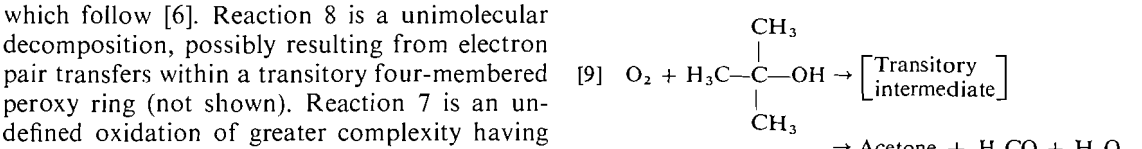

No attempt is made at this time to define the nature of the transitory intermediate. Although several structures could be postulated, the speculation is reserved for future papers.

Similarly, the oxidation of *sec*-butyl alcohol is second order, and the clearly indicated formation of intermediate ketones (Table 1) predisposes a mechanism similar to the tertiary alcohols with the formation of the corresponding ketone and presumably hydrogen peroxide as intermediates. However, no analytical evidence for the formation of hydrogen peroxide was obtained. If formed, it decomposes rapidly and is present in only zero to trace amounts. Although 2-butanone is rapidly oxidized, there is analytical evidence for its formation from *sec*-butyl alcohol (see Table 1). With isopropyl alcohol the stability of the intermediate acetone is such that it is formed nearly quantitatively at 200°, but at 250° further oxidation of the acetone is noted after 4 h.

n-Butyl alcohol oxidation is also kinetically second order and a mechanism similar to the above with an initial oxidation to the corresponding aldehyde is suggested. The carbon chain of the resulting aldehyde is rapidly

Can. J. Chem. Downloaded from www.nrcresearchpress.com by 210.87.254.6 on 09/05/12
For personal use only.

Can. J. Chem. Downloaded from www.nrcresearchpress.com by 210.87.254.6 on 09/05/12
For personal use only.

oxidized, carbon by carbon, to the end products, carbon dioxide and water.

With ethyl alcohol a distinct increase in acetic acid formation is noted at 250° as compared to 200° (Table 2). In explanation, the proposed intermediate acetaldehyde is rapidly oxidized to either acetic acid at 250° or to carbon dioxide at 200° via the enol intermediate as discussed for 2-butanone.

A radical-chain mechanism, although not totally eliminated from consideration, seems unlikely for alcohols as well as ketones. Radical–chain mechanisms in liquids are generally autocatalytic or require added initiators. Their rates are zero order in oxygen except at low oxygen concentrations. Peroxides necessary for the initiation step have not been detected; thus, if formed by any means, they decompose very rapidly. If the rate-determining step were

$$[11] \qquad RH + O_2 \rightarrow R\cdot + HO_2\cdot$$

an order of two would be observed. However, the activation energy of reaction 11 is much too high since the H—O_2 bond dissociation energy is 47 kcal/mol (19), and ΔH for [11] is roughly 40 kcal/mol or greater. The absence of reaction 11 in the homogeneous gas phase oxidative pyrolysis of ethane has been discussed (20). As indicated in the discussion on ketones, the radical–chain mechanism appears to be more likely under non-aqueous conditions and the non-chain mechanism is preferred in aqueous solutions due to the impact of solvent water.

Most oxidizing agents react with tertiary alcohols less readily than with secondary alcohols. With high pressure aqueous oxygen there is a conspicuous reversal among the butyl alcohols since the order is *tert* > iso > *sec* > prim. (Tables 2 and 3.) Further, the rate of oxidation of neopentyl alcohol is greater than that of 1-butanol. However, the enthalpies of activation follow the order *tert* $\geqq$ *sec* > iso $\geqq$ prim. At lower temperatures the tertiary butyl alcohol could become the slowest in rate since it has the greatest value of ΔH.

The entropies of activation $\Delta S^{\neq}$ in sequence are: *tert* > *sec* $\geqq$ iso > prim. Examination of the spatial characteristics of the four alcohols via Fisher–Hirschfelder models indicates qualitative sequential correlation with the several alcohols via mechanism 9. *tert*-Butyl alcohol is symmetrically compact and the oxygen may approach from any direction to form the activated complex by mechanism 9. In comparison the remaining molecules have smaller areas that are sensitive to oxygen attack. If the tertiary hydrogen of isobutyl alcohol is assumed to have greater reactivity than the secondary hydrogens of *n*-butyl alcohol, qualitative correlation with the observed entropies of activation can be made.

In conclusion this paper has presented an initial survey and has proposed mechanisms for high pressure aqueous oxidations of certain organic compounds. Research on the nature of these oxidations is being continued.

The concept of a basic study of high pressure aqueous oxidations was first proposed by Dr. Waldo Semon and the project was made possible by Dr. Semon's financial sponsorship of the Oxidation fellowship. The authors are further indebted to Dr. Semon for many excellent suggestions made during the course of the work.

The authors also wish to express their appreciation to Mr. Paul Norton, machinist, for the fabrication of the reactor and to Mr. John Thomas for the supplementary work on the oxidation of formaldehyde and ethylene glycol.

1. F. J. Zimmermann. U.S. Patent 2,842,058 (1958).
2. F. J. Zimmermann, U.S. Patent 2,903,425 (1959).
3. F. J. Zimmermann. Ind. Waters Waste. **6**, 102 (1961).
4. I. G. Pepelyaev, N. D. Punchenko, and V. V. Sboeva. Izv. Vyssh. Ucheb. Zaved. Stroit. Arkhitekt, **11**, 153 (1968).
5. Y. Hosaka. J. Chem. Soc. Jap. Ind. Chem. Sect. **57**, 197 (1954).
6. N. Ohta and T. Tezuka. J. Chem. Soc. Jap. Ind. Chem. Sect. **57**, 641–3 (1954).
7. N. Ohta and T. Tezuka. J. Chem. Soc. Jap. Ind. Chem. Sect. **57**, 723–5 (1954).
8. John N. Crosby. U.S. Patent 2,565,087 (1951).
9. W. G. Toland, Jr. U.S. Patent 2,587,666 (1952).
10. W. G. Toland, Jr. U.S. Patent 2,695,313 (1954).
11. H. A. Pray, C. D. Schweichert, and B. A. Minnich. Ind. Eng. Chem. **44** (1), 1146 (1952).
12. C. S. Foote. Acc. Chem. Res. **1**, 104 (1968).
13. J. E. Taylor. J. Am. Chem. Soc. **75**, 3912 (1953).
14. A. Gero. J. Org. Chem. **19**, 469, 1960 (1954); *cf.*, R. P. Bell and P. W. Smith. J. Chem. Soc. (B), Phys. Org. 241 (1966).
15. S. W. Benson. Thermochemical kinetics. John Wiley and Sons, Inc. 1968. p. 18.
16. J. Rouchaud and B. Lutete. Can. J. Chem. Eng. **47**, 157 (1969).
17. G. F. Zaikov, A. A. Vichutinskii, and Z. K. Maizus. Kinet. Katal. **8**, 675 (1967). *cf.* Chem. Abstr. **67**, 90321r (1967).
18. I. I. Rif, V. M. Potekhin, and V. A. Proskuryakov. Zh. Prikl. Khim. (Leningrad), **45**, 2132 (1972).
19. S. N. Foner and R. L. Hudson. J. Chem. Phys. **36**, 2681 (1962).
20. J. E. Taylor and D. M. Kulich. Int. J. Chem. Kinet. **5**, 455 (1973).

Dihydrothiophenes. III. Preparation of Some 3,4-Unsubstituted Examples

JOHN M. MCINTOSH AND RICHARD S. STEEVENSZ
Department of Chemistry, University of Windsor, Windsor, Ontario N9B 3P4

Received December 13, 1973

Using the reaction between four representative vinylphosphonium salts and three α-mercaptoaldehydes, 12 3,4-unsubstituted 2,5-dihydrothiophenes (**1**) were prepared. The reaction proceeds in excellent yields under mild conditions. The use of these compounds in the synthesis of dienes is indicated.

On a préparé 12 dihydro-2,5 thiophènes non substitués en position 3,4; ces synthèses impliquent la réaction de quatre sels représentatifs de vinylphosphonium avec trois α-mercaptoaldéhydes. La réaction se produit avec d'excellents rendements dans des conditions douces. On montre comment ces composés peuvent être utilisés pour la synthèse de diènes.
[Traduit par le journal]

Can. J. Chem., **52**, 1934 (1974)

Recently, we have reported (1, 2) a new route to conjugated dienes (**2**) using 2,5-dihydrothiophenes (**1**) as key intermediates (Scheme 1). As we have shown, these compounds are readily available from the reaction of vinylphosphonium salts and α-mercaptoketones. The synthetic advantages to this method have already been outlined (2).

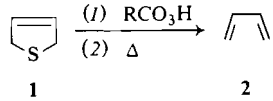

1 **2**

SCHEME 1

The dihydrothiophenes reported thus far have been derived from α-mercaptoketones and are substituted at the 3-position. As the final step in the reaction (Scheme 2) is a Wittig reaction, a process known to be dramatically subject to steric hindrance (3, 4), we had every reason to expect that employing α-mercaptoaldehydes in the reaction should afford excellent yields of **1**.

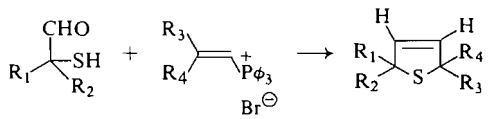

3-5 **6-9** **10-21**

SCHEME 2

These expectations were realized (Table 1). The reactions were run as previously described (2) using pyridine as solvent and preparing the vinyl salts by *in situ* isomerization of their allyl isomers when required.

The α-mercaptoaldehydes which frequently exist as highly insoluble dimers or polymers (2) were more difficult to prepare than the corresponding ketones but their reactions with the representative vinylphosphonium salts were more rapid. In most cases these reactions were essentially complete in a few hours at 100° but in others a longer reaction time was required for maximum yields (Table 1). Although all reactions were run using equimolar quantities of reactants it has been observed that a slight (10%) excess of the vinyl salt increased the yields dramatically (5).

As can be seen from Table 2, with the exception of compound **18**, the n.m.r. absorptions for the vinyl hydrogen atoms of the dihydrothiophenes occurred as sharp singlets. The chemical shifts of these appear to be dependent upon the degree of substitution at the 2,5-positions. We are pursuing this point. It should also be noted that the n.m.r. spectra provided no evidence for the presence of geometric isomers where these were possible. As the further conversion of the dihydrothiophenes to dienes occurs by a stereospecific pathway (2, 6) a highly stereoselective synthesis of compounds of type **1** would be of great importance. At present, we are engaged in a study of the reaction stereochemistry which will be reported at a later date.

Experimental

Unless otherwise noted, n.m.r. spectra were obtained on a JEOLCO C60HL spectrometer in deuteriochloroform and are reported in p.p.m. from TMS as internal standard. Gas–liquid chromatography analyses were carried out on an F and M Model 720 gas chromatograph utilizing an 8 ft × 0.375 in. 20% SE30 on Chromosorb W column. The flow rate of the helium carrier gas was 1 ml/s. Mass

Can. J. Chem. Downloaded from www.nrcresearchpress.com by 210.87.254.6 on 09/05/12
For personal use only.

TABLE 1. Products and yields of 2,5-dihydrothiophenes

Aldehyde	Salt[b]	Product	R_1	R_2	R_3	R_4	Time (h)	Yield (%)
3[a]	6	10	C_2H_5	H	H	H	2	70
3	7	11	C_2H_5	H	H	Me	2	70
3	8	12	C_2H_5	H	Me	Me	2	71
3	9	13	C_2H_5	H	Me	Ph	5	43
4[a]	6	14	C_5H_{11}	H	H	H	2	45
4	7	15	C_5H_{11}	H	H	Me	4	65
4	8	16	C_5H_{11}	H	Me	Me	12	95
4	9	17	C_5H_{11}	H	Me	Ph	20	50
5	6	18	$-(CH_2)_5-$		H	H	20	63
5	7	19	$-(CH_2)_5-$		H	Me	24	65
5	8	20	$-(CH_2)_5-$		Me	Me	46	95
5	9	21	$-(CH_2)_5-$		Me	Ph	48	54

[a]Reference 8.
[b]Reference 2.

TABLE 2. Indices of refraction and nuclear magnetic resonance spectra[a]

Compound	n_D^{25}	Nuclear magnetic resonance spectral data
10	1.5058	5.65 (s, 2), 4.08 (m, 1), 3.62 (m, 2), 1.61 (m, 2), 0.95 (t, 3, J = 6)
11	1.4898	5.60 (s, 2), 4.12 (m, 2), 1.63 (d, 3, J = 7), 0.98 (t, 3, J = 6)
12	1.4774	5.25 (s, 2), 4.18 (dd, 1, J = 7.5, 6), 1.65 (m, 2), 1.50 (s, 6), 0.95 (t, 3, J = 6)
13	1.5620	7.18 (m, 5), 5.68 (s, 2), 4.18 (dd, 1, J = 9), 1.88 (s, 3), 2.10–1.35 (m, 2), 0.92 (t, 3, J = 6)
14	1.4931	5.73 (s, 2), 4.35–3.89 (m, 1), 3.65 (m, 2), 1.95–0.65 (m, 8), 0.93 (t, 3, J = 6)
15	1.4851	5.60 (s, 2), 4.15 (m, 2), 2.00–0.80 (m, 8), 1.35 (d, 3, J = 7), 0.89 (t, 3, J = 6)
16	1.4759	5.49 (s, 2), 4.30–3.98 (m, 1), 1.80–0.90 (m, 8), 1.50 (s, 6), 1.02–0.63 (m, 3)
17	1.5361	7.19 (m, 5), 5.73 (s, 2), 4.43–4.03 (m, 1), 1.87 (s, 3), 1.75–1.08 (m, 8), 1.04–0.67 (m, 3)
18	1.5306	5.71 (m, 2), 3.69 (t, 2, J = 1), 1.70 (m, 10)
19	1.5166	5.61 (s, 2), 4.22 (q, 1, J = 6), 2.05–1.00 (m, 10), 1.50 (d, 3, J = 6)
20	1.5060	5.40 (s, 2), 1.97–0.92 (m, 10), 1.50 (s, 6)
21	1.5717	7.17 (m, 5), 5.68 (d, 2, J = 1), 2.18–0.88 (m, 10), 1.90 (s, 3)

[a]Tabulation follows the order chemical shift (δ), multiplicity, number of protons, coupling constant. Spectra run in $CDCl_3$.

spectra were obtained on a Varian MAT CH5-DF instrument. Unless otherwise noted, the drying agent used was anhydrous sodium sulfate and solvents were removed on a rotary evaporator at reduced pressure. Chromatography was performed using Fisher acidic alumina, 80–200 mesh, Brockman activity grade I. Microanalyses were performed by A. B. Gygli, Microanalysis Laboratory, Toronto, Ontario.

General Procedure (2)

If the allylic triphenylphosphonium salt was used, it was first isomerized to its vinyl isomer by heating in pyridine solution in the presence of 1 equiv of triethylamine for 45–60 min. If the vinyl salt was available, this isomerization could be omitted.

To a solution of the vinylphosphonium salt (0.01 mol) in 50 ml of dry pyridine and triethylamine (0.012 mol)

Can. J. Chem. Downloaded from www.nrcresearchpress.com by 210.87.254.6 on 09/05/12
For personal use only.

TABLE 3. Analytical data

Compound	Analysis (%) Calculated C	Calculated H	Found C	Found H	*m/e*
10	63.10	8.83	63.35	8.81	
11[a]	65.56	9.43	67.52	9.76	128
12	67.54	9.92	67.80	9.93	
13[a]	76.42	7.89	77.62	7.48	204
14	69.16	10.32	69.19	10.37	
15	70.52	10.65	70.83	10.37	
16	71.67	10.94	71.82	10.86	
17	77.99	9.00	77.01	9.44	
18	70.07	9.15	70.10	9.00	
19	71.37	9.58	71.64	9.62	
20[a]	72.46	9.95	71.16	9.52	182
21	77.63	8.25	77.82	8.47	

[a]The thermal instability prevented accurate elemental analysis.

was added a pyridine solution of 0.01 mol of the α-mercaptoaldehyde, dropwise with stirring. The system was purged with nitrogen and the mixture heated at gentle reflux for the time indicated in Table 1. The cooled solution was poured into 600 ml of water and extracted twice with 100 ml of ether and twice with 100 ml of pentane. The combined organic extracts were washed with 10% hydrochloric acid until the washings were acidic. The dried solution was reduced in volume to approximately 10 ml and chromatographed on alumina using pentane as eluant. This removed all phosphorous-containing and colored impurities. Removal of the solvent gave a product shown to be greater than 95% pure. Analytical samples were collected from g.l.c. Indices of refraction and n.m.r. spectra are shown in Table 2 and analytical data in Table 3. Except for the lack of carbonyl absorption, the i.r. spectra were uninformative.

α-Mercaptocyclohexanecarboxaldehyde (5) (As the Dimer)

To a suspension of 25 g (0.5 mol) of sodium sulfhydrate in 200 ml of ether was added a solution of 20 g (0.105 mol) of 1-bromocyclohexane carboxaldehyde (7) in 25 ml of ether. The addition was performed keeping the temperature of the reaction below 20°. After the final addition, stirring was continued for 20 h at ambient temperature. The mixture was filtered and the filtrate evaporated to afford an oil which was distilled to give 7.0 g (50%) of a clear colorless liquid, b.p. 40–45° (0.01 mm); i.r. (CCl_4) 3600, 3440, 2940, 2860, 1730(w), 1450 cm^{-1}; n.m.r. 5.18 (2H), 3.72 (2H), 2.3–0.9 (2OH); *m/e* (parent) 144; n_D^{25} 1.5459.

Anal. Calcd. for $C_7H_{12}OS$: C, 58.32; H, 8.39. Found: C, 58.41, H, 8.38.

The financial support of the National Research Council of Canada is most gratefully acknowledged.

1. J. M. McINTOSH and H. B. GOODBRAND. Tetrahedron Lett. 3157 (1973).
2. J. M. McINTOSH, H. B. GOODBRAND, and G. M. MASSE. J. Org. Chem. **39**, 202 (1974).
3. A. MAERCKER. Organic reactions. Vol. 14. Wiley, New York, N.Y. 1965. p. 270.
4. G. WITTIG and H. REIFF. Angew. Chem. Int. Ed. Engl. 7, 7 (1968).
5. G. M. MASSE and R. S. STEEVENSZ. Unpublished observations.
6. W. MOCK. J. Am. Chem. Soc. **88**, 2857 (1966); S. D. McGREGOR and D. M. LEMAL. J. Am. Chem. Soc. **88**, 2858 (1966).
7. I. HEILBRON, E. R. H. JONES, R. W. RICHARDSON, and F. SONDHEIMER. J. Chem. Soc. 737 (1949).
8. A. KIRRMANN, J. CANTACUZENE, and L. VIO. Rev. Chim. Acad. Rep. Populaire Roumaine, **7**, 1011 (1962); Chem. Abstr. 61, 8180a.

Can. J. Chem. Downloaded from www.nrcresearchpress.com by 210.87.254.6 on 09/05/12
For personal use only.

The Kinetics of Isotope Effects in a Model Solvolysis System Involving One Optically Active Ion Pair Intermediate

P. CHRISTIAN VOGEL

College of Pharmaceutical Sciences, Columbia University, New York, New York 10023[1]

Received December 5, 1972[2]

The derivation of the observed first-order rate constants from the "exact" integrated rate equations for the kinetic scheme of reaction 1 is presented. It is shown that the solvolytic exponential first-order rate constant is a special case of the polarimetric rate constant and that the optical activity of the product is determined by a multiplicative ratio of rate constants for the optically important reactions of the ion pair intermediate. A form of the integrated first-order polarimetric rate equation with a linearly independent parameter set is presented. The functions for the first-order rate constants derived using the steady state approximation are special cases of the functions derived from the exact equations, as are the functions for the first-order rate constants for two systems which involve pre-equilibria followed by a slow product forming step. These functions cannot all be derived one from the other. A differential analysis of observed isotope effects as functions of isotope effects on the rate constants for reactions involving the intermediates is presented.

La constante de vitesse observée de premier ordre est dérivée à partir des équations de vitesse obtenues par intégrale exacte pour le schéma cinétique de l'équation 1. La constante de vitesse solvolytique exponentielle de premier ordre est un cas spécial de la constante de vitesse polarimétrique. L'activité optique du produit est déterminée par un rapport multiplicatif des constantes de vitesse pour les réactions optiquement importantes de la paire d'ions intermédiaires. Une forme de l'équation intégrée de la vitesse polarimétrique de premier ordre est présentée avec un ensemble de paramètre linéairement indépendants. Dans le cas des constantes de vitesse de premier ordre, les fonctions dérivées en utilisant l'approximation de l'état stationnaire sont des cas spéciaux des fonctions dérivées des équations exactes; de même sont les fonctions pour les constantes de vitesse de premier ordre pour deux systèmes qui impliquent une prééquilibre, suivit d'une étape lente de formation de produit. Ces fonctions ne peuvent pas toutes être dérivées une de l'autre. On présente une analyse différentielle des effets isotopiques observés comme fonctions des effets isotopiques sur les constantes de vitesse pour les réactions impliquant les intermédiaires. [Traduit par le journal]

Can. J. Chem., **52**, 1937 (1974)

Ion pairs have been proposed as intermediates in the solvolyses of secondary alkyl esters with increasing frequency in the past several years (1–4). Generally, one or two different types of ion pairs are proposed to lie on the reaction coordinate between the unionized substrate and the free carbonium ion, if the free carbonium ion is included in the solvolysis scheme at all. The polarimetric and solvolytic kinetic data have uniformly been analyzed using the steady state approximation to obtain integrated rate equations, even though mechanistic arguements are advanced which the steady state assumption is clearly not designed to handle, such as pre-equilibria followed by a slow step which yields either the next ion pair or product. The fact that investigators are now analyzing observed kinetic isotope effects in these reactions in terms of the first-order rate constants derived using the steady state approximation calls for an examination of the validity of this approximation as well as the construction of a framework for discussing observed isotope effects as functions of isotope effects on the rates of reactions involving the intermediates. Such a discussion is presented herein for a model solvolysis system involving a single optically active ion pair intermediate which can undergo racemization and internal return in competition with unimolecular and bimolecular nucleophilic substitution.

Reaction 1 presents the solvolysis scheme chosen for this investigation. [RX] and [XR], etc. refer to enantiomeric pairs. The reactions

[1]Present address: Max Planck Institute für Chemie, Mainz, Germany.

[2]Revision received January 7, 1974.

Can. J. Chem. Downloaded from www.nrcresearchpress.com by 210.87.254.105 on 09/05/12
For personal use only.

Can. J. Chem. Downloaded from www.nrcresearchpress.com by 210.87.254.105 on 09/05/12
For personal use only.

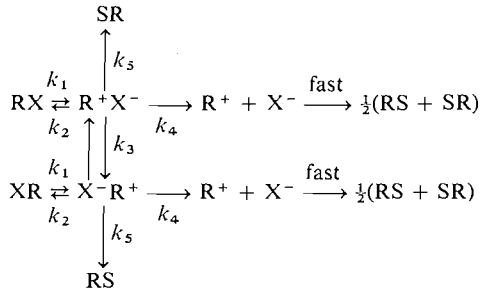

[1]

represented by k_1, k_2, k_3, and k_4 are unimolecular and first order, while that represented by k_5 is bimolecular, pseudo first order, and leads to product of inverted configuration. The reaction of solvent with free carbonium ion to form racemic product is assumed to be so fast as to be kinetically unimportant. This scheme is similar to that proposed by several investigators who need only a single ion pair intermediate to analyze their data (5, 6) and it is a special case of the more generalized solvolysis schemes involving two different ion pair intermediates which have been set up for more complex data analysis problems (1–4, 7). At zero time the concentrations of product and intermediate are zero and that of substrate is $[RX]_0 + [XR]_0$. The sum of the concentrations of the enantiomeric pairs is the chemical concentration of each pair while the difference is related to the optical activity of the pair by a multiplicative constant, α, the specific rotation of the enantiomer used as a reference. The integrated rate equations for the linear combinations of concentrations in reaction 1, derived using no approximations, are given in eqs. 2–6, where $[RX] + [XR] + [R^+X^-] + [X^-R^+] + [RS] + [SR] = [RX]_0 + [XR]_0$ (8)

$$[2]\quad ([RX] + [XR]) = ([RX]_0 + [XR]_0)(e^{-1/2pt})(\cosh(\tfrac{1}{2}qt) + ((p - 2k_1)/q)\sinh(\tfrac{1}{2}qt))$$

where $p = k_1 + k_2 + k_4 + k_5$

$q = (p^2 - 4k_1(k_4 + k_5))^{1/2}$

t = time

$$[3]\quad ([RX] - [XR]) = ([RX]_0 - [XR]_0)(e^{-1/2rt})(\cosh(\tfrac{1}{2}st) + ((r - 2k_1)/s)\sinh(\tfrac{1}{2}st))$$

where $r = k_1 + k_2 + 2k_3 + k_4 + k_5$

$s = (r^2 - 4k_1(2k_3 + k_4 + k_5))^{1/2}$

$$[4]\quad ([R^+X^-] + [X^-R^+]) = ([RX]_0 + [XR]_0)(e^{-1/2pt})(2k_1/q)\sinh(\tfrac{1}{2}qt)$$

$$[5]\quad ([R^+X^-] - [X^-R^+]) = ([RX]_0 - [XR]_0)(e^{-1/2rt})(2k_1/s)\sinh(\tfrac{1}{2}st)$$

$$[6]\quad ([SR] - [RS]) = ([RX]_0 - [XR]_0)k_\beta(1 - e^{-1/2rt}(\cosh(\tfrac{1}{2}st) + (r/s)\sinh(\tfrac{1}{2}st)))$$

$$k_\beta = k_5/(2k_3 + k_4 + k_5)$$

The integrated rate equations for the linear concentration combinations of reactant and product, derived using the steady state approximation, are given in eqs. 7–9, where $[RX] + [XR] + [SR] + [RS] = [RX]_0 + [XR]_0$ (8).

$$[7]\quad ([RX] + [XR]) = ([RX]_0 + [XR]_0)e^{-k_c t}$$

where $k_c = k_1(k_4 + k_5)/(k_2 + k_4 + k_5)$

$$[8]\quad ([RX] - [XR]) = ([RX]_0 - [XR]_0)e^{-k_\alpha t}$$

where $k_\alpha = k_1(2k_3 + k_4 + k_5)/(k_2 + 2k_3 + k_4 + k_5)$

$$[9]\quad ([SR] - [RS]) = ([RX]_0 - [XR]_0)k_\beta \times (1 - e^{-k_\alpha t})$$

Experimentally, the data indicate that the first-order rate constants are small, less than *ca.* 10^{-3} s^{-1} (concentration in liters), and that the concentration of the intermediate is experimentally undetectable.

Equations 2–6 are obviously not simple first-order integrated rate equations. However, the rate equations corresponding to eqs. 2–6 reduce to first-order rate equations as the values of the arguments of the hyperbolic functions become either very small or very large. The case in which these arguments are very small is not of interest in the study of solvolysis reactions, where half-lives are relatively long, but may well be of interest to those who study very fast reactions. When the value of q or s becomes large, the rate equations for the observable quantities become first order. Taking eq. 3 as a representative example, the corresponding rate equation when $(\frac{1}{2}st)$ is large reduces to the first-order form

$$\mathrm{d}\ln([RX] - [XR])/\mathrm{d}t = -\tfrac{1}{2}(r - s) = -k_{obs}$$

where k_{obs} is the experimentally observed first-order polarimetric rate constant analogous to k_α. k_{obs} can be expanded as a function of the k_i by transposing r and squaring.

$$k_1(2k_3 + k_4 + k_5) = rk_{obs} - k_{obs}^2$$

As r is greater than s which is very large and k_{obs} is experimentally less than unity (units of s^{-1}), the value of k_{obs}^2 can be neglected and a solution obtained for k_{obs}.

$$k_{obs} = k_1(2k_3 + k_4 + k_5)/(k_1 + k_2 + 2k_3 + k_4 + k_5)$$

From the above it may be seen that the quantity $k_1(2k_3 + k_4 + k_5)$ is small relative to $(k_1 + k_2 + 2k_3 + k_4 + k_5)$ and that either k_1 or $(2k_3 + k_4 + k_5)$ may be the determining factor in the small value of the observed rate constant. Thus, r and s are of nearly the same magnitude relative to $k_1(2k_3 + k_4 + k_5)$. A similar analysis applies to eq. 2, which is the solvolytic special case of eq. 3, and may be applied to eq. 6 using the experimental facts. The concentration of the intermediate will be small as t becomes large, since $\exp(-\frac{1}{2}(r - s)t)$ is less than unity and k_1 cannot be much greater than s.

Comparison of the expressions for k_{obs} and k_α shows that the steady state approximation is dependent on the value of k_1 being small relative to $(2k_3 + k_4 + k_5)$. When $(2k_3 + k_4 + k_5)$ is small relative to k_1 a pre-equilibrium is obtained, although it is hard to justify mechanistically. If there is a rapid pre-equilibrium with k_2, the rate

$$k_{pre\text{-}eq} = k_1(2k_3 + k_4 + k_5)/(k_1 + k_2)$$

constant for internal return, much greater than the other k_i, both k_α and $k_{pre\text{-}eq}$ reduce to the same function, $k_{int\text{-}ret}$. Note that k_α and $k_{pre\text{-}eq}$

$$k_{int\text{-}ret} = k_1(2k_3 + k_4 + k_5)/k_2$$

cannot be derived one from the other. It seems unwise, however, to make any blanket statements concerning the use of these rate constants to discuss individual experiments, since that is not the issue here. Rather, it appears that the expression for the observed first-order polarimetric rate constant derived from the "exact" integrated rate equations, k_{obs}, is better suited to general discussions of this type of solvolysis mechanism, since it will deal with both of the extreme mechanistic possibilities as well as with the mixed situation possible when k_1, k_2, and $(2k_3 + k_4 + k_5)$ are more nearly of the same magnitude.

The first-order integrated rate equation for optical activity as a function of time, derived from eqs. 3 and 6, is given in eq. 10. When one

$$[10] \quad \alpha = ([RX]_0 - [XR]_0)((\alpha_{RX} - \alpha_{SR}k_\beta) \times e^{-k_{obs}t} + \alpha_{SR}k_\beta)$$

makes the substitutions $\alpha_0 = \alpha_{RX}([RX]_0 - [XR]_0)$ and $\alpha_\infty = k_\beta\alpha_{SR}([RX]_0 - [XR]_0)$, the commonly used first-order integrated polarimetric rate equation is obtained. k_β, which appears in both the "exact" and steady state derivations, effectively determines the fraction of the reaction of the optically active ion pair which yields optically active product, and as such provides useful insight into the nature of the potential energy surface in the vicinity of the ion pair intermediate.

In calculating the value of the polarimetric rate constant for comparison with the solvolytic rate constant or determination of the isotope effect, the linearly independent parameter set ($[RX]_0 - [XR]_0$), k_{obs}, and k_β must be used, rather than the linearly dependent set of α_0, α_∞, and k_α, if the calculated quantities are to have well defined meanings (9). This importance in the choice of parameters for use in curve fitting is not always appreciated, particularly with the wide selection of "packaged" computer routines readily available. The development of current data collection techniques is such that rate constants can be derived from data fit to most first-order rate equations with a precision of 0.1% quite easily. However, the accuracy and, indeed, the meaning of rate constants so derived is a direct function of the choice of parameters used to fit the data. Thus, since the quantity $([RX]_0 - [XR]_0)$ appears in both α_0 and α_∞, the value of k_α fit to the data using the linearly dependent parameter set does not bear the same well defined relationship to the solvolytic rate constant k_{obs}(solv) as does the value of k_{obs} fit using the linearly independent parameter set. The exact difference between k_{obs} and k_α cannot be expressed in simple mathematical terms, since they are obtained by adjustment of other variables. However, this difference will become more pronounced as the optical activity in the product increases and both α_∞ and k_β differ increasingly from zero.

The effect of isotopic substitution in the alkyl ester reactant will alter the values of the k_i in eqs. 2–10, producing new functions for the dependence of concentrations on time (10).

Can. J. Chem. Downloaded from www.nrcresearchpress.com by 210.87.254.105 on 09/05/12
For personal use only.

Can. J. Chem. Downloaded from www.nrcresearchpress.com by 210.87.254.105 on 09/05/12
For personal use only.

The changes in the k_i, $dk_i = k_i^D - k_i^H$, will produce new values of the observed rate constants, $k_j^D = k_j^H + dk_j$. (Substitution of deuterium for hydrogen is assumed for the discussion, although the treatment is completely general.) Since the functions for the observed rate constants are single valued and continuous, the dk_j may be expanded as the total differential of the k_i. As

$$dk_j = \sum_i (\partial k_j/\partial k_i)\, dk_i$$

the theory of isotope effects deals with the ratio of rate constants for individual reactions and not the difference, it is necessary to expand the dk_i as functions of the rate constant ratios for the isotopically substituted molecules. Using

$$dk_i = k_i(\Delta k_i - 1)$$

$$\Delta k_i = k_j^D/k_i^H$$

the functions for k_{obs} and k_β, the equations expressing the effect of isotopic substitution on the observed rate constants as functions of the effect of isotopic substitution on the rate constants for reactions involving the intermediates are given in eqs. 11 and 12.

$$[11]\quad \Delta k_{obs} = \Delta k_1 + \frac{2k_3\Delta k_3 + k_4\Delta k_4 + k_5\Delta k_5}{2k_3 + k_4 + k_5} - \frac{k_1\Delta k_1 + k_2\Delta k_2 + 2k_3\Delta k_3 + k_4\Delta k_4 + k_5\Delta k_5}{k_1 + k_2 + 2k_3 + k_4 + k_5}$$

$$[12]\quad \Delta k_\beta = \Delta k_5 + 1 - \frac{2k_3\Delta k_3 + k_4\Delta k_4 + k_5\Delta k_5}{2k_3 + k_4 + k_5}$$

The solvolytic isotope effect is a special case of the observed polarimetric isotope effect in which k_3 and Δk_3 terms are omitted.

A limiting isotope effect will be observed as the consequence of two factors. First, there must be a maximum amount that the force constants about a particular position of isotopic substitution may change as the molecule passes from some initial to some transition state on the isotopically independent potential energy surface. Second, there must be a form of the equation for the isotope effect which is a function of the Δk_i alone, since the k_i's are functions of solvent composition and may vary widely with solvent changes. To examine the experimental data it is necessary to look at the solvolytic isotope effect, Δk_{obs} (solv), since values of the polarimetric rate constants obtained by fitting data using the independent parameter set are not currently available. (The function for this isotope effect, Δk_{obs} (solv), is eq. 11 with k_3 and Δk_3 omitted.) It is also useful to assume for the sake of compactness that one of the product forming steps, say k_4, is much faster than the other, although the lengthy general expression could be used. When there is a rapid pre-equilibrium with k_2 much greater than the other k_i, the limiting isotope effect is $\Delta k_1 - \Delta k_2 + \Delta k_4$, regardless of the relationship amongst the other k_i. In the steady state situation when k_2 is much less than k_4, the limiting isotope effect is Δk_1; in the pre-equilibrium situation when k_2 is much less than k_1, the limiting isotope effect is Δk_4.

While the foregoing is based on a series of approximations, first to the exact equations and then in the expansion of the observed isotope effects, none the less, this relatively uncomplex analysis may be used to provide a basis for quantitative discussion of what has intuitively been assumed about solvolytic secondary deuterium isotope effects for some time. Taking secondary alkyl brosylate solvolyses as an example, an estimate of the limiting value of Δk_1 of 1/1.15 has been obtained from the solvolysis of pinacolyl brosylate (11), in which rearrangement of the ion pair is faster than internal return via k_2. This compares with the limiting value of Δk_{obs} (solv) for brosylates of 1/1.21 in cases where internal return is not sterically or otherwise hindered (11, 12). The "theoretical minimum" value of Δk_{obs} (solv) for brosylates, calculated by assuming only a single transition state, is 1/1.22 (12). The authors conclude from a variety of mechanistic arguments that internal return via k_2 is important in these limiting solvolyses. On the basis of the foregoing discussion it is seen that such a conclusion arises logically from reaction 1, which further permits the quantitative estimate of $\Delta k_2 - \Delta k_4$ to be calculated as 0.04 (provided k_4 is the only product forming step). The fact that the limiting value of Δk_1 is so close to that of Δk_{obs}(solv) and both are so close to the theoretical minimum, makes the conclusion logical that force constant changes, and hence the isotope effects, associated with k_2, k_4, and k_5 are much smaller than those associated with k_1. Similar arguments can be advanced for other leaving

groups, although the estimate of Δk_1 is not so conveniently at hand.

These conclusions do not contradict those of Murr and co-worker, who have examined isotope effects in the more complicated two ion pair system by taking the ratios of the functions for the steady state rate constants and sorting out the ratios for the partitioning of the reactions of the ion pair intermediates (13). While this method avoids the approximations leading to eqs. 11 and 12, it introduces several others and the equations do not lend themselves to the use of isotope effect model calculations in creating a model of the ion pair, as eqs. 11 and 12 do, since the Δk_i can be calculated. A detailed comparison of the two methods will have to wait until a complete differential analysis is applied to the rate constants for the two ion pair system; however, the two methods are clearly complementary and both will contribute to the construction of models of the ion pair intermediates and to knowledge of the potential energy surface in the vicinity of the intermediates.

It is possible to discuss isotope effects which are not limiting within this mechanistic scheme but, as many investigators propose the existence of a second type of ion pair intermediate in these reactions, it seems prudent to wait until the proper differential analysis is available. However, the observation of a small isotope effect is consistant with the single ion pair model in which a pre-equilibrium exists with k_1 greater than k_2, the observed isotope effect being Δk_4 or Δk_5 or some combination of the two.

The calculation of the Δk_i presents the problem not only of the determination of the potential energy surface, but also of the determination of the internal coordinates of the ion pair as well as the transition states. The question of the extent to which solvent molecules are to be included in these models is unanswered. Thus it would be useful to know the solvent isotope effect on the limiting isotope effect, as well as on isotope effects in reactions which do not show limiting isotope effects. Within the approximation that the potential energy surface is unchanged by isotopic substitution, experiments of this type will provide the experimental data with which to calibrate the model calculations of the Δk_i.

To summarize, a general framework is presented for the quantitative discussion of kinetic isotope effects in a model solvolysis system involving a single, optically active ion pair intermediate. Also included is a rigorous derivation of the polarimetric and solvolytic curve fitting parameters which must be used to fit the data, if comparisons between rate constants derived from these two different data collection methods are to have well defined meanings. The equations used in this analysis are in the form required if model isotope effect calculations are to be used to aid in the creation of a model potential energy surface in the vicinity of the ion pair. Limiting isotope effects in some secondary alkyl brosylate solvolyses can be successfully discussed within this framework, although a general discussion will have to wait until a similar analysis is completed for the kinetic scheme with two different types of optically active ion pair intermediates.

The author wishes to thank Professor V. J. Shiner, Jr., for his comments during the course of this work.

1. V. J. SHINER, JR. *In* Isotope effects in chemical reactions. *Edited by* C. J. Collins and N. S. Bowman. Van Nostrand Reinhold, New York, N.Y. 1970.
2. R. A. SNEEN. Acc. Chem. Res. **6**, 46 (1973).
3. H. L. GOERING and H. HOPF. J. Am. Chem. Soc. **93**, 1224 (1971).
4. J. M. W. SCOTT and R. E. ROBERTSON. Can. J. Chem. **50**, 167 (1972).
5. J. M. SCOTT. Can. J. Chem. **48**, 3807 (1970).
6. R. E. ROBERTSON and B. ROSSAL. Can. J. Chem. **49**, 1441 (1971).
7. D. J. RABER, J. M. HARRIS, R. E. HALL, and P. v. R. SCHLEYER. J. Am. Chem. Soc. **93**, 4821 (1971).
8. A. A. FROST and R. G. PEARSON. Kinetics and mechanism. Wiley, New York, N.Y. 1961.
9. W. E. DEMING. Statistical adjustment of data. Dover, New York, N.Y. 1964.
10. C. J. COLLINS and N. S. BOWMAN. (*Editors*). Isotope effects in chemical reactions. Van Nostrand Reinhold, New York, N.Y. 1970.
11. V. J. SHINER, JR., R. D. FISHER, and W. DOWD. J. Am. Chem. Soc. **91**, 7748 (1969).
12. (*a*) V. J. SHINER, JR., M. W. RAPP, E. A. HALEVI, and M. WOLFSBERG. J. Am. Chem. Soc. **90**, 7171 (1968); (*b*) V. J. SHINER, JR. and W. DOWD. J. Am. Chem. Soc. **93**, 1029 (1971).
13. B. L. MURR and M. F. DONNELLY. J. Am. Chem. Soc. **92**, 6686, 6688 (1970).

Can. J. Chem. Downloaded from www.nrcresearchpress.com by 210.87.254.105 on 09/05/12
For personal use only.

The Determination of Traces of Bismuth by Solid State Luminescence

D. E. RYAN, H. ROLLIER, AND J. HOLZBECHER

Trace Analysis Research Centre, Department of Chemistry, Dalhousie University, Halifax, Nova Scotia B3H 4J1

Received November 13, 1973

Traces of Bi(III) are determined with good selectivity by measurement of the luminescence (λ_{ex} = 355 nm; λ_{em} = 430 nm) of CaO:Bi phosphor after co-precipitation with calcium oxalate and ignition at 850–900 °C. The detection limit is better than 0.01 μg Bi in 15 mg CaO; bismuth can be quantitatively recovered from 500 ml sample volumes and analysis is possible for 0.02 ng Bi/ml. The method has been successfully applied to the determination of trace amounts of bismuth added to synthetic blood and kidney samples.

Des traces de Bi(III) sont déterminées avec une bonne sélectivité par mesure de la luminescence (λ_{ex} = 355 nm; λ_{em} = 430 nm) de "phosphores" CaO:Bi, après coprécipitation avec de l'oxalate de calcium et calcination à 850–900 °C. La limite de détection est meilleure que 0.01 μg Bi par 15 mg CaO; le bismuth peut être collecté quantitativement à partir d'échantillons de 500 ml et l'analyse de 0.02 ng Bi/ml est possible. La méthode a été appliquée avec succès à la détermination de traces de bismuth ajoutées à des échantillons de sang et de rein synthétiques.

Can. J. Chem., **52**, 1942 (1974)

Introduction

Luminescence analysis of trace elements is generally limited in solution to non-transition element and non-heavy metal ions. Although this enhances the selectivity of fluorescence techniques, the failure of many metal ions to form fluorescent chelates seriously limits the applicability of spectrofluorometry. Many elements which fail to fluoresce as chelates, however, do form luminescent phosphors when incorporated into a crystal lattice; a recent communication (1) gave a preliminary report on the analytical potential of such luminescence. The present paper describes the determination of Bismuth(III) at the ng/ml level (and less) using the co-precipitation technique described previously (1); the determination of bismuth in practical samples is outlined.

Experimental

Apparatus and Reagents

Fluorometric measurements were made with a Turner Model 111 Fluorometer (fitted with CAMAG TLC Scanner) and with a Farrand Vis-UV Chromatogram Analyzer. Both instruments were standardized with a mixture of zinc sulfides, "phosphorescent" (Fisher) and "luminous" (B.D.H.). The sample cell was a blackened aluminum sheet with drilled holes (diameter, 5 mm). The sample powder was held in place on one side with a thin glass plate and on the other by masking tape.

A stock solution (1000 p.p.m. in ~5% HNO_3) was prepared by dissolution of bismuth metal (Merck) in 1:1 HNO_3 and dilution after boiling off nitrogen oxides; it was standardized by EDTA titration using xylenol orange (2) and analytical standards were prepared by dilution of the stock solution. The calcium chloride (Baker) solution contained 10 g of dihydrate per liter. The ammonium oxalate (Baker) solution contained 50 g of monohydrate per liter. The "synthetic blood" and "synthetic kidney" solutions contained major cations in concentrations given by Bowen (3).

Procedure

To 100 ml of solution containing 0.01–1.5 μg of Bi add 5 ml of 1:1 HNO_3, and pipet 4 ml of $(NH_4)_2C_2O_4$ solution and 4 ml $CaCl_2$ solution so that a reproducible amount of calcium oxalate (corresponding to about 15 mg CaO) is precipitated; add a few drops of methyl red indicator, heat to 80 °C, and precipitate by dropwise addition of 1:1 NH_3 until the color changes from red to yellow (stir rapidly during precipitation); allow the mixture to cool down to room temperature (about 1 h) and filter through a porous-base porcelain crucible. Wash with distilled water and dry at 200 °C for 1 h; transfer the precipitate to a microcrucible and ignite at 850–900 °C for 15 min (quantitative transfer is not crucial because the precipitate is essentially homogeneous). Allow to cool to room temperature in a desiccator. Grind and mix in an agate mortar, pack the cell and measure luminescence on a Farrand Vis-UV Chromatogram Analyzer (λ_{ex} = 355 nm; λ_{em} = 428 nm; aperture 0.75; filter 3-73; photomultiplier RCA IP21; gain 10.00). A typical calibration curve is shown in Fig. 1.

With the Turner Model 111 Fluorometer (excitation filter 7-60 and emission filter 2A), the lowest working range is 0.5–10 μg Bi. An increase in the concentration range of Bi requires a corresponding increase in the amount of collector to avoid saturation of the precipitate; thus, in the range of 0.5–10.0 μg Bi, 10 ml $(NH_4)_2C_2O_4$ solution + 10 ml $CaCl_2$ solution (giving a calcium oxalate precipitate corresponding to about 40 mg CaO) were used.

Results and Discussion

The fluorescence intensity is a linear function of bismuth concentration as long as there is no

Can. J. Chem. Downloaded from www.nrcresearchpress.com by 210.87.254.6 on 09/05/12
For personal use only.

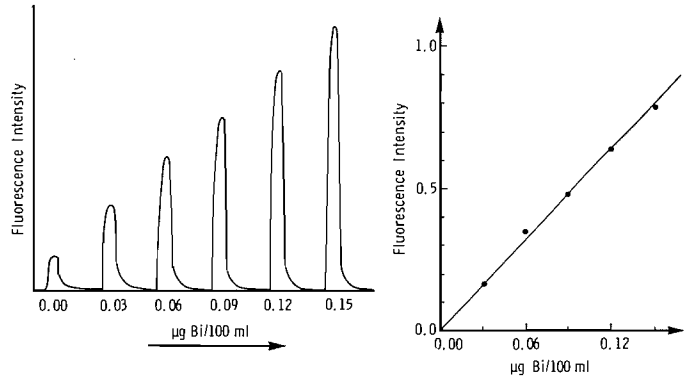

FIG. 1. Calibration curves for bismuth: graph on right is a re-plot of recorder scan on left.

saturation of the precipitate; the quantity of collector has to be adapted to the concentration range. Fifteen and 40 mg of CaO are satisfactory for the ranges 0.01–1.5 µg and 0.5–10 µg Bi, respectively.

The practical detection limit for 100 ml of sample solution is better than 0.1 p.p.b. (0.01 µg Bi collected) using the Farrand Vis-UV Chromatogram Analyzer. The relative standard deviation of six determinations of 0.1 µg Bi was 6%.

With the Turner Model 111 Fluorometer, the practical detection limit for 100 ml of sample solution is 5 p.p.b. (0.5 µg Bi collected). The relative standard deviation of six determinations of 2 µg Bi was 10%.

Factors Influencing Fluorescence

The highest luminescence intensity was obtained when samples were ignited at 850–900 °C for 15 min. Lower temperatures or shorter periods of time of ignition resulted in a greyish colored powder (carbon) and consequently low fluorescence readings; higher temperatures and longer periods of time increase volatilization of activator (1). The weight loss of precipitate upon ignition corresponds to complete conversion of calcium oxalate to calcium oxide.

No significant difference in fluorescence intensity was observed for samples containing 2.0 µg Bi when the volume of the sample was varied from 1 to 500 ml. Since the detection limit is 0.01 µg Bi collected, the practical concentration limit is 0.02 p.p.b. if 500 ml samples are available.

The fluorescence intensity of ignited samples exposed to the atmosphere decreases with time. When packed in the sample cell, the CaO:Bi phosphor exhibits more than 50% loss of luminescence upon standing overnight.

Bismuth (2.0 and 0.1 µg in 100 ml H_2O) was successfully determined in the presence of a 100-fold weight excess of Cd(II), Cu(II), Fe(III), Mg(II), Hg(II), Zn(II), bromide, and iodide. A ten-fold excess of Al(III), Pb(II), Ni(II) and Ag(I) and equivalent amounts of Co(II) and Mn(II) were also without interference. On the Turner Fluorometer, Cr(III) interfered even in equivalent amounts; the better spectral selectivity of the Farrand Analyzer allowed the presence of a 100-fold excess of Cr(III).

Applications

(*a*) The regular procedure was applied to 0.1 ml samples of synthetic blood (equal to 1 ml blood) diluted to 100 ml with water. Application of the procedure to such samples serves simply to demonstrate the potential of the method. The measurements were made on the Farrand Analyzer. In the 0.01–0.1 µg range, the bismuth added was determined with a maximum deviation of 30%; for amounts near 0.1 µg (and higher), the error was reduced to within the 6% standard deviation limit.

With the Turner fluorometer, the poorer sensitivity requires larger aliquots of blood and a higher concentration of interferents is introduced into the precipitate; a reprecipitation procedure was necessary to obtain acceptable results. In the procedure, the first calcium oxalate precipitate is dissolved in the crucible with 5 ml of 1:1 HNO_3. The sample is then transferred to a beaker, 100 ml of water and 10 ml of ammonium oxalate solution are added, and the precipitation with ammonia is repeated. Interference of at least a 1000-fold excess of Fe(III) and 100-fold excess of Cr(III) were thus removed but no improvement in interference levels was obtained for Mn(II), Ni(II), and Co(II).

Can. J. Chem. Downloaded from www.nrcresearchpress.com by 210.87.254.6 on 09/05/12
For personal use only.

The re-precipitation process was applied to 1 ml samples of synthetic blood (containing 19 900 μg Na; 16 900 μg K; 620 μg Ca; 410 μg Mg; 4750 μg Fe; 130 μg Zn; 10 μg Cu) diluted to 100 ml with water. For additions of 0.0, 5.0, and 10 μg of bismuth, the bismuth found was 0.0, 4.5, and 9.2 μg, respectively.

(*b*) Interference in the spectrophotometric determination of bismuth can be removed by extracting bismuth with diethyldithiocarbamate in the presence of EDTA, cyanide, and ammonia (4). As a test of the luminescence finish, the extraction process was applied to synthetic kidney samples containing known amounts of added bismuth. After extraction of the bismuth complex with carbon tetrachloride, the bismuth(III) was re-extracted with 1:1 HNO_3 and, after dilution, the usual co-precipitation procedure with calcium oxalate was followed. For bismuth additions of 0.0, 5.0, and 10 μg to one ml of synthetic kidney solution (containing 800 μg Na; 7800 μg K; 390 μg Ca; 550 μg Mg; 290 μg Fe; 210 μg Zn; 4 μg Mn; 12 μg Cu) diluted to 100 ml with water, 0.0, 5.2, and 11.0 μg of bismuth were found respectively. The results show that the solid state luminescence procedure can be applied after extraction of bismuth from complex matrices.

Results obtained by both the reprecipitation and extraction process are correct within ±10%. However, reprecipitation serves only to increase the amount of iron that can be tolerated and, if interferences such as cobalt, nickel, and manganese are present, the solvent extraction procedure is recommended.

It is a pleasure to thank the National Research Council of Canada for financial support.

1. D. E. RYAN, R. J. PRIME, J. HOLZBECHER, and R. E. YOUNG. Anal. Lett. **6**, 721 (1973).
2. S. KOTRLY and J. VRESTAL. Collect. Czech. Chem. Commun. **25**, 1148 (1960).
3. H. J. M. BOWEN. Trace Elements in Biochemistry. Academic Press, London. 1966.
4. K. L. CHENG, R. H. BRAY, and S. W. MELSTED. Anal. Chem. **27**, 24 (1955).

Can. J. Chem. Downloaded from www.nrcresearchpress.com by 210.87.254.6 on 09/05/12
For personal use only.

Distribution Function and Angular Deformations of a Model Related to Vitreous Ice and Liquid Water[1]

G. S. KELL

Division of Chemistry, National Research Council of Canada, Ottawa, Canada K1A 0R9

Received October 23, 1973

A random tetrahedral model, without bonding defects and in which the distance between nearest neighbors is constant, has been constructed to study the effect of angular variations from tetrahedral, and the observations have been interpreted in terms of vitreous ice and liquid water. The model was constructed to have relatively small deformations from tetrahedral, and the oxygen–oxygen–oxygen angles vary from 90 to 132°, with an interquartile width of 12°. The measured density is intermediate between that of hexagonal ice and liquid water and, because of the small angular deformations, provides an estimate both of the density of vitreous water and of the minimum density possible for a random tetrahedral system.

Un modèle non-cristallin tétraédrique, sans défauts et dans lequel la distance entre les sommets voisins est constante, a été fabriqué avec du plastique et du fil pour étudier la variation angulaire autour de l'angle tétraédrique, et l'effet de cette variation sur les propriétés de la glace vitreuse et de l'eau liquide. Le modèle met en évidence l'effet des déformations relativement faibles, et l'angle oxygène–oxygène–oxygène varie de 90 à 132°, avec une largeur interquartile de 12°. La densité obtenue est entre celles de la glace hexagonale et de l'eau liquide et, vu la faible déformation angulaire, donne un aperçu de la densité de l'eau vitreuse ainsi que du minimum de la densité d'un système non-cristallin tétraédrique.

Can. J. Chem., **52**, 1945 (1974)

Introduction

In four-coordinated amorphous materials (*e.g.* amorphous silicon, amorphous germanium, vitreous ice, liquid water), it is difficult to separate the observable features produced by variation of neighbor–neighbor–neighbor angle from those produced by variation of neighbor–neighbor distance or by coordination defects. This paper deals with the effect of one parameter, namely the variation of neighbor–neighbor–neighbor angles about tetrahedral, while neighbor–neighbor distances are held constant and coordination defects are absent. As the study was undertaken to elucidate the effect of the distribution of angle on the properties of vitreous ice and of liquid water, the results are considered in terms of those systems.

Liquid water is, at least in part, a hydrogen-bonded four-coordinated network, and vitreous ice has probably less angular distortion from tetrahedral and fewer coordination defects or interstitial molecules. Hydrogens are not represented in the model studied (which to that extent is really a model for amorphous silicon or germanium), so the distances are oxygen–oxygen nearest neighbor distances and the angles are those between oxygen–oxygen–oxygen nearest neighbors. As the preferred hydrogen bond O--H—O is either linear or very nearly so, neglect of the hydrogens is permitted at this level of approximation. The leading terms for the dependence of some property f on mean distance R between nearest neighbors, on deformation of oxygen–oxygen–oxygen angles from tetrahedral θ, and on effects due to the presence of non-hydrogen-bonded molecules as measured by parameter ξ, are given by

$$[1] \quad df = \left(\frac{\partial f}{\partial R}\right)_{\theta,\xi} dR + \left(\frac{\partial f}{\partial \theta}\right)_{R,\xi} d\theta + \left(\frac{\partial f}{\partial \xi}\right)_{R,\theta} d\xi + \cdots$$

If f is taken to be the density ρ, then $(\partial\rho/\partial R)_{\theta,\xi} = -3R^{-4}$.

Hexagonal ice, with a density of 0.917 g cm^{-3} at 0 °C and an oxygen–oxygen distance R_{OO} between nearest neighbors of 2.76 Å, has 0.644 molecules per R_{OO}^3. For liquid water, with density 1.000 g cm^{-3} at 0 °C, Narten and Levy (1)

[1]NRCC No. 13819.

Can. J. Chem. Downloaded from www.nrcresearchpress.com by 210.87.254.5 on 09/05/12
For personal use only.

Can. J. Chem. Downloaded from www.nrcresearchpress.com by 210.87.254.5 on 09/05/12
For personal use only.

now give the mean distance between neighboring oxygens of 2.84 Å at 4 °C (this distance changes sufficiently slowly with temperature that to its precision the same value applies at 0 °C and can be applied to the model, although the observed peak corresponds to more than four molecules, so that $R_{OO} \leq 2.84$ Å) though formerly they gave 2.82 Å (2). A value of $R_{OO} = 2.84$ Å gives a density of 0.766 molecules per R_{OO}^3, while $R_{OO} = 2.82$ Å gives 0.750 molecules per R_{OO}^3. Thus, while liquid water is 8% denser than ice I*h* in mass per unit volume, in terms of mass per R_{OO}^3, which is the most convenient way to compare the observed liquid with a model, liquid water is 18% denser than the solid. This 18% difference in density must be produced by the different angular distributions in the two phases. A search of the literature (3) failed to find an estimate for $(\partial\rho/\partial\theta)_{R,\xi}$, though this quantity can be determined for any tangible model.

To obtain the general features of the dependence of density on the angular relations about the molecules, measurements have been made on a model built according to rules strict enough that it should represent a situation that is reasonably well-defined mathematically. If statistical accuracy were the prime consideration, such a study would be better made with a computer so that greater numbers of vertices and larger distances could be handled accurately. However, in such a case the experimenter would not have an opportunity to gain the insight that comes from handling a tangible model. As well, the present model of flexible plastic tubing spontaneously relaxes to a state of minimum angular deformation energy, but this relaxation would not be easy to simulate on a computer. As the model is a static object, it can be regarded as an idealization of vitreous ice. It probably also shows certain features of the structures of liquid water as that structure affects phenomena with a time-scale shorter than 10^{-12} s.

The present model is most closely related to that of Ordway (4), though with differences in the construction rules, is close to the form visualized by Angell (5), and is also closely related to models for amorphous silicon, germanium, or other tetrahedrally coordinated systems, such as the model described for them by Polk (6). No illustration of the present model is shown as it is similar in general appearance to those published by Ordway and Polk. A vibrational analysis of smaller models of this sort has been given by Alben (7). Models that have bent bonds, such as those of Evans and King (8) or Bell and Dean (9), are more appropriate for oxide glasses such as silica or gemania.

Despite the wealth of observational and computational data now available for liquid water, there is still no general agreement about the basic physical processes that make the fluid water-like. Many authors see the presence of two states, called "hydrogen-bonded" and "non-hydrogen-bonded", as an important feature (10). For example, using this approach Murphy and Bernstein (11) have interpreted the Raman and infrared stretching regions of the liquid as showing two species having four and three hydrogen bonds. The present paper adopts the continuum approach which denies that the observations can be interpreted so simply, finding instead a range of molecular environments (3). The molecular dynamical calculations of Stillinger and Rahman (12) are in agreement with this view, and show no evidence to support theories that partition molecules into two classes. In a subsequent paper (13) the same authors discuss ring sizes in liquid water. Using reasonable definitions of a hydrogen bond, they find a broad distribution of ring sizes, rings with from three to eleven members being present; not every molecule participates in four hydrogen bonds. In contrast to that "realistic" result, in the present model every molecule participates in four hydrogen bonds, and rings are restricted to five, six, or seven members in the main model discussed. These restrictions, which give a model that is adequately defined mathematically, permit the evaluation of $(\partial\rho/\partial\theta)_R$. In the discussion we then examine the extent to which vitreous ice and liquid water can be understood in terms of this fully-bonded model.

The Model

The models were built of "Framework Molecular Models" manufactured by Prentice–Hall, Inc., Englewood Cliffs, N.J. The elements consisted of wire caltrops, or tetrahedra, with each leg 6 mm long, and of plastic tubing, cut to lengths of 60 mm. (For assemblies of up to 200 units this gives a model of such dimensions that the hand can easily be inserted to the center.) When assembled, the distance between vertices averaged 63 mm, with no distances measuring less than 62 mm nor more than 64 mm; of the 63 mm between vertices, 12 mm was filled with

Can. J. Chem. Downloaded from www.nrcresearchpress.com by 210.87.254.5 on 09/05/12
For personal use only.

wire from the tetrahedra and not free to bend, and the remaining 51 mm was free to bend. The small variations from 63 mm were produced by variations of the length of the tubing, by bending the tubing, and by the irregularities of the meeting of the tubing ends at the vertices. The model thus approaches that in which all dimensional changes are due to the bending O—O—O angles, and its measured properties were used to evaluate $(\partial f/\partial\theta)_{R,\xi}$ of eq. 1. During the building process the forces introduced by the newly-added vertices changed the geometry about the vertices already present, but because of the large number of bonds involved (for example there were about seventy bonds involved in the network to be deformed if the fourth neighbors of a newly added vertex were to move) only a small deformation took place at any but the closest vertices, and the addition of further vertices to the outer shell of a model containing 200 vertices would not produce a measurable change near the center. In addition to this fast relaxation as the model was built there was a slower one as the pieces of plastic tubing that were bent slowly took on a permanent set over a period of weeks or months. The first relaxation was wanted, and the second produced a change in the length of the bonds of only $\frac{1}{2}$ to 1% during a year, which is unimportant as the measurements were only made to the nearest millimeter and are only claimed accurate to 1%.

A model can be described in terms of R and θ, as in eq. 1, in terms of a radial distribution function, or in topological terms of ring size. It is control of ring size that is most convenient during the building process. Preliminary models were built to find rules for building models in which not much bending of the plastic tubing was needed when adding elements, with little density variation from place to place, and in which all bonds in the interior were completed. These models showed that 4-member rings produced strain that propagated for relatively long distances, so that their effects could probably be seen over distances greater than those of the present model. The distortion produced by a 4-member ring would increase the density as well. Therefore, the main model described here was built of 5, 6, and 7-member rings. That is, given a central vertex and two specified first neighbors, a shortest path can be taken from the central vertex, along the bond to a neighbor, to that molecule's neighbor in turn, etc., to return to the starting vertex through the other specified neighbor, giving a ring with at least 5 but not more than 7 members. The 5-member rings were nearly planar and easy to identify; 6-member rings tended to show either boat or chair conformation, with more or less distortion; 7-member rings usually encircled cavities, and the shortest path with 7 elements was not easier to identify without counting than paths with 8 or more steps.

As a result of the restriction on the permitted size of rings, the construction rules of Ordway (4) could not be followed. The model was built outward from a center cluster, checking the ring sizes at each addition, and regions were dismantled and rebuilt if necessary to meet the ring-size condition. Somewhat behind the additions, when it was clear that a region was not going to be dismantled, the vertices were numbered, and a table of connections was made. The network contained no interstitial elements and no free valences, so $d\xi$ of eq. 1 can be taken as zero. The completed model contained 170 numbered vertices, with a further 50, at greater distance, to ensure that all the numbered ones were held rigidly. Density measurements were made on shells of a sphere of radius $3.8R_{OO}$.

To investigate the bending of angles about a 4-member ring, a smaller model, with 33 numbered vertices and about 25 neighbors at greater distances to give rigidity, was built so that the distances, and hence the angles, at the vertices taking part in the 4-member ring could be determined, but the density was not found.

Observations

Density

Measurements of density made outward from the central vertex were still oscillating at radius $3.6R_{OO}$ where the sphere contained 130 vertices. This oscillation may arise in part from unnoticed variations in the construction techniques but appears chiefly due to intrinsic density fluctuations. The density of the model oscillated between 0.65 vertices/R_{OO}^3 and 0.73 vertices/R_{OO}^3, with 0.69 vertices/R_{OO}^3 as the most probable value.

In the introduction 0.644 molecules/R_{OO}^3 was given for the density of hexagonal ice, and 0.750 molecules/R_{OO}^3 for liquid water. The value for the present model lies midway between the two. As extreme deformations are absent from this model, and as deformations from tetrahedral

Can. J. Chem. Downloaded from www.nrcresearchpress.com by 210.87.254.5 on 09/05/12
For personal use only.

increase the density, expressed in molecules/R_{OO}^3, this value must be near the lower possible limit for a glassy form of water, and serve as an estimate of both the density of vitreous ice and of the minimum density that water tends toward as it is cooled.

If vitreous ice is related to the present model, its density should be intermediate between that of ice I*h* and liquid water at 0 °C. Ghormley and Hochanadel (14) reported a density of 0.94 ± 0.02 g cm^{-3} at 89 K, the same as that of ice I*h* at that temperature, while Seiber *et al.* (15) gave 0.81 ± 0.02 g cm^{-3}. As R_{OO} for vitreous ice is not expected to be less than that for hexagonal ice, these densities are lower than those predicted by the present model. We can speculate that in the condensation of the vapor not all hydrogen bonds are completed; this could produce both the lowered density and the enthalpy released when on warming the condensed amorphous ice transforms to ice I*c*. If the condensed material has, in fact, many uncompleted bonds, it is not the vitreous water to be expected on quenching liquid water, and the present model is closer to vitreous water.

Distribution of Five-member Rings

Topological parameters that were not controlled during the construction were the fraction of rings that were five-membered and their distribution on vertices. Of twenty-seven vertices in the interior that had complete rings about them; 2 had no five-member rings, 14 had only one, 4 had two, 5 had three, and 2 had four.

Vertices subtending 2 or 3 five-membered rings were found to have either 3 or 4 bonds involved. If only three, the local structure is like the corner of a pentagonal dodecahedron, particularly for the case of three five-member rings. This gives a bulky structure and a comparatively large cavity. Its ease of formation may well be related to the solvent properties of water, and small changes in the construction rules to increase or decrease the probability of 3 five-membered rings at a vertex would also have a considerable effect on the density.

Distribution Functions

A value of the mean density of the model is not needed to understand the number of vertices as a function of radial distance, but will be needed to calculate the pair distribution function $g(R/R_{OO})$. As the model is without bonding defects, each vertex has four first neighbors, at 63 ± 1 mm. The distribution of first neighbors is shown in Fig. 1*c*, and is seen to be close to a spike function at R_{OO}.

As any molecule can be reached by more than one path starting from a central molecule, for unique classification, neighbors are counted by the shortest path to reach them, and are counted once only; that is, first neighbors can be reached by traversing a single bond from the central vertex, and are not counted as higher neighbors, although they can perhaps be reached in four, five, or six steps around rings, or alternatively by longer paths extending further into the network.

Second Neighbors and Angular Deformations

As the smallest ring permitted has five members, each vertex has 12 second neighbors, with the distribution of distances shown in Fig. 1*a*. If R_{OO} is taken as constant, 63 mm for this calculation, the distances between second neighbors can be analyzed to give O—O—O angles. Let k be the central molecule, and i and j its first neighbors, and hence second neighbors of each other. The distances k to i and k to j are R_{OO}, and distances i to j is $a_{ij}R_{OO}$. If θ_{ij} is the angle between i and j subtended at k, by the law of cosines

$$\cos\theta_{ij} = 1 - \frac{a_{ij}^2}{2} \qquad [2]$$

Equation 2 was used to calculate the angles shown in Fig. 1*a* for second neighbors. In cubic ice θ_{ij} would be the tetrahedral angle, $\cos^{-1}(-\frac{1}{3}) \approx 109.47°$, throughout, and in hexagonal ice the angles are close to that value. In this model there is a considerable range of angles, from 90° (one of the five-member rings is so distorted that it has an angle of 90°) to 130°. This range is somewhat less than that found in the ices; in ice VI, in which every molecule is in three four-member rings, angles of 76° are found, and in ice V an angle of 135°.

The distribution curve for second neighbors shown in Fig. 1*a* is based on 60 measurements about 5 central molecules; the distribution about each of the five vertices is in approximate agreement with the mean curve given.

To obtain an independent estimate of the angular deviations from tetrahedral, the distances R_i, no longer assuming them constant, and R_{ij} were measured about ten vertices, to give information, shown in Fig. 2, to be compared to that of Fig. 1*a*. Three sides of each triangle were measured, the angle obtained,

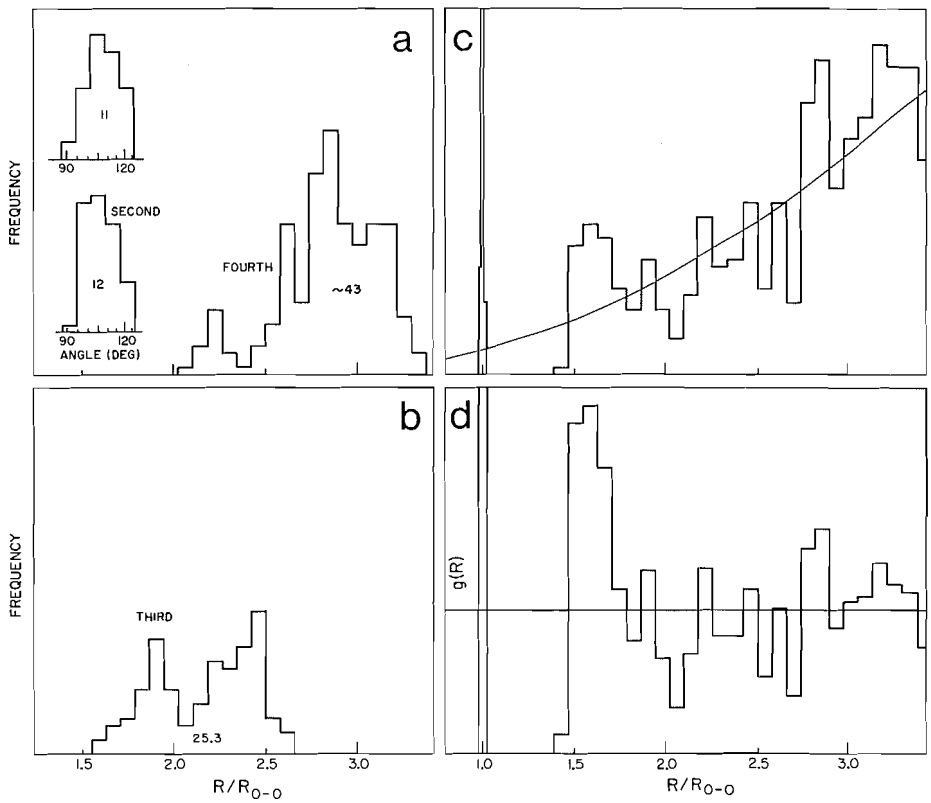

FIG. 1. Radial distribution in the model. (*a*) and (*b*) show the radial distribution of second neighbors, with the distribution of angles shown in the inset scale, and the radial distribution of third and fourth neighbors. The number under the peaks shows the number of neighbors included. In (*a*) the second-neighbor curve numbered 11 refers to the fragment built around a four-member ring whose vertices have only 11 second neighbors. The sum of all observations are given in (*c*), and this is expressed as the pair function $g(R/R_{OO})$ in (*d*). In the second-neighbor distribution of (*a*), distance is the primary measurement, and angles have been calculated by eq. 2.

shown in Fig. 2, and R/R_{OO} then calculated on the assumption that R_{OO} is constant at 63 mm. The sample differs from that shown in Fig. 1*a* because for Fig. 2 all six angles were determined at each vertex, while Fig. 1*a* measurements were made outwards from central vertices but (*i*) all six angles were not found at most first-neighbor vertices and (*ii*) while the distances needed to determine the distribution function were measured, R_{OO} was not found for every pair. For larger networks, where the central region over which complete measurements can be made is larger, the two measurements should give identical information.

The general form of the results shown in Fig. 2 is not much different from that of Fig. 1*a*. To be sure, an extreme angle of 132° was found in this group of measurements, making the total range observed from 90 to 132°. The quartiles of the data summarized in Fig. 1*a*, as determined from the raw data without the grouping shown in the figure, are at 99 and 111°, with an interquartile range of 12°, and the mean is 106°. It is not clear whether the displacement of these quartiles by about 3° downward from the values summarized in Fig. 2, *viz.* quartiles at 103 and 114°, with an interquartile range of 11° and a mean of 109°, reflects a sampling or a measurement error, though the latter should not exceed 1°.

In eq. 1 the variable θ is defined as some measure of the angular deformation from tetrahedral. It is not clear, however, whether the variable should be the mean angular deformation $\bar{\theta} = 6°$, or whether it should be the mean square angular deformation $\overline{\theta^2}$, which would be approximately proportional to the energy of deformation if deformations are small. If the angular distribution were Gaussian the root mean square angular deformation would be close to $1\frac{1}{2}$ times

Can. J. Chem. Downloaded from www.nrcresearchpress.com by 210.87.254.5 on 09/05/12
For personal use only.

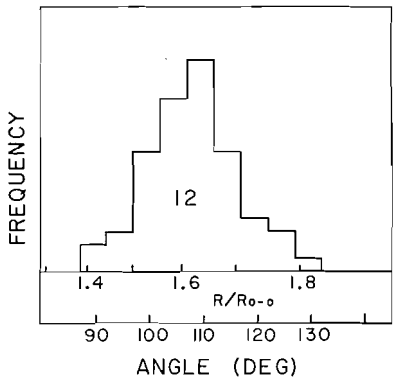

FIG. 2. Angular distribution about a vertex. The angles are the primary measurement, and distances have been calculated by eq 2 for comparison with Fig. 1*a*.

the mean angular deformation. The root mean square angular deformation was calculated from the data shown in Fig. 2 as 8.4°. However, here we assume that the deformations are small enough that effects are linear to experimental precision in $\bar{\theta}$.

In the approximation of small displacements from tetrahedral, the sum of the angular displacements from tetrahedral at a vertex is zero (16), but it is by no means clear that this approximation still holds for the magnitude of angular deformation in this model.

Only five of the six angles obtained by taking the four bonds about a central vertex in pairs are independent. Denote unit vectors from the central vertex to the neighboring vertices by $\boldsymbol{R}_1$, $\boldsymbol{R}_2$, $\boldsymbol{R}_3$, and $\boldsymbol{R}_4$. Three non-coplanar vectors can be taken as the basis set for a coordinate system, and the remaining vector can be expressed in terms of them.

$$[3] \quad \alpha_1\boldsymbol{R}_1 + \alpha_2\boldsymbol{R}_2 + \alpha_3\boldsymbol{R}_3 + \alpha_4\boldsymbol{R}_4 = 0$$

As is well known, if the scalar product of eq. 3 is taken in turn with $\boldsymbol{R}_1, \boldsymbol{R}_2, \boldsymbol{R}_3$, and $\boldsymbol{R}_4$, a set of the four simultaneous equations is obtained which is sufficient to determine the sixth angle if five are known. The magnitudes of the cosines of the six angles must meet the condition that the determinant of the coefficients is zero. If we write

$$\boldsymbol{R}_i \cdot \boldsymbol{R}_j = \cos\theta_{ij}$$

the determinant takes the form

$$[4] \quad \det \begin{vmatrix} 1 & \cos\theta_{12} & \cos\theta_{13} & \cos\theta_{14} \\ \cos\theta_{12} & 1 & \cos\theta_{23} & \cos\theta_{24} \\ \cos\theta_{13} & \cos\theta_{23} & 1 & \cos\theta_{34} \\ \cos\theta_{14} & \cos\theta_{24} & \cos\theta_{34} & 1 \end{vmatrix} = 0$$

which is quadratic in the cosine of any one angle.

To see if the shift of mean vertex angle from tetrahedral is a useful statistic, calculations were made using eq. 4, starting with five of the observed angles at a vertex, calculating the sixth, and finding the mean. As the computational error using eq. 4 is much less than the error of measurement, this gives means more precisely. Most means lay below the tetrahedral value but some were above, with $109.2_5°$ as the mean of the means. Melnyk (19) has shown that while the mean second neighbor distance is a maximum for the tetrahedral configuration, the mean angle is not so simple. The maximum mean angle corresponds to a square, and while there is a local maximum at the tetrahedral configuration, this is very narrow, and configurations not far from tetrahedral may give mean angles greater or less than tetrahedral. Accordingly, the mean angle is not a useful statistic for deformations of the magnitude present in this model.

Third and Higher Neighbors

In a model built according to the present rules, the numbers of third and higher neighbors can vary within limits. The number of third neighbors about ten vertices were: four cases of 24, two of 25, one of 26, and three of 27, with a mean of 25.3. Figure 1*b* shows the considerable width of the third-neighbor distribution, and that it has a double peak. This double distribution comes from vertices that are *cis* or *trans* to one another relative to the two vertices lying between them; that is, the *cis* peak represents third neighbors in rings of six or more members (a five-member ring does not have third neighbors in the present sense).

Statistics, shown in Fig. 1*a*, are no longer so

Can. J. Chem. Downloaded from www.nrcresearchpress.com by 210.87.254.5 on 09/05/12
For personal use only.

Can. J. Chem. Downloaded from www.nrcresearchpress.com by 210.87.254.5 on 09/05/12
For personal use only.

good for fourth neighbors, because of the size limitations of the model, but the five central vertices had 38 to 46 fourth neighbors, with a mean about 43. There is a small peak at 2.2 R_{OO} that again reflects *cis* configurations (in seven-member rings), but most vertices are found in a broad band centered near 3.0 R_{OO}.

Fifth neighbors are not shown separately; because of size limitations, measurements were possible only about the central vertex. The observations are included in the composite curve in Fig. 1*c*. The central vertex had 69 fifth neighbors, the closest at $2.75R_{OO}$, and the most distant at $4.08R_{OO}$. This distribution possibly showed two peaks, one near $3.2R_{OO}$ and another near $3.8R_{OO}$. The closest sixth neighbor was at $3.29R_{OO}$.

The most striking feature of the composite distribution function shown in Fig. 1*c* is that it has a great deal of structure near $3.5R_{OO}$, which corresponds, for water, to 10 Å. Inspection of the distribution functions for particular neighbors shows that the smallest radius at which there is probably extraneous structure due to inadequate statistics is in the third neighbor curve at $2.3R_{OO}$, and that there is a larger dip in the fourth neighbor curve at $2.7R_{OO}$. Yet the peak in Fig. 1*c* at $1.9R_{OO}$, which is the first third-neighbor peak, would have been considered spurious without the more detailed breakdown by shells. The exceptional degree of structure found compared with that from systems with varying R_{OO}, indicates the value of making measurements on a model of fixed R_{OO}.

Radial Distribution Function

If ρ_0 is the mean density of the model, found above to be 0.69 vertices/R_{OO}^3, the distribution function $F_0(r)$ would be expected to be

$$[5] \qquad F_0(r) = 4\pi\rho_0 r^2$$

where $r = R/R_{OO}$, and $\rho_0 = 0.69$ vertices/R_{OO} as given earlier. $F_0(r)$ is shown as the quadratic rising line in Fig. 1*c*. If the observed distribution function F is divided by F_0 the quotient is the radial distribution function $g(r)$ which is shown in Fig. 1*d*.

This radial distribution function may be compared with the ones observed for liquid water by Narten and Levy (2), the one measured by Polk (6) for a vitreous model with varying bond lengths, or the ones calculated by molecular dynamics by Stillinger and Rahman (12) from an assumed potential for water. The most striking feature is that the second-neighbor peak of the present r.d.f. is comparable in width to the first-neighbor peak of the other curves. If the resolution of the present r.d.f. were sufficiently degraded, it would resemble the r.d.f. obtained by scattering experiments.

Two limiting compressibilities can be distinguished for the model. Should the network be compressed shortening all bonds by the same fraction, angles would not change, and the force to shorten one bond would not be far from that in ice. (It must, of course, be recognized that if bond lengths were not constrained to equality they would change unequally on compression and angles would alter.) Another, larger compressibility would be obtained if the topology and angles were rearranged to give a denser form (even if R_{OO} were held constant). This larger compressibility is the one that is of greater interest.

Chay and Frank (17) have discussed the problems in obtaining the compressibility from the radial distribution function by the equation

$$[6] \quad kT\left(\frac{\partial\rho}{\partial P}\right)_T = 1 + \rho_0 \int_0^\infty [g(r) - 1]4\pi r^2 dr$$

where $r = R/R_{OO}$, and where the compressibility corresponds to both rearrangement of structure and shortening of bond length. However, eq. 6 cannot be used with the limited data shown in Fig. 1*d*. For water at 0 °C the l.h.s. of eq. 6 is about 0.06, which shows that the term on the r.h.s. with the integral must have a value of about −0.94. Indeed, the uncertainties of g are such that even the sign of the r.h.s. cannot be found from the data shown in Fig. 1*d*.

Discussion

The mean angular deformation from tetrahedral of $\theta = 6°$, determined for this model, may be compared with that from the mathematical model of Pople's (18), a mean angular deformation in liquid water at 0 °C of 26°, which Kell (3) revised downward to 16°. This latter number and the increase in density of the liquid from that of ice I*h* gives $(\partial\rho/\partial\theta) = 0.007_6$ molecules R_{OO}^{-3} deg^{-1}, while the 6° of the present model gives $(\partial\rho/\partial\theta) = 0.008$, so that the two approaches are in good agreement. In his model

Can. J. Chem. Downloaded from www.nrcresearchpress.com by 210.87.254.5 on 09/05/12
For personal use only.

Pople assumed that there were 11 second neighbors, that is that certain four-member rings were present, and 22 third neighbors, to be compared with the 12 (by definition) and 25 found here; this difference is related to the lower angular distortion of the present model.

The radial distribution function and other parameters reported here have been obtained from just one constructed model. However, once force constants for bending are introduced, whether the force constant for stretching is taken as infinite or not, there would be a different equilibrium structure at each temperature. As has already been shown (3), a temperature-dependent, defect-free structure can explain such properties of liquid water as the maximum density and the change of sign of $\partial\eta/\partial P$. A value of $\partial R/\partial T = 0.0006_0$ Å K^{-1} (for hexagonal ice the value is about 0.0001_3 Å K^{-1}) was used there, based on Narten and Levy (2). Hence, from eq. 1, using $\partial\rho/\partial\theta = 0.008$ molecules $R_{OO}{}^{-3}$ deg^{-1} found here, there is obtained $\partial\theta/\partial T = 0.08$ deg K^{-1}. Below the temperature of maximum density the effect of $\partial\theta/\partial T$, which gives a negative thermal expansion, is more important, while at higher temperatures the increase of bond length with temperature, which tends to decrease the density, is more important. We know from the ices that the oxygen–oxygen distance increases with angular deformation, so that, on this ground as well, the thermal expansion is expected to be positive at higher temperatures. The present numbers give $\partial R/\partial\theta = 0.007_5$ Å deg^{-1}.

If θ for liquid water at 0 °C is 16°, and $\partial\theta/\partial T =$ 0.08 deg K^{-1}, then the $\theta = 6°$ measured for this model corresponds to a temperature of 150 °K, an acceptable estimate of liquid water's glass-transition temperature, which is usually estimated to be between 130 and 160 °K. These values are only very rough and although the maximum density is reproduced, the change of thermal expansion with temperature is underestimated. The data are not sufficient to indicate whether a picture of liquid water based on the model fails, whether the model is adequate but higher-order terms are needed, or whether the picture and approximations are adequate but the numerical values are in error. Even with these uncertainties, we are able to predict that while below the glass-transition temperature the thermal expansion of vitreous ice must be about like that of ice, as the angular structure is frozen in, above that temperature angular deformations and structural rearrangements predominate up to the temperature of maximum density, and the thermal expansivity is everywhere negative.

Similarly, the pressure derivative of the viscosity $\partial\eta/\partial P$ is negative below 35 °C, and positive at higher temperatures. The present model would suggest, at least qualitatively, that the negative volume of activation at low temperatures is produced because as a molecule begins to move relative to its neighbors bonds are bent, and the volume decreases. At high temperatures, on the other hand, angular deformations are already larger, and a molecule can only move by increasing its local volume, and the volume of activation is positive.

Most lines of evidence suggest that liquid D_2O is more structured than H_2O, and certain solutes appear to enhance the degree of structure, the enhancement being greater in D_2O. It is by no means certain just what the structure is, but, as it is certainly non-periodic, it may be considered related to the random tetrahedral structure studied here, and the existence of a minimum density for the network then argues that the degree of liquid structure cannot increase indefinitely. If so, either indications of such a limit should be found in the properties of the structure-producing solutes at the lowest temperatures or the concept of structure is not useful in this context.

Three directions for further work can be seen, and in each of them the use of a computer would be profitable. They are: (*1*) the extension of the present kind of model-building to larger networks; (*2*) the determination of the features introduced by the positioning of hydrogen on the molecules; and (*3*) the study of the relation of the statistical properties of the networks to the properties of liquid and vitreous water.

(*1*) It would be necessary to study a large number of models, each larger than the present one, to establish relations between the distribution functions, angular deformations, and density, over a range of deformation parameters. A network twice the diameter of the present one would contain 1500 vertices, and would be hard to build, to handle, and to measure.

(*2*) In this model, as in the ices, hydrogens can be placed in such a way as to preserve the stoichiometry H_2O and to have one hydrogen on each bond. As two hydrogens can be placed about a tetrahedral vertex in six ways, giving rise to the residual entropy of ice of $R \ln \frac{3}{2}$, it would

be interesting to know the dipolar correlations, which have never been found for this sort of model.

(*3*) The present model represents a pretty drastic simplification of the structure of water, for the broadness of the first neighbor peak of the radial distribution function shows that large variations of R_{OO} occur in the liquid, and absence of bonding defects is also unrealistic. Nevertheless, studies of the present sort play an important role in establishing how much of the peculiar behavior of water can be explained in terms of non-quantum-mechanical concepts.

NOTE ADDED IN PROOF: Polk and Boudreaux have modified the previous Polk model (6) to give constant first-neighbor distances. Their radial distribution function shows features essentially similar to the present Fig. 1*c* out to $2.6R_{OO}$, and the standard deviation of their angular distribution is 9.1° in agreement with the average deviation of 6° found here. On the other hand, their density, based on a sphere of $5R_{OO}$ is only 1% less than that of the ice structure, compared with the 8% found here. The cause of this large disagreement is not apparent.

I wish to thank Dr. T. W. Melnyk, of the Department of Mathematics, Dalhousie University, Halifax, for showing me his treatment of mean angles, and the members of the High Pressure Section for their many discussions on this model.

1. A. H. NARTEN and H. A. LEVY. *In* Water: a comprehensive treatise. Vol. 1. *Edited by* F. Franks. Plenum Press, New York. 1972. p. 311.
2. A. H. NARTEN and H. A. LEVY. Science, **165**, 447 (1969).
3. G. S. KELL. *In* Water and aqueous solutions. *Edited by* R. A. Horne. John Wiley and Sons, New York. 1972. p. 331.
4. F. ORDWAY. Science, **143**, 800 (1964).
5. C. A. ANGELL. J. Phys. Chem. **75**, 3698 (1971).
6. D. E. POLK. J. Non-Crystalline Solids, **5**, 365 (1971).
7. R. ALBEN. Bull. Am. Phys. Soc. **18**, 766 (1973).
8. D. L. EVANS and S. V. KING. Nature, **212**, 1353 (1966).
9. R. J. BELL and P. DEAN. Nature, **212**, 1354 (1966).
10. C. M. DAVIS and J. JARZYNSKI. *In* Water and aqueous solutions. *Edited by* R. A. Horne, John Wiley and Sons, New York. 1972. p. 377.
11. W. F. MURPHY and H. J. BERNSTEIN. J. Chem. Phys. **76**, 1147 (1972).
12. F. H. STILLINGER and A. RAHMAN. J. Phys. Chem. **57**, 1281 (1972).
13. A. RAHMAN and F. H. STILLINGER. J. Am. Chem. Soc. **95**, 7943 (1973).
14. J. A. GHORMLEY and C. J. HOCHANADEL. Science, **171**, 62 (1971).
15. B. A. SEIBER, B. E. WOOD, A. M. SMITH, and P. R. MULLER. Science, **170**, 652 (1970).
16. E. B. WILSON, J. C. DECIUS, and P. C. CROSS. Molecular vibrations. McGraw-Hill Book Company Inc., New York. 1955. p. 140.
17. T. R. CHAY and H. S. FRANK. J. Chem. Phys. **57**, 2910 (1972).
18. J. A. POPLE. Proc. R. Soc. Lond. Ser. A, **205**, 163 (1951).
19. T. W. MELNYK. Private communication.
20. D. E. POLK and D. S. BOUDREAUX. Phys. Rev. Lett. **31**, 92 (1973).

Can. J. Chem. Downloaded from www.nrcresearchpress.com by 210.87.254.5 on 09/05/12
For personal use only.

Some Thermodynamic Properties of Indium Trichloride, Indium Hydroxide, and Indium Trioxide

ALAN N. CAMPBELL, ELINOR M. KARTZMARK, AND OM N. BHATNAGAR
Department of Chemistry, University of Manitoba, Winnipeg, Manitoba R3T 2N2

Received November 13, 1973

The equilibrium diagram of the system $InCl_3$–H_2O has been determined as far as it can be followed. From these freezing points, the activity coefficients at the freezing temperatures have been calculated. The heats of solution and of dilution of hydrated and of anhydrous indium chloride, in water, have been determined, as well as the heats of solution of indium hydroxide and of indium oxide (In_2O_3) in concentrated hydrochloric acid. From these data, the heat of the reaction: $2In(OH)_3 = In_2O_3 + 3H_2O$ and the molar enthalpies of $InCl_3$ and $In(OH)_3$ have been calculated.

Le diagramme déquilibre du système $InCl_3$–H_2O est établi aussi loin qu'il peut être suivi. Pour ces points de congélation, les coefficients d'activité aux températures de congélation sont calculés. Les chaleurs de solution et de dilution des chlorures d'indium hydraté et anhydre dans l'eau sont établies comme les chaleurs de solution de l'hydroxyde d'indium et de l'oxyde d'indium (In_2O_3) dans l'acide chlorhydrique concentré. De ces données, la chaleur de la réaction: $2In(OH)_3 = In_2O_3 + 3H_2O$ et les enthalpies molaires de $InCl_3$ et $In(OH)_3$ sont calculées. [Traduit par le journal]

Can. J. Chem., **52**, 1954 (1974)

Introduction

There appears to be a lack of precise information about indium trichloride. For instance, the only paper dealing with the hydrates of indium trichloride is the one by Ensslin, Ziemeck, and Schaepdryver (1) in which they claim the existence of several hydrates on evidence which appears to be very slender. The present communication deals with the equilibrium diagram of the system $InCl_3$–H_2O, as far as it can be followed, activity coefficients of aqueous solutions of indium chloride, the heats of solution and of dilution of hydrated and of anhydrous indium chloride as well as the heats of solution of indium hydroxide ($In(OH)_3$) and of indium trioxide (In_2O_3) in concentrated hydrochloric acid.

Experimental

Preparation of Indium Compounds

Indium Trichloride

We are indebted to Cominco of Trail, B.C. for solutions of pure indium chloride containing about 500 g of indium chloride per l. The solid hydrated salt is readily obtained by evaporation of this solution on the steam bath. Care must be observed not to remove all the water, or the anhydrous, or almost anhydrous, salt will be obtained. As the viscous solution cools, the indium chloride in solution reacts with water to form the hydrated salt. The expansion accompanying this is so great that the beaker usually cracks: it is therefore advisable to evaporate in a wide porcelain dish. As we have stated in the introduction, we have no certainty as to the composition of the hydrated form; it appears to vary within wide limits. The anhydrous form is obtained from the hydrated form by heating in a hot-air oven at 115°. The product is not quite pure: it contains 1 or 2% of insoluble material, no doubt hydroxide produced by hydrolysis.

Indium Hydroxide, $In(OH)_3$

Indium hydroxide is prepared from a solution of indium chloride by adding an excess of ammonia, filtering and washing with hot water and drying overnight at 110°.

Indium Sesquioxide, In_2O_3

The sesquioxide is prepared from the hydroxide by ignition at 650°. It is a chocolate brown powder at this temperature but becomes pale yellow on cooling.

Equilibrium Diagram and Activity Coefficients

The freezing points of dilute aqueous solutions were obtained by the ordinary freezing point technique, using a Beckmann thermometer, while more concentrated solutions were submitted to thermal analysis, using a copper–constantan thermocouple and a recording potentiometer. It was not possible to proceed beyond a concentration of 35.24 wt% $InCl_3$, because solutions containing more than this became extremely viscous, indeed vitreous at low temperatures. Cooling was produced by Dry Ice. Solutions at $-70°$ would not crystallize when inoculated with both crystals of ice and of hydrated indium trichloride. The eutectic was therefore not realizable.

Heats of Solution

We obtained from B.D.H. a sample of indium trichloride described on the label as "$InCl_3.3H_2O$", though our analysis corresponded to "$2.5H_2O$". This preparation was used to determine the heat of solution in very low concentration. For this purpose we used a very

Can. J. Chem. Downloaded from www.nrcresearchpress.com by 210.87.254.105 on 09/05/12
For personal use only.

Can. J. Chem. Downloaded from www.nrcresearchpress.com by 210.87.254.105 on 09/05/12
For personal use only.

TABLE 1

(*a*) Freezing points, apparent molecular weights, and *J*-functions of aqueous solutions of indium trichloride

Freezing point (°C)	$[InCl_3]$ wt. %	$[InCl_3]$ Molality	Apparent molecular weight	*J*
−0.072	0.3983	0.01808	102.5	0.4597
−0.181	1.0757	0.04916	111.6	0.5031
−0.272	1.7591	0.08095	122.4	0.5475
−0.471	3.0805	0.1499	125.4	0.5764
−1.540	8.525	0.4214	112.4	0.5072
−2.715	16.34	0.8831	133.7	0.5854
−6.064	25.58	1.554	105.3	0.4736
−10.09	35.24	2.460	100.2	0.4468
—	53.98	—	—	—

(*b*) Variation of activity coefficient with molality

Molality	Activity coefficient
0.05	0.203
0.10	0.138
0.15	0.110
0.20	0.095
0.25	0.084

TABLE 2. Heats of solution in kcal mol^{-1}

(*a*) B.D.H. prepared $InCl_3.3H_2O$ in water

Molality of solution × 10^3	ΔH
1.5939	−5.182
2.5603	−5.283
3.9317	−5.421
7.5948	−5.489
10.04	−6.273

(*b*) Anhydrous $InCl_3$ in water

Molality of solution	ΔH
0.05334	−21.49
0.07936	−23.14
0.1589	−21.31
0.3183	−22.88
0.5450	−22.02

accurate calorimeter, designed specifically for this purpose, and of which we have published a description elsewhere (2). For the more concentrated solutions, we used a simple calorimeter consisting of a Dewar flask, furnished with a heating coil and a mechanical stirrer. The input of electrical energy was measured in the usual way. This calorimeter has an accuracy of 2%, which, though poor by modern standards, was sufficient for our purpose. For the heats of mixing we used a mixing calorimeter, which we have previously described (3). Activities were obtained from the *J*-function ($J = 1 - (\Delta T/\nu mK)$, in the usual way.

Results

Freezing points, apparent molecular weights, and *J*-functions of aqueous solutions of indium trichloride are tabulated in Table 1*a*. The *J*-functions were plotted against molality and the values read off for smoothed molalities. From these values the activity coefficients were calculated in the usual way, with the results shown in Table 1*b*. These values are quite distinctly higher than those obtained by Hattox and de Vriess (4) for indium sulfate at corresponding concentrations; this may be due either to the difference in the electrolytes or in the methods of determination.

The heats of solution of B.D.H. prepared "$InCl_3.3H_2O$" and anhydrous $InCl_3$ in water are listed in Table 2*a* and *b*, respectively. Since the figures for the anhydrous salt show no definite trend with concentration, we thought it best to average the figures. Average $\Delta H = -22.17$ kcal.

The heats of dilution in cal per mol $InCl_3$ are shown in Table 3*a*. Adding these figures for heats of dilution to that for the heat of solution of anhydrous $InCl_3$ in water, the figures obtained for heats of solution at various concentrations are shown in Table 3*b*. According to Roth and

TABLE 3

(*a*) Heats of solution in cal per mol of $InCl_3$

Original solution		Final solution		
M	Moles H_2O per mol $InCl_3$	*M*	Moles H_2O per mol $InCl_3$	ΔH
7.528	7.37	2.243	24.74	−3481
5.360	10.37	2.772	20.04	−2173
2.779	19.99	1.250	44.44	−1645
2.243	24.74	1.0580	52.45	−987.9
1.278	43.47	0.6443	86.27	−912.7
1.058	52.45	0.6033	91.98	−729.1
0.7129	77.94	0.3385	164.1	−813
0.6033	92.09	0.2708	204.9	−408.6
0.2766	200.9	0.1587	350.1	−422.4

(*b*) Heats of solution at various concentration

Final molality	ΔH
0.2310	−22.17
0.6033	−21.44
1.058	−21.18
2.243	−20.00
7.528	−18.69

Buchner (5), the heat of solution of 1 mol $InCl_3$ in 11 900 moles of water, at 20°, is −23.25 kcal, a result in rather good agreement with ours, when the dilution is considered.

The heats of solution of indium hydroxide ($In(OH)_3$) and indium trioxide (In_2O_3) in concentrated HCl (37% HCl) are listed in Table 4.

Summary

Very little discussion of so purely practical a paper seems to us necessary. The very large negative values of the enthalpy of solution in water, of not only the anhydrous, but also of the hydrated, forms of indium chloride point to a profound interaction of the salt, or its ions, or both, with water. It is fashionable to speak of the "structure-breaking" or "structure-making" effect of a salt on water but it seems to us that so considerable a heat effect as described indicates a true chemical reaction between solute and solvent.

From the heats of solution of indium hydroxide and of indium trioxide in hydrochloric acid, the enthalpy of the reaction:

$$2\,In(OH)_3(s) = In_2O_3(s) + 3H_2O(l)$$

is obtained as −0.56 kcal. Taking the figure of −222.5 kcal, obtained by Becker and Roth (6) as the molar enthalpy of $In_2O_3(s)$, the molar enthalpy of $In(OH)_3(s)$ obtained is −213.45 kcal. The figure given in ref. 7 is −214 kcal, but such remarkable agreement can only be fortuitous.

Again, considering the solution of indium trioxide in HCl, it is possible to calculate the

$$In_2O_3(s) + 6HCl.aq = 2InCl_3.aq + 3H_2O(l)$$
$$\Delta H = -62.6\ \text{kcal}$$

enthalpy of $2InCl_3.aq$. From the heats of solution and dilution given in (8), we calculate this to be −177.5 kcal per mol of $InCl_3.aq$. Taking the value of ΔH for the reaction:

$$InCl_3(s) + aq = InCl_3.aq$$

as −23.25 (5), we find for $InCl_3(s)$ −154.25 kcal. This is to be compared with the figure of −128.5 obtained by Klemm and Brautigam (9), as the heat of solution of In, Cl_2, and $InCl_3$ in Herschkowitz's solution.

Can. J. Chem. Downloaded from www.nrcresearchpress.com by 210.87.254.105 on 09/05/12
For personal use only.

TABLE 4. Heats of solution of indium hydroxide ($In(OH)_3$) and indium trioxide (In_2O_3) in concentrated HCl

Molarity of solution	ΔH per mol of salt (kcal)	
Indium hydroxide		
0.349×10^{-3}	−31.577	In precision calorimeter: not suitable for high concentration. $\Delta H^\circ = -31.58$
0.958×10^{-3}	−31.560	
1.002×10^{-3}	−31.417	
2.211×10^{-3}	−31.356	
6.211×10^{-3}	−30.402	
0.025	−31.15	Approximately constant at $\Delta H = -31.67$ kcal
0.070	−32.06	
0.146	−31.71	
0.168	−31.38	
0.210	−30.89	
0.239	−32.90	
0.344	−31.26	
0.383	−31.97	
0.526	−31.72	
Indium trioxide		
0.548×10^{-3}	−62.811	In precision calorimeter $\Delta H^\circ = -62.6$
0.570×10^{-3}	−62.600	
0.670×10^{-3}	−62.400	
1.426×10^{-3}	−63.812	
2.028×10^{-3}	−63.873	
0.146	−63.03	Approximately constant at $\Delta H = -63.17$ kcal
0.158	−62.38	
0.0310	−64.35	
0.0529	−64.36	
0.0972	−64.13	
0.0214	−62.93	
0.1397	−64.23	
0.1569	−62.49	
0.1905	−61.41	
0.2584	−62.42	

1. F. ENSSLIN, B. ZIEMECK, and L. DE SCHAEPDRYVER. Z. Anorg. Chem. **254**, 293 (1947).
2. O. N. BHATNAGAR and A. N. CAMPBELL. Chem. Instr. **179**, (3) 4 (1973).
3. A. N. CAMPBELL, E. M. KARTZMARK, and S. C. ANAND. Can. J. Chem. **48**, 1579 (1970).
4. E. M. HATTOX and T. DE VRIESS. J. Am. Chem. Soc. **58**, 2126 (1936).
5. W. A. ROTH and A. BUCHNER. Z. Elektrochem. **40**, 88 (1934).
6. G. BECKER and W. A. ROTH. Zeit. Phys. Chem. **A161**, 72 (1932).
7. Selected values of chemical thermodynamic properties. Circular 500, N.B.S. 1952. Table 29. p. 170.
8. Thermal properties of aqueous uni-univalent electrolytes. U.S. Department of Commerce, National Bureau of Standards. pp. 50 and 66.
9. W. KLEMM and M. BRAUTIGAM. Z. Anorg. Chem. **163**, 232 (1927).

Can. J. Chem. Downloaded from www.nrcresearchpress.com by 210.87.254.105 on 09/05/12
For personal use only.

Complexes of Tantalum and Antimony Pentafluorides with Dimethyl Ether and Trimethylamine[1]

S. BROWNSTEIN AND MARJORIE JEAN FARRALL

Division of Chemistry, National Research Council of Canada, Ottawa, Canada K1A 0R9

Received September 17, 1973

Tantalum pentafluoride forms 1:1 and 1:2 complexes with dimethyl ether and trimethylamine. Antimony pentafluoride forms 2:1 and 1:1 complexes with dimethyl ether and trimethylamine. The rates of exchange of terminal and equatorial fluorines in the 1:1 TaF_5 – dimethyl ether adduct have been measured.

Le pentafluorure de tantale forme des complexes 1:1 et 1:2 avec l'éther méthylique et la triméthylamine. Le pentafluorure d'antimoine forme des complexes 2:1 et 1:1 avec l'éther méthylique et la triméthylamine. On a mesuré les vitesses d'échange des fluors terminaux et équatoriaux dans le produit d'addition 1:1 du TaF_5 avec l'éther méthylique. [Traduit par le journal]

Can. J. Chem., **52**, 1958 (1974)

Can. J. Chem. Downloaded from www.nrcresearchpress.com by 210.87.254.6 on 09/05/12
For personal use only.

Introduction

There has been considerable study, via fluorine resonance spectroscopy, of the complexes formed between oxygen or nitrogen containing organic compounds and Lewis acid fluorides (1–5). In some cases there have been studies of the rates of exchange between free and complexed species and details of exchange mechanism have been elucidated (1, 6, 7). The only reported study of tantalum pentafluoride complexes used the Lewis base itself as solvent which, because of rapid exchange, severely limited the amount of information which could be obtained (4). Results for antimony pentafluoride Lewis base adducts have generally been presented in a very abbreviated form (8), except for adducts with oxides of sulfur (9, 10). The aim of this investigation is a better understanding of the structures containing unequal amounts of acid and base and the mechanism of exchange in the 1:1 adducts.

Experimental

All samples were prepared by vacuum line techniques and solids were manipulated only in a vacuum dry box. Antimony pentafluoride was vacuum distilled and stored in a glass container closed by a stainless steel bellows valve. Aliquots were distilled into break-seal containers for weighing prior to sample preparation. Tantalum and niobium pentafluorides purchased from Ozark-Mahoning Ltd. were used without further purification. Sulfur dioxide and methylene chloride, used as solvents, were dried over phosphorus pentoxide and stored on the vacuum system. Sulfuryl chlorofluoride purchased from Cations Inc. was distilled directly into the sample containers. Dimethyl ether was dried over P_2O_5 and trimethylamine over KOH before use.

Fluorine resonance spectra were obtained on a Varian Associates HA-100D spectrometer operating at 94.1 MHz. Chemical shifts are reported as p.p.m. from internal $CFCl_3$. In samples with sulfuryl chlorofluoride as solvent, the solvent or SO_2F_2 as an impurity in it, were used as references and conversion made to the $CFCl_3$ scale assuming chemical shifts of −97.6 p.p.m. and −32.7 p.p.m., respectively. Temperature calibration and monitoring techniques used on this apparatus have been described (11). The theoretical spectra used to obtain exchange rates for the TaF_5 – dimethyl ether complex were calculated by a stochastic approach (12). The activation energy was obtained from a least squares treatment of the data. The quoted error is the estimated experimental error.

Results and Discussion

A 1:1 mixture of tantalum pentafluoride and dimethyl ether dissolved in methylene chloride shows, at very low temperature, the characteristic doublet and quintet of an AB_4 system. This strongly suggests an octahedral arrangement of ligands about tantalum with the dimethyl ether group occupying an apical position. The quintet from the apical fluorine has a chemical shift of −112.8 p.p.m. and the doublet of the four equatorial fluorines a chemical shift of −73.6 p.p.m. The spin coupling constant between the nonequivalent fluorines is 23.1 Hz, a value in good agreement with the *trans* coupling of 23.0 Hz in the $Ta_2F_{11}^-$ ion (13). As the temperature of the sample was raised the individual lines of the spin multiplets broadened and merged and these averaged lines further broadened. A representative collection of experimental and theoretical spectra for one sample are shown in Fig. 1.

[1]NRCC No. 13840.

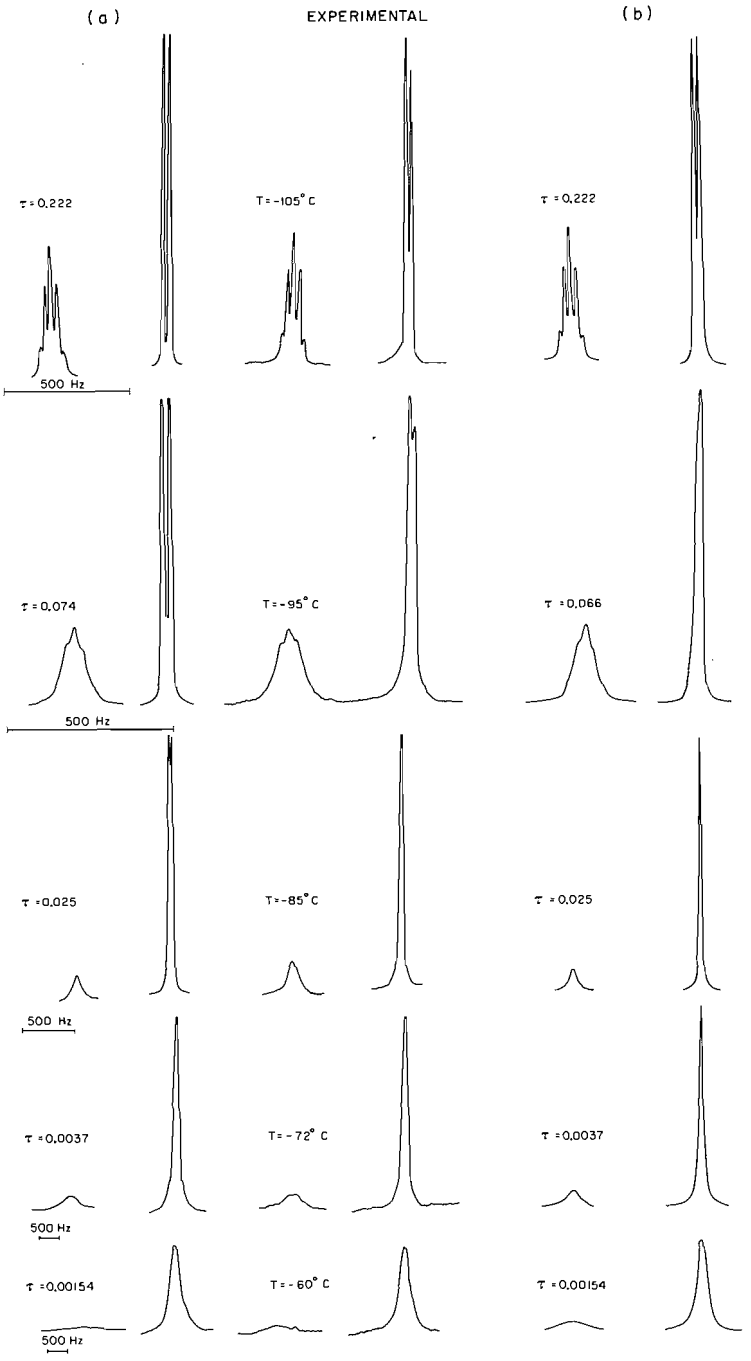

FIG. 1. Experimental and theoretical spectra for a methylene chloride solution 0.334 molal in TaF_5 and dimethyl ether. (*a*) Intramolecular mechanism, (*b*) intermolecular mechanism with a 0.2% excess of free TaF_5.

An excess of TaF_5 did not give any new species in solution. Therefore an attempt was made to determine the mechanism for fluorine exchange between equatorial and apical sites by varying the concentration of TaF_5 and its dimethyl ether complex. One possible mechanism for this exchange is intramolecular. In this case the average lifetime of an apical fluorine will be one quarter

Can. J. Chem. Downloaded from www.nrcresearchpress.com by 210.87.254.6 on 09/05/12
For personal use only.

Can. J. Chem. Downloaded from www.nrcresearchpress.com by 210.87.254.6 on 09/05/12
For personal use only.

that of an equatorial fluorine. Theoretical spectra calculated for this exchange mechanism are shown in Fig. 1. A second possible exchange mechanism is by an intermolecular route. This could occur either by dissociation of the complex and recombination of the dimethyl ether with the same or another TaF_5 molecule as in reaction 1, or, if excess TaF_5 is present, by reaction of the complex with TaF_5 according to reactions 2 or 3.[2]

[1] $$(CH_3)_2O{\cdot}TaF_5 \rightleftharpoons (CH_3)_2O + TaF_5$$

[2] $$(CH_3)_2O{\cdot}TaF_5 + TaF_5^* \rightleftharpoons (CH_3)_2O{\cdot}TaF_5^* + TaF_5$$

[3] $$(CH_3)_2O{\cdot}TaF_5 + TaF_5 \rightleftharpoons (CH_3)_2O{\cdot}TaF_4^+ + TaF_6^-$$

For the mechanisms of reactions 1 and 2 the average lifetimes of apical and equatorial fluorines will be equal when there is an excess of free TaF_5 present or if the complex is largely dissociated. The lifetimes of apical and equatorial fluorines exchanging by the mechanism of reaction 3 will be equal if there is a significant quantity of the ionic species but will be equivalent to those of intramolecular exchange if the equilibrium is far to the left.

The theoretical spectra of equal, or 1:4 lifetimes, are limiting cases. Although neither set is a perfect fit the experimental spectra correspond more closely to the intramolecular case, *i.e.* a ratio of lifetimes of 1:4. It is possible to calculate theoretical spectra for intermediate cases by including the resonance line of TaF_5 and varying the relative concentrations. Some representative results are listed in Table 1. Concentrations of free TaF_5 greater than about 4% do not cause further changes of much significance in the theoretical spectra.

The Kubo–Sack matrix, represented by **A**, is the sum of two matrices Ω and **D** (14–16). The Ω matrix only depends upon the chemical shifts while the **D** matrix depends upon the transition probabilities between sites and the lifetimes in these sites. The **D** matrices used to calculate theoretical spectra for intramolecular exchange and intermolecular exchange with equal effective concentrations of complex and TaF_5 are listed in Table 2. Sites 1 and 2 are the doublet, sites 3 to 7 the quintet, and site 8 is TaF_5.

For those samples containing a 1:1 ratio of TaF_5 to dimethyl ether the best fit between experimental and theoretical spectra was obtained with theoretical spectra including 0.2% of free TaF_5. A set of these spectra are included in Fig. 1. The lifetimes thus obtained are plotted in Fig. 2. For those samples containing an excess of TaF_5 the best agreement was obtained with 1.5% of free TaF_5. These lifetimes are also plotted in Fig. 2.

TABLE 1. Calculations of relative line widths as a function of concentration for a fixed exchange lifetime

$[TaF_5]_{free}$	Line width (Hz)	
$[TaF_5]_{complex}$	Doublet	Quintet
0.2	205	210
0.04	200	195
0.008	100	170
0.004	65	155
0.001	55	140
0.0002	45	155

Tantalum pentafluoride is sparingly soluble in methylene chloride at low temperatures. Therefore, with an excess of tantalum pentafluoride, its concentration in solution will not be known and will vary with temperature. The concentrations listed for Fig. 2 are those assuming complete solution and are for identification only in those samples containing excess TaF_5. The position of the equilibrium in reactions 1 and 3 will also be temperature dependent. This means that although it is possible to obtain lifetimes of the apical and equatorial fluorines as a function of temperature, one can only obtain rate constants if the exchange occurs by an intramolecular mechanism. An intramolecular mechanism, however, does not fit the theoretical spectra and must be discarded.

For the present system it is not possible to distinguish between the three proposed intermolecular exchange mechanisms on the basis of the theoretical spectra. From the slope of the temperature dependence of the lifetime, the Arrhenius activation energy for exchange may be calculated, although it does not necessarily correspond to a particular step in the exchange reaction. This index of exchange is 8 ± 1 kcal/mol for the samples with a 1:1 composition. Samples with an excess of TaF_5 have a lower activation energy for exchange with values of 6 ± 1 kcal/mol for a 2.5:1 ratio and 5 ± 1 kcal/mol for a 2:1 ratio. The difference between the latter two activation energies is probably not significant but their

[2]The authors wish to thank a referee for suggesting exchange according to reaction 3.

TABLE 2. Transition probability matrices for different exchange mechanisms

(*a*) Intramolecular exchange

	1	2	3	4	5	6	7
1	−0.25	0	0.016	0.062	0.094	0.062	0.016
2	0	−0.25	0.016	0.062	0.094	0.062	0.016
3	0.50	0.50	−1.0	0	0	0	0
4	0.50	0.50	0	−1.0	0	0	0
5	0.50	0.50	0	0	−1.0	0	0
6	0.50	0.50	0	0	0	−1.0	0
7	0.50	0.50	0	0	0	0	−1.0

(*b*) Intermolecular exchange

	1	2	3	4	5	6	7	8
1	−1.0	0	0	0	0	0	0	1.0
2	0	−1.0	0	0	0	0	0	1.0
3	0	0	−1.0	0	0	0	0	1.0
4	0	0	0	−1.0	0	0	0	1.0
5	0	0	0	0	−1.0	0	0	1.0
6	0	0	0	0	0	−1.0	0	1.0
7	0	0	0	0	0	0	−1.0	1.0
8	0.40	0.40	0.013	0.050	0.075	0.050	0.013	−1.0

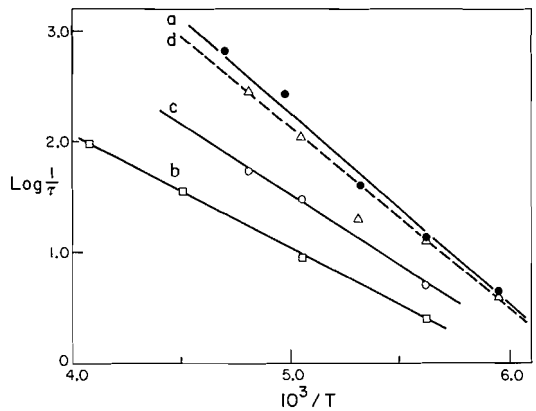

FIG. 2. Exchange rate as a function of temperature for methylene chloride solutions of the TaF_5 dimethyl ether complex at different concentrations. (*a*) 0.334 *m* TaF_5 and 0.334 *m* $(CH_3)_2O$. (*b*) 0.264 *m* TaF_5 and 0.132 *m* $(CH_3)_2O$. (*c*) 0.225 *m* TaF_5 and 0.09 *m* $(CH_3)_2O$. (*d*) 0.100 *m* TaF_5 and 0.098 *m* $(CH_3)_2O$.

difference from the 1 : 1 case is thought to be real. Since exchange by mechanism 1 must have a higher activation energy than for mechanisms 2 and 3, it is tentatively suggested that the 1 : 1 complex undergoes exchange by mechanism 1, but in the presence of excess TaF_5, the exchange occurs via mechanism 2 or mechanism 3.

It has been reported that with an excess of Lewis base, complexes with two equivalents of base for TaF_5 are sometimes formed and these are formulated as $[TaF_4L_4]^+[TaF_6]^-$ (4). With dimethyl sulfoxide as Lewis base and solvent, it was found that the intensities for the resonance lines from fluorine on tantalum in the positive species varied markedly with temperature. This was postulated to occur because of an equilibrium to give species with varying numbers of ligands attached to the positive tantalum species. The present results with dimethyl ether as Lewis base agree in principle with the earlier work, but the chemical shifts are sufficiently different as to cast some doubts upon the tentative assignments previously made. Because of the differences between the systems studied and the tentative nature of the assignments made previously, no attempt will be made to refute them. The results obtained in this study will be explained with reference to reactions 4–7, where L is dimethyl ether,

$$[4] \quad 2TaF_5 + 4L \rightarrow TaF_6^- + TaF_4L_4^+$$

$$[5] \quad TaF_4L^+ + L \rightarrow TaF_4L_2^+$$

$$[6] \quad TaF_4L_2^+ + L \rightarrow TaF_4L_3^+$$

$$[7] \quad TaF_4L_3^+ + L \rightarrow TaF_4L_4^+$$

K_4 is defined by

$$K_4 = \frac{[TaF_4L_4^+]}{[TaF_4L_3^+][L]}$$

and similarly for K_3. The equilibria and complexed species are slightly different than those

Can. J. Chem. Downloaded from www.nrcresearchpress.com by 210.87.254.6 on 09/05/12
For personal use only.

Can. J. Chem. Downloaded from www.nrcresearchpress.com by 210.87.254.6 on 09/05/12
For personal use only.

TABLE 3. Chemical shifts and equilibrium values for the complexed species $TaF_4L_4^+$, $TaF_4L_3^+$, and $TaF_4L_2^+$

T (°C)	$TaF_4L_4^+$ δ	Area	Concentration	K_4	$TaF_4L_3^+$ δ	Area	Concentration	K_3	$TaF_4L_2^+$ δ	Area	Concentration
(*i*) 0.162 *m* TaF_5 and 0.327 *m* $(CH_3)_2O$											
−85	−99.4	136	0.057	89	−81.3	53	0.022	400	−72.2	5	0.002
−65	−100.6	68	0.021	5	−81.4	181	0.055	170	−72.4	16	0.005
−45	−101.7	4	0.003	0.5	−81.9	91	0.070	9	−72.9	11	0.008
(*ii*) 0.328 *m* TaF_5 and 4.08 *m* $(CH_3)_2O$											
−85	−99.1										
−65	−100.3	137	0.153	4	−81.4	10	0.011				
−59	−100.7	31	0.141	2	−81.6	5	0.023				
−51	−101.4	20	0.126	1	−81.2	6	0.038				
(*iii*) Average values for all samples											
−105				1200 ± 600				—			
−85				40 ± 20				400 ± 200			
−65				4 ± 1				80 ± 70			
−45				0.5 ± 0.4				30 ± 20			

Can. J. Chem. Downloaded from www.nrcresearchpress.com by 210.87.254.6 on 09/05/12
For personal use only.

proposed previously (4). The only justification for this scheme is that it gives consistent values for K_3 and K_4 and no species are observed with fewer than six groups around tantalum. The chemical shift of TaF_6^- was found to be -39.6 and did not vary significantly with temperature nor solvent composition. The assignment of a particular line to one of the cationic species was done so that there would be a regular variation in chemical shift with number of ligands, and to be consistent with their concentration and temperature dependence.

The chemical shifts, relative areas, concentrations, and equilibrium constants as a function of temperature for two of six samples are listed in Table 3. The ratios of dimethyl ether to TaF_5 in these samples are at the two extremes of the range studied. Average values for the equilibrium constants are also listed.

Trimethylamine forms a 1:1 complex with tantalum pentafluoride. The chemical shifts of apical and equatorial fluorines are -89.3 and -77.5 p.p.m., and the coupling constant between them is 21 Hz. With an excess of TaF_5 to amine, only the spectrum of the 1:1 complex is observed. A sample prepared from two equivalents of trimethylamine and one of tantalum pentafluoride has only a simple sharp resonance at -68.5 p.p.m. even at -115 °C. It is suggested that rapid exchange is occurring for fluorine of TaF_6^- and $TaF_4 \cdot 4(CH_3)_3N^+$ since the weighted average of the chemical shifts of these species, with dimethyl ether as base, is -63.8 p.p.m. The 2:1 complex appears more stable relative to the 1:1 with trimethylamine as base than with dimethyl ether. Solutions prepared from equivalent amounts of $(CH_3)_3N$ and TaF_5 have peaks from both the 1:1 and 2:1 complexes. It did not appear useful to study exchange between apical and equatorial fluorines under these conditions.

Attempts to prepare complexes with boron trifluoride attached by a fluorine bridge bond to complexed tantalum pentafluoride failed. The BF_3 dimethyl ether and trimethylamine complexes were formed and TaF_5 liberated. This shows that TaF_5 forms weaker complexes with these ligands than does BF_3.

An equimolar mixture of antimony pentafluoride and dimethyl ether dissolved in SO_2ClF had the fluorine resonance spectrum of the 1:1 complex. The apical fluorine gives a quintet of lines at 134.4 and the equatorial fluorines a doublet at 123.3 with a spin-coupling constant of 101 Hz

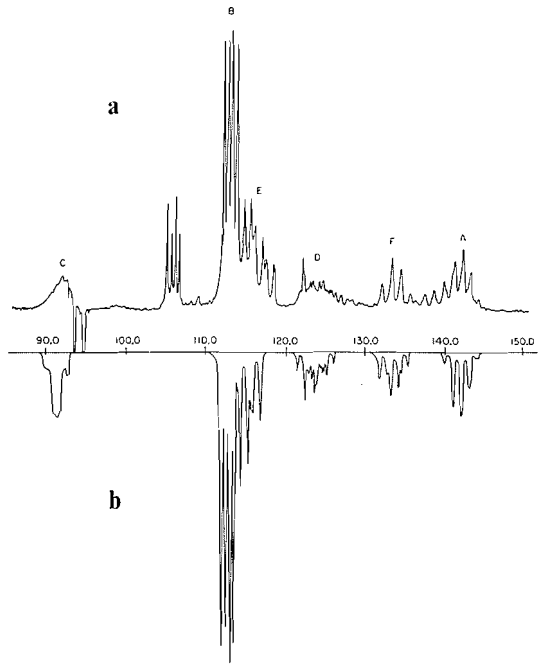

FIG. 3. The fluorine resonance spectrum of a sulfuryl chloride fluoride solution of 0.454 mmol dimethyl ether and 0.908 mmol antimony pentafluoride at -85 °C. (*a*) Experimental, (*b*) theoretical.

between them. In addition, there is a very weak multiplet at 114.1. These results are consistent with those reported for other complexes of antimony pentafluoride (8, 17). With an excess of dimethyl ether there was no evidence for formation of any complex containing two equivalents of Lewis base for each antimony pentafluoride.

A complex containing two molecules of antimony pentafluoride for each one of dimethyl ether has been identified and characterized from the fluorine resonance spectrum shown in Fig. 3. This molecule has the *cis* structure **1**, consistent

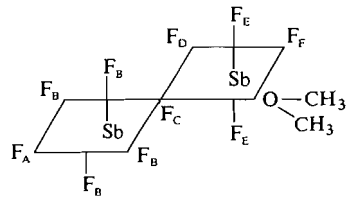

1

with that found for other antimony pentafluoride complexes (17). The parameters are listed in Table 4. The assignments were confirmed by double resonance experiments. Fluorine A would be a quintet from spin-coupling with the four equiv-

Can. J. Chem. Downloaded from www.nrcresearchpress.com by 210.87.254.6 on 09/05/12
For personal use only.

TABLE 4. Chemical shifts and coupling constants for **1**

Nucleus	Chemical shift[a]	Spin-coupling[b]
A	142.3	$J_{A-B} = 97$ $J_{A-C} = 13.5$
B	113.5	$J_{B-C} = 48$
C	92.0	$J_{C-D} = 85$ $J_{C-E} = 85$ $J_{C-F} = 13.5$
D	124.2	$J_{D-E} = 132$ $J_{D-F} = 85$
E	115.6	$J_{E-F} = 132$
F	134.2	

[a]In p.p.m. from $CFCl_3$.
[b]In Hz.

alent fluorines B. Fluorines B would be a doublet of doublets from spin-coupling with fluorine A and fluorine C. Upon irradiation of the resonance attributed to fluorine A, the one attributed to fluorine B collapsed to a doublet. It also collapsed to a doublet when the resonance attributed to fluorine C was irradiated. Similarly, the irradiation of fluorine B collapsed the fine structure found in the signal from fluorine A. Other pairs which were irradiated and behaved in a manner consistent with the above assignment were C–E and C–D. Unfortunately, the pairs D–E and D–F could not be handled in this manner because of overlapping from other parts of the spectrum produced by the double resonance technique. Since the system is not exactly first order, a final proof of assignment is the matching of the experimental spectrum with a theoretical one calculated from the assigned chemical shifts and spin-coupling constants. The theoretical spectrum was calculated by the program SIMEQ (18) and is shown in Fig. 3. It is a sum of separate systems AB_4C and CDE_2F therefore, the C resonance will be narrower than it should be.

There are various additional signals in these spectra from other species. The weak peak at 114.1 in the fluorine resonance spectrum of the 1:1 complex may be assigned to a small amount of complex containing two equivalents of antimony pentafluoride. The doublet at 105.8 in the 2:1 sample is from a 1:1 complex of SbF_5 with the solvent. The quintets of this complex gives the extra peaks in the region of the resonance of fluorine A. The doublet at 106.3 is not assigned. Its intensity is greatly reduced relative to the lines of the dimethyl ether complexes, both 1:1 and 1:2, in a solution prepared with 1.5 equivalents of SbF_5 for each equivalent of dimethyl ether.

Since it is possible to complex another molecule of SbF_5, via fluorine bridging, to antimony pentafluoride in its 1:1 complex with dimethyl ether, an attempt was made to complex other binary fluorides. It was found that there was no reaction between the SbF_5 – dimethyl ether complex and BF_3, NbF_5, TaF_5, or MoF_5. With phosphorous pentafluoride, a small amount of dimethyl ether is complexed by PF_5 in competition with SbF_5, but there is no evidence for a mixed complex containing two molecules of Lewis acid fluoride. The situation is more complicated with AsF_5, since in addition to the complex $AsF_5 \cdot (CH_3)_2O$, which has been observed previously (5), and a minor amount of the 2:1 SbF_5 – dimethyl ether species, another product is a complex with structure **2** and rapid exchange of the AsF_5 group between the

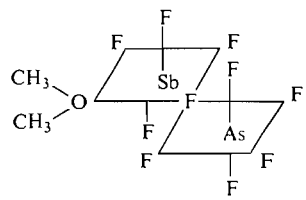

2

equatorial fluorines bonded to antimony. It is characterized by a doublet at 113.4 for the equatorial fluorines on antimony and a quintet at 122.9 for the bridging fluorine. (The spin-coupling constant between them is 107 Hz.) The fluorines bonded to arsenic alone all appear as a single line at 51.1. Evidently there is rapid averaging between the equatorial and apical fluorines on arsenic. *Cis* bonding with rapid averaging among the four equatorial fluorines on antimony is invoked to explain the lack of observed spin-coupling between the arsenic and antimony moieties. It is quite unlikely that the dimethyl ether is complexed to arsenic rather than antimony, since the various fluorines on arsenic would be likely to remain non-equivalent and not exchange rapidly on the n.m.r. time scale, with dimethyl ether complexed to the same central atom.

Efforts to study the system antimony pentafluoride – trimethylamine were frustrated by the inability to find an adequate, but inert, solvent. From the difference in solubility and fluorine resonance spectra, it appears that both 1:1 and

2:1 complexes of SbF_5 are formed with trimethylamine, but they have not been adequately characterized.

There is a marked difference in complexing behavior between the pentafluorides of antimony and tantalum, both in the same row of the periodic table, the former in group VA, and the latter group VB. In addition to a 1:1 complex, antimony pentafluoride forms a complex containing two equivalents of Lewis acid per equivalent of dimethyl ether, while tantalum pentafluoride forms a complex with two equivalents of dimethyl ether per equivalent of Lewis acid.

1. S. BROWNSTEIN, A. M. EASTHAM, and G. A. LATREMOUILLE. J. Phys. Chem. **67**, 1028 (1963).
2. A. G. MASSEY and A. J. PARK. J. Organometal. Chem. **5**, 218 (1966).
3. F. N. TEBBE and E. L. MUETTERTIES. Inorg. Chem. **6**, 129 (1967).
4. J. A. S. HOWELL and K. C. MOSS. J. Chem. Soc. (A), 2483 (1971).
5. L. LUNAZZI and S. BROWNSTEIN. J. Magnet. Res. **1**, 119 (1969).
6. A. C. RUTENBERG and A. A. PALKO. J. Phys. Chem. **69**, 527 (1965).
7. J. M. MILLER and M. ONZYSZCHUK. Can. J. Chem. **44**, 899 (1966).
8. E. L. MUETTERTIES. Advances in the chemistry of the coordination compounds. MacMillan, New York. 1961. p. 513.
9. J. BACON, P. A. W. DEAN, and R. J. GILLESPIE. Can. J. Chem. **47**, 1655 (1969).
10. J. BACON, P. A. W. DEAN, and R. J. GILLESPIE. Can. J. Chem. **48**, 3413 (1970).
11. S. BROWNSTEIN, E. C. HORSWILL, AND K. U. INGOLD. Can. J. Chem. **49**, 1350 (1971).
12. S. BROWNSTEIN and J. BORNAIS. Can. J. Chem. **46**, 225 (1968).
13. S. BROWNSTEIN. Inorg. Chem. **12**, 584 (1973).
14. R. KUBO. Nuovo Cimento, Suppl. **6**, 1063 (1957).
15. R. A. SACK. Mol. Phys. **1**, 163 (1958).
16. C. S. JOHNSON and C. G. MORELAND. J. Chem. Educ. **50**, 477 (1973).
17. P. A. W. DEAN and R. J. GILLESPIE. J. Am. Chem. Soc. **91**, 7260 (1969).
18. P. J. VAN DER HAAK. Private communication.

Can. J. Chem. Downloaded from www.nrcresearchpress.com by 210.87.254.6 on 09/05/12
For personal use only.

Isotope Effects on Chemical Equilibria. Part II. Some Further Secondary Isotope Effects of the Second Kind

DOUGLAS JAMES BARNES, PETER DAVID GOLDING, AND JOHN MARSHALL WILLIAM SCOTT

Chemistry Department and the Faculty of Medicine, Memorial University of Newfoundland, St. John's, Newfoundland A1C 5S7

Received October 9, 1973

The ratio of the dissociation constants $K_a(H)/K_a(D)$ has been measured conductimetrically for the isotopic pairs XCH_2COOH/XCD_2COOH where X = Cl, PhO, and PhS. Methods of calculating the ratio of the equilibrium constants are considered in some detail. Since the isotope effect varies with the nature of the X substituent it is concluded that the simple inductive description of these effects is not tenable.

On a mesuré les rapports de constantes de dissociation $K_a(H)/K_a(D)$ par conductimétrie pour chaque paire isotopique XCH_2COOH/XCD_2COOH dans lesquels X = Cl, PhO et PhS. On considère en détail les méthodes de calcul pour déterminer les rapports des constantes d'équilibre. Puisque l'effet isotopique varie avec la nature du substituant X on en conclu qu'une description de ce phénomène par un simple effet inductif n'est pas complète. [Traduit par le journal]

Can. J. Chem., **52**, 1966 (1974)

Introduction

In a previous communication (1) we reported isotope effects for the equilibria

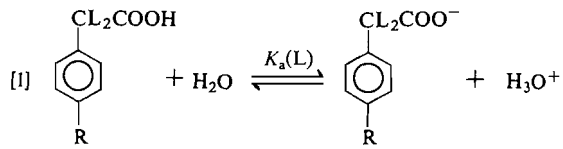

where R = MeO, H, and NO_2 and L represents hydrogen or deuterium. Although the $K_a(H)/K_a(D)$ ratios for the above equilibria were much smaller than anticipated from previous studies (1), two important observations emerged. Firstly the predicted value of the isotope effect for the pair $PhCH_2COOH/PhCD_2COOH$ based on $\sigma^*(D)$ is now closer to the observed value, *i.e.*, the inductive treatment is partially verified. Secondly, when combined with the data for acetic acid and acetic acid-d_3, the size of the isotope effect per deuterium appears to be variable and dependent on the strength of the protium acid (Fig. 1). An extrapolation of this correlation implies that the isotope effects might become inverse for acids with pK_a's less than that of 4-nitrophenylacetic acid. One of the purposes of this paper is to test such an extrapolation.

Whilst the discussion of some secondary isotope effects as inductive in nature has never been entirely convincing, an inductive effect of D *vs.* H

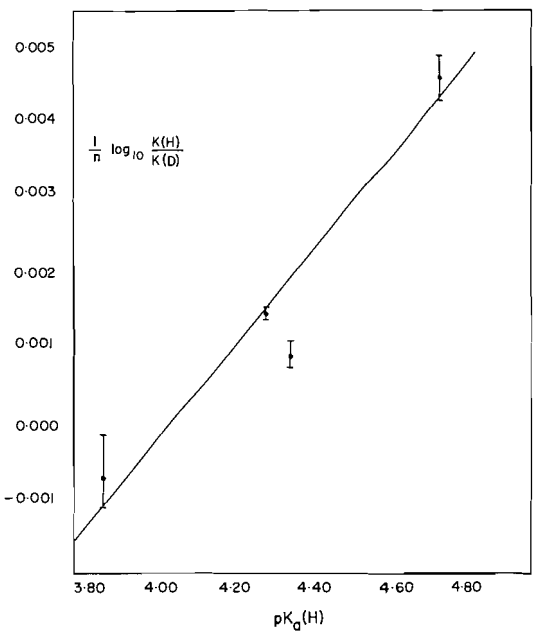

FIG. 1. Correlation of secondary isotope effects per deuterium against $pK_a(H)$. See ref. 1 for the data.

which is normal for some acids and in the opposite direction for others is hardly tenable within the conceptual framework of the inductive effect. Indeed, if such a situation arose the inductive description would have to be abandoned.

In order to definitely establish if such a correlation exists between pK_a and $K(H)/K(D)$ further

Can. J. Chem. Downloaded from www.nrcresearchpress.com by 210.87.254.40 on 09/05/12
For personal use only.

Can. J. Chem. Downloaded from www.nrcresearchpress.com by 210.87.254.40 on 09/05/12
For personal use only.

measurements are required, particularly on acids with pK_a's < 4. In the present paper we have further examined the problem of evaluating the equilibrium constants and the isotopic ratios from the conductance data. An attempt has been made to increase the precision of the conductance data as well as to provide an improved method for calculating $K_a(H)/K_a(D)$ without the determination of the equilibrium constant of either acid.

Experimental

General

All melting points and boiling points are uncorrected. Nuclear magnetic resonance (n.m.r.) spectra were obtained using a Varian A60 spectrometer. All organic solvents were distilled prior to use or were of known grade of purity.

Preparation and Purification of Materials

All the acids mentioned below were subjected to intensive purification by vacuum sublimation, zone refining, and recrystallization techniques. The samples were then dried *in vacuo* at a suitable temperature. Deuteration as judged by n.m.r. measurements was found to be >97% in all cases.

Phenylacetic acid: a commercial sample after purification had m.p. 76.2–76.6 °C (lit. m.p. 76.7 °C (2)).

Phenoxyacetic acid on purification had m.p. 98.9–99.5 °C (lit. m.p. 98.5–99.5 °C (3)).

Phenoxyacetic-α,α-d_2 acid was prepared by exchange (T = 125 °C) in a sealed tube using a mixture of D_2O, $(CH_3CH_2)_3N$. The purified acid had m.p. 99.1–99.5 °C.

Chloroacetic acid was prepared from Cl_2 and glacial acetic acid in the presence of red phosphorus[1] and purified (ref. 4, p. 428) to the point where the dichloro and trichloro acids were absent, m.p. 63.0–63.2 °C (lit. m.p. 63.0 °C (5)).

Chloroacetic-α,α-d_2 acid was prepared by chlorinating glacial acetic-d_3, m.p. 62.9–63.3 °C.

Phenylthioglycollic acid, a commercial sample, on purification had m.p. 62.8–63.5 °C (lit. m.p. 62.5–63.5 °C (3)).

Phenylthioglycollic-α,α-d_2 acid was obtained by exchange using conditions similar to the phenoxy acid preparation. The pure acid had m.p. 62.5–63.5 °C.

Potassium chloride was purified as previously reported (1).

Experimental Assembly and Technique

The measurements were made as in Part I with minor modifications. The regulation of the thermostat was improved by a Tronac Unit (PTC-1000A). Ten conductance cells of the Shedlovsky type (6) (cell constants (κ) in the range 0.08 → 0.4) were determined using three independent samples of potassium chloride. The potassium chloride solutions were prepared on the molal scale and were converted to the molar scale as previously described. The calculation of the cell constant also followed the procedure outlined in ref. 1. The individual cell constants were determined at least five times during the study and were reproducible to *ca.* 0.02%.

[1]Purified following the method described in Vogel (ref. 4, p. 193).

TABLE 1. Conductance data for phenylacetic acid at 25.051 °C

10^4c (molal)	Λ	10^5K_a	10^4c	Λ	10^5K_a
61.09	33.15	4.925	8.234	83.05	4.940
47.33	37.43	4.936	6.776	90.35	4.937
37.80	41.60	4.937	6.245	93.52	4.932
29.39	46.77	4.938	5.339	99.95	4.932
22.00	53.49	4.946	3.979	112.85	4.920
10.72	73.98	4.943	2.958	127.04	4.903
9.695	77.35	4.944	1.988	148.04	4.889

Concentration-equivalent conductance data for the acids chloroacetic, chloroacetic-α,α-d_2, phenoxyacetic, phenoxyacetic-α,α-d_2, phenylthioglycollic, phenylthioglycollic-α,α-d_2, and phenylacetic are listed in Tables 1 and 2. With the exception of $PhCH_2COOH$ and $PhCD_2COOH$ (see below) all conductivities were recorded at 25.000 ± 0.002 °C. The weight of water and each carboxylic acid sample was corrected to the true weight *in vacuo* following calculations described previously (1). The densities of the deuterated acids were assumed to be equal to their protium analogs in all cases. Unknown densities were determined by measuring both the dimensions of the fused material and its weight in air or a solvent of known density. Solidification of the acids was carried out by melting with slow cooling or by compression with a hydraulic press at *ca.* 3×10^4 pounds/inch^2.

Results

Thermodynamic equilibrium constants were evaluated by the Robinson and Stokes method (7) which is a variant of the Shedlovsky expression (8) (Tables 1 and 2). This method requires an accurate value of the equivalent conductance at infinite dilution (Λ_0) to calculate by successive approximations the equivalent conductance of the hypothetical completely ionized weak electrolyte at a finite concentration (c). The Λ_0 value quoted by Jeffrey and Vogel (9) for phenylacetic acid, and by Ives and co-worker for chloroacetic acid (10) were used in the calculations.[2,3] In the case of phenylacetic acid the limiting equivalent conductance had to be corrected to 25.051 °C using an expression developed by Laughton and Demayo (11)

$$[2] \qquad \Lambda_0 = -1122.08 + 4.9614T$$

Λ_0 ($PhSCH_2COOH$) was obtained from the data of Crockford and Douglas (12) by an extrapola-

[2]These Λ_0 values have been converted to the molal scale by the equation $\Lambda_0(\text{molar}) = \Lambda_0(\text{molal}/d_0)$.

[3]$\Lambda_0(H) = \Lambda_0(D)$. The validity of this assumption has been examined in the following discussion.

TABLE 2. Conductance data at 25.000 °C

10^4c (molal)	Λ	10^4K_a	10^4c (molal)	Λ	10^4K_a
Chloroacetic acid					
44.78	168.58	13.89	20.04	219.45	13.92
39.98	175.46	13.90	15.12	237.94	13.93
35.02	183.76	13.93	10.10	263.80	13.90
29.87	193.78	13.94	8.836	271.92	13.83
24.70	205.96	13.94	8.043	277.65	13.82
Chloroacetic-α,α-d_2 acid					
44.11	168.89	13.76	20.02	218.67	13.74
40.11	174.61	13.75	14.76	238.58	13.73
34.55	183.75	13.75	9.857	264.56	13.72
29.56	193.54	13.75	9.273	268.39	13.72
24.74	204.94	13.75	7.646	280.22	13.71
Phenoxyacetic acid					
50.19	122.56	7.245	9.059	222.70	7.260
40.29	133.64	7.253	7.980	230.62	7.235
30.09	149.35	7.267	7.082	238.21	7.231
20.10	172.69	7.267	5.923	249.48	7.220
9.817	217.43	7.249	5.005	259.87	7.203
Phenoxyacetic-α,α-d_2 acid					
50.55	121.65	7.164	9.045	222.03	7.172
40.00	133.42	7.175	7.986	229.72	7.139
30.16	148.59	7.185	6.994	238.25	7.143
20.06	172.07	7.176	5.841	249.51	7.123
10.02	215.36	7.168	5.059	258.40	7.109
Phenylthioglycollic acid					
50.08	81.74	2.800	15.12	134.20	2.807
45.37	85.33	2.802	9.942	157.22	2.807
40.24	89.86	2.804	9.033	162.80	2.807
34.96	95.42	2.806	8.096	169.27	2.807
30.19	101.51	2.807	6.895	178.91	2.803
25.04	109.70	2.808	6.008	187.39	2.801
19.85	120.55	2.808	5.027	198.49	2.795
Phenylthioglycollic-α,α-d_2 acid					
50.08	81.01	2.744	15.04	133.53	2.757
45.29	84.65	2.747	10.02	155.70	2.757
40.12	89.20	2.749	9.006	161.84	2.754
35.04	94.53	2.751	8.078	168.27	2.755
30.18	100.67	2.752	7.021	176.69	2.753
25.08	108.73	2.754	5.993	184.34	2.748
20.01	119.23	2.756	5.023	197.23	2.739

tion of a plot of Λ_c *vs.* $C^{1/2}$. No literature value of the equivalent conductance at infinite dilution was available for phenoxyacetic acid. As a result a value was developed from a Shedlovsky extrapolation–iteration method (SIM) for determining both Λ_0 and K_a simultaneously (13).

Average K_a values and related data for all seven acids are summarized in Table 3. A comparison with existing data can be made only for phenylacetic and chloroacetic acids. Within the accuracy of the phenylacetic acid data K_a (25.000 °C) is equal to K_a (25.051 °C).[4] This value is in excellent agreement with previous work on the acid, further confirming the reliability of the work. The thermodynamic equilibrium constant for chloroacetic acid is in agreement with the work of Shedlovsky and co-workers (14) but is

[4]Demayo found a 3.9% decrease in $K_a(PhCH_2COOH)$ from 20 to 40 °C.

Can. J. Chem. Downloaded from www.nrcresearchpress.com by 210.87.254.40 on 09/05/12
For personal use only.

TABLE 3. Comparison of equilibrium constants

Acid	$10^4 K_a$	Method*	Reference
$PhCH_2COOH$	0.4930±0.0016	RSM(*m*)	This work and ref. 9‡
	0.4923±0.0015 (Λ_0 = 379.6)†	RSM(*m*)	1
$ClCH_2COOH$	13.90 ±0.04 (Λ_0 = 390.8)†	RSM(*m*)	This work and ref. 10‡
	13.9	C(*c*)	15
	13.97	C(*c*)	14
	13.59	C(*c*)	10
	13.78	E.m.f.	16
	13.37	C.D.(*c*)	17
$ClCD_2COOH$	13.74 ±0.02 (Λ_0 = 390.8)†	RSM(*m*)	This work and ref. 10‡
$PhOCH_2COOH$	7.243 ±0.020 (Λ_0 = 381.3)§	RSM(*m*)	This work
	6.75	E.m.f.	18
$PhOCD_2COOH$	7.156 ±0.025 (Λ_0 = 381.3)§	RSM(*m*)	This work
$PhSCH_2COOH$	2.805 ±0.004 (Λ_0 = 381.1)	RSM(*m*)	This work and ref. 12
	2.76 ±0.04	C(*m*)	12
$PhSCD_2COOH$	2.751 ±0.005 (Λ_0 = 381.1)	RSM(*m*)	This work

*RSM, Robinson–Stokes method; C, conductance method; C.D., calorimetric determination; *c*, mol/l; m, mol/1000 g H_2O.
†Λ_0 (molal) used in RSM calculations
‡Literature ref. for Λ_0 (molar).
§Calculated using the Shedlovsky iteration method.

considerably higher than the equilibrium constant reported by Ives and Pryor (10). The latter authors suggest that the discrepancies may be due to hydrolytic decomposition, leading to unstable conductance readings. Neither of these factors were evident in this study or are reported by other investigators. No mention is made by Ives and Pryor of their method of drying the very hygroscopic acid. A moist sample of the acid would give a low value of the equilibrium constant.

Discussion

In a previous communication we reported that the classical method was more suitable for establishing absolute values of secondary isotope effects on chemical equilibria than a comparison of $K_a(H)/K_a(D)$ using the Robinson and Stokes method to calculate $K_a(H)$ and $K_a(D)$ separately. A small residual concentration dependence in K_a together with uncertainty in Λ_0 may be factors contributing to the relatively large deviations from the average value of the equilibrium constant.

The use of the RSM for calculating $K_a(D)$ depends on the assumption

[3] $$\Lambda_0^-(H) = \Lambda_0^-(D)$$

for isotopically substituted anions. Such an assumption has ample precedent (1) but was considered unsatisfactory by the referees who examined the first paper in the present series. A preliminary discussion of the problem was presented in ref. 1[5] but the central importance of this approximation to the present and previous work demands further comment.

The effect of isotopic substitution on the limiting equivalent conductance of ions is part of the wider problem of the effect of structure on this particular electrochemical quantity. To date available theories examine the problem in terms of the ion radius as the significant structural parameter (ref. 7, chapt. 6, 19). However the molecular anions related to the substituted acetic acids cannot be realistically characterized by a radius. More sophisticated theories of the hydrodynamic properties of spherical ions also relate the limiting equivalent conductance to the ion radius and include frictional forces arising from the viscous and dielectric properties of the solvent (20), the latter involving ion–dipole interactions. For nonspherical molecular anions the ion–dipole interactions must be replaced by dipole–dipole interactions between ion and solvent and differences in limiting equivalent conductance for isotopically substituted molecular ions would arise from differences in size between D and H and differences in dipole moments between C—H and C—D bonds. The Zwanzig theory (20) does not appear to have been developed beyond the

[5]See footnote 6, ref. 1.

Can. J. Chem. Downloaded from www.nrcresearchpress.com by 210.87.254.40 on 09/05/12
For personal use only.

TABLE 4. Comparison of isotope effects

Acid	Robinson and Stokes	Classical plot	Shedlovsky plot
$ClCH_2COOH/ClCD_2COOH$	1.012±0.0043	1.012±0.0008	1.012±0.0007
$PhOCH_2COOH/PhOCD_2COOH$	1.012±0.0063	1.011±0.0006	1.011±0.0007
$PhSCH_2COOH/PhSCD_2COOH$	1.020±0.0034	1.021±0.0003	1.021±0.0005

spherical ion – dipole description and thus is inadequate to cope with the molecular ion problem. We are therefore inclined to grossly simplify the problem and consider two anions, one which has a radius of 2 Å whilst the other has a radius which differs from 2 Å by 5×10^{-3} Å which is the maximum difference in length observed between C—H and C—D bonds (21). The former ion corresponds to the ion L = D and the latter L = H. The viscous force acting on the ion is inversely proportional to the radius of the ion, hence

$$[4] \quad \frac{\Lambda_0^-(D)}{\Lambda_0^-(H)} = \frac{r(H)}{r(D)} = \frac{2.0050}{2.0000} = 1.0025$$

The anion conductances $\Lambda_0^-(H)$ and $\Lambda_0^-(D)$ represent *ca.* 10% of the total limiting equivalent conductance since most of the current is carried by the counter-ion which is the proton. This reduces the isotope effect by an order of magnitude *i.e.* from 1.0025 to 1.00025.

Since (see ref. 1)

$$[5] \quad \frac{K(H)}{K(D)} = \frac{m(D)}{m(H)} \frac{\Lambda_0^2(D)}{\Lambda_0^2(H)}$$

the part of the isotope effect arising from the effect of isotopic substitution on the hydrodynamic properties of the ions is *ca.* 1 part in 5000. This, we emphasize again, is an upper limit and it is clear that the departure of the ratio $\Lambda_0^2(D)/\Lambda_0^2(H)$ from unity is not significant in this or the previous study.

Hydrogen bonding between the methylene H or D atoms and the solvent is neglected since we are unaware of any evidence which would establish the existance of such interactions. Current theories of the solubilities of neutral hydrocarbon molecules in water suggest that specific interactions between solute and solvent will be very weak and no isotope effect is likely to arise from this source.

The isotope effects $K(H)/K(D)$, calculated using both the Robinson and Stokes method and the classical plot method, are compared in Table 4. The latter method of presenting the data involves a comparison of the classical slopes from a linear correlation of the variables $1/\Lambda(L)$ and $\Lambda(L)c(L)$ for L = H and L = D

$$[6] \quad \frac{K_c(H)}{K_c(D)} = \frac{m(D)}{m(H)}$$

where $m(H)$ and $m(D)$ are the classical slopes for the deutero and protio acids and $\Lambda_0(H)$ is assumed to be equal to $\Lambda_0(D)$. Of the two methods of calculation the classical treatment superficially appears to provide a more precise value of the isotope effect. However, some uncertainty exists, a consequence of the fact that the activity and mobility terms are either implicitly ignored or are assumed to cancel.

In order to remedy this uncertainty the classical treatment was replaced by a modified extrapolation–iteration procedure. The data for each acid was fitted to the Shedlovsky–Kay equation (14)

$$[7] \quad \frac{1}{\Lambda(L)S[Z(L)]} = \frac{1}{\Lambda_0(L)} + \frac{\Lambda(L)c(L)S[Z(L)]f_\pm^2(L)}{K_a(L)\Lambda_0^2(L)}$$

where $\Lambda, \Lambda_0, c,$ and $f_\pm$ have their usual significance and the correction term $S[Z(L)]$ can be expressed as a power series in $Z(L)$:

$$[8] \quad S[Z(L)] = 1 + Z(L) + Z^2(L)/2 + Z^3(L)/8 + \ldots..$$

where Z is given by

$$[9]^6 \quad Z = \left(\frac{\alpha\Lambda_0(L) + \beta}{\Lambda_0(L)^{3/2}}\right)(\Lambda(L)c(L))^{1/2}$$

The Shedlovsky variables $1/\Lambda S[Z(L)]$ and $\Lambda c(L)S[Z(L)]f_\pm^2(L)$ can be correlated without iteration using a linear least squares analysis to yield a slope of $1/K_a(L)\Lambda_0^2(L)$. A comparison of $m(H)$ and $m(D)$, the slopes of the Shedlovsky equation, will reduce the isotope effect to a simple slope

[6]Fuoss and Accascina (22) replace the Robinson and Stokes symbols B_1 and B_2 by α and β (23).

Can. J. Chem. Downloaded from www.nrcresearchpress.com by 210.87.254.40 on 09/05/12
For personal use only.

TABLE 5. The Shedlovsky slope comparison method applied to the chloroacetic acid data

Λ_0	10^2m(H)	10^2m(D)	K(H)/K(D)
370	0.4726±0.0003	0.4780±0.0003	1.0114±0.0016
374	0.4725±0.0003	0.4779±0.0003	1.0114±0.0016
378	0.4724±0.0003	0.4778±0.0003	1.0114±0.0016
382	0.4723±0.0003	0.4777±0.0003	1.0114±0.0016
386	0.4722±0.0003	0.4776±0.0003	1.0114±0.0016
390	0.4721±0.0003	0.4775±0.0003	1.0114±0.0016
395	0.4720±0.0003	0.4774±0.0003	1.0114±0.0016

TABLE 6. The Shedlovsky comparison method

Acid pair	Cell number	Isotope effect, m(D)/m(H)
Phenoxyacetic	1	1.0104±0.0018
	2	1.0099±0.0016
	3	1.0104±0.0017
	4	1.0108±0.0017
	5	1.0109±0.0017
Chloroacetic	1	1.0114±0.0016
	2	1.0116±0.0016
	3	1.0116±0.0016
	4	1.0114±0.0016
	5	1.0116±0.0016
Phenylthioglycollic	1	1.0207±0.0013
	2	1.0209±0.0013
	3	1.0205±0.0013
	4	1.0211±0.0014
	5	1.0211±0.0013

ratio (see eq. 6). The K(H)/K(D) ratios evaluated from the Shedlovsky slope comparison method are summarized in Table 4 and are in excellent agreement with the classical plot and RSM values.

In situations where a literature value of Λ_0 is unavailable or is available but considered to be in error, eqs. 6 and 7 remain useful since a range of values can be systematically varied on either side of the true limiting equivalent conductance. The location of this range affords no difficulty since Λ_0 for carboxylic acids is relatively insensitive to the structure of the acid (see Table 3). The conductance data for each acid has been used to test the suitability of this method, however, only the results related to a single cell will be presented here. The slopes were generated from a linear correlation of the Shedlovsky variables with Λ_0 values ranging from 370 to 395, and are presented in Table 5. The corresponding K(H)/K(D) ratios determined in this way appear to be insensitive to the value of Λ_0 used to calculate the terms $1/S[Z(L)]$ and $S[Z(L)]/f_{\pm}^2(L)$.

Measurement of the conductance data for the protio and the deutero acids in the same cell enables a modification to the Shedlovsky slope comparison method detailed above. Replacement of Λ by $10^3\kappa/Rc$, where κ, R, and c have their usual meaning, followed by multiplication by $10^3\kappa$ gives

$$[10]\quad \frac{R(L)c(L)}{S[Z(L)]} = \frac{10^3\kappa}{\Lambda_0(L)} + \frac{10^6\kappa^2 S[Z(L)] f_{\pm}^2(L)}{R(L)K_a(L)\Lambda_0(L)}$$

with the slope m(L) obtained from the experimental variables $R(L)c(L)/S[Z(L)]$ and $S[Z(L)]f_{\pm}^2(L)/R(L)$. Hence m(L) is given by

$$[11]\quad m(L) = \frac{10^6\kappa^2}{K_a(L)\Lambda_0^2(L)}$$

Equation 11 shows that a comparison of the slopes for the H and D acids in a single cell will be virtually independent of the cell constant, which will only be required to calculate the small correction terms $1/S[Z(L)]$ and $S[Z(L)]/f_{\pm}^2(L)$. Single cell isotope effects evaluated in this way are reported in Table 6 for the three isotopic pairs.

Can. J. Chem. Downloaded from www.nrcresearchpress.com by 210.87.254.40 on 09/05/12
For personal use only.

Can. J. Chem. Downloaded from www.nrcresearchpress.com by 210.87.254.40 on 09/05/12
For personal use only.

Thus, although a value of κ and Λ_0 is required to calculate the correction terms, their main contribution to m(H) and m(D) cancels in the ratio of these quantities. The excellent agreement between K(H)/K(D) from the data for each cell (Table 6) and from three methods of calculation (Table 4), further confirms the accuracy of the cell constant determinations. Furthermore, the errors in the ratios are smaller for the combined data, probably a consequence of the fact that the larger the number of data points on the least squares fit the greater the degree of certainty in the value of the slope and thus K(H)/K(D). However, the discovery of the insensitivity of the method to the value of Λ_0 in calculating the isotope effect is far more interesting than the other conclusions drawn from Table 6. This insensitivity of the slopes and ratios to Λ_0 suggests that the Shedlovsky slope comparison method of calculation is the best for comparing thermodynamic equilibrium constants of isotopically substituted acids via conductance data.

The isotope effects for the substituted acetic acids XCH_2COOH/XCD_2COOH, X = Cl, PhO, and PhS are larger than those observed for the phenylacetic acids (X = 4-RC_6H_4 where R = MeO, H, and NO_2). The six effects we have investigated are however still less than those measured by Streitwieser and Klein (24) and Bates and co-workers (25) for the pair CH_3COOH/CD_3COOH. The new ratios are closer to those predicted by the simple inductive treatment (K(H)/K(D) = 1.02) but do not appear to follow the predictions of the correlation in Fig. 1. When the new K(H)/K(D) values are included the influence of the substituent on the isotope effects appears to be random. This observation cannot be reconciled with the inductive treatment presented in part I which requires the isotope effects to be constant, *i.e.* independent of X.

A rigorous statistical treatment of the isotope effects in terms of force constant – frequency changes between the acid and the related anion would involve the interaction terms absent in the simple inductive treatment. Such interaction terms would probably account for the alteration of the ratio K(H)/K(D) as X is structurally changed. Since the simple inductive treatment is incapable of accommodating our observations the inductive treatment of secondary isotope effects of the second kind has outgrown its utility.

The authors wish to thank the National Research Council of Canada for continued support and one of us (P. Golding) thanks the same body and Memorial University for post-graduate support. The authors would also like to offer their thanks to the personnel of the Technical Services unit at M.U.N. for assistance during various phases of this work.

1. D. J. Barnes and J. M. W. Scott. Can. J. Chem. **51**, 411 (1973).
2. Handbook of chemistry and physics. Chemical Rubber Publishing Co. 41st ed. Cleveland. 1959. p. 1255.
3. D. J. Pasto and R. Kent. J. Org. Chem. **30**, 2684 (1965).
4. A. I. Vogel. A textbook of practical organic chemistry. 3rd ed. Longmans, London. 1964.
5. E. H. Huntress. Organic chlorine compounds. John Wiley, New York. 1948. p. 173.
6. T. Shedlovsky. Physical methods of organic chemistry. 2nd ed. Part II. *Edited by* A. Weissberger. Interscience, New York. 1949.
7. R. A. Robinson and R. H. Stokes. Electrolyte solutions. Butterworth, London. 1961.
8. T. Shedlovsky. J. Franklin Inst. **225**, 739 (1938).
9. G. H. Jeffrey and A. I. Vogel. J. Chem. Soc. 166 (1934).
10. D. J. G. Ives and J. H. Pryor. J. Chem. Soc. 2104 (1955).
11. P. Laughton and A. Demayo. Private communication.
12. H. D. Crockford and T. B. Douglas. J. Am. Chem. Soc. **56**, 1472 (1934).
13. T. Shedlovsky and R. L. Kay. J. Phys. Chem. **60**, 151 (1956).
14. D. A. MacInnes, T. Shedlovsky, and L. G. Longsworth. Chem. Rev. **13**, 29 (1933).
15. M. Randell and C. F. Failey. Chem. Rev. **4**, 291 (1927).
16. D. D. Wright. J. Am. Chem. Soc. **56**, 314 (1934).
17. L. J. Minnick and M. Kilpatrick. J. Phys. Chem. **43**, 259 (1939).
18. N. V. Hayes and G. E. K. Branch. J. Am. Chem. Soc. **65**, 1555 (1943).
19. E. A. Moelwyn-Hughes. Physical chemistry. Pergamon Press, London, 1957. Chapt. 18, p. 834.
20. G. Atkinson and Y. Mori. J. Phys. Chem. **71**, 3523 (1967).
21. P. Laszlo and Z. Welvart. Bull. Soc. Chim. Fr. **7**, 2412 (1966).
22. R. Fuoss and F. Accasina. Electrolytic conductance. Interscience, New York. 1959. Chapt. 17.
23. E. J. King. Acid-base equilibria. The international encyclopedia of physical chemistry and chemical physics. Vol. 4. Pergamon Press, New York. 1965. Chapt. 2.
24. A. J. Streitwieser and H. S. Klein. J. Am. Chem. Soc. **85**, 2759 (1963).
25. R. A. Robinson, R. G. Bates, and M. Paabo. J. Phys. Chem. **70**, 540 (1966).

^{13}C Nuclear Magnetic Resonance Studies of Organometallic Compounds. V. Di- and Trimethylplatinum(IV) Derivatives[1]

HOWARD CHARLES CLARK, LEO ERNEST MANZER,[2] AND JOHN EDWARD HENRY WARD[3]

Department of Chemistry, The University of Western Ontario, London, Ontario N6A 3K7

Received December 6, 1973

The ^{13}C n.m.r. parameters for thirteen di- and trimethylplatinum(IV) derivatives have been obtained. It is shown that the ^{13}C shieldings and $^{1}J_{PtC}$ and $^{2}J_{PtCH}$ values of methyl groups both *cis* and *trans* to varied ligands consistently follow trends similar to those found for related methylplatinum(II) derivatives.

On a déterminé les paramètres en r.m.n. du ^{13}C pour treize dérivés di- et triméthylplatine (IV). On a trouvé que le déblindage du ^{13}C et les constantes de couplage $^{1}J_{PtC}$ et $^{2}J_{PtCH}$ pour les groupes méthyles *cis* et *trans* par rapport aux divers ligands suivent d'une façon régulière tendances trouvées pour les dérivés méthylplatine (II) correspondants. [Traduit par le journal]

Can. J. Chem., **52**, 1973 (1974)

Introduction

In our laboratories, carbon-13 nuclear magnetic resonance spectroscopy has provided important new information concerning the nature of the bonding in simple σ-bonded platinum(II) derivatives (1–4). From studies of three series of *trans*-methylplatinum(II) complexes (2), we presented evidence which firmly supports the rehybridization theory of the *trans*-influence (5–7). In contrast, our investigations of a series of *cis*-methylplatinum(II) derivatives (4) revealed that the n.m.r. *cis*-influence is neither strongly related to the n.m.r. *trans*-influence, nor is it apparently related to the rehybridization of platinum σ-orbitals in the platinum–carbon bonds. Finally, our ^{13}C n.m.r. examination of a series of *cis*-dimethylplatinum(II) derivatives (1) showed that when ligands both *cis* and *trans* to the methyl groups are simultaneously varied, the n.m.r. *trans*-influence rather than the n.m.r. *cis*-influence is dominant.

In order to test the generality of these results in more complex systems, we have obtained the ^{13}C n.m.r. parameters of a number of di- and trimethylplatinum(IV) derivatives of types **A**–**C**:

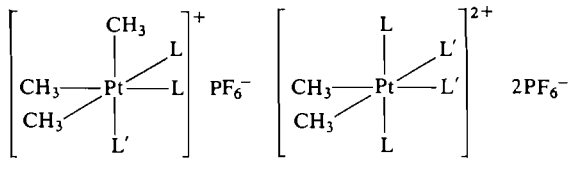

A **B**

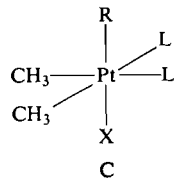

C

where L and L′ are neutral ligands and R and X are anionic substituents. The ^{13}C and ^{1}H n.m.r. parameters of the platinum–methyl, and other ligand carbons and protons are discussed and compared with the n.m.r. parameters of the related types of platinum(II) derivatives.

Experimental

The following chemicals were obtained commercially and used without further purification: anisonitrile, γ-picoline, triphenylarsine, and silver hexafluorophosphate.

fac-Trimethyliodobis(trimethylarsino)platinum(IV) was obtained by the method of Clark and Manzer (8), while ethylisocyanide was prepared by the method of Casanova *et al.* (9).

All reactions and recrystallizations were carried out using spectrograde solvents. Microanalyses were performed by Chemalytics Inc., Tempe, Arizona. Uncorrected melting points were determined on a Thomas Hoover Uni-melt capillary melting point apparatus.

The ^{13}C n.m.r. spectra were measured on a Varian XL-100-15 spectrometer operating in the pulsed Fourier transform mode at 25.2 MHz. All spectra were determined with noise-modulated proton decoupling. The spectra were taken on acetone, acetone-d_6, or chloroform-*d* solutions in 5 or 10 mm sample tubes and were calibrated using the solvent resonances as secondary standards (10). Computer analysis of a portion of one ^{13}C n.m.r. spectrum was performed with a Cyber 73 computer located at the University of Western Ontario and the LAØCØØN III program (a version of the least squares n.m.r. spectral fitting computer program described in ref. 11). The ^{1}H n.m.r. spectra were recorded on a Varian HA-100 spectrometer; the ^{1}H chemical shifts are reported with TMS as the internal standard.

[1]For the previous paper in this series see ref. 1.

[2]Present address: Central Research Department, Experimental Station, E.I. Du Pont de Nemours and Co., Wilmington, Delaware 19898.

[3]To whom correspondence should be addressed.

Can. J. Chem. Downloaded from www.nrcresearchpress.com by 210.87.254.6 on 09/05/12
For personal use only.

TABLE 1. Analytical data for the new complexes *fac*-$[(CH_3)_3Pt(As(CH_3)_3)_2L]^+PF_6^-$ **1–4**

Complex	L	Calcd. (%) C	Calcd. (%) H	Found (%) C	Found (%) H	Melting point (°C)[a]
1	*p*-$CH_3OC_6H_4CN$	26.9	4.52	27.1	4.27	120
2	γ-$CH_3C_5H_4N$	25.1	4.77	25.2	4.50	142
3	$(C_6H_5)_3As$	34.8	4.55	34.9	4.50	150
4	CH_3CH_2NC	21.2	4.74	21.2	4.53	130

[a]All compounds except **4** effervesce at this temperature, presumably giving off ethane and decomposing to the methylplatinum(II) derivatives *trans*-$[(CH_3)Pt(As(CH_3)_3)_2L]^+PF_6^-$. The compounds **1–3** resolidify and subsequently melt at the melting point of the platinum(II) derivatives (2).

The new cationic *fac*-$[(CH_3)_3Pt(As(CH_3)_3)_2L]^+PF_6^-$ complexes **1–4**, where L = *p*-$CH_3OC_6H_4CN$, γ-$CH_3C_5H_4N$, $(C_6H_5)_3As$, and CH_3CH_2NC, were prepared by procedures identical to that described for their cyclic carbene analog, where L = :$\overline{COCH_2CH_2CH_2}$ (8). References for the preparations of all other complexes are provided with the ^{13}C shielding data (*vide infra*). The analytical data for the new complexes are summarized in Table 1.

Results

The ^{13}C shieldings and ^{13}C–^{195}Pt and ^{13}C–^{31}P coupling constants obtained from the ^{13}C n.m.r. spectra of the platinum(IV) derivatives **1–13** are assembled in Tables 2 and 3. Since we have not determined the relative signs of the ^{13}C–^{195}Pt coupling constants, their absolute values, which are adequate for the arguments we will present later, are provided in Table 3.

In all cases, the high field resonances in the spectra were assigned to the carbons of the platinum–methyl groups of **1—13**, on the basis of their similarity with a host of related methylplatinum(II) derivatives (1, 2, 4). The central platinum–methyl resonances are flanked by widely spaced ^{195}Pt satellites of *ca.* one fourth intensity, whose separation appears to be sensitive to the nature of L, L′, R, and X.

The platinum–methyl region of the ^{13}C n.m.r. spectrum of the tris(dimethylphenylphosphine) complex **8**, shown in Fig. 1*A*, could not be rationalized by simple first-order spectral analysis arguments. On a first-order basis one would anticipate two small, equivalent coupling constants (*ca.* 6 Hz) (2, 14) for the coupling of the ^{13}C nucleus with the two *cis* ^{31}P nuclei, and one large ^{13}C—^{31}P coupling constant (*ca.* 105 Hz) (2, 14) for the ^{13}C coupling with the *trans*-^{31}P nucleus. Thus, the ^{13}C n.m.r. spectrum would appear as a doublet of triplets. However, the non-^{195}Pt coupled portion of the ^{13}C n.m.r. spectrum of the platinum–methyl groups consists of a doublet of quartets (as in Fig. 1*A*) suggesting that

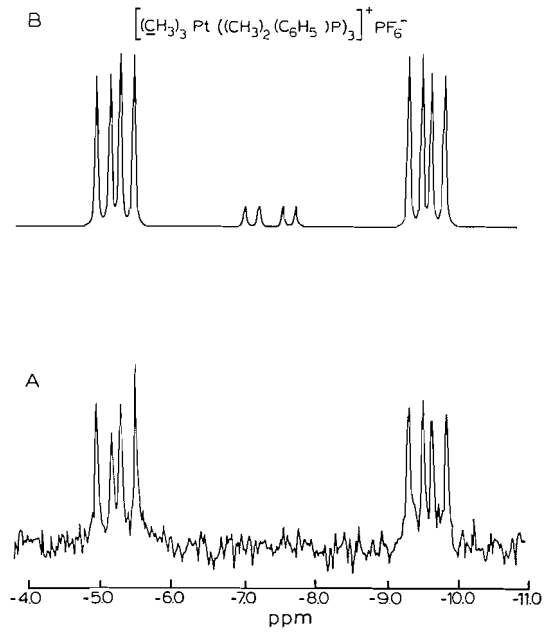

FIG. 1. Observed (*A*) and calculated (*B*) ^{13}C n.m.r. spectra for the non-^{195}Pt coupled platinum–methyl region of *fac*-$[(CH_3)_3Pt((CH_3)_2(C_6H_5)P)_3]^+PF_6^-$ **8**.

the spectrum is in fact second-order. The line frequencies and intensities were successfully duplicated when the signs of the two $^2J_{PPtC}$ values were assumed to be opposite.[4] The calculated spectrum is shown in Fig. 1*B*. Due to the relatively low signal-to-noise ratio of the spectrum, the positions of the four weak lines calculated between the two intense quartets could not be unequivocably established. Similarly, the ^{195}Pt satellites were weak, and the ^{13}C–^{195}Pt coupling constant could only be estimated from the few

[4]Cheney *et al.* (14) have recently shown that $^2J_{PPtC}$ (*cis*) and $^2J_{PPtC}$ (*trans*) have opposite signs in *cis*-$(CH_3)_2Pt^{II}((CH_3)_2(C_6H_5)P)_2$. This is also in accord with the results (15) of other workers.

Can. J. Chem. Downloaded from www.nrcresearchpress.com by 210.87.254.6 on 09/05/12
For personal use only.

Can. J. Chem. Downloaded from www.nrcresearchpress.com by 210.87.254.6 on 09/05/12
For personal use only.

TABLE 2. ^{13}C shieldings[a] for the platinum(IV) derivatives **1–13**

Complex	Type	L	L′ (R and X)	Solvent	Platinum methyls δ_C[b]	Platinum methyls δ_C[c]	L methyls	Other	Reference to preparation and ^1H n.m.r. data
1	**A**	$As(CH_3)_3$	*p*-$CH_3OC_6H_4CN$	$(CD_3)_2CO$	−13.0	+3.5	+7.0	δ_{OCH_3} 55.7, δ_{C_1} 99.7, $\delta_{C_{3,5}}$ 115.4, δ_{C_4} 164.9, δ_{CN} 120.0, $c_{2,6}$ 135.7	[d]
2	**A**	$As(CH_3)_3$	γ-$CH_3C_5H_4N$	$(CD_3)_2CO$	−14.4	+8.3	+7.1	δ_{CH_3} 20.4, $\delta_{C_{3,5}}$ 127.8, δ_{C_4} 150.6, $\delta_{C_{2,6}}$ 151.9	[d]
3	**A**	$As(CH_3)_3$	$(C_6H_5)_3As$	$(CD_3)_2CO$	+4.9	+2.4	+9.0	$\delta_{C_6H_5}$ 129.8–133.6[f]	[d]
4	**A**	$As(CH_3)_3$	CH_3CH_2NC	$(CD_3)_2CO$	−9.3	−2.0	+7.7	δ_{CH_3} 14.1, δ_{CH_2} 39.7, δ_{NC}[j]	[d]
5	**A**	$As(CH_3)_3$	$(CH_3)_2(C_6H_5)P$	$(CD_3)_2CO$	+0.3	−0.9	8.4	δ_{CH_3} 12.6, $\delta_{C_6H_5}$[j]	8
6	**A**	$P(CH_3)_2(C_6H_5)$	C_5H_4N	$(CD_3)_2CO$	−8.7	+12.1	+9.8	$\delta_{C_6H_5}$[j]	8
7	**A**	$P(CH_3)_2(C_6H_5)$	CH_3CH_2NC	$(CD_3)_2CO$	−4.3	+0.5	9.3–11.8[f]	δ_{CH_3} 13.9, δ_{CH_2} 39.9 δ_{NC}[e]	8
8	**A**	$P(CH_3)_2(C_6H_5)$	$P(CH_3)_2(C_6H_5)$	$(CD_3)_2CO$	−7.4	−7.4	+13.8[f]	$\delta_{C_6H_6}$[j]	8
9	**B**	$P(CH_3)_2(C_6H_5)$	*p*-$CH_3OC_6H_4CN$	CD_2Cl_2	−2.3		+8.8	δ_{OCH_3} 56.1, δ_{C_1} 97.5, $\delta_{C_{2,6}}$ 136.2, $\delta_{C_{3,5}}$ 115.4, δ_{C_4} 165.7, δ_{CN} 122.5, $\delta_{C_6H_5}$ 129.6–132.4	12
10	**B**	$P(CH_3)_2(C_6H_5)$	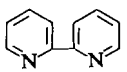	$(CD_3)_2CO$	−4.3		+6.1	$\delta_{C_{10}H_8N_2}$[j], $\delta_{C_6H_5}$[j]	12
11	**B**	$P(CH_3)_2(C_6H_5)$	CH_3CH_2NC	$(CD_3)_2CO$	−5.1		+10.6	δ_{CH_3} 13.0, δ_{CH_2} 40.9	12
12	**C**	$As(CH_3)_3$	CH_3^-, I^-	$(CH_3)_2CO$	−0.7[g]	+2.0[h]	+8.6		8
13	**C**	$As(CH_3)_3$	CH_3CO^-, Cl^-	$CDCl_3$		+3.5[i]	+8.6	δ_{CH_3CO} 36.4 δ_{CH_3CO} 193.2	13

[a]In p.p.m. (±0.1) (downfield positive) from TMS.
[b]*trans* to L′.
[c]*cis* to L′.
[d]This work, see Table 4.
[e]Signals not observed.
[f]Complex multiplet.
[g]*trans* to I^-.
[h]*cis* to I^-.
[i]*cis* to Cl^-.
[j]Signals not recorded.

Can. J. Chem. Downloaded from www.nrcresearchpress.com by 210.87.254.6 on 09/05/12
For personal use only.

TABLE 3. Coupling constant data[a] for the platinum(IV) derivatives **1–13**

Complex	Type	L	L′ (R and X)	Solvent	Platinum methyls				L methyls		Other
					$\lvert^1J_{PtC}\rvert^b$	$\lvert^2J_{PPtC}\rvert^b$	$\lvert^1J_{PtC}\rvert^c$	$\lvert^2J_{PPtC}\rvert^c$	$\lvert^2J_{PtEC}\rvert^d$	$\lvert^3J_{PPtPC}\rvert$	
1	**A**	$As(CH_3)_3$	*p*-$CH_3OC_6H_4CN$	$(CD_3)_2CO$	650(±2)		545(±2)		10(±4)		
2	**A**	$As(CH_3)_3$	γ-$CH_3C_5H_4N$	$(CD_3)_2CO$	595(±2)		570(±2)		10(±4)		
3	**A**	$As(CH_3)_3$	$(C_6H_5)_3As$	$(CD_3)_2CO$	523(±2)		543(±4)		5(±2)		
4	**A**	$As(CH_3)_3$	CH_3CH_2NC	$(CD_3)_2CO$	515(±2)		515(±2)		10(±4)		
5	**A**	$As(CH_3)_3$	$(CH_3)_2(C_6H_5)P$	$(CD_3)_2CO$	478(±5)	103(±5)	530(±5)	[e]	20(±4)		$^1J_{PCH} = 32(\pm2)$
6	**A**	$(CH_3)_2(C_6H_5)P$	C_5H_4N	$(CD_3)_2CO$	598(±2)	4(±2)	522(±2)	4(±2), 108(±2)	[e]		
7	**A**	$(CH_3)_2(C_6H_5)P$	CH_3CH_2NC	$(CD_3)_2CO$	514(±2)	7(±2)	462(±2)	6(±2), 108(±2)	[e]		
8	**A**	$(CH_3)_2(C_6H_5)P$	$(CH_3)_2(C_6H_5)P$	$(CD_3)_2CO$	484(±2)	5(±1),[f] 105(±1)[f]	484(±2)	5(±1),[f] 105(±1)[f]	[e]		$^2J_{PPtP} = 14(\pm1)$
9	**B**	$(CH_3)_2(C_6H_5)P$	*p*-$CH_3OC_6H_4CN$	CD_2Cl_2	560(±4)	5(±4)			20(±2)	20(±2)	
10	**B**	$(CH_3)_2(C_6H_5)P$	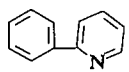	$(CD_3)_2CO$	528(±4)	4(±4)			22(±2)	20(±2)	
11	**B**	$(CH_3)_2(C_6H_5)P$	CH_3CH_2NC	$(CD_3)_2CO$	428(±4)	4(±2)			20(±2)	22(±2)	
12	**C**	$As(CH_3)_3$	CH_3^-, I^-	$(CH_3)_2CO$	623(±2)		556(±2)		7(±2)		
13	**C**	$As(CH_3)_3$	CH_3CO^-, Cl^-	$CDCl_3$			583(±2)		10(±2)		$^2J_{PtCOCH} = 22(\pm2)$ $^1J_{PtCO} = 851(\pm2)$

[a]In Hz.
[b]*trans* to L′.
[c]*cis* to L′.
[d]E is P or As.
[e]Coupling not observed.
[f]These coupling constants have opposite signs, as demonstrated by iterative spectral analysis.

Can. J. Chem. Downloaded from www.nrcresearchpress.com by 210.87.254.6 on 09/05/12
For personal use only.

^{195}Pt satellite signals that were well enough resolved.[5]

The ^{13}C resonances of the arsenic methyl groups span a range (*ca.* 7–9 p.p.m.) similar to that (*ca.* 7–10 p.p.m.) observed for series of related *trans*-methylplatinum(II) derivatives (2). Together with this, and the relative intensities of the signals, the assignments were readily carried out. The assignments of the signals from the phosphorus methyl groups were made in an analogous manner.

Where possible, the signals arising from the remaining ligands were specifically assigned by comparing their ^{13}C n.m.r. parameters with those derived from the related *trans*-methylplatinum(II) derivatives (2).

The ^1H n.m.r. data for the new complexes **1–4** are assembled in Table 4. Assignments of the ^1H chemical shifts and J_{PtH} values were based on arguments similar to those used to assign the ^{13}C n.m.r. parameters. The proton spectrum of the ethylisocyanide derivative **4** is particularly unusual because it exhibits coupling of both the methyl and methylene protons with the ^{14}N nucleus. Similar cases have been observed in only a few instances (17, 18).

Discussion

^{13}C and ^1H Nuclear Magnetic Resonance Data: General

The n.m.r. data obtained from complexes **1–13** reveal that with variations in ligands, substantial variations in the ^{13}C and ^1H n.m.r. parameters of the platinum–methyl groups may occur. For example, when anisonitrile in complex **1** is replaced by ethylisocyanide (complex **4**), the shielding of the platinum–methyl carbon *trans* to L′ decreases from −13.0 to −9.3 p.p.m., while the shieldings of the platinum–methyl carbons *cis* to L′ increase from +3.5 to −2.0 p.p.m. Concomitantly, the $^1J_{PtC}$ value of the ^{13}C nucleus *trans* to L′ decreases by 135 Hz, from 650(±2) to 515(±2) Hz, while the one bond ^{13}C–^{195}Pt coupling constant for the platinum–methyl carbons *cis* to L′ decreases by 30 Hz, from 545(±2) to 515(±2) Hz.

These coupling constant variations exemplify the changes we have observed for model platinum(II) derivatives (1, 2, 4), where we showed that the $^1J_{PtC}$ values of platinum–methyl groups *trans* to a varied ligand are considerably more sensitive than the $^1J_{PtC}$ values of those groups *cis* to a varied ligand.

From the $^1J_{PtC}$ values of the platinum–methyl groups of **1–5**, we may formulate an n.m.r. *trans*-influence series:

$$(CH_3)_2(C_6H_5)P > CH_3CH_2NC > (C_6H_5)_3As > \gamma\text{-}CH_3C_5H_4N > p\text{-}CH_3OC_6H_4CN$$

and an n.m.r. *cis*-influence series:

$$CH_3CH_2NC > (CH_3)_2(C_6H_5)P > (C_6H_5)_3As \approx p\text{-}CH_3OC_6H_4CN > \gamma\text{-}CH_3C_5H_4N$$

The n.m.r. *trans*-influence series is identical to that which we have observed for a series of complexes (with the same L′) of the type *trans*-$[(CH_3)Pt((CH_3)_2(C_6H_5)P)_2L]^+PF_6^-$ (2) and thus there is an excellent *qualitative* relationship between the n.m.r. *trans*-influences of the same ligands in both the platinum(II) and platinum(IV) derivatives.

There is also a generally good qualitative agreement of the n.m.r. *cis*-influence series above, with that observed for a series of *cis*-substituted methylplatinum(II) complexes of the type $[DIARSPt(CH_3)L]^+PF_6^-$ (4). For the latter complexes the ordering of the n.m.r. *cis*-influence series is:

$$CH_3CH_2NC > (C_6H_5)_3As > p\text{-}CH_3OC_6H_4CN > \gamma\text{-}CH_3C_5H_4N$$

In a similar fashion we can formulate n.m.r. *trans*-influence series for **6–8**:

$$(CH_3)_2(C_6H_5)P > CH_3CH_2NC > C_5H_4N$$

and **9–11**:

$$CH_3CH_2NC > \text{ 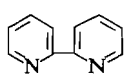 } > p\text{-}CH_3OC_6H_4CN$$

both of which are qualitatively identical with those *trans*-influence series which we have observed for related platinum(II) derivatives (2). Finally the n.m.r. *cis*-influence series for **6–8**:

[5]We should point out the similarity of the ^{13}C n.m.r. spectrum of the methylplatinum region of **8** with that obtained from the ^1H n.m.r. spectrum of the platinum hydride region of $[HPt(P(C_6H_5)_3)_3]^+(CF_3CO_2)_2H^-$ **14**, reported by Thomas *et al.* (16). These authors stated that the spectrum could almost completely be rationalized by invoking a chemical shift difference of 10 Hz between the *cis* and *trans* ^{31}P nuclei. From our results, it appears that $^2J_{PPtH}(cis)$ and $^2J_{PPtH}(trans)$ may well have opposite signs. Thus, the ^1H n.m.r. spectrum of the hydride region of **14** could possibly be completely accounted for without invoking the chemical shift difference of the *cis* and *trans* ^{31}P nuclei.

Can. J. Chem. Downloaded from www.nrcresearchpress.com by 210.87.254.6 on 09/05/12
For personal use only.

TABLE 4. ^{1}H n.m.r. chemical shifts[a] and coupling constants[b] for the new complexes *fac*-$[(CH_3)_3Pt(As(CH_3)_2L']^+PF_6^-$ **1–4**[c]

Complex	L	$\delta(CH_3)$[d]	$\lvert^2J(PtH)\rvert$[d]	$\delta(CH_3)$[e]	$\lvert^2J(PtH)\rvert$[e]	$\delta(As(CH_3)_3)$	$\lvert^3J(PtH)\rvert$	Other
1	*p*-$CH_3OC_6H_4CN$	0.81	75.6	1.01	60.0	1.58	7.4	$\delta(OCH_3)$ 3.94
2	γ-$CH_3C_5H_4N$	0.74	69.8	1.00	61.2	1.43	6.6	$\delta(CH_3)$ 2.46
3	$(C_6H_5)_3As$	1.06	63.0	0.97	59.9	1.39	7.2	
4	CH_3CH_2NC	0.48	61.6	1.27	60.7	1.68	7.6	$\delta(CH_3)$ 1.46, ^5J(PtH) 18.6, ^3J(NH) 2.9, J(HH) 7.2; $\delta(CH_2)$ 4.03, ^4J(PtH) 9.5, ^2J(NH) 2.3

[a]In p.p.m. (±0.005) from TMS.
[b]In Hz (±0.5).
[c]All spectra were obtained on acetone-d_6 solutions.
[d]*trans* to L'.
[e]*cis* to L'.

$CH_3CH_2NC > (CH_3)_2(C_6H_5)P > C_5H_4N$

is completely consistent with that observed for the *cis*-methylplatinum(II) derivatives (4) and the platinum(IV) complexes **1–5**. Thus, virtually identical qualitative trends are followed for the platinum(II) and platinum(IV) analogs.

^{13}C and ^{1}H Coupling Constants

Platinum Methyl Groups

First, we examined the ^{13}C n.m.r. parameters of **1–5** to determine the quantitative extent of the qualitative relationships just discussed. A plot of $^{1}J_{PtC}$ (CH_3 *trans* to L′, **1–5**) *vs.* $^{1}J_{PtC}$ (*trans*-$[(CH_3)Pt(As(CH_3)_3)_2L]^+PF_6^-$) is shown in Fig. 2. The linear regression analysis parameters[6] are summarized in eq. 1.[7]

[1] $^{1}J_{PtC}(CH_3$ *trans* to L′, **1–5**$)$
$= 0.89(\pm 0.05)\,^{1}J_{PtC}$(*trans*-$[(CH_3)Pt(As(CH_3)_3)_2L]^+PF_6^-$)
$+ 92.4(\pm 24.3)$
$r = 0.975$

The reasonably good linear correlation affirms our qualitative conclusion concerning the relationship of the $^{1}J_{PtC}$ values of methyl groups (*trans* to a varied ligand) for the platinum(II) and platinum(IV) analogs. Since the slope of the line deviates slightly from unity, it appears that the n.m.r. *trans*-influence in the platinum(IV) complexes **1–5** is not reflected as strongly as in the related platinum(II) complexes. In addition, since the plot does not pass through the origin, some other factors (in addition to those giving rise to $^{1}J_{PtC}$ in the platinum(II) complexes) appear to be manifest in the $^{1}J_{PtC}$ values of the platinum(IV)

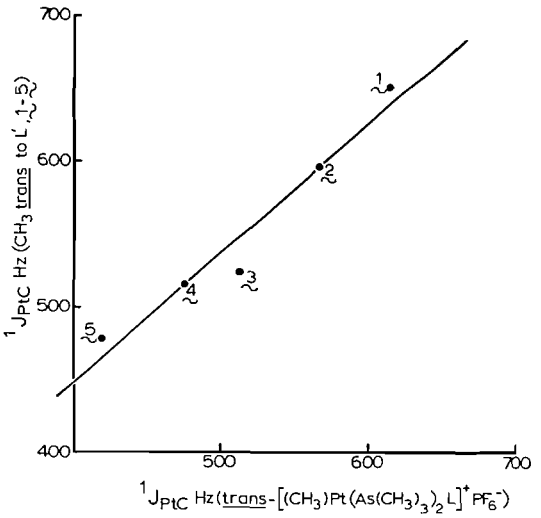

FIG. 2. Plot of $^{1}J_{PtC}$ for the methyl group *trans* to L′ in **1–5** *vs.* $^{1}J_{PtC}$ for the *trans*-$[(CH_3)Pt(As(CH_3)_3)_2L]^+PF_6^-$ analogs.

derivatives. Nevertheless the deviations just noted, while greater than the experimental uncertainty, are not particularly large in view of the low number of data points used. Thus, both classes of compounds may be used to provide a reasonably accurate measure of the n.m.r. *trans*-influence of a given ligand.

Next, we compared the $^{1}J_{PtC}$ values of the methyl groups *cis* to L′ for **1–5** with the corresponding one bond $^{13}C—^{195}Pt$ coupling constants of the *cis*-platinum(II) analogs [*DIARS*Pt-$(CH_3)L]^+PF_6^-$ (4). A plot of the appropriate four data points revealed a fair linear relationship. Linear regression analysis yielded eq. 2, with a correlation coefficient $r = 0.899$.

[2] $^{1}J_{PtC}$ (CH_3 *cis* to L′, **1–4**$)$
$= 0.60(\pm 0.08)\,^{1}J_{PtC}$-
([*DIARS*Pt$(CH_3)L]^+PF_6^-$)
$+ 277.5(\pm 43.4)$
$r = 0.899$

Thus, it seems that the n.m.r. *cis*-influence of a ligand in the platinum(IV) complexes **1–4** may be linearly related to the n.m.r. *cis*-influence of that ligand in the *DIARS* platinum(II) analogs.

We have previously suggested (4) that the n.m.r. *cis*-influence may be dependent on a ligand's "steric bulk". In **1–5**, L′ is juxtaposed to four *cis* substituents, while the ligand L in the [*DIARS*Pt$(CH_3)L]^+PF_6^-$ series is adjacent to two

[6]The average deviations of the slopes and intercepts for most of the linear equations presented here are calculated on the basis of the maximum possible error due to the inherent uncertainty of the experimental measurements. These errors have already been cited in Tables 2–4. It is worthwhile noting that these variations represent the maximum error in *precision* and that as such they may be generous estimates.

[7]For comparative purposes we require the $^{1}J_{PtC}$ value for *trans*-$[(CH_3)Pt(As(CH_3)_3)_2((CH_3)_2(C_6H_5)P)]PF_6^-$ **15**. While we have not prepared this analog, the ^{13}C n.m.r. spectrum of the related complex $[(CH_3)Pt((CH_3)_2(C_6H_5)P)_3]^+PF_6^-$ **16** has been obtained (2). Using the $^{1}J_{PtC}$ value of **16**, 457(±2) Hz, and the known relationship (2) between $^{1}J_{PtC}$ of the bis(arsine) and $^{1}J_{PtC}$ of the bis(phosphine) series: $^{1}J_{PtC}$(bis(arsine)) = 1.000 $^{1}J_{PtC}$(bis(phosphine)) − 37.7 we calculate $^{1}J_{PtC}$ for **15** to be 419 Hz.

Can. J. Chem. Downloaded from www.nrcresearchpress.com by 210.87.254.6 on 09/05/12
For personal use only.

Can. J. Chem. Downloaded from www.nrcresearchpress.com by 210.87.254.6 on 09/05/12
For personal use only.

cis substituents. When L and L′ are the same, the differing steric environments of the two series may give rise to substantially different ligand – *cis* substituent interactions, and thus different n.m.r. *cis*-influences for that ligand. For example, the twist angles or degree of "feathering" of the phenyl groups in the triphenylarsine derivatives may be substantially different for these two series of compounds. Similarly, the rotational preferences about the Pt—N bond in the γ-picoline derivatives may be different. These general considerations may be applied to all the ligands used in **1–4**. This proposal contrasts with the n.m.r. *trans*-influence theory, where the σ-donor properties of a ligand seem to be essentially independent of such steric considerations (2). Comparisons of the shieldings of the platinum–methyl carbons (*vide infra*) provide additional information concerning this problem. Nevertheless, there is a reasonable quantitative and a good qualitative relationship between the n.m.r. *cis*-influences of the ligands used in the platinum(II) and platinum(IV) complexes **1–4**.

In previous investigations, we examined the relationship between the $^1J_{PtC}$ and $^2J_{PtCH}$ values for platinum–methyl groups both *cis* (4) and *trans* (2) to a varied ligand L. Excellent linear relationships were observed in the latter case. A plot of $^2J_{PtCH}$ *vs.* $^1J_{PtC}$ for the methyl group *trans* to L′ in **1–5** and **12** is shown in Fig. 3. The linear regression analysis parameters are given in eq. 3.

[3] $^2J_{PtCH}$ (*trans* to L′, **1–5, 12**) =
$0.091(\pm 0.008)\ ^1J_{PtC}$ (*trans* to L′, **1–5, 12**)
$+ 16.0(\pm 4.9)$
$r = 0.988$

The excellent linear correlation may be taken as a demonstration that the factors affecting the $^1J_{PtC}$ values parallel, and thus are likely very similar to, those factors governing $^2J_{PtCH}$, within this series of compounds. We have already shown (2) that the common factor is probably α_{Pt}^2, the Pt(6s) orbital contribution to the Pt—C bond. Comparison of the slope of this plot with the slopes (*ca.* 0.12) for three series of *trans*-methylplatinum derivatives (2) reveals that the sensitivity of the *geminal* ^1H–^{195}Pt coupling constants is markedly less in the former case. Furthermore, the distinctly non-zero intercept of the plot for the platinum(IV) complexes indicates that the Fermi contact mechanism may not be the sole contributing factor to the $^1J_{PtC}$ and $^2J_{PtCH}$ values.

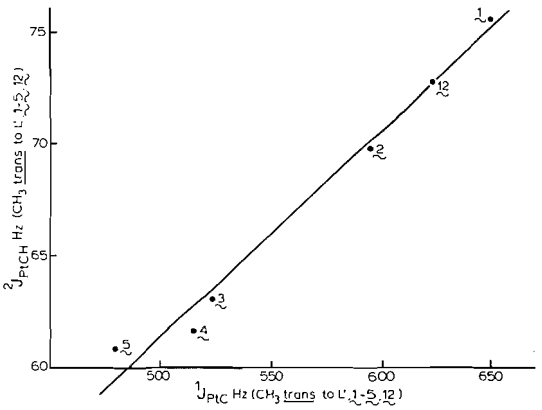

FIG. 3. Plot of $^2J_{PtCH}$ for the methyl group *trans* to L′ of **1–5** and **12** *vs.* $^1J_{PtC}$ for the methyl group *trans* to L′ of **1–5** and **12.**

Finally, we note that the charge of the complex does not appear to have a bearing on the slope or intercept of the line, as we have noted in other studies (2–4).

An analogous plot for the platinum–methyl groups *cis* to L′, revealed an apparently random scatter of points ($^2J_{PtCH}$ is essentially invariant). This feature is reminiscent of the same behavior of an analogous plot for the *cis*-methylplatinum derivatives [*DIARS*Pt(CH_3)L]$^+PF_6^-$ (4). Moreover a plot of $^1J_{PtC}$ (*trans* to L′) *vs.* $^1J_{PtC}$ (*cis* to L′) reveals again, a scattered array of data points, like a similar plot for the *DIARS* complexes. All this information supports the ideas that in these platinum(IV) derivatives, the n.m.r. *cis*-influence of a ligand is not strongly related to its n.m.r. *trans*-influence, nor is it clearly related to the rehybridization of platinum σ-orbitals in the platinum–carbon bonds.

Treatments similar to the quantitative methods just described for the trimethylplatinum(IV) complexes **1–5** may be applied to the trimethylplatinum(IV) derivatives **6–8** and the dimethylplatinum(IV) complexes **9–11**. Since there are only a few data points available for each type of plot, the linear regression analysis parameters shown in eqs. 4–6 are not necessarily completely characteristic of the relationships that exist for more complete series.

[4] $^1J_{PtC}$(**6–8**, *trans* to L′) = 0.8 $^1J_{PtC}$(*trans*-[(CH_3)Pt$((CH_3)_2(C_6H_5)P)_2$L]$^+PF_6^-$)
$+102$
$r = 0.992$

[5] $^2J_{PtCH}$(**6–8**, *trans* to L′) =
$0.11\ ^1J_{PtC}$(**6–8**, *trans* to L′) $+2.5$
$r = 0.966$

[6] $^2J_{PtCH}$(**9–11**, *trans* to L′) =
$0.08\ ^1J_{PtC}$(**9–11**, *trans* to L′) $+21.8$
$r = 0.964$

All the slopes of eqs. 3–5 are similar to those obtained for analogous plots for the complexes **1–5**. This provides added support for the notions that the n.m.r. *trans*-influence of a particular ligand in a platinum(IV) derivative parallels that in corresponding platinum(II) complexes, and that both $^1J_{PtC}$ and $^2J_{PtCH}$ for a platinum–methyl group *trans* to a varied ligand are mainly sensitive to variations in $\alpha_{Pt}{}^2$.

It is also interesting to compare the $^1J_{PtC}$ values of the platinum methyl groups between series **1–5** and **6–8**. A linear regression analysis[8] of the data yields eqs. 7 and 8.

[7] $^1J_{PtC}$(CH_3 *trans* to L′, **2**, **4**, **5**) =
$1.01\ ^1J_{PtC}$ (CH_3 *trans* to L′, **6–8**) -8.2
$r = 0.998$

[8] $^1J_{PtC}$ (CH_3 *cis* to L′, **2**, **4**, **5**) =
$0.93\ ^1J_{PtC}$ (CH_3 *cis* to L′, **6–8**) $+82.5$
$r = 0.995$

These equations support some important ideas: (*1*) the n.m.r. *cis*-influences of trimethylarsine and dimethylphenylphosphine are similar,[9] (*2*) the n.m.r. *trans*-influence of a ligand is regularly, but not strongly affected by variations in ligands *cis* to itself,[10] and (*3*) the n.m.r. *cis*-influence is outweighed by the n.m.r. *trans*-influence; eq. 8 reflects the substantial difference between the n.m.r. *trans*-influence of trimethylarsine and dimethylphenylphosphine.[11]

The ^{13}C—^{31}P coupling constants of the platinum–methyl groups require only brief comment. The $^2J_{PtPC}$ values for methyl groups *trans* to phosphorus all fall in the range $105(\pm5)$ Hz, while the corresponding coupling constants for platinum methyl groups *cis* to phosphorus all fall in the range $5(\pm2)$ Hz. These values are close to those observed for similar methylplatinum(II) phosphine derivatives (2, 14). The magnitudes of the remaining coupling constants in Table 3 are consistent with those observed in a variety of transition metal complexes. For example, the $^1J_{PtC}$ value ($851(\pm2)$ Hz) for the carbonyl carbon of the acyl derivative **13**, falls in the range 502–1070 Hz, observed for a variety of sp^2 hybridized carbons attached to platinum(II) (2, 3).

^{13}C Shieldings

A plot of the shieldings of the platinum–methyl carbons of the platinum(II) complexes *trans*-$[(CH_3)Pt(As(CH_3)_3)_2L]^+PF_6^-$ (2) with those of the methyl groups *trans* to L′ in **1–5** yields a fair linear relationship[12] shown in eq. 9.

---

[8]We have shown (2) that the n.m.r. *trans*-influences of γ-picoline and pyridine are identical. However, we have not shown that their n.m.r. *cis*-influences are the same, as would be expected on the basis of our steric arguments (4) proposed to account, in part, for the n.m.r. *cis*-influence. We have now obtained the $^1J_{PtC}$ value, $573(\pm2)$ Hz, of [*DIARS*Pt$(CH_3)(C_5H_5N)]^+PF_6^-$ **17** (19), the same as the corresponding coupling constant ($575(\pm2)$ Hz) in the γ-picoline analog (4). Thus, the n.m.r. *cis*-influences of γ-picoline and pyridine are identical. We assume this point in formulating eq. 8.

[9]This idea has arisen from previous ^{13}C n.m.r. studies by this group (2, 4).

[10]The same point was made earlier in the comparison of the $^1J_{PtC}$ values for the platinum–methyl groups *cis* to L′ in **1–4** with the $^1J_{PtC}$ value of the [*DIARS*Pt(CH_3)L]$^+PF_6^-$ analogs.

[11]The referees have commented on the relative magnitudes of the $^1J_{PtC}$ values in the corresponding Pt(II) and Pt(IV) systems. It has been noted (20) that the ratios of $^1J_{PtP}$ for Pt(IV):Pt(II) analogs are commonly in the range 0.56–0.68, close to 0.67, the ratio of the s-characters in six and four bond hybrids respectively. In contrast, the ratios of $^1J_{PtC}$ for the Pt(IV):Pt(II) complexes considered here fall in the range 1.02–1.14. This may be rationalized by the scheme described by Pidcock and co-workers (20, 21). In Pt(IV) *vs.* Pt(II) analogs, it appears that bonds to anionic ligands such as CH_3^- are significantly shorter, and bonds to neutral ligands are substantially longer. Thus, in the Pt(IV) complexes, relative to the Pt(II) analogs, s electron density would be concentrated in the Pt—CH_3 σ-bonding orbitals and higher $^1J_{PtC}$ values would be observed. The opposite effects would occur for Pt(IV)/Pt(II) analogs with neutral ligands such as phosphines. This argument may also be invoked to account for the reduced sensitivity of the $^1J_{PtC}$ values to changes in neutral ligands in the Pt(IV) complexes, as demonstrated by eqs. 1, 2, and 4.

[12]δ_C (-6.0 p.p.m.) for the platinum–methyl group of *trans*-$[(CH_3)Pt(As(CH_3)_3)_2(P(CH_3)_2(C_6H_5))]^+PF_6^-$ **14** was calculated from the analogous shielding ($+0.7$ p.p.m.) of $[(CH_3)Pt((CH_3)_2((C_6H_5)P)_3]^+PF_6^-$ **15** using the linear relationship (2)

δ_C (bis(arsine)) =
$1.04(\pm0.02)\ \delta_C$(bis(phosphine)) $-6.70(\pm0.18)$

Can. J. Chem. Downloaded from www.nrcresearchpress.com by 210.87.254.6 on 09/05/12
For personal use only.

[9] δ_C (*trans* to L′, **1–5**)
$= 0.81(\pm 0.02)\ \delta_C$ (*trans*-[$(CH_3)Pt(As(CH_3)_3)_2L]^+PF_6^-$)
$+ 7.4(\pm 0.1)$
$r = 0.917$

Thus, both the $^1J_{PtC}$ values for corresponding platinum–methyl groups in *trans*-methylplatinum(II) and *fac*-trimethylplatinum(IV) derivatives and the ^{13}C shieldings for those groups are linearly related.

Analysis of a similar plot of the platinum–methyl carbon shieldings of the series [*DIARS*Pt-$(CH_3)L]^+PF_6^-$ (4) with those shieldings of the platinum–methyl groups *cis* to L′ in **1–4** affords the linear regression analysis parameters in eq. 10.

[10] δ_C (CH_3 *cis* to L′, **1–4**) =
$0.88(\pm 0.04)\ \delta_C$ ([*DIARS*Pt$(CH_3)L]^+PF_6^-$)
$+ 11.6(\pm 0.1)$
$r = 0.994$

As was just shown for the *trans* platinum–methyl groups of **1–5**, linear trends exist between both the $^1J_{PtC}$ values and the methyl carbon shieldings of the related platinum(II) and platinum(IV) species. Moreover, this result suggests that the steric arguments proposed to account for the poorer linear correlation of the $^1J_{PtC}$ values for the methyl groups *cis* to a varied ligand in **1–4** and the *DIARS* derivatives may not be particularly important, and that a better relationship may be observed for an extended series of compounds.

We thank the National Research Council of Canada for financial support of this project, for the award of a post-doctoral fellowship to J.E.H.W., and for the award of a scholarship to L.E.M.

1. H. C. Clark, L. E. Manzer, and J. E. H. Ward. Can. J. Chem. **52**, 1165 (1974).
2. M. H. Chisholm, H. C. Clark, L. E. Manzer, J. B. Stothers, and J. E. H. Ward. J Am. Chem. Soc. **95**, 8574 (1973).
3. H. C. Clark and J. E. H. Ward. J. Am. Chem. Soc. In press.
4. H. C. Clark and J. E. H. Ward. Can. J. Chem. **52**, 570 (1974).
5. A. Pidcock, R. E. Richards, and L. M. Venanzi. J. Chem. Soc. A, 1707 (1966).
6. T. G. Appleton, H. C. Clark, and L. E. Manzer. Coord. Chem. Rev. **10**, 335 (1973).
7. F. R. Hartley. Chem. Soc. Rev. **2**, 163 (1973).
8. H. C. Clark and L. E. Manzer. Inorg. Chem. **12**, 362 (1973).
9. J. Casanova, Jr., R. E. Schuster, and N. D. Werner. J. Chem. Soc. 4280 (1963).
10. G. C. Levy and J. D. Cargioli. J. Magn. Reson. **6**, 143 (1972).
11. S. Castellano and A. A. Bothner-By, J. Chem. Phys., **41**, 3863 (1964).
12. H. C. Clark and L. E. Manzer. Inorg. Chem. **11**, 2749 (1972).
13. T. G. Appleton, H. C. Clark, and L. E. Manzer. J. Organomet. Chem. **65**, 275 (1974).
14. A. J. Cheney, B. E. Mann, and B. L. Shaw. Chem. Commun. 431 (1971).
15. J. G. Verkade. Coord. Chem. Rev. **9**, 80 (1972).
16. K. Thomas, J. T. Dumler, B. W. Renoe, C. J. Nyman, and B. M. Roundhill. Inorg. Chem. **11**, 1795 (1972).
17. H. C. Clark and L. E. Manzer. J. Organomet. Chem. **38**, C41 (1972).
18. H. C. Clark and L. E. Manzer. J. Organomet. Chem. **59**, 411 (1973).
19. H. C. Clark, K. J. Reimer, and J. E. H. Ward. Unpublished results.
20. G. G. Mather, A. Pidcock, and G. J. N. Rapsey. J. Chem. Soc. Dalton Trans. 2095 (1973) and references therein.
21. A. Pidcock. Private communication.

Can. J. Chem. Downloaded from www.nrcresearchpress.com by 210.87.254.6 on 09/05/12
For personal use only.

Methyl Cyclopentadienecarboxylate Formation in the Methanol Quenched Vapor Phase Thermolysis of Methyl Salicylate

O. A. MAMER

Mass Spectrometry Unit, Royal Victoria Hospital, Department of Experimental Medicine of McGill University, Montreal, Quebec

AND

K. G. RUTHERFORD AND R. J. SEIDEWAND[1]

Department of Chemistry, University of Windsor, Windsor, Ontario

Received December 14, 1973

Cyclopentadienylidenecarbonyl, the principle thermolytic fragment of methyl salicylate in the vapor phase, undergoes a rapid recombination with the methanol liberated in the initial fragmentation to yield monomeric methyl cyclopentadienecarboxylate. Reaction of this last ester with some dienophiles is reported, and, in the case of dimethyl acetylenedicarboxylate, adducts are obtained that suggest that the ester exists as a mixture of **1**- and **2**-substituted cyclopentadienes. No trace is found of a neutral fragment of mass 120 corresponding to the base peak in the 70 eV spectrum of methyl salicylate.

Le cylopentadiènylidènecarbonyl, fragment principal de la thermolyse du salicylate de méthyle en phase vapeur, se recombine rapidement avec le méthanol libéré dans la fragmentation initiale pour fournir le cyclopentadiènecarboxylate de méthyle à l'état monomérique. On rapporte des réactions de ce dernier ester avec quelques diénophiles et dans le cas de l'acétylènedicarboxylate de méthyle les produits d'additions obtenus indiquent que l'ester existe sous forme de mélange de cyclopentadiènes substitués en position 1 et en position 2. On ne trouve aucune trace d'un fragment neutre de masse 120 correspondant au pic de base dans le spectre du salicylate de méthyle à 70 eV. [Traduit par le journal]

Can. J. Chem., **52**, 1983 (1974)

Ortho-substituted aromatic compounds have been demonstrated by many workers to thermolyze in the vapor phase through many types of reaction pathways. Frequently a thermolysis is observed to occur via simultaneous and competing paths or by a pathway that significantly changes with increases in temperature, It may be surprising to note that a wide variety of these compounds have a thermolytic intermediate in common: cyclopentadienylidenecarbonyl (**1**). In this last group are *o*-nitroanisole (1), *o*-phenylenecarbonate (2, 3), diazotized *o*-aminophenol (4), salicylaldehyde (5), and *o*-hydroxyacetophenone (6). Methyl salicylate (**2**) has now been found to thermolyze exclusively to **1** with the apparent absence of any significant side reactions (Scheme 1).

An expected side reaction was one involving the elimination of methanol to yield keto-ketene **3**. Intermediate **3** has been observed spectroscopically in the photolysis at 77 °K of both 2-phenylbenzo-1,3-dioxan-4-one (7) and cyclic phthaloyl peroxide (8). The former compound yields methyl salicylate on photolysis in methanol at room temperature (7). Coumarandione has been shown to yield salicylic acid and other salicylate derivatives when photolyzed in water or other nucleophiles at room temperature, also suggesting the formation and subsequent solvolysis of **3** (9). Hence, it was thought that if we could detect ethyl salicylate in the ethanol quench of the thermolyzate of **2**, we would have compelling evidence for the thermolytic generation of **3**.

Figure 1 shows the effect of the furnace temperature on the normalized intensities of the major and significant masses detected in the furnace effluent when **2** is flash thermolyzed in a low pressure helium flow. In the range 400–750°, the intensity of the molecular ion of **2** (*m/e* 152) decreases approximately by 60% without a corresponding appearance of a fragment

[1]Present address: Dwight P. Joyce Research Center, The Glidden Durkee Division of SCM, 16651 Sprague Road, Strongsville, Ohio 44136.

Can. J. Chem. Downloaded from www.nrcresearchpress.com by 210.87.254.105 on 09/05/12
For personal use only.

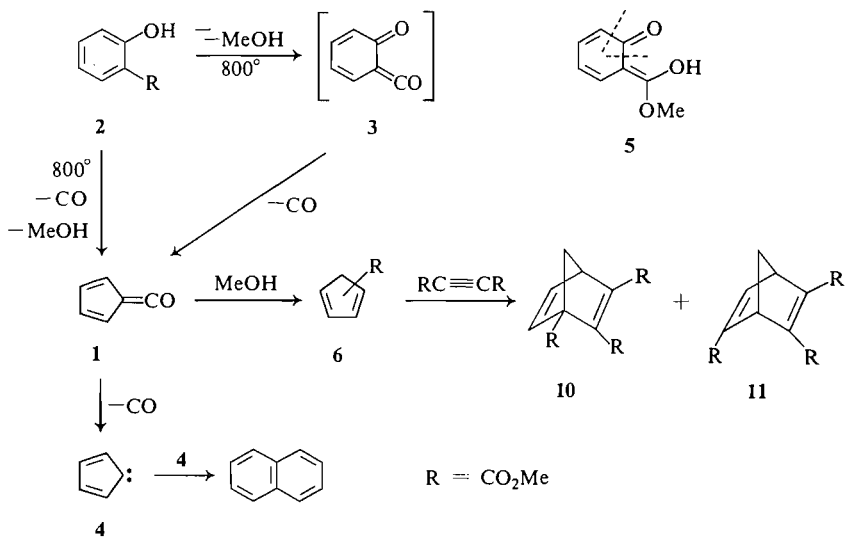

2 3 5 1 6 10 11 4

SCHEME 1. Composite reaction scheme for the thermolysis of methyl salicylate

mass. This suggests that **2** undergoes a thermally induced molecular rearrangement to a species having the same mass but less sensitivity for ionization than the cold form. Above 750° further losses in intensity of *m/e* 152 are met initially with increases in *m/e* 92 which is the molecular ion of **1**. With further increasing temperature, **1** undergoes decarbonylation yielding carbene **4** (*m/e* 64) which dimerizes to ultimately yield the naphthalene found in the preparative thermolyzate (below). This pattern of dependency of the intensities of *m/e* 92, 64, and 128 on furnace temperature is typical of those compounds that have a thermolytic route through **1**. This pathway was first proposed by DeJongh and Brent to account for the appearance of naphthalene in the thermolyzate of *o*-phenylenecarbonate (2).

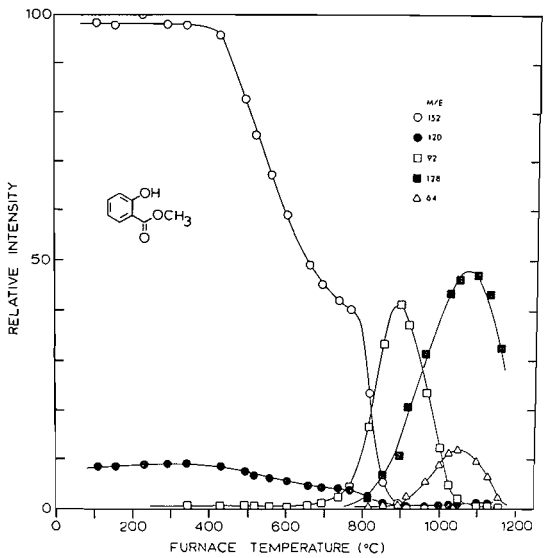

FIG. 1. Relative intensities of apparent molecular ions detected at 12 eV in the effluent stream of a quartz furnace at various temperatures. The ions are the molecular ions of the following species: *m/e* 152, methyl salicylate (**2**); *m/e* 92, cyclopentadienylidenecarbonyl (**1**); *m/e* 128, naphthalene; *m/e* 64, cyclopentadienylidene (**4**); *m/e* 120 is not a molecular ion but a low appearance potential fragment of **2** (see text).

The ratio of the intensities of *m/e* 120 to *m/e* 152 remains constant over the temperature interval 100–850° indicating that observable *m/e* 120 is derived solely as an electron-impact fragment of **2**. The absence of an accumulation at *m/e* 120 suggests that **3** is either very unstable as a neutral intermediate and does not survive the thermolytic conditions that give rise to large amounts of **1**, or it is not formed at all in the thermolysis of **2**. While it is not possible on the basis of these experiments to distinguish which of these two alternatives is fact, in either case, the thermolytic fragmentation of **2** deviates in a significant manner from the electron impact fragmentation in which *m/e* 120 is the base peak in the ionization energy range 18–70 eV and is derived from the molecular ion by the elimination of the elements of methanol (metastable confirmed).

Can. J. Chem. Downloaded from www.nrcresearchpress.com by 210.87.254.105 on 09/05/12
For personal use only.

Can. J. Chem. Downloaded from www.nrcresearchpress.com by 210.87.254.105 on 09/05/12
For personal use only.

The preparative thermolyzate of **2** that was quenched in ethanol yielded no trace of the ethyl salicylate that would have supported the thermolytic generation of **3**. Instead, an ethanol solution of monomeric methyl and ethyl cyclopentadienecarboxylates was obtained in 32 and 40% yields, respectively. Gas chromatographic analysis of the ethanol solution revealed a 4% yield of naphthalene and a 6% recovery of **2**.

The methyl ester could arise from the recombination of **1** with the methanol that is liberated with carbon monoxide in the furnace before the thermolyzate is quenched in the ethanol. An alternative explanation that the thermally induced rearrangement of **2** yields a species, perhaps similar to **5** that may decarbonylate without methanol elimination requires that a residue of mass 124 should be detectable in the furnace effluent as a primary thermal fragment. However *m/e* 124 shows no significant intensity changes with furnace temperature.

Both methyl and ethyl cyclopentadienecarboxylates yield pairs of adducts with dimethyl acetylenedicarboxylate that are easily separable on gas chromatography and have mass spectra in agreement with these assignments.

When the effluent was quenched in cold methanol, a nearly pure solution of methyl cyclopentadienecarboxylate (**6**, 75% yield based on **2** distilled into the furnace) was obtained that contained the small amounts of **2** and naphthalene as noted above.

The structures of the three principal dimers of this ester (**7**, **8**, and **9**) have been established (a brief review of this subject has been published by Franklin *et al.* (10)) and none of them appears to be formed simply and directly from methyl cyclopentadiene-5-carboxylate (*i.e.*, none of the dimers involves carbomethoxy substitutions on a methylene carbon atom) but rather from the 1-isomer acting as dienophile and both the 1- and 2-isomers serving as the diene.

The conditions of preparation and the lack of interfering contaminants suggested experiments to determine whether **6** is initially formed as the elusive 5-substituted isomer and whether it could be intercepted with a reactive dienophile in a 1–4 cycloaddition prior to dimerization or rearrangement to the more conjugated 1- and 2-isomers.

The addition of dimethyl acetylenedicarboxylate to the methanol quenched thermolyzate resulted in the formation of two adducts that

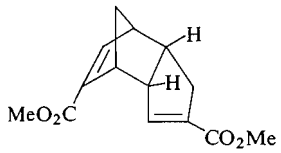

7

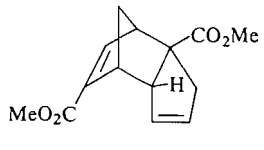

8

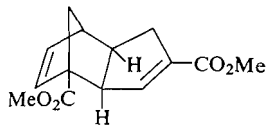

9

were identical to two of the four found in the similarly treated ethanol quench. These two adducts have mass spectra that display prominent molecular ions having isotopic abundances in accord with the molecular formulae of $C_{13}H_{14}O_6$. The spectra are too similar to permit unequivocal structure assignment. The n.m.r. spectra of the adducts isolated by preparative gas chromatography, however, are readily found to be the spectra of 2,3,4- and 2,3,5-tricarbomethoxynorbornadiene (**10** and **11**, respectively).

For the purposes of having a model compound on which to base the interpretation of the n.m.r. spectra of the dimethyl acetylenedicarboxylate adducts, 2,3-dicarbomethoxynorbornadiene was synthesized by the reaction of cyclopentadiene with excess acetylenedicarboxylic acid followed by esterification in methanol containing a trace of sulfuric acid. The 100 MHz n.m.r. spectrum ($CDCl_3$) was in agreement with what was expected for this model compound: τ 3.10 (m, 2, vinyl H), 6.08 (m, 2, bridgehead H), 6.25 (s, 6, OCH_3), 7.75 and 7.92 (AB quartet, 2, J_{AB} = 6.7 Hz and $J_{1,7} = J_{4,7}$ = 1.6 Hz, bridge H). Analysis of the AB quartet displayed by the bridge protons shows that each member is split further into triplets by the two bridgehead protons. In addition, the low-field half shows the broadening effect of long range coupling. From previous studies of the spin–spin coupling interactions in norbornene derivatives (11, 12) it appears reasonable to assign the proton *syn* to the carbomethoxy side of the norbornadiene ring and *anti* to the vinyl protons as the one at lower field and coupled weakly to the vinyl protons. Inspection of the n.m.r. spectrum of **10** (60 MHz, τ 3.04 (m, 2, vinyl H), 5.97 (m, 1, bridge-

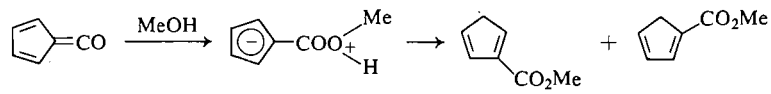

SCHEME 2. Reaction of cyclopentadienylidenecarbonyl with methanol

head H), 6.20 and 6.23 (two s, 9, OCH_3), 7.46 and 7.58 (AB quartet, 2, J_{AB} = 6.7 Hz and $J_{4,7}$ = 1.5 Hz, bridge H)) likewise shows a slightly greater amount of broadening in the lower field half of the bridge AB quartet. The doublet observed for the vinyl proton in **11** (60 MHz, τ 2.35 (broadened d, 1, J = 3.5 Hz, vinyl H), 6.0 (m, 2, bridgehead H), 6.21, 6.24, and 6.26 (three s, 9, OCH_3), 7.7 (m, 2, bridge H)) also shows slight broadening from long range coupling with presumably the *anti* bridge proton.

The addition of dimethyl maleate to the methanol quenched thermolyzate led to the formation of four tricarbomethoxynorbornene isomers as expected: *endo* or *exo* ester substitution at C-2 and C-3 as derived from the maleate, in combination with either C-4 or C-5 substitution of the third carbomethoxy group on the norbornene nucleus. While the four isomers were separable on analytical gas chromatography and had area ratios, in order of elution, 6:13:21:1, they could not be separated suitably on a preparative scale for n.m.r. All four displayed very similar mass spectra with molecular ions having isotopic abundances correct for the required $C_{13}H_{16}O_6$.

The difficulty of isolating adducts or dimers derived from the 5-isomer of **6** may stem from the possibility that the addition of methanol to **1** may not yield the 5-isomer as even a transient species at all. If the addition in methanol gives rise to a charge separated solvated species that has a carbomethoxycyclopentadienyl anionic nature, protonation of the charge delocalized cyclopentadienyl moiety would probably yield the conjugated 1- and 2-isomers directly (Scheme 2).

Further experiments are in progress which may yield the 5-isomer free of conditions favoring isomerization to the conjugated isomers.

Experimental

Methyl salicylate was subjected to thermolysis in two modes, both previously described in detail (5). Product identifications were made by comparisons of their gas chromatographic retention times and their mass spectra with those of standards when available, and by n.m.r. and mass spectral interpretation when standards were unavailable. An LKB 9000 combined gas chromatograph – mass spectrometer interfaced to a Varian SS-100 MS data system was used as described below.

Thermolytic Experiments

Thermolysis A

Methyl salicylate was slowly evaporated into a low pressure helium flow (approximately 0.1 Torr) and made to pass through a quartz reactor which was attached through a Becker-Ryhage helium separator to the mass spectrometer ion source. Before an experiment was carried out, the reactor temperature was cycled several times between 200° and the upper limit of 1150°.

The mass spectrometer was operated under the following conditions: ionizing energy, 12 eV at 60 × 10^{-6} A; accelerating potential 3.5 kV; source temperature, 290°; separator temperature, 280°; electron multiplier output filter cutoff at 120 Hz.

Experiments were started with the reactor temperature at approximately 100°. After each increment in reactor temperature, 2 min was allowed for thermal re-equilibration and then three slow scans were made in the range *m/e* 10–300 (6 s per scan) on line with the data system. After reaching the reactor limit of 1150°, the same schedule was followed with the reactor temperature decreasing. Each set of three scans was averaged and the standard deviations were calculated for each intensity in the averaged spectrum for each temperature. The standard deviations of the significant ions never exceeded 8% of their averaged intensities.

At the conclusion of an experiment, the data system presented the data as columns of *m/e* values and corresponding intensities with their associated standard deviations. Figure 1 is an example of the plotted results of a typical experiment.

Thermolysis B

On a semipreparative scale, methyl salicylate (10–20 mg, typically) was evaporated into argon (40 ml min^{-1}) and conducted through a nichrome filament reactor into a trap containing a trapping solvent (0.5 ml) at −78°. The contact time with the hot filaments (800° typically) was approximately 50 ms.

Trapping Solvent

(1) Ethanol. After 25 min of operation, the reactor was cooled and allowed to flood with argon to ambient pressure. An aliquot (2μl) of the ethanol solution of the thermolyzate (pale yellow and homogeneous), immediately analyzed by gas-chromatography – mass spectrometry was found to contain **6** (32%), ethyl cyclopentadienecarboxylate (40%), naphthalene (4%), and **2** (6% recovered).

Analytical conditions were as follows: injector port, 200°; column, 2 m × 6 mm glass packed with 3% OV-1 on Chromosorb W HP, temperature programmed from 30 + 5° min^{-1}; helium carrier, 40 ml min^{-1}; separator, 280°; ion source, 290°, 70 eV at 60 × 10^{-6} A.

Dimethyl acetylenedicarboxylate (50 mg) was added

Can. J. Chem. Downloaded from www.nrcresearchpress.com by 210.87.254.105 on 09/05/12
For personal use only.

to the cold thermolyzate and the mixture was then allowed to come to room temperature. Analysis by gas-chromatography – mass spectrometry after a few minutes showed the mixture to be unchanged from the initial analysis except for a very large peak due to the added acetylene. The mixture was further held at room temperature for 24 h and re-analyzed by gas-chromatography – mass spectrometry. Four new peaks appeared at longer retention time (area ratios, in order of elution 10:15:7:13) which had mass spectra consistent with their assignment as a pair of dimethyl acetylenedicarboxylate adducts for each of the methyl and ethyl esters of cyclopentadienecarboxylic acid. The two monomeric esters were still present in small quantities even after several days at room temperature suggesting that the adducts may thermally crack to a minor extent in the gas-chromatography injection port.

(2) Methanol. When methanol was substituted for the ethanol in the trap, and the thermolysis repeated, a single major peak was obtained on immediate gas-chromatography – mass spectrometry analysis of the cold thermolyzate solution which proved to be methyl cyclopentadienecarboxylate (75% yield). Small peaks due to methyl salicylate and naphthalene were still in evidence.

When allowed to react at room temperature for 24 h with dimethyl acetylenedicarboxylate, the methanol solution of the thermolyzate yielded two Diels–Alder adducts having nearly identical mass spectra and were the same as two of those detected in the ethanol solution above.

The two adducts were separated and collected by preparative gas-chromatography (6 ft × 0.5 in. 10% SE-30 on 60–80 mesh Chromosorb W) and their n.m.r. spectra were obtained in $CDCl_3$ at 60 MHz.

In separate experiments, methyl cyclopentadienecarboxylate was also made to react with dimethyl maleate (four adducts), diphenylacetylene (two adducts), and tetracyanoethylene. The last reagent appeared to yield unstable products that decomposed on attempted gas chromatography analysis.

The LKB 9000 gas chromatograph – mass spectrometer used in this work was granted by the Medical Research Council of Canada (Grant No. ME3720) to the Faculty of Medicine of McGill University. The authors gratefully recognize the assistance of Mr. David Hill of the University of Windsor Chemistry Department in the 60 MHz n.m.r. work and also Dr. Arthur Perlin of the McGill University Chemistry Department for the 100 MHz n.m.r. spectrum.

1. O. A. MAMER, R. J. KOMINAR, and F. P. LOSSING. Org. Mass Spectrom. **3**, 1411 (1970).
2. D. C. DEJONGH and D. A. BRENT. J. Org. Chem. **35**, 4204 (1970).
3. O. L. CHAPMAN and C. L. MCINTOSH. Chem. Commun. 770 (1971).
4. K. UNDHEIM, O. THORSTAD, and G. HVISTENDAHL. Org. Mass Spectrom. **5**, 73 (1971).
5. O. A. MAMER, Can. J. Chem. **49**, 3602 (1971).
6. O. A. MAMER. Can. J. Chem. **50**, 2513 (1972).
7. O. L. CHAPMAN and C. L. MCINTOSH. J. Am. Chem. Soc. **92**, 7001 (1970).
8. V. DVORAK, J. KOLC, and J. MICH. Tetrahedron Lett. **33**, 3443 (1972).
9. W. M. HORSPOOL and G. D. KHANDELWAL. J. Chem. Soc. D, 257 (1970).
10. W. E. FRANKLIN, C. H. MACK, and S. P. ROWLAND. J. Org. Chem. **33**, 626 (1968).
11. J. C. DAVIS, JR., and T. V. VAN AUKEN. J. Am. Chem. Soc. **87**, 3900 (1965).
12. P. M. SUBRAMANIAN, M. T. EMERSON, and N. L. LEBEL. J. Org. Chem. **30**, 2624 (1965).

Can. J. Chem. Downloaded from www.nrcresearchpress.com by 210.87.254.105 on 09/05/12
For personal use only.

Trajectory Studies of Atomic Recombination Reactions. VI. Recombination of Oxygen Atoms in Argon[1]

W. H. WONG AND G. BURNS

Lash Miller Chemical Laboratory, University of Toronto, Toronto, Ontario M5S 1A1

Received April 18, 1973

The recombination of oxygen in large excess of argon has been studied between 300 and 10 000 °K by trajectory calculations. Reasonable agreement between the computed results and the experimental rate data was obtained by assuming that the interaction between oxygen and argon atoms was 0.3 kcal/mol. The present calculation also showed that the radical-molecule-complex mechanism was the major route to recombination below 1000 °K. At higher temperatures, the energy-transfer mechanism predominated. The vibrational and rotational energy distributions of the nascent product from the energy-transfer mechanism at 10 000 °K were found to be much broader than that from the radical-molecule-complex mechanism at 300 °K. However, the total energy distributions of the nascent product, if expressed in units of kT, were similar in both cases.

La recombinaison de l'oxygène dans un large excès d'argon a été étudiée entre 300 et 10 000 °K par des calculs de trajectoire. Un accord raisonnable a été obtenu entre les résultats calculés et les données expérimentales de vitesse en admettant que l'interaction oxygène–argon était de 0.3 kcal/mol. Le présent calcul montre aussi que le mécanisme "complexe radical molécule" est la voie majeure de recombinaison au-dessous de 1000 °K. A des températures plus élevées, le mécanisme de transfert d'energie prédomine. Les distributions d'énergie vibrationnelle et rotationnelle du produit engendré par le mécanisme de transfert d'énergie à 10 000 °K, ont été trouvées plus larges que celles qui dérivent du mécanisme "complexe radical molécule" à 300 °K. Cependant, les distributions d'énergie totale du produit naissant, exprimées en unités kT, sont les mêmes dans les deux cas.

[Traduit par le journal]

Can. J. Chem., **52**, 1988 (1973)

Introduction

The kinetics of the recombination of oxygen atoms and its inverse process, the dissociation of oxygen molecules, has received considerable attention in recent years. A critical summary of experimental data for these reactions is available in the literature (1). In the present work, the recombination of oxygen atoms in an excess of argon is studied, using 3-D classical trajectory technique with Monte Carlo method of sampling, and the results are compared with the experiment. Somewhat similar calculations have been already performed on the recombination of bromine (2) and iodine (3) in different inert gases.

Computation Procedure

Two mechanisms have often been invoked in the discussions on atomic recombination reactions. One of them, the energy transfer (ET) mechanism (4), is described by a sequence

$$[1] \qquad O + O \rightleftarrows O_2^*$$

$$[2] \qquad Ar + O_2^* \rightarrow O_2 + Ar$$

in which the quasidimer O_2^* is a pair of unbound partners (5) with energy above the rotational barrier of the effective potential. The other is the radical molecule complex (RMC) mechanism (6–8), which involves bound as well as unbound intermediates and is summarized by a sequence

$$[1a] \qquad Ar + O \rightleftarrows ArO$$

$$[2a] \qquad O + ArO \rightarrow O_2 + Ar$$

where ArO denotes the bound and metastable species (9), as well as the quasidimers (5). The observed recombination rate constant is then

$$k_r \cong \sum_{i=1'}^{2'} K_i k_{2i}^{eq} f_i$$

where K is the equilibrium constant for the dimers, k_2^{eq} is the equilibrium, one-way flux for the reactions (3) [2] and [2a], and f is the redissociation correction factor, which takes

[1]Research sponsored, in part, by the Air Force Office of Scientific Research, Air Force Systems Command, USAF, under grant no. AFOSR-71-2016. The United States Government is entitled to reproduce and distribute reprints for Government purposes, notwithstanding any copyright notation hereon. Publication delayed at the request of authors.

Can. J. Chem. Downloaded from www.nrcresearchpress.com by 210.87.254.40 on 09/05/12
For personal use only.

Can. J. Chem. Downloaded from www.nrcresearchpress.com by 210.87.254.40 on 09/05/12
For personal use only.

into account that a fraction of the nascent recombination product redissociates rather than stabilizes to the observed product in subsequent collisions (2*b*, 3). The subscripts 1′ and 2′ denote quantities relevant to the ET mechanism and to the RMC mechanism, respectively. The calculation of each of these quantities is similar to that in ref. 3, and hence only a brief outline is given here.

The Equilibrium Constants for the Dimers

If a dimer is defined as a pair of atoms with energy u, (squared) orbital angular momentum q, and internuclear separation R, simultaneously obeying the following conditions

$$u_{min} \leqslant u < u_{max}$$

$$q_{min} \leqslant q < q_{max}$$

$$R_{min} \leqslant R < R_{max}$$

then the classical equilibrium constant for the dimers can be expressed as (5),

$$[3] \quad K = (kT)^{-1.5} g_A S \frac{\pi^{0.5}}{\mu} \times \int_{q_{min}}^{q_{max}} dq \int_{R_{min}}^{R_{max}} dR \int_{u_{min}}^{u_{max}} du \times [u - V_q(R)]^{-1/2} \exp(-u/kT)$$

In the above expression $V_q(R)$ is the effective potential, μ is the reduced mass, S is the symmetry number which is unity for like atoms and two for unlike atoms, and g_A is the electronic degeneracy factor for the reactions 1 and 1*a*. The above triple integral for the equilibrium constant of ArO dimers was evaluated by an asymptotic expansion (5, 9), and that for O_2^* quasidimers by Monte Carlo techniques.

The Two-Body Rate Constants

Since the velocities of the reacting species are described by Boltzmann distribution, the two-body rate constant can be expressed as

$$[4] \quad k_2 = g_B 4\pi \left(\frac{\mu}{2\pi kT}\right)^{3/2} \times \int_0^\infty v^3 \sigma(v) \exp\left(-\frac{uv^2}{2kT}\right) dv \cong g_B \langle v \rangle \langle \sigma \rangle$$

in which v and $\sigma(v)$ are the relative velocity of collision and the cross section leading to recombination, respectively. The angle-bracketed quantities are average values of the ensemble, and they were evaluated by Monte Carlo trajectories which simulated the collision process at a specified temperature T. The commonly accepted (10) overall electronic degeneracy factor, *i.e.*, $g_A g_B = 1/27$ was used.

Redissociation Correction

The nascent product of a recombination reaction is in general highly excited (2, 3). During subsequent collisions with the third body, these nascent molecules will either redissociate or will be stabilized to the observed product. The evolution of this nascent ensemble can formally be described by the master equation

$$[5] \quad \frac{\partial n(E,t)}{\partial t} = -Ln(E,t)$$

where $n(E,t)$ is the number of molecules with internal energy between E and $E + dE$ at time t. The evolution operator, L, acting on the ensemble effects dissociation as well as energy relaxation, and it can be expressed as

$$[6] \quad Ln(E,t) = 4\pi \left(\frac{\mu}{2\pi kT}\right)^{3/2} N_M \times \left[\int_0^\infty \{\sigma_{nR}(E,E') + \sigma_d(E)\} v^3 \times \exp\left(-\frac{\mu v^2}{2kT}\right) n(E,t)\, dv - \int_R dE' \int_0^\infty \sigma_{nR}(E',E) v^3 \times \exp\left(-\frac{\mu v^2}{2kT}\right) n(E',t)\, dv \right]$$

where $\sigma_{nR}(E,E')$ is the cross section for energy transfer from E to E', and $\sigma_d(E)$ is the dissociation cross section for the molecule with internal energy E. The subscript R indicates that the integration is over the entire energy space compatible with the dynamically stable molecule. Following the work of Gelb, Kapral, and Burns (11), we approximated the exponential form of the formal solution of [5] by a series of short time intervals of the order of mean collision time τ. After x such intervals, the approximate solution (11) is

$$[7] \quad f = \lim_{x \to \infty} \frac{\int_R n(E,x\tau)\, dE}{\int_R n(E,0)\, dE} = \lim_{x \to \infty} [N(0)]^{-1} \int_R n(E,0)(1 - L\tau)^x\, dE$$

Can. J. Chem. Downloaded from www.nrcresearchpress.com by 210.87.254.40 on 09/05/12
For personal use only.

where $N(0)$ is the total number of nascent molecules formed initially in single collisional events. The whole integral in the r.h.s. of 7 was evaluated by subjecting the product ensemble to successive collisions with the inert gas at the specified temperature. Even though the formal expression for the redissociation correction factor is the limiting value when x is very large, the number of collisions required to obtain the asymptotic value was generally below thirty. In most calculations it was assumed that if a molecule was stabilized by $5kT$ or more it will not redissociate. However, no such assumption was used when rate constants were calculated at 10 000 °K.

Results and Discussion

Recombination Rate Constants

The rate constants for the recombination of oxygen atoms in argon have been computed for a series of temperatures (300, 600, 2 000, 5 000, 8 000, 10 000 °K). The interaction potential for the recombining system was assumed to be the sum of pair-wise interactions:

$$V(R_{12},R_{23},R_{13}) = V_{12}(R_{12}) + V_{23}(R_{23}) + V_{13}(R_{13})$$

in which the subscripts indicate the quantities relevant to the interacting pair. The potential between two oxygen atoms was taken to be a Morse function with parameters deduced from spectroscopic constants (12), *i.e.* $D_e = 120.2$ kcal/mol; $r_e = 1.207$ Å; $\beta = 2.654$ Å^{-1}. The interaction between oxygen and argon atoms was represented by a Lennard–Jones (6-12) potential with $\varepsilon_\infty^{ArO} = 0.3$ kcal/mol and $\sigma_\infty^{ArO} = 2.9$ Å. This value of ε_∞^{ArO} is in fact the interaction between Ar and O_2, deduced from scattering experiments (13). Another set of Lennard–Jones parameters ($\varepsilon_\infty^{ArO} = 0.44$ kcal/mol, $\sigma_\infty^{ArO} = 2.82$ Å), which was employed by Keck and co-workers (10), was also used for calculations at several temperatures (300, 600, 1 000, 1 500, 2 000 °K).

The calculated rate constants are shown in Fig. 1, together with the experimental data obtained by Wray (14), Camac and Vaughan (15), Campbell and Thrush (16), and Watt and Myerson (17). The recombination rate constants of Wray (14), Camac and Vaughan (15) and Watt and Myerson (17) were obtained from dissociation rate constants, k_d, by assuming $k_r = k_d/K$, where K is the equilibrium constant for the $O_2 = 2O$ reaction.

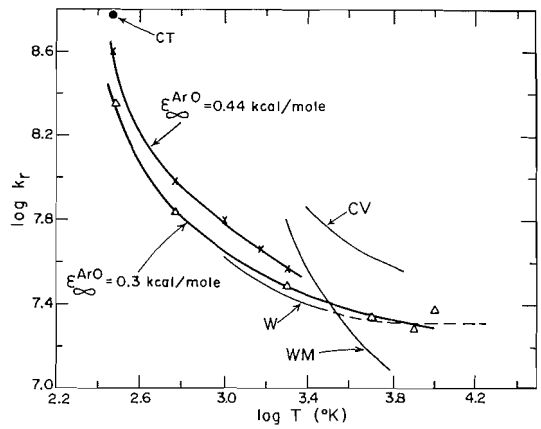

FIG. 1. Comparison of calculated and experimental recombination rate constants (l^2 mol^{-2} s^{-1}) of oxygen atom in argon. The computed curves are labelled by the value of the interaction parameter, ε_∞^{ArO}. The experimental data are from the following sources: CT, Campbell and Thrush, ref. 16; W, Wray, ref. 14; CV, Camac and Vaughan, ref. 15; WM, Watt and Myerson, ref. 17. The portion of Wray's data indicated by the dashed line was obtained from dissociation and the solid line from recombination.

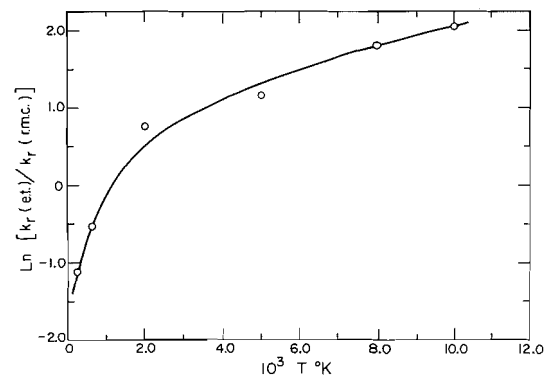

FIG. 2. The computed ratio of k_r(ET) to k_r(RMC).

As shown in Fig. 1, the calculated recombination rate constants agree reasonably well with the experimental data throughout the entire temperature range. Since the experimental data exhibit an appreciable scatter, no attempt was made to obtain a better fit. The ratio of contributions from the ET mechanism and from the RMC mechanism to the overall recombination is shown in Fig. 2. Consistent with the results of previous studies (2, 3), the ET mechanism was found to be the predominant route for recombination at high temperatures, while the RMC mechanism was the major contributor at low temperatures.

Can. J. Chem. Downloaded from www.nrcresearchpress.com by 210.87.254.40 on 09/05/12
For personal use only.

Another theoretical calculation on this recombination reaction has been performed within the framework of the modified phase-space theory (10). The agreement between our present results and the data computed from the phase-space theory, with the assumption that only the electronic ground state ($^3\Sigma_g^-$) was responsible for recombination, is fairly satisfactory within a temperature range of 300 to 3000 °K. However, above 3000 °K, the phase-space theory predicts a steeper negative temperature coefficient than that of the present work. It might be pointed out that an agreement between the present results and those of ref. 10 might well be somewhat coincidental. This is because the two calculations involve different approaches, and an agreement may just mean that various correction factors used cancel each other.

Reactive Initial Configurations

In order to understand better the mechanism of recombination, it is necessary to determine the dynamical variables which would most likely lead to reaction. Here we single out two initial variables of the collision: the relative translational energy and the impact parameter. Figure 3 shows the histograms for the distributions of impact parameters for those trajectories which lead to recombination via the ET mechanism at 10 000 °K and via the RMC mechanism at 300 °K. These temperatures were chosen because the ET mechanism predominates at 10 000 °K and the RMC at 300 °K. If every collision would have led to reaction, the histograms would have been a theoretical distribution of $f(b)db \sim bdb$, where b is the impact parameter. Such a distribution would have been defined by a diagonal which passes through the origin (Fig. 3). For purposes of comparison, the histograms were normalized in such a way that the enclosed areas were identical to that under the diagonal. It follows from Fig. 3 that the distribution of reactive impact parameters for the ET mechanism is broader than that for the RMC mechanism, even though both distributions are fairly wide. The distribution of impact parameters for the RMC mechanism peaks between 2.4 and 4.2 Å. For this reason, the average value of impact parameters leading to recombination via the RMC mechanism is slightly lower than that via the ET mechanism. This effect is certainly related to the fact that in the case of the RMC mechanism, a significant fraction of the ArO intermediates are bound and metastable

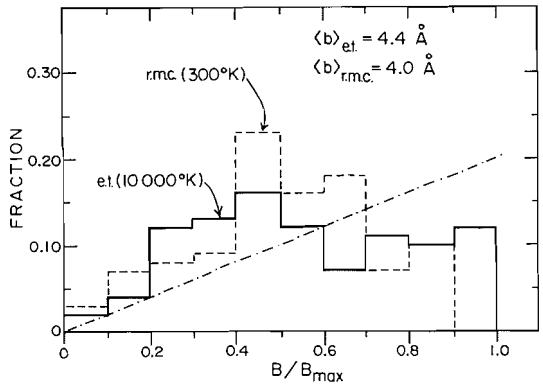

FIG. 3. Distribution of reactive impact parameters of the ET mechanism at 10 000 °K and of the RMC mechanism at 300 °K. The value of B_{max} is 8 Å. Trajectories with impact parameters sampled from 8 to 10 Å revealed no reaction from both mechanisms. The theoretical distribution, $f(b)db \sim bdb$, is shown by the dashed-dotted line.

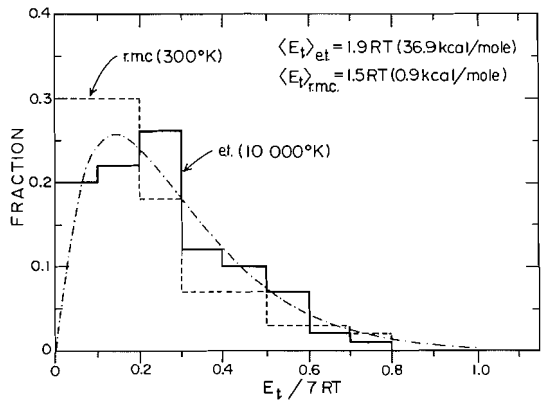

FIG. 4. Distributions of initial translational energy that leads to recombination in the ET mechanism at 10 000 °K and in the RMC mechanism at 300 °K. The dashed-dotted line is the Boltzmann distribution.

dimers which have a relatively small spatial extension.

The distributions of initial translational energies which lead to recombination are shown in Fig. 4. Since data at two different temperatures are compared, the energy is expressed in terms of RT. The low energy tail of the Boltzmann distribution is favorable in the case of the RMC mechanism. For the ET mechanism, no portion of the translational Boltzmann distribution is favored. Thus, the average translational energy, $\langle E_t \rangle$, for successful recombination via the RMC mechanism is only $1.5RT$ (0.9 kcal/mol at 300 °K) as compared to $1.9RT$ (37 kcal/mol at

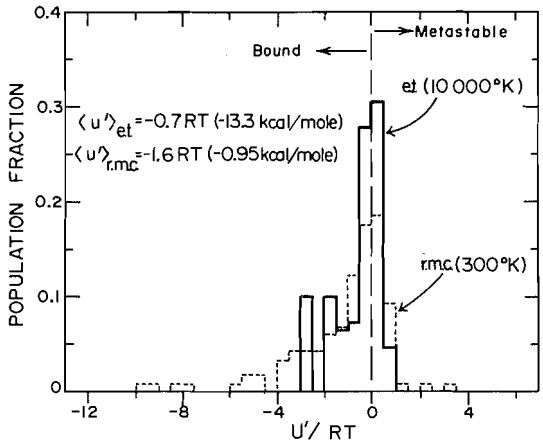

FIG. 5. Distributions of product total internal energy for the ET mechanism at 10 000 °K and for the RMC mechanism at 300 °K.

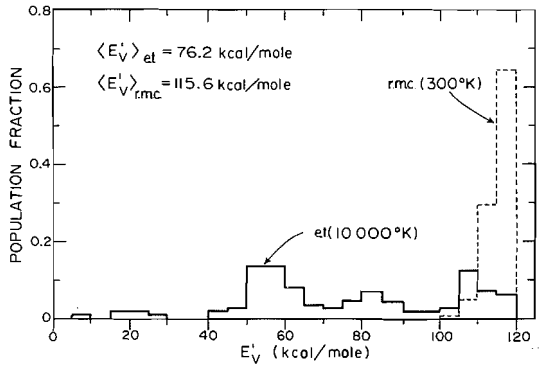

FIG. 6. Distributions of product vibration energy for the ET mechanism at 10 000 °K and for the RMC mechanism at 300 °K.

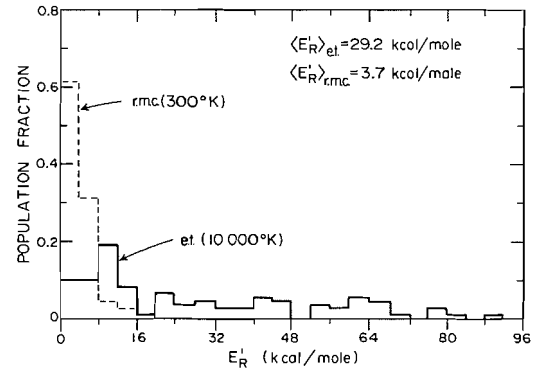

FIG. 7. Distributions of product rotational energy for the ET mechanism at 10 000 °K and for the RMC mechanism at 300 °K.

10 000 °K) for the ET mechanism. It appears that for the RMC mechanism a particle exchange process involves a delicate interplay of forces (18). For this reason, the $\langle E_t \rangle_{RMC}$ is relatively small. On the other hand, the ET mechanism involves a plain energy transfer process and occurs without particle exchange.

Product Energy Distributions

The nascent oxygen molecules produced in single collisional events were found to be in highly excited states, a result consistent with the findings on halogen recombination in previous studies (2, 3). The distributions of total internal energy u' of the nascent molecules obtained from the ET mechanism at 10 000 °K and from the RMC mechanism at 300 °K are shown in Fig. 5. The overwhelming majority of the nascent molecules formed at both temperatures have energies within $-2RT$ to $+1RT$ of the dissociation limit, with a substantial fraction being formed in the metastable states with positive internal energy. The average u' is $-1.6RT$ at 300 °K (*i.e.* −0.95 kcal/mol) and is $-0.7RT$ at 10 000 °K (*i.e.* −13.3 kcal/mol). Using the principle of detailed balancing, one may infer from these data, that the collisional dissociation predominately involves those reactant molecules which have a total internal energy very close to the dissociation limit.

The distributions of vibrational (E_v') and rotational (E_R') energies of the nascent oxygen molecules, produced in single collisional events, are shown in Figs. 6 and 7. It can be seen from these figures that the distributions from the two mechanisms are quite different. At 300 °K all nascent molecules have vibrational energy between 100 to 120 kcal/mol (the bottom of the Morse curve is taken as zero) and rotational energy below 10 kcal/mol. Both the vibrational and rotational energy distributions at 300 °K have pronounced peaks at the origins or their energy spectrum. The vibrational and rotational energy distributions of the ET mechanism at 10 000 °K, however, are very broad with no significant peak found in any energy range. Because of this difference in energy distributions, the average E_v' is very much lower, and the average E_R', very much higher at 10 000 °K than at 300 °K. It should be noted that it was also observed earlier (19), in agreement with present findings, that the product energy distribution resulting from reactive collisions broadens with increasing collision energy.

Can. J. Chem. Downloaded from www.nrcresearchpress.com by 210.87.254.40 on 09/05/12
For personal use only.

We would like to acknowledge the support of the Air Force Office of Scientific Research, U.S.A. This work was also supported in part by the National Research Council of Canada and the Defence Research Board of Canada, Grant No. 9530-54.

1. (*a*) K. L. WRAY. 10th Symp. (International) on Combustion. Academic Press, New York. 1965. p. 523; (*b*) F. KAUFMAN. Progr. Reaction Kinet. **1**, 1 (1961).
2. (*a*) A. G. CLARKE and G. BURNS. J. Chem. Phys. **55**, 4717 (1971); (*b*) A. G. CLARKE and G. BURNS. J. Chem. Phys. **56**, 4676 (1972); (*c*) A. G. CLARKE and G. BURNS. J. Chem. Phys. **58**, 1908 (1973); (*d*) W. H. WONG and G. BURNS. J. Chem. Phys. In press.
3. W. H. WONG and G. BURNS. J. Chem. Phys. **58**, 4459 (1973).
4. S. W. BENSON and T. FUENO. J. Chem. Phys. **36**, 1597 (1962).
5. S. K. KIM and J. ROSS. J. Chem. Phys. **42**, 263 (1965).
6. D. L. BUNKER and N. DAVIDSON. J. Am. Chem. Soc. **80**, 5090 (1958).
7. S. K. KIM. J. Chem. Phys. **46**, 123 (1967).
8. G. PORTER. Disc. Faraday Soc. **33**, 198 (1962).
9. D. E. STOGRYN and J. O. HIRSHFELDER. J. Chem. Phys. **31**, 1534 (1959).
10. V. H. SHUI, T. P. APPLETON, and J. C. KECK. 13th Symp. on Combustion. Academic Press, New York. 1971. p. 21.
11. A. GELB, R. KAPRAL, and G. BURNS. J. Chem. Phys. **56**, 4631 (1972).
12. G. HERZBERG. Spectra of diatomic molecules. 2nd ed. Van Nostrand, New York. 1965. p. 502.
13. F. P. TULLY and Y. T. LEE. J. Chem. Phys. **57**, 866 (1972).
14. (*a*) K. L. Wray. J. Chem. Phys. **37**, 1254 (1962). (*b*) K. L. WRAY. J. Chem. Phys. **38**, 1518 (1963).
15. M. CAMAC and A. VAUGHAN. J. Chem. Phys. **34**, 460 (1961).
16. I. M. CAMPBELL and B. A. THRUSH. Proc. Roy. Soc. A, **296**, 222 (1967).
17. W. S. WATT and A. L. MYERSON. J. Chem. Phys. **51**, 1638 (1969).
18. C. A. PARR, J. C. POLANYI, and W. H. WONG. J. Chem. Phys. **58**, 5 (1973).
19. J. C. POLANYI and W. H. WONG. J. Chem. Phys. **51**, 1439 (1969).

Can. J. Chem. Downloaded from www.nrcresearchpress.com by 210.87.254.40 on 09/05/12
For personal use only.

Can. J. Chem. Downloaded from www.nrcresearchpress.com by 210.87.254.5 on 09/05/12
For personal use only.

Conformational Isomerism and Oriented Polycrystal Formation of Dimethyl Carbonate[1]

J. E. KATON AND MARK D. COHEN

Department of Chemistry, Miami University, Oxford, Ohio 45056

Received February 5, 1974

It has been found that dimethyl carbonate exists in the liquid phase as a conformational equilibrium mixture. The conformers differ by rotation about the C—O bonds. The enthalpy difference of the two conformers is found experimentally to be 2.6 ± 0.5 kcal/mol. Dimethyl carbonate crystallizes in contact with alkali halide windows as an oriented polycrystalline film, as shown by polarized infrared spectra.

On trouve que les carbonate de méthyle existe à l'état liquide sous forme d'un mélange provenant d'un équilibre conformationnel. Les conformères diffèrent par la rotation autour des liens C—O. On a mesuré que la différence d'enthalpie des deux conformères serait de 2.6 ± 0.5 kcal/mol. Le carbonate de méthyle cristallise au contact d'une fenêtre d'halogénure alcalin sous forme d'un film polycristallin orienté; on a mis cette propriété en évidence par spectrométrie infrarouge polarisé. [Traduit par le journal]

Can. J. Chem., **52**, 1994 (1974)

Conformational isomerism in esters of organic carboxylic acids due to rotation about the C—O bond has been sought by many investigators. This area of research has been reviewed very recently by Jones and Owen (1). All detailed structural work on simple esters has indicated that they exist in the *cis* ester conformation and that there is no detectable amount of the *trans* conformer.

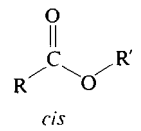

cis

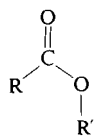

trans

Oki and Nakanishi (2) have presented evidence that *t*-butyl formate exists in a conformational equilibrium with the *cis* conformer being the more stable. This equilibrium has been confirmed by George *et al.* (3). Neither group detected evidence of a similar equilibrium in *t*-butyl acetate, however. In addition, Oki and Nakanishi (4) have reported that methyl *t*-butyl carbonate exists in a conformational equilibrium and that the *cis-trans* conformer (methyl group *cis*, *t*-butyl group *trans*) is more stable that the *cis-cis* conformer. Their data are not very conclusive, however.

We have recorded the infrared and Raman spectra of liquid dimethyl carbonate and the infrared spectra of crystalline dimethyl carbonate. Our results indicate that liquid dimethyl carbonate exists as a conformational equilibrium

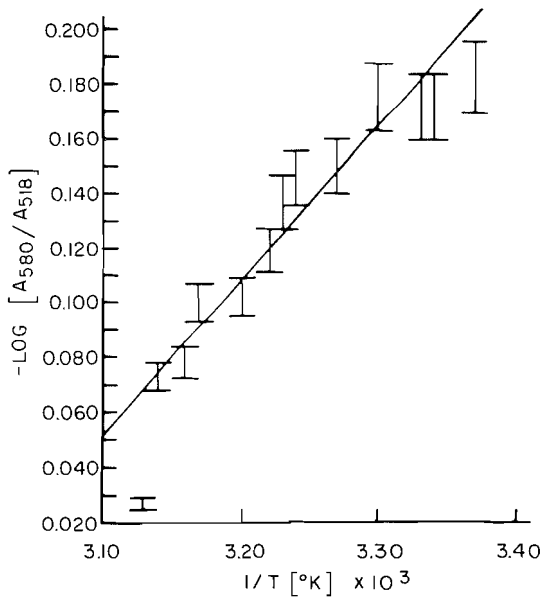

FIG. 1. Temperature dependence of the ratio of absorbances of the bands at 580 and 518 cm^{-1}.

[1]Supported in part by the U.S. Air Force under Contract No. F33715-73-C-5013.

Can. J. Chem. Downloaded from www.nrcresearchpress.com by 210.87.254.5 on 09/05/12
For personal use only.

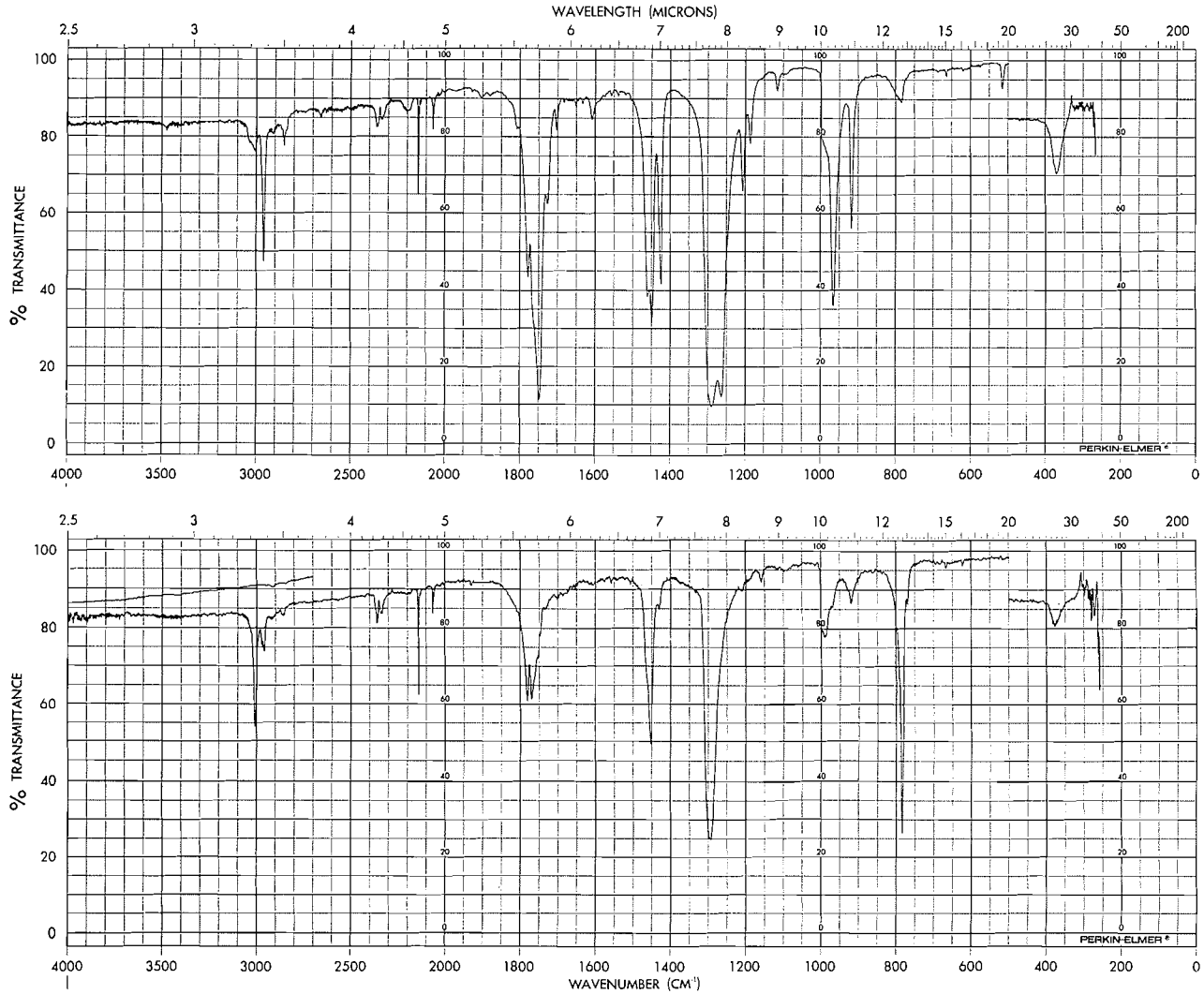

FIG. 2. Polarized infrared spectra of crystalline dimethyl carbonate at about −20 °C. The polarizer is oriented 90° apart in the upper and lower spectra.

mixture, although one conformer is present in quite low concentration. This indicates that simple esters are not locked into one conformation as has been proposed (see ref. 1) but that the relative energies of the two conformers differ so greatly in the simple esters that the concentration of the *trans* conformer is too small to be readily detected.

The infrared and Raman spectra of dimethyl carbonate in the vapor and liquid states have been reported (5) and are consistent only with the *cis-cis* structure. The Raman spectrum of the liquid has an unusual number of bands for one conformer, however. Comparison of the infrared spectrum of liquid dimethyl carbonate with that of the crystal shows that four weak bands disappear on crystallization. These occur at 1095, 863, 640, and 580 cm^{-1}. The liquid phase infrared spectrum was recorded on a Perkin-Elmer Model 180 spectrophotometer at a series of temperatures between 23 and 46 °C and the absorbance of the 580 cm^{-1} band compared with that of a band at 518 cm^{-1}. A graph of the log of the ratio of these two absorbances *vs.* $1/T$ is given in Fig. 1. The best straight line was drawn by the least-squares method and a slope of -0.568 ± 0.050 was obtained. This yields a value of ΔH of 2.60 ± 0.5 kcal/mol. The fact that such temperature dependence is obtained together with the fact that the 580 cm^{-1} band disappears on crystallization is strong evidence that it is associated with a second conformer. A Boltzmann distribution corresponding to this energy difference indicates a very low concentration of the second conformer (roughly 1%) but in dimethyl carbonate there exists a statistical weight factor which doubles this concentration, thereby making its detection more favorable.

Some time ago we reported that halogen containing organic molecules crystallized as oriented polycrystals when in contact with alkali halide windows and that this behavior was readily detected by infrared polarization studies (6). We have now found that a halogen atom is not necessary for this behavior to occur. Dimethyl carbonate exemplifies this behavior since it, too, readily crystallizes as an oriented polycrystalline film. Figure 2 shows the polarized infrared spectra of an oriented crystal film of dimethyl carbonate at about −20 °C. These spectra were obtained on a Perkin-Elmer Model 180 infrared spectrophotometer utilizing the standard polarizer accessory. The polarization is quite high indicating that orientation is quite high. Such behavior has also been found with other organic liquids which do not contain a halogen atom.

1. G. I. L. JONES and N. L. OWEN. J. Mol. Struct. **18**, 1 (1973).
2. N. OKI and H. NAKANISHI. Bull. Chem. Soc. Japan **43**, 2558 (1970).
3. W. O. GEORGE, D. V. HASSID, and W. F. MADDAMS, J. Chem. Soc. Perkin II, 952 (1973).
4. N. OKI and H. NAKANISHI. Bull. Chem. Soc. Japan **44**, 3419 (1971).
5. B. COLLINGWOOD, H. LEE, and J. K. WILMSHURST. Aust. J. Chem. **19**, 1637 (1966).
6. J. E. KATON, D. SINHA, M. G. GRIFFIN, and D. A. CONDIT, Can. J. Chem. **50**, 3255 (1972).

Can. J. Chem. Downloaded from www.nrcresearchpress.com by 210.87.254.5 on 09/05/12
For personal use only.

Selective-phase Ion Cyclotron Resonance Spectroscopy[1]

MELVIN B. COMISAROW AND ALAN G. MARSHALL
Department of Chemistry, University of British Columbia, Vancouver, Canada V6T 1W5

Received February 18, 1974

In-phase ("dispersion"), 90° out-of-phase ("absorption"), and "absolute-value" (square root of the sum of the squares of the "absorption" and "dispersion") ion cyclotron resonance (i.c.r.) spectra of CH_3^+ and CH_4^+ have been obtained by broad-band frequency-swept r.f. irradiation of an ionized methane sample, followed by broad-band detection, digitization of the transient i.c.r. response, Fourier transformation using a digital computer (1), and application of a linear phase correction across the F.t.-i.c.r. spectrum. The "absorption" spectrum is the same as would be obtained by conventional marginal-oscillator field-sweep i.c.r. detection and provides a means for identifying spurious "foldover" peaks; the "dispersion" response is not observable with a marginal oscillator detector. The principal advantages of the new "absolute-value" display are (*1*) the signal-to-noise ratio is significantly better than for the conventional "absorption" mode, at the expense of a slight broadening of the i.c.r. spectral line shape; and (*2*) "absolute-value" display will very likely be the method of choice in frequency-sweep F.t.-i.c.r. spectroscopy (2), in order to circumvent the complicated non-linear phase corrections which may otherwise be required to obtain an "absorption" mode display.

Les spectres de résonance ionique de cyclotron (r.i.c.) de CH_3^+ et CH_4^+ sont obtenus en phase ("dispersion"), déphasés de 90° ("absorption") et en "valeur absolue" (racine carrée de la somme des carrés de "l'absorption" et la "dispersion") par irradiation r.f. à bande large de balayage de fréquence d'un échantillon de méthane ionisé; on fait suivre d'une détection à bande large, d'une conversion numérique de la réponse r.i.c. temporaire, d'une transformation de Fourier utilisant un calculateur digital, et d'une application d'une correction linéaire de phase à travers le spectre F.t.-r.i.c. Le spectre "d'absorption" est le même que celui obtenu par une détection r.i.c. à balayage de champ d'un oscillateur marginal conventionnel; il fournit un moyen pour identifier des pics "de repli" parasites; la réponse de "dispersion" n'est pas observable avec un détecteur à oscillateur marginal. Les principaux avantages de l'étalement de la nouvelle "valeur absolue" sont: (*1*) le rapport signal-bruit est notablement meilleur que pour le mode conventionnel "d'absorption", aux dépens d'un léger élargissement de la forme de la raie spectrale du r.i.c.; et (*2*) l'étalement de la "valeur absolue" deviendra très probablement la méthode de choix en balayage de fréquence spectroscopique F.t.-r.i.c., afin d'éliminer les corrections compliquées de phase non-linéaire qui, autrement, peuvent être nécessaires à l'obtention d'un étalement de mode "d'absorption". [Traduit par le journal]

Can. J. Chem., **52**, 1997 (1974)

Prototype experiments (1, 2) have demonstrated that the frequency-sweep Fourier transform ion cyclotron resonance (F.t.-i.c.r.) technique provides a feasible means for obtaining i.c.r. spectra of specified signal-to-noise ratio and mass resolution, over a wide mass range, in an observation period which is two orders of magnitude shorter than that required in conventional i.c.r. mass spectroscopy. Now in conventional i.c.r. detection, a marginal oscillator operating at constant frequency (while the magnetic field is varied to bring different ions into resonance) effectively selects just the i.c.r. response which is 90° out-of-phase with the exciting radiation, and thus an "absorption"-mode spectral display is always obtained (3). However, in a typical F.t.-i.c.r. experiment, the phase of the i.c.r. signal depends on its location in the frequency spectrum in a reproducible but initially unknown fashion. The etiology and treatment of this condition will now be outlined, along with an additional optimization (use of absolute-value mode of spectral display) of signal-to-noise ratio which becomes possible with the F.t.-i.c.r. technique.

The F.t.-i.c.r. technique is based on a short-duration excitation (2) of i.c.r. responses over a given mass range, followed by detection and digitization of the i.c.r. transient response, with subsequent Fourier transformation of that digitized transient in a digital computer. Since the computer actually carries out both the sine and cosine transforms (4), the Fourier transformation

[1]Work supported by grants from the National Research Council of Canada (A 6614 and A 6178) and the Committee on Research, University of British Columbia (21-9220 and 21-9236).

Can. J. Chem. Downloaded from www.nrcresearchpress.com by 210.87.254.6 on 09/05/12
For personal use only.

Can. J. Chem. Downloaded from www.nrcresearchpress.com by 210.87.254.6 on 09/05/12
For personal use only.

process produces two (frequency-domain) spectra, each containing half as many points as the original (time-domain) transient. Ideally, these two spectra would correspond to the i.c.r. response which is either in-phase ("dispersion") or 90° out-of-phase ("absorption") with respect to an ordinary continuous-wave excitation at the resonant i.c.r. frequency for each ion. However in F.t.-i.c.r., the acquisition of i.c.r. transient response data begins *after* a fixed delay time, T_D, following completion of the excitation. Since that delay time corresponds to a number of cycles (and thus a number of degrees of phase angle) which is directly related to the frequency of the signal being digitized, it is logical that the frequency response resulting from Fourier transformation of that delayed transient will exhibit a phase shift which varies linearly across the frequency spectrum. The proper linear combination of sine and cosine transforms which generates a response of desired phase can be determined quickly by trial and error, using a simple first order phase correction (5); the F.t.-i.c.r. frequency spectrum will then consist of signals, all of which have the *same* phase. However, since the *initial* phase (*i.e.*, the phase angle at the beginning of the i.c.r. transient) is still arbitrary, it will in general be necessary to apply a further "zero-order" phase correction, which causes the same phase shift for each data point in the frequency spectrum. When the remaining electronics (r.f. transmitter, broad-band detector and amplifier, filter, etc.) exhibit constant or linear phase characteristics, or when the i.c.r. spectrum consists of two or fewer ions of different mass (as in the present example), it is always possible to produce an F.t.-i.c.r. spectrum of either all "absorption" or all "dispersion" signals. Because of the exceedingly large frequency bandwidth (50 kHz to 2 MHz for mass 15 to mass 500 at 2 tesla) in i.c.r., it is likely that such constant or linear phase conditions will not be met, and thus it may not always be possible to obtain a uniform "absorption" or "dispersion" frequency display.

The most obvious solution to the preceding dilemma is to compute the absolute-value spectrum, that is, the response which is obtained from the point-by-point square root of the sum of the squares of the sine and cosine transforms: the absolute-value spectrum will thus be completely insensitive to phase irregularities in the digitized i.c.r. response.

In order to demonstrate the above procedures, experimental i.c.r. data was generated as follows. CH_3^+ and CH_4^+ ions were created by application of a 70 eV electron beam pulse of 0.5 μA for 5 ms, to a sample of methane at 8×10^{-7} Torr. Ion cyclotron motion for both ions was excited by a 2.2 ms, 400 mV (p–p) r.f. electric field pulse whose frequency varied linearly from 100 to 200 kHz (bracketing the i.c.r. frequencies for CH_3^+ and CH_4^+ at 0.16 tesla) during the irradiation interval. The transient i.c.r. response voltage induced at the i.c.r. cell plates following the excitation pulse was then amplified by a broad-band (10 kHz to 3 MHz) r.f. amplifier, and mixed with the output of a second r.f. oscillator. The difference frequency, extracted with a 19 kHz low-pass filter, was then suitable for dig-

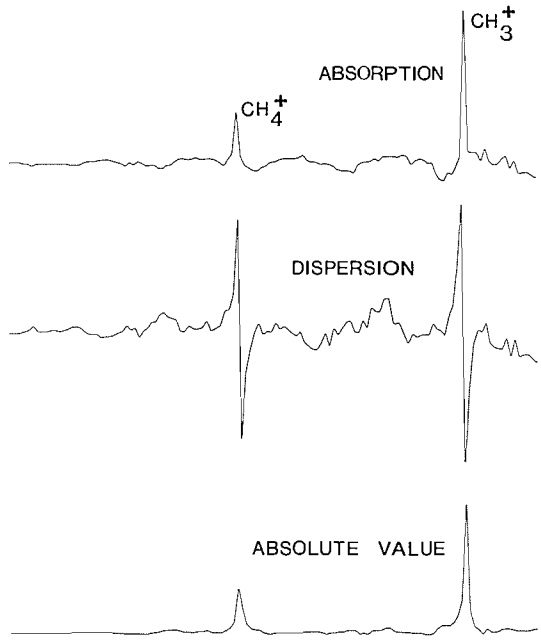

FIG. 1. Fourier transform ion cyclotron resonance spectra. Each spectrum was obtained by carrying out a discrete Fourier transformation on the same digitized 256-point i.c.r. transient response excited by a frequency-swept r.f. irradiation (see text). The top trace represents the i.c.r. response which is uniformly 90° out-of-phase with the excitation; middle trace is the in-phase response; bottom trace is the (point-by-point) square root of the sum of the squares of the two preceding traces. The spectral width is approximately 25 kHz, with zero frequency at the right. The reduction in intensity of the i.c.r. signal at higher displayed frequency (CH_4^+) is an artifact due to attenuation by the digitizer; the actual amplitudes of both i.c.r. signals would otherwise be about the same.

itizing at 50 kHz; discrete Fourier transformation of the digitized transient was then carried out by a digital computer, with the zero- and first-order phase corrections discussed above, to produce the three spectra shown in Fig. 1.

There are three significant uses for the phase-corrected F.t.-i.c.r. spectral display modes illustrated in Fig. 1. First, when it is possible to obtain a display exhibiting all "absorption" signals, for example, then the presence of any i.c.r. signals which are "folded-in" from higher frequency (6) is readily detected by their anomalous phase: this consideration may prove to be quite useful in cases for which only a segment of the total i.c.r. spectrum has been selected for examination. Second, the absolute-value display exhibits significantly better signal-to-noise than does the "absorption" display, at the cost of a slightly increased apparent i.c.r. line width: this feature should substantially reduce the number of transients which must be accumulated in signal-averaged F.t.-i.c.r. (7) using absolute-value spectral display. Finally, because the phase behavior across the i.c.r. spectrum is very likely to be non-linear, the absolute-value display will circumvent the otherwise time-consuming process of finding the phase corrections which are required to produce an F.t.-i.c.r. spectrum consisting of all "absorption" or all "dispersion" signals.[2]

The authors wish to express their thanks to C. E. Brion for his kind loan of the signal-averager (analog-to-digital converter plus memory) used in this study.

1. M. B. COMISAROW and A. G. MARSHALL. Chem. Phys. Lett. In press.
2. M. B. COMISAROW and A. G. MARSHALL. Chem. Phys. Lett. In press.
3. A. ABRAGAM, The principles of nuclear magnetism. Oxford, Clarendon Press. 1962. p. 78.
4. J. W. COOLEY and J. W. TUKEY. Math. Comp. **19**, 297 (1965).
5. J. W. COOPER, NIC-80/S-7202-D Computer Manual, Nicolet Instrument Corporation, 5225 Verona Road, Madison, Wisconsin 53711.
6. R. BRACEWELL. The Fourier transform and its applications. McGraw-Hill Book Co., New York. 1965.
7. M. B. COMISAROW and A. G. MARSHALL. To be published.
8. (*a*) D. WOBSCHALL, J. R. GRAHAM, and D. P. MALONE. Phys. Rev. **131**, 1565 (1963). (*b*) C. P. SLICHTER. Principles of magnetic resonance. Harper and Row. New York. 1963. pp. 28–44.

[2]For a discussion of dispersion and absorption modes in i.c.r. see ref. 8*a*, for a more general discussion with application to magnetic resonance, see ref. 8*b*.

Can. J. Chem. Downloaded from www.nrcresearchpress.com by 210.87.254.6 on 09/05/12
For personal use only.

Can. J. Chem. Downloaded from www.nrcresearchpress.com by 210.87.254.42 on 09/05/12
For personal use only.

Canadian Journal of Chemistry

Published by
THE NATIONAL RESEARCH COUNCIL OF CANADA

Journal canadien de chimie

Publié par
LE CONSEIL NATIONAL DE RECHERCHES DU CANADA

Volume 52 Number 11 June 1, 1974 Volume 52 numéro 11 1 juin 1974

Kinetics of Oxidation of Ferrocyanide by Iodate Ion

Y. SULFAB[1] AND (IN PART) HAMID A. ELFAKI

Chemistry Department, University of Khartoum, Khartoum, Sudan

Received April 30, 1973[2]

Y. SULFAB and HAMID A. ELFAKI. Can. J. Chem. **52**, 2001 (1974).

In the presence of vast excess of ferrocyanide, over the p*H* range 1.76–2.65, the reaction between iodate and ferrocyanide ions follows the rate law

$$\frac{-d[IO_3^-]}{dt} = \frac{k_a[H^+] + k_b[H^+]^2}{1 + K_1[H^+]}[Fe(CN)_6^{4-}][IO_3^-]$$

where k_a and k_b have values of $1.97 \times 10^3\ M^{-2}\ min^{-1}$ and $4.08 \times 10^5\ M^{-3}\ min^{-1}$, respectively, at an ionic strength of 1.18 *M* and a temperature of 25.0 ± 0.1 °C. K_1 is the formation constant of monoprotonated ferrocyanide. The "overall activation energy" of the reaction was found to be 15.8 kcal/mol. Rate-determining steps consistent with the kinetics have been proposed.

Y. SULFAB et HAMID A. ELFAKI. Can. J. Chem. **52**, 2001 (1974).

En présence d'un grand excès de ferrocyanure, à des pH allant de 1.76 à 2.65, l'équation de vitesse pour la réaction de l'iodate avec les ions ferrocyanures est

$$\frac{-d[IO_3^-]}{dt} = \frac{k_a[H^+] + k_b[H^+]^2}{1 + K_1[H^+]}[Fe(CN)_6^{4-}][IO_3^-]$$

dans laquelle k_a et k_b valent respectivement $1.97 \times 10^3\ M^{-3}\ min^{-1}$ et $4.08 \times 10^5\ M^{-3}\ min^{-1}$ pour une force ionique de 1.18 *M* et une température de 25.0 ± 0.1 °C. K_1 est la constante de formation du ferrocyanure monoprotoné. On a trouvé que l'énergie d'activation globale est égale à 15.8 kcal/mol. On propose des étapes qui pourraient contrôler la vitesse de la réaction et qui seraient en accord avec les données cinétiques. [Traduit par le journal]

Introduction

Oxidation of a number of metal ion complexes by the ClO_3^- ion in aqueous acidic solutions, have often invoked the suggestion that these reactions proceed via inner-sphere mechanisms (1). The observations (2, 3) that the ClO_3^- ion fails to oxidize the substitution-inert complexes, $(Fe(phen)_3^{2+})$ and $(Fe(CN)_6^{4-})$, supports the suggested mechanism. The behavior of the analogous IO_3^- ion is reported in this paper. It seems that the side reactions between iodide–iodate and iodide–ferricyanide as well as those between iodide and all the possible iodine oxidants produced during the course of reaction, have kept researchers from investigating the kinetics of this reaction, save a report by Reynolds (4) in his study of oxidation of $(Fe(CN)_6^{4-})$ by aqueous iodine.

[1]Present address: Chemistry Department, Kuwait University, Kuwait, Arabia.

[2]Revision received January 14, 1974.

Can. J. Chem. Downloaded from www.nrcresearchpress.com by 210.87.254.42 on 09/05/12
For personal use only.

Experimental

Analytical grade $K_2Fe(CN)_6 \cdot 3H_2O$ and KIO_3 were used without further recrystallization. A stock solution of KIO_3 was prepared according to Vogel (5), from which all dilutions were made up. Buffer solutions were made up from sodium hydrogen sulfate and sodium sulfate of known concentrations. Acetate and phosphate buffers were avoided, since these are known to catalyze the iodide–iodate reaction (6). Analytical grade $NaNO_3$ was used to keep the ionic strength constant in the different buffer solutions.

Boiled-out double-distilled water through which nitrogen was bubbled while cooling it to room temperature was used as a solvent and in all dilutions. Ferrocyanide solutions were used immediately after they were prepared.

An indented flask was used as a reaction vessel. With equal volumes of buffer and iodate solutions of known concentration in one compartment and ferrocyanide in the other, the vessel was allowed to stand for more than 30 min in a thermostat before the reactants were thoroughly mixed, and some of the reaction mixture quickly transferred to an absorption cell. The absorbance of the produced ferricyanide was then followed with time on a Unicam SP 700 spectrophotometer at 420 mμ. At this wavelength all the other species have negligible absorbance. The temperature was maintained constant in the cell-holder of the spectrophotometer by circulating water from the thermostat through the cell-holder cavity. The pH of the reaction mixtures was measured on a Pye pH meter Model 290.

Results

The stoichiometry of reaction 1

$$[1]\quad 6Fe(CN)_6^{4-} + IO_3^- + 6H^+ = 6Fe(CN)_6^{3-} + I^- + 3H_2O$$

was verified by observing the amount of ferricyanide produced at infinite time. The amount of ferricyanide produced agreed with that predicted from reaction 1. The ratio of ferricyanide formed to iodate initially present ranged from 5.93–6.00 at high ferrocyanide concentration.

It was found impossible to follow the reaction at relatively high iodate ion concentration ($5.0 \times 10^{-4}\ M$) and relatively low ferrocyanide ion concentration ($5.0 \times 10^{-4}\ M$) at pH 2.00 and ionic strength 1.18. Under such conditions autocatalysis is immediate. However, in the presence of vast excess of ferrocyanide over the iodate ion, the reaction follows first order kinetics over the iodate ion concentration 2.66×10^{-4} to $5.0 \times 10^{-5}\ M$. Plots of log $[IO_3^-]$ against time were typical first order curves to beyond 50% of reaction. The region over which the curve is linear decreases with increase of the initial iodate concentration and autocatalysis becomes evident. The pseudo first order rate constant (k_1 min^{-1}), as shown in Table 1, has an average value of 0.195 ± 0.004 min^{-1} under the specified conditions. Table 2 shows that the pseudo first order rate constant (k_1 min^{-1}) varies linearly with ferrocyanide concentration, thus showing a first order dependence on the total ferrocyanide ion concentration. The value of k_2 was obtained from $k_1/[Fe(CN)^{4-}]$.

In Table 3, variation of k_1 min^{-1} with the variation of pH, when all other factors are kept constant, is presented. Column 4 in Table 3 shows that the reaction is of the first order in $[H^+]$. k_3 is obtained from $k_1/[Fe(CN)_6^{4-}][H^+]$. It is, therefore, concluded that the kinetics of oxidation of ferrocyanide by iodate ions in aqueous acidic solutions follow the rate law [2].

$$[2]\quad \frac{-d[IO_3^-]}{dt} = k_3[IO_3^-][H^+][Fe(CN)_6^{4-}]$$

The results in Table 4 show that the rate of

TABLE 1. Order with respect to iodate ion*

$[IO_3^-]_0 \times 10^5$ (M)	$k_1 \times 10$ (min^{-1})
5.0	1.99
10.0	1.97
13.3	1.98
20.0	1.91
26.6	1.93

*$[Fe(CN)_6^{4-}]_0 = 1.00 \times 10^{-2}\ M$, p$H$ = 2.00, $T = 25.0 \pm 1$ °C, $\mu = 1.18\ M$.

TABLE 2. Variation of k_1 min^{-1} with $[Fe(CN)_6^{4-}]_0$*

$[Fe(CN)_6^{4-}]_0 \times 10^3$ (M)	k_1 (min^{-1})	k_2 (M^{-1} min^{-1})
4.0	0.079	19.8
6.5	0.124	19.1
8.0	0.160	20.0
10.0	0.195	19.5

*$[IO_3^-]_0 = 1.0 \times 10^{-4}\ M$, p$H$ = 2.00, $T = 25.0 \pm 0.1$ °C, $\mu = 1.18$.

TABLE 3. Variation of k_1, k_2, k_3 with pH

pH	k_1 (min^{-1})	k_2 (M^{-1} min^{-1})	$k_3 \times 10^{-3}$ (M^{-2} min^{-1})
1.769	0.326	32.6	1.92
2.00	0.195	19.5	1.95
2.102	0.151	15.1	1.91
2.245	0.109	10.9	1.90
2.645	0.044	4.4	1.94

*$[Fe(CN)_6^{4-}]_0 = 1.0 \times 10^{-2}\ M$, $[IO_3^-]_0 = 1.0 \times 10^{-4}\ M$, $T = 25.0 \pm 0.1$ °C, $\mu = 1.18$.

Can. J. Chem. Downloaded from www.nrcresearchpress.com by 210.87.254.42 on 09/05/12
For personal use only.

TABLE 4. Variation of the reaction rate with ionic strength

pH	μ	$k_3 \times 10^{-3}$ M^{-2} min^{-1}
2.00	1.18	1.92
1.844	0.955	2.18
1.955	0.733	2.35
2.095	0.511	2.78
2.40	0.288	3.44

*$[Fe(CN)_6^{4-}]_0 = 1.0 \times 10^{-2}$ M, $[IO_3^-]_0 = 1.0 \times 10^{-4}$ M, $T = 25.0 \pm 0.1$ °C.

TABLE 5. Influence of temperature on reaction rate

T (°C)	k_1 (min^{-1})
23.0	0.164
25.0	0.192
27.5	0.244
30.0	0.306
35.0	0.449

*$[Fe(CN)_6^{4-}]_0 = 1.0 \times 10^{-2}$ M, $[IO_3^-]_0 = 1.0 \times 10^{-4}$ M, $\mu = 1.18$, $pH = 2.00$.

the reaction increases with decrease of ionic strength. This, however, is not the expected behavior for a reaction between similarly charged ions and probably indicates a complicated mechanism. The variation of the reaction rate with temperature is shown in Table 5. The activation energy of the reaction as obtained from a plot of log k_1 *vs.* $1/T$ was found to be 15.8 kcal/mol.

Discussion

It has been known (7) for some time that ferrocyanide ions are extensively protonated in aqueous acidic solutions to form $HFe(CN)_6^{3-}$ and $H_2Fe(CN)_6^{2-}$. The thermodynamic dissociation constants of the mono- and diprotonated species are reported (8, 9) as 5.25×10^{-5} and 4.3×10^{-3} M at 25 °C, respectively. Lavison and Marcus (10) have determined these dissociation constants at $\mu = 1.0$ M and a temperature of 25 °C as 4.68×10^{-3} M and 0.32 M for the mono- and diprotonated species, respectively. The values of the dissociation constants at $\mu = 1.0$ M, $T = 25$ °C show that over the pH range 1.7–2.6, which corresponds to our acid variation, the monoprotonated species concentration varies from about 75–32% and that of the diprotonated species varies from about 4–0.2% of the total ferrocyanide initially present.

It is also known (11) that the iodate ion is appreciably protonated in aqueous acidic solutions and has a thermodynamic dissociation constant of 0.16 M at 25 °C. The value of the dissociation constant at $\mu = 1.0$ M, $T = 25$ °C is reported (12) as 0.514 M. Thus at our highest acid concentration about 3% of the total iodate is protonated.

From the above discussion it seems reasonable to suggest that the pre-equilibria [3–5]

[3] $$H^+ + Fe(CN)_6^{4-} \rightleftharpoons HFe(CN)_6^{3-} \quad K_1$$

[4] $$H^+ + HFe(CN)_6^{3-} \rightleftharpoons H_2Fe(CN)_6^{2-} \quad K_2$$

[5] $$H^+ + IO_3^- \rightleftharpoons HIO_3 \quad K'$$

play an important role in the kinetics of this reaction. The formation constants K_1, K_2, and K' have the values 214, 3.1, and 1.94 M^{-1} at $\mu = 1.0$ M and $T = 25$ °C, respectively. These values will not be far off if used at our ionic strength of 1.18 M.

We suggest [6–11] as possible rate-determining steps for the ferrocyanide–iodate reaction.

[6] $$Fe(CN)_6^{4-} + IO_3^- \xrightarrow{k_6} \text{Products}$$

[7] $$HFe(CN)_6^{3-} + IO_3^- \xrightarrow{k_7} \text{Products}$$

[8] $$Fe(CN)_6^{4-} + HIO_3 \xrightarrow{k_8} \text{Products}$$

[9] $$H_2Fe(CN)_6^{2-} + IO_3^- \xrightarrow{k_9} \text{Products}$$

[10] $$HFe(CN)_6^{3-} + HIO_3 \xrightarrow{k_{10}} \text{Products}$$

[11] $$H_2Fe(CN)_6^{2-} + HIO_3^- \xrightarrow{k_{11}} \text{Products}$$

From these steps the rate of the reaction may be expressed as in eq. 12

[12] $$\text{Rate} = \frac{k_6 + k_7K_1[H^+] + k_8K'[H^+] + k_9K_1K_2[H^+]^2 + k_{10}K_1K'[H^+]^2 + k_{11}K_1K_2K'[H^+]^3}{(1 + K_1[H^+] + K_1K_2[H^+]^2)(1 + K'[H^+])} \times [Fe(CN)_6^{4-}]_0[IO_3^-]_0$$

Thus from eq. [12] the reaction shows first order dependence on both ferrocyanide and iodate ions. The dependence of the second order rate constant k_2 on H^+ ions can be written as in eq. 13.

$$[13] \quad k_2 = \frac{k_b + (k_7K_1 + k_8K')[H^+] + (k_9K_1K_2 + k_{10}K_1K')[H^+]^2 + k_{11}K_1K_2K'[H^+]^3}{(1 + K_1[H^+] + K_1K_2[H^+]^2)(1 + K'[H^+])}$$

k_6 in eq. 13 may be taken as equal to zero since our results in Table 3 show that at $[H^+] = 0$, $k_2 = 0$. Furthermore the factors $K_1K_2[H^+]^2$ and $K'[H^+]$ in the denominator can be neglected as they are very small at our employed $[H^+]$. These approximations lead to eq. 14

$$[14] \quad k_2 = \frac{k_a[H^+] + k_b[H^+]^2 + k_c[H^+]^3}{1 + K_1[H^+]}$$

where

$$[15] \quad k_a = k_7K_1 + k_8K'$$

$$[16] \quad k_b = k_9K_1K_2 + k_{10}K_1K'$$

and

$$[17] \quad k_c = k_{11}K_1K_2K'$$

Equation 14 may be rearranged as in eq. 18

$$[18] \quad \frac{k_2(1 + K_1[H^+])}{[H^+]} = k_a + k_b[H^+] + k_a[H^+]^2$$

The plotting of $k_2(1 + K_1[H^+])/([H^+])$ *vs.* $[H^+]$ would give a straight line, with an intercept and a slope equal to k_a and k_b, respectively, only if the term $k_c[H^+]^2$ in eq. 18 is negligible. Our results in Table 3 when treated in this way give Fig. 1 from which $k_a = 1.97 \times 10^3\ M^{-2}\ min^{-1}$ and $k_b = 4.08 \times 10^5\ M^{-3}\ min^{-1}$. Thus, it could be concluded that reaction 11 is not of great importance under our experimental conditions and eq. 18 could be written as [19]

$$[19] \quad \frac{k_2(1 + K_1[H^+])}{[H^+]} = k_a + k_b[H^+]$$

which fits our kinetic results.

It is to be observed that it is not possible to distinguish either between paths [7] and [8] or between paths [9] and [10]. The fact that k_2 varies linearly with $[H^+]$ seems to be fortuitous.

The "overall activation energy" is most likely a composite figure with contributions from all rate-determining steps as well as the enthalpies of protonations of ferrocyanide and iodate ions.

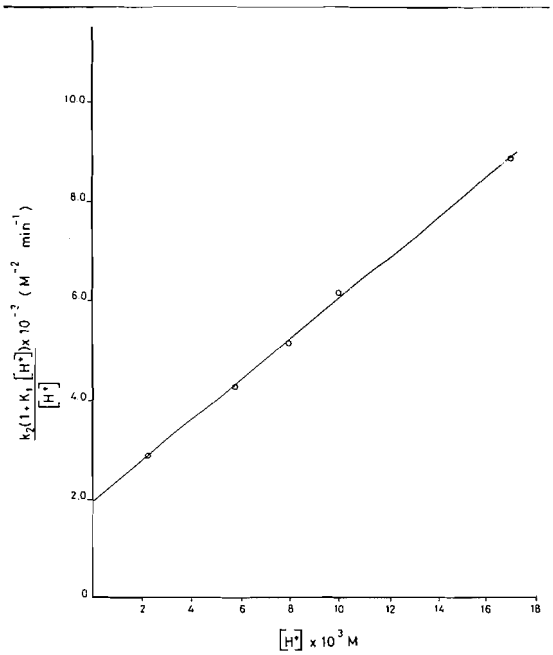

FIG. 1. Plot of $k_2(1 + K_1[H^+])/[H^+]$ *vs.* $[H^+]$. $\mu = 1.18\ M$, $T = 25\ °C$.

1. R. C. THOMPSON and G. GORDON. Inorg. Chem. **5**, 551, 562 (1965).
2. B. Z. SHAKHASHIRI and G. GORDON. J. Am. Chem. Soc. **91**, 1103 (1969).
3. Y. SULFAB and H. A. ELFAKI. Unpublished results.
4. W. L. REYNOLDS. J. Am. Chem. Soc. **80**, 1830 (1958).
5. A. I. VOGEL. A text book of quantitative inorganic Chemistry. 2nd ed. p. 360.
6. A. F. M. BARTON and G. A. WRIGHT. J. Chem. Soc. A, 2096 (1968).
7. I. M. KOLTHOFF. A. Anorg. Allg. Chem. **1**, 587 (1962).
8. J. JORDAN and G. J. EWING. Inorg. Chem. **1**, 587 (1962).
9. K. H. HSU and S. H. HO. Kexue Torgbao, 433 (1957) (Chem. Abs. 1961. 21953*b*).
10. S. A. LAVISON and R. A. MARCUS. J. Phys. Chem. **72**, 358 (1968).
11. A. D. PETHYBRIDGE and J. E. PRUE. Trans. Faraday Soc. **63**, 2019 (1967).
12. R. W. RAMETTE. J. Chem. Educ. **36**, 191 (1959).

Can. J. Chem. Downloaded from www.nrcresearchpress.com by 210.87.254.42 on 09/05/12
For personal use only.

Skeletal and Lattice Vibrations of Crystals of Dihalogenobis(pyridine)zinc(II)[1]

P. T. T. WONG

Division of Chemistry, National Research Council of Canada, Ottawa, Canada K1A 0R9

Received October 9, 1973

P. T. T. WONG. Can. J. Chem. **52**, 2005 (1974).

Detailed measurements of the low-frequency Raman spectra of the crystals of $[ZnPy_2Cl_2]$ and $[ZnPy_2Br_2]$ at room temperature, where Py is the pyridine molecule, and the far-infrared spectrum of the crystal of $[ZnPy_2Cl_2]$ at liquid nitrogen temperature have been made. The vibrational frequencies for the single molecule and for the complete crystal of these two complexes have been calculated and compared with the observed spectra, and the distribution of the potential energy of the normal modes has also been calculated to assist the refinement of the calculation and the interpretation of the spectra. Apparently, the skeletal Zn–ligand vibrations of the individual molecule couple with the lattice vibrations in the crystal, except for the normal modes at 326 cm^{-1} for $[ZnPy_2Cl_2]$ and at 250 cm^{-1} for $[ZnPy_2Br_2]$ which are dominated by the Zn–halogen stretching vibrations. Reasonably good Zn–ligand stretching force constants were obtained. The nature of the coordination bonds of these complexes has been discussed.

P. T. T. WONG. Can. J. Chem. **52**, 2005 (1974).

Des mesures détaillées de spectres Raman à basse fréquence sont faites pour des cristaux de $[ZnPy_2Cl_2]$ et $[ZnPy_2Br_2]$, à température de la pièce, et de spectres dans l'infra-rouge lointain du cristal $[ZnPy_2Cl_2]$, à température de l'azote liquide (Py: molécule de pyridine). Les fréquences vibrationnelles pour une molécule unique et pour le cristal entier de ces deux complexes sont calculées et comparées avec les spectres observés; la distribution de l'énergie potentielle des modes normaux est aussi calculée pour aider à l'étude plus fine du calcul et de l'interprétation des spectres. Apparemment, les vibrations du lien Zn–ligand du squelette de la molécule individuelle s'associent avec les vibrations du réseau dans le cristal à l'exception des modes normaux à 326 cm^{-1} pour $[ZnPy_2Cl_2]$ et à 250 cm^{-1} pour $[ZnPy_2Br_2]$ qui sont dominés par les vibrations d'élongation du lien Zn–halogène. On en déduit des constantes de force raisonnables pour l'élongation du lien Zn–ligand. La nature des liaisons de coordination de ces complexes est discutée.

[Traduit par le journal]

Introduction

The far-infrared spectra of the crystals of dichlorobis(pyridine)zinc(II), $[ZnPy_2Cl_2]$, and dibromobis(pyridine)zinc(II), $[ZnPy_2Br_2]$, at room temperature have been previously reported (1). A tentative interpretation for the metal–ligand skeletal modes was made on the basis of the frequency shift of the halogen sensitive bands. Those bands which were in the same frequency region for both compounds were assigned to the Zn–Py stretching and bending modes.

Recently, Nakamoto and co-workers (2) attempted to make an assignment for the Zn—Py vibrations of the $[ZnPy_2Cl_2]$ complex based on the isotope shift by using the zinc isotopes, ^{65}Zn and ^{68}Zn.

Obviously, neither of these methods is satisfactory. In both methods a gaseous molecule model was assumed, the interpretation was made on the basis of purely metal–ligand skeletal vibrations, and the effects of the lattice vibrations on the skeletal modes were neglected. The skeletal vibrational frequencies of the zinc complexes are below 350 cm^{-1} and the frequencies of the lattice vibrations of these crystals are also in this frequency region. It follows that the coupling between the skeletal and the lattice vibrations to some extent is expected. Therefore, to interpret correctly the metal–ligand vibrations of these crystals the vibrational modes of the crystal as a whole instead of the isolated molecule should be considered.

In the present work the detailed low-frequency Raman spectra of the crystals of the $[ZnPy_2Cl_2]$ and $[ZnPy_2Br_2]$ complexes at room temperature and the far-infrared spectrum of the crystal of the $[ZnPy_2Cl_2]$ complex at liquid nitrogen temperature were measured, and an attempt has been made to demonstrate the significant contribution of the lattice interaction to these low-frequency spectra. Spectra of the solutions of

[1]NRCC No. 13868.

Can. J. Chem. Downloaded from www.nrcresearchpress.com by 210.87.254.6 on 09/05/12
For personal use only.

Can. J. Chem. Downloaded from www.nrcresearchpress.com by 210.87.254.6 on 09/05/12
For personal use only.

TABLE 1. Observed and calculated frequencies for $[ZnPy_2Cl_2]$

	ν_{obs} (cm^{-1})			ν_{calcd} (cm^{-1})			
		Infrared					
Vibration	Raman	Reference 1	This work (100°K)	Crystal	Molecule	Molecular mode	Molecular assignment
ν_1	326.3	324.6	331.0	327.1, 327.1, 326.3, 326.3	325.7	(B_1)	Zn—Cl st.
ν_2	292.0	292.4	296.6	291.7, 291.6, 291.5, 291.4	287.3	(A_1)	Zn—Cl st., Cl—Zn—Cl bend.
ν_3	221.6	219.2	229.0	225.2, 224.8, 223.1, 222.7	219.2	(B_2)	Zn—Py st., Cl—Zn—Py bend.
ν_4	206.4	—	—	214.9, 214.6	—		
ν_5	200.1	201.1	206.0	203.9, 203.6	202.6	(A_1)	Cl—Zn—Cl bend., Zn—Cl st.
ν_6	162.6	—	166.0	160.1	—		
ν_7	151.7	152.6	154.5	158.8	—		
ν_8	—	142.4	143.4	141.4, 138.1, 132.5, 129.0	134.8	(A_1)	Zn—Py st., Cl—Zn—Cl bend.
ν_9	109.7	109.6	112.5	115.8, 112.7, 109.7, 109.3	104.4	(B_1)	Cl—Zn—Py bend., Zn—Py st.
ν_{10}	107.0	—	—	107.5, 107.3, 105.4, 105.0	100.2	(A_2)	Cl—Zn—Py bend.
ν_{11}	101.5	100.6	97.3	103.8, 103.3, 98.7, 96.9	99.2	(B_2)	Cl—Zn—Py bend.
ν_{12}	93.9	—	—	91.5	—		
ν_{13}	83.3	—	—	84.8	75.8	(A_1)	Py—Zn—Py bend.
ν_{14}	80.1	79.5	74.3	79.4	—		
ν_{15}	77.3	—	—	77.5	—		
ν_{16}	69.7	—	—	62.7	—		
ν_{17}	—	62.0	61.4	58.6	—		
ν_{18}	44.0	—	47.0	46.5	—		
	—	—	—	45.9	—		
	—	—	—	38.4	—		
	—	—	—	37.8	—		
ν_{19}	—	35.0	35.5	36.6	—		
	—	—	—	35.3	—		
	—	—	—	32.3	—		
ν_{20}	29.6	—	—	30.7	—		
ν_{21}	21.7	—	—	26.4	—		
	—	—	—	17.4	—		
	—	—	—	14.3	—		
	—	—	—	13.6	—		
ν_{22}	12.5	—	—	12.4	—		
ν_{23}	5.6	—	—	4.6	—		
	—	—	—	4.6	—		
	—	—	—	1.2	—		
	—	—	—	0.9	—		

Can. J. Chem. Downloaded from www.nrcresearchpress.com by 210.87.254.6 on 09/05/12
For personal use only.

these complexes should provide some information for this investigation. Unfortunately the intensity of the metal–ligand modes is so weak that no useful spectrum of these complexes has been obtained for this purpose. The approach in the present work was to do a series of frequency calculations for the isolated molecules of the $[ZnPy_2Cl_2]$ and $[ZnPy_2Br_2]$ complexes and for the whole crystals of them taking the zero-wave-vector lattice modes into account. With reasonable variation and restriction of the force constants on the basis of the best chemical and physical knowledge of them, the variation of the calculated frequencies, the inconsistency between the calculated frequencies for the isolated molecule and the observed ones, the influence of the lattice vibrations on the metal–ligand skeletal modes, and the reproducibility of the observed spectra were investigated.

Experimental Methods and Results

The preparation and the chemical analysis of the zinc complexes $[ZnPy_2X_2]$, where X is Cl or Br, have been reported elsewhere (1, 3).

The Raman spectra of the polycrystalline samples in capillary tubes were recorded with a Jarrell–Ash model 25–300 laser Raman spectrometer consisting of a Coherent Radiation model 52 argon ion laser, a 25–100 Czerny–Turner double monochromator, an ITT FW–130 photomultiplier tube and an electron-pulse-counting readout system. The spectrometer was calibrated against the standard emission lines of the neon and mercury lamps and the exciting line.

The 488.0 nm line at a power ~1 W was used for most of the spectra, and the 514.5 nm line at a power ~1 W was used to check them. The Raman emission of the samples was collected at 90° to the incident beam. At least twenty spectra were recorded for each compound in order to verify the weak features. The spectral slit width was 0.5–2 cm^{-1} and the scanning speed was 5 cm^{-1} min^{-1}.

The Raman spectra of the $[ZnPy_2Cl_2]$ and $[ZnPy_2Br_2]$ crystals in the frequency region below 350 cm^{-1} are shown in Figs. 1 and 2, and the frequencies of the Raman bands are listed in Tables 1 and 2.

Twenty peaks and shoulders were observed in the Raman spectrum of $[ZnPy_2Cl_2]$ and sixteen in the spectrum of $[ZnPy_2Br_2]$. The strongest band for $[ZnPy_2Cl_2]$ is at 29.6 cm^{-1}

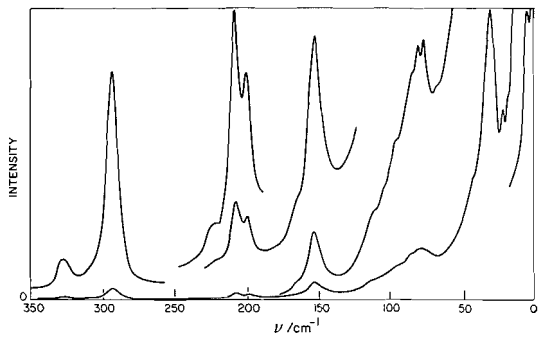

FIG. 1. The Raman spectrum of $[ZnPy_2Cl_2]$ crystal.

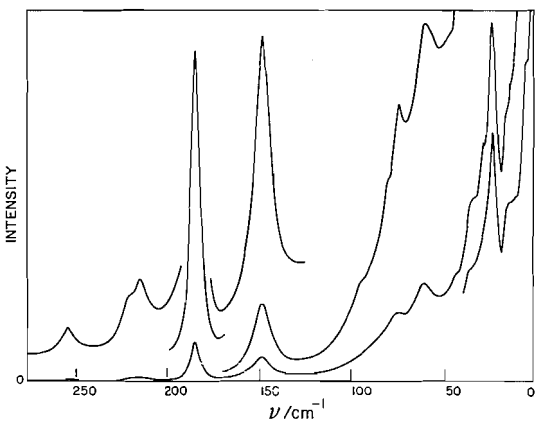

FIG. 2. The Raman spectrum of $[ZnPy_2Br_2]$ crystal.

and that for $[ZnPy_2Br_2]$ at 24.2 cm^{-1}. On the high frequency side of these bands there are three shoulders for $[ZnPy_2Br_2]$ and only one for $[ZnPy_2Cl_2]$, whereas on the low frequency side there are two sharp and weak peaks at 5.6 and 21.7 cm^{-1} and a shoulder at 12.5 cm^{-1} for $[ZnPy_2Cl_2]$, and the corresponding features for $[ZnPy_2Br_2]$ appear to be three shoulders at 3.9, 10, and 15 cm^{-1}. The three bands of highest frequency at 326.3, 292.0, and 221.6 cm^{-1} for $[ZnPy_2Cl_2]$, and 256.0, 221.6, and 218.0 cm^{-1} for $[ZnPy_2Br_2]$ are very weak. Two adjacent weak peeks at 206.4 and 200.1 cm^{-1} for $[ZnPy_2Cl_2]$ appear to be one band of intermediate intensity at 186.9 cm^{-1} in the spectrum of $[ZnPy_2Br_2]$. An intermediate band at 151.7 cm^{-1} for $[ZnPy_2Cl_2]$ has a shoulder on the high frequency side at 162.6 cm^{-1}. This band is asymmetric, and there could be an unresolved band on the low frequency side which corresponds to the infrared band at 142.4 cm^{-1}. A similar band is observed for $[ZnPy_2Br_2]$ at 150.5 cm^{-1} without any shoulder attached to it. A band at

Can. J. Chem. Downloaded from www.nrcresearchpress.com by 210.87.254.6 on 09/05/12
For personal use only.

TABLE 2. Observed and calculated frequencies for $[ZnPy_2Br_2]$

Vibration	ν_{obs} (cm^{-1})		ν_{calcd} (cm^{-1})			
	Raman	Infrared*	Crystal	Molecule	Molecular mode	Molecular assignment
ν_1	256.0	255.8	251.5, 251.5, 250.7, 250.7	249.0	(B_1)	Zn—Br st.
ν_2	221.6	—	227.2, 226.5, 226.3, 225.8	220.6	(A_1)	Zn—Br st., Br—Zn—Br bend.
ν_3	218.0	219.2	216.5, 216.5, 215.9, 215.9	212.5	(B_2)	Zn—Py st., Br—Zn—Py bend.
ν_4	186.9	—	178.1	—		
ν_5	—	183.1	176.3	—		
ν_6	150.5	151.1	140.8, 139.2	137.7	(A_1)	Zn—Py st., Zn—Br st.
ν_7	—	131.2	139.0, 137.2	—		
ν_8	—	104.4	101.6, 100.0	87.9	(A_1)	Br—Zn—Br bend., Zn—Py st.
ν_9	95.4	—	93.6, 93.5			
ν_{10}	82.7	—	91.0, 90.4, 84.8, 83.9	—		
ν_{11}	—	76.8	79.3, 77.4, 75.3, 74.0	—		
ν_{12}	75.4	—	71.2, 68.3, 66.7, 65.8	70.3	(B_1)	Br—Zn—Py bend.
ν_{13}	—	63.0	64.0	66.5	(A_2)	Br—Zn—Py bend.
	—	—	63.9	—		
ν_{14}	60.8	—	59.4	61.5	(B_2)	Br—Zn—Py bend.
	—	—	55.4	—		
ν_{15}	—	53.0	52.5	58.6	(A_1)	Py—Zn—Py bend.
ν_{16}	46.6	—	48.6	—		
	—	—	42.4	—		
	—	—	41.4	—		
	—	—	35.7	—		
	—	—	34.4	—		
ν_{17}	33.6	—	33.6	—		
	—	—	33.5	—		
ν_{18}	28.4	—	27.8	—		
ν_{19}	24.2	—	26.6	—		
	—	—	22.4	—		
ν_{20}	15.0	—	15.2	—		
	—	—	12.9	—		
ν_{21}	10.0	—	11.4	—		
	—	—	11.4	—		
ν_{22}	3.9	—	3.7	—		
	—	—	3.5	—		
	—	—	1.0	—		
	—	—	0.7	—		

*From ref. 1.

Can. J. Chem. Downloaded from www.nrcresearchpress.com by 210.87.254.6 on 09/05/12
For personal use only.

60.8 cm^{-1} for $[ZnPy_2Br_2]$ splits into two sharper bands at 80.1 and 77.3 cm^{-1} in the spectrum of $[ZnPy_2Cl_2]$. On the high frequency side of these bands, five shoulders are recognized for $[ZnPy_2Cl_2]$ and only two shoulders and a weak peak for $[ZnPy_2Br_2]$. On the low frequency side there is a shoulder for both $[ZnPy_2Cl_2]$ and $[ZnPy_2Br_2]$.

The far-infrared spectrum of the $[ZnPy_2Cl_2]$ crystal at ~ 100 °K was recorded in the frequency region 350–20 cm^{-1} with a Perkin–Elmer model 301 spectrophotometer which had been calibrated using water vapor, hydrogen cyanide, hydrogen chloride, and hydrogen bromide. The instrument was used in double beam mode in the frequency region 350–80 cm^{-1} and in single beam mode below 80 cm^{-1}. The resolution was about 2.5 cm^{-1}.

The sample for the far-infrared measurement was prepared as mull in Nujol with wedged high density polyethylene windows and was mounted on one of the sample holders in a multiple-sample low-temperature optical cell (4). On another sample holder, pure Nujol with the same wedged windows was mounted, which provided the background spectrum. The far-infrared spectra of the sample and the background were measured one after another by rotating the sample holder, and several spectra of both the sample and the background were recorded for each grating to verify the weak features. The spectrum of the $[ZnPy_2Cl_2]$ crystal obtained with the % transmittance scale was replotted on a linear optical density scale, after substracting the stray light and the background absorption by means of a computer program set up in this laboratory.

The far-infrared spectrum of $[ZnPy_2Cl_2]$ crystal at ~ 100 °K is shown in Fig. 3 and the frequencies of the observed bands are compared with those for room temperature in Table 1.

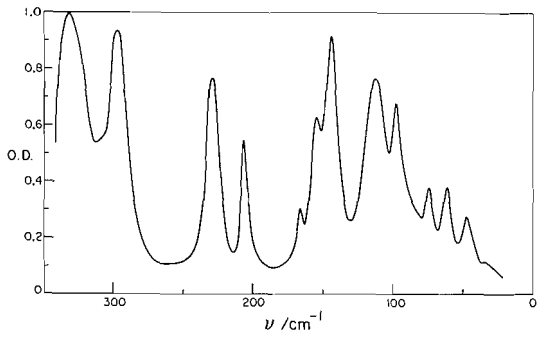

FIG. 3. The far-infrared spectrum of $[ZnPy_2Cl_2]$ crystal at 100 °K.

The half width of the infrared bands becomes narrower at 100 °K, and two new bands at 166 and 47 cm^{-1} are resolved. The room-temperature spectrum in the frequency region below ~ 100 cm^{-1} was poor (1), whereas at low temperature the features below 100 cm^{-1} became much better. At 100 °K the broad and weak band at 62 cm^{-1} of the room temperature spectrum is resolved into two sharp bands at 61.4 and 47 cm^{-1}, and the shoulder at ~ 100.6 cm^{-1} becomes a sharp band with the maximum at 97.3 cm^{-1}.

Analysis of the Spectra

Factor Group Analysis

The crystal structure of $[ZnPy_2Cl_2]$ has been reported by Porai-Koshits *et al.* on the basis of X-ray diffraction (5). The crystal belongs to the monoclinic-prismatic symmetry, $P2_1/c$ (C_{2h}^5), with four molecules per unit cell. The unit cell parameters are: $a = 8.44$ Å, $b = 17.5$ Å, $c = 8.25$ Å, and $\beta = 102°$. The determination of the structural parameters of the isolated molecule, $[ZnPy_2Cl_2]$, was not completed in their work and only the coordinates of the Zn atom and the two Cl atoms and the bond angles of Cl—Zn—Cl and N—Zn—Cl were given. No data concerning the Zn—N(ligand) distance and the positions of the pyridine rings in the molecule were reported.

The Zn—N(ligand) distances of a series of similar complex molecules of the tetrahedral configuration are 2.0–2.1 Å which are equal to the sum of the covalent radii (2.06 Å) within the limit of accuracy (6). Therefore in the present study the Zn—N distances in the $[ZnPy_2Cl_2]$ molecule are taken as 2.06 Å. Since previous studies showed that the coupling between the Zn—N vibration and the internal vibrations of the pyridine ring is negligible (1, 7, 8), the pyridine rings in the molecules will be considered as point masses at their center of gravity in the spectrum calculation in the following section. The coordinates of the two pyridine point masses of each molecule in the unit cell were calculated according to the coordinate system of Porai-Koshits *et al.* by means of a computer program.[2] The *b*-axis projection and the *c*-axis projection of the crystal structure are shown in Fig. 4.

Zannetti and Seppa (9) have also reported the crystal structure of $[ZnPy_2Cl_2]$ with slightly

[2]Supplied by Dr. E. J. Gabe, to whom I am indebted.

TABLE 3. Factor group analysis for optically active vibrations of $[ZnPy_2Cl_2]$ crystal

C_{2h}	Translational	Rotational	Pure translations	Skeletal	Spectral activity
A_g	3	3	0	9	Raman
B_g	3	3	0	9	Raman
A_u	2	3	1	9	Infrared
B_u	1	3	2	9	Infrared

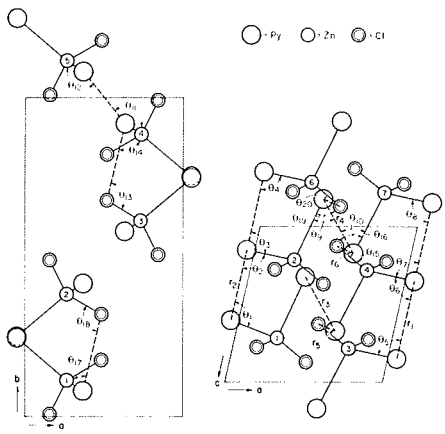

FIG. 4. The *c*-axis and *b*-axis projections of the structure of $[ZnPy_2Cl_2]$.

different parameters (a = 8.5 Å, b = 17.93 Å, c = 8.47 Å, β = 92°30′).

The result of the factor group analysis in Table 3 shows that $15A_g$ and $15B_g$ normal modes are Raman active, and $15A_u$ and $15B_u$ modes are infrared active, of which $6A_g$, $6B_g$, $5A_u$, and $4B_u$ normal modes belong to the lattice vibrations. However, since the lattice modes belong to the same symmetry classes as those of the skeletal modes, and their energy is close to some of the skeletal modes, coupling between them is expected. The symmetry analysis of the isolated $[ZnPy_2Cl_2]$ molecule shows that 9 skeletal vibrations are expected for each molecule, and they are classified as $4A_1$, $1A_2$, $2B_1$, and $2B_2$ symmetry species of the point group C_{2v}. All of them are Raman active, and 8 of them ($4A_1 + 2B_1 + 2B_2$) are infrared active. However, the molecules are all on C_1 sites in the crystal, and the A_2 mode becomes infrared active in the crystal.

Spectrum Calculation

The structural parameters of the $[ZnPy_2Cl_2]$ crystal reported by both Porai-Koshits *et al.* (5) and Zanetti and Seppa (9) are by no means precise. However, the structural parameters do not affect the calculated frequencies much. For instance, the change in the calculated frequencies with the error of 0.04 Å in the Zn—Cl distances is within 1 cm^{-1}. Therefore structural data of $[ZnPy_2Cl_2]$ and from Porai-Koshits *et al.* the Zn—N distance of 2.06 Å were adopted in the present calculation. Only those lattice potential constants for the atom pairs whose distances are shorter than 4.4 Å as shown by the projected dotted lines in Fig. 4 were taken into account in the calculation.

The Urey–Bradley force field of the following type was used to construct the $\mathbf{F}_R$ matrix in internal displacement coordinates,

$$
\begin{aligned}
2\bar{U} = {} & \sum_i \left[K_i + \sum_{j \neq i} (t_{ij}^2 F_{ij}' + s_{ij}^2 F_{ij}) \right] (\Delta r_i)^2 + \sum_{i<j} [H_{ij} - s_{ij}s_{ji}F_{ij}' + t_{ij}t_{ji}F_{ij}](r_{ij}\Delta\alpha_{ij})^2 \\
& + 2 \sum_{i<j} [-t_{ij}t_{ji}F_{ij}' + s_{ij}s_{ji}F_{ij}](\Delta r_i)(\Delta r_j) + 2 \sum_{i \neq j} [t_{ij}s_{ji}F_{ij}' + t_{ji}s_{ij}F_{ij}](r_j/r_i)^{1/2}(\Delta r_i)(r_{ij}\Delta\alpha_{ij}) \\
& + k_1[(\Delta r_1)^2 + (\Delta r_2)^2] + k_2[(\Delta r_3)^2 + (\Delta r_4)^2] + k_3[(\Delta r_5)^2 + (\Delta r_6)^2] \\
& + h_1[(\Delta\theta_1)^2 + (\Delta\theta_2)^2 + (\Delta\theta_3)^2 + (\Delta\theta_4)^2 + (\Delta\theta_5)^2 + (\Delta\theta_6)^2 \\
& + (\Delta\theta_7)^2 + (\Delta\theta_8)^2 + (\Delta\theta_9)^2 + (\Delta\theta_{10})^2 + (\Delta\theta_{11})^2 + (\Delta\theta_{12})^2] \\
& + h_2[(\Delta\theta_{13})^2 + (\Delta\theta_{14})^2 + (\Delta\theta_{15})^2 + (\Delta\theta_{16})^2 + (\Delta\theta_{17})^2 + (\Delta\theta_{18})^2 + (\Delta\theta_{19})^2 + (\Delta\theta_{20})^2]
\end{aligned}
$$

Can. J. Chem. Downloaded from www.nrcresearchpress.com by 210.87.254.6 on 09/05/12
For personal use only.

TABLE 4. Force constants for $[ZnPy_2X_2]$ crystals

Description	Symbol	$[ZnPy_2Cl_2]$ (mdyn Å^{-1})	$[ZnPy_2Br_2]$ (mdyn Å^{-1})
Zn—X stretching	K_1	1.13	0.922
Zn—Py stretching	K_2	0.68	0.73
X—Zn—X bending	H_1	0.23	0.075
Py—Zn—Py bending	H_2	0.085	0.085
X—Zn—Py bending	H_3	0.08	0.045
X---X repulsion	F_1	0.0055	0.022
Py---Py repulsion	F_2	0.0004	0.0004
X---Py repulsion	F_3	0.003	0.0112
Py---Py stretching	k_1	0.1	0.1
Py---Py stretching	k_2	0.12	0.12
X---Py stretching	k_3	0.32	0.65
Zn---Py---Py bending	h_1	0.02	0.02
Zn---Py---X bending Zn---X---Py bending	h_2	0.03	0.04

where

$$s_{ij} = (r_i - r_j \cos \alpha_{ij})/q_{ij}$$

$$s_{ji} = (r_j - r_i \cos \alpha_{ij})/q_{ij}$$

$$t_{ij} = (r_j \sin \alpha_{ij})/q_{ij}$$

$$t_{ji} = (r_i \sin \alpha_{ij})/q_{ij}$$

$$q_{ij} = r_i^2 + r_j^2 - 2r_i r_j \cos \alpha_{ij}$$

and K_{ij}, H_{ij}, and F_{ij} are the force constants of the skeletal bond stretching, angle bending, and repulsion between the nearest non-bonded atoms, respectively. The value of F_{ij}' was taken as $-0.1F_{ij}$ (11, 12). k and h are the lattice stretching and angle bending force constants, respectively. Totally thirteen force constants were introduced in the calculation, and their symbol and description are shown in Table 4.

The potential energy matrix $\mathbf{F_R}$ was transformed to the $\mathbf{F_X}$ matrix in Cartesian coordinates by means of the transformation matrix **B**, which was a 60 × 66 matrix. The $\mathbf{F_X}$ matrix thus obtained was a 60th-order matrix. The construction of the $\mathbf{F_R}$, the **B**, and the $\mathbf{F_X}$ matrices was carried out by means of the computer programs set up in this laboratory. The $\mathbf{G_X}$ matrix in Cartesian coordinates was a 60th-order diagonal matrix with the elements μ_1, μ_2, and μ_3 which are the reciprocal masses of Zn, Cl, and Py, respectively. These matrices are large, and they will not be reported in this paper, but are available from the author upon request.

The repulsion force constants F_1 and F_2 were obtained according to the Lennard–Jones 6–12 potential function as described by Shimanouchi and co-workers (13, 14). Since the distance between the nitrogen atoms of the two pyridine rings in each molecule is the shortest one, the repulsion force constant between two pyridine rings, F_2, was calculated assuming the repulsion only occurred between two nitrogen atoms. The repulsion force constant between chlorine and pyridine, F_3, was taken as the average value of F_1 and F_2. The resulting repulsion force constants were small, and contributed very little to the calculated frequencies. Therefore they were taken as the calculated values without further refinement.

The calculation procedure has been described before (10). The main feature is that before any calculation, the values of the force constants are restricted by the chemical and physical knowledge of them, then the force constants and the frequencies are adjusted within the restriction to best reproduce the observed spectrum.

A preliminary calculation was made taking the Zn—Cl stretching force constant as that of $[ZnCl_4]^{2-}$ (15), the Zn—Py stretching force constant as that obtained by the 1:1 model (1), and the bending force constants as 1/10 of the corresponding stretching force constants. Then, the force constants were refined.

The ν_1 and ν_2 bands are mainly contributed by the Cl—Zn stretching as shown by the potential energy distribution, consequently a good Cl—Zn stretching force constant was obtained without any difficulty. The refinement of the other force constants was not as straightforward. The ν_3 band is mainly due to the Zn—Py stretching and also a small amount of

Can. J. Chem. Downloaded from www.nrcresearchpress.com by 210.87.254.6 on 09/05/12
For personal use only.

Can. J. Chem. Downloaded from www.nrcresearchpress.com by 210.87.254.6 on 09/05/12
For personal use only.

Cl—Zn—Py bending. To refine the Zn—Py stretching force constant the Cl—Zn—Py bending force constant was adjusted at the same time. The values of the Cl—Zn—Py bending force constant was limited by the observed frequencies of the ν_9, ν_{10}, and ν_{11} bands, which contain mainly the Cl—Zn—Py bending. Moreover, about 50% of the energy of the ν_6, ν_7, and ν_8 bands is contributed by the Zn—Py stretching vibration, so the observed frequencies of these bands were also helpful for adjusting the Zn—Py stretching force constant. However, these bands contain a certain amount of the lattice stretching, and the calculated frequency of these bands could not fit any of the observed ones if the lattice stretching force constant, k_3, was not introduced into the calculation. A higher value of k_3 gave too high calculated frequencies of the ν_3 and ν_4 bands. If the k_3 value was kept high and the values of K_2 and H_3 were alternatively reduced, the calculated frequencies of the ν_3 and ν_4 bands could be adjusted well, but the calculated frequencies of the ν_5, ν_8, ν_{10}, and ν_{11} bands became too low. Consequently, the three force constants K_2, H_3, and k_3, were adjusted together to fit the frequencies of the ν_3, ν_4, ν_5, ν_6, ν_7, ν_8, ν_9, ν_{10}, and ν_{11} bands. The Cl—Zn—Cl bending force constant H_1 contributes an appreciable amount of the energy to the ν_2, ν_4, ν_5, and ν_8 modes. With a higher value of H_1 the calculated frequency of the ν_8 band fitted the observed one better, but the frequencies of the ν_2, ν_4, and ν_5 became too high, so this force constant was adjusted against the frequencies of all these bands. The Py—Zn—Py bending force constant, H_2, was refined according to the frequencies of the ν_{11}, ν_{12}, and ν_{13} modes. The lattice stretching force constant k_2 contributes essentially to the frequencies of the ν_{16} and ν_{17} modes and also appreciably to those of the ν_{12} and ν_9 modes. The calculated frequencies of the ν_{12}, ν_{16}, and ν_{17} modes with the value of the force constant, k_2, reported in Table 2, were low. They could be adjusted better, in principle, by increasing the value of k_2. However, the calculated frequency of the ν_9 mode became too high, if a higher value of k_2 was used. The lattice stretching vibrations with the force constant k_1 do not couple much with the skeletal modes, and dominate the low frequency bands, ν_{12}, ν_{13}, ν_{14}, ν_{15}, ν_{16}, ν_{17}, and ν_{18}. The refinement of this force constant was based on these frequencies. The observed normal modes in the frequency region below 38.4 cm^{-1} are almost completely contributed by the two lattice bending force constants, h_1 and h_2. The adjustment of these force constants was made according to the observed frequencies in this region. The value of h_2 was also limited by the observed frequencies of the ν_3, ν_4, and ν_9 modes.

The resulting force constants are given in Table 4, the calculated frequencies are compared with the experimental values in Table 1 and the calculated distribution of the potential energy among the internal coordinates is given in Table 5.[3] In order to investigate the effect of the lattice vibrations upon the skeletal vibrations of the complex molecules, the frequencies of the normal modes for an isolated molecule were also calculated simply by excluding the lattice stretching and bending force constants in the calculation and are shown in the last column of Table 1. This also provides a check on the calculation, since it shows that any particular skeletal mode which gives rise to several frequencies due to intermolecular coupling in the crystal yields a single frequency in the absence of the lattice force constants and four frequencies with exactly the same numerical value for each skeletal mole are obtained.

As seen in Table 1 the differences between the calculated and observed frequencies are within 5% except those for few very low frequency modes, of which the absolute difference is less than 5 cm^{-1}. Several calculated frequencies around the low frequency modes ν_{21} and ν_{23} were not observed in the Raman spectrum. This is probably due to the error in the calculation with insufficient number of lattice force constants in the model. On the other hand, it could be due to the poor Raman spectrum in this extremely low frequency region because it is close to the exciting laser line.

The significance of the force constants obtained in the present calculation is discussed briefly as follows. The Zn—Cl stretching force constant, K_1, is the strongest one and dominates the frequencies of the ν_1 and ν_2 bands, so its value is good. The Zn—Py stretching force constant, K_2, dominates the frequency of the ν_3 band and was refined together with the Cl—

[3]Photocopies of Tables 5 and 6 may be obtained at a nominal charge, upon request, from the Depository of Unpublished Data, National Science Library, National Research Council of Canada, Ottawa, Canada K1A 0S2.

Can. J. Chem. Downloaded from www.nrcresearchpress.com by 210.87.254.6 on 09/05/12
For personal use only.

Zn—Py bending force constant, H_3, according to the observed frequencies of the ν_3, ν_6, ν_7, ν_8, ν_9, ν_{10}, and ν_{11} bands, so these two force constants are also reasonably good. The repulsion force constants F_1, F_2, and F_3, were calculated directly by Shimanouchi's method and their values fit nicely in both the experimental and theoretical curves of the repulsion force constants of a series of similar compounds. The repulsion force constants thus obtained were small and did not affect much the values of the other force constants. The Py—Zn—Py bending force constant, H_2, was refined only according to the frequencies of the ν_{11}, ν_{12}, and ν_{13} bands, and the Cl—Zn—Cl bending force constant H_1, according to the frequencies of the ν_2, ν_4, ν_5, and ν_8 bands. Most of these modes contain a certain amount of lattice vibration, so the significance of these two bending force constants, H_1 and H_2, depends on that of the lattice force constants. In the present calculation, only those lattice stretching and bending vibrations with the distances among the Cl and Zn atoms and the Py point masses of the neighboring molecules in the crystal shorter than 4.4 Å were taken into account. Thirty-eight other distances among these neighboring atoms in the crystal are between 4.4 and 5 Å. The force constants of the lattice bending and stretching vibrations related to these distances were not included in the calculation, otherwise there were too many force constants to handle. Although these force constants are expected to be small, yet the contribution of all of them is high enough to affect the real values of the lattice force constants k_1, k_2, k_3, h_1, and h_2. Therefore the significance of the calculated values of these lattice force constants is uncertain.

The structural parameters of the $[ZnPy_2Br_2]$ crystal are not available in the literature, so the normal coordinate analysis for this crystal cannot be performed in detail at the present time. Since the configuration of the $[ZnPy_2Br_2]$ molecule is also tetrahedral (16), an approximate calculation for this crystal, assuming its crystal structure to be the same as that of the $[ZnPy_2Cl_2]$ crystal, has been carried out.

In this calculation only those force constants related to the motions of the Br atoms in the crystal have been re-adjusted, the Br---Br repulsion force constant was again obtained by the direct calculation, and the Zn—Py stretching force constant was increased to match the calculated and the observed frequencies of the ν_3 mode and others. The other force constants were directly transferred from the results for the $[ZnPy_2Cl_2]$ crystal. The highest frequency at 256 cm^{-1} is essentially the Zn—Br stretching frequency, so the Zn—Br stretching force constant was easily obtained. The Br—Zn—Br bending force constant was reduced to 0.075 mdyn/Å from the corresponding Cl—Zn—Cl bending force constant, otherwise the calculated frequency of the ν_2 mode and also those of the ν_9, ν_{10}, ν_{11}, ν_{12}, and ν_{13} modes were too high. The value of the lattice stretching force constant k_3 was adjusted to as high as 0.65 mdyn/Å in order to obtain reasonable calculated frequencies to match those of the observed ν_4, ν_5, and ν_6 modes.

The calculated frequencies, the force constants, and the distribution of the potential energy for the $[ZnPy_2Br_2]$ crystal are given in Tables 2, 4, and 6, respectively.[3]

Discussion

The normal vibrations of the crystals of $[ZnPy_2Cl_2]$ and $[ZnPy_2Br_2]$ can be interpreted directly from the distribution of the potential energy of the normal modes given in Tables 5 and 6, respectively.[3] For simplicity, only the frequencies of $[ZnPy_2Cl_2]$ are referred to in the following paragraphs.

The vibration with the highest frequency at 326.3 cm^{-1} is mainly the Zn—Cl stretching vibration. The second highest frequency vibration at 292 cm^{-1} is the Zn—Cl stretching vibration coupled with the Zn—Py stretching and the Cl—Zn—Cl bending vibrations. The normal mode at 221.6 cm^{-1} is mainly the Zn—Py stretching vibration and contains an appreciable amount of Py—Zn—Cl bending vibrations. The effect of the lattice vibrations on these three skeletal modes is weak. The other skeletal modes of the molecules in the crystal are more or less coupled with the lattice vibrations and each band of the isolated molecule splits into several due to the intermolecular coupling in the crystal. The observed bands at 206.4 and 200.1 cm^{-1} are the results of the splitting of the skeletal mode consisting of the Zn—Cl stretching, the Cl—Zn—Cl bending, and the Zn—Py stretching motions. The Raman bands at 162.6 and 151.7 cm^{-1} and the infrared band at 152.6 and 142.4 cm^{-1} are mainly due

Can. J. Chem. Downloaded from www.nrcresearchpress.com by 210.87.254.6 on 09/05/12
For personal use only.

to the Zn—Py stretching vibration. When the lattice vibration force constants are excluded in the calculation, the calculated frequency of this mode is 135 cm^{-1}, and it is impossible to raise the calculated frequency to fit the observed ones at 162.6 and 151.7 cm^{-1} with reasonable variation of the skeletal force constants. The observed bands at 109.7, 107.0, and 101.5 cm^{-1} correspond to the Py—Zn—Cl bending modes of the isolated molecule with the B_1, A_2, and B_2 symmetry, respectively, which weakly couple with the lattice vibrations. The Py—Zn—Py (A_1) bending mode of the isolated molecule is split into two at 93.9 and 83.3 cm^{-1} by the effects of the lattice Py---Py stretching and Zn---Py---Py bending motions. The observed frequencies at 80.1, 77.3, 69.7, and 44 cm^{-1} are mainly due to the lattice stretching vibrations which couple appreciably with the skeletal Py—Zn—Py and Py—Zn—Cl bendings. The bands at 62.0, 21.7, and 5.6 cm^{-1} are the lattice bending modes containing a small amount of skeletal bending. The other observed bands are dominated by the lattice bending vibrations.

Apparently lattice vibrations play a very important role on the vibrational spectra of $[ZnPy_2Cl_2]$ and $[ZnPy_2Br_2]$ crystals in the frequency range below 200 cm^{-1}. None of the observed bands in this frequency range is purely due to uncoupled skeletal vibration. If only an isolated molecule is considered, not only the very low frequency part of the spectrum, but also the observed bands at 206.4, 162.6, 151.7, and 152.6 cm^{-1} cannot be reproduced by any reasonable variation of the force constants or even the whole force field for the isolated molecule. On the other hand, when the calculation is done for the complete crystal, the calculated frequencies can be adjusted to yield an agreement with the observed ones within about 5%.

The Zn–halogen stretching force constant is 1.13 mdyn $Å^{-1}$ for $[ZnPy_2Cl_2]$ and 0.922 mdyn $Å^{-1}$ for $[ZnPy_2Br_2]$. The ratio of these force constants, K(Zn—Br)/K(Zn—Cl) is 0.82 which is close to those of a series of hexahalogeno complexes (14). This shows that the difference in bond character between Zn—Br and Zn—Cl in dihalogenobis(pyridin)zinc(II) complexes is almost the same as that in the hexahalogeno complexes and the effect of the pyridine ligands on the character of the Zn—Br and Zn—Cl bonds in these complexes is about the same.

The Zn—Py stretching force constant is 0.68 mdyn $Å^{-1}$ for $[ZnPy_2Cl_2]$ and 0.73 mdyn $Å^{-1}$ for $[ZnPy_2Br_2]$, which implies that the Zn—Py bond is stronger in the $[ZnPy_2Br_2]$ complex than that in the $[ZnPy_2Cl_2]$ complex. This is also indicated by the similarity of the ν_3 frequencies of these two complexes. The ν_3 mode is due to the Py—Zn stretching which couples slightly with the Py—Zn—X bending. If the bond strength of the Zn—Py bond is not stronger in the $[ZnPy_2Br_2]$ complex than in the $[ZnPy_2Cl_2]$ complex, the frequency of this mode of the $[ZnPy_2Br_2]$ complex should be lower because of this coupling. The difference in the Zn—Py bond strength between these two complexes is most likely the result of the effect of the Zn–halogen bonds. The charge transfer from the Br^- ions to the central Zn^{2+} ion via σ-bonding is more than that from the Cl^- ions due to the larger polarizability of the Br^- ions, which results in a higher electron density on the Zn^{2+} ion in the bromide complex and it in turn enhances the Zn—Py π-bond (3), so that the net bond strength of the Zn—Py bond in the bromide complex is stronger than that in the chloride complex. The Zn—Cl bond is stronger than the Zn—Br bond in these complexes. Therefore the dπ–dπ overlap in the Zn—Cl bond must be greater than that in the Zn—Br bond.

The Raman intensities of the skeletal modes are very low especially those of the high-frequency Zn—X and Zn—Py stretching modes. The low intensity of these modes indicates that the bond order of the Zn–ligand bonds is low (17), which is consistent with the results of the earlier work (1, 3, 18). Moreover, the delocalization character of the Zn–ligand bonds in these complexes (7) could also result in the low Raman intensities of the Zn–ligand modes. The electron density on the central metal atom drifts to or from the ligands during the vibrations and the net polarizability derivatives of the modes could become small. Probably this delocalization effect is quite important, since the intensity of the lattice bending mode at 29.6 cm^{-1} for $[ZnPy_2Cl_2]$ and the corresponding mode at 24.2 cm^{-1} for $[ZnPy_2Br_2]$ is strong, and apparently, the electron density migration discussed above would not occur in this mode.

I wish to thank Dr. E. Whalley for useful discussions.

1. P. T. T. Wong and D. G. Brewer. Can. J. Chem. **47**, 4589 (1969).
2. Y. Saito, M. Cordes, and K. Nakamoto. Spectrochim. Acta, **28**A, 1459 (1972).

3. P. T. T. WONG and D. G. BREWER. Can. J. Chem. **46**, 131 (1968).
4. P. T. T. WONG, J. E. BERTIE, and E. WHALLEY. Rev. Sci. Inst. **41**, 283 (1970).
5. M. A. PORAI-KOSHITS, L. O. ATOVMYAN, and G. N. TISHCHENKO. Zh. Strukt. Khim. **1**, 337 (1960).
6. A. V. ABLOV and E. D. RUCHKIN. Zh. Strukt. Khim. **4**, 50 (1963).
7. P. T. T. WONG and D. G. BREWER. Can. J. Chem. **46**, 139 (1968).
8. D. G. BREWER, P. T. T. WONG, and M. C. SEARS. Can. J. Chem. **46**, 3137 (1968).
9. R. ZANNETTI and R. SEPPA. Gazz. Chim. Ital. **90**, 328 (1960).
10. P. T. T. WONG and E. WHALLEY. J. Chem. Phys. **55**, 1830 (1971).
11. Y. MORINO, K. KUCHITSU, and T. SHIMANOUCHI. J. Chem. Phys. **20**, 726 (1952).
12. J. OVEREND and J. R. SCHERER. J. Chem. Phys. **32**, 1296 (1960).
13. T. SHIMANOUCHI. J. Chem. Phys. **17**, 848 (1949).
14. J. HIRAISHI, I. NAKAGAWA, and T. SHIMANOUCHI. Spectrochim. Acta, **20**, 819 (1964).
15. A. SABATINI and L. SACCONI. J. Am. Chem. Soc. **86**, 17 (1964).
16. R. H. H. CLARK and C. S. WILLIAMS. Inorg. Chem. **4**, 350 (1965).
17. D. A. LONG, Proc. R. Soc. Lond. **217**A, 203 (1953).
18. D. G. BREWER and P. T. T. WONG. Can. J. Chem. **44**, 1407 (1966).

Can. J. Chem. Downloaded from www.nrcresearchpress.com by 210.87.254.6 on 09/05/12
For personal use only.

Group V Chalcogenide Complexes of Boron Trihalides

P. M. BOORMAN AND D. POTTS

Department of Chemistry, The University of Calgary, Calgary, Alberta T2N 1N4

Received July 31, 1973

P. M. BOORMAN and D. POTTS. Can. J. Chem. **52**, 2016 (1974).

The preparation of the complexes $BX_3 \cdot R_3PY$ (X = Cl, Br, I; R = Me, Ph, cyclohexyl; Y = S, Se) is reported. The corresponding BF_3 adducts could not be isolated. The infrared spectra for all complexes are presented as well as the n.m.r. spectra for the methyl adducts. The shifts in ν(P—Y) upon co-ordination are amongst the largest ever reported for these ligands when they function as non-bridging species, and are in fact comparable to shifts observed in bridging situations. The spectral data are consistent with an increase in the B—Y bond strength as the atomic weight of X increases.

P. M. BOORMAN et D. POTTS. Can. J. Chem. **52**, 2016 (1974).

On rapporte la préparation des complexes $BX_3 \cdot R_3PY$ (X = Cl, Br, I; R = Me, Ph, cyclohexyle; Y = S, Se). Les produits d'addition du BF_3 correspondants n'ont pas pu être isolés. On présente les spectres infrarouges de tous les complexes de même que les spectres r.m.n. des produits d'addition de groupes méthyles. Les déplacements pour la fréquence ν(P—Y) lors de la coordination sont parmi les plus grands jamais rapporté pour ces ligands lorsqu'ils agissent comme des espèces ne créant pas de pont et ces déplacements sont de fait comparables à ceux observés dans des situations où il y a des ponts. Les données spectrales sont en accord avec une augmentation de la force du lien B—Y à mesure que le poid atomique de X augmente.

[Traduit par le journal]

Introduction

The Lewis base behavior of ligands of the type R_3PY (R = alkyl, phenyl; Y = S, Se) has been the subject of several recent reports (1–6). The P—Y stretching frequency is observed to decrease upon co-ordination and this has been attributed to either a weakening of the $p\pi \rightarrow d\pi$ bond ($Y \rightarrow P$) upon formation of a $M \leftarrow Y$ bond (3, 7), or a mass effect, considering the M—Y unit as a point mass (8). The latter argument has been disputed (1), and is inconsistent with published data for Ph_3PS complexes of a wide variety of metal halides (6). The effects of Lewis acids on the P—Y stretching frequencies of group V chalcogenide ligands are often complicated by the possibility of back donation of $p\pi$ (or $d\pi$) electrons of the Lewis acid to empty $d\pi$ sulfur (selenium) orbitals (9), and by the tendency of the R_3PY molecules to act in some cases as bridging ligands (1, 10). To date, few attempts have been made to study the effects of co-ordination on a wide variety of R_3PY ligands with a closely related series of Lewis acids. Consequently, we have synthesized a series of adducts containing the Lewis acids BCl_3, BBr_3, and BI_3 complexed to the ligands R_3PY (R = Ph, Me, Cy (cyclohexyl); Y = S, Se). No possibility of back donation of electrons from boron to sulfur or selenium exists in these complexes. Furthermore, the ligands are unlikely to adopt a bridging mode of co-ordination in complexes of formula BX_3L, since the co-ordination number of boron is unlikely to exceed four. The complexes $BX_3 \cdot Ph_3PY$ (X = Cl, Br; Y = S, Se) have been briefly reported by Schmidt and Block (11), but no spectral properties were described.

Experimental

All solvents were dried by standard procedures. The boron trihalides were obtained commercially and used without further purification. The chalcogenide ligands were prepared by literature methods (12, 13). All manipulations were carried out either in a dry box or in apparatus protected from atmospheric moisture by $CaCl_2$ guard tubes.

Boron Trichloride Adducts

Approximately 1 g of ligand was dissolved in 8 ml of dichloromethane in a 50 ml 3-necked flask. Carbon tetrachloride (20 ml) was then added and BCl_3 was passed through the solution, until precipitation of the complex ceased. The mixture was cooled to 0 °C and the solid isolated by filtration followed by drying *in vacuo*. The complexes $BCl_3 \cdot Cy_3PSe$ and $BCl_3 \cdot Ph_3PSe$ were not precipitated readily unless the solutions were cooled.

Boron Tribromide Adducts

Approximately 1 g of ligand in a 50 ml flask was dissolved in a dichloromethane – carbon tetrachloride mixture (1 : 3) and excess BBr_3 was then added. Precipitation of the complexes occurred readily in most cases and was completed by cooling to 0 °C. The compounds $BBr_3 \cdot Cy_3PSe$ and $BBr_3 \cdot Ph_3PSe$ were obtained only upon cooling. The solutions were filtered and the resulting solids dried *in vacuo*.

Can. J. Chem. Downloaded from www.nrcresearchpress.com by 210.87.254.5 on 09/05/12
For personal use only.

TABLE 1. Analytical data for complexes

Compound	Analysis (%) C Found	C Calcd.	H Found	H Calcd.	Halogen Found	Halogen Calcd.	Color
$BCl_3 \cdot Me_3PS$	16.05	15.99	3.95	4.03	46.97	47.20	Colorless
$BCl_3 \cdot Me_3PSe$	13.41	13.24	3.45	3.33	38.70	39.07	Colorless
$BCl_3 \cdot Cy_3PS$	50.18	50.29	7.79	7.74	24.62	24.80	Colorless
$BCl_3 \cdot Cy_3PSe$	45.52	45.34	6.93	6.98	22.18	22.36	Buff
$BBr_3 \cdot Me_3PS$	10.19	10.05	2.48	2.53	66.79	66.84	Colorless
$BBr_3 \cdot Me_3PSe$	8.87	8.88	2.32	2.24	58.90	59.11	Colorless
$BBr_3 \cdot Cy_3PS$	38.47	38.40	5.90	5.91	42.77	42.58	Colorless
$BBr_3 \cdot Cy_3PSe$	35.59	35.44	5.46	5.45	39.14	39.31	Buff
$BI_3 \cdot Me_3PS$	7.51	7.21	2.24	1.81	76.36	76.20	Orange
$BI_3 \cdot Me_3PSe$	6.70	6.59	1.79	1.66	69.79	69.66	Yellow
$BI_3 \cdot Cy_3PS$	30.84	30.71	4.68	4.72	54.44	54.08	Buff
$BI_3 \cdot Cy_3PSe$	28.84	28.79	4.34	4.43	50.51	50.70	Orange
$BI_3 \cdot Ph_3PS$	31.01	31.52	2.11	2.20	55.14	55.51	Orange
$BI_3 \cdot Ph_3PSe$	29.27	29.50	2.10	2.06	51.57	51.96	Yellow

Boron Triiodide Adducts

A 2 mol excess of BI_3 dissolved in 5 ml carbon tetrachloride was added to a dichloromethane – carbon tetrachloride mixture containing about 1 g of the chalcogenide ligand. Precipitation of the complexes occurred immediately in all cases. The mixtures were cooled to 0 °C, filtered, and the solids then washed twice with dry carbon tetrachloride, followed by drying *in vacuo*.

Infrared spectra were recorded on a Beckman IR 20-A spectrophotometer, either as Nujol mulls between CsI plates or as dichloromethane solutions using 1.0 mm KBr cells.

The n.m.r. spectra were determined in dichloromethane using a Varian Model A-60 spectrometer. Results are reported in τ values relative to tetramethylsilane as an internal standard.

Analyses were carried out by Alfred Bernhardt Laboratories, West Germany.

Results and Discussion

The adducts were isolated as powders upon addition of excess boron trihalide to a solution of the group V chalcogenide ligand dissolved in a dichloromethane – carbon tetrachloride mixture. Consistent with the increased acceptor strength of the boron trihalides in the order $BI_3 > BBr_3 > BCl_3$, the iodide complexes were formed much more readily than the analogous chlorides, and attempts to prepare corresponding BF_3 adducts were unsuccessful. The compounds are stable at room temperature but all are rapidly hydrolyzed by moisture. Analytical data for the new complexes reported in this work are provided in Table 1.

Infrared Spectra

The solid state infrared spectra of the compounds were recorded in the region 4000–300 cm^{-1}. Solution spectra in dichloromethane were obtained from 600 to 350 cm^{-1} for the complexes $BX_3 \cdot Me_3PY$ (X = Cl, Br, I; Y = S, Se). With the exception of P—Y stretching frequencies, little change in bands associated with ligand vibrations was observed upon co-ordination, therefore only values for ν(P—Y) are reported in Table 2. The assignments of these bands are after Zingaro (7). In all cases, adduct formation results in a value of ν(P—Y) lower than that found for the free ligand. These shifts to lower frequency, $\Delta\nu$(P—Y), for each complex are also shown in Table 2. Complexes containing Me_3PS as a non-bridging ligand have been found to exhibit values of $\Delta\nu$(P—S) in the order of 30 cm^{-1} (4, 14), while $\Delta\nu$(P—Se) for a variety of Me_3PSe adducts is in the range of 15–27 cm^{-1} (5, 15). The decreases in ν(P—Y) for these ligands upon co-ordination with BX_3 moieties are seen to be of significantly greater magnitude, being >40 cm^{-1} for the sulfide and at least 35 cm^{-1} for the selenide. Similarly, complexes formed for a variety of metal halides with Ph_3PS and Ph_3PSe show P—S (Se) frequencies some 40–50 and 15–20 cm^{-1} lower than observed in the free ligands (3, 8, 15), and again the BX_3 adducts containing these ligands have considerably larger values for $\Delta\nu$[P—S (Se)]. Few complexes containing Cy_3PS and Cy_3PSe have been reported. However, the decreases in ν[P—S (Se)] shown for the BX_3 adducts are of a magnitude comparable to those found for the four other ligands.

Can. J. Chem. Downloaded from www.nrcresearchpress.com by 210.87.254.5 on 09/05/12
For personal use only.

TABLE 2. P=S (Se) stretching frequencies for group V chalcogenide complexes

Complex	Frequencies (cm^{-1})* ν[(P—S)(Se)]	Δν[(P—S)(Se)]
Me_3PS	566 (569)†	
$BCl_3 \cdot Me_3PS$	523 (524)	43 (45)
$BBr_3 \cdot Me_3PS$	512 (518)	54 (51)
$BI_3 \cdot Me_3PS$	510 (506)	56 (63)
Me_3PSe	444 (445)	
$BCl_3 \cdot Me_3PSe$	409 (408)	35 (37)
$BBr_3 \cdot Me_3PSe$	403 (405)	41 (40)
$BI_3 \cdot Me_3PSe$	394 (395)	50 (50)
Cy_3PS	625	
$BCl_3 \cdot Cy_3PS$	568	59
$BBr_3 \cdot Cy_3PS$	565	62
$BI_3 \cdot Cy_3PS$	574	53
Cy_3PSe	550	
$BCl_3 \cdot Cy_3PSe$	519	31
$BBr_3 \cdot Cy_3PSe$	516	34
$BI_3 \cdot Cy_3PSe$	‡	
Ph_3PS	637	
$BCl_3 \cdot Ph_3PS$	573	64
$BBr_3 \cdot Ph_3PS$	571	66
$BI_3 \cdot Ph_3PS$	567	70
Ph_3PSe	562	
$BCl_3 \cdot Ph_3PSe$	531	31
$BBr_3 \cdot Ph_3PSe$	523	39
$BI_3 \cdot Ph_3PSe$	510	52

*Frequencies estimated to be accurate to within ±2 cm^{-1}.
†Frequencies obtained from dichloromethane solutions.
‡Bands obscured by B—I stretching vibrations.

Thus, excluding cases where the chalcogenide ligand is bridging, the decreases in ν[P—S (Se)] for the BX_3 adducts are amongst the largest yet to be observed. Since the solution spectra obtained for the Me_3PY complexes are quite similar to those observed for the solid state, these large values of Δν(P—Y) are unlikely to be the result of molecular interactions in the solids. It also seems unlikely that shifts in P—Y frequencies can be explained exclusively on the basis of mass effects. Of all the complexes of R_3PY ever reported, BCl_3 is the "lightest" acceptor species, and yet it causes one of the largest decreases in ν(P—Y). The most reasonable explanation for the large values of Δν(P—Y) is simply that the highly polarizing boron atom considerably decreases the electron density on the chalcogenide atom thereby decreasing the $p\pi \rightarrow d\pi$ interaction in the P—Y bond.

The decreases in ν(P—Se) for the selenide compounds are always seen to be less than those observed for ν(P—S) in the corresponding sulfide complexes. This behavior has been attributed to less extensive (P—Se)π-character in the free ligand and to decreased sensitivity of ν(P—Se), owing to the larger mass of Se with respect to S (3). Considering the $BX_3 \cdot R_3PS$ adducts, for a given halide the value of Δν(P—S) increases approximately in the order Me < Cy < Ph and this trend parallels the increase in $d\pi \leftarrow p\pi$ interaction expected in the P—S bond of the free ligand (7). Thus, coordination seems to lead to a large decrease in ν(P—S) when the free ligand has considerable $d\pi \leftarrow p\pi$ character in the P—S bond. A similar trend is not apparent in the selenide adducts.

For a given ligand, ν(P—Y) is seen to decrease in the order $BCl_3L > BBr_3L > BI_3L$. (The complex $BI_3 \cdot Cy_3PS$ is anomalous in this respect.) While this trend might be explained by a "mass effect" caused by the increasing atomic weight of the halogens, the general lack of dependence of P—Y stretching frequencies upon mass effects has already been discussed. Instead this behavior is thought to reflect a strengthening of the B—Y bonds as a result of the increasing Lewis acidity in the series $BCl_3 < BBr_3 < BI_3$. Such an effect is well documented (16), even though no entirely satisfactory explanation for the phenomenon is available (17). It is interesting to compare the values of ν(P—Y) observed in the BX_3 adducts with those for complexes containing the ligands as bridging species. The Cu(I) systems studied by Meek *et al.* are particularly interesting since both terminal and bridging Me_3PS have been observed here (10). Although Δν(PS) is definitely larger in the bridging case, the actual value (45 cm^{-1}) is about the same as in BCl_3Me_3PS, and rather smaller than that observed for BI_3Me_3PS (56 cm^{-1}). Clearly, the use of the change in PS stretching frequency to characterize bridging phosphine sulfides must be exercised with caution. Boorman and Reimer (1) have postulated the existence of bridging ligands in the complexes $[W_2Cl_8(Ph_3PS)_2]2Cl$, for which Δν(PS) was 96 cm^{-1}. Their conclusion appears to be justified since even in the case of BI_3Ph_3PS, Δν is only 70 cm^{-1}.

Comparison of the infrared spectra of all the complexes allowed us to tentatively locate the positions of the B—X stretching frequencies. These frequencies and their assignments are presented in Table 3. Amster and Taylor (18) have reported detailed spectral analyses for the compounds $Me_3N \cdot BX_3$ (X = F, Cl, Br) and our assignments for the BCl_3 and BBr_3 adducts are

Can. J. Chem. Downloaded from www.nrcresearchpress.com by 210.87.254.5 on 09/05/12
For personal use only.

TABLE 3. ν(B—X) for BX_3 adducts (X = Cl, Br, I)

	BCl_3				BBr_3				BI_3			
	E		A_1		*E*		A_1		*E*		A_1	
Ligand	^{10}B	^{11}B	^{10}B	^{11}B	^{10}B	^{11}B	^{10}B	^{11}B	^{10}B	^{11}B	^{10}B	^{11}B
Me_3PS	*	685	660	640	673	650	630	585 602	650	630	550	527
Cy_3PS	705	688	644	623	670	650	610	587	663	638	555	527
Ph_3PS	*	*	645	627	677	645 650	*	615	655	632	*	530
Me_3PSe	707	682	637	610	650	620	610	580	600	575	547	524 512
Cy_3PSe	705	694	615	597	657	627	627	560	605	585	548	516
Ph_3PSe	*	*	605	590	655 644	625 610	625 610	560	603	584	562	532

*Obscured by ligand vibrations.

based on this work. The *E* class of vibrations correspond to degenerate asymmetric B—X stretching modes while the A_1 class represent symmetric B—X stretching. Bands due to bending vibrations are generally weak (18) and were not observed in our spectra. Little spectroscopic data is available for BI_3 adducts, consequently the assignments for ν(B—I) were made by comparison with the BCl_3 and BBr_3 complexes. It should be noted that the Me_3N adducts were assumed to have C_{3v} symmetry whereas this situation will not be strictly true with our complexes, as a consequence of the non-linearity of the P—B bonds. In fact, most of the bands associated with B—X stretching were quite broad and occasionally split. Bands due to ν(^{10}B—X) had intensities approximately 1/4 that observed for ν(^{11}B—X). Unfortunately, no obvious correlation between ligand donor strength and ν(B—X) positions is evident. This could be the result of varying degrees of coupling between ν_{sym}(BX) and ν(BY). Bands due to boron–sulfur or boron–selenium stretching vibrations could not be located in our spectra.

N.M.R. Spectra

N.m.r. spectra were obtained for the complexes $BX_3 \cdot Me_3PY$ (X = Cl, Br, I; Y = S, Se) in dichloromethane at 30 °C. The results are presented in Table 4. Infrared spectra of these solutions confirmed that no free ligands are present. The P—C—H coupling constants for both ligands are seen to increase slightly upon adduct formation but remain constant as the nature of the Lewis acid is changed. τ values for the ligands also decrease upon co-ordination and continue to decrease slightly, but significantly, reflecting a decrease in shielding around the methyl protons as the acceptor power of BX_3 increases. While this trend is consistent with conclusions drawn from the infrared spectra indicating a strengthening of B—Y bonds in going from BCl_3 to BI_3, caution must be used in such interpretations due to the possibility of ligand exchange reactions, a well established phenomenon for $BX_3 \cdot L$ systems (19, 20). Preliminary n.m.r. work on solutions containing excess ligand shows that such exchange does occur. While more detailed exchange reaction studies are planned, we have found that the complexes $BCl_3 \cdot Me_3PS$, $BCl_3 \cdot Me_3PSe$, and $BBr_3 \cdot Me_3PSe$ exchange rapidly at 30 °C, while under similar conditions $BBr_3 \cdot Me_3PS$, $BI_3 \cdot Me_3PSe$, and $BI_3 \cdot Me_3PS$ have much slower rates of exchange, the iodide adduct being the slowest.

TABLE 4. N.m.r. spectra for the complexes $BX_3 \cdot Me_3PY$ (X = Cl, Br, I; Y = S, Se)

Complex	τ	*J*(P—C—H) Hz
Me_3PS	8.27	13.0
$BCl_3 \cdot Me_3PS$	7.93	13.5
$BBr_3 \cdot Me_3PS$	7.86	13.7
$BI_3 \cdot Me_3PS$	7.77	13.6
Me_3PSe	8.07	13.2
$BCl_3 \cdot Me_3PSe$	7.82	13.8
$BBr_3 \cdot Me_3PSe$	7.79	13.7
$BI_3 \cdot Me_3PSe$	7.75	13.7

Can. J. Chem. Downloaded from www.nrcresearchpress.com by 210.87.254.5 on 09/05/12
For personal use only.

These qualitative results provide further evidence of increasing strength in B—Y bonding in going from chloride to iodide complexes.

We thank the National Research Council of Canada for financial support.

1. P. M. BOORMAN and K. J. REIMER. Can. J. Chem. **49**, 2926 (1971).
2. P. M. BOORMAN, S. A. CLOW, D. POTTS, and H. WIESER. Inorg. Nucl. Chem. Lett. **9**, 941 (1973).
3. M. G. KING and G. P. MCQUILLAN. J. Chem. Soc. (A), 898 (1967).
4. A. M. BRODIE, S. H. HUNTER, G. A. RODLEY, and C. J. WILKINS. J. Chem. Soc. (A), 2039 (1968).
5. A. M. BRODIE, G. A. RODLEY, and C. J. WILKINS. J. Chem. Soc. (A), 2927 (1969).
6. W. VAN DER VEER and F. JELLINEK. Rec. Trav. Chim. **87**, 365 (1968).
7. R. A. ZINGARO. Inorg. Chem. **2**, 192 (1963).
8. J. A. W. DALZIEL, A. F. LE C. HOLDING, and B. E. WATTS. J. Chem. Soc. (A), 358 (1967).
9. R. A. ZINGARO and R. M. HEDGES. J. Phys. Chem. **65**, 1132 (1961).
10. J. A. TIETHOF, J. K. STALICK, and D. W. MEEK. Inorg. Chem. **12**, 1170 (1973).
11. M. SCHMIDT and H. D. BLOCK. Chem. Ber. **103**, 3705 (1970).
12. C. SCRETTAS and A. F. ISBELL. J. Org. Chem. **27**, 2573 (1962).
13. P. NICPON and D. W. MEEK. Inorg. Syn. **10**, 157 (1967).
14. D. W. MEEK and P. NICPON. J. Am. Chem. Soc. **87**, 4951 (1965).
15. P. NICPON and D. W. MEEK. Chem. Commun. 398 (1966).
16. (*a*) D. G. BROWN, R. S. DRAGO, and T. E. BOLLES. J. Am. Chem. Soc. **90**, 5706 (1968); (*b*) B. BENTON-JONES, M. E. A. DAVIDSON, J. S. HARTMAN, J. J. KLASSEN, and J. M. MILLER. J. Chem. Soc., Dalton, 2603 (1972).
17. F. A. COTTON and G. WILKINSON. Advanced inorganic chemistry. 3rd ed. Interscience, New York. 1972. p. 225.
18. R. L. AMSTER and R. C. TAYLOR. Spectrochim. Acta, **20**, 1487 (1964).
19. A. H. COWLEY and J. L. MILLS. J. Am. Chem. Soc. **91**, 2911 (1969).
20. J. FOGELMAN and J. M. MILLER. Can. J. Chem. **50**, 1262 (1972).

Can. J. Chem. Downloaded from www.nrcresearchpress.com by 210.87.254.5 on 09/05/12
For personal use only.

Cobalt(II) and Nickel(II) Complexes with Nitrogen, Sulfur, and Selenium Containing Heterocyclic Ligands

C. PRETI[1] AND G. TOSI

Istituto di Chimica Generale ed Inorganica, University of Modena, Modena, Italy

D. DE FILIPPO AND G. VERANI

Istituto Chimico Policattedra, University of Cagliari, Cagliari, Italy

Received September 26, 1973

C. PRETI, G. TOSI, D. DE FILIPPO, and G. VERANI. Can. J. Chem. **52**, 2021 (1974).

Cobalt(II) and nickel(II) halide complexes with thiomorpholin-3-thione and thiazolidine-2-selenone have been prepared. Infrared and far infrared spectra, electronic spectral studies, and magnetic susceptibility measurements indicate that the cobalt derivatives are tetrahedral in structure, nickel chloro- and bromo-thiomorpholin-3-thione derivatives are octahedral while $[Nits_2I_2]$ and all nickel thiazolidine-2-selenone complexes have a pseudo-tetrahedral symmetry. The probable site of bonding in the ligands is nitrogen in all the complexes studied here, except the nickel derivatives of thiazolidine-2-selenone. These results are confirmed by n.m.r. measurements. Spectroscopic parameters for the complexes have been calculated and compared against similar chromophores containing MN_2X_2 and MS_2X_2 chromophores.

C. PRETI, G. TOSI, D. DE FILIPPO, et G. VERANI. Can. J. Chem. **52**, 2021 (1974).

Les complexes des halogénures de cobalt(II) et de nickel(II) avec les thiomorpholine thione-3 et la thiazolidinesélénone-2 ont été préparés. Les spectres infrarouge et infrarouge lointoin, les études des spectres électroniques et les mesures de susceptibilité magnétique indiquent que les dérivés du cobalt ont une structure tétraédrique, que les dérivés nickel chloro et bromothiomorpholine thione-3 sont octaédriques alors que $[Nits_2I_2]$ et tous les complexes du nickel avec la thiazolidinesélénone-2 ont une symétrie pseudo-tétraédrique. Le site probable de liaison dans les ligands est l'azote dans tous les composés que nous avons étudiés, exceptés les dérivés du nickel avec de la thiazolidinesélénone-2. Ces résultats sont confirmés par des mesures r.m.n. Les paramètres spectroscopiques des complexes ont été calculés et comparés à ceux de chromophores similaires contenant les chromophores MN_2X_2 et MS_2X_2. [Traduit par le journal]

We have prepared several complexes of thiomorpholin-3-one

(tm = O=C—NH—CH_2—CH_2—S—CH_2)

and thiazolidine-2-thione

(ttz = S=C—NH—CH_2—CH_2—S)

with group VIB, VIII, IB, and IIB metals in order to study the competition among oxygen, nitrogen, and sulfur donor atoms in heterocyclic compounds in the coordination to the metal (1 and references therein).

In this paper we report the preparation and the characterization of thiomorpholin-3-thione

(ts = S=C—NH—CH_2—CH_2—S—CH_2)

and thiazolidine-2-selenone

(tzse = Se=C—NH—CH_2—CH_2—S)

[1]To whom correspondence should be addressed.

complexes with cobalt(II) and nickel(II) for comparison purposes in order to further our present knowledge and to gain new information concerning the behavior of the different ligands by substituting oxygen for sulfur in ts and sulfur for selenium in tzse.

By reaction of $MX_2 \cdot nH_2O$ salts (M = Co(II) or Ni(II), X = Cl, Br, I) with the ligands in refluxing chloroform, the compounds $[ML_2X_2]$ (L = ts or tzse) were obtained, except for the nickel chloro- and bromo-thiazolidine-2-selenone derivatives. In these cases only the 1:1 complexes $[NitzseX_2]$ for X = Cl or Br, separated out even with a metal:ligand ratio higher than 1:3. The compounds are micro-crystalline, high-spin and soluble in *N,N'*-dimethylformamide (DMF). Their analytical data and other physical characteristics are reported in Table 1.

All Co(II) and Ni(II) complexes behave as nonelectrolytes in *N,N'*-dimethylformamide solu-

TABLE 1. Analytical data and some physical properties

Complexes	Color	Found (%)			Calcd. (%)			Decomposition temperature (°C)	μ (B.M.)
		M	C	H	M	C	H		
$[Cots_2Cl_2]$	Dark green	14.9	24.6	3.6	14.9	24.3	3.6	132	4.6
$[Cots_2Br_2]\cdot 2H_2O$	Dark green	10.9	18.9	3.8	10.7	18.4	3.4	108	4.7
$[Cots_2I_2]$	Dark green	10.1	16.8	2.4	10.2	16.6	2.4	124	4.9
$[Nits_2Cl_2]$	Yellow-green	14.8	24.7	3.6	14.8	24.3	3.6	204	3.3
$[Nits_2Br_2]$	Brown-yellow	12.4	19.8	3.1	12.1	19.8	2.9	184	3.1
$[Nits_2I_2]\cdot 2H_2O$	Dark brown	9.5	15.7	2.7	9.6	15.6	2.9	160	3.2
$[Co(tzse)_2Cl_2]\cdot 2H_2O$	Turquoise	11.6	14.2	2.7	11.8	14.4	2.8	> 350	5.1
$[Co(tzse)_2Br_2]\cdot H_2O$	Dark green	10.7	12.5	2.0	10.4	12.7	2.1	300	4.6
$[Co(tzse)_2I_2]\cdot 2H_2O$	Dark green	8.5	10.6	1.7	8.6	10.6	2.1	224	4.6
$[NitzseCl_2]$	Olive green	20.0	12.2	1.9	19.9	12.2	1.7	> 350	3.6
$[NitzseBr_2]$	Dark brown	15.2	9.4	2.1	15.3	9.4	1.3	> 350	3.7
$[Ni(tzse)_2I_2]$	Black	9.1	11.2	1.8	9.1	11.2	1.6	> 350	3.9

TABLE 2. Electronic spectra*

Compound	Electronic spectra (cm^{-1})						*Dq*	*B'*	β
$[Cots_2Cl_2]$	7820	14300	16700	20830			467	722	0.75
$[Cots_2Br_2]\cdot 2H_2O$	5160	6375	7700	14100	15875	18850sh	451	670	0.69
$[Cots_2I_2]$	7300	13000	15150	17250sh	22250		430	643	0.66
$[Cotzse_2Cl_2]\cdot 2H_2O$	6900	13200	16130	22250			400	737	0.76
$[Cotzse_2Br_2]\cdot H_2O$	5160	6700	11640sh	15900	25650		387	732	0.76
$[Cotzse_2I_2]\cdot 2H_2O$	6620	13000	15625	21300			382	719	0.74
$[Nits_2Cl_2]$	5180	5820	8550	14300	26600		855	985	0.95
$[Nits_2Br_2]$	6850	8260	13700	24500			826	885	0.85
$[Nits_2I_2]\cdot 2H_2O$	5180	5820	7420	13700sh	15880		458	985	0.95
$[NitzseCl_2]$	5050	6890	12500				—	—	—
$[NitzseBr_2]$	4760	5130	6570	12200			—	—	—
$[Nitzse_2I_2]$	5130	6850	12050				—	—	—

*B is taken to be 967 cm^{-1} for the cobalt(II) ion and 1041 cm^{-1} for the nickel(II) ion.

tions, the small conductivity being due to a slight degree of decomposition.

Thiomorpholin-3-thione Derivatives

With the cobalt halides, complexes of essentially tetrahedral geometry are formed. Their magnetic moments and solid state electronic spectra (Table 2) are in accord with those expected for this stereochemistry, with Δ values of 4 300 cm^{-1} (X = I) to 4670 cm^{-1} (X = Cl). The bands at 15000 – 17000 cm^{-1} may be assigned as the $^4A_2(F) \rightarrow {}^4T_1(P)$ transition, the second at 7300 – 7800 cm^{-1} as the $^4A_2(F) \rightarrow {}^4T_1(F)$ transition. These bands on passing from the chloro- to the iodo-derivative are shifted towards lower energies. Using these frequencies we have calculated the values of Dq, B', and β by means of the equations proposed by Underhill and Billing (2). As already pointed out from the chloro- to the iodo-derivative the Dq values decrease from 467 to 430, while those of B' lie between 643 and 722. The magnetic moments at room temperature of the cobalt complexes are consistent with a tetrahedral configuration for high spin cobalt(II) derivatives (4.6, 4.7, 4.9 for chloro-, bromo-, and iodo-derivatives, respectively).

Passing from the free ligand i.r. spectrum to those of the complexes (Table 3) we observe that the bands II and III of the —N—C=S group, according to Rao's nomenclature (3), are shifted moderately towards lower wave numbers while band I does not move.

The ν(NH) in the complexes is shifted towards lower wave numbers of about 200 cm^{-1} using as reference the value of 3380 cm^{-1} for ν(NH) for the free ligand in chloroform solution, or of about 50 cm^{-1} using the 3225 cm^{-1} value obtained from the solid phase spectrum of the free ligand. The low value of the solid free ligand

TABLE 3. Infrared spectral data of thiomorpholin-3-thione derivatives

Compounds	ν(N—H)	—N—C=S			ν(C—S)		ν(M—X)	ν(M—N)
		I	II	III	Asym.	Sym.		
ts solid	3225s	1590vs, 1560vs	1345vs	1100vs	700w	620w	—	—
ts $CHCl_3$ sol.	3380s	1580vs, 1570vs	1335vs	—	—	—	—	—
ts CS_2 sol.	3380s	—	1338, 1325vs	1108vs	690w	670m	—	—
$[Cots_2Cl_2]$	3210vs	1590vs, 1560vs	1350vs	1095vs	725s	690w	310m, 290ms	250m
$[Cots_2Br_2]\cdot 2H_2O$	3160vs	1550vs	1330vs	1090vs	715w	620w	238s, 218m	246m
$[Cots_2I_2]$	3150s	1590sh, 1550vs	1345w, 1325ms	1090vs	710s	660w	208m	245m
$[Nits_2Cl_2]$	3100s	1545vs	1330vs	1095vs	720s	655m	183s, 155ms	222m
$[Nits_2Br_2]$	3070s	1590vs, 1550vs	1350s	1090vs	710vw	680mw	157vs, 120s	230m
$[Nits_2I_2]\cdot 2H_2O$	3200vs	1580s, 1550vs	1335s	1085s	720w	680w	205m	212m

spectrum arises from extensive hydrogen bonding which disappear after dissolution in chloroform. According to Singh and Rivest (4) a sharp NH band in the metal derivatives is indicative of absence of hydrogen bonding and a comparison of these values with the ν(NH) solution frequency of the ligand could be used to suggest a coordination through the nitrogen atom.

In our complexes sharp bands are present in the range 3150 – 3210 cm^{-1} and a comparison with the ν(NH) value of 3380 would be indicative of a M—N coordination, but we prefer to use electronic spectra to confirm this hypothesis.

Analysis of the electronic spectra of tetrahedral cobalt(II) complexes allows us to a determination of mode of bonding. By comparison of Dq and B' values reported for CoL_2X_2 complexes and for CoL_4^{2+} cations and CoX_4^{2-} anions (5, 6), we can see that for CoS_4 chromophores Dq lies in the range 316–425 cm^{-1} and B' in the range 600–664 cm^{-1}. The corresponding ranges for CoN_4 chromophores are 467–538 and 700–757 cm^{-1} for Dq and B' values respectively. The Dq and B' values for CoL_2X_2 complexes may be calculated by taking averages of Dq and B' values of the CoL_4^{2+} and CoX_4^{2-} ions, using the "law of average environment" (6). Table 2 shows that Dq and B' values of our complexes are in very good agreement with the literature data for CoL_2X_2 derivatives containing cobalt–nitrogen bonds.

Working on this hypothesis, the halogen independent bands at 250, 246, and 245 cm^{-1} for chloro-, bromo-, and iodo-derivative respectively, can be attributed to the ν(Co—N) vibrations, according to literature data (7–9). Some strong bands are present in the spectra of cobalt(II) derivatives in the range 400–200 cm^{-1}, at 310m and 290ms cm^{-1} for $[Cots_2Cl_2]$, at 238s and 218m cm^{-1} for $[Cots_2Br_2]$, and at 208m cm^{-1} for $[Cots_2I_2]$. They may be attributed to metal–halogen stretching, by comparison with the spectra of pseudotetrahedral cobalt(II) complexes (7–13).

Moreover, the vibrations stretching attributed to the prevailing contributions of ν(C—S) are found at higher wave numbers. It is clear that the coordination center is the nitrogen atom of the ts molecule. The full infrared spectra in the range 500–70 cm^{-1} are reported in Table 6.

The nickel derivatives show different properties as the size of the halogen increases. The chloro- and bromo-derivatives are yellow-green and dark yellow respectively as opposed to the dark brown iodo-derivative, and are less soluble than the iodo-derivative. It is known from literature data that the nickel(II) compounds of general formula $[NiL_2X_2]$ possess a different stereochemistry on passing from chlorine to iodine. The dark brown iodo-derivatives have a pseudo-tetrahedral symmetry, whereas the yellow chloro- and very often the bromo-derivatives have a pseudo-octahedral environment with bridging halides.

The reflectance spectra of $[Nits_2X_2]$ (X = Cl, Br) complexes show three major bands at 26600 – 24500 cm^{-1}, ~14000 cm^{-1}, and 8000 cm^{-1}, and all these are very weak in intensity. This is characteristic of octahedral nickel(II) complexes. These bands in O_h symmetry may be assigned to the transitions $^3A_2(F) \rightarrow {}^3T_1(P)\ \nu_3$; $^3A_2(F) \rightarrow {}^3T_1(F)\ \nu_2$; $^3A_2(F) \rightarrow {}^3T_2(F)\ \nu_1$. As the ν_3 is very wide it is difficult to apply the method proposed by Eilbek and co-workers (14) who

calculated the ligand field parameters from the visually estimated frequency of the center of gravity of the band. In order to avoid errors arising from this uncertain assignment and the ratios ν_2/ν_1 being equal to 1.66, range usually accepted for octahedral nickel(II) complexes (15), we have preferred to evaluate Dq, B', and β parameters from ν_1 and ν_2 values only. It may be further noted that ν_3 band is calculated to be equal to $12Dq + 15B'$ and resulted 25035 cm^{-1} and 23200 cm^{-1} for chloro- and bromo-derivatives, respectively. This is in quite good agreement with the observed bands.

A pseudo-tetrahedral structure has been assigned to the complex $[Nits_2I_2]$ on the basis of its electronic spectrum (2, 13, 16, 17). The $^3T_1 \rightarrow {}^3T_2$ transition (ν_1) appears as a symmetrical band near 5800 cm^{-1}. The medium strong band at 7400 cm^{-1} can be attributed to the $^3T_1 \rightarrow {}^3A_2$ transition (ν_2), while the band present at 15800 cm^{-1}, accompanied by a shoulder at 13700 cm^{-1} may be assigned to the ν_3 transition $^3T_1 \rightarrow {}^3T_1(P)$. The Dq value is 458 cm^{-1} and B' is 985 cm^{-1}. These values have been calculated using only ν_2 and ν_3 values, the assignment of ν_1 being very often ambiguous because of the presence of vibrations due to the ligand itself in the region near 5000 cm^{-1}.

The magnetic moments at room temperature of chloro- and bromo-nickel(II) complexes lie within the range usually observed for octahedral nickel(II) compounds. The magnetic moment of the iodo-derivative is near the lower limit of the range normally accepted for nickel(II) in a tetrahedral stereochemistry (18).

As for infrared spectra, the bands I, II, and III of the —N—C=S group and the ν(NH) stretching behave as in cobalt(II) derivatives. In particular the ν(NH) appears in the nickel(II) complexes as a sharp band at 3100, 3070, and 3200 cm^{-1} for chloro-, bromo-, and iodo-derivative, respectively. The stretching symmetric and antisymmetric of ν(C—S) shows positive shifts (Table 3).

Comparison of the electronic spectra of our complexes with those of derivatives involving Ni—S bonds and Ni—N bonds confirms that $[Nits_2X_2]$ derivatives are *N*-bonded, being the band energies at higher values than in *S*-bonded derivatives (6, 19). This fact strongly supports the infrared results that the coordination must therefore take place via the nitrogen atom. New medium strong bands appear at 222, 230, and 212 cm^{-1} for chloro-, bromo-, and iodo-derivative which could be attributed to a nickel–nitrogen interaction (8). As for the nickel–halide stretching vibrations, they are found at 183s and 155ms cm^{-1} for $[Nits_2Cl_2]$ and at 157s and 120s cm^{-1} for $[Nits_2Br_2]$ in good agreement with literature data for nickel(II) octahedral complexes (20, 21). The medium band at 205 cm^{-1} in $[Nits_2I_2]$ is due to ν(Ni—I) according to nickel–iodide values for pseudo-tetrahedral complexes (7).

The medium absorption bands present in the range 3480–3460 cm^{-1} ν(OH) and 1650–1630 cm^{-1} δ(HOH) in $[Cots_2Br_2]\cdot 2H_2O$ and $[Nits_2I_2]\cdot 2H_2O$, respectively, clearly confirm the presence of water of crystallization. Evidence that this water is purely lattice water is given by the absence of the typical bands of coordinated water. In fact, when the water is coordinated to a metal, besides the three fundamental modes of the free molecule, other vibrational modes such as wagging, twisting, and rocking are activated (22). Furthermore this water is lost near 95–100 °C while the coordinated water is lost near 150–160 °C.

N.M.R. Measurements

The thiomorpholin-3-thione has been extensively studied by means of n.m.r. techniques in a previous paper (1). The proton resonance of the NH-group was identified in the range 8.53–9.17 p.p.m. moving towards higher fields on decreasing the concentration. The extrapolated value at zero concentration is 8.36 p.p.m. This variation of the NH-proton resonance chemical shift might be explained in terms of intermolecular hydrogen bonds. In all the cobalt(II) and nickel(II) complexes the NH-group proton resonance was identified at 10.30 and 10.40 p.p.m., respectively. This chemical shift of about 2 p.p.m. towards lower field is ascribed to the electronic withdrawing of the metal from the nitrogen atom and the deshielding effect supports the hypothesis that the studied complexes are *N*-bonded.

Characterization of Thiazolidine-2-selenone (tzse)

The i.r. spectrum of tzse, recorded in $CHCl_3$ solution or in the solid phase, shows ν(NH) at 3400vs cm^{-1} for chloroform solution or at

TABLE 4. Most important bands of thiazolidine-2-selenone derivatives

Compounds	ν(N—H)	Selenoamide I	ν(C=Se) +δ(NCSe)	ν(C—S) Asym.	ν(C—S) Sym.	ν(M—X)*	ν(M—L)
tzse {solid	3110vs	1515vs	1285vs	705ms	655ms	—	—
tzse {$CHCl_3$ sol.	3400vs						
$[Cotzse_2Cl_2]\cdot 2H_2O$	3130vs	1530vs	1310vs	715s	660ms	321m, 305m	252m
$[Cotzse_2Br_2]\cdot H_2O$	3140s	1520vs	1300vs	695m	660ms	238m, 215m	250m
$[Cotzse_2I_2]\cdot 2H_2O$	3230m	1505vs	1290vs	695w	665w	206ms	255s
$[NitzseCl_2]$	3400vs	1560m	1310m	710w	—	$204m_b$, $154m_b$ $268m_t$, $240s_t$	180ms
$[NitzseBr_2]$	3350vs	1510m	1295ms	700w	660w	$158m_b$, $148m_b$ $200m_t$	171ms
$[Nitzse_2I_2]$	3350vs	1550m	1310w	690w	660w	$210m_t$	176ms

*b = bridging; t = terminal.

TABLE 5. *Dq* and *B'* values of the complexes

	ts*		ttz†(16)		tzse‡		ε-Thiocaprolactam (26)		Triphenylarsine oxide (27)		Triphenylphosphine oxide (28)		Dimethylacetamide (29)	
Compound	*Dq*	*B'*	*Dq*	*B'*	*Dq*	*B'*	*Dq*	*B'*	*Dq*	*B'*	*Dq*	*B'*	*Dq*	*B'*
CoL_2Cl_2	467	722	460	660	400	737	387	651	327	753	327	760	322	797
CoL_2Br_2	451	670	410	710	387	732	366	656	325	727	318	754	303	788
CoL_2I_2	430	643	360	710	382	719	340	640	321	717	305	—	307	745

*ts = thiomorpholin-3-thione.
†ttz = thiazolidine-2-thione.
‡tzse = thiazolidine-2-selenone.

3110vs in the solid state. The band B (23) or selenoamide band I, having a predominant C=N character, appears at 1515vs cm^{-1}, while the band, due to ν(C=Se) + δ(NCSe), is found at 1285vs cm^{-1}. The stretching modes attributed to the prevailing contribution of symmetric and asymmetric ν(C—S) are at 705ms and 655ms cm^{-1} (Table 4). The n.m.r. spectrum recorded in DMSO-d_6 solution shows two multiplets in the range between 3.30 and 3.95 p.p.m. (having TMS as internal reference). The proton resonance of the NH-group was identified at 10.80 p.p.m.

Thiazolidine-2-selenone Derivatives

An essentially tetrahedral geometry may be assigned to the compounds $[Cotzse_2X_2]$ (X = Cl, Br, I) on the basis of their electronic spectra (Table 2) and magnetic moments (Table 1). In the solid state spectra the bands showed the high intensities characteristic of this geometry. The spectra consist of a band in the range 15600 – 16150 cm^{-1} accompanied by a weaker band on the low-energy side of the stronger band in the chloro-derivative, and by a shoulder in the bromo-derivative. Strong absorptions are observed in the region 6600–6900 cm^{-1}. The first band may be identified with the $^4A_2 \rightarrow {}^4T_1(P)$ transition and the second with the $^4A_2 \rightarrow {}^4T_1(F)$ transition (24).

Using the ν_3 and ν_2 values we have calculated the crystal field parameters (2). *Dq* decreases in the order Cl > Br > I and this order is consistent with the generally accepted sequence of ligands in the spectrochemical series. In order to find out the position of the ligand in the spectrochemical series, the *Dq* values of the complexes were compared with the *Dq* values of known tetrahedral halide complexes of cobalt(II). Table 5, which lists the *Dq* and *B'* values of the complexes, suggests the following order for the ligands in the spectrochemical series: thiomorpholin-3-tione > thiazolidine-2-thione > thiazolidine-2-selenone > ε-thiocaprolactam > triphenylphosphine oxide > triphenylarsine oxide > dimethylacetamide. The *B'* values are of the order of 74–76% of the free ion value (967 cm^{-1}), suggesting that there is a considerable orbital overlap. The nephelauxetic parameter β shows an order Cl ≃ Br > I.

TABLE 6. Far i.r. (500–70 cm^{-1}) absorption bands

Compound	Far infrared spectra
ts	395ms, 370s, 361sh, 329s, 320sh, 194m, 160sh, 140ms, 86m, 70m
tzse	550s, 510s, 324s, 231ms, 92m, 71mw
$[Cots_2Cl_2]$	470mw, 400ms, 375mw, 360ms, 345ms, 325s, 310m, 290ms, 250m
$[Cots_2Br_2]\cdot 2H_2O$	500m, 475m, 390s, 360s, 330s, 300sh, 246m, 238s, 218m
$[Cots_2I_2]$	400s, 375w, 360s, 300vw, 245m, 222sh, 208m
$[Cotzse_2Cl_2]\cdot 2H_2O$	321m, 305m, 252m, 90m, 70m
$[Cotzse_2Br_2]\cdot H_2O$	315m, 250m, 238m, 215m, 90m, 70m
$[Cotzse_2I_2]\cdot 2H_2O$	470sh, 425w, 315ms, 255s, 206ms, 91m, 72m
$[Nits_2Cl_2]$	415s, 355s, 310w, 250m, 222m, 183s, 155ms, 110m
$[Nits_2Br_2]$	490m, 415vw, 400m, 380vw, 350ms, 230m, 220m, 188sh, 170ms, 157vs, 120s
$[Nits_2I_2]\cdot 2H_2O$	490w, 400w, 350m, 212m, 205m
$[NitzseCl_2]$	400m, 320sh, 314m, 268m, 240s, 222ms, 204m, 180ms, 154m, 88m, 70m
$[NitzseBr_2]$	500w, 400w, 320w, 250m, 200m, 171ms, 158m, 148m, 89m, 72m
$[Nitzse_2I_2]$	324m, 231m, 210m, 176ms, 89m, 72m

The most important bands present in the i.r. spectra of the ligand and its complexes in the region 4000–70 cm^{-1} are reported in Tables 4 and 6. The ν(NH) shows in cobalt complexes a negative shift of *ca.* 270 cm^{-1} having as reference the value of 3400 cm^{-1} for the free ligand in chloroform solution; working in Nujol mulls this absorption falls at 3110 cm^{-1} because of the presence of intermolecular hydrogen bonds.

While the bands due to the bonds involving sulfur and selenium atoms show positive shifts or are at the same wave numbers as in the free ligand, the large negative shift of ν(NH) seems to suggest that the nitrogen atom is involved in the coordination bond.

Using the "law of average environment" as already done for cobalt(II) ts derivatives, taking averages of *Dq* and *B'* values of CoL_4^{2+} and CoX_4^{2-} ions, and comparing our values against similar chromophores containing MN_2X_2 and MS_2X_2 chromophores, with selenium having the same soft character of sulfur, we can conclude that the cobalt(II) tzse derivatives contain cobalt–nitrogen bonds.

The medium strong bands present at 321 and 305 cm^{-1} for $[Cotzse_2Cl_2]\cdot 2H_2O$, 238 and 215 cm^{-1} for $[Cotzse_2Br_2]\cdot H_2O$ and 206 cm^{-1} for $[Cotzse_2I_2]\cdot 2H_2O$ can be attributed to ν(CoX), in good agreement with literature data and thiomorpholin-3-thione cobalt complexes (7, 8, 10–13).

In our spectra strong bands near 230 cm^{-1} are not present, where ν(CoS) was found for pyridine thiols cobalt derivatives (5). New bands for chloro-, bromo-, and iodo-derivative appear at 252m, 250m, and 255s cm^{-1} respectively, clearly due to ν(CoN) stretching modes (7–9). The same values have been found in the $[Cots_2X_2]$ complexes.

In all the complexes medium strong bands appear in the range 3450–3400 and 1630–1620 cm^{-1} due to ν(OH) and δ(HOH) thus confirming the presence of crystallization water. As already pointed out this water is lattice water being lost in the range 95–100 °C and because the vibrational modes of coordinated water are not present in the expected ranges (22).

The solid state electronic spectra of nickel(II) derivatives are consistent with a pseudo-tetrahedral symmetry (Table 2). The band present in the range 12000 – 12500 cm^{-1} is attributed to the ν_3 transition $^3T_1 \rightarrow {}^3T_1(P)$ and the ν_2 transition $^3T_1 \rightarrow {}^3A_2$ appears in the range 6500 – 6900 cm^{-1}, while the $^3T_1 \rightarrow {}^3T_2$ transition (ν_1) appears at 5000 cm^{-1}. The magnetic moments at room temperature lie in the range 3.6–3.9 B.M. These values, lower than 4.1 B.M., are expected when the effects of distortion are operative as in our complexes.

The nickel derivatives show the ν(NH) stretching as a broad band at 3400 – 3350 cm^{-1}, while the selenoamide I, ν(C═Se) + δ(NCSe) and symmetric and asymmetric ν(C—S) behave as in cobalt derivatives. In the far infrared

region, the values found at 204 and 154 cm^{-1} for [$NitzseCl_2$] and 158 and 148 cm^{-1} for [$NitzseBr_2$] are typical for halide bridged nickel(II) complexes (20, 21). The stretching modes for ν(NiX) (X = Cl, Br) for terminal halides lie at 268 and 240 cm^{-1} for chloro- and 200 cm^{-1} for bromo-derivative (20, 21). The compound [$Nitzse_2I_2$] shows an absorption band at 210 cm^{-1} clearly due to ν(NiI). Furthermore, no bands are present in the range 230–220 cm^{-1} typical for ν(NiN), as already observed in ts complexes. In all the three complexes studied here new medium strong bands appear at 180, 171, and 176 cm^{-1} for chloro-, bromo-, and iodo-derivatives respectively. Any assignment is, however, at the moment impossible because of the lack of literature data concerning the position of ν(NiSe).

The n.m.r. spectra of cobalt and nickel complexes in DMSO-d_6, as in the case of ts derivatives have broad bands because of the presence of a paramagnetic center and a detailed analysis of the individual band is, therefore, impossible. It is clear, however, that in cobalt complexes there is a shift of the NH-proton resonance of about 1.5 p.p.m. towards lower field. This fact strongly supports that tzse cobalt(II) derivatives are *N*-bonded in good agreement with the electronic spectra and i.r. conclusions. In the nickel(II) complexes the NH resonance appears broadened, but at the same value as in the free ligand, 10.80 p.p.m.

Experimental

Preparation of Thiomorpholin-3-thione

ts was prepared by treating thiomorpholin-3-one with an excess of P_4S_{10} slurry in refluxing benzene as previously described (1), m.p. 141–141.5 °C.

Preparation of Thiazolidine-2-selenone

tzse was prepared by reaction of NaHSe and 1,3-thiazolidine-2-methylthiol in absolute ethanol for 1 or 2 h at room temperature. Ethanol was distilled and from the cooled solution the ligand separated out as white crystals. The crude product was recrystallized from chloroform/petroleum ether 30–50 °C, m.p. 125–126 °C.

Anal. Calcd. for C_3H_5NSSe (166.10): C, 21.7; H, 3.0. Found: Mol. wt. 170; C, 21.7; H, 3.0.

Preparation of Complexes

All compounds were obtained by reaction of $MX_2 \cdot nH_2O$ (M = Co, Ni; X = Cl, Br, I) in refluxing stirred chloroform solution of the ligand for 48 h for the ts derivatives and for 2–4 h for the tzse ones.

I.R. Measurements

The i.r. spectra have been recorded in the range 4 000 – 200 cm^{-1} with Perkin–Elmer 457 and 225 spectrophotometers as KBr discs or in $CHCl_3$ solution. The far i.r. spectra (400–70 cm^{-1}) have been recorded as Nujol mulls between polyethylene sheets on a Hitachi Perkin–Elmer FIS 3 spectrophotometer.

Visible and U.V. spectra

Solid state electronic spectra have been recorded with a Beckman DK2A spectrophotometer by the method of Venanzi and co-workers (25).

Magnetic Susceptibility Measurements

These were carried out by use of the Gouy method. Molecular susceptibilities were corrected for diamagnetism of the component atoms by use of the Pascal's constants.

Conductivity Measurements

These measurements were carried out with a WTW, LBR type conductivity bridge for 10^{-3} *M N,N'*-dimethylformamide solutions at 25 ± 0.1 °C. All the complexes are non-electrolytes.

N.M.R. Spectra

The n.m.r. spectra (for the thiazolidine-2-selenone and cobalt(II) and nickel(II) derivatives) were measured in DMSO-d_6 solutions with a Jeol JNM-C 60 HL instrument at 60 MHz.

Molecular Weight Determination

Molecular weight determination was carried out by an Hitachi Perkin–Elmer 115 instrument in methanol solution at 25 °C.

We thank Dr. G. Colombini for his experimental work and the Consiglio Nazionale delle Ricerche of Italy for financial support.

1. D. De Filippo, A. Lai, C. Preti, E. F. Trogu, and G. Verani. J. Inorg. Nucl. Chem. **36**, 73 (1974).
2. A. E. Underhill and D. E. Billing. Nature, **210**, 834 (1966).
3. C. N. R. Rao and R. Venkataraghavan. Spectrochim. Acta, **18**, 541 (1962).
4. P. P. Singh and R. Rivest. Can. J. Chem. **46**, 2361 (1968).
5. B. P. Kennedy and A. B. P. Lever. Can. J. Chem. **50**, 3488 (1972).
6. A. B. P. Lever. Inorganic electronic spectroscopy. Elsevier, Amsterdam. 1968.
7. W. J. Eilbeck, F. Holmes, C. E. Taylor, and A. E. Underhill. J. Chem. Soc. (A), 128 (1968).
8. M. J. M. Campbell, D. W. Card, R. Grzeskowiak, and M. Goldstein. J. Chem. Soc. Dalton, 1687 (1972).
9. J. Reedijk. Rec. Trav. Chim. **90**, 117 (1971).
10. E. J. Duff, M. N. Hughes, and K. J. Rutt. J. Chem. Soc. (A), 2354 (1968).
11. E. J. Duff, M. N. Hughes, and K. J. Rutt. J. Chem. Soc. (A), 2101 (1969).
12. C. E. Taylor and A. E. Underhill. J. Chem. Soc. (A), 368 (1969).
13. W. J. Eilbeck, F. Holmes, C. E. Taylor, and A. E. Underhill. J. Chem. Soc. (A), 1189 (1968).
14. W. J. Eilbeck, F. Holmes, C. E. Taylor, and A. E. Underhill. J. Chem. Soc. (A), 128 (1968).

15. L. SACCONI. Trans. Metal Chem. **4**, 199 (1968).
16. D. DE FILIPPO and C. PRETI. J. Chem. Soc. (A), 1904 (1970).
17. S. L. HOLT and R. L. CARLIN. J. Am. Chem. Soc. **86**, 3017 (1964).
18. B. N. FIGGIS and J. LEWIS. Progr. Inorg. Chem. **6**, 37 (1964).
19. J. R. ALLAN, D. H. BROWN, and M. LAPPIN. J. Inorg. Nucl. Chem. **32**, 2287 (1970).
20. C. POSTMUS, J. R. FERRARO, A. QUATTROCHI, K. SHOBATAKE, and K. NAKAMOTO. Inorg. Chem. **8**, 1851 (1969).
21. M. GOLDSTEIN and W. D. UNSWORTH. Spectrochim. Acta A, **28**, 1107 (1972).
22. K. NAKAMOTO. Infrared spectra of inorganic and coordination compounds. Wiley, New York. 1963.
23. K. JENSEN and P. H. NIELSEN. Acta Chem. Scand. **20**, 597 (1966).
24. R. L. CARLIN. Trans. Metal Chem. **1**, 1 (1968).
25. G. DYER, J. G. HARTLEY, and L. M. VENANZI. J. Chem. Soc. (A), 1293 (1965).
26. S. K. MADAN and C. GOLDSTEIN. J. Inorg. Nucl. Chem. **28**, 1251 (1966).
27. D. M. L. GOODGAME, M. GOODGAME, and F. A. COTTON. Inorg. Chem. **1**, 239 (1962).
28. F. A. COTTON, D. M. L. GOODGAME, and M. GOODGAME. J. Am. Chem. Soc. **83**, 4690 (1961).
29. S. K. MADAN and A. M. DONOHUE. J. Inorg. Nucl. Chem. **28**, 1617 (1966).

Constituents of *Solidago* Species. Part VI.[1] The Constitution of Diterpenoids from a Chemically Distinct Variety of *Solidago serotina*

ROBERT MCCRINDLE[2] AND ETSU NAKAMURA

Chemistry Department, University of Guelph, Guelph, Ontario

Received January 16, 1974

ROBERT MCCRINDLE and ETSU NAKAMURA. Can. J. Chem. **52**, 2029 (1974).

One known (**1**) and eight new (**3**, **5**, **6***a*, **7**, **8***a*, **15**, **16**, and **19***b*) diterpenoids have been isolated from a chemically distinct subgroup within the species *Solidago serotina* Ait. The constitution and stereochemistry of the new compounds are deduced from their spectroscopic properties and chemical reactions. Of key importance are the conversions of (*i*) **6***a* and **8***a* into **8***b*, which has been synthesized from methyl kolavenate (**9**); (*ii*) **1** and **15** into **3**; and (*iii*) **15** and **19***b* into **16**. Also discussed are the cleavages of the epoxides **10** and **15** with boron trifluoride which result in rearrangement, the products being **12** and a mixture of **16**, **17***a*, and **17***b*, respectively.

ROBERT MCCRINDLE et ETSU NAKAMURA. Can. J. Chem. **52**, 2029 (1974).

On a isolé neuf diterpénoïdes à partir d'un sous groupe chimiquement distinct à l'intérieur de l'espèce de *Solidago serotina* Ait; parmi ces composés un était déjà connu (**1**) et huit sont nouveaux (**3**, **5**, **6***a*, **7**, **8***a*, **15**, **16** et **19***b*). On a déduit la constitution et la stéréochimie des nouveaux composés à partir de leurs réactions chimiques et de leurs propriétés spectroscopiques. Les réactions suivantes sont de prime importance: (*i*) **6***a* et **8***a* peuvent être transformés en **8***b* que l'on a synthétisé à partir du kolavénate de méthyle (**9**); (*ii*) **1** et **15** peuvent être transformés en **3**; (*iii*) **15** et **19***b* peuvent être transformés en **16**. On discute aussi des résultats obtenus lors de l'ouverture des époxydes **10** et **15** par le trifluorure de bore alors que des réarrangements se produisent; les produits sont respectivement **12** et un mélange de **16**, **17***a* et **17***b*.

[Traduit par le journal]

In recent papers (1, 2) we have assigned structures to 11 new diterpenoids from the roots of *Solidago serotina* Ait. We have now discovered several clones of this species[3] which, although almost indistinguishable morphologically from the plants studied earlier (1, 2), elaborate an entirely different set of diterpenoids. In the present paper the constitution and stereochemistry of these nine compounds are assigned.

Column chromatography over silica gel of an ether extract of ground, dried roots obtained from the clones discussed above and then preparative t.l.c. of the individual fractions afforded nine neutral diterpenoids. No related acidic constituents were detected in the extract. The nine compounds will be discussed in a sequence, least polar first, which corresponds to their relative chromatographic polarities on silica gel.

[1]For part V see ref. 1.

[2]To whom correspondence should be addressed.

[3]Dr. Jean R. Beaudry, Département des Sciences biologiques, Université de Montréal, Montréal, Québec, to whom we are grateful for the identification of this taxon, has informed us that, contrary to footnote 3 in ref. 2, the name used here is preferred rather than *S. gigantea* Ait. var. *serotina* (Kuntze) Cronq.

Compound A

The least polar compound, the oily furano-olefin **1**, $[\alpha]_D$ −48°, was a minor component of the extract. The presence of the β-substituted furan ring, inferred from its color reaction with Ehrlich's reagent, was confirmed by the presence of the typical (see for example ref. 2) resonance pattern arising from the three aromatic protons at τ 2.75, 2.89, and 3.82 in its n.m.r. spectrum. In addition, this spectrum reveals the presence of one olefinic proton (τ 4.83, m) and four methyl groups: two tertiary (τ 9.01 and 9.26), one secondary (τ 9.15, d, J = 5.5 Hz), and the remaining one on an olefinic bond (τ 8.44, broad s). These structural components are readily accommodated in a clerodane skeleton (**2**) and immediately suggested the identity of this furano-olefin as **1** or a stereoisomer. Direct comparison of compound A with an authentic sample of **1**, prepared (3) from hardwickiic acid, showed the two to be identical. The isolation of **1** from the bulbs of *Annona coriacea* has been recorded (4).

Compound B

The next constituent **3**, m.p. 93–94°, $[\alpha]_D$ −19°, was readily recognized as a close relative of com-

Can. J. Chem. Downloaded from www.nrcresearchpress.com by 86.111.144.194 on 09/06/12
For personal use only.

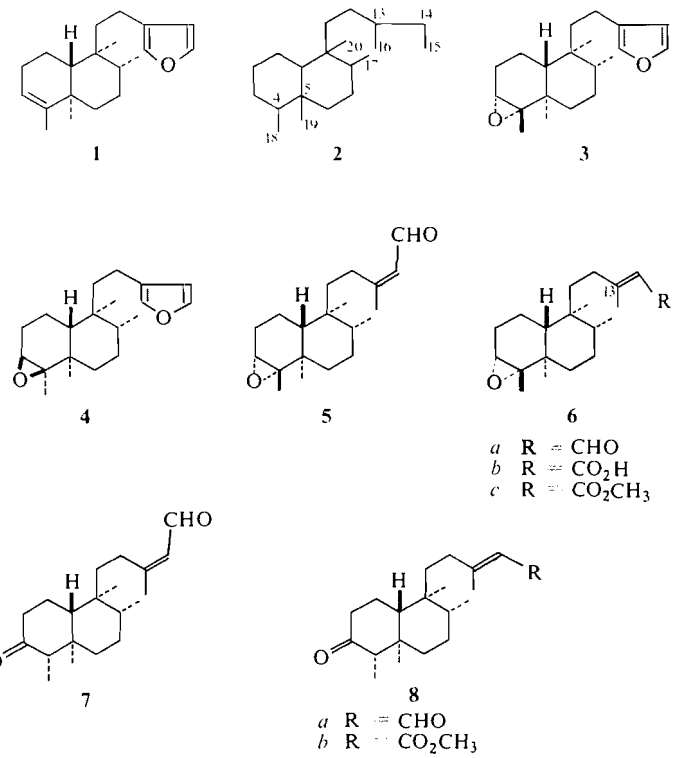

pound A. Thus it also gives a positive test with Ehrlich's reagent and has resonances in its n.m.r. spectrum assignable to one β and two α furan protons and four methyl groups. The n.m.r. spectrum also indicates the difference between the two compounds, the resonances attributable to a proton and a methyl group on an olefinic bond in compound A being replaced by those of a proton (τ 7.20) and a methyl group (τ 8.88) attached to an epoxide ring in compound B. The α-orientation of this ring was inferred from the multiplicity (3) of the H-3 resonance (broad s, $W_{1/2}$ = 4 Hz), thus allowing a tentative assignment of structure, **3**, to the compound. Confirmation of this assignment was readily obtained by epoxidation of compound A. As anticipated (3), the major product was the oily epoxide **4** formed by attack of the reagent on the less hindered β-face of ring A in **1**. However the minor, slightly less polar product, the α-epoxide (**3**) was identical with compound B.

Compounds C–F

The next four compounds (**5**, **6***a*, **7**, **8***a*) are all oily, unstable α,β-unsaturated aldehydes, two of which bear in addition an epoxy ring while the other two contain ketonic carbonyl groups. The difference within the pairs of compounds arises from geometric isomerism around the olefinic bond.

Compound C, **5**, was obtained as a very minor constituent of the extract. Because of a lack of material it was not submitted for elemental analysis, however a structure can be assigned with assurance on the basis of its spectroscopic properties and close similarity to compound D. The conjugated carbonyl system results in i.r. and u.v. absorption at 1675 cm^{-1} and 238 nm, respectively, and n.m.r. doublets (J = 7.5 Hz) from the aldehydic (τ 0.22) and vinylic (τ 4.23) protons. Also discernible in the n.m.r. spectrum are resonances attributable to an epoxide proton (τ 7.25) and five methyl groups, of which one is secondary while two are on quaternary carbon atoms. One (τ 8.92) of the remaining two is attached to the epoxide ring and the other (τ 8.10) to the olefinic bond. The chemical shift of the latter indicates (5) that it is *trans* to the aldehyde group.

The spectroscopic data obtained for compound D, **6***a*, match closely those of the previous compound, except that the methyl attached to C-13 now resonates at τ 7.85 since it is *cis* to the aldehyde group. Indeed the n.m.r. spectra of com-

Can. J. Chem. Downloaded from www.nrcresearchpress.com by 86.111.144.194 on 09/06/12
For personal use only.

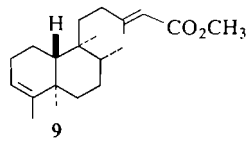

9

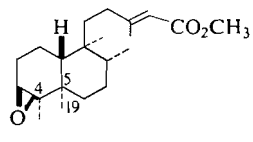

10

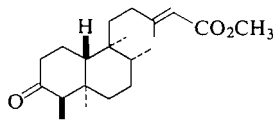

11

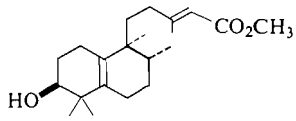

12

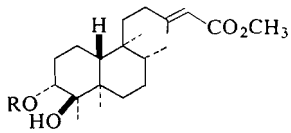

13

a R = $COCCl_3$
b R = H

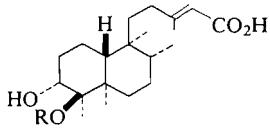

14

pounds B (**3**), C (**5**), and D (**6***a*) are all remarkably similar apart from the resonances arising from the functionalized portion of the side chain. The obvious conclusion, that the decalin moiety of compounds C and D have a constitution and relative stereochemistry identical to that of B, was substantiated for D by a chemical correlation (see below) with methyl kolavenate of well defined (6) structure and absolute stereochemistry.

The n.m.r., u.v., and i.r. spectra of compound E (**7**), which was also isolated in quantities insufficient for elemental analysis, suggest a close structural relationship with compound C. The replacement of the C-3, C-4 epoxide in the latter by a C-3 ketone is readily deduced from the appearance of a new i.r. carbonyl band at 1705 cm^{-1} and the substitution of the resonances arising from the proton and methyl group attached to the epoxide by an additional secondary methyl group (τ 9.16, d). This resonance is readily distinguished from that of the other secondary methyl group (τ 9.20, d) since the former is not broadened by "virtual coupling", there being no hydrogen atoms on C-3 or C-5.

Compound F (**8***a*) bears the same relationship to D as E does to C. In F, the C-4 secondary methyl group gives rise to a very clean doublet in its n.m.r. spectrum at τ 9.17 in deuteriochloroform and at τ 9.07 in benzene. The magnitude of this downfield shift defines (7) clearly the orientation of this methyl group as equatorial (α). The structures proposed for D and F (and presumably also those of C and E) were confirmed by conversion of both into the keto-ester **8***b* which was also obtained from methyl kolavenate (**9**) as follows.

The known epoxide **10**[4] was prepared (8) from methyl kolavenate. An attempt was then made to convert **10** with boron trifluoride etherate into the keto-ester **11**, which on treatment with sodium methoxide – methanol was expected to furnish the desired C-4 epimer (**8***b*). However as feared on mechanistic grounds, bearing in mind the stereochemical relationship of the C_5—C_{19} and C_4—O bonds, **10** on exposure to the Lewis acid formed no detectable amount of the keto-ester **11** but only the alcohol **12**. A second approach for the preparation of **8***b* from **10** was successful. Reaction of the epoxide (**10**) with trichloroacetic acid resulted in the expected (9) *trans*-diaxial opening of the ring and formation of the trichloroacetate **13***a* which was then converted with sodium boro-

[4]This compound appeared homogeneous on t.l.c. and n.m.r. examination but, bearing in mind the outcome (see above) of the epoxidation of **1**, it probably contained a small proportion of the α-epoxide.

Can. J. Chem. Downloaded from www.nrcresearchpress.com by 86.111.144.194 on 09/06/12
For personal use only.

Can. J. Chem. Downloaded from www.nrcresearchpress.com by 86.111.144.194 on 09/06/12
For personal use only.

hydride into the diol **13***b*. This proved a much more compliant substrate, since on exposure to boron trifluoride it afforded the desired ketone **8***b*. In this case, migration of the C-3 hydride to a C-4 cation, resulting from acid-catalyzed heterolysis of the tertiary hydroxyl group, competes favorably with methyl migration from C-5 since the former process is assisted by formation of the C-3 ketone. The stereochemistry at C-4 in **8***b* can be assigned with assurance since the migrating hydride has the β-orientation. Oxidation of compound F with selenium dioxide – hydrogen peroxide in *tert*-butyl alcohol (10) and then methylation yielded the same keto-ester (**8***b*) providing unambiguous proof of the structure of F as **8***a*.

In an attempt to substantiate our conclusion concerning the structure (**6***a*) of compound D, its transformation into the diol **13***b* prepared earlier from methyl kolavenate (see above) was undertaken. The projected route involved oxidation of **6***a* to the corresponding acid **6***b* and formation of the diol, or a derivative, by acid-catalyzed opening of the epoxide ring in the derived ester **6***c*. In the event, an unexpectedly convenient correlation of **6***a* with a known compound was achieved. Thus, oxidation of compound D with selenium dioxide – hydrogen peroxide and then methylation yielded, rather than the expected epoxy-ester **6***c*, the keto-ester **8***b* already prepared from compound F and methyl kolavenate. Presumably, an acidic selenium species reacts with the epoxide moiety forming a derivative (**14**) of the diol, which then decomposes to the ketone.

Compound G

Compound G (**15**), an oil of $[\alpha]_D$ −21°, was the major diterpenoid constituent in the plant. It was readily formulated as a β-substituted $\Delta^{\alpha,\beta}$-butenolide, a structural feature frequently found (11) in diterpenoids from *Solidago* species. The presence of this functional group accounts for absorption at 214 nm in the u.v., and 1775 and 1750 cm^{-1} in the i.r., and resonances at τ 4.27 (olefinic proton) and 5.37 (—CH_2O—). The remainder of the n.m.r. spectrum is nearly identical with that of compound B, except for the signals due to the three furan protons in the latter. This led to the assignment of structure **15** to the compound. Indeed, reduction of compound G with diisobutyl aluminum hydride provided sound evidence for this assignment since it afforded, in addition to a complex mixture of more polar materials, compound B (**3**).

Compound H

The penultimate constituent, **16**, an oil of $[\alpha]_D$ +22°, was only slightly more polar than that (**15**) immediately preceding it. Its spectral characteristics in general but particularly a comparison of its n.m.r. spectrum with those of compounds F (**8***a*) and G (**15**) indicated that it should be assigned the structure **16**. The sign and magnitude (see Experimental) of the benzene-induced shift of the resonance arising from the secondary methyl group at C-4 represents important confirmatory evidence for the α-orientation of this group. In an attempt to confirm the above assignment, compound G of proven structure (**15**) was treated with boron trifluoride in the expectation that at least some **16** would form. Ketone formation was expected in this case since the C-5 methyl group is *cis* to the C_4—O bond and might be expected to compete less favorably with the C-3 hydride in migration than in **10** (see above). However, when this reaction of **15** was carried out only a trace of a compound tentatively identified as **16** formed, the two major products being the rearranged hydroxy-butenolides **17***a* and **17***b*.[5] Comment should be made on the observations that with boron trifluoride the β-epoxide **10** gives almost exclusively the $\Delta^{5,10}$-olefin (**12**) while the α-epoxide **15** furnishes the $\Delta^{5,6}$ (**17***a*)- and $\Delta^{5,10}$ (**17***b*)-olefins in approximately equal amounts. One possible explanation is that in the former case, as the epoxide ring opens, the C-3 oxygen function is utilized (**18** or a related species) in stabilizing the incipient cation at C-5 resulting from methyl migration to C-4. In this situation the oxygen atom is suitably disposed to remove the C-10 proton in an intramolecular process, forming the tetrasubstituted olefin. In the case of an α-epoxide, a mechanism of this type is impossible sterically and thus *either* the C-10 *or* the C-6 β-proton, both of which are *trans*-antiparallel to the C-5 methyl in **15**, is removed in an intermolecular reaction.

Since cleavage of the epoxide ring in **15** with boron trifluoride did not produce significant amounts of the ketone **16**, we turned to a reaction sequence analogous to that which had proved successful in the correlation of **8***b* and **10**. Treatment of **15** with trichloroacetic acid afforded the

[5]When tissue of the variety of *S. serotina* dealt with in this paper is stored for several weeks at −10° before extraction, these extracts contain **17***a* and **17***b* whereas extracts of freshly collected roots do not.

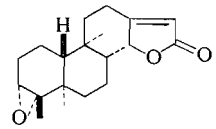

15

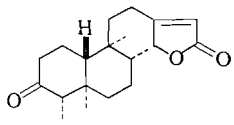

16

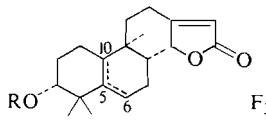

17

a $\Delta^{5,6}$; R = H

b $\Delta^{5,10}$; R = H

c $\Delta^{5,10}$; R = $COCH_3$

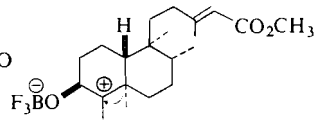

18

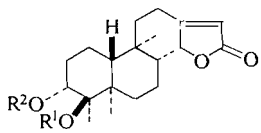

19

a R^1 = $COCCl_3$; R^2 = H

b R^1 = H; R^2 = H

c R^1 = H; R^2 = $COCH_3$

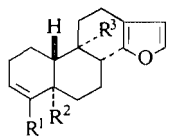

20

a R^1 = R^2 = CH_3; R^3 = CO_2H

b R^1 = R^3 = CH_3; R^2 = CO_2H

c R^1 = CO_2H; R^2 = R^3 = CH_3

trichloroacetate **19***a*, m.p. 130–131°. Reduction of this compound with sodium borohydride yielded, rather than the desired diol (**19***b*), a much more polar material which appeared on spectral evidence to have been formed by reductive cleavage of both the trichloroacetate group and the butenolide ring. However, the trichloroacetate itself was smoothly converted with boron trifluoride into the desired ketone (**16**). The outcome of this reaction sequence provides convincing proof of the structure of **16**, including the configuration at C-4, since the **19***a* → **16** transformation involves migration of a β-hydride from C-3 to C-4.

Compound I

The final constituent, the diol **19***b* was obtained as an oil, $[\alpha]_D$ −9°. However, the corresponding monoacetate (**19***c*) crystallized readily and had m.p. 206–209°, $[\alpha]_D$ −24°. The i.r. and n.m.r. spectra of these compounds indicated the presence of the functional groups included in **19***b* and **19***c*, while the lack of i.r. absorption resulting from intramolecular hydrogen bonding between the two hydroxyl groups in **19***b* was taken as proof of their *trans* relationship. Treatment of the diol with boron trifluoride furnished the known ketone **16** and provided convincing evidence for the structure (**19***b*) assigned to the former.

Experimental

Melting points are uncorrected and were determined on a Kofler hot-stage apparatus. Specific rotations refer to chloroform solutions and were measured on a Bendix Ericsson ETL-NPL automatic polarimeter. For analytical and preparative t.l.c., chromatoplates were spread with Kieselgel G (Merck). Gas–liquid chromatography was carried out with a Varian Aerograph 1200 gas chromatograph using a stainless steel column (1/8 in. × 10 ft) packed with 20% carbowax 20M and nitrogen as carrier gas (with a flow rate of 25 ml/min) at 200°. Light petroleum was of b.p. 60–80°. Microanalyses were by Dr. A. Woon-Fat or Mr. H. S. McKinnon, Guelph. Infrared spectra were recorded for carbon tetrachloride solutions

Can. J. Chem. Downloaded from www.nrcresearchpress.com by 86.111.144.194 on 09/06/12
For personal use only.

Can. J. Chem. Downloaded from www.nrcresearchpress.com by 86.111.144.194 on 09/06/12
For personal use only.

on a Beckmann 1R5A or 1R12 spectrophotometer and u.v. spectra in ethanol on a Unicam S.P. 800 spectrophotometer. Proton magnetic resonance spectra were run on a Varian Associates A-60A spectrometer using carbon tetrachloride as solvent, unless otherwise stated, and tetramethylsilane as internal standard. Mass spectra were run on a Varian Associates CH7 instrument.

Isolation Procedure

(*i*) The ground, air-dried (2 days) roots (150 g) of *Solidago serotina* Ait.[6] were continuously extracted with ether for 6 h in a Soxhlet apparatus. The extract (5.7 g), which showed one intense and one faint spot on analytical t.l.c. when sprayed with Ehrlich reagent and a very complex spot pattern with sulfuric acid and heating, was chromatographed over a silica gel (Baker) column (170 g) in light petroleum. Nine fractions were collected, the last two, eluted with ethyl acetate and ethyl acetate – acetic acid (9:1), being discarded since they were essentially devoid (n.m.r.) of terpenoids.

Fraction I (110 mg), eluted with light petroleum, on preparative t.l.c. (light petroleum, run twice) afforded the minor furanoid compound, the furano-olefin **1** (38 mg). This oil, after distillation *in vacuo*, had $[\alpha]_D$ −48° (*c*, 1.85) and was identical (n.m.r., mass spectrum, and t.l.c. on both silica gel and silica gel – silver nitrate, 22:3) to the furano-olefin obtained from junceic (**20***a*, (3)), maingayic (**20***b*, (12)), and hardwickiic (**20***c*, (12)) acids.

Fraction II (277 mg), eluted with ethyl acetate – light petroleum (1:49), contained the major furanoid component, compound B (**3**), which was purified by preparative t.l.c. (ethyl acetate – light petroleum, 1:10). The resulting solid (110 mg) crystallized from methanol and had m.p. 93–94°, $[\alpha]_D$ −19° (*c*, 0.76); ν_{max} 887 and 873 cm^{-1}; τ 2.75, 2.89, 3.82 (all m, 1H, furan protons), 7.20 (s, 1 H-3, $w_{1/2}$ = 4 Hz), 8.88 (s, 3 H-18), 8.98 (s, 3 H-19), 9.18 (d, 3 H-17, *J* = 6 Hz), and 9.33 (s, 3 H-20).

Anal. Calcd. for $C_{20}H_{30}O_2$: C, 79.42; H, 10.00. Found: C, 79.43; H, 9.90.

Fractions III (252 mg), IV (207 mg), and V (199 mg), eluted with ethyl acetate – light petroleum (1:19, 1:9, and 1:4, respectively), contained compounds C–G. The three fractions were combined and submitted to repeated preparative t.l.c. (ethyl acetate – light petroleum, 1:4). This furnished all five compounds as oils which were purified further by distillation *in vacuo*. Compound C, the epoxy-aldehyde **5** (17 mg) had ν_{max} 1675 cm^{-1}; λ_{max} 238 nm (ε 8900); τ 0.22 (d, 1 H-15, *J* = 7.5 Hz), 4.23 (d, 1 H-14, *J* = 7.5 Hz), 7.25 (s, 1 H-3, $w_{1/2}$ = 4.5 Hz), 8.10 (d, 3 H-16, *J* = 1 Hz), 8.92 (s, 3 H-18), 9.01 (s, 3 H-19), 9.17 (d, 3 H-17, *J* = 6 Hz), and 9.32 (s, 3 H-20). Compound D, the epoxy-aldehyde **6***a* (54 mg) had ν_{max} 1675 cm^{-1}; λ_{max} 237 nm (ε 8500); τ 0.18 (d, 1 H-15, *J* = 7.5 Hz), 4.26 (d, 1 H-14, *J* = 7.5 Hz), 7.21 (s, 1 H-3, $w_{1/2}$ = 4.5 Hz), 7.85 (d, 3 H-16, *J* = 1 Hz), 8.90 (s, 3 H-18), 8.98 (s, 3 H-19), 9.16 (d, 3 H-17, *J* = 6 Hz), and 9.32 (s, 3 H-20).

Anal. Calcd. for $C_{20}H_{32}O_2$: C, 78.90; H, 10.59. Found: C, 79.01; H, 10.50.

Compound E, the keto-aldehyde 7 (28 mg) had ν_{max} 1705 and 1675 cm^{-1}; λ_{max} 238 (ε 8600); τ 0.05 (d, 1 H-15, *J* = 7.5 Hz), 4.15 (d, 1 H-14, *J* = 7.5 Hz), 8.05 (d, 3 H-16, *J* = 1 Hz), 9.16 (d, 3 H-18, *J* = 6 Hz), 9.20 (d, 3 H-17, *J* = 6 Hz), 9.23 (s, 3 H-19), and 9.27 (s, 3 H-20). Compound F, the keto-aldehyde **8***a* (38 mg) had ν_{max} 1705 and 1675 cm^{-1}; λ_{max} 238 (ε 8500); τ 0.10 (d, 1 H-15, *J* = 7.5 Hz), 4.18 (d, 1 H-14, *J* = 7.5 Hz), 7.82 (d, 3 H-16, *J* = 1 Hz), 9.17 (d, 3 H-18, *J* = 6.5 Hz), 9.21 (d, 3 H-17, *J* = 6 Hz), 9.23 (s, 3 H-19), and 9.27 (s, 3 H-20); τ (C_6D_6) 8.35 (d, 3 H-16, *J* = 1 Hz), 9.07 (d, 3 H-18, *J* = 6.5 Hz), 9.36 (d, 3 H-17, *J* = 6 Hz), 9.43 (s, 3 H-20), and 9.52 (s, 3 H-19).

Anal. Calcd. for $C_{20}H_{32}O_2$: C, 78.90; H, 10.59. Found: C, 79.13; H, 10.72.

Compound G, the epoxy-butenolide **15** (149 mg) was also obtained as the major constituent (550 mg) of fraction VI (1.15 g), eluted with ethyl acetate – light petroleum (3:7) from which it was separated by preparative t.l.c. (ethyl acetate – light petroleum, 1:4, run twice). In addition, this preparative t.l.c. afforded compound H, the keto-butenolide **16** (58 mg). The epoxy-butenolide **15** after distillation *in vacuo* had $[\alpha]_D$ −21° (*c*, 1.88); ν_{max} 1775 and 1750 cm^{-1}; λ_{max} 214 nm (ε 9900); *m/e* 318 (M); τ 4.27 (m, 1 H-14, $w_{1/2}$ = 4 Hz), 5.37 (d, 2 H-16, J_{obs} = 1.5 Hz), 7.20 (m, 1 H-3, $w_{1/2}$ = 3.5 Hz); 8.89 (s, 3 H-18), 8.98 (s, 3 H-19), 9.18 (d, 3 H-17, *J* = 6 Hz), and 9.31 (s, 3 H-20).

Anal. Calcd. for $C_{20}H_{30}O_3$: C, 75.43; H, 9.50. Found: C, 75.42; H, 9.82.

The keto-butenolide **16** was distilled *in vacuo* and had $[\alpha]_D$ +22° (*c*, 2.37); ν_{max} 1775, 1750, and 1705 cm^{-1}; λ_{max} 211 (ε 12 800); *m/e* 318 (M); τ ($CDCl_3$) 4.10 (m, 1 H-14, $w_{1/2}$ = 4.5 Hz), 5.20 (d, 2 H-16, *J* = 2 Hz), 9.08 (d, 3 H-18, *J* = 6.5 Hz), 9.13 (d, 3 H-17, *J* = 6 Hz), 9.18 (s, 3 H-19), and 9.23 (s, 3 H-20); τ (C_6D_6) 4.43 (m, 1 H-14, $w_{1/2}$ = 4 Hz), 5.92 (d, 2 H-16, *J* = 2 Hz), 9.03 (d, 3 H-18, *J* = 6.5 Hz), 9.37 (d, 3 H-17, *J* = 6 Hz), 9.41 (s, 3 H-20), and 9.50 (s, 3 H-19).

Anal. Calcd. for $C_{20}H_{30}O_3$: C, 75.43; H, 9.50. Found: C, 75.21; H, 9.51.

Fraction VII (1.64 g), eluted with ethyl acetate – light petroleum (1:1), furnished by preparative t.l.c. (ethyl acetate – light petroleum, 5:6), further amounts of **15** (410 mg) and **16** (40 mg) and in addition compound **I**, the diol-butenolide **19***b* (162 mg). This compound was obtained as an oil which had $[\alpha]_D$ −9° (*c*, 1.25); ν_{max} 3630, 1785, and 1760 cm^{-1}; λ_{max} 212 (ε 9500); τ ($CDCl_3$) 4.13 (m, 1 H-14, $w_{1/2}$ = 4 Hz), 5.22 (d, 2 H-16, *J* = 1.5 Hz), 6.40 (s, 1 H-3, $w_{1/2}$ = 5.5 Hz), 7.12 (m, —O*H*, lost on D_2O exchange), 8.75 (s, 3 H-18), 8.87 (s, 3 H-19), 9.18 (d, 3 H-17, *J* = 6 Hz), and 9.22 (s, 3 H-20). Treatment of the diol with acetic anhydride – pyridine yielded the corresponding diol monoacetate **19***c*, which was purified by preparative t.l.c. (ethyl acetate – light petroleum, 1:3) and then crystallization from light petroleum. It had m.p. 206–209°; $[\alpha]_D$ −24° (*c*, 1.16), ν_{max} 3500, 1775, 1750, and 1730 cm^{-1}; τ ($CDCl_3$) 4.14 (m, 1 H-14, $w_{1/2}$ = 4 Hz), 5.22 (m, 2 H-16 + 1 H-3), 7.93 (s, —OCOC*H*$_3$), 8.88 (s, 3 H-18), 8.90 (s, 3 H-19), 9.18 (d, 3 H-17, *J* = 6 Hz), and 9.22 (s, 3 H-20).

[6]Voucher specimen number 73-10, Professeur Jean R. Beaudry, Département des Sciences Biologiques, Université de Montréal. This plant material was located and collected by Mr. A. B. Anderson, Department of Botany and Genetics, University of Guelph.

Can. J. Chem. Downloaded from www.nrcresearchpress.com by 86.111.144.194 on 09/06/12
For personal use only.

Anal. Calcd. for $C_{22}H_{34}O_5$: C, 69.81; H, 905. Found: C, 69.75; H, 9.28.

(*ii*) When an extractive from root tissue which had been stored at $-10°$ for 2 weeks was treated as above two additional compounds **17***a* and **17***b* were isolated. Extracts of fresh tissue contained no detectable quantities of these compounds which both have polarities on t.l.c. (ethyl acetate – light petroleum, 1:4, run twice) very similar to that of **16**. They were identified by direct comparison with samples prepared from **15** by treatment with boron trifluoride (see below).

Epoxidation of the Furano-olefin ***1***

The furano-olefin **1** (38 mg) was reacted in the dark with *m*-chloroperbenzoic acid (25 mg) in carbon tetrachloride (20 ml) at 20° for 3 h. The resulting solution was washed with aqueous sodium carbonate (10%; twice) and the solvent removed *in vacuo*. Preparative t.l.c. (ether – light petroleum, 1:40, run thrice) furnished the less polar component, the oily β-epoxide **4** (19 mg), which had $[\alpha]_D$ $-35°$ (*c*, 0.91); τ 2.78, 2.90, 3.86 (all m, 1 H, furan protons), 7.29 (m, 1 H-3, $w_{1/2}$ = 7 Hz), 8.87 (s, 3 H-18), 8.96 (s, 3 H-19), 9.18 (d, 3 H-17, J = 5.5 Hz), and 9.32 (s, 3 H-20); g.l.c. retention time, 21.4 min.

Anal. Calcd. for $C_{20}H_{30}O_2$: C, 79.42, H, 10.00. Found: C, 79.24; H, 10.22.

The more polar, minor α-epoxide **3** (1.5 mg) was identical (mass spectroscopy, t.l.c., g.l.c. retention time of 23.4 min) with compound B.

Conversion of the Epoxy-ester ***10*** *into the Keto-ester* ***8b***

The epoxide **10** (1.04 g, (8)) of methyl kolavenate was exposed to trichloroacetic acid (0.52 g) in carbon tetrachloride (30 ml) at 20° for 4.5 h. The resulting solution was washed with aqueous sodium bicarbonate, dried, and the solvent evaporated. Chromatography of the residue over silica gel (150 g) and elution with ethyl acetate – light petroleum (3:17) afforded the trichloroacetate **13***a*, which even after further purification by preparative t.l.c. (ethyl acetate – light petroleum, 1:4) failed to crystallize. It (470 mg) had τ 4.38 (m, 1 H-14, $w_{1/2}$ = 4 Hz), 5.21 (m, 1 H-3, $w_{1/2}$ = 5.5 Hz), 6.37 (s, 3H, $—CO_2CH_3$), 7.87 (d, 3 H-16, J = 1 Hz), 8.82 (s, 3 H-18), 8.90 (s, 3 H-19), 9.19 (d, 3 H-17, J = 5.5 Hz), and 9.26 (s, 3 H-20). Reaction of this trichloroacetate (390 mg) with excess sodium borohydride in ethanol (50 ml) at 20° for 3 h furnished the diol **13***b* (192 mg). Purification by preparative t.l.c. (ethyl acetate – light petroleum, 1:1) afforded an oil which had τ ($CDCl_3$) 4.33 (m, 1 H-14), 6.35 (s, 3H, $—CO_2CH_3$), 6.44 (m, 1 H-3), 7.86 (d, 3 H-16), J = 1 Hz); 8.78 (s, 3 H-18), 8.88 (s, 3 H-19), 9.21 (d, 3 H-17, J = 6 Hz), and 9.26 (s, 3 H-20).

Anal. Calcd. for $C_{21}H_{36}O_4$: C, 71.55; H, 10.29. Found: C, 71.09; H, 10.51.

The diol (126 mg) was treated with boron trifluoride etherate (2 ml) in anhydrous benzene (10 ml) at 20° for 30 min. The solution was diluted with ethyl acetate (20 ml) and washed with aqueous sodium bicarbonate, then brine, and dried. Preparative t.l.c. (ethyl acetate – light petroleum, 1:5, run twice) of the oil remaining after evaporation of the solvent afforded the ketone **8***b* which crystallized from light petroleum. It (44 mg) had m.p. 88–89°; $[\alpha]_D$ +22° (*c*, 2.86) ν_{max} 1710 and 1705 cm^{-1}; λ_{max} 220 (ε 12 000); τ 4.40 (m, 1 H-14), 6.38 (s, 3H, $—CO_2CH_3$), 7.85 (d, 3 H-16, J = 1 Hz), 9.16 (d, 3 H-18, J = 6 Hz), 9.23 (s, 3 H-19), 9.24 (d, 3 H-17, J = 5.5 Hz), and 9.27 (s, 3 H-20); τ (C_6D_6) 4.13 (m, 1 H-14), 6.48 (s, 3H, $—CO_2CH_3$), 7.77 (d, 3 H-16, J = 1 Hz), 9.06 (d, 3 H-18, J = 6.5 Hz), 9.32 (d, 3 H-17, J = 5.5 Hz), 9.42 (s, 3 H-20), and 9.49 (s, 3 H-19).

Anal. Calcd. for $C_{21}H_{34}O_3$: C, 75.41; H, 10.25. Found: C, 75.38; H, 10.39.

Conversion of the Keto-aldehyde ***8a*** *into the Keto-ester* ***8b***

The keto-aldehyde (37 mg) was dissolved in *tert*-butyl alcohol (5 ml) containing selenium dioxide (12.8 mg). A solution (0.5 ml, 1%) of hydrogen peroxide in *tert*-butyl alcohol was then added and the reaction mixture kept at 20°. Three further portions (0.5 ml each) of the hydrogen peroxide solution were added at *ca.* 5-h intervals. After a total of 30 h, ethanol (2 ml) and then ethyl acetate (40 ml) were added. The solution was washed with brine, dried, and the solvent evaporated. The residue in ether was treated briefly with a slight excess of diazomethane and the product submitted to preparative t.l.c. (ethyl acetate – light petroleum, 1:3, run twice). The material from two bands of very similar polarity was recovered. The major (12.5 mg), more polar, component crystallized from light petroleum and was identical (t.l.c., m.p., mixture m.p., n.m.r., and $[\alpha]_D$) with the keto-ester **8***b* prepared from methyl kolavenate (see above). An unidentified more polar component (10.5 mg) was also obtained.

Conversion of the Epoxy-aldehyde ***6a*** *into the Keto-ester* ***8b***

The epoxy-aldehyde **6***a* (35 mg) was reacted with selenium dioxide (11.2 mg) and hydrogen peroxide (0.5 ml, 1% solution) in *tert*-butyl alcohol as described above. Preparative t.l.c. (ethyl acetate – light petroleum, 1:3, run twice) afforded the keto-ester **8***b* (10.4 mg) and two unidentified more polar products (3 mg and 10.8 mg). The first of these three was identical (same criteria as above) with the sample of **8***b* prepared from methyl kolavenate.

Treatment of Epoxy-ester ***10*** *with Boron Trifluoride*

The epoxy-ester **10** (65 mg) was treated with boron trifluoride etherate (0.5 ml) in anhydrous benzene (10 ml) at 20° for 15 min. The resulting solution was diluted with ethyl acetate (40 ml), extracted with aqueous sodium bicarbonate, then brine, and dried. Evaporation of solvent left an oil which was submitted to preparative t.l.c. (ethyl acetate – light petroleum, 1:6). This afforded only one component (47 mg), the oily alcohol **12**. After distillation *in vacuo* it had ν_{max} 3600 and 1705 cm^{-1}; τ 4.41 (m, 1 H-14), 6.38 (s, 3H, $—CO_2CH_3$), 6.54 (t, 1 H-3, J_{obs} = 4.5 Hz), 7.86 (d, 3 H-16, J = 1 Hz), 9.00 (s, 6H, quaternary C—CH_3's), 9.12 (d, 3 H-17, J = 6 Hz), and 9.14 (s, 3H, quaternary C—CH_3).

Anal. Calcd. for $C_{21}H_{34}O_3$: C, 75.41; H, 10.25. Found: C, 75.12; H, 10.40.

Reduction of the Epoxy-butenolide ***15*** *with Diisobutyl Aluminum Hydride*

Diisobutyl aluminum hydride in hexane (20%, 2 ml) was added to the epoxy-butenolide **15** (120 mg) in dry tetrahydrofuran (10 ml) and the solution kept at $-20°$ for 1 h. Acetone (2 ml) was added and the solution allowed to warm up to 20°. It was then diluted with ethyl

acetate (20 ml) and washed with aqueous sodium sulfate. Preparative t.l.c. (ether – light petroleum, 1:30, run twice) of the oily residue (110 mg) from evaporation of the organic layer afforded the epoxy-furan **3** (14.5 mg) identical ($[\alpha]_D$, n.m.r., mass spectroscopy, t.l.c., g.l.c. retention time of 23.4 min) with material of natural provenance.

*Treatment of Epoxy-butenolide **15** with Boron Trifluoride*

Reaction of the epoxy-butenolide (307 mg) with boron trifluoride-etherate (2 ml) in anhydrous benzene (20 ml) at 20° for 15 min and work-up (dilution with ethyl acetate and washing with water) afforded an oily product. This gave two spots of very similar polarity on analytical t.l.c. (ethyl acetate – light petroleum, 1:4, run twice). The mixture was submitted to preparative t.l.c. (same solvent, run seven times). The plates showed two barely resolved bands. The upper half of the less polar band furnished the hydroxy-butenolide **17***a* (51 mg) which crystallized from light petroleum and had m.p. 120–122°; ν_{max} 3600, 1780, and 1750 cm^{-1}; *m/e* 318 (M); τ 4.22 (m, 1 H-14), 4.48 (m, 1 H-6, $w_{1/2}$ = 7 Hz), 5.28 (m, 2 H-16), 6.58 (m, 1 H-3, $w_{1/2}$ = 7 Hz), 7.33 (s, —O*H*, lost on D_2O exchange), 8.90 (s, 3 H-19), 8.98 (s, 3 H-18), 9.14 (d, 3 H-17, J = 6 Hz), and 9.27 (s, 3 H-20); τ ($CDCl_3$ with a *ca* 0.1 *M* ratio of Eu(DPM)$_3$ to **17***a*) 7.92 (s, 3 H-19), 8.43 (s, 3 H-18), 8.93 (s, 3 H-20), and 9.02 (d, 3 H-17, J = 6 Hz).

Anal. Calcd. for $C_{20}H_{30}O_3$: C, 75.43; H, 9.50. Found: C, 75.36; H, 9.56.

The lower half of the more polar band yielded the hydroxy-butenolide **17***b* (87 mg) as an oil. This after distillation *in vacuo* had τ 4.21 (m, 1 H-14), 5.27 (m, 2 H-16), 6.62 (m, 1 H-3), 7.40 (s, —O*H*, lost on D_2O exchange), 8.97, 9.06, 9.12 (all s, 3H, quaternary C—CH_3's), and 9.13 (d, 3 H-17, J = 5.5 Hz). The derived (acetic anhydride – pyridine) acetate **17***c* was also obtained as an oil. After purification by preparative t.l.c. (ethyl acetate – light petroleum, 1:5, run twice) and then distillation *in vacuo* it had ν_{max} 1775, 1750, and 1730 cm^{-1}; τ 4.22 (m, 1 H-14), 5.32 (m, 2 H-16), 5.44 (t, 1 H-3, J_{obs} = 4.5 Hz), 7.99 (s, 3H, —OCOCH_3), 8.99, 9.05, 9.13 (all s, 3H, quaternary C—CH_3's), and 9.12 (d, 3 H-17, J = 5.5 Hz).

Anal. Calcd. for $C_{22}H_{32}O_4$: C, 73.30; H, 8.95. Found: C, 73.05; H, 8.80.

The intermediate chromotoplate area between the two regions dealt with above yielded an oil (94 mg) which was acetylated and the products separated by preparative t.l.c. (ethyl acetate – light petroleum, 1:4, run twice). This afforded a mixture (n.m.r. evidence) of the acetates (70 mg) of **17***a* and **17***b*, and as a more polar constituent, the keto-butenolide **16** (8 mg). This sample was identical (t.l.c., n.m.r., mass spectra) with **16** of natural provenance (see above).

*Conversion of the Epoxy-butenolide **15** into the Keto-butenolide **16***

The epoxy-butenolide **15** (152 mg) was treated with trichloroacetic acid (100 mg) in chloroform (5 ml) at 20° for 3 h. The resulting solution was diluted with chloroform (10 ml) and extracted with brine. Preparative t.l.c. (ethyl acetate – light petroleum, 1:3) of the residue (155 mg) from evaporation of the organic layer afforded the trichloroacetate **19***a* (58 mg) and a mixture (t.l.c. and and n.m.r. evidence) of **16**, **17***a*, and **17***b* (88 mg). The trichloroacetate crystallized from ethyl acetate – light petroleum and had m.p. 130–131°; ν_{max} 3630, 1783, and 1760 cm^{-1}; τ 4.19 (m, 1 H-14, $w_{1/2}$ = 5.5 Hz), 5.29 (d, 2 H-16, J_{obs} = 1.5 Hz), 5.41 (m, 1 H-3, $w_{1/2}$ = 6 Hz), 7.18 (m, —O*H*, lost on D_2O exchange), 8.31 (s, 3 H-18), 8.77 (s, 3 H-19), 9.18 (s, 3 H-20) and 9.20 (d, 3 H-17, J = 6 Hz).

Anal. Calcd. for $C_{22}H_{31}O_5Cl_3$: C, 54.84; H, 6.48. Found: C, 54.92; H, 6.54.

Treatment of this trichloroacetate (10 mg) with a slight excess of sodium borohydride in ethanol at 20° for 2 h afforded only material of much greater polarity than the diol **19***b* on t.l.c. (ethyl acetate – light petroleum, 1:2).

The trichloroacetate (17 mg) was exposed to boron trifluoride etherate (0.5 ml) in dry benzene (5 ml) at 20° for 25 min. Water was then added and the product recovered by extraction into ethyl acetate. It was purified by preparative t.l.c. (ethyl acetate – light petroleum, 1:3, run thrice) and identified as the keto-butenolide **16** (11 mg) by n.m.r., t.l.c., and $[\alpha]_D$.

*Treatment of Dihydroxy-butenolide **19***b* with Boron Trifluoride*

Reaction of the diol **19***b* (81 mg) with boron trifluoride etherate (0.5 ml) in anhydrous benzene at 20° for 12 min and work-up with water – ethyl acetate as above furnished an oil. This was submitted to preparative t.l.c. (ethyl acetate – light petroleum, 2:5, run five times) and yielded as the major component, the oily keto-butenolide **16** (23 mg). This material was identical (same criteria as above) with **16** of natural provenance.

We thank Dr. A. Ohsuka for a sample of methyl kolavenate and for providing us with unpublished data concerning the diterpenoid constituents of *Solidago altissima* L. We are also indebted to the National Research Council of Canada for an operating grant.

1. M. S. Henderson, R. McCrindle, and D. McMaster. Can. J. Chem. **51**, 1346 (1973).
2. T. Anthonsen, M. S. Henderson, A. Martin, R. D. H. Murray, R. McCrindle, and D. McMaster. Can. J. Chem. **51**, 1332 (1973).
3. M. S. Henderson, R. D. H. Murray, R. McCrindle, and D. McMaster. Can. J. Chem. **51**, 1322 (1973).
4. M. Ferrari, F. Pelizzoni, and G. Ferrari. Phytochemistry, **10**, 3267 (1971).
5. L. M. Jackmann and S. Sternhell. Applications of nuclear magnetic resonance spectroscopy in organic chemistry. Pergamon Press, Oxford. 1969. p. 171.
6. R. Misra, R. C. Pandey, and Sukh Dev. Tetrahedron Lett. 2681 (1968).
7. J. D. Connolly and R. McCrindle. Chem. Ind. 379 (1965); N. S. Bhacca and D. H. Williams. Tetrahedron, **21**, 2021 (1965).
8. S. Kusumoto, T. Okazaki, A. Ohsuka, and M. Kotake. Bull. Chem. Soc. Jap. **42**, 812 (1969).
9. G. Berti, F. Bottari, and A. Marsili. Tetrahedron, **25**, 2939 (1969).
10. C. W. Smith and R. T. Holm. J. Org. Chem. **25**, 764 (1957).
11. T. Anthonsen and R. McCrindle. Acta Chem. Scand. **23**, 1068 (1969); T. Anthonsen and G. Bergland, Acta Chem. Scand. **25**, 1924 (1971); T. Okazaki, A. Ohsuka, and M. Kotake. J. Chem. Soc. Jap. 584 (1973).
12. K. Kawazu, C. Nishino, R. McCrindle, and D. McMaster. Agr. Biol. Chem. **36**, 1245 (1972).

Can. J. Chem. Downloaded from www.nrcresearchpress.com by 86.111.144.194 on 09/06/12
For personal use only.

The Aldol Condensation of Acetaldehyde: the Equilibrium Constant for the Reaction and the Rate Constant for the Hydroxide Catalyzed RetroAldol Reaction

J. PETER GUTHRIE

Department of Chemistry, University of Western Ontario, London, Ontario N6A 3K7

Received November 28, 1973

J. PETER GUTHRIE. Can. J. Chem. **52**, 2037 (1974).

An indirect thermochemical estimate of the equilibrium constant for the aldol condensation of acetaldehyde suggested that this reaction was much less irreversible than has been believed. The rate of the hydroxide catalyzed retroaldol reaction has been measured; $k_{21} = 2.8 \times 10^{-3}$ M^{-1} s^{-1} at 25°, so that the equilibrium constant is 4.0×10^{2} M^{-1}. The γ value for acetaldehyde as addend is 0.40. The enthalpy change for the aldol reaction is -9.84 kcal/mol.

J. PETER GUTHRIE. Can. J. Chem. **52**, 2037 (1974).

Un estimé thermochimique indirect de la constante d'équilibre pour la condensation aldolique de l'acétaldéhyde suggère que cette réaction est beaucoup moins irréversible qu'on le croyait. La vitesse de la réaction de rétroaldolisation catalysé par les ions hydroxydes est de $k_{21} = 2.8 \times 10^{-3}$ M^{-1} s^{-1} à 25°, ce qui implique une constante d'équilibre de 4.0×10^{2} M^{-1}. La valeur γ lorsque l'acétaldéhyde s'additionne est de 0.40. Le changement d'enthalpie pour la réaction aldolique est de -9.84 kcal/mol. [Traduit par le journal]

Condensation of acetaldehyde with itself is one of the simplest and most thoroughly studied (1–6) examples of the aldol reaction. This

$$[1] \qquad 2CH_3CHO \underset{k_{21}}{\overset{k_{12}}{\rightleftharpoons}} CH_3CH(OH)CH_2CHO$$

$$[2] \qquad CH_3CH(OH)CH_2CHO \underset{k_{32}}{\overset{k_{23}}{\rightleftharpoons}} CH_3CH{=}CHCHO$$

condensation is usually described as "irreversible" (6–8). For reasons of experimental practicality the reaction has been studied in rather concentrated solutions[1] and these studies have had to contend with the notorious (6,7,9) complexity of the acetaldehyde–water–hydroxide system. Nevertheless it is curious that the statement that the self condensation of acetaldehyde is "irreversible" is so widely accepted, since all the information needed to evaluate the equilibrium constant is available in the literature. The standard free energy change for the self condensation of acetaldehyde in aqueous solution can be calculated in a straightforward manner, using available thermochemical data. It might be pointed out that thermochemical calculations of this sort are a potentially very useful, but much neglected, tool for the investigation of mechanisms of organic reactions. Comparison of the thermochemically estimated equilibrium constant and the known rate constant for the condensation step (k_{12}) (1,5) led to the conclusion that the rate of the retroaldol step (k_{21}) should be readily measured for dilute solutions; this proved to be the case.

[1]Concentrations from 0.02 (6) to 1.40 (4) M have been used.

Results and Discussion

The thermochemical calculations summarized in Table 1 lead to the conclusion that for reaction 1, $\Delta G^0 = -2.40$ kcal/mol, $\Delta H^0 = -9.84$ kcal/mol, and that $K_1 = 57$ M^{-1} at 25 °C.

It should be borne in mind that thermochemical values for species in aqueous solution in Table 1, and the ΔG^0 and ΔH^0 values for the aldol condensation refer to species at equilibrium with respect to covalent hydration of the aldehyde groups; values for the free aldehydes would be slightly different.

When crotonaldehyde is added to aqueous hydroxide solution, equilibrium 2 is rapidly established; there then follows a slow disappearance of the rest of the crotonaldehyde[2] (10) (see Fig. 1). By working at very low initial concentrations of crotonaldehyde, complications

[2]The Russian authors (10) observed two phase kinetics but did not evaluate a rate constant for the second phase, nor did they identify this step as dealdolization. They worked at 2.14×10^{-3} M crotonaldehyde and also observed slow formation of a new chromophore absorbing at 280 nm.

Can. J. Chem. Downloaded from www.nrcresearchpress.com by 210.87.254.5 on 09/05/12
For personal use only.

TABLE 1. Thermodynamic properties at 298 °K

Compound	ΔH_f^0 (g)	S^0 (g)	ΔG_f^0 (g)	ΔG_f^0 (aq)[a]	ΔH_f^0 (aq)[a]
CH_3CHO	−39.76[b]	63.15[b]	−31.86[b]	−33.35[c,d]	−49.88[d,e]
$CH_3CH{=}CHCHO$	−24.03[f]	77.05[g] (80.35)[m]	−10.16[h] (−11.14)[m]	−12.58[d,i] (−13.56)[m]	−35.03[d,j]
$CH_3CH(OH)CH_2CHO$				−69.10[d,k] (−70.25)[m]	−109.60[d,l]

[a]For 1 *M* aqueous solution with an infinitely dilute reference state.
[b]See ref. 15.
[c]Calculated using activity coefficient data from ref. 16.
[d]These values refer to the equilibrium mixture of free aldehyde and hydrate.
[e]See ref. 17.
[f]See ref. 18.
[g]Estimated, after ref. 15, from the value for S^0 of *trans*-2-pentene.
[h]Calculated using the H_f^0 (g) and S^0 (g) values shown.
[i]Calculated from solubility in ref. 19, and vapor pressure (estimated by the method of Has and Newton in ref. 20).
[j]Calculated using a heat of solution measured using a simple Dewar type calorimeter, and H_f^0 (l) from ref. 18.
[k]Calculated using the equilibrium constant for reaction 2 in ref. 21.
[l]Calculated using the heat of hydration from ref. 21.
[m]Calculated using the values of K_1 and K_2 evaluated in this work.

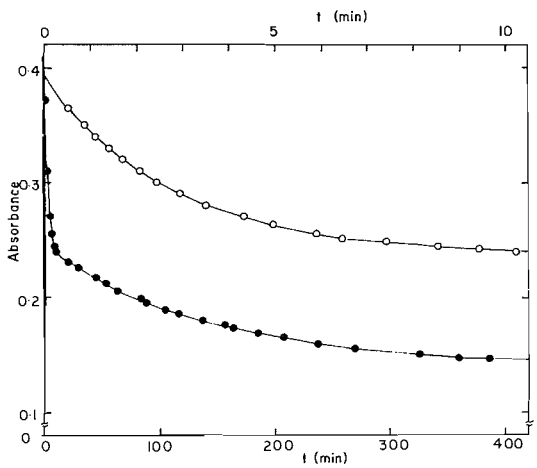

FIG. 1. Absorbance at 225 nm as a function of time when crotonaldehyde is added to 0.1 *N* NaOH at 25°; initial crotonaldehyde concentration was 1.56×10^{-5} *M*. (●) lower abscissa, (○) upper abscissa; experimental points: the lines are those determined by least-squares fit to a two exponential rate law.

due to polymerization can be avoided and the k_{12} step is negligible with respect to the k_{21} step. Under these conditions, with hydroxide concentration fixed, the kinetic equations can be solved (11) to give the rigorously correct equation for the concentration of crotonaldehyde at time t:

$$[3]\quad [C]_t = [C]_0\left\{\frac{k_{32}(\lambda_1 - k_{21})}{\lambda_1(\lambda_1 - \lambda_2)}\,e^{-\lambda_1 t} + \frac{k_{32}(k_{21} - \lambda_2)}{\lambda_2(\lambda_1 - \lambda_2)}\,e^{-\lambda_2 t}\right\}$$

where λ_1 and λ_2 are given by

$$[4]\quad \lambda_{1,2} = \tfrac{1}{2}\{k_{32} + k_{23} + k_{21} \pm ([k_{32} + k_{23} + k_{21}]^2 - 4\,k_{32}\,k_{21})^{\frac{1}{2}}\}$$

When $k_{21} \ll k_{23}$, k_{32}, we can make the useful approximation that

$$[5]\quad \lambda_1 \simeq k_{32} + k_{23}$$

$$[6]\quad \lambda_2 \simeq k_{32}\,k_{21}/(k_{32} + k_{23})$$

and

$$[7]\quad [C]_t = [C]_0\left\{\frac{1}{1 + k_{23}/k_{32}}\,e^{-\lambda_1 t} + \frac{1}{1 + k_{32}/k_{23}}\,e^{-\lambda_2 t}\right\} = \alpha\,e^{-\lambda_1 t} + \beta\,e^{-\lambda_2 t}$$

Then

$$K_2 = k_{23}/k_{32} = \beta/\alpha$$

and

$$k_{21} = \lambda_2/(1 + K_2)$$

A complication arises in concentrated alkali solutions from ionization of the carbonyl hydrate of 3-hydroxybutanal; this hydrate might be expected to be a slightly stronger acid than acetaldehyde hydrate ($pK_a = 13.57$ (12)) because of possible intramolecular hydrogen bonding in the anion. Such ionization would affect the apparent equilibrium constant for addition of water to crotonaldehyde and the apparent rate constants k_{21} and k_{23}, which refer to the total concentration of 3-hydroxybutanal, its hydrate, and the hydrate anion. It may be shown that the apparent equilibrium constant for hydration of crotonaldehyde will then be a function of hydroxide ion concentration

Can. J. Chem. Downloaded from www.nrcresearchpress.com by 210.87.254.5 on 09/05/12
For personal use only.

TABLE 2. Kinetic results[a]

[NaOH]	$\alpha^{b,c}$	$10^3 \times \lambda_1{}^{b,d}$	$\beta^{b,c}$	$10^4 \times \lambda_2{}^{b,d}$	$K_2{}^{app e}$	$10^3 \times k_{23}{}^{d,f}$	$10^3 \times k_{32}{}^{d,g}$	$10^4 \times k_{21}{}^{d,h}$
0.100	0.148	6.38	0.105	1.16	0.709	2.65	3.73	1.98
0.0667	0.112	4.22	0.0869	0.899	0.776	1.85	2.38	1.59
0.0333	0.108	2.07	0.0955	0.406	0.885	0.968	1.10	0.766

[a]In aqueous solution, 25.0 ± 0.1 °C, ionic strength 0.1 *M* (KCl), initial [crotonaldehyde] = 1.56×10^{-5} *M*, followed at 225 nm.
[b]The kinetic data were fitted to the equation, absorbance = $A_\infty + \alpha e^{-\lambda_1 t} + \beta e^{-\lambda_2 t}$ by a non-linear least-squares procedure, see ref. 22, using a computer program written for this purpose.
[c]In absorbance units.
[d]In s^{-1}.
[e]Dimensionless: $\beta/\alpha = K_2{}^{app}$ = [crotonaldehyde]/[3-hydroxybutanal].
[f]The corresponding second-order rate constant, corrected for ionization of 3-hydroxybutanal hydrate, is 0.035 ± 0.002 M^{-1} s^{-1}.
[g]The corresponding second-order rate constant is 0.035 ± 0.002 M^{-1} s^{-1}.
[h]The corresponding second-order rate constant, corrected for ionization of 3-hydroxybutanal hydrate, is 0.0028 ± 0.0002 M^{-1} s^{-1}.

$$K_2{}^{app} = K_2{}^0/(1 + a[OH^-])$$

and that

$$k_{21} = k_{21}{}^0/(1 + a[OH^-])$$

$$k_{23} = k_{23}{}^0/(1 + a[OH^-])$$

where a is a constant.

From the kinetic results in Table 2, correcting for ionization of 3-hydroxybutanal hydrate, the second-order rate constant for hydroxide ion catalyzed decomposition of 3-hydroxybutanal is 2.8×10^{-3} M^{-1} s^{-1}; combined with the value for k_{12} of 1.11 M^{-2} s^{-1} evaluated by Bell (1,5) this leads to a value of 4.0×10^2 M^{-1} for the equilibrium constant for the aldol condensation of acetaldehyde with itself. In terms of free energy this corresponds to −3.55 kcal, which differs from the thermochemical estimate by 1.15 kcal, which is rather more than one would expect; nonetheless, the thermochemical estimate would have been more useful and informative than a statement that the reaction is "irreversible". Using the values of K_1 and K_2 evaluated in this work, the thermochemical calculation can be performed in the other direction, leading to values shown in Table 1 and in particular to a revised value for the standard entropy of gaseous crotonaldehyde.

With the equilibrium constant for the addition of acetaldehyde to acetaldehyde in hand, it can be compared with other equilibrium constants for addition to acetaldehyde; the available values are given in Table 3, along with the γ values for the addends; γ is a measure of the tendency to add to a carbonyl (13). The equilibrium constants for the addends other than acetaldehyde can be fitted to the equation:[3]

[3]For hydrogen peroxide the observed equilibrium constant was divided by statistical factor of 2 (13).

TABLE 3. Equilibrium constants for addition to acetaldehyde[a]

Addend	γ^b	$K(M^{-1})$
H_2O	−3.58	1.9×10^{-2}[c]
$HOCH_3$	−2.22	7.0×10^{-1}[d]
H_2O_2	−0.64	4.8×10^{1}[e]
CH_3CHO	+0.40[f]	4.0×10^{2}[f,h]
HCN	+2.44	3.7×10^{4}[g]

[a]In aqueous solution at 25°.
[b]From ref. 13 unless otherwise stated.
[c]See ref. 23.
[d]See ref. 24.
[e]See ref. 25.
[f]Evaluated in this work as described in the text.
[g]See ref. 26.
[h]Calculated for addition of acetaldehyde, at equilibrium with respect to hydration, to free acetaldehyde to give 3-hydroxybutanal, at equilibrium with respect to hydration. The hydration correction and the statistical correction (since 2 molecules of acetaldehyde react) cancel each other almost exactly.

[8] $$\log K = 1.04\gamma + 2.15$$

By interpolation, using this equation, γ for acetaldehyde is 0.40.

Finally it should be pointed out that, although in the present case the rate constant for the retroaldol reaction was readily measurable, the thermochemical methods used to obtain the initial estimate of the equilibrium constant for the aldol reaction would have led to a reliable estimate even if the reaction had been much more nearly irreversible. Thus thermochemical calculations can be a more powerful tool than direct measurement for the evaluation of equilibria, since they are subject to fewer limitations. It is surprising that they are used so seldom by organic chemists.

Experimental

Crotonaldehyde was freshly distilled before being used for kinetics or thermochemical measurements; inorganic chemicals were reagent grade.

Can. J. Chem. Downloaded from www.nrcresearchpress.com by 210.87.254.5 on 09/05/12
For personal use only.

The heat of solution of crotonaldehyde was measured using a simple Dewar type calorimeter, calibrated in the normal way (14). Crotonaldehyde (4.00 ml) was injected by syringe into 400 ml of 0.1 *N* aqueous HCl in the calorimeter. The heat of solution so determined was 1.8_2 kcal/mol at ca. 24 °C.

Sodium hydroxide solutions for kinetics were diluted as necessary with 0.1 *M* KCl. Reaction was initiated by adding 20 μl of a dilute aqueous solution of crotonaldehyde and followed at 225 nm; reactions were carried out in 1-cm cells in the thermostatted (25.0 ± 0.1 °C) cell compartment of a Gilford Model 240 spectrophotometer.

I thank the National Research Council of Canada for financial support of this work.

1. R. P. Bell. J. Chem. Soc. 1637 (1937).
2. K. F. Bonhoeffer and W. D. Walters. Z. Phys. Chem. A**181**, 441 (1938).
3. A. Broche and R. Gilbert. Bull. Soc. Chim. Fr. 131 (1955).
4. R. P. Bell and M. J. Smith. J. Chem. Soc. 1691 (1958).
5. A. Broche. Colloque national de cinetique. Strasbourg. 1953.
6. R. P. Bell and P. T. McTigue. J. Chem. Soc. 2983 (1960).
7. L. C. Gruen and P. T. McTigue. Aust. J. Chem. **17**, 953 (1969).
8. W. P. Jencks. Progr. Phys. Org. Chem. **2**, 106 (1969).
9. M. Vogel and D. Rhum. J. Org. Chem. **31**, 1775 (1966).
10. V. A. Terent'ev, V. S. Markevich, and N. E. Stirel. Russ. J. Org. Chem. **3**, 434 (1967).
11. A. A. Frost and R. G. Pearson. Kinetics and mechanism. Wiley, New York. 1961. pp. 173–177.
12. R. P. Bell and D. P. Onwood. Trans. Faraday Soc. **58**, 1557 (1962).
13. E. G. Sander and W. P. Jencks. J. Am. Chem. Soc. **90**, 6154 (1968).
14. F. Daniels, J. W. Williams, P. Bender, R. A. Alberty, and C. D. Cornwell. Experimental physical chemistry. 6th Ed. McGraw-Hill, New York. 1962.
15. D. R. Stull, E. F. Westrum, Jr., and G. C. Sinke. The chemical thermodynamics of organic compounds. Wiley, New York. 1967.
16. S. G. d'Avila and R. S. F. Silva. J. Chem. Eng. Data, **15**, 421 (1970).
17. F. D. Rossini, D. D. Nagman, W. H. Evans, S. Levine, and I. Jaffe. Selected values of chemical thermodynamic properties. National Bureau of Standards circular No. 500. U.S. Government Printing Office, Washington, D. C. 1952.
18. J. D. Cox and G. Pilcher. Thermochemistry of organic and organometallic compounds. Academic Press, New York. 1970.
19. Handbook of chemistry and physics. 37th Ed. Chemical Rubber Publishing Co., Cleveland, Ohio. 1955.
20. Handbook of chemistry and physics. 48th Ed. Chemical Rubber Publishing Co., Cleveland, Ohio. 1955. pp. D106-107.
21. S. Winstein and H. J. Lucas. J. Am. Chem. Soc. **59**, 1461 (1973).
22. W. E. Wentworth. J. Chem. Educ. **42**, 96, 162 (1965).
23. J. L. Kurz. J. Am. Chem. Soc. **89**, 3524 (1967).
24. J. P. Guthrie. J. Am. Chem. Soc. **95**, 6999 (1973).
25. P. L. Kooijman and W. L. Ghijsen. Rec. Trav. Chim. **66**, 205 (1947).
26. G. Schlesinger and S. L. Miller. J. Am. Chem. Soc. **95**, 3729 (1973).

Can. J. Chem. Downloaded from www.nrcresearchpress.com by 210.87.254.5 on 09/05/12
For personal use only.

Carbon-13 Nuclear Magnetic Resonance Spectra of 1,4-Oxathiane Derivatives

WALTER A. SZAREK[1] AND DOLATRAI M. VYAS
Department of Chemistry, Queen's University, Kingston, Ontario K7L 3N6
AND
ANNE-MARIE SEPULCHRE, STEPHAN D. GERO, AND GABOR LUKACS
Institut de Chimie des Substances Naturelles, C.N.R.S., 91190 Gif-sur-Yvette, France

Received January 10, 1974

WALTER A. SZAREK, DOLATRAI M. VYAS, ANNE-MARIE SEPULCHRE, STEPHAN D. GERO, and GABOR LUKACS. Can. J. Chem. **52**, 2041 (1974).

The carbon-13 n.m.r. spectra of a series of 1,4-oxathianes, including the 4-oxide and 4,4-dioxide of 1,4-oxathiane, are reported. The results corroborated conclusions reached previously, on the basis of proton n.m.r. studies, concerning the conformational equilibria. The work also permitted a structural differentiation of the two nucleosides 6-chloro-9-(1,4-oxathian-2-yl)-9*H*-purine (**1**) and 6-chloro-9-(1,4-oxathian-3-yl)-9*H*-purine (**2**).

WALTER A. SZAREK, DOLATRAI M. VYAS, ANNE-MARIE SEPULCHRE, STEPHAN D. GERO, et GABOR LUKACS. Can. J. Chem. **52**, 2041 (1974).

Les spectres de r.m.n. du ^{13}C d'une série d'oxathianne-1,4 ainsi que l'oxyde en position 4 et le dioxyde de l'oxathianne-1,4 sont décrits et discutés. L'équilibre conformationnel de ces composés, étudié antérieurement par la r.m.n. du proton, se trouve confirmé. Ce travail a permis en outre la différentiation structurale des deux nucléosides 6-chloro-9-(1,4-oxathiann-2-yl)-9*H*-purine (**1**) et 6-chloro-9-(1,4-oxathiann-3-yl)-9*H*-purine (**2**).

Introduction

In a recent communication, the synthesis of two nucleoside derivatives of 1,4-oxathiane, namely,6-chloro-9-(1,4-oxathian-2-yl)-9*H*-purine (**1**) and 6-chloro-9-(1,4-oxathian-3-yl)-9*H*-purine (**2**) was reported (1). A tentative differentiation of the regioisomers **1** and **2** was based solely on

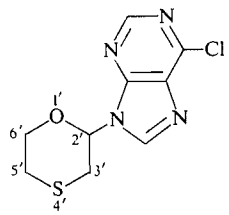

1

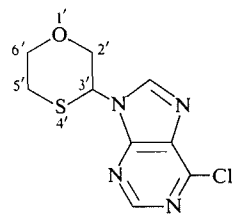

2

their proton magnetic resonance (p.m.r.) spectra. In the present work, a study by carbon-13 magnetic resonance (c.m.r.) spectroscopy of these compounds and a related series of 1,4-oxathianes has corroborated the structures assigned to **1** and **2**. A further stimulus for the present study was provided by the investigations by Zefirov *et al.* (2) of the conformational equilibria of 2-substituted 1,4-oxathianes using p.m.r. spectroscopy; it was felt that c.m.r. spectroscopy would be an effective tool for such investigations, since carbon-13 chemical shifts are more sensitive to steric, conformational, and electronic changes in a molecule.

It is known that anisotropy effects have an important bearing on proton chemical shifts but much less so on those for ^{13}C (3, 4). However, Perlin *et al.* (5) have shown in the carbohydrate series that changes induced in proton chemical shifts (deshielding) are intimately associated with the shielding state of the carbon to which the proton is bonded. The anisotropy of various functional groups, such as C=C (6), C≡N (7), and S=O (8), has afforded valuable structural and stereochemical information. For example, a detailed study of proton chemical shift changes induced in penicillins and cephalosporins (9) as a result of oxidation at sulfur has yielded information on the configuration of the S=O bond and the conformations of both the thiazolidine and thiazine rings. Sulfoxide anisotropy effects in substituted 1,4-oxathianes obtained from carbohydrate precursors (10), 1,2-oxathiane

[1]To whom inquiries should be addressed.

Can. J. Chem. Downloaded from www.nrcresearchpress.com by 210.87.254.5 on 09/05/12
For personal use only.

TABLE 1. Carbon-13 chemical shifts for 1,4-oxathiane derivatives*†

Compound	Carbon 2	3	5	6	OCH_3	O—CO—*C*H_3	O—*C*O—CH_3	CH_3
3	68.5	27.0	27.0	68.5				
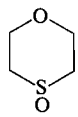 **4**	59.0	46.2	46.2	59.0				
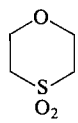 **5**	66.0	52.8	52.8	66.0				
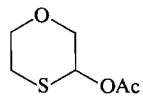 **6**	70.9	67.9‡	23.3	67.6‡	—	21.0	169.1	
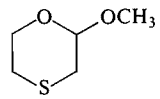 **7**	98.9	30.2	26.0	65.1	55.3	—	—	
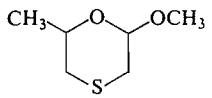 **8**	95.1	29.3	31.9	64.3	54.6	—	—	21.5

*In p.p.m. from tetramethylsilane (TMS) in chloroform-*d*.
†1,4-Dithiane gave a single line at 29.1 p.p.m. and 1,4-dioxane at 67 p.p.m.
‡Confirmed by single frequency off-resonance decoupling (SFORD).

2-oxide (8), and trimethylene sulfite (11) have been well studied. The above work prompted an investigation of the changes in ^{13}C and proton chemical shifts in the series 1,4-oxathiane (**3**), 1,4-oxathiane 4-oxide (**4**), and 1,4-oxathiane 4,4-dioxide (**5**).

Some recent applications of c.m.r. spectroscopy of relevance to the work described in this article include structural and conformational studies on carbohydrates (5, 12–14), nucleosides (15), sulfur heterocycles (16), and penicillins (17).

Results and Discussion

The c.m.r. and p.m.r. data for compounds **3**, **4**, and **5** are given in Tables 1 and 2, respectively. The ^{13}C chemical shift assignments for these compounds were readily made by a comparison with the observed shifts for 1,4-dithiane and 1,4-dioxane. One notable feature is an upfield shift of $\sim$2 p.p.m. in the c.m.r. signal for C-3 and -5 in compound **3** relative to that in 1,4-dithiane. The origin of this effect has been discussed by Perlin *et al.* (5) in connection with

Can. J. Chem. Downloaded from www.nrcresearchpress.com by 210.87.254.5 on 09/05/12
For personal use only.

TABLE 2. Proton magnetic resonance data for compounds **3**, **4**, and **5***†

Compound	Hydrogen					
	H-2ax	H-2eq	H-6ax	H-6eq	H-3's	H-5's
3‡	← τ 6.08 →				← τ 7.38 →	
4	τ 5.62	τ 6.18	τ 5.62	τ 6.18	← τ 7.13 →	
5	← τ 5.87 →				← τ 6.90 →	

$J_{2ax,2eq} = J_{6ax,6eq} = 13$ Hz
$J_{2ax,3ax} = J_{5ax,6ax} = 9$ Hz
$J_{2eq,3eq} = J_{5eq,6eq} = 3.5$ Hz
$J_{2eq,3ax} = J_{5ax,6eq} = 4.5$ Hz
$J_{2eq,6eq} \approx 0.5$ Hz

*In chloroform-*d* with internal TMS standard.
†1,4-Dithiane gave a singlet at τ 7.13 in chloroform-*d*, and 1,4-dioxane at τ 6.33.
‡Proton magnetic resonance data for compound 3 in carbon tetrachloride are given in ref. 30.

various carbohydrates. Similar effects in *trans*-fused bicyclic hexopyranoside derivatives (18) and dioxanes (19) have been reported.

The 60 MHz p.m.r. spectrum of 1,4-oxathiane 4-oxide (**4**) (20) in chloroform-*d* is shown in Fig. 1. The 1-proton multiplet centered at τ 5.62 was assigned to the axial hydrogens at C-2 and -6 on the basis of the observed 9-Hz coupling, a value which is consistent with a *trans*-diaxial relationship to the adjacent hydrogens; an analogous assignment has been made by Harpp and Gleason (8) in the case of 1,2-oxathiane 2-oxide. The 1-proton multiplet at higher field, namely τ 6.18, was then assigned to the equatorial hydrogens at C-2 and -6. The observed deshielding of the axial hydrogens is consistent with an axial S=O bond, which can affect the hydrogens at C-2 and -6 by its acetylene-like anisotropy. The axial hydrogens at these positions are especially subject to a deshielding effect, since they occupy *syn*-axial positions with respect to the axial exocyclic S=O bond. The multiplets at τ 5.62 and 6.18 were analyzed as illustrated in Fig. 1 and documented in Table 2. The unresolved 4-proton multiplet centered at τ 7.13 was assigned to the hydrogens at C-3 and -5.

^{13}C and proton chemical shift correlation diagrams for the series 1,4-oxathiane (**3**), 1,4-oxathiane 4-oxide (**4**), and 1,4-oxathiane 4,4-dioxide (**5**) are given in Fig. 2. One interesting feature is that in the sulfoxide **4** the axial hydrogens at C-2 and -6 are deshielded, whereas, as evidenced by the ^{13}C chemical shifts, these

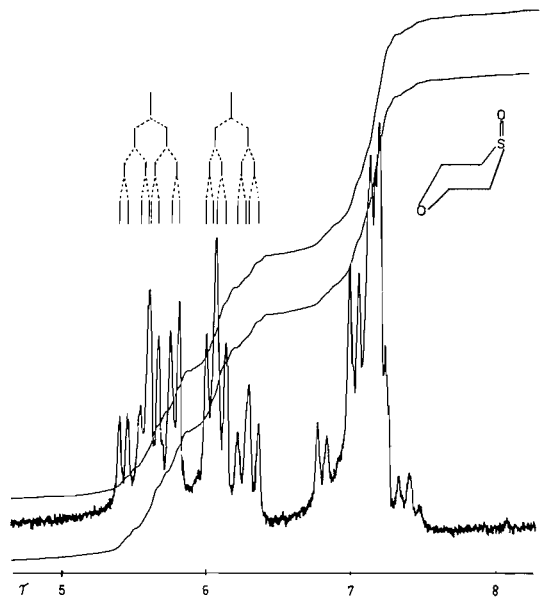

FIG. 1. The p.m.r. spectrum (60 MHz) of 1,4-oxathiane 4-oxide (**4**) in chloroform-*d*.

Can. J. Chem. Downloaded from www.nrcresearchpress.com by 210.87.254.5 on 09/05/12
For personal use only.

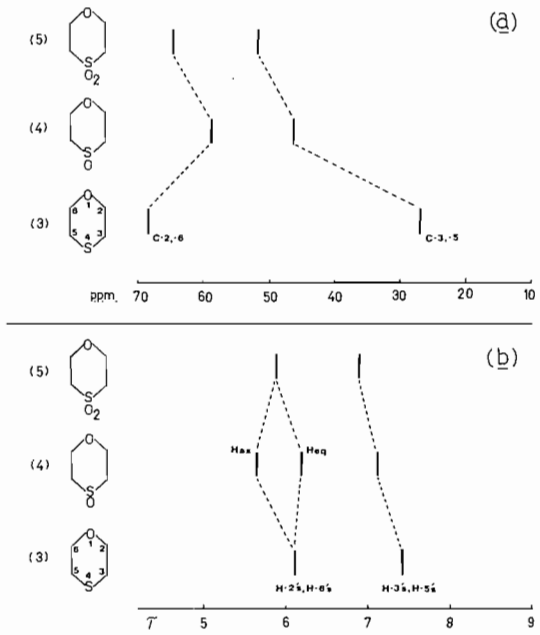

FIG. 2. ^{13}C (*a*) and proton (*b*) chemical shift correlations for 1,4-oxathiane (**3**), 1,4-oxathiane 4-oxide (**4**), and 1,4-oxathiane 4,4-dioxide (**5**).

carbons are themselves shielded (~10 p.p.m.). Such inverse effects have been observed previously by Perlin *et al.* (5) in the monosaccharide series; also, a nearly identical shift has been recently observed by Buchanan *et al.* (16*b*) in the case of epimeric trimethylene sulfites (axial S=O and equatorial S=O). The large downfield shift of 20 p.p.m. in the ^{13}C chemical shifts of C-3 and -5 in **4** relative to those of the corresponding carbons in 1,4-oxathiane (**3**) may be attributed to the β effect (21) of the oxygen of the S=O bond, the diminished electron density at these carbons as a result of inductive withdrawal by the sulfoxide oxygen and a hybridization change at sulfur (16*a*, 22). The decreased charge density at C-3 and -5 in **4** is even reflected in the proton shifts (Fig. 2*b*); the hydrogens at these carbons are deshielded (0.25 p.p.m. downfield shift) with respect to the corresponding hydrogens in 1,4-oxathiane (**3**). Conversion of the sulfoxide **4** into the sulfone **5** results in a downfield shift in ^{13}C chemical shifts of C-2 and -6, and a concomitant downfield shift in ^{13}C and proton chemical shifts at C-3 and -5. In both **4** and **5**, C-2 and -6 are shielded with respect to the corresponding carbons in 1,4-oxathiane (**3**). In the case of **4** it is clear that the axial S=O bond has a very large influence on the shieldings of C-2 and -6; this may presumably be attributed to the γ steric effect (van der Waals' repulsive interactions) (compare ref. 23). A theoretical model for the γ effect based on charge polarization has been proposed (24). However, the local anisotropic contributions to the shieldings cannot be disregarded, since a lower shielding of C-2 and -6 was observed in the case of **5** (see Fig. 2*a*), in spite of the fact that the non-bonded interactions between the axial S=O bond and the axial hydrogens at C-2 and -6 should be essentially the same as those in **4**. The lower shielding in the case of **5** may perhaps be attributed to a diminished anisotropy of the axial S=O bond in the sulfone **5** with respect to the S=O anisotropy in the sulfoxide **4**; in the sulfone **5** the shielding zone of the equatorial S=O bond may counteract the deshielding zone of the axial S=O bond. The downfield shifts at C-3 and -5 reflect the greater positive character of the sulfur in the sulfone with respect to that in the sulfoxide.

^{13}C chemical shift data for 3-acetoxy-1,4-oxathiane (**6**) (1), 2-methoxy-1,4-oxathiane (**7**) (2), and (2*R*,6*S*)-2-methoxy-6-methyl-1,4-oxathiane (**8**) (25) are given in Table 1 and data for the 1,4-oxathiane nucleoside derivatives **1** and **2** are given in Table 3. Zefirov *et al.* (2) have estimated the conformational equilibrium of 2-substituted 1,4-oxathianes by p.m.r. spectroscopy and assuming the chair conformation for these systems (26). In Table 4 are summarized data on the conformational equilibrium of compounds **1**, **2**, **6**, **7**, and **8** obtained in the present work by p.m.r. spectroscopy. A ^{13}C chemical shift correlation diagram for these compounds is given in Fig. 3; it is known (21) that carbon shieldings depend, at least in part, on molecular geometry and conformation.

The ^{13}C chemical shift assignments in the 2-acetoxy derivative **6** were facilitated by comparison of the spectrum with that of 1,4-oxathiane (**3**); the C-3 and -6 assignments were confirmed by single frequency off-resonance decoupling (SFORD). The 3.6 p.p.m. upfield shift of the signal for C-5 in **6** (relative to **3**) can be considered to arise from the 1,3-diaxial non-bonded interaction (5) between the axial proton at C-5 and the axial acetoxy group at C-3; p.m.r. spectroscopy has shown that the conformational equilibrium contains ~90% of the conformer having the 3-acetoxy group axially disposed (see Table 4). The presence of the acetoxy group at

Can. J. Chem. Downloaded from www.nrcresearchpress.com by 210.87.254.5 on 09/05/12
For personal use only.

TABLE 3. Carbon-13 chemical shifts for 6-chloro-9-(1,4-oxathian-2-yl)-9*H*-purine (**1**) and 6-chloro-9-(1,4-oxathian-3-yl)-9*H*-purine (**2**)*†

	Carbon								
Compound	2′	3′	5′	6′	2	4	5	6	8
1	82.0	31.1	25.9	70.2	151.5	150.6‡	131.1	150.1‡	142.0
2	71.1	49.4	24.1	68.1	151.5	150.8	131.0	150.8	143.7

*In p.p.m. from tetramethylsilane (TMS) in chloroform-*d*.
†Chemical shifts obtained for the purine ring carbons of 6-chloropurine (15) measured in methyl sulfoxide are as follows: 150.3 (C-2), 152.4 (C-4), 132.2 (C-5), 152.4 (C-6), 146.4 (C-8).
‡Assignments for peak positions marked with‡ may be reversed.

TABLE 4. Conformational equilibrium data for substituted 1,4-oxathianes in chloroform-*d**

Compound	Chemical shift of H_x (τ)	Form of signal H_x	J_{AX+BX} (Hz)	% axial conformer (I_a or II_a)†
1	3.95	Quartet	11.5	~25
2	4.43	Broad signal	~6	~90
6‡	4.60	Broad signal	~6	~90
7§	5.80	Triplet	~9	~50
8¶	5.40	Broad signal	~5.5	~95

*The position of conformational equilibrium was estimated using the equation of Zefirov *et al.* (2): $|J_{AX} + J_{BX}| = N\Sigma J_1 + (1 - N)\Sigma J_{11} = N(J_{ae} + J_{ee}) + (1 - N)(J_{aa} + J_{ee})$ for which $J_{aa} = 11$ Hz, $J_{ae} = J_{ee} = 2.5$ Hz (for 1,4-oxathianes only).
†For 2-substituted 1,4-oxathianes, the conformational equilibrium under consideration is

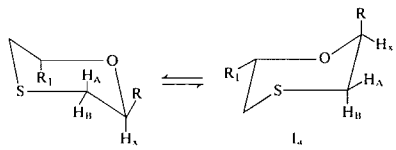

8 R_1 = CH_3
7 R_1 = H
1 R_1 = H

For 3-substituted 1,4-oxathianes, the conformational equilibrium is

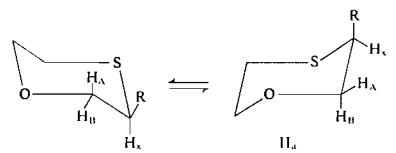

‡Full p.m.r. data for this compound will be published later (see also ref. 1).
§Proton magnetic resonance data for this compound in carbon tetrachloride and acetonitrile have also been reported (2).
¶Proton magnetic resonance data for this compound in carbon tetrachloride have also been reported (25).

C-3 in **6** causes a large downfield shift of the C-3 signal (relative to **3**), namely 41 p.p.m., and exercises a small "downfield effect" on C-2.

The ^{13}C chemical shift assignments in the 2-methoxy derivative **7** were relatively straightforward. The C-2 and -5 assignments were readily made, since the C-5 signal in **7** had barely shifted (relative to **3**), but the C-2 signal experienced a large downfield shift (30 p.p.m.) because of the presence of the methoxyl group at C-2. Since the conformational equilibrium of **7** contains approximately equal proportions of the two chair conformers (see Table 4), the 3 p.p.m. downfield shift of the C-3 signal may be attributed to a "downfield effect" exercised by both the axial and equatorial methoxyl group. In the case of C-6, only the axial conformer contributes to its shielding, resulting from a 1,3-

Can. J. Chem. Downloaded from www.nrcresearchpress.com by 210.87.254.5 on 09/05/12
For personal use only.

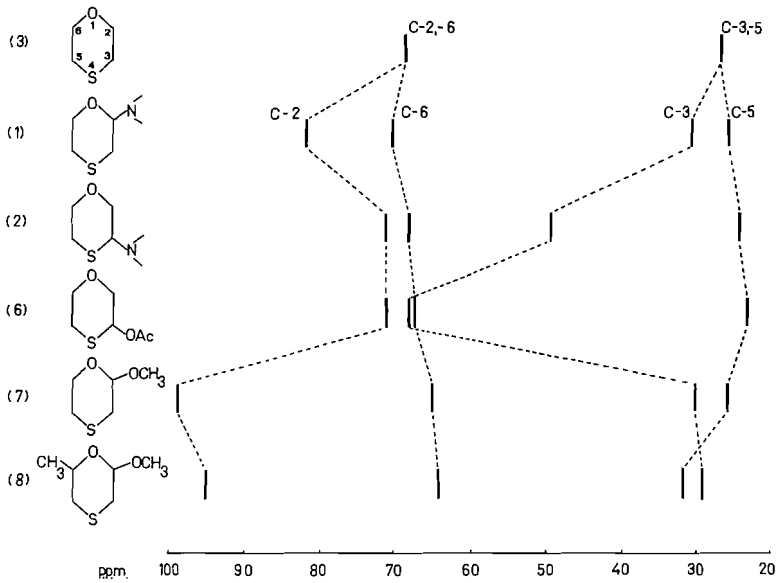

FIG. 3. ^{13}C chemical shift correlations for substituted 1,4-oxathianes. Only the carbon atoms of the oxathiane ring are included.

diaxial non-bonded interaction, as reflected by the observed upfield shift of 3.5 p.p.m.

In contrast to **7**, (2*R*,6*S*)-2-methoxy-6-methyl-1,4-oxathiane (**8**) exists in chloroform-*d* solution almost entirely in the conformer with the methoxyl group axially disposed (see Table 4), a phenomenon clearly manifested by the ^{13}C chemical shifts of C-2 and -6. Thus, there is an upfield shift of ~4 p.p.m. of the C-2 signal in the case of compound **8** relative to the corresponding signal for **7** (see Fig. 3). This upfield shift would be expected on the basis of the previous observation (5) that an axial oxygen atom is associated with increased shielding of the ^{13}C nucleus to which it is bonded and on the fact that the preponderant (~95%) conformer of **8** is that having an axial methoxyl whereas in the case of **7** the two conformers exist in approximately equal proportions. Another salient feature of the c.m.r. spectrum of **8** is the observation that the presence of the methyl group at C-6 barely affects the chemical shift of C-6 relative to the corresponding signal in compound **7**; a downfield shift might have been expected (α effect). The observation of the essentially identical C-6 chemical shifts in **7** and **8** suggests that the α effect may be counteracted by the shielding effect of a 1,3-diaxial nonbonded interaction between an axial methoxyl group at C-2 and an axial hydrogen atom at C-6, and hence corroborates the previous conclusions regarding the conformational equilibrium in these compounds. In the case of compound **8**, unlike that in **6**, the C-3 and -5 assignments could not be made by SFORD. Nevertheless, unambiguous assignments were made in the following manner. If in compound **8** a full equatorial β effect is exercised on C-5 by the methyl group at C-6, then the C-5 chemical shift in **8** should be ~7–8 p.p.m. lower, as estimated from a 1,3-dioxane model (19), then the observed chemical shift of C-5 in **7** (26.02 p.p.m.). However, since compound **8** exists only slightly in the conformation having the methyl group in the axial orientation, and since the axial β effect of a methyl group is smaller than the equatorial β effect (5), then the actual β effect exercised on C-5 in **8** should be only slightly smaller than a full equatorial β effect. Thus, the signal in the c.m.r. spectrum of **8** at 31.91 p.p.m. was assigned to C-5.

The structural differentiation of the nucleosides **1** and **2** could be readily made by comparison of their c.m.r. spectra with that of 1,4-oxathiane (**3**) (see Fig. 3). Interestingly, the two regioisomers show different conformational preferences in chloroform-*d* solution (Table 4), as determined from their p.m.r. spectra (1). In the case of **1**, there is a preponderance of the conformer having the purine moiety in an equatorial

Can. J. Chem. Downloaded from www.nrcresearchpress.com by 210.87.254.5 on 09/05/12
For personal use only.

orientation, whereas in the case of **2**, there is a preponderance of the axial form. A rationalization for this difference in terms of attractive (27) or repulsive nonbonded interactions between lone pairs on the oxygen, sulfur, and the nitrogen atom at position 9 of the purine ring is under investigation and will be reported separately. Zefirov *et al.* (2) have accounted for the conformational behavior of some 2-substituted 1,4-oxathianes and 1,4-dioxanes on the basis of the anomeric effect and a repulsive interaction picturesquely referred to as the "hockey-sticks" effect.

Experimental

The nucleosides **1** and **2**, and 3-acetoxy-1,4-oxathiane (**6**), were samples prepared in a previous work by Vyas and Szarek (1). 1,4-Oxathiane (**3**) and 1,4-dithiane were obtained from Aldrich Chemical Co., Inc., Milwaukee, Wisconsin. 1,4-Oxathiane 4-oxide (**4**) was synthesized according to the procedure of Leonard and Johnson (20). The 4,4-dioxide (**5**) was prepared by treatment of compound **3** with 2 equiv. of sodium metaperiodate in aqueous methanol in the dark at room temperature for 5 days, followed by extraction with chloroform, and concentration of the chloroform solution; recrystallization of the residue from chloroform – petroleum ether (b.p. 60–80°) gave **5** as white needles, m.p. 130° in agreement with the literature value (28). 2-Methoxy-1,4-oxathiane (**7**) was synthesized according to the procedure of Parham *et al.* (29); (2*R*,6*S*)-2-methoxy-6-methyl-1,4-oxathiane (**8**) was synthesized according to the procedure of Buck *et al.* (25).

Proton magnetic resonance spectra were recorded at 60 MHz on a Bruker HX-60 spectrometer with tetramethylsilane (TMS) as the locking signal; c.m.r. spectra were recorded in chloroform-*d* solution on a Bruker Fourier transform spectrometer at 22.6 MHz; chemical shifts are given in p.p.m. downfield from TMS: $\delta^{TMS} = \delta^{CDCl_3} + 76.9$ p.p.m.

The authors are grateful to the National Research Council of Canada for their generous financial support. They also wish to thank Professors J. K. N. Jones and E. Lederer for their interest and encouragement.

1. D. M. Vyas and W. A. Szarek. Carbohydr. Res. **30**, 225 (1973).
2. N. S. Zefirov, V. S. Blagoveshchensky, I. V. Kazimirchik, and N. S. Surova. Tetrahedron, **27**, 3111 (1971).
3. P. C. Lauterbur. J. Am. Chem. Soc. **83**, 1838 (1961).
4. J. B. Stothers. Carbon-13 NMR spectroscopy. Academic Press, New York, N.Y. 1972.
5. A. S. Perlin, B. Casu, and H. J. Koch. Can. J. Chem. **48**, 2596 (1970).
6. D. M. Vyas and G. W. Hay. Can. J. Chem. **49**, 3755 (1971).
7. J. C. Muller, J. P. Fleury, and U. Schiedegger. Org. Magn. Res. **2**, 77 (1970).
8. D. N. Harpp and J. G. Gleason. J. Org. Chem. **36**, 1314 (1971).
9. P. V. Demarco and R. Nagarajan. *In* Cephalosporins and penicillins. *Edited by* E. H. Flynn. Academic Press, Inc., New York. 1972. Chap. 8.
10. K. W. Buck, A. B. Foster, W. D. Pardoe, M. H. Qadir, and J. M. Webber. Chem. Commun. 759 (1966).
11. C. H. Green and D. G. Hellier. J. Chem. Soc. Perkin II, 458 (1972).
12. A. S. Perlin and B. Casu. Tetrahedron Lett. 2921 (1969).
13. L. D. Hall and L. F. Johnson. Chem. Commun. 509 (1969).
14. D. E. Dorman and J. D. Roberts. J. Am. Chem. Soc. **92**, 1355 (1970).
15. A. J. Jones, D. M. Grant, M. W. Winkley, and R. K. Robins. J. Am. Chem. Soc. **92**, 4079 (1970).
16. (*a*) H. J. Reich and J. E. Trend. J. Org. Chem. **38**, 2637 (1973); (*b*) G. W. Buchanan, J. B. Stothers, and G. Wood. Can. J. Chem. **51**, 3746 (1973).
17. R. A. Archer, R. D. G. Cooper, P. V. Demarco, and L. F. Johnson. Chem. Commun. 1291 (1970).
18. E. Conway, R. D. Guthrie, S. D. Gero, G. Lukacs, A.-M. Sepulchre, E. W. Hagaman, and E. Wenkert. Tetrahedron Lett. 4879 (1972).
19. A. J. Jones, E. L. Eliel, D. M. Grant, M. C. Knoeber, and W. F. Bailey, J. Am. Chem. Soc. **93**, 4772 (1971); F. G. Riddell, J. Chem. Soc. B, 331 (1970); G. M. Kellie and F. G. Riddell. J. Chem. Soc. B, 1030 (1971).
20. N. J. Leonard and C. R. Johnson. J. Org. Chem. **27**, 283 (1962).
21. G. W. Buchanan and J. B. Stothers. Can. J. Chem. **47**, 3605 (1969).
22. R. A. Archer, R. D. G. Cooper, and P. V. Demarco. Chem. Commun. 1291 (1970).
23. G. Wood, G. W. Buchanan, and M. H. Miskow. Can. J. Chem. **50**, 521 (1972).
24. D. M. Grant and B. V. Cheney. J. Am. Chem. Soc. **89**, 5315 (1967).
25. K. W. Buck, F. A. Fahim, A. B. Foster, A. R. Perry, M. H. Qadir, and J. M. Webber. Carbohydr. Res. **2**, 14 (1966).
26. R. S. Mcewen and G. A. Sim. J. Chem. Soc. 271 (1967).
27. N. D. Epiotis. J. Am. Chem. Soc. **95**, 3087 (1973).
28. A. E. Cashmore. J. Chem. Soc. **123**, 1738 (1923).
29. W. E. Parham, I. Gordon, and J. D. Swalen. J. Am. Chem. Soc. **74**, 1824 (1952).
30. W. B. Smith and B. A. Shoulders. J. Phys. Chem. **69**, 579 (1965).

Can. J. Chem. Downloaded from www.nrcresearchpress.com by 210.87.254.5 on 09/05/12
For personal use only.

The Preparation and Crystal Structure of $[I_2]^+[Sb_2F_{11}]^-$

C. G. DAVIES, R. J. GILLESPIE, P. R. IRELAND, AND JOY M. SOWA

Department of Chemistry, McMaster University, Hamilton, Ontario L8S 4M1

Received November 13, 1973

C. G. DAVIES, R. J. GILLESPIE, P. R. IRELAND, and JOY M. SOWA. Can. J. Chem. **52**, 2048 (1974).

The crystal structure of the compound $I_2^+Sb_2F_{11}^-$ has been determined from three-dimensional X-ray counter data. Crystals are monoclinic with $a = 13.283(5)$, $b = 8.314(3)$, $c = 5.571(2)$ Å; $\beta = 103.75(2)°$; $V = 579.5$ Å^3; $Z = 2$ and $D_c = 3.92$ g cm^{-3}. The structure has been refined in the space group $C2$ with a final conventional R factor of 0.055 for 365 independent reflections with $I \geq 3\sigma(1)$. The structure consists of discrete I_2^+ cations and $Sb_2F_{11}^-$ anions, each with a crystallographic two-fold rotation axis through the center. The I—I bond length is 2.557(4) Å while the Sb—F bridge length is 2.00(1) Å with a bridge angle of 166(3)° in the symmetric anion.

C. G. DAVIES, R. J. GILLESPIE, P. R. IRELAND et JOY M. SOWA. Can. J. Chem. **52**, 2048 (1974).

La structure du cristal du composé $I_2^+Sb_2F_{11}^-$ est déterminée par un compteur de données de rayons-x à trois dimensions. Les cristaux sont monocliniques avec: $a = 13.283$ (5), $b = 8.314(3)$, $c = 5.571(2)$ Å; $\beta = 103.75(2)°$; $V = 597.5$ Å^3; $Z = 2$ et $D_c = 3.92$ g cm^{-3}. La structure est raffinée dans le groupe d'espace $C2$ avec un facteur conventionnel final R de 0.055 pour 365 réflexions indépendantes avec $I \geq 3\sigma(1)$. La strucutre consiste en cations I_2^+ et anions $Sb_2F_{11}^-$ distincts ayant chacun un axe cristallographique de rotation d'ordre 2, passant par le centre. La distance du lien I—I est 2.557(4) Å alors que la longueur du pont Sb—F est 2.00(1) Å; l'angle du pont à l'anion symétrique est 166.3°. [Traduit par le journal]

Introduction

The I_2^+ cation has been characterized in solution in the acids HSO_3F and $H_2S_2O_7$ by conductimetric, spectrophotometric, and magnetic measurements (1) and by Raman spectroscopy (2). The frequency of the I_2^+ stretching vibration (238 cm^{-1}) suggested that the cation has a stronger and shorter bond than the I_2 molecule which has a stretching frequency of 213 cm^{-1} and a bond length of 2.66 Å (3). A dark blue solid was prepared by Kemmitt *et al.* (4) from I_2, IF_5, and SbF_5 and was formulated by them as $I_2^+Sb_2F_{11}^-$, however, it melted over a considerable range and it seems probable that it contained impurities such as $IF_4^+SbF_6^-$ and SbF_3. We have now prepared the dark blue crystalline compound $I_2^+Sb_2F_{11}^-$ in a pure state by the oxidation of iodine with SbF_5 in liquid sulfur dioxide as solvent and we have determined its structure by X-ray crystallography.

Experimental

Crystal Preparation

SbF_5 (9.93 mmol) in dried liquid SO_2 was added to finely ground I_2 (3.47 mmol) and stirred for one week at room temperature. White SbF_3 precipitated from the blue solution and was removed by filtering through sintered glass. Removal of the solvent by distillation yielded a dark blue crystalline solid, $I_2^+Sb_2F_{11}^-$. This compound melts sharply at 122–123 °C. It is moisture sensitive and was handled in a dry atmosphere. The preparation is described by the equation

$$2I_2 + 5SbF_5 \xrightarrow[20\,°C]{SO_2} 2I_2^+Sb_2F_{11}^- + SbF_3$$

Anal. Calcd. for $I_2^+Sb_2F_{11}^-$: I, 35.93; Sb, 34.48; F, 29.59. Found: I, 36.73; Sb, 35.27; F, 27.63.

Raman Spectrum

Crystals of $I_2^+Sb_2F_{11}^-$ sealed in a melting point tube were studied at room temperature using 6328 Å He–Ne excitation. An intense I_2^+ resonance Raman spectrum with a fundamental at 238 cm^{-1} and two overtones was observed which agrees with spectra reported earlier for I_2^+ in fluorosulfuric acid solution (2). No anion peaks were observed.

Crystal Data f.w. = 706.30

$I_2Sb_2F_{11}$ is monoclinic with $a = 13.283(5)$, $b = 8.314(3)$, $c = 5.571(2)$ Å; $\beta = 103.75(2)°$; $V = 597.5$ Å^3; $Z = 2$ and $D_c = 3.92$ g cm^{-3}.

No experimental density was obtained because of the sensitivity of the compound to moisture. Single crystal precession photographs revealed the systematic absences: hkl, $h + k = 2n + 1$, indicating one of the C centered space groups $C2$, Cm, or $C2/m$. After some initial ambiguity, the structure was ultimately refined in the space group $C2$.

Can. J. Chem. Downloaded from www.nrcresearchpress.com by 210.87.254.5 on 09/05/12
For personal use only.

TABLE 1. Structural parameters* for $I_2^+Sb_2F_{11}^-$ ($U_{ij} \times 10^2$)

Atom	X	Y	Z	U or U_{11}	U_{22}	U_{33}	U_{12}	U_{13}	U_{23}
I	0.0733(1)	0.0	0.8871(5)	5.3(1)	6.2(2)	6.7(2)	−0.7(4)	3.6(1)	0.0(4)
Sb	0.3558(1)	−0.006(1)	0.5437(5)	4.1(1)	3.3(1)	7.1(2)	−0.2(3)	3.3(1)	−0.2(4)
F(1)	0.5	0.022(7)	0.5	7.1(1.1)					
F(2)	0.224(1)	0.009(7)	0.588(4)	6.8(6)					
F(3)	0.316(2)	0.136(4)	0.256(6)	7.4(9)					
F(4)	0.342(3)	−0.179(5)	0.350(7)	9.9(1.2)					
F(5)	0.415(3)	−0.119(6)	0.815(8)	11.5(1.4)					
F(6)	0.390(2)	0.180(4)	0.733(6)	7.9(9)					

*x, y, and z are atomic coordinates expressed as fractions of the cell edges. The isotropic temperature factor U is from the expression $\exp[-U(\sin^2\theta)/\lambda^2]$ and the form of the anisotropic thermal ellipsoid is $\exp[-2\pi^2(h^2a^{*2}U_{11} + ... + 2hka^*b^*U_{12} + ...)]$ Least-squares-estimated standard errors in the least significant digits are given in parentheses.

X-Ray Measurements

A small, approximately spherical crystal (radius 0.08 mm) was sealed in a thin-walled quartz capillary and used for intensity measurements on a Syntex PĪ diffractometer equipped with MoK_α ($\lambda = 0.71069$ Å) radiation. Cell parameters were obtained from a least squares refinement using 10 high angle reflections in the region $25° < 2\theta < 35°$. Intensity data were collected by the θ–2θ scan technique with scan rates varying from 2.0 to 24.0°/min (in 2θ) so that the weaker reflections were examined most slowly to minimize counting errors. Stationary background counts with a time equal to half the scan time for each reflection were made at each end of the scan range. The scan width varied from 2° at low 2θ to 2.5° for the higher angle data. Two standards were regularly checked to monitor the stability of the crystal and its alignment, but no significant time dependent trends were observed. Reflections within a unique quadrant with $2\theta < 50°$ were measured, resulting in 365 reflections with intensities greater than three times their standard deviation based on counting statistics. The linear absorption coefficient for the material is 99.0 cm^{-1} for the MoK_α radiation used, and a spherical absorption approximation seemed the most appropriate. Lorentz, polarization, and spherical absorption corrections were applied to the data.

Solution and Refinement of the Structure

Reflection statistics were strongly in favor of a non-centric space group, and $C2$ was arbitrarily chosen for preliminary refinement. The positions of the iodine and antimony atoms were readily located from inspection of the three dimensional Patterson function. With the y coordinate of the iodine atom arbitrarily fixed at zero to define the origin, full matrix least squares refinement of all other positional and isotropic temperature parameters for the two atoms gave a conventional agreement index $R_1(R_1 = \Sigma\Delta/\Sigma|F_o|$ where $\Delta = ||F_o| - |F_c||)$ of 0.17. A difference Fourier synthesis revealed the remaining six fluorine atoms including a bridging atom at a special position on the two-fold rotation axis. Refinement with anisotropic thermal parameters for the two heavy atoms and isotropic parameters for the fluorine atoms (a total of 40 variables), converged at $R_1 = 0.057$.

The refined $Sb_2F_{11}^-$ unit had an approximate mirror plane normal to the two-fold axis of the space group $C2$. Trial refinements were therefore attempted in the space groups Cm and $C2/m$ with the appropriate parameters constrained because of special position requirements. Refinement in Cm resulted in the same R_1 of 0.057, but an increase in the number of variable parameters to 48 and an unreasonable distorted geometry discounted this space group. Only 25 variable parameters were necessary to refine the model in the centric space group $C2/m$, again including anisotropic thermal parameters for the iodine and antimony atoms and isotropic parameters for the fluorine atoms. This model demanded a linear symmetric bridge between the two antimony atoms. A satisfactory refinement was achieved with R_1 converging at 0.065. However, use of Hamilton's R ratio test (5) showed that this was a significantly poorer result than that obtained in the $C2$ refinement and the highly symmetric model could be properly rejected. Refinements for all three models were found to have no significant effect on the I—I bond length.

Unit weights were initially used in all refinements. An examination of the data showed however that a weighting scheme was necessary to achieve the condition that $\Sigma w\Delta^2$ be approximately independent of $|F_o|$ and $(\sin\theta)/\lambda$. An empirical scheme of the form $\sqrt{w} = (A + BF_o + CF_o^2)^{-1}$ was calculated with final values of A, B, and C of 0.511, 0.348, and 0.002, respectively. Using this scheme refinement converged at $R_1 = 0.055$ while the weighted agreement index R_2 ($R_2 = (\Sigma w\Delta^2/\Sigma wF_o^2)^{1/2}$) decreased from 0.068 with unit weights, to 0.062. The largest shift of any parameter divided by its estimated standard deviation was 0.04 in the final cycle. The top four peaks in a final difference Fourier (1 — 2e/Å) were all within 0.8 Å of the iodine atom. No systematic trends indicating the need for an extinction correction were evident in the data.

Atomic scattering factors for iodine, antimony, and fluorine with anomalous dispersion corrections for the iodine and antimony atoms were taken from ref. 6. All calculations were performed on a CDC 6400 computer using the series of programs in the XRAY 71 system (7) and our own programs. The final atomic positional coordinates and temperature factors are presented in Table 1. A tabulation of observed and calculated structure factors is available.[1]

[1]A listing of observed and calculated structure factor amplitudes is available, at a nominal charge, from the Depository of Unpublished Data, National Science Library, National Research Council of Canada, Ottawa, Canada K1A 0S2.

Can. J. Chem. Downloaded from www.nrcresearchpress.com by 210.87.254.5 on 09/05/12
For personal use only.

Can. J. Chem. Downloaded from www.nrcresearchpress.com by 210.87.254.5 on 09/05/12
For personal use only.

Results and Discussion

Figure 1 shows a projection of the structure down the *b* axis while Table 2 lists selected bond lengths and angles. The shortest I---F contact is 2.89 Å indicating that the structure is essentially ionic.

The two symmetry related iodine atoms are 2.557(4) Å apart in the cation compared with an I—I distance of 2.66 Å in the iodine molecule. This shortening can be correlated with the change in frequency of the Raman band from 213 cm^{-1} for iodine to 238 cm^{-1} for the cation. For the analogous bromine molecule and cation (8) a similar reduction in bond length from 2.27 to 2.15 Å is accompanied by an increase in Raman frequency from 317 to 368 cm^{-1} (Table 3). Although the Cl_2^+ ion is not known as a stable species either in solution or in the solid state the stretching frequency and bond length (Table 3) have been obtained from its electronic spectrum in the gas state at low pressure (9). The stronger and shorter bond in the X_2^+ cations compared with the X_2 neutral molecules is consistent with the removal of an electron from an antibonding π^* orbital in the formation of the cation.

Several structures containing the $Sb_2F_{11}^-$ ion have recently been determined and the parameters that we have found for this ion are quite similar to those found previously (Table 4). The increased length of the bridging Sb—F bond has the usual effect of distorting the octahedral environment around the antimony atom. The four fluorine atoms F(3), F(4), F(5), and F(6) remain coplanar with a maximum deviation of 0.006 Å but the plane is displaced 0.14 Å towards the bridge bond and away from the antimony atom. This can be attributed to the longer and weaker Sb—F bridge bond exerting smaller repulsions on the four neighboring Sb—F bonds than the shorter and stronger Sb—F bond that is *trans* to the bridge. One

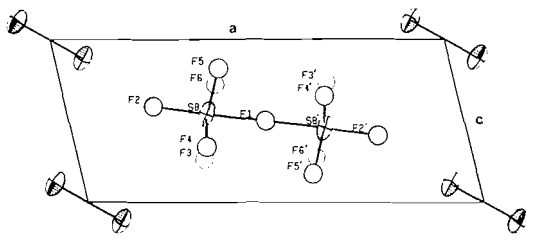

FIG. 1. Projection of structure down the *b* axis.

TABLE 2. Selected bond distances and angles for $I_2^+Sb_2F_{11}^-$

Bond	Distance (Å)	Bonds	Angle (deg)
Intramolecular			
I—I′	2.557(4)	Sb—F(1)—Sb′	166(3)
Sb—F(1)	2.001(7)	F(1)—Sb—F(2)	169(2)
—F(2)	1.83(2)	—F(3)	85(2)
—F(3)	1.96(4)	—F(4)	89(2)
—F(4)	1.78(4)	—F(5)	86(2)
—F(5)	1.80(4)	—F(6)	82(2)
—F(6)	1.87(4)	F(2)—Sb—F(3)	90(2)
		—F(4)	99(2)
Intermolecular		—F(5)	99(2)
I—F(2)	2.89(2)	—F(6)	89(2)
		F(3)—Sb—F(4)	91(2)
		—F(5)	170(2)
		—F(6)	87(2)
		F(4)—Sb—F(5)	93(2)
		—F(6)	171(2)
		F(5)—Sb—F(6)	88(2)

TABLE 3. Stretching frequencies, absorption maxima, and bond lengths of the halogen molecules and the diatomic halogen cations (3)

Species	Stretching frequency (cm^{-1})	Principal absorption (nm)	Bond length (Å)
Cl_2	564.9	330	1.98
Cl_2^+	645.6	—	1.89
Br_2	320	410	2.27
Br_2^+	360	510	2.15
I_2	213	500	2.66
I_2^+	238	646	2.56

interesting difference between the structure of the $Sb_2F_{11}^-$ ion found in the present case and those found previously is that the ion has a symmetric fluorine bridge (there is indeed a twofold crystallographic rotation axis passing through the bridging fluorine) whereas the $Sb_2F_{11}^-$ ions in the compounds $XeF_3^+Sb_2F_{11}^-$, $XeF^+Sb_2F_{11}^-$, and $BrF_4^+Sb_2F_{11}^-$ have asymmetric fluorine bridges (10–13). The extent of this asymmetry increases with increasing interaction between the cation and the $Sb_2F_{11}^-$ ion as shown by the length of the shortest cation–anion contact. This interaction also manifests itself in a lengthening of the Sb—F bond involved. All the data are consistent with an increasing interaction between the cation and the anion in the series I_2^+, XeF_3^+, XeF^+, BrF_4^+ indicating that the cations become increasingly acidic, *i.e.*, in-

TABLE 4. Comparison of $[Sb_2F_{11}]^-$ anions

Compound	Sb—F_1 bridge‡ distances (Å)	Bridge angle Sb—F_1—Sb (deg)	Shortest F_2-cation distance (Å)	Sb—F_2 distance	Mean Sb—F terminal distance (Å)	Reference
$SbCl_4^+Sb_2F_{11}^-$	2.01(7), 2.01(7)	155(4)	3.0	—	1.87(7)	13
$I_2^+Sb_2F_{11}^-$	2.00(1), 2.00(1)	166(3)	2.89	1.83(2)	1.85	This work
$XeF_3^+Sb_2F_{11}^-$	2.01(1), 2.04(1)	155.4(2)	2.50	1.90	1.85	10
$XeF^+Sb_2F_{11}^-$	1.98(4), 2.05(4)	150	2.35	1.93	1.83	11
$(Br_2^+)SbF_5Sb_2F_{11}^-$	1.97(4), 2.10(3)	148(3)	2.10* (2.86†)	1.97	1.83	8
$BrF_4^+Sb_2F_{11}^-$	1.94(12), 2.14(12)	173(6)	2.24	1.86	1.81	12

*$Sb_2F_{11}^-$ --- SbF_5 distance.
†Br_2^+ --- $Sb_3F_{16}^-$ distance.

‡

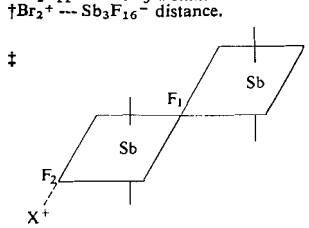

creasingly good electron pair acceptors in this order. The long cation–anion contact distance in $I_2^+Sb_2F_{11}^-$, although rather shorter than the sum of the van der Waals radii, indicates that any interaction between these two ions is very small and accordingly one may consider that in this case one has an essentially "free" symmetrical $Sb_2F_{11}^-$ ion. A similar negligible interaction has been found between Br_2^+ and $Sb_3F_{16}^-$ (8). There also appears to be a tendency for the angle at the bridging fluorine of $Sb_2F_{11}^-$ to decrease with increasing anion–cation interaction although the F-bridge angle of $Sb_2F_{11}^-$ in $BrF_4^+Sb_2F_{11}^-$ is not consistent with this trend. Possibly this is related to the continuous chain-like structure of this latter compound but in any case it is difficult to give any simple explanation of these bridging bond angles. The cation–anion interaction involves a movement of the fluorine involved in this interaction towards the central atom of the cation and some donation of charge to this atom. This in turn involves some loss of electron density at the antimony atom of this half of the $Sb_2F_{11}^-$ which accordingly becomes more positive and attracts the fluorine of the bridge more strongly than the other antimony resulting in the observed asymmetry. It is interesting to note that the structure of the anion $Sb_3F_{16}^-$ is consistent with the above discussion. This anion may be regarded as an $Sb_2F_{11}^-$ ion interacting with an SbF_5 molecule which, like the cations above, is a strong Lewis acid. This interaction involves the formation of a fluorine bridge by one end of the $Sb_2F_{11}^-$ unit and a consequent appearance of an asymmetry of the fluorine bridge of $Sb_2F_{11}^-$. The observed parameters are quite consistent with the others in Table 4 and imply that as an electron pair acceptor SbF_5 is stronger than XeF^+ but weaker than BrF_4^+. This conclusion raises the question of the validity of describing $BrF_5 2SbF_5$ as the ionic compound $BrF_4^+Sb_2F_{11}^-$ as the bonding must be regarded as less "ionic" than that in the $Sb_3F_{16}^-$ ion and indeed as Lind and Christe (12) point out the structure of $BrF_5 \cdot 2SbF_5$ closely resembles that of polymeric SbF_5. In summary it may be stated with some certainty that in the series of compounds $XeF_3^+ \cdot Sb_2F_{11}^-$, $XeF^+ \cdot Sb_2F_{11}^-$, $SbF_5 \cdot Sb_2F_{11}^-$, and $BrF_4^+ \cdot Sb_2F_{11}^-$ there is an increasingly strong covalent interaction between the anion and the cation, that is, an increasing tendency for a fluorine of the "anion" to donate an electron pair into the valence shell of the central atom of the "cation".

We thank the National Research Council of Canada for their support of this work. One of us (J.S.) also thanks the Government of Ontario for the award of an Ontario Graduate Fellowship.

1. R. J. GILLESPIE and J. B. MILNE. Inorg. Chem. **5**, 1577 (1966).
2. R. J. GILLESPIE and M. J. MORTON. J. Mol. Spectrosc. **30**, 178 (1969).
3. R. J. GILLESPIE and M. J. MORTON. Q., Rev. **25**, 553 (1971).

Can. J. Chem. Downloaded from www.nrcresearchpress.com by 210.87.254.5 on 09/05/12
For personal use only.

4. R. D. W. KEMMITT, M. MURRAY, V. M. MCRAE, R. D. PEACOCK, M. C. R. SYMONS, and T. A. O'DONNELL. J. Chem. Soc. A, 862 (1968).
5. W. C. HAMILTON. Acta Cryst. **18**, 502 (1965).
6. International tables for X-ray crystallographers. Kynock Press, Birmingham. 1962.
7. J. M. STEWART, F. A. KUNDELL, and J. C. BALDWIN. XRAY 71 system of crystallographic programs. University of Maryland, Technical Report. 1971.
8. A. J. EDWARDS, G. R. JONES, and R. J. C. SILLS. Chem. Commun. 1527 (1968); A. J. EDWARDS and G. R. JONES. J. Chem. Soc. A, 2318 (1971).
9. F. P. HUBERMAN. J. Mol. Spectrosc., **20**, 29 (1966).
10. P. E. MCKEE, C. J. ADAMS, A. ZALKIN, and N. BARTLETT. J. Chem. Soc. Chem. Commun. 26 (1973).
11. V. M. MCRAE, R. D. PEACOCK, and D. R. RUSSELL. Chem. Commun. 62 (1969).
12. M. D. LIND and K. O. CHRISTE. Inorg. Chem. **11**, 608 (1972).
13. H. B. MILLER, H. W. BAIRD, C. L. BRAMLETT, and W. K. TEMPLETON. Chem. Commun. 262 (1972).

Can. J. Chem. Downloaded from www.nrcresearchpress.com by 210.87.254.5 on 09/05/12
For personal use only.

Reversible Inhibition of Carboxypeptidase A. II.[1] Inhibition of Esterase Activity by Dicarboxylic Acid Anions

JOHN W. BUNTING AND CHESTER D. MYERS

Department of Chemistry, University of Toronto, Toronto, Ontario M5S 1A1

Received January 9, 1974

JOHN W. BUNTING and CHESTER D. MYERS. Can. J. Chem. **52,** 2053 (1974).

Reversible inhibition of the hydrolysis of *O*-hippuryl-L-3-phenyllactic acid by carboxypeptidase A has been studied for a series of decarboxylic acids at 25°, p*H* 7.5, and ionic strength 0.2. All inhibitors studied displayed either strictly competitive or partially competitive inhibition kinetics. For the series $CO_2H(CH_2)_nCO_2H$, strictly competitive inhibition was observed for $n = 1, 3, 4, 8, 10$, whereas partially competitive inhibition occurs for $n = 2, 5, 6, 7$. A series of 11 alkyl- and aryl-substituted malonic acids were all strictly competitive inhibitors; for a series of six alkylmalonic acids the inhibition constants are correlated with the Hansch π-parameter by the equation $-\log K_i = 2.25\pi + 1.75$; arylmalonic acids are poorer inhibitors than expected on the basis of their π-parameters, in accord with a similar observation for monocarboxylic acids. Phthalic acid is a strictly competitive inhibitor ($K_i = 1.7$ m*M*), whereas the isomeric isophthalic and terephthalic acids cause relatively little inhibition even at 0.1 *M*; maleic acid is a partially competitive inhibitor, whereas the isomeric fumaric acid gives only 15% inhibition at 0.1 *M*. Homophthalic acid and 2,2-dimethyl- and 3,3-dimethylglutaric acids were also investigated.

The characteristics of partially competitive inhibition displayed by all dicarboxylic acids and also monomethyl succinate and succinamic acid are consistent with a scheme which assumes the formation of an $E.I_2$ complex. The observed specificity of dicarboxylic acid binding is used to postulate a schematic diagram for binding of these species to the enzyme, and an interpretation of this diagram is suggested on the basis of the crystallographically determined structure of the enzyme.

JOHN W. BUNTING et CHESTER D. MYERS. Can. J. Chem. **52,** 2053 (1974).

On a étudié l'inhibition réversible de l'hydrolyse de l'acide *O*-hippuryl phényl-3 L-lactique par la carboxypeptidase A pour une série d'acides dicarboxyliques à 25°, à p*H* 7.5 et à une force ionique de 0.2. Tous les inhibiteurs étudiés présentent une cinétique d'inhibition qui est soit strictement compétitive soit partiellement compétitive. On a observé une inhibition strictement compétitive pour les séries $CO_2H(CH_2)_nCO_2H$ où $n = 1, 3, 4, 8, 10$, pendant qu'on a observé une inhibition partiellement compétitive pour $n = 2, 5, 6, 7$. Une série de 11 acides maloniques substitués par des groupes alcoyles et aryles sont tous des inhibiteurs strictement compétitifs; les constantes d'inhibition pour une série de six acides alcoylmaloniques sont reliées avec le paramètre π de Hansch par l'équation $-\log K_i = 2.25\ \pi + 1.75$; les acides arylmaloniques sont des inhibiteurs plus faibles que ce que l'on s'attendait en se basant sur leurs paramètres π ce qui est en accord avec une observation similaire pour les acides monocarboxyliques. L'acide phtalique est un inhibiteur strictement compétitif ($K_i = 1.7$ m*M*), tandis que les acides isomères isophtaliques et téréphtaliques produisent une inhibition relativement faible même à 0.1 *M*. On a aussi étudié l'acide homophtalique et les acides diméthyl-2,2 et diméthyl-3,3 glutariques.

Les caractéristiques des inhibitions partiellement compétitives produites par tous les acides dicarboxyliques ainsi que par le monosuccinate de méthyle et l'acide succinamique sont en accord avec un schéma qui suppose la formation d'un complexe $E.I_2$. La spécificité de la liaison d'un acide dicarboxylique est utilisée pour postuler un diagramme schématique pour la fixation de ces espèces à l'enzyme, et une interprétation de ce diagramme est suggérée en se basant sur la structure de l'enzyme déterminée de façon cristallographique.

[Traduit par le journal]

We recently reported (1) a detailed study of the reversible inhibition by carboxylic acid anions of the hydrolysis of *O*-hippuryl-L-3-phenyllactic acid by bovine carboxypeptidase A. As part of our continuing investigation of the influence of inhibitor structure on the form and extent of the reversible inhibition of this enzyme, we now wish to report the extension of this study to the anions of dicarboxylic acids. During the course of this work, reports (2, 3) have appeared of the unusually strong competitive inhibition of both the peptidase and esterase activities of this enzyme

[1]For Part I, see ref. 1.

Can. J. Chem. Downloaded from www.nrcresearchpress.com by 210.87.254.42 on 09/05/12
For personal use only.

Can. J. Chem. Downloaded from www.nrcresearchpress.com by 210.87.254.42 on 09/05/12
For personal use only.

by L-benzylsuccinic acid ($K_i = 4.5 \times 10^{-7}$ *M* at p*H* 7.5, 25°). Our present study suggests that dicarboxylic acid anions, in general, are somewhat more potent inhibitors than might have been expected from analogy with related monocarboxylic acids, and furthermore, that the inhibition constants of these species display informative structural dependences.

Experimental

Materials

All carboxylic acids, except those indicated below, were obtained commercially and recrystallized to constant melting points in agreement with literature values. Once recrystallized oxalic acid (m.p. 190°, lit (4) m.p. 189.5°) gave 71% inhibition at 0.1 *M* inhibitor concentration. However, upon repeated recrystallization, this inhibition gradually decreased to zero at this concentration and so the inhibition initially observed is presumably due to a small amount of unidentified impurity.

The diethyl esters of propylmalonic acid and isopropylmalonic acid were prepared from diethyl malonate and propyl iodide and isopropyl bromide, respectively, by the method of Adams and Kamm (5). These esters, and also a commercial preparation of diethyl phenethylmalonate, were hydrolyzed to give the corresponding dipotassium salts by treatment with a stoichiometric amount of potassium hydroxide in methanolic solution overnight. After removal of the methanol on the rotary evaporator, the salts were recrystallized several times from 50% aqueous methanol. The samples of those salts that were used in the inhibition studies were pure by p.m.r. spectroscopy.

O-Hippuryl-L-3-phenyllactic acid was purchased from Fox Chemical Company, Los Angeles, California. Stock solutions of bovine carboxypeptidase A (Worthington Biochemical Corporation (Code COA)) were prepared from a toluene suspension of the crystalline enzyme as previously described (1).

Methods

All reactions were studied at 25°, ionic strength 0.2, p*H* 7.5. Sodium chloride was used to adjust the total ionic strength of the reaction solutions to 0.2. The enzymic hydrolysis of *O*-hippuryl-L-3-phenyllactic acid was followed on the p*H*-stat as previously described (1). Extraction of competitive inhibition constants from the experimental data for the dependence of initial velocity on substrate concentration at constant inhibitor concentration was also carried out as described previously (1). Inhibition constants from the dependence of initial velocity on inhibitor concentration at constant substrate concentration (2.0×10^{-4} *M*) were calculated by the method of Dixon (6) after linear least-squares fitting of the data.

Results

The percentage inhibition of the hydrolysis of *O*-hippuryl-L-3-phenyllactic acid by carboxypeptidase A by the dicarboxylic acids $CO_2H(CH_2)_n$-CO_2H (n = 0–8, 10) at constant inhibitor concentration ($I = 0.04$ *M*) is plotted as a function of n in Fig. 1. This dependence clearly passes

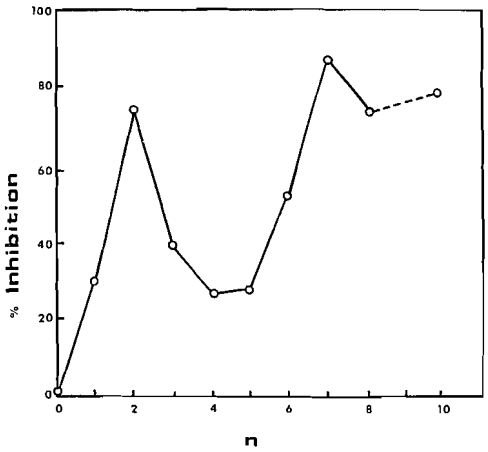

FIG. 1. Inhibition of the hydrolysis of *O*-hippuryl-L-3-phenyllactic acid ($S = 2.0 \times 10^{-4}$ *M*) by dicarboxylic acids, $CO_2H(CH_2)_nCO_2H$, ($I = 0.04$ *M*) at p*H* 7.5, ionic strength 0.2.

through maxima at $n = 2$ and $n = 7$. Reciprocal plots (E/v *vs.* $1/S$) of the dependence of initial velocity (v/E) on substrate concentration (S) for each of the above anions (*e.g.* Figs. 2 and 3) indicate that all are competitive inhibitors. Inhibition constants (K_i) calculated from these data are collected in Table 1 and are compared with inhibition constants that were obtained from Dixon plots (E/v *vs.* I) (Fig. 4). For malonic ($n = 1$), glutaric ($n = 3$), adipic ($n = 4$), sebacic ($n = 8$), and dodecanedioic ($n = 10$) acids, the Dixon plots are quite linear and there is a close correspondence between the K_i values obtained by these two methods. However, for the succinic ($n = 2$), pimelic ($n = 5$), suberic ($n = 6$), and azelaic ($n = 7$) acids, the Dixon plots are nonlinear (Fig. 5), and furthermore, the K_i values obtained from the Lineweaver–Burk plots show a dependence on inhibitor concentration. This latter observation is typical of partially competitive inhibition and has also been observed previously for some monocarboxylic acid anions (1).

We have explored the influence of hydrophobic side chains in dicarboxylic acid anions on the reversible inhibition of carboxypeptidase A by making use of a series of substituted malonic acids. All substituted malonic acids that were examined proved to be strictly competitive inhibitors and K_i values calculated from Lineweaver–Burk plots and Dixon plots for each inhibitor are given in Table 2. Again, a close agreement between inhibition constants determined in the two ways is apparent. For comparison,

Can. J. Chem. Downloaded from www.nrcresearchpress.com by 210.87.254.42 on 09/05/12
For personal use only.

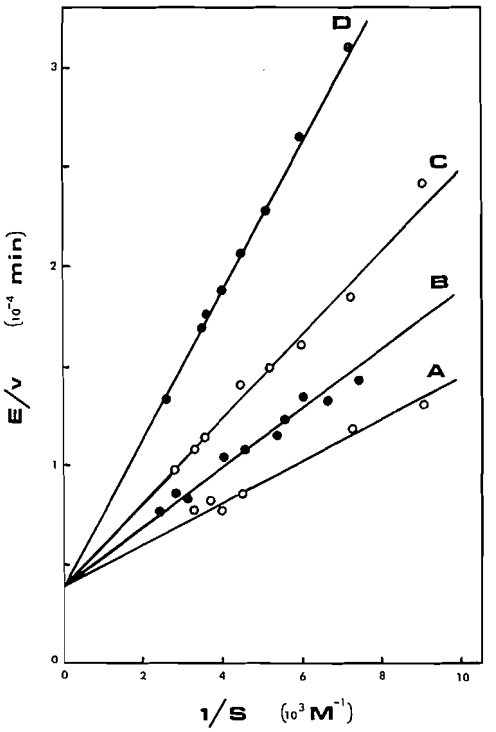

FIG. 2. Inhibition of the hydrolysis of *O*-hippuryl-L-3-phenyllactic acid by dicarboxylic acids: (*A*) glutaric acid (0.0409 *M*); (*B*) malonic acid (0.0926 *M*); (*C*) sebacic acid (0.0199 *M*); (*D*) sebacic acid (0.0398 *M*).

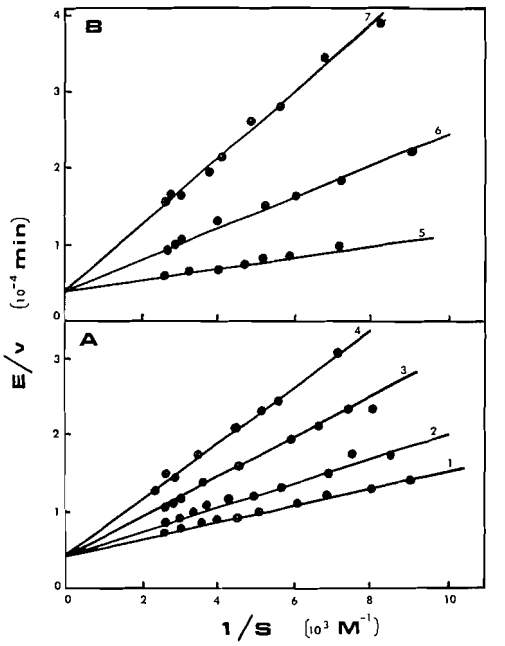

FIG. 3. Inhibition of the hydrolysis of *O*-hippuryl-L-3-phenyllactic acid by dicarboxylic acids: (*A*) succinic acid ((*1*) 0.0120 *M*, (*2*) 0.0199 *M*, (*3*) 0.0298 *M*, (*4*) 0.0398 *M*); (*B*) azelaic acid ((*5*) 0.00995 *M*, (*6*) 0.0199 *M*, (*7*) 0.0299 *M*).

Table 2 also includes inhibition constants for monocarboxylic acids having corresponding hydrophobic groups. In all cases, the dicarboxylic acids ($RCH(CO_2H)_2$) are stronger inhibitors than the corresponding monocarboxylic acids (RCH_2CO_2H).

A comparison of the inhibitory properties towards carboxypeptidase A of some other dicarboxylic acids (Table 3) indicates a strong dependence on the substitution pattern. Thus, phthalic acid is a relatively strong competitive inhibitor, K_i = 1.7 m*M*, whereas isophthalic and terephthalic acids show little inhibition even at 0.1 *M* (34 and 18%, respectively, at $S = 2.0 \times 10^{-4}$ *M*). Phthalic acid is also a stronger inhibitor than benzoic acid (K_i = 6.0 m*M* (1)). Homophthalic acid is also approximately a threefold stronger inhibitor than phthalic acid.

Maleic acid, a *cis*-1,2-dicarboxylic acid, displays partially competitive inhibition and is a much stronger inhibitor than its *trans*-isomer, fumaric acid, for which less than 15% inhibition is observed at 0.1 *M* inhibitor concentration. At this latter concentration, maleic acid shows close to 100% inhibition. 3,3-Dimethylglutaric acid is a 10-fold poorer inhibitor than 2,2-dimethylglutaric acid, although both are considerably stronger inhibitors than glutaric acid.

In Table 4 and Fig. 6, the results of a study of the reversible inhibition of carboxypeptidase A by monomethyl succinate and succinamic acid (succinic acid monoamide) are presented. These two derivatives are partially competitive inhibitors as is succinic acid itself.

We have previously (7) analyzed the partially competitive inhibition of carboxypeptidase A by monocarboxylic acid anions in terms of Scheme 1. For this scheme, plots of $1/K_i$ *vs.* *I* and E/v *vs.* I^2 are predicted (7) to be linear under suitable conditions[2] according to eqs. 1 and 2. (K_i is the inhibition constant calculated from plots of E/v

[2]The complete form of the rate equation for Scheme 1 is

$$E/v = \frac{1 + K_s/S}{k_2} + \frac{K_s I}{Sk_2}\frac{(K_i' + K_i'')}{K_i'K_i''} + \frac{K_s I^2}{Sk_2 K_i' K_{ii}'}$$

This reduces to eq. 2 provided that the term in *I* is small relative to the other terms.

TABLE 1. Competitive inhibition of carboxypeptidase A by $CO_2H(CH_2)_nCO_2H$[a]

Acid	n	Inhibitor concentration (M)	% inhibition[b]	K_i[c] (M)	K_i[d] (M)
Malonic	1	0.0926	54	2.1×10^{-2}	1.5×10^{-2}
Succinic	2	0.0120	49	5.02×10^{-3}	[e]
		0.0199	58	4.76×10^{-3}	
		0.0298	68	3.86×10^{-3}	
		0.0398	78	3.43×10^{-3}	
Glutaric	3	0.0409	36	1.7×10^{-2}	1.7×10^{-2}
Adipic	4	0.0900	50	2.4×10^{-2}	2.5×10^{-2}
Pimelic	5	0.0600	52	1.5×10^{-2}	[e]
		0.0900	74	1.3×10^{-2}	
Suberic	6	0.0248	41	9.6×10^{-3}	[e]
		0.0397	56	7.8×10^{-3}	
		0.0792	86	3.0×10^{-3}	
Azelaic	7	0.00995	28	6.7×10^{-3}	[e]
		0.0199	58	3.8×10^{-3}	
		0.0299	73	2.2×10^{-3}	
Sebacic	8	0.0199	63	3.1×10^{-3}	3.8×10^{-3}
		0.0398	74	3.8×10^{-3}	
Dodecanedioic	10	0.00987	60	3.5×10^{-3}	2.8×10^{-3}

[a]At pH 7.5, 25°, ionic strength 0.2.
[b]At $S = 2.0 \times 10^{-4}$ M.
[c]From reciprocal plot at indicated inhibitor concentration.
[d]From Dixon plot at $S = 2.0 \times 10^{-4}$ M.
[e]Non-linear Dixon plot.

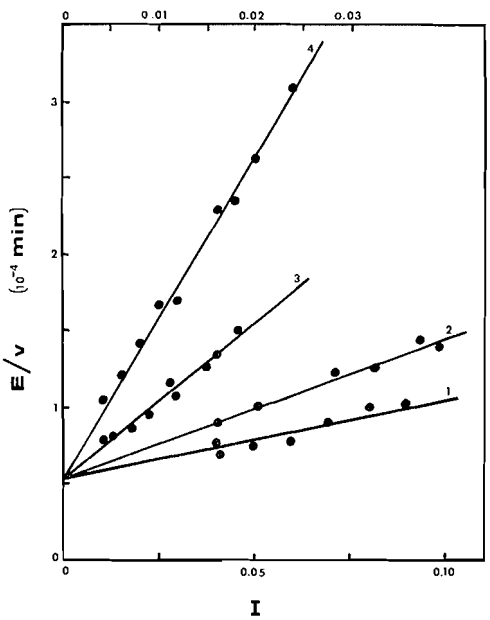

FIG. 4. Inhibition of the hydrolysis of *O*-hippuryl-L-3-phenyllactic acid (2.0×10^{-4} M) by dicarboxylic acids: (*1*) adipic acid (lower abscissa); (*2*) glutaric acid (lower abscissa); (*3*) 1,10-dodecanedioic acid (upper abscissa); (*4*) sebacic acid (lower abscissa).

vs. $1/S$ at inhibitor concentration I by assuming

$$[1] \qquad \frac{1}{K_i} = \frac{K_i' + K_i''}{K_i' K_i''} + \frac{I}{K_i' K_{ii}'}$$

$$[2] \qquad \frac{E}{v} = \frac{1 + K_s/S}{k_2} + \frac{K_s I^2}{S k_2 K_i' K_{ii}'}$$

that strictly competitive inhibition is operative; *i.e.* as in Tables 1–4). Such plots for succinic acid, monomethyl succinate, and succinamic acid are shown in Figs. 7 and 8, and appear quite linear. Values for $K_i' K_i''/(K_i' + K_i'')$ and $K_i' K_{ii}'$ are collected in Table 5 and the agreement between the independent evaluations of the product $K_i' K_{ii}'$ via eqs. 1 and 2 is quite reasonable.

Plots of $1/K_i$ *vs.* I and E/v *vs.* I^2 for the other partially competitive inhibitors observed in this study are also linear and the values of the product $K_i' K_{ii}'$ evaluated from each plot are also included in Table 5. In general, for each inhibitor there is good agreement within experimental error between these independent evaluations of $K_i' K_{ii}'$ and this is further evidence in support of Scheme 1 for the partially competitive inhibition of this enzyme.

Can. J. Chem. Downloaded from www.nrcresearchpress.com by 210.87.254.42 on 09/05/12
For personal use only.

TABLE 2. Competitive inhibition of carboxypeptidase A by substituted malonic acids $(R_1R_2C(CO_2H)_2)^a$

No.	R_1	R_2	K_i $(M)^b$	K_i $(M)^c$	K_i for $R_1R_2CHCO_2H^d$
1	H	H	2.1×10^{-2}	1.5×10^{-2}	5.3×10^{-2}
2	CH_3	H	1.4×10^{-3}	1.4×10^{-3}	5.1×10^{-3}
3	CH_3	CH_3	3.9×10^{-4}	3.7×10^{-4}	1.6×10^{-3}
4	C_2H_5	H	2.5×10^{-5}	2.8×10^{-5}	8.0×10^{-4}
5	C_2H_5	C_2H_5	6.5×10^{-5}	5.8×10^{-5}	—
6	n-C_3H_7	H	5.3×10^{-6}	7.5×10^{-6}	2.1×10^{-4}
7	i-C_3H_7	H	6.3×10^{-5}	5.8×10^{-5}	1.2×10^{-4}
8	n-C_4H_9	H	1.0×10^{-5}	1.1×10^{-5}	2.7×10^{-4}
9	C_6H_5	H	1.6×10^{-4}	1.6×10^{-4}	5.2×10^{-4}
10	$C_6H_5CH_2$	H	2.9×10^{-5}	3.2×10^{-5}	1.7×10^{-4}
11	$C_6H_5(CH_2)_2$	H	1.7×10^{-5}	1.7×10^{-5}	5.8×10^{-4}

[a]At p*H* 7.5, 25°, ionic strength 0.2.
[b]From *E*/v *vs.* 1/*S* at constant inhibitor concentration.
[c]From Dixon plot at $S = 2.0 \times 10^{-4}$ *M*.
[d]From ref. 1.

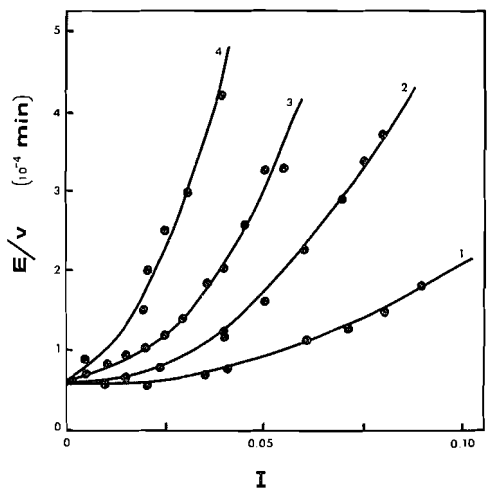

FIG. 5. Inhibition of the hydrolysis of *O*-hippuryl-L-3-phenyllactic acid (2.0×10^{-4} *M*) by dicarboxylic acids: (*1*) pimelic acid; (*2*) suberic acid; (*3*) succinic acid; (*4*) azelaic acid.

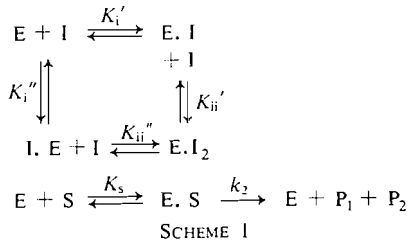

SCHEME 1

Discussion

In several cases, the inhibition constants that we have obtained in the present study may be compared with similar data recently obtained by

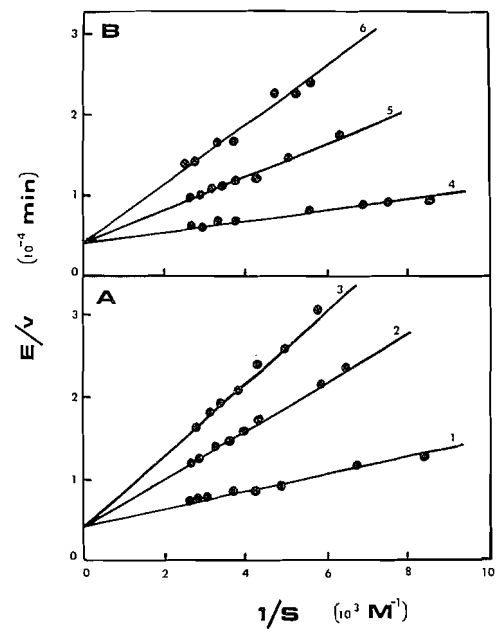

FIG. 6. Inhibition of the hydrolysis of *O*-hippuryl-L-3-phenyllactic acid: (*A*) monomethyl succinate ((*1*) 0.015 *M*, (*2*) 0.0197 *M*, (*3*) 0.0295 *M*); (*B*) succinamic acid ((*4*) 0.0855 *M*, (*5*) 0.142 *M*, (*6*) 0.185 *M*).

Byers and Wolfenden (3) against the peptide substrate, *N*-carbobenzoxyglycylglycyl-L-phenylalanine at ionic strength 0.75 but otherwise similar conditions to those used in the present study. Thus for benzylmalonic acid our value of $K_i = 3.0 \times 10^{-5}$ *M* is in reasonable agreement with the reported value of 6×10^{-5} *M* (3). The reported (3) inhibition constants for succinic (K_i =

Can. J. Chem. Downloaded from www.nrcresearchpress.com by 210.87.254.42 on 09/05/12
For personal use only.

TABLE 3. Competitive inhibition of carboxypeptidase A by dicarboxylic acids[a]

Acid	Concentration (M)	% inhibition[b]	K_I (M)[c]	K_I (M)[d]
Phthalic	9.96×10^{-3}	61	1.7×10^{-3}	1.7×10^{-3}
Isophthalic	0.090	34	(5.0×10^{-2})[e]	—
Terephthalic	0.090	18	(1.1×10^{-1})[e]	—
Homophthalic	2.80×10^{-3}	58	5.4×10^{-4}	6.6×10^{-4}
2,2-Dimethylglutaric	2.00×10^{-3}	61	3.5×10^{-4}	3.0×10^{-4}
3,3-Dimethylglutaric	0.030	70	3.4×10^{-3}	3.2×10^{-3}
Maleic	0.020	46	6.2×10^{-3}	[f]
	0.030	65	4.3×10^{-3}	
	0.040	73	3.3×10^{-3}	
Fumaric	0.10	< 15		

[a]At pH 7.5, 25°, ionic strength 0.2.
[b]At $S = 2.0 \times 10^{-4}$ M.
[c]From E/v *vs.* $1/S$ at indicated inhibitor concentration.
[d]From Dixon plot at $S = 2.0 \times 10^{-4}$ M.
[e]Calculated assuming competitive inhibition.
[f]Non-linear Dixon plot.

TABLE 4. Inhibition of carboxypeptidase A by succinic acid derivatives[a]

Inhibitor	Concentration (M)	% inhibition[b]	K_I (M)
Monomethyl succinate	0.0150	40	6.2×10^{-3}
	0.0197	52	4.8×10^{-3}
	0.0295	71	3.1×10^{-3}
	0.0346	77	2.7×10^{-3}
Succinamic acid	0.0855	25	6.5×10^{-2}
	0.142	62	2.3×10^{-2}
	0.185	71	2.0×10^{-2}

[a]At pH 7.5, 25°, ionic strength 0.2.
[b]At $S = 2.0 \times 10^{-4}$ M.

TABLE 5. Parameters for partially competitive inhibition of carboxypeptidase A

Inhibitor	$K_I'K_I''/(K_I' + K_I'')$	$K_I'K_{II}'$[a]	$K_I'K_{II}'$[b]
Succinic acid	6.7×10^{-3}	2.8×10^{-4}	1.5×10^{-4}
Succinamic acid	[c]	3.8×10^{-3}	3.3×10^{-3}
Monomethyl succinate	[c]	9.1×10^{-5}	8.9×10^{-5}
Pimelic acid			9.1×10^{-4}
Suberic acid	1.3×10^{-2}	4.4×10^{-4}	3.1×10^{-4}
Azelaic acid	[c]	7.1×10^{-5}	5.1×10^{-5}
Maleic acid	[c]	1.5×10^{-4}	1.8×10^{-4}

[a]From $1/K_I$ *vs.* I according to eq. 1.
[b]From E/v *vs.* I^2 according to eq. 2.
[c]Intercept according to eq. 1 is too small to allow an accurate estimate of this parameter.

5×10^{-4} M), maleic ($K_i = 3 \times 10^{-4}$ M), and fumaric ($K_i = 3 \times 10^{-3}$ M) acids are based on the amount of inhibitor required to produce 50% inhibition and also presumably assume strictly competitive inhibition. We have shown that for succinic and maleic acids, inhibition towards our ester substrate corresponds to partially competitive inhibition and so the earlier estimates of K_i for these two inhibitors may not be reliable. However, fumaric acid is an extremely poor inhibitor in our study and this suggests important differences in the binding of this inhibitor relative to the different substrates used in this study and the previous study (3).

Our interpretation of the phenomenon of partially competitive inhibition (Scheme 1) requires the presence of at least two different binding sites on this enzyme for inhibiting anions. Experi-

Can. J. Chem. Downloaded from www.nrcresearchpress.com by 210.87.254.42 on 09/05/12
For personal use only.

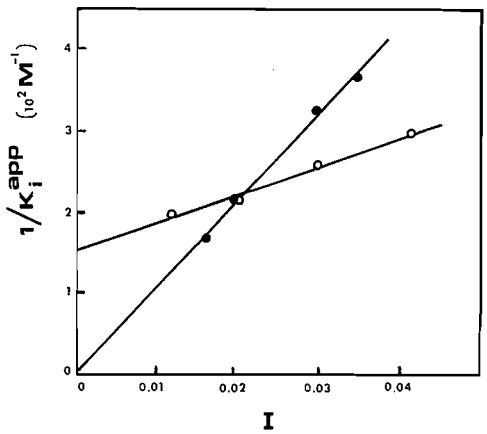

FIG. 7. Dependence of $1/K_i^{app}$ on I for succinic acid (○) and monomethyl succinate (●).

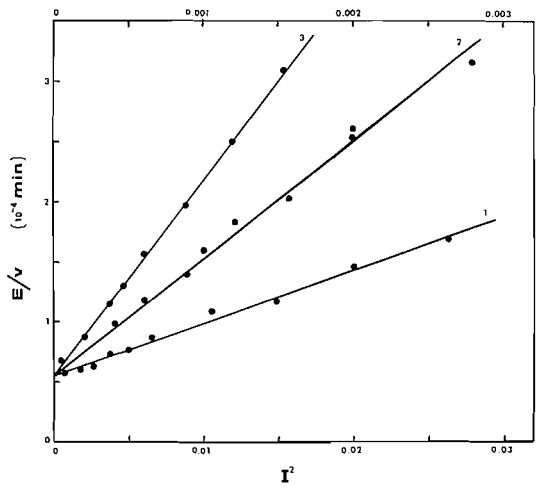

FIG. 8. Dependence of E/v on I^2 for: (*1*) succinamic acid (lower abscissa); (*2*) succinic acid (upper abscissa); (*3*) monomethyl succinate (upper abscissa). All inhibitors at $S = 2.0 \times 10^{-4}$ *M*.

mental evidence for the binding of two (or more) carboxylate ion inhibitors to one carboxypeptidase A molecule is available from both X-ray crystallographic (8) and spectroscopic (9, 10) studies. Thus our postulate of an $E.I_2$ species has experimental support; however, the dependence of partially competitive inhibition on the structure of the inhibitor species is somewhat puzzling. Consideration of the data in Table 1 indicates that succinic acid displays partially competitive inhibition but its next lower and higher homologs seem to be strictly competitive inhibitors. Pimelic, suberic, and azelaic acids each display partially competitive inhibition but the two highest homologs examined, sebacic and dodecanedioic acids, seem to be strictly competitive inhibitors.[3]

The observation of partially competitive inhibition kinetics according to Scheme 1 will be very dependent, of course, on the relative values of the various inhibition constants defined by this scheme. These inhibition constants will in turn depend upon the inhibitor specificity characteristics of the two binding sites. If K_{ii}' and K_{ii}'' are both much larger than K_i' and K_i'', respectively, then deviations of the Dixon plots from linearity will only occur at quite high percentage inhibitions, and consequently, partially competitive inhibition may not be experimentally observable in this case. Additionally, it should be noted that even when $E.I_2$ species are not formed in any appreciable amounts, Scheme 1 predicts that the inhibition constants obtained from strictly competitive inhibition may only be apparent inhibition constants if significant amounts of both E.I and I.E species are present. This apparent inhibition constant, $K_i^{app} = K_i'K_i''/(K_i' + K_i'')$, reduces to $K_i^{app} = K_i'$ for $K_i'' \gg K_i'$ (*i.e.* predominant formation of E.I) and to $K_i^{app} = K_i''$ for $K_i' \gg K_i''$ (*i.e.* predominant formation of I.E). Furthermore, K_i^{app} represents a minimum value for both K_i' and K_i''.

If we were to ignore the succinic acid result, then the remaining alkanedioic acid data in Table 1 might be simply interpreted according to Scheme 1 by assuming that the lower homologs (C_3–C_6) predominantly bind to the enzyme to produce the E.I species (*i.e.* $K_i' \ll K_i''$ and $K_i' \ll K_{ii}'$), whereas the higher two homologs (C_{10} and C_{12}) bind preferentially at a different site to produce I.E (*i.e.* $K_i'' \ll K_i'$ and $K_i'' \ll K_{ii}''$). The C_7–C_9 homologs might then be expected to show intermediate behavior, with all dissociation constants in Scheme 1 being sufficiently similar in magnitude for these inhibitors that significant amounts of each of E.I, I.E, and $E.I_2$ are present in equilibrium with one another. Consequently, partially competitive inhibition would only be apparent in these latter cases. This interpretation implies that the E.I binding site shows a preference for small dicarboxylic acid species, while the I.E binding site is specific for much larger dicarboxylic acid inhibitors. Since

[3]There is no evidence for mixed inhibition by these higher homologs as was previously observed for nonanoic and decanoic acids (1).

Can. J. Chem. Downloaded from www.nrcresearchpress.com by 210.87.254.42 on 09/05/12
For personal use only.

formation of both E.I and I.E is competitive with substrate binding, it is further required that either each inhibitor binding site should overlap with a portion of the substrate binding site sufficiently to preclude substrate binding, or alternatively, that inhibitor binding should otherwise block access of the substrate to the catalytically active site (*e.g.* by a conformational change in the enzyme upon inhibitor binding).

An alternative interpretation is also apparent. Thus, the E.I site might show little specificity and so be able to bind all the alkanedioic acids examined, whereas the I.E site might show much more restrictive specificity requirements and be only able to accommodate the C_7–C_9 homologs. Under these circumstances, significant amounts of the $E.I_2$ species would only be formed for the C_7–C_9 homologs and so only these dicarboxylic acids would show partially competitive inhibition kinetics.

As noted above, the observation of partially competitive inhibition for succinic acid does not fit well into the foregoing hypotheses. The simplest way of accounting for this discrepancy seems to be to suggest that there is yet another binding site on the enzyme molecule and that this site is highly specific for succinic acid and its derivatives. In this regard, it should be noted that in addition to succinic acid itself, both monomethyl succinate and succinamic acid also display partially competitive inhibition characteristics (Table 5 and Figs. 7 and 8). For succinic acid, K_i^{app} as defined above can be evaluated from the ordinate intercept of the $1/K_i$ *vs.* I plot (Fig. 7). However, for the succinic acid ester and amide this intercept is indistinguishable from zero within experimental error. This indicates that K_i^{app} (and hence K_i' and K_i'') is much greater for these derivatives than for succinic acid itself. This is in accord with the observation of Byers and Wolfenden (3) that L-benzylsuccinic acid is bound 14 times more strongly than its monomethyl ester.

The simplest interpretation of these data would seem to be that the succinate dianion is bound much more strongly than succinic acid monoanions. However, Byers and Wolfenden (3) have rationalized the pH dependence (pH 5.4–10.1) of K_i for L-benzylsuccinic acid in terms of the inhibitor monoanion (HI^-) binding to an enzyme species EH but not to the deprotonated species E^- (pK_a = 9.0). The introduction of the catalytically important protonation of EH to give EH_2^+ (pK_a = 6.2) (11) gave a poor fit to the experimental data for pH < 6.5 (3). In this regard, we wish to point out that for pH > 6.5, the pH dependence of K_i can be equally well explained in terms of the binding of the inhibitor dianion (I^{2-}) to EH_2^+, since in this pH region the binding of I^{2-} to EH_2^+ or of HI^- to EH will generate the same pH dependence for the observed K_i. The experimental deviations from the predicted pH dependence for K_i in the region pH = 5.4–6.5 may then be rationalized by assuming that HI^- may also bind to EH_2^+ as indicated in Scheme 2.

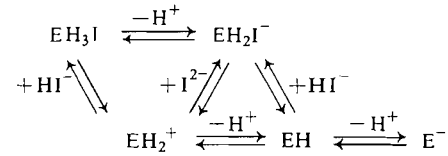

SCHEME 2

We feel that Scheme 2 is a more reasonable interpretation of the data of Byers and Wolfenden (3), since it does not ignore the ionization constant of pK_a = 6.2 for formation of the EH_2^+ species which has been demonstrated (11) to be catalytically important. Furthermore, Scheme 2 is more consistent with the kinetically required scheme for peptide substrate binding (in the monoanionic form) to both EH_2^+ and EH species but not to E^- (11). It is clear that the pH dependence of K_i from Scheme 2 does not allow a decision on whether the enzyme–inhibitor complex EH_2I^- is produced at pH 7.5 by binding of I^{2-} to EH_2^+ or of HI^- to EH or by a mixture of both processes. Therefore, we are unable at the present time to determine whether the dicarboxylic acids included in the present study are binding to the enzyme in the monoanionic or dianionic forms. All K_i values in the present study are expressed in terms of the dianions since these species predominate at pH 7.5.[4]

We have recently shown (1) that for the monocarboxylic acid inhibitors, RCH_2CO_2H, the inhibition constant is linearly related by eq. 3 to Hansch's π-parameter which is a measure of the hydrophobicity (13, 14) of RCH_2. This is consis-

[4]The most weakly acidic second dissociation among all the dicarboxylic acids included in the present study is that of maleic acid (pK_a = 6.2 (12)). If it should seem desirable at a later date, all the inhibition constants reported in this work may, of course, be converted into terms of the monoanionic species by making use of the second ionization constants of these dicarboxylic acids.

Can. J. Chem. Downloaded from www.nrcresearchpress.com by 210.87.254.42 on 09/05/12
For personal use only.

Can. J. Chem. Downloaded from www.nrcresearchpress.com by 210.87.254.42 on 09/05/12
For personal use only.

[3] $$-\log K_i = 1.77\pi + 0.50$$

tent with RCH_2 being accomodated in a hydrophobic pocket in or near the active site of the enzyme with the usual favorable energetic consequences that are associated with "hydrophobic bonding" (15). One would predict that the introduction of a highly polar substituent into RCH_2 should reduce the affinity of this group for the hydrophobic pocket of the enzyme and so give rise to a considerable increase in the dissociation constant K_i. This effect would be even further magnified if a charged substituent were introduced. By assuming that the second carboxyl group in $RCH(CO_2H)_2$ is not involved in a specific bonding interaction with the enzyme, one may use the correlation line in eq. 3 to estimate the difference in K_i values for pairs of mono- and dicarboxylic acids having the same R group. Thus, taking $\pi_{CO_2H} = -0.67$ (14),

$$\log K_i (RCH(CO_2H)_2) - \log K_i (RCH_2CO_2H)$$
$$= 1.77 (\pi_{RCH_2} - \pi_{RCH(CO_2H)})$$
$$= 1.77 (\pi_H - \pi_{CO_2H})$$
$$= 1.20$$

Thus, the assumption that the same linear free energy relationship is applicable to mono- and dicarboxylic acid inhibitors predicts that K_i for a dicarboxylic acid will be 16-fold greater for the dicarboxylic acid than for the corresponding monocarboxylic acid. From the data in Table 2, it is clear that in all cases K_i actually decreases upon introduction of a second carboxyl group. The above calculation is based upon the assumption that the monoanion of the dicarboxylic acid binds to the enzyme; the K_i values in Table 2 refer to dianion binding and correction of these to represent monoanion binding would further increase the discrepancy between the calculated and experimental K_i values approximately 100-fold ($pK_a = 5.7$ for dianion formation from malonic acid (12)). Thus, it is clear that the second carboxyl group is involved in a specific interaction in the binding of the inhibitor species to the enzyme.

The K_i values of Table 2 for substituted malonic acids are plotted in Fig. 9 as a function of the π value of the substituent. For alkylmalonic acids up to propylmalonic acid, a linear correlation is apparent and least-squares fitting gives eq. 4 (correlation coefficient 0.962).

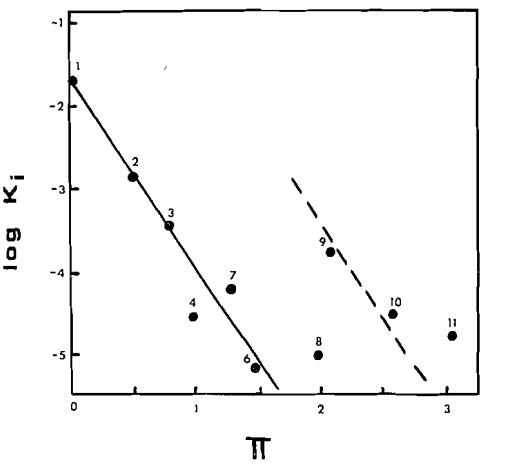

FIG. 9. Dependence of $\log K_i$ on π for substituted malonic acids. Individual acids are indicated by the numbers in Table 2.

[4] $$-\log K_i = 2.25\pi + 1.75$$

The phenyl- and benzylmalonic acids can be considered to lie on a line of similar slope, with eq. 5 being applicable. Equation 5 is similar to the equa-

[5] $$\log K_i \text{ (aliphatic)} - \log K_i \text{ (aromatic)} = -2.7$$

tion previously used to compare aliphatic and aromatic monocarboxylic acids ($\log K_i$ (aliphatic) $- \log K_i$ (aromatic) $= -1.9$ (1)), although the difference in the binding constants of aliphatic and aromatic moieties with equal π values is increased a further sixfold in the dicarboxylic acids.

The butylmalonic and phenethylmalonic acids show significant positive deviations from the lines in Fig. 9. Similar deviations were observed for substituents of this size or larger in the monocarboxylic acid series (1) and are believed to result from the hydrophobic substituent becoming too large to fit in its energetically most favorable conformation into the hydrophobic pocket of the enzyme. The fact that these deviations from the π-correlation occur at the same size alkyl or aralkyl substituent in both the mono- and dicarboxylic acid inhibitors is evidence in favor of the binding of the hydrocarbon moieties of these two groups of inhibitors at the same enzyme site. It should be noted that dimethylmalonic acid seems to fall reasonably close to the correlation line in Fig. 9; however, the diethylmalonic acid binds 100-fold less strongly than predicted by eq. 4 (*i.e.* K_i (predicted) $= 6 \times 10^{-7}$ *M*) and this

Can. J. Chem. Downloaded from www.nrcresearchpress.com by 210.87.254.42 on 09/05/12
For personal use only.

presumably reflects the inability of the two ethyl groups to enter the hydrophobic site without serious distortion of other binding interactions.

The large pre-π factor of eq. 4 is noteworthy, and is even greater than that previously observed for the monocarboxylic acids (eq. 3). We have previously (1) suggested a possible interpretation for the unusually high values for these pre-π factors. The similarities in the pre-π factors in eqs. 3 and 4 and the applicability of an equation such as eq. 5 to both mono- and dicarboxylic acid inhibitors, give further support to the above suggestion that the hydrophobic moieties of both series of inhibitors are binding to the same site on the enzyme.

As discussed above, the comparison of K_i values for corresponding mono- and dicarboxylic acids in Table 2 suggests that the presence of the second carboxyl group makes a significant contribution to the binding of the inhibiting ion. This may be interpreted as binding via simultaneous interactions of the carboxyl groups (or carboxylate ions) with suitable binding sites on the enzyme which are indicated schematically as S_1 and S_2 in Fig. 10. If the inhibitor does bind in the dianionic form as indicated, then it is clear that S_1 and S_2 would most likely be cationic in nature. However, a similar situation could be readily envisaged for binding of a dicarboxylic acid monoanion, in which one of the neutral carboxyl groups is bound to S_1 or S_2 (charge unspecified) via hydrogen bonding or dipolar interactions. The observed importance of hydrophobic interactions in binding of substituted malonic acids (Fig. 9) can be accommodated by the introduction of a hydrophobic pocket in the vicinity of the sites S_1 and S_2 as is schematically indicated in Fig. 10.

The relatively strong binding of phthalic acid but not the isomeric isophthalic and terephthalic

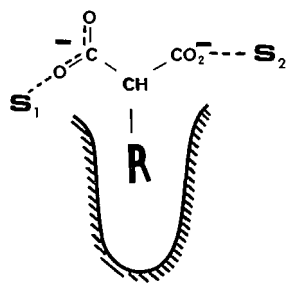

FIG. 10. Schematic diargam for binding of dicarboxylic acid inhibitors to carboxypeptidase A (see text).

acids can also be accounted for in terms of the above description of inhibitor binding. Thus, it may be assumed that the separation of the carboxyl groups in phthalic acid is suitable to allow a close interaction with S_1 and S_2, while at the same time allowing the phenyl ring to be oriented so that it extends into the hydrophobic pocket to some extent. In isophthalic and terephthalic acids the carboxyl groups are further apart and these two molecules do not have the rotational flexibility that is available in the saturated acids to allow suitable conformational changes to occur for optimal binding. Any attempt at optimizing the interactions of the carboxyl groups of these two acids with S_1 and S_2 would lead to less penetration of the aromatic ring into the hydrophobic pocket, relative to that which is possible for phthalic acid. Consequently, the hydrophobic interactions would be less important for the binding of these two inhibitors. The threefold stronger binding of homophthalic acid than of phthalic acid might be accounted for in terms of the methylene group allowing a deeper penetration of the aromatic ring into the hydrophobic pocket, with a resultant increase in favorable hydrophobic interactions.

The above interpretations and schematic diagram of inhibitor binding are based solely on the observed inhibitor specificities in Tables 2 and 3, and do not depend upon a knowledge of the actual structure of the active site region of the enzyme. Such information is available,[5] however, and it is of interest to compare the above schematic representation of the inhibitor binding site with the structure of the enzyme as elucidated crystallographically by Lipscomb and co-workers (8, 16, 17). These studies have shown that the interactions indicated in Fig. 11 are involved in the binding of glycyl-L-tyrosine and similar interactions are postulated to be involved in the productive binding of substrate molecules (18–20). The close relationship between Figs. 10 and 11 is quite apparent. Thus the carboxylate group and carbonyl group of the hydrolyzable peptide bond interact with positively charged sites on the enzyme, while the side chain of the *C*-terminal amino acid is located in a hydrophobic pocket.

[5]Obviously, this information was available to us prior to our construction of Fig. 10 and so it can be argued that we are not able to objectively interpret the inhibitor specificity data. However, we have not been able to construct any other schematic diagram which accounts for the observed inhibitor specificity data.

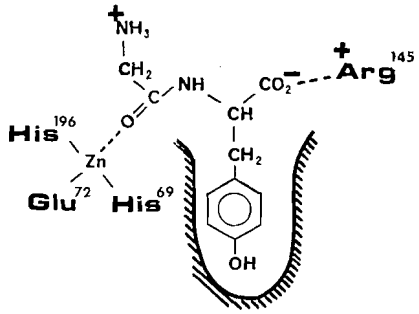

FIG. 11. Binding of glycyl-L-tyrosine to carboxypeptidase A as deduced by X-ray crystallography (see refs. 16 and 17).

It is therefore very tempting to equate S_1 and S_2 of Fig. 10 with Arg-145 and the zinc ion of Fig. 11. This is further suggested by the competitive nature of the inhibition that is observed, and also by the fact that L-benzylsuccinic acid is more than a tenfold stronger inhibitor than its lower and higher homologs, benzymalonic and benzylglutaric acids respectively (3). This latter observation suggests that a two-atom separation between the carboxyl groups is optimal for binding to S_1 and S_2, which is in accord with the separation between the carboxylate and peptide carbonyl groups of glycyl-L-tyrosine which results in binding to Arg-145 and the zinc ion.

This research was supported by an operating grant from the National Research Council of Canada and by the award of a Walter C. Sumner Memorial Fellowship to C.D.M.

1. J. W. BUNTING and C. D. MYERS. Can. J. Chem. **51**, 2639 (1973).
2. L. D. BYERS and R. WOLFENDEN. J. Biol. Chem. **247**, 606 (1972).
3. L. D. BYERS and R. WOLFENDEN. Biochemistry, **12**, 2070 (1973).
4. D. D. PERRIN, W. L. F. ARMAREGO, and D. R. PERRIN. Purification of laboratory chemicals. Pergamon Press, Oxford. 1966. p. 228.
5. R. ADAMS and O. KAMM. Org. Synth. Coll. Vol. 1. 250 (1947).
6. M. DIXON. Biochem. J. **55**, 170 (1953).
7. J. W. BUNTING and C. D. MYERS. Biochim. Biophys. Acta, **341**, 222 (1974).
8. T. A. STEITZ, M. L. LUDWIG, F. A. QUIOCHO, and W. N. LIPSCOMB. J. Biol. Chem. **242**, 4662 (1967).
9. S. A. LATT and B. L. VALLEE. Biochemistry, **10**, 4263 (1971).
10. L. FRETTO and E. H. STRICKLAND. Biochim. Biophys. Acta, **235**, 473 (1971).
11. D. S. AULD and B. L. VALLEE. Biochemistry, **9**, 4352 (1970).
12. G. KORTUM, W. VOGEL, and K. ANDRUSSON. Pure App. Chem. **1**, 187 (1960).
13. T. FUJITA, J. IWASA, and C. HANSCH. J. Am. Chem. Soc. **86**, 5171 (1964).
14. A. LEO, C. HANSCH, and D. ELKINS. Chem. Rev. **71**, 525 (1971).
15. M. H. KLAPPER. Prog. Bioorganic Chem. **2**, 55 (1973).
16. W. N. LIPSCOMB, G. N. REEKE, JR., J. A. HARTSUCK, F. A. QUIOCHO, P. H. BETHGE, M. L. LUDWIG, T. A. STEITZ, H. MUIRHEAD, and J. C. COPPOLA. Brookhaven Symp. Biol. **21**, 24 (1968).
17. W. N. LIPSCOMB, G. N. REEKE, JR., J. A. HARTSUCK, F. A. QUIOCHO, and P. H. BETHGE. Phil. Trans. Roy. Soc. London, Ser. B, **257**, 177 (1970).
18. W. N. LIPSCOMB. Acc. Chem. Res. **3**, 81 (1970).
19. F. A. QUIOCHO and W. N. LIPSCOMB. Adv. Protein Chem. **25**, 1 (1971).
20. J. A. HARTSUCK and W. N. LIPSCOMB. *In* The enzymes. 3rd Ed. Vol. 3. *Edited by* P. D. Boyer. Academic Press, New York. 1971. p. 1.

Can. J. Chem. Downloaded from www.nrcresearchpress.com by 210.87.254.42 on 09/05/12
For personal use only.

Identification d'un nouveau alcaloïde de canneberges

KRZYSZTOF JANKOWSKI, SIMONE GODIN ET NIVEN E. CUNDASAWMY

Département de Chimie, Université de Moncton, Moncton, Nouveau-Brunswick

Reçu le 9 mai, 1973[1]

KRZYSZTOF JANKOWSKI, SIMONE GODIN et NIVEN E. CUNDASAWMY. Can. J. Chem. **52**, 2064 (1974).

La structure d'un nouveau alcaloïde des canneberges, méthyl-12-octahydro-1,2,3,4,6,7,12,12b-indolo[2,3-*a*]quinolizine, a été établie à l'aide de la spectroscopie de masse et par la synthèse.

KRZYSZTOF JANKOWSKI, SIMONE GODIN, and NIVEN E. CUNDASAWMY. Can. J. Chem. **52**, 2064 (1974).

The structure of a new cranberry alkaloid, 12-methyl-1,2,3,4,6,7,12,12b-octahydroindolo[2,3-*a*]quinolizine was established using mass spectroscopy and by synthesis.

Nous avons décrit dans les publications précédentes les trois nouveaux alcaloïdes (1, 2) séparés à partir des extraits des Canneberges du Nouveau-Brunswick. Ces alcaloïdes, appelés les Cannaguinines (**1***a–c*), se caractérisent par la présence

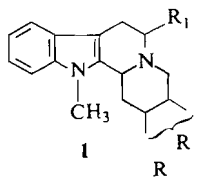

1

	R	R_1
a	$-C\equiv C-COOCH_2-$	H
b	$-C\equiv C-COOH$, CH_2OH	$COOCH_3$
c	$-C\equiv C-COOH$, CH_2OH	H

du système de *N*-méthylindole et le squelette de la tétrahydro-β-carboline. Nous avons cherché à réaliser la synthèse du quatrième alcaloïde, isolé en très petites quantités (<2.0 mg),[2] la méthyl-12-octahydro-1,2,3,4,6,7,12,12b-indolo-[2,3-*a*]quinolizine (**2**) pour ainsi prouver sa structure.

D'abord, la condensation, selon Gribble (3) du chlorhydrate de la tryptamine avec l'aldéhyde glutarique dans l'eau, suivie par la réduction avec du $NaBH_4$ a donné une octahydro-1,2,3,4,6,7,12,12b-indolo[2,3-*a*]quinolizine (**3**). Ensuite nous avons procédé à la *N*-méthylation avec l'excès d'iodure de méthyle en présence de $NaNH_2$ dans l'éthanol. La méthylation a donné le produit **2** (schéma 1), dont l'identification a été basée sur l'étude comparative avec le même produit d'origine naturelle. La comparaison du R_f du produit **2** naturel, 17.4, et synthétique, 17.0, (chromatographie sur couche mince, benzène–éthanol 9:1) a été le premier indice qualitatif de leur identité. Les spectres u.v. et i.r. du produit **2** naturel et synthétiques ont été identiques. Les composés **2** et **3** se prêtent difficilement à une étude par r.m.n. car ils sont insolubles dans la plupart des solvants organiques utilisés dans cette spectroscopie. Malgré cette difficulté, on a enregistré le spectre du produit **2** synthétique en le comparant avec le spectre du produit **3**. On a constaté que le signal du groupement N—H (à 7.6) a été remplacé à cause de la méthylation par le signal N—CH_3 (à 3.5) caractéristique pour les dérivés *N*-méthylindole ou *N*-méthylpyrrole (4). Les signaux de quatre protons aromatiques ont été légèrement déplacés vers le champ plus bas pour le produit **2**. Le changement du solvent ne change pas visiblement le spectre ($CDCl_3$ contre DMSO-d_8).

Les fragmentations principales du produit **2** naturel et synthétique et le produit modèle **3** ont été résumés dans le tableau 1. D'abord, les ions moléculaires intenses et le fragment du type $M^+/2$ ont été observés. Les fragments 100% pour les trois produits ont correspondu à une formule $M^+ - 1$ avec perte d'un hydrogène, 12b. Cette fragmentation, très typique pour les alcaloïdes tétrahydro-β-carboliniques (5–8), a été supportée pour le produit **2** naturel, le fragment à *m/e* 239, par une masse exacte trouvée 239.1547 correspondante à une formule moléculaire $C_{16}H_{19}N_2$. La perte de CH_2 ou CH_3 à partir d'un ion moléculaire a ensuite été détectée. Les séries des fragments dénotées dans le tableau 1 corres-

[1]Révision reçue le 25 janvier, 1974.

[2]Séparation des alcaloïdes par la chromatographie sur couche mince préparative, est décrite dans nos articles précédents (1, 2).

Can. J. Chem. Downloaded from www.nrcresearchpress.com by 210.87.254.6 on 09/05/12
For personal use only.

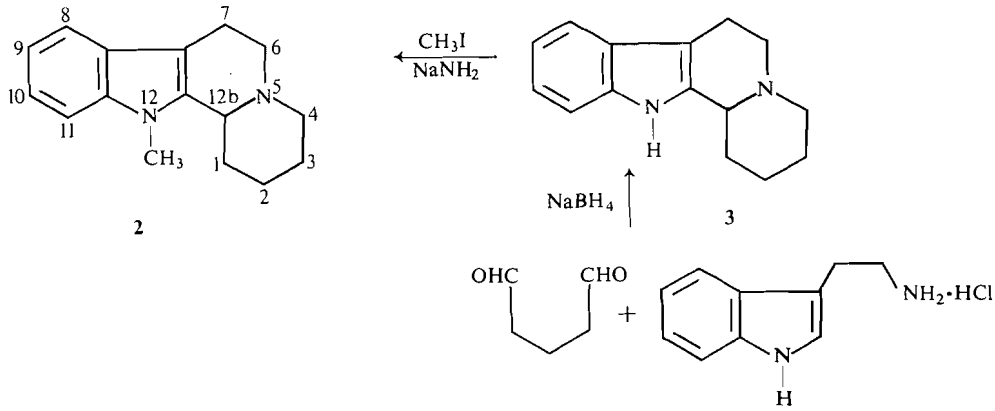

2 3

SCHÉMA I

TABLEAU 1. Spectroscopie de masse de composés **2** et **3**

m/e (intensité relative %)			
2[a]	**2**[b]	**3**	Fragment
240 (44.5)	240 (42.9)	226 (68.1)	M^+
239 (100.0)	239 (100.0)	225 (100.0)	M^+-1
226 (13.1)	226 (10.8)	—	M^+-14
225 (17.2)	225 (15.6)	—	M^+-15
212 (4.1)	212 (3.2)	198 (6.3)	M^+-28
211 (10.1)	211 (9.5)	197 (22.9)	$M^+-1-C_2H_4$
198 (4.0)	198 (3.7)	184 (5.6)	$M^+-C_3H_6$
196 (2.5)	196 (1.8)	182 (6.9)	$M^+-H_2-C_3H_6$
184 (14.7)	184 (12.8)	170 (15.9)	$M^+-C_4H_8$
183 (21.5)	183 (20.0)	169 (28.6)	$M^+-1-C_4H_8$
182 (10.2)	182 (10.1)	168 (12.6)	[c]
170 (10.1)	170 (9.5)	156 (9.9)	$M^+-C_4H_8N$
168 (4.0)	168 (3.5)	154 (8.3)	[c]
159 (8.1)	159 (8.0)	144 (7.8)	[c]
158 (6.1)	158 (6.0)	143 (9.1)	[c]
157 (4.1)	157 (3.5)	142 (7.3)	[c]
143 (6.0)	143 (6.0)	129 (7.1)	$M^+-C_4H_8N-C_2H_3$
120 (4.3)	120 (4.0)	113 (6.6)	$M^+/2$

[a]Naturel.
[b]Synthétique.
[c]Ces fragments peuvent être obtenus par quelques voies compétitives.

pondent à l'aromatisation successive (par exemple, 184, 193, 182) ou aux clivages retro-Diels–Alder (184, 170).

Les fragmentations ont été supportés abondamment par les ions métastables. Nous avons dénoté seulement les ions métastables communs aux processus de fragmentations de produits **2** et **3** (tableau 2). L'étude des ions métastables complète les travaux précédents sur les fragmentations des alcaloïdes indoliques (9).

Partie expérimentale

Les points de fusion ont été déterminés sur un appareil Fisher-Johns, et n'ont pas été corrigés. De l'alumine Woelm (activité III) a été utilisée pour la chromatographie sur colonne et du gel de silice G (Macherey & Nagel Co.) a été utilisé pour la chromatographie sur couche mince. Les solvants ont été purifiés selon les méthodes habituelles. Les spectres de masse ont été enregistrés à l'aide de l'appareil AEI-MS-902 (température 150 °C, 56–61 eV), les spectres i.r. (pastilles KBr) à l'aide de l'appareil Perkin-Elmer 467, les spectres u.v. (éthanol 95%) à l'aide de l'appareil Beckmann DB et les spectres r.m.n. avec l'appareil Varian T-60 (δ. p.p.m.). Analyse élémentaire a été faite sur Coleman Carbon-Hydrogen Analyser, model 33.

Méthyl-12-octahydro-1,2,3,4,6,7,12,12b-indolo[2,3-a]quinolizine (2)

Sur une période de 10 min. 4.5 g d'une solution aqueuse 25% d'aldéhyde glutarique (Aldrich Chemical Co.) ont

Can. J. Chem. Downloaded from www.nrcresearchpress.com by 210.87.254.6 on 09/05/12
For personal use only.

TABLEAU 2. Ions métastables $A \xrightarrow{m^*} B$

	A	B	m^* Obs. (8)	m^* Calc.	Type de la fragmentation
2[a]	239	211	186.4	186.2	
3	225	197	172.6	172.5	
2	240	196	160.0	160.2	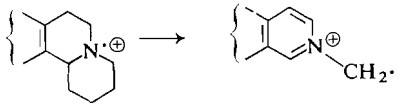
3	226	182	146.6	146.4	
2	239	183	140.4	140.1	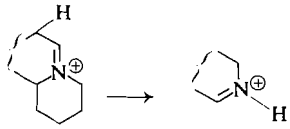
3	225	169	126.9	126.9	
2	239	158	104.6	104.4	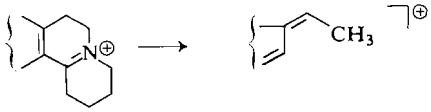
3	225	144	92.4	92.1	
2	170	143	120.5	120.3	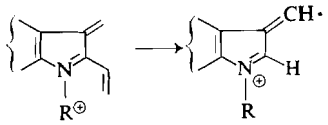
3	156	129	106.7	106.6	

R = H, CH_3

[a]Le produit 2 naturel.

été ajoutés à une solution agitée de 1.5 g de chlorhydrate de tryptamine (Aldrich Chemical Co.) dans l'eau glacée (1500 ml). La solution a été agitée pendant 1 h à 0–5 °C et ensuite laissée sous atmosphère d'azote à la température de la pièce pendant 10 jours. La solution jaune a été refroidie dans un bain de glace, diluée avec 600 ml d'éthanol aqueux 95% et traitée avec 24.0 g de $NaBH_4$ (en 10 portions) pendant 10 min. La solution a été agitée à 0–5 °C pendant 1 h et ensuite à la température de la pièce pendant 8 h. Le mélange a été rendu fortement basique avec du NaOH 6 *N*. L'extraction a été faite avec du CH_2Cl_2. L'extrait a été lavé avec du NaCl aqueux saturé, séché avec du Na_2CO_3 anhydre et évaporé sous vide. Une mousse jaune a été chromatographiée sur 100 g d'alumine basique d'activité III, avec élution de benzène. Les fractions de 25 ml ont été recueillies; 170 mg du produit **3**, p.f. 151–152°, recristallisé avec l'éther ont été récupérés de la fraction 3. Une portion (35 mg) de produit **3** ont été dissout dans l'éthanol (2 ml) auquel ont été ajouté 0.5 ml d'iodure de méthyle et 15 mg d'amidure de sodium. Un reflux a été fait pendant 2 h. La solution a ensuite été filtrée, le filtrat évaporé sous vide et recrystallisé avec l'éther. Le produit **2**, p.f. 168–170 °C (**2** naturel p.f. 166–168 °C), a été isolé; rendement, 8 mg; *i.r.* (cm^{-1}) 2925, 2880, 2860, 2830, 2800, 1705, 1618, 1548, 1452, 1130, 1285, 1245, 1010, 730; u.v. (nm/log ε) 214 (4.3), 272 (3.4), 279 (3.6), 289 (3.2), 298 (3.05); r.m.n.[3] produit **2** synthétique: 3.5 (N—CH_3), 6.9–7.5 (ϕ); (le spectre du **3**: 7.6 (N*H*), 7.0–7.4 (ϕ), 2.7–3.0 (H-4, H-6), 2.6 (H-12β), 2.4 (H-7), 1.3–1.9 (H-1, H-2, H-3)).

Anal. calc. pour le produit **2**, $C_{16}H_{20}N_2$ (240.2): C, 79.76; H, 8.39. Trouvé: C, 79.82; H, 8.25.

Nous remercions le Conseil national de recherches du Canada et le Conseil de recherches de l'Université de Moncton pour l'aide financière apportée sous forme d'une subvention de recherche.

1. K. JANKOWSKI, J. BOUDREAU et I. JANKOWSKA. Experientia, **27**, 1141 (1971).
2. K. JANKOWSKI. Experientia, **29**, 551 (1973).
3. G. W. GRIBBLE. J. Org. Chem. **37**, 1833 (1972).

[3]Microtube $CDCl_3$.

Can. J. Chem. Downloaded from www.nrcresearchpress.com by 210.87.254.6 on 09/05/12
For personal use only.

4. L. M. JACKMAN et S. STERNHELL. Application of nuclear magnetic resonance spectroscopy in organic chemistry. 2nd Ed. Pergamon Press, New York. 1969. p. 178–179.
5. H. BUDZIKIEWICZ, C. DJERASSI et D. H. WILLIAMS. Structure elucidation of natural products by mass spectrometry. Vol. I. Holden-Day Inc., San Francisco. 1964. pp. 77–83.
6. L. D. ANTONACCIO, N. A. PEREIRA, B. GILBERT, H. VORBRUEGGEN, H. BUDZIKIEWICZ, J. M. WILSON, L. J. DURHAM et C. DJERASSI. J. Am. Chem. Soc. **84**, 2161 (1962).
7. B. GILBERT, J. A. BRISSOLESE, N. FINCH, W. I. TAYLOR, H. BUDZIKIEWICZ, J. M. WILSON et C. DJERASSI. J. Am. Chem. Soc. **85**, 1523 (1963).
8. B. GILBERT, L. D. ANTONACCIO et C. DJERASSI. J. Org. Chem. **27**, 4702 (1962).
9. K. BIEMANN. Mass spectroscopy, organic chemical applications. McGraw-Hill, New York. 1962. p. 156.

Can. J. Chem. Downloaded from www.nrcresearchpress.com by 210.87.254.6 on 09/05/12
For personal use only.

Oxidation of CO to CO_2 in Melts Containing V_2O_5 and Alkali Oxides

A. BLOCK-BOLTEN, B. J. M. BERTRAND,[1] AND S. N. FLENGAS

Department of Metallurgy and Materials Science, University of Toronto, Toronto, Ontario M5S 1A4

Received October 29, 1973

A. BLOCK-BOLTEN, B. J. M. BERTRAND, and S. N. FLENGAS. Can. J. Chem. **52**, 2068 (1974).

The conversion of CO to CO_2 in the presence of V_2O_5 dissolved in a melt containing K_2O and other alkali metal oxides was investigated in the temperature range 440 to 640 °C.

The results indicate that CO may be oxidized to CO_2 with a high overall reaction efficiency in a system of reactors connected in series. Molten salt solutions have the advantage, over solid "catalysts" in that they operate without being poisoned. The oxidizing capacity of these solutions is limited only by the depletion of V_2O_5 in the melts due to reaction and by the presence of large amounts of insoluble V_2O_4 solid which is a reaction product. The melts may be reactivated by treatment with oxygen.

A. BLOCK-BOLTEN, B. J. M. BERTRAND et S. N. FLENGAS. Can. J. Chem. **52**, 2068 (1974).

On a étudié dans l'intervalle de température de 440 à 640 °C la conversion du CO en CO_2 en présence de V_2O_5 en solution dans une masse fondue contenant du K_2O et d'autres oxydes de métaux alcalins.

Les résultats montrent que le CO peut être oxydé en CO_2 dans un système de réacteurs reliés en série et avec une grande efficacité globale de la réaction. Les solutions de sels fondus ont l'avantage, sur les "catalyseurs" solides, de fonctionner sans être empoisonnées. Le pouvoir d'oxydation de ces solutions est limité seulement par la diminution de V_2O_5 dans les produits fondus due à sa réaction, et par la présence d'une grande quantité de V_2O_4 solide et insoluble produit par la reaction. Les produits fondus peuvent être réactivés par traitement à l'oxygène.

[Traduit par le journal]

Introduction

The use of V_2O_5 for the oxidation of SO_2 is part of a well established industrial process.

The oxidation process may be understood in terms of the redox reaction

$$[1] \qquad V_2O_{4(s)} + \tfrac{1}{2}O_{2(g)} \rightarrow V_2O_{5(s \text{ or } l)}$$

The V_2O_5–V_2O_4 system is ill-defined. On the V_2O_5 side of the V_2O_5–V_2O_4 subsystem a eutectic temperature is indicated at 660 °C and at a composition of 15 mol% V_2O_4. Liquidus temperatures at compositions 28.5, 35, 36.6, 37.8, and 40.0 mol% are respectively 685, 700, 750, 800, and 850 °C (1). Other authors have also investigated this system (2–5). At higher temperatures between 953 and 1081 °C the liquidus has been determined by Suito and Gaskell (2). However, the liquidus tie line is ill-defined and uncertain.

The system K_2O–V_2O_5 forms liquid solutions at low temperatures which have a low melting eutectic at a temperature of 390 °C at a composition of 40 mol% K_2O (6–9). Solid V_2O_4, on the other hand, appears to have little solubility in these melts.

[1]Present Address: Canadian Copper Refineries, Montreal East, Quebec.

In the present investigation the oxidation of CO was measured according to the reaction

$$[2] \qquad \underset{\text{(liquid solution with } K_2O)}{V_2O_5} + \underset{\text{(gas)}}{CO} \rightarrow \underset{\text{(in saturated liquid solution } K_2O\text{–}V_2O_5\text{–}V_2O_4)}{V_2O_4} + \underset{\text{(gas)}}{CO_2}$$

followed by the re-oxidation reaction which allows the recovery of the oxidizing agent.

$$[3] \qquad \underset{\text{(in saturated liquid solution } K_2O\text{–}V_2O_5\text{–}V_2O_4)}{V_2O_4} + \tfrac{1}{2}O_2 \rightarrow \underset{\text{(in liquid solution)}}{V_2O_5}$$

These two reactions have to be conducted separately due to the explosive nature of the mixtures of CO and oxygen above 600 °C. The oxidation of CO to CO_2 by solid V_2O_5 has been the subject of several investigations (10–36). Oxidation of some hydrocarbons in the presence of a molten phase containing vanadium compounds was reported (37) but carbon monoxide oxidation was not studied. The oxidation of CO in molten salt solutions containing V_2O_5 as a solute has not yet been reported. The CO system was chosen because of the potential use of V_2O_5 in pollution control devices.

Can. J. Chem. Downloaded from www.nrcresearchpress.com by 210.87.254.40 on 09/05/12
For personal use only.

Can. J. Chem. Downloaded from www.nrcresearchpress.com by 210.87.254.40 on 09/05/12
For personal use only.

Experimental

The system consisted of two Inconel tube reactors of 60 mm diameter and 50 cm high which were connected in series as shown in Fig. 1. Gas mixtures of CO and of inert gas such as argon, were introduced into reactor 1 containing the V_2O_5–K_2O melt, and the CO_2 produced was retained in the ascarite weighing bottles. A three way stopcock allowed the gas stream to be directed into either of the two ascarite traps so that a continuous analysis of the reaction product could be made for same reaction time intervals. The exit gas, containing the unreacted CO was then introduced into reactor 2 and the analysis procedure could be repeated in ascarite tube number 3. For experiments with pure CO, the analysis of the reacted gas mixture was done continuously every 10 min. For the dilute mixtures containing CO and argon, and at low temperatures, the reaction efficiency decreased and the reaction time had to be extended considerably. For example, in the extreme case of a mixture containing 0.1% CO, each ascarite bottle was used continuously for about 3 h. Both reactors were kept at the same temperature for temperatures between 440 and 640 °C and a comparison between the reaction efficiencies in reactors 1 and 2 could be made. The weight of melt in each reactor was 440 g, representing 3 g-mol of V_2O_5–K_2O mixture containing 60 mol% V_2O_5. A reduced melt containing V_2O_4 could be re-oxidized to V_2O_5 by bubbling pure O_2 through the melt.

The gas mixtures of CO and argon were premixed, commercially available, gases from Matheson of the following compositions in CO expressed as volume %: 0.11%, 9%, 18%, 25%, 35%, 60%, and pure CO. Gas flow rates were measured using calibrated floating ball type flowmeters connected in series with the reactor and thus the rate of CO feed per unit time was known and could be varied between 15 and 110 ml/min.

Each reactor was equipped with a set of baffles for the purpose of increasing the residence time of the gas in the melt and the efficiency of mixing. Inconel alloy was found to resist corrosion and was used for periods of several months without any sign of deterioration.

The melt of eutectic composition was prepared by fusion of the appropriate amounts of V_2O_5 and K_2CO_3 according to the reaction

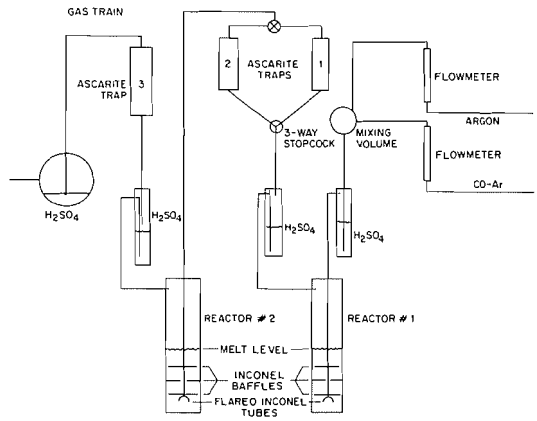

FIG. 1. Schematic diagram of the gas train and of the reactors.

[4] V_2O_5 (solid) + K_2CO_3 (solid) $\rightarrow$ $(V_2O_5$–$K_2O)$ (melt) + CO_2 (gas)

For this reaction solid K_2CO_3 was slowly added to the initially solid V_2O_5 at about 600 °C to prevent the violent evolution of CO_2.

The completion of this displacement reaction was measured from the weight loss in an open crucible due to the CO_2 evolution, and was found to proceed with a 100% efficiency at 575 °C.

Results and Discussion

Reaction efficiencies may be expressed in two different ways. The "conversion rate" R_C represents the conversion of CO to CO_2 in g or g-mol per unit time for a given CO content in the ingoing gas mixture and is calculated as

[5] $$R_C = \Delta n/\Delta t$$

The "relative" reaction efficiency η_R is calculated as

[6] $$\eta_R = \frac{\Delta n \text{ (mol of CO reacted in time } \Delta t)}{\Delta n_t \text{ (total mol of CO passed through reactor during same period of time)}} \times 100$$

The quantity Δn_t is obtained from the known flow rate during the period of time Δt. R_C is related to η_R by the expression $R_C = \eta_R f/100$ where f is the flow rate of the ingoing gas in g-mol/h.

The plot of log R_C *vs.* $1/T$ is shown in Fig. 2 (curve 1) for pure CO at a flow rate of 57 ml/min. At each temperature, the rate obtained at 10 min intervals for a total of 5 measurements was plotted *vs.* time. The reaction indicated a slow start for the first 10 min and reached a steady state rate which is reported herein. The points on this graph represent separate experiments for which pure CO was passed through a newly re-oxidized melt.

The graph indicates that the CO_2 conversion rate increases with temperature. The apparent activation energy for the process calculated by least squares from the expression $(\mathrm{d} \log R_C)/\mathrm{d}T = \Delta E_{APP}/2.303\,RT^2$ is 11 800 cal/g-mol ($\pm$70: standard deviation) which is reasonable for a diffusion process through a liquid phase.

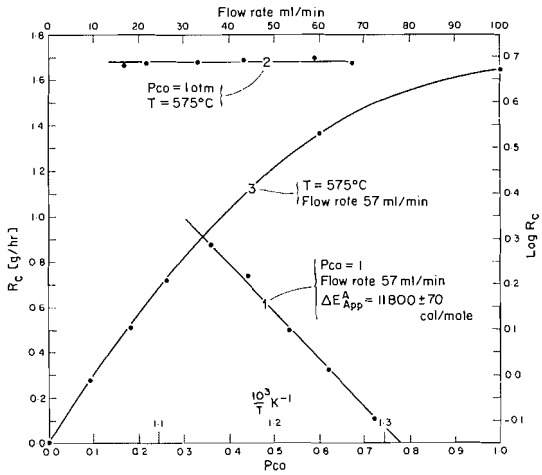

FIG. 2. Curve *1*, log R_C *vs.* $10^3/T$ plot; curve *2*, flow rate dependence of conversion rate R_C at constant temperature; curve *3*, dependence of R_C on partial pressure of CO at 575 °C.

At 575 °C R_C was found to be independent of flow rate within the range of 10 to 70 ml/min (curve 2, Fig. 2).

In addition the conversion rate R_C is independent of V_2O_5 depletion in the melt, at least for the initial stages of the reaction where the melt is present in excess.

The dependence of the steady state values of the conversion rate R_C on the partial pressure of CO in a gas mixture is given in Fig. 2, curve 3, for constant flow rate and temperature. The conversion rate R_C decreases with decreasing CO content and the dependence of R_C *vs.* P_{CO} becomes almost linear for low CO contents. For the latter gas diffusion processes could also be expected to interfere with the overall reaction mechanism. It is of interest that in the range 0 to 18% CO which is the CO content in car exhaust mixtures (38), reaction efficiencies are still high. This is shown more clearly when relative efficiencies η_R are used instead of the conversion rates R_C.

In Fig. 3, curve 1, the relative efficiency, which is a measure of total conversion, is plotted against percent CO in feed gas.

The curve indicates a maximum of 42% conversion at about 20% CO content and even for very low CO contents (like 0.11%) the efficiency decreases to only 29.9%. Higher CO contents have similar efficiencies.

The conversion efficiency of a gas mixture leaving reactor No. 1, and re-reacted in reactor No. 2, indicated exactly the same result. It is therefore possible to remove CO for a pollutant gas mixture by using a number of reactors in series.

The effect of flow rate in the relative reaction efficiency η_R obtained at steady state in a reactivated melt is also shown in Fig. 3, curve 2. It is clearly indicated that the percent conversion decreases with increasing flow rate due to the effect of decreasing residence time of the gas mixture in the melt.

The effect of continuous use of a melt was also investigated in a total depletion experiment, whereby the same melt in one reactor only was allowed to oxidize pure CO until no further oxidation could take place due to the complete conversion of V_2O_5 into V_2O_4.

Figure 4 shows the plot of conversion rate R_C with time for a total reaction time of 148 h, at a flow rate of 108 ml/min and a temperature of 440 °C. At this low temperature conversion rates are very low as indicated by the results in Fig. 3. The melt weight was again 440 g, or 3 mol, of mixture and contained some Cs_2O.

The curve in Fig. 4, indicates an unexpected initial increase in conversion rate followed by a decrease as the melt becomes depleted in V_2O_5. Finally the conversion rate appears to increase again when it is least expected and all V_2O_5 has been consumed. The latter, coincided (32) with the breakdown of carbon monoxide into CO_2

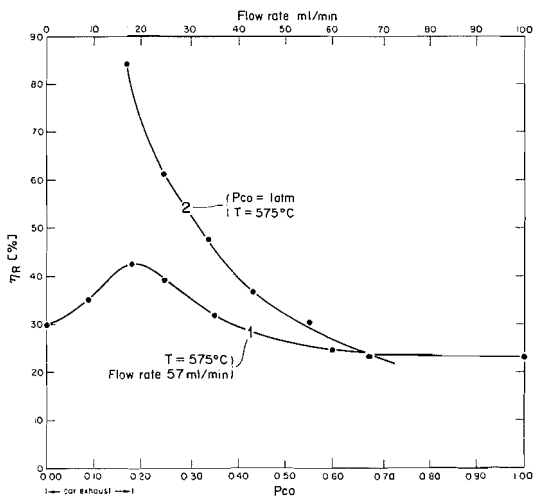

FIG. 3. Curve *1*, relative reaction efficiency η_R versus partial pressure of CO at 575 °C; curve *2*, dependence of η_R on flow rate at constant temperature.

Can. J. Chem. Downloaded from www.nrcresearchpress.com by 210.87.254.40 on 09/05/12
For personal use only.

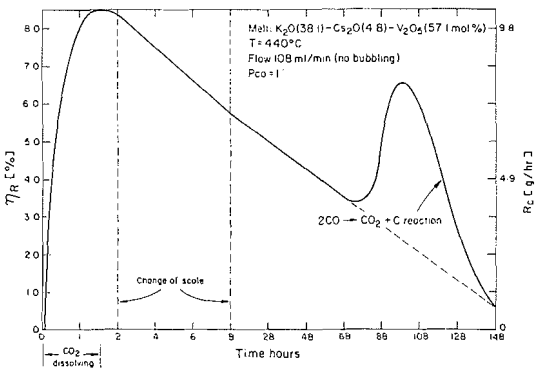

FIG. 4. Relative reaction efficiency *vs.* time during a depletion experiment.

according to the reaction $2CO \rightarrow C + CO_2$ with the appearance of large amounts of soot in the reactor.

It appears that the initial low conversion rate could be associated with the solubility of CO_2 in the melts. Thus, the CO_2 initially produced is retained in the melt and is not available for detection in the ascarite trap. However, once the melt has been saturated, then further reaction is producing CO_2 which is detected by the ascarite trap. Additions of small amounts of other oxides appear to have an effect on reaction efficiencies (35, 36). Additions of 5 mol% of Cs_2O (K_2O, 38.1; Cs_2O, 4.8; V_2O_5, 57.1 mol%) enhance the efficiency of the reactor, while the presence of 5 mol% Li_2O representing a melt composition of (K_2O, 39.6; Li_2O, 4.9; V_2O_5, 55.5 mol%) appear to retard the initial stages of the reaction. The conversion rate for the high CO partial pressures investigated appears to be dependent upon the diffusion of dissolved V_2O_5 in the liquid phase. V_2O_4 is produced as an insoluble phase and is not expected to affect the reaction kinetics providing that the appearance of a compact solid layer can be avoided.

Chemical control or adsorption at the gas liquid interface do not appear to be rate determining because of the positive temperature dependence of the conversion rate. It should be noted that thermodynamic calculations on reaction 2 indicate that the free energies become less negative at higher temperatures. The process would then be expected to be less efficient at higher temperatures, which is opposite to the observed kinetic trends.

The trends in the depletion experiment, namely the initial increase in reaction efficiency may be explained as follows.

The oxidation reactions may be written

[7] (V_2O_5) (in melt) $+ CO$ (gas) $\rightarrow (V_2O_4)$ (solid) $+ CO_2$ (gas)

followed by

[8] CO_2 (gas) $+ O^{2-}$ (in melt) $\rightleftarrows CO_3^{2-}$ (in melt)

The equilibrium reaction 8 justifies the solubility of CO_2 in a melt under an external pressure of CO_2 gas.

The solubility of CO_2 would also be enhanced by the basicity of the oxide melt. Hence, the addition of the more basic oxide Cs_2O appears to increase the retaining capacity of the melt. The increased basicity is attributed to the large ionic size of cesium and to the lower coulombic attraction of a Cs^+ for an O^{2-} anion. Thus, the "free" O^{2-} concentration in the Cs_2O doped melts is expected to be higher, and reaction 8 should be shifted to the right in the direction of increased CO_2 solubility.

Conclusions

The results indicate that the system is capable of oxidizing CO with a reasonably high efficiency in CO compositions representing the pollutant gas mixture emitted by the exhaust of motor vehicles. The advantages of a fused salt catalyst, as compared to solid V_2O_5 may be described by the constant renewal of gas to liquid interface within the melt during bubbling, and the absence of poisoning. In addition the entire volume of the melt participates in the reaction and localized heating or cooling effects due to exothermic and endothermic reactions, respectively, are avoided. Such a melt must be operated at the optimum temperature of about 550 to 575 °C, as at higher temperatures V_2O_5 has a high vapor pressure and volatilizes. At lower temperatures, the reaction becomes more favorable thermodynamically but slow kinetically. The appearance of the solid V_2O_4 product in large quantities should be avoided by frequent reoxidation cycles. The eutectic composition $V_2O_{5(0.6)}$–$K_2O_{(0.4)}$ melting at 390 °C is necessary because it allows a melt to be operated at the desired temperature range well below the melting temperature for pure V_2O_5 which is 685 °C.

Can. J. Chem. Downloaded from www.nrcresearchpress.com by 210.87.254.40 on 09/05/12
For personal use only.

The authors are grateful to the National Research Council of Canada for a research grant in support of this work. Participation of Mr. Klaus Meyer in the initial stages of this work is also acknowledged.

1. A. BURDESE. Ann. Chim. Rome, **47**, 785 (1957).
2. H. SUITO and D. R. GASKELL. Met. Trans. **2**, 3299 (1971).
3. A. A. FOTIEV and V. L. VOLKOV. Russ. J. Phys. Chem. **45**, 1516 (1971).
4. T. TODA, K. KOSUGE, and S. KACHI. Nippon Kagaku Zasshi. **87**, 1311 (1966).
5. K. KOSUGE. J. Phys. Chem. Solids, **28**, 1613 (1967).
6. F. HOLTZBERG, A. REISMAN, M. BERRY, and M. BERKENBLIT. J. Am. Chem. Soc. **78**, 1538 (1956).
7. V. V. ILARIONOV, R. P. OZEROV, and E. V. KILDISHEVA. Zhur. Neorg. Khim. **1**, 779 (1956).
8. M. POUCHARD, J. GALY, L. RABARDEL, and P. HAGENMÜLLER. C. R. Acad. Sc. Paris Ser. C. **264**, 1943 (1967).
9. J. LUKACS and C. STRUSIEVICI. Rev. Roum. Chim. **12**, 1347 (1967).
10. C. F. TIPPER and B. H. WILLIAMS. Öl-Gasfeuer, **10**, 1078 (1965).
11. Texaco Development Corp. French Patent, 1,400,504, Cl.B; May 28, 1965.
12. L. C. HARDISON. U.S. Patent 3,544,264, Cl.23-2; Dec. 1, 1970.
13. E. L. FORCE and R. J. AYEN. A. I. Ch.E. Symp. Ser. 1972, **68**(126). 80 (Eng).
14. H. WOZNIAK and J. SZYLICKI, Zesz. Nauk. Uniw. Poznan. Mat. Fiz. Chem. **10**, 67 (1967).
15. P. W. SNYDER, W. A. STOVER, and H. G. LASSEN. Status report on HC/CO oxidation catalysts. Proc. Am. Petrol. Inst., Div. Refin. **52**, 721 (1972).
16. S. M. ARIYA and M. P. MOROZOV. Zh. Obsh. Khim. **32**, 2081 (1962).
17. T. SEYIAMA, A. SUENAGA, and W. SAKAI. Nippon Kagaku Zasshi, **82**, 292 (1961).
18. K. TARAMA, S. TERANISHI, and T. YASUI. Kôgyô Kagaku Zasshi, **60**, 1222 (1957).
19. K. TARAMA, S. TERANISHI, and T. YASUI. Nippon Kagaku Zasshi, **81**, 1034 (1960).
20. H. KAKIOKA, V. DUCARME, and S. J. TEICHNER. J. Chim. Phys. Physicochim, Biol. **68**, 1726 (1971).
21. H. KAKIOKA, V. DUCARME, and S. J. TEICHNER. Kinet. Katal. **14**, 78 (1973).
22. H. KAKIOKA, V. DUCARME, and S. J. TEICHNER, J. Chim. Phys. Physicochim. Biol. **68**, 1722 (1971).
23. S. YOSHIDA. Shokubai, Tokyo, **10**, 90 (1968).
24. M. YA. KON, V. A. SHVETS, and V. B. KAZANSKII. Kinet. Katal. **13**, 735 (1972).
25. E. A. PASTUKHOV and N. A. VATOLIN. Trudy Inst. Met. Akad. Nauk. SSSR. Ural N.T. **27**, 127 (1972).
26. G. K. BORESKOV, V. I. MARSHNEVA, and V. D. SOKOLOVSKII. Dokl. Akad. Nauk. SSSR, **199**, 1091 (1971).
27. M. YA. KON, V. A. SHVETS, and V. B. KAZANSKII. Dokl. Akad. Nauk. SSSR, **203**, 624 (1972).
28. V. P. ELYUTIN, YA. A. PAVLOV, V. P. POLYAKOV, and S. B. SHEBOLDAEV. Isvestia Akad. Nauk. SSSR, Neorg. Mater. **6**, 37 (1970).
29. M. F. HUGHES and G. R. HILLS. J. Phys. Chem. **59**, 388 (1955).
30. M. YA. KON, V. A. SHVETS, and V. B. KAZANSKII. Kinet. Katal. **14**, 403 (1973).
31. V. I. MARSHNEVA, G. K. BORESKOV, and V. D. SOKOLOVSKII. Kinet. Katal. **13**, 393 (1972).
32. V. P. ELYUTIN, YU. A. PAVLOV, V. P. POLYAKOV, and S. B. SHEBOLDAEV. IZV. Vyssh. Ucheb. Zav. Chern. Met. **12**, 5 (1969).
33. N. A. STUKANOVSKAYA, L. G. SVINTSOVA, V. A. YUZO, G. P. KORNEICHUK and V. A. ROITER. Katal. Katal **6**, 18 (1970).
34. N. A. STUKANOVSKAYA, N. A. BOLDYREVA, and V. A. ROITER. Katal. Katal. **7**, 47 (1971).
35. M. NAGANO, A. KATO, I. MOCHIDA, and T. SEIYAMA. Yogyo Kyokai Shi, **78**, 401 (1970).
36. I. TADAO, M. ARAMATA, and R. FURUICHI. Nippon Kagaku Kaisshi, (6), 1068 (1972).
37. N. I. VOLYNKIN. Zh. Prikl. Khim. **44**, 1853 (1971).
38. W. A. GRUSE. Motor fuels. Reinhold Publishing Co., New York. 1967. p. 21.

Can. J. Chem. Downloaded from www.nrcresearchpress.com by 210.87.254.40 on 09/05/12
For personal use only.

A Kinetic Model of the Accommodation Pumping Phenomenon

GRAHAM RICHARD BRANTON AND STEPHEN ALAN RYCE

Department of Chemistry, University of Victoria, Victoria, British Columbia V8W 2Y2

Received November 22, 1973

GRAHAM RICHARD BRANTON and STEPHEN ALAN RYCE. Can. J. Chem **52**, 2073 (1974).

A simple kinetic model of the accommodation pumping phenomenon is developed. This model is consistent with the earlier suggestion that the extent to which specular reflection occurs from smooth Pyrex surfaces is dependent upon the velocity of the atoms. It is shown that the upper limit for the pump ratio (P_A/P_B) is 2, but that in any real situation this ratio would be less than this value. The model is used to show that the deviation of the thermal transpiration ratio from the ideal value, $(T_1/T_2)^{1/2}$, should be the same as the accommodation pumping ratio for the same tubing with the same temperature difference.

GRAHAM RICHARD BRANTON et STEPHEN ALAN RYCE. Can. J. Chem. **52**, 2073 (1974).

Un modèle cinétique simple de l'adaptation du phénomène de pompage est développé. Ce modèle est en accord avec la suggestion antérieure: la mesure à laquelle une réflexion apparaît à partir des surfaces lisses du pyrex est dépendante de la vitesse des atomes. Il est établi que la limite supérieure du rapport de pompe (P_A/P_B) est égale à 2, mais que dans n'importe quelle situation réelle ce rapport serait inférieur à cette valeur. Le modèle est utilisé pour montrer que la déviation de la valeur idéale du rapport de transporisation thermique $(T_1/T_2)^{1/2}$, doit être le même que le rapport d'adaptation de pompage pour la même canalisation avec la même différence de températures.

[Traduit par le journal]

Introduction

In recent studies Hobson and co-workers (1–5) described a new development in vacuum pumping termed accommodation pumping, which is operative in the free-molecular and transition flow region. It is postulated by Hobson that the observed pumping action is a consequence of the difference in thermal accommodation between warm gas molecules impinging upon cold surfaces and cold molecules striking warm surfaces.

A typical pump consists of volumes A and B connected by a U-tube made of Pyrex glass. The arm of the pump connected to B is smooth (untreated), whereas the tubulation adjoining A is "atomically rough" (leached in HCl). With the assembly at a uniform temperature no pressure difference exists between volumes A and B, *i.e.*, $P_A = P_B$. However, when the U-tube is partially immersed in a cold bath at temperature T_1, a pumping action develops such that $P_A > P_B$.

Following the notation of Hobson we have

$$[1] \qquad P_A/P_B = a^n$$

where a is the pressure or pump-ratio for a single stage pump as described above, and n is the number of pump stages in series.

An atomistic interpretation of the phenomenon is that molecules arriving at a rough surface from both warm and cold regions are highly accommodated. On the smooth surfaces of the U-tube, however, collisions of warm molecules with cold surfaces are more likely to result in specular reflection than collisions of cold molecules with warm surfaces (1, 6). Thus in the temperature transition region in the smooth arm of the U-tube, molecules on the average maintain more readily their velocity component in the direction leading to volume A.

An analysis of the pressure changes in accommodation pumps was made by Hobson (7) by comparing the action of a 28-stage Pyrex accommodation pump with that of blanks of identical geometrical dimensions. Hobson's experiments confirmed the validity of his earlier postulate (1) of a model of an accommodation pump as a pipe with unequal conductances in two directions. In the following we derive for accommodation pumping a model in which the observed pumping ratio is related in kinetic terms to the behavior of the molecules or atoms in the gas phase.

Model

The basis of our model is the supposition that when a constant ratio $P_A/P_B = a$ has been

Can. J. Chem. Downloaded from www.nrcresearchpress.com by 210.87.254.105 on 09/05/12
For personal use only.

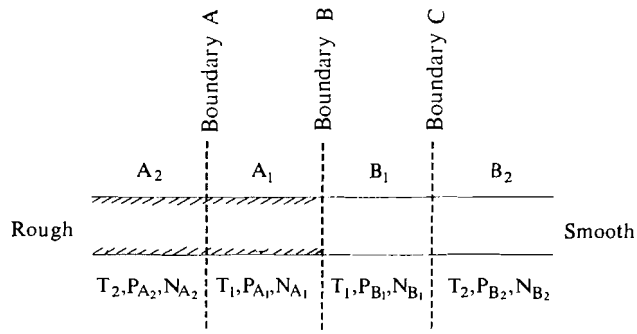

FIG. 1. Schematic of the 4 compartments of an accommodation pump. N_{A_1}, N_{A_2}, N_{B_1}, N_{B_2} are the number of atoms per cm^3 which are fully accommodated in compartments A_1, A_2, B_1, B_2, respectively.

reached, an equilibrium exists in the pump whence the net mass flow through any cross sectional boundary of the tube is zero. Conveniently the pump is divided into 4 compartments (see Fig. 1), A_2, A_1 rough and B_2, B_1 smooth. Compartments A_2 and B_2 are at temperature T_2, A_1 and B_1 are at temperature T_1, with $T_2 > T_1$. The compartments are separated by three hypothetical sharp boundaries: A between A_2 and A_1, B between B_2 and B_1, and C between A_1 and B_1. We define the boundaries to be sharp in the sense that abrupt changes of state (P, T) exist, but that the diffusion of molecules across the boundaries is uninhibited.

Incomplete accommodation at any surfaces would lead to a fraction of the atoms (or molecules) after having crossed a particular boundary to proceed and to cross the next boundary prior to accommodation. Let γ_{2B_1} = the fraction of atoms which having crossed B proceed to cross C; γ_{1A_1} = the fraction of atoms which having crossed C proceed to cross A; γ_{2A_1} = the fraction of atoms which having crossed A proceed to cross C; γ_{1B_1} = the fraction of atoms which having crossed C proceed to cross B.

We neglect the Maxwellian distribution of energies of the atoms at temperatures T_2 and T_1 and use expression 2 (8) for the number of atoms striking unit area in unit time.

$$[2] \qquad \frac{dN}{dt} = \tfrac{1}{4}N\bar{c}$$

where N is the number of atoms per cm^3 and $\bar{c}$ is the average speed, $\bar{c} = (8RT/\pi M)^{1/2}$. At equilibrium there is no net mass flow across any of the boundaries. For boundary A:

$$[3] \quad \tfrac{1}{4}N_{A_2}\bar{c}_2 = \tfrac{1}{4}N_{A_1}\bar{c}_1 + \gamma_{1A_1}(\tfrac{1}{4}N_{B1}\bar{c}_1 + \gamma_{2B_1}\tfrac{1}{4}N_{B_2}\bar{c}_2)$$

Similar equations may be written for boundaries B and C.[1]

These equations may be rearranged to give

$$[4] \qquad \frac{N_{A_2}}{N_{B_2}} = \frac{(1 + \gamma_{2B_1})}{(1 + \gamma_{1B_1})} \cdot \frac{(1 + \gamma_{1A_1})}{(1 + \gamma_{2A_1})}$$

where

$$[5] \qquad \frac{N_{A_2}}{N_{B_2}} = \frac{P_{A_2}}{P_{B_2}} = a$$

The phenomenon of thermal transpiration (9) may be treated in an exactly similar manner to the above where a tube F connects two volumes E and D at temperatures T_2 and T_1 respectively (see Fig. 2).

At equilibrium there is no net flow across the boundaries and equations of the same form as [3] may be written in order to express the equilibria at boundaries D and E. Hence

$$\frac{N_D}{N_E} = \frac{\bar{c}_2(1 + \gamma_{2F})}{\bar{c}_1(1 + \gamma_{1F})}$$

i.e.

$$[6] \qquad \frac{P_D}{P_E} = \left(\frac{T_1}{T_2}\right)^{1/2} \cdot \frac{(1 + \gamma_{2F})}{(1 + \gamma_{1F})}$$

Hobson (6) has shown that the ideal thermal transpiration law

$$[7] \qquad \frac{P_D}{P_E} = \left(\frac{T_1}{T_2}\right)^{1/2}$$

applies when section F is leached Pyrex glass with a reasonable length at temperature T_1

[1]For simplicity it has been assumed that the probability of an atom crossing A (B) having previously crossed C is the same regardless of whether it was accommodated in B_1 (A_1). Whilst this is not strictly accurate the error introduced will be small since the product of the two γ terms will be very small.

Can. J. Chem. Downloaded from www.nrcresearchpress.com by 210.87.254.105 on 09/05/12
For personal use only.

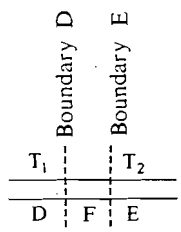

FIG. 2. Schematic for thermal transpiration model.

($T_1 < T_2$). This means that when $\gamma_{2F} = \gamma_{2A_1}$ and $\gamma_{1F} = \gamma_{1A_1}$ the ratio $(1 + \gamma_{2A_1})/(1 + \gamma_{1A_1})$ is unity, *i.e.* the leached Pyrex surface behaves the same to all atoms regardless of their velocity. Equation 4 may then be rewritten as

$$[8] \qquad \frac{N_{A_2}}{N_{B_2}} = \frac{P_{A_2}}{P_{B_2}} = a = \frac{(1 + \gamma_{2B_1})}{(1 + \gamma_{1B_1})}$$

Thus if $a \neq 1$, $\gamma_{2B_1} \neq \gamma_{1B_1}$, *i.e.* the behavior of the smooth Pyrex surface towards atoms must depend on their velocities. The limiting situation would be when all low velocity atoms (T_1) are accommodated (*i.e.* $\gamma_{1B_1} = 0$, the cosine law of diffuse reflection being obeyed) and when all high velocity atoms (T_2) are reflected specularly (*i.e.* $\gamma_{2B_1} = 1$, the atoms lose no forward momentum on collision with the walls). Thus the maximum theoretical value which a may have is 2, and is less than 2 in any real situation.

If for thermal transpiration the two volumes D and E are joined by a smooth Pyrex tube eq. 6 becomes

$$[9] \qquad \frac{P_D}{P_E} = \left(\frac{T_1}{T_2}\right)^{1/2} \cdot \frac{(1 + \gamma_{2B_1})}{(1 + \gamma_{1B_1})}$$

From eq. 9 it may be readily seen that the extent to which the thermal transpiration pressure ratio deviates from the ideal value (given by eq. 7) should be the same as the pumping ratio for a single stage accommodation pump. Precise quantitative comparisons, of the deviation of the thermal transpiration ratio from the ideal value and the pumping ratio for a single stage accommodation pump, are difficult since both critically depend on the exact state of the smooth Pyrex surface (4); however, qualitative comparisons may be undertaken.

For helium with $T_1 = 77$ K and $T_2 = 298$ K, using tubing of internal diameter in the range 8–22 mm, the pump ratio (for accommodation pumping) varies within the range 1.16–1.25 (1, 4, 10). The thermal transpiration data of Hobson and co-workers (9), obtained using the "tube" system, may be used to obtain a value for the factor by which the observed thermal transpiration ratio deviates from the ideal value (given by eq. 7). For helium with $T_1 = 77.4$ K and $T_2 = 295$ K, using tubing of internal diameter 11.3–19 mm, this factor is found to be in the range 1.14–1.22. Thus for helium the values of $(1 + \gamma_{2B_1})/(1 + \gamma_{1B_1})$ obtained from accommodation pumping and thermal transpiration experiments are in very good qualitative agreement.

The comparison may at present only be extended to other gases on a very qualitative basis since there is relatively little information currently available. From the data given by Edmonds and Hobson (9), for thermal transpiration, neon should behave in a very similar manner to helium, whilst argon and xenon show much smaller deviations from the ideal thermal transpiration ratio. This is again in good agreement with the data from accommodation pumping when it is found (Hobson (1) and our own results) that helium and neon have very similar pumping ratios (differing by only 1 or 2% from each other) whereas argon and xenon have much smaller values (about 1.07 for argon and xenon against ~1.2 for helium and neon).

Conclusion

The simple kinetic model outlined appears to explain satisfactorily the data observed for accommodation pumps where the ratio may be compared with the phenomenon of thermal transpiration. As suggested previously the accommodation pumping phenomenon arises from differences in the extent to which specular reflection occurs from smooth Pyrex surfaces depending on the velocity of the atoms. In the present model it is not essential to propose completely diffuse reflection from a leached Pyrex surface, but merely that the accommodation at the leached surface is sufficient that the extent to which specular reflection occurs is independent of the velocity of the incident atoms.

This model predicts an upper limit for the value of the pump ratio $a = 2$ for a pump operating in an idealized mode. Idealized in the sense, that in the smooth arm of the pump all hot molecules are specularly reflected from cold surfaces and on the other hand all cold molecules are completely accommodated. For a 20-stage pump at $a = 2$, $P_A/P_B \cong 10^6$. The best values obtained by Hobson and ourselves are only

Can. J. Chem. Downloaded from www.nrcresearchpress.com by 210.87.254.105 on 09/05/12
For personal use only.

$a \cong 1.3$, yielding a value of $P_A/P_B \cong 200$ in a 20-stage pump. Whilst the limiting theoretical value of the pump ratio cannot be attained in any real situation, the large difference between this limiting value and present experimental values appears to be sufficient to make a search for a better system than Pyrex – leached Pyrex, worthwhile.

We are grateful for the hospitality extended to S.A.R. at the Chemistry Department, University of Sussex. Thanks are also due to the National Research Council of Canada for financial support to both authors.

1. J. P. HOBSON. J. Vac. Sci. Technol. **7**, 351 (1970).
2. J. P. HOBSON. Bulletin of the radio and electrical engineering division, National Research Council of Canada, **20**, 2 (1970).
3. J. P. HOBSON. Vacuum, **21**, 527 (1971).
4. J. P. HOBSON and A. W. PYE. J. Vac. Sci. Technol. **9**, 252 (1972).
5. B. G. BAKER, J. P. HOBSON, and A. W. PYE. J. Vac. Sci. Technol. **10**, 241 (1973).
6. J. P. HOBSON. J. Vac. Sci. Technol. **6**, 257 (1969).
7. J. P. HOBSON. J. Vac. Sci. Technol. **8**, 290 (1971).
8. M. KNUDSEN. The kinetic theory of gases. John Wiley and Sons, Inc., New York. 1934.
9. T. EDMONDS and J. P. HOBSON. J. Vac. Sci. Technol. **2**, 182 (1965).
10. I. H. DOETSCH and S. A. RYCE. Can. J. Chem. **50**, 957 (1972).

Can. J. Chem. Downloaded from www.nrcresearchpress.com by 210.87.254.105 on 09/05/12
For personal use only.

Composés d'addition de SbF_5 avec H_2O et HF. Formation d'ions hydronium

B. BONNET, J. ROZIERE, R. FOURCADE ET G. MASCHERPA

Laboratoire des Acides Minéraux, associé au C.N.R.S. n° 79, Université des Sciences et Techniques du Languedoc, 34060 Montpellier, France

Reçu le 21 décembre 1973

B. BONNET, J. ROZIERE, R. FOURCADE et G. MASCHERPA. Can. J. Chem. **52**, 2077 (1974).

Une étude par analyse thermique différentielle des solutions de SbF_5 dans H_2O et HF, a permis de déterminer les traitements thermiques nécessaires à l'obtention des phases stables cristallisées: $SbF_5.2H_2O$, $4SbF_5.5H_2O$, $SbF_5.H_2O$, $3SbF_5.2H_2O$ et $SbF_5.HF.2H_2O$.

Tous ces composés ont été caractérisés par leurs spectres de diffraction des rayons X sur poudre.

Les spectres de vibration de $SbF_5.2H_2O$ et $SbF_5.HF.2H_2O$ sont en bon accord avec une structure ionisée; ces composés doivent être respectivement formulés $H_3O^+SbF_5OH^-$ et $H_5O_2^+SbF_6^-$. Les autres hydrates sont de simples complexes donneur-accepteur de structure $H_2O \rightarrow SbF_5$, où les molécules d'eau supplémentaires sont liées par liaisons hydrogène à l'eau coordinée à l'antimoine.

B. BONNET, J. ROZIERE, R. FOURCADE, and G. MASCHERPA. Can. J. Chem. **52**, 2077 (1974).

A differential thermal analysis study of solutions of SbF_5 in H_2O and HF has enabled us to determine the thermal treatments required to obtain the stable crystalline phases: $SbF_5.2H_2O$, $4SbF_5.5H_2O$, $SbF_5.H_2O$, $3SbF_5.2H_2O$, and $SbF_5.HF.2H_2O$.

The SbF_5 adducts were characterized by X-ray powder diagrams.

The vibrational spectra of $SbF_5.2H_2O$ and $SbF_5.HF.2H_2O$ are consistent with the ionic structures $H_3O^+SbF_5OH^-$ and $H_5O_2^+SbF_6^-$.

The other hydrates are simple donor-acceptor complexes with the structure $H_2O \rightarrow SbF_5$, in which one water molecule is coordinated to the SbF_5 and the others are bound by hydrogen bonds to the coordinated water molecule.

Introduction

Les pentahalogénures des éléments du groupe V de la classification périodique sont des acides de Lewis forts, susceptibles de donner des complexes d'addition avec de nombreux composés; en solution ces complexes peuvent jouer le rôle de catalyseur, notamment dans les réactions de Friedels et Craft (1).

Ainsi l'eau et les ions fluorures jouent le rôle de base vis-à-vis de SbF_5, en favorisant l'apparition d'espèces protonnées.

Ce travail fait partie de l'étude systématique, entreprise au Laboratoire des Acides Minéraux, sur les systèmes MX_n–H_2O et MX_n–H_2O–HX[1] en tant que milieux formateurs d'hydrates du proton $(H_2O)_nH^+$. Nous présentons ici les résultats de l'étude des systèmes SbF_5–H_2O et SbF_5–HF–H_2O effectuée par analyse thermique, diffraction des rayons X et spectroscopie de vibration infrarouge et Raman.

[1] MX_n pouvant être GaX_3, BF_3, $SbCl_5$. Travaux en cours de publication.

Partie expérimentale

Purification de SbF_5

Le pentafluorure d'antimoine commercial utilisé est purifié par une double rectification dans un appareillage en verre Pyrex; les têtes et queues de distillation sont éliminées à chaque passage, seule la fraction de distillat passant à 141 °C est conservée.

L'agressivité et la très forte hygroscopicité de SbF_5 rendent sa manipulation délicate et nécessitent l'utilisation à l'abri de l'humidité, des échantillons fraîchement distillés. Dans ces conditions il n'est pas à craindre une attaque de l'appareillage, soit lors de la purification de SbF_5, soit dans la préparation des échantillons analysés.

Préparation des mélanges SbF_5–H_2O

La réaction de SbF_5 sur l'eau est très exothermique et les mélanges doivent être réalisés à froid, à la température de l'air liquide. Pour une composition déterminée, la quantité d'eau nécessaire est introduite par fractions successives, le mélange étant homogénéisé lentement par augmentation progressive de la température.

Préparation du composé $SbF_5.HF.2H_2O$

Tous les essais de préparation à partir des trois composés SbF_5, HF et H_2O se sont soldés par des échecs; la réaction est trop violente, ce qui entraîne la décomposition et la volatilisation partielle de l'échantillon. Par contre la

Can. J. Chem. Downloaded from www.nrcresearchpress.com by 210.87.254.40 on 09/05/12
For personal use only.

Can. J. Chem. Downloaded from www.nrcresearchpress.com by 210.87.254.40 on 09/05/12
For personal use only.

réaction est contrôlable à partir des deux monohydrates du pentafluorure d'antimoine et du fluorure d'hydrogène.

$$SbF_5.H_2O + HF.H_2O \rightarrow SbF_5.HF.2H_2O$$

La réaction est réalisée à basse température, dans un appareillage en polycarbonate.

Analyse thermique

La méthode utilisée est l'analyse thermique différentielle à l'échauffement, méthode particulièrement adaptée à l'étude d'échantillons aisément vitrifiables et aussi difficilement cristallisables que sont ces solutions de SbF_5 dans H_2O. Après vitrification à la température de l'air liquide du produit analysé, les phases stables du système sont cristallisées par des traitements thermiques appropriés, au détriment des espèces métastables qui cristallisent parfois spontanément lors du refroidissement. Tous ces traitements et l'analyse à l'échauffement des produits parfaitement cristallisés sont réalisés sur des échantillons mis en tubes scellés, afin d'éviter tout risque d'hydratation.

Diffraction des rayons X

Toutes les phases stables mises en évidence par analyse thermique ont été caractérisées par leur spectre de diffraction X sur poudre. Les diffractogrammes ont été enregistrés à température ambiante à l'aide d'un diffractomètre à compteur Philips PW 1380 en utilisant la raie K_α du cuivre, sur des échantillons finement broyés et protégés de l'humidité ambiante par une mince feuille de polyéthylène.

Spectroscopie de vibration

Les spectres infrarouges ont été enregistrés de 4000 à 180 cm^{-1} à l'aide d'un spectromètre Perkin–Elmer 180, à température ambiante et à la température de l'air liquide. Les échantillons analysés étaient parfaitement cristallisés selon le protocole mis au point par analyse thermique. Ils étaient prélevés en boîte sèche et introduits finement pulvérisés entre des faces de chlorure d'argent ou de silicium, selon le domaine de fréquence étudié.

L'appareillage Raman utilisé était constitué des spectromètres PH0 et PH1 de la Coderg, équipés respectivement de laser à argon ionisé et à hélium–néon. Les échantillons finement broyés étaient contenus dans des tubes Pyrex placés dans un cryostat refroidi à l'air liquide. Le phénomène de diffusion particulièrement intense dans le cas de ces composés, ne nous a pas permis d'étudier le domaine de fréquence au-dessus de 1000 cm^{-1} par spectroscopie Raman.

Résultats

Analyse thermique

Le système SbF_5–H_2O a été étudié dans le domaine de concentration de 30 à 60% en moles de SbF_5. Pour des concentrations plus riches en eau il y a hydrolyse. Au-delà de 60% en moles de SbF_5, on obtient systématiquement des verres au refroidissement; des recuits de plusieurs mois à la température de −32 °C sont alors nécessaires à l'obtention de phases stables parfaitement cristallisées.

Dans le domaine étudié des recuits systématiques, au-dessus de la température de dévitrification, nous ont permis d'obtenir les hydrates sous leur forme stable. Ainsi le monohydrate ne cristallise pas spontanément au refroidissement et c'est l'eutexie métastable E_M à 59 °C qui est observée (Fig. 1); cet invariant est éliminé par traitement thermique au profit du monohydrate.

Le diagramme de phase met en évidence l'existence: de trois hydrates à fusion congruente: $4SbF_5.5H_2O$ (T_f^0 = 128.0 °C), $SbF_5.H_2O$ (T_f^0 = 117.5 °C) et $3SbF_5.2H_2O$ (T_f^0 = 122.3 °C); d'un hydrate à fusion non congruente: $SbF_5.2H_2O$ (T_θ^0 = 36.5 °C).

Seul le composé $4SbF_5.5H_2O$ présente une transformation à l'état solide à 93 °C.

$$4SbF_5.5H_2O\ (\alpha) \rightleftarrows 4SbF_5.5H_2O\ (\beta)$$

Dans le cas de ce composé il a été très difficile de déterminer sa stoechiométrie. Cependant l'évolution des températures de fin de fusion d'échantillons de compositions voisines de celles du composé 4/5 et les diagrammes de Tammann des équilibres invariants adjacents ont permis de confirmer sa composition.

Les différentes eutexies mises en évidence sont rapportées dans le tableau 1.

Le diagramme de phase ne révèle pas de différence marquée de stabilité entre les différents composés. Ainsi le dihydrate a le point de fusion (non congruent) le plus bas (36.5 °C) alors que les autres hydrates fondent normalement dans des domaines de température compris entre

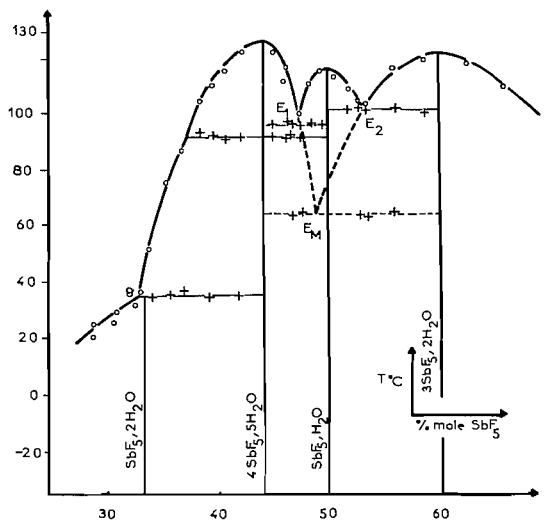

FIG. 1. Diagramme de phases du système SbF_5–H_2O.

TABLEAU 1. Coordonnées eutectiques

Equilibre eutectique	Température eutectique (°C)	Composition eutectique (% en mole de SbF_5)
Liq. $E_1 \rightleftarrows 4SbF_5.5H_2O(s) + SbF_5.H_2O(s)$	97 ± 1	47.2 ± 0.2
Liq. $E_2 \rightleftarrows SbF_5.H_2O(s) + 3SbF_5.2H_2O(s)$	103 ± 1	53.5 ± 0.5
Liq. $E_M \rightleftarrows 4SbF_5.5H_2O(s) + 3SbF_5.2H_2O(s)$	59 ± 1	48.0 ± 0.5

117.5 et 128.0 °C. Ceci n'est pas surprenant car les températures de fusion de la plupart des hydrates d'acides (au sens de Lewis ou de Brönsted) décroissent lorsque le nombre de molécules d'eau associées croît.

Radiocristallographie

Les différentes valeurs des angles de réflexion, des distances réticulaires correspondantes, ainsi que l'intensité relative des raies caractéristiques de ces composés sont consignées aux archives de ce journal.[2] Chaque spectre est nettement individualisé mais, en l'absence d'étude complète sur monocristaux, aucun n'a pu être indexé.

Spectroscopie infrarouge et Raman

Nous avons représenté sur les figs. 2 et 3 les spectres infrarouges et Raman à température ambiante de ces hydrates (excepté pour le composé $3SbF_5.2H_2O$) et du complexe $SbF_5.HF.2H_2O$.

Les fréquences observées et leurs attributions probables sont rapportées sur les tableaux 2 et 3. Ces attributions ont été facilitées par l'obtention des spectres des homologues deutériés.

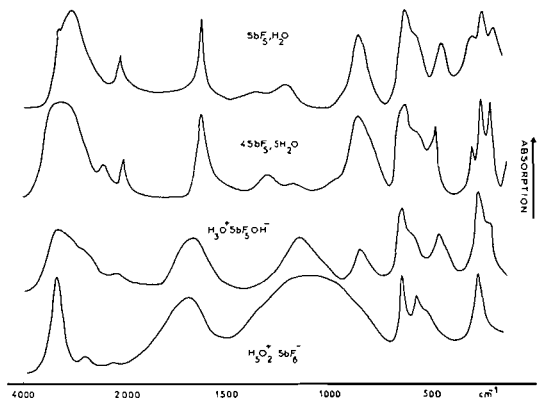

FIG. 2. Spectres infrarouges à température ambiante.

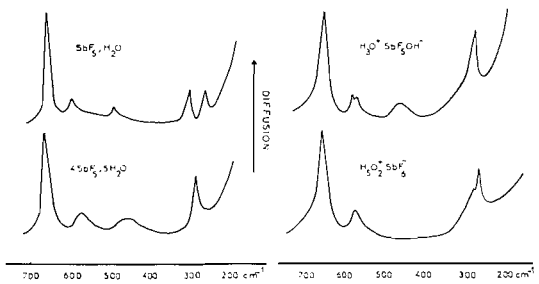

FIG. 3. Spectres Raman à température ambiante.

Discussion

Les résultats expérimentaux ont permis de confirmer l'existence des deux hydrates signalés dans la littérature: le dihydrate par Ruff (2) et le monohydrate mis en évidence d'une part par Dean et Gillespie (3), en solution dans SO_2 et, d'autre part, par Commeyras et Olah (4) dans le solvant acide fluorosulfurique.

Le composé $SbF_5.2H_2O$ serait probablement l'hydroxopentafluoroantimonate d'oxonium $H_3O^+SbF_5OH^-$ alors que $SbF_5.H_2O$ paraît être, d'après les auteurs précédents, un composé moléculaire d'addition $H_2O \rightarrow SbF_5$, du moins en solution dans les solvants considérés. Dean et Gillespie envisagent en outre la possibilité d'existence d'une réaction de redistribution des coordinats autour de l'antimoine selon la réaction

$$2(SbF_5.H_2O) \rightleftarrows SbF_4(OH_2)_2^+ + SbF_6^-$$

L'existence de la forme ionisée selon la réaction d'autodissociation

$$2(SbF_5.H_2O) \rightleftarrows H_3O^+ + Sb_2F_{10}OH^-$$

faisant intervenir un pont Sb—O—Sb analogue au pont B—O—B observé dans le complexe $NO_2^+(BF_3)_2OH^-$ est tout aussi possible (5).

Le monohydrate

L'absence dans le spectre infrarouge du mono-

[2]La série complète des tableaux à un prix nominal, en s'adressant au Dépôt données non publiées, Bibliothèque scientifique national, Conseil national de recherches du Canada, Ottawa, Canada K1A 0S2.

Can. J. Chem. Downloaded from www.nrcresearchpress.com by 210.87.254.40 on 09/05/12
For personal use only.

Can. J. Chem. Downloaded from www.nrcresearchpress.com by 210.87.254.40 on 09/05/12
For personal use only.

TABLEAU 2. Valeurs (en cm^{-1}) des fréquences d'absorption infrarouge*

$SbF_5.H_2O$	$4SbF_5.5H_2O$	Attributions	$H_3O^+SbF_5OH^-$	Attributions	$H_5O_2^+SbF_6^-$	Attributions
3280 ép	3200 TF	$2\delta(H_2O)$ et ν_s, $\nu_{as}(H_2O)$	3460 TF 3200 ép	ν(OH) de SbF_5OH^- et de	3460 TF 3250 ép	ν_s et $\nu_{as}(H_2O)$
3120 TF			2700 ép	H_3O^+ (ν_1 et ν_3)	3140 ép	
2500 ép	2400 f				2800–2600 f	Combinaisons
2220 ép	—	Combinaisons	2200 f	Combinaisons	2200 f	
2045 m	2040 m		2050 f			
1630 TF	1630 TF	$\delta(H_2O)$	1680 TF	$\nu_4(H_3O^+)$	1700 TF	$\delta(H_2O)$
					2000–800 TF, TL	ν_{as}(OHO)
1330 f	1320 f	Combinaisons				
1225 f	1235 f		1180 F	$\nu_2(H_3O^+)$	1140 F	δ ou γ(OHO)
875 F	865 F	$\rho(H_2O)$ ou $W(H_2O)$	860 m	δ(OH) de SbF_5OH^-	1060 ép 880 ép	$\rho(H_2O)$ et $W(H_2O)$
640 TF	655 TF		660 ép		668 TF	$\nu_3(SbF_6^-)$
565 ép	575 ép	$\nu(OSbF_5)$	640 TF			
460 m	470 m		570 ép	$\nu(OSbF_5)$	565 F	$\nu_2(SbF_6^-)$
320 ép	330 f		550 ép 470 F		485 ép	$\zeta(H_2O)$
265 F	270 F	$\delta(OSbF_5)$				
200 m	210 F		270 TF 230 ép	$\delta(OSbF_5)$	280 F	$\nu_4(SbF_6^-)$

*TF = très fort, TL = très large, F = fort, m = moyen, f = faible, ép = épaulement.

TABLEAU 3. Valeurs (en cm^{-1}) des fréquences de diffusion Raman*

$SbF_5.H_2O$	$4SbF_5.5H_2O$	Attributions	$H_3O^+SbF_5OH^-$	Attributions	$H_5O_2^+SbF_6^-$	Attributions
658 TF	664 TF		657 TF		658 TF	$\nu_1(SbF_6^-)$
595 m	570 m	$\nu(OSbF_5)$	578 m	$\nu(OSbF_5)$		
494 f	470 f		565 m 458 m		570 m	$\nu_2(SbF_6^-)$
300 F	282 F	$\delta(OSbF_5)$	283 F	$\delta(OSbF_5)$	280 ép	$\nu_5(SbF_6^-)$
258 F	—		—		270 F	

*TF = très fort, F = fort, m = moyen, f = faible, ép = épaulement.

Can. J. Chem. Downloaded from www.nrcresearchpress.com by 210.87.254.40 on 09/05/12
For personal use only.

hydrate des bandes caractéristiques de l'ion oxonium (6), en particulier celles correspondant aux vibrations de déformation ν_4 et ν_2 et qui sont généralement larges et relativement intenses, permet d'écarter la structure $H_3O^+Sb_2F_{10}OH^-$ proposée précédemment.

Les bandes observées sont très caractéristiques des modes de vibrations d'une molécule d'eau coordinée à un acide de Lewis. En particulier on retrouve les trois domaines principaux des vibrations de valence ν_s et $\nu_{as}(H_2O)$ sous la forme d'une bande large à 3120 cm^{-1}, de la vibration de déformation $\delta(H_2O)$ à 1630 cm^{-1}, des modes de rotation plane $\rho(H_2O)$ ou de balancement $W(H_2O)$ de la molécule d'eau vers 875 cm^{-1}.

Les vibrations ν(OH) se situent à une fréquence relativement basse, nettement inférieure par exemple à celle de l'harmonique $2\delta(H_2O)$, ce qui est particulièrement rare dans le cas des spectres de l'eau coordinée.

On peut noter à titre de comparaison les fréquences ν(OH) observées pour le monohydrate de $SbCl_5$ à 3350 cm^{-1} (7), de BF_3 à 3340 cm^{-1} (8), de $GaCl_3$ et $GaBr_3$ à 3290 cm^{-1} (9). Il est admis généralement que la formation de liaison de coordination métal–oxygène a pour effet d'affaiblir les liaisons OH des molécules d'eau, et l'évolution des fréquences ν(OH) dans les hydrates précédents semble en accord avec les acidités relatives des différents halogénures.

Le pentafluorure d'antimoine, acide de Lewis très fort, doit présenter une affinité particulièrement élevée vis-à-vis de l'eau. On doit donc attendre une liaison Sb—O forte et, corrélativement, une augmentation du pouvoir accepteur des atomes de fluor qui seront susceptibles de former des liaisons hydrogène relativement fortes.

Il est probable que les deux effets: coordination de l'atome d'oxygène sur le métal et formation de liaisons OH...F concourent à l'affaiblissement des liaisons OH et donc à l'abaissement des fréquences ν(OH).

Dans le cas de ce complexe, les vibrations de libration sont observées à des fréquences plus élevées que pour les hydrates précédents et celà, aussi, peut être relié à l'augmentation de la force de la liaison M—O (10) ou aux liaisons hydrogène.

En ce qui concerne le squelette, il est difficile de localiser la (ou les) vibration (s) SbO. Les fréquences infrarouges et Raman observées sont assez proches de celles de l'ion SbF_6^- (11). Cependant, l'apparition de bandes dans le domaine 450–500 cm^{-1} (dans le cas de $SbF_5.H_2O$: i.r., 460 cm^{-1}; Raman, 494 cm^{-1}) d'intensités moyennes en infrarouge et faibles en Raman, peut être reliée à la formation d'une liaison antimoine–oxygène, puisque les spectres de SbF_6^- dans ce même domaine sont exempts de bandes. Toutefois il nous semble que l'attribution à une vibration SbO ne puisse être exclusive car cette vibration doit être fortement couplée aux autres modes du squelette et que, par exemple, la bande la plus intense en Raman à 658 cm^{-1} puisse être mieux décrite comme le mode $\nu_s(OSbF_5)$. Dans ce domaine, on peut remarquer la similitude du spectre infrarouge du monohydrate avec celui du squelette $OSbF_5$ du complexe $SbF_5.SO_2$ (12) et l'on peut penser que leurs structures sont voisines.

Les autres bandes observées peuvent donc se répartir en vibrations de valence du squelette $\nu(OSbF_5)$ et en vibrations de déformation $\delta(OSbF_5)$.

Comme il a été dit précédemment, les fréquences de vibrations du squelette ne sont pas assez éloignées de celles de SbF_6^- pour permettre d'écarter la structure ionique $SbF_4(H_2O)_2^+$ SbF_6^- définitivement. Cependant, l'étude en spectroscopie de vibration de la série des monohydrates des acides $MX_n.H_2O$ (7–9) montre que dans tous les cas c'est le composé $H_2O \rightarrow MX_n$ qui a été isolé et caractérisé. On ne connaît à l'heure actuelle qu'une structure analogue avec SbF_5, celle du composé d'addition $OSO \rightarrow SbF_5$.

Le composé $4SbF_5.5H_2O$

L'étude des spectres infrarouges et Raman de cet hydrate montre l'existence de motifs $OSbF_5$, très voisins de ceux obtenus dans le cas du monohydrate. Cette analogie entre ces deux composés est confirmée d'ailleurs par certaines observations faites sur leurs propriétés physiques. En particulier, ce sont deux composés à fusion nettement congruente, dont les températures de fusion sont très voisines (T_f^0 4/5 = 128 °C; T_f^0 mono = 117 °C): le composé 4/5 cristallisant cependant plus facilement.

L'aspect général du spectre infrarouge montre par comparaison avec celui du monohydrate, un élargissement considérable de la bande de déformation de la molécule d'eau. Le même phénomène est observable sur la vibration de valence $\nu(H_2O)$, ce qui semble indiquer l'intervention de plusieurs modes νOH provenant de différents types de molécules d'eau.

Il semble donc que la structure du composé 4/5

Can. J. Chem. Downloaded from www.nrcresearchpress.com by 210.87.254.40 on 09/05/12
For personal use only.

soit très proche de celle du monohydrate, la molécule d'eau supplémentaire étant simplement liée aux autres par des liaisons hydrogène.

Le composé $SbF_5.2H_2O$

Le complexe MX_n–H_2O peut être considéré comme un acide de Brönsted fort et la réaction $SbF_5.H_2O + H_2O$ peut alors conduire à un composé complètement ionisé $H_3O^+SbF_5OH^-$. Ce phénomène n'est pas général; ainsi dans l'état liquide le complexe $BF_3.2H_2O$ peut être considéré comme le composé $H_3O^+BF_3OH^-$ (13) alors que dans l'état solide ce n'est pas le cas (14). Les formes moléculaires $(MX_n.H_2O)H_2O$ y sont très souvent obtenues.

Cependant, il est remarquable de constater que les solutions aqueuses concentrées de certains acides minéraux forts, tels l'acide perchlorique et l'acide nitrique en particulier se comportent de façon inverse. Les acides partiellement ionisés dans l'état liquide donnent dans l'état solide les composés $H_3O^+ClO_4^-$ et $H_3O^+NO_3^-$ (15, 16).

L'ion oxonium est caractérisé par trois domaines principaux d'absorption. Les deux premiers domaines (1200–1000 et 1700–1600 cm^{-1}) sont parfaitement définis et attribuables aux vibrations de déformation. Le troisième domaine qui correspond aux vibrations de valence ν_1 et ν_3 semble beaucoup varier (3400–2500 cm^{-1}) en fonction de l'environnement de H_3O^+ et donc de la présence de liaisons hydrogène; il dépendra par conséquent de l'acide considéré. Aussi il n'est pas surprenant que les attributions dans le domaine des vibrations de valence soient contreversées (17–19).

Ce sont donc les vibrations de déformation qui vont nous servir à caractériser l'ion oxonium.

Sur le spectre infrarouge on observe deux bandes intenses, relativement larges vers 1700 et 1180 cm^{-1} caractéristiques de la présence de H_3O^+ et que l'on attribue aux vibrations de déformation ν_4 et ν_2.

Le domaine des vibrations de valence ν(OH) est plus complexe car on y attend les vibrations ν(OH) de SbF_5OH^-, ainsi que les vibrations ν_1 et ν_3 de l'ion H_3O^+. Ce domaine est relativement étendu, en particulier vers les basses fréquences, ce qui indique de fortes interactions en particulier par liaisons hydrogène.

Dans le cas des vibrations du squelette, les valeurs des fréquences observées sont en bon accord avec celles données pour quelques sels d'hydroxofluoroantimonate alcalins étudiés par Kolditz et Nussbücker (20). Ces auteurs attribuent la fréquence de la vibration SbO à 560 cm^{-1}. On peut remarquer cependant que tous les composés étudiés et en particulier SbF_6^-, ont des fréquences de vibrations au voisinage de 560 cm^{-1}. Les bandes observées à 470 cm^{-1} en infrarouge et à 468 cm^{-1} en Raman paraissent donc plus caractéristiques de la liaison SbO. Il semble toutefois que comme pour les hydrates précédents, cette vibration soit fortement couplée aux autres modes du squelette.

Ainsi, la position et la largeur des bandes dans le domaine des vibrations de déformation semblent donc caractéristiques de la présence de l'ion H_3O^+. Par conséquent, à l'inverse des dihydrates $BF_3.2H_2O$ et $GaBr_3.2H_2O$ nous ne sommes pas en présence de l'entité moléculaire $(MX_n.H_2O)H_2O$, mais plutôt d'un composé ionique dont la formule fait intervenir l'ion oxonium H_3O^+.

Le composé $SbF_5.HF.2H_2O$

Les acides forts complexes comme HPF_6, $HAsF_6$, HSF_6 sont susceptibles de former avec des bases organiques oxygénées (R_nO) des complexes de stoechiométrie 2:1, dans lesquels le proton est généralement solvaté par les molécules de la base (R_nO---H^+---OR_n); le cation ainsi formé étant susceptible de comporter une liaison hydrogène courte et symétrique. Les spectres infrarouges de tels complexes sont en effet caractéristiques de composés faisant intervenir des liaisons hydrogène fortes et courtes (21). En particulier, il apparaît une absorption large et intense au-dessous de 1800 cm^{-1}, qui peut être associée aux mouvements du proton dans ces liaisons hydrogène.

Dans le complexe $HF.SbF_5.2H_2O$, la présence de l'ion $(H_2O)_2H^+$ ou $H_5O_2^+$ peut être envisagée indirectement par la mise en évidence de l'ion SbF_6^-. Nous avons comparé dans le tableau 4 les fréquences observées pour ce complexe à celles de composés faisant intervenir l'ion SbF_6^-.

En fait, l'observation d'une très large absorption entre 2000 et 800 cm^{-1} caractéristique d'une liaison hydrogène très courte et très forte constitue une preuve plus directe de sa présence.

Le spectre infrarouge est très comparable à ceux obtenus pour quelques dihydrates d'acide minéraux forts ou sels de dioxonium par l'un d'entre nous (22).

A l'heure actuelle en se basant sur les structures radiocristallographiques de dihydrates

TABLEAU 4. Fréquences (en cm^{-1}) de diffusion Raman de quelques hexafluoroantimonates

$K^+ SbF_6^-$†	$NO^+SbF_6^-$†	$NO_2^+SbF_6^-$†	$H_5O_2^+SbF_6^-$‡	Attributions
661	658	661	658	ν_1 (Raman)
575	570*	576*	570	ν_2 (Raman)
		568*		
655	660	660	668	ν_3 (Infrarouge)
270	275	275	280	ν_4 (Infrarouge)
294	294	294	280	ν_5 (Raman)
278	284	283	270	

*Indique une vibration active aussi en infrarouge.
†Référence 11.
‡Ce travail.

d'acides forts relativement nombreuses (23–26), on peut considérer que l'ion $H_5O_2^+$ est constitué de deux groupes H_2O relié par un pont hydrogène très court ($\simeq$2.41 Å). On peut donc décomposer les vibrations de l'ion dioxonium

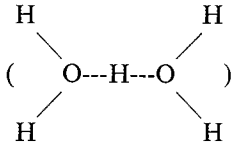

en vibrations caractéristiques des groupes terminaux: $\nu_s(H_2O)$, $\nu_{as}(H_2O)$, $\delta(H_2O)$ et modes de librations $\rho(H_2O)$, $W(H_2O)$, $\zeta(H_2O)$ d'une part et, d'autre part, celles de la liaison hydrogène $\nu_{as}(OHO)$, $\nu_s(OHO)$, δ et $\gamma(OHO)$ (27). Dans le spectre infrarouge, la bande large et intense entre 2000 et 800 cm^{-1} peut être associé à la vibration $\nu_{as}(OHO)$; une fréquence aussi basse (vers 1000 cm^{-1}) pour $\nu_{as}(OHO)$ dans le cas de l'ion dioxonium a déjà été observé par Gillard et Wilkinson dans une série de sels complexes de type $[Co(en)_2Cl_2]Cl_2H_5O_2$ (28). L'une des vibrations $\delta(OHO)$ ou $\gamma(OHO)$ peut être considérée comme responsable de la bande à 1140 cm^{-1}. La fréquence relativement basse de $\nu_{as}(OHO)$ et une fréquence de vibration de déformation aussi élevée, sont le signe de la présence d'une liaison hydrogène très forte.

Généralement, l'ion dioxonium est fortement lié par liaisons hydrogène avec l'anion. La fréquence relativement élevée du maximum à 3460 cm^{-1} pour les vibrations $\nu_s(H_2O)$ et $\nu_{as}(H_2O)$ des groupes terminaux dans le cas de $H_5O_2^+SbF_6^-$ et la faible largeur de la bande, sont le signe d'une interaction anion–cation très faible. Ce phénomène est observé pour les ν(OH) terminales de l'ion dioxonium associé à des anions tels que $SbCl_6^-$, $GaBr_4^-$, $GaCl_4^-$, qui sont respectivement observées à 3480, 3450 et 3440 cm^{-1} (22). Etant donné son volume et son faible pouvoir accepteur, l'ion SbF_6^- n'est susceptible de former que des liaisons hydrogène faibles avec $H_5O_2^+$. Ce point remarquable illustre parfaitement le rôle que joue un gros anion globulaire dans la stabilisation des hydrates du proton.

Conclusion

Les spectres de vibration des composés étudiés peuvent être interprétés sur la base des trois équations suivantes

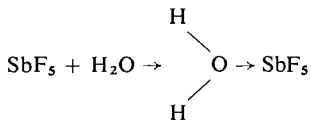

$$SbF_5.H_2O + H_2O \rightarrow H_3O^+ + SbF_5OH^-$$

$$SbF_5.H_2O + HF.H_2O \rightarrow H_5O_2^+ + SbF_6^-$$

Ces résultats sont à rapprocher des solubilités observées dans SO_2 pour ces composés. Les deux formes ioniques sont très peu solubles dans ce solvant peu polaire (29); par contre, les deux autres hydrates non ionisés $SbF_5.H_2O$ et $4SbF_5.5H_2O$ y sont très fortement solubles.

Dans le cas du monohydrate on a un simple complexe donneur–accepteur, l'antimoine occupant le centre d'un octaèdre déformé. Ce composé se comporte comme un acide fort; l'addition d'une deuxième molécule d'eau conduit à la formation de l'ion oxonium et à l'anion SbF_5OH^-. En présence d'ions fluorures et de molécules d'eau, c'est bien l'ion hexafluoroantimonate SbF_6^- qui se forme associé à l'ion dioxonium. Ces deux derniers composés semblent donc conduire à la formation d'espèces ioniques et en particulier à la formation d'ions hydronium. Mais si dans le dihydrate de SbF_5 l'ion H_3O^+ interagit fortement avec l'anion SbF_5OH^-, dans le deuxième complexe $SbF_5.HF.2H_2O$ les liaisons hydrogène sont très faibles et les espèces ioniques SbF_6^- et $H_5O_2^+$ sont mieux individualisées.

Can. J. Chem. Downloaded from www.nrcresearchpress.com by 210.87.254.40 on 09/05/12
For personal use only.

Des résultats analogues ont été obtenus par Olofsson (30) dans les systèmes $SbCl_5$–H_2O et $SbCl_5$–HCl, en présence de bases faibles.

1. G. OLAH, R. DEMEMBER et R. H. SCHLUSBERG. J. Am. Chem. Soc. **91**, 2112 (1969).
2. O. RUFF. Ber. **39**, 4310 (1906).
3. P. A. W. DEAN et R. J. GILLESPIE. J. Am. Chem. Soc. **91**, 7264 (1969).
4. A. COMMEYRAS et G. OLAH. J. Am. Chem. Soc. **91**, 2929 (1969).
5. R. FOURCADE. Thèse U.S.T.L. Montpellier, France. 1971.
6. J. ROZIERE et J. POTIER. J. Inorg. Nucl. Chem. **35**, 1170 (1973).
7. G. PICOTIN. Thèse 3e cycle U.S.T.L. Montpellier, France. 1973.
8. G. CADE. Thèse 3e cycle U.S.T.L. Montpellier, France. 1973.
9. M. T. BORIES, J. ROZIERE et A. POTIER. Chem. Commun. 213 (1971).
10. G. BRUN. Rev. Chim. Miné. **5**, 899 (1968).
11. A. M. QURESHI et F. AUBKE. Can. J. Chem. **48**, 3117 (1970).
12. J. W. MOORE, H. BAIRD et H. B. MILLER. J. Am. Chem. Soc. **90**, 1358 (1968).
13. N. N. GREENWOOD et R. L. MARTIN. J. Chem. Soc. **3**, 1915 (1951).
14. P. T. FORD et R. E. RICHARDS. J. Chem. Soc. **3**, 3870 (1956).
15. P. A. GIGUERE. Rev. Chim. Miné. **3**, 627 (1966).
16. R. E. RICHARDS et J. A. S. SMITH. Trans. Faraday Soc. **47**, 1261 (1951).
17. C. C. FERRISO et D. F. HORNIG. J. Chem. Phys. **23**, 1464 (1955).
18. R. SAVOIE et P. A. GIGUERE. J. Chem. Phys. **41**, 2698 (1964).
19. D. E. BETHELL et N. SHEPPARD. J. Chem. Phys. **21**, 1421 (1953).
20. V. L. KOLDITZ et B. NUSSBÜCKER. Z. Anorg. Allg. Chem. **335**, 191 (1965).
21. D. COOK. Chem. Ind., 608 (1963).
22. J. ROZIERE. Thèse U.S.T.L. Montpellier, France. 1973, N°CNRS: AO 8634.
23. J. OLOVSSON et I. LUNDGREN. Acta Cryst. **23**, 966 (1967).
24. J. OLOVSSON. J. Chem. Phys. **49**, 1063 (1968).
25. I. LUNDGREN. Acta Cryst. **26**, 1893 (1970).
26. J. M. WILLIAMS. Inorg. Nucl. Chem. Lett. **3**, 297 (1967).
27. J. ROZIERE et J. POTIER. J. Mol. Struct. **12**, 979 (1972).
28. R. D. GILLARD et G. WILKINSON. J. Chem. Soc. 1640 (1964).
29. L. F. AUDRIETH et J. KLEINBERG. Non aqueous solvents. J. Wiley, New York. 1953. p. 211.
30. G. OLOFSSON et I. OLOFSSON. Tetrahedron, **29**, 1711 (1973).

Can. J. Chem. Downloaded from www.nrcresearchpress.com by 210.87.254.40 on 09/05/12
For personal use only.

Acid Catalyzed Rearrangements of Structurally Constrained Tricarbonyl(*trans*-pentadienyl)iron Cations[1]

C. R. JABLONSKI[2] AND T. S. SORENSEN

Department of Chemistry, The University of Calgary, Calgary, Alberta T2N 1N4

Received October 17, 1973

C. R. JABLONSKI and T. S. SORENSEN. Can. J. Chem. **52**, 2085 (1974).

Both the tricarbonyl(1,4-dimethylene-*cis*,*cis*,*trans*,*cis*-hexa-1,3-dienyl)iron (secondary) and the tricarbonyl(1,4-dimethylene-5-methyl-*cis*,*cis*,*trans*-hexa-1,3-dienyl)iron (tertiary) cations, which cannot convert to a ^5h-*cis* pentadienyl system via a simple bond rotation, can be prepared at low temperature in strong acid media from their related alcohol complexes. The secondary as well as the tertiary ions rearrange to give the thermodynamically more stable tricarbonyl-(1-alkylcyclohexa-1,3-dienyl)iron cation via an acid catalyzed pseudo first order process. The rate of rearrangement of the secondary ion is much faster than that of the tertiary ion indicating a substantial amount of residual positive charge on the exocyclic (β) carbon in the complexed *trans*-pentadienyl carbonium ions.

C. R. JABLONSKI et T. S. SORENSEN. Can. J. Chem. **52**, 2085 (1974).

Partant des complexes des alcools correspondants et travaillant à basse température et dans un milieu fortement acide, on a pu préparer chacun des cations du (diméthylène-1,4 *cis*,*cis*,*trans*,*cis* hexadiène-1,3 yl) fer (secondaire) tricarbonyle et du (diméthylène-1,4 méthyl-5 *cis*,*cis*,*trans* hexadiène-1,3 yl) fer (tertiaire) tricarbonyle qui ne peuvent être transformés en un système ^5h-*cis* pentadiényle par le moyen d'une simple rotation. L'ion secondaire de même que le tertiaire se réarrangent pour donner le cation thermodynamiquement le plus stable (alkyl-1 cyclohexa-diène-1,3 yl) fer tricarbonyle grâce à un processus de pseudo premier ordre catalysé par les acides. Le réarrangement de l'ion secondaire est beaucoup plus rapide que celui de l'ion tertiaire indiquant qu'une quantité importante de charge positive résiduelle existe sur le carbone (β) exocyclique dans les carbocations complexés *trans*-pentadiényle. [Traduit par le journal]

The fact that acyclic tricarbonyl(*trans*-pentadienyl)iron cations (**1**) are ubiquitous in their rearrangement to give the related *pentahapto*-tricarbonyl(*cis*-pentadienyl)iron cations (**2**) has been amply demonstrated (1–3).

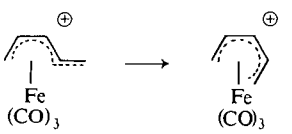

1 **2**

Protonated tricarbonyl(*trans*,*trans*-2,4-hexadienal)iron complexes (**3**), which have been shown to be excellent models for the parent ions (**1**), show similar reactions (4, 5).

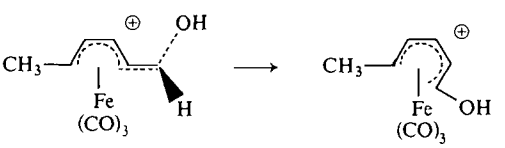

3 **4**

The obvious structural relationships of the ions **1** and **3** with the profusely studied, yet still controversial (6) ferrocenyl ion (**5**) has initiated

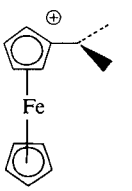

5

considerable discussion regarding the electronic structure of the *trans*-pentadienyl ion **1**. Intimately involved with any discussion of the electronic structure of **1** and **3** is a consideration of the driving force for the rearrangements **1** → **2** and **3** → **4**.

We have previously shown (3) that related *trans–cis* tricarbonyl(pentadienyl)iron cation pairs (*e.g.* **1** and **2**) rapidly equilibrate and that in special circumstances conversion to a *pentahapto*-tricarbonyl(*cis*-pentadienyl)iron complex is no guarantee of thermodynamic stability. It was of immediate interest then to investigate the stabilization modes available to tricarbonyl (*trans*-

[1]Presented in part at the XIV ICCC, Toronto, Ontario, June 22–28, 1972. Abstracts p. 130.

[2]Present address: Department of Chemistry, The University of Western Ontario, London, Ontario.

Can. J. Chem. Downloaded from www.nrcresearchpress.com by 210.87.254.42 on 09/05/12
For personal use only.

pentadienyl)iron cations in which a direct conversion to a ^{5}*h-cis* ion is structurally prohibited.

The tricarbonyl (1,4-dimethylenepenta-1,3-dienyl)iron cations (**6**) are examples of such ions[3]

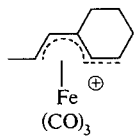

7

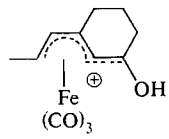

8

and we report here their preparation from alcoholic precursors (**9**) and their medium dependant rearrangements leading ultimately to the thermodynamically very stable tricarbonyl(cyclohexadienyl)iron cations **10**.

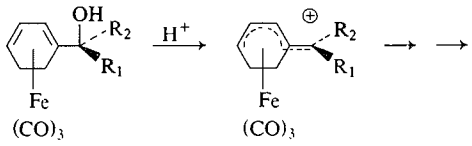

9 6

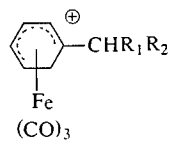

10

Preparation of the Alcohol Precursors

Generation of the desired cation complexes with known stereochemistry (**6**, $R_1 \neq R_2$) at the exocyclic carbon requires both the stereospecific *exo* departure of the leaving group (7) and the stereospecific synthesis of the (diastereomeric) alcohol complexes **9**. Since sodium borohydride reduction of a number of tricarbonyl(*trans*-hexa-2,4-dienone)iron complexes has been shown to proceed nearly stereospecifically (7, 8) to give the Ψ-*endo*[4] epimer (**11** → **12**) (*c.f.* however ref. 9) attention was focused on the preparation of the cyclic analog, tricarbonyl(dihydroacetophenone)-iron, **13**.

In principle, conjugated 1-substituted 1,3-

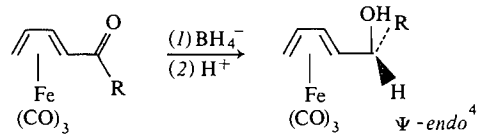

11 12

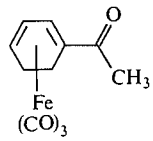

13

cyclohexadiene complexes could be prepared directly via $Fe(CO)_5$ catalyzed rearrangement of the Birch reduction products of aromatic substrates (11), electrophilic substitution of the parent tricarbonyl(cyclohexa-1,3-diene)iron complexes (12), or indirectly via complexation of the dienone ligand. In view of the variety of products available from both direct methods, we chose the latter alternative.

Dihydroacetophenone (13) was prepared via a modification of the dihydrobenzaldehyde synthesis of Langenbeck *et al.* (14) rather than via the rather lengthy literature method (13). The synthesis followed the route shown in Scheme 1.

Critical to the overall success of Scheme 1 is the preparation of quantities of the dieneamine **14** in good yield. Extensive polymerization results unless a catalytic amount of *o*-quinone or naphthoquinone is added (15) and the pyrolysis carried out as quickly as possible.

Photochemical reaction of **17***a* and *b* with iron pentacarbonyl gave the expected products. Ketone **17***b* was, however, more satisfactory since the aldehyde complex **18** readily decomposes and the pure complex is freed from unreacted ligand with difficulty.

Borohydride reduction of the ketone complex **13** was found to proceed with nearly complete stereospecificity while, in contrast, reaction of the aldehyde complex **18** with methyllithium gave a mixture of two epimeric alcohols in nearly equal amounts (t.l.c. analysis).

It is apparent that the smaller steric requirements of the aldehyde moiety do not force a strong conformational preference resulting in a loss of stereospecificity (7, 8, 16). In accord with these results are recent p.m.r. investigations of protonated aldehyde complexes which show that the parent aldehyde complexes exist in nearly a

[3]Lillya and co-workers have previously reported the constrained ion **7** and the related protonated ketone complex **8** (2, 4).

[4]Ψ-*endo* refers to the C_1 epimer which has —OH nearest iron in the most stable conformation. Ψ-*exo* is however most stable with —OH farthest from iron (7*a*, 10).

Can. J. Chem. Downloaded from www.nrcresearchpress.com by 210.87.254.42 on 09/05/12
For personal use only.

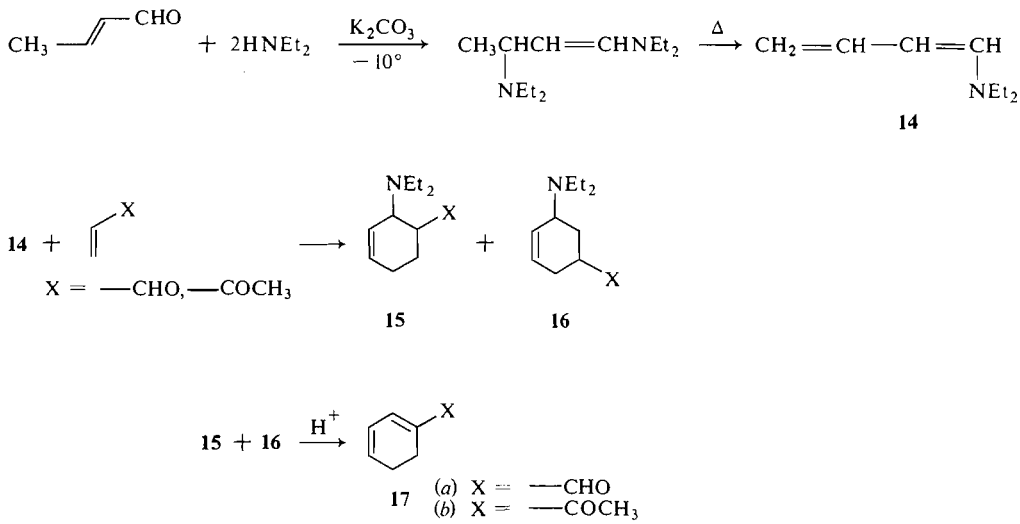

SCHEME 1

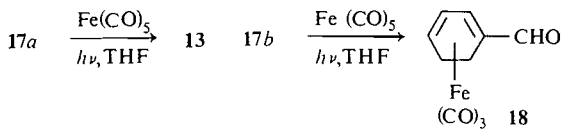

1:1 ratio of *s-cis* and *s-trans* isomers (5). A similar lack of stereospecificity has been noted for the reaction of acyclic tricarbonyl(penta-2,4-dienal)-iron complexes with alkyllithiums (1).

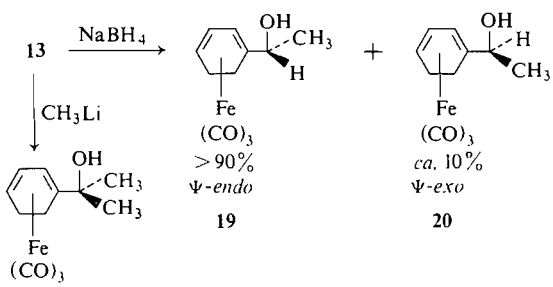

The configuration at C_1 for the major product received from borohydride reduction of **13** is affirmed as Ψ-*endo* by its characteristic chromatographic behavior (7, 8). Thus the major product (assigned as **19**) of the above reduction shows an R_f value (silica gel thin layer plates) identical with the higher R_f product obtained from the reaction of aldehyde **18** with methyllithium. Since both i.r. and p.m.r. spectral data of similar epimeric pairs are routinely nearly indistinguishable, the above t.l.c. test is considered conclusive.

Reaction of ketone **13** with methyllithium gave a single alcoholic product achiral at C_1. Spectral parameters and analysis were consistent with the expected tertiary alcohol structure **21**.

Preparation and Reaction of the Carbonium Ions

Dissolution of the Ψ-*endo* alcohol complex **19** in a 1:3 mixture of FSO_3H:SO_2ClF held at −120° resulted in a yellow solution which gave the p.m.r. spectrum shown in Fig. 1. When this solution was warmed, a rearrangement occurred giving a p.m.r. spectrum identical with that obtained by dissolving **19** in 100% FSO_3H at −78° or in 96% H_2SO_4 at 0° (Fig. 2).

We interpret these observations in terms of a thermally induced rearrangement of the expected tricarbonyl(1,4-dimethylene-*cis*,*cis*,*trans*,*cis*-hexa-1,3-dienyl)iron cation **22** to the tricarbonyl-(1-ethylcyclohexa-1,3-dienyl)iron cation **23**.

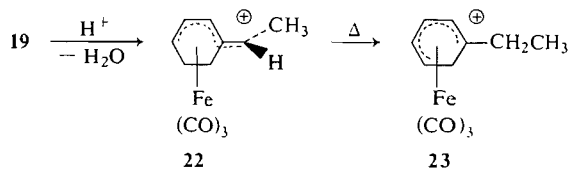

Assignment of the *trans*-pentadienyl (3) structure (**22**) to the spectrum shown in Fig. 1 resulted from a consideration of: (*a*) the propensity for *exo* departure of the leaving group in similar systems (7, 8), (*b*) our earlier observations of retention of stereochemistry at C_1 and along the dienyl backbone when acyclic alcohol complexes are treated in the same fashion, and (*c*) a detailed

Can. J. Chem. Downloaded from www.nrcresearchpress.com by 210.87.254.42 on 09/05/12
For personal use only.

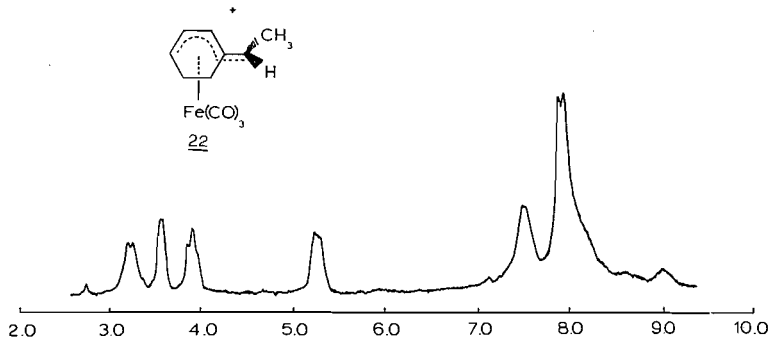

FIG. 1. Proton magnetic resonance spectrum of ion **22** in FSO_3H/SO_2ClF at *ca.* $-120°$.

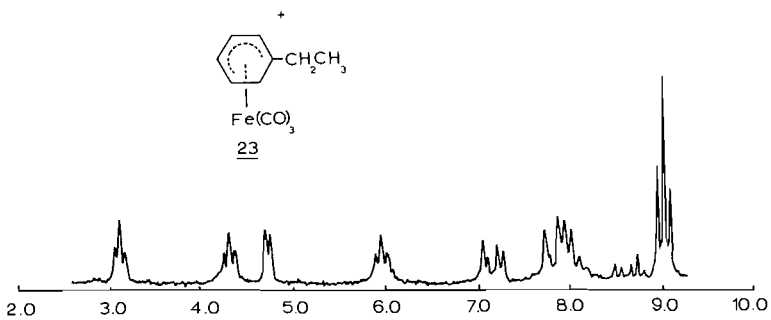

FIG. 2. Proton magnetic resonance spectrum of ion **23** in FSO_3H at *ca.* $-60°$.

consideration of the p.m.r. parameters (*c.f.* Table 3).

The cyclohexadienyl ion **23** shows a p.m.r. spectrum (Fig. 2) closely resembling previously reported ions of similar structure (17) and is completely assigned with the aid of double resonance experiments.

The tricarbonyl(1-ethylcyclohexa-1,3-dienyl)-iron cation **23** may be isolated as its PF_6^- or BF_4^- salt. Samples of **23**—BF_4 prepared by adding HBF_4 to **19** gave a p.m.r. spectrum (in liquid SO_2) identical with that shown in Fig. 2. The isolated salt is quite stable as is found to be the case for the parent tricarbonyl(cyclohexa-1,3-dienyl)iron cation and decomposes only at temperatures above 200° (N_2 filled capillary). The infrared spectrum of the isolated salt shows two CO stretching bands at relatively high frequency (2050 and 2115 cm^{-1} assigned to the doubly degenerate E and the A_1 modes assuming local symmetry C_{3v}) confirming the cationic nature of the ligand (18).

In more weakly acidic media where an appreciable amount of free secondary alcohol remains, the formation of ion **23** is accompanied by the production of protonated bis ethers. The ratio of the protonated bis ether to **23** is markedly dependent upon the acidity of the medium as one would expect. Complete cleavage to the carbonium ion is observed in very strongly acidic media (100% FSO_3H). Table 1 shows the medium dependence of oxonium ion formation.

In more weakly acidic media, both the presence of free secondary alcohol and the inability to cleave ethers (19) combine and result in the observation of **24** formed via nucleophilic attack of the oxygen lone pair at the exocyclic carbonium ion. Ion **24** was also observed in $FSO_3H:SO_2ClF$ mixtures which contained only sufficient acid to dissolve the alcohol complex.

The structure assigned to ion **24** is consistent with its p.m.r. spectrum (see Experimental) and

TABLE 1. Medium dependence of oxonium ion formation

% H_2SO_4	24:23*
84	4.5
89	2.6
92	1.1
96	0.4

*Calculated by direct integration of the n.m.r. spectra at 0°.

Can. J. Chem. Downloaded from www.nrcresearchpress.com by 210.87.254.42 on 09/05/12
For personal use only.

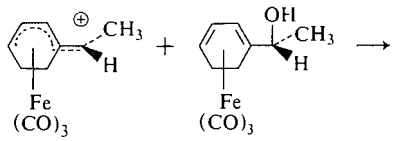

22 19

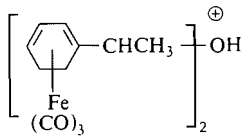

24

is further confirmed by the isolation of the parent diastereomeric ethers **25** by careful aqueous quenching of an 84% H_2SO_4 solution containing **24**. Thin layer chromatographic analysis of the aqueous quench products revealed the presence of at least five products. Two of the products (A and B) are formed in major amounts and have high and very similar R_f values. Preparative thin layer chromatography separated a mixture of A and B from the remaining products but could not resolve the mixture further. Proton magnetic resonance and mass spectral investigation concluded with the assignment of A and B as a diastereomeric mixture of the bis ethers **25**.

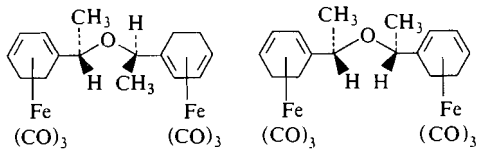

25

The stereochemistry of the isolated ethers must have been previously defined in the ion **24** which therefore must also be present as a mixture of diastereomers with very similar p.m.r. spectra.

The mass spectrum of a third product C, showed a molecular ion at $m/e = 510$ indicating its isomeric nature with respect to **25**. Proton magnetic resonance parameters are consistent with but do not demand a mixed ether structure **26**.

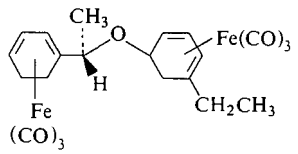

26

The low R_f values of the remaining products D and E were highly reminiscent of tricarbonyl-(dienol)iron complexes. Examination by thin layer chromatography (silica gel with $CHCl_3$ and benzene elution) showed that D and E were identical with the two crude alcoholic products obtained from reaction of the ketone **13** with sodium borohydride or the aldehyde **18** with methyllithium. Alcohol D had a higher R_f value and was present in only trace amounts.

Epimerization at C_1 leading to product E (identified as **20** by the above t.l.c. test) could have occurred via rotation of the exocyclic bond in the carbonium ion **22** or via an addition-elimination mechanism involving the formation of a triene intermediate.[5]

Thus p.m.r. spectra obtained by dissolving alcohol **21** in a ca. 1:3 FSO_3H:SO_2ClF mixture held at $-120°$ in a pentene slush bath were, unlike the secondary carbonium ions described above, nearly temperature independent in the range from -120 to $0°$ although peaks corresponding to a new ionic species slowly appeared at the upper level of the temperature range.[6] In addition, identical spectra could be generated at temperatures as high as $0°$ in 95% H_2SO_4 or D_2SO_4 (*c.f.* Fig. 3).

The spectrum in Fig. 3 is assigned the tricarbonyl(5-methyl-1,4-dimethylene-*cis*,*cis*,*trans*,*cis*-hexa-1,3-dienyl)iron cation structure **27**. This tertiary ion shows two distinct methyl absorptions in the appropriate region while the low field multiplet at 3.2 τ corresponding to H-5 in **22** (*c.f.* Fig. 1) is notably absent in Fig. 3. The assignments of Figs. 1 and 3 as **22** and **27** are then internally consistent. Assignments of all the dienyl protons in ion **27** were confirmed by double resonance experiments.

The observed magnetic nonequivalence of the methyl groups in **27** implies a restricted rotation about the exocyclic double bond, a situation recently confirmed for the related ferrocenyl ion (21). An increase in temperature to $+10°$ (95% H_2SO_4) did not result in any obvious signs of signal averaging resulting from rapid (on the n.m.r. time scale) bond rotation. Further increases in temperature led to a deterioration in the p.m.r. spectrum due to decomposition concomitant with a rapid rearrangement to give a new ion (see discussion below).

[5]The results of exocyclic bond rotation have been observed in the related ferrocenyl system and it has been shown that addition-elimination is not operative (20).

[6]Higher temperatures in this medium led to sample decomposition.

Can. J. Chem. Downloaded from www.nrcresearchpress.com by 210.87.254.42 on 09/05/12
For personal use only.

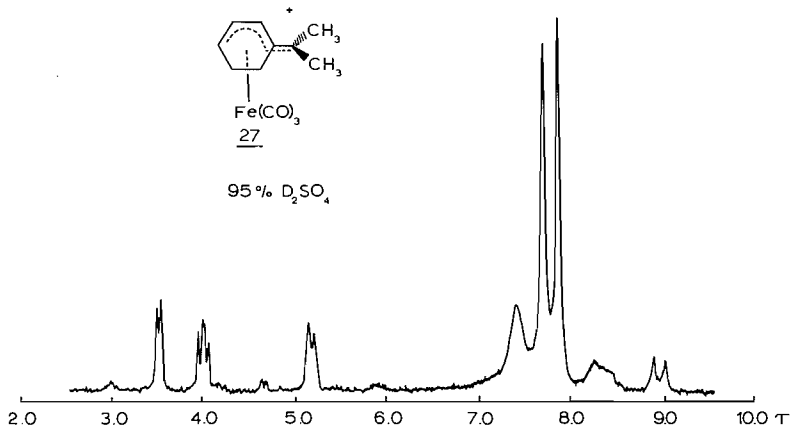

FIG. 3. Proton magnetic resonance spectrum of ion **27** in H_2SO_4 at 0°.

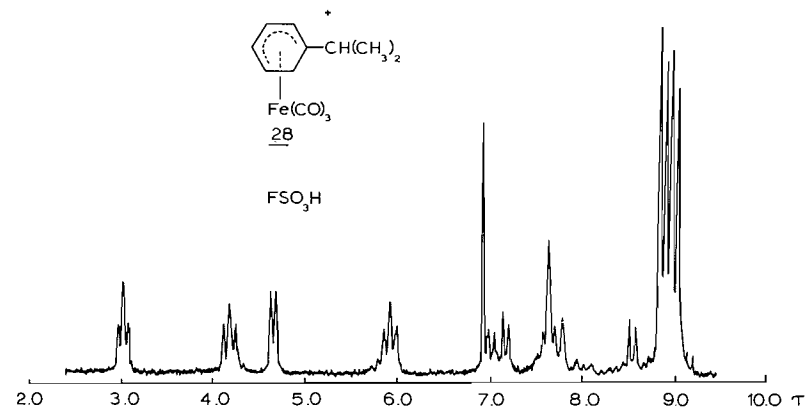

FIG. 4. Proton magnetic resonance spectrum of ion **28** in FSO_3H at −50°.

Attempted preparation of the ion **27** in 100% FSO_3H at −78° was unsuccessful even when precautions were taken to prevent excessive local heating resulting from slow dissipation of the heat of formation. In each case the p.m.r. spectrum obtained (Fig. 4) was identical with that resulting from warming 95% H_2SO_4 solutions of **27**.

Double resonance experiments allowed the complete assignment of Fig. 4 as the isomeric tricarbonyl(1-isopropylcyclohexa-1,3-dienyl)iron cation **28** formed by a rearrangement analogous to that observed for the secondary ions **22** → **23**.

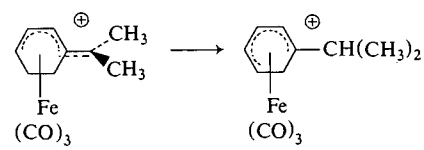

27 **28**

The ease of the rearrangement **27** → **28** in the strong acid FSO_3H as compared to the weaker acid 95% H_2SO_4 implies a strong rate depen-

TABLE 2. Pseudo first-order rate constants for the rearrangement **27** → **28**

% H_2SO_4*	$k \times 10^5$ (s^{-1})† at +5.0 ± 0.5°	r
93.0	2.4±2‡	0.9822
95.1	6.2±2	0.9894
97.1	8.2±2	0.9971
	8.4±2	0.9987
98.2	22 ±2	0.9912
99.3	51.3±2 (39)§	0.9958
	50.8±2 (37)	0.9939

*Corrected for the water formed in the protonation reactions; ROH + H^+, R^+ + H_2O, *s.f.* ref. 39.
†Least squares analysis.
‡Error calculated assuming a 5% analytical error in the concentration data.
§The larger rate constant is that for the total disappearance of **27**. The rate constant in parentheses is that for the formation of **28**.

Can. J. Chem. Downloaded from www.nrcresearchpress.com by 210.87.254.42 on 09/05/12
For personal use only.

TABLE 3. Proton magnetic resonance parameters for the tricarbonyl (1,4-dimethylenehexa-1,3-dienyl)iron cations

	Chemical shift (τ)					Coupling constant	
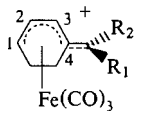	R_1	R_2	H_1	H_3	H_2	J_{23}	J_{12}
22 $R_1 = H$, $R_2 = CH_3$	3.24	7.97	5.27	3.59	3.92		
27 $R_1, R_2 = CH_3$	7.71	7.88	5.14	3.51	3.98	6.5	4.8

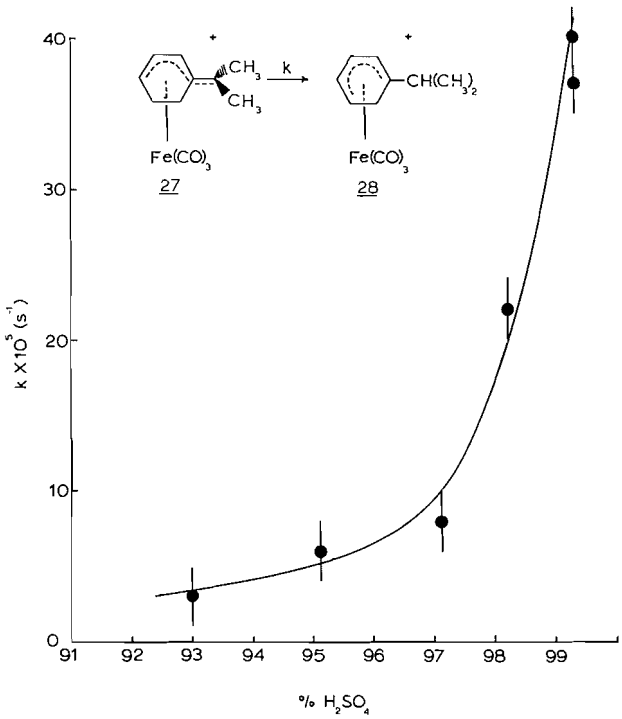

FIG. 5. Acid dependence of the pseudo first-order rate constant for the conversion of **27** → **28** in H_2SO_4.

dence on solvent acidity and a kinetic study was undertaken in order to clarify the nature of this effect. The rate of rearrangement as monitored by the increase in the p.m.r. signal corresponding to the isopropyl group in **28** was found to be cleanly first order. The pseudo first order rate constants at +5° are given in Table 2 and a plot of $\%H_2SO_4$ *vs.* k_1 is shown in Fig. 5.

Samples of **28** prepared by dissolving alcohol **21** in 95% D_2SO_4 followed by thermal rearrangement at 0° showed as the only detectable change, a collapse of the double doublet corresponding to the isopropyl group and a disappearance of the methinyl signal. These changes are consistent with complete, specific deuterium uptake at the methinyl position. Similarly, the p.m.r. spectrum obtained by dissolving the secondary alcohol **19** in D_2SO_4 showed a collapse of the triplet due to the methyl group to a doublet resulting from the incorporation of a single deuterium atom at the methylene position.

The rearrangement of ion **27** in 99% H_2SO_4, but inexplicably not in more weakly acidic media or in 100% FSO_3H, is accompanied by the formation of a second rearranged ion. Rate studies show that the new ion is formed from **27** at

Can. J. Chem. Downloaded from www.nrcresearchpress.com by 210.87.254.42 on 09/05/12
For personal use only.

constant ratio with respect to **28** indicating a parallel reaction (*c.f.* Table 2). This new ion, which is never the exclusive product, shows a p.m.r. spectrum with multiplets at τ 2.3, 3.8, 2.98, 5.68 in addition to well defined singlets at 8.08 and 8.50. A plausible structure is the ring expanded ion **29** formed from **27**, a reaction which has precedence in the literature (22, 23). Complete assignments of **29** are given in the experimental section.

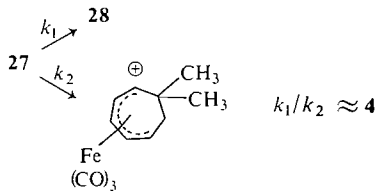

29

Discussion

Overall irreversibility in the rearrangements of both the secondary (**22** → **23**) and tertiary (**27** → **28**) systems contrasts with the behavior of related secondary and tertiary acyclic dienyl complexes (3) and suggests an even more formidable driving force for the formation of *pentahapto cis* dienyl cation complexes. This strong preference for *cis-pentahapto* complexes most likely derives from the enforced planarity without concomitant steric strain in the cyclohexadienyl moiety compared to an acyclic dienyl system.

Since both cyclohexadienyl ions **23** and **28** are most probably of similar thermodynamic stability, the qualitative differences in the rates of rearrangement of the constrained *trans* pentadienyl ions (secondary ≫ tertiary) is consistent with substantial residual carbonium ion character at the β-carbon in both **22** and **27**. The tetrahapto structure **30** is then an important contributor to the overall structure.

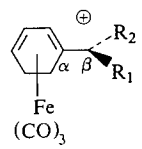

30

That there is greater electron release to the β-carbon in the —$Fe(CO)_3$ derivatives than in the related uncomplexed carbonium ions has been demonstrated (7).[7] Since, however, neither kinetic (7) studies nor the results in this paper are able to critically distinguish vertical and non-vertical (25) processes, the actual mode of electron release remains obscure.

It is, nevertheless, becoming increasingly clear that the α-ferrocenyl ion is best described by a slightly bent static structure and that its stability derives from a mesomeric electron release of some nature (6*c*, 26). X-Ray data on the related α-cyclobutadienyl-$Fe(CO)_3$ cation also shows that there is no direct bonding between the electron deficient center and iron (27).

In view of the universal observation that tricarbonyl(diene) iron complexes are twisted along the termini of the diene moiety (28) so as to provide better orbital overlap, similar twisted structures are likely for the *trans* ions **22** and **27** (**31**).

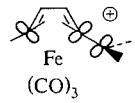

31

Movement of the electron deficient β-carbon atom towards the "interannular" region allows for increased overlap with particularly electron rich filled orbitals (29). Since mesomeric effects are not particularly sensitive to small deformations, conjugative electron release from diene electrons is simultaneously possible.

Both the medium dependence and deuterium uptake observed in the isomerizations **22** → **23** and **27** → **28** are inconsistent with a direct isopolar sigmatropic [1,6] hydrogen migration (30–32) or an intramolecular rearrangement of a stable hydridic intermediate. The results do suggest a mechanism involving a rate determining proton transfer from solvent which may occur with a concerted or synchronous intermolecular loss of a proton from a hydridic intermediate (Scheme 2).

The rate determining step is proton addition to the uncomplexed double bond which directly generates the stable cyclohexadienyl complex (33).

Whitesides and co-workers (34) have shown

[7]This conclusion must be tempered with the realization that transition state structures for solvolytic reactions may be different from that of the actual carbonium ions (24).

Can. J. Chem. Downloaded from www.nrcresearchpress.com by 210.87.254.42 on 09/05/12
For personal use only.

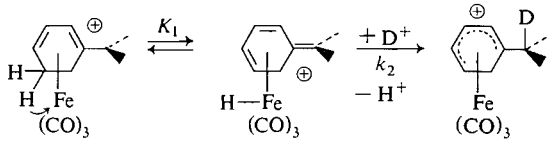

32

SCHEME 2

that in CD_3CO_2D deuterium incorporation into tricarbonyl(cyclohexa-1,3-diene)iron is stereospecifically *endo*.[8] This stereoelectronic preference for *endo* proton elimination to give a tricarbonyl (cyclohexadienyl)iron cation complex implies that H-*endo* is lost in the formation of the hydridic intermediate **32**.

The cationic intermediate hydride **32** then suffers protonation on the exocyclic double bond. Protonation at C-β gives directly the observed cyclohexadienyl ions. Protonation at C-α occurs with **27** which gives a tertiary intermediate but not with **22** which would lead to a secondary ion. Intermediate **33** then undergoes a ring opening reaction which leads directly to a cycloheptadienyl product.

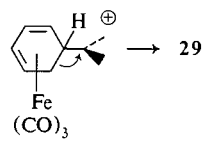

33

Integration of p.m.r. spectra of ion **27** in D_2SO_4 on samples which were incompletely isomerized showed no detectable deuterium incorporation into the ring methylene positions so that H/D exchange of **32** with solvent and/or protonation of the complexed double bond are slow.

The protonation step in Scheme 2 may occur with initial formation of a dication (36) which rapidly eliminates a proton or with concomitant loss of H^+ in a concerted or synchronous fashion.

Equally consistent with these results is an alternative mechanism involving initial protonation to form a dication intermediate **34**. If the loss of a proton from **34** is rate controlling, the function of solvent is to furnish an equilibrium concentration of the conjugate acid **34**. If, on the other hand, $k_2 \gg k_{-1}$ the formation of **34** becomes rate limiting (*c.f.* Scheme 3).

[8]Recent work indicates, however, that protonation of tricarbonyl-(tropone) iron is non-stereospecific in H_2SO_4 but stereospecifically *exo* in CF_3CO_2H (35).

[1] 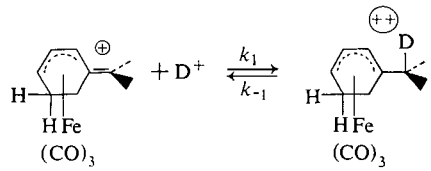

34

[2] 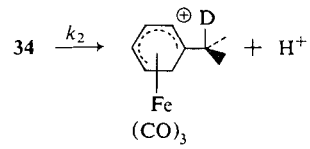

SCHEME 3

Attempts to observe a hydridic signal in the p.m.r. spectrum of solutions of **27** in order to test Scheme 2 were unsuccessful. Although this evidence favors Scheme 3 it must be interpreted with caution since (*a*) the reactive hydrido-intermediate (**32**) need not be present in concentrations sufficient to be detected via. n.m.r. and (*b*) the observation of transition metal hydrides by n.m.r. is subject to several further restraints (37).

It should be emphasized that neither Scheme 2 nor Scheme 3 accounts for the apparently discontinuous results obtained when the solvent system is changed from H_2SO_4 to the much stronger acid FSO_3H.

Experimental

General

Reactions carried out under inert atmosphere used the general technique described by Shriver (38). Nitrogen was passed through a column containing one pound of BTS catalyst (available from BASF corp., # R 3-11) held at 150° before use. Drying of the nitrogen stream was accomplished by bubbling through 96% H_2SO_4.

All boiling points (b.p.) and melting points (m.p.) are uncorrected. Melting points were taken on a Kofler micro heating stage except for organometallic compounds with m.p. greater than 80°. These and other air sensitive samples were determined in nitrogen-filled capillaries in an oil bath.

Infrared (i.r.) spectra were recorded on a Perkin–Elmer instrument (model 337) and were calibrated using the 1601 cm^{-1} band of polystyrene. Frequencies are reported in $cm^{-1} \pm 10$.

Ultraviolet (u.v.) spectra were recorded using a Perkin–Elmer model 202 spectrophotometer and band positions are reported in nm followed by the molar absorptivity (ε).

Proton magnetic resonance (p.m.r.) spectra were recorded using a Varian Associates A-60 or HA-100 spectrometer equipped with a variable temperature probe. Spectra were recorded using the HA-100 spectrometer

Can. J. Chem. Downloaded from www.nrcresearchpress.com by 210.87.254.42 on 09/05/12
For personal use only.

Can. J. Chem. Downloaded from www.nrcresearchpress.com by 210.87.254.42 on 09/05/12
For personal use only.

in the field sweep mode with internal tetramethylsilane (TMS) or tetramethylammonium chloride internal reference. Acid spectra used solvent signal for locking. Double resonance experiments were carried out in the frequency sweep mode. Spectra are reported in tau (τ) units ± 0.02. Samples were approximately 10% (w/v or v/v) in deuterochloroform ($CDCl_3$) or acid. Deuterochloroform samples were filtered through Celite (Johns–Manville, L-665-A) into nitrogen-filled n.m.r. tubes immediately before observation. Carbonium ion samples were generated in carefully degassed acid solutions and all transfers were made using nitrogen-filled pipettes. Tubes were either sealed or stoppered with a tight-fitting plastic cap.

The tricarbonyl(diene)iron complexes are generally air stable for periods of up to a few hours thus allowing most work up operations to proceed as normal. Samples are, however, best stored in a freezer in nitrogen-filled containers. Samples stored in this manner showed only limited signs of decomposition over a three year period.

Analytical thin layer chromatography (t.l.c.) experiments were carried out on Eastman Chromatogram sheets (# 6060 Silica gel with indicator) or Camag precoated t.l.c. plates (# 31179 DSF-A with indicator). Visualization was accomplished with a u.v. light or by the ferric thiocyanate method. The latter consists of initial oxidation with iodine followed by heating in a 100° oven for 5 min. The plates were then sprayed with a 10% solution of potassium thiocyanate in water. Organometallic compounds of iron are revealed as red–brown spots.

Preparative t.l.c. experiments were carried out on 1 m plates with either 1 or 2 mm layers of silica gel (E. Merck AG, # 7747 with indicator). Best results were obtained with *ca.* 300 mg of crude material on 1 mm plates.

Sample Preparation for Kinetic Runs

Cationic samples in acid solution were in general prepared as described in the Experimental section taking particular care to ensure the absence of all traces of oxygen. This is especially important for the slower reactions. Ions were generally prepared at as low a temperature as possible (−78° for FSO_3H and −10 to −20° for H_2SO_4) and then frozen in liquid nitrogen or Dry Ice – acetone bath until insertion in the n.m.r. probe.

Kinetics

First order rate constants were obtained by monitoring the decrease in concentration of reactant or increase in concentration of product as calculated from peak area data. Peak areas were expressed referenced to either an internal standard, usually tetramethylammonium chloride or to a weighted total peak area of reactant and product.

Plots of ln C vs. t according to the general expression for first order kinetics (1) showed good linearity.

$$\ln C' = -kt + \ln C_0 \qquad [1]$$

where C_0 = reactant concentration at time = 0, C' = reactant concentration at time = t, k = rate constant (s^{-1}), t = time (s).

Temperatures for kinetic runs carried out directly in the n.m.r. probe were calibrated using a copper–constantan thermocouple immersed in an n.m.r. tube containing methanol and inserted into the probe. Temperature readings were taken immediately preceding and following a kinetic run and the drift was well within 1° and usually with 0.5°.

*Preparation of Diethylaminobutadiene (**14**), (13, 14)*

Crotonaldehyde (1630.0 g, 2.3 mol) was added dropwise at 0–5° with stirring under a nitrogen atmosphere to 485 ml (4.7 mol) of diethyl amine dissolved in 750 ml of ether. During the addition 100 g of anhydrous K_2CO_3 was added in small portions. The reaction mixture was then filtered and the ether removed under reduced pressure (10 mm). Naphthoquinone (0.1 g) was added to the resulting brown oil which was pyrolyzed at 135°/20 mm. The pyrolysis was carried out by dropping the crude diamine adduct obtained above into a heated 500 ml flask which was half filled with glass helices and fitted with a take-off head. The crude product was collected at 60–100°/20 mm and was then redistilled through a column packed with helices to give the title dienamine as a light yellow oil. Diethylaminobutadiene rapidly darkens at room temperature and is best stored in the cold. The yield is 167 g (58%).

P.m.r. ($CDCl_3$) 3.77 (m, 1, H_3), 3.84 (d, 1, H_1), 4.48 (dd, 1, H_2), 5.31 (d, 1, H_4-*trans*), 5.54 (d, 1, H_4-*cis*), 6.94 (q, 2, —CH_2—), 8.88 (t, 3, —CH_3). $J_{34cis} = 10.3$, $J_{4cis4trans} = 2.0$, $J_{34trans} = 16.7$, $J_{23} = 10.1$, $J_{12} = 13.1$, $J_{-CH_2CH_3} = 7.0$. I.r. (neat) 3090, 3045, 2975, 2940, 2370, 1640, 1400, 1250, 1205, 1160, 1110, 990, 922, 845, and 650 cm^{-1}.

*Preparation of $\Delta^{1,3}$-Dihydrobenzaldehyde (**17a** X = —CHO) (14)*

Diethylaminobutadiene (12 g, 0.096 mol) was added dropwise at room temperature to a stirred solution of 5 g (0.089 mol) of acrolein in 18 ml of ether. The rate of addition was adjusted so as to maintain a gentle reflux. After the addition was complete, the reaction mixture was allowed to stir at room temperature for an additional 1.0 h and was then filtered. Removal of solvent at 25°/10 mm gave a yellow oil.

The crude diethylaminotetrahydrobenzaldehyde obtained as above was added to 100 ml of cold (0°) 5% HCl. After a few minutes a light yellow oil appeared. Steam distillation followed by ether extraction, drying (K_2CO_3), and removal of solvent at aspirator pressure gave a yellow oil which was distilled at 75–77°/16 mm to give 5.7 g (59%) of the title compound.

P.m.r. ($CDCl_3$) 0.48 (s, 1, —CHO), 3.24 (d, 1, H_2), 3.78 (m, 2, H_3 and H_4), 7.66 (m, 4, —CH_2CH_2—). I.r. (neat) aldehyde band at 1770 and olefinic band at 1560.

*Preparation of Tricarbonyl ($\Delta^{1,3}$-dihydrobenzaldehyde)-iron (**18**)*

A nitrogen-filled, water-jacketed one liter flask fitted with a magnetic stirrer and Hg sealed gas vent was charged with 5.5 g (0.052 mol) of $\Delta^{1,3}$-dihydrobenzaldehyde, 10.3 g (0.052 mol, 7.05 ml) of $Fe(CO)_5$, and 700 ml of tetrahydrofuran (freshly distilled from a blue solution of benzophenone ketyl). The clear yellow reaction mixture was then photolyzed with water cooling (8–9°) with a Westinghouse 250 W sunlamp. After 10 h the solvent and unreacted $Fe(CO)_5$ were removed with the aid of a water aspirator (Hood!). The residue was fractionated at 0.05 mm through a short path set up. The fraction boiling at 90–95° was collected to give 4.5 g (35%) of the title aldehyde complex as an orange oil which solidified upon standing. Several recrystallizations from pentane gave the product with m.p. 87.5–88°.

P.m.r. ($CDCl_3$) τ 0.79 (s, 1, —CHO), 4.13 (d, 1, H_2),

TABLE 4. Proton magnetic resonance parameters for the tricarbonyl(cyclohexadienyl)iron cations

	Chemical shift (τ)				Coupling constant		
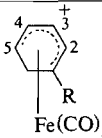	H_5	H_2	H_3	H_4	J_{23}	J_{34}	J_{45}
23 R = $-CH_2CH_3$	5.94	4.71	3.09	4.28	5.5	5–6	5–6
28 R = $-CH(CH_3)_2$	5.89	4.64	2.99	4.17	5.0	5–6	5–6

4.57 (dd, 1, H_3), 6.41 (m, 1, H_4), 7.7–8.8 (m, 4, $-CH_2CH_2-$). J_{23} = 4. J_{34} = 7. I.r. (neat) showed strong carbonyl bands at 2070 and 2000 cm^{-1} and an aldehyde band at 1700 cm^{-1}.

Anal. Calcd. for $C_{10}H_8O_4Fe$: C, 48.38; H, 3.22. Found: C, 46.41; H, 3.91. (Sample decomposition led to poor analysis.)

Preparation of $\Delta^{1,3}$-Dihydroacetophenone (17a, X = $-COCH_3$), (13)

Methyl vinyl ketone (20.0 g, 0.286 mol) was slowly added to a solution of 35.7 g (0.286 mol) of diethylaminobutadiene in 100 ml of benzene. The addition is slightly exothermic. The solution was then refluxed for a period of 4 h. Removal of solvent with the aid of a water aspirator gave a yellow oil which was distilled through a 10 cm column packed with glass helices. The fraction boiling at 75–76°/14 mm was collected to give 15.7 g (45%) of the product ketone as a colorless oil.

The 2,4-dinitrophenylhydrazone obtained as purple needles from acetic acid had m.p. 182–184° (reported 194°). Further recrystallization from 95% ethanol gave the product with m.p. 194–195°.

P.m.r. ($CDCl_3$) τ 3.09 (m, 1, H_3), 3.85 (m, 2, H_4 and H_5), 7.67 (m, $-CH_2CH_2-$), 7.72 (s, —, $-CH_3$). I.r. (neat) showed enone bands at 1665 and 1575 cm^{-1}.

Preparation of Tricarbonyl ($\Delta^{1,3}$-dihydroacetophenone)iron (13)

A solution of 12.0 g (0.097 mol of $\Delta^{1,3}$-dihydroacetophenone (**17a**) X = $-COCH_3$) and 39.2 g (0.2 mol, 26.9 ml) of $Fe(CO)_5$ in 700 ml of dry tetrahydrofuran (freshly distilled from a blue solution of benzophenone ketyl) was photolyzed at 8–9° under a nitrogen atmosphere in a water-jacketed one liter flask with a Westinghouse 250 W sunlamp. After 48 h, the solvent and unreacted $Fe(CO)_5$ were removed at aspirator pressure (Hood!) and the resulting red oil was distilled at 98°/0.025 mm to give 17.0 g (66%) of the title ketone complex as a red orange oil which solidified upon cooling. Several recrystallizations from pentane gave the product as lemon yellow plates, m.p. 26–27°.

P.m.r. ($CDCl_3$) τ 3.94 (d, 1, H_2), 4.60 (dd, 1, H_3), 6.58 (m, 1, H_4), 7.5–8.6 (m, —, $-CH_2CH_2-$), 7.79 (s, 3, $-CH_3$). J_{23} = 4.5, J_{34} = 6. I.r. (neat) showed strong carbonyl bands at 2055 and 1990 cm^{-1} and a ketone band at 1680 cm^{-1}.

Anal. Calcd. for $C_{11}H_{10}O_4Fe$: C, 50.38; H, 3.82. Found: C, 49.62; H, 3.64.

Preparation of Tricarbonyl (Ψ-endo-1-(α-hydroxyethyl)-cyclohexa-1,3-diene)iron (19)

A solution of 6.19 g (23.8 mol) of tricarbonyl ($\Delta^{1,3}$-dihydroacetophenone)iron (**13**) in 15 ml of methanol was added dropwise at room temperature under a nitrogen atmosphere to 6.0 g (150 mol) of sodium borohydride in 100 ml of water. After stirring for 2 h at room temperature, the reaction was poured onto 400 ml of water and extracted with three 100 ml portions of ether. The combined organic extracts were dried over K_2CO_3. Removal of solvent with the aid of a water aspirator left an orange oil. Thin layer chromatography analysis showed the crude product to be greater than 90% of the desired Ψ-*endo* epimer. Crystallization from pentane gave yellow needles which were sublimed at 30°/10^{-3} mm to give 5.87 g (94%) of the title complex as a lemon yellow solid with m.p. 44–45°.

P.m.r. ($CDCl_3$) τ 4.54 (d, 1, H_2), 4.78 (dd, 1, H_3), 6.10 (m, 1, —C—H), 6.83 (m, 1, H_4), 7.85–8.7 (m, 5, $-CH_2CH_2-$ and —OH), 8.56 (d, 3, $-CH_3$). J_{23} = 4.2, J_{34} = 6.6, $J_{4-CH_2(endo)}$ = 3.2, $J_{4-CH_2(exo)}$ = 12.8. I.r. (neat) showed strong carbonyl bands at 2040 and 1960 cm^{-1} and alcohol bands at 3450 and 3620 cm^{-1}.

Anal. Calcd. for $C_{11}H_{12}O_4Fe$: C, 50.00; H, 4.54. Found: C, 49.96; H, 4.56.

Preparation of the Tricarbonyl(1-ethylcyclohexa-1,3-dienyl)iron Cation (23)

Solid tricarbonyl (Ψ-*endo*-1-(α-hydroxyethyl)-cyclohexa-1,3-diene)iron (**19**) (80 mg) was added to a stirred solution of 0.8 ml of fluorosulfonic acid held at −78° in a nitrogen-filled Schlenk tube. The resulting lemon yellow solution was transferred to a precooled n.m.r. tube which had been previously filled with nitrogen.

The p.m.r. spectrum of the acid solution prepared as above is shown in Fig. 2. Proton magnetic resonance parameters are given in Table 4.

The same ion can be prepared in 96% H_2SO_4 at 0°. Ultraviolet (96% H_2SO_4) showed λ_{max} at 219 (13 600) and 290 (sh) (1600).

Preparation of the Tricarbonyl(1,4-dimethylene-cis,cis, trans,cis-hexa-1,3-dienyl)iron Cation (22)

Approximately 0.3 ml of dry SO_2ClF (Allied Chemicals, code 1990936) was condensed at −78° into an n.m.r. tube which had been previously filled with nitrogen. Then enough nitrogen saturated FSO_3H was added to give a *ca.* 1:4 FSO_3H:SO_2ClF mixture. The solution was stirred with a coiled platinum wire and cooled to −119° in a

Can. J. Chem. Downloaded from www.nrcresearchpress.com by 210.87.254.42 on 09/05/12
For personal use only.

Can. J. Chem. Downloaded from www.nrcresearchpress.com by 210.87.254.42 on 09/05/12
For personal use only.

n-propyl chloride slush bath. A solution of 60 mg of tricarbonyl (Ψ-*endo*-1-α-hydroxyethyl)-cyclohexa-1,3-diene)iron (**19**) in a minimal amount of $CDCl_3$ was added from a microliter syringe under a countercurrent of nitrogen. The reaction mixture was then stirred with a coiled platinum wire until homogeneous.

The p.m.r. spectrum of the acid solution obtained above is shown in Fig. 1.

Reaction of Tricarbonyl (Ψ-endo-1-(α-hydroxyethyl)-cyclohexa-1,3-diene)iron (19) with 84% H_2SO_4

Solid tricarbonyl (Ψ-*endo*-1-(α-hydroxyethyl)-cyclohexa-1,3-diene)iron (**19**) (80 mg) was added to a stirred solution of 0.6 ml of 84% H_2SO_4 held at 0° in a nitrogen-filled Schlenk tube. The resulting p.m.r. spectrum showed the presence of the previously described tricarbonyl(1-ethylcyclohexa-1,3-dienyl)iron cation (**23**) as well as a new product which was assigned the protonated ether structure (**24**).

Ion (**24**) can also be obtained by adding alcohol (**19**) to a FSO_3H/SO_2ClF solution containing sufficient acid to give a homogeneous solution.

P.m.r. (84% H_2SO_4) τ 3.78 (m, 2, H_2 and 1-H on ethyl), 4.00 (t?, 1, H_3), 5.13 (d, 1, H_4), 7.3 (m, 2, *endo* methylene ring protons), 7.5–8.5 (m, 5, *endo* methylene ring protons and $—CH_3$).

Preparation of the bis-α-(Tricarbonyl(1-ethyl-cyclohexa-1,3-diene)iron) Ethers (25)

Solid tricarbonyl (Ψ-*endo*-1-(α-hydroxyethyl)-cyclohexa-1,3-diene)iron (**19**) (1.0 g) was added to a stirred solution of 2.0 ml of 84% H_2SO_4 held at 0° in a nitrogen-filled Schlenk tube. The bright red solution was allowed to stir at 0° for 1.0 h and was poured onto 100 g of ice. Extraction with two 100 ml portions of chloroform followed by drying ($MgSO_4$) and removal of solvent gave a yellow oil. Preparative t.l.c. workup, eluting with benzene, gave, as the major products, a diastereomeric mixture of the title ethers. Two other minor products were isolated and assigned (in order of decreasing R_f values) the isomeric ether structure (**77**) and the epimeric alcohol tricarbonyl (Ψ-*exo*-1-(α-hydroxyethyl)-cyclohexa-1,3-diene)-iron prepared above.

P.m.r. ($CDCl_3$)-bis-ethers **25** τ 4.78 (m, 4, H_2 and H_3), 6.48 (q, 2, 1-H on ethyl), 6.82 (m, 2, H_4), 8.1–8.9 (m, 14, ring methylene protons and CH_3. I.r. (KBr disk) 2900, 2045, 1970, 1185, 1058, 1025, 970, 620, and 552 cm^{-1}. Mass spectrum showed $M^{+\cdot}$ at m/e = 510 and significant peaks at 454, 426, 342, 292, 286, 264, 247, 234, 219, 191, 164, 160, 106, 91, 79, 77, and 56.

P.m.r. ($CDCl_3$) isomeric ether **26** τ 4.45–5.1 (m, 2, —), 6.2–6.9 (m, 5, —), 8.0–9.0 (m, 15, —). I.r. (neat) 2970, 2940, 2870, 1970, 1190, 2045, 1088, 620, and 560 cm^{-1}. Mass spectrum showed $M^{+\cdot}$ at m/e = 510 and significant peaks at 454, 426, 342, 292, 264, 247, 236, 208, 162, 135, 107, 91, 79, 77, and 56.

P.m.r. ($CDCl_3$) tricarbonyl (Ψ-*exo*-1-(α-hydroxyethyl)-cyclohexa-1,3-diene)iron (**20**), 4.57 (m, —, H_2), 4.77 (m, —, H_3), 6.07 (m, —CH), 6.77 (m, —, H_4), 8.03–8.80 (m, —, ring methylene protons, $—CH_3$ and —OH).

Preparation of Tricarbonyl(1-(α-hydroxyisopropyl)-cyclohexa-1,3-diene)iron (21)

A solution of 5.0 g (19.1 mmol) of tricarbonyl ($\Delta^{1,3}$-dihydroacetophenone)iron (**13**) in 20 ml of anhydrous ether was added under a nitrogen atmosphere to a stirred solution of 20.0 ml (54 mmol) of a 2.7 *M* solution of methyllithium in 80 ml of anhydrous ether held at −78°. After the addition was complete the reaction mixture was allowed to stir at −78° for 2.0 h. Warming to −10° followed by careful addition of 10 ml of water gave a dark emulsion which was extracted with four 50 ml portions of ether. The combined ether extracts were washed with water until the washings became clear and finally dried over K_2CO_3. Removal of solvent left a dark oil which was distilled through a short path apparatus at 91°/0.05 mm to give the title alcohol as a yellow oil which solidified upon standing. Sublimation at 50°/10^{-3} mm followed by recrystallization from pentane gave the title complex as lemon yellow prisms m.p. 63–63.5°. The yield after recrystallization is 40%.

P.m.r. ($CDCl_3$) τ 4.32 (d, 1, H_2), 4.82 (dd, 1, H_3), 6.93 (m, 1, H_4), 8.1–8.8 (m, —, ring methylene protons), 8.50, 8.58 (s, s, 3, 3, $—CH_3$'s). J_{23} = 4.2, J_{34} = 6.6, J_{24} = 1.5. I.r. (CCl_4) showed strong carbonyl bands at 2050 and 1975 cm^{-1} and an alcohol band at 3635 cm^{-1}.

Anal. Calcd. for $C_{12}H_{14}O_4Fe$: C, 51.79; H, 5.03. Found: C, 51.29; H, 5.20.

Preparation of the Tricarbonyl(1,4-dimethylene-5-methyl-cis,cis,trans-hexa-1,3-dienyl)iron Cation (27)

Following the procedure used for the preparation on ion **22** a solution of 80 mg of tricarbonyl(1-(α-hydroxy-isopropyl)-cyclohexa-1,3-diene)iron (**21**) in a minimal amount of $CDCl_3$ was added to 0.5 ml of a *ca.* 1:4 solution of FSO_3H:SO_2ClF held at −119°. The reaction mixture was stirred with a coiled platinum wire until homogeneous.

The p.m.r. spectrum of the orange solution prepared above is shown in Fig. 3. Proton magnetic resonance parameters are given in Table 3.

Preparation of the Tricarbonyl(1-isopropylcyclohexa-1,3-dienyl)iron Cation (28)

Solid tricarbonyl(1-(α-hydroxyisopropyl)-cyclohexa-1,3-diene)iron (**21**) (80 mg) was added to a stirred solution of 0.7 ml of 96% H_2SO_4 held in a nitrogen-filled Schlenk tube at 0°. The red solution was then transferred to a n.m.r. tube by means of a precooled, nitrogen-filled pipette. Immediate p.m.r. observation shows the presence of ion **27** described above, however a slow rearrangement to the title ion **28** occurs at temperatures greater than +20°. After *ca.* 0.5 h an approximate 1:1 mixture is formed. Identical spectra were obtained in H_2SO_4 of varying concentrations, but the rate of rearrangement, **27** → **28** was changed.

The p.m.r. spectrum of the title ion is shown in Fig. 4. Proton magnetic resonance parameters are given in Table 4.

We acknowledge with gratitude the financial support received from the National Research Council of Canada and the Killam Foundation.

1. J. E. MAHLER and R. PETTIT. J. Am. Chem. Soc. **85**, 3955 (1963); J. E. MAHLER, D. R. GIBSON, and R. PETTIT. J. Am. Chem. Soc. **85**, 3959 (1963).
2. C. P. LILLYA and R. A. SAHATJIAN. J. Organomet. Chem. **25**, C 67 (1970).

3. T. S. SORENSEN and C. R. JABLONSKI. J. Organomet. Chem. **25**, C 62 (1970).
4. C. P. LILLYA and R. A. SAHATJIAN. J. Organomet. Chem. **32**, 371 (1971).
5. M. BROOKHART and D. L. HARRIS. J. Organomet. Chem. **42**, 441 (1972).
6. (*a*) M. ROSENBLUM and F. W. ABBATE. Am. Chem. Soc. Adv. Chem. **62**, 532 (1967); (*b*) M. CAIS. Rec. Chem. Prog. **27**, 177 (1966); (*c*) T. D. TURBITT and W. E. WATTS. J. Organomet. Chem. **49**, C 30 (1973).
7. (*a*) N. A. CLINTON and C. P. LILLYA. J. Am. Chem. Soc. **92**, 3058 (1970); (*b*) N. A. CLINTON and C. P. LILLYA. J. Am. Chem. Soc. **92**, 3065 (1970).
8. D. E. KUHN and C. P. LILLYA. J. Am. Chem. Soc. **94**, 1682 (1972).
9. M. I. FORMAN. J. Organomet. Chem. **39**, 161 (1972).
10. E. A. HILL and J. H. RICHARDS. J. Am. Chem. Soc. **83**, 4216 (1961).
11. A. J. BIRCH, P. E. CROSS, J. LEWIS, D. A. WHITE, and S. B. WILD. J. Chem. Soc. A, 332 (1968).
12. E. O. GREAVES, G. R. KNOX, and P. L. PAUSON. J. Chem. Soc. D, 1124 (1969), R. E. GRAF and C. P. LILLYA. J. Chem. Soc. Chem. Commun. 271 (1973).
13. E. R. H. JONES and F. SONDHEIMER. J. Chem. Soc. 615 (1949).
14. W. LANGENBECK, O. GODDE, L. WESCHSKY, and R. SCHALLER. Chem. Ber. **75**, 233 (1942).
15. W. LANGENBECK. Ger. Pat. # 715544. 1941.
16. A. F. KLUGE and C. P. LILLYA. J. Org. Chem. **36**, 1977 (1971).
17. D. JONES, L. PRATT, and G. WILKINSON. J. Chem. Soc. 4458 (1962).
18. R. PETTIT and G. F. EMERSON. Adv. Organomet. Chem. **1**, 1 (1964); G. F. EMERSON, R. PETTIT, and J. E. MAHLER. J. Chem. Educ. **40**, 175 (1963)
19. D. JAQUES and J. A. LEISTEN. J. Chem. Soc. 2683 (1964); R. L. BURWELL JR. Chem. Rev. **54**, 615 (1954).
20. T. D. TURBITT and W. E. WATTS. J. Chem. Soc. Chem. Commun. 182 (1973).
21. N. M. D. BROWN, T. D. TURBITT, and W. E. WATTS. J. Organomet. Chem. **46**, C 19 (1972).
22. G. E. HERBERICH and J. SCHWARZER. Chem. Ber. **103**, 2016 (1970); G. E. HERBERICH, G. GREISS, and H. F. HEIL. J. Organomet. Chem. **22**, 723 (1970).
23. R. C. KERBER and D. J. EHNTHOLT. J. Am. Chem. Soc. **95**, 2927 (1973).
24. E. A. HILL and R. WIESNER. J. Am. Chem. Soc. **91**, 509 (1969).
25. J. M. JERKUNICA and T. G. TRAYLOR. J. Am. Chem. Soc. **93**, 6278 (1971); T. G. TRAYLOR, H. J. BERWIN, J. JERJUNICA, and M. L. HALL. Pure Appl. Chem. **30**, 599 (1972).
26. S. L. LUPAN, M. KAPON, M. CAIS, and F. H. HERBSTEIN. Angew. Chem. Int. Ed. **11**, 1025 (1972).
27. R. E. DAVIS, H. D. SIMPSON, N. GRICE, and R. PETTIT. J. Am. Chem. Soc. **93**, 6688 (1971).
28. R. EISS. Inorg. Chem. **9**, 1650 (1970); G. MAGLIO, A. MUSCO, and R. PALUMBO. J. Organomet. Chem. **32**, 127 (1971).
29. D. F. HUNT, C. P. LILLYA, and M. D. RAUSCH. J. Am. Chem. Soc. **90**, 2561 (1968).
30. F. G. COWHERD and J. L. von ROSENBURG. J. Am. Chem. Soc. **91**, 2157 (1969).
31. M. A. CAIRNS, J. F. NIXON, and B. WILKINS. J. Chem. Soc. D, 86 (1972).
32. A. P. HUMPHRIES and S. A. R. KNOX. J. Chem. Soc. Chem. Commun. 326 (1973).
33. M. BROOKHART, E. R. DAVIS, and D. L. HARRIS. J. Am. Chem. Soc. **94**, 7853 (1972).
34. T. H. WHITESIDES and R. W. ARHART. J. Am. Chem. Soc. **93**, 2250 (1971).
35. D. F. HUNT, G. C. FARRANT, and G. T. RODEHEAVER. J. Organomet. Chem. **38**, 349 (1972).
36. D. A. T. YOUNG, J. R. HOLMES, and H. D. KAESS. J. Am. Chem. Soc. **91**, 6968 (1969).
37. J. E. BERCAW, R. H. MARVICH, L. G. BELL, and H. H. BRINTZINGER. J. Am. Chem. Soc. **94**, 1219 (1972); B. Pesee. (*Editor*). Nuclear magnetic resonance in chemistry. Academic Press, New York. 1965. pp. 35–53.
38. D. F. SHRIVER. The manipulation of air sensitive compounds. Part II. McGraw–Hill Co., New York. 1969.
39. T. S. SORENSON, I. J. MILLER, and C. M. URNESS. Can. J. Chem. **48**, 3374 (1970).

Can. J. Chem. Downloaded from www.nrcresearchpress.com by 210.87.254.42 on 09/05/12
For personal use only.

Carbonyl Ylides and the Rearrangement of (+)-*trans*-2,3-Diisopropenyloxirane

JEAN-CLAUDE PALADINI AND R. J. CRAWFORD

Department of Chemistry, University of Alberta, Edmonton, Alberta T6G 2G2

Received December 27, 1973

JEAN-CLAUDE PALADINI and R. J. CRAWFORD. Can. J. Chem. **52**, 2098 (1974).

The kinetics of the gas phase racemization and rearrangement of 2,3-diisopropenyloxirane have been determined. Comparison with the kinetic data for 2,3-divinyloxirane allows us to exclude the mechanism for the formation of vinyldihydrofuran wherein an inward conrotatory ring opening comprises the first step. The mechanism proposed consists of an isomerization about the carbon–oxygen bond of the carbonyl ylide to form an isomeric intermediate which then undergoes a disrotatory five-centered ring closure to produce 2-isopropenyl-4-methyl-2,3-dihydrofuran.

JEAN-CLAUDE PALADINI et R. J. CRAWFORD. Can. J. Chem. **52**, 2098 (1974).

La cinétique en phase gazeuse de la racémisation du diisopropényl-2,3-époxyde (+), et de sa conversion en isopropényl-2-méthyl-4-dihydro-2,3-furanne a été étudiée et comparée à celle du divinyl-2,3-époxyde. La formation du dihydrofuranne pourrait s'expliquer par une suite de deux réactions électrocycliques concertées, ou par un mécanisme comportant trois étapes dont l'une impliquerait la rotation non concertée autour de la liaison C—O des ylures de carbonyle intermédiaires. Les résultats que nous avons obtenus sont en accord avec cette dernière hypothèse.

Introduction

In a recent study on the racemization and rearrangement of (+)-2,3-divinyloxirane we observed that all of the products were racemic (1). Our results on the formation of vinyldihydrofuran were in agreement with the proposal of Paladini and Chuche (2) that isomerization of the carbonyl ylide intermediate followed by an electrocyclic ring closure represented a feasible path. We report, herein, a study of (+)-*trans*-2,3-diisopropenyloxirane. In using the isopropenyl group we expect a minimal change in electronic factors affecting the stability of the reactants and the carbonyl ylide intermediate (the methyl groups are at the nodes of the highest occupied molecular orbital of the carbonyl ylide). It is anticipated that steric factors will significantly destabilize those forms of the carbonyl ylide (*e.g.* **3***b*)[1] produced by moving the bulkier isopropenyl group inward as opposed to those forms produced by moving them outwards (*e.g.* **2***b*). Form **3** can readily undergo disrotatory ring closure to dihydrofuran (**6**) whereas **2** cannot. As a consequence if dihydrofuran formation occurs by oxirane ring opening as **1** → **3** then, on going from **1***a* to **1***b*, we would expect the ratio $k_1/(k_2 + k_3)$ to increase dramatically.

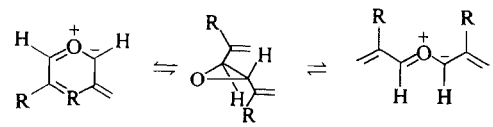

3 **1** **2**

a R = H

b R = CH_3

Results

Chiral **1***b* was prepared from *erythro*-4-chloro-2,5-dimethyl-1,5-hexadien-3-ol (**4**) by conversion to the half ester of phthalic acid followed by resolution of its brucine salt and the formation of **1***b* by alkaline saponification of the chloro half ester (**5**) (Scheme 1).

Kinetics of the Racemization and Conversion of 1b to 6 and 7 (Scheme 2)

Samples of **1***b* were degassed and sealed into ampoules in a manner such that at 200° the pressure would not exceed 700 Torr. The samples were then heated for the appropriate times and then analyzed by gas chromatography using a Hewlett Packard 3370A electronic integrator. Table 1 gives the data and the observed product

[1]Other conformations of **2** and **3** produced by the thermally allowed conrotatory ring opening of the oxirane **1** exist and the same considerations apply. The forms **2** and **3** are merely chosen as representative.

Can. J. Chem. Downloaded from www.nrcresearchpress.com by 210.87.254.6 on 09/05/12
For personal use only.

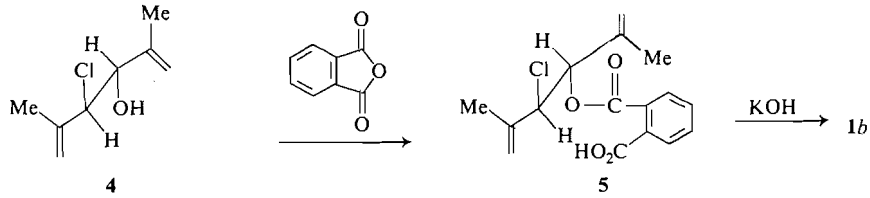

SCHEME 1

TABLE 1. Rate constants and product proportions for the reactions of **1***b*

Temperature (±0.04°)	$10^5 (k_2 + k_3)$ (s^{-1})	% **6**	% **7**
180.53		77.6±0.2*	22.4±0.2
199.55	2.35±0.03	76.8±0.2	23.6±0.2
210.41	5.80±0.06	76.1±0.2	23.9±0.2
221.55	15.2 ±0.2	75.5±0.3	24.5±0.3
240.16		74.4±0.3	25.6±0.3

*The error quoted is the standard deviation of five analyses.

TABLE 2. Rate constants for the racemization of (+)-**1***b*

Temperature (±0.03°)	$10^5 k_\alpha$ (s^{-1})	$10^5 (k_2 + k_3)$* (s^{-1})	$10^5 k_1$ (s^{-1})
156.72	2.47±0.03	0.035	1.22
165.12	5.21±0.06	0.086	2.56
171.63	9.80±0.09	0.168	4.81
181.02	21.7 ±0.2	0.432	10.6

*Extrapolated from plot of rate data in Table 1.

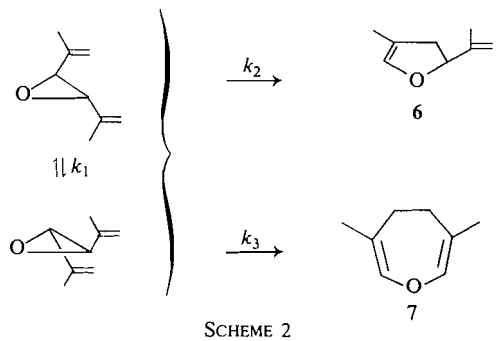

SCHEME 2

proportions. A sample run is given in the experimental section.

Samples of (+)-**1***b* were degassed in Pyrex break-seals in a manner analogous to that described earlier (1). The rate constants for the observed racemization, k_α, and that for the rate of interconversion of enantiomers, k_1, where $2k_1 = k_\alpha - (k_2 + k_3)$, are recorded in Table 2. The activation parameters for k_1, k_2, and k_3 are given in Table 3.

Experimental

The i.r. spectra were obtained on a Perkin-Elmer 421 Spectrophotometer and the n.m.r. spectra were obtained using a Varian A-60. All rotations were measured in a thermostated cell on a Perkin-Elmer Model 141 Polarimeter. Preparative gas chromatography (g.c.) was carried out using a Nester Faust Model 850 Prepkromat.

Preparation of erythro-4-Chloro-2,5-dimethyl-1,5-hexadien-3-ol (4)

A stream of dry hydrogen chloride was passed through a solution of 2,3-diisopropenyloxirane (**1***b*) (3) (9.74 g, 78.5 mmol) in ether (300 ml) cooled to −50°. The reaction was followed by t.l.c. Upon completion of the reaction the excess hydrogen chloride was removed by a stream of nitrogen. The solution was then neutralized with cold aqueous sodium bicarbonate and the product isolated by drying over magnesium sulfate followed by removal of the ether. The product was not distilled lest it undergo an allylic rearrangement. Proton magnetic resonance of **4** (10% w/w in carbon tetrachloride) δ: 1.75. (3*H*, triplet); 1.85 (3*H*, triplet); 2.5 (*H*, removed with D_2O); 6.08 (H_3, doublet); 6.30 (H_4, doublet); $H_{1,6}$ 4.9 to 5.11 (4*H*, multiplet); $J_{3,4}$ = 9 Hz. Infrared spectrum (carbon disulfide) cm^{-1}: 3540 s (OH), 3080 s (CH_2), 1630 ms (C=C).

Can. J. Chem. Downloaded from www.nrcresearchpress.com by 210.87.254.6 on 09/05/12
For personal use only.

TABLE 3. Activation parameters for the reactions of **1***b* and (+)-**1***b* as in Scheme 2

	log A	E_a (kcal mol^{-1})	$\Delta H^{\ddagger}$ (kcal mol^{-1})	$\Delta S^{\ddagger}$ (cal deg^{-1} mol^{-1})
k_1	12.74	34.7±0.5	33.8±0.5	−3±1*
k_2	13.30	39.0±0.9	38.1±0.9	0±1
k_3	13.58	40.7±0.7	39.8±0.7	1±1

*At T = 150° for comparison with data in ref. 1.

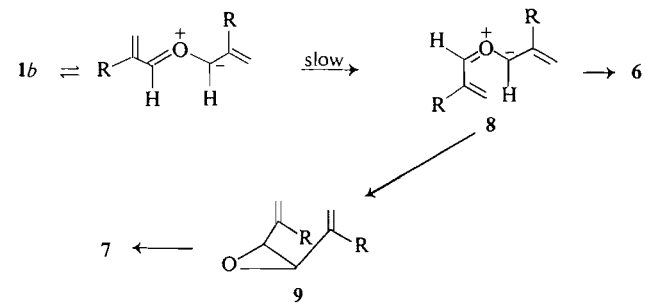

SCHEME 3

Resolution of **4** *by the Phthalate Half Ester (***5***)*

A solution of phthalic anhydride (12.58 g, 85 mmol) in 17 ml of pyridine was allowed to stand for 12 h with the chlorohydrin **4** (13.6 g, 85 mmol). After heating for 1 h at 80°, the solution was cooled in an ice water bath and ether added. After washing with concentrated hydrochloric acid the ether layer was separated and the solvent evaporated. The remaining syrup was taken up in a sodium carbonate solution extracted with ether, cooled, and then acidified. After extraction with chloroform the solvent was removed and the half ester **5** was recrystallized from benzene and pentane; yield 54%, m.p. 102°.

Anal. Calcd. for $C_{16}H_{17}ClO_4$: C, 62.24; H, 5.55; Cl, 11.48. Found: C, 62.27; H, 5.60; Cl, 11.51.

Brucine (27.62 g, 65 mmol) was added to a refluxing solution of the half ester **5** (36 g, 116 mmol) in dry acetone (100 ml). The solid residue was removed by rapid filtration and the filtrate cooled to produce the brucine salt (51.2 g). After three further recrystallizations from boiling acetone the salt had a constant m.p. 162–168°. Upon treatment of the salt with hydrochloric acid (100 ml of 5%) the solution was extracted six times with ether. Upon evaporation to dryness the ester **5** was produced, $[\alpha]_D^{20}$ −2.315°; yield 6.6 g (19%).

A solution of the half ester (3.18 g, 10.29 mmol) in ethylene glycol was added dropwise, under reduced pressure (15 Torr), to a solution of potassium hydroxide (6 g, 105 mmol) in hot (60°) ethylene glycol (75 ml). The organic material in the vacuum trap was dried over potassium carbonate to yield 1 g (85%) of *trans*-2,3-diisopropenyloxirane. The oxirane was further purified by preparative gas chromatography (15% Carbowax 1500 on Chromosorb W, 80–100 mesh, 200 × 0.9 cm, 50°) $[\alpha]_{598}^{22.5}$ +4.133°, $[\alpha]_{365}^{22.5}$ +40.627° (*c* 4.8185 g/100 g of solution, 2-propanol).

*Kinetics of Racemization of (+)-***1***b*

The procedure used to observe the racemization of (+)-**1***b* is the same as that described earlier for that of (+)-2,3-divinyloxirane (1). A sample run at 165.12 ± 0.03° consists of the following data: 10^4 s, $[\alpha_t]/[\alpha]_0$; 0.450, 0.7676; 0.744, 0.6534; 0.840, 0.6136; 1.08, 0.5615; 1.32, 0.4893; 1.536, 0.445; 1.812, 0.3812; 2.046, 0.3317; infinity tube 3 days, 0.000°. These results yield k_α = (5.21 ± 0.06) × 10^{-5} s^{-1}.

Kinetics of the Rearrangement of **1***b to* **6** *and* **7**

The procedure used is the same as that described earlier for **1***a* (1). A sample run at 199.55 ± 0.02° for the rate of disappearance of **1***b* is: 10^4 s, $[1b]^t/[1b]^0$; 1.44, 0.723; 1.98, 0.635; 2.52, 0.556; 3.07, 0.498; 3.60, 0.433; 4.14, 0.379; 4.67. 0.341; 5.05, 0.307. These results yield $k_2 + k_3$ = (2.35 ± 0.03) × 10^{-5} s^{-1}.

Discussion

A possible mode of formation of the vinyldihydrofuran, **6**, consists of **1***b* undergoing the preferred (4,5) conrotatory ring opening of the oxirane ring to produce **3***b* then by a five-centered disrotatory ring closure to produce **6**. The intermediate **2***b* cannot lead directly to **6** since the groups R and H are *trans* and must have a *cisoid* arrangement (as in **3**) to produce **6**. As a consequence we would expect that the rate of racemization via **2***b* should be decreased only slightly but that the rate of formation of **6**, if it requires the inward conrotatory ring opening as exemplified by **3**, should decrease very sharply. From Table 3 we can calculate that at 150° the

Can. J. Chem. Downloaded from www.nrcresearchpress.com by 210.87.254.6 on 09/05/12
For personal use only.

rate constant ratio k_1/k_2 is 42.4 for **1***b* compared with 19.4 for **1***a*. There is no significant difference between these rate ratios ($\delta\Delta G^{\ddagger} \simeq 0.6$ kcal mol^{-1}) and thus we can conclude that the mode of conrotatory ring opening exemplified by **3** cannot be of significance in forming **6**. The racemization rate constant for **1***a*, at 150°, is only 4.7 times greater than that for **1***b*, again suggesting that substitution has had little effect. It is more likely that a path, similar to that suggested by Paladini and Chuche (2) for the rearrangement of 2-phenyl-3-vinyloxirane, is operative for **1***a* and **1***b*; such a path is outlined in Scheme 3. Support for this comes from the observation that the intermediate **8** by a conrotatory three-centered closure gives rise to the *cis* oxirane **9** which is known to rearrange rapidly to **7** (3). In such a case the substitution of hydrogen by methyl on going from **1***a* to **1***b* should not greatly affect the ratio $k_1/(k_2 + k_3)$, which is 10.7 for **1***a* and 33.8 for **1***b*. We conclude that the rate-determining step in the sequence is the isomerization about the carbon–oxygen bond of the carbonyl ylide to form **8**.

The authors wish to acknowledge the financial assistance of the National Research Council of Canada and the Canada Council. We wish to express our appreciation of discussion with Prof. Rolf Huisgen and Prof. Josselin Chuche. J-C. P. wishes to express his gratitude to the Fondation de la Vocation (France) for its support.

1. V. VUKOV, H. TOKUNAGA, and R. J. CRAWFORD. Can. J. Chem. **51**, 3718 (1973).
2. J. C. PALADINI and J. CHUCHE. Tetrahedron Lett. 4383 (1971).
3. J. C. POMMELET, N. MANISSE, and J. CHUCHE. Tetrahedron, **28**, 3929 (1972).
4. H. J. H. MACDONALD and R. J. CRAWFORD. Can. J. Chem. **50**, 428 (1972).
5. H. HAMBERGER and R. HUISGEN. Chem. Commun. 1190 (1971); A. DOHMEN, H. HAMBERGER, R. HUISGEN, and V. MARKOWSKI. Chem. Commun. 1192 (1971).

Can. J. Chem. Downloaded from www.nrcresearchpress.com by 210.87.254.6 on 09/05/12
For personal use only.

The Modular Structure of Lignin

M. WAYMAN AND T. I. OBIAGA

Department of Chemical Engineering and Applied Chemistry, University of Toronto, Toronto, Ontario M5S 1A4

Received November 21, 1973

M. WAYMAN and T. I. OBIAGA. Can. J. Chem. **52**, 2102 (1974).

A kinetic investigation of the polymerization of lignin-like polymers of coniferyl alcohol (DHP) using horseradish peroxidase as the phenol oxidase revealed the product to have a bimodal distribution of molecular weight. A peak representing material of low molecular weight M_w 3000–4000 was first formed, followed by the formation of a second peak in the molecular weight range 80 000–100 000 whose growth appeared to proceed at the expense of the first.

Alkaline degradation of lignins isolated from spruce and hemlock also gave products having a bimodal distribution of molecular weight, with peaks at the same values as found for the synthetic lignin. Lignin isolated during alkaline pulping of finely divided wood showed the presence of the same two components of high and low molecular weight.

From these results, we have constructed models for the formation of lignin and for its degradation during an alkaline pulping of wood. The lignin macromolecule as it occurs in wood may well be material of narrow molecular weight distribution with d.p. about 500. It is proposed that this macromolecule is an assembly of subassemblies, or modules, each of d.p. about 20. Lignin formation is seen to proceed by enzyme dehydrogenation of the monomers first producing free radicals as described by Freudenberg, the free radicals reacting by a step condensation to form the modules, followed by intermodular addition polymerization to form the lignin macromolecules. Lignin degradation in pulping reactions involves first the nonrandom homolytic chain depolymerization of the macromolecule to yield free-radical carrying modules, which, after stabilization against recondensation by the pulping chemicals, break down to lower oligomers and monomers by a step depolymerization reaction.

M. WAYMAN et T. I. OBIAGA. Can. J. Chem. **52**, 2102 (1974).

L'alcool coniféryle (DHP), sous l'influence de la peroxydase du raifort agissant comme oxydase des phénols, se transforme en un polymère ressemblant à la lignine; une étude cinétique de cette polymérisation révèle que le produit a une distribution bimodale de la masse moléculaire. Un premier maximum correspondant à des produits de faibles poids moléculaires, M_w 3000–4000 se forme en premier lieu; un second sommet correspondant aux substances de poids moléculaires allant de 80 000–100 000 apparait ensuite et il semble que sa croissance se fait aux dépends du premier.

La dégradation alcaline des lignines isolées du sapin et de la ciguë donne aussi des produits ayant une distribution bimodale de la masse moléculaire, avec des maxima aux mêmes valeurs que celles trouvées pour la lignine synthétique. La lignine isolée lors de la pulpation alcaline du bois finement fractionné montre la présence des mêmes composantes de hauts et faibles poids moléculaires.

A l'aide de ces résultats, nous avons construit des modèles pour la formation de la lignine et pour sa dégradation lors d'une pulpation alcaline du bois. La macromolécule de lignine, telle qu'elle existe dans le bois, peut bien être une matière de distribution étroite de la masse moléculaire avec un d.p. d'environ 500. On propose que cette macromolécule est un ensemble formé à partir de sous-ensembles, ou modules ayant chacun un d.p. d'environ 20. La formation de lignine semble découler d'une déshydrogénation enzymatique des monomères produisant en premier lieu des radicaux libres tels que décrit par Freudenberg; ces derniers réagissent ensuite par condensation pour former les modules, et ceux-ci par des réactions de polymérisation par additions intermoléculaires formeraient les macromolécules de lignine. La dégradation de la lignine dans les réactions de pulpation implique au début une dépolymérisation homolytique ordonnée de la chaine de la macromolécule pour donner des modules portant des radicaux libres; ceux-ci, stabilisés par les produits chimiques de la pulpation pour éviter une recondensation combrisent en oligomères et monomères plus petits par une réaction de dépolymérisation par étape. [Traduit par le journal]

Introduction

Studies of the lignin molecule have recently taken on new importance deriving from two principal sources of interest. In response to rising wood costs and in the interests of conservation, there has been an expansion of high yield wood pulping processes. The products of such processes contain a significant proportion

Can. J. Chem. Downloaded from www.nrcresearchpress.com by 210.87.254.40 on 09/05/12
For personal use only.

Can. J. Chem. Downloaded from www.nrcresearchpress.com by 210.87.254.40 on 09/05/12
For personal use only.

of lignin, up to 20% or more. The presence of lignin affects the behavior and usefulness of the woodpulp. Lignin is a hydrophobic, relatively rigid polymer, and for some purposes, it may need to be modified to increase flexibility and hydrophilic properties. Knowledge of its molecular structure would be of assistance in guiding such practical work. A second impetus to these studies has come from increasing concern over pollution. Large quantities of lignin, millions of tons annually in each of the major pulp-producing countries, are discharged into streams. There is as yet little understanding of the pathways of lignin degradation in nature and this is an active field of research. An understanding of the structure of the lignin macromolecule would be useful in such work also. These new impulses have been added to the continued interest in the chemistry of lignin, a renewable natural resource in contrast to other evidently exhaustible nonrenewable resources.

The term "lignin" as used in the preceding paragraph has been used in its generic sense, the composition of natural lignins differing with plant species, with location within the plant, and even within the cell wall (1). The polymers are each composed of at least three different monomers, coniferyl alcohol, sinapyl alcohol, and *p*-hydroxycinnamic alcohol. The monomers are linked in a variety of ways and are frequently partially oxidized, giving rise to several different functional groups (2). The general mechanism whereby the monomers polymerize has been described by Freudenberg (2), Harkin (3), and others (4). It is now reasonably clear that free radicals are formed from the monomers by a dehydrogenase enzyme, that these have several mesomeric forms, and that they react with each other to form dimers, oligomers ("lignols"), and ultimately the lignin macromolecule. Similarly in the work of Kleinert (5), there is evidence that the initial step in the degradation of lignins in pulping reactions involves thermolysis to form free radicals.

It is not clear that the mechanisms which have been identified as initial apply consistently or in uniform fashion to the building of complete lignin macromolecules or to their degradation. In studies of molecular weight distribution during degradation of lignins by fungi, Brown and co-workers (6) have observed molecular size groupings, rather than a uniform continuum of molecular weight distribution. Forss and Fremer (7) have proposed, based on consideration of the course of sulfite pulping reactions, that the lignin macromolecule is composed of repeating units. There is considerable disagreement over the size of lignin macromolecules, a very wide range of molecular weights being reported (8).

In the present work, an effort has been made to identify the size of lignin macromolecules and how this varies during synthesis and degradation. To this end, a synthetic lignin, a dehydrogenase polymer of coniferyl alcohol (DHP), has been made *in vitro*, and molecular weight and its distribution has been followed during the synthesis. The principal tool used has been gel permeation chromatography (g.p.c.). Further, lignins have been isolated from two wood species, a spruce and a hemlock, by physical means, assisted in some cases by cellulase. These milled wood lignins (MWL) have been analysed by g.p.c. as isolated and during simulated pulping reactions. Finally, wood of these species has been pulped in small laboratory equipment and the dissolved lignins have been analyzed for molecular weight and its distribution during the course of pulping. By study of the resulting data, a model has been formulated of the structure of the lignin macromolecule.

Experimental

(a) Dehydrogenase Polymers of Coniferyl Alcohol (DHP)

Synthetic lignin-like polymers of coniferyl alcohol were prepared by controlled polymerization using horseradish peroxidase as the phenol oxidase and adding a dilute solution of hydrogen peroxide into the reaction mixture according to the method of Freudenberg (9). The coniferyl alcohol, m.p. 73–75 °C, was prepared by the reduction of ethyl ferulate. Ethyl ferulate was prepared by the ethylation of ferulic acid in the presence of dicyclohexylcarbodiimide (10). The ethyl ferulate was reduced using $LiAlH_4$, according to Freudenberg's method (11). Coniferyl alcohol was polymerized at p*H* 5.5 and 20 ± 0.1 °C over several days. In a 4-l resin kettle in a constant temperature bath was placed 5 mg crystalline horseradish peroxidase enzyme (3100 units/mg; Worthington Biochemical Co., Freehold, N.J.) in 10 ml 0.1 *M* citrate buffer p*H* 5.5, and the solution made up to 400 ml. Into the resin kettle were pumped simultaneously two solutions, the first made by dissolving 0.8 g crystalline coniferyl alcohol in a minimum of acetone and making up to 400 ml with distilled water, and the second being 0.025 or 0.05% H_2O_2 in distilled water. The miniature Beckman metering pumps, activated by Zenith Electric Company time switches, were calibrated to deliver 400 ml each 24 h. The reactants were stirred constantly. After 48 h, a further 4 mg peroxidase in 10 ml citrate buffer was added and the p*H* readjusted to 5.5. The addition of coniferyl alcohol and peroxide continued at the same rate for 60 h. At that point, the addition of coniferyl alcohol was

Can. J. Chem. Downloaded from www.nrcresearchpress.com by 210.87.254.40 on 09/05/12
For personal use only.

discontinued and the rate of flow of peroxide solution was reduced to half. Additions of enzyme and p*H* adjustment were continued at 12-h intervals. At the end of the reactions or after harvesting a sample from the reactor, 1% NaCN was added to deactivate the enzyme and the milky white suspension of DHP was centrifuged at 15 000 r.p.m. The precipitate was resuspended in water and recentrifuged four times. It was then dissolved in 90:10 dioxane–water, filtered through glass fiber, and the clear solution was then freeze-dried to yield the fluffy cream-colored polymers.

In this manner, two DHP samples were prepared, DHP 125 using 0.025% H_2O_2 solution for 7 days, whereas for DHP 122, 0.05% H_2O_2 solution was used for 6 days. Samples were withdrawn from the reaction mixture at intervals for molecular weight determinations.

(b) Milled Wood Lignins (MWL)

The preparation of the MWL used in these experiments has been described in detail (12). Groundwood pulps of eastern spruce (*Picea mariana*, B S and P)[1] and western hemlock (*Tsuga heterophylla*, Sarg)[2] were used. Prior to milling, the pulps were extracted with various solvents and dried (13). The milling period varied from 7 to 21 days. Then 5 g of the milled wood and 5 g of a cellulase, Onozuka, S.S.[3] (14), were suspended in 250 ml of sodium acetate – acetic acid buffer of p*H* 4.7 in a 500 ml flask and shaken mechanically for 72 h at 46 °C. The mixture was centrifuged at 12 000 r.p.m. to separate the precipitate which was then washed thoroughly with water and reprecipitated twice with ether from 90:10 acetic acid – water. The lignin was washed again with water and then dissolved in 90:10 dioxane–water, centrifuged, and the clear solution freeze-dried.

Some of these samples were heated with NaOH or with a solution containing NaOH and Na_2S in simulated "pulping" by a procedure very similar to that described for wood in the next section. A sample of spruce MWL was heated in 90:10 dioxane–water solution at 160 °C and the product freeze-dried.

(c) Alkaline Pulping of Wood

Wood chips or groundwood of the same two species were pulped by alkaline sodium sulfide (the kraft pulping process) or by sodium hydroxide (the soda process). Laboratory reagent grade NaOH pellets and crystalline Na_2S were used. Boiled, nitrogen-flushed distilled water was used to make 0.5 *N* NaOH. The Na_2S crystals were washed under a blanket of nitrogen and dissolved to 20 g/l, again using boiled, nitrogen-flushed distilled water. The stock solution of Na_2S was stored in a dark bottle at 4 °C and fresh solution made up every 2 weeks. Pulping was carried out in 15 ml glass vials placed in 30 ml stainless steel bombs (10), in a silicone oil bath maintained at the desired temperature ±0.5 °C. In order to maintain approximately constant solution compositions, dilute solutions were used. For 50 mg wood, 10 ml of a solution containing 10 mg active alkali, that is NaOH + $\frac{1}{2}Na_2S$ calculated as Na_2O, were used. When using the soda process, there was no Na_2S present and when using the kraft process 25% of the active alkali was in the form of the sulfide.

The time required for the bombs to attain temperature was less than 2 min. At the appropriate time, the bomb was cooled rapidly and the contents washed with water and filtered. The solution was acidified with 0.5 *N* HCl to p*H* 3. The lignin precipitated in this way was centrifuged at 15 000 r.p.m. for 5 min, washed three times by resuspension with water, and the residue dissolved in a small volume of 90:10 dioxane–water and freeze-dried.

(d) Gel Permeation Chromatography (g.p.c.)

The analytical system, which consisted of K25/45 column packed with Sephadex G100 swollen in dimethyl sulfoxide, has been described in detail (15). The same paper describes the calibration of the column using narrow molecular weight fractions of lignin in the ultracentrifuge. The same conditions of operation were used in this work and the data, taken from the plot of absorbance at 280 nm using a Beckman DU spectrophotometer and an ultramicro cell of capacity 0.08 ml and 10 mm light path length for continuous flowthrough, was used to compute molecular weight averages and the distribution curves. The computer programs employed to calculate the various coefficients of molecular weight are given in ref. 10.

During the synthesis of DHP 125, two g.p.c. columns were used in series, the first packed with Sephadex G50 and the second with Sephadex G15. These were not calibrated for molecular weight but were adequate for demonstrating molecular weight distribution.

Results

The elemental composition and methoxyl content of DHP 122 and the MWLs are given in Table 1. The analytical data for DHP 122 are in good agreement with expectation, an analysis for a spruce MWL by Bjorkman and Person (21) being included for comparison. The other MWLs were prepared here by ball milling for 12 days followed by cellulase treatment (14). These are low in methoxyl content. This has been attributed to carbohydrate and polyphenolic contamination (14), although the possibility of demethylation is not excluded. This isolation process is preferred because of the high yield of lignin, resulting in a more representative sample.

The polymer, DHP 122, was analyzed on the calibrated Sephadex G100 column. Table 2 gives the molecular weight averages obtained for the sample at various stages of synthesis. Figure 1 shows the changes in molecular weight distribution occurring during synthesis. After 12 h of synthesis, a peak appeared at an elution volume of about 170 ml, with a slight shoulder at about 120 ml. On the third day after synthesis was begun, the 170 ml peak had shifted to about

[1]From Ontario Paper Company Ltd., Thorold, Ontario.
[2]From British Columbia Forest Products Ltd., Vancouver, B.C.
[3]Purchased from Kamematsu-Gosho Ltd., Tokyo.

TABLE 1. Elemental compositions and molecular weights of MWL and DHP

Sample designation	Wood Species	Yield[a] (%)	Analysis (%) C	H	O[b]	OCH_3	M_n	M_w	M_w/M_n
DHP 122	—	—	62.94	6.04	29.97	15.96	8 500	31 400	3.7
B and P[c]	Spruce	—	63.96	6.14	29.84	15.74	—	—	—
ES-12DE	Spruce	56	57.47	6.07	34.60	11.02	11 200	36 000	3.2
WH-12DE	Hemlock	57	58.60	6.33	33.53	11.60	10 600	33 500	3.2
Azhar *et al.*[d]	Hemlock	100	—	—	—	11.40	60 600	77 000	1.3

[a]Based on Klason lignin (16).
[b]By difference.
[c]Reference 21, included for comparison.
[d]Reference 14.

TABLE 2. Molecular weights during synthesis of DHP 122

Synthesis time (h)	M_n	M_w	M_w/M_n
12	2500	3 600	1.5
72	5000	11 000	2.2
144	8500	31 400	3.7

145 ml and the shoulder now appeared as a second peak at about 55 ml. The weight average molecular weights had increased from 3600 at 12 h to 11 000 on the third day. The polydispersity index increased also in the same period from 1.5 to 2.2. After 6 days of synthesis, the 145 ml peak experienced no further shift in position. Rather, its relative size decreased while that of the 55 ml peak increased. The weight average molecular weights and the polydispersity index also increased to 31 400 and 3.65, respectively. The bimodal distribution of molecular weight which was found from the early hours of synthesis thus became much more pronounced as the synthesis proceeded.

From the calibration curve (15), the peak at 55 ml represents lignin of M_w about 80 000, while the peak at 145 ml corresponds to M_w 3600.

The changes in molecular weight distribution occurring during the synthesis of the second coniferyl alcohol dehydrogenase polymer, DHP 125, are presented in Fig. 2. The analyses were carried out in two g.p.c. columns packed with Sephadex G50 and G15 gels connected in series. This analytical method was used in an attempt to detect the changes in molecular weight distribution at the early stages of the synthesis when changes in the low molecular weight region would presumably be dominant. The columns were not calibrated to yield quantitative molecular weights and the results depict only changes in molecular weight distribution during synthesis. Coniferyl alcohol appeared with a peak elution volume at 250 ml. After one day of synthesis, this peak elution volume had shifted to a markedly lower elution volume at about 190 ml indicating the formation of higher molecular weight material. In addition, a very slight shoulder appeared at an elution volume of about 125 ml, representing still higher molecular weight. After two days of synthesis, the shoulder at 125 ml elution volume had grown into a distinct second peak, resulting in a bimodal distribution curve. This bimodal distribution of molecular weight persisted throughout the rest of the synthesis time with the positions of the two peaks remaining the same, while the second peak increased in size relative to the first as the synthesis proceeded.

The molecular weight and its distribution of a spruce MWL is shown in Fig. 3. This preparation of MWL was made by milling for 12 days, followed by treatment with cellulase. The yield was 56% of the lignin present in the wood. The molecular weight averages were $M_n = 11\,000$, $M_w = 36\,000$ and the poly-dispersity index $M_w/M_n = 3.3$. There is a sharp peak in M_w at about 80 000 and a smaller peak at M_w about 3600. Figure 3 also repeats the molecular weight distribution curve for DHP 122 taken after 6 days of polymerization and demonstrates the general agreement of the peak positions.

The molecular weight and its distribution of a hemlock MWL isolated in very high yield by Azhar *et al.* (14) is shown in Fig. 4. This MWL was made similarly to the spruce MWL shown in Fig. 3 by 12 days of milling followed by cellulase treatment. It was obtained in an apparent yield of 100% based on the lignin of the wood

Can. J. Chem. Downloaded from www.nrcresearchpress.com by 210.87.254.40 on 09/05/12
For personal use only.

Can. J. Chem. Downloaded from www.nrcresearchpress.com by 210.87.254.40 on 09/05/12
For personal use only.

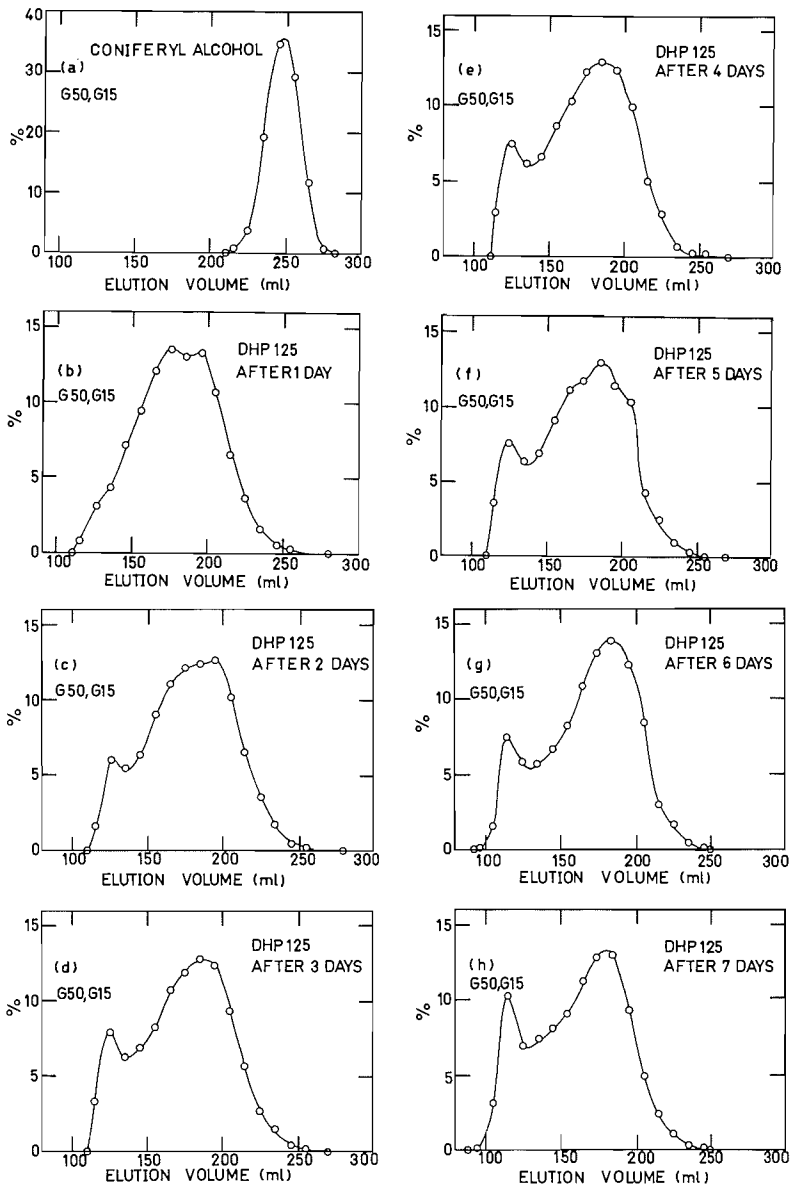

FIG. 1. Molecular weight and its distribution during synthesis of DHP 122, a dehydrogenase polymer of coniferyl alcohol.

(16) but was contaminated with carbohydrates and polyphenols, and had a low methoxyl content. The molecular weight averages for this MWL are much higher than for any other lignins examined, being M_n 60 000 and M_w 77 000, and the polydispersity index M_w/M_n of 1.27 is also the lowest found. The sharp high molecular weight peak in the distribution curve lies at about M_w 100 000 and there is very little if any lignin at higher M_w. There was no lignin below M_w of about 10 000 in this sample. This MWL may be the least altered in macromolecular properties of any yet isolated from wood. Other samples of cellulase MWL isolated by the authors (10) at 44 to 57% yield had M_w 33 000 (hemlock) and 36 000 (spruce) and a broader distribution, M_w/M_n being about 3.0. These lignins also display a sharp peak in their distribution curves

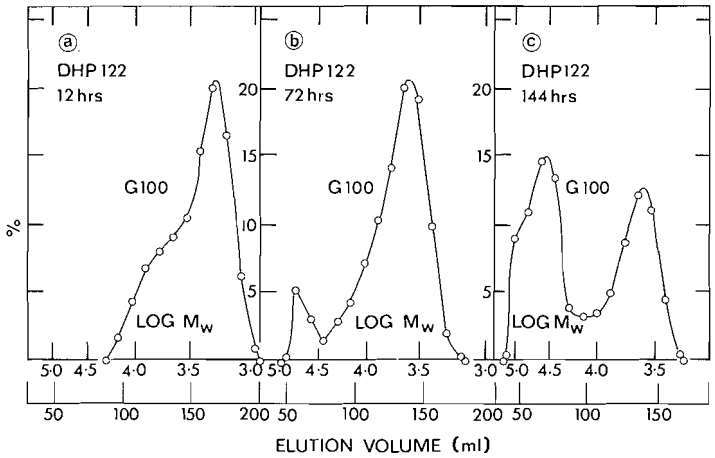

FIG. 2. Molecular weight and its distribution during synthesis of DHP 125, a dehydrogenase polymer of coniferyl alcohol.

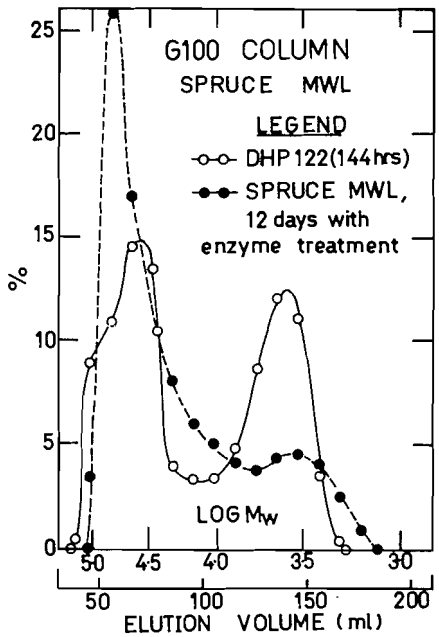

FIG. 3. Comparison of molecular weights and their distributions of a spruce milled wood lignin and a dehydrogenase polymer of coniferyl alcohol.

at M_w 80 000 to 100 000 but contain substantial quantities of lignin of lower M_w, down to about 2500. The presence of the lower M_n lignin is attributed to degradation during milling.

Figure 5 illustrates the effect of heating a spruce MWL dissolved in 90:10 dioxane–water at 160 °C for 120 min on the molecular weight distribution. The low molecular weight peak at about M_w 4000 has increased considerably in size, although the peak position has not changed. The high molecular weight peak has decreased in size and has also shifted towards a somewhat higher molecular weight, from about M_w 80 000 to 100 000. Figure 6 illustrates the effect of heating the same MWL in dilute NaOH solution (simulated "soda pulping") at 160 °C for increasing periods of time from 15–120 min. The curves show a growth in the low molecular weight peak and a decrease in the high molecular weight peak with increasing reaction time. In addition, at 30 min and thereafter, the same shift in high molecular weight peak position found in dioxane–water was also found in dilute NaOH.

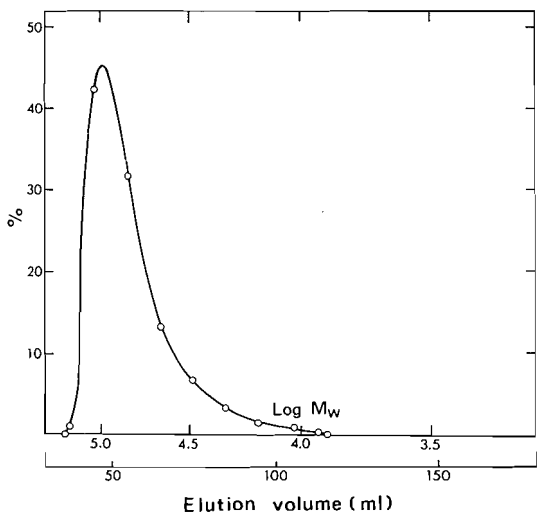

FIG. 4. Molecular weight and its distribution of a hemlock milled wood lignin.

Can. J. Chem. Downloaded from www.nrcresearchpress.com by 210.87.254.40 on 09/05/12
For personal use only.

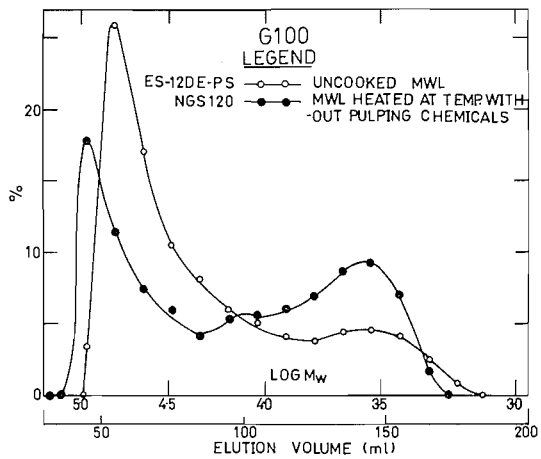

FIG. 5. Spruce MWL, molecular weight and its distribution as prepared, and on heating for 2 h at 160 °C in aqueous dioxane.

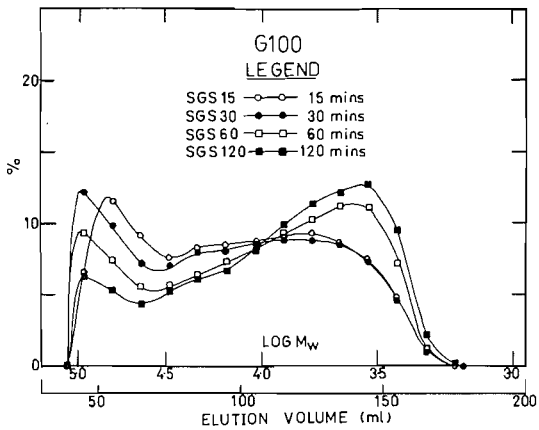

FIG. 6. Spruce MWL, molecular weight and its distribution during simulated "soda pulping" at 160 °C.

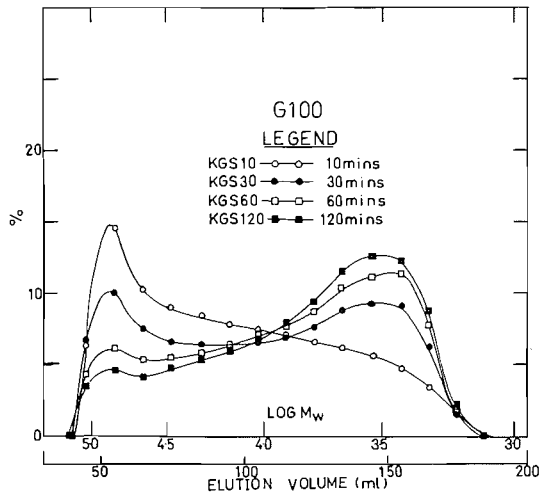

FIG. 7. Spruce MWL, molecular weight and its distribution during simulated "kraft pulping" at 160 °C.

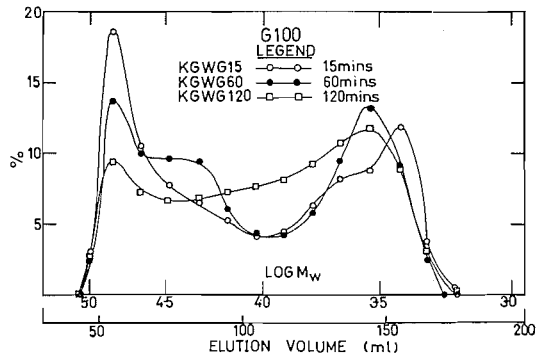

FIG. 8. Molecular weight and its distribution of dissolved lignin during kraft pulping of hemlock groundwood at 160 °C.

On the other hand, when a solution of NaOH plus Na_2S was used (Fig. 7, simulated "kraft pulping") the high peak remained at about M_w 80 000 although again the growth of the low molecular weight peak and the decrease in the high molecular weight were observed.

In Fig. 8 is shown the molecular weight and its distribution of lignins dissolved during the kraft pulping of hemlock groundwood. The three curves show the effects of pulping at 160 °C for 15, 60, and 120 min. The generally bimodal distribution of molecular weight is maintained, the high molecular weight peak remaining at about M_w 80 000 and the low molecular weight peak at about M_w 2500 to 3500. The M_w 80 000 peak decreased with time of pulping and the relative importance of the lower molecular weight peak increased. It appeared that the low molecular weight peak increased at the expense of the high molecular weight peak. Other examples of the effect of alkaline pulping of wood are given in (10) and (17). In these other examples, while pulping of groundwood generally follows the pattern shown here, pulping of wood chips follows a different sequence, in which lower molecular weight lignin is first found in the pulping solution and higher molecular weight lignin appears later. The difference is attributed to the physical structure of wood and the path followed by the chemicals in reaching the lignin. The bimodal molecular weight distribution and the relative constancy of the peak positions are nevertheless observed.

Can. J. Chem. Downloaded from www.nrcresearchpress.com by 210.87.254.40 on 09/05/12
For personal use only.

Can. J. Chem. Downloaded from www.nrcresearchpress.com by 210.87.254.40 on 09/05/12
For personal use only.

Discussion

The Modular Structure of Lignin

Bimodal molecular weight distribution is shown on almost all of the figures, with a high molecular weight peak at M_w 80 000 to 100 000 and a low molecular weight peak at M_w 3000 to 4000. The hemlock MWL samples shown on Fig. 4 have only the high peak with very little lignin of M_w below about 20 000. This leads us to the tentative suggestion that the hemlock lignin macromolecule as it occurs in wood has a rather narrow molecular weight distribution with a sharp peak at about 100 000. Since the monomeric weight for softwood lignins is about 180, this would suggest d.p. about 550.

Very early during the synthesis of coniferyl alcohol DHP a peak is formed at M_w about 3600, that is, d.p. of 20. A second high molecular weight peak at about M_w 80 000, that is, d.p. 440, is established soon thereafter. This new peak grows at the expense, as it were, of the first, without accumulation of material in the intermediate range.

During degradation, either by hydrolysis or in alkaline solution, the reverse process appears to take place. As the reaction proceeds, the lower molecular weight peak grows at the expense of the high molecular weight peak. While some product of intermediate molecular weight is formed, this may be regarded as transitional. The dominant reaction appears to be the degradation of macromolecule of d.p. about 440 to 550 to a polymer of d.p. about 20, with the formation of little or no intermediate polymer.

The evidence of this work suggests that the lignin macromolecule is an assembly of subassemblies of d.p. about 20. This is consonant with the earlier suggestions of Forss and Fremer (7), Bolker and Brenner (18), and Brown and coworkers (6).

The subassemblies, for which we prefer the term modules, are made up of about 20 aromatic monomers derived from the three alcohols previously named and with a variety of functional groups which are the result of dehydrogenation, oxidation, hydration, and condensation reactions as described by Freudenberg (2) and Freudenberg and Neish (4). The bonds between the modules in the macromolecule are formed with more difficulty and are broken more easily than the bonds between the monomers of which the modules are composed.

Lignin Synthesis and Degradation

The following is a schematic representation of lignin synthesis and degradation:

Scheme 1 follows the generally accepted pathway of lignin synthesis up to the formation of modules and proposes that thereafter the lignin macromolecule is formed by intermodular addition polymerization. This would explain the formation of the peak at d.p. about 20 observed early in DHP synthesis and the subsequent formation and growth of the peak at d.p. about 440.

Kleinert (5) has proposed that the initial step in the breakdown of the lignin macromolecule in pulping reactions is a random thermal homolytic depolymerization. From the present work we conclude that the first step in the homolysis of the lignin macromolecule consists of the breaking of the bonds between the modules and is to that extent not random. This would explain the formation and growth of the peak at d.p. about 20 observed during the experiments on degradation of MWL and pulping of hemlock groundwood. McNelis (19) used the term "unzipping" to describe coupling reactions of 2,6-xylenols in which one oligomer chain polymerizes at the expense of other chains. He suggested its possible application in "probing the structure of other aromatic polyethers such as lignin". The term appears to be particularly apt in the present context. We regard the "unzipping" mechanism as applicable to the formation of the modules of d.p. about 20. Further degradation to oligomers of lower d.p. may well proceed by a step depolymerization reaction, producing a disperse mixture of products and eventually monomers.

In Kleinert's proposal, the first products of thermal homolysis of the lignin macromolecule are free radicals. These are then stabilized against recondensation by the pulping chemicals. In the event that free radical stabilization is not fast enough, however, condensation reactions involving the free radicals may take place. Our results lend support to Kleinert's hypothesis. In lignin degradation reactions in which water or sodium hydroxide acted as the free radical stabilizers, we observed a shift of the high molecular weight peak to a still higher value. No such shift was found when sulfide-containing solutions were used. The greater reactivity of sulfides in alkaline lignin degradation is well established in industrial practice and has been

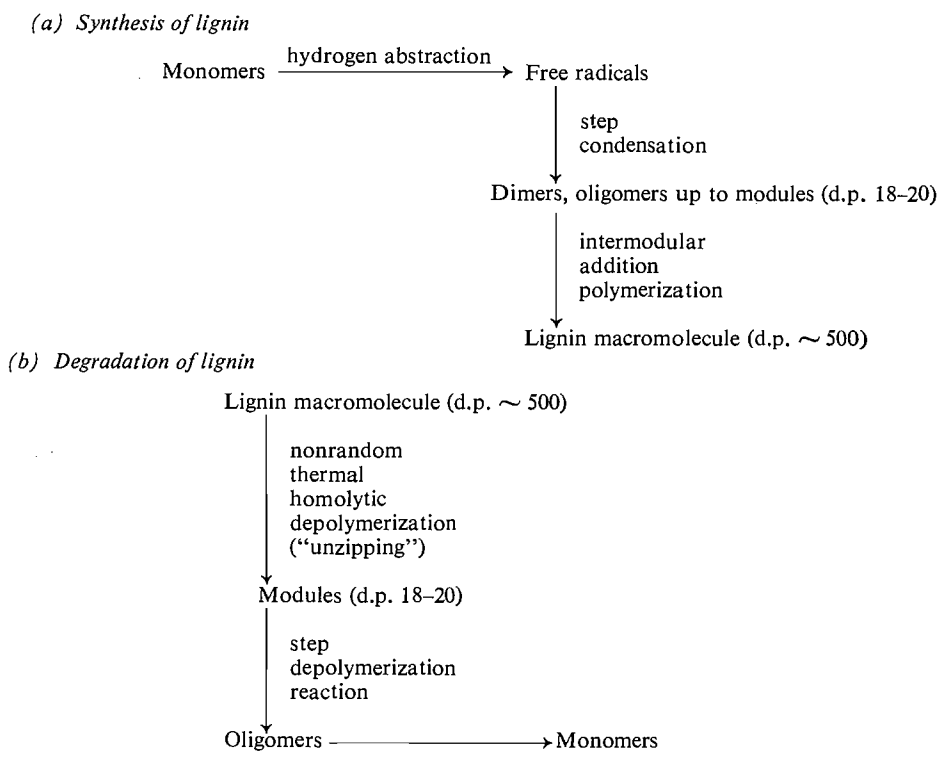

SCHEME 1

attributed by the present authors to the stabilization of the free radicals by a resonance mechanism (20). Sulfide sulphur is highly suited for this by virtue of its ability to expand its valence electrons into 3d orbitals not available to hydroxyl oxygen, hence kraft pulping solutions are more efficient than soda pulping solutions.

This work was supported by a grant from the National Research Council of Canada. One of us, T. I. Obiaga, would like to thank the Canadian Commonwealth Scholarship and Fellowship Committee for a fellowship held during much of the period of this week. The authors also thank Dr. Eric Kvasnicka for assistance in the preparation of the coniferyl alcohol.

1. K. V. SARKANEN and H. L. HERGERT. Lignins. *Edited by* K. V. Sarkanen and C. H. Ludwig. Wiley-Interscience. 1971. Chapt. III.
2. K. FREUDENBERG. Wood chemistry. Butterworths. 1962; Lignin structure and reactions. Advances in Chemistry Series No. 59. American Chemical Society. 1966.
3. J. M. HARKIN. Oxidative coupling of phenols. *Edited by* W. I. Taylor and A. R. Battersby. Marcel Dekker. 1967. Chapt. VI.
4. K. FREUDENBERG and A. C. NEISH. Constitution and biosynthesis of lignin. Springer-Verlag, New York Inc. 1968.
5. T. N. KLEINERT. Tappi, **49**, 126 (1966); **50**, 120 (1967).
6. W. BROWN, E. B. COWLING, and S. I. FALKEHAG. Svensk Papperstidn. **71**, 811 (1968).
7. K. FORSS and K-E. FREMER. Paperi Puu, **47**, 443 (1965).
8. D. A. I. GORING. Lignins. *Edited by* K. V. Sarkanen and C. H. Ludwig. Wiley-Interscience. 1971. p. 700.
9. K. FREUDENBERG. Biochemistry of wood. *Edited by* K. Kratzl and G. Billek. Pergamon. 1959. p. 121–136; K. FREUDENBERG and B. LEHMANN. Ber. **93**, 1354 (1960); K. FREUDENBERG. Science, **148**, 595 (1964).
10. T. I. OBIAGA. Ph.D. Thesis. University of Toronto, Toronto, Ontario. 1972.
11. K. FREUDENBERG. Ber. **85**, 1181 (1952).
12. M. WAYMAN and T. I. OBIAGA. Tappi. In press.
13. M. R. AZHAR and M. WAYMAN. Pulp Pap. Mag. Can. **71**, 47 (1970).
14. M. R. AZHAR, J. POLCIN, and W. H. RAPSON. Paper presented at the annual convention of the Technical Assoc. of the Pulp and Paper Industry, New York, 1971.
15. T. I. OBIAGA and M. WAYMAN. J. Appl. Poly. Chem. In press.
16. TAPPI Standard T-13. Technical Association of the Pulp and Paper Industry, New York. 1954.
17. T. I. OBIAGA and M. WAYMAN. Svensk Papperstidn. **76**, 699 (1973).
18. H. I. BOLKER and H. S. BRENNER. Science **170**, 173 (1970).
19. E. MCNELIS. J. Org. Chem. **31**, 1255 (1966).
20. T. I. OBIAGA and M. WAYMAN. Pulp Pap. Mag. Can. **70**, 64 (1969).
21. A. BJORKMAN and B. PERSON. Svensk. Papperstidn. **60**, 243 (1957).

Can. J. Chem. Downloaded from www.nrcresearchpress.com by 210.87.254.40 on 09/05/12
For personal use only.

1,4-Diphenyl-1,4-butadiyl Diradicals from Thermolysis of *cis*- and *trans*-3,6-Diphenyl-3,4,5,6-tetrahydropyridazine[1,2]

KARL R. KOPECKY AND JOSÉ SOLER

Department of Chemistry, University of Alberta, Edmonton, Alberta T6G 2G2

Received January 10, 1974

KARL R. KOPECKY and JOSÉ SOLER. Can. J. Chem. **52**, 2111 (1974).

Reduction of 3,6-diphenyl-2,3,4,5-tetrahydropyridazine with sodium amalgam in ethylene glycol at 130° produces a 1:2 mixture of *cis*- and *trans*-3,6-diphenylpiperidazine (*cis*- and *trans*-**4**) from which *trans*-**4** was obtained by fractional crystallization. Oxidation of *cis*- and *trans*-**4** with oxygen gave *cis*- and *trans*-3,6-diphenyl-3,4,5,6-tetrahydropyridazine (*cis*- and *trans*-**1**). For thermolysis of *trans*-**1** at 62.5° $E_a = 25.3 \pm 1.1$ kcal/mol and $\Delta S^{\ddagger} = 0.4 \pm 3$ e.u. At 63° the relative yields of styrene, *cis*- and *trans*-1,2-diphenylcyclobutane (*cis*- and *trans*-**7**) formed from *cis*-**1** are 55.3, 30.1, and 18.6% and those formed from *trans*-**1** are 59.1, 1.7, and 39.2%, respectively. For the 1,4-diphenyl-1,4-butadiyl diradical from thermolysis of *cis*-**1** $k_{cleav}/k_{rot} = 1.1$ and $k_{cyc}/k_{rot} = 1.5$ whereas for that of *trans*-**1** $k_{cleav}/k_{rot} = 10$ and $k_{cyc}/k_{rot} = 14$. At 205° *cis*-**7** decomposes to yield a 4.8:1 ratio of styrene:*trans*-**7**. This is near the ratio expected if the initial geometries of the diradicals produced from *cis*-**1** and *cis*-**7** are similar.

KARL R. KOPECKY et JOSÉ SOLER. Can. J. Chem. **52**, 2111 (1974).

La réduction da la diphényl-3,6-tétrahydro-2,3,4,5-pyridazine avec l'amalgame de sodium dans l'éthylène glycol à 130° donne un mélange de *cis*- et *trans*-diphényl-3,6-piperidazine (le *cis*- et *trans*-**4**) dans le rapport 1:2. A partir de ce mélange le *trans*-**4** a été obtenu par crystallization fractionnée. L'oxidation du *cis*- et *trans*-**4** par l'oxygène donne le *cis*- et *trans*-diphényl-3,6-tétrahydro-3,4,5,6-pyridazine (le *cis*- et *trans*-**1**). Pour la thermolyse du *trans*-**1** à 62.5° on a trouvé $E_a = 25.3 \pm 1.1$ kcal/mol et $\Delta S^{\ddagger} = 0.4 \pm 3$ cal/mol. A 63° les rendements relatifs de styrène, de *cis*- et *trans*-diphényl-1,2-cyclobutane (le *cis*- et *trans*-**7**) formés à partir du *cis*-**1** sont 55.3, 30.1 et 18.6% et ceux, formés à partir du *trans*-**1**, sont 59.1, 1.7 et 39.2% respectivement. Pour le diradical diphényl-1,4-butadiyl-1,4 provenant de la thermolyse du *cis*-**1** on a obtenu $k_{rupture}/k_{rotation} = 1.1$ et $k_{cyclization}/k_{rotation} = 1.5$ et pour le diradical provenant du *trans*-**1** les valeurs sont $k_{rupture}/k_{rotation} = 10$ et $k_{cyclization}/k_{rotation} = 14$. A 205° le *cis*-**7** se décompose en donnant un mélange de styrène:*trans*-**7** dans le rapport 4.8:1. Ceci est presque le rapport attendu si les géométries initiales des diradicaux produit à partir du *cis*-**1** et du *cis*-**7** sont voisines.

Recently, *cis*-3,6-diphenyl-3,4,56-tetrahydropyridazine, *cis*-**1**, was prepared and thermolized in connection with a study of the mechanism of the thermal initiation of styrene polymerization (1). Because of interest in the stereochemistry of azoalkane decompositions (2) and in reactions of 1,4-diradicals (3) *trans*-**1** has been prepared and thermolyzed. The relative rates of rotation, cyclization, and decomposition to styrene of the 1,4-diphenyl-1,4-butadiyl diradicals derived from *cis*- and *trans*-**1** can be determined now.

Results

The preparations of *trans*-**1** and of related compounds are outlined in Scheme 1. Of the several methods which were used to reduce 3,6-diphenyl-2,3,4,5-tetrahydropyridazine **3** the one which gave the most useful yields of *trans*-3,6-diphenylpiperazine, *trans*-**4**, was treatment of **3** with sodium amalgam in ethylene glycol at 130°. A mixture containing *cis*- and *trans*-**4** in a ~1:2 ratio together with unreacted **3** was formed. This mixture could be separated readily by chromatography of the monocarbomethoxy derivatives, *cis*- and *trans*-1-carbomethoxy-3,6-diphenylpiperidazine, *cis*- and *trans*-**5**, and 2-carbomethoxy-3,6-diphenyl-2,3,4,5-tetrahydropyridazine **6** which were formed by treatment of the crude reaction mixture with methyl chloroformate. Saponification of *cis*- and *trans*-**5** followed by decarboxylation afforded the pure hydrazines. These were oxidized readily by oxygen to the azo compounds. Pure *trans*-**4** could be obtained also from the reduction of **3** by fractional crystallization.

[1]Presented at the 56th Canadian Chemical Conference of the Chemical Institute of Canada, Montreal, Quebec, June, 1973. Abstract 212.

[2]This research was supported in part by the National Research Council of Canada.

Can. J. Chem. Downloaded from www.nrcresearchpress.com by 210.87.254.6 on 09/05/12
For personal use only.

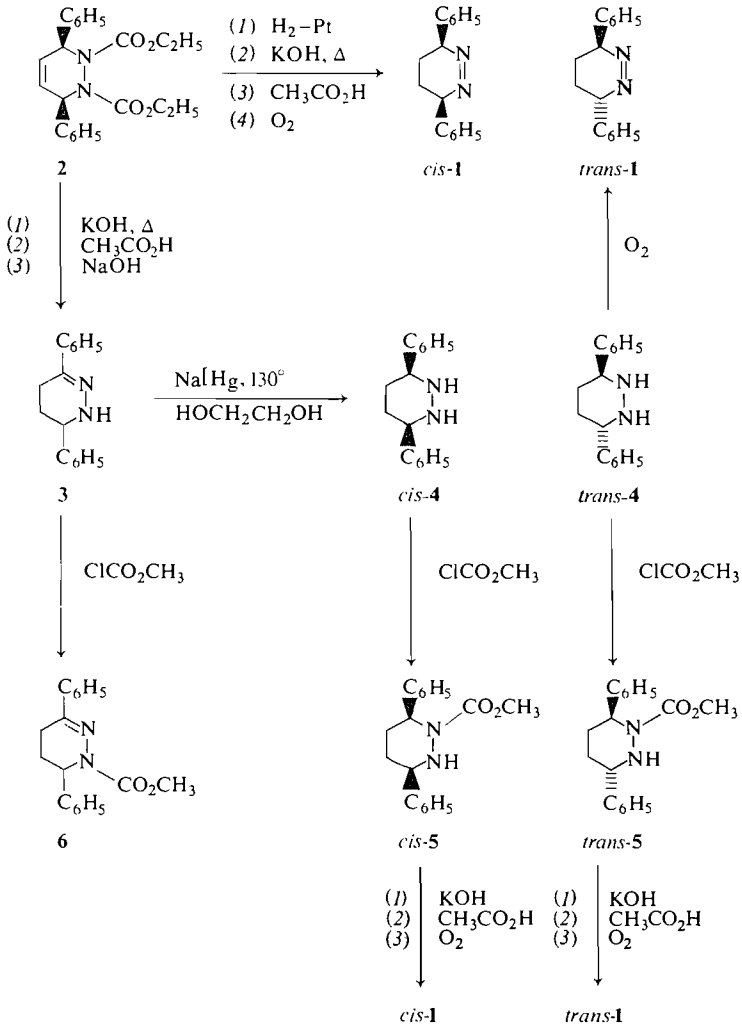

SCHEME 1

Examination by t.l.c. of the crude monocarbomethoxy derivatives *cis*- and *trans*-**5** obtained by treatment of the hydrazines *cis*- and *trans*-**4** separately with methyl chloroformate showed that each isomer, and, therefore, the corresponding azo compound, was contaminated with undetectable amounts (<0.5%) of the other.

The assignment of stereochemistry to *cis*- and *trans*-**1** is based on the assumption that the Diels–Alder adduct **2** of *trans,trans*-1,4-diphenyl-1,3-butadiene and diethyl azodicarboxylate, in which the phenyl groups are *cis* (4), is converted without isomerization to *cis*-**1**. Therefore, the isomeric azo compound, which is obtained from the major product of the reduction of **3**, must be *trans*-**1**. In support of this conclusion the n.m.r. spectrum of *trans*-**1** has a much more simple pattern than does that of *cis*-**1** as would be expected from the higher symmetry of *trans*-**1**. The spectrum of *trans*-**1** has a sharp singlet for the phenyl protons at τ 2.7 and one set of signals for the methylene protons centered at τ 8.1, whereas that of *cis*-**1** has two broad multiplets for the phenyl protons between τ 2.4 and 2.9 and two sets of multiplets for the methylene protons centered at τ 7.9 and 8.7.

The rates and activation parameters of thermolysis of *cis*- and *trans*-**1** given in Table 1 indicate that *trans*-**1** thermolyzes about 5–6 times as rapidly as does *cis*-**1**. The difference in the rates of decomposition of *cis*- and *trans*-**1** is

Can. J. Chem. Downloaded from www.nrcresearchpress.com by 210.87.254.6 on 09/05/12
For personal use only.

TABLE 1. Kinetic data for thermolysis[a] of *cis*- and *trans*-**1** in ethylbenzene

Compound	Temperature (°C)	$k_{obs} \times 10^4$ (s^{-1})	% N_2	% **3**[b]	$k_{corr} \times 10^4$[c] (s^{-1})
trans-**1**[d]	62.4	5.53	95	1	5.48
	62.6	5.30	95	2	5.20
	44.8	0.730	92	5.5	0.690
	44.8	0.633	94	5.5	0.600
	80.0				34.9[e]
cis-**1**	64.7				1.0[f]
	79.5				5.6[f]

[a]For *cis*-**1** at 79.5° $\Delta H^{\neq} = 26.7 \pm 1.2$ kcal/mol, $\Delta S^{\neq} = 2.4 \pm 4$ e.u. (1). For *trans*-1 at 62.5° $\Delta H^{\neq} = 24.6 \pm 1.1$ kcal/mol, $\Delta S^{\neq} = -0.4 \pm 3$ e.u.
[b]Determined from the u.v. spectrum of the solution after thermolysis.
[c]$k_{corr} = k_{obs} \times 0.01$ %-hydrocarbon.
[d]Solvent contained 2% ethyldiisopropylamine.
[e]Extrapolated.
[f]From ref. 1.

TABLE 2. Product distribution in the thermolysis of *cis*- and *trans*-**1** in benzene

Compound	Temperature (°C)	Relative yields (mol %)[a] Styrene	*cis*-7	*trans*-7
cis-**1**	280[b]	66.8	21.3	11.9
	133	61.3	24.9	13.7
	63	55.3	30.1	14.6
trans-**1**	280[b]	66.5	2.0	31.4
	133	61.7	1.9	36.4
	63	59.1	1.7	39.2

[a]The values are averages of at least two separate runs, each analyzed in triplicate. Errors are estimated to be ±0.5%.
[b]Temperature of the injection port of the gas chromatograph into which solutions of *cis*- and *trans*-**1** were injected.

greater than has been observed with diastereomeric pairs of acyclic azo compounds (5). The enthalpies of activation for the thermolysis of *cis*- and *trans*-**1** and that (27.5 kcal/mol) of *trans*-3,5-diphenyl-1-pyrazoline (6) are considerably lower than that (32 kcal/mol) of the acyclic analogue 1,1′-diphenylazoethane (7). It may be that the factors which cause acyclic *cis* azo compounds to thermolize much more rapidly than their *trans* isomers (8) also affect the thermolysis of these cyclic azo compounds.

The product distributions obtained on thermolysis of *cis*- and *trans*-**1** are given in Table 2. That of *cis*-**1** agrees well with values obtained previously (1, 9). Styrene and *cis*- and *trans*-1,2-diphenylcyclobutane, *cis*- and *trans*-**7**, account for >98% of the starting materials in each case. A small amount, <0.5%, of another product, reported to be 1-phenyltetralin (9), was detected from both isomers but not identified. In addition, ~1% of hydrazone was formed in

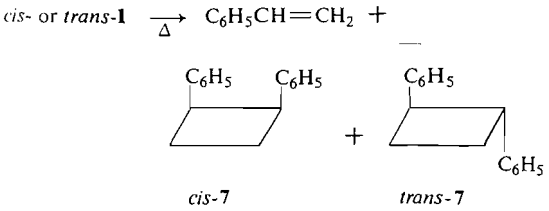

those reactions which were carried out in solution at 133 and 63°.

The thermolysis of *cis*-**7** produces styrene and *trans*-**7** (10). These experiments were not made under conditions suitable for comparison with the results of the thermolysis of *cis*- and *trans*-**1** so that the thermolysis of *cis*-**7** was reexamined. At 205° in benzene the decomposition of 0.1 *M* *cis*-**7** is 45% complete after 1 h. The ratio of styrene to *trans*-**7** is 4.8 and falls slowly to 4.7 after 9.5 h when 2% of *cis*-**7** remain. This ratio of styrene to *trans*-**7** is somewhat higher than the reported ratio of ~4:1 obtained at 165° (10*c*).

Can. J. Chem. Downloaded from www.nrcresearchpress.com by 210.87.254.6 on 09/05/12
For personal use only.

Can. J. Chem. Downloaded from www.nrcresearchpress.com by 210.87.254.6 on 09/05/12
For personal use only.

The rate of disappearance of *cis*-**7** at 205° is $\sim 1 \times 10^{-4}$ s^{-1} which compares well with a value of 1.1×10^{-4} s^{-1} calculated from the reported activation parameters (10*c*). Control experiments showed that after 1 h at 205° negligible amounts of *trans*-**7** would have decomposed to styrene and that negligible amounts of styrene would have polymerized or dimerized to *trans*-**7**.

Discussion

Thermolysis of cis- and trans-1

Although the styrene produced from thermolysis of *cis*- and *trans*-**1** might be formed by a concerted, thermally allowed route (11) *cis*- and *trans*-**7** definitely are not formed in the same way. There is only a small effect of temperature on the ratio of cleavage to cyclization products in the thermolysis of both azo compounds. This would be unlikely if the styrene were formed by a concerted route directly from the azo compounds while *cis*- and *trans*-**7** were formed by another pathway. Such different modes of decomposition would very likely have quite different activation parameters. Thus the azo compounds appear to decompose by only one path. Recent evidence for one bond cleavage in certain azo compounds (8*b* and *c*, 12) makes it necessary to consider such a process here. There is evidence from the effect of pressure on the rate of thermolysis of *cis*-**1** that both C—N bonds are breaking simultaneously (9). Also, the relative amounts of *cis*- and *trans*-**7** formed from the two azo compounds indicate that these materials are not formed by intramolecular radical displacement of N_2 (13) in a species, such as **8**, in which only one C—N

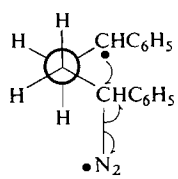

8

bond is broken. Otherwise, one might expect more *trans*-**7** to be formed from *cis*-**1** than is observed since this would require fewer overall rotations than would the formation of *trans*-**7** from *trans*-**1** by such an internal displacement. The results from the thermolysis of *cis*-**7** indicate that the diradical produced from this material, which cannot contain nitrogen, must have properties very similar to the material formed initially from *cis*-**1**. If the same initial diradical were produced from thermolysis of both *cis*-**1** and *cis*-**7** one can predict from the data in Table 2 that the ratio styrene: *trans*-**7** formed from *cis*-**7** at 205° should be ~5.1. This is quite close to the actual value of 4.8. Thus, it is quite likely that all the products of thermolysis of *cis*- and *trans*-**1** are formed by way of 1,4-diphenyl-1,4-butadiyl diradicals. The calculations below assume that these are formed directly by simultaneous cleavage of both C—N bonds.

Reactions of the Diradicals

The diradicals formed by simultaneous cleavage of both C—N bonds will have initial conformations at least approximating those given in Scheme 2. That formed from thermolysis of *cis*-**7** will have the initial conformation as shown for *cis*-DR. It is most probable that the ratio of conformers of *trans*-DR formed by interconversion of *cis*-DR is different from that formed directly from *trans*-**1** and that these two conformers undergo the several reactions indicated with somewhat different rate constants. The relative rates of interconversion, cleavage, and cyclization given in Table 3 were calculated (14) with the assumption that both conformers of *trans*-DR undergo these reactions with the same rates. This may distort the values of the relative rates a bit but there seems to be no other way of handling the data. However, this should still allow a good comparison of the relative rates of reaction of *cis*- and *trans*-DR to be made.

The rate constants k_1 and k_2 are the rate constants for the interconversion of one diradical into the other. Since rotation about either the C_1—C_2 or the C_3—C_4 bond will interconvert the diradicals the actual rate constants for rotation about one of these bonds are $\frac{1}{2}k_1$ and $\frac{1}{2}k_2$. Thus, for each diradical the rate of cyclization to the cyclobutane is faster than the rate of rotation about the C_1—C_2 or C_3—C_4 bonds by factors of ~14 for *trans*-DR and ~1.5 in *cis*-DR at 63°. The ratio of the rate of cleavage to the rate of rotation is $k_4/\frac{1}{2}k_2 \sim 10$ for *trans*-DR but that for *cis*-DR is only $k_5/\frac{1}{2}k_1 \sim 1$. Certainly the suggestion (15) that barriers to rotation might be greater than barriers to cleavage in singlet 1,4-diradicals is not generally applicable.

For both of the diradicals the rate of rotation of the radical center is much smaller relative to the rate of cyclization (coupling) than it is for

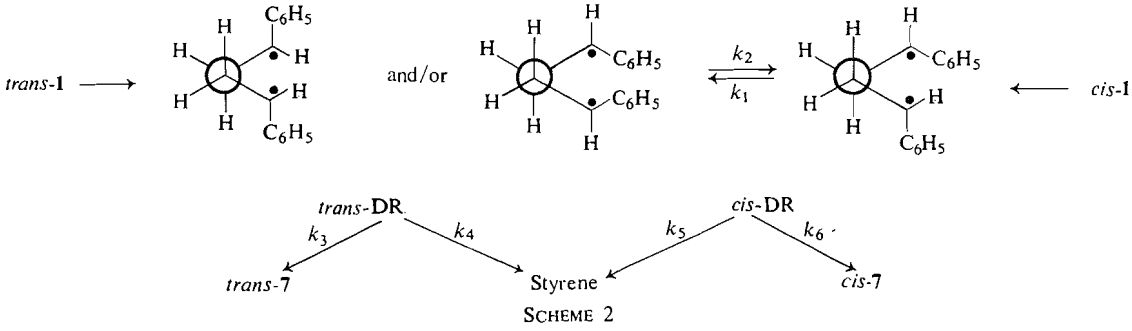

SCHEME 2

TABLE 3. Relative rates[a] of interconversion, cyclization, and cleavage of the 1,4-diphenyl-1,4-butadiyl diradicals derived from *cis*- and *trans*-**1**[b]

Temperature (°C)	k_5/k_6	k_4/k_3	k_2/k_3	k_1/k_6	$\frac{k_1/k_6}{k_2/k_3}$
63	0.56±0.01	0.73±0.03	0.15±0.01	1.27±0.04	8.8±0.6
133	0.78±0.01	0.81±0.02	0.21±0.01	1.57±0.02	7.4±0.4
280°	1.02±0.04	1.00±0.03	0.31±0.02	1.85±0.04	6.0±0.5

[a]Rate constants are those depicted in Scheme 2.
[b]Errors determined from estimated experimental errors in Table 2. Only values of product distributions from present work were used.

caged radical pairs formed from thermolysis of acyclic azo compounds whose structures are otherwise closely analogous to those of *cis*- and *trans*-**1** (2*b* and *c*). It has been suggested that diradicals from cyclic azo compounds cyclize faster than caged radical pairs from acyclic azo compounds couple because the latter are born with an intervening nitrogen molecule, which must diffuse away before coupling can occur, while the former are not (2*b*). Superimposed on this could be the slower rate of rotation about the C_1—C_2 and C_3—C_4 bonds which may be intrinsic to singlet diradicals (15).

Another way of analyzing the relative rates of rotation and cyclization in *cis*- and *trans*-DR is by means of the retention ratios *p*, *trans*-**7**/*cis*-**7** from *trans*-**1**; *q*, *cis*-**7**/*trans*-**7** from *cis*-**1**; and their product, *pq* (16). Selectivity is lost as temperature increases: *pq* = 48 at 63°, 36 at 133°, and 28 at 280°. The product *pq* derived from the present system is much higher than those derived from diradicals produced by alkene dimerization (3*a*,17) but not as high as that obtained on thermolysis of *meso*- and *dl*-3,6-diethyl-3,6-dimethyl-3,4,5,6-tetrahydropyrazoline **9** (3*b*) where *pq* > 1800 at 145°. Steric hindrance to cyclization of the diradicals formed from *meso*- and *dl*-**9** must be as great or greater

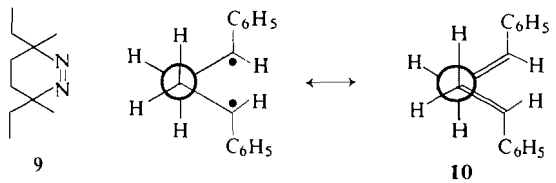

9 **10**

than that of *cis*- and *trans*-DR, especially of *trans*-DR, so that it is necessary to look elsewhere for the large difference in the *pq*'s. Two possible factors come to mind, both of which result from the stabilization of the benzylic diradicals by delocalization of the odd electrons into the benzene rings. First, such diradicals would be less reactive and might couple more slowly than unstabilized diradicals. Second, this delocalization could cause the alkenic contributing structure (15), for example, **10**, of the diradicals to be less important in *cis*- and *trans*-DR than it is in the aliphatic diradicals thus decreasing the barrier to rotation about the C_1—C_2 and C_3—C_4 bonds in the former relative to the latter diradicals.

The 1,4-diphenyl-1,4-butadiyl diradical can be produced in yet a third way, as well as from *cis*- and *trans*-**1** and *cis*-**7**. Pure styrene dimerizes slowly to form *cis*- and *trans*-**7** in a ratio of ~1:2 at 110° (18) by a reaction which is inde-

Can. J. Chem. Downloaded from www.nrcresearchpress.com by 210.87.254.6 on 09/05/12
For personal use only.

TABLE 4. Nuclear magnetic resonance spectra[a] of some 3,6-diphenylpyridazine derivatives

Compounds	Protons			
	Aromatic	Benzylic	Methylene	Other
cis-**1**[b]	2.4–2.85(m)	6.0(m,$w_{1/2}=20$)	7.8–8.1(m,2H) 8.5–8.9(m,2H)	
trans-**1**[b]	2.7(s)	5.4(m,$w_{1/2}=18$)	7.8–8.3(m)	
cis-**4**	2.5–2.8(m)	5.95(m,$w_{1/2}=8$)	7.9–8.1(m)	NH: 6.7(s)
trans-**4**	2.65(s)	6.2(m,$w_{1/2}=15$)	7.7–8.2(m)	NH: 6.6(s)
3	2.2–2.4(m), 2.6–2.8(m)	5.9(d of d), $J=5.5$ and 8.5	7.2–7.5(m,2H) 7.7–7.8 (m,2H)	NH: 4.4(b)
cis-**5**	2.6–2.8(m)	4.5(t,$J=4$, 1H), 6.1(t,$J=6$, 1H)	7.5–7.9(m,2H) 8.0–8.3(m,2H)	NH: 5.5(s) CH_3: 6.2(s)
trans-**5**	2.5–2.8	4.75(t,$J=5$, 1H) 5.90(t,$J=5$, 1H)	7.8–8.0(m)	NH: 5.7(s) CH_3: 6.35(s)
6	2.15–2.35(m) 2.6–2.9(m)	4.4(m,$w_{1/2}=8$)	7.7–7.9(m)	CH_3: 6.2(s)

[a]In deuteriochloroform; chemical shifts in τ values, *J* and half-widths in Hz; s = singlet, d = doublet, t = triplet, m = multiplet, b = broad.
[b]In carbon tetrachloride containing some ethyldiisopropylamine.

pendent of the process which leads to the thermal polymerization of styrene (10*c*,19). It is very doubtful that this dimerization can be a concerted reaction (20). It has been noted (1) that the initial conformation of the diradical produced from styrene must be different from that formed from *cis*-**1**. The present results show that it is different from that from *trans*-**1** as well. It thus appears that an extended (21) form of the diradical is produced initially. If this then converted to *cis*- and *trans*-DR with equal probability *cis*- and *trans*-**7** would be formed in a 1:2 ratio which is the same as would be obtained from the thermolysis of equal amounts of *cis*- and *trans*-**1**.

It should be mentioned that theoretical calculations indicate that there is no energy minimum for the simple 1,4-butadiyl diradical between cyclobutane and two molecules of ethylene (22). If such a situation were generally true for 1,4-diradicals calculation of the relative rates of reaction for such species would be meaningless (23). However, there is such a large body of data on reactions which involve 1,4-diradicals which can be analyzed in a reasonable and self-consistent manner by assuming that the diradicals behave as true intermediates that we feel justified in continuing this practice for *cis*- and *trans*-DR as well.

Experimental

Melting points were taken with a Reichert hot-stage melting point apparatus and are uncorrected. Nuclear magnetic resonance spectra were recorded on Varian analytical spectrometers, Models A-60 and A-56/60, and are listed in Table 4. Ultraviolet spectra were recorded on a Bausch and Lomb Spectronic 600 spectrophotometer which was calibrated with holmium oxide. Analyses by gas chromatography were carried out with an Aerograph 202 gas chromatograph using a 9.5 ft × ¼ in. stainless steel column packed with 20% SF-96 on 60–80 Chromosorb P. Elemental analyses were performed by Mrs. Darlene Mahlow and Mrs. Andrea Dunn.

3,6-Diphenyl-2,3,4,5-tetrahydropyridazine (3)

A solution of 32 g (0.57 mol) of potassium hydroxide in 100 ml methanol was added to 15 g (0.04 mol) *cis*-3,6-diphenyl-1,2-dicarboethoxy-1,2,3,6-tetrahydropyridazine **2** (24) dissolved in 175 ml boiling methanol. The resulting mixture was heated under reflux under nitrogen for 24 h and cooled. The white precipitate which formed was collected on a filter and then dissolved in 150 ml water. The stirred solution was acidified with acetic acid and stirred at 20° for ½ h. The mixture was then made alkaline to phenolphthalein with a solution of potassium hydroxide. After a short while the mixture was decolorized with a few drops of ammonium chloride solution. The precipitate was filtered, washed with water, and dried to give 7.6 g of **3**, m.p. 160–161° (lit. (25) m.p. 157–159°).

Evaporation of the methanolic filtrate and treatment of the resulting solid as above gave another 1.4 g of **3**, m.p. 155–159°. Total yield 95%.

trans-3,6-Diphenylpiperidazine (trans-4)

A solution of 20 g (0.085 mol) of **3** in 1 l of ethylene glycol at 130° was stirred vigorously while three portions of 50 g (0.26 g-atom) each of 4% sodium amalgam were added at 20 min intervals. Stirring was continued for 30 min after the last addition and the clear yellow solution was decanted from the mercury and cooled to 0° under nitrogen. After 3 h the precipitate was filtered and dried to give 5.2 g of material which was mainly unreacted **3** together with some *trans*-**4**. The filtrate was diluted with

Can. J. Chem. Downloaded from www.nrcresearchpress.com by 210.87.254.6 on 09/05/12
For personal use only.

Can. J. Chem. Downloaded from www.nrcresearchpress.com by 210.87.254.6 on 09/05/12
For personal use only.

700 ml of concentrated ammonium chloride solution and the resulting mixture extracted twice with 1 l ether. The extracts were combined, concentrated, and the concentrate cooled to 0° under nitrogen. The crystals of the hydrazine were filtered. The filtrate was successively concentrated, cooled, and freed from precipitate several more times in this way until hydrazone **3** began to precipitate. A total of 5.6 g, 28%, hydrazine was collected which was recrystallized from 1:1 ether–pentane to give cotton-like crystals, m.p. 134–135°. A sample of this material was converted to the monocarbomethoxy derivative *trans*-**5** with methyl chloroformate. The crude product was shown by t.l.c. to be free of *cis*-**5**. Control experiments showed that 0.5% *cis*-**5** could have been detected clearly.

Evaporation of the mother liquor yielded 5.3 g of a mixture of hydrazone **3**, *trans*-**4**, and oily *cis*-**4**. Total recovery of material was 85%.

Hydrazine *trans*-**4** is stable as a solid if kept at −10° but in solution is oxidized rapidly by air. Samples of *trans*-**4** can also be separated from hydrazone and *cis*-**4** by column chromatography on silica gel using ether as eluent.

trans-3,6-Diphenyl-3,4,5 6-tetrahydropyridazine (trans-1)

A solution of 650 mg *trans*-**4** in 200 ml benzene was stirred in the dark under oxygen in a neutralized 500-ml erlenmeyer flask for 2 h. The solution was concentrated to 125 ml and 300 ml heptane was added to the concentrate. The resulting solution was concentrated to about 200 ml and cooled to 0° to give 285 mg yellow crystals of *trans*-**1**, sinter 80–85°, m.p. 94–95° with gas evolution; λ_{max}(cyclohexane) 382 nm, ε 166. The absorption peak is broader, half width 40 nm, than that of *cis*-**1** and an absorption tail extends to the visible, ε_{400} 0.56.

Solid *trans*-**1** can be stored at −10° for several weeks without change. In solution it is reasonably stable in hydrocarbon solvents if neutralized glassware is used. It isomerizes slowly to the hydrazone **3** in methanol but does so within a minute in carbon tetrachloride or chloroform. Addition of small amounts of ethyldiisopropylamine to the latter solvents stops the isomerization for at least a day.

cis-3,6-Diphenyl-3,4,5,6-tetrahydropyridazine (cis-1)

This material was prepared as described previously (1). Its properties were identical to those reported except for the u.v. spectrum which was now found to be λ_{max}(cyclohexane) 377 nm, ε 178, half-width 30 nm, (lit. (1) λ_{max}(cyclohexane) 385 nm, ε 363). Recently reported values of the u.v. spectrum of *cis*-**1** also appear to be in error (26). As reported previously this material is also very readily isomerized to the hydrazone **3**. As in the case of *trans*-**1** addition of ethyldiisopropylamine to solutions of the azo compound drastically reduces the rate of isomerization.

cis-1-Carbomethoxy-3,6-diphenylpiperidazine (cis-5) and trans-1-Carbomethoxy-3,6-diphenylpiperidazine (trans-5)

The hydrazone **3** (4.5 g) in 250 ml ethylene glycol was treated with 55 g 4% sodium amalgam as described above. The cooled reaction mixture was poured into 250 ml concentrated ammonium chloride solution and the resulting mixture extracted with 500 ml ether. The ether layer was washed with 2 × 100 ml ammonium chloride solution, dried ($MgSO_4$), and filtered. The filtrate was cooled to 0° under nitrogen, 35 ml pyridine was added followed by dropwise addition with stirring of 30 ml methyl chloroformate in 25 ml ether. This mixture was allowed to warm to 20°, stirred for 1 h, and filtered. The filtrates were washed with 3 × 100 ml saturated sodium chloride solution, dried, and concentrated. The residue was taken up in 50 ml benzene and the resulting solution concentrated. This was repeated until the pyridine was removed. Finally, the oily residue was chromatographed on 400 g silica gel using 1:1 ether–hexane as eluent. First eluted after **3** was *cis*-**5** which was crystallized from ether to give 0.8 g, 15%, of product, m.p. 61–63°.

Anal. Calcd. for $C_{18}H_{20}N_2O_2$: C, 72.95; H, 6.80; N, 9.45. Found: C, 72.69; H, 6.85; N, 9.57.

A solution of 510 mg *cis*-**5** and 1.0 g potassium-hydroxide in 5 ml ethanol was heated to reflux for 4 h under nitrogen, cooled, and diluted with 20 ml water. The resulting solution was treated with 1.5 ml acetic acid, stirred for ½ h, and made alkaline with potassium hydroxide solution, and then extracted with 100 ml ether. The dried ($MgSO_4$) ether solution was concentrated to give 347 mg (88%) *cis*-**4** as an oil that could not be induced to crystallize. A portion of this oil was dissolved in a small amount of ether and the resulting solution was allowed to stand overnight. The precipitate which formed was collected, washed with cold ether and shown to be pure *cis*-**1** (m.p. mixture m.p., n.m.r. spectrum).

Further elution of the chromatography column removed *trans*-**5** and **6** together which were separated by fractional crystallization from ether (*trans*-**5** crystallizes rapidly, **6** more slowly) to give 1.1 g (18%) of *trans*-**5**, m.p. 121–122°, and 0.95 g (17%) of **6**.

Anal. Calcd. for $C_{18}H_{20}N_2O_2$ (*trans*-**5**): C, 72.95; H, 6.80; N, 9.45. Found: C, 73.22; H, 6.79; N, 9.53.

Using the same procedure as used for the preparation of *cis*-**5**, 380 mg *trans*-**5** was saponified using potassium hydroxide and the resulting salt decarboxylated with acetic acid. The reaction mixture was made alkaline with potassium hydroxide and the resulting precipitate filtered, washed with water, and dried under vacuum to give 280 mg (90%) of *trans*-**4**, identical (m.p., mixture m.p., n.m.r. spectrum) with material prepared as described above. A portion of the material was dissolved in ether and the solution allowed to stand overnight. This solution was shaken with water, dried and concentrated. The resulting crystals were shown to pure *trans*-**1** (m.p., mixture m.p., and n.m.r. spectrum).

2-Carbomethoxy-3,6-diphenyl-2,3,4,5-tetrahydropyridazine (6)

A solution of 0.5 g **3** in a solution of 10 ml ether and 10 ml pyridine was treated with 2 ml methyl chloroformate in 5 ml ether as described above for the preparation of *cis*- and *trans*-**5**. The product, 0.12 g (20%) was isolated as described above and recrystallized from ether, m.p. 112–113.5°.

Anal. Calcd. for $C_{18}H_{18}N_2O_2$: C, 73.44; H, 6.16; N, 9.52. Found: C, 73.32; H, 6.27; N, 9.52.

Product and Rate Studies

Decompositions of *cis*- and *trans*-**1** and the analysis of the decomposition products were carried out as described (1). Samples of *cis*- and *trans*-**1** were decomposed and analyzed in parallel. The results are listed in Table 2.

The rate of decomposition of *trans*-**1** was measured in the same way as described (1) for *cis*-**1** except that the solvent, ethylbenzene, contained 2% ethyldiisopropylamine which greatly decreased the amount of isomeriza-

TABLE 5. Product distribution from thermolysis of *cis*-1,2-diphenylcyclobutane, *cis*-**7**, in benzene at 205°

Time (h)	Product Distribution (relative mol %)		
	cis-**7**	*trans*-**7**	Styrene
0.17	94.7	Trace	5.3
1	55.4	7.7	36.8
2	34.2	11.1	54.6
4	17.8	14.4	67.7
9.5	1.9	17.3	80.7
21	—	17.8	82.2

tion of *trans*-**1** to the hydrazone **3**. The amount of hydrazone formed was determined by u.v. spectroscopy.

Thermolysis of cis-1,2-Diphenylcyclobutane (cis-7)

Benzene solutions 0.1 *M* in *cis*-**7** and in chlorobenzene as internal standard were placed in several heavy-walled 1-mm i.d. tubes and degassed to 10^{-3} mm. The tubes were sealed and placed in a bath of boiling benzyl alcohol (205.5 ± 0.5°). Tubes were removed after appropriate intervals and the contents were analyzed by gas chromatography. Results are presented in Table 5.

Control experiments showed that after 17 h at 205° a benzene solution initially 0.2 *M* in styrene contained 67% of the initial styrene, 1.5% *trans*-**7**, and no *cis*-**7**. Another experiment indicated that after the same treatment a solution initially 0.1 *M* in *trans*-**7** now contained 70% of the initial amount of *trans*-**7** and 17% styrene.

1. K. R. KOPECKY and S. EVANI. Can. J. Chem. **47**, 4041 (1969).
2. (*a*) P. D. BARTLETT and J. D. MCBRIDE. Pure Appl. Chem. **15**, 89 (1967); (*b*) K. R. KOPECKY and T. GILLAN. Can. J. Chem. **47**, 2371 (1969); (*c*) F. D. GREENE, M. A. BERWICK, and J. C. STOWELL. J. Am. Chem. Soc. **92**, 867 (1970).
3. (*a*) P. D. BARTLETT and K. E. SCHUELLER. J. Am. Chem. Soc. **90**, 6077 (1968); (*b*) P. D. BARTLETT and N. A. PORTER. J. Am. Chem. Soc. **90**, 5317 (1968); (*c*) H. R. GERBERICH and W. D. WALTERS. J. Am. Chem. Soc. **83**, 4884 (1961); (*d*) H. E. O'NEAL and S. W. BENSON. J. Phys. Chem. **72**, 1866 (1968); (*e*) N. C. YANG and S. P. ELLIOT. J. Am. Chem. Soc. **91**, 7550 (1969).
4. (*a*) J. C. BRELIERE and J. M. LEHN. Chem. Commun. 426 (1965); (*b*) B. J. PRICE, R. V. SMALLMAN, and F. O. SUTHERLAND. Chem. Commun. 319 (1966); (*c*) R. DANIELS and K. R. ROSEMAN. Tetrahedron Lett. 1335 (1965); (*d*) B. H. KORSCH and N. V. RIGGS. Tetrahedron Lett. 5897 (1966); (*e*) B. J. PRICE, I. O. SUTHERLAND, and F. G. WILLIAMSON. Tetrahedron, **22**, 3477 (1966); (*f*) J. E. ANDERSON and J. M. LEHN. Tetrahedron, **24**, 137 (1968).
5. (*a*) C. G. OVERBERGER and M. B. BERENBAUM. J. Am. Chem. Soc. **73**, 2618 (1951); (*b*) C. G. OVERBERGER, W. F. HALE, M. B. BERENBAUM, and A. B. FIRESTONE. J. Am. Chem. Soc. **76**, 6185 (1954); (*c*) S. E. SCHEPPELE and S. SELTZER. J. Am. Chem. Soc. **90**, 358 (1968).
6. J. W. TIMBERLAKE and B. K. BANDLISH. Tetrahedron Lett. 1393 (1971).
7. S. G. COHEN, S. J. GROSZOS, and D. B. SPARROW. J. Am. Chem. Soc. **72**, 3947 (1950).
8. (*a*) T. MILL and R. S. STRINGHAM. Tetrahedron Lett. 1853 (1969); (*b*) N. A. PORTER and M. O. FUNK. Chem. Commun. 263 (1973); (*c*) N. A. PORTER and L. J. MARNETT. J. Am. Chem. Soc. **95**, 4361 (1973).
9. R. C. NEUMAN, JR. and E. W. ERTLEY. Tetrahedron Lett. 1225 (1972).
10. (*a*) R. M. DODSON and A. G. ZIELSKE. J. Org. Chem. **32**, 28 (1967); (*b*) W. G. BROWN. Makromol. Chem. **128**, 130 (1969); (*c*) K. KIRCHNER and K. BUCHOLZ. Angew. Makromol. Chem. **13**, 127 (1970).
11. R. B. WOODWARD and R. HOFFMANN. Angew. Chem. Int. Ed. Engl. **8**, 781 (1969).
12. (*a*) S. SELTZER and F. T. DUNNE. J. Am. Chem. Soc. **87**, 2628 (1965); (*b*) W. A. PRYOR and K. SMITH. J. Am. Chem. Soc. **92**, 5403 (1970); (*c*) A. TSOLIS, S. G. MYLOKANIS, M. T. NIEH, and S. SELTZER. J. Am. Chem. Soc. **94**, 829 (1972); (*d*) R. J. CRAWFORD and K. TAKAGI. J. Am. Chem. Soc. **94**, 7406 (1972); (*e*) S. W. BENSON and H. E. O'NEAL. Nat. Stand. Data Ref. Ser. Natl. Bur. Stand. No. 21 (1970), pp. 31–34.
13. (*a*) W. R. ROTH and M. MARTIN. Ann. **702**, 1 (1967); (*b*) A. L. ALLRED and R. L. SMITH. J. Am. Chem. Soc. **89**, 7133 (1967); (*c*) P. B. CONDIT and R. G. BERGMAN. Chem. Commun. 4 (1971).
14. R. G. BERGMAN and W. L. CARTER. J. Am. Chem. Soc. **91**, 7411 (1969).
15. L. M. STEPHENSON and T. A. GIBSON. J. Am. Chem. Soc. **94**, 4599 (1972).
16. L. K. MONTGOMERY, K. E. SCHUELLER, and P. D. BARTLETT. J. Am. Chem. Soc. **86**, 622 (1964).
17. (*a*) P. D. BARTLETT and G. E. H. WALLBILLICH. J. Am. Chem. Soc. **91**, 409 (1969); (*b*) P. D. BARTLETT, K. HUMMEL, S. P. ELLIOT, and R. A. MINNS. J. Am. Chem. Soc. **94**, 2898 (1972).
18. W. G. BROWN. J. Am. Chem. Soc. **90**, 1916 (1968).
19. M. H. HALL. Ph.D. Thesis, University of Alberta, Edmonton, Alberta, 1971.
20. P. D. BARTLETT, G. M. COHEN, S. P. ELLIOTT, K. HUMMEL, R. A. MINNS, C. M. SHARTS, and F. Y. FUKUNAGA. J. Am. Chem. Soc. **74**, 2899 (1972).
21. (*a*) P. D. BARTLETT, C. J. DEMPTSTER, L. K. MONTGOMERY, K. E. SCHUELLER, and G. E. H. WALLBILLICH. J. Am. Chem. Soc. **91**, 405 (1969); (*b*) P. D. BARTLETT. Quart. Rev. Chem. Soc. **24**, 473 (1970).
22. R. HOFFMANN, S. SWAMINATHAN, B. G. ODELL, and R. GLEITER. J. Am. Chem. Soc. **92**, 7091 (1970).
23. L. SALEM and C. ROWLAND. Angew. Chem. Int. Ed. Engl. **11**, 92 (1972).
24. K. ALDER and H. NIKLAS. Ann. **585**, 81 (1954).
25. S. G. COHEN, S. HSIAO, E. SAKLAD, and C. H. WONG. J. Am. Chem. Soc. **79**, 4400 (1957).
26. H. RAU. Angew. Chem. Int. Ed. Engl. **12**, 224 (1973).

Can. J. Chem. Downloaded from www.nrcresearchpress.com by 210.87.254.6 on 09/05/12
For personal use only.

The Synthesis and Stereochemistry of (±)-(4a,13b-*trans*)-2,3,4,4a,8,9,13b,14-Octahydro-1*H*-benzo[6,7]cyclohepta[1,2,3-*de*]pyrido[2,1-*a*]-isoquinoline Hydrochloride (Taclamine Hydrochloride[1]), a Novel Psychotropic Agent

FRANÇOIS T. BRUDERLEIN, LESLIE G. HUMBER, AND KAREL PELZ

Chemistry Department and Chemical Development Department, Ayerst Research Laboratories, Montreal, Quebec

Received September 28, 1973

FRANÇOIS T. BRUDERLEIN, LESLIE G. HUMBER, and KAREL PELZ. Can. J. Chem. **52**, 2119 (1974).

Two synthetic routes to (±)-(4a,13b-*trans*)-2,3,4,4a,8,9,13b,14-octahydro-1*H*-benzo[6,7]cyclohepta[1,2,3-*de*]pyrido[2,1-*a*]isoquinoline hydrochloride (**1**) (taclamine hydrochloride) are described. Configurational assignments have been made on the basis of n.m.r. spectral interpretations and mechanistic considerations.

FRANÇOIS T. BRUDERLEIN, LESLIE G. HUMBER et KAREL PELZ. Can. J. Chem. **52**, 2119 (1974).

Deux synthèses du chlorhydrate de la (±)-(4a,13b-*trans*)-2,3,4,4a,8,9,13b,14-octahydro-1*H*-benzo[6,7]cyclohepta[1,2,3-*de*]pyrido-[2,1-*a*]isoquinoline (**1**) (chlorhydrate de taclamine) sont présentées. L'interprétation des mécanismes de formation et de la spectroscopie r.m.n. permettent d'en déterminer la stéréochimie.

Can. J. Chem. Downloaded from www.nrcresearchpress.com by 210.87.254.40 on 09/05/12
For personal use only.

(±)-(4a,13b-*trans*)-2,3,4,4a,8,9,13b,14-Octahydro-1*H*-benzo[6,7]cyclohepta[1,2,3-*de*]pyrido[2,1-*a*]isoquinoline hydrochloride (**1**) (taclamine hydrochloride) is a novel psychotropic agent exhibiting actions characteristic of anti-anxiety drugs in experimental animals. Preliminary pharmacological results have been described (1) and a full paper is in preparation. In this report we describe the synthesis and stereochemistry of taclamine hydrochloride.

The synthesis of taclamine·HCl **1** has been accomplished through two independent pathways (see Scheme 1). In the first, 10,11-dihydro-5*H*-dibenzo[*a*,*d*]cyclohepten-5-ylmethylamine (**2**) (2) was condensed with δ-valerolactone to give the hydroxyamide **3**, which on treatment with phosphorous oxychloride undergoes a double cyclization to afford the pentacyclic pyridoisoquinolinium salt **4**. Reduction of **4** with hydrogen and platinum, or, with sodium borohydride generates the 4a,13b-*cis* isomer of taclamine free base which was converted to the hydrochloride salt **5**. On the other hand, reduction of **4** with zinc and hydrochloric acid affords predominately the 4a,13b-*trans* isomer, **1**. (See discussion of stereochemistry below.) The isomeric nature of the two reduction products was confirmed by the oxidation of each, with mercuric acetate, to the common precursor, the pyridoisoquinolinium salt **4**.

The second pathway for the synthesis of taclamine·HCl involved the addition of methyl vinyl ketone to 1,7,8,12b-tetrahydrobenzo-[1,2]-cyclohepta[3,4,5-*de*]isoquinoline hydrochloride (**6**) (3). A mixture of the 4a,13b-*trans*- and 4a,13b-*cis*-pentacyclic amino ketones **7***a* and **8***a*, respectively, were formed in a ratio of 6:1. The mixture was readily separated into its components by column chromatography and the amino ketones **7***a* and **8***a* were converted to **1** and **5**, respectively, through desulfurization of the corresponding ethylenethioketal derivatives, **7***b* and **8***b*. The pure ethylenethioketal derivatives, **7***b* and **8***b* were also obtained by column chromatographic separation of the mixture of **7***b* and **8***b* obtained by direct treatment of the amino ketone mixture (**7***a* and **8***a*) with ethanedithiol and boron trifluoride etherate.

Configurational assignments at the 4a and 13b centers of **1** and **5** were made by interpretation of their n.m.r. spectra and, independently, by a consideration of the stereochemical controls operative in the reductions of the iminium salt **4**. Thus, the isomer **5** obtained via catalytic hydrogenation of **4** is assigned a 4a,13b-*cis* relative configuration since examination of molecular models shows that the substrate for reduction, **4**, contains an iminium center, which causes rings C, D, and E to be virtually coplanar while the phenyl ring A is located on the α-side at the

[1]Nonproprietary name selected by the U.S. Adopted Names Council. This compound has also been designated AY-22,214.

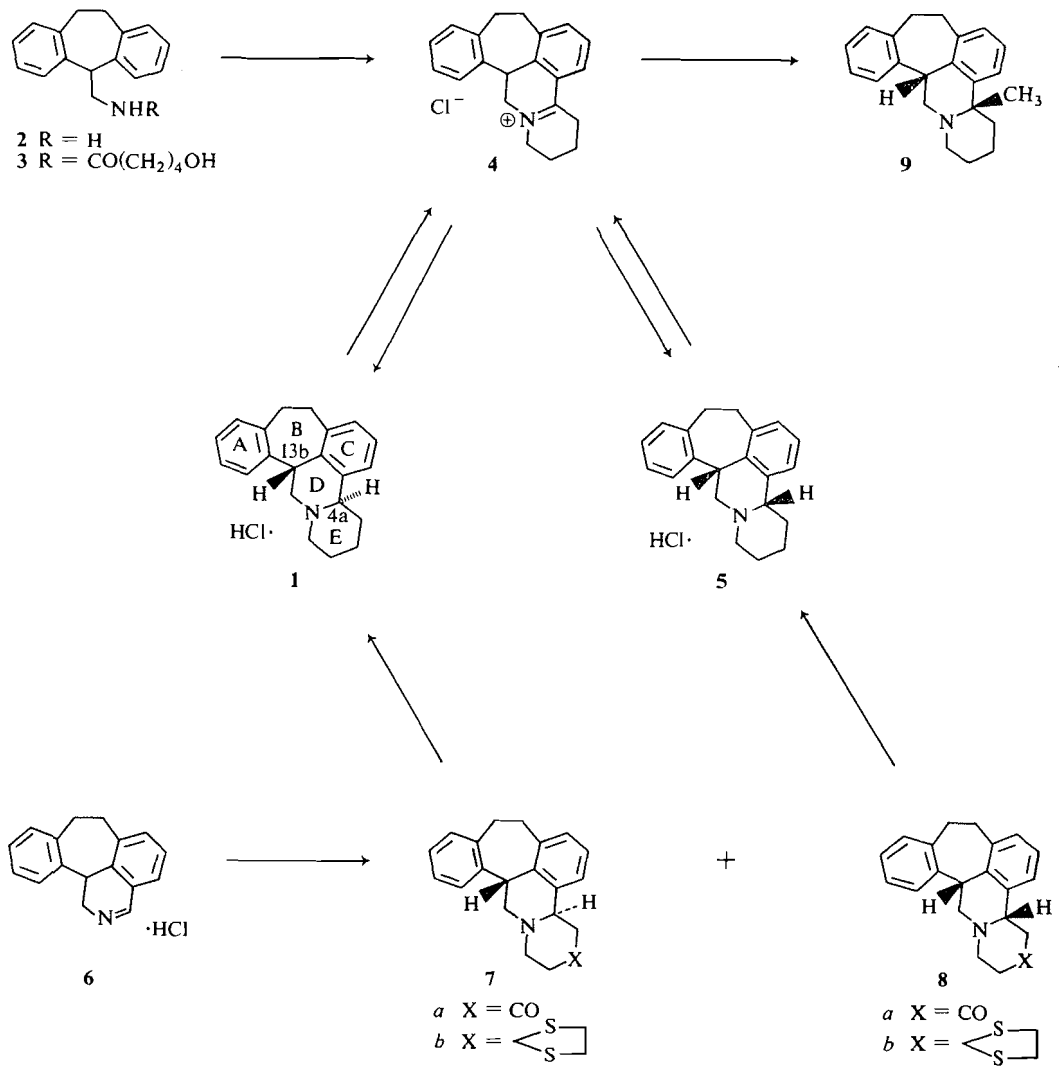

SCHEME 1

CDE plane and is oriented to it by an angle of about 100°. Absorption to the catalyst will take place from the less-hindered β-face of the molecule whence hydrogen will be delivered, generating a 4a,13b-*cis* relative configuration. The other isomer, **1**, obtained by zinc and hydrochloric acid reduction consequently is assigned a 4a,13b-*trans* relative configuration.

The i.r. spectra of **1** and **5** as their free bases show only weak absorption in the Bohlmann band region at 2700–2800 cm^{-1} and the low intensity of these bands makes their use unreliable for configurational assignments. The n.m.r. spectra, in contrast, show pronounced differences which can be readily interpreted. The preferred conformation of the 4a,13b-*trans* isomer **1** is shown in Fig. 1*A* in the form of the base along with the Newman projection obtained by viewing the C_{14}—C_{13b} axis. Of particular significance are the dihedral angles of 35 and 146° between the C_{13b}-proton and those at C_{14}. The C_{13b}-proton should consequently appear as a triplet in the isomer obtained by metal–acid reduction. Experimentally the n.m.r. spectrum of the metal–acid reduction product shows a one-proton band as a triplet centered at 4.9 δ which is assigned to the benzylic C_{13b}-proton and allows a 4a,13b-*trans* configurational

Can. J. Chem. Downloaded from www.nrcresearchpress.com by 210.87.254.40 on 09/05/12
For personal use only.

Can. J. Chem. Downloaded from www.nrcresearchpress.com by 210.87.254.40 on 09/05/12
For personal use only.

assignment for taclamine·HCl, **1**. Similarly, examination of the preferred conformation of the free base of the 4a,13b-*cis* isomer, **5**, (see Fig. 1*B*) reveals that the dihedral angles in question are 20 and 90°, and consequently the C_{13b}-proton should appear as a doublet as is observed experimentally, centered at 4.5 δ.

The assignment of 4.9 and 4.5 δ bands in the n.m.r. spectra to the 13b-protons of **1** and **5**, respectively, is confirmed by the appearance of a 4.4 δ band in the spectrum of the 4a-methyl derivative **9**. Compound **9** was obtained by the reaction of methyl magnesium iodide with the iminium salt **4**, and is expected to be formed by attack of the Grignard reagent from the least hindered β-face of the molecule, generating a 4a,13b-*cis* relationship of the groups at these centers. Thus, the absorption of the C_{13b}-proton of **9** (4.4 δ) occurs at about the same position as that of the corresponding proton in the *cis* isomer **5** (4.5 δ). The large downfield shift of the C_{13b}-proton, to 4.9 δ, in the *trans* isomer **1** is probably due to the deshielding of this proton by the nitrogen lone pair in **1** (see Fig. 1*A*).

The configurational assignments for the amino ketones **7***a* and **8***a* are consistent with their conversions to **1** and **5**, respectively. In addition the n.m.r. absorption of the C_{13b}-proton appears as a triplet in **7***a*, and as a doublet in **8***a* consistent with the patterns seen for *cis* isomers in this series (*viz.* **1** and **8***b*) and for *trans* isomers (*viz.* **5** and **7***b*).

Experimental

Melting points were taken on a Thomas-Hoover apparatus and are corrected. Analyses were done by Mr. W. Turnbull and staff of Ayerst Research Laboratories. The n.m.r. spectra were recorded on a Varian A-60-A instrument. All new compounds gave i.r. and n.m.r. spectra consistent with their respective structures.

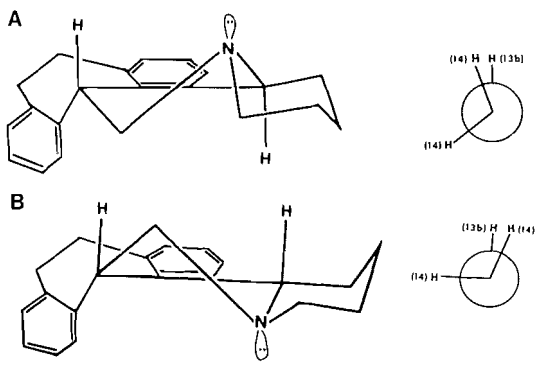

FIG. 1. Molecular models of **1** and **5**.

N-(10,11-Dihydro-5H-dibenzo[a,d]cyclohepten-5-ylmethyl)-5-hydroxyvaleramide (3)

A mixture of **2** (2) (20 g, 0.09 mol) and δ-valerolactone (12.5 g, 0.125 mol) was heated for 3 h at 150°. After cooling, the solid was recrystallized from benzene to give 24 g (83%) of **3**, m.p. 104–106°.

Anal. Calcd. for $C_{21}H_{25}NO_2$: C, 77.99; H, 7.79; N, 4.33. Found: C, 78.23; H, 7.74; N, 4.36.

1,2,3,4,8,9,13b,14-Octahydro[6,7]cyclohepta[1,2,3-de]pyrido[2,1-a]isoquinolinium Chloride (4)

Method A

To a solution of **3** (24 g, 0.074 mol) in 400 ml of toluene, phosphorus oxychloride (150 ml) was added and the reaction mixture was refluxed for 3 h. After cooling, petroleum ether (b.p. 60–80°) was added and the solvent was decanted. The residual oil was dissolved in benzene, quickly washed with water, a 10% aqueous sodium hydroxide solution and water again, dried, and finally refluxed for 40 min. The precipitate was recrystallized from acetone to give 10.1 g (42%) of **4**, m.p. 220–223°; u.v. (EtOH) λ 283 (ε 10 660); i.r. (Nujol) 3350 (OH), 1645 cm^{-1} (C=N). This compound could be obtained only in a hydrated form for which good analysis could not be obtained.

Anal. Calcd. for $C_{21}H_{22}ClN{\cdot}1\frac{1}{2}H_2O$: C, 71.88; H, 7.17; Cl, 10.09; N, 3.99; H_2O, 7.7. Found: C, 71.44; H, 7.00; Cl, 9.94; N, 3.62; H_2O, 8.2.

Method B

Compound **5** (1.5 g, 0.005 mol), and mercuric acetate (9.3 g, 0.029 mol) were dissolved in a mixture of 15 ml of tetrahydrofuran, 12 ml of acetic acid, and 50 ml of water and heated on a steam bath for 1 h. The hot solution was filtered and the filtrate concentrated under vacuum, made basic with a 10% aqueous sodium hydroxide solution, and extracted with ether. The dried ethereal solution was then treated with gaseous hydrogen chloride and the precipitate was crystallized from acetone to give 0.9 g (60%) of **4**, identical with the sample obtained according to method A. The same product was also obtained using **1** as starting material.

(±)-(4a,13b-cis)-2,3,4,4a,8,9,13b,14-Octahydro-1H-benzo[6,7]cyclohepta[1,2,3-de]pyrido[2,1-a]isoquinoline Hydrochloride (5)

Method A

Sodium borohydride (0.5 g, 0.013 mol) was added portionwise to a solution of **4** (1 g, 0.003 mol) in methanol and the mixture was refluxed for 1 h. The solvent was removed under vacuum, the residue treated with water, and extracted with ether to give 0.74 g (90%) of **5** free base, m.p. 132–134° (hexane); n.m.r. ($CDCl_3$) δ, 4.5 (d, 13b-H, J = 4 Hz).

Anal. Calcd. for $C_{21}H_{23}N$: C, 87.15; H, 8.01; N, 4.84. Found: C, 86.98; H, 8.31; N, 4.63.

The corresponding hydrochloride melts at 235–236° (acetone).

Anal. Calcd. for $C_{21}H_{23}N{\cdot}HCl$: N, 4.30; Cl, 10.88. Found: N, 4.34; Cl, 11.19.

Method B

Catalytic hydrogenation of **4** (1.3 g, 0.004 mol) in 50 ml of ethanol in presence of 50 mg of platinum oxide at room temperature and under normal pressure gave, after removal of the solvent, dissolution in hexane, and

Can. J. Chem. Downloaded from www.nrcresearchpress.com by 210.87.254.40 on 09/05/12
For personal use only.

filtration through alumina, 0.9 g (84%) of **5** free base, identical with the product obtained using method A.

Method C

To a refluxing solution of **8***b* (2 g, 0.005 mol) in 200 ml of tetrahydrofuran, 20 g of Raney Ni were added portionwise. The mixture was stirred and refluxed for 4 h. The Ni was removed, washed with 100 ml of tetrahydrofuran, and the pooled solutions were concentrated to 150 ml, then poured into water and extracted with ether. After drying and evaporating the solvent an oil (1.5 g) which crystallized slowly was isolated. Recrystallization from hexane gave 1 g (65.5%) of pure **5** free base, identical with samples obtained using methods A or B.

1,2,4,4a,8,9,13b,14-Octahydro-3H-benzo[6,7]cyclohepta[1,2,3-de]pyrido[2,1-a]isoquinolin-3-ones(7a and 8a)

A mixture of **6**·HCl (2) (32 g, 0.119 mol) and methyl vinyl ketone (26 g, 0.372 mol) was heated on a steam bath for 30 min. The mixture first became homogenous then gave a semisolid mass. This material was triturated with ether, dissolved in a 10% aqueous sodium hydroxide solution, and extracted with ethyl acetate. After drying and evaporating the solvent, crystallization from acetone–hexane gave 19 g (52.8%) of a mixture of 7*a* and **8***a*, m.p. 150–155°. Chromatography of this mixture on silica gel and eluting with chloroform–benzene (1:4) gave 2.8 g of **8***a*, m.p. 202–203° (acetone–hexane); n.m.r. ($CDCl_3$) δ 4.6 (d, 13b-H, J = 4 Hz).

Anal. Calcd. for $C_{21}H_{21}NO$: C, 83.13; H, 6.98; N, 4.62. Found: C, 83.30; H, 7.17; N, 4.46.

Using $CHCl_3$ as eluant 16 g of 7*a*, m.p. 163–165° (acetone–hexane) were isolated; n.m.r. ($CDCl_3$) δ 4.8 (t, 13b-H, J = 10 Hz).

Anal. Calcd. for $C_{21}H_{21}NO$: C, 83.13; H, 6.98; N, 4.62. Found: C, 83.08; H, 7.22; N, 4.41.

1,2,4,4a,8,9,13b,14-Octahydrospiro[3H-benzo[6,7]cyclohepta[1,2,3-de]pyrido[2,1-a]isoquinolin-3,2′-[1,3]dithiolanes] (7b and 8b)

A solution of a mixture of 7*a* and **8***a* (39 g, 0.129 mol) in 750 ml of acetic acid, 39 ml of ethanedithiol and 39 ml of boron trifluoride etherate was left overnight at room temperature. After pouring it into water and extracting with ether, the organic layer was neutralized with a 10% aqueous sodium carbonate solution, dried, and concentrated to give 37 g (76%) of a crystalline material, m.p. 218–220°. Chromatography of this mixture on silica gel using $CHCl_3$ as eluant gave **8***b*, m.p. 150° (methanol–hexane), followed by 7*b*, m.p. 225–230° (methanol–hexane) using methanol as eluant, in a ratio similar to that of the original mixture of 7*a* and **8***a*.

7*b*: n.m.r. ($CDCl_3$) δ 4.83 (t, 13b-H, J = 13 Hz).

Anal. Calcd. for $C_{23}H_{25}NS_2$: C, 72.78; H, 6.64; N, 3.69. Found: C, 72.88; H, 6.60; N, 3.39.

8*b*: n.m.r. ($CDCl_3$) δ 4.5 (d, 13b-H, J = 4 Hz).

Anal. Calcd. for $C_{23}H_{25}NS_2$: C, 72.78; H, 6.64; N, 3.69. Found: C, 72.68; H, 7.01; N, 3.56.

*(±)-(4a,13b-trans)-2,3,4,4a,8,9,13b,14-Octahydro-1H-benzo[6,7]cyclohepta[1,2,3-de]pyrido]2,1-a]isoquinoline hydrochloride (**1**)*

Method A

A suspension of **4** (2 g, 0.006 mol), 4 g of Zn dust in 150 ml of ethanol and 40 ml of concentrated hydrochloric acid was stirred and heated on a steam bath for 1 h. The ethanol was removed under vacuum and the remainder of the mixture was made basic with concentrated ammonium hydroxide and then extracted with benzene. The benzene extract was dried and concentrated to dryness. The crude base (1.2 g) was dissolved in 10 ml of benzene and absorbed on a column of 120 g of neutral alumina (activity II). By elution with hexane 325 mg (19.7%) of **5** free base, m.p. 132–134° was first isolated; elution with benzene gave 800 mg (48.5%) of **1** free base m.p. 90–92° (hexane); n.m.r. ($CDCl_3$) δ 4.9 (t, 13b-H, J = 14 Hz).

Anal. Calcd. for $C_{21}H_{23}N$: C, 87.15; H, 8.01; N, 4.84. Found: C, 87.46; H, 8.13; N, 4.63.

The hydrochloride salt of **1** was crystallized from isopropanol–acetone, m.p. 270–272°.

Anal. Calcd. for $C_{21}H_{23}N$·HCl: C, 77.40; H, 7.42; N, 4.30; Cl, 10.88. Found: C, 77.56; H, 7.52; N, 4.30; Cl, 10.92.

Method B

In the same way as described for the preparation of **5** (method C), 7*b* (1.9 g, 0.005 mol) was treated with 20 g of Raney Ni to give 1.2 g (83%) of **1** free base, which was converted directly to the corresponding hydrochloride **1** identical with the product obtained by using the method above.

*(±)-(4a,13b-cis)-4a-Methyl-2,3,4,4a,8,9,13b,14-octahydro-1H-benzo[6,7]cyclohepta[1,2,3-de]pyrido[2,1-a]isoquinoline (**9**)*

Compound **4** (4 g, 0.0114 mol) was added portionwise to a solution of methylmagnesium iodide in ether (100% excess) and the reaction mixture was refluxed for 40 min. The excess of the Grignard reagent was destroyed by adding slowly a saturated solution of ammonium chloride in water (150 ml). The organic phase was separated, dried, and concentrated to give 2.5 g of an oil, which was chromatographed over alumina (neutral, activity I) using benzene as eluant. After crystallization from hexane 2.3 g (66.3%) of **9**, m.p. 119–120°, were isolated; n.m.r. ($CDCl_3$) δ 1.3 (s, 4a-CH_3), 4.4 (d, 13b-H, J = 5 Hz).

Anal. Calcd. for $C_{22}H_{25}N$: C, 87.08; H, 8.30; N, 4.62. Found: C, 87.00; H, 8.45; N, 4.76.

The corresponding hydrochloride melts at 270° (methanol–ether).

Anal. Calcd. for $C_{22}H_{25}N$·HCl: C, 77.71; H, 7.71; N, 4.72; Cl, 10.43. Found: C, 77.50; H, 7.75; N, 4.69; Cl, 10.58.

The authors wish to thank Miss R. Liechti, Mr. B. Berger, and Mr. N. Sideridis for their valuable technical assistance.

1. K. Voith and F. Herr. Abstract of papers, fifth international congress on pharmacology, San Francisco, 1972. Abstr. No. 1457. p. 243.
2. L. G. Humber, M. A. Davis, R. A. Thomas, R. Otson, and J. R. Watson. J. Heterocycl. Chem. **3**, 247 (1966).
3. L. G. Humber, M. A. Davis, G. Beaulieu, and M.-P. Charest. Can. J. Chem. **46**, 2981 (1966).

Reactions of Aralkyl and Unsaturated Chloramines: The Nitrenium Ion Question[1]

O. E. EDWARDS, G. BERNATH,[2] J. DIXON,[2] J. M. PATON,[2] AND D. VOCELLE[2]

Division of Biological Sciences, National Research Council of Canada, Ottawa, Canada K1A 0R6

Received December 5, 1973

O. E. EDWARDS, G. BERNATH, J. DIXON, J. M. PATON, and D. VOCELLE. Can. J. Chem. **52**, 2123 (1974).

Evidence for intermolecular electrophilic halogenation of aromatic rings and olefinic double bonds by aliphatic chloramines at low p*H*, and for homolytic cyclization of unsaturated chloramines in neutral medium is presented. Independent proof of structure and stereochemistry of derivatives of 6-azabicyclo[3.2.1]octane and 2-azabicyclo[2.2.2]octane was provided. No evidence for involvement of nitrenium ions in the chloramine reactions was observed.

O. E. EDWARDS, G. BERNATH, J. DIXON, J. M. PATON et D. VOCELLE. Can. J. Chem. **52**, 2123 (1974).

L'évidence, d'un processus d'halogénation électrophile intermoléculaire par les chloramines aliphatiques en milieu acide, est démontrée pour les composés contenant des cycles aromatiques ou des doubles liaisons à caraitire oléfinique. Nous démontrons aussi que la cyclisation thermique des chloramines non saturées, en milieu neutre, procède de façon homolitique. Des preuves de la structure et de la stéréochimie des dérivés de l'aza-6 bicyclo[3.2.1]octane et de l'aza-2 bicyclo[2.2.2]octane sont présentées.

Aucune évidence de l'implication d'un ion nitrénium dans ces réactions de chloramines ne fut observée. [Traduit par le journal]

Some time ago we concluded that nitrenium ions (R_2N^+) could be generated from aliphatic chloramines using silver ions in polar solvents (1). However, subsequent work showed that the reactions were mainly homolytic (2) and that near room temperature simple aliphatic chloramines do not react at an appreciable rate with silver ions. It occurred to us that if there were any tendency for silver-promoted ionization of the N—Cl bond as in eq. 1, the presence of a nucleophilic aromatic ring might assist in the ionization and result in amination of the ring. Again, however, mixtures of silver nitrate and *N*-chloropiperidine with 2-methoxynaphthalene or anisole in methanol reacted very slowly at room temperature. A mixture of diethylchloramine and silver perchlorate in anisole was inert at room temperature, and at 65° no diethylaminoanisoles were produced.

$$[1] \qquad R_2\ddot{N}Cl\cdots Ag^+ \rightarrow R_2\ddot{N}^+ + AgCl$$

In order to enhance the chance of electrophilic attack on the aromatic nucleus by developing nitrenium ions, we next examined the reactions of *N*-chloro-2′-methylamino-3-methoxyphenylethane (**1**) and *N*-chloro-3′-methylamino-3-methoxyphenylpropane (**2**). These proved inert at room temperature to silver perchlorate in benzene, and silver nitrate in methanol or acetonitrile, provided the p*H* was above 5. Reaction of **1** and **2** with silver perchlorate in benzene was slow (*ca.* 20% per hour) even at reflux temperature and only traces of tertiary amines were formed.

At low p*H* electrophilic chlorination of the aromatic nuclei became rapid. Anisole and *N*-chloropiperidine in methanol containing *p*-toluenesulfonic acid gave *O*- and *p*-chloroanisoles in the ratio 1:2. This is the ratio for attack on the nucleus by cationic chlorine as distinct from homolytic chlorination (3). 2-Methoxynaphthalene gave 1-chloro-2-methoxynaphthalene in high yield under similar conditions and chloramines **1** and **2** gave mixtures of nuclear chlorinated products.

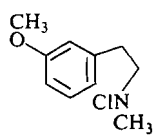

1

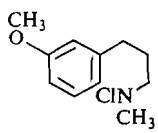

2

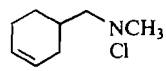

3

Thus we had again failed to demonstrate any tendency of aliphatic N—Cl bonds to ionize toward nitrenium ions even with silver ion assistance and the proximity of nucleophilic aromatic nuclei. However, Gassman and co-workers have claimed that nitrenium ions are important in a variety of chloramine solvolyses in hot polar solvents (4, 5*a*). Among these cases were reports of a π route to azabicyclic compounds (*e.g.* eq.

[1]Issued as NRCC No. 13880. Presented in part at the Symposium on Heterocyclic Chemistry, Poznan, July 24–26, 1972.

[2]NRCC Postdoctorate Fellows.

Can. J. Chem. Downloaded from www.nrcresearchpress.com by 210.87.254.40 on 09/05/12
For personal use only.

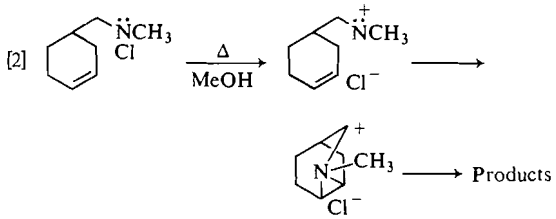

2). Since such cyclic products could have arisen by (*a*) electrophilic chlorination followed by cyclization or (*b*) by homolytic fission of the N—Cl bonds followed by cyclization, we decided to reexamine these reactions.

At room temperature in methanol *N*-chloro-4-methylaminomethylcyclohexene (**3**) was inert in the presence of silver salts provided the p*H* was above 5. At reflux temperature the initial reaction was slow and the major product (70%) was parent amine.

When chloramine **3** was treated at 5 °C with *p*-toluenesulfonic acid in methanol a rapid reaction ensued. Unless more than 1 molar equiv. of acid was present the reaction ended when the acid was neutralized by products. With excess acid, the chloramine reacted completely in 2 h at room temperature. The mixture of salts of the initial products was converted to the free bases, then a methanol solution of these refluxed. The bases **4** (if present) and **5** cyclized to give *N*-methyl-4-

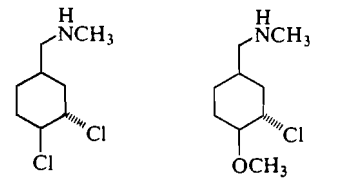

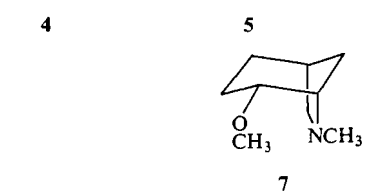

endo-chloro-6-azabicyclo[3.2.1]octane (**6**) and *N*-methyl-4-*endo*-methoxy-6-azabicyclo[3.2.1]octane (**7**). The remaining base, which did not cyclize, was separated and characterized as its *N*-acetyl derivative. It was assigned the structure *N*-methyl-*cis*-4-chloro-*trans*-3-methoxy-1-aminomethylcyclohexane (**8**) on the basis of analysis, spectra, and the failure to cyclize. The location of the substituents is surmised on mechanistic grounds (see Discussion).

The best yield of **6** was 7%. Its structure and stereochemistry were deduced from its failure to

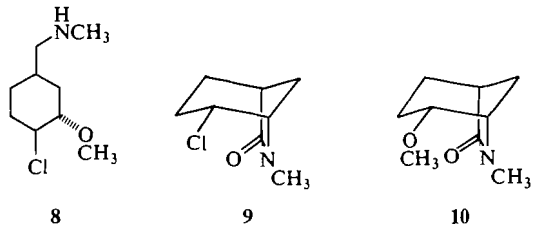

cyclize, and its oxidation to the γ-lactam **9** (ν_{max} ($CHCl_3$) 1690 cm^{-1}). The best yield of **7** was 32%. Its nonidentity with the *trans* isomer (see below) and its oxidation to a γ-lactam (**10**) proved its structure and stereochemistry.

If the total base from the acid-catalyzed reaction of **3** in methanol was isolated under mild conditions, then acetylated, the only tertiary base found was **6** (7.5%). It was shown that the *N*-acetyl fraction contained derivatives of **5** and **8**.

When *N*-chloro-*N*-methyl-5-aminomethylcycloheptene (**11**) was decomposed by *p*-toluenesulfonic acid in methanol and the basic products refluxed in methanol very little bicyclic material formed. A 0.02% yield of the chlorobicyclic base **12** (*N*-methyl-*cis*-4-chloro-6-azabicyclo[3.2.2]-nonane) was isolated as its perchlorate but the small amount of methoxybicyclic base was not obtained pure. The main products were secondary bases, isolated as their *N*-acetyl derivatives. The mixture analyzed approximately correctly for **13** (and/or **14**) and its n.m.r. spectrum was consistent with these structures.

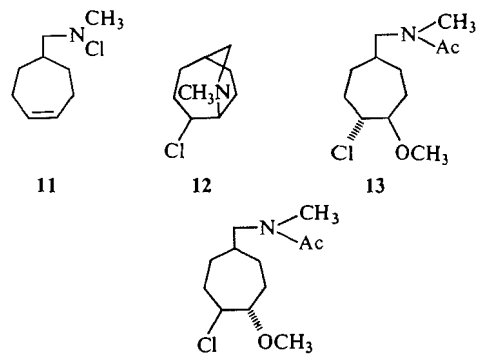

We next studied the thermolysis of **3** and **11** in pure methanol under nitrogen. In each case the reactions at reflux temperature showed a marked induction period (1–3 h before reaction began) followed by fairly rapid decomposition of the chloramine (Fig. 1). This is characteristic of homolytic reactions. In accord with this, the presence of around 1 mol% of benzoyl peroxide eliminated the induction period (Fig. 1). In the

Can. J. Chem. Downloaded from www.nrcresearchpress.com by 210.87.254.40 on 09/05/12
For personal use only.

Can. J. Chem. Downloaded from www.nrcresearchpress.com by 210.87.254.40 on 09/05/12
For personal use only.

case of **3** the product composition was identical with or without the peroxide. However, in the case of **11** the product ratios changed moderately when the initiator was present. If the thermolysis was conducted under oxygen the reaction was markedly slowed (Fig. 1) and the major product became parent secondary amine.

The main products from **3** were the same as described by Gassman and Dygos (5), *N*-methyl-4-*endo*-chloro-6-azabicyclo[3.2.1]octane (**6**) (13%), *N*-methyl-4-*exo*-methoxy-6-azabicyclo[3.2.1]octane (**15**) (18%), *N*-methyl-*trans*-6-methoxy-2-azabicyclo[2.2.2]octane (**16**) (27%), and parent amine (14%). In addition traces of two volatile tertiary bases, probably **17** and **18**, and 15% of higher boiling bases were produced.

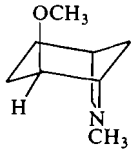

15

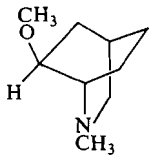

16

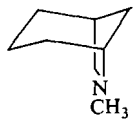

17

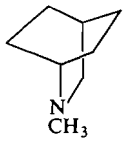

18

The structure and stereochemistry that had been assigned to **15** and **16** (5) was confirmed by independent synthesis from cyclohex-1-ene-3-carboxylic acid using acyl nitrene cyclization (6) (Scheme 1).

The ring system in **17** and **20** was deduced on the basis of the carbonyl stretching frequency (γ- and δ-lactam, respectively) (7).

The cycloheptene analogue **11** similarly gave parent amine (3.5%), the bicyclic chloro base **12** (4.5%), and a methoxy bicyclic base (25%). By

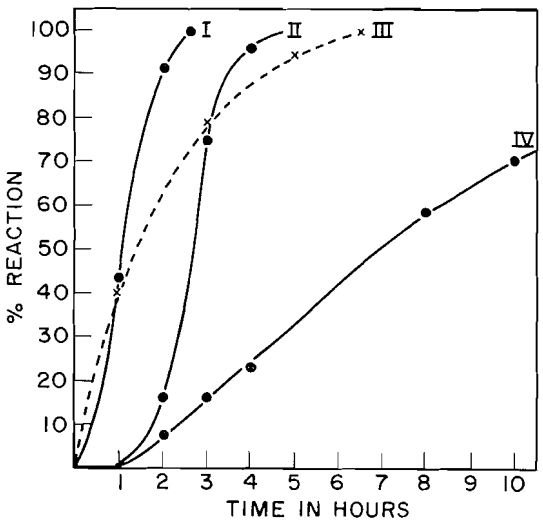

FIG. 1. Reaction of **3** in methanol: (I) reflux, 1 mol % perbenzoic acid, N_2; (II) reflux, N_2; (III) Ag^0, 25 °C, N_2; (IV) reflux, O_2.

analogy to the cyclohexene case this was assigned the structure *N*-methyl-*trans*-4-methoxy-6-azabicyclo[3.2.2]nonane (**21**).

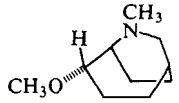

21

In view of the relatively efficient production of amine radicals from medium ring chloramines by Tollens' silver reported earlier, the action of this reagent on a number of the above-mentioned chloramines was studied. In all cases the major product was the parent amine.

Discussion

The electrophilic chlorinations are mainly understandable in terms of transfer of positive chlo-

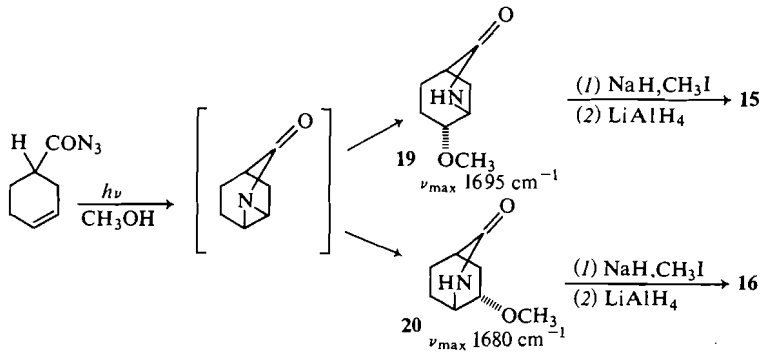

SCHEME 1

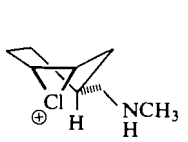

22 23

rine from protonated chloramine to aromatic rings or double bonds (eqs. 3 and 4).

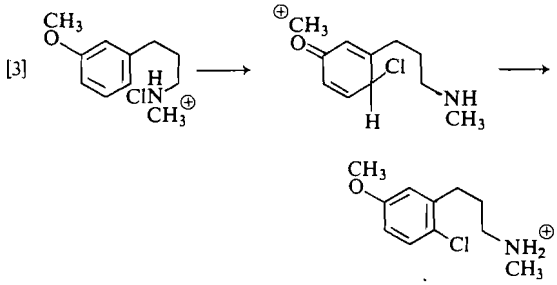

[3]

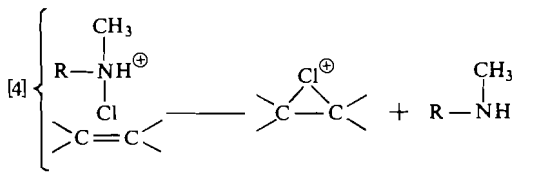

[4]

Diaxial opening by methanol of the two chloronium ions **22** and **23** from **3** would give the two methoxy–chloro bases **5** and **8**, respectively. The fact that both are formed in similar yields shows that intermolecular reaction is dominant.

We cannot exclude the possibility that some chlorine was produced as the reactions progressed, formed by the action of chloramines on small amounts of chloride ion produced in cyclization reactions. Indeed, the hydrochloride of *N*-methyl-4-aminomethylcyclohexene in methanol containing *p*-toluenesulfonic acid reacted rapidly with chlorine, giving after work-up the three main products found in the acid-catalyzed reaction of the chloramine. However, the minor amounts, if any, of **7** and **8** in the thermal and benzoyl peroxide-initiated reactions show that free chlorine plays no significant role in these reactions.

The chlorobicyclic base **6** could arise in the acid-catalyzed reactions by cyclization of **4**, which could arise by chloride ion attack on chloronium ions **22** or **23**. Since, however, **6** is the only bicyclic product formed unless the basic products are heated in methanol, this would demand that **4** would cyclize very much faster than **5**. An alternate possibility is that a small homolytic

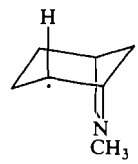

24

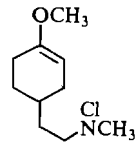

25

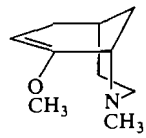

26

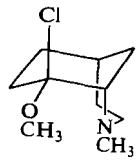

27

component of reaction leads to the bicyclic radical **24**, which gives both the *cis*- and *trans*-chloro compounds. The latter could be lost during work-up (via aziridinium ion to water-soluble hydroxy base).[3]

While our studies of the acid-catalyzed reactions of **3** were in progress, Gassman and Dygos (*5b*) published an account of similar reactions of **3** in aqueous acid. However, they interpreted the reactions as involving discrete Cl^+ ions. The recent observations of Waegell and co-workers on chloramines containing enol ether functions (8) parallel nicely the above electrophilic chlorination of **3**. Surprisingly, however, they encountered predominant electrophilic chlorination in the thermal reaction of **25** in methanol without added acid. This is probably a consequence of the high nucleophilic potential of the enol ether. Contrary to their conclusions, however, we consider the origin of the bicyclic enol ether **26** formed during the initial reaction to be the chloromethoxy compound **27** produced in a radical process.

Neale and Marcus described acid catalyzed intermolecular electrophilic chlorination of olefins by chloramines but interpret these as Cl^+ ion reactions rather than direct transfer of chlorine from protonated chloramine to olefin (9). However, Hickinbottom and co-workers (10) have presented evidence that chlorination of aromatic nuclei by protonated *N*-chloroacetanilides in the absence of chloride ion is direct electrophilic chlorination. Chloroaminations of double bonds catalyzed by aluminum chloride have been described by Kovacic and Lowery (11) and Waegell and co-workers (12). Whereas these reactions could be interpreted as involving initial

[3]Prof. J. D. Hobson (personal communication) and co-workers have observed this selective loss in related work.

Can. J. Chem. Downloaded from www.nrcresearchpress.com by 210.87.254.40 on 09/05/12
For personal use only.

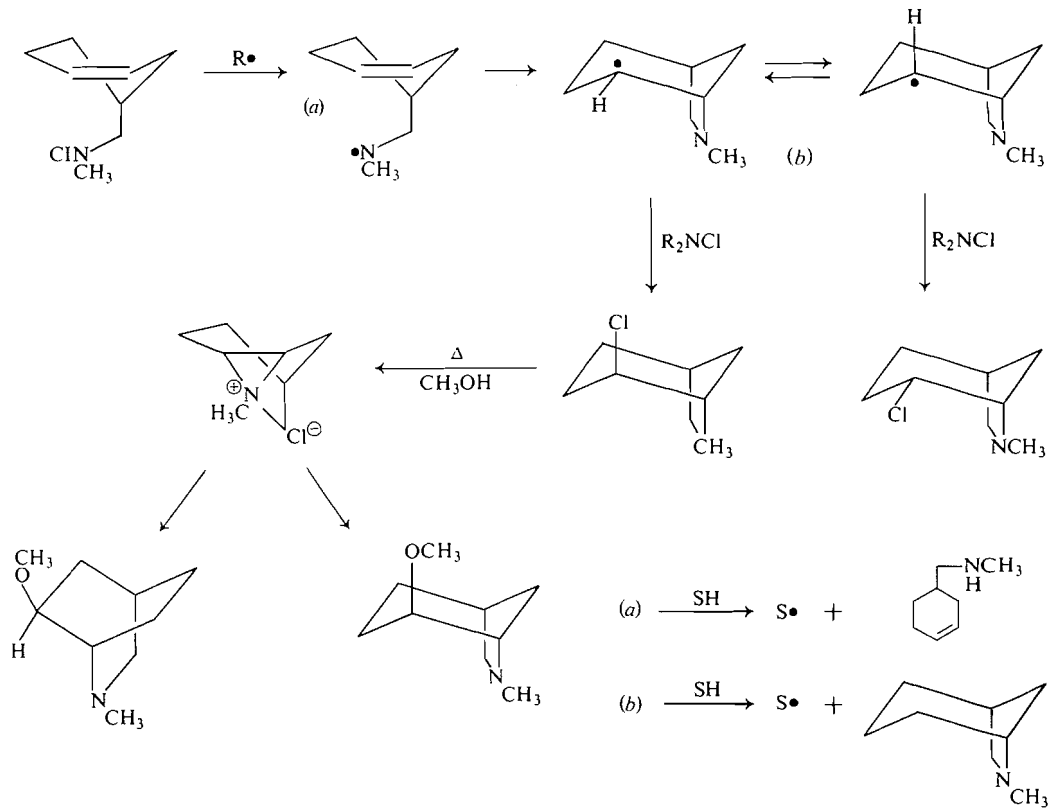

SCHEME 2

attack by Cl^+ ions (13), addition as nitrenium ion – $AlCl_4^-$ pairs is also possible in view of the molecular rearrangements observed under the influence of the same catalyst (14–20).

It is clear from the complete difference in the methoxybicyclic products between the acid-catalyzed and thermal reactions of **2** and **11** that a different mechanism is operative in the latter. The observed induction period, the retardation by oxygen, and the acceleration of reaction by radical sources such as benzoyl peroxide demonstrate that the thermal reactions are homolytic. The mechanism in Scheme 2 accounts for all the observed products and their stereochemistry. Hobson and co-workers have reached the same conclusion in their work on cyclooctene derivatives (21). They also showed that oxygen or *N*,*N*-diphenylpicrylhydrazyl markedly slowed the thermal decomposition. Parallel cyclizations of **3** and its close relatives have been described by Surzur and co-workers (22) using redox systems or photolysis to generate the nitrogen-centered radical, and by Chow and Perry (23) using photolysis of the related *N*-chloro- and *N*-nitrosoamides.

We conclude that nitrenium ions are not formed from simple aliphatic chloramines near room temperature, even when double bonds or aromatic rings are available to provide anchimeric assistance, and silver ions are present to assist ionization. In addition, no heterolytic fission takes place at 60–80 °C, decomposition at these temperatures only being initiated by traces of adventitious radicals. Possible homolytic mechanisms can be written for other reactions considered to involve nitrenium ions. For example, arenesulfonyloxy radicals have been shown to be good electrophilic reagents (24), hence the *N*-tosyloxyoxindole reactions (25) may be formulated as in eq. 5. However, the molecular rearrangements observed by Gassman (26), Kovacic and co-workers (19), Wasserman and co-workers (20), and by Rautenstrauch (27) seem best explained as involving assisted ionizations in the $>N^+\cdots Cl^-$ sense.

We had hoped that silver metal would provide

Can. J. Chem. Downloaded from www.nrcresearchpress.com by 210.87.254.40 on 09/05/12
For personal use only.

[5] 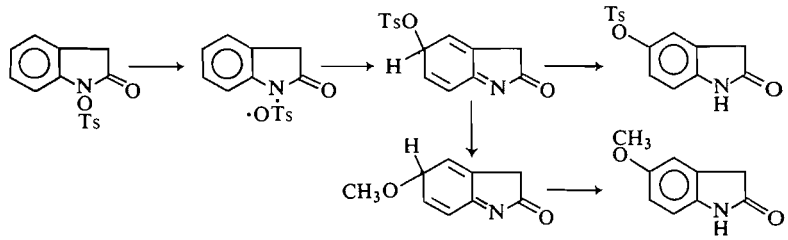

us with a room temperature preparation of the various nitrogen radicals, as in the reactions with medium ring chloramines (2). However, the major products were the parent secondary amines. This could have been rationalized if the initial nitrogen-centered radicals were reduced by excess silver to the anion (eq. 6).[4] This is in ac-

$$[6]\quad >N\cdots Cl + Ag^0 \rightarrow >N\cdot + AgCl \xrightarrow{Ag^0} >N^- + Ag^+$$

cord with our observation of reduction of succinamidyl radical to the anion by silver (28). However, nearly 1 equiv. of silver chloride was produced (few chain reactions) and no other Ag(I) products were formed. Hence we must conclude that most of the nitrogen-centered radicals produced in this way are unable to cyclize before abstracting hydrogen from solvent and that the reduction shown in eq. 6 does not take place.

Mass Spectra

We had hoped that electron impact mass spectra would distinguish between the bicyclo[3.2.1] and bicyclo[2.2.2] structures, and possibly between the epimers **7** and **15**. In actuality, the spectra of all three components (**7**, **15**, and **16**) were very similar down to *m/e* 82 (Table 1). Since

TABLE 1. Relative abundance of ions

	Base		
m/e	**7**	**15**	**16**
155	15	14	29
140	25	33	81
97	6	9	40
96	21	26	49
94	12	14	27
82	100	100	100
72	140	165	23
57	175	159	35

[4]We thank Prof. J. D. Hobson who independently suggested this possibility.

this ion most probably has the structure **28** (see also refs. 29 and 30), we were unable to convincingly account for its formation from **16**, hence we proved the structure of **16** as described above. The probable origin of the more abundant ions with higher masses is outlined in Scheme 3. It now

28

appears that the ions at *m/e* 72 and 57 are the most characteristic features from the two bicyclo[3.2.1] bases. These ions are unimportant for the parent heterocycle (29) and of low abundance in the spectrum of **16**. We account for them as shown in Scheme 4. The stereochemistry of the methoxyl group in **7** and **15** only makes a small difference in the fragmentation (see also ref. 29). As anticipated on the basis of more advantageous stereoelectronic factors, the ratio of *m/e* 140 to the parent ion was higher for the *trans* isomer (2.3) than for the *cis* (1.7).

Experimental

The i.r. spectra were obtained using a Perkin-Elmer model 257 grating spectrometer, and n.m.r. spectra on a Varian A60A spectrometer. Mass spectra were obtained using a Perkin Elmer-Hitachi single-focussing instrument. The g.l.c. analyses of amines were done using a 6 ft × ¼ in. column of OS-138 (polyphenyl ether, 20%) on Chromosorb and preparative separations using a 6 ft × 3/8 in. column with the same packing. The yields were calculated on the assumption that peak areas using a thermal conductivity detector were proportional to the mol fraction of the very similar molecules being separated.

Anisole Reactions

(*i*) Two grams of diethylchloramine was added to a solution of 4 g of anhydrous silver perchlorate in 30 ml of anisole. Only a trace of silver perchlorate precipitated in 17 h at room temperature in the dark. In 3 h at 65° a heavy precipitate formed which consisted of 1.9 g of silver chloride and 3.3 g of amine perchlorate. The latter was converted to the base which was extracted into ether. On evaporation no base higher boiling than diethylamine was found.

(*ii*) A solution of 1.08 g of anisole (10 mmol) and 3.8 mg of *p*-toluenesulfonic acid (20 mmol) in 40 ml of methanol

Can. J. Chem. Downloaded from www.nrcresearchpress.com by 210.87.254.40 on 09/05/12
For personal use only.

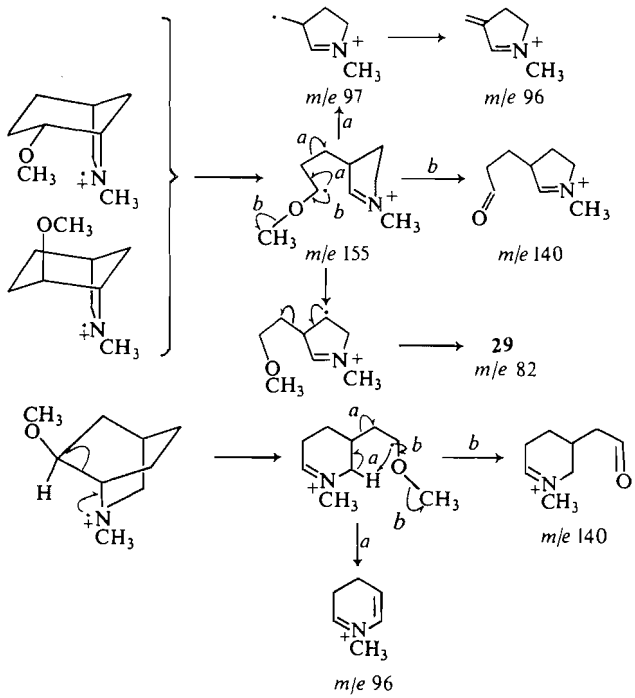

SCHEME 3

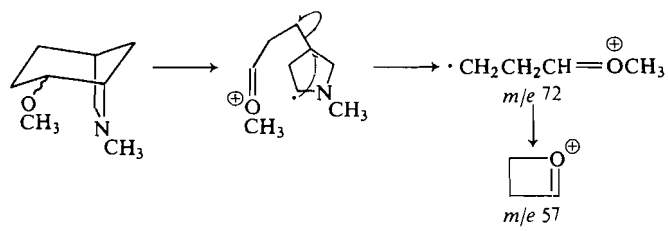

SCHEME 4

and 5 ml of water was prepared. To this was added 1.18 g of *N*-chloropiperidine (10 mmol) in 5 ml of methanol and the mixture stirred under nitrogen in the dark. After 1 h 25% and after 5 h, 70% of the chloramine had reacted. The mixture was left overnight at room temperature, the bulk of the methanol removed under reduced pressure, and the product extracted into ether. The ether was washed with water, then with sodium carbonate solution, dried, and evaporated. The 600 mg of product recovered were demonstrated by n.m.r. spectroscopy to consist of *O*-chloroanisole (δ OCH_3 3.87) and *p*-chloroanisole (δ OCH_3 3.79) in the ratio 1:2.

2-Methoxynaphthalene and N-Chloropiperidine

(*i*) With $AgNO_3$ in methanol: to a solution of 1.58 g (10 mmol) of 2-methoxynaphthalene and 1.185 g (10 mmol) of *N*-chloropiperidine in 40 ml of methanol and 5 ml of water was added 1.7 g (10 mmol) of silver nitrate. A very slow reaction ensued (*ca.* 25% per day at first). After 1 week only a trace of chloramine was identified among the less-volatile product.

(*ii*) A solution of 1.58 g (10 mmol) of 2-methoxynaphthalene and 1.185 g of *N*-chloropiperidine in 45 ml of methanol and 5 ml of water was stirred under nitrogen for 5 h. No reaction occurred. Addition of 20 mmol of *p*-toluenesulfonic acid in 10 ml of methanol induced rapid reaction. In 10 min at room temperature only 5% of the *N*-chloropiperidine remained. After 1 h the bulk of the solvent was removed under reduced pressure, the product extracted into ether. the ether washed with sodium carbonate solution, then water, dried, and distilled. The 1.85 g of crude product was shown by t.l.c. separation of an aliquot to contain 1.64 g (85%) of 1-chloro-2-methoxynaphthalene, m.p. 68–69° (lit. (31, 32) m.p. 69°).

2′-Methylamino-3-methoxyphenylethane

This was prepared by reduction of the corresponding amide by lithium aluminum hydride in refluxing tetrahydrofuran. It gave a hydrochloride which crystallized as fine needles from ethanol – ethyl acetate, m.p. 119–120°.

Anal. Calcd. for $C_{10}H_{16}ClNO$: C, 59.70; H, 7.96; N, 6.96. Found: C, 59.82; H, 7.87; N, 6.97.

Can. J. Chem. Downloaded from www.nrcresearchpress.com by 210.87.254.40 on 09/05/12
For personal use only.

Can. J. Chem. Downloaded from www.nrcresearchpress.com by 210.87.254.40 on 09/05/12
For personal use only.

3'-Methylamino-3-methoxy-1'-phenylpropane

This was prepared as described for the lower homologue. Its hydrochloride had m.p. 106–107°.

Anal. Calcd. for $C_{11}H_{18}ClNO$: C, 61.25; H, 8.35; N, 6.50. Found: C, 61.43; H, 8.29; N, 6.43.

Reactions of N-Chloro-2'-methylamino-3-methoxyphenylethane (1)

(a) With Silver Nitrate in Methanol

A solution of 1.45 g of silver nitrate in 30 ml of methanol (heating) was stirred with powdered calcium carbonate to give a p*H* of near 6, then filtered. A portion (20 ml) of this was added to 431 mg (2.16×10^{-3} mol) of the chloramine (**1**). No reaction took place in 1 h at room temperature. The solution was then placed in a bath at 64° under nitrogen. The extent of reaction was: 1 h, 18%; 2 h, 43%; 3 h, 59%; 4¾ h, 78%. The heating was continued for a further 6 h to ensure complete reaction. The product isolated consisted of 259 mg of silver chloride (1 equiv. = 280 mg), 66 mg of neutral oil (aldehyde and amides), and bases which after acetylation gave 20 mg of tertiary base and 270 mg of *N*-acetyl derivative. The latter was shown by n.m.r. to be essentially pure *N*-acetyl derivative of the parent amine.

Comparable results were obtained when the reaction was done in air.

(b) With Silver Perchlorate in Benzene

A solution of 500 mg of anhydrous silver perchlorate and 329 mg (1.65×10^{-3} mol) of the chloramine in 12 ml of dry benzene gave a clear solution. No silver chloride formed in 2 h at room temperature. After 3 h at 65°, 45% of the chloramine had reacted. Reaction was nearly complete after a further 6 h heating. Silver chloride and a brown methanol-soluble solid had separated. The products isolated were 139 mg of silver chloride (1 *M*equiv. is 220 mg), 67 mg of ether-soluble neutral oil, and bases which on acetylation gave 104 mg of *N*-acetyl derivative of the parent base and 33 mg of tertiary base. In each case the neutral and tertiary base products were mixtures and because of the low yields the components were not identified.

(c) With Silver Perchlorate in Acetonitrile

One gram of anhydrous silver perchlorate was dissolved in 5 ml of acetonitrile (freshly filtered through Activity 1 alumina). The solution was added to 10 ml of dry acetonitrile containing 309 mg (1.55×10^{-3} mol) of chloramine **1**. No reaction was detected in 2 h at room temperature but after 17 h in the dark, 32% of the chloramine had reacted. Subsequent heating at 50 °C for 4 h completed decomposition of the chloramine. The products isolated were 172 mg of silver chloride (70 mol %), 81 mg of ether-soluble neutral product (amides), 14 mg of "tertiary base", and 84 mg of parent amine.

Reactions of N-Chloro-3'-methylamino-3-methoxy-1'-phenylpropane (2)

(a) With Silver Nitrate in Methanol

A solution of 888 mg of silver nitrate in 30 ml of methanol containing 1 g of powdered calcium carbonate was stirred for 20 min, then filtered. The solution was added to 0.581 g (2.73×10^{-3} mol) of the chloramine (**2**). No silver chloride separated and iodimetry showed that the chloramine was unchanged after 5 h at room temperature in diffuse light. After a further 15 h at room temperature, 4.5% of the chloramine had reacted. The mixture was then heated in a bath at 60° in semidarkness. The extent of reaction was: 1.5 h, 37%; 3 h, 58%; 6 h, 76%. It was then left for 63 h at room temperature, when only a trace of oxidizing material was left. The suspension was filtered, giving 282 mg of silver chloride (1 equiv. = 353 mg). Dilute hydrochloric acid was added to the filtrate to precipitate the excess silver ions. After filtration, the solution was adjusted to p*H* 3 and the bulk of the methanol removed under reduced pressure below room temperature. The product was separated into 101 mg of aldehyde (ν_{max} 1740 cm^{-1}, C*H*O signal a doublet at δ 9.4), 347 mg of parent amine and 28 mg of tertiary base.

(b) With Silver Perchlorate in Benzene

A solution of 1.5 g of anhydrous silver perchlorate in 20 ml of hot benzene was filtered to remove a trace of brown solid. The filtrate was added to 0.555 g (2.6×10^{-3} mol) of chloramine **2**. No silver halide formed at room temperature. In a bath at 70°, 48% of the chloramine reacted in 1.25 h, 60% in 2.25 h, and 97% in 6 h. A brown solid deposited on the walls. The products isolated from the solid and solution were silver chloride contaminated with a methanol-insoluble brown solid, 68 mg of methanol soluble ether insoluble solid and 396 mg of bases. The latter were shown by acetylation to contain 19 mg of tertiary bases and 377 mg of parent base.

(d) With Acid in Methanol

A solution of 1.11 g (5.2 mmol) of **2** and 1.9 g (10 mmol) of *p*-toluenesulfonic acid hydrate in 30 ml of methanol was left at room temperature. In 15 min, 85% of the chloramine had decomposed. After complete reaction (1 h) the products were separated by acetylation into tertiary base (*ca.* 50 mg) and *N*-acetyl secondary bases (950 mg). The latter was analyzed for chlorine.

Anal. Calcd. for $C_{13}H_{18}ClNO$: Cl, 13.86. Found: Cl, 14.06%.

Acid Catalyzed Reactions of Chloramine (3)

(*a*) A methanol solution (53 ml) containing 1.99 g (1.25×10^{-2} mol) of chloramine **3** was cooled in an ice bath. Over a period of 5 min 5 g of *p*-toluenesulfonic acid hydrate was added to the stirred chloramine solution. After a further 15 min the reaction mixture was removed from the ice bath and allowed to come to room temperature. After a total time of 1.3 h only a trace of chloramine remained (iodimetry). The remaining solution (1 ml removed for titrations) was evaporated to a syrup on a rotating evaporator. The residue was diluted with water, neutralized with sodium carbonate, made strongly alkaline with sodium hydroxide solution, then thoroughly extracted with ether. The 2.02 g of faintly yellow base was dissolved in 100 ml of methanol then the solution refluxed under nitrogen for 16.5 h during which time 3.54×10^{-3} g-atom of chloride ion was formed (29% of theory). The solution was acidified with hydrochloric acid, the methanol removed under reduced pressure and the base recovered as before. The 1.61 g of base and 2 ml of acetic anhydride was heated on the steam bath for 30 min. The excess anhydride was destroyed using methanol, then the methanol and methyl acetate removed *in vacuo*. The residue was separated into 702 mg of tertiary base and 1.05 g of *N*-acetyl derivative. The base contained three

components by g.l.c. on OS-138, corresponding to a trace of parent amine and the *cis*-methoxy base **7** and *cis*-chloro base **6** in the ratios 4.4:1. The yield of **7** was 30% and that of **6**, 7% based on chloramine used. The perchlorate of the tertiary base crystallized from ethyl acetate containing a trace of alcohol giving 761 mg of moderately pure salt of **7** (24%).

(*b*) In a run comparable to *a* using 8.7 mmol of chloramine **3** the total basic product was distilled over a short path up to 140° under 12 mm pressure. The residue weighed 263 mg. The distillate (975 mg) was acetylated, giving 509 mg (2.18 mmol, 25%) of the *N*-acetyl derivative of **8** and tertiary bases. The latter was estimated by g.l.c. to contain 92 mg (0.58 mmol, 7%) of **6** and 430 mg (2.8 mmol, 32%) of **7**. To prepare analytic specimens of the tertiary bases they were separated using an OS-138 column at 180°. The fractions were further purified as their perchlorates.

(*c*) The acid-catalyzed reaction of **3** was carried out as in *a* (97% reaction in 1.3 h). The basic products were then isolated and acetylated with acetic anhydride. The tertiary base was separated from the *N*-acetyl derivatives. It proved to be nearly pure chlorobicyclic base **6** (7.5% yield) by g.l.c. on OS-138 (picrate m.p. 215°, perchlorate m.p. 223°).

The *N*-acetyl derivative gave one main peak on g.l.c. analysis (SE-30 column) but contained a small amount of compound with longer retention time. It was distilled *in vacuo*. When 919 mg of the *N*-acetyl derivative was refluxed for 44 h in 3 ml of 6 *N* sulfuric acid the hydrolysis was incomplete. Ether extraction of the acid solution gave 109 mg of *N*-acetyl derivative. The acid layers gave 459 mg of base. The base was refluxed in methanol for 8 h, then separated into secondary and tertiary bases by acetylation (376 mg of *N*-acetyl derivative, 115 mg of fairly pure methoxybicyclic base **7**).

*cis-4-Methoxy-6-methyl-6-azabicyclo[3.2.1]octane (**7**)*

The main tertiary base from the acid catalyzed reactions gave a perchlorate which crystallized as blades from methanol – ethyl acetate, m.p. 121–122°.

Anal. Calcd. for $C_9H_{18}ClNO_5$: C, 42.28; H, 7.10; N, 5.48. Found: C, 42.26; H, 7.21; N, 5.40.

*cis-4-Chloro-6-methyl-6-azabicyclo[3.2.1]octane (**6**)*

The minor tertiary base from the acid-catalyzed reactions gave a perchlorate which crystallized from methanol – ethyl acetate, m.p. 224°.

Anal. Calcd. for $C_8H_{15}Cl_2NO_4$: C, 36.92; H, 5.81; N, 5.39; Cl, 27.31. Found: C, 36.82; H, 5.87; N, 5.31; Cl, 26.94.

The base gave n.m.r. signals at δ 3.79 (t, J = 8 Hz, with small secondary coupling), 3.05 (s, 1H), 2.93 (s, 1H), and 2.50 (s, 3H). The spectrum coincided with that of a sample of the same base, provided by Prof. Y. L. Chow.

N-Acetyl-cis-4-chloro-trans-3-methoxy(methylaminomethyl)cyclohexane

The derivative from run *a* distilled over a short path at a bath temperature of 120° under 0.01 mm as a colorless oil. It gave p.m.r. signals at δ 2.12 ($NCOCH_3$), 2.97 and 3.05 ($N—CH_3$), 3.43 (OCH_3), and 4.32 br ($CHOCH_3$). In pyridine at 60 °C the $N—CH_3$ pair of signals collapsed to a sharp singlet.

Anal. Calcd. for $C_{11}H_{20}ClNO_2$: C, 56.53; H, 8.56; N, 5.99, Cl, 15.19. Found: C, 56.37; H, 8.70; N, 5.89; Cl, 15.32.

*cis-4-Methoxy-6-methyl-7-oxo-6-azabicyclo[3.2.1]octane (**10**)*

A portion (200 mg) of the perchlorate of **7**, m.p. 120°, was dissolved in 8 ml of acetone, 0.2 ml of acetic acid, and 0.4 ml of water. After addition of 100 mg of anhydrous sodium acetate the mixture was heated to give a clear solution. This was cooled to room temperature, then 348 mg of powdered potassium permanganate added over 1.5 h with stirring. The small excess was destroyed with sodium sulfite solution and the manganese dioxide removed by filtration. The acetone was removed under reduced pressure, the residual liquid diluted with 1 ml of water then basified using sodium carbonate. The product was extracted into methylene chloride giving 127 mg of oil. This was separated using preparative t.l.c. (10% methanol in chloroform, silica gel) into 68 mg of nearly pure γ-lactam **10** and 51 mg of nearly pure *N*-formyl derivative. A third amide, probably the de(*N*-methyl)lactam was present as a minor component. The lactam from several runs was purified further by preparative t.l.c. then distillation over a short path at 75° under 0.01 mm.

Anal. Calcd. for $C_9H_{15}NO_2$: C, 63.88; H, 8.94; N, 8.28. Found: C, 63.63; H, 8.79; N, 8.11.

It had ν_{max} ($CHCl_3$) 1685 cm^{-1} and gave n.m.r. signals at δ 3.07 (NCH_3) and 3.45 (OCH_3). The *N*-formyl derivative had ν_{max} ($CHCl_3$) 1660 cm^{-1} and gave an n.m.r. signal at δ 3.45 (OCH_3).

*cis-4-Chloro-6-methyl-7-oxo-6-azabicyclo[3.2.1]octane (**9**)*

The base was liberated from 169 mg of the perchlorate of the chlorobicyclic base **6**. It was dissolved in a mixture of 4 ml of acetone, 0.1 ml of acetic acid, and 0.2 ml of water. A total of 322 mg of powdered potassium permanganate was added to the stirred solution during 0.75 h. After an extra 0.5 h of reaction time the mixture was worked up as for lactam **10**. The 98 mg of product was estimated by t.l.c. separation to contain 15 mg of γ-lactam **9**, 58 mg of *N*-formyl derivative and 17 mg of other amides.

The γ-lactam from several runs was combined, purified from *N*-formyl derivative by 1.5 h hydrolysis in 6 *N* sulfuric acid, and then distilled over a short path at 70° under 0.1 mm. It had ν_{max} ($CHCl_3$) 1690 cm^{-1} and gave an n.m.r. signal at δ 3.18 ($N—CH_3$). Its n.m.r. spectrum was nearly identical to that of a chlorolactam from which had been assigned the same structure by Chow and Perry (23). We thank Prof. Chow for a copy of the spectrum.

Action of Chlorine in Methanol on 4-Methylaminomethylcyclohexene Hydrochloride

Chlorine was bubbled into a solution of 3 g of *p*-toluenesulfonic acid hydrate in 50 ml of methanol at 0–5 °C until it contained 3.5×10^{-2} mol of available chlorine (iodimetry). To the stirred solution was added 1.1 g of 4-methylaminomethylcyclohexene hydrochloride. The reaction mixture was removed from the cooling bath, then left for a total time of 3 h at room temperature. After removal of methanol under reduced pressure, the base (1.05 g) was recovered (aqueous NaOH, ether), dissolved in 55

Can. J. Chem. Downloaded from www.nrcresearchpress.com by 210.87.254.40 on 09/05/12
For personal use only.

Can. J. Chem. Downloaded from www.nrcresearchpress.com by 210.87.254.40 on 09/05/12
For personal use only.

ml of methanol, and the solution refluxed for 22 h. In this time 75 mg of chloride ion (38% of 1 equiv.) was produced. The base was recovered, acetylated, and the tertiary bases (164 mg) analyzed by g.l.c. on an OS-138 column. The ratio of the areas of the two peaks corresponding to *cis*-chlorobicyclic base **6** and *cis*-methoxybicyclic base **7** was 1:1.1.

Action of Chlorine in Water on 4-Methylaminomethylcyclohexene Hydrochloride

Chlorine was bubbled into a cooled solution of 1.24 g of the base hydrochloride, 1 ml of concentrated hydrochloric acid, and 1 g of sodium chloride in 20 ml of water until the weight had increased by 564 mg. The mixture was left for 2 h at room temperature, at which time no free chlorine was left (KI–starch). The solution was reduced to 10 ml under reduced pressure and the base isolated (NaOH, ether). The 1.15 g of base was dissolved in 40 ml of pure dioxane and 10 ml of water. The solution was heated at 80 °C under nitrogen for 16.5 h, cooled, acidified with hydrochloric acid, then taken to small volume under reduced pressure. The 964 mg of bases were isolated (NaOH, ether), then adsorbed from 1:1 ether–hexane onto 20 g of neutral alumina (activity I); 60 ml of 1:1 ether–hexane eluted 102 mg of pure chlorobicyclic base **6**, characterized as its perchlorate (overall yield 7%). The mixture of more strongly adsorbed hydroxy bases was not characterized.

N-Acetyl-4-methylaminomethylcyclohexene

This was prepared by acetylation of 4-methylaminomethylcyclohexene, followed by distillation at 120°, 0.01 mm. It gave n.m.r. signals at δ 2.12 ($NCOCH_3$), 2.98, and 3.08 ($N—CH_3$), 3.25, 3.33, 3.43 (2H multiplet, $CH_2—N$), and 5.8 (narrow 2H multiplet, vinyl hydrogens). In pyridine at 60° the *N*-methyl signals collapsed to a sharp singlet but the CH_2N signals remained complex even at 100°.

Thermolysis of N-Chloro-4-methylaminomethylcyclohexene (3)

The chloramine was prepared by addition of a solution of 644 mg of 4-methylaminomethylcyclohexene hydrochloride (m.p. 202°) to excess aqueous alkaline sodium hypochlorite solution below 20 °C, 1 h stirring followed by extraction into pentane. The pentane solution was washed with water, a small volume of 0.1 *N* sulfuric acid, then with sodium carbonate solution. The solvent was removed on a rotating evaporator below room temperature. The colorless oil was dissolved in 20 ml of methanol (freshly purified by double distillation over sodium hydroxide then over *p*-toluenesulfonic acid). The p*H* of the solution, which contained 3.8×10^{-3} mol of the chloramine (iodimetry) was 6.8 (glass electrode). The solution was split in two parts.

(*a*) The methanol solution (6.5 ml) was refluxed under pure nitrogen while shielded from light. After 2 h no reaction had taken place but after 4.7 h 96.5% of the chloramine had reacted (iodimetry). (In other runs the induction period varied between 1 and 3 h.) After a further 45 min reflux the mixture was left overnight at room temperature. The p*H* was now 5.7. After being acidified with hydrochloric acid the solution was reduced to a syrup *in vacuo* below room temperature. The residue was separated into a small amount of sweet smelling neutral oil and a mixture of bases. Gas–liquid chromatography analysis on an OS-138 column at 180° showed the base composition to be nearly identical to that from *b*.

(*b*) Benzoyl peroxide (7 mg, 2.9×10^{-5} mol) was added to 13 ml of the methanol solution of the chloramine (2.5×10^{-3} mol). The mixture was refluxed under pure nitrogen. In 2 h 68.5% of the chloramine had reacted. After 4.5 h reaction was complete. After standing at room temperature overnight the reaction mixture had p*H* 5.8. It was worked up as in *a*. The neutral product gave a nearly identical g.l.c. pattern (SE-30 column) to that from *a* and the g.l.c. of the bases (OS-138 at 180°) was nearly identical to that from *a*.

The neutral products had ν_{max} 1732 cm^{-1}. The bases were distilled over a short path up to 140° under 12 mm pressure. The viscous residue weighed 75 mg. The 278 mg of distillate was analyzed using an OS-138 column at 180°. The bases were, in order of emergence: two tertiary bases (3%) (probably 6-methyl-6-azabicyclo[3.2.1]octane and 2-methyl-2-azabicyclo[2.2.2]octane); parent amine (14%); *trans*-4-methoxy-6-methyl-6-azabicyclo[3.2.1]octane (**15**) (18%); *trans*-6-methoxy-2-methyl-2-azabicyclo[2.2.2]octane (**16**) (27%); and *cis*-4-chloro-6-methyl-6-azabicyclo[3.2.1]octane (**6**) (13%). In several runs the total base was acetylated and the *N*-acetyl derivative identified as *N*-acetyl-4-methylaminomethylcyclohexene (15% recovery).

The bases were separated by preparative g.l.c. on an OS-138 column or by chromatography on a t.l.c. silica gel column (ratio 100:1) using 10% diethylamine in benzene as developing solvent, and the abundant ones characterized as salts.

trans-4-Methoxy-6-methyl-6-azabicyclo[3.2.1]octane (15)

This gave a crystalline perchlorate separating from ethyl acetate as thin plates, m.p. 130°. It proved identical with the salt of the *N*-methyl base prepared from *trans*-4-methoxy-6-azabicyclo[3.2.1]octane-7-one.

Anal. Calcd. for $C_9H_{18}ClNO_5$: C, 42.28; H, 7.10; N, 5.48. Found: C, 42.42; H, 7.33; N, 5.32.

trans-6-Methoxy-2-methyl-2-azabicyclo[2.2.2]octane (16)

The perchlorate of this base did not crystallize readily from ethyl acetate hence the picrate was prepared. This crystallized as stout needles from methanol, m.p. 176–178°.

Anal. Calcd. for $C_{15}H_{20}N_4O_8$: C, 46.87; H, 5.25; N, 14.58. Found: C, 46.73; H, 5.29; N, 14.55.

Thermolysis of Chloramine 3 in Acetonitrile

A solution of 4.8 mmol of chloramine **3** in 20 ml of acetonitrile (dried over molecular sieve, distilled) was flushed with nitrogen, then refluxed under nitrogen. In 1 h the chloramine had completely reacted. Methanol (5 ml) was added and the mixture refluxed under nitrogen for 1.5 h. The weakly basic solution was acidified using hydrochloric acid and evaporated to near dryness. The residue yielded 176 mg of neutral product (ν_{max} 3030, 2720, 1733, and 1660 cm^{-1}) and 453 mg of base. Gas–liquid chromatography on an OS-138 column showed this to be mainly parent amine, but also to contain some of the bicyclic amines **6**, **15**, and **16**. The bases were acetylated, and the product separated into neutral *N*-acetyl derivative (237 mg) and 130 mg of tertiary bases. Gas–liquid chromatog-

Can. J. Chem. Downloaded from www.nrcresearchpress.com by 210.87.254.40 on 09/05/12
For personal use only.

raphy on the OS-138 column confirmed the presence of the bicyclic amines **6**, **15**, and **16** and two minor tertiary amines with short retention time, probably the bicyclic bases **17** and **18**.

Thermolysis in an Oxygen Atmosphere

Simultaneous refluxing of aliquots of a 0.15 *M* solution of chloramine **3** in methanol under pure nitrogen and pure oxygen are compared in Fig. 1. The reaction under oxygen was 89% complete after 16.5 h refluxing. The basic products were acetylated, giving a 49% yield of the *N*-acetyl derivative of the parent amine and 16% of a mixture of the same tertiary amines produced in the reactions under nitrogen.

Action of Silver on Chloramine 3 in Methanol

(*a*) A solution of 1.65×10^{-3} mol of the chloramine in 15 ml of purified methanol was prepared and flushed with nitrogen. Water and methanol-washed Tollens' silver from 626 mg of silver nitrate was added, and the suspension again flushed with nitrogen. The mixture was heated under reflux in an oil bath. A rapid reaction ensued. After 1 h 93% of the chloramine had reacted. Refluxing was continued for 1 h more to complete reaction. The solids were removed by filtration, the basic filtrate was acidified using hydrochloric acid, and then evaporated to small volume. The bases were liberated and extracted into ether. Gas–liquid chromatography on an OS-138 column at 180° showed the major product to be parent secondary amine. Acetylation, followed by base–neutral separation, gave 122 mg of *N*-acetyl derivative and 57 mg of tertiary base. The latter gave five peaks on the OS-138 column, corresponding to the three bicyclic bases **6**, **15**, and **16** and two readily eluted minor bases (probably **17** and **18**). The solids contained 195 mg (1.36 mmol) of silver chloride.

(*b*) Chloramine **3** (2.2 mmol) and Tollens' silver from 1.02 g of silver nitrate (washed with water and methanol) in 15 ml of pure methanol were stirred under nitrogen. The extent of reaction was: 1.3 h, 67%; 3 h, 87%; 5.5 h, 99%. The base recovered from the reaction was shown by g.l.c. to be mainly parent amine. The solids contained 255 mg of silver chloride (1.78 mmol).

Action of Silver Perchlorate in Methanol on Chloramine (3)

A solution of 1.29 of silver perchlorate in 15 ml of methanol (p*H* approximately 1) was adjusted to p*H* 6 (by cautious addition of sodium methoxide). After removal of 47 mg of silver oxide by filtration the volume was readjusted to 15 ml and the solution added to the chloramine prepared from 0.30 g of the hydrochloride of 4-methylaminomethylcyclohexene. After 3 h in the dark at room temperature no reaction had taken place. The reaction mixture was then heated under nitrogen in a bath at 65°. The extent of reaction was: 1 h, 22%; 2 h, 65%. The mixture was left overnight at room temperature, then reaction completed by 2 h reflux. The p*H* of the solution was now 3, and 178 mg of silver chloride had precipitated (AgCl/chloramine = 0.95). The rest of the silver was precipitated using hydrochloric acid, the suspension filtered, the bulk of the solvent removed, then the base recovered. Gas–liquid chromatography on the OS-138 column showed it to consist of at least nine products, with parent amine being the dominant one (70%). Three peaks corresponding to the bases **6**, **15**, and **16** were present.

Photolysis of 3-Cyclohexenecarbonyl Azide

A solution of 3.4 g of the azide in 125 ml of methanol at 5 °C was irradiated through a Vycor glass sleeve using a 100 W Hanovia high pressure immersion lamp in a central well. The azide was completely decomposed in 3 h. The methanol and some volatile products were evaporated on a rotating evaporator. The residue was distilled over a short path under 0.5 mm pressure. A mobile oil (965 mg) distilled at a bath temperature of 75–80°. It had an ester odor and had ν_{max} 3435, 1715, and 1511 cm^{-1}. Gas–liquid chromatography on an OS-138 column at 235° showed it to be mainly one compound, presumably the expected methyl urethane.

The bulk of the remaining product distilled at bath temperatures between 80 and 135°. It consisted mainly of amides (broad i.r. absorption centered at 1690 cm^{-1}). Gas–liquid chromatography on an OS-138 column at 190° showed it to consist of three main components, the *N*-methoxy amide of 3-cyclohexenecarboxylic acid and the γ- and δ-lactams **19** and **20**. These were separated on preparative t.l.c. plates, developing with 5% methanol in chloroform.

For larger preparative runs the lactam mixture after distillation was oxidized with potassium permanganate in acetone to remove unsaturated products, then the γ- and δ-lactams were separated on columns of t.l.c. silica gel.

N-Methoxy-3-cyclohexenecarboxamide

The yield of this product was estimated to be 17%. After distillation over a short path at 90°, 0.2 mm, then recrystallization from ethyl acetate–hexane it melted at 71–74°. It had ν_{max} 3400, 3220, 2840, and 1669 cm^{-1} and n.m.r. signals at δ 5.80 (barely resolved doublet, 2H) and 3.83 (3H).

Anal. Calcd. for $C_8H_{13}NO_2$: C, 61.91; H, 8.44; N, 9.03. Found: C, 61.94; H, 8.56; N, 8.97.

trans-4-Methoxy-6-azabicyclo[3.2.1]octan-7-one (19)

The γ-lactam (yield 4.6%) crystallized as thick plates from ethyl acetate – hexane mixtures. It had m.p. 83–85°, ν_{max} 3435, 3220, and 1695 cm^{-1}, and gave n.m.r. signals at δ 3.85 and 3.50 (broad 1H singlets, hydrogens on C-1 and C-7, respectively) and a 3H singlet at δ 3.41 (OCH_3).

Anal. Calcd. for $C_8H_{13}NO_2$: C, 61.91; H, 8.44; N, 9.03. Found: C, 62.11; H, 8.54; N, 9.01.

trans-4-Methoxy-6-methyl-6-azabicyclo[3.2.1]octan-7-one

The γ-lactam **19** (105 mg), 205 mg of sodium hydride powder, and 480 mg of methyl iodide in 4 ml of dry dioxane was heated at 70° under nitrogen for 3 h. The solution was filtered through sintered glass. The filtrate was evaporated to small volume on a rotating evaporator at 40°. The 104 mg of crude product had no N—H absorption, ν_{max} 1690 cm^{-1}, and gave only one peak on g.l.c. on an SE-30 column at 200°. It gave n.m.r. signals at δ 2.87 (NCH_3) and 3.39 (OCH_3).

trans-4-Methoxy-6-methyl-6-azabicyclo[3.2.1]octane (15)

The above *N*-methyllactam (100 mg) was dissolved in 4 ml of dry dioxane, 365 mg of powdered lithium aluminum hydride added, the system flushed with nitrogen, then the

Can. J. Chem. Downloaded from www.nrcresearchpress.com by 210.87.254.40 on 09/05/12
For personal use only.

mixture placed in a bath at 100° for 1 h. The mixture was cooled, ether added, followed by methanol to destroy excess lithium aluminum hydride. After addition of 1 ml of saturated sodium sulfate solution, the suspension was filtered through celite. The filtrate was taken to p*H* 3 using hydrochloric acid, then evaporated to dryness. The base was liberated and converted to its perchlorate. This crystallized from ethyl acetate giving 64 mg, m.p. 125°. After recrystallization from ethyl acetate this melted at 129° and showed no mixture m.p. depression with the perchlorate m.p. 130° from the thermolysis of chloramine **3** in methanol.

The base was converted to its methiodide using methyl iodide in ether. This had m.p. 206° and did not depress the m.p. of a sample of the corresponding methiodide (m.p. 199°, mixture m.p. up to 202°) from thermolysis of chloramine **3** in methanol kindly supplied by Prof. P. Gassman (5).

Anal. Calcd. for $C_{10}H_{20}INO$: C, 40.41; H, 6.78; N, 4.71. Found: C, 40.44; H, 6.83; N, 4.69.

*trans-6-Methoxy-2-azabicyclo[2.2.2]octan-3-one (**20**)*

The δ-lactam (yield 2.3%) crystallized from ethyl acetate – hexane as needles, m.p. 120°. It had ν_{max} 3430, 3220, and 1680 cm^{-1} and gave an n.m.r. signal at δ 3.39 (OCH_3).

Anal. Calcd. for $C_8H_{13}NO_2$: C, 61.91; H, 8.44; N, 9.03. Found: C, 62.03; H, 8.61; N, 9.08.

trans-6-Methoxy-2-methyl-2-azabicyclo[2.2.2]octan-3-one

A mixture of 108 mg of δ-lactam **20**, 210 mg of sodium hydride powder and 467 mg of methyl iodide in 5 ml of dioxane was heated (under nitrogen) in a bath at 70° for 3 h. The suspension was filtered and the filtrate evaporated on a rotating evaporator. The residual oil gave one peak on g.l.c. analysis using the SE-30 column at 200°. It contained no NH, had ν_{max} 1668 cm^{-1}, and gave n.m.r. signals at δ 2.99 (NCH_3) and 3.37 (OCH_3).

*trans-6-Methoxy-2-methyl-2-azabicyclo[2.2.2]octane (**16**)*

The *N*-methyl δ-lactam (*ca.* 130 mg) was reduced with lithium aluminum hydride as for γ-lactam. The base gave 177 mg of picrate. After one recrystallization from methanol it formed stout needles, m.p. 175–178°. It proved identical (mixture m.p., i.r. spectra of major mulls) with the 178° picrate from thermolysis of chloramine **3** in methanol. The base was converted to its methiodide, m.p. 208°. This did not depress the m.p. of a sample of the corresponding methiodide (m.p. 200°, mixture m.p. 202°) from thermolysis of chloramine **3** in methanol (5), kindly provided by Prof. Gassman.

Anal. Calcd. for $C_{10}H_{20}INO$: C, 40.41; H, 6.78; N, 4.71. Found: C, 40.67; H, 6.86; N, 4.73.

A sample of the base assigned the above structure was kindly provided by Prof. Gassman. It was converted to its picrate which after recrystallization from methanol had m.p. 173–175.5°. It gave no mixture m.p. depression with the above picrate.

N-Methylcyclohept-4-enecarboxamide

This was prepared from cyclohept-3-enecarbonyl chloride and ice-cold saturated aqueous methyl amine. After recrystallization from acetone – ethyl acetate mixture it had m.p. 126–128°.

5-Methylaminomethylcycloheptene

Reduction of *N*-methylcyclohept-3-enecarboxamide using excess lithium aluminum hydride in refluxing dioxane for 1 h gave the base which was characterized as its hydrochloride. After recrystallization from methanol – ethyl acetate it had m.p. 204–206° (evacuated capillary).

Anal. Calcd. for $C_9H_{18}ClN$: C, 61.52; H, 10.32; Cl, 20.18. Found: C, 61.25; H, 10.51; Cl, 19.39.

*Thermolysis of N-Chloro-5-methylaminomethylcycloheptene (**11**)*

The chloramine was prepared from the secondary amine using excess sodium hypochlorite, then extracted into pentane. A solution of 1.07 g (6.09 mmol) of the chloramine was dissolved in 25 ml of methanol (distilled from sodium hydroxide, then from *p*-toluenesulfonic acid).

(*a*) After flushing with nitrogen 12.5 ml of the chloramine solution was refluxed under nitrogen while shielded from light. The decomposition rate was: 1.5 h, 0%; 3.5 h, 8.6%; 5 h, 16%; 8 h, 50%; 11 h, 86%; 15 h, 99%. The p*H* of the solution was now 5.6. It was adjusted to p*H* 2 using hydrochloric acid then evaporated to near dryness. The residue was extracted with ether, to give 4 mg of neutral product with ν_{max} 2720 and 1730 cm^{-1}. The salts gave 230 mg of base. Gas–liquid chromatography on OS-138 at 196° showed it to contain four major components with peak areas in order of emergence in the ratios 0.25:3.1:1:0.16.

(*b*) 12.5 ml of the chloramine solution containing 10 mg of perbenzoic acid was refluxed under nitrogen while shielded from light. The decomposition rate was: 1.5 h, 11%; 3.5 h, 72%; 6.5 h, 100%. The p*H* of the solution was now 5.2. Work-up as in *a* gave a small amount of neutral product identical to that in *a* and 329 mg of base. It contained the same bases as obtained from run *a* but in different ratio: (relative areas of peaks) 1.07:1.51:1:0.17. The second peak corresponded to the parent secondary base.

The bases from *a* and *b* were combined and acetylated using acetic anhydride. Base–neutral separation gave 357 mg of *N*-acetyl derivative (mainly the derivative of the parent amine) and 225 mg of tertiary base.

The tertiary bases contained at least six components but three predominated, corresponding to the first, third, and fourth peaks from the total bases with relative areas 0.08:1:0.14. Gas–liquid chromatographic separation of the product from larger runs enabled characterization of the two most abundant tertiary amines in order of emergence as *trans*-4-methoxy-6-methyl-6-azabicylco[3.2.2]-nonane (**21**) and *cis*-4-chloro-6-methyl-6-azabicyclo-[3.2.2]nonane (**12**).

*trans-4-Methoxy-6-methyl-6-azabicyclo[3.2.2]nonane (**21**)*

This base did not readily give a crystalline perchlorate but gave a picrate, m.p. 182°, which was sparingly soluble in methanol. The yield in the benzoyl peroxide catalyzed reactions averaged approximately 25%.

Anal. Calcd. for $C_{16}H_{22}N_4O_8$: C, 48.24; H, 5.57; N, 14.07. Found: C, 48.09; H, 5.65; N, 13.96.

The n.m.r. spectrum of the base contained signals for the *N*-methyl and methoxyl groups at δ 2.50 and 3.39. A

Can. J. Chem. Downloaded from www.nrcresearchpress.com by 210.87.254.40 on 09/05/12
For personal use only.

doublet at δ 3.1 (J = 3 Hz) can be attributed to the N—CH_2—CH group. The hydrogens on C-1 and C-7 resonated close to δ 2.7 and 3.5, respectively.

*cis-4-Chloro-6-methyl-6-azabicyclo[3.2.2]nonane (**12**)*

This formed a perchlorate which crystallized from methanol – ethyl acetate as short needles, m.p. 246°.

Anal. Calcd. for $C_9H_{17}Cl_2NO_4$: C, 39.43; H, 6.27; N, 5.11; Cl, 25.86. Found: C, 39.54; H, 5.70; N, 4.98; Cl, 25.86.

The yield in the benzoyl peroxide catalyzed reactions approximated 4.5%.

*Acid-catalyzed Reaction of Chloramine **7** in Methanol*

p-Toluenesulfonic acid hydrate (2.5 g) was added cautiously with external cooling to a solution of 1.75 g (10.1 mmol) of chloramine 7 in 50 ml of methanol. The reaction was 94% complete in 10 min and 97% complete in 20 min. After a total reaction time of 45 min the methanol was evaporated under reduced pressure. Water was added to the residue, which was adjusted to pH 4 using sodium carbonate, then left overnight. The solution was then made strongly acid with dilute sulfuric acid, and extracted twice with ether. The ether was back-washed with acid, dried, and distilled, leaving 14 mg of neutral oil with ν_{max} 1732 cm^{-1}. The aqueous layers were basified with sodium hydroxide and thoroughly extracted with ether, yielding 1.80 g of colorless oil. This contained four bases with moderate retention times on the OS-138 column. Their peak areas in order of emergence were 0.09:0.15:1:3.5. The total base mixture was dissolved in 25 ml of methanol. The solution was refluxed for 1 h then left for 47 h at room temperature. No ionic halogen was produced. Acetic anhydride acetylated the fourth and most abundant base, giving 1.75 g of neutral *N*-acetyl derivative (77% yield, corrected for samples removed for analysis) and a small amount of tertiary base. The latter gave 54 mg of the perchlorate of *cis*-4-chloro-6-azabicyclo[3.2.2]-nonane (**12**) (see above). No pure compound was isolated from the remaining 100 mg of noncrystalline perchlorate.

The N-Acetylated Secondary Amine

The *N*-acetyl product was distilled over a short path at a bath temperature of 150–160° under 0.5 mm pressure, giving a faintly colored viscous oil. It gave n.m.r. signals at δ 3.53 (3H, OCH_3), 3.10, and 3.01 (3H, NCH_3) and 2.17 (3H, $COCH_3$).

Its n.m.r. spectrum corresponded to the expectation for *N*-acetyl-*trans*-4-chloro-*cis*-5-methoxy-1-methylaminomethylcycloheptane (δ 2.1 ($COCH_3$); 2.99, 3.09 (NCH_3); 3.52 (OCH_3); two broad 1H signals centered near 3.5 and 4.2) and it gave a single g.l.c. peak (SE-30 at 226°) superimposed on a weak broad signal. It analyzed approximately correctly.

Anal. Calcd. for $C_{12}H_{22}ClNO_2$: C, 58.18; H, 8.89; N, 5.66; Cl, 14.33. Found: C, 57.45; H, 9.12; N, 5.39; Cl, 13.81.

We thank Prof. J. D. Hobson for communicating results prior to publication, Prof. P. G. Gassman for reference samples, Prof. Y. L. Chow for reference spectra, M. Lesage and R. Kolt for technical assistance, H. Seguin for microanalyses, and B. Cougle for mass spectra.

1. O. E. Edwards, D. Vocelle, J. W. ApSimon, and F. Haque. J. Am. Chem. Soc. **87**, 678 (1965).
2. O. E. Edwards, D. Vocelle, and J. W. ApSimon. Can. J. Chem. **50**, 1167 (1972).
3. D. R. Harvey and R. O. C. Norman. J. Chem. Soc. 3604 (1961).
4. P. G. Gassman, F. Hoyda, and J. H. Dygos. J. Am. Chem. Soc. **90**, 2716 (1968).
5. G. Gassman and J. H. Dygos. Tetrahedron Lett. (*a*) 4745 (1970); (*b*) 4749 (1970).
6. I. Brown, O. E. Edwards, J. M. McIntosh, and D. Vocelle. Can. J. Chem. **47**, 2751 (1969).
7. O. E. Edwards, M. Chaput, F. H. Clarke, and T. Singh. Can. J. Chem. **32**, 785 (1954).
8. R. Tadayoni, A. Heumann, R. Furstoss, and B. Waegell. Tetrahedron Lett. 2879 (1973).
9. R. S. Neale and N. L. Marcus. J. Org. Chem. **32**, 3273 (1967); **33**, 3457 (1968).
10. A. H. El Nadi, W. J. Hickinbottom, and S. Wasif. J. Chem. Soc. (B), 1131 (1970).
11. P. Kovacic and M. K. Lowery. J. Org. Chem. **34**, 911 (1969).
12. A. Heumann, R. Furstoss, and B. Waegell. Tetrahedron Lett. 933 (1972).
13. P. Kovacic, M. K. Lowery, and K. W. Field. Chem. Rev. **70**, 639 (1970).
14. P. Kovacic, M. K. Lowery, and P. D. Roskos, Tetrahedron, **26**, 529 (1970).
15. P. Kovacic, J.-H. Liu, P. D. Roskos, and E. M. Levi. Chem. Commun. 1034 (1970).
16. T. A. Kling, M. B. Nazareno, and P. Kovacic. J. Am. Chem. Soc. **94**, 2157 (1972).
17. T. A. Kling, R. E. White, and P. Kovacic. J. Am. Chem. Soc. **94**, 7416 (1972).
18. S. J. Padegimos and P. Kovacic. J. Org. Chem. **37**, 2672 (1972).
19. R. D. Fisher, T. D. Bogard, and P. Kovacic. J. Am. Chem. Soc. **95**, 3646 (1973).
20. H. H. Wasserman, H. W. Adickes, and O. E. de Ochoa. J. Am. Chem. Soc. **93**, 5586 (1971).
21. J. W. Bastable, J. D. Hobson, and W. D. Riddell. J. Chem. Soc. Perkin I, 2205 (1972).
22. J.-M. Surzur, L. Stella, and R. Nouguier. Tetrahedron Lett. 903 (1971).
23. Y. L. Chow and R. A. Perry. Tetrahedron Lett. 531 (1972).
24. M. Kobayashi, M. Sekiguchi, and H. Minato. Tetrahedron Lett. 393 (1972).
25. P. G. Gassman and G. A. Campbell. Chem. Commun. 1437 (1971).
26. P. G. Gassman. Acc. Chem. Res. **3**, 26 (1970).
27. V. Rautenstrauch. Chem. Commun. 1122 (1969).
28. O. E. Edwards, D. H. Paskovic, and A. H. Reddoch. Can. J. Chem. **51**, 978 (1973).
29. R. Furstoss, A. Heumann, and B. Waegell. Org. Mass Spectrom. **6**, 1207 (1972).
30. J. E. Dewhurst, J. J. Kaminski, and J. H. Supple. J. Heterocycl. Chem. **9**, 507 (1972).
31. Ng. Ph. Buu-Hoi. Rec. Trav. Chim. **73**, 197 (1954).
32. E. C. Rakunas de Alvarez. Rev. Fac. Cienc. Quim. Univ. Nacl. Eva Peron, **26**, 57 (1951); Chem. Abstr. **50**, 2551 (1956).

A Synthesis of 1-Alkyl-3,5-dimethoxybenzenes

KEITH BAILEY

Research Laboratories, Health Protection Branch, Health and Welfare Canada, Ottawa K1A 0L2

Received January 28, 1974

KEITH BAILEY. Can. J. Chem. **52**, 2136 (1974).

The reaction of 3,4,5-trimethoxybenzaldehyde or 3,4,5-trimethoxyphenyl methyl ketone with alkyl magnesium halides gives secondary or tertiary carbinols. These are converted in good yields into 1-alkyl-3,5-dimethoxybenzenes by reaction with dissolving sodium in alcohols.

KEITH BAILEY. Can. J. Chem. **52**, 2136 (1974).

Les réactions du triméthoxy-3,4,5 benzaldéhyde ou de la triméthoxy-3,4,5 phényl méthyl cétone avec les halogénures de méthylmagnésium conduisent aux alcools secondaires ou tertiaires correspondants. La réaction de ces derniers avec du sodium dissous dans les alcools conduit avec de bons rendements aux alkyl-1 diméthoxy-3,5 benzène.

[Traduit par le journal]

Syntheses of many plant products including cannabinoids (1–4) and their homologues depend largely on the availability of 1-alkyl-3,5-dihydroxybenzenes (**1**) (5). Although syntheses of such resorcinol homologues were described several years ago (6–10), they remain somewhat inaccessible and the current interest in cannabinoids and other plant products has spurred further investigations (2, 11–13). A simple synthesis of 1-alkyl-3,5-dimethoxybenzenes (**2**), which are readily demethylated to the 3,5-dihydroxybenzenes (2, 9, 11), is described here. It involves the Grignard reaction of an alkyl magnesium halide

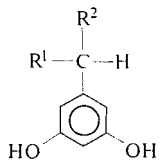

1

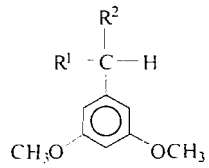

2

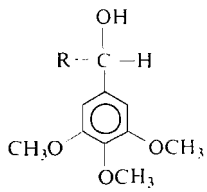

3

with 3,4,5-trimethoxybenzaldehyde or 3,4,5-trimethoxyphenyl methyl ketone (which are more readily available than their 3,5-dimethoxy counterparts) to give a carbinol (**3**; R^1 = H or CH_3) which is simultaneously 4-demethoxylated and reduced in the side chain to give the dimethoxybenzenes (**2**; R^1 = H or CH_3) by the action of dissolving sodium in *t*-butanol. The last step is an extension and improvement of a reaction described by Asahina (6) in which dimethoxybenzenes (**2**; R^1 = H) were prepared from 3,4,5-trimethoxyphenyl alkyl ketones with dissolving sodium in alcohol. If the resorcinol derivatives (**1**) are desired, it is not generally necessary to purify the intermediates **2** and **3**. Typical procedures are described in the Experimental section.

When the reaction was first investigated, Asahina's procedure (6) (add sodium pieces and ethanol or isopropanol to 3,4,5-trimethoxyphenyl alkyl ketones) was applied to the carbinol. A number of 1-alkyl-3,5-dimethoxybenzenes were prepared (**2**; R^1 = H, R^2 = CH_3; R^1 = H, R^2 = *n*-C_3H_7; R^1 = H, R^2 = *n*-C_4H_9; R^1 = H, R^2 = *n*-C_5H_{11}; R^1 = H, R^2 = C_6H_5; R^1 = CH_3, R^2 = *n*-C_3H_7; R^1 = CH_3, R^2 = *n*-C_4H_9; R^1 = CH_3, R^2 = *n*-C_6H_{13}; R^1 = CH_3, R^2 = cyclohexyl; R^1 = CH_3, R^2 = C_6H_5) but the yields were only fair (about 75% isolated, about 60% pure). A more satisfactory practice (see

TABLE 1. Effect of change in alcohol on reduction* of **3** (R^1 = H, R^2 = *n*-C_5H_{11})

Alcohol	Isolated crude yield (%)	Purity (%)
Methanol	99	77
Ethanol	83	67
i-Propanol	92	85
t-Butanol	92	93

*For conditions, see Experimental; purity was estimated by g.l.c. assuming equal response factors.

Can. J. Chem. Downloaded from www.nrcresearchpress.com by 210.87.254.105 on 09/05/12
For personal use only.

TABLE 2. Effect of change in proportion of sodium on reduction* of 3 (R^1 = H, R^2 = n-C_5H_{11})

Quantity of 3 (mmol)	Quantity of sodium (mmol)	Crude yield (%)	Purity (%)
1.2	43	83	98
2.4	43	92	93
5.0	43	97	61

*See footnote, Table 1.

TABLE 3. Yields of 2 on reduction* of different carbinols 3

3	Crude yield 2 (%)	Purity of 2 (%)
R^1 = H, R^2 = n-C_3H_7	89	86
R^1 = H, R^2 = n-C_5H_{11}	92	93
R^1 = H, R^2 = cyclohexyl	100	54
R^1 = H, R^2 = C_6H_5	93	84
R^1 = CH_3, R^2 = cyclohexyl	89	50
R^1 = CH_3, R^2 = C_6H_5	96	57

*See footnote, Table 1.

Experimental) was to generate sodium sand (14), cover it with a little benzene, add the carbinol, and then the alcohol. The effect of changing the alcohol on the reduction of 3 (R^1 = H, R^2 = n-C_5H_{11}) was investigated with the results shown in Table 1. *t*-Butanol had the advantage of a good yield of material which was sufficiently pure for subsequent transformation. The effects of changing the ratio of sodium to carbinol are shown in Table 2; a molar ratio of about 20:1 (about half that employed by Asahina (6)) afforded a good yield of reasonably pure product. Yields of 2 from different carbinols (3) are shown in Table 3. Starting materials of approximately 95% purity, estimated by gas–liquid chromatography (g.l.c.) were employed in investigating the yields presented in the tables.

A frequent by-product of the synthesis of 3 was the olefin corresponding to its dehydration. Investigations on 1-(3,4,5-trimethoxyphenyl)-hexene as an example showed that it was converted into 2 (R^1 = H, R^2 = n-C_5H_{11}) under the reduction conditions and so in practical syntheses the crude Grignard product (3) was usually used without purification.

The progress of the reduction of the carbinols was monitored by g.l.c. and the formation of an "intermediate" was noted. A small amount was isolated by column chromatography of the products from the reduction of 3 (R^1 = H, R^2 = n-C_5H_{11}) and identified spectroscopically and by comparison with material synthesized from 3,5-dimethoxybenzaldehyde as the 4-demethoxylated product 2 (R^1 = OH, R^2 = n-C_5H_{11}). (These products can be converted into 2 by dehydration (refluxing xylene) followed by hydrogenation or into 1 by simultaneous demethylation and dehydration with pyridine hydrochloride (2) followed by hydrogenation.)

Experimental

Proton magnetic resonance (p.m.r.) spectra were determined at 60 MHz for solutions in deuteriochloroform containing tetramethylsilane as internal reference, with a Varian A60A spectrometer. Infrared (i.r.) spectra were determined on natural films or Nujol mulls with a Unicam SP1000 spectrophotometer. Gas–liquid chromatography was performed on a Varian Aerograph 1520 with 6 ft long × 3/16 in. i.d. glass columns containing 5% OV-7 on 80–100 mesh Chromosorb W, injection port, and flame ionization detector at 275°, nitrogen flow 30 ml/min, and an appropriate oven temperature (175–225°, depending on retention time).

Preparation of Carbinols (3)

Typically, magnesium turnings (1.725 g, 0.0725 mol) were covered with dry ether (25 ml) and bromoalkane (1 g) was added to initiate formation of the Grignard reagent. The bromoalkane (to total 0.075 mol) in dry ether (25 ml) was then added and the mixture heated under reflux with stirring until no magnesium remained. A solution of 3,4,5-trimethoxybenzaldehyde or 3,4,5-trimethoxyphenyl methyl ketone (0.05 mol) in dry benzene (75 ml) was added dropwise and the mixture was stirred under

Can. J. Chem. Downloaded from www.nrcresearchpress.com by 210.87.254.105 on 09/05/12
For personal use only.

reflux for 2 h and then allowed to cool. Hydrochloric acid (1.5 *N*, 50 ml) was added cautiously. The aqueous layer was separated and extracted with benzene (50 ml) and the organic phases were combined, dried ($MgSO_4$), and concentrated to furnish the carbinol (**3**). In the case of **3** (R^1 = H), the products were usually of reasonable purity (*ca.* 90%) and were used in the reduction step (6). For the purposes of quantitative investigation, carbinols **3** (R^1 = H, R^2 = cyclohexyl, and $R^1 = CH_3$, $R^2 = C_6H_5$) were purified by recrystallization from mixtures of hexane with chloroform and **3** ($R^1 = CH_3$, R^2 = cyclohexyl) was purified by adsorption onto a column of silica gel and elution with chloroform. The carbinols **3** (R^1 = H or CH_3) had very similar i.r. spectra with absorption at *ca.* 3450, 1590, 1505, 1415, 1325, 1235, 1130, 1005, and 935 cm^{-1}. Their p.m.r. bands included δ *ca.* 3.9 (OCH_3) and for **3** (R^1 = H) at 6.55 (Ar*H*) and *ca.* 4.3–4.6 (benzylic *H*, multiplicity and position depending on R^2) and for **3** ($R^1 = CH_3$) at 6.67 (Ar*H*) and 1.57 (benzylic CH_3) p.p.m.

Reduction of Carbinols (3)

Typically, sodium sand (1 g, 43 mmol) was prepared (14) in a round bottom flask and covered with dry benzene (5 ml). The carbinol (2.5 mmol) was added. A two-neck adaptor with a condenser and dropping funnel were fitted. The mixture was stirred magnetically and kept at 80–85° on an oil bath. The alcohol (15 ml) was added (methanol or ethanol were added dropwise to keep the ensuing reaction moderate but *t*-butanol could be added safely in one steady portion). The mixture was stirred at 80–85° for 3–4 h (extended periods did not significantly improve the yields), inspected for the disappearance of all sodium, and then poured into water (300 ml). The mixture was acidified (HCl) and extracted with ether (3 × 50 ml). The extract was dried ($MgSO_4$) and concentrated. The products **2** (R^1 = H or CH_3) had similar i.r. spectra with absorption bands at *ca.* 1605, 1595, 1200, 1150, 1060, and 830 cm^{-1} (by-products **2**; R^1 = OH, had ν_{max} 3400, 1605, 1595, 1200, 1150, 1060, and 840 cm^{-1}). Their p.m.r. bands included δ 6.33 (Ar*H*), 3.77 (OCH_3), *ca.* 2.3–2.6 (benzylic protons, multiplicity and position depending on R^1 and R^2) and for **2** ($R^1 = CH_3$) 1.20 (doublet, benzylic CH_3) p.p.m. (by-products **2**; R^1 = OH, had δ *ca.* 6.50 (Ar*H* at 2 and 6), 6.38 (Ar*H* at 4), 3.78 (OCH_3) and *ca.* 4.5 (benzylic proton, multiplicity and position depending on R^2) p.p.m.).

In experiments where the proportion of sodium was changed, the volume of *t*-butanol was kept constant. The products **2** could be purified by adsorption on to silica gel and elution with chloroform in hexane, and their conversion into **1** accomplished with pyridine hydrochloride (2).

The technical assistance of M D. Legault and Mlle D. Verner is gratefully acknowledged.

1. R. Mechoulam, P. Braun, and Y. Gaoni. J. Am. Chem. Soc. **89**, 4552 (1967).
2. T. Petrzilka, W. Haefliger, and C. Sikemeier. Helv. Chem. Acta, **52**, 1109 (1969).
3. R. K. Razdan and G. R. Handrick. J. Am. Chem. Soc. **92**, 6061 (1970).
4. L. Crombie and R. Ponsford. J. Chem. Soc. C, 796 (1971).
5. R. Mechoulam. Science, **168**, 1159 (1970).
6. Y. Asahina. Chem. Ber. **69**, 1643 (1936).
7. C. M. Suter and A. W. Weston. J. Am. Chem. Soc. **61**, 232 (1939).
8. R. M. Anker and A. H. Cook. J. Chem. Soc. 311 (1945).
9. R. Adams, K. H. Chen, and S. Loewe. J. Am. Chem. Soc. **67**, 1534 (1945).
10. F. Korte and H. Sieper. Justus Liebigs Ann. Chem. **630**, 71 (1960).
11. P. Baeckstrom and G. Sundstrom. Acta Chem. Scand. **24**, 716 (1970).
12. R. S. Marmor. J. Org. Chem. **37**, 2901 (1972).
13. J. R. Cannon, P. K. Cheong, C. J. Fallick, B. H. Hamilton, I. A. McDonald, and G. Vinciguerra. Aust. J. Chem. **26**, 799 (1973).
14. L. F. Fieser. Organic experiments. D. C. Heath and Co., Boston. 1964. pp. 142–143.

Can. J. Chem. Downloaded from www.nrcresearchpress.com by 210.87.254.105 on 09/05/12
For personal use only.

Complex Formation in Ether–Chloroform Systems: Comparison of Thermodynamic and Spectroscopic Results

NEIL F. PASCO AND DAVID V. FENBY
Department of Chemistry, University of Otago, Dunedin, New Zealand
AND
LOREN G. HEPLER
Department of Chemistry, University of Lethbridge, Lethbridge, Alberta T1K 3M4
Received November 16, 1973

NEIL F. PASCO, DAVID V. FENBY, and LOREN G. HEPLER. Can. J. Chem. **52**, 2139 (1974).
A number of procedures for evaluation of equilibrium constants and standard enthalpies of complex formation from equilibrium liquid–vapor and calorimetric results have been applied to ether–chloroform systems. The results are compared with published spectroscopic values.

NEIL F. PASCO, DAVID V. FENBY et LOREN G. HEPLER. Can. J. Chem. **52**, 2139 (1974).
Nous avons appliqué à des systèmes d'ether-chloroforme un certain nombre de procédés d'évaluation des constantes d'équilibre et des enthalpies standards de complexation à partir d'équilibres liquide-vapeur et de résultats calorimétriques. Nous avons ensuite comparé les résultats avec ceux des valeurs spectroscopiques déjà publiées.

Introduction

Reliable values for the thermodynamic properties associated with complex formation in liquid systems are needed for many chemical and biochemical studies, and are also required for testing such extrathermodynamic relationships as the Badger–Bauer equation (1).

Equilibrium constants for complex formation are commonly evaluated from results of spectroscopic measurements made on solutions in which concentrations of the reactants are varied. The standard enthalpy of complex formation can then be evaluated from the temperature dependence of the equilibrium constant and the van't Hoff equation

$$\Delta H^0 = RT^2 (\partial \ln K/\partial T)_p$$

Even with equilibrium constants obtained from results of careful experiments and data analysis, these ΔH^0 values are subject to appreciable uncertainty (2). These uncertainties are often largest for the moderately weak hydrogen bonded or charge transfer complexes that are of considerable practical and theoretical importance.

Several calorimetric methods for evaluation of K and ΔH^0 for complex formation have been reviewed recently (3). Most of these methods possess the advantage that they yield ΔH^0 without recourse to the van't Hoff equation. In this paper we report results of applications of some of these methods to various ether–chloroform systems and compare our K and ΔH^0 values with results of earlier spectroscopic investigations of these same systems.

Theory

We are here concerned with liquid mixtures formed by mixing N_A moles of ether A with N_B moles of chloroform. On the basis of spectroscopic, thermodynamic, and other information, it is already known that complex formation takes place between the unlike molecules as represented by

[1] $$A + B = AB$$

It will be assumed that any further complex formation between the like and/or unlike molecules is relatively insignificant.

The three chemical species (A, B, AB) are assumed to form an ideal solution so that all deviations from ideality in the systems under consideration are attributed entirely to the formation of the complex. This "ideal associated solution" model (4) is also invoked in spectroscopic studies (for example, in the work of Baker *et al.* (5) that is referred to in the next section) and is by no means peculiar to the thermodynamic methods under discussion here.

Letting z_i represent the *equilibrium* mole fraction of the chemical species i, we have

Can. J. Chem. Downloaded from www.nrcresearchpress.com by 210.87.254.6 on 09/05/12
For personal use only.

Can. J. Chem. Downloaded from www.nrcresearchpress.com by 210.87.254.6 on 09/05/12
For personal use only.

[2] $$z_A + z_B + z_{AB} = 1$$

The equilibrium constant for the reaction represented by eq. 1 is

[3] $$K = z_{AB}/z_A z_B$$

Combining eqs. 2 and 3 and rearranging leads to

[4] $$(1 - z_A - z_B)/z_A z_B = K$$

Since the three chemical species are assumed to form an ideal solution, each equilibrium mole fraction is equal to the corresponding activity a_i so that eq. 4 becomes

[5] $$(1 - a_A - a_B)/a_A a_B = K$$

According to this equation, a plot of $(1 - a_A - a_B)/a_A$ *vs.* a_B or of $(1 - a_A - a_B)/a_B$ *vs.* a_A should be linear through the origin with slope K. Or a plot of $(1 - a_A - a_B)/a_A a_B$ *vs.* a_A or a_B should be linear with intercept K and zero slope. Activities we use for evaluation of K in this way have been derived from liquid–vapor equilibrium studies.

The molar enthalpy of mixing ΔH_m is related to a measured enthalpy of mixing Q and the stoichiometric numbers of moles N of A and B by

[6] $$\Delta H_m = Q/(N_A + N_B)$$

For an ideal associated solution we also have

[7] $$Q = n_{AB}\Delta H^0$$

in which n_{AB} represents the equilibrium number of moles of AB formed and ΔH^0 represents the molal enthalpy of formation of the complex. Thus we also have

[8] $$\Delta H_m = n_{AB}\Delta H^0/(N_A + N_B)$$

Algebraic manipulations with eqs. 2, 3, and 8 with mass balance equations ($N_A = n_A + n_{AB}$ and $N_B = n_B + n_{AB}$) lead to the two following equations:

[9] $$x_B = \frac{(1 + K)z_B}{1 + Kz_B(2 - z_B)}$$

[10] $$\Delta H^0 = \Delta H_m(1 + Kz_B)/(1 - x_B)Kz_B$$

Using an independently determined value of K in eq. 9, we can calculate values of x_B at selected values of z_B. Then use of these values of K, z_B, and x_B with molar enthalpies of mixing ΔH_m in eq. 10 permits evaluation of the enthalpy of complex formation ΔH^0.

Equations 5, 9, and 10 are abbreviated forms of equations first derived by McGlashan and Rastogi (6) for systems in which both AB and AB_2 complexes are formed. Our equations can be obtained from theirs by setting the equilibrium constant for formation of AB_2 equal to zero. The McGlashan–Rastogi method has been used to obtain equilibrium constants and enthalpies for formation of AB and AB_2 complexes in several systems (6–9).

All discussion above has centered on separate evaluation of K and ΔH^0 for complex formation. It is also possible to combine eqs. 9 and 10 to obtain

[11] $$x_B(1 - x_B)/\Delta H_m = -(K + 1)\Delta H_m/K(\Delta H^0)^2 + (K + 1)/K\Delta H^0$$

According to eq. 11, a plot of $x_B(1 - x_B)/\Delta H_m$ *vs.* ΔH_m will be linear. Values of *both* K and ΔH^0 can be obtained from the slope and the intercept. We have reported previously (10) another derivation of eq. 11 and applied this equation to complex formation in the triethylamine–chloroform system. It was emphasized there (10) that eq. 11 can be usefully applied only to those systems for which ΔH_m for the equimolar mixture is more exothermic than about 1.5 kJ mol^{-1}.

Results

Here we report results of our evaluations of K and ΔH^0 based on various thermodynamic measurements and equations and compare these values with those derived previously from results of spectroscopic measurements.

Beath and Williamson (11) have reported molar enthalpies of mixing at 298 °K for a number of ether + chloroform mixtures. Applying eq. 11 to their ΔH_m results leads us to the K values listed in Table 1 and also to the ΔH^0 values listed in Table 2. Experimental results reported for mixtures of (iso-$C_5H_{11})_2O$ and (n-$C_6H_{13})_2O$ with $HCCl_3$ do not cover enough of the mole fraction range to allow application of eq. 11.

Constant pressure vapor–equilibrium measurements have been reported (12) for $(C_2H_5)_2O$ + $HCCl_3$ over the temperature range 310.5–335.5 °K. We have applied eq. 5 to each result and obtained by extrapolation the K at 298 °K reported in Table 1. (The large scatter precludes reliable calculation of ΔH^0 by way of the van't Hoff equation.)

For mixtures of (n-$C_3H_7)_2O$ with $HCCl_3$, isothermal vapor pressures at 298 °K are available

TABLE 1. Equilibrium constants for complex formation in ether–chloroform systems at 298 °K

Ether	Source of equilibrium constant K		
	Equation 11[a]	Equation 5	Spectroscopy
$(C_2H_5)_2O$	1.4	1.4[b]	1.46 ± 0.04[c]
$(n\text{-}C_3H_7)_2O$	1.0	1.02[d]	1.2[e]
$(iso\text{-}C_3H_7)_2O$	2		2.41[e], 2.06 ± 0.08[c]
$(n\text{-}C_4H_9)_2O$	0.7		
$(tert\text{-}C_4H_9)_2O$	0.6		1.33[e]
$(n\text{-}C_5H_{11})_2O$	0.6		1.02[e]
$(n\text{-}C_6H_{13})_2O$		1.1[f]	

[a]Based on calorimetric ΔH_m values (11).
[b]Based on vapor–liquid equilibrium data for 310.5–335.5 °K extrapolated to 298 °K.
[c]Based on n.m.r. measurements on solutions of ether and $HCCl_3$ in CCl_4 (15).
[d]Based on vapor pressures at 298 °K (13).
[e]Based on n.m.r. measurements (5).
[f]Approximate value obtained as described in the text.

TABLE 2. ΔH^0/kJ mol^{-1} values for complex formation in ether–chloroform systems

Ether	ΔH^0 (kJ mol^{-1})		
	Equation 11[a]	Equation 10[c]	Spectroscopy K and $(\partial \ln K/\partial T)_p$[b]
$(C_2H_5)_2O$	−14.9	−14.6 (1.46)	
$(n\text{-}C_3H_7)_2O$	−14	−12 (1.2)	−10.8
$(iso\text{-}C_3H_7)_2O$	−14	−14.1 (2.06)	−11.7
$(n\text{-}C_4H_9)_2O$	−16		
$(tert\text{-}C_4H_9)_2O$	−14	−9 (1.33)	−7.9
$(n\text{-}C_5H_{11})_2O$	−15	−12 (1.02)	−10.0
$(n\text{-}C_6H_{13})_2O$		−10 (1.1)	

[a]Based on calorimetric ΔH_m values (11).
[b]Based on n.m.r. measurements (5).
[c]K values in parentheses are taken from Table 1.

(13). A plot of $(1 - a_A - a_B)/a_A a_B$ *vs.* a_B (suggested by eq. 5) is linear with a small positive (~0.2) slope. Following McGlashan and Rastogi (6), this slope might be interpreted as the equilibrium constant K_2 for formation of an AB_2 complex. The equilibrium constant for formation of AB as listed in Table 1 corresponds to the intercept at $a_B = 0$.

For mixtures of $(n\text{-}C_6H_{13})_2O$ with $HCCl_3$, we have isothermal vapor pressures at 278.68 °K (14). In this case, however, a plot of $(1 - a_A - a_B)/a_A a_B$ *vs.* a_B is linear with a positive (~0.7) slope. The approximate K value listed in Table 1 was obtained by assuming that K at 278.68 °K is given by the intercept at $a_B = 0$ and then using the van't Hoff equation (with $\Delta H^0 = -10$ kJ mol^{-1}) to obtain K at 298 °K.

Equilibrium constants based on thermodynamic eqs. 5 and 11 are independent of each other in that they are evaluated independently from different kinds of experimental results. Agreement between these independent values is generally good.

The spectroscopic equilibrium constants listed in Table 1 were obtained from n.m.r. measurements. Uncertainties listed are those given in the original publications.

Use of eq. 10 for evaluation of ΔH^0 of complex formation requires independently determined values of K. Our results listed in Table 2 have been obtained by using the equilibrium constants given in parentheses with the molar enthalpies of mixing reported by Beath and Williamson (11).

The "spectroscopic" ΔH^0 values listed in Table 2 were obtained by application of the van't Hoff equation to equilibrium constants derived from n.m.r. measurements at different temperatures. Uncertainties have been estimated (5) as about 10%.

Tables 1 and 2 show that the equilibrium con-

Can. J. Chem. Downloaded from www.nrcresearchpress.com by 210.87.254.6 on 09/05/12
For personal use only.

stants and enthalpies of complex formation evaluated from thermodynamic measurements are generally in good agreement with those based on spectroscopic measurements. Although we have no means for precise quantitative assessment of the accuracies of the various tabulated values, we can make some useful generalizations as follows.

It is reasonable to begin on the basis that the "best" values of K and ΔH^0 will be those derived in such a way that a "set" of experimental data is interpreted in terms of a minimum number of parameters. Secondly, we also expect that "best" values will be those that are not based on any differentiation procedure because such procedures inevitably magnify experimental uncertainties. On the basis of these generalizations, it follows that K values based on spectroscopic measurements or on thermodynamic activity measurements and eq. 5 are likely to be "better" than K values based on eq. 11, which requires simultaneous evaluation of K and ΔH^0. We also conclude that ΔH^0 values based on calorimetric enthalpies and eq. 10 (independent K) are likely to be "better" than those based on eq. 11 (simultaneous evaluation of K and ΔH^0) or on application of the van't Hoff equation (differentiation) to equilibrium constants determined spectroscopically (or in any other way) at several temperatures.

Although our discussion above indicates that simultaneous evaluation of both K and ΔH^0 from enthalpies of mixing by way of eq. 11 is not the "best" way to obtain either K or ΔH^0, values actually obtained in this way seem to be of satisfactory accuracy for several systems as shown here and previously (10).

1. R. M. BADGER and S. H. BAUER. J. Chem. Phys. **5**, 839 (1937).
2. E. J. KING. Acid–base equilibria. Pergamon Press, Oxford. 1965.
3. D. V. FENBY and L. G. HEPLER. Chem. Soc. Rev. In press.
4. I. PRIGOGINE and R. DEFAY. Chemical thermodynamics. *Translated by* D. H. Everett. Longmans Green, London. 1954.
5. J. R. BAKER, I. D. WATSON, and A. G. WILLIAMSON. Aust. J. Chem. **24**, 2047 (1971).
6. M. L. MCGLASHAN and R. P. RASTOGI. Trans. Faraday Soc. **54**, 496 (1958).
7. E. R. KEARNS. J. Phys. Chem. **65**, 314 (1961).
8. K. W. MORCOM and D. N. TRAVERS. Trans. Faraday Soc. **61**, 230 (1965).
9. D. V. FENBY and L. G. HEPLER. J. Chem. Thermodyn. **6**, 185 (1974).
10. L. G. HEPLER and D. V. FENBY. J. Chem. Thermodyn. **5**, 471 (1973).
11. L. A. BEATH and A. G. WILLIAMSON. J. Chem. Thermodyn. **1**, 51 (1969).
12. J. KOHOUTEK. Coll. Czech. Chem. Commun. **25**, 288 (1960).
13. L. A. BEATH, I. D. WATSON, and A. G. WILLIAMSON. Proc. 1st Int. Conf. Calorimetry and Thermodynamics, Warsaw. 1969. p. 773.
14. N. F. PASCO. Ph.D. Thesis, University of Otago, Dunedin, New Zealand. 1973.
15. B. B. HOWARD, C. F. JUMPER, and M. T. EMERSON. J. Mol. Spectrosc. **10**, 117 (1963).

Can. J. Chem. Downloaded from www.nrcresearchpress.com by 210.87.254.6 on 09/05/12
For personal use only.

Electric Field Gradients in Alkali Halide Molecules

JEAN-PIERRE LAPLANTE[1] AND ANDRE D. BANDRAUK

Département de Chimie, Université de Sherbrooke, Sherbrooke, Québec J1K 2R1

Received October 12, 1973

JEAN-PIERRE LAPLANTE and ANDRE D. BANDRAUK. Can. J. Chem. **52**, 2143 (1974).

The electric field gradient q has been calculated from Hartree–Fock wavefunctions for the molecules LiF, LiCl, LiBr, NaF, NaCl, NaBr, KF, and KCl. It is found that σ and π electrons behave quite differently. Exchange distortions are of great importance for a proper understanding of σ contributions to q. Polarizations of π electrons into the bonding region are also considerable. These effects are responsible for failures of classical models and are further discussed using calculated density difference diagrams.

JEAN-PIERRE LAPLANTE et ANDRE D. BANDRAUK. Can. J. Chem. **52**, 2143 (1974).

Le présent article rapporte les résultats de calculs *ab initio* du gradient de champ électrique q pour la série de molécules ioniques-type LiF, LiCl, LiBr, NaF, NaCl, NaBr, KF et KCl. Ces gradients ont été obtenus à l'aide de fonction d'onde de type Hartree–Fock. Ces résultats démontrent clairement que les électrons σ et π se comportent d'une façon très différente dans ces molécules. Les distorsions d'échange présentes se révèlent aussi d'importance majeure pour une compréhension adéquate de la contribution des électrons σ à la valeur de q. La polarisation des électrons π dans la région de liaison est aussi considérable. L'ensemble de ces effets s'avère donc responsable de la faillite des modèles classiques pour l'interprétation de q. La discussion est appuyée des diagrammes de différence de densité correspondants.

Introduction

The theoretical interpretation of the electric field gradient q in a molecule is of interest as it is a direct measure of the charge distribution. This follows from the fact that the interaction e^2qQ, called the quadrupole coupling constant, between a nuclear quadrupole moment Q and the field gradient q of a molecular charge distribution ρ, is a weak interaction such that first-order perturbation theory is adequate (1). Experimentally e^2qQ is determined from various hyperfine structures in resonance experiments of the microwave type (1, 2). The field gradient q is also an intrinsic part of the theoretical expression for the force constant of a diatomic molecule (3).

In this article we examine various models used to interpret q in ionic molecules, in particular, the alkali halides. Considerable theoretical work (4) has been done using a simple model based on ions with polarizable charge distributions. The problem then becomes the perturbation of an ion with a nuclear quadrupole moment by the field of an external point charge. The expression for the field gradient of simple ions with closed-shells configurations appears as

$$[1] \qquad q^{\pm} = \mp\frac{2}{R^3}(1 - \gamma_\infty{}^{\pm})$$

where superscripts $\pm$ indicate positive and negative ions correspondingly. The factor $\gamma_\infty{}^{\pm}$ represents the effect of the deformation of the closed shells of the ion by the external charge on the value of q. If the distorted electron distribution opposes the field gradient of the external charge, then $\gamma_\infty{}^{\pm}$ is positive and there is a *shielding* effect, while if the distorted distribution enhances the field gradient, then $\gamma_\infty{}^{\pm}$ is negative and there is an *antishielding* effect. The perturbation of the external charge will produce radial and angular excitations of the ionic charge distribution. The former, *e.g.*, $p \rightarrow np$, are antishielding and the latter ($s \rightarrow d$, $p \rightarrow f$) are shielding (at the halogen nucleus and conversely at the alkali). The polarizable ion model first developed by Sternheimer gives reasonable results for q^+ (alkali nucleus) but less so for q^- (halogen nucleus) as shown in Table 1. Thus at the halogen nucleus, the model often predicts the wrong sign.

Certain attempts have been made to rectify the model by introducing covalency (5), but with little success (6). The introduction of overlap (7) improved the model somewhat but not enough at the halogen. De Wijn (8) recently obtained some success by suppressing the antishielding of σ electrons and considering instead dipolar $p_\pi \rightarrow d_\pi$ polarizations at the halide ion. Experimental values of q^- are used to obtain an ionic degree i

[1]NRCC Postgraduate Fellow.

Can. J. Chem. Downloaded from www.nrcresearchpress.com by 210.87.254.5 on 09/05/12
For personal use only.

TABLE 1. Values of electric field gradients q at alkali and halogen nuclei, at $R = R_e$ (in 10^{15} e.s.u.)

Molecule	R_e (a.u.)	At nucleus	q Experiment*	q This work†	q Sternheimer‡	q De Wijn§
LiF	2.88770	Li	−0.3	−0.121	−0.20	−0.25
		F		−0.902	6.33‖	
LiCl	3.82500	Li	−0.1	−0.070	−0.08	−0.14
		Cl	0.53	0.387	6.3	
LiBr	4.06550	Li	−0.1	−0.070	−0.07	−0.11
		Br	1.5	1.848	10.1	
NaF	3.62883	Na	−1.0	−1.274	−0.73	−0.9
		F		−0.362	3.19	
NaCl	4.46090	Na	−0.7	−0.823	−0.39	−0.6
		Cl	0.785	0.637	3.82	
NaBr	4.72800	Na	−0.6	−0.585	−0.33	−0.5
		Br	2.4	3.104	6.4	
KF	4.10348	K	−1.2	−1.966	−1.45	−1.7
		F		−1.350	2.21	
KCl	5.03900	K	−0.9	−1.431	−0.79	−1.1
		Cl	−0.01	−0.326	2.7	

*These values are taken from refs. 8 and 9.
†Another series of *ab initio* calculations has been done by Matcha (see ref. 10*b*). His results are in general the same as ours.
‡Calculated from γ_∞ given in ref. 8.
§Taken from ref. 8.
‖Calculated from γ_∞ given in ref. 22.

which is then used to calculate q^-. The values of q^+ predicted by de Wijn are also reported in Table 1 and are seen to improve the Sternheimer values of q^+. De Wijn's model has been further refined by Peters and Todd (9). These authors retain antishielding effects and adjust the degree of p_π polarization to give correct coupling constants. There remains therefore the problem of ascertaining the real behavior of σ and π electron densities in these molecules.

We report here calculations of q and its different components for various internuclear distances from tabulated Hartree–Fock wavefunctions of LCAO–MO–SCF type (10). These functions were also used to produce molecular density diagrams in addition to density difference diagrams with respect to the free atoms and ions (Figs. 1–4). These diagrams are useful in visualizing the electronic redistributions which occur upon bond formation and have been used previously for this purpose (11).

The general result which emanates from these calculations is that p_σ electrons behave quite differently from p_π electrons. It is precisely this difference in σ and π behavior in the molecule which renders difficult the elaboration of any simple model for the calculation of ionic electric field gradients.

Calculations

For a closed-shell diatomic molecule AB, with a ground state electronic wave function ψ expressed as a determinant of molecular orbitals ψ_i, we can write the expectation value of q_A, the field gradient at nucleus A as

$$[2] \qquad q_A = \frac{2Z_B}{R^3} - \sum_i 2\left\langle \psi_i \left| \frac{3\cos^2\theta_A - 1}{r_A^3} \right| \psi_i \right\rangle$$

Z_B is the charge on nucleus B, r_A is the distance of an electron from nucleus A, and θ_A is the angular position of the electron with respect to the molecular axis. ψ_i, the doubly-filled orthonormal molecular orbitals can be further written as $\psi_i = \phi_{A_i} + \phi_{B_i}$, *i.e.*, a sum of atomic functions centered on the nuclei ($\phi_{A_i} = \sum_P C_{P_i}\chi_{P_i}$, $\phi_{B_i} = \sum_q C_{q_i}\chi_{q_i}$, where the χ's are Slater-type orbitals). This permits one to attribute four contributions to the field gradient: nuclear, atomic, overlap, and shielding, *i.e.* we have

$$[3] \qquad q_A = \frac{2Z_B}{R^3} - q_{AT} - q_{ov} - q_{SH}$$

Can. J. Chem. Downloaded from www.nrcresearchpress.com by 210.87.254.5 on 09/05/12
For personal use only.

Can. J. Chem. Downloaded from www.nrcresearchpress.com by 210.87.254.5 on 09/05/12
For personal use only.

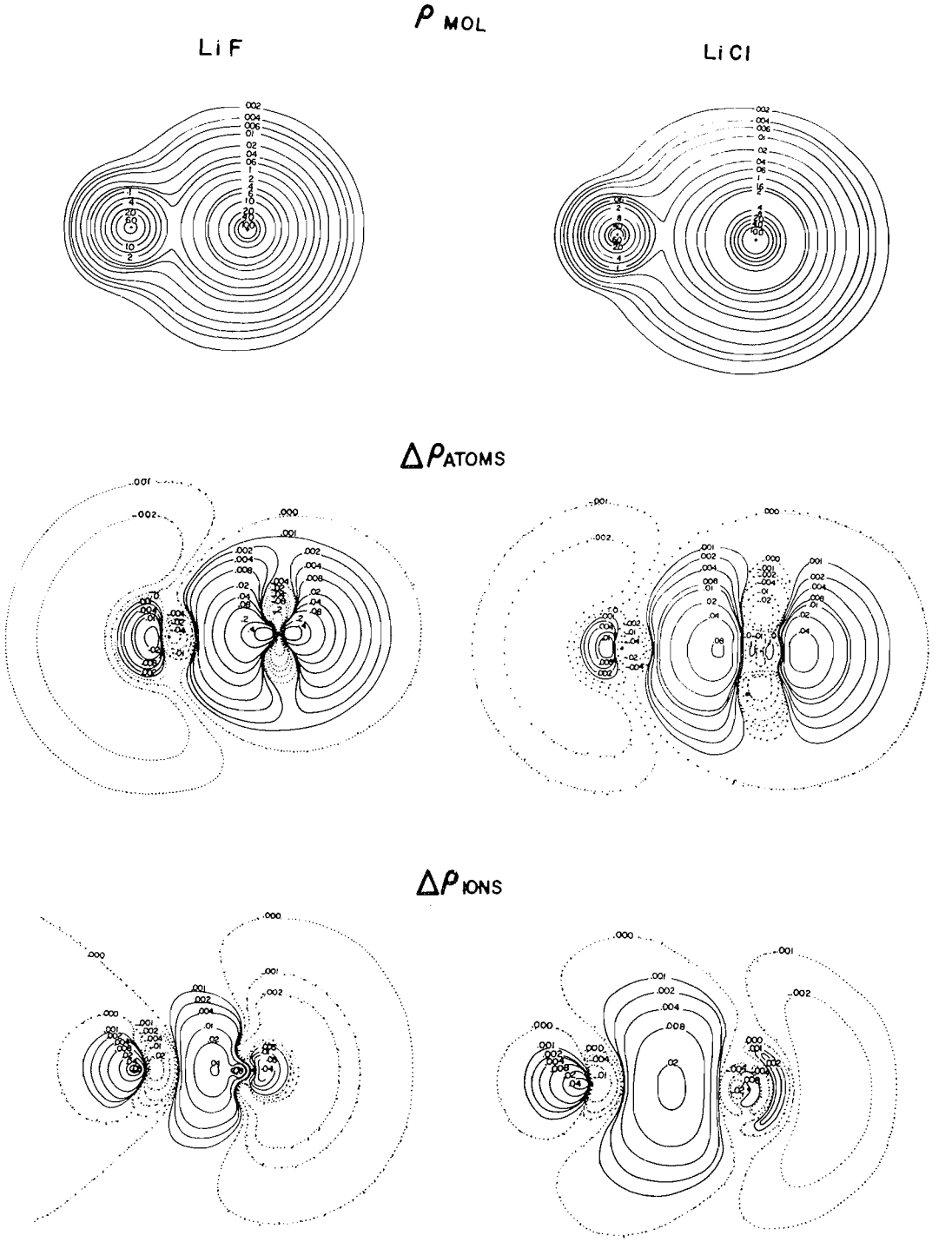

FIG. 1. Contour maps, at $R = R_e$, of the total molecular charge distribution ρ_{mol}, of the density difference distributions $\Delta\rho_{atoms}$, $\Delta\rho_{ions}$, defined by: $\Delta\rho_{atoms}(r) = \rho_{mol}(r) - [\rho_A(r) + \rho_B(r)]$ $\Delta\rho_{ions}(r) = \rho_{mol}(r) - [\rho_{A^+}(r) + \rho_{B^-}(r)]$. All contours are in atomic units and at the same scale.

Can. J. Chem. Downloaded from www.nrcresearchpress.com by 210.87.254.5 on 09/05/12
For personal use only.

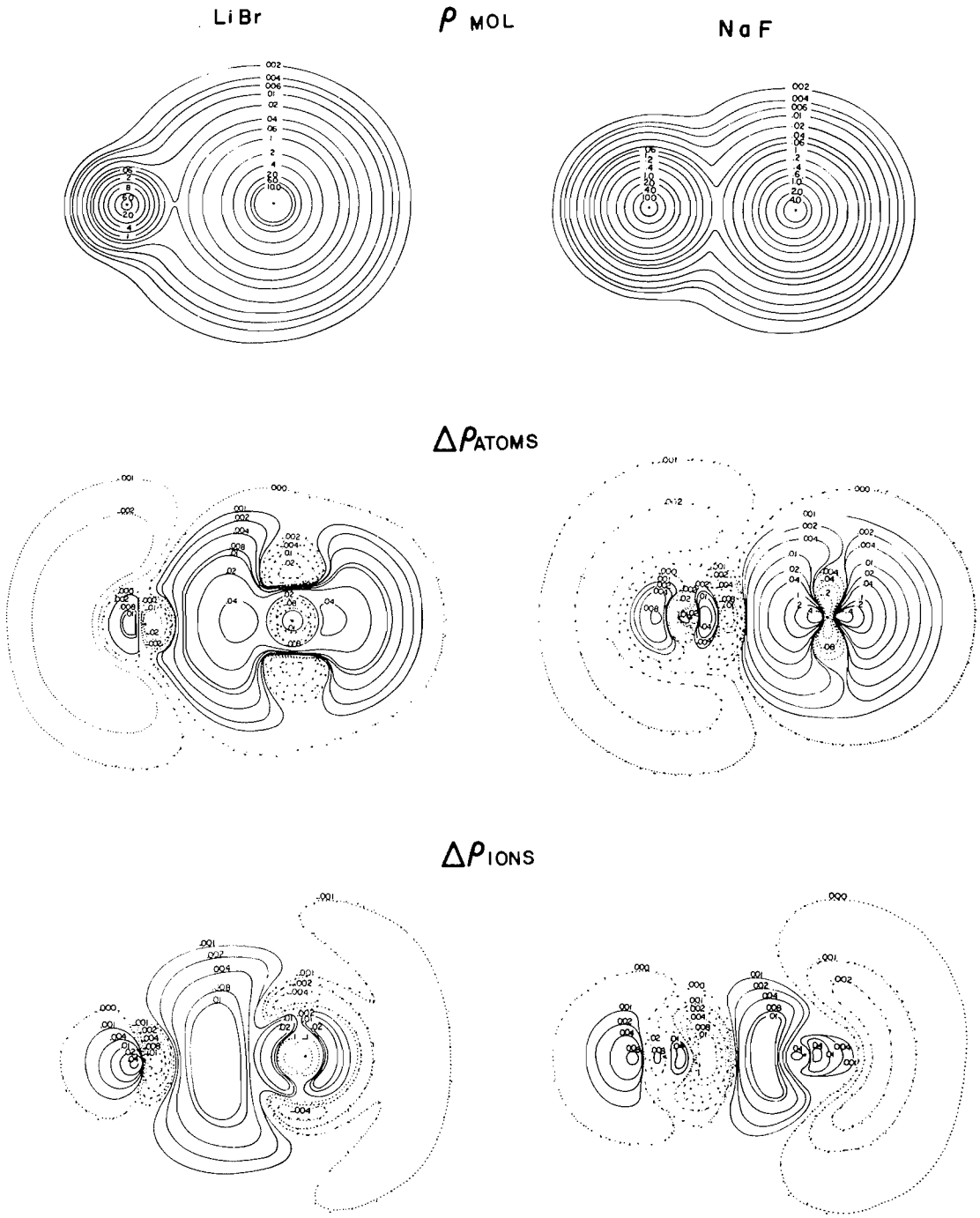

FIG. 2. Contour maps of ρ_{mol}, $\Delta\rho_{atoms}$, and $\Delta\rho_{ions}$ for LiBr and NaF, at $R = R_e$.

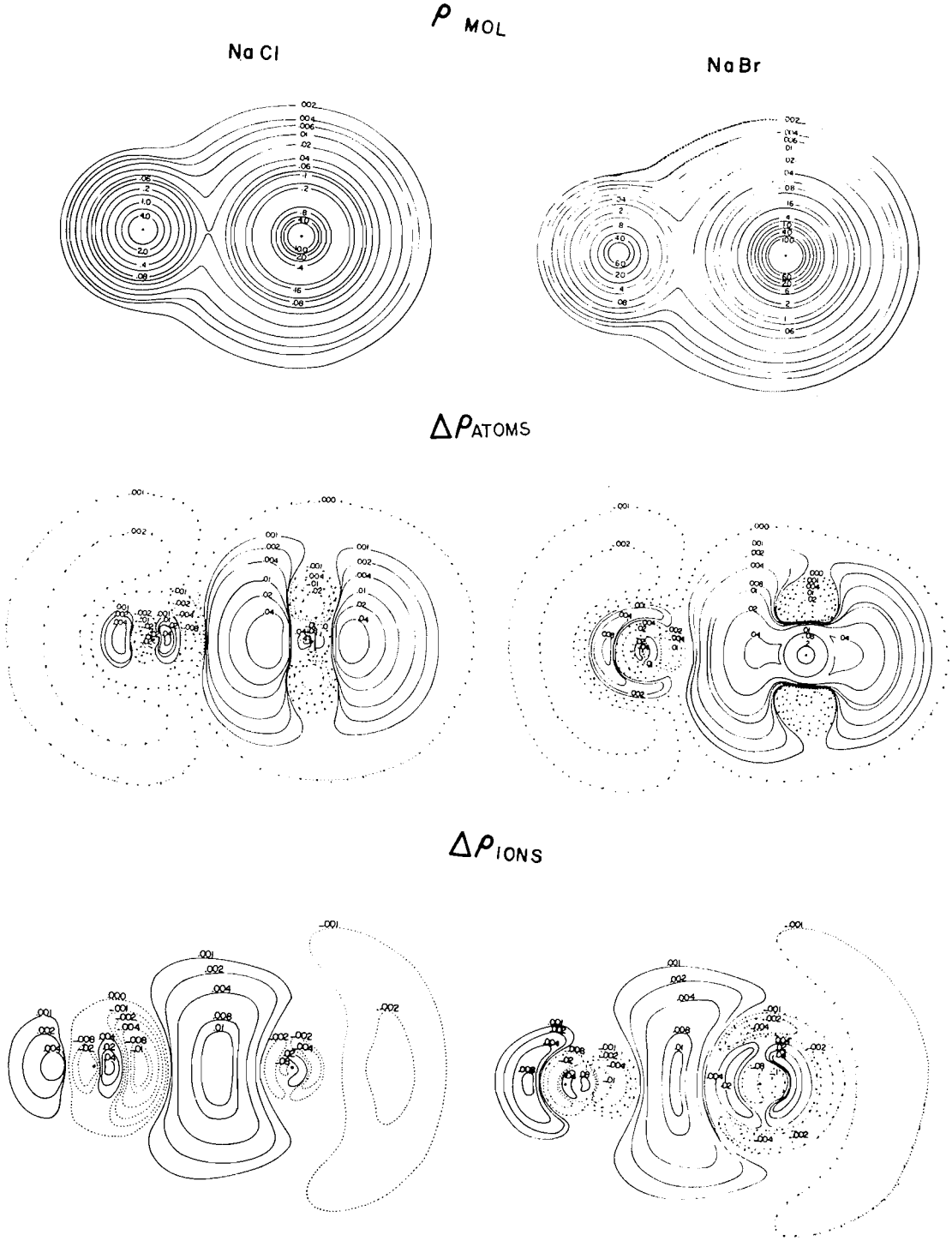

FIG. 3. Contour maps of ρ_{mol}, $\Delta\rho_{atoms}$, and $\Delta\rho_{ions}$ for NaCl and NaBr, at $R = R_e$.

Can. J. Chem. Downloaded from www.nrcresearchpress.com by 210.87.254.5 on 09/05/12
For personal use only.

Can. J. Chem. Downloaded from www.nrcresearchpress.com by 210.87.254.5 on 09/05/12
For personal use only.

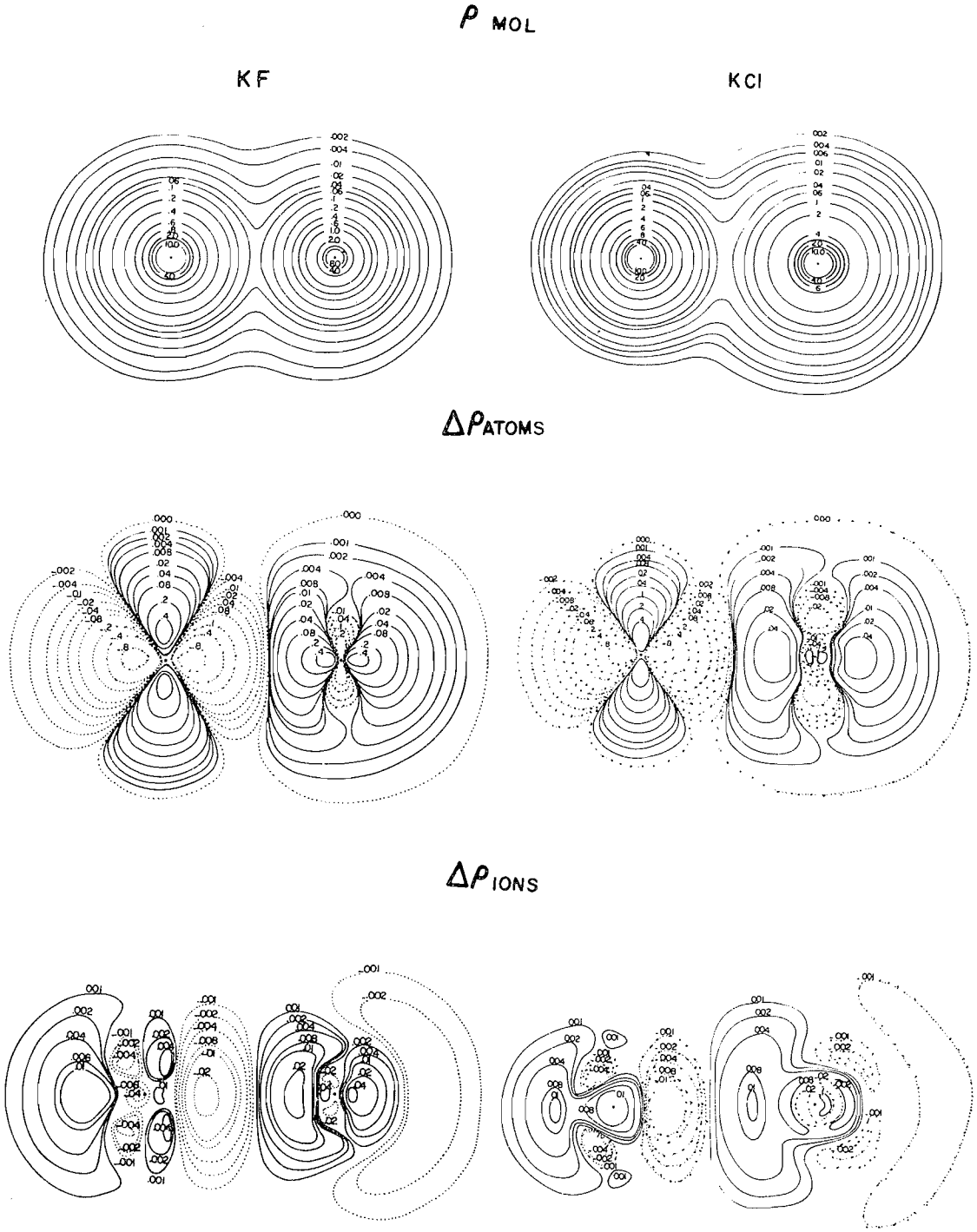

FIG. 4. Contour maps of ρ_{mol}, $\Delta\rho_{atoms}$, and $\Delta\rho_{ions}$ for KF and KCl, at $R = R_e$.

TABLE 2. *Ab initio* values of atomic contributions at alkali nuclei, at $R = R_e$ (in a.u. = e/a_0^3)

Molecule	q_{AT}^{σ}	q_{AT}^{π}	q_{AT}	$(R^3/2)q_{AT} \simeq -\gamma^+(R)$	$-\gamma_\infty{}^+$
LiF	−0.020	−0.002	−0.022	−0.263	−0.26
LiCl	−0.007	−0.002	−0.009	−0.257	−0.26
LiBr	0.001	−0.004	−0.003	−0.092	−0.26
NaF	27.502	−27.132	0.370	8.838	4.55
NaCl	27.403	−27.157	0.240	10.910	4.55
NaBr	26.906	−26.732	0.174	9.209	4.55
KF	263.938	−263.359	0.579	20.010	15.0
KCl	263.374	−262.950	0.424	27.124	15.0

TABLE 3. *Ab initio* values of atomic contributions at halogen nuclei at $R = R_e$ (in a.u. = e/a_0^3)

Molecule	q_{AT}^{σ}	q_{AT}^{π}	q_{AT}	$(R^3/2)q_{AT} \simeq \gamma^-(R)$	$\gamma_\infty{}^-$
LiF	10.494	−10.133	0.361	4.344	−22.5
NaF	10.229	−10.078	0.151	3.615	−22.5
KF	10.589	−10.131	0.458	15.814	−22.5
LiCl	169.887	−169.986	−0.099	−2.758	−53
NaCl	169.802	−169.988	−0.186	−8.251	−53
KCl	168.587	−168.475	0.112	7.164	−53
LiBr	2354.790	−2355.320*	−0.530	−17.813	−107
NaBr	2354.228	−2355.141	−0.913	−48.242	−107

*The q_{AT}^{π} term at Br^- includes the contribution q_{AT}^{δ}: LiBr, −52.128 a.u., NaBr, −52.148 a.u. These contributions being almost constant, are included in q_{AT}^{π}.

where q_{AT} is due to the atomic charge density $2\sum_i \phi_{A_i}{}^2$, q_{ov} to the overlap charge density $4\sum_i \phi_{A_i}\phi_{B_i}$, and finally q_{SH} to the density $2\sum_i \phi_{B_i}{}^2$ which shields nucleus B from nucleus A. For a purely ionic alkali halide, one would have $q_{SH}{}^{\pm} = (2/R^3)(Z_B \pm 1)$ and $q_{ov} = 0$. We may therefore rewrite eq. [3] as

$$[4] \qquad q^{\pm}(R) = -\frac{2}{R^3}\{\alpha_{\pm}(R) + \beta_{\pm}(R)\}$$

with

$$[5] \qquad \alpha_{\pm}(R) = \pm 1 + \frac{R^3}{2} q_{AT}{}^{\pm}(R)$$

$$\beta_{\pm}(R) = \Delta Z_B{}^{\mp}(R) + \frac{R^3}{2} q_{ov}{}^{\pm}(R)$$

The term $\alpha_{\pm}$ contains the ionic charge (± 1) of the ion B in addition to the quadrupolar polarization of the ion A as measured by the operator $(3\cos^2\theta_A - 1)/r_A{}^3$. This polarization, given by $(R^3/2)q_{AT}{}^{\pm}$, is therefore approximately the equivalent of the antishielding factor $\gamma_\infty{}^{\pm}$.[2] The term $\beta_{\pm}$ represents all deviations from a true ionic model ($\beta_{\pm} = 0$ for a perfect ionic molecule), $\Delta Z_B{}^{\mp}(R)$ corresponds to an ionic defect of the ion B due to incomplete shielding of nucleus **B** by the electron charge situated on it: $\Delta Z_B{}^{\mp} = 2\sum_i \int \phi_{B_i}{}^2 dv_i - (Z_B \pm 1)$. For a perfect ion, $\Delta Z_B{}^{\mp} = 0$.

Table 1 reports our calculated values of the total q. In general these results are fairly close to the experimental results which depend on not too well known values of nuclear quadrupole moments Q and thus may not be too reliable (12). The experimental results further correspond to $v = 0$ values which may introduce a further discrepancy due to different R_e values. Finally, there remains always the question of accuracy near the nuclei of the wavefunctions used. An exact wavefunction will contain all polarizations to all orders. Correlated or configuration interaction wavefunctions would therefore be useful to explain the divergences if these exist. For closed shell systems, one electron properties such as q are expected to be correct to first order in the correlation error following Brillouin's theorem for Hartree–Fock functions. As will be shown later, the present functions are nevertheless sufficient to pinpoint the most important contributions to the field gradients.

The various contributions to $\alpha_{\pm}(R)$ and $\beta_{\pm}(R)$ are reported in Tables 2–7 and are further described in the next sections. The variation of these terms as a function of internuclear distance

[2] If $\beta_{\pm} \ll \alpha_{\pm}$, we have $(R^3/2)q_{AT}{}^{\pm} \cong \mp \gamma_\infty{}^{\pm}$.

Can. J. Chem. Downloaded from www.nrcresearchpress.com by 210.87.254.5 on 09/05/12
For personal use only.

Can. J. Chem. Downloaded from www.nrcresearchpress.com by 210.87.254.5 on 09/05/12
For personal use only.

TABLE 4. *Ab initio* values of overlap contributions at alkali nuclei at $R = R_e$ (in a.u. $= e/a_0^3$)

Molecule	q_{ov}^{σ}	q_{ov}^{π}	q_{ov}	$(R^3/2)q_{ov}$
LiF	0.030	0.011	0.041	0.491
LiCl	0.026	0.006	0.032	0.907
LiBr	0.022	0.006	0.028	0.952
NaF	−0.014	0.008	−0.006	−0.155
NaCl	−0.002	0.005	0.003	0.116
NaBr	−0.001	0.006	0.005	0.273
KF	0.006	0.006	0.012	0.430
KCl	0.005	0.004	0.009	0.581

TABLE 5. *Ab initio* values of overlap contributions at halogen nuclei, at $R = R_e$ (in a.u. $= e/a_0^3$)

Molecule	q_{ov}^{σ}	q_{ov}^{π}	q_{ov}	$(R^3/2)q_{ov}$
LiF	0.076	−0.077	−0.001	−0.009
NaF	0.053	−0.050	0.003	0.060
KF	0.057	−0.063	−0.007	−0.228
LiCl	0.015	−0.002	0.013	0.371
NaCl	0.013	−0.002	0.011	0.490
KCl	0.007	−0.002	0.005	0.349
LiBr	0.005	−0.017	−0.012	−0.397
NaBr	−0.013	−0.013	−0.026	−1.382

TABLE 6. *Ab initio* values of shielding contributions at alkali nuclei, at $R = R_e$ (in atomic units of charge)*

Molecule	q_{SH}^{σ}	σ_{def}†	q_{SH}^{π}	π_{def}	q_{SH}	$\Delta Z_B^- = \sigma_{def} + \pi_{def}$
LiF	6.403	0.403	2.818	−1.182	9.221	−0.779
NaF	6.327	0.327	3.177	−0.823	9.504	−0.496
KF	6.240	0.240	3.253	−0.747	9.493	−0.507
LiCl	10.604	0.604	6.351	−1.649	16.955	−1.045
NaCl	10.470	0.470	6.770	−1.230	17.240	−0.760
KCl	10.591	0.591	6.929	−1.071	17.520	−0.480
LiBr	16.807	0.807	14.201	−1.799	31.008‡	−0.992
NaBr	16.599	0.599	14.576	−1.424	31.175	−0.825

*All values are multiplied by $R^3/2$ to give effective charges.
†$\sigma_{def} = q_{SH}^{\sigma}$ − number of σ electrons in ion B. $\pi_{def} = q_{SH}^{\pi}$ − number of π electrons in ion B.
‡q_{SH}^{δ} (LiBr : 4.06; NaBr : 4.05) is not included as these are perfect shielding and do not contribute to the defect.

TABLE 7. *Ab initio* values of shielding contributions at halogen nuclei, at $R = R_e$ (in atomic units of charge)*

Molecule	q_{SH}^{σ}	σ_{def}†	q_{SH}^{π}	π_{def}	q_{SH}	$\Delta Z_B^+ = \sigma_{def} + \pi_{def}$
LiF	2.015	0.015	−0.002	−0.002	2.013	0.013
LiCl	2.038	0.038	0.009	0.009	2.047	0.047
LiBr	2.046	0.046	0.022	0.022	2.068	0.068
NaF	6.298	0.298	3.693	−0.307	9.991	−0.009
NaCl	6.236	0.236	3.804	−0.196	10.040	0.040
NaBr	6.226	0.226	3.837	−0.163	10.064	0.064
KF	10.559	0.559	7.228	−0.772	17.787	−0.213
KCl	10.424	0.424	7.496	−0.504	17.921	−0.079

*All values are multiplied by $R^3/2$ to give effective charge.
†$\sigma_{def} = q_{SH}^{\sigma}$ − number of σ electrons in ion B. $\pi_{def} = q_{SH}^{\pi}$ − number of π electrons in ion B.

Can. J. Chem. Downloaded from www.nrcresearchpress.com by 210.87.254.5 on 09/05/12
For personal use only.

is represented in Figs. 5 and 6 and is discussed later. A quick perusal of these tables and figures reveals that the atomic term, q_{AT}, or $(R^3/2)q_{AT}$ in effective charges, is always the most important term. The deviation term, $\beta_{\pm}(R)$, being the sum of overlap contribution and the shielding defect, is usually of the order of 5% of the atomic term and is therefore quite negligible when compared to the atomic contribution.

Interpretation of Field Gradients

$q^+(R)$, Alkali Field Gradient

Tables 2, 4, and 6 report the atomic, overlap, and shielding contributions of the field gradient $q^+(R)$ at the various alkali ions M^+. For each case, σ and π contributions are separated to accentuate the different polarizations. These results are further complemented by Fig. 5 for a relative comparison of the importance of the terms $\alpha_+(R)$ and $\beta_+(R)$.

q_{AT} (Table 2)

The first observation is the negative values for Li^+ which correspond to a shielding effect, whereas for Na^+ and K^+ one has positive values, corresponding to antishielding. This difference stems from different types of polarizations which occur in the M^+ cases. Thus in Li^+, a detailed study of the wavefunction shows that quadrupolar polarizations are produced by quadrupolar excitations of the angular type ($s \rightarrow d$) *à la* Sternheimer (13). This creates a displacement of the alkali core density behind and also perpendicular to the direction of the molecular axis (Fig. 1). In the case of Na^+ and K^+, the quadrupolar polarizations which prevail are those of the $2p^6$ and $3p^6$ electron shells respectively. Detailed calculations show inner shells remain quite unpolarized, *i.e.*, spherical. The polarizations of the outer shells of Na^+ and K^+ are antishielding, *i.e.* q_{AT} positive as they increase the electric field gradient. The net atomic contributions reflect a large discrepancy between σ and π polarizations, the σ electrons overcoming the π electrons as a result of mainly radial excitations of the type $p \rightarrow np$ (17). This is further substantiated by the $\Delta\rho$ diagrams of Figs. 2, 3, and 4 where p-like polarizations are found on both sides of the Na and K nuclei. It is to be noticed that our values of γ^+ do not correlate well with the Sternheimer values except in the case of LiF and LiCl. Furthermore, in the sodium series, one has q_{AT} larger in the order NaF > NaCl > NaBr, reflecting to some extent the effect of internuclear distance. This produces random values of γ^+, indicating that γ^+ does not correlate well with this effect.

$q_{ov} + q_{SH}$ (Tables 4 and 6)

Overlap contributions increase as one passes from LiF to LiBr. This is counterbalanced by a total *undershielding* of the density at X^-. In the sodium and potassium series, overlap contributions are smaller than in the former series. In general, the overlap contributions tend to cancel out the ionic defect of the halide ion. A diagram of the overlap density (15) in LiF indicates that this overlap density is in fact closer to the halogen nucleus and should be thus more properly attributed to F^-. This therefore explains partly the above cancellation effect. Thus the net defect $\beta_+(R)$ becomes negligible compared to $\alpha_+(R)$, the atomic polarization, as the ionic sizes increase. However, as in q_{AT}, σ and π densities shield each nucleus differently, σ densities being closer to the alkali *overshield* the halide nucleus, whereas π densities *undershield* this same nucleus as a result of their particular geometric distribution. In LiF, this introduces an appreciable defect (Fig. 5) and is therefore responsible for the difference between the calculated q_{Li^+} and the Sternheimer value.

Polarizations and Pauli repulsions are responsible for the different σ and π contributions to the field gradient. In the Li series as depicted in Figs. 1 and 2, there is a net backpolarization of the cation density as required by the Hellmann–Feynman theorem (16). This backpolarization is in large part due to Pauli repulsions and has been considered previously by Benson and Van der Hoff (14). For Na^+ and K^+ the $\Delta\rho$ diagrams clearly demonstrate quenching of radial excitations in front of these alkali nuclei, thus enhancing the antishielding effect. These diagrams also indicate definite polarizations of p_π density towards the bonding region. Thus the larger σ backpolarization is counterbalanced by an inpolarization of the π density. This effect is obviously related to the ionic sizes as can be seen by comparing the ρ diagrams. Thus KF, as an example, seems to be nearly symmetric in size. This is not surprising as the classical ionic radii of K^+ and F^- are nearly identical (18). These radii can be fairly well reproduced from the ρ diagrams by measuring the distance from any nucleus outwards to the 0.002 contour (11).

Can. J. Chem. Downloaded from www.nrcresearchpress.com by 210.87.254.5 on 09/05/12
For personal use only.

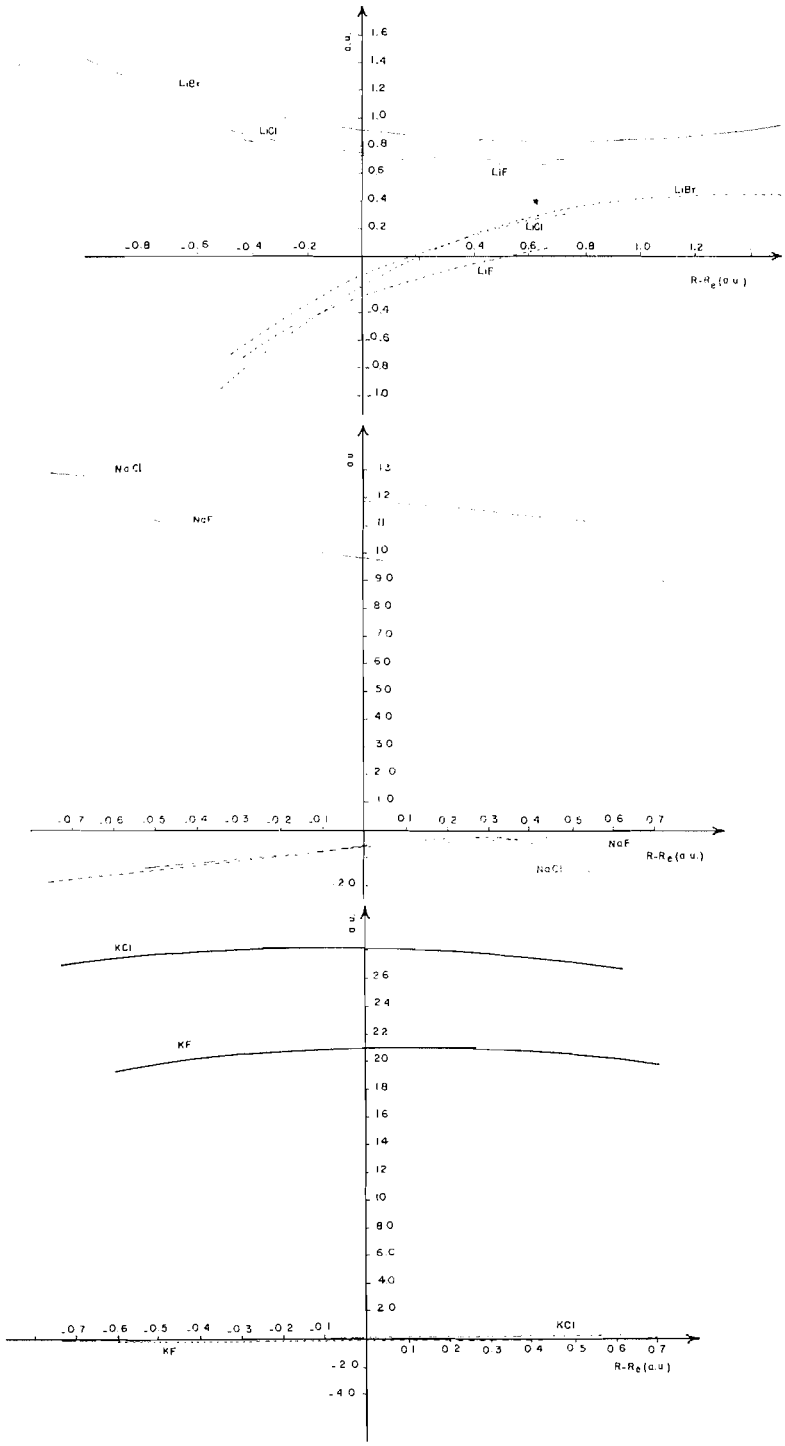

FIG. 5. Dependence on internuclear distance R of α_+ (solid curves) and β_+ (dashed curves) terms, for Li^+, Na^+, and K^+, in homolog series. Values are in atomic charge units.

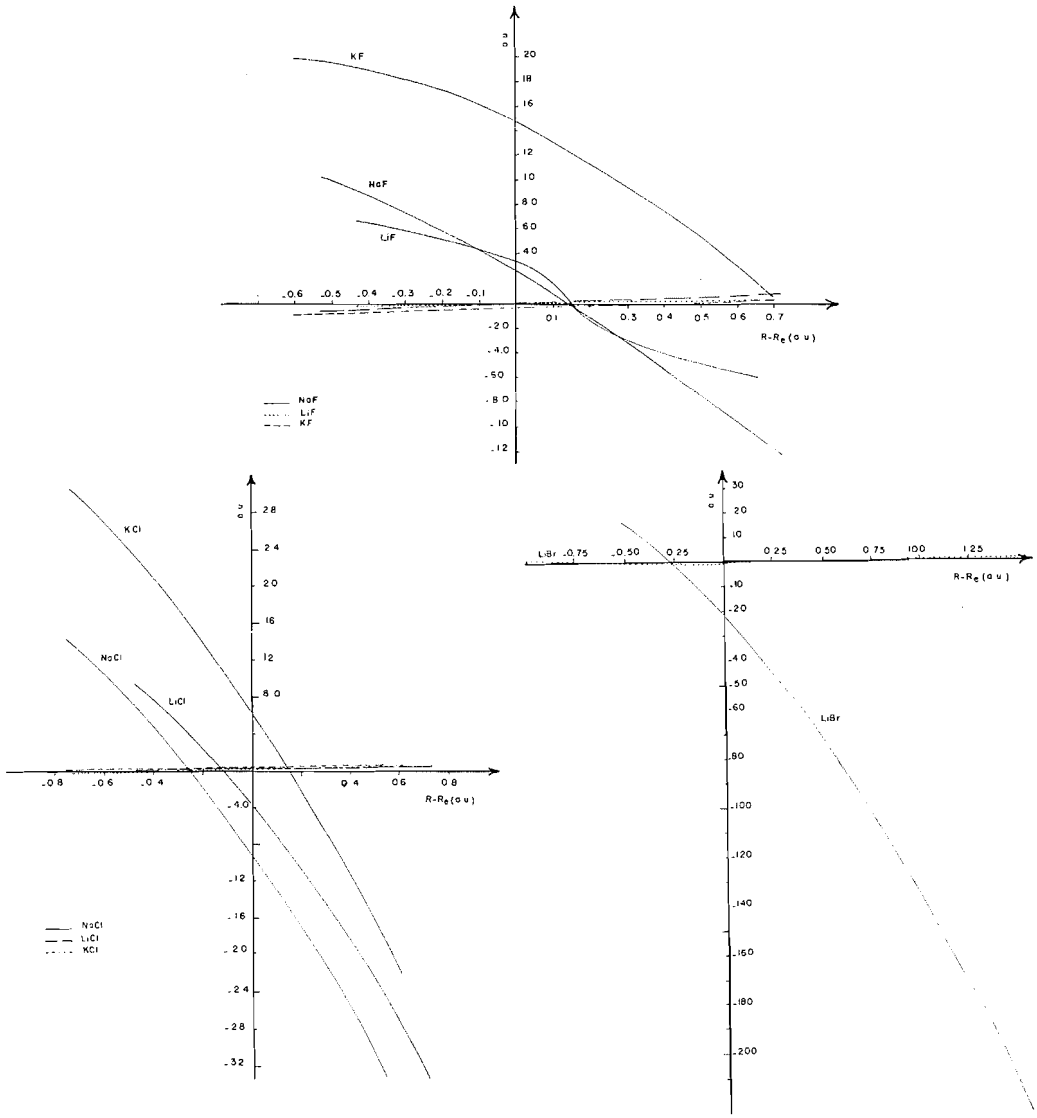

FIG. 6. Dependence on internuclear distance R of α_- (solid curves) and β_- (dashed curves) terms, for F^-, Cl^-, and Br^-, in homolog series. Values are in atomic charge units.

$q^-(R)$, Halide Field Gradient

The different contributions of $q^-(R)$ are given in Tables 3, 5, and 7. These various contributions are further regrouped in the terms $\alpha_-(R)$ the classical term, and $\beta_-(R)$ the deviation term. These are drawn schematically in Fig. 6.

q_{AT} (Table 3)

The unusual shorter bond lengths in the fluorides introduce a shielding (γ_{F^-} positive) by the F^- charge density as opposed to an antishielding predicted by the Sternheimer theory. This shielding by the F^- density comes from a large difference in polarizations of the σ and π densities. In the chloride, one has shielding in KCl and very weak antishielding in LiCl and NaCl. The Sternheimer freely polarizable model again overestimates the antishielding effect. The stronger shielding in KCl and KF is most certainly associated with the larger K^+ ionic radius which enhances the difference between σ and π polarizations. In the case of the bromides, the

Can. J. Chem. Downloaded from www.nrcresearchpress.com by 210.87.254.5 on 09/05/12
For personal use only.

Can. J. Chem. Downloaded from www.nrcresearchpress.com by 210.87.254.5 on 09/05/12
For personal use only.

introduction of 3d orbitals do not complicate the analysis. In fact, a detailed study of the orbital contribution shows that the latter are negligibly polarized in comparison to 4p orbitals. The whole antishielding effect can be imputed to the atomic polarization of the $4p^6$ shell of the Br^- ion. These polarizations are again exaggerated in the Sternheimer model, predicting much larger antishielding effects. This leads to the conclusion that antishielding is in fact *quenched* in these molecules.

$q_{ov} + q_{Sfl}$ (Tables 5 and 7)

Overlap contributions are negligible in the fluorides except in KF, which as explained in the previous section is due to the similar ionic radii of K^+ and F^-. In the halides and bromides, overlap effects become more appreciable but these are still quite negligible compared to the magnitude of the atomic polarizations. Of interest is the fact that the shielding defects $\Delta Z_B{}^+$ (Table 7) of the core electron density of the M^+ ions are quite negligible. Thus the alkali ions M^+ behave as near perfect ions from the halogen end of the molecule. This indicates that the LCAO expansion of the Hartree–Fock wavefunctions is quite faithful to the ionic model in terms of electron distribution. In general, the total ionic defect $\beta_-(R)$ is negligible compared to the atomic polarizations reflected in $\alpha_-(R)$ (Fig. 6). A consideration of the inner polarizations of the X^- charge density reveals these to be negligible, so that polarizations of X^- outer shells in the presence of a hindering M^+ core seems to be the appropriate model.

The hindering presence of M^+ core is reflected in the unusual strong shielding effects of the F^- polarizations. We emphasize that this behavior is quite contrary to the Sternheimer theory, which would predict a net antishielding due to radial excitations of the F^- density via the attractive potential of the M^+ ion. In the halides and bromides, the calculations show a much weaker antishielding than predicted by the Sternheimer theory. Evidently, radial excitations are being quenched. This is clearly evident in the $\Delta\rho_{atom}$ and $\Delta\rho_{ion}$ diagrams for these molecule (Figs. 1–4). The p_σ-like density along the internuclear axis is squashed by the presence of the M^+ core. This is most certainly due to Pauli exclusion forces as exemplified by the charge redistribution in two of the atoms (19). There is a large increase of density in front of the halogen nucleus which *augments* the absolute value of $q_{AT}{}^\sigma$. There is also evident a polarization into the bond of p_π-like density, which manifests itself as an increase in front of the halogen nucleus but now in a perpendicular direction. This polarization will tend to diminish $|q_{AT}{}^\pi|$. As this contribution is negative (Table 3), the net result will be to further enhance the shielding effect, *i.e.*, make q_{AT} more positive. This behavior of the π density is therefore more or less in accord with the proposals of de Wijn (8) and Peters and Todd (9). However, the decisive factor is the *increase in shielding* of the p_σ density due to a *compression* of this density in the region of the halide nucleus by exchange repulsions. This conjecture is supported by the ρ and $\Delta\rho$ diagrams. As an example, the last ρ spherical contour is 0.04 in NaBr as compared to 0.06 in LiBr. In this latter molecule, $\Delta\rho_{atom}$ is more indented by the Li^+ core than in NaBr. Similarly in $\Delta\rho_{ion}$ the density increase with respect to free Br^- is less diffuse in LiBr and more concentrated in the σ region. It would seem that the close proximity of Li^+ to Br^- results in a larger contraction of the halide electron density, thus decreasing the antishielding of the latter. Increasing constraints, such as shorter internuclear distances (LiBr as compared to NaBr) quench the σ polarizations much more and therefore increase the shielding or conversely reduce the antishielding (Table 3).

Variation of $q^\pm(R)$ as a Function of R

From the expression [1], one readily obtains the derivative

$$[6] \qquad \frac{dq^\pm}{dR} = \pm\frac{6}{R^4}(1 - \gamma_\infty{}^\pm)$$

where $\gamma_\infty{}^\pm$ is assumed constant as in the Sternheimer model (1). From the values of $\gamma_\infty{}^\pm$ in Table 2, one predicts that dq^+/dR should be positive, as is observed in most experimental cases, *i.e.*, an increase in q with vibrational quantum number. The situation is quite different at the halogen ion, as emphasized by de Wijn (8). The values of $\gamma_\infty{}^-$ in Table 3 predict that dq^-/dR should be negative, contrary to experimental values which give positive values for this derivative. In this section we will show how this contradiction may be resolved.

From expression [5] we have two terms that contribute to $q^\pm(R)$. Firstly there is $\alpha_\pm(R)$ which corresponds to $(1 - \gamma^\pm(R))$, *i.e.*, the classical term except that we now allow for variation of $\gamma(R)$. Secondly, there is $\beta_\pm(R)$, the ionic defect made up of overlap contributions and incomplete shielding effects of the adjacent charge distribution.

TABLE 8. *Ab initio* values of slopes dq_{AT}^{σ}/dR, dq_{AT}^{π}/dR, and their ratio, at halogen nuclei, at $R = R_e$ (in a.u. $= e/a_0^4$)

Molecule	dq_{AT}^{σ}/dR	dq_{AT}^{π}/dR	$(dq_{AT}^{\sigma}/dR)/(dq_{AT}^{\pi}/dR)$
LiF	−1.025	−0.291	3.5
NaF	−0.628	−0.228	2.8
KF	−0.618	−0.172	3.6
LiCl	−0.945	−0.220	4.3
NaCl	−0.69	−0.09	7.7
KCl	−0.58	−0.145	4.0
LiBr	−1.87	−0.527	3.6

TABLE 9. *Ab initio* values of slopes dq_{AT}^{σ}/dR, dq_{AT}^{π}/dR and their ratio at Na^+ and K^+ cations, at $R = R_e$ (in a.u. $= e/a_0^4$)

Molecule	(dq_{AT}^{σ}/dR)	(dq_{AT}^{π}/dR)	$(dq_{AT}^{\sigma}/dR)/(dq_{AT}^{\pi}/dR)$
NaF	−0.313	−0.056	5.6
NaCl	−0.149	−0.036	4.1
KF	−0.318	−0.106	2.9
KCl	−0.173	−0.082	2.1

These two terms are schematized in Fig. 5, from which it is seen that for the alkali ions, $\alpha_+(R)$ is fairly constant. This indicates that $\gamma^+(R)$ is indeed the asymptotic Sternheimer parameter $\gamma_\infty{}^+$. In addition, as pointed out already in the preceding section, $\beta_+(R)$ diminishes in importance for the larger cations. The one exception arises for the lithium series, where as the internuclear distance decreases, this term increases in importance. At these shorter distances, the halide ion cannot be treated as a point charge any more. For the sodium and potassium series, the atomic polarizations at M^+ far outweigh the non-classical contributions contained in $\beta_+(R)$.

Turning to the halide ions, Fig. 6 shows that the picture has drastically changed. The non-classical term, $\beta_-(R)$, is completely negligible in all cases, so that one is left only with the polarizations of the anion. The rapid variation of $\alpha_-(R)$ as opposed to a near invariance of $\alpha_+(R)$ is due to two main causes with increasing R: (*i*) expansion of the contracted p_σ halogen density, thus antishielding the halogen nucleus, *i.e.* $dq_{AT}^{\sigma}/dR < 0$; (*ii*) depolarization and backtransfer of the p_π density from which $dq_{AT}^{\pi}/dR < 0$. Considering $\beta_-(R)$ as completely negligible, then $q^-(R)$ may be expressed following expression [4] as

$$[7] \qquad \frac{dq^-(R)}{dR} = \frac{-6}{R^4} - \frac{dq_{AT}^-}{dR}$$

The values of the components dq_{AT}^{σ}/dR and dq_{AT}^{π}/dR are given in Table 8. These components counteract the negative contribution from the M^+ ion charge, *i.e.*, $-dq_{AT}/dR$ is always positive. Putting in values of R_e for various molecules into eq. 7, it is easy to see that the atomic term in fact overwhelms the M^+ ionic charge term, thus rendering $dq^-(R)/dR$ always positive.

The p_π depolarization is in accord with the corrections proposed by de Wijn (8) and Peters and Todd (9) to the simple antishielding model. However both theories *incorrectly* treat the p_σ depolarizations. In de Wijn's theory, dq_{AT}^{σ}/dR is assumed negligible whereas in the Peters and Todd model, $\gamma_\infty{}^-$ is retained following the Sternheimer model. Table 8 establishes conclusively that it is the density in the last occupied p_σ orbital of the halide ion which is in major part responsible for the *deshielding* of the halogen nucleus with increasing R. On the average, the p_σ contribution to dq^-/dR is four times that of the p_π density.

It is interesting to notice that this same effect occurs at the cations Na^+ and K^+ with last occupied p shells (see Table 9). This effect is about ten times smaller than in the anions, as expected from the smaller polarizabilities of the former. Nevertheless, it is evident that the p_σ density is depolarizing, thus decreasing q_{AT} and the p_π density is returning, therefore diminishing q_{AT} further. These effects can be seen concretely in the relaxation density diagrams about F^- for bond extension of LiF as reported in ref. 3. There is evidently a net increase of p_π density and a net decrease of p_σ density near the fluorine nucleus.

Can. J. Chem. Downloaded from www.nrcresearchpress.com by 210.87.254.5 on 09/05/12
For personal use only.

Can. J. Chem. Downloaded from www.nrcresearchpress.com by 210.87.254.5 on 09/05/12
For personal use only.

Conclusion

The main purpose of our work has been to clarify the discrepancies between experimental values and those obtained from classical models for the electric field gradient in alkali halide molecules. Our calculations and density diagrams show that quenching and even contraction effects invalidate any simple polarizable model in these molecules.

Our results affirm the major importance of the atomic polarizations as measured by q_{AT} in the total value of the field gradient q. Furthermore, the value of q_{AT} largely depends only on the difference of the contribution from the last occupied p_σ and p_π orbitals of the ion in question. For cations, the size of the ion determines its field gradient. Thus in Na^+ and K^+, the introduction of p shells renders these two ions antishielding as opposed to Li^+. The antishielding of these two larger ions is much larger than predicted by the Sternheimer theory. Exclusion repulsion effects are in large measure responsible for a larger p_σ contribution, causing a contraction of this density near the nucleus. The variation of $q^+(R)$ at the alkali ion is small. This is indicative of a fairly constant antishielding factor $\gamma^+(R)$. The antishielding model recovers therefore a certain measure of respectability with this last observation.

For the halogen ions, there is usually a large difference in p_σ and p_π contributions, indicative of quite different polarizabilities. In addition, $q^-(R)$ at the halogen nucleus is a very sensitive function of R. It has been shown that, in fact, it is the σ electrons which are most responsible for this effect. These electrons contribute on the average four times as much as π electrons to $dq^-(R)/dR$. The p_σ electrons seem to expand or decontract as the internuclear distance increases, thus increasing the electric field gradient. Backtransfer of p_π density to the anion also enhances this effect, but only one-fourth as much.

Any satisfactory theory of the field gradient at the halide ion and at larger cations such as Cs^+ and Rb^+ must consider the σ-quenching and π-polarizations separately in alkali halide molecules. Brumer and Karplus (20) in a perturbation calculation have recently shown that the inclusion of exchange distortions in the classical ion model gives rise to saturations of polarizabilities. This is the equivalent of the quenching and even compression effect on σ densities as observed by us. There is however one more effect which must be added, an effect which is also noticeable in the $\Delta\rho$ diagrams. Ruedenberg (21) has suggested that in molecules there is usually a contraction or clustering of valence electron density about the nuclei. This efficiently lowers the potential energy of the electrons in a molecule. It may well be that the large increase of density in the σ region with its unusual effects on field gradients is in large measure due to such contraction effects thus invalidating further any simple polarizable model.

We thank the National Research Council of Canada for a graduate fellowship to J.P.L. and also for a computing grant to A.D.B. which enabled us to pursue the calculations reported here.

1. T. P. Das and E. L. Hahn. Nuclear quadrupole resonance spectroscopy. Academic Press Inc., New York. 1958.
2. C. H. Townes and A. L. Schawlow. Microwave spectroscopy. McGraw-Hill Co., New York. 1955.
3. R. F. W. Bader and A. D. Bandrauk. J. Chem. Phys. **49**, 1666 (1968).
4. H. M. Foley, R. M. Sternheimer, and D. Tycko. Phys. Rev. **91**, 934 (1954); J. A. Smith. J. Chem. Educ. **48**, 39 (1971).
5. C. H. Townes and B. P. Dailey. J. Chem. Phys. **17**, 782 (1949).
6. E. G. Wikner and T. P. Das. Phys. Rev. **115**, 357 (1959).
7. T. P. Das and M. Karplus. J. Chem. Phys. **30**, 845 (1959).
8. H. W. de Wijn. J. Chem. Phys. **44**, 810 (1966).
9. A. W. Peters and J. E. Todd. J. Chem. Phys. **57**, 1129 (1972).
10. (*a*) A. D. McLean and M. Yoshimine. Tables of linear molecule wavefunctions. IBM, San Jose, California. 1967; (*b*) R. L. Matcha. J. Chem. Phys. **47**, 4595 (1967); **47**, 5295 (1967); **48**, 335 (1968); **49**, 1264 (1968); **53**, 485 (1970); **53**, 4490 (1970).
11. R. F. W. Bader and A. D. Bandrauk. J. Chem. Phys. **49**, 1653 (1968).
12. H. Kopfermann. Nuclear moments. Academic Press, New York. 1958.
13. R. M. Sternheimer. Phys. Rev. **95**, 736 (1964).
14. G. C. Benson and M. E. Van der Hoff. J. Chem. Phys. **22**, 469 (1954).
15. R. F. W. Bader and W. H. Henneker. J. Am. Chem. Soc. **87**, 3068 (1965).
16. A. D. Bandrauk. Ph.D. Thesis. McMaster University, Hamilton, Ontario. 1968. p. 132.
17. R. M. Sternheimer. Phys. Rev. **84**, 244 (1951).
18. R. T. Sanderson. Inorganic chemistry. Reinhold Publishing Corp., New York. 1967.
19. R. F. W. Bader and H. J. T. Preston. Can. J. Chem. **44**, 1131 (1966); B. M. Deb. Rev. Mod. Phys. **45**, 22 (1973).
20. P. Brumer and M. Karplus. J. Chem. Phys. **58**, 3903 (1973).
21. K. Ruedenberg. Rev. Mod. Phys. **34**, 326 (1962).
22. R. M. Sternheimer. Phys. Rev. **132**, 1637 (1963).

Aldol Type Condensations of β-Keto Ester Dianions

STUART NICHOLAS HUCKIN AND LARRY WEILER[1]

Department of Chemistry, University of British Columbia, Vancouver, British Columbia V6T 1W5

Received December 18, 1973

STUART NICHOLAS HUCKIN and LARRY WEILER. Can. J. Chem. **52**, 2157 (1974).

The dianion of methyl acetoacetate reacts with ketones and aldehydes to yield δ-hydroxy-β-keto esters. These hydroxy esters can be dehydrated to the corresponding γ,δ-unsaturated-β-keto esters which are useful in annelation reactions to form cyclic β-keto esters. The dianion of methyl acetoacetate does not appear to undergo conjugate addition to simple α,β-unsaturated ketones, instead only carbonyl addition occurs.

STUART NICHOLAS HUCKIN et LARRY WEILER. Can. J. Chem. **52**, 2157 (1974).

Le dianion de l'acétoacétate de méthyle réagit avec les cétones et les aldéhydes pour fournir des esters δ hydroxylés β-cétoniques. Ces esters hydroxylés peuvent se déshydrater pour conduire aux β-cétoesters nonsaturés correspondant qui sont utiles dans des réactions d'annélation conduisant à des esters β-cétoniques cycliques. Le dianion de l'acétoacétate de méthyle réagit avec les cétones α,β nonsaturés simple pour conduire uniquement à des produits d'addition; il ne semble pas que l'addition conjuguée se produise. [Traduit par le journal]

Recently we have been interested in utilizing the basic four carbon unit of β-keto esters (**1**) as

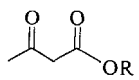

1

a foundation for an array of synthetic reactions. The introduction of this unit is relevant to the synthesis of a range of natural products, particularly the acetogenins (1). We have already described the ready generation of dianions from β-keto esters (2) and the alkylation (2, 3) and acylation (4, 5) of these intermediates. Now we would like to present some details of the reaction of these dianions with aldehydes and ketones.[2]

The dianion **2** can be prepared from methyl acetoacetate in a variety of ways; however, the most efficient method we have developed involves treating the β-keto ester with 1 equiv. of sodium hydride to generate the monoanion and subsequently treatment with 1 equiv. of *n*-butyllithium produces the dianion **2** (2, 3). This reaction

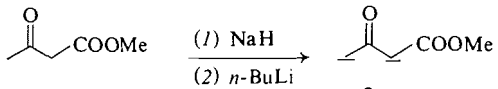

2

can be performed in a range of solvents (7) but most of the present results are for reactions in tetrahydrofuran. Not unexpectedly dianion **2** reacts with an electrophile at the terminal γ-carbon (8). One of the reactions of particular use in our proposed synthesis of some aromatic antibiotics was the aldol type condensation of **2** shown in reaction 1.

We found that dianion **2** did react with a series of aldehydes and ketones to give the addition product **4** in reasonable yields for most substrates investigated (Table 1). The spectral data for each reaction product was compatible only with the δ-hydroxy-β-keto ester structure **4**, another ex-

TABLE 1. Addition of dianion **2** to ketones and aldehydes

3		Yield of **4** (%)[a]
R	R′	
CH_3	H	26
CH_3CH_2	H	73
$CH_3CH_2CH_2CH_2$	H	36
$(CH_3)_3C$	H	82
C_6H_5	H	89
o-$CH_3OC_6H_4$	H	73
2,3-$(CH_3O)_2C_6H_3$	H	68
2-Furyl	H	68
CH_3	CH_3	70
CH_3CH_2	CH_3	56
—$(CH_2)_5$—		63
—$(CH_2)_4$—		25
C_6H_5	CH_3	77
o-$CH_3OC_6H_4$	CH_3	79
C_6H_5	C_6H_5	93

[a]Isolated yield.

[1]Author to whom correspondence should be addressed.

[2]A preliminary communication of a portion of this work has appeared (6).

Can. J. Chem. Downloaded from www.nrcresearchpress.com by 210.87.254.5 on 09/05/12
For personal use only.

[1] 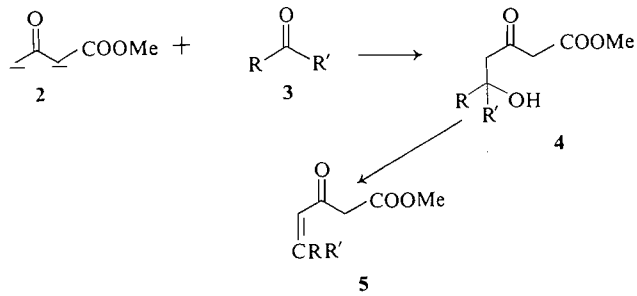

ample of reaction at the more nucleophilic terminal carbon in a multiple anion (1–8). In the case of acetaldyde, pentanal, and cyclopentanone a large amount of methyl acetoacetate was recovered. It may be that proton transfer is a competing side reaction in these cases, since self-condensation products of cyclopentanone were also formed in the reaction of **2** and cyclopentanone. Similar difficulties involving proton transfer have been reported during the reaction of dianions from β-diketones with ketones and aldehydes (9). Earlier it has been found that reaction of the dianion from ethyl acetoacetate with benzophenone gave the corresponding δ-hydroxy-β-keto ester in 50% (10). Using the above method this product was obtained in 81% from ethyl acetoacetate or 93% from methyl acetoacetate.

With some of the aromatic aldehydes and ketones, difficulty was encountered when attempts were made to purify the adducts **4** by distillation. Many of these products were liquids and they were readily purified by chromatography for spectral analysis; however, they were converted to the corresponding trimethylsilyl ethers (**6**) for further spectral analyses and elemental analyses. These ethers were readily distilled and could easily be hydrolyzed back to **4** by refluxing in methanol for a short period.

A brief study of the temperature dependence of this aldol addition was made, using the reaction of dianion **2** with propanal as the model. At temperatures below 0 °C, the reaction became very sluggish and finally at −78° only 11% of the desired product could be isolated after 1-h reaction period (79% recovery of methyl acetoacetate). When the reaction was performed at 25° for ½ h adduct **4** ($R = C_2H_5$; $R' = H$) was isolated in 57% yield. Whereas, this same product was isolated in 73% yield after 10 min reaction time at 0°. A similar temperature dependence was noted for alkylation (2, 3, 7) and acylation (4, 5, 7) of **2**.

The dianion **2** could also be generated from methyl acetoacetate and **2** equiv. of lithium diisopropylamide, and subsequent reaction with benzophenone gave **4** ($R = R' = C_6H_5$) in 62%. Hence, it would appear that the dilithio intermediate **2** does not have the same reactivity as the sodio lithio intermediate **2**. Lithium bis(trimethylsilyl)amide was not a sufficiently strong enough base to generate the dianion **2**. The lower basicity of lithium bis(trimethylsilyl)amide compared to lithium dialkylamides parallels the lower basicity of silylamines compared to alkylamines (11). This has been attributed to dπ–pπ bonding between the nitrogen lone pairs and the adjacent silicon atom.

Several procedures were investigated to convert the adducts **4** into the corresponding unsaturated keto esters **5**. Treatment of these adducts (**4**) with phosphorus oxychloride in pyridine, *p*-toluenesulfonic acid in refluxing benzene, and refluxing 10% aqueous sulfuric acid gave complex mixtures of products. However, it was found that treatment of the product **4** with anhydrous hydrogen chloride in chloroform resulted in smooth conversion to the unsaturated keto ester (**5**). In those adducts (**4**) in which $R \neq R'$ a mixture of two isomeric unsaturated products (**5**) was obtained, these were not separated but estimates of the relative amounts of two isomers were obtained from the n.m.r. spectra (7). Recently synthetic interest in simple γ,δ-unsaturated-β-keto esters (**5**) has been revived and these esters appear to be very useful in annelation reactions to synthesize cyclic β-keto esters (12). Together with the renewed interest in these esters (**5**), was a need for an efficient synthesis of these materials; the above dianion route provides an efficient route to all but the simplest (**5**, $R = R' = H$) of these esters. Stork and Guthikonda have also developed an efficient route to these esters, which is outlined in eq. 2 (12).

We also undertook a limited study of the

Can. J. Chem. Downloaded from www.nrcresearchpress.com by 210.87.254.5 on 09/05/12
For personal use only.

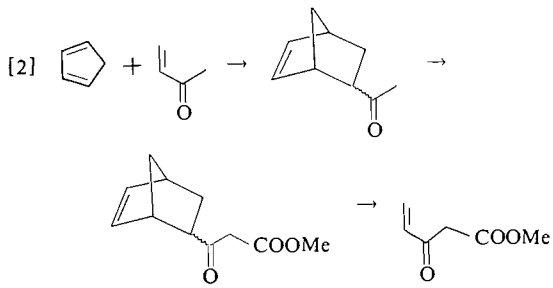

possible conjugate addition of dianion **2** to α,β-unsaturated ketones. However, dianion **2** gave only carbonyl addition products with methyl vinyl ketone and cyclohex-2-enone. Addition of a variety of stoichiometries of cuprous iodide again gave only carbonyl addition products, although it is believed that some form of copper dianion complex was formed, as evidenced by the dissolution of the cuprous iodide and formation of a brown solution. The failure of the conjugate addition is attributed to the high nucleophilic reactivity of dianion **2**. It was found, however, that under acid work-up the initially formed carbonyl adduct of **2** and cyclohex-2-enone rearranged to the secondary alcohol **7**.

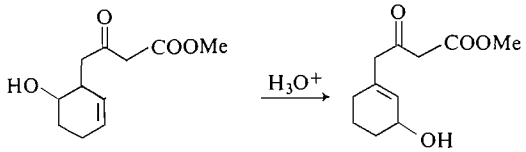

7

Experimental[3]

Aldol Reactions of the Dianion of β-Keto Esters

Methyl 5-Hydroxy-5-methyl-3-oxohexanoate (4a)

Sodium hydride (0.465 g, 11.0 mmol), as a 57% mineral oil dispersion, was weighed into an oven-dried 50 ml flask and tetrahydrofuran (*ca.* 25 ml) was distilled directly into this flask from lithium aluminum hydride. The flask was equipped with a magnetic stirrer, stoppered (septum cap), cooled in ice to 0 °C, and flushed with nitrogen. Methyl acetoacetate (1.161 g, 10.0 mmol) was added dropwise to the cooled slurry and the reaction allowed to stir for 10 min after the addition was complete. A solution of *n*-butyllithium (5 ml, 2.1 *M* in hexane, 10.5 mmol) was added dropwise to the solution and the reaction allowed to stir at 0° for a further 10 min. Acetone (0.638 g, 11.0 mmol) was added in one portion and the reaction allowed to stir for 10 min at 0° before being quenched with concentrated hydrochloric acid (*ca.* 2 ml). The reaction was worked up by the addition of water (10 ml) and diethyl ether (35 ml). The aqueous layer was separated and further extracted with ether (2 × 35 ml). The organic extracts were combined, washed with saturated sodium chloride solution (6 × 15 ml), dried over anhydrous sodium sulfate, and filtered. The solvents were removed by evaporation under reduced pressure and distillation of the resulting oil gave 1.162 g (72%) of **4a**, b.p. 51–52° (14 mm); i.r. ($CHCl_3$) 3500, 1740, and 1705 cm^{-1}; n.m.r. ($CDCl_3$) δ 3.76 (s, 3H), 3.48 (s, 2H), 3.27 (broad s, exchangeable D_2O, 1H), 2.70 (s, 2H), and 1.30 p.p.m. (s, 6H); mass spectrum, *m/e* (relative intensity) 174(4), 159(48), 128(71), 116(100), 85(62), 59(87), and 43(87).

Anal. Calcd. for $C_8H_{14}O_4$: C, 55.16; H, 8.10. Found: C, 54.97; H, 8.32.

Methyl 5-Hydroxy-5-methyl-3-oxoheptanoate (4b)

This compound was prepared by the same procedure as that employed in the preparation of methyl 5-hydroxy-5-methyl-3-oxohexanoate (**4a**). The reagents used in the preparation were: sodium hydride (0.467 g, 11.0 mmol), as a 57% mineral oil dispersion, methyl acetoacetate (1.161 g, 10.0 mmol), *n*-butyllithium (5 ml, 10.5 mmol), as a 2.1 *M* solution in hexane, and 2-butanone (0.792 g, 11.0 mmol), which gave 1.052 g (56%) of **4b**, b.p. 88–89° (14 mm); i.r. (neat film) 3500, 1740, and 1705 cm^{-1}; n.m.r. ($CDCl_3$) δ 3.77 (s, 3H), 3.51 (s, 2H), 3.15 (broad s, exchangeable D_2O, 1H), 2.71 (s, 2H), 1.60 (distorted q, J = 8 Hz, 2H), 1.27 (s, 3H), and 0.92 p.p.m. (distorted t, J = 8 Hz, 3H); mass spectrum, *m/e* (relative intensity) 188(0.2), 170(10), 159(49), 128(75), 116(50), 85(47), 73(47), and 43(100).

Anal. Calcd. for $C_9H_{16}O_4$: C, 57.43; H, 8.57. Found: C, 57.27; H, 8.71.

Methyl 4-(1-Hydroxycyclohexyl)-3-oxobutanoate (4c)

This compound was also prepared by the same procedure as that employed in the preparation of methyl 5-hydroxy-5-methyl-3-oxohexanoate (**4a**). The reagents used in the preparation were: sodium hydride (0.465 g, 11.0 mmol), as a 57% mineral oil dispersion, methyl acetoacetate (1.161 g, 10.0 mmol), *n*-butyllithium (5 ml, 10.5 mmol), as a 2.1 *M* solution in hexane, and cyclohexanone (1.078 g, 11.0 mmol), which gave 1.348 g (63%) of **4c**, b.p. 95–96° (0.3 mm); i.r. (neat film) 3500, 1740, and 1705 cm^{-1}; n.m.r. ($CDCl_3$) δ 3.75 (s, 3H), 3.50 (s, 2H), 3.11 (broad s, exchangeable D_2O, 1H), (s, 2H), and 1.52 p.p.m. (m, 10H); mass spectrum, *m/e* (relative intensity) 214(3), 196(18), 182(12), 138(61), 123(40), 122(47), 116(44), 98(63), 95(60), 80(53), 69(69), 55(84), and 43(100).

Anal. Calcd. for $C_{11}H_{18}O_4$: C, 61.66; H, 8.47. Found: C, 61.84; H, 8.47.

Methyl 4-(1-Hydroxycyclopentyl)-3-oxobutanoate (4d)

This compound was prepared by the same procedure as that employed in the preparation of methyl 5-hydroxy-5-methyl-3-oxohexanoate (**4a**). The reagents used in the preparation were: sodium hydride (0.466 g, 11.0 mmol), as a 57% mineral oil dispersion, methyl acetoacetate (1.161 g, 10.0 mmol), *n*-butyllithium (5 ml, 10.5 mmol), as a 2.1 *M* solution in hexane, and cyclopentanone (0.924 g, 11.0 mmol), which gave 0.502 g (25%) of **4d**, b.p. 67–68° (0.3 mm); i.r. (neat film) 3500, 1740, and 1705 cm^{-1}; n.m.r. (CDCl) δ 3.77 (s, 3H), 3.52 (s, 2H), 3.10 (broad s, exchangeable D_2O, 1H), 2.90 (s, 2H), and 1.72 p.p.m. (m, 8H); mass spectrum, *m/e* (relative intensity) 200(4), 182(12), 159(89), 126(62), 116(89), 109(51), 198(65), 101(84), 85(89), 84(98), 67(62), 59(62), 55(100), and 43(100).

[3]See refs. 3, 5, or 7 for general details.

Can. J. Chem. Downloaded from www.nrcresearchpress.com by 210.87.254.5 on 09/05/12
For personal use only.

Can. J. Chem. Downloaded from www.nrcresearchpress.com by 210.87.254.5 on 09/05/12
For personal use only.

Anal. Calcd. for $C_{10}H_{16}O_4$: C, 59.98; H, 8.05. Found: C, 60.14; H, 7.94.

Methyl 5-Hydroxy-3-oxoheptanoate (4e)

This compound was prepared by the same procedure as that employed in the preparation of methyl 5-hydroxy-5-methyl-3-oxohexanoate (**4***a*). The reagents used in the preparation were: sodium hydride (0.465 g, 11.0 mmol), as a 57% mineral oil dispersion, methyl acetoacetate (1.161 g, 10.0 mmol), *n*-butyllithium (5.0 ml, 10.5 mmol), as a 2.1 *M* solution in hexane, and propanal (0.639 g, 11.0 mmol), which gave 1.270 g (73%) of **4***e*, b.p. 86–87° (0.5 mm); i.r. (neat film) 3500, 1740, and 1705 cm^{-1}; n.m.r. ($CDCl_3$) δ 4.00 (m, 1H), 3.76 (s, 3H), 3.52 (s, 2H), 2.66 (m, 2H), 2.43 (broad s, exchangeable D_2O, 1H), 1.45 (m, 2H), and 0.95 p.p.m. (m, 3H); mass spectrum, *m/e* (relative intensity) 174(1), 156(6), 145(17), 116(16), 114(38), 101(32), 83(59), 71(49), 69(53), 59(52), and 43(100).

Anal. Calcd. for $C_8H_{14}O_4$: C, 55.16; H, 8.10. Found: C, 54.95; H, 8.09.

Methyl 5-Hydroxy-3-oxononanoate (4f)

This compound was prepared by the same procedure as that employed in the preparation of methyl 5-hydroxy-5-methyl-3-oxohexanoate (**4***a*). The reagents used in the preparation were: sodium hydride (0.465 g, 11.0 mmol), as a 57% mineral oil dispersion, methyl acetoacetate (1.161 g, 10.0 mmol), *n*-butyllithium (5 ml, 10.5 mmol), as a 2.1 *M* solution in hexane, and pentanal (0.946 g, 11.0 mmol), which gave 0.727 g (36%) of **4***f*, b.p. 55–56° (0.2 mm); i.r. (neat film) 3500, 1740, and 1705 cm^{-1}; n.m.r. (CDCl) δ 4.00 (m, 1H), 3.76 (s, 3H), 3.50 (s, 2H), 2.66 (m, 2H), 2.42 (broad s, exchangeable D_2O, 1H), and 1.52–0.77 p.p.m. (m, 9H); mass spectrum, *m/e* (relative intensity) 202(1), 184(9), 145(38), 127(9), 116(36), 113(35), 101(23), 97(14), 85(27), 84(19), 58(32), and 43(100).

Anal. Calcd. for $C_{10}H_{18}O_4$: C, 59.39; H, 8.97. Found: C, 59.19; H, 8.96.

Methyl 5-Hydroxy-3-oxohexanoate (4g)

This compound was prepared by the same procedure as that employed in the preparation of methyl 5-hydroxy-5-methyl-3-oxohexanoate (**4***a*). The reagents used in the preparation were: sodium hydride (0.465 g, 11.0 mmol), as a 57% mineral oil dispersion, methyl acetoacetate (1.161 g, 10.0 mmol), *n*-butyllithium (5 ml, 10.5 mmol), as a 2.1 *M* solution in hexane, and acetaldehyde (0.484 g, 11.0 mmol), which gave 0.416 g (26%) of **4***g*, b.p. 42–43° (0.3 mm); i.r. ($CHCl_3$) 3500, 1740, and 1705 cm^{-1}; n.m.r. (CCl_4) δ 4.10 (m, 1H), 3.70 (s, 3H), (s, 2H), 3.00 (broad s, exchangeable D_2O, 1H), 2.62 (m, 2H), and 1.12 p.p.m. (m, 3H); mass spectrum, *m/e* (relative intensity) 160(40), 142(54), 127(33), 116(60), 101(73), 85(42), 59(64), and 43(100).

Anal. Calcd. for $C_7H_{12}O_4$: C, 52.49; H, 7.55. Found: C, 52.65; H, 7.39.

Methyl 5-Hydroxy-6,6-dimethyl-3-oxoheptanoate (4h)

This compound was prepared by the same procedure as that employed in the preparation of methyl 5-hydroxy-5-methyl-3-oxohexanoate (**4***a*). The reagents used in the preparation were: sodium hydride (0.465 g, 11.0 mmol), as a 57% mineral oil dispersion, methyl acetoacetate (1.161 g, 10.0 mmol), *n*-butyllithium (5 ml, 10.5 mmol), as a 2.1 *M* solution in hexane, and 2,2-dimethylpropanol (0.946 g, 11.0 mmol), which gave 1.654 g (82%) of **4***h*, b.p. 68–69° (0.2 mm); i.r. ($CHCl_3$) 3500, 1740, and 1705 cm^{-1}; n.m.r. (CCl_4) δ 3.70 (s, 3H), 3.63 (m, 1H), 3.42 (s, 2H), 3.00 (broad s, exchangeable D_2O, 1H), 2.58 (m, 2H), and 0.87 p.p.m. (s, 9H); mass spectrum *m/e* (relative intensity) 202(1), 184(10), 170(22), 155(23), 145(90), 127(42), 116(48), 115(48), 113(92), 111(94), 101(60), 56(96), 83(87), 71(100), 69(94), 59(77), 55(100), and 43(100).

Anal. Calcd. for $C_{10}H_{18}O_4$: C, 59.39; H, 8.97. Found: C, 59.15; H, 8.95.

Methyl 5-Hydroxy-5-(2-methoxyphenyl)-3-oxohexanoate (4i)

This compound was prepared by the same procedure as that employed in the preparation of **4***a*. The reagents used were: sodium hydride (0.465 g, 11.0 mmol), as a 57% mineral oil dispersion, methyl acetoacetate (1.161 g, 10.0 mmol), *n*-butyllithium (5 ml, 10.5 mmol), as a 2.1 *M* solution in hexane, and *o*-methoxyacetophenone (1.650 g, 11.0 mmol), which gave 2.550 g of pale yellow oil. Purification of this oil was achieved by t.l.c.: crude **4***i* (544 mg) was chromatographed on a 20 × 20 cm silica coated plate, adsorbant thickness 0.9 mm, using a mixture of chloroform and ethyl acetate (9:1, v/v) as eluent. After elution, the band lying in the region R_f 0.25–0.33 was removed and extracted with ether (15 ml). The solvent was removed by evaporation under reduced pressure to give 471 mg (73%) of **4***i*; i.r. ($CHCl_3$) 3500, 1740, and 1705 cm^{-1}; u.v. (CH_3OH) 276, 270, and 264 nm (shoulder); n.m.r. (CCl_3) δ 7.70–6.70 (m, 4H), 4.10 (broad s, exchangeable D_2O, 1H), 3.82 (s, 3H), 3.63 (s, 3H), 3.33–1.65 (m, 4H), and 1.50 p.p.m. (s, 3H); mass spectrum (*a*) high resolution calcd. for $C_{14}H_{18}O_5$: 266.1154 a.m.u.; found: 266.1135 a.m.u.; (*b*) *m/e* (relative intensity) 266(10), 251(8), 234(16), 208(10), 159(34), 151(78), 135(94), 115(52), 91(25), 77(80), 59(47), and 43(100).

Methyl 5-(2-Methoxyphenyl)-3-oxo-5-trimethylsiloxyhexanoate (6i). Methyl 5-hydroxy-5-(2-methoxyphenyl)-3-oxohexanoate (**4***i*) (0.257 g, 0.99 mmol), chlorotrimethylsilane (0.108 g, 1.00 mmol), and hexamethyldisilazane (0.081 g, 0.50 mmol) were dissolved in dry pyridine (*ca.* 5 ml) and the solution stirred for 10 min. A fine white precipitate was thrown down and this was filtered off and washed with ether (3 × 10 ml). The washings were added to the filtrate and the solvents removed by evaporation under reduced pressure. The resulting oil was distilled under high vacuum to give 0.176 g (65%) of **6***i*, b.p. 83–85° (0.3 mm); i.r. ($CHCl_3$) 1740, 1705, and 1075 cm^{-1}; n.m.r. (CCl_4, ext TMS) 7.55–6.67 (m, 4H), 3.80 (s, 3H), 3.53 (s, 3H), 3.20 (m, 2H), 2.80 (m, 2H), 1.67 (2, 3H), and 0.00 p.p.m. (s, 9H); mass spectrum, *m/e* (relative intensity) 338(3), 323(2), 308(2), 265(2), 223(98), 173(35), 151(19), 135(80), 115(17), 105(46), 91(19), 75(100), 59(30), and 43(76).

Anal. Calcd. for $C_{17}H_{26}O_5Si$: C, 60.33; H, 7.74. Found: C, 60.20; H, 7.49.

Hydrolysis of Methyl 5-(2-Methoxyphenyl)-3-oxo-5-trimethylsiloxyhexanoate (6i). Methyl 5-(2-methoxyphenyl)-3-oxo-5-trimethylsiloxyhexanoate (**6***i*) (0.170 g, 0.50 mmol) was dissolved in methanol (10 ml) and the solution heated to reflux. After a period of 30 min at reflux the solution was cooled and filtered. The methanol was removed by evaporation under reduced pressure and the resulting oil purified by preparative t.l.c., using a 20 × 20 cm silica coated plate, adsorbant thickness 0.5 mm, and employing a mixture of chloroform and ethyl acetate (9:1, v/v) as eluent. The band lying

Can. J. Chem. Downloaded from www.nrcresearchpress.com by 210.87.254.5 on 09/05/12
For personal use only.

in the region R_f 0.25–0.33 was removed and extracted with ether. The solvent was removed by evaporation under reduced pressure to give 95 mg (71%) of methyl 5-hydroxy-5-(2-methoxyphenyl) 3-oxohexanoate (**4*i***), which showed identical i.r. and n.m.r. spectra to **4*i*** obtained above.

Methyl 5-(2-Methoxyphenyl)-3-oxohex-4-enoate (5i). Chloroform (*ca.* 10 ml) was saturated with anhydrous hydrogen chloride, by direct passage of the gas through the solvent. Methyl 5-hydroxy-5-(2-methoxyphenyl)-3-oxohexanoate (**4*i***) (0.051 g, 0.19 mmol) was dissolved in this chloroform and the solution stirred for 30 min. The solution was washed with saturated sodium hydrogen carbonate solution (4 × 5 ml) and with saturated sodium chloride solution (2 × 5 ml), dried over anhydrous sodium sulfate, and filtered. The chloroform was removed by distillation to give 0.040 g (85%) of a mixture of *Z* and *E* isomers of **5*i*** (ratio of isomers, *Z*:*E* 1.0:2.3, by n.m.r.); i.r. ($CHCl_3$) 1740, 1680, and 1600 cm^{-1}; u.v. (CH_3OH) 320 (shoulder) and 278 nm; n.m.r. (CCl_4) δ 7.40–6.67 (m, 4H), 6.20 (m, 0.7H, *E*), 6.10 (m, 0.3H, *Z*), 3.82 (s, 3H), 3.70 (d, J = 1 Hz, 2.1H, *E*), 3.60 (d, J = 1 Hz, 0.9H, *Z*), 3.40 (s, 2H), 2.43 (d, J = 1 Hz, 2.1H, *E*), and 2.12 p.p.m. (d, J = 1 Hz, 0.9H, *Z*); mass spectrum: (*a*) high resolution calcd. for $C_{14}H_{16}O_4$: 248.1048 a.m.u.; found: 248.1064 a.m.u.; (*b*) *m/e* (relative intensity) 248(2), 217(14), 189(3), 175(11), 160(13), 159(100), 150(5), 136(17), 119(4), 115(4), 105(6), 91(9), 77(4), 69(2), 59(2), and 43(22).

Methyl 5-Hydroxy-3-oxo-5-phenylpentanoate (4j)

This compound was prepared by the same procedure as that employed in the preparation of methyl 5-hydroxy-5-(2-methoxyphenyl)-3-oxohexanoate (**4*i***). The reagents used in the preparation were: sodium hydride (0.466 g, 11.0 mmol), as a 57% mineral oil dispersion, methyl acetoacetate (1.161 g, 10.0 mmol), *n*-butyllithium (4.5 ml, 10.6 mmol), as a 2.35 *M* solution in hexane, and benzaldehyde (1.168 g, 11.0 mmol), which gave 2.553 g of crude **4*j***, as a yellow oil. The crude product was purified by chromatography on a silica gel (200 g) column using a mixture of chloroform and ethyl acetate (9:1 v/v) as eluent. The major component from the chromatography was **4*j*** (1.973 g, 89%); i.r. ($CHCl_3$) 3500, 1740, and 1705 cm^{-1}; u.v. (CH_3OH) 280 (shoulder), 264, 258, 252, and 247 nm; n.m.r. (CCl_4) δ 7.22 (s, 5H), 5.05 (m, 1H), 3.65 (s, 3H), 3.33 (s, 2H), 3.30 (broad s, exchangeable D_2O, 1H), and 2.79 p.p.m. (m, 2H); mass spectrum: (*a*) high resolution calcd. for $C_{12}H_{14}O_4$: 222.089 a.m.u.; found: 222.086 a.m.u.; (*b*) *m/e* (relative intensity) 222(20), 204(74), 190(21), 188(18), 162(30), 149(58), 131(77), 116(86), 107(98), 106(88), 105(90), 91(32), 85(53), 84(72), 77(94), 58(90), 51(78), and 43(100)

Methyl 3-Oxo-5-phenyl-5-trimethylsiloxypentanoate (6j). This compound was prepared by the same procedure as that employed in the preparation of methyl 5-(2-methoxyphenyl)-3-oxo-trimethylsiloxyhexanoate (**6*i***). The reagents used were: methyl 5-hydroxy-3-oxo-5-phenylpentanoate (**4*j***) (0.208 g, 0.93 mmol), chlorotrimethylsilane (0.108 g, 1.00 mmol), and hexamethyldisilazane (0.080 g, 0.50 mmol), which gave 0.153 g (52%) of **6*j***, b.p. 60–62° (0.2 mm); i.r. ($CHCl_3$) 1740, 1705, and 1080 cm^{-1}; n.m.r. (CCl_4, ext TMS) δ 7.23 (s, 5H), 5.20–4.87 (m, 1H), 3.63 (s, 3H), 3.27 (s, 2H), 2.93–2.27 (m, 2H), and 0.00 p.p.m. (s, 9H); mass spectrum, *m/e* (relative intensity) 294(1), 279(4), 264(3), 249(8), 221(16), 204(51), 189(12), 179(53), 162(34), 149(38), 144(52), 131(62), 117(45), 116(66), 105(76), 91(68), 85(54), 77(82), 69(62), 59(100), and 43(83).

Anal. Calcd. for $C_{15}H_{22}O_4Si$: C, 61.19; H, 7.53. Found: C, 61.40; H, 7.32.

Methyl 5-Hydroxy-5-(2-methoxyphenyl)-3-oxopentanoate (4k)

This compound was prepared by the same procedure as that employed in the preparation of methyl 5-hydroxy-5-(2-methoxyphenyl)-3-oxohexanoate (**4*i***). The reagents used were: sodium hydride (0.465 g, 11.0 mmol), as a 57% mineral oil dispersion, methyl acetoacetate (1.160 g, 10.0 mmol), *n*-butyllithium (4.5 ml, 10.6 mmol), as a 2.34 *M* solution in hexane, and *o*-methoxybenzaldehyde (1.498 g, 11.0 mmol), which gave 2.830 g of crude **4*k*** as a yellow oil. Purification of this oil was achieved by t.l.c.: crude **4*k*** (374 mg) was chromatographed on a 20 × 20 cm silica coated plate, adsorbant thickness 0.9 mm, using a mixture of chloroform and ethyl acetate (9:1 v/v) as eluent. After elution, the band lying in the region R_f 0.2–0.3 was removed and extracted with ether (20 ml). The solvent was removed by evaporation under reduced pressure to give 243 mg (73%) of **4*k***; i.r. ($CHCl_3$) 3600, 1740, and 1705 cm^{-1}; n.m.r. (CCl_4) δ 7.50–6.67 (m, 4H), 5.30 (m, 1H), 3.83 (s, 3H), 3.68 (s, 3H), 3.50 (broad s, exchangeable D_2O, 1H), 3.36 (s, 2H), and 2.77 p.p.m. (m, 2H); u.v. (CH_3OH) 276, 271, and 257 nm; mass spectrum: (*a*) high resolution: calcd. for $C_{13}H_{16}O_5$: 252.099 a.m.u.; found: 252.102 a.m.u.; (*b*) *m/e* (relative intensity) 252(4), 234(36), 203(26), 179(16), 175(19), 161(43), 151(44), 137(60), 133(100), 127(36), 121(51), 116(39), 105(58), 91(47), 85(65), 77(54), 59(50), and 43(70).

Methyl 5-(2-Methoxyphenyl)-3-oxo-5-trimethylsiloxypentanoate (6k). This compound was prepared by the same procedure as that employed in the preparation of methyl 5-(2-methoxyphenyl)-3-oxo-5-trimethylsiloxyhexanoate (**6*i***). The reagents used in the preparation were: methyl 5-hydroxy-5-(2-methoxyphenyl)-3-oxopentanoate (**4*k***) (149 mg, 0.59 mmol), chlorotrimethylsilane (69 mg, 0.64 mmol), and hexamethyldisilazane (52 mg, 0.32 mmol), which gave 138 mg (71%) of **6*k***, b.p. 64–65° (0.5 mm); i.r. ($CHCl_3$) 1740, 1705, and 1070 cm^{-1}; n.m.r. (CCl_4, ext TMS) δ 7.47–6.60 (m, 4H), 5.43 (m, 1H), 3.80 (s, 3H), 3.63 (s, 3H), 3.30 (s, 2H), 2.63 (m, 2H), and 0.00 p.p.m. (s, 9H); mass spectrum, *m/e* (relative intensity) 324(7), 306(45), 293(10), 266(8), 251(15), 241(31), 209(97), 199(24), 195(17), 179(25), 173(95), 161(33), 145(25), 135(53), 127(24), 115(37), 105(53), 91(69), 85(20), 77(68), 75(92), 73(100), 60(22), 59(66), and 43(88).

Anal. Calcd. for $C_{16}H_{24}O_5Si$: C, 59.23; H, 7.46. Found: C, 59.46; H, 7.48.

Methyl 5-(2-Furyl)-5-hydroxy-3-oxopentanoate (4l)

This compound was prepared by the same procedure as that employed in the preparation of methyl 5-hydroxy-5-methyl-3-oxohexanoate (**4*a***). The reagents used in the preparation were sodium hydride (0.463 g, 11.0 mmol), as a 57% mineral oil dispersion, methyl acetoacetate (1.160 g, 10.0 mmol), *n*-butyllithium (4.5 ml, 10.6 mmol), as a 2.34 *M* solution in hexane, and 2-furfuraldehyde (1.061 g, 11.0 mmol), which gave 1.445 g (68%) of **4*l***, b.p. 82–84° (0.1 mm); i.r. ($CHCl_3$) 3600, 1740, and 1710 cm^{-1}; n.m.r. (CCl_4) δ 7.32 (m, 1H), 6.23 (m, 2H), 5.05 (m, 1H), 3.82 (broad s, exchangeable D_2O, 1H), 3.69 (s, 3H), 3.42 (s, 2H), and 2.93 p.p.m. (m, 2H); mass spectrum, *m/e* (relative intensity) 212(12), 194(11), 149(11), 121(50),

Can. J. Chem. Downloaded from www.nrcresearchpress.com by 210.87.254.5 on 09/05/12
For personal use only.

116(30), 101(13), 97(75), 96(71), 95(76), 69(26), 65(21), 59(35), and 43(100).

Anal. Calcd. for $C_{10}H_{12}O_5$: C, 56.60; H, 5.70. Found: C, 56.66; H, 5.35.

Methyl 5-Hydroxy-3-oxo-5-phenylhexanoate (4m)

This compound was prepared by the same procedure as that employed in the preparation of methyl 5-hydroxy-5-(2-methoxyphenyl)-3-oxohexanoate (**4***i*). The reagents used were: sodium hydride (0.461 g, 11.0 mmol), as a 57% mineral oil dispersion, methyl acetoacetate (1.163 g, 10 mmol), *n*-butyllithium (4.5 ml, 10.6 mmol), as a 2.34 *M* solution in hexane, and acetophenone (1.318 g, 11.0 mmol), which gave 2.801 g of crude **4***m* as a yellow oil. Purification of this oil was achieved by t.l.c.: 563 mg of crude **4***m* was chromatographed on a 20 × 20 cm silica coated plate, adsorbant thickness 0.9 mm, using a mixture of chloroform and ethyl acetate (9:1 v/v) as eluent. After elution, the band lying in the region R_f 0.25–0.40 was removed and extracted with ether (20 ml). The solvent was removed under reduced pressure to give 367 mg of **4***m* (77% yield); i.r. ($CHCl_3$) 2550, 1740, and 1705 cm^{-1}; u.v. (CH_3OH) 294 (shoulder), 278, and 273 nm; n.m.r. (CCl_4) δ 7.30 (m, 5H), 3.85 (broad s, exchangeable D_2O, 1H), 3.63 (s, 3H), 3.25 (m, 2H), 2.67 (m, 2H), and 1.65 p.p.m. (s, 3H); mass spectrum: (*a*) high resolution calcd. for $C_{13}H_{16}O_4$: 236.104 a.m.u.; found: 236.105 a.m.u.; (*b*) *m/e* (relative intensity) 236(2), 221(5), 218(5), 190(6), 170(2), 159(11), 145(12), 127(17), 121(64), 120(95), 116(88), 106(50), 105(88), 101(45), 85(95), 77(100), 74(95), 69(64), 59(97), and 43(100).

Methyl 3-Oxo-5-phenyl-5-trimethylsiloxyhexanoate (6m). This compound was prepared by the same procedure as that employed for the preparation of methyl 5-(2-methoxyphenyl)-3-oxo-5-trimethylsiloxyhexanoate (**6***i*). The reagents used were: methyl 5-hydroxy-3-oxo-5-phenylhexanoate (**4***m*) (305 mg, 1.30 mmol), chlorotrimethylsilane (155 mg, 1.43 mmol), and hexamethyldisilazane (115 mg, 0.72 mmol), which gave 242 mg (61%) of **6***m*, b.p. 82–83° (0.3 mm); i.r. ($CHCl_3$) 1740, 1705, and 1075 cm^{-1}; n.m.r. (CCl_4, ext TMS) δ 7.20 (m, 5H), 3.57 (s, 3H), 3.03 (m, 2H), 2.53 (m, 2H), 1.66 (s, 3H), and 0.00 p.p.m. (s, 9H); mass spectrum, *m/e* (relative intensity) 308(1), 295(9), 279(7), 264(9), 250(4), 233(11), 221(5), 211(6), 185(100), 179(11), 169(46), 156(28), 146(12), 126(17), 113(48), 101(31), 91(9), 77(26), and 73(62).

Anal. Calcd. for $C_{16}H_{24}O_4Si$: C, 62.30; H, 7.84. Found: C, 62.33; H, 7.77.

Methyl 5-(2,3-Dimethoxyphenyl)-5-hydroxy-3-oxopentanoate (4n)

This compound was prepared by the same procedure as that employed for the preparation of methyl 5-hydroxy-5-(2-methoxyphenyl)-3-oxohexanoate (**4***i*). The reagents used were: sodium hydride (0.466 g, 11.0 mmol), as a 57% mineral oil dispersion, methyl acetoacetate (1.162 g, 10.0 mmol), *n*-butyllithium (4.5 ml, 10.6 mmol), as a 2.34 *M* solution in hexane, and 2,3-dimethoxybenzaldehyde (1.823 g, 11.0 mmol), which gave 3.044 g of crude **4***n*, as a pale brown oil. Purification of **4***n* was achieved by t.l.c.: 306 mg of crude **4***n* was chromatographed on a 20 × 20 cm silica coated plate, adsorbant thickness 0.9 mm, using a mixture of chloroform and ethyl acetate (9:1 v/v) as eluent. After elution, the band lying in the region R_f 0.30–0.40 was removed and extracted with ether (20 ml). The solvent was removed by evaporation under reduced pressure to give 194 mg of **4***n* (68% yield); i.r. ($CHCl_3$) 3550, 1740, and 1705 cm^{-1}; u.v. (CH_3OH) 264 (shoulder), 256, 252, and 246 nm; n.m.r. (CCl_4) δ 6.93 (m, 3H), 5.20 (m, 1H), 4.03 (broad s, exchangeable D_2O, 1H), 3.80 (s, 6H), 3.67 (s, 3H), 3.37 (s, 2H), and 2.77 p.p.m. (m, 2H); mass spectrum: (*a*) high resolution calcd. for $C_{14}H_{18}O_6$: 282.110 a.m.u.; found: 282.111 a.m.u.; (*b*) *m/e* (relative intensity) 282(19), 264(7), 250(15), 233(11), 222(2), 217(2), 209(5), 205(4), 191(9), 182(3), 191(9), 182(3), 167(100), 166(46), 151(21), 139(22), 137(21), 116(11), 107(11), 91(7), 85(10), 77(21), 69(9), 59(15), and 43(73).

Methyl 5-(2,3-Dimethoxyphenyl)-3-oxo-5-trimethylsiloxypentanoate (6n). This compound was prepared by the same procedure as that employed for the preparation of methyl 5-(2-methoxyphenyl)-3-oxo-5-trimethylsiloxyhexanoate (**6***i*). The reagents used were: methyl 5-(2,3-dimethoxyphenyl)-5-hydroxy-3-oxopentanoate (**4***n*) (173 mg, 0.61 mmol), chlorotrimethylsilane (74 mg, 0.68 mmol), and hexamethyldisilazane (55 mg, 0.34 mmol) which gave 114 mg (53%) of **6***n*, b.p. 89–91° (0.4 mm); i.r. ($CHCl_3$) 1740, 1705, and 1075 cm^{-1}; n.m.r. (CCl_4, ext TMS) δ 6.87 (m, 3H), 5.42 (m, 1H), 3.80 (s, 6H), 3.63 (s, 3H), 3.29 (s, 2H), 2.70 (m, 2H), and 0.00 p.p.m. (s, 9H); mass spectrum, *m/e* (relative intensity 354(16), 323(8), 304(4), 241(14), 236(100), 223(4), 209(8), 193(22), 183(47), 165(24), 151(13), 149(11), 135(13), 121(25), 115(21), 105(11), 91(11), 89(19), 75(44), 73(52), 59(17), and 43(11).

Anal. Calcd. for $C_{17}H_{26}O_6Si$: C, 57.60; H, 7.40. Found: C, 57.80; H, 7.29.

Methyl 5-Hydroxy-3-oxo-5,5-diphenylpentanoate (4p)

This compound was prepared by the same procedure as that employed for the preparation of methyl 5-hydroxy-5-(2-methoxyphenyl)-3-oxohexanoate (**4***i*). The reagents used were: sodium hydride (0.466 g, 11.0 mmol), as a 57% mineral oil dispersion, methyl acetoacetate (1.160 g, 10.0 mmol), *n*-butyllithium (4.5 ml, 10.6 mmol), as a 2.35 *M* solution in hexane, and benzophenone (2.003 g, 11.0 mmol), which gave 3.124 g of a semisolid. Recrystallisation from a hexane–ether mixture gave a first crop of **4***p* (1.831 g). Subsequent concentration of the mother liquors gave a second crop of **4***p* (0.321 g) and finally chromatography of the residual solution on silica gel (50 g) using chloroform as eluent gave 0.622 g of **4***p*, to total 2.774 g (93%) of product as colorless needles, m.p. 77–79 °C; i.r. ($CHCl_3$) 3550, 1740, and 1710 cm^{-1}; u.v. (CH_3OH) 253 (785), 259 (820), 265 (685), and 269 nm (52); n.m.r. (CCl_4) δ 7.27 (m, 10H), 4.43 (broad s, exchangeable D_2O, 1H), 3.67 (s, 3H), 3.40 (s, 2H), and 3.27 p.p.m. (s, 2H); mass spectrum, *m/e* (relative intensity) 298(6), 207(22), 189(14), 184(66), 183(98), 165(11), 154(18), 116(10), 105(100), 91(19), 77(85), 69(22), 59(45), 51(59), and 43(60).

Anal. Calcd. for $C_{18}H_{18}O_4$: C, 72.47; H, 6.08. Found: C, 72.47; H, 6.05.

Ethyl 5-Hydroxy-3-oxo-5,5-diphenylpentanoate (4q)

This compound was prepared by the same procedure as that employed for the preparation of methyl 5-hydroxy-5-(2-methoxyphenyl)-3-oxohexanoate (**4***a*). The reagents used were: sodium hydride (0.465 g, 11.0 mmol), as a 57% mineral oil dispersion, ethyl acetoacetate (1.303 g, 10.0 mmol), and benzophenone (2.001 g, 11.0 mmol), which gave 3.642 g of a yellow oil. This oil was dissolved in cyclohexane and addition of a small quantity of methanol to the solution precipitated **4***q* (2.510 g, 81%) as colorless needles, m.p. 68–69 °C (lit. (10) m.p. 68.5–69.5 °C).

Can. J. Chem. Downloaded from www.nrcresearchpress.com by 210.87.254.5 on 09/05/12
For personal use only.

Methyl 4-(1-Hydroxycyclohex-2-enyl)-3-oxobutanoate (4r)

This compound was prepared by the same procedure as that employed for the preparation of methyl 5-hydroxy-5-methyl-3-oxohexanoate (**4***a*). The reagents used were: sodium hydride (0.467 g, 11.0 mmol), as a 57% mineral oil dispersion, methyl acetoacetate (1.162 g, 10.0 mmol), *n*-butyllithium (4.5 ml, 10.6 mmol), as a 2.35 *M* solution in hexane, and cyclohex-2-enone (0.962 g, 10.0 mmol), which gave 2.210 g of pale yellow oil. Careful distillation of this oil in base-washed apparatus gave 1.229 g (58%) of **4***r*, b.p. 83–85 °C (0.1 mm) as a colorless oil which rapidly darkened on standing; i.r. (CCl_4) 3600, 1740, 1705, and 1630 cm^{-1}; n.m.r. (CCl_4) δ 5.67 (m, 2H), 3.70 (s, 3H), 3.40 (s, 2H), 2.83 (broad s, exchangeable D_2O, 1H), 2.67 (s, 2H), and 2.10–1.46 p.p.m. (m, 6H); mass spectrum: (*a*) high resolution calcd. for $C_{11}H_{16}O_4$: 212.1048 a.m.u.; found: 212.1063 a.m.u.; (*b*) *m/e* (relative intensity) 212(8), 197(12), 194(13), 180(15), 169(23), 136(27), 135(100), 134(15), 121(85), 108(58), 97(85), 96(54), 91(46), 84(38), 79(69), 77(58), 68(69), 55(43), and 43(77).

Attempted Conjugate Addition of Dianion 2 to Cyclohex-2-enone

Sodium hydride (0.465 g, 11.0 mmol), as a 57% mineral oil dispersion, was weighed into an oven-dried 50 ml flask and tetrahydrofuran (*ca.* 25 ml) was distilled, from lithium aluminum hydride, directly into this flask. The flask was equipped with a magnetic stirrer, stoppered (septum cap), cooled in ice to 0 °C, and flushed with nitrogen. Methyl acetoacetate (1.160 g, 10.0 mmol) was added dropwise to the cooled slurry and the reaction allowed to stir for 10 min after the addition was complete. A solution of *n*-butyllithium (4.5 ml 2.35 *M* in hexane, 10.6 mmol) was added dropwise to the solution and the mixture allowed to stir for an additional 10 min, to allow complete formation of the dianion. Cuprous iodide (4.208 g, 22.0 mmol), dried at 110° *in vacuo* (0.1 mm) for 20 h prior to use, was weighed under dry conditions into a 100 ml flask and tetrahydrofuran distilled directly into this flask from lithium aluminum hydride. The flask was equipped with a magnetic stirrer, stoppered (septum cap), and flushed with nitrogen. Both the solution of dianion and the cuprous iodide suspension were cooled in a Dry Ice – acetone slurry to −78 °C. The dianion solution was transferred, via a stainless steel cannula, in a dropwise manner to the flask containing the cuprous iodide. The resulting dark brown mixture was stirred for 1 h at the end of which time most of the solid had dissolved. Cyclohex-2-enone (0.963 g, 10.0 mmol) dissolved in tetrahydrofuran (*ca.* 5 ml) was added to the reaction which was maintained at −78 °C for an additional hour before being allowed to warm to 0 °C. The reaction was quenched by dropwise addition of it to a vigorously stirred mixture of ether (50 ml) and hydrochloric acid (12 ml, 2 *M* solution). The aqueous phase was separated and further extracted with ether (2 × 35 ml). The ethereal extracts were combined, washed with saturated sodium chloride solution (6 × 25 ml), dried over anhydrous sodium sulfate, and filtered. The solvents were removed by evaporation under reduced pressure and the resulting oil chromatographed on silica gel using a mixture of hexane, ether and acetic acid as eluent. The major fractions were identified, by comparison of i.r. and n.m.r. spectra with authentic or previously prepared materials, as methyl acetoacetate (0.708 g, 61%), cyclohex-2-enone (0.564 g, 59%), methyl 4-(1-hydroxycyclohex-2-enyl)-3-oxobutanoate (**4***r*) (0.360 g, 17%), and methyl 4-(3-hydroxycyclohex-1-enyl)-3-oxobutanoate (0.276 g, 13%).

Methyl 5-Hydroxy-5-methyl-3-oxohept-6-enoate (4s)

This compound was prepared by the same procedure as that employed in the preparation of methyl 5-hydroxy-5-methyl-3-oxohexanoate (**4***a*). The reagents used in the preparation were: sodium hydride (0.466 g, 11.0 mmol), as a 57% mineral oil dispersion, methyl acetoacetate (1.163 g, 10.00 mmol), *n*-butyllithium (4.5 ml, 10.6 mmol), as a 2.35 *M* solution in hexane, and methyl vinyl ketone (0.661 g, 11.0 mmol), which gave 1.450 g (78%) of **4***s*, b.p. 101–103 °C (0.3 mm); i.r. ($CHCl_3$) 3550, 1740, 1705, and 1630 cm^{-1}; n.m.r. (CCl_4) δ 5.87 (m, 1H), 5.10 (m, 2H), 3.72 (s, 3H), 3.36 (s, 2H), 3.20 (broad s, exchangeable D_2O, 1H), 2.20 (m, 2H), and 1.27 p.p.m. (s, 3H); mass spectrum (*a*) high resolution, calcd. for $C_9H_{14}O_4$: 186.0891 a.m.u.; found: 186.0921 a.m.u; (*b*) *m/e* (relative intensity) 186(1), 171(1), 168(3), 139(4), 127(6), 116(15), 101(10), 97(9), 95(8), 85(20), 84(14), 74(12), 71(31), 69(16), 59(26), 55(60), and 43(100).

Base Dependency Study

(a) Generation of Dianion 2 by means of Lithium Diisopropylamide

Diispropylamine (1.129 g, 11.3 mmol), which has been dried by distillation and stored over potassium hydroxide pellets prior to use, was weighed into a 50 ml oven dried flask and tetrahydrofuran (*ca.* 25 ml) distilled directly into this flask from lithium aluminum hydride. The flask was equipped with a magnetic stirrer, stoppered (septum cap), cooled in ice, and flushed with nitrogen. *n*-Butyllithium (5 ml, 11.75 mmol), as a 2.35 *M* solution in hexane, was added dropwise to the solution and the reaction allowed to stir for 10 min after the addition was complete, to ensure complete formation of the amide. Methyl acetoacetate (0.638 g, 5.5 mmol) was added dropwise to solution and after a further 10 min, benzophenone (1.003 g, 5.5 mmol) dissolved in tetrahydrofuran (5 ml) was added. The reaction was quenched after 10 min by addition of concentrated hydrochloric acid (2 ml) and worked up by the addition of ether (50 ml) and water (15 ml). The aqueous phase was separated and further extracted with ether (2 × 35 ml). The ethereal extracts were combined, washed with ether (50 ml) and water (15 ml). The aqueous phase was separated and further extracted with ether (2 × 35 ml). The ethereal extracts were combined, washed with saturated sodium chloride solution (4 × 35 ml), dried over anhydrous sodium sulfate and filtered. The solvents were removed by evaporation under reduced pressure to give a semisolid which was recrystallised from a mixture of hexane and ether to give 0.827 g of methyl 5-hydroxy-3-oxo-5,5-diphenylpentanoate (**4***p*). Chromatography of the mother liquors on silica gel using chloroform as eluent gave an additional 0.184 g of **4***p*, to total 1.011 g (62%) as colorless needles, m.p. 77–79 °C.

(b) Attempted Generation of Dianion 2 by Means of Lithium Bis(trimethylsilyl)amide

Lithium bis(trimethylsilyl)amide was prepared from hexamethyldisilazane and *n*-butyllithium (13) and dissolved in tetrahydrofuran. This solution was standardised by titration against hydrochloric acid to determine its total base equivalence. An aliquot of this solution, which

had been found to be 1.52 *M* (5 ml, 7.60 mmol) was diluted to 25 ml with tetrahydrofuran and transferred to a 50 ml oven dried flask. The flask was equipped with a magnetic stirrer, stoppered (septum cap), cooled in ice, and flushed with nitrogen. Methyl acetoacetate (0.420 g, 3.62 mmol) was added dropwise to the solution of base and the reaction allowed to stir for 1 h after the addition was complete. Benzophenone (0.655 g, 3.65 mmol) dissolved in tetrahydrofuran (3 ml) was added to the reaction which was quenched after a further 15 min by addition of concentrated hydrochloric acid (0.75 ml). The reaction was worked up by the addition of ether (25 ml) and water (5 ml). The aqueous layer was separated and further extracted with ether (2 × 25 ml). The ethereal extracts were combined, washed with saturated sodium chloride solution (4 × 25 ml), dried over anhydrous sodium sulfate, and filtered. The solvents were removed by evaporation under reduced pressure to a pale yellow oil. Vapor phase chromatography analysis indicated that this oil was mainly methyl acetoacetate contaminated with hexamethyldisilazane and benzophenone, and distillation at reduced pressure gave essentially pure methyl acetoacetate (0.352 g, 84%). No product could be detected by v.p.c. or t.l.c. either in the crude oil or the residue from the distillation, that was not starting materials or hexamethyldisilazane.

Temperature Dependency Study

The dianion of methyl acetoacetate was generated as outlined above and then treated with propanal at low and room temperature.

Reaction of Dianion **2** *with Propanal at −78 °C*

The solution of dianion **2** was cooled to −78 °C in a Dry Ice – acetone slurry and propanal (0.640 g, 11.0 mmol) added. The reaction was stirred at −78 °C for 1 h and then allowed to warm to 0 °C before being quenched with concentrated hydrochloric acid (2 ml). The reaction was worked up by the addition of ether (25 ml) and water (5 ml). The aqueous phase was separated and further extracted with ether (2 × 35 ml). The ethereal extracts were combined, washed with saturated sodium chloride solution (6 × 25 ml), dried over sodium sulfate, and filtered. The solvents were removed by evaporation at reduced pressure and the resulting oil distilled under high vacuum to give methyl acetoacetate (0.915 g, 79% recovery), identified by v.p.c. analysis and by its i.r. spectrum, and methyl 5-hydroxy-3-oxoheptanoate (**4***e*) (0.191 g, 11%), identified by comparison of its i.r. and n.m.r. spectra with those of previously prepared **4***e*.

Reaction of Dianion **2** *with Propanal at 25 °C*

The solution of dianion **2** was allowed to warm to room temperature before propanal (0.641 g, 11.0 mmol) was added. The reaction was stirred at room temperature for ½ h before being quenched with concentrated hydrochloric acid (2 ml). The reaction was worked up in an identical manner to the previous low temperature reaction to give 0.993 g (57%) of **4***e*, b.p. 48–49 °C (0.2 mm), which showed identical i.r. and n.m.r. spectra to that prepared previously.

We are grateful to the University of British Columbia and the National Research Council of Canada for support of this work.

1. J. H. RICHARDS and J. B. HENDRICKSON. The biosynthesis of steroids, terpenes and acetogenins. W. A. Benjamin, New York, N.Y. 1964.
2. L. WEILER. J. Am. Chem. Soc. **92**, 6702 (1970).
3. S. N. HUCKIN and L. WEILER. J. Am. Chem. Soc. **96**, 1082 (1974).
4. S. N. HUCKIN and L. WEILER. Tetrahedron Lett. 2405 (1972).
5. S. N. HUCKIN and L. WEILER. Can. J. Chem. In press.
6. S. N. HUCKIN and L. WEILER. Tetrahedron Lett. 4835 (1971).
7. S. N. HUCKIN. Ph. D. Thesis, University of British Columbia, Vancouver, British Columbia, 1973.
8. T. M. HARRIS and C. M. HARRIS. Org. React. **17**, 155 (1969).
9. (*a*) R. J. LIGHT and C. R. HAUSER. J. Org. Chem. **26**, 1716 (1961); (*b*) S. D. WORK and C. R. HAUSER. J. Org. Chem. **28**, 725 (1963).
10. J. F. WOLFE, T. M. HARRIS, and C. R. HAUSER. J. Org. Chem. **29**, 3249 (1964).
11. (*a*) E. A. EBSWORTH and N. SHEPARD. J. Inorg. Nucl. Chem. **9**, 95 (1959); (*b*) M. A. FINEMAN and R. DAIGNAULT. J. Inorg. Nucl. Chem. **9**, 205 (1959).
12. G. STORK and R. N. GUTHIKONDA. Tetrahedron Lett. 2755 (1972).
13. E. H. AMINOO-NEIZER, R. A. SHAW, D. O. SKOVLIN, and B. C. SMITH. J. Chem. Soc. 2997 (1965).

Can. J. Chem. Downloaded from www.nrcresearchpress.com by 210.87.254.5 on 09/05/12
For personal use only.

The Effect of the Excess Kinetic Energy of the $O(^1D)$ Atoms from the Flash Photolysis of N_2O on their Reaction with N_2O [1]

H. ALLAN WIEBE[2] AND GEORGE PARASKEVOPOULOS

Division of Chemistry, National Research Council of Canada, Ottawa, Canada K1A 0R9

Received October 26, 1973

H. ALLAN WIEBE and GEORGE PARASKEVOPOULOS. Can. J. Chem. **52,** 2165 (1974).

In order to investigate the suggested involvement of kinetically "hot" $O(^1D)$ atoms in their reaction with N_2O, $O(^1D)$ atoms with a maximum excess kinetic energy in the range 25–47 kcal/g-atom were produced by flash photolysis of N_2O in the absence and presence of inert deactivators of kinetic energy such as He and Ne. The following reactions take place:

[1] $$N_2O + h\nu \rightarrow O(^1D) + N_2$$

[2*a*] $$O(^1D) + N_2O \rightarrow N_2 + O_2$$

[2*b*] $$\rightarrow 2NO$$

NO and N_2 were determined directly in each experiment, the former spectrophotometrically, the latter by gas-solid chromatography. The ratio N_2/NO was found to be independent of the addition of the inert moderators, indicating that k_{2a}/k_{2b} is not affected by the excess kinetic energy of the $O(^1D)$ atoms. The calculated value of k_{2a}/k_{2b} is $1.0 \pm 0.1_7$.

H. ALLAN WIEBE et GEORGE PARASKEVOPOULOS. Can. J. Chem. **52,** 2165 (1974).

Afin de pouvoir évaluer l'hypothèse selon laquelle des atomes $O(^1D)$ cinétiquement chauds sont impliqués lors de leur réaction avec N_2O, nous avons produit des atomes $O(^1D)$ avec un excès maximum d'énergie cinétique, de l'ordre de 25 à 47 kcal/g-atome, par une photolyse éclair de N_2O en l'absence et présence de gaz inertes tels que He et Ne qui agissent comme désactivateurs d'énergie cinétique. Les réactions suivantes ont lieu:

[1] $$N_2O + h\nu \rightarrow O(^1D) + N_2$$

[2*a*] $$O(^1D) + N_2O \rightarrow N_2 + O_2$$

[2*b*] $$\rightarrow 2\,NO$$

On détermine directement NO et N_2 dans chaque expérience, le premier de façon spectrophotométrique et le second par chromatographie gaz–solide. Le rapport N_2/NO est indépendant de l'addition de modérateurs inertes, ce qui indique que k_{2a}/k_{2b} n'est pas influencé par l'excès d'énergie cinétique des atomes $O(^1D)$. La valeur calculée de k_{2a}/k_{2b} est de $1.0 \pm 0.1_7$.
[Traduit par le journal]

Introduction

The photolysis of N_2O by light of wavelength 1850–2300 Å gives electronically excited oxygen atoms mainly in the $O(^1D)$ state (1). The $O(^1D)$ atoms subsequently react rapidly with N_2O to give N_2, O_2, and NO

[1] $$N_2O + h\nu \rightarrow O(^1D) + N_2$$

[2*a*] $$O(^1D) + N_2O \rightarrow N_2 + O_2$$

[2*b*] $$\rightarrow 2NO$$

Previous observations (1, 2) have established that [1] is the only important primary process in that wavelength region. It has also been well established (3–6) that [2*a*] and [2*b*] are the only important processes occurring with a possible minor contribution (2–3%) from the spin forbidden process [3*b*]

[3*b*] $$O(^1D) + N_2O \rightarrow O(^3P) + N_2O$$

The relative rate k_{2a}/k_{2b} has been determined several times (3–5, 7) and there are small discrepancies between the reported values and disagreement as to whether it depends on the excess kinetic energy of the $O(^1D)$ atoms.

Thus, Heicklen and co-workers photolyzed N_2O at 2139 Å (3), and 2139 and 1849 Å (5) and using the method of chemical difference they

[1]NRCC No. 13886.

[2]NRCC Postdoctorate Fellow 1971–1972. Present address: Atmospheric Environment Service, Department of the Environment, Downsview, Ontario.

Can. J. Chem. Downloaded from www.nrcresearchpress.com by 210.87.254.5 on 09/05/12
For personal use only.

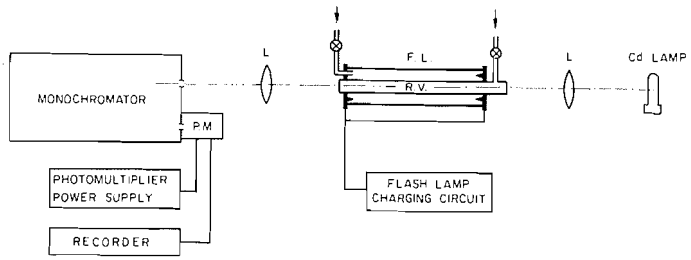

FIG. 1. Schematic diagram of the apparatus. F.L. flash lamp; R.V., reaction vessel; L, lenses; P.M., photomultiplier.

determined the quantum yield of O_2 from which they calculated k_{2a}/k_{2b} values of 0.59 ± 0.01 and 0.69 ± 0.05. The maximum available translational energy of the $O(^1D)$ atoms at these wavelengths is 25.2 and 44.0 kcal/g-atom. When they added He to remove the translational energy the ratio k_{2a}/k_{2b} became 0.83 ± 0.06. From these experiments they concluded that the value of the ratio depends on the excess translational energy of the $O(^1D)$ atoms and that it is 0.90 ± 0.10 and 0.65 ± 0.07, respectively, for $O(^1D)$ atoms without and with excess translational energy.

On the other hand Preston and co-workers (4) determined the same ratio using three different experimental techniques *i.e.* photolysis of NO_2–N_2O mixtures at 2420 and 2288 Å, flash photolysis of O_3–N_2O mixtures ($\lambda \sim 2500$ Å), and photolysis of N_2O at 2288 Å. They obtained k_{2a}/k_{2b} values of 1.01 ± 0.06, 0.99 ± 0.06, and 1.08 ± 0.19, respectively. Since in these experiments the maximum available excess kinetic energy varied from 0.1 to 25.6 kcal/g-atom they concluded that the value of the ratio k_{2a}/k_{2b} is 1.00 ± 0.04 and is not affected by the excess translational energy of the $O(^1D)$ atoms.

More recently Ghormley *et al.* (7) obtained a value for the ratio of 0.72 ± 0.02 from the flash photolysis of O_3 ($\lambda > 2300$ Å) in mixtures of O_2 and N_2O. Although the $O(^1D)$ atoms in their system should have a maximum excess kinetic energy in the range 6–20 kcal/g-atom they compare their value with the values of 0.83 and 1.01 for thermalized $O(^1D)$ atoms.

The measured values of the ratio k_{2a}/k_{2b} differ more than the estimated experimental error in each measurement. The discrepancies are not perhaps large, yet reactions 2*a* and 2*b* are important to atmospheric chemistry. Moreover the photolysis of N_2O has been used extensively for the production of $O(^1D)$ atoms in laboratory studies. In these studies the rate of N_2 production from reaction 2*a* has been used to determine primary quantum yields of $O(^1D)$ production in the photolysis of various oxides, as well as the relative rates of $O(^1D)$ reactions with other gases in experiments in which various added gases compete with N_2O for $O(^1D)$. In all these measurements it is important to know accurately the relative rate k_{2a}/k_{2b}. Further independent determinations using different techniques are therefore necessary. In the present work $O(^1D)$ atoms were produced by flash photolysis of N_2O ($\lambda \sim$ 1800–2300 Å) both in the absence and presence of inert[3] deactivators of translational energy such as He and Ne, and the N_2 and NO produced in reactions 2*a* and 2*b* were measured directly.

Experimental

The block diagram of the experimental arrangement is shown in Fig. 1. The all quartz reaction vessel with plane end-windows (50 cm long, 2.5 cm i.d., 195.0 cc volume) was mounted in the center of a flash lamp of annular design (11, 12). The vessel was connected to a mercury-free high vacuum system. The flash lamp was filled with dry air, a 75 μF capacitance was charged to 8 kV, the air was then evacuated and the discharge triggered when the breakdown pressure of air was reached, producing a reproducible 2400 J light pulse of about 20 μs duration to half-peak height.

The NO was analyzed photoelectrically in absorption by the attenuation of the 2267 Å line (γ(0,0) band of NO). The intensity of the 2267 Å cadmium line emitted by a cadmium lamp (Philips 93107 E) was monitored by a Philips 150 UVP photomultiplier mounted at the exit slit (40μ wide, bandwidth ~ 0.35 Å) of a 1 m Czerny–Turner scanning spectrophotometer (Jarrell–Ash). The photocurrents before and after the flash were registered on a potentiometric recorder. For the quantitative measurement of NO and in order that the absorption varied linearly with the NO pressure the γ-band was pressure broadened before the measurement by addition of He or Ne to a total pressure of 1 atm. The He or Ne were added before or after the flash depending on whether the reac-

[3]Previous work has shown that He (2, 8) and Ne (9, 10) do not interact with $O(^1D)$ to any significant extent.

Can. J. Chem. Downloaded from www.nrcresearchpress.com by 210.87.254.5 on 09/05/12
For personal use only.

Can. J. Chem. Downloaded from www.nrcresearchpress.com by 210.87.254.5 on 09/05/12
For personal use only.

tion took place in the presence or absence of He or Ne. A calibration was made in which the absorbance (log I_0/I_{tr}) of known amounts of NO (0.050 to 0.225 Torr) was determined in the presence of 1 atm of He. Pressures of NO were measured in a small volume using a sulfuric acid manometer. The gas was then expanded into the cell. The expansion ratio was 67 ± 0.11. Helium was then added to the cell to a total pressure of 1 atm. The data were expressed in a form of the Beer–Lambert law.

$$\text{NO (Torr)} = \alpha \log (I_0/I_{tr})$$

The least square value of α was found to be $\alpha = 1.205$, standard deviation = ±0.014. A plot of log (I_0/I_{tr}) against the NO pressure is shown in Fig. 2, and it may be seen that the variation of the absorbance with NO pressure is linear in the pressure range of the experiments.

The noncondensable gases (N_2, O_2, He, or Ne) were collected by a Toepler pump after passing through two liquid nitrogen traps and a solid nitrogen trap (capable of trapping NO), and were transferred *in toto* into the 200 cc glass loop of the gas chromatographic line. The loop was connected to the He carrier stream by a four way stopcock. The N_2 and O_2 were separated on a 14 ft column packed with 40/60 mesh molecular sieve 5A, operated at 0 °C and equipped with a thermistor detector. Only N_2 was determined since O_2 was partly lost by reaction with NO in the cold traps. Quantitative determination of N_2 was based on peak area measurements. The calibration of the thermistor response for N_2 was made with known amounts of N_2, measured in the same manner as that of NO, diluted in an atmosphere of He, and transferred from the reaction vessel to the chromatographic line in the same manner as in the actual experiments. The flow of the He carrier gas was such that all the gas in the loop was introduced into the column in about 1 min; the O_2 and N_2 peaks were well separated but somewhat broadened. For the majority of the experiments with He–N_2 mixtures the error in the N_2 determinations was found to be about 6%. In the few experiments with Ne–N_2 mixtures, N_2 was not completely separated from Ne (the N_2 peak appeared at the tail of the large Ne peak) and although calibrations were made with similar Ne–N_2 mixtures the error in the N_2 determination was perhaps as large as 15%.

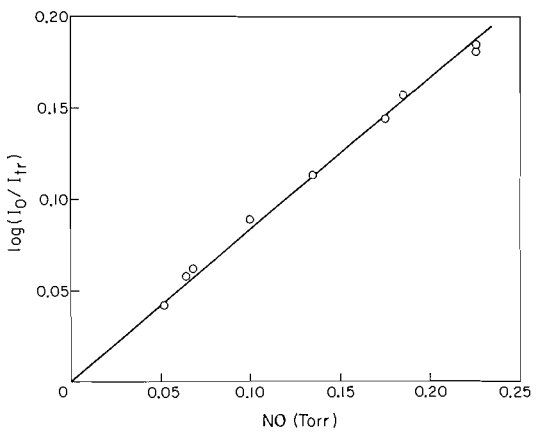

FIG. 2. Plot of absorbance of NO, log (I_0/I_{tr}), against partial pressure of NO diluted in 1 atm of He.

Matheson nitrous oxide (stated purity 98% minimum) was degassed at −196 °C and distilled *in vacuo* from a Dry Ice – acetone bath. It was further degassed at −196 °C before each experiment. Canadian Oxygen He (stated purity 99.95 minimum), and Matheson purified Ne (stated purity 99.99) were passed through molecular sieve at −196 °C.

Results and Discussion

Little is known about the factors affecting the partitioning of energy, in excess of the minimum required to break a bond, into translational and internal degrees of freedom of the fragments following photodissociation. Busch and Wilson (13) found that in the photodissociation of NO_2 and NOCl approximately 60–70% of the excess energy goes into translation of the fragments. The wavelength distribution of the photolysis flash light is continuous and the energy available for dissociation can only be estimated for the range between the onset of absorption by the N_2O and the lower wavelength limit of transmission for the quartz reaction vessel (~1800 Å). The lowest wavelengths available are in the region 1800–1850 Å (separate experiments showed that 12.0 Torr of H_2O, which does not absorb above 1900 Å (14), flashed under the same conditions in the presence of an excess of CO gave 16.0μ ± 10% of OH per flash as determined from the amount of CO_2 formed). The upper wavelength limit is of course the onset of absorption of light by N_2O *i.e.*, 2300 Å (14). From the energies of the photons at these wavelengths (1800–2300 Å) and assuming that all the excess energy goes into translation of the O(¹D) and N_2 fragments, we estimate that the O(¹D) atoms in our system have a maximum kinetic energy in the range 25–47 kcal/g-atom.

The experiments were made at room temperature (25 ± 2 °C). For the reactions 1, 2*a*, and 2*b*, with the usual steady-state assumption the following expression is obtained

$$\frac{k_{2a}}{k_{2b}} = \frac{R_{N_2}}{R_{NO}} - \frac{1}{2}$$

where R_{N_2} and R_{NO} are the rates of production of N_2 and NO respectively. R_{N_2}/R_{NO} is the ratio of the yields of N_2 and NO. The measured yields of N_2 and NO and the calculated values of the ratios N_2/NO and k_{2a}/k_{2b} are given in Table 1. The average values of N_2/NO in the absence and presence of He were, 1.47 ± 0.12

TABLE 1. Yields of N_2 and NO from the flash photolysis of N_2O in the absence and presence of He and Ne

N_2O (Torr)	N_2 (Torr)	NO (Torr)	$\frac{N_2}{NO}$	$\frac{k_{2a}}{k_{2b}}$
N_2O flashed without He				
79.9	0.163	0.108	1.51	1.01
80.6	0.194	0.121	1.60	1.10
76.4	0.169	0.130	1.30	0.80
79.2	0.184	0.117	1.57	1.07
81.3	0.184	0.126	1.46	0.96
79.2	0.175	0.133	1.32	0.82
77.7	0.182	0.120	1.52	1.02
	Average values		1.47	0.97
	Standard deviation		0.12	
N_2O flashed with 678 ± 5 Torr of He				
82.7	0.204	0.126	1.62	1.12
81.4	0.195	0.119	1.64	1.14
77.8	0.175	0.120	1.46	0.96
81.3	0.218	0.135	1.61	1.11
82.7	0.196	0.138	1.42	0.92
79.1	0.171	0.122	1.40	0.90
80.4	0.157	0.116	1.35	0.85
	Average values		1.50	1.00
	Standard deviation		0.12	
N_2O flashed with 671 Torr of Ne				
80.4	0.293	0.184	1.59	1.09
80.4	0.234	0.164	1.43	0.93
81.7	0.223	0.157	1.42	0.92

and 1.50 ± 0.12 from which k_{2a}/k_{2b} was calculated to be 0.97 ± 0.12 and 1.00 ± 0.12 respectively. Essentially the same values were obtained when 671 Torr of Ne were added (Table 1). The quoted errors are standard deviations. Care was taken to eliminate non-random errors. From a realistic assessment of the possible uncertainty of every measurement involved (pressure, absorbance, gas chromatography) and taking into account the propagation of errors in the calculation of the final results (15) we estimated the possible random error of the N_2/NO to be ±0.17. Within this error our results show that the ratio k_{2a}/k_{2b} in our system is entirely unaffected by the addition of He or Ne, which are good deactivators of translational excitation, indicating that the excess translational energy of the $O(^1D)$ atoms does not affect the relative rates of reactions 2*a* and 2*b*. The mean value of the two sets of experiments is $k_{2a}/k_{2b} = 1.0 \pm 0.1_7$, in good agreement with the value of 1.00 ± 0.04 obtained by Preston and co-workers (4) by different techniques.

As those workers have noted (4), the ratio k_{2a}/k_{2b} for the reaction of ground state oxygen atoms, $O(^3P)$, has also been found to be close to unity in the majority of determinations (16–19), although values higher than unity have also been reported (20). The activation energies for the two pathways are the same or nearly so for the reaction with $O(^3P)$ (16–18, 21) and evidently (22) are both very small or negligible in the case of reaction with $O(^1D)$ (the rate constant of $O(^1D) + N_2O$ approaches collision efficiency (22)). If similar transition complexes are involved in the two cases, the values of k_{2a}/k_{2b} for $O(^3P)$ and $O(^1D)$ would be expected to be very close.

The authors are grateful to Dr. R. J. Cvetanović for his interest in this work, his advice and encouragement.

1. K. F. PRESTON and R. F. BARR. J. Chem. Phys. **54**, 3347 (1971).
2. G. PARASKEVOPOULOS and R. J. CVETANOVIĆ. J. Am. Chem. Soc. **91**, 7572 (1969).
3. R. GREENBERG and J. HEICKLEN. Int. J. Chem. Kinet. **2**, 185 (1970).
4. P. M. SCOTT, K. F. PRESTON, R. J. ANDERSEN, and L. M. QUICK. Can. J. Chem. **49**, 1808 (1971).
5. R. SIMONAITIS, R. I. GREENBERG, and J. HEICKLEN. Int. J. Chem. Kinet. **4**, 497 (1972).
6. G. PARASKEVOPOULOS, V. B. SYMONDS, and R. J. CVETANOVIĆ. Can. J. Chem. **50**, 1838 (1972).
7. J. A. GHORMLEY, R. L. ELLSWORTH, and C. J. HOCHANADEL. J. Phys. Chem. **77**, 1341 (1973).
8. H. YAMAZAKI and R. J. CVETANOVIĆ. J. Chem. Phys. **41**, 3703 (1964).
9. M. CLERK, A. REIFFSTECK, and B. LESIGNE. J. Chem. Phys. **50**, 3721 (1969).
10. H. YAMAZAKI. Can. J. Chem. **48**, 3269 (1970).
11. P. M. SCOTT and R. J. CVETANOVIĆ. J. Chem. Phys. **54**, 10 (1965).
12. P. C. GOODFRIEND and H. P. WOODS. Rev. Sci. Instr. **36**, 10 (1965).
13. G. E. BUSCH and K. R. WILSON. J. Chem. Phys. **56**, 3626, 3655 (1972).
14. K. WATANABE, M. ZELIKOFF, and E. C. Y. INN. Absorption coefficients of several atmospheric gases. Geophysics Research Directorate, Air Force Cambridge Research Center, Cambridge, Mass. Report No. 53–23. 1953.
15. E. M. PUGH and G. H. WINSLOW. The analysis of physical measurements. Addison–Wesley, Reading, Mass. 1966.
16. D. GUTMAN, R. L. BELFORD, A. J. HAY, and R. PANCIROV. J. Phys. Chem. **70**, 1793 (1966).
17. S. C. BARTON and J. E. DOVE. Can. J. Chem. **47**, 521 (1969).
18. H. HEINRICI and S. H. BAUER. J. Chem. Phys. **50**, 1333 (1969).
19. A. A. BORISOV. Kinet. Katal. **9**, 482 (1968).
20. D. MILKS and R. A. MATULA. Fourteenth Symposium (International) on Combustion. The Combustion Institute. 1973. p. 83.
21. F. KAUFMAN, N. J. GERRI, and R. E. BOWMAN. J. Chem. Phys. **25**, 106 (1956).
22. R. J. CVETANOVIĆ. *In* Chemical kinetic data survey. N.B.S. Interim Report 73–206. 1973.

Can. J. Chem. Downloaded from www.nrcresearchpress.com by 210.87.254.5 on 09/05/12
For personal use only.

Can. J. Chem. Downloaded from www.nrcresearchpress.com by 210.87.254.5 on 09/05/12
For personal use only.

The High Temperature and Dilute Acid (HTDA) Procedure as a General Method of Replacing Aromatic Hydrogen by Deuterium. II[1-3]

NICK H. WERSTIUK AND TONY KADAI

Department of Chemistry, McMaster University, Hamilton, Ontario

Received September 11, 1973

NICK H. WERSTIUK and TONY KADAI. Can. J. Chem. **52**, 2169 (1974).

The preparation of aniline-d_5, phenol-d_5, and benzoic acid-d_5 utilizing the conditions of high temperature and dilute acid (HTDA) is described.

NICK H. WERSTIUK et TONY KADAI. Can. J. Chem. **52**, 2169 (1974).

On décrit la préparation de l'aniline-d_5, du phénol-d_5 et de l'acide benzoique-d_5 utilisant les conditions de haute température et d'acide dilué déjà proposées. [Traduit par le journal]

As a continuation of our studies on the development of the high temperature (200–300°) and dilute acid procedure (1, 2) as a general method for the deuteration and tritiation of aromatic compounds, we have studied H–D exchange in aniline (**1**), phenol (**2**), and benzoic acid (**3**). The results are listed in Tables 1, 2 and 3, respectively.

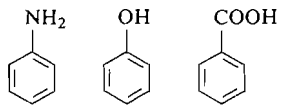

1 2 3

Entry 1 of Table 1 shows that under the HTDA conditions (24 h), at 175° no appreciable exchange occurs at the *meta* positions in aniline. When the temperature is increased to 300° (entry 2) aniline is converted into phenol and ammonium chloride, likely via nucleophilic aromatic substitution involving the anilinium salt. Even at 275° after 24 h (entry 3) some conversion to phenol (31%) occurs. As described in entries 4 and 6, at 250° the exchange at the *ortho* and *para* positions is rapid[4] followed by slow *meta* exchange with complete equilibration (95% exchange) resulting in *one* cycle after 54 h.

The HTDA procedure thus also provides a unique, likely quantitative method for the deamination of aromatic amines and the conversion of aromatic oxy and thio ethers to phenols.

Thus by an appropriate choice of temperature and reaction time aniline-d_5 or -d_7[4] and phenol-d_5 or -d_6 can be prepared in one step directly from aniline. Thus tritiated aniline and phenol can also be prepared using the HTDA procedure. Certainly, deuterated and tritiated substituted anilines and phenols can also now be prepared via the HTDA conditions. The procedure also provides a unique route to ^{18}O labelled phenols. In a typical large-scale preparation (entries 7 and 8, Table 1) freshly recrystallized aniline hydrochloride (20 g, 0.15 mol) was stirred with D_2O (50 ml, 2.5 mol) at room temperature for several hours and the D_2O was distilled off under vacuum and recovered for use in the first cycle of subsequent exchanges. The aniline hydrochloride was dissolved in D_2O (60 ml, 2.6 mol) and the solution was sealed in a glass tube after being degassed three times via freeze–pump–thaw cycles. The tube was heated at 250° in a 2 l Parr pressure apparatus containing H_2O to equalize the internal pressure. After 48 h the D_2O and traces of phenol were distilled off under vacuum to yield a yellowish solid (16.4 g, 82%). The solid was heated at 250° with a fresh batch of D_2O

[1]Patent pending.

[2]Presented in part at the Conference on Stable Isotopes in Chemistry, Biology and Medicine, Argonne, Illinois, May, 1973.

[3]Publication delayed at authors request.

[4]Exchange occurs readily at the *ortho* and *para* positions when aniline hydrochloride is heated at 100° in D_2O (3). Aniline-d_7 has been prepared in 70% yield by nitration of benzene-d_6 followed by reduction of the nitrobenzene-d_5 (4) or by treating aniline with activated platinum in D_2O at 140° for 3 days (5).

TABLE 1. H–D exchange in aniline hydrochloride in D_2O

Entry*	Conditions		D/molecule 1†	% exchange in aromatic ring	Position			% yield	
	Temp. (°C)	Time (h)			*o*	*m*	*p*	**1**	**2**
1	175	24	2.85	57	1.90	0.0	0.95	86	—
2	300	48	—	—				0	—¶
3‡	275	24	—	—				44	31
4	250	12	3.60	72	1.85	0.80	0.95	74	1
5	250	35	4.60	92	1.90	1.75	0.95	72	3
6	250	54	4.75	95	1.90	1.90	0.95	69	4
7§	250	48	4.15	83	1.75	1.55	0.85	82	—¶
8‖	250	50	4.85	97	1.95	1.95	0.95	72	—¶

*Typically, a solution of recrystallized substrate in water was degassed three times and heated in a sealed tube.
†Determined by n.m.r. integral analysis by using the back-exchanged amino group as an internal standard.
‡Run in H_2O.
§The amino protons were first exchanged by washing with D_2O at room temperature.
‖The crude deuterated **1** from entry 7 was used in this run.
¶Not determined.

TABLE 2. H–D exchange in phenol in 4% (v/v) concentrated HCl–D_2O

Entry	Conditions		D/molecule* 2†	% exchange in aromatic ring	Position†		% recovery
	Temp. (°C)	Time (h)			*o* + *p*	*m*	
1	175	72	3.05	61	2.7	0.2	—‡
2	200	48	3.90	78	2.7	1.3	95

*Determined mass spectrometrically after O–D was washed out.
†Determined by n.m.r. integral analysis.
‡Not determined.

TABLE 3. H–D exchange in benzoic acid in 4% (v/v) concentrated HCl–D_2O

Entry	Conditions		D/molecule* 3	% exchange in aromatic ring	% recovery
	Temp. (°C)	Time (h)			
1	175	72	0	0	>95
2	250	65	3.40	68	>95
3	275	75	4.70	94	>95

*Determined by n.m.r. integral analysis using the back exchanged O–H as internal standard.

(60 ml) for 50 h and the D_2O was reclaimed by vacuum distillation. H_2O (80 ml) was added to the remaining solid and the solution was basified with concentrated aqueous NaOH and extracted with ether (5 × 20 ml). The ether extract was washed with 5% HCl (5 × 20 ml). The aqueous HCl phase was basified with concentrated NaOH, saturated with solid NaCl, and extracted with ether (5 × 30 ml). The ether extract was washed with water and dried. Vacuum distillation (b.p. 43–44°, 2 mm) gave 10.3 g (72%) of aniline-d_5. Nuclear magnetic resonance area intergral analysis showed that all aromatic positions had been equilibrated with 97% overall exchange.

Table 2 lists the preliminary results obtained with phenol which establish that phenol and therefore certainly substituted phenols may be deuterated and therefore also tritiated using the HTDA conditions.

In order to establish the complete generality of the HTDA exchange procedure, benzoic acid (**3**) which is deactivated to electrophilic aromatic substitution was examined. The results are listed in Table 3. The data in entries 1, 2, and 3 establish that a one cycle HTDA exchange can be used successfully to deuterate and therefore tritiate in high yield aromatic nuclei which contain electron withdrawing groups.

With regard to the mechanism of exchange, protonation–deprotonation of the aromatic nu-

Can. J. Chem. Downloaded from www.nrcresearchpress.com by 210.87.254.5 on 09/05/12
For personal use only.

cleus is likely involved. In the case of phenol, exchange may occur both through protonation of phenol or the phenoxide anion.

We are presently continuing our studies on other aromatic and polyaromatic systems with emphasis on the preparation of labelled biologically active materials.

Financial support by the National Research Council of Canada is very gratefully acknowledged.

1. N. H. WERSTIUK and T. KADAI. Chem. Commun. 1349 (1971).
2. N. H. WERSTIUK and T. KADAI. Can. J. Chem. **51**, 1485 (1973).
3. A. P. BEST and L. L. WILSON. J. Chem. Soc., 239 (1946).
4. A. RIEKER and P. ZIEMER. Z. Naturforsch. **20B**, 640 (1965).
5. R. R. FRASER and R. N. RENAUD. J. Am. Chem. Soc. **88**, 4365 (1966).

Can. J. Chem. Downloaded from www.nrcresearchpress.com by 210.87.254.5 on 09/05/12
For personal use only.

Methyl Radicals in Solid Acetonitrile: Decay or No Decay[1]

FREDERICK PETER SARGENT, MARSHALL GRANT BAILEY, AND EDWARD MICHAEL GARDY

Research Chemistry Branch, Atomic Energy of Canada Limited, Whiteshell Nuclear Research Establishment, Pinawa, Manitoba R0E 1L0

Received March 4, 1974

FREDERICK PETER SARGENT, MARSHALL GRANT BAILEY, and EDWARD MICHAEL GARDY. Can. J. Chem. **52**, 2171 (1974).

A comparison of both the e.s.r. spectra and the thermal stability of the radicals produced in γ radiolysis and 185 nm photolysis of acetonitrile shows that the former are not free methyl radicals. The initial species formed by γ radiolysis can be converted by photobleaching into a methyl radical weakly associated with a cyanide ion. The methyl radical of this CH_3---CN^- pair decays via hydrogen abstraction, whereas the free methyl radicals produced by 185 nm photolysis of acetonitrile are quite stable at 77 K. We ascribe the low energy of activation for the hydrogen abstraction reaction in the γ irradiated samples not primarily to quantum mechanical tunnelling but to perturbation by the cyanide ion.

FREDERICK PETER SARGENT, MARSHALL GRANT BAILEY, et EDWARD MICHAEL GARDY. Can. J. Chem. **52**, 2171 (1974).

On montre, par comparaison des spectres r.p.e. et de la stabilité thermique des radicaux produits par radiolyse γ et photolyse à 185 nm de l'acétonitrile, que les produits formés dans le premier cas ne sont pas des radicaux méthyles libres. Les premières espèces formées par radiolyse γ peuvent être transformées par photodécoloration en un radical méthyle faiblement associé avec un ion cyanure. Le radical méthyle de cette paire CH_3---CN^- est détruit par abstraction d'hydrogène, tandis que les radicaux méthyles libres produits par photolyse à 185 nm de l'acétonitrile sont assez stables à 77 K. La faible énergie d'activation pour la réaction d'abstraction d'hydrogène dans les échantillons irradiés par les rayons γ ne dépend pas principalement d'un franchissement de tunnel relevant de la mécanique quantique, mais plutôt d'une perturbation par l'ion cyanure. [Traduit par le journal]

γ-Radiolysis of solid acetonitrile at low temperatures yields methyl and $\cdot CH_2CN$ radicals together with a light sensitive species (1, 2). The latter has been shown to be an electron trapped on two acetonitrile molecules (3). It is destroyed on exposure of the irradiated sample to visible light but a corresponding increase in the number of methyl radicals is observed (1, 2). These decay exponentially and irreversibly by hydrogen atom abstraction to give $\cdot CH_2CN$ as in reaction 1

$$[1] \qquad \cdot CH_3 + CH_3CN \rightarrow CH_4 + \cdot CH_2CN$$

The energy of activation for this reaction derived from the decay rates at 77 and 87 K was 6 kJ/mol (1, 2). This is in marked contrast to the value of 42 kJ found in the gas phase at high temperatures (373–573 K) (4).

[1]AECL No. 4477.

cleus is likely involved. In the case of phenol, exchange may occur both through protonation of phenol or the phenoxide anion.

We are presently continuing our studies on other aromatic and polyaromatic systems with emphasis on the preparation of labelled biologically active materials.

Financial support by the National Research Council of Canada is very gratefully acknowledged.

1. N. H. WERSTIUK and T. KADAI. Chem. Commun. 1349 (1971).
2. N. H. WERSTIUK and T. KADAI. Can. J. Chem. **51**, 1485 (1973).
3. A. P. BEST and L. L. WILSON. J. Chem. Soc., 239 (1946).
4. A. RIEKER and P. ZIEMER. Z. Naturforsch. **20B**, 640 (1965).
5. R. R. FRASER and R. N. RENAUD. J. Am. Chem. Soc. **88**, 4365 (1966).

Can. J. Chem. Downloaded from www.nrcresearchpress.com by 210.87.254.6 on 09/05/12
For personal use only.

Methyl Radicals in Solid Acetonitrile: Decay or No Decay[1]

FREDERICK PETER SARGENT, MARSHALL GRANT BAILEY, AND EDWARD MICHAEL GARDY

Research Chemistry Branch, Atomic Energy of Canada Limited, Whiteshell Nuclear Research Establishment, Pinawa, Manitoba R0E 1L0

Received March 4, 1974

FREDERICK PETER SARGENT, MARSHALL GRANT BAILEY, and EDWARD MICHAEL GARDY. Can. J. Chem. **52**, 2171 (1974).

A comparison of both the e.s.r. spectra and the thermal stability of the radicals produced in γ radiolysis and 185 nm photolysis of acetonitrile shows that the former are not free methyl radicals. The initial species formed by γ radiolysis can be converted by photobleaching into a methyl radical weakly associated with a cyanide ion. The methyl radical of this CH_3---CN^- pair decays via hydrogen abstraction, whereas the free methyl radicals produced by 185 nm photolysis of acetonitrile are quite stable at 77 K. We ascribe the low energy of activation for the hydrogen abstraction reaction in the γ irradiated samples not primarily to quantum mechanical tunnelling but to perturbation by the cyanide ion.

FREDERICK PETER SARGENT, MARSHALL GRANT BAILEY, et EDWARD MICHAEL GARDY. Can. J. Chem. **52**, 2171 (1974).

On montre, par comparaison des spectres r.p.e. et de la stabilité thermique des radicaux produits par radiolyse γ et photolyse à 185 nm de l'acétonitrile, que les produits formés dans le premier cas ne sont pas des radicaux méthyles libres. Les premières espèces formées par radiolyse γ peuvent être transformées par photodécoloration en un radical méthyle faiblement associé avec un ion cyanure. Le radical méthyle de cette paire CH_3---CN^- est détruit par abstraction d'hydrogène, tandis que les radicaux méthyles libres produits par photolyse à 185 nm de l'acétonitrile sont assez stables à 77 K. La faible énergie d'activation pour la réaction d'abstraction d'hydrogène dans les échantillons irradiés par les rayons γ ne dépend pas principalement d'un franchissement de tunnel relevant de la mécanique quantique, mais plutôt d'une perturbation par l'ion cyanure. [Traduit par le journal]

γ-Radiolysis of solid acetonitrile at low temperatures yields methyl and $\cdot CH_2CN$ radicals together with a light sensitive species (1, 2). The latter has been shown to be an electron trapped on two acetonitrile molecules (3). It is destroyed on exposure of the irradiated sample to visible light but a corresponding increase in the number of methyl radicals is observed (1, 2). These decay exponentially and irreversibly by hydrogen atom abstraction to give $\cdot CH_2CN$ as in reaction 1

$$[1] \qquad \cdot CH_3 + CH_3CN \rightarrow CH_4 + \cdot CH_2CN$$

The energy of activation for this reaction derived from the decay rates at 77 and 87 K was 6 kJ/mol (1, 2). This is in marked contrast to the value of 42 kJ found in the gas phase at high temperatures (373–573 K) (4).

[1]AECL No. 4477.

Can. J. Chem. Downloaded from www.nrcresearchpress.com by 210.87.254.6 on 09/05/12
For personal use only.

LeRoy *et al.* (5) have suggested that the low energy of activation for reaction 1 at low temperatures is due to quantum mechanical tunnelling. In view of this we have reinvestigated the rates of reaction 1 at several low temperatures to determine the validity of the assumed (1, 2) Arrhenius behavior. We have also prepared methyl radicals in acetonitrile at 77 K by methods other than γ radiolysis and measured their decay rates. Our results show that although the γ radiolysis produced methyl radicals which decay in accord with the Arrhenius temperature–rate law, it is possible to photochemically generate methyl radicals in acetonitrile which do not decay at 77 K. This together with differences in the coupling constants of the radicals generated by the two techniques has prompted a reconsideration of the identity of the radicals formed.

Experimental

The acetonitrile was of spectrograde quality and was dried with anhydrous magnesium sulfate on a vacuum line. Dried degassed samples were prepared under vacuum by distillation from the storage vessel into the sample tubes which were sealed off and then γ irradiated in the dark at 77 K. Typical irradiation times were about 20 min corresponding to a dose of about 0.2 MRads. The samples were examined in a Varian V4500 electron spin resonance (e.s.r.) spectrometer. The dark spectrum of methyl radicals was used to set up the spectrometer. The specimen was then illuminated to generate additional methyl radicals (1). Their decay was monitored by means of the high field line of relative intensity three. The temperature was varied by immersing the samples in different refrigerants such as liquid nitrogen, argon, air, and oxygen. Boiling points were corrected for atmospheric pressure changes (6). The decays were shown to be exponential over several half-lives but normally were followed only for two half-lives.

Photolyses were performed at 185 nm with a low pressure (resonance) mercury lamp and also, in experiments with added *N,N,N′,N′*-tetramethyl-*p*-phenylenediamine (TMPD), at 366 nm with a high pressure 100 W mercury lamp and filter system.

Results

γ-*Radiolysis*

γ-Radiolysis of acetonitrile at 77 K followed by illumination gave an e.s.r. spectrum similar to that previously reported, namely a quartet with a separation of 21.8 ± 0.2 G and a center line, which were assigned to methyl and CH_2CN radicals respectively (1). The quartet species decayed exponentially as shown in Fig. 1 and the line due to $\cdot CH_2CN$ increased correspondingly. The decays were measured in liquid nitrogen, argon, oxygen, and air and typical values are shown in Table 1. It was found that there was a large scatter of half-lives for a given coolant. For data obtained on different days, $t_{1/2}$ values in liquid nitrogen varied from 28 to 33 min, whereas the values observed for a given day were constant to within 3%. These differences were found to correlate with changes in atmospheric pressure, and the scatter was much less after a pressure correction (6) was applied to the boiling points of the liquid. We also found that a large error can arise from the absorption of air by liquid nitrogen when left open to the atmosphere. This may explain the low $t_{1/2}$ values previously reported of 24.4 (1) and 26.6 min (2). Our present decay data obeyed the Arrhenius relation as shown in Fig. 2 from which the energy of activa-

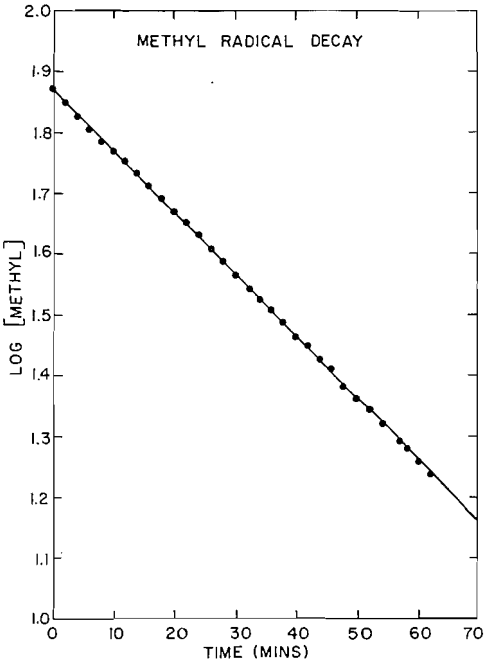

FIG. 1. The decay of methyl radicals in γ irradiated acetonitrile at 77 K.

TABLE 1. The rate constants and half lives for methyl radical decay in γ irradiated acetonitrile at various temperatures

Temperature (K)	k (min^{-1})	$t_{1/2}$ (min)
77	0.022	31.0
80	0.033	20.7
87	0.078	8.9
90	0.108	6.4

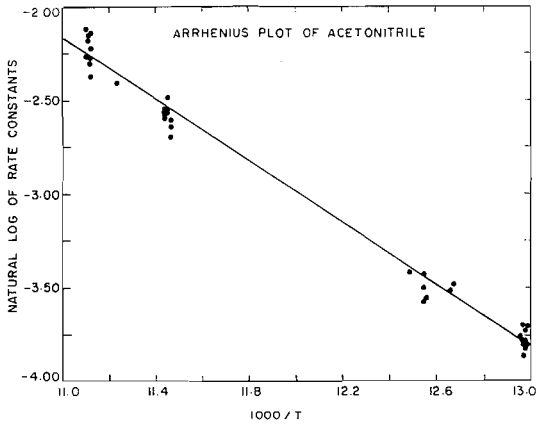

FIG. 2. The rates of decay of methyl radicals in γ irradiated acetonitrile as a function of temperature. An Arrhenius plot.

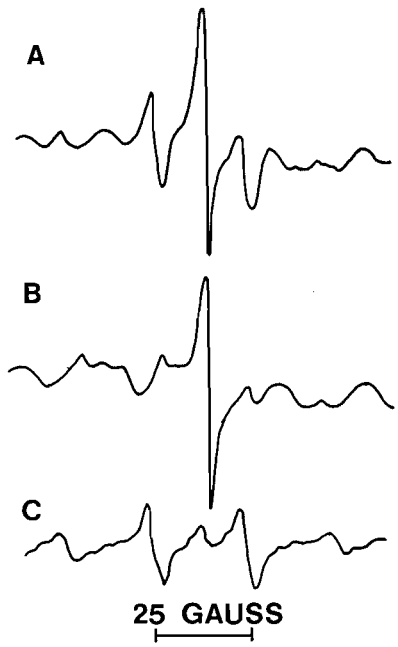

FIG. 3. The e.s.r. spectra observed in solid acetonitrile at 77 K (*A*) immediately following photolysis at 185 nm, (*B*) sample warmed to 120 K, (*C*) the difference spectrum of (*A*) and (*B*).

tion is 7.0 kJ (1.7 kcal). Within experimental error, the same value was found for samples which had not been dried or outgassed.

Having established that the decay of methyl radicals in γ irradiated acetonitrile does have a very low energy of activation, we attempted to produce these radicals in this matrix by other means.

CH_3I Photolysis

The photolysis of methyl iodide in acetonitrile at 77 K with 254 nm light did not produce an appreciable yield of methyl radicals. The e.s.r. spectrum primarily showed the presence of $\cdot CH_2CN$. This probably arises from the generation of "hot" methyl radicals which rapidly abstract hydrogen from the acetonitrile as in reactions 2 and 3.

[2] $$h\nu(254) + CH_3I \rightarrow CH_3^* + I$$

[3] $$CH_3^* + CH_3CN \rightarrow CH_4 + \cdot CH_2CN$$

TMPD Photolysis

The 366 nm photolysis of degassed *N,N,N',N'*-tetramethyl-*p*-phenylenediamine (TMPD) acetonitrile solutions yielded very weak e.s.r. spectra. In aerated samples, however, a sharp quartet of 21.8 G was observed superimposed on the broad singlet due to $TMPD^+$. At 77 and 87 K this quartet decayed at the same rates as the one in the γ irradiated samples. We therefore presume that the same radical is present in both systems.

185 nm Photolysis

Acetonitrile is transparent at 254 nm, but does absorb the 185 nm line of the low pressure mercury lamp. Exposure of samples of this lamp using Suprasil Dewars and sample tubes gave the e.s.r. spectrum shown in Fig. 3*a*. This has features which are due to a methyl radical quartet. However, these do *not* decay at 77 K and the sample had to be warmed to 120 K to give the spectrum in Fig. 3*b*. Subtraction of these two spectra gave the quartet of Fig. 3*c* and a hyperfine coupling of 22.8 G. This species is quite different from the one observed in the γ radiolysis samples which not only decayed but had a hyperfine coupling of 21.8 G.

Discussion

Our results can be summarized as follows. γ-Radiolysis of solid acetonitrile and 366 nm photolysis of the TMPD–acetonitrile system both yield a radical which exhibits a quartet e.s.r. spectrum with a proton hyperfine coupling constant of about 22 G. This species decays at 77 K by reaction 1 and the energy of activation is 7 kJ rather than the gas phase value of 40 kJ. However, the quartet species produced by the 185 nm photolysis did not decay and had a different proton coupling constant of about 23 G.

Can. J. Chem. Downloaded from www.nrcresearchpress.com by 210.87.254.6 on 09/05/12
For personal use only.

Can. J. Chem. Downloaded from www.nrcresearchpress.com by 210.87.254.6 on 09/05/12
For personal use only.

The latter is closer to that normally accepted for methyl radicals (7). We therefore assign the 23 G species in the 185 nm photolysis to the normal "free" methyl radical.

What then is the nature of the radical observed in the γ irradiated and TMPD photolysis, *i.e.* the unstable 22 G species? This radical arises from the reactions of electrons as in [4] which also produces cyanide ion.[2]

[4] $$CH_3CN + e \rightarrow CH_3\cdot + CN^-$$

We suggest that the methyl radicals so formed are not entirely free but are weakly associated with the cyanide ion. Evidence for the association of radicals with ions as a result of dissociative electron capture by methyl halides has been presented by Sprague and Williams (8). For methyl bromide in deuterated acetonitrile, the e.s.r. spectrum showed a bromine hyperfine coupling of about 55 G together with a methyl proton coupling of 20.6 G, attributable to a methyl radical associated with a bromide ion. Similar association of the anion with the radical has been suggested to explain the perturbation of the benzyl radical optical spectrum in irradiated ethane glasses containing benzyl halides (9, 10). Therefore, we suggest that the photobleached, γ irradiated samples and the TMPD photolyzed samples each contain methyl radical – cyanide ion pairs.

Now to explain the difference in stability of the free methyl radical in comparison with the CH_3---CN^- pairs, it would certainly appear that the presence of the cyanide ion reduces the energy requirements for reaction 1. The low energy of activation observed for this hydrogen abstraction reaction may well be due to perturbation of the methyl radical by the cyanide ion. Considering this perturbation in terms of orbital hybridization the methyl group in the CH_3---CN^- pairs is likely to be intermediate between sp^2 and sp^3. The sp^3 character should decrease the energy of activation for [1], since at least part of the barrier is due to the conversion of the methyl group from sp^2 in the radical to sp^3 in methane. Andrews and Pimentel (11) estimate that the latter amounts to about 20 kJ (5 kcal).

As in the case of CH_3---Br^-, the magnitude of the proton hyperfine coupling for the proposed CH_3---CN^- pair is smaller than the free methyl radical coupling of 23 G. Pyramidal deformation of planar sp^2 methyl has been shown theoretically to lead to a decrease in this coupling (12). Delocalization of the unpaired electron and the influence of the negative charge in CH_3---CN^- could also affect the hyperfine coupling.

Conclusions

The low energy of activation observed for reaction 1 in γ irradiated solid acetonitrile is not entirely due to a tunnelling effect. It is, at least in part, caused by the close proximity of the cyanide ion which not only lowers the energy requirements but also decreases the methyl radical hyperfine coupling constant.

We grately thank our colleagues in the Research Chemistry Branch for many helpful discussions.

1. F. P. Sargent. Can. J. Chem. **48**, 1780 (1970).
2. E. D. Sprague and F. Williams. J. Am. Chem. Soc. **93**, 787 (1971).
3. K. Takeda and F. Williams. Mol. Phys. **17**, 677 (1969).
4. M. H. J. Wijnen. J. Chem. Phys. **22**, 1074 (1954).
5. R. J. LeRoy, E. D. Sprague, and F. Williams. J. Phys. Chem. **76**, 546 (1972).
6. G. K. White. Experimental techniques in low temperature physics. The Claredon Press, Oxford. 1968. p. 367.
7. R. W. Fessenden. J. Phys. Chem. **71**, 74 (1967).
8. E. D. Sprague and F. Williams. J. Chem. Phys. **54**, 5425 (1971).
9. J. B. Gallivan and W. H. Hamill. Trans. Faraday Soc. **61**, 1960 (1965).
10. B. Brocklehurst and M. I. Savadatti. Nature, **212**, 1231 (1966).
11. L. Andrews and G. C. Pimentel. J. Chem. Phys. **47**, 3637 (1967).
12. S. Y. Chang, E. R. Davidson, and G. Vincow. J. Chem. Phys. **52**, 5596 (1970).

[2]The situation is undoubtedly more complicated than reaction 4 suggests. Probably $(CH_3CN)_2^-$ is first formed and this is photobleached to give CH_3---CN^-.

EDITOR'S NOTE

The manuscript of a Communication contesting the conclusions reached in the above Communication has been received from Dr. Ffrancon Williams.

Can. J. Chem. Downloaded from www.nrcresearchpress.com by 210.87.254.40 on 09/05/12
For personal use only.

Canadian Journal of Chemistry

Published by
THE NATIONAL RESEARCH COUNCIL OF CANADA

Journal canadien de chimie

Publié par
LE CONSEIL NATIONAL DE RECHERCHES DU CANADA

Volume 52 Number 12 June 15, 1974

Volume 52 numéro 12 15 juin 1974

Revision of the Shannon and Prewitt Effective Ionic Radii of Tetravalent Elements

OSVALD KNOP AND JOHN S. CARLOW[1]

Department of Chemistry, Dalhousie University, Halifax, Nova Scotia B3H 3J5

Received June 6, 1973[2]

OSVALD KNOP and JOHN S. CARLOW. Can. J. Chem. **52**, 2175 (1974).

A new empirical set of "effective ionic" radii for tetravalent atoms in 6-coordination has been constructed. It is based on $V^{1/3}$ *vs.* r plots for isostructural series of M^{4+} compounds of high symmetry. The radius values resulting from a non-linear least-squares refinement of all the data have been adjusted to coincide with the Shannon and Prewitt set of radii at Ti^{4+} and Sn^{4+}. Evidence is presented for the existence of a cusp at Bk in the $r^{vi}(M^{4+})$ *vs.* atomic number curve for M^{4+}(5f).

OSVALD KNOP et JOHN S. CARLOW. Can. J. Chem. **52**, 2175 (1974).

Un nouvel ensemble de rayons ioniques effectifs a été déduit pour les atomes quadrivalents de coordinence six. Cet ensemble est obtenu par un calcul de moindres carrés itératif à partir des correlations $V^{1/3}$–r pour des composés de M^{4+} isostructuraux de haute symétrie. Les valeurs de r ainsi obtenues sont ajustées afin qu'elles coïncident avec celles pour Ti^{4+} et Sn^{4+} publiées par Shannon et Prewitt. L'existence d'un point de rebroussement pour l'élément Bk dans la courbe des $r^{vi}(M^{4+})$ en fonction du nombre atomique pour la série M^{4+}(5f) est mis en évidence.

In our recent study (1, 2) of the cubic pyrophosphates of tetravalent elements, $M^{4+}P_2O_7$, we wished to see whether a linear correlation exists between the lattice parameters a_0 and the effective ionic radii $r(M^{4+})$. These pyrophosphates form a very complete series in that the end members correspond to the smallest (Si) and the second-largest (Th) 6-coordinated tetravalent atoms known. Shannon and Prewitt's (S.P.) (3) set of empirical ionic radii seemed the obvious choice for the test. However, in the S.P. $r^{vi}(M^{4+})$ list the values for Pu and Ce are marked as uncertain and no value is given for U; the S.P. $r^{viii}(M^{4+})$ series, which is complete for the larger atoms, begins only at Hf (Table 1). An $r^{vi}(M^{4+})$ set was therefore obtained by subtracting 0.12 Å from the S.P. $r^{viii}(M^{4+})$ values and combining the result with the S.P. $r^{vi}(M^{4+})$ radii. The corrected $r^{viii}(Pb^{4+})$ value (0.82 Å compared with $r^{vi}(Pb^{4+})$ = 0.775 Å) was out of line and was disregarded; the corrected $r^{viii}(Th^{4+})$ value, 0.92 Å, was 0.08 Å lower than the S.P. $r^{vi}(Th^{4+})$ value, 1.00 Å.

The a_0 *vs.* $r^{vi}(M^{4+})$ plot, for the pyrophosphate series Ti, Hf, Zr, Pu, Ce, U, Th, based on this new set of radii seemed to indicate that either the values for U and Th were too high or the a_0 values for α-UP_2O_7 and α-ThP_2O_7 were too low. The spread in the Si, Ge, Sn, Pb group was even greater, and it was difficult to assess to what extent the scatter was attributable to uncertainties in the values of the radii.

An attempt was therefore made to improve the

[1]Killam Postdoctoral Fellow, 1972–1974.
[2]Revision received February 7, 1974.

TABLE 1. Empirical "ionic" M^{4+} radii for 6-coordination, in Å[a]

M	G	A	Z	S.P.(6)	S.P.(8)	This work[b] r	This work[b] r''
Si	0.39	0.42	0.38	0.400R†		0.449(6)	
Ge	0.53	0.53		0.540R†		0.541(3)	
Ti	0.64	0.68	0.60	0.605R†		0.605(2)[c]	
Ru	0.65	0.67		0.620R		0.618(2)	
Pt		(0.65)		0.63R		0.629(2)	
Re				0.63R		0.662(6)[c]	
Sn	0.74	0.71		0.690R†		0.690(2)[c]	
Hf		0.78		0.71R	0.83	0.716(3)	
Zr	0.87	0.79	0.77	0.72R	0.84	0.731(3)	
Pb	0.84	0.84	0.84	0.775R	0.94R	0.778(3)	
Dy							0.78[c]
Tb		0.81		0.76R	0.88	0.790(6)[c]	
Cf						0.818(6)[d]	
Nd							0.83[c]
Bk					0.93R	0.827(7)	0.828
Cm					0.95R	0.833(6)	0.832
Am		0.92	0.89		0.95	0.839(6)	0.839
Pr	1.00	0.92		0.78?	0.96R	0.842(6)	
Pu		0.93	0.90	0.80?	0.96	0.848(6)	0.849
Ce	1.02	0.94	0.92	0.80?	0.97R	0.854(6)	
Np		0.95	0.92		0.98R	0.863(6)	0.862
U	1.05	0.97	0.93		1.00R†	0.879(7)	0.878
Pa		0.98	0.96		1.01	0.892(7)	0.897
Th	1.10	1.02	0.99	1.00	1.04R	0.922(8)	0.919
Po					1.08R	0.938(30)[d]	

[a]G, Goldschmidt; A, Ahrens; Z, Zachariasen; S.P.(6) and S.P.(8), "effective ionic" radii for 6- and 8-coordination respectively (3). For correlation of S.P. and *r* see text. R associated with the S.P. radii indicates that the value has been obtained from radius *vs.* volume plots; "those values for which at least 5 structural determinations resulted in radii differing by no more than ±0.01 Å are marked †" (3).

[b]*r*, results of the least-squares refinement of the master plot; *r''*, smoothed values from parabolic least-squares fits of *r* *vs.* atomic number (Fig. 3).

[c]See text.

[d]Uncertainty estimated from the error limits quoted for the lattice parameter in the original paper.

self-consistency of the $r^{vi}(M^{4+})$ set relying on $V^{1/3}$ *vs.* *r* plots alone. The isostructural series of compounds were limited to series of oxidic compounds with simple crystal structures of high symmetry (and preferably of high M site symmetry), and advantage was taken of lattice-parameter values more recent than those available to S.P. or not included in their compilation. Initially the a_0 or $V^{1/3}$ values for a few of the oxide series were plotted against the S.P. r^{vi} or r^{viii} values. The plots for the individual series were then combined to a master plot against r^{vi} utilizing the great *r* range of the two perovskite series, and the r^{vi} values were adjusted graphically to give the best overall agreement. The resulting provisional $r^{vi}(M^{4+})$ set was found to give reasonable linear correlations also for several fluoride series. The master plot was therefore extended to accommodate a total of 11 "oxide", 13 fluoride, and 2 chloride series, and best $r^{vi}(M^{4+})$ values were obtained from the entire aggregate of data by non-linear least squares starting from the provisional radii. Each lattice-parameter value to be used was scrutinized and assigned a weight that was deemed justified by the reported experimental conditions and evaluation procedure.[3] The refinement included the following compounds (structure type, space group, and site symmetry of the M atom are shown):

MO_2 (rutile, $P4_2/mnm$, *mmm*): Si (4, 5), Ge (6, 7), Ti (8), Ru (9, 10), Pt (orthorhombic) (11), Sn (6, 12), Pb (6, 13, 14).

MO_2 (fluorite, $Fm3m$, $m3m$): Tb (15, 16), Cf (17), Bk (18, 19), Cm (20–22), Am (23, 24), Pr (15, 16), Pu (23, 25, 26), Ce (26, 27), Np (23), U (28–30), Pa (23), Th (23, 26, 31). The PaO_2 preparation of ref. 32 was of uncertain composition and was not included. The lattice parameter of α-PoO_2 has been taken to be 5.64(1) Å; the difficulty in deciding on the most likely value is

[3]While individual references are not made to sources of the lattice-parameter values cited in Wyckoff's (6) compilation, almost all the pertinent papers were consulted in the original.

Can. J. Chem. Downloaded from www.nrcresearchpress.com by 210.87.254.40 on 09/05/12
For personal use only.

Can. J. Chem. Downloaded from www.nrcresearchpress.com by 210.87.254.40 on 09/05/12
For personal use only.

described in ref. 33, which appears to be the only source of $a(\alpha\text{-}PoO_2)$ available to date. The values for Cf, Cm, and Am have been corrected for expansion due to self-irradiation damage.

AMO_3 (perovskite, *Pm3m*, *m3m*):
$SrMO_3$: Ti (34), Ru (orthorhombic) (6, 35), Sn (6, 36), Hf (6, 37), Zr (6, 38), Pb (orthorhombic) (39, 40), Am (pseudocubic) (24), Pu (orthorhombic or monoclinic) (39, 41), Ce (6), U (orthorhombic ?) (42), Th (6).
$BaMO_3$: Ti (tetragonal) (6, 34), Sn (6, 43), Hf (37), Zr (6, 44), Pb (orthorhombic) (6, 45, 46), Tb (rhombohedral) (47, 48), Am (24), Pr (orthorhombic) (6, 47), Pu (39, 49), Ce (orthorhombic) (6, 47), U (6, 50), Pa (51), Th (6, 31, 52). The Pr and Tb preparations of ref. 47 were slightly deficient in oxygen and the Pu preparation of ref. 49, in Ba.

$A_2M_2O_7$ (pyrochlore, *Fd3m*, $\bar{3}m$):
$Er_2M_2O_7$: Ge (53), Ti (54), Ru (55), Pt (56), Sn (57), Pb (58).
$Gd_2M_2O_7$: Ge (53), Ti (54), Ru (55), Pt (56), Sn (57) Hf (59), Pb (58). The lattice parameter for Zr varies from *ca.* 10.52 to 10.535 Å, depending on the method of preparation and the firing conditions as well as on the actual degree of order in the structure (fluorite ↔ pyrochlore).[4]
$Sm_2M_2O_7$: Ti (54), Ru (55), Pt (56), Sn (57), Hf (59), Zr (59), Pb (58).

$MSiO_4$ (zircon, $I4_1/amd$, $\bar{4}2m$): Hf (60, 61), Zr (6, 61, 62), Am (24); U, Th (6).

$MGeO_4$ (scheelite, $I4_1/a$, $\bar{4}$): Hf, Zr, Ce, Th (6, 61); Am (24), U (6).

MOS (PbFCl, *P4/nmm*, *4mm*): α-Pu, $Pu_{0.5}U_{0.5}$ (63); U, Th (6); Np (6, 63). The Pa preparation (6, 23) was not stoichiometric.

$M(SO_4)_2.4H_2O$ (*Fddd*, 222): Zr, Ce, Pu (6). (*Pnma*, *m*): Pu, U (6).

$MOCl_2$ (*Pbam*, *m*): Pa (64, 65); Np, U, Th (64).

A_2MX_6 (β-$(NH_4)_2SiF_6$, $P\bar{3}m1$, $\bar{3}m$):
K_2MF_6: Ge, Pt (66); Ti (67), Ru (6).
$(NH_4)_2MF_6$: Si, Ti (6); Ge (66); Sn, Pb (68).
Rb_2MF_6: Pt (66); Ge, Ti, Hf, Zr (6).
Cs_2MF_6: Pt (66); Ti, Ru, Hf, Zr (6).
Cs_2MCl_6: Ce (69), Np (70), Pa (71); Pu, U, Th (6).

K_2MF_6 (K_2PtCl_6, *Fm3m*, *m3m*): Si (6, 72); Ti, Ru (6).

α-K_2MF_6 (cubic): Np (73); U, Th (6).

Rb_2MF_6 (K_2ZrF_6, *Cmcm*, *mm*): U (74, 75); Cm, Am, Pu, Np (74).

$LiMF_5$ ($I4_1/a$, 1): Pu, Np (76, 77); U (77, 78); Pa (77, 79); Cm, Am, Th (77).

$Na_7M_6F_{31}$ ($R\bar{3}$, 1): Zr (80), Pr (81); Pu, Np (76, 77, 82); Pa (77, 79, 82); Cm, Am, U, Th (77, 82).

$BaMF_6$ ($TlSbF_6$, $R\bar{3}m$, $\bar{3}m$): Si (6, 83); Ge, Ti, Ru, Pt, Sn, Pb (6).

AMF_6 (LaF_3, $P\bar{3}c1$, "2"):
$SrMF_6$: U, Th (6, 84); Pu, Ce, Np (84).
$PbMF_6$: U, Th (6, 84); Ce, Np (84).

MF_4 (UF_4, *C2/c*, 2 and 1): Bk (85); Cm, Am, Pu, Np, U, Th (6, 86); Pr (87); Pa (79, 86, 88); Hf, Zr, Tb, Ce (6).

Computations were carried out on the CDC 6400 installation at the Dalhousie Computer Centre using a Fortran program based on a corrected version of the routine originally supplied by Powell and Macdonald (98). This routine allows for errors in both $V^{1/3}$ and $r^{vi}(M^{4+})$ coordinates during the fitting procedure. In order to define a scale for $r^{vi}(M^{4+})$ not all the radii could be allowed to vary; $r^{vi}(Ti^{4+})$ and $r^{vi}(Sn^{4+})$ were therefore fixed at their S.P. values. The refined values r of the radii are listed in Table 1 and the parameters describing the best straight lines for the individual series, in Table 2.

The final set gives good linear correlations for all the series examined (Figs. 1 and 2). The uncertainty limits quoted for the $r^{vi}(M^{4+})$ values are the 1σ values of the least-squares refinement. For the Ti^{4+} and Sn^{4+} radii, which were entered at fixed values, error estimates were unobtainable from the computation. Separate estimates were therefore made for these two radius values by repeating the computation, this time with a different pair of radius values (Ge and Hf) locked at their newly refined values.

The refined set of radii is as self-consistent as can be constructed at present, but it can undoubtedly be improved as more reliable lattice-parameter values for some of the compounds become available. On the other hand, there are $V^{1/3}$ values one can hardly expect to be bettered, yet they do not fit the respective regression lines well enough, *e.g.* $BaTiO_3$, $BaSnO_3$, and some of the transition-element MO_2 rutiles. In these cases the poor fit is inherent and reflects departures from the "normal" degree of ionic character of M in these oxides, or else too large a volume available to the M atom in a rigid structural framework imposed by the size of the anion atoms. In the fluorites of Fig. 2, however, the large deviations of some of the $V^{1/3}$ values from the best straight lines are almost certainly due to insufficient experimental accuracy;[5] occasionally confusion between Å and kX may still exist. Moreover, significant differences commonly occur between lattice-parameter values as determined from powder patterns and those obtained from single-crystal diffractometry, *e.g.* for $LiUF_5$ (77, 78), Rb_2UF_6 (74, 75), $PaOCl_2$ (64, 65). These differences may be real and may result from the vagaries of crystal growth (*cf.* for

[4]C. Ayasse. Unpublished results.

[5]For example, the internal consistency of the available a_0 values for the cubic $A_2{}^+M^{4+}X_6$ halides isostructural with K_2PtCl_6 is surprisingly poor and these series could not be included in the refinement, even though they are quite extensive and otherwise well suited.

TABLE 2. Coefficients of the equations of the best straight lines, $V_1^{1/3} = pr^{vi}(M^{4+}) + q$, in Figs. 1 and 2*

Series	p	$\sigma(p)$	q (Å)	$\sigma(q)$ (Å)
MO_2 (rutile)	1.8483	0.0471	2.0183	0.0305
MO_2 (fluorite)	1.7363	0.1230	1.9251	0.1014
MOS	1.7790	0.2208	2.1122	0.1900
$SrMO_3$	1.5195	0.0461	2.9872	0.0313
$BaMO_3$	1.5237	0.0466	3.0799	0.0319
$Sm_2M_2O_7$	1.2074	0.0373	3.3327	0.0246
$Gd_2M_2O_7$	1.2742	0.0569	3.2725	0.0374
$Er_2M_2O_7$	1.2611	0.0330	3.2346	0.0213
$MSiO_4$ (zircon)	1.4556	0.0629	2.9663	0.0459
$MSiO_4$ (scheelite)	1.3632	0.0567	2.9770	0.0414
$M(SO_4)_2.4H_2O$	1.4314	0.0672	4.8817	0.0502
$MOCl_2$	1.8278	0.3043	2.8772	0.2680
$LiMF_5$	1.7053	0.1617	2.9869	0.1370
$Na_7M_6F_{31}$	1.7154	0.0813	3.1660	0.0628
K_2MF_6 (trigonal)	0.8481	0.0477	4.5826	0.0290
K_2MF_6 (K_2PtCl_6)	0.8189	0.0739	4.7567	0.0413
α-K_2MF_6 (cubic)	1.4772	0.2398	4.6328	0.2104
$(NH_4)_2MF_6$ (trigonal)	0.8512	0.0214	4.7754	0.0139
Rb_2MF_6 (trigonal)	1.1991	0.1057	4.5314	0.0690
Rb_2MF_6 (K_2ZrF_6)	0.8130	0.2693	4.7276	0.2303
Cs_2MF_6 (trigonal)	1.1724	0.1394	4.7744	0.0919
Cs_2MCl_6 (trigonal)	1.6006	0.2206	5.2546	0.1907
$SrMF_6$	0.6546	0.0916	3.1824	0.0796
$BaMF_6$	0.7507	0.0500	4.3791	0.0298
$PbMF_6$	0.5950	0.1038	3.2933	0.0905
MF_4	2.2492	0.1152	2.2874	0.0899

*Use r values of Table 1. V_1, unit-cell volume per one M atom.

example $CuCl_2.2H_2O$ (89) or $K_2CuCl_4.2H_2O$ (90, 91)) or from variable stoichiometry. Compounds of the actinides present yet another problem. Crystal structures containing these α-emitters undergo expansion due to self-irradiation damage, and owing to the strong activity of the shorter-lived nuclides and the very small quantities of material used in the preparation of some of the samples and X-ray specimens, the stoichiometry cannot always be regarded as dependable. In some cases the lattice parameters have been corrected for the effects of radiation damage, but the uncertainty due to possible non-stoichiometry is less tractable.

The present value of $r^{vi}(Tb^{4+})$ is based on three compounds only. The unit-cell volume available for TbF_4 is unreliable and one of the $BaTbO_3$ preparations is stated to have been slightly non-stoichiometric.

For Cf and Po a single $V^{1/3}$ value each were available; the radii were calculated from the equation of the best straight line for the fluorite series. The Po value in particular is uncertain (see above). No suitable oxidic compound could be found for Re^{4+} and this element was therefore not included in the refinement. However, the radius values calculated from $V^{1/3}$ of K_2ReF_6, Rb_2ReF_6, and Cs_2ReF_6 (6) were in close agreement and averaged to 0.662 Å (Fig. 2).

Only the $SrMO_3$ and $BaMO_3$ perovskite series are sufficiently extensive to bridge the gap between the compounds of the large (from Tb on) elements and those of the small ones (up to Sn). Unfortunately both series contain a number of a_0 values of poor accuracy, and so the correlation of the large with the small radii leaves something to be desired.

The MO_2 fluorite series, which has been the mainstay of various $V^{1/3}$ *vs.* r and similar correlations, is of more limited usefulness than is usually thought. It does not include Zr and Hf. Pure cubic ZrO_2 and HfO_2 exist only at very high temperatures (92, 93) or as metastable thin oxide coatings of uncertain stoichiometry on the metals (94). In the former case extrapolation of a_0 to room temperature is of no value, in the latter case accurate information is not available. The $V^{1/3}$ values of the other forms of ZrO_2 and HfO_2 do not fit the fluorite regression line, and extrapolation from cubic solid solutions of other

Can. J. Chem. Downloaded from www.nrcresearchpress.com by 210.87.254.40 on 09/05/12
For personal use only.

Can. J. Chem. Downloaded from www.nrcresearchpress.com by 210.87.254.40 on 09/05/12
For personal use only.

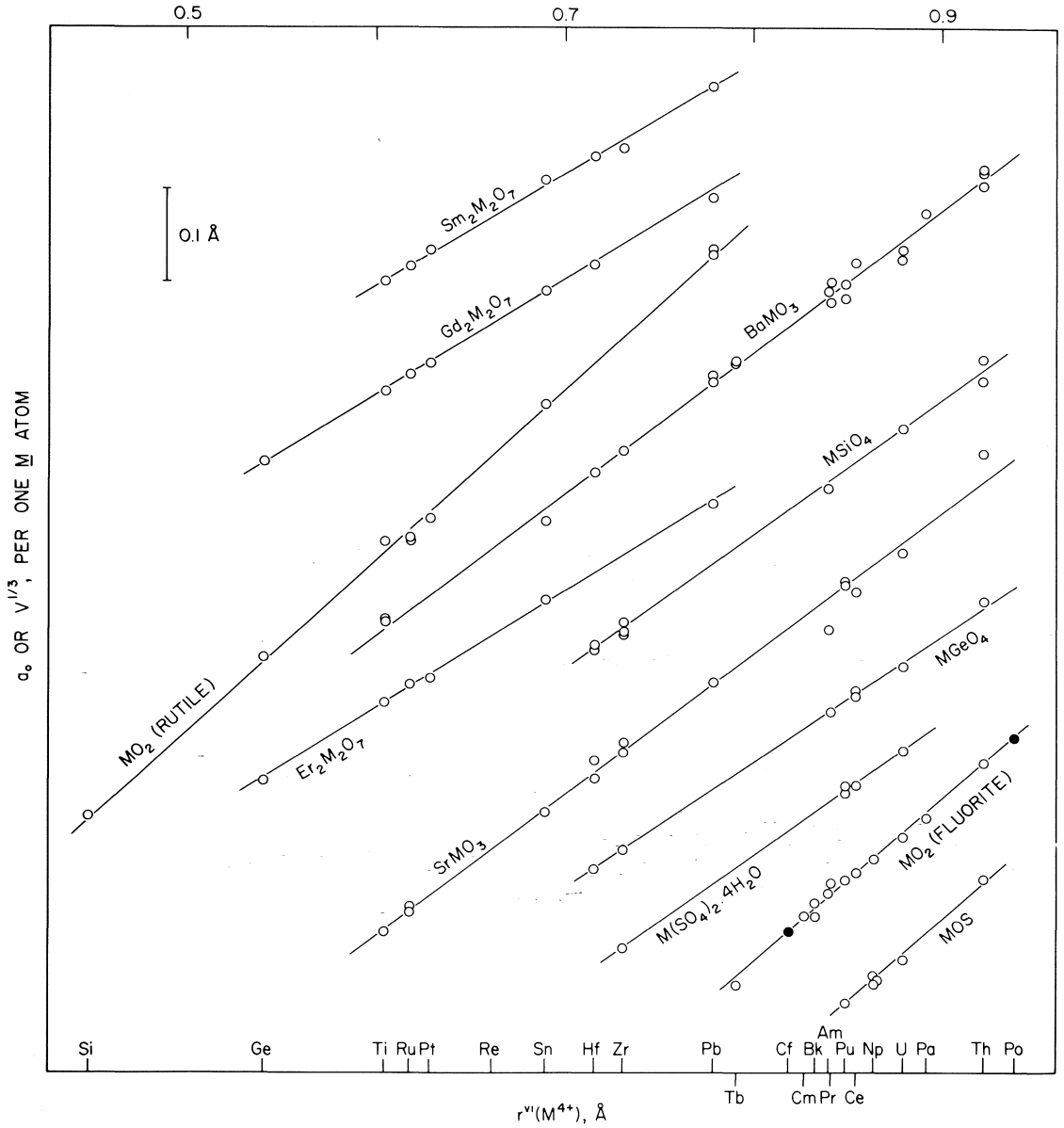

FIG. 1. Plot of a_0 or $V^{1/3}$ of oxidic compounds against $r^{VI}(M^{4+})$ of Table 1. Diameter of circles, 0.01 Å. The equations of the straight lines are specified in Table 2. Full circles, compounds not included in the least-squares refinement (Cf and Po).

oxides in zirconia and hafnia is uncertain. The a_0 values cited for cubic ZrO_2 and HfO_2 by Wyckoff (6) and used by S.P. are over 40 years old (95). They were obtained by extrapolation over a considerable composition range from cubic solid solutions of CeO_2 in ZrO_2 (5.065(10) kX?) and HfO_2 ("probable" value, 5.115(10) kX?) and must be viewed as artefacts of doubtful value for the purpose in hand. This explains the deviation of ZrO_2 from the fluorite plot queried in ref. 96.

The S.P. values for 8-coordination are on the average 0.116 Å higher than the r values of Table 1, notable exceptions being Pb, Tb, and Po. The S.P. values for 6-coordination for Si to Pb agree quite well with ours, with the exception

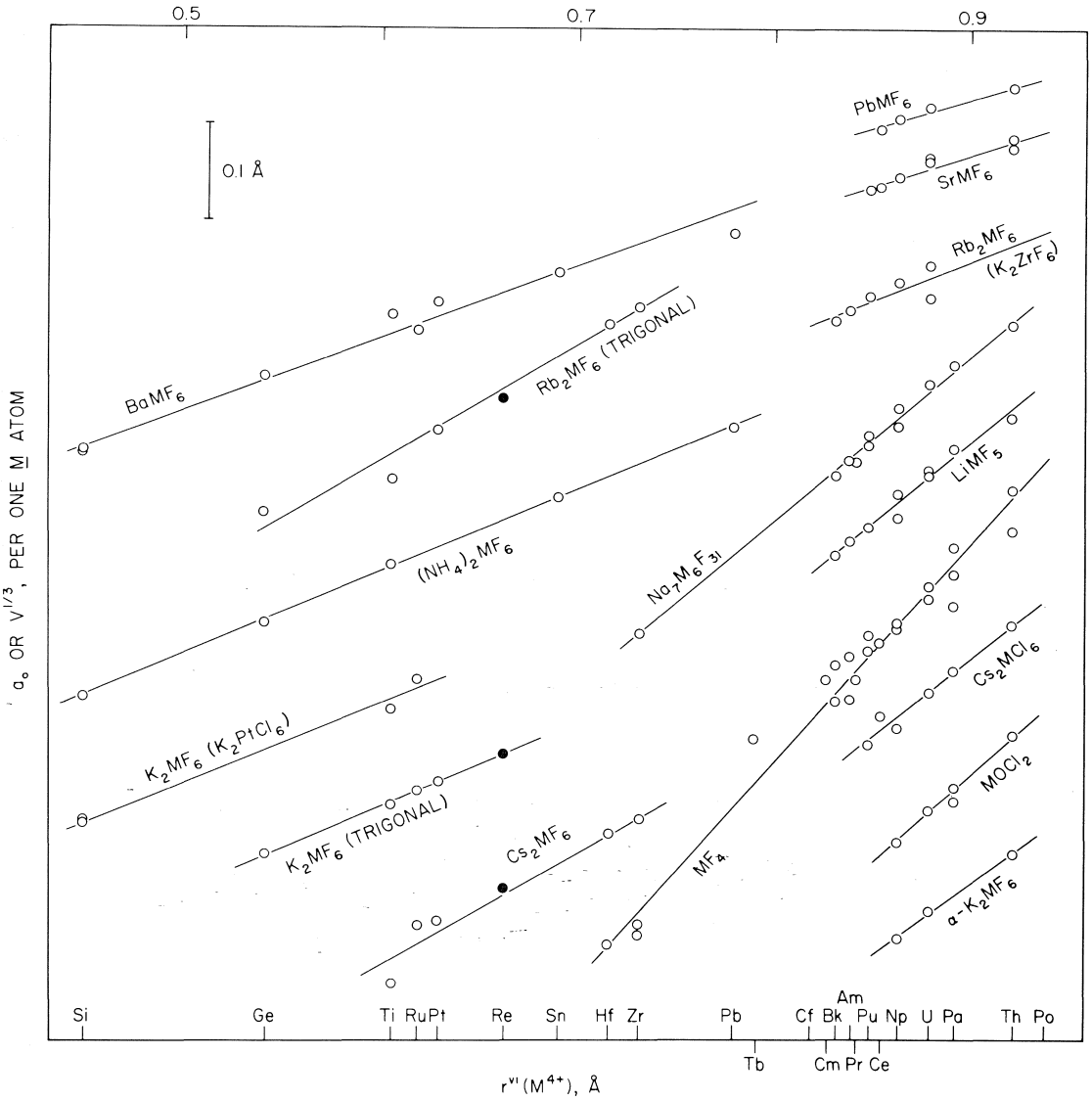

FIG. 2. Plot of a_0 or $V^{1/3}$ of fluorides and chlorides against $r^{vi}(M^{4+})$ of Table 1. Diameter of circles, 0.01 Å. The equations of the straight lines are specified in Table 2. Full circles, compounds not included in the least-squares refinement (Re).

of Si and the value for Re, which was not refined. However, for Tb and Th the differences are much larger.

Adoption of values other than those of S.P. for $r^{vi}(Ti^{4+})$ and $r^{vi}(Sn^{4+})$ would necessitate rescaling of the r values of Table 1 to the new pair of reference points, but the transformed set $r' = mr + n$ would be as consistent with the above aggregate of $V^{1/3}$ data as the r set. Self-consistency is in fact the main claim of the r set to usefulness. The r values can therefore be used to advantage for checking on accuracy of lattice parameters and stoichiometry from $V^{1/3}$ *vs.* r plots (*cf.* discussion in ref. 96). For this purpose radii such as ours, *i.e.* derived directly from the variation of $V^{1/3}$ with r, are preferable to similar sets of numbers derived from interatomic distances by subtracting a constant value for the radius of the anion; the latter propagate the often not inconsiderable uncertainties in positional parameters and suffer from difficulties arising from the anisotropy of the M atoms in sites of symmetry lower than cubic.

The effect of covalency is implicit in any

Can. J. Chem. Downloaded from www.nrcresearchpress.com by 210.87.254.40 on 09/05/12
For personal use only.

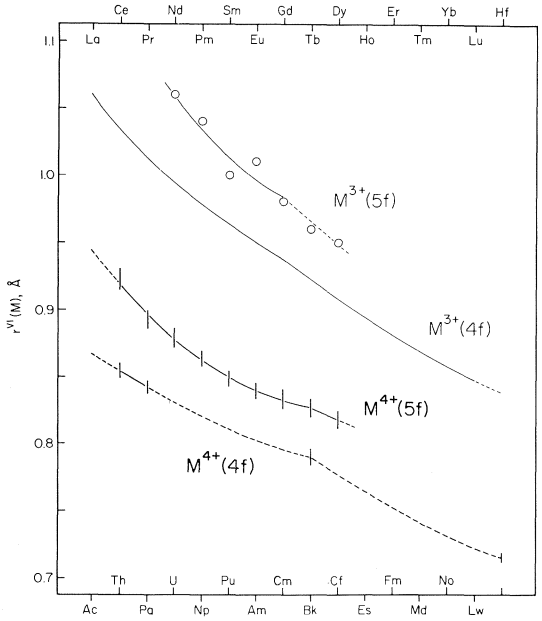

FIG. 3. Effective ionic radii r^{vi}(M) plotted against atomic number. M^{4+}: Table 1. M^{3+}: lanthanons, Templeton and Dauben (*cf.* ref. 3); actinides, Shannon and Prewitt (3) (open circles). The curves are sections of parabolas obtained by least-squares fitting wherever sufficient points are available. The length of the vertical lines represents the 1σ interval resulting from the composite least-squares fit including all the series of Figs. 1 and 2.

empirical set of "ionic" radii. If the variation with M of the degree of covalency in an isostructural series significantly differs from that in the series of Figs. 1 and 2, discrepancies can be expected. Search for a set of "universal" $r^{vi}(M^{4+})$ to be used for prediction of interatomic distances in the most general circumstances is bound to prove illusory.

When the $r^{vi}(M^{4+})$ values of the actinides are plotted against the atomic number (Fig. 3), the resulting curve for Th to Bk is satisfactorily fitted to a parabola[6] and shows a cusp at Bk. This cusp is typical of half-filled shells: it is well known from the Ln^{3+} series where it occurs at Gd (Fig. 3), and in the 3d series it takes the form of a local maximum at d^5 in the curves for high-spin M^{2+} and M^{3+}. In the M^{3+}(5f) series its existence at Cm cannot be demonstrated as convincingly because of the insufficient accuracy of the available r^{vi} values (*cf.* Fig. 3). At present the existence of the cusp in the curve for M^{4+}(5f) depends on the r^{vi} value for Cf^{4+}. This value has been derived from a *single* unit-cell volume, that for the fluorite $^{249}CfO_2$ ($t_{\frac{1}{2}}$ = 360 years), and so the cusp might be regarded as spurious. However, any subsequent revision of $r^{vi}(Cf^{4+})$ is expected to produce merely a change in the initial slope of the second half of the curve while preserving the cusp.

On the assumption that the branches of the r^{vi} *vs.* atomic number curves of Fig. 3 are reasonably fitted by sections of parabolas, the r^{vi} values for Ce^{4+}, Pr^{4+}, and Tb^{4+} define the first branch of the M^{4+}(4f) curve. Assuming further that the difference in the r^{vi} values for M^{4+}(4f) and M^{3+}(4f) diverges linearly from Tb^{4+} to Hf^{4+}, the second branch of the M^{4+}(4f) is obtained. The resulting tentative curve makes it possible to estimate r^{vi} values for Nd^{4+} and Dy^{4+} (Table 1); stabilization of these oxidation states in mixed oxide perovskites has recently been announced by Jacobson *et al.* (97).

NOTE ADDED IN PROOF: Professor K. W. Bagnall has drawn our attention to the recently published lattice parameters of CfF_4 (99). Inclusion of this compound increases the $r^{vi}(Cf^{4+})$ value slightly, from 0.818 to 0.821 Å. The value which would be expected if the Cf^{4+} point were on the continuation of the Th^{4+} – Bk^{4+} curve of Fig. 3 is 0.827 Å. The new r^{vi}-(Cf^{4+}) value thus still supports the existence of a cusp at Bk^{4+}.

Thanks are due to Dr. H. Brunner for advice on refinement techniques. The costs of computing were defrayed by the National Research Council of Canada through a grant in aid of research.

[6]The smoothed r'' values from this plot are compared in Table 1 with the corresponding r values. The agreement of r'' and r is excellent, within $\pm$0.003 Å except for Pa. This suggests that $r(Pa^{4+})$ is too low. The difference between the high and the low values of $V^{1/3}$ (per one M atom) is 0.061 Å for PaF_4 and 0.013 Å for $PaOCl_2$. Discounting the two low values would raise $r(Pa^{4+})$ to about 0.895 Å and bring the radius closer to $r''(Pa^{4+})$. The uncertainty of the available $a(BaPaO_3)$ value is estimated to be $\pm$0.02 Å (51).

1. C.-H. HUANG, O. KNOP, D. A. OTHEN, F. W. D. WOODHAMS, and R. A. HOWIE. Can. J. Chem. To be published.
2. F. W. D. WOODHAMS, R. A. HOWIE, and O. KNOP. Can. J. Chem. In press.
3. R. D. SHANNON and C. T. PREWITT. Acta Cryst. B **25**, 925 (1969); B **26**, 1046 (1970).
4. S. M. STISHOV and N. V. BELOV. Dokl. Akad. Nauk SSSR, **143**, 951 (1962).
5. E. C. T. CHAO, J. J. FAHEY, J. LITTLER, and D. J. MILTON. J. Geophys. Res. **67**, 419 (1962).

Can. J. Chem. Downloaded from www.nrcresearchpress.com by 210.87.254.40 on 09/05/12
For personal use only.

Can. J. Chem. Downloaded from www.nrcresearchpress.com by 210.87.254.40 on 09/05/12
For personal use only.

6. R. W. G. WYCKOFF. Crystal structures. 2nd ed. Vols. 1–4. Interscience, New York. 1963–1968.
7. H. E. SWANSON, N. T. GILFRICH, M. I. COOK, R. STINCHFIELD, and P. C. PARKS, U.S. Natl. Bur. Stand. Circ. 539, **8** (1959).
8. H. E. SWANSON, H. F. MCMURDIE, M. C. MORRIS, and E. H. EVANS. U.S. Natl. Bur. Stand. Monogr. 25, **7** (1969).
9. C.-E. BOMAN. Acta Chem. Scand. **24**, 116 (1970).
10. D. B. ROGERS, R. D. SHANNON, A. W. SLEIGHT, and J. L. GILSON. Inorg. Chem. **8**, 841 (1969).
11. R. D. SHANNON. Solid State Commun. **6**, 139 (1968).
12. H. E. SWANSON and E. TATGE. U.S. Natl. Bur. Stand. Circ. 539, **1** (1953).
13. J. S. WHITE, JR. Miner. Rec. **1**, 75 (1970).
14. J. LECIEJEWICZ and I. PADLO. Naturwiss. **49**, 373 (1962).
15. A. F. CLIFFORD. Proc. 3rd Conf. Rare Earth Res. 45 (1964).
16. G. BRAUER and B. PFEIFFER. Angew. Chem. **74**, 716 (1962); Proc. 4th Conf. Rare Earth Res. 573 (1965).
17. R. D. BAYBARZ, R. G. HAIRE, and J. A. FAHEY. J. Inorg. Nucl. Chem. **34**, 557 (1972).
18. J. R. PETERSON and B. B. CUNNINGHAM. Inorg. Nucl. Chem. Lett. **3**, 327 (1967).
19. R. G. HAIRE. Proc. 10th Rare Earth Res. Conf., Carefree, Arizona, April 30 – May 3, 1973. *Edited by* C. J. Kevane and T. Moeller. CONF-730402-Pl, USAEC, Tech. Inf. Center, Oak Ridge, Tenn. p. 882.
20. J. R. PETERSON and J. FUGER. J. Inorg. Nucl. Chem. **33**, 4111 (1971).
21. M. NOÉ and J. FUGER. Inorg. Nucl. Chem. Lett. **7**, 421 (1971).
22. W. C. MOSLEY. J. Inorg. Nucl. Chem. **34**, 539 (1972).
23. P. A. SELLERS, S. FRIED, R. E. NELSON, and W. H. ZACHARIASEN. J. Am. Chem. Soc. **76**, 5935 (1954).
24. C. KELLER. Adv. Chem. Ser. **71**, 228 (1967).
25. B. RILEY. Sci. Ceram. **5**, 83 (1970).
26. R. N. R. MULFORD and F. H. ELLINGER. J. Phys. Chem. **62**, 1466 (1958).
27. D. J. M. BEVAN, W. W. BARKER, and R. L. MARTIN. Proc. 4th Conf. Rare Earth Res. 441 (1965).
28. K. SUZUKI, K. MARUYA, and T. KUBOTA. Chem. Abstr. **61**, 14137g (1964).
29. L. N. GROSSMAN, L. E. LEWIS, and D. M. ROONEY. J. Nucl. Mat. **21**, 302 (1967).
30. I. F. FERGUSON and P. G. T. FOGG. J. Chem. Soc. 3679 (1957).
31. J. FAVA, G. LE FLEM, M. DEVALETTE, L. RABARDEL, J.-P. COUTURES, M. FOËX, and P. HAGENMULLER. Rev. Int. Hautes Temp. Refract. **8**, 305 (1971).
32. T. STCHOUZKOY, R. MUXART, H. PEZERAT, and J. DHERS. Rev. Chim. Miner. **5**, 1085 (1968).
33. K. W. BAGNALL and R. W. M. D'EYE. J. Chem. Soc. 4295 (1954).
34. H. E. SWANSON, R. K. FUYAT, and G. M. UGRINIC. U.S. Natl. Bur. Stand. Circ. 539, **3** (1954).
35. D. D. KHANOLKAR. Curr. Sci. (India), **30**, 52 (1961).
36. H. E. SWANSON, H. F. MCMURDIE, M. C. MORRIS, and E. H. EVANS. U.S. Natl. Bur. Stand. Monogr. 25, **8** (1970).
37. V. N. STREKALOVSKII, Z. S. VOLCHENKOVA, and S. F. PAL'GUEV. Izv. Akad. Nauk SSSR, Neorg. Mater. **2**, 1230 (1966); Inorg. Mater. **2**, 1049 (1966).
38. H. E. SWANSON, M. I. COOK, T. ISAACS, and E. H. EVANS. U.S Natl. Bur. Stand. Circ. 539, **9** (1960).
39. C. KELLER. Nukleonik, **4**, 271 (1962).
40. R. D. SHANNON. J. Solid State Chem. **3**, 184 (1971).
41. D. M. CHACKRABURTTY and N. C. JAYADEVAN. Ind. J. Phys. **38**, 585 (1964).
42. C. BRISI. Ric. Sci., Suppl. **30**, (12), 2376 (1960).
43. H. E. SWANSON, M. C. MORRIS, E. H. EVANS, and L. ULMER. U.S. Natl. Bur. Stand. Monogr. 25, **3** (1964).
44. G. TILLOCA and M. PEREZ Y JORBA. Rev. Int. Hautes Temp. Refract. **1**, 331 (1964).
45. R. D. SHANNON and P. E. BIERSTEDT. J. Am. Ceram. Soc. **53**, 635 (1970).
46. T. NITTA, K. NAGASE, S. HAYAKAWA, and Y. IIDA. J. Am. Ceram. Soc. **48**, 642 (1965).
47. A. J. JACOBSON, B. C. TOFIELD, and B. E. F. FENDER. Acta Cryst. B **28**, 956 (1972).
48. E. BANKS, S. J. LAPLACA, W. KUNNMANN, L. N. CORLISS, and J. M. HASTINGS. Acta Cryst. B **28**, 3429 (1972).
49. D. M. CHACKRABURTTY, N. C. JAYADEVAN, and C. K. SIVARAMAKRISHNAN. Acta Cryst. **16**, 1060 (1963).
50. W. RÜDORFF and F. PFITZER. Z. Naturforsch. **9**b, 568 (1954).
51. C. KELLER. J. Inorg. Nucl. Chem. **27**, 321 (1965).
52. S. BRADSTREET and Y. HARADA. U. S. DEPT. Com., Office Tech. Serv., PB Rept. **160**, 623 (1960).
53. R. D. SHANNON and A. W. SLEIGHT. Inorg. Chem. **7**, 1649 (1968).
54. O. KNOP, F. BRISSE, and L. CASTELLIZ. Can. J. Chem. **47**, 971 (1969).
55. F. BERTAUT, F. FORRAT, and M.-C. MONTMORY. C.R. **249**, 829 (1959).
56. A. W. SLEIGHT. Mater. Res. Bull. **3**, 699 (1968).
57. F. BRISSE and O. KNOP. Can. J. Chem. **46**, 859 (1968).
58. A. W. SLEIGHT. Inorg. Chem. **8**, 1807 (1969).
59. F. BRISSE. Ph.D. Thesis. Dalhousie University, Halifax, Nova Scotia. 1967.
60. D. J. SALT and G. HORNUNG. J. Am. Ceram. Soc. **50**, 549 (1967).
61. G. BAYER. J. Less-Common Met. **26**, 255 (1972).
62. H. E. SWANSON, R. K. FUYAT, and G. M. UGRINIC. U.S. Natl. Bur. Stand. Circ. 539, **4** (1955).
63. J.-P. MARCON. C.R. C**264**, 1475 (1967); C**265**, 235 (1967).
64. K. W. BAGNALL, D. BROWN, and J. F. EASEY. J. Chem. Soc. A, 288 (1968).
65. R. P. DODGE, G. S. SMITH, Q. JOHNSON, and R. E. ELSON. Acta Cryst. B **24**, 304 (1968).
66. H. E. SWANSON, N. T. GILFRICH, and M. I. COOK. U.S. Natl. Bur. Stand. Circ. 539, **6** (1956).
67. H. E. SWANSON, N. T. GILFRICH, and M. I. COOK. U.S. Natl. Bur. Stand. Circ. 539, **7** (1957).
68. R. L. DAVIDOVICH and T. A. KAIDALOVA. Zh. Neorg. Khim. **16**, 2539 (1971); (Engl. transl.) **16**, 1354 (1971).
69. T. KAATZ and M. MARCOVICH. Acta Cryst. **21**, 1011 (1966).
70. K. W. BAGNALL and J. B. LAIDLER. J. Chem. Soc. A, 516 (1966).
71. D. BROWN and P. J. JONES. J. Chem. Soc. A, 243 (1967).
72. J. A. SKARULIS and J. B. SEIBERT. J. Chem. Eng. Data, **15**, 37 (1970).
73. C. E. THALMAYER and D. COHEN. Adv. Chem. Ser. **71**, 256 (1967).
74. T. K. KEENAN. Inorg. Nucl. Chem. Lett. **3**, 463 (1967).
75. F. H. KRUSE. J. Inorg. Nucl. Chem. **33**, 1625 (1971).

76. C. KELLER and H. SCHMUTZ. Inorg. Nucl. Chem. Lett. **2**, 355 (1966).
77. R. A. PENNEMAN, T. K. KEENAN, and L. B. ASPREY. Adv. Chem. Ser. **71**, 248 (1967).
78. G. BRUNTON. Acta Cryst. **21**, 814 (1966).
79. L. B. ASPREY, F. H. KRUSE, and R. A. PENNEMAN. Inorg. Chem. **6**, 544 (1967).
80. J. H. BURNS, R. D. ELLISON, and H. A. LEVY. Acta Cryst. B **24**, 230 (1968).
81. L. B. ASPREY and T. K. KEENAN. J. Inorg. Nucl. Chem. **16**, 260 (1961).
82. T. K. KEENAN. Inorg. Nucl. Chem. Lett. **2**, 211 (1966).
83. H. E. SWANSON, M. C. MORRIS, and E. H. EVANS. U.S. Natl. Bur. Stand. Monogr. 25, **3** (1964).
84. M. SALZER (1966). Quoted in D. Brown, Halides of the lanthanides and actinides. Wiley-Interscience, London. p. 77 and ref. 303.
85. L. B. ASPREY and T. K. KEENAN. Inorg. Nucl. Chem. Lett. **4**, 537 (1968).
86. T. K. KEENAN and L. B. ASPREY. Inorg. Chem. **8**, 235 (1969).
87. L. B. ASPREY, J. S. COLEMAN, and M. J. REISFELD. Adv. Chem. Ser. **71**, 122 (1967).
88. D. BROWN and P. J. JONES. J. Chem. Soc. A, 719 (1967).
89. Å. ENGBERG. Acta Chem. Scand. **24**, 3510 (1970).
90. R. CHIDAMBARAM, Q. O. NAVARRO, A. GARCIA, K. LINGGOATMODJO, S.-C. LIN, I.-H. SUH, A. SEQUEIRA, and S. SRIKANTA. Acta Cryst. B **26**, 827 (1970).
91. H. E. SWANSON, H. F. MCMURDIE, M. C. MORRIS, E. H. EVANS, B. PARETZKIN, J. D. DEGROOT, and S. J. CARMEL. U.S. Natl. Bur. Stand. Monogr. 25, **9**, 34 (1971).
92. A. G. BOGANOV, V. S. RUDENKO, and L. P. MAKAROV. Dokl. Akad. Nauk SSSR, **160**, 1065 (1965).
93. D. K. SMITH and C. F. CLINE. J. Am. Ceram. Soc. **45**, 249 (1962).
94. M. DENOUX. C.R. **260**, 5003 (1965).
95. L. PASSERINI. Gazz. Chem. Ital. **60**, 762 (1930).
96. R. D. SHANNON and C. T. PREWITT. J. Inorg. Nucl. Chem. **32**, 1427 (1970).
97. A. J. JACOBSON, B. C. TOFIELD, and B. E. F. FENDER. Proc. 10th Rare Earth Res. Conf., Carefree, Arizona. April 30 – May 3, 1973. *Edited by* C. J. Kevane and T. Moeller. CONF-730402-P1, USAEC, Tech. Inf. Center, Oak Ridge, Tenn. p. 194.
98. D. R. POWELL and J. R. MACDONALD. Comput. J. **15**, 148 (1972).
99. R. G. HAIRE and L. B. ASPREY. Inorg. Nucl. Chem. Lett. **9**, 869 (1973).

Can. J. Chem. Downloaded from www.nrcresearchpress.com by 210.87.254.40 on 09/05/12
For personal use only.

The Crystal Structure of Tripotassium bis(Oxalato)dioxovanadate(V) Trihydrate

Date of receipt of article: November 9, 1973.

R. E. DREW, F. W. B. EINSTEIN,[1] AND SUSAN E. GRANSDEN

Department of Chemistry, Simon Fraser University, Burnaby 2, British Columbia V5A 1S6

R. E. DREW, F. W. B. EINSTEIN, and SUSAN E. GRANSDEN. Can. J. Chem. **52**, 2184 (1974).

The potassium salt of bis(oxalato)dioxovanadate(V), $K_3[V(O)_2(C_2O_4)_2]\cdot 3H_2O$ crystallizes in a triclinic lattice with space group $P\bar{1}$. Two formula units make up the asymmetric unit which has dimensions $a = 7.851(2)$, $b = 11.603(2)$, $c = 7.778(2)$ Å, $\alpha = 94.26(1)$, $\beta = 110.07(1)$, $\gamma = 91.25(1)°$. Three-dimensional single-crystal X-ray diffraction counter data was refined by full-matrix least-squares techniques to $R = 0.039$. Hydrogen atomic parameters were included in the 213 variables used. A total of 3869 reflections was measured of which 85.4% were classed observed by the criterion $I \geq 2.3\sigma$. The 563 unobserved reflections were included in the final cycle of structure-factor calculations but were not used in the refinement.

The anion has irregular octahedral geometry with the two double-bonded oxygen atoms (V=O, 1.628(2) and 1.639(2) Å) *cis* to each other. The V—O (oxalate) bonds are of two significantly different types: (*i*) those that are *trans* to each other (2.009(2), 1.995(2) Å) and (*ii*) those that are *trans* to oxo ligands (2.158(2), 2.230(2) Å). The non-coplanar oxalate ligands are twisted about the C—C single bonds (1.550(3) and 1.551(4) Å), while the terminal C—O bonds average to 1.226(9) Å, and the inner ones to 1.274(16) Å. The anions exhibit an approximate non-crystallographic two-fold axis, though distortions from regularity are found. These distortions may best be attributed to hydrogen bonding with the three water molecules and, to a much lesser extent, by contact with the potassium ions.

R. E. DREW, F. W. B. EINSTEIN et SUSAN E. GRANSDEN. Can. J. Chem. **52**, 2184 (1974).

Le sel de potassium du bis(oxalato)dioxovanadate(V), $K_3[V(O)_2(C_2O_4)_2]\cdot 3H_2O$ cristallise dans un réseau triclinique avec un groupe d'espace $P\bar{1}$. Deux unités forment le motif asymétrique qui a pour dimensions $a = 7.851(2)$, $b = 11.603(2)$, $c = 7.778(2)$ Å, $\alpha = 94.26(1)$, $\beta = 110.07(1)$, $\gamma = 91.25(1)°$. Les données du compteur de diffraction de rayons-X du cristal unique tridimensionnel sont raffinée par les techniques de matrice entière de moindres carrés à $R = 0.039$. Les paramètres de l'hydrogène atomique sont compris dans les 213 variables utilisées. Un total de 3869 réflexions sont mesurées parmi lesquelles 85.4% sont classées d'après le critère $I \geq 2.3\sigma$. Les 565 réflexions non-observées sont comprises dans le cycle final des calculs du facteur de structure mais ne sont pas utilisées dans le raffinement.

L'anion a une géométrie octaédrique irrégulière avec deux atomes d'oxygène doublement liés (V=O, 1.628(2) et 1.639(2) Å) en position *cis*. Les liens V—O (oxalates) sont de deux types notablement différents: (*i*) ceux qui sont *trans* l'un par rapport à l'autre (2.009(2), 1.995(2) Å) et (*ii*) ceux qui sont *trans* par rapport aux ligands oxo (2.158(2), 2.30(2) Å). Les ligands oxalates non-coplanaires sont enroulés autour des liaisons simples C—C (1.550(3) et 1.551(4) Å), alors que la longueur moyenne des liens terminaux C—O est de 1.226(9) Å et ceux de l'intérieur de 1.274(16) Å. Les anions représentent un axe approximatif, non-cristallographique, d'ordre 2, bien que des distorsions par rapport à la régularité soient trouvées. Ces distorsions sont le mieux attribuées aux liaisons d'hydrogène avec trois molécules d'eau et, dans une moindre mesure au contact avec les ions potassium. [Traduit par le journal]

Introduction

In an attempt to further study the structural chemistry of the peroxovanadates (1), crystals of what was initially thought to be the monoperoxovanadate salt $K_3[VO(O_2)(C_2O_4)_2]\cdot 2H_2O$ were prepared. The bright red color, usually characteristic of the monoperoxo compound, and the approximate agreement between calculated and observed densities (2.16 and 2.20(5) g/cm^3, respectively), led us to believe that the expected product had been obtained. Single-crystal diffraction studies however, revealed the compound to be $K_3[V(O)_2(C_2O_4)_2]\cdot 3H_2O$.

Experimental

Preparation

Crystals were prepared by reacting divanadium pentoxide, V_2O_5 (0.9094 g, 5 mmol) with oxalic acid (1.2604 g, 10 mmol), potassium oxalate (1.8424 g, 10 mmol), and potassium hydroxide (0.5611 g, 10 mmol) in 40 ml of 15% H_2O_2. The resulting deep red solution was allowed to stand until the chunky orange–red crystals formed. The crystal used for data collection was ground to an approxi-

[1]Author to whom correspondence should be addressed.

Can. J. Chem. Downloaded from www.nrcresearchpress.com by 210.87.254.42 on 09/05/12
For personal use only.

Can. J. Chem. Downloaded from www.nrcresearchpress.com by 210.87.254.42 on 09/05/12
For personal use only.

mate sphere with extreme dimensions varying between 0.60 and 0.50 mm.

Data Collection

Precession and Weissenberg photographs of a number of reciprocal lattice layers, which were not conveniently related to the final reduced cell chosen, indicated that the salt crystallized in a triclinic lattice, with space group $P\bar{1}$. Precise cell parameters were determined by least-squares refinement of 30 reflections in the range $54° < 2\theta < 60°$ measured on the computer controlled Picker four-circle diffractometer ($\lambda MoK\alpha_1 = 0.70926$ Å). The density was measured in toluene at 22 °C, using a berman balance. Crystal data are:

$K_3[V(O)_2(C_2O_4)_2]\cdot 3H_2O$ f.w. = 430.3
Triclinic, $a = 7.851(2)$, $b = 11.603(2)$, $c = 7.778(2)$ Å, $\alpha = 94.26(1)°$, $\beta = 110.07(1)°$, $\gamma = 91.25(1)°$, $V = 662.85$ Å^3, $\rho_o = 2.20(5)$ g/cm^3, $\rho_c = 2.16$ g/cm^3, $Z = 2$, $F(000) = 206$, $T = 22$ °C, $\mu MoK\alpha = 20.4$ cm^{-1}.

The intensity of 3869 unique reflections was measured and 563 were classed unobserved by the criterion $I < 2.3\sigma$; $\sigma = \sqrt{N}$ where N is the scan count plus the total normalized background count. The unobserved reflections were not used in the least-squares refinement although they were included in the final structure-factor calculation. Data was collected within the sphere $2\theta < 60°$ at a scan speed of 2°/min in 2θ with a θ–2θ scan width of $1.05 + (180/\pi)(2 \tan\theta)(\delta\lambda/\lambda)°$. The background intensity was determined by the normalization of two 10 s stationary background counts measured at the scan limits. The take-off angle was 2.5° and the crystal was positioned 28 cm from the detector. Niobium-filtered MoKα radiation was used. Two standard reflections were measured every 70 reflections. No systematic change in their intensity was apparent and the largest departure from their average was only 2.8%. A very small splitting of certain reflections led us to suspect a possible crack or fissure in the crystal, but careful remeasurement of selected intensities indicated the integrated scan intensities were unaffected.

No corrections for spherical absorption were made since for $\mu r = 0.60$, the maximum angular change would be a 3% decline in intensity. Lorentz and polarization factors were applied to the data and structure factor amplitudes derived. Normalized structure factors were calculated and E statistics suggested a centrosymmetric structure.

Determination and Refinement of Structure

The structure was solved using symbolic addition techniques (2, 3). The origin was fixed by arbitrarily assigning phases to three of the stronger E's,

3	−9	1	($E = 3.200$)
−3	12	0	($E = 3.148$)
4	−3	4	($E = 2.974$)

and the symbolic addition procedure was used to complete the phasing. The procedure led to two promising alternative solutions and one of these yielded a satisfactory electron density map. Two cycles of structure-factor least-squares refinement followed by electron density difference maps yielded the remaining atomic positions. Two more cycles of full-matrix refinement, including all non-hydrogen atoms, brought the conventional R value[2] down to 0.074. Additional refinement and another difference map showed clear indications of anisotropic motion of the potassium, vanadium, and oxygen atoms in the anion. In the subsequent refinement these atoms were given anomalous scattering factors, and anisotropic thermal motion parameters were varied, the R value immediately dropped to 0.050 ($R_w = 0.067$).[3] The next two difference maps showed the hydrogen atoms as major features. These were allowed to refine and the R decreased to 0.045. All three water oxygen atoms were allowed to move anisotropically and several more cycles of refinement were done using counter weights. (Prior to this, unit weights had been used.) Shifts in the final cycle were not larger than 0.05σ in magnitude, and the conventional R value was 0.039; R_w (including unobserveds) = 0.053. The scattering factors for the nonhydrogen atoms, including anomolous scattering, were taken from ref. 4, while the scattering factors for the hydrogen atoms were taken from a table of Stewart *et al.* (5). The function minimized was $\Sigma w(|F_o| - |F_c|)^2$.

The final electron density difference map revealed no significant features. The largest feature was a trough of −0.31(12) e/Å^3 near the vanadium atom, followed by some small peaks near oxalate oxygen atoms.

Results

Attempts to describe the anion as a whole, each oxalate group, or only those atoms bonded directly to the vanadium atom, as a rigid body (6), indicated that none of these groups can be described in this manner. Mean planes through the oxalate groups and through the oxygen atoms coordinated to the vanadium were examined. None of these groups are coplanar within the precision of the structure determination.

The final positional and thermal parameters are listed in Table 1, while the interatomic distances and angles are listed in Table 2. Errors in the interatomic distances and angles were calculated from the inverse matrix and include correlation between atomic parameters and errors in the cell dimensions. The structure is illustrated by the packing diagram, Fig. 1, in which one anion is represented by 50% probability thermal ellipsoids. A selection of the best (non-planar) weighted least-squares planes are given in Table 3. Calculations were carried out on an IBM 370/155 using programs listed in ref. 1.

Discussion

The $[V(O)_2(C_2O_4)_2]^{3-}$ anion has a slightly irregular octahedral geometry in which the two oxo ligands are *cis* to each other. As previously discussed by Hoard and co-workers (7), these two oxygens have short V—O bonds (average =

[2]The R value is defined as $\Sigma(|F_o| - |F_c|)/\Sigma|F_o|$.

[3]The R_w value is defined as $[\Sigma w(|F_o| - |F_c|)^2/\Sigma wF_o^2]^{1/2}$.

Can. J. Chem. Downloaded from www.nrcresearchpress.com by 210.87.254.42 on 09/05/12
For personal use only.

TABLE 1. Final atomic parameters

(*a*) Fractional coordinates*

Atom	*x*	*y*	*z*
V	18601(5)	29257(3)	15450(5)
K(1)	−72510(8)	47963(5)	57086(8)
K(2)	−73112(7)	22797(4)	15893(7)
K(3)	3240(8)	17253(5)	58820(8)
O(1)	−72(3)	3518(2)	3169(3)
O(2)	−3411(3)	2857(2)	2510(3)
O(3)	−857(3)	1363(2)	1933(3)
O(5)	−3679(3)	1804(2)	−868(3)
O(7)	−1280(3)	−525(2)	1108(3)
O(9)	−4006(3)	−34(2)	−2070(3)
C(1)	−1684(4)	474(2)	856(3)
C(3)	−3286(3)	760(2)	−859(3)
O(4)	−2958(3)	4292(2)	202(3)
O(6)	−600(3)	3016(2)	−512(3)
O(8)	−3402(3)	5238(2)	−2296(3)
O(10)	−994(4)	3765(2)	−3162(3)
C(2)	−2674(3)	4499(2)	−1287(4)
C(4)	−1299(4)	3696(2)	−1731(4)
O(W1)	−6813(3)	3200(3)	−1558(3)
O(W2)	−5204(4)	2642(3)	5270(4)
O(W3)	−7463(4)	−24(3)	5130(4)
H(11)	−666(8)	385(5)	−103(8)
H(12)	−582(7)	288(5)	−127(7)
H(21)	−497(8)	215(5)	607(8)
H(22)	−435(7)	253(5)	490(7)
H(31)	−712(7)	13(4)	423(7)
H(32)	−645(6)	−8(4)	589(6)

*Fractional atomic coordinates $\times 10^5$ for V and K, $\times 10^4$ for O and C, and $\times 10^3$ for H.

(*b*) Thermal motion parameters ($\times 10^4$)

Atom	U_{11}*	U_{22}	U_{33}	U_{12}	U_{13}	U_{23}
V	219(2)	235(2)	222(2)	5(1)	23(1)	−15(1)
K(1)	360(3)	274(3)	325(3)	20(2)	−52(2)	1(2)
K(2)	298(3)	259(2)	268(2)	21(2)	−1(2)	3(2)
K(3)	424(3)	277(3)	275(3)	30(2)	4(2)	38(2)
O(1)	339(9)	368(10)	278(9)	−111(8)	11(7)	−22(7)
O(2)	337(10)	369(10)	457(11)	−32(8)	175(9)	−43(8)
O(3)	291(8)	243(8)	205(7)	33(6)	−37(6)	0(6)
O(5)	298(9)	246(8)	304(9)	63(7)	−70(7)	7(7)
O(7)	505(11)	239(8)	281(9)	65(8)	−14(8)	42(7)
O(9)	390(10)	293(9)	284(9)	17(7)	−82(7)	−60(7)
C(1)	263(11)	261(10)	157(9)	11(8)	17(8)	15(8)
C(3)	234(10)	256(10)	212(10)	11(8)	5(8)	9(8)
O(4)	305(9)	277(8)	375(10)	88(7)	123(8)	19(7)
O(6)	298(9)	341(4)	298(9)	150(7)	88(7)	102(7)
O(8)	329(9)	267(4)	474(11)	110(7)	54(8)	99(8)
O(10)	722(15)	566(13)	319(10)	363(12)	212(10)	165(9)
C(2)	199(10)	200(10)	322(12)	11(8)	3(9)	−18(8)
C(4)	282(11)	248(11)	233(10)	88(9)	10(9)	4(8)
O(W1)	322(10)	431(12)	397(11)	−10(9)	99(9)	−3(9)
O(W2)	478(14)	640(16)	322(11)	60(11)	53(10)	49(10)
O(W3)	336(11)	734(16)	358(11)	8(10)	48(10)	92(11)

*Anisotropic thermal parameters. The form of the anisotropic thermal ellipsoid is: $\exp[-2\pi^2(a^{*2}h^2U_{11} + b^{*2}k^2U_{22} + c^{*2}l^2U_{33} + 2a^*b^*hkU_{12} + 2a^*c^*hlU_{13} + 2b^*c^*klU_{23})]$.

TABLE 1. (*Concluded*)

Atom	U_{iso}† (× 10^2)	Atom	U_{iso}† (× 10^2)
H(11)	11(2)	H(12)	8(2)
H(21)	11(2)	H(22)	9(2)
H(31)	9(2)	H(32)	6(2)

†Isotropic thermal parameters. The expression for the thermal sphere is: $\exp[-8\pi^2\bar{U}^2\sin^2\theta/\lambda^2)]$.

TABLE 2. Interatomic distances and angles

(*a*) Bonded contacts

Bond	Distance (Å)	Bond	Distance (Å)
V—O(1)	1.628(2)	V—O(2)	1.639(2)
V—O(3)	1.995(2)	V—O(4)	2.009(2)
V—O(5)	2.230(2)	V—O(6)	2.158(2)
C(1)—O(3)	1.287(3)	C(2)—O(4)	1.290(4)
C(3)—O(5)	1.257(3)	C(4)—O(6)	1.263(3)
C(1)—O(7)	1.220(3)	C(2)—O(8)	1.221(3)
C(3)—O(9)	1.240(3)	C(4)—O(10)	1.224(4)
C(1)—C(3)	1.550(3)	C(2)—C(4)	1.551(4)
O(W1)—H(11)	0.82(6)	O(W1)—H(12)	0.84(5)
O(W2)—H(21)	0.85(6)	O(W2)—H(22)	0.83(6)
O(W3)—H(31)	0.87(6)	O(W3)—H(32)	0.82(4)

(*b*) Interatomic angles

Bonds	Angle (deg)	Bonds	Angle (deg)
O(1)—V—O(6)	92.67(9)	O(2)—V—O(5)	89.33(9)
O(1)—V—O(3)	90.86(9)	O(2)—V—O(4)	92.26(9)
O(1)—V—O(4)	102.24(9)	O(2)—V—O(3)	100.72(9)
O(1)—V—O(5)	162.77(9)	O(2)—V—O(6)	161.25(9)
O(5)—V—O(3)	76.11(7)	O(6)—V—O(4)	76.25(7)
O(5)—V—O(4)	87.38(7)	O(6)—V—O(3)	86.60(7)
O(1)—V—O(2)	104.35(10)	O(5)—V—O(6)	75.59(8)
O(3)—V—O(4)	158.75(7)		
V—O(3)—C(1)	120.5(2)	V—O(4)—C(2)	119.7(2)
V—O(5)—C(3)	113.8(2)	V—O(6)—C(4)	115.3(2)
O(3)—C(1)—O(7)	124.7(2)	O(4)—C(2)—O(8)	125.1(3)
O(3)—C(1)—C(3)	114.5(2)	O(4)—C(2)—C(4)	113.5(3)
O(7)—C(1)—C(3)	120.8(2)	O(8)—C(2)—C(4)	121.4(3)
O(5)—C(3)—O(9)	127.2(3)	O(6)—C(4)—O(10)	126.7(3)
O(5)—C(3)—C(1)	114.6(2)	O(6)—C(4)—C(2)	113.8(3)
O(9)—C(3)—C(1)	118.2(2)	O(10)—C(4)—C(2)	119.6(2)

(*c*) Non-bonded contacts, edges of the anion coordination octahedron

Contact	Distance (Å)	Contact	Distance (Å)
O(1)–O(2)	2.580(3)	O(5)–O(6)	2.698(3)
O(2)–O(5)	2.751(3)	O(1)–O(6)	2.763(3)
O(2)–O(4)	2.642(3)	O(1)–O(3)	2.594(3)
O(2)–O(3)	2.807(3)	O(1)–O(4)	2.841(3)
O(5)–O(4)	2.932(3)	O(6)–O(3)	2.850(3)
O(5)–O(3)	2.611(3)	O(6)–O(4)	2.575(3)

Can. J. Chem. Downloaded from www.nrcresearchpress.com by 210.87.254.42 on 09/05/12
For personal use only.

TABLE 2. (*Concluded*)

(*d*) Environment of the potassium ions (contacts <3.3 Å)

Contact	Distance (Å)	Symmetry transformation*	Contact	Distance (Å)	Symmetry transformation*	Contact	Distance (Å)	Symmetry transformation*
K(1)–O(10)	2.706(3)	3	K(2)–O(7)	2.729(2)	7	K(3)–O(7)	2.704(2)	8
K(1)–O(1)	2.725(2)	4	K(2)–O(6)	2.734(2)	4	K(3)–O(10)	2.757(3)	5
K(1)–O(W1)	2.861(3)	5	K(2)–O(W2)	2.766(3)	1	K(3)–O(W3)	2.815(3)	9
K(1)–O(8)	2.869(3)	3	K(2)–O(9)	2.828(2)	7	K(3)–O(W3)	2.856(3)	10
K(1)–O(8)	2.898(2)	5	K(2)–O(W1)	2.823(3)	1	K(3)–O(W1)	2.863(3)	2
K(1)–O(2)	2.914(2)	6	K(2)–O(8)	2.898(2)	3	K(3)–O(3)	2.882(2)	1
K(1)–O(W2)	3.062(3)	1	K(2)–O(2)	2.944(2)	1	K(3)–O(1)	3.018(2)	1
K(1)–O(1)	3.192(3)	6	K(2)–O(3)	3.062(2)	4			
K(1)–O(4)	3.224(2)	6	K(2)–O(1)	3.158(3)	4			

*Figures in this column refer to the following set of symmetry transformations with respect to the oxygen atoms: (1) x,y,z; (2) $x+1, y, z+1$; (3) $\bar{x}-1, \bar{y}+1, \bar{z}$; (4) $x-1, y, z$; (5) $x, y, z+1$; (6) $\bar{x}-1, \bar{y}+1, \bar{z}+1$; (7) $\bar{x}-1, \bar{y}, \bar{z}$; (8) $\bar{x}, \bar{y}, \bar{z}+1$; (9) $\bar{x}-1, \bar{y}, \bar{z}+1$; (10) $x+1, y, z$. (11) $-1-x, -y, -1-z$.

(*e*) Hydrogen bonding parameters†

Bond	Distance (Å)	Symmetry transformation*	Bond	Distance (Å)
O(W1)—O(4)	3.051(3)	3	H(11)—O(4)	2.26(6)
O(W1)—O(5)	2.892(3)	1	H(12)—O(5)	2.07(6)
O(W2)—O(5)	3.069(4)	5	H(21)—O(5)	2.31(6)
O(W2)—O(2)	2.965(4)	1	H(22)—O(2)	2.27(6)
O(W3)—O(9)	2.984(4)	11	H(31)—O(9)	2.14(6)
O(W3)—O(9)	2.838(4)	5	H(32)—O(9)	2.02(4)

*Figures in this column refer to symmetry transformations of oxygen atoms (see section (*d*)).
†The angles involved lie in the following ranges: H—O—H, 97(4)–109(5); O—H···O, 141(5)–172(4); H···O—C, 96(2)–143(2).

1.633 Å) which indicate strong multiple bond character. The remaining four metal–oxygen bonds are longer (1.995(2) to 2.230(2) Å) and fall into two groups depending on whether or not they are *trans* to a V=O bond. The *trans* bonds are significantly longer (2.158(2) and 2.230(2) Å) than the other pair (2.009(2) and 1.995(2) Å), a good illustration, as mentioned by Hoard *et al.* (7–10), of the structural *trans* effect. This σ bond strength weakening is reflected throughout the rest of the anion as the strongest of the inner C—O bonds are adjacent to the weaker of the V—O bonds. The terminal carbon–oxygen bond lengths average to 1.226(9) Å, which is slightly shorter than the inner C—O bonds (average = 1.274(16) Å) but comparable to the C=O double bond lengths found in many aldehydes and ketones (11). The carbon–carbon bond exhibits no double bond character at all, as was also found in oxalic acid dihydrate (12).

There are certain similarities and differences between the anion in the present structure and in the ammonium salt previously studied (7). In both cases, the anion exhibits approximate non-crystallographic two-fold symmetry through the vanadium atom, although the deviations from symmetry are not the same in both cases. Both show double bond character in the VO_2^+ moiety and an O—V—O angle which is larger than 90°. However, the average V=O bond length in the present structure is shorter (0.009(4) Å) than in the previous one. This would be consistent with the slight increase in O—V—O angle from 103.8(1)° to 104.4(1)° and with the observation that the hydrogen bonding to the vanadyl oxygen atoms is stronger in the ammonium salt. In each case, the longer of the non-equivalent V=O bonds is the one which has the stronger hydrogen bond to it.

The oxalate groups all contain planar "CO_2" fragments which, in the case of the potassium salt, are twisted about the C—C bond by 3.8(2) and 7.9(2)°, so that the ligand as a whole is not planar. The C—C bond is slightly shorter in the ammonium salt. The inner C—O bond lengths are comparable in the two structures and these

Can. J. Chem. Downloaded from www.nrcresearchpress.com by 210.87.254.42 on 09/05/12
For personal use only.

TABLE 3. The equations of the least-squares mean planes*

Plane	Equation	χ^2
1: O(1),O(3),O(4),O(5)	$0.831x + 0.103y - 0.546z + 1.659 = 0$	627
2: O(2),O(3),O(4),O(6)	$-0.491x - 0.446y - 0.748z + 1.098 = 0$	26
3: O(1),O(2),O(5),O(6)	$-0.359x + 0.877y - 0.318z - 3.209 = 0$	35430

*The normal equation of a plane in the form $Ax + By + Cz + D = 0$, expressed in Ångströms, referring to the orthogonalized set of axes x, y, z (corresponding to a, b, and c, respectively), the direction cosines of the normal to the plane, A, B, and C, and the distance of the plane from the origin, D.

Displacement of vanadium from planes

Plane	Displacement (Å)
1	−0.236(1)
2	−0.256(1)
3	0.025(1)

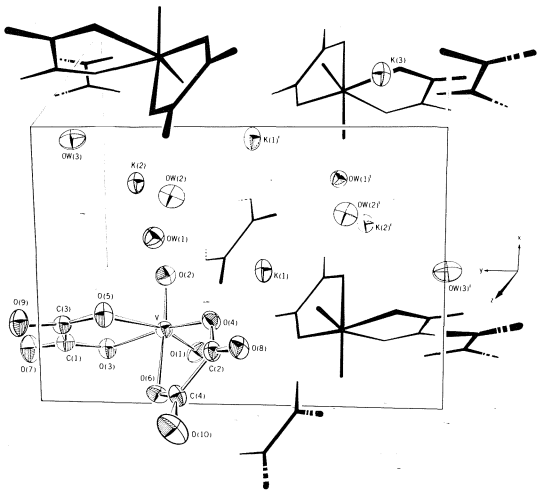

FIG. 1. The unit cell of tripotassium bis(oxalato)-dioxovanadate(V) trihydrate showing the atomic labelling.

too fall into two groups, depending on the length of the V—O bond adjacent to them. Minor variations in length can be attributed to hydrogen bonding. The outer oxalate oxygens are the atoms most influenced by the environment of the anion. In the potassium salt, only one bond length is different from the rest and it is to an oxygen which is involved in hydrogen bonding to two water molecules. In the ammonium salt, those oxygens which are strongly hydrogen bonded also have bond lengths of ~1.24 Å, and the one which is less strongly affected by water molecules has a bond length of only 1.22 Å.

The potassium ions have irregular environments; in one case there are seven adjacent oxygen atoms and in the other two there are nine (see Table 2). The actual polyhedra are, as may be expected, highly irregular; the distortions involve both distance and angular effects.

We wish to thank the National Research Council of Canada for their support which made this work possible.

We also wish to thank the Department of Chemistry for arranging a summer scholarship which provided support for one of us (S.E.G.).

1. R. E. DREW and F. W. B. EINSTEIN. Inorg. Chem. **12**, 829 (1973).
2. J. KARLE and I. L. KARLE. Acta Crystallogr. **21**, 849 (1966).
3. D. SAYRE. Acta Crystallogr. **5**, 60 (1952).
4. International tables of X-ray crystallography. Vol. III. Kynoch Press, Birmingham, England. 1965. Section 3.3.
5. R. F. STEWART, E. R. DAVIDSON, and W. T. SIMPSON. J. Chem. Phys. **42**, 3175 (1965).
6. V. SCHOMAKER and K. N. TRUEBLOOD. Acta Crystallogr. B**24**, 63 (1968).
7. W. R. SCHEIDT, C. C. TSAI, and J. L. HOARD. J. Am. Chem. Soc. **93**, 3867 (1971).
8. W. R. SCHEIDT. Inorg. Chem. **12**, 1758 (1973).
9. W. R. SCHEIDT, D. M. COLLINS, and J. L. HOARD. J. Am. Chem. Soc. **93**, 3873 (1971).
10. W. R. SCHEIDT, R. COUNTRYMAN, and J. L. HOARD. J. Am. Chem. Soc. **93**, 3878 (1971).
11. L. E. SUTTON. Tables of interatomic distances and configurations. The American Chemical Society, London. 1958. p. 517.
12. (*a*) P. COPPENS, T. M. SABINE, R. G. DELAPLANE, and J. A. IBERS. Acta Crystallogr. B**25**, 2451 (1969); (*b*) R. G. DELAPLANE and J. A. IBERS. Acta Crystallogr. B**25**, 2423 (1969); (*c*) P. COPPENS and T. M. SABINE. Acta Crystallogr. B**25**, 2442 (1969).

Can. J. Chem. Downloaded from www.nrcresearchpress.com by 210.87.254.42 on 09/05/12
For personal use only.

FOR ERRATA SEE
V.53(10)1975 P.1536

Sur l'existence des composés P_4Se_x($x \leq 3$) et $P_4Se_{3-n}S_n$($n = 1, 2$)

YVES MONTEIL ET HENRI VINCENT

Laboratoire de Physico-Chimie Minérale I, Associé au C.N.R.S. n°116, Service du Professeur Cueilleron, Université Claude Bernard, 43 boulevard du 11 novembre 1918, 69621, Villeurbanne, France

Reçu le 23 janvier, 1973

YVES MONTEIL et HENRI VINCENT. Can. J. Chem. **52**, 2190 (1974).

Le diagramme de phases P rouge – P_4Se_3 est étudié systématiquement par analyse thermique différentielle et radiocristallographie. P_4Se_3 qui est le seul composé binaire dans ce domaine, existe sous trois formes allotropiques: $P_4Se_3\alpha$ se transforme à 82 °C en $P_4Se_3\beta$ qui se transforme à 192 °C en $P_4Se_3\gamma$; les formes β et γ étaient inconnues. Nous avons évalué les chaleurs de transformation des différentes variétés allotropiques ainsi que la chaleur de fusion du P_4Se_3.

Dans le diagramme ternaire P–S–Se, la coupe isoplèthe P_4Se_3–P_4S_3 est une section quasi-binaire. On observe un eutectique à 170 °C pour une concentration molaire de 5% en P_4Se_3. Dans l'étude de cette section isoplèthe, il n'apparaît pas de composé mixte du type $P_4Se_{3-n}S_n$ avec n entier, égal à 1 ou 2.

YVES MONTEIL and HENRI VINCENT. Can. J. Chem. **52**, 2190 (1974).

The phase diagram of P(red) + P_4Se_3 was studied systematically by differential thermal analysis and X-ray crystallography. P_4Se_3, which is the sole binary compound in the system, exists as three allotropic forms: $P_4Se_3\alpha$ transforms at 82 °C into $P_4Se_3\beta$ which is transformed at 192 °C into $P_4Se_3\gamma$; the β- and γ- forms were unknown. The heats of the allotropic transformations were evaluated as well as the heat of fusion of P_4Se_3.

In the ternary diagram P–S–Se the isopleth P_4Se_3–P_4S_3 is a quasi-binary section. An eutectic is observed at 170 °C with a concentration of 5% in P_4Se_3. No mixed compound of the type $P_4Se_{3-n}S_n$ (n an integer = 1 or 2) was found during the study of this isopleth.

[Journal translation]

Ce travail se situe dans une étude sur les chalcogénures binaires et ternaires du phosphore entreprise au Laboratoire. Nous avons étudié les combinaisons phosphore–soufre (1) mais les combinaisons phosphore–sélénium et phosphore–soufre–sélénium sont mal connues. Depuis longtemps on sait que le phosphore se combine au sélénium et au soufre par simple fusion des éléments (2–4).

Si l'existence des composés binaires P_4Se_3, P_4Se_5 et P_4Se_{10} ne paraît pas faire de doute (5–7), bien que le caractère vitreux de P_4Se_{10} rende son identification très délicate, celle des composés P_4Se, P_4Se_2 et P_4Se_6 n'est qu'aléatoire (8–10). Les combinaisons ternaires décrites par Meyer (8), en 1902, sont du type $P_4Se_{3-n}S_n$ avec n entier égal à 1 ou 2.

Ces résultats fragmentaires nous ont conduit à entreprendre l'étude du diagramme de phases phosphore rouge – sélénium. Nous présentons dans cet article les résultats obtenus pour la partie correspondant au domaine P rouge – P_4Se_3. Nous avons étudié dans le système ternaire P–S–Se, la coupe P_4S_3–P_4Se_3 qui se présente comme une section quasi-binaire. L'étude des diagrammes a été faite par analyse thermique différentielle et par radiocristallographie. Préalablement nous nous sommes intéressés à la préparation du produit de départ: le triséléniure de tétraphosphore P_4Se_3.

Préparation de P_4Se_3

Le triséléniure de tétraphosphore, P_4Se_3, a déjà été préparé soit en phase solide, soit en solution:

La première méthode de préparation due à Meyer (8) consiste à fondre des mélanges stoechiométriques de phosphore, blanc ou rouge, avec du sélénium. Le composé P_4Se_3 est obtenu par distillation sous atmosphère de CO_2 à 300–400°C; Behrens et Haschka (11) purifient ce composé par sublimation sous vide. Tout récemment P_4Se_3 a été préparé par fusion de P_4Se_{10} avec le phosphore rouge (12).

La seconde méthode de préparation consiste à chauffer en solution dans la tétraline, un mélange de phosphore blanc et de sélénium. Elle a été mise en oeuvre par Mai (13) et reprise et modifiée par Irgolic *et al.* (14).

Le produit préparé par la méthode de Mai est soluble dans le sulfure de carbone alors que celui obtenu d'après la méthode de Meyer ne l'est pas. En se basant sur cette seule différence de solu-

Can. J. Chem. Downloaded from www.nrcresearchpress.com by 210.87.254.40 on 09/05/12
For personal use only.

Can. J. Chem. Downloaded from www.nrcresearchpress.com by 210.87.254.40 on 09/05/12
For personal use only.

bilité dans le sulfure de carbone, Mai a supposé l'existence de deux formes allotropiques de P_4Se_3; d'autre part la mesure des C_p de $PySe_3$ laisse supposer l'existence d'une transition cristalline vers 350 °K (17). Aucune confirmation de cette hypothèse n'ayant été apportée par la suite il nous a paru important d'étudier la préparation de P_4Se_3.

Pour notre part nous avons préparé P_4Se_3 par traitement thermique du mélange stoechiométrique de phosphore rouge et de sélénium, en tube scellé, à des températures supérieures à 250 °C. Nous avons constaté que quelque soit la durée du traitement et sa température, la masse réactionnelle n'est jamais constituée de P_4Se_3 pur. Il est indispensable de purifier ce produit, soit par sublimation sous vide, soit par extraction dans l'appareil de Soxhlet par le sulfure de carbone. Avec cette seconde méthode nous obtenons P_4Se_3 sous forme de très beaux cristaux de couleur orange. Le composé ainsi obtenu fond à 246 °C, son diagramme de rayons X peut être indexé à partir des paramètres de la maille orthorhombique déterminés par Keulen et Vos (5).

Description du diagramme de phases P rouge – P_4Se_3

Les matériaux sont préparés en ampoules scellées sous vide par mélange de phosphore rouge et de triséléniure de tétraphosphore. Le chauffage de ces échantillons, dont le poids est de l'ordre de 1 gramme, est alors effectué dans un four à des températures légèrement inférieures à 600 °C pour les composés riches en phosphore et, à 300 °C, pour le domaine avoisinant le triséléniure de tétraphosphore. Après refroidissement, les échantillons sont broyés, caractérisés systématiquement par diffraction de rayons X et introduits dans les cellules d'analyse thermique différentielle.

L'interprétation des courbes d'analyse thermique différentielle conduit sans aucune ambiguité à l'établissement du diagramme représenté sur la figure 1. L'eutectique est observé à 164 °C pour une composition voisine de 67% en atomes de phosphore.

Le phosphore rouge fond à 590 °C. Nous observons à 440 ± 10 °C un accident thermique correspondant à une transformation du phosphore qui passe de la forme amorphe P(I) à la forme P(II) cristallisée dans le système hexagonal. Nous n'avons pas mis en évidence l'existence d'autre phénomène thermique dû à cet élément.

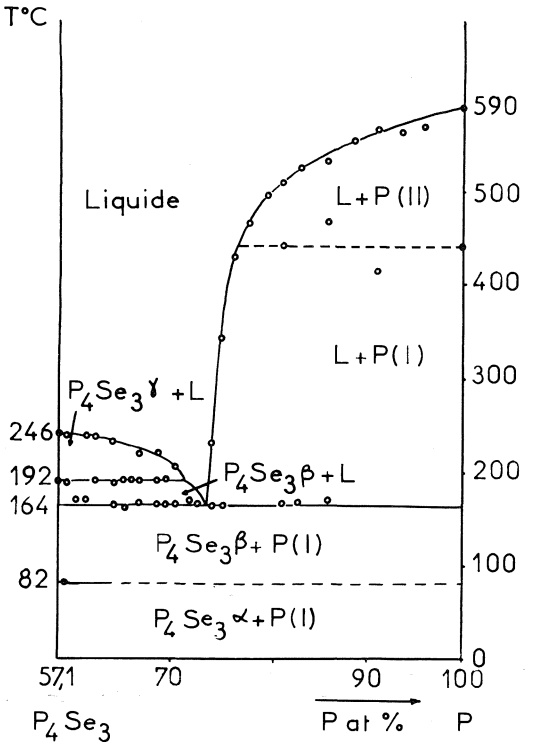

FIG. 1. Diagramme de phases du système P rouge – P_4Se_3.

Le composé P_4Se_3 fond à 246 °C. Un palier se manifeste à 192 °C que nous pouvons attribuer sans aucun doute à une transition du P_4Se_3.

Cette étude ne permet pas de retrouver de séléniure plus riche en phosphore que P_4Se_3 tel que P_4Se_2 ou P_4Se.

Différentes variétés allotropiques de P_4Se_3

Le diagramme de phases du système P rouge – P_4Se_3 permet de mettre en évidence à 192 °C l'existence d'une transformation allotropique de P_4Se_3.

D'autre part, lorsqu'on soumet à l'analyse thermique différentielle un produit obtenu directement par sublimation ou par recristallisation par le sulfure de carbone, on observe un accident thermique supplémentaire à 82 °C.

Ces résultats s'expliquent par l'existence de trois variétés allotropiques de P_4Se_3: une variété α, stable à basse température qui subit une transformation en forme β à 82 °C, qui elle même donne la variété γ à 192 °C.

Au cours de l'échauffement d'un échantillon de $P_4Se_3\alpha$ on observe successivement les trois es-

TABLEAU 1

hkl	d (Å) Obs.	d (Å) Calc.	I obs.	hkl	d (Å) Obs.	d (Å) Calc.	I obs.
012	8.80	8.78	m	048	2.20	2.20	m
111	7.25	7.22	f	342	2.15	2.15	tf
004	6.55	6.57	f	055		2.15	
020	5.90	5.90	f	328		2.15	
014	5.75	5.74	m	344	2.07	2.07	tf
120	5.05	5.05	F	425		2.07	
114	4.95	4.95	TF	345	2.02	2.02	tf
024	4.39	4.39	f	254		2.02	
006		4.38		162	1.91	1.91	tf
204	3.91	3.91	f	256		1.91	
116	3.78	3.78	f	064	1.88	1.88	tf
032		3.77		163		1.88	
220	3.76	3.76	f	158		1.88	
221	3.70	3.72	f	520	1.85	1.85	m
214		3.72		257		1.85	
026	3.52	3.52	f	164		1.85	
223	3.45	3.45	tf	437	1.81	1.81	tf
034	3.38	3.38	m	165		1.81	
008	3.28	3.29	m	523		1.81	
311	3.12	3.11	F	263	1.785	1.785	tf
312	3.06	3.04	TF	258		1.784	
303		3.04		438	1.75	1.75	tf
225		3.06		356		1.75	
217	2.88	2.88	m	533	1.715	1.712	tf
140	2.82	2.82	m	167		1.715	
142	2.76	2.76	F	526	1.705	1.704	m
305		2.76		534	1.685	1.687	tf
323	2.71	2.705	f	266		1.684	
037		2.72		364	1.628	1.629	m
137	2.60	2.62	f	540		1.626	
324		2.61		528	1.612	1.612	tf
045	2.55	2.57	f	365	1.602	1.602	tf
316		2.55		544	1.58	1.58	tf
333	2.41	2.41	f	456		1.58	
317		2.405		460	1.53	1.53	tf
237	2.37	2.37	m	461		1.53	
146		2.37		625	1.505	1.500	tf
411		2.37		463		1.507	
422	2.22	2.22	tf	458		1.506	
153		2.22					
054		2.22					

$P_4Se_3\alpha$: orthorhombic, *Pmnb*, $a = 9.74$ Å, $b = 11.80$ Å, $c = 26.30$ Å.

pèces; au refroidissement le passage de la forme β à la forme α n'est pas observé. Ceci explique que nous n'avons pas observé la transformation de $P_4Se_3\alpha$ en $P_4Se_3\beta$ dans l'étude du diagramme de phases précédemment décrit.

La transformation de la forme β en sa forme γ est réversible. Nous n'avons pas pu isoler la variété γ du P_4Se_3 à la température ambiante par des trempes à la température de l'air liquide.

Nous avons pu évaluer les enthalpies de transformation des différentes variétés allotropiques du P_4Se_3 et son enthalpie de fusion, par mesure des aires des pics obtenus par analyse thermique différentielle. Nous avons utilisé comme étalon pour ces mesures, l'enthalpie de fusion de l'acide benzoïque qui fond à température proche des phénomènes étudiés.

Nous avons obtenu pour la transformation du $P_4Se_3\alpha$ en $P_4Se_3\beta$ à 82 °C la valeur: $\Delta H = 20 \pm 2$ kcal mol^{-1}.

Nous avons toujours trouvé cette même valeur élevée, que le $P_4Se_3\alpha$ soit obtenu par sublimation sous vide ou par dissolution dans le sulfure de carbone.

Can. J. Chem. Downloaded from www.nrcresearchpress.com by 210.87.254.40 on 09/05/12
For personal use only.

TABLEAU 2.

$P_4Se_3\beta$ (Cubique, a = 16.25 Å)				$P_4Se_3\gamma$ (Cubique, a = 17.81 Å)			
	d (Å)		I		d (Å)		I
hkl	Obs.	Calc.	obs.	*hkl*	Obs.	Calc.	obs.
220	5.77	5.75	f	211	7.25	7.25	m
221	5.43	5.42	TF	310	5.62	5.63	F
310	5.14	5.17	F	222	5.17	5.15	F
311	4.92	4.90	m	320	4.90	4.93	m
222	4.70	4.69	f	400	4.47	4.45	m
320	4.55	4.50	f	411	4.20	4.20	m
321	4.37	4.34	m	332	3.80	3.80	f
322	3.94	3.94	f	422	3.60	3.64	m
421	3.55	3.54	f	333	3.39	3.43	f
332	3.46	3.46	f	511		3.43	
422	3.35	3.32	f	521	3.25	3.25	f
431	3.18	3.18	F	441	3.10	3.10	f
333	3.12	3.12	m	522		3.10	
432	3.02	3.01	m	433	3.05	3.05	F
520		3.01		530		3.05	
521	2.96	2.96	tf	541	2.75	2.75	tf
441	2.81	2.82	tf				
522		2.82					
433	2.78	2.78	f				
530		2.78					
531	2.74	2.74	tf				
442	2.70	2.70	tf				
600		2.70					
610	2.66	2.67	tf				
640	2.25	2.25	tf				
821	1.95	1.95	tf				
742		1.95					

Nous n'avons pas observé de dégradation thermique ou chimique du composé après cette transformation. Le point de fusion du composé P_4Se_3 ne varie pas après plusieurs chauffages. N'ayant pas pu obtenir de monocristal de la forme β du P_4Se_3 nous ne sommes pas en mesure de dire si cette chaleur de transformation élevée correspond à un changement structural important.

L'enthalpie de la transformation du $P_4Se_3\beta$ en $P_4Se_3\gamma$ à 192 °C est égale à

$$\Delta H = 1.5 \pm 0.15 \text{ kcal mol}^{-1}$$

L'enthalpie de fusion du P_4Se_3 a pour valeur à 246 °C:

$$\Delta H = 4.0 \pm 0.4 \text{ kcal mol}^{-1}$$

L'étude radiocristallographique de P_4Se_3 a mis nettement en évidence l'existence de ses trois variétés allotropiques.

En l'absence de monocristal de la forme β du P_4Se_3 nous avons pu indexer son diagramme de poudre de rayons X dans le système cubique. Le paramètre de la maille cubique à la valeur suivante: a = 16.23 Å.

Le diagramme de rayons X obtenu pour la forme γ du P_4Se_3 peut aussi être indexé dans le système cubique avec comme valeur du paramètre de maille: a = 17.81 Å. Dans les tableaux 1 et 2 nous donnons l'indexation des diagrammes de rayons X des trois variétés allotropiques de P_4Se_3.

Nous avons également caractérisé les formes α et β du P_4Se_3 par spectrométrie infra-rouge. Seule la forme α est soluble dans le sulfure de carbone et, de plus, comme ce même solvant favorise la transformation de la forme β en forme α, il ne nous a pas été possible d'opérer en solution.

Comme les produits n'absorbent pas au-dessus de 600 cm^{-1}, nous représentons sur la fig. 2, les spectres d'absorption infrarouge des formes α et β du P_4Se_3 dans le domaine 600–250 cm^{-1} obtenus par pastillage dans le bromure de césium.

Le spectre de la forme α du P_4Se_3 est en accord avec les résultats donnés par Irgolic *et al.* (14). Le

Can. J. Chem. Downloaded from www.nrcresearchpress.com by 210.87.254.40 on 09/05/12
For personal use only.

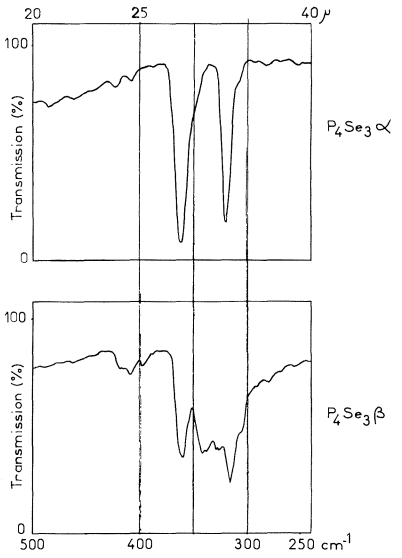

FIG. 2. Spectres infra-rouge des formes α et β du P_4Se_3 rencontrées à température ambiante.

spectre de la forme β du P_4Se_3 est établi pour la première fois.

Il n'a pas été possible de passer de la forme β du P_4Se_3 à sa forme α par traitement thermique.

Par contre la transformation est possible si on ensemence avec la forme α du P_4S_3, isotype de la forme α du P_4Se_3.

Etude de la section P_4Se_3–P_4S_3

Meyer (8) avait caractérisé les combinaisons ternaires P_4Se_2S et P_4SeS_2 par la valeur de leurs points de fusion. Mai (13) prétendait pour sa part que ces 2 combinaisons n'étaient en fait que des mélanges de P_4Se_3 et de P_4S_3.

Nous savons aussi que les formes α des trisséléniure et trisulfure de tétraphosphore cristallisent dans le même système cristallin, orthorhombique, avec le même groupe d'espace et elles possèdent la même structure moléculaire tétraédrique dérivée de celle du phosphore blanc (2, 15) (Fig. 3*a*).

Après avoir entrepris l'étude des 2 systèmes binaires P–S (1) et P–Se (16) il nous a paru intéressant d'essayer d'obtenir des combinaisons ternaires que nous pouvons représenter par la formule $P_4Se_{3-n}S_n$. Nous avons donc étudié systématiquement les interactions entre P_4Se_3 et P_4S_3 ce qui nous a amené à entreprendre dans le système ternaire P–S–Se, l'étude de la section isoplèthe P_4Se_3–P_4S_3 (Fig. 3*b*). Le composé P_4S_3 est préparé à partir de P_4S_{10} et de phosphore rouge ou à partir de soufre et de phosphore rouge. Le produit est purifié soit, par extraction au sulfure de carbone et recristallisé dans ce même solvant, soit par sublimation sous vide.

Les échantillons pour l'analyse thermique différentielle ont été préparés à partir des mélanges de $P_4Se_3\alpha$ et de $P_4S_3\alpha$, chauffés à 300 °C et refroidis lentement. Les diagrammes de rayons X des produits obtenus ne décèlent que l'existence des seuls composés P_4Se_3 et P_4S_3.

Nous représentons sur la figure 4 les résultats de l'analyse thermique différentielle. La coupe isoplèthe P_4Se_3–P_4S_3 est une section quasi-binaire. Nous observons un palier à 192 °C qui correspond à la transition $P_4Se_3\beta$–$P_4Se_3\gamma$ et un autre à 40 °C qui correspond à la transformation $P_4S_3\alpha$–$P_4S_3\beta$. Le diagramme présente aussi un palier à 56 °C, pour des concentrations molaires comprises entre 60 et 100% en P_4Se_3; ce dernier est attribué à la transformation $P_4Se_3\alpha$–$P_4Se_3\beta$. Les clichés de rayons X pris à différentes températures dans ce domaine de concentration confirment ce résultat. L'abaissement de la température de transition de 82 à 56 °C étant dû vraisemblablement à l'existence d'une solution solide terminale. Cette transformation n'avait pas été observée lors du tracé du diagramme de phases correspondant au domaine P rouge – P_4Se_3 ce qui nous permet de conclure que la présence de $P_4S_3\alpha$ favorise l'obtention de la forme α de P_4Se_3.

La fusion de P_4S_3 se produit à 173 °C, celle de P_4Se_3 à 246 °C.

Nous avons observé l'eutectique pour une température de 170 °C dans un domaine de concentration limité et de plus la forme aplatie des courbes de liquidus sur le palier eutectique rend la détermination de sa composition difficile. Le diagramme de Tammann ne nous est d'aucun secours car le phénomène thermique de l'eutectique est indiscernable de celui de la fusion, les pics correspondants se recouvrant en grande partie ou totalement. Nous pouvons situer néanmoins la composition de l'eutectique à 5% en moles de P_4Se_3 par rapport à celles de P_4S_3 et P_4Se_3.

Le diagramme montre que dans les conditions de l'étude aucune phase intermédiaire ne se manifeste entre P_4Se_3 et P_4S_3.

Conclusions

L'étude du diagramme de phases phosphore–sélénium, dans le domaine phosphore rouge –

Can. J. Chem. Downloaded from www.nrcresearchpress.com by 210.87.254.40 on 09/05/12
For personal use only.

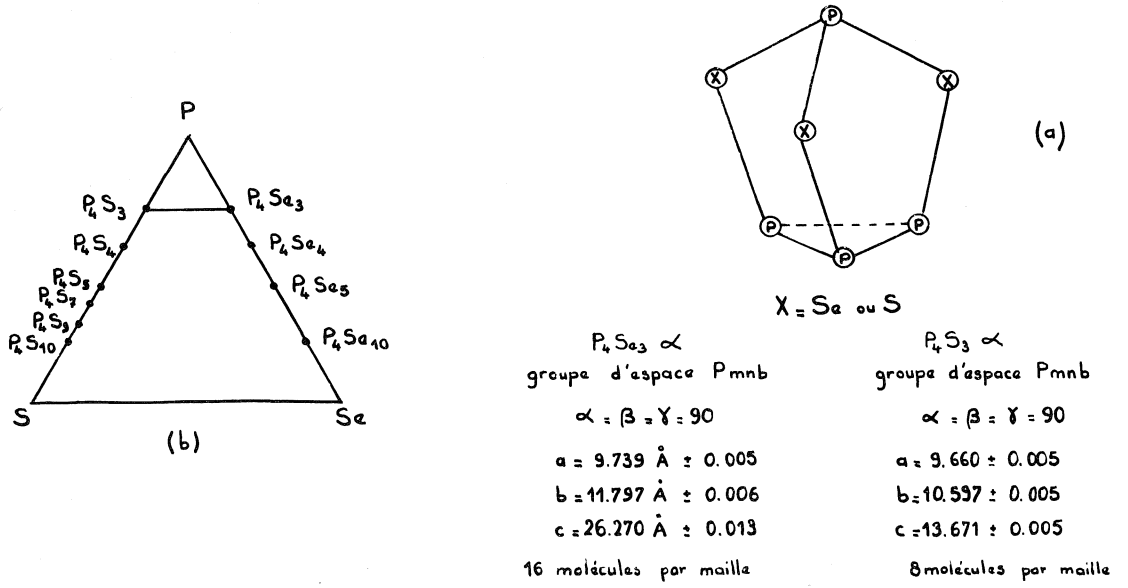

FIG. 3. (*a*) Données cristallographiques concernant les formes α de P_4S_3 et P_4Se_3. (*b*) Schématisation dans le ternaire P–S–Se de la coupe isoplèthe P_4S_3–P_4Se_3.

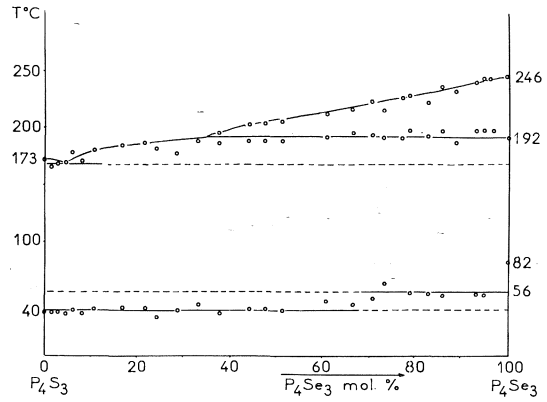

FIG. 4. Diagramme de phases de la coupe P_4Se_3–P_4S_3.

triséléniure de tétraphosphore, montre que le triséléniure de tétraphosphore (P_4Se_3) est le composé binaire sélénié le plus riche en phosphore; on ne retrouve pas l'existence des mono- et diséléniure de tétraphosphore (P_4Se, P_4Se_2).

P_4Se_3 fond à 246 °C; il existe sous 3 variétés allotropiques. Les diagrammes de rayons X des formes inédites β et γ du P_4Se_3 peuvent être indexés suivant des systèmes cubiques. Si la forme α du P_4Se_3 est celle qui est stable à température ambiante, nous devons noter qu'après fusion du composé, nous le rencontrons sous sa seule forme β. Nous avons obtenu le passage de la forme β du P_4Se_3 à sa forme α par le traitement par le sulfure de carbone, par sublimation ou par ensemencement avec la forme α du P_4S_3. Le spectre infrarouge de la forme β du P_4Se_3 très différent de celui de sa forme α, peut être un moyen d'identification commode des deux variétés allotropiques.

Dans le système ternaire phosphore–soufre–sélénium, la coupe isoplèthe P_4Se_3–P_4S_3 est une section quasi-binaire. Au cours de son étude nous n'avons pas rencontré de composés mixtes de formule $P_4Se_{3-n}S_n$ cités précédemment par Meyer.

Partie expérimentale

Synthèse de P_4Se_3

Le sélénium gris en poudre (provenance Merck, pureté indiquée 99.5%) et le phosphore rouge en poudre (provenance Merck, pureté indiquée 99%) sont utilisés sans purification particulière. Un mélange de 6.2 g de P rouge et de 11.85 g de Se est placé dans un tube en Pyrex. Le tube est ensuite scellé sous vide avant d'être chauffé pendant 12 h à 350 °C et refroidi pendant 8 heures à la température ambiante. Le contenu du tube est alors recueilli, placé dans un appareil de Soxhlet, et extrait par 250 cm^3 de CS_2 durant 6 heures. On recueille dans le solvant une partie de P_4Se_3 qui a cristallisée, puis l'autre partie après évaporation du solvant sous vide. Le produit obtenu est la forme α du P_4Se_3 qui est la seule forme soluble dans CS_2, le Se et le P rouge étant insolubles.

Quantité obtenue: 14.4 g (rendement 80%); spectre de Debye–Scherrer: voir Tableau 1; spectre d'absorption i.r.: bandes intenses vers 357 et 315 cm^{-1}.

Can. J. Chem. Downloaded from www.nrcresearchpress.com by 210.87.254.40 on 09/05/12
For personal use only.

Synthèse de P_4S_3

On traite 12.4 g de phosphore rouge et 9.6 g de soufre (provenance: Prolabo, pureté indiquée: 99.8%) ou 13.3 g de P_4S_{10} (provenance Coignet, pureté indiquée 99%) et 8.7 g de P rouge à 300 °C pendant 12 heures en tube scellé. Après refroidissement, le P rouge et les sulfures de phosphore autres que P_4S_3 étant insolubles dans le sulfure de carbone, le P_4S_3 est extrait dans l'appareil de Soxhlet par 250 cm^3 de sulfure de carbone durant 12 heures. On recueille ainsi la forme α du P_4S_3, ce produit est encore sublimé juste avant son emploi. Rendement 98%.

Spectre de Debye–Scherrer: raies intenses à 5.71; 4.95; 3.14; 2.69 Å. Spectre d'absorption en i.r.: bandes intenses vers 485, 440 et 423 cm^{-1}.

Analyse thermique différentielle

Les manipulations d'analyse thermique différentielle ont été réalisées à l'aide de deux appareillages:

(*i*) un appareil construit au laboratoire dont la tête de mesure en acier inoxydable, supportée par un tube en alumine, permet de détecter les effets thermiques par des couples "thermocoax" (chromel–alumel). Un dispositif à vis, permet de centrer la tête de mesure dans le four. Les effets thermiques dus aux différentes transformations sont enregistrés par un appareil Meci X_1, X_2 précédé d'un amplificateur Setaram. Les échantillons, dont le poids est d'environ 1 g sont placés dans les ampoules en verre Pyrex, scellées sous vide, dont le fond possède un doigt de gant dans lequel vient se loger l'extrémité du thermocouple.

(*ii*) un microanalyseur thermique Setaram dont la tête de mesure comprend 3 thermocouples identiques placés suivant les sommets d'un triangle équilatéral. Chaque thermocouple est constitué par un microcreuset de forme tronconique qui est la soudure du couple Pt/Pt–Rh. Le microcreuset de 25 microlitres est destiné à recevoir directement l'échantillon. A cause de la grande agressivité du phosphore, du sélénium et du trisélénure de tétraphosphore pour le platine, nous avons dû placer les échantillons dans de petites ampoules de silice. Nous les avons fabriquées à partir d'un tube de 4 mm de diamètre. L'extrêmité de l'ampoule est légèrement étirée et rodée extérieurement afin d'obtenir la forme tronconique de la coupelle en platine. Lors du scellement sous vide, l'extrêmité de l'ampoule est maintenue dans un bloc métallique refroidi à la température de l'air liquide pour éviter le détitrage de l'échantillon. Les ampoules scellées, d'environ 1 cm de hauteur, nous ont imposé de relever le chapeau de la sonde en y adjoignant une pièce en acier inoxydable. Cette pièce de forme cylindrique percée d'un trou permet de maintenir en place l'ampoule contenant l'échantillon. Cette modification n'a pas apporté de perturbation dans la détermination des effets thermiques. La quantité de produit étudié est de 20 mg environ.

Radiocristallographie

Les diagrammes de rayons X à différentes températures ont été effectués dans deux appareils:

(*i*) une chambre de Guinier–Lenne munie d'un monochromateur (radiation CuKα). Le produit est déposé sur une platine ce qui nécessite de travailler sous atmosphère d'azote et de ne pas étudier de composé volatil.

(*ii*) une chambre de Rigaku–Denki dans laquelle l'échantillon peut être placé dans un tube de Lindemann, pour des températures inférieures à 350 °C ce qui permet d'étudier les composés volatils.

Spectroscopie infrarouge

L'appareil utilisé est un spectrophotomètre Perkin–Elmer, modèle 457. Les pastilles en bromure de césium contiennent 3% en poids du composé à étudier.

1. H. Vincent. Bull. Soc. Chim. **12**, 4517 (1972).
2. J. Berzelius. Schw. J. **23**, 309 (1818).
3. E. Beckmann et H. Pfeiffer. Z. Phys. Chem. **22**, 614 (1897).
4. A. Stock et K. Thiel. Ber. **38**, 2720 (1905).
5. E. Keulen et A. Vos. Acta Cryst. **12**, 323 (1959).
6. G. J. Penney et G. M. Sheldrick. J. Chem. Soc. A, 245 (1971).
7. M. V. Kudchadker, R. A. Zingaro et K. J. Irgolic. Can. J. Chem. **46**, 8, 1417 (1968).
8. J. Meyer, Z. anorg. Chem. **30**, 249 (1902).
9. O. Hahn. J. pr. Chem. **93**, 430 (1864).
10. P. L. Robinson et W. E. Scott. Z. anorg. Chem. **210**, 57 (1933).
11. H. Behrens et G. Haschka. Ber. **94**, 1191 (1961).
12. V. A. Maroni et R. V. Schablaske. J. Inorg. Nucl. Chem. **33**, 3182 (1971).
13. J. Mai. Chem. Ber. **59**, 1888 (1926); **61**, 1807 (1928).
14. K. Irgolic, R. A. Zingaro et M. V. Kudchadker. Inorg. Chem. **4**, 1421 (1965).
15. Y. C. Leung, J. Waser, S. van Houten, A. Vos, G. A. Wiegers et E. H. Wiebenga. Acta Cryst. **10**, 574 (1957).
16. Y. Monteil et H. Vincent. Communication à l'Assemblée Annuelle de la Société Chimique de France, Marseille. Mai 1973.
17. H. L. Clever, E. F. Westrum, Jr., and A. W. Cordes. J. Phys. Chem. **69**, 4, 1214 (1965).

Can. J. Chem. Downloaded from www.nrcresearchpress.com by 210.87.254.40 on 09/05/12
For personal use only.

Crystal Structure of Hexamethylcyclotriphosphazene–Iodine (1:1 Adduct)

PETER L. MARKILA AND JAMES TROTTER

Department of Chemistry, University of British Columbia, Vancouver 8, British Columbia

Received November 26, 1973

PETER L. MARKILA and JAMES TROTTER. Can. J. Chem. **52**, 2197 (1974).

Crystals of the title compound, $N_3P_3Me_6.I_2$, are triclinic, $a = 10.707(13)$, $b = 8.873(5)$, $c = 8.871(6)$ Å, $\alpha = 96.65(6)$, $\beta = 103.91(12)$, $\gamma = 97.81(12)°$, $Z = 2$, space group $P\bar{1}$. The structure was determined with MoKα diffractometer data by Patterson and Fourier syntheses, and was refined by full-matrix least-squares methods to $R = 0.053$ for 1934 observed reflexions. One atom of the iodine molecule is weakly bonded to nitrogen, N—I = 2.417(7), I—I = 2.823(1) Å, N—I—I = 177.8(2)°. The six-membered phosphazene ring is slightly non-planar, with a chair conformation. The two P—N bonds involving the nitrogen atom bonded to iodine are longer, mean 1.64 Å, than the other four P—N bonds, mean 1.598 Å. Other mean dimensions are: P—C = 1.789 Å, N—P—N = 114.7, P—N—P = 124.0, C—P—C = 104°.

PETER L. MARKILA et JAMES TROTTER. Can. J. Chem. **52**, 2197 (1974).

Le composé cité dans le titre cristallise dans le système triclinique, $a = 10.707(13)$, $b = 8.873(5)$, $c = 8.871(6)$ Å, $\alpha = 96.65(6)$, $\beta = 103.91(12)$, $\gamma = 97.81(12)°$, $Z = 2$, groupe spatial $P\bar{1}$. La structure a été déterminée sur la base des observations diffractométriques recueillies par le rayon MoKα à l'aide des synthèses de Patterson et de Fourier, et a été affinée par la méthode de moindres carrés (matrice complète) jusqu'à un indice $R = 0.053$ pour 1934 réflexions observées. Un atome de la molécule d'iode est faiblement lié à l'azote, N—I = 2.417(7), I—I = 2.823(1) Å, N—I—I = 177.8(2)°. Le cycle hexagonal du phosphazène est légèrement gauche et affecte la conformation de la chaise. Les deux liaisons P—N(I_2) sont plus longues, 1.64 Å en moyenne, que les autres liaisons P—N, 1.598 Å en moyenne. Les autres dimensions moyennes sont les suivantes: P—C = 1.789 Å, N—P—N = 114.7, P—N—P = 124.0, C—P—C = 104°.

Introduction

Detailed structural information is available for several cyclophosphazene derivatives in which the bonding in the ring has been disturbed by protonation (1–3), or by complexing with a transition metal (4–6). We now describe the first structural study of a compound in which the ring has been perturbed by formation of a charge transfer complex, $N_3P_3Me_6.I_2$. The crystal structure of the parent compound has not been determined.

Experimental

Crystals of $N_3P_3Me_6.I_2$ (14) are purple fragments, usually elongated along *b*. Unit-cell and intensity data were measured as for $[N_3P_3(NMe_2)_6H]_2CoCl_4$ (3) and $[NP(NMe_2)_2]_3$ (7). Unit-cell and space group data were obtained from film and diffractometer measurements. The unit-cell parameters were refined by a least-squares treatment of $\sin^2\theta$ values for 30 reflections measured on a diffractometer with MoKα radiation.

Intensities were measured on a Datex-automated General Electric XRD 6 diffractometer, with a scintillation counter, MoKα radiation (Zr filter and pulse height analyzer), and a θ–2θ scan at $2°\ min^{-1}$ over a range of $(1.80 + 0.86 \tan\theta)$ degrees in 2θ, with 20 s background counts being measured at each end of the scan. Data were measured to $2\theta = 45°$ (minimum interplanar spacing 0.93 Å). A check reflection was monitored every 50 reflections throughout the data collection. Lorentz and polarization corrections were applied, and the structure amplitudes derived. The crystal had dimensions of *ca.* $0.4 \times 0.6 \times 0.4$ mm and was mounted with *b* parallel to the goniostat axis; no absorption correction was made. Of the 2259 independent reflections measured, 325 had intensities less than $3\sigma(I)$ above background where $\sigma^2(I) = S + B + (0.05S)^2$ with S = scan count and B = background count. These reflections were classified as unobserved.

$C_6H_{18}I_2N_3P_3$ f.w. = 479.0

Triclinic, $a = 10.707(13)$, $b = 8.873(5)$, $c = 8.871(6)$ Å, $\alpha = 96.65(6)$, $\beta = 103.91(12)$, $\gamma = 97.81(12)°$, $V = 800.8$ Å^3, ρ_{obs} was not measured, $Z = 2$, $\rho_{calc} = 1.99$, $F(000) = 452$ (20 °C, MoKα, $\lambda = 0.7107$ Å, $\mu = 43\ cm^{-1}$). Space group $P1(C_1^1)$ or $P\bar{1}(C_i^1)$.

Structure Analysis

Intensity statistics suggested space group $P\bar{1}$, which was confirmed by the structure analysis. The structure was determined by Patterson and Fourier syntheses, and was refined by full-matrix least-squares methods, with minimization of $\Sigma w(F_o - F_c)^2$, and final weights $w = [0.553 + 0.391|F_o| - 0.017|F_o|^2 + 0.0002|F_o|^3]^{-1}$ for the observed reflexions, $w = 0$ for the unobserved reflexions. Hydrogen atoms were included in positions calculated with staggered arrangements of bonds (C—H = 1.0 Å, $B = 5$ Å^2), but were not refined. The

Can. J. Chem. Downloaded from www.nrcresearchpress.com by 210.87.254.40 on 09/05/12
For personal use only.

Can. J. Chem. Downloaded from www.nrcresearchpress.com by 210.87.254.40 on 09/05/12
For personal use only.

TABLE 1

(*a*) Final positional ($\times 10^4$) with standard deviations in parentheses

Atom	*x*	*y*	*z*
I(1)	5665(1)	−2030(1)	7128(1)
I(2)	3567(1)	−4508(1)	6515(1)
P(1)	7575(2)	1576(2)	8881(2)
P(2)	9911(2)	2785(2)	8182(2)
P(3)	8502(2)	−0098(2)	6508(2)
N(1)	7515(7)	0023(8)	7630(8)
N(2)	8907(7)	2773(8)	9251(8)
N(3)	9746(7)	1248(8)	6966(8)
C(1)	7390(10)	0960(11)	10672(10)
C(2)	6184(11)	2476(13)	8146(15)
C(3)	11532(8)	3145(12)	9441(11)
C(4)	9864(10)	4395(11)	7147(11)
C(5)	9045(8)	−1908(9)	6567(10)
C(6)	7605(9)	−0202(13)	4507(10)
H(1)	8110	0387	11088
H(1′)	7426	1876	11461
H(1″)	6528	0266	10470
H(2)	6211	2774	7102
H(2′)	5362	1734	8033
H(2″)	6208	3414	8903
H(3)	11658	2285	10067
H(3′)	12175	3220	8791
H(3″)	11666	4137	10170
H(4)	8987	4289	6390
H(4′)	10026	5367	7914
H(4″)	10554	4437	6560
H(5)	9531	−1968	7666
H(5′)	8273	−2759	6213
H(5″)	9634	−2017	5854
H(6)	7229	−0761	4376
H(6′)	8201	−0317	3805
H(6″)	6882	−1111	4221

(*b*) Anisotropic thermal parameters (Å^2 $\times$ 10^2) with standard deviations in parentheses*

Atom	U_{11}	U_{22}	U_{33}	U_{12}	U_{13}	U_{23}
I(1)	3.55(4)	4.41(4)	4.53(4)	−0.16(3)	0.58(2)	0.27(3)
I(2)	5.19(5)	5.99(5)	10.04(6)	−1.90(4)	1.98(4)	−1.40(4)
P(1)	3.63(11)	3.39(11)	3.74(11)	0.26(9)	0.90(9)	−0.42(9)
P(2)	3.34(11)	2.45(10)	3.88(11)	−0.03(8)	0.50(9)	0.07(9)
P(3)	3.55(11)	2.75(11)	3.06(10)	0.32(9)	0.67(8)	0.03(8)
N(1)	4.12(38)	2.95(35)	4.62(39)	−1.04(30)	1.78(31)	−1.12(31)
N(2)	4.99(43)	3.35(37)	4.68(39)	−0.11(32)	1.90(33)	−1.35(32)
N(3)	4.32(39)	3.79(38)	4.86(40)	−0.14(32)	2.47(33)	−0.58(32)
C(1)	6.46(60)	5.47(57)	4.28(49)	−0.08(48)	2.21(44)	−0.42(44)
C(2)	5.68(65)	6.18(69)	10.08(86)	1.79(56)	0.33(59)	0.18(63)
C(3)	3.64(48)	6.45(62)	4.77(50)	−0.13(45)	−0.27(39)	0.37(46)
C(4)	6.13(60)	4.68(55)	5.60(55)	0.71(47)	0.47(46)	1.85(47)
C(5)	3.99(46)	2.51(42)	5.95(52)	−0.02(36)	1.03(40)	0.11(38)
C(6)	5.54(56)	7.64(69)	3.18(44)	0.82(52)	−0.14(40)	0.77(46)

*t.f. = $\exp -2\pi^2 10^{-2} (U_{11}h^2a^{*2} + \ldots + 2U_{12}hka^*b^* + \ldots)$.

TABLE 2. Bond lengths (Å) and angles (deg), with standard deviations in parentheses

Bond	Distance (Å)	Bond	Distance (Å)
I(1)—I(2)	2.823(1)	N(3)—P(3)	1.600(7)
I(1)—N(1)	2.417(7)	P(1)—C(1)	1.785(9)
N(1)—P(1)	1.650(7)	P(1)—C(2)	1.805(11)
N(1)—P(3)	1.623(7)	P(2)—C(3)	1.787(8)
N(2)—P(1)	1.597(7)	P(2)—C(4)	1.786(9)
N(2)—P(2)	1.596(7)	P(3)—C(5)	1.783(8)
N(3)—P(2)	1.599(7)	P(3)—C(6)	1.789(8)

Bonds	Angle (deg)	Bonds	Angle (deg)
I(2)—I(1)—N(1)	177.8(2)	C(2)—P(1)—N(1)	111.1(5)
I(1)—N(1)—P(1)	118.5(3)	C(2)—P(1)—N(2)	108.8(5)
I(1)—N(1)—P(3)	117.3(3)	C(3)—P(2)—N(2)	108.4(4)
		C(3)—P(2)—N(3)	108.5(4)
N(1)—P(1)—N(2)	113.9(3)	C(4)—P(2)—N(2)	110.7(4)
N(2)—P(2)—N(3)	115.7(3)	C(4)—P(2)—N(3)	109.3(4)
N(3)—P(3)—N(1)	114.6(3)	C(5)—P(3)—N(3)	109.1(4)
		C(5)—P(3)—N(1)	108.4(4)
P(1)—N(2)—P(2)	123.4(4)	C(6)—P(3)—N(3)	111.0(4)
P(2)—N(3)—P(3)	124.2(4)	C(6)—P(3)—N(1)	109.1(4)
P(3)—N(1)—P(1)	124.5(4)		
		C(1)—P(1)—C(2)	106.5(5)
C(1)—P(1)—N(1)	107.5(4)	C(3)—P(2)—C(4)	103.5(5)
C(1)—P(1)—N(2)	108.7(4)	C(5)—P(3)—C(6)	104.0(5)

final $R = 0.053$ for the 1934 observed reflexions and a final difference synthesis showed no anomalous features. Positional and thermal parameters are given in Table 1, and measured and calculated structure factors have been placed in the Depository of Unpublished Data.[1]

Discussion

The phosphazene ring (Fig. 1) is slightly non-planar, with a chair conformation, the ring atoms being alternately above and below the (unweighted) mean plane by an average of 0.06 Å. Such minor deviations from planarity are typical of the situation in other cyclotriphosphazenes, and the displacements have been ascribed to intra- and intermolecular steric effects (7).

The I_2 molecule lies approximately in the mean ring plane, and one of the iodine atoms is bonded to a nitrogen atom (Fig. 1), the N—I—I grouping being close to linear, 177.8(2)° (Table 2). The N—I bond distance, 2.417(7) Å, is considerably greater than the sum of the covalent radii, 2.03 Å, very much less than the sum of the van der Waals radii, 3.65 Å, and slightly longer than the corresponding distances, 2.26–2.31 Å, in

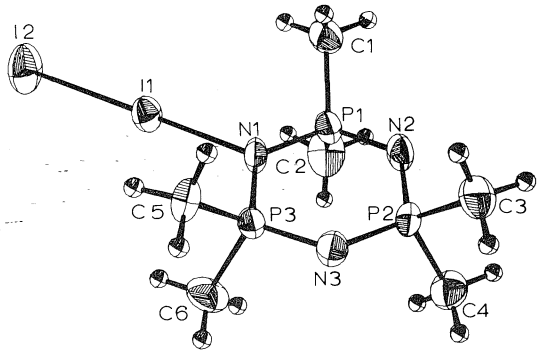

FIG. 1. View of the molecule of the $N_3P_3Me_6.I_2$ complex; H atoms are at calculated positions.

charge-transfer complexes of I_2 or ICl with pyridine (8), trimethylamine (9, 10), and γ-picoline (11). The N—I bond in the present structure therefore appears to represent a charge-transfer interaction which involves donation of the nitrogen non-bonding electron-pair into an antibonding orbital of the I_2 molecule. The longer N—I bond, in comparison with the complexes in refs. 8–11, suggests a weaker interaction in the present case, so that the cyclophosphazene is a poorer electron donor than the other molecules. This is in accord with the involvement of the lone-pair electrons of the nitrogen atom in

[1]The structure factor table is available, at a nominal charge, from the Depository of Unpublished Data, National Science Library, National Research Council of Canada, Ottawa, Canada K1A 0S2.

Can. J. Chem. Downloaded from www.nrcresearchpress.com by 210.87.254.40 on 09/05/12
For personal use only.

one of the two π-systems of the phosphazene ring (12).

The I—I bond length, 2.823(1) Å, is greater than in the free I_2 molecule, 2.67 Å, but close to the distance of 2.83 Å in trimethylamine.I_2 (9) and γ-picoline.I_2 (11). The increases in bond length in comparison with the free molecule support the donation of electrons into antibonding orbitals of the I_2 molecule. The linear N—I—I grouping is found in the present compound and in the other complexes.

The P—N bonds involving the nitrogen atom bonded to iodine, 1.650(7) and 1.623(7), mean 1.64 Å, are lengthened in comparison with the other four bonds, 1.596–1.600(7), mean 1.598 Å, and with bonds in unperturbed phosphazene rings, *e.g.* 1.596 Å in $N_4P_4Me_8$ (13). This is again in accord with the involvement of nitrogen lone-pair electrons in bonding to iodine, with a resulting reduction in their availability for ring π-bonding. The elongated bonds are not as long as the corresponding bonds in protonated rings, 1.67–1.69 Å (1–4) but are more comparable to those in rings complexed to metal atoms, 1.62–1.63 Å (4–6), an indication of the relative electron accepting powers of H^+, I_2, and the metal atoms.

The mean P—N—P and N—P—N angles are 124.0 and 114.7° respectively, slightly closer to the values in a parent cyclotriphosphazene, $N_3P_3(NMe_2)_6$, 123.0 and 116.7° (7), than are the values in the corresponding protonated ring, $N_3P_3(NMe_2)_6H^+$, 128 and 111° (3). The angles involving the nitrogen bonded to iodine differ slightly from the others (Table 2), but the differences are barely significant.

The P—C bonds are all equivalent, mean length 1.789 Å, and mean C—P—C is 104.7°. Intermolecular contacts correspond to van der Waals interactions; the shortest distances are 3.58 and 3.67 Å for N(3)...C(6) and N(2)...C(4) respectively.

We thank Professor N. L. Paddock and Mr. T. W. J. Mah for crystals, the University of British Columbia Computing Centre for assistance, and the National Research Council of Canada for financial support.

1. J. TROTTER and S. H. WHITLOW. J. Chem. Soc. A, 460 (1970).
2. N. V. MANI and A. J. WAGNER. Acta Cryst. B**27**, 51 (1971).
3. A. L. MACDONALD and J. TROTTER. Can. J. Chem. **52**, 734 (1974).
4. J. TROTTER and S. H. WHITLOW. J. Chem. Soc. A, 455 (1970).
5. W. C. MARSH and J. TROTTER. J. Chem. Soc. A, 1482 (1971).
6. W. HARRISON and J. TROTTER. J. Chem. Soc. Dalton Trans. 61 (1973).
7. S. J. RETTIG and J. TROTTER. Can. J. Chem. **51**, 1295 (1973).
8. O. HASSEL and C. RØMMING. Acta Chem. Scand. **10**, 696 (1956); **11**, 195 (1957).
9. K. O. STRØMME. Acta Chem. Scand. **13**, 268 (1959).
10. O. HASSEL and H. HOPE. Acta Chem. Scand. **14**, 391 (1960).
11. O. HASSEL, C. RØMMING, and T. TUFTE. Acta Chem. Scand. **15**, 967 (1961).
12. D. P. CRAIG and N. L. PADDOCK. *In* Nonbenzenoid aromatics, Vol. 2. Academic Press, New York. 1971.
13. M. W. DOUGILL. J. Chem. Soc. 5471 (1961).
14. N. L. PADDOCK and T. W. J. MAH. To be published.

Can. J. Chem. Downloaded from www.nrcresearchpress.com by 210.87.254.40 on 09/05/12
For personal use only.

Thermodynamique de composés azotés. I. Etude calorimétrique des enthalpies de sublimation des trois acides aminobenzoïques

RAPHAËL SABBAH, RAYMOND CHASTEL ET MARC LAFFITTE

Centre de Recherches de Microcalorimétrie et de Thermochimie du C.N.R.S. – 26, Rue du 141ème R.I.A., 13003 Marseille, France

Reçu le 30 octobre 1973

RAPHAËL SABBAH, RAYMOND CHASTEL et MARC LAFFITTE. Can. J. Chem. **52**, 2201 (1974).

La mesure des enthalpies de sublimation des trois acides aminobenzoïques a été faite aux trois températures 367.35, 376.75 et 389.95 K en utilisant un microcalorimètre Tian–Calvet équipé d'une cellule d'effusion.

Nous avons pu obtenir les enthalpies de référence de sublimation à 298.15 K en utilisant les courbes $(\Delta H_{sub})_m(T) = f(T)$. Celles-ci sont égales à (104.9 ± 1.0), (128.0 ± 3.2) et (116.1 ± 3.7) kJ mol^{-1} respectivement pour les acides amino-2, amino-3 et amino-4 benzoïques.

A partir des contributions énergétiques apportées par le noyau benzénique et les deux fonctions acide et amine, que l'on trouve dans la littérature, nous avons pu calculer l'enthalpie de sublimation de l'isomère *para*. La comparaison du résultat obtenu avec la valeur expérimentale montre que les contributions utilisées sont correctes.

En utilisant certaines données structurales, nous avons essayé d'interpréter les différences que l'on observe pour les enthalpies de sublimation des isomères *ortho* et *méta* par rapport au dérivé *para*.

Enfin, à titre indicatif et approximatif, nous avons calculé la pression de vapeur saturante de ces acides aux trois températures ci-dessus mentionnées ainsi que le libre parcours moyen de leurs molécules.

RAPHAËL SABBAH, RAYMOND CHASTEL, and MARC LAFFITTE. Can. J. Chem. **52**, 2201 (1974).

The measurement of enthalpies of sublimation of three aminobenzoic acids was made at 367.35, 376.75, and 389.95 K using a Tian–Calvet microcalorimeter equipped with an effusion cell.

From the curves $(\Delta H_{sub})_m(T) = f(T)$, it was possible to obtain the values for the standard enthalpies of sublimation of the compounds at 298.15 K: (104.9 ± 1.0), (128.0 ± 3.2), and (116.1 ± 3.7) kJ mol^{-1}, respectively, for the 2-aminobenzoic acid, the 3-aminobenzoic acid, and the 4-aminobenzoic acid.

The experimental $(\Delta H_{sub}{}^0)_m$ (298.15 K) values can be accounted for quantitatively from the various contributions (benzene ring, amine, and carboxylic group) obtained from similar compounds.

With the help of structural data, we have tried to explain the differences between the enthalpies of these compounds.

We also report here the calculated saturation vapor pressure of these acids, as well as the mean free path of their molecules, at the three temperatures given above.

Introduction

La connaissance de l'enthalpie de changement d'état permet, d'une part, le calcul de l'enthalpie de formation d'un composé à l'état gazeux et, d'autre part, la détermination directe de l'énergie du réseau cristallin de ce composé. Au laboratoire, nous utilisons ces deux possibilités.

Le peu de données énergétiques concernant la liaison C—N nous a incités à nous intéresser à quelques composés la renfermant. Pour commencer, nous avons étudié les trois acides aminobenzoïques pour lesquels nous n'avons trouvé, dans la littérature, aucune indication concernant leurs enthalpies de combustion et de changement d'état.

Des résultats partiels relatifs à la combustion (1) et à la sublimation (2) de ces acides ont été communiqués.

Dans ce mémoire, il est question de la mesure de leurs enthalpies de sublimation et de l'interprétation des résultats obtenus.

Partie experimentale

Produits

Les acides aminobenzoïques que nous avons utilisés sont des produits Fluka. Comme leur degré de pureté est inférieur à 99%, nous les avons purifiés par sublimation.

Can. J. Chem. Downloaded from www.nrcresearchpress.com by 210.87.254.40 on 09/05/12
For personal use only.

TABLEAU 1.

Dérivé	Degré de pureté (mol %)	T (K)	Nombre de mesures	$(\Delta H_{sub})_m$ (T) (kJ mol^{-1})	$(\Delta H_{sub}{}^0)_m$ (298.15 K) (kJ mol^{-1})	p_{sat} (T)* (Torr)	$\lambda(T)$* (mm)
Acide amino-2 benzoïque	99.96	367.35	5	100.6±0.3		5.10^{-2}	0.3
		376.75	6	99.0±0.2	104.9±1.0	11	0.1
		389.95	5	99.2±1.2		63	0.02
Acide amino-3 benzoïque	99.95	367.35	7	123.0±3.3		1.10^{-3}	11
		376.75	10	122.4±3.3	128.0±3.2	4	3
		389.95	9	121.6±2.7		13	1
Acide amino-4 benzoïque	99.94	367.35	8	113.9±4.2		3.10^{-3}	5
		376.75	7	114.6±3.5	116.1±3.7	5	3
		389.95	5	113.5±2.2		12	1

*La reproductibilité des mesures est en moyenne de ±3.5%.

Le degré de pureté des échantillons expérimentés a été déterminé par analyse thermique (méthode de Skau). Les résultats ont été consignés dans le tableau 1.

Appareillage et technique opératoire

L'appareillage que nous avons utilisé a été décrit dans un mémoire précédent (3). Comme les acides aminobenzoïques ont, à 298.15 K, des pressions de vapeur trop faibles, nous avons été obligés d'élever la température du calorimètre jusqu'à 360 K.[1] A cette température, la pression de vapeur saturante des trois acides est comprise entre 10^{-2} et 10^{-3} Torr et les thermogrammes obtenus sont utilisables.

Toutes nos expériences ont été faites à 367.35, 376.75 et 389.95 K. Ces températures ont été déterminées à l'intérieur de la cellule calorimétrique en utilisant un thermocouple chromel–alumel étalonné. La précision sur les valeurs de T est de 0.05 K.

A chacune de ces températures et pour chacun des composés, nous avons respecté les conditions d'effusion moléculaire (3).

Afin d'ouvrir et de fermer à volonté l'orifice de la cellule d'effusion, le montage décrit (3) comporte un obturateur solidaire d'une tige métallique. Celle-ci traverse la ligne de vide et est en contact avec le milieu extérieur. La présence de cette tige crée un drain thermique entre la cellule calorimétrique où $T \geq 360$ K et la salle thermorégulée où $T = 293$ K.

Dans un premier temps, nous avons opéré comme indiqué précédemment (3). On déclanchait l'opération d'évaporation en manoeuvrant la tige porte-obturateur, c'est-à-dire en la remontant d'environ 10 mm. Cette opération entraînait la brusque élimination de la conduction de chaleur le long de la tige vers l'extérieur ce qui avait pour effet de décaler de façon importante la position du zéro expérimental en l'envoyant hors de l'échelle de mesure. L'utilisation des thermogrammes devenait alors délicate. Aussi, avons-nous été obligés d'opérer différemment.

Nous avons, tout d'abord, vérifié qu'il n'y avait pas de perte de masse appréciable de l'échantillon placé dans la cellule d'effusion pendant plusieurs heures à la température de l'expérience. Nous avons alors utilisé la technique opératoire suivante. Une masse connue d'échantillon est placée dans la cellule d'éffusion. Celle-ci est mise en place dans la cellule calorimétrique. On n'obture pas l'orifice d'effusion. L'ensemble est laissé sous pression atmosphérique pendant le temps de stabilisation thermique (1 à 3 h). Lorsque l'équilibre thermique est atteint, nous créons progressivement le vide dans toute l'installation. La sublimation démarre. Le thermogramme que nous enregistrons comprend à la fois un effet endothermique dû au phénomène de détente de la colonne d'air qui emplit la cellule calorimétrique et un second effet, toujours endothermique, dû à la sublimation.

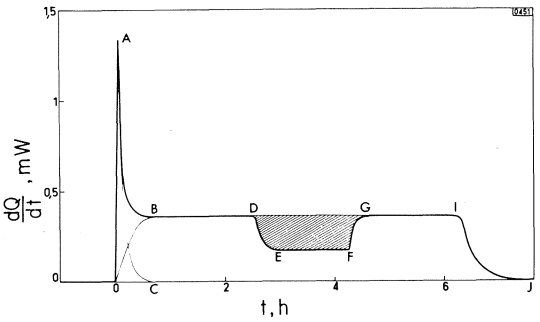

FIG. 1. Exemple de thermogramme enregistré au cours d'une sublimation.

Plusieurs expériences, faites en l'absence de substance dans la cellule d'effusion, ont montré que l'effet endothermique, dû à la détente de la colonne d'air, se traduit par un thermogramme très aigu dont la surface est proportionnelle à la hauteur du pic. La connaissance de cette relation permet de distinguer, dans une expérience de sublimation, la part d'énergie propre à chacun des deux effets.

La fig. 1 représente un thermogramme enregistré au cours d'une sublimation. Nous avons tracé, en traits fins, les deux effets décrits précédemment. Le triangle curviligne OAC représente l'effet de détente de la colonne d'air, la courbe OB, le début de la sublimation de l'é-

[1]Notons, toutefois, que le dérivé amino-2 benzoïque ayant une pression de vapeur plus élevée que les deux autres dérivés, commence à se sublimer, de façon appréciable, à 353 K.

Can. J. Chem. Downloaded from www.nrcresearchpress.com by 210.87.254.40 on 09/05/12
For personal use only.

Can. J. Chem. Downloaded from www.nrcresearchpress.com by 210.87.254.40 on 09/05/12
For personal use only.

chantillon contenu dans la cellule d'effusion. L'aire OBDGIJO représente son enthalpie de sublimation. L'aire hachurée DEFGD représente l'énergie dissipée dans le calorimètre par effet Joule pendant l'étalonnage.

Resultats[2]

Les courbes $(\Delta H_{sub})_m(T) = f(T)$ sont des droites (fig. 2). Leur extrapolation graphique fournit les valeurs de $(\Delta H_{sub})_m$ (298.15 K) (voir tableau 1). Bien qu'elle ait été appliquée à un ensemble de trois couples de valeurs pour chaque composé, la méthode des moindres carrés confirme les résultats obtenus par extrapolation graphique.

Compte tenu des faibles pressions de vapeur de ces acides, nous avons vérifié que $(\Delta H_{sub})_m$ $(p_{sat}, T) = (\Delta H_{sub}{}^0)_m$ $(p = 1$ atm, $T)$.

Nous avons montré, dans notre précédent mémoire (3), que lorsque a/A est de l'ordre de 10^{-2} (a = aire de l'orifice d'effusion et A = aire émissive), la pression qui règne à l'intérieur de la cellule d'effusion est effectivement la pression de vapeur saturante (p_{sat}). Dans ce travail, ce rapport varie de 0.133×10^{-3} (pour $a = 1.77 \times 10^{-8}$ m^2) à 1.92×10^{-2} (pour $a = 2.55 \times 10^{-6}$ m^2).

A titre indicatif et approximatif,[3] nous avons calculé, aux différentes températures, la pression $p = p_{sat}$ qui règne à l'intérieur de la cellule d'effusion ainsi que le libre parcours moyen des molécules en utilisant les relations suivantes:

$$p(T) = \frac{dm}{adt}\left(\frac{2\pi RT}{M}\right)^{1/2}\frac{1}{F}$$

$$\lambda(T) = \frac{1}{\sqrt{2\pi d^2 n}}$$

$p(T)$ = pression mesurée par effusion à la température T, dm/dt = masse de substance effusée par unité de temps, R = constante des gaz parfaits, M = masse molaire du composé, F = facteur de Clausing, d = diamètre d'une molécule, n = nombre de molécules par unité de volume.

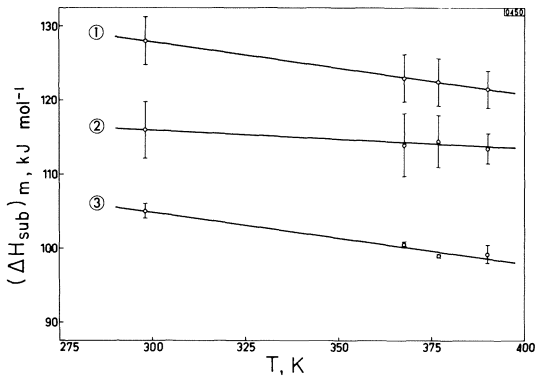

FIG. 2. Variation de l'enthalpie de sublimation des trois acides aminobenzoïques en fonction de la température: (*1*) acide amino-3 benzoïque; (*2*) acide amino-4 benzoïque; (*3*) acide amino-2 benzoïque.

Les résultats sont consignés dans le tableau 1. On remarquera que la reproductibilité (σ) des mesures de $(\Delta H_{sub})_m(T)$ est comprise entre 1 et 3.2%. Pour la calculer, nous avons utilisé la relation $\sigma = \pm\Sigma(g - \bar{g})/N$ dans laquelle g et $\bar{g}$ représentent respectivement la grandeur mesurée et sa valeur moyenne pour un nombre N de mesures. Pour l'intervalle de pressions qui nous intéresse, les valeurs de $(\Delta H_{sub})_m(T)$ que l'on trouve dans la littérature sont généralement obtenues par voie indirecte, c'est-à-dire à partir de mesures de pressions de vapeur en fonction de la température et en appliquant la loi de Clapeyron. L'incertitude qui accompagne ces valeurs est généralement comprise entre 5 et 10% suivant la pression.

Discussion

Plusieurs études effectuées sur des familles de composés bien définis ont eu pour but de déterminer, à partir de l'enthalpie de sublimation (ou de vaporisation), la contribution apportée à celle-ci par les différents chaînons qui constituent les molécules (4–11).

Il est bien connu qu'à l'état solide et en solution dans l'eau, les acides aminés peuvent exister sous forme de zwittérions. Ce caractère semble général pour les acides aminés dont la chaîne carbonée est aliphatique. Par contre, lorsque l'atome d'azote est lié à un noyau aromatique, les acides aminés existent à la fois sous formes moléculaire et zwittérionique (12–15).

Dans la littérature, nous n'avons, malheureuse-

[2]Notations utilisées: $(\Delta H_{sub})_m(T)$: enthalpie molaire de sublimation d'un composé à la température T et sous la pression de vapeur saturante p_{sat}. $(\Delta H_{sub}{}^0)_m(T)$: enthalpie molaire (de référence) de sublimation d'un composé à la température T et sous la pression de 1 atm. $P_{sat}(T)$: pression de vapeur saturante à l'équilibre solide–vapeur à la température T. dQ/dt: puissance mise en jeu lors d'une sublimation. $\lambda(T)$: libre parcours moyen d'une molécule à la température T.

[3]Car le temps et le diamètre de l'orifice d'effusion sont déterminés avec incertitude.

TABLEAU 2.

Dérivé	T_f (°C)*	$(\Delta H_{fus})_m$ (kJ mol^{-1})†	ρ (g cm^{-3})‡
Acide amino-2 benzoïque	146.1	20.38	1.412
Acide amino-3 benzoïque	177.9	21.84	1.511
Acide amino-4 benzoïque	187.0	20.92	1.374

*Référence 28.
†Référence 27.
‡Référence 29.

Can. J. Chem. Downloaded from www.nrcresearchpress.com by 210.87.254.40 on 09/05/12
For personal use only.

ment, pas trouvé d'étude radiocristallographique pour l'acide amino-3 (dérivé *méta*). Cependant, Gopal *et al.* (16) ont montré, par spectroscopie i.r., que ce composé se trouve à l'état de zwittérion dans le cristal. Les acides amino-2 (dérivé *ortho*) et amino-4 (dérivé *para*) existent sous forme moléculaire en solution dans l'eau et à l'état solide (17). Toutefois, une récente étude du dérivé *ortho*, faite par Brown (18) par diffraction de rayons X, semble indiquer dans le cristal, à côté des formes moléculaires, la présence de zwittérions.

Toutes les études qui ont été faites sur la structure cristalline des trois acides aminobenzoïques montrent l'existence de liaisons hydrogène intermoléculaires. Seul le dérivé *ortho* présente une liaison intramoléculaire (18). Cette particularité est justifiée par les observations suivantes: (*1*) Des trois isomères, le dérivé *ortho* a la pression de vapeur saturante la plus forte quelle que soit la température (voir tableau 2). (*2*) Comparé au dérivé *para*, l'acide *ortho* aminobenzoïque est moins soluble dans l'eau et dans l'alcool éthylique (19). (*3*) Respectivement par spectroscopie i.r. et u.v., Peltier et Pichevin (20) d'une part, Dearden et Forbes (21) d'autre part, ont montré que le dérivé *ortho* présente une chélation.

Comme dans le réseau cristallin, le dérivé *para* se trouve à l'état moléculaire et ne présente pas de liaison intramoléculaire, nous avons cherché à retrouver son enthalpie molaire de sublimation à partir des contributions énergétiques apportées par le noyau benzénique et les deux fonctions acide et amine. Afin de tenir au mieux compte des interactions que peuvent avoir le noyau benzénique et les fonctions au sein du cristal, nous avons cherché à calculer ces contributions à partir de grandeurs énergétiques de molécules ayant une nature chimique voisine de celles qui nous intéressent. Dans le cas présent, le problème se simplifie du fait que nous possédons l'enthalpie de sublimation de l'acide benzoïque (22): celle-ci est égale à (89.74 ± 0.62) kJ mol^{-1}. Il suffit donc d'ajouter à cette valeur la contribution de chaînon NH_2.

Nous avons déterminé cette contribution en considérant les deux composés suivants: benzène et aniline et en recherchant dans la littérature les principales données qui nous permettaient de déterminer leur enthalpie de sublimation. Pour le benzène, cette enthalpie est (43.93 ± 0.84) kJ mol^{-1}. Pour l'aniline, qui est liquide à 298.15 K, son enthalpie de vaporisation, à cette température, est (55.834 ± 0.029) kJ mol^{-1} (23). Comme l'aniline fond à (267.13 ± 0.05) K (24), il est nécessaire de calculer cette enthalpie à cette température. Pour cela, nous avons utilisé les résultats obtenus par Hatton *et al.* (24) pour l'enthalpie de vaporisation de l'aniline à 298.15 et 333 K. Ces auteurs trouvent respectivement 55.764 et 52.576 kJ mol^{-1}, ce qui revient à considérer une variation dans la valeur de l'enthalpie de vaporisation de 91.50 J mol^{-1} K^{-1}. Nous trouvons pour l'enthalpie de vaporisation de l'aniline, à 267.13 K, la valeur 58.67 kJ mol^{-1}. Pour avoir l'enthalpie de sublimation de l'aniline, il suffit alors d'appliquer la relation $(\Delta H_{sub}{}^0)_m(T_f) = (\Delta H_{vap}{}^0)_m(T_f) + (\Delta H_{fus}{}^0)_m$. Comme l'enthalpie de fusion $(\Delta H_{fus}{}^0)_m$ de l'analine est comprise entre 10.54 kJ mol^{-1} (24) et 10.56 kJ mol^{-1} (25), nous trouvons pour $(\Delta H_{sub}{}^0)_m(T_f)$ la valeur 58.67 + 10.55 = 69.22 kJ mol^{-1}.

La contribution du chaînon NH_2 est donc de 69.22 − 43.93 = 25.29 kJ. L'enthalpie de sublimation du dérivé *para*, calculée à partir des différentes contributions, est 89.74 + 25.29 = 115.03 kJ mol^{-1}. Sa comparaison avec la valeur expérimentale (116.1 ± 3.7) kJ mol^{-1} montre que notre démarche est raisonnable.

Le dérivé *ortho* a pour enthalpie de sublimation une valeur inférieure de 11.2 kJ mol^{-1} à celle du dérivé *para*. Cette différence doit être attribuée au fait que la molécule d'acide amino-2 benzoïque présente moins de liaisons hydrogène

Can. J. Chem. Downloaded from www.nrcresearchpress.com by 210.87.254.40 on 09/05/12
For personal use only.

intermoléculaires que les deux autres dérivés. En effet, comme nous l'avons vu au début de cette discussion, elle est la seule à posséder une liaison hydrogène intramoléculaire et celle-ci ne participe pas à l'énergie du réseau cristallin. Dans une étude faite sur les deux isomères *ortho* et *para* de l'acide hydroxybenzoïque, Davies et Jones (8) avaient montré que l'enthalpie de sublimation du dérivé *ortho* était inférieure de 20.9 kJ mol^{-1} à celle du dérivé *para*. En comparant cette différence à la nôtre, nous sommes amenés à admettre que la chélation est moins forte dans l'acide amino-2 benzoïque qu'elle ne l'est dans l'acide hydroxy-2 benzoïque. Nous trouvons une confirmation à cette explication dans le travail de Peltier et Pichevin (20). En étudiant une série d'acides benzoïques substitués par spectroscopie i.r., ces auteurs montrent que le groupe OH apparaît nettement plus chélaté que le groupe NH_2.

En ce qui concerne l'acide amino-3 benzoïque, son enthalpie de sublimation est supérieure de 11.9 kJ mol^{-1} à celle de l'acide amino-4 benzoïque. Il nous est possible d'expliquer cette différence de la façon suivante. Comme l'isomère *méta* se trouve à l'état de zwittérion dans le cristal et qu'il n'existe pas de composé sous forme zwittérionique à l'état gazeux, il y a lieu de considérer, au moment de la sublimation, le passage, dans le cristal, de cet acide de la forme zwittérionique à la forme moléculaire. Ce passage, qui se traduit par un transfert de proton, met en jeu une certaine quantité d'énergie qui serait, dans le présent cas, de 11.9 kJ mol^{-1}. Takagi *et al.* (26) ont estimé que l'énergie liée au transfert de proton dans le cristal de glycine est de 29.3 à 41.8 kJ mol^{-1}.

Enfin, comme la masse volumique (ρ) et l'enthalpie de fusion $(\Delta H_{fus})_m$ du dérivé *méta* sont supérieures à celles des deux autres dérivés (voir tableau 2), nous pensons que l'existence de zwittérion dans le cristal doit renforcer les interactions électrostatiques, ce qui a pour effet de rendre l'édifice cristallin plus compact.

1. J. DELAFONTAINE, R. SABBAH et M. LAFFITTE. Communic. réunion des sections du sud de la Soc. chim. Fr. Bordeaux, 23–25 novembre 1972. Bull. Soc. chim. Fr. (1973), 5b, 45.
2. R. SABBAH, R. CHASTEL et M. LAFFITTE. Communic. 3ème Confér. internat. de thermodynam. chim. IUPAC. Baden, Autriche. 3–7 septembre 1973, **1**, 30.
3. R. SABBAH, R. CHASTEL et M. LAFFITTE. Thermochim. Acta, **5**, 117 (1972).
4. K. KUSANO et I. WADSO. Acta Chem. Scand. **25**, 219 (1971).
5. E. G. LOVERING et O. M. NOR. Can. J. Chem. **40**, 199 (1962).
6. J. B. GREENSHIELDS et F. D. ROSSINI. J. Phys. Chem. **62**, 271 (1958).
7. A. BONDI. J. Chem. Eng. Data, **8**, 371 (1963).
8. M. DAVIES et J. I. JONES. Trans. Faraday Soc. **50**, 1042 (1954).
9. M. DAVIES et B. KYBETT. Trans. Faraday Soc. **61**, 1608 (1965).
10. R. S. BRADLEY et T. G. CLEASBY. J. Chem. Soc. 1681, 1690 (1953).
11. D. P. BACCANARI, J. A. NOVINSKI, Y. C. PAN, M. M. YEVITZ et H. A. SWAIN. Trans. Faraday Soc. **64**, 1201 (1968).
12. H. H. JAFFE. J. Am. Chem. Soc. **77**, 4445 (1955).
13. R. W. GREEN et H. K. TONG. J. Am. Chem. Soc. **78**, 4896 (1956).
14. H. P. STEPHENSON et H. SPONER. J. Am. Chem. Soc. **79**, 2050 (1957).
15. L. D. TAYLOR. J. Org. Chem. **27**, 4064 (1962).
16. L. GOPAL, C. I. JOSE et A. B. BISWAS. Spectrochim. Acta, **23**A, 513 (1967).
17. A. THEORET. Spectrochim. Acta, **27**A, 11 (1971).
18. C. J. BROWN. Proc. R. Soc. A, **302**, 185 (1968).
19. C. D. HODGMAN. (*Editor*). Handbook of chemistry and physics. The Chemical Rubber Publishing Co., Cleveland, Ohio (1963).
20. D. PELTIER et A. PICHEVIN. Bull. Soc. Chim. Fr. 1141 (1960).
21. J. C. DEARDEN et W. F. FORBES. Can. J. Chem. **38**, 1837 (1960).
22. R. CHASTEL, F. STECKEL et H. TACHOIRE. Proc. Int. Conf. Calorimetry Thermodynamics, 1st, Warszawa, 1969. Warszawa, Polish scientific publishers (s.d). p. 155.
23. K. KUSANO et I. WADSO. Bull. Chem. Soc. Jap. **44**, 1705 (1971).
24. W. E. HATTON, D. L. HILDEBRANDT, G. C. SINKE et D. R. STULL. J. Chem. Eng. Data, **7**, 229 (1962).
25. G. S. PARKS, H. M. HUFFMAN et M. BARMORE. J. Am. Chem. Soc. **55**, 2733 (1933).
26. S. TAKAGI, H. CHIHARA et S. SEKI. Bull. Chem. Soc. Jap. **32**, 84 (1959).
27. D. H. ANDREWS, G. LYNN et J. JOHNSTON. J. Am. Chem. Soc. **48**, 1274 (1926).
28. P. LAZZEL et J. JOHNSTON. J. Phys. Chem. **32**, 1331 (1928).
29. F. K. BEILSTEINS (*Editor*). Handbuch der organischen Chemie, Vierte Auflage, Zweites Ergïzungswerk, Vierzehnter Band, Springer–Verlag, Berlin 1951, p. 246.

Crystal and Molecular Structure of the *N*-Methyldiethanolaminogallane Dimer, $[CH_3N(CH_2CH_2O)_2GaH]_2$

STEVEN J. RETTIG, ALAN STORR, AND JAMES TROTTER

Department of Chemistry, University of British Columbia, Vancouver, British Columbia V6T 1W5

Received January 24, 1974

STEVEN J. RETTIG, ALAN STORR, and JAMES TROTTER. Can. J. Chem. **52**, 2206 (1974).

Crystals of the *N*-methyldiethanolaminogallane dimer are orthorhombic, $a = 19.112(4)$, $b = 9.947(2)$, $c = 7.709(2)$ Å, $Z = 4$, space group $P2_12_12_1$. The structure was determined by Patterson and Fourier synthesis and was refined by full-matrix least-squares procedures to a final R of 0.056 for 1477 observed reflections. The structure provides the first[1] known crystallographic example of pentacoordinate gallium, the dimerization of $MeN(CH_2CH_2O)_2GaH$ occurring via the formation of a four-membered Ga_2O_2 ring. The coordination about the gallium is distorted trigonal bipyramidal with an angle of 151.2(4)° between the axial substituents. The mean bond distances are: Ga—N, 2.192(5), and Ga—O, 2.018(2) for axial ligands; Ga—O, 1.847(2), 1.960(8), and Ga—H, 1.41(4) for equatorial ligands; O—C, 1.419(14), C—N, 1.470(7), C—C, 1.520(12), and C—H, 1.00(13) Å. The molecule has C_2 symmetry to within experimental error. There are possible C—H...O hydrogen bonds (C...O, 3.13(1)-3.44(1) Å) in the structure.

STEVEN J. RETTIG, ALAN STORR et JAMES TROTTER. Can. J. Chem. **52**, 2206 (1974).

Les cristaux du dimère du *N*-méthyldiéthanolaminogallane sont orthorhombiques; le groupe d'espace est $P2_12_12_1$ avec $a = 19.112(4)$, $b = 9.947(2)$, $c = 7.709(2)$ Å et $Z = 4$. La structure est déterminée par les techniques de Patterson et de Fourier et elle est affinée à l'aide d'une matrice entière des moindres carrés, pour 1477 réflexions observées, à une valeur finale de R de 0.056. La structure fournit le premier[1] exemple cristallographique connu de gallium pentacoordonné; la dimérisation du $MeN(CH_2CH_2O)_2GaH$ se produit par la formation d'un cycle à quatre de Ga_2O_2. La coordination du gallium est de forme bipyramide trigonale déformée avec un angle de 151.2(4)° entre les substituants axiaux. Les distances moyennes des liaisons sont: Ga—N, 2.192(5), et Ga—O, 2.018(2) pour les ligands axiaux: Ga—O, 1.847(2), 1.960(8) et GaH, 1.41(4) pour les ligands équatoriaux; O—C, 1.419(14), C—N, 1.470(7), C—C, 1.520(12) et C—H, 1.00(13) Å. La molécule a une symétrie C_2 dans les limites de l'erreur expérimentale. Il y a les ponts hydrogène C—H...O, (C...O, 3.13(1)–3.44(1) Å) possibles dans la structure.

[Traduit par le journal]

Introduction

Trimethylamine-gallane is known to react with compounds containing active hydrogen to eliminate molecular hydrogen and trimethylamine and form coordinatively unsaturated intermediates which then undergo cyclization to give oligomers whose size depends upon a balance between steric, mechanistic, and valency angle effects (1–3). The present work is part of an extension of this type of reaction involving aminoalcohols where the active hydrogen is attached to oxygen and/or nitrogen atoms. The title compound is derived from *N*-methyldiethanolamine and trimethylamine-gallane reacted in 1:1 molar ratio. In the title compound four coordination about the gallium atom can be achieved in monomer units, analogous to similar boron compounds (4–7), by coordination of two oxygen atoms, one nitrogen atom, and the remaining hydrogen atom, after elimination of two moles of hydrogen and one mole of trimethylamine from the reaction sphere. The metal is indeed coordinated to these atoms but instead of discrete monomer units a novel dimerization through bridging oxygen atoms is realized, to give a distorted trigonal bipyramidal arrangement about each five-coordinate gallium atom (**1**).

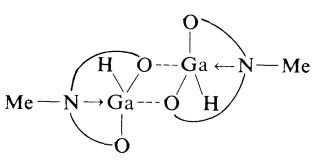

1

[1]A brief description of the structure of the five-coordinate Ga(III) complex: chlorobis-(8-hydroxy-2-methyl-quinolato)gallium(III) by Dymock and Palenik (26) appeared after this manuscript had been submitted for publication.

Can. J. Chem. Downloaded from www.nrcresearchpress.com by 210.87.254.40 on 09/05/12
For personal use only.

TABLE 1. Results of Hamilton's test

Parameter compared	Value for enantiomorph (A)	(B)	(B/A)	Significance level*
Conventional R (observed F)	6.126	6.210	1.0137	>99.5
Conventional R (all F)	6.491	6.573	1.0125	>99.5
Weighted R (observed F)	8.738	8.878	1.0161	>99.5
Weighted R (all F)	9.162	9.232	1.0145	>99.5

*This is the % probability that enantiomorph (A) is the correct absolute configuration.

Experimental

The *N*-methyldiethanolaminogallane dimer was prepared by reacting *N*-methyldiethanolamine (0.226 g, 1.9 mmol) with trimethylamine-gallane (0.250 g, 1.9 mmol) in benzene solvent. Hydrogen (84.5 ml; 3.77 mmol) was evolved at room temperature to leave the product in benzene as a clear solution:

$$MeN(CH_2CH_2OH)_2 + Me_3NGaH_3 \rightarrow MeN(CH_2CH_2O)_2GaH + 2H_2 + Me_3N$$

Removal of all volatiles gave a white air-sensitive solid.

Anal. Calcd. for $MeN(CH_2CH_2O)_2GaH$: Ga, 37.1; hydrol. H, 0.53. Found: Ga, 36.9; hydrol. H, 0.54.

The compound was redissolved in benzene and the solution cooled to 5 °C. Large colorless crystals were deposited from solution after a prolonged period of time. Crystals suitable for X-ray analysis were positioned in capillaries under a nitrogen atmosphere to avoid the rapid hydrolysis which occurred in contact with moist air. The capillaries were then flame sealed.

The crystal chosen for study was mounted with the $[\bar{2}11]$ vector parallel to the goniostat axis and had dimensions of *ca.* 0.3 × 0.3 × 0.5 mm. Unit-cell and space group data were obtained from film and diffractometer measurements. The unit-cell parameters were refined by a least-squares treatment of $\sin^2\theta$ values for 30 reflections measured on a diffractometer with CuKα radiation. Crystal data are:

$C_{10}H_{24}Ga_2N_2O_4$ f.w. = 375.8

Orthorhombic, $a = 19.112(4)$, $b = 9.947(2)$, $c = 7.709(2)$ Å, $V = 1465.5(5)$ Å^3, $Z = 4$, $\rho_c = 1.703(1)$ g cm^{-3}, $F(000) = 768$ (20 °C, CuKα, $\lambda = 1.5418$ Å, $\mu = 49.7$ cm^{-1}). Absent reflections: $h00$, $h \neq 2n$, $0k0$, $k \neq 2n$, and $00l$, $l \neq 2n$ define uniquely the space group $P2_12_12_1$ (D_2^4, No. 19).

Intensities were measured on a Datex-automated General Electric XRD 6 diffractometer, with a scintillation counter, CuKα radiation (nickel filter and pulse height analyzer), and a θ–2θ scan at 2° min^{-1} over a range of (1.80 + 0.86 tan θ) degrees in 2θ, with 20 s background counts being measured at each end of the scan. Data were measured to $2\theta = 145°$ (minimum interplanar spacing 0.81 Å). A check reflection was monitored every 40 reflections throughout the data collection. The r.m.s. deviation of the intensity of the check reflection from its initial value was 2.2% and the final intensity was 1.014 times the initial value. Lorentz and polarization corrections were applied, and the structure amplitudes were derived. No absorption correction was attempted due to the irregularity of the crystal surface (in particular reentrant angles). Of the 1697 independent reflections measured, 180 had intensities less than $3\sigma(I)$ above background where $\sigma^2(I) = S + B + (0.05S)^2$ with S = scan count and B = background count, corrected to time of scan. These reflections were classified as unobserved.

Structure Analysis

The positions of the two gallium atoms were determined from the three-dimensional Patterson function. Three cycles of full-matrix least-squares refinement of the positional and isotropic thermal parameters of the gallium atoms gave $R = 0.27$. A difference map revealed the positions of all the C, N, and O atoms. All the non-hydrogen atoms were refined isotropically for three cycles giving $R = 0.096$ and then anisotropically for two cycles giving $R = 0.076$. A difference map revealed the positions of the gallium H atoms and 12 of the 16 methylene protons. The remaining hydrogen atoms were started in calculated positions. The hydrogen atoms were included in all subsequent cycles of refinement with isotropic temperature factors. The refinement was concluded after four more cycles with $R = 0.056$ for 1477 observed reflections (40 reflections were given zero weight in the final stages of refinement due to suspected extinction or counter errors).

The absolute configuration of the complex (for the particular crystal used) has been determined through the anomalous scattering of the non-hydrogen atoms. Enantiomorph (A) is represented by the coordinates in Table 2 referred to a right-handed axial system and enantiomorph (B), the mirror image of (A), was generated by changing the x coordinates of (A) to $1 - x$. Both enantiomorphs were refined and Hamilton's test (8) applied to the resulting R factor ratios. Enantiomorph (A) was clearly indicated as correct. The results of Hamilton's test are compiled in Table 1.

The least-squares refinement was based on the minimization of $\Sigma w(F_o - F_c)^2$. The scattering factors of ref. 9 were used for the non-hydrogen atoms and those of ref. 10 for the hydrogen atoms. Anomalous scattering factors from ref. 11 were used for Ga, O, N, and C atoms. The anisotropic thermal parameters employed in the refinement are U_{ij} in the expression:

$$f = f^0 \exp[-2\pi^2(U_{11}h^2a^{*2} + U_{22}k^2b^{*2} + U_{33}l^2c^{*2} + 2U_{12}hka^*b^* + 2U_{13}hla^*c^* + 2U_{23}klb^*c^*)]$$

where f^0 is the tabulated scattering factor and f is that corrected for thermal motion. The weighting scheme: $w = 1$ if $|F_o| \leq 11$; $w = (11/|F_o|)^2$ if $|F_o| > 11$, and $w = 0.49$ for the unobserved reflections gave constant

Can. J. Chem. Downloaded from www.nrcresearchpress.com by 210.87.254.40 on 09/05/12
For personal use only.

Can. J. Chem. Downloaded from www.nrcresearchpress.com by 210.87.254.40 on 09/05/12
For personal use only.

average values of $w(F_o - F_c)^2$ over ranges of $|F_o|$ and was employed in the final stages of refinement. A final difference map showed maximum fluctuations of 0.8 e/Å^3 in the vicinity of the gallium atoms and 0.35 e/Å^3 elsewhere.

On the final cycle of refinement the mean parameter shift was 0.29σ, the largest shifts were 0.85σ for non-hydrogen and 1.70σ for hydrogen atoms, both of which were associated with the C(10) methyl group. The final positional and thermal parameters are given in Tables 2 and 3 respectively. Measured and calculated structure factor amplitudes have been placed in the Depository of Unpublished Data.[2]

Thermal Motion and Correction of Molecular Geometry

The ellipsoids of thermal motion for the non-hydrogen atoms are shown in Fig. 1. The thermal motion has been analyzed in terms of the rigid-body modes of translation (**T**), libration (**L**), and screw (**S**) motion using the computer program MGTLS (12). The r.m.s. standard deviation in the temperature factors U_{ij} is 0.0042 Å^2 which indicates that the thermal motion of the molecule as a whole (r.m.s. $\Delta U_{ij} = 0.0054$ Å^2) is adequately described by the rigid-body parameters in Table 4. The indicated modes of motion are physically reasonable; the translational and librational motions are both somewhat anisotropic. The orientation of the principal axes of **L** is nearly coincident with that of the principal axes of inertia, the largest librational motion occurring about the least axis of inertia.

The appropriate bond distances and angles have been corrected for libration (13, 14), using shape parameters q^2 of 0.08 for all the atoms involved, and appear in Tables 5 and 6, respectively.

Results and Discussion

The X-ray analysis has provided the first known crystallographic example of pentacoordinate gallium as well as the first reported Ga—H distances. The numbering scheme is shown in Fig. 1, in which the molecule is viewed along its approximate C_2 axis. Figure 2 shows the coordination about the gallium atoms and Fig. 3 shows the crystal structure viewed along *c*. Ga—N and Ga—O bond distances in related four and six-coordinate structures are compiled in Table 7. The dihedral angles in the five fused rings of the molecule are given in Table 8. Selected inter- and intramolecular contacts are listed in Table 9.

The molecule has C_2 symmetry within the limits of experimental error. The bond distances, valence angles, and dihedral angles averaged assuming C_2 symmetry also appear in the appropriate tables and will be employed in the discussion of the molecular geometry. The molecule exhibits, in part, the structure expected for the monomeric boron analog (on the basis of the

TABLE 2. Final positional parameters (fractional × 10^4, Ga × 10^5, H × 10^3) with estimated standard deviations in parentheses

Atom	*x*	*y*	*z*
Ga(1)	41623(5)	20988(9)	38421(13)
Ga(2)	40777(5)	27950(8)	76738(12)
O(1)	4292(3)	1238(5)	6085(7)
O(2)	3291(4)	2739(6)	3234(10)
O(3)	4335(3)	3645(5)	5470(8)
O(4)	3170(4)	2235(6)	8000(9)
N(1)	3704(4)	126(7)	3277(10)
N(2)	3662(4)	4807(7)	8153(11)
C(1)	3999(6)	−794(8)	4579(14)
C(2)	4036(6)	−97(8)	6316(13)
C(3)	2961(5)	424(9)	3574(18)
C(4)	2800(5)	1779(9)	2715(16)
C(5)	3837(9)	−343(12)	1516(18)
C(6)	4032(5)	5690(8)	6919(15)
C(7)	4118(6)	4996(8)	5206(13)
C(8)	2928(5)	4611(9)	7696(15)
C(9)	2686(5)	3265(9)	8447(17)
C(10)	3763(7)	5237(11)	9954(16)
H(Ga1)	475(5)	217(9)	282(11)
H(Ga2)	461(4)	268(7)	899(9)
H(1A)	445(5)	−90(10)	430(14)
H(1B)	365(5)	−151(9)	463(12)
H(2A)	426(8)	−81(14)	713(18)
H(2B)	353(5)	5(11)	653(15)
H(3A)	290(6)	34(12)	476(18)
H(3B)	258(6)	−27(10)	312(13)
H(4A)	273(4)	165(8)	141(11)
H(4B)	241(10)	194(17)	304(26)
H(5A)	342(10)	−102(20)	142(29)
H(5B)	380(8)	32(18)	76(22)
H(5C)	426(5)	−41(10)	131(13)
H(6A)	460(6)	566(13)	735(15)
H(6B)	375(7)	641(13)	679(17)
H(7A)	443(7)	548(14)	467(18)
H(7B)	377(7)	490(12)	460(15)
H(8A)	289(5)	434(11)	629(17)
H(8B)	276(11)	516(19)	859(28)
H(9A)	263(6)	318(11)	997(15)
H(9B)	213(6)	290(11)	795(14)
H(10A)	334(8)	598(19)	990(22)
H(10B)	340(9)	453(17)	1086(24)
H(10C)	431(6)	548(12)	1021(15)

[2]The structure factor table is available, at a nominal charge, from the Depository of Unpublished Data, National Science Library, National Research Council of Canada, Ottawa, Canada K1A 0S2.

TABLE 3. Final thermal parameters and their estimated standard deviations

(*a*) Anisotropic thermal parameters ($U_{ij} \times 100$ Å^2)

Atom	U_{11}	U_{22}	U_{33}	U_{12}	U_{13}	U_{23}
Ga(1)	5.47(6)	3.23(5)	4.90(6)	−0.30(4)	0.36(4)	0.20(4)
Ga(2)	5.16(6)	2.86(5)	4.97(6)	0.08(4)	−0.27(4)	0.14(4)
O(1)	5.8(3)	3.1(2)	4.7(3)	0.5(2)	0.0(3)	0.2(2)
O(2)	7.5(4)	2.9(3)	8.1(4)	−0.1(3)	−1.9(3)	1.4(3)
O(3)	6.3(3)	2.8(2)	5.1(3)	−0.9(2)	0.1(3)	0.2(2)
O(4)	6.5(3)	3.1(3)	7.5(4)	−0.1(3)	1.0(3)	0.4(3)
N(1)	5.7(4)	3.1(3)	5.5(4)	−0.1(3)	−0.5(3)	0.3(3)
N(2)	5.6(4)	2.9(3)	6.3(4)	0.1(3)	0.5(3)	0.5(3)
C(1)	6.5(6)	3.2(4)	6.5(5)	0.7(4)	−0.9(5)	−0.1(4)
C(2)	6.8(6)	3.6(4)	5.3(5)	−0.1(4)	−0.6(4)	0.6(4)
C(3)	5.8(5)	3.7(4)	9.0(8)	−0.1(4)	−0.5(5)	0.7(5)
C(4)	5.9(5)	4.2(4)	8.3(7)	−0.1(4)	−1.8(5)	1.1(4)
C(5)	9.3(10)	4.9(5)	7.1(7)	−0.4(6)	0.6(7)	−0.8(5)
C(6)	6.3(6)	2.7(4)	7.6(6)	−0.5(4)	0.7(5)	0.0(4)
C(7)	6.3(5)	3.7(4)	6.0(5)	−0.7(4)	1.0(5)	1.0(4)
C(8)	5.8(5)	3.5(4)	7.1(6)	−0.5(3)	0.5(4)	0.9(4)
C(9)	6.0(5)	3.8(4)	9.0(7)	0.6(4)	1.8(5)	1.4(4)
C(10)	10.1(9)	4.2(5)	6.6(6)	0.5(5)	−0.4(6)	−1.4(5)

(*b*) Isotropic thermal parameters

Atom	B (Å^2)	Atom	B (Å^2)
H(Ga1)	3.9(19)	H(Ga2)	2.3(13)
H(1A)	4.3(21)	H(6A)	7.0(29)
H(1B)	3.0(17)	H(6B)	5.4(28)
H(2A)	8.8(30)	H(7A)	6.5(29)
H(2B)	3.6(21)	H(7B)	4.3(28)
H(3A)	4.8(27)	H(8A)	2.6(23)
H(3B)	4.0(20)	H(8B)	11.9(52)
H(4A)	1.7(12)	H(9A)	3.0(24)
H(4B)	12.3(51)	H(9B)	10.2(23)
H(5A)	17.4(50)	H(10A)	13.7(44)
H(5B)	8.0(40)	H(10B)	4.7(47)
H(5C)	2.1(18)	H(10C)	5.2(24)

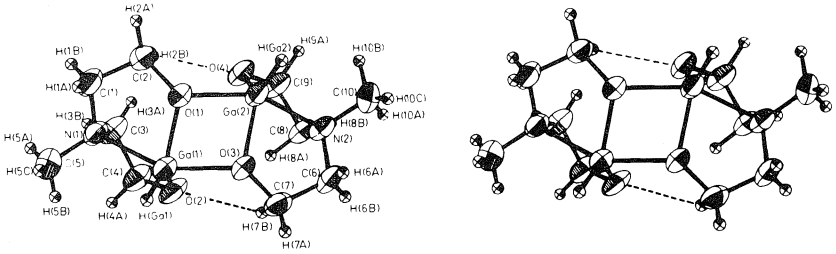

FIG. 1. A stereo view of the molecule along the C_2 axis showing the atom numbering and 50% probability thermal ellipsoids for the non-hydrogen atoms. Broken lines show possible C—H...O hydrogen bonds.

structures of triethanolamine borate (5), *B,B*-diphenylboroxazolidine (6), and *B,B*-bis(*p*-fluorophenyl)boroxazolidine (7), and supporting chemical evidence (4)) in that the $MeN(CH_2CH_2O)_2$ acts as a tridentate ligand, the nitrogen and two oxygen atoms all being coordinated to the same gallium atom. Here the similarity to the boron compounds ends as dimerization occurs through bridging oxygen atoms, creating a four-membered Ga_2O_2 ring which results in the formation of a molecule possessing a system of five fused rings. A polymeric structure might be

Can. J. Chem. Downloaded from www.nrcresearchpress.com by 210.87.254.40 on 09/05/12
For personal use only.

TABLE 4. Rigid-body thermal parameters for all non-hydrogen atoms

L ($\times 10$ deg^2)	49(9)	−14(9)	−4(8)
		157(21)	46(13)
			69(15)

Principal axes of L

r.m.s. amplitude	Direction cosines ($\times 10^3$)		
4.2°	−108	914	392
2.2	−506	288	−833
2.2	−856	−286	430

Principal axes of reduced T

r.m.s. amplitude	Direction cosines ($\times 10^3$)		
0.23Å	−1	−268	−963
0.22	997	−73	20
0.16	−76	−960	267

Displacement of axes from intersecting (Å)

Parallel to L_1	0.65
Parallel to L_2	−0.53
Parallel to L_3	−0.32

Effective screw translations (Å)

Parallel to L_1	0.036
Parallel to L_2	−0.039
Parallel to L_3	−0.031

Fractional coordinates of unique origin ($\times 10^4$)

x	3862
y	2358
z	5740

Fractional coordinates of center of gravity ($\times 10^4$)

x	3818
y	2462
z	5721
r.m.s. ΔU_{ij} (Å^2)	0.0054

*Axes of reference are orthogonal Angstrom axes. E.s.d.'s of components of L are given in parentheses in units of the last place shown.

expected of the compound produced by the reaction of trimethylamine-gallane and *N*-methyldiethanolamine even though gallium has a high tendency to form four-membered rings with oxygen (15, 16). Thus polymerization through nitrogen or oxygen atoms (*i.e.* the $MeN(CH_2CH_2O)_2$ acting as a bridging ligand) to form large heterocycles with tetrahedral coordination about the gallium atoms was originally suspected.

The resulting structure contains pentacoordinate gallium atoms with distorted trigonal bipyramidal geometry. The nitrogen and two oxygen atoms of each $MeN(CH_2CH_2O)_2$ ligand occupy respectively an axial and two equatorial positions about the associated gallium atom. One of the oxygen atoms bridges the two gallium atoms, occupying an axial position of the second gallium atom. The remaining equatorial site is occupied by the hydrogen atom (see Fig. 2).

The axial Ga—N distance of 2.192(5) Å is longer than the observed distances for tetrahedral (mean 1.97 Å) and for octahedral gallium (mean 2.12 Å) shown in Table 7. The distance compares well with a sterically similar bond in octahedral $GaH(EDTA).H_2O$ (17) of 2.182(5) Å and the axial Al—N distance of 2.18 Å in $AlH_3(NMe_3)_2$ (18). The bond nevertheless appears to be weaker than a normal single bond as a result of steric strain as in the related amino-alcohol boron compounds (5–7). The three types of Ga—O bonds are all significantly different. The equatorial non-bridging distance is 1.847(2) Å and for the bridging oxygen the equatorial distance is 1.960(8) and the axial is 2.018(2) Å. The equatorial bonds involve sp^2 hybrids at the gallium atoms which reduces the covalent radius of gallium to 1.21 Å for these bonds. The expected equatorial Ga—O distance is then about 1.87 Å. The mean Ga—O distances in related four-coordinate and octahedral complexes are 1.96 and 1.959 Å respectively. In this structure the 1.847 Å "terminal" Ga—O distance corresponds to a strong bond while the bridge bonds, 1.960 and 2.018 Å, seem to be of nearly equal strength considering that one is axial and the other equatorial and both these distances are within the range of previously reported Ga—O bond lengths (see Table 7). Using an effective radius of 0.23 Å for hydrogen (19), the expected Ga—H bond length is 1.44 Å in good agreement with the mean Ga—H distance of 1.41(4) Å.

The distortion of the trigonal bipyramid occurs as a deformation of the angle between the axial groups from the ideal 180 to 151.2(4)°. The equatorial GaOOH groups are both planar within experimental error and the mean O—Ga—O, 119.3(2)°, and O—Ga—H angles, 120.3°, are close to the expected 120°. The equatorial – Ga – axial angles range from 76° (in the four-membered ring) to 104° (mean N—Ga—H), each 14° from the ideal 90°. The angular distortions are a result of the steric constraints inherent in the fused ring system.

The four-membered Ga_2O_2 ring is non-planar with all intra-annular dihedral angles equal within experimental error, the mean value being 21.6°. Angles in the ring are 76.0(3) at Ga and 100.0(2)° at O. The ring is different from the

Can. J. Chem. Downloaded from www.nrcresearchpress.com by 210.87.254.40 on 09/05/12
For personal use only.

TABLE 5. Bond lengths (Å) with estimated standard deviations in parentheses

(*a*) Non-hydrogen atoms

Bond	Distance (Å)		Bond	Distance (Å)		
	Uncorrected	Corrected		Uncorrected	Corrected	Mean*
Ga(1)—O(1)	1.945(6)	1.952	Ga(2)—O(3)	1.960(6)	1.967	1.960(8)
Ga(1)—O(2)	1.843(7)	1.848	Ga(2)—O(4)	1.839(7)	1.845	1.847(2)
Ga(1)—O(3)	2.012(6)	2.016	Ga(2)—O(1)	2.016(6)	2.019	2.018(2)
Ga(1)—N(1)	2.193(7)	2.196	Ga(2)—N(2)	2.184(7)	2.187	2.192(5)
O(1)—C(2)	1.427(10)	1.429	O(3)—C(7)	1.422(10)	1.424	1.427(3)
O(2)—C(4)	1.398(11)	1.399	O(4)—C(9)	1.422(11)	1.424	1.412(13)
N(1)—C(1)	1.471(12)	1.475	N(2)—C(6)	1.475(12)	1.479	1.477(2)
N(1)—C(3)	1.468(13)	1.471	N(2)—C(8)	1.460(12)	1.464	1.468(4)
N(1)—C(5)	1.458(15)	1.460	N(2)—C(10)	1.466(14)	1.468	1.464(4)
C(1)—C(2)	1.510(14)	1.512	C(6)—C(7)	1.499(14)	1.501	1.507(6)
C(3)—C(4)	1.533(13)	1.535	C(8)—C(9)	1.531(12)	1.533	1.534(1)

(*b*) Bonds involving hydrogen atoms

Bond	Distance (Å)	Bond	Distance (Å)
Ga(1)—H(Ga1)	1.37(8)	Ga(2)—H(Ga2)	1.45(7)
C(1)—H(1A)	0.90(10)	C(6)—H(6A)	1.14(12)
C(1)—H(1B)	0.98(9)	C(6)—H(6B)	0.90(13)
C(2)—H(2A)	1.04(14)	C(7)—H(7A)	0.87(14)
C(2)—H(2B)	0.99(10)	C(7)—H(7B)	0.82(12)
C(3)—H(3A)	0.93(14)	C(8)—H(8A)	1.12(13)
C(3)—H(3B)	1.06(11)	C(8)—H(8B)	0.94(20)
C(4)—H(4A)	1.02(8)	C(9)—H(9A)	1.18(11)
C(4)—H(4B)	0.81(19)	C(9)—H(9B)	1.20(11)
C(5)—H(5A)	1.05(20)	C(10)—H(10A)	1.10(18)
C(5)—H(5B)	0.89(18)	C(10)—H(10B)	1.21(16)
C(5)—H(5C)	0.83(9)	C(10)—H(10C)	1.09(12)

*Average of corrected bonds related by the C_2 axis, numbers in parentheses is r.m.s. deviation from the mean.

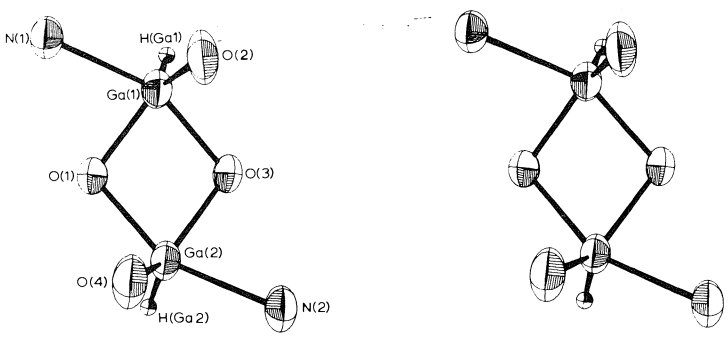

FIG. 2. A view of the coordination about the gallium atoms.

planar centrosymmetric Ga_2O_2 ring in the octahedral complex $[Ga_2(OH)_2Cl_2(C_{14}H_{17}N_3)_2]Cl_2 . H_2O$ (16) in which there is one strong and one weak Ga—O bond (1.908 and 2.017 Å).

The difference between the "terminal" and "bridging" oxygen atoms is carried into the five-membered GaOCCN rings which have distinct geometries which may be ascribed to steric and electronic differences between the two classes of rings. The mean dihedral angles in each type of ring are compared with those obtained from energy minimization calculations (20) in Table 8. The conformational differences between the two types of five-membered rings are small yet the rings with the "bridging" oxygen atoms (A rings) have a conformation which is closest to

Can. J. Chem. Downloaded from www.nrcresearchpress.com by 210.87.254.40 on 09/05/12
For personal use only.

TABLE 6. Bond angles (deg) with estimated standard deviations in parentheses

(*a*) Non-hydrogen atoms

Bonds	Angle (deg)		Bonds	Angle (deg)		
	Uncorrected	Corrected		Uncorrected	Corrected	Mean*
O(1)—Ga(1)—O(2)	119.5(3)	119.5	O(3)—Ga(2)—O(4)	119.1(3)	119.1	119.3(2)
O(1)—Ga(1)—O(3)	76.2(2)	76.2	O(3)—Ga(2)—O(1)	75.8(2)	75.7	76.0(3)
O(1)—Ga(1)—N(1)	80.4(3)	80.4	O(3)—Ga(2)—N(2)	80.9(3)	80.9	80.7(3)
O(2)—Ga(1)—O(3)	92.5(3)	92.5	O(4)—Ga(2)—O(1)	92.4(3)	92.4	92.5(1)
O(2)—Ga(1)—N(1)	84.1(3)	84.0	O(4)—Ga(2)—N(2)	84.9(3)	84.9	84.5(5)
O(3)—Ga(1)—N(1)	150.9(3)	150.8	O(1)—Ga(2)—N(2)	151.6(3)	151.6	151.2(4)
Ga(1)—O(1)—Ga(2)	100.1(2)	100.2	Ga(2)—O(3)—Ga(1)	99.7(2)	99.8	100.0(2)
Ga(1)—O(1)—C(2)	118.5(5)	118.5	Ga(2)—O(3)—C(7)	117.3(6)	117.3	117.9(6)
Ga(2)—O(1)—C(2)	124.8(5)	124.7	Ga(1)—O(3)—C(7)	125.8(6)	125.7	125.2(5)
Ga(1)—O(2)—C(4)	116.4(5)	116.4	Ga(2)—O(4)—C(9)	115.4(5)	115.3	115.9(6)
Ga(1)—N(1)—C(1)	105.6(5)	105.5	Ga(2)—N(2)—C(6)	105.2(5)	105.2	105.4(2)
Ga(1)—N(1)—C(3)	100.1(5)	100.1	Ga(2)—N(2)—C(8)	100.7(5)	100.8	100.5(4)
Ga(1)—N(1)—C(5)	113.7(7)	113.6	Ga(2)—N(2)—C(10)	112.3(6)	112.3	113.0(7)
C(1)—N(1)—C(3)	113.0(8)	112.9	C(6)—N(2)—C(8)	112.6(8)	112.6	112.8(2)
C(1)—N(1)—C(5)	111.6(8)	111.7	C(6)—N(2)—C(10)	112.0(8)	112.0	111.9(2)
C(3)—N(1)—C(5)	112.2(9)	112.3	C(8)—N(2)—C(10)	113.2(9)	113.2	112.8(5)
N(1)—C(1)—C(2)	109.7(7)	109.8	N(2)—C(6)—C(7)	110.2(7)	110.3	110.1(3)
N(1)—C(3)—C(4)	107.7(8)	107.7	N(2)—C(8)—C(9)	108.4(8)	108.4	108.1(4)
C(1)—C(2)—O(1)	109.5(7)	109.4	C(6)—C(7)—O(3)	109.9(8)	109.9	109.7(3)
C(3)—C(4)—O(2)	110.0(8)	110.1	C(8)—C(9)—O(4)	110.0(8)	110.0	110.1(1)

(*b*) Angles involving hydrogen atoms

Bonds	Angle (deg)	Bonds	Angle (deg)
O(1)—Ga(1)—H(Ga1)	115(4)	O(3)—Ga(2)—H(Ga2)	118(3)
O(2)—Ga(1)—H(Ga1)	125(4)	O(4)—Ga(2)—H(Ga2)	123(3)
O(3)—Ga(1)—H(Ga1)	101(4)	O(1)—Ga(2)—H(Ga2)	103(3)
N(1)—Ga(1)—H(Ga1)	105(4)	N(2)—Ga(2)—H(Ga2)	102(3)
N(1)—C(1)—H(1A)	106(7)	N(2)—C(6)—H(6A)	105(6)
N(1)—C(1)—H(1B)	102(5)	N(2)—C(6)—H(6B)	104(8)
C(2)—C(1)—H(1A)	103(7)	C(7)—C(6)—H(6A)	98(6)
C(2)—C(1)—H(1B)	109(5)	C(7)—C(6)—H(6B)	109(8)
H(1A)—C(1)—H(1B)	126(8)	H(6A)—C(6)—H(6B)	129(10)
O(1)—C(2)—H(2A)	125(8)	O(3)—C(7)—H(7A)	113(9)
O(1)—C(2)—H(2B)	103(6)	O(3)—C(7)—H(7B)	102(9)
C(1)—C(2)—H(2A)	104(7)	C(6)—C(7)—H(7A)	104(9)
C(1)—C(2)—H(2B)	100(7)	C(6)—C(7)—H(7B)	118(8)
H(2A)—C(2)—H(2B)	113(11)	H(7A)—C(7)—H(7B)	110(12)
N(1)—C(3)—H(3A)	105(7)	N(2)—C(8)—H(8A)	109(5)
N(1)—C(3)—H(3B)	118(6)	N(2)—C(8)—H(8B)	94(12)
C(4)—C(3)—H(3A)	119(8)	C(9)—C(8)—H(8A)	98(6)
C(4)—C(3)—H(3B)	107(5)	C(9)—C(8)—H(8B)	98(12)
H(3A)—C(3)—H(3B)	101(9)	H(8A)—C(8)—H(8B)	146(15)
O(2)—C(4)—H(4A)	117(4)	O(4)—C(9)—H(9A)	104(6)
O(2)—C(4)—H(4B)	114(13)	O(4)—C(9)—H(9B)	107(5)
C(3)—C(4)—H(4A)	110(4)	C(8)—C(9)—H(9A)	118(6)
C(3)—C(4)—H(4B)	103(13)	C(8)—C(9)—H(9B)	115(5)
H(4A)—C(4)—H(4B)	103(15)	H(9A)—C(9)—H(9B)	103(8)
N(1)—C(5)—H(5A)	98(12)	N(2)—C(10)—H(10A)	94(9)
N(1)—C(5)—H(5B)	111(10)	N(2)—C(10)—H(10B)	107(9)
N(1)—C(5)—H(5C)	112(7)	N(2)—C(10)—H(10C)	111(6)
H(5A)—C(5)—H(5B)	111(14)	H(10A)—C(10)—H(10B)	89(11)
H(5A)—C(5)—H(5C)	133(13)	H(10A)—C(10)—H(10C)	124(11)
H(5B)—C(5)—H(5C)	91(12)	H(10B)—C(10)—H(10C)	125(10)

*Mean of angles related by the C_2 axis, number in parentheses is the r.m.s. deviation from the mean.

Can. J. Chem. Downloaded from www.nrcresearchpress.com by 210.87.254.40 on 09/05/12
For personal use only.

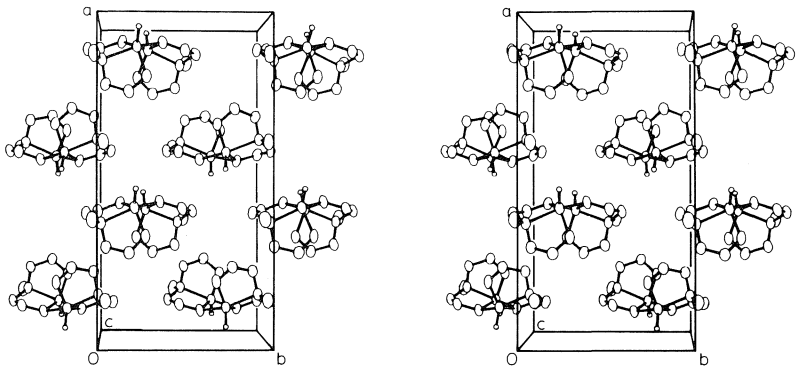

FIG. 3. The packing arrangement viewed along *c*.

TABLE 7. Comparison of Ga—O and Ga—N bond distances

Compound	Ga coordination number	Distance (Å)		Reference
		Ga—O	Ga—N	
GaN	4		1.94	21
$(H_2GaNCH_2CH_2)_3$	4		1.97	2
$[D_2Ga(N_2C_3H_3)]_2$	4		1.980	3
$[(CH_3)_2GaOH]_4$	4	1.94, 1.98		22
$(CH_3)_3NGaH_3$	4		1.97	23
$[CH_3N(CH_2CH_2O)_2GaH]_2$	5	1.843–2.019	2.187, 2.196	This work
$[Ga_2(OH)_2Cl_2(C_{14}H_{17}N_3)_2]Cl_2.H_2O$	6	1.908, 2.017	2.083–2.132	16
$GaH(EDTA).H_2O$	6	1.924–1.996	2.097, 2.182	17
$[GaCl_2(bipy)_2]^+[GaCl_4]^-$	6		2.097, 2.105	24
$GaCl_3(terpy)$	6		2.034–2.115	25

TABLE 8. Intra-annular dihedral angles (deg)

(*a*) Five-membered rings

Bond	ω_{obs}	Bond	ω_{obs}	Mean	ω_{calc}
Ga(1)—O(1)	2.1(5)	Ga(2)—O(3)	3.4(5)	2.8(7)	5.0
O(1)—C(2)	−25.0(8)	O(3)—C(7)	−26.4(8)	−25.7(7)	−29.8
C(2)—C(1)	43.3(8)	C(7)—C(6)	44.1(8)	43.7(4)	43.0
C(1)—N(1)	−39.8(7)	C(6)—N(2)	−39.2(7)	−39.5(3)	−40.0
N(1)—Ga(1)	21.4(5)	N(2)—Ga(2)	20.1(5)	20.8(7)	21.8
Ga(1)—O(2)	1.2(5)	Ga(2)—O(4)	2.7(5)	2.0(8)	1.3
O(2)—C(4)	−27.5(8)	O(4)—C(9)	−28.3(8)	−27.9(4)	−27.1
C(4)—C(3)	50.3(9)	C(9)—C(8)	49.6(9)	50.0(4)	42.3
C(3)—N(1)	−44.1(7)	C(8)—N(2)	−42.6(7)	−43.4(8)	−41.6
N(1)—Ga(1)	25.3(6)	N(2)—Ga(2)	23.5(5)	24.4(11)	25.0

(*b*) Four-membered ring

Bond	ω_{obs}
Ga(1)—O(1)	−21.3(2)
O(1)—Ga(2)	22.0(2)
Ga(2)—O(3)	−21.2(2)
O(3)—Ga(1)	21.9(2)

Can. J. Chem. Downloaded from www.nrcresearchpress.com by 210.87.254.40 on 09/05/12
For personal use only.

TABLE 9. (*a*) Selected intra- and intermolecular contacts

Intramolecular		Intermolecular*	
Atoms	Distance (Å)	Atoms	Distance (Å)
C(2)...C(3)	2.99(2)	O(4)...C(3)[1]	3.44(1)
C(7)...C(8)	3.00(1)	Ga(1)...H(10C)[2]	3.41(12)
C(4)...C(5)	3.04(2)	Ga(2)...H(6A)[2]	3.30(12)
C(9)...C(10)	3.07(2)	Ga(2)...H(5B)[3]	3.46(18)
C(2)...H(3A)	2.52(12)	Ga(2)...H(2A)[4]	3.48(15)
C(7)...H(8A)	2.58(11)	O(1)...H(6A)[2]	2.50(12)
C(3)...H(2B)	2.55(11)	O(2)...H(10B)[5]	2.57(17)
C(9)...H(10B)	2.68(18)	C(4)...H(9A)[5]	2.56(11)
H(2B)...H(3A)	1.84(17)	C(9)...H(4A)[3]	2.79(8)
H(7B)...H(8A)	2.20(16)	H(1B)...H(9B)[1]	2.40(14)
H(9A)...H(10B)	2.10(19)	H(4A)...H(9A)[5]	1.90(15)

(*b*) Gallium coordination sphere

Atoms	Distance (Å)	Atoms	Distance (Å)
Ga(1)...Ga(2)	3.038(2)	O(1)...O(3)	2.442(8)
O(1)...O(2)	3.273(8)	O(3)...O(4)	3.275(9)
O(1)...N(1)	2.678(10)	O(3)...N(2)	2.695(10)
O(2)...O(3)	2.787(9)	O(4)...O(1)	2.785(9)
O(2)...N(1)	2.716(9)	O(4)...N(2)	2.728(9)
O(1)...H(Ga1)	2.82(8)	O(3)...H(Ga2)	2.92(7)
O(2)...H(Ga1)	2.86(9)	O(4)...H(Ga2)	2.90(8)
O(3)...H(Ga1)	2.63(8)	O(1)...H(Ga2)	2.73(7)
N(1)...H(Ga1)	2.87(9)	N(2)...H(Ga2)	2.86(7)

(*c*) Possible C—H...O hydrogen bonds†

D—H...A	D...A	H...A	∠DHA	∠XAH
C(7)—H(7B)...O(2)	3.14(1)	2.56(12)	129(10)	82(3), 158(3)
C(2)—H(2B)...O(4)	3.13(1)	2.55(11)	118(8)	88(3), 154(2)
C(3)—H(3B)...O(4)[1]	3.44(1)	2.43(11)	160(8)	144(3), 101(3)

*Superscripts refer to atoms at positions: [1] $1/2 - x, -y, z - 1/2$; [2] $1 - x, y - 1/2, 3/2 - z$; [3] $x, y, 1 + z$; [4] $1 - x, 1/2 + y, 3/2 - z$; [5] $x, y, z - 1$.
†The H...O...H angle at O(4) is 59(3)°.

that calculated for $\omega_1 = 5.0°$ while those containing the "terminal" oxygens (B rings) have a conformation nearest to that calculated for $\omega_1 = 25.0°$. Both ring types show the same strain relative to the minimum energy conformations but the B rings show higher strain (4.0° r.m.s. deviation between ω_{calc} and ω_{obs} compared to 2.4° for the A rings), this occurring primarily in the twist about the C—C bonds.

Bond angles in the A rings range from 80.7(3)° at Ga to 117.9(6)° at O and in the B rings from 84.5(5)° at Ga to 115.9(6)° at O with mean values of 104.8 and 103.8° in A and B rings respectively compared to the calculated value of 104.2° (20) and observed values in BOCCN rings of 104.8 (6) and 104.9° (7). The C—O, C—C, and C—N distances are 1.427(3), 1.507(6), and 1.477(2) Å in the A rings and 1.412(13), 1.534(1), and 1.468(4) Å in the B rings. The differences in the bond lengths and angles in the two types of rings are a result of steric and electronic differences between the corresponding atoms in the ring, and to some extent are indicative of the charge distribution in the molecule. The mean C—O, C—C, and C—N distances in the two structures with BOCCN rings (6, 7) are 1.416(3), 1.500(6), and 1.488(3) Å. The mean N—C (methyl) distance of 1.464(4) Å in the present structure is as expected. The mean angle at nitrogen is 109.4° but the individual angles all differ significantly from the mean and range from 100.5(4)° for Ga—N—C (B ring) to 113.0(7)° for Ga—N—C (methyl). The angle at N between the A and B rings is 112.8(2)°. The

Can. J. Chem. Downloaded from www.nrcresearchpress.com by 210.87.254.40 on 09/05/12
For personal use only.

distortion of the nitrogen tetrahedron results from steric constraints imposed by the fused-ring system.

The mean C—H distance of 1.00(13) Å is as expected for X-ray data (19). All angles involving hydrogen atoms (R—C—H, R = N, O, C, H) are within three standard deviations of the mean value of 109°.

The crystal structure consists of discrete $[CH_3N(CH_2CH_2O)_2GaH]_2$ molecules which are separated by normal van der Waals distances, the shortest of which are listed in Table 9, except for one C—H...O interaction (C...O = 3.44(1) Å) which may correspond to a weak hydrogen bond. There are also two possible intramolecular C—H...O hydrogen bonds present (related by the two-fold rotation axis) which are indicated by broken lines in Fig. 1. The geometrical data for these C—H...O interactions are given in Table 9. The asymmetry introduced by the intermolecular O(4)...H(3B)—C(3) interaction is a reasonable explanation for the difference between the C(4)—O(2), 1.399, and C(9)—O(4), 1.424 Å, bond distances (which represents the largest deviation from C_2 symmetry in the molecule). The non-bonded contacts in the gallium coordination spheres and other intramolecular non-bonded contacts which correspond to steric interactions within the molecule are also listed in Table 9.

The infrared spectrum of the title compound in benzene solution showed a very strong Ga—H stretching absorption at 1900 cm^{-1} with a weak shoulder at 1810 cm^{-1}. A medium intensity band at 770 cm^{-1} is assigned to the Ga—H wagging mode. The low frequency spectrum displayed a number of absorptions attributable to "Ga—O", "Ga—N", and ring modes (615 sh, 595 vs, 540 vs, 510 vs, 420 s, 390 s, 380 sh) but no assignment of this part of the spectrum is attempted at this time.

Coates and Hayter (15), by chemical tests, postulated that dimerization in $[Me_2NCH_2CH_2OGaMe_2]_2$ probably occurs via a four-membered Ga_2O_2 ring leaving the gallium atoms four-coordinate and the normally stronger nitrogen donor atoms not utilized in coordinate-type bonding. It is tempting, as a result of the present study, to postulate that in the above dimer five-coordinate gallium atoms might again be featured, the bonding about the metal atoms again involving both nitrogen and oxygen atoms to give a fused-ring system. This possibility is under study for the analogous gallane dimer, $[Me_2NCH_2CH_2OGaH_2]_2$.

We thank the National Research Council of Canada for financial support, and the University of British Columbia Computing Centre for assistance.

1. A. Storr, B. S. Thomas, and A. D. Penland. J. Chem. Soc. Dalton, 328 (1972).
2. W. Harrison, A. Storr, and J. Trotter. J. Chem. Soc. Dalton, 1554 (1972).
3. D. F. Rendle, A. Storr, and J. Trotter. J. Chem. Soc. Dalton, 2252 (1973).
4. H. K. Zimmermann. Adv. Chem. Ser. No. **42**, 23 (1964).
5. Z. Taira and K. Osaki. Inorg. Nucl. Chem. Lett. **7**, 509 (1971).
6. S. Rettig and J. Trotter. Can. J. Chem. **51**, 1288 (1973).
7. S. Rettig and J. Trotter. Acta Cryst. B**30**, Submitted for publication.
8. W. C. Hamilton. Acta Cryst. **18**, 502 (1965).
9. D. T. Cromer and J. B. Mann. Acta Cryst. A**24**, 321 (1968).
10. R. F. Stewart, E. R. Davidson, and W. T. Simpson. J. Chem. Phys. **42**, 3175 (1965).
11. D. T. Cromer and D. Liberman. J. Chem. Phys. **53**, 1891 (1970).
12. V. Schomaker and K. N. Trueblood. Acta Cryst. B**24**, 63 (1968).
13. D. W. J. Cruickshank. Acta Cryst. **9**, 747, 754 (1956).
14. D. W. J. Cruickshank. Acta Cryst. **14**, 896 (1961).
15. G. E. Coates and R. G. Hayter. J. Chem. Soc. 2519 (1953).
16. K. Dymock, G. J. Palenik, and A. J. Carty. Chem. Commun., 1218 (1972).
17. C. H. L. Kennard. Inorg. Chim. Acta, **1**, 347 (1967).
18. C. W. Heitsch, C. E. Nordman, and R. W. Parry. Inorg. Chem. **2**, 508 (1963).
19. M. R. Churchill. Inorg. Chem. **12**, 1213 (1973).
20. J. B. Hendrickson. J. Am. Chem. Soc. **83**, 4537 (1961); **85**, 4059 (1963).
21. R. Juza and H. Hahn. Z. Anorg. Chem. **239**, 282 (1938).
22. G. S. Smith and J. L. Hoard. J. Am. Chem. Soc. **81**, 3907 (1959).
23. J. L. Calderon, F. A. Cotton, and A. Shaver. J. Organometal. Chem. **37**, 127 (1972).
24. R. Restivo and G. J. Palenik. Chem. Commun. 867 (1969).
25. G. Beran, A. J. Carty, H. A. Patel, and G. J. Palenik. Chem. Commun. 222 (1970).
26. G. J. Dymock and K. Palenik. Chem. Commun. 884 (1973).

Can. J. Chem. Downloaded from www.nrcresearchpress.com by 210.87.254.40 on 09/05/12
For personal use only.

Homogeneous Catalysis of Hydrogen Isotope Exchange between D_2 and Ethanol by Chlorotris(triphenylphosphine)rhodium(I). I. in Benzene–Ethanol[1]

GRAEME STRATHDEE AND RUSSELL GIVEN

Research Chemistry Branch, Atomic Energy of Canada Limited, Whiteshell Nuclear Research Establishment, Pinawa, Manitoba R0E 1L0

Received October 22, 1973

GRAEME STRATHDEE and RUSSELL GIVEN. Can. J. Chem. **52**, 2216 (1974).

The kinetics and mechanism of D_2–C_2H_5OH exchange catalyzed by chlorotris(triphenylphosphine)rhodium(I) have been studied in 50 volume percent benzene–ethanol. In this mixed solvent, the rate of exchange was low and was limited by the rate of transfer of deuterium from dideuteridochlorotris(triphenylphosphine)rhodium(III) to the solvent, and not by the rate of activation of D_2. The activation energy for the overall process was relatively low, 35 kJ mol^{-1}. In addition, new data have been presented for the catalysis of H_2–D_2 exchange in benzene by $RhCl(PPh_3)_3$. Analysis of the apparent HD:D_2 isotope effect that is observed during D_2–C_2H_5OH exchange suggests that this effect originates with the relative stabilities of the D_2, HD, and H_2 adducts with $RhCl(PPh_3)_3$, or by control of the HD and H_2 product distribution by the H_2–D_2 equilibration reaction.

GRAEME STRATHDEE et RUSSELL GIVEN. Can. J. Chem. **52**, 2216 (1974).

On a étudié, pour une solution à 50% par volume d'éthanol dans le benzène, la cinétique et le mécanisme de l'échange D_2–C_2H_5OH catalysé par le chlorotris(triphénylphosphine)rhodium(I). Dans ce solvant mixte, le taux d'échange est bas et limité par le taux de transfert du deutérium du dideutério chlorotris(triphénylphosphine)rhodium(III) au solvant et non par le taux d'activation du deutérium. L'énergie d'activation pour la réaction globale est relativement basse soit 35 kJ par mole. De plus on présente de nouvelles données pour l'échange H_2–D_2 dans le benzène catalysé par $RhCl(PPh_3)_3$. Une analyse de l'effet isotopique apparant HD:D_2 qui est observé durant l'échange D_2–C_2H_5OH indique que l'origine de cet effet est la stabilité relative des composés d'addition de D_2, HD et H_2 avec $RhCl(PPh_3)_3$ ou un contrôle de la distribution des produits de HD et H_2 par une réaction d'équilibre entre H_2 et D_2.

[Traduit par le journal]

Introduction

The major stimulus for this work has been the need for novel catalysts which actively promote deuterium exchange for application in improved processes for the enrichment of deuterium. This isotope of hydrogen is an essential nuclear material, but must be concentrated from its natural abundance level of about 120–155 p.p.m. in hydrogenous molecules to greater than 99.9% as D_2O for use as a reactor moderator and coolant. To accomplish this, deuterium is preferentially enriched in one component of a binary mixture by equilibration (1). Although proton exchange reactions occur spontaneously between many pairs of molecules, other reactions, particularly those of practical importance, must be catalyzed. For example, conventional supported or oxide-promoted metal catalysts have been employed to accelerate the transfer of D between hydrogen and water (H_2–H_2O) (2, 3). Also, the strongly basic hydroxide (4), amide (5), and methylamide (6) anions respectively promote H_2–H_2O, H_2–NH_3, and H_2–CH_3NH_2 exchange in solution. In contrast, complexes of the transition metal ions, which are known to catalyze many conversions involving hydrocarbons, (7, 8), have not been systematically examined for their abilities to enhance the rates of H–D isotope exchange between hydrogenous molecules.

During the course of this work, Eberhardt *et al.* (9) reported that several complexes of Rh, Ru, Ir, and Os promote D transfer between D_2 and —OH functions in methanol, ethanol, and acetic acid. Homogeneous catalysts active for D_2–H_2O exchange include $Co(CN)_5^{3+}$ (10), and $RuCl_6^{3+}$ (11). Recently, Hirabayashi and Yasumori have discussed the kinetics of the D_2–CH_3OH exchange reaction catalyzed by a Pt(II)–Sn(II) complex (12). More complexes have not been studied because ready reduction to the

[1]AECL No. 4478.

Can. J. Chem. Downloaded from www.nrcresearchpress.com by 210.87.254.6 on 09/05/12
For personal use only.

Can. J. Chem. Downloaded from www.nrcresearchpress.com by 210.87.254.6 on 09/05/12
For personal use only.

metal occurs unless appropriate stabilizing ligands are present. Many ligands which confer stability also inhibit H–D exchange.

Two types of catalyzed D-exchange experiments are discussed in this paper: (*i*) exchange of D_2 with the hydroxyl group of C_2H_5OH to yield HD and H_2 as products and (*ii*) equilibration of H_2 and D_2 to yield HD without transfer of D to the solvent. Our preliminary experiments established that $RhCl(PPh_3)_3$, an important homogeneous olefin hydrogenation catalyst, promoted D_2 exchange with ethanol in 50 vol% solutions with either C_6H_6 or $CHCl_3$ as co-solvent. Rates were about 10 times greater in $CHCl_3$–C_2H_5OH than in C_6H_6–C_2H_5OH, but the former system is complex. This is the topic of a separate paper. In 1:1 C_6H_6–C_2H_5OH, we particularly desired to obtain detailed information on the component reactions of the catalyst hydrogenation equilibrium:

$$[1] \qquad RhCl(PPh_3)_3 + H_2 \overset{K_1}{\rightleftarrows} RhH_2Cl(PPh_3)_3$$

and to investigate the utility of D tracer techniques for this purpose. This approach has the advantage of avoiding the complexities of additional equilibria present in, say, solutions with olefins. Wherever possible, data and conclusions presented in this paper are related to those of authors who have studied the performance of this catalyst for other classes of reactions.

Experimental

$RhCl(PPh_3)_3$ was obtained from Strem Chemicals and used as received.

Anal. Calcd. for $C_{54}H_{45}ClP_3Rh$: C, 70.0; H, 4.9; Cl, 3.8; P, 10.0; Rh, 11.1. Found: C, 70.2; H, 4.9; Cl, 3.8; P, 10.0; Rh, 10.5.

Hydrogen and deuterium gases were treated as previously described (10). The 1:1 mixture of H_2 and D_2 obtained from Matheson was used as received, since contact with the usual de-oxygenation catalysts caused equilibration. Solvents were distilled, degassed, and stored under N_2 as before (10). Other reagents were used as received.

Exchange reactions were conducted in this way: (*i*) the desired quantity of catalyst was weighed into the reaction flask in air, (*ii*) the flask was evacuated on a vacuum line and filled with the appropriate gases (for experiments in which reduced partial pressures of D_2 or H_2–D_2 were required, N_2 was added to yield a final total pressure of about 1 atm), (*iii*) C_6H_6 was injected to completely dissolve the complex, and (*iv*) the D_2–ROH exchange was commenced upon injection of the ethanol or other alcohol. The glass reactor had a volume of 93.3 ml, solutions were magnetically stirred at 2900 ± 100 r.p.m., and the temperature was controlled to better than 0.1 K. Gaseous samples were removed by syringe through a septum and isolating stopcock, and analyzed on a CEC-21-130 mass spectrometer.

For both the D_2–C_2H_5OH and H_2–D_2 exchange reactions, data are reported as initial rates of disappearance of D_2.

$$[2] \qquad -d[D_2]/dt = \ln [(n_o - n_e)/(n_t - n_e)]\, A/t = k_{D_2}' A = k_{D_2} [D_2]$$

where n_o, n_t, and n_e represent the mol% D_2 at $t = 0$, $t = t$ s, and at equilibrium respectively. A is the gas:liquid ratio in mol D_2 per liter defined as: initial D_2, mmol ÷ volume of solution, ml. The experimental rate constant k_{D_2}' was obtained from the slope of a plot of log D_2 against time. The rate constant in solution, $k_{D_2} = k_{D_2}'$ (total D_2)/(dissolved D_2). Post-reaction v.p.c. analysis of the solvent gave no evidence of C_6H_6 hydrogenation products C_6H_{10} or C_6H_{12}, therefore no metallic Rh was present.

Hydrogen partial pressures have been used interchangeably with corresponding solubilities in the text. To permit ready conversion, the solubility of H_2 in 1:1 C_6H_6–C_2H_5OH at 298 K is 31.1 mol H_2 l^{-1} MPa^{-1} (13).

Results

A typical set of experimental data for D_2–C_2H_5OH exchange is shown in Fig. 1 as a plot of log mol% D_2, HD, and H_2 in the gas phase as a function of time. Since exchange rates were low, the extent of conversion of D_2 was generally about 20% over 5 h. This varied, of course, with the concentration of $RhCl(PPh_3)_3$, initial D_2, and temperature. In every case the log D_2 *vs.*

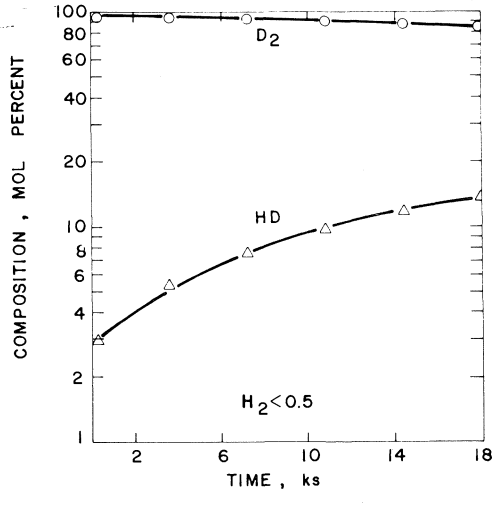

FIG. 1. Typical D_2–C_2H_5OH experimental data. Conditions: solvent: 50 vol% C_6H_6–C_2H_5OH; gas volume, 72.9 ml; solution volume, 20.0 ml; $p(D_2)$ initial, 88 kPa; $RhCl(PPh_3)_3$, 200 mg; T, 303.1 K.

time data fell on good straight lines. From this, it was concluded that the distribution of catalytically active species did not change significantly during the period of observation. Expression of results as initial rates, defined by eq. 2, was therefore justified.

(1) The Dependence of Exchange Rate on the Concentrations of Rhodium and Initial D_2

The increase in the overall exchange rate was almost proportional to total rhodium concentration. These data are presented in Fig. 2*A*. In comparison, Fig. 2*B* shows the marked dependence of the exchange rate on initial dissolved D_2 (approximately the total hydrogen concentration). These rates are extremely low, particularly compared to those for uptake of H_2 by $RhCl(PPh_3)_3$ (13, 14) or for the hydrogenation of terminal olefins under identical conditions (15) which are greater than 10 $\mu M\ s^{-1}$ at 1 m*M* Rh and 2.5 m*M* H_2. This suggests that the rate determining step in the overall exchange process is not the activation of D_2, HD, or H_2 but is related to the transfer of D from the adduct $RhD_2Cl(PPh_3)_3$ to the protic solvent. This topic will be developed later in the discussion.

It has been assumed that the overall reaction 3 was dominant in 1:1 C_6H_6–C_2H_5OH.

[3] $$D_2 + C_2H_5OH \rightarrow HD + C_2H_5OD$$

We have demonstrated that reaction 3 was the main D-exchange reaction in $CHCl_3$–C_2H_5OH by i.r. observation of the disappearance of the —OH absorption at 3620 cm^{-1} and appearance of the —OD band at 2670 cm^{-1} upon bubbling D_2 through a 1% solution of C_2H_5OH in $CHCl_3$ containing 5 m*M* $RhCl(PPh_3)_3$. Reaction rates were too slow in C_6H_6–C_2H_5OH to permit a similar observation. There is no evidence in literature that $RhCl(PPh_3)_3$ promotes D_2–C_6H_6 isotope exchange, or that the *ortho*-hydrogens of the triphenylphosphine ligands are exchanged under these experimental conditions.

(2) The Effect of Temperature on the Exchange Rate

Exchange reaction rates were measured between 290 and 308 K and these data are shown in Fig. 3. Measurements were not made at lower temperatures because rates were too slow (a typical experimental half-life for D_2 was 1.5×10^5 s at 290 K). Within this range the activation energy for the overall exchange process was only 35 kJ mol^{-1}. This value is considerably lower than the activation energy of 95.8 kJ mol^{-1} reported by Osborn *et al.* for cyclohexene reduction catalyzed by $RhCl(PPh_3)_3$ in C_6H_6 (15).

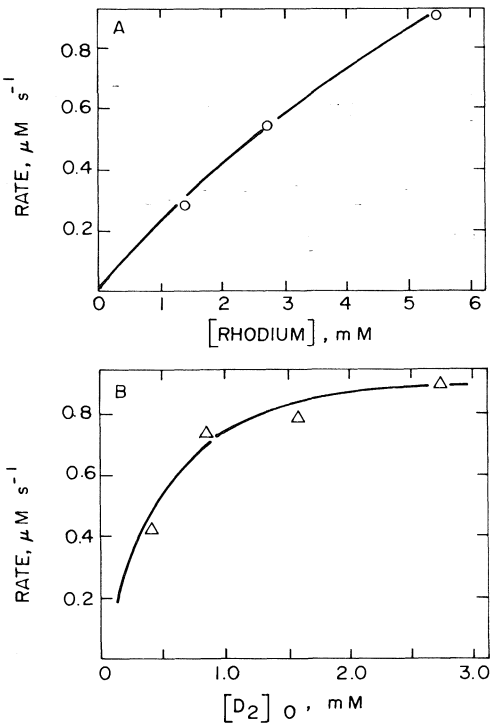

FIG. 2. The dependence of the overall D_2 exchange rate in 1:1 C_6H_6–C_2H_5OH on the total rhodium (*A*) and initial deuterium (*B*) concentration. Conditions: (*A*): $[D_2]_0$: 2.73 m*M*; *T*: 298 K; (*B*): [Rh]: 5.5 m*M*; *T*: 298 K.

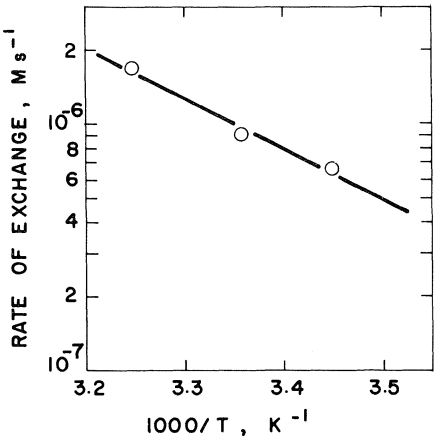

FIG. 3. Temperature dependence of the D_2–C_2H_5OH exchange rate.

Can. J. Chem. Downloaded from www.nrcresearchpress.com by 210.87.254.6 on 09/05/12
For personal use only.

Additional analysis of the activation energy is included in the discussion.

(3) H–D Isotope Effects during D_2–C_2H_5OH Exchange

The apparent kinetic isotope effects, $2k_{HD}/k_{D_2}$, were calculated by an iterative curve fitting technique assuming that sequential first order conversions occurred (16):

$$[4] \qquad D_2 \xrightarrow{k_{D_2}} HD \xrightarrow{k_{HD}} H_2$$

$$[5] \qquad [D_2] = [D_2]_0 \exp(-k_{D_2}t)$$

$$[6] \qquad [HD] = \frac{k_{D_2}[D_2]_0}{k_{HD} - k_{D_2}} [\exp(-k_{D_2}t) - \exp(-k_{HD}t) + [HD]_0 \exp(-k_{HD}t)]$$

$$[7] \qquad [H_2] = \left[\frac{[D_2]_0}{k_{HD} - k_{D_2}}\right] \times [k_{D_2} \exp(-k_{HD}t) - k_{HD} \exp(-k_{D_2}t)] - [HD]_0 \exp(-k_{HD}t) + [D_2]_0 + [HD]_0 + [H_2]_0$$

The computer program minimized the standard deviation between the observed and calculated HD yield and allowed for the possibility that the initial concentrations of HD and H_2 might be significant. This was found essential to avoid large variances in the computed values of k_{HD} and k_{D_2}. In this way apparent kinetic isotope effects were calculated from experiments with D_2 conversions ranging from 10–35%.

The values of $2k_{HD}/k_{D_2}$ calculated in this way are shown in Table 1 for three experiments in which the rhodium concentration was fixed and the total hydrogen partial pressure was 13.3, 26.6, and 53.3 kPa, respectively. The standard deviation reported for each ratio of rate constants is relatively large because only 5–7 data points were available. The differences between the experimental and calculated yields of HD or H_2 were usually less than 0.5 mol% which was approximately the magnitude of the experimental error in analysis of the gas mixtures.

(4) The H_2–D_2 Exchange Reaction in C_6H_6

Equilibration of a 1:1 mixture of H_2 and D_2 to yield HD, reaction 8, is catalyzed by $RhCl(PPh_3)_3$ in C_6H_6.

$$[8] \qquad H_2 + D_2 \rightleftarrows 2HD$$

TABLE 1. The apparent H–D kinetic isotope effect

[Rh] (m*M*)	[D_2] (m*M*)	D_2 Exchange rate ($\mu M\ s^{-1}$)	$\frac{2k_{HD}}{k_{D_2}} \pm \sigma$
5.4	0.41	0.43	1.11±0.09
5.4	0.83	0.73	0.97±0.08
5.5	1.55	0.90	1.14±0.02

Since the atom fraction of deuterium in the gas phase $(2D_2 + HD)/2(D_2 + HD + H_2)$ remained unchanged during the period of the experiment, no transfer of D to other protic molecules occurred. The H_2–D_2 reaction was not due to traces of metallic rhodium since no C_6H_6 hydrogenation products could be detected by v.p.c. analysis. Rhodium is an extremely effective catalyst for C_6H_6 hydrogenation (17). There was no D-exchange during blank experiments without $RhCl(PPh_3)_3$ in solution.

The H_2–D_2 equilibration rates had poor reproducibility, and differed by as much as a factor of two in successive apparently identical experiments. Also, erratic rate variations were detected even during individual runs. These effects may have originated with contaminants, but there was no correlation with trace hydrocarbon impurities in either the C_6H_6 or the commercial 1:1 gas mixture which was used as received. The usual catalytic deoxygenation procedures equilibrate H_2–D_2 streams. Gas mixtures prepared from separately purified H_2 and D_2 gave similar results.

These experiments show that $RhCl(PPh_3)_3$ promotes H_2–D_2 exchange. The dependence of exchange rate on the total rhodium and initial D_2 concentrations is illustrated in Fig. 4. Fixed $[D_2]_0 = 1.3$ m*M* and fixed [Rh] = 1.35 m*M*, in the respective experimental sets. These log–log plots yield the apparent reaction orders +0.9 in rhodium and −0.7 in D_2. Excess triphenylphosphine did not inhibit the reaction, although a slow increase of rate to the usual limiting value occurred during the 0.5 h following the addition of 25 mol PPh_3 per mol Rh. This behavior was unexpected in view of the poisoning effect which excess PPh_3 has on the olefin hydrogenation reaction (15).

The D_2 exchange rates $(-d[D_2]/dt)$ are dependent on T^{-1} in the manner shown in Fig. 5. An activation energy, calculated from the tangent to the curve at 1/298 K is 42 kJ mol^{-1}.

Can. J. Chem. Downloaded from www.nrcresearchpress.com by 210.87.254.6 on 09/05/12
For personal use only.

Can. J. Chem. Downloaded from www.nrcresearchpress.com by 210.87.254.6 on 09/05/12
For personal use only.

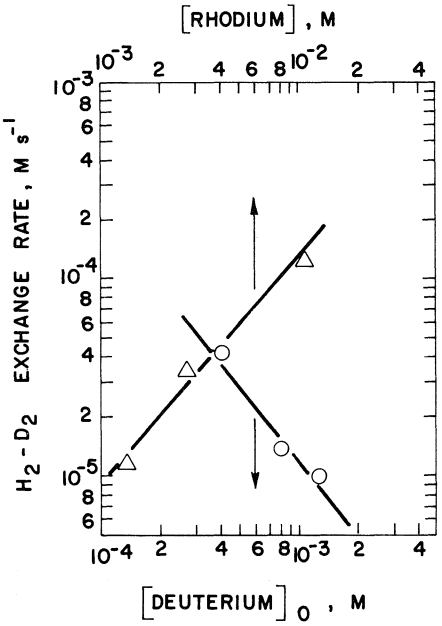

FIG. 4. The dependence of the 1:1 H_2–D_2 exchange rate on [Rh] and $[D_2]_0$ in C_6H_6 at 298 K. ⊙, Fixed [Rh] = 1.35 mM; △, fixed $[D_2]_0$ = 1.3 mM.

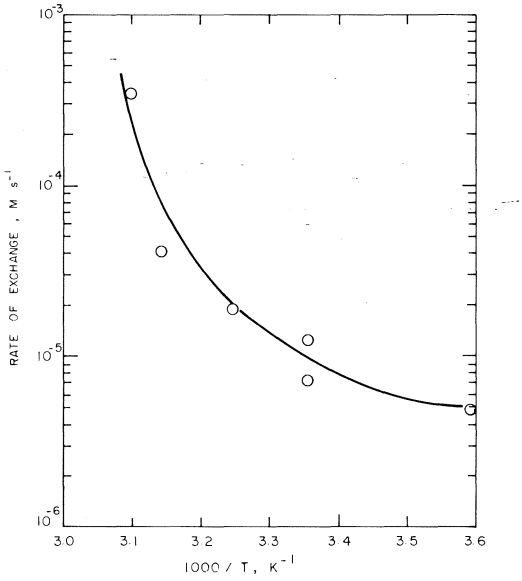

FIG. 5. Temperature dependence of the H_2–D_2 exchange rate at $[D_2]_0$ = 1.3 mM, [Rh] = 1.35 mM in C_6H_6.

Discussion

In the following discussion, the present understanding of the function of $RhCl(PPh_3)_3$ as a homogeneous catalyst is reviewed, a mechanism is proposed for the catalysis of the D_2–C_2H_5OH exchange reaction, and the origin of the apparent kinetic isotope effect defined by $2k_{HD}/k_{D_2}$ is considered. Comments are also made on the significance of the H_2–D_2 exchange reaction.

(1) The Uptake of Hydrogen by $RhCl(PPh_3)_3$

This topic has been thoroughly reviewed recently by James (8), and will therefore not be discussed at length here. The purpose of this section is to emphasize that the component reactions of reaction 1 cannot be rate-limiting in the D_2 exchange experiments reported above.

It is well known that $RhCl(PPh_3)_3$ activates H_2 or D_2 by oxidative addition to yield a dihydride or a dideuteride adduct respectively. The dominant equilibrium in solutions containing up to about 5 mM total rhodium is represented by reaction 1. This process of reversible uptake of hydrogen by $RhCl(PPh_3)_3$ was first described by Wilkinson and co-workers (15). The ^{31}P n.m.r. study of the hydrogenated catalyst in CH_2Cl_2 by Meakin *et al.* (18) established that the dominant species was $RhH_2Cl(PPh_3)_3$ and not $RhH_2Cl(PPh_3)_2$, solvent. The configuration of the dideuteride is shown in Fig. 6. The two Rh—D bonds are not equivalent.

Spectroscopic methods have shown that this dihydride exists in equilibrium with hydrogen and the parent complex in various solvents including C_6H_6, CH_2Cl_2, and $CHCl_3$ (15, 18). There is some evidence that the rate and equilibrium constants for the overall catalyst hydrogenation reaction 1 are solvent dependent, although the values reported for K_1, determined from kinetic (19) or spectroscopic data (18) or from the amount of absorbed (15, 20) or reversibly bound hydrogen (13), differ substantially. Nevertheless, there is general agreement that the component reaction rates are rapid, and their specific rates k_1 and k_{-1} which yield K_1 $(= k_1/k_{-1})$ are large. It is probable that rates of hydrogen uptake by $RhCl(PPh_3)_3$ reported by Strohmeier and co-worker for toluene solutions (14) and by us for benzene solutions (13) have been limited by H_2 mass transfer and therefore true specific rates cannot be derived from these data. However, we have estimated a lower limit

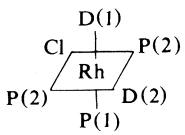

FIG. 6. Configuration of $RhD_2Cl(PPh_3)_3$ (18).

Can. J. Chem. Downloaded from www.nrcresearchpress.com by 210.87.254.6 on 09/05/12
For personal use only.

for the rate of uptake of H_2 by residual $RhCl(PPh_3)_3$ upon attainment of equilibrium 1 by a solution 1.25 mM in Rh, 2.6 mM in H_2, and at 298 K of 1.6×10^{-5} $M\,s^{-1}$ (13). This value is low compared with the limiting rate for hydrogenation of 1-heptene in C_6H_6 under similar conditions of Rh concentration and H_2 pressure of 7.9×10^{-5} $M\,s^{-1}$ obtained by Osborn *et al.* (15).

In contrast it may be seen from Fig. 2*A* that the D_2–C_2H_5OH exchange rate in 50% C_6H_6–C_2H_5OH is only 2.7×10^{-7} $M\,s^{-1}$. This is about 100 times slower than the rate expected for H_2 (or D_2) uptake. It is therefore considered that neither D_2 activation nor subsequent release of HD or H_2 from the catalyst can be rate limiting in the C_6H_6–C_2H_5OH solvent system.

(2) The Mechanism of D_2 Exchange with 1:1 C_6H_6–C_2H_5OH Catalyzed by $RhCl(PPh_3)_3$

Although n.m.r. experiments indicate that the two Rh—D bonds are not equivalent (18), it will be shown that it is unnecessary to specifically account for this in the kinetic analysis.

Since the rates of reversible hydrogen uptake are up to two orders of magnitude more rapid than the overall rates of D_2–C_2H_5OH exchange then the transfer of deuterium from Rh—D bonds of either $RhD_2Cl(PPh_3)_3$ or $RhHDCl(PPh_3)_3$ to the hydroxy group of C_2H_5OH must be rate determining. Because C_2H_5OH was present in at least a 2000-fold excess, the exchange of Rh—D bonds may be considered pseudo-first order. If the non-equivalence of the Rh—D sites in the dideuteride is taken into account, and they are labelled Rh—D′ and Rh—D″ respectively, then

$$[9] \quad -d[D_2]/dt = d[RhD_2]/dt = k_x'[Rh—D'] + k_x''[Rh—D'']$$

Two possibilities must be considered to simplify expression 9: (*i*) either $k_x' > k_x''$. that is, one of the two Rh—D bonds is more labile for D-transfer to the solvent than the other or (*ii*) $k_x' = k''_x$ and they are equally exchangeable. Since in (*ii*) the probability of a dual exchange event during the adduct lifetime would be exceedingly small, this case is equivalent to and indistinguishable from (*i*). The present data do not establish which alternative is correct. For either possibility the rate determining step becomes

$$[10] \quad -d[D_2]/dt = k_x\,[Rh—D]$$

Using reaction 1, the following expression is easily derived for the overall initial rate of exchange

$$[11] \quad -d[D_2]_0/dt = \frac{k_x K_1 [D_2]_0 [Rh]_0}{1 + K_1[D_2]_0}$$

where $[D_2]_0$ = total concentration of dissolved hydrogen $[H_2 + HD + D_2)$, and $[Rh]_0$ = total rhodium concentration. The constants k_x and K_1 refer to the rate determining reaction 10 and equilibrium 1 respectively.

A plot of $(d[D_2]/dt)^{-1}$ *vs.* $[D_2]_0^{-1}$, Fig. 7, yields $k_x = 2.3 \times 10^{-4}\,s^{-1}$ and $K_1 = 5.2 \times 10^3$ M.

(2.1) Rate Constant k_x

This determination of k_x is significant, not only because it is the first value reported for the specific rate of exchange of $RhD_2Cl(PPh_3)_3$ with a protic solvent, but also because it corresponds to the frequency at which some olefins hydrogenate at this complex. A connection may therefore exist between the rate of exchange of the Rh—D bond, and the rate of transfer to a Rh-activated olefin. For example, with 1 M cyclohexene in C_6H_6, the frequency of hydrogenation is $1.25 \times 10^{-4}\,s^{-1}$ (15).

(2.2) Equilibrium Constant K_1

Several values have already been reported in the literature for the equilibrium constant K_1. These, with the experimental methods and solvents used in each case, are compared in Table 2. In C_6H_6, the estimates based on H_2 uptake by $RhCl(PPh_3)_3$ (13, 15) or on the H_2 recoverable from $RhH_2Cl(PPh_3)_3$ by our inert gas purging technique (13) are substantially greater than those calculated from u.v.–visible spectrometric

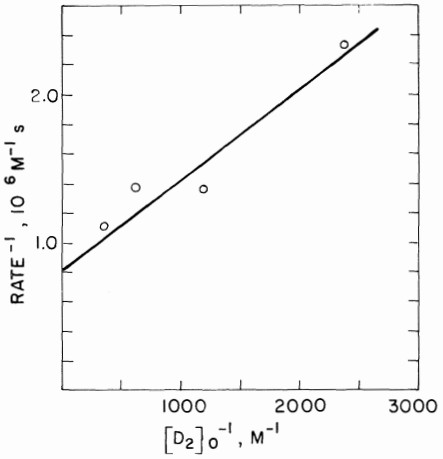

FIG. 7. Plot of $(D_2$–C_2H_5OH exchange rate$)^{-1}$ against $[D_2]_0^{-1}$.

TABLE 2. Summary of reported values for K_1

Method	Solvent	T(K)	K_1 (M^{-1})	Reference
Kinetic analysis	C_6H_6	303	500	19
H_2 uptake	C_6H_6	298	>6400*	13, 15
	Toluene	298	660	14
Ultraviolet–visible spectrometry	CH_2Cl_2	299	800	18
	C_6H_6	299	800	
H_2 reversibly bound	C_6H_6	298	>2300	13
	CH_2Cl_2	298	>1900	
D_2 exchange	C_6H_6–C_2H_5OH	298	5200	This work

*Assuming $[RhH_2Cl(PPh_3)_3]/[RhCl(PPh_3)_3] > 19$ when measured uptake is 1 mol H_2/mol Rh, *i.e.* 5% experimental error.

studies (18) or from analysis of the kinetics of cyclohexene hydrogenation catalyzed by $RhCl(PPh_3)_3$ (19). Since each experimental method possessed satisfactory precision, the variations in magnitude of K_1 suggest that reaction 1 does not completely describe hydrogenated solutions of $RhCl(PPh_3)_3$. It is possible that significant dimer formation, either of $[RhCl(PPh_3)_2]_2$ or $[RhH_2Cl(PPh_3)_2]_2$ (15), occurs. Also, the relative purity of each system is not known with certainty. The sensitivity of solutions of $RhCl(PPh_3)_3$ to O_2 is well established (8, 21, 22), and could give rise to the tabulated discrepancies.

In view of the different values of K_1 reported for C_6H_6 solutions, a discussion of subtle effects of solvent on K_1 based on these data is not justified. A comparison of our present determination of $K_1 = 5200\ M^{-1}$, from D_2 exchange data in 1:1 C_6H_6–C_2H_5OH, with the lower values of K_1 in C_6H_6 alone must be made with caution. These results suggest that the dideuteride (or the dihydride) is thermodynamically more stable in this mixed solvent than in C_6H_6 solution. This may partially explain the enhanced olefin hydrogenation rates observed in C_6H_6–C_2H_5OH solutions noted by Hussey and Takeuchi (23).

(2.3) Activation Energy

The true activation energy for the rate determining step, eq. 10, can be obtained by analysis of the temperature dependence of reaction 8:

$$[12]\quad \frac{d\ln(\text{Rate})}{d(1/T)} = \frac{d\ln k_x}{d(1/T)} - \frac{d\ln}{d(1/T)}\left[\frac{1}{1 + 1/K_1[H_2]}\right]$$

where $[H_2]$ represents the total concentration of H_2, HD, and D_2 and equals $[D_2]_0$. From expression 12 one obtains:

$$[13]\quad \frac{d\ln(\text{Rate})}{d(1/T)} = -\frac{1}{R}\left[E_x^{\ddagger} - \frac{\Delta H_1 + \Delta H_s}{1 + K_1[H_2]}\right]$$

in which R is the gas constant, $E_x^{\ddagger}$ is the activation energy for reaction 10, ΔH_1 is the enthalpy of reaction 1, and ΔH_s is the enthalpy of solution for H_2 in 1:1 C_6H_6–C_2H_5OH.

Our measured value for ΔH_s is +2.0 kJ mol^{-1}. Neither ΔH_1 nor K_1 are known precisely, but may be estimated from existing data. Since we have detected only a slight difference in the amount of H_2 reversibly bound as $RhH_2Cl(PPh_3)_3$ between 278 and 313 K in C_6H_6 solution (13), it is unlikely that ΔH_1 is greater than 40 kJ mol^{-1}. At 88 kPa total H_2, $K_1[H_2]$ is not less than 4, therefore the term $[\Delta H_1 + \Delta H_s]/[1 + K_1[H_2]]$ should be approximately 8.4 kJ mol^{-1}. Thus, the true activation energy for the rate-controlling D-transfer reaction 10 should be 35.1 kJ mol^{-1} (the apparent activation energy calculated from data in Fig. 3) plus 8.4 kJ mol^{-1} = 43.5 kJ mol^{-1}.

The value is substantially less than the activation energy of 95.8 kJ mol^{-1} reported by Osborn *et al.* (15), or even their revised value of 77.8 kJ mol^{-1} (24), for the rate determining step in the $RhCl(PPh_3)_3$-catalyzed hydrogenation of cyclohexene in C_6H_6. The detailed rate limiting process in the present case must therefore differ considerably from that proposed by Osborn *et al.* for C_6H_{10} hydrogenation, namely the loss of weakly bound solvent (S) from the intermediate

Can. J. Chem. Downloaded from www.nrcresearchpress.com by 210.87.254.6 on 09/05/12
For personal use only.

$RhH_2Cl(PPh_3)_2S$ prior to olefin activation. In view of the n.m.r. study of Meakin *et al.* (18) the departing ligand S may instead be the labile triphenylphosphine, P(1) in Fig. 6.

It is conceivable that a similar process precedes the actual exchange of D between Rh—D and C_2H_5OH, that is, activation of C_2H_5OH at the metal center occurs following PPh_3 dissociation or displacement. However, because of the considerable difference in activation energies noted above, and because the rate constant for exchange of the labile PPh_3 is extremely large, about 400 s^{-1} (18), compared to that for reaction 10, 2.3×10^{-4} s^{-1}, we prefer a route which does not require coordination of the C_2H_5OH molecule to the Rh atom. A four center intermediate of this type may be involved.

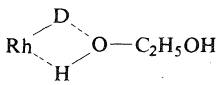

(2.4) Activation Entropy

A comparison of D_2 exchange with olefin hydrogenation catalyzed by $RhCl(PPh_3)_3$ suggests that the low reaction rates observed in the former case are due to a large negative entropy of activation. With 1.25 m*M* $RhCl(PPh_3)_3$ and 2.6 m*M* dissolved H_2 (or D_2), the rate of D_2 exchange in 1:1 C_6H_6–C_2H_5OH was about 7×10^{-3} times slower than the rate of hydrogenation of 1 *M* cyclohexene in C_6H_6 obtained by Osborn *et al.* (15). Since the respective activation energies for these processes are 43.5 and 77.8 kJ mol^{-1}, the activation entropy for the exchange reaction must be -145 J mol^{-1} K^{-1}, compared to $+11$ J mol^{-1} K^{-1} for cyclohexene reduction in C_6H_6 obtained by Jardine *et al.* (24).

We suggest that this large negative activation entropy is associated with the transition state structure proposed in section 2.3. In the case of olefin hydrogenation, the activation entropy is low in polar solvent mixtures and with sterically hindered double bonds (24). The activation entropy for D_2 exchange is low by those standards, therefore additional structuring of the transition state must arise with effects other than those related to the substrate–solvent exchange at the active site. The four-center intermediate suggested in section 2.3 may fulfill this requirement.

(3) (H–D) Isotope Effects

The observed isotope effects, $2k_{HD}/k_{D_2}$, could originate with either the relative thermodynamic stabilities of the H_2, HD, and D_2 adducts, or because the H_2–D_2 reaction occurred rapidly and concurrently. Each possibility would yield the same observed product distribution, and neither can be excluded. The differences between the solubilities of H_2, HD, and D_2 are insufficient to account for these isotope effects.

(3.1) The Relationship between the Thermodynamic Stabilities of the H_2, HD, and D_2 Adducts and the H–D Isotope Effect

If the hydrogen isotope dependence of constant K_1 is taken into account, then from reaction 1 it may be written

$$[14] \qquad [RhD_2] = K_1^{D_2}[Rh][D_2]$$

$$[15] \qquad [RhHD] = K_1^{HD}[Rh][HD]$$

$$[16] \qquad [RhH_2] = K_1^{H_2}[Rh][H_2]$$

where RhD_2, RhHD, and RhH_2 represent $RhD_2Cl(PPh_3)_3$, $RhHDCl(PPh_3)_3$, and $RhH_2Cl(PPh_3)_3$ respectively. Since

$$[17] \quad [Rh]_0 = [Rh] + [RhD_2] + [RhHD] + [RhH_2]$$

then

$$[18] \quad [Rh] = [Rh]_0/(1 + K_1^{D_2}[D_2] + K_1^{HD}[HD] + K_1^{H_2}[H_2])$$

in which $[Rh]_0$ = total rhodium and $[Rh] = [RhCl(PPh_3)_3]$.

From eqs. 2 and 10, the relationship between the experimental and mechanistic rate constants is given by

$$[19] \quad d[D_2]/dt = -k_{D_2}[D_2] = -k_x^{D_2}[RhD_2]$$

$$[20] \quad d[HD]/dt = k_{D_2}[D_2] - k_{HD}[HD] = k_x^{D_2}[RhD_2] - k_x^{HD}[RhHD]$$

At high conversions of D_2 (>90%), $k_{D_2}[D_2] \ll k_{HD}[HD]$, and this approximation holds

$$[21] \quad d[HD]/dt = -k_{HD}[HD] = -k_x^{HD}[RhHD]$$

that is, the slope of a plot of log (mol% HD) against time may be used to obtain k_{HD} directly from experimental data. The calculation outlined in section 3 of the results will yield a value for k_{HD} identical with that obtained from data taken only at low conversions.

By substitution of eq. 18 into [14] and [15], and then in [19] and [21] respectively it may be shown that

$$[22] \qquad 2k_{HD}/k_{D_2} = 2k_x^{HD}K_1^{HD}/k_x^{D_2}K_1^{D_2}$$

Can. J. Chem. Downloaded from www.nrcresearchpress.com by 210.87.254.6 on 09/05/12
For personal use only.

Can. J. Chem. Downloaded from www.nrcresearchpress.com by 210.87.254.6 on 09/05/12
For personal use only.

This expression relates the experimentally determinable k_{D_2} and k_{HD} to the corresponding rate constants which have fundamental significance.

An observable D-exchange event occurs only with transfer of D from a Rh—D bond to the solvent. Exchange of Rh—H with solvent —OH will not be detectable by these experiments. Thus, the rate constant k_x refers only to D-transfer and for our purposes can exhibit no primary H–D isotope effect. It is conceivable that k_x might differ for a D_2 and HD adduct (identified by $k_x^{D_2}$ and k_x^{HD} respectively). We have assumed that the effect of having a D compared to an H atom at the adjacent *cis*-position in the complex is negligible, therefore

$$[23] \qquad k_x^{D_2} = 2k_x^{HD}$$

This statement holds for cases (*i*) and (*ii*) discussed in section 2. It follows from eq. 22 that the experimental isotope effect $2k_{HD}/k_{D_2}$ is a direct measure of the ratio of equilibrium constants $K_1^{HD}/K_1^{D_2}$ for uptake of HD and D_2 by $RhCl(PPh_3)_3$.

Siegel and Ohrt have calculated $K_1^{H_2}/K_1^{D_2} = 1.38$ at 303 K, using the vibrational partition functions known for H_2 and D_2, and estimated for $RhH_2Cl(PPh_3)_3$ and $RhD_2Cl(PPh_3)_3$ (26). In a similar way, $K_1^{HD}/K_1^{D_2} = 1.25$ may be calculated if it is assumed that the Rh—H and Rh—D stretching frequencies are 2035 and 1461 cm^{-1} respectively and the RhHD bending frequency is 717 cm^{-1}. It must be recognized that these equilibrium constant ratios have been obtained from an extremely simple model in which replacement of Rh—H by Rh—D was considered to have no effect on other metal–ligand normal modes. The uncertainty associated with the ratios reported here is likely to be about 10%.

The experimental values reported for $2k_{HD}/k_{D_2}$ in Table 1 closely approximate the calculated value $K_1^{HD}/K_1^{D_2} = 1.25 \pm 0.1$ reported here. Interpretation of the tabulated data as direct measures of $K_1^{HD}/K_1^{D_2}$ must be made with caution in view of the possible effect of the H_2–D_2 reaction discussed in the following section.

(3.2) The Effect of the H_2–D_2 Reaction on the Observed Isotope Effect

Under comparable experimental conditions, say rhodium concentration = 1.35 m*M* and total dissolved hydrogen (H_2 + HD + D_2) = 2.6 m*M*, it may be seen from Figs. 2 and 4 that the rate of H_2–D_2 equilibration in C_6H_6 will exceed the rate of D_2–C_2H_5OH exchange by at least a factor of 10. Therefore, if the H_2–D_2 reaction occurs in 1:1 C_6H_6–C_2H_5OH at a comparable rate, the HD and H_2 product distribution must be at least partially controlled by the magnitude of the equilibrium constant for reaction 8. Using a value of $K_8 = 3.26$ at 298 K (27), and assuming instant equilibration of H_2, HD, and D_2 during D_2–C_2H_5OH exchange, the theoretical value we have calculated for $2k_{HD}/k_{D_2}$ is 1.14. Experimental data reported in Table 1 agree well with this number.

In view of the magnitudes of the standard deviations associated with the determination of experimental values of $2k_{HD}/k_{D_2}$ and the approximations inherent in the calculation of $K_1^{HD}/K_1^{D_2}$ discussed in section 3.1, it cannot be established whether the observed H–D isotope effect arises only because of the relative stabilities of the H_2, HD, and D_2 adducts with $RhCl(PPh_3)_3$, or because of the H_2–D_2 reaction, or for both reasons.

(4) The H_2–D_2 Reaction

Previously, Osborn *et al.* have shown that H_2–D_2 exchange may be catalyzed by $RhCl(PPh_3)_3$ in C_6H_6 (15). The data presented in Fig. 4 clearly show that the initial rate of the H_2–D_2 equilibration reaction is inversely dependent on D_2 (or total hydrogen) concentration and approximately first order in rhodium. These observations can be explained if the dihydride or dideuteride does not take part in the mechanism of H_2–D_2 exchange. Our data suggest that the simultaneous activation of H_2 and D_2, or the bimolecular collision process suggested by Osborn *et al.* (15) do not occur. Each route would require participation of a dihydride. Since excess triphenylphosphine did not poison the catalyst for H_2–D_2 exchange it is unlikely that loss of PPh_3 from the catalytically active species preceded activation of H_2 and D_2. It has been previously emphasized that our solutions were not contaminated by suspended metallic rhodium, which is an excellent catalyst for H_2–D_2 exchange (17).

If $RhCl(PPh_3)_3$ and $RhH_2Cl(PPh_3)_3$ are the the main Rh-containing species in C_6H_6 solution, and no other labile rhodium hydrides form to permit H_2–D_2 exchange to proceed by alternate activation of an H_2 and a D_2 molecule, (*c.f.* the function of $RhH(CO)(PPh_3)_3$ (28)) then our data suggest that H_2–D_2 exchange must occur in the

presence of $RhCl(PPh_3)_3$ without formal Rh—D or Rh—H bond formation. The function of the catalyst may be to lower the symmetry and activation barriers (29), and thereby to accelerate scrambling of the H_2—D_2 bonds.

(5) Summary

The rate-limiting step in the exchange of D_2 with 1:1 C_6H_6–C_2H_5OH catalyzed by $RhCl(PPh_3)_3$ was shown to be the transfer of D from a Rh—D bond to the solvent. This may have occurred without coordination of C_2H_5OH to the rhodium(III) dideuterido intermediate. The experimentally observed H–D isotope effect arose either because the adducts with $RhCl(PPh_3)_3$ decreased in thermodynamic stability in the sequence $H_2 > HD > D_2$, or because the exchange reaction product distribution was controlled by the H_2–D_2 equilibration step.

The authors wish to thank David M. Garner for calculating the apparent H–D isotope effects, and Drs. Norman H. Sagert, E. Allan Symons, and M. Tomlinson for their comments and helpful discussion.

1. H. London. Separation of isotopes. George Newnes Limited, London. 1961.
2. N. H. Sagert and R. M. L. Pouteau. Can. J. Chem. **49**, 3411 (1971); **50**, 3686 (1972).
3. J. H. Rolston and J. W. Goodale. Can. J. Chem. **50**, 1900 (1972).
4. J. M. Flournoy and W. K. Wilmarth. J. Am. Chem. Soc. **83**, 2257 (1961).
5. W. K. Wilmarth and J. C. Dayton. J. Am. Chem. Soc. **75**, 4553 (1953).
6. E. Rochard and J. Ravoire. J. Chim. Phys. Physicochim. Biol. **68**, 1183 (1971).
7. G. N. Schrauzer. (*Editor*). Transition metals in homogeneous catalysis. Dekker, New York. 1971.
8. B. R. James. Homogeneous hydrogenation. Wiley, New York. 1973. Chapt. 11.
9. G. G. Eberhardt, M. E. Tadros, and L. Vaska. J. Chem. Soc. Chem. Commun. 290 (1972).
10. G. G. Strathdee and M. J. Quinn. Can. J. Chem. **50**, 3144 (1972).
11. J. Halpern and B. R. James. Can. J. Chem. **44**, 671 (1966).
12. K. Hirabayashi and I. Yasumori. J. Chem. Soc. Faraday I, **69**, 595 (1973).
13. G. G. Strathdee and R. M. Given. J. Catal. **30**, 30 (1973).
14. W. Strohmeier and R. Endres. Z. Naturforsch. B, **26**, 362 (1971).
15. J. A. Osborn, F. H. Jardine, J. F. Young, and G. Wilkinson. J. Chem. Soc. A, 1711 (1966).
16. A. A. Frost and R. G. Pearson. Kinetics and mechanism: a study of homogeneous chemical reactions. Wiley, New York. 1961.
17. P. N. Rylander. Catalytic hydrogenation over platinum metals. Academic Press, New York. 1967. p. 309.
18. P. Meakin, J. P. Jesson, and C. A. Tolman. J. Am. Chem. Soc. **94**, 3240 (1972).
19. S. Siegel and D. Ohrt. Inorg. Nucl. Chem. Lett. **8**, 15 (1972).
20. R. L. Augustine and J. V. Peppen. Chem. Commun. 497 (1970).
21. D. D. Lehman, D. F. Shriver, and I. Wharf. Chem. Commun. 1486 (1970).
22. R. W. Mitchell, J. D. Ruddick, and G. Wilkinson. J. Chem. Soc. A, 3224 (1971).
23. A. S. Hussey and Y. Takeuchi. J. Org. Chem. **35**, 643 (1970).
24. F. H. Jardine, J. A. Osborn, and G. Wilkinson. J. Chem. Soc. A, 1574 (1967).
25. M. W. Cook, D. N. Hanson, and B. J. Alder. J. Chem. Phys. **26**, 748 (1957).
26. S. Siegel and D. W. Ohrt. Chem. Commun. 1529 (1971).
27. G. C. Bond. Catalysis by metals. Academic Press, New York. 1962. p. 151.
28. D. Evans, G. Yagupsky, and G. Wilkinson. J. Chem. Soc. A, 2660 (1968).
29. R. G. Pearson. Acc. Chem. Res. **4**, 152 (1971).

Can. J. Chem. Downloaded from www.nrcresearchpress.com by 210.87.254.6 on 09/05/12
For personal use only.

Homogeneous Catalysis of Hydrogen Isotope Exchange Between D_2 and Ethanol by Chlorotris(triphenylphosphine)rhodium(I). II. In Chloroform–Ethanol[1]

GRAEME STRATHDEE AND RUSSELL GIVEN

Research Chemistry Branch, Atomic Energy of Canada Limited, Whiteshell Nuclear Research Establishment, Pinawa, Manitoba R0E 1L0

Received October 22, 1973

GRAEME STRATHDEE and RUSSELL GIVEN. Can. J. Chem. **52**, 2226 (1974).

The kinetics and mechanism of D_2 exchange catalyzed by $RhCl(PPh_3)_3$ have been studied in chloroform–ethanol solutions. Interpretation of the results was complicated by a side reaction of the solvent to yield HCl, $RhHCl_2(PPh_3)_2$, C_2H_5Cl, CH_2Cl_2, Ph_3PO, and other phosphorus(V) species. Computer simulation of the exchange reaction was used to show that the observed inverse isotope effect $2k_{HD}/k_{D_2} = 0.85$ could arise only if the rate determining step was the activation of D_2, HD, and H_2 by $RhCl(PPh_3)_3$.

The D_2 exchange reaction rate was extremely dependent on solvent composition and decreased 30 times between 6 and 96 mol% C_2H_5OH. The activation energy for D_2 exchange was 101 ± 9 kJ mol^{-1} at 58 mol% C_2H_5OH, and 86 ± 8 kJ mol^{-1} at 6 mol% C_2H_5OH. These data suggested that solvent–catalyst bonding interactions were important.

GRAEME STRATHDEE et RUSSELL GIVEN. Can. J. Chem. **52**, 2226 (1974).

On a étudié, pour des solutions d'éthanol dans le chloroforme la cinétique et le mécanisme de l'échange du deutérium catalysé par le $RhCl(PPh_3)_3$. L'interprétation des résultats est compliquée par une réaction secondaire du solvant qui fournit HCl, $RhHCl_2(PPh_3)_2$, $C_2H_5Cl_2$, Ph_3PO et d'autres espèces du phosphore (V). On a utilisé des simulations par ordinateur de la réaction d'échange afin de montrer que l'effet isotopique inverse qui a été observé pour $2k_{HD}/k_{D_2} = 0.85$ peut se produire seulement si l'étape déterminante de la réaction est l'activation de D_2, HD et H_2 par $RhCl(PPh_3)_3$.

Le taux de la réaction d'échange avec le deutérium dépend au plus au point sur la composition du solvant et diminue par un facteur de 30 entre 6 et 96 moles pourcent de C_2H_5OH. L'énergie d'activation pour l'échange du D_2 est de 101 ± 9 kJ par mole à 58 moles pourcent de C_2H_5OH, et 86 ± 8 kJ moles à 6 moles pourcent de C_2H_5OH. Ces données indiquent que les interactions solvant–catalyseur sont importantes. [Traduit par le journal]

Introduction

Enrichment of deuterium to produce heavy water may be accomplished by preferential concentration of deuterium in the bonds of one component of a two-component mixture at equilibrium. Most H–D isotope exchange reactions must be catalyzed to obtain sufficiently high rates, and catalysts which function efficiently in the liquid phase are of particular interest to us. Some transition-metal complexes promote exchange of deuterium between D_2 and protic solvents and are therefore potentially useful for this application.

In a previous paper (1), the kinetics and mechanism of the exchange of deuterium between D_2 and the hydroxyl group of ethanol catalyzed by $RhCl(PPh_3)_3$ in 1:1 benzene–ethanol have been discussed. We have found that the behavior of this catalyst in chloroform–ethanol solutions is considerably different. Whereas in the former case, the rate of transfer of deuterium from the dideuterido adduct, $RhD_2Cl(PPh_3)_3$, to ethanol was found to be rate-limiting, in chloroform–ethanol the slow step is the activation of D_2 by $RhCl(PPh_3)_3$

$$[1] \qquad D_2 + RhCl(PPh_3)_3 \rightleftarrows RhD_2Cl(PPh_3)_3$$

Data on the apparent H–D isotope effect and the sensitivity of the overall D_2 exchange reaction rate to solvent composition are presented to support this conclusion.

In addition, aspects of a complex side reaction of $RhCl(PPh_3)_3$ with $CHCl_3$–C_2H_5OH have been investigated. Hydrogen chloride was produced and led to formation of the monohydride:

$$[2] \qquad RhCl(PPh_3)_3 + HCl \rightleftarrows RhHCl_2(PPh_3)_3$$

The kinetics of D_2 exchange with this mixed solvent are interpreted in terms of competition between equilibria 1 and 2.

[1]AECL No. 4479.

Can. J. Chem. Downloaded from www.nrcresearchpress.com by 210.87.254.6 on 09/05/12
For personal use only.

Can. J. Chem. Downloaded from www.nrcresearchpress.com by 210.87.254.6 on 09/05/12
For personal use only.

Experimental

The techniques by which $RhCl(PPh_3)_3$, D_2 gas and solvents were purified or handled were identical to those already described (1).

Exchange reaction data are reported as initial rates defined as

$$[3] \qquad -d[D_2]/dt = \ln [(n_0 - n_e)/(n_t - n_e)]\, A/t$$

where n_0, n_t, and n_e represent the mol% D_2 in the gas phase at $t = 0$, $t = t$ s, and at equilibrium. A is the gas:liquid ratio given by: initial D_2, mmol ÷ volume of solution, ml.

The reactions between $RhCl(PPh_3)_3$ and 10 vol% C_2H_5OH in $CHCl_3$ were performed in Pierce Chemical Company Reacti-Vials sealed with Mininert Teflon valves. Weighing the containers before and after runs confirmed that no solvent distilled out of these flasks at 328 K. Volatile liquid products from these reactions were separated by v.p.c. on a Poropak R column at 423 K with a carrier gas flow of 0.4 ml s^{-1}. Mass spectra of eluted components were obtained with a Varian CH7 spectrometer. The n.m.r. spectrometer was a Perkin–Elmer R12A, which thermoregulated samples at 311 K.

The HCl generated upon dissolution of $RhCl(PPh_3)_3$ in $CHCl_3$–C_2H_5OH was measured with a glass–AgCl/Ag electrode couple mounted in a glass cell which could be purged with either N_2 or H_2. The HCl concentrations were read from a calibration plot of electrode e.m.f. against HCl concentration in 50 vol% $CHCl_3$–C_2H_5OH (2).

The hydrogenation of 1-butene was followed upon injection of 195 μmol into the exchange-reaction cell at the conclusion of a D_2 exchange experiment. Standard conditions were: total hydrogen (H_2 + HD + D_2) = 88 kPa; solution volume = 20.0 ml; T = 303 K. Rates were calculated from the slopes of plots of log mol fraction 1-butene against time.

Results

Overall exchange reaction rates and apparent H–D isotope effects were obtained from each set of experimental data. Results for a typical experiment are shown in Fig. 1. In general, the plots of log D_2 against time were linear for up to 6 h, or more than 90% conversion of D_2. The distribution of catalytically active species therefore did not change significantly during the period of observation and presentation of data as initial rates, defined by eq. 3, was satisfactory. The zero-time intercept of the D_2 data was usually identical to the D_2 fraction of the feed gas except in experiments in which ethanol-stabilized (0.05 vol%) chloroform was employed. In these experiments the extrapolated value of the initial D_2 composition was only about 90%. This effect was traced to a large enhancement of exchange rate in dilute solutions of C_2H_5OH in $CHCl_3$ and is discussed in section 3.

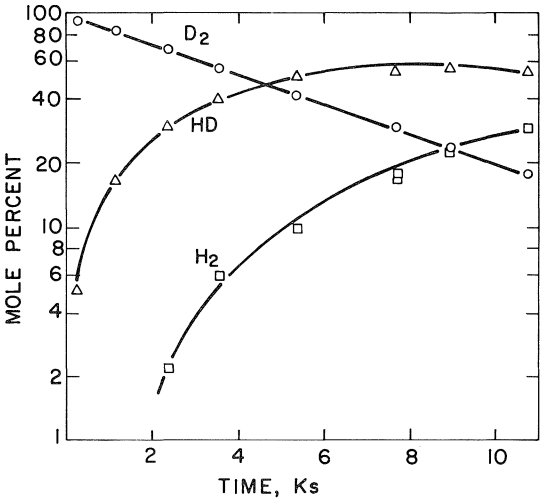

FIG. 1. Typical D_2 exchange data. Conditions: solvent = 1:1 $CHCl_3$–C_2H_5OH; gas volume = 72.9 ml; solution volume = 20.0 ml; $P(D_2)$ = 88 kPa; $RhCl(PPh_3)_3$ = 200 mg; T = 303 K.

The overall exchange reaction catalyzed by $RhCl(PPh_3)_3$ was shown to be

$$[4] \qquad D_2 + C_2H_5OH \rightarrow HD + C_2H_5OD$$

by i.r. observation of the disappearance of the —OH absorption at 3620 cm^{-1} and simultaneous appearance of the —OD band at 2670 cm^{-1} upon bubbling D_2 through a 1% solution of C_2H_5OH in $CHCl_3$ containing 5 mM $RhCl(PPh_3)_3$. Subsequent conversion of HD to H_2 occurred in the same manner.

If experiments were run for sufficient time, direct measurement of the apparent H–D isotope effect $2k_{HD}/k_{D_2}$ for the overall exchange reaction 4 could be made either by direct comparison of the rates of decay of HD or D_2 or from the HD maximum assuming sequential first-order decay kinetics for D_2 and HD (1). For example, in Fig. 1 the HD maximum is 53 ± 1 mol%, therefore $2k_{HD}/k_{D_2} = 0.85 \pm 0.05$. An apparent inverse H–D isotope effect of this magnitude was found in all cases.

(1) The Dependence of Exchange Rate on the Concentrations of Rhodium and Initial D_2

Data are presented in Fig. 2 for initial D_2 exchange rates in 1:1 $CHCl_3$–C_2H_5OH. These overall rates are at least a factor of 10 greater than those in 1:1 C_6H_6–C_2H_5OH under comparable conditions. Considerable curvature is evident in Fig. 2*A* at low total rhodium concen-

TABLE 1. Reaction of C_2H_5OH and $CHCl_3$ to yield C_2H_5Cl and CH_2Cl_2 in the presence of $RhCl(PPh_3)_3$ at 323 K

$RhCl(PPh_3)_3$ added (μmol)	Initial rate of production ($\mu M\ s^{-1}$)		Final composition	
	CH_2Cl_2	C_2H_5OH	CH_2Cl_2/Rh	C_2H_5Cl/Rh
27.0	0.9	0.5	1.2	3.6
54.1	1.8	0.9	1.6	3.8
108.0	5.6	1.9	2.3	4.6

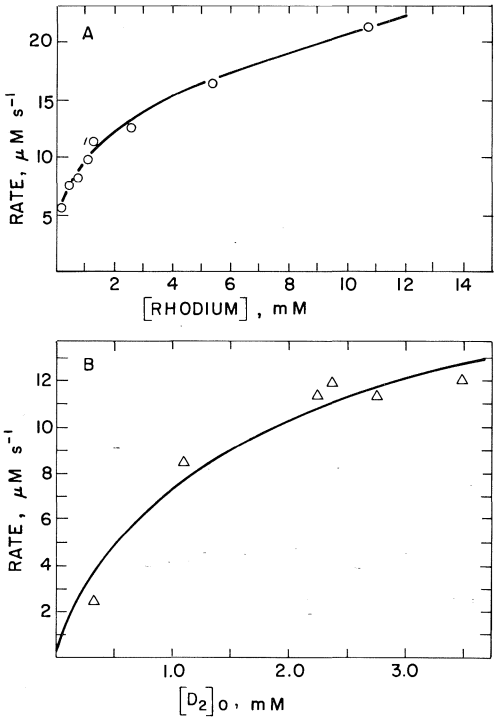

FIG. 2. The dependence of the overall deuterium exchange rate in 50% $CHCl_3$–C_2H_5OH on the total rhodium (*A*) and initial deuterium (*B*) concentrations. Experimental conditions: (*A*): $[D_2]_0 = 2.77$ m*M*; $T = 303$ K; (*B*): [Rh] = 1.35 m*M*; $T = 303$ K.

trations, in contrast to the almost linear dependence of the exchange rate on total rhodium in 1:1 C_6H_6–C_2H_5OH. The fall-off in D_2 exchange rate at higher concentrations is likely due to the reduction in the fraction of catalytically active rhodium available to participate in reaction 1 because of the generation of HCl by the side-reaction discussed below and competition from reaction 2.

(2) The Reaction of $RhCl(PPh_3)_3$ with $CHCl_3$–C_2H_5OH

Direct evidence for the presence of $RhHCl_2(PPh_3)_2$ was obtained during a repetition of the n.m.r. experiment of Osborn *et al.* (3), in which the reversibility of the hydrogenation equilibrium, reaction 1, was observed upon alternately saturating a 0.1 *M* $RhCl(PPh_3)_3$ solution in $CHCl_3$ with H_2 and purging with N_2. A broad residual resonance centered at 26.5 τ *vs.* $(CH_3)_4Si$ remained when the $RhH_2Cl(PPh_3)_3$, characterized by the broad doublet maxima 21.5, 18.8 τ and the singlet at 28.2 τ, was dissociated by flushing H_2 from the solution. Due to sensitivity limitations of our spectrometer, and the low concentration of the monohydride, estimated to be less than 0.02 *M*, good resolution of the usual doublet of triplets expected for this species was not achieved. However, the following experiments confirmed the preliminary identification.

Analysis of 10 vol% C_2H_5OH–$CHCl_3$ solutions of $RhCl(PPh_3)_3$, which had been reacted for up to 20 h, by v.p.c.-m.s. at 323 K showed that two quite unexpected products, dichloromethane and chloroethane, were major new components of the reaction mixture. These apparently had formed by a $RhCl(PPh_3)_3$-catalyzed conversion of $CHCl_3$ and C_2H_5OH respectively, since the yield of CH_2Cl_2 and C_2H_5Cl exceeded the initial total rhodium concentration. The C_2H_5OH–$CHCl_3$ solvent composition was selected to simplify v.p.c. analysis, and is not critical.

Results of kinetic studies and the composition of the final reaction mixtures are summarized in Table 1. In these experiments 25 to 100 mg $RhCl(PPh_3)_3$ were reacted with 1.0 ml total volume of 10% C_2H_5OH–$CHCl_3$ under N_2. Rates for formation of CH_2Cl_2 and C_2H_5Cl were obtained from plots of the quantities of

Can. J. Chem. Downloaded from www.nrcresearchpress.com by 210.87.254.6 on 09/05/12
For personal use only.

Can. J. Chem. Downloaded from www.nrcresearchpress.com by 210.87.254.6 on 09/05/12
For personal use only.

each component present *vs.* time. These data were linear over a 6 h period. In each case, solution colors had faded from the deep red of $RhCl(PPh_3)_3$ to bright yellow characteristic of $RhHCl_2(PPh_3)_2$.

After reaction, the n.m.r. spectrum of the solution most concentrated in Rh contained a doublet of triplets centered at 26.5 τ. Injection of 1 mol anhydrous HCl per mol Rh to this sample developed a sharp well-resolved spectrum of authentic $RhHCl_2(PPh_3)_2$ with identical parameters to the product of reaction with the solvent: a multiplet centered at 26.5 τ, $J_{Rh-H} = 13$ Hz, $J_{P-H} = 21$ Hz. From the data in Table 1, it may readily be seen that neither were initial rates of production of CH_2Cl_2 and C_2H_5Cl equivalent nor were final yields of these components simply stoichiometric.

In addition, we found that in the presence of a large excess of triphenylphosphine (PPh_3:Rh = 35), no CH_2Cl_2 formed, but quantitative conversion of ethanol to chloroethane was achieved. No other volatiles, such as chloroethylenes or chloroethanes, were detected. A solid residue, collected by pumping off the solvents, was extracted with diethylether. Evaporation and vacuum drying of this filtered solution gave a white solid, m.p. 79–80 °C. The mass spectrum of this material showed that triphenylphosphine and triphenylphosphine oxide were major components, by comparison with authentic spectra of these materials. Also, it suggested that the species triphenylphosphine dichloride, Ph_3PCl_2 (m.w. = 333), and triphenylphosphine dichloromethylene, $Ph_3P{=}CCl_2$ (m.w. = 345), were present since minor peaks occurred at *m/e* 330–332 and 344–346.

By substitution of $CHCl_3$ and C_2H_5OH with D-labelled solvents in appropriate experiments, we found by ^1H n.m.r. analyses that $RhHCl_2(PPh_3)_2$ formed only in the presence of C_2H_5OH. Chloroethane and methylene chloride were detected in the usual quantities in every case. No deuterium exchange occurred with, nor was there activation of, alkane C—H bonds of $CHCl_3$ or C_2H_5OH. These data may indicate that $RhCl(PPh_3)_3$ can specifically activate alcoholic hydroxy bonds. Further evidence of preferential solvation of the catalyst by C_2H_5OH is presented in the following section.

It was not feasible to confirm by the same methods that these reactions occurred under the conditions employed to study the D_2 exchange reactions. However, about 1.0 m*M* free HCl was detected with the glass–AgCl/Ag electrodes in a 1.0 m*M* solution of $RhCl(PPh_3)_3$ in 1:1 $CHCl_3$–C_2H_5OH at 298 K under N_2. About a three-fold increase of HCl concentration was noted upon saturating the solution with H_2. Similar reactions with the solvent therefore occur at low rhodium concentrations.

(3) The Effect of $CHCl_3$–C_2H_5OH Solvent Composition on the D_2 Exchange Rate

In some exchange experiments we observed that the first sample of solvent-free gas removed from the reaction flask contained only 90–95% D_2, compared to the feed D_2, which was generally 98+% D_2. This was shown by infrared spectroscopy to be due to very rapid exchange of D_2 with the 0.05 vol% C_2H_5OH stabilizer present in the $CHCl_3$. The reaction was complete a couple of minutes after dissolution of the catalyst.

The considerable effect of solvent composition on the rate of D_2–C_2H_5OH exchange is shown in Fig. 3. Also included are data which illustrate the effect of solvent composition on the rate of hydrogenation of 1-butene. It may be seen that, between 6 and 96 mol% C_2H_5OH in $CHCl_3$, the rate of D_2–C_2H_5OH exchange decreases by a factor of about 30. In comparison,

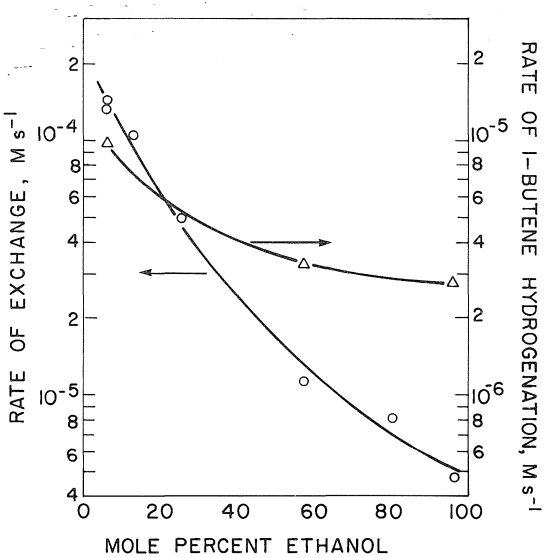

FIG. 3. The effect of $CHCl_3$–C_2H_5OH solvent composition on the rate of 1-butene hydrogenation at T = 303 K; $P(D_2)_0$ = 88 kPa.

Can. J. Chem. Downloaded from www.nrcresearchpress.com by 210.87.254.6 on 09/05/12
For personal use only.

the rate of 1-butene hydrogenation drops by only a factor of 3.4. Little significance can be attached to the relative magnitudes of the rates of these two types of reaction, since the solution concentration of 1-butene was low. It should be noted that the solubility of H_2 is less in pure $CHCl_3$ than in C_2H_5OH, 0.027 and 0.035 μM Pa^{-1} respectively (5), and on this basis alone a relative increase in rate for both these reactions of up to 1.3 would be expected upon replacing $CHCl_3$ by C_2H_5OH.

The possibility that the rate enhancement in $CHCl_3$-rich solution originated with a change in activation energy was considered, and tested by comparing $E^{\ddagger}$ for the exchange reactions in 5 and 50 vol% C_2H_5OH in $CHCl_3$. Rates in the former solvent were greater by a factor of 10, and this enhancement appears to be associated with a reduction in the enthalpy of activation, rather than an increase in the entropy of activation which could arise with solvent restructuring. This topic is considered further in section 4.

(4) The Temperature Dependence of the Rates of D_2–C_2H_5OH Exchange Reactions

A comparison of the effect of temperature on D_2 exchange rates is shown in Fig. 4 for $RhCl(PPh_3)_3$ in three different solvent mixtures, and for $RhBr(PPh_3)_3$ in 50 vol% $CHCl_3$–C_2H_5OH. Experimental rates have been plotted as a function of $1/T$, since derivation of specific rate constants would require the assumption of a reaction mechanism which may not hold for each system.

The considerable curvature in rate data with T^{-1} for both the chloro and bromo complexes in 50 vol% $CHCl_3$–C_2H_5OH is additional evidence for the side reactions discussed in section 2. The relative loss of catalytic activity is likely associated with the considerable decrease in the reversibly bound H_2:Rh ratio with increasing temperature as discussed separately (2). An example of these data is included in Table 2. It has not been possible to explain quantitatively the kinetics in terms of competing equilibria, reactions 1 and 2, since HCl is irreversibly produced by reactions discussed in section 2. However, qualitatively, we believe this interpretation is correct, and that the relative fall-off in D_2 exchange rate is a result of increased formation of the thermodynamically more stable $RhHCl_2(PPh_3)_2$ species compared to $RhH_2Cl(PPh_3)_3$ at the elevated temperatures in $CHCl_3$–C_2H_5OH.

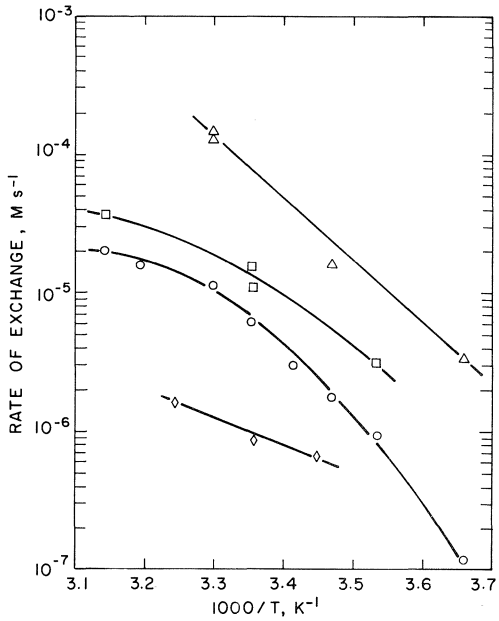

FIG. 4. D_2 exchange rates as a function of $T(K^{-1})$. Notation: $RhCl(PPh_3)_3$ in: ⊙ 50 vol% C_2H_5OH–$CHCl_3$; △ 5 vol% C_2H_5OH–$CHCl_3$; ◇ 50 vol% C_6H_6–C_2H_5OH; ⊡ $RhBr(PPh_3)_3$ in 50 vol% C_2H_5OH–$CHCl_3$. Conditions: $P(D_2)_0$ = 88 kPa; [Rh] = 1.30 ± 0.05 mM.

TABLE 2. The effect of temperature on the reversibly bound H_2:Rh ratio in 50% $CHCl_3$–C_2H_5OH. [Rh] = 2.6 mM; $P(H_2)$ = 88 kPa

Temperature (K)	Mol H_2:mol Rh
273	0.38
303	0.22
323	0.03

Nuclear magnetic resonance experiments showed that addition of an equimolar quantity of anhydrous HCl to $RhH_2Cl(PPh_3)_3$ in $CHCl_3$ yielded the monohydride.

$RhCl(PPh_3)_3$ is at least 10 times more active in 5 vol% compared to 50 vol% C_2H_5OH in $CHCl_3$. Activation energies, $E^{\ddagger}$, between 273–303 K were 86 ± 8 and 101 ± 9 kJ mol^{-1} respectively, and were calculated from the slope of the best straight line through the linear portion of each set of data. This difference is significant, and is more than enough to account for the observed rate enhancement (a factor of 10 increase in rate requires $E^{\ddagger}$ to decrease by 5.7 kJ mol^{-1} at 298 K). Unfortunately, data are not sufficiently precise to establish if an increase in the entropy of activation has accompanied the

Can. J. Chem. Downloaded from www.nrcresearchpress.com by 210.87.254.6 on 09/05/12
For personal use only.

comparatively large decrease in $E^{\neq}$ in going from 50 to 5 vol% C_2H_5OH–$CHCl_3$.

With $RhBr(PPh_3)_3$, the exchange rate was approximately twice that for the $RhCl(PPh_3)_3$ catalyzed reaction, but the activation energy was similar. A more precise comparison is not justified, since both sets of data exhibit curvature in Fig. 4. The increase in rate was probably due to electronic or steric changes upon replacement of Cl by Br, but because an undetermined amount of solvent decomposition occurred in these solutions as well, the extent of chloride exchange or HCl adduct formation cannot be assessed.

Data for $RhCl(PPh_3)_3$-catalyzed D_2 exchange in 1:1 C_6H_6–C_2H_5OH have been included in Fig. 4 for comparison. It may be seen that both the overall exchange rates and the activation energy, approximately 35 kJ mol^{-1} (1), are lower under experimental conditions which were identical except for solvent type and composition.

(5) H–D Isotope Effects

(5.1) In 1:1 $CHCl_3$–C_2H_5OH

It has already been stated that in 1:1 $CHCl_3$–C_2H_5OH the isotope effect defined as $2k_{HD}/k_{D_2}$ was 0.85 ± 0.05.

As seen in the previous sections, the analysis of the catalytic function of $RhCl(PPh_3)_3$ in $CHCl_3$–C_2H_5OH solution was obscured by the occurrence of a complex side reaction. We have not fully defined this process quantitatively, therefore reliable analytical expressions for the distribution of catalytically active species have not been written. Instead, the origin of the H–D isotope effect has been investigated by computer simulation of the D_2 exchange reactions. Two important basic assumptions were made: (*i*) that a fixed portion of the catalyst participates in the reversible hydrogenation equilibrium, eq. 1, and (*ii*) that no other Rh-containing species are catalytically active. These points are discussed later.

The model is illustrated schematically in Fig. 5 in which the species RhD^1D^2, RhH^1D^2, RhD^1H^2, and RhH^1H^2 are notations for the D_2, HD, and H_2 adducts of $RhCl(PPh_3)_3$ respectively. The non-equivalent Rh—H (or D) bonds are labelled 1 and 2 respectively. Provision was made for adjustment of rate constants for uptake and release of D_2 (k_1 and k_4), HD (k_2 and k_5), or H_2 (k_3 and k_7). Also the rate of pseudo-first-order decay of Rh—D at site 1 or

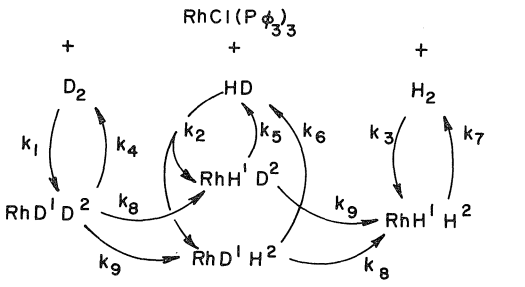

FIG. 5. The general mechanism assumed for $RhCl(PPh_3)_3$-catalyzed D_2–C_2H_5OH exchange. Notation: k_i's are identical with those used in Table 3. Other ligands have been omitted from the hydride species for clarity.

2 was variable by rate constants k_8 or k_9 respectively. Numerical integration of the set of differential equations shown in Table 3 yielded gas-phase compositions in D_2, HD, and H_2, and the concentrations of catalyst species, as a function of time (4). The effect of changing constants k_1 to k_9 was assessed by comparison of calculated and experimental data. Constants k_1 to k_9 are the same in Table 3 and Fig. 5.

The experimental isotope effect $2k_{HD}/k_{D_2}$ could only be obtained with this program if $k_1 > k_2 > k_3$. Since there is a thermodynamic requirement that $K_1^{D_2} < K_1^{HD} < K_1^{H_2}$, that is, $k_1/k_4 < k_2/k_5 \sim k_2/k_6 < k_3/k_7$, then it is necessary that $k_4 > k_5 = k_6 > k_7$. Use of input rate constants which met these criteria yielded a satisfactory fit to experimental data. Variation of the gas solubility constants so that $H_{D_2}:H_{HD}:H_{H_2} = 1.025:1.00:0.975$ made no significant difference to the calculated H–D isotope effects.

It was also necessary that $k_8 \gg k_9$, since in the limiting case if $k_8 = k_9$ and the rate of transfer of deuterium from the Rh—D bonds to the

TABLE 3. Set of differential expressions used to simulate $RhCl(PPh_3)_3$-catalyzed exchange experiments*

$$dc_1/dt = (-k_1c_1c_4 + k_4c_5)/(1 + V_G/RTV_LH_1)$$
$$dc_2/dt = (-k_2c_2c_4 + k_5c_6 + k_6c_7)/(1 + V_G/RTV_LH_2)$$
$$dc_3/dt = (-k_3c_3c_4 + k_7c_8)/(1 + V_G/RTV_LH_3)$$
$$dc_4/dt = -k_1c_1c_4 - k_2c_2c_4 - k_3c_3c_4 + k_4c_5 + k_6c_7 + k_7c_8$$
$$dc_5/dt = k_1c_1c_4 - k_4c_5 - k_8c_5 - k_9c_5$$
$$dc_6/dt = 0.5k_2c_2c_4 - k_5c_6 + k_8c_5 - k_9c_6$$
$$dc_7/dt = 0.5k_2c_2c_4 - k_6c_7 + k_9c_5 - k_8c_7$$
$$dc_8/dt = k_3c_3c_4 - k_7c_8 + k_8c_7 + k_9c_6$$

*$c_1 = [D_2]$; $c_2 = [HD]$; $c_3 = [H_2]$; $c_4 = [RhCl(PPh_3)_3]$; $c_5 = [RhD^1D^2Cl(PPh_3)_3]$; $c_6 = [RhH^1D^2Cl(PPh_3)_3]$; $c_7 = [RhD^1H^2Cl(PPh_3)_3]$; $c_8 = [RhH^1H^2Cl(PPh_3)_3]$; V_G = volume of gas phase, in liters; V_L = volume of solution, in liters; R = gas constant; T = absolute temperature; H_i = solubility constant for D_2, HD, H_2 when $i = 1, 2, 3$ respectively.

solvent was made rapid with respect to hydrogen activation, then the calculation showed that negligible amounts of HD formed because dual transfer events of the type

$$[5] \qquad RhD^1D^2 \overset{k_8,\ k_9}{\rightleftharpoons} RhH^1H^2$$

were important. This was obviously not the case experimentally.

Two conclusions were drawn: (*i*) the rate-controlling step for D_2 exchange in $CHCl_3$–C_2H_5OH must be the hydrogen activation step (*i.e.* D_2, HD, H_2) and (*ii*) only one of the two Rh—D bonds was labile for D-transfer.

(6) The H_2–D_2 Equilibration Reaction in $CHCl_3$

Reaction 6 is catalyzed by 1.3 m*M* $RhCl(PPh_3)_3$ in $CHCl_3$ at 44 kPa partial pressure of both H_2 and D_2 at 298 K at a rate of 39 μ*M* D_2 s^{-1}. If ethanol-stabilized $CHCl_3$ is used, the initial rapid exchange of D_2 with the 0.05 vol% C_2H_5OH is detectable as a change in the atom fraction of D in the gas phase.

$$[6] \qquad H_2 + D_2 \rightleftarrows 2HD$$

The D_2–C_2H_5OH exchange reaction product distribution is not governed by the occurrence of the H_2–D_2 reaction. This point is considered in section 4 of the discussion.

Discussion

The catalytically active species and the kinetics and mechanism of $RhCl(PPh_3)_3$-catalyzed D_2–C_2H_5OH exchange with $CHCl_3$ as co-solvent are discussed, and compared with the 1:1 C_6H_6–C_2H_5OH case (1). The bases for the pronounced solvent composition dependence of the D_2 exchange reaction, the inverse H–D isotope effect, and the solvent decomposition reaction are also considered.

(1) $RhCl(PPh_3)_3$ in $CHCl_3$–C_2H_5OH

It has been assumed in the previous text that reaction 1 was the dominant reversible catalyst-hydrogenation equilibrium in $CHCl_3$–C_2H_5OH. The following evidence supports this assumption: (*i*) Osborn *et al.* (3) found by n.m.r. spectrometry that the same dihydride formed in $CDCl_3$ and in several basic solvents, (*ii*) Meakin, *et al.* showed by ^{31}P n.m.r. experiments that the dihydride also formed in H_2-saturated CH_2Cl_2 and that it existed in the conformation shown in Fig. 6 (6), (*iii*) addition of C_2H_5OH to C_6H_6 solutions of $RhH_2Cl(PPh_3)_3$ enhanced olefin hydrogenation rates (7) suggesting that equilibrium constant K_1 was probably not grossly affected by the presence of the alcohol component. Therefore, although we have not directly confirmed that reaction 1 occurs in 1:1 $CHCl_3$–C_2H_5OH, there is strong evidence to support this claim.

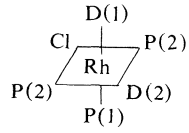

FIG. 6. Configuration of $RhD_2Cl(PPh_3)_3$ (6).

We know from separate experiments that a smaller mole fraction of $RhCl(PPh_3)_3$ participates in reaction 1 in 1:1 $CHCl_3$–C_2H_5OH than in C_6H_6 or in CH_2Cl_2 alone. Direct measurement of reversibly bound H_2 by an inert gas stripping technique yielded data, some of which are summarized in Table 2, which showed, for example, that at 303 K and 88 kPa H_2 only 0.22 mol H_2 per mol Rh could be recovered (2). In comparison, 0.85 mol H_2 was bound per mol Rh in C_6H_6 solution under identical conditions.

Depending on the amount of free $RhCl(PPh_3)_3$, about 0.7 mol fraction Rh was present as the monohydride $RhHCl_2(PPh_3)_2$ formed by reaction 2 at 303 K and 88 kPa H_2. The HCl was generated by a catalyzed side-reaction involving the solvent and $RhCl(PPh_3)_3$. Sacco *et al.* (8) have shown that HCl will add to $RhCl(PPh_3)_3$ to yield α and β stereoisomers, each of which loses some HCl in solution. On the basis of n.m.r. data, Baird and co-workers (9) concluded that the monohydride was a bis(triphenylphosphine) adduct, and that it was unstable with respect to HCl dissociation. Since Sacco *et al.* have also noted that the Rh—H bond will not exchange with DCl in D_2O (in the presence of excess ligand), we have concluded that the monohydride itself is catalytically inactive for the D_2–C_2H_5OH reaction.

These results suggest that the three main species in $CHCl_3$–C_2H_5OH solution were $RhCl(PPh_3)_3$, $RhH_2Cl(PPh_3)_3$, and $RhHCl_2(PPh_3)_2$, the concentrations of which were governed by reactions 1 and 2 and the extent of HCl generation. It is likely that PPh_3 dissociates from both $RhCl(PPh_3)_3$ and $RhH_2Cl(PPh_3)_2$ to some degree, although not to the extent suggested originally by Osborn *et al.* (3).

Can. J. Chem. Downloaded from www.nrcresearchpress.com by 210.87.254.6 on 09/05/12
For personal use only.

Can. J. Chem. Downloaded from www.nrcresearchpress.com by 210.87.254.6 on 09/05/12
For personal use only.

Arai and Halpern have reported the equilibrium constant $K_7 = 1.4 \times 10^{-4}\ M$ in C_6H_6 at 298 K (10) for

$$[7] \qquad RhCl(PPh_3)_3 \overset{K_7}{\rightleftarrows} RhCl(PPh_3)_2 + PPh_3$$

Meakin *et al.* concluded that loss of PPh_3 from $RhH_2Cl(PPh_3)_3$ was small, probably less than 5% (6) in the concentrated solutions required by their n.m.r. studies. Thus, dissociation of PPh_3 is not thermodynamically favored in either case. However, the rates of PPh_3 exchange are rapid (6, 11), therefore from the kinetic standpoint, these equilibria cannot be neglected. The half-life for free and complexed PPh_3 on $RhCl(PPh_3)_3$ has been estimated from n.m.r. data as $>10^{-2}$ s (11) and on $RhH_2Cl(PPh_3)_3$ as $>10^{-3}$ s (6). These values may be compared with $t_{1/2}$ for H_2 on the dihydride in C_6H_6 of about 30 s, calculated by using $K_1 = 2300\ M^{-1}$ and $k_{-1} = 0.023\ s^{-1}$ when [Rh] = 4.0 mM and $[H_2]$ = 2.5 mM at 298 K (2). Rates of exchange of PPh_3 with these catalytically important species are clearly rapid with respect to the rate of activation and dissociation of H_2. The sensitivity of the D_2 exchange reaction to excess PPh_3 is likely related to these factors.

(2) The Side-reaction Involving Solvent

This complex reaction may be a catalyzed analog of the known replacement of alcoholic hydroxy groups by chlorine which can occur in CCl_4 in the presence of PPh_3 (12). There was no reaction between $CHCl_3$, C_2H_5OH, and PPh_3 without $RhCl(PPh_3)_3$. In an attempt to explain our observations, the following mechanism is proposed

$$[8] \quad PPh_3 + CHCl_3 \xrightarrow{RhCl(PPh_3)_3} (Ph_3PCl)^+\ CHCl_2^- \xrightarrow{C_2H_5OH} Ph_3PO + C_2H_5Cl \leftarrow (Ph_3PCl)^+\ OC_2H_5^- + CH_2Cl_2$$

This sequence is based on the scheme employed by Hooz and Gilani to explain the ROH–CCl_4–PPh_3 reaction (13), and accounts for the greater initial rate of formation of CH_2Cl_2 compared to C_2H_5Cl. Since excess PPh_3 would be expected either to inhibit any ligand dissociation from $RhCl(PPh_3)_3$ or to displace weakly interacting $CHCl_3$ molecules from the solvation shell of $RhCl(PPh_3)_3$, we suggest that the following process occurs

$$[9] \quad (PPh_3)_3RhCl + C_2H_5OH \rightarrow (Ph_3P)_3RhH(OC_2H_5)Cl$$

Reaction of this intermediate with $CHCl_3$ and PPh_3 could yield Ph_3PCl_2, $Ph_3P{=}CCl_2$, $Ph_3P{=}O$, and C_2H_5Cl, without formation of CH_2Cl_2.

Our data do not permit determination of the stoichiometries of these reactions, or more explicit descriptions of the function of $RhCl(PPh_3)_3$ as the catalyst for these reactions. In particular, it is not known if $RhHCl_2(PPh_3)_2$ is formed by reaction 2 from free HCl, or if the Rh—H bond formed by cleavage of the O—H bond of ethanol is retained and Cl^- added by a ligand exchange step, say, with the intermediate proposed in reaction 9.

An important point which we have been unable to clarify experimentally is the reason for the apparently more rapid generation of HCl under the conditions used for D_2 exchange compared to those used to study the solvent metathesis at 323 K. As noted, the decay of D_2 in exchange experiments was accurately first-order, therefore no loss of catalytic activity with time occurred. This would not be expected if the concentration of the inactive $RhHCl_2(PPh_3)_2$ increased with time. The apparently rapid solvent decomposition and establishment of reaction 2 in dilute solution may be related to the PPh_3 dissociation equilibrium, reaction 7. This could not be tested by addition of excess PPh_3, since the course of the side-reaction changed considerably. The sensitivity of the D_2 exchange reaction to solvent composition may indicate that solvation of $RhCl(PPh_3)_3$ is critical. This phenomenon, and the solvent side-reaction perhaps originate from the same basis.

(3) Effects of Solvent Composition

The dependence of the kinetics and mechanism of the D_2 exchange reaction on solvent composition and on the nature of the components is pronounced. In our D_2 exchange experiments, progressive replacement of $CHCl_3$ by C_2H_5OH reduced the rate by a factor of 30 (Fig. 3). Both the dipole moment and the dielectric constant of C_2H_5OH are greater than those for $CHCl_3$ (14), and on this basis one must conclude that if D_2 activation is rate determining in this solvent, then a reduction in polarity of the transition state relative to the initial states of D_2 and $RhCl(PPh_3)_3$ must occur. That is, the increased solvation ability of the solvent inhibits activation of D_2. This behavior is contrary to the effect of solvent on the rate of activation of H_2 by IrCl-

Can. J. Chem. Downloaded from www.nrcresearchpress.com by 210.87.254.6 on 09/05/12
For personal use only.

$(CO)(PPh_3)_2$ observed by Vaska and Werneke (15). In our system, preferential solvation of $RhCl(PPh_3)_3$ by C_2H_5OH, perhaps due to hydrogen bonding with nonbonding d electrons on the Rh, could explain this phenomenon.

It is interesting to speculate on the possible connection of the solvent-dependence of the exchange reaction and the complex side-reaction discussed in section 2. Each reaction requires some activation of solvent molecules. In the former case, proton transfer between $RhD_2Cl(PPh_3)_3$ and C_2H_5OH might occur by either of these four-center intermediates:

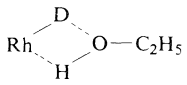

1

or

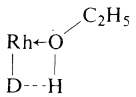

2

In **1**, which we prefer, hydrogen bonding of the —OH group to, say, nonbonding d electrons on the rhodium might permit the close approach illustrated. However, the hydrido ligand should possess a net negative charge, and close approach of an oxygen atom may be impossible. If, on the other hand, ethanol enters the coordination sphere of Rh(III), perhaps at the labile triphenylphosphine site P(1) in Fig. 6 (6), proton exchange can be facilitated if the —OH bond is effectively weakened. In section 2 of the results it was noted that the hydrido ligand in $RhHCl_2(PPh_3)_2$ was originally the hydroxyl proton of ethanol. Since it is unlikely that any Rh species would be sufficiently basic to abstract a proton from C_2H_5OH, perhaps proton activation by coordination of ethanol to $RhCl(PPh_3)_3$ occurred. Thus, there is some evidence that the D_2 exchange and solvolytic phenomena have a common basis.

Olefin hydrogenation rates are particularly low in $CHCl_3$ solutions of $RhCl(PPh_3)_3$ (7), although the dihydride readily forms in this solvent. It has been suggested that this inhibition is due to blocking of the active site on $RhH_2Cl(PPh_3)_3$ generated, presumably, by dissociation of a PPh_3 ligand (6). In view of the D_2 exchange data presented in this paper, the slow hydrogenation rates in $CHCl_3$ may arise with a change of the rate-limiting step from H_2 transfer from the dihydride to the olefin (as in C_6H_6 (3)) to H_2 activation by $RhCl(PPh_3)_3$.

(4) Mechanism of the D_2 Exchange Reaction

In section 5.1 of the results a computer simulation of the overall exchange reaction was described. It was emphasized that agreement between the observed and calculated H–D isotope effects, $2k_{HD}/k_{D_2}$, could only be obtained if it was assumed that the activation of D_2 (or HD and H_2) was rate-determining. Thus, the present $CHCl_3$–C_2H_5OH system differs considerably from the 1:1 C_6H_6–C_2H_5OH case.

In comparison, we have shown that in 1:1 C_6H_6–C_6H_5OH the rate-determining step must be the transfer of D from the labile Rh—D bond to the hydroxyl group. Also, the experimental isotope effect, $2k_{HD}/k_{D_2} = 1.1$, must originate either because of (*i*) the decreasing relative thermodynamic stabilities of the H_2, HD, and D_2 adducts or because of (*ii*) control of the HD and H_2 product distribution by the H_2–D_2 reaction, reaction 6 (1). Factors (*i*) and (*ii*) cannot dominate in $CHCl_3$–C_2H_5OH, since the observed isotope effect is only $2k_{HD}/k_{D_2} = 0.85$.

It is a fundamental requirement that the H_2, HD, and D_2 dihydrides have the indicated stabilities and this must give rise to a normal H–D isotope effect in the sequence $2k_{HD} > k_{D_2}$. Thus, if the simple model shown in Fig. 5 is valid then a true inverse kinetic isotope effect of at least the magnitude shown must exist in the hydrogen activation step. The effect of reaction 6 on the isotope effect must be negligible, perhaps because the rate of H_2–D_2 equilibration is low in the presence of excess ethanol.

In Fig. 3 it may be seen that the rate of D_2–C_2H_5OH exchange was considerably more sensitive to solvent composition than was the rate of hydrogenation of 1-butene. Both Osborn *et al.* (3) and Ohrt (16) have argued that the H–D isotope effect in the rate-determining step in the hydrogenation of terminal olefins, at least in C_6H_6 solution, must arise with the rate-limiting transfer of H_2 (or D_2) to the olefin. If the controlling step is the same in $CHCl_3$–C_2H_5OH, then our data suggest that D_2 exchange and olefin hydrogenation do not have a common basis. This is additional experimental support for the validity of the present model, since the four coordinate $RhCl(PPh_3)_3$ should exhibit greater variation in reactivity with solvent type than should the coordinately saturated

intermediate $RhH_2Cl(PPh_3)_3$ which must exist in the hydrogenation case.

The apparent inhibition of the D_2-exchange reaction in C_2H_5OH-rich solvent mixtures may be related to the greater solvent–catalyst H-bonding interaction expected between C_2H_5OH and $RhCl(PPh_3)_3$ than between $CHCl_3$ and this species. It is known that $RhCl(PPh_3)_3$ behaves as a hard base towards certain electron acceptors (17), although there is no direct evidence to support the present assumption that the complex will act in a similar manner towards hydrogen-bonding solvents. Presumably, the relatively large decrease of the D_2 exchange rate with small increases in C_2H_5OH concentration was a reflection of a specific bonding interaction with $RhCl(PPh_3)_3$.

The authors wish to thank their colleagues for helpful discussions, particularly M. Tomlinson and Dr. N. H. Sagert, and D. Bell of the Analytical Science Branch for deuterium analyses.

1. G. G. STRATHDEE and R. M. GIVEN. Can. J. Chem. This issue.
2. G. G. STRATHDEE and R. M. GIVEN. J. Catal. **30**, 30 (1973).
3. J. A. OSBORN, F. H. JARDINE, J. F. YOUNG, and G. WILKINSON. J. Chem. Soc. A, 1711 (1966).
4. G. G. STRATHDEE and M. J. QUINN. Can. J. Chem. **50**, 3144 (1972).
5. W. F. LINKE. Solubilities of inorganic and metal organic compounds. Vol. 1. Am. Chem. Soc. 1958. p. 1088.
6. P. MEAKIN, J. P. JESSON, and C. A. TOLMAN. J. Am. Chem. Soc. **94**, 3240 (1972).
7. A. S. HUSSEY and Y. TAKEUCHI, J. Org. Chem. **35**, 643 (1970).
8. A. SACCO, R. UGO, and A. MOLES. J. Chem. Soc. A, 1670 (1966).
9. M. C. BAIRD, J. T. MAGUE, J. A. OSBORN, and G. WILKINSON. J. Chem. Soc. A, 1347 (1967).
10. H. ARAI and J. HALPERN. Chem. Commun. 1571 (1971).
11. D. R. EATON and S. R. SUART. J. Am. Chem. Soc. **90**, 4170 (1968).
12. N. S. ISAACS and D. KIRKPATRICK. Chem. Commun. 443 (1972).
13. J. HOOZ and S. S. H. GILANI. Can. J. Chem. **46**, 86 (1968).
14. Handbook of chemistry and physics, 49th ed. The Chemical Rubber Company, Cleveland, Ohio, 1968.
15. L. VASKA and M. F. WERNEKE. Trans. N.Y. Acad. Sci. **31**, 70 (1972).
16. D. W. OHRT. Ph.D. Thesis. University of Arkansas, Fayetteville, Arkansas. 1972.
17. D. F. SHRIVER. Acc. Chem. Res. **3**, 231 (1970).

Can. J. Chem. Downloaded from www.nrcresearchpress.com by 210.87.254.6 on 09/05/12
For personal use only.

Complex Fluoroanions in Solution. V. Vanadium Pentafluoride[1]

S. BROWNSTEIN AND G. LATREMOUILLE

Division of Chemistry, National Research Council of Canada, Ottawa, Canada K1A 0R9

Received November 6, 1973

S. BROWNSTEIN and G. LATREMOUILLE. Can. J. Chem. **52**, 2236 (1974).

Vanadium pentafluoride is associated at low temperature in solution. It reacts with NbF_6^- and TaF_6^- to give complex fluoroanions and with BF_4^-, PF_6^-, AsF_6^-, and SbF_6^- to possibly yield complex fluoroanions.

S. BROWNSTEIN et G. LATREMOUILLE. Can. J. Chem. **52**, 2236 (1974).

A base température et en solution, le pentafluorure de vanadium est associé. Il réagit avec NbF_6^- et TaF_6^- pour fournir des fluoroanions complexes et avec BF_4^-, PF_6^-, AsF_6^- et SbF_6^- pour donner possiblement des fluoroanions complexes. [Traduit par le journal]

Can. J. Chem. Downloaded from www.nrcresearchpress.com by 210.87.254.40 on 09/05/12
For personal use only.

Introduction

There have been studies of the association of binary pentafluorides in the gas (1), liquid (2, 3), and solid phases (4). Vanadium pentafluoride exists almost exclusively as the monomer in the gas phase and primarily as the monomer in the liquid above 100 °C (1, 3). At lower temperatures the liquid is predominantly associated (3). The structural arrangement in the solid is endless chains of VF_5 in an octahedral arrangement joined by *cis* fluorine bridges (4). Complex fluoroanions of vanadium have not been positively identified in solution although they are widespread for its sister elements niobium and tantalum (5).

Fluorine magnetic resonance spectroscopy has identified the structure of liquid antimony pentafluoride to be endless chains in an octahedral arrangement joined by *cis* fluorine bridges (2). Rapid averaging on the n.m.r. time scale yields single lines devoid of structural information, even at low temperatures, for the other pentafluorides which have been studied. There have been no reports of the fluorine resonance spectrum of VF_5, although that attributed to $AgVF_6$ has been described (6). Fluorine resonance spectroscopy has been very useful in characterizing a variety of complex fluoroanions (5, 7).

Experimental

All sample preparation and handling was done with standard vacuum line techniques on a Pyrex vacuum line or, with non-volatile solids, using a vacuum dry box. Vanadium pentafluoride, purchased from Ozark-Mahoning Ltd., had the vapor above the solid pumped away several times and was then used without further purification. Small amounts were transferred under vacuum to break-seal equipped vials, sealed under vacuum, and weighed. Except during weighing and transferring operations the glass container with its VF_5 was stored in Dry Ice and used within three days of preparation. No evidence of attack by VF_5 on the glass vessels was found when these precautions were carefully followed. The break–seal container would then be sealed to an appropriate apparatus to prepare the sample under study. Reagent and solvent purification and storage were accomplished as previously described (5, 8). Sulfuryl chlorofluoride, purchased from Cationics, Inc., was used as received. All samples were stored at Dry Ice temperature and never allowed to reach ambient temperature. Silver hexafluorovanadate was prepared from silver and vanadium pentafluoride in bromine trifluoride as solvent, using a quartz apparatus, according to a literature procedure (9). Establishment of the purity of this compound will be described in the next section.

Fluorine resonance spectra were obtained on a Varian Associates HA-100D spectrometer operating at 94.1 MHz. Chemical shifts are reported as p.p.m. from internal $CFCl_3$. In those cases where SO_2ClF is used as solvent, the solvent peak is used as reference and is assumed to have a chemical shift of −99.7 p.p.m. X-Ray powder photographs were taken with nickel filtered CuKα radiation in 114.6 mm diameter Debye–Scherer cameras.

Results and Discussion

Vanadium pentafluoride is soluble in sulfuryl chlorofluoride to give a solution whose fluorine resonance spectrum at −75 °C has a single broad line at −484 p.p.m. in addition to the resonance of the solvent. By −135 °C this has altered to three lines at −630, −535, and −13 p.p.m. with intensity ratios of two, two, and one with some hint of structure in all three lines. This spectrum is shown in Fig. 1. Lower temperatures, necessary to resolve the fine structure,

[1]NRCC No. 13902.

TABLE 1. Experimental and theoretical elemental compositions

	Analysis (%)					
	Ag		V		F	
Compound	Calcd.	Found	Calcd.	Found	Calcd.	Found
$AgVF_6$	39.5	40.4	18.7	18.8	41.8	39.6
$AgVF_4(OH)_2$	40.1	40.2	19.0	18.8	28.3	33
$AgVF_5OH$	39.8		18.8		35.1	
$AgVF_4O$	43.0		20.3		30.3	

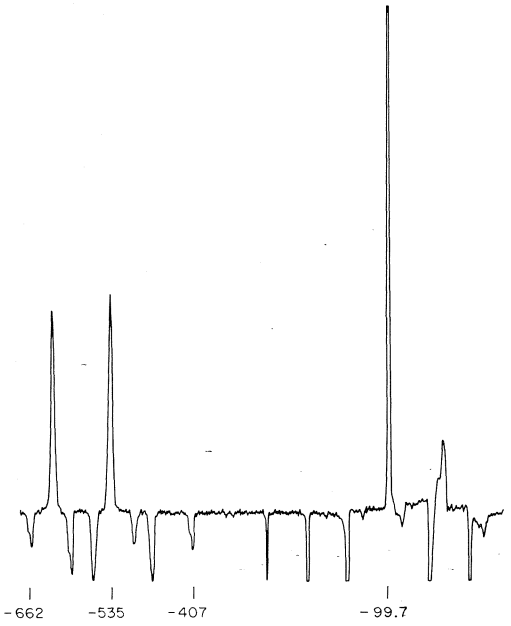

FIG. 1. The fluorine resonance spectrum of a sulfuryl chlorofluoride solution of VF_5 at -135 °C.

could not be obtained with this solvent. The fluorine resonance spectrum of VF_5 may be readily interpreted as arising from chains, either linear or cyclic, of VF_5 molecules in an octahedral configuration and joined by *cis*-fluorine bridges. The bridging fluorine is at highest field, as in $Ta_2F_{11}^-$ and $Nb_2F_{11}^-$, in contrast to the results for SbF_5 and $Sb_2F_{11}^-$ (5, 7). The weighted average for the chemical shifts of the three types of fluorine atoms is -469 p.p.m., in good agreement with the averaged chemical shift found at higher temperature. It therefore is possible to assert that the structure of VF_5 in solution at low temperature is similar to that found in the solid.

In an attempt to reproduce the fluorine resonance spectrum of $AgVF_6$ in acetonitrile (6), only a single sharp line was found at -345 p.p.m. Similar results were obtained for $AgVF_6$ in SO_2. If the solid $AgVF_6$ was briefly exposed to the atmosphere and then pumped under vacuum before preparation of the acetonitrile solution a line appeared at -130 p.p.m. with $J_{^{19}F-^{51}V} = 88$ Hz in the fluorine resonance spectrum in addition to that at -345 p.p.m. These values are in agreement with the 88 Hz previously reported for this species. If the solid sample of $AgVF_6$ was allowed to remain exposed to the air for a longer time before pumping and sample preparation the sharp line disappeared and only the highly structured line remained. A fluorine resonance spectrum of the intermediate case is shown in Fig. 2, along with a fully resolved spectrum of the structured region. It seems clear that the spectrum previously attributed to $AgVF_6$ arises from a hydrolysis product. The composition $AgVF_4(OH)_2$ is proposed for the hydrolysis product with the two hydroxyl ligands occupying axial positions.

On the basis of elemental analyses, listed in Table 1, the hydrolyzed compound could be $AgVF_4(OH)_2$, $AgVF_5OH$, or $AgVF_4O$, although the agreement is not very good for $AgVF_4O$. It is difficult to prepare a sample of $AgVF_6$ without some hydrolysis so the low experimental value for fluorine in $AgVF_6$ is not surprising.

Further support for the composition of the hydrolysis product is derived from X-ray powder diffraction data. There is a contradiction in the literature concerning the crystal structure of $AgVF_6$. Cox has reported that it is cubic and isomorphous with $AgSbF_6$ (10), while Sharp and co-workers report it to be tetragonal and isomorphous with $AgNbF_6$ (11). We have found the pattern for $AgVF_4(OH)_2$ fits the description of Cox and is isomorphous with the pattern of an authentic sample of $AgSbF_6$. Fluorine and

Can. J. Chem. Downloaded from www.nrcresearchpress.com by 210.87.254.40 on 09/05/12
For personal use only.

Can. J. Chem. Downloaded from www.nrcresearchpress.com by 210.87.254.40 on 09/05/12
For personal use only.

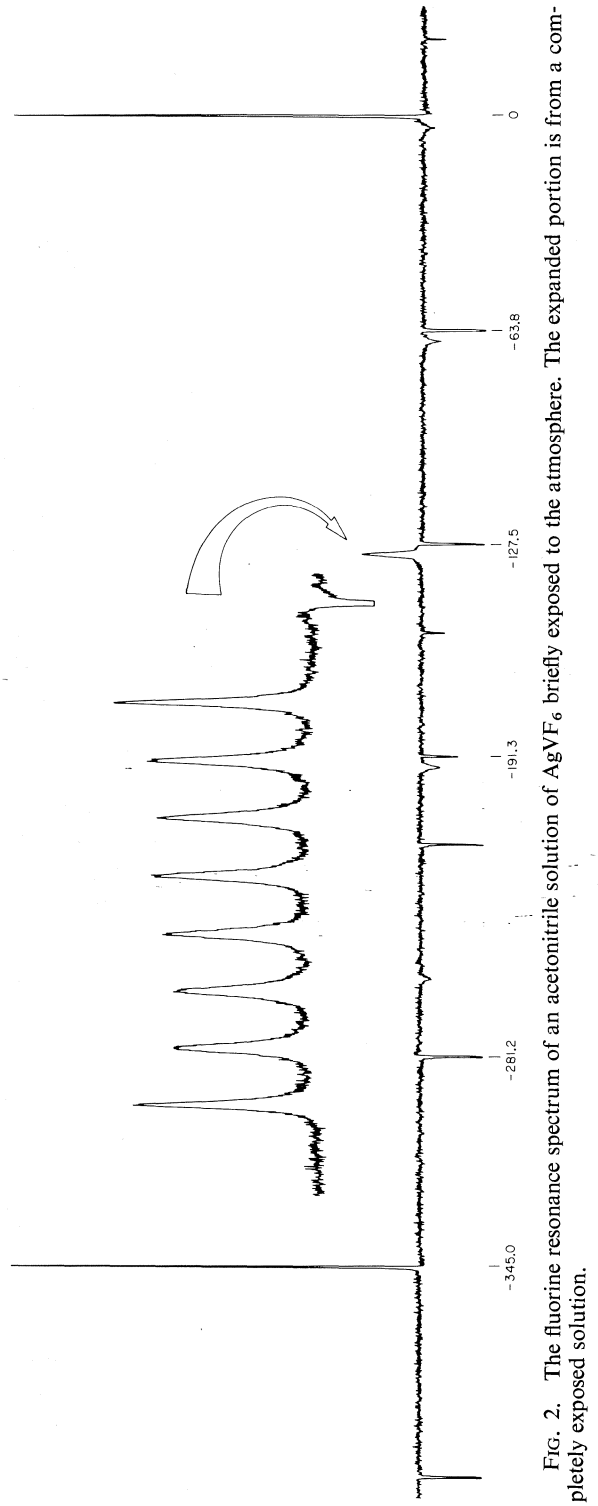

FIG. 2. The fluorine resonance spectrum of an acetonitrile solution of $AgVF_6$ briefly exposed to the atmosphere. The expanded portion is from a completely exposed solution.

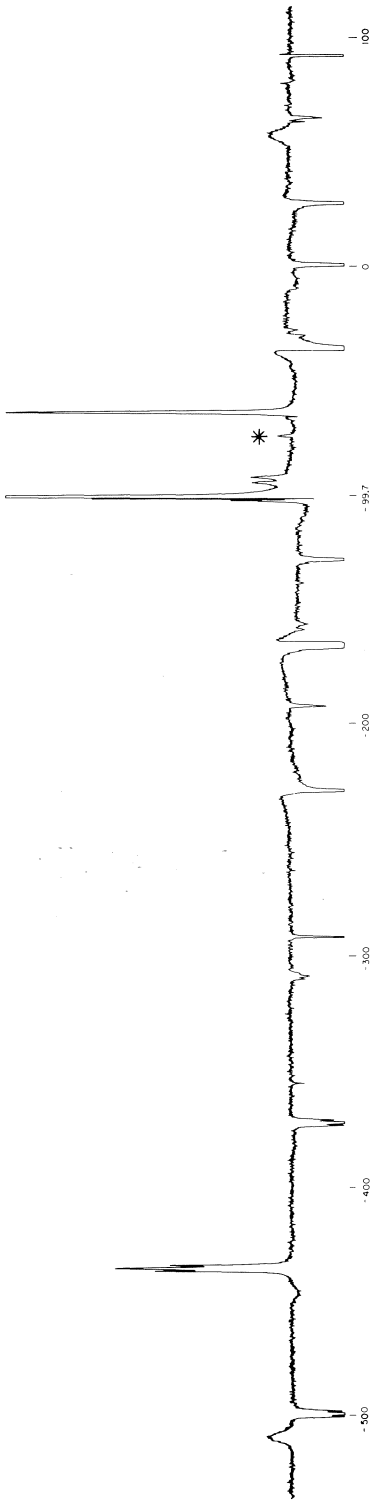

FIG. 3. The fluorine resonance spectrum of an equimolar sulfuryl chlorofluoride solution of $(TBA)TaF_6$ and VF_5 at -130 °C.

Can. J. Chem. Downloaded from www.nrcresearchpress.com by 210.87.254.40 on 09/05/12
For personal use only.

TABLE 2. Fluorine chemical shifts of group V species

Element	$\delta(MF)_5$	$\delta(MF_6^-)$	$\Delta\delta$
P	65.8*	71.0*	5.2
As	57.0*	61.7*	4.7
Sb	106.7†	117.9†	11.2
V	−484	−345	139
Nb	−162‡	−104‡	58
Ta	− 99.6‡	− 40.4‡	59.2

*Reference 8.
†Reference 7.
‡Reference 5.

oxygen are practically indistinguishable by X-ray methods in compounds containing both. Therefore since $AgSbF_6$ and $AgVF_4(OH)_2$ are isomorphous, and SbF_6^- is known to be octahedral, $VF_4(OH)_2^-$ must also be octahedral. These results exclude $AgVF_4O$ but not $AgVF_5$-OH from consideration as the hydrolysis product. It was not possible to prepare a capillary for X-ray study which did not contain a significant quantity of $AgVF_4(OH)_2$ so the results of Sharp and co-workers can be neither confirmed nor denied.

The only vanadium hydroxide fluoride species in which all fluorines would be magnetically equivalent are $VF_4(OH)_2^-$ with the proposed structure or $VF_2(OH)_4^-$ with the fluorines occupying axial positions. The former structure is the only one satisfying both the analytical and magnetic resonance results. If rapid motional averaging occurs a single fluorine resonance line could be obtained from VF_5OH^-. Such averaging is not normally observed for monosubstituted octahedrally coordinated fluoride species. The species VF_5OH^- may be excluded since V—F spin coupling is clearly observed. It follows that the rate of quadrupole induced relaxation of the vanadium spin states is low and therefore that the electric field gradient about the vanadium nucleus is small. There must be a high symmetry about vanadium which is not likely for VF_5OH^-.

The new values for the chemical shifts of VF_5 and VF_6^- reported here are now consistent with the difference in chemical shift found for MF_5 and MF_6^- where M is a Group V element (5). A complete compilation for these elements is given in Table 2.

The fluorine resonance spectrum of an equimolar solution of (TBA)TaF_6 and VF_5 in sulfuryl chlorofluoride at −130 °C is shown in Fig. 3. On the basis of results obtained with other polyfluoroanions the spectrum may be assigned to structure **1** where M is tantalum and

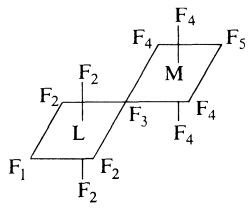

1

L is vanadium (5). The broadened line at −510.5 p.p.m. is assigned to the terminal fluorine on vanadium (F_1). It is broadened by spin coupling to F_2 and F_3 with values such that fine structure cannot be resolved. The triplet at −435.4 is assigned to the four equatorial fluorines on vanadium (F_2). The splitting arises from almost equal spin couplings of about 120 Hz to F_1 and F_3. The line at 57.5 is assigned to the bridging fluorine (F_3), which is broadened by spin coupling with F_1, F_2, and F_5. The sharp line at −63.4 is assigned to the equatorial fluorines on tantalum (F_4) and the doublet at −92.6 to the terminal fluorine on tantalum (F_5). It is split into a doublet by a spin coupling of 223 Hz with F_3. Some confirmation of this assignment comes from double resonance studies where F_1 is irradiated and F_2 collapsed to a broadened structureless line. F_1 is also affected by irradiation of F_2. It is not possible to determine the value of the spin coupling constant between F_1 and F_3 but it must be less than 400 Hz, the width of F_1 at half height.

One feature of the fluorine resonance spectrum of $VTaF_{11}^-$ which is unique for the group VB elements is the absence of observable spin coupling for J_{3-4} and J_{4-5}. A compilation of the fluorine resonance parameters for all the species of structure **1** where L and M are group V elements is presented in Table 3. The chemical shifts and remaining spin couplings in $VTaF_{11}^-$ are normal for these elements. The line marked with an asterisk in Fig. 3 is from the equatorial

TABLE 3. Fluorine resonance parameters for the species LMF_{11}^-

L	M	δ_1 (p.p.m.)	δ_2	δ_3	δ_4	δ_5	J_{1-2} (Hz)	J_{1-3} (Hz)	J_{2-3} (Hz)	J_{3-4} (Hz)	J_{3-5} (Hz)	J_{4-5} (Hz)
As	As (12)	85.0	48.6	21.1	48.6	85.0	127	~0	51			
Sb	Sb (7)	136.4	114.6	93.4	114.6	136.4	100	~0	60			
Nb	Nb (5)	−191.0	−145.9	56.0	−145.9	−191.0	70	200	70			
Ta	Ta (5)	−115.1	− 72.0	80.8	− 72.0	−115.1	23.0	165	41.8			
P	Sb (13)	83.4	86.2		159.1	112.0						
As	Sb (8)	92.9	50.5	118	118	138.9	126	~0	47			112
As	Ta (5)		62.7*		− 76.1	−122.3						
Sb	Nb (5, 14)	131.5	117.7	101.7	−156.5	−205						
Sb	Ta (5)	134.0	117.3	99.6	− 78.6	−125.7	90	~0	40	43	172	23
V	Nb	−507.5	−431.8		−135.3	−170.5	123	<80	123	~0	275	~0
V	Ta	−510.5†	−435.4	57.5	− 63.4	− 92.6	120	—	120	~0	223	~0
Nb	Ta (5)	−196.6	−149.5	70.8	− 69.1	−109.0	70		70	190		25

*An averaged value including a contribution from the apical fluorine.
†The width at half height is 400 Hz.

TABLE 4. The effect of a binary fluoride upon the chemical shift of a probe nucleus

Chemical shift for fluoride	Probe nucleus equatorial F on Ta	Terminal F on Ta	Equatorial F on Nb	Terminal F on Nb
MoF_5*	−58.6	−89.9	−161.1	−194.4
VF_5	−63.4	−92.6	−135.3	−170.5
WF_4	−65.6	−94.6	−138	
NbF_5	−69.4	−108.7	−145.5	−191.3
TaF_5	−72.0	−115.1	−149.4	−197.4
AsF_5	−76.1	−122.3		
SbF_5	−78.6	−125.7	−156.5	−205

*Reference 15.

fluorines of $Ta_2F_{11}^-$ in low concentration. Although it has not been possible thus far to determine rate constants for exchange of non-equivalent fluorines in the complex fluoroanions it is possible to say in a qualitative fashion that the lowest temperatures are required to slow down exchange of fluorines bonded to vanadium and therefore that they are the most mobile.

The fluorine resonance spectrum of an equimolar sulfuryl chlorofluoride solution of TBA(NbF_6) and VF_5 is very similar, except for chemical shift changes, to the analogous tantalum system. Fluorine resonance parameters for $VNbF_{11}^-$ assigned in the way just described are also listed in Table 3 and show a close similarity to those with M equal to tantalum. In this case the quintet of F_1 is poorly resolved allowing a lower limit to be set on J_{1-3} than was possible for $VTaF_{11}^-$.

It has been demonstrated that the chemical shift of a given fluorine bonded to tantalum or niobium in a complex fluoroanion can serve as an indicator of the electron withdrawing capability of the other central element in the complex fluoroanion (14). Vanadium pentafluoride appears to be a much weaker electron withdrawing group than the pentafluorides of the other group V elements. This is shown in Table 4.

The fluorine resonance spectra of the reaction products formed from vanadium pentafluoride and the tetra-*n*-butylammonium salts of BF_4^-, PF_6^-, AsF_6^-, and SbF_6^- all have a broad line at about −460 p.p.m. from fluorine bonded to vanadium and another line at 147.0, 70.6, 61.5, and 117.2, respectively, from fluorine bonded to the other central element. A phosphorus–fluorine spin coupling of 748 Hz was observed for fluorine bonded to phosphorus in its complex fluoroanion with vanadium. The broad lines were all observed at temperatures just above the freezing points of the solutions. At somewhat higher temperatures the line from fluorine on vanadium sharpens presumably because of more rapid exchange of non-equivalent fluorines. It is reasonably certain that the complex fluoroanion

Can. J. Chem. Downloaded from www.nrcresearchpress.com by 210.87.254.40 on 09/05/12
For personal use only.

is formed in each case since the spectrum of VF_5 or VF_6^- does not correspond with the ones that were observed. The fluorine resonance spectra for the other half of the complex fluoroanion are close to those observed for the appropriate simple fluoroanion and not to the binary fluoride. The inability to slow down the fluorine exchange sufficiently to observe lines and fine structure from the non-equivalent fluorines prevents a more positive characterization of these species.

Vanadium pentafluoride appears to form complexes more readily than the other group V elements since it forms complexes with all the simple fluoroanions which were tried. The exchange rate between the non-equivalent fluorines in the vanadium complex fluoroanions is faster than for its sister elements since these are the only cases where the exchange could not be sufficiently slowed by lowering the temperature. There does not appear to be a parallel between the electron withdrawing ability of the pentafluoride in a complex fluoroanion and its complexing ability. Although VF_5 does not withdraw electrons strongly from the other half of the complex fluoroanion it readily forms complexes.

1. M. J. VASILE, G. R. JONES, and W. E. FALCONER. Chem. Commun. 1355 (1971).
2. C. J. HOFFMANN, B. E. HOLDER, and W. L. JOLLY. J. Phys. Chem. **62**, 364 (1958).
3. H. H. CLAASSEN and H. SELIG. J. Chem. Phys. **44**, 4039 (1966).
4. A. J. EDWARDS and G. R. JONES. J. Chem. Soc. A, 1651 (1969).
5. S. BROWNSTEIN. Inorg. Chem. **12**, 584 (1973).
6. J. A. S. HOWELL and K. C. MOSS. J. Chem. Soc. A, 2483 (1971).
7. J. BACON, P. A. W. DEAN, and R. J. GILLESPIE. Can. J. Chem. **48**, 3413 (1970).
8. S. BROWNSTEIN. Can. J. Chem. **47**, 605 (1969).
9. H. J. EMELEUS and V. GUTMANN. J. Chem. Soc. 2979 (1949).
10. B. COX. J. Chem. Soc. 876 (1956).
11. R. D. W. KEMMITT, D. R. RUSSELL, and D. W. A. SHARP. J. Chem. Soc. 4408 (1963).
12. P. A. W. DEAN, R. J. GILLESPIE, R. HULME, and D. A. HUMPHREYS. J. Chem. Soc. A, 341 (1971).
13. S. BROWNSTEIN. Unpublished results.
14. P. A. W. DEAN and R. J. GILLESPIE. Can. J. Chem. **49**, 1736 (1971).
15. S. BROWNSTEIN. Can. J. Chem. **51**, 2530 (1973).

Can. J. Chem. Downloaded from www.nrcresearchpress.com by 210.87.254.40 on 09/05/12
For personal use only.

The Photobromination of (+)-1-Cyano-2-methylbutane

DENNIS D. TANNER, TOMOKI C. S. RUO, AND E. V. BLACKBURN
Department of Chemistry, The University of Alberta, Edmonton, Alberta T6G 2G2
Received November 16, 1973

DENNIS D. TANNER, TOMOKI C. S. RUO, and E. V. BLACKBURN. Can. J. Chem. **52**, 2242 (1974).

The photobromination of (±)-1-cyano-2-methylbutane with molecular bromine, under varying conditions, yields a mixture of three monobrominated products: 1-cyano-1-bromo-2-methylbutane (relative yield 78–95%), 1-cyano-3-bromo-2-methylbutane (relative yield 1–5%), and 1-cyano-2-bromo-2-methylbutane (relative yield 4–17%). The production of the major monobrominated product is proposed to arise by an acid catalyzed ionic reaction. When the bromination of (+)-1-cyano-2-methylbutane was carried out in the presence of solid *N*-bromosuccinimide as well as molecular bromine, the three monobrominated products were formed in relative yields that reflected a free radical bromination reaction: (+)-1-cyano-1-bromo-2-methylbutane (5–14%), (±)-1-cyano-2-bromo-2-methylbutane (68–85%), and (+)-1-cyano-3-bromo-2-methylbutane (10–19%).

The inability to obtain active 1-cyano-2-bromo-2-methylbutane from these bromination reactions may not be due to the fundamental nature of the bromination of a substrate at a chiral center but may be due to the instability of this particular tertiary bromide.

DENNIS D. TANNER, TOMOKI C. S. RUO et E. V. BLACKBURN. Can. J. Chem. **52**, 2242 (1974).

La photobromination du (±)-cyano-1 méthyl-2 butane avec du brome moléculaire sous diverses conditions conduit à un mélange de trois produits monobromés: le cyano-1 bromo-1 méthyl-2 butane (rendement relatif 78 à 95%), cyano-1 bromo-3 méthyl-2 butane (rendement relatif 1–5%), et cyano-1 bromo-2 méthyl-2 butane (rendement relatif 4–17%). On suggère que la formation prépondérante du produit monobromé majeur provient d'une réaction ionique acido-catalysée. Quand la bromuration du (+)-cyano-1 méthyl-2 butane est effectuée en présence de *N*-bromosuccinimide de solide en même temps que du brome moléculaire, les trois produits monobromés se forment avec des rendements relatifs qui réflètent une réaction de bromuration radicalique; (+)-cyano-1 bromo-1 méthyl-2 butane (5–14%) (±)-cyano-1 bromo-2 méthyl-2 butane (68–85%) et (+)-cyano-1 bromo-3 méthyl-2 butane (10–19%).

Le fait que le cyano-1 bromo-2 méthyl-2 butane est obtenu inactif lors de ces réactions de bromuration peut être du à la nature fondamentale de la bromuration d'un substrat ayant un centre chiral, mais elle peut aussi être du à l'instabilité de ce type particulier de bromure tertiaire. [Traduit par le journal]

Introduction

The formation of free radicals at asymmetric centers by hydrogen abstraction generally leads, after their transfer reactions, to optically inactive products (1, 2). Exceptions to this generalization are the bromination by a number of free radical brominating agents (*viz.*, *t*-butyl hypobromite (3), *N*-bromosuccinimide (4), and molecular bromine (2, 3)) of (+)-1-chloro-2-methylbutane (3) and (+)-1-bromo-2-methylbutane (2–4).

The retention of activity by the brominated products has been attributed to the formation of an intermediate halogen bridged radical, **i**. The formation of this bridged species was presumed to occur by the assisted removal of the tertiary hydrogen atom by the neighboring halogen atom (5, 6).

It has been suggested that this picture of the bromination pathway has several limitations. When the active bromide was brominated and the starting material was reisolated after the reaction, it was found that the starting bromide had racemized to a small extent (2). The principle of microscopic reversibility demands that racemization of the starting material (6–14% of the radicals formed) must arise from the formation of an open radical, which then undergoes rotation, closes again to a bridged radical, and transfers with hydrogen bromide. It was suggested that this sequence of reactions, although possible, was highly unlikely (2). The structure of the intermediate β-bromo and -chloro radicals have, likewise, been modified since both the e.s.r. spectra of the radicals themselves (7–9), or the CIDNP spectra of their transfer products (10), have shown them not to be symmetrically bridged and it has been suggested that a better representation of these intermediates is a partially bridged struc-

Can. J. Chem. Downloaded from www.nrcresearchpress.com by 210.87.254.5 on 09/05/12
For personal use only.

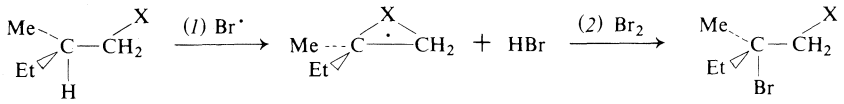

i

ture, **ii** (9), or a hyperconjugatively frozen structure, **iii** (7, 8).

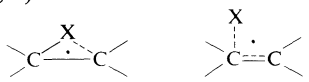

ii iii

An alternative to the bridged structure has been proposed to explain the stereochemical results obtained from the liquid phase photobromination of (+)-1-cyano-2-methylbutane to yield (+)-1-cyano-2-bromo-2-methylbutane. It was suggested by the authors (11) that, under the high concentration of bromine necessary for the observation of the retention of optical activity in the three 1-substituted-2-methylbutanes which have been studied, the abstracting species was, in fact, the $Br_3\cdot$ radical rather than the bromine atom and that upon abstraction both molecular bromine and an alkyl radical are formed as a geminate pair. Accordingly, the retention of activity was due to a rapid cage reaction between them which was faster than the molecular rotation of the radical (11).

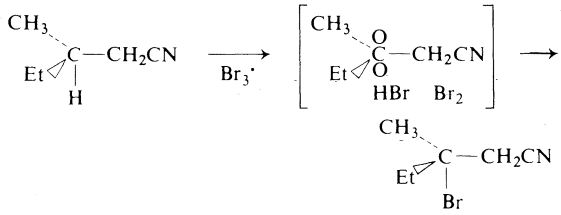

It was subsequently pointed out (2) that a bridged cyano group was not as unlikely as Haag and Heiba (11) had first proposed and that there was considerable precedent for considering such an intermediate. An anomaly was also commented on: that the sign of the rotation of the (+)-bromocyanide, contrary to what was reported, would be predicted by Brewster's rules (12) to be inverted to a (−)-bromocyanide if the conversion had taken place with a retention of absolute configuration.[1]

[1]It is recognized, however, that a molecule with two polar groups on adjacent carbon atoms may exhibit strong dipolar interactions or solvent interactions favoring or disfavoring a particular conformation and the observed rotation may be quite different from what is predicted. When the magnitude of the rotation is small, even an inversion of sign may be observed.

Discussion and Results

The photoinitiated reaction of 1-cyano-2-methylbutane (**1**) with molecular bromine (2:1 or 10:1) yielded three monobromination products, 1-cyano-1-bromo-2-methylbutane (**2**), 1-cyano-2-bromo-2-methylbutane (**3**), and 1-cyano-3-bromo-2-methylbutane (**4**). Contrary to the

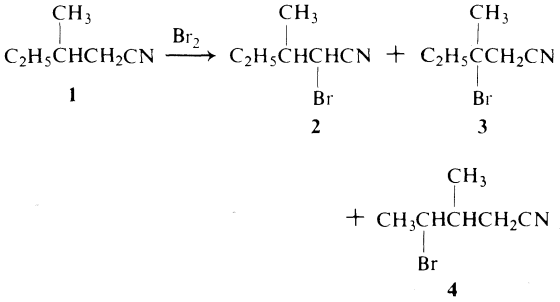

previous study (11), where only **3** was reported, the major isomeric monobromide obtained from the bromination was 1-cyano-1-bromo-2-methylbutane (**2**), 95%. The minor isomers **3** and **4** were formed in a relative yield of 4 and 1%, respectively. The absolute yields of the three monobromides were low and ranged from 71% at 2:1 (RCN:Br_2) to 57% at 10:1 (RCN:Br_2) ratios of substrate to bromine.

It was apparent from the isomer distribution obtained from the bromination of **1** with molecular bromine that a radical bromination was not leading to the production of the major product **2**, since the expected product of radical bromination would result from the substitution of the tertiary hydrogen. A likely explanation for the formation of **2** was an acid-catalyzed α-bromination of the methylene position adjacent to the activating cyano group. The ionic bromination was not found to be extremely rapid under the conditions employed (>0.5–2 days).

The ionic bromination could be greatly minimized by the addition of solid *N*-bromosuccinimide (NBS) to the reaction mixture. The NBS functions as a source of molecular bromine which forms by the reaction of the hydrogen bromide produced in the reaction with the NBS. Photobromination of **1** using mixtures of solid NBS and bromine in carbon tetrachloride (RCN:Br_2:

Can. J. Chem. Downloaded from www.nrcresearchpress.com by 210.87.254.5 on 09/05/12
For personal use only.

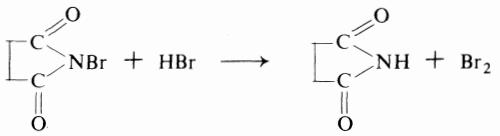

1

NBS, 6:1:5) gave a 29% yield of the three monobrominated products in the ratio of **2**:**3**:**4** of 5:85:10, when the reaction was carried out so that 60.2% of the active bromine was consumed. This method of bromination was, in fact, similar to the method used by Haag and Heiba in their original report (11) of the bromination of (+)-1-cyano-2-methylbutane.[2]

The two chiral isomeric monobromides (+)-1-cyano-3-bromo-2-methylbutane and (+)-1-cyano-1-bromo-2-methylbutane which are formed in minor amounts during the bromine–NBS brominations were synthesized by independent reactions and isolated by preparative g.l.p.c.

Since the mechanism of the *t*-butyl hypobromite bromination of alkanes proceeds by a free radical chain, carried by the less selective (relative to bromine) *t*-butoxy radical (13), it was anticipated that a more random distribution of products would be obtained from its use as the reagent for brominating (+)-1-cyano-2-methylbutane. The bromination of (+)-1-cyano-2-methylbutane with *t*-butyl hypobromite (2:1 mol ratio) yielded upon g.l.p.c. analysis five monobrominated products in the ratio of 19:32:39:4:6. The compounds corresponding to the first two peaks were (+)-1-cyano-1-bromo-2-methylbutane and presumably the inactive 1-cyano-2-bromo-2-methylbutane. The compound corresponding to peak 3 was (+)-1-cyano-3-bromo-2-methylbutane ($[\alpha]_{546}^{26}$ +9.40).

The chiral monobromide, (+)-1-cyano-1-bromo-2-methylbutane, was synthesized from (+)-1-cyano-2-methylbutane ($[\alpha]_{546}^{24}$ +8.97) with phosphorus tribromide and bromine and was found to have a rotation of ($[\alpha]_{546}^{27}$ +6.62).

The photoinitiated bromination of (+)-1-cyano-2-methylbutane with mixtures of molecular bromine and NBS was carried out in the same manner as the bromination of the racemic mixture of that cyanide. Fractional distillation of the product mixture, after the destruction of the excess brominating agent, yielded unreacted starting material (37–40°/8 mm) and a fraction boiling at 52–53°/1 mm. Gas–liquid partition chromatography analysis of this fraction showed it to be primarily 1-cyano-2-bromo-2-methylbutane. The reisolated starting material was purified by preparative g.l.p.c. and was found to be racemized 3–4%. The fraction containing 1-cyano-2-bromo-2-methylbutane was redistilled using a 10 in. Vigreux column and a fraction boiling at 48–49°/1.2 mm was collected. Gas–liquid partition chromatography analysis of this fraction showed the presence of small amounts of (+)-1-cyano-1-bromo-2-methylbutane (1.4%) and (+)-1-cyano-3-bromo-2-methylbutane (7.0%) as well as the desired 2-brominated isomer.

No attempt was made to isolate the tertiary bromide from the reaction mixture by preparative g.l.p.c. since the attempted isolation of (−)-1,2-dibromo-2-methylbutane in this manner led to extensive racemization, while distillation allowed its isolation (2). Furthermore, g.l.p.c. treatment of **3** leads to small amounts (~3%) of products resulting from the elimination of hydrogen bromide. The tertiary bromide, (±)-1-cyano-2-bromo-2-methylbutane, could be synthesized and obtained as a pure material from the reaction of anhydrous hydrogen bromide and a mixture of 1-cyano-2-methyl-1-butene and 1-cyano-2-methyl-2-butene. The product, **3**, was found to be unstable and decomposed, giving off hydrogen bromide, upon standing for several days; however, with some care, it was possible to store the pure material.

A synthetic mixture made up of 1.36% of (+)-1-cyano-1-bromo-2-methylbutane and 6.95% of (+)-1-cyano-3-bromo-2-methylbutane and 91.69% of (±)-1-cyano-2-bromo-2-methylbutane was analyzed by g.l.p.c. The chromatogram of the synthetic mixture was identical to that obtained from an analysis of the redistilled fraction obtained from the bromination of the active cyanide (see Fig. 1).

A comparison of the specific rotation obtained for this fraction with that of the synthetic mixture showed them to be identical; the calculated rotation expected from the synthetic mixture was, likewise, found to be identical to that which was observed (see Table 1).

The conditions used to isolate the tertiary bromocyanide were the same as those used to

[2]In a private communication with Dr. Heiba, we have been informed that their reactions were carried out with added NBS and solid K_2CO_3, and that the mention of these additives was inadvertently omitted from their paper and that they were anxious to have this oversight corrected in the literature.

Can. J. Chem. Downloaded from www.nrcresearchpress.com by 210.87.254.5 on 09/05/12
For personal use only.

TABLE 1. Optical rotation of reactants and products in the NBS–Br_2 bromination of (+)-1-cyano-2-methylbutane, **1***a*[a]

	$[\alpha]_\lambda$				
	1*a* (at 24°)			Synthetic mixture[d] of **2***a*, **3**, and **4***a* (at 26°)	
λ (nm)	Before reaction	After reaction[b]	Isolated **3**[c] (at 27°)	Observed	Calcd.
589	+ 7.65	+ 7.40	+0.038	+0.036	+0.038
578	+ 7.98	+ 7.63	+0.039	+0.039	+0.040
546	+ 8.97	+ 8.61	+0.046	+0.048	+0.046
436	+14.83	+14.45	+0.078	+0.077	+0.076
365	+22.40	+21.70	+0.120	+0.122	+0.120

[a]All rotations were obtained in carbon tetrachloride.
[b]Recovered material had racemized 3–4%.
[c]The isolated material was contaminated with 1.4% of **2***a* and 7.0% of **4***a*, see Fig. 1.
[d]A synthetic mixture 1.36% of **2***a*, 91.69% of **3**, and 6.95% of **4***a*. The calculated rotations were obtained using values for **2***a* and **4***a* listed in Table 2.

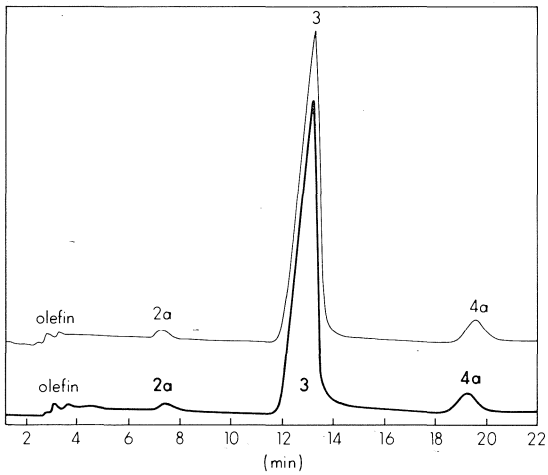

FIG. 1. The g.l.p.c. chromatogram of an isolated fraction of **3** from the bromination (NBS–Br_2) of **1***a* compared to the chromatogram of a synthetic mixture of **3** and added **2***a* and **4***a*: reaction mixture, dark line; synthetic mixture, heavy line.

isolate active (−)-1,2-dibromo-2-methylbutane, without racemization (2). Since the bromination of (+)-1-cyano-2-methylbutane produced minor amounts of two other (+)-chiral monobromides, which could not be removed by distillation, and since the impurities which contaminated the isolated 1-cyano-2-bromo-2-methylbutane accounted for the entire observed rotation of the reaction mixture; we are forced to the conclusion that, in our hands, the bromination of (+)-1-cyano-2-methylbutane leads to inactive (±)-1-cyano-2-bromo-2-methylbutane.

Our observation may not be due to the fundamental nature of the bromination of a substrate at a chiral center, but may very well be due to the instability of this particular tertiary bromide (**3**).

Experimental

Materials

Bromine was washed with concentrated sulfuric acid and distilled from phosphorus pentoxide before use. *N*-Bromosuccinimide (>97% pure by iodometric titration); (−)-2-methybutanol, $[\alpha]_{546}^{27}$ −6.55 (Aldrich Chemical Company, Inc.); trichlorofluoromethane (Freon 11); and spectroanalyzed carbon tetrachloride (Fisher Scientific Company) were used without further purification.

Instruments

Preparative g.l.p.c. was carried out on a Hewlett Packard HP-402 all-glass system gas chromatograph and an Aerograph 202 using a 10 ft × 1/4 in. glass column packed with 10% Carbowax 20M TPA or 10% DEGS on 60–80 mesh Chromosorb P AW. Gas–liquid partition chromatography analyses of product ratios were carried out on an Aerograph HY-FI 600 D (10 ft × 1/8 in. glass column) and an Aerograph 202 (10 ft × 1/4 in. glass column) instruments using isothermal conditions. Rotations were recorded on a Perkin-Elmer 141 automatic polarimeter.

(+)-1-Cyano-2-methylbutane (1a)

The active cyanide was prepared by the treatment of the *p*-toluene sulfonate ester of (−)-2-methylbutanol ($[\alpha]_{546}^{27}$ −6.55) (2) with potassium cyanide.

The tosylate (60 g, 0.25 mol) and a solution of potassium cyanide (86 g, 1.32 mol) in diethylene glycol (80 g) was heated at reflux for 3 h. Fractional distillation of the product mixture yielded 18 g (72%) of pure (+)-1-cyano-2-methylbutane, b.p. 152–154°/699 mm (lit. (14) b.p. 151.4–152.6°/743 mm), n_D^{23} 1.4075 (lit. (14) n_D^{25} 1.4070). The specific rotation of the active cyanide (CCl_4) is listed in Table 2 (lit. (11) $[\alpha]_{548.1}$ +7.98). The optical rotation of **1***a* after reisolation by g.l.p.c. gave the same rotation; i.r. ν_{max} (liquid film) 2970 (s), 2940 (s), 2880 (s), 2860 (sh), 2240 (m), 1460 (s), 1425 (m), 1380 (m), 1350 (w), 1345 (w), 1155 (w), and 970 (w) cm^{-1}; n.m.r. τ (CCl_4) 7.77 (2H; d; 2-H), 8.0–8.8 (3H, m, 3- and 4-H), 8.93 (3H, d, 3-CH_3), and 9.06 (3H, t, 5-H).

Anal. Calcd. for $C_6H_{11}N$: C, 74.17; H, 11.41. Found: C, 74.08; H, 11.21.

Can. J. Chem. Downloaded from www.nrcresearchpress.com by 210.87.254.5 on 09/05/12
For personal use only.

TABLE 2. Specific rotation of (+)-1-cyano-2-methylbutane (**1***a*), (+)-1-cyano-1-bromo-2-methylbutane (**2***a*), and (+)-1-cyano-3-bromo-2-methylbutane (**4***a*) in CCl_4

λ (nm)	$[\alpha]_\lambda$ **1***a* (at 24°)	**2***a* (at 27°)	**4***a* (at 26°)
589	+ 7.65	+ 5.64	+ 7.88
578	+ 7.98	+ 5.89	+ 8.18
546	+ 8.97	+ 6.62	+ 9.40
436	+14.83	+10.48	+15.85
365	+22.40	+15.09	+25.21

1-Cyano-2-methyl-1-butene and 1-Cyano-2-methyl-2-butene

The method of Whyte and Cope (15) was used to synthesize a mixture of these olefins. A benzene solution (150 ml) of methyl ethyl ketone (225 g, 3.1 mol), cyanoacetic acid (245 g, 2.9 mol), glacial acetic acid (90 g, 1.5 mol), and ammonium acetate (46.6 g, 0.6 mol) was heated under a Dean–Stark trap until all of the water had separated. The solvent benzene was removed by distillation and the crude mixture was heated at 145° for 5 h. The reaction products were then distilled at 80 mm. The distillate was washed with water and then dried over anhydrous sodium sulfate. Redistillation gave 149 g (54%) of a mixture of 1-cyano-2-methyl-1-butene and 1-cyano-2-methyl-2-butene, b.p. 82–84°/50 mm; n_D^{23} 1.4396; i.r. ν_{max} (liquid film) 2243 ($-CH_2CN$), 2220 ($-\underset{|}{C}=CHCN$), 1627 ($\diagdown C=C \diagup$).

Anal. Calcd. for C_6H_9N: C, 75.74; H, 9.54. Found: C, 75.79; H, 9.64.

(±)-1-Cyano-2-bromo-2-methylbutane

Anhydrous hydrogen bromide was bubbled through a stirred solution of 31 g (0.33 mol) of a mixture of 1-cyano-2-methyl-1-butene and 1-cyano-2-methyl-2-butene in 220 ml of ether at 0° for 6 h. The reaction mixture was washed with water, 5% sodium bicarbonate, water, and dried over anhydrous sodium sulfate. Distillation under reduced pressure gave 35.3 g (61%) of (±)-1-cyano-2-bromo-2-methylbutane, b.p. 70.5–71°/5 mm (lit. (16), b.p. 85–86°/13 mm), n_D^{23} 1.4745 (lit. (16) n_D^{22} 1.4772; i.r. ν_{max} (liquid film) 2980 (s), 2940 (s), 2920 (sh), 2880 (s), 2840 (sh), 2240 (m), 1455 (s), 1500 (sh), 1430 (m), 1415 (s), 1385 (s), 1345 (w), 1315 (w), 1300 (w), 1285 (w), 1240 (w), 1150 (w), 1115 (s), 1110 (sh), 1088 (m), 1015 (w) cm^{-1}; n.m.r. τ (CCl_4 solution) 7.07 (2H, s, 2-H), 8.05 (2H, q, 4-H), 8.15 (3H, s, 3-CH_3), 8.89 (3H, t, 5-H).

The pure material could be stored for days in the dark at 0°. If left to stand on the bench top for several days it fumed and gave off hydrogen bromide.

Anal. Calcd. for $C_6H_{10}BrN$: C, 40.93; H, 5.72; Br, 45.39; N, 7.96. Found: C, 40.90; H, 5.83; Br, 45.50; N, 7.94.

(+)-1-Cyano-1-bromo-2-methylbutane

A mixture of (+)-1-cyano-2-methylbutane (13.6 g, 0.14 mol), bromine (24.6 g, 0.15 mol), and 2 ml of phosphorus tribromide was heated at 80° for 4 h. The reaction mixture was allowed to cool to room temperature and then was distilled under reduced pressure (water pump). The distillate was washed with water, 5% sodium bicarbonate, and water again, and dried over anhydrous magnesium sulfate. Redistillation gave 16.3 g (66%) of (+)-1-cyano-1-bromo-2-methylbutane, b.p. 94°/25.5 mm, n_D^{25} 1.4644. The specific rotation is given in Table 1; n.m.r. τ (CCl_4) 5.74 (1H, d, 2-H), 8.70–7.90 (3H, m, 3- and 4-H), 8.82 and 8.79 (3H, d and d, 3-CH_3),[3] 8.98 and 9.01 (3H, t and t, 5-H)[3]; i.r. ν_{max} (liquid film) 2238 cm^{-1} ($-C\equiv N$).

Anal. Calcd. for $C_6H_{10}BrN$: C. 40.93; H, 5.72; Br, 45.39; N, 7.96. Found: C, 40.61; H, 5.84; Br, 45.53; N, 7.91.

Bromination of (+)-1-Cyano-2-methylbutane with t-Butyl Hypobromite

A mixture (2:1 mol ratio) of (+)-1-cyano-2-methylbutane and *t*-butyl hypobromite (13) (94% pure by iodometric titration) was sealed in a degassed Pyrex ampoule. The ampoule was thermostated at 25° and irradiated with a 100 W incandescent lamp until colorless (4 h). Gas–liquid partition chromatography analysis of the reaction mixture using an Aerograph 202 gas chromatograph equipped with a 1/4 in. × 10 ft 10% Carbowax 20M TPA on 60–80 mesh Chromosorb P AW glass column (135° isothermal) indicated five monobromo-1-cyano-2-methylbutanes and a small amount (~5%) of a high boiling component, besides *t*-butyl alcohol and unreacted starting material. Gas chromatography – mass spectral analysis of the reaction mixture showed the first five products to be monobromides. They were present in the following ratio: 19:32:39:4:6. The compounds corresponding to peaks 1, 2, and 3 were isolated by preparative g.l.p.c. using a 1/4 in. × 10 ft glass column packed with 10% DEGS on Chromosorb P AW. Peaks 1 and 2 were identified as corresponding to 1-cyano-1-bromo-2-methylbutane and 1-cyano-2-bromo-2-methylbutane by a comparison of their g.l.p.c. retention times, and their ^1H n.m.r. and i.r. spectra with those of authentic samples. Nuclear magnetic resonance showed the compound corresponding to peak 3 to be a 1-cyano-3-bromo-2-methylbutane. Its specific rotation is listed in Table 1. ^1H n.m.r. τ (CCl_4) 8.86 and 8.79 (3H, d and d, 3-CH_3),[3] 8.29 and 8.26 (3H, d and d, 4-CH_3),[3] 8.20–7.70 (1H, m, $-\underset{|}{CH}-$), 7.62 and 7.53 (2H, q and q, $-CH_2-$),[3] 5.92 and 5.81 (1H, quintet and octet, $-CHBr-$); i.r. (in CCl_4) 2245 cm^{-1} ($-C\equiv N$).

Anal. Calcd. for $C_6H_{10}BrN$: C, 40.93; H, 5.72; Br, 45.39; N, 7.96. Found: C, 40.99; H, 5.86; Br, 45.36; N, 8.20.

Peaks 4 and 5 corresponded presumably to 1-cyano-2-(bromomethyl)butane and 1-cyano-4-bromo-2-methylbutane. Both of these compounds had parent ions at *m/e* 175 and 177 ($C_6H_{10}BrN$), 93 and 95 (CH_2Br), and base peak at 55 (C_4H_7).

Photobromination of (±)-1-Cyano-2-methylbutane with Molecular Bromine

The brominations were carried out under a helium atmosphere and were isolated from the air by a dioctyl-

[3]Chemical shifts and couplings that are reported are for the mixture of *erythro* and *threo* isomers.

Can. J. Chem. Downloaded from www.nrcresearchpress.com by 210.87.254.5 on 09/05/12
For personal use only.

TABLE 3. Bromination of (±)-1-cyano-2-methylbutane (**1**) with molecular bromine

Reaction	Mole ratio **1**:Br_2	Temperature (°C)	Relative yields of monobromides	Yield (%)
1	2:1	24	**2** 95 **3** 4 **4** 1	
2	2:1	40	**2** 93 **3** 5 **4** 2	
3	13:1	24	**2** 78 **3** 17 **4** 5	
4	13:1	40	**2** 87 **3** 10 **4** 3	
5	2:1	25	**2** 93 **3** 5.6 **4** 1.4	66.3 3.8 0.9
6	4.5:1	25	**2** 90 **3** 7 **4** 3	53.1 4.1 1.8
7	10:1	25	**2** 92 **3** 6.2 **4** 1.8	52.4 3.5 1.1

phthalate bubbler (2). Mixtures of (±)-1-cyano-2-methylbutane and molecular bromine (under a helium atmosphere) were placed in a thermostated Pyrex water bath and were irradiated using incandescent light. The solution which was stirred continually was irradiated until the bromine color had been discharged. A copious evolution of hydrogen bromide was observed to bubble out through the dioctylphthalate. The reaction mixture was washed with aqueous sodium thiosulfate solution, 5% sodium bicarbonate, and dried over anhydrous sodium sulfate. The reaction mixtures were subjected to g.l.p.c. analysis, using the DEGS column. The major product (>90%) was 1-cyano-1-bromo-2-methylbutane which was isolated and identified by the comparison of its g.l.p.c. retention time, and n.m.r. and i.r. spectra with those of an authentic sample. The minor products, 1-cyano-2-bromo-2-methylbutane and 1-cyano-3-bromo-2-methylbutane, were identified by a comparison of their g.l.p.c. retention times on two columns (DEGS and Carbowax). The conditions used and the relative yields of products are listed in Table 3 (reactions 1–4).

The brominations were repeated in degassed, sealed Pyrex ampoules. The solutions were irradiated until the bromine color was discharged. The tubes were opened and a known amount of chlorobenzene and *o*-dichlorobenzene was added. The reaction mixture was washed with aqueous sodium thiosulfate solution, saturated sodium bicarbonate, and dried over anhydrous sodium sulfate. The solutions were then subjected to g.l.p.c. analysis on the HY-FI g.l.p.c. using a 1/8 in. × 10 ft glass column packed with 10% Carbowax 20M TPA on 60–80 mesh Chromosorb P AW (135°, isothermal). The absolute yield of the products was obtained (Table 3, reactions 5–7) by using standard calibration curves for the g.c. response of the products and starting material *vs.* chlorobenzene and *o*-dichlorobenzene.

Bromination of (+)-1-Cyano-2-methylbutane (1a) with NBS and Molecular Bromine

The reactions were carried out in degassed, sealed Pyrex ampoules with constant shaking (see Table 4, reactions 1–2) or with continual stirring (see Table 4, reactions 3–6). The thermostated reaction mixtures were irradiated using 2 × 140 W Hanovia Utility lamps from 68–365 h. At the end of the reaction solid NBS remained in the bottom of the reaction vessel. The reaction solutions were washed with aqueous sodium thiosulfate solution, water, saturated sodium bicarbonate, water again, and dried over anhydrous sodium sulfate, and analyzed by g.l.p.c. using the 1/8 in. × 10 ft glass column packed with 10% Carbowax 20M TPA. The results and reaction conditions are given in Table 4.

Reaction mixtures (Table 4, 3–6) were distilled under reduced pressure (60 mm) to remove the carbon tetrachloride solvent and the unbrominated starting material (37–40°/8 mm); finally the fraction boiling at 52–53°/1 mm was collected and was found by g.l.p.c. analysis to be primarily 1-cyano-2-bromo-2-methylbutane. This fraction was redistilled and collected at 48–49°/1.2 mm. Gas–liquid partition chromatography analysis of the redistilled fraction (48–49°/1.2 mm) showed small amounts of **2***a* (1.4%) and **4***a* (7.0%), see Fig. 1. The rotation of this mixture is listed in Table 1. A synthetic mixture of 1.36% of **2***a*, 6:95% of **4***a*, and 91.69% of **3** was made and its

Can. J. Chem. Downloaded from www.nrcresearchpress.com by 210.87.254.5 on 09/05/12
For personal use only.

TABLE 4. Bromination of (+)-1-cyano-2-methylbutane (**1***a*) with NBS and molecular bromine in carbon tetrachloride

Reactants in CCl_4			Reaction	Temperature	Products
1*a* (*M*)	Br_2 (*M*)	NBS (10^2 mol/100 ml)	No.	(°C)	(**2***a*:3:**4***a*)
4.34	0.54	10.9	1	25	6:80:14
			2	25	14:68:18
3.73	0.45	9.3	3	21	10:71:19
			4	21	12:70:18
2.50	0.32	15.7	5	22	5:80:15
2.23	0.36	16.3	6	33	5:80:10

observed rotation was compared with that of the material collected by distillation from the reactions, see Table 1. The g.l.p.c. analysis of the synthetic mixture was also compared to this isolated fraction, see Fig. 1.

The reisolated unreacted starting material was purified by preparative g.l.p.c. on a 1/4 in. × 10 ft glass column packed with 10% Carbowax 20M TPA and its specific rotation was compared to the starting material, **1***a*, see Table 1.

Small amounts of olefin (< 3%) were formed during the analysis of 1-cyano-2-bromo-2-methylbutane. The amount of olefin was found to be variable and was shown to be formed from the decomposition of **3**, since the g.l.p.c. isolated material when reanalyzed still showed a small amount of olefin.

The absolute yield was determined for the reaction (Table 4, reaction 6) by reanalysis of the mixture, after the addition of a known amount of chlorobenzene and *o*-dichlorobenzene. The extent of reaction was determined by iodometric titration. The reaction mixture was washed with water, sodium bicarbonate solution, again with water, and dried over anhydrous sodium sulfate. The reaction mixture was analyzed by g.l.p.c. (Carbowax 20M TPA) The absolute yield of the three monobromides (Table 4, reaction 6) was found to be 29% based on the active bromine consumed (60%)

The authors wish to thank the National Research Council of Canada and the University of Alberta for their generous support of this work.

1. H. C. BROWN, M. S. KHARASH, and T. H. CHAO. J. Am. Chem. Soc. **62**, 3435 (1940).
2. D. D. TANNER, H. YABUUCHI, and E. V. BLACKBURN. J. Am. Chem. Soc. **93**, 4802 (1971).
3. P. S. SKELL, D. L. TULEEN, and P. D. READIO. J. Am. Chem. Soc. **85**, 2849 (1963).
4. P. S. SKELL, D. L. TULEEN, and P. D. READIO, J. Am. Chem. Soc. **85**, 2850 (1963).
5. W. A. THALER. Methods in free-radical chemistry. **2**, Marcel Dekker, New York. 1969. p. 121.
6. L. KAPLAN. Bridged free radicals. Marcel Dekker, Inc., New York. 1972.
7. A. R. LYONS and M. C. R. SYMONS. J. Am. Chem. Soc. **93**, 7330 (1971).
8. M. C. R. SYMONS. J. Am. Chem. Soc. **94**, 8589 (1972).
9. K. S. CHEN, I. H. ELSON, and J. K. KOCHI. J. Am. Chem. Soc. **95**, 5341 (1973).
10. J. H. HARGIS and P. B. SHEVLIN. Chem. Commun. 179 (1973).
11. W. O. HAAG and E. I. HEIBA. Tetrahedron Lett. 3679 (1965).
12. J. H. BREWSTER. J. Am. Chem. Soc. **81**, 5475 (1959).
13. C. WALLING and A. PADWA. J. Org. Chem. **27**, 2976 (1962).
14. Dictionary of organic compounds. Vol. 4. Eyre and Spottiswoode, London. 1965. p. 2341.
15. D. E. WHYTE and A. C. COPE. J. Am. Chem. Soc. **65**, 1999 (1943).
16. G. BOULARAND and R. VESSIERE. Bull. Soc. Chim. Fr. 1706 (1967).

Can. J. Chem. Downloaded from www.nrcresearchpress.com by 210.87.254.5 on 09/05/12
For personal use only.

Photochemical Ring Enlargements of Two α-Cyanocycloalkanones[1]

G. K. CHIP AND T. R. LYNCH

Department of Chemistry and Scarborough College, University of Toronto, West Hill, Ontario M1C 1A4

Received November 19, 1973

G. K. CHIP and T. R. LYNCH. Can. J. Chem. **52**, 2249 (1974).

The photochemical transformations undergone by 2-cyano-2-methylcycloheptanone (**1**) and 2-cyano-2-methylcyclohexanone (**2**) have been studied in methanol and aqueous dioxane. In the former solvent, **1** is isomerized to three products in the ratio 78:8:13, corresponding to the enals **3***a* and **3***b*, and a new ring expansion product **4**, respectively. In aqueous dioxane, the cyclic imide **6** was obtained in 18% yield. Cycloalkanone **2** in methanol produces four products in the ratio 61:30:7:1, these being the isomeric enals **8***a* and **8***b*, the ester **9**, and the ring expansion product **10**. No imide related to **6** could be obtained from irradiation of **2** in aqueous dioxane.

G. K. CHIP et T. R. LYNCH. Can. J. Chem. **52**, 2249 (1974).

On a étudié, dans le méthanol et le dioxanne aqueux, les transformations photochimiques subies par la cyano-2 méthyl-2 cycloheptanone (**1**) et la cyano-2 méthyl-2 cyclohexanone (**2**). Dans le premier solvant, **1** s'isomérise en trois produits présents dans le rapport 78:8:13 et ces produits sont respectivement les énals **3***a* et **3***b* et le nouveau produit d'extention **4**. Dans le dioxanne aqueux, on obtient l'imide cyclique **6** avec un rendement de 18%. Dans le méthanol, la cycloalkanone **2** conduit à quatre produits dans le rapport 61:30:7:1; ces produits sont respectivement les énals isomères **8***a* et **8***b*, l'ester **9** et le produit d'extention **10**. Aucune imide de structure similaire à **6** n'a pu être obtenue lors de l'irradiation de **2** dans le dioxanne aqueux.

[Traduit par le journal]

The photochemical reactions undergone by cyclic ketones have for some time been of widespread interest (2), the principal products being carboxylic acid derivatives (3), enals (2), and cyclic ethers (4, 5). Acyl alkyl diradical intermediates (6, 7) are commonly invoked and may arise from either the singlet or triplet excited states of the ketone (4, 8, 9).

Photochemical ring enlargements of synthetic interest have recently been discovered, employing cycloalkanones with appropriate substituents in the 2-position as substrates. Thus, 2-vinyl- and 2-ethynylcycloalkanones on irradiation lead to a two-carbon expansion (10, 11), whereas the analogous 2-cyclopropyl and 2-oxiranyl cases enlarge the carbocyclic ring by three atoms (12, 13). Other one-atom reactions involving introduction of an additional carbon (14, 15), nitrogen (16–18), and oxygen (4, 5) into a ring are also known.

Recently, we have shown that simultaneously generated acyl and α-cyanoalkyl radicals combine predominantly on the nitrogen of the alkyl intermediate to give, in the presence of water, *N*-acylamides (19); it is assumed that an *N*-acylketenimine is first formed which subsequently undergoes rapid addition of water (Scheme 1). We were curious as to whether this same mode of recombination would occur when the radical pair were joined by a carbon chain. We have consequently studied the photochemistry of 2-cyano-2-methylcycloheptanone (**1**) and 2-cyano-2-methylcyclohexanone (**2**), both of which would be expected to undergo the Norrish Type I cleavage indicated to give examples of the desired diradicals. The irradiation of these cycloalkanones was also of interest since few cycloalkanones with two different substituents in the 2-position have been so examined and, relative to cyclopentanones and -hexanones, cycloheptanones have received little attention.

The ketone **1** was synthesized by the known

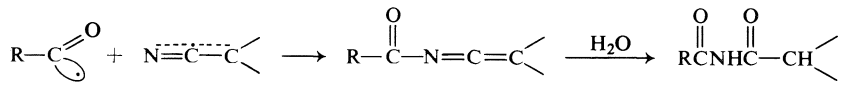

SCHEME 1

[1]A preliminary account of part of this work has appeared previously (1).

Can. J. Chem. Downloaded from www.nrcresearchpress.com by 210.87.254.42 on 09/05/12
For personal use only.

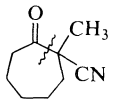

1

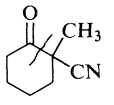

2

Thorpe cyclization of suberonitrile to 2-cyanocycloheptanone (20) followed by *C*-methylation with methyl iodide. 2-Cyano-2-methylcyclohexanone was obtained by a literature method (21).

Photolysis of a 5% solution of **1** in methanol under nitrogen caused the formation of three products in the ratio 78:8:13,[2] which were isolated by preparative g.l.c. The first and second components were identified as the *Z* and *E* aldehydes **3***a* and **3***b* (Scheme 2), respectively. In their i.r. spectra, each exhibited carbonyl and conjugated nitrile absorptions at 1720 and 2210 cm^{-1}, respectively, while the carbon–carbon double bond stretch appeared at 1640 cm^{-1} for the *Z* aldehyde and at 1660 cm^{-1} for the *E* isomer. The n.m.r. spectra are also consistent with the structural assignments and the isomers were distinguished by the relative positions of the single vinyl proton in each case, δ 6.17 p.p.m. for the *Z* isomer and δ 6.35 p.p.m. for the *E* isomer. This means of discrimination is in accord with two previous reports on the n.m.r. spectra of a number of acrylonitrile derivatives where the authors have observed that the β-vinyl hydrogen *cis* to the nitrile group absorbs *ca.* 0.1–0.15 p.p.m. further downfield than the β-vinyl hydrogen *trans* to the cyano function (22, 23).

Attempts to obtain analytical data on the 2,4-DNP derivatives of the aldehydes were unsuccessful, thus, accurate mass measurement of the molecular ion peaks was resorted to. For the *Z* and *E* aldehydes, the measured masses were 151.099439 and 151.099589, respectively, in good agreement with the calculated value of 151.099714 for $C_9H_{13}NO$.

The third product obtained from the irradiation of **1** was a colorless oil of molecular formula $C_{10}H_{17}NO_2$ (from accurate mass measurement: observed 183.12575, calculated 183.12592). The incorporation of a solvent molecule in this product was suggested by a three-proton singlet at δ 3.7 p.p.m. in the n.m.r. spectrum. Other features of the spectrum were a methyl doublet (J = 7 Hz) at 1.18 p.p.m., together with two multiplets totalling 11 hydrogens in the region 1.3–2.7 p.p.m. A structure consistent with these data, and the product hoped for at the genesis of this work, is the hexahydro-9-methoxyazonin-2-one, **4**. Added support is provided by the i.r. spectrum of this oil, which exhibits two strong overlapping bands at 1690 and 1660 cm^{-1}, assigned to the carbonyl and imino functions, respectively. These values compare reasonably well with those of 1710 and 1665 cm^{-1} reported for the dihydroazepin-2-one system **5** (24).

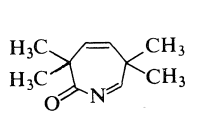

5

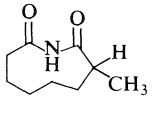

6

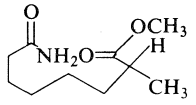

7

The results from the irradiation of the ketone **1** in a 1:1 water–dioxane medium were most gratifying, particularly since they provided a further elegant demonstration of the ring enlargement previously observed in methanol solution. Gas–liquid chromatographic examination of the photolysis product indicated the presence of the enals **3***a* and **3***b* together with a third product in 18% absolute yield and of long retention time. This was subsequently isolated by crystallization of the crude product from methanol and found to be a $C_9H_{15}NO_2$ compound, m.p. 138.5–139.5°, whose i.r. spectrum exhibited a sharp weak band at 3340 cm^{-1} indicative of the presence of an >N—H group, together with strong carbonyl

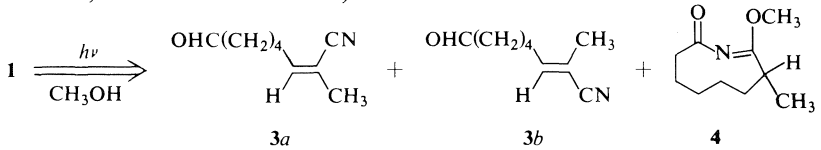

3*a* **3***b* **4**

SCHEME 2

[2]From g.l.c. peak areas.

Can. J. Chem. Downloaded from www.nrcresearchpress.com by 210.87.254.42 on 09/05/12
For personal use only.

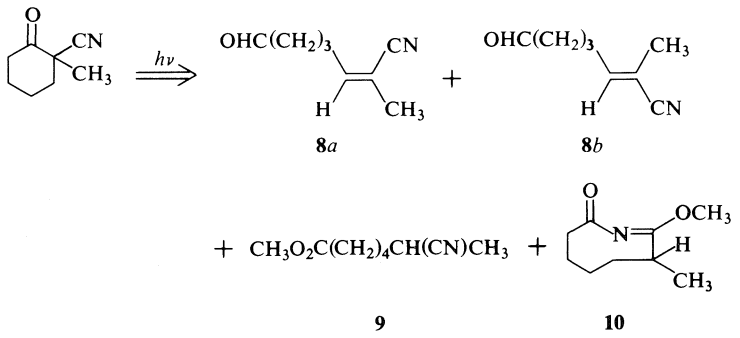

SCHEME 3

absorption at 1690 cm^{-1}. The n.m.r. spectrum had one exchangeable proton at δ 8.27 p.p.m., three- and eight-hydrogen multiplets at δ 2.83 and 1.7 p.p.m., respectively, together with a methyl doublet (J = 6 Hz) at 1.23 p.p.m. These spectra are quite consistent with the structure of this product being that of the cyclic imide **6**. Of course, this observation greatly enhances one's confidence in the correctness of the assignment of the structure **4** to the photoproduct in methanol.

Since **4** is one of the two possible O-methyl iminoethers related to **6**, we attempted the acid (2 *N* HCl) hydrolysis of **4** to **6** using the conditions previously reported for a related acyclic example (25). In the event, no **6** could be detected, the i.r. spectrum of the product suggesting the formation of an amide ester, possibly **7**, and thus the occurrence of preferential ring opening. Because of the small amount of **4** available, no further work on the hydrolysis product was possible. However, we were interested to observe that **6** itself did not survive these hydrolytic conditions.

Irradiation of a 10% methanol solution of 2-cyano-2-methycyclohexanone (**2**) led to the formation of four products in the ratio 61:30:7:1. The first two were the *Z* and *E* isomeric aldehydes **8***a* and **8***b* (Scheme 3), respectively, characterized by satisfactory elemental analyses on their 2,4-DNP derivatives and by their spectra. The isomers were distinguished by the chemical shifts of the vinyl protons, δ 6.17 p.p.m. for that of the *Z* compound, 6.33 p.p.m. for the *E* isomer. The third product was identified as the ester **9** by comparison with an authentic sample (26).

The fourth product was isolated only in small quantities but the assignment to it of structure **10** appears secure on the basis of the following. Both the i.r. (ν_{max} ($CHCl_3$) 1690 (m), 1660 cm^{-1} (s)) and n.m.r. (δ ($CDCl_3$) 1.22 (3H, d, J = 7 Hz), 1.5–2.6 (9H, two multiplets), and 3.7 p.p.m. (3H, s)) spectra are remarkably similar to those of the O-methyl iminoether **4** isolated from irradiation of **1**. In addition, alkaline hydrolysis of this photoproduct gave an oil whose i.r. and n.m.r. spectra corresponded very closely to those of an authentic sample of 2-methylheptanedioic acid (26). Methylation of the hydrolysis product gave material identical with the dimethyl ester of 2-methylheptanedioic acid. Irradiation of the cyclohexanone **2** in water–dioxane was found to give none of the anticipated cyclic imide.

Thus, our investigations have shown that the photochemical ring enlargement reaction of 2-cyanocycloalkanones is realizable in at least two cases and that it can provide either iminoethers or imides depending upon the solvent. However, the yields of these expansion products are significantly less than in the related cases reported by Carlson (10–13). The poorer yield of the eight-membered iminoether **10** relative to its nine-membered homolog **4** can be interpreted in terms of the relative ring strains in the precursor ketenimines (27).

The *Z*/*E* enal ratio from both **1** and **2** is in accord with the stereochemistry of enals observed in previous cases (28, 29). Enal/ester ratios of 1.7:2.9 have been reported for the photolysis in methanol for a number of 2-alkyl substituted cyclohexanones (30). For 2-cyano-2-methylcyclohexanone, this ratio is much larger, approximately 13. While conformational factors in the diradical almost certainly will play a role in controlling the relative amounts of enal and ester, it would appear very reasonable that the conjugation available in the product α,β-unsaturated nitrile would provide a driving force favoring this product over the alternative ketene (which leads to ester). Studies on 2-phenylcycloalkanones appear to support this argument (29).

Finally, it may be mentioned that in some re-

Can. J. Chem. Downloaded from www.nrcresearchpress.com by 210.87.254.42 on 09/05/12
For personal use only.

lated cases ring enlargement does not occur, *e.g.* 2-acetyl-2-methyl- and 2-benzoylcyclohexanone have been found to provide no ring expanded products on irradiation (31, 32). In contrast, a number of cyclic nonenolizable β-diketones are known to transform to enol lactones but without increase in ring size (33, 34).

Experimental

Spectroscopic and chromatographic instruments employed in this work have been described elsewhere (19).

Syntheses

(a) Suberonitrile

Finely powdered potassium cyanide (19.5 g, 0.3 mol) was added to a solution of 1,6-dibromohexane (Eastman, 24.4 g, 0.1 mol) in 95% ethanol (50 ml) and the mixture was refluxed overnight. When cool, the precipitated solids were dissolved by the addition of a small amount of water and the aqueous mixture was then extracted three times with ether (total, 300 ml); the combined ether extracts were washed successively with water, 5% aqueous sodium hydroxide, and water, and then dried. The manipulations above were all performed in a well-ventilated fume hood, using rubber gloves. The ether was distilled off, and the residue fractionated to give the desired suberonitrile (12 g, 90% yield) b.p. 140–145°/1 mm (lit. (35) b.p. 185°/15 mm). Gas–liquid chromatography indicated this material to be *ca.* 95% pure and it was employed in the next step.

(b) 2-Cyanocycloheptanone

The method of Iwanoff (20) was employed. The ethylmagnesium anilide (36) from *N*-methylaniline was prepared by dropwise addition of ethyl bromide (27.3 g, 0.25 mol) in anhydrous ether (100 ml) over 0.5 h to agitated magnesium turnings (7.2 g, 0.3 mol) in anhydrous ether (20 ml) in a carefully dried three-necked flask cooled in an ice bath, employing a dry nitrogen stream to exclude air. The reaction was moderately vigorous and the solution was stirred for a further 0.5 h after the ethyl bromide addition was complete. Then *N*-methylaniline (26.8 g, 0.25 mol) in anhydrous benzene (100 ml) was added over 0.5 h to the Grignard solution prepared as above and maintained at room temperature, the solution subsequently being stirred for a further 0.5–0.75 h, and then was heated to reflux.

Suberonitrile (23.12 g, 0.17 mol) in 250 ml of a 1:1 benzene–ether mixture was then added at the rate of 1 drop/0.5 min to this refluxing anilide solution; the addition required about 8 h. After refluxing overnight the cooled solution was treated with ice-cold 15% aqueous hydrochloric acid; the benzene–ether layer was separated and washed with a further 100 ml aliquot of 15% aqueous hydrochloric acid. The combined aqueous layers were extracted three times with ether (total, 300 ml), and then the combined organic layers were washed with water and dried. The solvents were distilled off, and the residue distilled to give 2-cyanocycloheptanone (8.1 g, 35%), b.p. 69–72°/0.05 mm (lit. (20) b.p. 135–136°/10 mm); ν_{max} ($CHCl_3$) 2250 (m), 1710 cm^{-1} (s); δ ($CDCl_3$) 3.8 (1H, m), 2.6 (2H, m), 1.4–2.2 p.p.m. (8H, br).

(c) 2-Cyano-2-methylcycloheptanone

Sodium metal (0.69 g, 0.03 g-atom) was dissolved in anhydrous ethanol (12 ml) followed by the addition of 2-cyanocycloheptanone (4.07 g, 0.027 mol) with stirring. After a few minutes, the sodium salt of the ketone separated, and stirring was continued for a further 20 min. Methyl iodide (7.66 ml, 0.054 mol) was then added dropwise; the reaction was not noticeably exothermic and after a further 15 min stirring, the mixture was warmed in an oil bath for 12 h. The ethanol was then removed, water added, and the solution extracted three times with ether; the combined ether extracts were washed twice with 2% aqueous sodium hydroxide, then with water, and dried. Distillation provided 2-cyano-2-methylcycloheptanone (3.3 g, 72%), b.p. 61–63°/0.15 mm, of *ca.* 99% purity by g.l.c.; ν_{max} ($CHCl_3$) 2240 (m), 1718 cm^{-1} (s); δ ($CDCl_3$) 3.7 (2H, m), 1.8 (8H, br), 1.5 p.p.m. (3H, s). A 2,4-dinitrophenylhydrazone derivative, m.p. 145–145.5°, was prepared (37).

Anal. Calcd. for $C_{15}H_{17}N_5O_4$: C, 54.38; H, 5.14; N, 21.14. Found: C, 54.22; H, 5.11; N, 20.94.

(d) 2-Cyanocyclohexanone

Finely powdered potassium cyanide (38 g, 0.58 mol) was added to a solution of 2-chlorocyclohexanone (26.5 g, 0.2 mol; obtained by the method of Newman *et al.* (38)) in 95% ethanol (100 ml) and after stirring for 20 min, the solution was refluxed for 40 min, cooled, poured into ice water, and the aqueous mixture was acidified with 15% aqueous hydrochloric acid to Congo Red p*H*, then extracted with ether. After drying, the ether was distilled off, and the residue fractionated to give the product (13.5 g, 55%), b.p. 87°/0.5 mm (lit. (39) b.p. 129–131°/7 mm); semicarbazide, m.p. 155–156° (lit. (40) m.p. 162°); ν_{max} ($CHCl_3$) 2250 (w), 1720 cm^{-1} (s); δ ($CDCl_3$) 3.8 (1H, m), 2.8–1.4 (8H, br).

(e) 2-Cyano-2-methylcyclohexanone

Sodium metal (1.2 g, 0.05 g-atom) was dissolved in anhydrous ethanol (10 ml) and 2-cyanocyclohexanone (6.15 g, 0.05 mol) added with stirring. A mildly exothermic reaction took place with the appearance of a white precipitate. Methyl iodide (11.36 g, 0.08 mol) was then dropped in and the mixture warmed on the water bath for 0.5 h. At the end of this time, all solid material had disappeared. The solvent was then removed, water added, and the mixture extracted with ether. The aqueous layer was saturated with sodium chloride and again extracted. The combined ether layers were washed twice with water, dried, and the solvent distilled. The residue was fractionated twice to give the desired product, b.p. 88–92°/15 mm (lit. (21) b.p. 94°/13 mm) which was contaminated with a small amount of 2-chlorocyclohexanone. Highly pure 2-cyano-2-methylcyclohexanone was produced by preparative g.l.c. on a 20 ft × 1/4 in. 5% SE-30 column. The purified material was a colorless liquid; ν_{max} ($CHCl_3$) 2240 (m), 1723 cm^{-1} (s); δ ($CDCl_3$) 3.9–1.7 (8H, complex), 1.4 p.p.m. (3H, s); semicarbazone, m.p. 200–202° (lit. (41) m.p. 201–202°).

(f) Methyl 6-Cyanoheptanoate

2-Methylcyclohexanone peroxide was obtained by reaction of 2-methylcyclohexanone with 30% hydrogen peroxide (42) and converted by the method of Minisci and Portolani (26) to the desired product which was iso-

Can. J. Chem. Downloaded from www.nrcresearchpress.com by 210.87.254.42 on 09/05/12
For personal use only.

Can. J. Chem. Downloaded from www.nrcresearchpress.com by 210.87.254.42 on 09/05/12
For personal use only.

lated in poor yield as an oil; ν_{max} ($CHCl_3$) 3000 (v br), 1710 cm^{-1} (s); δ ($CDCl_3$) 10.9 (s), 2.4 (m), 1.6 (m), 1.3 (d, J = 7 Hz). Methylation of this acid with diazomethane gave the methyl ester, a pure sample of which was prepared by preparative g.l.c.; ν_{max} ($CHCl_3$) 2250 (w), 1735 cm^{-1} (s); δ ($CDCl_3$) 3.67 (3H, s), 2.35 (3H, m), 1.9–1.4 (6H, br), 1.31 (3H, J = 7 Hz).

(g) 2-Methylheptanedioic Acid and its Dimethyl Ester

6-Cyanoheptanoic acid was hydrolyzed with aqueous ethanolic potassium hydroxide solution, and the crude acid was obtained as an oil by acidification and ether extraction, followed by solvent removal. A portion crystallized from ether, m.p. 49–50° (lit. (26) m.p. 56–57°). The oil had ν_{max} ($CHCl_3$) 3000 (br), 1705 cm^{-1} (s); δ ($CDCl_3$) 11.2 (2H, s), 2.3 (3H, m), 1.5 (6H, br), 1.1 p.p.m. (3H, d, J = 7 Hz).

Treatment of this diacid with diazomethane in ether gave the dimethyl ester, obtained as a colorless oil, ν_{max} ($CHCl_3$) 1725 cm^{-1} (s), δ ($CDCl_3$) 3.65 (6H, s), 2.3 (3H, m), 1.4 (6H, br), 1.13 p.p.m. (3H, d, J = 7 Hz).

Irradiations

Photochemical studies were performed employing a Hanovia 450 W high pressure lamp in a quartz water-cooled jacket. All samples were irradiated in Pyrex; small scale solutions were degassed by several freeze–thaw cycles on a high-vacuum line, then sealed, while preparative scale ones had oxygen-free nitrogen continuously bubbled through for the irradiation period. Products were isolated using either a 10 ft or 20 ft × 1/4 in. 5% SE-30 column in a Varian Aerograph Model 700 gas chromatograph.

*(a) 2-Cyano-2-methylcycloheptanone (**1**) in Methanol*

A solution of **1** (1.03 g) in methanol (20 ml) was irradiated for 64 h, after which time most of the starting material had been consumed. The solvent was removed and the yellow oil remaining subjected to preparative g.l.c. to give:

*Compound **3a***: colorless oil; ν_{max} ($CHCl_3$) 2850, 2710, 2210, 1720, 1640 cm^{-1}; δ ($CDCl_3$) 9.92 (1H, t, $J \approx 1$ Hz), 6.17 (1H, m), 2.4 (4H, m), 1.93 (3H, s, fine splitting), 1.5 (4H, m); mass spectrum, m/e 151 (10%, M^+, accurate mass measurement, 151.099439; calcd. for $C_9H_{13}NO$, 151.099714), 123 (27%), 122 (24%), 108 (28%), 106 (29%), 94 (100%), 81 (45%), 64 (46%), 55 (53%), 53 (56%), 41 (100%), 39 (69%); 2,4-DNP, m.p. 88–92°;

*Compound **3b***: colorless oil, ν_{max} ($CHCl_3$) 2850, 2710, 2210, 1720, 1660 cm^{-1}; δ ($CDCl_3$) 9.95 (1H, t, $J \approx 1$ Hz), 6.35 (1H, m), 2.6–1.2 (8H, br), 1.87 (3H, s); mass spectrum, very similar to that of **3a** (accurate mass measurement on m/e 151 peak, 151.099589; calcd. for $C_9H_{13}NO$, 151.099714).

*Compound **4***: colorless oil; ν_{max} ($CHCl_3$) 1690, 1660 cm^{-1}; δ ($CDCl_3$) 3.70 (3H, s), 2.5 (3H, m), 1.5 (8H, m), 1.18 (3H, d, J = 7 Hz); mass spectrum, m/e 183 (37%, $M^{+\cdot}$, accurate mass measurement, 183.12575; calcd. for $C_{10}H_{17}NO_2$, 183.12592), 154 (11%), 140 (52%), 126 (100%), 112 (75%), 97 (12%), 87 (58%), 70 (20%), 69 (20%), 55 (60%), 41 (85%), 39 (35%).

Aqueous hydrolysis (3 *N* hydrochloric acid – dioxane) of a sample of **4** at room temperature overnight gave material with ν_{max} ($CHCl_3$) 3500 (w), 3410 (w), 1735 (s), 1690 (s), 1600 cm^{-1} (m); δ ($CDCl_3$) 3.66 (3H, s), 2.2 (3H, br), 1.3 (8H, br), 1.1 (3H, d, J = 7 Hz).

(b) 2-Cyano-2-methylcycloheptanone in Aqueous Medium

A solution of **1** (0.21 g) in 1:1 dioxane–water (20 ml) was irradiated for 27 h. The cloudy solution was evaporated to dryness and the residue was crystallized from methanol to give **6** as white crystals, m.p. 139–139.5° (33 mg, 14%); ν_{max} ($CHCl_3$) 3340, 1690 cm^{-1}; δ ($CDCl_3$) 8.27 (1H, br, exchangeable), 2.8 (3H, br), 1.7 (8H, br), 1.23 (3H, d, J = 7 Hz), mass spectrum, m/e 169 (11%, $M^{+\cdot}$), 152 (52%), 142 (16%), 126 (22%), 113 (96%), 98 (74%), 82 (46%), 73 (63%), 69 (51%), 59 (74%), 55 (100%), 41 (100%), 39 (35%);

Anal. Calcd. for $C_9H_{15}NO_2$: C, 63.88; H, 8.93; N, 8.23. Found: C, 64.07; H, 9.08; N, 8.15.

Solution of a sample of this photoproduct in 3 *N* hydrochloric acid – dioxane at 20° overnight yielded, after work-up, an oily product with ν_{max} ($CHCl_3$) 3500 (w), 3410 (w), 1710 (s), 1660 (s), 1600 cm^{-1} (w).

*(c) 2-Cyano-2-methylcyclohexanone (**2**) in Methanol*

A solution of this ketone (1 g) in methanol (10 ml) was irradiated for 36 h, by which time about 75% of the starting material had been consumed. Preparative g.l.c. gave:

*Compound **8a***: ν_{max} ($CHCl_3$) 2820, 2720, 2210, 1720, 1640 cm^{-1}; δ ($CDCl_3$) 10.00 (1H, t, $J \approx 1$ Hz), 6.17 (1H, m), 2.5 (4H, m), 1.93 (3H, s, fine splitting), 1.9 (2H, m); mass spectrum, m/e 137 (7%, $M^{+\cdot}$), 108 (15%), 94 (80%), 93 (29%), 81 (21%), 67 (17%), 58 (90%), 53 (21%), 43 (100%); a 2,4-DNP derivative, m.p. 113.5–5.114.0°, was obtained (37).

Anal. Calcd. for $C_{14}H_{15}N_5O_4$: C, 52.99; H, 4.73; N, 22.08. Found: C, 52.89; H, 4.77; N, 22.01.

*Compound **8b***: ν_{max} ($CHCl_3$) 2820, 2720, 2210, 1720, 1640 cm^{-1}; δ ($CDCl_3$) 9.95 (1H, t, $J \approx 1$ Hz), 6.33 (1H, m), 2.7–1.5 (6H, m), 1.87 (3H, s, fine splitting); mass spectrum, apart from variations in peak intensities, identical to that of **8a**; a 2,4-DNP derivative, m.p. 83–85° was obtained (37).

Anal. Calcd. for $C_{14}H_{15}N_5O_4$: C, 52.99; H, 4.73; N, 22.08. Found: C, 53.02; H, 4.72; N, 21.93.

*Compound **9***: i.r. and n.m.r. spectra identical with those of an authentic sample previously described.

*Compound **10***: ν_{max} ($CHCl_3$) 1690, 1660 cm^{-1}; δ ($CDCl_3$) 3.70 (3H, s), 2.5 (3H, br), 1.67 (6H, br), 1.22 p.p.m. (3H, d, J = 7 Hz); a sample (12 mg) was hydrolyzed by refluxing for 3 h in 10% aqueous potassium hydroxide solution to which a little methanol had been added. Work-up gave a semisolid whose i.r. and n.m.r. spectra were practically superimposable on those of an authentic sample of 2-methylheptanedioic acid. Treatment of this semisolid with diazomethane in ether gave a product whose i.r. and n.m.r. spectra and g.l.c. retention times (on 5 ft × 1/8 in. 3% SE-30 and Carbowax columns) were identical to those of a sample of the dimethyl ester of 2-methylheptanedioic acid.

The authors are grateful to the National Research Council of Canada for partial support of this work.

1. G. K. Chip and T. R. Lynch. Chem. Commun. 641 (1973).
2. R. Srinivasan. Adv. Photochem. **1**, 83 (1963).
3. G. Quinkert. Angew. Chem. Int. Ed. Engl. **4**, 211 (1965).
4. D. R. Morton and N. J. Turro. J. Am. Chem. Soc. **95**, 3947 (1973).
5. P. Yates. Pure Appl. Chem. **16**, 93 (1968).
6. J. A. Barltrop and J. D. Coyle. Chem. Commun. 1081 (1969).
7. P. Dowd, A. Gold, and K. Sachdev. J. Am. Chem. Soc. **92**, 5724 (1970).
8. P. J. Wagner and R. W. Spoerke. J. Am. Chem. Soc. **91**, 4437 (1969).
9. G. L. Closs and C. E. Doubleday. J. Am. Chem. Soc. **94**, 9248 (1972).
10. R. G. Carlson, R. L. Coffin, W. W. Cox, and R. S. Givens. Chem. Commun. 501 (1973).
11. R. G. Carlson and D. E. Henton. Chem. Commun. 674 (1969).
12. R. G. Carlson and E. L. Biersmith. Chem. Commun. 1049 (1969).
13. R. G. Carlson, J. H.-A. Huber, and D. E. Henton. Chem. Commun. 223 (1973).
14. A. Sonada, I. Moritani, J. Miki, T. Tsuji, and S. Nishida. Bull. Chem. Soc. Jap. **45**, 1777 (1972).
15. W. G. Dauben, G. W. Shaffer, and E. J. Deviny. J. Am. Chem. Soc. **92**, 6273 (1970).
16. S. T. Reid and J. N. Tucker. Chem. Commun. 1609 (1971).
17. S. Sato. Bull. Chem. Soc. Jap. **41**, 2524 (1968).
18. T. Sasaki, S. Eguchi, and T. Toru. Chem. Commun. 1239 (1970).
19. T. R. Lynch, F. N. MacLachlan, and J. S. Suschitzky. Can. J. Chem. **51**, 1378 (1973).
20. C. Iwanoff. Chem. Ber. **87**, 1600 (1954).
21. K. V. Auwers, Th. Bahr, and E. Frese. Ann. **441**, 68 (1925).
22. G. S. Reddy, J. H. Goldstein, and L. Mandell. J. Am. Chem. Soc. **83**, 1300 (1961).
23. A. N. Kurtz, W. E. Billups, R. B. Greenlee, H. F. Hamil, and W. T. Pace. J. Org. Chem. **30**, 3141 (1965).
24. T. Sasaki, S. Eguchi, and M. Ohno. J. Am. Chem. Soc. **92**, 3192 (1970).
25. R. Scarpati and M. L. Graziano. J. Heterocycl. Chem. **9**, 1087 (1972).
26. F. Minisci and A. Portolani. Gazz. Chim. Ital. **89**, 1941 (1959).
27. W. J. Ball and S. R. Landor. J. Chem. Soc. 2298 (1962).
28. C. C. Badcock, M. J. Perona. G. O. Pritchard, and B. Rickborn. J. Am. Chem. Soc. **91**, 543 (1969).
29. A. A. Baum. Tetrahedron Lett. 1817 (1972).
30. J. D. Coyle. J. Chem. Soc. (B), 1736 (1971).
31. H. Nozaki, Z. Yamaguti, T. Okada, R. Noyori, and M. Kawanisi. Tetrahedron, **23**, 3993 (1967).
32. C. L. McIntosh. Can. J. Chem. **45**, 2267 (1967).
33. T. Okada, K. Kamogawa, M. Kawanisi, and H. Nozaki. Bull. Chem. Soc. Jap. **43**, 2908 (1970).
34. H. Kato, N. Miyamoto, M. Kawanisi, and H. Nozaki. Tetrahedron, **26**, 2975 (1970).
35. Dictionary of organic compounds. Eyre and Spottiswoode, London. 1965.
36. V. Grignard and J. Colonge. C. R. Acad. Sci. Fr. **194**, 929 (1933).
37. R. L. Shriner, R. C. Fuson, and D. Y. Curtin. The systematic identification of organic compounds. 4th ed. J. Wiley, New York. 1956. p. 129.
38. M. S. Newman, M. D. Farbman, and H. Hipsher. Org. Synth. Coll. Vol. 3. J. Wiley, New York. 1955. p. 188.
39. R. E. Myer. Helv. Chim. Acta, **16**, 129 (1933).
40. M. Mousseron, J. Jullien, and Y. Jolchine. Bull. Soc. Chim. Fr. 1209 (1950).
41. W. R. Schleigh and F. D. Popp. J. Chem. Soc. (C), 760 (1966).
42. N. A. Milas, S. A. Harris, and P. C. Panagiotakos. J. Am. Chem. Soc. **61**, 2430 (1939).

Can. J. Chem. Downloaded from www.nrcresearchpress.com by 210.87.254.42 on 09/05/12
For personal use only.

The Reaction of Iminophosphoranes with Dimethylformamide

JOSEPH M. MUCHOWSKI[1]
Bristol Laboratories of Canada, Candiac, Quebec
Received December 27, 1973

JOSEPH M. MUCHOWSKI. Can. J. Chem. **52**, 2255 (1974).
It is shown that aliphatic iminophosphoranes react with dimethylformamide to produce *N,N*-dimethyl-*N'*-alkylformamidines.

JOSEPH M. MUCHOWSKI. Can. J. Chem. **52**, 2255 (1974).
On démontre que les iminophosphoranes aliphatiques réagissent avec la diméthylformamide pour conduire aux *N,N*-diméthyle *N'*-alkylformamidines. [Traduit par le journal]

Can. J. Chem. Downloaded from www.nrcresearchpress.com by 210.87.254.42 on 09/05/12
For personal use only.

Iminophosphoranes, the isoelectronic analogs of phosphonium ylides (phosphoranes), have been known for more than five decades (1) and their chemistry has been studied in considerable detail (2–4). Whereas the reaction of iminophosphoranes with aldehydes and ketones is well known (2,4,5), to our knowledge, no reaction of these ylides with amides has heretofore been described.

When an aliphatic, cycloaliphatic, or benzylic iminophosphorane[2] (generated *in situ* (eq. 1) from an alkyl azide and triphenylphosphine (1, 5)) was heated under reflux in anhydrous dimethylformamide (DMF), a slow ($t_{1/2}^{153°} \sim 2$ days) reaction took place to give the corresponding *N,N*-dimethyl-*N'*-alkylformamidine[3] and triphenylphosphine oxide, presumably via a four-centered transition state (eq. 2). Under similar conditions aromatic iminophosphoranes failed to yield *N'*-arylformamidines, and no reaction occurred between dimethylacetamide and simple aliphatic iminophosphoranes. These observations show that the amide reactivity and the iminophosphorane nucleophilicity are two important factors which determine the success or failure of the above reaction. Further details concerning the scope and mechanism of this new reaction will be described in due course.

[1] $RN_3 + (C_6H_5)_3P \rightarrow (C_6H_5)_3P{=}N{-}R + N_2$

[2] $(C_6H_5)_3P{=}N{-}R + (CH_3)_2NCHO \rightarrow$
$\left[(C_6H_5)_3{-}P(-O{-}CH{=}N(CH_3)_2){-}N{-}R\right] \rightarrow$
$RN{=}CH{-}N(CH_3)_2 + (C_6H_5)_3P{=}O$

[3] $RNH_2 + [(CH_3)_2N{-}CHCl]^+Cl^- \xrightarrow{-(C_2H_5)_3N} RN{=}CH{-}N(CH_3)_2$

Experimental

The synthesis of *N,N*-dimethyl-*N'*-(2-phenethyl)formamidine is typical. To a solution of triphenylphosphine (2.65 g) in anhydrous DMF (20 ml) was added 2-phenethyl azide (1.47 g (7)). When the vigorous gas evolution had subsided (0.5 h), the solution was heated at reflux temperature under a positive pressure of dry nitrogen for 93 h. The cooled solution was poured into ice water (100 ml) and concentrated hydrochloric acid (5 ml), and the mixture was extracted with dichloromethane. The aqueous phase was made strongly basic with sodium hydroxide solution (10 *N*, 10 ml) and the amidine was extracted into benzene. The extract was washed well with water, dried over sodium sulfate, and evaporated *in vacuo*. Evaporative distillation (80°/0.01 mm) of the residue gave a colorless oil (1.20 g, 68%) which was identical to an authentic specimen prepared from 2-phenethylamine and dimethylformamide dichloride (6). The picrate had m.p. 138.5–140° (lit.(8) m.p. 141–142°), undepressed on admixture with the picrate prepared from the authentic amidine.

If the reaction was interrupted after 3 h, a small amount (< 10% yield) of the amidine could be isolated

[1]Present address: Syntex, S.A., Division de Investigacion, Calle Carretera Mexico-Toluca No. 2822, Apartado Postal 10–820, Mexico 10, D.F.

[2]Among others, the iminophosphoranes derived from *n*-octyl, cyclohexyl, and benzyl azides gave results analogous to those described herein for 2-phenethyl azide.

[3]The isolated yields of amidines after 4 days at reflux temperature were 60–70%. Comparable yields were obtained in much shorter times if the reactions were conducted in sealed ampoules at 180°. The amidines were identified by direct comparison with authentic specimens synthesized from dimethylformamide dichloride (6) and the requisite primary amine (eq. 3).

All new compounds were fully characterized by spectroscopic techniques and elemental analyses.

but evaporation of the dichloromethane extract of the acidified reaction solution gave the hydrochloride salt (m.p. 181–184°) of the iminophosphorane, as its hemibenzene solvate, in 80% yield (after crystallization from 2:1 benzene:dichloroethane).

Anal. Calcd. for $C_{26}H_{24}NP \cdot HCl \cdot \frac{1}{2}C_6H_6$: C, 76.19; H, 6.18; N, 3.07. Found: C, 76.29; H, 6.24; N, 2.99.

The author gratefully acknowledges the proficient technical assistance of Mr. F. Franco.

1. H. STAUDINGER and J. MEYER, Helv. Chim. Acta, **2**, 635 (1919).
2. A. W. JOHNSON. Ylid chemistry. Academic Press, New York. 1966. pp. 217–238.
3. S. TRIPPET. *In* Organophosphorous chemistry. Vol. 1. The Chemical Society, London. 1970. pp. 207–213.
4. S. TRIPPET. *In* Organophosphorous chemistry. Vol. 2. The Chemical Society, London. 1971. pp. 187–190.
5. A. W. JOHNSON and S. C. K. WONG. Can. J. Chem. **44**, 2793 (1966).
6. H. H. BOSSHARD, R. MORY, M. SCHMID, and H. ZOLLINGER. Helv. Chim. Acta, **42**, 1653 (1959).
7. P. A. S. SMITH and B. B. BROWN. J. Am. Chem. Soc. **73**, 2435 (1951).
8. H. BREDERECK, R. GOMPER, K. KLEMM, and H. REMPFER. Ber. **92**, 837 (1959).

Can. J. Chem. Downloaded from www.nrcresearchpress.com by 210.87.254.42 on 09/05/12
For personal use only.

The Addition of *N*-Bromoacetamide to 2,3-Unsaturated Nitro Sugars, a New Approach to 2,3-Diamino Sugars. Synthesis of Derivatives of 2,3-Diamino-2,3-dideoxy-D-mannose and -D-talose[1]

HANS H. BAER AND WERNER RANK

Department of Chemistry, University of Ottawa, Ottawa, Canada K1N 6N5

Received February 4, 1974

HANS H. BAER and WERNER RANK. Can. J. Chem. **52**, 2257 (1974).

The methyl 4,6-*O*-benzylidene-2,3-dideoxy-3-nitrohex-2-enopyranosides having the α-D-*erythro* (**1**), α-D-*threo* (**10**), β-D-*erythro* (**19**), and β-D-*threo* (**24**) configurations react smoothly with *N*-bromoacetamide (NBA) in the presence of sodium acetate in acetone or aqueous acetone. The main products are 2-acetamido-3-bromo-2,3-dideoxy-3-nitrohexose derivatives (**2**, **11**, **20**, **25**, and **26**). Depending on the amount of sodium acetate provided, varying proportions of 2-*O*-acetyl-3-bromo-3-deoxy-3-nitrohexose derivatives (**3**, **12**, and **21**) are formed also. The reactions are highly stereoselective in that the acetamido or acetoxy substituent appears to enter exclusively in the position *trans* to the anomeric methoxyl group. Generally the nitro group in the addition products appears to be oriented equatorially. An exceptional case is the reaction of **24**, which gives two C-3 epimers (**25** and **26**). Borohydride reduction of **3**, **12**, and **21** results in loss of the bromo and acetoxy substituents leading to known, saturated 2,3-dideoxy-3-nitro derivatives (**4**, **13**, and **23**). Compounds **2**, **11**, **20**, **25**, and **26** are debrominated by sodium borohydride to give vicinal acetamidonitro derivatives having the following configurations: α-D-*manno* (**5**, from **2**), α-D-*talo* (**14**, from **11**), β-D-*gluco* (**22**, from **20**), and β-D-*galacto* (**27**, from **25** and **26**). Compound **5** was converted by standard reaction sequences into methyl 2,3-diacetamido-2,3-dideoxy-α-D-mannopyranoside (**8**) and its 4,6-diacetate **9**. Compound **14** was similarly converted into the corresponding derivatives (**16** and **17**) of hitherto unknown 2,3-diamino-2,3-dideoxy-D-talose.

HANS H. BAER et WERNER RANK. Can. J. Chem. **52**, 2257 (1974).

Les méthyl-4,6-*O*-benzylidène-2,3-didéoxy-3-nitro-hex-2-ènopyranosides possédant les configurations α-D-*érythro* (**1**), α-D-*thréo* (**10**), β-D-*érythro* (**19**) et β-D-*thréo* (**24**) réagissent dans des conditions douces avec la *N*-bromoacétamide en présence d'acétate de sodium soit dans l'acétone ou l'acétone aqueuse. Les produits principaux de la réaction sont les dérivés 2-acétamido-3-bromo-2,3-didéoxy-3-nitro (**2**, **11**, **20**, **25** et **26**). Suivant la quantité d'acétate de sodium mise en jeu, des quantités variables des 2-*O*-acétyl-3-bromo-3-déoxy-3-nitro-hexopyranosides (**3**, **12** et **21**) sont aussi formés. Les réactions sont hautement stéréosélectives; les substituants acétamido ou acétoxyle semblent entrer exclusivement en position *trans* par rapport au groupe méthoxy anomérique. Dans les produits d'addition, le groupe nitro semble généralement en position équatoriale. Un cas exceptionnel est celui de la réaction du composé **24** qui conduit aux deux produits épimères en C-3 (**25** et **26**). La réduction des produits **3**, **12** et **21** par le borohydrure de sodium enlève les substituants bromo et acétoxyle conduisant ainsi aux dérivés saturés connus, les 2,3-didéoxy-3-nitro-hexopyranosides (**4**, **13** et **23**). La débromation, par le borohydrure de sodium, des composés **2**, **11**, **20**, **25** et **26** fournit des dérivés acétamido-nitro vicinaux ayant les configurations suivantes: α-D-*manno* (**5**, à partir de **2**), α-D-*talo* (**14**, à partir de **11**), β-D-*gluco* (**22**, à partir de **20**) et β-D-*galacto* (**27**, à partir de **25** et **26**). Le composé **5** a été converti par une suite de réactions standards en méthyl-2,3-diacétamido-2,3-didéoxy-α-D-mannopyranoside (**8**) et en son 4,6-diacétate (**9**). Le composé **14** a été converti de la même façon dans les dérivés correspondants (**16** et **17**) d'un sucre inconnu jusqu'ici, le 2,3-diamino-2,3-didéoxy-D-talose.

A preceding article (1) reported on syntheses of *gem*-halonitro sugars, for which *N*-bromoacetamide (NBA) was employed as an efficient reagent for bromination of saturated nitro glycosides. In conjunction with these studies, interest arose in the question as to how unsaturated nitro sugars would behave towards that reagent. It was found (2, 3) that α-nitroalkene groupings smoothly add NBA in the presence of sodium acetate, to give β-acetamido-α-bromo-α-nitroalkane systems. In the examples studied, which comprised 1-nitro-2-phenylethylene and a 5,6-unsaturated 6-nitrohexofuranose

[1]Part XXXIII in a series on reactions of nitro sugars. For Part XXXII see ref. 3.

Can. J. Chem. Downloaded from www.nrcresearchpress.com by 210.87.254.6 on 09/05/12
For personal use only.

Can. J. Chem. Downloaded from www.nrcresearchpress.com by 210.87.254.6 on 09/05/12
For personal use only.

derivative, the nitro group was situated on a terminal carbon atom and NBA therefore proceeded to substitute the α-hydrogen atom present, producing β-acetamido-α,α-dibromo-α-nitro compounds. We now report applications of the NBA addition to carbohydrates containing an endocyclic α-nitroalkene moiety, *viz.*, 2,3-unsaturated 3-nitrohexopyranosides, in which such further substitution is of course not possible.

The four stereoisomeric methyl 4,6-*O*-benzylidene-2,3-dideoxy-3-nitrohex-2-enopyranosides having the α-D-*erythro* (**1**), α-D-*threo* (**10**), β-D-*erythro* (**19**), and β-D-*threo* (**24**) configurations readily reacted with NBA in aqueous acetone at room temperature when at least a catalytic amount of sodium acetate was provided. With one exception, a single acetamido adduct was obtained in high yield in each case, which indicated a high degree of stereoselectivity of the addition. These adducts, which possessed the structure of methyl 2-acetamido-4,6-*O*-benzylidene-3-bromo-2,3-dideoxy-3-nitrohexopyranosides (**2**, **11**, **20**, **25**, and **26**), were the main reaction products. Depending on the amount of catalyst employed, varying proportions of corresponding 2-acetoxy derivatives (**3**, **12**, and **21**) arose as by-products, which evidently was due to acetate ion competing with the reactive acetamido species for addition to the double bond. In every case the configuration generated at C-2 in the product proved to be governed by that of C-1 in the substrate, in such a way that a 1,2-*trans* arrangement was formed. Thus, in the α-D-glycosides **1** and **10** the acetamido (or acetoxy) group entered axially and in the β-D-glycosides **19** and **24**, equatorially. The configuration of the geminally substituted carbon atom C-3 could not be established rigorously. However, it is known that a nitro group situated at C-3 of a pyranose ring strongly prefers to assume the equatorial orientation in kinetically controlled nitronate protonation as well as when thermodynamic factors prevail (4) and we have argued on the basis of chemical and spectroscopic evidence that such preference very likely applies to the formation of 3-halogeno-3-nitro derivatives also (1). In the NBA additions here considered, the mechanism probably involves an initial nucleophilic attack of the acetamido moiety on C-2 which leads to intermediate anion formation at C-3; subsequent attack of Br^+ may occur from either direction (so that 2,3-*cis* or 2,3-*trans* addition can be the result) but will normally take place axially. The configurations depicted for, and names assigned to, most of the new bromonitro derivatives were therefore based on these assumed preferences. (The C-3 epimers **25** and **26** represented a special case; see later). The assignments received support from n.m.r. data.

Reaction of the α-D-*erythro* glycoside **1** with NBA in acetone solution containing a catalytic amount of sodium acetate gave in 76% yield the acetamido derivative **2**, which was termed[2] methyl 2-acetamido-4,6-*O*-benzylidene-3-bromo-2,3-dideoxy-3-nitro-α-D-altropyranoside. Only a trace of by-product was detected by t.l.c. but its proportion increased strongly when a large excess of sodium acetate was used. Under such conditions, 62.5% of **2** and 33.5% of the second product were isolated. The latter proved to be the known (1) methyl 2-*O*-acetyl-4,6-*O*-benzylidene-3-bromo-3-deoxy-3-nitro-α-D-altropyranoside (**3**). In this connection, further observations concerning the previously noted instability of **3** were made. Thus, attempted recrystallization of the compound from hot ethyl acetate regenerated **1** in reversal of the bromoacetoxylation. Treatment of **3** with sodium borohydride, which in similar instances had simply replaced the bromine by hydrogen (1, 5), produced the 2,3-dideoxy-3-nitro glycoside **4**. A likely explanation for this is that abstraction of bromine was followed by elimination of the acetoxy group to give intermediary **1** which is known (6) to be reduced to **4** rapidly. By contrast, action of sodium borohydride upon the acetamido derivative **2** removed the bromine without loss of the C-2 substituent, to give a high yield of methyl 2-acetamido-4,6-*O*-benzylidene-2,3-dideoxy-3-

[2]Following a suggestion by Professor D. Horton, Columbus, Ohio, and pending adoption of an official international rule of nomenclature, we denote configurations of sugars that bear unequal geminal substituents on a ring carbon in this way: the substituent of a higher priority according to the Cahn–Ingold–Prelog rule (here Br) is thought of as replacing the hydroxyl group and the substituent of lower priority (here NO_2) is thought of as replacing the corresponding ring hydrogen, in a parent sugar, and the established configurational notation of the parent sugar so defined is used to describe the derivative (1). Hence the orientation of the nitro group in 3-bromo-3-deoxy-3-nitro-D-altrose is the same as in 3-deoxy-3-nitro-D-mannose although the absolute configuration of C-3 is reversed.

Can. J. Chem. Downloaded from www.nrcresearchpress.com by 210.87.254.6 on 09/05/12
For personal use only.

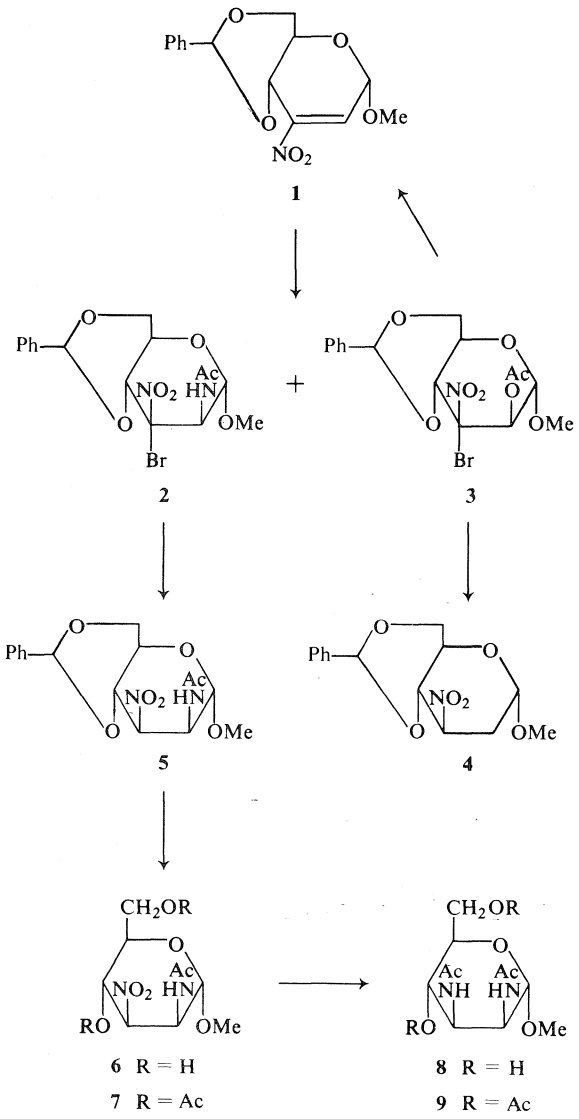

nitro-α-D-mannopyranoside (**5**).[3] Debenzylidenation of **5** with acid gave chromatographically homogeneous but amorphous methyl 2-acetamido-2,3-dideoxy-3-nitro-α-D-mannopyranoside (**6**) which was characterized by its crystalline 4,6-diacetate **7**. Catalytic hydrogenation of **6** in an acid medium followed in turn by *N*- and *O*-acetylation afforded methyl 2,3-diacetamido-2,3-dideoxy-α-D-mannopyranoside (**8**) and the known (8) 4,6-diacetate **9** thereof. The reaction sequence thus provided chemical proof for the configuration at C-2 in **2** as well as for the α-D-*manno* configuration of **5**–**8**.

The addition of NBA to the α-D-*threo* glycoside **10** gave methyl 2-acetamido-4,6-*O*-benzylidene-3-bromo-2,3-dideoxy-3-nitro-α-D-idopyranoside (**11**) and methyl 2-*O*-acetyl-4,6-*O*-benzylidene-3-bromo-3-deoxy-3-nitro-α-D-idopyranoside (**12**) in yields of 83 and 15%, respectively. Treatment of **11** and **12** with sodium borohydride proceeded in full analogy to the previous series. Thus, the *O*-acetyl compound **12** suffered elimination and reduction leading to the 2,3-dideoxy-3-nitro glycoside **13** which had previously been obtained (6) by borohydride reduction of **10**, whereas the acetamido compound **11** was debrominated in high yield to furnish methyl 2-acetamido-4,6-*O*-benzylidene-2,3-dideoxy-3-nitro-α-D-talopyranoside (**14**). Debenzylidenation of **14** gave the acetamidonitro glycoside **15**. The latter was catalytically hydrogenated under conditions of *N*-acetylation to produce methyl 2,3-diacetamido-2,3-dideoxy-α-D-talopyranoside (**16**), and *O*-acetylation of **16** gave the 4,6-diacetate **17**, the first derivatives of 2,3-diamino-2,3-dideoxy-D-talose to be recorded in the literature. Exhaustive hydrolysis of **16** with hydrochloric acid appeared to succeed according to spectroscopic evidence, but the reducing diamino sugar dihydrochloride failed to crystallize. *N*-Acetylation of the hydrolysis product likewise did not yield a crystalline derivative although i.r. and n.m.r. data of the product were consistent with a diacetamido sugar.

Since none of the products derived from **11** was known, structural proof was required. It was sufficient, however, to elucidate the steric arrangements at C-2 and -3 since those at the remaining centers were not in question. Hence, only the α-D-*talo*, α-D-*galacto*, α-D-*ido*, and α-D-*gulo* configurations had to be considered. Of these, the two last-mentioned ones could be regarded as highly unlikely as far as **14** and the subsequent products were concerned: they would comprise an axial C-3 substituent in the $_1C^4$ chair conformation (the more stable chair for

[3]Compound **5** proved identical with a minor by-product that had been obtained (7) in the reaction of methyl 2-*O*-acetyl-4,6-*O*-benzylidene-3-deoxy-3-nitro-α-D-glucopyranoside with ammonia. Some n.m.r. data and a chemical analogy had suggested the α-D-*manno* configuration for that by-product but a definitive assignment was held in abeyance. Unambiguous proof of configuration is furnished by the present work.

Can. J. Chem. Downloaded from www.nrcresearchpress.com by 210.87.254.6 on 09/05/12
For personal use only.

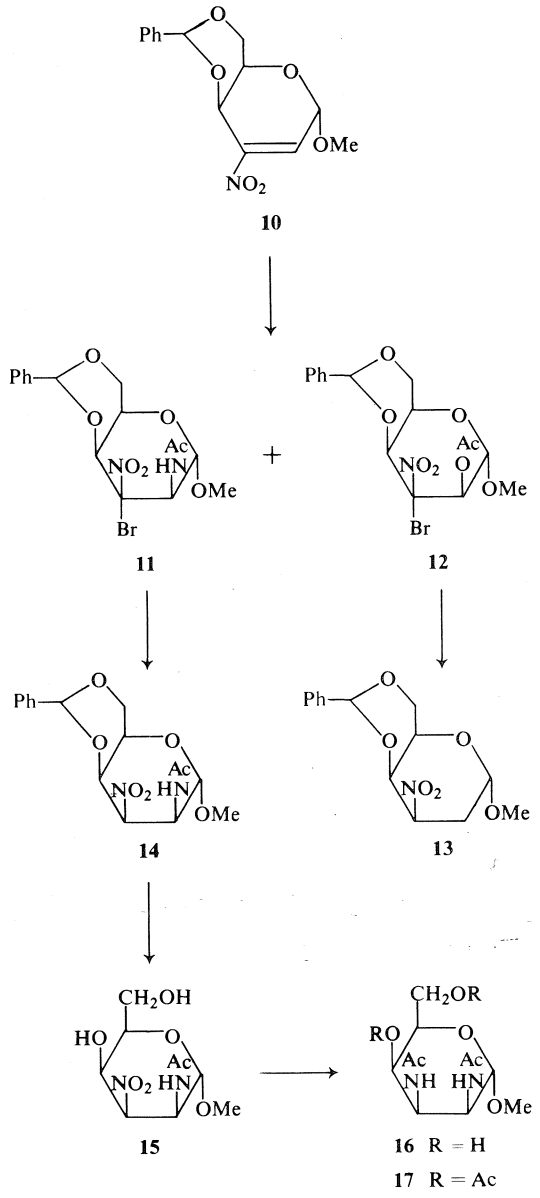

α-D-pyranosides) whereas, regardless of the original arrangement at the geminally substituted C-3 in **11**, reductive removal of the bromine atom by borohydride would most certainly lead to an equatorial nitro group.[4] The u.v. spectrum of the benzylidene acetal **14** in alcoholic 0.01 *N* KOH solution showed absorption at 250 nm with a very high intensity (ε 21 000) which was indicative of especially facile nitronate formation and hence pointed to the D-*talo* configuration, with two axial substituents flanking the nitro group (9). The n.m.r. spectrum of **14** was consistent therewith and it definitely ruled out the α-D-*galacto* configuration as no large splittings in the order of 10 Hz, that could have been attributed to 2,3-diaxial ring protons, were present in any of the signals. The α-D-*talo* configuration was further supported by the chemical shifts of the acetyl protons of **17**. In $CDCl_3$ solution the signals occurred at τ 7.88 7.98, 7.98, and 8.11 and were therefore attributable to an axial acetoxy, an axial acetamido, a primary C-6 acetoxy, and an equatorial acetamido group.[5] Final proof was obtained by chemical means. Boron trifluoride-catalyzed acetylation of **15** gave, instead of the 4,6-diacetate expected, an unsaturated monoacetate (**18**). The nitroolefinic nature of **18** was revealed by characteristic absorptions in the i.r. (ν_{max} 1530 cm^{-1}) and u.v. (λ_{max} 247 nm with ε 5000, in chloroform[6]). The n.m.r. spectrum demonstrated the presence of an olefinic proton (H-4, doublet at τ 2.64) and the remaining signals also agreed with the proposed structure. The ease with which **15** underwent elimination during acid-catalyzed acetylation was indicative of the *talo* configuration as it paralleled a similar tendency observed (10) in methyl 3,6-dideoxy-3-nitro-α-L-talopyranoside but had no counterpart in related compounds possessing other configurations. Finally, an identical nitroolefin **18** was obtained from the α-D-*manno* derivative **7** by dehydroacetoxylation with slightly basic silica gel in refluxing chloroform. This fact proved that **18** was methyl 2-acetamido-6-*O*-acetyl-2,3,4-trideoxy-3-nitro-α-D-*threo*-hex-3-enopyranoside, and it showed that **7** and **15** had the same configuration at C-2. Conse-

[4]Compare the results of such debrominations recorded earlier (1) and later in the present article.

[5]This pattern was inconsistent with the α-D-*galacto* and α-D-*ido* configurations, though not with the α-D-*gulo* configuration. The acetyl proton signals of the isomer **9** appeared at τ 7.94, 7.96, 7.99, and 8.12 in accordance with the equatorial acetoxy, axial acetamido, primary C-6 acetoxy, and equatorial acetamido groups in the D-*manno* configuration. For references to the rule that permits such assignments and for a discussion of its applicability to other compounds described in this article, see a subsequent paragraph.

[6]Upon addition of 0.1*N* methanolic sodium methoxide (0.1 ml) to the $10^{-4}M$ solution of the sample (3 ml), a bathochromic shift to λ_{max}257 nm took place and the absorbance increased to 10 100. This is interpreted as resulting from nucleophilic addition of methoxide ion to give a saturated glycoside nitronate.

Can. J. Chem. Downloaded from www.nrcresearchpress.com by 210.87.254.6 on 09/05/12
For personal use only.

quently the α-D-*galacto* and α-D-*gulo* configurations were eliminated for **15**, and the α-D-*talo* configuration remained for **14**–**17** as the only one that was compatible with all the pieces of chemical and spectroscopic evidence accumulated.

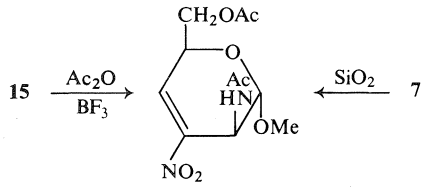

18

Addition of NBA to the β-D-*erythro* glycoside **19** in the presence of excess sodium acetate produced methyl 2-acetamido-4,6-*O*-benzylidene-3-bromo-2,3-dideoxy-3-nitro-β-D-allopyranoside (**20**) and its previously described (1) 2-acetoxy analog **21** in yields of 55 and 24%, respectively. For both products the equatorial orientation of the C-2 substituent was indicated by diaxial proton coupling (8 Hz) between H-1 and H-2. Reduction with sodium borohydride converted **20** into methyl 2-acetamido-4,6-*O*-benzylidene-3-deoxy-3-nitro-β-D-glucopyranoside (**22**), and **21**, into methyl 4,6-*O*-benzylidene-2,3-dideoxy-3-nitro-β-D-*arabino*-hexopyranoside (**23**), in complete analogy to the corresponding reactions mentioned earlier on. The known compounds **22** and **23**, which have served as useful intermediates in amino sugar syntheses, have been made in high yields from **19** by more direct methods (4*a*, 6, 11). No further work was therefore devoted to the reaction of **19** with NBA and the question of a possible influence of the sodium acetate concentration on the product ratio was not pursued. The highly stereoselective introduction of substituents at C-2 in the direction opposite to the aforedescribed examples, was, however, noted with interest.

Addition of NBA to the β-D-*threo* glycoside **24** also proceeded very smoothly. Only a catalytic amount of sodium acetate was applied in this case, and no acetoxybromo adduct was detected. The product consisted of approximately equal proportions of two acetamidobromo isomers which were isolated by column chromatography, each in about 45% yield. Both isomers exhibited an anomeric proton doublet with a splitting of 9 Hz, which indicated 1,2-*trans* diaxial ring hydrogen atoms and hence,

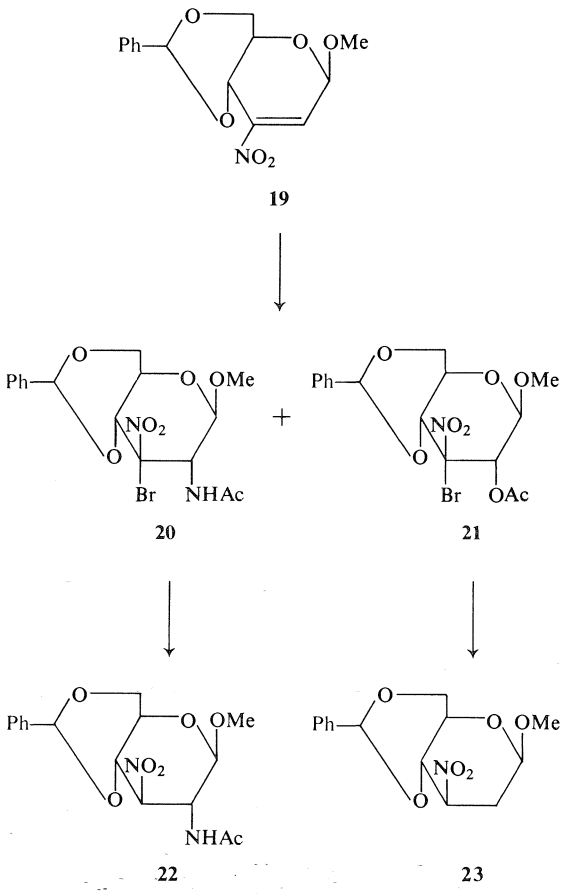

19 **20** **21** **22** **23**

an equatorial substituent at C-2. The stereoisomerism of the two adducts must therefore be due to different orientations at C-3, *i.e.*, the β-D-*gulo* (**25**) and β-D-*galacto* (**26**) configurations must hold. For reasons given below, the more slowly moving product was judged to be **25**, and the faster moving one was assigned formula **26**. Treatment of either compound with sodium borohydride led to the same product of debromination, namely, the known (12) methyl 2-acetamido-4,6-*O*-benzylidene-2,3-dideoxy-3-nitro-β-D-galactopyranoside (**27**), which constituted chemical proof for configurational identity at C-2 and epimerism at C-3. Rebromination of **27** gave in 80% yield the slow-moving bromonitro compound (**25**) while only a trace of the fast-moving isomer (**26**) seemed to arise. It is a reasonable assumption supported by evidence that nitro glycosides of the type of **27** are brominated axially (1); the finding just mentioned thus provided grounds for the formula allocation made.

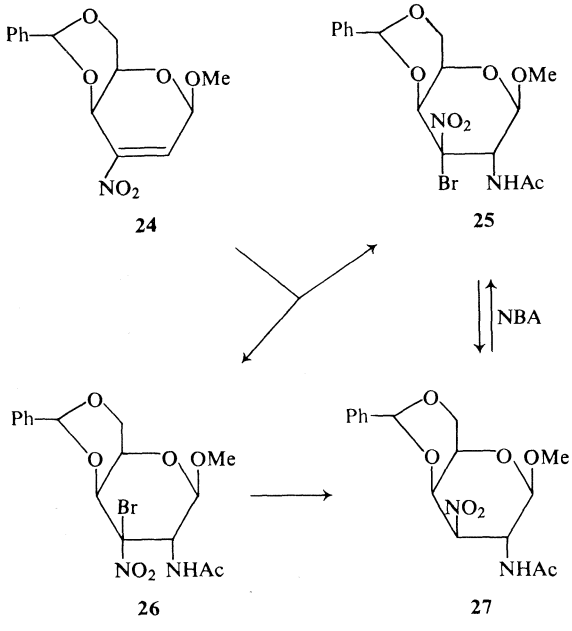

Discussion of Nuclear Magnetic Resonance Data

In addition to the n.m.r. parameters already mentioned, some further spectral features deserve comment. In the series of 4,6-*O*-benzylidene-3-deoxy-3-halo-3-nitro pyranosides studied previously it was noted that the chemical shift of the characteristic benzylidene methine proton singlet in the region of τ 4.2–4.5 is quite sensitive to the configurations at C-3 and -4. When compared with the position in the corresponding nonhalogenated compounds (all of which possess an equatorial nitro group at C-3), the methine signal upon halogenation at C-3 was moderately but significantly shifted downfield (by 0.1–0.2 p.p.m.) in some of the cases but remained virtually unaffected in others. This could be reconciled with all other considerations when the downfield shift was taken to indicate a *gauche* orientation between the C-3—halogen and the C-4—oxygen bonds while absence of such shift was taken to signify an *anti* orientation of these bonds (1). Similar observations were again made in the present series of compounds (Table 1). Thus, downfield shifts of 15, 12, and 21 Hz were found in the bromonitro compounds **2**, **20**, and **26** as compared to the bromine-free compounds **5**, **22**, and **27**, respectively. On the other hand, comparison of **11** and **25** with **14** and **27**, respectively, revealed only insignificant differences in the methine proton shifts. These findings reinforce the configurational assignments made for C-3.[7]

Another point of interest concerns the chemical shifts of acetyl proton resonances. In peracetylated pyranoses and aminopyranoses as well as their methyl glycosides, axial *O*-acetyl groups resonate at lowest field (τ 7.80–7.87), axial acetamido, equatorial *O*-acetyl, and primary (C-6) *O*-acetyl groups resonate in an intermediate range (τ 7.89–8.01), and equatorial acetamido groups give signals at highest field (τ 8.03–8.10 or sometimes slightly higher) in the most commonly employed solvent, chloroform-*d* (14–17). Better separation of signals is observed in dimethylsulfoxide-d_6 solution where the corresponding ranges have been reported (17) to be τ 7.86–7.89, 7.95–8.10, and 8.21–8.27. Very similar resonance ranges apply to peracetylated inositols, inosamines, and related cyclohexane derivatives (18, 19). The shift ranges have been verified on a multitude of examples in many laboratories and are now generally regarded as reliable stereochemical indicators for compounds of the types mentioned. We have used the principle to confirm the configurations of **9** and **17** (see above). Ambiguity may of course arise if acetyl signals happen to fall very close to range bounds. A case in point is the axial-acetamido signal (τ 8.02) of the nitro compound **7** which hardly differs from the equatorial-acetamido signal (τ 8.03) of the β-D-*gluco* isomer (11*b*) although normally a nitro group does not tend to cause serious deviations. However, certain functionalities such as free hydroxyl groups, halogens, sulfonate esters, and particularly, aryl substituents present in the molecule invalidate the aforementioned acetyl resonance ranges as a basis for ready stereochemical correlations (16–18). This is clearly illustrated by the benzylidenated nitro and bromonitro sugars listed here (Table 1) and earlier (Table 1 of ref. 1). Perusal of the tables will show that, although in several instances the signals do occur within the "normal" regions, they fall outside in many cases.

[7]Unfortunately, for the new bromonitro 2-acetate **12** there exists no exact counterpart for comparison. However, its τ-value of 4.41, besides being very similar to that of **11**, is close also to those of the bromine-free compounds **13** (τ 4.43, ref. 1) and methyl 4,6-*O*-benzylidene-3-deoxy-3-nitro-α-D-talopyranoside (τ 4.42, ref. 13; all data refer to $CDCl_3$ solutions). This lends support to the assumed configuration.

Can. J. Chem. Downloaded from www.nrcresearchpress.com by 210.87.254.6 on 09/05/12
For personal use only.

TABLE 1. Chemical shifts (τ) of 100 MHz n.m.r. signals[a]

Compound	$PhCHO_2$	OCH_3	*O*—Ac	*N*—Ac	H-1	H-2	Other signals
2	4.21	6.64		8.04	5.33s	4.69d[b,c]	3.50d (N—H)
2*	4.19	6.68		8.19	5.30s	4.96d[b,c]	1.35d (N—H), 5.19d (8Hz, H-4?)
3	4.21	6.61	8.00		5.29s	4.35s	
5	4.36	6.61		8.01	5.32s		4.0m (N—H), 4.9m (H-2, -3)
5*	4.32	6.66		8.15	5.34s		1.6m (N—H), 4.94q (4, 10Hz, H-3)
7		6.60	7.90, 7.96	8.01	5.31s	~4.95	4.95 (H-3), 4.35t (10Hz, H-4)
9		6.63	7.94, 7.99	7.96, 8.12			5.12t (10Hz, H-4)
11	4.37	6.60		8.31	5.17s	4.81d[b,c]	3.27d (N—H), 5.17s (H-4), 5.7q (AB pattern, H-6, 6′), 5.82s (H-5)
12	4.41	6.59	8.03		5.08s	4.27s	5.22s (H-4), 5.5–5.9 (H-5, -6, 6′)
14	4.38	6.60		8.25	[d]	[d]	[d]
14*	4.24	6.67		8.31	[e]	[e]	[e]
17		6.63	7.88, 7.98	7.98, 8.11	5.40s		~3.75m (2N—H), ~4.6q (narrow, H-4)
18		6.56	7.92	8.03	5.12s	4.83d[b,f]	2.64d (2Hz, H-4), 4.2d (N—H), 5.3–5.8(H-5, -6, 6′)
20	4.38	6.54		8.02	5.49d	4.97q	4.0d[c] (N—H)
20*	4.15	6.60		8.19			
21	4.39	6.51	7.93		5.37d	4.47d	
22*	4.27	6.63		8.22	5.37d		4.99t (H-3)
25	4.32	6.56		7.93	5.38d	4.93q[c,g]	5.32s (H-4), 5.85q (AB pattern, H-6, 6′)
25*	4.30	6.62		8.15	5.52d		5.0-5.2 (H-2, -4), ~5.8 (H-5, -6, 6′)
26*	4.14	6.64		8.11			5.1–5.3 (H-1, -2, -4), 5.85 (H-6, 6′), 6.17 (H-5)
27*	4.35	6.64		8.24	5.5–5.8		4.72q (4, 11Hz, H-3), 5.24q (narrow, H-4)

[a]Data refer to $CDCl_3$ solutions except for compounds marked by an asterisk (*) which were measured in DMSO-d_6 solution. The substituent resonances were all singlets of the expected intensity. For ring protons, multiplicities are indicated as s (singlet, or apparent singlet in case of very small splitting), d (doublet), t (triplet), q (quartet), and m (multiplet).
[b]Singlet after D_2O exchange.
[c]$J_{2,NH}$ = 10 Hz.
[d]τ 3.05d (N—H); 4.99 and 5.14, centers of narrow 2-proton signals (H-1, -2, -3, -4); 5.7, center of 2-proton AB-quartet (H-6, 6′); 6.26s (H-5).
[e]τ 3.1d (N—H); 4.67q (narrow, H-3); 4.94d (~1 Hz, H-4); 5.25 (H-1 singlet over H-2 multiplet); 5.80s (H-6, 6′); 6.26s (H-5).
[f]$J_{2,NH}$ = 8 Hz.
[g]Doublet after D_2O exchange; $J_{1,2}$ = 8 Hz.

Especially striking examples are provided by **11** and **14** whose axial acetamido groups resonate upfield even of the "normal" equatorial-acetamido range, and by **25** and **26** whose equatorial acetamido groups, conversely, resonate below that range. Obviously a more detailed analysis is needed before the conformational significance of these data can be evaluated. On the other hand, the chemical shifts of the anomeric methoxyl signals do not appear to be subject to similar disturbances. In most of the compounds described here and earlier (1), these signals occur in the range τ 6.40–6.56 (β-glycosides) and τ 6.55–6.66 (α-glycosides) ($CDCl_3$ solutions),[8] in line with expectations (15).

[8]Exceptions exist in α-glycosides presumed to have an axial nitro group at C-3; an unusually high τ-value is observed (1).

Conclusion

Amination of the α- and β-D-*erythro* nitroolefins **1** and **19** (and of their preparative precursors, the corresponding saturated α- and β-D-glucopyranoside 2-acetates) with ammonia provides an excellent route to vicinal aminonitro sugars from which 2,3-diamino sugars can easily be prepared (4*a*, 7, 11*b*). However, in both anomeric series the predominant reaction products so obtainable possess the D-*gluco* configuration and only small proportions of D-*manno* isomers are formed.[9] The present work

[9]In remarkable contrast to this general steric course of the amination, addition of anthranilic acid to **19** under special reaction conditions yielded 56% of an adduct possessing the β-D-*manno* configuration, and this did provide the basis for a reasonably convenient synthesis of 2,3-diamino-2,3-dideoxy-D-mannose (20). Similar reaction of anthranilic acid with **1** gave only the α-D-*gluco* adduct (21).

Can. J. Chem. Downloaded from www.nrcresearchpress.com by 210.87.254.6 on 09/05/12
For personal use only.

Can. J. Chem. Downloaded from www.nrcresearchpress.com by 210.87.254.6 on 09/05/12
For personal use only.

has demonstrated that NBA lends itself as a vehicle for high-yielding aminations which in their stereoselectivity depend on the anomeric configuration of the substrate. Especially in view of the synthesis of the α-D-*manno* glycosides **5**–**9** the new approach represents a useful complement and improvement. The same pertains to the reactions of the D-*threo* nitroolefins **10** and **24**. Amination of the former with ammonia has never been tried, and the sequence here described provides a first access to hitherto unknown 2,3-diamino-2,3-dideoxy-D-talose. A modified procedure of amination of **24** had given, in 35–38% yield, the β-D-*galacto* derivative **27** which was subsequently converted into derivatives of 2,3-diamino-2,3-dideoxy-D-galactose (12). In the sequence **24** → **25** + **26** → **27** the overall yield was 85% (and might be even higher if separation of **25** and **26** is omitted), which clearly endows the new method with superior preparative appeal.

Experimental

For general preparative techniques and instruments used see preceding articles of this series (*e.g.*, refs. 1, 6, 7, 10, 13). Optical rotations were measured at room temperature, and unless otherwise indicated, the solvent was chloroform (*c*, 0.5–1). Infrared data refer to Nujol mulls. Column chromatography was performed on silica gel (70–325 mesh, a product of E. Merck AG, Darmstadt), and the following solvent systems (v/v) were employed: A, chloroform–acetone (7:3); B, carbon tetrachloride – ethyl acetate (7:3); C, the same (4:3); D, chloroform–methanol (4:1); E, the same (8:1).

*Methyl 2-Acetamido-4,6-O-benzylidene-3-bromo-2,3-dideoxy-3-nitro-α-D-altropyranoside (**2**) and Methyl 2-O-Acetyl-4,6-O-benzylidene-3-bromo-3-deoxy-3-nitro-α-D-altropyranoside (**3**)*

(a) Reaction with Catalytic Amount of Sodium Acetate

A 50-mg sample of the nitro olefin **1** (ref. 22; see also footnote 9 in ref. 21), NBA (35 mg), and sodium acetate (2 mg) were stirred in acetone (4 ml), at room temperature. After 2 h the mixture was processed by the addition of water (6 ml) and evaporation of most of the acetone. A white precipitate was collected, washed with cold water, and dried. Thin-layer chromatography with solvent A showed a main product spot (**2**) and only traces of a faster moving product (presumably **3**). Two recrystallizations from ethyl acetate – petroleum ether gave **2** (56.5 mg, 76%) melting at 125–126° and at 127–129° after another recrystallization from ethanol–water; $[\alpha]_D$ +46°, ν_{max} 3260 (NH), 1660, 1530 (amide), and 1560 cm^{-1} (NO_2).

Anal. Calcd. for $C_{16}H_{19}BrN_2O_7$ (431.3): C, 44.60; H, 4.44; N, 6.51; Br, 18.50. Found: C, 44.32; H, 4.59; N, 6.63; Br, 18.68.

(b) Reaction with Excess Sodium Acetate

A solution of **1** (293 mg) in acetone (20 ml) was mixed with a solution of NBA (200 mg) in aqueous, saturated sodium acetate (15 ml), and the mixture was vigorously stirred for 7 h. Water (30 ml) was then added, and removal of acetone by partial evaporation gave a white solid (dry weight 425 mg) that showed two strong spots (**2** and **3**) on t.l.c. with solvent A. The products were separated on a 20-g silica gel column by use of solvent A. The fast-moving fractions gave crystalline **3** (145 mg, 33.5%); m.p. 152–153°; $[\alpha]_D$ +10.5°; ν_{max} 1760 (OAc) and 1570 cm^{-1} (NO_2). Comparison of spectra and physical constants established the identity with **3** described earlier; reported (1), m.p. 152–153°; $[\alpha]_D$ +12.3°. Recrystallization of the product from hot ethyl acetate converted it into **1**, m.p. 181–182°; $[\alpha]_D$ −97.5°; ν_{max} 1525 cm^{-1} (nitroalkene) without carbonyl band (lit. (22) m.p. 183°; $[\alpha]_D$ −93° (in ethyl acetate)).

The slow-moving fractions eluted from the above column gave 270 mg (62.5%) of **2**, m.p. 127–129° upon recrystallization from ethanol–water.

*Methyl 4,6-O-Benzylidene-2,3-dideoxy-3-nitro-α-D-arabinohexopyranoside (**4**)*

A solution of **3** (100 mg) and sodium borohydride (30 mg) in ethanol (20 ml) was stirred in an ice bath for 1 h and then acidified with 2 *N* acetic acid. Upon addition of water (20 ml) and partial evaporation of the ethanol a white precipitate was obtained, which was washed with water. Recrystallization from ethanol–water gave 59.5 mg (87%) of **4**; m.p. 109–110°, unchanged on admixture of authentic **4** (6, 22). The identity was ascertained by comparison of i.r. spectra.

*Methyl 2-Acetamido-4,6-O-benzylidene-2,3-dideoxy-3-nitro-α-D-mannopyranoside (**5**)*

A mixture of **2** (150 mg), sodium borohydride (150 mg), and ethanol (10 ml) was stirred at room temperature for 1 h. Acidification with 2 *N* acetic acid, dilution with water (20 ml), and partial evaporation produced a white solid which was washed with cold water, dried, and recrystallized from chloroform – *n*-pentane. There was obtained 112 mg (91%) of **5**; m.p. 121–123°; $[\alpha]_D$ +14.8°; ν_{max} 3300–3200 (NH), 1665 (amide I), 1560–1530 cm^{-1} (NO_2 and amide II). The i.r. spectrum was identical in every detail with that of a product previously obtained and referred to (7) as "by-product **6**" (m.p. 123–125° and $[\alpha]_D$ +16° for a sample shown to contain some chloroform of crystallization; the exhaustively dried compound melted at 186–187° and gave correct microanalytical data for $C_{16}H_{20}N_2O_7$).

*Methyl 2-Acetamido-4,6-di-O-acetyl-2,3-dideoxy-3-nitro-α-D-mannopyranoside (**7**)*

Compound **5** (600 mg) was stirred with 90% trifluoroacetic acid (5 ml) for 30 min at room temperature. Evaporation with successive additions of several portions of water, and eventually ethanol, gave the debenzylidenated compound (**6**) as a colorless syrup which exhibited a single, slow-moving spot on t.l.c. (solvent A). All attempts at crystallization failed. Part of the material (100 mg) was acetylated with acetic anhydride (3 ml) by use of 3 drops of boron trifluoride etherate as a catalyst (30 min at ambient temperature). The reaction mixture was poured into ice water to give an amorphous precipitate which was filtered off, washed with cold water, and dried. Reprecipitation from ethyl acetate

Can. J. Chem. Downloaded from www.nrcresearchpress.com by 210.87.254.6 on 09/05/12
For personal use only.

solution with petroleum ether gave chromatographically pure **7** showing $[\alpha]_D$ +38°; ν_{max} 3300 (NH), 1745 (OAc), 1665 (amide I), 1560 (NO_2), and 1535 cm^{-1} (amide II).

Anal. Calcd. for $C_{13}H_{20}N_2O_9$ (348.3): C, 44.83; H, 5.79; N, 8.05. Found: C, 44.75; H, 5.89; N, 8.19.

*Methyl 2,3-Diacetamido-2,3-dideoxy-α-D-mannopyranoside (**8**)*

A solution of syrupy **6** (300 mg; see the preceding section) and platinum dioxide (200 mg) in water (50 ml) and 0.1 *N* hydrochloric acid (11.6 ml) was shaken for 2.5 days at 25° with hydrogen under pressure (4 atm). Removal of the catalyst, evaporation of the solution, and evaporation of several portions of added ethanol from the residue gave a colorless syrup. For *N*-acetylation, the syrup was dissolved in water (10 ml), and methanol (1 ml), acetic anhydride (0.5 ml), and Dowex-1 × 8 (carbonate form) were added. The mixture was stirred at room temperature for 90 min. Evaporation of the filtered solution gave a colorless syrup which crystallized from ethanol–ether to afford **8** (243 mg, 77%); m.p. 248–250°; $[\alpha]_D$ +4.8° (*c* 0.4, in water); ν_{max} 3520, 3470, 3300 (NH, OH), 1640 and 1540 cm^{-1} (amide).

Anal. Calcd. for $C_{11}H_{20}N_2O_6$ (276.3): C, 47.82; H, 7.30; N, 10.14. Found: C, 47.55; H, 7.43; N, 9.97.

*Methyl 2,3-Diacetamido-4,6-di-O-acetyl-2,3-dideoxy-α-D-mannopyranoside (**9**)*

The compound **8** (100 mg) was treated with acetic anhydride (1 ml) in pyridine (4 ml) for 16 h at 25°. Azeotropic evaporation with toluene and ethanol, followed by crystallization of the residue from benzene – petroleum ether, furnished 109 mg (83%) of **9**; m.p. 199–201°; $[\alpha]_D$ +84°; ν_{max} 3300 (NH), 1745 (OAc), 1640, and 1545 cm^{-1} (amide) (lit. (8) m.p. 200–202°; $[\alpha]_D$ +89.2°).

*Methyl 2-Acetamido-4,6-O-benzylidene-3-bromo-2,3-dideoxy-3-nitro-α-D-idopyranoside (**11**) and Methyl 2-O-Acetyl-4,6-O-benzylidene-3-bromo-3-deoxy-3-nitro-α-D-idopyranoside (**12**)*

A 200-mg sample of the nitro olefin **10** (13) dissolved in acetone (16 ml) was added to a solution of NBA (200 mg) and sodium acetate (10 mg) in water (10 ml). The reaction mixture was stirred at room temperature for 2.5 h during which a white precipitate appeared. Addition of water (25 ml) and subsequent removal of acetone by partial evaporation produced further quantities of precipitate. The material was isolated, washed with cold water, dried, and shown by t.l.c. (solvent C) to consist of two easily separable, main components. They were separated on a 20-g silica gel column using solvent A. The fast-moving, minor component (**12**) was obtained as crystals (46 mg, 15.6%) melting at 225–226°; $[\alpha]_D$ +31.5°; ν_{max} 1760 (OAc) and 1565 cm^{-1} (NO_2).

Anal. Calcd. for $C_{16}H_{18}BrNO_8$ (432.3): C, 44.50; H, 4.20; Br, 18.45. Found: C, 44.63; H, 4.01; Br, 18.74.

The slow-moving, major component (**11**) was isolated as crystals (245 mg, 83%) melting at 175–176°; $[\alpha]_D$ +19.1°; ν_{max} 3460 (NH), 1705, 1500 (amide I and II), 1570 cm^{-1} (NO_2).

Anal. Calcd. for $C_{16}H_{19}BrN_2O_7$ (431.3): C, 44.60; H, 4.44; Br, 18.50. Found: C, 44.74; H, 4.56; Br. 18.37.

*Methyl 4,6-O-Benzylidene-2,3-dideoxy-3-nitro-α-D-lyxo-hexopyranoside (**13**)*

Treatment of **12** (165 mg) with sodium borohydride (40 mg) in ethanol (30 ml) for 30 min at 0° was followed by work-up as described for the preparation of the isomer **4**. It yielded 95 mg (85%) of **13**, m.p. 103–105°. Identity with an authentic sample (6, 22) was established by a mixture melting point and comparison of the i.r. spectra.

*Methyl 2-Acetamido-4,6-O-benzylidene-2,3-dideoxy-3-nitro-α-D-talopyranoside (**14**)*

Compound **11** (80 mg) was treated with sodium borohydride (20 mg) in ethanol (10 ml) at 0°. The debromination appeared complete after 5 min (t.l.c. with solvent A). After 10 min the mixture was worked up as described for the isomer **5**. Recrystallization of the product from chloroform – petroleum ether gave 55 mg (85%) of **14**; m.p. 205°; $[\alpha]_D$ +55.3°; ν_{max} 3450 (NH), 1695, 1510 (amide I and II), 1560 cm^{-1} (NO_2).

Anal. Calcd. for $C_{16}H_{20}N_2O_7$ (352.3): C, 54.54; H, 5.72; N, 7.95. Found: C, 54.39; H, 5.74; N, 7.80.

*Methyl 2-Acetamido-2,3-dideoxy-3-nitro-α-D-talopyranoside (**15**)*

Compound **14** (220 mg) was debenzylidenated with trifluoroacetic acid in the same manner as **5**. The product crystallized on trituration with ether to give 153 mg (93%) of **15**; m.p. 119–120°, raised to 120–121° by recrystallization from chloroform–ether; $[\alpha]_D$ +52.5° (*c* 0.6, water); ν_{max} 3400, 3200 (NH, OH), 1655, 1540 (amide I and II), 1540 cm^{-1} (NO_2).

Anal. Calcd. for $C_9H_{16}N_2O_7$ (264.2): C, 40.90; H, 6.10; N, 10.60. Found: C, 40.95; H, 5.94; N, 10.77.

*Methyl 2,3-Diacetamido-2,3-dideoxy-α-D-talopyranoside (**16**)*

A solution of **14** (400 mg) in methanol (40 ml) was hydrogenated in the presence of acetic anhydride (2.4 ml) with prereduced platinum oxide (400 mg) as the catalyst. Ordinary temperature and pressure was used. Hydrogen consumption ceased after 5 h and work-up then afforded a syrup that crystallized from ethanol–ether. The product was purified by passage over a small silica gel column using solvent D as the eluent, and subsequently recrystallized from ether. The yield was 289 mg (69%); m.p. 218–219°; $[\alpha]_D$ +11.8° (*c* 0.8, water).

Anal. Calcd. for $C_{11}H_{20}N_2O_6$ (276.3): C, 47.82; H, 7.30; N, 10.14. Found: C, 47.68, H, 7.29; N, 9.98.

*Hydrolysis of **16***

The glycoside **16** (150 mg) was refluxed with half-concentrated hydrochloric acid (15 ml) for 16 h. The dark brown solution was evaporated, and water was evaporated repeatedly from the residue in order to remove remnant acid. The dark syrup was then dissolved in water, and the solution was decolorized with acid-washed activated charcoal and evaporated to give a colorless, hygroscopic syrup that could not be crystallized. It reduced Fehling solution strongly, gave a ninhydrin positive spot ($R_{glucosamine\text{-}HCl}$ 0.86) in paper chromatography (23) and exhibited no methoxyl and acetyl signals in an n.m.r. spectrum in D_2O. One may, therefore, assume that complete hydrolysis of **16** to 2,3-diamino-2,3-dideoxy-D-talose dihydrochloride had taken place.

Can. J. Chem. Downloaded from www.nrcresearchpress.com by 210.87.254.6 on 09/05/12
For personal use only.

Part of the syrup (50 mg) was *N*-acetylated by the usual procedure (24); compare the preparation of **8**, above. The syrupy product was chromatographed on a column of silica gel (20 g) with chloroform–methanol (1:1). A material (35 mg) was eluted which was homogeneous on t.l.c. but failed to crystallize. It reduced Fehling solution, showed strong amide i.r. bands at 1650 and 1530 cm^{-1} (neat film), and exhibited 2 strong n.m.r. signals attributable to *N*-acetyl groups (60 MHz spectrum in D_2O).

*Methyl 2,3-Diacetamido-4,6-di-O-acetyl-2,3-dideoxy-α-D-talopyranoside (**17**)*

Compound **16** (100 mg) was acetylated with acetic anhydride (1 ml) and pyridine (4 ml) at room temperature. The reaction mixture was evaporated with added toluene and ethanol, and the syrupy product was passed over a small silica gel column by means of solvent E and then crystallized from benzene – petroleum ether. The yield was 99 mg (76%); m.p. 85–89°; $[\alpha]_D$ +107.5°. The n.m.r. spectrum revealed benzene of crystallization to be present in the sample, and the microanalysis was acceptable assuming this amounted to 0.5 mol/mol.

Anal. Calcd. for $C_{15}H_{24}N_2O_8 \cdot 0.5C_6H_6$ (399.4): C, 54.13; H, 6.81, N, 7.01. Found: C, 53.76; H, 7.09; N, 7.10.

*Methyl 2-Acetamido-6-O-acetyl-2,3,4-trideoxy-3-nitro-α-D-threo-hex-3-enopyranoside (**18**)*

*(a) From **15***

To a mixture of **15** (100 mg) and acetic anhydride (3 ml) was added boron trifluoride etherate (3 drops). The reaction mixture was kept at ambient temperature for 30 min and then poured into ice water whereby solid **18** separated. The product was isolated, washed well with cold water, and dried: yield, 93 mg (85%); m.p. 159–161°, raised to 162–163° by recrystallization from ethyl acetate – petroleum ether; $[\alpha]_D$ +82.5°.

Anal. Calcd. for $C_{11}H_{16}N_2O_7$ (288.3): C, 45.85; H, 5.59; N, 9.71. Found: C, 45.72; H, 5.64; N, 9.91.

*(b) From **7***

A solution of **7** (30 mg) in dry chloroform (10 ml) was refluxed for 1 h in the presence of 30 mg of silica gel (from a fresh supply, "for column chromatography", p*H* of aqueous slurry ~7–7.5). The filtered solution was evaporated to give a syrup which crystallized from ethyl acetate – petroleum ether, affording 15 mg of **18**, m.p. 162–163°. The i.r. and n.m.r. spectra of the products obtained from **7** and **15** were identical.

*Methyl 2-Acetamido-4,6-O-benzylidene-3-bromo-2,3-dideoxy-3-nitro-β-D-allopyranoside (**20**) and Methyl 2-O-Acetyl-4,6-O-benzylidene-3-bromo-3-deoxy-3-nitro-β-D-allopyranoside (**21**)*

A solution of 293 mg of the nitro olefin **19** (11*a*, 25) in acetone (20 ml) was mixed with a saturated, aqueous sodium acetate solution (15 ml) containing NBA (200 mg). The mixture was stirred at room temperature for 5 h, then diluted with water (20 ml), and partially evaporated to remove acetone. The white precipitate was washed with water and dried (393 mg). It contained two components that were readily separable on a silica gel column (20 g) with solvent A. The faster moving component (**21**) was isolated as crystals (102 mg, 24%), m.p. 224–225° after recrystallization from ethyl acetate – petroleum ether. An undepressed mixture m.p. and comparison of i.r. and n.m.r. spectra proved the identity of the product with previously prepared **21**, (lit. (1) m.p. 223–225°).

The slower fractions from the column yielded 237 mg (55%) of crystalline **20**. After recrystallization from ethyl acetate – petroleum ether it melted at 205–206° and showed $[\alpha]_D$ −70°; ν_{max} 3300 (NH), 1645, 1545 (amide I and II), 1560 cm^{-1} (NO_2).

Anal. Calcd. for $C_{16}H_{19}BrN_2O_7$ (431.3): C, 44.60; H, 4.44; H, 6.51; Br, 18.50. Found: C, 44.67; H, 4.56; N, 6.32; Br, 18.78.

*Methyl 2-Acetamido-4,6-O-benzylidene-2,3-dideoxy-3-nitro-β-D-glucopyranoside (**22**)*

Debromination of **20** (50 mg) using sodium borohydride (50 mg) in ethanol (10 ml) yielded, after 30 min at room temperature, the known glycoside **22** (36 mg, 88%); m.p. 309–311° as reported (11*b*). The i.r. and n.m.r. spectra were identical with those of an authentic sample.

*Methyl 4,6-O-Benzylidene-2,3-dideoxy-3-nitro-β-D-arabino-hexopyranoside (**23**)*

Reaction of **21** (100 mg) with sodium borohydride (50 mg) in ethanol (20 ml) for 1 h at room temperature afforded 65 mg (96%) of **23** melting at 144–146°, undepressed upon admixing an authentic sample (6, 11*a*). The i.r. spectrum of the product was identical with that of the sample.

*Methyl 2-Acetamido-4,6-O-benzylidene-3-bromo-2,3-dideoxy-3-nitro-β-D-gulopyranoside (**25**) and -β-D-galactopyranoside (**26**)*

To a solution of 293 mg of the nitro olefin **24** (25, 26) in acetone (20 ml) was added NBA (300 mg) and sodium acetate (10 mg) in water (5 ml). The reaction mixture was stirred overnight at room temperature. Two new, more slowly moving products were formed (t.l.c. with solvent A). Dilution of the mixture with water (30 ml) and evaporation of the acetone produced a white precipitate which was washed with cold water and dried (441 mg). Chromatography on silica gel (20 g) with solvent A effected separation of the two products, the faster moving one being **26** (196 mg, 45.5%) and the slower one, **25** (187 mg, 43.4%).

Recrystallized from ethanol, the β-D-*gulo* isomer **25** showed m.p. 190–191°; $[\alpha]_D$ −20.5° (*c*, 0.4 in dimethylformamide); ν_{max} 3320 (NH), 1670, 1525 (amide I and II), 1565 cm^{-1} (NO_2).

Anal. Calcd. for $C_{16}H_{19}BrN_2O_7$ (431.3): C, 44.60, H, 44.44; N, 6.51; Br, 18.50. Found: C, 44.43; H, 4.59; N, 6.36; Br, 18.38.

The β-D-*galacto* isomer **26** was recrystallized from ethyl acetate – petroleum ether; m.p. 188–189° decomp.; $[\alpha]_D$ +86.6° (*c*, 0.9 in chloroform); ν_{max} 3320 (NH), 1670, 1540 (amide I and II), 1570 cm^{-1} (NO_2).

Anal. Calcd. for $C_{16}H_{19}BrN_2O_7$ (431.3): C, 44.60, H, 4.44; N, 6.51; Br, 18.50. Found: C, 44.90; H, 4.62; N, 6.38; Br, 18.33.

*Methyl 2-Acetamido-4,6-O-benzylidene-2,3-dideoxy-3-nitro-β-D-galactopyranoside (**27**)*

Compounds **25** and **26** (64 mg each) were separately reduced in like manner, with sodium borohydride (50 mg) in ethanol (10 mg) in an ice bath. Processing of the reaction mixtures as described previously gave

crystalline products (51 and 50 mg, 97 and 95%) that were identical according to t.l.c., i.r. spectra (ν_{max} 3300, 1655, 1550–1545 cm^{-1}), decomposition points of 288–289° (after recrystallization from nitromethane), and $[\alpha]_D$ values of +34.5° and +36.7° (*c* 0.5, in dimethylformamide). The i.r. spectra were identical with that obtained from an authentic sample of **27** (12).

For *rebromination*, a solution of **27** (40 mg) in acetone (15 ml) was stirred for 10 min at room temperature with NBA (40 mg) and saturated aqueous sodium acetate solution (1 ml). Thin-layer chromatography with solvent A revealed complete disappearance of **27** and formation of a product having the same R_f value as **25**. Work-up of the reaction mixture and recrystallization of the crude product from ethanol furnished 39.5 mg (80.5%) of **25**, m.p. 188–191°, unchanged on admixture of **25** from **24**. The identity was confirmed by i.r. spectra.

Support of this work by the National Research Council of Canada is gratefully acknowledged. W.R. thanks the Province of Ontario for a Postgraduate Scholarship 1969–1971. We wish to express our appreciation for the excellent services continually obtained over the past 12 years from Mikroanalytisches Laboratorium F. Bernhardt, 5251 Elbach/Engelskirchen, West Germany.

1. H. H. BAER and W. RANK. Can. J. Chem. **51**, 2001 (1973).
2. W. RANK and H. H. BAER. Tetrahedron Lett. In press.
3. W. RANK and H. H. BAER. Carbohydr. Res. In press.
4. (*a*) H. H. BAER. Adv. Carbohydr. Chem. Biochem. **24**, 69 (1969); (*b*) H. H. BAER and J. KOVÁŘ. Can. J. Chem. **49**, 1940 (1971).
5. D. C. IFFLAND and G. X. CRINER. J. Am. Chem. Soc. **75**, 4047 (1953).
6. H. H. BAER and W. RANK. Can. J. Chem. **50**, 1292 (1972).
7. H. H. BAER and F. RAJABALEE. Carbohydr. Res. **12**, 241 (1970).
8. R. D. GUTHRIE and D. MURPHY. J. Chem. Soc. 6956 (1965).
9. H. H. BAER and W. RANK. Can. J. Chem. **49**, 3197 (1971).
10. H. H. BAER and C. W. CHIU. Can. J. Chem. **52**, 111 (1974).
11. H. H. BAER and T. NEILSON. (*a*) Can. J. Chem. **43**, 840 (1965); (*b*) J. Org. Chem. **32**, 1068 (1967).
12. H. H. BAER and K. S. ONG. J. Org. Chem. **34**, 560 (1969).
13. H. H. BAER and W. RANK. Can. J. Chem. **50**, 1216 (1972).
14. R. U. LEMIEUX, R. K. KULLNIG, H. J. BERNSTEIN, and W. G. SCHNEIDER. J. Am. Chem. Soc. **80**, 6098 (1958).
15. L. D. HALL. Adv. Carbohydr. Chem. **19**, 51 (1964).
16. D. HORTON, J. B. HUGHES, J. S. JEWELL, K. D. PHILIPS, and W. N. TURNER. J. Org. Chem. **32**, 1073 (1967).
17. F. W. LICHTENTHALER, G. BAMBACH, and P. EMIG. Chem. Ber. **102**, 994 (1969).
18. F. W. LICHTENTHALER and P. EMIG. Carbohydr. Res. **7**, 121 (1968).
19. A. HASEGAWA and H. Z. SABLE. J. Org. Chem. **33**, 1604 (1968).
20. H. H. BAER and F. KIENZLE. J. Org. Chem. **34**, 3848 (1969).
21. H. H. BAER, F. RAJABALEE, and F. KIENZLE. J. Org. Chem. **34**, 4204 (1969).
22. H. H. BAER and F. KIENZLE. Can. J. Chem. **45**, 983 (1967).
23. F. G. FISCHER and H. DÖRFEL. Z. Physiol. Chem. **301**, 224 (1955).
24. S. ROSEMAN and J. LUDOWIEG. J. Am. Chem. Soc. **76**, 301 (1954).
25. H. H. BAER. Methods Carbohydr. Chem. **6**, 302 (1972).
26. H. H. BAER, F. KIENZLE, and T. NEILSON. Can. J. Chem. **43**, 1829 (1965).

Can. J. Chem. Downloaded from www.nrcresearchpress.com by 210.87.254.6 on 09/05/12
For personal use only.

Virial Partitioning of Charge Distributions and Properties of Diatomic Hydrides; NaH↔HCl

R. F. W. BADER AND R. R. MESSER

Department of Chemistry, McMaster University, Hamilton, Ontario L8A 4M1

Received January 7, 1974

R. F. W. BADER and R. R. MESSER. Can. J. Chem. **52**, 2268 (1974).

The virial partitioning method is applied to the ground states of the AH diatomic hydrides (A = Na, Mg, Al, Si, P, S, Cl) in their neutral and charged forms. This is a spatial partitioning of a molecular system, the partitioning surfaces, which in this instance divide each molecule into an (A) and an (H) fragment, being determined by the topographical features of the electronic charge distribution. The kinetic and potential energies of the virial fragments are well-defined quantities and in addition, satisfy the quantum mechanical virial relationship. Most important, virial fragments faithfully reflect the chemistry of the individual elemental components of molecular systems, the fragments and their properties remaining nearly constant or changing when in different systems, in accordance with chemical expectations.

The populations of (H) in combination with (A) are used to order the first- and second-row elements (neutral and charged) in their abilities to abstract or donate charge relative to hydrogen. This ordering is of general interest as the population of (H) in AH changes little on passage to the general (most stable) polyatomic AH_n. The virial equations are used to relate the kinetic energy of binding in AH to the changes in the potential energies and total energies of each fragment. One finds, in comparison of first- and second-row results, that the nature of the most important stabilizing interactions in the formation of AH change in a similar manner across the two rows of elements, but the change in the second-row set occurs two members to the right with respect to the first-row set.

R. F. W. BADER et R. R. MESSER. Can. J. Chem. **52**, 2268 (1974).

On applique la méthode de partition virielle aux formes neutres et chargées des états fondamentaux des hydrures diatomiques AH (A = Na, Mg, Al, Si, P, S, Cl). C'est une partition spatiale d'un système moléculaire, la partition de surfaces, qui dans cette circonstance divise chaque molécule en un fragment (A) et un fragment (H), déterminés par les caractères topographiques de la distribution de la charge électronique. Les énergies cinétiques et potentielles des fragments viriels sont des quantités bien définies et de plus satisfont la mécanique quantique virielle. Plus important encore, les fragments viriels réflètent fidèlement la chimie des composants élémentaires individuels des systèmes moléculaires, les fragments et leurs propriétés restent presque constants ou changent avec les différents systèmes conformément aux prévisions chimiques.

On utilise les populations de (H) en combinaison avec (A) pour classer les éléments de la première et de la deuxième rangée (neutres et chargés) selon leur habilité par rapport à l'hydrogène d'arracher ou donner la charge. Ce classement est d'un intérêt général sachant que la population de (H) dans AH change peu lorsque l'on passe au produit polyatomique général (plus stable) AH_n. On utilise les équations virielles pour établir un rapport entre l'énergie cinétique de liaison dans AH et les changements dans les énergies potentielles et les énergies totales de chaque fragment. En comparant les résultats de la première et de la seconde rangée, on trouve que la nature des interactions de stabilisation les plus importantes dans la formation de AH change de façon similaire à travers les deux rangées d'éléments, mais le changement dans le groupe de la deuxième rangée a lieu sur deux membres à droite par rapport au groupe de la première rangée. [Traduit par le journal]

Introduction

We give here the results obtained through the application of the virial partitioning method to some properties of the second-row hydrides (NaH → HCl) in their ground and positively and negatively charged states. Particular attention is given to the partitioning of the total and binding energies of the ground state systems, the latter quantities being employed in a comparative study of the binding in the first- and second-row hydride systems.

The virial partitioning method (1, 2) divides the total (real) space of a molecular system into separate fragment volumes in a manner determined by the topographical features of the electronic charge distribution. A partitioning surface

Can. J. Chem. Downloaded from www.nrcresearchpress.com by 210.87.254.105 on 09/05/12
For personal use only.

Can. J. Chem. Downloaded from www.nrcresearchpress.com by 210.87.254.105 on 09/05/12
For personal use only.

separating adjacent fragments is defined by that collection of gradient paths traced out by the vectors $\nabla\rho(\boldsymbol{x})$, which pass through the null point $\nabla\rho(\boldsymbol{x}) = 0$ between a pair of adjacent nuclear centers and terminate at another null point, generally at infinity. In the present examples, an internuclear null point in $\nabla\rho(\boldsymbol{x})$ corresponds to a saddle point in the charge distribution. Such surfaces, termed zero-flux surfaces, are illustrated in Figs. 1 to 3 for various second-row AH systems. Since it is a property of the vector $\nabla\rho(\boldsymbol{x})$ that it be normal to contour lines of constant density, the surfaces are unique in that only one surface passes through a given internuclear null point. All gradient paths not passing through such a null point terminate at a nucleus (3).[1]

It has been demonstrated that a fragment bounded by a zero-flux surface $S(\boldsymbol{x})$, one satisfying the relationship

$$[1] \qquad d\rho(\boldsymbol{x})/d\boldsymbol{n} = 0, \quad \forall \boldsymbol{x} \in S(\boldsymbol{x})$$

(where $\boldsymbol{n}$ is the vector normal to $S(\boldsymbol{x})$ at each $\boldsymbol{x}$) has a well-defined kinetic energy. In addition, it has been demonstrated that the kinetic energy of such a fragment satisfies the virial relationship (1, 2).[2] That is, for a fragment (A)

$$[2] \qquad -2T(\mathrm{A}) = V'(\mathrm{A}) + V''(\mathrm{A}) + V_n(\mathrm{A})$$

where $T(\mathrm{A})$ is the kinetic energy of (A), $V'(\mathrm{A})$ is the attractive interaction of the charge density in (A) with all of the nuclei in the system, $V''(\mathrm{A})$ is the self-repulsion of the electrons in (A) and one-half of the repulsion of the electrons in (A) with all the remaining electrons in the system, and $V_n(\mathrm{A})$ is the nuclear virial of the fragment.

[1]For further details on the properties and determination of the partitioning surfaces see ref. 3.

[2]The proof that the virial relationship, eq. 2, holds for a fragment bounded by a zero-flux surface is numerical and confined to Hartree–Fock wave functions (as used in this study) (2). Recently, Mazziotti *et al.* (4) have provided a theoretical proof for the existence of a regional stationary principle and hence a regional virial theorem for a fragment of a molecular system. Their surface condition, also a zero-flux condition but more complicated than that stated in eq. 1, is derived for and stated in terms of the exact wave function. However, in the words of these authors, " ... in most cases the surfaces determined by it (their surface condition) should be similar to those determined by Bader's condition." In view of the excellent numerical accuracy obtained for eq. 2 using fragments defined by eq. 1, the exact surface requirements may reduce to or approximate even more closely those of eq. 1 when the exact wave function is approximated by a Hartree–Fock function.

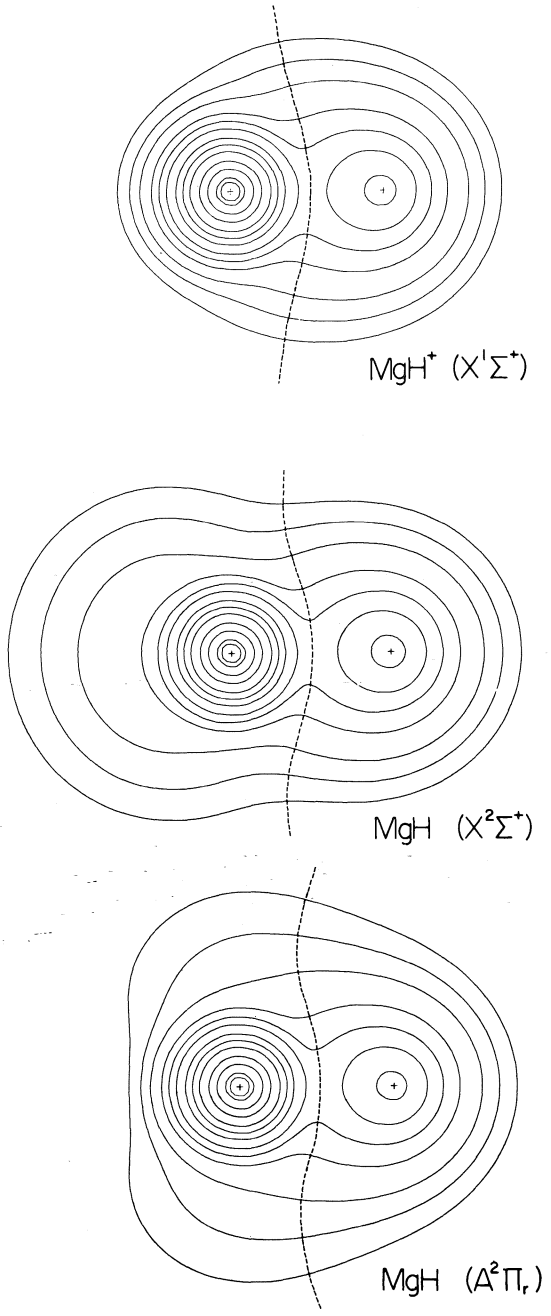

FIG. 1. Contour maps of the electronic charge distribution functions for states of the MgH system illustrating the three classes of hydride charge distributions: $MgH^+(X^1\Sigma^+)$ (Class I); $MgH(X^2\Sigma^+)$ (Class II); $MgH(A^2\Pi_r)$ (Class III). The contours in this figure and Figs. 2 and 3 (in a.u.) increase in value from the outermost contour inwards in steps of 2×10^n, 4×10^n, 8×10^n. The smallest contour value is 0.002 with n increasing in steps of unity to yield a maximum contour value of 20.

Can. J. Chem. Downloaded from www.nrcresearchpress.com by 210.87.254.105 on 09/05/12
For personal use only.

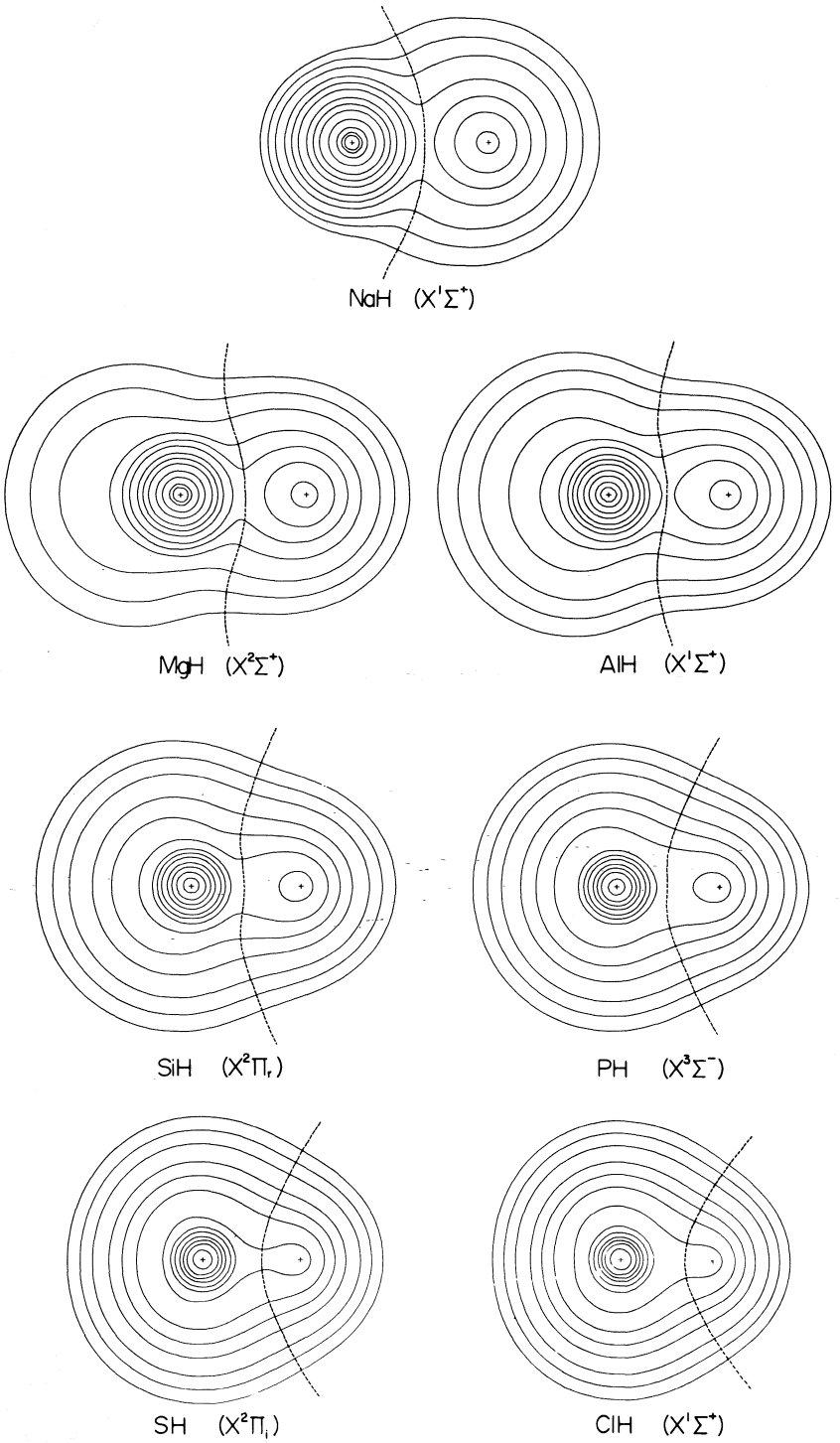

FIG. 2. Contour maps of the electronic charge distribution functions for neutral ground state hydrides. The virial partitioning surfaces are indicated by dashed lines.

Can. J. Chem. Downloaded from www.nrcresearchpress.com by 210.87.254.105 on 09/05/12
For personal use only.

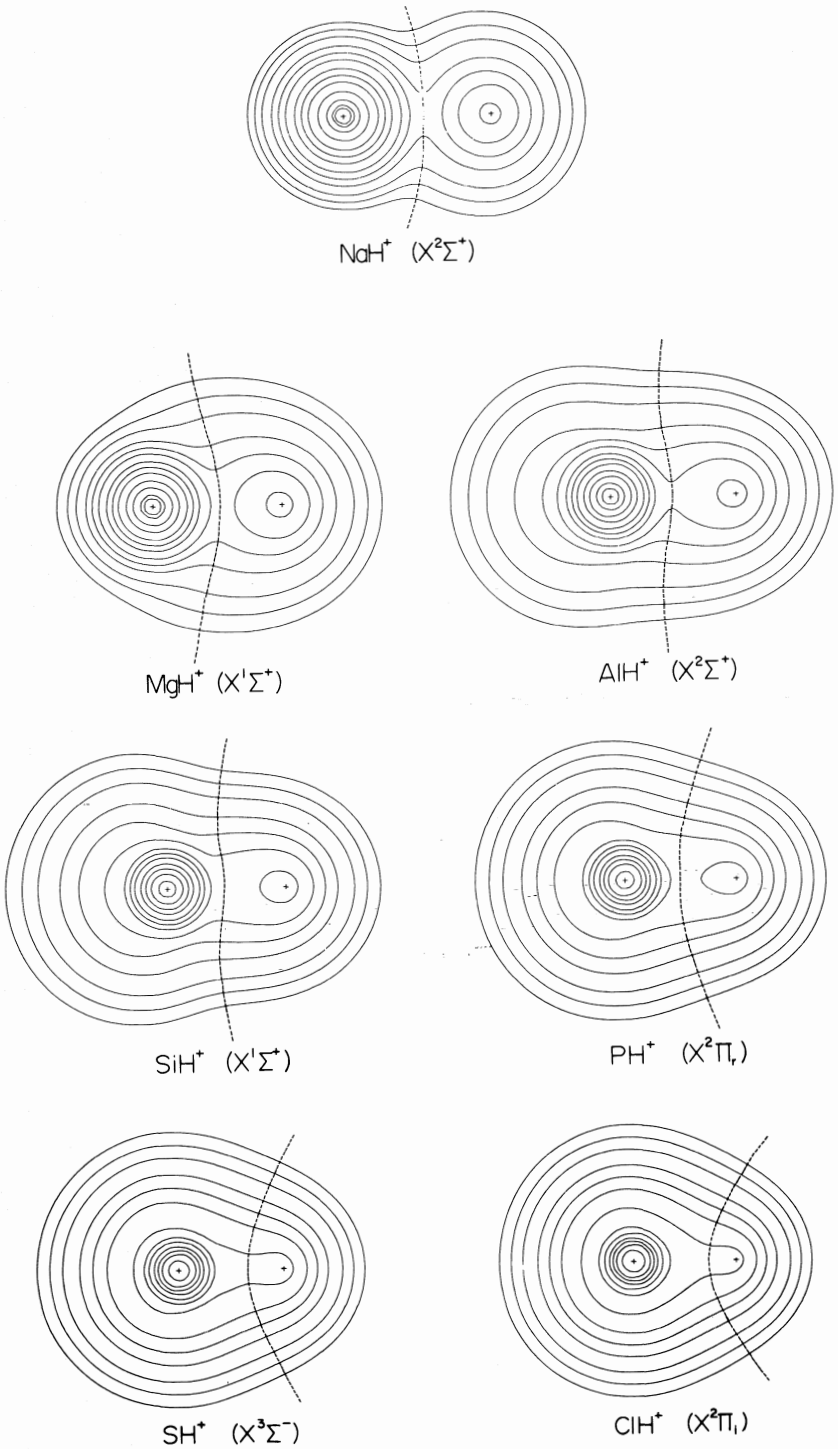

FIG. 3. Contour maps of the electronic charge distribution functions for the ground states of the positively charged second-row diatomic hydrides. The virial partitioning surfaces are indicated by dashed lines.

Can. J. Chem. Downloaded from www.nrcresearchpress.com by 210.87.254.105 on 09/05/12
For personal use only.

(Reference 5 provides a detailed summary of the contributions to the total virial of a fragment.)

The virial of the force on a particle is simply the quantum mechanical average of the dot product of the force and the position vector of the particle. The virials of the attractive forces exerted on the electrons by the nuclei and of the electron–electron repulsive forces, reduce to their corresponding potential energy contributions, V' and V''. A nucleus experiences repulsive forces exerted by the nuclei in the system and, if the molecule is not in an equilibrium geometry (energy minimum or maximum), an external force will be required to hold the nucleus in its position. The Hellmann–Feynman force exerted on a nucleus by the charge distribution is equal and opposite to the sum of the nuclear repulsive forces and the external force exerted on the same nucleus. Thus, minus the sum of the virials of the Hellmann–Feynman forces exerted on all the nuclei will equal the sum of the nuclear virials, a sum which in turn is equal to the total of the nuclear repulsive potential energies plus the virials of the external forces. *Thus, one may spatially partition the nuclear virials by spatially partitioning the forces exerted on the nuclei by the molecular charge distribution.* In a diatomic molecule, the nuclear virial of a fragment is minus the sum of the virials of the forces exerted on each of the nuclei by the charge density in the fragment (2, 5). When all the nuclei are in their equilibrium positions, the external forces vanish and the nuclear virial for the total system and for each fragment reduces to just the nuclear–nuclear repulsive contribution. In this case, the further virial relationship is

$$-T(\mathrm{A}) = E(\mathrm{A}) \qquad [3]$$

where

$$E(\mathrm{A}) = T(\mathrm{A}) + V'(\mathrm{A}) + V''(\mathrm{A}) + V_n(\mathrm{A})$$

is the total energy of the fragment (A). Thus, in the absence of external forces, one may partition the total energy of a system and assign an energy to each separate spatial region of a molecule which is bounded by a surface of zero-flux.

The physical significance of virial partitioning is based upon the following observations (1, 2). The extent to which the properties of a fragment of a molecular system are additive between different systems is determined by the extent to which the charge distribution of the fragment is unchanged between the systems. Since the virial partitioning method defines a fragment in terms of the topographical features of the charge distribution, it naturally accounts for the constancy of the properties of a fragment in different bonding environments in those cases where its charge distribution exhibits only small differences between two systems. Furthermore, as a consequence of the definition of the fragment boundaries, the differences between the charge distributions of a given fragment in different systems are minimized. *Thus, the virial partitioning method yields chemically identifiable fragments by maximizing the retention of the distribution of charge and hence of properties for each fragment between different systems.*

We have also found evidence that the charge distribution of a fragment is determined by the virial of all the forces exerted on it (1, 2). To the extent that the total virial of a fragment remains unchanged in two different systems, regardless of the changes in the individual force contributions to the virial, the charge density and the properties of the fragment remain unaltered. Since each fragment obeys the virial relationship, any change in its virial and the energetic consequences of the accompanying change in its charge distribution are quantitatively determined by the change in its kinetic energy.

To exemplify some of the above concepts we compare in Table 1 the electronic populations and kinetic energies of (H) fragments in a number of diatomic AH and polyatomic AH_n systems. Each entry gives the population N(H) and kinetic energy T(H) of the (H) fragment in AH and the change in these quantities when AH is changed to AH_n. The three-dimensional distribution of electronic charge in the (H) fragment is very similar in any of the AH–AH_n pairs of systems. This is evidenced by the small differences in their populations, a population being simply the integral of the charge distribution over the volume of the fragment. Correspondingly, the kinetic energies and hence total energies of the (H) fragments for a given pair of systems differ only by small amounts. These relatively small changes in $\rho(\boldsymbol{x})$, N(H), and T(H) are found in spite of large changes in the individual forces exerted on the (H) fragment as the system changes from AH to AH_n. For example, the change in the electron–nuclear attractive potential exerted on the (H) fragment in passage from BeH to BeH_2 is -228 kcal/mol. However, the sum of the changes in the electron–electron and nuclear repulsive contributions is of almost equal magnitude and opposite sign and hence the change in the total

TABLE 1. Comparison of charge and kinetic energies of (H) fragments* in AH and AH_n

Fragment	N(H) (e^-)	ΔN(H) (e^-)	T(H) = $-E$(H) (kcal/mol)	ΔT(H) (kcal/mol)
BeH–BeH_2	1.868	−0.007	484	−6
BH–BH_3	1.754	−0.042	557	−7
NH–NH_3	0.677	+0.041	310	+8
OH–H_2O	0.415	+0.022	230	+9

*N(H) and T(H) refer to populations and kinetic energies of (H) in AH. ΔN(H) and ΔT(H) are the differences between (H) in AH and an (H) fragment in AH_n, $\Delta N(H) = N(H)_{AH} - N(H)_{AH_n}$. E(H) for a free H atom is −314 kcal/mol.

virial of (H) is relatively small. In this way the virial definition of a fragment accounts for the fact that the properties of a hydrogen in BeH are similar to those in BeH_2.

We are not implying that the differences which do exist are not chemically important, they are. What we are saying is that we can quantitatively account for changes in properties and relate these changes to a change in the virial of a fragment and ultimately to the changes in the individual potential contributions which compose the virial. Perhaps most important of all, since the total virial of all the forces exerted on a fragment often changes by only small amounts, we can account for the observation that fragments or groups of fragments in molecular systems can have characteristic sets of properties which vary between relatively narrow limits.

While an (H) fragment bonded to a given A nucleus exhibits such a set of characteristic properties, it is also clear from the results in Table 1 that the properties of (H) are quite different for combination with different A. When bound to beryllium or boron, the (H) gains electronic charge and is more stable than an isolated H atom, while when bound to nitrogen or oxygen, the (H) loses electronic charge and is less stable.

A study of the changes in population and energy of (H) in combination with various (A) provides a quantitative probe of the relative bonding properties of (A). The charge distribution of (H) is a maleable one, and unlike a fluorine fragment for example, sensitive to changes in the virial of the external forces exerted on it. The populations and values of the electron–nuclear attractive interactions for (A) and (H) in AH parallel nicely one's chemical intuition and notions based on concepts such as electronegativity. Indeed the populations of (A) in combination with (H) may be used to predict the populations of (A) and (A′) in combination with each other (5). Thus, while the present study is restricted to the diatomic hydrides, much of the information so obtained will be of a general nature, applicable to polyatomic systems. From the nature of the data in Table 1, it is clear that the population of (H) in PH, for example, will provide a reasonable estimate of the net charge expected for (H) in PH_3. A parallel study has been given for the first-row diatomic hydrides (5). The results of that study are used here in an extensive inter-row comparison of properties.

The Charge Distributions

In earlier studies (6, 7) we have characterized and compared the general properties of the total charge distributions of first- and second-row diatomic hydrides and presented a discussion of the binding in these compounds in terms of the density difference distribution function $\Delta\rho(\boldsymbol{x})$,

$$\Delta\rho(\boldsymbol{x}) = \rho(\boldsymbol{x})[\text{molecule}] - \rho(\boldsymbol{x})[\text{atoms}]$$

and the forces exerted on the nuclei by the charge distribution. The results of these studies provide both parallel and alternative points of view to the more quantitative results obtained from the virial partitioning method. The nonbonded charge of a fragment, a concept introduced in the earlier studies (6, 7), is the electron population of the volume of space lying on the nonbonded side of a plane, drawn through the nucleus of the fragment, perpendicular to the internuclear axis. While the position and shape of this defining surface is somewhat arbitrary, the resulting population does refer to a well-defined spatial region, and as noted in the following discussion, to a region whose properties are sensitive to the type of binding in the system. An associated nonbonded radius was also defined as the distance along the molecular axis from the nucleus to the point where the nonbonded charge density has fallen to the value of 0.002 a.u. In general, the 0.002 a.u. contour defines a volume of space which envelopes 98 to 99% of the total electronic charge of the system,

Can. J. Chem. Downloaded from www.nrcresearchpress.com by 210.87.254.105 on 09/05/12
For personal use only.

Can. J. Chem. Downloaded from www.nrcresearchpress.com by 210.87.254.105 on 09/05/12
For personal use only.

and the molecular dimensions determined by this contour agree well with experimental values of van der Waals or nonbonded radii (8). Since the virial partitioning method yields a total population for each fragment (denoted by N(A) for a fragment (A)), the nonbonded population may be subtracted from the total population of a fragment, to yield a bonded population. Correspondingly, a bonded radius may be defined as the distance from the nucleus of the fragment to the null point ($\nabla\rho(\boldsymbol{x}) = 0$) on the internuclear axis. A classification of the charge distributions of AB (B $\neq$ H) molecules in terms of their bonded and nonbonded charges and associated radii has been previously given (9). In this earlier scheme, a molecule was partitioned by a *planar* surface through the internuclear null point. It was found that all diatomic charge distributions could be grouped into four classes, each class possessing a characteristic set of properties in terms of their bonded and nonbonded populations and associated radii. The same classification is found to hold for fragments defined by the surfaces of zero-flux, where now all members of a given class are found to possess a zero-flux surface of similar shape.

Figure 1 illustrates the three basic types of charge distributions which diatomic hydrides may possess, all illustrated for the MgH system.[3] The ground state of $MgH^+(^1\Sigma^+)$ is typical of charge distributions with a large extent of charge transfer from one fragment to the other (in this case A $\rightarrow$ H) and in which the number of valence electrons of the donor fragment is equal to or less than the number of vacancies in the acceptor. In such cases the (A) fragment approaches in terms of its bonded and nonbonded radii and charges the limiting tight "core" distribution of the A^+ or A^{2+} ion, and the zero-flux surfaces are paraboloid in shape, with arms which, in general, sweep back to encompass the electropositive fragment. Typical members of such Class I systems are NaH($X^1\Sigma^+$), LiH($X^1\Sigma^+$), LiF($X^1\Sigma^+$), BeO-($X^1\Sigma^+$).

In Class II systems, as typified by the ground state of $MgH(^2\Sigma^+)$, the number of valence electrons of the donor fragment (Mg) exceeds the number of vacancies in the acceptor fragment (H). In such systems, the remaining valence charge density of the donor fragment is strongly polarized into its nonbonded region in the form of a relatively diffuse distribution. The nonbonded population of the donor fragment exceeds its bonded population, and both the nonbonded population and its radius exceed those of the corresponding free atom values. The nonbonded population of (Mg) in MgH(X) is 5.93 indicating that over 90% of the unpaired valence charge density of magnesium is localized in the nonbonded region of the fragment. The transfer of charge from one fragment to the other in such Class II systems is reflected in the initial paraboloid nature of the zero-flux surface. However, the diffuse valence density remaining on (A) extends into the outer reaches of the internuclear region, causing a reversal in the curvature of the outer arms of the surface $S(\boldsymbol{x})$. A partitioning surface similar to that shown for MgH(X) (Fig. 1) is always found for systems with the above characteristics for the distribution on (A). It is the type of surface which defines fragments with chemically active unshared electrons; (C) of CO($X^1\Sigma^+$), (B) of BF($X^1\Sigma^+$), for example.

Class III systems exhibit the same general properties as do systems in Class II and differ only in that the diffuse valence density on (A) is present as an equatorial rather than as an axial distribution, as typified by MgH($A^2\Pi$) obtained from MgH($X^2\Sigma^+$) by a $\pi \leftarrow \sigma$-type transition. The generality of these Class definitions and the similarities which can exist between compounds of first- and second-row elements are illustrated by a comparison of the charge distributions of these three states of the MgH system with those for the corresponding states of the BeH system (Fig. 1 of ref. 5), and of the BeF system (Fig. 1 of ref. 2).

From the properties of the surfaces illustrated in Fig. 2 for the ground state molecules, NaH is a Class I system, with charge transfer from (A) $\rightarrow$ (H), and MgH, AlH, SiH, and PH are all in Class II, again with charge transfer (A) $\rightarrow$ (H). SH and ClH are Class I systems. SH is transitional with a small charge transfer (S) $\rightarrow$ (H). In HCl the charge transfer is (H) $\rightarrow$ (Cl). The net charge on each (A) fragment, defined as $C(\text{A}) = Z_\text{A} - N(\text{A})$ ($= -C(\text{H})$ for these neutral systems) is listed in Table 2. The sharp transition from Class I to II occurs at corresponding members of the first- and second-row hydrides, at BeH in the first-row and MgH in the second. The characteristics of

[3]All wave functions used in this and previous studies are close to the Hartree–Fock limit. The functions for AH are from ref. 10, for SH^- from ref. 11, and the remainder from ref. 13.

TABLE 2. Virial partitioning of ground-state dipole moment*

AH(X)	$C(A)$ $Z_A - N(A)$	μ(A)	μ(H)	μ(CT)	μ(AH)
LiH	+0.911	−0.001	+0.387	−2.747	−2.361
BeH	+0.868	+1.520	+0.571	−2.203	−0.112
BH	+0.754	+1.950	+0.493	−1.761	+0.682
CH	+0.032	+0.807	−0.121	−0.068	+0.618
NH	−0.323	+0.183	−0.176	+0.633	+0.640
OH	−0.585	−0.224	−0.148	+1.073	+0.701
FH	−0.760	−0.449	−0.104	+1.317	+0.764
NaH	+0.810	+0.017	+0.133	−2.890	−2.739
MgH	+0.796	+1.701	+0.302	−2.602	−0.599
AlH	+0.825	+2.274	+0.360	−2.568	+0.066
SiH	+0.795	+1.976	+0.428	−2.285	+0.119
PH	+0.579	+1.464	+0.317	−1.569	+0.212
SH	+0.094	+0.587	−0.009	−0.239	+0.339
ClH	−0.241	−0.006	−0.103	+0.581	+0.471

*A negative value for μ implies the direction A^+H^- for the dipole. The units are atomic units; 1 a.u. = 2.542 D.

Class II persist in both series of molecules (number of valence electrons on A > single vacancy on H) until the direction of charge transfer is reversed, to (H) → (A). This occurs at NH in the first-row and ClH in the second-row. In both series, the member immediately preceding this change, is transitional in its behavior. Thus, the extents of charge transfer in CH and SH are very small but still in the direction (A) → (H), $C(C) = +0.03$ and $C(S) = +0.09$. The partitioning surfaces, however, are typical of Class I and similar to the following members in each series with charge transfer (H) → (A).[4]

The transition from electron donor to electron acceptor relative to hydrogen occurs two elements to the right in the second-row as compared to the first-row. In addition, the transition in both rows of elements is marked by an element, carbon or sulfur, with electron acceptor ability only slightly less than that of hydrogen. In both these systems the disparity between the bonded and nonbonded populations on (A) drops in value reflecting a more even sharing of the valence charge density over the (A) and (H) fragments. In the earlier study of the second-row AH series (7), it was noted that the influence of the A nucleus and its KL (ten-electron) core was similar in its effect in determining the distribution of charge in AH to its first-row congener with its smaller K (two-electron) core one or two members to the left. The nearly spherical core distribution on A in AH and their decrease in size with increasing nuclear charge on A are very evident in Fig. 2. The above observations indicate that the greater shielding of the nuclear charge afforded by a KL core compared to that obtained from a K core is such that the effective field exerted on the valence charge density by a sulfur nucleus with sixteen positive charges is (approximately) comparable to the field exerted by the six positive charges of a carbon nucleus. Beyond a sphere of radius determined by the 0.001 a.u. contour of a core density (*i.e.*, a sphere containing in excess of 99.9% of the core electrons) the screening effect of the core density should be essentially 100% effective. Thus, beyond this sphere, the effective field of a sulfur nucleus and core is equivalent to +6 charges compared to +4 charges for a carbon nucleus and core. The field of the sulfur nucleus is, however, still only comparable to that of carbon nucleus because the size of the sulfur core (as determined by the 0.001 or 0.002 a.u. contour) is approximately 0.5 a.u. larger than the carbon K core.

In the first-row series, $C(A) \geqslant +0.75$ for LiH to BH and then exhibits a sharp drop at CH. In the second-row, $C(A) \geqslant +0.80$ from NaH to SiH,

[4]Since (H) has no core electrons, its behavior in Class I systems in which it is the electron donor differs from the general behavior given above. For example, when in combination with an extreme electron withdrawing fragment, F^+ or Ne^+, the charge density is so tightly bound to A that the internuclear null point $\nabla\rho(x) = 0$ vanishes and the volume of (H) reduces to zero. That is, FH^+ and NeH^+ are not partionable and the charge distributions of both systems approach those of the corresponding united atoms. Thus, when acting as an electropositive fragment, the (H) fragment vanishes in the extreme limit of charge transfer, while other (A) approach the limiting core distribution characteristic of A^+ or A^{2+}, etc.

Can. J. Chem. Downloaded from www.nrcresearchpress.com by 210.87.254.105 on 09/05/12
For personal use only.

TABLE 3. Virial partitioning of ground-state neutral and charged diatomic hydrides*†

AH		R	N(F)	V'(F)	V''(F)	V_n(F)	T(F)
NaH	$X^1\Sigma^+$	3.566	10.190	−390.4717	66.5279	0.2909	161.8264
			1.810	−6.7776	2.8440	2.7866	0.5736
MgH	$X^2\Sigma^+$	3.271	11.204	−479.2303	79.9716	0.2503	199.5042
			1.796	−8.0763	3.3567	3.4218	0.6489
AlH	$X^1\Sigma^+$	3.114	12.175	−578.7089	95.1105	0.1526	241.7229
			1.825	−9.4225	3.9193	4.0220	0.7406
SiH	$X^2\Pi$	2.874	13.205	−689.5592	112.0727	0.2301	288.6282
			1.795	−10.7479	4.4953	4.6458	0.8034
PH	$X^3\Sigma^-$	2.708	14.420	−813.6910	131.7975	0.9189	340.4873
			1.579	−10.7023	4.4956	4.6456	0.7805
SH	$X^2\Pi$	2.551	15.906	−952.7586	154.9379	2.9019	397.4594
			1.094	−7.9278	3.2990	3.3958	0.6165
ClH	$X^1\Sigma^+$	2.4087	17.241	−1103.9825	180.2272	4.5535	459.6009
			0.759	−5.9831	2.4757	2.5199	0.4938
NaH^+	$X^2\Sigma^+$	3.566	10.039	−389.6610	64.7799	1.4389	161.7211
			0.961	−3.9535	1.3349	1.5649	0.5269
MgH^+	$X^1\Sigma^+$	3.116	10.402	−476.0927	77.0505	0.4394	199.3014
			1.598	−7.6218	2.9969	3.4121	0.6064
AlH^+	$X^2\Sigma^+$	3.027	11.403	−575.0482	91.6669	0.3433	241.5190
			1.597	−8.7011	3.4123	3.9620	0.6634
SiH^+	$X^1\Sigma^+$	2.874	12.329	−684.7759	107.8545	0.1608	288.3803
			1.671	−10.3904	4.1108	4.7119	0.7839
PH^+	$X^2\Pi$	2.693	13.539	−808.1064	126.8109	0.9027	340.1964
			1.460	−10.2247	4.0580	4.6523	0.7572
SH^+	$X^3\Sigma^-$	2.551	15.125	−947.4796	149.5335	3.3639	397.2911
			0.875	−6.4111	2.5090	2.8504	0.5259
ClH^+	$X^2\Pi$	2.485	16.436	−1097.1989	173.6650	4.8695	459.3322
			0.564	−4.4042	1.6952	1.9201	0.3944
SiH^-	$X^3\Sigma^-$	2.861	14.088	−693.2491	115.5968	0.2561	288.6980
			1.912	−11.0848	4.8809	4.5990	0.8039
PH^-	$X^2\Pi$	2.668	15.282	−817.6832	135.8564	0.8394	340.4937
			1.717	−11.4154	5.0217	4.7538	0.8199
SH^-	$X^1\Sigma^+$	2.551	16.728	−957.1878	159.6998	2.5360	397.4760
			1.272	−9.0417	3.9616	3.7316	0.6743

*Increasing ability of $A^{+,0,-}$ to withdraw charge from (H), all C(H) > 0: $Li^+ < Na^+ < S^+ < N^- < Cl < C^+ < N < O^- < Cl^+ < O \sim N^+ < F < O^+ < F^+$. Increasing ability of $A^{+,0,-}$ to donate charge to (H), all C(H) < 0: $C < S < C^- < S^- < B^+ < P^+ < P < Al^+ \sim Mg^+ < Si^+ < P^- < B < Be^+ < Si \sim Mg < Na < Al < Be < Li < Si^-$.

†(F) denotes either an (A) or (H) fragment. The properties of (A) are listed above those for (H) in each system.

and shows a less dramatic drop through $C(P) = +0.6$ to a near zero-value at SH. The decrease in electronegativity associated with the increased core size is both exhibited and quantified by the C(A) values. In the second-row elements, only Cl acts as an acceptor of electronic charge in combination with H, and the extent of charge transfer is only about one-third as great as that found in HF. Note, however, that NaH and MgH are anomalous in that the net charges on (Na) and (Mg) are *less* than those found for (Li) and (Be).

The charge distributions of ground state AH^+ are illustrated in Fig. 3. Since (Na) in NaH approximates the tightly bound core of Na^+, approximately 85% of the charge lost on ionization of NaH comes from (H). (See Table 3 for N(A) and N(H) values for AH and AH^+.) In MgH and the remaining members, just the reverse situation is found. Ionization in these systems is confined largely to the loss of the diffuse (and loosely bound) nonbonded valence density on (A). Note that the ionization of MgH corresponds to a

Can. J. Chem. Downloaded from www.nrcresearchpress.com by 210.87.254.105 on 09/05/12
For personal use only.

Downloaded from www.nrcresearchpress.com by 210.87.254.105 on 09/05/12
For personal use only.

great reduction in extension of the density into the nonbonded region of (Mg) and the partitioning surface assumes a shape characteristic of Class I for MgH^+. Thus, the transition from Class I to Class II is shifted one place to the right in AH^+ compared to AH, as a result of the ionization of MgH being largely restricted to the removal of the single nonbonded electron on (Mg). Correspondingly, in the first-row series, BeH^+ possess a Class I distribution (5). The net charge on (H) remains negative in sign on ionization of any of the Class II systems. Ionization of the transitional member SH does, however, yield a net positive charge on (H) and SH^+ is a well-defined Class I system. Instead, the distribution for PH^+ is the transitional member for the change to Class II from I in the AH^+ series.

Since each ground state AH^+ dissociates into $A^+(X) + H(^2S)$, the populations of (H) in AH and AH^+ may be employed directly to compare the electron attracting ability of A with A^+ relative to hydrogen. Thus, Cl^+ is between N and O in its ability to withdraw electrons from (H) and S^+ is less effective in this regard than is neutral Cl. The negative ions considered here also dissociate to yield $H(^2S)$, or

$$H(^2S) + A^-(X) \rightarrow AH^-(X)$$

We have listed at the end of Table 3 the first- and second-row A^+, A, and A^- in a series, the order being determined by the population of (H) in combination with them. For convenience, the series is broken into two; the first denoting an increasing ability of $A^{+,0,-}$ to withdraw charge from (H) for the combinations in which $C(H) > 0$ and the second, the increasing ability of $A^{+,0,-}$ to donate charge to (H) for those combinations in which $C(H) < 0$.

The fragment contributions to the molecular dipole moments illustrate the same inter-row trends in the charge distributions of the two AH series. When a neutral diatomic system is partitioned into fragments, its dipole moment μ may be expressed as (9)

$$\mu(AH) = \mu_C + \mu(A) + \mu(H)$$

where the charge transfer contribution μ_C

$$\mu_C = C(H)\cdot R = -C(A)\cdot R$$

results from the transfer of charge from one fragment to the other and $\mu(A)$ and $\mu(H)$ are the fragment or "atomic" dipole contributions

$$\mu(A) = -\int_A z_A \rho(x) d\tau$$

$$\mu(H) = -\int_H z_H \rho(x) d\tau$$

Only in systems composed of nearly spherical fragment distributions, such that $\mu(A)$ and $\mu(B)$ approach zero, will the dipole moment approach the value anticipated on the basis of the charge transfer. As expected (see Table 2), the fragment dipole contributions are smallest for the (Li) and (Na) fragments in the Class I distributions, as these approach most nearly the tight core distributions of their corresponding ions. The more diffuse (H) fragments in LiH and NaH exhibit a significant polarization in a direction counter to the charge transfer component and hence even in these two systems the observed dipole moment does not reflect the total extent of charge transfer. The transition from the tight (A) distributions of Class I to the diffuse back-polarized (A) distributions of Class II is clearly marked by the dramatic increase in the fragment dipoles observed for the (Be) and (Mg) fragments, a phenomenon which persists in (B) of BH in the first-row and up to and including (P) of PH in the second-row series. In all the Class II systems, the observed dipole moment provides no indication of the extent of charge transfer A → H which is present in these systems. In BeH and MgH, μ is greatly reduced in value from μ_C and for the remainder of the Class II systems, μ is dominated by the fragment dipoles, yielding a moment whose direction is opposed to that generated by the charge transfer contribution. Clearly, in Class II systems, the extent or direction of the charge transfer cannot be inferred from a knowledge of μ alone. In the transitional cases CH and SH, the (A) fragment dipole moment is less than half of that for the preceding member and the (H) moments are reversed in sign. For the remaining members of both series, HCl and NH, OH and HF, all Class I systems, the dipole is again dominated by the charge transfer contribution.

Virial Partitioning of Binding Energies

Since each fragment of a system obeys the virial relationship during the entire course of a chemical reaction, the virial theorem may be applied separately to the energy changes experienced by each fragment yielding

$$[4] \quad -2\Delta T(A) = \Delta V'(A) + \Delta V''(A) + \Delta V_n(A)$$

Can. J. Chem. Downloaded from www.nrcresearchpress.com by 210.87.254.105 on 09/05/12
For personal use only.

TABLE 4. Changes in fragment energies on bond formation for ground state diatomic hydrides*†

AH(X)	$\Delta T(A) = -\Delta E(A)$ (kcal/mol)	$\Delta V_A'(A)$ (a.u.)	$\Delta V_H'(A)$ (a.u.)	$\Delta V''(A)$ (a.u.)	$\Delta V_n(A)$ (a.u.)	$\Delta T(H) = -\Delta E(H)$ (kcal/mol)	$\Delta V_H'(H)$ (a.u.)	$\Delta V_A'(H)$ (a.u.)	$\Delta V''(H)$ (a.u.)	$\Delta V_n(H)$ (a.u.)
NaH	−24.7	2.1003	−2.8517	0.5143	0.3157	+46.2	−0.4525	−5.3251	2.8440	2.7864
MgH	−66.9	3.1122	−3.3079	0.1570	0.2519	+93.5	−0.5377	−6.5386	3.3567	3.4218
AlH	−98.4	3.4868	−3.7131	0.3642	0.1757	+151.0	−0.6356	−7.7872	3.9196	4.0220
SiH	−139.0	4.1639	−4.3296	0.3669	0.2416	+190.4	−0.6626	−9.0853	4.4953	4.6458
PH	−129.3	3.5344	−5.0272	1.0192	0.8856	+176.1	−0.5782	−9.1241	4.4956	4.6455
SH	−12.3	0.1036	−5.9928	3.0590	2.8694	+73.1	−0.2812	−6.6466	3.2990	3.3958
ClH	+84.6	−2.6694	−6.9769	4.8487	4.5280	−3.9	−0.0207	−4.9624	2.4757	2.5198

*The atomic values used in the calculation of the differences Δ were obtained using the wave functions of Clementi (14).

†In general, LCAO-MO-SCF wave functions, even those close to the Hartree–Fock limit, do not exactly satisfy the Hellmann–Feynman and virial theorems (2). For the purposes of discussing energy changes the small errors in $\overline{V}_n$ (for the Hellmann–Feynman theorem) and in the relationship $\overline{T} = -\overline{E}$ (the virial theorem) have been removed by scaling the T values to satisfy the relationship $T = -E$ and the V_n values were then chosen to satisfy the virial relationship for each fragment.

Can. J. Chem. Downloaded from www.nrcresearchpress.com by 210.87.254.105 on 09/05/12
For personal use only.

For the particular case of partitioning the energy of bond formation, Δ will denote the value of a property for a fragment in the molecule minus its value in the free atomic state. Since each molecule is at its equilibrium separation, no external forces act on the nuclei and the further virial relationship

$$[5] \qquad \Delta T(\mathrm{A}) = -\Delta E(\mathrm{A})$$

will apply. Equation 5 is a statement of the well-known result that the change in energy for the passage of the system from one equilibrium state to another will be less than zero, *i.e.*, stabilizing, only if there is an *increase* of equal magnitude in the kinetic energy of the system. While the total kinetic energy must increase for the formation of a chemical bond, the change in kinetic energy for just a fragment of a system may be greater or less than zero. Thus, from the sign of $\Delta T(\mathrm{A})$ in eq. 5, one may determine whether a given fragment is stabilized or destabilized in the formation of the molecule. If $\Delta T(\mathrm{A}) > 0$, then $\Delta E(\mathrm{A}) < 0$, the fragment is increased in stability while if $\Delta T(\mathrm{A}) < 0$, $\Delta E(\mathrm{A}) > 0$, and the fragment is destabilized in the formation of the molecule. Equation 4 relates the change in $\Delta T(\mathrm{A})$ to the change in the virial of all the forces, attractive and repulsive, exerted on the fragment. Thus, through the use of eq. 4, one may relate the change in the stability of the fragment to the changes in the individual potential energy contributions. This approach has been previously applied to the charge redistributions and energy changes associated with the formation of the first-row hydrides (5), and to the corresponding changes associated with nucleophilic displacement reactions (12).

The attractive potential interaction of the charge density in fragment (A) with all of the nuclei in a system $V'(\mathrm{A})$ may be written as a sum over the separate nuclear contributions. In a diatomic system AH, for example

$$V'(\mathrm{A}) = V_{\mathrm{A}}'(\mathrm{A}) + V_{\mathrm{H}}'(\mathrm{A})$$

where $V_{\mathrm{A}}'(\mathrm{A})$ is the interaction of the A nucleus with the charge density in (A) and $V_{\mathrm{H}}'(\mathrm{A})$ is the corresponding contribution from the proton, external to (A). The change in $V'(\mathrm{A})$ on bond formation may be similarly summed,

$$\Delta V'(\mathrm{A}) = \Delta V_{\mathrm{A}}'(\mathrm{A}) + \Delta V_{\mathrm{H}}'(\mathrm{A})$$

where $\Delta V_{\mathrm{A}}'(\mathrm{A})$ measures the difference between the interaction of the A nucleus with the charge density in fragment (A) and in the free atom A. $\Delta V_{\mathrm{H}}'(\mathrm{A}) \equiv V_{\mathrm{H}}'(\mathrm{A})$ is the new interaction of the proton with the charge density in (A). In general, both the changes in electron–electron repulsion V'' and the nuclear repulsion V_n for a fragment are greater than zero on bond formation and hence the stabilization, if present, occurs because of a decrease in V'. The breakdown of $\Delta V'$ described above allows one to assign this increase in stability to the interactions of specific nuclei with particular localizations of charge within the system.

The electron–electron repulsion term $V''(\mathrm{A})$ can also be partitioned into intra- and interfragment contributions; $V_{\mathrm{A}}''(\mathrm{A})$ being the self-repulsion of the electrons in (A) and $V_{\mathrm{B}}''(\mathrm{A})$ being the repulsion of the electrons in (A) with those in (B). Such a partitioning of $V''(\mathrm{A})$ requires a six-dimensional integration of $\Gamma^{(2)}(x_1,x_2)$ bounded by the surface $S(\boldsymbol{x})$. While we have performed such integrations in a number of specific cases, they are, in general, too time-consuming (and hence too expensive) to determine in all cases.

The electron populations, the kinetic and potential energies of the (A) and (H) fragments in the ground states of AH, AH^+, and some AH^- are listed in Table 3. All these quantities are calculated from wave functions close to the Hartree–Fock limit, all from a common set of (optimized) basis functions and all of identical quality (10, 11). The populations of the fragments will probably differ by no more than a few one-hundredths of an electronic charge from those calculated using a fully correlated wave function. The Hartree–Fock energies contain a correlation error. A full discussion of the magnitude and trend of this error in the AH series is given by Cade and Huo (10). The partitioning of the energies as presented in Table 3 may be used to study any physical process involving these molecules at the Hartree–Fock level, *i.e.*, at a level which will indicate the principal trends in the behavior of the systems in this series.[5]

The necessary data for determining the charge and energy changes responsible for the binding in the second-row diatomic hydrides are given in Table 4. While the changes in the individual potential energy contributions for each fragment are relatively large (and reported in a.u.), the re-

[5]The Hartree–Fock calculated and experimental values of D_e (the latter in parentheses) in eV are: NaH, 0.932 (2.3); MgH, 1.15 (2.3); AlH, 2.36 (3.0); SiH, 2.23 (3.32); PH, 2.03 (3.3); SH, 2.63 (3.70); HCl, 3.48 (4.616). The values are from ref. 10.

Can. J. Chem. Downloaded from www.nrcresearchpress.com by 210.87.254.105 on 09/05/12
For personal use only.

sultant changes in the total and kinetic energies of each fragment are all of normal chemical magnitude, and are reported in kcal/mol. In the molecules, NaH ↔ SH, characterized by a transfer of charge from (A) → (H), one finds $\Delta T(A) < 0$ and $\Delta T(H) > 0$. In these systems, the (A) fragments are destabilized relative to the corresponding free A atoms and the binding arises from the charge transferred to and its subsequent stabilization in the (H) fragment. Both the destabilization of (A) and the stabilization of (H) are a maximum for SiH followed by a sharp drop in both effects at SH, the system exhibiting the smallest net charge transfer. Only in the case of HCl, where 0.24 e^- are transferred from (H) → (Cl) is the (A) fragment stabilized with respect to the A atom. The (H) fragment in HCl is only slightly increased in energy.

The pattern of the changes in stability of the second-row elements in formation of AH parallels those found for the first-row elements, with the transitional member again found two places to the right, at SH compared to CH. In the molecules in which there is a significant charge transfer (A) → (H), the systems NaH ↔ PH (or LiH ↔ BH in first-row), $\Delta V_A'(A)$ is large and greater than zero because of the reduced amount of charge density in (A). While the interaction of the proton with the remaining charge density on (A) in these systems is stabilizing, $\Delta V_H'(A) < 0$, the magnitude of this effect is too small to counteract the increases in $\Delta V_A'(A)$, $\Delta V''(A)$, and $\Delta V_n(A)$. Thus, the (A) fragments are destabilized by the transfer of charge from (A) → (H). Why is the charge transferred from (A) → (H) if the result is a destabilizing increase in $\Delta V_A'(A)$? A partial explanation is found in the surprisingly large negative values obtained for $\Delta V_A'(H)$, the interaction of the A nucleus with the charge density in (H). For the systems under discussion in both first- and second-row, *the interaction of the A nucleus with the charge density transferred to (H) is comparable to or greater than that obtained when the same density was centered on (A) in the atomic state*. This result is directly related to the loosely bound nature of the diffuse valence density on the elements Na to P (or Li to B) and makes understandable the considerable extent of charge transfer, (A) → (H), which persists up to and includes phosphorous. Consider AlH for example. The loss of 0.83 e^- from (Al) and the redistribution of the density remaining in this fragment, causes an increase in $V_A'(A)$ of 3.49 a.u. The interaction of the aluminum nucleus with the 1.83 e^- in (H) decreases the energy by −7.79 a.u. One may assign a fraction (0.83/1.83) of this decrease in energy to the interaction of the aluminum nucleus with the charge transferred from (Al) → (H). This yields a value of −3.53 a.u. as compared to the increase of 3.49 a.u. in $V_A'(A)$. The very large magnitude of the interaction of the A nucleus with the charge distribution on (H) is a result of the very pronounced polarization of the density in (H) towards (A). This interaction is the major source of stability in just those molecules LiH ↔ BH and NaH ↔ PH for which (H) possesses a large positive fragment dipole (see Table 2). In these systems, the increase in stability arising from this interaction is approximately twice as great as the increase in stability resulting from the interaction of the proton with the charge density of (A), and many times the magnitude of the only other stabilizing interaction, that of the proton with the charge density in (H).

The extent of charge transfer in CH, the transitional member of the first-row, is only 0.032 e^-, (C) → (H). The remarkable aspect of the binding in CH is the extent to which the energy changes for the two fragments approach the limiting case of the binding between two identical fragments, in spite of the great dissimilarities in their total populations. Thus, one finds that all of the changes in the potential interactions, changes resulting primarily from a redistribution of charge within each fragment are approximately the same for both fragments. Of these changes, the largest ones are the stabilizing interactions of each nucleus with the charge distribution of the other fragment, $\Delta V_H'(C) \sim \Delta V_C'(H)$.

Of the second-row set of molecules, SH approaches this behavior most closely. The charge transfer in SH is approximately three times that in CH and SH, while transitional in its binding, does not approach the limiting homopolar case as closely as does CH. Because of the small transfer of charge in SH, $\Delta V_A'(A)$ is only slightly positive, and much less in value than that for the preceding case, PH. For the same reason $\Delta V_H'(H)$ is smaller in magnitude than for PH. As in CH the principal stabilizing interactions are $\Delta V_A'(H)$ and $\Delta V_H'(A)$ and both are of the same order of magnitude, while in the preceding members $|\Delta V_A'(H)| \sim 2|\Delta V_H'(A)|$.

Since the transfer of charge from (A) → (H) is sharply decreased in SH compared to the preceding members, the polarization of the charge

Can. J. Chem. Downloaded from www.nrcresearchpress.com by 210.87.254.105 on 09/05/12
For personal use only.

distribution in the (S) fragment away from the proton is reduced (recall the trend in the μ(A) values). Consequently, the antibinding force exerted on the sulfur nucleus by the charge density in (S) is markedly decreased.[6] In SH, the increases in the nuclear–nuclear and electron–electron repulsive potentials are of the same order of magnitude for both (H) and (S), while in the preceding members, they were all much larger for (H) than for (A). This sudden break is directly determined by the sudden decrease in the extent of charge transfer and in the consequent polarizations which occur at SH.[7]

HCl is the only member of the second-row set for which the direction of charge transfer is (H) → (A), and the charge transferred, 0.24 e^-, is less than the 0.32 e^- transferred in NH, the corresponding member of the first-row set. In this case, as with NH, OH, and FH, the (A) fragment is stabilized and the (H) fragment destabilized, the latter to only a minor extent in HCl and NH, but increasingly so in OH and FH. The dominant interaction for all these molecules is the attraction of the proton for the charge density in (A). HCl is the first system in the second-row set for which this interaction exceeds $\Delta V_A'$(H), the attraction of the A nucleus for the density of (H). The interaction $\Delta V_A'$(H) continues to decrease in magnitude for OH and HF, while the magnitudes of $\Delta V_H'$(A) and $\Delta V_A'$(A) continue to increase as the extent of charge transfer (H) → (A) increase in the order HCl, HN, HO, HF.

In summary, there is an extensive transfer of charge from (A) → (H) in LiH, BeH, BH and in NaH, MgH, AlH, SiH, and PH. The largest single stabilizing interaction in all of these systems is the interaction of the A nucleus with the charge density of the (H) fragment. This interaction is maximized in BH in the first-row and in PH in the second-row. The net negative field exerted by the (H) fragment induces a pronounced polarization of the charge distribution of the (A) fragment. In LiH and NaH, in which the (A) fragments consist of tightly bound core distributions, this polarization is most pronounced in the regions close to the lithium and sodium nuclei.[8] In the remaining members, the polarization consists of a diffuse extension of the unshared valence density into the nonbonded region of the (A) fragment. As a result of this polarization and the antibinding force it exerts on the A nucleus, the contribution of the nuclear repulsive virial to the (A) fragment is small in value and the destabilization of the (A) fragments in these systems resulting from the transfer of charge to (H) is considerably lessened. Thus, in these systems V_n(H) > V_n(A) and V_n(H) attains its maximum value for the complete

[6]The force exerted on a nucleus by the charge density in the fragment containing that nucleus may be binding (*i.e.*, the direction of the force is towards the other nucleus) or antibinding (the direction of the force is away from the other nucleus). As explained in detail in ref. 5, a binding force on the nucleus in (A) gives a positive contribution to V_n(A) while an antibinding force gives a negative contribution to V_n(A). This is a very important point, as it explains how polarizations of the charge distribution into nonbonded regions are energetically not only feasible, but favorable. Polarization of charge density into a nonbonded (or antibinding) region of a fragment (A) necessarily reduces the magnitude of its interaction with a neighboring nucleus B, the interaction V_B'(A). The same polarization, however, yields a negative (stabilizing) contribution to V_n(A). Thus, the localization of charge density in nonbonded regions of space, an effect prevalent throughout almost all chemical systems with the exception of H_2 and H_2^+, is understandable as it leads to a local lowering of the energy via the nuclear virial contribution to the total energy field of the system.

[7]$\Delta V''$(A) is understandably small for all systems with charge transfer (A) → (H). However, it reaches a distinct minimum for the formation of BeH and MgH. A partitioning of $\Delta V''$ for both (A) and (H) into intra- and inter-fragment contributions for BeH yields the following values (in a.u.); $\Delta V_{Be}''$(Be) ≡ V_{Be}''(Be) − V''(Be atom) = −0.9417, $\Delta V_H''$(Be) ≡ $\Delta V_{Be}''$(H) = 0.9947, $\Delta V_H''$(H) = 0.5205. The *decrease* in the self-repulsion of the electrons on Be is particularly large because the loss of charge to (H) in this case (and for MgH) effectively separates the only valence pair present on the A atom. In addition, the subsequent polarization of the remaining valence electron into an extended nonbonded distribution reduces its repulsion with the core electrons on A. The decrease in $\Delta V_{Li}''$(Li) in the formation of LiH is only one-half as large as for (Be) ($\Delta V_{Li}''$(Li) = −0.4885) since the only contribution is a decrease in the valence-core electron repulsions. $\Delta V_A''$(A) increases in value for elements past Be and Mg presumably because the localization of the remaining pairs of valence electrons in the nonbonded region of (A) results in an increase in their self-repulsions.

[8]In referring to the polarization of a charge distribution, one must specify with respect to which operator the polarization is measured. For example, the (Li) fragment is very slightly polarized in the direction A → H in terms of the average value of z_{Li}, z_{Li} being the coordinate directed along the internuclear axis with origin at the Li nucleus. In terms of the electric field which the (Li) fragment distribution exerts on the Li nucleus, the average of z_{Li}/r_{Li}^2, the (Li) fragment is strongly polarized in the direction away from (H). Clearly, the electronic dipole moment operator z weights most heavily density relatively far removed from the origin (nucleus) while the electric field (the force operator) z/r^2 weights density in the immediate vicinity of the nucleus.

series at BH in the first-row and at PH in the second-row.

The transfer of charge (A) → (H) is sharply reduced at CH and SH to less than 0.1 e^-. The polarizations of the (C) and (S) fragments into their nonbonded regions are correspondingly reduced from that found for the preceding set. The result of these effects is that the individual potential energy changes, both stabilizing and destabilizing, are more nearly equal for the (A) and (H) fragments in both systems. In particular, the interaction of the proton with the charge density in (C) or (S) is as important as the interaction of the A nucleus with the charge density of (H) in the binding of these systems.

In HCl, NH, OH, and HF the charge transfer is (H) → (A), increasing in the indicated order. In these systems, the charge distributions of the (A) fragments are polarized towards the (H) fragments which bear a net positive charge. The nuclear repulsive virial is here greater for (A) than for (H). The dominant stabilizing interaction in all of these systems is the interaction of the proton with the charge density of (A) and in NH, OH, and HF, the interaction of the A nucleus with the same density becomes increasingly important. The (A) fragment is stabilized and the (H) fragment destabilized in these four molecules.

Thus, the largest single stabilizing interaction changes from $V_A'(H)$ in those systems characterized by charge transfer (A) → (H), to $V_A'(H)$ and $V_H'(A)$ being equally important in those systems with small charge transfer, to $V_H'(A)$ and $V_A'(A)$ in those systems in which charge is transferred from (H) → (A).

1. R. F. W. Bader and P. M. Beddall. J. Chem. Phys. **56**, 3320 (1972).
2. R. F. W. Bader, P. M. Beddall, and J. Peslak, Jr. J. Chem. Phys. **58**, 557 (1973).
3. G. Runtz. Ph.D. Thesis, McMaster University, Hamilton, Ontario. 1973.
4. A. Mazziotti, R. G. Parr, and G. Simons. J. Chem. Phys. **59**, 939 (1973).
5. R. F. W. Bader and P. M. Beddall. J. Am. Chem. Soc. **95**, 305 (1973).
6. R. F. W. Bader, I. Keaveny, and P. E. Cade. J. Chem. Phys. **47**, 3381 (1967).
7. P. E. Cade, R. F. W. Bader, W. H. Henneker, and I. Keaveny. J. Chem. Phys. **50**, 5313 (1969).
8. R. F. W. Bader, W. H. Henneker, and P. E. Cade. J. Chem. Phys. **46**, 3341 (1967).
9. R. F. W. Bader, P. M. Beddall, and P. E. Cade. J. Am. Chem. Soc. **93**, 3095 (1971).
10. P. E. Cade and W. M. Huo. J. Chem. Phys. **47**, 649 (1967).
11. P. E. Cade. J. Chem. Phys. **47**, 2390 (1967).
12. R. F. W. Bader, A. J. Duke, and R. R. Messer. J. Am. Chem. Soc. **95**, 7715 (1973).
13. P. E. Cade. Private communication.
14. E. Clementi. Tables of atomic functions. International Business Machines Corporation. 1965.

Can. J. Chem. Downloaded from www.nrcresearchpress.com by 210.87.254.105 on 09/05/12
For personal use only.

One Step Synthesis of Thietane 1,1-Dioxide Derivatives from α-Amino Ketoximes[1]

SHI-CHOW CHEN
Department of Chemistry, National Chung-Hsing University, Taichung, Taiwan
AND
YUAN L. CHOW
Department of Chemistry, Simon Fraser University, Burnaby 2, British Columbia

Received January 14, 1974

SHI-CHOW CHEN and YUAN L. CHOW. Can. J. Chem. **52**, 2283 (1974).

One step conversion of cyclic α-amino ketoximes to 2-(ω-cyanoalkyl)-2-dialkylaminothietane 1,1-dioxides was described. The n.m.r. studies of the thietane 1,1-dioxides, using a combination of $Eu(fod)_3$ shift reagent and decoupling technique, indicates the *trans* orientation of the substitution groups on the thietane ring.

SHI-CHOW CHEN et YUAN L. CHOW. Can. J. Chem. **52**, 2283 (1974).

On décrit une méthode permettant de transformer, en une étape, des cétoximes α-aminés cycliques en (ω-cyanoalkyl)-2 dialkylamino-2 thiétanne dioxyde-1,1. Des études par r.m.n. du thiétanne dioxyde-1,1, utilisant le réactif $Eu(fod)_3$ et des techniques de découplage, indiquent que les substituants de noyau thiétanne ont une relation *trans*. [Traduit par le journal]

Mechanistic aspects of the α-amino oxime ester cleavage reaction under basic conditions have been extensively studied by Grob and his coworkers (1) and other groups (2, 3). Electronically, the reaction is essentially a Beckman type reaction but is greatly facilitated by the participation of the electron pair of the amino group strategically located at the position α to the oxime group. The cleavage reaction when coupled with an efficient synthesis of α-amino oximes through nitrosamine photoaddition to a carbon–carbon double bond (4), constitutes an alternative method of double bond degradation. Application of the method to the cleavage reaction of a cyclic α-amino ketoxime, such as α-piperidinocyclohexanone oxime (**1**) obtained from a nitrosopiperidine photoaddition to cyclohexene, however, does not give the expected 4-cyanopentanal (**3**) in a synthetically useful yield due to the fact that the aldehyde undergoes secondary aldol condensations under the cleavage conditions (5). It is reasoned that if the intermediate enamine **2***b* can be intercepted *in situ* with a sulfene, it should be possible to obtain a more stable thietane derivative. This would also provide a new route to synthesis of thietane compounds. Generation of sulfenes from methanesulfonyl chloride and the analogs by a base treatment has been well established (6). Cycloaddition of a sulfene, generated *in situ*, to an enamine has been reported by various groups in recent years (*6d*, 7).

Results and Discussion

The required α-aminocyclohexanone oximes **1**, **5**, **6**, and **9** were prepared from our previous studies of nitrosamine photoaddition to appropriate olefins (4, 8). When a mixture of methanesulfonyl chloride and oxime **1** were allowed to react in anhydrous pyridine, 2-(3′-cyanopropyl)-3-piperidinothietane 1,1-dioxide (**4**) was isolated in 38% yield. The molecular formula of **4** was established by the mass spectrum and analysis and its functional groups indicated by the i.r. absorptions at 2250, 1300, 1140, and 1150 cm^{-1}. The thietane dioxide ring protons in the n.m.r. spectra were extensively coupled with each other and the pattern could not be clarified by decoupling experiments. However, their chemical shifts were consistent with those of published thietane dioxides (7). Under similar conditions, the corresponding thietane dioxides **7** and **8** were synthesized from *anti,cis*-3-piperidino-5-*tert*-butylcyclohexanone oxime (**5**)(4) and *anti,trans*-2-dimethylamino-*tert*-butylcyclohexanone oxime (**6**) (5). These thietane dioxides exhibited the expect-

[1]Taken in part from the Ph.D. Thesis submitted by S. C. Chen, Simon Fraser University, Burnaby 2, British Columbia, 1970.

Can. J. Chem. Downloaded from www.nrcresearchpress.com by 210.87.254.42 on 09/05/12
For personal use only.

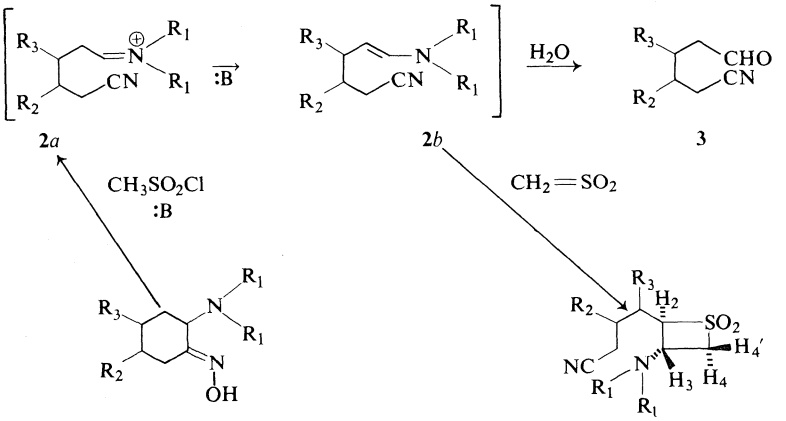

1 R = —$(CH_2)_5$—; $R_2 = R_3 = H$
5 R_1 = —$(CH_2)_5$—; $R_2 = (CH_3)_3C$—; $R_3 = H$
6 $R_1 = CH_3$—; $R_2 = H$; $R_3 = (CH_3)_3C$—

4 R_1 = —$(CH_2)_5$—; $R_2 = R_3 = H$
7 R_1 = —$(CH_2)_5$—; $R_2 = (CH_3)_3C$—; $R_3 = H$
8 $R_1 = CH_3$—; $R_2 = H$; $R_3 = (CH_3)_3C$—

SCHEME 1

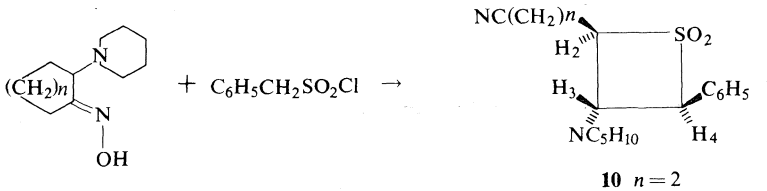

1 $n=2$
9 $n=1$

10 $n=2$
11 $n=1$

SCHEME 2

ed spectroscopic data that can be correlated to those of **4**.

It is obvious methanesulfonyl chloride serves dually to form the sulfonate of the oximes and to generate sulfene. The cleavage of the former gives the transient immonium salt **2***a* which is deprotonated by the base to give the necessary enamine **2***b*. Thus in one step thietanes **4**, **7**, and **8** are formed in reasonable yields (Scheme 1). The yield of thietanes were much higher (*ca.* 70%) when phenylmethanesulfonyl chloride was used as shown in the conversion of oximes **1** and **9** to **10** and **11** (Scheme 2). Obviously the facile phenysulfene generation (6*d*) caused the improved yield of **10** and **11**.

Whereas the stereochemistry of the thietane dioxide derivatives is related directly to that of the enamine it has remained unresolved in most of the known cases (6*d*). In the present study, an extensive application of n.m.r. decoupling studies has not been successful in unraveling the orientation of the thietane dioxide ring protons since the magnitudes of *cis* and *trans* proton–proton coupling constants are indistinguishable from each other; for example, J_{23} and J_{34} in **10** were shown to be 8–8.5 Hz (Table 1). Upon the reasonable assumption that the amino group coordinates most strongly with a lanthamide shift reagent[2] among other functional groups in the thietane dioxide derivatives (9, 10), $Eu(fod)_3$ can be utilized to induce differential n.m.r. shifts of the ring protons. This technique has been applied widely to determine the steroechemistry of various organic molecules (9) and recently of thietane derivatives (7*a*) with various success. On addition of incremental amounts of $Eu(fod)_3$ to a $CDCl_3$ solution of **10**, H_2, H_3, and H_4 were shifted downfield (Table 1). Clearly H_2 and H_4 must be oriented *cis* to the piperidine ring and exhibit much larger induced shifts, $\Delta\delta$, than H_3 does.

[2]$Eu(fod)_3$ is the abbreviation of tris(7,7-dimethyl-3,3,2,2,1,1,1-heptafluoro-4,6-octanedionato)europium-(III).

Can. J. Chem. Downloaded from www.nrcresearchpress.com by 210.87.254.42 on 09/05/12
For personal use only.

TABLE 1. Nuclear magnetic resonance parameters of thietane **10***

$Eu(fod)_3$ (mg)	Chemical shifts (τ)			Coupling constant†	
	H_2	H_3	H_4	$J_{23} + J_{34}$	J_{34}
0	5.74	6.94	4.76	8.0 + 9.0	8.5
20	5.54	6.82	4.58	8.5 + 8.5	8.5
40	4.99	6.45	4.13	8.5 + 8.5	8.5
60	4.43	6.04	3.64	7.5 + 8.8	8.2
80	3.91	5.66	3.19	7.8 + 8.5	8.5
100	3.44	5.32	2.78	7.5 + 8.8	8.2
Δδ‡	2.30	1.62	1.98		

*The spectra were recorded with a Varian XL-100 using $COCl_3$ solution containing the thietane (69 mg/ml) and internal TMS standard.
†J_{34} was obtained from the doublet of the H_4 signal and $J_{23} + J_{34}$ was the triplet spacings of the H_3 signal.
‡Cumulative induced shift.

This allowed us to conclude that **10** had an all-*trans* configuration of the substituents on the thietane dioxide ring. It should be added that the splitting patterns of the H_3 and H_4 signals were not visibly changed on complexation[3] with $Eu(fod)_3$ (Table 1), suggesting that the coupling constants of the thietane dioxide ring protons were not significantly altered in a $Eu(fod)_3$ complex.

The extensive overlapping of H_2, H_3, and H_4 protons in the n.m.r. spectrum of thietane dioxide **4** makes an interpretation of its spectrum impossible. Taking advantage of the above observations, this complex n.m.r. spectrum has been resolved by addition of $Eu(fod)_3$ to an interpretable one in which all the thietane ring protons are converted to first-order coupling patterns. On addition of 190 mg of $Eu(fod)_3$ (see the Experimental) H_2 and H_4 were shifted downfield by 2.15 and 1.77 p.p.m. while the corresponding shifts for H_3 and H_4' were shifted downfield by 1.35 and 1.45 p.p.m. This information was consistent with the *trans* orientation of the C_2-alkyl and C_3-piperidine groups as shown in **4**. Decoupling experiments carried out with the sample containing $Eu(fod)_3$ gave $J_{23} = 7.5$ Hz, $J_{34}(H) = 8.5$, and $J_{34}(H') = 7.5$ Hz. If these coupling constants also prevail for **4** in the absence of $Eu(fod)_3$ as suggested[3] by the finding in **10**, it may be concluded that spin–spin interactions for *cis*- and *trans*-protons in thietane dioxide rings are about the same magnitude and consequently, are unsuitable for elucidation of the ring stereochemistry.

[3]Proton coupling constants in nitrosamines appear to remain unchanged in their $Eu(fod)_3$ complexes (10).

In the present work the yields of the thietanes are nowhere near quantitative and the balance of the starting material has not been accounted for. However all the isolated thietane dioxides invariably possess the substituent groups on all thietane rings in the *trans* configuration. This suggests that the cycloaddition is a highly stereoselective process. Assuming a stepwise mechanism for this reaction, it is likely that during the ring formation process the bulky groups, such as piperidino, phenyl, and alkyl groups, stagger themselves around the ring to avoid undue steric crowding. The steric effects may account for the observed stereoselectivity.

Experimental

Nuclear magnetic resonance spectra were recorded in $CDCl_3$ with TMS as an internal standard with a Varian A-56/60 or a XL-100 spectrometer. The n.m.r. signals were reported as τ values and with coupling patterns expressed as m(multiplet), d(doublet), t(triplet), and q(quartet). Infrared spectra were taken neat or in Nujol mulls with a Perkin-Elmer 457 Grating Infrared Spectrophotometer, mass spectra with a Perkin-Elmer EMU-6E instrument. Melting points were determined in capillaries and were not corrected.

2-(3′-Cyanopropyl)-3-piperidinothietane 1,1-Dioxide (4)

Methanesulfonyl chloride (2.5 g, 22 mmol) was added dropwise during 1/2 h to a stirred solution of 2-piperidinocyclohexanone oxime (**1**) (846 mg, 4.3 mmol) in pyridine (10 ml) cooled in an ice bath. The reaction was maintained for additional 3 h. After decomposition with ice flakes the dark brown mixture was basified with sodium carbonate to p*H* 10 and extracted with chloroform (30 ml × 3). The chloroform extract was washed with water and dried (Na_2SO_4), and then concentrated to give a viscous liquid (864 mg) which was chromatographed over a silicic acid column (40 g). The first chloroform eluent (300 ml) gave a trace of an unidentified liquid. The second eluent (700 ml) from the same solvent gave a colorless gummy substance

Can. J. Chem. Downloaded from www.nrcresearchpress.com by 210.87.254.42 on 09/05/12
For personal use only.

(420 mg) which crystallized on treatment with ether. Recrystallization three times from ether afforded an analytical sample of **4** as fine needles, m.p. 79–80° (dec.); mass spectrum *m/e* (%) 256 (10), 202 (54), 178 (84), and 177 (100).

Anal. Calcd. for $C_{12}H_{20}N_2SO_2$: C, 56.23; H, 7.86; N, 10.90. Found: C, 56.13; H, 7.92; N, 10.62.

A $CDCl_3$ solution of **4** (80 mg/ml) exhibited the following n.m.r. signals: τ 5.86 (m, H_2), *ca.* 6.10 (m, H_4 and H_4'), 7.35 (m, H_3). On successive addition of $Eu(fod)_3$ to the solution these signals shift downfield; at 190 mg of $Eu(fod)_3$ content, it showed the signals at τ 3.71 (m, H_2), 4.25 (dd, J = 13 and 7.5 Hz, H_4'), 4.65 (dd, J = 13 and 8.5 Hz, H_4), and 6.03 (m, H_3). On irradiation at H_3, the τ 4.25 and 4.65 signals collapsed to a AB quartet and the τ 3.71 signal collapsed to a poorly resolved double doublet (J = 11 and 6 Hz). The H_2 proton signal (τ 3.71) was shown to be coupled with a pair of the magnetically nonequivalent protons at the τ 6.9 and 6.5 region which was assigned to the neighboring methylene protons.

2-(2′-tert-Butyl-3′-cyanopropyl)-3-piperidinothietane 1,1-Dioxide (7)

Oxime **5** (170 mg, 0.67 mmol) was allowed to react with methanesulfonyl chloride (0.5 ml, *ca.* 6.7 mmol) in pyridine (3 ml) according to the method described above. Chromatography gave an amorphous product (94 mg 43%) of **7**: i.r. 2245, 1315, 1140, and 1110 cm^{-1}; n.m.r. τ 5.75 (m, 1H), 6.05 (m, 2H), 7.15 (m, 1H), and 9.00 (s, 9H); mass spectrum *m/e* 312, 234.

2-(3′-Cyanopropyl-1′-tert-butyl propyl)-3-dimethylaminothietane 1,1-Dioxide (8)

Oxime **6** (220 mg, 0.94 mmol) was allowed to react with methanesulfonyl chloride (1 ml, *ca.* 13 mmol) in pyridine (4 ml) in the usual method as described above. Chromatographic purification gave adduct **8** (115 mg, 45%) as a colorless liquid: i.r. 2230, 313, 1130, and 1015 cm^{-1}; n.m.r. τ 5.83 (m, 1H), 6.10 (m, 2H), 7.20 (m, 1H), 7.75 (s, 6H), and 9.10 (s, 9H); mass spectrum *m/e* 272, 194.

2-(3′-Cyanopropyl)-3-piperidino-4-phenylthietane 1,1-Dioxide (10)

To a solution of oxime **1** (500 mg, 2.6 mmol) in pyridine (5 ml) cooled in ice bath, phenylmethanesulfonyl chloride (970 mg, 5.2 mmol) was added portionwise while the solution was stirred with a magnetic stirrer. The mixture was then stirred overnight at −10° and was worked up to give crude adduct **10** (600 mg, 71%). An analytical sample recrystallized from CCl_4 had m.p. 130–131° (dec.); i.r. (Nujol) 2255, 1620, 1490, 1290, 1150, and 1120 cm^{-1}; n.m.r. 2.60 (s, 5H), 4.76 (d, J = 8 Hz, H_4), 5.74 (m, H_2), and 6.94 (t, J = 8 and 8.5 Hz, H_3).

Anal. Calcd. for $C_{18}H_{24}N_2SO_2$: C, 65.02; H, 7.27; N, 8.42. Found: C, 64.88; H, 7.41; N, 8.20.

On irradiation of H_3, H_2 became an unresolved double doublet due to couplings with the magnetically nonequivalent methylene protons and H_4 became a narrow doublet (J = 1 Hz) due to the long range coupling with H_2. To a $CDCl_3$ solution of **10** (69 mg/ml) successive portions of $Eu(fod)_3$ were added and spectra recorded; the chemical shifts are summarised in Table 1.

2-(2′-Cyanoethyl)-3-piperidino-4-phenylthietane 1,1-Dioxide (11)

Oxime **9** (300 mg, 1.6 mmol) was allowed to react with phenylmethanesulfonyl chloride (628 mg, 3.2 mmol) in pyridine (2 ml) under the conditions similar to those described above. Adduct **11** (342 mg, 65%) was recrystallized from $CHCl_3$–CCl_4 as colorless crystals: m.p. 163–164° (dec.); i.r. 2250, 1600, 1490, 1300, 1140, and 1110 cm^{-1}; n.m.r. τ 2.60 (5H), 4.70 (d, J = 8 Hz, H_4), 5.70 (m, H_2), and 6.95 (t, J = 8 Hz, H_3); mass spectra *m/e* 318, 254, 164 (30%), and 124 (100%).

Anal. Calcd. for $C_{17}H_{22}N_2SO_2$: C, 64.12; H, 6.69; N, 8.79. Found: C, 64.20; H, 7.14; N, 8.48.

The authors are grateful to the National Research Council of Canada, Ottawa for financial support.

1. C. A. Grob, H. P. Fischer, and E. Renk. Helv. Chim. Acta, **46**, 1190 (1963).
2. M. Ohno, N. Naruse, S. Torimitsu, and I. Terasawa. J. Am. Chem. Soc. **88**, 3168 (1966).
3. K. Lunkwitz, W. Prizkow, and G. Schmidt. J. Prakt. Chem. **37**, 319 (1968).
4. Y. L. Chow, S. C. Chen, K. S. Pillay, and R. A. Perry. Can. J. Chem. **50**, 1051 (1972).
5. S. C. Chen. Ph.D. Dissertation, Simon Fraser University, British Columbia, 1970.
6. (*a*) T. J. Wallace. Quart. Rev. **20**, 67 (1966); (*b*) J. E. King and T. Durst. J. Am. Chem. Soc. **87**, 5686 (1965); (*c*) W. E. Truce and R. W. Campbell. J. Chem. Soc. **88**, 3599 (1966); (*d*) G. Opitz. Angew. Chem. Int. Ed. **6**, 107 (1967).
7. (*a*) C. T. Goralski and T. E. Evans. J. Org. Chem. **37**, 2080 (1972); (*b*) I. J. Borowitz. J. Am. Chem. Soc. **86**, 1146 (1964); (*c*) G. Opitz and H. Adolph. Angew. Chem. Int. Ed. **1**, 113 (1962).
8. Y. L. Chow. Acc. Chem. Res. **6**, 354 (1973).
9. (*a*) I. Armitage, G. Dunsmore, L. D. Hall, and A. G. Marshall. Can. J. Chem. **50**, 2119 (1972); (*b*) J. K. M. Saunders and D. H. Williams. J. Am. Chem. Soc. **93**, 641 (1971).
10. R. A. Perry and Y. L. Chow. Can. J. Chem. **52**, 315 (1974).

Can. J. Chem. Downloaded from www.nrcresearchpress.com by 210.87.254.42 on 09/05/12
For personal use only.

Excess Volumes, Ultrasonic Velocities, and Adiabatic Compressibilities for Binary Cycloalkanol Mixtures at 25 °C[1]

OSAMU KIYOHARA[2], JEAN-PIERRE E. GROLIER,[3] AND GEORGE C. BENSON
Division of Chemistry, National Research Council of Canada, Ottawa, Canada K1A 0R6

Received December 6, 1973

OSAMU KIYOHARA, JEAN-PIERRE E. GROLIER, and GEORGE C. BENSON. Can. J. Chem. **52**, 2287 (1974).

Molar excess volumes and ultrasonic velocities were determined for the systems cyclopentanol + cyclohexanol, cyclopentanol + cycloheptanol, and cyclohexanol + cycloheptanol at 25 °C. Values of the adiabatic compressibilities were calculated from the experimental results.

OSAMU KIYOHARA, JEAN-PIERRE E. GROLIER et GEORGE C. BENSON. Can. J. Chem. **52**, 2287 (1974).

Les volumes molaires d'excès et les célérités ultrasonores ont été déterminés pour les systèmes cyclopentanol + cyclohexanol, cyclopentanol + cycloheptanol et cyclohexanol + cycloheptanol à 25 °C. Les valeurs des compressibilités adiabatiques ont été calculées à partir des résultats expérimentaux.

Can. J. Chem. Downloaded from www.nrcresearchpress.com by 210.87.254.5 on 09/05/12
For personal use only.

Introduction

The thermodynamic properties of binary alcohol systems usually exhibit significant deviations from ideality. These arise not only from differences in molecular size but also from changes in hydrogen bonding. In some cases, varying cancellation between contributions differing in sign leads to complex forms for the excess thermodynamic functions.

Although many binary alcohol systems formed from normal and/or branched alcohols have been studied extensively, there do not appear to have been any previous studies of binary mixtures of cycloalkanols. In order to investigate the volume behavior of the latter, volumes of mixing and velocities of ultrasound propagation were measured for the three binary systems formed from the alcohols cyclopentanol (c-PeOH), cyclohexanol (c-HxOH), and cycloheptanol (c-HpOH) at 25 °C. From these data, accurate values of the adiabatic compressibility of the mixtures were derived. These values are of interest since it has been found for a number of systems that the variations of the excess adiabatic compressibility with composition are similar to those of the excess volume (1–3). Furthermore, it has been suggested that the excess adiabatic compressibility is approximately proportional to the strength of the interaction between unlike molecules in a mixture (3).

There is also a general requirement for compressibilities of mixtures, along with other basic thermodynamic data, in order to convert heat capacities and excess enthalpies measured at constant pressure to values at constant volume. The latter are usually more directly comparable to theoretical estimates.

Experimental

Component Liquids

Sources of the primary materials were as follows: cyclopentanol and cycloheptanol (purity 99%) from Aldrich Chemical Corp. Inc., cyclohexanol (laboratory reagent) from British Drug Houses Ltd. The cyclopentanol and cyclohexanol were purified chromatographically. A column (6 ft long and 0.75 in. o.d.) packed with Chromosorb W containing 25% Apiezon L was used for cyclopentanol. The same column followed by a second one (of similar size) packed with Chromosorb W containing 25% Carbowax 20M was used for cyclohexanol. The cycloheptanol was distilled and the fraction with boiling range 184–185 °C was collected. Densities of the cycloalkanols, measured at 25 °C with an Anton Paar densimeter (4) are given in Table 1. The error of the density values is estimated to be less than $\pm 5 \times 10^{-6}$ g cm^{-3}. Densities taken from the compilation by Timmermans (5) are included in Table 1 for comparison.

Measurements of Excess Volume

Values of the molar excess volume at constant pressure

---

[1]NRCC No. 13931.

[2]National Research Council of Canada Postdoctorate Fellow 1971–1973. Present address: Department of Chemistry, Université de Sherbrooke, Sherbrooke, Québec J1K 2R1.

[3]Visiting French Scientist 1972–1973, attached to C.N.R.S. (Paris) from the Université de Clermont-Ferrand, Clermont-Ferrand, France.

TABLE 1. Properties of pure components at 25 °C

Component	Density ρ (g cm^{-3}) Experimental	Density ρ (g cm^{-3}) Literature	Sound velocity u (m s^{-1}) Experimental	Sound velocity u (m s^{-1}) Literature	Adiabatic compressibility* κ_s (TPa^{-1})
c-PeOH	0.942965	0.94293 (5)	1435.03		514.97
c-HxOH	0.945363	0.94542 (5)	1464.53	1454.0 (13) 1462.0 (14) 1453.5 (15)	493.18
c-HpOH	0.954842		1511.86		458.19

*Calculated from experimental results for ρ and u.

and 25.00 ± 0.01 °C were determined dilatometrically using a successive dilution technique (6). During a run the temperature was controlled to ±0.001 °C. The error of results for equimolar mixtures is estimated to be less than ±0.0005 cm^3 mol^{-1}.

Measurements of Ultrasonic Velocity

Method and Equipment

Velocity measurements were made with r.f. pulses, using the pulse-echo-overlap method in a multiple echo mode. In this method, the velocity is determined by measuring the time interval between a pair of echoes of an ultrasonic wave. The echoes are converted to electrical pulses by a transducer, and are applied to the Y-axis of a cathode ray oscilloscope (c.r.o.). The X-axis of the c.r.o. is driven sinusoidally by a continuous wave (c.w.) generator with variable frequency (f_{cw}). When the echoes observed on the c.r.o. are overlapped, the delay time (t) between echoes is a simple multiple (m) of the reciprocal of the c.w. frequency (*i.e.* $t = m/f_{cw}$) and the sound velocity (u) is given by L/t, where L is the difference between the distances travelled by the echoes. A block diagram of our pulse-echo-overlap apparatus is shown in Fig. 1. Since the equipment is very similar to that described by Papadakis (7), only a brief outline is given here.

The c.w. frequency which is applied to the X-axis of the c.r.o. is also applied to a frequency divider which divides it by 100 or 1000. The reduced frequency activates a delayed pulser which triggers the pulsed r.f. generator. This excites the transducer (through the Hybridge circuit) at a repetition rate which is sufficiently low for the train of echoes in the sample to die out before the next burst is triggered. The same pulser also triggers the c.r.o. and two other delayed pulsers which are connected to the Z-terminal of the c.r.o. All of the pulsers are synchronized with the phase of the c.w. frequency. A network attached to the Hybridge balances the impedance of the transducer at the operating frequency. The Hybridge circuit couples the pulsed r.f. generator to the transducer and passes echo pulses to the c.r.o. The pulsers connected to the Z-terminal of the c.r.o. are adjusted to intensify the display of two selected echoes. The other pulser can be adjusted to center the display on the c.r.o. screen. When the echoes are overlapped correctly, the frequency of the c.w. generator is measured with the counter. Several overlaps are possible within the frequency range of the c.w. generator; these occur at integer multiples of the lowest possible overlap frequency.

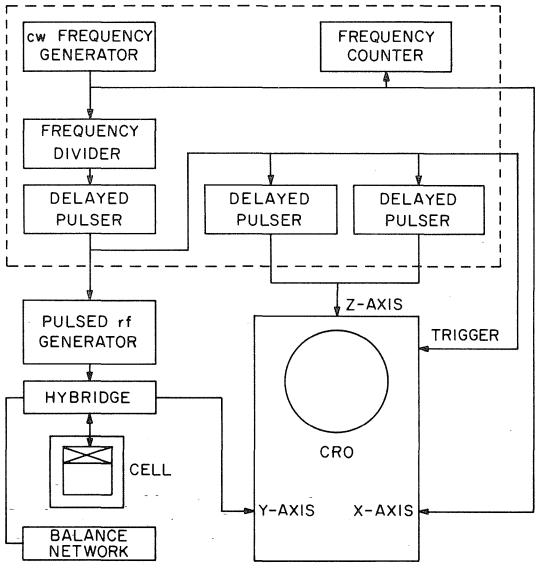

FIG. 1. Block diagram of pulse-echo-overlap apparatus. The units contained in the broken outline make up Panametrics Ultrasonic Time Intervalometer System 5054. The other units are as follows: Arenberg PG-650 pulsed r.f. generator; Alford 1236C Hybridge; Panametrics custom-built balance network; Tektronix 545A oscilloscope with Type L plug-in unit; cell with transducer (see Fig. 2).

Ultrasonic Cell

The cell, shown in Fig. 2, is cylindrical in shape (i.d. 1.8 cm) and made of brass. It has a double wall through which water from a thermostat (controlled to ±0.002 °C) is circulated. The temperature within the cell is monitored with a quartz digital thermometer. The cell is mounted at an angle to facilitate the injection of samples without any air space. A broadband transducer (diameter 1.4 cm) is held with O-ring seals at the lower end of the cell and the face of the transducer is gold plated to protect it from the organic solvents. All of our measurements were made with the r.f. generator operating at 2.11 MHz which is close to the resonant frequency of the transducer. The top end of the cell is closed by a plane brass reflector which can be removed to facilitate cleaning the cell. The cell was calibrated by measuring the difference between the

Can. J. Chem. Downloaded from www.nrcresearchpress.com by 210.87.254.5 on 09/05/12
For personal use only.

TABLE 2. Experimental values of the molar excess volume for binary cycloalkanol mixtures at 25 °C

c-PeOH + c-HxOH		c-PeOH + c-HpOH		c-HxOH + c-HpOH	
x_1	V^E (cm^3 mol^{-1})	x_1	V^E (cm^3 mol^{-1})	x_1	V^E (cm^3 mol^{-1})
0.0396	0.0062	0.0147	0.0008	0.0173	−0.0004
0.0651	0.0105	0.0365	0.0015	0.0216	−0.0006
0.0961	0.0148	0.0678	0.0017	0.0463	−0.0012
0.1417	0.0196	0.1030	0.0015	0.0554	−0.0014
0.1896	0.0247	0.1485	0.0008	0.0882	−0.0024
0.2446	0.0284	0.2002	−0.0003	0.1105	−0.0031
0.2941	0.0314	0.2568	−0.0027	0.1336	−0.0038
0.3473	0.0333	0.3167	−0.0056	0.1798	−0.0054
0.4005	0.0345	0.3752	−0.0084	0.1897	−0.0058
0.4492	0.0349	0.4273	−0.0109	0.2471	−0.0079
0.4931	0.0346	0.4757	−0.0126	0.2493	−0.0080
0.5301	0.0341	0.5186	−0.0139	0.3045	−0.0103
0.5336	0.0342	0.5583	−0.0148	0.3209	−0.0107
0.5736	0.0331	0.5871	−0.0155	0.3602	−0.0120
0.6163	0.0320	0.5945	−0.0156	0.4134	−0.0133
0.6609	0.0304	0.6261	−0.0162	0.4456	−0.0139
0.7081	0.0280	0.6673	−0.0166	0.4978	−0.0145
0.7558	0.0252	0.7081	−0.0164	0.5386	−0.0147
0.8044	0.0213	0.7489	−0.0159	0.5434	−0.0147
0.8467	0.0180	0.7828	−0.0147	0.5685	−0.0147
0.8874	0.0142	0.8236	−0.0130	0.5926	−0.0146
0.9228	0.0100	0.8612	−0.0112	0.5968	−0.0145
0.9546	0.0062	0.8958	−0.0089	0.6249	−0.0144
0.9769	0.0035	0.9276	−0.0063	0.6471	−0.0140
0.9921	0.0015	0.9572	−0.0034	0.6498	−0.0139
		0.9782	−0.0013	0.7173	−0.0126
		0.9911	−0.0003	0.7844	−0.0105
				0.8527	−0.0079
				0.9174	−0.0047
				0.9378	−0.0040
				0.9675	−0.0023
				0.9717	−0.0018
				0.9877	−0.0006

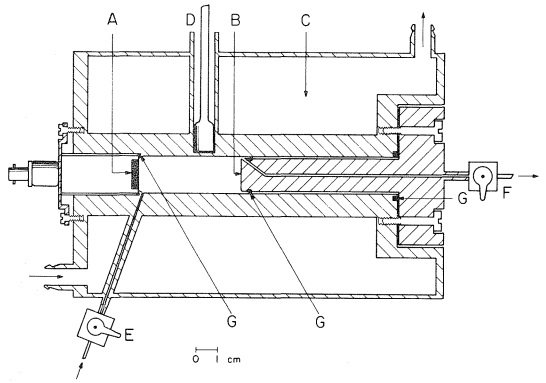

FIG. 2. Schematic drawing of the ultrasonic cell. A, Panametrics Type 5070 VIP transducer; B, fixed reflector unit; C, double-walled jacket; D, Hewlett Packard 2801A quartz thermometer; E, inlet valve; F, outlet valve; G, O-ring.

travel times for the first and second echoes in triply distilled, partially degassed water at 25.00 ± 0.01 °C. Calculation of the distance between the transducer and the reflector was based on the value of the velocity for pure water reported by Del Grosso and Mader (8) (1496.687 m s^{-1} at 25 °C).

Measurements in Mixtures

Binary mixtures of the cycloalkanols were prepared by weight and corrections were applied for the effect of buoyancy. The mole fractions are estimated to be accurate to better than 1 × 10^{-3} mol%. Velocities of ultrasound in the mixtures were measured at 25.00 ± 0.01 °C. The results were reproducible to less than 0.07 m s^{-1}, but their absolute error may be about ten times greater due to uncertainties in the mode of sound propagation within the cell. The occurrence of multi-mode guided wave propagation is possible since, in order to keep the volume of the cell small, the diameter of the cylinder is only a little larger than the diameter of the transducer. Some idea of the magnitude of the error due to guided waves can be obtained from the work of Lastovka and Carome

Can. J. Chem. Downloaded from www.nrcresearchpress.com by 210.87.254.5 on 09/05/12
For personal use only.

TABLE 3. Coefficients and standard errors for least squares representations of V^E, Δu, and κ_s^E

System	Function	a_1	a_2	a_3	σ
c-PeOH + c-HxOH	V^E (cm^3 mol^{-1})	0.13855	0.01792	0.02496	0.00022
	Δu (m s^{-1})	8.097	−0.585	−2.467	0.056
	κ_s^E (TPa^{-1})	−2.556	0.376	1.830	0.039
c-PeOH + c-HpOH	V^E (cm^3 mol^{-1})	−0.05375	0.06986	0.02397	0.00033
	Δu (m s^{-1})	30.775	−0.776	−0.353	0.033
	κ_s^E (TPa^{-1})	−11.441	1.006	0.189	0.022
c-HxOH + c-HpOH	V^E (cm^3 mol^{-1})	−0.05778	0.01934	0.01799	0.00018
	Δu (m s^{-1})	4.157	0.036	−0.541	0.029
	κ_s^E (TPa^{-1})	−1.029	0.057	0.424	0.019

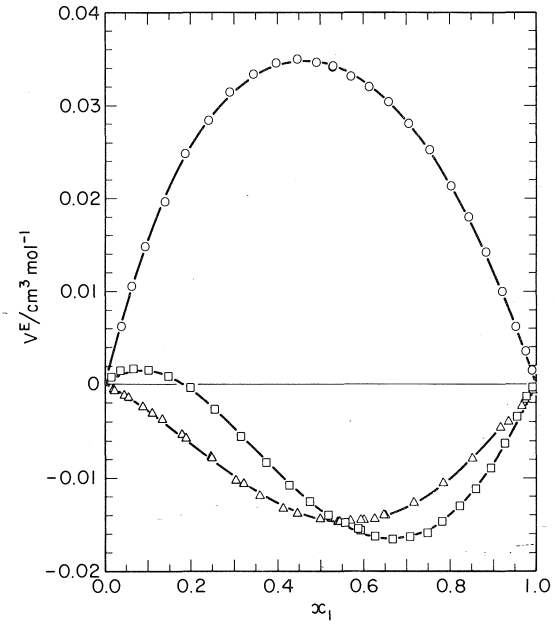

FIG. 3. Molar excess volumes at 25 °C. Experimental results: ○, c-PeOH + c-HxOH; □, c-PeOH + c-HpOH; △, c-HxOH + c-HpOH. Curves are least squares fits using coefficients from Table 3.

(9), who found that the velocity of sound in water was lower than the free-field value by about 2.5 m s^{-1} when determined with ultrasonic pulses at 2 MHz in a cylindrical wave guide with inner diameter equal to that of the transducer. Since it is difficult to estimate accurately the effect of interference of guided waves in our cell, no explicit corrections were applied. The procedure of calibrating the cell with water allows empirically for guided-mode propagation. Although this allowance is not exact, it should provide good relative values of the velocities over the restricted range encountered in the present mixtures. We believe that ±1 m s^{-1} is a reasonable estimate of the absolute accuracy of the velocities.

Results and Discussion

Excess Volumes

Values of the molar excess volume, V^E, measured for the three binary systems cyclopentanol(1) + cyclohexanol(2), cyclopentanol(1) + cycloheptanol(2), and cyclohexanol(1) + cycloheptanol(2) at 25 °C, are listed in Table 2. In all cases, x_1 is the mole fraction of the component with the lower molecular weight. The results are also presented graphically in Fig. 3. The method of least squares was used to fit the empirical form

$$[1] \quad V^E = x_1(1 - x_1) \sum_{p=1}^{n} a_p(1 - 2x_1)^{p-1}$$

to each set of results. For each system the optimum number of coefficients was ascertained from an examination of the variation with n, of the standard error of estimate

$$[2] \quad \sigma_v = [\Sigma(V_{obs}^E - V_{calcd})^2/(n_{obs} - n)]^{1/2}$$

where the sum is taken over the n_{obs} results. The values obtained for the coefficients a_p are given in Table 3 along with the standard error for each representation. The curves in Fig. 3 were calculated from eq. 1 using these values of the coefficients.

The excess volumes for the present cycloalkanol systems differ in two respects from those observed previously for binary *n*-alkanol systems (6, 10). The latter usually correspond to expansions when mixtures are formed at 25 °C and the values of V^E increase with increasing difference between the numbers of carbon atoms in the component molecules. Qualitatively, the V^E results for the cycloalkanol systems are more similar to those for the corresponding binary cycloalkane systems (11, 12). Thus it appears that the main contribution to V^E arises from the difference in the cyclic groups and that contributions associated with changes in hydrogen bonds are relatively less important.

Ultrasonic Velocities

Ultrasonic velocities, u, measured for the pure

Can. J. Chem. Downloaded from www.nrcresearchpress.com by 210.87.254.5 on 09/05/12
For personal use only.

Can. J. Chem. Downloaded from www.nrcresearchpress.com by 210.87.254.5 on 09/05/12
For personal use only.

TABLE 4. Ultrasonic velocities, densities, and adiabatic compressibilities for binary cycloalkanol mixtures at 25 °C

x_1	u (m s^{-1})	ρ (g cm^{-3})	κ_s (TPa^{-1})	κ_s^E (TPa^{-1})
c-PeOH + c-HxOH				
0.09998	1462.05	0.945016	495.04	−0.05
0.20888	1459.53	0.944680	496.92	−0.30
0.28158	1457.80	0.944474	498.21	−0.47
0.40239	1454.53	0.944158	500.62	−0.56
0.50176	1451.69	0.943917	502.71	−0.59
0.55464	1450.18	0.943795	503.82	−0.64
0.55870	1450.05	0.943786	503.92	−0.63
0.60052	1448.75	0.943693	504.87	−0.61
0.70297	1445.48	0.943475	507.28	−0.53
0.74732	1443.99	0.943386	508.37	−0.46
0.80436	1442.05	0.943277	509.80	−0.38
0.81963	1441.39	0.943249	510.28	−0.26
0.88597	1439.06	0.943133	512.00	−0.14
c-PeOH + c-HpOH				
0.06556	1508.63	0.954225	460.45	−0.63
0.11492	1506.07	0.953758	462.24	−1.07
0.20604	1500.99	0.952883	465.81	−1.78
0.31054	1494.53	0.951846	470.35	−2.37
0.38669	1489.40	0.951058	473.99	−2.66
0.44263	1485.43	0.950457	476.83	−2.80
0.51665	1479.81	0.949630	480.88	−2.83
0.55378	1476.93	0.949200	482.97	−2.85
0.61699	1471.76	0.948441	486.76	−2.75
0.70004	1464.63	0.947389	492.06	−2.50
0.78093	1457.23	0.946297	497.64	−2.08
0.88859	1446.64	0.944732	505.79	−1.17
0.94308	1441.03	0.943888	510.19	−0.62
c-HxOH + c-HpOH				
0.09737	1507.61	0.954037	461.16	−0.08
0.20387	1502.85	0.953142	464.53	−0.13
0.25823	1500.40	0.952677	466.27	−0.16
0.29760	1498.60	0.952336	467.56	−0.18
0.40435	1493.77	0.951389	471.06	−0.27
0.50250	1489.12	0.950487	474.46	−0.26
0.56792	1485.97	0.949868	476.78	−0.24
0.59103	1484.88	0.949645	477.59	−0.24
0.68898	1480.12	0.948678	481.16	−0.21
0.78217	1475.56	0.947723	484.62	−0.19
0.83664	1472.76	0.947150	486.76	−0.10
0.88362	1470.43	0.946646	488.57	−0.08

cycloalkanols at 25 °C are given in Table 1, along with values for cyclohexanol from the literature (13–15). Acoustic relaxation absorption, attributed to polar-equatorial type rotational isomers, has been reported for cyclohexanol at 0.12 MHz (16). Under the present operational conditions, no difficulty was encountered in observing first and second echoes in all of the cycloalkanols and their mixtures and it is assumed that the value of the sound velocity at 2.11 MHz is a good approximation to the equilibrium thermodynamic (low frequency) value.

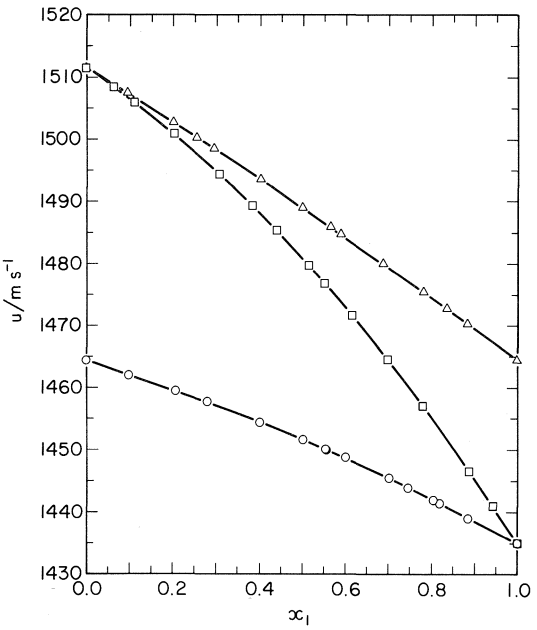

FIG. 4. Ultrasonic velocities at 25 °C. Experimental results: ○, c-PeOH + c-HxOH; □, c-PeOH + c-HpOH; △, c-HxOH + c-HpOH. Curves are least squares fits using eq. 3 and coefficients from Table 3.

Results for the binary mixtures are summarized in Table 4 and the velocities are plotted in Fig. 4 as a function of the mole fraction of component 1. The deviation of the ultrasonic velocity for a mixture, from additivity on a mole fraction basis is

$$[3] \qquad \Delta u = u - \sum x_i u_i^0$$

where u_i^0 is the ultrasonic velocity for pure component i. Values of Δu were fitted with a polynomial expression similar to eq. 1. The coefficients and standard errors for these representations are listed in Table 3. The values of Δu are positive for the 3 systems and, for equimolar mixtures, decrease in the order c-PeOH + c-HpOH, c-PeOH + c-HxOH, and c-HxOH + c-HpOH. Most of the binary alcohol systems which have been studied previously also exhibit positive deviations; these systems include mixtures formed from normal, branched, and cyclic alcohols (1, 15).

Adiabatic Compressibilities

Adiabatic compressibilities, κ_s, were obtained from the ultrasonic velocities and densities, ρ, according to the equation

[4] $$\kappa_s = (\rho u^2)^{-1}$$

Values for the pure components are given in Table 1. In the case of mixtures, the density required in eq. 4 was calculated from the relations

[5] $$\rho = \sum M_i x_i / V_m$$

[6] $$V_m = V_m^0 + V^E$$

and

[7] $$V_m^0 = \sum x_i V_i^0$$

where M_i and $V_i^0 (\equiv M_i \rho_i^0)$ are respectively the molecular mass and molar volume of pure component i. Results for the densities and adiabatic compressibilities of the mixtures are listed in Table 4. The relative error in the values of κ_s is estimated to be less than 0.01%.

Also included in Table 4 are values of the excess adiabatic compressibility κ_s^E defined by the expression

[8] $$\kappa_s^E = \kappa_s - \sum \phi_i^0 \kappa_{s,i}^0$$

where $\kappa_{s,i}^0$ is the adiabatic compressibility of pure component i, and the volume fraction

[9] $$\phi_i^0 = x_i V_i^0 / V_m^0$$

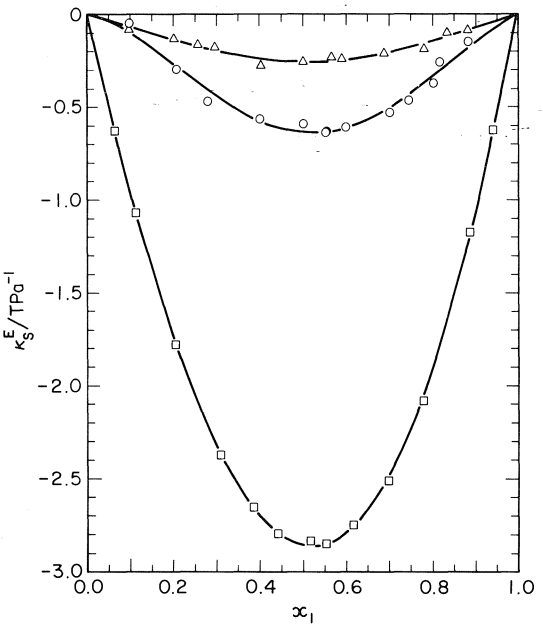

FIG. 5. Excess adiabatic compressibilities at 25 °C. ○, c-PeOH + c-HxOH; □, c-PeOH + c-HpOH; △, c-HxOH + c-HpOH. Curves are least squares fits using coefficients from Table 3.

refers to the unmixed state. The values of κ_s^E are plotted in Fig. 5. Values of the coefficients and standard errors of least squares representations of κ_s^E by the same polynomial form as used for V^E and Δu are listed in Table 3.

It should be noted that the term "excess compressibility" has been used to denote several thermodynamically different quantities (17–19). The importance of the proper definition of excess functions has been discussed by Missen (20). In our usage, "excess compressibility" refers to the deviation of the compressibility of the mixture from that of an ideal Raoult solution model at the same temperature and pressure. The quantity

[10] $$-\frac{1}{V_m}\left(\frac{\partial V^E}{\partial p}\right)_s = \kappa_s - \sum \phi_i^* \kappa_{s,i}^0$$

with

[11] $$\phi_i^* = x_i V_i^0 / V_m$$

is frequently called the excess compressibility (17, 21). The difference between this and κ_s^E is

[12] $$\delta\kappa_s^E = \kappa_s^E + \frac{1}{V_m}\left(\frac{\partial V^E}{\partial p}\right)_s = -\frac{V^E}{V_m}\sum \phi_i^0 \kappa_{s,i}^0$$

For the present systems, the approximate expression

[13] $$(\delta\kappa_s^E/\mathrm{TPa}^{-1}) \simeq -5.0(V^E/\mathrm{cm}^3\ \mathrm{mol}^{-1})$$

provides a good estimate of the numerical value of this difference. It amounts to about 0.18 TPa^{-1} for an equimolar mixture of c-PeOH + c-HxOH.

The excess adiabatic compressibilities are negative for all of the present cycloalkanol systems; similar behavior has been observed for most of the hydrogen bonded systems studied previously (1–3, 15). Fort and Moore (3) found that the excess compressibility decreased and became increasingly negative as the strength of the interaction between unlike molecules increased, and that the excess volume showed a similar variation. In the present systems, the difference in the sizes of the component molecules facilitates the close approach of unlike molecules most in c-PeOH + c-HpOH mixtures, and leads to the largest reduction in compressibility through the formation of mixed hydrogen bonds. However size alone cannot explain in

Can. J. Chem. Downloaded from www.nrcresearchpress.com by 210.87.254.5 on 09/05/12
For personal use only.

detail the results obtained for the cycloalkanol systems, since the curves in Figs. 3 and 5 fall in different orders. Evidently the excess properties of these systems depend on a balance between opposing effects. Several theoretical treatments (22–24) lead to relations between the excess volume and the excess compressibility of mixtures in which the molecules interact primarily through dispersive forces, but none of these are applicable to the present systems in which both components are capable of forming hydrogen bonds.

We are indebted to Dr. E. P. Papadakis (Panametrics Inc., Waltham, Mass.) for discussions of the pulse-echo-overlap technique. We also thank Mr. C. J. Halpin and Mr. P. J. D'Arcy for their assistance in all phases of the experimental work.

1. F. Danusso. Atti. accad. nazl. Lincei, Rend., Cl. sci. fis., mat. e nat. **17**, 114 (1954).
2. F. Danusso. Att. accad. nazl. Lincei, Rend., Cl. sci. fis., mat. e nat. **17**, 370 (1954).
3. R. J. Fort and W. R. Moore. Trans. Faraday Soc. **61**, 2102 (1965).
4. O. Kiyohara and G. C. Benson. Can. J. Chem. **51**, 2489 (1973).
5. J. Timmermans. Physico-chemical constants of pure organic compounds. Vol. I. Elsevier Press Inc., New York. 1950.
6. H. D. Pflug and G. C. Benson. Can. J. Chem. **46**, 287 (1968).
7. E. P. Papadakis. J. Acoust. Soc. Am. **42**, 1045 (1967).
8. V. A. Del Grosso and C. W. Mader. J. Acoust. Soc. Am. **52**, 1442 (1972).
9. J. B. Lastovka and E. F. Carome. J. Acoust. Soc. Am. **35**, 1279 (1963).
10. G. C. Benson and H. D. Pflug. J. Chem. Eng. Data, **15**, 382 (1970).
11. B. J. Levien. J. Chem. Thermodyn. **5**, 679 (1973).
12. M. B. Ewing and K. N. Marsh. Proc. 3rd Int. Conf. Chem. Thermodyn. Baden, Austria. 1973. p. 168.
13. G. W. Willard. J. Acoust. Soc. Am. **19**, 235 (1947).
14. T. Kishimoto and O. Nomoto. J. Phys. Soc. Jap. **9**, 1021 (1954).
15. G. W. Marks. J. Acoust. Soc. Am. **41**, 103 (1967).
16. J. Karpovich. J. Chem. Phys. **22**, 1767 (1954).
17. I. Prigogine and R. Defay. Chemical thermodynamics. (*Translated by* D. H. Everett.) Longmans Green and Co., London. 1954. Chapt. 24.
18. I. Prigogine. The molecular theory of solutions. North Holland Publishing Co., Amsterdam. 1957. Chapt. 1, Section 7.
19. M. J. Blandamer and D. Waddington. Adv. Mol. Relax Process, **2**, 1 (1970).
20. R. W. Missen. Ind. Eng. Chem. Fundam. **8**, 81 (1969).
21. G. A. Holder and E. Whalley. Trans. Faraday Soc. **58**, 2108 (1962).
22. J.-P. Poupko. Bull. Acad. R. Belg. Class. Sci. **41**, 991 (1955).
23. J. Barriol and P. Boule. C. R. Acad. Sci. Paris, Ser. C. **267**, 1433 (1968).
24. P. Boule, J. Barriol, J.-P. Herbeuval, and M.-L. Gaulard. J. Chim. Phys. **69**, 58 (1972).

Can. J. Chem. Downloaded from www.nrcresearchpress.com by 210.87.254.5 on 09/05/12
For personal use only.

Deuteron Relaxation Study of the Reorienting Methyl Groups in *p*-Azoxyanisole

M. WISZNIEWSKA, RONALD Y. DONG, AND E. TOMCHUK
Department of Physics, The University of Winnipeg, Winnipeg, Manitoba R3B 2E9
AND
E. BOCK
Parker Chemistry Laboratory, The University of Manitoba, Winnipeg, Manitoba R3T 2N2

Received November 8, 1973

M. WISZNIEWSKA, RONALD Y. DONG, E. TOMCHUK, and E. BOCK. Can. J. Chem. **52,** 2294 (1974).

The deuteron spin–lattice relaxation times were measured in the nematic and isotropic phases of *p*-azoxyanisole$(CD_3)_2$. An apparent activation energy for the methyl group reorientation in the isotropic phase is obtained. The quadrupole coupling constant along the C—D bond is found to be 147 ± 8 kHz.

M. WISZNIEWSKA, RONALD Y. DONG, E. TOMCHUK, et E. BOCK. Can. J. Chem. **52,** 2294 (1974).

On a mesuré les temps de relaxation spin–réseau du deutérium dans des phases nématiques et isotropiques du *p*-azoxyanisole $(CD_3)_2$. On a obtenu une énergie apparente d'activation pour la réorientation du groupe méthyle dans la phase isotropique. On a trouvé que la constante de couplage quadrupolaire le long du lien C—C est de 147 ± 8 kHz.

[Traduit par le journal]

Introduction

Proton spin–lattice relaxation has been used extensively to study liquid crystals by many authors (1, 2). Since there are many inequivalent protons in each molecule, the spectrum and interspin dynamical relationships are complicated. In our continuing effort to study molecular dynamics in liquid crystals, we have investigated the reorienting motions of methyl groups in a partially-deuterated nematic *p*-azoxyanisole, PAA$(CD_3)_2$ (a molecule with CD_3 replacing the CH_3 groups in PAA) by measuring the deuteron spin–lattice relaxation time T_1(D) both in its nematic and isotropic liquid phases. The possible effect of the reorienting methoxy groups on the proton T_1 in the isotropic phase of PAA has recently been discussed (3) while relating the n.m.r. and dielectric relaxation data. The present study enables us to isolate the methyl end groups from the rest of this rod-like molecule. An apparent activation energy for the reorienting methyl groups in the isotropic phase of PAA was determined. In addition, we report here a determination of the deuteron quadrupolar coupling constant along the C—D bond in PAA-$(CD_3)_2$ using the effective correlation times τ_{eff} for the methyl group reorientation obtained by isotopic dilution studies (4).

Experimental

The deuterated sample of PAA was obtained from Dr. Chas. G. Wade, Texas. The sample was sealed in a vacuum by the freeze–melt method with the nematic–isotropic transition (T_c) at ~131 °C.

The T_1(D) measurements were made at a Larmor frequency $\omega_L/2\pi$ = 9 MHz with a Bruker B-KR322S pulsed spectrometer using 180°–τ–90° sequences. The accuracy in our measurements is about 5%. The temperatures of the sample were maintained by a nitrogen gas flow with a temperature gradient across the sample (length ~2 cm) of the order of 0.5 °C.

Results and Discussion

The deuteron spin–lattice relaxation times T_1(D) of PAA$(CD_3)_2$ are presented in Fig. 1 as a function of the reciprocal temperature. In the nematic phase of PAA, the molecules are free to rotate around their molecular axes. In addition, there are thermal oscillations of the entire molecule about its preferred local alignment (*i.e.* director) due to the orientational order fluctuations (1, 5). Furthermore, the rotation of methyl groups around their C_3 axes is known to be fast (*i.e.* $\omega_L\tau \ll 1$ where τ is a correlation time for the C_3 rotation) both in the nematic and isotropic phases (2). Another degree of freedom to the methyl groups is the reorientations of their C_3 axes around the ring-carbon–oxygen bonds which are also known to be fast (6) in the nematic phase. The deuterons of the CD_3 groups are relaxed to some extent by each of the above molecular motions in the nematic phase of PAA$(CD_3)_2$. In the isotropic phase, an additional relaxation mechanism due to the presence of rapid molecular tumbling (*i.e.* rotational diffusion of the whole molecule) is a major con-

Can. J. Chem. Downloaded from www.nrcresearchpress.com by 210.87.254.5 on 09/05/12
For personal use only.

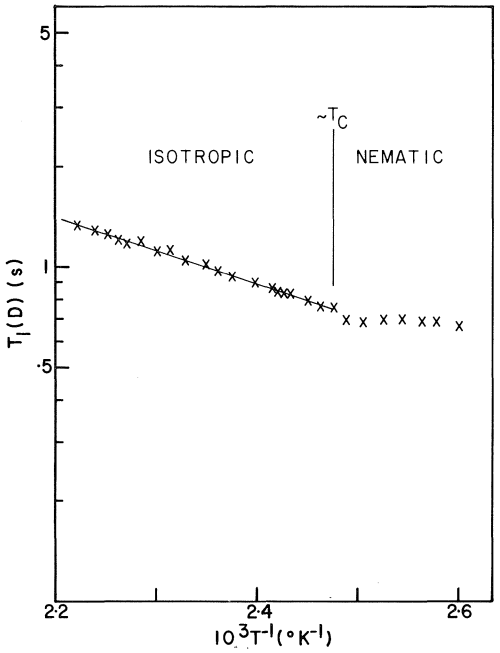

FIG. 1. Deuteron relaxation time T_1(D) of PAA$(CD_3)_2$ at 9 MHz *vs* reciprocal temperature.

tributor to the deuteron spin relaxation. The T_1(D) in this phase therefore reflects a reorientation of the CD_3 groups which is a combination of several degrees of motional freedom. Thus the slope of T_1(D) *vs.* T^{-1} in the isotropic phase (Fig. 1) gives an *apparent* activation energy (E_a = 4.6 kcal/mol) for the complicated reorientations of the methyl groups in this phase. By assuming the effective correlation time τ_{eff} determined for the CH_3 groups in PAA($\tau_{eff} = 3.5 \times 10^{-12}$ s at 136 °C (4)) being equal to that of the CD_3 groups, one obtains $\tau_{eff} = 1.3 \times 10^{-14} \exp(E_a/RT)$ s in the isotropic phase of PAA$(CD_3)_2$. The above assumption is correct only under certain conditions (7), but probably holds well in the present case.

T_1(D) shows no clear discontinuity at T_c and is found to be independent of temperature in the nematic phase within the experimental error. This temperature dependence is in contrast with that in the isotropic phase. We believe this arises from the disappearance of molecular tumbling and the onset of long range orientational order fluctuations below T_c in the nematic phase, since these are the motions which show differences in the two phases and gradual changes near T_c. It should be noted that the orientational order fluctuations are known to give a weak temperature dependent spin relaxation rate (5). The apparent activation energy in the isotropic phase can therefore be attributed mostly to the process of molecular tumbling.

The expression for T_1^{-1}, due to the modulation of quadrupole coupling by molecular motion, is given, for $I = 1$, in the short correlation time limit by (8)

$$[1] \qquad \frac{1}{T_1} = \frac{3\pi^2}{2}\left(1 + \frac{\eta^2}{3}\right)\left(\frac{e^2qQ}{h}\right)^2 \tau_{eff}$$

where η is the asymmetry parameter, (eq) the largest value of the field gradient in the molecular frame and e^2qQ/h the quadrupole coupling constant in Hz. η is usually small for C—D bonds (9) and is assumed to be zero. Using $\tau_{eff} = 5.1 \times 10^{-12}$ and 3.5×10^{-12} s at 120 and 136 °C (4), we obtained from eq. 1 and our T_1(D) measurements in both the nematic and isotropic phases an average value for the quadrupole coupling constant along the C—D bond of 147 ± 8 kHz if (eq) is assumed to be constant in our temperature range. This value lies in the range of values for the quadrupole coupling constants along C—D bond obtained in other compounds (10).

We are grateful to Dr. Chas. G. Wade for lending us a sample of PAA$(CD_3)_2$. The financial assistance of the National Research Council of Canada, the University of Winnipeg, and the Faculty of Graduate Studies of the University of Manitoba is gratefully acknowledged. We are also grateful to Mr. E. Samulatis and Mr. K. Krebs for their technical assistance.

1. G. H. BROWN, J. W. DOANE, and V. D. NEFF. Crit. Rev. Solid State Sci. **1**, 303 (1970). G. R. LUCKHURST. Magnetic resonance spectroscopy of non-amphiphilic systems. *In* Liquid crystalline systems. *Edited by* G. W. Gray and P. A. Winsor. Van Nostrand, Princeton. 1974.
2. R. Y. DONG, W. F. FORBES, and M. M. PINTAR. J. Chem. Phys. **55**, 145 (1971).
3. P. L. NORDIO, G. RIGATTI, and U. SEGRE. Chem. Phys. Lett. **19**, 295 (1973).
4. E. T. SAMULSKI, C. R. DYBOWSKI, and CHAS. G. WADE. Mol. Cryst. Liq. Cryst. **22**, 309 (1973); Phys. Rev. Lett. **29**, 340, 1050 (1972).
5. P. PINCUS. Solid State Commun. **7**, 415 (1969). J. W. DOANE and D. L. JOHNSON. Chem. Phys. Lett. **6**, 291 (1970). J. J. VISINTAINER, J. W. DOANE, and D. L. FISHEL. Mol. Cryst. Liq. Cryst. **13**, 69 (1971).
6. R. BLINC, D. E. O'REILLY, E. M. PETERSON, G. LAHAJNAR, and I. LEVSTEK. Solid State Commun. **6**, 839 (1968).
7. E. TOMCHUK, J. J. CZUBRYT, E. BOCK, and N. CHATTERJEE. J. Magn. Reson. **12**, 20 (1973).
8. A. ABRAGAM. The principles of nuclear magnetism. Oxford, England. 1961.
9. J. C. ROWELL, W. D. PHILIPS, L. R. MELBY, and M. PANAR. J. Chem. Phys. **43**, 3442 (1965).
10. M. D. ZEIDLER. Ber. Bunsenges. Phys. Chem. **69**, 659 (1965).

Can. J. Chem. Downloaded from www.nrcresearchpress.com by 210.87.254.5 on 09/05/12
For personal use only.

Essai de calcul des paramètres d'anisotropie des liaisons C—C, C—H, C=C et C=O par régression multi-linéaire sur des données expérimentales résonance magnétique nucléaire

JOHN W. APSIMON

Department of Chemistry, Carleton University, Ottawa, Canada K1S 5B6

JOSÉ ELGUERO ET ALAIN FRUCHIER

Laboratoire de Synthèse et d'Etude physicochimique d'Hétérocycles azotés, Université des Sciences et Techniques du Languedoc, Place Eugène Bataillon, 34060 Montpellier cedex, France

ET

DIDIER MATHIEU ET ROGER PHAN-TAN-LUU

Laboratoire de Traitement de l'Information et de Prospective, Institut Universitaire de Technologie, Rue de la Fourane, 13100 Aix-en-Provence, France

Reçu 17 septembre 1973

JOHN W. APSIMON, JOSÉ ELGUERO, ALAIN FRUCHIER, DIDIER MATHIEU ET ROGER PHAN-TAN-LUU. Can. J. Chem. **52**, 2296 (1974).

L'emploi d'une méthode statistique de traitement des données numériques a permis de mettre en évidence l'impossibilité de calculer les susceptibilités magnétiques et les anisotropies des liaisons C—C et C—H à partir des déplacements chimiques de la littérature réunis par Simon et coll. (22), car ni le modèle de McConnell ni celui d'ApSimon n'est compatible avec les valeurs expérimentales.

Par contre, on a pu déterminer la valeur et l'intervalle de confiance des anisotropies des liaisons C=C et C=O et du terme électrique de la liaison C=O.

JOHN W. APSIMON, JOSÉ ELGUERO, ALAIN FRUCHIER, DIDIER MATHIEU, AND ROGER PHAN-TAN-LUU. Can. J. Chem. **52**, 2296 (1974).

A statistical treatment has allowed us to demonstrate the impossibility of calculating the magnetic susceptibilities and the anisotropies of the C—C and C—H bonds from the collection of chemical shifts reported by Simon and co-workers (22) as we have found the model of McConnell and the ApSimon to be inconsistent with experimental values.

Nevertheless, we have been able to determine the values and confidence limits for the magnetic anisotropies of the C=C and C=O bonds and the electric field term for the C=O bond.

Introduction

Dans deux travaux préliminaires (1, 2) concernant l'étude par résonance magnétique nucléaire de l'effet longue distance de l'anisotropie magnétique du groupe méthyle en libre rotation, nous n'avons pu retrouver par le calcul l'effet produit par le remplacement d'un proton par un méthyle sur les déplacements chimiques des autres protons dans le cycle pyrazoline-2.

Pour expliquer l'écart entre la valeur calculée et la valeur observée, nous avons proposé une série d'hypothèses, dont la plus simple était que les paramètres des liaisons C—C et C—H utilisés dans l'équation proposée par ApSimon et coll. (3) n'étaient pas corrects. En effet, si la méthode itérative décrite par ces auteurs pour le calcul de $\Delta\chi^{CC}$ et $\Delta\chi^{CH}$, qui tient compte d'une correction pour les courtes distances, est très intéressante, les valeurs numériques obtenues ne peuvent pas être acceptées car les droites de régression $\Delta\sigma_{calc} = f(\Delta\sigma_{exp})$ ont des pentes très différentes de l'unité et des ordonnées à l'origine différentes de zéro. Ceci provient du fait que ces auteurs, utilisant un modèle mathématique du type [1] ont imposé $C = 0$:

$$[1] \qquad a_i\Delta\chi^{CC} + b_i\Delta\chi^{CH} + C = \Delta\sigma_i$$

Les droites de régression obtenues montrent que $C \neq 0$ et que, par conséquent, les paramètres calculés sont erronés.

D'autre part, de nombreux auteurs (3–20) ont déja essayé de calculer des paramètres d'anisotropie (tableau 1) des liaisons C—C et C—H. La plupart utilisent des séries homogènes comprenant un faible nombre de composés. On remarque que les valeurs différent nettement selon les auteurs. Faut-il en déduire que les valeurs ne sont valables qu'à l'intérieur des séries pour lesquelles

elles ont été déterminées? Notons, de plus, qu'il est très rare (les valeurs publiées par Jackman et Sternhell (20) constituent une exception) de trouver les intervalles de confiance des paramètres calculés.

L'objet du présent travail est, dans une première partie, d'essayer de calculer de nouvelles valeurs des paramètres d'anisotropie des liaisons C—C et C—H en utilisant un programme de régression multi-linéaire, REGMUL (21), et des ensembles de valeurs expérimentales publiées par Simon et coll. (22) d'une part et par l'un d'entre nous (3) d'autre part. Nous avons aussi repris, dans une deuxième partie, les calculs effectués précédemment (19, 23–25) afin de calculer la signification des paramètres des liaisons C=C et C=O.

Description du programme REGMUL

Soit le modèle mathématique

$$\eta = \beta_0 + \sum \beta_n x_n$$

Pour chaque groupe de valeurs des variables indépendantes x_n on dispose expérimentalement d'une valeur Y, mesure de η, telle que $E[Y] = \eta$. On peut écrire:

$$Y = a_0 + \sum a_n x_n + \varepsilon$$

équation dans laquelle a_0 et a_n sont des estimations de β_0 et β_n (26).

Le programme accepte comme données les variables dépendantes et indépendantes ainsi que le niveau de signification α utilisé pour les différents tests statistiques. Tous nos calculs ont été effectués avec $\alpha = 0.05$.

Lors de l'estimation des coefficients a_n les trois méthodes habituelles sont utilisables: stepwise, backward elimination ou moindres carrés classique. Si le modèle mathématique impose que $a_0 = 0$, la signification de a_0 est testée. Ce n'est que dans le cas où a_0 n'est pas significative que le modèle avec $a_0 = 0$ est utilisé.

En plus de l'étude statistique classique, le programme teste la validité du modèle par analyse de variance si l'on a une estimation de l'erreur expérimentale. Il effectue aussi une étude des résidus comprenant notamment l'étude de l'alternance des signes avant et après classement de la variable dépendante. Ceci permet d'étudier l'influence possible d'un facteur extérieur au modèle. Nous noterons enfin que le calcul des fonctions de probabilité (Loi normale, loi de Student–Fisher, loi de Fisher–Snedecor et loi binomiale) est fait par sous-programmes inclus dans le programme principal (24).

Liaisons C—C et C—H

(i) Principe de la méthode

On admet généralement que le remplacement d'une liaison C—H par un groupe méthyle provoque sur un proton voisin un $\Delta\sigma$, d'origine purement magnétique, donné par [2]:

$$[2] \qquad \Delta\sigma_T = \Delta\sigma^{CC} + \Delta\sigma^{Me} - \Delta\sigma^{CH}$$

Deux méthodes peuvent être utilisées pour le calcul des termes de l'équation 2:

Méthode 1

Chaque terme est calculé au moyen de l'équation de McConnell. On peut alors écrire:

$$[3] \quad \Delta\sigma_i = \Delta\chi^{CC}.TGC_i + \Delta\chi^{CH}.(TGM_i - TGH_i)$$

Dans cette équation, $\Delta\sigma_i$ représente, en p.p.m., la variation des déplacements chimiques provoquée par l'introduction du groupe méthyle, et TGC, TGH et TGM les termes géométriques[1] reliant la position du proton où l'on mesure $\Delta\sigma_i$ à la liaison C—C, à la liaison C—H et aux trois liaisons C—H en libre rotation du groupe méthyle, respectivement.

$$TGC = \frac{1 - 3\cos^2\gamma}{3R^3}$$

$$TGH = \frac{1 - 3\cos^2\gamma'}{3R'^3}$$

Les paramètres γ ey γ', ainsi que R et R' sont définis dans la fig. 1. Nous noterons que TGC = TGH si les dipoles ponctuels représentant les liaisons C—C et C—H sont à la même distance de l'atome de carbone. La valeur de TGM est obtenue au moyen de la méthode décrite par ApSimon et coll. (3) (voir Appendice):

$$TGM = \left\langle \frac{1 - 3\cos^2\theta\varphi}{3R^3\varphi} \right\rangle$$

Les intégrales elliptiques nécessaires sont calculées numériquement par un sous-programme utilisant la transformation de Landens, écrit d'après le sous-programme CELI2 (28). Le système d'équation 3 sera résolu par régression multi-linéaire sur le modèle mathématique [4]:

[1]Nous avons adopté pour les termes géométriques une notation simplifiée différente de celle utilisée dans les précédents articles de la série (25, 27).

TABLEAU 1. Anisotropies des liaisons CC et CH exprimées en 10^{-30} cm^3 molécule^{-1}

Référence	CC	CH
Bothner-By et Naar-Colin (4)	5.5	0
Narasimhan et Rogers (5)	6.65	0
Musher (6)	8.3	0
Musher (7)	8.33	0
Moritz et Sheppard (8)	7.0	0
Huisgen et coll. (9)	8.1	0
Homer et Callaghan (10)	7.3	0
Hall (11)	6.5	0
Yamaguchi et Brownstein (12)	6.37	0
Zurcher (13)	3.24–6.18	0–2.5
Tillieu (14)	2.05	0.4–2.5
Zurcher (15)	1.74	−1.24
Davies (16)	6.68	5.02
Pople (17)	18.3	11.3
Reddy et Goldstein (18)	16.7	
ApSimon et coll., Méthode 1 (3)	21.33	12.57
ApSimon et coll., Méthode 2 (3)	13.98	11.00
ApSimon et coll., Méthode 2, valeurs modifiées (19)	11.26	7.54
Jackman et Sternhell (20)	16.0	11.6
Jackman et Sternhell (20)	12.4	10.6
Jackman et Sternhell (20)	25.8 ± 7.4	13.7 ± 6.0

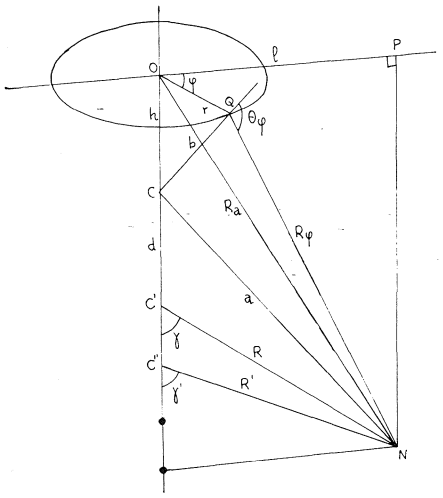

FIG. 1. OP = l; OC = h; OQ = r; CQ = b; CN = a; ON = R_a; QN = R; C′N = R (C′ = position du centre du dipole representant la liaison C—C); C″N = R' (C″ = position du centre du dipole representant la liaison C—H); CC′ = d.

$$[4]\quad \Delta\sigma_i = A_0 + B_0.\mathrm{TGC}_i + C_0(\mathrm{TGM}_i - \mathrm{TGH}_i) + \varepsilon$$

Si la constante A_0 est trouvée proche de 0 et si les résidus sont aléatoires, nous pourrons dire que le modèle représenté par [4] est convenable et que B_0 et C_0 sont des estimations satisfaisantes de $\Delta\chi^{CC}$ et $\Delta\chi^{CH}$ respectivement.

Méthode 2

Chaque terme de l'équation 2 est calculé en ajoutant le terme en $1/R^5$ introduit par ApSimon et coll. (3) à l'équation de McConnell. Si l'équation de McConnell ne permet d'atteindre que les anisotropies des liaisons, l'équation d'ApSimon peut, en principe, permettre d'atteindre les susceptibilités longitudinales et transversales. On peut écrire:

$$[5]\quad \Delta\sigma_i = {\chi_L}^{CC}(\mathrm{TGC}_i + \mathrm{SC.DGC}_i) + {\chi_T}^{CC}(-\mathrm{TGC}_i + \mathrm{SC.RGC}_i) + {\chi_L}^{CH}[\mathrm{TGM}_i - \mathrm{TGH}_i + \mathrm{SH}(\mathrm{DGM}_i - \mathrm{DGH}_i)] + {\chi_T}^{CH}[\mathrm{TGH}_i - \mathrm{TGM}_i + \mathrm{SH}(\mathrm{RGM}_i - \mathrm{RGH}_i)]$$

SC et SH représentent les carrés des demi-longueurs des dipoles des liaisons C—C et C—H respectivement. TGC, TGH et TGM ont la même définition que précédemment. Les autres constantes sont définies de la façon suivante:

$$\mathrm{DGC} = (-1/2 + 5\cos^2\gamma - 35\cos^4\gamma/6)/R^5$$

$$\mathrm{RGC} = (-1 + 5\sin^2\gamma - 35\sin^4\gamma/6)/R^5$$

$$\mathrm{DGH} = (-1/2 + 5\cos^2\gamma' - 35\cos^4\gamma'/6)/R'^5$$

TABLEAU 2. Comparaison des valeurs calculées suivant l'ensemble I et l'ensemble II

	Ensemble I	Ensemble II
A	-1.234 ± 0.065	-1.286 ± 0.043
B	0.0107 ± 0.0006	0.0107 ± 0.0004
K	-30.0 ± 5.8	-16.0 ± 5.3
L	0.28 ± 0.05	0.26 ± 0.05
CC	0.912	0.643
si $\Delta\chi^{CH} = 0$	$\Delta\chi^{CC} = 24.3 \pm 6.0$	$\Delta\chi^{CC} = 12.5 \pm 4.5$
si $A_0 = 0$	$\Delta\chi^{CC} = 26.0 \pm 6.1$	$\Delta\chi^{CC} = 24.3 \pm 5.6$

$$RGH = (-1 + 5\sin^2\gamma' - 35\sin^4\gamma'/6)/R'^5$$

$$DGM = 3\langle(-1/2 + 5\cos^2\theta_\varphi - 35\cos^4\theta_\varphi/6)/R^5\rangle$$

$$RGM = 3\langle(-1 + 5\sin^2\theta_\varphi - 35\sin^4\theta_\varphi/6)/R^5\rangle$$

Le détail du calcul des deux derniers termes est en appendice. Comme précédemment, le système d'équations 5 surdéterminé sera résolu par régression multi-linéaire sur le modèle [6]:

$$[6] \quad \Delta\sigma_i = A_0 + B_0W_i + C_0X_i + D_0Y_i + E_0Z_i + \varepsilon$$

afin d'obtenir des estimations correctes des susceptibilités longitudinales et transversales.

(ii) Données expérimentales

Comme valeurs de $\Delta\sigma_i$ nous avons utilisé:

Ensemble I: 25 des 26 valeurs utilisées par Simon et coll. (22) pour obtenir la première droite (Fig. 1, p. 108 de la réf. 22). Le point 16 (tableau 5, p. 110 de la réf. 22) n'a pas été considéré car il s'agit de l'effet d'un méthyle sur un autre méthyle.

Ensemble II: 54 des 57 valeurs utilisées par Simon et coll. (22) pour sa deuxième corrélation (Fig. 3, p. 112 de la réf. 22). Les points 16 et 57 ont été exclus pour la raison exposée précédemment. Le point 55 l'a été aussi car il s'agit de l'effet d'un *N*-méthyle.

Ensemble III: 19 valeurs utilisées par ApSimon *et al.* (3) (tableau 1, p. 2351 de la réf. 3).

Les paramètres R et γ ont été mesurés (3) sur des modèles Dreiding et tous les autres calculés à partir d'eux.

(iii) Résultats et discussion

Nous avons utilisé dans tous les cas la méthode d'élimination des variables après test de leur signification.

Calcul des paramètres d'anisotropie: Aussi bien avec l'ensemble I qu'avec l'ensemble II, la première régression effectuée avec le modèle [4] ne conduit pas à des coefficients significatifs. Le calcul est alors automatiquement recommencé en supprimant les variables TGC_i et l'équation finale est:

$$[7] \quad K(TGM_i - TGH_i + L = \Delta\sigma_i$$

Ceci peut sembler dénué de sens. Toutefois on remarque que la matrice de corrélation des variables montre un bon coefficient (0.993) entre les variables TGC_i et $(TGM_i - TGH_i)$. Une relation [8] peut donc être écrite:

$$[8] \quad TGC_i = A(TGM_i - TGH_i) + B$$

Toute l'information étant contenue dans une seule des deux séries de variables, il est normal que soit éliminée de la régression la série dont le coefficient a la plus faible signification. Le coefficient calculé, K, ne représente alors pas $\Delta\chi^{CH}$ mais une combinaison linéaire de $\Delta\chi^{CC}$ et $\Delta\chi^{CH}$ [9]:

$$[9] \quad K = A\Delta\chi^{CC} + \Delta\chi^{CH}$$

Les valeurs de K, L, A et B sont indiquées dans le tableau 2 ainsi que les coefficients de corrélation CC entre variables dépendante calculée et expérimentale pour les deux ensembles I et II; nous y avons ajouté les valeurs de $\Delta\chi^{CC}$ dans l'hypothèse où $\Delta\chi^{CH}$ serait nul. On peut remarquer, d'autre part, que le couple de valeurs de Jackman et Sternhell (20) ($\Delta\chi^{CC} = 25.8 \pm 7.4$ et $\Delta\chi^{CH} = 13.7 \pm 6.0$) (tableau 1) est compatible avec l'équation 9 si l'on utilise les coefficients K et A de l'ensemble II (tableau 2).

Etant donné que les variables TGM_i sont calculées de façon non analytique, il est difficile de justifier mathématiquement la relation 8 que nous considèrerons comme une relation empirique, au même titre que celle proposée par Simon et coll. (22) ($\Delta\sigma = f(R)$); elle n'est probablement valable que dans un domaine limité de valeurs de R et γ.

On constate dans le tableau 2 que si les valeurs de A, B et L peuvent être considérées comme égales pour les deux ensembles, il n'en est pas de même pour K. Comme d'après les équations 4, 7 et 8, on peut écrire:

$$[10] \qquad \Delta\chi^{CC} = (L - A_0)/B$$

on pourrait penser que $\Delta\chi^{CC}$ est mieux défini que $\Delta\chi^{CH}$. Or, dans la première étape de la régression, la valeur de A_0 bien que significative, est entachée d'une erreur assez grande, et est différente pour les deux ensembles. L'équation 10 ne peut donc permettre de calculer une valeur de $\Delta\chi^{CC}$ convenant aux deux ensembles.

Le modèle [3] de l'équation de McConnell impose que A_0 soit nul, mais il n'est acceptable qu'au prix d'approximations importantes car, aussi bien d'après la somme des carrés des déviations que d'après les coefficients de corrélation, celui de l'équation 7 est supérieur. Le modèle $A_0 = 0$, bien que séduisant car conduisant au moyen de l'équation 10 à des valeurs de $\Delta\chi^{CC}$ cohérentes pour les deux ensembles (tableau 2), doit être rejeté car non satisfaisant sur le plan statistique.

Il n'est d'ailleurs pas étonnant que les ensembles I et II conduisent à des coefficients différents car le second est beaucoup plus hétérogène que le premier. En effet, alors que dans l'ensemble I les protons et méthyles considérés sont fixés à des carbones sp^3, l'ensemble II contient, en plus de l'ensemble I, des composés de toutes sortes (aromatiques, cyclopropanes, etc...) dans lesquels la composante non magnétique du $\Delta\sigma_{obs}$ est probablement plus importante. La qualité plus mauvaise de l'ensemble II apparait nettement dans les coefficients de corrélation du tableau 2, qui montrent que 83% de la régression est du à $(TGM_i - TGH_i)$ pour l'ensemble I et seulement 41% pour l'ensemble II.

Par contre, avec l'ensemble III, on trouve deux valeurs significatives avec un coefficient de corrélation de 0.948:

$$[11] \qquad \Delta\chi^{CC} = 44.1 \pm 7.9$$

et

$$\Delta\chi^{CH} = 37.6 \pm 8.2$$

mais la constante A_0 du modèle [4] n'est pas nulle et vaut -0.13 ± 0.05 p.p.m. Ces valeurs sont tellement différentes de celles publiées dans la réf. 3 que nous en avons cherché la raison. Il s'avère tout d'abord que les valeurs publiées dans ref. 3 ont été calculées en supposant *a priori* que $A_0 = 0$. Ceci n'est statistiquement pas justifié. En effet, avec les facteurs géométriques et les $\Delta\sigma$ expérimentaux corrigés au moyen du terme correctif pour les courtes distances calculé avec des susceptibilités dues à Davies (16) (réf. 3, p. 2343), on trouve:

$$[12] \qquad \Delta\chi^{CC} = 29.3 \pm 7.1$$

et

$$\Delta\chi^{CH} = 18.3 \pm 5.5$$

avec un coefficient de corrélation de 0.913 et une constante A_0 de -0.10 ± 0.07 p.p.m. au lieu des valeurs:

$$[13] \qquad \Delta\chi^{CC} = 23.14$$

et

$$\Delta\chi^{CH} = 13.51$$

précédemment publiées dans (3) avec l'hypothèse $A_0 = 0$. En utilisant les $\Delta\sigma$ expérimentaux non corrigés, déja employés pour calculer les valeurs [11], et les coefficients géométriques ayant servi au calcul des valeurs [12], on trouve:

$$[14] \qquad \Delta\chi^{CC} = 32.1 \pm 7.0$$

et

$$\Delta\chi^{CH} = 19.7 \pm 5.4$$

avec un coefficient de corrélation de 0.928 et une constante A_0 de -0.10 ± 0.07 p.p.m. Ces valeurs [14] devraient, en principe, être identiques aux valeurs [11]. Nous avons alors constaté que la différence provient uniquement des termes géométriques TGM du méthyle en libre rotation. Les méthodes de calcul étant rigoureusement identiques, la différence est due aux paramètres R_a, a et l (définis dans l'Appendice) qui ont été mesurés sur des modèles Dreiding dans la réf. 3 et calculés ici à partir de R et γ. Parmi ces trois paramètres, l'un (l) découle des deux autres (R_a et a). C'est pourquoi leur calcul à partir de R et γ nous semble préférable à leur mesure qui risque de donner trois valeurs non seulement incohérentes entre elles mais aussi inconsistantes avec les paramètres R et γ utilisés pour le calcul de TGC et TGH. C'est ce qui est arrivé notamment pour le point 2 dont le coefficient TGM précédemment trouvé est très loin de celui provenant de R et γ (tableau 3).

Essai de calcul des susceptibilités longitudinales et transversales. Posons:

TABLEAU 3. Comparaison des termes géométriques du méthyl en libre rotation de la réf. 3 et calculées ici*

Du tableau 2 de la réf. 3	R	γ	R_a	a	l	Coef. géom. TGM
1	3.6	21	4.57 (4.35)	4.33 (4.20)	1.29 (1.23)	0.3288 (0.6809)
2	2.6	96	2.69 (2.51)	2.63 (2.45)	2.59 (2.55)	−0.2858 (−1.7250)
3	4.0	37	4.86 (4.61)	4.64 (4.46)	2.41 (2.44)	0.2787 (0.4602)
4	3.8	48	4.55 (4.44)	4.35 (4.30)	2.82 (2.98)	0.3043 (0.3909)
5	2.4	66	2.97 (2.90)	2.80 (2.77)	2.19 (2.20)	1.1220 (1.3340)
6	2.8	31	3.72 (3.68)	3.48 (3.47)	1.44 (1.49)	0.5146 (0.6627)
7	4.1	36	4.97 (4.83)	4.74 (4.67)	2.41 (2.53)	0.2643 (0.3897)
8	3.7	71	4.15 (4.11)	4.02 (3.98)	3.50 (3.43)	0.1823 (0.2125)
9	4.1	75	4.48 (4.29)	4.36 (4.24)	3.96 (3.98)	0.0509 (−0.0834)
11	2.4	68	2.94 (2.82)	2.78 (2.71)	2.23 (2.22)	1.1400 (1.4170)
12	2.6	58	3.26 (3.15)	3.08 (3.01)	2.20 (2.12)	0.8334 (1.1700)

*Nous rappelons entre parenthèses les valeurs du tableau 2 situé à la page 2352 de la réf. 3.

$$W_i = \mathrm{TGC}_i + \mathrm{SC.DGC}_i$$

$$X_i = \mathrm{SC.RGC}_i - \mathrm{TGC}_i$$

$$Y_i = \mathrm{TGM}_i - \mathrm{TGH}_i + \mathrm{SH}(\mathrm{DGM}_i - \mathrm{DGH}_i)$$

$$Z_i = \mathrm{TGH}_i - \mathrm{TGM}_i + \mathrm{SH}(\mathrm{RGM}_i - \mathrm{RGH}_i)$$

L'équation 5 devient alors:

$$[15] \quad \Delta\sigma_i = W_i\chi_L{}^{CC} + X_i\chi_T{}^{CC} + Y_i\chi_L{}^{CH} + Z_i\chi_T{}^{CH}$$

La régression est effectuée sur le modèle représenté par l'équation 6. Avec aucun des trois ensembles, on n'a trouvé des coefficients significatifs.

Ensemble I: La matrice de corrélation entre les variables indépendantes montre qu'en fait elles ne sont pas indépendantes:

	W	X	Y	Z
W	1.000	−0.991	−0.997	0.609
X		1.000	0.983	−0.530
Y			1.000	−0.670
Z				1.000

Les variables X_i et Z_i sont successivement éliminées pour arriver finalement à l'équation 16:

$$[16] \quad \Delta\sigma_i = KW_i + LY_i + M$$

avec

$$K = -66.7 \pm 54.8$$

$$L = -101.4 \pm 60.6$$

$$M = 0.79 \pm 0.49$$

et un coefficient de corrélation multiple de 0.93.

Etant donné l'imprécision attachée aux coefficients K, L et M, et surtout leur peu de relation avec les paramètres cherchés, on peut conclure qu'il n'est pas possible, avec cet ensemble I, d'atteindre les susceptibilités longitudinales et transversales des liaisons C—C et C—H.

Ensemble II: La matrice de corrélation est très semblable à celle de l'ensemble I. Les variables X_i, Y_i et Z_i sont successivement retirées de la régression pour arriver à l'équation 17 avec un coefficient de corrélation multiple de 0.63.

$$[17] \quad \Delta\sigma_i = NW_i + P$$

avec

$$N = 12.6 \pm 4.3$$

et

$$P = 0.12 \pm 0.05$$

Le coefficient N, bien que mieux défini que les coefficients K et L de l'ensemble I, ne permet pas d'atteindre les paramètres cherchés.

Il nous a alors semblé intéressant de voir si l'introduction d'une contrainte arbitraire dans le calcul des χ_L et χ_T pouvait conduire à des solutions plus satisfaisantes. Nous avons pour cela introduit les susceptibilités moyennes (29)[2]

$$[18] \qquad 1/3(\chi_L{}^X + 2\chi_T{}^X) = SM^X$$

avec

$$SM^{CC} = -6.2$$

et

$$SM^{CH} = -6.41$$

On obtient alors l'équation 19 en combinant [15] et [18]:

$$[19] \quad (X_i - 2W_i)\chi_T{}^{CC} + (Z_i - 2Y_i)\chi_T{}^{CH} = \Delta\sigma_i - 3W_iSM^{CC} - 3Y_iSM^{CH}$$

Le résultat final de la régression est l'équation 20:

$$[20] \quad T(Z_i - 2Y_i) + R = \Delta\sigma_i - 3W_iSM^{CC} - 3Y_iSM^{CH}$$

Comme précédemment, le coefficient T représente, grâce à la bonne corrélation existant entre les variables $(X_i - 2W_i)$ et $(Z_i - 2Y_i)$ (le coefficient de corrélation est 0.96 pour les deux ensembles), une combinaison linéaire [21] entre $\chi_T{}^{CC}$ et $\chi_T{}^{CH}$:

$$[21] \qquad T = A\chi_T{}^{CC} + \chi_T{}^{CH}$$

et

$$R = B\chi_T{}^{CC} + K$$

Les valeurs de T, R, A et B sont pour les deux ensembles:

Ensemble I

$$T = 12.4 \pm 2.1$$

et

$$R = 0.60 \pm 0.06$$

$$A = -1.47 \pm 0.18$$

et

$$B = -0.056 \pm 0.005$$

Ensemble II

$$T = 7.4 \pm 2.1$$

et

$$R = 0.51 \pm 0.07$$

$$A = -1.59 \pm 0.12$$

et

$$B = -0.057 \pm 0.004$$

On voit que ces résultats ne permettent pas, non plus, d'atteindre les susceptibilités longitudinales et transversales.

Avec l'ensemble III, si l'on introduit les susceptibilités moyennes (avec les réserves exprimées précédemment), on peut effectuer la régression sur le modèle de l'équation 19. On trouve alors: $\chi_T{}^{CC} = -12.1 \pm 2.9$ et $\chi_T{}^{CH} = -12.5 \pm 3.8$ avec un coefficient de corrélation de 0.906 et une constante égale à -0.13 ± 0.10 p.p.m. D'après l'équation 18 on calcule: $\chi_L{}^{CC} = 5.6 \pm 5.8$ et $\chi_L{}^{CH} = 5.6 \pm 7.6$ en supposant les susceptibilités moyennes non entachées d'erreur. Ces valeurs, bien que non significatives, permettent de calculer des paramètres d'anisotropie: $\Delta\chi^{CC} = 17.7 \pm 8.7$ et $\Delta\chi^{CH} = 18.1 \pm 11.4$. Nous noterons encore que la non-nullité de la constante rend le modèle utilisé non conforme à celui de l'équation théorique 3.

Paramètres de la liaison C=C

Nous rappellerons brièvement le modèle utilisé, décrit dans la réf. 19:

$$[22] \quad \Delta\sigma_i = a_i\Delta\chi_1{}^{C=C} + b_i\Delta\chi_2{}^{C=C} - (e_i + f_i - c_i)\Delta\chi^{CH} - d_i\Delta\chi^{CC}$$

$\Delta\chi_1{}^{C=C}$ est l'anisotropie entre l'axe normal au plan nodal des orbitales π et à l'axe de la liaison C=C, $\Delta\chi_2{}^{C=C}$ est l'anisotropie entre l'axe de la liaison C=C et l'axe situé dans le plan nodal, perpendiculaire au précédent et passant au milieu de la liaison. Les paramètres géométriques a, b, c, d, e et f ont été définis au bas des tableaux 4, 5 et 6 de la référence 19. Dans ce précédent travail, il avait été montré que les valeurs de $\Delta\chi^{CC}$ et

[2]Il est permis d'être sceptique quant à la signification des paramètres obtenus en utilisant les susceptibilités moyennes. En effet, d'après Dorfman (30), ces dernières ne peuvent pas être considérées comme des quantités physiques mais plutôt comme des incréments permettant le calcul des susceptibilités moléculaires. Dans cette hypothèse, il est tout-à-fait incorrect de relier ces incréments à des paramètres, obtenus par des mesures r.m.n., qui ne sont pas, eux non plus, des quantités physiques mais des valeurs permettant de prévoir des variations de déplacements chimiques.

$\Delta\chi^{CH}$ calculées dans la référence 3 par la méthode 2 sont meilleures que celles obtenues par la méthode 1 (3). Nous avons dans le présent travail posé ces deux paramètres inconnus et les avons calculé:

$$\Delta\chi_1^{C=C} = -12.9 \pm 3.8$$
$$\Delta\chi_2^{C=C} = -15.2 \pm 6.4$$
$$\Delta\chi^{CC} = 15.0 \pm 4.4$$
$$\Delta\chi^{CH} = 13.4 \pm 9.4$$

avec un coefficient de corrélation de 0.952 et une constante non significative qui a été posée nulle comme le modèle [22] l'impose. Ces résultats confirment que $\Delta\chi^{CH}$ est le paramètre le moins bien défini. Il serait d'autre part imprudent d'attacher aux valeurs de $\Delta\chi^{CC}$ et $\Delta\chi^{CH}$ ainsi calculées un caractère de généralité. Il s'agit simplement des valeurs les plus cohérentes avec le modèle [22] et avec les points expérimentaux considérés.

Paramètres de la liaison C=O

Dans ce cas, le modèle mathématique décrit dans les références 24 et 25 est:

$$[23]\quad \Delta\sigma = \Delta\chi_1^{C=O}\langle g_1^M(CO)\rangle + \Delta\chi_2^{C=O}\langle g_2^M(CO)\rangle + K^{C=O}\langle g^E(CO)\rangle - \Delta\chi^{CH}[\langle g^M(CH_\alpha)\rangle + \langle g^M(CH_\beta)\rangle]$$

Les trois premiers termes représentent l'effet du groupe carbonyle introduit et les deux derniers l'effet des deux liaisons C—H enlevées. $\Delta\chi_1^{C=O}$ est l'anisotropie entre l'axe normal au plan nodal des orbitales π et à l'axe de la liaison C=O, $\Delta\chi_2^{C=O}$ est l'anisotropie entre l'axe σ de la liaison C=O et l'axe situé dans le plan nodal des orbitales π et perpendiculaire au précédent et $K^{C=O}$ est une constante proportionnelle au moment dipolaire électrique de la liaison C=O.

Les facteurs géométriques ont été définis précédemment (24, 25). Nous avons utilisé ceux obtenus à partir de mesures aux rayons X sur le squelette de l'androstérone, considéré comme un bon modèle pour les 20 couples (androstanes et androstanones) étudiés. Ces facteurs ont été donnés dans le tableau 2, p. 1331 de la réf. 25. L'effet du carbonyle en 17 sur le méthyle 18 ainsi que l'effet du carbonyle en 11 sur le méthyle 19 n'ont pas été considérés pour les raisons déja indiquées (25).

La première étape de la régression montre que la constante n'est pas significative et peut donc être posée nulle comme le modèle [23] l'exige. Les valeurs des paramètres d'anisotropie sont:

$$\Delta\chi_1^{C=O} = -31.2 \pm 2.8$$
$$\Delta\chi_2^{C=O} = -23.5 \pm 8.6$$
$$K^{C=O} = -6.2 \pm 2.5$$
$$\Delta\chi^{CH} = 5.5 \pm 8.5$$

Le coefficient $\Delta\chi^{CH}$ n'étant pas significatif, les facteurs géométriques des liaisons C—H peuvent être supprimés de la régression. On obtient alors de nouvelle valeurs:

$$\Delta\chi_1^{C=O} = -31.1 \pm 2.8$$
$$\Delta\chi_2^{C=O} = -19.6 \pm 6.3$$
$$K^{C=O} = -7.4 \pm 1.7$$

avec un coefficient de corrélation de 0.989. Dans ce cas, il semble que la contribution des liaisons C—H aux $\Delta\sigma$ expérimentaux soit négligeable, mais ce n'est pas suffisant pour généraliser, à partir de cette expérience particulière, la valeur $\Delta\chi^{CH} = 0$.

Conclusion

Une méthode générale de régression multilinéaire nous a permis de rechercher une corrélation entre les variations de déplacements chimiques provoqués par le remplacement d'un proton par un groupe méthyle sur un proton voisin, et les paramètres géométriques de la molécule, au moyen des modèles mathématiques proposés par McConnell d'une part et ApSimon et coll. d'autre part.

On constate d'abord qu'aucun des deux modèles, dans le cas des liaisons C—C et C—H, n'est parfaitement compatible avec les résultats expérimentaux puisqu'une constante significative non nulle nécessaire à la régression doit être ajoutée au modèle. De plus, il arrive souvent qu'aucun des coefficients ne soit significatif. Il nous a donc été impossible, avec les données r.m.n. expérimentales dont nous disposions, d'atteindre les paramètres d'anisotropie des liaisons C—C et C—H. Une explication plausible est que l'influence de l'anisotropie de ces liaisons est suffisament faible pour n'être pas significative, compte tenu, d'une part de l'imprécision des $\Delta\sigma$ expérimentaux (puisqu'une même géométrie peut conduire à des valeurs très différentes), et d'autre part à la diffi-

culté d'obtenir des paramètres géométriques convenables. En effet, si les erreurs de mesure à partir des modèles moléculaires ont été réduites au maximum par utilisation d'instruments de mesure adéquats (31), rien ne prouve que le modèle soigneusement mesuré représente correctement la géométrie exacte de la molécule étudiée.

Quant à la possibilité de calculer les susceptibilités longitudinales et transversales au moyen de l'équation d'ApSimon et coll., elle est à exclure car seul le terme correctif peut permettre ce calcul. Il serait donc nécessaire de disposer de points expérimentaux particuliers pour lesquels ce terme ne serait pas négligeable devant les imprécisions expérimentales. Il nous semble donc que, même en admettant une contribution purement magnétique à la variation des déplacements chimiques ainsi que la validité des deux modèles ci-dessus, celui d'ApSimon et coll. est beaucoup trop élaboré pour être utilisé de façon courante, et qu'il devrait être réservé aux cas pour lesquels la précision des mesures serait telle que l'équation de McConnell ne constituerait plus un modèle suffisant.

La conclusion ultime de ce travail est qu'il faut être très critique vis-à-vis de toute valeur numérique provenant d'un traitement de données expérimentales par la méthode des moindres carrés lorsqu'une analyse statistique de la validité des résultats n'est pas effectuée. Le calcul des intervalles de confiance nous a, en effet, permis de montrer qu'il est possible de calculer, à partir de données r.m.n., les paramètres d'anisotropie des liaisons C═C et C═O avec une précision acceptable. Notons bien que cela ne prouve pas que ces valeurs représentent physiquement des anisotropies de liaisons. Elles doivent plutôt être considérées comme des nombres permettant dans certains cas de prévoir l'influence de ces liaisons sur les déplacements chimiques de protons voisins. Il faut donc être prudent en essayant de généraliser la validité de telle ou telle valeur (32).

Partie expérimentale

Les calculs ont été effectués sur l'ordinateur IBM 360-40 du Centre de Calcul de l'Université des Sciences et Techniques du Languedoc ainsi que sur l'ordinateur IBM 1130 du Centre de Calcul de l'Université de Provence. Le programme REGMUL (Fortran IV) peut être envoyé sur demande.

Appendice

(Voir la fig. 1 pour la définition des paramètres géométriques.)

Nous rappellerons tout d'abord les résultats d'ApSimon et coll. (3):

$$\left\langle \frac{\cos^2\theta_\varphi}{R_\varphi^3} \right\rangle = \frac{1}{4b^2}\left\langle \frac{1}{R_\varphi} \right\rangle - \frac{a^2-b^2}{2b^2}\left\langle \frac{1}{R_\varphi^3} \right\rangle + \frac{(a^2-b^2)^2}{4b^2}\left\langle \frac{1}{R_\varphi^5} \right\rangle$$

On peut écrire:

$$\left\langle \frac{1}{R_\varphi} \right\rangle = \frac{2K}{\pi\sqrt{m}}$$

$$\left\langle \frac{1}{R_\varphi^3} \right\rangle = \frac{2E}{\pi n\sqrt{m}}$$

$$\left\langle \frac{1}{R_\varphi^5} \right\rangle = \frac{2H}{\pi n^2\sqrt{m}}$$

Dans ces équations, K et E sont les intégrales elliptiques de premier et second ordre. H, h, n et m sont définis de la façon suivante:

$$h = R_a^2 + r^2$$

$$n = h - 2rl$$

$$m = h + 2rl$$

et

$$H = \frac{4hE - nK}{3m}$$

Nous avons étendus ici ces calculs afin d'obtenir la correction aux courtes distances sur le méthyle en libre rotation:

$$\left\langle \frac{\cos^2\theta_\varphi}{R_\varphi^5} \right\rangle = \frac{(a^2-b^2)^2}{4b^2}\left\langle \frac{1}{R_\varphi^7} \right\rangle - \frac{a^2-b^2}{2b^2}\left\langle \frac{1}{R_\varphi^5} \right\rangle + \frac{1}{4b^2}\left\langle \frac{1}{R_\varphi^3} \right\rangle$$

$$\left\langle \frac{\cos^4\theta_\varphi}{R_\varphi^5} \right\rangle = \frac{1}{16b^4}\left\langle \frac{1}{R_\varphi} \right\rangle - \frac{a^2-b^2}{4b^4}\left\langle \frac{1}{R_\varphi^3} \right\rangle + \frac{3(a^2-b^2)^2}{8b^4}\left\langle \frac{1}{R_\varphi^5} \right\rangle - \frac{(a^2-b^2)^3}{4b^4}\left\langle \frac{1}{R_\varphi^7} \right\rangle + \frac{(a^2-b^2)^4}{16b^4}\left\langle \frac{1}{R_\varphi^9} \right\rangle$$

$$\left\langle \frac{\sin^2\theta_\varphi}{R_\varphi^5} \right\rangle = \left\langle \frac{1}{R_\varphi^5} \right\rangle - \left\langle \frac{\cos^2\theta_\varphi}{R_\varphi^5} \right\rangle$$

$$\left\langle \frac{\sin^4\theta_\varphi}{R_\varphi^5} \right\rangle = \left\langle \frac{1}{R_\varphi^5} \right\rangle - 2\left\langle \frac{\cos^2\theta_\varphi}{R_\varphi^5} \right\rangle + \left\langle \frac{\cos^4\theta_\varphi}{R_\varphi^5} \right\rangle$$

Les deux intégrales nécessaires sont:

$$\left\langle \frac{1}{R_\varphi^{\,7}} \right\rangle = \frac{2I}{\pi n^3 \sqrt{m}} \quad \text{avec} \quad I = \frac{8hH - 3nE}{5m}$$

$$\left\langle \frac{1}{R_\varphi^{\,9}} \right\rangle = \frac{2J}{\pi n^4 \sqrt{m}} \quad \text{et} \quad J = \frac{12hI - 5nH}{7m}$$

Note. Les paramètres a, l, et R_a peuvent, soit être mesurés directement sur les modèles Dreiding comme l'ont fait ApSimon et coll. (3, 31), soit être calculés en fonction des paramètres R et γ au moyen des équations suivantes:

$$a = (d^2 + R^2 + 2dR\cos\gamma)^{1/2}$$

$$l = R\sin\gamma$$

$$R_a = [(d + h)^2 + R^2 + 2(d + h)R\cos\gamma]^{1/2}$$

Le Dr. K. J. Toyne (Department of Chemistry, The University, Hull, England) nous a informé récemment avoir effectué un travail similaire sur la liaison C=O (33, 34). Nous le remercions d'avoir accepté de discuter et de comparer nos résultats avec les siens.

1. J. ELGUERO, A. FRUCHIER, et R. GIL. Bull. Soc. Chim. Fr. 4403 (1968).
2. J. ELGUERO et A. FRUCHIER. Bull. Soc. Chim. Fr. 496 (1970).
3. J. W. APSIMON, W. G. CRAIG, P. V. DEMARCO, D. W. MATHIESON, L. SAUNDERS et W. B. WHALLEY, Tetrahedron, **23**, 2339 (1967).
4. A. A. BOTHNER-BY et C. NAAR-COLIN. Ann. N.-Y. Acad. Sci. **70**, 833 (1958).
5. P. T. NARASIMHAN et M. T. ROGERS. J. Chem. Phys. **31**, 1302 (1959).
6. J. I. MUSHER. J. Chem. Phys. **35**, 1159 (1961).
7. J. I. MUSHER. Mol. Phys. **6**, 93 (1963).
8. A. G. MORITZ et N. SHEPPARD. Mol. Phys. **5**, 361 (1962).
9. R. SUSTMANN, R. HUISGEN et H. HUBER. Chem. Ber. **100**, 1802 (1967).
10. J. HOMER et D. CALLAGHAN. J. Chem. Soc. A, 439 (1968).
11. L. D. HALL. Tetrahedron Lett. 1457 (1964).
12. Y. YAMAGUCHI et S. BROWNSTEIN. J. Phys. Chem. **68**, 1572 (1964).
13. R. F. ZURCHER. Helv. Chim. Acta, **44**, 1755 (1961).
14. J. TILLIEU. Ann. Phys. Paris, **2**, 471 et 631 (1957).
15. R. F. ZURCHER. J. Chem. Phys. **37**, 2421 (1962).
16. D. W. DAVIES. Mol. Phys. **6**, 489 (1963).
17. J. A. POPLE. Discuss. Faraday Soc. **34**, 68 (1962).
18. G. S. REDDY et J. H. GOLDSTEIN. J. Chem. Phys. **38**, 2736 (1963).
19. J. W. APSIMON, W. G. CRAIG, P. V. DEMARCO, D. W. MATHIESON, L. SAUNDERS et W. B. WHALLEY. Tetrahedron, **23**, 2357 (1967).
20. L. M. JACKMAN et S. STERNHELL. Applications of NMR spectroscopy in organic chemistry. Pergamon Press, Oxford. 1969.
21. D. MATHIEU. Thèse, Université de Provence. 1971.
22. E. PRETSCH, H. IMMER, C. PASCUAL, K. SCHAFFNER et W. SIMON. Helv. Chim. Acta, **50**, 105 (1967).
23. J. W. APSIMON, W. G. CRAIG, P. V. DEMARCO, D. W. MATHIESON et W. B. WHALLEY. Tetrahedron, **23**, 2375 (1967).
24. J. W. APSIMON, P. V. DEMARCO, D. W. MATHIESON, W. G. CRAIG, A. KARIM, L. SAUNDERS et W. B. WHALLEY. Tetrahedron, **26**, 119 (1970).
25. J. W. APSIMON et H. BEIERBECK. Can. J. Chem. **49**, 1328 (1971).
26. N. R. DRAPER et H. SMITH. Applied regression analysis. J. Wiley and Sons, New York. 1966.
27. J. W. APSIMON, H. BEIERBECK et D. K. TODD. Can. J. Chem. **50**, 2351 (1972).
28. Scientific Subroutine Package, IBM Application Programme, H 20-0205-3.
29. P. PASCAL, A. PACAULT et J. HOARAU. C. R. Acad. Sci. Paris, **233**, 1078 (1951).
30. YA. G. DORFMAN. Diamagnetism and the chemical bond. Edward Arnold Ltd., London. 1965. chapitre IV.
31. J. W. APSIMON, P. V. DEMARCO et A. RAFFLER. Chem. Ind. 1792 (1966).
32. F. H. A. RUMMENS. J. Magn. Reson. **6**, 550 (1972).
33. A. K. DAVIS, D. W. MATHIESON, P. D. NICKLIN, J. R. BELL et K. J. TOYNE. Tetrahedron Lett. 413 (1973).
34. K. J. TOYNE. Tetrahedron, **29**, 3889 (1973).

Kinetic and Equilibrium Studies of the Reactions of 2,4,6-Trinitrotoluene and 2,4,6-Trinitrotoluene-d_3 with Sodium and Potassium *t*-Butoxide in *t*-Butanol

ERWIN BUNCEL, ALBERT RICHARD NORRIS,[1] KENNETH EDWIN RUSSELL, AND HAROLD WILSON

Department of Chemistry, Queen's University, Kingston, Ontario

Received October 30, 1973

ERWIN BUNCEL, ALBERT RICHARD NORRIS, KENNETH EDWIN RUSSELL, and HAROLD WILSON. Can. J. Chem. **52,** 2306 (1974).

The reactions of 2,4,6-trinitrotoluene (TNT) and 2,4,6-trinitrotoluene fully deuterated at the methyl position (TNT-d_3) with sodium and potassium *t*-butoxide in *t*-butanol have been studied. With TNT as the substrate, proton abstraction by ion-paired sodium or potassium *t*-butoxide appears to be the predominant reaction in solution. With sodium *t*-butoxide as base, the forward rate constant for proton abstraction at 30.0 °C ($k_{f,ip}$) is 6000 ± 400 M^{-1} s^{-1} while $\Delta H^{\ddagger}$ and $\Delta S^{\ddagger}$ for the reaction are 4.2 ± 0.3 kcal mol^{-1} and −27 ± 2 cal deg^{-1} mol^{-1}, respectively. With TNT-d_3 as the substrate, formation of a TNT-d_3 – *t*-butoxide ion σ-complex occurs simultaneously with deuteron abstraction. Specific rate constants for the two processes have been determined at 30.0 °C. Initial rate studies establish a hydrogen–deuterium kinetic isotope effect of 8 ± 1 for the formation of the anion in *t*-butanol.

ERWIN BUNCEL, ALBERT RICHARD NORRIS, KENNETH EDWIN RUSSELL et HAROLD WILSON. Can. J. Chem. **52,** 2306 (1974).

On a étudié les réactions du trinitro-2,4,6 toluène (TNT) et du trinitro-2,4,6 toluène complètement deutérié en position méthyle (TNT-d_3) avec les *tert*-butylates de sodium ou de potassium dans le *tert*-butanol. Avec le TNT comme substrat, il semble que l'enlèvement d'un proton, par un *tert*-butylate de potassium ou de sodium sous forme de paire d'ions, soit la réaction prédominante dans la solution. Lorsque le *tert*-butylate de sodium est utilisé comme base, la constante de vitesse pour l'enlèvement du proton à 30 °C ($k_{f,ip}$) est de 6000 ± 400 M^{-1} s^{-1}; les $\Delta H^{\ddagger}$ et $\Delta S^{\ddagger}$ de la réaction sont respectivement de 4.2 ± 0.3 kcal mol^{-1} et −27 ± 2 cal deg^{-1} mol^{-1}. Lorsque le substrat est le TNT-d_3, la formation d'un complexe σ entre le TNT-d_3 et l'ion *tert*-butylate se produit simultanément avec l'enlèvement d'un deutérium. On a déterminé les constantes de vitesse spécifique pour les deux réactions à 30 °C. Des études sur les vitesses initiales ont permis d'établir que dans le *tert*-butanol, l'effet isotopique cinétique hydrogène–deutérium, pour la formation de l'anion, est de 8 ± 1.

[Traduit par le journal]

Introduction

In the corresponding alcohol, and with base in excess, alkoxide ion reacts with 2,4,6-trinitrotoluene (TNT) and 2,4,6-trinitrotoluene fully deuterated at the methyl position (TNT-d_3) to yield two main products. The predominant nitroaromatic species at equilibrium is the purple anion **1** (X = H or D) resulting from proton or deuteron transfer from the substrate to the alkoxide ion. During the early stages of the reaction a σ-complex is also formed by attack of the alkoxide ion (Y^-) either at the C-1 or -3 position of the substrate to yield **2***a* (X = H or D) or **2***b* (X = H or D), respectively.

The extent to which σ-complex formation occurs and the rates of its formation and decomposition are markedly dependent on the solvent–base pair (1, 2). With ethoxide ion in ethanol, the extent of σ-complex formation is slight and the rates of formation and decomposition of the σ-complex are large compared to the rate of formation of the purple anion. As a result, kinetic data relating to the formation of the purple anion can be analyzed readily to yield both the equili-

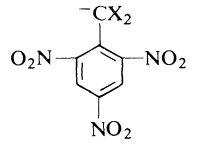

1

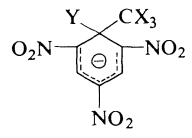

2*a*

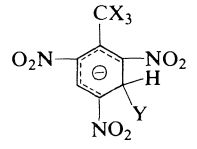

2*b*

[1]Author to whom all correspondence should be addressed.

Can. J. Chem. Downloaded from www.nrcresearchpress.com by 210.87.254.40 on 09/05/12
For personal use only.

Can. J. Chem. Downloaded from www.nrcresearchpress.com by 210.87.254.40 on 09/05/12
For personal use only.

brium constant for σ-complex formation and the specific rate constant for proton transfer. With isopropoxide ion in isopropanol, the rates of proton transfer and σ-complex formation are comparable in magnitude and it is not possible to choose reaction conditions such that one of the processes is predominant.

In the reactions of the alkali-metal alkoxides with TNT and TNT-d_3 in the higher alcohols, ion-pairing effects have to be taken into account. Thus, with sodium isopropoxide in isopropanol both "free" and "ion-paired" isopropoxide ions exist in solution and these species possess different reactivities in proton transfer and σ-complex formation (2). Ion-pairing effects may also contribute to changes in the relative stabilities of the purple anion and the σ-complex.

The results of kinetic and equilibrium studies of sulfite ion and cyanide ion σ-complex formation with TNT and 1,3,5-trinitrobenzene (TNB) (3, 4), and of σ-complex formation between TNB and the lyate ions of methanol, ethanol, *n*-propanol, isopropanol, *n*-butanol, isobutanol, and *t*-butanol in the corresponding solvents (5) led us to expect both a small equilibrium constant and a relatively small forward rate constant for formation of the TNT – *t*-butoxide ion σ-complex. On the other hand, ion-pairing effects were expected to be more pronounced in *t*-butanol than in any of the alcohols used previously. It seemed possible therefore that studies of the reactions of TNT and TNT-d_3 with alkali-metal *t*-butoxides in *t*-butanol might yield more detailed information concerning the reactivities of "ion-paired" and "free" lyate ions in proton and deuteron transfer reactions. The results of studies of the reactions of TNT and TNT-d_3 with sodium and potassium *t*-butoxide in *t*-butanol are presented here.

Experimental

Materials

The preparation and purification of TNT and TNT-d_3 were as previously described (1, 2). Reagent grade *t*-butanol was refluxed over Linde 4Å Molecular Sieve for several hours then distilled under nitrogen. Only the middle fraction of the distillate was retained. Solutions of sodium *t*-butoxide and potassium *t*-butoxide were prepared and standardized as previously described (5).

Procedure

The equipment and the procedures used in carrying out kinetic measurements and in obtaining equilibrium constants for formation of the purple anion have been described previously (1, 2, 5).

Results

The addition of a 2×10^{-5} *M* solution of TNT in *t*-butanol to a *t*-butanol solution of sodium or potassium *t*-butoxide (4×10^{-3} *M*) results in the rapid formation of a purple colored species. The purple color then gradually fades and is replaced by a stable yellow colored species ($\lambda_{max} \simeq$ 395 nm). With all the reaction conditions the same, but with TNT-d_3 as the substrate, the reaction mixture passes through an initial purple stage before turning brown and then yellow in color. The absorption maximum of the final solution again occurs at approximately 395 nm. At base concentrations above 1×10^{-2} *M*, the rate of conversion of either TNT or TNT-d_3 to the yellow species becomes competitive with the rate of formation of the purple species; consequently, most of the kinetic results described here were obtained in runs carried out at base concentrations below 1×10^{-2} *M*.

Attempts were made to measure the equilibrium constant associated with formation of the purple species employing solutions 3.0×10^{-5} to 1.5×10^{-4} *M* in TNT and 6.0×10^{-5} to 5.0×10^{-3} *M* in base. As the equilibrium constant (K) associated with the formation of the purple species is large, accurate values of the absorbance associated with the purple species (A_∞) obtained under conditions of low ratios of base concentration to TNT concentration are required in order to obtain accurate values of K (6). Over the range of TNT concentrations which could be used in the stopped-flow experiments, A_∞ values at the lowest base concentrations employed (6.0×10^{-5} to 5.0×10^{-4} *M*) were not reproducible, possibly because of neutralization of some of the base by absorbed carbon dioxide. At higher concentrations of base (5.0×10^{-4} to 5.0×10^{-3} *M*) the fading reaction (the conversion of purple species to yellow species) was sufficiently fast that the errors associated with the extrapolation of the absorbance *vs.* time curve of the fade reaction back to the time of mixing were comparable to the changes in A_∞ expected as a result of changes in the base concentration. Because of the difficulties in obtaining accurate A_∞ values the studies yielded only upper and lower limits on K (as defined by eq. 1) at 30.0 °C. These are 10^6 and 5×10^4 M^{-1}, respectively.

$$[1] \quad K = \frac{[TNT^-]}{\{[TNT]_0 - [TNT^-]\}\{[MOR]_0 - [TNT^-]\}}$$

Can. J. Chem. Downloaded from www.nrcresearchpress.com by 210.87.254.40 on 09/05/12
For personal use only.

In eq. 1, MOR represents sodium or potassium *t*-butoxide, [TNT^-] represents the equilibrium concentration of the purple species, and [ ]$_0$ represents the total (stoichiometric) concentration of the species indicated.

In the kinetic studies the reaction of TNT with potassium *t*-butoxide (KOR) at 30.0 °C was monitored at three wavelengths (420, 520, and 650 nm) whereas the reaction of TNT with sodium *t*-butoxide (NaOR) was followed at 430, 520, and 630 nm over the range of temperatures 30–50 °C. For each base, at each base concentration employed and each wavelength at which absorbances (A) were measured, plots of log ($A_\infty - A_t$) *vs.* time were linear to at least 80% completion of reaction. For a given concentration of either base, the slopes of the log ($A_\infty - A_t$) *vs.* time plots ($\equiv k_{obs}/2.303$) were, within experimental error, independent of the wavelengths at which values of A were measured. At the same [MOR]$_0$, temperature, and [TNT]$_0$, k_{obs} for the TNT–NaOR reaction was always less than the k_{obs} for the TNT–KOR reactions (Fig. 1).

For the TNT–KOR reaction the plot of k_{obs} *vs.* [KOR]$_0$ at 30.0 °C was linear and passed through the origin (Fig. 1). There was also a good linear correlation between log k_{obs} and the indicator acidity function H_r^{BuOH} (7). Plots of k_{obs} *vs.* [NaOR]$_0$ were linear at all temperatures. However, unlike the corresponding plots for the TNT–KOR reaction, they did not pass through the origin but crossed the X-axis at a small positive value (see Fig. 1 for comparative plots of 30.0 °C). The magnitude of the intercept on the X-axis was found to decrease with increasing temperature, as indicated in Fig. 2. The slopes of the k_{obs} *vs.* [NaOR]$_0$ plots at various temperatures are listed in Table 1. A linear log k_{obs} *vs.* H_r^{BuOH} relationship was also observed for the TNT–NaOR reaction.

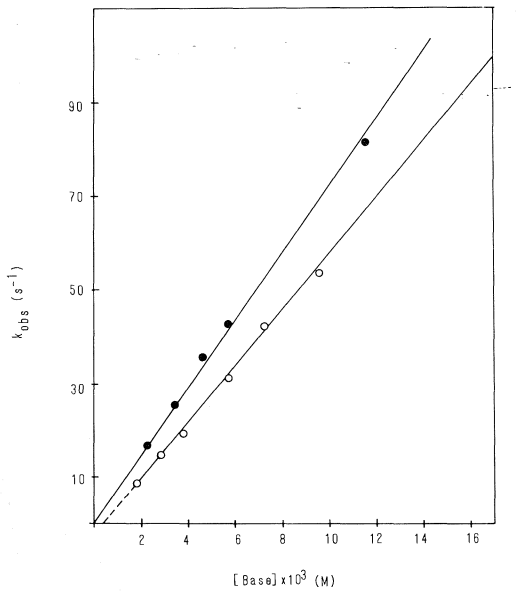

FIG. 1. Plots of k_{obs} *vs.* [Base] for the reactions of 2,4,6-trinitrotoluene with potassium *t*-butoxide (●) and sodium *t*-butoxide (○) in *t*-butanol. T = 30.0 °C. Absorbances recorded at 520 nm.

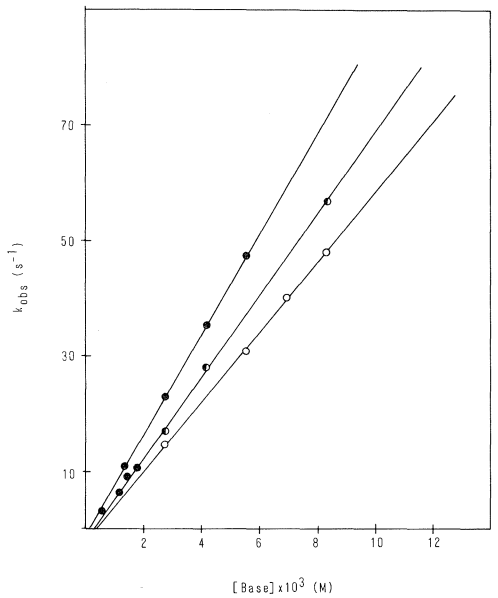

FIG. 2. Plots of k_{obs} *vs.* [Base] for the reaction of 2,4,6-trinitrotoluene with sodium *t*-butoxide in butanol at 30.0 (○), 34.9 (◐), and 44.9 °C (●). Absorbances recorded at both 430 and 520 nm.

The addition of various amounts of $NaBPh_4$ to reaction mixtures containing a fixed [TNT]$_0$ and [NaOR]$_0$ had no apparent effect on the value of k_{obs} for the reaction (Table 2). The only noticeable effect of increasing the total salt concentration was to increase the value of A_∞ at 420 nm and to decrease the value of A_∞ at 650 nm (Table 2). These changes in A_∞ values were not, however, proportional to the concentration of added $NaBPh_4$. Thus, there was a sharp decrease in A_∞ at 650 nm from 0.551 (no added salt) to 0.405 on making the solution 5×10^{-3} M in $NaBPh_4$ and further additions of $NaBPh_4$ caused no further change in A_∞.

A series of TNT–NaOR reactions at 30.0 °C

Can. J. Chem. Downloaded from www.nrcresearchpress.com by 210.87.254.40 on 09/05/12
For personal use only.

TABLE 1. Slopes of the k_{obs} *vs.* $[NaOR]_0$ plots at various temperatures for the 2,4,6-trinitrotoluene – sodium *t*-butoxide reaction[a]

Temperature (°C)	Slope (M^{-1} s^{-1})
30.0	6000 ± 400
30.2	6200 ± 400[b]
34.9	7100 ± 300
35.0	6900 ± 200
39.6	7800 ± 300
40.1	8000 ± 300[c]
40.5	8100 ± 300[b]
44.2	8600 ± 400
44.9	8800 ± 400
49.9	9600 ± 500[b]

[a]k_{obs} based on calculations employing absorbance changes at 520 nm unless indicated otherwise.
[b]Absorbance change monitored at 630 nm.
[c]Absorbance change monitored at 340 nm.

were carried out at a total concentration of NaOR plus $NaBPh_4$ equal to 4.69×10^{-3} *M* but varying concentration of NaOR (9.40×10^{-4} to 4.69×10^{-3} *M*). In all cases, linear log $(A_\infty - A_t)$ *vs.* time plots were obtained using absorbance data recorded at either 650 or 420 nm. Values of k_{obs} were, within experimental error, independent of the wavelength used to monitor the reaction (Table 2). Linear k_{obs} *vs.* $[NaOR]_0$ plots were obtained which, as in the case of runs not carried out at a fixed total salt concentration, did not pass through the origin. The slopes of the k_{obs} *vs.* $[NaOR]_0$ plots at 30.0 °C were 7300 ± 500 M^{-1} s^{-1}.

Kinetic Studies Employing TNT-d_3 as the Substrate

In the reactions of TNT-d_3 with KOR at 30.0 °C, plots of log $(A_\infty - A_t)$ *vs.* time were not linear when the absorbances were recorded at 520 and 650 nm and the range of base concentrations employed was 1.15×10^{-3} to 1.15×10^{-2} *M*. For the same range of base concentrations linear log $(A_\infty - A_t)$ *vs.* time plots to 60–70% completion of reaction could be obtained when absorbances were measured at 430 nm. The resulting plot of k_{obs} *vs.* $[KOR]_0$ was linear (slope = 1800 ± 100 M^{-1} s^{-1}) and passed through the origin.

In the TNT-d_3 – NaOR reaction at 30.0 °C, plots of log $(A_\infty - A_t)$ *vs.* time, utilizing absorbance values measured at 650 nm, were not linear at any of the base concentrations employed in the runs (1.0×10^{-4} to 1.15×10^{-2} *M*). When absorbances were recorded at 430 and 520 nm, plots of log $(A_\infty - A_t)$ *vs.* time were markedly curved in those runs in which the $[NaOR]_0$ was less than 2×10^{-3} *M* but showed no curvature for runs in which the $[NaOR]_0$ was greater than 5×10^{-3} *M*. For a given base concentration above 5×10^{-3} *M*, k_{obs}^{430}, the pseudo first-order rate constant based on absorbance changes recorded at 430 nm, was always greater than k_{obs}^{520}, the pseudo first-order rate constant based on absorbance changes recorded at 520 nm. The plot of k_{obs}^{430} *vs.* $[NaOR]_0$ was linear with a positive intercept. A plot of k_{obs}^{520} *vs.* $[NaOR]_0$ was also linear but intercepted the X-axis at a small positive value of approximately the same magnitude (4×10^{-4} *M*) as observed in the case of the k_{obs} *vs.* [NaOR] plots for the TNT–NaOR reaction. The slopes of the two lines were 1650 ± 150 and 1340 ± 100 M^{-1} s^{-1}, respectively.

Studies of the TNT-d_3 – NaOR reaction at a fixed total salt concentration of 4.69×10^{-3} *M* but varying $[NaOR]_0$ over the range 9.4×10^{-4} to 4.69×10^{-3} *M* yielded linear log $(A_\infty - A_t)$ *vs.* time plots for absorbance data recorded at 650 nm but non-linear log $(A_\infty - A_t)$ *vs.* time plots for absorbance data recorded at 420 nm (contrast to runs carried out at variable salt concentrations). The k_{obs}^{650} *vs.* $[NaOR]_0$ plot for this system at 30.0 °C was linear with slope 800 ± 100 M^{-1} s^{-1} and showed a small positive intercept on the X-axis.

Initial rate measurements of the TNT–NaOR and TNT-d_3 – NaOR reactions were carried out at 30.0 °C at a number of wavelengths in the visible region. The results are given in Table 3.

Discussion

Equilibrium Studies Employing TNT and TNT-d_3 as the Substrates

The purple species formed in the reaction of TNT or TNT-d_3 with NaOR or KOR in *t*-butanol shows an absorption maximum at 520 nm (ε 13 500 ± 500 M^{-1} cm^{-1}) and a shoulder with mid-point at approximately 650 nm (ε 6700 ± 500 M^{-1} cm^{-1}). The spectrum is identical to that recorded for the purple species formed in the reaction of TNT with ethoxide ion in ethanol (1, 8) and is similarly ascribed to anion **1** (X = H or D).

The formation of **1** (X = H) in the reactions of

Can. J. Chem. Downloaded from www.nrcresearchpress.com by 210.87.254.40 on 09/05/12
For personal use only.

TABLE 2. Values of k_{obs} for the 2,4,6-trinitrotoluene – sodium *t*-butoxide reaction at $T = 30.0$ °C

$[NaOR]_0 \times 10^3$ (M)	$[NaBPh_4] \times 10^3$ (M)	A_∞^{665}	A_∞^{435}	k_{obs}^{665} (s^{-1})	k_{obs}^{435} (s^{-1})
(i) fixed concentration of base, variable total salt concentration					
2.08	0	0.551	0.539	12.0	13.4
2.08	5.2	0.404	0.647	12.2	12.5
2.08	10.4	0.414	0.647	14.3	12.5
2.08	15.6	0.405	0.619	14.3	14.5
2.08	23.9	0.404	0.574	11.6	12.5
(ii) fixed total salt, variable base concentration					
0.94	3.75	—	—	2.90	2.65
1.41	3.28	—	—	6.79	6.44
2.35	2.34	—	—	14.96	13.40
3.28	1.41	—	—	23.16	20.67
4.22	0.47	—	—	30.20	26.62
4.69	0	—	—	30.10	31.21

TABLE 3. Results of initial rate[a] studies of the 2,4,6-trinitrotoluene- and 2,4,6-trinitrotoluene-d_3 – sodium *t*-butoxide reactions.[b] $T = 30.0$ °C

λ(nm)	$(IR)_H \times 10^{-7}$ (M^{-2} s^{-1})	$(IR)_D \times 10^{-7}$ (M^{-2} s^{-1})	$(IR)_H/(IR)_D$	$(IR)_H/\varepsilon_T l$ (M^{-1} s^{-1})	$(IR)_D/\varepsilon_T l$ (M^{-1} s^{-1})	$k_{f_H} - k_{f_D}$[c] (M^{-1} s^{-1})
375	6.94	1.29	5.37	7120	1325	5795
395	5.42	1.83	2.96	5420	1830	3590
415	5.07	3.02	1.67	5136	3059	2077
435	5.68	5.00	1.14	5483	4827	656
455	7.93	5.20	1.53	5768	3782	1986
475	12.00	6.24	1.92	6318	3286	3032
495	11.95	4.85	2.46	4939	2004	2935
515	17.82	6.18	2.88	6614	2294	4320
535	15.43	6.60	2.34	5630	2408	3222
555	13.07	4.84	2.70	5581	2067	3514
575	10.00	2.86	3.49	5863	1667	4196
595	7.80	2.42	3.22	5331	1654	3677
615	8.34	1.10	7.58	5874	778	5096
665	6.81	0.82	8.30	5536	667	4869

[a]Initial rates: $(IR)_H = (dA/dt)_{t=0}/[TNB]_0[NaOR]_0$; $(IR)_D = (dA/dt)_{t=0}/[TNT\text{-}d_3]_0[NaOR]_0$; errors in initial rates can be as high as 10%.
[b]$[TNT]_0 = 2.996 \times 10^{-5}$ M, $[NaOR]_0 = 2.40 \times 10^{-3}$ M; $[TNT\text{-}d_3]_0 = 2.835 \times 10^{-5}$ M, $[NaOR]_0 = 4.80 \times 10^{-3}$ M.
[c]$((IR)_H - (IR)_D)/\varepsilon_T l = k_{f_H} - k_{f_D}$.

TNT with the lyate ions of methanol, ethanol, *n*-propanol, isopropanol, and *n*-butanol in the corresponding alcohols is characterized by a linear log K *vs.* E_T plot with slope -0.55 ± 0.05 (data in Table 4). The value of log K, for the case in which the lyate ion is *t*-butoxide, is significantly lower (4 log K units) than might have been expected on the basis of the E_T value of *t*-butanol. Entirely analogous behavior has been observed in the formation of σ-complex **3** as a result of reaction of the lyate ions of methanol, ethanol, *n*-propanol, isopropanol, *n*-butanol, isobutanol, and *t*-butanol with 1,3,5-trinitrobenzene (TNB) in the corresponding alcohols (5).

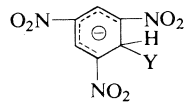

3

Y = CH_3O, C_2H_5O, *n*- and iso-C_3H_7O, *n*-, iso-, and *t*-C_4H_9O

The lower than expected value of K (~4 log K units) in the formation of **3** (Y = *t*-C_4H_9O) in *t*-butanol was attributed to steric effects associated with the addition of the *t*-butoxide group at a ring carbon of TNB (5). However, while there are undoubtedly greater steric effects associated

TABLE 4. Equilibrium constants (K) for purple anion formation from TNT and ε values of the purple anion at 520 nm[a]

Solvent	E_T[b]	$K(M^{-1})$	ε (M^{-1} cm^{-1})
Methanol	64.6	6.7±0.3	13 500±350
Ethanol	61.2	2069±105	13 000±270
n-Propanol	60.0	6500±500	13 200±200
n-Butanol	59.2	12 300±1000	13 100±300
Isopropanol	57.2	240 000±40 000	13 600±200
t-Butanol	51.1	$>5\times10^4$ $<10^6$	13 200±500

[a]T = 25.0 °C in all cases except *t*-butanol where T = 30.0 °C.
[b]E_T values determined using 1-(*p*-hydroxyphenyl)-2,4,6-triphenylpyridinium betaine as described in ref. 4.

with the reaction of *t*-butoxide ion with TNT than with the reaction of methoxide, ethoxide, *n*-propoxide, isopropoxide, and *n*-butoxide with TNT, it seems unlikely that the steric effects associated with the TNT – *t*-butoxide reaction to form **1** (X = H) are as large as those associated with the TNB – *t*-butoxide reaction to form σ-complex **3** (Y = *t*-C_4H_9O). The explanation previously offered for this effect must therefore be reexamined.

A possible alternate explanation for the observed behavior is that, in the lower alcohols, dissociation of metal alkoxide is essentially complete under all the reaction conditions employed and the reaction being studied is between a solvated alkoxide ion and the substrate. With TNT as the substrate, the measured K for reaction 2 is

$$\text{[2]} \qquad \text{TNT} + \text{Y}^- \underset{k_{b,i}}{\overset{k_i}{\rightleftharpoons}} \mathbf{1}\ (\text{X} = \text{H}) + \text{HY}$$

thus equal to $k_i/k_{b,i}$, where k_i is the specific rate constant for reaction of the substrate and the solvated alkoxide ion (Y^-) and $k_{b,i}$ is the specific rate constant for the reversion of **1** (X = H) to the substrate. In the case of NaOR or KOR in *t*-butanol, dissociation of the base may be very slight so that the reaction being investigated could be between an ion-pair $\{M^+...^-OR\}$ and the substrate (eq. 3). In that event, the measured

$$\text{[3]} \qquad \text{TNT} + \{\text{M}^+...^-\text{OR}\} \underset{k_{b,ip}}{\overset{k_{ip}}{\rightleftharpoons}} \{\mathbf{1}...\text{M}^+\} + \text{HOR}$$

K is equal to $k_{ip}/k_{b,ip}$ where k_{ip} is the specific rate constant for reaction of the substrate and the ion-pair and $k_{b,ip}$ is the specific rate constant for reversion to substrate of the species formed in the forward reaction. If the measured equilibrium constants for the systems in which Y = CH_3O, C_2H_5O, *n*-C_3H_7O, *iso*-C_3H_7O, and *n*-C_4H_9O and in which Y = *t*-C_4H_9O, refer to different processes it is not surprising that they cannot be correlated by the solvent parameter E_T.

Kinetic Studies Employing TNT as the Substrate

Under the conditions employed in the kinetic studies of the TNT–MOR reactions ($[MOR]_0/[TNT]_0 \geqslant 50:1$) conversion of TNT to the anion appeared to be quantitative. The A_∞ value at any wavelength was independent of the concentration of added base and directly proportional to the initial TNT concentration. These results are completely in accord with the large equilibrium constants (K) associated with these reactions.

In general, plots of log ($A_\infty - At$) *vs.* time were linear to a greater percent completion for the reactions in the TNT–KOR system and values of k_{obs} were more reproducible in the TNT–KOR system, particularly at low values of $[MOR]_0$. In addition, plots of k_{obs} *vs.* $[KOR]_0$ always passed through the origin whereas plots of k_{obs} *vs.* $[NaOR]_0$ consistently showed a positive intercept on the X-axis.

It is possible that plots of k_{obs} *vs.* $[NaOR]_0$ plots have a lower slope at low $[NaOR]_0$ than at high $[NaOR]_0$, *i.e.* they "curve into" the origin. Such behavior might be indicative of a second reaction pathway involving free *t*-butoxide ion becoming more dominant at low base concentrations. Unfortunately, attempts to define more precisely the form of the k_{obs} *vs.* $[NaOR]_0$ plots at concentrations of base $<2\times10^{-3}$ M were not successful because, at the low temperatures (30 to 35 °C) and the lower base concentrations, the k_{obs} values could no longer be obtained with a high degree of reproducibility. A number of workers have noted similar problems with regard to reproducibility in other studies involving the reactions of sodium *t*-butoxide in *t*-butanol (9, 10).

Can. J. Chem. Downloaded from www.nrcresearchpress.com by 210.87.254.40 on 09/05/12
For personal use only.

Can. J. Chem. Downloaded from www.nrcresearchpress.com by 210.87.254.40 on 09/05/12
For personal use only.

Linear k_{obs} *vs.* $[MOR]_0$ plots were observed for both bases. If there was a small degree of dissociation of the alkali-metal *t*-butoxide in solution and the rate-determining step in the formation of **1** (X = H) was between TNT and the free *t*-butoxide ion, a linear k_{obs} *vs.* $[MOR]_0^{1/2}$ plot would be expected. Our observations indicate therefore that the main mode of conversion of TNT to **1** (X = H) does not take place via this mechanism. However, the results cannot rule out some small contribution to anion formation via reaction of TNT with free *t*-butoxide ion (RO^-).

The slopes of the k_{obs} *vs.* $[KOR]_0$ and k_{obs} *vs.* $[NaOR]_0$ plots at 30.0 °C are 7000 ± 400 and 6200 ± 400 M^{-1} s^{-1}, respectively. The magnitudes of the slopes of these plots represent true specific rate constants only if both bases are completely dissociated under the reaction conditions used and all reaction in both cases occurs via the free RO^- ion or if no dissociation occurs and all reaction proceeds via the ion-pair $\{M^+...^-OR\}$. For the two cases the slopes of the k_{obs} *vs.* $[MOR]_0$ plots would represent the specific rate constants associated with the abstraction of proton by the free ion (k_{RO^-}) and by the ion-pair ($k_{\{M^+...^-OR\}}$), respectively. Complete dissociation of the MOR species under our reaction conditions is highly unlikely (11, 12) so we are left with the proposition that the ion-paired species $\{M^+...^-OR\}$ is the prime reactant in both cases. It is unlikely that the greater slope in the case of the TNT–KOR reaction is a consequence of the slope being a composite function containing contributions from both k_{RO^-} and $k_{\{M^+...^-OR\}}$, since this would require that NaOR be more extensively dissociated than KOR, and that the free ion have a lower reactivity than the ion-pair. The slightly different values for the slopes of the k_{obs} *vs.* $[MOR]_0$ plots for M = Na^+ and M = K^+ may simply reflect the difference in the ability of Na^+ and K^+ to stabilize the transition state for proton abstraction, as indicated in structure **4**.

Initial rate studies of the TNT–NaOR reaction in *t*-butanol at 30.0 °C yielded a mean value of $(IR)_H/\varepsilon_T l$ of 5750 ± 550 M^{-1} s^{-1} (Table 3). In view of the error limits associated with initial rate studies, this value is in satisfactory agreement with the value of 6000 ± 400 M^{-1} s^{-1} obtained from the k_{obs} *vs.* $[NaOR]_0$ plot. The latter value is however considered to be a far more reliable rate constant for the TNT–NaOR reaction

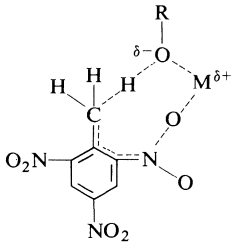

4

at 30.0 °C. The initial rate studies also indicate that if formation of σ-complex **2** (X = H, Y = *t*-C_4H_9O) (eq. 4)

$$\text{TNT} + \{M^+...^-OR\} \underset{k_b'}{\overset{k_f'}{\rightleftharpoons}} \sigma\text{-complex } \mathbf{2} \qquad [4]$$

is occurring simultaneously with the formation of **1** (X = H) then the extent of σ-complex formation is small even in the initial stages of the reaction.

If log *K* *vs.* E_T plots hold equally well for both the formation of σ-complex **3** (Y = OR) and σ-complex **2** (X = H; Y = OR) an upper limit on log *K* of approximately 2 would be predicted for reaction 4. Since log *K* for the formation of the purple anion (reaction 2) is $\geqslant 10^{4.7}$, the amount of σ-complex **2** present at equilibrium would be predicted to be small. The measured ε values at 520 and 650 nm of the purple species in *t*-butanol support this prediction. Within experimental error the ε values at 520 and 650 nm are the same as those recorded for the purple species formed in methanol and ethanol, solvents in which the extent of σ-complex formation is known to be very small (1).

An upper limit on log *K* for reaction 4 of approximately 2 is also indicated by the kinetic results since, if log *K* was larger than this, curvature in the k_{obs} *vs.* $[MOR]_0$ would have been expected over the range of base concentrations used in the kinetic experiments. No curvature was noted in any of the k_{obs} *vs.* $[MOR]_0$ plots.

Bethell and Cockerill have reported linear k_{obs} *vs.* H_r^{BuOH} plots for the reactions of alkali-metal butoxides with 9-bromofluorene, 9-bromo-9,9′-bifluorenyl, and 4-nitrodiphenylmethyl chloride (13–15). No significance was attached to the magnitudes of the slopes (1.0, 0.7, and 0.82) of the respective plots. For the first two reactions changes of alkali-metal cation from K^+ to Na^+ in a medium having the same H_r^{BuOH} halved the reaction rate, whereas for the last reaction, rates of proton abstraction in a medium having

Can. J. Chem. Downloaded from www.nrcresearchpress.com by 210.87.254.40 on 09/05/12
For personal use only.

a given value of H_r^{BuOH} were independent of the nature of the cation. Based on these observations Bethell and Cockerill tentatively suggested (15) that dependence of k_{obs} values on H_r^{BuOH} alone might be characteristic of reactions in which carbanion formation is rate limiting while dependence of k_{obs} on the cation at a given value of H_r^{BuOH} might be indicative of a process involving a carbanion as reactant. In the present systems the slopes of the log k_{obs} *vs.* H_r^{BuOH} plots are both 1.01 ± 0.05. However, at a given value of H_r^{BuOH}, k_{obs} for the NaOR–TNT reaction is some 30% greater than the k_{obs} for the KOR–TNT reaction.

For the TNT–NaOR reaction the apparent first-order rate constants obtained from the slopes of the k_{obs} [NaOR]$_0$ plots were evaluated at various temperatures and activation parameters for the proton transfer calculated in the normal way. The resulting $\Delta H^{\ddagger}$ and $\Delta S^{\ddagger}$ values are 4.2 ± 0.3 kcal mol^{-1} and -27 ± 2 cal deg^{-1} mol^{-1}. Employing an identical procedure, Jarczewski and Leffek (16) obtained a $\Delta H^{\ddagger}$ of 7.1 ± 0.9 kcal mol^{-1} for proton abstraction from di(4-nitrophenyl)methane by sodium *t*-butoxide in *t*-butanol.[2] Enthalpies of activation associated with a number of proton abstraction reactions involving ethoxide and isopropoxide ion commonly have values in the 10–13 kcal mol^{-1} range (16–19). This observation led the authors to suggest that the smaller $\Delta H^{\ddagger}$ characterizing their proton abstraction reaction was a consequence of the fact that the major barrier to reaction of alkoxide ion is desolvation of the ion and that this process will require less energy in the sodium *t*-butoxide case since this base exists predominantly as ionic aggregates which presumably are not as well solvated. The large negative entropy of activation associated with proton abstraction from TNT by sodium *t*-butoxide in *t*-butanol is fully in accord with this postulate.

Kinetic Studies Employing TNT-d_3 as the Substrate

Our studies indicate that the reactions of TNT-d_3 with NaOR and KOR are subject to complications which are not present in the corresponding reactions of TNT with these two bases. Under none of the reaction conditions employed could linear log $(A_\infty - A_t)$ *vs.* time plots be obtained from absorbance data simultaneously recorded at three different wavelengths. In runs at constant [TNT-d_3]$_0$ and constant [MOR]$_0$, in which linear log $(A_\infty - A_t)$ *vs.* time plots were obtained from absorbances recorded at two different wavelengths, the slopes of the plots ($\equiv k_{obs}/2.303$) differed. When the TNT-d_3 – NaOR reaction was studied at a constant total concentration of salt equal to 4.69×10^{-3} *M*, linear log $(A_\infty - A_t)$ *vs.* time plots could only be obtained from absorbance data recorded at one wavelength (650 nm). For a given [NaOR]$_0$ the k_{obs} so obtained was approximately one-half the k_{obs} recorded in the absence of added salt. This behavior is in marked contrast to that observed in the case of the TNT–NaOR reaction. For these reasons it is doubtful whether the k_{obs} values obtained in the studies of the TNT-d_3 – NaOR and TNT-d_3 – KOR reactions are valid rate constants and that the slopes of the k_{obs} *vs.* [MOR]$_0$ plots have proper significance.

The results of the initial rate studies of the TNT-d_3 – NaOR reaction confirm that it is more complex than the TNT–NaOR reaction and yield evidence concerning the source of this complexity. If only the rate of deuteron transfer is being measured by the initial rate technique, $(IR)_D/\varepsilon_T l$ should be a constant at all wavelengths, as is $(IR)_H/\varepsilon_T l$ in the case of the TNT–NaOR reaction (Table 3). However, it is obvious that $(IR)_D/\varepsilon_T l$ is not a constant. The fact that minimum values of this quantity are obtained in the 400–440 nm region, while maximum values of this quantity are obtained in the 600–700 nm region, suggests that complications arise because of simultaneous formation of the TNT-d_3 – *t*-butoxide σ-complex **2** (X = D, Y = *t*-C_4H_9O), since this species should have its maximum and minimum absorbances in the 400–440 and 600–700 nm regions, respectively (2). In view of the results obtained in the studies of other TNT- and TNT-d_3 – alkoxide ion reactions, the formation of a TNT-d_3 σ-complex is not an unexpected reaction (1, 2).

The ratio $(IR)_H/(IR)_D = 8.3$ at 650 nm is taken as being close to the true isotope effect (k_f^H/k_f^D) for anion formation in this system since, at this wavelength, absorbance is almost entirely due to TNT or TNT-d_3 anion (2, 8). If it is assumed that σ-complex formation and proton abstraction are occurring simultaneously in

[2]The calculation of $\Delta H^{\ddagger}$ and $\Delta S^{\ddagger}$ using the above procedure ignores the fact that as the temperature increases the dielectric constant of *t*-butanol decreases and the degree of ion-association increases (7). Bethell and Cockerill (7) have shown that the basicity of a *t*-butanol solution halves when the temperature is raised from 30 to 50 °C.

the reaction, then in the simplest case

$$[5]\quad \frac{(IR)_H - (IR)_D}{\varepsilon_T l} = (k_f^H - k_f^D) + (k_{f'}^H - k_{f'}^D)\varepsilon_\sigma/\varepsilon_T$$

$\varepsilon_\sigma/\varepsilon_T$ is approximately zero in the 600–700 nm region and the quantity $(k_{f'}^H - k_{f'}^D)$ is expected to be small. The initial rate data obtained at 650 nm yield therefore a $k_f^D = 670\ M^{-1}\ s^{-1}$ at 30 °C. In view of the errors associated with the initial rate studies, and the uncertainty ($\pm 10\%$) in the kinetic isotope effect, a realistic value for k_f^D would be $800 \pm 200\ M^{-1}\ s^{-1}$ at 30 °C. The value of k_f^D obtained in this fashion compares well with the value of the slope of the k_{obs} *vs.* $[NaOR]_0$ plot obtained in studies of the TNT–NaOR reaction at a constant salt concentration of $4.69 \times 10^{-3}\ M$.

If one assumes that reactions 3 and 4 are taking place simultaneously in solution and that $k_{ip} = 800\ M^{-1}\ s^{-1}$, $k_f' = 1400\ M^{-1}\ s^{-1}$,[3] $k_{b,ip} \ll 1\ s^{-1}$ and $k_b' = 1\ s^{-1}$ it is possible, using known values of ε_T and ε_σ at the different wavelengths, to calculate absorbance as a function of time at the different wavelengths. Calculations using the computer reproduce qualitatively the variations in $(IR)_D$ with wavelength reported in Table 3, though quantitative agreement is not very good. Thus, for the reaction conditions cited in Table 3, values of $(IR)_D$ at 420, 520, and 650 nm are calculated to be 6.20, 4.98, and 0.93, respectively, whereas the observed values are 5.00, 6.60, and 0.82. The differences in the calculated and observed initial rate values are perhaps not that serious in that the calculated initial rate values depend markedly on the input values of k_f' and are dependent as well (but to lesser extent) on the input values of k_{ip}, k_b', ε_T, and ε_σ.

A reaction sequence (eq. 6) involving the formation of the anion via the σ-complex can also be envisaged.

$$[6]\quad \text{TNT-}d_3 + \{M^+ \ldots {}^-OR\} \underset{k_b'}{\overset{k_f'}{\rightleftharpoons}} \sigma\text{-complex } \mathbf{2} \underset{k_b}{\overset{k_f}{\rightleftharpoons}} \text{TNT-}d_3^-$$

For the k_f' and k_b' values quoted above, $k_f = 800\ M^{-1}\ s^{-1}$ and $k_b \ll 1\ s^{-1}$, a sigmoidal absorbance *vs.* time plot is predicted for absorbances recorded at 650 nm. A careful check of oscilloscope traces of absorbance at 650 nm *vs.* time showed no indication of this type of behavior.

The computer-calculated absorbances as a function of time for reactions 3 and 5 taking place simultaneously in solution can also be used to construct log $(A_\infty - A_t)$ *vs.* time plots. For the range of base concentrations employed in the studies of the TNT-d_3 – NaOR and TNT-d_3 – KOR reactions, plots of log $(A_\infty - A_t)$ *vs.* time, based on the calculated absorbance values at 650 nm, are not linear. Similar plots based on the calculated absorbance values at 420 and 520 nm are linear, but k_{obs}^{420} values are always slightly greater than the k_{obs}^{520} values. This corresponds exactly to the experimental observations.

Similar computer calculations were carried out for the TNT–NaOR reaction using $k_{ip} = 6000\ M^{-1}\ s^{-1}$, $k_f' = 1400\ M^{-1}\ s^{-1}$, $k_{b,ip} \leqslant 1\ s^{-1}$, and $k_b' = 1\ s^{-1}$. For the range of base concentrations employed, plots of log $(A_\infty - A_t)$ *vs.* time, based on the calculated absorbances at 420, 520, and 650 nm as a function of time, are all linear. Values of k_{obs}^λ are found to decrease in the order $k_{obs}^{420} > k_{obs}^{520} > k_{obs}^{650}$ but the differences in the k_{obs}^λ values are much smaller than in the case of the TNT-d_3 – NaOR reaction and well within the experimental error associated with the measurement of k_{obs}. The results of the calculations are therefore in accord with our observation that in the TNT–NaOR and TNT–KOR systems, k_{obs} is independent of the wavelength at which absorbances are recorded.

Financial support by the National Research Council of Canada is acknowledged. The authors are indebted to Dr. P. J. Sheridan and Dr. R. Tucker for measurements of the equilibrium constants for formation of the purple anion in a number of the TNT–alkoxide ion–alcohol systems.

[3]This is an approximate value only based on the results of the initial rate studies in the TNT- and TNT-d_3 – NaOR reactions and on considerations of log k *vs.* E_T plots for these and related reactions.

1. E. Buncel, A. R. Norris, K. E. Russell, and R. Tucker. J. Am. Chem. Soc. **94**, 1646 (1972).
2. E. Buncel, A. R. Norris, K. E. Russell, P. Sheridan, and H. Wilson. Can. J. Chem. In press.
3. A. R. Norris. Can. J. Chem. **45**, 175 (1967).
4. L. H. Gan and A. R. Norris. Can. J. Chem. **52**, 8 (1974).
5. L. H. Gan and A. R. Norris. Can. J. Chem. **49**, 2490 (1971).
6. D. A. Deranleau. J. Am. Chem. Soc. **91**, 4050 (1969).
7. D. Bethell and A. F. Cockerill. J. Chem. Soc. (B), 913 (1966).
8. C. F. Bernasconi. J. Org. Chem. **36**, 1671 (1971).

Can. J. Chem. Downloaded from www.nrcresearchpress.com by 210.87.254.40 on 09/05/12
For personal use only.

9. L. F. BLACKWELL, P. D. BUCKLEY, K. W. JOLLEY, and A. K. H. MACGIBBON. J. Chem. Soc. Perkin II, 169 (1973).
10. R. A. MORE O'FERRALL. J. Chem. Soc. (B), 268 (1970).
11. J. BARTHEL, R. WACHTER, and M. KNERR. Electrochim. Acta, **16**, 723 (1971).
12. D. J. CRAM. Fundamentals of carbanion chemistry. Academic Press, New York, N.Y. 1965. p. 35.
13. D. BETHELL. J. Chem. Soc. 666 (1963).
14. D. BETHELL and A. F. COCKERILL. J. Chem. Soc. (B), 917 (1966).
15. D. BETHELL and A. F. COCKERILL. J. Chem. Soc. (B), 920 (1966).
16. A. JARCZEWSKI and K. T. LEFFEK. Can. J. Chem. **50**, 24 (1972).
17. E. F. CALDIN and J. C. TRICKETT. Trans. Faraday Soc. 772 (1954).
18. E. F. CALDIN and G. LONG. Proc. Roy. Soc. A **228**, 263 (1955).
19. E. F. CALDIN, M. KASPARIAN, and G. TOMALIN. Trans. Faraday Soc. **64**, 2802 (1968).

Can. J. Chem. Downloaded from www.nrcresearchpress.com by 210.87.254.40 on 09/05/12
For personal use only.

Tricyclic Analogs of the Prodines

MARCEL MÉNARD, PIERRE RIVEST, LEE MORRIS, JACQUES MEUNIER, AND YVON G. PERRON
Bristol Laboratories of Canada, Candiac, Quebec

Received January 19, 1974

MARCEL MENARD, PIERRE RIVEST, LEE MORRIS, JACQUES MEUNIER, and YVON G. PERRON. Can. J. Chem. **52**, 2316 (1974).

A search for an analgesic with the potency of β-prodine and with the quality of analgesia associated with the benzomorphans led to the preparation of the octahydrobenz[*f*] isoquinoline system, a system where β-prodine is bridged in a manner related to the benzomorphans. Three different syntheses of this system are described. They permit access to a variety of substitution patterns as well as to the possible stereoisomers. The hybrid β-prodine–benzomorphan system displayed interesting CNS activity.

MARCEL MENARD, PIERRE RIVEST, LEE MORRIS, JACQUES MEUNIER et YVON G. PERRON. Can. J. Chem. **52**, 2316 (1974).

La recherche d'un analgésique aussi puissant que la β-prodine mais d'une pureté d'action correspondant à celle des benzomorphanes nous a amené à préparer le système tricyclique octahydrobenz[*f*]isoquinoline. Dans ce système les deux cycles de la β-prodine sont pontés à la manière des benzomorphanes. Trois synthèses ont été développées permettant l'accès aux différents stéréoisomères et à une variété de substitution. Ce système hybride β-prodine–benzomorphane possède des propriétés pharmacologiques intéressantes.

The enhanced analgesic activity of β-prodine **1** over its α-isomer **2** (1) (Fig. 1) has been discussed in terms of increased contact with the receptor surface due to axial phenyl group conformation (2), restricted rotation favoring coplanarity of the phenyl and piperidine rings (3), and increased ability of the β-isomer to penetrate the blood–brain barrier (4). Extensive structure–activity relationship in this area has shown that these explanations cannot fully account for the observed difference in potency. At present the accepted view (5) is that the analgesic receptor, although unique, is flexible enough to accommodate a wide variety of structures, the observed analgesia being related to the ability of the drug to reach the receptor site and to achieve ionic binding with the receptor.

In an attempt to obtain an analgesic with a level of activity equal or superior to β-prodine but with a quality of analgesia associated with many benzomorphans (*e.g.* **3**; low physical dependance) we have prepared two series of compounds, **4** and **24**, in which the phenyl and methyl groups of the prodines are incorporated into an additional ring thus fixing both the conformation of the phenyl group and the angle between the phenyl and the piperidine planes. The two rings become linked in a manner similar to the benzomorphans, the junction being shifted by one carbon atom. In addition, a change in the

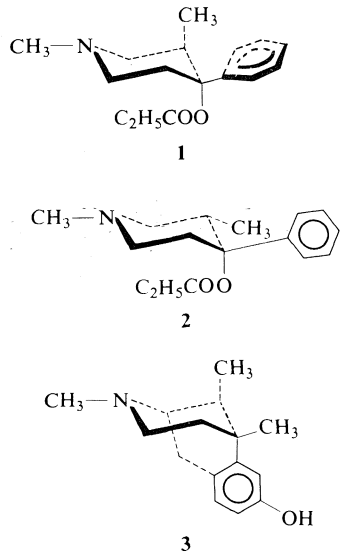

FIG. 1. Analgetic potency of the prodines and benzomorphans.

ED_{50}: 1.2 mg/kg (1)

ED_{50}: 5 mg/kg ED_{50}: 8.9 mg/kg (6)

stereochemistry of the new ring junction as well as an increase in the number of methylenes linking the methyl and phenyl groups result in a convenient variation of the angle between the two planes (Fig. 2).

In structure **4***b* the aromatic and piperidine

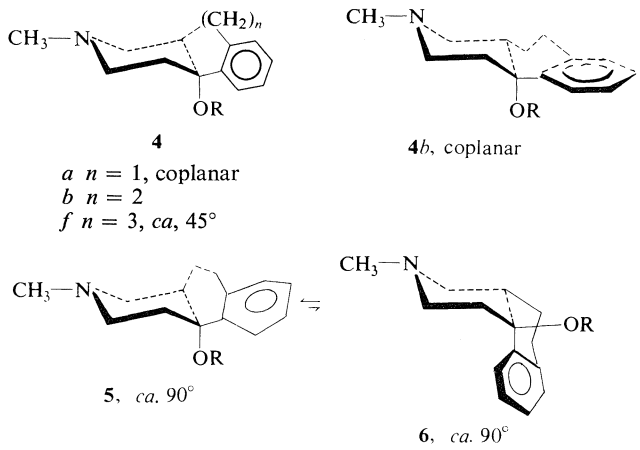

FIG. 2. The approximate angle between the planes of the aromatic and piperidine ring (from Drieding models) in tricyclic prodine analogs.

rings are frozen in a spatial arrangement that is almost identical to the conformation of β-prodine believed to confer the higher potency to the β-isomer (4). In **4***a* the two rings are still roughly parallel but the aromatic group is pushed backward in the plane as compared to **4***b*. The angles between the two planes in **4***f* and in the *cis* compound **5** are roughly 45 and 90°, thus providing the whole range of spatial arrangement. The conformation represented by **6** would mimic the phenylpiperidine arrangement found in the benzomorphans **3** but, at least in solution in deuteriochloroform, there is spectral evidence that the *cis* series exists exclusively in the conformation depicted by structure **5**. Structures such as **4** and **5** bearing an axial 4-OH would be stabilized, through the corresponding skew-boat conformation, by bonding of the OH to the lone pair of the nitrogen (3).

The 1,3-dipolar cycloaddition reaction of nitrones to conjugated olefins (7) provided a facile entry to compounds of type **4** as shown in Scheme 1 (Table 1). Since this type of cylcoaddition is stereospecific (8), the *trans* ring fusion desired for **4** was established at this early stage. Yields of the cycloaddition of *N*-methyl nitrone to unsaturated esters **7** were reasonable (60–80%) with the exception of **7***f* (17%). The seven-membered ring series *f* was abandoned after unfruitful attempts to improve this yield. The resulting isoxazolidines **8** were found to be versatile intermediates since they also provided other analogs, **10** and **12**, of meperidine and prodilidine. Reductive cleavage of the N—O bond afforded a quantitative yield of the aminoesters **9**. Although they are stable for short periods at room temperature the amino esters **9** spontaneously underwent cyclization to the lactams **11** and **13** upon warming. Treatment with a formaldehyde solution converted the aminoester **9***d* to the oxazine **10**, an analog of meperidine where the C-3 carbon atom of the piperidine moiety is replaced by an oxygen atom. When the reductive cleavage of **8***d* was carried out in the presence of formaldehyde the tertiary amine **9***e* was the sole product of the reaction. The lactams **11** and **13** were readily reduced by lithium aluminum hydride to the aminoalcohols **12** and **4**.

Esterification of the aminoalcohols **12** and **4** proved to be quite difficult and could not be achieved in the case of **4***a*. Under the conventional acylation conditions for tertiary alcohols (9) attempted esterification resulted in elimination to unsaturated amines as exemplified by **14** (Scheme 2). However we finally found out that the alcohols **12***a* and **4***b* were readily acylated by propionyl chloride, without base, in benzene solution at or below room temperature to give the esters **12***c* and **4***c* as hydrochlorides which could be precipitated from the reaction mixture by the addition of anhydrous ether.

The change in the n.m.r. chemical shift of the H-10 proton in **14***c*, **4***b*, and **4***c* constitutes a further confirmation of the correctness of these structures. In **14***c*, H-10 is part of the bulk of the 4 aromatic protons centered at 2.38 δ. The axial OH at position 10b in **4***b* shifts the H-10 proton downfield to 7.328. In **4***c* this shift is even more pronounced and H-10 appears as a multiplet centered at 7.72 δ.

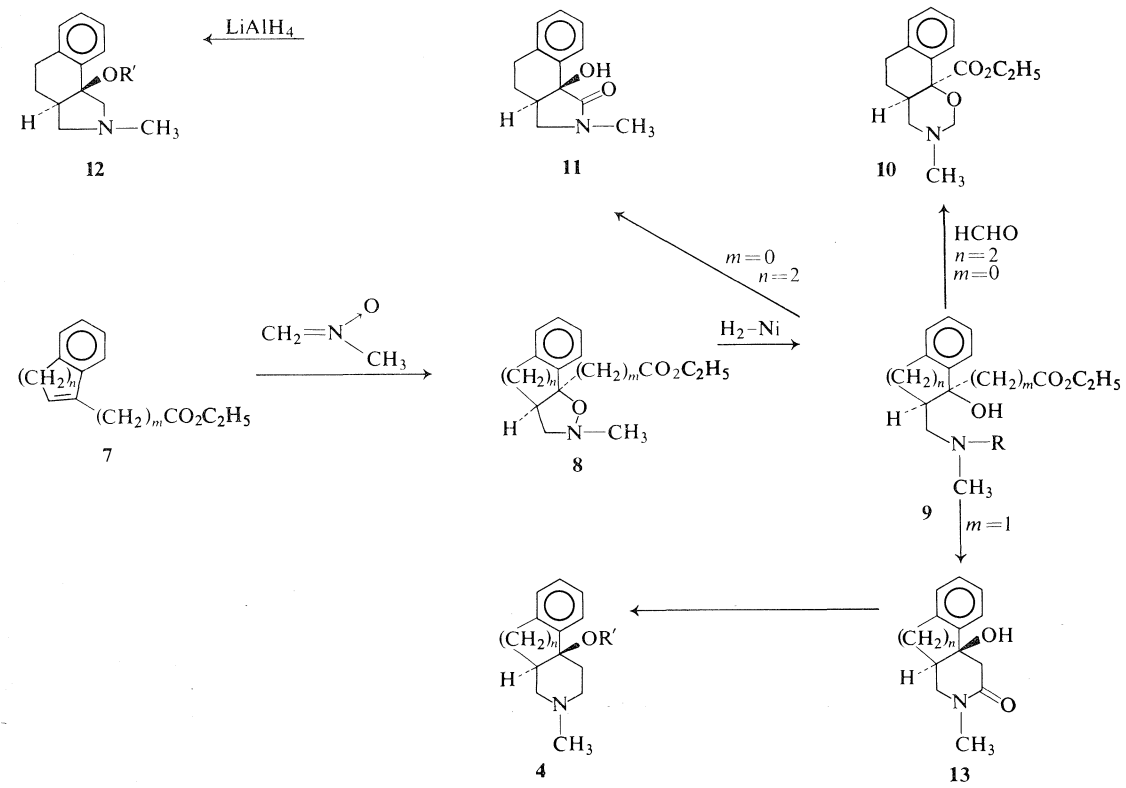

a $n = 1$; $m = 1$; $R' = H$
b $n = 2$; $m = 1$; $R = R' = H$
c $n = 2$; $m = 1$; $R = CH_3$; $R' = C_2H_5CO$
d $n = 2$; $m = 0$; $R = H$
e $n = 2$; $m = 0$, $R = CH_3$
f $n = 3$; $m = 1$; $R' = H$

SCHEME 1

Alternatively the tertiary alcohols of type **4***b* could be produced cheaply as shown in Scheme 2 by aminomethylation (10) of 1-methyl-3,4-dihydronaphthalene (**15**) followed by hydrobromic acid addition across the double bond of the unsaturated amines **14**. Solvolysis in water at low temperature afforded the alcohols **18** (**18***c* = **4***b*). Yields of the aminomethylation reaction were considerably lower with ammonium chloride (17%) than with methylamine hydrochloride (51%) but the former has the advantage of providing the secondary amine **14***a* which can be alkylated with the desired alkyl halide. The aminoalcohol **18***e* obtained in this manner posseses pharmacological properties related to those of haloperidol.

The *cis*-fused tricyclic analogs of prodine (**5**) were prepared as outlined in Scheme 3. In fact this scheme provides higher yields of the *trans*-isomer. This suited our purposes because at this stage we had found out that the presence of the axial proton at position 4a in **4** in a *trans* configuration with respect to the alcohol or ester group at 10b, rendered elimination so easy that the pharmacological activity of the ester **4***c* represented the resultant of the combined activities of the ester **4***c* and its elimination product **14***c*. Accordingly we wished to block this elimination by incorporating an angular methyl group at 4a in the original structure **4**. Also at this time we were interested in finding how the presence of a phenolic group in the aromatic ring would affect the activity. In the benzomorphan class of analgesics a phenolic group at position 3 enhances the analgesic potency severalfold (5). Since there was some uncertainty

TABLE 1. Physical constants of compounds outlined in Scheme 1

Compound	Melting or boiling point (°C)	Solvent	Yield (%)	Formula	Analysis (%) Calcd. C	Calcd. H	Calcd. N	Found C	Found H	Found N
4*a*	167–168	EtOAc		$C_{13}H_{17}NO$	76.81	8.43	6.89	76.36	8.47	7.00
4*b*	163–165	Petroleum ether	85	$C_{14}H_{19}NO$	77.38	8.81	6.45	76.95	8.76	6.42
4*c*[a]	174–175	EtOH–Et_2O	42	$C_{17}H_{24}ClNO_2$	65.90	7.81	4.52	65.82	7.73	4.65
8*a*[c]	96–97	C_6H_{12}	65	$C_{14}H_{17}NO_3$	68.00	6.93	5.66	67.57	6.61	5.51
8*b*	117–8/0.2		80	$C_{16}H_{21}NO_3$	69.79	7.69	5.09	70.38	7.79	4.93
8*d*	71–73	EtOH–H_2O	80	$C_{15}H_{19}NO_3$	68.94	7.33	5.36	68.82	7.28	5.42
8*f*	138–40/0.3		17	$C_{17}H_{23}NO_3$	70.56	8.01	4.84	70.31	8.08	5.47
11	184–186	EtOAc	45	$C_{13}H_{15}NO_2$	71.86	6.96	6.45	71.77	6.87	6.45
12*a*	145–146	EtOAc	90	$C_{13}H_{17}NO$	76.81	8.43	6.89	77.32	8.48	6.84
12*c*[b]	156–158	EtOH–Et_2O	45	$C_{18}H_{23}NO_6$	61.87	6.63	4.09	61.62	6.61	3.94
13*a*	216–217	EtOH		$C_{13}H_{15}NO_2$	71.86	6.96	6.45	71.65	6.91	6.38
13*b*	225–227	EtOH	89	$C_{14}H_{17}NO_2$	72.70	7.41	6.06	72.76	7.42	5.95
13*f*	166–167	MeOH–H_2O		$C_{15}H_{19}NO_2$	73.44	7.81	5.71	73.30	7.81	5.60

[a]HCl salt.
[b]Oxalic acid salt.
[c]Methyl ester.

TABLE 2. Physical constants of compounds outlined in Scheme 3

Compound	Melting or boiling point (°C)	Solvent	Formula	Analysis (%) Calcd. C	Calcd. H	Calcd. N	Found C	Found H	Found N
20*a*			Not purified[d]						
20*b*	126–127.5		Not purified[d]						
20*c*	101–102	MeOH	$C_{16}H_{19}NO_4$	66.42	6.62	4.84	66.44	6.66	4.71
20*d*	106–107	MeOH	$C_{16}H_{19}NO_4$	66.42	6.62	4.84	66.53	6.64	4.79
21*a*	211–213	*i*-PrOH–EtOAc	$C_{14}H_{17}NO_2$	72.70	7.41	6.06	72.69	7.37	5.84
21*b*	240–242	EtOH–H_2O	$C_{15}H_{19}NO_3$	68.94	7.33	5.36	69.29	7.45	5.40
21*c*	166–167	EtOAc	$C_{15}H_{19}NO_3$	68.94	7.33	5.36	68.69	7.34	5.50
21*d*	216–217	EtOAc	$C_{15}H_{19}NO_3$	68.94	7.33	5.36	68.70	7.29	5.66
22*a*			Not purified[d]						
22*b*	170–171	EtOAc – Petroleum ether	$C_{15}H_{21}NO_2$	72.84	8.56	5.66	72.42	8.49	5.59
22*c*	166–167	EtOAc	$C_{15}H_{21}NO_2$	72.84	8.56	5.66	73.40	8.71	5.77
22*d*	Oil[d]								
23*a*			Not purified[d]						
23*b*[c]	221–222	MeOH–Et_2O	$C_{16}H_{24}ClNO_2$	64.53	8.12	4.70	64.46	8.26	4.63
23*c*	152–153	MeOH–H_2O	$C_{16}H_{23}NO_2$	73.53	8.87	5.36	73.61	9.03	5.35
23*d*[c]	210–211	MeOH–Et_2O	$C_{16}H_{24}ClNO_2$	64.53	8.12	4.70	64.55	8.20	4.53
24*a*[c]	194–196[a]	MeOH–Et_2O	$C_{18}H_{26}ClNO_2$	66.76	8.09	4.33	66.96	8.14	4.29
24*b*[c]	164–166[b]	MeOH–Et_2O	$C_{19}H_{28}ClNO_3$	64.49	7.98	3.96	64.61	8.07	3.86
24*c*[c]	195–196	MeOH–Et_2O	$C_{19}H_{28}ClNO_3$	64.49	7.98	3.96	64.46	8.02	4.17
24*d*[c]	167–168	MeOH–Et_2O	$C_{19}H_{28}ClNO_3$	64.49	7.98	3.96	64.57	8.04	3.99

[a]Melts with evolution of a gas, resolidifies, and melts again at 210–230°.
[b]Melts with evolution of a gas, resolidifies, and melts again at 231–232°.
[c]Hydrochloric acid salt.
[d]Crude product used in the next step.

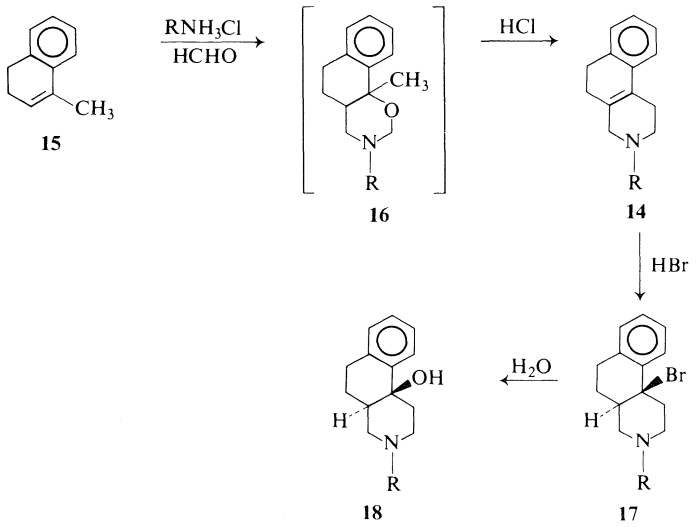

a R = H
b R = C_6H_5CO
c R = CH_3
d R = CH_2—CH_2—3-indolyl
e R = *p*-$FC_6H_4CO(CH_2)_3$

SCHEME 2

as to which of the position 7 or 9 in **4** would correspond to the 3 position of **3** an example of both series was desired. All of these were available through Scheme 3.

Nucleophilic addition of lithioacetonitrile to the ketones **19** gave mixtures of the isomeric *cis*-(OH, CH_3) and *trans*-cyano alcohols **20**, (Table 2) with the *trans*-isomer predominating in all cases. Although the isomers could be easily separated by fractional crystallization or column chromatography no effort was made to obtain the pure *cis*-isomers with the exception of **20***c*, which was selected to study the structure–activity relationships in relation to the stereochemistry of the new ring junction. Catalytic hydrogenation of the nitrile group resulted in spontaneous cyclization of the intermediate aminoesters to the lactams **21**. Reduction of **21** with lithium aluminum hydride afforded the aminoalcohols **22** which were methylated and acylated with propionyl chloride as described for **4***c*. The resulting esters **24**, with the angular 4a-methyl group, were considerably more stable than **4***c* but unfortunately not stable enough to resist the conditions required [HBr; pyridine·HCl (14); BBr_3 (11); $\phi_2\overline{P}$ (12); EtSNa (13)] to achieve their *O*-demethylation. Either no *O*-dealkylation was observed or the main reaction product was the unsaturated amine **25**.

The stereochemistry of compounds **19**–**24** was assigned from a study of their n.m.r. spectra. The series **21***d*, **22***d*, and **23***d* shows a doublet for H-10 (J_{8-10} = 3 Hz) centered at the chemical shift indicated in Table 3. This doublet is shifted downfield in the series **21***c*, **22***c*, and **23***c* by *ca.* 17 Hz indicating a closer proximity of H-10 to the oxygen function at 10b. The doublets (J_{7-8} = 8.5 Hz) centered at 7–7.1 δ for H-7 and the doublets of doublets (J_{7-8} = 8.5 Hz; J_{8-10} = 3 Hz) centered at 6.7–6.8 δ for H-8 are not affected by the change of stereochemistry. Examination of molecular models reveals that H-10 and O-10b are in a *cisoid* conformation in a *cis* structure like **5** while the two groups are more remote in a *trans* structure like **4**. This deshielding of the H-10 proton in the *cis* series also provides some evidence that, in solution in deuteriochloroform, **5** and not **6** is the most stable conformation since there is no possible interaction between H-10 and O-10b in **6**. In the open-chain intermediates **20** a *cis* relation between the cyanomethyl group and methyl group at 2 deshields the 2-methyl by *ca.* 12 Hz. On the other hand, when it is the methoxy carbonyl group that is *cis* to the cyanomethyl group it is the ester-methyl which is shifted downfield by *ca.* 14 Hz.

Because of the instability of **4***c* it is difficult to

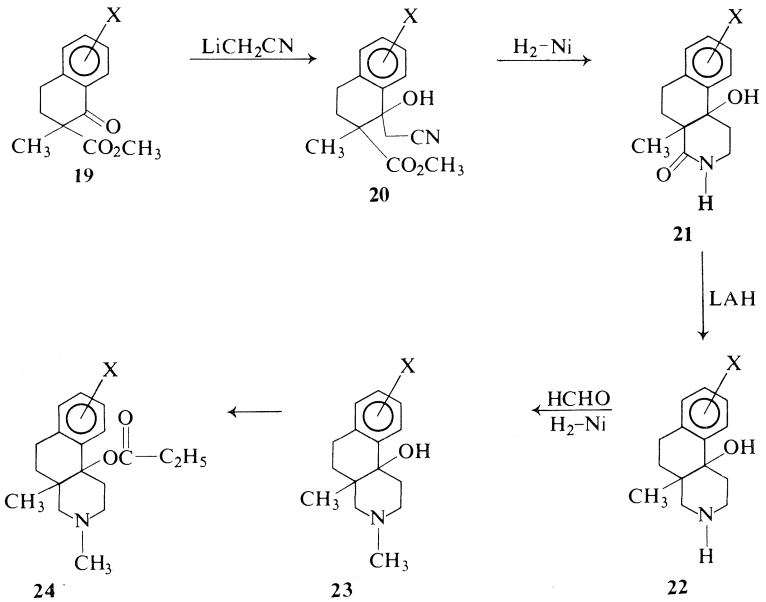

a X = H, *trans* (OH, CH_3)
b X^1 = 5-OCH_3, *trans* (OH, CH_3)
c X = 7-OCH_3, *cis* (OH, CH_3)
d X = 7-OCH_3, *trans* (OH, CH_3)

SCHEME 3

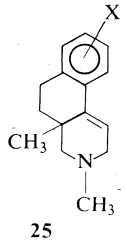

25

assess its analgesic activity with certainty. Orally it is a potent antidepressant of the MAO inhibitor type which indicates that it is rapidly degraded to **14**. Parenterally it shows analgesia which slowly changes to the type of activity exhibited by **14**. The inclusion of a methyl group at position 4a of **4***c* does stabilize the molecule but it also reduces the analgesic potency (**4***a*, **24***a*). The presence of a methoxyl group on the aromatic moiety of **24***a* improves the potency but, unexpectedly, the position of substitution is not critical (**24***b*, **24***d*). Since the alcohol **23***b* is a stronger analgesic than the corresponding ester **24***b* this series seems to bear a closer relation to the benzomorphans than to the prodines.

[1]Numbering refers to 5- or 7-methoxytetralone as starting material.

TABLE 3. Nuclear magnetic resonance data. Chemical shifts, in δ units, (TMS)

Compound	C—CH_3	CO_2CH_3	CH_2CN	O—CH_3
20*a*	1.50	3.62	2.80[a]	—
20*b*	1.49	3.63	2.78[a]	3.80
20*d*	1.43	3.60	2.71[a]	3.80
20*c*	1.28	3.83	2.81[b]	3.83

Compound	C—CH_3	O—CH_3	H_7	H_8	H_{10}
21*c*	1.28	3.82	7.11	6.82	7.30
21*d*	0.99	3.78	7.11	6.82	7.02
22*c*	0.81	3.76	7.01	6.73	7.19
22*d*	0.81	3.76	7.08	6.73	6.90
23*c*	0.88	3.77	7.02	6.70	7.13
23*d*	0.95	3.70	7.03	6.70	6.88

[a]Multiplet.
[b]Singlet.

The most surprising observation is that a change from *trans* to *cis* in the stereochemistry of the ring bridging the piperidine and the phenyl ring does not alter the analgesic activity (**24***d*, **24***c*). This is in marked contrast with the prodine series where the superiority of the *cis* over the *trans* geometry for activity is well established (5). On the other hand compound **10**, where the

replacement of the carbon atom at position 3 of the piperidine ring by an oxygen atom is not likely to alter the conformation of the system with regard to **4***c* and **24***d*, is completely devoid of analgesic activity. Obviously, as already stressed out by Portoghese and Larson (4), factors other than the purely geometrical contribution play a major role in the ability of a molecule to reach and interact with the analgesic receptor (Table 4).

Other intermediates in this tricyclic series of compounds exhibited interesting CNS activity as shown in Table 5.

Experimental

Melting points, determined on a Fisher Mel-Temp, are not corrected. All compounds possessed i.r. and n.m.r. spectra consistent with their structure. The i.r. spectra were determined on a Unicam SP200-G grating spectrophotometer. The n.m.r. spectra were obtained on a Varian A-60A spectrometer with TMS as internal standard and in deuteriochloroform. Combustion analyses were performed by Microtech Laboratories.

N-Methylnitrone (17)

A mixture of paraformaldehyde (9.3 g, 0.31 mol HCHO), *N*-methyl hydroxylamine hydrochloride (25.0 g, 0.30 mol), and anhydrous potassium carbonate (90.0 g, 0.65 mol) in dry benzene (500 ml) was stirred at room temperature for 5 h. The solids were removed by filtration and washed with methylene chloride. Concentration of the filtrates on the rotary evaporator left the crude nitrone as a yellowish semisolid.

TABLE 4. Analgesic potency[a]

Compound	ED_{50}[b] (mg/kg)
4*c*	20
22*b*	30
23*b*	3
24*a*	32
24*b*	13
24*c*	14
24*d*	11

[a]Phenylquinone writhing test, mice, subcutaneous administration (15).
[b]Effective dose: 50% of the mice under test.

TABLE 5. Antireserpine activity[a]

Compound	ED_{50}[b] (mg/kg)
4*b*	1
4*c*	1
14*a*	2.5
14*c*	<0.25

[a]Ability to reverse reserpine-induced hypothermia in mice (16).
[b]Effective dose, 50% of the mice under test, oral administration.

Cycloaddition of N-Methylnitrone to the Olefins 7

A mixture of the above crude nitrone and the olefin **7** (0.2 mol) (18) in benzene or toluene (500 ml) was stirred at room temperature or heated under reflux as specified below. The cooled solution was extracted with 10% hydrochloric acid and the aqueous layer made basic with concentrated ammonium hydroxide. Extraction with methylene chloride, drying, and concentration left an oily residue which was purified by crystallization or distillation. The unreacted olefin was recovered from the original benzene or toluene solution: **7***b* (18*a*) and **7***d* (18*b*); benzene, room temperature 48 h; **7***a* (18*a*), benzene, reflux, 6 days; **7***f* (18*c*), toluene, reflux, 60 h.

*Reductive Cleavage of the Isoxazolidines **8** to the Aminoalcohols **9***

The ixoxazolidine **8** (0.02 mol) in absolute ethanol (100 ml) was hydrogenated, in a Parr Shaker, at an initial pressure of 60 p.s.i. of hydrogen in the presence of Raney nickel (*ca.* 5 g). One equivalent of hydrogen was absorbed in a few minutes. The catalyst was removed by filtration over Celite and the filtrates were concentrated on the rotary evaporator at room temperature. The crude residue was used immediately without further purification.

An analytical sample of the oxalate salt of **9***d* was prepared in ether. Recrystallization of the solid from alcohol–water gave colorless crystals, m.p. 221–223°.

Anal. Calcd. for $C_{17}H_{23}NO_7$:C, 57.78; H, 6.56; N, 3.96. Found: C, 57.63; H, 6.54; N, 3.93.

*trans(2-Dimethylaminomethyl-1-hydroxy)-1-ethoxycarbonyl-1,2,3,4-tetrahydronaphthalene (**9e**)*

The isoxazolidine **8***b* (5.0 g, 0.019 mol) in absolute methanol (100 ml) was hydrogenated as described above in the presence of paraformaldehyde (3.0 g, 0.099 mol) and Raney nickel (*ca.* 5 g). The residue left after removal of the catalyst and solvent was crystallized in petroleum ether (90–120°) to give **9***e* as white crystals, m.p. 57–60°; yield 4.2 g, 79%.

Anal. Calcd. for $C_{16}H_{23}NO_3$: C, 69.26; H, 8.36; N, 5.05. Found: C, 69.03; H, 8.38; N, 4.92.

4a,10b-cis-10b-Ethoxycarbonyl-3-methyl-3,4,4a,5,6,10b-hexahydro-2H-naphth[2,1-e]-1,3-oxazine (10)

The isoxazolidine **8***b* (5.0 g, 0.019 mol) was hydrogenated as described above. After removal of the catalyst, paraformaldehyde (2.0 g, 0.066 mol) was added to the filtrates and the solution was heated under reflux for 2 h. Concentration on the rotary evaporator, dissolution in ether, and treatment with an excess of dry hydrogen chloride afforded **10** as a crystalline hydrochloride, m.p. 228–230° (ethanol); yield 4.15 g, 70%.

Anal. Calcd. for $C_{16}H_{22}ClNO_3$: C, 61.63; H, 7.11; N, 4.49. Found: C, 61.42; H, 7.05; N, 4.48.

*Cyclization of the Aminoesters **9** to the Lactams **11** and **13***

The crude aminoester **9** was dissolved in toluene, a few milligrams of *p*-toluenesulfonic acid were added, and the solution was heated under reflux for 3 h. After cooling, the solution was washed with 10% hydrochloric acid, dried, and concentrated on the rotary evaporator. The

solid residue was recrystallized in the solvent specified in Table 1.

*Reduction of the Lactams **11** and **13***

The lactam (0.05 mol) in dry THF or dioxane (75 ml) was added dropwise to a stirred slurry of lithium aluminum hydride (5.0 g, 0.13 mol) in the same solvent (75 ml). The mixture was heated under reflux for 18 h, cooled (0–5°), and treated in succession with water (5.0 ml), 20% sodium hydroxide solution (3.75 ml), and water (17.5 ml). The solids were removed by filtration and washed with methylene chloride. Concentration of the filtrates on the rotary evaporator left an oil which was crystallized in the solvent specified in Table 1.

*Esterification of the Alcohols **4b** and **12a***

A solution of the alcohol **4***b* or **12***a* (0.01 mol) and freshly distilled propionyl chloride (2.0 ml, 2.81 g, 0.03 mol) in dry benzene (15 ml) was stirred at room temperature for 2 h. Anhydrous ether was added to complete the crystallization of the ester hydrochloride. After standing at 0° for 1 h the hygroscopic solid was collected by filtration. The ester **4***c* was purified by recrystallization. The ester **12***c* was dissolved in methylene chloride and the solution neutralized at 0° with a saturated sodium carbonate solution, washed with brine, dried, and concentrated to leave an oil. The oil was dissolved in ether and treated with an excess of a solution of oxalic acid in ether to give the oxalic acid salt of **12***c* as a white nonhydroscopic solid.

*1,2,3,4,5,6-Hexahydrobenz[f]isoquinoline (**14a**)*

A mixture of 3,4-dihydro-1-methylnaphthalene (14.4 g, 0.1 mol), 37% formaldehyde solution (34.0 g, 0.43 mol), and ammonium chloride (10.8 g, 0.2 mol) in glacial acetic acid (35 ml) was stirred on the steam-bath for 18 h, diluted with ice-cold water (150 ml), washed with ether (3 × 75 ml), and neutralized with a 50% sodium hydroxide solution. Extraction with methylene chloride and concentration yielded 24.0 g of crude **16**.

The residue was dissolved in concentrated hydrochloric acid (250 ml), heated under reflux for 2 h, cooled, washed with ether (5 × 100 ml), and neutralized with a 50% sodium hydroxide solution. Extraction with ether, drying, and concentration gave an oil which was purified by distillation to afford pure **14***a*, b.p. 120°/0.1 mm; yield 3.2 g, 17%.

An hydrochloric acid salt was prepared for analytical purposes, m.p. 204–205° dec.

Anal. Calcd. for $C_{13}H_{16}ClN$: C, 70.41; H, 7.27; N, 6.32. Found: C, 70.60; H, 7.31; N, 6.47.

*1,2,3,4,5,6-Hexahydro-3-methylbenz[f]isoquinoline (**14c**)*

(*a*) A mixture of 3,4-dihydro-1-methyl naphthalene (86.0 g, 0.6 mol), 37% formaldehyde solution (200 g, 2.4 mol), and glacial acetic acid was stirred vigorously a 60–65° for 1/2 h. Monomethylamine hydrochloride (81.0 g, 1.4 mol) was added by small portions while keeping the temperature at 70°. After the end of the addition, the mixture was stirred for 3 h at 70°, diluted with ice-cold water, washed with ether (5 × 100 ml), made basic with a 50% sodium hydroxide solution, and extracted with ether (5 × 100 ml). Drying and concentration of the ether extracts gave crude **16***c* (116.2 g) as a yellow oil.

The above was dissolved in concentrated hydrochloric acid (100 ml) and heated under reflux for 2 h. Work-up as above gave an oil (99.5 g) which was purified by distillation to provide **14***c* as a slightly colored viscous oil b.p. 120–130°/0.05 mm; yield 61.5 g, 51%.

A solid hydrochloride was prepared for analytical purposes, m.p. 208–209° (ethanol–ether).

Anal. Calcd. for $C_{14}H_{18}ClN$: C, 71.32; H, 7.70; N, 5.94. Found: C, 71.18; H, 7.68; N, 6.00.

(*b*) By methylation of **14***a*: methylation of **14***a* by the normal formaldehyde – formic acid method (19) gave an oil identified as **14***c* by comparison (i.r., n.m.r., t.l.c.) with an authentic sample.

(*c*) By elimination from **4***b*: a mixture of the alcohol **4***b* (2.0 g, 0.0092 mol) and freshly distilled propionyl chloride (2.0 ml, 2.81 g, 0.03 mol) in benzene (25 ml) was heated under reflux for 18 h. Addition of ether gave a white solid which was recrystallized in isopropanol–ether to give crystals, m.p. 208–209° identical (i.r., mixture m.p.) with authentic **14***a*.

*3-Benzoyl-1,2,3,4,5,6-hexahydrobenz[f]isoquinolines (**14b**)*

A solution of benzoyl chloride (1.6 g, 0.0114 mol) in chloroform (10 ml) was added dropwise to a cooled (0–5°) and stirred mixture of the amine **14***a* (2.0 g, 0.0108 mol) and 10% sodium hydroxide solution (5 ml). After a 30 min stirring period at room temperature, the phases were decanted, the aqueous phase re-extracted with chloroform, and the combined chloroform extracts were dried and concentrated. The semisolid residue was recrystallized in ethylacetate – petroleum ether to give **14***b* as a white solid, m.p. 93–95°; yield 2.3 g, 73%.

Anal. Calcd. for $C_{20}H_{19}NO$: C, 83.01; H, 6.62; N, 4.84. Found: C, 82.76; H, 6.69; N, 4.79.

*3-[4′-(p-Fluorophenyl)-4′-butyryl]-1,2,3,4,5,6-hexahydrobenz[f]isoquinoline (**14e**)*

A mixture of the amine **14***a* (2.0 g, 0.0108 mol), triethylamine (2.0 g, 0.0197 mol), γ-chloro-*p*-fluorobutyrophenone (2.5 g, 0.0125 mol), and dry toluene (10 ml) was stirred and heated under reflux for 18 h. After cooling the mixture was washed with water, the aqueous phase re-extracted with toluene, and the combined organic phases dried and concentrated to leave an oil. The oil was dissolved in ether and the hydrochloride of **14***e* was precipitated with dry hydrogen chloride. After washing with ether, the solid was dissolved in water, neutralized with a 10% sodium hydroxide solution, and extracted with methylene chloride. Drying and concentration left a yellow oil which was crystallized in petroleum ether to give **14***e* as a white solid, m.p. 73–74°; yield 1.9 g, 51%.

Anal. Calcd. for $C_{23}H_{24}FNO$: C, 79.05; H, 6.92; N, 4.01. Found: C, 79.10; H, 6.99; N, 4.05.

*10b-Hydroxy-1,2,3,4,4a,5,6,10b-octahydro-4a,10b-trans-benz[f]isoquinoline (**18a**)*

A solution of the amine **14***a* (5.0 g, 0.027 mol) in glacial acetic acid (35 ml) was cooled to 10° and saturated with dry hydrogen bromide during 4 h while maintaining the temperature at 10–20°. After standing at room temperature for 18 h the solution was diluted with ether (250 ml) and the precipitated solid was collected by filtration, dissolved in water (25 ml), stirred for 2 h at room temperature, cooled to 5°, neutralized with a 50% sodium

hydroxide solution, and extracted with methylene chloride. Drying and concentration left a solid which was crystallized in carbon tetrachloride to give **18***a* as white crystals, m.p. 173–175°; yield 2.25 g, 50%.

Anal. Calcd. for $C_{13}H_{17}NO$: C, 76.81; H, 8.43; N, 6.89. Found: C, 76.20; H, 8.39; N, 6.99.

*3-(β-Ethyl-3′-indolyl)-10b-hydroxy-1,2,3,4,4a,5,6,10b-octahydro-4a,10b-trans-benz[f]isoquinoline (**18***d*)

A solution of 3-indoleglyoxylyl chloride (20) (2.0 g, 0.00965 mol) in chloroform (30 ml) was added dropwise to a cooled (0–5°) and stirred mixture of the amine **18***a* (2.0 g, 0.00985 mol), 20% sodium hydroxide solution (2 ml), water (5 ml), and chloroform (10 ml). The mixture was stirred 0.5 h at 0° and then 1 h at room temperature The solid was collected by filtration and recrystallized in ethanol to give the 3-indoleglyoxylamide as a white solid, m.p. 200–204°; yield 2.7 g, 75%.

The above solid was reduced in dioxane with lithium aluminum hydride (1.0 g) under the normal conditions (18 h, reflux). The oily reaction residue was dissolved in $CHCl_3$–ether and treated with an excess of dry hydrogen chloride. The solid was recrystallized in methanol–ether to give **18***d* as white crystals, m.p. 246–248° dec; yield 2.3 g, 61%.

Anal. Calcd. for $C_{23}H_{27}ClNO_2$: C, 72.14; H, 7.11; N, 7.32. Found: C, 72.24; H, 7.24; N, 7.02.

*3-[4′-(p-Fluorophenyl)-4′-butyryl]-10b-hydroxy-1,2,3,4,4a,5,6,10b-octahydro-4a,10b-trans-benz(f)-isoquinoline (**18***e*)

A mixture of the amine **18***a* (3 g, 0.0148 mol), γ-chloro-*p*-fluorobutyrophenone (4.0 g, 0.02 mol), potassium carbonate (3.0 g, 0.0217 mol), and dry toluene (30 ml) was stirred and heated under reflux for 48 h. After cooling the solids were removed by filtration, washed with toluene, and the combined filtrates concentrated. The residual oil was dissolved in ethanol and acidified with 10% hydrochloric acid. The solid hydrochloride was recrystallized in dilute ethanol to give **18***e* as white crystals, m.p. 211–221°; yield 3.7 g, 62%.

Anal. Calcd. for $C_{23}H_{27}ClFNO_2 \cdot \frac{1}{2}H_2O$: C, 66.90; H, 6.84; N, 3.39. Found: C, 67.00; H, 6.56; N, 3.50.

*1-Cyanomethyl-1-hydroxy-2-methoxycarbonyl-2-methyl-1,2,3,4-tetrahydronaphthalenes (**20**)*

A solution of acetonitrile (4.1 g, 0.1 mol) in dry THF (100 ml) was added dropwise under nitrogen to a solution of *n*-butyllithium (69 ml of a 1.6 *M* solution in hexane, 0.11 mol) in dry THF (70 ml) kept at −78°. After stirring at −78° for 1 h, a solution of the ketone **19***a* (21), **19***b* (22), or **19***c* (23) (0.1 mol) in THF (150 ml) was added rapidly (5 min), the cooling bath removed, and the solution stirred for 0.5 h, poured into a mixture of crushed ice (*ca.* 400 g) and concentrated hydrochloric acid (100 ml), and the layers separated. The aqueous phase was extracted with ether (4 × 75 ml) and the combined organic layers dried and concentrated to leave an oil (100%). Chromatography over activity 2 alumina, eluting with ether, gave in succession the unreacted ketone **19** (0–30%), the *trans*-isomer (30–66%), the *cis*-isomer (15–30%), and byproduct (0–30) identified as 2-cyanoacetyl-2-methyl-1-tetralone.

Compound **20***a* could be isolated, without chromatography, by crystallization of the reaction residue in methanol; yield 60–75%. The *cis*-isomer was not characterized.

Compound **20***b* was isolated in a 25% yield. The *cis*-isomer (9%) and the byproduct (32%) were not characterized. Mixed fractions and unreacted ketone accounted for 32%.

Compound **20***c* was obtained in 12% yield; **20***d* in 15%; byproduct in 20%; unreacted ketone in 20%. The byproduct was recrystallized in methanol to give a white solid m.p. 143–144°, characterized as 2-cyanoacetyl-7-methoxy-2-methyl-1-tetralone.

Anal. Calcd. for $C_{15}H_{15}NO_3$: C, 70.02; H, 5.88; N, 5.44. Found: C, 70.03; H, 5.94; N, 5.46.

*10b-Hydroxy-4a-methyl-1,2,3,4,4a,5,6,10b-octahydro-4-oxobenz[f]isoquinolines (**21**)*

A solution of the cyanoesters **20** (0.05 mol) in absolute methanol (100 ml) was hydrogenated in a Parr Shaker in the presence of Raney nickel (*ca.* 7 g) until 2 equiv. of hydrogen had been absorbed (2–4 h). The catalyst was removed by filtration over Celite, washed with methanol, and the filtrates were concentrated on the rotary evaporator to leave the lactams **21** as white solids which were purified by recrystallization; yield 85–95%.

*10b-Hydroxy-4a-methyl-1,2,3,4,4a,5,6,10b-octahydrobenz-[f]-isoquinoline (**22**)*

The lactams **21** (0.055 mol) in dioxane (300 ml) were reduced with lithium aluminum hydride (7.32 g, 0.193 mol) in dioxane (100 ml) as described above for **11** and **13**. The crude reaction residue was purified by crystallization; yields 80–90%.

*3,4a-Dimethyl-10b-hydroxy-1,2,3,4,4a,5,6,10b-octahydrobenz[f]isoquinolines (**23**)*

A solution of the secondary amines **22** (0.051 mole) and paraformaldehyde (3.3 g, 0.102 mol) in absolute methanol (200 ml) was hydrogenated in a Parr Shaker in the presence of Raney nickel (*ca.* 10 g) at an initial pressure of 60 p.s.i. of hydrogen. When 1 equiv. of hydrogen was absorbed (20–60 min) the catalyst was removed by filtration over Celite, washed with methanol, and concentrated on the rotary evaporator. The residue was purified either by crystallization or through a hydrochloride prepared in ether.

*3,4a-Dimethyl-1,2,3,4,4a,5,6,10b-octahydro-10-b-propionyloxybenz[f]-isoquinolines (**24**)*

The tertiary alcohols **23** were esterified with freshly distilled propionyl chloride as described above for **4** and **12**. The resulting hydrochloric acid salts were purified by crystallization; yields 50%.

*3,4a-Dimethyl-9-hydroxy-2,3,4,4a,5,6-hexahydrobenz[f]-isoquinoline (**25***d*)

(*a*) A mixture of the alcohol **23***d* (0.52 g, 0.002 mol) and dry pyridine hydrochloride (6.0 g, 0.05 mol) was heated, under a vacuum of 20 mm Hg, at 185° for 2 h. After cooling, the mixture was dissolved in water (50 ml) and washed with ether (2 × 25 ml). The aqueous phase was made basic with concentrated ammonium hydroxide and extracted with methylene chloride. Drying and concentration of the extracts left the unsaturated amine **25***d* as at crude brown solid, m.p. 168–170°; 0.48 g; δ 1.05 (singlet, C—CH_3), δ 2.44 (singlet, N—CH_3), δ 5.9 (multiplet, C-1).

Anal. Calcd. for $C_{15}H_{20}ClNO$: C, 67.78; H, 7.58; N, 5.27. Found: C, 67.72; H, 7.72; N, 5.13.

(*b*) The alcohol **23***d* (1.3 g, 0.005 mol) kept 1.5 h at 100° with 48% hydrobromic acid gave a 87% yield of **25***d*.

We wish to thank Dr. R. Martel of Bristol-Candiac and Dr. A. W. Pircio of Bristol-Syracuse for the pharmacological data and Dr. B. Belleau for fruitful discussions.

1. A. H. BECKETT, A. F. CASY, G. KIRK, and J. WALKER. J. Pharm. Pharmacol. **9**, 939 (1957).
2. A. H. BECKETT and A. F. CASY. J. Pharm. Pharmacol. **6**, 986 (1954).
3. A. F. CASY. J. Med. Chem. **11**, 188 (1968); J. Chem. Soc. 2491 (1969).
4. P. S. PORTOGHESE and D. L. LARSON. J. Pharm. Sci. **57**, 711 (1968).
5. A. F. CASY. *In* Progress in medicinal chemistry. Vol. 7. *Edited by* G. P. Ellis and G. B. West. Meredith Corporation, New York. 1970. pp. 229–284.
6. J. H. AGER, S. E. FULLERTON, and E. L. MAY. J. Med. Chem. **6**, 322 (1963).
7. R. HUISGEN. Angew. Chem. Int. Ed. **2**, 565 (1963); J. HAMER and A. MACALUSO. Chem. Rev. **64**, 473 (1974); B. R. DELPIERRE and M. LAMCHEN. Quart. Rev. **19**, 329 (1965).
8. W. OPPOLZER and K. KELLER. Tetrahedron Lett. 1117 (1970).
9. A. ZIERING and J. LEE. J. Org. Chem. **12**, 911 (1947); A. POHLAND and H. R. SULLIVAN. J. Am. Chem. Soc. **75**, 4458 (1953).
10. C. J. SCHMIDLE and R. C. MANSFIELD. J. Am. Chem. Soc. **77**, 5698 (1955).
11. F. W. BACHELOR, A. A. LOMAN, and L. R. SNOWDON. Can. J. Chem. **48**, 1554 (1970).
12. F. G. MANN and M. J. PRAGNELL. J. Chem. Soc. 4120 (1965).
13. G. I. FEUTRILL and R. N. MIRRINGTON. Tetrahedron Lett. 1327 (1970).
14. J. C. SHEEHAN, W. F. ERMAN, and P. A. CRUICKSHANK. J. Am. Chem. Soc. **79**, 147 (1957).
15. E. SIEGMUND, R. CADMUS, and G. LU. Proc. Soc. Exp. Biol. Med. **95**, 729 (1957); H. BLUMBERG, P. S. WOLF, and H. B. DAYTON. Proc. Soc. Exp. Biol. Med. **118**, 763 (1965).
16. S. GARATINI, A. GIACHETTI, A. JORI, L. PIARI, and L. VALZELLI. J. Pharm. Pharmacol **14**, 509 (1962).
17. C. W. BROWN and M. A. T. ROGERS. British Patent No. 850, 418 (1960); Chem. Abstr. **55**, 6498 (1961).
18. (*a*) H. AHMED and N. CAMPBELL. J. Chem. Soc. 4115 (1960); (*b*) M. F. ANSELL and G. T. BROOKS. J. Chem. Soc. 201 (1961). (*c*) A. G. ANDERSON JR. and S. Y. WANG. J. Org. Chem. **19**, 277 (1954).
19. R. I. ICKE and B. WISEGARVER. Org. Synth. Col. Vol. III. p. 723.
20. J. L. NEUMEYER, U. V. MOYER, and J. E. LEONARD. J. Med. Chem. **12**, 450 (1969).
21. W. E. BACHMANN and D. G. THOMAS. J. Am. Chem. Soc. **63**, 598 (1941).
22. W. E. BACHMANN and N. L. WENDLER. J. Am. Chem. Soc. **68**, 2580 (1956).
23. J. H. HUNTER and J. KORMAN. J. Am. Chem. Soc. **69**, 2124 (1947).

Quaternary Bases from *Hunteria eburnea* Pichon

R. H. BURNELL, A. CHAPELLE, AND M. F. KHALIL
Département de Chimie, Université Laval, Québec 10, Québec

Received April 13, 1972[1]

R. H. BURNELL, A. CHAPELLE, and M. F. KHALIL. Can. J. Chem. **52,** 2327 (1974).

A re-examination of the quaternary alkaloids of *Hunteria eburnea* has shown the presence of antirhine β-methochloride **6**, dihydroantirhine β-methochloride **7** (originally called H. alkaloid J), and pleiocarpamine methochloride **5** (H. alkaloid F). A novel structure (**1**) has been forwarded for hunteracine chloride (bromide).

R. H. BURNELL, A. CHAPELLE et M. F. KHALIL. Can. J. Chem. **52,** 2327 (1974).

On a réexaminé les alcaloïdes quaternaires de *Hunteria eburnea*: on y retrouve le β-méthochlorure d'antirhine **6**, le β-méthochlorure de dihydroantirhine **7** (originalement appelé alcaloïde J de H.) et le méthochloride de pléiocarpamine **5** (alcaloïde F de H.). On propose une nouvelle structure (**1**) pour le chlorure (bromure) de l'huntéracine. [Traduit par le journal]

Can. J. Chem. Downloaded from www.nrcresearchpress.com by 210.87.254.105 on 09/05/12
For personal use only.

Previous workers (1) investigating the quaternary bases extracted from the bark of *Hunteria eburnea* Pichon identified (or established structures for) six alkaloids and referred to six other compounds isolated in quantities insufficient for complete characterization. One of the salts described in some detail (hunteracine) analyzed for $C_{20}H_{25}N_2OCl$ and was assumed to contain among its structural members:

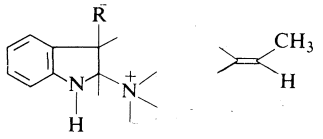

with the suggestion that R might be a hydroxyl group. The promise of an original structure prompted our isolation of more of this quaternary base. Elemental analyses of both the chloride and the bromide convinced us that the original molecular formula should be changed to $C_{18}H_{23}N_2OCl$ and the 283 *m/e* molecular ion in the mass spectrum supported our findings. The u.v. absorption and n.m.r. spectrum of the base chloride confirmed the partial structure and the changes in the n.m.r. on hydrogenation (to saturate the ethylidene moiety) were as expected. Hunteracine chloride (or bromide) proved remarkably stable; for instance, it could be purified by sublimation under reduced pressure and survived a variety of conditions normally used to degrade alkaloid salts. Several reactions attempted in basic medium produced a tertiary base in varying amounts and this proved to be a pseudoindoxyl, obtained in very limited quantities by earlier workers (1). The best yields were obtained by refluxing the salt for short periods with potassium hydroxide in ethanol and elemental analysis (with mass spectral confirmation) established the molecular formula $C_{18}H_{22}N_2O$. The fragmentation of hunteracine cation and hunteracine pseudoindoxyl in the mass spectrum afforded major peaks at 122 and 108 *m/e*; numerous examples have shown these to be indicative of the presence of an ethylidene piperidine moiety (n.m.r. confirms the ethylidene side chain).

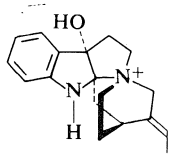

1

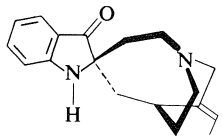

2

To eliminate the ambiguity that chemical degradation would probably engender it was decided to determine the structure by X-ray diffraction. In a preliminary report (2) the structure **1** was advanced for the hunteracine cation (discrepancy index 8.4%) and full details will be published shortly. From this structure the pseudoindoxyl must be **2**.

A plausible biogenetic origin for hunteracine would be via stemmadenine (**3**) necessitating degradative removal of the ester and carbinol functions and hydroxylation at the β-position of the indole. Transannular attack by the elec-

[1]Revision received February 28, 1974.

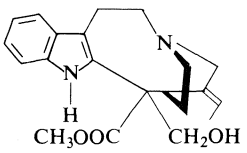

3

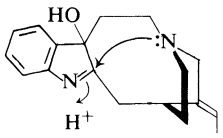

4

tron pair of the basic nitrogen on either an indolenine or indolenium double bond would afford hunteracine (as in **4**). Hunteracine chloride appears to be the first indole alkaloid wherein the C-2. of the indole moiety is incorporated in a quinuclidine system (in this case quinuclidinium).

Among the other quaternary bases incidentally isolated, we identified the alkaloid F which on demethylation afforded pleiocarpamine, identical with a sample provided by Dr. M. Hesse (Zurich). This is the first alkaloid isolated from this species as both the quaternary **5** and tertiary base (3) contrary to the suggestion (1) that yohimboid precursors afford the quaternary alkaloids of *H. eburnea* while the tertiary bases belong to the aspidosperma-eburnea type.

The properties of another quaternary chloride suggested it to be antirhine methochloride but comparison with a sample obtained from Dr. S. R. Johns (Melbourne) did not establish identity despite great simularity. This appeared to be another example of N_b diastereomers, already noted for the hunterburnines (1). In fact, demethylation of the new quaternary alkaloid with sodium thiophenoxide afforded a tertiary base showing all the properties reported for antirhine and conversion to the methochloride (via the methiodide) gave a product in all ways identical with the sample from Dr. Johns.

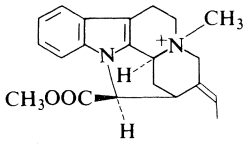

5

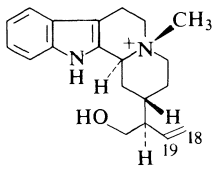

6

Previous studies by Sawa and Matsumura (4) have shown that laboratory *N*-methylation of tertiary bases with the antirhine skeleton gives only one product (the α-methochloride) and since in our case the natural salt is not the same as the laboratory derivative, we feel the alkaloid is antirhine β-methochloride **6**. None of the products referred to in earlier *H. eburnea* investigations resemble antirhine β-methochloride but hydrogenation of the natural alkaloid afforded a dihydro derivative, $C_{20}H_{29}N_2OCl$ (**6**) (no 18,19 double bond) identical with the product of unknown structure called H. alkaloid J. We also isolated the latter from the plant. The *O*-acetyl derivative of natural alkaloid J proved more soluble than the alcohol and afforded a clear n.m.r. spectrum showing the *N*-methyl singlet at 3.2 δ (in CF_3COOH). After demethylation with thiophenoxide, reaction with methyl iodide, and exchanging the cation to chloride, the new methochloride showed the *N*-methyl singlet at 3.5 δ (in CF_3COOH). This agrees with earlier findings (4, 5) which show that *N*-methyl peaks in the n.m.r. spectra of *trans*-quinolizidinium salts (β-metho salts in our case) are found at higher field than the *cis*-isomers.

Experimental

The methanol extract (8 kg) of the root and stem bark of *H. eburnea* was fractionated following essentially the method given by Taylor and co-workers (1). In our hands higher concentrations of water in acetone were needed to elute the products from the cellulose columns. The various chromatograms afforded the amounts shown in Table 1.

Hunteracine Chloride (1)

Recrystallised from ethanol, m.p. 343° (dec.), $[\alpha]_D$ −90° (c 0.1, in aqueous methanol); λ_{max} (EtOH) 234 (3.95) and 289 (3.49) nm (no change in acid or base); i.r. peaks at 3440, 3150 and 1620 (C=C) cm^{-1}; n.m.r.: 1.67 (3H, d: CH_3—CH=C) and 5.20 (1H, m. C=C*H*—) δ; mass spectrum: 283 (M^+), 282 (base peak), 266, 265, 172, 159, 158, 146, 137, 130, 124, 122, 121, and 108 *m/e*.

Anal. Calcd. for $C_{18}H_{23}N_2OCl$: C, 67.8; H, 7.3; N, 8.8; O, 5.0; Cl, 11.1. Found: C, 67.8; H, 7.3; N, 8.7; O, 5.0; Cl, 11.2.

The anion was exchanged on Permatit Isopor SRA-66 bromide form resin in 50% aqueous acetone to give the *bromide*, m.p. 340° (dec.) after recrystallisation from acetone–water.

Anal. Calcd. for $C_{18}H_{23}N_2OBr$: C, 59.5; H, 6.3; N, 7.7; O, 4.4; Br, 22.0. Found: C, 59.6; H, 6.3; N, 7.9; O, 4.5; Br, 22.2.

Dihydrohunteracine Chloride

Hunteracine chloride (70 mg) was hydrogenated over Adams' catalyst in 90% ethanol. After 1 mol of hydrogen, uptake ceased and the product showed m.p. 313–315° (dec.) from ethanol. The n.m.r. spectrum now showed: 0.90 (3H, t J = 6.5 Hz) δ and lacked peaks in the vinyl region.

Anal. Calcd. for $C_{18}H_{25}N_2OCl$: C, 67.5; H, 7.8; N, 8.7; O, 5.0; Cl, 11.1. Found: C, 67.5; H, 7.9; N, 8.7; O, 5.0; Cl, 11.1.

Hunteracine Pseudoindoxyl (2)

Hunteracine chloride (220 mg) was refluxed with potassium hydroxide (250 mg) in ethanol (50 ml) for 30 min. After filtration and elimination of most of the ethanol the basic tertiary base (155 mg), as fine very pale

Can. J. Chem. Downloaded from www.nrcresearchpress.com by 210.87.254.105 on 09/05/12
For personal use only.

TABLE 1. Summary of chromatographic data

Alkaloid	Yield (mg) from chromatogram*					Remarks
	A	B	C	D	Total	
Hunteracine chloride (1)	400	560	520	250	1730	
Yohimbol methochloride	700	—	900	400	2000	
Hunterburnine α-methochloride	100	—	30	40	170	
Huntrabrine methochloride	15	—	—	—	15	
Hunterburnine α-methochloride	20	—	—	50	70	
Pleiocarpamine methochloride (5)	—	960	—	—	960	≡ Alkaloid F
Akuammicine methochloride	—	20	—	—	20	
Antirhine α-methochloride (**6**)	—	500	900	200	1600	Not previously reported
Dihydroantirhine β-methochloride	—	—	630	350	980	≡ Alkaloid J

*Briefly, the origins of the samples are the following: A, crude chlorides; B, chlorides extracted with CH_2Cl_2; C, chlorides *not* extracted with CH_2Cl_2 or adsorbed on charcoal; D, chlorides not extracted with CH_2Cl_2, desorbed from charcoal.

yellow needles, was isolated by extraction, m.p. 235° (dec.), from ethanol, $[\alpha]_D$ −355° (c 0.1, in ethanol); λ_{max} (EtOH) 229 (4.35) and 380 (3.48) nm; i.r. spectrum: 3400, 3200, 1692, 1625 cm^{-1}; mass spectrum: 282 (M^+), 281, 238, 237, 236, 210, 201, 196, 185, 183 (base peak), 158, 130, 122, and 108 *m/e*.

Anal. Calcd. for $C_{18}H_{22}N_2O.C_2H_5OH$: C, 73.1; H, 8.6; N, 8.5; O, 9.7. Found: C, 73.5; H, 8.3; N, 8.8; O, 9.4.

Antirhine β-Methochloride (6)

From ethanol, m.p. 306° (dec.), $[\alpha]_D$ +75° (c, 0.04, in ethanol); λ_{max} (EtOH) 222 (4.84), 272 (3.85) and 289 (3.80) nm; n.m.r. spectrum (D_2O): 7.1–7.7 (4H, m aromatic protons), 5.54 (3H, m vinyl protons); mass spectrum: 311 (M^+), 310, 296, 295, 265, 239, 225 (base peak), 223, 197, 184, 169, 156, and 143 *m/e*.

Anal. Calcd. for $C_{20}H_{27}N_2OCl$: C, 69.2; H, 7.8; N, 8.1; O, 4.6; Cl, 10.2. Found: C, 69.0; H, 7.9; N, 8.1; O, 4.4; Cl, 10.2.

O-Acetylantirhine β-Methochloride

This product, m.p. 306° (dec.) was prepared from antirhine β-methochloride (130 mg) using acetic anhydride (1 ml) and pyridine (2 ml) in a sealed tube at 85° for 40 h; i.r. spectrum: 3130, 1740, 1245 cm^{-1}; n.m.r. spectrum showed the CH_3CO— resonance at 1.87 δ and a singlet at 3.305 (N—CH_3); mass spectrum gave 352 *m/e* as M^+.

Anal. Calcd. for $C_{22}H_{29}N_2OCl$: C, 67.9; H, 7.2; O, 8.2; Cl, 9.1. Found: C, 67.7; H, 7.7; O, 8.1; Cl, 9.2.

Dihydroantirhine β-Methochloride (H. alkaloid J)

Antirhine β-methochloride (100 mg) in ethanol (50 ml) was shaken under hydrogen (50 p.s.i.) in the presence of 10% palladium–charcoal (15 mg). The dihydro derivative crystallized from ethanol, m.p. 305° (dec.), $[\alpha]_D$ +71.4° (c 0.13, in water), and was identical with *H. alkaloid J* which was obtained from the extraction; λ_{max} (EtOH) 220 (4.59), 272 (3.88), 282 (sh. 3.87), and 289 nm; i.r. peaks at 3390 and 3150 cm^{-1}; n.m.r.: methyl triplet 1.2 δ (J = 7 Hz and *N*-methyl 3.20 δ; *m/e* 312 (M^+).

Anal. Calcd. for $C_{20}H_{29}N_2OCl$: C, 68.9; H, 8.3; N, 8.0; O, 4.6; Cl, 10.2. Found: C, 68.7; H, 8.1; N, 8.1; O, 4.5; Cl, 10.3.

Sealed tube acetylation afforded *O-acetyldihydroantirhine β-methochloride*, m.p. 303° (dec.), $[\alpha]_D$ +68° (c, 0.1 in aqueous methanol); i.r. 3130, 1722, 1245 cm^{-1}; *m/e* 355 (M^+); n.m.r. spectrum (CF_3COOH) showed *N*-methyl at 3.2, and CH_3CO at 2.32 δ.

Antirhine α-Methochloride (Des-N-methylation and N-Methylation)

Antirhine β-methochloride (221 mg) and sodium thiophenoxide (235 mg) were stirred together in ethanol (40 ml) for 20 min. The sodium chloride was removed by filtration and the solvent evaporated. The residue was dissolved in methyl ethyl ketone (100 ml) and refluxed under nitrogen for 36 h. Evaporation and extraction afforded the tertiary base, *antirhine* (135 mg) as pale yellow needles, m.p. 112–115°, $[\alpha]_D$ −2° (c, 0.1 in chloroform) (lit. (6) m.p. 112–114°, $[\alpha]_D$ −2° all other physical data were in agreement with those published).

Antirhine α-Methiodide, m.p. 288–290° (dec.) $[\alpha]_D$ −24.4 (c 0.1 in ethanol) formed rapidly and almost quantitatively from methanol containing methyl iodide (n.m.r.: three proton —$\overset{+}{N}$—CH_3 singlet at 3.42 δ). The methiodide was passed over a column of Permutit Isopor SRA-66 (chloride form) in 50% aqueous acetone and the product crystallized from methanol–water giving *antirhine α-methochloride*, m.p. 325–328° (dec.), $[\alpha]_D$ −17.9° (c 0.27 in aqueous methanol). Comparison with a sample kindly supplied by Dr. S. R. Johns (Melbourne) confirmed the identity of the product (i.r., t.l.c., u.v., and mass spectrum).

Dihydroantirhine α-Methochloride

Demethylation of dihydroantirhine α-methochloride (with thiophenoxide) and treatment with methyl iodide gave *dihydroantirhine α-methiodide*, m.p. 296–298° (dec.), which was converted to the α-methochloride on ion exchange resin. Recrystallization from ethanol–water, m.p. 310–312° (dec.), $[\alpha]_D$ −8° (c 0.13, in aqueous ethanol). The other physical characteristics of the α-isomer were very similar to the β-isomer except the more prominent Bohlmann bands in the i.r. (2840 cm^{-1}) and the N—CH_3 peak in the n.m.r. (now at 3.5 δ, taken in trifluoroacetic acid).

Pleiocarpamine Methochloride (≡ H, Alkaloid F) (5)

Recrystallized from ethanol–water, m.p. 242–243° (dec.), $[\alpha]_D$ +165° (c 0.5, in aqueous methanol); λ_{max} 223 (4.47), 274 (3.92), 283 (sh 3.87) and 292 (sh 3.75) nm; i.r. spectrum: 3460, 3410, and 1737 cm^{-1}; n.m.r. peaks at 6.9–8 (arom), 5.65 (1H *d*), 4.99 (1H *d*), 3.70 (CH_3OOC—),

Can. J. Chem. Downloaded from www.nrcresearchpress.com by 210.87.254.105 on 09/05/12
For personal use only.

3.18 ($\overset{+}{N}$—CH_3) and 1.58 (3H *d* CH_3—CH=) δ; mass spectrum: 375, 374, *373* (base peak), 337, *314*, 313, 283, *180*, *122*, *108* *m/e*. (Note incorporation of halide, see ref. 7.)

Anal. Calcd. for $C_{21}H_{25}N_2O_2Cl$. H_2O: C, 64.5; H, 7.2; N, 7.0; O, 12.3; Cl, 9.1. Found: C, 64.3; H, 7.0; N, 7.1; O, 12.5; Cl, 9.4.

The *methiodide* (prepared by ion exchange), m.p. 230° (dec.) showed mass spectrum peaks at 464, 405, 337, 180, 128, 122 *m/e*.

Demethylation (thiophenoxide method) gave the tertiary base, pleiocarpamine, m.p. 158°, $[\alpha]_D$ +134° (c 0.2, in chloroform). Compared with a sample kindly sent by Dr. M. Hesse (Zurich) the two products were identical (m.p., mixture m.p., t.l.c., i.r., and mass spectrum).

We thank the National Research Council of Canada for operating and equipment grants.

1. M. F. Bartlett, B. Korzun, R. Sklar, A. F. Smith, and W. I. Taylor. J. Org. Chem. **28**, 1445 (1963).
2. R. H. Burnell, A. Chapelle, M. F. Khalil, and P. H. Bird. Chem. Commun. 772 (1970).
3. M. F. Bartlett, R. Sklar, A. F. Smith, and W. I. Taylor. J. Org. Chem. **28**, 2197 (1963).
4. Y. K. Sawa and H. Matsumura. Tetrahedron, **25**, 5319 (1969).
5. T. M. Moynehan, K. Schofield, R. A. Y. Jones, and A. R. Katritsky. J. Chem. Soc. 2637 (1962).
6. W. Jordan and P. J. Scheuer. Tetrahedron, **21**, 3731 (1965).
7. S. R. Johns, J. A. Lamberton, and J. L. Occolowitz. Aust. J. Chem. **20**, 1463 (1967).

Can. J. Chem. Downloaded from www.nrcresearchpress.com by 210.87.254.105 on 09/05/12
For personal use only.

Studies Relating to Aziridine Antitumor Antibiotics. Part II.[1] ^{13}C and ^{1}H Nuclear Magnetic Resonance Spectra of Mitomycin C and Structurally Related Streptonigrin

J. WILLIAM LOWN AND ASHER BEGLEITER[2]

Department of Chemistry, University of Alberta, Edmonton, Alberta

Received November 15, 1973

J. WILLIAM LOWN and ASHER BEGLEITER. Can. J. Chem. **52**, 2331 (1974).

Double irradiation experiments in the 100 MHz n.m.r. spectrum of mitomycin C allowed determination of vicinal coupling constants which provide information on the conformation of the antibiotic in solution. The natural abundance ^{13}C spectrum and comparison with selected model compounds allowed assignment of the carbon resonances of mitomycin C. The ^{13}C chemical shifts of the quinone ring carbons in mitomycin C have a bearing on the proposed stabilization *in vivo*. Similar studies on the antitumor antibiotic streptonigrin bearing the common aminoquinone moiety gave indications of conjugative interactions similar to those established for mitomycin C.

J. WILLIAM LOWN et ASHER BEGLEITER. Can. J. Chem. **52**, 2331 (1974).

Des expériences de double irradiation du spectre r.m.n. à 100 MHz de la mitomycine C permettent de déterminer les constantes de couplage vicinales; celles-ci apporteront de l'information sur la conformation de l'antibiotique en solution. On attribue les positions de résonance des divers carbones de la mitomycine C à l'aide de son spectre de ^{13}C en abondance naturelle et par comparaison avec quelques composés modèles. Les déplacements chimiques du ^{13}C du noyau quinonique de la mitomycine C apportent un appui à la stabilisation proposée *in vivo*. Au cours d'études semblables sur la Streptonigrine, antibiotique antitumoral portant le même groupe amino-quinone, on a obtenu des résultats indiquant la présence d'interactions par conjugaison similaires à celles établies pour la mitomycine C. [Traduit par le journal]

Can. J. Chem. Downloaded from www.nrcresearchpress.com by 210.87.254.40 on 09/05/12
For personal use only.

Mitomycin C and related structures of the mitosane class are potent antibiotics (1) and have found clinical use in Japan as antineoplastic agents (2). Considerable interest has been shown recently in their attempted total synthesis (3), the synthesis of analogs (4), and their biosynthesis from *Streptomyces verticallatus* (5). We report spectroscopic studies including the natural abundance ^{13}C spectrum of mitomycin C and the structurally related streptonigrin which pertain to the proposed stabilization of the former antibiotic *in vivo* (7) and which should assist in possible further biosynthetic studies employing the incorporation of ^{13}C labelled substrates and in characterizing synthetic analogs. Information is also obtained from the spin-decoupled ^{1}H n.m.r. spectrum on the conformation of mitomycin C in solution.

A 100 MHz p.m.r. spectrum of mitomycin C in pyridine-d_5, (see Fig. 1), together with double irradiation experiments permitted assignment of all the proton signals and determination of the proton–proton coupling constants. The C-10 methylene protons at 5.00 and 5.36 have unequal couplings of 10.5 and 4.5 Hz to the C-9 methine proton at 3.96. In addition the dihedral angle of H—C_2—C_3—H is 90° since the vicinal coupling constant $J_{23} = 0$, consonant with the molecular geometry for the solid phase indicated by X-ray analysis for the *N*-brosyl derivative of the related antibiotic mitomycin A (7 substituent CH_3O instead of —NH_2) (7) and $J_{23'} = 2.5$ Hz. The observed value of $J_{12} = 4.5$ Hz is also consistent with *cis*-coupled aziridine ring protons. The broad signals in the region δ 3.7–4.6 (3H) were exchangeable with deuterium oxide and are ascribed to NH and NH_2 protons.

This information on the conformation of mitomycin C in solution is of interest in connection with its proposed mode of antibacterial action *i.e.* of intercalation and cross-linking of the complementary strands of DNA by bifunctional alkylation through reactive centers C-10 and -1 at specific sites in the macromolecule (currently considered to be O-6 positions of guanine) (8).

A ^{13}C noise decoupled n.m.r. spectrum in

[1]For Part I see ref. 29.

[2]NRCC Studentship holder 1970 to present.

TABLE 1. ^{13}C chemical shifts in p.p.m. from TMS of antibiotics as 0.224 *M* solutions in pyridine-d_5 at 25.15 MHz[a]

Mitomycin C		Streptonigrin	
Chemical shift	Assignment	Chemical shift	Assignment
178.6 s	8	181.1 s	5
176.8 s	5	176.9 s	8
158.0 s	10a	168.3 s	CO_2H
156.0 s	5a	161.0 s	6,5a
150.0 s	7	154.2 s	
111.0 s	9a	150.0 s	6′
107.0 s	6	147.1 s	5′
104.5 s	8a	144.9 s	10′
62.7 t	10	141.9 s	2′
50.7 t	3	138.6 s	12′
49.7 (q)	9a—OCH_3	137.8 s	4′
44.5 d	9	137.1 s	
36.8 d	1	135.9 s	
32.8 d	2	135.3 s	3′
8.7 q	6—CH_3	133.5 d	1
		130.7 s	11′
		127.4 s	
		126.2 d	2
		125.4 d	8′
		116.4 s	7′
		105.1 d	9′
		60.5 q	—OCH_3
		60.1 q	
		56.1 q	7—OCH_3
		17.8 q	CH_3

[a]Lock signal pyridine-d_5. Chemical shift data using a 4K data set are accurate to ±0.05 p.p.m.

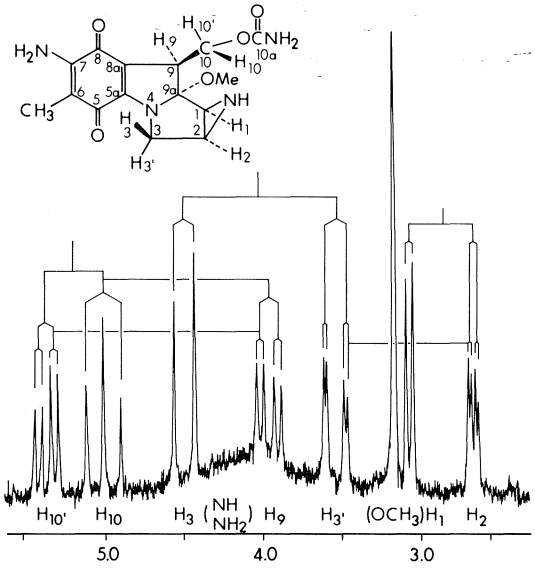

FIG. 1. 100 MHz p.m.r. spectrum of mitomycin C in pyridine-d_5.

natural abundance was obtained at 25.15 MHz on a 0.224 *M* solution of mitomycin C in pyridine-d_5 (see Table 1). All 15 carbon atoms are clearly distinguishable (singlets). The spectrum can be divided into three regions, low field carbonyl carbons, middle range quinone ring and quaternary carbons, and saturated carbons at high field. The following carbons could be assigned readily: δ 158.0 (10a, *cf.* ethyl carbamate carbonyl 158.4); 62.7 (10, *cf.* **2***d*—CH_2OCONH_2 63.9 (see also (21)); 8.7 (6-CH_3, *cf.* CH_3 signal of model **2***e* at 9.2).

In contrast, the poor agreement for the positions of the quinone ring carbon signals with those of the quinone models (see Table 2) **1***a–c* as well as the poor agreement of the C-5 and -8 carbonyl resonances of mitomycin C with those of **1***a–c* signified an unusual structure for the quinone moiety of mitomycin C. The stability of the oxidized form of the mitomycins has been attributed to resonance between forms A and B which results in partial withdrawal of electrons

Can. J. Chem. Downloaded from www.nrcresearchpress.com by 210.87.254.40 on 09/05/12
For personal use only.

TABLE 2. ^{13}C chemical shifts in p.p.m. from TMS in pyridine-d_5 at 25.15 MHz

Structure	Quinone ring carbons				Pyrr(ol)idine ring		CH_3	Carbonyl	Additional resonances	
	2	3	5	6	1′	2′				
1*a* Benzoquinone		136.6						187.4		
1*b* 2,5-Dimethylquinone	145.7	133.6					15.2	187.9		
1*c* Tetramethylquinone	140.4						12.2	187.0		
2*a*	103.7	153.7			53.4	25.7	12.4	183.7		
2*b*[e]	99.9	149.8			50.9	24.4		180.5		
2*c*	102	154.8			59.8	125.6	11.7	183.4		
2*d*	102.4	154.7	102.9	154.7	53.2 53.5	24.6 25.6	12.2	183.6, 158.2[a]	45[b]	63.9[c]
2*e*[d]	149.4	101.7					9.2	179.3		
3*a* 6-(4′-Bromophenyl)-3,6-diazabicyclo-[3.1.0]hexane					48.3	44.7				
3*b* 6-(4′-Nitrophenyl)-3,6-diazabicyclo-[3.1.0]hexa-2,4-dione						42.8				

[a]C=O of 2-side chain
[b]C_1' of 2-side chain
[c]C_2' of 2-side chain
[d]Solvent $(CD_3)_2SO$
[e]Solvent $CDCl_3$

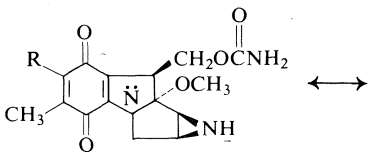

A ↔ B

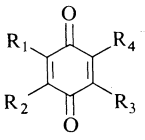

a $R_2 = R_4 = CH_3$; $R_1 = R_3$ = Pyrrolidine
b $R_2 = R_4 = H$; $R_1 = R_3$ = Pyrrolidine
c $R_2 = R_4 = CH_3$; $R_1 = R_3$ = 3-Pyrroline
d $R_2 = CH_3$; $R_4 = CH_2CH_2OCONH_2$; $R_1 = R_3$ = Pyrrolidine
e $R_2 = R_4 = CH_3$; $R_1 = R_3 = NH_2$

from N-4 into the quinone ring and consequent stabilization of the 9*a*-methoxy substituent, an otherwise good leaving group (6). NADP-dependent enzymatic reduction of mitomycins to the hydroquinone form is considered to release the indole nitrogen pair to promote expulsion of the bridgehead alkoxy group (6a). Pullman and Pullman have pointed out the strong conjugative interaction of groups directly attached to the quinone ring (6b).

Since similar conjugative interaction has been established in simple aminoquinones by other spectroscopic means (9), we sought information on this (A ↔ B) interaction and confirmation of the ^{13}C signals of mitomycin by examining further model compounds **2** and **3** (see Table 2). The introduction of the 2,5 nitrogen substituents particularly the amino groups in **2***e* in these quinones produced much better agreement in the line positions for C-8 and -5 carbonyls at 178.6 and 176.8, respectively. Model **2***e* permits the assignment of C-7 at 150 and C-5a at 156.0, and of C-6 and -8a ring carbons at 104.5 and 107.0, although at present the latter pair may not be discriminated further. Comparison of models **3***a* and *b* indicates an upfield shift of the aziridine carbons due to an adjacent oxygen function. On this basis C-1 and -2 in mitomycin C were tentatively assigned values of 36.8 and 32.8, respectively. The 62.66 p.p.m. absorption became a triplet by off-resonance decoupling confirming its assignment as C-10. The only other triplet signal at 50.67 is therefore unambiguously

Can. J. Chem. Downloaded from www.nrcresearchpress.com by 210.87.254.40 on 09/05/12
For personal use only.

assigned to C-3, also assigned by reference to models **2***a* and *b*. Two signals appeared as doublets at 49.7 and 8.7 and they may well be actual quartets. The latter information together with the methyl assignment in **2***e* confirms the 6-CH_3 carbon assignment and therefore the 49.7 peak was ascribed to the 9*a*-methoxy carbon. The line position is also in excellent agreement with literature values of 51.0 p.p.m. for methoxy groups (10).

Three signals appeared as doublets at 44.5, 36.8, and 32.8 p.p.m. corresponding to the required three methines in mitomycin C. The high field pair at 36.8 and 32.8 were assigned to the aziridine carbonyls 1 and 2, permitting the assignment of C-9 at 44.5 p.p.m. The eight signals which remained as singlets as required by the structure have all been assigned.

The presence of the *o*-aminoquinone moiety in mitomycin C, as well as in the antineoplastic agents streptonigrin **4** (11) and actinomycin **5** (11) (and the structurally related aurantins (12)), as well as in the *ansa*-antibiotics rifamycin **6** (13) and geldanamycin (14), increases the interest in these assignments.

Streptonigrin is an antibiotic which is derived from *Streptomyces flocculus* (11). Streptonigrin and mitomycin C are similar in a number of important respects (15, 16): (*a*) both contain the aminoquinone moiety; (*b*) both selectively inhibit net DNA synthesis in bacterial cells (17); (*c*) both initiate bacterial DNA degradation; (*d*) both induce lysogenic bacteria; and (*e*) DNA synthesis, as measured by phage production can be restored by phage infection or induction in the presence of either antibiotic.

Although there is as yet no firm evidence on the mode of antitumor activity of streptonigrin (18), the primary cytotoxic activity appears to be connected with inhibition of DNA synthesis, as in the case of mitomycin. When salmon sperm and *Escherichia coli* DNA were treated with streptonigrin at concentrations of 15 μg/ml the thermal denaturation temperature was increased (19). Significantly the viscosity of DNA was not affected by the drug unless it was first reduced to the hydroquinone form in the presence of DNA which is precisely what happens with mitomycin. This points to the biological significance of the common aminoquinone moiety in these drugs. Therefore a ^{13}C n.m.r. spectrum of streptonigrin in pyridine-d_5 was obtained and the assignments are summarized in Table 2. All

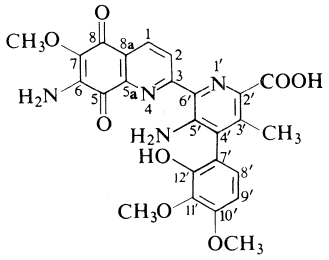

4

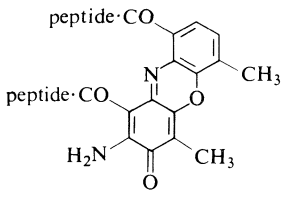

5

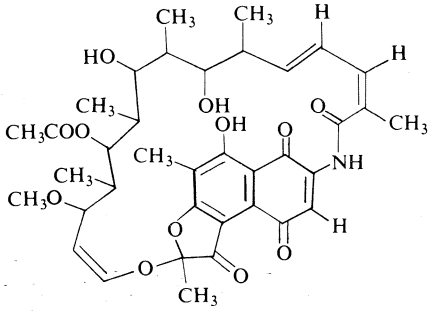

6

25 carbons are clearly visible and several firm assignments could be made *viz.* CH_3 at 17.8 (quartet) and three —OCH_3 groups at 60.5, 60.1, and 56.1 (quartets, *cf.* comparable signal in mitomycin C). Four signals only displayed doublet multiplicity as required by **4**, 133.5, 126.2, 125.4, and 105.1. Of these the latter two are ascribed tentatively to 8′ and 9′, respectively, on the basis of substituent shift predictions from 2,3-dimethoxy-6-phenylphenol as a model (20). The ^{13}C spectrum of picolinic acid served to establish the position of the carboxyl carbon (at 167.8 in good agreement with that in streptonigrin at 168.3) and as a base for substituent shift predictions, also the general positions for carbons on pyridine rings. Further assignments were made possible on the basis of substituent shift predictions from 5-amino-4,6-diphenyl-3-methyl-2-picolinic acid. It is recognized that the additivity relationships for four substituents have severe

Can. J. Chem. Downloaded from www.nrcresearchpress.com by 210.87.254.40 on 09/05/12
For personal use only.

Can. J. Chem. Downloaded from www.nrcresearchpress.com by 210.87.254.40 on 09/05/12
For personal use only.

limitations so they are used only as a guide in the line assignments.

These results now permit the assignment of the quinone carbonyls in streptonigrin at 181.1 and 176.9. The similarity in the positions with those of the aminoquinone model **2***e* as well as those of mitomycin suggests a similar conjugative interaction of the 7-NH_2 function in streptonigrin. Details of the synthesis of mitomycin analogs based on structures **2** and the application of the spectroscopic results in this paper to their characterization will be described in a subsequent paper.

Experimental

Melting points were determined on a Fisher-Johns apparatus and are uncorrected. The i.r. spectra were recorded on a Perkin-Elmer Model 421 spectrophotometer and only the principal, sharply defined peaks are reported. The n.m.r. spectra were recorded on a Varian HA-100 analytical spectrometer. The spectra were measured on approximately 10–15% (w/v) solutions in $CDCl_3$, with tetramethylsilane as a standard. Line positions are reported in p.p.m. from the reference.

Noise decoupled ^{13}C n.m.r. spectra in natural abundance were obtained at 25.15 MHz in 12 mm spinning tubes in pyridine-d_5 solution on a Varian HA-100-15 instrument using tetramethylsilane as internal reference. Typically for mitomycin C a total of 4000 scans were made for multiscan averaging and accumulated with an interfaced Digitab FTS/NMR 3 data system. Additional ^{13}C spectra were determined at 22.63 MHz in 10 mm spinning tubes in the Fourier mode using a Bruker HFX-90 spectrometer in conjunction with a Nicolet-1085, 20 K memory computer. The spectrometer features a deuterium lock system, a BSV-2 random noise (800 Hz band-width) proton decoupler, and a BSV-2 pulse generator-amplifier. Mass spectra were determined on an Associated Electrical Industries MS-9 double focusing high resolution mass spectrometer. The ionization energy, in general, was 70 eV. Peak measurements were made by comparison with perfluorotributylamine at a revolving power of 15 000. Kieselgel DF-5 (Camag, Switzerland) and Eastman Kodak precoated sheets were used for t.l.c. Microanalyses were carried out by Mrs. D. Mahlow of this department.

Materials

Commercial mitomycin C (Calbiochem Inc.) was used and characterized spectroscopically as follows. Infrared spectrum ν_{max} (Nujol): 1595; 1720 ($OCONH_2$); 1700 (quinone C=O), 3260, 3300, 3420 cm^{-1} (NH,NH_2). Absorption spectrum λ_{max} (CH_3CN (log ε): 540 (3.43); 359 (5.37); 350 (5.32); 240 (sh) (5.03)). Mass spectrum: base peak 334 ($M - CH_3OH$).

Pure streptonigrin was kindly supplied by Dr. H. B. Wood, Division of Cancer Treatment, National Institutes of Health.

*2,5-Dimethyl-3,6-bis(pyrrolidino)-1,4-benzoquinone (**2a**)*

This compound was prepared in 17% yield following the procedure of Crosby and Lutz (22), m.p. 149–150.5° (lit. (23) m.p. 149–150°).

*2,5-Bis(pyrrolidino)-1,4-benzoquinone (**2b**)*

This compound was prepared in 62% yield essentially by the procedure of Crosby and Lutz (22), m.p. 245–250° (dec.) (lit. (24) m.p. 238–240°).

*2,5-Dimethyl-3,6-bis(3-pyrrolino)-1,4-benzoquinone (**2c**)*

This compound was prepared by a literature procedure (22). Upon heating it changed from a purple to a white solid between 164–172° and melted at 242.5–244.5°.

Anal. Calcd. for $C_{16}H_{18}N_2O_2$ (mol. wt. 270.1368): C, 71.09; H, 6.71; N, 10.36. Found 270.1360, (mass spectrum): C, 70.89; H, 6.48; N, 9.96.

The i.r. spectrum ν_{max} ($CHCl_3$): 1610 cm^{-1} (C=O). The ^1H n.m.r. spectrum δ_{TMS} ($CDCl_3$): 2.02 (s, 6H, CH_3); 4.54 (s, 8H, methylenes); 5.85 (s, 4H, vinyl).

*2-(2′-Carbamoyloxyethyl)-5-methyl-3,6-bis(pyrrolidino)-1,4-benzoquinone (**2d**)*

A solution of 0.40 g (2 mmol) of freshly crushed cupric acetate monohydrate and 0.85 g (12 mmol) of pyrrolidine in 20 ml of methanol was purged with oxygen. While bubbling oxygen through the reaction mixture, a solution of 0.418 g (2 mmol) of 2-(2′-carbamoyloxymethyl)-5-methyl-1,4-benzoquinone (25) was added at such a rate that the temperature remained between 20–30°. Oxygenation was continued for 1 h after all the quinone had been added. The solution was concentrated to *ca.* 5 ml and chromatographed on a column of neutral alumina (Woelm), eluting with methanol. The first fraction was collected and evaporated affording 0.367 g (53% yield) of **2***d* as an oil.

Mol. Wt. Calcd. for $C_{18}H_{25}N_3O_4$: (347.1845). Found (mass spectrum): 347.1847.

The ^1H n.m.r. spectrum δ_{TMS} ($CDCl_3$): 1.94 (s, 3H, CH_3); 1.89 and 2.04 (2m, 4H each, H_3 and H_4 of pyrrolidine rings); 2.85 (t, 2H, H_A, J_{AB} = 2.5 Hz); 3.36 and 3.74 (2m, 4H each, H_2 and H_5 of pyrrolidine rings); 3.95 (t, 2H, H_B).

*2,5-Diamino-3,6-dimethyl-1,4-benzoquinone (**2e**)*

This compound was prepared by the procedure of Zee-Cheng and Cheng (4*b*), m.p. 309–310° (lit. (4*b*) m.p. 310–312°).

*6-(4′-Bromophenyl)-3,6-diazabicyclo[3.1.0]hexane (**3a**)*

This compound was prepared in 48% yield by an adaption of a procedure due to Oida *et al.* (26) using a Pyrex filtered 200 W Hanovia high pressure mercury lamp for 6 h, m.p. 114–115.5° (lit. (27) m.p. 115–116°).

*6-(4′-Nitrophenyl)-3,6-diazabicyclo[3.1.0]hexa-2,4-dione (**3b**)*

This compound was prepared in 30% yield by the procedure of Davis and Rondesveldt (28), m.p. 243–245° (lit. (28) m.p. 245°).

This research was supported by grants to J. W. L. from the National Research Council of Canada and the National Cancer Institute of Canada and by the Chemistry Department, University of Alberta. We thank Dr. A. Hogg and Mr. R. Swindlehurst for the mass and n.m.r. spectra. We also wish to thank Dr. T. Nakashima for careful ^{13}C spectra.

Can. J. Chem. Downloaded from www.nrcresearchpress.com by 210.87.254.40 on 09/05/12
For personal use only.

1. (*a*) T. HATO, Y. SANO, R. SUGAWARA, A. MATSUMAE, K. KANAMORI, T. SHIMA, and T. HOSHI. J. Antibiot. (Tokyo), Ser. A, **9**, 141 (1956); (*b*) S. WAKAKI, H. MARUMO, T. TOMIOKA, G. SHIMIZU, E. KATO, H. KAMADA, S. KUDO, and Y. FUJIMOTO. Antibiot. Chemother. **8**, 228 (1958); (*c*) S. WAKAKI. Cancer Chemother. Rep. **13**, 79 (1961); (*d*) J. S. WEBB, D. B. COSULICH, J. H. MOWAT, J. B. PATRICK, R. W. BROSCHARD, W. E. MEYER, R. P. WILLIAMS, C. F. WOLF, W. FULMOR, C. PIDACKS, and J. E. LANCASTER. J. Am. Chem. Soc. **84**, 3185 (1962).
2. (*a*) W. FRANK and A. E. OSTERBERG. Cancer Chemother. Rep. **9**, 114 (1960); (*b*) K. SUGIURA. Cancer Chemother. Rep. **13**, 51 (1961); (*c*) A. E. EVANS. Cancer Chemother. Rep. **14**, 1 (1961); (*d*) J. S. EVANS, E. A. MUSSER, and J. E. GRAY. Antibiot. Chemother. **11**, 445 (1961).
3. (*a*) W. A. REMERS and M. J. WEISS. J. Med. Chem. **11**, 737 (1968) and papers cited therein; (*b*) R. W. FRANCK and J. AUERBACH. J. Org. Chem. **36**, 31 (1971); (*c*) T. HIRATA, Y. YAMADA, and M. MATSUI. Tetrahedron Lett. 4107, (1969); (*d*) T. TAKADA, and S. OHKI. Chem. Pharm. Bull. (Japan), **19**, 977 (1971); (*e*) T. TAKADA, S. KUNUGI, and S. OHKI. Chem. Pharm. Bull. (Japan), **19**, 982 (1971); (*f*) T. TAKADA and M. AKIBA. Chem. Pharm. Bull. (Japan), **20**, 1785 (1972).
4. (*a*) A. I. MEYERS, T. A. NARWID, and E. W. COLLINGTON. J. Heterocycl. Chem. **8**, 875 (1971); (*b*) K-Y. ZEE-CHENG and C. C. CHENG. J. Med. Chem. **13**, 264 (1970); (*c*) L. MANDELL and E. C. ROBERTS. J. Heterocycl. Chem. **2**, 479 (1965).
5. U. HORNEMANN and M. J. AIKMAN. Chem. Commun. 88 (1973); U. HORNEMANN, J. P. KEHRER, C. S. NUNEZ, and R. L. RANIERI. J. Am. Chem. Soc. **96**, 320 (1974).
6. (*a*) W. SZYBALSKI and V. N. IYER. The mitomycins and porfiromycins. Antibiotics I. *Edited by* D. Gottleib and P. D. Shaw. Springer-Verlag Publishers, New York. 1967. p. 227; (*b*) B. PULLMAN and A. PULLMAN. Quantum biochemistry. Interscience Publishers, New York. 1963. p. 482.
7. A. TULINSKY. J. Am. Chem. Soc. **84**, 3188 (1962).
8. (*a*) Reference 6*a*, p. 225; (*b*) M. N. LIPSETT and A. WEISSBACH. Biochemistry, **4**, 206 (1965); (*c*) W. SZYBALSKI and V. N. IYER. Fed. Proc. **23**, 946 (1964); (*d*) W. SZYBALSKI and V. N. IYER. Microb. Genet. Bull. No. 21, 16 (1964); (*e*) V. N. IYER and W. SZYBALSKI. Science, **145**, 55 (1964); (*f*) A. WEISSBACH and A. LISIO. Biochemistry, **4**, 196 (1965); (*g*) H. A. WHITE and J. R. WHITE. J. Elisha Mitchell Sci. Soc. **81**, 37 (1965); (*h*) V. N. IYER and W. SZYBALSKI. Proc. Natl. Acad. Sci. U.S. **50**, 355 (1963); (*i*) W. C. SUMMERS and W. SZYBALSKI. Rad. Res. **25**, 246 (1965); (*j*) W. C. SUMMERS and W. SZYBALSKI. J. Mol. Biol. **26**, 107 (1967); (*k*) W. C. SUMMERS and W. SZYBALSKI. J. Mol. Biol. **26**, 227 (1967).
9. (*a*) H. S. VERTER and J. ROGERS. J. Org. Chem. **31**, 987 (1966); (*b*) S. DAHNE, J. RANFT, and H. PAUL. Tetrahedron Lett. 3355 (1964).
10. (*a*) J. B. STOTHERS. Carbon-13 nmr spectroscopy. Academic Press, New York. 1972. p. 196; (*b*) G. C. LEVY and G. L. NELSON. Carbon-13 nuclear magnetic resonance for organic chemists. Wiley-Interscience, New York. 1972. p. 79.
11. K. V. RAO, K. BIEMANN, and R. B. WOODWARD. J. Am. Chem. Soc. **85**, 2532 (1963).
12. (*a*) M. B. BITTEEVA. Mikrobiologika, **31**, 492 (1962); (*b*) Y. O. SAZYKIN and G. N. VARISOVA. Fed. Proc. **23**, 380 (1964); (*c*) G. P. GEORGIEV, O. P. SAMARINA, M. I. LERMAN, M. N. SMIRNOV, and A. N. SEVERTZOV. Nature, **200**, 1291 (1963).
13. P. SENSI. Res. Progr. Org. Biol. Med. Chem. **1**, 337 (1964).
14. K. SASAKI, K. L. RINEHART, JR., G. SLOMP, M. F. GROSTIC and E. C. OLSON. J. Am. Chem. Soc. **92**, 7591 (1970).
15. M. LEVINE. Virology, **13**, 493 (1961).
16. M. SEKIGUCHI and Y. TAKAGI. Nature, **183**, 1134 (1959).
17. (*a*) M. LEVINE and M. BORTHWICK. Virology, **21**, 568 (1963); (*b*) M. LEVINE and M. BORTHWICK. Bacterial Proc. 153 (1963).
18. Reference 6*a*, p. 229.
19. H. L. WHITE and J. R. WHITE. Biochem. Biophys. Acta, **123**, 648 (1966).
20. J. B. STOTHERS. Carbon-13 nmr spectroscopy. Academic Press. New York. 1972. p. 197.
21. L. F. JOHNSON and W. C. JANKOWSKI. Carbon-13 nmr spectra. Wiley-Interscience, New York. 1972.
22. A. H. CROSBY and R. E. LUTZ. J. Am. Chem. Soc. **78**, 1233 (1956).
23. D. W. CAMERON and R. G. F. GILES. J. Chem. Soc. C, 1461 (1968).
24. A. MARXER. Helv. Chim. Acta, **38**, 1473 (1955).
25. H. NAKAO and M. ARAKAWA, Chem. Pharm. Bull. (Japan), **20**, 1962 (1972).
26. S. OIDA, H. KUWANO, Y. OHASHI, and E. OHKI. Chem. Pharm. Bull. (Japan), **18**, 2478 (1970).
27. P. SCHEINER. Tetrahedron, **24**, 2757 (1968).
28. S. J. DAVIS and C. S. RONDESVELDT, JR. Chem. Ind. 845 (1956).
29. J. W. LOWN, T. ITOH, and N. ONO. Can. J. Chem. **51**, 856 (1973).

Radioisomerization and Photoisomerization of Liquid 2-Butenes in the Presence of Sulfur Compounds

GUY J. COLLIN, PATRICK M. PERRIN, AND FRANÇOIS X. GARNEAU

Département des Sciences Pures, Université du Québec à Chicoutimi, Chicoutimi, Québec G7H 2B1

Received October 5, 1973

GUY J. COLLIN, PATRICK M. PERRIN, and FRANÇOIS X. GARNEAU. Can. J. Chem. **52**, 2337 (1974).

The liquid phase radiolysis and photolysis of *cis*- and *trans*-2-butenes were studied in the presence of various additives. A very efficient isomerization of 2-butenes was achieved by the addition of thiols of low molecular weight (hydrogen sulfide, methyl and isopropyl mercaptans). In the absence of molecular oxygen, we have observed G values (*trans*-2-butene) of the order of 90 000. On the other hand, little or no isomerization occurred in the presence of carbon disulfide, sulfur hexafluoride, and *tert*-dodecylmercaptan. Although the majority of the additives have no effect on the 2-butene:hydrogen sulfide system, conjugated diolefins block the isomerization reaction. These diolefins disappear from the reaction mixture.

GUY J. COLLIN, PATRICK M. PERRIN et FRANÇOIS X. GARNEAU. Can. J. Chem. **52**, 2337 (1974).

La radiolyse et la photolyse en phase liquide des *cis*- et *trans*-butène-2 ont été étudiées en présence de différents additifs. L'addition de dérivés thiols légers (hydrogène sulfuré, méthyl et isopropyl mercaptans) isomérisent les deux 2-butènes l'un dans l'autre dans un mécanisme très efficace. En l'absence d'oxygène moléculaire, on a relevé des rendements G (*trans*-butène-2) de l'ordre de 90 000. Par contre, le bisulfure de carbone, l'hexafluorure de soufre et le *tert*-dodecylmercaptan n'ont pas ou peu d'effet en faveur de l'isomérisation. Alors que la majorité des impuretés ajoutées sont sans effet sur le système butène-2: hydrogène sulfuré, les dioléfines conjuguées bloquent l'isomérisation. Ces dioléfines conjuguées disparaissent du milieu réactionnel.

Introduction

The synthesis of thiols by radiochemical and photochemical methods is well known (1–5). The mechanism of this synthesis in the presence of large quantities of hydrogen sulfide is the following:

[1] $$H_2S + h\nu \rightarrow HS + H$$

[2] $$HS + RCH = CH_2 \rightarrow RCH{-}CH_2SH$$

[3] $$RCHCH_2SH + H_2S \rightarrow RCH_2CH_2SH + HS$$

[4] $$2\,RCHCH_2SH \rightarrow RCH(CH_2SH)CH(CH_2SH)R$$

In the course of the study of the vacuum u.v. photolysis of olefins in the presence of small quantities of hydrogen sulfide, the main reaction observed was that of the *cis–trans* isomerization of the olefins (6):

[5] $$HS + \textit{cis}\text{-}2\text{-}C_4H_8 \rightleftharpoons C_4H_8SH$$

[6] $$C_4H_8SH \rightleftharpoons \textit{trans}\text{-}2\text{-}C_4H_8 + SH$$

Recently, we have shown that the isomerization reaction was also important in the near u.v. gas phase photolysis of *cis*-2-butene in the presence of 10% hydrogen sulfide (7). In the present work we have studied the radiolysis and photolysis of *cis*- and *trans*-2-butenes in the liquid phase and in the presence of low percentages of sulfur compounds. The G values and the effect of certain pre-selected additives were used to determine the mechanism of the isomerization reaction.

Experimental

The near u.v. experiments were carried out using a Hanovia high pressure quartz mercury-vapor lamp. Samples were prepared in a Pyrex tube fitted with a high-vacuum stopcock. The radiolytical and analytical techniques have for the most part been described as well as the amount of energy and the rate of absorption of energy used (6). All the irradiations were done at room temperature. G values were calculated from the energy absorbed by 2-butene. A column of *n*-octane – porasil C 120/150 mesh was also used to separate the *cis*- and *trans*-2-butenes. *cis*-2-Butene (99.0%) and *trans*-2-butene (99.0%) (Matheson of Canada Ltd.) were used as received after being degassed. *cis*-2-Butene contained *trans*-2-butene (0.50%) and 1,3-butadiene ($\simeq$110 p.p.m.). *trans*-2-Butene contained *cis*-2-butene (0.35%) and 1,3-butadiene ($\simeq$210 p.p.m.). *tert*-Dodecylmercaptan (B.D.H. technical) was used as received after being degassed.

Can. J. Chem. Downloaded from www.nrcresearchpress.com by 210.87.254.40 on 09/05/12
For personal use only.

Can. J. Chem. Downloaded from www.nrcresearchpress.com by 210.87.254.40 on 09/05/12
For personal use only.

Results

The addition of a small amount of hydrogen sulfide to either *cis*-2-butene or *trans*-2-butene has a marked effect on the yield of the isomer of the compound irradiated (Fig. 1). The absolute yield of the isomer increases as a function of the time of irradiation and thereby as a function of the total amount of energy absorbed. In the case of *cis*-2-butene, the system tends to evolve rapidly towards a stationary state close to the thermodynamic equilibrium. The isomerization of *trans*-2-butene seems to be much slower. As a function of the percentage of hydrogen sulfide, the final ratio of *trans*/(*cis* + *trans*) reaches a maximum at a hydrogen sulfide/*cis*-2-butene ratio of the order of 0.02–0.03 (Fig. 2). With methylmercaptan, the maximum is reached at a methylmercaptan/*cis*-2-butene ratio of the order of 0.04–0.06 (Fig. 2). Most of the additives are without notable action on the isomerization with the exception of oxygen (Table 1) and pentadienes (Table 2). Moreover, *trans*-1,3-pentadiene disappears from the reaction mixture with a *G* value greater or equal to 100 depending on its initial concentration. 1,4-Pentadiene has a lesser effect than *trans*-1,3-pentadiene. Finally, by changing the nature of the sulfur derivative, it is observed that the property of isomerization is common to derivatives with the formula RSH; sulfur hexafluoride and carbon disulfide do not, or to only a slight extent, favor isomerization in comparison with that obtained with hydrogen sulfide and low molecular weight thiols (Table 3).

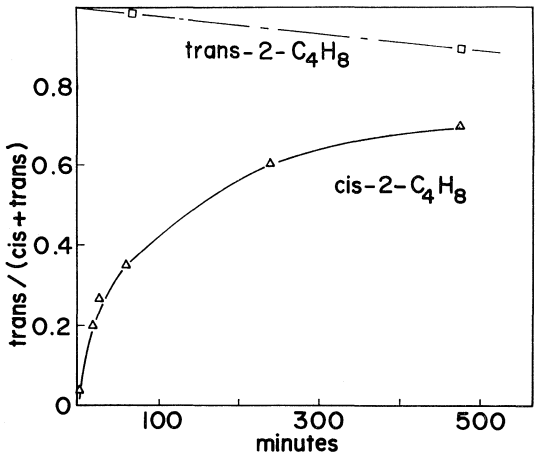

FIG. 1. Radiolysis of liquid *cis*-2-butene (△) and *trans*-2-butene (□) in the presence of hydrogen sulfide. The variation of the final *trans*/(*cis* + *trans*) ratio *vs.* the irradiation time ($H_2S/2\text{-}C_4H_8 = 0.033$).

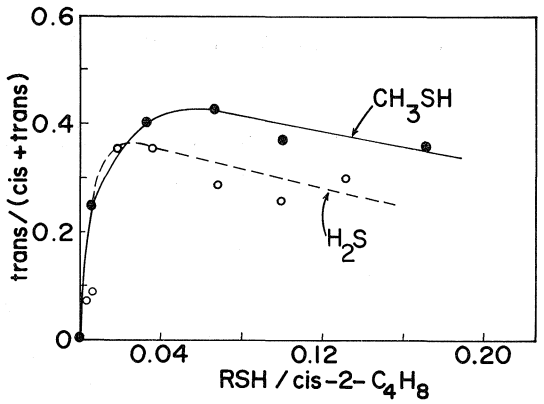

FIG. 2. Radiolysis of liquid hydrogen sulfide: *cis*-2-butene mixtures. The variation of the final composition *vs.* the RSH/*cis*-2-C_4H_8 ratio (irradiation time, 30 min.); CH_3SH, ●; H_2S, ○.

TABLE 1. Radiolysis of liquid *cis*-2-butene:Hydrogen Sulfide: additive (100:3.3:*x*)[a] mixtures

Additives (*x*)	*G* (*trans*-2-butene)[c]
—[b]	4.0[b]
—	80 000 ± 15%
O_2(100 Torr)	≃0.0
SF_6(10)	60 000
CH_3Cl(20)	70 000
CH_3OH (5)	75 000
N_2O (2)	50 000
$CH_3C{\equiv}CH$ (25)	78 000
C_6H_6(1–3)	70 000–58 000
$CH_3C_6H_5$ (1)	89 000
CH_3COCH_3 (3)	89 000
CH_3OCH_3 (0.7)	100 000

[a]In the absence of hydrogen sulfide, the *G* (*trans*-2-butene) values are lower than 100.
[b]Radiolysis of pure *cis*-2-butene, from ref. 20.
[c]Irradiation time, 30 min.

The isomerization was also shown to be an important reaction in the photolysis of liquid *cis*-2-butene in the presence of hydrogen sulfide in the near u.v. region. In addition, we have observed that in this system tert-dodecylmercaptan does not favor the isomerization reaction.

Discussion

The presence of a small amount of hydrogen sulfide catalyzes to an important extent the radioisomerization of *cis*-2-butene to *trans*-2-butene and vice versa. The amount of 2-butene measured after the irradiations is essentially identical to that contained in the samples before irradiation. There would then be very few sulfur addition products, although the irradiated

TABLE 2. Radioisomerization of liquid *cis*-2-butene:hydrogen sulfide: pentadiene (100:3.3:*x*) mixtures[a]

	G	
Pentadiene x	*trans*-2-C_4H_8	*trans*-1,3-C_5H_8
trans-1,3-Pentadiene		
1.16[b]	500 ± 100	−940 ± 100
0.33	2400 ± 500	−270 ± 75
0.13	4100 ± 500	−100 ± 30
1,4-Pentadiene		
3.45[c]	11 800 ± 1000	[d]
0.66[c]	32 000	< 10
0.13[c]	44 500	< 10

[a]Irradiation time, 30 min.
[b]*G* (*cis*-1,3-pentadiene) = 9 ± 2.
[c]*G* (−(1,4-pentadiene)) < 100.
[d]Not measured.

TABLE 3. Radioisomerization of *cis*-2-butene in the presence of sulfur compounds[a]

Additives (3.3%)	*G* (*trans*-2-C_4H_8)
SF_6	< 100
CS_2	400 ± 80
H_2S	80 000
CH_3SH	87 000
$(CH_3)_2CHSH$	42 000
$(CH_3)_3CSH$	5500

[a]Irradiation time, 30 min.

samples have a pronounced odor of sulfur compounds. The shape of the curve (Fig. 2) is similar to that observed in the gas phase. First of all, between 0 and 3% hydrogen sulfide in *cis*-2-butene, the yield of *trans*-2-butene increases regularly to reach a maximum value. For concentrations of hydrogen sulfide greater than 4%, the yield in the *trans* isomer decreases slowly, contrary to the results obtained in the gas phase. This decrease may be explained by the formation of mercaptans (reaction 3). It should be noted however that the process of initiation of the reaction is different from that indicated above. In the radiolysis experiments and in the presence of low concentrations of hydrogen sulfide, the majority of incident energy is absorbed by the 2-butene. Then the mechanism of initiation is probably as shown in reactions 7 and 8, where R is a free radical, H the hydrogen atom, and R′R″ a neutral molecule.

[7] $$2\text{-}C_4H_8 \rightsquigarrow R, H, R'R''$$

[8] $$R + H_2S \rightarrow RH + HS$$

Effect of Various Additives

In radiochemistry, the reaction processes are *a priori* more varied than those obtained in the photolysis at 8.4 eV (8). The electronic scavengers such as methyl chloride (9) and sulfur hexafluoride (10–12) have no notable effect on the isomerization in the presence of hydrogen sulfide (Table 1). The slight influence of nitrous oxide is probably caused by the small amount of oxygen formed by the radiodecomposition of the nitrous oxide (13). The fact that methanol has no effect casts doubt on the intervention of positive ions (at least those having a long enough lifetime in the system). The complete absence of isomerization in the presence of molecular oxygen is indicative of a radical mechanism of isomerization (14). Finally, the observation that the isomerization is an important reaction when the source of radiation is u.v. light, lends further support to a non-ionic mechanism.

Very few organic compounds intervene in the mechanism of isomerization. In the absence of hydrogen sulfide, benzene, toluene, acetone, and dimethyl ether have but little effect and if the isomerization occurs (15), it does so with yields much below those observed in the presence of hydrogen sulfide (Table 1). We can then conclude that the isomerization mechanism is particular to hydrogen sulfide and its derivatives.

Diolefins have a strong negative effect (Table 2), as was previously observed in gas phase vacuum u.v. photochemistry (6). In the case of *trans*-1,3-pentadiene, the low *G* value of *cis*-1,3-pentadiene and the large negative *G* values for the *trans* isomer are suggestive of the intermediacy of a resonance stabilized addition com-

Can. J. Chem. Downloaded from www.nrcresearchpress.com by 210.87.254.40 on 09/05/12
For personal use only.

Can. J. Chem. Downloaded from www.nrcresearchpress.com by 210.87.254.40 on 09/05/12
For personal use only.

plex (16), which may further react with hydrogen

[9] $HS + trans\text{-}1,3\text{-}C_5H_8 \rightarrow C_5H_8SH$

sulfide to give addition products. The disappearance of the conjugated diolefins is in accordance with a kinetic chain mechanism. In the case of 1,4-pentadiene its influence was less than that of 1,3-pentadiene. The effect of the former is probably related to the mobility of the doubly allylic hydrogen atoms of this compound.

The irradiation of *cis*-2-butene in the presence of sulfur compounds other than hydrogen sulfide was also studied (Table 3). Carbon disulfide also initiates the isomerization but with much lower yields. The sulfur atoms formed by the radiodecomposition of the disulfide are probably responsible for this isomerization as is the case in the gas phase (17). Sulfur hexafluoride has little or no effect. However, methanethiol was observed to be an initiator of comparable efficiency to hydrogen sulfide. This was shown by a comparison of the extent of isomerization at low concentrations of the sulfur compounds (Fig. 2). At higher concentrations, comparisons are difficult due to the increasing importance of competing reactions.

2-Propanethiol is a good initiator for the isomerization. In contrast, 2-methyl-2-propanethiol initiates the isomerization to a lesser extent. A study of molecular models shows that rotation about the central C—C bond of the complex $C_4H_8SC(CH_3)_3$ should be difficult because of steric hindrance. The same situation probably holds true for *tert*-dodecylmercaptan.

Isomerization of trans-2-Butene

In the gas phase, it was shown that *cis*-2-butene isomerized about three times faster than *trans*-2-butene. In the liquid phase, the observed rate of isomerization of *trans*-2-butene is at least an order of magnitude smaller than that of *cis*-2-butene (Fig. 1). This difference can be explained either by a thermal effect or by the presence of impurities in the reaction mixture. The addition of the thiyl radical to 2-butene is exothermic. The reverse reaction is then endothermic. The high frequency of collisions in the liquid phase possibly allows a deactivation of the intermediate complex (HSC_4H_8). It is, however, more likely that this difference may be explained by the presence of different quantities of 1,3-butadiene in the two 2-butenes before irradiation. Other work is in progress to study this point.

Thermochemistry and Kinetics

Calculations of the thermicity of the addition reactions of thiyl radicals to *cis*-2-butene were carried out using the method of Pitts and coworkers (18). All these reactions were shown to be exothermic by about 11 kcal mol^{-1} (19).

The radiochemistry of liquid 2-butenes is known (20), and the yields of free radicals were measured. The total yield of free radicals is of the order of 3.0/100 eV (21). If it is only these free radicals which react with the hydrogen sulfide, it is then possible to estimate the chain length of the isomerization mechanism. The values of the chain lengths are then three times smaller than the *G* (isomerization) values.

We wish to thank the Université du Québec à Chicoutimi and the National Research Council of Canada for their financial support of this work.

1. F. W. Stacey and J. F. Harris, Jr. Organic reactions. Vol. 13 (4). J. Wiley & Sons, New York, N.Y. 1965. p. 191.
2. W. E. Vaughan and F. F. Rust. J. Org. Chem. **7**, 472 (1942).
3. C. Walling and W. Helmreich. J. Am. Chem. Soc. **81**, 1144 (1959).
4. K. Sugimoto, W. Ando, and S. Oae. Bull. Chem. Soc. Jap. (*a*) **37**, 365 (1964); (*b*) **38**, 224 (1965); (*c*) **38**, 226 (1965).
5. O. P. Strausz, T. Hikiba, and H. E. Gunning. Can. J. Chem. **43**, 717 (1965).
6. (*a*) G. J. Collin and P. M. Perrin. Can. J. Chem. **50**, 2400 (1972); (*b*) G. J. Collin, P. M. Perrin, and C. M. Gaucher. Can. J. Chem. **50**, 2391 (1972).
7. F. X. Garneau. Unpublished results.
8. G. J. Collin and P. M. Perrin. Can. J. Chem. **50**, 2823 (1972).
9. F. Fiquet-Fayard. Actions Chim. Biol. Radiat. VIII Serie, (1965).
10. W. J. Holtslander and G. R. Freeman. J. Phys. Chem. **71**, 2562 (1967); G. R. Freeman. Radiat. Res. Rev. **1**, 1 (1968).
11. C. S. Munday, J. T. Richards, G. Scholes, and M. Simic. Chem. Ioniz. Excit. 151 (1967).
12. G. W. Klein and R. H. Schuler. J. Phys. Chem. **77**, 978 (1973).
13. A. R. Anderson. *In* Fundamental processes in radiat. Chem. *Edited by* P. Ausloos. J. Wiley & Sons Inc., New York. 1968. p. 312.
14. D. M. Graham and J. F. Soltys. Can. J. Chem. **48**, 2173 (1970).
15. R. B. Cundall and P. A. Griffiths. J. Am. Chem. Soc. **85**, 1211 (1963); Disc. Faraday Soc. **36**, 111 (1964).
16. D. M. Graham and J. F. Soltys. Can. J. Chem. **47**, 2719 (1969).
17. M. W. Schmidt and E. K. C. Lee. J. Chem. Phys. **51**, 2124 (1969).
18. J. L. Sprung, H. Akimoto, and J. N. Pitts, Jr. J. Am. Chem. Soc. **93**, 4358 (1971).
19. D. H. Fine and J. B. Westmore. Can. J. Chem. **48**, 395 (1970).
20. P. C. Kaufman. J. Phys. Chem. **67**, 1671 (1963).
21. R. A. Holroyd and G. W. Klein. J. Phys. Chem. **69**, 194 (1965).

Réactions des ions iso-$C_4H_8^+$ et t-$C_4H_9^+$ avec l'isobutène en phases liquide et gazeuse

G. J. COLLIN[1]

Département des Sciences Pures, Université du Québec à Chicoutimi, Chicoutimi, Québec G7H 2B1

Reçu le 5 décembre 1973

G. J. COLLIN. Can. J. Chem. **52**, 2341 (1974).

On a étudié la radiolyse en phases liquide et gazeuse du néopentane. En phase liquide on a montré que l'ion iso-$C_4H_8^+$ réagit au moins aussi vite avec l'isobutène qu'avec le méthylcyclopentane. L'ion t-$C_4H_9^+$ réagit au moins 10 fois plus vite avec l'isobutène et la réaction principale est la réaction de transfert de proton en résonnance avec l'isobutène. Moins de 5% des ions t-$C_4H_9^+$ s'additionnent sur l'isobutène. En phase gazeuse, la réaction de condensation est plus importante que la réaction de transfert de proton en résonnance, puisque le transfert de proton ne compte que pour environ 30% du total: k(addition)/k(transfert) $\simeq 2.35 \pm 0.15$. Enfin le transfert d'un deutéron en résonnance est environ 2.9 fois plus lent que le transfert d'un proton.

G. J. COLLIN. Can. J. Chem. **52**, 2341 (1974).

The radiolysis of neopentane has been studied in gas and liquid phases. It was shown that, in the liquid phase, the iso-$C_4H_8^+$ ion reacts at least as quickly with isobutene as with methylcyclopentane. The t-$C_4H_9^+$ ion reacts at least 10 times more rapidly with isobutene and the main reaction is one of resonant transfer of a proton with isotubene; fewer than 5% of the t-$C_4H_9^+$ ions add to isobutene. In the gas phase, the condensation reaction is more important than that of resonant proton transfer since proton transfer represents only 30% of the total reaction: k(addition)/k(transfer) $\simeq 2.35 \pm 0.15$. Finally, the resonant transfer of a deuteron occurs about 2.9 more slowly than proton transfer. [Journal translation]

Introduction

La radiolyse du néopentane est bien connue. Ce système présente des qualités qui permettent une interprétation relativement simple des processus chimiques initiés par le rayonnement. Citons, par exemple, la symétrie de la molécule, le nombre limité de liaisons différentes, et la faible réactivité du néopentane lui-même. C'est donc un système approprié pour étudier l'effet des intercepteurs, des impuretés, ou même des produits issus de la radiolyse sur la radiolyse elle-même. Nous ne reviendrons pas ici sur les réactions radicalaires engendrées dans ce système qui ont fait l'objet d'un travail excellent (1), ni sur l'effet de l'isobutène sur ces réactions radicalaires (1). Nous voulons porter notre attention sur les réactions ioniques engendrées dans ce système, et de l'influence de l'isobutène sur ces réactions. Cette étude fait donc suite à celle des réactions ioniques dans le néopentane pur (2*a*). Nous étendrons enfin cette étude aux réactions entre l'ion tertiobutyle et l'isobutène en phase gazeuse.

[1]Chercheur invité (1968–1969). Radiation Chemistry Section, National Bureau of Standards, Washington, D.C. 20234. Ce travail a été en partie subventionné par la Commission de l'énergie atomique des Etats-Unis.

Méthode expérimentale

La plupart des techniques expérimentales ont été décrites (2). Il suffit de rappeler que la vitesse de dose absorbée par le néopentane est de 0.53×10^{19} eV mol^{-1} s^{-1} sauf dans les cas indiqués. Toutes les irradiations ont été faites à la température de la chambre. Tous les échantillons contiennent de l'oxygène. La pression est de 100 Torr d'oxygène mesurés à 77 °K. La solubilité de l'oxygène dans ces conditions est d'environ 0.3% (3). L'analyse chromatographique des échantillons irradiés et les analyses par spectrométrie de masse ont été, elles aussi, décrites ailleurs (2).

Résultats

Les rendements indiqués sont exprimés en valeurs G(X) où G(X) est le nombre de molécules du produit X formées par 100 eV d'énergie absorbés par le néopentane.

(*A*) En phase liquide, les résultats présentés completent ceux qui ont déjà été publiés (2*a*) et ils sont rappelés dans les trois tableaux et les deux premières figures de ce texte. Il faut mentionner seulement que l'addition d'isobutène-d_0 au mélange néopentane:méthylcyclopentane-d_{12}:tétrachlorure de carbone:oxygène (100:9.2:2.8:0.3) fait décroître tous les rendements en isobutane sauf celui de l'iso-C_4H_{10} (fig. 1). Par contre, il y a augmentation du rendement en chlorure de t-butyle (t-C_4H_9Cl) (fig. 2). Ces

Can. J. Chem. Downloaded from www.nrcresearchpress.com by 210.87.254.5 on 09/05/12
For personal use only.

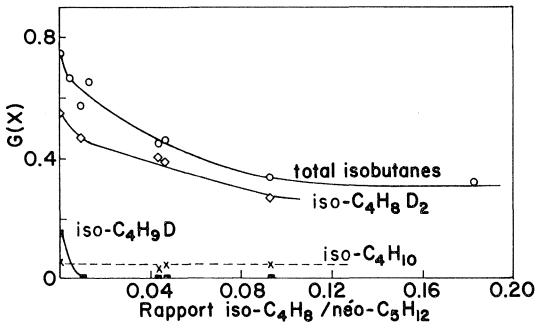

FIG. 1. Radiolyse du néopentane liquide: néo-C_5H_{12}:cyclo-$C_5D_9CD_3$:CCl_4:O_2 (100:9.2:2.8:0.3). Variation des rendements en isobutane avec le pourcentage d'isobutène ajouté.

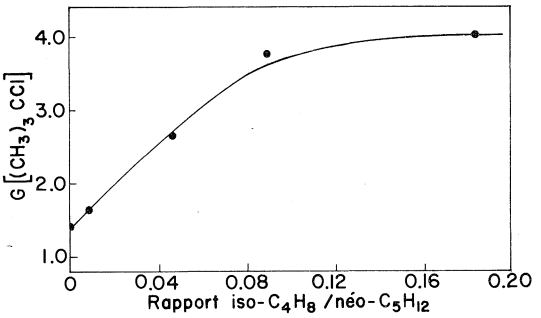

FIG. 2. Radiolyse du néopentane liquide: néo-C_5H_{12}:cyclo-$C_5D_9CD_3$:CCl_4:O_2 (100:9.2:2.8:0.3). Variation du rendement en chlorure de tertiobutyle avec le pourcentage d'isobutène ajouté.

analyses sont complétées par les analyses isotopiques des isobutanes (tableau 1) et des chlorures de *t*-butyles (tableau 2) obtenus dans différentes conditions. On a également montré la formation de composés en C_8, avec des rendements G relativement faibles (tableau 3).

(*B*) En phase gazeuse l'addition de méthylcyclopentane au mélange néopentane:isobutène-d_8 (100:1.0:4–8) augmente les rendements en isobutane-d_0 et -d_8 (fig. 3). En outre l'irradiation du mélange néo-C_5H_{12}:iso-C_4D_8:O_2 (100:0.40:4.5) donne les résultats suivants: G(iso-C_4D_7H) = 0.11 ± 0.02, G(iso-C_4H_8) = 1.0 ± 0.1 et G(isobutanes) ≤ 0.02. L'irradiation du mélange néo-C_5H_{12}:iso-C_4D_8:cyclo-$C_5D_9CD_3$:O_2 (100:3.8:0.9:9.4) donne les résultats suivants: G(iso-C_4H_9D) = 0.92 et G(iso-C_4D_9H) = 0.22. De la même façon, dans le mélange néo-C_5H_{12}:iso-C_4D_8:cyclo-$C_5H_9CH_3$:O_2 (100:1.0:1.0:4.8), G(iso-$C_4D_8H_2$) = 0.18 et G(iso-C_4H_{10}) = 0.52. Enfin, dans le mélange néo-C_5H_{12}:cyclo-$C_5D_9CD_3$:iso-C_4D_8:O_2 (100:3.8:0.9:4.6), G(iso-C_4H_9D) = 0.98 et G(iso-C_4D_9H) = 0.22.

TABLEAU 1. Radiolyse du neopentane liquide, néo-C_5H_{12}:cyclo-$C_5D_9CD_3$:CCl_4:O_2:Additif (100: 9.1: 2.8: 0.3: *x*)

	Analyse des isobutanes			
Additif (*x*)	-d_0	-d_1	-d_2	-d_{10}
—	0.05	0.15	0.55	0.00
iso-C_4H_8(0.41)	0.05	0.00	0.48	0.00
iso-C_4D_8(0.55)	0.00	0.02	0.46	0.20
iso-C_4D_8(1.38)	0.00	0.05	0.29	0.30

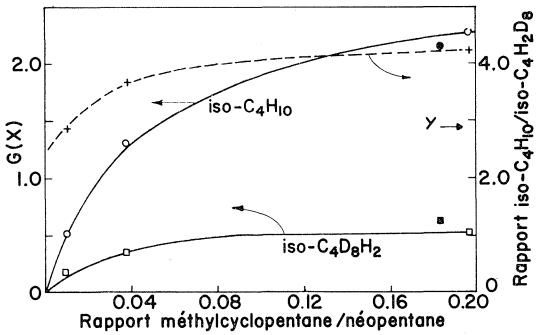

FIG. 3. Radiolyse du néopentane gazeux: néo-C_5H_{12}:iso-C_4D_8:O_2 (100:1.0:4–8). Variation des rendements G(X) en isobutane et du rapport y = iso-C_4H_{10}/iso-$C_4H_2D_8$ en fonction du pourcentage de méthylcyclopentane-d_0 ajouté. Les points ■, ● et y correspondent à une expérience où le méthylcyclopentane est -d_{12}: ■ = iso-C_4D_{10} et ● = iso-C_4H_9D.

Discussion

(A) En phase liquide

Les ions iso-$C_4H_8^+$

Dans la radiolyse du néopentane liquide pur, le rendement en ion iso-$C_4H_8^+$ est de l'ordre de 0.9 (2*a*). En présence de méthylcyclopentane ces ions réagissent par transfert d'ion H_2^- pour donner l'isobutane

[1] iso-$C_4H_8^+$ + cyclo-$C_5D_9CD_3$ → $(CH_3)_2CDCH_2D + C_6D_{10}^+$

Cependant cette réaction ne devient importante qu'en présence de tétrachlorure de carbone. Cet additif intercepte les électrons et augmente ainsi le temps de vie de chaque ion. Dans ces conditions, cette réaction est relativement importante puisque l'ion est tout à fait inerte vis-à-vis du néopentane et le rendement en iso-$C_4H_8D_2$ augmente (2*a*). Egalement il faut noter que des résultats similaires ont été obtenus en phase gazeuse (4). En ajoutant de l'isobutène perprotoné au mélange précédent, le rendement en isobutane-d_2 décroît (fig. 1). Il y a donc lieu d'ad-

Can. J. Chem. Downloaded from www.nrcresearchpress.com by 210.87.254.5 on 09/05/12
For personal use only.

Can. J. Chem. Downloaded from www.nrcresearchpress.com by 210.87.254.5 on 09/05/12
For personal use only.

TABLEAU 2. Radiolyse du néopentane liquide

	Mélanges irradiés*						Rendements en chlorure de *t*-butyle		
N°	néo-C_5H_{12}	néo-C_5D_{12}	iso-C_4H_8	iso-C_4D_8	cyclo-$C_5D_9CD_3$	CCl_4	$(CH_3)_3CCl$	$(CD_3)_2C(CD_2H)Cl$	$(CD_3)_3CCl$
A	100	100	—	—	—	5	0.89	0.00†	0.50
B	100	100	—	—	100	5	0.89	0.00†	0.47
C	100	—	—	0.92	—	9.2	0.67	2.78†	0.16
D	100	—	—	4.0	—	9.2	0.24	2.66†	0.16
E	100	—	—	0.55	9.2	2.8	0.49	0.39†	0.05
F	100	—	—	1.38	9.2	2.8	0.16	← 1.06 →	
G	100	—	0.18	—	9.2	2.8	100‡	0.00	0.00
H	—	100	0.54	—	—	3.6	100‡	← 97 →	

*Le mélange contient toujours de l'oxygène: O_2/néo-C_5H_{12} = 0.3%.
†G(*t*-C_4H_8DCl) = 0.00.
‡Analyses relatives à $G'((CH_3)_3CCl) = 100$.

TABLEAU 3. Radiolyse du néopentane liquide,* (néo-C_5H_{12}:CCl_4:O_2:additifs) (100:3.3:0.3:x)

Additifs (x)		G(C(C)(C)—C—C—C)†	G(C(C)(C)—C—C=C—C)†	G(C(C)(C)—C—C(C)—C)†	
iso-C_4H_8	cyclo-$C_5H_9CH_3$				$G(C_8?)$‡
—	—	0.05	0.006	0.05	0.05
1.33	—	0.13	0.12	0.021	0.024
2.0	—	0.13	0.12	0.016	0.016
1.33	0.66	0.21	0.04	0.033	0.05
2.0	0.66	0.21	0.04	0.024	0.05

*Vitesse de dose: 2.0×10^{17} eV mol^{-1} s^{-1}; temps d'irradiation 1140 min.
†Temps de rétention déterminés relativement en utilisant les résultats de Hirely et Hipton (12).
‡Temps de rétention correspondant à un C_8, mais l'identification en est incertaine.

mettre que les ions iso-$C_4H_8^+$ réagissent avec cet additif.

[2] iso-$C_4H_8^+$ + iso-C_4H_8 → Autre produit que iso-C_4H_{10}

et d'après les pourcentages relatifs de méthylcyclopentane et d'isobutène on peut estimer que les constantes de vitesse des réactions 1 et 2 sont semblables: $k_2 = 5.4 \times 10^{-10}$ cm^3 $molécule^{-1}$ s^1 (5). Cependant, en irradiant le mélange en présence d'isobutène-d_8 (tableau 1), l'isobutane-d_{10} devient important. On ne peut, sur la seule base de l'énergie directement absorbée par l'isobutène-d_8, expliquer les rendements importants en isobutane-d_{10}. D'autre part le rendement en isobutane-d_2 diminue. Il y a donc diminution de l'importance relative de la réaction 1. Sur la base des résultats présentés ici, il est spéculatif de vouloir préciser la nature du mécanisme réactionnel responsable. On peut cependant expliquer les résultats en admettant un transfert de charge en résonnance suivi de la réaction 1 où l'ion isobutène est alors perdeutéré (6).[2]

[3][3] iso-$C_4H_8^+$ + iso-C_4D_8 → iso-C_4H_8 + iso-$C_4D_8^+$

[4] iso-$C_4D_8^+$ + cyclo-$C_5D_9CD_3$ → iso-C_4D_{10} + $C_6D_{10}^+$

Les ions t-$C_4H_9^+$

En l'absence d'intercepteurs hydrocarbonés, les ions t-$C_4H_9^+$ sont particulièrement inertes dans le néopentane (2*a*). En fait, il semble qu'ils sont, pour la majorité, interceptés par des ions négatifs, surtout si le milieu contient du tétrachlorure de carbone.

[5] $(CH_3)_3C^+ + CCl_4^-(Cl^-) \rightarrow (CH_3)_3CCl + CCl_3$

Cette réaction est en accord avec les résultats isotopiques des chlorures de tertiobutyles formés. Pour le mélange néo-C_5H_{12}:néo-C_5D_{12}, le chlorure de tertiobutyle est d_0 ou d_9 (exp. A, tableau 2). L'addition de méthylcyclopentane-d_{12} ne change pas les rendements des chlorures produits (exp. B). On doit cependant noter la présence d'isobutane-d_1, probablement formé à travers la réaction suivante (voir fig. 1)

[6] $(CH_3)_3C^+$ + cyclo-$C_5D_9CD_3$ → $(CH_3)_3CD + C_5D_{11}^+$

Cependant l'importance de cette réaction est négligeable. Bien que le rendement $G((CH_3)_3C^+) = 2.4$, le rendement maximum obtenu en isobutane-d_1, est de 0.15. L'addition d'isobutène-d_0 supprime complètement cette formation (fig. 1)

[7] $(CH_3)_3C^+$ + iso-C_4H_8 → Autre produit que $(CH_3)_3CD$

La réaction 7 a une constante de vitesse au moins de deux ordres supérieurs à celle de la réaction 6 (fig. 1). Cependant la formation de chlorure de tertiobutyle n'est pas compromise. Au contraire elle semble augmenter au fur et à mesure de l'augmentation de la concentration en isobutène (fig. 2). Il semble que la présence d'isobutène permette la transformation de tous les ions primaires en chlorure de tertiobutyle puisque le rendement $G(C_4H_9Cl)$ tend vers 4. L'analyse de ces chlorures, lorsque l'isobutène est perdeutéré,

[2]Ce système se complique par la possibilité de la réaction inverse: irradiation directe du méthylcyclopentane (7–9).

cyclo-$C_5D_9CD_3^+$ + iso-C_4D_8 → $C_6D_{10}^+$ + iso-C_4D_{10} (ou iso-$C_4D_8H_2$ avec l'ion cyclo-$C_5H_9CH_3^+$).

[3]Il ne peut y avoir de transfert d'atome de deutérium de l'iso-C_4D_8 vers l'ion iso-$C_4H_8^+$ car alors on trouverait du chlorure de tertiobutyle-d_1 (exp. C et D, tableau 2).

Can. J. Chem. Downloaded from www.nrcresearchpress.com by 210.87.254.5 on 09/05/12
For personal use only.

Can. J. Chem. Downloaded from www.nrcresearchpress.com by 210.87.254.5 on 09/05/12
For personal use only.

montre la présence de trois composés: $(CH_3)_3CCl$, $(CD_3)_2(CD_2H)CCl$ et $(CD_3)_3CCl$ et l'importance relative du chlorure-d_8 décroît avec la croissance de la concentration en isobutène-d_8 (exp. C et D, tableau 2). Cela montre l'existence d'un transfert de proton en résonnance entre l'ion $t\text{-}C_4H_9^+$ et l'isobutène.

[8] $(CH_3)_3C^+ + \text{iso-}C_4D_8 \rightarrow \text{iso-}C_4H_8 + (CD_3)_2(CD_2H)C^+$

[9] $(CD_3)_2(CD_2H)C^+ + \text{iso-}C_4D_8 \rightarrow \text{iso-}C_4D_7H + (CD_3)_3C^+$

Ces réactions sont suivies de la réaction de formation des chlorures correspondants: réaction 5. Cependant l'augmentation de la formation de l'ion $(CD_3)_2(CD_2H)C^+$ n'entraîne pas nécessairement une augmentation des chlorures correspondants, puisqu'il faut tenir compte de la possibilité de réactions de condensation sur l'isobutène (voir plus loin). Il faut noter le faible rendement en $t\text{-}C_4D_9Cl$. Il est probablement le résultat de deux phénomènes qui concourent à la formation limitée des ions $(CD_3)_3C^+$. Tout d'abord, à chaque étape de transfert d'un proton (ou d'un deutéron), il correspond une étape d'addition de l'ion tertiobutyle sur l'isobutène et une étape de neutralisation par les ions négatifs. En outre le transfert d'un ion D^+ est *a priori* plus lent que le transfert d'un ion H^+ (effet isotopique). Ces deux raisons se conjuguent pour faire en sorte que la formation des ions $(CD_3)_3C^+$ est de peu d'importance.

On doit en outre penser aux réactions de condensation ioniques sur l'isobutène. Viswanathan et Kevan ont rapporté avoir injecté des ions $t\text{-}C_4H_9^+$ produits en phase vapeur dans de l'isobutène liquide (10). Sans revenir sur les réserves déjà émises à propos de ce travail (5), ces auteurs ont indentifié au moins quatre hydrocarbures en C_8. Nous avons retrouvé trois de ces hydrocarbures; nous n'avons cependant pas pu indentifier le quatrième (tableau 3). Néanmoins, les produits observés en présence d'oxygène sont sensibles à la présence d'isobutène seul ou combiné avec le méthylcyclopentane. En présence d'oxygène qui est un excellent intercepteur radicalaire, ces produits peuvent être formés par voie ionique, en dedans ou en dehors de la trace (spur), mais aussi par voie radicalaire, à l'intérieur de la trace.

En présence d'isobutène, l'ion $t\text{-}C_4H_9^+$ s'additionne sur la double liaison. L'ion de condensation formé peut alors, soit abstraire un ion hydrure (H^-), soit transférer un proton sur une autre molécule d'isobutène.

[10] $(CH_3)_3C^+ + \text{iso-}C_4H_8 \rightarrow$ 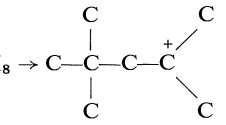

[11] 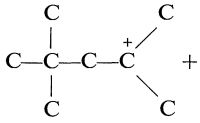 $+ MH \rightarrow M^+ +$ Triméthyl-2,2,4-pentane

[12] 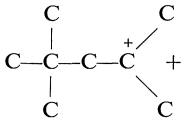 $+ \text{iso-}C_4H_8 \rightarrow$ 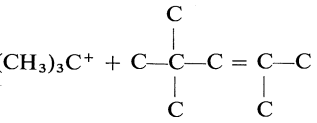

En présence d'isobutène seul, l'augmentation du triméthyl-2,4,4-pentène-2 est en accord avec la réaction 12. Puisque le triméthylpentène peut être formé dans d'autres réactions, $G([12])$ est inférieur à 0.11. En présence de méthylcyclopentane et d'isobutène, l'augmentation du rendement en triméthylpentane montre que la réaction 11 est prépondérante, d'autant que les rendements obtenus ne varient pas avec une variation des concentrations relatives des additifs: $G([11]) \doteq 0.08$.

La formation des autres composés en C_8 est moins facile à expliquer. Néanmoins, il a déjà été proposé qu'ils peuvent résulter de l'addition de l'ion $t\text{-}C_4H_9^+$ sur le carbone central de l'isobutène suivie d'une isomérisation très rapide de l'ion (10).

[13] $(CH_3)_3C^+ + \text{iso-}C_4H_8 \rightarrow$ 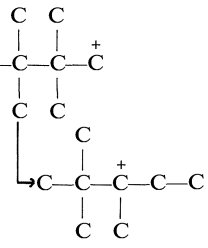

Il est évidemment possible que d'autres condensations ioniques interviennent, donnant lieu à la formation de composés en C_{12} (10). Cependant, il n'en reste pas moins que les réactions de condensation apparaissent relativement peu im-

portantes comparativement aux processus de neutralisation ion–ion (réaction 5).

(B) En phase gazeuse

La chimie des ions $t\text{-}C_4H_9^+$ en phase gazeuse est assez bien connue. Dans le milieu inerte qu'est le néopentane, les ions $t\text{-}C_4H_9^+$ reagissent avec le méthylcyclopentane pour donner l'isobutane: $k_{14} = 1.2 \times 10^{-10}$ cm^3 molécule^{-1} s^{-1} (2). La réaction avec l'isobutène-d_8 est encore plus rapide: $k_{15} = 9.0 \times 10^{-10}$ cm^3 molécule^{-1} s^{-1} (2).

[14] $(CH_3)_3C^+ + \text{cyclo-}C_5H_9CH_3 \rightarrow \text{iso-}C_4H_{10} + C_6H_{11}^+$

[15] $(CH_3)_3C^+ + \text{iso-}C_4D_8 \rightarrow \text{Produits}$

Là encore, les résultats montrent sans ambiguités le transfert de proton en résonnance entre l'ion $t\text{-}C_4H_9^+$ et l'isobutène-d_8. L'irradiation du mélange néo-C_5H_{12}:iso-C_4D_8:O_2 (100:0.40:4.5) produit l'isobutène-d_0 et -d_7 (voir Résultats). En admettant une valeur $G((CH_3)_3C^+) = 3.0$ dans la radiolyse du néopentane (11) et que les seules réactions possibles pour l'ion $(CH_3)_3C^+$ sont les réactions 8 et 16, le rapport des constantes de vitesse k_{16}/k_8 est alors égal au rapport $[G((CH_3)_3C^+) - G(\text{iso-}C_4H_8)]/G(\text{iso-}C_4H_8) = 2.0 \pm 0.3$.

[16] $(CH_3)_3C^+ + \text{iso-}C_4D_8 \rightarrow C_8H_9D_8^+$

Le rapport est cependant imprécis, car l'analyse de l'isobutène-d_0 dans une masse importante d'isobutène-d_8 n'est pas aisée. De la même façon, les ions $t\text{-}C_4D_8H^+$ produits dans la réaction 8 réagissent avec l'isobutène-d_8: réactions 9, 17 et 18.

[17] $(CD_3)_2(CD_2H)C^+ + \text{iso-}C_4D_8 \rightarrow \text{iso-}C_4D_8 + (CD_3)_2(CD_2H)C^+$

[18] $(CD_3)_2(CD_2H)C^+ + \text{iso-}C_4D_8 \rightarrow \text{Add}^+$

Dans ce système le rendement $G((CD_3)_2(CD_2H)C^+)$ est égal à l'unité. On peut en outre estimer que le rapport k_8/k_{17} est égal à 9.0. En effet, alors que l'ion $t\text{-}C_4H_9^+$ a 9 atomes d'hydrogène disponible, l'ion $(CD_3)_2(CD_2H)C^+$ n'en a qu'un. Par conséquent, et puisque le rapport k_{16}/k_8 est égal à 2.0, le rendement $G([17]) \simeq 0.04$. Le rendement mesuré $G([9]) = 0.11$ puisque $G(\text{iso-}C_4D_7H) = 0.11$, et le rapport $k_9/k_{17} \simeq 2.8$. Il y a donc un effet isotopique tel que le rapport k_{H^+}/k_{D^+} (où k_{H^+} et k_{D^+} représentent les constantes de vitesse de transfert d'un proton et d'un deutéron de l'ion tertiobutyle vers l'isobutène) est égal à 2.9.

En irradiant différents mélanges néo-C_5H_{12}:iso-C_4D_8:cyclo-$C_5H_9CH_3$:O_2 (100:0.9:x:4–8), on trouve que les rendements en isobutane-d_0 et -d_8 croissent avec la concentration de méthylcyclopentane (fig. 3). En ne tenant compte que des réactions 8, 14, 16, 18 et 19 pour la disparition des ions $t\text{-}C_4H_9^+$ et $t\text{-}C_4HD_8^+$,

[19] $(CD_3)_2(CD_2H)C^+ + \text{cyclo-}C_5H_9CH_3 \rightarrow \text{iso-}C_4H_2D_8 + C_6H_{11}^+$

on obtient que les vitesses de formation des isobutane-d_0 et -d_8 sont telles que

$$\frac{V_{\text{iso-}C_4H_{10}}}{V_{\text{iso-}C_4D_8H_2}} = \left(\frac{k_{14}}{k_{19}}\right) \times \frac{k_{18}[\text{iso-}C_4D_8] + k_{19}[\text{cyclo-}C_5H_9CH_3]}{k_8[\text{iso-}C_4D_8]} = R$$

R est donc une fonction croissante de la concentration en méthylcyclopentane (voir fig. 3). Le rapport k_{14}/k_{19} est probablement égal à l'unité puisqu'il s'agît essentiellement de la même réaction: celle d'un transfert d'ion hydrure (H^-) vers l'ion tertiobutyle (2). En outre si le méthylcyclopentane-d_0 est remplacé par son homologue perdeutéré, le transfert de l'ion D^- est moins rapide que celui de l'ion H^-: $k_{19(H)} \simeq 1.6\ k_{19(D)}$ (2). Donc pour une même concentration, la valeur de R décroît lorsque le méthylcyclopentane-d_0 est remplacé par son homologue perdeutéré (voir fig. 3). Enfin, la valeur de R tend vers le rapport k_{18}/k_8, lorsque la concentration de méthylcyclopentane tend vers zéro: $R_0 \simeq 2.4 \pm 0.2$. De la même façon, l'irradiation des deux derniers mélanges (voir Résultats) permet de calculer une valeur du rapport k_{16}/k_8 égale à 2.35 ± 0.15. On vérifie aussi que les vitesses des réactions 16 et 18 sont semblables. Par contre, on n'a pas pu mesurer d'isobutane-d_{10} lorsque le méthylcyclopentane est perdeutéré. Cela montre que le transfert de deutéron (D^+) entre l'ion $t\text{-}C_4D_8H^+$ et l'isobutène-d_8 est de peu d'importance (réaction 9).

Nous voulons exprimer nos remerciements au professeur P. Ausloos qui a bien voulu commenter ce travail. L'aide apportée par l'OTAN a été vivement appréciée.

Can. J. Chem. Downloaded from www.nrcresearchpress.com by 210.87.254.5 on 09/05/12
For personal use only.

1. R. A. HALROYD. J. Am. Chem. Soc. **65**, 1352 (1961).
2. (*a*) G. J. COLLIN et P. AUSLOOS. J. Am. Chem. Soc. **93**, 1336 (1971); (*b*) P. AUSLOOS et S. G. LIAS. J. Am. Chem. Soc. **92**, 5037 (1970).
3. C. B. KRETSCHMERE, J. NOVA KAWSKA et R. WEIBE. Ind. Eng. Chem. **38**, 506 (1946).
4. S. G. LIAS et P. AUSLOOS. J. Am. Chem. Soc. **92**, 1840 (1970); J. HERMAN, K. HERMAN et P. AUSLOOS. J. Chem. Phys. **52**, 28 (1970).
5. L. W. SIECK, S. G. LIAS, L. HELLNER et P. AUSLOOS. J. Res. Natl. Bur. Stand. **76**A, 115 (1972).
6. P. AUSLOOS et S. G. LIAS. Chem. Ioniz. Excitation, 77 (1967).
7. P. AUSLOOS et S. G. LIAS. J. Chem. Phys. **43**, 127 (1965).
8. A. A. SCALA, S. G. LIAS et P. AUSLOOS. J. Am. Chem. Soc. **88**, 5701 (1966).
9. P. AUSLOOS, A. A. SCALA et S. G. LIAS. J. Am. Chem. Soc. **89**, 3677 (1967).
10. N. S. VISWANATHAN et L. KEVAN. J. Am. Chem. Soc. **89**, 2482 (1967).
11. S. G. LIAS et P. AUSLOOS. J. Chem. Phys. **43**, 2748 (1965).
12. R. A. HIRELY et R. E. HIPTON. J. Gas Chromatogr. **6**, 203 (1968).

Can. J. Chem. Downloaded from www.nrcresearchpress.com by 210.87.254.5 on 09/05/12
For personal use only.

Can. J. Chem. Downloaded from www.nrcresearchpress.com by 210.87.254.40 on 09/05/12
For personal use only.

Cis–Trans Conformational Dependence of the Carboxylate p*K* in Glycylsarcosine[1]

R. A. MORTON
Department of Biology, McMaster University, Hamilton, Ontario L8S 4K1
AND
S. S. DANYLUK
Division of Biological and Medical Research, Argonne National Laboratory, Argonne, Illinois 60439

Received January 25, 1974

R. A. MORTON et S. S. DANYLUK. Can. J. Chem. **52**, 2348 (1974).

A study is reported of the influence of p*D* upon the 220 MHz proton n.m.r. spectrum of the dipeptide glycylsarcosine (Gly-Sar) in D_2O at 23 °C. Variation of p*D* produces characteristic changes in chemical shifts for Gly-Sar and an analysis of the p*D* – chemical shift curves shows that the carboxyl p*K* differs significantly in *cis* and *trans* conformers, having values of 3.01 ± 0.03 and 3.39 ± 0.03, respectively. From a consideration of molecular models and theoretical calculations, it is concluded that the p*K* difference arises from a closer juxtaposition of terminal carboxyl and amino groups in the *cis* isomer.

R. A. MORTON and S. S. DANYLUK. Can. J. Chem. **52**, 2348 (1974).

On rapporte les spectres r.m.n. du proton du dipeptide glycylsarcosine (Gly-Sar); on a déterminé ces spectres à 220 MHz en solution dans D_2O à 23 °C. En faisant varier le p*D* de la solution, on observe des changements caractéristiques des déplacements chimiques du Gly-Sar; une analyse des courbes reliant le p*D* avec les déplacements chimiques montre que les p*K* des groupements carboxyliques diffèrent d'une manière appréciable suivant la nature *cis* ou *trans* des conformères qui ont respectivement des p*K* de 3.01 ± 0.03 et 3.39 ± 0.03. A partir de considérations basées sur les modèles moléculaires et des calculs théoriques, on peut conclure que les différences de p*K* proviennent du fait que dans l'isomère *cis* les groupes amino et carboxyle terminaux sont plus rapprochés. [Traduit par le journal]

Introduction

Most recent theoretical calculations of polypeptide conformation (for example see refs. 1–3) assume a *trans* conformation for the peptide bond. However, *cis–trans* rotational isomerism cannot be ruled out, and several theoretical and experimental studies (4–12) of model amides have examined this question in detail. In general, these have confirmed the existence of a *cis* amide bond in both linear (13–16) and cyclic peptides (17–19) containing prolyl residues. A dynamic equilibrium between *cis* and *trans* conformations of proline-containing polypeptides such as poly (Pro),[2] poly (Pro-Gly), and poly (Gly-Gly-Pro-Gly) has also been inferred from n.m.r. measurements (20, 21). Numerous examples of *cis-trans* isomerism have further been reported for *N*-substituted amino acid derivatives including *N*-methyldialanine (22), *N*-acetylsarcosine, polysarcosine (23), *N*-acetyl-*N*-methyl-L-alanine methyl ester (24), and poly *N*-methyl-L-alanine (25). Stabilization of the *cis* isomer is apparently induced to some degree by a bulky substituent group at the *N*-amide position.

Among additional factors which can contribute to stabilities and isomer populations are the presence of electrostatic interactions in the oligomer, i.e. zwitterion effects, intra- and intermolecular hydrogen bonding, and ionic strength and p*H* of the solvent. A careful study of the influence of these factors is warranted, and in this work we report on the effect of p*H* change upon the *cis–trans* equilibrium for the dipeptide glycylsarcosine (Gly-Sar). The results show that the p*K* for the reaction in eq. 1 differs signifi-

[1] 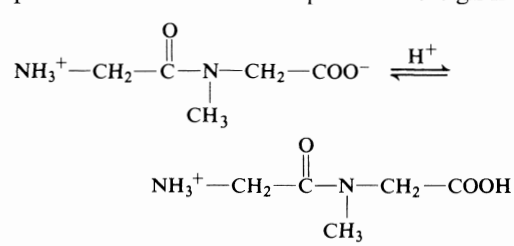

cantly in the two isomers and is traceable to differences in intramolecular electrostatic inter-

[1]Work supported by the U.S. Atomic Energy Commission.

[2]Abbreviations used: Pro, L-proline; Gly, glycine; Sar, sarcosine; TSP, sodium trimethylsilylpropionate-d_4.

Can. J. Chem. Downloaded from www.nrcresearchpress.com by 210.87.254.40 on 09/05/12
For personal use only.

actions between terminal amino and carboxyl groups.

Materials and Methods

Chemicals

Glycylsarcosine was purchased from two sources, Cyclo Chemical Company and Sigma Chemical (St Louis). The purity, as checked by thin-layer chromatography and 220 MHz n.m.r. spectra, was better than 95% and no further purification was carried out. Deuterated materials were purchased from Merck, Sharp and Dohme of Canada.

Preparation of Solutions

Gly-Sar solutions (0.15–0.20 *M*) were prepared in D_2O and adjusted to the desired p*D* by titrating with DCl or KOD. The p*H* was measured with a Radiometer Model 28 meter and type G2222 electrodes calibrated with the usual standard buffers. p*D* values were calculated by the equation $pD = pH + 0.4$ (26).

Nuclear Magnetic Resonance Measurements

Proton n.m.r. spectra were measured at 200 MHz with a Varian 220 spectrometer. Internal TSP (0.005 *M*) was used as reference and shifts were measured by the audio-side-band method (27).

Results

The 220 MHz proton spectrum of Gly-Sar consists of duplicate sets of signals for all of the Sar and Gly CH_2 and CH_3 protons, as would be expected for an equilibrium mixture of *cis* and *trans* isomers. One set of signals (*cis* isomer) has lower signal intensities than the second set, as is evident in the CH_2 region of the spectrum shown in Fig. 1. Higher temperatures produced a coalescence of the two sets of signals and indicated that at 23 °C the spectra are characteristic of a slow exchange limit.

Assignments of the signals can be made from a consideration of p*H* effects and correlations with chemical shifts of other amides. Titration of the carboxyl group leads to the largest chemical shift changes for CH_2 protons α to the ionizing group and forms the basis for an assignment of CH_2 signals at 3.99 and 3.90 p.p.m. to the Sar residue. Confirmation of this assignment was made by preparation and examination of the spectrum for Gly(d_2)-Sar. An assignment of signals to *cis* and *trans* isomers is based on extensive data (28) which show that signals for

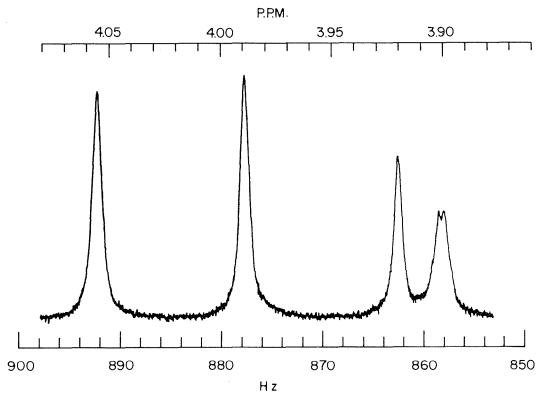

FIG. 1. The 220 MHz n.m.r. spectrum of glycylsarcosine in D_2O, pD = 4.4, temperature 23 °C, internal reference TSP at 0 Hz. Only the —CH_2— region is shown.

N—CH_3 groups *cis* to amide carbonyls in methyl amides are located up-field relative to those in a *trans* orientation. Accordingly, the present results indicate that the *trans* isomer in Gly-Sar predominates (mol fraction ≈0.70). A summary of our assignments of extrapolated chemical shift values for cation and zwitterion is given in Table 1.

Titration of the carboxyl group causes marked shift changes for both *cis* and *trans* Sar-CH_2 protons, Fig. 2, with Δδ for the former (0.3 p.p.m.) being largest (see Table 1). Smaller but measurable shift changes occur for Gly-CH_2 and Sar-NCH_3 signals in both isomers. The shift to higher field with increasing p*D* is consistent with an increased shielding arising from the negatively charged carboxylate group. Also, the observed S-shaped δ–p*D* curves follow the pattern expected for a simple ionization equilibrium, eq. 1. The shift to higher field is accompanied by an increase in *cis* isomer population from 21 ± 3% at pD = 1.4 to 40 ± 1% at pD = 4.

Discussion

From the curves in Fig. 2, it is apparent that the carboxylate p*K* is different in the *cis* and *trans* isomers of Gly-Sar. A numerical determination of individual p*K* values can be made by fitting the observed δ–p*D* curve to the equation, $pD = pK + N \log A/B$, where A/B is the ratio of zwitterion to cation calculated from the shift data. An excellent fit of calculated (solid lines) and observed points (Fig. 2) was obtained for all four sets of —CH_2— shifts and the final least-square fit p*K* and *N* values are listed in

TABLE 1. Gly-Sar chemical shifts in D_2O (23 °C)

	—CH_2—		
	Glycyl	Sarcosine	N—CH_3
Trans conformation			
Zwitterion	892 (4.05)	873 (3.97)	666 (3.03)
Cation	902 (4.10)	928 (4.22)	680 (3.09)
p*D* shift	10 (0.05)	55 (0.25)	14 (0.06)
Cis conformation			
Zwitterion	858 (3.90)	860 (3.91)	655 (2.98)
Cation	871 (3.96)	933 (4.24)	661 (3.00)
p*D* shift	13 (0.06)	73 (0.33)	6 (0.03)

NOTE: Chemical shifts are downfield relative to TSP in Hz or (p.p.m.) and are the extrapolated values used for the p*K* determination. The approximate p*D* value which applies to the cation is 1.4; for the zwitterion it is 5.0.

TABLE 2. Least-squares fit of chemical shift data (23 °C)

	Trans		*Cis*	
	p*K*	*N*	p*K*	*N*
Sarcosine —CH_2—	3.45 ± 0.03	0.90 ± 0.04	3.00 ± 0.03	0.92 ± 0.05
Glycyl —CH_2—	3.39 ± 0.06	0.97 ± 0.10	3.03 ± 0.05	0.89 ± 0.08
N—CH_3	3.34 ± 0.05	0.81 ± 0.09	3.03 ± 0.06	1.03 ± 0.12
Mean	3.39 ± 0.03		3.01 ± 0.03	

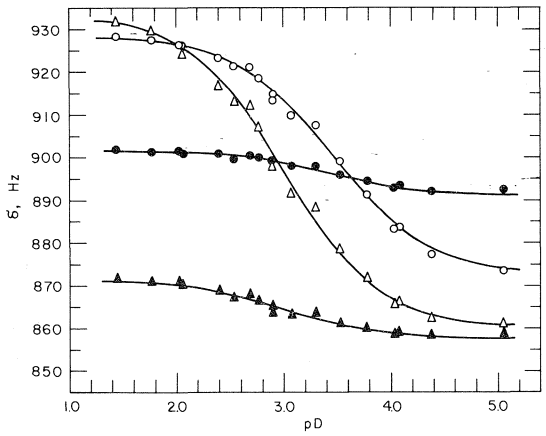

FIG. 2. The effect of p*D* on the chemical shift of the methylene protons of glycyl-sarcosine in D_2O. Temperature 23 °C. Symbols: —▲—, *cis*-glycyl; —△—, *cis*-sarcosine; —●—, *trans*-glycyl; —○—, *trans*-sarcosine.

Table 2. The close agreement among the three independently determined p*K* values (*i.e.*, Sar-CH_2, Gly-CH_2, and NCH_3) for individual isomers confirms the validity of the model. From the data the p*K* difference between isomers is 0.38 ± 0.04 at 23 °C with the *cis* isomer being a somewhat stronger acid.

The most reasonable explanation for the carboxylate p*K* difference is the effect of intramolecular electrostatic interaction between carboxyl and positively charged amino groups. A variety of experimental and theoretical evidence indicates that dipeptide derivatives (usually model dipeptides without charged groups) exist in a compact, folded conformation which brings the ends of the molecule together (22, 29–34). It has also been known for some time that a number of physical properties, *e.g.* p*K* (35–37), and dielectric constant (38, 39), of small, optically pure peptides differ from those for optically mixed isomers, *i.e.*, LL or DD compared with LD or DL. These differences have been interpreted (40) in terms of a slightly smaller average end-to-end separation in the mixed peptide as opposed to the pure one. A similar conformational property may account for the *cis–trans* p*K* difference of Gly-Sar, *i.e.*, the *cis* isomer must be more compact in order to have a lower carboxylate p*K*.

In order to determine whether a conformation effect could result in sufficient difference in charge separation to explain the observed p*K* shift, combined molecular model and semi-empirical conformational calculations of non-

Can. J. Chem. Downloaded from www.nrcresearchpress.com by 210.87.254.40 on 09/05/12
For personal use only.

Can. J. Chem. Downloaded from www.nrcresearchpress.com by 210.87.254.40 on 09/05/12
For personal use only.

bonded interaction energy (E_i) were carried out on Gly-Sar. The calculations were based on: (*a*) a Lennard-Jones (6–12) function for Van der Waals interactions using the constants given by Scheraga in ref. 1; (*b*) a torsional energy of the form $E_T = A/2\,(1 - \cos 3\psi)$ where ψ is the dihedral angle. The energy barriers were taken as 1 kcal/mol; (*c*) an electrostatic interaction energy of the form $e_i e_j / R_{ij} D_e$ where e_i and e_j were monopole charges located at atomic centres separated by R_{ij}. For the charges we distributed $+1.0\,e$ among the atoms of the amino group, $-1.0e$ among the atoms of the carboxyl group, and charges of $-0.2\,e$, $+0.3\,e$, $-0.1\,e$ on peptide O, C, and N respectively. Calculations were done with several values of D_e. Bond lengths and bond angles were held constant at values determined from the known crystal structures of Gly-Gly (41) and cyclo-$(Sar)_4$ (42). Both the models and calculations confirmed that the amino and carboxyl groups could come much closer together in the *cis* than in the *trans* isomer.

With a value of $D_e = 6$, we estimated an average charge separation ($\bar{R}_i$) of 5.1 Å in the most probable *trans* conformation and a value of 3.3 Å for the most probable *cis* conformation. In this calculation $\bar{R}_i$ was taken as the average distance between the six pairs of amino hydrogens and carboxylate oxygens (H^+—O^-) in the conformation of lowest energy.

A quantitative estimate of the resultant pK difference can be made using the Bjerrum equation (43), where k = Boltzmann constant, e =

$$[2] \quad pK_{cis} - pK_{trans} \approx \frac{e^2}{2.303kT}\frac{1}{D_e}\left(\frac{1}{R_c} - \frac{1}{R_t}\right)$$

electronic charge, T = absolute temperature, D_e = effective dielectric constant, R = charge separation.

Kirkwood and Westheimer (44) showed that eq. 2 can be derived by considering the molecule as a charged dielectric cavity within the solvent. For charges located near the cavity perimeter, D_e approaches (or even exceeds) the solvent dielectric constant. To estimate ΔpK from eq. 2 we calculated $\bar{R}_t$ and $\bar{R}_c$ as follows. For each isomer we obtained 4000 conformations by random choice of dihedral angles (keeping the peptide bond fixed at either 180 or 0°). The non bonded interaction energy (E_i) was calculated as described above and the average charge separation was obtained from eq. 3. The value of $\bar{R}_i$

$$[3] \quad \bar{R} = \frac{\sum_i \bar{R}_i \exp(-E_i/0.6)}{\sum \exp(-E_i/0.6)}$$

for each conformation was obtained as described above. In this way we found $\bar{R}_t = 5.92$ Å and $\bar{R}_c = 5.13$ Å. With $D_e = 80$, these values give $\Delta pK = 0.08$, while to obtain $\Delta pK = 0.38$, D_e must be about 16.5.

The calculations and models clearly showed that a low energy, folded conformation of the *cis* isomer can be obtained if amino, carboxyl, and methyl groups are precisely oriented. The calculated energy of this conformation relative to more extended conformations (similar to the low energy conformation found for *trans* Gly-Sar) depends on the choice of Van der Waals and electrostatic parameters. Several calculations were carried out using different choices. The values presented above represent a relatively conservative example. We have concluded therefore that the electrostatic effect is able to account for the major part of the observed pK difference between *cis* and *trans* Gly-Sar isomers.

The importance of the electrostatic interaction energy in determining the relative stabilities of *cis* and *trans* Gly-Sar is also indicated by the population shift from ~20% *cis* in the cation to ~40% *cis* in the zwitterion. An estimate of the difference in zwitterion electrostatic interaction energy (along the lines of eq. 1 with $D_e = 16$) showed that it is of the right order of magnitude to account for the observed population shift. Madison and Schellman (13) have observed a similar population shift for proline dipeptides.

Finally, we would like to draw attention to the nonequivalence of the glycyl-CH_2 protons which was observed only in the zwitterion of the *cis* isomer (Fig. 1). Chemical shift nonequivalence of methylene hydrogens in dipeptides containing glycine has been previously reported (45, 46), and attributed to electric field gradients produced by dipolar ions or aromatic groups. This view is consistent with our interpretation of the conformational difference between *cis* and *trans* isomers of Gly-Sar.

A part of this study was done while R.A.M. was a Faculty Research Participant at Argonne National Laboratory, and the support from the Argonne Center for Educational Affairs is gratefully acknowledged. Some of the n.m.r. measurements were completed with the assistance of the Canadian 220 MHz NMR Centre.

1. H. A. SCHERAGA. Adv. Phys. Org. Chem. **6**, 103 (1968).
2. G. N. RAMACHANDRAN and V. SASISEKHARAN. Adv. Prot. Chem. **23**, 283 (1968).
3. A. M. LIQUORI. Q. Rev. Biophys. **2**, 65 (1969).
4. R. C. NEUMAN, D. N. ROARK, and V. JONAS. J. Am. Chem. Soc. **89**, 3412 (1967).
5. P. T. INGLEFIELD, E. KRAKOWER, L. W. REEVES, and R. STEWART. Mol. Phys. **15**, 65 (1968).
6. K. RABINOVITZ and A. PINES. J. Am. Chem. Soc. **91**, 1585 (1969).
7. E. A. ALLAN, R. F. HOBSON, L. W. REEVES, and K. N. SHAW. J. Am. Chem. Soc. **94**, 6604 (1972).
8. T. DRAKENBERG and S. FORSEN. J. Phys. Chem. **74**, 1 (1970).
9. J. SANDSTROM. J. Phys. Chem. **71**, 2318 (1967).
10. P. R. ANDREWS. Biopolymers, **10**, 2253 (1971).
11. T. DRAKENBERG, K.-I. DAHLQVIST, and S. FORSEN. J. Phys. Chem. **76**, 2178 (1972).
12. P. N. SKANCKE and I. AANESLAND. Acta Chem. Scand. **26**, 2614 (1972).
13. V. MADISON and J. SCHELLMAN. Biopolymers, **9**, 511 (1970).
14. C. M. DEBER, F. A. BOVEY, J. P. CARVER, and E. R. BLOUT. J. Am. Chem. Soc. **92**, 6191 (1970).
15. V. J. HRUBY, A. I. BREWSTER, and J. A. GLASEL. Proc. Natl. Acad. Sci. U.S. **68**, 450 (1971).
16. W. A. THOMAS and M. K. WILLIAMS. Chem. Commun. 994 (1972).
17. D. A. TORCHIA, S. C. K. WONG, C. M. DEBER, and E. R. BLOUT. J. Am. Chem. Soc. **94**, 609 (1972).
18. D. A. TORCHIA, S. C. K. WONG, C. M. DEBER, and E. R. BLOUT. J. Am. Chem. Soc. **94**, 616 (1972).
19. C. M. DEBER, D. A. TORCHIA, S. C. K. WONG, and E. R. BLOUT. Proc. Natl. Acad. Sci. U.S. **69**, 1825 (1972).
20. D. A. TORCHIA and F. A. BOVEY. Macromolecules, **4**, 246 (1971).
21. D. A. TORCHIA. Biochemistry, **11**, 1462 (1972).
22. V. F. BYSTROV, S. L. PORTNOVA, V. J. TESTLIN, V. T. IVANOV, and YU A. OVCHINNIKOV. Tetrahedron, **25**, 493 (1969).
23. F. A. BOVEY, J. J. RYAN, and F. P. HOOD. Macromolecules, **1**, 305 (1968).
24. M. GOODMAN and M. FRIED. J. Am. Chem. Soc. **89**, 1264 (1967).
25. F. CONTI and P. DE SANTIS. Biopolymers, **10**, 2581 (1971).
26. P. K. GLASOE and F. A. LONG. J. Phys. Chem. **64**, 188 (1960).
27. J. T. ARNOLD and M. E. PACKARD. J. Chem. Phys. **19**, 1608 (1951).
28. F. A. L. ANET and A. J. R. BOURN. J. Am. Chem. Soc. **87**, 5250 (1965).
29. S. MIZUSHIMA, T. SHIMANOUCHI, M. TSABOR, and T. AKAKAWA. J. Am. Chem. Soc. **79**, 5357 (1957).
30. M. AVIGNON, P. V. HUONG, J. LASCOMBE, M. MARRAUD, and J. NEEL. Biopolymers, **8**, 69 (1969).
31. M. AVIGNON and P. VAN HUONG. Biopolymers, **9**, 427 (1970).
32. G. GOVIL and A. SARAN. J. Chem. Soc (A), 3624 (1971).
33. B. MAIGRET, B. PULLMAN, and M. DREYFUS. J. Theoret. Biol. **26**, 321 (1970).
34. J. NEEL. Pure and Appl. Chem. **31**, 201 (1972).
35. E. ELLENBOGEN. J. Am. Chem. Soc. **74**, 5198 (1952).
36. E. ELLENBOGEN. J. Cell Comp. Physiol. **47** (Suppl. 1), 151 (1956).
37. N. C. LI, G. W. MILLER, N. SOLONY, and B. T. GILLIS. J. Am. Chem. Soc. **82**, 3737 (1960).
38. P. M. HARDY, G. W. KENNER, and R. C. SHEPPARD. Tetrahedron, **19**, 95 (1963).
39. J. BEACHHAM, V. T. IVANOV, G. W. KENNER, and R. C. SHEPPARD. Chem. Commun. 386 (1965).
40. S. LANDE. Biopolymers, **7**, 879 (1969).
41. R. PARTHASARATHY. Acta Cryst. B**25**, 509 (1969).
42. P. GROTH. Acta Chem. Scand. **24**, 780 (1970).
43. N. BJERRUM. Z. Physik. Chem. **106**, 219 (1923).
44. J. B. KIRKWOOD and F. H. WESTHEIMER. J. Chem. Phys. **6**, 506 (1938).
45. V. J. MORLINO and R. B. MARTIN. J. Am. Chem. Soc. **89**, 3107 (1967).
46. A. NAKAMURA and O. JARDETZKY. Proc. Natl. Acad. Sci. U.S. **58**, 2212 (1967).

Can. J. Chem. Downloaded from www.nrcresearchpress.com by 210.87.254.40 on 09/05/12
For personal use only.

Can. J. Chem. Downloaded from www.nrcresearchpress.com by 210.87.254.42 on 09/05/12
For personal use only.

The Total Synthesis of a Hexacyclic Relay for the Alkaloid Napelline

KAREL WIESNER, PAK-TSUN HO, AND CONNIE SHII JEOU (PAN) TSAI
Natural Products Research Center, University of New Brunswick, Fredericton, New Brunswick

Received March 1, 1974

KAREL WIESNER, PAK-TSUN HO, and CONNIE SHII JEOU (PAN) TSAI. Can. J. Chem. **52**, 2353 (1974).

The total synthesis of the racemic compound **12** and its identification with the corresponding optically active derivative prepared from lucidusculine is described.

KAREL WIESNER, PAK-TSUN HO et CONNIE SHII JEOU (PAN) TSAI. Can. J. Chem. **52**, 2353 (1974).

On décrit la synthèse totale du composé racémique **12** et son identification avec le dérivé correspondant optiquement actif préparé à partir de la lucidusculine.

[Traduit par le journal]

We have described recently a simple and stereospecific synthesis of the intermediate **1** (1). In the present Communication we wish to disclose the conversion of this material to the hexacyclic polysubstituted lactame **12** and the identification of this compound with the corresponding optically active derivative of napelline. The method which we have used for this purpose was worked out some time ago on a model system (2).

The phenol **1** was converted quantitatively to the crotyl derivative **2**[1] by treatment with crotylchloride and potassium carbonate in dimethyl formamide at 80 °C for 3.5 h; m.p. 201 °C; n.m.r.: singlet (3H) τ 8.66 (C—CH_3), doublet (3H) τ 8.23 (CH=CH—CH_3), multiplet (2H) τ 5.51 (—O—CH_2—), multiplet (2H) τ 4.19 p.p.m. (—CH=CH—). Compound **2** was heated for 2 h to 180–185 °C in an evacuated and sealed tube. The product **3** (m.p. 273–276 °C) was a mixture of two methyl epimers and it was obtained in a yield of 81.5%.

The phenol **3** was methylated in dimethylformamide with methyl iodide and potassium carbonate at 75–80 °C for 40 min. The methyl ether **4** (m.p. 196–198 °C) was obtained in a 88% yield; i.r.: 1700 (ketone), 1670 cm^{-1} (amide); n.m.r.: doublet (3H) τ 8.79 (CH—CH_3), singlet (3H) τ 6.14 (—OCH_3), two singlets and a multiplet (1H each) τ 4.86, 5.08, 3.93 (vinyl protons), two singlets (1H each) τ 2.83, 3.03 p.p.m. (aromatic protons).

A solution of the olefin **4** and osmic acid in tetrahydrofuran was stirred for 1 h. An aqueous solution of sodium periodate was then added and stirring continued for 20 min. The keto aldehyde **5** (m.p. 151–152 °C) was obtained in a yield of 80%; i.r.: 1725 (aldehyde), 1705 (ketone), 1670 cm^{-1} (amide); n.m.r.: doublet (1H) τ −0.03 p.p.m. (aldehyde proton). The diketal **6** (m.p. 257–263 °C) was prepared by the standard method in a quantitative yield; n.m.r.: two doublets (1H) τ 4.90, 4.96 (acetal protons of the two epimers), two multiplets (4H each) τ 5.86, 6.13 p.p.m. (dioxolane protons).

Reduction of the diketal **6** with lithium in liquid amonia followed by addition of methanol and work-up yielded a dihydro derivative and unreduced **6**. This material was immediately dissolved in a mixture of benzene and acetone (1:1) and stirred with *p*-toluenesulphonic acid for 24 h at room temperature. Besides a 50% yield of an aromatic ketal aldehyde, from which the starting material **6** is readily obtainable, a 50% yield of the crystalline (m.p. 319–325 °C) diastereoisomeric mixture **7** was obtained; i.r.: 1725 (aldehyde), 1670 cm^{-1} (α,β-unsaturated ketone and lactam); n.m.r.: doublet (1H) τ 0.26 (aldehyde proton), doublet (1H) τ 3.56 (olefinic proton), multiplet (4H) τ 6.00 p.p.m. (dioxolane protons); u.v.: λ_{max}(EtOH) 239 nm (ε = 9600).

[1]The i.r., n.m.r., and mass spectra of all compounds have been recorded and are in agreement with the structures assigned. Only specially relevant spectral data are reported. All crystalline compounds gave correct elemental analyses.

Can. J. Chem. Downloaded from www.nrcresearchpress.com by 210.87.254.42 on 09/05/12
For personal use only.

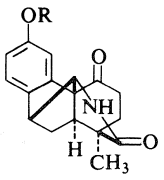

1 R = H

2 R = —CH_2—CH=CH—CH_3

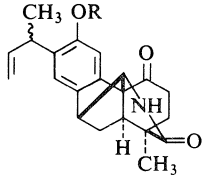

3 R = H

4 R = CH_3

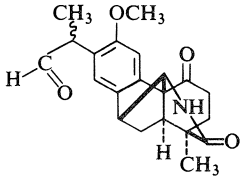

5

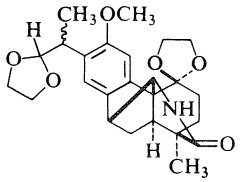

6

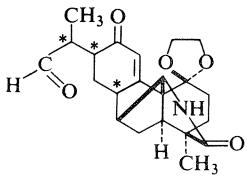

7

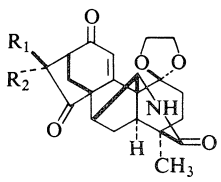

8 R_1 = CH_3; R_2 = H

9 R_1 = H; R_2 = CH_3

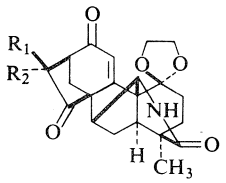

10 R_1 = CH_3; R_2 = H

11 R_1 = H; R_2 = CH_3

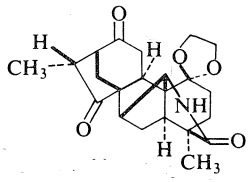

12

The diastereoisomeric mixture **7** was now dissolved in methanolic potassium hydroxide (0.5%), stirred at room temperature under nitrogen for 6 h, and the products of the vinylogous aldole condensation were purified by preparative t.l.c. They were obtained in a yield of 75% and were immediately oxidized with chromium trioxide – pyridine in methylene dichloride. The total yield of the resulting diketones (**8**, **9**, **10**, **11**) after purification was 92%.

In our model experience (2) the skeletal structure corresponding to **8** and **9** was the thermodynamically controlled single product. In the present case, on the other hand, the isomers **10** and **11** were more stable but the isomers **8** and **9** were formed more rapidly. Under the conditions described in this Communication the ratio (**8** + **9**)/(**10** + **11**) was about 6:4. We believe that the shortening of the synthesis which we accomplished by the use of a crotyl residue (instead of an allyl as in the model) had cost us the full stereospecificity of the C/D ring construction. The four diketones were readily separated by chromatography and purified by recrystallization.

Compound **8** (m.p. 292–294 °C) was identical by t.l.c., mass, and infrared spectra with the optically active material (m.p. 206–208 °C) of the same structure prepared from napelline (3); i.r.: 1745 (five-membered ketone), 1672 cm^{-1} (lactame and α,β-unsaturated ketone); n.m.r.: singlet (1H) τ 4.1 (vinyl proton), doublet (3H) τ 8.66, 8.81 (*exo*-CH—CH_3), singlet (3H) τ 8.81 p.p.m. (C—CH_3); u.v.: λ_{max}(EtOH) 232, 272 nm (ε = 8234, 5553). Compound **9** (m.p. 324 °C): i.r.: 1740 (five-membered ketone), 1670 cm^{-1} (α,β-unsaturated ketone and lactame); n.m.r.: singlet (1H) τ 4.1 (vinyl proton), doublet (3H)

τ 8.91, 9.03 (*endo*-CH—CH_3), singlet (3H) τ 8.80 p.p.m. (C—CH_3). Ultraviolet and mass spectra of compounds **8** and **9** were identical. Compound **9** was hydrogenated on 10% palladium on charcoal in ethanol. The diketo ketal **12** (m.p. 319 °C) was obtained in a quantitative yield. This material was identical (t.l.c., i.r., n.m.r., and mass spectra) with the corresponding optically active compound of the same structure (m.p. 245–248 °C) obtained from napelline (3).

We wish to thank the National Research Council, Ottawa, and the Hoffmann-La Roche Company, Dorval, Quebec, and Nutley, New Jersey (U.S.A.) for the generous support of these investigations.

1. K. Wiesner, P. T. Ho, D. Chang, Y. K. Lam, C. S. J. Pan, and W. Y. Ren. Can. J. Chem. **51**, 3978 (1973).
2. K. Wiesner, A. Deljac, T. Y. R. Tsai, and M. Przybylska. Tetrahedron Lett. **14**, 1145 (1970).
3. K. Wiesner, P. T. Ho, C. S. J. Tsai, and Y. K. Lam. Can. J. Chem. This issue.

Can. J. Chem. Downloaded from www.nrcresearchpress.com by 210.87.254.42 on 09/05/12
For personal use only.

The Total Synthesis of Racemic Napelline

Karel Wiesner, Pak-tsun Ho, Connie Shii Jeou (Pan) Tsai, and Yiu-Kuen Lam

Natural Products Research Center, University of New Brunswick, Fredericton, New Brunswick

Received April 19, 1974

Karel Wiesner, Pak-Tsun Ho, Connie Shii Jeou (Pan) Tsai, and Yiu-Kuen Lam. Can. J. Chem. **52**, 2355 (1974).

Lucidusculine **1** was converted into the lactame **5**. This compound is identical with the corresponding racemate described in the accompanying Communication. The synthesis of napelline **2** from the lactame **5** is discussed. The process completes the first (formal) total synthesis of a racemic hexacyclic polysubstituted aconite alkaloid.

Karel Wiesner, Pak-Tsun Ho, Connie Shii Jeou (Pan) Tsai et Yiu-Kuen Lam. Can. J. Chem. **52**, 2355 (1974).

On transforme la lucidusculine **1** en la lactame **5**. Ce composé est identique au racémate correspondant décrit dans la communication qui accompagne cet article. On présente une discussion de la synthèse de la napelline **2** à partir de la lactame **5**. Le processus complète la première synthèse totale (formelle) de l'alcaloïde aconite polysubstitué hexacyclique et racémique. [Traduit par le journal]

In the accompanying Communication (1) we have described the total synthesis of the racemic hexacyclic lactames **5** and **8**. We report now the preparation of the optically active form of these compounds from lucidusculine (2) **1** and the conversion of (optically active) **5** to the alkaloid napelline **2** (2).

Lucidusculine **1** was converted quantitatively to napelline **2** (m.p. 165 °C) by reduction with lithium aluminum hydride in tetrahydrofuran at 0 °C. Hydrogenation of napelline with platinum oxide in acetic acid gave dihydronapelline **3** (2) (m.p. 175 °C) in a yield of 70%. Treatment of **3** with mercuric acetate in aqueous acetic acid at 60 °C for 3 h gave a mixture of products which was oxidized with chromium trioxide in pyridine at room temperature for 36 h. The triketolactam **4**[1] (m.p. 284 °C) was isolated in a yield of 16.5%; i.r.: 3400 (NH), 1742 (five-membered ketone), 1706 (six-membered ketone), 1672 cm^{-1} (lactam); n.m.r.: singlet (3H) τ 8.74 (C—CH_3), doublet (3H) τ 8.99 p.p.m. (*endo*-CH—CH_3).

The diketo ketal **5** (m.p. 248 °C) was prepared by treatment of **4** with *p*-toluenesulfonic acid and ethylene glycol in boiling benzene for 2 h in a yield of 71%; i.r.: 1738 (five-membered ketone), 1710 (six-membered ketone), 1670 cm^{-1} (lactam); n.m.r.: broad singlet (4H) τ 5.96 (dioxolane protons), singlet (3H) τ 8.85 (C—CH_3), doublet

[1]The i.r., n.m.r., and mass spectra of all compounds have been recorded and are in agreement with the structures assigned. All crystalline compounds gave correct elemental analyses.

τ 8.91, 9.03 (*endo*-CH—CH_3), singlet (3H) τ 8.80 p.p.m. (C—CH_3). Ultraviolet and mass spectra of compounds **8** and **9** were identical. Compound **9** was hydrogenated on 10% palladium on charcoal in ethanol. The diketo ketal **12** (m.p. 319 °C) was obtained in a quantitative yield. This material was identical (t.l.c., i.r., n.m.r., and mass spectra) with the corresponding optically active compound of the same structure (m.p. 245–248 °C) obtained from napelline (3).

We wish to thank the National Research Council, Ottawa, and the Hoffmann-La Roche Company, Dorval, Quebec, and Nutley, New Jersey (U.S.A.) for the generous support of these investigations.

1. K. Wiesner, P. T. Ho, D. Chang, Y. K. Lam, C. S. J. Pan, and W. Y. Ren. Can. J. Chem. **51**, 3978 (1973).
2. K. Wiesner, A. Deljac, T. Y. R. Tsai, and M. Przybylska. Tetrahedron Lett. **14**, 1145 (1970).
3. K. Wiesner, P. T. Ho, C. S. J. Tsai, and Y. K. Lam. Can. J. Chem. This issue.

Can. J. Chem. Downloaded from www.nrcresearchpress.com by 210.87.254.105 on 09/05/12
For personal use only.

The Total Synthesis of Racemic Napelline

Karel Wiesner, Pak-tsun Ho, Connie Shii Jeou (Pan) Tsai, and Yiu-Kuen Lam

Natural Products Research Center, University of New Brunswick, Fredericton, New Brunswick

Received April 19, 1974

Karel Wiesner, Pak-Tsun Ho, Connie Shii Jeou (Pan) Tsai, and Yiu-Kuen Lam. Can. J. Chem. **52**, 2355 (1974).

Lucidusculine **1** was converted into the lactame **5**. This compound is identical with the corresponding racemate described in the accompanying Communication. The synthesis of napelline **2** from the lactame **5** is discussed. The process completes the first (formal) total synthesis of a racemic hexacyclic polysubstituted aconite alkaloid.

Karel Wiesner, Pak-Tsun Ho, Connie Shii Jeou (Pan) Tsai et Yiu-Kuen Lam. Can. J. Chem. **52**, 2355 (1974).

On transforme la lucidusculine **1** en la lactame **5**. Ce composé est identique au racémate correspondant décrit dans la communication qui accompagne cet article. On présente une discussion de la synthèse de la napelline **2** à partir de la lactame **5**. Le processus complète la première synthèse totale (formelle) de l'alcaloïde aconite polysubstitué hexacyclique et racémique. [Traduit par le journal]

In the accompanying Communication (1) we have described the total synthesis of the racemic hexacyclic lactames **5** and **8**. We report now the preparation of the optically active form of these compounds from lucidusculine (2) **1** and the conversion of (optically active) **5** to the alkaloid napelline **2** (2).

Lucidusculine **1** was converted quantitatively to napelline **2** (m.p. 165 °C) by reduction with lithium aluminum hydride in tetrahydrofuran at 0 °C. Hydrogenation of napelline with platinum oxide in acetic acid gave dihydronapelline **3** (2) (m.p. 175 °C) in a yield of 70%. Treatment of **3** with mercuric acetate in aqueous acetic acid at 60 °C for 3 h gave a mixture of products which was oxidized with chromium trioxide in pyridine at room temperature for 36 h. The triketolactam **4**[1] (m.p. 284 °C) was isolated in a yield of 16.5%; i.r.: 3400 (NH), 1742 (five-membered ketone), 1706 (six-membered ketone), 1672 cm^{-1} (lactam); n.m.r.: singlet (3H) τ 8.74 (C—CH_3), doublet (3H) τ 8.99 p.p.m. (*endo*-CH—CH_3).

The diketo ketal **5** (m.p. 248 °C) was prepared by treatment of **4** with *p*-toluenesulfonic acid and ethylene glycol in boiling benzene for 2 h in a yield of 71%; i.r.: 1738 (five-membered ketone), 1710 (six-membered ketone), 1670 cm^{-1} (lactam); n.m.r.: broad singlet (4H) τ 5.96 (dioxolane protons), singlet (3H) τ 8.85 (C—CH_3), doublet

[1]The i.r., n.m.r., and mass spectra of all compounds have been recorded and are in agreement with the structures assigned. All crystalline compounds gave correct elemental analyses.

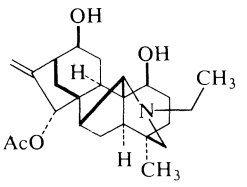

1

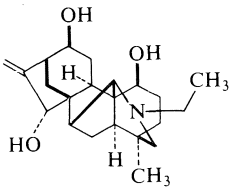

2

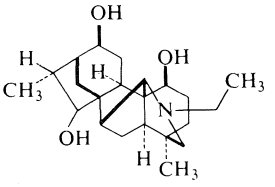

3

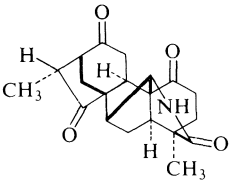

4

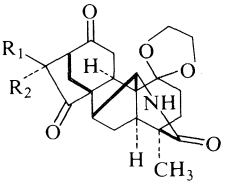

5 $R_1 = H$; $R_2 = CH_3$

6 $R_1 = CH_3$; $R_2 = H$

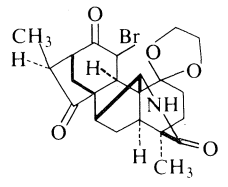

7

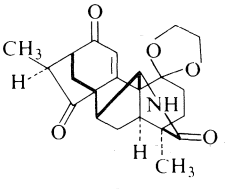

8

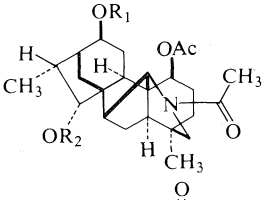

9 $R_1 = R_2 = C(=O)—CH_3$

10 $R_1 = R_2 = H$

11 $R_1 = C(=O)—CH_3$, $R_2 = H$

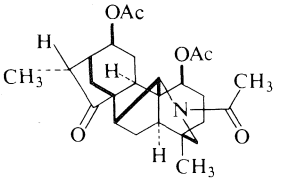

12

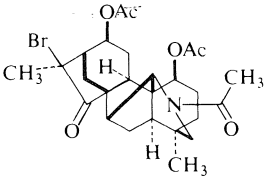

13

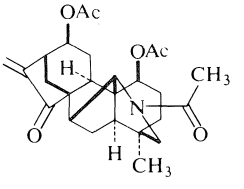

14

(3H) τ 8.99 p.p.m. (*endo*-CH—CH_3). The identity of this optically active material and the synthetic racemic compound (m.p. 319 °C) is reported in the accompanying Communication (1).

Refluxing with methanolic potassium hydroxide, converted the diketo ketal **5** to an equilibrium mixture (4:6, separated by preparative t.l.c.) of the starting material and the epimer **6** (m.p. 249 °C); n.m.r.: singlet (3H) τ 8.78 (C—CH_3), doublet (3H) τ 8.83 p.p.m. (*exo*-CH—CH_3). Compound **6** was brominated with bromine in a mixture of ether and chloroform in the presence of hydrogen chloride at 0 °C. The monobromo ketone **7** (m.p. 229 °C) was obtained in a yield of 92%; n.m.r.: doublet (1H) τ 5.03 (CH—*CH*—Br), doublet (3H) τ 8.79 p.p.m. (*exo*-CH—CH_3). Dehydrobromination of **7** with lithium bromide and lithium carbonate in dimethylformamide at 140 °C for 1 h gave 85% of the unsaturated ketone **8** (m.p. 208 °C); i.r.: 1745 (five-membered ketone), 1672 cm^{-1} (lactam and α,β-unsaturated ketone); n.m.r.: singlet (1H) τ 4.10 (vinyl proton), doublet (3H) τ 8.73 (*exo*-CH—CH_3), singlet (3H) τ 8.81 p.p.m. (C—CH_3); u.v.: λ_{max}(EtOH) 232, 272 nm (ε =

Can. J. Chem. Downloaded from www.nrcresearchpress.com by 210.87.254.105 on 09/05/12
For personal use only.

8234, 5553). (For the identity of compound **8** and the corresponding totally synthetic racemate *cf.* (1).) Hydrogenation of **8** on 10% palladium on charcoal in ethanol gave back quantitatively the diketone **6**.

In order to complete the synthesis of napelline, compound **5** was converted to the triketone **4** in 60% aqueous acetic acid at 80 °C in a quantitative yield. Reduction of **4** with lithium aluminum hydride in boiling dioxane under nitrogen for 22 h yielded a trihydroxyamine, which was immediately acetylated with acetic anhydride in pyridine and gave compound **9** (m.p. 189 °C) in a yield of 20% (after recrystallization); i.r.: 1730 (acetate), 1626 cm^{-1} (amide); n.m.r.: two singlets (3H) τ 7.82, 7.88 (—N(—CO—CH_3)—), singlets (3H each) τ 7.91, 7.93, 7.98 (3-O—CO—CH_3), doublet (3H) τ 9.08 (CH—CH_3), singlet (3H) τ 9.14 p.p.m. (C—CH_3).

Alkaline hydrolysis of **9** with potassium carbonate in aqueous methanol at room temperature gave a mixture from which the oily dihydroxy acetate **10** was isolated by preparative t.l.c. in a yield of 45%; i.r.: 1733 (acetate), 1625 cm^{-1} (amide); n.m.r.: broad singlet (1H) τ 4.93 (—C*H*—OAc), singlet (3H) τ 7.92 p.p.m. (—O—CO—CH_3). Compound **10** was acetylated with acetic anhydride in pyridine at 5 °C for 7 h. The oily hydroxy diacetate **11** was obtained in an almost quantitative yield and it was purified by preparative t.l.c.; n.m.r.: singlet (3H) τ 7.93 (—O—CO—CH_3), singlet (3H) τ = 8.00 (—O—CO—CH_3), doublet (3H) τ 8.96 (CH—CH_3), singlet (3H) τ 9.14 p.p.m. (C—CH_3).

Compound **11** was oxidized with chromium trioxide – pyridine in methylene dichloride at room temperature. The oily ketone **12** was obtained in a yield of 77% and was homogeneous by t.l.c. in several solvent systems; i.r.: 1739 (five-membered ketone and acetate), 1633 cm^{-1} (amide); n.m.r.: singlet (3H) τ 7.91 (—O—CO—CH_3), singlet (3H) τ 7.94 (—O—CO—CH_3), doublet (3H) τ 8.80 p.p.m. (CH—CH_3). Compound **12** was dissolved in a mixture of ether and chloroform containing hydrogen chloride and treated with bromine at room temperature to yield 82% of the oily bromo ketone **13**; n.m.r.: singlet (3H) τ 8.04 p.p.m. (—CBr—CH_3). Dehydrobromination of **13** with lithium bromide and lithium carbonate in dimethylformamide at 145 °C for 1 h led to the formation of the unsaturated ketone **14** in a yield of 62%. It was homogeneous in t.l.c.; i.r.: 1735 (acetate), 1731 (α,β-unsaturated ketone), 1643 (double bond), 1628 cm^{-1} (amide); n.m.r.: two broad singlets (2H) τ 3.91, 4.39 p.p.m. (methylenic protons); u.v.: λ_{max}(EtOH) 225 nm (ε = 11 830).

Finally, reduction of **14** with lithium aluminum hydride in dioxane at 60 °C for 2 h yielded napelline **2** (m.p. 165 °C). The synthetic compound was identical (mixture m.p., t.l.c., i.r. in KBr, n.m.r., and mass spectrum) with an authentic sample of napelline **2**. Thus, the first total synthesis of napelline is formally completed.

We wish to thank the National Research Council of Canada, and the Hoffmann-La Roche Company, Dorval, Quebec, and Nutley, New Jersey (U.S.A.) for the generous support of these investigations. We also thank Professor Shô Itô, Tohoku University, Japan, for providing us with the large amount of lucidusculine needed for these studies.

1. K. Wiesner, Pak-tsun Ho, and C. S. J. (Pan) Tsai, Can. J. Chem. This issue.
2. S. W. Pelletier. Chemistry of the alkaloids. Van Nostrand Reinholt Company, New York, 1970.

Can. J. Chem. Downloaded from www.nrcresearchpress.com by 210.87.254.105 on 09/05/12
For personal use only.

Canadian Journal of Chemistry

Published by
THE NATIONAL RESEARCH COUNCIL OF CANADA

Journal canadien de chimie

Publié par
LE CONSEIL NATIONAL DE RECHERCHES DU CANADA

Volume 52 Number 13 July 1, 1974 Volume 52 numéro 13 1 juillet 1974

The Behavior of 1-Phenyl-2-benzimidazolinethione and 1-Phenyl-2-benzimidazolinone upon Electron Impact and Pyrolysis

DENIS C. K. LIN, MICHAEL L. THOMSON, AND DON C. DEJONGH[1]

Department of Chemistry, University of Montreal, P.O. Box 6210, Branch A, Montreal, Quebec H3C 3V1

Received February 4, 1974

DENIS C. K. LIN, MICHAEL L. THOMPSON, and DON C. DEJONGH. Can. J. Chem. **52**, 2359 (1974).

The mass spectra of 1-phenyl-2-benzimidazolinethione (**3**) and 1-phenyl-2-benzimidazolinone (**4**) have been compared with their pyrolysis products and similarities have been found. In the 70 eV mass spectrum of **3**, the base peak results from the loss of H•; at low ionizing voltages, this path and a competing path, loss of S, are the only ones which remain. At 650° in a stream of N_2, 1-phenylbenzimidazole (**8**, 20%) formed from the loss of S and benzimidazo-[2,1-*b*]benzothiazole (**5**, 11%) formed by loss of H_2. The major fragmentation paths in the mass spectrum of **4** are loss of CHO• and NCO•. At 950°, phenazine (**6**, 35%) formed by loss of CH_2O, and carbazole (**7**, 14%) formed by loss of HNCO. In each pyrolysis, 65–70% of the starting material was recovered or accounted for.

DENIS C. K. LIN, MICHAEL L. THOMPSON et DON C. DEJONGH. Can. J. Chem. **52**, 2359 (1974).

On rapporte les spectres de masse de la phenyl-1 benzimidazolinethione-2 (**3**) et de la phenyl-1 benzimidazolinone-2 (**4**), tel qu'obtenus par impact électronique. On compare ces spectres avec les produits de pyrolyse des composés **3** et **4**. Dans le spectre de masse du composé **3**, pris à 70 eV, le pic de base se forme par perte de H•; à basses énergies des électrons, ce dernier est accompagné de l'ion moléculaire ainsi que d'un pic résultant de l'élimination de S. La pyrolyse du composé **3** à 650° dans un courant d'azote conduit à la formation de phenyl-1 benzimidazole (**8**, 20%) par perte de S et à la formation de benzimidazo[2,1-*b*]benzothiazole (**5**, 11%) par perte de H_2. Les patrons majeurs de fragmentation trouvés dans le spectre de masse du composé **4** résultent de la perte de CHO• et de la perte de NCO•. Les produits de la pyrolyse du composé **4** à 950° sont la phénazine (**6**, 35%) formée par la perte de CH_2O et le carbazole (**7**, 14%) formé par la perte de HNCO. Dans chaque cas, les produits formés ainsi que les produits originaux récupérés représentent de 65 à 70% des produits de départ.

Introduction

A considerable number of publications have appeared on the subject of pyrolysis at short contact times in the gas phase (1) and several of them have included a comparison of the pyrolysis products with those products which would be expected from an interpretation of the mass spectra of the starting material. We have been working in this area for several years (2) and report some of our recent results in this article.

A project under study in our laboratory is a comparison of the mass spectra and pyrolyses of molecules related to benzothiazole, benzoxazole, and benzimidazole (2, 3). Results obtained from 2-benzimidazolinethione (**1**) and 2-benzimidazolinone (**2**) were included in our recent reports (2, 3). Now, we have observed from the mass spectra of their *N*-phenyl deriva-

[1]To whom correspondence should be addressed.

Can. J. Chem. Downloaded from www.nrcresearchpress.com by 210.87.254.6 on 09/05/12
For personal use only.

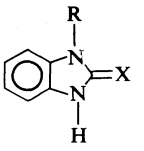

1 X = S: R = H
2 X = O; R = H
3 X = S; R = C_6H_5
4 X = O; R = C_6H_5

tives (**3** and **4**) that the phenyl group has a major influence on fragmentation of the molecular ions of these compounds. This observation has led us to study the pyrolyses of **3** and **4** in order to see if this influence is also important there.

In this article we report the mass spectrum, photolysis, and pyrolysis of 1-phenyl-2-benzimidazolinethione (**3**) and the mass spectrum and pyrolysis of 1-phenyl-2-benzimidazolinone (**4**). The mass spectrum of **4** has been published previously (4). High-resolution data and metastable-ion peaks are discussed in the schemes and text, along with certain features of the spectra obtained at low ionizing voltages.

Infrared spectra and dipole moments provide evidence for the presence of the keto structure of **2** (5). Thus, we will use the keto and thioketo forms in our discussion, rather than the tautomeric enol and thiol forms, even though there is no evidence that either form is preferred in the molecular ions.

Pyrolyses were performed by sublimation of the samples into a stream of N_2 which passed through an unpacked quartz tube surrounded by a 12 in. furnace (3, 6). Generally, a N_2 flow rate of 0.25 l/min and a system pressure of about 2 Torr were used. The pyrolyses were repeated several times at the same and different temperatures. Where possible, pyrolysis products were isolated and identified by physical as well as spectroscopic characteristics.

Results

1-Phenyl-2-benzimidazolinethione (3)

The 70 eV mass spectrum of **3** is summarized in Scheme 1. The (M − H) peak is the base peak

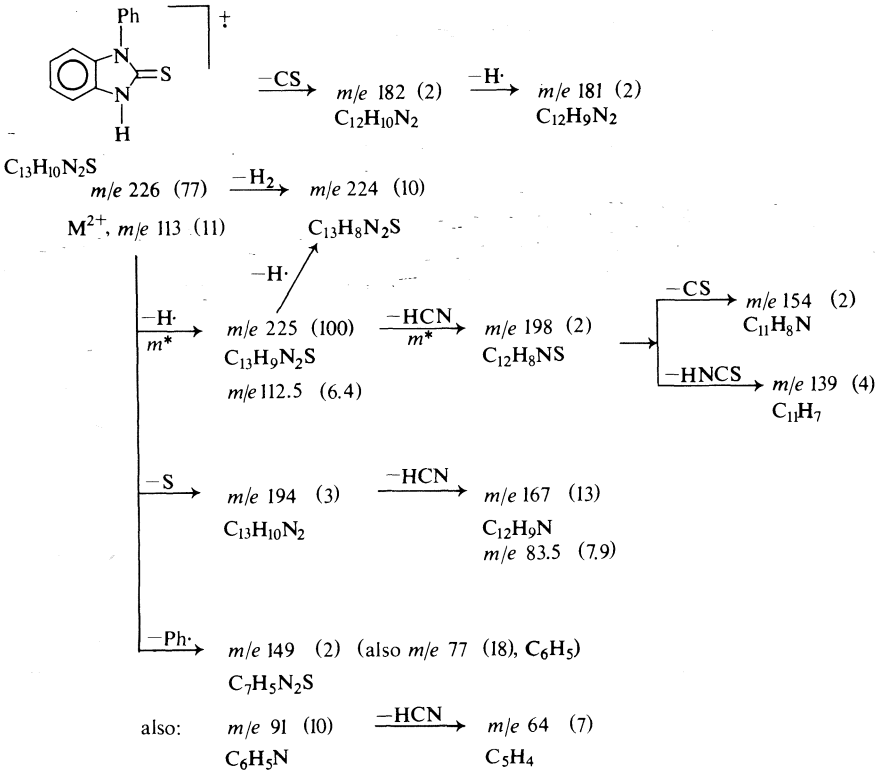

SCHEME 1[2]

[2]The elemental compositions are the result of exactmass measurements. The values in parentheses are relative intensities and *m** denotes the presence of a metastable-ion peak.

Can. J. Chem. Downloaded from www.nrcresearchpress.com by 210.87.254.6 on 09/05/12
For personal use only.

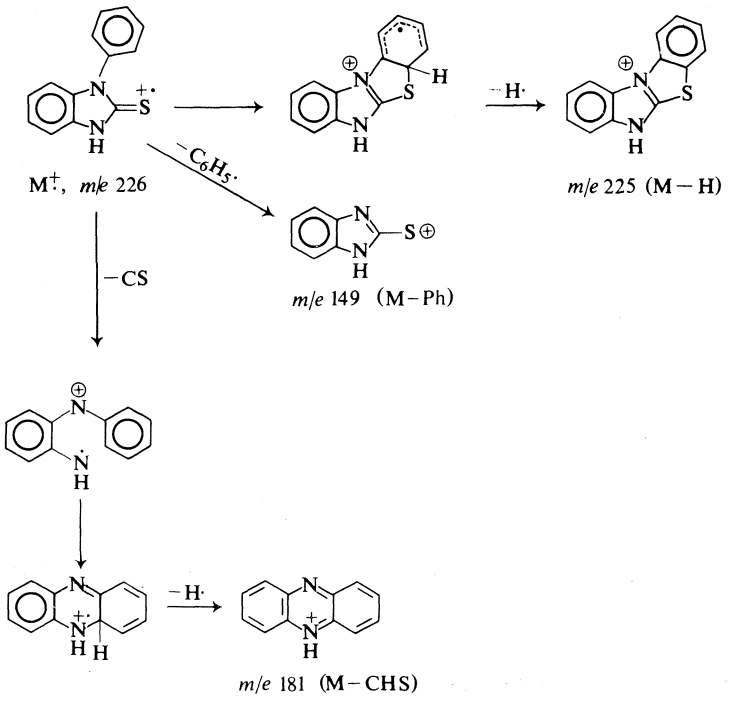

SCHEME 2

at 15 eV as well as at 70 eV. The peaks at *m/e* 224 (M − 2H) and at *m/e* 194 (M − S) are the only other fragment-ion peaks found at 15 eV. In fact, the peak at *m/e* 194 is present at electron voltages as low as 12 eV. Minor paths found at 70 eV begin by the loss of CS and by the loss of C_6H_5·. An abundant loss of H· is not observed in the mass spectrum of **1**; however in that case the loss of S is the lowest-energy path (3). There is no metastable-ion peak for formation of the peak at *m/e* 224 either from the peaks at *m/e* 226 or 225. So, it cannot be determined that the peak at *m/e* 224 forms by a one-step and/or a two-step path.

The fragmentations proposed in Scheme 2 can account for the formation of these ions. The structure proposed for the ion at *m/e* 225 corresponds to the protonated form of benzimidazo-[2,1-*b*]benzothiazole (**5**) and the structure proposed for the ion at *m/e* 181 corresponds to protonated phenazine (**6**). The peak at *m/e* 194 can be represented by the molecular ions of 1- and/or 2-phenylbenzimidazole (**8** and **9**). The loss of HCN from *m/e* 194 could give the molecular ion of carbazole (**7**) at *m/e* 167 (eq. 1).

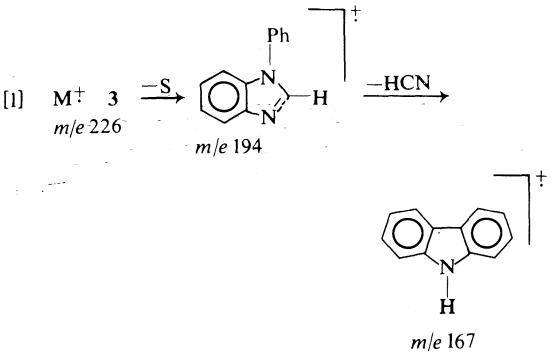

Compound **3** was pyrolyzed at 650, 800, and 950°. At 650°, 46.5% of starting compound was recovered. In addition, a 20% yield (based on unrecovered **3**) of 1-phenylbenzimidazole (**8**) and an 11% yield of benzimidazo[2,1-*b*]benzothiazole (**5**) were obtained (eq. 2).

Compound **8** forms by loss of S from **3** with migration of H from N to C. In the formation of **5**, the phenyl ring becomes bonded to the sulfur atom and H_2 is lost.

At 950°, the recovery of **3** decreased to 23.1% and the yield of **5** increased to 24%. On the other hand, the yield of **8** decreased to <0.5% but carbazole (**7**, 3%) and 2-phenylbenzimidazole (**9**, 11%) were now present among the pyrolysis products. Trace amounts of phenazine (**6**),

Can. J. Chem. Downloaded from www.nrcresearchpress.com by 210.87.254.6 on 09/05/12
For personal use only.

[2] 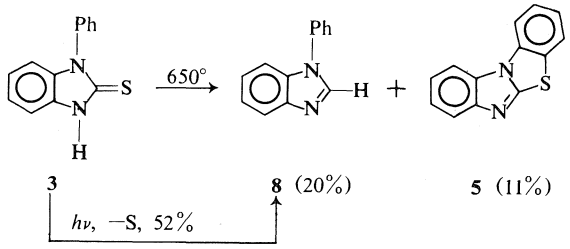

cyanocarbazole, 1- and 2-cyanonaphthalenes, 2-cyanoaniline, naphthalene, and benzonitrile were identified in addition.

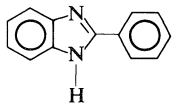

9

Also we photolyzed **3** in order to compare its behavior with the results obtained upon pyrolysis and electron impact. The only product found was 1-phenylbenzimidazole (**8**), formed by the loss of S, in 52% yield. *t*-Butyl alcohol was used as the solvent.

In summary, the lowest energy fragmentations of **3** upon electron impact are loss of H· and loss of S from the molecular ions. Pyrolysis of **3** at 650° produces benzimidazo[2,1-*b*]benzothiazole (**5**) by a loss of H_2 and 1-phenylbenzimidazole (**8**) by loss of S. Only compound **8** is observed upon photolysis of **3** in *t*-butyl alcohol.

1-Phenyl-2-benzimidazolinone (4)

The 70 eV mass spectrum of **4** is summarized in Scheme 3. The major fragmentation paths begin with loss of HCO· and with loss of NCO·. There are broad metastable-ion peaks present for each of these fragmentations. At 12 eV, the relative intensities of *m/e* 181 and 168 are 6 and 4%, respectively; also, there are very minor peaks present at *m/e* 209 and 167. The ions at *m/e* 181 can be represented as protonated phenazine and those at *m/e* 168 and 167 as protonated carbazole and carbazole (**7**), respectively.

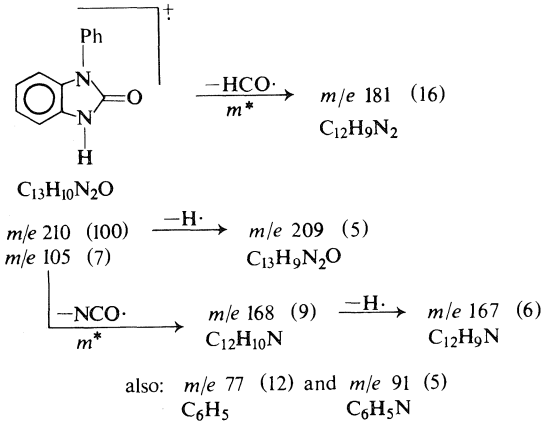

SCHEME 3

Compound **4** was pyrolyzed at 950° and 16.3% was recovered. The major products and their yields (based on unrecovered starting material) were phenazine (**6**, 35%) and carbazole (**7**, 14%) (eq. 3).

[3] 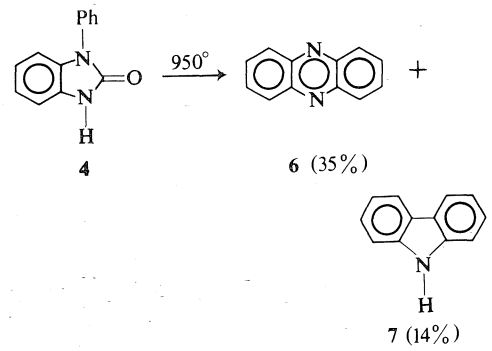

A number of minor products were obtained also, *viz.* diphenylamine (1%), 1- and 2-cyanonaphthalenes (2.5%), naphthalene (2%), benzonitrile (3%), and phenylisocyanate (2%). The last product was isolated as *N*-phenylcarbamate, after having reacted with ethanol during the work-up.

In summary, compound **4** loses CHO· and NCO· in the mass spectrometer. Pyrolysis of **4** gives phenazine, after loss of CH_2O (probably as CO and H_2) and carbazole, after loss of HNCO.

Discussion

At low ionizing voltages only two decompositions of the molecular ions of **3** are observed: loss of S and loss of H·. The products formed in the pyrolysis of **3** can be explained by similar decompositions. The formation of 1-phenylbenzimidazole (**8**) can arise by a desulfurization of the C=S bond; there is a neighboring hydrogen which can rearrange to the developing

Can. J. Chem. Downloaded from www.nrcresearchpress.com by 210.87.254.6 on 09/05/12
For personal use only.

Can. J. Chem. Downloaded from www.nrcresearchpress.com by 210.87.254.6 on 09/05/12
For personal use only.

electron-deficient center. Compound **8** is a major product isolated from the pyrolysis of **3** and the only product isolated from photolysis in *t*-butyl alcohol.

Precedents can be found for the pyrolytic and photolytic desulfurization of the C=S bond. For example, 2,6-diphenyl-4*H*-pyran-4-thione (**10**) undergoes photodesulfurization, giving the dimer **11** in 80% yield, (eq. 4) (7). This dimerization

[4] 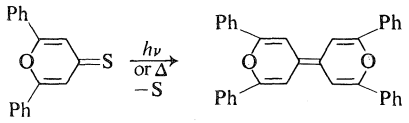

10 **11**

with desulfurization was also observed upon the heating of **10**. Another example, 1-(3-methyl-2-thioureido)pyridinium hydroxide inner salt (**12**) gives, in practically quantitative yield, pyridine and sulfur, (eq. 5) (8). Methyl cyanamide has

[5] 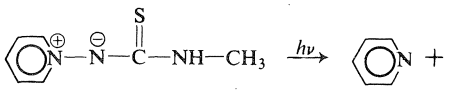

12

$$S + [N{\equiv}C{-}NH{-}CH_3]$$

been proposed as the undetected component. An initial loss of sulfur has been proposed as the most likely pathway. The molecular ion of **12** loses sulfur giving an ion $C_7H_9N_3$ which readily forms the pyridinium ions at *m/e* 79 by losing the elements of methyl cyanamide. Thus, the mass-spectral fragmentation pattern is consistent with the photochemical reaction.

The other product (**5**) formed in the pyrolysis of **3** results from the addition of the thermally excited thioketo group to the aromatic ring (eq. 6). The photoaddition of thiocarbonyl com-

[6] 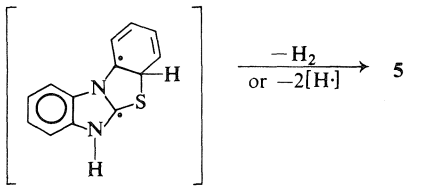

pounds to olefins is well known (9). Also, **8** could be formed photolytically from **3** in *t*-butyl alcohol by the photoexcitation of the thiocarboxyl group, (eq. 7). A similar scheme has been proposed to explain the photoreduction reactions of thiobenzophenones in solvents which have easily extractable hydrogens (10). In the

[7] 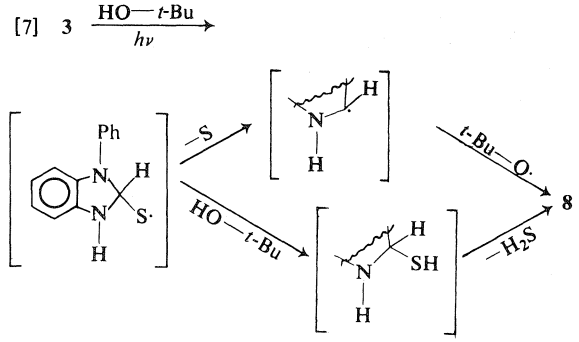

photodimerization with elimination of sulfur of 4*H*-pyran-4-thiones, the presence of H_2S was detected (7*b*).

In comparison, pyrolysis of **1** at 950° gave a 70% yield of products resulting from the loss of S (3). The loss of S from the molecular ions and from the (M + H) ions in the chemical-ionization mass spectrum is the lowest-energy fragmentation. The major pyrolysis product is benzimidazole (**8**, NH in place of N—Ph) (62.5%); this isomerizes to 2-cyanoaniline (7.5%) under the pyrolytic conditions. There is no pathway for **1** which is similar to the loss of H· from the molecular ions of **3** or to the formation of **5** from **3**.

At 1000°, 2-benzimidazolinone (**2**) gave a 14% yield of $C_6H_4N_2$ isomers, resulting from the loss of CO and H_2. The intermediate shown in eq. 8

[8] 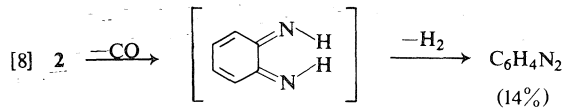

was invoked to explain these results (2). The major product isolated from the pyrolysis of **4** can be explained by the same type of intermediate. However, in this case an internal cyclization occurs before the H_2 is lost (eq. 9). The loss

[9] 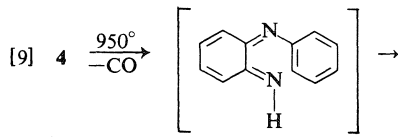

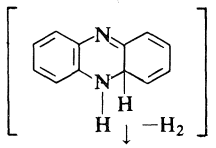

6 (35%)

of CHO· is one of the two major fragmentation pathways in the mass spectrum of **4**. Decarbonylation under pyrolytic conditions has frequently been observed. (1, 2).

The other product, carbazole (**7**), formed in 14% yield in the pyrolysis of **4** is the result of the loss of HNCO. Also, a major fragmentation in the mass spectrum of **4** is the loss of NCO·. To explain the formation of **7**, the initial cleavage of the carbonyl carbon – *N*-phenyl bond can be proposed (eq. 10). If the phenyl group partici-

[10] **4** $\xrightarrow{\Delta}$ 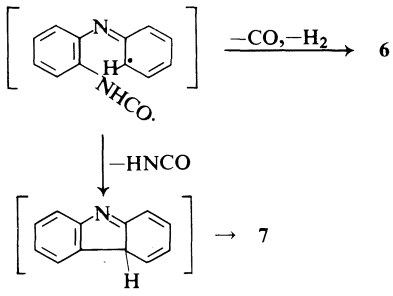 **6**

pates in the loss of HNCO, **7** can be formed. On the other hand, decarbonylation leads to the reactions shown in eq. 9.

The compounds **3** and **4** therefore join the list of compounds (1–3) whose pyrolytic and electron-impact fragmentations are similar. The lowest-energy paths in their mass spectra can be compared with the pyrolysis products. The reactions seem to be governed by the elimination of small, neutral species such as CO, S, H_2, and HNCO. The *N*-phenyl group intramolecularly traps reactive intermediates to give stable polycyclic products in relatively high yields, a path which is not available to compound **1** and **2**. In each pyrolysis, 65–70% of the starting material was accounted for.

These and other similarities among high-energy processes provide possibilities of finding useful synthetic applications and evidence for novel reaction intermediates, as well as the possibility of studying interesting decomposition pathways.

Experimental Section

Melting points were determined by the open capillary method using a MEL-TEMP apparatus and were corrected. Infrared spectra were recorded with a Beckman IR8 spectrometer and a Perkin-Elmer Infracord. Nuclear magnetic resonance spectra were taken on a Varian T-60 spectrometer using 1% TMS as an internal standard. Ultraviolet spectra (1 cm path) were determined on a Bausch and Lamb Spectronic 505. Low-resolution mass spectra were obtained from a Hitachi RMU-6D mass spectrometer. Electron voltage readings were taken directly from the dial since more precise values were not needed. Combined g.c.–m.s. data were determined with a LKB 9000 instrument.

Exact-mass data were obtained from an AEI MS-902 mass spectrometer linked to a PDP-8 computer. All experimental values agreed with the calculated values within ±0.0015 mass units. Metastable ions were observed in the low-resolution spectra and, in certain cases, sought with the AEI MS-902 spectrometer operating in the defocused mode.

The ion source of the RMU-6D was maintained at 250° and the MS-902, at 150°. Since pyrolysis of the compounds studied does not begin until approximately 600°, pyrolysis in the source cannot account for the fragmentations observed.

The gas-chromatographic (g.c.) work was carried out using a Hewlett-Packard 5752B Research Chromatograph with a thermal conductivity detector. Columns were prepared with 0.25 in. copper tubing and 60/80 mesh Chromosorb W as a solid support, unless otherwise stated. A total of 10 g.c. columns was used; during the initial stages of analysis of the pyrolysis mixtures, most of the columns were tried. However, only the column that gave the best separations is reported for each analysis. Comparison of the areas under the peaks of the pyrolysis products with the areas under the peaks of solutions of known concentrations of the same compound was used to determine yields. Analysis were performed by Midwest Microlab, Inc., Indianapolis, Indiana.

Chemicals

2-Aminodiphenylamine, benzotriazole, 2-phenylbenzimidazole (**9**), phenazine (**6**), 1-cyanoaniline, and benzonitrile were purchased from Aldrich; 1- and 2-cyanonaphthalene were purchased from Eastman Kodak; carbazole (**7**), diphenylamine, and naphthalene were purchased from Fisher.

1-Phenyl-2-benzimidazolinethione (3)

Compound **3** was prepared by modifying a procedure published by Allen and Deacon (11). A mixture of 18.8 g of 2-aminodiphenylamine, 18.4 g of potassium ethyl xanthate, 100 ml of ethanol, and 20 ml of H_2O was refluxed with stirring for 3 h. After the first 10 min of refluxing, 4 g of carbon was added cautiously to the ethanol solution. The hot reaction mixture was filtered by gravity to remove the carbon. Approximately 500 ml of warm H_2O and 10 ml of glacial acetic acid were added to the ethanolic solution. The off-white crystals were recrystallized from ethanol, yielding 12 g of 1-phenyl-2-benzimidazolinethione (**3**): m.p. 196–197° (lit. (12) 194°); yield 52%. The i.r. spectrum ($HCCl_3$) contains absorption bands at 3475, 2350, and 1217 cm^{-1}. The mass spectrum is summarized in Scheme 1 and discussed in the text.

Anal. Calcd. for $C_{13}H_{10}N_2S$: C, 69.03; H, 4.42. Found: C, 69.32; H, 4.47.

1-Phenyl-2-benzimidazolinone (4)

Compound **4** was prepared from 2-aminodiphenylamine by the procedure of Simonov and Pozhanskii (13). Toluene was used for recrystallization; yield: 5.0 g, (34%); m.p. 202–203° (lit. (13, 14) m.p. 202–203°); i.r.

Can. J. Chem. Downloaded from www.nrcresearchpress.com by 210.87.254.6 on 09/05/12
For personal use only.

TABLE 1. Pyrolyses of 1-phenyl-2-benzimidazolinethione (**3**)*

	% recovered at		
	650°	800°	950°
1-Phenyl-2-benzimidazolinethione (**3**)	46.5	37.0	23.1
(Starting amount of **3**, g)	(0.80 and 1.27)	(1.41 and 1.46)	(1.01, 1.14, and 1.82)
Benzimidazo[2,1-*b*]benzothiazole (**5**)	6.0	15.0	18.7
2-Phenylbenzimidazole (**9**)	—	<0.5	8.7
Cyanocarbazole	—	<0.5	2.0
1-Phenylbenzimidazole (**8**)	10.8	5.9	<0.5
Carbazole (**7**)	—	1.0	2.3
Phenazine (**6**)	—	Trace	<0.5
1-Cyanonaphthalene	—	Trace	1.2
2-Cyanonaphthalene	—	Trace	0.7
2-Cyanoaniline	—	<0.5	2.5
Naphthalene	—	Trace	1.0
Benzonitrile	—	<0.5	3.7
Total	63.3	60.9	64.9

*A N_2 flow rate of 0.20–0.25 l/min and system pressure of 0.7–2.0 Torr were used.

spectrum ($HCCl_3$) contains absorption bands at 3390, 3060, 1705, 1600, 1500, and 1380 cm^{-1}.

Anal. Calcd. for $C_{13}H_{10}N_2O$: C, 74.29; H, 4.76. Found: C, 74.12; H, 5.01.

1-(2-Benzothiazolyl)benzotriazole

1-(2-Benzothiazolyl)benzotriazole was prepared from benzotriazole by the method used by Orth and Soedigdo (15); yield 4.3 g (34%); m.p. 174° (lit. (15) m.p. 174°); λ_{max} (EtOH) 322, 275 sh, 268, 245, and 228.5 nm.

Anal. Calcd. for $C_{13}H_8N_4S$: C, 61.89; H, 3.19; N, 22.21; S, 12.71. Found: C, 61.68; H, 3.33; N, 22.36; S, 13.05.

Benzimidazo[2,1-b]benzothiazole (5)

Benzimidazo[2,1-b]benzothiazole (**5**) was prepared photolytically from 1-(2-benzothiazolyl)benzotriazole (1 g) according to the method of Hubert (16) using a 450 W high-pressure Hg lamp; yield, 0.17 g (18%); λ_{max} (EtOH) 300, 291, 283, 263 sh, 242, and 222 nm; mass spectrum, *m/e* 224 ($C_{13}H_8N_2S$, 100), 223 ($C_{13}H_7N_2S$, 16), 198 ($C_{12}H_8NS$, 8), 192 ($C_{13}H_8N_2$, 3), 180 ($C_{12}H_8N_2$, 3), 179 ($C_{12}H_7N_2$, 5), 166 ($C_{12}H_8N$, 3), 134 (C_7H_4NS, 3), 122 (C_6H_4NS, 6), 112 ($C_{13}H_8N_2S$ (doubly charged), 30), 96 (C_5H_4S, 10), and 90 (C_6H_4N, 8); molecular ion, *m/e* 224.0405. Calcd. for $C_{13}H_8N_2S$, *m/e* 224.0408.

Pyrolysis Apparatus and Procedure

The pyrolysis apparatus and procedure have been described previously (3, 6). The sample (approximately 1 g) in a stream of nitrogen passed through a quartz tube heated by an electric furnace 12 in. long. The flow rate was 0.25 l/min at 2.5 Torr. A series of traps was placed between the quartz tube and the pump. Approximately 1 h was required for the passage of each $\frac{1}{2}$ g of sample through the tube. A solution was made of the material in the traps in a volumetric flask; g.l.p.c. and t.l.c. were used to separate the compounds in this solution.

Photolysis Apparatus and Procedure

The apparatus (Hanovia) used for photolysis consisted of a quartz immersion well, a 450 W high-pressure mercury lamp, an appropriate power supply, various filters, and a 500 ml reaction-vessel jacket. The compounds were dissolved in appropriate solvents and placed in the reaction vessel. During photolysis the apparatus was cooled by running water through the immersion well. The reactions were followed by the u.v. spectrum of the reaction solutions. The photolysis was stopped when no more changes in the u.v. spectrum were observed. Then the solvent of a measured amount of reaction solution was evaporated off in vacuum and the residue was made into a solution in a volumetric flask for analysis.

Pyrolysis of 1-Phenyl-2-benzimidazolinethione (3)

The conditions and results for the pyrolyses of 1-phenyl-2-benzimidazolinethione (**3**) are summarized in Table 1. The percentages shown are averages of different trials at the same temperature; good agreement was obtained among the different runs.

In each case, three traps were employed: the first was air cooled and the next two were cooled with liquid nitrogen. The traps were washed with acetone and chloroform. The g.c. column used was 6 ft, 10% SE 54 on Chromosorb G 60/80. The cyanonaphthalenes were better separated on a 6 ft column of 3% OV 225 on Chromosorb W 80/100. The temperature was programmed between 100° (1 min) and 260° (hold) at 10°/min. The column used for g.c./m.s. was a 6 ft glass column of 3% OVI Chrom HP 80/100. The starting material did not elute from the g.c. columns well and was recovered by extracting all the other compounds using heptane from the residue of a known amount of the pyrolysis solution. The concentration of 1-phenylbenzimidazole (**8**) was estimated from u.v. data (17). The exact position of the cyano group on the cyanocarbazole ring was not determined; analysis by g.c. showed that it had a different retention time from 9-cyanocarbazole, which was synthesized for comparison (18). The concentration of cyanocarbazole was estimated using carbazole (**7**) as a standard. All other products were identified by comparison with authentic materials. 2-Cyanoaniline had a tendency to react on standing with acetone to form an anil, *o*-cyano-*N*-isopropylideneaniline.

Can. J. Chem. Downloaded from www.nrcresearchpress.com by 210.87.254.6 on 09/05/12
For personal use only.

Photolysis of 1-Phenyl-2-benzimidazolinethione (3)

1-Phenyl-2-benzimidazolinethione (0.2 g) in 400 ml of *t*-butyl alcohol was used for photolysis. A Vycor filter was used. The reaction was stopped after an irradiation time of 1 h. A quantity of 300 ml of reaction solution was evaporated to make up a 25 ml solution using chloroform. Analysis by g.c. was made using a 6 ft column, 10% SE 54. The only product was 1-phenylbenzimidazole (**8**). The yield was estimated to be 51.8% from its u.v. absorption.

Pyrolysis of 1-Phenyl-2-benzimidazolinone (4)

The temperature used in the pyrolyses of 1-phenyl-2-benzimidazolinone (**4**) was 950°. The N_2 flow rate was 0.20–0.25 l/min. The system pressure was 0.5–2.5 Torr. The columns used for g.c. analysis were the same as those used in the analysis of the pyrolyses of **3**. The average percentages of the products recovered from the two runs (0.94 and 1.26 g of starting material (**4**)) were: 1-phenyl-2-benzimidazolinone (**4**), 16.3%; phenazine (**6**), 29.6%; carbazole (**7**), 12.0%; diphenylamine, 0.7%; 1-cyanonaphthalene, 1.1%; 2-cyanonaphthalene, 0.9%; ethyl *N*-phenylcarbamate, 2.0%; naphthalene, 1.8% and benzonitrile, 2.4%. The total percentage recovered was 66.8%. Agreement between the two runs was good. Ethyl *N*-phenylcarbamate was synthesized for comparison by mixing phenylisocyanate (Matheson, Coleman and Bell) with excess absolute ethanol which then was left to evaporate at room temperature. The ethyl *N*-phenylcarbamate was recrystallized in hexane (m.p. 53°, (lit. (19) m.p. 53°)). All the other products were identified by comparison with authentic materials and their concentrations, including starting material (**4**), were estimated by g.c.

We thank the National Research Council of Canada for its financial support. We also thank Dr. O. A. Mamer, Royal Victoria Hospital, Montreal, for the use of the LKB 9000 GC/MS combination and Mr. A. S. Blair, University of Montreal, for his assistance in obtaining the high-resolution mass-spectral data.

1. H. J. Hageman and U. E. Wiersum. Chem. Brit. **9**, 206 (1973).
2. M. L. Thomson and D. C. DeJongh. Can. J. Chem. **51**, 3313 (1973).
3. D. C. DeJongh and M. L. Thomson. J. Org. Chem. **38**, 1356 (1973).
4. T. Kametani, S. Hirata, S. Shibuya, and M. Shio. Org. Mass Spectrom. **4**, 395 (1970).
5. V. V. Kalmykov, V. E. Blokhin, and K. V. Aglitskaya. Tr. Voronezh. Gos. Univ., **73**, 67 (1969); Chem. Abstr. **74**, 47608 (1971).
6. D. C. DeJongh, D. C. K. Lin, and M. L. Thomson. *In* Advances in mass spectrometry. Vol. 6. *Edited by* A. R. West. Applied Science Publishers, Barking, England. 1974. Chapt. 12.
7. (*a*) N. Ishibe, M. Odani, and K. Teramura. Chem. Commun. 371 (1970); (*b*) N. Ishibe, M. Sunami, and M. Odani. Tetrahedron, **29**, 2005 (1973).
8. K. T. Potts and R. Dugas. Chem. Commun. 732 (1970).
9. A. Ohno, Y. Ohnishi, and G. Tsuchihashi. J. Am. Chem. Soc. **91**, 5038 (1969).
10. G. Oster, L. Citarel, and M. Goodman. J. Am. Chem. Soc. **84**, 703 (1962).
11. J. A. Van Allen and B. D. Deacon. Organic syntheses. Vol. IV. Wiley, New York, N.Y. 1963. p. 569.
12. D. F. Duffin and J. D. Kendall. J. Chem. Soc. 361 (1956).
13. A. M. Simonov and A. F. Pozhanskii. J. Gen. Chem. USSR, **33**, 2289 (1963); Zh. Obshch. Khim. **33**, 2350 (1963).
14. L. Rosnati. Gajz. Chim. Ital. **86**, 257 (1956).
15. R. E. Orth and S. Soedigdo. J. Heterocycl. Chem. **2**, 486 (1965).
16. A. J. Hubert. J. Chem. Soc. (C), 1334 (1969).
17. J. P. Phillips, J. C. Dacons, and R. G. Rice (*Editors*). Organic electronic spectral Data. Vol. VII. Wiley Interscience, New York. 1964–1965, p. 447.
18. C. Wentrup. Tetrahedron, **27**, 367 (1971).
19. Handbook of Chemistry and Physics, 50th Ed. R. C. Weast (*Editor*). The Chemical Rubber Co. Cleveland, Ohio. 1969. p. C-232.

Can. J. Chem. Downloaded from www.nrcresearchpress.com by 210.87.254.6 on 09/05/12
For personal use only.

The Mechanism of the Transition Metal-catalyzed Reaction of 1,1′-Carbonyldipyrazoles with Aldehydes and Ketones

L. K. PETERSON, E. KIEHLMANN, A. R. SANGER, AND K. I. THÉ
Department of Chemistry, Simon Fraser University, Burnaby 2, British Columbia
Received October 30, 1973

L. K. PETERSON, E. KIEHLMANN, A. R. SANGER, and K. I. THÉ. Can. J. Chem. **52**, 2367 (1974).

The metal-catalyzed reaction of 1,1′-carbonyldipyrazoles with aldehydes or ketones to give 1,1′-alkylidenedipyrazoles and carbon dioxide, the latter being derived from the amide carbonyl group as shown by labeling experiments, is sensitive to electronic and to steric substituent effects. Under comparable reaction conditions, 1,1′-carbonyldiimidazole, *N*-acetylpyrazole, and 1-pyrazole-*N*,*N*-diethylcarbonamide do not react with acetone while pyrazole-1-carbo(*N*′-phenylhydrazide) yields an anilino isocyanate dimer. These results are interpreted in terms of a mechanism that involves coordination of the metal ion at the 2,2′-nitrogen atoms of the pyrazole rings and heterolytic cleavage of an amide bond, followed by formation of a carbamate intermediate, decarboxylation, and metal ion exchange. Unsymmetrically substituted 1,1′-carbonyldipyrazoles were found to equilibrate thermally with their respective symmetrical analogs by an intermolecular exchange mechanism.

L. K. PETERSON, E. KIEHLMANN, A. R. SANGER et K. I. THÉ. Can. J. Chem. **52**, 2367 (1974).

La réaction, catalysée par les métaux, des carbonyl-1,1′ dipyrazoles avec les aldéhydes et les cétones conduit aux alkylidène-1,1′ dipyrazoles avec élimination de CO_2; on a montré par des expériences de marquages que le CO_2 provient du groupe amide du carbonyle et que la réaction dans son ensemble est sensible à des effets stériques et électroniques des substituants. Dans des conditions comparables le carbonyl-1,1′ diimidazole, le *N*-acétylpyrazole et le *N*,*N*-diéthylcarbonamide pyrazole-1 ne réagissent pas avec l'acétone alors que le carbo(*N*′-phénylhydrazide)pyrazole-1 conduit à un dimère de l'isocyanate d'aniline. On interprète ces résultats en terme d'un mécanisme qui impliquerait la coordination de l'ion métallique par les atomes d'azote en position 2,2′ des noyaux pyrazoles et une coupure hétérolytique du lien amide suivi par la formation d'un carbamate intermédiaire, d'une décarboxylation et d'un échange d'ion métallique. On a trouvé que les carbonyl-1,1′ dipyrazoles substitués d'une façon non-symétrique s'équilibrent thermiquement avec leurs analogues symétriques respectifs par un mécanisme d'échange intermoléculaire. [Traduit par le journal]

Introduction

The metal-catalyzed reaction of 1,1′-carbonyldipyrazole (**1**), 1,1′-carbonylbis(3-methylpyrazole) (**2**), and 1,1′-carbonylbis(3,5-dimethylpyrazole) (**3**) with various aldehydes and ketones has been reported (1, 2) to give 1,1′-alkylidenedipyrazoles in high yield (eq. 1). This procedure represents a convenient one-step route to these products which are also accessible via the reaction of pyrazole or alkali metal pyrazolides with geminal dihaloalkanes, acetals, or ketals (3, 4). Mechanistically, the latter process (eq. 2) is a typical example of a nucleophilic displacement at saturated carbon, with pyrazole or the pyrazolide anion serving as nucleophile. The reagents shown in eq. 1, on the other hand, are not generally considered as good nucleophiles which, in conjunction with the necessity for a transition metal catalyst and aprotic reaction conditions, suggests a completely different mechanism for the replacement of the carbonyl group of the heterocyclic urea analogs **1**, **2**, and **3** by the hydrocar-

[1] 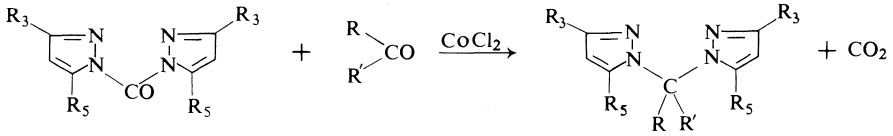

1 $R_3=R_5=H$
2 $R_3=CH_3$; $R_5=H$
3 $R_3=R_5=CH_3$

4

R and R′ = H, alkyl, or aryl

Can. J. Chem. Downloaded from www.nrcresearchpress.com by 210.87.254.5 on 09/05/12
For personal use only.

TABLE 1. Nuclear magnetic resonance chemical shifts of 1,1′-carbonyl- and 1,1′-alkylidenedipyrazoles (eq. 1)

Compound (R, R′, R_3, R_5)	H-3 or Me-3	H-4	H-5 or Me-5
1	2.10q	3.40q	1.27q
2	7.63s	3.68d	1.37d
3	7.75s	3.95m	7.52d
4*a* (Me, Me, Me, H)	7.72s	3.98	2.78d
4*b* (H, Me, Me, H)	7.78s	4.00	2.55d
4*c* (Me, Me, Me, Me)	7.77s	4.17	8.32d
4*d* (Cyclobutyl*, Me, Me)	7.78s	4.22	8.13d

*R—R′ = —$(CH_2)_3$—.

[2] $2py—M + CR_2X_2 \rightarrow py—CR_2—py + 2MX$

M = H, Na, or K
X = Cl, Br, I, or OCH_3 py =
R = H or alkyl

bon moiety of an aldehyde or ketone. We now report a detailed mechanistic study of this novel reaction.

Results and Discussion

Elucidation of the reaction mechanism (eq. 1) required (*a*) determination of the organic product structures and (*b*) identification of the carbon atom source of the carbon dioxide. The latter problem was solved by performing the catalytic reaction of **1** with acetone in the presence of acetone-2-^{14}C, separating the carbon dioxide from the alkylidenedipyrazole (**4**, R = R′ = CH_3), and measuring the extent of ^{14}C incorporation into each product. Since essentially all of the radiocarbon was found in the 2,2′-dipyrazolylpropane, the source of the CO_2 carbon is clearly the carbonyl group of **1**.

The structures of several alkylidenedipyrazoles, as identified by spectroscopic means, have been reported (1, 2). However, it remained to be shown whether it is the amide (N-1) or the amino nitrogen atoms (N-2) of the two methyl-substituted pyrazole rings of **2** which become bonded to the hydrocarbon moiety (**4**, >CRR′) of the product. The solution of this problem, however, proved difficult because of the well-known thermal isomerization of *N*-acylpyrazoles (5, 6). Since thermal stability is closely related to steric substituent effects (5), the isomer with the acylated nitrogen atom more remote from the larger substituent is generally preferred.

Interestingly, the reaction of sodium 3(5)-methylpyrazolide with phosgene gives only one isomer, 1,1′-carbonylbis(3-methylpyrazole) (**2**), this structural assignment being based on the presence of *broad* CH_3 singlet at τ 7.63 (2). By contrast, the CH_3-5 signal (τ 7.52) of 1,1′-carbonylbis(3,5-dimethylpyrazole) (**3**) is a sharp doublet which collapses to a singlet when the sample is irradiated at the H-4 resonance frequency. We have also observed that in 1,1′-carbonyldipyrazole the H-3 bands are broader than and upfield relative to the H-5 bands. The data summarized in Table 1 show the consistency of our assignments and are in agreement with chemical shifts reported in the literature (7) for similar pyrazole derivatives. The catalytic reaction of **2** with acetone also gave but one isomer (eq. 3), the broad singlet absorption observed for the pyrazole-bonded methyl group, again signifying that the original amide nitrogens of **2** are bonded to the alkylidene carbon of the product.
Thus, the N-2 atoms of the two reagent pyrazole rings can be ruled out as nucleophilic centers toward the aldehyde or ketone carbonyl group unless a rapid and difficult-to-detect thermal isomerization step intervenes.

A systematic investigation of structural variations in the aldehyde or ketone component has demonstrated that the reaction is sensitive to electronic and steric substituent effects.

In contrast to the less bulky aldehydes and ketones discussed earlier (1), methyl isopropyl ketone, methyl isobutyl ketone, and *p*-dimethylaminobenzaldehyde were found to react with **1** only on heating to 90–170° for prolonged time periods, while with diisopropyl ketone, chloral, hexachloroacetone, and hexafluoracetone no CO_2 evolution was observed even after 16 h at

Can. J. Chem. Downloaded from www.nrcresearchpress.com by 210.87.254.5 on 09/05/12
For personal use only.

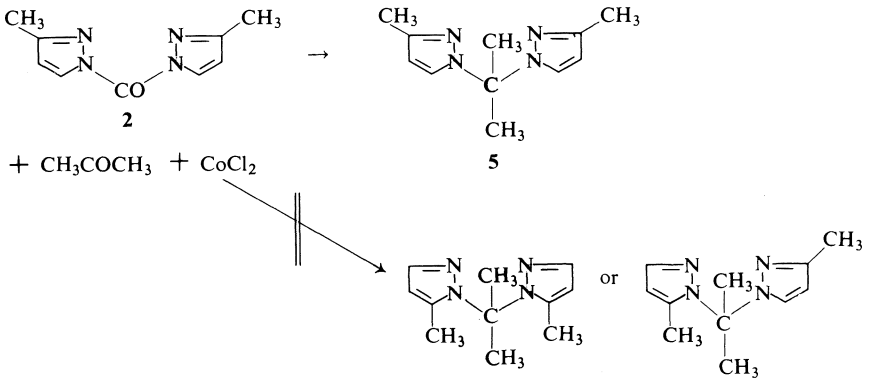

[3]

160°. Under similar conditions, methyl *tert*-butyl ketone, *p*-nitrobenzaldehyde, *p*-methoxyacetophenone, and *p*-nitroacetophenone, respectively, yielded 40–80% of the theoretically expected quantity of carbon dioxide, although none of the expected alkylidenedipyrazoles could be isolated or detected by spectroscopic means, presumably due to the formation of unidentified decomposition products. These results are in agreement with our previously reported findings that 3-methyl- and 4-methylcyclohexanone, but not 2-methylcyclohexanone or acetophenone, react with **1** and $CoCl_2$ at room temperature (1) and that the introduction of methyl groups into the pyrazole rings (**1**→**2**→**3**) drastically reduces the reactivities of the corresponding carbonyldipyrazoles. Competitive experiments with several pairs of structurally similar aldehydes and ketones competing for a limited amount of 1,1′-carbonyldipyrazole have confirmed these reactivity trends, *i.e.*, preferred or exclusive formation of the sterically least hindered alkylidenedipyrazole. Thus, using the pairs CH_3CHO–CH_3COCH_3, CH_3COCH_3–Et_2CO, C_6H_5CHO–CH_3COCH_3, C_6H_5CHO–*p*-$CH_3OC_6H_4CHO$, C_6H_5CHO–*p*-$Me_2NC_6H_4$-CHO, and *p*-ClC_6H_4CHO–*p*-$Me_2NC_6H_4CHO$, the product was derived exclusively from the first-listed carbonyl compound in each case whereas with CH_3COCH_3–CH_3COEt, CH_3-$COEt$–Et_2CO, and C_6H_5CHO–*p*-ClC_6H_4CHO, product mixtures containing the corresponding 1,1′-alkylidenedipyrazoles in the approximate ratios 2:1, 10:1, and 1:1, respectively, were obtained.

Studies using amides and diamides related to 1,1′-carbonyldipyrazole have provided further information about the mechanism. Thus, the compounds *N*-acetylpyrazole, pyrazole-1-*N*,*N*-diethylcarbonamide, and 1,1′-carbonyldiimidazole all fail to react with acetone in the presence of cobalt(II) chloride, the starting materials being recovered in each case; since these compounds and their derivatives are generally known to be *more* reactive than their corresponding pyrazole analogs in most hydrolytic, aminolytic, and dissociative cleavage reactions (8–10), we interpret their inertness toward acetone in terms of an unfavorable geometric arrangement of donor atoms for chelation with cobalt(II). This conclusion is further supported by (*a*) the exclusive formation of **5** from **2** (eq. 3); (*b*) the fact that in the absence of a transition metal catalyst **1** does not react with aldehydes or ketones (1); and (*c*) our finding that in compound **6**, the phenyl-substituted rather than the amide NH proton experiences a strong downfield shift on complexation with mercuric chloride (eq. 4) (11). These results strongly suggest that the more basic amino nitrogens (N-2) of the pyrazole rings of **1**, **2**, and **3** are the preferred coordination sites (12) in an intermediate catalytic complex.

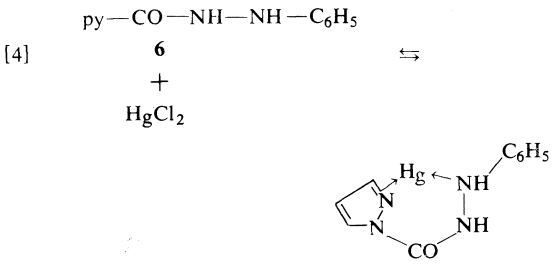

[4]

It is also noteworthy that the phenylhydrazide **6** did not react with acetone and $CoCl_2$ at temperatures below 50° but, on heating to 90°, gave pyrazole and an *N*-anilino isocyanate dimer (eq. 5) whose spectral characteristics are consistent

Can. J. Chem. Downloaded from www.nrcresearchpress.com by 210.87.254.5 on 09/05/12
For personal use only.

[5] $C_6H_5-NH-NH-CO-py \xrightarrow{\Delta} \left[O=C=\overset{\oplus}{N}H-NH-C_6H_5 + py^{\ominus}\right]$

proton transfer ↓

$C_6H_5-NH-N(CO-N-C_6H_5)(CO-NH)$ (7) ← dimerization — $[O=C=N-NH-C_6H_5] + pyH$

with the 1,2,4-triazole formulation **7** (13). This observation and the previously reported dissociation of other heterocyclic carboxamides into isocyanates and the respective azoles (10) are indicative of an analogous thermal ionization process (first step of eq. 5) occurring in the metal-catalyzed reaction of carbonyldipyrazoles with aldehydes or ketones (*vide infra*). Thus, on the basis of the experimental evidence cited above, we propose the following mechanism (Scheme 1) for the reaction shown in eq. 1.

Coordination of the transition metal ion at the N-2 nitrogen atoms of the two pyrazole rings of **1** leads to the formation of complex **9** (1) and renders the organic ligand more reactive toward ionization. Although this effect may be partially due to the electron-withdrawing action of the metal ion as a Lewis acid, other yet unknown factors must also be of significance since only Fe(II), Co(II), Ni(II), and Cu(I) but not Cr(III), Cu(II), Ag(I), Mn(II), Zn(II), Hg(II), and Fe(III) were found to be catalytically active. Subsequent cleavage of one amide bond gives a species that is not only stabilized by bonding to the metal but also by resonance delocalization of the positive charge developing on the carbonyl carbon to the adjacent amide nitrogen of the second pyrazole ring. Otting and Staab (10) report that the dissociation into azole and phenylisocyanate is greater for imidazole-1-carboxanilide in solution that for 3,5-dimethylpyrazole-1-carboxanilide; in our case we find the opposite reactivity trend: 1,1′-carbonyldiimidazole is inert toward acetone and $CoCl_2$, and we attribute this difference to the favorable geometry of the pyrazole structures for chelation at N-2 and N-2′. The third step is believed to involve addition of the ionic fragments, held together by chelation, to the aldehyde or ketone to give a carbamate intermediate which is structurally similar to the monoalkoxymonopyrazolylalkanes isolated by Trofimenko (3) from the reaction of pyrazole with certain ketals. Although all our attempts to isolate and characterize such an intermediate have failed,we consider structure **10** more likely and more stable than the alternative β-lactone of carbamic acid formed by 1,2-cycloaddition of the carbonyl compound across the C=N double bond of the isocyanate (14). Carbamic acid esters derived from imidazoles and pyrazoles (8, 15) readily eliminate dioxide, presumably via an incipient carbonium ion, since their decomposition rate has been reported (16) to parallel the relative stability order of the carbonium ions formed by

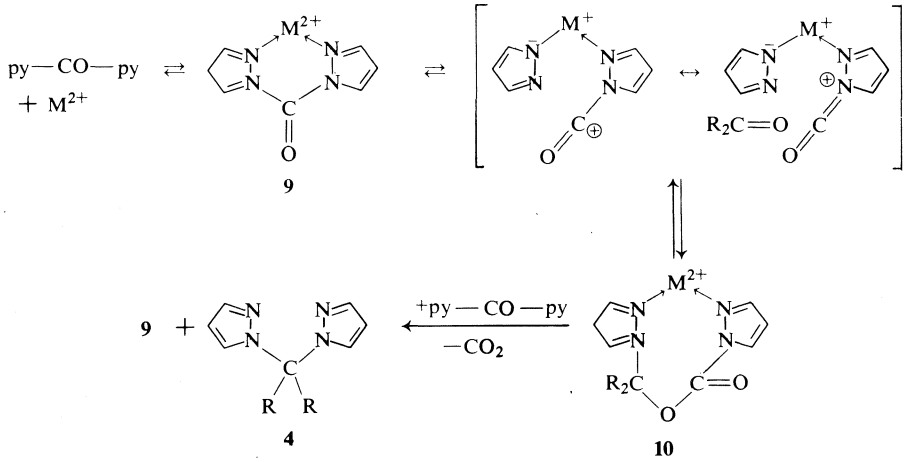

SCHEME 1

Can. J. Chem. Downloaded from www.nrcresearchpress.com by 210.87.254.5 on 09/05/12
For personal use only.

Can. J. Chem. Downloaded from www.nrcresearchpress.com by 210.87.254.5 on 09/05/12
For personal use only.

heterolytic cleavage of the C—O single bond; carbon-14 labelling experiments carried out with several compounds of this type (17) are in agreement with our finding that the CO_2 carbon derives exclusively from the amide carbonyl group. Finally, transfer of the metal ion to a second reagent molecule (**1**) gives the observed 1,1′-alkylidenedipyrazole (**4**).

To determine whether the decarboxylation–metal exchange step (Scheme 1) is intra- or intermolecular, we prepared several unsymmetrical 1,1′-carbonyldipyrazoles (eq. 6). In the absence of competing processes, the intra- and intermolecular pathways would give particular alkylidenedipyrazole products, characteristic of the mechanism, in the reactions with acetone and $Co(II)Cl_2$ of (*a*) unsymmetrical carbonyldipyrazoles and (*b*) mixtures of symmetrical carbonyldipyrazoles.

[6] R-py—CO—Cl + R′-py—H → R-py—CO—py-R′ + $Et_3N{\cdot}HCl$

11 R-py = 1-pyrazolyl; R′-py = 3-methyl-1-pyrazolyl

12 R-py = 1-pyrazolyl; R′-py = 3,5-dimethyl-1-pyrazolyl

13 R-py = 3-methyl-1-pyrazolyl; R′-py = 3,5-dimethyl-1-pyrazolyl

Although **12** and **13** appear to be stable compounds in the solid state under anhydrous conditions, n.m.r. spectroscopic analyses showed that they equilibrated with their symmetrical analogs when dissolved or when heated above the melting point (eq. 7). Pyrazolyl-1-carbonyl chloride gave

[7] 2 R-py—CO—py-R′ ⇄ $(R\text{-py})_2CO + (R'\text{-py})_2CO$

1 and phosgene by a similar process. Partial ionization is probably again involved in this intermolecular exchange of the heterocyclic moieties, possibly via a six-membered ring (**14**) as transition state, since the similar imidazolyl-1-carboxanilide dissociates into phenyl isocyanate and imidazole only in solution but not in the solid state (10).

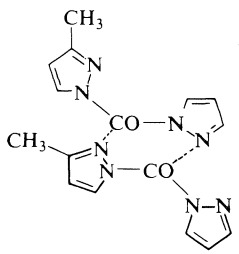

14

Clearly, the equilibration process precludes product analysis as a means of distinguishing between the intra- and intermolecular routes. Preliminary kinetic measurements, however, have shown that the cobalt(II)-catalyzed reaction of **2** with excess acetone is second order in the carbonyldipyrazole component, obeying the integrated rate eq. 8 where *b* is the concentration of **2** at time zero, *t* the time, and *P* the carbon dioxide pressure (at times *t* and infinity, respectively) at constant volume.

[8] $bk = P_t/t(P_{inf} - P_t) = 3.03 \pm 0.23\ s^{-1}$

This result suggests that the last step of the mechanism (Scheme 1) is slow and bimolecular, *i.e.*, a second carbonyldipyrazole molecule is involved either in the rate-determining decarboxylation of the carbamate intermediate followed by rapid metal ion exchange, or in the rate-determining metal ion exchange preceded by a rapid unimolecular decarboxylation step.

To clarify further the catalytic role of the transition metal salt, we are planning more detailed studies of the kinetics of the above reactions, as well as X-ray crystallographic studies of the structures of selected carbonyl- and alkylidenedipyrazoles and their metal complexes.

Experimental

Compounds were manipulated under anhydrous conditions, using a nitrogen-filled dry box or a high vacuum system. Solvents were rigorously dried and distilled before use (18). Elemental analyses were performed by the departmental analyst. Melting points are uncorrected. Infrared spectra were determined with a Perkin Elmer 457 spectrophotometer, mass spectra with a double focusing RMU-6E Hitachi Perkin Elmer instrument, and n.m.r. spectra with a Varian A56/60 or Varian XL100 spectrometer, using $CDCl_3$ as solvent and with TMS as internal standard, unless otherwise specified.

Preparation of Carbonyldipyrazoles

To obviate the intermediate synthesis of a sodium pyrazolide salt (1), a number of preparative routes were explored, using an excess of the pyrazole or triethylamine, as hydrogen chloride acceptor, and phosgene, in the solvents THF, benzene, and toluene. The following procedure was found to be most satisfactory: a mixture of $COCl_2$ (3.55 mmol), 3-methylpyrazole (7.07 mmol), and Et_3N (7.07 mmol) was allowed to react in THF (~150 ml) for 30 min. The precipitate was filtered, the solvent was removed under vacuum, and the product (**2**) was purified by sublimation. The above method also gave good yields (80–90%) of **1** and **3** when pyrazole or 3,5-dimethylpyrazole were used in place of 3-methylpyrazole. In the latter case, the residue, after removal of THF, was contaminated with 3,5-dimethylpyrazole hydrochloride;

TABLE 2. Reactions of **1** with carbonyl compounds

Carbonyl compound(s)	Temperature (°)	Time (h)	CO_2 yield (%)	Product structure (R, R′)*
$CH_3COCH(CH_3)_2$†	130	16	95	**4***e* (Me, *i*-Pr)
$CH_3COCH_2CH(CH_3)_2$†	90	16	68	**4***f* (Me, *i*-Bu)
p-$CH_3OC_6H_4CHO$	25	0.1	100	**4***g* (H, *p*-$CH_3OC_6H_4$)
p-ClC_6H_4CHO	170	16	89	**4***h* (H, *p*-ClC_6H_4)
p-$(CH_3)_2NC_6H_4CHO$	170	16	99	**4***i* (H, *p*-$(CH_3)_2NC_6H_4$)
CH_3CHO and CH_3COCH_3	80		100	**4***j* (H, Me)
CH_3COCH_3 and $CH_3COCH_2CH_3$	25		92	**4***k* (Me, Me) (70%) and **4***l* (Me, Et) (30%)
CH_3COCH_3 and $(CH_3CH_2)_2CO$	160	16	100	**4***k* (Me, Me)
$CH_3COCH_2CH_3$ and $(CH_3CH_2)_2CO$	160	16	93	**4***l* (Me, Et) (90%) and **4***m* (Et, Et) (10%)
CH_3COCH_3 and C_6H_5CHO	100	16	100	**4***n* (H, C_6H_5)‡
C_6H_5CHO and *p*-$CH_3OC_6H_4CHO$	90	16	90	**4***n* (H, C_6H_5)‡
C_6H_5CHO and *p*-$(CH_3)_2NC_6H_4CHO$	150	16	90	**4***n* (H, C_6H_5)‡
C_6H_5CHO and *p*-ClC_6H_4CHO	150	16	100	**4***n* (H, C_6H_5) (56%) and **4***h* (H, *p*-ClC_6H_4) (44%)‡,§
p-ClC_6H_4CHO and *p*-$(CH_3)_2C_6H_4CHO$	160	16	100	**4***h* (H, *p*-ClC_6H_4)

*See eq. 1 ($R_3 = R_5 = H$).
†Catalyst $Fe_3(CO)_{12}$, reagent ketone used as solvent.
‡Sublimed after trituration in hexane.
§Vapor phase chromatography analysis (5% SE-30, 150°) of the crude mixture gave **4***n*:**4***h* = 52:48.

the product was readily separated from this impurity by extraction with benzene and purified by sublimation.

*Reaction of 1,1′-Carbonyldipyrazole (**1**) with Acetone-2-^{14}C*

Freshly dried tetrahydrofuran (approximately 5 ml) and 250 μCi of acetone-2-^{14}C (5 μCi/mmol, New England Nuclear Corporation) diluted with unlabelled acetone (2.34 mmol) were condensed into a reaction tube containing 1,1′-carbonyldipyrazole (1.17 mmol) and dry $COCl_2$ (4 mg). The vessel was sealed and agitated for about 1 h at −70° and then 26 h at room temperature. Upon fractionation, the mixture gave CO_2 (1.18 mmol) and a solid residue of 2,2′-dipyrazolylpropane which was purified by sublimation. The carbon dioxide was trapped in a solution (1:2 v/v) of ethanolamine in methyl cellosolve (19). The scintillation media used were (*a*) a toluene–methyl cellosolve solution (2:1 v/v) containing 5.5 g/l of 2,5-diphenyloxazole (DPO) for CO_2 and (*b*) a toluene solution containing DPO (4 g/l) and *p*-bis[2-(5-phenyloxazolyl)]benzene (50 mg/l). The solutions were counted on a Beckman LS-200B Liquid Scintillation System to give 20 counts min^{-1} $mmol^{-1}$ for CO_2 and 1.63×10^8 counts min^{-1} $mmol^{-1}$ for the 2,2′-dipyrazolylpropane.

*Reactions of **1** with Carbonyl Compounds*

The procedure used has been described before (1, 2) and the experimental parameters specific to the new reactions reported in this paper are listed in Table 2. Unless marked otherwise, $CoCl_2$ was used as catalyst and dry THF as solvent. In the competitive experiments, equimolar amounts of the two carbonyl compounds (1–5 mmol) and 1,1′-carbonyldipyrazole were employed in the molar ratio $1:1:x$ where $x = 0.5$–1.0. In those cases where both possible alkylidenedipyrazoles were formed, the composition of the sublimed product mixture was determined by n.m.r. analysis.

Characterization of New 1,1′-Alkylidenedipyrazoles (Table 2)

4*e*: m.p. 35–36°; mass spectrum, P_{obs} 204, P_{calcd} 204.

Anal. Calcd. for $C_{11}H_{16}N_4$: C, 64.68; H, 7.89; N, 27.43. Found: C, 64.65; H, 7.99; N, 27.68.

The n.m.r. spectrum, τ 9.15 (d, 6H, $(CH_3)_2C$, $J = 6.8$ Hz), 7.70 (s, 3H, CH_3Cpy_2), 6.50 (sept., 1H, $CHMe_2$, $J = 6.8$ Hz), 3.75 (q, 2H, 4-H; $J_{34} = 1.8$ Hz; $J_{45} = 2.5$ Hz), 2.45 (q, 2H, 5-H; $J_{35} = 0.7$ Hz; $J_{45} = 2.5$ Hz), 2.25 (q, 2H, 3-H; $J_{34} = 1.8$ Hz; $J_{35} = 0.7$ Hz).

4*f*: mass spectrum, P_{obs} 218, P_{calcd} 218.

Anal. Calcd. for $C_{12}H_{18}N_4$: C, 66.02; H, 8.31; N, 25.66. Found: C, 65.78; H, 8.43; N, 26.01.

The n.m.r. spectrum, τ 9.18 (d, 6H, $(CH_3)_2C$; $J = 6.4$ Hz), 8.37 (m, 1H, $CHMe_2$), 7.71 (s, 3H, CH_3Cpy_2), 7.33 (d, 2H, CH_2; $J = 5.9$ Hz), 3.77 (q, 2H, 4-H; $J_{34} = 1.8$ Hz; $J_{45} = 2.6$ Hz), 2.62 (q, 2H, 5-H; $J_{35} = 0.7$ Hz; $J_{45} = 2.6$ Hz), 2.48 (q, 2H, 3-H; $J_{34} = 1.8$ Hz; $J_{35} = 0.7$ Hz).

4*g*: m.p. 52–53°; mass spectrum, P_{obs} 254, P_{calcd} 254.

Anal. Calcd. for $C_{14}H_{14}N_4O$: C, 66.13; H, 5.55; N, 22.03. Found: C, 66.33; H, 5.63; N, 22.23.

The n.m.r. spectrum, τ 6.20 (s, 3H, CH_3O), 3.70 (q, 2H, 4-H; $J_{34} = 1.9$ Hz; $J_{45} = 2.5$ Hz), 3.10 (m, 4H, C_6H_4), 2.50 (q, 2H, 5-H; $J_{35} = 0.7$ Hz; $J_{45} = 2.5$ Hz), 2.40 (q, 2H, 3-H; $J_{34} = 1.9$ Hz; $J_{35} = 0.7$ Hz), 2.30 (s, 1H, $CHpy_2$).

Can. J. Chem. Downloaded from www.nrcresearchpress.com by 210.87.254.5 on 09/05/12
For personal use only.

Can. J. Chem. Downloaded from www.nrcresearchpress.com by 210.87.254.5 on 09/05/12
For personal use only.

4*h*: m.p. 81.5–82.5°; mass spectrum, P_{obs} 258 and 260, P_{calcd} 258 and 260.

Anal. Calcd. for $C_{13}H_{11}ClN_4$: C, 60.35; H, 4.29; N, 21.66. Found: C, 60.49; H, 4.30; H, 21.80.

The n.m.r. spectrum, τ 3.67 (q, 2H, 4-H; J_{34} = 1.8 Hz; J_{45} = 2.4 Hz), 2.88 (m, 4H, C_6H_4), 2.47 (q, 2H, 5-H; J_{35} = 0.6 Hz; J_{45} = 2.4 Hz), 2.38 (q, 2H, 3-H; J_{34} = 1.8 Hz; J_{35} = 0.6 Hz), 2.30 (s, 1H, C*H*py_2).

4*i*: m.p. 84.5–85.5°; mass spectrum, P_{obs} 267, P_{calcd} 267.

Anal. Calcd. for $C_{15}H_{17}N_5$: C, 67.39; H, 6.41; N, 26.20. Found: C, 67.35; H, 6.36; N, 26.57.

The n.m.r. spectrum, τ 7.13 (s, 6H, $(CH_3)_2N$), 3.78 (q, 2H, 4-H; J_{34} = 1.8 Hz; J_{45} = 2.4 Hz), 3.24 (m, 4H, C_6H_4), 2.57 (q, 2H, 5-H; J_{35} = 0.7 Hz; J_{45} = 2.4 Hz), 2.45 (q, 2H, 3-H; J_{34} = 1.8 Hz; J_{35} = 0.7 Hz), 2.36 (s, 1H, C*H*py_2).

*Preparation of Pyrazole-1-carbonyl Chloride (**15**)*

A mixture of pyrazole (6.7 mmol), Et_3N (6.6 mmol), and phosgene (6.8 mmol) in THF (~50 ml) was stirred at room temperature for 30 min; the solution was filtered and the filtrate was fractionated under vacuum, the product being held mainly at −63°. The product, **15**, slowly decomposed into **1** and $COCl_2$ during handling and was extremely lachrymatory in the open air; a sample heated at 80° was converted quantitatively into **1** and $COCl_2$. A freshly prepared sample gave spectral data consistent with the given formulation, which was corroborated by subsequent conversions of **13** into identifiable products, yield 50–60%; m.p. 52–54 °C.

Anal. Calcd. for $C_4H_3ClN_2O$: C, 36.82; H, 2.30; N, 21.50. Found: C, 35.60; H, 2.15; N, 20.98.

The i.r. spectrum, ν(C—H), 3120, 3065 cm^{-1}; ν(C=O), 1830, 1770, 1720 cm^{-1}; ν(C=N), 1540 cm^{-1}.

The n.m.r. spectrum, τ 2.12 (q, 1H, 4-H; J_{45} = 3.3 Hz; J_{34} = 1.3 Hz), 0.59 (s, broad, 1H, 3-H), and 0.15 (d, 1H, 5-H; J_{45} = 3.3 Hz).

*Reactions of **15** with Amino Compounds*

Because of its instability, samples of pyrazole-1-carbonyl chloride were freshly prepared *in situ* in THF, according to the method described above, and allowed to react, without further purification, with appropriate quantities of protic reagents and triethylamine. The reaction with Et_2NH is described in detail and is typical of the procedure followed with phenylhydrazine, *N,N*-dimethylhydrazine, imidazole, 3-methylpyrazole, and 3,5-dimethylpyrazole.

*Preparation of Pyrazole-1-N,N-diethylcarbonamide (**16**)*

A solution of **15** (1.1 mmol) in THF (50 ml) was treated with a mixture of Et_2NH (1.1 mmol) and Et_3N (1.1 mmol) in THF (50 ml). After 1 h, the solution was filtered and solvent was removed under vacuum; the solid residue, **16**, was purified by sublimation (yield, 40%). In the i.r. spectrum, ν(C=O) was observed at 1690 cm^{-1}, while the parent ion (P_{obs} 167, P_{calcd} 167) was observed in the mass spectrum; n.m.r. spectrum, τ 8.51 (t, 6H, CH_2CH_3; J = 7.3 Hz), 5.90 (q, 4H, CH_2; J = 7.3 Hz), 2.50 (q, 1H, 4-H; J_{45} = 3.0 Hz; J_{34} = 1.7 Hz), 0.50 (d, 1H, 3-H; J_{34} = 1.7 Hz), 0.02 (d, 1H, 5-H; J_{45} = 3.0 Hz). The crude product showed mass spectral impurity bands attributable to **1** and $(Et_2N)_2CO$.

*Pyrazole-1-carbo-(N′-phenylhydrazide) (**6**)*

Procedure as above; yield 50%; m.p. 145 °C (dec.); mass spectrum, P_{obs} 202, P_{calcd} 202; n.m.r. spectrum, τ 2.70 (s, broad, 1H, C_6H_5NH), 2.32 (q, 1H, 4-H; J_{34} = 1.7; J_{45} = 2.8 Hz), 0.81 (s, broad, 1H, 3-H), 0.19 (d, 1H, 5-H; J_{45} = 2.8 Hz), −0.75 (s, broad, 1H, CONH), and a complex pattern in the region 1.2–1.9 due to phenyl proton resonances.

At temperatures above 90 °C, **6** was observed to decompose, with elimination of pyrazole, yielding a product with analytical and spectral data consistent for $(C_6H_5NHNCO)_2$ (**7**); mass spectrum, P_{obs} 268, P_{calcd} 268.

Anal. Calcd. for $C_{14}H_{12}N_4O_2$: C, 62.68; H, 4.51; N, 20.88. Found: C, 63.29; H, 4.58; N, 21.10.

Pyrazole-1-carbo-N,N-dimethylhydrazide

Procedure as above, but purification by crystallization from a petroleum ether – acetone mixture, giving pale green crystals, yield 50–60%; m.p. 50–57 °C; mass spectrum, P_{obs} 154, P_{calcd} 154; n.m.r. spectrum, τ 4.55 (s, 6H, NMe_2), 2.35 (q, 1H, 4-H; J_{34} = 1.0 Hz; J_{45} = 2.6 Hz), 1.64 (d, 1H, 3-H; J_{34} = 1.0 Hz), 1.42 (s, broad, 1H, N—H), 1.23 (d, 1H, 5-H; J_{45} = 2.6 Hz). In the presence of D_2O, the signal at 1.42 disappeared, due to exchange. The i.r. spectrum, ν(N—H), 3315 cm^{-1}; ν(C=O), 1745 cm^{-1}; ν(C—H), 2800 cm^{-1}.

*Pyrazole-1-carbo-1′-imidazolide (**17**)*

The reaction of **15** with imidazole was found to give a difficult-to-separate mixture of **17**, **1**, and carbonyldiimidazole; both imidazole and pyrazole were found to react with **17** producing carbonyldiimidazole and **1**, respectively. The approximate yield of product was 70–80%; m.p. 53–56 °C; mass spectrum, P_{obs} 162, P_{calcd} 162. The i.r. spectrum, ν(C—H), 3100–3170 cm^{-1}; ν(C=O), 1740 cm^{-1}; ν(C=N), 1532 cm^{-1}; n.m.r. spectrum, τ 3.45 (q, 1H, 4-H; J_{45} = 2.8 Hz; J_{34} = 1.5 Hz), 3.14 (d, 1H, 4′-H; $J_{4'5'}$ = 1.4 Hz), 2.69 (d, 1H, 3-H; J_{34} = 1.4 Hz), 2.60 (d, 1H, 5′-H; $J_{4'5'}$ = 1.4 Hz), 2.35 (d, 1H, 5-H; J_{45} = 2.8 Hz), 2.08 (s, 1H, 2′-H). The solution of **17** in $CDCl_3$ was unstable; after 1 day at room temperature, absorptions attributable to **1** were observed.

*3-Methylpyrazole-1-carbo-1′-pyrazolide (**11**)*

The reaction of **15** with 3-methylpyrazole gave a pale yellow liquid, with i.r. and n.m.r. spectra consistent for a mixture of **1**, **11**, and **2**; the same spectra were obtained for the product of a group-exchange reaction between **1** and **2** in THF (reverse of eq. 7, R=H; R′=Me).

Because of rapid disproportionation in solution or when melted, to produce the symmetric end-members, compound **11** could not be isolated in the pure state. However, by subtracting bands due to **1** and **2** from the composite spectrum, the n.m.r. spectrum for **11** is τ 7.64 (s, 3H, 3′-Me), 3.68 (d, 1H, 4′-H; J_{45} = 2.9 Hz), 3.47 (q, 1H, 4-H; J_{34} = 1.5 Hz; J_{45} = 2.9 Hz), 2.13 (q, 1H, 3-H; J_{34} = 1.5 Hz; J_{35} = 0.6 Hz), 1.38 (d, 1H, 5′-H; J_{45} = 2.9 Hz), 1.31 (q, 1H, 5-H; J_{45} = 2.9 Hz; J_{35} = 0.6 Hz). The same equilibration was detected when a mixture of **1** and **2**, dissolved in dry benzene, was injected into a gas chromatography column (5 ft × 1/8 in. 5% SE-30 on 70/80 Varaport 30) at 120°. While the pure components gave rise to peaks at 4.2 and 11.0 min, respectively, three peaks with retention times of 4.2, 6.9, and 11.0 min were observed for the binary mixture, suggesting the formation of 3-methylpyrazole-1-carbo-1′-pyrazolide (**11**) on the column.

3,5-Dimethylpyrazole-1-carbo-1′-pyrazolide (12)

As in the previous case, the reaction of **15** with 3.5-dimethylpyrazole gave a mixture of **12**, **1**, and **3**, usually obtained as a viscous liquid; if the solvent is quickly removed from the reaction medium, however, comparatively pure crystals of **12** are obtained. In a separate n.m.r. experiment, the equilibration of **1** and **3**, in solution in $CDCl_3$, to yield **12** was observed over a period of 2 days. The following absorptions were assigned to **12**: τ 7.71 (s, overlapping bands, 3′-Me), 7.51 (2, overlapping bands, 3-Me), 7.50 (d, 3H, 5′-Me), 4.17 (m, 1H, 4′-H), 3.72 (d, 1H, 4-H), 1.41 (d, 1H, 5-H).

3,5-Dimethylpyrazole-1-carbo-1′-(3′-methylpyrazolide) (13)

An equimolar mixture (9.5 mmol) of phosgene, Et_3N, and 3,5-dimethylpyrazole in THF (60 ml) was allowed to react at room temperature for 30 min, then treated with a solution of methylpyrazole (9.5 mmol) and Et_3N (9.5 mmol) in THF (20 ml). After stirring for 60 min, the mixture was filtered and solvent was removed under vacuum from the filtrate, leaving white crystals and a colorless liquid, which were separated by distillation under vacuum. The n.m.r. spectrum of a solution of the product in $CDCl_3$ was consistent for a mixture of **2**, **3**, and **13**. In a separate n.m.r. experiment, a mixture of **2** and **3** in $CDCl_3$ was observed to equilibrate over a period of several days, with formation of **13**. Allowing for overlap and coincidence of some absorptions in the mixture, the following spectrum was assigned to **13**: τ 7.74 (s, 3-Me), 7.63 (s, 3′-Me), 7.43 (d, 5′-Me), 3.93 (m, 4′-H), 3.70 (4-H), 1.47 (d, 5-H).

Reactions of 6, 16, 17, and 1,1′-Carbonyldiimidazole with Acetone

In a typical experiment, **16** (2.33 mmol), anhydrous cobalt chloride (~0.01 g), and dry acetone (~15 ml) were sealed together in a reaction tube. After 5 days at room temperature, the deep blue solution was fractionated, revealing the absence of CO_2; the components were sealed together once more and heated at 110° for 7 days. Again, no CO_2 was detected upon separating the products.

In a similar fashion, the possibility of a cobalt(II)-catalyzed reaction between acetone and (*a*) **6**, (*b*) **17**, and (*c*) carbonyldiimidazole was investigated.

In case *a*, no CO_2 was produced, even at 100 °C; at the higher temperatures, however, the formation of pyrazole and $(C_6H_5NHNCO)_2$ was noted. In case *b*, the slow evolution of CO_2, at room temperature, was observed, and **4** (R=R′=Me) was identified spectroscopically as one component of the liquid residue.

Kinetics of the $CoCl_2$-catalyzed Reaction of 2 with Acetone

Excess acetone (approximately 10 ml) was condensed into a vessel containing 0.400 g (2.11 mmol) of 1,1′-carbonylbis(3-methylpyrazole) (**2**) and 10 mg of dry $CoCl_2$ and the reaction flask was immediately connected to a mercury-filled manometer tube. At a temperature of 16 ± 0.5° and constant volume, the carbon dioxide pressure was measured at 13 time intervals over a period of 135 min (approximately three half-lives) and an "infinity" reading was obtained after 30 h. Graphical determination of the reaction rate at various times *t* followed by a plot of log rate *vs.* log [**2**] gave a kinetic order of approximately two, and all pressure readings taken after the initial 6 min were found to fit the integrated second-order rate law shown in eq. 8. During the first 6 min of the reaction, some reagent (**2**) remained undissolved thus causing major rate deviations.

We wish to express our sincere thanks to Mrs. M. Belluce, Mr. F. Slawson, and Mr. R. Wojtyk for their technical assistance and to the National Research Council of Canada for the financial support of these investigations.

1. K. I. Thé and L. K. Peterson. Can. J. Chem. **51**, 422 (1973).
2. K. I. Thé, L. K. Peterson, and E. Kiehlmann. Can. J. Chem. **51**, 2448 (1973).
3. S. Trofimenko, J. Am. Chem. Soc. **92**, 5118 (1970).
4. H. Reimlinger, A. Noels, J. Jadot, and A. v. Overstraeten. Chem. Ber. **103**, 1954 (1970).
5. R. Fusco. Pyrazoles, *In* The chemistry of heterocyclic compounds, pyrazoles, pyrazolidines, indazoles and condensed rings. *Edited by* A. Weissberger. Interscience, New York. 1967. p. 137.
6. A. N. Kost and I. I. Grandberg. Adv. Heterocycl. Chem. **6**, 419 (1966).
7. (*a*) J. K. Williams. J. Org. Chem. **29**, 1377 (1964); (*b*) C. L. Habraken and J. A. Moore. J. Org. Chem. **30**, 1892 (1965); (*c*) J. A. Moore and C. L. Habraken. J. Am. Chem. Soc. **86**, 1456 (1964); (*d*) L. G. Tensmeyer and C. Ainsworth. J. Org. Chem. **31**, 1878 (1966).
8. H. A. Staab. Angew. Chem. **74**, 407 (1962).
9. H. A. Staab. Justus Liebigs Ann. Chem. **622**, 31 (1959).
10. W. Otting and H. A. Staab. Justus Liebigs Ann. Chem. **622**, 23 (1959).
11. Unpublished results.
12. S. Trofimenko. J. Am. Chem. Soc. **88**, 1842 (1966).
13. W. S. Wadsworth and W. D. Emmons. J. Org. Chem. **32**, 1279 (1967).
14. H. Ulrich. Cycloaddition reactions of heterocumulenes. Academic Press, New York. 1967. p. 160.
15. (*a*) H. A. Staab and A. Mannschreck. Chem. Ber. **95**, 1284 (1962); (*b*) K. von Auwers and H. Stuhlmann. Chem. Ber. **59**, 1043 (1926); (*c*) K. von Auwers and E. Cauer. Chem. Ber. **61**, 2402 (1928).
16. K. B. Wiberg and T. M. Shryne. J. Am. Chem. Soc. **77**, 2774 (1955).
17. (*a*) H. A. Staab and G. Maleck. Chem. Ber. **99**, 2955 (1966); (*b*) L. Otvos, J. Marton, and J. Meisel-Agoston. Tetrahedron Lett. 15, (1960).
18. A. Weissberger. Technique of organic chemistry. Vol. VIII. Organic Solvents. Interscience Publishers, Inc., N.Y. 1955.
19. H. Jeffay and J. Alvarez. Anal. Chem. **33**, 612 (1961).

Can. J. Chem. Downloaded from www.nrcresearchpress.com by 210.87.254.5 on 09/05/12
For personal use only.

^{121}Sb Mössbauer Spectroscopy: Stereochemical Activity of the 5s Electrons in some Sb(III) Halide Complexes

JACK G. BALLARD AND THOMAS BIRCHALL

Department of Chemistry, McMaster University, Hamilton, Ontario L8S 4M1

AND (in part)

JOHN B. MILNE AND W. DUNCAN MOFFETT

Department of Chemistry, University of Ottawa, Ottawa, Canada K1N 6N5

Received November 29, 1973

JACK G. BALLARD, THOMAS BIRCHALL, JOHN B. MILNE, and W. DUNCAN MOFFETT. Can. J. Chem. **52**, 2375 (1974).

The ^{121}Sb Mössbauer spectra of a number of SbX_4^- and $Sb_2X_9^{3-}$ salts have been recorded. Only SbF_4^-, $SbCl_4^-$, and $Sb_2F_9^{3-}$ show significantly large quadrupole splittings with the 5s electrons being stereochemically active.

JACK G. BALLARD, THOMAS BIRCHALL, JOHN B. MILNE et W. DUNCAN MOFFETT. Can. J. Chem. **52**, 2375 (1974).

On a enregistré les spectres Mössbauer du ^{121}Sb pour un certain nombre de sels du SbX_4^- et du $Sb_2X_9^{3-}$. Il n'y a que les sels SbF_4^-, $SbCl_4^-$ et $Sb_2F_9^{3-}$ qui montrent de larges couplages quadrupolaires impliquant des électrons 5s comme éléments stéréochimiquement actifs.

[Traduit par le journal]

Introduction

According to the VSEPR theory of Gillespie (1), the geometry about the central antimony atom in complexes of Sb(III) would be strongly influenced by the 5s electrons. For the most part, structural predictions based upon this simple theory are borne out in practice. However, a few exceptions are known, in which the lone pair is not stereochemically active. In $TeBr_6^{2-}$, $TeCl_6^{2-}$ (2), and $(NH_4)_2Sb_2Br_{12}$ (3) the 5s electron pair appears to have no distorting effect upon the six surrounding ligands. In all of these examples, the XMX angles are 90° but there is a significant lengthening of the M—X bond. Mössbauer studies on these compounds (4–7) have shown that this nonactivity of the 5s electrons produces a marked effect on the chemical isomer shift of the Te and Sb nuclei. Participation of the 5s electrons in the bonding scheme would lead to a distorted environment and produce a quadrupole split spectrum. Such distortions have been claimed for the $Co(NH_3)_6SbX_6$ and $Cs_3Sb_2X_9$ systems (7) though the original report (6) concluded that the Sb(III) environments in $Co(NH_3)_6SbCl_6$ and $Rb_4Sb_2Cl_{12}$ were undistorted. This was subsequently confirmed by Schroeder and Jacobson (8) to be the case for $Co(NH_3)_6SbCl_6$. They found Cl—Sb—Cl angles of 90° and all Sb—Cl distances equal at 2.643 Å, considerably longer than Donaldson's estimate of 2.52 Å (7). Furthermore, the NaCl-like structure of this salt indicates that there will be no contribution to the quadrupole splitting parameter from a lattice contribution.

In view of this, it seemed essential that the Mössbauer data for $M_3Sb_2X_9$ (7) and $MSbX_4$ (9) be checked in order that any structural conclusions drawn, particularly from small values of quadrupole coupling constants, be based on well-established data. We here report our ^{121}Sb Mössbauer data for $Cs_3Sb_2X_9$ (X = Cl, Br, I) and $MSbX_4$ (X = F, Cl, Br, I), together with new data on some other $[Sb_2X_9]^{3-}$ and $[SbX_4]^-$ salts. The results are discussed in terms of the known and likely structures.

Experimental

The sodium tetrafluoroantimonate(III) was prepared from antimony trioxide and sodium carbonate in excess HF as described previously (10). The series of complexes SbX_4^- (X = Cl, Br, I) were prepared by the treatment of the trihalide with a solution of tetraalkylammonium or pyridinium halide in various solvents as described in ref. 11. The bis-*n*-butylammonium tetraiodoantimonate(III) was prepared by adding the solution of antimony(III) iodide in concentrated HI slowly, with vigorous stirring, to a large excess of the solution of bis-*n*-butylammonium iodide in concentrated HI (12).

Hexamminecobalt nonafluorodiantimonate(III) was prepared from a 0.2 *M* solution of $Co(NH_3)_6F_3$ and a

Can. J. Chem. Downloaded from www.nrcresearchpress.com by 210.87.254.5 on 09/05/12
For personal use only.

Can. J. Chem. Downloaded from www.nrcresearchpress.com by 210.87.254.5 on 09/05/12
For personal use only.

solution of Sb_2O_3 in 49% HF. $Co(NH_3)_6F_3$ was prepared by dissolving 0.01 mol of $Co(NH_3)_6Cl_3$ in water and adding a saturated solution of AgF (Ozark Mahoning), 0.03 mol. The precipitated AgCl was filtered off and the resulting solution was concentrated to 50 ml by pumping on the vacuum line. Sb_2O_3 (0.01 mol) was dissolved in a minimum amount of 48% HF (J. T. Baker) and the solution was filtered to remove any suspended particles. Addition to the $Co(NH_3)_6F_3$ solution yielded a good crop of dark orange crystals after cooling in dry ice. The crystals were collected at the pump, washed with a small quantity (a few mls) of cold ethanol, and dried under vacuum.

Anal. Calcd.: NH_3, 17.73; Sb, 42.32; F, 29.71. Found: NH_3, 17.89; Sb, 42.15; F, 29.47.

The caesium nonahalodiantimonate(III) compounds were prepared from antimony trihalide and caesium halide in concentrated hydrogen halide solution as described in ref. 14. *N*-Butylammonium nonachlorodiantimonate(III) was prepared by addition of a solution of antimony trichloride in concentrated HCl to a solution of the amine in concentrated HCl yielding a white precipitate which was filtered and washed in ether and dried under vacuum. Tetramethylammonium nonabromodiantimonate(III) dibromine was prepared as described in ref. 15. Pyridinium nonabromodiantimonate(III) dibromide was prepared from pyridine and antimony tribromide in concentrated HBr (16). The *n*-butyl and *i*-butylammonium nonaiodoiantimonate(III) compounds were prepared by addition of an excess of the respective amine in concentrated HI to a solution of antimony(III) iodide in concentrated HI (12).

Antimony analyses were in good agreement with the formulae given.

The Mössbauer spectra were recorded on apparatus previously described (10). The source was $Ba^{121}SnO_3$ (0.5 mCi) obtained from New England Nuclear Ltd. All spectra are reported relative to InSb at 4 °K and calibrated with iron foil at room temperature, and were recorded with the source at room temperature and the sample at 4 °K. The samples were finely powdered with 8–10 mg of Sb per cm^2. The spectra were computer fitted to an eight-line quadrupole split pattern as previously described (10), as well as to a one-line Lorentzian pattern.

Results and Discussion

The problems involved in obtaining meaningful Mössbauer parameters from ^{121}Sb spectra have been discussed (17) and great care must be exercised to ensure that the data are meaningful. Clearly the peak maximum cannot be taken as the isomer shift in cases where there is a finite quadrupole interaction (7, 17, 18). The error incurred would be smaller if a single Lorentzian fit was used instead of the peak maximum, since the Lorentzian fit would be weighted to more positive or negative velocities depending upon the sign of the e^2qQ. Where there is a large splitting, a single line fit would be inferior to one of eight-lines. However, for situations with $e^2qQ \geqslant \sim 10$ mm/s, the asymmetry of the spectrum is obvious and one would only use the more complex fitting procedure. Where e^2qQ is ~ 6 mm/s or less, the asymmetry is not obvious unless the isomer shift of the sample is close to that of the source material so that relatively slow sweep velocities can be employed, and it will be much more difficult to evaluate a meaningful coupling constant. The effect of changing e^2qQ upon the shape of the absorption envelope has been demonstrated by Donaldson *et al.* (7), but their simulated spectra are misleading in that they are all centered at 0 mm/s. In fact, their Sb(III) spectra all have shifts at ~ -19 mm/s from the source, so that these spectra approximate more to a single Lorentzian and make the abstraction of meaningful quadrupole coupling constants very difficult indeed. Since a splitting of +6.8 mm/s was claimed (7) for $Co(NH_3)_6SbCl_6$, when previous workers (6) found none and subsequent X-ray analysis (8) showed O_h symmetry about antimony, one must view with some skepticism the small e^2qQ values reported for the Sb(III) halide complexes (7, 9).

Table 1 contains data which illustrate the points discussed above. It includes Mössbauer parameters for some compounds which have been previously examined by us (10) and others (7, 9) together with some new data. All of our results were obtained under identical conditions; previous reporters have used a variety of conditions and standards (7, 9, 10).

The complexes studied are of two types, namely $MSb(III)X_4$ and $M_3Sb(III)_2X_9$ (X = F, Cl, Br, and I). Only in the cases where there is a large e^2qQ value do the isomer shift values, calculated by the two fitting procedures, differ appreciably. The spectra of $NaSbF_4$ (10) and $Co(NH_3)_6Sb_2F_9$ can clearly only be realistically fitted to the eight-line pattern without incurring serious errors. In these two cases, the line width of the single Lorentzian fit is more than double the natural width (2.1 mm/s) and the width calculated from the eight-line fit. From a visual examination the spectra of $NaSbF_4$ (10) and $Co(NH_3)_6Sb_2F_9$ (Fig. 1) are also clearly asymmetric. $C_5H_5NHSbCl_4$ is also visually asymmetric and has an unacceptably high line width from the single line fit. The eight-line fit does give a fairly large quadrupole coupling constant but surprisingly the isomer shifts calculated by the two methods are not appreciably different. This is, perhaps, a reflection of the quality of this particular spectrum. For all of the other compounds,

TABLE 1. ^{121}Sb Mössbauer parameters for some antimony(III) halides

Compound	Eight Lorentzians			One Lorentzian	
	Isomer shift* (±0.1 mm/s)	e^2qQ (±2 mm/s)	Line width (mm/s)	Isomer shift (mm/s)	Line width (mm/s)
$NaSbF_4$	−5.73	+18.3	2.6	−5.20	5.4
	−5.48†	+18.6†	3.9†		
$(C_2H_5)_4NSbCl_4$	−8.17	+8.9	2.6	−8.09	3.8
	−7.47†	+10.6†	3.3†		
$(C_4H_9)_4NSbBr_4$	−8.15	+4.6	3.7	−8.18	3.9
$(C_4H_9)_4NSbI_4$	−7.37	—	2.7	−7.28	3.3
	−6.88†	−3.3†	3.4†		
$C_5H_5NHSbCl_4$	−8.10	+11.3	3.6	−7.95	4.9
	−7.98†	+9.1†	2.2†		
$(n\text{-}C_4H_9)_2NH_2SbI_4$	−7.38	—	2.7	−7.37	3.8
$Co(NH_3)_6Sb_2F_9$	−6.30	+15.9	2.9	−5.86	5.3
$Cs_3Sb_2Cl_9$	−9.67	+7.7	2.8	−9.50	3.7
	−10.9‡	+6.8‡	3.0‡		
$Cs_3Sb_2Br_9$	−8.97	—	3.3	−8.97	3.4
	−10.3‡	+6.4‡	2.9‡		
$Cs_3Sb_2I_9$	−8.35	+2.9	2.5	−8.36	2.7
	−9.7‡	+5.0‡	3.2‡		
$[(CH_3)_4N]_3Sb_2Br_9Br_2$	−8.50	+3.8	2.8	−8.50	3.0
$(n\text{-}C_4H_9NH_3)_3Sb_2Cl_9$	−9.16	+8.2	2.9	−9.14	3.9
$(C_5H_5NH)_5Sb_2Br_9Br_2$	−8.22	+7.2	2.8	−8.16	3.6
$(i\text{-}C_4H_9NH_3)_3Sb_2I_9$	−8.05	+7.5	2.0	−7.95	2.9
$(n\text{-}C_4H_9NH_3)_3Sb_2I_9$	−8.09	+1.8	2.7	−8.14	3.5

*Relative to InSb at 4 °K.
†Reference 9.
‡Reference 7.

the isomer shift values computed by the two procedures do not differ by more than 0.1 mm/s indicating that the presence of a "small" quadrupole splitting does not, in practice, affect the isomer shift parameter significantly at the high velocities employed. There does appear to be a correlation between the difference in the two line widths and the calculated quadrupole coupling constants. The greater the difference in width, the larger the coupling constant and a comparison of the data obtained by both fitting procedures should perhaps be made before drawing structural conclusions. In our view, there will always be a large error in the quadrupole splitting parameter, probably $\sim \pm 2$ mm/s, when large sweep velocities are employed in recording ^{121}Sb spectra.

The quadrupole coupling constants reported here are, apart from $Cs_3Sb_2Br_9$, in reasonable agreement with those of the previous workers (7, 9) bearing in mind the above discussion. Our computer program would not give a reproducible value for the e^2qQ of $Cs_3Sb_2Br_9$ and this, together with the line width comparison, suggests to us that the value is much smaller than the +6.4 mm/s reported earlier (7). Similarly the SbI_4^- salts must also have negligible quadrupole splittings. Agreement with literature isomer shifts is good for $NaSbF_4$ and $C_5H_5NHSbCl_4$, but poor for $(C_2H_5)_4NHSbCl_4$ and $(C_4H_9)_4NSbI_4$ where the values (9) are up to 0.7 mm/s more positive than those reported here. The situation is even worse for the $Cs_3Sb_2X_9$ series where our shifts are up to 1.3 mm/s more positive than those of Donaldson *et al.* (7). Brill *et al.* (13) find that $(CH_3NH_3)_3Sb_2Br_9$ has an isomer shift of −8.20 mm/s, very close to the value we find for $(C_5H_5NH)_5Sb_2Br_9Br_2$ which gives us some confidence in our results.

In both series of compounds the order of negative chemical isomer shifts, *i.e.*, Cl > Br > I > F can be explained in terms of the probable structures of the compounds and the relative electronegativities of the halogens. Each of the anions in $NaSbF_4$ and $C_5H_5NHSbCl_4$ is halogen bridged to adjacent anions, but the two structures are quite different. $NaSbF_4$ has a chain structure (19, 20), with F bridges linking the ions to give

Can. J. Chem. Downloaded from www.nrcresearchpress.com by 210.87.254.5 on 09/05/12
For personal use only.

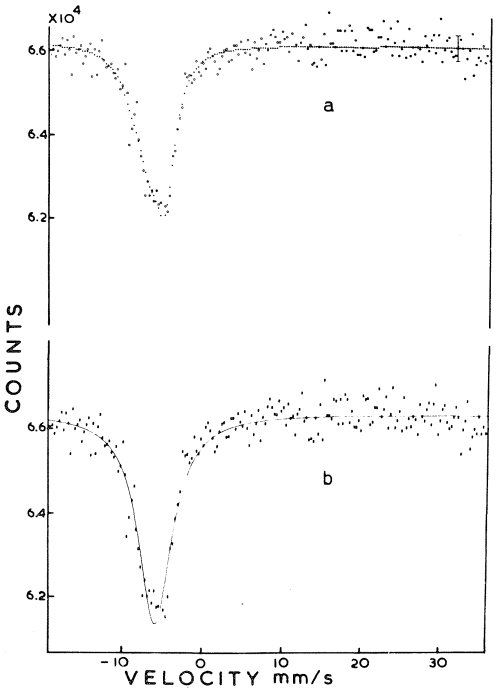

FIG. 1. ^{121}Sb Mössbauer spectra of $Co(NH_3)_6Sb_2F_9$ using (*a*) eight-line quadrupole split pattern, and (*b*) single-line Lorentzian pattern. ○, experimental counts; +, computed counts.

five fluorines about the Sb(III) with the sixth coordination site being occupied by a lone pair of electrons. The effect is a distorted Sb environment and an effective removal of 5s electron density, both of which are apparent in the Mössbauer parameters (10). Pyridinium tetrachloroantimonate(III) also has anions linked by halogen bridges in an infinite chain (21) but, two chlorines of each $SbCl_4^-$ are bridging. This results in an octahedral arrangement of six chlorines about the antimony, two at 2.380 Å, two at 2.630 Å, and two at 3.126 Å. Donaldson *et al.* (9) consider that the two longest Sb—Cl distances are non-bonding and discussed their data in terms of a trigonal bipyramidal (t.b.p.) arrangement of four chlorines and a lone pair about antimony. This appears most unrealistic since even the longest Sb—Cl distance is 0.9 Å less than the sum of van der Waals radii (22) and indicates a significant bonding interaction. Furthermore, in a t.b.p. arrangement, the Cl—Sb—(Cl) angles should be at ~90° and ~120° (1), whereas only 90° bond angles are found in $SbCl_4^-$ (21). The X-ray results show that the Sb environment has no space to accommodate a localized non-bonding electron pair, as it has in SbF_4^-, and it is logical to infer that the 5s pair remains in an essentially spherical orbital (21). The result is a high s electron density on Sb and a more negative isomer shift for $SbCl_4^-$ compared to SbF_4^-, where the 5s electrons are clearly involved in the bonding scheme. The isomer shifts of the remainder of the SbX_4^- salts can most reasonably be explained if one assumes that they all have similar structures, *i.e.*, six halogens about an Sb(III) having a stereochemically inactive pair of 5s electrons. As the electronegativity of X decreases, the s electrons become more shielded by p and d bonding electrons, the s electron density decreases and a more positive isomer shift is observed. We find the isomer shift of the SbI_4^- salts to be close to that reported for SbI_3 (23), and to be in the same region as $[Sb_2I_9]^{3-}$ in both of which the Sb is six coordinate (13). Rationalization of the quadrupole coupling constants is much more difficult because of the large errors involved. Clearly, where the 5s electrons are involved in the bonding (SbF_4^-) a large splitting occurs. In the other SbX_4^- cases, the coupling must arise from the asymmetry created by the different Sb—X bond lengths, *e.g.*, 2.380, 2.630, and 3.126 Å in $SbCl_4^-$. This asymmetry would be expected to decrease as the halogen size and hence the Sb—X distance increases and indeed the trend is to smaller e^2qQ values from Cl to I. These trends are also paralleled in the $[Sb_2X_9]^{3-}$ series with F > Cl > Br > I.

In the $Sb_2X_9^{3-}$ series, a number of X-ray crystallographic determinations have been completed (16–19). The bromide salts all have anions composed of two octahedra sharing a face to give an ion with D_{3h} symmetry. Each antimony is in an octahedral environment with the only obvious place for the 5s electrons being a spherical orbital about the antimony. The Sb—Br distances are longer than in the parent $SbBr_3$ being 2.63 and 3.00 Å for the terminal and bridging bonds respectively. Taken together, these facts account for the large negative shifts obtained. With the exception of the $Sb_2F_9^{3-}$ salt, the other $Sb_2X_9^{3-}$ ions must have the same structure as the bromide and these ions will also almost certainly be found to have longer Sb—X bonds than the parent trihalide.

The nonafluoride is anomalous with a much more positive isomer shift and a large quadrupole coupling constant indicating that it has a structure different from the other $Sb_2X_9^{3-}$ ions.

Can. J. Chem. Downloaded from www.nrcresearchpress.com by 210.87.254.5 on 09/05/12
For personal use only.

Can. J. Chem. Downloaded from www.nrcresearchpress.com by 210.87.254.5 on 09/05/12
For personal use only.

As in other fluoride structures, where the central atom also possesses a lone pair, *e.g.*, XeF_6, the short M—F bonds result in steric crowding which prevents the 5s electron pair from remaining in a spherical orbital and it becomes involved in the bonding. In the $[Sb_2X_9]^{3-}$ ion where X = F, the stereochemical effect of the 5s electrons dominates; the distorted Sb environment results in a large e^2qQ and a more positive isomer shift than than for the other $[Sb_2X_9]^{3-}$ ions. X-Ray analysis confirms that two Sb—X—Sb bridge bonds have been broken to give an ion consisting of two octahedra sharing a corner with each octahedron composed of four terminal fluorines, one bridging fluorine, and a lone pair of electrons (24). The fluorine bridge was found to be asymmetric and the ion therefore has two slightly different antimony environments which cannot be distinguished by Mössbauer spectroscopy. The parameters quoted in Table 1 for this ion were obtained by fitting the spectrum to only one antimony site.

It has been noted in both Sb and Sn compounds that the chemical isomer shift of an ion is influenced by the counter-ion (6, 25). Where there is interaction between a polarizing cation and a ligand attached to a Mössbauer nucleus, the effective electronegativity of the ligand is changed and this change will be transmitted to the Mössbauer nucleus and result in a change in isomer shift. Such an effect appears evident in our results. The isomer shifts of the compounds having a cation with an active hydrogen, *i.e.*, $R_3\overset{+}{N}—H$, are, with one exception, more positive than those that do not have this feature. We believe that this is an indication of hydrogen bonding between the N—H and the halogen of the anion. This in turn means that there is less p–d electron withdrawal from the antimony nucleus, an increase in shielding, and hence a reduction in s electron density. This effect is most noticeable in the $[Sb_2X_9]^{3-}$ salts where there is more likelihood that the X—Sb bonding orbitals are composed of p and d character only.

Thanks are due to the National Research Council of Canada for financial support.

1. R. J. GILLESPIE. Molecular geometry. Van Nostrand Reinhold, London. 1972.
2. I. D. BROWN. Can. J. Chem. **42**, 2758 (1964).
3. S. L. LAWTON and R. A. JACOBSON. Inorg. Chem. **5**, 743 (1966).
4. T. C. GIBB, R. GREATREX, N. N. GREENWOOD, and A. C. SARMA. J. Chem. Soc. A, 212 (1970).
5. G. G. LONG, R. J. TULBANE, and L. H. BOWEN. Abstr. 158th Am. Chem. Soc. Meeting, New York. September, 1969.
6. T. BIRCHALL, B. DELLA VALLE, E. MARTINEAU, and J. B. MILNE. J. Chem. Soc. A, 1855 (1971).
7. J. D. DONALDSON, M. J. TRICKER, and B. W. DALE. J. Chem. Soc. Dalton, 893 (1972).
8. D. R. SCHROEDER and R. A. JACOBSON. Inorg. Chem. **12**, 210 (1973).
9. J. D. DONALDSON, J. T. SOUTHERN, and M. J. TRICKER. J. Chem. Soc. Dalton, 2637 (1972).
10. T. BIRCHALL and B. DELLA VALLE. Can. J. Chem. **49**, 2808 (1971).
11. G. Y. AHLIJAH and M. GOLDSTEIN. J. Chem. Soc. A, 326 (1970).
12. R. D. WHEALY and J. B. BLACKSTOCK, JR. J. Inorg. Nucl. Chem. **26**, 243 (1964).
13. T. B. BRILL, P. E. GARROU, and G. G. LONG, JR. Inorg. Nucl. Chem. **33**, 3285 (1971).
14. H. YAMATERA and K. NAKATSU. Bull. Chem. Soc. Jap. **27**, 244 (1954).
15. C. R. HUBBARD and R. A. JACOBSON. Inorg. Chem. **11**, 2247 (1972).
16. S. K. PORTER and R. A. JACOBSON. J. Chem. Soc. A, 1359 (1970).
17. J. A. GABRIEL and S. L. RUBY. Nucl. Inst. Methods, **36**, 23 (1965).
18. T. C. GIBB, B. A. GOODMAN, and N. N. GREENWOOD. Chem. Commun. 774 (1970).
19. A. BYSTROM, S. BÜCHLAND, and K. A. WILHELM. Ark. Kemi, **6**, 77 (1953).
20. S. H. MASTIN and R. R. RYAN. Inorg. Chem. **10**, 2793 (1970).
21. S. K. PORTER and R. A. JACOBSON. J. Chem. Soc. A, 1356 (1970).
22. L. PAULING. Nature of the chemical bond, 3rd Ed. Cornell University Press, Ithaca, New York. 1960. p. 260.
23. L. BOWEN, J. G. STEVENS, and G. G. LONG. J. Chem. Phys. **51**, 2010 (1969).
24. D. R. SCHROEDER and R. A. JACOBSON. Inorg. Chem. **12**, 306 (1973).
25. J. D. DONALDSON and B. J. SENIOR. J. Chem. Soc. A, 1798 (1966).

Infrared Studies of Water in Crystalline Hydrates: Location of Hydrogen Atoms and Evidence for a Bifurcated Hydrogen Bond in $K_2SnCl_4.H_2O$ [1]

MICHAEL FALK AND CHUNG-HSI HUANG

Atlantic Regional Laboratory, National Research Council of Canada, Halifax, Nova Scotia B3H 3Z1

AND

OSVALD KNOP

Department of Chemistry, Dalhousie University, Halifax, Nova Scotia B3H 3J5

Received January 31, 1974

MICHAEL FALK, CHUNG-HSI HUANG, and OSVALD KNOP. Can. J. Chem. **52**, 2380 (1974).

Infrared spectra of polycrystalline $K_2SnCl_4 \cdot H_2O$ at different degrees of deuteration were recorded between 4000 and 300 cm^{-1} at temperatures between 30 and -160 °C. The spectra are consistent with the crystal structure proposed by Kamenar and Grdenić. The water molecules are all equivalent and asymmetric. They are sufficiently well separated from one another for the dynamic coupling of vibrations to be negligible. Both hydrogens of the water molecule participate in hydrogen bonding; one of the hydrogen bonds is weak and bifurcated. Positional parameters of the hydrogen atoms have been calculated using supplementary information from available n.m.r. studies. Infrared spectral characteristics of water molecules engaged in bifurcated hydrogen bonding are discussed.

MICHAEL FALK, CHUNG-HSI HUANG et OSVALD KNOP. Can. J. Chem. **52**, 2380 (1974).

Les spectres infrarouges de $K_2SnCl_4 \cdot H_2O$ polycrystallin ont été enregistrés entre 4000 et 300 cm^{-1} à différentes températures et degrés de deutération. Les spectres sont en accord avec la structure cristalline proposée par Kamenar et Grdenić. Les molécules d'eau sont toutes équivalentes et asymétriques. Les distances entre les molécules d'eau sont suffisamment grandes pour que le couplage dynamique de leurs vibrations soit négligeable. Les deux hydrogènes de la molécule d'eau participent aux liaisons hydrogène; une de ces liaisons est faible et bifurquée. Les paramètres de position des atomes d'hydrogène ont été calculés en utilisant de données r.m.n. fournies par la littérature. Les caractéristiques spectrales infrarouge des molécules d'eau qui participent aux liaisons hydrogène bifurquées, sont discutées.

In the crystal structure proposed for $K_2SnCl_4.H_2O$ in 1939 by Brasseur and de Rassenfosse (1, 2) (B.R.) the water oxygen was placed at a center of symmetry in a unit cell of space-group symmetry *Pnma* (No. 62). Fourteen years later Itoh *et al.* (3, 4) attempted to complete the B.R. structure by determining the positions of the hydrogen atoms from a proton magnetic resonance (p.m.r.) study of single crystals of this hydrate. Being unable to reconcile their results with the B.R. structure, they assumed the structure of $K_2SnCl_4.H_2O$ to be similar to that of $K_2HgCl_4.H_2O$, which they studied at the same time, and accordingly changed the space group *Pnma* to *Pbam* (No. 55), without commenting on the difference in the conditions that govern observable reflections in the two space groups (5). The water oxygens were now placed in equipoint 4(*f*) of *Pbam*, of symmetry C_2-2, necessitating the equivalence of the two hydrogens of a water molecule and hence the equivalence of the H...Cl bonds in which the hydrogen atoms were considered to engage. McGrath and Silvidi (6, 7), who re-examined the hydrate by p.m.r. and obtained results only slightly different from those of refs. 3 and 4, adopted the B.R. structure as modified by Itoh *et al.* and described the hydrogen bonds explicitly as being to two Cl atoms of the same type, Cl(III)...H—O—H...Cl(III). However, a subsequent re-investigation by X-ray diffraction led Kamenar and Grdenić (8) to propose for $K_2SnCl_4.H_2O$ a crystal structure (K.G.) substantially different from the B.R. structure, though having the same space group, *Pnma* (Table 1). Obviously if the positions of the non-hydrogenic atoms in the K.G. structure are essentially correct, a re-interpretation of the p.m.r. results of refs. 3, 4, 6, and 7 is needed, especially as Kamenar and Grdenić made no reference to the p.m.r. studies.

In the following we shall (*i*) examine the compatibility of the K.G. structure with the available p.m.r. evidence, with a view to locating the H

[1]NRCC No. 13929.

Can. J. Chem. Downloaded from www.nrcresearchpress.com by 210.87.254.6 on 09/05/12
For personal use only.

TABLE 1. Positional parameters and site symmetries of atoms in $K_2SnCl_4.H_2O$ (*Pnma**) (8)

Atom	Equipoint	Site symmetry	*x*	*y*	*z*
Sn	4(*c*)	*m*	0.988	1/4	0.000
K	8(*d*)	*1*	0.185	0.982	0.370
Cl(1)	4(*c*)	*m*	0.192	1/4	0.112
Cl(2)	8(*d*)	*1*	0.944	0.448	0.207
Cl(3)	4(*c*)	*m*	0.734	1/4	0.901
O	4(*c*)	*m*	0.960	1/4	0.559

*Converted from the original description in *Pbnm* to the tabulated standard setting *Pnma* (ref. 5; *cf.* also ref. 2). Unit-cell dimensions (8): $a = 12.05(3)$ Å, $b = 9.14(2)$ Å, $c = 8.24(2)$ Å; $Z = 4$. Uncertainties in the values of the positional parameters are stated to be comparable to those reported for the determination of the structure of $SnCl_2.2H_2O$ (10), *i.e.* leading to standard errors of ± 0.03 Å in interatomic distances and $\pm 1°$ in bond angles. An arbitrary uncertainty of ± 0.09 Å in the distances, and $\pm 3°$ in the angles, has been assumed for the purposes of the present work.

atoms correctly, and (*ii*) discuss new information obtained by us from a study of the i.r. spectra of the water molecule in partially deuterated polycrystalline samples of $K_2SnCl_4.H_2O$.

Conclusions Possible from the K.G. Structure Alone

The four oxygen atoms in the unit cell are located in mirror planes parallel to 010 (Fig. 1 and Table 1) and are equivalent. The shortest O...O separation is *ca.* 4.8 Å, which precludes the existence of O—H...O bonds and leaves hydrogen bonding of the O—H...Cl type as the only possibility. Each oxygen atom has six Cl neighbors at distances shorter than 3.78 Å, the upper limit postulated for effective O—H...Cl hydrogen bonding (9), and a seventh Cl at 3.92(9) Å. The immediate cation environment of an oxygen atom consists of two K atoms at 2.81 Å, well within the range of observed K...OH_2 distances (9), and an Sn atom at a distance of 3.65 Å, which is much greater than the Sn...O distance normally observed for water coordinated to an Sn atom, *ca.* 2.15 Å (10).

The K.G. structure requires the water molecule to be of symmetry C_s. Depending on the orientation of the molecule relative to the mirror plane, the following situations are consistent with the structure (*cf.* Fig. 1 for identification of atoms).

(*1*) The two hydrogen atoms are mirror images. Then all the hydrogens in the unit cell are equivalent, in equipoint 8(*d*) of *Pnma*, and there are two possibilities for hydrogen bonding: (*1a*) $Cl(2)^B$...H—O^A—H′...$Cl(2)^{B'}$, with O...Cl distances of 3.42(9) Å and a Cl...O...Cl angle of *ca.* 64°; (*1b*) $Cl(2)^C$...H—O^A—H′...$Cl(2)^{C'}$, with O...Cl distances of 3.56(9) Å and a Cl...O...Cl angle of *ca.* 102°.

(*2*) The two hydrogens are situated in the mirror plane and are nonequivalent, each belonging to a different equipoint 4(*c*). Any hydrogen bond that could form would lie in the mirror plane. The bonds could be either *normal* (O^A—H...$Cl(3)^D$, O...Cl = 3.32(9) Å, *or* O^A—H...$Cl(1)^F$, O...Cl = 3.52(9) Å) or *bifurcated* (O^A—H...*B*, O...*B* = 2.90(8) Å, *or* O^A—H...*C*, O...*C* = 2.25(9) Å, where *B* and *C* are the projections of $Cl(2)^B$ and

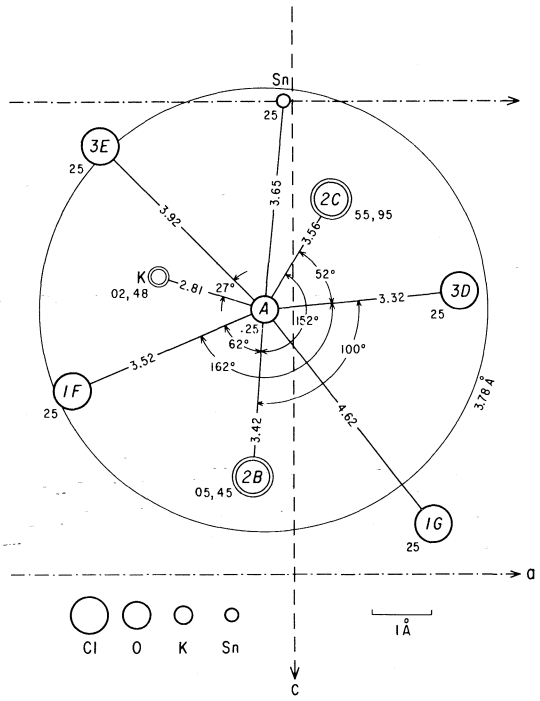

FIG. 1. Immediate environment of an oxygen atom (*A*) of a water molecule in $K_2SnCl_4.H_2O$ according to ref. 8. The original description in space group *Pbnm* has been converted to the standard setting *Pnma*. The fractional coordinates shown have been multiplied by 100; the interatomic distances are in Å. Double circles represent atoms related by a mirror plane parallel to 010.

Can. J. Chem. Downloaded from www.nrcresearchpress.com by 210.87.254.6 on 09/05/12
For personal use only.

$Cl(2)^C$ respectively onto the mirror plane).[2] Only one of the different combinations of these four possible H-bonds, $Cl(3)^D...H—O^A—H...B$, is consistent with the assumption that the H-bond acceptor angle is within 35° of 108°, the mean H—O—H angle in hydrates (9); it involves one normal and one bifurcated hydrogen bond.

For both (*1*) and (*2*) there exists also a range of configurations involving hydrogen atoms which are uncommitted, *i.e.* not engaged in H...Cl contacts shorter than 2.80 Å, the postulated cut-off distance for effective O—H...Cl bonding (9).

Conclusions from the K.G. Structure and Proton Magnetic Resonance Evidence

The length r of the H—H vector in the water molecule and the acute angle[3] α which H–H makes with the α-axis were estimated from p.m.r. studies to be, respectively, 1.62 Å and $\pm 50.5°$ (3, 4), and 1.59 Å and $\pm 52°$ (6, 7). The angle β of the H–H vector with the b-axis was stated (7) to be 90°, *i.e.* the vector lies in a plane parallel to 010. This information immediately eliminates possibilities (*1a*) and (*1b*), and is sufficient to specify the positions of the two hydrogen atoms with some accuracy. Taking the mean of the two experimental values for r, 1.61(2) Å, and α, $\pm 51.2(11)°$, and assuming that both O—H distances are 0.98 Å (9), the positional parameters of the two hydrogen atoms H(1) and H(2) of O^A are calculated as (0.038, 1/4, 0.593) and (0.955, 1/4, 0.440) respectively (Fig. 2). The O^A—H(1)...Cl-(3)^D and O^A—H(2)...B angles corresponding to these parameters would then be about 166° and 180° respectively.

The results of the p.m.r. studies are thus consistent with the K.G. structure. If this is taken as evidence for the correctness of both, no further experimental work is needed and the crystal structure of $K_2SnCl_4.H_2O$ can be regarded as established, albeit with not very high accuracy. However, the conclusion that the O^A—H(2)...B bond is bifurcated provides incentive for further study. The spectroscopic behavior of bifurcated hydrogen bonds is practically unknown. Only four cases

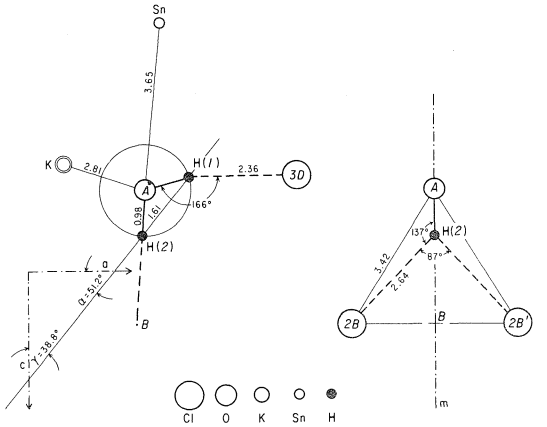

FIG. 2. Proposed location of the hydrogen atoms belonging to oxygen A in $K_2SnCl_4.H_2O$ (see Fig. 1). *Left*, projection on 010. *Right*, detail of the bifurcated hydrogen bond (m, mirror plane||010).

of water molecules forming such bonds have been clearly demonstrated in inorganic crystalline hydrates by neutron diffraction (*cf.* Table III, p. 74 of ref. 9), and the i.r. spectrum has been reported for only one of them. $K_2SnCl_4.H_2O$ appeared to offer a possibility for an i.r. study of the bifurcated H-bond that is unusually free from complications. Furthermore, confirmation by additional means of the correctness of the $K_2SnCl_4.H_2O$ structure derived above seemed desirable, and for this i.r. spectra of partially deuterated material are well suited.

Experimental

Preparation

$K_2SnCl_4.H_2O$ was prepared from a saturated aqueous solution of KCl and an aqueous solution of stannous chloride acidified with HCl. The two solutions were mixed at room temperature in a K:Sn ratio of approximately 2:1 or with the KCl in large excess. After a few minutes large white, opaque crystals began to form. Their habit was the same as described in ref. 11 for $K_2SnCl_4.2H_2O$, but chlorine and water analyses showed clearly that the composition corresponded to the formula $K_2SnCl_4.H_2O$, in agreement with ref. 2 and earlier reports quoted therein. Some of the crystals were recrystallized from a nearly saturated solution of KCl at room temperature without change of composition. If the recrystallization was from warm concentrated HCl, the product was mostly the colorless transparent, well-developed octahedral crystals of K_2SnCl_6.

After the first two or three crops of the $K_2SnCl_4.H_2O$ crystals were collected, the mother liquor, which had turned yellowish, was warmed up to dissolve any remaining solids and allowed to crystallize. The transparent to white hair-like crystals that separated were $KSnCl_3.H_2O$; their appearance agreed with the descrip-

[2]The seventh Cl atom, $Cl(3)^E$, is unlikely to act as a H-acceptor, both because its distance from O^A exceeds the above upper limit of 3.78 Å and because the O^A...$Cl(3)^E$ vector makes an angle of only 27° with the bisector of the two O^A...K directions.

[3]The angles formed by the H–H vector with the crystallographic axes have been renamed to conform with the standard setting *Pnma* (Fig. 2).

Can. J. Chem. Downloaded from www.nrcresearchpress.com by 210.87.254.6 on 09/05/12
For personal use only.

TABLE 2. Interplanar spacings d (in Å) and estimated powder diffractometer intensities* I of $K_2SnCl_4.H_2O$ and $KSnCl_3.H_2O$

$K_2SnCl_4.H_2O$				$KSnCl_3.H_2O$			
d	I	d	I	d	I	d	I
6.62	s	2.382	m	7.80	s	2.557	w
5.84	w	2.294	m	6.31	m	2.534	w
4.90	vw	2.265	m	6.05	vw	2.515	w
4.48	w	2.221	vw	5.75	vw	2.496	vw
4.23	vw	2.149	w	4.63	m	2.450	w
4.07	w	2.130	m	4.32	w	2.426	w
3.74	s	2.048	m	4.21	w	2.413	w
3.58	m	2.017	m	4.08	w	2.385	s
3.56	s	1.985	w	3.80	vw	2.319	w
3.36	w	1.939	m	3.58	s	2.277	w
3.03	s	1.916	m	3.55	m	2.258	w
2.974	m	1.885	w	3.46	vw	2.241	w
2.936	s	1.869	vw	3.41	s	2.179	s
2.845	w			3.29	w	2.100	vw
2.827	m			3.16	w	2.058	vw
2.796	m			3.09	m	2.043	w
2.702	s			3.07	s	2.017	w
2.656	w			2.982	vw	1.998	vw
2.609	w			2.909	m	1.988	vw
2.556	w			2.823	m	1.935	vw
2.487	m			2.748	s	1.896	vw
2.410	m			2.614	w	1.860	m

*CuKα; focussing monochromator after specimen.

tion in ref. 11.[4] Their X-ray powder diffraction pattern was completely different from that of $K_2SnCl_4.H_2O$ (Table 2). The formula $KSnCl_3.H_2O$ was confirmed by analyzing for Cl and H_2O. Weak additional features in the i.r. spectra of $KSnCl_3.H_2O$ showed occasionally the presence of small amounts of $K_2SnCl_4.H_2O$.

After the bulk of the $KSnCl_3.H_2O$ crystals was removed from the mother liquor, by now quite yellow, the solution was again warmed up and allowed to crystallize. This time only the characteristic octahedral, transparent crystals of K_2SnCl_6 appeared.

To prepare deuterated specimens, saturated solutions of KCl in H_2O–D_2O mixtures of different isotopic compositions were mixed with HCl solutions of stannous chloride at room temperature. Anhydrous $SnCl_2$ and DCl were used for the highest degree of deuteration. The crystals formed were quickly dried by pressing between filter papers and sealed in sample vials. Owing to the rapid H–D exchange with atmospheric moisture the highest degree of deuteration attained was about 92%.

Authentication

The water contents were determined (in triplicate) by thermogravimetric analysis. Chlorine was determined as AgCl (precipitation in the dark under vigorous stirring) by the Volhard method using dry reagent-grade KCl as a standard. Several determinations gave the following results (in wt%):

Anal. Calcd. for $K_2SnCl_4.H_2O$: H_2O, 5.05; Cl, 39.75. Found: H_2O, 5.0(1); Cl, 40.0(3).

Anal. Calcd. for $K_2SnCl_4.2H_2O$: H_2O, 9.62; Cl, 37.84.

Anal. Calcd. for $KSnCl_3.H_2O$: H_2O, 6.38; Cl, 37.69. Found: H_2O, 6.2(1); Cl, 37.9(3).

X-Ray powder diffraction patterns were obtained both photographically (114.6 mm Straumanis-type camera) and with a Philips diffractometer fitted with a focussing monochromator after the rotated specimen. In the latter case smear mounts were prepared by mixing the finely ground sample powder with silicone grease and pressing the thick paste into a shallow counterbore in a lucite slug to be fitted into the specimen holder. For powder photography the CuKα radiation ($\lambda\alpha_1 = 1.54056$ Å, $\lambda\alpha_2 = 1.54440$ Å) was filtered with Ni. Advantage was taken of having analyzed samples of $KSnCl_3.H_2O$ to characterize this compound by its powder diffraction pattern (Table 2) and i.r. spectra (Fig. 3).

Infrared spectra

Infrared spectra were recorded from 4000 to 300 cm^{-1} using both the Nujol mull and the KCl pellet techniques, with a Perkin-Elmer model 521 grating spectrophotometer. Careful calibration made it possible to measure the frequencies of sharp spectral features to within 0.5 cm^{-1}. Low-temperature spectra were obtained using a Model VLT-2 variable temperature cell (Research and Industrial Instruments Co., London).

The mulls were mounted between two KBr or CsBr

[4]On occasion the few crystals of $K_2SnCl_4.H_2O$ that had formed initially acted as crystallization nuclei for $KSnCl_3.H_2O$ and were eventually completely enveloped by the latter material.

Can. J. Chem. Downloaded from www.nrcresearchpress.com by 210.87.254.6 on 09/05/12
For personal use only.

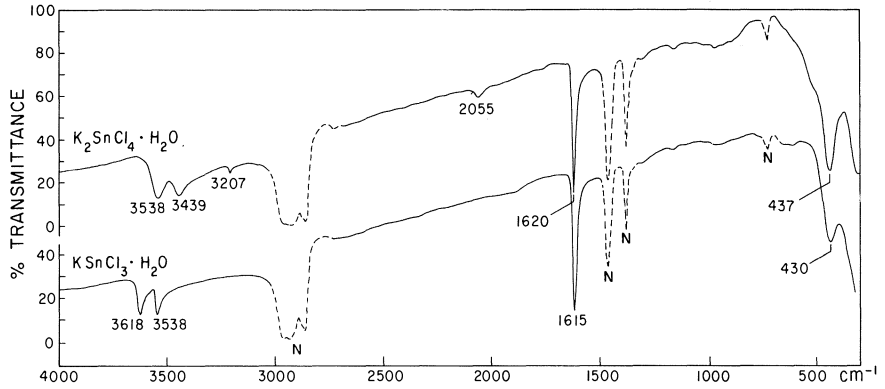

FIG. 3. Survey spectra of undeuterated $K_2SnCl_4.H_2O$ and $KSnCl_3.H_2O$ at room temperature (Nujol mulls) *N* denotes major features of the nujol spectrum.

plates; with the latter it was possible to record spectra down to 250 cm^{-1}. The KCl pellets of $K_2SnCl_4.H_2O$ were prepared by pressing mixtures of the finely ground sample powder with freshly dried KCl in an evacuable die. The mulls had the advantage that almost no moisture was introduced during the preparation, while small amounts of atmospheric moisture invariably found their way into the KCl pellets. With $KSnCl_3.H_2O$ only mulls could be used. as pressing the powder with excess KCl resulted in the formation of $K_2SnCl_4.H_2O$. Pressing powdered $SnCl_2.2H_2O$ (or $SnCl_2$ containing a trace of moisture) with excess KCl resulted in mixtures of $K_2SnCl_4.H_2O$ and $KSnCl_3.H_2O$.

Results and Discussion

Vibrational Assignments

Spectra of Nujol mulls and KCl pellets were essentially the same. Figure 3 shows a typical survey spectrum of $K_2SnCl_4.H_2O$ and includes a spectrum of $KSnCl_3.H_2O$ in a form suitable for identification purposes.[5,6] Figures 4 and 5 show the spectrum in regions of stretching and bending fundamentals of the water molecule at different degrees of deuteration. At lower temperatures all bands become sharper and undergo small frequency shifts. Table 3 summarizes band assignments and the shifts of frequencies with temperature. The most interesting effect of temperature is

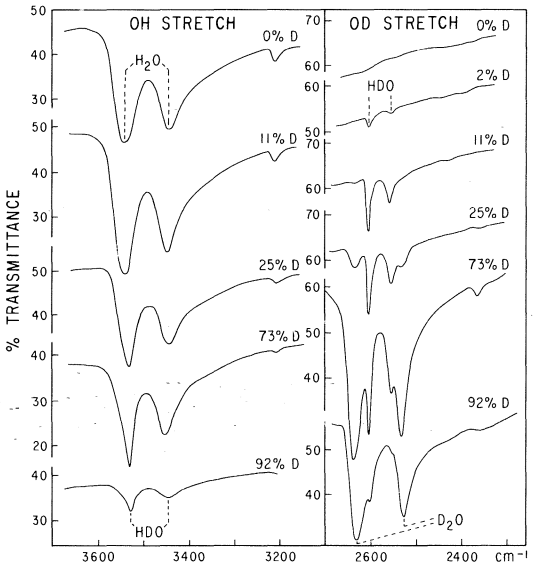

FIG. 4. Spectra of $K_2SnCl_4.H_2O$ at room temperature: stretching fundamentals of water at different degrees of deuteration.

in the region of water librations (Fig. 6 and discussion below).

At low isotopic concentrations of H_2O and D_2O the bending fundamentals of these species are sharp singlets at 1620 and 1192 cm^{-1} respectively, with a half-width of only about 3 cm^{-1} at -150 °C and about 6 cm^{-1} at room temperature. These frequencies are due to the essentially independent motions of water molecules whose nearest water-molecule neighbors belong to other isotopic species. The fact that these frequencies are singlets proves that all water molecules in the structure are equivalent (*cf.* ref. 9).

[5]The spectrum presented as that of "$KSnCl_3.xH_2O$" in Nyquist and Kagel's catalogue of i.r. spectra of inorganic compounds (ref. 12, spectrum No. 764) is in fact that of $K_2SnCl_4.H_2O$. In the recent Raman study of $KSnCl_3.H_2O$ and $K_2SnCl_4.H_2O$ by Davies and Tench (13) the identity of the material investigated was correct, but the spectra are limited to the frequency region below about 325 cm^{-1}.

[6]The structural conclusions based on a study of the i.r. spectra of $KSnCl_3.H_2O$ at different degrees of deuteration will be described in a subsequent paper.

Can. J. Chem. Downloaded from www.nrcresearchpress.com by 210.87.254.6 on 09/05/12
For personal use only.

TABLE 3. Vibrational assignments for water in $K_2SnCl_4.H_2O$*

		HOH		HOD		DOD	
		30 °C	−160 °C	30 °C	−160 °C	30 °C	−160 °C
OH stretch	OH(2)	3538	3543	3529	3535		
	OH(1)	3439	3436	3453	3444		
2 × bend		3207	3218				
OD stretch	OD(2)			2604	2608	2632	2632
	OD(1)			2554	2546	2530	2525
Bend + libration		2055	2071				
Bend		1620	1622	1430 1423	1435 1424	1192	1193
Librations		~525 437	530 458 427	~440 367	~430 ~380 ~330	318	384 ~332 ~305

*Frequencies are in cm^{-1}.

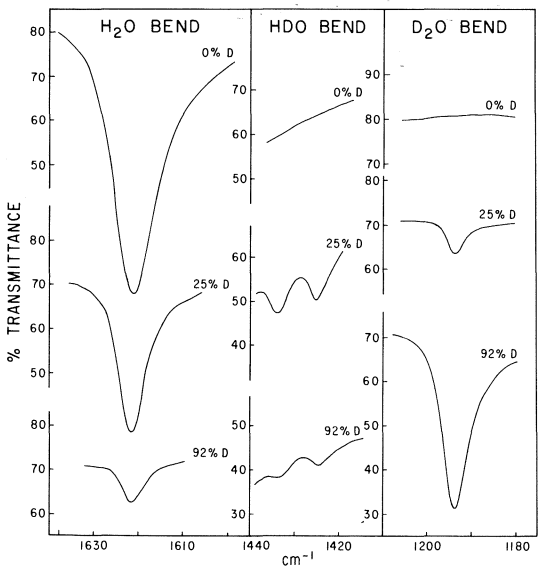

FIG. 5. Spectra of $K_2SnCl_4.H_2O$ at room temperature: bending fundamentals of water at different degrees of deuteration.

In pure undeuterated (or highly deuterated) crystals dynamic coupling of vibrations of the four water molecules in the unit cell would be expected to yield two i.r.-active H_2O (or D_2O) bending fundamentals, of species B_{2u} and B_{3u} (Fig. 7). However, the H_2O and D_2O bending fundamentals remain sharp and single at high isotopic concentrations; the half-widths increase only slightly, to about 6 cm^{-1} at −150 °C and about 8 cm^{-1} at room temperature. The frequencies of these bands are independent of isotopic content. Similar observations apply to the two stretching fundamentals of H_2O and D_2O (Fig. 4). From this it is concluded that dynamic coupling of stretching and bending fundamentals of water is negligible, which implies that the water molecules are isolated from one another and probably do not share common neighbors (*cf.* ref. 14).

The stretching and bending fundamentals of HDO are well-separated *doublets*. Again there is no observable change of frequency with isotopic

Can. J. Chem. Downloaded from www.nrcresearchpress.com by 210.87.254.6 on 09/05/12
For personal use only.

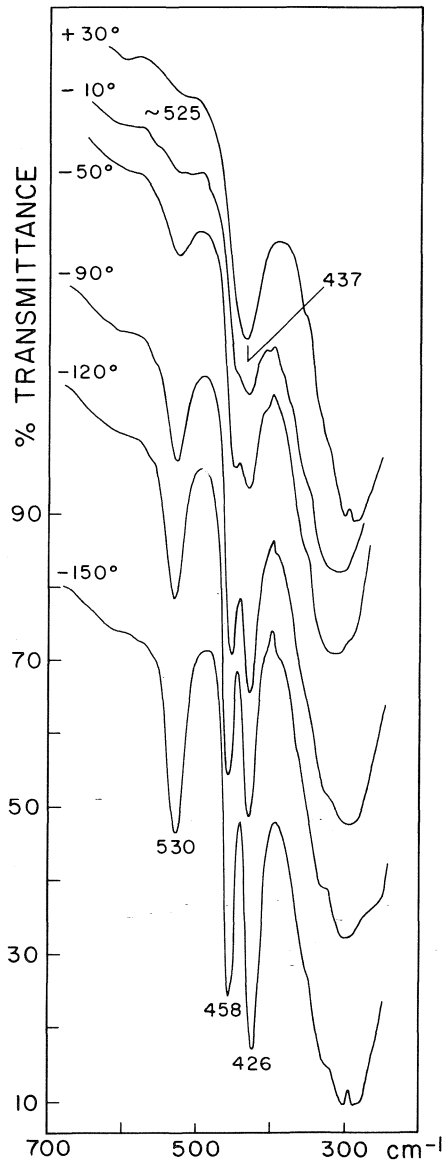

FIG. 6. Spectra of undeuterated $K_2SnCl_4.H_2O$ at different temperatures in the region of libration of water molecules.

concentration of HDO, which indicates negligible dynamic coupling. Doubling of the HDO fundamentals is indicative of an asymmetric force field in the water molecule.

The values of the stretching frequencies of isotopically isolated HDO are 3529 and 3453 cm^{-1} for OH, and 2604 and 2554 cm^{-1} for OD stretching. These frequencies point to participation of both H atoms of the water molecule in hydrogen bonding; however, the bonding must be very

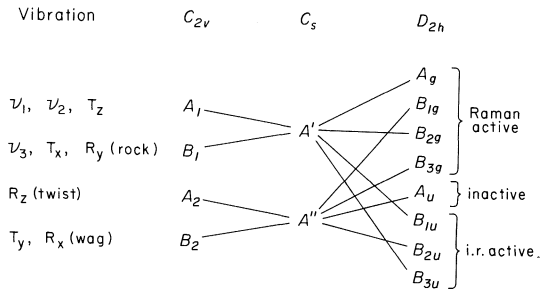

Fig. 7. Correlation table for H_2O fundamentals in $K_2SnCl_4.H_2O$ under the symmetry of the free molecule (C_{2v}), symmetry of the site (C_s; mirror plane = symmetry plane of the H_2O molecule), and the symmetry of the unit cell (factor group D_{2h}).

weak (*cf.* ref. 9). In the following and in Table 3 we shall identify the H atom which gives rise to the lower OH frequency (and presumably is somewhat more strongly H-bonded) with H(1) and the other H atom, with H(2). For H_2O (and D_2O) the description of the two stretching fundamentals as individual OH(1) and OH(2) stretching modes is only approximate though more nearly correct, in view of the strongly asymmetric force field, than the description in terms of "symmetric" and "antisymmetric" stretching modes.

The value of $d\nu/dT$ is positive for the stretching of OH(1) and negative for the stretching of OH(2). This is characteristic of a water molecule engaged simultaneously in a nearly straight, O—H(1)...Cl, and in a highly bent, O—H(2)...Cl, hydrogen bond; increasing thermal motion tends to bend the straight bond, thus raising the OH(1) frequency, and to straighten the bent bond, thus lowering the OH(2) frequency (*cf.* ref. 15).

A water molecule in a crystal structure has three degrees of freedom corresponding to librational motion. However, the libration about an axis approximately coinciding with the HOH bisector is usually of very low i.r. intensity; this "twist" mode is i.r.-inactive for H_2O in sites of C_{2v} symmetry. The other two librations, "wag" and "rock", have intensities which vary widely depending on the force field in the crystal (*cf.* ref. 14).

The spectrum of $K_2SnCl_4.H_2O$ in the librational region contains three intense bands at liquid-nitrogen temperature: at 530, 458, and 427 cm^{-1} for H_2O and at 384, 332, and 305 cm^{-1} for D_2O.[7] These bands are clearly identified as

[7]The corresponding HDO motions could not be completely enumerated because of interference from H_2O and D_2O bands.

Can. J. Chem. Downloaded from www.nrcresearchpress.com by 210.87.254.6 on 09/05/12
For personal use only.

librations by the frequency shift on deuteration, the frequency ratios averaging 1.40, very close to $\sqrt{2}$ expected for pure motion of hydrogen atoms. The possibility that the two lower frequencies are due to dynamic coupling is unlikely because other water vibrations show negligible coupling and because of the absence of absorption at intermediate frequency, which would be expected for isotopically isolated H_2O or D_2O molecules at lower isotopic concentrations. The appearance of all three librational fundamentals of the water molecule points to an extremely asymmetric force field. The gradual weakening of the 530 cm^{-1} band and the convergence of the 458 and 427 cm^{-1} bands at increasing temperature (Fig. 6) implies a diminution of molecular asymmetry through increased thermal motion, attested to independently by the temperature variation of HDO stretching frequencies.

A detailed description of the motion corresponding to each of the three librational fundamentals is not possible, nor can we identify the one in-plane and two out-of-plane librational motions from the present i.r. results obtained with polycrystalline specimens.

Environment of the Water Molecule in $K_2SnCl_4.H_2O$

Analysis of the i.r. spectrum has shown that: (*a*) all the water molecules are equivalent; (*b*) the water molecules are isolated from one another and probably do not share common neighbors; (*c*) the environment of the water molecule is highly asymmetric, the asymmetry decreasing somewhat with increasing temperature; (*d*) both hydrogens of the water molecule participate in hydrogen bonding, but one of the hydrogen bonds is considerably weaker and probably highly bent.

Conclusion (*c*) contradicts the structure proposed for $K_2SnCl_4.H_2O$ by Itoh *et al.* (3, 4): placing the water oxygen in equipoint 4(*f*) of *Pbam*, of symmetry C_2-2, implies equivalence of the two hydrogens of the water molecule. However, all four conclusions are compatible with the environment of H_2O which results when the K.G. structure is combined with the p.m.r. evidence (*cf.* above), *i.e.* essentially that of Fig. 2. While a more accurate location of the H atoms by neutron diffraction will be welcome, it is evident that H(1) participates in a "normal" hydrogen bond to $Cl(3)^D$, and H(2) in a bifurcated hydrogen bond to $Cl(2)^B$ and $Cl(2)^{B'}$.

The *symmetric* bifurcated hydrogen bond is an interesting feature of the structure. Only one other case of a water molecule participating in such a bond appears to be known, that of $H_2O(2)$ in $NiCl_2.6H_2O$ (16). The bifurcated H-bonds in the two compounds have almost identical geometries, when one takes account of the difference of *ca.* 0.40 Å between the van der Waals radii of chlorine and oxygen:

Compound	H-acceptor atom, *X*	Angle O—H...*X* (deg)	H...*X* distance (Å)
$NiCl_2.6H_2O$	Oxygen	139	2.27
$K_2SnCl_4.H_2O$	Chlorine	137	2.64

In both instances the other H atom of the water molecule participates in a normal H-bond of average length and the coordination of the remaining nearest neighbors about the H_2O molecule is approximately tetrahedral. However, in the Ni compound the two electron-acceptor neighbors are OH groups of other water molecules, while in $K_2SnCl_4.H_2O$ they are two potassium ions.

Do Bifurcated Hydrogen Bonds Have Characteristic Spectral Features?

$K_2SnCl_4.H_2O$ appears to be the first crystalline hydrate which contains a bifurcated hydrogen bond and whose i.r. spectrum has been examined in detail. It affords an opportunity to enquire whether or not it is possible to recognize the presence of a bifurcated H-bond from spectral features which may be characteristic of it. This is a question of a wider interest than might at first appear, for weak and highly bent hydrogen bonds in crystals tend to approach, or achieve, the bifurcated geometry (9), and spectral evidence would be desirable for the presumed occurrence of bifurcated H-bonds as intermediate transition states during molecular rotations of H_2O molecules in liquid water.

Several of the features observed in the i.r. spectrum of water in $K_2SnCl_4.H_2O$ are unusual: (*i*) the relatively high stretching frequency of OH(2), (*ii*) the negative value of dv/dT for OH(2), (*iii*) the nearly equal intensities of the three libration fundamentals, and (*iv*) the large effect of temperature on the relative intensities of the libration fundamentals. It has previously been shown that (*i*) and (*ii*) are associated with weak and highly bent H-bonds (9), while (*iii*) and (*iv*) appear to indicate the presence of a highly asymmetric force

Can. J. Chem. Downloaded from www.nrcresearchpress.com by 210.87.254.6 on 09/05/12
For personal use only.

field. Thus none of the individual spectral features of $K_2SnCl_4.H_2O$ are uniquely attributable to bifurcation, but *observed together*, (*i*) to (*iv*) may prove to be characteristic of it. Whether or not these combined features constitute a reliable diagnostic can only be determined when the spectra of further hydrates containing bifurcated H-bonds have been examined.

One may ask next whether O_wH groups of water molecules participating in bifurcated H-bonds show any characteristic deviations from the well-known correlation between the OH (or OD) stretching frequency and the $O_w...X$ distance (the ν–R correlation) (9). On the one hand, bifurcated H-bonds are highly bent and hence weaker than straight bonds of the same $O_w...X$ distance, so a shift toward higher frequencies may be expected relative to O_wH groups engaged in "normal" H-bonds. On the other hand, *two* H-bond acceptor atoms are involved, leading to a stronger bond, hence a frequency *lowering* would be expected. When the stretching frequencies of isotopically isolated HDO in $K_2SnCl_4.H_2O$ are entered in the ν–R plot, such as the one in Fig. 17 on p. 106 of ref. 9, it is found that the points for OH(1) and OH(2) lie about 1.5σ off the ν–R regression line toward low frequencies (*i.e.* greater interatomic distances). These deviations we consider too small to be significant, particularly as the deviation is about the same for both the normal and the bifurcated OH group. This would suggest that the expected opposing frequency shifts compensate almost exactly, at least in the symmetrically bifurcated case.

Some i.r. data are available for $BaCl_2.2H_2O$, which contains two crystallographically distinct water molecules, $H_2O(1)$ with two "normal" H-bonds and $H_2O(2)$ with one "normal" and one bifurcated bond (17). Although this hydrate has been the subject of several spectroscopic studies, serious problems of frequency assignment unfortunately remain, in particular in the libration region, for which several sets of alternative band assignments have been proposed (for review see Table XII on p. 109 of ref. 9). The stretching frequencies of isotopically isolated HDO have been reported briefly by Schiffer and Hornig (18) and more fully by Brink (19), but corresponding frequencies in the two sets differ by as much as 36 cm^{-1}. Choosing the more recent data of Brink and assigning the highest stretching frequency to hydrogen H(4), which forms the bifurcated bond, leads to a good fit in the ν–R correlation, well within one standard deviation. Brink's results also show that the value of $d\nu/dT$ for the stretching of the bifurcated OH group is negative, in contrast to the positive $d\nu/dT$ values for the remaining three OH groups. Additional i.r. results for $BaCl_2.2H_2O$ as well as for the several other hydrates known to contain bifurcated and nearly-bifurcated H-bonds (Table III, p. 74 of ref. 9) are clearly desirable.

NOTE ADDED IN PROOF: The unit cell dimensions of $K_2SnCl_4.H_2O$ have been redetermined using a single-crystal diffractometer on a crystal from the same batch as used for our i.r. study. The new values are 12.0316(9), 9.1300(13), and 8.2517(7) Å. The differences between these values and those quoted in Table 1 are too small to warrant recalculating the interatomic distances in the paper. We are indebted to Dr. P. S. White for providing us with this information.

We wish to thank Miss Gwen H. Thomas for carrying out the early stages of the experimental work, and Mr. Ping F. Seto for his excellent and many-faceted assistance with this investigation.

1. H. BRASSEUR and A. DE RASSENFOSSE. Z. Krist. **101**A, 389 (1939).
2. H. BRASSEUR and A. DE RASSENFOSSE. Nature, **143**, 332 (1939).
3. J. ITOH, R. KUSAKA, Y. YAMAGATA, R. KIRIYAMA, H. IBAMOTO, T. KANDA, and Y. MASUDA. J. Phys. Soc. Jap. **8**, 287 (1953).
4. J. ITOH, R. KUSAKA, Y. YAMAGATA, R. KIRIYAMA, and H. IBAMOTO. J. Phys. Soc. Jap., **8**, 293 (1953).
5. International tables for X-ray crystallography. Vol. 1. The Kynoch Press, Birmingham. 1952.
6. A. A. SILVIDI and J. W. MCGRATH. Bull. Am. Phys. Soc. Ser. II, **4**, 471 (1959).
7. J. W. MCGRATH and A. A. SILVIDI. J. Chem. Phys. **34**, 322 (1961).
8. B. KAMENAR and D. GRDENIĆ. J. Inorg. Nucl. Chem. **24**, 1039 (1962).
9. M. FALK and O. KNOP. Water: a comprehensive treatise. Vol. 2. *Edited by* F. Franks. Plenum Press, New York. 1973. Chapt. 2.
10. B. KAMENAR and D. GRDENIĆ. J. Chem. Soc. 3954 (1961).
11. G. M. RICHARDSON. Am. Chem. J. **14**, 89 (1892).
12. R. A. NYQUIST and R. O. KAGEL. Infrared spectra of inorganic compounds. Academic Press, New York and London. 1971.
13. J. E. D. DAVIES and I. R. TENCH. Inorg. Nucl. Chem. Lett. **7**, 491 (1971).
14. G. H. THOMAS, M. FALK, and O. KNOP. Can. J. Chem. **52**, 1029 (1974).
15. G. BRINK and M. FALK. Can. J. Chem. **48**, 2096 (1970).
16. R. KLEINBERG, J. Chem. Phys. **50**, 4690 (1969).
17. V. M. PADMANABHAN, W. R. BUSING, and H. A. LEVY. Acta Cryst. **16**, A26 (1963).
18. J. SCHIFFER and D. F. HORNIG. *In* Molecular dynamics and structure of solids. *Edited by* R. S. Carter and J. J. Rush. Natl. Bur. Stand. Special Publ. No. 301. 1969. p. 257.
19. G. BRINK. Spectrochim. Acta, **28**A, 1151 (1972).

Can. J. Chem. Downloaded from www.nrcresearchpress.com by 210.87.254.6 on 09/05/12
For personal use only.

Electronic and Vibrational Relaxation in Sulfur Dioxide Vapor

ROBERT B. CATON AND A. R. GANGADHARAN

Department of Chemistry, Scarborough College, University of Toronto, West Hill, Ontario M1C 1A4

Received December 17, 1973

ROBERT B. CATON and A. R. GANGADHARAN. Can. J. Chem. **52**, 2389 (1974).

Vibrational relaxation in the A^1B_1 and a^3B_1 excited electronic states of sulfur dioxide vapor has been observed by direct spectroscopic means. The effects of vibrational relaxation on the phosphorescence quantum yield have been investigated in the pressure range from 0.6 to 200 mTorr of pure sulfur dioxide and in mixtures of sulfur dioxide with He, N_2, CO_2, and SF_6. Phosphorescence persists at the lowest pressure reached for excitation at 302.0 or 313.1 nm, contrary to previous reports. The mechanism for the production of sulfur dioxide phosphorescence for the wide bandwidth excitation used here (185–370 cm^{-1}) is consistent with recent evidence for two fluorescing species provided by Brus and McDonald from laser-excitation experiments.

ROBERT B. CATON et A. R. GANGADHARAN. Can. J. Chem. **52**, 2389 (1974).

On a observé à l'aide de méthodes spectroscopiques directes la relaxation vibrationnelle des états électroniques excités $\tilde{A}^1B_1$ et $\tilde{a}^3B_1$ du dioxyde de soufre à l'état de vapeur. On a étudié les effets de la relaxation vibrationnelle sur le rendement quantique de phosphorescence pour l'intervalle de pressions de 0.6 à 200 mTorr de dioxyde de soufre pur et pour des mélanges de dioxyde de soufre avec He, N_2, CO_2 et SF_6. Contrairement à ce qui a été rapporté précédemment, la phosphorescence des excitations à 302.0 et 313.1 nm persiste jusqu'à la plus basse pression atteinte. Le mécanisme proposé pour expliquer la phosphorescence du dioxyde de soufre provoqué par une excitation par de grande largeur de bande telle qu'utilisée ici (185–370 cm^{-1}), est en accord avec les résultats obtenus récemment par Brus et McDonald lors d'expériences d'excitation par laser et qui suggéraient l'existence de deux espèces fluorescentes.

[Traduit par le journal]

Introduction

Calvert and co-workers (1–3) have studied unresolved emission from the low-lying excited electronic states of SO_2 stimulated either by a broad-band light source or by various laser lines. Recently, Brus and McDonald (4) reported fluorescence lifetime measurements made at several wavelengths with a narrow-bandwidth (3 cm^{-1}) tunable laser source, using cutoff or wide-bandpass filters to isolate SO_2 fluorescence. Implications of the vibronic structure of SO_2 emission, in both fluorescence and phosphorescence, reported by Greenough and Duncan (5) and by Mettee (6), however, have received little attention.

Recently, Sidebottom *et al.* (1) detected what appeared to be vibrational relaxation effects on the fluorescence lifetime and quantum yield of the $\tilde{A}^1B_1$ state of SO_2. Their interpretation of these results is that for levels with excess vibrational energy between 5329 and 9356 cm^{-1}, lower-lying vibronic states of excited singlet SO_2 undergo more rapid radiationless relaxation than do higher-lying states. The fluorescence lifetime appeared to increase with decreasing wavelength of the exciting light. This trend is opposite to that observed by Douglas (7).

Another uncertainty in the SO_2 literature concerns the zero-pressure fluorescence quantum yield. Mettee (6) found that the fluorescence yield determined by extrapolating Stern–Volmer graphs to zero-pressure is essentially unity at exciting wavelengths from 265.0 to 313.0 nm. Rao and Calvert (8) came to the conclusion that the wavelength-dependent fluorescence quantum yield is significantly less than unity for all relevant wavelengths. Brus and McDonald (4), however, demonstrated that SO_2 fluorescence excited in the 300 nm region is characterized by two emitting "states", one short-lived and one long-lived. On the basis of the work of Brus and McDonald, Calvert (9) has reinterpreted his group's previous results to be consistent with a fluorescence quantum yield of 1.0 for isolated SO_2 molecules. Thus, the phosphorescent $\tilde{a}^3B_1$ state must be populated from $\tilde{A}^1B_1$ by collisional perturbation. The mechanism and energy dependence of populating the $\tilde{a}^3B_1$ state have not yet been described clearly.

In the hope of clarifying these processes we

Can. J. Chem. Downloaded from www.nrcresearchpress.com by 210.87.254.105 on 09/05/12
For personal use only.

Can. J. Chem. Downloaded from www.nrcresearchpress.com by 210.87.254.105 on 09/05/12
For personal use only.

have recorded vibronically resolved emission spectra from the $\tilde{A}^1B_1$ ($^1SO_2$, fluorescence) and $\tilde{a}^3B_1$ ($^3SO_2$, phosphorescence) states of SO_2 at pressures of pure SO_2 between 6×10^{-4} and 2×10^{-2} Torr and in mixtures of SO_2 with various quenching gases. We have used these spectra to compute fluorescence and phosphorescence quantum yields as functions of pressure.

Experimental

The materials used were commercial cylinder gases: Anhydrous grade SO_2 (99.98%), High purity He (99.995%), Prepurified N_2 (99.997%), SF_6 (99.8%), and Extra Dry grade CO_2 (99.8%). All materials were manipulated and admitted to the emission cell in a grease-free, mercury-free vacuum system.

The apparatus for exciting and observing SO_2 emission was similar to that described by Parmenter and Schuyler (10). A 15 cm long White cell formed the excitation arm. The detection arm of the cell was 35 cm long, 10 cm in diameter, and fitted with spherical mirrors. An MKS Baratron capacitance manometer was connected directly to the emission cell, whereby absolute pressure down to 0.2 mTorr could be measured with 1% accuracy, according to the manufacturer's specifications. When experimental conditions, such as outgassing and temperature variations, are taken into account, we estimate that for the duration of the experiments results of which are reported below, the uncertainty in our pressure reading was about 30% at 0.6 mTorr, improving to 5% at 7 mTorr and to 1% at 20 mTorr.

The 289.4, 296.7, 302.0, or 313.1 nm pressure-broadened lines from a 200 W Hg/Xe compact-arc lamp were selected by a ½ m monochromator. The bandpass of this instrument was between 1.6 and 3.2 nm for various experiments (about 185 to 370 cm^{-1} at these wavelengths).

The detecting system was a Spex 3/4 m spectrometer, coupled with a cooled EMI 6256S photomultiplier tube, and an Ortec photon-counting unit with analog output through a linear ratemeter. A 0.5 nm bandpass was used during the recording of all spectra.

All of the emission quantum yields which we measured were relative yields. They were computed either by integrating band areas or by measuring band heights in vibronically resolved spectra. Phosphorescence peaks were corrected for the underlying fluorescence contribution. In the case of emission from pure SO_2, the relative yields were computed by dividing the band area (or band height) by the SO_2 pressure, assuming the absorbed light intensity to vary linearly with pressure. This assumption was shown to be valid in our cell up to about 200 mTorr at 313.1 nm and up to about 100 mTorr at the other wavelengths.

In the case of SO_2 mixed with buffer gases, the relative yield was taken as the ratio of the band area to that of the pure SO_2 band. The selected phosphorescence band was scanned with 1 or 5 mTorr of SO_2 in the cell. Quenching gases were admitted to the cell in increments through a micrometer needle value. When equilibrium was reached, as demonstrated by the stabilization of emission intensity, the peak was scanned again for each increment of quenching gas. The selected phosphorescence band was normally that at 415.3 nm, which is assigned as the $\tilde{a}^3B_1$ (000) $\rightarrow$ $\tilde{X}^1A_1$ (110) transition (5). This band was incompletely resolved from the (000) $\rightarrow$ (030) band to shorter wavelengths (413.2 nm), but since they both originate in the vibrationless level in the excited triplet state, their pressure dependence is identical. We monitored this band because it is the most intense band in the phosphorescence spectrum and because this region of the spectrum is free from the resonance fluorescence bands (26) which appear interlaced with the phosphorescence bands at low pressure. See Fig. 1*c*. All of our reported phosphorescence quantum yields, then, refer to the zero-point level of the $\tilde{a}^3B_1$ state.

Although we have measured only relative phosphorescence quantum yields, those reported below have been converted to absolute yields by normalizing our data to Mettee's absolute yields (6, 27). Our relative values were converted by fitting pseudo-Stern–Volmer plots to the raw data which were the basis of Fig. 9 in ref. 6. This procedure seems reasonable, since there is consistent agreement about the absolute phosphorescence yields measured by Mettee and by Rao *et al.* (11).

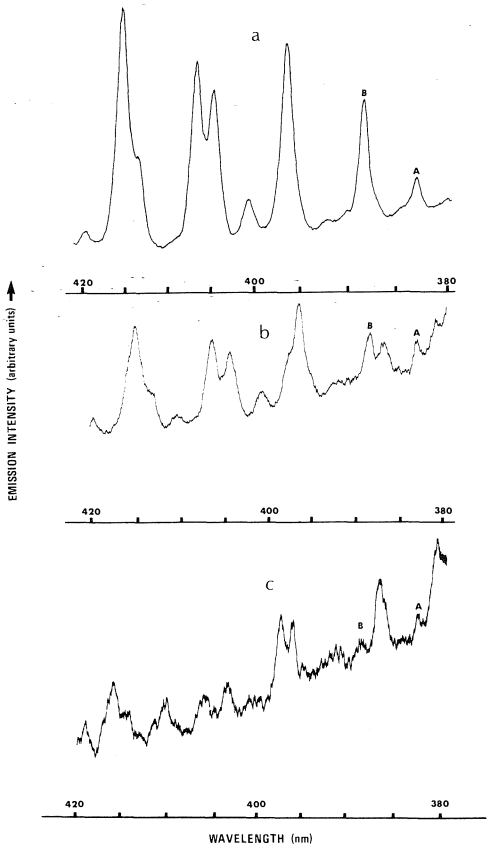

FIG. 1. Phosphorescence spectra of pure SO_2 vapor at (*a*) 102 mTorr, (*b*) 10 mTorr, (*c*) 3 mTorr. The band marked A is $\tilde{a}^3B_1(010)$–$\tilde{X}^1A_1(000)$; B is $\tilde{a}^3B_1(000)$–$\tilde{X}^1A_1(000)$.

Can. J. Chem. Downloaded from www.nrcresearchpress.com by 210.87.254.105 on 09/05/12
For personal use only.

Results

The Phosphorescence Spectrum and Vibrational Relaxation in the $\tilde{a}^3B_1$ State

Figure 1 depicts part of the 313.1 nm excited emission spectrum originating from the $\tilde{a}^3B_1$ state of SO_2 at three stages of relaxation. The high-pressure spectrum (*a*) is that of the vibrationally-equilibrated $^3B_1$ state. The bands marked A and B are the (010)–(000) and (000)–(000) transitions, respectively, of the $\tilde{a}^3B_1$–$\tilde{X}^1A_1$ system (12, 13). The relative intensity of these two bands changes markedly as the pressure is reduced, as shown in Fig. 1*b* and *c*. Figure 2 shows the pressure dependence of the ratio of intensities of bands A and B, demonstrating that equilibrium in the bending mode (ν_2) does not obtain below about 30 mTorr. That is, the ratio of intensities persists at a value of about 0.2 from 30 mTorr to higher pressures, in good agreement with a prediction of 0.21 from the product of the Boltzmann factor for ν_2 with the ratio of Franck–Condon factors from the absorption spectrum.

If we assume that the SO_2–SO_2 collision frequency at 30 mTorr is the characteristic number of collisions necessary to bring about equilibration and that the initial excess of vibrational energy in the $^3B_1$ state is given by the difference between the energy of the exciting line and the zero-point energy of the $^3B_1$ state, we can compute the average amount of vibrational energy removed per collision. In the case of 313.1 nm excitation, the maximum excess vibrational energy is about 6170 cm^{-1}. At 30 mTorr, a $^3SO_2$ molecule undergoes about 200 collisions during its lifetime. Thus, an intermolecular collision removes an average of 30 cm^{-1}, and about 12 collisions at maximum, are required to remove one quantum of the bending mode in the triplet state (ν_2 = 360 cm^{-1}).

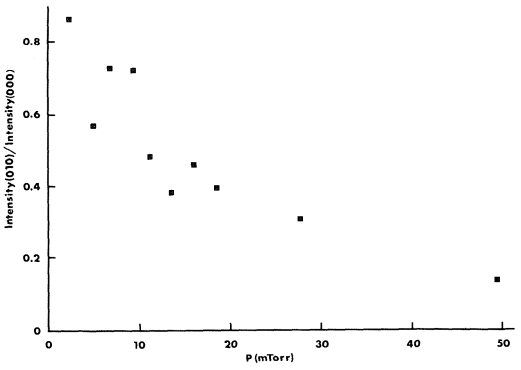

FIG. 2. Relative intensity of the (010)–(000) and (000)–(000) phosphorescence bands, marked A and B in Fig. 1, respectively, *vs.* pressure of SO_2.

The Fluorescence Spectrum and Vibrational Relaxation in the $\tilde{A}^1B_1$ State

Figure 3 presents fluorescence spectra excited by 313.1 nm radiation of two different pressures. In Fig. 4, we have plotted the ratio of the intensity of the resonance fluorescence band which teminates in the (100) level of the ground state (marked R in Fig. 3) to the intensity at the maximum of the fluorescence envelope for 289.4, 296.7, 302.0, and 313.1 nm excitation. Figure 4, then, represents a rough measure of the redistribution of fluorescence intensity as the resonance emission diminishes and the equilibrated fluorescence increases with increasing pressure. This graph can be interpreted similarly to Fig. 2 to give the amount of excess vibrational energy in the $^1B_1$ state which is removed by an SO_2–SO_2 collision. The pressure at which equilibrium appears to obtain for 302.0 and 313.1 nm excitation is about 10 mTorr, where SO_2 singlets undergo about 5 hard-sphere collisions during their lifetime. If we take 28 238 cm^{-1} as the energy of the zero-point level in $\tilde{A}^1B_1$ (14), the excess vibrational energy at 302.0 and 313.1 nm is 4875 and 3701 cm^{-1}, respectively. Thus, each SO_2–SO_2 collision removes a mean of about 900 cm^{-1} of vibrational energy.

For comparison, we note that McClelland and

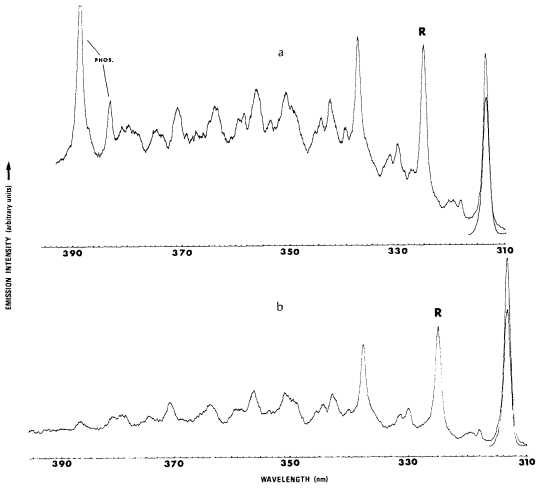

FIG. 3. Fluorescence spectra of pure SO_2 vapor at (*a*) 56 mTorr, (*b*) 1 mTorr. The band marked R is the resonance transition which terminates in $\tilde{X}^1A_1(100)$.

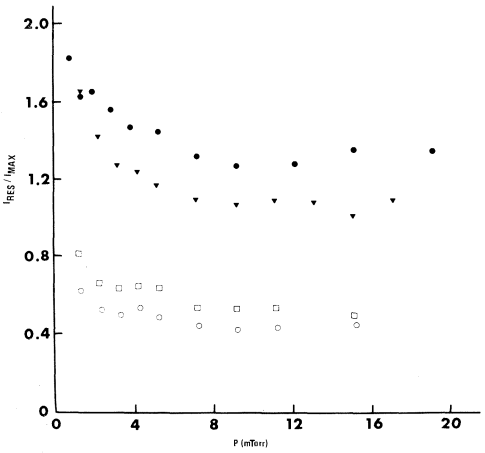

FIG. 4. Relative intensity of resonance fluorescence and emission maxima for pure SO_2 taken as the ratio of the intensity of the (initially-excited level) $\rightarrow \tilde{X}^1A_1(100)$ band, marked R in Fig. 3, to that of the maximum in the emission envelope *vs.* pressure. ●, 313.1 nm; ▼, 302.0 nm; □, 296.7 nm; ○, 289.4 nm excitation.

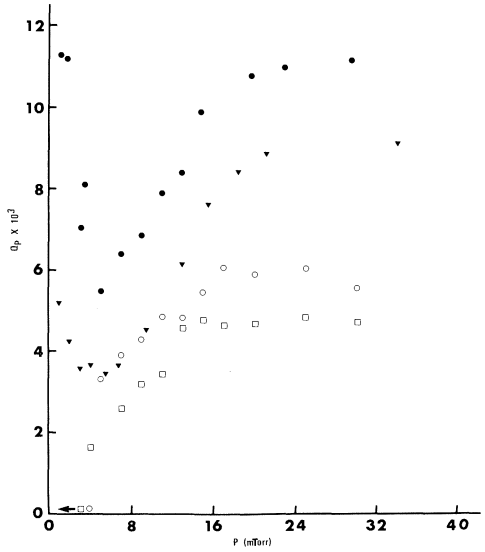

FIG. 5. Absolute phosphorescence quantum yield from the zero-point level of pure SO_2 vapor, Q_P, *vs.* pressure. Relative yields from this work normalized to Mettee's (6) data. Symbols refer to the same wavelengths as in Fig. 4. The arrow indicates essentially zero phosphorescence at all pressures below the last data points for 296.7 and 289.4 nm excitation.

Yardley (15) have found that the fluorescent state of biacetyl loses about 730 cm^{-1} of vibrational energy per collision between excited and ground state biacetyl molecules by an unspecified relaxation mechanism.

Phosphorescence Quantum Yields

The phosphorescence quantum yields for 289.4, 296.7, 302.0, and 313.1 nm excitation, normalized to Mettee's absolute yield data as outlined in the Experimental section, are presented as functions of pressure in Fig. 5. It is clear from this figure that the pressure dependence of Q_P for 289.4 and 296.7 nm excitation is qualitatively different from that for 302.0 and 313.1 nm excitation. We should bear in mind that all of the Q_P's in Fig. 5 refer to the zero-point level of the $^3B_1$ state, since this was the only level which could be monitored consistently at all pressures.

Figures 6 and 7 represent the relative phosphorescence quantum yield for 313.1 nm excitation for various quenching gases added to 1 and 5 mTorr of SO_2, respectively.

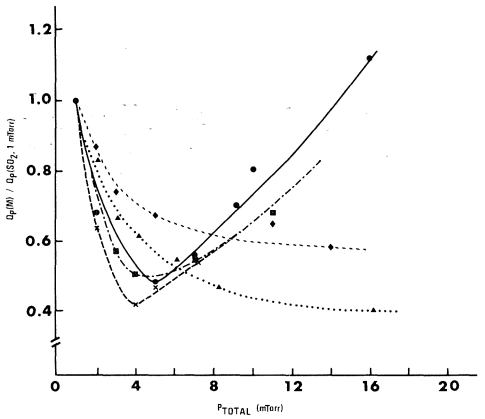

FIG. 6. Relative phosphorescence quantum yield of SO_2 for various foreign gases added to 1 mTorr SO_2 *vs.* total pressure. ● (—), SF_6; ■ (– - –), SO_2; X(- - -), CO_2; ◆ (▌▌▌), He; ▲ (···), N_2. The lines are for guidance only. 313.1 nm excitation.

Discussion

Vibronic Structure in the Relaxation Mechanism

In terms of the traditional kinetic emission mechanism which has been proposed by several authors, the following scheme seems to pertain to primary photophysical processes in SO_2 vapor:

[1] $SO_2 + h\nu_{abs} \rightarrow {}^1SO_2{}^m$

[2] ${}^1SO_2{}^m + M \rightarrow {}^1SO_2{}^n + M,\ n = m - 1, ..., 0$

[3*a*] ${}^1SO_2{}^m + M \rightarrow SO_2 + M$

Can. J. Chem. Downloaded from www.nrcresearchpress.com by 210.87.254.105 on 09/05/12
For personal use only.

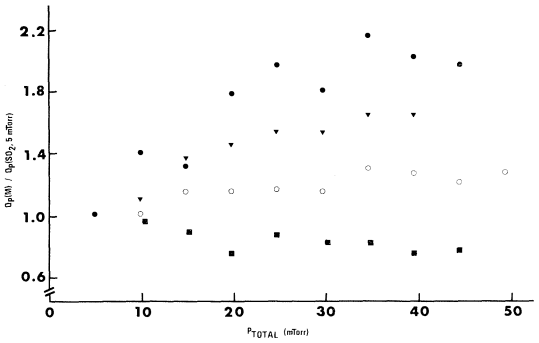

FIG. 7. Relative phosphorescence quantum yield of SO_2 for various foreign gases added to 5 mTorr SO_2 *vs.* total pressure. ●, SF_6; ▼, CO_2; ○, N_2; ■, He. 313.1 nm excitation.

[3*b*] $^1SO_2{}^n + M \rightarrow SO_2 + M$

[4] $^1SO_2{}^m + M \rightarrow {}^3SO_2{}^p + M$

[5] $^1SO_2{}^n + M \rightarrow {}^3SO_2{}^q + M$

[6] $^3SO_2{}^p + M \rightarrow {}^3SO_2{}^q + M, q = p - 1, ..., 0$

[7*a*] $^3SO_2{}^p + M \rightarrow SO_2 + M$

[7*b*] $^3SO_2{}^q + M \rightarrow SO_2 + M$

[8] $^1SO_2{}^{m,n} \rightarrow SO_2 + h\nu_{fl}$

[9] $^3SO_2{}^{p,q} \rightarrow SO_2 + h\nu_{phos}$

[10*a*] $^1SO_2{}^m \rightarrow SO_2$

[10*b*] $^1SO_2{}^n \rightarrow SO_2$

[11*a*] $^1SO_2{}^m \rightarrow {}^3SO_2{}^p$

[11*b*] $^1SO_2{}^n \rightarrow {}^3SO_2{}^q$

[12*a*] $^3SO_2{}^p \rightarrow SO_2$

[12*b*] $^3SO_2{}^q \rightarrow SO_2$

M represents either SO_2 or an added gas. *m*, *n*, *p*, and *q* represent vibrational quantum numbers for unspecified normal modes.

It is clear from our work that steps 2, 4, 5, and perhaps 6 and 7 are important in regulating the channels by which electronic relaxation occurs in SO_2. Certainly step 6 occurs, as the data of Fig. 2 show, but whether step 7 influences the mechanism of electronic relaxation in the low pressure region is not clear. Wampler *et al.* (3) have convincing evidence that step 7*a* is much faster than step 7*b* when $q = 0$, but in the low pressure region of the present work (≤ 15 mTorr) where new phenomena appear, neither step 7*a* nor step 7*b* is important, that is, bimolecular quenching of $^3B_1$ is a slow and unimportant process.

In the following discussion, we assume by inference from Figs. 4 and 5 that electronic relaxation out of various vibrational states of $^1SO_2$ implies relaxation into $^3B_1$, along with other final states. This correlation is suggested by the fact that the onset of a marked change in the $^3B_1$ emission yield occurs at essentially the same pressure as the onset of vibrational relaxation arrest in $^1SO_2$.

The rates of intersystem crossing for steps 4 and 5, that is, for different vibrational levels of $^1SO_2$, appear to be quite different. Vibrational relaxation of $^1SO_2$ from the initial levels populated by 289.4 and 296.7 nm radiation enhances the intersystem crossing process to $^3B_1$. Vibrational relaxation from the initial levels reached by 302.0 and 313.1 nm radiation diminishes intersystem crossing to $^3B_1$. The data for 289.4 and 296.7 nm are consistent with the observations of Sidebottom *et al.* (1) that the non-radiative contribution to the $^1SO_2$ fluorescence lifetime increases with exciting wavelength up to 298.0 nm. That is, in the wavelength region common to the two studies, the decrease in non-radiative decay of $^1SO_2$ as the excess vibrational energy increases observed by Sidebottom *et al.* correlates with the decrease in phosphorescence quantum yield which we have found.

In this regard the 302.0 and 313.1 nm data are most illuminating. At these wavelengths, vibrational relaxation brings about the opposite effect on the quantum yield, namely the $^3B_1$ quantum yield increases when the vibrational relaxation of $^1SO_2$ is arrested. This trend is consistent with Douglas' observation (7) that the non-radiative contribution to the fluorescence lifetime of $^1SO_2$ increased with decreasing wavelength in an unspecified range. This qualitatively different behavior is strongly suggestive that a resonance, or at least some structure, occurs in the spectrum of the non-radiative relaxation rate of $^1SO_2$ into $^3SO_2$.

If we combine our results with those of Sidebottom *et al.* (1), we can locate very approximately the region of strongest coupling between the $^1B_1$ and $^3B_1$ manifolds. Sidebottom *et al.* observed that the lifetime of the unrelaxed singlet state decreases with increasing wavelength of excitation between 266.0 (± 10) nm and 298.0 (± 14) nm. Our data imply that the non-radiative process which populates the $^3B_1$ mani-

Can. J. Chem. Downloaded from www.nrcresearchpress.com by 210.87.254.105 on 09/05/12
For personal use only.

Can. J. Chem. Downloaded from www.nrcresearchpress.com by 210.87.254.105 on 09/05/12
For personal use only.

fold increases in importance as the energy of the vibronic level approaches that of the level populated in direct absorption at either 313.1 (±16) nm or 302.0 (±16) nm. If the non-radiative processes which decrease the singlet lifetime and increase the triplet quantum yield are related (as we have presumed), then the region of maximum interaction between the singlet and triplet manifolds, or between these two manifolds and some other manifold, is bracketed about the level corresponding to the absorption band at 300 nm. This level coincides with the maximum intensity in the magnetic rotation spectrum observed by Hardwick (16), but not with the maximum intensity of the normal absorption spectrum, which occurs at shorter wavelengths.

Thus, Renner–Teller coupling between the $^1B_1$ and $^1A_1$ components of a $^1\Delta_g$ linear state, which Hardwick invokes to account for the appearance of the magnetic rotation effect in quasi-linear $^1B_1$ SO_2, may also provide the channel necessary for efficient radiationless relaxation of $^1B_1$ during collisional perturbations. Whether an intermediate state, as suggested by Sidebottom *et al.* (1), is involved cannot be determined from this work.

Zero Pressure Phosphorescence Quantum Yield

We turn now to the question of the significance of the non-zero intercept of the Q_P *vs.* P graphs for 302.0 and 313.1 nm excitation (Fig. 5). In terms of the relaxation mechanism, steps 1–12, a non-zero phosphorescence quantum yield at zero pressure implies that step 11 occurs to an appreciable extent. A phosphorescence quantum yield of zero at zero pressure, as obtains for 289.4 and 296.7 nm excitation, implies that step 11 is unimportant and that collisional perturbation (steps 4 and 5) is the only mechanism of $^3B_1$ production.

Even at the lowest pressure for which we have phosphorescence quantum yield data, 0.6 mTorr, neither singlet nor triplet SO_2 molecules are collision-free during their lifetime. From the usual kinetic molecular theory parameters and a typical lifetime of about 50 μs, one computes that a $^1SO_2$ molecule undergoes about 0.3 collision during its lifetime at 0.6 mTorr. The longest lifetime measured by Brus and McDonald (4), 532 μs for 319.8 nm excitation, would lead to a collision number of about 3 at 0.6 mTorr. Similarly for a typical lifetime of 1 ms, a $^3B_1$ molecule undergoes about 6 collisions at the same pressure. We would have to extend our data to two orders of magnitude lower in pressure to be able to conclude confidently what happens in a truly isolated $^1SO_2$ molecule. We can state, however, that under conditions for which a $^1SO_2$ molecule undergoes a relatively small number of collisions, the quantum yield from the zero point level of $\tilde{a}^3B_1$ is ≥ 0.01 for excitation by 302.0 or 313.1 nm radiation and near zero for excitation at 289.4 and 296.7 nm at the lowest pressure which we reached. Because of the complications in the mechanism caused by vibrational relaxation, the Q_P *vs.* P relationship cannot be written in a simple algebraic form, and extrapolation of the ≤ 5 mTorr data to zero pressure is unwarranted.

We can construct a more useful interpretation of the low pressure phosphorescence quantum yield data if we use a stationary-state model, rather than the customary time-dependent model. Douglas (7) and Gelbart and Freed (17) have suggested that the standard kinetic scheme, that is a sequence of transitions between pure electronic states, is of little value in interpreting the relaxation dynamics of small molecules like SO_2. In the "mixed-state relaxation theory" of Gelbart and Freed, the stationary rovibronic states, expressed as linear combinations of Born–Oppenheimer (BO) states replace the pure BO states implied by the notation in our scheme, steps 1–12.

Our data for SO_2 cannot be rationalized by the simple model which Gelbart and Freed (17) and Gelbart and Cazes (18) construct to account for the observed relaxation kinetics of CH_2. The SO_2 data are complicated by the slow vibrational relaxation of the emitting states and by the large number of vibrational quanta excited in the region of strong interaction. The relaxation dynamics must then be described by coupling amongst many mixed rovibronic states of the sort

$$[13]\quad |evr\rangle = c_1(v'r')|^1B_1{}^{v'r'}\rangle + c_2(v''r'')|^3B_1{}^{v''r''}\rangle + c_3(v'''r''')|^1A_1{}^{v'''r'''}\rangle + \ldots$$

The coupling mechanism involves, presumably, both the Renner–Teller coupling between the excited and ground state singlets suggested by Gardner (19) and elaborated by Hardwick (16) and (vibronic) spin–orbit coupling between the two BO singlet manifolds and the BO triplet manifold(s) of vibronic states.

Can. J. Chem. Downloaded from www.nrcresearchpress.com by 210.87.254.105 on 09/05/12
For personal use only.

There may be additional electronic states located near the $^1B_1$ and $^3B_1$ states, such as $^3B_2$ and $^3A_2$, which contribute to the expansion [13] and influence the pathways of electronic relaxation (3, 13). It seems inappropriate, therefore, to speculate about the specific vibronic interactions which might be responsible, especially since rotational interactions, which we did not resolve, may be as important in SO_2 as they appear to be in the excited states of NO_2 (20, 21).

The following model suggests itself. Let us assume, for the moment, that the two sets of lifetimes measured by Brus and McDonald characterize not two different states but sets of strongly coupled and weakly coupled (rotational) levels of a state which is primarily $^1B_1$ in electronic character. We envision a mechanism whereby collisions induce the $^1B_1 \rightarrow {}^1A_1$ internal conversion followed by or simultaneous with intersystem crossing to $^3B_1$, which then relaxes vibrationally and eventually emits from its lower-lying vibrational states.

According to Hardwick's analysis (16), the strongest Renner–Teller coupling between $\tilde{A}^1B_1$ and $\tilde{X}^1A_1$ occurs in the vicinity of $v_2' = 19$, 20, 21. The energy of the initial level reached by 302.0 nm radiation is in the center of this strong coupling region, whereas that reached at 313.1 nm is below and those reached at 289.4 and 296.7 nm are above this region. It seems reasonable to assume that levels above those populated at 289.4 nm and below those populated at 313.1 nm are weakly coupled, since the magnetic rotation spectrum is weak in those regions.

The two exit channels, steps 2 and 4 or 5 in our scheme, compete as the SO_2 molecule relaxes vibrationally and electronically. A large number of collisional coupling matrix elements is required to represent the dynamics of the vibrational relaxation intersystem crossing processes involving sets of cascading levels. That is, vibrational–rotational relaxation modifies the sets of quantum numbers $v'r'$; $v''r''$, etc. in [13] and the nature of the mixed-state changes, likewise the electronic relaxation dynamics. This would lead to a distribution of relaxation rates and multi-exponential transient fluorescence decay. If we confine ourselves to a scheme which involves only the two kinds of levels, strongly and weakly coupled, we can account for the observed behavior of the phosphorescence quantum yield qualitatively, as follows.

First, we note that the levels which we call strongly coupled are quenched at a rate which is an order of magnitude greater than gas-kinetic and a factor of 20 greater than the quenching rate for the weakly coupled levels (4). Vibrational cascade (step 2) from the initially populated levels at 289.4 or 296.7 nm will enhance Q_P through the participation of the lower-lying, strongly-coupled levels. Eventually, the cascade process slows down, since the relaxation probability is roughly proportional to the vibrational quantum number, and a steady-state distribution of vibrational energy is achieved through competition between the slow exit channel [5] and the slow relaxation channel [2] for small values of the quantum numbers. In this situation, Q_P is expected to increase linearly with pressure (see below). Figure 5 exhibits these characteristics roughly.

Cascade from the initially populated levels at 302.0 or 313.1 nm, which we postulate have energies equal to or less than the strongly coupled levels, will diminish Q_P until the above mentioned steady-state situation leads to the expected linear increase of Q_P with pressure. Figure 5 again has the proper characteristics for these two wavelengths. This so-called steady-state distribution of vibrational energy in the singlet manifold is achieved by competition between steps 2 and 5 (as well as [3], of course). That such a frozen, non-thermal distribution obtains is suggested by the appearance of the fluorescence spectrum, Fig. 3. There is clearly a red-shift of the fluorescence maximum with increasing pressure, but the limiting, high-pressure distribution of vibronic intensity appears not to approximate thermal equilibrium.

We cannot improve upon this qualitative scheme with the available information; further detailed rovibronic matrix elements need to be determined experimentally or computed theoretically in order to carry out a detailed analysis of the relaxation dynamics. In the Gelbart–Freed model, relaxation in SO_2 proceeds only by intermolecular perturbations which have been enhanced by intramolecular coupling such as we have mentioned, in agreement with the original Bixon and Jortner model (22). All of our evidence is consistent with their model.

Phosphorescence Yield from $\tilde{a}^3B_1(000)$

A further comparison of our results with other work concerns step 12 of the mechanism. Here again we must choose between the spectroscopic

Can. J. Chem. Downloaded from www.nrcresearchpress.com by 210.87.254.105 on 09/05/12
For personal use only.

state (or mixed-state) model and the usual kinetic (or sequential) model to represent relaxation of the BO $^3B_1$ state. We choose to use the language of the sequential model in order to expedite comparison with previous work. Horowitz and Calvert (23) and Strickler and co-workers (28) agree that the emitting levels of $\tilde{a}^3B_1$, primarily the zero-point level, undergo apparent first-order radiationless relaxation to a surprisingly large extent. Both of these laboratories find $k_9/(k_9 + k_{12})$ to be about 0.065. On the basis of a mechanism which includes steps 1, 3, 5, and 8–12, that is, which involves the relaxed singlet and excludes bi-molecular triplet quenching, the phosphorescence quantum yield depends linearly upon pressure (concentration) as follows

$$[14] \quad Q_P = Q_P^0 + Q_E k_5[SO_2]/(k_8 + k_{10} + k_{11})$$

$Q_E \equiv k_9/(k_9 + k_{12})$ is the parameter of interest, and Q_P^0 is the "spontaneous" phosphorescence yield. The portion of our Q_P *vs.* P graphs (Fig. 5) between 5 and 15 mTorr is, in fact, roughly linear. Substituting the best values of the rate constants of Calvert *et al.* in eq. 14 for excitation near 300 nm gives slope [14] = $Q_E \times 1.59 \times 10^5$ l mol^{-1}.

A least-squares fit to the linear portion of our Q_P *vs.* P graph for 313.1 nm excitation gives

$$[15] \quad Q_P = (3 \pm 2) \times 10^{-3} + 8.3 \times 10^3 \text{ l mol}^{-1}[SO_2]$$

Equating the slope of [14] to the slope of [15], we obtain $Q_E = 0.05$, in good agreement with the above quoted value. There seems to be no reason to expect such an admixture of the ground state into the (000) level of $\tilde{a}^3B_1$, since this level seems to be entirely free of rotational perturbations according to the high-resolution analysis of Brand *et al.* (12). The intercept of [15], Q_P^0, is not significant, except that it is near zero, as it should be if the weakly coupled, long-lived vibrational states of $\tilde{A}^1B_1$ relax to $\tilde{a}^3B_1$ only under the influence of collisions (step 5).

Foreign Gas Quenching

The results depicted in Fig. 6 indicate that the relative efficiencies for the production of $^3B_1$ phosphorescence by collision with the added gases CO_2 and N_2 are roughly the same as those found by Wampler *et al.* (2). The relative efficiencies of CO_2, SF_6, N_2, and He for the production of phosphorescence are essentially the same as for the quenching of $^1SO_2$ fluorescence reported by Mettee (24). This correlation provides additional evidence that fluorescence quenching and phosphorescence inducement are directly connected. Paralleling Mettee's results on $^1SO_2$ quenching (22), CO_2 and SF_6 are about as efficient as SO_2 in producing $^3SO_2$; whereas, N_2 and He are significantly less effective. Our data for CO_2 suggest that, in fact, its efficiency in $^3SO_2$ production is slightly greater than that of SO_2 itself. This result agrees with Greenough and Duncan's conclusion (5) that CO_2 is about 10% more efficient than SO_2 in quenching $^1SO_2$ fluorescence. The SF_6 and CO_2 curves in Fig. 6 level off at higher pressures and behave like the SO_2 curves of Fig. 5. The N_2 and He curves were not followed to higher pressures to determine whether they behave similarly to CO_2 and SF_6.

When the foreign gases are added to the system in which $^1SO_2$ is vibrationally relaxed, represented by Fig. 7, the efficiency of phosphorescence enhancement increases in the order He, N_2, CO_2, SF_6. Similar data for 302.0 nm excitation follow the same pattern.

These data imply that whereas CO_2 appears to be slightly more effective than SF_6 at inducing intersystem crossing from the vibrationally excited mixed state, on the basis of the quantum yield asymptotes, SF_6 is about 50% more effective than CO_2 in inducing intersystem-crossing in the mixed state in which the singlet component is vibrationally relaxed. Intersystem crossing means, in this context, collision-induced enhancement of the coupling between the singlet and triplet components of the mixed state. The reason for this behavior is not clear, since the relative vibrational and electronic quenching cross-sections of these two molecules are not known separately. Mettee (24) found that the quenching efficiency toward $^1SO_2$ correlated best with the polarizability of the collision partner, implying an electronic quenching mechanism. The fact that CO_2 and SF_6 behave somewhat differently toward vibrationally relaxed and excited $^1SO_2$ suggests that a vibrational energy transfer mechanism (v–v) may also be involved. More specific data from narrow-bandwidth experiments are necessary to quantify these observed differences.

It is clear from our results that different vibrational levels of $\tilde{A}^1B_1$, and perhaps of $\tilde{a}^3B_1$ as

Can. J. Chem. Downloaded from www.nrcresearchpress.com by 210.87.254.105 on 09/05/12
For personal use only.

well, have significantly different relaxation pathways. This suggests caution in the interpretation of many of the kinetic data which have been published, since they are not detailed enough to refer to well-defined rovibronic states.

Possible Diffusion Effects

A possibility which we must consider is whether diffusion, that is, a wall effect, plays a role in producing the observed, pressure-dependent phenomena. The vibrational relaxation effects depicted in Figs. 2 and 4 cannot be the result of wall effects, since relative intensities of bands in the same emission system have been plotted. Diffusion might be expected to decrease the phosphorescence quantum yields in Fig. 5 by removing emitting $^3B_1$ molecules from the field of detection, which is opposite to the trend of our data. Sidebottom *et al.* (1) and Otsuka and Calvert (25) have discussed the effects of SO_2 diffusion in their much smaller emission cell. Brus and McDonald (4) also discuss SO_2 diffusion. We calculate that at 1 mTorr, $^1SO_2$ molecules diffuse about 6 cm during their maximum lifetime of about 500 μs. Because of the size and geometry of our cell (see Experimental) and because we detect emission primarily from the center of a large illuminated area, we would not expect diffusion to the walls to enhance the $^3B_1$ yield through collision induced intersystem crossing, since $^1SO_2$ would have to hit the wall and return to the detection region as $^3SO_2$, a distance of at least 10 cm.

The strongest argument against attributing our results to diffusional effects is the quite different behavior of the 296.7 and 302.0 nm excited levels. The lifetimes of the long-lived fluorescing species measured by Brus and McDonald (4) near these wavelengths are 184 μs (296.2 nm) and 308 μs (304.4 nm). This difference in lifetimes would lead to a diffusion distance ratio of only $(308/184)^{1/2} \approx 1.3$, which is certainly not great enough to produce the observed differences in Q_P pressure dependence.

Since diffusion is expected to decrease the apparent $^3B_1$ phosphorescence yield, our data would tend to underestimate rather than overestimate the low pressure quantum yield. We also underestimate Q_P by monitoring only the zero-point level of the $^3B_1$ state, since as Fig. 2 shows, the fraction of phosphorescent intensity which originates from excited vibrational levels of $^3B_1$ increases as the pressure decreases below 30 mTorr. Correcting for this effect is expected to increase Q_P for each wavelength by about the same factor.

NOTE ADDED IN PROOF: The results in Fig. 5 have been confirmed by experiments performed in a 35 cm diameter spherical cell with a large illuminated area. This supports the conclusion that diffusion effects were not responsible for the low-pressure upturn in Q_P.

Conclusion

General trends in various relaxation parameters for SO_2 excited electronic states (first and second order rate constants, quantum yields) which have been deduced in experiments without spectroscopic analysis may be misleading. The existence of resonances, or fine structure, in the spectra of these parameters for SO_2 or SO_2/foreign gas systems may explain some of the confusing discrepancies amongst the published results referred to in the Introduction.

Since our quantum yield data refer only to the zero-point level in $\tilde{a}^3B_1$, we can say little about the total absolute quantum yield from all vibronic levels at $\tilde{a}^3B_1$. Our data, however, established a lower bound to the overall yield in this pressure regime, as discussed in the section on the zero pressure phosphorescence yield. This limitation does not affect the details of our arguments.

This work was supported in part by the National Research Council of Canada. We also thank Drs. L. E. Brus, J. L. Hardwick, and S. J. Strickler for preprints of their papers.

1. H. W. SIDEBOTTOM, K. OTSUKA, A. HOROWITZ, J. G. CALVERT, B. R. RABE, and E. K. DAMON. Chem. Phys. Lett. **13**, 337 (1972).
2. F. B. WAMPLER, J. B. CALVERT, and E. K. DAMON. Int. J. Chem. Kinet. **5**, 107 (1973).
3. F. B. WAMPLER, K. OTSUKA, J. G. CALVERT, and E. K. DAMON. Int. J. Chem. Kinet. **5**, 669 (1973).
4. L. E. BRUS and J. R. MCDONALD. Chem. Phys. Lett. **21**, 283 (1973).
5. K. F. GREENOUGH and A. B. F. DUNCAN. J. Am. Chem. Soc. **83**, 555 (1961).
6. H. D. METTEE. J. Chem. Phys. **49**, 1784 (1968).
7. A. E. DOUGLAS. J. Chem. Phys. **45**, 1007 (1966).
8. T. N. RAO and J. G. CALVERT. J. Phys. Chem. **74**, 681 (1970).
9. J. G. CALVERT. Chem. Phys. Lett. **20**, 484 (1973).
10. C. S. PARMENTER and M. W. SCHUYLER. J. Chem. Phys. **52**, 5366 (1970).

11. T. N. RAO, S. S. COLLIER, and J. G. CALVERT. J. Am. Chem. Soc. **91**, 1609 (1969).
12. J. C. D. BRAND, V. T. JONES, and C. DI LAURO. J. Mol. Spectrosc. **40**, 616 (1971).
13. J. C. D. BRAND, V. T. JONES, and C. DI LAURO. J. Mol. Spectrosc. **45**, 404 (1973).
14. J. C. D. BRAND and R. NANES. J. Mol. Spectrosc. **46**, 194 (1973).
15. G. M. MCCLELLAND and J. T. YARDLEY. J. Chem. Phys. **58**, 4368 (1973).
16. J. L. HARDWICK. Ph.D. Thesis, Georgia Institute of Technology, Atlanta, Georgia. 1972.
17. W. M. GELBART and K. F. FREED. Chem. Phys. Lett. **18**, 470 (1973).
18. W. M. GELBART and D. CAZES. Chem. Phys. Lett. **15**, 37 (1972).
19. P. J. GARDNER. Chem. Phys. Lett. **4**, 167 (1969).
20. P. B. SACKETT and J. T. YARDLEY. J. Chem. Phys. **57**, 152 (1972).
21. C. G. STEVENS, M. W. SWAGEL, R. WALLACE, and R. N. ZARE. Chem. Phys. Lett. **19**, 465 (1973).
22. M. BIXON and J. JORTNER. J. Chem. Phys. **50**, 3284 (1969).
23. A. HOROWITZ and J. G. CALVERT. Int. J. Chem. Kinet. **4**, 175 (1972).
24. H. D. METTEE. J. Phys. Chem. **73**, 1071 (1969).
25. K. OTSUKA and J. G. CALVERT. J. Am. Chem. Soc. **93**, 2581 (1971).
26. R. B. CATON. Unpublished results.
27. H. D. METTEE. Private communication.
28. S. J. STRICKLER, J. P. VIKESLAND, and H. D. BIER. J. Chem. Phys. **60**, 664 (1974).

Can. J. Chem. Downloaded from www.nrcresearchpress.com by 210.87.254.105 on 09/05/12
For personal use only.

Studies on *N,N′*-Diimidyl Systems by Nuclear Magnetic Resonance Spectroscopy

SHIVA MOHAN VERMA, KUMAR OM PRAKASH SINHA, AND CHENNUPATI KOTESWARA RAO

Department of Chemistry, Banaras Hindu University, Varanasi-221005, India

Received September 6, 1973

SHIVA MOHAN VERMA, KUMAR OM PRAKASH SINHA, and CHENNUPATI KOTESWARA RAO. Can. J. Chem. **52**, 2399 (1974).

A number of *N,N′*-diimidyl compounds, which possess asymmetry about the imidyl planes, have been synthesized and characterized by n.m.r. and i.r. spectroscopy. The n.m.r. spectra of the compounds were found to be temperature dependent and provide evidence for the hindered rotation about the N—N′ bond. This characteristic feature has been utilized to establish the proposed structures of the products. The asymmetric "cage moieties" have been found useful for the detection of noncoplanar ground states proposed for this system.

SHIVA MOHAN VERMA, KUMAR OM PRAKASH SINHA et CHENNUPATI KOTESWARA RAO. Can. J. Chem. **52**, 2399 (1974).

On a synthétisé et caractérisé par spectroscopie r.m.n. et i.r. un certain nombre de composés *N,N′*-diimidylés qui possèdent de l'asymétrie autour des plans imidyles. On a trouvé que les spectres r.m.n. de ces composés dépendent de la température et ces résultats indiquent que la rotation est empêchée autour du lien *N,N′*. On a utilisé ces caractéristiques pour établir les structures proposées pour ces produits. On a trouvé utile les "portions en demi cage" asymétriques (asymetric "cage moieties") pour détecter les états fondamentaux non coplanaires proposés pour ce système. [Traduit par le journal]

Can. J. Chem. Downloaded from www.nrcresearchpress.com by 178.218.224.3 on 09/06/12
For personal use only.

Hindered rotation about the N—N′ bond in tetraacylhydrazine systems of the type **1** have been rationalized (1–4) in terms of nonbonding repulsions between the carbonyls at the two nitrogens. The nonbonding repulsive interactions in *N,N′*-diimidyl systems of the type **2** could be much stronger than those in *N′,N′*-diacyl-*N*-aminoimide systems **1** studied so far, where the two carbonyls at the exocyclic nitrogen are free to change their conformations about the N′—CO bonds. Hence it is reasonable to presume such nonplanar ground states and restricted rotation about the N—N′ bond in *N,N′*-diimidyl systems also. X-Ray analysis (5) of *N,N′*-bisuccinimidyl has indicated a 65° dihedral angle between the two imide ring planes while the n.m.r. spectrum (6) failed to show hindered rotation because of symmetry in the molecule. Introduction of some magnetic asymmetry about one of the succinimidyl planes may differently affect the two methylene groups of the other ring and thus the detection of nonplanar ground states by n.m.r. spectroscopy may be achieved. *N,N′*-Biscamphorimidyl has been shown (7) to assume nonplanar ground states due to hindered rotation about the N—N′ bond. Hedaya *et al.* (8) used u.v., i.r., and n.m.r. spectroscopy to distinguish between *N,N′*-diimides and *N,N′*-diisoimides. We report the preparation of some *N,N′*-diimidyl compounds of type **2** and characterization by their temperature dependent n.m.r. spectra.

Compounds with Cyclopentadiene – Maleic Anhydride Adduct Cage Moiety

The n.m.r. spectrum of the *N*-citraconimidyl-[2.2.1]bicyclo-5-heptene-2,3-*endo*-dicarboximide (**2***a*), in $CDCl_3$, shows a slightly broad doublet at δ 2.20 for the *N′*-ring methyl protons, a multiplet at δ 6.66 for the *N′*-ring proton, and normal resonances at δ 6.42 (2H, t),[1] 1.73 (2H, q), and 3.50 (4H, m) for the cage olefinic, methylene, and methine protons, respectively. On higher resolution (50 Hz sweep width), the methyl doublet splits into two interlacing doublets of slightly different intensities (Δν = 1 Hz) due to hindered rotation about the N—N′ bond. Since these protons are far away from the effective magnetic zone of the cage moiety, the signals are not well resolved. However, when nitrobenzene is used as solvent, the *N′*-ring methyl signal appears as a sharp pair of doublets (Δν = 1.6 Hz at 45°) since the methyl group in the two conformers about the N—N′ bond could be affected dif-

[1]The brackets include the number of hydrogens responsible for the signal and the shape of the signal abbreviated as s = singlet, d = doublet, t = triplet, q = quartet, and m = multiplet. In case of multiplicity due to restricted rotation, the ligand of the signal shape is preceded by the *number* of such signals observed.

Can. J. Chem. Downloaded from www.nrcresearchpress.com by 178.218.224.3 on 09/06/12
For personal use only.

ferently by the solvent. The spectrum is temperature dependent and the two doublets move closer as the temperature is raised and coalesce at 95°. This behavior is evidence of hindered rotation about the N—N′ bond and supports a nonplanar type **2** structure.

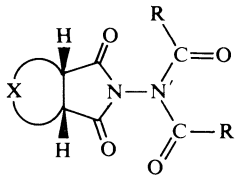

X = A chain of four carbons

1

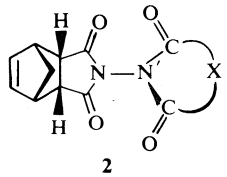

2

a X = —CH=C(CH$_3$)—
b X = —CH=CH—
c X = —CH$_2$—CH$_2$—
d X = —CH$_2$—CH$_2$—CH$_2$—

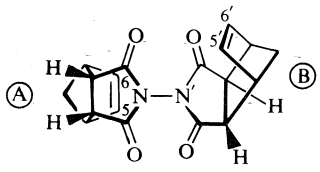

3

The other *N*,*N*′-diimidyl compounds, **2***b–d*, show simple n.m.r. spectra in $CDCl_3$ but when studied in nitrobenzene, the *N*′-ring protons show temperature-dependent multiplicity of signals, thus holding the validity of the above arguments in favor of the proposed structures.

The n.m.r. spectrum of the *N*,*N*′-bis[2.2.1]-bicyclo-5-heptene-2,3-*endo*-dicarboximidyl (**3**), in $CDCl_3$, is similar to that of its simple anhydride. It shows a normal triplet at δ 6.35 for all the four olefinic protons, an AB type quartet at δ 1.70 for both the methylene groups, and a multiplet at δ 3.45 for all the eight methine protons. In a noncoplanar conformation about the N—N′ bond, the C_5-proton in cage A is not magnetically identical with the C_6-proton, because these two protons lie one above and the other below the succinimidyl plane of the cage **B** and similar observation holds with the other protons, except the methylene groups. Therefore, a complicated n.m.r. spectrum could be expected for this compound but the observed simplicity of the spectrum is probably because the protons in each cage moiety are held far away from the magnetic asymmetry of the other cage moiety.

Compounds with Anthracene – Maleic (Citraconic) Anhydride Adduct Cage Moieties

Since the cage moieties of the compounds **4***a–c* are magnetically more asymmetric about the succinimidyl plane when compared to **3**, it is expected that the protons of each cage may be substantially magnetically affected by the other cage. The n.m.r. spectrum of *N*,*N*′-bis-9,10-dihydroanthracene-9,10-*endo*-α-methyl-α, β-succinimidyl (**4***a*), in $CDCl_3$, shows the following resonances: C_{11} and $C_{11'}$ (methyls) δ 1.18 (6H, 2s); C_{12} and $C_{12'}$ δ 2.71 (2H, 2d); C_{10} and $C_{10'}$ δ 4.43 (2H, 2s); C_9 and $C_{9'}$ δ 4.78 (2H, 2d); and C_{1-8} and $C_{1'-8'}$ (aromatic) δ 7.37 (16H, m). It is evident that each set of protons exhibits two signals. A rotation by 180° about the N—N′ bond in structure **4** gives the other stable conformation of the molecule where the magnetic environments of the corresponding protons are changed. Thus the two signals for each set of protons correspond to the two stable conformers. The spectrum of this compound in nitrobenzene exhibits a similar pattern (Δν = 5 Hz for the cage methyl at 45°) and is temperature dependent, thus supporting structure **4**. Similar observations were made for **4***b* dissolved in nitrobenzene. It shows splitting for all the cage protons of the two cage moieties (Δν = 8.5 Hz for the cage methyl at 45°). The well resolved signals of the asymmetric cage were found to be temperature dependent, which supports the proposed structure and the nonplanar ground states about the N—N′ bond.

Compound **4***c* in nitrobenzene shows the following n.m.r. signals: C_{9-10} and $C_{9'-10'}$ δ 5.03 (4H, m) and C_{11-12} and $C_{11'-12'}$ δ 3.45 (4H, m). The two conformers about the N—N′ bond in this compound are identical as observed with compound **3**. The complex nature of the signals of each set of protons (*i.e.* methine protons), unlike the spectrum of the corresponding *N*-aminoimide (**1**), probably results from the multiplicity due to slow rotation about the N—N′ bond, along with the many-fold spin couplings.

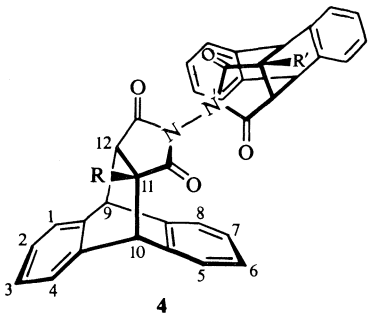

4

a R = R′ = CH_3
b R = CH_3; R′ = H
c R = R′ = H

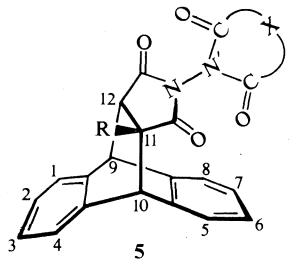

5

a R = CH_3; X = —CH=C(CH_3)—
b R = H; X = —CH=C(CH_3)—
c R = CH_3; X = —CH_2—CH_2—
d R = H; X = —CH_2—CH_2—
e R = CH_3; X =

The spectrum of compound **5***a* in $CDCl_3$ shows a doublet for the *N*-citraconimidyl ring methyl protons at δ 2.08 (J = 1.5 Hz) and a quartet for its olefinic proton at δ 6.53 (J = 1.5 Hz) along with other normal cage proton resonances. The spectrum of compound **5***b*, in $CDCl_3$, is very similar to that of **5***a* and shows a doublet at δ 2.05 (3H, J = 2 Hz) and a quartet at δ 6.58 (1H, J = 2 Hz) for *N*-citraconimidyl ring methyl and olefinic protons, respectively, along with normal resonances for the other protons. However, the spectrum of each of these compounds in nitrobenzene shows two doublets for the *N'*-ring methyl protons (Δν = 10 Hz) and two (poorly resolved) quartets for the olefinic proton, which are temperature dependent. The similarity between the spectra of these two compounds suggests that the signal multiplicity of **5***a*, in nitrobenzene, is not due to the presence of the cage methyl group but it is due to hindered rotation and nonplanar ground states about the N—N′ bond. Though the spectra of compounds **5***c* and **5***d* in $CDCl_3$ are deceptively simple as both show broad singlets of 4H intensity for their *N*-succinimidyl protons at δ 2.75 and 2.80, respectively, along with other normal resonances for the cage protons, they exhibit temperature dependent A_2B_2 pattern when studied in nitrobenzene (the two innermost signals separated by 1.75 Hz at 45° move closer to 0.75 Hz at 120°) and thus support the proposed structures.

The spectrum of compound **5***e* in $CDCl_3$ shows, along with normal resonances for all other protons, a broad signal at δ 6.3 for the C_5 and C_6, olefinic protons, whereas the corresponding *N*-aminoimide showed (2) a sharp triplet-like signal. Therefore this broadness could be assigned to the differential magnetic effect of the anthracene adduct cage on these protons in the nonplanar conformation about the N—N′ bond.

Thus the *N,N'*-diimidyl systems could be characterized by their temperature dependent n.m.r. spectra and hindered internal rotation.

Experimental

Nuclear magnetic resonance spectra were recorded on a Varian A-60D spectrometer equipped with a variable temperature controller (Model No. V-6040). The spectral data were recorded using TMS as internal reference standard. Proper care was taken, while recording the variable temperature n.m.r. spectra of the compounds, to establish a genuine exchange process. Movement of the signals with the temperature was considered not to be due to the differential effects of the solvent because the temperature-dependent signals of these compounds moved closer and never apart, as the temperature was raised. Exchange is, of course, preceded by a broadening of the resonance signals of different conformers and due care was taken to ensure that this broadening was not due to loss of homogeneity of the magnetic field within the heated probe. Coalescence of the *N'*-ring methyl proton signals of the compound **2***a* was observed at 95°; in other compounds, coalescence could not be observed up to 120° but exchangeable signals showed a definite movement, *e.g.* for compound **4***b* in nitrobenzene, the Δν values of the methyl proton signals were found to be 8.5 and 6 Hz at 45 and 120°, respectively. *N'*-Ring methylene and methine protons in **2***b–c* and **5***c–d*, which appear to be singlets in $CDCl_3$, show narrow multiplets in nitrobenzene and sharpen when the temperature is raised.

Infrared spectra were recorded in Nujol medium on a Perkin Elmer-257 spectrophotometer. The characteristic i.r. bands, elemental analyses, and the melting points are included in Table 1.

Preparation of Compounds[2]

Compounds 2a–d and 3

Compound **2***a* was prepared by refluxing the *N*-amino-

[2]All compounds were recrystallized from ethanol.

Can. J. Chem. Downloaded from www.nrcresearchpress.com by 178.218.224.3 on 09/06/12
For personal use only.

TABLE 1. Melting points, elemental analyses, and characteristic i.r.* bands of the compounds

Compound	Melting point (°C)	Analysis (%) Carbon Found	Carbon Calcd.	Hydrogen Found	Hydrogen Calcd.	Infrared bands C=O stretching (cm^{-1})
2*a*	159–160	61.58	61.76	4.27	4.41	1730s
2*b*	205–207	60.54	60.46	3.96	3.87	1745s, 1725s
2*c*	197–199	59.65	60.00	4.46	4.61	1720s
2*d*	237–239	61.56	61.31	5.35	5.11	1725s
3	285–287	66.62	66.66	4.83	4.93	1735s
4*a*	323–326	78.95	79.17	4.78	4.86	1780w, 1745s
4*b*	334–337	78.76	79.00	5.01	4.63	1780w, 1740s
4*c*	370–373	78.64	78.81	4.32	4.41	1780w, 1740s
5*a*	261–263	72.28	72.36	4.75	4.52	1810w, 1740s (broad)
5*b*	278–280	72.59	71.87	4.82	4.16	1820w, 1740s (broad)
5*c*	289–291	70.96	71.50	4.76	4.66	1785w, 1740s (broad)
5*d*	296–299	70.35	70.95	4.92	4.30	1810w, 1755s, 1735s
5*e*	238–240	74.16	74.66	5.38	4.88	1780w, 1745s

*s = strong, w = weak.

[2.2.1]bicyclo-5-heptene-2,3-*endo*-dicarboximide (2) with equimolecular quantity of maleic anhydride in dry toluene, using Dean–Stark water separator, for about 6 h. The reaction mixture was filtered hot, the solvent evaporated, and the residue washed with water and petroleum ether. The other compounds (**2***b–d* and **3**) were obtained in the same way from *N*-amino[2.2.1]bicyclo-5-heptene-2,3-*endo*-dicarboximide and the appropriate anhydrides.

Compounds **4***a–c*

Compound **4***a* was prepared by refluxing *N*-amino-9,10-dihydroanthracene-9,10-*endo*-α-methyl-α,β-succinimide (4) with an equimolecular quantity of anthracene – citraconic anhydride adduct in dry toluene for 4 h. Compound **4***b* was prepared similarly from *N*-amino-9,10-dihydroanthracene-9,10-*endo*-α-methyl-α,β-succinimide and anthracene – maleic anhydride adduct. Compound **4***c*[3] was prepared from equimolar quantities of *N*-amino-9,10-dihydro-anthracene-9,10-*endo*-α,β-succinimide (1) and anthracene – maleic anhydride adduct following the above procedures.

Compounds **5***a and b*

N-Amino-9,10-dihydroanthracene-9,10-*endo*-α-methyl-α,β-succinimide and *N*-amino-9,10-dihydroanthracene-9,10-*endo*-α,β-succinimide, on heating with citraconic anhydride in equimolar proportions at 120° for 2 h, gave **5***a* and *b*, respectively.

Compounds **5***c and d*

Equimolar proportions of *N*-amino-9,10-dihydroanthracene-9,10-*endo*-α-methyl-α,β-succinimide and succinic anhydride were refluxed in dry toluene for 4 h to yield the compound **5***c*. The compound **5***d* was prepared similarly from *N*-amino-9,10-dihydroanthracene-9,10-*endo*-α,β-succinimide and succinic anhydride.

Compound **5***e*

Equimolecular amounts of *N*-amino-9,10-dihydro-anthracene-9,10-*endo*-α-methyl-α,β-succinimide and cyclopentadiene-maleic anhydride adduct were refluxed in dry benzene for 4 h to yield the compound **5***e*.

The authors thank Prof. G. B. Singh for his keen interest and the C.S.I.R. for the award of a research fellowship to C.K.R.

1. B. H. KORSCH and N. V. RIGGS. Tetrahedron Lett. 5897 (1966).
2. S. M. VERMA and C. KOTESWARA RAO. Tetrahedron, **28**, 5029 (1972).
3. N. V. RIGGS and S. M. VERMA. Aust. J. Chem. **23**, 1913 (1970); S. M. VERMA and O. SUBBA RAO. Aust. J. Chem. **26**, 1963 (1973).
4. S. M. VERMA and K. O. P. SINHA. Ind. J. Chem. **11**, 1138 (1973).
5. G. S. D. KING. J. Chem. Soc. (B), 1224 (1966).
6. R. FOSTER and C. A. FYFE. Spectrochim. Acta, **21**, 1785 (1965).
7. S. M. VERMA and RAJENDRA PRASAD. J. Org. Chem. **38**, 1004 (1973).
8. E. HEDAYA, R. L. HINMAN, and S. THEODOROPULOS. J. Org. Chem. **31**, 1311, 1317 (1966).

[3]Synthesized earlier by a different procedure by Hedaya *et al.* (8).

Can. J. Chem. Downloaded from www.nrcresearchpress.com by 178.218.224.3 on 09/06/12
For personal use only.

An Investigation of σ and π Contributions to Long-range ^1H–^1H Coupling Constants in Planar Aromatic Derivatives Using CNDO and INDO Molecular Orbital Calculations[1]

IAN R. PEAT[2] AND WILLIAM F. REYNOLDS[3]

Department of Chemistry, University of Toronto, Toronto, Ontario M5S 1A1

Received January 14, 1974

IAN R. PEAT and WILLIAM F. REYNOLDS. Can. J. Chem. **52**, 2403 (1974).

Molecular orbital calculations of coupling constants based on finite perturbation theory in the CNDO/2 and INDO approximations have been carried out for styrene, benzaldehyde, and naphthalene. INDO calculations have also been carried out in which one-center exchange integrals involved in σ–π interaction are omitted (INDO(σ) calculations). Both CNDO and INDO(σ) constants give reasonable estimates of σ contributions to long-range ^1H–^1H couplings, with the former giving better results when strongly stereospecific σ contributions are present. INDO calculations also give reasonable, but generally overestimated, π contributions to these couplings.

IAN R. PEAT et WILLIAM F. REYNOLDS. Can. J. Chem. **52**, 2403 (1974).

On a effectué, pour le styrène, le benzaldéhyde et le naphtalène, des calculs d'orbitales moléculaires des constantes de couplage en faisant appel à la théorie des perturbations définies dans les approximations CNDO/2 et INDO. On a aussi effectué des calculs INDO dans lesquels les intégrales d'échange impliquées dans l'interaction σ–π ont été négligés (calcul INDO(σ)). Les résultats obtenus pour les constantes, tant par la méthode CNDO et de l'INDO (σ), correspondent à des approximations raisonables des contributions σ dans les couplages ^1H–^1H à longue distance; la première méthode donne des meilleurs résultats quand des contributions σ stéréospécifiques sont présentes. Des calculs INDO donnent aussi des valeurs raisonnables pour les contributions π à ces couplages; ces valeurs sont toutefois généralement trop élevées. [Traduit par le journal]

Introduction

Molecular orbital calculations based on finite perturbation theory (1) in the INDO (2) and CNDO/2 (3) approximations have proved to be a particularly useful method for determining the relative importance of σ and π contributions to long-range ^1H–^1H coupling constants (4–13).

Two approaches have been used to separate σ and π contributions to ^1H–^1H couplings in planar conjugated systems. As a result of the neglect of one-center exchange integrals in the CNDO/2 approximation, these calculations only predict contributions from σ coupling pathways in planar systems. By contrast, INDO calculations include one-center exchange integrals and thus allow estimation of not only σ contributions but also π contributions arising via a spin polarization mechanism (14). Thus, one approach has been to use J(CNDO) as a measure of σ contributions and J(INDO) − J(CNDO) as a measure of π contributions (7, 12). However, this approach is not strictly valid because the different parameters used for the CNDO calculations lead to contributions to J(INDO) − J(CNDO) which are neither σ or π contributions but rather artifacts of the calculation (12, 13).

Bacon and Maciel have suggested an alternative, theoretically more valid, approach to the problem (4). They performed INDO calculations for butadiene and derivatives with and without one-center exchange integrals leading to the σ–π exchange interaction (*i.e.* those involving $C(2p_z)$ atomic orbitals). This allows factoring out of the contribution to the coupling constant which is transmitted through the π electron system via σ–π exchange. Thus the modified INDO calculations (INDO(σ)) give σ contributions with INDO − INDO(σ) giving π contributions (INDO(π)). It should be stressed that this

[1]Taken in part from the Ph.D. Thesis of I. R. Peat, University of Toronto, 1973.

[2]Gulf Oil Fellowship Holder 1971–1973. Current address: Department of Chemistry, Florida State University, Tallahassee, Florida 32306, U.S.A.

[3]To whom correspondence should be addressed.

Can. J. Chem. Downloaded from www.nrcresearchpress.com by 210.87.254.105 on 09/05/12
For personal use only.

Can. J. Chem. Downloaded from www.nrcresearchpress.com by 210.87.254.105 on 09/05/12
For personal use only.

TABLE 1. Experimental and calculated ring-proton side-chain proton coupling constants (in Hz) in styrene and benzaldehyde

Coupling constant[a]	Styrene					Benzaldehyde				
	J(CNDO)	J(INDO(σ))	J(INDO(π))[b]	J(INDO)	J_{exp}[c]	J(CNDO)	J(INDO(σ))	J(INDO(π))[b]	J(INDO)	J_{exp}[d]
J_{27}	+0.19	−0.14	−0.14	−0.28	—	+0.53	+0.48	−0.28	+0.20	
$\langle J_{27},J_{67}\rangle$	+0.06	−0.32	−0.21	−0.52	−0.51±0.03	+0.40	+0.24	−0.34	−0.10	−0.10
J_{67}	−0.07	−0.49	−0.28	−0.77	−0.47	+0.27	−0.01	−0.39	−0.40	
J_{28}	+0.03	−0.05	+0.45	+0.40	—					
$\langle J_{28},J_{68}\rangle$	−0.19	−0.28	+0.45	+0.18	<0.07					
J_{68}	−0.41	−0.50	+0.45	−0.05	−0.15					
J_{29}	+0.16	+0.16	+0.34	+0.50	—					
$\langle J_{29},J_{69}\rangle$	+0.04	+0.02	+0.31	+0.35	+0.15±0.04					
J_{69}	−0.08	−0.12	+0.32	+0.20	<0.07					
J_{37}	+0.11	+0.10	+0.13	+0.23	<0.07	+0.02	−0.02	+0.22	+0.20	
$\langle J_{37},J_{57}\rangle$	+0.45	+0.53	+0.25	+0.77	+0.35±0.02	+0.46	+0.58	+0.33	+0.90	+0.38
J_{57}	+0.78	+0.95	+0.36	+1.31	+0.7	+0.90	+1.17	+0.43	+1.60	
J_{38}	+0.03	+0.03	−0.22	−0.19	<0.07					
$\langle J_{38},J_{58}\rangle$	+0.02	+0.02	−0.22	−0.20	<0.07					
J_{58}	0.00	0.00	−0.22	−0.22	—					
J_{39}	+0.20	+0.25	−0.14	+0.11	0.10[e]					
$\langle J_{39},J_{59}\rangle$	+0.11	+0.14	−0.17	−0.03	<0.07					
J_{59}	+0.02	+0.02	−0.20	−0.18	—					
J_{47}	−0.01	−0.03	−0.21	−0.24	−0.25	+0.00	−0.02	−0.27	−0.29	−0.03
J_{48}	−0.01	−0.01	+0.31	+0.30	+0.26					
J_{49}	−0.01	−0.01	+0.31	+0.30	+0.27					

[a]Numbering from **1** and **2**.
[b]J(INDO(π)) = J(INDO) − J(INDO(σ)).
[c]Data from refs. 5, 20, 21.
[d]Data from ref. 15.
[e]Magnitude only but assumed positive (see text).

Can. J. Chem. Downloaded from www.nrcresearchpress.com by 210.87.254.105 on 09/05/12
For personal use only.

approach allows factoring out of contributions due to σ–π exchange only in cases of planar molecules (4).

This approach has not been tested beyond the original publication (4). Consequently we decided to carry out CNDO, INDO(σ), and INDO calculations for a series of planar aromatic molecules, both to test the relative validity of CNDO and INDO(σ) calculations to estimate σ contributions to coupling constants in these derivatives and also to estimate the relative importance of σ and π pathways for coupling constants in these derivatives. This represented an extension of our previous investigation of conjugated dienes and diynes using CNDO and INDO calculations (13). Compounds chosen for investigation were styrene, benzaldehyde, and naphthalene since accurate experimental results were available for all three derivatives (5, 15, 16). Previous theoretical investigations of coupling constants in these derivatives included INDO calculations for styrene (5) and CNDO and INDO calculations for benzaldehyde (6). Results of the present investigation are reported below.

Details of Calculations

CNDO and INDO finite perturbation calculations were performed using a modified version (8) of a standard CNINDO program (17). For the INDO(σ) calculations, the program was further modified to allow exclusion of specific one-center integrals.[4] Calculations were performed on an IBM 370 computer. Standard bond lengths and bond angles (14) were used for the calculations. In the INDO(σ) calculations, all one-center integrals involving $C(2p_z)$ atomic orbitals on all carbons (*i.e.* those orbitals forming the π electron system) were omitted.

Results and Discussion

(a) Styrene

Results of CNDO, INDO(σ), and INDO finite perturbation calculations of ring proton – vinyl proton coupling constants are summarized in Table 1. The numbering of protons is given in **1**. Results of INDO calculations agree very closely with those obtained previously with a different version of the INDO finite perturbation program (5).

[4]Further details of program modifications are available on request from the authors.

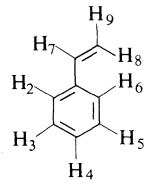

1

CNDO and INDO(σ) calculations both indicate insignificant σ contributions to long-range couplings involving the *para* proton (J_{47}, J_{48}, J_{49}). INDO(π) contributions are in excellent agreement with the experimental results for 3-bromostyrene and 2,5-dichlorostyrene, confirming the previous conclusion that these couplings are transmitted exclusively through the π electron system (5).

By contrast, there are σ contributions to many of the long-range couplings involving *meta* (H_3,H_5) and *ortho* (H_2,H_6) protons. The CNDO and INDO(σ) calculations confirm the presence of the expected (5, 18, 19) stereospecific σ contribution to J_{57}, transmitted through the all-*trans* "zig-zag" pathway. This large σ contribution is overestimated by the INDO(σ) calculations. The INDO calculations also appear to overestimate to the π contributions to J_{37} and J_{57} since the near zero values of J_{37} in 2,5-dichlorostyrene and 2-bromostyrene (5) indicate negligible π contributions. The CNDO results, however, are in excellent agreement with the experimental results. Both CNDO and INDO(σ) calculations indicate a (positive) σ contribution to J_{39} and insignificant σ contributions to other *meta* proton to β-vinyl proton couplings (J_{38}, J_{58}, J_{59}). The experimental results support this conclusion since of all the coupling constants of this type in the various styrenes which have been investigated (5, 20), only J_{39} in 2,5-dichlorostyrene (5) has a measurable magnitude. J_{39} has a magnitude of 0.10 Hz. Since the corresponding coupling in naphthalene (J_{27}) equals +0.10 Hz, it is believed that J_{39} is also positive, as indicated by the INDO calculation (+0.11 Hz). The INDO calculations also indicate nearly equal π contributions (*ca.* −0.2 Hz) to J_{38}, J_{39}, J_{58}, and J_{59}. In the case of J_{39} and J_{59}, the combination of a positive σ contribution (to J_{39}) and negative π contributions could lead to the observed near zero values for these couplings (see Table 1). However, this cannot account for the small values for J_{38} and J_{58}. The π contributions to these two couplings may be overestimated by the

Can. J. Chem. Downloaded from www.nrcresearchpress.com by 210.87.254.105 on 09/05/12
For personal use only.

INDO calculations. Alternatively, π contributions to all four couplings may be overestimated since π contributions to all couplings should be similar because nearly identical π pathways are involved.

Of the couplings involving the *ortho* protons, the most interesting are J_{68} and J_{69}. J_{68} in 2,5-dichlorostyrene is negative even though a positive π electron contribution is expected. Both CNDO and INDO(σ) calculations indicate that this is due to a negative σ electron contribution. The negative coupling has been attributed to a direct or through-space interaction of the proximate protons (see **1**) (5). In support of this mechanism, CNDO calculations in which the C(1)—C(α)—C(β) angle is opened to 130° show that $J(\text{CNDO})_{68}$ changes from −0.41 Hz to −0.10 Hz as the distance between H_6 and H_8 is increased (21). More surprisingly $J(\text{CNDO})_{69}$ is also negative (−0.08 Hz) but becomes positive (+0.03 Hz) for ∠C(1)—C(α)—C(β) = 130° (21). It is not clear whether this represents some type of stereospecific σ contribution or a through-space mechanism transmitted by the intervening proton, H_8.

INDO calculations quantitatively reproduce the magnitude of the averaged coupling constant $\langle J_{27}, J_{67}\rangle$. INDO(σ) and CNDO calculations give opposite signs for σ contributions but both indicate substantial π contributions. Both calculations indicate a stereospecific σ effect, leading to difference values of J_{27} and J_{67}. However, this may be due to some inadequacy in the calculations since experimental results for both 2,5-dichlorostyrene (5) and 3-vinyl-6-methylpyridine and 4-vinylpyridine (22) indicate that $J_{27} \simeq J_{67}$.

(b) Benzaldehyde

The results of CNDO, INDO, and INDO(σ) calculations for benzaldehyde are summarized in Table 1. Since the pattern of results resembles in many ways that for styrene and since CNDO and INDO results for benzaldehyde have previously been reported (6), only differences between styrene and benzaldehyde will be discussed in detail. The numbering of benzaldehyde protons is given in **2**.

Just as in styrene, the INDO calculations quantitatively predict the average value of J_{27} and J_{67} in benzaldehyde. Both CNDO and INDO(σ) calculations indicate that the marked change in $\langle J_{27}, J_{67}\rangle$ from styrene to benzaldehyde (−0.51 Hz to −0.10 Hz) is due to a more significantly more positive σ contribution to this coupling in benzaldehyde. By contrast, the π electron contribution is predicted to be more negative in benzaldehyde.

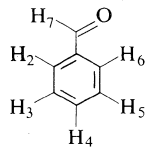

2

The CNDO calculations correctly predict a negligible change in $\langle J_{37}, J_{57}\rangle$ from styrene to benzaldehyde. By contrast, the INDO calculations predict a significant change in the magnitude of this coupling. As in styrene, the CNDO calculations are in much better agreement with the magnitude $\langle J_{37}, J_{57}\rangle$ than either INDO(σ) or INDO calculations.

J_{47} changes from −0.26 Hz to −0.03 Hz from styrene to benzaldehyde. The small value of J_{47} in benzaldehyde suggests a negligible π contribution to this coupling. However, the calculations indicate similar σ and π contributions with excellent agreement between experimental and calculated results for styrene. Thus they provide no explanation for the surprisingly small J_{47} coupling in benzaldehyde.

(c) Naphthalene

CNDO, INDO(σ) and INDO calculations for naphthalene are summarized in Table 2 with numbering of protons given in **3**. INDO calculations not only reproduce the signs of all the experimental intra- and inter-ring coupling constants but also accurately reproduce the magnitudes of most of these couplings.

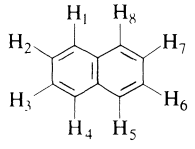

3

The CNDO and INDO(σ) calculations both indicate that the *ortho* and *meta* intra-ring coupling constants are transmitted primarily through the σ electron system, as normally assumed (22). They also indicate a substantial σ contribution to the *para* coupling constants (J_{14}, J_{58}), contrary to the usual assumption that this coupling is transmitted primarily through the π electron system (23).

TABLE 2. Experimental and calculated ^1H–^1H coupling constants (in Hz) for naphthalene

Coupling constants[a]	J(CNDO)	J(INDO(σ))	J(INDO(π))	J(INDO)	J_{exp}[b]
$J_{12},J_{34},J_{56},J_{78}$	+7.21	+7.92	+0.13	+8.05	+8.28
J_{23},J_{67}	+7.86	+8.83	−0.24	+8.59	+6.85
$J_{13},J_{24},J_{57},J_{68}$	+1 95	+1.99	−0.05	+1.94	+1.24
J_{14},J_{58}	+0.64	+0.82	+0.96	+1.78	+0.74
J_{15},J_{48}	+0.89	+1.09	+0.72	+1.81	+0.85
$J_{16},J_{25},J_{38},J_{47}$	−0.01	−0.04	−0.40	−0.44	−0.10
$J_{17},J_{28},J_{35},J_{46}$	+0.15	+0.14	+0.41	+0.55	+0.23
J_{18},J_{45}	+0.15	−0.20	−0.39	−0.59	−0.45
J_{26},J_{37}	+0.01	+0.01	+0.39	+0.40	+0.25
J_{27},J_{36}	+0.21	+0.26	−0.24	+0.02	+0.10

[a]Labelling shown in 3.
[b]Ref. 16.

TABLE 3. Comparison of experimental values for corresponding coupling constants in naphthalene and styrene

Naphthalene		Styrene	
Coupling constant	J_{exp} (Hz)[a]	Coupling constant	J_{exp} (Hz)[b]
J_{15}	+0.85	J_{57}	+0.7
J_{16}	−0.10	J_{47}	−0.25
J_{17}	+0.23	J_{29}	+0.15±0.04[c]
J_{18}	−0.45	J_{27}	−0.51±0.04[c]
J_{26}	+0.25	J_{49}	+0.27
J_{27}	+0.10	J_{39}	0.10[d]

[a]Ref. 16.
[b]Refs. 5, 20, 21.
[c]Average for two planar conformations of vinyl group (5).
[d]Magnitude only.

All of the inter-ring coupling constants can be related to corresponding values in styrene (see Table 3). Both experimental and calculated couplings closely parallel those for styrene, suggesting that similar mechanisms are operative. The close similarity of experimental results is particularly striking. Since naphthalene is certainly a planar molecule, this close parallel suggests that styrene is almost certainly also planar or nearly planar. Although the planarity of styrene has been questioned (12), available experimental evidence suggests that it is planar (5). $J_{15}(J_{48})$ shows a strong σ contribution just as J_{57} does in styrene. Again the actual magnitude is best predicted by the CNDO calculation, suggesting that the INDO calculations overestimate both σ and π contributions to this coupling. For $J_{27}(J_{36})$ both CNDO and INDO(σ) calculations indicate a stereospecific σ contribution of *ca.* +0.2 Hz just as in the case of J_{39} for styrene. The experimental evidence supports this since J_{27} = +0.10 Hz, whereas it should be negative if π contributions dominate. The close parallel with styrene suggests that J_{39} for styrene (magnitude = 0.10 Hz) is also positive.

The calculations also indicate a positive σ contribution to $J_{17}(J_{28}, J_{35}, J_{46})$ of 0.1–0.2 Hz, identical to the contribution to J_{29} for styrene. Again the experimental results support this conclusion. Finally, both the calculations and experimental results indicate dominant π electron contributions to $J_{16}(J_{25}, J_{38}, J_{47})$ and $J_{18}(J_{45})$, as in the case of J_{47} and J_{27} in styrene.

Although the calculations parallel the experimental results, there does appear to be a persistent tendency of the INDO calculations to overestimate π contributions to inter-ring couplings. This is most apparent for J_{15} and to a lesser degree for J_{16}, J_{17}, and J_{26}. It would also account for the underestimation of J_{27} where σ and π contributions are opposite in sign.

To summarize, CNDO and INDO(σ) calcula-

Can. J. Chem. Downloaded from www.nrcresearchpress.com by 210.87.254.105 on 09/05/12
For personal use only.

tions usually give similar and apparently reasonable estimates of contributions to long-range ^1H–^1H couplings in planar aromatic derivatives. The sole exception is for $^5J_{H,H}$ couplings of the type **4**. INDO(σ) and INDO calculations per-

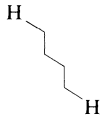

4

sistently overestimate this coupling while CNDO calculations give much more reasonable values.

INDO calculations also generally give reasonable estimates of π contributions to these couplings, when J(INDO) − J(INDO(σ)) is taken as estimate of π contributions. However, the calculations often overestimate the magnitudes of the π contributions. The INDO(π) calculations predict nearly equal π contributions to couplings involving similar π electron structures (*e.g.* J_{38}, J_{39}, J_{58}, J_{59} for styrene, also see ref. 4), as expected. By contrast, J(INDO) − J(CNDO) often predicts markedly different π contributions for these sets of couplings (13). Thus J(INDO(π)) appears to give a more reliable estimate of π coupling contributions than J(INDO) − J(CNDO). Consequently the combination of INDO(σ) and INDO calculations appears to be superior to CNDO plus INDO calculations for separating σ and π contributions to ^1H–^1H coupling constants in planar conjugated systems. An alternative, empirical procedure which may be even better when large σ contributions are present is to take J(CNDO) as a measure of σ contributions (see previous paragraph) and J(INDO(π)) as a measure of π contributions. However this has the disadvantage of requiring three instead of two calculations.

For the aromatic derivatives investigated, most long-range coupling constants are transmitted predominantly through the π electron system. However, a number of stereospecific σ contributions were noted, particularly those involving either all-*trans* coupling pathways or spatially proximate protons.

Financial support from the National Research Council of Canada is gratefully acknowledged. I.R.P. thanks Gulf Oil Canada, Ltd. for a Fellowship.

1. J. A. Pople, J. W. McIver, Jr., and N. S. Ostlund. J. Chem. Phys. **49**, 2960 (1968); **49**, 2965 (1968).
2. J. A. Pople and G. A. Segal. J. Chem. Phys. **43**, S136 (1965).
3. J. A. Pople, D. L. Beveridge, and P. A. Dobosh. J. Chem. Phys. **47**, 2026 (1967).
4. M. Bacon and G. E. Maciel. Mol. Phys. **21**, 257 (1971).
5. M. Barfield, C. J. Macdonald, I. R. Peat, and W. F. Reynolds. J. Am. Chem. Soc. **93**, 4195 (1971).
6. R. Wasylishen and T. Schaefer. Can. J. Chem. **49**, 3216 (1971).
7. L. Ernst, H. M. Hutton, and T. Schaefer. Can. J. Chem. **50**, 1863 (1972).
8. C. J. Macdonald, G. K. Hamer, I. R. Peat, and W. F. Reynolds. Can. J. Chem. **50**, 2035 (1972).
9. R. Wasylishen and T. Schaefer. Can. J. Chem. **50**, 274 (1972).
10. R. Wasylishen and T. Schaefer. Can. J. Chem. **50**, 1852 (1972).
11. M. Barfield and S. Sternhell. J. Am. Chem. Soc. **94**, 1905 (1972).
12. J. B. Rowbotham and T. Schaefer. Can. J. Chem. **51**, 953 (1973).
13. I. R. Peat and W. F. Reynolds. Can. J. Chem. **51**, 2968 (1973).
14. D. L. Beveridge and J. A. Pople. Approximate molecular orbital theory. McGraw-Hill Book Company, New York, N.Y. 1970.
15. R. J. Kostelnik, M. P. Williamson, D. E. Wisnosky, and S. M. Castellano. Can. J. Chem. **47**, 3313 (1969).
16. R. W. Crecely and J. H. Goldstein. Org. Magn. Res. **2**, 613 (1970).
17. Quantum Chemistry Program Exchange Program 141.
18. G. J. Karabatsos and F. M. Vane. J. Am. Chem. Soc. **85**, 3887 (1963).
19. T. Schaefer, R. Schwenk, C. J. Macdonald, and W. F. Reynolds. Can. J. Chem. **46**, 2187 (1968).
20. I. R. Peat and W. F. Reynolds. Submitted to Can. J. Chem.
21. I. R. Peat. Ph.D. Thesis, University of Toronto, Toronto, Ont., 1973.
22. J. B. Rowbotham and T. Schaefer. Can. J. Chem. **52**, 136 (1974).
23. M. Barfield and B. Chakrabarti. Chem. Rev. **69**, 759 (1969).

Can. J. Chem. Downloaded from www.nrcresearchpress.com by 210.87.254.105 on 09/05/12
For personal use only.

Organic Sulfur Mechanisms. 16. Competing Reverse Diels–Alder and Desulfonylation–Rearrangement Reactions in the Thermolysis of a Cyclic Sulfone[1]

JAMES FREDERICK KING, RUDYARD MENDIOLA ENANOZA, AND ERROL GEORGE LEWARS

Department of Chemistry, University of Western Ontario, London, Ontario N6A 3K7

Received October 30, 1973

JAMES FREDERICK KING, RUDYARD MENDIOLA ENANOZA, and ERROL GEORGE LEWARS. Can. J. Chem. **52**, 2409 (1974).

2,2-Dioxido-4-phenyl-2-thiabicyclo[2.2.2]octa-5,7-diene-5,6-dicarboxylic anhydride (**4**) on heating gives about equal amounts of a biphenyl (**5**) and a cycloheptatriene (**6**), derived respectively from a reverse Diels–Alder reaction and a desulfonylation accompanied by allylic rearrangement followed by further rearrangement. This contrasts with our earlier observation that the corresponding dimethyl ester (**1***a*) gives only the reverse Diels–Alder products. Possible factors affecting the course of the reaction of such species are discussed.

JAMES FREDERICK KING, RUDYARD MENDIOLA ENANOZA et ERROL GEORGE LEWARS. Can. J. Chem. **52**, 2409 (1974).

Par chauffage de l'anhydride de l'acide dioxido-2,2 phényl-4 thia-2 bicyclo[2.2.2]octadiène-5,7 dicarboxylique-5,6 (**4**), on obtient des quantités égales de biphényle (**5**) et de cycloheptatriène (**6**) qui proviennent respectivement d'une réaction de Diels–Alder renversée et d'une réaction de désulfonylation accompagnée par un réarrangement allylique et suivie d'autres réarrangements. Ces résultats sont en opposition avec nos observations antérieures selon lesquelles l'ester diméthylique correspondant (**1***a*) conduit uniquement aux produits de réaction de Diels–Alder renversée. On discute des facteurs qui peuvent affecter le cours de la réaction de telles espèces. [Traduit par le journal]

We have recently shown that thermolysis of the cyclic sulfone **1***a* gives dimethyl biphenyl-2,3-dicarboxylate (**2***a*) and sulfene (**3**), the latter being detected by trapping experiments (1). Very recently Fischer and Lin (2) reported that the action of heat on the parent bicyclic sulfone (**1***b*) surprisingly gave only a small amount of the phthalate (**2***b*) and sulfene, the principal reaction being a desulfonylation with rearrangement to a mixture of dimethyl cycloheptatrienedicarboxylates. In this note we wish to point out that another comparatively minor structural change, namely conversion of the diester group to the cyclic anhydride as in **4**, also leads to a pronounced decrease in the tendency to yield the reverse Diels–Alder reaction with formation of **5** and sulfene (**3**), and a corresponding increase in the extent of desulfonylation–rearrangement.

Saponification of **1***a* gives the dicarboxylic acid which on gentle treatment with trifluoroacetic anhydride gives the cyclic anhydride (**4**). The structure of **4** follows from its mode of synthesis taken with (*a*) the presence of bands at 1850, 1785, 1325, and 1115 cm^{-1} (showing the presence of the cyclic anhydride and sulfone groupings) and (*b*) an n.m.r. spectrum with AB and ABX patterns very similar to those in the spectrum of **1***a* (1). When **4** is heated above 100° it readily yields a mixture containing the biphenyl anhydride (**5**) (3) and a yellow crystalline solid shown by the following evidence to have in all probability structure **6**.

Elemental analysis and the appearance of a molecular ion peak at *m/e* 238 established the molecular formula $C_{15}H_{10}O_3$. The i.r. spectrum showed bands at 1840, 1815, 1775, and 1765 cm^{-1} ascribable to a five-membered ring anhydride; the u.v. spectrum had bands at 337 (ε 11 400), 290 (ε 14 900), and 265 nm (shoulder,ε 14 900). The n.m.r. spectrum showed in addition to the phenyl multiplet, an AMX pattern ($\delta_A \sim$ 7.5 (obscured by the phenyl hydrogens), δ_M 6.72, δ_X 5.55 p.p.m., J_{AM} = 6.2, J_{MX} = 8.0 Hz) with H_X also coupled to a methylene group at 3.05 p.p.m. (J = 7.4 Hz); this clearly requires the array C=CH—CH=CH—CH_2 with the additional specification that H_A be in a strongly deshielded environment. There are only two phenylcycloheptatrienedicarboxylic anhydride structures with this structural fragment; these are

[1]For Part 15 see ref. 11.

Can. J. Chem. Downloaded from www.nrcresearchpress.com by 210.87.254.42 on 09/05/12
For personal use only.

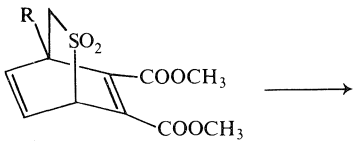

1 *a* R = Ph
b R = H

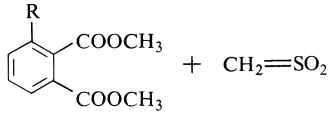

2 3

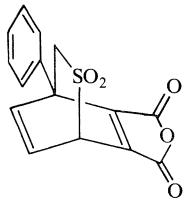

4

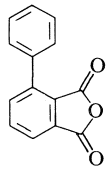

5

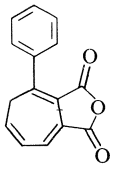

6

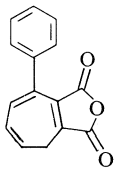

7

shown as **6** and **7**. In our view **6** accounts more readily than **7** for the downfield position of the H_A signal, but since this argument seemed insufficient to prove the point further evidence was obtained from the n.m.r. spectrum of the corresponding dimethyl ester in the presence of $Eu(fod)_3$. The ester, obtained by basic hydrolysis of the anhydride followed by esterification of the diacid with diazomethane, showed n.m.r. bands very similar to those in the spectrum of the anhydride except that H_A of the AMX pattern was not obscured by the absorption of the phenyl group. In the presence of $Eu(fod)_3$ the $H_A$signal shifted from 7.58 to 14.65 p.p.m. while the methylene doublet moved from 2.68 to 4.66 p.p.m., observations which in our opinion clearly favor the 1-phenyl-substituted structures (*e.g.* **6**) for the anhydride and the diester over the 3-phenyl structures (*e.g.* **7**). The assignment of the peaks in the above spectrum was carefully checked by decoupling experiments, a precaution taken partly because of the complexity in the 7.9 and 9.3 p.p.m. regions arising from the splitting of the original phenyl singlet in the presence of the shift reagent.

Thermolysis of **4** at ~120° leads to roughly equal amounts of **5** and **6**. At higher temperatures increasingly larger proportions of the biphenyl (**5**) are isolated, but when account is taken of greater stability of **5** under the conditions of the reaction and work-up, it would appear that the two products **5** and **6** are formed at approximately the same rate. The preparation of **6**, incidentally, may be carried out directly from the diacid derived from hydrolysis of **1***a*, simply by refluxing with acetic anhydride.

As Fischer and Lin have pointed out (2) for the analogous reaction of **1***b*, the formation of the cycloheptatriene from the bicyclic sulfone system can be rationalized as in the scheme **4** → **8** → **6**; thermal extrusion of sulfur dioxide accompanied by allylic rearrangement is followed by valence isomerization of the norcaradiene (**8**) to the cycloheptatriene (**6**). Thermal desulfonylation with rearrangement in allylic sulfones was first reported by La Combe and Stewart (4), who presented evidence for a cyclic concerted process at lower temperatures, with incursion of a free radical mechanism at higher temperatures. We have observed the analogous rearrangement of 2-propenesulfonyl ("allylsulfonyl") chloride to allyl chloride on flash thermolysis; these conditions are such that a radical recombination mechanism is exceedingly unlikely, and in agreement with this, a deuterium labelling experiment showed the extrusion of sulfur dioxide to be accompanied by an allylic rearrangement (5).

The proposed reaction **4** → **8** may also be regarded as homologous to the well-known cheletropic reaction of 2,5-dihydrothiophene 1,1-dioxide (butadiene sulfone) to give sulfur dioxide and butadiene; the transformation **4** → **8** differs only in that a substituted vinylcyclopropane is formed instead of butadiene. The reaction of butadiene sulfones shows the stereospecificity expected of a cheletropic reaction (6, 7), even with 1,3-dihydrobenzo[*c*]thiophene 2,2-dioxide (8), which is particularly well arranged to display any tendency to react by a free radical process. This analogy argues in favor of a cyclic, concerted mechanism for the reaction **4** → **8**, which in terms of the Woodward–Hoffmann rules for pericyclic reactions (9) may be regarded as a thermally allowed $[{}_{\pi}2_s + {}_{\sigma}2_s + {}_{\sigma}2_s]$ process.

One obvious question obtrudes: Why does one

Can. J. Chem. Downloaded from www.nrcresearchpress.com by 210.87.254.42 on 09/05/12
For personal use only.

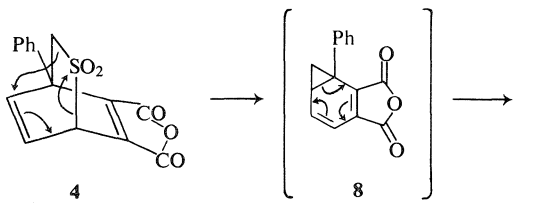

4 8

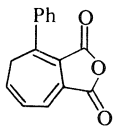

6

9 10

substrate (**1***a*) give the reverse Diels–Alder reaction, while a closely related compound (**1***b*) gives almost entirely the extrusion–rearrangement and another (**4**) gives both? From the previous paragraph it seems reasonable to discuss the desulfonylation–rearrangement in terms of a cyclic, concerted mechanism, the transition state for which may be approximated by **9**; the corresponding stage of the reverse Diels–Alder process is given by **10**. It is obvious that in the reaction of **1***a* the phenyl group is capable of conjugative stabilization of **10** (R = Ph) but not **9** (R = Ph) and this may well be the major factor responsible for the occurrence of the reverse Diels–Alder reaction as the principal thermal reaction of **1***a* but not **1***b*. The partial incursion of the desulfonylation–rearrangement process with **4** could conceivably also be due in part to essentially the same thing. The presence of the cyclic anhydride system leads to a nonbonding repulsion between the phenyl group and the adjacent carbonyl oxygen. In the diester (**1***a*) the same interaction may be alleviated by rotation of the carbomethoxyl group, whereas in the anhydride (**4**) only the phenyl group is capable of being rotated. The conformation of the phenyl group that minimizes the interaction with the carbonyl group is, however, the conformation least favorable for stabilization of **10** and hence this effect would lead to an increase in the energy of the transition state **10** in the reaction of **4** relative to **1***a*.

The above, however, cannot be the only influence at work since **4** thermolyzes *more readily* than **1***a*. An important factor in this could be the fusion of the cyclic anhydride system to an already strained unsaturated system, which would lead to greater angle strain in the anhydride (**4**) than in the diester (**1***a*) and which may be partly released on going to either **9** or **10**. It is also conceivable that this same angle strain deriving from the cyclic anhydride grouping or else the nonbonding repulsion between the phenyl and carbonyl groups (or both) actually lowers the energy of **9** relative to **10** in the reaction of **4**. We do not know enough about the geometry of **9** or **10** to discuss these possibilities fruitfully at present except to note that the phenyl–carbonyl interaction in **8** is clearly less than in **5** (or **2***a*) and to the extent that (*a*) the transition states **9** and **10** resemble these products and (*b*) the phenyl–carbonyl repulsion is greater in **4** than in **1***a*, this could be a factor contributing to the observed results.

Experimental

Melting points were determined with a Gallenkamp melting point apparatus and are uncorrected. The i.r. spectra were determined with a Beckman IR-20A spectrometer, u.v. spectra with a Cary Model 14 spectrometer, n.m.r. spectra with a Varian T-60 or HA-100 spectrometer, and mass spectra (m.s.) with a Varian M-66 instrument. Camag DF5 silica gel was used for t.l.c. Solvents were removed from solutions with a Büchi rotary evaporator in conjunction with a water aspirator.

2,2-Dioxido-4-phenyl-2-thiabicyclo[2.2.2]octa-5,7-diene-5,6-dicarboxylic Anhydride (4)

A suspension of the diester (**1***a*) (0.2 g, 0.56 mmol) in sodium hydroxide solution (5%, 24 ml, 31 mmol) was heated at 83–86° with constant stirring for 10 h. The resulting lemon-yellow solution was allowed to cool to room temperature and then acidified to about p*H* 1 with 12 *N* hydrochloric acid solution. Water was removed leaving a yellow solid residue which was taken up in acetone and filtered. The filtrate was evaporated to dryness and the residue was dried *in vacuo* (0.2 mm) at room temperature for 24 h. The faintly yellow crystals were recrystallized from acetone and pentane to give the diacid (0.15 g, 81%); i.r. (KBr): 1695, 1700 cm^{-1} (COOH), no absorption due to CO_2CH_3. To a solution of the diacid (0.1 g, 0.33 mmol) in acetone (10 ml) was added trifluoroacetic anhydride (1.0 ml, 7.0 mmol) prepared by the method of Schmidt and Staab (10). After stirring for 7.5 h the reaction mixture was concentrated at 25° to a white solid residue which was recrystallized from methylene chloride – pentane to yield colorless needles of the anhydride **4** (0.084 g, 89%); m.p. 174–174.5° dec.; i.r. (KBr): 1850, 1785, 1325, 1115 cm^{-1}, no sign of COOH absorption. The n.m.r. spectrum showed a multiplet (5H) at 7.49 (Ph), an ABX pattern with δ_A 6.98, δ_B 6.85, δ_X 5.47, J_{AB} = 7.6, J_{AX} = 7.4, and J_{BX} = 0.3 Hz, and an AB pattern with δ_A 3.64, δ_B 3.29, and J_{AB} = 11.0 Hz.

Anal. Calcd. for $C_{15}H_{10}O_5S$: C, 59.60; H, 3.34; S, 10.59. Found: C, 59.88; H, 3.30; S, 10.73.

Can. J. Chem. Downloaded from www.nrcresearchpress.com by 210.87.254.42 on 09/05/12
For personal use only.

TABLE 1. Thermolysis of 2,2-dioxido-4-phenyl-2-thiabicyclo[2.2.2]octa-5,7-diene-5,6-dicarboxylic anhydride ("sulfone-anhydride", **4**)

Amount of sulfone anhydride (**4**) (mmol)	Temperature (°C)	Time (min)	Observed yield		Recovery in the control after heating* (%)		Estimated conversion (%)	
			5	**6**	**5**	**6**	**5**	**6**
1.29	118–123	210	16†	15†	100	83	22†	27†
3.81	150–155	25	34	25	92	80	54	46
2.09	188–190	25	28	21	89	58	43	52

*Recovery in the controls on chromatography was 73% for **5** and 69% for **6** (average of three runs each). The values in the "estimated conversion" columns were obtained by assuming the same percentage recovery for each compound on both heating and chromatography as in the control experiments.

†Incomplete conversion; unreacted starting material was evident on t.l.c.

*1-Phenyl-1,3,5-cycloheptatriene-2,3-dicarboxylic Anhydride (**6**) from the Diester (**1a**)*

To a solution of the diester (**1a**) (0.5 g, 1.44 mmol) in *p*-dioxane (10 ml) was added with stirring a solution of sodium hydroxide pellets (0.160 g, 4.0 mmol) in water (5 ml). After stirring at room temperature for 12 h the mixture was acidified with 12 *N* hydrochloric acid and then sodium chloride (*ca.* 1 g) was added and the resulting two layers were separated. The dioxane layer was dried over anhydrous sodium sulfate and then evaporated to dryness. Acetic anhydride (5 ml) was added to the residue and the mixture was refluxed at 145° for 30 min, after which the lemon-yellow solution turned dark orange. The reaction mixture was then evaporated leaving an orange oil which was crystallized from methylene chloride – pentane to give yellow needles of **6**. The mother liquor was concentrated to near dryness and then saturated with pentane to give an additional yield of 0.03 g (total yield 0.10 g, 25%). The two crops were combined and carefully recrystallized from methylene chloride – pentane to give well-formed yellow needles (*ca.* 0.070 g), m.p. 179–181°. The i.r. spectrum showed carbonyl bands appearing as a doublet of doublets at 1840, 1815, 1775, and 1765 cm^{-1}, with no sign of bands due to a sulfonyl group. The u.v. spectrum: λ_{max} (CH_2Cl_2) 337 (ε 11 400), 290 (ε 14 900), 265 nm (sh, ε 14 900). The n.m.r. spectrum showed peaks which after integration and the appropriate decoupling experiments could be unambiguously assigned as follows: 7.4–7.8 (m, 5H, phenyl group), an AMX pattern, $\delta_A \sim 7.5$ (partly obscured by the phenyl multiplet), δ_M 6.72, δ_X 5.55 p.p.m., $J_{AM} = 6.2$ and $J_{MX} = 8.0$ Hz, and a doublet at 3.08 p.p.m. (2H) due to a methylene group coupling with H_X ($J = 7.4$ Hz).

Anal. Calcd. for $C_{15}H_{10}O_3$: C, 75.62; H, 4.23. Found: C, 75.65; H, 4.26.

The mass spectrum shows the parent peak at *m/e* 238.1 (calcd.: 238.06); M + 1/M = 16.48% (calcd.: 16.48%); M + 2/M = 2.20% (calcd.: 0.6%).

*Biphenyl-2,3-dicarboxylic Anhydride (**5**) from Dimethyl Biphenyl-2,3-dicarboxylate (**2a**)*

A suspension of dimethyl biphenyl-2,3-dicarboxylate (**2a**) (0.069 g, 0.255 mmol) in sodium hydroxide solution (5%, 9.5 ml, 12.5 mmol) was heated at 83° with constant stirring for 7 h. The clear solution was allowed to come to room temperature and then neutralized with 12 *N* hydrochloric acid solution. Evaporation to dryness followed by extraction with acetone (25–30 ml) gave the diacid which was then dried *in vacuo* (0.2 mm) for 3 h. The crude diacid was dissolved in acetic anhydride (*ca.* 1.5 ml) with warming and the resulting solution was heated under reflux at 120° for 5 h. Evaporation of the solvent followed by recrystallization from methylene chloride – pentane solvent mixture gave colorless needles of compound **5** (0.048 g, 85%); m.p. 145–146°, (lit. m.p. (3) 146–146.5°); n.m.r. ($CDCl_3$) δ 8.0 (3H, m), 7.6 p.p.m. (5H, s, Ph); i.r. (CH_2Cl_2) 1855, 1775 cm^{-1}, no sign of OH absorption; u.v. λ_{max} (cyclohexane) 274 (ε 13 000), 305 (ε 2020), 317 nm (2100).

*Thermolysis of the Sulfone Anhydride (**4**)*

An accurately weighed sample of anhydride **4** was placed in a Pyrex tube (0.55 × 10 cm), then swept with nitrogen and evacuated, sealed *in vacuo*, and finally half immersed in an oil bath which was equilibrated at the desired temperature. After being heated for the specified time (see Table 1) and then chilled at 3° for *ca.* 1 h, the Pyrex tube was opened and the dark brown solid mixture dissolved in methylene chloride (1–2 ml) and then chromatographed on a silica gel column (1 × 10 cm). Successive eluants used were the following: 1:1 chloroform – pentane, chloroform, 1:1 chloroform – methylene chloride, methylene chloride, and methanol (50 ml each). Separation was monitored by u.v. and t.l.c. The main products were identified as compounds **5** and **6** by t.l.c., comparison of spectra (i.r. and u.v. of each compound and n.m.r. of reaction mixture), and mixture m.p. determination. Sulfur dioxide was detected by its odor and reaction to p*H* paper. The yields were determined using subtractive u.v. analysis in the 335 and 250 nm regions which correspond to the absorption maxima of compound **6** and **5**, respectively. The "estimated conversion" values given in Table 1 were obtained by adjusting for attrition on the silica gel column and in the reaction mixture as follows. In separate control experiments, the recovery of compounds **5** and **6** from the silica gel column (1 × 10 cm) and the thermolysis reaction conditions was determined spectrophotometrically by means of subtractive u.v. analysis. In the latter case **5** and **6** were determined without prior chromatographic separation. For compound **6** a calibration curve was used for more precise measurement of absorptivity. The results are summarized in Table 1.

Can. J. Chem. Downloaded from www.nrcresearchpress.com by 210.87.254.42 on 09/05/12
For personal use only.

Dimethyl 1-Phenyl-1,3,5-cycloheptatriene-2,3-dicarboxylate from the Anhydride (6)

To a solution of the anhydride (**6**) (33.1 mg, 0.139 mmol) in tetrahydrofuran (5 ml) was added by means of a syringe 0.816 *M* sodium hydroxide solution (0.19 ml, 0.153 mmol) and the resulting mixture was heated at 60° for 1 h and then stirred at room temperature for 2 h. The reaction mixture was then acidified with 0.1 *N* hydrochloric acid solution to p*H* 3 and saturated with sodium chloride (0.5 g). The organic layer was separated, dried over anhydrous magnesium sulfate, and concentrated to a yellowish gum which was dried at 0.2 mm for 12 h. The diacid was then esterified with an ethereal solution of diazomethane, the solvent removed, and the product crystallized from methylene chloride – pentane to give yellow prisms of the dimethyl ester, m.p. 116–118° (18.4 mg, 45%); ν_{max} 1720 cm^{-1}; n.m.r. ($CDCl_3$): δ 7.58 (1H, d, J_{AM} = 5.5), 7.10 (5H, s), 6.26 (1H, dd, J_{AM} = 5.5, J_{MX} = 9.5), 5.65 (1H, dt, J = 7.0, J_{MX} = 9.5), 3.66 (3H, s), 3.35 (3H, s), 2.68 p.p.m. (2H, d, J = 7.0 Hz); *m/e* M^+ 284.1047 (calcd. for $C_{17}H_{16}O_4$ 284.10476). The n.m.r. spectrum ($CDCl_3$) of the dimethyl ester (18.4 mg, 6.5 × 10^{-2} mmol) in the presence of Eu(fod)$_3$, *i.e.* tris(1,1,1,2,2,-3,3-heptafluoro-7,7-dimethyl-4,6-octadiene)europium-(III), (115.8 mg, 11 × 10^{-2} mmol) showed: δ 14.65 (1H, d, J_{AM} = 5.5), 9.3 (2H, m), 7.9 (3H, m), 8.51 (3H, s), 7.37 (1H, dd, J_{AM} = 5.5, J_{MX} = 9.5), 6.92 (1H, dt, J_{MX} = 9.5, J = 7.0), 6.66 (3H, s), 4.66 (2H, d, J = 7.0); appropriate decoupling experiments confirmed the above coupling patterns.

We thank the National Research Council of Canada for financial support of this work.

1. J. F. KING and E. G. LEWARS. Chem. Commun. 700 (1972); Can. J. Chem. **51**, 3044 (1973).
2. N. H. FISCHER and H. N. LIN. J. Org. Chem. **38**, 3073 (1973).
3. C. M. ATKINSON and C. J. SHARPE. J. Chem. Soc. 2858 (1959).
4. E. M. LA COMBE and B. STEWART. J. Am. Chem. Soc. **83**, 3457 (1961).
5. J. F. KING and D. R. K. HARDING. Chem. Commun. 959 (1972).
6. S. D. MCGREGOR and D. M. LEMAL. J. Am. Chem. Soc., **88**, 2858 (1966).
7. W. L. MOCK. J. Am. Chem. Soc. **88**, 2857 (1966).
8. J. R. DU MANOIR, J. F. KING, and R. R. FRASER. Chem. Commun. 541 (1972).
9. R. B. WOODWARD and R. HOFFMANN. Angew. Chem. Int. Ed. **8**, 781 (1969).
10. O. T. SCHMIDT and W. STAAB. Chem. Ber. **87**, 388 (1954).
11. J. F. KING and J. R. DU MANOIR. Can. J. Chem. **51**, 4082 (1973).

Can. J. Chem. Downloaded from www.nrcresearchpress.com by 210.87.254.42 on 09/05/12
For personal use only.

Barrier to Internal Rotation in 2,6-Dichlorobenzal Iodide and some α, α′-*m*-Xylyl Halides. Experimental Evidence for the Transition State Conformation in Benzal Halides

JAMES PEELING, J. BRIAN ROWBOTHAM, LUDGER ERNST, AND TED SCHAEFER

Department of Chemistry, University of Manitoba, Winnipeg, Manitoba R3T 2N2

Received February 14, 1974

JAMES PEELING, J. BRIAN ROWBOTHAM, LUDGER ERNST, and TED SCHAEFER. Can. J. Chem. **52**, 2414 (1974).

The barriers to internal rotation in the α,α′-di-X-2,4,5,6-dichloro-*m*-xylenes (X = Cl, Br, I) are determined by proton magnetic resonance bandshape analyses. Their magnitudes are experimental evidence for the calculated conformation of the activated rotational state of the benzal halides, in which the C—H bond of the side chain is predicted to lie in a plane perpendicular to the aromatic nucleus. The synthesis and the barrier to rotation in 2,6-dichlorobenzal iodide are reported.

JAMES PEELING, J. BRIAN ROWBOTHAM, LUDGER ERNST et TED SCHAEFER. Can. J. Chem. **52**, 2414 (1974).

On a déterminé, par l'analyse de la forme des bandes de r.m.n., les barrières à la rotation interne dans les α,α′-di-X dichloro *m*-xylènes-2,4,5,6. On déduit des valeurs observées que les molécules existent dans la conformation calculée pour l'état rotationnel activé des halogénures de benzal dans lesquels le lien C—H de la chaîne latérale serait dans un plan perpendiculaire au noyau aromatique. On rapporte la synthèse et les barrières à la rotation dans l'iodure de dichloro-2,6 benzal. [Traduit par le journal]

Introduction

A recent analysis (1) of the long-range spin–spin coupling constants in benzal fluoride and its dichloro derivatives shows that its ground state conformation is **1** and that the barrier to internal rotation is substantially less than 0.5 kcal/mol, in agreement with an *ab initio* molecular orbital prediction of 0.18 kcal/mol (2) for the barrier and

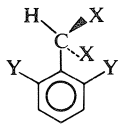

1

X = F, Cl, Br, I

Y = H, Cl, Br

of **1** as the low energy form. As the size of the substituents X and Y in **1** increases, the barrier naturally rises (3) until for 2,6-dichlorobenzal iodide the free energy of activation, $\Delta G^{\ddagger}$, becomes $21.0_5 \pm 0.1_0$ kcal/mol near 377 °K (see below).

All compounds **1** have the indicated ground state conformation, as have those in which two or three $CHCl_2$ groups are spaced by at least one ring halogen substituent (4). Molecular models and approximate potential energy calculations (5) suggest a high energy conformation, **2**, in which a C—X bond eclipses the C—Y bond.

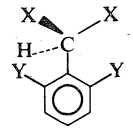

2

More accurate classical calculations (3, 6) predict **3** as the high energy form and give reasonably

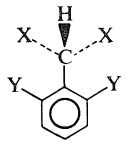

3

X = Cl, Br, I

Y = Cl, Br

good agreement with the observed barriers to internal rotation.[1] However, the computational

[1]CNDO/2 and INDO computations (7*a*) in this laboratory using the geometries predicted by the classical model, yield **3** as the *low* energy conformation.

Can. J. Chem. Downloaded from www.nrcresearchpress.com by 210.87.254.5 on 09/05/12
For personal use only.

Can. J. Chem. Downloaded from www.nrcresearchpress.com by 210.87.254.5 on 09/05/12
For personal use only.

complexities demand some approximations (6) and consequently it seems desirable to obtain experimental evidence for **3** as the transition state in the internal rotation process. This can be done by the following indirect approach.

Of course, the high energy form is not observable. However, if **3** is the transition state for the CHX_2 group, the eclipsed conformation **2** being of lower energy, it follows that the benzyl halide, **4**, whose transition state is the eclipsed

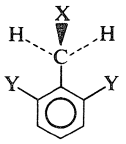

4

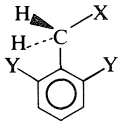

5

conformation, **5**, must have a *considerably* lower barrier to internal rotation than do the benzal halides. This conclusion is reasonable because the calculations predict that **6** (0°,60° interaction) has a substantially lower potential energy than **7** (30°,30° interaction). Furthermore, a

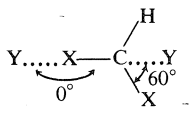

6

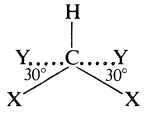

7

60°,60° interaction as in **1** represents a near-zero potential energy (see calculations below), so that the eclipsed form **5** for the benzyl halide will hardly be of higher energy than **6** for the benzal halide.

The barrier in the symmetrical benzyl halide, **4**, is not accessible to line-shape fitting methods. Therefore the more complex compounds **8**, **9**, **10**,

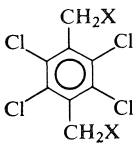

8

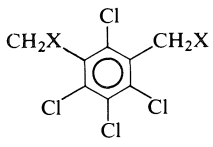

9

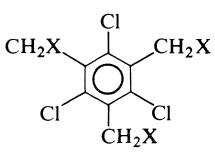

10

were prepared. Insofar as the CH_2X groups within a given molecule can take on independent orientations, the protons in different methylene groups (**8** and some forms of **10**) or within the same methylene group (**9** and some forms of **10**) need not be isochronous. Thus, for **9** the two forms **11** and **12** can display two distinct $[AB]_2$

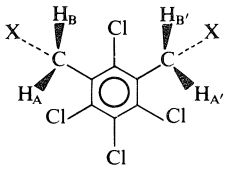

11 *cis*

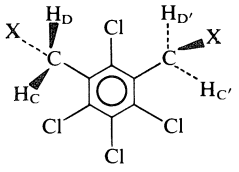

12 *trans*

proton magnetic resonance spectra. Rapid rotation of the CH_2X groups on the time scale defined by the extent of the anisochronicity within one $[AB]_2$ spectrum *and* between the two $[AB]_2$ spectra leads to a single peak A_4 and the line shape at intermediate rotational rates contains an extractable rate constant.

For reasons described below, only $\Delta G^{\ddagger}$ could be found and that only for **9** (X = Cl, Br, I). Yet the results suffice as an indirect demonstration of the conformation of the rotational transition state in the benzal halides. In addition, the barrier to rotation in the 2,6-dichlorobenzal iodide is measured and calculated.

Experimental

Preparation of Compounds

(a) 2,6-Dichlorobenzal Iodide (7b)

2,6-Dichlorobenzaldehyde (10 g), 20 ml of hydrazine hydrate, and 50 ml of CCl_4 were refluxed for 1.5 h. On cooling, white needles precipitated and the mixture was filtered after the addition of 50 ml of H_2O. The needles were washed with H_2O, dried by suction, and were added to 30 ml of CCl_4 and 70 ml of $N(CH_3)_3$. On addition of 25 g of I_2 in ether, a gas evolved rapidly. The solution was washed with 100 ml volumes of 5% aqueous $Na_2S_2O_3$, 3 *N* HCl, 5% aqueous K_2CO_3, and H_2O. The solution was dried over K_2CO_3, filtered, the solvent boiled off, leaving a red oil which was extracted twice with 50 ml portions of absolute ethanol. The product was a brown powder.

(b) The α,α′-Dihaloxylene Derivatives

Compounds **8** (X = Cl) and **9** (X = Cl) were obtained from Aldrich; compound **10** (X = Cl) was prepared from mesitylene (4). The bromine derivatives of **8**, **9**, and **10** (X = Br) were prepared by slow addition of an aqueous solution of KBr to boiling acetone solutions of the corresponding chlorides. After refluxing for 2 h the solution was poured into water and the precipitate was collected and recrystallized from ethanol (for the bromine derivative

TABLE 1. Physical characteristics of ring chlorinated α,α′-xylyl halides and α,α′,α′′-mesityl halides

Compound*	Melting point (°C)	Mol % (solvent)	Chemical shift† (p.p.m.)
p-Cl	178–180	1 (toluene-d_8)	4.260
p-Br	211–212	1 (toluene-d_8)	4.125
p-I	> 300	Insoluble	—
m-Cl	138–140	1 (toluene-d_8)	4.301
m-Br	158–160	1 (toluene-d_8)	4.124
m-I	180.5–181.5	1 (toluene-d_8)	4.051
Mesityl-Cl	159–161	1 (CS_2)	4.847
Mesityl-Br	180–181	1 (CS_2)	4.720
Mesityl-I	219.5–221.5	0.25 (CS_2)	4.637

*p-Cl means α,α′,2,3,5,6-hexachloro-*p*-xylene, *m*-I means α,α′,-diiodo-2,4,5,6-tetrachloro-*m*-xylene etc.
†Relative to internal tetramethylsilane at 32 °C.

of **10** the exchange was repeated four times, recrystallization from CCl_4).

For the iodine derivatives of **8**, **9**, and **10**, acetone solutions of the chlorides were added to acetone solutions of NaI and the mixtures were poured into water. The precipitate was collected and recrystallized from CCl_4. Chemical shift and m.p. data for these compounds are collected in Table 1.

Proton Magnetic Resonance Spectra

(a) 2,6-Dichlorobenzal Iodide

A 7 mol% solution in 1,2,3-trichloropropane, containing a small amount of hexamethyldisilane, was not sealed for reasons of safety. Proton magnetic resonance spectra were calibrated on an HA100D spectrometer at sweep rates of 0.02 or 0.05 Hz/s. The homogeneity of the magnetic field was monitored by the appearance of those resonance peaks (methine and the two outer peaks of H_4 corresponding to αα and ββ spin states of H_3 and H_5) whose width was independent of the exchange rate. Temperatures were measured as described previously (8). Fairly rapid decomposition occurred above about 110 °C.

(b) The α,α′-Dihaloxylene Derivatives

Solutions of **9** (X = Br, I) (1 mol%) in toluene-d_8, containing a very small amount of CH_2Cl_2 for monitoring magnet homogeneity and tetramethylsilane as a locking material, were used at temperatures down to −90 °C. For X = Cl, a 0.5 mol% solution in toluene-d_8 was used for reasons of solubility. No other suitable low-temperature solvent was found for **9**.

For **8** (X = I) no solvent was found; but for **8** (X = Cl, Br) very dilute solutions in toluene-d_8 could be cooled to −80 °C. Some broadening of the spectral peak at −80 °C may have arisen, not from a rate process, but from partial precipitation of the solute.

The solubility of **10** (X = Cl, Br, I) at low temperatures was insufficient for spectral work.

Results and Discussion

2,6-Dichlorobenzal Iodide

(a) Spectral Parameters at Low Rotation Rates

Near ambient temperatures the rate of conversion from **13** to its superimposable mirror image **14** is low enough for observation of an ABCD proton spectrum at 100 MHz (see Fig. 1). The spectral parameters at 33.0 and 50.6 °C are given in Table 2 as obtained from the program LAME (9). To within experimental error the spin–spin coupling constants are temperature independent. The shift between H_A and H_B, whose Larmor frequencies define the sites between which exchange occurs, does not change over this temperature range. The resonance frequency of H_D is the same in **13** and **14** and therefore its peaks do not broaden at intermediate exchange rates. The two outer peaks of H_C are not broadened by

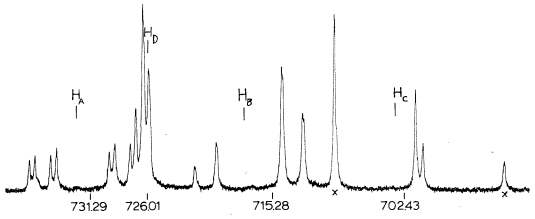

FIG. 1. The proton magnetic resonance spectrum at 100 MHz and 50.6 °C of a 7 mol% solution of 2,6-dichlorobenzal iodide in 1,2,3-trichloropropane. The solution was undegassed and the chemical shift scale is in Hz to low field of internal hexamethyldisilane. The labelling refers to structure **13** of the text.

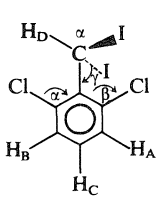

13

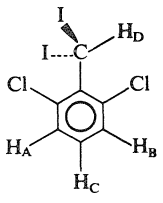

14

Can. J. Chem. Downloaded from www.nrcresearchpress.com by 210.87.254.5 on 09/05/12
For personal use only.

TABLE 2. Spectral parameters and free energies of rotational activation for 2,6-dichlorobenzal iodide, 7 mol % in 1,2,3-trichloropropane

Parameter	Value at 33.0 °C	Value at 50.6 °C
ν_A*	732.24 (0.006)†	731.29 (0.005)
ν_B	716.21 (0.006)	715.28 (0.006)
ν_C	703.68 (0.007)	702.43 (0.006)
ν_D	725.384 (0.007)	726.01 (0.005)
$^4J_{AB}$‡	1.28 (0.008)	1.27 (0.007)
$^3J_{AC}$	8.07 (0.008)	8.10 (0.008)
$^3J_{BC}$	8.12 (0.008)	8.11 (0.007)
$^5J_{AD}$	0.54 (0.008)	0.53 (0.007)
$^5J_{BD}$§	−0.01 (0.008)	−0.02 (0.007)
$^6J_{CD}$§	−0.02 (0.008)	−0.04 (0.007)
Root mean square error	0.0123	0.0110
Largest error	0.035	0.022
Lines assigned	32	32

T (°K)	k (s^{-1})	$\Delta G^{\ddagger}$ (kcal/mol)
366.5	2.25 ± 0.15	21.02 ± 0.08
378.9	6.25 ± 0.75	20.98 ± 0.11
390.2	11.5 ± 1.5	21.16 ± 0.11

*In Hz at 100 MHz to low field of internal hexamethyldisilane.
†Probable errors, to be multiplied by a factor of 3 to 5.
‡In Hz.
§Not necessarily different from zero.

the rate process because they correspond to αα and ββ states for H_A and H_B. These H_C peaks and the H_D peaks serve as convenient measures of the linewidth corrections, T_2, applicable to the exchange-broadened spectra.

(b) Free Energy of Activation ($\Delta G^{\ddagger}$)

Decomposition occurs fairly rapidly above 110 °C. Exchange-broadened spectra were obtained at 93.3, 105.7, and 117.0 °C, coalescence occurring above 120 °C. Rate constants were obtained by matching complete spectral lineshapes with those calculated by the program DNMR2 (10, 11). Rate constants and $\Delta G^{\ddagger}$ values at the three temperatures are given in Table 2. The errors are the linearized relative statistical errors (12), including those arising from uncertainties in both the rate constants and in the temperatures. Slow decomposition occurred at temperatures above 90 °C, so that insufficient data could be collected for a reliable determination of $\Delta H^{\ddagger}$ and $\Delta G^{\ddagger}$. However, in 2,4,6-tribromobenzal bromide $\Delta S^{\ddagger}$ is zero within experimental error (3) and one may assume a similar value for 2,6-dichlorobenzal iodide.

(c) Comparison with Potential Energy Calculations

The method of calculation (6) allows the deformation of the bond angles indicated in **13**, the stretching of the C—C_α bond, and for the nonbonded interactions via a 6–12 potential. The results[2] are given in Table 3. The calculated barrier of 21.7 kcal/mol is 3% higher than the observed value of $21.0_5 \pm 0.1_0$ kcal/mol.

When ω = 60°, a C—I bond eclipses a C—Cl bond (see **6**) and the potential energy relative to the ground state is then 76% of the transition state energy at ω = 90° (see **7**). When ω = 30°, one C—I bond lies in a plane perpendicular to the aromatic ring and the energy is 34% of the transition energy. To zero order the energy of the transition state for a CH_2I group should then be 55% of that for a CHI_2 group, when both are flanked by C—Cl bonds on the ring. Thus the barrier for a CH_2I group may lie near 21.0 × 0.55 = 11.5 kcal/mol, while for CH_2Cl it may be near 15.3 × 0.55 = 8.4 kcal/mol (3). These

[2]Details of the calculations are available from the authors.

Can. J. Chem. Downloaded from www.nrcresearchpress.com by 210.87.254.5 on 09/05/12
For personal use only.

TABLE 3. Conformational energy calculations for 2,6-dichlorobenzal iodide.*

ω (deg)	$l_{C_1-C_\alpha}$	Bond angles (deg) α	β	γ	E_{nb}	E_1	E_θ	E	E_{rel}
0	1.510	124	125	113	−1.00	0.08	1.57	0.65	0.00
30	1.525	122	131	118	1.48	0.31	6.16	7.95	7.30
60	1.545	124	135	121	4.58	0.84	11.85	17.28	16.62
90	1.560	133	133	121	6.79	1.41	14.15	22.35	21.70

*Definitions of symbols used: $l_{C_1-C_\alpha}$ = bond length C_1—C_α in Å; E_{nb} = sum of nonbonded interactions; E_1 = energy for deformation of C_1—C_α bond; E_θ = sum of bond bending energies; $E = E_{nb} + E_1 + E_\theta$ in kcal/mol; ω = 0° when the C_α—H bond lies in plane of aromatic ring. Further definitions are given in the explanation of structure **13** in the text.

values are high enough for extraction by a line-shape analysis and are the subject of the next section.

Barriers to Rotation in m-C_6Cl_4 $(CH_2X)_2$ (X = Cl, Br, I)

(a) Spectral Characteristics and Assignments

In principle, **11** and **12** each possess ABB′A′, *i.e.* $[AB]_2$ resonance spectra (13). Their appearance will be dominated by the large $^2J_{AB}$ coupling within a methylene group because the coupling between protons in different groups is at least ten times smaller than $^2J_{AB}$ (14, 15).

In the event, at low enough temperatures the spectrum of each compound displays an AB quartet and, superimposed on the low-field tall peak of this quartet, there occurs a peak of relatively low intensity. The linewidths are about 1 Hz, suggesting the presence of unresolved long-range coupling between protons in different methylene groups. The quartet with a relatively large internal shift may be assigned to one conformer, **11** or **12**, and the single peak must then represent a tightly coupled AB quartet from the other, less abundant, conformer. A probable assignment can be made as follows.

Electric fields (16, 17) from the bond dipoles in **11** and **12** can cause relative chemical shifts of the methylene protons of less than 0.01 p.p.m. A detailed consideration of molecular sizes and packing, and of aromatic solvent induced shifts (18) suggests that the magnetic anisotropy of the toluene-d_8 solvent molecules causes the internal chemical shifts in **11** and **12** and that H_B in the *cis* form experiences a net shift to high field. Such considerations are consistent with the observation of no internal chemical shift in **8** at considerably lower temperatures than those needed for spectral coalescence in **11**. Intramolecular electric fields are again insufficient as causes of internal shifts in **8** and the barrier to rotation will be almost identical in the *meta* and *para* isomers, buttressing effects being rather small in even more crowded compounds (5, 19, 20).

The above interpretation of the observed shifts implies the higher stability of the *cis* form, **11**, at the temperatures in Table 4. Intramolecular electric fields or nonbonded interactions (17) are not large enough to reproduce the ΔG^0 values in Table 4 but the more polar form, **11**, is stabilized by the aromatic solvent by as much as 0.5 kcal/mol (21–26). The ΔG^0 values in Table 4 are then expected and observed to increase in the order Cl > Br > I. The *cis* form, **11**, is then more stable than the *trans* form, **12**.

(b) Extraction of Rate Constants and Rotational Barriers

The chemical shifts and proton–proton coupling constants of the methylene protons are given in Table 4. The latter are no doubt negative and their magnitudes have the same relative order as those in the corresponding methyl halides (27) and in some benzyl halide derivatives (28). The relative stabilities are presented as ΔG^0 values, obtained by simulation of the well-defined quartet and subtraction of this area from the total area of the observed spectrum.

The exchange process occurs between c, t, c', and t' (Scheme 1) and the spectral types of each form are indicated as ABB′A′ etc. The complexity of the process and the moderate quality of the spectra dictated an approximate treatment of the data, yielding $\Delta G^{\ddagger}$ at the coalescence temperature of the well-defined quartet. The exchange broadened spectra were simulated with the program ABXFIT (29) and the fitting method gave the rate of interconversion of c and c'. At equilibrium one has $p_c k_{ct} = p_t k_{tc} = p_c k_{ct'} = k' = p_t k_{tc'}$, etc. The sum of the fractional populations, p, is unity and therefore the rate of the AB exchange is

$$k_{AB} = p_c k_{ct} + p_t k_{tc'} + p_c k_{ct'} + p_t k_{t'c'} = 4k'$$

Can. J. Chem. Downloaded from www.nrcresearchpress.com by 210.87.254.5 on 09/05/12
For personal use only.

TABLE 4. Spectral parameters, relative populations, and rate data for α,α′-dihalo-2,4,5,6-tetrachloro-*m*-xylenes

Parameter	Value		
	Cl (°K)	Br (°K)	I (°K)
ν_B*	378.9 (161)	372.7 (196)	368.3 (226)
ν_A	390.7	383.9	379.1
ν	382.3	375.9	371.4
$\lvert J_{AB}\rvert$ (Hz)	11.8 ± 0.5	11.2 ± 0.2	10.1 ± 0.2
$G_t^0 - G_c^0$ (kcal/mol)	1.260 ± 0.100 (185)	0.845 ± 0.015 (215)	0.680 ± 0.080 (240)
k_{ct} (s^{-1})†	11.6 ± 5.9 (185)	11.5 ± 2.9 (215)	12.5 ± 3 (240)
k_{tc} (s^{-1})	375 ± 125	82.5 ± 21	52 ± 13
$\Delta G_{ct}^{\ddagger}$ (kcal/mol)	9.5 ± 0.2	11.1 ± 0.1	12.4 ± 0.1
$\Delta G_{tc}^{\ddagger}$ (kcal/mol)	8.2 ± 0.2	10.3 ± 0.1	11.7 ± 0.1

*Shift in Hz at 100 MHz to low field of internal TMS, temperature in brackets; the center of the resonance of the less abundant isomer is given as ν.
†The subscripts *ct* refer to the *cis* and *trans* isomers, **11** and **12**, of these compounds; see also Scheme 1.

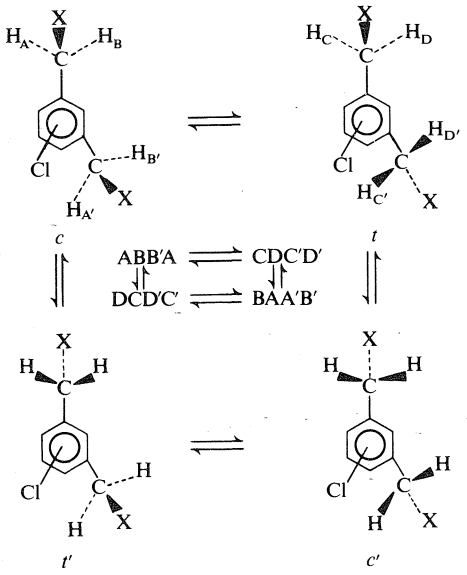

SCHEME 1

Noting that, for example, k_{ct} is the rate constant for the conversion of *c* to *t* ,the rate constants and $\Delta G^{\ddagger}$ values in Table 4 can be deduced.

Generous errors of 25 to 33% in the rate constants and of ±2 °C in the temperatures were treated by Binsch's method (12) to obtain the quoted errors in $\Delta G^{\ddagger}$. For the reasons given above, the ΔG^0 values will likely decrease as the temperature increases, so that $\Delta G_{ct}^{\ddagger}$ and $\Delta G_{tc}^{\ddagger}$ will likely converge at higher temperatures.

(c) Comparison of Benzal and m-Xylyl Halide Barriers.

The mean $\Delta G^{\ddagger}$ values for the *m*-xylyl halides amount to 60% of $\Delta G^{\ddagger}$ values for the corresponding benzal halides (3). Thus, $\Delta G^{\ddagger}$ in 2,6-dichlorobenzal iodide is 21.0_5 kcal/mol and $(\Delta G_{ct}^{\ddagger} + \Delta G_{tc}^{\ddagger})/2$ is 12.0_5 kcal/mol in α,α′-diiodo-2,4,5,6-tetrachloro-*m*-xylene. The $\Delta G^{\ddagger}$ values are measured at widely different temperatures for the various compounds (3) and we take the constant ratio of 60% for X = Cl, Br, I as a strong indication of very small $\Delta S^{\ddagger}$ magnitudes in the hindered internal rotations. Therefore the potential energy calculations can be equated to $\Delta G^{\ddagger}$ values with some confidence.

In our opinion these results are evidence for the conformation, **3** or **7**, of the activated rotational state of the benzal halides.

We are grateful to the National Research Council of Canada for financial assistance.

1. J. B. ROWBOTHAM, A. F. JANZEN, J. PEELING, and T. SCHAEFER. Can. J. Chem. **52**, 481 (1974).
2. W. J. HEHRE, L. RADOM, and J. A. POPLE. J. Am. Chem. Soc. **94**, 1496 (1972).
3. J. PEELING, L. ERNST, and T. SCHAEFER. Can. J. Chem. **52**, 849 (1974).
4. J. PEELING, B. W. GOODWIN, T. SCHAEFER, and J. B. ROWBOTHAM. Can. J. Chem. **51**, 2110 (1973).
5. B. H. BARBER and T. SCHAEFER. Can. J. Chem. **49**, 789 (1971).
6. A. MANNSCHRECK and L. ERNST. Chem. Ber. **104**, 228 (1971).
7. (*a*) J. A. POPLE and D. L. BEVERIDGE. Approximate molecular orbital theory. McGraw-Hill Book Co., New York. 1970; (*b*) A. PROSS and S. STERNHELL. Aust. J. Chem. **23**, 989 (1970).
8. J. PEELING, T. SCHAEFER, and C. M. WONG. Can. J. Chem. **48**, 2839 (1970).
9. C. W. HAIGH and J. M. WILLIAMS. J. Mol. Spectrosc. **32**, 398 (1969).
10. G. BINSCH. J. Am. Chem. Soc. **91**, 1304 (1969).
11. Quantum chemistry program exchange. Indiana University, Bloomington, Ind. Program. 140.

Can. J. Chem. Downloaded from www.nrcresearchpress.com by 210.87.254.5 on 09/05/12
For personal use only.

12. A. STEIGEL, J. SAUER, D. A. KLEIER, and G. BINSCH. J. Am. Chem. Soc. **94**, 2770 (1972).
13. C. W. HAIGH. J. Chem. Soc. A, 1682 (1970).
14. C. J. MACDONALD and W. F. REYNOLDS. Can. J. Chem. **48**, 1002 (1970).
15. R. E. WASYLISHEN and T. SCHAEFER. Can. J. Chem. **50**, 1852 (1972).
16. A. D. BUCKINGHAM. Can. J. Chem. **38**, 300 (1960).
17. W. F. REYNOLDS and D. J. WOOD. Can. J. Chem. **51**, 2659 (1973).
18. R. WASYLISHEN, T. SCHAEFER, and R. SCHWENK. Can. J. Chem. **48**, 2885 (1970).
19. J. PEELING, B. W. GOODWIN, T. SCHAEFER, and C. WONG. Can. J. Chem. **49**, 1489 (1971).
20. M. A. H. STEWART, T. SCHAEFER, H. M. HUTTON, and C. M. WONG. Can. J. Chem. **49**, 1085 (1971).
21. R. J. ABRAHAM and T. M. SIVERNS. J. Chem. Soc. Perkin Trans. II, 1587 (1972).
22. R. J. ABRAHAM and Z. L. ROSSETTI. J. Chem. Soc. Perkin Trans. II, 583 (1973).
23. R. J. ABRAHAM and M. A. COOPER. J. Chem. Soc. B. 202 (1967).
24. R. J. ABRAHAM. J. Phys. Chem. **73**, 1192 (1969).
25. P. LASZLO. Prog. N.M.R. Spectrosc. **3**, 231 (1967).
26. E. L. ELIEL and O. HOFER. J. Am. Chem. Soc. **95**, 8041 (1973).
27. H. J. BERNSTEIN and N. SHEPPARD. J. Chem. Phys. **37**, 3012 (1962).
28. C. A. CUPAS, J. M. BOLLINGER, and M. HASLANGER. J. Am. Chem. Soc. **90**, 5502 (1968).
29. B. J. FUHR, B. W. GOODWIN, H. M. HUTTON, and T. SCHAEFER. Can. J. Chem. **48**, 1558 (1970).

Can. J. Chem. Downloaded from www.nrcresearchpress.com by 210.87.254.5 on 09/05/12
For personal use only.

Polymorphism in *n*-Alkylammonium Halides. A Wide Line Nuclear Magnetic Resonance Study of the Chlorides C_{11}—C_{15}

J. TSAU AND D. F. R. GILSON

Chemistry Department, McGill University, P.O. Box 6070, Station A, Montreal, Quebec H3C 3G1

Received January 29, 1974

J. TSAU and D. F. R. GILSON. Can. J. Chem. **52**, 2421 (1974).

Wide line n.m.r. studies of the *n*-alkylammonium chlorides C_{12}—C_{15} show a nonreversible behavior which parallels that observed using differential scanning calorimetry. For samples which have been heated above the nonreversible transition the temperature dependence of the line width and second moment resemble that of the shorter chain compounds of this series; one transition due to the onset of chain rotation and a second higher temperature transition due to more extended motion probably of a translational nature. A change in crystal structure is proposed in order to explain the nonreversibility.

J. TSAU et D. F. R. GILSON. Can. J. Chem. **52**, 2421 (1974).

Les études de la bande large en r.m.n. des chlorures de *n*-alkylammonium C_{12}—C_{15} montrent un comportement non-réversible qui est du même type que celui observé par calorimétrie à balayage différentiel. La dépendance de la largeur de bande et du moment secondaire par rapport à la température pour les échantillons chauffés au-dessus de la transition non-réversible ressemble à ce qui a été observé pour les composés à chaîne plus courte de cette série; une première transition est due au début de rotation de la chaîne et une deuxième est due à un mouvement plus développé probablement de nature translationnelle. On propose un changement dans la structure cristalline en vue d'expliquer la non-réversibilité.

[Traduit par le journal]

Can. J. Chem. Downloaded from www.nrcresearchpress.com by 86.111.144.194 on 09/06/12
For personal use only.

Introduction

Fragmentary evidence for the existence of solid–solid phase transitions in the homologous series of *n*-alkylammonium halides has existed for many years but there have been few systematic investigations of the nature of these transitions (1–3). The reported X-ray structural studies are limited almost entirely to room temperature measurements of the (001) long spacings (4–8), and only *n*-propyl– and *n*-pentylammonium chlorides (9, 10) and *n*-dodecylammonium bromide (7) appear to have been studied in any greater detail. In general the chlorides are tetragonal up to a chain length of about 10 carbon atoms and either monoclinic (C_{12},C_{14},C_{15},C_{16}) or orthorhombic (C_{13},C_{18}) thereafter. Differential scanning calorimetric (d.s.c.) studies (2) showed that several thermal transitions exist for each compound and that these occur below room temperature for chain lengths up to C_9 and above room temperature for the longer members of the series. On the basis of this evidence it seems probable that one of the thermal transitions involves a change from, at low temperature, a monoclinic or orthorhombic form to a tetragonal structure at higher temperature. Such a transition has been observed for *n*-propylammonium chloride (9). The lowest temperature d.s.c. transitions showed an odd–even chain length alternation in transition temperature, which is a well known phenomenon (11, 12) for such homologous series, particularly for melting temperatures. For the *n*-alkylammonium chloride series C_3 to C_{10} the low temperature transitions correlated approximately with the lower of two line width and second moment transitions observed by wide line n.m.r. methods (3) although the n.m.r. transitions were at about 10–20° lower temperature. This n.m.r. transition is due to the onset of molecular re-orientation about the chain axis. The higher temperature n.m.r. transition involves a more extensive molecular motion, which must be of a translational nature as the second moments are too low to be explained by rotation alone.

The d.s.c. results for transition temperatures and enthalpies of the longer chain *n*-alkylammonium chlorides depend upon the thermal history of the sample. A single transition, with a large enthalpy change, was observed the first time the sample was heated but on cooling and on subsequent reheating cycles three smaller enthalpy transitions occurred at temperatures

TABLE 1. Transition temperatures, second moments. and enthalpies for the nonreversible transitions

Chain length (C atoms)	n.m.r. transition temperature (°K)	Second moment (G^2)		d.s.c. transition temperature (°K)	ΔH_{trans} (kcal/mol)
		Before	After		
12	334	17.3	2.5	333	7.39
13	341	13.4	5.3	320	2.46
14	341	13.4	3.7	343	7.21
15	334	15.8	6.0	337	6.86

TABLE 2. Experimental second moments and transition temperature ranges for the reversible transitions

Chain length (C atoms)	Second moment at 77 °K (G^2)	Transition temperature range (°K)	Second moment (G^2)		Transition temperature range (°K)	Second moment (G^2)	
			Before	After		Before	After
11	24.0	262–269	15.6	9.1	336–350	4.7	2.5
12	27.7	289–295	20.3	8.1	334–350	5.8	2.4
13	26.0	261–282	18.4	9.1	328–359	5.5	2.4
14	27.0	—*	—*	—*	—*	—*	—*
15	26.5	237–281	20.8	8.0	325–380	6.4	3.1

*Not studied.

different from the original scan. The present paper describes the results of a wide line n.m.r. study of the *n*-alkylammonium chlorides which have transitions above room temperature, extending the series up to C_{15}.

Experimental

The *n*-alkylammonium chlorides were prepared by passing hydrogen chloride gas into a solution of the amine in chloroform or ether followed by recrystallization three times from chloroform. Wide line n.m.r. spectra were obtained as described previously (3). Second moments were computer calculated from the experimental derivative curves, using a program written in this laboratory, and corrected for finite modulation width.

Results

The most notable feature of the temperature dependence of the line widths and second moments, with the exception of *n*-undecylammonium chloride, is the nonreversible behavior. When samples, which have not been previously heated, are heated from ambient temperature the line widths and second moments undergo sharp transitions from second moment values in the range 13 to 18 G^2 down to about 3 to 6 G^2, Table 1, but on cooling this initial behavior is not reversed and the transitions occur in two stages and at lower temperatures. If the samples are then re-heated the line widths and second moments follow the path observed for the cooling direction. This temperature dependence now resembles that previously observed for the lower members of the series (3): a gradual decrease from second moments of 24 to 28 G^2 at 77 °K to values in the range of 15 to 20 G^2, followed by a sharp transition to 8 to 9 G^2 and a broader transition at still higher temperatures to second moments of less than 3 G^2.

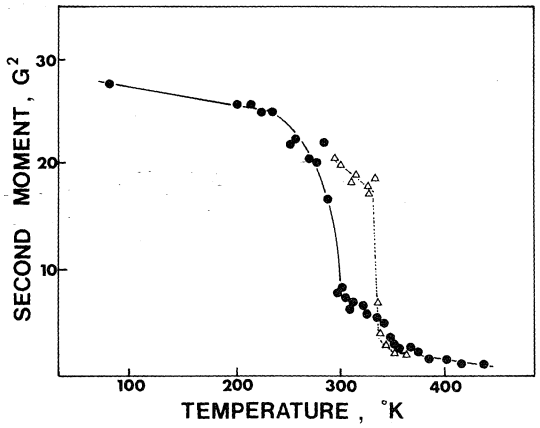

FIG. 1. The temperature dependence of the second moment of *n*-dodecyclammonium chloride. The triangles indicate the initial heating cycle.

As an example, this temperature dependence is shown in Fig. 1 for *n*-dodecylammonium chloride and second moments and transition temperature ranges are given for this series in Table 2.

Can. J. Chem. Downloaded from www.nrcresearchpress.com by 86.111.144.194 on 09/06/12
For personal use only.

Can. J. Chem. Downloaded from www.nrcresearchpress.com by 86.111.144.194 on 09/06/12
For personal use only.

TABLE 3. Theoretical second moments (G^2)

Chain length	Rigid	End-methyl rotation	Chain rotation
11	29.33	26.44	8.27
12	29.14	26.49	8.32
13	28.97	26.55	8.35
14	28.82	26.59	8.38
15	28.70	26.62	8.41

Discussion

The approximate theoretical second moments, Table 3, were estimated in the same manner as for the shorter chain members (3); the intramolecular contribution was calculated using standard bond lengths and angles, and the intermolecular second moment based upon values observed or calculated for similar long chain compounds. The experimental second moments at 77 °K are in good agreement with the values calculated for a rigid chain with end-methyl rotation. A more extensive motion develops with increasing temperature, probably chain torsion plus wagging, until the first transition when chain rotation commences. For the samples which had not been previously heated the low value of the second moment above this transition indicates the presence of additional motions, which must be of a translational nature, and there is no intermediate stage where chain rotation alone ocurs. If a heating cycle has occurred, then a plateau is reached, where, over a certain temperature region, chain rotation occurs without other extensive motions and the second transition follows at a higher temperature. In this high temperature phase the line is still broad in comparison with a liquid and there is no narrow component of modulation width at the center of the absorption signal. This latter is in contrast to the observations reported on salts of *n*-alkylcarboxylic acids (13), which otherwise behave in very similar fashion.

This behavior is now seen to be general for all the *n*-alkylammonium chlorides, C_3–C_{15}; only end-methyl rotation occurs at low temperatures, then, after some torsional chain motions, the chains rotate about their long axes and this is followed by a translational motion which must involve groups of molecules within which some order must be maintained. In general the observed d.s.c. transitions occur in or near the temperature region of the second n.m.r. transition whereas chain rotation occurs at lower temperatures, prior to the region of the thermal effects.

The temperatures of the nonreversible n.m.r. transitions correlate extremely well with those of the nonreversible d.s.c. transitions, Table 1. The enthalpies of these transitions are large (2), greater than the enthalpies of fusion, except for *n*-tridecylammonium chloride. This compound has an orthorhombic crystal structure (6) instead of the monoclinic form observed for the others. The difference in transition enthalpies may reflect this structural difference.

These results now permit an explanation of the X-ray structural results and of inconsistencies between them. Gordon *et al.* (7) reported (001) spacings for *n*-dodecylammonium chloride and bromide of 17.9 and 35.8 Å, respectively, whereas Kertes *et al.* (8) found spacings of 35.3 and 17.7 Å. This discrepancy was attributed by Kertes *et al.* to the occurrence of twinning. Gordon *et al.* also observed that *n*-dodecylammonium chloride underwent a transition at 59 °C to another monoclinic or triclinic form, with a double sheet arrangement and on cooling did not return to the previous form but had a slightly different (001) spacing. No other details of the thermal history of the samples were reported by either group.

The important criterion resulting from the d.s.c. and n.m.r. measurements appears to be whether samples have been heated above the nonreversible transition. For chain lengths less than 10 carbon atoms the transitions occur at or below room temperature and unless suitable experimental precautions are taken these compounds will unavoidably be heated above the transition. This may have inadvertently occurred for *n*-undecylammonium chloride in the present studies (the lowest transition is at 304 °K) and thus the nonreversible transition was not observed. If the longer chain compounds are heated, to remove solvent for instance, they will return to a different crystal structure upon cooling to room temperature. The reported X-ray results for *n*-dodecylammonium chloride and bromide suggest that this change may involve a doubling of the (001) spacing (7, 8). The transition temperature of 59 °C reported by Gordon *et al.* (7) agrees with the d.s.c. and n.m.r. values but the (001) spacing was described as only "slightly different," not doubled. X-Ray studies are presently being undertaken for this series of alkylammonium chlorides with controlled experimental condi-

tions to determine the (001) distances at different temperatures.

Thus we believe that two different crystal structures can exist for those members of the series which have transitions sufficiently far above room temperature. One form can be obtained by crystallization below the lowest transition and the other by heating the first above the transition. The enthalpy difference between the two may be small but conversion back to the original form will be slow if a large activation energy exists. The n.m.r. line narrowing process will occur at different temperatures because the potential barrier hindering chain reorientation depends upon the intermolecular contact distances, which differ in the two crystal lattices. Similarly the thermal transitions must also be dependent on the crystal structure.

Financial support from the National Research Council of Canada is gratefully acknowledged. J.T. acknowledges the award of a National Research Council Studentship 1966–1969.

1. P. CHEVALIER and C. SANDORFY. Paper presented at the International Symposium on Molecular Structure and Spectroscopy, Tokyo, 1962. C. Sandorfy, personal communication.
2. J. TSAU and D. F. R. GILSON. J. Phys. Chem. **72**, 4082 (1968).
3. J. TSAU and D. F. R. GILSON. Can. J. Chem. **51**, 1990 (1973).
4. S. B. HENDRICKS. Z. Krist. **68**, 189 (1928).
5. J. D. BERNAL. Nature, **129**, 870 (1932); Z. KRIST. **83**, 153 (1932).
6. G. L. CLARK and C. R. HUDGENS. Science, **112**, 309 (1950).
7. M. GORDON, E. STENHAGEN, and V. VAND. Acta Cryst. **6**, 739 (1953).
8. A. S. KERTES, A. GUTMANN, and I. MAYER. J. Appl. Cryst. **4**, 93 (1971).
9. M. V. KING and W. N. LIPSCOMB. Acta Cryst. **3**, 222 (1950).; Acta Cryst. **3**, 227 (1950).
10. C. SOUTHARD, R. T. MILNER, and S. B. HENDRICKS. J. Chem. Phys. **1**, 95 (1932).
11. E. F. WESTRUM JR. and J. P. MCCULLOUGH. *In* Physics and chemistry of the organic solid state. Vol. 1. *Edited by* D. Fox, M. M. Labes, and A. Weissberger. Interscience Publishers, New York, N.Y. 1963. Chapt. 1.
12. A. R. UBBELOHDE. Melting and crystal structure. Clarendon Press, London. 1965.
13. B. A. DUNELL and W. R. JANZEN. Wiss. Z. Friedrich-Schiller Univ. Jena, **14**, 191 (1965).

Can. J. Chem. Downloaded from www.nrcresearchpress.com by 86.111.144.194 on 09/06/12
For personal use only.

The Methyl Ethers of 2-Amino-2,6-dideoxyglucopyranose (Quinovosamine)[1]

MALCOLM B. PERRY AND VIRGINIA DAOUST

Division of Biological Sciences, National Research Council of Canada, Ottawa, Canada K1A 0R6

Received January 24, 1974

MALCOLM B. PERRY and VIRGINIA DAOUST. Can. J. Chem. **52**, 2425 (1974).

The 3-, 4-, and 3,4-dimethyl ethers of 2-amino-2,6-dideoxyglucose have been synthesized. 3,4-Di-*O*-methyl-L-rhamnal on treatment with nitrosyl chloride gave dimeric 2-deoxy-3,4-di-*O*-methyl-2-nitroso-α-L-rhamnopyranosyl chloride which on reduction and *N*-acetylation afforded 2-acetamido-2,6-dideoxy-3,4-di-*O*-methyl-L-glucose and 2-acetamido-2,6-dideoxy-4-*O*-methyl-L-glucose. 2-Acetamido-2,6-dideoxy-3-*O*-methyl-D-glucose was made from methyl 2-acetamido-2-deoxy-3-*O*-methyl-α-D-glucopyranoside by the reduction of its 6-deoxy-6-iodo derivative, prepared from synthesized methyl 2-acetamido-4-*O*-acetyl-2-deoxy-3-*O*-methyl-6-*O*-(*p*-tolylsulfonyl)-α-D-glucopyranoside, to yield the required 6-deoxy-L-glucose derivative.

MALCOLM B. PERRY et VIRGINIA DAOUST. Can. J. Chem. **52**, 2425 (1974

On a synthétisé les méthoxy-3, méthoxy-4 et diméthoxy-3,4 amino-2 didéoxy-2,6 glucose. Le traitement du di-*O*-méthyl-3,4 L-rhamnal par le chlorure de nitrosyle fourni le dimère du chlorure de déoxy-2 di-*O*-méthyl-3,4 nitroso-2 α-L-rhamnopyranosyle qui par réduction et *N*-acétylation fourni l'acétamido-2 didéoxy-2,6 di-*O*-méthyl-3,4 L-glucose et l'acétamido-2 didéoxy-2,6 *O*-méthyl-4 L-glucose. On a préparé l'acétamido-2 didéoxy-2,6 *O*-méthyl-3 D-glucose à partir de l'acétamido-2 déoxy-2 *O*-méthyl-3 α-D-glucopyranoside de méthyle par réduction de son dérivé déoxy-6 iodo-6 qui peut être préparé à partir de l'acétamido-2 *O*-acétyl-4 déoxy-2 *O*-méthyl-3 *O*-(*p*-tolylsulfonyl-6) α-D-glucopyranoside de méthyle pour conduire au dérivé déoxy-6 L-glucose désiré. [Traduit par le journal]

2-Amino-2,6-dideoxy-D-glucose (D-quinovosamine) is a component of several bacterial polysaccharides (1–5). In our work on the determination of the structures of some quinovosamine containing lipopolysaccharides obtained from strains of *Pseudomonas aeruginosa* (6) using methylation analysis methods, we were prompted to prepare, for use as reference compounds, the methyl ethers of the aminoglycose in order to facilitate the identification of these materials in the fission products of the methylated polysaccharides.

The 3,4-di- and 4-methyl ethers of 2-amino-2,6-dideoxy-L-glucose were made using the general synthetic procedure for aminoglycoses which was developed by Lemieux and co-workers (7*a* and *b*) and involves reduction of the acetyl derivatives of 2-deoxy-2-nitrosoglycopyranosyl chlorides. It was found that nitrosyl chloride reacted with 3,4-di-*O*-methyl-L-rhamnal to give the expected crystalline dimeric 2-deoxy-3,4-di-*O*-methyl-2-nitroso-α-L-rhamnopyranosyl chloride. The nuclear magnetic resonance (n.m.r.) parameters for this compound were in close agreement with those found for the dimeric tri-*O*-acetyl-2-deoxy-2-nitroso-α-D-glucopyranosyl chloride (8) in keeping with the expected *cis* addition of the nitrosyl chloride to the rhamnal derivative and they were consistent with the assigned structure of the product. Reduction of the 2-deoxy-3,4-di-*O*-methyl-2-nitroso-α-L-rhamnopyranosyl chloride with zinc–copper couple in acetic acid – acetic anhydride solution, followed by de-*O*-acetylation of the product, gave a mixture of 2-acetamido-2,6-dideoxy-3,4-di-*O*-methyl-L-glucose (41%) and 2-acetamido-2,6-dideoxy-4-*O*-methyl-L-glucose (59%). While it was expected (7*a*) that the aminoglycose produced in this reduction would have the amino group in the equatorial orientation (*i.e. gluco*), the production of the 4-*O*-methyl derivative by elimination of the 3-*O*-methyl substituent from the precursor is of note. Similar elimination of 3-*O*-substituents were observed in the reduction of the nitrosyl chloride adducts of tri-*O*-acetyl-3-*O*-methyl-D-glucal and of 1 → 3 linked disaccharides.

The mixture of the two acetamidoglycoses was fractionated by cellulose column chromatography to yield pure crystalline 2-acetamido-2,6-dideoxy-3,4-di-*O*-methyl-L-glucose and 2-acetamido-2,6-dideoxy-4-*O*-methyl-L-glucose. The identity of the di-*O*-methyl glycose was esta-

[1]NRCC No. 13973.

Can. J. Chem. Downloaded from www.nrcresearchpress.com by 210.87.254.6 on 09/05/12
For personal use only.

Can. J. Chem. Downloaded from www.nrcresearchpress.com by 210.87.254.6 on 09/05/12
For personal use only.

blished by the fact that it had identical chromatographic and physical properties to a sample of 2-acetamido-2,6-dideoxy-3,4-di-*O*-methyl-L-glucose prepared by direct methylation of 2-acetamido-2,6-dideoxy-L-glucose (9) which differed from those of the correspondingly-prepared, epimeric 2-acetamido-2,6-dideoxy-3,4-di-*O*-methyl-L-mannose derivative. The 2-acetamido-2,6-dideoxy-4-*O*-methyl-L-glucose had a methoxyl value and also chromatographic properties corresponding to a mono-*O*-methyl derivative; after methylation and hydrolysis of the product with dilute hydrochloric acid, it gave 2-amino-2,6-dideoxy-3,4-di-*O*-methyl-L-glucose hydrochloride thus establishing its *gluco* configuration. The position of the methoxyl group at C4 was inferred from the fact that it had chromatographic and physical properties distinct from those of the corresponding 3-*O*-methyl glycose. 2-Amino-2,6-dideoxy-3,4-di-*O*-methyl-L-glucose and 2-amino-2,6-dideoxy-4-*O*-methyl-L-glucose hydrochlorides were obtained crystalline by hydrolysis of the parent 2-acetamido-2-deoxyglucoses with dilute hydrochloric acid.

2-Acetamido-2,6-dideoxy-3-*O*-methyl-D-glucose was made from methyl 2-acetamido-2-deoxy-3-*O*-methyl-α-D-glucopyranoside (10). Mono tosylation and acetylation of the latter compound afforded crystalline methyl 2-acetamido-4-*O*-acetyl-2-deoxy-3-*O*-methyl-6-*O*-(*p*-tolylsulfonyl)-α-D-glucopyranoside which on heating with sodium iodide in acetone gave methyl 2-acetamido-4-*O*-acetyl-2,6-dideoxy-6-iodo-3-*O*-methyl-α-D-glucopyranoside. This compound on catalytic reduction gave crystalline methyl 2-acetamido-4-*O*-acetyl-2,6-dideoxy-3-*O*-methyl-α-D-glucopyranoside which on hydrolysis with dilute hydrochloric acid gave crystalline 2-amino-2,6-dideoxy-3-*O*-methyl-D-glucose hydrochloride, convertible by *N*-acetylation (11) to crystalline 2-acetamido-2,6-dideoxy-3-*O*-methyl-D-glucose.

The chromatographic and physical properties of the 3,4-di-, 3-, and 4-methyl ethers of 2-acetamido-2,6-dideoxyglucose and their amino hydrochloride derivative are recorded together with the gas-chromatographic relative retention times of the corresponding acetylated 2-acetamido-2,6-dideoxyglucitol methyl ethers prepared by borohydride reduction and acetylation of the parent glycoses (12, 13).

Experimental

Paper chromatography was performed by the descending method (14) on Whatman No. 1 filter paper using either (A) pyridine – ethyl acetate – water (2:5:5 v/v, top layer) or (B) 1-butanol – ethanol – water (4:1:5 v/v, top layer) as the mobile phase. Glycoses were detected with either (*a*) 2% silver nitrate in acetone followed by 3% sodium hydroxide in ethanol (15), (*b*) 2% *p*-anisidine hydrochloride in ethanol (16), or (*c*) 2% ninhydrin in acetone. The rates of movement of the glycoses are quoted relative to L-rhamnose (R_{Rh}) or to 2-amino-2-deoxy-D-glucose hydrochloride (R_{GN}).

Thin-layer chromatography (t.l.c.) was done on silica gel G coated plates using benzene–methanol (10:1 v/v) and compounds located by heating developed plates, sprayed with 10% sulfuric acid in ethanol, at 130 °C for 20 min have their mobilities quoted relative to the solvent front (R_f).

Gas–liquid partition chromatography (g.l.p.c.) was carried out using a Hewlett–Packard model 402 chromatograph with a hydrogen flame detector and fitted with glass U-tubes (4 ft × 6 mm × 3 mm internal diameter) packed with either (A) 10% (w/w) neopentylglycol sebacate polyester on 80–100 mesh acid washed Chromosorb W or (B) 3% (w/w) ECNSS-M on 100–120 mesh Gas-Chrom Q (Applied Science Labs., State College, Pa.). Retention times are quoted relative to methyl 2,3,4,6-tetra-*O*-(trimethylsilyl)-α-D-glucopyranoside (T_{GS}) or to penta-*O*-acetyl-L-arabinitol (T_A).

Melting points were determined on a Fisher-Johns apparatus and are corrected. Solutions were concentrated under reduced pressure and below 40 °C. Optical rotations were determined at 20 °C using a Perkin–Elmer 141 polarimeter. Nuclear magnetic resonance (n.m.r.) spectra were recorded at 60 MHz with a Varian A-60A spectrometer with tetramethylsilane (τ 10.00) as an internal standard in chloroform-*d* solutions. Molecular weight determinations were made on chloroform solution using a Mechrolab osmometer model 301A.

2-Amino-2,6-dideoxy-3,4-di-O-methyl-L-glucose and 2-Amino-2,6-dideoxy-4-O-methyl-L-glucose

(*a*) *3,4-Di-O-methyl-L-rhamnal*

L-Rhamnal (17) (20 g) was dissolved in a mixture of dry *N*-dimethylformamide (100 ml) and methyl iodide (100 ml), and silver oxide (50 g) was added in four portions over 3 h to the cooled stirred mixture which was then stirred overnight. Following the addition of ether (1.5 l), the reaction mixture was filtered and the ether filtrate was washed with water (5 × 1 l). The dried (anhydrous Na_2SO_4) ether solution on concentration gave 3,4-di-*O*-methyl-L-rhamnal (21 g) as a syrup which had $[\alpha]_D$ + 32.4° (*c*, 7 in chloroform) and gave a single spot on t.l.c. with R_f 0.75, (n.m.r. OMe τ 6.40 and 6.57).

Anal. Calcd. for $C_8H_{14}O_3$: C, 60.74; H, 8.92; OMe, 39.24. Found: C, 60.71; H, 9.00; OMe, 39.03.

(*b*) *Dimeric 2-Deoxy-3,4-di-O-methyl-2-nitroso-α-L-rhamnopyranosyl Chloride*

A solution of 3,4-di-*O*-methyl-L-rhamnal (20 g) in dry ethyl acetate (140 ml) was contained in a three-neck flask fitted with a thermometer and gas injection and outlet tubes. The magnetically stirred solution was flushed with nitrogen and then cooled to −40 °C using a Dry Ice – acetone bath. A slow stream of nitrosyl chloride gas was passed through the cooled solution over 15 min and the mixture was then flushed with nitrogen over 20 min while the mixture was allowed to warm to 0 °C. On keeping the solution for 10 min at 0 °C, the dimeric 2-deoxy-3,4-di-*O*-

Can. J. Chem. Downloaded from www.nrcresearchpress.com by 210.87.254.6 on 09/05/12
For personal use only.

methyl-2-nitroso-L-rhamnopyranosyl chloride crystallized out and it was collected by filtration, washed with a little cold ethyl acetate, and then dried *in vacuo* over phosphorus pentoxide and potassium hydroxide. The product (19.8 g) gave a single spot on t.l.c. (R_f 0.89) and had m.p. 136–137 °C and $[\alpha]_D$ −300° (*c*, 3 in chloroform). Nuclear magnetic resonance data: τ 3.42 (1-proton doublet, $J_{1,2}$ 4.0 Hz, H-1), 4.72 (1-proton quartet, $J_{2,3}$ 10.2 Hz, H-2), 6.34 (6-proton singlet, OMe), 8.65 (3-proton doublet, $J_{5,6}$ 6.4 Hz, H-6). Attempts to recrystallize the product caused decomposition.

Anal. Calcd. for $C_{16}H_{28}Cl_2N_2O_8$ (mol. wt. 447.3): C, 42.96; H, 6.31; Cl, 15.85; N, 6.26; Found (mol. wt. 445, osmometric): C, 42.88; H, 6.31; Cl, 15.7; N, 6.21.

(*c*) *Reduction of Dimeric 2-Deoxy-3,4-di-O-methyl-2-nitroso-α-L-rhamnopyranosyl Chloride*

Zinc–copper couple (11 g) (Ventron Corp., Congress St., Beverly, Massachusetts) was added to a stirred solution of dimeric 2-deoxy-3,4-di-*O*-methyl-2-nitroso-α-L-rhamnopyranosyl chloride (6 g) in glacial acetic acid (120 ml) containing acetic anhydride (16 ml) and the mixture was stirred vigorously at room temperature for 2 d. Following the addition of more zinc–copper couple (11 g), acetic acid (50 ml), and acetic anhydride (8 ml) the mixture was stirred for a further 2 d. The reaction mixture was filtered, the residue was washed with chloroform (700 ml), and the combined filtrate and washings were washed successively with water, saturated sodium bicarbonate solution, and water and the dried (anhydrous Na_2SO_4) chloroform solution was concentrated to a partially crystalline mass (5.0 g). This residue (4.9 g) was dissolved in 70% aqueous methanol (55 ml) and, following the addition of triethylamine (14 ml), the mixture was kept at 20 °C overnight. The concentrated solution was dissolved in water (30 ml), treated with charcoal (*ca.* 2 g), filtered, and the filtrate was concentrated to a syrup (3.52 g).

Paper chromatographic examination of the product (solvent A) revealed two spots with R_{Rh} 1.93 and 1.57 (visual ratio 1:1) corresponding in mobility with 2-acetamido-2,6-dideoxy-3,4-di-*O*-methyl-L-glucose and 2-acetamido-2,6-dideoxy-4-*O*-methyl-L-glucose, respectively. Gas–liquid partition chromatography of the trimethylsilylated (18) product (column A, 190 °C) gave four peaks having T_{GS} 4.03 and 4.96 (TMS derivative of the 3,4-di-*O*-methylglycose, 41%) and 3.45 and 5.65 (TMS derivative of the 4-*O*-methylglycose, 59%).

The product (3 g) was fractionated by cellulose column (4 × 40 cm) chromatography using 1-butanol – water (10:1 v/v) as the mobile phase to yield the chromatographically pure components:

(1) 2-Acetamido-2,6-dideoxy-3,4-di-O-methyl-L-glucose

2-Acetamido-2,6-dideoxy-3,4-di-*O*-methyl-L-glucose (1.03 g) was the first compound eluted from the column. It gave a single spot on paper chromatography with R_{Rh} 1.93 (solvent A) and was obtained crystalline (0.88 g) from ethanol solution. The pure compound had m.p. 211–213 °C and $[\alpha]_D$ −56.3 → −17.2° (*c*, 0.14 in water).

Anal. Calcd. for $C_{10}H_{19}NO_5$: C, 51.49; H, 8.21; N, 6.01; OMe, 26.61. Found: C, 51.30; H, 8.10; N, 6.20; OMe, 26.40.

The g.l.p.c. (column A, 190 °C) of the trimethylsilylated crystalline 2-acetamido-2,6-dideoxy-3,4-di-*O*-methyl-L-glucose gave a single peak with T_{GS} 4.03 whereas the trimethylsilylated product prepared from the glucose equilibrated in water gave two peaks having T_{GS} 4.03 (87%) and 4.96 (13%) corresponding in retention times with the TMS derivatives of 2-acetamido-2,6-dideoxy-3,4-di-*O*-methyl-L-glucose prepared by a small scale Haworth type methylation of 2-acetamido-2,6-dideoxy-L-glucose (9).

2-Amino-2,6-dideoxy-3,4-di-O-methyl-L-glucose hydrochloride. A portion of crystalline 2-acetamido-2,6-dideoxy-3,4-di-*O*-methyl-L-glucose (0.5 g) was hydrolyzed with 3 *N* hydrochloric acid (15 ml) at 100 °C for 2.5 h and, following concentration, the residue was twice concentrated with toluene to remove HCl. The residue was dissolved in hot ethanol, decolorized with charcoal, filtered, and on keeping the ethanol solution at 2 °C, crystalline 2-amino-2,6-dideoxy-3,4-di-*O*-methyl-L-glucose hydrochloride (0.43 g) was obtained which gave a single ninhydrin positive spot on paper chromatography (R_{GN} 3.87, solvent B) and had m.p. 200–205 °C (dec.) and $[\alpha]_D$ −99.1 → −80.6° (*c*, 0.3 in water).

Anal. Calcd. for $C_8H_{18}ClNO_4$: C, 42.20; H, 7.97, Cl, 15.57; N, 6.15; OMe, 27.26. Found: C, 41.62; H, 7.77; Cl, 15.78; N, 5.95; OMe, 27.19.

(2) 2-Acetamido-2,6-dideoxy-4-O-methyl-L-glucose

The second fraction eluted from the column was 2-acetamido-2,6-dideoxy-4-*O*-methyl-L-glucose (1.50 g) obtained as crystals (1.2 g) from ethanol solution which gave a single spot on paper chromatography (R_{Rh} 1.75, solvent A) and had m.p. 211–213 °C and $[\alpha]_D$ −72.3 → −26.15° (*c*, 0.14 in water).

Anal. Calcd. for $C_9H_{17}NO_5$: C, 49.30; H, 7.82; N, 6.39; OMe, 14.16. Found: C, 49.20; H, 7.68; N, 6.13; OMe, 14.16.

Gas–liquid partition chromatography (column A, 190 °C) of the trimethylsilylated crystalline 2-acetamido-2,6-dideoxy-4-*O*-methyl-L-glucose gave a single peak with T_{GS} 3.45 whereas the trimethylsilylated product of the glycose equilibrated in water gave two peaks with T_{GS} 3.45 (57%) and 5.65 (43%).

A portion of the 2-acetamido-2,6-dideoxy-4-*O*-methyl-L-glucose (70 mg) after Haworth type methylation in aqueous dioxane (19) and subsequent hydrolysis of the product (3 *N* HCl, 3 h at 100 °C) afforded crystalline 2-amino-2,6-dideoxy-3,4-di-*O*-methyl-L-glucose (45 mg) having m.p. and mixture m.p. 201–205 °C and identical chromatographic properties and i.r. spectra to the authentic glycose.

2-Amino-2,6-dideoxy-4-O-methyl-L-glucose hydrochloride. A portion of 2-acetamido-2,6-dideoxy-4-*O*-methyl-L-glucose (0.5 g) was hydrolyzed with 3 *N* hydrochloric acid (20 ml) for 2 h at 100 °C. Subsequent concentration and dissolution of the residue in ethanol afforded crystalline 2-amino-2,6-dideoxy-4-*O*-methyl-L-glucose hydrochloride (0.41 g) which gave a single ninhydrin positive spot on paper chromatography (solvent B) with R_{GN} 2.74 and had m.p. 197–200 °C (dec.) and $[\alpha]_D$ −99.8 → −61.6° (*c*, 0.2 in water).

Anal. Calcd. for $C_7H_{16}ClNO_4$: C, 39.35; H, 7.55; Cl, 16.59; N, 6.56; OMe, 14.52. Found: C, 39.21; H, 7.51; Cl, 16.80; N, 6.70; OMe, 14.39.

2-Acetamido-2,6-dideoxy-3-O-methyl-D-glucose

(*a*) *Methyl 2-Acetamido-2-deoxy-3-O-methyl-6-O-(p-tolylsulfonyl)-α-D-glucopyranoside*

p-Toluenesulfonyl chloride (9 g) was added over 30 min

Can. J. Chem. Downloaded from www.nrcresearchpress.com by 210.87.254.6 on 09/05/12
For personal use only.

to a stirred solution of methyl 2-acetamido-2-deoxy-3-*O*-methyl-α-D-glucopyranoside (10) (6 g) in dry pyridine (90 ml) and the mixture was kept at room temperature for 18 h. Water (6 ml) was added to the stirred reaction mixture and, after 2 h the mixture was diluted with chloroform (1.2 l). The chloroform solution was washed successively with cold 3 *N* hydrochloric acid (*ca.* 350 ml), cold saturated sodium bicarbonate solution (*ca.* 100 ml), and cold water (*ca.* 100 ml) and the dried (anhydrous Na_2SO_4) chloroform solution was concentrated to a syrup (8.7 g). Crystalline methyl 2-acetamido-2-deoxy-3-*O*-methyl-6-*O*-(*p*-tolylsulfonyl)-α-D-glucopyranoside (7.2 g), obtained from methanol solution of the product, had m.p. 159–160 °C and $[\alpha]_D$ +99° (*c*, 0.2 in chloroform).

Anal. Calcd. for $C_{17}H_{25}NO_8S$: C, 50.61; H, 6.25; N, 3.47; S, 7.95. Found: C, 50.41; H, 6.23; N, 3.43; S, 7.79.

(*b*) *Methyl 2-acetamido-4-O-acetyl-2-deoxy-3-O-methyl 6-O-(p-tolylsulfonyl)-α-D-glucopyranoside*

Methyl 2-acetamido-2-deoxy-3-*O*-methyl-6-*O*-(*p*-tolylsulfonyl)-α-D-glucopyranoside (5 g) dissolved in dry pyridine (25 ml) was treated with acetic anhydride (7 ml) and the mixture was kept at 70 °C for 1 h. The mixture was poured into stirred ice-water (1 l) containing acetic acid (25 ml) and, after 4 h at 2 °C, the precipitated product (5.6 g) was collected by filtration. Two recrystallizations of the product from methanol solution afforded crystalline methyl-2-acetamido-4-*O*-acetyl-2-deoxy-3-*O*-methyl-6-*O*-(*p*-tolylsulfonyl)-α-D-glucopyranoside (5 g) which had m.p. 172–173 °C and $[\alpha]_D$ +113° (*c*, 2.2 in chloroform).

Anal. Calcd. for $C_{19}H_{27}NO_9S$: C, 51.22; H, 6.11; N, 3.14; S, 7.20. Found: C, 50.98; H, 6.09; N, 3.12; S, 6.90.

(*c*) *Methyl 2-Acetamido-4-O-acetyl-2,6-dideoxy-6-iodo-3-O-methyl-α-D-glucopyranoside*

A mixture of methyl 2-acetamido-4-*O*-acetyl-2-deoxy-3-*O*-methyl-6-*O*-(*p*-tolysulfonyl)-α-D-glucopyranoside (5 g) and sodium iodide (5 g) in dry acetone (90 ml) was heated in a sealed tube at 100 °C for 7 h. The cooled reaction mixture was filtered to remove the crystalline sodium *p*-toluenesulfonate and the filtrate was diluted with chloroform (200 ml). The chloroform solution was washed with 10% sodium thiosulfate solution (10 ml) and with water (30 ml), dried (anhydrous Na_2SO_4), and concentrated to a crystalline mass (5.2 g). Recrystallization of the product from methanol gave pure methyl 2-acetamido-4-*O*-acetyl-2,6-dideoxy-6-iodo-3-*O*-methyl-α-D-glucopyranoside (4.5 g) which had m.p. 226–227 °C and $[\alpha]_D$ +86° (*c*, 0.15 in chloroform).

Anal. Calcd. for $C_{12}H_{20}NO_6I$: C, 35.92; H, 5.02; N, 3.49; I, 31.63. Found: C, 36.10; H, 5.10; N, 3.41; I, 31.7.

(*d*) *Methyl 2-acetamido-4-O-acetyl-2,6-dideoxy-3-O-methyl-α-D-glucopyranoside*

Methyl 2-acetamido-4-*O*-acetyl-2,6-dideoxy-6-iodo-3-*O*-methyl-α-D-glucopyranoside (4 g) in methanol (40 ml) containing diethylamine (1.3 ml) was treated with fresh Raney nickel (2 g) and the compound was reduced by vigorous shaking for 2 h under a hydrogen atmosphere of 40 p.s.i. pressure. The filtered reaction mixture was concentrated to a solid which was taken up in hot methanol (*ca.* 10 ml) and, on keeping the solution at 0 °C, crystalline methyl 2-acetamido-4-*O*-acetyl-2,6-dideoxy-3-*O*-methyl-α-D-glucopyranoside (2.2 g) was obtained which had m.p. 185–186 °C and $[\alpha]_D$ +103° (*c*, 0.18 in chloroform).

Anal. Calcd. for $C_{12}H_{21}NO_6$: C, 52.35; H, 7.69; N, 5.09. Found: C, 52.14; H, 7.70; N, 4.96.

(*e*) *2-Amino-2,6-dideoxy-3-O-methyl-D-glucose Hydrochloride*

Methyl 2-acetamido-4-*O*-acetyl-2,6-dideoxy-3-*O*-methyl-α-D-glucopyranoside (2 g) was hydrolyzed with 3 *N* hydrochloric acid (30 ml) for 2 h at 100 °C and, following concentration, the residue was kept *in vacuo* over sodium hydroxide. The residue was dissolved in hot methanol, decolorized with a little charcoal, filtered, and the filtrate was diluted with acetone. On keeping the solution at 2 °C it afforded crystalline 2-amino-2,6-dideoxy-3-*O*-methyl-D-glucose hydrochloride (1.6 g) which gave a single spot on paper chromatography (R_{GN} 2.28, solvent B) and had m.p. 197–210 °C (dec.) and $[\alpha]_D$ +99.7 → +73.8° (*c*, 0.54 in water).

Anal. Calcd. for $C_7H_{16}ClNO_4$: C, 39.35; H, 7.55; Cl, 16.59; N, 6.56; OMe, 14.52. Found: C, 39.39; H, 7.61; Cl, 16.71; N, 6.42; OMe, 14.61.

(*f*) *2-Acetamido-2,6-dideoxy-3-O-methyl-D-glucose*

N-acetylation (11) of 2-amino-2,6-dideoxy-3-*O*-methyl-D-glucose hydrochloride (0.5 g) afforded crystalline 2-acetamido-2,6-dideoxy-3-*O*-methyl-D-glucose (0.44 g) from ethanol solution which gave a single spot on paper chromatography (R_{Rh} 1.52, solvent A) and had m.p. 212–214 °C and $[\alpha]_D$ +42.9 → 0° (*c*, 0.17 in water).

Anal. Calcd. for $C_9H_{17}NO_5$: C, 49.30; H, 7.82; N, 6.39; OMe, 14.16. Found: C, 49.13; H, 7.84; N, 6.23; OMe, 13.99.

Gas–liquid partition chromatography of the trimethylsilylated crystalline glycose gave a single peak with T_{GS} 5.46 (column A, 190 °C) whereas the trimethylsilylated product prepared from the glycose equilibrated in water gave two peaks having T_{GS} 5.46 (56%) and 7.05 (44%).

Gas–Liquid Partition Chromatography of the Acetate Derivatives of the Methyl Ethers of 2-Acetamido-2,6-dideoxyglucitol

The 3-, 4-, and 3,4-dimethyl ethers of 2-acetamido-2,6-dideoxyglucose or their amine hydrochloride derivatives (10 mg) in water (2 ml) were reduced by the addition of sodium borohydride (15 mg) and, after 12 h, the excess borohydride was destroyed by acidification with acetic acid. The mixtures were concentrated to dryness and the residues were evaporated repeatedly with methanol (6 × 15 ml). The final residues were treated with acetic anhydride (0.8 ml) and kept at 130 °C for 2 h. Samples (1–5 μl) of the solutions were taken for direct injection on column B at 200 °C. Each derivative gave a single peak and had the relative retention values recorded: 2-acetamido-tetra-*O*-acetyl-2,6-dideoxy-L-glucitol, T_A 4.20; 2-acetamido-tri-*O*-acetyl-2,6-dideoxy-4-*O*-methyl-D-glucitol, T_A 3.24; 2-acetamido-tri-*O*-acetyl-2,6-dideoxy-3-*O*-methyl-L-glucitol, T_A 2.42; 2-acetamido-di-*O*-acetyl-2,6-dideoxy-3,4-di-*O*-methyl-L-glucitol, T_A 1.25.

1. E. J. SMITH. Biochem. Biophys. Res. Commun. **15**, 593 (1964).
2. O. LÜDERITZ, J. GMEINER, B. KICKHÖFEN, H. MEYER, and R. WHEAT. J. Bacteriol. **95**, 490 (1968).
3. R. R. COLWELL, E. J. SMITH, and G. B. CHAPMAN. Can. J. Microbiol. **14**, 165 (1968).
4. N. SUZUKI, A. SUZUKI, and A. FUKASAWA. J. Jap. Biochem. Soc. **42**, 130 (1970).
5. S. G. WILKINSON and K. A. CARBY. J. Gen. Microbiol. **66**, 221 (1971).
6. R. LOWE, M. B. PERRY, B. B. DIENA, F. E. ASHTON,

and R. WALLACE. Abst. 41st Can. Public Health Assn., Toronto, Nov. 1973.
7. (*a*) R. U. LEMIEUX and T. L. NAGABHUSHAN. Can. J. Chem. **46**, 401 (1968). (*b*) R. U. LEMIEUX, Y. ITO, K. JAMES, and T. L. NAGABHUSHAN. Can. J. Chem. **51**, 7 (1973).
8. R. U. LEMIEUX, T. L. NAGABHUSHAN, and I. K. O'NEILL. Can. J. Chem. **46**, 413 (1968).
9. M. B. PERRY and V. DAOUST. Carbohydr. Res. **27**, 460 (1973).
10. A. NEUBERGER. J. Chem. Soc. 50 (1941).
11. S. ROSEMAN and J. LUDOWIEG. J. Am. Chem. Soc. **76**, 301 (1954).
12. M. B. PERRY and A. C. WEBB. Can. J. Chem. **47**, 4091 (1969).
13. M. B. PERRY and V. DAOUST. Can. J. Biochem. **51**, 1335 (1973).
14. S. M. PARTRIDGE. Biochem. J. **42**, 238 (1948).
15. W. E. TREVELYAN, D. P. PROCTER, and J. S. HARRISON. Nature, **166**, 444 (1950).
16. L. HOUGH, J. K. N. JONES, and W. H. WADMAN. J. Chem. Soc. 1702 (1950).
17. W. ROTH and W. PIGMAN. *In* Methods in carbohydrate chemistry. Vol. 2 Academic Press Inc. 1963. p. 405.
18. M. B. PERRY. Can. J. Biochem. **42**, 451 (1964).
19. W. O. CUTLER, W. N. HAWORTH, and S. PEAT. J. Chem. Soc. 1979 (1937).

Can. J. Chem. Downloaded from www.nrcresearchpress.com by 210.87.254.6 on 09/05/12
For personal use only.

Redox Behavior of Diazotized Amines in Aprotic Solvents[1]

R. M. ELOFSON, F. F. GADALLAH, A. A. CANTÚ, AND K. F. SCHULZ

Research Council of Alberta, Edmonton, Alberta T6G 2C2

Received May 3, 1973[2]

R. M. ELOFSON, F. F. GADALLAH, A. A. CANTÚ, and K. F. SCHULZ. Can. J. Chem. **52**, 2430 (1974).

The redox behavior of diazotized aromatic and aliphatic amines is discussed. The half-wave potentials of their cathodic and/or anodic waves is correlated with their chemical reactivity. The effect of redox reactions on the stability of the nitrogen moiety of diazo compounds is elaborated. The lability of nitrogen in the resulting ion-radical species is suggested as a key to fixation of nitrogen via redox schemes.

R. M. ELOFSON, F. F. GADALLAH, A. A. CANTÚ et K. F. SCHULZ. Can. J. Chem. **52**, 2430 (1974).

On discute des propriétés oxydo–réductrices des amines aliphatiques et aromatiques diazotées. Une corrélation existe entre leur réactivité chimique et leur potentiel de demi-vague de leurs vagues cathodiques et/ou anodiques. On élabore une théorie sur l'effet des réactions d'oxydo–réduction sur la stabilité de la portion azotée des composés diazo. On suggère que la labilité de l'azote dans les espèces ion-radical qui en résultent est la cause de la fixation de l'azote par l'intermédiaire de schémas d'oxydo–réduction. [Traduit par le journal]

Can. J. Chem. Downloaded from www.nrcresearchpress.com by 210.87.254.105 on 09/05/12
For personal use only.

Introduction

This laboratory has reported the polarographic behavior of diazotized aromatic amines in sulfolane (1) and in subsequent papers (2–4) applied the electrochemical data to a number of physical organic and synthetic problems. More recently, some of the chemical consequences of that work have been reviewed (5). In the meantime, following a discussion with a colleague,[3] we decided to investigate the polarography of diazoalkanes and diazoacetic ester in sulfolane (6).

The enormous differences in half-wave potentials among these compounds are shown in Table 1 and Fig. 1. Also shown in Table 1, last column, are the *solution phase* electron affinities (from Hg) and the solution phase ionization potentials (to Hg), defined according to the processes

[1] $\text{ox(soln)} + e^{(-)}\text{(Hg)} \rightarrow \text{red(soln)} + \overline{\text{EA}}\text{[ox(soln)]}$

and

[2] $\bar{I}_p\text{[red(soln)]} + \text{red(soln)} \rightarrow \text{ox(soln)} + e^{(-)}\text{(Hg)}$

Through the Matsen equation (7), these values are related to the half-wave potentials *vs.* SCE[4]

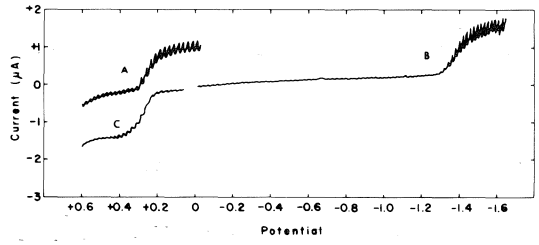

FIG. 1. Polarographic waves of 0.00066 *M* diazo compounds in 0.1 *M* solution of tetrabutylammonium perchlorate in sulfolane: (*A*) benzenediazonium tetrafluoroborate; (*B*) diazoacetic ester; (*C*) diazomethane.

by

[3] $\overline{\text{EA}} = \xi_{1/2}^{\text{red}} + 0.53 \text{ eV}$

[4] $\bar{I}_p = \xi_{1/2}^{\text{ox}} + 0.53 \text{ eV}$

Discussion

The well defined a.c. polarograms, together with the usual line shape analysis of the d.c. polarograms, show that the electrochemical reactions of diazomethane and benzenediazonium ion proceed by way of a reversible one-electron transfer. The reduction of diazoacetic ester has not been investigated as fully but from examination of the diffusion constant it clearly involves one electron, and as suggested by Hoijtink and co-workers (8), the observed potential must be considered a measure of the energy required to add one electron to the molecule. Electrochemical reduction of diazoacetic ester at a controlled

---

[1]Contribution No. 633 from the Research Council of Alberta, Edmonton, Alberta.

[2]Revision received March 15, 1974.

[3]O. E. Edwards, National Research Council, Ottawa, private communication.

[4]Since this is an aqueous SCE, an additive correction factor must be considered to allow for the difference in liquid junction potential.

TABLE 1. Half-wave potentials, current type, ionization potentials, and/or electron affinity of some diazo compounds

Compound	$\xi_{1/2}$ *vs.* SCE (V)	Current type	$\bar{I}_p$* (eV)	$\overline{EA}$* (eV)
Benzenediazonium tetrafluoroborate	+0.260	Cathodic		+0.79
Diazoacetic ester	−1.380 (> +0.8)	Cathodic (Anodic)	> +1.33	−0.85
Diazodiphenylmethane	−1.700 +0.80 (+0.95)†	Cathodic Anodic (Anodic)	1.33 (1.48)	−1.17
Diazomethane	+0.270 (+1.70)†	Anodic (Anodic)	+0.80 (+2.23)	
more negative than	> −2.8	Cathodic		< −2.27

*Calculated from eqs. 3 and 4.
†See refs. 9–11.

potential of −1.5 V *vs.* SCE produced ethyl acetate and nitrogen.

The results indicate that the benzenediazonium cation is a powerful electrophile, diazoacetic ester is less strong, and that diazomethane is an electron donor.[5] The nucleophilicity of diazomethane is well established.

The oxidation potentials at a rotating Pt electrode of a large number of diazoalkanes were studied by Jugelt and co-workers (9–11). Their attempt to relate the potentials to the reaction rate with benzoic acid failed in the case of diazomethane. The potential Jugelt and co-workers (11) reported for diazomethane (1.70 V) compared to what they found for, say, diphenyldiazomethane (0.95 V) is in reverse order to the observed reactivities of these compounds toward benzoic acid.

At the mercury electrode the oxidation potential of diazomethane is 0.27 V (Fig. 1), corresponding to a reactivity several orders of magnitude faster than the diphenyl derivative, and more in line with the observed reactivity. The two electrodes gave similar oxidation potentials for diphenyldiazomethane. Jugelt believed the oxidation of diazomethane occurring at 1.70 V at a platinum electrode to be irreversible. The oxidation at 0.27 V at the mercury electrode is, on the other hand, apparently reversible. The reason for the discrepancy is not clear at this time.

The polarogram of diphenyldiazomethane (Fig. 2) has two components: an anodic wave coinciding with the mercury dissolution wave at about 0.8 V and a cathodic wave at −1.7 V. The cathodic wave corresponds, roughly, to a one-electron transfer. The mercury drop-rate becomes irregular, suggesting attack of the electrode by the radical anion. Reduction of diazodiphenylmethane (0.1 *M* in 0.1 *M* solution of Bu_4NBF_4 in sulfolane) on a mercury pool at −2 V *vs.* SCE produced a 40% yield of diphenylmethane and N_2 but no ammonia. However, due to resonance stabilization, the diazodiphenyl radical couples with a diphenylmethyl radical to give azodiphenylmethane (detected by mass spectrometry in residue) which is further reduced to produce diphenylaminomethane in 20% overall yield (g.l.c. and mass spectrometer compare with

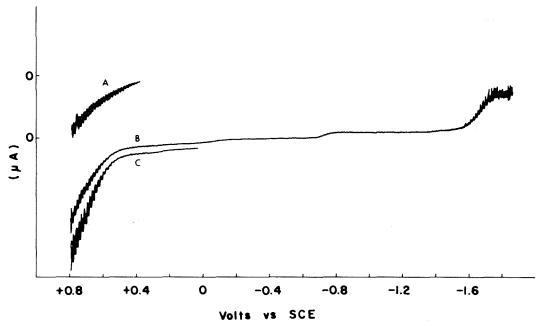

FIG. 2. Polarography of (*A*) 0.1 *M* tetrabutylammonium perchlorate in sulfolane; (*B*) 0.00066 *M* diazodiphenyl methane added; (*C*) 0.0013 *M* diazodiphenylmethane added.

[5]For the purpose of orientation of the reader, convention states that the more positive the cathodic potential ($E_{1/2}$) of a compound, the more electrophilic it should be; the more negative the anodic potential the more nucleophilic it should be. The linear correlation of half-wave potentials with electrophilicity of substituted benzenediazonium compounds in coupling reaction was demonstrated in ref. 5*a* based on results previously published by R. M. Elofson and co-workers (5*b*) and H. Zollinger (5*c*).

Can. J. Chem. Downloaded from www.nrcresearchpress.com by 210.87.254.105 on 09/05/12
For personal use only.

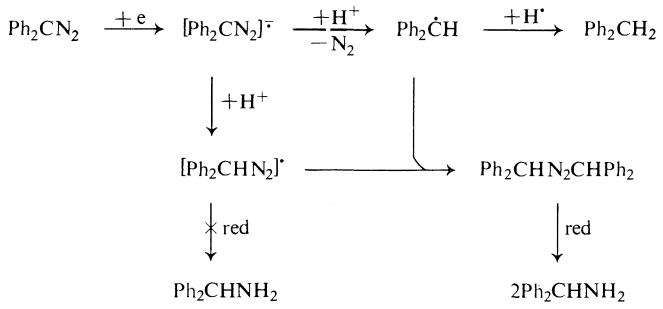

SCHEME 1

authentic sample). The absence of ammonia eliminates the possibility of cleavage of the N=N bond in the diazodiphenylmethyl radical. A simple version of the suggested mechanism is shown in Scheme 1.

The electrode reaction, verified by charge distribution analysis from all-Valence-Electron SCF[6] calculation on the diazomethane system, is presumably given by:

[5] 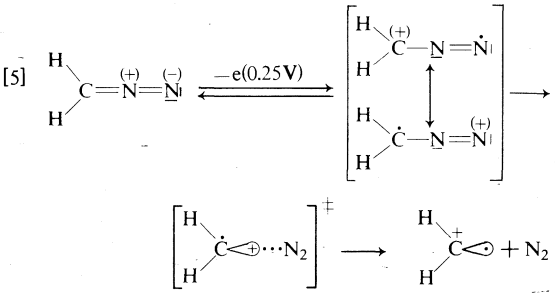

The existence of the radical cation of methylene was demonstrated experimentally by the following electrochemical oxidation of diazomethane: a 0.001 *M* solution of diazomethane in sulfolane (0.1 *M* solution of Bu_4NClO_4) at a mercury anode and +0.3 V *vs.* SCE in the presence of pyridine produced >80% yield of methyl pyridinium ion ($E_{1/2} = -1.36$ V *vs.* SCE agrees with authentic sample). The suggested mechanism is shown by eq. 6. It is not clear yet which happens first, the abstraction of H· or coupling with pyridine. The spin state of the methylene if

[6] 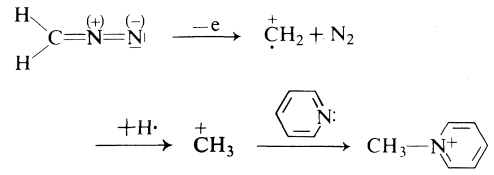

produced in the pyridine reaction is not known at present. Methylation of other substrates by diazomethane is probably affected by a similar mechanism.

The wide range in redox potentials of this class of compounds can be rationalized on the basis of charge distribution changes in the redox process and the subsequent nitrogen release. In terms of acceptance or donation of an electron the following mechanisms rationalize and unify diazo chemistry.

The C_6H_5 moiety gains aromaticity on reduction, hence the strong electrophilicity of benzenediazonium cation [7]. The stability of phenyl radical accounts for its discriminatory properties [2]. The gain in energy, if any, by the diazoester upon reduction is *minimal* [12]. The ester is a very weak electrophile. Diazomethane cannot add an electron as in [8], at least up to the limit of energy available in polarography, instead it loses one [5]. In the absence of a suitable acceptor, radical chain polymerization to polymethylene occurs after nitrogen release (12). The reported coupling reactions between diazomethane and β-substituted α-naphthol (13, 14) do not suggest that reactions of the type shown in [8] can proceed. Nesnow and Shapiro (13) and Pyrek and Achmatowicz (14) propose methyldiazonium cation as the reacting species. Steric factors and media effects (formation of an "intimate ion pair" between diazomethane and α-naphthol in media of low dielectric constant (14)) may lead to the formation of the aliphatic

[6] S. Fraga, University of Alberta, Edmonton, Alberta, private communication. The SCF calculations were performed for diazomethane and the benzenediazonium cation. Charge distributions for the corresponding reduced or oxidized radicals were acquired via the virtual orbital approximation and Koopman's theorem, respectively (17). For diphenyldiazomethane and diazoacetic ester, the relevant canonical structures are inferred.

Can. J. Chem. Downloaded from www.nrcresearchpress.com by 210.87.254.105 on 09/05/12
For personal use only.

Can. J. Chem. Downloaded from www.nrcresearchpress.com by 210.87.254.105 on 09/05/12
For personal use only.

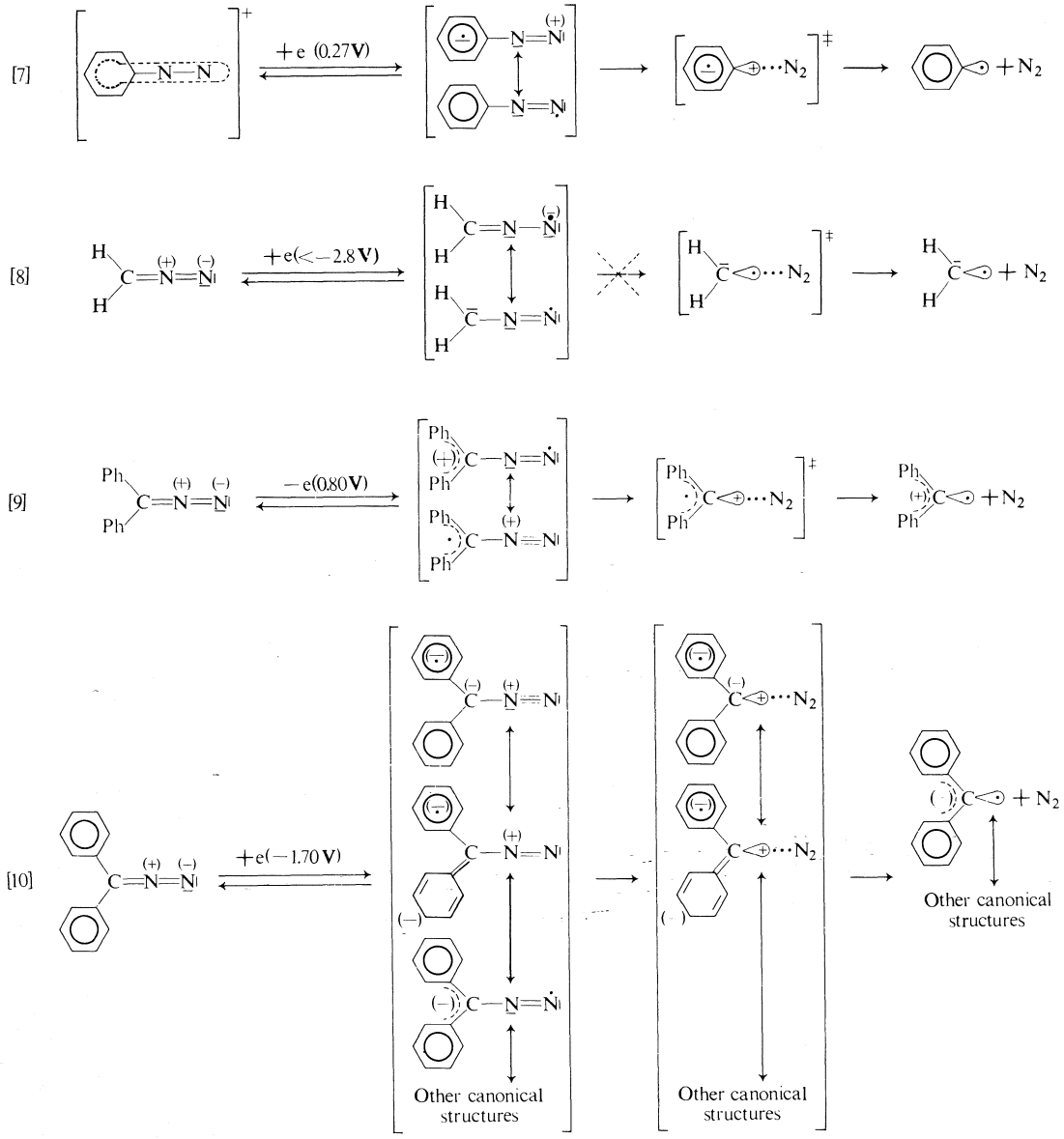

diazonium cation. More likely, the intimate ion pair of Pyrek and Achmatowicz is actually a cyclic complex, involving a proton bridge (Fig. 3) then the complex might decay rupturing either the O—H bridge bond to give azo coupling with activated 4-position or the C—N bond to yield the methylated compound. Whether hydrogen bonding by the phenolic hydrogen, in effect, raises the electrophilicity of diazomethane sufficiently to permit reduction and coupling is a moot point.

Resonance stabilization of the resultant radical makes diphenyldiazomethane [10] and diazoacetic ester easier to reduce [9] than diazomethane. The oxidation of diazomethane proceeds more readily than that of diphenyldiazomethane, due, at least in part, to the greater solvation energy of the smaller radical cation.[7] The oxidation potential of diazoacetic ester [11] was not found polarographically, due to the limits of polarography (dissolution of Hg). That

[7]For an introduction to the effect of ionic radius on solvation energies, see ref. 18.

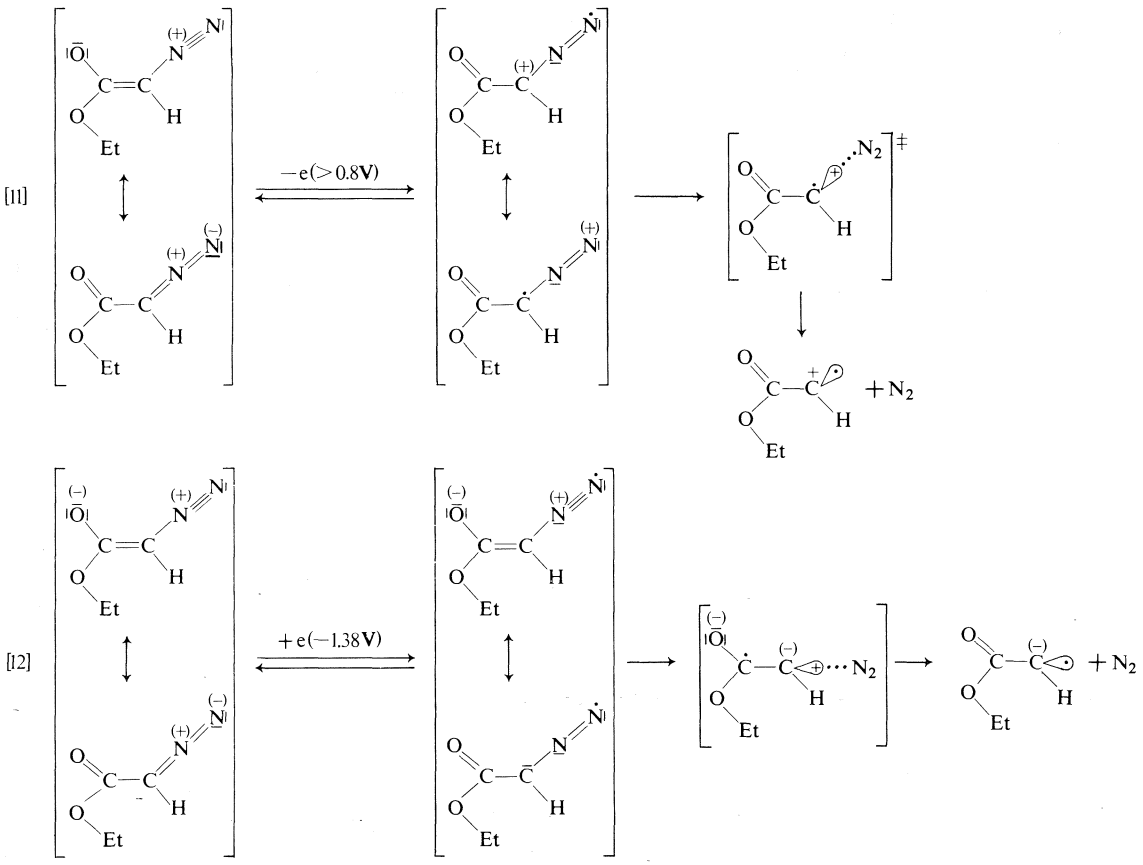

oxidation does occur is inferred from its chemical reactivity (15).

Polarographic measurements suggest that the decomposition of aryl diazonium salts in aqueous protic media (rather than aprotic) is fundamentally different from the decomposition of diazoalkanes.[8] The former involves primary attack by a proton as the oxidizing agent. Diazoacetic ester and diazo ketone may act as either electron acceptors or donors. They produce alkanes with H^+ and alcohols with OH^-. Both reactions may occur simultaneously. A note of caution is in order. The redox potentials presented here are determined in a single aprotic solvent, sulfolane. Because of solvation, quantitative correlations may not be completely satisfactory in other solvents but a knowledge of solvation effects will enable useful qualitative correlations to be made (18). Useful polarographic measurements cannot be made in wholly non-polar solvents and polarographic results in protic media must be handled with caution.

Finally, it should be noted that the nitrogen moieties on diazomethane and benzenediazonium are reasonably stable in sulfolane solution. Decomposition is effected by electron transfer *to* benzenediazonium but *from* diazomethane. In either case, electron transfer results

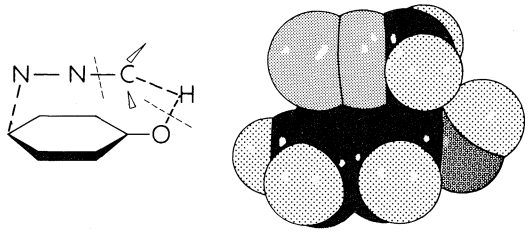

FIG. 3. The cyclic complex between diazomethane and phenol.

[8]The electrode reactions in protic media of benzene diazonium salts and diazo ketones have been investigated in detail, and yield respectively phenyl hydrazine and ammonia. Diazoacetic ester in aqueous alcohol at p*H* 4.7 yields ammonia and the ester. Diazomethane has not been investigated in protic media.

Can. J. Chem. Downloaded from www.nrcresearchpress.com by 210.87.254.105 on 09/05/12
For personal use only.

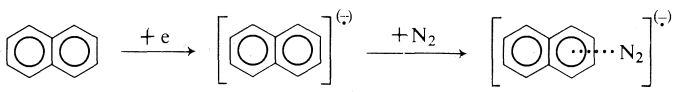

[13]

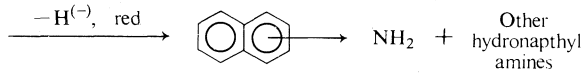

in destabilization of the molecule and release of nitrogen and a cation or anion radical.

The lability of the diazo radicals in aromatic and aliphatic systems leads to consideration of the counter reaction, *i.e.* nitrogen fixation. The work done by several workers involving the reaction between molecular nitrogen and anion radicals in the presence and absence of catalysts under mild conditions (16) could be explained as redox like charge-transfer reactions. The presence of a hydride transfer agent in the system effectively reverses the diazonium decomposition [13].

Experimental

All polarographic measurements were performed by a PAR Model 170, Electrochemistry System. Each diazotized amine was dissolved in a solution of 0.1 *M* tetrabutylammonium perchlorate in sulfolane.

1. R. M. ELOFSON and F. F. GADALLAH. J. Org. Chem. **34**, 854 (1969).
2. F. F. GADALLAH and R. M. ELOFSON. J. Org. Chem. **34**, 3335 (1969).
3. R. M. ELOFSON and F. F. GADALLAH. J. Org. Chem. **36**, 1769 (1971).
4. R. M. ELOFSON, F. F. GADALLAH, and K. F. SCHULZ. J. Org. Chem. **36**, 1526 (1971).
5. (*a*) R. M. ELOFSON, F. F. GADALLAH, and K. F. SCHULZ. Halifax Meeting, Chemical Institute of Canada, May 30–June 2, 1971; (*b*) R. M. ELOFSON, R. L. EDSBERG, and P. A. MECKERLY. J. Electrochem. Soc. **97**, 166 (1950); (*c*) H. ZOLLINGER. Helv. Chim. Acta, **36**, 1730 (1953).
6. M. BAILES and L. L. LEVESON. J. Chem. Soc. B, 34 (1970).
7. F. A. MATSEN. J. Chem. Phys. **24**, 602 (1956).
8. ATEN I. C. BULHKER and C. J. HOIJTINK. Trans. Faraday Soc. **55**, 324 (1959).
9. F. PRAGST and W. JUGELT. Electrochim. Acta, **15**, 1543 (1970).
10. W. JUGELT and F. PRAGST. Angew. Chem. Int. Ed. **7**, 290 (1968).
11. L. BERSECK, W. JUGELT, F. PRAGST, and D. SCHMIDT. J. Prakt. Chem. **312**, 117 (1970).
12. H. STAUD and H. GAULE. Ber. **49**, 1897 (1916).
13. S. NESNOW and R. SHAPIRO. J. Org. Chem. **34**, 2011 (1969).
14. JAN ST. PYREK and O. ACHMATOWICZ, JR. Tetrahedron Lett. 2651 (1970).
15. G. BREDIG and P. F. RIPLEY. Ber. **40**, 4015 (1907).
16. M. E. VOLPIN, A. A. BELYI, V. P. SHUR, N. A. KATKOV, I. M. NEKAEVA, and R. V. KUDRYAVTSEV. Chem. Commun. 246 (1971).
17. M. J. S. DWAR. The molecular orbital theory of organic chemistry. McGraw-Hill Co., New York, 1969.
18. E. A. COTTON and G. WILKINSON. Advanced inorganic chemistry. Interscience Publishers, New York, 1967. P. 42 ff.

Can. J. Chem. Downloaded from www.nrcresearchpress.com by 210.87.254.105 on 09/05/12
For personal use only.

Anisotropic Conductivity and Phase Transformation Studies in Potassium Chromate Crystals

MAHADEVA NATARAJAN AND ETALO A. SECCO

Department of Chemistry, St. Francis Xavier University, Antigonish, Nova Scotia

Received December 20, 1973

MAHADEVA NATARAJAN and ETALO A. SECCO. Can. J. Chem. **52**, 2436 (1974).

Electrical conductivity measurements on single crystals of potassium chromate indicate anisotropic behavior in the directions $\perp$ and $\parallel$ to the c_0 axis. The cation migration energy, estimated from the conductivity *vs.* $1/T$ plots, is slightly higher than the usual value in potassium halides, suggesting the possibility of a different conduction mechanism. The defect formation energy, ~2.20 eV, is comparable to known values in ionic solids. The phase transformation near 660 °C appears to be a first order transition associated with appreciable hysteresis.

MAHADEVA NATARAJAN et ETALO A. SECCO. Can. J. Chem. **52**, 2436 (1974).

Des mesures de conductivité électrique sur des cristaux uniques de chromate de potassium indiquent un comportement anisotrope dans les directions $\perp$ et $\parallel$ à l'axe c_0. L'énergie de migration du cation est évaluée à partir de graphiques de la conductivité par rapport à $1/T$; elle est légèrement plus grande que la valeur usuelle des halogénures de potassium suggérant ainsi la possibilité d'un mécanisme différent de conduction. L'énergie de formation des défauts, ~2.20 eV, est comparable à des valeurs connues dans des solides ioniques. La transformation de phase près de 660 °C apparaît être une transition de premier ordre associée à une hystérésis appréciable. [Traduit par le journal]

Introduction

Potassium chromate which exists in orthorhombic form (space group, *Pnam* with $a_0 = 7.663 \pm 0.003$ Å, $b_0 = 10.391 \pm 0.003$ Å, and $c_0 = 5.919 \pm 0.003$ Å) transforms to hexagonal form ~660 °C with the lattice constants, $a_0 = 6.125 \pm 0.005$ Å and $c_0 = 8.245 \pm 0.007$ Å at 705 °C (1). The transition enthalpy and entropy were given as 5500 ± 3500 cal mol^{-1} and 5.70 ± 3.50 cal mol^{-1} deg^{-1}. The variation of orthorhombic lattice constants with temperature, observed by Pistorius (1), indicates appreciable anisotropic thermal expansion in the three axial directions. The magnitudes of the transition enthalpy and entropy together with the change in the molar volume, ΔV, (~1.87 cm^3 mol^{-1}) at the transition point suggest that the phase change in K_2CrO_4 is likely to be a first order type and that it might be associated with hysteresis effects (2).

In this paper, we report the study of phase transition in potassium chromate single crystals, employing differential thermal analysis (DTA) and electrical conductivity measurements. Studies were also made on polycrystalline powder samples for comparison with single crystal data.

Experimental

Single crystals of potassium chromate were prepared by slow evaporation of an aqueous solution of AR grade (99.96%) K_2CrO_4. Seed crystals were washed and allowed to grow by hanging in saturated K_2CrO_4 solution; crystals grew to sizes of ~10 mm × 5 mm.

Differential thermal analysis curves were recorded on a DuPont 900 Thermo-analyzer, using the DuPont 1200 °C DTA cell with Al_2O_3 as the inert reference standard and a constant heating rate of 20°/min (3).

Electrical conductivity measurements were made on single crystals $\parallel$ and $\perp$ to the long axis (b_0), in a stainless steel conductivity cell as previously described (4). The cell was heated in a cylindrical furnace at a rate of ~30°/h. The crystal was held between two platinum discs by a spring-loaded support. The conductivity was measured in air at 1 kHz as a function of increasing temperature employing a General Radio 1608-A Impedance bridge. Chromel–alumel thermocouples were used for temperature measurements. Conductivity measurements were also made on a sintered polycrystalline pellet specimen.

Results and Discussion

Differential Thermal Analysis

The orthorhombic–hexagonal phase transformation in K_2CrO_4 takes place at ~682 °C in single crystals (Fig. 1). The heating and cooling DTA curves clearly indicate that the transition is reversible and that the change is a sharp one occurring in a narrow temperature range. The smaller hysteresis observed in the single crystal indicates that thermal equilibrium is more easily established than in compact powders. The sharpness of the heating curves together with the observed hysteresis effects further confirm our

Can. J. Chem. Downloaded from www.nrcresearchpress.com by 210.87.254.40 on 09/05/12
For personal use only.

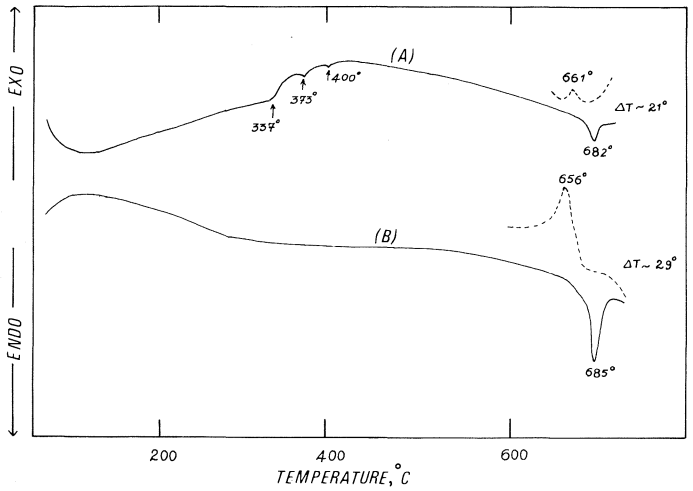

FIG. 1. Differential thermal analysis curves for (*a*) single crystal embedded in aluminum oxide, and (*b*) polycrystalline powder sample of potassium chromate. Solid lines are the heating curves (at 20 °C per min); broken lines represent cooling curves. The transition temperature appears at 675 °C for the powder at a heating rate of 10°/min.

earlier view that the phase transition is a first order type.

We note the two additional endotherms at ~373 and 400 °C, in the single crystal specimen; in a well ground powdered sample these endotherms are not observed. As mentioned for thallium chromate (5, 6), these effects might arise from distortions in the lattice.

Electrical Conductivity

The results of electrical conductivity measurements on single crystals and powder specimens of potassium chromate are shown in Fig. 2, where the logarithm of electrical conductivity, σ, is plotted against reciprocal of absolute temperature, T. The open circles (curve 1) refer to measurements on the crystal along the c_0 axis. The room temperature conductivity remains constant up to ~250 °C and rises slowly until at ~375 °C there is a sharp rise. The activation energy, 0.24 eV, in this region is comparable to activation energy values in Tl_2CrO_4 and Ag_2CrO_4 (6). Above this region, the conductivity is essentially linear with slope value of $\sim 0.9 \pm 0.1$ eV. This energy refers to the cation migration energy, E_c^m, of K^+ ions. Both theoretical estimates and experimental results in potassium halides have given for E_c^m, values between 0.60 and 0.78 eV (7). The slightly higher value of 0.90 eV for the migration energy in potassium chromate might be due to different host lattice (orthorhombic) symmetry (8). The transition is indicated by a "knee" at ~658 °C, above which the conductivity rises sharply with a large activation energy of ~4.3 eV.

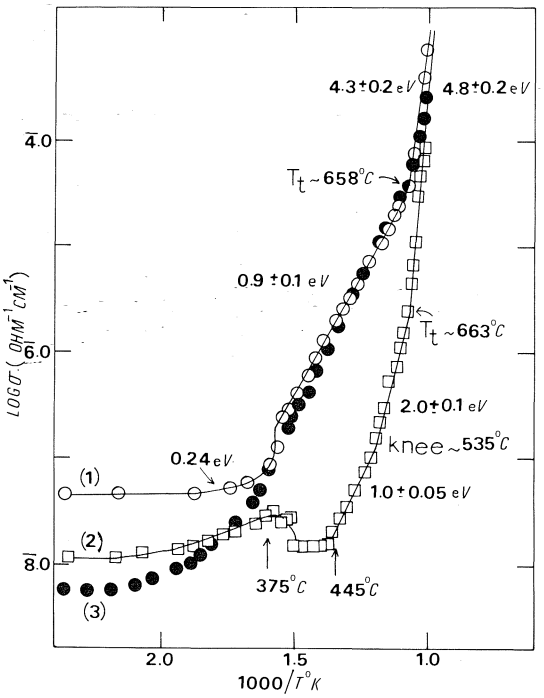

FIG. 2. Logarithm of electrical conductivity, σ, *vs.* reciprocal of absolute temperature, T. Measurements along the c_0 axis are shown by open circles; open squares refer to data $\perp$ to the c_0 axis, and filled circles refer to measurements on powder sample.

Conductivity measurements $\perp$ to the c_0 axis (curve 2) are shown by open squares. The room

Can. J. Chem. Downloaded from www.nrcresearchpress.com by 210.87.254.40 on 09/05/12
For personal use only.

temperature conductivity is lower than in the ∥ direction, indicating appreciable anisotropic conduction in the crystal. The ratio $\sigma_{\parallel}/\sigma_{\perp}$, 4.8, slowly narrows to about 2.5 at 315 °C. Above this temperature the conductivity behavior along each direction is quite different. The conductivity in the ⊥ direction shows a marked decrease between 375 and 445 °C. These two effects are consistent with the two weak irreversible endotherms in the thermal analysis curves (Fig. 1), and resembles the anomalous conductivity and thermal behavior in thallium chromate (5, 6). But unlike thallium chromate, no anomaly in the temperature variation of the lattice dimensions is observed (1). The conductivity curve above 450 °C, is linear with a "knee" at ~535 °C. The activation energy of 1.0 eV below the "knee", might include the cation migration energy, E_c^m while above the "knee" the activation energy is ~2.0 eV. Assuming that this activation energy is equal to the sum of half the defect formation energy, E^s, and the cation migration energy, E_c^m, we find the defect formation energy, E^s, to be ~2.2 eV. While this latter value is comparable to E^s values in alkali halides (in the *Fm3m* structure) we are unable to confirm this value since there are insufficient data in the literature on low symmetry systems like potassium chromate. The defect formation energies in the *Pm3m* and *Fm3m* forms of cesium chloride have been shown to be different from theoretical (9) and experimental (10) studies. Thus, it is not yet clearly known whether defect formation energies are structure-sensitive and if so to what extent. The activation energy of 2.0 eV in the intrinsic region above the "knee" in potassium chromate is close to values observed in thallium and silver chromates (6).

The orthorhombic–hexagonal transformation is indicated by a break in the conductivity plot at ~663 °C above which there is a sharp increase in the conductivity in the solid. The anisotropy in conductivity increases with temperature and it is reasonable to suppose that the anisotropy will disappear at temperatures near the melting point. The energy of activation of ~4.8 eV in the high temperature region is slightly higher than the value in the ∥ direction. The increased conductivity in the high temperature form could arise from various contibutions such as anionic conduction, an increased number of vacancies, and a loosening of the lattice.

Conductivity measurements on a sintered polycrystalline sample (curve 3, filled circles) show a somewhat different behavior below 375 °C, above which the conductivity merges with curve 1. The absence of any anomaly in the conductivity of the sintered sample corroborates the DTA curve on the powder specimen.

The present study clearly reveals the existence of anisotropic electrical conductivity in a low-symmetry system like potassium chromate. The close agreement between polycrystalline data and single crystal measurements above the intrinsic region suggests that careful measurements on powder samples could be quite useful in cases where single crystals are unobtainable. The fairly large cationic migration energy in a low symmetry system like potassium chromate could be due to different transport mechanism(s) in such structures. While this may be a conjecture, it would be interesting to explore such possibilities. Diffusion data on these low symmetry solids would lead to a better understanding of the transport phenomena in these crystals. We thus look forward to more experimental and theoretical studies on the transport properties in low symmetry solids.

The authors are grateful to the National Research Council of Canada and the University Council for Research for financial support during the investigation. The authors are grateful to the referees for very helpful comments and suggestions.

1. C. W. F. T. Pistorius. Z. Phys. Chem. Neue Folge. **35**, 109 (1962).
2. M. Natarajan. Ph.D. Thesis. Indian Institute of Technology, Kanpur, India. 1970.
3. O. K. Srivastava and E. A. Secco. Can. J. Chem. **45**, 579 (1967); P. Ramamurthy and E. A. Secco. Can. J. Chem. **47**, 2185 (1969).
4. P. N. Mehrotra. Ph.D. Thesis. Indian Institute Technology, Kanpur, India. 1968.
5. N. I. Bashilova. J. Inorg. Chem. USSR, **9**, 57 (1964).
6. M. Natarajan and E. A. Secco. Can. J. Chem. **52**, 712 (1974).
7. M. Hartmanová. Fys. cas. **22**, 1–2 (1972).
8. S. Radhakrishna and K. P. Pande. Phys. Stat. Solidi (a), **16** (2), 433 (1973).
9. (*a*) I. M. Boswarva. Phil. Mag. **16**, 827 (1967); (*b*) I. M. Boswarva and A. B. Lidiard. Phil. Mag. **16**, 803 (1967).
10. M. Natarajan, B. Prakash, and C. N. R. Rao. J. Chem. Soc. A, 2291 (1971).

Can. J. Chem. Downloaded from www.nrcresearchpress.com by 210.87.254.40 on 09/05/12
For personal use only.

Synthesis and ^{19}F Nuclear Magnetic Resonance Spectra of Fluorosubstituted Bis(arene)chromium Complexes

MICHAEL J. MCGLINCHEY AND TEONG-SENG TAN

Department of Chemistry, McMaster University, Hamilton, Ontario L8S 4M1

Received January 9, 1974

MICHAEL J. MCGLINCHEY and TEONG-SENG TAN. Can. J. Chem. **52**, 2439 (1974).

A series of substituted bis(fluorobenzene)chromium complexes, $(C_6H_4FX)_2Cr$, where X is H, F, Cl, CH_3, or CF_3, have been synthesized by cocondensing Cr atoms and fluoroarenes. The ^{19}F chemical shifts of these compounds correlate well with those of the corresponding C_6F_5X system suggesting that the overall electron-withdrawing effect of a π-bonded Cr on each ring is similar to the effect of four ring fluorine substituents.

MICHAEL J. MCGLINCHEY et TEONG-SENG TAN. Can. J. Chem. **52**, 2439 (1974).

La cocondensation d'atomes de chrome et de fluoroarènes permet de synthétiser une série de complexes de bis(fluorobenzène substitué) chrome de formule $(C_6H_4FX)_2Cr$ dans lesquels X est égal à H, F, Cl, CH_3 ou CF_3. Une bonne corrélation existe entre le déplacement chimique du ^{19}F de ces composés et ceux des systèmes C_6F_5X correspondants; ce résultat suggère que l'effet électroaffinitaire global du chrome lié par des électrons π sur chacun des cycles est semblable à l'effet de quatre substituants fluor sur le cycle. [Traduit par le journal]

Can. J. Chem. Downloaded from www.nrcresearchpress.com by 178.218.224.3 on 09/06/12
For personal use only.

Introduction

The upfield chemical shift of protons in arene–metal π-complexes relative to those of the free arenes is well-known and has been ascribed to a number of factors *viz.*, decrease in the aromatic ring current, the magnetic anisotropy of the metal–arene bond, and the electron-withdrawing effect of the metal carbonyl moiety (1–3). In contrast, the chemical shifts of fluorine atoms on aromatic rings π-bonded to zero-valent metals have received very little attention. To our knowledge, the only such compounds for which ^{19}F chemical shifts have been reported are fluorobenzene-tricarbonyl chromium and hexafluorobenzene tris(trifluorophosphine)chromium where upfield shifts of $\sim$20 p.p.m. relative to the free arenes were observed on complexation (2, 4). It has been pointed out (2) that such shifts are too large to be attributable to either a decrease in the ring current (which should cause a change comparable to that observed with protons, *i.e.*, 1–2 p.p.m.) (5), or to the magnetic anisotropy of the metal–ring bond. They suggest that the strongly electron-withdrawing $Cr(CO)_3$ group causes an increase in the electronegativity of the aromatic ring carbons leading to a partial $sp^2 \rightarrow sp^3$ rehybridization; this in turn distorts the symmetry of the fluorine valence electrons and so alters the Ramsey paramagnetic term which is known to be a dominant factor in the shielding of fluorine nuclei (2).

It has not been possible to synthesize fluorosubstituted bis(arene)chromium complexes because the conventional route pioneered by Fischer and Hafner (6) fails when the arene has functionalities possessing lone pairs of electrons; presumably the arene forms a complex with the Lewis acid $AlCl_3$ which is the catalyst for the process. However, the very recent syntheses of fluorosubstituted bis(arene)chromium complexes by cocondensation of the appropriate fluoroarene with atomic chromium vapor (4, 7) appeared to offer an ideal opportunity to investigate ^{19}F chemical shifts in π-bonded arene–metal systems.

Consequently, a series of substituted bis(fluorobenzene)chromium complexes of general formula $(C_6H_4FX)_2Cr$, where X is H, F, Cl, CH_3, or CF_3,[1] have been prepared and their ^{19}F n.m.r. spectra recorded.

Experimental

Nuclear magnetic resonance spectra were recorded on a Varian DP-60 spectrometer and mass spectra on a C.E.C. 21-110-B spectrometer. Melting points (decomposition points for most of these complexes) are uncorrected. Elementary analyses were performed by Gygli Microanalysis Laboratory, Toronto.

Chromium vapor was produced by electrical heating (10 V, 45 A) of finely-crushed Cr chips in a conical

[1]Attempts to prepare the bis(bromofluorobenzene)-chromium compounds failed, and $CrBr_3$ was isolated in good yield; this presumably reflects the weakening of the carbon–halogen bond as one descends the group.

TABLE 1. Physical data for bis(arene)chromium complexes

Arene	Color	Melting point (°C)	Yield (%)	C (%)		H (%)	
				Calcd.	Found	Calcd.	Found
C_6H_5F	yellow-green	96–98	19	59.02	59.27	4.10	3.99
o-$C_6H_4F_2$	orange	74	17	51.43	51.69	2.86	3.14
m-$C_6H_4F_2$	brown	82	18	51.43	51.64	2.86	2.61
p-$C_6H_4F_2$	red-brown	71	12	51.43	51.71	2.86	3.01
o-C_6H_4FCl	brown	74	23	46.00	45.76	2.55	2.30
m-C_6H_4FCl	brown	59	17	46.00	45.89	2.55	2.39
p-C_6H_4FCl	light brown	104	17	46.00	45.80	2.55	2.46
o-$CH_3 \cdot C_6H_4F$	olive green	70–73	16	61.77	61.66	5.15	5.02
m-$CH_3 \cdot C_6H_4F$	black	88	16	61.77	62.03	5.15	4.98
p-$CH_3 \cdot C_6H_4F$	dark green	62–65	21	61.77	61.71	5.15	5.28
m-$CF_3 \cdot C_6H_4F$	red-brown	41	20	44.21	44.42	2.11	2.30

tungsten spiral coated with alundum cement; this was mounted between two water-cooled stainless steel electrode supports in an evacuated apparatus similar to that previously described (8). Substrate vapor was led into the system through an inlet tube with holes suitably positioned such that the substrate and metal vapor cocondensed in the same region on the cold (−196 °C) walls of the reaction flask. Since 20% of the metal vaporized fails to reach the walls, being intercepted by the electrode supports and the inlet ring, the weight of chromium available for reaction is only 80% of the weight loss of the crucible, and yields are calculated accordingly.

In a typical experiment, *p*-chlorofluorobenzene (25.0 g, 192 mmol) was cocondensed with chromium vapor (312 mg, 6 mmol) over a 65 min period. The reaction flask was allowed to warm to room temperature and the excess unreacted arene was removed *in vacuo*. The lower portion of the flask was surrounded by a 60 °C water bath while the upper part of the flask was encircled by several coils of water-cooled Tygon tubing. Bis(*p*-chlorofluorobenzene)chromium (320 mg, 1.03 mmol; 17%) collected in the upper part of the reaction flask as red-brown microcrystals which were resublimed and identified by mass and n.m.r. spectra and by microanalysis.

The remaining compounds were all prepared analogously and the relevant data is presented in Tables 1–3. All the compounds are air stable for several days at least except for the fluorotoluene complexes which have only moderate stability; in solution, however, they all decompose quite rapidly unless oxygen is rigorously excluded. They are soluble in aromatic solvents and moderately soluble in methanol, but they decompose rapidly in chlorinated solvents.

The mass spectra of these bis(fluorobenzene)chromium complexes show not only the expected P and (P-arene) peaks, but also peaks rationalizable on the basis of migration of fluorine to chromium and loss of the remainder of the ring. This is also observed with CF_3 groups and gives rise to ions of the type $[(\text{arene})Cr{-}CF_3]^+$.

Discussion

Taft *et al.* (9, 10) have demonstrated that ^{19}F n.m.r. chemical shifts may be used as a sensitive probe to investigate electronic properties of aromatic systems. Although this method has been criticized on theoretical grounds (11, ref. 4, pp. 53–67) it nevertheless fulfills the criterion of being empirically useful. It is well-established that the ^{19}F chemical shifts of *m*- and *p*-substituted fluorobenzenes correlate well with σ_I and with $\sigma_I + \sigma_R^0$ respectively, where σ_I and σ_R^0 are the Taft inductive and resonance parameters derived from reactivity considerations.

The most obvious effect on complexation is an upfield shift of 40–50 p.p.m. relative to the free arene, but there is little correlation between the shifts of the free and complexed arenes (see Table 3) indicating considerable modification of the electron density distribution upon complexation. For the case of the bis(1-fluoro-3-X-benzene)chromium series there is no simple correlation between chemical shift and σ_I; in fact the data best fit the expression

$$[1] \quad \Delta_m^F(\text{complex}) = -9.1(\sigma_I + 1.25\sigma_R^0) + 162.4$$

where Δ_m^F(complex) is the chemical shift of the fluorine atoms in the complex measured in p.p.m. upfield of $CFCl_3$, and σ_I and σ_R^0 are the Taft inductive and resonance parameters of the *m*-substituent X. One must stress that this does not necessarily imply a large contribution from a resonance interaction since, classically at least, this is difficult to visualize; this is merely an empirical correlation that fits the experimental data.

This correlation of ^{19}F chemical shift with a combination of both σ_I and σ_R^0 for a *meta*-substituent is reminiscent of the pentafluoro-

Can. J. Chem. Downloaded from www.nrcresearchpress.com by 178.218.224.3 on 09/06/12
For personal use only.

Can. J. Chem. Downloaded from www.nrcresearchpress.com by 178.218.224.3 on 09/06/12
For personal use only.

TABLE 2. Mass spectral data for bis(arene)chromium complexes

		Relative intensities		
m/e	Assignment	ortho	meta	para
Difluorobenzenes				
280	$C_{12}H_8F_4Cr^+$	16.7	100	61.2
261	$C_{12}H_8F_3Cr^+$	0.7	5.7	0.6
185	$C_6H_4F_3Cr^+$	12.1	3.2	0.4
166	$C_6H_4F_2Cr^+$	18.8	70.6	26.1
147	$C_6H_4FCr^+$	2.8	5.6	3.2
114	$C_6H_4F_2^+$	100	60.3	100
95	$C_6H_4F^+$	62.5	22.1	8.2
76	$C_6H_4^+$	30.4	27.9	23.7
Chlorofluorobenzenes				
312/314/316	$C_{12}H_8F_2Cl_2Cr^+$	98.7	100	3.0
293/295/297	$C_{12}H_8FCl_2Cr^+$	0.8	1.4	0.1
277/279	$C_{12}H_8F_2ClCr^+$	48.5	46.5	8.0
258/260	$C_{12}H_8FClCr^+$	0.9	0.2	0.1
217/219/221	$C_6H_4FCl_2Cr^+$	4.7	7.9	3.0
201/203	$C_6H_4F_2ClCr^+$	13.0	3.5	1.2
182/184	$C_6H_4FClCr^+$	100	79.2	88.0
163/165	$C_6H_4ClCr^+$	0.3	1.5	1.2
147	$C_6H_4FCr^+$	20.1	15.3	12.1
130/132	$C_6H_4FCl^+$	96.9	51.1	100
111/113	$C_6H_4Cl^+$	31.8	20.2	12.0
95	$C_6H_4F^+$	84.4	45.4	42.5
76	$C_6H_4^+$	51.7	56.5	13.7
Fluorotoluenes				
272	$C_{14}H_{14}F_2Cr^+$	58.5	40.9	47.5
257	$C_{13}H_{11}F_2Cr^+$	0.1	0.1	0.4
253	$C_{14}H_{14}FCr^+$	1.3	0.1	0.3
181	$C_7H_7F_2Cr^+$	16.1	1.0	8.2
162	$C_7H_7FCr^+$	100	90.0	64.9
110	$C_7H_7F^+$	52.7	4.6	100
95	$C_6H_4F^+$	0.7	0.1	1.4
91	$C_7H_7^+$	70.0	100	36.2
Meta-fluorobenzotrifluoride				
380	$C_{14}H_8F_8Cr^+$		1.0	
361	$C_{14}H_8F_7Cr^+$		0.02	
304	$C_8H_4F_8Cr^+$		0.02	
285	$C_8H_4F_7Cr^+$		0.03	
235	$C_7H_4F_5Cr^+$		0.07	
216	$C_7H_4F_4Cr^+$		7.7	
197	$C_7H_4F_3Cr^+$		4.8	
164	$C_7H_4F_4^+$		9.8	
145	$C_7H_4F_3^+$		100	
126	$C_7H_4F_2^+$		19.5	
114	$C_6H_4F_2^+$		6.3	
95	$C_6H_4F^+$		19.5	
69	CF_3^+		2.8	
52	Cr^+		4.3	

TABLE 3. Nuclear magnetic resonance chemical shifts* of arenes and complexes

Arene	Free	Complex	Δ†
C_6H_5F	113.1	160.6	47.5
o-$C_6H_4F_2$	139.0	180.3	41.3
m-$C_6H_4F_2$	110.1	162.8	52.7
p-$C_6H_4F_2$	119.5	161.3	41.8
o-C_6H_4FCl	119.0	163.7	44.7
m-C_6H_4FCl	113.0	161.1	48.1
p-C_6H_4FCl	119.0	161.3	42.3
o-$CH_3 \cdot C_6H_4F$	118.1	166.7	48.6
m-$CH_3 \cdot C_6H_4F$	114.0	164.3	50.3
p-$CH_3 \cdot C_6H_4F$	118.6	166.3	47.7
$C_6H_5 \cdot CF_3$	63.7	58.9	−4.8
m-$CF_3 \cdot C_6H_4F$	64.1	57.8	−6.3
	110.3	157.0	46.7
m-$C_6H_4(CF_3)_2$	64.5	58.7	−5.8

*All p.p.m. values were obtained from 2% solutions in C_6H_6 containing $CFCl_3$ as standard.
†Shift from free arene values on complexation.

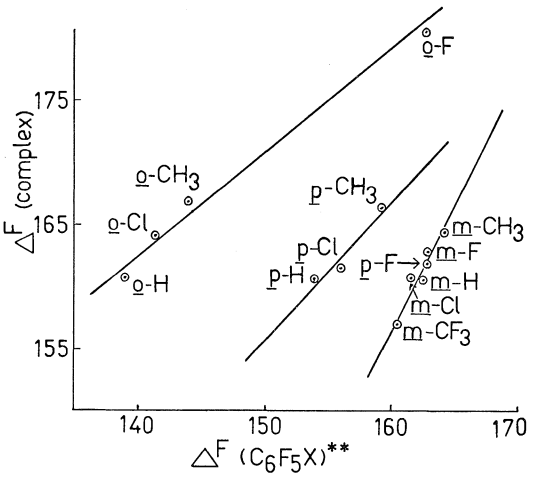

FIG. 1. Plot of chemical shifts of substituted C_6F_5X against chemical shifts of bis(fluoroarene)chromium complexes, measured in p.p.m. to high field of $CFCl_3$. (**), Data taken from ref. 12.

phenyl system (12) in which the chemical shifts of the fluorines *meta* to the substituent X follow the equation

$$[2] \quad \Delta_m^F(C_6F_5X) = -5.3(\sigma_I + 1.35\sigma_R^0) + 162.9$$

This apparent similarity of the dependence of the shifts of *meta*-fluorines on a similar combination of σ_I and σ_R^0 in two such different systems prompted us to see if there were any direct correlation between chemical shifts of corresponding fluorines in the two systems. Indeed the plot of ^{19}F chemical shifts of the complexes $(C_6H_4FX)_2Cr$ *vs.* the chemical shifts of fluorine atoms in the same position relative to the same substituent in the C_6F_5X system shows a good correlation (see Fig. 1), and these data are summarized below

$$[3] \quad \Delta_o^F(\text{complex}) = 0.76[\Delta_0^F(C_6F_5X)] + 55.7$$

$$[4] \quad \Delta_m^F(\text{complex}) = 1.94[\Delta_m^F(C_6F_5X)] - 154.6$$

$$[5] \quad \Delta_p^F(\text{complex}) = 1.18[\Delta_p^F(C_6F_5X)] - 22.2$$

A notable anomaly in Fig. 1 is the *p*-fluoro substituent which falls (probably coincidentally) directly on the *meta*-substituent line. A possible rationale may lie in the fact that, of the substituents studied in the present work, only the fluoro has a very large resonance effect and so its effective σ_R^0 will be more drastically modified by a reduction of π-electron density in the complexed ring than are the Taft parameters of the other substituents. However, such reasoning must remain speculative until pK_a or other such data are available for bis(arene)chromium systems.

The proton n.m.r. spectra for the halogen-substituted bis(arene)chromiums show many interesting features such as reduced ring proton coupling constants and large substituent chemical shifts. We are presently studying these compounds at 220 MHz in order to present unambiguous assignments and substituent chemical shifts in the near future.

Conclusions

Although the ability of substituents to deliver their inductive, resonance, and presumably steric effects in the bis(fluorobenzene)chromium and pentafluorophenyl rings is not identical, there does seem to be enough similarity to postulate that the chemistry of the two ring systems should be analogous. In particular, one would anticipate that nucleophilic substitution reactions should occur in, for example, bis(*p*-difluorobenzene)chromium to parallel those already known for hexafluorobenzene (13). Indeed, our preliminary investigations indicate that the fluorines in the complex are replaceable by methoxide. Hopefully, we may thus open up routes to many hitherto unavailable derivatives which cannot be made directly by the cocondensation method because the arenes are involatile, and which cannot be made conventionally be-

Can. J. Chem. Downloaded from www.nrcresearchpress.com by 178.218.224.3 on 09/06/12
For personal use only.

cause the arenes have substituents with lone pairs which interact with the $AlCl_3$ catalyst.

Finally, it is noteworthy that CF_3 groups directly bonded to π-complexed rings undergo small downfield shifts relative to the CF_3 resonance in benzotrifluoride (see Table 3), but no simple rationale is apparent.

We thank the National Research Council of Canada and McMaster University Science and Engineering Research Board for financial support. We also thank Mr. J. I. A. Thompson for technical assistance.

1. R. V. EMANUEL and E. W. RANDALL. J. Chem. Soc. A, 3002 (1969).
2. V. S. KHANDKAROVA, S. P. GUBIN, and B. A. KVASOV. J. Organometal. Chem. **23**, 509 (1970).
3. A. WU, E. R. BIEHL, and P. C. REEVES. J. Organometal. Chem. **33**, 53 (1971).
4. R. MIDDLETON, J. R. HULL, S. R. SIMPSON, and P. L. TIMMS. J. Chem. Soc. Dalton, 120 (1973).
5. J. W. EMSLEY and L. PHILIPS. Prog. Nucl. Magn. Reson. spectrosc. **7**, 45 (1971).
6. E. O. FISCHER and W. HAFNER. Z. Naturforsch. **10**B, 665 (1955).
7. P. S. SKELL, D. L. WILLIAMS-SMITH, and M. J. MCGLINCHEY. J. Am. Chem. Soc. **95**, 3337 (1973).
8. P. L. TIMMS. Adv. Inorg. Chem. Radiochem. **14**, 121 (1972).
9. R. W. TAFT. J. Am. Chem. Soc. **79**, 1045 (1957).
10. R. W. TAFT, E. PRICE, I. R. FOX, I. C. LEWIS, K. K. ANDERSEN, and G. T. DAVIS. J. Am. Chem. Soc. **85**, 3146 (1963).
11. M. J. S. DEWAR and A. P. MARCHAND. J. Am. Chem. Soc. **88**, 3318 (1966).
12. I. J. LAWRENSON. J. Chem. Soc. 1117 (1965).
13. R. E. BANKS. Fluorocarbons and their derivatives. Oldbourne Press, London. 1964. p. 140.

Can. J. Chem. Downloaded from www.nrcresearchpress.com by 178.218.224.3 on 09/06/12
For personal use only.

Comments on the 14-12-8-6 Potential Function

ROBERTO EMILIO CALIGARIS[1] AND OSVALDO HÉCTOR SCALISE

Departamento de Física, Facultad de Ciencias Exactas, Universidad Nacional de La Plata, c.c. 67, La Plata, Argentina

JOSÉ RAUL GRIGERA[2]

Departamento de Bioquímica, Facultad de Ciencias Exactas, Universidad Nacional de La Plata, Argentina

AND

VEDENE H. SMITH, JR. AND AJIT J. THAKKAR

Department of Chemistry, Queen's University, Kingston, Ontario K7L 3N6

Received March 13, 1974

ROBERTO EMILIO CALIGARIS, OSVALDO HÉCTOR SCALISE, JOSÉ RAUL GRIGERA, VEDENE H. SMITH, JR., and AJIT J. THAKKAR. Can. J. Chem. **52**, 2444 (1974).

Argon second and third virial coefficients for the recently proposed 14–12–8–6 potential are calculated and compared with experiment. The influence of the coefficients in the longrange dispersion energy on both of the virial coefficients is discussed.

ROBERTO EMILIO CALIGARIS, OSVALDO HÉCTOR SCALISE, JOSÉ RAUL GRIGERA, VEDENE H. SMITH, JR. et AJIT J. THAKKAR. Can. J. Chem. **52**, 2444 (1974).

On calcule et compare avec l'expérience les deuxième et troisième coefficients viriel de l'argon pour les potentiels 14–12–8–6 proposés récemment. On discute de l'influence des coefficients dans la dispersion d'énergie à longue distance sur les deux coefficients viriel.

[Traduit par le journal]

Can. J. Chem. Downloaded from www.nrcresearchpress.com by 210.87.254.6 on 09/05/12
For personal use only.

Introduction

The recent availability[3] of molecular beam measurements, both of the total and differential cross-sections, and spectroscopic data has occasionally resulted in the relative neglect of virial coefficients as a test of interatomic potentials proposed for argon.

In this note we examine the 14-12-8-6 potential from the point of view of second and third virial coefficients and dispersion coefficients. The 14-12-8-6 potential was recently used[4] by Kalos and Grosser (3) as a trial potential for fitting the angular distribution of Ar + Ar scattering. It is given by[5]

$$[1] \quad U(x) = \varepsilon C_6^*(1 + Ax^{-2})(x^{-12} - x^{-6})$$

where $x = r/\sigma$, $C_6^* = C_6/\varepsilon\sigma^6$, σ is the slow collision diameter, ε the depth of the potential well, C_6 the coefficient of the r^{-6} term, and A a mixing coefficient.

Second Virial Coefficients

Second virial coefficients were evaluated by numerical integration of the expression

$$[2] \quad B^* = B/b_0 = -3\int_0^\infty x^2 f(x)\mathrm{d}x$$

where $f(x) = -1 + \exp(-U(x)/kT)$ and $b_0 = 2\pi N\sigma^3/3$. The smoothed values given by Dymond and Smith (4) were used for comparison with experiment.[6]

A comparison of calculated and experimental second virial coefficients is made in Fig. 1 for

[1]Member of Carrera del Investigador Científico of the Consejo Nacional de Investigaciones Científicas y Técnicas, Argentina.

[2]Member of the Carrera del Investigador Científico of the Comisión de Investigaciones Científicas de La Provincia de Buenos Aires, Argentina.

[3]For recent reviews, see refs. 1 and 2.

[4]Kalos and Grosser (3) also tried a number of Lennard–Jones (12,6) potentials, but they are not considered in detail because they are completely inconsistent with experimental second virial coefficients. Standard deviations from the smoothed data of Dymond and Smith (4) range from 32 to 109 cm^3/mol.

[5]Note that the expression given in ref. 3 contains a

$$U(x) = \varepsilon C_6^*(1 - Ax^{-2})(x^{-12} - x^{-6})$$

misprint. This is evident from the fact that the potential function has only one zero at finite separations.

[6]The data point at 400 °K (-0.9 ± 0.5 cm^3/mol) was omitted because the percentage uncertainty in this value is an order of magnitude greater than that in the remaining values. Three sets of standard deviations are presented in Table 1. SD1 includes all points, SD2 all points except that at 81 °K, and SD3 all points except those at 81 and 85 °K. This procedure was adopted because we have found that nearly all potential functions fit the data better if the points at 81 and 85 °K are omitted. This suggests that these data could be in error as has been independently suspected (5). New measurements at these temperatures would be useful.

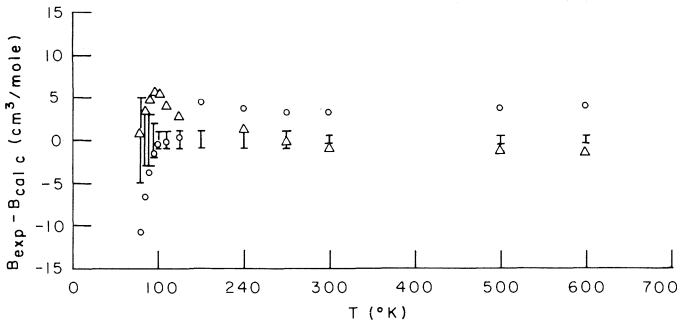

FIG. 1. Comparison between theoretical and experimental second virial coefficients. ○, 14–12–8–6 potential number 7. △, 14–12–8–6 potential number 1. Error bars set by Dymond and Smith (4).

two of the seven 14-12-8-6 potentials listed in Table 1.

Of the six 14-12-8-6 potentials given by Kalos and Grosser (3), only No. 1 and No. 4 (see Table 1) give satisfactory agreement with the second virial data. However No. 4 has too large a slow-collision diameter and gave poorer agreement (3) with spectroscopic data than No. 1.

The C_6 values of the 14-12-8-6 potentials given by Kalos and Grosser (3) were fixed to an older estimate of Dalgarno (6) which, however, lies outside the rigorous bounds given by Starkschall and Gordon (7). Similarly none of these potentials predict a value of the C_8/C_6 ratio that lies within the bounds recently given by Starkschall and Gordon (8). In fact No. 2 is the only one that predicts a C_8/C_6 ratio which is of the right *order of magnitude*.

It may be recalled that when the parameters of the similar 11-6-8 potential (9) were modified (5) to obtain relatively better agreement with the known values of the dispersion coefficients, the fit to the virial data was noticeably worsened (SD3 changed from 0.82 to 4.18 cm^3/mol while $C_6 \times 10^{60}$ improved from 21.6 to 52.9 erg cm^6 and C_8/C_6 improved from 103 to 28.2 $Å^2$). In order to determine the effects of improving agreement between the known values of the dispersion coefficients and those predicted by the 14-12-8-6 potential, we obtained a new set of parameters for the 14-12-8-6 potential by the following procedure. The values of C_6 and C_8/C_6 were fixed to the accurate semiempirical values (7, 8) and the third parameter was determined by fitting to experimental second virial coefficients. The parameters of the resulting potential (No. 7) are shown in Table 1 and a comparison between experimental second virial coefficients and those calculated from No. 7 is made in Fig. 1. It can be seen that agreement with the virial data is reasonable. Hence it seems that it is easier to simultaneously fit second virial coefficient data and values of the dispersion coefficients with the 14-12-8-6 potential than it was with the 11-6-8 potential.

Third Virial Coefficients

In this section, we consider only the better of the 14-12-8-6 potentials (Nos. 1 and 7 of Table 1). For the calculation of the third virial coefficients we consider the usual additive third virial coefficients and contributions due to the multipole expansion of the non-additive third-order interaction energy (10). It is sufficient to take into account the non-additive terms up to and including the dipole–dipole–quadrupole term (11).

The additive, C_{add}, and non-additive, ΔC, contributions to the third virial coefficient may be written as:

$$[3] \quad C_{add}^* = C_{add}/b_0^2 = -6 \int_0^\infty rf(r) \int_0^\infty sf(s) \int_{|r-s|}^{r+s} tf(t)\mathrm{d}t\mathrm{d}s\mathrm{d}r$$

and

$$[4] \quad \Delta C = \Delta C_{ddd} + 3\Delta C_{ddq}$$

where

$$[5] \quad \Delta C_{ijk} = Z_{ijk}\delta C_{ijk}$$

with

$$[6] \quad \delta C_{ijk}^* = \delta C_{ijk}/b_0^2 = 6/T^* \int_0^\infty re(r) \times \int_0^\infty se(s) \int_0^\infty te(t)W_{ijk}\mathrm{d}t\mathrm{d}s\mathrm{d}r$$

In eq. 6 the W_{ijk} are geometrical factors given by Bell (10) and $e(x) = f(x) + 1$. The Z_{ijk} are interaction coefficients which depend solely

Can. J. Chem. Downloaded from www.nrcresearchpress.com by 210.87.254.6 on 09/05/12
For personal use only.

Can. J. Chem. Downloaded from www.nrcresearchpress.com by 210.87.254.6 on 09/05/12
For personal use only.

TABLE 1. Comparison of 14-12-8-6 potentials for argon

Number	Reference	ε/k (°K)	σ (Å)	r_m (Å)	A [a]	$C_6 \times 10^{60}$ (erg cm^6)	C_8/C_6 (Å^2)	ΔB (cm^3/mol) [b]		
								SD1	SD2	SD3
1	3(10) [c]	147	3.40	3.77	1.26	62.2	14.6	3.50	3.65	3.68
2	3(33)	148	3.15	3.52	0.36	62.2	3.57	8.76	7.00	5.72
3	3(34)	152	3.35	3.71	1.14	62.2	12.8	10.7	10.4	9.75
4	3(43)	141	3.50	3.88	1.64	62.2	20.1	3.06	3.15	3.28
5	3(31)	145	3.60	3.98	2.27	62.2	29.4	18.3	17.2	15.6
6	3(30)	141	3.35	3.72	0.97	62.2	10.9	9.47	7.65	6.27
7	[d]	148.7	3.202	3.569	0.458	64.8	4.69	4.65	3.65	3.22
Semiempirical		142 [h]	3.32 [e]			64.8 [f]	4.67 [g]			
		(±5)	(±0.04)			(±1.9)	(±0.70)			

[a] Mixing coefficient.
[b] Standard deviations from second virial coefficient data. SDl includes all points, SD2 all points except that at 81 °K, and SD3 all points except those at 81 and 85 °K.
[c] Numbers in parentheses indicate the number given to the potential in ref. 3.
[d] Present work.
[e] Reference 20.
[f] Reference 7.
[g] Reference 8.
[h] Reference 21.

TABLE 2. Reduced third virial coefficient integrals for the 14-12-8-6 potential function

	$A = 1.26$, $C_6^* = 1.98345$			$A = 0.458$, $C_6^* = 2.9299$		
T^*	C_{add}^*	δC_{ddd}^*	$3\delta C_{ddq}^*$	C_{add}^*	δC_{ddd}^*	$3\delta C_{ddq}^*$
0.8	0.1405	26.93	65.95	−0.2587	28.93	70.62
0.9	0.5010	19.05	45.16	0.3394	20.32	48.09
1.0	0.5962	14.41	33.25	0.5410	15.28	35.23
1.1	0.6001	11.44	25.78	0.5948	12.07	27.21
1.2	0.5736	9.407	20.79	0.5921	9.890	21.87
1.3	0.5396	7.949	17.27	0.5689	8.328	18.12
1.4	0.5064	6.860	14.69	0.5399	7.167	15.37
1.5	0.4767	6.022	12.73	0.5111	6.275	13.29
1.6	0.4514	5.359	11.21	0.4847	5.572	11.68
1.7	0.4300	4.823	9.991	0.4616	5.006	10.40
1.8	0.4122	4.382	9.002	0.4416	4.541	9.353
1.9	0.3975	4.014	8.185	0.4245	4.153	8.494
2.0	0.3852	3.702	7.500	0.4099	3.825	7.775
2.2	0.3667	3.204	6.420	0.3870	3.303	6.643
2.4	0.3538	2.824	5.611	0.3704	2.906	5.796
2.6	0.3448	2.525	4.984	0.3582	2.594	5.142
2.8	0.3385	2.284	4.484	0.3492	2.344	4.622
3.0	0.3340	2.086	4.078	0.3424	2.139	4.200
3.5	0.3273	1.718	3.334	0.3315	1.758	3.429
4.0	0.3241	1.463	2.829	0.3253	1.496	2.907
4.5	0.3222	1.277	2.464	0.3213	1.304	2.531
5.0	0.3208	1.135	2.189	0.3183	1.158	2.247

upon the atomic species involved in the interaction. The index ddd indicates the dipole–dipole–dipole contribution while the index ddq indicates the dipole–dipole–quadrupole contribution.

In Table 2, we list the calculated results corresponding to the additive and non-additive terms for potentials number 1 and 7. Comparison with experiment is made in Fig. 2. The third virial coefficients predicted by potential No. 1 are similar to those predicted by the Bobetic–Barker–Maitland–Smith (B.B.M.S.) potential (11) and the agreement with experiment is good.

Previous calculations of $C(T)$, for the Barker–Pompe potential (12), the M.S.V. III potential (13), the B.B.M.S. potential (11), and the R.M.M.V. potential (14), along with the present results for potential number 1 could lead to the conclusion that any potential function for argon which incorporates theoretically calculated dispersion coefficients and fits second virial coefficients will predict third virial coefficients in good agreement with experimental data. On the other hand, potentials, such as the Lennard–Jones (12,6) and the previously mentioned 11-6-8, which do not reproduce the theoretical C_6 give third virial coefficients in poor agreement with experiment (15, 16).

However, the third virial coefficients for potential number 7 are in poor agreement with experiment despite the fact that this potential provides a reasonable fit to second virial coefficients and includes the correct C_6 and C_8 coefficients. Thus it is clear that the above criteria alone are not sufficient to ensure accurate third virial coefficients.

Now the third virial coefficients for the square-well potential (17, 18) suggest that calculated values of $C(T)$ for any potential will be too low if the width of the well is not wide enough. As Mason and Spurling point out (18), this conclusion is illusory if non-additive contributions are not taken into account because neglect of the latter leads to the same sort of deviations. However in the case of the 14-12-8-6 potential we have calculated non-additive triple-dipole and dipole–dipole–quadrupole contributions and the third virial coefficients are still too low. Assuming that other non-additive contributions are negligible, as indicated by previous calculations (11, 19), we are tempted to conclude that the well of the 14-12-8-6 potential number 7 is too narrow. However we note that the third virial coefficient is also highly sensitive to the slow collision diameter, σ, because σ^6 appears in the expression for the third virial coefficient. Com-

Can. J. Chem. Downloaded from www.nrcresearchpress.com by 210.87.254.6 on 09/05/12
For personal use only.

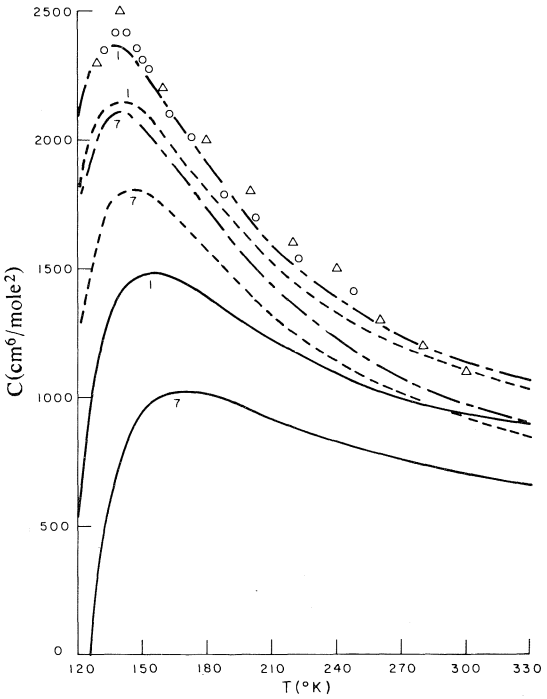

FIG. 2. Comparison between theoretical and experimental third virial coefficients. Curves numbered 1 and 7 refer to 14-12-8-6 potentials number 1 and 7 respectively. —, C(additive); ---, C(additive + ddd term); -.-.-., C(additive + ddd term + ddq term). Experimental data: ○, ref. 22; △, ref. 23.

paring Present's estimate (20) of σ with the σ for potential number 7, we see that the latter is too small and this is another factor contributing to the low calculated values of $C(T)$.

Thus we see that a potential function that incorporates theoretically calculated dispersion coefficients and fits second virial coefficients need not predict third virial coefficients in agreement with experiment. $C(T)$ is also sensitive to the shape of the well, most notably to its width.

1. G. C. MAITLAND and E. B. SMITH. Chem. Soc. Rev. **2**, 181 (1973).
2. P. R. CERTAIN and L. W. BRUCH. Intermolecular forces. *In* Theoretical chemistry. *Edited by* W. Byers Brown. Butterworths, London, England. 1972.
3. F. KALOS and A. E. GROSSER. Can. J. Chem. **50**, 892 (1972).
4. J. H. DYMOND and E. B. SMITH. The virial coefficients of gases. The Clarendon Press, Oxford, England. 1969.
5. H. J. M. HANLEY, J. A. BARKER, J. M. PARSON, Y. T. LEE, and M. KLEIN. Mol. Phys. **24**, 11 (1972).
6. A. DALGARNO. Adv. Chem. Phys. **12**, 143 (1967).
7. G. STARKSCHALL and R. G. GORDON. J. Chem. Phys. **54**, 663 (1971).
8. G. STARKSCHALL and R. G. GORDON. J. Chem. Phys. **56**, 2801 (1972).
9. M. KLEIN and H. J. M. HANLEY. J. Chem. Phys. **53**, 4722 (1970); H. J. M. HANLEY and M. KLEIN. J. Phys. Chem. **76**, 1743 (1972).
10. R. J. BELL. J. Phys. B, At. Mol. Phys. **3**, 751 (1970).
11. R. E. CALIGARIS. Mol. Phys. **25**, 1465 (1973).
12. C. H. J. JOHNSON and T. H. SPURLING. Aust. J. Chem. **24**, 2205 (1971).
13. C. H. J. JOHNSON and T. H. SPURLING. J. Chem. Phys. **57**, 1804 (1972).
14. R. E. CALIGARIS, O. H. SCALISE, and J. R. GRIGERA. To be published.
15. H. W. GRABEN and R. FOWLER. Phys. Rev. **177**, 288 (1969).
16. R. E. CALIGARIS and A. E. RODRIGUEZ. J. Phys. B, At. Mol. Phys. **6**, L 24 (1973).
17. T. KIHARA. Rev. Mod. Phys. **25**, 831 (1953).
18. E. A. MASON and T. H. SPURLING. The virial equation of state. Pergamon, New York. 1969.
19. R. FOWLER and H. W. GRABEN. J. Chem. Phys. **56**, 1917 (1972).
20. R. D. PRESENT. J. Chem. Phys. **58**, 2659 (1973).
21. R. J. LEROY. J. Chem. Phys. **57**, 573 (1972).
22. A. MICHELS, J. M. LEVELT, and A. DEGRAAF. Physica, **24**, 659 (1958).
23. J. M. H. LEVELT SENGERS, M. KLEIN, and J. S. GALLAGHER. A.I.P. Handbook. McGraw-Hill, New York. 1972.

Can. J. Chem. Downloaded from www.nrcresearchpress.com by 210.87.254.6 on 09/05/12
For personal use only.

The Hydrogen Bond Energies in $ClHCl^-$ and $Cl^-(HCl)_n$

R. YAMDAGNI AND P. KEBARLE

Chemistry Department, University of Alberta, Edmonton, Alberta T6G 2G2

Received February 13, 1974

R. YAMDAGNI and P. KEBARLE. Can. J. Chem. **52**, 2449 (1974).

The equilibrium constants for the gas phase reactions: $Cl^-(HCl)_n = Cl^-(HCl)_{n-1} + HCl$, $(n, n-1)$ were measured at different temperatures with a pulsed electron beam high pressure mass spectrometer. This allowed determination of $\Delta G_{n,n-1}^0$, $\Delta H_{n,n-1}^0$, and $\Delta S_{n,n-1}^0$ for reactions with $n = 1$ to $n = 4$. The enthalpy change for the reaction: $(ClHCl)^- = Cl^- + HCl$ was $\Delta H_{1,0}^0 = 23.7$ kcal/mol. This value is much higher than the literature value of 14.2 kcal/mol based on Born cycles. The stabilities of the $Cl^-(HCl)_n$ clusters are compared with those of $OH^-(H_2O)_n$ and $Cl^-(H_2O)_n$ measured earlier. It is found that the $(ClHCl)^-$ is nearly as stable as the $(HOHOH)^-$ species but that the stabilities of the higher $Cl^-(HCl)_n$ clusters decreases much more rapidly than that of $OH^-(H_2O)_n$. The initial strong interaction in (ClHCl) is assumed to be due to the high polarizability of Cl. For large n this effect becomes unimportant. Cl^-HOH is much more weakly bound than $(ClHCl)^-$, however, at high n the $Cl^-(H_2O)_n$ interactions become more favorable.

R. YAMDAGNI et P. KEBARLE. Can. J. Chem. **52**, 2449 (1974).

On mesure avec un spectromètre de masse à haute pression à faisceau de pulsation d'électrons les constantes d'équilibre à différentes températures pour les réactions en phase gazeuse: $Cl^-(HCl)_n = Cl^-(HCl)_{n-1} + HCl$, $(n, n-1)$. Par cela on détermine $\Delta G_{n,n-1}^0$, $\Delta H_{n,n-1}^0$ et $\Delta S_{n,n-1}^0$ pour les réactions avec $n = 1$ jusqu'à $n = 4$. Le changement d'enthalpie pour la réaction: $(ClHCl)^- = Cl^- + HCl$ est $\Delta H_{1,0}^0 = 23.7$ kcal/mol. Cette valeur est plus élevée que celle basée sur les cycles de Born trouvée dans la littérature (14.2 kcal/mol). On compare les stabilités des agglomérations $Cl^-(HCl)_n$ avec celles mesurées précédemment $OH^-(H_2O)_n$ et $Cl^-(H_2O)_n$. On trouve que $(ClCHl)^-$ est presque aussi stable que les espèces $(HOHOH)^-$ mais que les stabilités des groupes de plus haut degré $Cl^-(HCl)_n$ décroissent plus rapidement que celle de $OH^-(H_2O)_n$. On attribue les fortes interactions initiales dans (ClHCl) à la haute polarisabilité du Cl. Cet effet devient sans importance lorsque la valeur de n est élevée. Cl^-(HOH) est plus faiblement lié que $(ClHCl)^-$, cependant, pour une grande valeur de n les interactions $Cl^-(H_2O)_n$ deviennent plus favorables. [Traduit par le journal]

Introduction

The bond energies and properties of the strongly hydrogen bonded halide systems XHX^- have been subject to a number of investigations (1–9). The studies can be roughly divided into: estimates of the bond energies based on Born type cycles involving some extra thermodynamic evaluations (1–4), crystallographic investigations of crystals containing the bihalide ion (5) (quantum mechanical) calculations (6), and studies of the infrared spectra of the XHX^- in condensed phases (2, 7–9).

It appears that the bond energies for FHF^- and $ClHCl^-$ are still very uncertain. Not too long ago a study of strongly hydrogen bonded species Cl^-—HR was made in this laboratory (10). The species HR were compounds like: HOH, CH_3OH, C_6H_5OH, CH_3COOH, etc. The studies were based on measurement of the gas phase ionic equilibria 1

$$[1] \qquad (ClHR)^- = Cl^- + HR$$

observed with a special high pressure ion source mass spectrometer. This work showed that ΔG^0, and ΔH^0, increased with the *gas phase* acidity of HR. This regularity fitted an earlier observation (11) that the strength of the interactions B^-—HOH increased with the gas phase basicity of B^-. It was therefore postulated (10, 11) that hydrogen bonding to charged species in the gas phase increases in strength with the gas phase basicity of the (partial) proton acceptor and acidity of the proton donor.

Agreement with the rule was later observed in several systems in this (12–16) and other laboratories (17, 18). The above rule is particularly useful if the base B^- is kept constant and the nature of the acid HR varied or *vice versa*. It is less useful for prediction of the bonding energies in symmetric species like $(XHX)^-$ where the base and conjugate base (of the acid) are

Can. J. Chem. Downloaded from www.nrcresearchpress.com by 210.87.254.40 on 09/05/12
For personal use only.

Can. J. Chem. Downloaded from www.nrcresearchpress.com by 210.87.254.40 on 09/05/12
For personal use only.

identical. Nevertheless an extrapolation of the regularities observed for the non-symmetric cases B^-HR and one symmetric case (11, 12) $(HOHOH)^-$ allowed crude estimates for symmetric species to be made (10). The prediction for ΔH_1^0 involving the species $(ClHCl)^-$ was 22 kcal/mol. This value was in agreement with a value of 24 kcal obtained by extrapolations (10) of bond energies for the higher clusters $Cl^-(HCl)_n$ measured in this laboratory (19),[1] but in serious disagreement with the value of 14.2 kcal/mol obtained by McDaniel and Valleé (3) from Born type cycles.

The present work describes measurements of the temperature dependence for the gas phase equilibria $(n,n-1)$ which permit the evaluation

$$(ClHCl)^- = Cl^- + HCl \qquad (1,0)$$

$$Cl^-(HCl)_n = Cl^-(HCl)_{n-1} + HCl \qquad (n,n-1)$$

not only of $\Delta H_{1,0}^0$ but also of the binding energies for the higher clusters.

Experimental

The measurements were made with the pulsed electron beam high pressure mass spectrometer described earlier (12, 20). The present measurements were done with pure HCl gas from 1–4 Torr and with mixtures of HCl 0.1–0.6 Torr and some 4–5 Torr buffer gas like CH_4 or N_2. The gases passed in slow flow through the ion source. The measurements were made in the presence of some 0.01 Torr CCl_4 whose presence greatly increased the intensity of the signal. The reaction sequence assumed to occur is: (*a*) near thermalization of primary and secondary electrons created by the electron pulse; (*b*) dissociative electron capture $e + CCl_4 = Cl^- + CCl_3$; (*c*) establishment of clustering equilibria $(n, n-1)$ at some level of n depending on concentration and temperature. The negative ions escaping from a small sampling slit in the ion source were separated with a magnetic mass spectrometer. The ion counting system included a multiscaler whose sweep was started by the electron pulse. The time resolved ion profiles after the pulse could be observed in this manner. At low HCl concentrations the approach to equilibrium was slow (several hundreds of μs) and could be observed. Generally the HCl concentrations were so selected as to lead to a more rapid approach to equilibrium, assumed to occur when the observed ion count rate ratios became constant. The ion count rates in this stationary range were assumed proportional to the equilibrium ion concentration in the ion source. The equilibrium constant expression $K_{n,n-1} = (I_{n-1}[HCl])/I_n$ was used where I is the ion count rate.

[1]Quoted in ref. 10 as "Can. J. Chem. In press." but subsequently withdrawn.

Results and Discussion

The equilibrium constants measured for the 1,0 equilibrium are shown in Fig. 1. Similar independence of HCl pressure was observed also for the higher cluster equilibria. The Van't Hoff plots of all the equilibrium constants determined in the present work are shown in Fig. 2. The resulting ΔG^0, ΔH^0, and ΔS^0 values are summarized in Table 1. The errors given in Table 1 correspond to standard deviation from least squares plot. Past experience has shown that the actual error is generally larger. Comparison between ΔG^0 values at a given temperature have proven reliable to about 0.3 kcal (a factor of 2 in value of K). However, the ΔH values have been found to be reliable only to about ± 2 kcal. This is due to the somewhat restricted temperature range which is accessible with present technique, difficulties of measuring accurately the temperature of the gas in the ion source, and other systematic errors of less tractable origin.

The present experimental value for $\Delta H_{1,0}^0$ (Table 1) is seen to be equal to 23.7 kcal/mol. This is in good agreement with the previous estimates from this laboratory (10) but in disagreement with the value of 14.2 kcal/mol of McDaniel and Valleé (3). We believe that the value of McDaniel and co-worker is erroneous, probably because of the inadequacy of the extra-

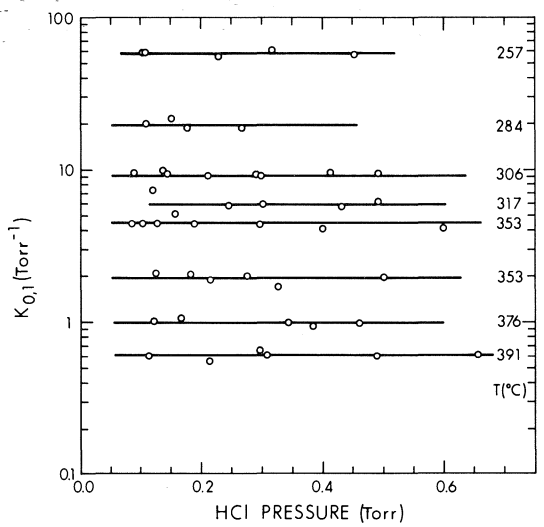

FIG. 1. Equilibrium constants $K_{0,1}$ for reaction: $Cl^- + HCl = (ClHCl)^-$ (note $K_{0,1} = 1/K_{1,0}$) in function of temperature and HCl pressure. Measurements in presence of 4–5 Torr CH_4 or N_2. Standard state 1 Torr.

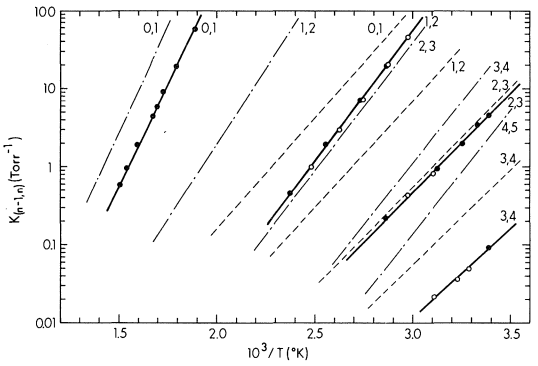

FIG. 2. Van't Hoff plots of equilibrium constants $K_{n-1,n}$ for reactions: —, $Cl^-(HCl)_{n-1}+HCl=Cl^-(HCl)_n$. The equilibria, ·····, $OH^-(H_2O)_{n-1} + H_2O = OH^-(H_2O)_n$ and - - -, $Cl^-(H_2O)_{n-1}+H_2O=Cl^-(H_2O)_n$ measured in earlier work (11, 12) are also shown for comparison purposes.

thermodynamic assumptions involved in the cycle used.

The relative strengths of the interactions in $Cl^-(HCl)_n$ and the only other symmetric species measured (11, 12), $OH^-(HOH)_n$, can be most directly compared in the Van't Hoff plots given in Fig. 2. This comparison is preferable since it involves ΔG differences at the temperature of determination which should be the most accurate. The 0,1 interaction for the OH^- is only slightly stronger than that for the formation of Cl^-HCl, the principle difference being in the ΔS^0 values (Table 1). Interestingly the 1,2 interaction for the $Cl(HCl)_n$ system which is very much weaker than that for the $OH^-(HOH)_n$ (Fig. 2 and Table 1). In fact the 1,2 chlorine interaction is comparable to the 2,3 interaction for the hydroxy system (Fig. 2). The relatively more rapid decrease of stability for the Cl system continues as n is increased further. Thus the 3,4 plot is much lower than the 2,3 plot for the OH^- system (Fig. 2). A similar trend is observed for the $\Delta G_{n,n-1}{}^0$ (300 °K) values, Table 1, which are based on relatively long extrapolations for the plots with low n. These findings may be rationalized as follows. Previous work (15, 16) has shown that hydrogen bonding remains the dominant interaction in many systems involving protic solvent (clustering) molecules. Thus it was found (15) that the species $(CH_3)_2OH^+O(CH_3)_2$ was very stable but that the addition of one more dimethyl ether molecule led to a very unstable cluster presumably because there were no H bonding positions available for the third molecule. For the present systems we might expect that the $OH^-(H_2O)_n$ will be totally H bonded system for all n. For higher n such structures are three dimensional with considerable charge dispersal, the center of the charge being near the center of the cluster (21, 15, 16). The situation for $Cl^-(HCl)_n$ should be somewhat different. The $(ClHCl)^-$ will be linear. The large Cl radius should affect the stability adversely. On the other hand since the dichloride has a high negative charge density, the high polarizability of Cl should be important. This is in agreement with the observed nearly equal $\Delta H_{1,0}{}^0$ for the dihalide and dihydroxide systems. The addition of further HCl molecules might initially lead to a further buildup of the linear chain. However, the large Cl radius and the decreasing importance of the polarizability should probably make these structures progressively less stable compared with the hydroxy hydrates. A reorganization into a central Cl^- ion solvated by a shell of HCl molecules might be expected of some higher n. The present data do not give an indication whether or when such a reorganization occurs. However, they do show the expected progressively worsening bonding relative to the hydroxy system.

The $Cl^-(H_2O)_n$ data (Fig. 2 and Table 1) show that the binding free energy is initially (n = 1) much weaker than that for $Cl(HCl)_n$.

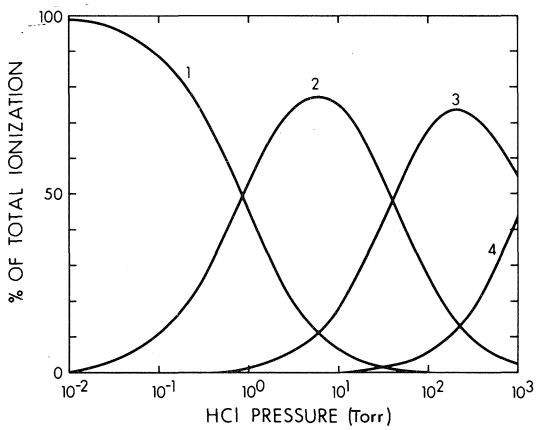

FIG. 3. Calculated distribution of $Cl^-(HCl)_n$ clusters for 127 °C and different pressures of HCl. Equilibrium data from Table 1 were used for calculation. Numbers above curves equal to n. $K_{0,1} \approx 100\,000$ (standard state 1 Torr) at 127 °C. Therefore Cl^- (n = 0) becomes equal in concentration to $Cl^-(H_2O)$ at some 10^{-5} Torr.

Can. J. Chem. Downloaded from www.nrcresearchpress.com by 210.87.254.40 on 09/05/12
For personal use only.

Can. J. Chem. Downloaded from www.nrcresearchpress.com by 210.87.254.40 on 09/05/12
For personal use only.

TABLE 1. Thermodynamic data* (from measurement of gas phase equilibria $Cl^-(HCl)_n = Cl^-(HCl)_{n-1} + HCl$; $(n,n-1)$. Data for $Cl^-(H_2O)_n$ and $OH^-(H_2O)_n$ given for comparison)

	ΔH^0				ΔS^0				$\Delta G_{298}{}^0$			
System	(1,0)	(2,1)	(3,2)	(4,3)	(1,0)	(2,1)	(3,2)	(4,3)	(1,0)	(2,1)	(3,2)	(4,3)
$Cl^-(HCl)_n$	23.7 ±0.2	15.2 ±0.2	11.7 ±0.3	10.3 ±0.7	23.5 ±0.4	24.4 ±0.4	23.4 ±0.8	26.7 ±2.0	16.7 ±0.3	7.9 ±0.2	4.7 ±0.3	2.4 ±1.0
$Cl^-(H_2O)_n$†	13.1	12.7	11.7	11.1	16.5	20.8	23.2	25.8	8.2	6.5	4.5	3.4
$OH^-(H_2O)_n$	24.0‡	17.9‡	15.1§	14.2§	20.8‡	21.2‡	24.8§	29.5§	17.8‡	11.5‡	7.7§	5.4§

*All energy values in kcal/mol, entropy in e.u., standard state 1 atm.
†Arshadi *et al.* (11*a*).
‡Payzant *et al.* (12).
§Arshadi and Kebarle (11*b*).

This was explained earlier as being due to the higher gas phase acidity of HCl. As n is increased the differences decrease. A crossover occurs after the addition of 3 molecules with $\Delta G_{4,3}{}^{0}$ for $Cl(H_2O)$ becoming larger than $\Delta G_{4,3}{}^{\circ}$ Cl(HCl). This result is similar to that already discussed above. Water becomes the preferred solvent at high n since the high polarizability of Cl becomes less important at low charge densities.

The presence of $Cl^{-}(HCl)_n$ clusters is of direct significance to the interpretation of the results for the gas phase radiolysis (22) of HCl. The present data (Table 1) permits the evaluation of the relative cluster concentrations for a variety of temperatures and pressures. An example of such calculated distributions is given in Fig. 3 which shows that for 127 °C the data permits the prediction of the clusters for pressures from 10^{-5} to 10^{3} Torr.

1. J. A. KETELAAR. Rec. Trav. Chim. **60**, 523 (1941).
2. T. C. WADDINGTON. Trans. Faraday Soc. **54**, 25 (1958); T. C. WADDINGTON. J. Chem. Soc. 1708 (1958).
3. D. H. MCDANIEL AND R. E. VALLÉE. Inorg. Chem. **2**, 996 (1963).
4. S. A. HARREL and D. H. MCDANIEL. J. Am. Chem. Soc. **86**, 4497 (1969).
5. L. W. SCHROEDER and J. A. IBERS. J. Inorg. Chem. **7**, 594 (1968).
6. P. A. KOLLMAN and L. C. ALLEN. J. Inorg. Chem. **92**, 6101 (1970).
7. J. C. EVANS and G. Y. S. LO. J. Phys. Chem. **70**, 11 (1966).
8. J. W. NIBLER and G. C. PIMENTEL. J. Chem. Phys. **47**, 710 (1967).
9. D. E. MILLIGAN and M. JACOX. J. Chem. Phys. **53**, 2034 (1970).
10. R. YAMDAGNI and P. KEBARLE. J. Am. Chem. Soc., **93**, 7139 (1971).
11. (*a*) M. ARSHADI, R. YAMDAGNI, and P. KEBARLE. J. Phys. Chem. **74**, 1475 (1970). (*b*) M. ARSHADI and P. KEBARLE. J. Phys. Chem. **74**, 1483 (1970).
12. (*a*) J. D. PAYZANT, R. YAMDAGNI, and P. KEBARLE. Can. J. Chem. **49**, 3308 (1971); (*b*) R. YAMDAGNI, J. D. PAYZANT, and P. KEBARLE. Can. J. Chem. **51**, 2507 (1973).
13. R. YAMDAGNI and P. KEBARLE. J. Am. Chem. Soc. **95**, 3504 (1973).
14. J. PAYZANT, A. J. CUNNINGHAM, and P. KEBARLE. Can. J. Chem. **51**, 3242 (1973).
15. E. P. GRIMSRUD and P. KEBARLE. J. Am. Chem. Soc. **95**, 7939 (1973).
16. K. HIRAOKA, E. P. GRIMSRUD, and P. KEBARLE. J. Am. Chem. Soc. In press.
17. L. K. BLAIR, P. C. ISOLANI, and J. M. RIVEROS. J. Am. Chem. Soc. **95**, 1057 (1973).
18. R. T. MCIVER JR., J. A. SCOTT, and J. M. RIVEROS. J. Am. Chem. Soc. **95**, 2706 (1973).
19. R. YAMDAGNI and P. KEBARLE. Unpublished work.
20. A. J. CUNNINGHAM, J. D. PAYZANT, and P. KEBARLE. J. Am. Chem. Soc. **94**, 7627 (1972).
21. M. D. NEWTON and S. EHRENSON. J. Am. Chem. Soc. **93**, 4971 (1971).
22. D. E. WILSON and D. A. ARMSTRONG. Radiat. Res. Rev. **2**, 297 (1970).

Can. J. Chem. Downloaded from www.nrcresearchpress.com by 210.87.254.40 on 09/05/12
For personal use only.

Spin-labelled Ligands

C. T. CAZIANIS AND D. R. EATON

Department of Chemistry, McMaster University, Hamilton, Ontario L8S 4M1

Received November 14, 1973

C. T. CAZIANIS and D. R. EATON. Can. J. Chem. **52,** 2454 (1974).

A spin-labelled ligand is defined as a molecule with two functional groups, one of which provides a Lewis base site suitable for complexing to a metal ion. The second functional group comprises a site bearing an unpaired electron. The possible utility of such compounds in coordination chemistry has been explored. The spin density distribution in 4-pyridyl-*t*-butyl nitroxide provides information on the relative electron accepting abilities of different metal ions in various ligand environments. A method for measuring the rates of very rapid ligand exchange reactions is also suggested.

C. T. CAZIANIS et D. R. EATON. Can. J. Chem. **52,** 2454 (1974).

On défini un coordinat à spin marqué comme une molécule possédant deux groupes fonctionnels un desquels peut servir de site basique dans le sens de Lewis pour la formation d'un complexe avec un ion métallique. Le deuxième groupe fonctionnel est formé d'un site portant un électron non pairé. On a étudié les utilisations que l'on peut faire de tels composés en chimie de la coordination. La distribution des densités de spin dans le radical pyridyl-4 *tertio*-butyl nitroxyde fournit des informations sur les capacités relatives d'acceptation d'électrons de différents ions métalliques dans divers environnements du coordinat. On suggère une méthode pour mesurer les vitesses de réactions d'échange très rapide des coordinats.

[Traduit par le journal]

Introduction

Electron spin resonance provides a powerful technique for the study of the molecular and electronic structure of molecules. If atoms possessing nuclear spin moments are present the resulting hyperfine coupling pattern is particularly valuable since it permits investigation of the spin density distribution within the molecule. There is however a major limitation to the widespread use of the method, namely the molecule under study must be paramagnetic. The majority of molecules which offer interesting problems involving bonding or structure do not fulfil this condition. The technique of spin labelling has been introduced into biological chemistry in an attempt to extend the range of molecules amenable to study by e.s.r. (1). A variety of enzymes and other biologically active molecules have been chemically modified by the introduction of a paramagnetic substituent (the spin label) hopefully in the vicinity of the active site. The intent of the present work was to utilize the spin labelling concept in a study of metal ligand bonding.

We define a spin-labelled ligand as a molecule containing two functional groups, one of which possesses an electron pair suitable for donation to a metal ion. The other functional group must possess an unpaired electron. Ideally the two functions must be connected, but not too closely connected. We wish to use the radical function as a probe for electronic changes at the Lewis base site. If the unpaired electron is too well removed from the site of interaction with the metal it will obviously be an insensitive probe. If on the other hand the Lewis base and radical functions are combined in the same group the ligand metal bonding may be very different from that of the unlabelled ligand. A number of e.s.r. studies involving radical ligands of this latter type have been reported.[1] In some cases, *e.g.* *o*-semiquinones (2) and alkyl nitroxides (3–6, 11) the unpaired electrons remain essentially localized on the ligand. In other cases *e.g.* *o*-phenanthrolene (7) negative ions and dithiolate (8) ions the interactions with the metal ion are sufficiently strong to lead to complete delocalization and it becomes debatable whether it is more correct to describe the compound as a complex of a radical with a metal ion in a high oxidation state or a complex of a non-radical ligand with a metal in a lower oxidation state. Thus for example V(dipy-

[1]Very recently e.s.r. spectra of the chelate complexes of Zn, Cd, and Hg with 4,4,5,5-tetramethyl-2-(2 pyridyl)-Δ^2-imidazoline-1-oxyl have been reported (21).

Can. J. Chem. Downloaded from www.nrcresearchpress.com by 210.87.254.40 on 09/05/12
For personal use only.

Can. J. Chem. Downloaded from www.nrcresearchpress.com by 210.87.254.40 on 09/05/12
For personal use only.

ridyl)$_3$ could be described as a complex of V^{3+} with three radical anions, a complex of V^0 with three neutral diamagnetic ligands, or any intermediate combination. In contrast to the above examples, the Lewis base and radical functions have been intentionally separated in the present study and molecules of this latter type may be described as "spin-labelled ligands."

Pyridine was chosen for the Lewis base part of the molecule. It has the advantages of readily forming complexes with a wide variety of metal ions and of possessing a π system which can form a link with the radical group. Both semidione groups and nitroxide groups have been used to provide the spin label. Both are capable of forming relatively stable radicals. The second proved to be more useful than the first for our purposes.

Synthesis and Electron Spin Resonance Spectra of Ligands

Radicals with structures **1** and **2** have been prepared. Radical **1** can be obtained by exposing

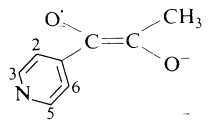

1

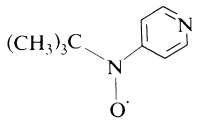

2

a solution of pyridyl ethyl ketone in dimethyl sulfoxide containing potassium *t*-butoxide to a trace of oxygen. The mechanism by which reactions of this type lead to the formation of semidione radicals has been discussed by Russell (9). The resulting e.s.r. spectrum is shown in Fig. 1. Forty-five of the possible 108 lines are resolved and the analysis is straightforward. The derived hyperfine coupling constants are $a_N = 1.6$ G, $a_{H,3,5} = 0.3$ G, $a_{H,2,6} = 1.9$ G, and $a_{CH_3} = 2.6$ G. These constants may be compared with those reported for the radical containing a phenyl group (9) rather than a pyridyl group: $a_4 = 1.84$ G, $a_{3,5} = 0.53$ G, $a_{2,6} = 1.59$ G, and $a_{CH_3} = 3.43$ G. The latter have been shown to be consistent with spin densities calculated by the McLachlan method and the similarity with those obtained for radical **1** confirms the correctness of the assignment. We may also assume by analogy with the phenyl compound that radical **1** has a *trans* configuration. Chelation of a metal ion with the semidione oxygens is therefore unlikely.

Radical **2** was prepared by the reaction sequence:

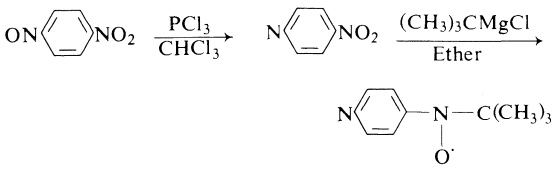

The preparation of the analogous *p*-tolyl radical has been reported by the reaction of *t*-butyl magnesium bromide with *p*-nitrotoluene (10). Electron spin resonance spectra were obtained by adding a few drops of the ethereal solution to an appropriate solvent. The resulting spectra are well resolved and analysis is again straightforward. No splitting is observed from the protons of the *t*-butyl group. Sixty-three of the predicted 81 lines arising from the remaining magnetic nuclei can be observed. A typical spectrum is shown in Fig. 2. It proved convenient to prepare metal complexes of this radical in several different solvents. The extent of the variation of hyperfine coupling constants with solvent is apparent from the data in Table 1.

Complexing of Radicals with Metal Ions

Only very limited success was achieved in forming metal complexes of the semidione **1**. Addition of the ether and trimethylamine complexes of the very strong Lewis acid BF_3 to a solution of the radical in DMSO lead to the observation of a complex e.s.r. spectrum. The lack of symmetry of this spectrum suggests that more than one species is present and prevented analysis. A number of attempts were made to produce Zn complexes by adding various Zn salts and labile complexes to the radical in DMSO or DMSO/THF mixtures. These experiments lead to destruction of the radical. The problem probably lies in the ready oxidation of semidiones except in strongly basic solution. Addition of metal ions removes the base ($(CH_3)_3CO^-$) followed immediately by oxidation of the radical. This occurs even in solutions which have been very carefully deoxygenated on a vacuum line. An attempt was also made to produce complexed radicals by oxidation of the compound

but this also proved unsuccessful.

Can. J. Chem. Downloaded from www.nrcresearchpress.com by 210.87.254.40 on 09/05/12
For personal use only.

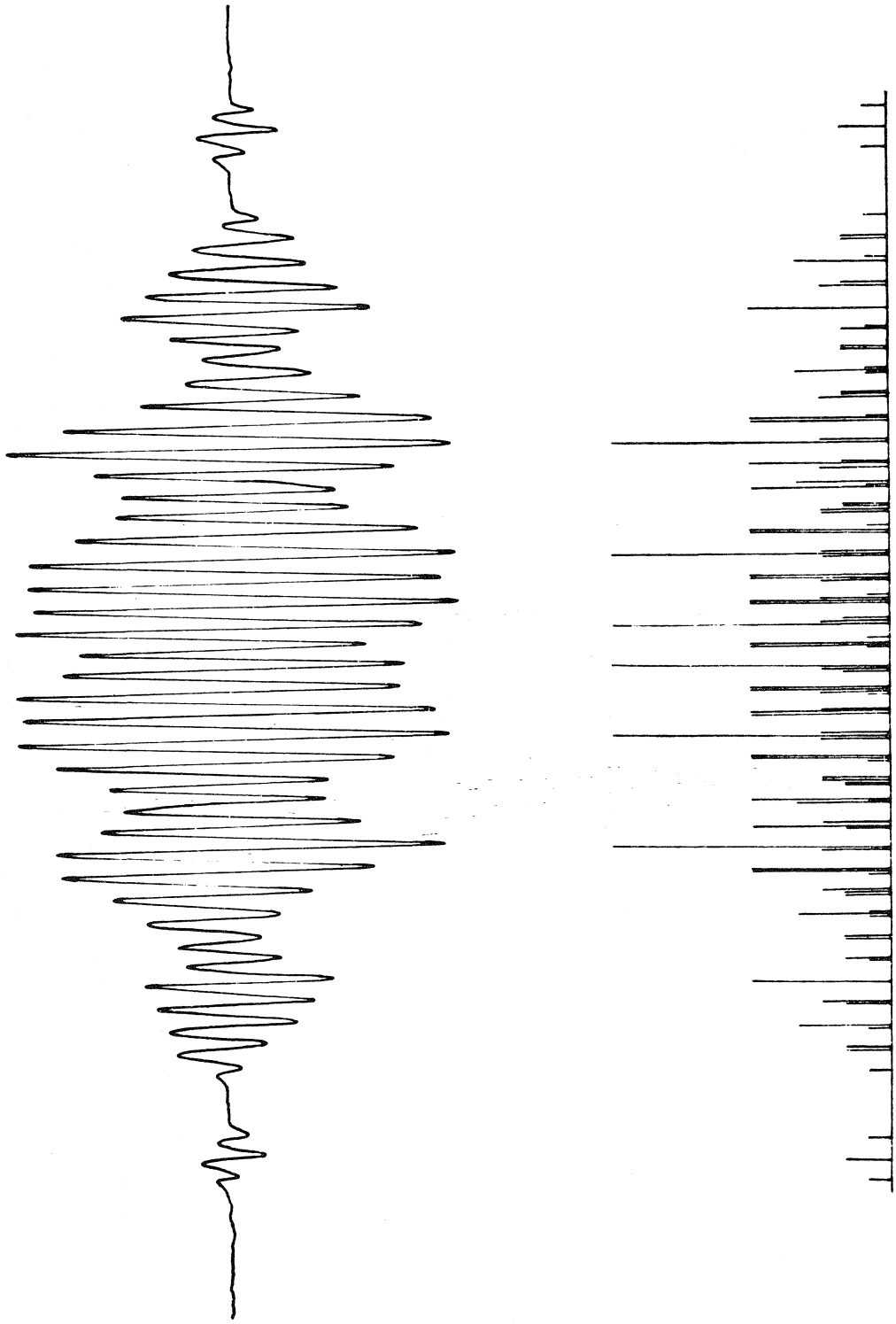

FIG. 1. Electron spin resonance spectrum of 4-pyridyl propane-1,2 semidione radical in DMSO solution. Calculated spectrum below.

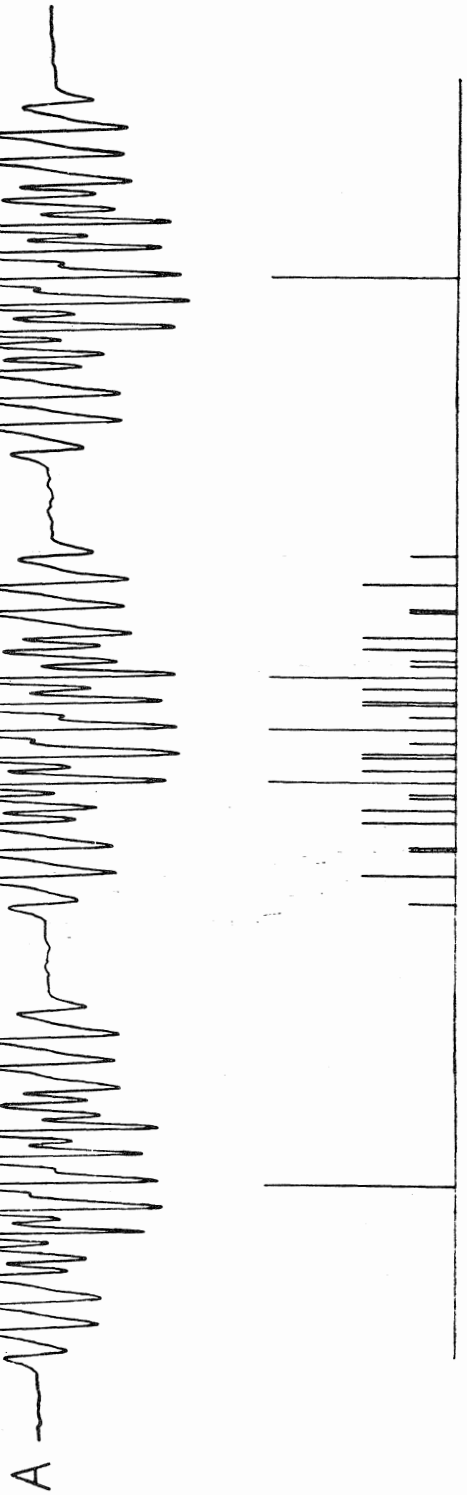

FIG. 2. Electron spin resonance spectrum of 4-pyridyl-*t*-butyl nitroxide radical in benzene/THF mixture. Calculated spectrum below.

Can. J. Chem. Downloaded from www.nrcresearchpress.com by 210.87.254.40 on 09/05/12
For personal use only.

TABLE 1. Hyperfine coupling constants (G) of 4-pyridyl-*t*-butyl nitroxide radical

Radical	*a* (position)				Solvent
	a_2^N	a_6^N	$a_{4,8}^H$	$a_{5,7}^H$	
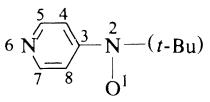	10.57	1.26	2.17	0.63	Benzene
	10.70	1.23	2.16	0.63	1,4-Dioxane
	10.52	1.23	2.16	0.64	Benzene/THF (11:1)
	10.74	1.23	2.16	0.63	Dioxane/THF (11:1)

FIG. 3. Electron spin resonance spectra of 4-pyridyl-*t*-butyl nitroxide in benzene/THF mixture: (*A*) free radical; (*B*) complex with $HgCl_2$; (*C*) complex with $ZnCl_2$; (*D*) complex with $Pd(NO_3)_2$.

Experiments with the nitroxide labelled ligand proved more fruitful. The stability of this radical is unaffected by the presence of metal compounds except in one or two special cases. The results obtained fall into six different classes.

(*1*) Addition of the metal compound leads to no change in the e.s.r. spectrum of the radical. In this class fall complexes such as $Co(acac)_3$ for which replacement of the chelating acetylacetonate would not be expected. Any change due to the presence of the spin-labelled ligand in the second sphere is apparently too small to observe. Similarly the radical will apparently not replace phosphine in $Pd(P\phi_3)_2Cl_2$ or pyridine in $Copy_3(NCS)_2Cl$ to any observable extent. Neither could we find evidence for increase in the metal coordination number on the addition of $Pt(acac)_2$, $Pd(acac)_2$ or zinc phthalocyanine.

(*2*) Addition of excess of the metal compound leads to the appearance of a single new e.s.r. spectrum. Examples are shown in Fig. 3. Results in this class were obtained with a variety of zinc compounds, with mercury halides, with cadmium iodide, and with palladium nitrate. The hyperfine coupling constants obtained from the analysis of these spectra are presented in Table 2. There are two possibilities which could lead to results of this type. Either all the spin-labelled ligand is complexed to the metal ion or some is complexed and some is free and the ligand exchange rate is sufficiently fast to give an averaged e.s.r. spectrum. In these experiments the ratio of metal ion concentration ($\sim 10^{-1}$ *M*) to radical concentration ($\sim 10^{-4}$ *M*) is very large and none of the competing ligands is as strong a Lewis base as pyridine. The first possibility seems therefore the

Can. J. Chem. Downloaded from www.nrcresearchpress.com by 210.87.254.40 on 09/05/12
For personal use only.

TABLE 2. Hyperfine coupling constants (G) and experimental spin-densities of 4-pyridyl-*t*-butyl nitroxide in the presence of metal compounds

Metal compound	*a* (position)[a]				ρ_2^N (exptl.)[b]
	a_2^N	a_6^N	$a_{4,8}^H$	$a_{5,7}^H$	
—	10.52[c]	1.23[c]	2.16[c]	0.64[c]	0.207[c]
$Zn(TU)_2Cl_2$[e]	9.47	1.60	2.12	0.49	0.142
CdI_2	9.38	1.63	2.15	0.51	0.136
$ZnCl_2$	9.28	1.60	2.12	0.49	0.130
$ZnBr_2$	9.24	1.60	2.12	0.49	0.127
ZnI_2	9.14	1.63	2.13	0.49	0.121
$HgCl_2$	9.85	1.55	2.14	0.57	0.165
HgI_2	9.87	1.56	2.16	0.57	0.167
$Pd(NO_3)_2$	9.14	2.03	2.16	0.54	0.121
$Zn(\phi NH_2)_2Cl_2$[d]	9.25	1.60	2.12	0.49	0.128
$Zn(\phi NH_2)_2Br_2$[d]	9.20	1.60	2.12	0.49	0.125

[a]Obtained in benzene/THF, 11:1 mixture. Numbering system as in Table 1.
[b]Calculated using eq. 1.
[c]H.C.C's of the uncomplexed radical.
[d]Obtained in 1,4-dioxane/THF (10:1).
[e]TU = thiourea.

more likely but the second cannot be entirely ruled out. If the rapidly exchanging free ligand were present only in small concentration it would of course produce only a small modification of the complexed ligand spectra.

(*3*) The observed e.s.r. spectrum arises from at least two paramagnetic species. Such spectra are complex and generally unsymmetrical about the center. In these cases analysis is not feasible. This type of spectrum was observed on the addition of $Zn(\phi NH_2)_2I_2$, $Znpy_2Br_2$, $Znpy_2(SCN)_2$, $Pd(hfac)_2$ (hfac ≡ hexafluoroacetylacetone), $Zn(hfac)_2(H_2O)_2$, and $Pd(tfac)_2$ (tfac ≡ trifluoroacetylacetone). The most likely explanation in these cases is that free and complexed radicals are present and that the rate of exchange is slow on the e.s.r. time scale. Two different environments for complexed ligands (*e.g.*, neutral and cationic complexes) represents another possibility.

(*4*) A single e.s.r. spectrum is observed but some of the lines are preferentially broadened. An example of such a spectrum is shown in Fig. 4*A*. $Zn(acac)_2H_2O$ and $Znpy_2(CNO)_2$ show this effect. A rate process involving the radical is indicated and rapid ligand exchange is the most plausible suggestion. The condition for such broadening is that $\tau(\omega_A - \omega_B) \sim 0.1$ where τ is the average lifetime of the radical in a given environment and $(\omega_A - \omega_B)$ is the difference in frequency of a transition for the environments A and B.

(*5*) If the metal compound to which the spin-labelled ligand is attached is already paramagnetic interaction between the unpaired electron

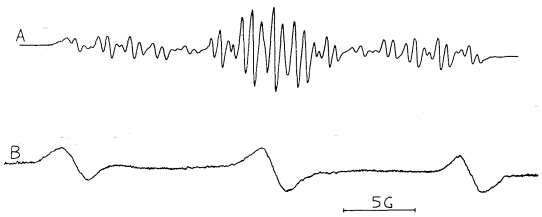

FIG. 4. Electron spin resonance spectra of 4-pyridyl-*t*-butyl nitroxide. (*A*) Complex with $Zn(acac)_2H_2O$. (*B*) Complex with $Ni(hfac)_2$. (a_N = 14 G).

of the ligand and those on the metal must be anticipated. Both changes in the coupling constants and in the electron spin relaxation time can occur. A spectrum obtained by addition of Ni(II)hexafluoroacetylacetonate to the labelled ligand is shown in Fig. 4*B*. Cobalt(II) hexafluoroacetylacetonate gives similar results except that the lines are broader and show signs of additional partly resolved hyperfine coupling.

(*6*) With some very strong Lewis acids such as BF_3 and $AlCl_3$ it appears that catalytic rearrangement of the radical occurs. These rearrangement reactions will be discussed in a subsequent publication.

Discussion

Hyperfine coupling constants and spin densities obtained from the analysis of spectra in the second class in the above summary are shown in Table 2. It is apparent that there are significant changes in the spin density distribution of the radical. Most notably the ^{14}N coupling involving the nitroxide nitrogen has diminished by up to

Can. J. Chem. Downloaded from www.nrcresearchpress.com by 210.87.254.40 on 09/05/12
For personal use only.

TABLE 3. Theoretical spin densities[a] and corresponding hyperfine coupling constants[b] in 4-pyridyl-*t*-butyl nitroxide as a function of the coulomb integral, $\delta(N)_{(Ring)}$, of the pyridine nitrogen atom

λ	δ(N) ring	P_1^{π}	P_2^{π}	P_3^{π}	$P_{4,8}^{\pi}$	$P_{5,7}^{\pi}$	P_6^{π}	a_6^N (theoretical)
1.20	0.50	0.6253	0.2459	−0.0557	0.0890	−0.0388	0.0843	—
1.20	0.60	0.6310	0.2368	−0.0503	0.0842	−0.0337	0.0822	—
1.20	0.70	0.6364	0.2268	−0.0444	0.0793	−0.0284	0.0797	—
1.20	0.80	0.6417	0.2176	−0.0388	0.0744	−0.0230	0.0767	—
1.20	0.90	0.6447	0.2084	−0.0329	0.0695	−0.0174	0.0733	—
1.20	1.00	0.6514	0.1998	−0.0269	0.0645	−0.0117	0.0700	—
1.00	0.50	0.5909	0.2383	−0.0421	0.0925	−0.0313	0.0902	1.15G
1.00	0.70	0.6017	0.2215	−0.0319	0.0838	−0.0217	0.0849	1.23G
1.00	1.00	0.6179	0.1968	−0.0166	0.0707	−0.0073	0.0769	1.34G

[a]McLachlan calculations (ref. 12). Numbering as in Table 1.
[b]Values obtained using eq. 2, (ref. 14).

1.3 G and the ^{14}N coupling of the pyridine nitrogen has increased by up to 0.8 gauss. This behavior may be compared with that observed for metal complexes formed with the nitroxide oxygen (4–6, 11). In these cases the hyperfine coupling with the nitroxide nitrogen has been markedly increased due to enhanced contribution of the valence bond structure **4**. The present

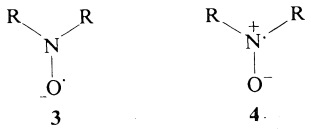

3 **4**

spectra, showing the opposite effect, *i.e.* diminished coupling with the nitroxide nitrogen, clearly arise from complexing with the pyridine nitrogen. As a further check the phenyl *t*-butyl nitroxide radical was prepared and its e.s.r. spectrum examined in the presence and absence of metal compounds. In no case did any of the metal compounds of Table 2 cause any significant change in the e.s.r. spectrum demonstrating that the pyridyl nitrogen is necessary for complex formation. This conclusion has been further confirmed by molecular orbital calculations of the spin density distribution using the McLachlan method (12). The results of these calculations are shown in Table 3. The model used is based on the premise that complex formation removes charge from the pyridine nitrogen thereby increasing its effective coulomb integral but that the remaining parameters are unchanged. Increasing the coulomb integral on the pyridine nitrogen clearly decreases the spin density on the nitroxide nitrogen (ρ_2 in Table 3). The relationship between the nitrogen hyperfine coupling constant and the p_{π} nitrogen spin density has been the subject of some discussion in the literature. Eames and Hoffman (6) have proposed the equation[2]

$$[1] \qquad a_N = Q\rho_N^{\pi} + q$$

where $Q = 16$ G and $q = 7.2$ G. This equation gives $\rho_N^{\pi} \sim 0.5$ for the *t*-butyl nitroxide radical which agrees well with arguments based on proton hyperfine coupling constants in related radicals. Using this formula the nitrogen spin density of the uncomplexed spin-labelled ligand is 0.21 consistent with substantial delocalization to the pyridine ring and in good agreement with the calculated spin densities in Table 3. On complexation the spin density falls by an additional 20–80%. This corresponds to changes of the order 0.5β in the pyridine nitrogen coulomb integral. We can therefore associate the smallest ^{14}N coupling constant with the largest amount of electron withdrawal by the metal ion from the pyridine. This qualitative conclusion is independent of the specific method used to calculate the spin densities and of the specific relationship between the spin densities and the nitrogen hyperfine coupling constant. The differences among the various metal complexes are significant as is apparent from the spectra of Fig. 3. We note particularly the sequence $a_N(HgI_2) = 9.87$ G, $a_N(CdI_2) = 9.38$ G, and $a_N(ZnI_2) = 9.14$ G.

Clearly Zn withdraws electrons more effectively than Cd which in turn is more effective than Hg as would be anticipated from the electronegativities of the elements. The various zinc compounds are presumably solvated by THF under the conditions employed. Replacement of THF by thiourea apparently decreases the

[2]A more sophisticated relationship was later suggested by Cohen and Hoffman (22).

Can. J. Chem. Downloaded from www.nrcresearchpress.com by 210.87.254.40 on 09/05/12
For personal use only.

Can. J. Chem. Downloaded from www.nrcresearchpress.com by 210.87.254.40 on 09/05/12
For personal use only.

electron affinity of the zinc as might be anticipated on the basis that a Zn—S bond is likely to be more covalent than a Zn—O bond. The sequence of the a_N's for the zinc halides Cl > Br > I is the opposite to what might have been expected on the basis of the electronegativity of the halogens. However anomalous orders for the halogens have also been observed in n.m.r. studies of the electron withdrawing abilities of complexed metal ions (13) and it is apparent that simple considerations of electronegativities do not always suffice to account for charge density distributions in complexes. These results indicate that the Pd compound has a very small $a_{N_0}{}^N$ and hence a large metal electron affinity. We must assume planar Pd coordination since the metal salt is diamagnetic and this should perhaps not be compared with the tetrahedral zinc compounds. The spin density distribution within the pyridyl ring differs somewhat from that of the other complexes most notably in the high value for the pyridyl nitrogen coupling. It is possible that metal–ligand π bonding is important for a square planar complex in which case a calculation simply changing the coulomb integral of the nitrogen would be inappropriate. It is apparent that with the present small number of compounds examined extensive discussion of trends in the charge distributions is inappropriate and that these results merely serve to illustrate the potentialities of the method.

We have also noted changes in the pyridine nitrogen hyperfine coupling constants. The interpretation here is a little more complicated since such coupling constants depend on the spin densities on both the nitrogen and the adjacent carbon atoms. Henning (14) has studied a number of nitrogen containing aromatic radicals and proposed the equation

$$[2] \qquad a_N = Q_1\rho_N{}^\pi + Q_2\,(\rho_{C_1}{}^\pi + \rho_{C_2}{}^\pi)$$

where C_1 and C_2 refer to the adjacent carbon atoms and $Q_1 = 19.1 \pm 1.7$ G and $Q_2 = 9.1 \pm 1.7$ G. Experimentally a_N changes from 1.26 G in the uncomplexed radical to 1.5–2.0 G in the complexes. The spin density calculations in Table 3 show that both ρ_N and ρ_C of the adjacent carbons decrease with increasing nitrogen coulomb integral. The carbon spin densities are however negative so that the net result is that the calculated a_N increases from 0.904 G to 1.124 G for an increase of 0.5β in the nitrogen coulomb integral, *i.e.* a change of approximately 20%. The absolute calculated values of a_N are somewhat low but from the experimental increase on complexation of approximately 25–75% we would again deduce an increase in the nitrogen coulomb integral of better than 0.5β. Thus the changes in the pyridine nitrogen coupling are entirely consistent with those of the nitroxide nitrogen. The nitroxide nitrogen however obviously provides a more sensitive probe of the charge withdrawing properties of the metal ion.

Finally we note the line broadening effects illustrated in Fig. 4*A*. These are attributed to rapid exchange between free and complexed ligand. Line broadening due to rate processes has been extensively discussed in the e.s.r. literature (15) and has been used to study cases of restricted rotation, electron transfer, proton transfer, and fluxional ion pairing. In the present case the central set of lines arising from transitions for which m_1 for the nitroxide nitrogen is zero is much less broadened than the outer sets of lines for which $m_1 = \pm 1$. This effect is clearly shown in Fig. 4*A*. A modulation of the nitroxide nitrogen hyperfine coupling by the exchange process is implied. Since free and complexed ligands have substantially different coupling constants ligand exchange is indicated. It is necessary that the complexed ligand should have a lifetime such that $\tau(\omega_A - \omega_B) \sim 1$ implying lifetimes of 10^{-6}–10^{-7} s. The correctness of this interpretation is further confirmed by the observation that broadened spectra similar to that shown in Fig. 4*A* can be obtained by adding small amounts of water or DMSO to solutions of the nitroxide radical complexed to zinc chloride. In this case the exchange is between complexed ligand and the added coordinating solvent. There is precedence for the observation of extremely fast ligand exchange for pyridine ligands. Thus Corden and Rieger (16) have studied the broadening of the e.s.r. spectra of Cu(II)bis(di-*n*-butyldithiocarbamate) on the addition of amines and Farmer *et al.* (17) have reported a study of a similar process using Cu(II)bis(*t*-diethyldithiocarbamate). Both groups interpret their results using a theory derived from the modified Bloch equations leading to line widths given by an equation of the type

$$T_2{}^{-1} = T_{20}{}^{-1} + P_A{}^2 P_B \tau_B (\omega_A - \omega_B)^2$$

and arrive at values for τ_B, the lifetime of complexed ligand, of the order of 10^{-9} s. In the present case we report the inverse of these experiments, *i.e.* the exchange is between a paramagnetic ligand and a diamagnetic metal rather than

between a diamagnetic ligand and a paramagnetic metal. An implication of this model is that the smaller hyperfine coupling constants of the exchanging spectra should be intermediate between those of the free and complexed ligand. Analysis of the central multiplet of spectrum 4*A* shows that this is true.

Conclusion

The intention of the present study was to investigate the potential utility of spin-labelled ligands in inorganic chemistry. Two of the areas uncovered seem to show promise. It has been demonstrated that the hyperfine coupling constants of a complexed radical are sensitive to the Lewis acid involved and that they may be used as a measure of the strength of this Lewis acid. A rather direct interpretation in terms of the change in effective coulomb integral of the donor atom is possible. Further, this can be done using ligands only slightly perturbed, from those commonly occurring in a large variety of metal complexes. The observation with the Pd complex suggests that more detailed studies of metal–ligand bonding, *e.g.*, evaluations of the importance of π bonding, may be possible. Secondly, a method for the study of very fast ligand exchange reactions is suggested. Such studies need not be confined to paramagnetic metals as is the case with previous e.s.r. work or to simple ligands in aqueous solution suitable for temperature jump or ultrasonic relaxation techniques. Potentially the spin-labelled ligand approach has also a number of practical advantages in the form of sharper lines, the absence of quadrupolar broadening and of effects due to anisotropy in the **g** tensors. It should be possible in favorable conditions to measure rapid ligand exchange rates leading to lifetimes as short as 10^{-8} s.

Experimental

Electron spin resonance spectra were obtained with a JEOLCO-JES-3BS-X spectrometer operating at 9400 MHz (X band). All experiments were carried out at room temperature. Samples were deoxygenated before spectra were obtained using standard vacuum techniques. The field calibration was performed by recording simultaneously the e.s.r. spectrum of the sample and that of a dilute aqueous solution of peroxylamine disulfonate the coupling constant of which has been given by Windle and Wiersama (18).

Preparation of 4-Pyridyl-t-butyl Nitroxide (19, 20)

Commercially available 4-nitropyridine-1-oxide was first purified by recrystallization from acetone. To 1 g of pure 4-nitropyridine-1-oxide (m.p. 159 °C) suspended in 15 ml of ice cold chloroform, 1.9 ml of PCl_3 were added and the mixture heated for 1 h at 70–80 °C. After cooling the resulting solution was diluted with water, made alkaline with NaOH, and the 4-nitropyridine extracted with chloroform. The chloroform solution was dried over anhydrous Na_2SO_4 and evaporated to dryness. The residue was recrystallized from petroleum ether to give 4-nitropyridine as pale yellow crystals (m.p. 48 °C). To a solution of 1.24 g of this product in 100 ml of dry ether was added a freshly prepared ethereal solution containing 0.03 mol of *t*-butyl magnesium chloride. After neutralization with ammonium chloride the radical was extracted with ether and dried over Na_2SO_4. The ethereal solution was concentrated under vacuum and the product stored over Na_2SO_4.

We are indebted to the National Research Council of Canada for financial support of this research.

1. O. H. Griffith and A. S. Waggoner. Acc. Chem. Res. **2**, 17 (1969).
2. (*a*) D. R. Eaton. Inorg. Chem. **3**, 1268 (1964); (*b*) G. A. Abakumov, G. A. Razuvaev, and E. S. Klimov. Dokl. Akad. Nauk. S.S.S.R. **201**, 624 (1971).
3. W. Beck, K. Schmidtner, and H. J. Keller. Chem. Ber. **100**, 503, 3363 (1967).
4. G. A. Abakumov, V. D. Tikhonov, and G. A. Razuvaev. Dokl. Akad. Nauk. S.S.S.R. **187**, 571 (1969).
5. G. A. Razuvaev, V. D. Tikhonov, and G. A. Abakumov. Bull. Akad. Nauk. S.S.S.R. Chem. 1634 (1970).
6. T. B. Eames and B. M. Hoffman. J. Am. Chem. Soc. **93**, 3141 (1971).
7. S. I. Weissman and I. M. Brown. J. Am. Chem. Soc. **85**, 2528 (1963).
8. G. N. Schrauzer. Acc. Chem. Res. **2**, 72 (1969).
9. G. A. Russell. Semidione radical anions. *Edited by* E. T. Kaiser and L. Kevan. Interscience, New York. 1968. p. 87.
10. H. Lemaire, Y. Marechal, R. Ramassenl, and A. Rassat. Bull. Soc. Chim. 372 (1965).
11. B. M. Hoffman and T. B. Eames. J. Am. Chem. Soc. **91**, 5168 (1969).
12. A. D. McLachlan. Mol. Phys. **3**, 233 (1960).
13. W. J. Louch and D. R. Eaton. To be published.
14. J. C. M. Henning. J. Chem. Phys. **44**, 2139 (1966).
15. P. D. Sullivan and J. R. Bolton. Adv. Magn. Reson. **4**, 39 (1970).
16. B. J. Corden and P. H. Rieger. Inorg. Chem. **10**, 263 (1971).
17. J. B. Farmer, F. G. Herring, and R. L. Tapping. Can. J.Chem. **50**, 2079 (1972).
18. J. J. Windle and A. K. Wiersama. J. Chem. Phys. **39**, 1139 (1963).
19. L. F. Fieser and M. Fieser. Reagents for organic synthesis, p. 876, John Wiley, New York. 1967. p. 876.
20. M. S. Kharasch and O. Reinmuth. Grignard reactions of non-metallic substances. Prentice Hall, New York, 1954. p. 26.
21. R. E. Wagner, J. N. Helbert, R. D. Bates, and E. H. Poindexter. Chem. Commun. 748 (1973).
22. A. H. Cohen and B. M. Hoffman. J. Am. Chem. Soc. **95**, 2061 (1973).

Can. J. Chem. Downloaded from www.nrcresearchpress.com by 210.87.254.40 on 09/05/12
For personal use only.

Lewis Acid Catalyzed Rearrangements of Nitroxide Radicals

C. T. Cazianis and D. R. Eaton

Department of Chemistry, McMaster University, Hamilton, Ontario L8S 4M1

Received November 14, 1973

C. T. Cazianis and D. R. Eaton. Can. J. Chem. **52,** 2463 (1974).

The interaction of nitroxide radicals with the Lewis acids, aluminum chloride and boron trifluoride has been investigated using e.s.r. and n.m.r. techniques. Three types of reaction have been demonstrated. Initially a paramagnetic complex with the nitroxide group is formed. This can then dimerize or polymerize to a diamagnetic complex. Concurrently rearrangement of *t*-butyl groups to *s*-butyl groups can occur giving a further series of radicals and complexes. The rearrangements are analogous to the well known carbonium ion rearrangements induced by Lewis acid catalysts. Relative equilibrium constants and rates for the various reactions are discussed in a qualitative manner.

C. T. Cazianis et D. R. Eaton. Can. J. Chem. **52,** 2463 (1974).

On a examiné, utilisant les techniques de la r.p.e. et de la r.m.n. les interactions entre les radicaux nitroxydes et des acides de Lewis tels que le chlorure d'aluminium et le trifluorure de bore. On a mis en évidence trois types de réactions. Au début un complexe paramagnétique se forme avec le groupe nitroxyde. Celui-ci peut alors se dimériser ou se polymériser pour former un complexe diamagnétique. Concurremment des réarrangements des groupes *tertio*-butyles en groupes butyles secondaires peuvent se produire donnant naissance à une nouvelle série de radicaux et de complexes. Les réarrangements sont semblables à ceux, bien connus, que subissent les carbocations sous l'influence de catalyseurs acide de Lewis. On discute, d'une façon qualitative, des constantes d'équilibre et des vitesses relatives des diverses réactions.

[Traduit par le journal]

Can. J. Chem. Downloaded from www.nrcresearchpress.com by 178.218.224.3 on 09/06/12
For personal use only.

Introduction

In a previous paper (1) we reported the synthesis and use of certain radicals as spin labelled ligands. In particular, interactions of a molecule in which a pyridine moiety acted as the Lewis base and a *t*-butyl nitroxide group provided the spin label were studied with a variety of metal compounds. In the large majority of cases the resulting e.s.r. spectrum could be interpreted in terms of complexing of the pyridine nitrogen with the metal. In the case of the strong Lewis acids $AlCl_3$ and BF_3 we obtained e.s.r. spectra which could not be readily interpreted along these lines. It seemed possible that with strong Lewis acids interaction with the oxygen of the nitroxide group was occurring. Electron spin resonance studies of such complexes have indeed been reported (2–4) but their relevance to the interpretation of the spectra mentioned above was not clear. We have therefore further investigated the reactions of several nitroxide radicals with strong Lewis acids. In the course of these studies it became apparent that some of the e.s.r. spectra observed did not arise from the nitroxide radical introduced into the system. The present paper therefore presents evidence for Lewis acid catalyzed rearrangements of nitroxide radicals.

Results

The radical initially used in these studies has the structure **1**

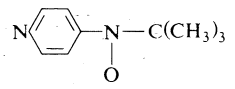

1

In the presence of $AlCl_3$ an e.s.r. spectrum consisting of 14 broad lines is obtained. In the presence of BF_3 the spectrum is essentially similar except that an additional quartet splitting with intensity ratios 1:3:3:1 is observed. This can be reasonably assigned to the fluorine atoms. This latter spectrum is shown in Fig. 1 and the former in Fig. 5*A*. These spectra are anomalous in two respects: (*a*) we were unable to find a reasonable combination of coupling constants which, allowing for overlapping lines, would reproduce the observed spectrum. The basic problem is that radical **1** should give a spectrum with an odd number of lines whereas the observed spectra clearly have an even number of lines; (*b*) the e.s.r. spectra are much weaker than those obtained with other metal complexes and the spectrum decays with time. Other complexes seem quite stable. In order to clarify these results the

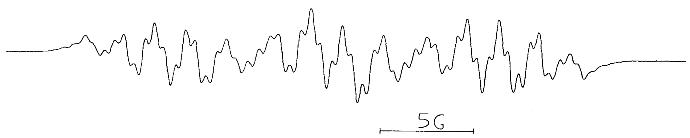

FIG. 1. Electron spin resonance spectrum of 4-pyridyl-*t*-butyl nitroxide radical in 1,4-dioxane/THF mixture in the presence of excess $(C_2H_5)_2OBF_3$.

spectrum of the simpler radical **2** was investigated in the presence of BF_3 and $AlCl_3$. In this case only complexing with the oxygen of the nitroxide group is possible

$(CH_3)_3$ C—N—C $(CH_3)_3$
|
O

2

The e.s.r. spectrum comprises a simple triplet which is shown in Fig. 2*A*. Eames and Hoffman (4) have described the preparation of complexes of this radical with BF_3 using a technique of distilling excess BF_3 into a solution of the radical in toluene. In order to duplicate the conditions used to obtain the spectrum of Fig. 1 a rather different approach was adopted. Initially a solution of the diethyl ether addition compound of boron trifluoride in 1,4-dioxane was added incrementally to a solution of radical **2** in the same solvent. It was observed that the e.s.r. spectrum of radical **2** decreased in intensity with the addition of BF_3 but that a new weaker spectrum appeared. This second spectrum consists of three triplets and is shown in Fig. 2*B*. With a large excess of BF_3 this latter spectrum also disappeared. The original spectrum with approximately its original intensity can be regenerated by adding triethylamine to the final solution. Presumably triethylamine, a strong base, preferentially complexes with the BF_3 and restores the *status quo*. The rate of reaction of di-*t*-butyl nitroxide with BF_3 appears to be relatively slow since the intensity of the e.s.r. signal

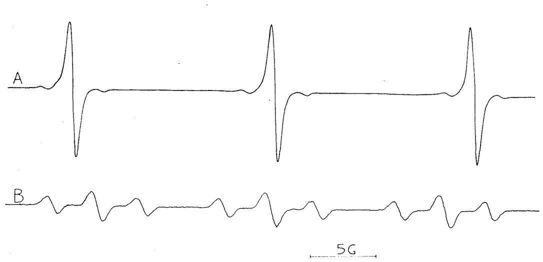

FIG. 2. (*A*) Electron spin resonance spectrum of di-*t*-butyl nitroxide radical in 1,4-dioxane. (*B*) Electron spin resonance spectrum obtained by adding excess $(C_2H_5)_2OBF_3$ to di-*t*-butyl nitroxide in 1,4-dioxane.

continues to fall for some time after an aliquot of the BF_3/ether solution is added. In the experiments in which triethylamine was added to the solution with excess BF_3 no regeneration of the second e.s.r. spectra was observed but since radical **2** is much more intense than the second spectrum the latter may still be present. It seemed likely that the solution with excess BF_3 was diamagnetic. This was confirmed by measuring the magnetic susceptibility using the n.m.r. method. The susceptibility falls from ~1.45 B.M. to zero on adding BF_3/ether solution. As expected this solution also gave a sharp line n.m.r. spectrum shown in Fig. 3*A*. This proton spectrum shows the CH_2 and CH_3 groups of the diethyl ether and an additional intense peak assigned to the *t*-butyl protons originating from radical **2**. A number of weaker peaks in the methyl region are also apparent indicating that a mixture of diamagnetic species is probably formed. The ether chemical shifts have reverted from their positions in the BF_3/ether complex (Fig. 3*B*) towards the positions found for free ether (Fig. 3*C*) confirming that the reaction proceeds by displacement of the ether of the BF_3/ether complex.

Similar experiments were carried out with $AlCl_3$. In this case it proved more convenient to use tetrahydrofuran as a solvent. The e.s.r. results were exactly analogous to those with BF_3 including the observation of the spectrum of Fig. 2*B*. However some further information resulted from an attempt to examine the e.s.r. spectra in CCl_4. An excess of $AlCl_3$ was added to a solution of the radical in CCl_4. A yellow precipitate appeared immediately. After decanting the CCl_4 this precipitate was found to be soluble in benzene. On standing the solution separated into two layers the upper layer being yellow in color and the lower layer deep red. The yellow solution was found to be diamagnetic but the red solution gave the e.s.r. spectrum shown in Fig. 4. This spectrum has 18 lines of equal intensity and can be readily analyzed on the basis of a ^{14}N hyperfine coupling constant of 20.1 G and a $^{27}Al(I = 5/2)$ hyperfine coupling constant of 11.5 G. It is

Can. J. Chem. Downloaded from www.nrcresearchpress.com by 178.218.224.3 on 09/06/12
For personal use only.

Can. J. Chem. Downloaded from www.nrcresearchpress.com by 178.218.224.3 on 09/06/12
For personal use only.

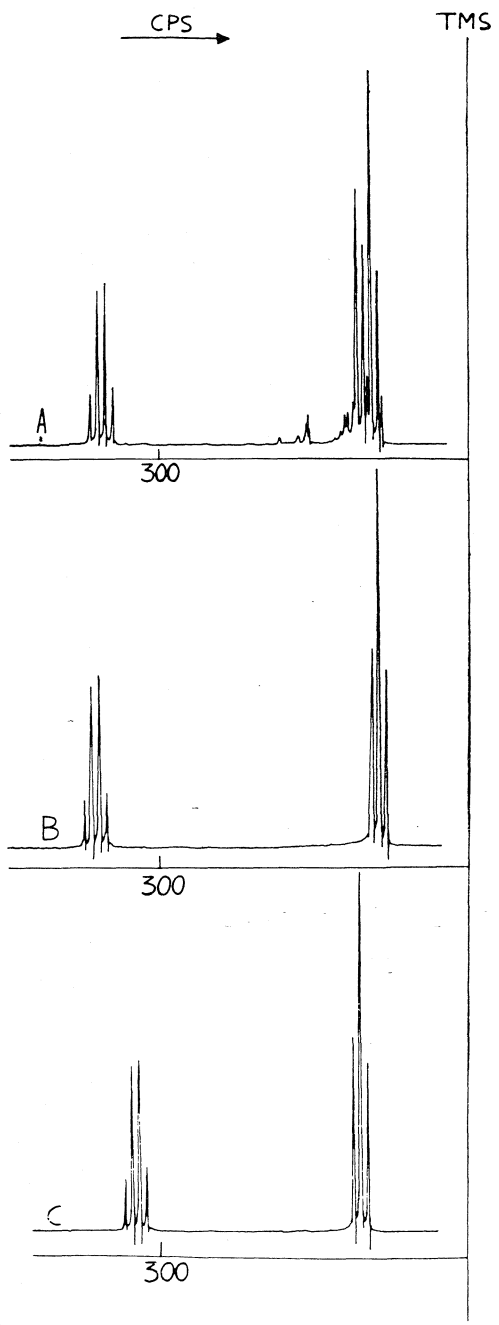

FIG. 3. 100 MHz n.m.r. spectra of benzene solutions containing (*A*) di-*t*-butyl nitroxide and excess $(C_2H_5)_2OBF_3$; (*B*) $(C_2H_5)_2OBF_3$; (*C*) $(C_2H_5)_2O$.

in fact the spectrum of the $AlCl_3$ complex reported by Eames and Hoffman (4). The significant observation is that reaction with $AlCl_3$ leads to two products only one of which is paramagnetic. It is reasonable to assume the formation of a complex between the Lewis acid and the free radical is the initial reaction and that rapid precipitation from CCl_4 has enabled us to isolate this intermediate. The $AlCl_3$ complex has only limited stability in benzene since the spectrum disappears in 45–60 min.

There remains the question of the assignment of the spectra shown in Figs. 1 and 2*B*. The possibilities in the second case are quite limited. It is obviously a nitroxide radical showing hyperfine coupling with the nitrogen and two additional nuclei of spin 1/2. The latter can only be protons. Protonation of di-*t*-butyl nitroxide has been reported (5). The proton is located on the oxygen atom and gives rise to a hyperfine coupling of 3.3 G. However this would only account for coupling with one proton and it is accompanied by a large increase in the ^{14}N coupling constant. We observe coupling with two protons and a decrease in the ^{14}N coupling. Coupling to protons on the carbon adjacent to the nitrogen is therefore suggested. The observed couplings to a CH_2R group in this position vary from 8–10 G (6) whereas those for CHR_2 groups are in the range 3–4 G (6). A value of 3.6 G is found in this case. These arguments suggest the di-*s*-butyl nitroxide radical **3**.

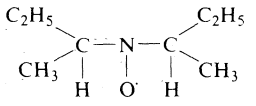

3

The e.s.r. spectrum of this radical has been reported in the literature (7). The reported coupling constants $a_N = 13.4$ G and $a_H = 3.8$ G (obtained in benzene) agree satisfactorily with those found in the present experiments, $a_N = 13.2$ G and $a_H = 3.62$ G (obtained in dioxane). No other assignment of the radical seems plausible.

By analogy the spectra obtained with the pyridine nitroxide radical **1** might be expected to be derived from **4**.

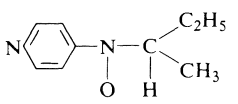

4

This radical has not been reported previously and it was therefore synthesized by the reaction of γ-nitropyridine with *s*-butyl magnesium chloride. It was obtained only in low yield and the in-

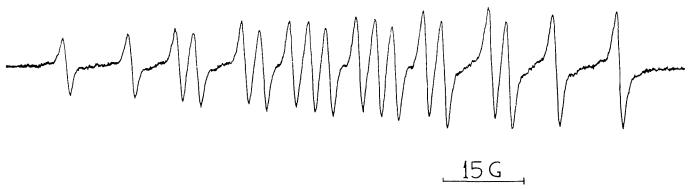

FIG. 4. Electron spin resonance spectrum of di-*t*-butyl nitroxide $AlCl_3$ complex in benzene.

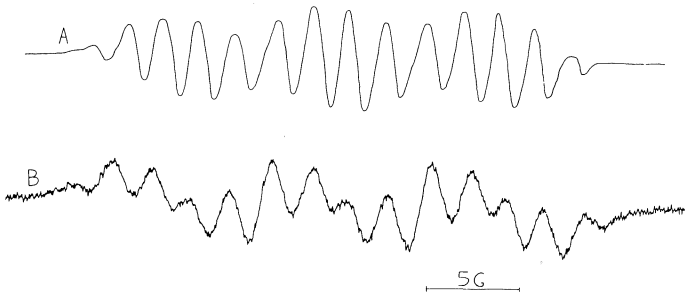

FIG. 5. (*A*) Electron spin resonance spectrum of 4-pyridyl-*t*-butyl nitroxide in the presence of excess $AlCl_3$ in 1,4-dioxane. (*B*) Electron spin resonance spectrum of 4-pyridyl-*s*-butyl nitroxide in the presence of $ZnCl_2$ in 1,4-dioxane.

completely resolved spectrum cannot be analyzed in detail. The nitrogen coupling constant of 9.4 G can however be readily picked out and assigned to the nitroxide group. Some difficulty was experienced obtaining reasonable spectra of this radical in the presence of metal compounds since the initial radical spectrum is relatively weak. A fairly well resolved spectrum was however obtained with zinc chloride. This spectrum proved to be virtually identical to that obtained initially with radical **1** and $AlCl_3$. The two are shown together in Fig. 5. In both cases the nitrogen hyperfine coupling constant has been reduced to 8.3 G as expected for metal complexing on the pyridine nitrogen. We therefore assign spectrum 5*A* to

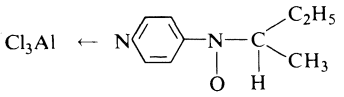

and spectrum 1 to the analogous BF_3 adduct with some confidence. Both spectra can be reasonably analyzed on this basis since an even number of lines is predicted. The coupling constants obtained from the various spectra discussed in this section are gathered together in Table 1.

Discussion

It is apparent that strong Lewis acids can interact with nitroxide radicals in several ways. The present studies provide evidence for three different reactions namely: (*1*) the formation of paramagnetic adducts of the type reported by Eames and Hoffman (4); (*2*) the formation of diamagnetic adducts presumably involving dimers or polymers of the radical;[1] (*3*) rearrangement of the alkyl groups to give different radicals.

The third type of reaction is established by the identification of e.s.r. spectra arising from radicals containing *s*-butyl groups. We considered the possibility that such radicals might have been present as impurities in the original *t*-butyl radicals. Samples of di-*t*-butyl nitroxide were examined very carefully to check this possibility. Several of the lines of the *s*-butyl radical occur in positions well away from the e.s.r. lines of the *t*-butyl radical. No signs of absorption at these frequencies could be observed. In the spectra used the ^{15}N satellites of di-*t*-butyl nitroxide were observed with a signal-to-noise ratio better than 10:1. ^{15}N has a spin of 1/2 and an isotopic abundance of 0.365%. Each line therefore corresponds to an abundance of 0.18%. We deduce therefore

[1]It has been reported that 2,2,6,6-tetramethylpiperidine nitroxide can be oxidized to give a diamagnetic compound $[TMPN^+{\equiv}O]_2SnX_6^{2-}$ by reaction with Sn(IV) halides (14). Since neither BF_3 nor $AlCl_3$ is an oxidizing agent an analogous explanation of the diamagnetism observed in the present reactions seems unlikely.

Can. J. Chem. Downloaded from www.nrcresearchpress.com by 178.218.224.3 on 09/06/12
For personal use only.

Can. J. Chem. Downloaded from www.nrcresearchpress.com by 178.218.224.3 on 09/06/12
For personal use only.

TABLE 1. Radicals produced by the reaction of nitroxides with $AlCl_3$ and BF_3 in 1,4-dioxane

Original radical + MX_3	Radical product	Hyperfine coupling constants (G) a_{NO}^{N}	a_{CH}^{H}	a^{Al}
$(t\text{-Bu})_2NO^{\cdot}$ + BF_3	$(s\text{-Bu})_2NO^{\cdot}$	13.2	3.62	—
$(t\text{-Bu})_2NO^{\cdot}$ + $AlCl_3$	$(s\text{-Bu})_2NO^{\cdot}$	13.2	3.62	—
$(t\text{-Bu})_2NO^{\cdot}$ + $AlCl_3$	$(t\text{-Bu})_2N\dot{O} \rightarrow AlCl_3$*	20.1	—	11.5
$(s\text{-Bu})_2NO^{\cdot}$ + —	—	13.39†	3.84†	—
$(t\text{-Bu})_2NO^{\cdot}$ + —	—	15.2	—	—

Original radical + Lewis acid	Radical product	Hyperfine coupling constants (G)‡ a_2^{N}	a_6^{N}	$a_{4,8}^{H}$	$a_{5,7}^{H}$	a_{CH}^{H}	a^{Al}	a^{B}	a^{F}
(Py)—N(O·)—(*t*-Bu) + $AlCl_3$	$Cl_3Al \leftarrow$ 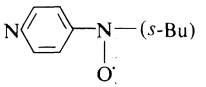	8.3	~2	~2	Not observed	~2	Not observed	—	—
(Py)—N(O·)—(*t*-Bu) + BF_3	$F_3B \leftarrow$ 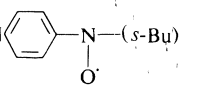	8.3	~2	~2	Not observed	~2	—	Not observed	~0.5
(Py)—N(O·)—(*s*-Bu) + $ZnCl_2$	$Cl_2Zn \leftarrow$ 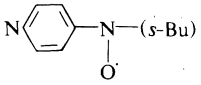	8.5	~2	~2	Not observed	~2	—	—	—
(Py)—N(O·)—(*s*-Bu) + —	—	9.4		Not resolved					

*In benzene.
†Reference 7.

‡Numbering system 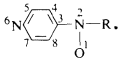 .

Can. J. Chem. Downloaded from www.nrcresearchpress.com by 178.218.224.3 on 09/06/12
For personal use only.

that any *s*-butyl impurity is present in a concentration of less than 0.03%. This is insufficient to account for the observed spectra.

It is reasonable that the initial reaction in each case is formation of an adduct with the Lewis acid, *e.g.*

$$R_2NO + AlCl_3 \rightarrow R_2NO \rightarrow AlCl_3$$

Abakumov *et al.* (2) suggested that such adducts involved π bonding to the N—O bond but Hoffman and Eames (3, 4) and other authors (8) prefer a σ donor bond. The latter seems more reasonable. The electronic structure of such adducts can be discussed either in terms of valence bond or molecular orbital theory. In the former terms the radical has two principal contributing structures:

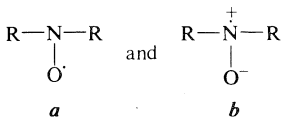

a *b*

Complexation with a Lewis acid greatly increases the contribution of **b**. This is manifested by a large increase in the ^{14}N hyperfine coupling constant, *e.g.*, from 15.2 to 20.1 G in the case of the aluminum chloride adduct with di-*t*-butyl nitroxide. In molecular orbital terms the effect of complexation may be represented by an increase in the coulomb integral of the oxygen and a Hückel calculation reproduces the increase in the N spin density quite satisfactorily. Eames and Hoffman (4) have considered the molecular orbital diagram in more detail and have calculated N spin densities from the equation

$$[1] \qquad a_N = Q\rho_N^{\pi} + q$$

where $Q = 16.0$ G and $q = 7.2$ G. We wish to suggest that the increased polarity of the N—O bond provides a rationale for the subsequent reactions.

A possible reaction to give a diamagnetic species is

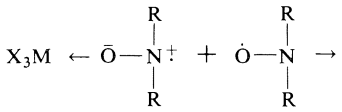

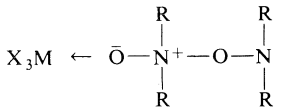

The Lewis acid must be involved in the diamagnetic complex since the n.m.r. experiments show that ether is no longer bound to BF_3. More than one radical could be complexed to $AlCl_3$ but not to BF_3. The n.m.r. shows a single intense peak for the *t*-butyl group but this observation does not necessarily have structural significance since there may be exchange processes operative which are fast on the n.m.r. time scale. The weaker peaks could arise from higher polymers. Since nitroxide radicals show little or no tendency to dimerize in the absence of Lewis acids it seems reasonable to attribute the process to the enhanced dipole of the N—O bond which results from complexation.

Rearrangements of alkyl groups catalyzed by strong Lewis acids are well known. They frequently occur for example during the alkylation of benzene using the Friedel Crafts reaction with $AlCl_3$ as a catalyst. Perhaps the most pertinent report is that of Roberts *et al.* (9) who observed the isotope position rearrangement of *t*-butyl chloride on treatment with $AlCl_3$. They proposed a carbonium ion mechanism with the secondary butyl carbonium ion acting as an intermediate, *i.e.*

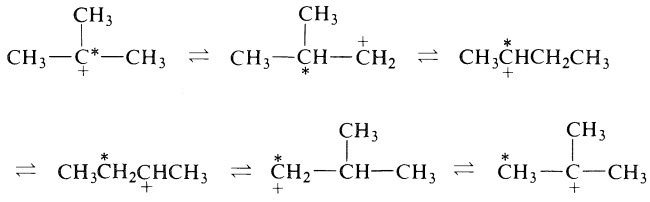

The existence of carbonium ions in solutions of alkyl halides with $AlCl_3$ or BF_3 seems to be uncertain. Thus Olah and Olah (10) referring to studies with *t*-butyl chloride comment on the basis of n.m.r. evidence that the shifts "could be attributed only to weak-donor–acceptor complexes and not to carbonium ions." Alkyl fluorides and very strong Lewis acids such as SbF_5 unambiguously produce carbonium ions and the rearrangements of these ions have been directly

Can. J. Chem. Downloaded from www.nrcresearchpress.com by 178.218.224.3 on 09/06/12
For personal use only.

studied by n.m.r. (11). In any event whether $AlCl_3$ produces discrete carbonium ions or not it seems clear that its key function in catalyzing alkyl rearrangements is to withdraw charge from the carbon atom.

In the present case the e.s.r. data clearly show that complexation with $AlCl_3$ withdraws a substantial amount of charge from the nitrogen. The change in spin density calculated from eq. 1 suggests that this withdrawal amounts to approximately 1/3 of an electron. This effect will certainly be reflected in a more positive charge on the adjacent carbon. Rearrangement of the alkyl group can then proceed in a manner exactly analogous to that suggested by Roberts *et al.* (9) for *t*-butyl chloride except that only the first two steps are necessary. The present results do not provide any further evidence as to whether there is any carbonium ion intermediate. Any mechanism which suffices to explain the $AlCl_3$ catalyzed rearrangement of alkyl halides will suffice to explain the present rearrangement.

We therefore postulate the following reaction scheme to describe the interactions of Lewis acids with nitroxide radicals.

$$\begin{array}{ccccc} R_2NO + MX_3 & \overset{1}{\rightleftharpoons} & R_2NOMX_3 & \overset{2}{\rightleftharpoons} & (R_2NO)_{2n}(MX_3)_m \\ & & \Big\Updownarrow 5 & & \\ R_2'NO + MX_3 & \overset{3}{\rightleftharpoons} & R_2'NOMX_3 & \overset{4}{\rightleftharpoons} & (R_2'NO)_{2n}(MX_3)_m \end{array}$$

The species observed depend on the equilibrium constants for these various reactions and the rates at which equilibrium is attained. The observations are consistent with the equilibrium constant for complex formation (reaction 1) being smaller in polar solvents such as dioxane than in nonpolar solvents such as benzene or toluene. The dependence of this equilibrium constant on solvent is demonstrated by the observation that the addition of DMSO to a diamagnetic di-*t*-butyl nitroxide/$AlCl_3$ solution in benzene leads to the regeneration of the di-*t*-butyl nitroxide e.s.r. spectrum. It also appears that reactions 1, 3, and 5 are fast but 2 and 4 are relatively slow and solvent dependent. Thus in 1,4-dioxane the dimerization reaction is fairly fast and this factor, combined with the smaller equilibrium constant for complex formation, does not allow sufficient buildup of the intermediate paramagnetic complex to permit observation by e.s.r. In the less polar solvents the equilibrium is more favorable and dimerization is apparently much slower so that e.s.r. spectra of complexed radicals are observed although they decay slowly with time. The same considerations apply to the isomeric *s*-butyl compounds. The latter differ however in the important respect that the overall equilibrium of reactions 3 and 4 is significantly further to the left than that of reactions 1 and 2. Thus under conditions in which sufficient $AlCl_3$ has been added to convert di-*t*-butyl nitroxide completely to the diamagnetic dimer there is still sufficient di-*s*-butyl nitroxide present to give a reasonably intense e.s.r. spectrum. It is this latter factor which allows the isomerization to be observed in spite of the fact that the equilibrium concentration of the *s*-butyl-isomer is considerably less than that of the *t*-butyl isomer. We also infer that the isomer with one *t*-butyl and one *s*-butyl group has equilibrium constants similar to those of the di-*t*-butyl compound and is not observed for this reason.

Finally we turn to the original observations involving the pyridyl radical **1**. The considerations here are similar but with the additional complication that complexing to the pyridine nitrogen can also occur. Apparently the addition to radical **1** of sufficient $AlCl_3$ or BF_3 to form the pyridine complex also suffices to completely dimerize the compound. The e.s.r. spectrum of the expected complex was therefore not observed. However a smaller amount of the *s*-butyl isomer has been formed by rearrangement, this is less susceptible to dimerization, and sufficient free radical is present to form a pyridyl complex. It is interesting to note that the e.s.r. characteristics of the radicals obtained by interaction of the Lewis acid with the pyridine nitrogen mirror those of complexes involving the nitroxide group. Thus with the BF_3 pyridine complex the coupling constant of the nitroxide nitrogen is reduced, ^{19}F coupling is observed but no ^{11}B coupling occurs. For the nitroxide complex the ^{14}N coupling is enhanced, ^{11}B coupling is quite large but ^{19}F coupling is absent. Assignment of the Lewis base site is therefore unambiguous.

Experimental

The preparation of radical **1** has been described previously (1). Di-*t*-butyl nitroxide was obtained by a standard method (12) and purified by distillation (b.p. 52–54°C at 11 mm Hg pressure). Radical samples were degassed on a vacuum line before measuring the e.s.r. spectra. Aluminum trichloride was purchased from Baker and Adamson and boron trifluoride etherate from Matheson Coleman and Bell. Electron spin resonance spectra were obtained using a JEOL spectrometer operating at 9K MHz. It

proved convenient to use di-*t*-butyl nitroxide as a calibration standard based on the line separations given by Faber *et al.* (13).

We are indebted to Dr. J. J. McCullough for the preparation of the di-*t*-butyl nitroxide, to Dr. J. Warkentin for helpful discussions of rearrangement reactions, and to the National Research Council of Canada for financial support of this research.

1. C. T. CAZIANIS and D. R. EATON. Can. J. Chem. This issue.
2. (*a*) G. A. ABAKUMOV, V. D. TIKHONOV, and G. A. RAZUVAEV. Dokl. Chem. **187**, 561 (1969). (*b*) G. A. RAZUVAEV, V. D. TIKHONOV, and G. A. ABAKUMOV. Bull. Akad. Nauk. S.S.S.R. Chem. 1634 (1970).
3. B. M. HOFFMAN and T. B. EAMES. J. Am. Chem. Soc. **91**, 5168 (1969).
4. T. B. EAMES and B. M. HOFFMAN. J. Am. Chem. Soc. **93**, 3141 (1971).
5. B. M. HOFFMAN and T. B. EAMES. J. Am. Chem. Soc. **91**, 2169 (1969).
6. B. H. J. BIELSKI and J. M. GEBICKI. Atlas of electron spin resonance spectra. Academic Press, New York. 1967. pp. 380–404.
7. J. C. BAIRD. J. Chem. Phys. **37**, 1879 (1962).
8. R. A. ZELONKA and M. C. BAIRD. J. Am. Chem. Soc. **93**, 6066 (1971).
9. J. D. ROBERTS, R. E. MCMAHON, and J. S. HINE. J. Am. Chem. Soc. **72**, 4237 (1950).
10. G. A. OLAH and J. A. OLAH. Carbonium ions, Vol. 2. *Edited by* G. A. Olah and R. Schleyer. Interscience, New York. 1970. p. 720.
11. M. SAUNDERS and E. L. HAGEN. J. Am. Chem. Soc. **90**, 2436 (1968).
12. A. K. HOFFMAN, A. M. FELDMAN, E. GELBLUM, and W. G. HODGSON. J. Am. Chem. Soc. **86**, 639 (1964).
13. J. FABER, W. MARKLEY, and J. A. WEIL. J. Chem. Phys. **46**, 1652 (1967).
14. Y. TAKAYA, G. MATSUBAYSHI, and T. TANAKA. Inorg. Chim. Acta, **6**, 339 (1972).

Can. J. Chem. Downloaded from www.nrcresearchpress.com by 178.218.224.3 on 09/06/12
For personal use only.

Simultaneous Electron Spin – Nuclear Spin Transitions in Solid Solutions of Methyl Radicals

C. T. CAZIANIS AND D. R. EATON

Department of Chemistry, McMaster University, Hamilton, Ontario L8S 4M1

Received December 10, 1973

C. T. CAZIANIS and D. R. EATON. Can. J. Chem. **52**, 2471 (1974).

The e.s.r. spectra of methyl radicals produced by the ultraviolet irradiation of Tl(III) acetate show satellites attributed to simultaneous electron spin – nuclear spin transitions involving a proton of a neighboring water molecule. Measurement of the relative intensities of the satellites and the main transitions allows the average separation of the interacting proton from the unpaired electron to be calculated. Such measurements have been carried out over the temperature range −180 to −120 °C. The implications regarding the environment of the methyl radical in the ice matrix are briefly discussed.

C. T. CAZIANIS et D. R. EATON. Can. J. Chem. **52**, 2471 (1974).

Les spectres r.p.e. des radicaux méthyles produits par irradiation ultraviolet de l'acétate de Tl(III) montrent des satellites qui sont attribués à des transitions simultanées spin électronique/spin nucléaire impliquant un proton d'une molécule d'eau environnante. Des mesures d'intensités relatives des satellites et des transitions principales permettent de calculer la distance moyenne entre les protons interagissant et les électrons non-pairés. On a fait ces mesures à diverses températures entre −180 et −120 °C. On discute brièvement des implications que l'on peut en déduire concernant l'environnement des radicaux méthyles dans une matrice de glace.

[Traduit par le journal]

Introduction

Second order transitions due to simultaneous changes in the spin state of a single proton and the spin state of the unpaired electron are occasionally observed in e.s.r. spectra. They are induced by a weak dipole–dipole coupling between the electron magnetic moment and the magnetic moment of the neighboring proton. These transitions were first detected as satellites accompanying the main lines of atomic hydrogen produced in γ-irradiated frozen acids (1, 2). A theoretical treatment has been given by Trammell *et al.* (3) who also predicted a second and even a third set of satellites corresponding to two and three neighboring protons simultaneously changing state. This was confirmed experimentally by Köhnlein and Venable (4) who observed additional sets of lines in the e.s.r. spectra of atomic hydrogen at high microwave power levels. There have been only two instances, however, in which the satellites appear in e.s.r. spectra of free radicals, *i.e.* the e.s.r. spectra of γ-irradiated single crystals of thymidine (5) and of barbituric acid dihydrate (6). In neither case was an absolute determination of which protons in the crystal give rise to the satellite lines possible, but in the case of barbituric acid dihydrate it was assumed that the protons of the water molecules in the hydrated crystal are responsible for the effect. In the present work, experimental evidence for the occurrence of second order transitions in the e.s.r. spectrum of methyl radicals is reported. These transitions are attributed to the flipping of a single proton of a nearby solvent molecule to which the electron spin is weakly coupled through dipole–dipole interaction. The effective single proton distance from the carbon nucleus of the methyl radical has been estimated as a function of temperature.

Preliminary Observations

In the process of examining the photochemistry of Tl(III) acetate (7), the e.s.r. spectra of methyl radicals (produced during the u.v.-irradiation of $Tl(OCOCH_3)_3$ in 10% H_2SO_4 at −196 °C) were obtained, they showed clearly satellite lines accompanying the main absorption lines. The separation of the satellites from the main hyperfine lines, in frequency units, is close to the proton resonance frequency for the particular magnetic field strength at which the observation is made. Thus the observed separation of 4.85 G compared favorably with the theoretically predicted value of 4.95 G for magnetic field 3250 G. Also, power-saturation experiments indicated that (*a*) the intensity ratio of the satellite to the

Can. J. Chem. Downloaded from www.nrcresearchpress.com by 210.87.254.105 on 09/05/12
For personal use only.

Can. J. Chem. Downloaded from www.nrcresearchpress.com by 210.87.254.105 on 09/05/12
For personal use only.

main transition increases on increasing the microwave power (this is in agreement with previous experimental observations) (1, 2). This effect is illustrated in Figs. 1*A* and *B*; (*b*) no additional sets of satellites appeared even at high microwave power.

It was therefore confirmed that the observed satellites correspond to a single proton concurrently changing state with the change in spin state of the electron. A solution of $Tl(OCOCH_3)_3$ in 10% H_2SO_4 (where H_2O has now been replaced by D_2O) was irradiated and its e.s.r. spectrum recorded at -196 °C. This spectrum is shown in Fig. 1*C*. The fact that satellite lines are not present in this spectrum indicates that the dipole–dipole coupling is to a deuteron rather than to a proton (in this case the separation of the satellites is reduced by a factor $g_D/g_H = 0.153$ and therefore the satellites cannot be resolved). This observation shows that the nuclei which give rise to the satellites are protons on the water molecules.

The Effective Proton–Electron Separation as a Function of Temperature

In their theoretical treatment, Trammell *et al.* (3) have derived expressions in which the intensity ratio of the satellites to the main absorption line is related to the average distance of the flipping protons from the nucleus on which the spin density is concentrated. The single proton distance for randomly oriented systems is given by

$$[1] \qquad \frac{T_1}{2T_2} \approx \frac{3}{20}\left\langle \sum_i \frac{g_e^2\beta_e^2}{H^2 r_i^6} \right\rangle$$

where T_1, T_2 are the intensities of the satellite and the main line, respectively, H is the applied field, and r_i represents the distance of the ith flipping proton from the nucleus on which the spin density is concentrated.

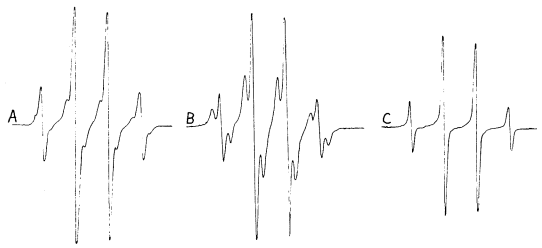

FIG. 1. (*A*) Methyl radical e.s.r. spectrum obtained after 1 h irradiation of 0.1 *M* Tl(III) acetate in 10% H_2SO_4 at 77 °K. Microwave power attenuation 17 DB. (*B*) As in *A* but microwave attenuation 8 DB. (*C*) Spectrum in D_2O. Microwave attenuation 8 DB.

In order to obtain the correct experimental ratio $T_1/2T_2$, it is necessary to correct for saturation effects and also for overlap of the lines. This was achieved as follows: a sample of $Tl(OCOCH_3)_3$ in 10% H_2SO_4 was irradiated for $\sim$1 h. This gives a very intense and noise free spectrum. Using always the same irradiated sample, seven sets of e.s.r. spectra of the low field central line of the methyl radical ($H \cong$ 3250 G) were recorded at seven different temperatures ranging from -182 to -122 °C at 10 °C intervals. Each set consisted of seven spectra obtained at different microwave power levels, but otherwise recorded under the same instrumental conditions. Each experimental spectrum was analyzed on the basis of a corresponding computer-calculated spectrum. This calculation was made on the following assumptions: (*a*) the spectrum is composed of three lines each represented by the derivative of a Gaussian curve with two adjustable parameters, the amplitude and width; (*b*) the two satellite lines on each side of the main line are of equal intensity; (*c*) the separation of the satellites from the main line is constant and taken to be 4.85 G (experimental value); (*d*) all three lines have the same linewidth (peak to peak).

A computer program was written to generate simulated e.s.r. spectra of various relative line intensities and line widths, to compare the simulated spectra with an experimental spectrum, and to determine the parameters corresponding to optimum agreement (8). Thirty data points from each experimental spectrum were used to make this comparison. The intensities of the main line and the satellite lines corresponding to optimum fit were obtained directly from the calculated spectrum. An example of a spectrum fit is shown in Fig. 2*A*.

The variation of the saturation behavior of the satellites and the main transition is illustrated in Fig. 2*B*, where the intensities obtained in the above manner are plotted against the microwave power. Figure 2*C* shows a plot of the intensity ratio *vs.* microwave power. From this plot the corrected value of $T_1/2T_2$ is obtained by extrapolating to zero power.

These ratios were substituted in eq. 1 to obtain an effective single-proton distance, defined as

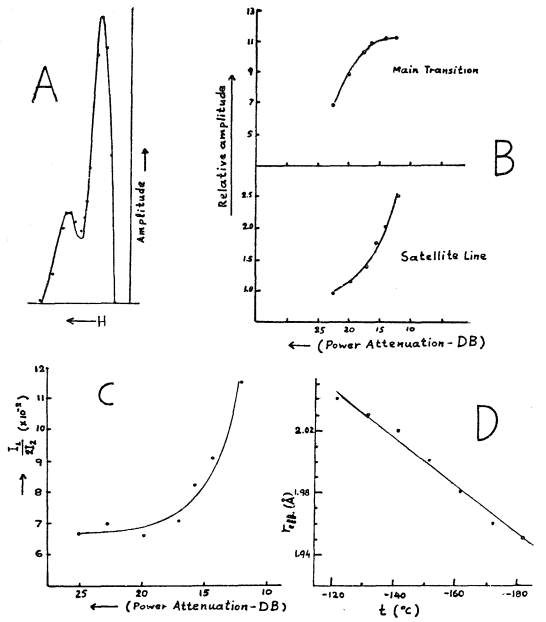

FIG. 2. (*A*) Comparison of calculated and observed e.s.r. spectra of one-half the low field central line of the CH_3 radical. The points are experimental. (*B*) Microwave power saturation of the main line and satellites. (*C*) Plot $T_1/2T_2$ *vs.* power attenuation. (*D*) Variation of r_{eff} with temperature.

$$[2] \qquad r_{eff} = \left[\left\langle \sum_i \frac{1}{r_i^6} \right\rangle\right]^{-1/6}$$

The plot of r_{eff} *vs.* temperature is shown in Fig. 2*D*. A linear increase of r_{eff} with temperature is apparent.

Discussion

The previous reports of the observation of satellite lines in e.s.r. spectra have referred to either hydrogen atoms or to complex organic radicals obtained by γ-irradiation of single crystals. The present results are of interest in that they refer to a small radical of known geometry and because it has proved possible to study the effects as a function of temperature. From the method of producing the radicals, we initially considered it possible that the interacting proton was located on a neighboring acetate ion since the reaction

$$CH_3\cdot + CH_3COO^- \rightarrow CH_4 + \cdot CH_2COO^-$$

had to be postulated to occur in acetate photochemistry at low temperatures (9). However, the disappearance of the satellites when the irradiation is carried out in D_2O demonstrates that this is not the case and that the interaction is with a solvent proton. The calculated internuclear separation of 1.95 Å between the methyl carbon and the solvent proton at −182 °C may be compared with the value of 1.73 Å obtained from atomic hydrogen satellites (3). This relatively short separation places some clear limitations on the nature of the radical's environment. The interacting proton cannot be in the plane of the methyl radical since the C—H bond length of 1.1 Å plus the hydrogen Van der Waals radius of 1.0 Å clearly will not allow the observed internuclear separation. A much more plausible model is one in which the proton is situated perpendicular to the plane of the methyl radical. There is undoubtedly some tumbling motion of the CH_3 radical in the lattice which would have to be considered in a quantitative calculation. The lines of the CH_3 spectrum are always quite sharp but it is not clear that this implies free rotation about all axes since the g and a_H anisotropies are both small (10). Examination of a molecular model of the ice crystal shows that the observed separation is consistent with that of a proton perpendicular to the plane of the radical for either the case where a $CH_3\cdot$ radical has been substituted for a H_2O molecule in the lattice or for the case where a CH_3 radical has been introduced in one of the open "cages" in the ice lattice. We are not able to postulate a specific site. The increase in the separation to 2.04 Å at −122 °C on warming can be correlated with the expansion of the ice lattice. At temperatures higher than −100 °C methyl radicals are no longer observed. Presumably diffusion and subsequent recombination of the radicals becomes possible at this temperature. We have attempted no detailed analysis of this temperature dependence but the observation of these satellites would seem to offer an interesting approach to the study of crystal lattice behavior.

Experimental

Electron spin resonance spectra were obtained using a JEOLCO-JES-3BS-X spectrometer operating at 9400 MHz (X-band). Experimental details pertaining to the photolysis of metal acetates have been described elsewhere (7).

We are indebted to Dr. C. Charalambous of the Department of Electrical Engineering, McMaster University, for aid and advice in the computer simulation of

Can. J. Chem. Downloaded from www.nrcresearchpress.com by 210.87.254.105 on 09/05/12
For personal use only.

e.s.r. spectra and to the National Research Council of Canada for financial support of this reasearch.

1. H. ZELDES and R. LIVINGSTON. Phys. Rev. **96**, 1702 (1954).
2. R. LIVINGSTON, H. ZELDES, and E. H. TAYLOR. Disc. Faraday Soc. **19**, 166 (1955).
3. G. T. TRAMMEL, H. ZELDES, and R. LIVINGSTON. Phys. Rev. **110**, 630 (1958).
4. W. KÖHNLEIN and J. H. VENABLE. Nature, **215,** 618 (1967).
5. B. PRUDEN, W. SNIPES, and W. GORDY. Proc. Nat. Acad. Sci. **53**, 917 (1965).
6. W. SNIPES and W. BERNHARD. J. Chem. Phys. **43**, 2921 (1965).
7. C. T. CAZIANIS and D. R. EATON. To be published.
8. R. FLETCHER. Computer J. **13**, 317 (1970).
9. K. HEUSLER and H. LOELINGER. Helv. Chim. Acta, **52**, 1495 (1969).
10. J. JANEKA, H. M. VYAS, and M. FUJIMOTO. J. Chem. Phys. **54**, 3229 (1971).

Can. J. Chem. Downloaded from www.nrcresearchpress.com by 210.87.254.105 on 09/05/12
For personal use only.

L'oxydation chromique et les esters chromiques

JEAN-CLAUDE RICHER ET JEAN-MARIE HACHEY[1,2]
Département de chimie, Université de Montréal, Montréal, Québec
Reçu le 4 octobre, 1973

JEAN-CLAUDE RICHER et JEAN-MARIE HACHEY. Can. J. Chem. **52**, 2475 (1974).

Des vitesses de décomposition d'esters chromiques dérivés de cyclanols aliphatiques secondaires ainsi que les vitesses d'oxydation de ces cyclanols par des esters chromiques dérivés d'alcools tertiaires ont été mesurées dans le benzène anhydre. Les résultats obtenus sont comparés à ceux d'autres chercheurs pour des réactions en solvants polaires. Un mécanisme est proposé pour expliquer les résultats obtenus.

JEAN-CLAUDE RICHER and JEAN-MARIE HACHEY. Can. J. Chem. **52**, 2475 (1974).

Rates of decomposition of chromic acid esters derived from secondary alicyclic alcohols and rates of oxidation of these cyclanols by chromic esters derived from tertiary alcohols have been measured in anhydrous benzene. The results obtained are compared to those of other workers for reactions held in polar solvents. A mechanism is suggested to explain the observed results.

Can. J. Chem. Downloaded from www.nrcresearchpress.com by 210.87.254.5 on 09/05/12
For personal use only.

Introduction

C'est à Beckmann (1) que l'on doit les premières observations sur l'existence d'intermédiaires lors de l'oxydation chromique. Dès 1889, ce chercheur signale que durant l'oxydation chromique du menthol, il y a formation d'un composé cristallin rouge qui se décompose en menthone à 53 °C. Depuis lors, de nombreux chercheurs ont observé de tels intermédiaires durant l'oxydation chromique d'alcools. (Pour un résumé, voir la réf. 2).

Le chromate de ditertiobutyle est un oxydant doux et spécifique couramment utilisé (3–8). En 1967, Matsuura et Suga (9) publient un article de revue sur l'oxydation de composés organiques par cet ester chromique; ils font une rétrospective des travaux ayant trait à l'oxydation d'alcools primaires, d'alcools secondaires et de composés ayant des groupements méthyléniques activés.

Dans ce travail, nous étudions d'abord le mécanisme de décomposition d'esters chromiques dérivés de cyclanols secondaires puis nous étendons notre étude à l'oxydation de cyclanols secondaires par des esters chromiques dérivés d'alcools tertiaires. Les réactions sont faites dans le benzène anhydre avec divers cyclanols aliphatiques secondaires et des esters chromiques dérivés de différents alcools aliphatiques tertiaires.

[1]Les résultats rapportés dans le présent travail sont extraits en partie de la thèse soumise par M. Jean-Marie Hachey en vue de l'obtention du grade de Ph.D., Faculté des sciences, Université de Montréal, janvier 1972.

[2]Adresse actuelle: Département des sciences pures, Université du Québec à Chicoutimi, Chicoutimi, Québec.

Esters chromiques dérivés d'alcools secondaires

Synthèse et caractérisation d'esters chromiques dérivés d'alcools secondaires cycliques

La synthèse des esters chromiques est une adaptation de la méthode générale décrite par Wienhaus (10). Un léger excès de CrO_3 solide est mis en contact avec un alcool secondaire dans un solvant apolaire (benzène, CCl_4). Après 2 ou 3 min d'agitation, l'excès de CrO_3 est séparé de la solution par décantation; la solution est ensuite séchée sur Na_2SO_4 anhydre puis décantée. Après évaporation du solvant, l'ester chromique présente les caractéristiques suivantes. Spectre u.v.: une large bande vers 385 nm et une moins large vers 285 nm. Spectre i.r.: la bande —OH est absente. Apparition de bandes Cr—O vers 985 et 960 cm^{-1}. Après quelques minutes, une bande carbonyle commence à se développer. Spectre r.m.n.: disparition totale du signal attribuable au proton hydroxyle. Quelque 20 min plus tard, une seconde détermination du spectre r.m.n. laisse voir une diminution dans l'intensité du signal de l'hydrogène carbinolique et l'apparition graduelle d'un signal vers 2.00 p.p.m. correspondant aux protons méthyléniques en position α du carbonyle.

Identification des produits de la réaction

Les produits de la réaction de décomposition dans un solvant non polaire (benzène, CCl_4)

TABLEAU 1. Vitesses de décomposition d'esters chromiques dérivés de cyclanols secondaires*

Alcools	$k_1 \times 10^5$ (s^{-1})	$k_2 \times 10^3$ (l mol^{-1} s^{-1})	Vitesses relatives
Cyclopentanol (**1**)	4.40±0.12	5.91±0.18	1.22
Cyclohexanol (**2**)	3.58±0.04	4.84±0.06	1.00
Cycloheptanol (**3**)	6.38±0.07	8.60±0.09	1.78
Cyclooctanol (**4**)	7.59±0.15	10.31±0.28	2.13
Cyclooctanol deutéré (**5**)	1.97±0.06	2.67±0.08	0.55
Cyclononanol (**6**)	6.01±0.07	8.16±0.12	1.69
Cyclodécanol (**7**)	5.19±0.06	6.98±0.12	1.44

*Conditions: $[Alcool]_0 \simeq 7.1 \times 10^{-3}$ *M*; $[Ester\ chromique]_0 \simeq 0.38 \times 10^{-3}$ *M*; $T = 25$ °C.

d'un ester chromique dérivé d'un alcool secondaire cyclique sont la cétone correspondante, l'excès d'alcool et un composé insoluble du chrome réduit (composition voisine de CrO_2). Ces résultats sont identiques à ceux rapportés par Leo et Westheimer (11) pour la décomposition du chromate de diisopropyle dans le benzène.

Vitesse de décomposition d'esters chromiques dérivés d'alcools secondaires cycliques

Toutes les mesures cinétiques furent effectuées dans le benzène anhydre en présence d'un excès d'alcool secondaire selon un rapport de concentrations molaires alcool:Cr(VI) de 20:1. La vitesse de la réaction fut mesurée à 24.05 ± 0.03 °C au maximum d'absorption de l'ester chromique.

Les tableaux 1 et 2 donnent les moyennes de trois ou quatre mesures avec l'écart maximum observé; les vitesses relatives sont données par rapport à k_2 pour le cyclohexanol.

La variation des vitesses relatives en fonction de la grandeur du cycle, par rapport au cyclohexanol, est donnée dans la fig. 1. La fig. 2 montre la variation des vitesses relatives de décomposition d'esters chromiques dérivés de cyclanols secondaires.

Discussion

A la fig. 1, les résultats de ce travail sont comparés aux résultats (milieu H_2O–$HClO_4$) de Kuivila et Becker (12) et aux résultats (milieu AcOH–H_2O) de Richer et Hoa (13). La séquence des vitesses suit la même tendance pour les trois études. La fig. 1 indique que plus le milieu est polaire, plus les écarts sont prononcés entre les vitesses d'oxydation du cyclohexanol et celle des cyclanols homologues supérieurs.

La fig. 2 permet de comparer les résultats

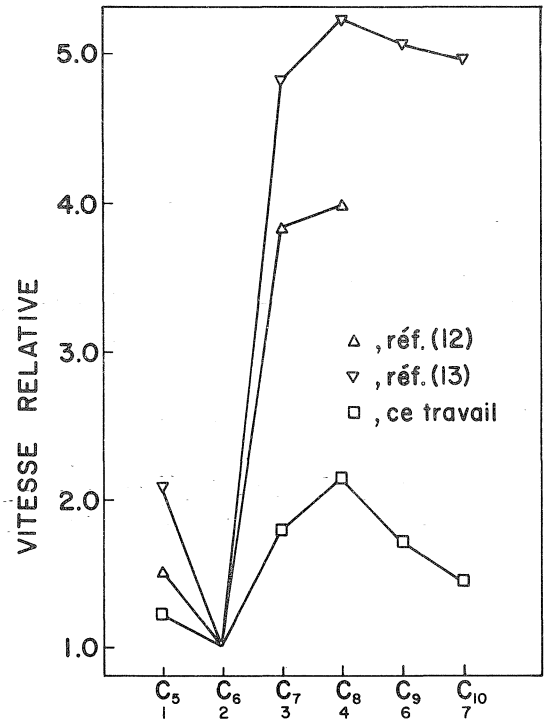

FIG. 1. Vitesses relatives d'oxydation chromique de cyclanols secondaires. Conditions: réf. 12: $T = 40.0 \pm 0.01$ °C, $[acide\ chromique]_0$ 0.001–0.002 *M*, $[Alcool]_0$ variable, $[HClO_4]$ 0.10–0.25 *M*, force ionique 0.40, solvant H_2O; réf. 13: $T = 25.10$ °C, $[acide\ chromique]_0 \sim 3.0 \times 10^{-3}$ *N*, $[Alcool]_0 \simeq 2 \times 10^{-2}$ *M*, solvant AcOH:H_2O (3:1).

résumés au tableau 2, aux résultats (milieu AcOH–H_2O) de Richer, Eliel *et al.* (14, 15) et à ceux de Richer et Gilardeau (16). L'examen de la fig. 2 permet également de constater qu'un milieu non polaire (favorisant un mécanisme cyclique intramoléculaire) contribue à atténuer les écarts entre les vitesses d'oxydation.

Can. J. Chem. Downloaded from www.nrcresearchpress.com by 210.87.254.5 on 09/05/12
For personal use only.

TABLEAU 2. Vitesses de décomposition d'esters chromiques dérivés de cyclohexanols secondaires diversement alkylés*

Alcools		$k_1 \times 10^5$ (s^{-1})	$k_2 \times 10^3$ ($l\ mol^{-1}\ s^{-1}$)	Vitesses relatives
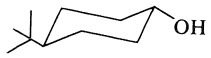 **8**	(*trans*)	2.93±0.04	3.96±0.05	0.82
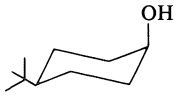 **9**	(*cis*)	5.58±0.12	7.55±0.17	1.56
10	(*cis*)	5.15±0.09	6.99±0.12	1.44
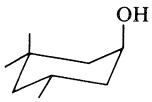 **11**	(*trans*)	7.43±0.24	10.09±0.34	2.08

*Conditions: $[Alcool]_0 \simeq 7.1 \times 10^{-3}\ M$; $[Ester\ chromique]_0 \simeq 0.38 \times 10^{-3}\ M$; $T = 25\ °C$.

Plusieurs explications peuvent être avancées sur le fait que les différences dans les vitesses d'oxydation sont plus importantes dans le cas de la réaction bimoléculaire (en solvant polaire). En premier lieu, il faut souligner que l'oxydation chromique en solvants polaires (*e.g.* AcOH–H_2O) procède par un mécanisme bien différent (pour une revue, voir la réf. 2) de celui opérant lors de la décomposition d'esters chromiques dérivés d'alcools secondaires et conduite en solvants apolaires. En effet, dans un solvant polaire, le Cr(VI) est ultimement réduit en Cr(III) et il y a participation du Cr(V) et du Cr(IV) à l'oxydation (2). En solvant apolaire, le Cr(VI) est réduit en Cr(IV) (11). De plus, dans le mécanisme bimoléculaire, l'eau serait un meilleur agent nucléophile que l'oxygène lié au chrome dans l'ester chromique (22). Il semble également que le solvant polaire (AcOH–H_2O) soit plus sensible à la stéréochimie de l'alcool à oxyder que ne l'est l'oxygène de l'ester chromique dans un solvant apolaire. Enfin, il est également permis de soupçonner une influence spécifique selon la nature et la composition du solvant polaire sur l'équilibre alcool – demiester chromique et/ou l'équilibre alcool – diester chromique et/ou l'équilibre demiester chromique – diester chromique.

Conclusions

La conclusion la plus importante découle de l'observation suivante: la formation d'esters chromiques comme intermédiaires lors de l'oxydation est confirmée par des méthodes spectroscopiques (i.r., u.v. et r.m.n.).

Les résultats présents traitant de la décomposition d'esters chromiques dérivés de cyclohexanols secondaires diversement alkylés (réactions en milieu non polaire) (*cf.* fig. 2) montrent, dans l'ensemble, une bonne concordance avec les travaux antérieurs (réactions en milieu polaire) (14, 15). Ce fait confirmerait l'influence prépondérante des effets stériques telle que suggérée par Richer *et al.* (14, 15).

Les résultats de ce travail sur la décomposition (réactions en milieu non polaire) d'esters chromiques dérivés d'une série homologue de cyclanols secondaires supportent bien la comparaison (voir fig. 1) avec les travaux publiés dans le passé (réactions en milieu polaire) (12, 13). Le présent travail constitue donc une confirmation supplémentaire de la théorie des

Can. J. Chem. Downloaded from www.nrcresearchpress.com by 210.87.254.5 on 09/05/12
For personal use only.

Can. J. Chem. Downloaded from www.nrcresearchpress.com by 210.87.254.5 on 09/05/12
For personal use only.

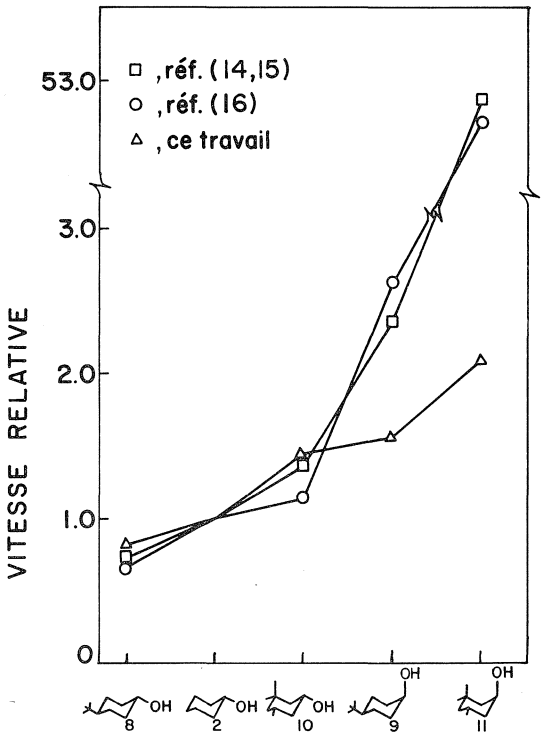

FIG. 2. Vitesses relatives d'oxydation chromique de cyclohexanols diversement alkylés. Conditions: réf. 14, 15: $T = 25\,^{\circ}C$, [acide chromique]$_0$ $\sim 5 \times 10^{-3}$ N, [Alcool]$_0$ = (1.0 à 3.0) 10^{-2} M, solvant AcOH: H_2O (3:1); réf. 16: $T = 25\,^{\circ}C$, [acide chromique]$_0$ $\sim 1.0 \times 10^{-3}$ M, [Alcool]$_0$ $\simeq 1.0 \times 10^{-2}$ M, solvant AcOH:H_2O (3:1).

tensions internes (I-strain) de Brown *et al.* (17) pour un changement de covalence de 4 (*i.e.* sp^3) à 3 (*i.e.* sp^2) dans les cycles moyens.

La nature apolaire du solvant, la faible valeur de l'effet isotopique cinétique ainsi que la formation d'un oxyde de chrome réduit de composition voisine de CrO_2 s'accorderaient très bien avec le mécanisme illustré dans les conclusions générales et caractérisé par la décomposition cyclique intramoléculaire de l'ester chromique.

Les esters chromiques dérivés d'alcools tertiaires comme agents oxydants

Identification des produits de la réaction

L'oxydation, dans le benzène anhydre, d'un excès de cyclanol secondaire par un ester chromique dérivé d'un alcool tertiaire conduit à un mélange réactionnel contenant la cétone correspondante, l'excès d'alcool secondaire non réagi, l'alcool tertiaire provenant de l'ester chromique ainsi qu'un précipité brun d'oxyde de chrome réduit (vraisemblablement le CrO_2) et/ou un mélange d'oxydes de chrome approchant cette composition.

Ces observations sont conformés à celles décrites dans la littérature (8, 18) lors de l'oxydation d'un alcool par un ester chromique dérivé d'un alcool tertiaire.

L'analyse gravimétrique, les tests de solubilité, la décomposition thermique en Cr_2O_3 avec dégagement d'oxygène et l'aspect physique s'accordent bien avec la description du CrO_2 donné dans la littérature (19, 20). Les produits organiques sont analysés par chromatographie en phase gazeuse et i.r.

Vitesses d'oxydation chromique de cyclanols secondaires au moyen d'esters chromiques dérivés d'alcools tertiaires

Les vitesses d'oxydation chromique sont calculées à partir du taux de diminution dans l'absorption du Cr(VI); la longueur d'onde ayant été préalablement fixée au maximum d'absorption. Des mesures effectuées à longueur d'onde variable et balayages lents et répétés confirment les résultats obtenus à longueur d'onde constante. La méthode utilisée est décrite dans la partie expérimentale. Les valeurs indiquées sont des vitesses moyennes pour trois ou quatre mesures; l'écart maximum observé est indiqué dans chaque cas.

Influence de l'excès d'alcool à oxyder sur la vitesse d'oxydation

Le cas étudié fut celui de l'oxydation du cyclohexanol par le chromate de diadamantyle-1. Les résultats du tableau 3 sont en accord avec plusieurs travaux antérieurs (14, 16, 19) où il est possible de constater que la vitesse d'oxydation diminue avec augmentation de la concentration de l'excès d'alcool à oxyder.

Influence de la pyridine sur la vitesse d'oxydation

Le cas examiné fut celui de l'oxydation du

TABLEAU 3. Vitesses d'oxydation du cyclohexanol par le chromate de diadamantyle-1

Rapport molaire [Alc]$_0$/[Cr(VI)]$_0$	$k_1 \times 10^5$ (s^{-1})	$k_2 \times 10^3$ ($l\,mol^{-1}\,s^{-1}$)
11	1.94±0.05	4.79±0.11
20	0.88±0.04	1.14±0.05
39	0.41±0.03	0.26±0.03

TABLEAU 4. Vitesses d'oxydation d'alcools par divers esters chromiques

Alcools	$k_1 \times 10^5$ (s^{-1})	$k_2 \times 10^3$ (l mol^{-1} s^{-1})	Vitesses relatives	k_H/k_D
	(a) Oxydations par le chromate de ditertiobutyle			
2	1.84±0.03	2.37±0.04	1.00	
4	4.92±0.06	6.31±0.08	2.66	2.13
5	2.30±0.03	2.97±0.04	1.25	
8	1.23±0.05	1.59±0.07	0.67	
9	2.46±0.07	3.17±0.09	1.34	
10	2.27±0.06	2.92±0.07	1.23	
11	2.55±0.06	3.29±0.07	1.39	
	(b) Oxydations par le chromate de di(méthyl-3 pentyl-3)			
2	1.47±0.03	1.90±0.04	1.00	
4	3.10±0.06	3.97±0.07	2.09	2.01
5	1.53±0.06	1.98±0.07	1.04	
	(c) Oxydations par le chromate de di(méthyl-3 hexyl-3)			
2	1.44±0.06	1.86±0.08	1.00	
4	2.92±0.06	3.72±0.05	2.00	2.05
5	1.41±0.06	1.82±0.08	0.98	
	(d) Oxydations par le chromate de di(méthyl-3 heptyl-3)			
2	1.38±0.03	1.78±0.04	1.00	
4	2.79±0.07	3.58±0.09	2.01	2.20
5	1.26±0.06	1.63±0.08	0.91	
	(e) Oxydations par le chromate de diadamantyle-1			
1	1.02±0.03	1.26±0.04	1.11	
2	0.88±0.04	1.14±0.05	1.00	
3	1.48±0.05	1.90±0.06	1.67	
4	1.65±0.03	2.12±0.04	1.86	
6	1.42±0.03	1.83±0.04	1.61	
7	1.35±0.03	1.73±0.04	1.52	
12	1.00±0.03	1.29±0.04	1.13	
13	0.92±0.03	1.19±0.04	1.04	

*Conditions: $[Alcool]_0 \simeq 7.7 \times 10^{-3}$ M; $[Ester\ chromique]_0 \simeq 0.38 \times 10^{-3}$ M; $T = 25$ °C.

cyclohexanol par le chromate de ditertiobutyle à 24.05 ± 0.03 °C. Les concentrations initiales en alcool et en ester chromique étaient évidemment les mêmes que celles utilisées pour les autres réactions d'oxydation. Les résultats observés permettent de conclure que l'addition d'un léger excès de pyridine (15.6×10^{-3} M) n'affecte pas, de façon sensible, la vitesse d'oxydation. En effet, nous avons mesuré $k_1 = (1.84 \pm 0.03)\ 10^{-5}$ s^{-1} et $k_2 = (2.37 \pm 0.04)\ 10^{-3}$ l mol^{-1} s^{-1} que la réaction soit faite avec ou sans pyridine. Les résultats obtenus permettent de suggérer que l'ester chromique se décompose selon un mécanisme cyclique intramoléculaire. En effet, une décomposition bimoléculaire de l'ester chromique aurait vraisemblablement été affectée (accélérée) par l'addition de pyridine.

Influence de la nature de l'alcool sur la vitesse d'oxydation

Les résultats des vitesses d'oxydation de différents alcools par divers esters chromiques dérivés d'alcools tertiaires sont résumés au tableau 4. La fig. 3 illustre la variation des vitesses relatives d'oxydation de quelques cyclohexanols diversement alkylés. Une comparaison entre les vitesses d'oxydation de ces alcools par le $(t\text{-Bu})_2CrO_4$ et les vitesses de décomposition pour les esters chromiques secondaires dérivés de ces alcools laisse voir sensiblement la même tendance. La fig. 3 fait également ressortir le fait suivant: la décomposition d'un ester chromique dérivé d'un alcool secondaire se fait plus rapidement que l'oxydation de ce même alcool par un ester chromique dérivé d'un alcool ter-

Can. J. Chem. Downloaded from www.nrcresearchpress.com by 210.87.254.5 on 09/05/12
For personal use only.

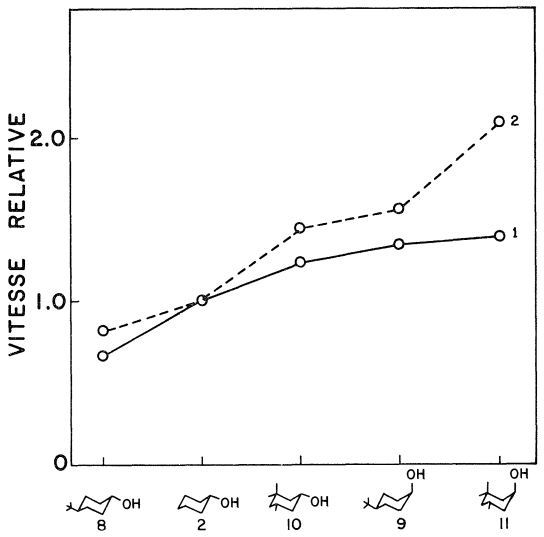

FIG. 3. Vitesses relatives d'oxydation par $(t\text{-Bu})_2CrO_4$ (trait plein (*1*)). Vitesses relatives de décomposition d'esters chromiques secondaires (traites espacés (*2*)).

tiaire. Ces observations s'expliquent facilement de la manière suivante: lors de l'oxydation par le $(t\text{-Bu})_2CrO_4$, la réaction se fait évidemment en deux étapes: d'abord transestérification puis réduction du Cr(VI) en Cr(IV) (voir fig. 3, tracé *1*). Par contre, la réduction du Cr(VI) en Cr(IV) (voir fig. 3, tracé *2*) se fait directement; l'ester chromique dérivé de l'alcool secondaire étant déjà formé lors de la mesure du taux de disparition du Cr(VI).

Influence de la nature de l'ester chromique sur la vitesse d'oxydation

Les résultats obtenus (voir tableau 4) lors de l'oxydation de cyclanols par divers esters chromiques permettent de dégager les points suivants. Tout d'abord, la vitesse d'oxydation est sensiblement réduite lorsque l'encombrement stérique est accru dans l'agent oxydant c'est-à-dire, l'ester chromique. En second lieu, la séquence des vitesses relatives d'oxydation (par des esters chromiques dans un solvant apolaire) suit assez bien la tendance observée lors d'oxydations par l'acide chromique dans l'acide acétique aqueux. Les écarts pourraient être expliqués, d'une part, par la participation de la transestérification à la cinétique et, d'autre part, par le fait que dans le benzène, la décomposition unimoléculaire de l'ester chromique selon un mécanisme cyclique à cinq atomes est la plus vraisemblable. De plus, il faut se rappeler que le mécanisme de l'oxydation chromique en solvants polaires (*e.g.* AcOH—H_2O) (pour une revue voir la réf. 2) est différent du mécanisme prévalant en solvant apolaire.

Sur l'effet isotopique cinétique

Nos résultats exposés au tableau 4 permettent de constater que l'effet isotopique est légèrement supérieur dans le cas de la décomposition d'un ester chromique dérivé d'un cyclanol secondaire (3.86) que dans celui de l'oxydation d'un cyclanol secondaire par un ester chromique dérivé d'un alcool tertiaire ($\sim$2).

Ce fait pourrait s'expliquer par la participation de la transestérification à la cinétique lors de l'oxydation par un ester chromique dérivé d'un alcool tertiaire. Ces résultats se comparent bien à ceux observés par Rocek *et al.* (21) qui ont constaté un effet isotopique k_H/k_D de 2.0 pour une oxydation faite dans AcOH 60% en présence d'AcONa; les auteurs en concluent que, dans ces conditions, l'estérification et la décomposition de l'ester contribuent à la cinétique.

Les faibles valeurs de l'effet isotopique observées dans notre étude permettent de confirmer l'hypothèse de Rocek et ses collaborateurs (21) en faveur d'une décomposition unimoléculaire de l'ester chromique. Selon ces auteurs, le déplacement d'un atome d'hydrogène dans un petit cycle devrait donner des effet isotopiques plus petits que ceux observés lors d'une décomposition bimoléculaire.

Ces résultats s'accordent également avec les travaux de Mosher *et al.* (22) traitant de l'oxydation d'α-phényléthanols par le $(t\text{-Bu})_2CrO_4$ dans le benzène anhydre. En effet, cet auteur trouve un effet isotopique k_H/k_D de 3.30 à 25.85 °C et 3.09 à 34.5 °C.

Conclusions générales

Les résultats observés dans ce travail permettent de tirer les conclusions suivantes: (*i*) la réaction, dans un solvant apolaire anhydre tel le benzène ou le CCl_4, entre l'anhydride chromique et un alcool secondaire alicyclique conduit à l'ester chromique correspondant dont la présence est appuyée par les spectres u.v., i.r. et r.m.n. Ces observations confirment donc la formation de l'ester chromique préalablement à l'oxydation; (*ii*) les produits de la réaction à 24.05 °C, dans un solvant apolaire anhydre (benzène, éther de pétrole), entre un excès de cyclanol secondaire et un ester chromique dérivé d'alcool tertiaire sont la cétone correspondante, l'alcool tertiaire provenant de l'ester chromique, un précipité

Can. J. Chem. Downloaded from www.nrcresearchpress.com by 210.87.254.5 on 09/05/12
For personal use only.

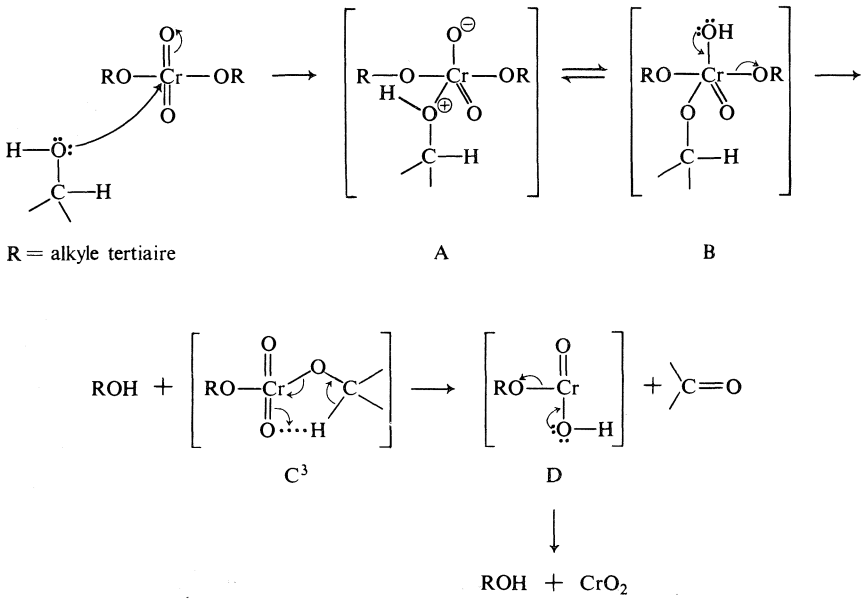

SCHÉMA 1. Mécanisme suggéré

brun d'oxyde de chrome de composition voisine de CrO_2 et l'excès d'alcool secondaire retrouvé intact; (*iii*) la vitesse d'oxydation chromique diminue avec une augmentation de la concentration de l'excès d'alcool à oxyder; (*iv*) la vitesse d'oxydation chromique diminue avec augmentation de l'encombrement stérique de l'ester chromique utilisé comme agent oxydant; (*v*) la nature apolaire du solvant, la faible valeur de l'effet isotopique cinétique ainsi que l'absence de catalyse basique en présence de pyridine s'accorderaient très bien avec le mécanisme suivant caractérisé par la participation de la transestérification à la cinétique et la décomposition cyclique intramoléculaire de l'ester chromique.

Mécanisme de l'oxydation d'un alcool secondaire par un ester chromique dérivé d'un alcool tertiaire

Ce mécanisme (représenté dans le schéma 1) se fait en deux étapes: (*i*) transestérification; (*ii*) oxydation de l'alcool.

Partie expérimentale

Les points de fusion ont été déterminés sur un microscope chauffant de la compagnie Reichert (Autriche) à l'aide d'un thermomètre calibré.

Les spectres i.r. ont été pris sur un spectrophotomètre de la cie "Beckman", modèle I.R. 8 à double faisceau, entre deux plaques de NaCl. Les produits liquides sont examinés sans solvant et sous forme de film; les solides sont mis en suspension sous forme d'émulsion dans le Nujol.

Les indices de réfraction ont été mesurés sur un refractomètre de type Abbe de la cie Karl Zeiss.

Les analyses par chromatographie en phase gazeuse (c.p.g.) furent effectuées de la façon suivante. Alcools tertiaires: appareil de la cie "F & M" à détection par ionisation de flamme; colonne en cuivre (14 pd × ¼ po) contenant 10% d'"hyprose" sur chromosorb "P"; gaz porteur: 60 ml He/min; 140 °C. Alcools secondaires: appareil de la cie "Microtek" à détection par conductivité thermique; colonne en cuivre (12 pd × ¼ po) contenant 10% de silicone "SE-30" sur "Chromport-XXX"; gaz porteur: 60 ml He/min; 180–200 °C.

Les spectres u.v. furent déterminés de la façon suivante: spectres u.v. de caractérisation: spectrophotomètre "Bausch & Lomb", modèle Spectronic 505; solvant, pentane; spectres u.v. de cinétique: les vitesses d'oxydation chromique furent mesurées à l'aide d'un spectrophotomètre "Perkin-Elmer", modèle 4000-A à double faisceau équipé de compartiments thermostatés. spectres r.m.n.: spectrophotomètre "Varian", modèle A-60; solvant, CCl_4; standard interne TMS.

Esters chromiques dérivés d'alcools secondaires

Synthèse et propriétés des alcools secondaires

Les alcools secondaires utilisés au cours de ce travail

[3]Dans le cas de la décomposition d'un ester chromique dérivé d'un alcool secondaire, la réaction se fait évidemment à partir de l'intermédiaire "C". Cet intermediaire pourrait s'écrire

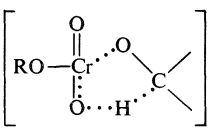

Can. J. Chem. Downloaded from www.nrcresearchpress.com by 210.87.254.5 on 09/05/12
For personal use only.

étaient, en majorité, disponibles au laboratoire. Certains alcools furent synthétisés par réduction de la cétone correspondante par $LiAlH_4$ suivie d'une hydrolyse acide selon la méthode décrite par Roberts et Sauer (25). La pureté de tous ces alcools fut assurée par les méthodes traditionnelles: distillation ou recristallisation, spectre i.r., indice de réfraction, chromatographie en phase gazeuse. Les propriétés physiques et les caractéristiques spectrales de tous ces produits s'accordent bien avec les données de la littérature (26, 27).

Synthèse et caractérisation d'esters chromiques dérivés d'alcools secondaires cycliques

L'expérience a démontré que les conditions expérimentales suivantes étaient optima pour la préparation d'esters chromiques dérivés d'alcools secondaires. Quelque 40 à 50 mg d'alcool secondaire à estérifier sont dissous dans 3–5 ml de CCl_4 à la température ambiante. Un excès de CrO_3 solide (généralement une quantité équimolaire; une molécule de CrO_3 réagissant avec deux molécules d'alcool) est alors ajouté à la solution de l'alcool et l'agitation est maintenue durant 2–3 min à la température de la pièce. Dès l'addition des premiers cristaux de CrO_3 solide, la solution se colore rapidement jaune-rouge. Après l'agitation, l'excès de CrO_3 est séparé de la solution par décantation. La solution est ensuite séchée par Na_2SO_4 anhydre durant environ 3 min. L'ester chromique fraîchement préparé présente alors les caractéristiques spectrales décrites plus haut.

Vitesse de décomposition d'esters chromiques dérivés d'alcools secondaires

(a) Identification des produits de la réaction

Un excès d'alcool secondaire (0.3–0.5 g) en solution dans 10 ml de benzène anhydre est mis en présence de CrO_3 solide dans des conditions semblables à celles qui existent lors de la mesure d'une vitesse de décomposition. L'agitation est maintenue durant 3–5 min puis la solution est séchée sur Na_2SO_4 anhydre. Les seuls produits organiques observés par c.p.g. après concentration de la solution par évaporation du solvant sous pression réduite sont la cétone correspondante et l'excès d'alcool de départ; le spectre i.r. confirme cette observation. Il y a aussi formation d'un précipité brun-noir (oxyde de chrome réduit, composition voisine de CrO_2).

(b) Procédé expérimental

Des essais préliminaires nous ont permis de constater que les conditions expérimentales suivantes étaient optima: avant chaque série de mesures de vitesse, une solution benzénique de l'alcool étudié est préparée (les concentrations sont de l'ordre de 15.5×10^{-3} mol l^{-1}). La méthode consiste à prélever, au moyen d'une pipette, 5.0 ml de la solution benzénique de l'alcool qui sont ensuite transférés dans un ballon de 25 ml contenant déjà 5.0 ml de benzène anhydre. Ensuite, quelques cristaux de CrO_3 anhydre (conservé dans un flacon renfermant du $CaCl_2$ anhydre), sont ajoutés et l'agitation est assurée par une barre magnétique. L'agitation est poursuivie durant 3–5 min jusqu'à ce que l'absorption de la solution soit de 1.2 (absorption correspondant à une concentration de 0.38×10^{-3} M en ester chromique et évaluée par calibration); la compensation est faite avec du benzène pur. Lorsque la solution donne cette absorption, elle est transférée dans une fiole conique de 10 ml puis séchée sur Na_2SO_4 anhydre durant 5 min. La solution est ensuite à nouveau transférée dans une cellule en quartz puis placée dans un compartiment thermostaté. Afin de s'assurer du thermostatage, un délai de 10 min est observé avant le début d'une mesure. De cette façon, le temps écoulé depuis la mise en contact de l'alcool et du CrO_3 et le début d'une mesure varie entre 1000 et 1200 s. (L'excès d'alcool à oxyder par rapport à l'ester chromique secondaire est alors de l'ordre de 20:1; ces concentrations initiales sont comparables à celles prévalant lors de l'oxydation d'un alcool secondaire par un ester chromique dérivé d'un alcool tertiaire).

(c) Mesures

Une constante de vitesse (k_1) est calculée à partir du taux de disparition du Cr(VI) à 385 nm ($T = 24.05 \pm 0.03$ °C). Un facteur de conversion permettant de calculer la concentration en ester chromique à partir de l'absorption en u.v. est déterminé. La concentration initiale de l'alcool est calculée en faisant la différence entre la concentration totale de l'alcool secondaire mise en solution et la concentration calculée d'ester chromique. Une constante (k_2) est obtenue en divisant k_1 par la concentration initiale de l'alcool.

Esters chromiques dérivés d'alcools tertiaires comme agents oxydants

Identification des produits de la réaction

L'oxydation d'un excès de cyclanol secondaire par un ester chromique dérivé d'un alcool tertiaire, dans des conditions comparables à celles qui prévalent lors de la mesure d'une vitesse d'oxydation, donne la cyclanone correspondante, le cyclanol en excès, l'alcool tertiaire utilisé pour la synthèse de l'ester chromique et un précipité brun-noir de composition voisine de CrO_2. Les produits organiques sont analysés par chromatographie en phase gazeuse; le spectre i.r. confirme la présence de cétone et d'alcool.

Stabilité des esters chromiques utilisés comme agents oxydants

Il s'agit essentiellement de préparer un ester chromique dérivé d'un alcool tertiaire, de le sécher puis de mesurer le taux de diminution dans l'absorption du Cr(VI) à la longueur d'onde d'absorption maximum (λ_{max}). La méthode générale utilisée est décrite ici dans le cas du chromate de ditertiobutyle. A l'aide d'une spatule, 0.0014 g de *t*-BuOH sont pesés dans un ballon jaugé de 25 ml. Le ballon jaugé est ensuite rincé en utilisant trois portions de 2 ml de benzène anhydre afin de tout transférer le *t*-BuOH dans un ballon de 25 ml muni d'une barre magnétique. L'excès de CrO_3 solide (conservé dans un flacon renfermant du $CaCl_2$ anhydre) est alors introduit au moyen d'une spatule. L'agitation est ensuite poursuivie durant 3–5 min. La solution benzénique colorée jaune (ester chromique) est décantée de l'excès de CrO_3 solide, ce résidu est rincé trois fois par 2 ml de benzène anhydre afin de tout en extraire l'ester chromique. La solution benzénique de l'ester est séchée sur Na_2SO_4 anhydre pendant 3–5 min. La solution est ensuite séparée du Na_2SO_4 par décantation et celui-ci rincé à trois reprises par 1 ml de benzène anhydre; toute la solution est ensuite transférée dans un ballon jaugé de 25 ml lequel est ensuite rempli jusqu'au trait de jauge avec du benzène anhydre. Une celle en quartz de 1 cm est ensuite remplie de la solution de l'ester, une autre cellule remplie de benzène pur assure la compensation pour le solvant. Afin de s'assurer du thermostatage, un délai de 600 s est observé avant le début d'une mesure. Dans une première étape, le

Can. J. Chem. Downloaded from www.nrcresearchpress.com by 210.87.254.5 on 09/05/12
For personal use only.

maximum d'absorption est déterminé puis la longueur d'onde est fixée à cette valeur pour l'étape suivante qui consiste à mesurer le taux de diminution dans l'absorption pour un laps de temps donné; on obtient ainsi une constante de vitesse moyenne k_1; k_2 est obtenu en divisant k_1 par la concentration initiale de l'alcool à oxyder. Le taux de diminution dans l'absorption de l'ester chromique tertiaire est mesuré avant chaque série de mesures et sa valeur est évidemment retranchée de celle observée lors de l'oxydation chromique.

Vitesses d'oxydation chromique de cyclanols secondaires au moyen d'esters chromiques dérivés d'alcools tertiaires

La méthode générale utilisée est décrite ici dans le cas de l'oxydation du cyclohexanol par le chromate de ditertiobutyle. Le cyclanol secondaire à oxyder est pesé dans un ballon de 25 ml. Ensuite, 5.0 ml (prélevés à l'aide d'une pipette) de la solution benzénique de l'ester chromique sont ajoutés à l'alcool secondaire et le mélange est agité vigoureusement durant 30 s. Il s'agit d'abord de déterminer la longueur d'onde au maximum d'absorption (λ_{max}) du mélange réactionnel.

Ensuite, la fréquence est fixée à cette valeur pour l'étude cinétique. Le chronomètre est mis en marche dès le contact alcool secondaire – ester chromique et 600 s se seront écoulées avant le début de la mesure du taux de disparition du Cr(VI). L'expérience a montré qu'une même valeur est obtenue pour la constante de vitesse à ± 20 nm du maximum du mélange; cette observation s'explique facilement par la largeur des bandes. De plus, des constantes de vitesse calculées à longueur d'onde constante ont été corroborées par d'autres calculées à longueur d'onde variable et balayages répétés à intervalles définis.

(a) Mesure d'une vitesse d'oxydation à longueur d'onde variable et balayage répété

Dans le but de vérifier les valeurs de constantes de vitesses obtenues à longueur d'onde constante, des mesures ont été faites à longueur d'onde variable et balayages répétés à intervalles définis. Les concentrations initiales respectives d'alcool secondaire et d'ester chromique sont évidemment les mêmes que lors des mesures à longueur d'onde constante.

(b) Influence de la pyridine sur la vitesse d'oxydation

Le cas examiné fut celui de l'oxydation du cyclohexanol par le chromate de ditertiobutyle. La pyridine utilisée était évidemment anhydre et classifiée "reagent"; elle fut distillée avant l'usage puis conservée sur tamis moléculaire.

Mesure de la stabilité de l'ester chromique en présence de pyridine. Il s'agissait simplement de mesurer le taux de diminution dans l'absorption du Cr(VI) pour le $(t\text{-Bu})_2\text{CrO}_4$ en présence de pyridine dans le benzène anhydre. Il a été observé que l'addition de 0.0185 g de pyridine dans 15 ml de solution benzénique de l'ester chromique n'affecte pas de façon sensible le taux de diminution dans l'absorption du Cr(VI). Dans cette mesure, la concentration en pyridine était 15.60×10^{-3} M et la concentration en ester chromique 0.39×10^{-3} M.

Mesure de la vitesse d'oxydation du cyclohexanol par le chromate de ditertiobutyle en présence de pyridine Le cyclohexanol est pesé (0.0039 g) dans un ballon de 25 ml. A l'aide d'une pipette, 5.0 ml de la solution benzénique de $(t\text{-Bu})_2\text{CrO}_4$ dont la concentration est 0.39×10^{-3} M sont ajoutés au cyclohexanol puis le mélange est agité durant une minute. Le chronomètre est mis en marche dès le contact entre le cyclohexanol et le $(t\text{-Bu})_2\text{CrO}_4$. Le ballon est de nouveau agité durant une minute. Le mélange est finalement transféré dans une cellule en quartz de 1 cm puis dans un compartiment thermostaté. La compensation optique est faite avec une solution de pyridine (15.60×10^{-3} M) dans le benzène. Un délai de 600 s s'écoule avant le début d'une mesure.

(c) Influence de la nature de l'ester chromique sur la vitesse d'oxydation

Les réactions sont effectuées et les vitesses sont mesurées selon la méthode générale décrite ci-dessus à 24.05 °C dans le benzène "reagent" anhydre.

Les auteurs remercient vivement le Conseil National de Recherches du Canada, la compagnie C.I.L. et le Conseil de Recherches pour la Défense pour leur aide financière.

1. E. BECKMANN. Ann. **250**, 322 (1889).
2. H. O. HOUSE. Modern synthetic reactions. 2e ed. Benjamin, California, 1972. pp. 257–291.
3. R. OPPENAUER et H. OBERRAUCH. Anals. Asoc. Quim. Argentina, **37**, 246 (1949).
4. W. J. MURRAY et E. P. STEVENSON. Chem. Abstr. **33**, 9323 (1939).
5. D. GINSBURG et J. PAPO. J. Chem. Soc. 516 (1951).
6. T. SUGA, K. KIHARA et T. MATSUURA. Bull. Chem. Soc. Jap. **38**, (6), 893 (1965).
7. T. SUGA, K. KIHARA et T. MATSUURA. Bull. Chem. Soc. Jap. **38**, (7), 1141 (1965).
8. T. SUGA et T. MATSUURA. Bull. Chem. Soc. Jap. **38**, (9), 1503 (1965).
9. T. MATSUURA et T. SUGA. Yuki Gosei Kagaku Kyokai Shi, **25** (3), 214 (1967). Chem. Abstr. **67**, 10852b (1967).
10. H. WIENHAUS. Ber. **47**, 322 (1914).
11. A. LEO et F. H. WESTHEIMER. J. Am. Chem. Soc. **74**, 4383 (1952).
12. H. G. KUIVILA et W. J. BECKER. J. Am. Chem. Soc. **74**, 5329 (1952).
13. J. C. RICHER et N. T. HOA. Can. J. Chem. **47**, 2479 (1969).
14. J. C. RICHER, L. A. PILATO et E. L. ELIEL. Chem. Ind. (London), 2007 (1961).
15. E. L. ELIEL, S. H. SHROETER, T. J. BRETT, F. J. BIROS et J. C. RICHER. J. Am. Chem. Soc. **88**, 3327 (1966).
16. J. C. RICHER et C. GILARDEAU. Can. J. Chem. **43**, 538 (1965).
17. H. C. BROWN et M. GERSTEIN. J. Am. Chem. Soc. **72**, 2926 (1950); J. C. BROWN, R. S. FLETCHER et R. B. JOHANNESEN. J. Am. Chem. Soc. **73**, 212 (1951); H. C. BROWN et M. BORKOWSKI. J. Am. Chem. Soc. **74**, 1894 (1952).
18. H. H. ZEISS et D. W. PEASE, JR. J. Am. Chem. Soc. **78**, 3182 (1956).
19. A. LEO et F. H. WESTHEIMER. J. Am. Chem. Soc. **74**, 4383 (1952).
20. C. DUVAL, J. LECOMPTE et C. WADIER. C. R. **257** (25). 3766 (1963); F. J. DARNELL et W. H. CLOUD. Bull. Soc. Chim. Fr. **4**, 1164 (1965); G. LORTHIOIR et A. MICHEL. Bull. Soc. Chim. Fr. **4**, 1166 (1965); D. RODBELL et R. DE VRIES. Mater. Res. Bull. **2** (4), 491

Can. J. Chem. Downloaded from www.nrcresearchpress.com by 210.87.254.5 on 09/05/12
For personal use only.

(1967); R. M. CHRENKO et D. S. RODBELL. Phys. Lett. A **24** (4), 211 (1967).
21. J. ROCEK, F. H. WESTHEIMER, A. ESCHENMOSER, L. MOLDOVANYI et J. SCHREIBER. Helv. Chim. Acta, **45**, 2554 (1962).
22. B. W. FARNUM, S. A. FARNUM et W. A. MOSHER. Proc. N. Dak. Acad. Sci. **20**, 79 (1966).
23. J. D. ROBERTS et C. W. SAUER. J. Am. Chem. Soc. **71**, 3925 (1949).
24. S. WINSTEIN et N. J. HOLNESS. J. Am. Chem. Soc. **77**, 5562 (1955).
25. G. V. D. THIERS. J. Am. Chem. Soc. **79**, 5585 (1957); C. R. NOLLER et R. ADAMS. J. Am. Chem. Soc. **48**, 1080 (1926); H. P. UNGNADE et D. NIGHTINGALE. J. Am. Chem. Soc. **66**, 1218 (1944); J. BOESEKEN et C. J. A. HANAGRAAF. Rec. Trav. Chim. **61**, 69 (1942); H. H. ZEISS et M. TSUTSUI. J. Am. Chem. Soc. **75**, 897 (1953); L. RUZICKA et H. A. BOEKENAGEN. Helv. Chim. Acta, **14**, 1319 (1931); A. T. BLOOMQUIST, L. H. LIU et J. C. BOHRER. J. Am. Chem. Soc. **74**, 3643 (1952); M. KOBELT, P. BARMAN, V. PRELOG et L. RUZICKA. Helv. Chim. Acta, **32**, 256 (1949); E. L. ELIEL et R. S. RO. J. Am. Chem. Soc. **79**, 5992 (1957); E. G. PEPPIATT et R. J. WICKER. Chem. Ind. (London), 716 (1955).

Can. J. Chem. Downloaded from www.nrcresearchpress.com by 210.87.254.5 on 09/05/12
For personal use only.

The Nucleophilic Displacement of the Nitrate Group. 1. The Hydrolysis of a Series of Benzyl Nitrates in Water

KALAVELIL MATTHEW KOSHY[1] AND ROSS ELMORE ROBERTSON

The University of Calgary, Calgary, Alberta T2N 1N4

Received September 10, 1973

KALAVELIL MATTHEW KOSHY and ROSS ELMORE ROBERTSON. Can. J. Chem. **52**, 2485 (1974).

The temperature dependence of the rates of hydrolysis of a series of substituted benzyl nitrates in water provided estimates of the heat capacities of activation. These values varied with the substituent over a wide range ($-28 \rightarrow -101$ cal mol^{-1} deg^{-1}).

An approximate parallelism has been found to exist between the ΔC_p^* values and kinetic α-deuterium effects obtained for the nitrates and chlorides.

While recognizing the existence of specific factors contributing to individual differences, the relative values of these parameters for the individual members of the two series provide a useful measure of the ionic character of the transition state.

KALAVELIL MATTHEW KOSHY et ROSS ELMORE ROBERTSON. Can. J. Chem. **52**, 2485 (1974).

On a mesuré en solution aqueuse les vitesses d'hydrolyse d'une série de nitrates benzyliques substitués; un examen de la relation entre ces vitesses et la température a permis de déterminer les capacités calorifiques d'activation. Ces valeurs varient avec le substituant entre -28 et -101 cal mol^{-1} deg^{-1}.

Un certain parallélisme existe entre les valeurs de ΔC_p^* et les effets cinétiques du deutérium en α sur les réactions des nitrates et des chlorures.

Tout en reconnaissant l'existence de facteurs spécifiques contribuant à des différences individuelles, les valeurs relatives de ces paramètres pour des produits individuels des deux séries s'avèrent une mesure utile du caractère ionique de l'état de transition.

[Traduit par le journal]

Introduction

The chemistry of nitrate esters has been reviewed by Boschan *et al.* (1) and more recently by Connon (2). The hydrolysis of benzyl nitrates under basic conditions was found to involve both displacement and "carbonyl elimination" reactions, giving as products, benzyl alcohols and benzaldehydes (3). Electron withdrawing substituents favored the "carbonyl elimination" reaction while electron donors favored substitution. Separate rate constants for the two reactions were reported by Baker and Heggs (3). Under neutral conditions the mechanism appeared to be less complicated, benzyl alcohol being the only product (4), a fact subsequently confirmed by us.

This "clean" solvolysis of benzyl nitrates in water prompted an investigation with a view to determining the temperature dependence of the rates and kinetic α-deuterium effects for a series of substituted benzyl nitrates for comparison with similar data for benzyl chlorides (5). These comparisons are especially useful since the conclusions derived from the two sources *viz.* the activation parameters, in particular the heat capacity of activation, and α-deuterium effect provide a useful basis for the discussion of differences in mechanism.

[1]Present address: Department of Chemistry, University of Saskatchewan, Saskatoon, Saskatchewan.

Experimental

Materials

Water

Ordinary distilled water was passed through an ion exchange resin (Fisher Research Grade Rexyn I-300) and subsequently redistilled.

Nitrate Esters

All nitrate esters were prepared either by (*i*) the homogeneous method of Ferris and co-workers (6) or (*ii*) the heterogeneous method of Baker and Heggs (3). Both methods are based on the reactions between benzyl halides and silver nitrate. For the less reactive halides the homogeneous method was the method of choice.

Benzyl nitrate. Method *i*. The product was fractionally distilled: b.p. 63° (1 mm); n.m.r. $_{TMS}CCl_4$ δ 7.32 (s, 5, aryl), 5.31 (s, 2, methylene).

4-Methylbenzyl nitrate. 4-Methylbenzyl alcohol obtained by the reduction of ethyl *p*-toluate (prepared from pure *p*-toluic acid) by lithium aluminum hydride, was converted to the corresponding chloride by thionyl chloride. The nitrate was prepared from this by method *ii*: b.p. 70° (0.4 mm); n.m.r. $_{TMS}CCl_4$ δ 7.22 (s, 4, aryl), 5.3 (s, 2, methylene), 2.36 (s, 3, methyl).

Can. J. Chem. Downloaded from www.nrcresearchpress.com by 210.87.254.40 on 09/05/12
For personal use only.

Can. J. Chem. Downloaded from www.nrcresearchpress.com by 210.87.254.40 on 09/05/12
For personal use only.

4-Chlorobenzyl nitrate. A commercial sample of 4-chlorobenzyl chloride was purified by distillation under reduced pressure and converted to the nitrate by method *i*: b.p. 72° (2 mm); n.m.r. $_{TMS}CCl_4$ δ 7.35 (s, 4, aryl), 5.38 (s, 2, methylene).

4-Nitrobenzyl nitrate. Prepared from purified 4-nitrobenzyl chloride by method *i*. The product purified by recrystallization: m.p. 67–68°; n.m.r. $_{TMS}CCl_4$ δ 7.4–8.4 (m, 4, aryl), 5.5 (s, 2, methylene).

4-Trifluoromethylbenzyl nitrate. 4-Trifluoromethylbenzyl bromide (Air Products & Chemicals Inc.) was converted to the nitrate by method *i*: b.p. 56° (0.3 mm); n.m.r. $_{TMS}CCl_4$ δ 7.32–7.77 (m, 4, aryl) 5.41 (s, 2, methylene).

3-Methoxybenzyl nitrate. 3-Methoxybenzyl chloride prepared from 3-methoxybenzyl alcohol (Aldrich) was converted to the nitrate by method *i*: b.p. 70° (0.2 mm); n.m.r. $_{TMS}CCl_4$ δ 6.67–7.39 (m, 4, aryl), 5.27 (s, 2, methylene), 3.75 (s, 3, methoxy).

Rate Measurements

Rate measurements were made by a conductance method which has been described previously (7). Temperature control was good to $\sim\pm 0.002$ °C and the temperatures were measured by a platinum resistance thermometer and an L & N Type G-1 Mueller Bridge. Before starting rate measurements on a given compound, the conductance cells were washed with acetone and steamed for 3 h to get rid of materials adsorbed on the walls. Doubly distilled water containing a trace of KNO_3 as backing electrolyte was introduced and the filled cells were placed in a constant temperature bath in the temperature range of study for at least 24 h. After this preliminary conditioning, the cells were not allowed to dry out, the spent solution from one kinetic run being replaced by a fresh solution immediately prior to a new rate determination. This technique was designed to minimize errors due to adsorption on the walls.

Product Determination

In each case a neutral equivalent determination of the acid produced by the hydrolysis confirmed the assumption that 1 mol of nitric acid was produced for each mole of nitrate ester reacting. For this latter purpose, the hydrolysis had to be carried out under heterogeneous conditions but this was not considered to have a significant bearing on the above conclusions.

The products of hydrolysis for 4-methylbenzyl nitrate and 4-nitrobenzyl nitrate (compounds representing the two ends of the reactivity scale for our series) were extracted with ether and were found to contain only the respective alcohols by n.m.r. and g.l.c.

Further, the amounts of NO_2^- ion produced during the hydrolysis of all the nitrate esters were estimated by a sensitive method (8). In all cases, the amount of NO_2^- found corresponded to less than 0.01% "carbonyl elimination."

Insofar as could be judged by the products, it was concluded that the benzyl nitrates hydrolyzed in water remarkably free from side reactions.

Results and Discussion

In Table 1 we give a typical set of temperature–rate data for benzyl nitrate.

Values of specific rate constants for each benzyl nitrate (the average of four replicate runs) for a series of temperatures covering a range of about 30° were fitted to the empirical equation

$$\log_{10} k = A_1 + A_2/T + A_3 \log_{10} T$$

The values of the constants A_1, A_2, and A_3 are reported in Table 2. These constants permit the calculation of the specific rate constant at any desired temperature within the experimental range and with less accuracy beyond that range. The activation parameters were derived on the

TABLE 1. Pseudo first-order rate data for the hydrolysis of benzyl nitrate in water[a]

Temperature (°C)	Rate $\times 10^{-4}$ (s^{-1})	Estimated[b] error $\times 10^{-6}$
41.475	0.5261	0.1
41.475	0.5240	0.1
41.475	0.5237	0.1
46.059	0.9517	0.2
46.059	0.9551	0.1
46.059	0.9503	0.1
46.059	0.9533	0.1
48.257	1.252	0.5
48.257	1.250	0.5
49.747	1.514	0.2
49.747	1.516	0.2
49.747	1.517	0.2
49.747	1.514	0.2
54.067	2.565	0.9
54.067	2.556	1.2
54.067	2.561	0.9
55.805	3.138	0.4
55.853	3.151	0.5
59.417	4.760	1.5
59.417	4.761	1.2
59.417	4.776	1.5
59.417	4.773	1.3
60.666	5.483	0.2
60.666	5.477	0.2
60.666	5.477	0.2
64.700	8.568	0.4
64.700	8.565	0.6
68.281	12.540	1.0
68.281	12.590	0.6
69.075	13.700	4.3
69.075	13.770	2.4
77.837	33.170	5.4
77.837	33.220	5.6
77.837	33.030	7.7
80.987	44.550	12.7
80.987	44.540	11.5
81.177	45.610	9.8
81.177	45.540	9.8
81.177	45.540	9.8
81.467	47.170	8.7
81.467	47.250	7.8
81.467	46.760	9.9

[a]These data were obtained in part by Dr. Jan Han Ong.
[b]Calculated deviation from LMS plot.

TABLE 2. Empirical constants[a] for the interpolation of rates

Compound	A_1	$-A_2$	$-A_3$	T_1/T_2 (°C)[b]
Benzyl nitrate	103.0797	9858.501	30.43700	41–81
p-Chlorobenzyl nitrate	90.72482	9341.646	26.24825	46–79
3-Methoxybenzyl nitrate	67.20602	8149.836	18.35576	35–64
p-Methylbenzyl nitrate	161.3484	12174.42	50.04481	10–41
p-Nitrobenzyl nitrate	61.19654	7900.292	16.97718	73–90
p-Trifluoromethylbenzyl nitrate	49.47034	7202.352	13.00073	58–89

[a]For the equation $\log_{10} k = A_1 + (A_2/T) + A_3 \log_{10} T$.
[b]T_1/T_2 define experimental temperature range.

TABLE 3. Enthalpies and entropies of activation for the solvolysis in water of benzyl nitrates at 50 °C

Compound	$\Delta H^{\ddagger}$ (cal mol^{-1})	$\Delta S^{\ddagger}$ (cal mol^{-1} deg^{-1})	$\Delta C_p^{\ddagger}$ (cal mol^{-1} deg^{-1})
Benzyl nitrate	24.9±0.0	1.1±0.1	−62±1
4-Chlorobenzyl nitrate	25.2±0.1	0.9±0.3	−54±7
3-Methoxybenzyl nitrate	24.9±0.0	−0.4±0.0	−38±2
4-Methylbenzyl nitrate	22.9±0.1	−3.5±0.3	−101±5
4-Trifluoromethylbenzyl nitrate	24.0±0.2	−9.4±0.6	−28±8
4-Nitrobenzyl nitrate	24.6±0.4	−9.3±1.1	−35±12

basis of transition state theory and are discussed in terms of this formalism. Were the temperature coefficient of the Arrhenius activation energy substituted as an empirical parameter, the conclusions would not be altered. The derived pseudothermodynamic values are collected in Table 3.

Because the value of the temperature coefficient of $\Delta H^{\ddagger}$ is sensitive to mechanistic complexity and because alternative reaction paths yielding identical products are possible in the solvolysis of nitrate esters (2), it is obvious that the identification of the specific reaction path or paths that the solvolysis of benzyl nitrates follows is essential for a meaningful interpretation of our results. The fact that the solvolytic product in all the cases consisted of at least 99.9% of the corresponding benzyl alcohol rules out, for all practical purposes, the possibility of "carbonyl elimination." However, the formation of benzyl alcohols can, in principle, proceed by displacement of the NO_3^- group from the α-carbon atom or by nucleophilic attack on nitrogen (2). That the former is the predominant mechanism in a number of cases is evident from the relatively large α-deuterium effect and its near constancy with temperature[2] and the large value of the Hammett reaction constant. These two mechanistic indicators are consistent with C—O bond fission and the development of considerable carbonium ion character at the transition state. From the limited data available it would appear that the rate data for the hydrolysis of a series of substituted benzyl nitrates, as in the case of the corresponding chlorides, show considerable departure for a single Hammett plot.

The temperature coefficient of the apparent enthalpy of activation ($\Delta C_p^{\ddagger}$) for the hydrolysis of such compounds in water (in the absence of such spurious effects as impurities (9)) has been shown to be dependent to the extent of about −30 cal mol^{-1} deg^{-1} on factors other than the structural properties of the water system. More negative values of this coefficient reflect the degree of solvent reorganization in the activation process and are traceable to the nature of initial state solvation, the nature of the groups being displaced and the degree of charge development at the transition state. Benzenesulfonate and methanesulfonate ions disturb water structure very little in comparison to the displacement of a halide ion (*cf.* the value of $\Delta C_p^{\ddagger} = -40$ cal mol^{-1} deg^{-1} found for the hydrolysis of 3-methyl-2-butylmethane sulfonate with the corresponding value of −80 cal mol^{-1} deg^{-1} for displacement of the bromide (10). The value of $\Delta C_p^{\ddagger}$ for hydrolysis of *t*-butyl chloride is −81 cal mol^{-1} deg^{-1} and about the same value was

[2]See Table 4; the temperature effect within the noted temperature range is not greater than 1–2% of the observed effect.

Can. J. Chem. Downloaded from www.nrcresearchpress.com by 210.87.254.40 on 09/05/12
For personal use only.

TABLE 4. Heat capacities of activation and kinetic α-deuterium effect for the solvolysis of benzyl nitrates and benzyl chlorides in water

Compound	$-\Delta C_p^{\ddagger}$ (cal mol^{-1} deg^{-1})	k_H/k_D [a] (per two deuterium atoms)	T_1/T_2
4-Methylbenzyl nitrate	101 ± 5	1.384 ± 0.003 [c]	24–44
4-Methylbenzyl chloride	79 ± 3 [b]	1.279 ± 0.002 [b]	19–40
4-Chlorobenzyl nitrate	54 ± 7	1.252 ± 0.003 [c]	60–71
Benzyl nitrate	62 ± 1	1.240 ± 0.003 [c]	49–74
3-Methoxybenzyl nitrate	38 ± 2	1.238 ± 0.002	35–64
Benzyl chloride	41 ± 5 [d]	1.095 ± 0.002 [b]	54–78
4-Chlorobenzyl chloride	48 ± 9 [b]	1.061 ± 0.003 [b]	60–80
4-Nitrobenzyl nitrate	35 ± 12		
4-Trifluoromethylbenzyl nitrate	28 ± 8	0.976 ± 0.002	70–90

[a]Average of k_H/k_D values measured at three different temperatures.
[b]From ref. 5.
[c]From ref. 19.
[d]From ref. 20.

obtained for 4-methylbenzyl chloride (5). From the available data, compounds tending to hydrolyze by an ionizing mechanism in water are dependent on the nature of the ionizing group and in the range of about $-80 \rightarrow -100$ for the halides and, as will be shown in this and in subsequent papers, to be $-100 \rightarrow -150$ cal mol^{-1} deg^{-1} for the displacement of the nitrate group.

The less negative values of $\Delta C_p^{\ddagger}$ found for the hydrolysis of the 4-Cl, 4-NO_2, and 4-CF_3 benzyl nitrates (Table 4) lie in the same range as the earlier value for the hydrolysis of methyl nitrate (-44 cal mol^{-1} deg^{-1}) reported by McKinley-McKee and Moelwyn-Hughes (11) and these values are also in the same range as the values found by Heppolette and Robertson for the hydrolysis of the methyl halides (12). In all of these latter examples the component of $\Delta C_p^{\ddagger}$ to be attributed to structure breaking of the solvent at the transition state is small. There is some indication that at low levels of charge development at the transition state, charge distribution in the nitrate group leads to less solvent interaction than in the case of the halides, a characteristic of the sulfonate ions (13). As the mechanism shifts to a more limiting state, the developing nitrate ion, as might be expected, gives evidence of being a better structure breaker than the halides. Thus, the values of $\Delta C_p^{\ddagger}$ for the unsubstituted and the 4-methylbenzyl nitrates are about -20 cal mol^{-1} deg^{-1} more negative than we found for the corresponding benzyl chlorides (5). In view of the lower values noted above where bond making was important, these latter differences are indicative not of initial state differences but of differences in the degree of solvent reorganization at the transition state. The more negative values can be attributed in part to the greater "structure breaking" characteristic of the fully charged nitrate ion compared to that of the halides (14) in aqueous solution ($\Delta S_0(Cl^-) = 19$ e.u. and $\Delta S_0(NO_3^-) = 40.5$ e.u. with reference to $\Delta S_0(H^+) = -5.5$ e.u.) (15).

The kinetic α-deuterium isotope effect has been shown to provide an alternative indication of the extent of bond fission at the transition state independent of solvation (16–18). Values of this rate ratio, k_H/k_D, for the benzyl nitrates (19) together with corresponding data for the chlorides (5) and the $\Delta C_p^{\ddagger}$ values are collected in Table 4. In general, the α-deuterium effects for the hydrolysis of the nitrates are somewhat larger than for the displacement of the corresponding chloride, the limiting value probably being a little less than found for the displacement of a tosylate (21). Similarly, for a very different reason, the values of $\Delta C_p^{\ddagger}$ are more negative for 4-methyl and unsubstituted benzyl nitrates where solvent structure-breaking is significant on activation. Both of these effects in a general way reflect the degree of bond fission at the transition state, hence, it is reasonable that a positive correlation should be found between these two different parameters within the same series. In view of the differences cited above, it may seem surprising that the series of benzyl chlorides and nitrates taken together should approximate to a smooth curve (Fig. 1). 3-Methoxybenzyl nitrate shows a rather large deviation from this correlation due to its $\Delta C_p^{\ddagger}$ being more positive than expected. The modifica-

Can. J. Chem. Downloaded from www.nrcresearchpress.com by 210.87.254.40 on 09/05/12
For personal use only.

TABLE 5. $\Delta\Delta H^{\ddagger}$ and $\Delta\Delta S^{\ddagger}$ [a] values and relative rates for displacement of NO_3^- and Cl^- from Y-$C_6H_4CH_2$-X

Y	Temperature (°C)	$\Delta\Delta H^{\ddagger}$ (cal mol^{-1})	$\Delta\Delta S^{\ddagger}$ (cal mol^{-1} deg^{-1})	k_{NO_3}/k_{Cl}
4-Me	25	2700	10.50	
	50	2530	8.65	1.5
4-Cl	50	4600	11.1	0.7
H	50	4450	13.3	0.7
3MeO				0.8
4NO_2	50	2780	6	0.3
	75	3468	8	

[a] $\Delta\Delta X^{\ddagger} = \Delta X^{\ddagger}_{NO_3^-} - \Delta X^{\ddagger}_{Cl^-}$.

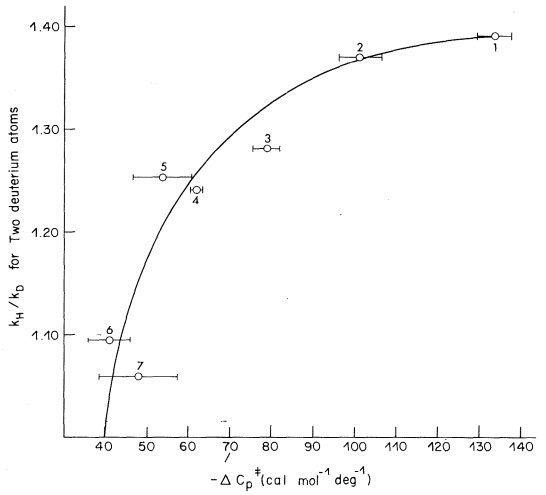

FIG. 1. Correlation of kinetic α-deuterium effect with s$C_p^{\ddagger}$.

tion of the solvation pattern of the initial state and the transition state (22) by the methoxy group which can strongly interact with the solvent may be responsible for this smaller magnitude of $\Delta C_p^{\ddagger}$. Similar deviations from regular behavior have been reported for the solvolysis of 4-methoxybenzenesulfonyl chloride (23) and for the ionization of 4-methoxybenzoic acid (24).

In spite of the accuracy with which $\Delta H^{\ddagger}$ and $\Delta S^{\ddagger}$ are determined in this study, the quantitative interpretation of differences in these parameters arising from *para* substitution presents obvious difficulties. These are most apparent if we examine differences in $\Delta H^{\ddagger}$ for displacement of the nitrate and chloride ions from each of the substituted benzylic compounds (Table 5).

From Table 5 it is apparent that the relative rates of displacement of the two ions ($k_{NO_3^-}/k_{Cl^-}$) are not greatly different for each pair. These rate ratios are much less, for example, than that reported by Lucas and Hammett (25) for the corresponding displacement from *t*-butyl where a ratio of 50 was found. Kevill and Suthoff (26) reported this ratio to be 2890 for the relative rates of decomposition of the latter pair in acetonitrile, though this ratio need not be significant in the present comparison. In both of the latter studies on displacement from the *t*-butyl group, the difference in the rates of reaction was found to be due to the more positive entropy of activation, favoring the nitrate, the differences in $\Delta H^{\ddagger}$ being small. In aqueous ethanol, Baker and Heggs (3) found that the variation in $\Delta H^{\ddagger}$ for solvolysis of a series of benzyl nitrates was in the order of ± 0.3 kcal, the differences in the rate arising to a much larger degree from differences in the apparent entropy of activation, hence presumably, to solvation differences. Part of this solvent dependent difference may be attributed to the structural character of water and to the greater structure-breaking ability of the nitrate compared to the chloride ion. Such a combination will result in more positive values of $\Delta H^{\ddagger}$ and $\Delta S^{\ddagger}$ in the activation processes involving displacement of the nitrate ion compared to the displacement of the chloride ion. Such an explanation will account for part of the observed difference and implies a more negative value of $\Delta C_p^{\ddagger}$ as already noted. Where bond making is more important and the transition state is characterized by a low degree of ionic character (compare the $\Delta\Delta H^{\ddagger}$ and k_{NO_3}/k_{Cl} values for methyl with 4-nitro, Table 5), reorganization of the solvent becomes less important and some other factor must account for the observed differences in $\Delta H^{\ddagger}$ and $\Delta S^{\ddagger}$ and the similarity in the values of $\Delta C_p^{\ddagger}$. Wold and Exner begin their most recent paper on the statistics of enthalpy–entropy relationship

Can. J. Chem. Downloaded from www.nrcresearchpress.com by 210.87.254.40 on 09/05/12
For personal use only.

with the statement "few concepts in chemistry have reached a state of such confusion as the enthalpy–entropy relationship" (27). While the compensation law to which these authors refer differs from the comparison made above, their conclusion would seem applicable here.

1. R. BOSCHAN, R. MERROW, and R. W. VAN DOLAH. Chem. Rev. **55**, 485 (1955).
2. N. W. CONNON. Eastman Organic Chemical Bulletin. Vol. **42**, No. 2. 1970.
3. J. W. BAKER and T. G. HEGGS. J. Chem. Soc. 616 (1955).
4. J. W. BAKER and A. J. NEALE. J. Chem. Soc. 608 (1955).
5. K. M. KOSHY, R. E. ROBERTSON, and W. M. J. STRACHAN. Can. J. Chem. **51**, 2958 (1973).
6. A. F. FERRIS, K. W. MCLEAN, I. G. MARKS, and W. D. EMMONS. J. Am. Chem. Soc. **75**, 4078 (1953).
7. R. E. ROBERTSON and S. E. SUGAMORI. J. Am. Chem. Soc. **91**, 7254 (1969).
8. APHA, AWWA, and FSIWA. Standard methods for the examination of water, sewage and industrial wastes. American Public Health Association Inc., New York. 1955.
9. L. J. BRUBACHER, L. TREINDL, and R. E. ROBERTSON. J. Am. Chem. Soc. **90**, 4611 (1968).
10. Y. INOMOTO, R. E. ROBERTSON, and G. SARKIS. Can. J. Chem. **47**, 4599 (1969).
11. J. S. MCKINLEY-MCKEE and E. A. MOELWYN-HUGHES. Trans. Faraday Soc. **48**, 247 (1952).
12. R. L. HEPPOLETTE and R. E. ROBERTSON. Proc. Roy. Soc. A, **252**, 273 (1959).
13. H. M. R. HOFFMANN. J. Chem. Soc. 6753 (1965).
14. H. S. FRANK and W. Y. WEN. Dis. Faraday Soc. **24**, 113 (1957).
15. R. W. GURNEY. Ionic processes in solution. McGraw-Hill Book Company Inc., New York. 1953.
16. V. J. SHINER, JR. *In* Isotope effects in chemical reactions. A.C.S. Monograph No. 157. *Edited by* C. J. Collins and N. S. Bowman. Van Nostrand Reinhold Co., New York. 1971.
17. A. STREITWIESER, JR., R. C. FAHEY, R. H. JAGOW, and S. SUZUKI. J. Am. Chem. Soc. **80**, 2326 (1958).
18. S. SELTZER. J. Am. Chem. Soc. **83**, 2625 (1961).
19. K. M. KOSHY and R. E. ROBERTSON. J. Am. Chem. Soc. **96**, 914 (1974).
20. J. M. W. SCOTT and R. E. ROBERTSON. J. Chem. Soc. 1596 (1961).
21. J. M. HARRIS, R. E. HALL, and P. v. R. SCHLEYER. J. Am. Chem. Soc. **93**, 2551 (1971).
22. R. E. ROBERTSON. *In* Progress in physical organic chemistry. Vol. 4. Interscience Publishers, New York. 1967. p. 213.
23. R. E. ROBERTSON and B. ROSSALL. Can. J. Chem. **49**, 1441 (1971).
24. J. W. LARSON and L. G. HEPLER. *In* Solute solvent interactions. *Edited by* J. F. Coetzee and C. D. Ritchie. Marcel Dekker, Inc., New York. 1969.
25. G. R. LUCAS and L. P. HAMMETT. J. Am. Chem. Soc. **64**, 1928 (1945).
26. D. N. KEVILL and R. F. SUTHOFF. J. Am. Chem. Soc. 366 (1969).
27. S. WOLD and O. EXNER. Chemica Scripta, **3**, 5 (1973).

Can. J. Chem. Downloaded from www.nrcresearchpress.com by 210.87.254.40 on 09/05/12
For personal use only.

Photolysis of Di-tert-butyl Peroxide in Solution

EDUARDO LISSI[1]

Departamento de Química, Universidad Técnica del Estado, Santiago, Chile

Received November 27, 1973

EDUARDO LISSI. Can. J. Chem. **52**, 2491 (1974).

Di-tert-butyl peroxide has been photolyzed at 3130 Å in carbon tetrachloride solution in the presence of cyclohexane. The quantum yield of free tert-butoxy radicals was 1.9 ± 0.1, independent of the hydrocarbon concentration. Unlike results obtained in the gas phase at 2537 Å, no evidence for the quenching of the excited peroxide molecule could be detected.

EDUARDO LISSI. Can. J. Chem. **52**, 2491 (1974).

On a effectué la photolyse à 3130 Å du peroxyde de tert-butyle en solution dans le tétrachlorure de carbone en présence de cyclohexane. Le rendement quantique de radicaux libres tert-butoxy est de 1.9 ± 0.1; ce rendement est indépendant de la concentration d'hydrocarbure. Contrairement aux résultats obtenus en phase gazeuse à 2537 Å, on n'a pu détecter aucun signe de désactivation des molécules excitées de peroxyde. [Traduit par le journal]

Can. J. Chem. Downloaded from www.nrcresearchpress.com by 210.87.254.42 on 09/05/12
For personal use only.

The photolysis of di-tert-butyl peroxide in solution has been frequently employed as a clean tert-butoxy radical source (1). Nevertheless, recent results obtained by Yip and Pritchard on the gas phase photolysis of di-tert-butyl peroxide at 2537 Å cast doubts about the simplicity of its photodecomposition (2). In this work it was found that the quantum yield of reaction 1

[1] $$P^* \rightarrow 2\ t\text{-BuO}^\bullet$$

where P* stands for an excited peroxide molecule, is pressure dependent when hydrocarbons (propane or cyclopropane) are employed as pressurizing gases. At 1 mol/l hydrocarbon concentration, the tert-butoxy radical quantum yield drops to nearly 0.5 (from a value of two obtained at low pressure). Yip and Pritchard postulated that reaction 2

[2] $$P^* + M \rightarrow P + M$$

competes with the decomposition of the excited peroxide molecule. Since reaction 2 should have to be particularly important in solution, we have reinvestigated the photodecomposition of di-tert-butyl peroxide in carbon tetrachloride in the presence of different concentrations of cyclohexane.

Photolyses were carried out in a "merry-go-round" apparatus. Since a medium pressure mercury lamp was employed and the reaction tubes were made of Pyrex, most of the absorbed radiation was in the 3130 Å region. Acetone and tert-butanol were analyzed by gas–liquid chromatography.

Actinometries were carried out employing 2-pentanone as standard. A value of 0.3 was taken for the acetone quantum yield in *n*-hexane (3).

The obtained results can be summarized as follows: (*i*) At 22°, the tert-butanol quantum yield was 1.9 ± 0.1, independent of cyclohexane concentration in the 0.095 to 9.3 mol/l range. (*ii*) At 74°, absolute quantum yields were not determined but ($\phi_{acetone} + \phi_{tert\text{-}butanol}$) was constant (less than 7% variation) when the cyclohexane concentration was changed from 0.03 to 1.2 mol/l. (*iii*) At 78°, the total product quantum yield was independent of di-tert-butyl peroxide concentration and light intensity. (*iv*) At 74°, $\phi_{tert\text{-}butanol}/\phi_{acetone}$ was linear with cyclohexane concentration.

Point (*iii*) shows that under our experimental conditions an induced peroxide decomposition must be minimal. This is in agreement with results obtained in similar systems (4).

Points (*i*) and (*iv*) indicate that reaction 3

[3] $$P^* \rightarrow \text{acetone} + \text{products}$$

is negligible in the 20 to 74° temperature range. In fact, we obtain that at 20° the quantum yield of reaction 3 must be lower than 0.02. This result agrees with qualitative data reported previously for the photolysis of di-tert-butyl peroxide in solution at 40° (5), and with the results obtained

[1]Present address: Departmento de Físico Química, Facultad de Ciencias, Universidad de Buenos Aires, Ciudad Universitaria, Buenos Aires, Argentina.

in the gas photolysis at 2537 Å (2). Furthermore, the results obtained at 74° are compatible with a simple mechanism comprising reactions 1, 4, and 5

[4] $t\text{-BuO}^{\bullet} + c\text{C}_6\text{H}_{12} \rightarrow t\text{-BuOH} + c\text{C}_6\text{H}_{11}^{\bullet}$

[5] $t\text{-BuO}^{\bullet} \rightarrow \text{acetone} + \text{CH}_3^{\bullet}$

The data obtained at 74° give $k_4/k_5 = 8.0$ l/mol.

Points (*i*) and (*ii*) are the most relevant to the present discussion. They indicate that reaction 2 cannot be important under our experimental conditions, even in neat cyclohexane. The value 1.9 obtained for the tert-butanol quantum yield at room temperature is particularly meaningful since it is compatible with a unity quantum yield for reaction 1 and the estimated cage recombination of tert-butoxy radicals in a solvent like carbon tetrachloride (6). The results obtained in the present work are then significantly different from those obtained in the gas phase by Yip and Pritchard (2). The reason for this difference is not clear since the fact that the wavelengths used were different is not expected to lead to different behavior in the high pressure limit. Further work would be necessary to elucidate this point.

1. H. B. HEMBEST, J. A. W. REID, and C. J. M. STIRLING. J. Chem. Soc. 5239 (1961); 1217 (1964); W. J. MAGUIRE and R. C. PINK. Trans. Faraday Soc. **63**, 1907 (1967); A. G. DAVIES and B. P. ROBERTS. J. Chem. Soc. D, 699 (1969); A. G. DAVIES, D. GRITTER, and B. P. ROBERTS. Perkin Trans. II, 993 (1972); A. G. DAVIES, B. P. ROBERTS, and J. C. SCAIANO. J. Organometal. Chem. **42**, C27 (1972).
2. C. K. YIP and H. O. PRITCHARD. Can. J. Chem. **50**, 1531 (1972).
3. J. C. DALTON and N. J. TURRO. Ann. Rev. of Phys. Chem. **21**, 499 (1970).
4. W. PRYOR. Tetrahedron Lett. 1201 (1963).
5. H. B. HENBEST, J. A. W. REID, and C. J. M. STIRLING. J. Chem. Soc. 1220 (1964).
6. T. G. TRAYLOR and H. KIEFER. J. Am. Chem. Soc. **89**, 6667 (1967).

Can. J. Chem. Downloaded from www.nrcresearchpress.com by 210.87.254.42 on 09/05/12
For personal use only.

Carbon-13 Nuclear Magnetic Resonance Spectra of Carcinogenic Polynuclear Hydrocarbons. I. 3-Methylcholanthrene and Related Benzanthracenes[1]

RICHARD S. OZUBKO[2] AND GERALD W. BUCHANAN[3]

Department of Chemistry, Carleton University, Ottawa, Canada K1S 5B6

AND

IAN C. P. SMITH

Division of Biological Sciences, National Research Council of Canada, Ottawa, Canada K1A 0R6

Received February 6, 1974

RICHARD S. OZUBKO, GERALD W. BUCHANAN, and IAN C. P. SMITH. Can. J. Chem. **52**, 2493 (1974).

Carbon-13 chemical shifts are reported for a series of carcinogenically active and related inactive polynuclear hydrocarbons. Resonance assignments for complex systems such as 3-methylcholanthrene, dibenzanthracenes, benz[*a*]anthracene and its 7-methyl and 7,12-dimethyl derivative, have been made primarily from a study of simpler models, including phenanthrene, triphenylene, and anthracene. Selective proton decoupling has been employed extensively. Quaternary carbon assignments have been aided by deuterium isotope shift and spin–lattice relaxation time measurements. Vicinal C—D couplings have been found to be unreliable as means of assignment for quaternary carbons.

RICHARD S. OZUBKO, GERALD W. BUCHANAN et IAN C. P. SMITH. Can. J. Chem. **52**, 2493 (1974).

On rapporte les déplacements chimiques du ^{13}C pour une série d'hydrocarbures polynucléaires dont quelques uns sont cancérigènes. L'attribution des positions de résonance dans les systèmes complexes tels le méthyl-3 cholanthrène les dibenzanthracènes, le benz[*a*]anthracène et ses dérivés méthyl-7 et diméthyl-7,12 sont fait principalement par comparaison avec des modèles plus simples tels que le phénanthrène, le triphénylène et l'anthracène. On a utilisé d'une façon extensive les découplages sélectifs de proton. On a attribué les résonances des carbones quaternaires à l'aide de mesures de déplacements dus aux effets isotopiques du deutérium et aux mesures de temps de relaxation spin–réseau. On trouve que les constantes de couplage vicinal C—D ne sont pas satisfaisantes pour déterminer les déplacements chimiques des atomes de carbone quaternaires. [Traduit par le journal]

Introduction

During the past decade a great deal of attention has been directed toward the elucidation of proton n.m.r. spectra of polycyclic condensed benzenoid hydrocarbons. Initial attempts (1–8) at 60 and 100 MHz were incomplete due to peak overlap and spectral complexity. Subsequent examinations at 220 MHz combined with iterative computer analysis have furnished reliable proton data for a series of benzanthracenes, benzpyrenes, and 3-methylcholanthrene (9, 10).

The cancer-inducing properties of many of these molecules (11, 12) make them the object of theoretical interest. Numerous theories relating electronic structure, chemical reactivity, and carcinogenic power of alternant hydrocarbons have been advanced (11, 13 and references therein). It is in connection with the electronic structures of these systems that the carbon-13 n.m.r. parameters are of greatest interest. Potentially the ^{13}C chemical shifts should yield more valuable information regarding local electronic properties at carbon than the shieldings of the bonded protons. Accordingly we have obtained and analyzed the Fourier transform ^{13}C spectra of a series of benzanthracenes, and that for the most potent carcinogenic hydrocarbon known, 3-methylcholanthrene.

Results and Discussion

The numbering scheme (14) and structures for the fifteen compounds included in the present study are presented in Fig. 1.

Assignments of resonance positions were accomplished using a variety of techniques. Initially resonances for quaternary carbons can be separated from those for carbons bearing

[1]NRCC No. 13972.
[2]NRCC Postgraduate Scholar 1972–present.
[3]To whom correspondence should be addressed.

Can. J. Chem. Downloaded from www.nrcresearchpress.com by 210.87.254.5 on 09/05/12
For personal use only.

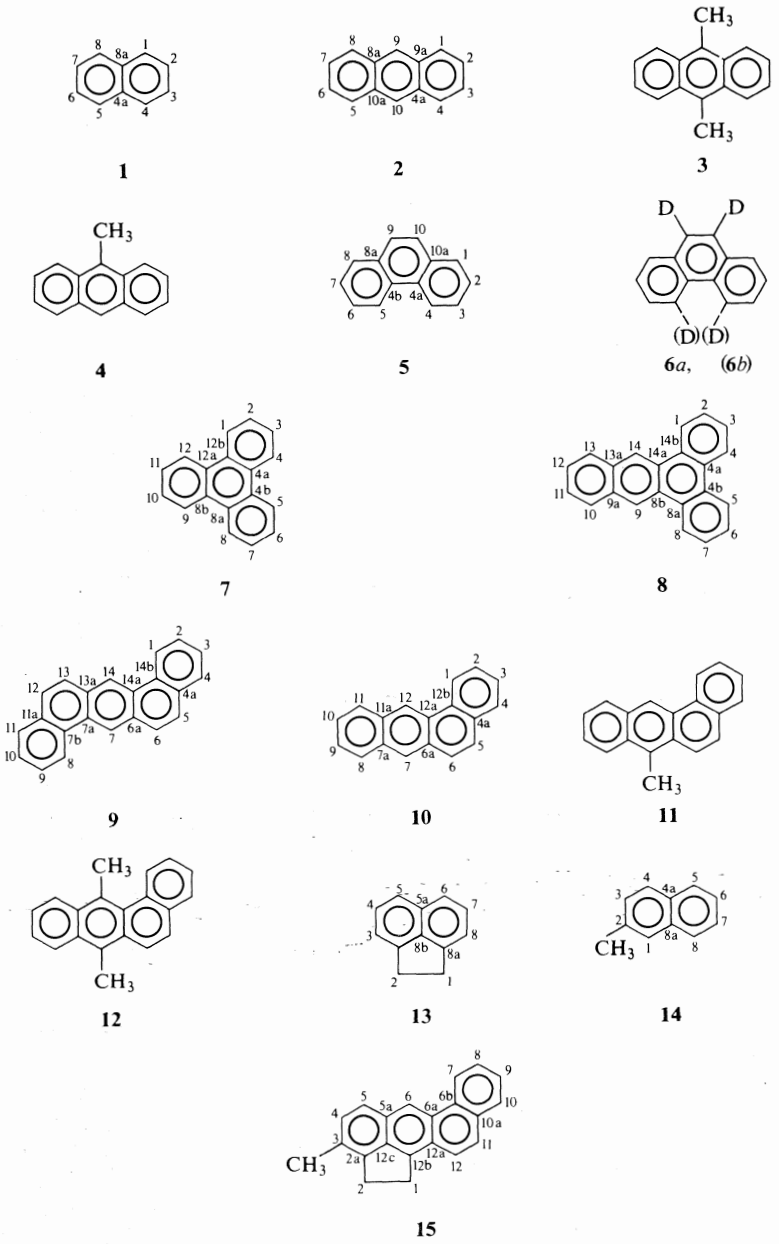

FIG. 1. Numbering scheme for polynuclear hydrocarbons.

directly bonded hydrogens by the retention of singlet structure for the former in off-resonance decoupling experiments. Furthermore a reduced nuclear Overhauser enhancement for quaternary centres is evident. In cases where assigned proton data are available, specific ^1H decoupling using the graphical method of Birdsall, *et al.* (15) was employed. This method is particularly applicable to closely spaced ^{13}C signals. Extensive use was made of model compounds, empirical chemical shift additivity correlations, and, occasionally, deuterium substitution.

Ring carbon shifts for compounds **1**–**8**, **9**–**12**, and **13**–**15** are presented in Tables 1, 2, and 3, respectively, while methyl carbon data are collected in Table 4.

Can. J. Chem. Downloaded from www.nrcresearchpress.com by 210.87.254.5 on 09/05/12
For personal use only.

TABLE 1. ^{13}C shieldings for **1–8** (δ_c from TMS ± 0.1)

	Compound								
Position	**1**	**2**	**3**	**4**	**5**	***6a***	***6b***	**7**	**8**
C-1	127.7	128.3	125.3	124.6d	128.5	128.5	128.5	123.2	123.4a
C-2	125.6	125.2	124.6	125.3d	126.5	126.5	126.5	127.1	127.4b
C-3	125.6	125.2	124.6	125.2d	126.5	126.5	126.4	127.1	127.6b
C-4	127.7	128.3	125.3	129.0	122.6	122.6	122.3	123.2	123.6a
C-4a	133.3	131.6	129.9	131.5	130.3	130.3	130.2	129.7	130.1c
C-4b					130.3	130.3	130.2	129.7	130.1c
C-5	127.7	128.3	125.3	129.0	122.6	122.6	122.3	123.2	123.6a
C-6	125.6	125.2	124.6	125.2d	126.5	126.5	126.4	127.1	127.6b
C-7	125.6	125.2	124.6	125.3d	126.5	126.5	126.5	127.1	127.4b
C-8	127.7	128.3	125.3	124.6d	128.5	128.5	128.5	123.2	123.4a
C-8a	133.3	131.6	129.9	130.1	132.0	131.9	132.0	129.7	130.2c
C-8b								129.7	128.5
C-9		126.1	128.3	130.0	126.9	126.7	126.9	123.2	122.0
C-9a		131.6	129.9	130.1					132.3
C-10		126.1	128.3	124.8	126.9	126.7	126.9	127.1	128.1
C-10a		131.6	129.9	131.5	132.0	131.9	132.0		
C-11								127.1	126.0
C-12								123.2	126.0
C-12a								129.7	
C-12b								129.7	
C-13									128.1
C-13a									132.3
C-14									122.0
C-14a									128.5
C-14b									130.2c

NOTE: a–d indicate groups of resonances where specific assignments cannot be made due to proximity.

All spectra were recorded using $CDCl_3$ solutions.

Ring Carbon Chemical Shifts

Results for naphthalene (**1**) in $CDCl_3$ are similar to those reported for CS_2 solutions (16). For anthracene (**2**) however, the C-9,10 shifts in $CDCl_3$ are *ca.* 6 p.p.m. upfield from those in benzene solution as determined by Grant and co-workers (17). We have repeated this experiment and find the previous results for anthracene in C_6D_6 to be in error. Correct chemical shifts for C-9,10 and C-1,4,5,8 of **2** are δ 126.9 and 128.7, respectively. Values for C-2,3,6,7 and C-9a,10a are close to those in $CDCl_3$, and the aromatic solvent induced shifts for **2** are all less than 1 p.p.m. Our assignments for **2** agree with those recently reported by Gunther (18).

For 9,10-dimethylanthracene (**3**), the most remarkable effect of methyl substitution is the 3.0 p.p.m. upfield displacement of C-1,4,5,8 relative to that observed in **2**. A "γ" relationship exists between the methyl carbons and the C-1,4,5,8 positions, respectively. Apparently this is a further example of the now well-established upfield γ ^{13}C steric shift (19–22) for which a theoretical model based on charge polarization has been proposed (22). Nonbonded interactions between the methyl protons and protons at C-1,4,5,8 no doubt will perturb the electron distribution at these positions and increase their shielding. Employing **3** as a model and with selective decoupling, chemical shifts for **4** can then be assigned.

Previous work on phenanthrene (**5**) (16, 23) has not permitted clear distinction between the resonances for quaternary centers 4a,4b *vs.* 8a,10a. By examination of the 9,10- and 4,5-dideuterio derivatives ***6a*** and ***6b***, respectively, these resonances can be assigned with confidence. The most useful phenomenon in this respect is the isotope shift (24) of carbons adjacent to the deuterium-bearing carbon; it is generally in the upfield direction by 0.12 ± 0.04 p.p.m., and that of the next-nearest carbon is insignificant. In the ^{13}C spectrum of the 9,10-dideuterio derivative (***6a***), the chemical shift of the pair of quaternary carbons resonating at 132.0 p.p.m. in **5** has shifted upfield by 0.05 p.p.m. Conversely, in the 4,5-dideuterio deriva-

Can. J. Chem. Downloaded from www.nrcresearchpress.com by 210.87.254.5 on 09/05/12
For personal use only.

Can. J. Chem. Downloaded from www.nrcresearchpress.com by 210.87.254.5 on 09/05/12
For personal use only.

TABLE 2. ^{13}C shieldings for **9–12** (δ_c from TMS ± 0.1)

	Compound			
Position	**9**	**10**	**11**	**12**
C-1	122.8	122.8	123.6	130.2
C-2	126.9	126.7a	126.8	126.3f
C-3	126.7	126.6a	126.8	126.4f
C-4	128.6	128.5b	128.3	127.4
C-4a	132.0	131.9	131.7e	132.2h
C-5	127.1	126.9	126.9	125.5
C-6	127.4	126.9	123.1	123.8
C-6a	129.1	131.9	131.5e	133.2h
C-7	122.1	127.2	131.0	129.0h
C-7a	130.8	131.8	129.8	129.1h
C-7b	130.2			
C-8	122.8	128.3b	124.4	124.9g
C-9	126.9	125.6c	125.2	125.3
C-10	126.7	125.7c	125.7	125.1
C-11	128.6	127.6b	129.3	124.7g
C-11a	132.0	128.8	128.7	129.1h
C-12	127.1	121.4	120.3	127.7h
C-12a		130.5d	130.9	131.3h
C-12b		130.6d	130.5	130.5h
C-13	127.4			
C-13a	129.1			
C-14	122.1			
C-14a	130.8			
C-14b	130.2			

NOTE: a–h indicate groups of resonances where specific assignments cannot be made.

tive ***6b*** an 0.07 p.p.m. upfield displacement is noted for the quaternary carbons resonating at 130.3 p.p.m. in **5**. In both deuterio compounds the resonance of the alternate pair of quaternary carbons changes by less than 0.01 p.p.m. relative to that in **5**. Identical concentrations of **5**, ***6a***, and ***6b*** have been used and therefore we assign the resonances in **5** at 132.0 and 130.3 p.p.m. to pairs of carbons 8a,10a and 4a,4b, respectively. These are further substantiated by the relative values of spin–lattice relaxation times (T_1) in these compounds (*vide infra*).

An alternate possibility for assigning the resonances of quaternary carbons 4a, 4b, 8a, and 10a is to utilize the observation that geminal $^{13}C—^{2}H$ couplings (J_{CC^2H}) are usually small (<0.15 Hz), whereas the corresponding *vicinal* ($J_{^{13}CCC^2H}$) couplings vary between zero and >1 Hz depending upon the dihedral angle. Such an approach is not applicable to ***6a*** because each of quaternary carbons 4a, 4b, 8a, and 10a is *trans* to one or the other deuterium. Only a slight difference in couplings due to different paths, might be expected. In fact the resonance at 131.9 p.p.m. (attributed to 8a and 10a above) is visibly tripled with a splitting of *ca.* 1.3 Hz, whereas that at 130.3 p.p.m. (attributed to 4a and 4b above) is a single line of width *ca.* 1.1 Hz (coupling $\leqslant 0.4$ Hz). Thus the coupling pathway $^{2}H_{10}C_{10}C_9C_{8a}$ is more effective than $^{2}H_9C_9C_{8a}C_{4b}$. In contrast, in compound ***6b*** the deuterium at position 4 has a dihedral angle of *ca.* 180° with C_{10a} and 0° with C_{4b}. Thus, depending on the symmetry of the relationship linking the vicinal couplings and dihedral angles, approximately equal and large ($\geqslant 1$ Hz) ^{2}H

TABLE 3. ^{13}C shieldings for **13–15** (δ_c from TMS ± 0.1)

	Compound		
Position	**13**	**14***	**15**
C-1	30.2	126.7	29.7_3b
C-2	30.2	134.7	29.6_9b
C-2a	145.6		143.2
C-3	118.9	127.7	128.3
C-4	127.5	127.4	130.7
C-4a		131.6	
C-5	122.0	127.4	122.8
C-5a	131.4		127.4
C-6	122.0	124.8	116.3
C-6a			131.7c
C-6b			129.9
C-7	127.5	125.2	123.3
C-8	118.9	126.9	126.4d
C-8a	145.6	133.2	
C-8b	139.0		
C-9			126.5d
C-10			128.6
C-10a			131.9c
C-11			125.9d
C-12			123.8
C-12a			125.3
C-12b			142.7
C-12c			137.7

NOTE: b–d indicate groups of resonances where specific assignments cannot be made.
*Reference 28.

TABLE 4. ^{13}C shieldings for methyl carbons (δ_c p.p.m. from TMS ± 0.1)

	Compound					
Position	**3**	**4**	**11**	**12**	**14***	**15**
2					21.4	
3						18.6
7			14.1	14.2		
9	14.0	13.8				
10	14.0					
12				21.0		

*Saturated solution in $CDCl_3$.

Can. J. Chem. Downloaded from www.nrcresearchpress.com by 210.87.254.5 on 09/05/12
For personal use only.

couplings to both C_{4b} and C_{10a} (or C_{4a} and C_{8a}) are expected. In the ^{13}C spectra of ***6b*** the resonance at 132.0 p.p.m. (attributed to 8a and 10a) has a width of *ca.* 2.5 Hz (coupling $\leqslant$ 0.8 Hz) and that at 130.2 p.p.m. (attributed to 4a and 4b) has a width of *ca.* 1.8 Hz (coupling $\leqslant$ 0.6 Hz), demonstrating that the *trans* arrangement leads to a slightly greater coupling as observed in ^1H—^1H vicinal couplings (25). Accordingly, the small magnitude of the vicinal ^{13}C—^2H couplings and their sensitivity to the nature of the path, make them unreliable means of assignment of quaternary carbons in these molecules.

Shifts for triphenylene (**7**) in $CDCl_3$ are reasonably close to those previously reported in CS_2 (20). Triphenylene constitutes a useful model for the C-1 to C-8 region of dibenz[*a*,*c*]anthracene (**8**). Shieldings at carbons 1, 2, 3, 4, 4a, 4b, 5, 6, 7, 8, 8a, and 14b of **8** are remarkably similar to those for corresponding carbons of **7**. Specific assignments within several groups of resonances are not possible due to small chemical shift differences. These are denoted by letters in the tables. The quaternary centers 9a and 13a of **8** were assigned by analogy with those in anthracene, leaving the higher field quaternary resonance at δ 128.5 to be associated with C-8b and -14a. The C-9,14 protons appear as a singlet at lowest field and therefore specific decoupling permitted clear assignment of the resonance at δ 122.0 to these carbons. It is interesting that these carbons appear *ca.* 4 p.p.m. to higher field than C-9,10 of anthracene, presumably due to the γ steric interaction involving C-1 and -8, respectively.

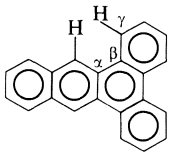

The assignment for C-10,13 of **8** is by analogy with C-1,4,5,8 of **2**. Similarly C-11,12 of **8** are close in resonance position to C-2,3,6,7 of **2**.

The ^1H n.m.r. spectrum of dibenz[*a*,*h*]anthracene (**9**) has been completely assigned at 220 MHz (9). As a result, specific ^1H decoupling permits clear assignment of resonances for the methine carbons 1–14. Presumably the γ steric shift is responsible for the high-field resonances for C-1,8 and C-7,14. The validity of the model compound approach can be tested here. It is likely that the environment of C-4,11 in **9** is similar to C-1,8 of **5** and the chemical shifts for these carbons are found to be within 0.3 p.p.m. Likewise, the environments of C-5,6,12,13 of **9** should most closely approximate that of C-9,10 of phenanthrene and a close correspondence in their shieldings is noted. Accordingly we feel justified in using the model compound approach in further assignments.

In considering the quaternary carbon resonances of **9** extensive use of the simpler model compounds was employed. It is expected that 4a,11a of **9** will be similar to 8a,10a of **5** and therefore the chemical shift at 132.0 is assigned to these positions. Analogously the 7b,14b carbons of **9** are given a value of 130.2, using 4a,4b of **5** as a model. The 8b,14a quaternary carbons of **8** were used to assign the resonance at 130.8 to the 7a,14a carbons of **9**. By elimination the remaining resonance at 129.1 must correspond to C-6a,13a of **9**.

Details of the ^1H n.m.r. spectrum of benz[*a*]anthracene (**10**) have been published (9) and from these, specific ^1H decoupling allows definite assignment of the C-1,7 and 12 resonances. Once more the 1 and 12 carbons are shifted upfield due to the γ effect. Shielding for C-2 and -3 are nearly identical and are close to those for C-2 and -3 of **5** and **9**. The double intensity resonance at 126.9 was attributed to C-5 and -6 by analogy with C-9,10 of **5**. Protons at C-9 and -10 of **10** appear at the highest field position (9) and specific ^1H decoupling sharpens ^{13}C resonances at δ 125.6 and 125.7. Again, predictions based on the C-2,3,6,7 resonances for **1** and **2** would lend credence to the applicability of model compounds. Unambiguous assignments are not possible for the remaining methine carbon resonances at δ 127.6, 128.3, and 128.5. One might expect, however, that C-1 of **5** would serve as a model for C-4 of **10** and that C-8 and -11 of **10** should have a similar shift to C-1 of **2**. These expectations are realized.

Quaternary carbon assignments for **10** have been made in the following manner. C-12a and -12b are designated as appearing at 130.5 and/or 130.6, respectively, due to the similarity with C-4a,4b of **5**. Remarkably, C-4a and -6a of **10** appear at the identical position (131.9) to 8a and 10a of **5**. Carbon 7a should be similar to 4a, 8a, 9a, and 10a in **2** leaving the remaining resonance at 128.8 to be associated with 11a.

Can. J. Chem. Downloaded from www.nrcresearchpress.com by 210.87.254.5 on 09/05/12
For personal use only.

Knowledge of the ^1H spectral parameters (9) for 7-methyl benz[*a*]anthracene (**11**) facilitated specific decoupling experiments. Substitution of the methyl group at C-7 causes notable changes relative to **10** only at the C-6, -7, and -8 carbons. The 3.7 p.p.m. downfield shift at C-7 is consistent with the empirically established trends of alkyl substitution on ^{13}C shieldings (20). The upfield shifts of *ca.* 4 p.p.m. at C-6 and C-8 are presumably due to the γ steric shift mentioned earlier.

In the 7,12-dimethyl benz[*a*]anthracene (**12**), the most remarkable observation is the 6.6 p.p.m. downfield shift at C-1 relative to C-1 of **11**. Apparently this constitutes another example of the recently reported deshielding "δ" effect whereby substantial downfield shifts are found in compounds containing spatially interacting δ functions (26, 27). The 6.6 p.p.m. effect in **12**

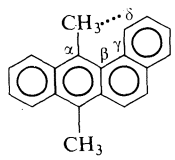

vs. **11** is the same as that observed for the methyl groups of 1,8-dimethylnaphthalene relative to the 1,4-dimethyl derivative (26).

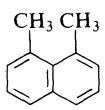

The upfield shift of 3.6 p.p.m. at C-11 of **12** relative to **11** is again attributed to a γ steric shift. For the quaternary centers of **12** only the 4a resonance can be clearly assigned and remaining designations must be regarded as tentative.

Shieldings for acenaphthene[4] (**13**) and 2-methylnaphthalene (**14**) have been previously reported and discussed (20, 28). These constitute particularly important model compounds for 3-methylcholanthrene (**15**).

The ^1H spectrum of **15** in CS_2 has been published and complete assignments have been made (9). In $CDCl_3$ solution the overall spectral appearance is similar to that in CS_2, however only three resonances are sufficiently isolated to enable specific ^1H decoupling of the carbon resonances. Initially the H-6 proton is a singlet at lowest field and specific decoupling shows that C-6 appears at δ 116.3. Relative to C-6 of acenaphthene (**13**) an upfield shift of 5.7 p.p.m. is evident which can be attributed to the γ effect of the 7 position in **15**. The proton at C-7 appears as a doublet at next lowest field in the spectrum and specific decoupling indicates a shift of 123.3 p.p.m. for C-7. Predictably this is very close to the shieldings for C-1 of **7**–**11**. The aromatic proton at highest field in the spectrum of **15** is that bonded to C-4. The resonance at δ 130.7 is associated with this position from specific decoupling. If one employs C-4 of **13** as a model and allows for a downfield shift of 2.1 p.p.m. from *ortho* methyl substitution (compare **1** and **14**), the predicted shift for C-4 of **15** is (127.5 + 2.1) = 129.6, in reasonable agreement with that found. Similarly using **13** as a model and considering the influence of *meta* substitution in **14** *vs.* **1**, a shielding of 121.7 is predicted for C-5 of **15**, again within 1 p.p.m. of the observed shift.

Resonances for C-8,9 of **15** were assigned by analogy to C-2,3 of phenanthrene (**5**) as was C-10 of **15** which is similar to C-1 of **5**. For C-11, appearing at 125.9, the resonance of C-9,10 of **5** (126.6) was used as a model but we cannot clearly distinguish this from the 8,9 resonances of **15**. For C-12 of **15** a shift of 123.8 p.p.m. is found, *i.e.* 2.8 p.p.m. to higher field than C-9,10 of **5**. A γ steric interaction with the C-1 position is deemed responsible for this effect. Surprisingly, the C-1,2 resonances of **15** are shielded by only 0.5 p.p.m. relative to C-1,2 of **13**, despite the apparent existence of γ steric interactions of C-1 and -2 of **15** with C-12 and the 3-methyl group, respectively.

Quaternary carbon assignments for the 2a, 12b, and 12c positions of **15** were made by analogy with **13** and in light of the known deshielding effects of *ortho* methyl substitution (20). For C-3 of **15**, the C-3,8 resonance of **13** at 118.9 was taken as a starting point and then combined with the known deshielding of 9.1 p.p.m. for C-1 of toluene relative to benzene, to predict a shift of 128.0 p.p.m., in good agreement with the observed 128.3. Assignment of the δ 131.9 resonance to C-10a of **15** is made by analogy with C-8a,10a of **5** and C-4a,6a of **10**. Similarly the peak at 129.9 p.p.m. is attributed to C-6b of **15** based on the chemical shift of C-4a,4b of **5**.

The C-12a resonance for **15** was assigned using C-6a of **10** (δ 131.9) as a reference point. Then the effects of the ethano bridge and methyl substitution were evaluated by comparing

[4]We thank Professor J. B. Stothers for communicating shieldings for **13** recorded in $CDCl_3$ solution.

Can. J. Chem. Downloaded from www.nrcresearchpress.com by 210.87.254.5 on 09/05/12
For personal use only.

C-3,8 of **13** (δ 118.9), and C-7 of **14** (δ 125.2), respectively, with C-2,3 of **1** (δ 125.6). The predicted chemical shift for C-12a is therefore 124.8 p.p.m. (*i.e.* 131.9 − 6.7 − 0.4), and justifies its association with the high-field resonance at δ 125.3. In a similar manner, C-6a of **15** is deemed to resonate at δ 131.7, employing C-12a of **10** as a reference point and comparing **1** with **13** and **14**. The remaining resonance at δ 127.4 is left to be associated with C-5a.

Methyl Carbon Chemical Shifts

In Table 4 it is interesting to note the similarity of the methyl shieldings for **3**, **4**, **11**, and the C-7 methyl group of **12** (14.0 ± 0.2 p.p.m.). The downfield shift of 6.8 p.p.m. for the C-12 methyl of **12** is attributed to the δ interaction (26, 27) with C-1 as described earlier. Notably the magnitude of the δ effect is comparable at C-1 and -12.

For 2-methylnaphthalene (**14**) the shielding of 21.4 p.p.m. is close to that observed for toluene (20). The upfield shift of 2.8 p.p.m. for the 3-methyl group of **15** likely arises from a γ interaction involving the C-2 methylene function, although it is puzzling that the phenomenon is not reciprocal at C-2.

Interestingly the methyl carbon shielding for 1-methylnaphthalene is 19.1 p.p.m. (23). This upfield shift of 2.3 p.p.m. relative to **14** suggests that steric repulsions between the CH_3 hydrogens and the *peri* hydrogen of the adjacent ring are operative. Similar interactions in **3**, **4**, **11** and for C-7 of **12** probably contribute to the high field resonance positions observed for the methyls.

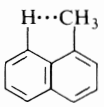

Spin–Lattice Relaxation Times (T_1)

The recent work of Levy (29) has demonstrated that ^{13}C T_1's may allow distinction between various types of nonprotonated carbons based on the distances to nearby protons. Values for mescaline-d_3 are indicated below. Relaxation of mescaline is dominated by the $^{13}C—^{1}H$ dipole–dipole mechanism.

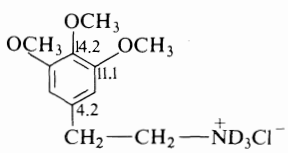

Accordingly C-4 with no *ortho* protons has the longest T_1 (14.2 s) while those for C-3 and -5 are somewhat shorter. For C-1, with two *ortho* protons and the CH_2 protons, relaxation is fastest.

In an attempt to put our assignments for quaternary carbons on a firmer basis, T_1 measurements were carried out. Results are presented in Fig. 2 for **5**, **6***a*, **6***b*, and **8**. The greater standard deviations for compounds **6***a*, **6***b*, and **8** are due to poorer signal-to-noise ratios in the spectra, a consequence of the smaller amounts of these compounds available.

For phenanthrene (**5**) the resonance at 132.0 p.p.m. had a T_1 significantly shorter (≥twice the standard deviation) than that of the resonance at 130.3 p.p.m. This is consistent with the assignment shown in Fig. 2, in which C-10a (8a) has two geminal hydrogens and C-4a (4b) has only one. Confirmation of this comes from the data for 9,10-dideuteriophenanthrene (**6***a*) in which one of the hydrogens geminal to C-10a has been replaced by deuterium, whose dipole–dipole coupling to ^{13}C is only *ca.* 10% of that of ^{1}H. This should substantially decrease its contribution to ^{13}C relaxation. The T_1 values for C-10a and -4a are equal (within the standard deviation), in agreement with the presence of only one geminal hydrogen. A similar argument applies to the T_1 values for 4,5-dideuteriophenanthrene (**6***b*). In this case the T_1 values for C-4a (4b) could not be determined accurately within a reasonable time due to their great length. However, the data clearly indicate that the resonance assigned to C-10a (8a) relaxes substantially faster than that assigned to C-4a (4b), as expected for

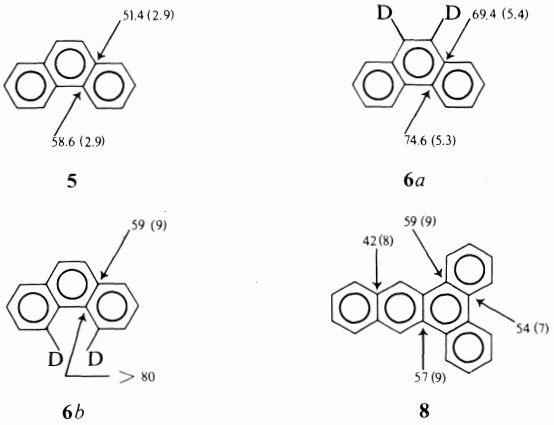

FIG. 2. Spin–lattice relaxation times for designated carbons (in seconds). Standard deviations are indicated in parenthesis.

Can. J. Chem. Downloaded from www.nrcresearchpress.com by 210.87.254.5 on 09/05/12
For personal use only.

TABLE 5. Carcinogenic properties of hydrocarbons

Compound	Activity
1–5, 7, 8	0
9	Mild
10	Mild
11	Mild
12	Potent
13	0
14	0
15	Very potent

two hydrogens geminal to C-10a (8a) and none to C-4a (4b). Thus the T_1 data are in complete accord with the assignments made on the basis of deuterium isotope shifts (*vide supra*).

The T_1 values for dibenz[*a*,*c*]anthracene (**8**) allow distinction of one ambiguous quaternary resonance (132.3 p.p.m.) from the other three (128.5, 130.1, and 130.2 p.p.m.). The shorter T_1 value is attributable to C-13a (9a) which has two geminal hydrogens.

Carbon Shieldings and Carcinogenic Activity

Table 5 lists the known cancer inducing properties of compounds **1–15** (11, 12). It is interesting to compare the chemical shifts for structurally related inactive compounds such as phenanthrene (**5**) with active materials such as dibenz[*a*,*h*]anthracene (**9**). Assignments for these molecules are unambiguous from deuteration and specific decoupling, respectively.

It has been suggested (11, 13) that the activity of **9** is due to the presence of a bond which is active for addition reactions (K region shown below). It is now apparent, however, that an active K region, although a necessary condition for carcinogenic potency, is not a sufficient one.

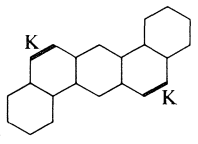

9

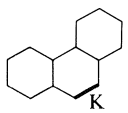

5

^{13}C shieldings for K region carbons of **9** are nearly identical (within 1 p.p.m.) to those for C-9,10 of **5** which implies no large differences in electron density at K region carbons of active and inactive materials.

Recent ^1H n.m.r. results of Clin and Lemanceau (30) indicate that the noncarcinogenic dibenz[*a*,*j*]acridine forms only 1:1 complexes with benzene, whereas the carcinogenic dibenz[*a*,*c*]acridine may form 1:2 complexes. This being the case, it may be possible to distinguish between active and inactive hydrocarbon sites using solvent induced chemical shifts, and such experiments are in progress.

Results for related epoxides and benzpyrenes will be the subject of future reports.

Experimental

Materials

Compounds **1** and **2** were obtained from Fisher Scientific Co. Ltd., Montreal, Quebec and were used without further purification. Samples of **3**, **4**, **5**, **7**, **8**, **9**, **10**, **11**, **12**, and **15** were purchased from K and K Laboratories Inc., Plainview, New York.

Spectra

Nuclear magnetic resonance spectra of ^{13}C in natural abundance were obtained by the pulsed Fourier transform technique at 25.16 MHz on a Varian XL-100-15 spectrometer. The free-induction decays were stored in a Varian 620/L computer (16K memory) and were Fourier transformed after a sufficient number had been accumulated. Before transformation all interferograms were smoothed with an exponential function to enhance signal-to-noise. The maximum number of data points used in accumulating the interferograms was 8192. The spectral widths varied with the resolution required.

Samples were studied in tubes of 12 mm outer diameter with concentrations on the range 0.09 to 0.40 *M* in $CDCl_3$; (concentration effects on chemical shifts are small in this range). The deuterium of the solvent was used as a field-frequency lock and all chemical shifts are expressed as downfield from internal TMS. Routinely, spectra were recorded with complete proton noise decoupling at a probe temperature of 32 °C. For the specific decoupling experiments, proton irradiation was carried out at low decoupler power (104 dB) with no noise modulation. The decoupler was calibrated by irradiating the protons of TMS under low power conditions.

Spin–lattice relaxation times were measured using a pulse sequence of $(90° - HS - \tau - 90° - AT - HS)_n$ where τ is a variable internal and HS is a 20 ms pulse to spoil the homogeneity along the z axis (31). The 16K T_1 program was supplied by Ellis and Peters.[5] The experimental points were fitted to be best straight line satisfying the relationship $\ln(\delta_\infty - \delta_\tau) = -\tau/T_1$ and standard deviations were calculated accordingly.

G. W. Buchanan thanks the National Cancer Institute of Canada and the National Research Council of Canada for financial support. We thank Drs. L. C. Leitch and R. Renaud for samples of deuterated compounds **6***a* and **6***b*.

1. P. DURAND, J. PARELLO, and N. P. BUN-HOI. Bull. Soc. Chim. Fr. 2438 (1963).
2. J. D. MEMORY and T. B. COBB. J. Chem. Phys. **38**, 1453 (1963).

[5]P. D. Ellis and C. S. Peters. Private communication. December 1973.

3. R. H. MARTIN, N. DEFAY, F. GEERTS-EVRARD, and S. DELAVARENNE. Tetrahedron, **20**, 1073 (1964).
4. T. J. BATTERHAM, L. TSAI, and H. ZIFFER. Aust. J. Chem. **18**, 1959 (1965).
5. J. D. MEMORY, C. W. PARKER, and J. C. HALSEY. J. Chem. Phys. **45**, 3567 (1966).
6. C. MACLEAN, J. H. VAN DER WAALS, and E. L. MACKOR. Mol. Phys. **1**, 247 (1958).
7. J. S. WAUGH and R. W. FESSENDEN. J. Am. Chem. Soc. **79**, 846 (1957).
8. T. B. COBB and J. D. MEMORY. J. Chem. Phys. **47**, 2020 (1967).
9. K. D. BARTLE, D. W. JONES, and R. S. MATTHEWS. Spectrochim. Acta, **25**A 1603 (1969).
10. C. W. HAIGH and R. B. MALLION. J. Mol. Spect. **29**, 478 (1969).
11. A. PULLMAN and B. PULLMAN. Cancerisation par les substances chimiques et structure moléculaire. Masson, Paris. 1955.
12. P. DAUDEL and R. DAUDEL. Chemical carcinogenesis and molecular biology. John Wiley and Sons Ltd., New York. 1966.
13. E. CAVALIERI and M. CALVIN. Proc. Nat. Acad. Sci. U.S.A. **68**, 1251 (1971).
14. Definitive rules for nomenclature of organic chemistry, A. IUPAC, 1957.
15. B. BIRDSALL, N. J. M. BIRDSALL, and J. FEENEY. Chem. Commun. 316 (1972).
16. T. D. ALGER, D. M. GRANT, and E. G. PAUL. J. Am. Chem. Soc. **88**, 5397 (1966).
17. R. J. PUGMIRE, D. M. GRANT, M. J. ROBINS, and R. K. ROBINS. J. Am. Chem. Soc. **91**, 6381 (1969).
18. H. GUNTHER., H. SCHMICKLER, and G. JIKELI. J. Magn. Res. **11**, 1333 (1973).
19. G. W. BUCHANAN, D. A. ROSS, and J. B. STOTHERS. J. Am. Chem. Soc. **88**, 4301 (1966).
20. J. B. STOTHERS. Carbon-13 NMR spectroscopy. Academic Press, New York, N.Y. 1972.
21. N. K. WILSON and J. B. STOTHERS. Topics in stereochemistry. Vol. 8. *Edited by* E. L. Eliel and N. L. Allinger. Interscience, New York, N.Y. 1973.
22. D. M. GRANT and B. V. CHENEY. J. Am. Chem. Soc. **89**, 5315 (1967).
23. L. F. JOHNSON and W. C. JANKOWSKI. Carbon-13 NMR spectra. John Wiley and Sons, New York, N.Y. 1972.
24. R. A. BELL, C. L. CHAN, and B. G. SAYER. Chem. Commun. 67 (1972).
25. M. KARPLUS. J. Chem. Phys. **30**, 11 (1959).
26. S. H. GROVER, J. P. GUTHRIE, J. B. STOTHERS, and C. T. TAN. J. Magn. Res. **10**, 227 (1973).
27. G. W. BUCHANAN, J. B. STOTHERS, and G. WOOD. Can. J. Chem. **51**, 3746 (1973).
28. D. DODDRELL and P. R. WELLS. J. Chem. Soc. Perkin II, 1333 (1973).
29. G. C. LEVY. Acc. Chem. Res. **6**, 161 (1973).
30. B. CLIN and A. LEMANCEAU. C.R. Acad. Sc. Paris, Serie C, **276**, 323 (1973).
31. G. G. MACDONALD and J. S. LEIGH, JR. J. Magn. Res. **9**, 358 (1973).

Can. J. Chem. Downloaded from www.nrcresearchpress.com by 210.87.254.5 on 09/05/12
For personal use only.

Etude de l'influence de l'ionicité du milieu réactionnel sur les propriétés texturales de gels d'oxyde de titane

HENRY BRUSSET, HENRI-GEORGES MENDELBAUM ET CHANTAL FLICOTEAUX

Ecole Centrale des Arts et Manufactures, Institut de Chimie, Grande Voie des Vignes, 92 Chatenay -Malabry, France

Reçu le 5 novembre 1973

HENRY BRUSSET, HENRI-GEORGES MENDELBAUM et CHANTAL FLICOTEAUX. Can. J. Chem. **52**, 2502 (1974).

Une étude systématique a été effectuée, concernant l'influence de deux facteurs: l'acidité et la présence d'un solvant dans le milieu réactionnel de synthèse des gels d'oxyde de titane. Cette étude montre que dans un milieu acide aqueux l'évolution des propriétés texturales est liée à la concentration en ions H^+ dissociés. La présence d'un solvant, tels que le butanol ou le benzène de basse constante diélectrique dans un milieu réactionnel acide, atténue l'évolution des propriétés texturales en diminuant la dissociation ionique de l'acide. Nos résultats peuvent expliquer les mesures apparemment divergentes de la littérature.

HENRY BRUSSET, HENRI-GEORGES MENDELBAUM, and CHANTAL FLICOTEAUX. Can. J. Chem. **52**, 2502 (1974).

A systematic study has been made of the influence of two factors on the synthesis of titanium dioxide gels: (*i*) the acidity of the reaction medium and (*ii*) the presence of a solvent. This study demonstrates that, in an aqueous acid medium, the development of textural properties is related to the concentration of free hydrogen ions. The presence in an acid reaction medium of a solvent, such as butanol or benzene, of low dielectric constant, inhibits the development of the structural properties by lowering the ionic dissociation of the acid. Our results provide an explanation for the apparently divergent measurements in the literature.

[Journal translation]

Introduction

L'influence de l'acidité du milieu réactionnel sur la texture des gels d'oxyde de titane a suscité deux courants d'opinions. La première tendance suppose que l'acidité du milieu réactionnel influence le mode d'association des particules de sol lors de la coagulation des gels. Ainsi Gregg et Pope (1) en utilisant du butylate de titane pur et des solutions d'acide sulfurique plus ou moins concentrées, ont observé une évolution de la surface spécifique et du volume poreux en fonction de la concentration en acide sulfurique bien que le diamètre de pore reste sensiblement constant.

L'autre tendance suggère que l'acidité du milieu réactionnel entraine peu ou pas de variations des propriétés texturales. En effet, Harris et Whitaker (2) en hydrolysant des solutions de butylate de titane à 20% en poids dans le benzène par divers mélanges tampons, ont constaté une légère variation du diamètre de pore passant par un maximum lorsque le p*H* est voisin de 4. De même Vicarini *et al.* (3) en faisant réagir des solutions de butylate de titane à 10% en poids dans le butanol avec de l'acide acétique plus ou moins concentré, n'ont pas observé de variations sensibles de la surface spécifique et du volume poreux en fonction de l'acidité du milieu réactionnel.

Nous avons pensé que cette divergence d'opinion pouvait provenir du fait que les auteurs ont opéré avec des acides de forces différentes et surtout dans un milieu réactionnel acide soit en absence (1), soit en présence (2, 3) d'un solvant tel que le benzène ou le butanol.

C'est pourquoi nous avons étudié l'effet de l'influence du milieu ionisant en présence ou en absence d'un alcool (tel que le butanol) sur les propriétés texturales des gels ainsi synthétisés. Nous nous sommes placés dans des conditions opératoires aussi voisines que possible de celles utilisées par Gregg et Pope (1) puis Vicarini *et al.* (3), afin de tenter de comprendre la diversité des résultats trouvés dans la littérature.

Parmi les méthodes de préparation de gels d'oxyde de titane, nous avons choisi celle de Gregg et Pope (1) qui présente de nombreux avantages par rapport aux autres méthodes. Elle peut s'effectuer à température ambiante, soit en présence, soit en absence de butanol, et avec une quantité d'eau déterminée. Les caractéristiques texturales des produits ainsi synthétisés sont déterminées par une étude d'adsorption d'azote à

Can. J. Chem. Downloaded from www.nrcresearchpress.com by 178.218.224.3 on 09/06/12
For personal use only.

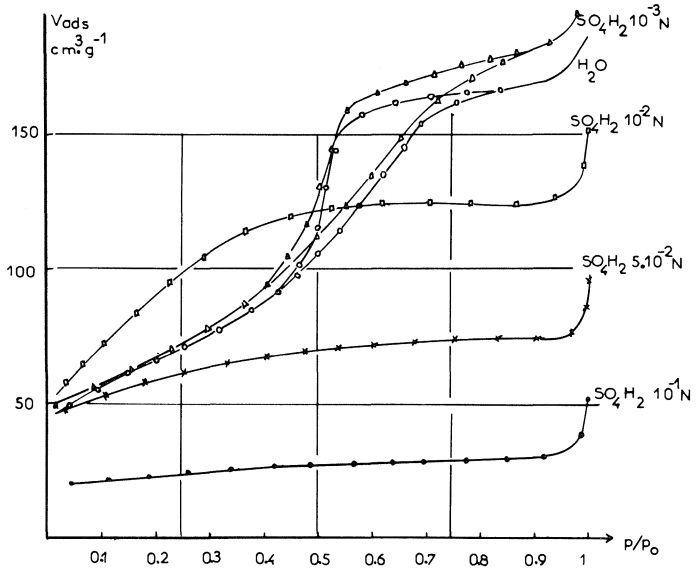

FIG. 1. Isothermes d'adsorption d'azote à −195 °C sur des gels d'oxyde de titane préparés en solutions sulfuriques (en absence de butanol).

−195 °C. La pureté des produits de départ et les méthodes de calcul employées sont analogues à celles décrites précédemment (4).

Influence de l'acidité du milieu réactionnel en absence de butanol

Toutes nos préparations sont éffectuées sans butanol et à température ambiante par addition goutte à goutte de butylate de titane, soit à diverses solutions d'acide sulfurique dont la concentration est comprise entre 10^{-3} N et N, soit à diverses solutions d'acide acétique dont la concentration est comprise entre 10^{-1} N et N. Le tout est placé sous courant d'azote et sous agitation pendant quelques heures. Le domaine de concentration utilisé a été choisi de façon à se replacer dans des conditions opératoires aussi voisines que possible de celles employées par divers auteurs de la littérature (1, 3). Seule la solution d'acide sulfurique normale n'a pas donné naissance à un précipité. Dans les autres cas les précipités gélatineux sont mis à décanter pendant une nuit. Ils sont ensuite lavés à l'eau distillée de pH = 5.9 et séchés à l'étuve à 110 °C pendant 24 h. Les solides ainsi obtenus, étudiés par diffraction des rayons X et le rayonnement $K\alpha_1$ du cuivre, présentent un faible état de cristallisation se traduisant par un fond continu important et la présence des raies diffuses de l'anatase.

Une étude par adsorption d'azote à −195 °C sur ces solides préalablement dégazés à 110 °C sous un vide de 10^{-2} Torr pendant 18 h, montre que les isothermes d'adsorption évoluent du type I au type IV de la classification de Brunauer *et al.* (5) lorsque la concentration en acide sulfurique ou en acide acétique décroit (voir figs. 1, 3 et 4). Les résultats de nos mesures d'adsorption sont rassemblés dans le tableau 1. Un calcul statistique sur un grand nombre de mesures nous a permis de déterminer que les valeurs moyennes indiquées dans ce tableau sont connues à 5% près avec une probabilité de 95% (8).

Ce tableau nous montre qu'il existe une bonne concordance entre les surfaces spécifiques calculées par les méthodes B.E.T. (5) et B.J.H. (6). Par ailleurs la présence ou l'absence de butanol n'influence pas les propriétés texturales des gels d'oxyde de titane synthétisés en milieu neutre (4). En effet dans les deux cas, les surfaces respectives sont 220 $m^2 g^{-1}$ (4) et 238 $m^2 g^{-1}$ et les diamètres de pores respectifs supposés cylindriques sont de 42 Å (4) et 44 Å.

Par contre il est possible d'observer une évolution de la surface spécifique, du volume microporeux, du volume poreux total et du diamètre de pore lorsque la concentration initiale en ions H^+ dissociés (avant réaction avec le butylate) varie (voir fig. 2). En effet, la surface spécifique et le volume microporeux passent par un maximum

Can. J. Chem. Downloaded from www.nrcresearchpress.com by 178.218.224.3 on 09/06/12
For personal use only.

Can. J. Chem. Downloaded from www.nrcresearchpress.com by 178.218.224.3 on 09/06/12
For personal use only.

TABLEAU 1. Influence de l'acidité du milieu réactionnel en absence de butanol*

Nature des produits de départ	$\bar{S}_{BET}$ ($m^2\ g^{-1}$)	$\bar{S}_{BJH}$ ($m^2\ g^{-1}$)	$\bar{V}_\mu$ ($cm^3\ g^{-1}$)	$\bar{V}_p$ ($cm^3\ g^{-1}$)	$\frac{\bar{V}_\mu \times 100}{\bar{V}_p}$ (%)	$\bar{D}_{BJH}$ pores cylindres (Å)	$\bar{D}_c = 4V_p/S$ pores cylindres (Å)	$\bar{D}_s = 6V/S$ pores sphères (Å)	$\bar{D}_p = 6/\rho S$ particules sphères (Å)	Type d'isotherme
$(BuO)_4Ti$ + SO_4H_2 10^{-1} N $\lvert H^+\rvert$ dissocié 6×10^{-2}	114	93	0.032	0.049	64	< 20	17	26	135	I
SO_4H_2 5×10^{-2} N $\lvert H^+\rvert$ dissocié 4×10^{-2}	218	226	0.086	0.106	80	< 20	20	30	66	I
SO_4H_2 10^{-2} N $\lvert H^+\rvert$ dissocié 8×10^{-3}	317	295	0.124	0.194	64	24	24	37	48	I
CH_3COOH 1.4 N $\lvert H^+\rvert$ dissocié 5×10^{-3}	356	338	0.130	0.180	74	20	20	30	43	I
CH_3COOH N $\lvert H^+\rvert$ dissocié 4×10^{-3}	337	314	0.130	0.160	81	20	19	29	46	I
SO_4H_2 10^{-3} N $\lvert H^+\rvert$ dissocié 10^{-3}	242	236	0.099	0.272	36	42	45	67	64	IV
CH_3COOH 10^{-1} N $\lvert H^+\rvert$ dissocié 10^{-3}	242	241	0.100	0.180	58	35	30	45	64	IV
H_2O	238	236	0.099	0.263	37	43	44	66	65	IV

*$\bar{S}_{BET}$ = valeur moyenne de la surface spécifique calculée par la méthode de Brunauer *et al.* (5). $\bar{S}_{BJH}$ = valeur moyenne de la surface cumulative des pores calculées par la méthode de Barrett *et al.* (6). $\bar{V}_\mu$ = valeur moyenne du volume microporeux calculé par la méthode de Dubinin *et al.* (7). $\bar{V}_p$ = valeur moyenne du volume poreux total d'azote adsorbé à l'état liquide pour une pression relative $p/p_0 = 0.975$. $\bar{D}_{BJH}$ = valeur moyenne du diamètre de pore calculé par la méthode de Barrett *et al.* (6). $\bar{D}_c = 4V_p/S$ valeur moyenne du diamètre des pores supposés cylindriques. $\bar{D}_p = 6/\rho S$ valeur moyenne du diamètre des particules supposées sphériques. $\bar{D}_s = 6V_p/S$ valeur moyenne du diamètre des pores supposés sphériques.

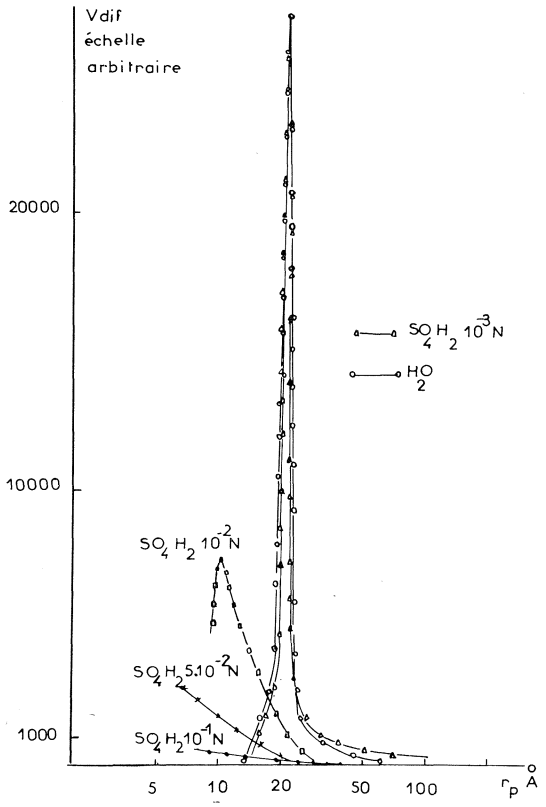

FIG. 2. Distributions des rayons de pore de gels d'oxyde de titane préparés en solutions sulfuriques (en absence de butanol).

lorsque la concentration en acide sulfurique est voisine de 10^{-2} N (soit 8×10^{-3} ion g H^+/l) et celle en acide acétique voisine de 1.4 N (soit 5×10^{-3} ion g H^+/l). Ils décroissent ensuite et possèdent une valeur sensiblement constante lorsque l'hydrolyse est effectuée en présence d'eau distillée. Le volume poreux total V_p croît lorsque la concentration en acide diminue.

Il est intéressant de noter que le passage d'une isotherme du type I au type IV correspond à un changement de texture des gels. En effet, à ce stade, on observe une décroissance du volume microporeux V_μ et de la surface spécifique, et une forte croissance du diamètre de pore de 20 à 40 Å pour un modèle cylindrique, et de 30 à 60 Å pour un modèle sphérique. Le diamètre des pores devient sensiblement égal à celui des particules. Néanmoins le diamètre des particules est sensiblement constant sauf pour une concentration en acide sulfurique égale à 10^{-1} N pour laquelle le diamètre des particules est de 135 Å.

Un phénomène analogue a été observé par Coudurier et coll. (9) lors d'une étude de l'évolution de la surface spécifique de gels de silice préparés entre $pH = 3.7$ et $pH = 10.3$. Ces auteurs ont constaté une augmentation de la surface spécifique lorsque le pH croît de 3.7 à 5, puis une décroissance de cette surface lorsque le pH continue à croître. Par ailleurs ils ont observé que pour un $pH = 4$, l'isotherme d'adsorption était du type I de la classification de Brunauer *et al.* (5) et caractéristique d'une texture microporeuse. Par contre pour un $pH = 7$, l'isotherme était du type IV de la classification de Brunauer *et al.* (5) et le diamètre des pores était du même ordre de grandeur que le diamètre des particules mesurées par microscopie électronique.

Discussion

(*1*) Comparons nos résultats à ceux obtenus par Gregg et Pope (1) qui ont étudié l'influence de l'acidité du milieu réactionnel dans des conditions sensiblement identiques aux nôtres. Tous nos résultats sont rassemblés dans le tableau 2.

Pour les concentrations en $SO_4H_2 \geqslant 10^{-2}$ N nous obtenons ainsi que ces auteurs une croissance rapide de la surface spécifique et du volume poreux total lorsque la concentration en ions H^+ dissociés diminue. Le diamètre des pores reste sensiblement constant et de l'ordre de 20 Å pour une modèle cylindrique.

Toutefois lorsque la concentration est $\leqslant 10^{-3}$ N, nous obtenons une diminution de la surface spécifique, une croissance du volume poreux total et une brusque augmentation du diamètre de pore qui devient de l'ordre de 40 Å pour un modèle cylindrique (fig. 2). Par contre Gregg et Pope (1) ont observé une croissance simultanée de la surface spécifique et du volume poreux total. Ceci peut s'expliquer par une progression du nombre de micropores dont la taille reste sensiblement constante et de l'ordre de 20 Å. Cette différence de résultats pour les faibles concentrations en acide pourrait provenir du fait que ces auteurs ont travaillé avec de l'eau distillée décarbonatée contenant très peu d'ions SO_4^{2-}, alors que nous avons opéré avec de l'eau distillée non décarbonatée présentant un $pH = 5.9$.

(*2*) Mais comment expliquer le changement de texture observé lors du passage d'une isotherme du type I à une isotherme du type IV si le volume poreux total croît et le diamètre des particules demeure sensiblement constant?

Reportons nous aux travaux effectués par Leontev *et al.* (11), Sullivan et Cole (10) et Gregg

Can. J. Chem. Downloaded from www.nrcresearchpress.com by 178.218.224.3 on 09/06/12
For personal use only.

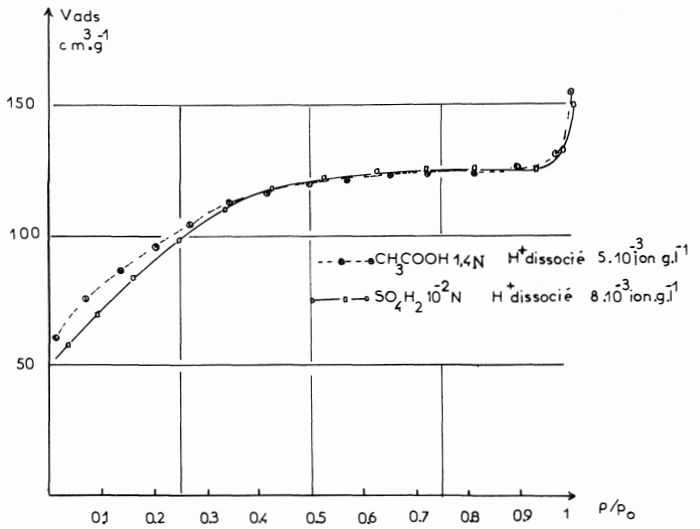

FIG. 3. Comparaison des isothermes d'adsorption d'azote sur deux gels d'oxyde de titane préparés en milieux ionisants voisins (en absence de butanol) 5 et 8 $\times$ 10^{-3} ion g l^{-1}.

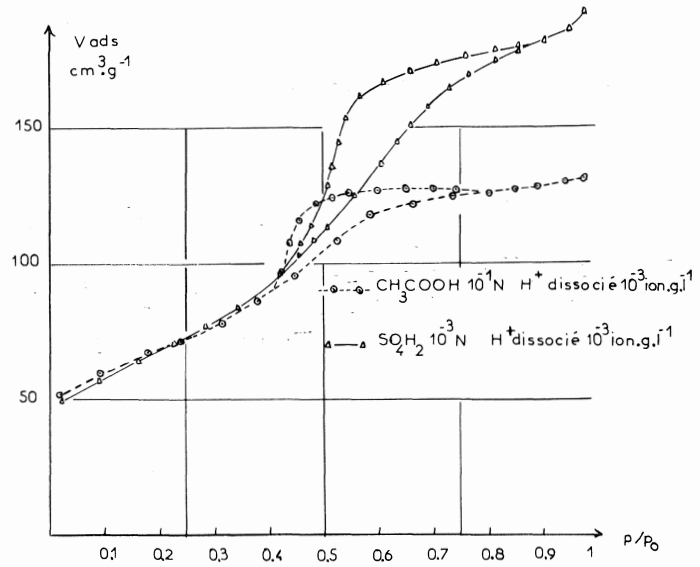

FIG. 4. Comparaison des isothermes d'adsorption d'azote sur deux gels d'oxyde de titane préparés en milieux ionisants voisins faibles soit 10^{-3} ion g l^{-1} (en absence de butanol).

et Pope (1) sur l'oxyde de titane colloïdal. Ces auteurs ont montré que les gels d'oxyde de titane étaient constitués par des agrégats de particules. Or Gregg et Pope (1) ont émis l'hypothèse selon laquelle l'acidité du milieu réactionnel affecterait le mode d'association des particules donc la compacité de l'agrégat. Un milieu fortement acide favoriserait une texture compacte évoluant vers une texture plus lâche lorsque l'acidité du milieu réactionnel diminue.

Considérons nos résultats et plaçons nous en milieu fortement acide. Empilons soit des particules de 135 Å, soit des particules de 60 Å, suivant un modèle hexagonal compact. Les longueurs des interstices laissés entre particules jointives varient entre 10 et 40 Å (4). Dans les deux cas les longueurs sont sensiblement du même ordre de grandeur que le diamètre des pores trouvés expérimentalement soit 20 à 30 Å.

Par contre lorsque la concentration en ions H^+

Can. J. Chem. Downloaded from www.nrcresearchpress.com by 178.218.224.3 on 09/06/12
For personal use only.

TABLEAU 2. Comparaison de l'évolution des propriétés textural de gels d'oxyde de titane synthétisés en milieu sulfurique aqueux

Auteurs	Produits de départ		SO_4H_2 (10^{-1} N)	SO_4H_2 (10^{-2} N)	SO_4H_2 (10^{-3} N)	SO_4H_2 ($<10^{-9}$ N)	H_2O distillée pH = 5.9
Gregg et Pope (1)	Isopropylate de titane	S_{BET} ($m^2\ g^{-1}$)	4	316	430	493	
	Butylate de titane	S_{BET} ($m^2\ g^{-1}$) Lecture sur courbe	50	390	554	485–520	
Nos résultats	Butylate de titane	S_{BET} ($m^2\ g^{-1}$)	114	317	242		238
Gregg et Pope (1)	Isopropylate de titane	V_p ($cm^3\ g^{-1}$)	Non mesuré	0.147	0.247	0.175	
Nos résultats	Butylate de titane	V_p ($cm^3\ g^{-1}$)	0.049	0.194	0.272		0.263
Gregg et Pope (1)	Isopropylate de titane	$D_c = 4V_p/S$ (Å)	Non mesuré	19	21	14	
Nos résultats	Butylate de titane	$D_c = 4V_p/S$ (Å)	17	24	45		43

dissociés diminue, il pourrait y avoir une évolution vers une texture plus lâche et apparition d'une isotherme du type IV. Empilons des particules de 60 Å suivant un modèle moins dense ou cubique simple. Les longueurs des interstices laissés entre les particules jointives varient entre 25 et 60 Å, ce qui est compatible avec nos résultats expérimentaux donnant un diamètre de pore compris entre 40 et 60 Å suivant le modèle géométrique adopté.

(*3*) Si nous comparons les résultats obtenus à partir d'une solution d'acide acétique 1.4 N et ceux obtenus à partir d'une solution d'acide sulfurique 10^{-2} N dont les concentrations initiales en ions H^+ dissociés (avant réaction avec $(BuO)_4Ti$) sont respectivement de l'ordre de 5×10^{-3} et 8×10^{-3} ion g l^{-1}. Les gels ainsi synthétisés présentent des isothermes intermédiaires entre le type I et le type IV, et possèdent des textures poreuses analogues (fig. 3).

De même comparons les textures des gels synthétisés soit en présence d'acide acétique 10^{-1} N, soit en présence d'acide sulfurique 10^{-3} N, ce qui correspond à une même concentration initiale en ions H^+ dissociés (avant réaction avec $(BuO)_4Ti$) de l'ordre de 10^{-3} ion g l^{-1}. Les isothermes de ces solides sont du type IV, les surfaces spécifiques sont identiques et de l'ordre de 240 $m^2\ g^{-1}$, les diamètres de pores respectifs sont de 36 et 42 Å. Par contre, le volume poreux total du gel préparé en présence d'acide acétique est inférieur au volume poreux total du gel synthétisé en présence d'acide sulfurique. Ceci peut s'expliquer par la présence d'un petit nombre de pores de grandes tailles qui interviennent fortement dans le volume poreux total et n'ont que peu d'influence sur la surface spécifique qui reste constante (fig. 4).

On peut donc penser qu'il règne une certaine similitude entre les gels synthétisés soit en présence d'acide sulfurique, soit en présence d'acide acétique lorsque les concentrations en ions H^+ dissociés sont du même ordre de grandeur.

Ainsi nos résultats expérimentaux montrent une évolution des propriétés texturales des gels d'oxyde de titane en fonction de la concentration en ions H^+ dissociés en absence de butanol.

Influence de l'acidité du milieu réactionnel en présence de butanol

Toutes nos préparations sont effectuées à température ambiante par addition goutte à goutte d'une solution de butylate de titane (20% en poids dans le butanol) à diverses solutions d'acide sulfurique (10^{-3} à 10^{-1} N) ou d'acide acétique (10^{-1} N à N). Après séchage, les solides ainsi obtenus présentent un faible état de cristallisation et les raies diffuses de l'anatase.

Le tracé des isothermes d'adsorption à -195 °C sur ces solides, nous montre un décalage systématique des courbes présentant un volume adsorbé plus important qu'en milieu acide aqueux

Can. J. Chem. Downloaded from www.nrcresearchpress.com by 178.218.224.3 on 09/06/12
For personal use only.

Can. J. Chem. Downloaded from www.nrcresearchpress.com by 178.218.224.3 on 09/06/12
For personal use only.

TABLEAU 3. Influence de l'acidité du milieu réactionnel en présence de butanol

Nature des produits de départ	$\bar{S}_{BET}$ ($m^2\ g^{-1}$)	$\bar{S}_{BJH}$ ($m^2\ g^{-1}$)	$\bar{V}_\mu$ ($cm^3\ g^{-1}$)	$\bar{V}_p$ ($cm^3\ g^{-1}$)	$\frac{\bar{V}_\mu \times 100}{\bar{V}_p}$ (%)	$\bar{D}_{BJH}$ pores cylindres (Å)	$\bar{D}_c = 4V_p/S$ pores cylindres (Å)	$\bar{D}_s = 6V_p/S$ pores sphères (Å)	$\bar{D}_p = 6/\rho S$ particules sphères (Å)	Type d'isotherme
$(BuO)_4Ti$ + BuOH SO_4H_2 10^{-1} N	215	206	0.076	0.105	73	$\simeq 20$	19	29	71	I
SO_4H_2 5×10^{-2} N	271	276	0.114	0.186	88	$\simeq 20$	27	41	57	I–IV
SO_4H_2 10^{-2} N $\lvert H^+\rvert$ dissocié 8×10^{-3}	259	264	0.108	0.230	47	39	36	53	59	IV
CH_3COOH N $\lvert H^+\rvert$ dissocié 4×10^{-3}	262	250	0.110	0.220	50	39	34	50	59	IV
SO_4H_2 10^{-3} N $\lvert H^+\rvert$ dissocié 10^{-3}	238	243	0.099	0.264	38	40	44	66	65	IV
CH_3COOH 10^{-1} N $\lvert H^+\rvert$ dissocié 10^{-3}	245	268	0.100	0.245	41	41	40	60	63	IV
H_2O	249	247	0.098	0.283	35	41	45	68	62	IV

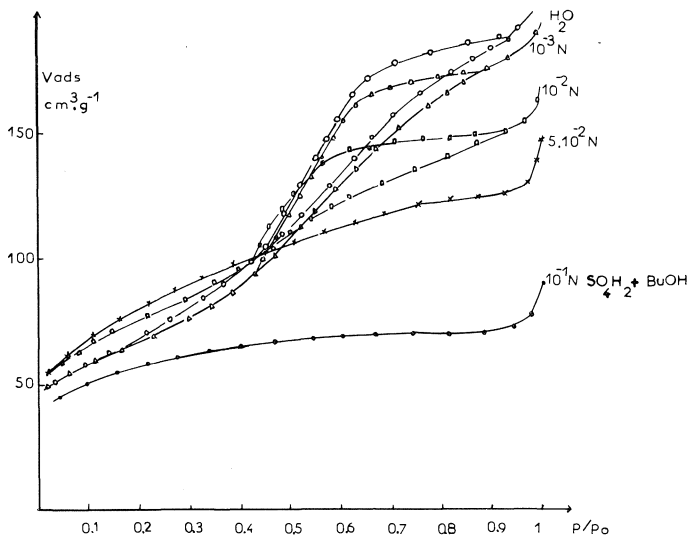

FIG. 5. Isothermes d'adsorption d'azote à −195 °C sur des gels d'oxyde de titane préparés en solutions sulfuriques (en présence de butanol).

pour les faibles pressions relatives et les fortes concentrations en acide, ainsi qu'une évolution plus rapide des isothermes du type I vers des isothermes du type IV de la classification de Brunauer *et al.* (5) (fig. 5).

Ainsi lorsqu'on est en présence de butanol, le passage d'une isotherme du type I à une isotherme du type IV de la classification de Brunauer *et al.* (5) a lieu pour des concentrations respectives en acide sulfurique et en acide acétique de l'ordre de 10^{-2} *N* et *N*. Par contre dans un milieu réactionnel exempt de butanol, il s'effectue pour des concentrations respectives en acide sulfurique et en acide acétique de l'ordre de 10^{-3} et 10^{-1} *N*.

Nos résultats d'adsorption sont regroupés dans le tableau 3. Nous pouvons constater que la surface spécifique et le volume microporeux subissent une évolution parallèle mais beaucoup plus atténuée qu'en milieu aqueux. Ainsi dans un milieu réactionnel contenant de l'acide sulfurique et du butanol, lorsque la concentration en ions H^+ dissociés diminue, la surface spécifique croît de 215 à 271 $m^2\ g^{-1}$ puis décroit légèrement. Par contre en milieu sulfurique aqueux, lorsque la concentration en ions H^+ dissociés diminue, la surface spécifique croît de 110 à 317 $m^2\ g^{-1}$, puis décroît ensuite. Il en est de même du volume microporeux.

Le volume poreux total d'azote adsorbé en milieu acide contenant du butanol est légèrement supérieur à celui obtenu en milieu acide aqueux pour des concentrations initiales en acide identiques. Le diamètre des particules reste sensiblement constant et du même ordre de grandeur que le diamètre des pores (modèle sphérique) excepté pour une concentration en acide sulfurique égale à 10^{-1} *N*.

Par ailleurs le tableau 3 montre que les gels syn-

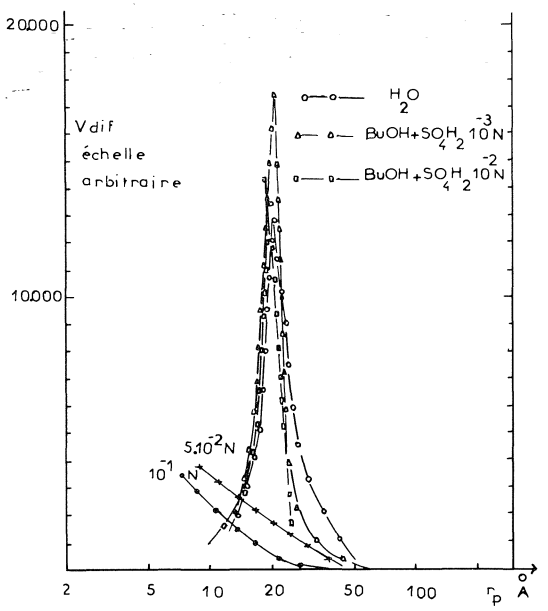

FIG. 6. Distributions des rayons de pores de gels d'oxyde de titane préparés en solutions sulfuriques (en présence de butanol).

Can. J. Chem. Downloaded from www.nrcresearchpress.com by 178.218.224.3 on 09/06/12
For personal use only.

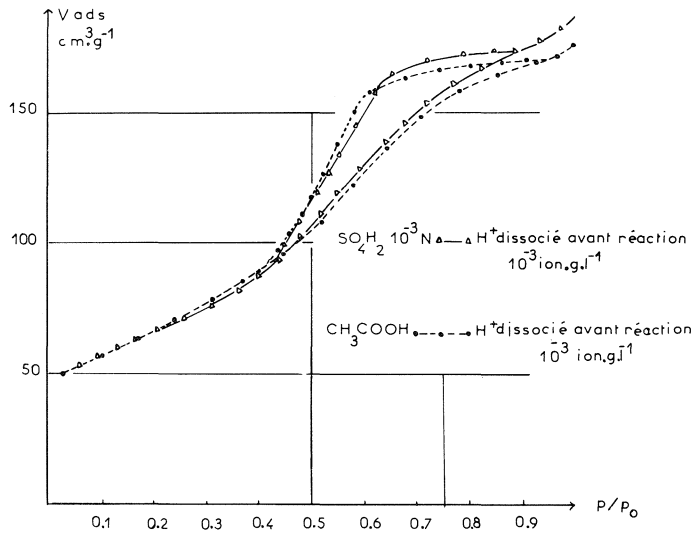

FIG. 7. Comparaison des isothermes d'adsorption d'azote à −195 °C sur deux gels d'oxyde de titane préparés en milieux ionisants voisins (en présence de butanol) 4×10^{-3} et 8×10^{-3} ion g l^{-1}.

thétisés en milieu butanol-acide présentent une disparition plus rapide des micropores de diamètre inférieur à 32 Å (modèle cylindrique) qu'en milieu sulfurique aqueux (figs. 2, 6).

Discussion

Vicarini *et al.* (3) ont travaillé dans un domaine de concentration en acide acétique compris entre 10^{-1} *N* et *N*, ce qui correspond à un domaine en ions H^+ dissociés avant réaction compris entre 10^{-3} et 4×10^{-3} ion g l^{-1}. Ils ont obtenu des surfaces spécifiques comprises entre 95 et 118 m^2 g^{-1} et des volumes poreux compris entre 0.25 et 0.21 cm^3 g^{-1}.

Nos résultats obtenus en milieu acétique et en présence de butanol sont identiques à ceux donnés par le milieu sulfurique en présence de butanol voir tableau 3. En effet il existe une bonne concordance des surfaces spécifiques, des volumes poreux et des diamètres de pores quels que soient l'acide et la concentration considérés (figs. 7 et 8). Par ailleurs il n'est pas possible de mettre en évidence une variation sensible des propriétés texturales des gels d'oxyde de titane dans le domaine de concentration envisagé.

En résumé: (*a*) Nous constatons que la présence de butanol dans un milieu réactionnel acide diminue les variations des propriétés texturales des gels ainsi synthétisés par rapport aux variations observées en milieu acide aqueux. (*b*) Les résultats sont reproductibles quel que soit l'acide (SO_4H_2 ou CH_3COOH) pour une même concentration en ions H^+ dissociés.

Par ailleurs Harris et Whitaker (2) ont synthétisé des gels d'oxyde de titane à partir de solutions de butylate de titane à 20% en poids dans le benzène, qu'ils ont hydrolysées par diverses solutions tampons dont le p*H* était compris entre 2.3 et 10.5. Ces auteurs n'ont pas observé de variation systématique de la surface et du volume poreux, sauf pour un p*H* supérieur à 8.5 où se manifeste une décroissance très importante de la surface spécifique. Toutefois ces auteurs ont remarqué qu'en milieu acide le diamètre des pores était inférieur à 32 Å (modèle cylindrique). Par contre lorsque le gel était synthétisé dans un milieu réactionnel exempt d'acide, de base ou de tampons, le diamètre de pore était de l'ordre de 40 Å (modèle cylindrique). Nos résultats permettent également d'expliquer cette faible variation.

On peut penser que l'influence de l'ionicité du milieu réactionnel est atténuée par la présence d'un solvant tel que le benzène de faible constante diélectrique, jouant le même rôle que le butanol.

En effet, il est bien connu (12) que si un solvant S est mis en présence d'un acide HA, il peut se former un complexe SHA qui, suivant la constante diélectrique ε_r du solvant, peut se dissocier en SH^+ et A^-. En fait on mesure une constante globale d'acidité car on ne peut distinguer HA de SHA.

[1] $$K_a = \alpha_s K_D$$

Can. J. Chem. Downloaded from www.nrcresearchpress.com by 178.218.224.3 on 09/06/12
For personal use only.

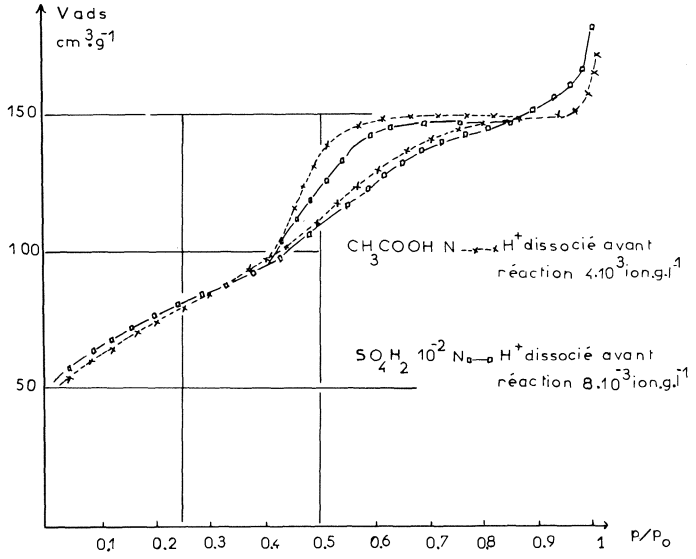

FIG. 8. Comparaison des isothermes d'adsorption d'azote sur deux gels d'oxyde de titane préparés en milieux ionisants voisins faibles (en présence de butanol) soit 10^{-3} ion g l^{-1}.

où α_s = fraction solvolysée de l'acide HA qui dépend du caractère du solvant et K_D = constante de dissociation de SHA qui dépend de la constante diélectrique du solvant.

Or il existe une relation due à Denison et Ramsey (14) basée sur la théorie de Bjerrum (13) qui permet de relier pK_D à la constante diélectrique du solvant ε_r.

$$[2] \qquad pK_D = pK_0 + \frac{B}{\varepsilon_r(r_1 + r_2)}$$

B = facteur de proportionnalité indépendant de la constante diélectrique et r_i = rayons des ions solvatés.

On voit donc que si ε_r est grand, ce qui est le cas de l'eau ($\varepsilon_r = 78.5$), le second terme de l'expression est petit, donc pK_D est petit ainsi que pK_a. Comme $pK_D = -\log K_D$, la constante de dissociation K_D est grande, et par voie de conséquence la constante K_a de l'acide est grande. Par contre, lorsque ε_r est faible, ce qui est le cas du butanol où $\varepsilon_r = 17.1$ et du benzène où $\varepsilon_r = 2.3$, la valeur de pK_D croît, donc il lui correspond une constante de dissociation K_D plus faible que dans l'eau, et par conséquent une constante d'acidité plus faible.

Donc on peut penser que la présence de butanol ou de benzène dans le milieu réactionnel atténue l'ionicité. Or nous avons observé que les propriétés texturales dépendent étroitement de l'ionicité du milieu.

Conclusion

Compte tenu de nos résultats expérimentaux et de ceux mentionnés dans la littérature, cette étude nous a conduit à montrer que les propriétés texturales des gels d'oxyde de titane étaient liées à la concentration en ions H^+ dissociés dans le milieu réactionnel. Par ailleurs la présence d'un solvant de faible constante diélectrique (comme le butanol ou le benzène) dans le milieu réactionnel atténue les variations des propriétés texturales en diminuant la dissociation ionique de l'acide.

Ceci nous permet d'expliquer, non seulement les résultats de Gregg et Pope (1) qui ont observé une évolution des propriétés texturales en fonction de la concentration en acide fort (H_2SO_4) du milieu aqueux de synthèse, mais aussi ceux de Vicarini et coll. (3) et ceux de Harris et Whitaker (2) qui n'ont pas observé d'évolution sensible des propriétés texturales en fonction de la concentration en acide faible (CH_3COOH) en présence de butanol, ou dans des milieux tampons divers en présence de benzène.

1. S. J. GREGG et M. I. POPE. Kolloid Z. **174**, 27 (1961).
2. M. R. HARRIS et G. WHITAKER. J. Appl. Chem. **13**, 198 (1963); J. Appl. Chem. **12**, 490 (1962).
3. M. A. VICARINI, G. A. NICOLAON, S. J. TEICHNER. Bull. Soc. Chim. Fr. **5**, 1651 (1970).
4. CH. FLICOTEAUX. Thèse de 3eme cycle. Paris. 1973. H. G. MENDELBAUM et C. FLICOTEAUX. Congrès

Can. J. Chem. Downloaded from www.nrcresearchpress.com by 178.218.224.3 on 09/06/12
For personal use only.

International sur l'emploi des ordinateurs en génie chimique. F.E.G.C. 24–27 avril, 1973. Paris.
5. S. BRUNAUER, P. H. EMMETT et L. TELLER. J. Am. Chem. Soc. **60**, 309 (1938).
6. E. P. BARRETT, L. G. JOYNER et P. P. HALENDA. J. Am. Chem. Soc. **73**, 373 (1951).
7. M. M. DUBININ, B. P. BERING et V. V. SERPINSKY. J. Colloid Interface Sci. **21**, 378 (1966).
8. H. BRUSSET, J. J. P. MARTIN, H. G. MENDELBAUM. Bull. Soc. Chim. Fr. **7**, 2346 (1967).
9. M. COUDURIER, B. BAUDRU et J. B. DONNET. Bull. Soc. Chim. Fr. **9**, 3144 (1971).
10. W. F. SULLIVAN et S. S. COLE. J. Am. Ceram. Soc. **42**, 127 (1959).
11. E. A. LEONTEV, V. M. LUK'YANOVICH, I. F. NEIMARK. Izv. Akad. Nauk. S.S.S.R. **9**, 1037 (1958).
12. M. GARRIC. Cours de chimie, Tome I. édition Dunod. Paris. 1970.
13. F. MADAULE-AUBRY. Bull. Soc. Chim. Fr. **4**, 1456 (1966).
14. J. J. DENISON et J. B. RAMSEY. J. Am. Chem. Soc. **77**, 2615 (1955).

Can. J. Chem. Downloaded from www.nrcresearchpress.com by 178.218.224.3 on 09/06/12
For personal use only.

The Near-ultraviolet Absorption Spectrum of Diimide in Liquid Ammonia and its Decomposition between −65 and −38 °C[1]

R. A. Back and C. Willis

Division of Chemistry, National Research Council of Canada, Ottawa, Canada K1A 0R6

Received March 8, 1974

R. A. Back and C. Willis. Can. J. Chem. **52**, 2513 (1974).

The near-ultraviolet absorption spectrum of diimide in liquid ammonia at −50 °C is shifted about 500 Å to the red compared with the gas-phase spectrum, with λ_{max} = 4000 Å. The spectrum is also broadened and the vibrational structure largely obscured. It is suggested that hydrogen bonding is responsible for these changes.

Diimide is much more stable in liquid ammonia between −65 and −38 °C than in the gas phase at room temperature. A first-order decay is observed with Arrhenius parameters of $A = 1.9 \times 10^3$ s^{-1} and E = 6.6 kcal/mol; this is always preceded by a more rapid, higher-order initial decay which may be related to the rapid decomposition observed during vaporization.

R. A. Back et C. Willis. Can. J. Chem. **52**, 2513 (1974).

Le spectre d'absorption, dans le proche ultraviolet, de la diimide dans l'ammoniac liquide à −50 °C est déplacé d'environ 500 Å vers le rouge lorsqu'on le compare au spectre en phase gazeuse; λ_{max} = 4000 Å. On observe que le spectre est élargi et que la structure vibrationnelle est obscurcie. On suggère que les ponts hydrogènes sont responsables de ces changements.

La diimide est beaucoup plus stable dans l'ammoniac liquide entre −65 et −38 °C qu'en phase gazeuse à température de la pièce. On a déterminé les taux de décomposition du premier ordre et établi les paramètres d'Arrhenius qui sont $A = 1.9 \times 10^3$ s^{-1} et E = 6.6 kcal/mol. Cette décomposition est toujours précédée par une décomposition plus rapide d'un ordre plus élevé qui est relié à la décomposition rapide que l'on observe durant la vaporisation.

[Traduit par le journal]

Introduction

In a recent study (1) of its physical and chemical properties, diimide (N_2H_2) was trapped at −196 °C together with a 5- to 10-fold excess of ammonia. On warming, the solid mixture melted at about −65 °C to a pale yellow liquid. The yellow color persisted for many minutes at temperatures between −65 and −25 °C, suggesting that under these conditions diimide was appreciably more stable than in the gas phase at room temperature. The present paper reports the measurement of the absorption spectrum of diimide in liquid ammonia, and a brief spectrophotometric study of its decomposition at temperatures from −65 to −38 °C.

Experimental

Diimide–ammonia mixtures containing about 15% diimide were prepared by a microwave discharge through hydrazine vapor as described previously (1). For each experiment, several (4–10) small batches were prepared, rapidly vaporized, and recondensed one after another at −196 °C on a small "cold finger" attached to the top of a 1 × 1 cm spectrophotometer cell. This was fitted in an insulated brass block cooled by a liquid refrigerant circulated from a low-temperature thermostat, and mounted in the light path of a single-beam Heath spectrophotometer. When the desired amount of diimide had been collected, enough additional ammonia was condensed to fill the cell above the level of the light beam. The cold finger was then warmed until the diimide–ammonia mixture melted and flowed down into the thermostatted cell, and the spectrophotometric measurements were begun. During the decomposition the cell was attached to a manometer to avoid excessive pressure increase. No product analysis was undertaken, and pressure changes were not recorded since their interpretation is complex (1).

Results and Discussion

Figure 1 shows the near-u.v. absorption spectrum of diimide in liquid ammonia at −50 °C, and for comparison, the spectrum of the vapor (1, 2). The absorption in liquid ammonia is shifted to the red by about 500 Å, broadened considerably, and the sharp vibrational structure observed in the gas phase is almost completely lost. The shift to the red seems anomalously large for a simple polar-solvent effect and is opposite in direction to the blue shift expected for a $\pi^* \leftarrow n$ transition. There is evidence from the infrared spectrum (3) and from the vapor pressure of diimide–ammonia mixtures (1) that

[1]NRCC No. 13963.

Can. J. Chem. Downloaded from www.nrcresearchpress.com by 210.87.254.5 on 09/05/12
For personal use only.

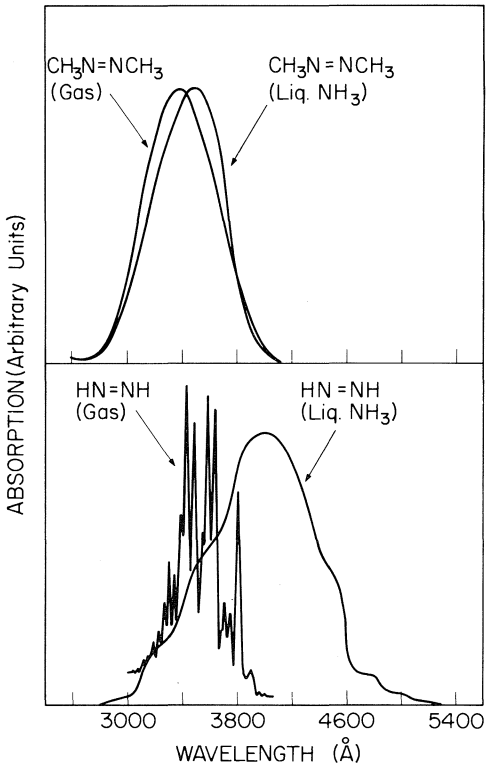

FIG. 1. Absorption spectra of N_2H_2 and $(CH_3)_2N_2$ in liquid ammonia (slits, 30 μ; T, −50 °C), and in the gas phase (1, 2, 4).

the two components interact strongly, probably through hydrogen bonding, and the large red shift and broadening of the present spectrum can reasonably be attributed to the same cause. To test this hypothesis, a liquid ammonia solution of azomethane, which should be much less hydrogen-bonded, was prepared and its absorption spectrum measured at −50 °C; this is shown in Fig. 1, together with the gas-phase spectrum (4). Again, a shift to the red is observed, but much smaller than with diimide. This suggests that bonding of the diimide hydrogens to the NH_3 lone pairs is much more important than the bonding of the NH_3 hydrogens to the lone pairs of azomethane or diimide, as might be expected from the strong intramolecular interaction between the two lone pairs in *azo* compounds (5) which would make them less available for intermolecular interactions.

Figure 2 shows typical first-order plots of the disappearance of diimide in liquid ammonia at −65, −58, and −38 °C. Optical density at 4000 Å is plotted, rather than N_2H_2 concentration, since the extinction coefficient is not known; optical densities in the single-beam instrument were based on final values of the transmitted intensity attained after complete decay of the diimide in each experiment. Differences in the initial optical densities have no significance, simply reflecting different amounts of diimide condensed into the cell.

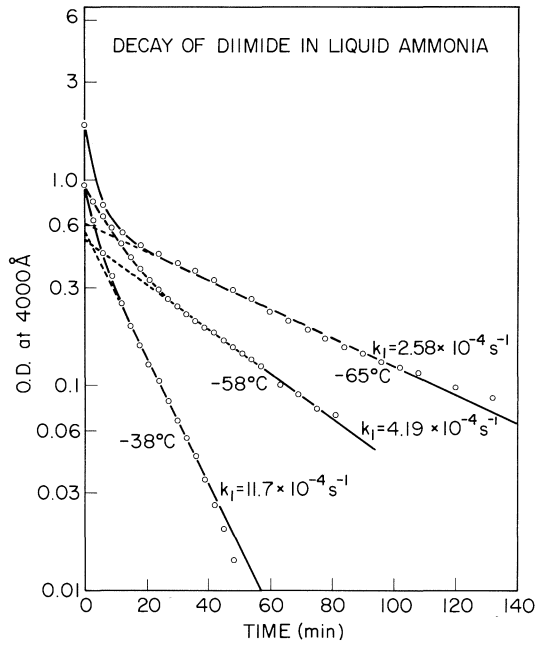

FIG. 2. First-order plots of diimide decay in liquid ammonia.

In all the experiments a rapid initial disappearance with an order greater than one was observed, followed by a simple first-order decay; these features are evident in Fig. 2. The lifetime of diimide, as expected, is much longer than in the gas phase at 22 °C, and decreases with increasing temperature. Figure 3 shows an Arrhenius plot of the first-order rate constant derived from the linear portions of the curves in Fig. 2, or similar ones, from which Arrhenius parameters of $A = 1.9 \times 10^3$ s^{-1} and $E = 6.6$ kcal/mol were obtained. Also plotted in Fig. 3 is a value of the rate constant obtained in the gas phase at 22 °C (1); this lies below an extrapolation of the low-temperature data. The gas-phase decomposition showed an activation energy of about 20 kcal between 22 and 200 °C, and rather complex kinetics (1).

It is evident from Fig. 2 that a major portion of the diimide disappeared in the rapid initial

Can. J. Chem. Downloaded from www.nrcresearchpress.com by 210.87.254.5 on 09/05/12
For personal use only.

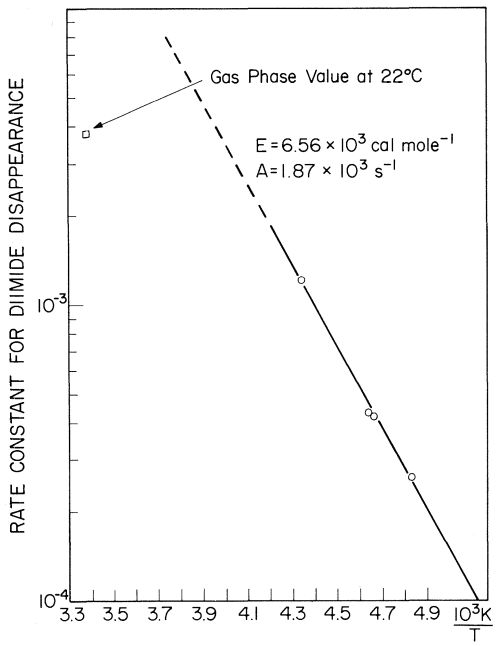

FIG. 3. Arrhenius plot of first-order rate constants for diimide decay.

decay, which may well correspond to the rapid partial decomposition previously observed to accompany the vaporization of diimide (1). This is probably a bimolecular process and may involve the *cis* isomer of diimide (1), and it appears that extrapolation of the rates observed in the present experiments to the higher temperatures and much higher concentration present in the transient liquid phase formed during vaporization could account for the very rapid decomposition in the latter system (1).

The slower first-order decay in liquid ammonia is probably similar in nature to the gas-phase decomposition, and may involve *trans–cis* isomerization as a rate-controlling step (1), although the activation energy of 6.6 kcal is much lower than any reasonable estimate for the energy barrier for isomerization (6).

The authors wish to thank Mr. J. Parsons for his assistance in some of these experiments.

1. C. WILLIS and R. A. BACK. Can. J. Chem. **51**, 3605 (1973).
2. R. A. BACK, C. WILLIS, and D. A. RAMSAY. Can. J. Chem. **52**, 1006 (1974).
3. V. E. BONDYBEY and J. W. NIBLER. J. Chem. Phys. **58**, 2125 (1973).
4. J. G. CALVERT and J. N. PITTS. Photochemistry. Wiley, New York. 1966.
5. M. B. ROBIN, R. R. HART, and N. A. KUEBLER. J. Am. Chem. Soc. **89**, 1564 (1967).
6. N. C. BAIRD and J. R. SWENSON. Can. J. Chem. **51**, 3097 (1973).

Can. J. Chem. Downloaded from www.nrcresearchpress.com by 210.87.254.5 on 09/05/12
For personal use only.

The Crystal Structure of Levoglucosan Triacetate

F. LEUNG AND R. H. MARCHESSAULT

Department of Chemistry, Université de Montréal, Montreal 101, Quebec

Received December 14, 1973

F. LEUNG and R. H. MARCHESSAULT. Can. J. Chem. **52**, 2516 (1974).

The crystal structure of the acetylated levoglucosan (1,6-anhydro-2,3,4-triacetylglucose) was determined by X-ray crystallography. The crystal data are: $P2_12_12_1$, $a = 10.916$, $b = 8.318$, $c = 15.612$ Å. It was found that the pyranose ring of the molecule has the 1C(D) chair conformation with the acetate groups occupying the axial positions. The orientation of the acetate groups with respect to the pyranose ring was discussed in conjunction with other acetylated carbohydrate structures.

F. LEUNG et R. F. MARCHESSAULT. Can. J. Chem. **52**, 2516 (1974).

On a déterminé la structure cristalline du levoglucosane acétylé (anhydro-1,6 triacétyl-2,3,4 glucose) à l'aide de la diffraction de rayon-X. Les données cristallographiques sont: $P2_12_12_1$, $a = 10.916$, $b = 8.318$, $c = 15.612$ Å. On trouve que le noyau pyrannose de la molécule a une conformation chaise 1C(D) dans laquelle les groupes acétates se trouvent dans des positions axiales. On discute de l'orientation des groupes acétates par rapport au noyau pyrannose par comparaison avec d'autres structures de carbohydrates acétylés. [Traduit par le journal]

Introduction

The crystal structures of 1,6-anhydro-β-glucopyranose (levoglucosan) **1** and 1,6:2,3-dianhydro-β-gulopyranose **2** have been reported recently (1, 2) and the importance of the anhydro sugars in carbohydrate chemistry has been outlined by these investigators. Furthermore, since a trimethyl substituted derivative of **1** was the first stereoregularly polymerized carbohydrate monomer (3), it would be helpful to examine the crystal structure of such derivatives in order to understand the steric and strain factors which may be involved in the selective opening of the anhydro ring.

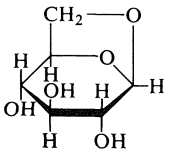

1

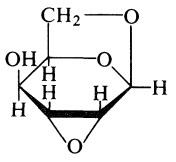

2

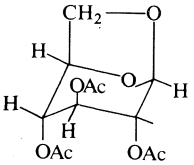

3a

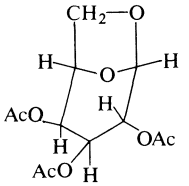

3b

In a recent study of the crystal structure of xylobiose hexaacetate (4) it was found that the orientation of the acetate group with respect to the pyranose ring was relatively constant for different positions on the ring and also insensitive to the conformation of the disaccharide itself. This confirms the predicted (5, 6) preference for a planar trans conformation of the acetoxyl groups, wherein the C(A)—O(A) bond is nearly eclipsed with the C—H bond of the ring as shown in Fig. 1. The limited amount of data concerning the favoured orientation of acetoxyl groups was mentioned by Corfield *et al.* (7) whose comments concerning the acetoxyl groups of tri-*O*-acetyl-β-D-arabinopyranosyl bromide are very much in line with some of the generalization which will be made in this study concerning the acetate groups in completely substituted 1,6-anhydro-β-D-glucopyranose, ***3a***.

We observed that the powder diffraction pattern of the sample crystallized from the melt is different from that of the sample crystallized from solution. Examination of molecular models shows that the molecule readily assumes either the "chair" form ***3a*** or the "boat" form ***3b*** which

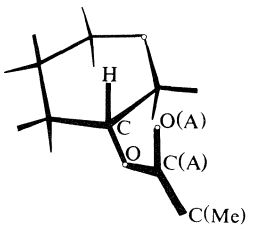

FIG. 1. A diagram showing the orientation of the acetate group with respect to the pyranose ring.

Can. J. Chem. Downloaded from www.nrcresearchpress.com by 210.87.254.40 on 09/05/12
For personal use only.

places the acetate groups in axial or equatorial positions, respectively; the present study aims to establish the form in the solution grown crystal. The 1C(D) ring conformation which places the 2, 3, and 4 substituents in the axial position was found for levoglucosan (1). Nikitin *et al.* (8) have observed changes in the i.r. spectra of levoglucosan which they have interpreted in terms of a "chair–boat" transition.

Experimental

Suitable crystals were obtained by recrystallizing the compound from 1:1 water–methanol solution. The crystal data are:

$C_{12}H_{16}O_8$ m.p. 108 °C f.w. = 288

Space group $P2_12_12_1$, $a = 10.916(3)$, $b = 8.318(3)$, $c = 15.612(6)$ Å, $D_m = 1.45$ g/cc, $D_c = 1.44$ g/cc, $Z = 4$, $\mu = 11.0$ cm^{-1} (CuKα, $\lambda = 1.5418$ Å). The cell parameters were determined from diffractometer measurements using 12 reflections and refined by a least-squares procedure. The intensity data were collected on a Picker FACS-1 diffractometer using CuKα (Ni-filtered) radiations. The crystal used for data collection had the dimensions of 0.7 × 0.5 × 0.3 mm. A 2θ-scanning mode was used during data collection. A total of 1408 independent reflections were recorded within the range of $2 \leqslant 2\theta \leqslant 130°$. There are 115 reflections with net counts less than 10% of the background; these reflections were considered to be unobserved and were excluded from structure refinement. No absorption correction was applied in the data reduction procedure. Normalized structure factors were generated by the K-curve method (9).

Structure Solution and Refinement

The structure was solved using the multi-solution TANFOR program[1] which involved direct application of the tangent formula (10) in an interative manner. The following reflections with the corresponding phases were chosen as the starting set:

h	k	l	$\|E\|$	Phase(deg)
0	1	4	3.24	90
7	6	0	2.94	90
10	0	5	2.53	90
9	4	4	2.80	±45, ±135
7	1	8	2.50	±45, ±135
8	2	6	2.27	+45, +135

[1]The computer programs used were locally modified versions of the following: F. R. Ahmed and C. P. Huber, NRC-2 (data reduction); M. Drew, TANFOR (tangent formula); A. Zalkin, FORDAP (Fourier and *E*-map); R. J. Doedens and J. A. Ibers, NUCLS (least-squares refinement) with block-diagonal option introduced by J. Sygusch; R. Shinono and S. S. C. Chu, BONDLA (bond length and angles); M. E. Pippy and F. R. Ahmed, NRC-22 (best least-squares planes); P. R. Sundararajan, BOND (torsional angles); C. K. Johnson, ORTEP (drawings).

All reflections (206) with $|E| \geq 1.40$ were used in the application of the tangent formula. A total of 32 different sets of phases were obtained, corresponding to the 32 different combinations of initial phases allocated to the above reflections. For the set with the lowest R_{Karle} (0.25), 157 phases were determined. The *E*-map computed using these 157 reflections revealed all the nonhydrogen atoms of the molecule.

The atomic coordinates estimated from the *E*-map were refined by full-matrix least squares with individual isotropic thermal parameters. All observed reflections were given equal weights during this refinement procedure. The isotropic refinement converged to an R factor of 0.14, where R is defined as $\sum(||F_o| - |F_c||)/\sum|F_o|$. The refinement was continued with anisotropic thermal parameters, an R factor of 0.08 was obtained. At this stage, a difference map was computed with all the observed reflections, it showed all the hydrogen atoms of the molecule. The refinement was then continued with the hydrogen atoms included and each assigned isotropic thermal parameters. The following weighting function was used. It was obtained by making

$$\omega = \frac{1}{(1.494 + 0.01\,F_o + 0.0001\,F_o^2)^2}$$

the average $\omega\Delta^2$ (where $\Delta = |F_o| - |F_c|$) similar in magnitude over the whole range $|F_o|$. The atomic scattering factors used for the hydrogens and nonhydrogen atoms were taken from Stewart *et al.* (11) and Cromer and co-worker (12), respectively. The hydrogen atoms and the nonhydrogen atoms were refined isotropically and anisotropically respectively. After several cycles of block-diagonal least-squares refinement, convergence was reached at an R factor of 0.048 for observed reflections only. The final positional and thermal parameters are listed in Table 1. Final F_o and F_c values have been placed in the Depository for Unpublished Data.[2]

Results and Discussion

The bond lengths, bond angles, and atomic labelling of the molecule are illustrated in Fig. 2. The bond lengths of the molecule are in good agreement with those in **1** (1). The difference in bond lengths between the two molecules is less than 0.01 Å with the exception of the equatorial

[2]Copies of F_o and F_c listing are available, at a nominal charge, from the Depository of Unpublished Data, National Science Library, National Research Council of Canada, Ottawa, Canada K1A 0S2.

Can. J. Chem. Downloaded from www.nrcresearchpress.com by 210.87.254.40 on 09/05/12
For personal use only.

Can. J. Chem. Downloaded from www.nrcresearchpress.com by 210.87.254.40 on 09/05/12
For personal use only.

TABLE 1. (*a*) Final atomic coordinates and thermal parameters of non-hydrogen atoms. The temperature factor used was exp $(-(h^2\beta_{11} + k^2\beta_{22} + l^2\beta_{33} + 2hk\beta_{12} + 2hl\beta_{13} + 2kl\beta_{23}))$. The estimated standard deviations are in parentheses

Atom	x	y	z	β_{11}	β_{22}	β_{33}	β_{12}	β_{13}	β_{23}
C1	0.2860(3)	−0.1273(4)	−0.2546(2)	0.0069(3)	0.0142(5)	0.0050(2)	−0.0001(3)	0.0003(2)	−0.0002(3)
C2	0.2755(3)	−0.1021(4)	−0.1587(2)	0.0065(3)	0.0137(5)	0.0046(1)	−0.0006(3)	0.0004(2)	0.0006(2)
C3	0.3271(3)	0.0617(4)	−0.1309(2)	0.0071(3)	0.01480(5)	0.0041(1)	0.0002(3)	0.0005(2)	−0.0005(2)
C4	0.3144(3)	0.1919(4)	−0.1996(2)	0.0052(2)	0.0111(4)	0.0062(2)	0.0003(3)	0.0009(2)	0.0010(3)
C5	0.3228(3)	0.1253(4)	−0.2899(2)	0.0067(3)	0.0145(5)	0.0053(2)	0.0000(3)	0.0003(2)	0.0020(3)
C6	0.4411(3)	0.0331(4)	−0.3071(2)	0.0071(3)	0.0168(6)	0.0053(2)	0.0003(4)	0.0016(2)	0.0006(3)
C7	0.1091(4)	−0.1504(5)	−0.0621(3)	0.0094(4)	0.0201(7)	0.0052(2)	−0.0033(5)	0.0021(2)	−0.0002(3)
C8	−0.0278(4)	−0.1431(7)	−0.0547(3)	0.0103(4)	0.0325(11)	0.0068(2)	−0.0042(6)	0.0032(3)	−0.0018(5)
C9	0.5123(4)	0.1377(5)	−0.0611(2)	0.0111(4)	0.0201(7)	0.0044(2)	−0.0029(5)	0.0014(2)	0.0010(3)
C10	0.6461(4)	0.1044(7)	−0.0545(3)	0.0103(4)	0.0309(11)	0.0064(2)	−0.0021(6)	−0.0022(3)	0.0024(4)
C11	0.1761(3)	0.4120(4)	−0.1994(3)	0.0084(3)	0.0129(5)	0.0078(2)	0.0014(4)	−0.0011(2)	0.0001(3)
C12	0.0474(3)	0.4591(5)	−0.1837(3)	0.0094(4)	0.0204(8)	0.0086(3)	0.0061(5)	−0.0013(3)	−0.0025(4)
O1	0.4118(2)	−0.1278(3)	−0.2782(2)	0.0087(2)	0.0142(4)	0.0059(1)	0.0013(3)	0.0017(1)	−0.0003(2)
O2	0.1455(2)	−0.1044(3)	−0.1418(2)	0.0078(2)	0.0179(4)	0.0046(1)	−0.0016(3)	0.0010(1)	0.0010(2)
O3	0.4567(2)	0.0340(3)	−0.1149(2)	0.0071(2)	0.0172(4)	0.0051(1)	0.0005(3)	−0.0010(1)	−0.0002(2)
O4	0.1933(2)	0.2568(3)	−0.1862(2)	0.0058(2)	0.0133(3)	0.0082(1)	0.0013(2)	0.0011(1)	−0.0001(2)
O5	0.2322(2)	0.0014(3)	−0.3004(2)	0.0071(2)	0.01839(4)	0.0049(1)	−0.0005(3)	0.0000(1)	0.0004(2)
O6	0.1810(3)	−0.1886(5)	−0.0083(2)	0.01609(4)	0.0386(9)	0.0051(1)	−0.0014(5)	−0.0003(2)	0.0048(3)
O7	0.4578(3)	0.2458(4)	−0.0258(2)	0.0152(4)	0.0263(6)	0.0069(2)	−0.0010(5)	−0.0009(2)	−0.0047(3)
O8	0.2551(3)	0.4952(5)	−0.2222(4)	0.0111(3)	0.0167(5)	0.0260(6)	0.0010(3)	0.0032(4)	0.0076(5)

(*b*) Atomic coordinates and isotropic thermal parameters of hydrogen atoms

Atom	x	y	z	B (Å^2)
H(1)	0.248(3)	−0.237(4)	−0.270(2)	3.9(7)
H(2)	0.314(3)	−0.204(4)	−0.132(2)	2.9(6)
H(3)	0.291(4)	0.116(5)	−0.079(3)	6.0(10)
H(4)	0.373(3)	0.271(4)	−0.191(2)	2.8(6)
H(5)	0.306(3)	0.217(4)	−0.327(2)	3.2(7)
H(1,6)	0.513(3)	0.066(4)	−0.270(2)	3.9(8)
H(2,6)	0.464(3)	0.016(5)	−0.371(2)	4.5(8)
H(1m2)	−0.073(7)	−0.188(9)	−0.096(5)	12(2)
H(2m2)	−0.062(9)	−0.174(10)	0.003(5)	17(3)
H(3m2)	−0.038(5)	−0.022(7)	−0.040(4)	10(2)
H(1m3)	0.701(6)	0.217(8)	−0.069(4)	11(2)
H(2m3)	0.661(8)	0.032(13)	−0.103(7)	21(4)
H(3m3)	0.657(6)	0.042(8)	−0.016(4)	12(2)
H(1m4)	−0.010(6)	0.388(8)	−0.193(4)	12(2)
H(2m4)	0.026(4)	0.533(6)	−0.227(3)	8(1)
H(3m4)	0.029(5)	0.521(7)	−0.139(3)	10(1)

TABLE 2. Mean values of bond lengths and angles of acetate groups attached to carbohydrates and related molecules. The weighted averages are calculated based on the number of acetate groups in each of the compounds

Compound	No. of acetate groups	Bond length (Å) C=O	C—O	CH_3—C	Bond angles (deg) CH_3—C—O	CH_3—C=O	O—C=O
A*	6	1.195	1.336	1.496	111.7	125.0	123.3
B†	3	1.170	1.367	1.493	111.3	126.7	122.3
C‡	1	1.180	1.334	1.488	112.2	124.3	123.4
D§	3	1.183	1.363	1.513	111.3	126.7	121.4
E‖	2	1.185	1.346	1.492	111.1	124.7	124.2
This work	3	1.189	1.343	1.490	111.2	126.8	122.0
Weighted average		1.186	1.348	1.496	111.4	125.8	122.7

*(1 → 4)-β-D-Xylobiose hexaacetate (4).
†Tri-*O*-acetyl-β-D-arabinopyranosyl bromide (7).
‡3′-*O*-Acetyl-4-thiothymidin (13).
§1-*O*-(*p*-Bromobenzenesulphonyl)-4,5,7-tri-*O*-acetyl-2,6-anhydro-3-deoxy-D-glucoheptitol (14).
‖Cytosamine triacetate (15); one of the acetate groups is not attached to the pyranose ring and is therefore excluded.

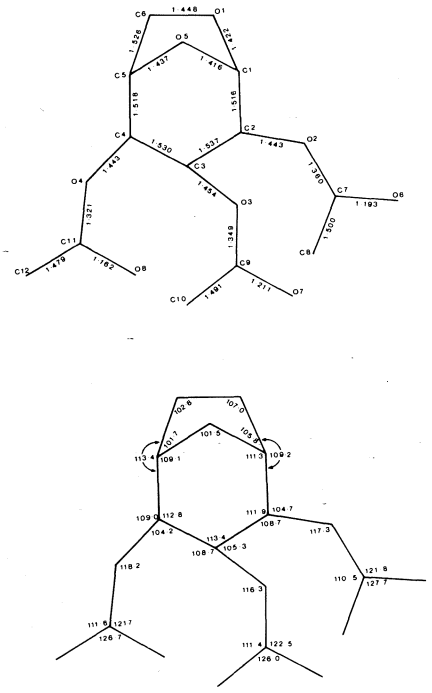

FIG. 2. Bond lengths and bond angles of 1,6-anhydro-2,3,4-tri-*O*-acetyl-β-D-glucopyranose. Maximum standard deviation for C—C bond is 0.006 Å and for C—O bond is 0.005 Å. Maximum e.s.d. for bond angles is 0.4°.

C—O bonds, which are 0.016–0.028 Å longer. The bond lengths and angles of the acetate groups are well in line with those attached to other carbohydrate ring systems (4, 7, 13–15). The mean values of bond lengths and angles for the acetate groups are tabulated in Table 2 together with those in some other carbohydrate rings. The angle CH_3—C—O (111.2°) is much less than 120°. This observation is consistent for all 18 acetate groups in 6 different structural analyses. The smallest values reported for this angle is 107.8° (14). Such distortion of the bond angles were not found in the cases of acetic acid (16) and the acetate acidium ion (17).

The pyranose ring of the molecule has the 1C(D) chair conformation with the acetate groups occupying the axial positions at C2, C3, and C4. A stereoscopic view of the molecule is shown in Fig. 3. The best least-squares planes for the pertinent parts of the molecule are shown in Table 3. The acetate groups show much less deviations from coplanarity than C1, C2, C4, and C5 in the pyranose ring and C1, C5, C6, and O1 in the anhydride ring. It is evident from Table 3 that the deviations from coplanarity for the pyranose ring in the acetylated molecule are almost 10 times larger than those obtained for the unacetylated molecule. The distance of C3 from the mean plane is decreased by 0.054 Å.

The torsional angles of the molecule are listed in Table 4. The sign conventions used are those of IUPAC (18). The torsional angles of the pyranose ring are in good agreement with those of the unacetylated molecule **1** (1). In no case do

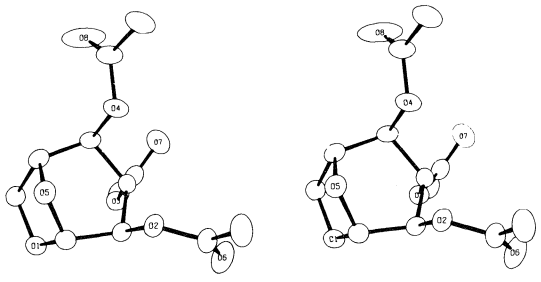

FIG. 3. A stereoscopic view of 1,6-anhydro-2,3,4-tri-*O*-acetyl-β-D-glucopyranose.

Can. J. Chem. Downloaded from www.nrcresearchpress.com by 210.87.254.40 on 09/05/12
For personal use only.

TABLE 3. Least-squares planes in 1,6-anhydro-2,3,4-tri-*O*-acetyl-β-D-glucopyranose. The values in parentheses are those of 1,6-anhydro-β-D-glucopyranose, **1**, (1). Equation for plane: $Ax + Bg + Cz = D$, where x, y, z are in Å

	Atoms in "best" plane	Atoms out of "best" plane	Distance from "best" plane, Å (P)	Estimated standard deviation in P	Constants	
Pyranose ring	C1		0.010 (0.001)	0.003 (0.003)	−0.9827 (0.501)	*A*
	C2		−0.009 (−0.001)	0.003 (0.003)	0.1497 (0.477)	*B*
	C4		0.009 (0.001)	0.003 (0.003)	−0.1089 (0.722)	*C*
	C5		−0.010 (−0.001)	0.003 (0.003)	−2.8037 (2.638)	*D*
		C3	−0.406 (−0.460)	0.003 (0.003)		
		O5	0.826 (0.820)	0.002 (0.002)		
Anhydride ring	C1		0.018 (0.012)	0.004 (0.004)	−0.2844 (0.049)	*A*
	C5		−0.017 (−0.011)	0.004 (0.003)	−0.2077 (−0.563)	*B*
	C6		0.026 (0.017)	0.004 (0.004)	−0.9359 (0.825)	*C*
	O1		−0.028 (−0.018)	0.003 (0.002)	3.0343 (1.599)	*D*
		O5	0.632 (0.623)	0.003 (0.002)		
Acetates	O2		−0.001	0.003	−0.0599	*A*
	C7		0.003	0.004	−0.9494	*B*
	C8		−0.001	0.006	−0.3082	*C*
	O6		−0.001	0.004	1.4123	*D*
	O3		0.004	0.002	0.1802	*A*
	C9		−0.011	0.004	0.6092	*B*
	O7		0.005	0.003	−0.7722	*C*
	C10		0.003	0.005	2.4530	*D*
	O4		0.002	0.003	−0.2276	*A*
	C11		−0.007	0.003	−0.1928	*B*
	O8		0.003	0.006	−0.9545	*C*
	C12		0.002	0.005	1.8805	*D*

they differ by more than 5°. These small deviations can be attributed to the slight "flattening" of the pyranose ring. In conclusion, the effect of the acetylation on levoglucosan are (*a*) to lessen the coplanarity of the atoms C1, C2, C4, and C5 due to nonbonded interaction of the axial acetate groups; (*b*) to "flatten" the pyranose ring such that the distance of C3 from the mean plane defined by C1, C2, C4, and C5 is decreased by 0.05 Å; and (*c*) to leave the geometry of the anhydride ring unchanged.

The orientation of the acetate groups with respect to the pyranose ring is shown in the Newman projections of Fig. 4. In all three cases, the carbon(acetate)–oxygen bond makes a dihedral angle of approximately 30° with the carbon(ring)–hydrogen bond. In other acetylated carbohydrate rings (4, 7, 13–15), the value of this dihedral angle varies from 0 to 43°. The distribution of acetate groups *vs.* this dihedral angle magnitude is shown in Table 5. The calculations are based on nonhydrogen positions; the ring-hydrogen positions were estimated assuming sp^3 hybridization of the carbon atoms. With the data available at the present moment, one may

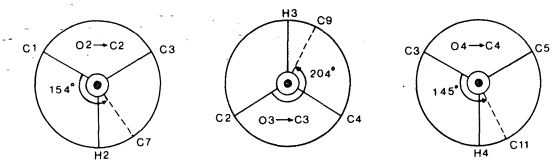

FIG. 4. Orientation of the acetate groups (Newman projection) in 1,6-anhydro-2,3,4-tri-*O*-acetyl-β-D-glucopyranose.

conclude that there is a "high probability" that the acetate groups in sugars lie in "near eclipsing" positions[3] as shown in Fig. 1.

It is interesting to note that the tri-*O*-acetyllevoglucosan assumes the same 1C(D) conformation as in levoglucosan. Thus in spite of the bulky acetate groups, and perhaps because of their planarity, their substituents are able to occupy the axial positions as required by the 1C(D) chair. This was proposed by Hall and

[3]It should be noted that our use of the word "eclipsing" is in terms of the standard terminology which uses four contiguous atoms, in this case: C(A)—O—C—H (*cf.* Fig. 1). Some authors (7) refer to "eclipsing" of C=O in carbohydrate acetates with the ring C—H but this involves five atoms.

Can. J. Chem. Downloaded from www.nrcresearchpress.com by 210.87.254.40 on 09/05/12
For personal use only.

TABLE 4. Torsional angles of levoglucosan triacetate. The conventions used are of Klyne and Prelog (18)

Bonds	Angles (deg)	Bonds	Angles (deg)
C2—C1—O1—C6	−96.4	C3—C4—C5—C6	−56.8
C2—C1—O5—C5	75.3	C3—C4—C5—O5	55.7
O1—C1—C2—C3	62.7	C3—C4—O4—C11	144.8
O1—C1—C2—O2	−179.7	C5—C4—O4—C11	−94.5
O1—C1—O5—C5	−43.2	O4—C4—C5—C6	−172.1
O5—C1—C2—C3	−53.7	O4—C4—C5—O5	−59.6
O5—C1—C2—O2	63.8		
O5—C1—O1—C6	23.4	C4—C5—C6—O1	86.6
		C4—C5—O5—C1	−75.4
C1—C2—C3—C4	30.3	C6—C5—O5—C1	44.6
C1—C2—C3—O3	−88.4	O5—C5—C6—O1	−30.4
C1—C2—O2—C7	153.6		
C3—C2—O2—C7	−86.7	C5—C6—O1—C1	4.7
O2—C2—C3—C4	−84.9		
O2—C2—C3—O3	156.5	C8—C7—O2—C2	178.9
		O6—C7—O2—C2	−0.6
C2—C3—C4—C5	−32.0		
C2—C3—C4—O4	86.1	C10—C9—O3—C3	−176.0
C2—C3—O3—C9	−156.1	O7—C9—O3—C3	1.8
C4—C3—O3—C9	82.1		
O3—C3—C4—C5	84.7	C12—C11—O4—C4	179.6
O3—C3—C4—O4	−157.2	O8—C11—O4—C4	0.9

TABLE 5. The distribution of acetate groups (4, 7, 13–15) *vs.* the dihedral angle magnitude (the angle between two planes defined by H, C, O, and the atoms C, O, C(A) in Fig. 1)

Dihedral angle (deg)	No. of acetate groups
0–5	4
6–10	3
11–15	3
16–20	1
21–25	2
26–30	1
31–35	1
36–40	1
41–45	1
	Total 17*

*The acetate group attached to C6 of the glucose unit (14) was eliminated from this survey.

co-worker (19) and Horton and co-worker (20) based on n.m.r. data. Proton n.m.r. studies (21) also assign the same conformation to the tri-*O*-methyl derivative. Since the latter polymerizes stereoregularly under the influence of PF_5 catalyst while the tri-*O*-acetyl derivative does not (22) polymerize at all. It would seem that there is no correlation between the stable monomer conformation and the mechanism responsible for the stereoregular polymerization.

1. Y. J. PARK, H. S. KIM, and G. A. JEFFREY. Acta Cryst. B, **27**, 220 (1971).
2. B. BERKING and N. C. SEEMAN. Acta Cryst. B, **27**, 1752 (1971).
3. C. C. TU and C. SCHUERCH. Polym. Lett. **1**, 163 (1963).
4. F. LEUNG and R. H. MARCHESSAULT. Can. J. Chem. **51**, 1215 (1973).
5. S. M. GABBAY, P. R. SUNDARARAJAN, and R. H. MARCHESSAULT. Biopolymers, **11**, 79 (1972).
6. A. SARKO and R. H. MARCHESSAULT. J. Am. Chem. Soc. **89**, 6454 (1967).
7. P. W. R. CORFIELD, J. D. MOKREN, P. L. DURETTE, and D. HORTON. Carbohydr. Res. **23**, 158 (1972).
8. V. N. NIKITIN, I. YU, LEVDIK and M. A. IVANOV. J. Struct. Chem. **9**, 901 (1968).
9. J. KARLE and H. HAUPTMAN. Acta Cryst. **11**, 757 (1958).
10. J. KARLE and I. L. KARLE. Acta Cryst. **21**, 849 (1966).
11. R. F. STEWART, E. R. DAVIDSON, and W. T. SIMPSON. J. Chem. Phys. **42**, 3175 (1965).
12. D. T. CROMER and J. T. WALKER. Acta Cryst. **18**, 104 (1965).
13. W. SAENGER and D. SUCK. Acta Cryst. B, **27**, 2105 (1971).
14. A. CAMERMAN and J. TROTTER. Acta Cryst. **18**, 197 (1965).
15. J. SYGUSCH, F. BRISSE, and S. HANESSIAN. Acta Cryst. 1974. In press.
16. R. E. JONES and D. H. TEMPLETON. Acta Cryst. **11**, 484 (1958).
17. P. G. JONSSON and I. OLOVSSON. Acta Cryst. B, **24**, 559 (1968).
18. W. KLYNE and V. PRELOG. Experientia, **16**, 521 (1960).
19. L. D. HALL and L. HOUGH. Proc. Chem. Soc. 382 (1962).
20. D. HORTON and J. D. WANDER. J. Org. Chem. **32**, 3780 (1967).
21. A. TRACEY. B.Sc. Thesis. University of British Columbia, British Columbia. 1967.
22. E. R. RUCKEL and C. SCHUERCH. J. Org. Chem. **31**, 2233 (1966).

Can. J. Chem. Downloaded from www.nrcresearchpress.com by 210.87.254.40 on 09/05/12
For personal use only.

Hydride Reductions of 1-Phenyl-1-nonen-3-one: Mass Spectrometry of 1-Phenyl-1-nonen-3-ols and Relative Stereochemistry of the Diastereoisomeric 4-Dimethylaminomethyl-1-Phenyl-1-nonen-3-ols[1]

WESLEY GORDON TAYLOR AND JONATHAN RICHARD DIMMOCK[2]

College of Pharmacy, University of Saskatchewan, Saskatoon, Saskatchewan S7N 0W0

Received August 7, 1973[3]

WESLEY GORDON TAYLOR and JONATHAN RICHARD DIMMOCK. Can. J. Chem. **52**, 2522 (1974).

The metal hydride reduction products of some styryl ketones and dimethylaminomethyl Mannich bases have been investigated. Sodium borohydride selectively attacked the carbonyl carbon atom to give the desired allylic alcohols. Reduction of 1-phenyl-1-nonen-3-one with lithium aluminum hydride gave 1-phenyl-3-nonanol which represents the conjugate addition product. Fragmentations of 1-phenyl-1-nonen-3-ol were compared to the modes of mass spectral breakdown of 4-phenyl-3-buten-2-ol, an allylic alcohol which is known to behave like a saturated ketone on electron bombardment. Peaks corresponding to the McLafferty ion and the loss of a methyl radical from this rearrangement product were observed. Certain Mannich bases were reduced to diastereoisomeric allylic amino alcohols. The separation, ^{1}H n.m.r. spectroscopy, and relative stereochemistry of the diastereoisomers are discussed.

WESLEY GORDON TAYLOR et JONATHAN RICHARD DIMMOCK. Can. J. Chem. **52**, 2522 (1974).

On a examiné les produits de la réduction par les hydrures métalliques de quelques styryles cétones et de leurs bases de Mannich diméthylaminométhylées. Le borohydrure de sodium attaque d'une façon sélective le groupement carbonyle et conduit aux alcools allyliques désirés. La réduction de la phényl-1 nonèn-1 one-3 par l'hydrure double de lithium et d'aluminium conduit aux phényl-1 nonanol-1; ceci correspond au produit d'addition conjugué. On a comparé les modes de fragmentations du phényl-1 nonèn-1 ol-3 avec les modes de coupures en spectrométrie de masse du phényl-4 buten-3 ol-2, un alcool allylique connu pour réagir comme une cétone saturée lors du bombardement électronique. On a pu observer les pics correspondants à l'ion de McLafferty et à celui correspondant à la perte d'un radical méthyle provenant du produit de réarrangement. Certaines bases de Mannich se réduisent en aminoalcools allyliques diastéréoisomères. On discute de la séparation, de la r.m.n. du proton et de la stéréochimie relative des diastéréoisomères. [Traduit par le journal]

Introduction

The synthesis and mass spectral characteristics of the α, β-ethylenic ketones **1** required for this work have been reported (1). Nuclear substituted dimethylaminomethyl Mannich bases **2** were prepared (2) and these water-soluble styryl ketones have been evaluated for *in vitro* and *in vivo* anticancer activity by established procedures (3). In attempts to alter the polarized olefinic system in the conjugated ketones while maintaining the rigid stereochemistry of the ethylenic bond, the allylic alcohols **3** and allylic amino alcohols **4** were prepared (Scheme 1) for testing in experimental tumor screens.[4]

Current interest in unsaturated alcohols as possible anticancer agents has stemmed from the requirements for an allylic ester functional group in tumor-inhibitory members of the pyrrolizidine alkaloids (4). These allylic aminoesters are thought to function as biological alkylating agents by a mechanism involving alkyl oxygen ester fission to give stable carbonium ions (5). More recently, Willette and Driscoll (6) have studied synthetic allylic esters as acyclic model compounds of the pyrrolizidine alkaloids. For the same reason, we have prepared and tested[4] a series of substituted allylic esters, two of which (**3***b*-*p*-nitrobenzoate and **4***a*-*p*-nitrobenzoate) are described herein.

Based on early literature reports, the choice of metal hydride reducing agent for synthesizing unsaturated alcohols from cinnamyl derivatives is sodium borohydride (7) because lithium aluminum hydride may lead to reduction of the ethylenic bond (8). Conjugate addition by sodium

[1]Presented in part at the Nineteenth Canadian Conference on Pharmaceutical Research, University of Alberta, Edmonton, Alberta, August 1972.

[2]To whom inquiries should be directed.

[3]Revision received March 25, 1974.

[4]The antineoplastic activity and other pharmacological activities of these alcohols will be reported elsewhere.

Can. J. Chem. Downloaded from www.nrcresearchpress.com by 210.87.254.42 on 09/05/12
For personal use only.

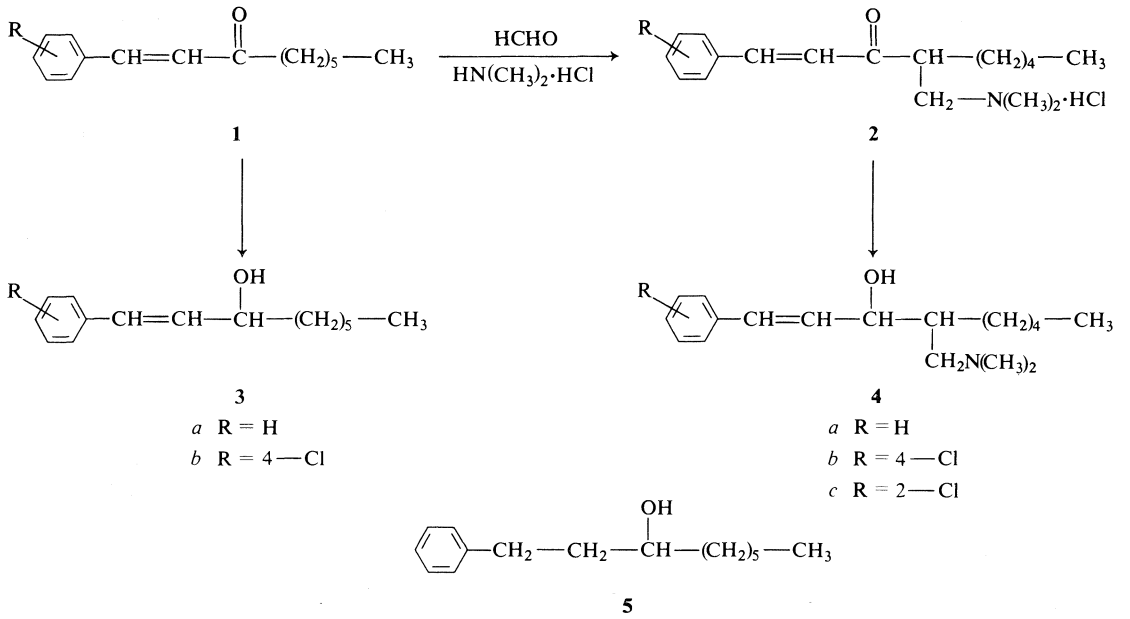

SCHEME 1

borohydride to give saturated alcohols, however, represented a substantial competing process in a more recent study of the metal hydride reductions of β-alkyl-α,β-unsaturated ketones (9). In fact, lithium aluminum hydride emerged as a better agent than sodium borohydride for preparing a series of allylic alcohols. To clarify the pattern of reduction with our olefinic ketones, and since the reduction of Mannich bases **2** is complicated by the formation of diastereoisomeric amino alcohols, we initially examined the styryl ketone **1***a* to determine a suitable reducing agent for preparing allylic alcohols from α,β-unsaturated ketones of these two particular types.

Results and Discussion

Reductions

Four metal hydrides were chosen for this study (Table 1) and they are listed in order of decreasing reducing power (10). Gas–liquid chromatography was employed in order to examine the ratio of carbonyl addition **3***a* to conjugate addition **5** products. It was found that lithium aluminum hydride reduction of the unsaturated ketone **1***a* gave the saturated alcohol **5** (>99%). As expected, olefinic proton signals were absent from the n.m.r. spectrum and i.r. spectroscopy revealed the absence of carbonyl stretching bands with hydroxyl stretching appearing at 3350 cm^{-1}.

As seen in Table 1, sodium borohydride proved to be the best reducing agent for synthesizing 1-phenyl-1-nonen-3-ol (**3***a*) from **1***a*. Reduction mixtures from the lithium borohydride and sodium trimethoxyborohydride experiments analyzed as multi-component mixtures although *ca.* 80% of **3***a* was detected by g.l.c. By avoiding reflux temperatures, sodium borohydride converted **1***a* to the allylic alcohol **3***a* (99%) whereas the saturated alcohol **5** represented 6% of the mixture when the methanol–water medium was heated under reflux prior to product isolation. Iqbal and Jackson (11) have likewise shown that the reductions of α,β-unsaturated ketone systems with sodium borohydride gave more of the allylic relative to the saturated alcohol when low reaction temperatures are employed. The aqueous methanol media is also desirable in order to prevent solvent addition to the β-carbon atom (9).

Sodium borohydride smoothly reduced the 4-chloro ketone **1***b* to the allylic alcohol **3***b* (Scheme 1). The crude reduction mixture showed 97% of one component (g.l.c.) with 3% representing unreduced ketone and less than 0.5% of an unidentified component.

Mass Spectrometry

The fragmentation in **3***a* and *b* were somewhat predictable by reference to reported work (12, 13)

Can. J. Chem. Downloaded from www.nrcresearchpress.com by 210.87.254.42 on 09/05/12
For personal use only.

Can. J. Chem. Downloaded from www.nrcresearchpress.com by 210.87.254.42 on 09/05/12
For personal use only.

TABLE 1. Reductions of 1-phenyl-1-nonen-3-one

Metal hydride	Reducing agent/1-phenyl-1-nonen-3-one (mol)	Conditions		Solvent	Product analysis (%)*		
		Initial	Final		**3***a*†	**5**‡	Yield§ (%)
$LiAlH_4$	0.02/0.02	0° 20 min	3 h reflux	Et_2O	1	99	71
$LiBH_4$	0.01/0.01	0° 20 min	3 h reflux	Et_2O	85‖	2.5	77
$NaBH(OCH_3)_3$	0.052/0.01	0° 20 min	3 h reflux	Et_2O	79¶	2	70
$NaBH_4$	0.02/0.02	0° 30 min	24 h room temperature	MeOH–H_2O	99	1	77
$NaBH_4$	0.02/0.02	0°, then 24 h room temperature	8 h reflux	MeOH–H_2O	94	6	66

*By g.l.c. on the crude reduction products.
†1-Phenyl-1-nonen-3-ol, retention time 8.4 min.
‡1-Phenyl-3-nonanol, retention time 4.7 min. Authentic mixtures (2.0 and 4.0%) of **5** in **3***a* analyzed within ±0.2% of the expected values assuming an equal detector response factor for the two alcohols.
§Reported yields are based on crude material.
‖The remainder was a component with retention time of 11.4 min (2%), unreduced ketone (2.5%), and other lower retention time peaks (8%).
¶Also detected was a component with a retention time of 11.4 min (6%), unreduced ketone (6%), and several lower retention time peaks (7%).

Can. J. Chem. Downloaded from www.nrcresearchpress.com by 210.87.254.42 on 09/05/12
For personal use only.

on the mass spectra of other allylic alcohols. In this context, the alcohols gave spectra (Figs. 1 and 2) which were characteristic of unsaturated alcohol and saturated ketone mixtures.

In the first case, an allylic bond cleavage product which represented the base peak was observed. This ion (*a*) subsequently lost water to give peaks at *m/e* 115 and 149 for **3***a* and **3***b*, respectively. The removal of an *ortho* hydrogen atom in the allylic ion (*a*) has been considered as one route to (*a* − H_2O) (Scheme 2). In contrast to the ion (*a* − H_2O) process, the emanation of 18 mass units from the allylic alcohol molecular ions was not a favorable fragmentation (<2%) but the saturated alcohol **5**, Fig. 3, gave the (M − H_2O) ion at *m/e* 202 (23%). The α-cleavage ion (*a*), *m/e* 135, from **5** also expelled water to give an important peak at *m/e* 117.[5]

The generation of a saturated ketone molecular ion from the allylic alcohol molecular ion followed by fragmentation accounted for most of the remaining products (Scheme 2). In the case of 4-phenyl-3-buten-2-ol (*m/e* 105 = 100%; *m/e* 115 = 35%; *m/e* 133 = 35%), the two rearranged hydrogen atoms originated from the secondary carbon atom and the hydroxyl group (12). Fragment ions from **3***a* and **3***b* included the acylium ion (a_r), isomeric with the base peak (*a*), in addition to the McLafferty ion (b_r). The latter ion decomposed either to ion (a_r) by an unusual loss of a methyl group (14, 15) or to a substituted tropylium ion (*c*). Prominent peaks for the loss of one and two hydrogen atoms from ion (*c*) were

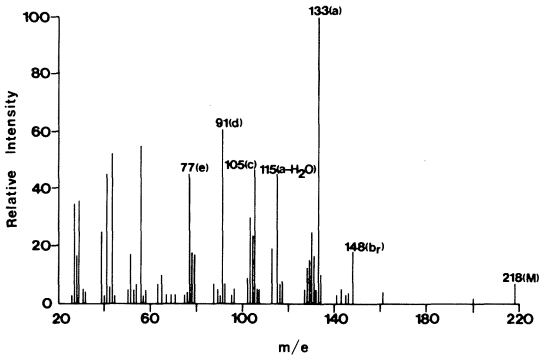

FIG. 1. Mass spectrum (70 eV) of **3***a*.

[5]Exact mass measurements and metastable transitions of the ions involved in the major fragmentation pathways of **3***a*, **3***b*, and **5** are available from the Depository of Unpublished Data, National Science Library, National Research Council of Canada, Ottawa, Canada K1A 0S2.

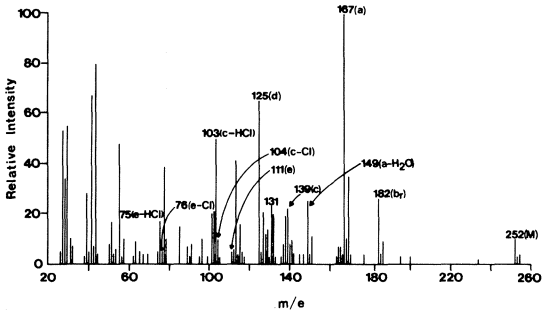

FIG. 2. Mass spectrum (70 eV) of **3***b*.

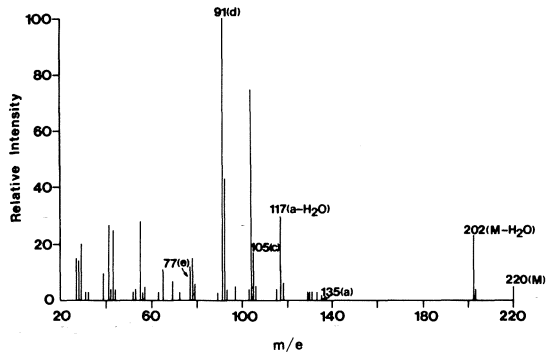

FIG. 3. Mass spectrum (70 eV) of **5**.

noted. With **3***b*, ion (*c*) and the phenyl cation (*e*) decomposed by losing a chlorine atom or hydrogen chloride. Peaks at *m/e* 131 and 132 may be due to the loss of hydrogen chloride or a chlorine atom from the McLafferty rearrangement product (1). Fragments in the region *m/e* 127 to 130 are unique to the allylic alcohols discussed since these ions were suppressed in the mass spectra of **5** (Fig. 3) and of 4-phenyl-2-butanone (12).

Stereochemistry

Since sodium borohydride selectivity reduced the carbonyl group of the ketones **1** and of related nonasymmetric α,β-unsaturated amino ketones (16, 17), this reagent was used to convert the available racemic Mannich bases **2** to the desired allylic amino alcohols **4** (Scheme 1). Reduction conditions were initially developed for **2***a* and, even after the required 3 h heating under reflux, there was obtained no evidence for sodium borohydride reduction of the ethylenic bond. The n.m.r. spectrum on crude **4***a* clearly revealed that diastereoisomeric allylic alcohols were present. In addition to the 10 lines evidenced from δ 5.85–6.87, the methine protons at C-3 appeared at δ 4.23 (ragged triplet) and at δ 3.98 (doublet of

Can. J. Chem. Downloaded from www.nrcresearchpress.com by 210.87.254.42 on 09/05/12
For personal use only.

TABLE 2. Nuclear magnetic resonance data for diastereoisomeric allylic amino alcohols

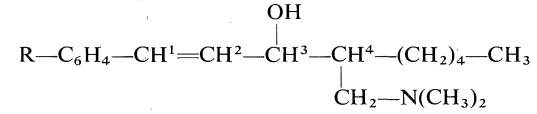

	Isomer	Ratio of isomers (%)	δ H^1	δ H^2	$J_{H}1_{H}2$	$J_{H}1_{H}3$	$J_{H}2_{H}3$	δ H^3	$W_{H}3$	$J_{H}3_{H}4$	Footnote reference
4*a*											
R = H	*threo*	67	6.63	6.08	15.5	1	4.5	4.23	9	3.5	*
			(6.77)	(6.20)	(15.5)	—	(4.5)	(4.77)	(10)	(4.5)	†
	erythro	33	6.52	6.02	15.5	—	6.5	3.98	16	8	*
			(6.60)	(6.15)	(15.5)	—	(7)	(4.17)	(18)	(9)	†
4*b*											
R = 4-Cl	*threo*	65	6.32	5.83	15	1	4.0	4.05	9	4	‡
			(6.80)	(6.27)	(16)	—	(4.5)	(4.87)	(11)	(6.5)	†
	erythro	35	6.15	5.73	15	—	6.0	3.78	16	7.5	‡
			(6.63)	(§)	(16)	—	(7.0)	(4.22)	(18)	(9)	†
4*c*											
R = 2-Cl	*threo*	70	‖	6.10	15.5	‖	4.5	4.28	10	3.5–5	‡
			‖	(6.15)	(15.5)	‖	(4.5)	(4.77)	(10)	(5.5)	†
	erythro	30	‖	6.00	15.5	‖	6.5	4.03	16	8	‡¶

*As 0.5 *M* solutions of the free base in carbon tetrachloride (D_2O added). The coupling constants and half-bandwidth measurements are expressed in Hz.
†In parentheses are given the corresponding values found in deuterochloroform for the hydrochloride salt (*threo* isomer) and the maleate salt (*erythro* isomer).
‡Data from the mixture of free bases.
§The lower field portion of this doublet of doublets was obscured by olefinic proton signal of maleic acid.
‖The H^1 signal appeared with the aromatic proton multiplet and hindered the observation of allylic coupling between H^1 and H^3. $J_{H}1_{H}3$ was identified in the other *threo* isomers by irradiating the H^3 signal.
¶An attempt at isolating the minor isomer as the maleate salt was unsuccessful. The n.m.r. data was then derived from the free base mixture.

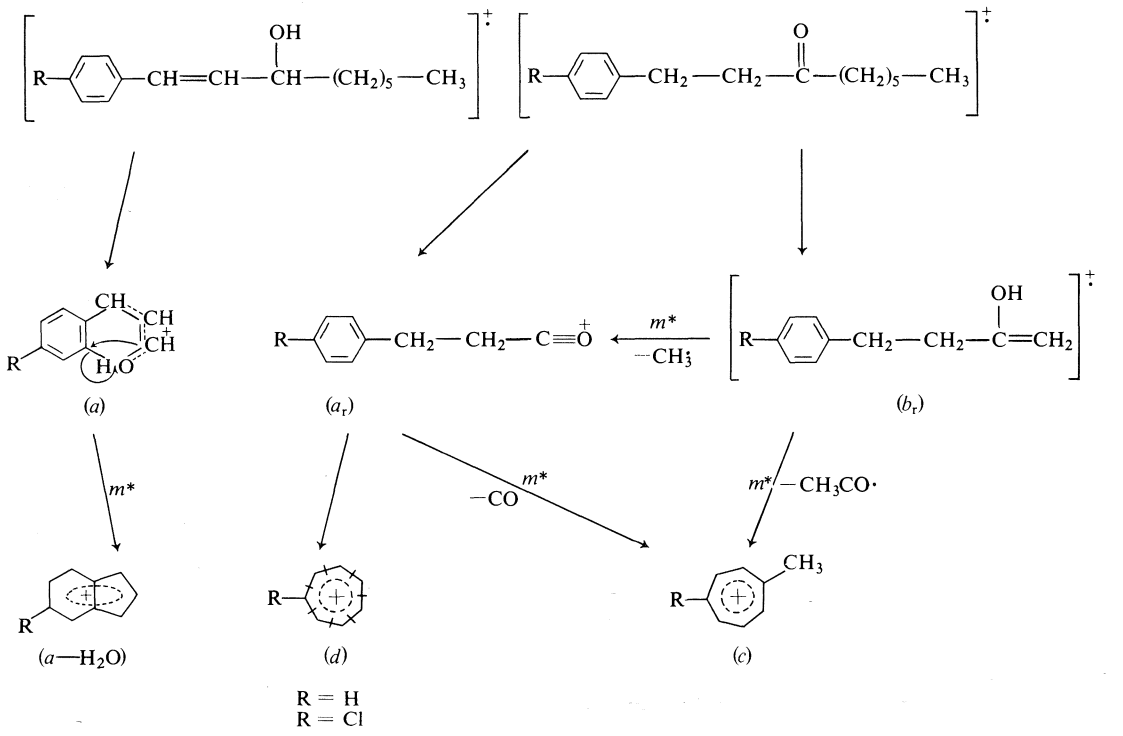

SCHEME 2

doublets). On integration of H-3, the diastereoisomeric ratio of the amino alcohols was found to be 67:33.[6] Pertinent n.m.r. data for the three pairs of diastereoisomers are collected in Table 2.

Assignments of relative configurations to acyclic diastereoisomers (18, 19) has become possible from the Karplus (20) relationship between the magnitude of J and the dihedral angle separating vicinal protons. In the present work, assignments to **4** are made using i.r. and n.m.r. spectroscopy. Application is also made to the *RS* nomenclature wherein the **3***R*,**4***S*/**3***S*,**4***R* and **3***R*,**4***R*/**3***S*,**4***S* isomers implies, respectively, the *erythro* and *threo* configurations (21).

Because intramolecular hydrogen bonded conformational preferences of acyclic diastereoisomers may contribute more to conformational preferences which are constructed by considering nonbonded steric interactions of adjacent substituents (22, 23), it was important to confirm that the amino alcohols were internally hydrogen bonded. The i.r. spectra of both diastereoisomeric bases **4***a* revealed broad absorptions corresponding to the bonded hydroxyl stretching band.[7] Diluted solutions of the aminoalcohols showed a strong i.r. band at 3220 cm^{-1} (*threo* isomer) and at 3185 $\pm$ 5 cm^{-1} (*erythro* isomer) down to a concentration of 0.005 *M*. A weak free hydroxyl stretching band appeared near 3600 cm^{-1}. The bonded and free hydroxyl stretching bands did not change dramatically in intensity and in position with changes in concentration thus providing evidence[8] that the diastereoisomers were both

[6]The unsubstituted alcohols **4***a* were resolved on a Carbowax column (peak area ratio of 73:27) but identical retention times for the diastereoisomeric chlorinated alcohols **4***b* and **4***c* precluded the use of g.l.c. to estimate the isomer ratios. These ratios were determined by integrating the H-3 signals in the free base mixtures.

[7]The i.r. spectra in carbon tetrachloride were determined at the following molar concentrations (cell thickness in parentheses): 0.50 (0.1 mm); 0.10 (0.25 mm); 0.025 (1.0 mm); 0.010 (2.5 mm); 0.005 (5.0 mm).

[8]In the related 3-dimethylamino-2-methyl-1-phenyl-1-propanol system, Angiolini and Gottarelli (24) based their conformational analysis on the hydrogen bonded tetrahydro-1,3-oxazine-like ring system. Rather than making configurational assignments to **4** based on axial–equatorial relationships of H-3, and H-4, we have considered "pure" staggered rotomers depicting *trans* ($\Phi = 180°$) and *gauche* ($\Phi = 60°$) orientations of the carbon–hydrogen bonds at C-3 and C-4.

Can. J. Chem. Downloaded from www.nrcresearchpress.com by 210.87.254.42 on 09/05/12
For personal use only.

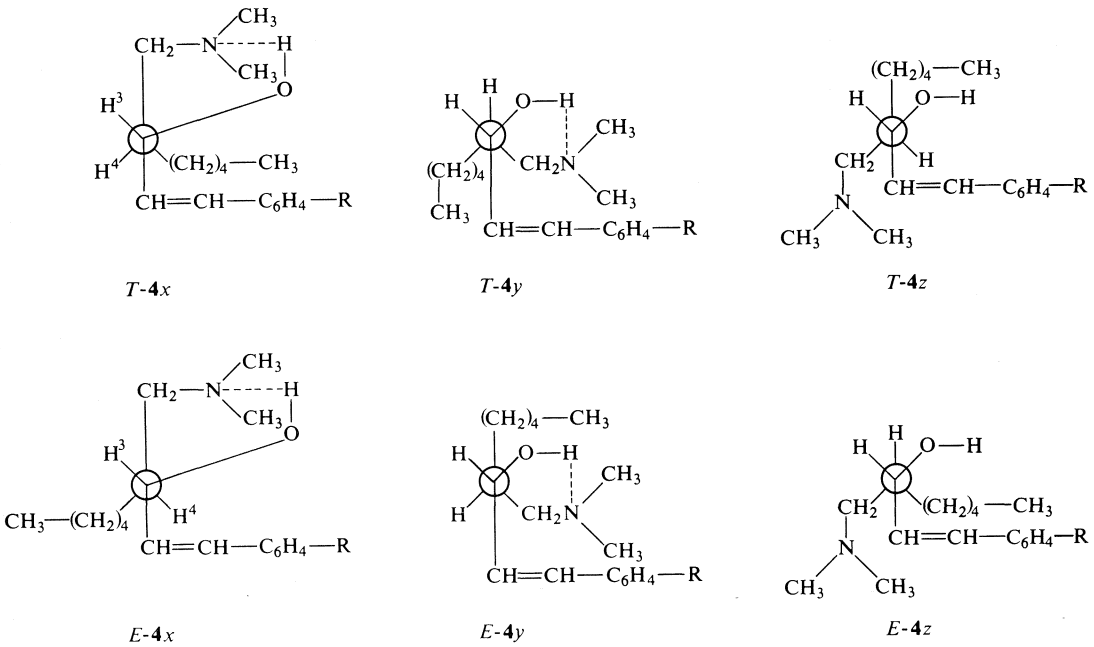

FIG. 4. Newman projections of (3*R*,4*R*)-4-dimethylaminomethyl-1-phenyl-1-nonen-3-ol (*T*-**4**) and (3*R*,4*S*)-4-dimethylaminomethyl-1-phenyl-1-nonen-3-ol (*E*-**4**).

intramolecular hydrogen bonded in the nonpolar solvent.

Derivation of $J_{H^3H^4}$ for the major isomers (*threo* in Table 2) was based on half-bandwidth measurements of the H-3 signal (9–10 Hz) minus the sum of the coupling to H-3 by H-1 (1 Hz) and H-2 (4–4.5 Hz). The 3.5–5 Hz coupling constants suggested a *gauche* orientation of the protons at C-3 and at C-4.

The rotomers *T*-**4***z* and *E*-**4***z* (Fig. 4) cannot assume a hydrogen-bonded conformation and they can be eliminated as preferred conformations of either diastereoisomer. Although rotomer *E*-**4***y* has the *gauche* relationship of H-3 and H-4, *E*-**4***y* is not as stable as *E*-**4***x* since the latter rotamer has bulky substituents flanked by hydrogen atoms. Therefore the major isomer, having as a preferred conformation rotamer *T*-**4***x* has the **3***R*,**4***R* (*threo*) configuration.

For the minor isomer, the n.m.r. data (Table 2) are in agreement with this diastereoisomer having the **3***R*,**4***S* (*erythro*) relative configuration. Since the H-3 signal gave four lines (J = 6.0–6.5 Hz; J = 7.5–8.0 Hz) and a $J_{H^2H^3}$ of 6.0–6.5 Hz was seen in the doublet of doublets of the H-2 signal, $J_{H^3H^4}$ was equal to 7.5–8.0 Hz. A *trans* relationship of H-3 and H-4 in a conformational preference of the diastereoisomer was suggested. This is shown in Fig. 4 as rotomer *E*-**4***x*.

Half-bandwidths of H-3 for the diastereoisomeric salts were consistently similar to the same signals for the free bases (Table 2). A much lesser degree of conformational homogeneity is indicated for *threo*-**4***a* methiodide (see Experimental) which gave a half-bandwidth of 14 Hz compared to half-bandwidths of 9 Hz for the corresponding tertiary amine and 10 Hz for the hydrochloride salt.

Experimental

Elemental analyses on the compounds reported in this work were performed by F. B. Strauss, Microanalytical Laboratories, Oxford, England. Melting points and boiling points are uncorrected. Nuclear magnetic resonance spectra were obtained with a Varian T-60 spectrometer. The spectra were run at room temperature with tetramethylsilane providing the internal standard. Infrared absorption spectra were recorded on a Unicam SP-200G spectrophotometer. Mass spectra were determined on an MS-12 spectrometer operated by Mr. D. Bain, Department of Chemistry, University of Saskatchewan, Saskatoon. Gas–liquid chromatography was performed on a Pye Series 104 chromatograph which was equipped with a flame ionization detector. The 5 ft × 0.25 in. o.d. glass column contained 4% Carbowax 20 M adsorbed onto Chromosorb G, 100–120 mesh. The carrier flow rate was 75 cm³/min (nitrogen) with the gas chromatograph operating at 220°.

Preparation of 1-Phenyl-3-nonanol (5)

Using the quantities and conditions given in Table 1, lithium aluminum hydride reduction of (*E*)-1-phenyl-1-

Can. J. Chem. Downloaded from www.nrcresearchpress.com by 210.87.254.42 on 09/05/12
For personal use only.

Can. J. Chem. Downloaded from www.nrcresearchpress.com by 210.87.254.42 on 09/05/12
For personal use only.

nonen-3-one gave, after adding water, filtering and evaporating *in vacuo* the dried ($MgSO_4$) ether extracts, a colorless oil which was distilled through an air condenser packed with 10 cm of Raschig rings: b.p. 136–138°/1.0 mm (lit. (25) b.p. for **5** is 95–97°/0.5 mm).

Anal. Calcd. for $C_{15}H_{24}O$: C, 81.76; H, 10.98. Found: C, 81.44; H, 10.91.

*Preparation of (E)-1-Phenyl-1-nonen-3-ols (**3**)*

(*E*)-1-Phenyl-1-nonen-3-one (4.326 g, 0.02 mol) was dissolved in methanol (30 ml) and cooled to 0°. Sodium borohydride (0.757 g, 0.02 mol) in water (12 ml; adjusted to p*H* 8.5 with aqueous NaOH) was added dropwise with stirring for 30 min. The reaction was continued at 0° for 1 h, stirred at room temperature for 24 h, evaporated *in vacuo*, and the resulting semisolid was suspended in p*H* 4 water (75 ml). The solution was extracted with ether, washed with water, and dried ($MgSO_4$). Evaporation under reduced pressure gave an oil which was distilled *in vacuo* to give 2.37 g of **3***a*, b.p. 128° (0.80 mm) (lit. (26) b.p. 156–157°/2.0 mm). The distillates, which solidified on cooling, furnished an analytical sample, m.p. 28–29°, as a white solid (from hexane); n.m.r. (CCl_4) gave doublets (J = 16 Hz) at δ 6.45 and 6.02 for C(H)=C(H) with other signals as expected.

Anal. Calcd. for $C_{15}H_{22}O$: C, 82.51; H, 10.16. Found: C, 82.10; H, 10.05.

(*E*)-1-(*p*-Chlorophenyl)-1-nonen-3-ol (**3***b*) was prepared by the above procedure from (*E*)-1-(*p*-chlorophenyl)-1-nonen-3-one (5.015 g, 0.02 mol) and sodium borohydride (0.76 g, 0.02 mol). The crude product was recrystallized from hexane to give **3***b* (2.89 g, 57%) as a white solid with m.p. 42–43°.

Anal. Calcd. for $C_{15}H_{21}ClO$: C, 71.27; H, 8.375. Found: C, 70.95; H, 8.16.

(*E*)-1-(*p*-Chlorophenyl)-1-nonen-3-ol *p*-nitrobenzoate was prepared from **3***b* (2.53 g, 0.01 mol, in 20 ml anhydrous pyridine) and *p*-nitrobenzoyl chloride (2.28 g, 0.012 mol) by stirring at 5° for 30 min then at 22° for 17 h. The reaction mixture was poured into ice and 5 ml of 10% hydrochloric acid was added. The aqueous suspension was extracted with ether. The ether extracts were washed successively with 5% hydrochloric acid, 10% sodium carbonate, then water, and dried ($MgSO_4$). Evaporation *in vacuo* gave a yellow syrup which crystallized on cooling. Three recrystallizations from petroleum ether (b.p. 60–80°) gave the desired ester (0.27 g, 6.7%) as a white powder: m.p. 58–59°; i.r. (KBr) 1715 (C=O) and 965 cm^{-1} (C(H)=C(H)); n.m.r. (CCl_4) δ 8.13 (s, 4, *p*-$NO_2C_6H_4$), 7.20 (s, 4, *p*-ClC_6H_4), 6.60 (d, 1, J = 15 Hz, C_1H), 6.08 (dd, 1, J = 15 Hz, J = 6.5 Hz, C_2H), 5.57 (q, 1, J = 6.5 Hz, C_3H), 2.10–1.10 (m, 10, $(CH_2)_5$), and 0.87 p.p.m. (m, 3, C_9H_3); mass spectrum *m/e* 401 (M^+).

Anal. Calcd. for $C_{22}H_{24}ClNO_4$: C, 65.75; H, 6.02; N, 3.49. Found: C, 66.00; H, 5.88; N, 3.53.

*Preparation of 4-Dimethylaminomethyl-1-phenyl-1-nonen-3-ols (**4**) (Table 2)*

A solution of (*E*)-4-dimethylaminomethyl-1-phenyl-1-nonen-3-one hydrochloride (30.99 g, 0.10 mol) in methanol (150 ml) was cooled at 0°. Sodium borohydride (3.785 g, 0.10 mol) in p*H* 8.5 water (60 ml) was added dropwise and, after stirring for 1 h at 5–8°, the mixture was heated under reflux for 3 h. The reaction vessel was cooled (ice bath) and the p*H* adjusted to 5 with ethanolic hydrochloric acid. Solvent evaporation *in vacuo* gave a white semisolid which, after dissolving in water (200 ml), was extracted with ether. The p*H* of the cold aqueous solution was adjusted to 10 by addition of aqueous sodium hydroxide solution. Following extraction of the free bases with ether, the ether extracts were washed with water and dried ($MgSO_4$). Evaporation of the ether under reduced pressure afforded a colorless oil (23.14 g, 84% yield of the mixture of diastereoisomers (**4***a*)).

Amino alcohols **4***b* were similarly prepared (12.40 g, 71%) by reducing (*E*)-1-(*p*-chlorophenyl)-4-dimethylaminomethyl-1-nonen-3-one hydrochloride (19.4 g, 0.0565 mol) with sodium borohydride (2.14 g, 0.0565 mol). As the free base, (*E*)-1-(*o*-chlorophenyl)-4-dimethylaminomethyl-1-nonen-3-one (9.50 g, 0.031 mol) gave the alcohols **4***c* (6.43 g, 67%) on reduction with sodium borohydride (1.46 g, 0.039 mol) in methanol.

*(a) Derivatives of **4**a*

(*i*) The mixture of diastereoisomeric aminoalcohols (20.65 g) was stirred in ether (350 ml) and ethanolic hydrochloric acid was added until the p*H* was adjusted to 6. On cooling, a product precipitated which was recrystallized from acetone to furnish *threo*-**4***a* hydrochloride (9.03 g, 39%) as white crystals: m.p. 126°; i.r. (KBr) 3335 (OH) and 970 cm^{-1} (C(H)=C(H)); mass spectrum *m/e* 275 (M^+ − HCl).

Anal. Calcd. for $C_{18}H_{30}ClNO$: C, 69.31; H, 9.70; N, 4.49. Found: C, 69.50; H, 9.68; N, 4.55.

(*ii*) A mixture of diastereoisomeric alcohols (2.0 g, 0.0073 mol) was dissolved in absolute ethanol (2 ml) and methyl iodide (2.07 g, 0.015 mol) was added. The reaction mixture was heated under reflux for 1 h. Evaporation *in vacuo* gave a tan semisolid which crystallized on cooling. Recrystallization from absolute ethanol gave *threo*-**4***a* methiodide (0.91 g, 38%) as an off-white powder: m.p. 112.5–113.5°; i.r. (KBr) 3360 (OH) and 970 cm^{-1} (C(H)=C(H)).

Anal. Calcd. for $C_{19}H_{32}INO$: C, 54.67; H, 7.73; I, 30.41; N, 3.36. Found: C, 54.68; H, 7.71; I, 30.63; N, 3.40.

No attempt was made to isolate the *erythro* isomer of **4***a* as the methiodide.

(*iii*) The ether mother liquor from *i* was evaporated *in vacuo* to give a light yellow oil (9.46 g). From a 5.0 g portion of this oily mixture the free bases were liberated. The mixture (0.55 g, 0.002 mol) was stirred in ether (65 ml) and maleic acid (0.23 g, 0.002 mol) was added. On cooling, the deposited product (0.579 g, m.p. 83–90°) was recrystallized from acetone to give *erythro*-**4***a* maleate (0.30 g, 38%): m.p. 98°; i.r. (KBr) 3290 (OH) and 975 cm^{-1} (C(H)=C(H)); mass spectrum *m/e* 275 (M^+ − $C_4H_4O_4$).

Anal. Calcd. for $C_{22}H_{33}NO_5$: C, 67.49; H, 8.50; N, 3.58. Found: C, 67.45; H, 8.45; N, 3.56.

(*iv*) To a chilled (−5°) solution of *threo*-**4***a* free base (2.75 g, 0.010 mol) in 50 ml ether was added *p*-nitrobenzoyl chloride (2.23 g, 0.012 mol). After the addition

had been completed (30 min), the reaction mixture was stirred (ice bath) for 1 h and ether (50 ml) was added. Esterification was continued for 42 h. A product was collected, washed with ether, and recrystallized from acetone to give *threo*-**4***a* *p*-nitrobenzoate hydrochloride. On thin layer silica gel plates (*n*-butanol – glacial acetic acid – water 12:3:5 v/v/v) the compound migrated as one spot. Another recrystallization from acetone did not alter the m.p. of 136°; i.r. (KBr) 1725 (C=O) and 960 cm^{-1} (H C=C H); n.m.r. ($CDCl_3$) δ 12.50–11.67 (broad s, 1, $\overset{+}{N}H$, exchanged with D_2O), 8.27 (s, 4, *p*-$NO_2C_6H_4$), 7.33 (m, 5, phenyl *H*), 6.83 (d, 1, J = 14 Hz, C_1H), 6.57–5.90 (m, 2, C_2H and C_3H), 3.63–2.70 (m, 8, $CH_2\overset{+}{N}(CH_3)_2$), 2.70–2.20 (broad s, 1, C_4H), 1.97–1.10 (m, 8, $(CH_2)_4$), and 0.90 p.p.m. (m, 3, C_9H_3); mass spectrum *m/e* 424 (M^+ – HCl).

Anal. Calcd. for $C_{25}H_{33}ClN_2O_4$: C, 65.13; H, 7.21; N, 6.08. Found: C, 64.92; H, 7.18; N, 6.21.

(*b*) *Derivatives of* **4***b* *and* **4***c*

(*i*) A diastereoisomeric mixture of **4***b* (12.16 g) was stirred in ether and the p*H* was adjusted to 6 with ethanolic hydrochloric acid. A product was precipitated with ether, dried, and recrystallized from acetone to give *threo*-**4***b* hydrochloride (5.05 g, 37%): m.p. 151–152°; i.r. (KBr) 3315 (OH) and 975 cm^{-1} (H C=C H); mass spectrum *m/e* 309 (M^+ – HCl).

Anal. Calcd. for $C_{18}H_{29}Cl_2NO$: C, 62.42; H, 8.44; N, 4.04. Found: C, 62.58; H, 8.46; N, 4.04.

(*ii*) The ether mother liquor from *i* was evaporated *in vacuo* and the free bases liberated as previously described. To the mixture (2.33 g, 0.0075 mol) in ether (150 ml) was added maleic acid (0.87 g, 0.0075 mol). Crystals were precipitated by adding cold ether to give, after recrystallization from ethyl butyrate, *threo*-**4***b* maleate (1.48 g, 46%) melting at 103–105°. An analytical sample had m.p. 109–110°; i.r. (KBr) 3290 (OH) and 975 cm^{-1} (H C=C H); mass spectrum *m/e* 309 (M^+ – $C_4H_4O_4$).

Anal. Calcd. for $C_{22}H_{32}ClNO_5$: C, 62.03; H, 7.57; N, 3.29. Found: C, 62.20; H, 7.64; N, 3.22.

(*iii*) The hydrochloride salts of **4***c* were formed on 5.06 g of the free base mixture to give, after recrystallization from ethyl acetate, *threo*-**4***c* hydrochloride (2.07 g, 46.5%) as white crystals: m.p. 113–114°; i.r. (KBr) 3335 (OH) and 970 cm^{-1} (H C=C H); mass spectrum *m/e* 309 (M^+ – HCl).

Anal. Calcd. for $C_{18}H_{29}Cl_2NO$: C, 62.42; H, 8.44; N, 4.04. Found: C, 62.26; H, 8.43; N, 4.22.

(*iv*) Separation of *erythro*-**4***c* from the diastereoisomeric mixture was unsuccessful giving, after adding equimolar amounts of maleic acid to the mixture of free bases (2.77 g, 0.0089 mol) in ether, an insoluble oil which failed to crystallize by storage under vacuum in a desiccator.

Grateful acknowledgment is made to the Medical Research Council of Canada for providing a studentship to one of us (W.G.T.). Our thanks are also extended to Smith Kline and French Laboratories, Philadelphia, Pennsylvania, for financial support of this work.

1. P. J. Smith, J. R. Dimmock, and W. G. Taylor. Can. J. Chem. **50**, 871 (1972).
2. J. R. Dimmock and W. G. Taylor. J. Pharm. Sci. **63**, 69 (1974).
3. Cancer Chemotherapy Rep. **25**, 1 (1962).
4. C. C. J. Culvenor, J. Pharm. Sci. **57**, 1112 (1968).
5. C. C. J. Culvenor, A. T. Dann, and A. T. Dick. Nature, **195**, 570 (1962).
6. R. E. Willette and R. C. Driscoll. J. Med. Chem. **15**, 110 (1972).
7. S. W. Chaikin and W. G. Brown. J. Am. Chem. Soc. **71**, 122 (1949).
8. F. A. Hochstein and W. G. Brown. J. Am. Chem. Soc. **70**, 3484 (1948).
9. M. R. Johnson and B. Rickborn. J. Org. Chem. **35**, 1041 (1970).
10. E. Schenker. *In* Newer methods of preparative organic chemistry. Vol. IV. *Edited by* W. Foerst. Academic Press, New York, N.Y. 1968. p. 198.
11. K. Iqbal and W. R. Jackson. J. Chem. Soc. C, 616 (1968).
12. B. Willhalm and A. F. Thomas. Org. Mass Spectrom. **1**, 627 (1968).
13. M. Kraft and G. Spiteller. Org. Mass Spectrom. **1**, 617 (1968).
14. H. Budzikiewicz, C. Djerassi, and D. H. Williams. Mass spectrometry of organic compounds. Holden-Day, Inc., San Francisco. 1967. pp. 158–159.
15. Y. M. Sheikh, A. M. Duffield, and C. Djerassi. Org. Mass Spectrom. **4**, 273 (1970).
16. C. D. Blanton and W. L. Nobles. J. Pharm. Sci. **52**, 46 (1963).
17. G. F. Hennion and G. G. King. J. Chem. Eng. Data, **12**, 275 (1967).
18. C. A. Kingsbury. J. Org. Chem. **33**, 1128 (1968).
19. K. Bailey. Can. J. Chem. **48**, 3597 (1970).
20. M. Karplus. J. Chem. Phys. **30**, 11 (1959).
21. M. Hanack. *In* Conformational theory. Vol. 3. *Edited by* A. T. Blomquist. Academic Press, New York, N.Y. 1965. p. 333.
22. J. B. Hyne. Can. J. Chem. **39**, 2536 (1961).
23. J. C. Randall, R. L. Vaulx, M. E. Hobbs, and C. R. Hauser. J. Org. Chem. **30**, 2035 (1965).
24. L. Angiolini and G. Gottarelli. Tetrahedron, **26**, 421 (1970).
25. M. L. Poutsma and P. A. Ibarbia. J. Org. Chem. **34**, 2848 (1969).
26. V. I. Pansevich-Kolyada and B. K. Bogush. Vesti Akad. Navuk, Belarus. SSR, Ser. Khim, Navuk. 55 (1967); Chem. Abstr. **68**, 2746a (1968).

Can. J. Chem. Downloaded from www.nrcresearchpress.com by 210.87.254.42 on 09/05/12
For personal use only.

Can. J. Chem. Downloaded from www.nrcresearchpress.com by 210.87.254.42 on 09/05/12
For personal use only.

Canadian Journal of Chemistry

Published by
THE NATIONAL RESEARCH COUNCIL OF CANADA

Journal canadien de chimie

Publié par
LE CONSEIL NATIONAL DE RECHERCHES DU CANADA

Volume 52 Number 14 July 15, 1974

Volume 52 numéro 14 15 juillet 1974

Crystal and Molecular Structure of 4,4-Dimethyl-2,2-diphenyl-1,3-dioxa-4-azonia-2-boranatacyclopentane

STEVEN J. RETTIG AND JAMES TROTTER

Department of Chemistry, University of British Columbia, Vancouver, British Columbia V6T 1W5

AND

W. KLIEGEL

Institut für Pharmazeutische Chemie der Technischen Universität, 33 Braunschweig, Bundesrepublik Deutschland

Received February 20, 1974

STEVEN J. RETTIG, JAMES TROTTER, and W. KLIEGEL. Can. J. Chem. **52**, 2531 (1974).

Crystals of 4,4-dimethyl-2,2-diphenyl-1,3-dioxa-4-azonia-2-boranatacyclopentane are orthorhombic, $a = 17.043(3)$, $b = 6.289(1)$, $c = 13.024(2)$ Å, $Z = 4$, space group $Pna2_1$. The structure was determined by direct methods, and was refined by full-matrix least-squares procedures to $R = 0.071$ for 1100 reflections with $I \geq 3\sigma(I)$. Bond angles in the five-membered ring, which has a distorted half-chair conformation, range from 101.5(4) for OBO to 107.1(4)° for NOB. Bond lengths are: mean B—C, 1.632(8), B—O, 1.506(7) and 1.556(8), N—O, 1.409(5), C—O, 1.378(9), C—N, 1.467–1.509(7–10), mean C—C(aromatic), 1.395(25) Å. The structure consists of discrete molecules separated by normal van der Waals distances.

STEVEN J. RETTIG, JAMES TROTTER et W. K. KLIEGEL. Can. J. Chem. **52**, 2531 (1974).

Les cristaux du diméthyl-4,4 diphényl-2,2 dioxa-1,3 azonia-4 boranata-2 cyclopentane sont orthorhombiques, $a = 17.043(3)$, $b = 6.289(1)$, $c = 13.024(2)$ Å, $Z = 4$, groupe d'espace $Pna2_1$. La structure est déterminée par les méthodes directes; elle est raffinée par la technique des moindres carrés (matrice entière) à une valeur $R = 0.071$ pour 1100 réflexions avec $I > 3\sigma(I)$. Les angles des liaisons dans le cycle à cinq, qui a une conformation demi-chaise déformée, s'étalent entre 101.5(4) pour OBO à 107.1 (4)° pour NOB. Les longueurs de liaisons sont: moyenne pour B—C, 1.632(8), B—O, 1.506(7) et 1.556(8), N—O, 1.409(5), C—O, 1.378(9), C—N, 1.467–1.509(7–10), moyenne pour C—C aromatique, 1.395(25) Å. La structure se compose de molécules distinctes séparées par des distances de van der Waals normales.

[Traduit par le journal]

Introduction

From the reaction of *N*-hydroxydialkylamine (**1**) and formaldehyde an addition can be expected either at the nitrogen or at the oxygen atom to give **2** or **4**. The addition products, originally regarded as *N*-hydroxymethyloxydialkylamines (**4**) by Zinner and Ritter (1, 2), react with diphenylboron-supplying reagents (Ph_2B—X) to yield crystalline compounds which were initially assigned the structure **5** containing intramolecular N→B coordination. This assignment was based on the earlier studies of the "boroxazolidines" by Weidmann and co-workers (3–5) and was subsequently employed for compounds of this type (6–10).

There is, however, some evidence which indicates that the alternate structures **2** and **3** are probably favored over the originally proposed structures **4** and **5**:

(*1*) The alkylation of *N*-hydroxydialkylamines normally leads to tertiary amine oxides.

(*2*) *N*-Oxides show stronger basicity and pos-

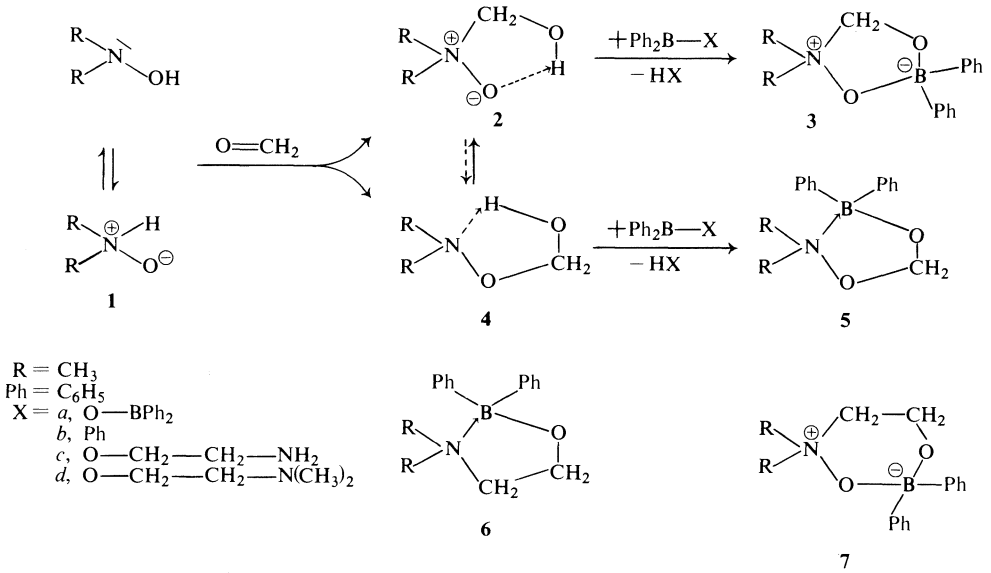

sess better nucleophilic or donor qualities than the isomeric *N*-alkyloxyamines (11, 12). A hydrogen bridge chelate of the type **2** should therefore be more stable than **4**.

(*3*) If both forms **2** and **4** existed, possibly in a state of equilibrium, the reaction with an electrophilic reagent such as Ph_2B—X should shift the (hypothetical) equilibrium to the side of the better donor molecule, *i.e.* the *N*-oxide (**2**).

(*4*) The *N*-oxide form not only facilitates the approach of the Lewis acid Ph_2B—X to the donor (oxygen) atom but also results in a sterically favored chelate structure (**3**).

(*5*) Ethanolamine esters of diphenylborinic acid are intramolecular N→B coordinated cyclic complexes (6), as recently proved conclusively for Ph_2B—O—$CH_2CH_2NH_2$ (13) and (p-$FC_6H_4)_2B$—O—$CH_2CH_2NH_2$ (14). Despite the stability of these "boroxazolidines" (3–5, 15) the rechelation of the applied examples (**6**, R = H, CH_3) was possible with the formaldehyde adduct. This also supports structures **2** and **3** since it is not very plausible that a weakly basic *N*-hydroxymethyloxydialkylamine, HO—CH_2ONR_2 (**4**), in an equimolar quantity can displace the isosteric but more basic aminoalcohol HO—CH_2CH_2-NR_2.

(*6*) Finally there exists an analogy between **3** and the diphenyl boron chelates (**7**) of *N*-(2-hydroxyalkyl)dialkylamine-*N*-oxides and other similar cyclic boron–nitrogen–betaines (16–20) which are closely related to **3** both in means of preparation and in their chemical and physical behavior.

These considerations and also the chemical and physical data obtained to date are consistent with the betaine-type chelate **3**, but do not provide unambiguous proof. To this end the full X-ray crystallographic study of the homologue with R = CH_3 has been carried out.

Experimental

4,4-Dimethyl-2,2-diphenyl-1,3-dioxa-4-azonia-2-boranatacylopentane (3)

A solution of *N*-hydroxydimethylamine (5 mmol) in 5 ml of ethanol was mixed with an aqueous solution of formaldehyde (40%, 5 mmol). After addition of: (*a*) 2.5 mmol oxybisdiphenylborane, or (*b*) 5.0 mmol triphenylborane, or (*c*) 5.0 mmol *B*-(2-aminoethyloxy)diphenylborane, or (*d*) 5.0 mmol *B*-(2-dimethylaminoethyloxy)diphenylborane, the mixture was heated until initial boiling and then allowed to cool. During the cooling or after the dissolution of the boron component the precipitation began.

Yields: (*a*) 99%, (*b*) 90%, (*c*) 98%, (*d*) 85%. M.p. 191–192 °C (acetonitrile); Lit. m.p. (6): 191–192 °C (ethanol)

Anal. Calcd. for $C_{15}H_{18}BNO_2$ (mol. wt. 255.1): C, 70.62; H, 7.11; B, 4.24; N, 5.49. Found: C, 70.96; H, 7.21; B, 4.18; N, 5.45.

^{1}H-n.m.r. (100 MHz, d_6-DMSO/TMS) τ(p.p.m.): 6.84 s (6, CH_3), 5.25 s (2, CH_2), 2.6–3.1 m (10, Ph). ^{11}B-n.m.r. (32.1 MHz, DMSO): δ(BF_3OEt_2) = −11.1 p.p.m.

Crystals suitable for X-ray analysis were obtained by recrystallization from 3:1 acetone – carbon tetrachloride. The crystal used for data collection was bounded by the (001), (010), and (100) planes a distances of 0.14, 0.35, and 0.14 mm from an internal origin and was mounted with *b* parallel to the goniostat axis. Unit-cell and space

Can. J. Chem. Downloaded from www.nrcresearchpress.com by 210.87.254.42 on 09/05/12
For personal use only.

Can. J. Chem. Downloaded from www.nrcresearchpress.com by 210.87.254.42 on 09/05/12
For personal use only.

group data were obtained from film and diffractometer measurements. The unit-cell parameters were refined by a least-squares treatment of $\sin^2\theta$ values for 27 reflections measured on a diffractometer with CuKα radiation. Crystal data are:

$C_{15}H_{18}BNO_2$ f.w. = 255.1

Orthorhombic, $a = 17.043(3)$, $b = 6.289(1)$, $c = 13.024(2)$ Å, $V = 1395.9(5)$ Å^3, $\rho_m = 1.225$ (flotation in aqueous KI), $Z = 4$, $\rho_x = 1.214(1)$ g cm^{-3}, $F(000) = 544$ (20 °C, CuKα, $\lambda = 1.5418$ Å, $\mu = 6.4$ cm^{-1}). Absent reflections: $0kl$, $k + l \neq 2n$ and $h0l$, $h \neq 2n$, space group $Pna2_1$ (C_{2v}^9, No. 33).

Intensities were measured on a Datex-automated General Electric XRD 6 diffractometer, with a scintillation counter, CuKα radiation (nickel filter and pulse height analyzer), and a θ–2θ scan at 2° min^{-1} over a range of $(1.80 + 0.86 \tan\theta)$ degrees in 2θ, with 20 s background counts being measured at each end of the scan. Data were measured to $2\theta = 145°$ (minimum interplanar spacing 0.81 Å). The r.m.s. deviation of the intensity of the check reflection, measured every 40 reflections throughout the data collection, from its initial value was 2.4%. The final intensity was 1.045 times the initial value. Lorentz, polarization, and absorption corrections were applied, and structure factor amplitudes were derived. Of 1450 independent reflections measured, 324 had intensities less than $3\sigma(I)$ above background where $\sigma^2(I) = S + B + (0.06S)^2$ with S = scan count and B = background count, corrected to time of scan. These reflections were given zero weight in the refinement.

Structure Analysis

The systematic absences allow space groups $Pna2_1$, or $Pnma$; with only four molecules in the unit cell $Pnma$ is precluded on symmetry considerations. The structure was solved by direct methods, 158 reflections with normalized structure factor $|E| \geq 1.55$ being used in the symbolic addition procedure for non-centrosymmetric crystals (21). The phases of the 5 5 0, 8 3 0, and 14 2 1 reflections were fixed to define the origin and the enantiomorph was fixed by allowing one of the symbol phases to take only values between 0 and π. During a manual expansion, carried out among the 75 reflections with largest $|E|$ values, it became apparent that there were eight reflections from which the three symbol phases could be chosen. After several unsuccessful runs, a combination of symbol phases which gave a promising set of trial phases was found. The three symbol phases; 1 1 11, 3 1 13, and 1 4 8; along with the origin determining phases comprise the basic starting group given in Table 1.

TABLE 1. Basic starting set of reflections for $C_{15}H_{18}BNO_2$

h	k	l	$\|E\|$	Phase (mc)	
5	5	0	3.28	0	Origin determining
8	3	0	2.07	0	
14	2	1	1.99	0	
1	1	11	2.66	a	
3	1	13	2.62	b	
1	4	8	2.44	c	

Eight starting sets were generated by allowing symbols a and b to have initial values of ± 250 mc and c to have initial values of 125 and 375 mc (thereby fixing the enantiomorph). These sets were used as input to a computer program which determines phases using the tangent formula (22, 23). The values of overall t, overall α, Q, and Rk on the final cycle for each of the sets are given in Table 2. Set 4, which had the lowest value of Rk, was expanded to 185 reflections with $|E| \geq 1.50$ by starting with the same symbol values as in set 4. The final value of Rk was 0.23 with 180 phases assigned. An $|E|$-map based on these 180 phases gave positions for the 19 non-hydrogen atoms among the 40 highest peaks.

Two cycles of full-matrix least-squares refinement of the positional and isotropic thermal parameters of the non-hydrogen atoms gave $R = 0.156$. This was followed by two cycles of anisotropic refinement which reduced R to 0.103. A difference map at this point revealed the positions of seven of the ten phenyl hydrogen atoms. The remaining hydrogen atom positions were calculated and all 18 hydrogen atoms were included in subsequent cycles of refinement with isotropic thermal parameters. The refinement was concluded at $R = 0.071$ for 1100 reflections with $I \geq 3\sigma(I)$ (26 reflections which had $|F_o - F_c| \geq 3\sigma(F)$ were removed from the data set in the final stages of refinement due to suspected extinction or counter errors). The standard deviation of a reflection of unit weight was 2.020.

The least-squares refinement was based on the minimization of $\Sigma w(F_o - F_c)^2$. The scattering factors for the O, N, C, and B atoms were taken from ref. 24 and those for the hydrogen atoms from ref. 25. The anisotropic temperature factors employed in the refinement are U_{ij} in the expression

$$f = f^o \exp[-2\pi^2(U_{11}h^2a^{*2} + U_{22}k^2b^{*2} + U_{33}l^2c^{*2} + 2U_{12}hka^*b^* + 2U_{13}hla^*c^* + 2U_{23}klb^*c^*)]$$

where f^o is the tabulated scattering factor and f is that corrected for thermal motion. The weighting scheme, $w = 1/\sigma^2(F)$ where $\sigma^2(F)$ is derived from the previously defined $\sigma^2(I)$, gave constant average values of $w(F_o - F_c)^2$ over ranges of $|F_o|$ and was employed in the final stages of refinement.

On the final cycle of refinement no parameter shift was greater than 0.33σ for non-hydrogen atoms except for the y coordinates of methyl carbon atoms C(2) and C(3) which shifted by 0.80σ. The shifts were less than 1.5σ for the methyl hydrogens and less than 1.0σ for the remaining hydrogen atoms. The final positional and thermal parameters appear in Tables 3 and 4 respectively. Observed and calculated structure factors have been placed in the Depository of Unpublished Data.[1]

Thermal Motion and Correction of Molecular Geometry

The ellipsoids of thermal motion for the non-hydrogen atoms are shown in Fig. 1. The thermal

[1]The structure factor table is available, at a nominal charge, from the Depository of Unpublished Data, National Science Library, National Research Council of Canada, Ottawa, Canada K1A 0S2.

TABLE 2. Results for the eight starting sets in the phase determination procedure

Set	*a*(mc)	*b*(mc)	*c*(mc)	*t*	α	*Q*	*Rk*	*N*
1	250	250	125	0.69	158	0.30	0.30	146
2	250	250	375	0.72	158	0.27	0.31	144
3	250	−250	125	0.69	165	0.30	0.35	141
4	250	−250	375	0.68	160	0.31	0.24	154
5	−250	250	125	0.69	160	0.30	0.30	145
6	−250	250	375	0.71	163	0.28	0.34	143
7	−250	−250	125	0.71	163	0.28	0.28	149
8	−250	−250	375	0.58	135	0.41	0.36	141

TABLE 3. Final positional parameters (fractional × 10^4, × 10^3 for H atoms) with estimated standard deviations in parentheses

Atom	*x*	*y*	*z*
O(1)	3418(2)	4469(6)	1466(4)
O(2)	3126(2)	962(6)	915
N	3315(2)	977(7)	1968(4)
C(1)	3207(4)	3249(14)	2300(6)
C(2)	4138(4)	108(17)	2051(7)
C(3)	2771(5)	−431(22)	2513(6)
C(4)	2139(3)	3904(9)	385(4)
C(5)	1578(4)	2389(11)	255(7)
C(6)	801(3)	2872(13)	39(7)
C(7)	571(3)	4941(11)	−20(5)
C(8)	1100(3)	6539(13)	91(6)
C(9)	1907(3)	6006(10)	308(5)
C(10)	3584(3)	3654(9)	−463(5)
C(11)	3659(3)	1995(10)	−1166(5)
C(12)	4062(4)	2244(13)	−2085(6)
C(13)	4409(4)	4265(14)	−2305(6)
C(14)	4327(4)	5879(14)	−1610(7)
C(15)	3922(3)	5542(12)	−688(6)
B	3054(3)	3323(11)	570(5)
H(1A)	354(4)	364(11)	307(6)
H(1B)	255(4)	340(12)	255(5)
H(2A)	434(5)	129(11)	159(8)
H(2B)	422(9)	2(21)	298(14)
H(2C)	425(5)	−177(14)	170(7)
H(3A)	242(11)	−13(29)	228(16)
H(3B)	311(4)	−248(10)	226(5)
H(3C)	285(7)	−43(16)	336(10)
H(5)	170(3)	99(9)	23(4)
H(6)	47(3)	149(7)	−25(4)
H(7)	5(4)	525(11)	−25(5)
H(8)	91(3)	796(9)	12(4)
H(9)	220(6)	706(17)	53(8)
H(11)	342(5)	50(12)	−116(7)
H(12)	404(3)	129(9)	−259(5)
H(13)	479(5)	459(11)	−292(7)
H(14)	443(6)	776(13)	−186(7)
H(15)	384(4)	685(10)	−33(5)

motion has been analyzed in terms of the rigid-body modes of translation (**T**), libration (**L**), and screw (**S**) motion using the computer program MGTLS (26). Four analyses were carried out: the 19 non-hydrogen atoms were considered first, then each of the phenyl groups along with the boron atom, and finally the five-membered ring and attached carbon atoms which failed to give a positive-definite **L** tensor. The results of the analyses of the two phenyl groups appear in Table 5.

The r.m.s. standard deviation in the temperature factors U_{ij} is 0.0035 Å^2 which indicates that the molecule as a whole (r.m.s. $\Delta U_{ij} = 0.0124$ Å^2) is not a good rigid-body whereas the thermal motion of the phenyl groups is adequately described by the rigid-body parameters (r.m.s. $\Delta U_{ij} = 0.0052$ and 0.0046 Å^2). Both groups show somewhat anisotropic translational motion and anisotropic librational motion, particularly the C(4)—C(9), B group (see Table 5). The principal axes of **L** are oriented as expected: the largest oscillations, L_1, correspond to rotations about the B—C bonds, the angles between the L_1 axes and the B—C bonds being 7.3 (C(4)) and 8.9° (C(10)). The unique origins (26) are in the expected locations for both groups, lying between the B and attached phenyl C atoms.

The appropriate bond distances and angles in the phenyl groups have been corrected for libration (27, 28) using shape parameters q^2 of 0.08 for all atoms. Both corrected and uncorrected bond lengths and angles appear in Tables 6 and 7 respectively.

Results and Discussion

The X-ray analysis has shown that the betaine-type structure (**3**) is correct. Figure 1 shows a general view of the molecule and the crystallographic numbering scheme. Figure 2 shows the packing arrangement viewed along *b*. Intra-annular torsion angles defining the conformation of the five-membered ring are given in Table 8 and some weighted least-squares mean planes through the molecule in Table 9. Nonbonded intra- and intermolecular contacts are listed in Table 10. Henceforth, the molecules $(C_6H_5)_2BOCH_2CH_2NH_2$ and $(p\text{-}FC_6H_4)_2BOCH_2CH_2$-

Can. J. Chem. Downloaded from www.nrcresearchpress.com by 210.87.254.42 on 09/05/12
For personal use only.

Can. J. Chem. Downloaded from www.nrcresearchpress.com by 210.87.254.42 on 09/05/12
For personal use only.

TABLE 4. Final thermal parameters and their estimated standard deviations

(*a*) Anisotropic thermal parameters ($U_{ij} \times 1000$ Å^2)

Atom	U_{11}	U_{22}	U_{33}	U_{12}	U_{13}	U_{23}
O(1)	47(2)	75(3)	46(2)	−12(2)	−13(2)	3(2)
O(2)	46(2)	68(3)	38(2)	−4(2)	−10(2)	3(2)
N	35(2)	60(3)	34(2)	2(2)	−5(2)	5(2)
C(1)	67(4)	101(6)	57(4)	−1(4)	−9(3)	3(4)
C(2)	48(3)	142(7)	60(4)	39(4)	−18(3)	−4(5)
C(3)	65(4)	187(11)	46(4)	−33(6)	14(3)	26(5)
C(4)	37(2)	59(3)	33(2)	−11(2)	1(2)	−1(2)
C(5)	51(3)	44(4)	104(5)	3(2)	−19(3)	14(4)
C(6)	38(3)	87(5)	101(5)	−11(3)	−18(3)	11(4)
C(7)	34(2)	80(4)	47(3)	2(3)	−6(2)	0(3)
C(8)	45(3)	84(5)	66(4)	23(3)	−5(3)	−13(3)
C(9)	39(3)	57(4)	58(3)	4(2)	−4(2)	−5(3)
C(10)	29(2)	67(3)	42(3)	3(2)	−11(2)	11(3)
C(11)	41(3)	56(4)	49(3)	9(2)	−3(2)	5(3)
C(12)	53(3)	85(5)	58(4)	29(3)	2(3)	6(4)
C(13)	39(3)	123(6)	60(4)	12(4)	13(3)	14(4)
C(14)	45(3)	91(5)	86(5)	0(3)	17(3)	29(4)
C(15)	41(3)	75(4)	56(3)	−10(3)	−8(2)	11(3)
B	37(3)	52(3)	42(3)	−7(2)	−5(2)	3(3)

(*b*) Isotropic thermal parameters

Atom	B (Å^2)	Atom	B (Å^2)
H(1A)	3.8(16)	H(6)	2.0(9)
H(1B)	5.3(15)	H(7)	5.1(13)
H(2A)	6.0(18)	H(8)	3.1(11)
H(2B)	15.0(44)	H(9)	11.9(27)
H(2C)	8.8(21)	H(11)	5.6(16)
H(3A)	22.2(67)	H(12)	3.0(12)
H(3B)	4.3(14)	H(13)	7.1(17)
H(3C)	11.2(30)	H(14)	9.2(25)
H(5)	2.5(9)	H(15)	4.4(13)

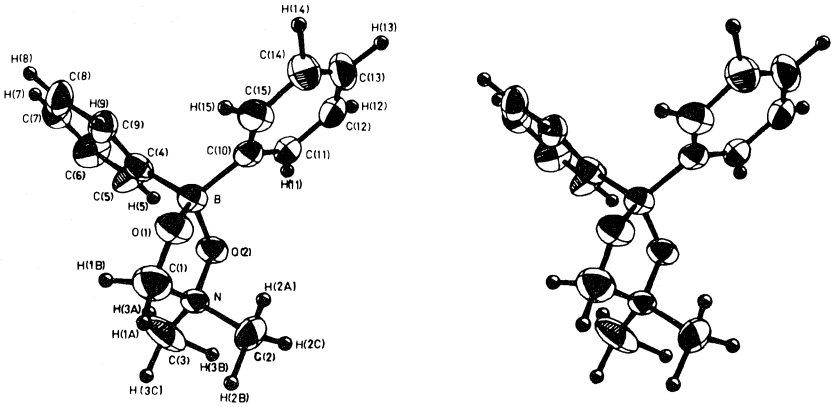

FIG. 1. A stereoscopic view of the molecule showing crystallographic numbering scheme. 50% probability ellipsoids are shown for the non-hydrogen atoms.

TABLE 5. Rigid-body thermal parameters*

	C(4)–C(9), B			C(10)–C(15), B		
L (deg^2)	104(17)	−18(7)	26(10)	23(9)	−2(5)	−12(9)
		9(7)	−5(5)		13(6)	0(6)
			17(5)			33(14)
Principal axes of L						
r.m.s. amplitude	Direction cosines (× 10^3)			r.m.s. amplitude	Direction cosines (× 10^3)	
10.7°	949	−171	264	6.4°	−562	26	827
3.0	268	2	−963	4.0	−702	512	−495
2.5	165	985	48	3.5	−436	−859	−269
Principal axis of reduced T						
r.m.s. amplitude	Direction cosines (× 10^3)			r.m.s. amplitude	Direction cosines (× 10^3)	
0.22 Å	45	−998	36	0.22 Å	152	−857	−492
0.19	998	46	32	0.20	407	508	−759
0.17	−33	35	999	0.14	901	−84	426
Displacement of axes from intersecting (Å)						
Parallel to L_1	0.74			1.60		
Parallel to L_2	0.13			0.55		
Parallel to L_3	0.40			−0.03		
Effective screw translations (Å)						
Parallel to L_1	0.014			0.002		
Parallel to L_2	−0.005			0.000		
Parallel to L_3	−0.053			−0.004		
Fractional coordinates of unique origin (× 10^4)						
x	2412			3051		
y	4353			3786		
z	329			−388		
Fractional coordinates of center of gravity						
x	1572			3871		
y	4296			3851		
z	227			−1132		
r.m.s. ΔU_{ij} (Å^2)	0.0052			0.0046		

*Axes of reference are orthogonal angstrom axes. E.s.d.'s of components of L are given in parentheses in units of the last places shown.

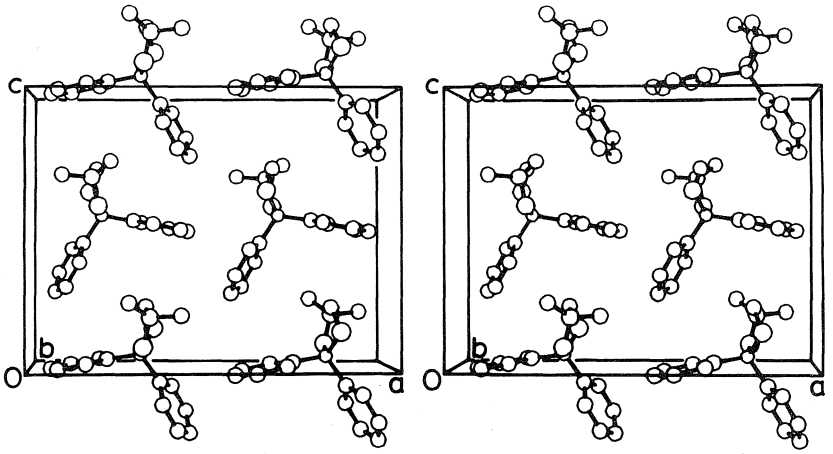

FIG. 2. The packing arrangement viewed along b, hydrogen atoms have been omitted for clarity.

Can. J. Chem. Downloaded from www.nrcresearchpress.com by 210.87.254.42 on 09/05/12
For personal use only.

TABLE 6. Bond lengths (Å) with estimated standard deviations in parentheses

(*a*) Non-hydrogen atoms

Bond	Distance (Å)		Bond	Distance (Å)	
	Uncorrected	Corrected		Uncorrected	Corrected
O(1)—C(1)	1.378(9)	—	C(5)—C(6)	1.388(9)	1.391
O(2)—N	1.409(5)	—	C(6)—C(7)	1.361(10)	1.377
O(1)—B	1.506(7)	—	C(7)—C(8)	1.359(10)	1.372
O(2)—B	1.556(8)	—	C(8)—C(9)	1.443(8)	1.446
C(4)—B	1.620(7)	1.624	C(10)—C(11)	1.394(8)	1.402
C(10)—B	1.634(8)	1.639	C(10)—C(15)	1.353(9)	1.363
C(1)—N	1.505(10)	—	C(11)—C(12)	1.390(9)	1.396
C(2)—N	1.509(7)	1.551*	C(12)—C(13)	1.431(10)	1.441
C(3)—N	1.467(9)	1.520*	C(13)—C(14)	1.367(11)	1.374
C(4)—C(5)	1.360(8)	1.373	C(14)—C(15)	1.401(10)	1.406
C(4)—C(9)	1.383(8)	1.399			

(*b*) Bonds involving hydrogen atoms

Bond	Distance (Å)	Bond	Distance (Å)
C(1)—H(1A)	1.18(7)	C(6)—H(6)	1.10(5)
C(1)—H(1B)	1.17(7)	C(7)—H(7)	0.95(7)
C(2)—H(2A)	1.02(9)	C(8)—H(8)	0.95(6)
C(2)—H(2B)	1.22(18)	C(9)—H(9)	0.88(11)
C(2)—H(2C)	1.28(9)	C(11)—H(11)	1.02(8)
C(3)—H(3A)	0.70(20)	C(12)—H(12)	0.89(6)
C(3)—H(3B)	1.45(6)	C(13)—H(13)	1.05(9)
C(3)—H(3C)	1.11(13)	C(14)—H(14)	1.24(8)
C(5)—H(5)	0.90(5)	C(15)—H(15)	0.96(6)

*Riding motion correction only.

NH_2 will be referred to as **6***a* and **6***b*, respectively.

The conformation of the five-membered ring is nearly the same as that of the isosteric "boroxazolidine" ring in **6***b*, four of the five torsion angles being equal within experimental error while the last differs by 2.5° (4 standard deviations). Atoms C(1) and N both lie on the same side of the OBO plane, displaced −0.75 and −0.31 Å from the plane. The observed torsion angles in the ring are in good agreement with those obtained from energy minimization calculations for $\omega_1 = 10°$ (29), also given in Table 8. The observed magnitudes of the torsion angles are slightly smaller than the calculated values since the mean angle in the ring, 104.6°, is slightly greater than the calculated value of 104.2° but in good agreement with the values of 104.8 and 104.9° in the structures **6***a* and **6***b*. The individual values range from 101.5(4) at B to 107.1(4)° at O(2). The angle at B is slightly, but significantly, greater than the mean value of 99.8(1)° in the boroxazolidines.

The bond distances in the five-membered ring differ from their expected values as a result of steric strain and electron distribution in the molecule, analogous to that occurring in systems with N → B interactions (see e.g. 30 and 31). The O(1)—C(1) bond, 1.378(9) Å, is significantly shorter than the usual value of 1.426 Å as well as the values of 1.413 in **6***a* and 1.418 Å in **6***b*. The C(1)—N bond, 1.505(10) Å, is somewhat longer than those in **6***a* and **6***b* (1.485 and 1.491 Å) but is not significantly longer than a normal $C(sp^3)$—$N(sp^3)$ bond. The N—O(2) distance of 1.409(5) Å is significantly longer than the sum of covalent radii (1.36 Å) but lies in the range of 1.34–1.44 Å usually observed for N—O single bonds (32, 33). The two B—O distances, 1.506(7) and 1.556(8) Å, are significantly different. The pattern of one bond close to the normal value and one on the order of 0.1 Å longer than normal also occurs in the boroxazolidines **6***a* and **6***b* where the B—O distances (1.484 and 1.471 Å) are normal while the B—N bonds (1.653 and 1.652 Å) are each on the order of 0.1 Å longer

Can. J. Chem. Downloaded from www.nrcresearchpress.com by 210.87.254.42 on 09/05/12
For personal use only.

TABLE 7. Bond angles (deg) with estimated standard deviations in parentheses

(*a*) Non-hydrogen atoms

Bonds	Uncorrected angle (deg)	Bonds	Angle (deg) Uncorrected	Corrected
C(1)—O(1)—B	103.8(4)	B—C(4)—C(5)	122.5(5)	122.1
N—O(2)—B	107.1(4)	B—C(4)—C(9)	120.1(4)	119.9
O(2)—N—C(1)	105.0(4)	C(9)—C(4)—C(5)	117.4(5)	118.0
O(2)—N—C(2)	106.4(4)	C(4)—C(5)—C(6)	122.8(6)	122.5
O(2)—N—C(3)	108.8(5)	C(5)—C(6)—C(7)	119.7(6)	119.5
C(1)—N—C(2)	115.9(6)	C(6)—C(7)—C(8)	120.7(5)	121.2
C(1)—N—C(3)	110.9(7)	C(7)—C(8)—C(9)	118.8(6)	118.5
C(2)—N—C(3)	109.6(7)	C(8)—C(9)—C(4)	120.5(6)	120.3
O(1)—B—O(2)	101.5(4)	B—C(10)—C(11)	119.7(5)	119.6
O(1)—B—C(4)	113.8(5)	B—C(10)—C(15)	121.8(5)	121.7
O(1)—B—C(10)	110.5(4)	C(15)—C(10)—C(11)	118.4(6)	118.5
O(2)—B—C(4)	109.5(4)	C(10)—C(11)—C(12)	121.8(6)	121.7
O(2)—B—C(10)	108.4(4)	C(11)—C(12)—C(13)	118.5(7)	118.5
C(4)—B—C(10)	112.4(4)	C(12)—C(13)—C(14)	119.0(6)	119.1
O(1)—C(1)—N	105.7(6)	C(13)—C(14)—C(15)	120.4(7)	120.3
		C(14)—C(15)—C(10)	121.9(7)	121.9

(*b*) Angles involving hydrogen atoms

Bonds	Angle (deg)	Bonds	Angle (deg)
O(1)—C(1)—H(1A)	116(4)	C(5)—C(6)—H(6)	113(2)
O(1)—C(1)—H(1B)	115(3)	C(7)—C(6)—H(6)	126(2)
N—C(1)—H(1A)	112(4)	C(6)—C(7)—H(7)	118(4)
N—C(1)—H(1B)	106(4)	C(8)—C(7)—H(7)	120(4)
H(1A)—C(1)—H(1B)	102(5)	C(7)—C(8)—H(8)	118(3)
N—C(2)—H(2A)	90(4)	C(9)—C(8)—H(8)	123(3)
N—C(2)—H(2B)	101(7)	C(8)—C(9)—H(9)	122(7)
N—C(2)—H(2C)	116(4)	C(4)—C(9)—H(9)	116(7)
H(2A)—C(2)—H(2B)	126(9)	C(10)—C(11)—H(11)	130(5)
H(2A)—C(2)—H(2C)	115(6)	C(12)—C(11)—H(11)	108(5)
H(2B)—C(2)—H(2C)	107(8)	C(11)—C(12)—H(12)	123(4)
N—C(3)—H(3A)	100(16)	C(13)—C(12)—H(12)	118(4)
N—C(3)—H(3B)	100(2)	C(12)—C(13)—H(13)	126(4)
N—C(3)—H(3C)	114(6)	C(14)—C(13)—H(13)	115(4)
H(3A)—C(3)—H(3B)	119(17)	C(13)—C(14)—H(14)	121(4)
H(3A)—C(3)—H(3C)	122(17)	C(15)—C(14)—H(14)	116(4)
H(3B)—C(3)—H(3C)	100(6)	C(14)—C(15)—H(15)	126(4)
C(4)—C(5)—H(5)	121(3)	C(10)—C(15)—H(15)	111(4)
C(6)—C(5)—H(5)	115(3)		

TABLE 8. Intra-annular torsion angles (deg), five-membered ring

Bond	Angle (deg) Observed	Calculated
B—O(1)	34.3(5)	36.4
O(1)—C(1)	−42.3(5)	−43.9
C(1)—N	33.7(5)	34.8
N—O(2)	−10.5(5)	−12.3
O(2)—B	−13.4(4)	−15.0

than normal. The exocyclic C—N distances have been corrected for riding motion and are equal within experimental error. Bearing in mind that the riding model approach usually overcorrects, it still appears that these bonds are somewhat longer than normal (see Table 6).

The two phenyl rings are planar within experimental error (see Table 9). Two hydrogen atoms, H(6) and H(14), are significantly displaced from their respective mean planes, probably as a result of inaccuracy in the hydrogen atom positions

Can. J. Chem. Downloaded from www.nrcresearchpress.com by 210.87.254.42 on 09/05/12
For personal use only.

Can. J. Chem. Downloaded from www.nrcresearchpress.com by 210.87.254.42 on 09/05/12
For personal use only.

TABLE 9. Weighted least-squares mean planes

(*a*) Distances (Å) of relevant atoms from the mean planes

Plane *1*: C(4)–C(9)			Plane *2*: C(10)–C(15)		
Atom	*d*	d/σ	Atom	*d*	d/σ
C(4)	−0.001	0.1	C(10)	0.005	0.5
C(5)	−0.004	0.5	C(11)	0.006	0.0
C(6)	0.012	1.3	C(12)	−0.007	0.1
C(7)	−0.009	1.3	C(13)	−0.007	0.4
C(8)	0.007	0.8	C(14)	0.007	1.2
C(9)	0.000	0.0	C(15)	−0.006	1.1
B	0.070	10.5	B	0.105	18.0
H(5)	0.088	1.6	H(11)	0.062	0.8
H(6)	0.285	6.1	H(12)	0.143	2.5
H(7)	0.116	1.7	H(13)	−0.137	1.7
H(8)	−0.104	1.9	H(14)	0.357	3.7
H(9)	−0.195	1.8	H(15)	0.150	2.5

(*b*) Equations of planes $lX + mY + nZ = p$*

Plane	*l*	*m*	*n*	*p*
1	0.1930	−0.0163	−0.9811	0.1760
2	−0.8458	0.2917	−0.4468	−4.2290

*The dihedral angle between the planes is 74°. *X*, *Y*, *Z* are orthogonal angstrom coordinates derived as follows:

$$\begin{pmatrix} X \\ Y \\ Z \end{pmatrix} = \begin{pmatrix} a & 0 & 0 \\ 0 & b & 0 \\ 0 & 0 & c \end{pmatrix} \begin{pmatrix} x \\ y \\ z \end{pmatrix}$$

due to thermal effects. The boron atom is significantly displaced from both phenyl mean planes, by 0.07 from the C(4)—C(9) plane and by 0.11 Å from the C(10)—C(15) plane, representing a slight folding of the phenyl groups away from each other. The dihedral angle between the mean planes is 74°. The two phenyl groups are not equivalent, the rings being rotated unequally about the B—C bonds. The dihedral angles C(9)[C(4)—B]O(1), C(15)[C(10)—B]O(1), C(5)[C(4)—B]O(2), and C(11)[C(10)—B]O(2) are −52.1(6), 39.9(6), 17.9(6), and −33.4(6)° respectively. The orientation of the phenyl groups represents a minimization of intra- and intermolecular steric interactions.

The corrected C—C bond lengths in the phenyl groups range from 1.363 to 1.446 with a mean value of 1.395 Å. There is a significant variation in the individual bond distances, the C(10—C(17) bond, 1.363 Å, being significantly shorter and the C(8)—C(9), 1.446, and C(12)—C(13), 1.441 Å, bonds significantly longer than the normal value of 1.394 Å (32, 33). The means over chemically equivalent groups of bonds (as they are removed from the boron substituent) are 1.384, 1.410, and 1.391 Å. This pattern is different from that observed in the two boroxazolidine structures (13, 14) where the bond lengths decrease as they are removed from the boron substituent. The B—C distances are equal within experimental error and their mean value, 1.632 Å, is longer than in the structures **6***a* (1.616) and **6***b* (1.621) but shorter than in the tetraphenyl borate anion (1.631–1.648(8) Å) (34).

The angles in the phenyl rings have values ranging from 118.0 to 122.5°, showing some significant deviations from 120°. The mean angle at the carbon atom carrying the boron group is 118.3° and the other mean values are 121.6, 119.2, and 120.2° for atoms *ortho*, *meta*, and *para* to the boron group. These angular deviations have the same pattern as those in **6***a* and **6***b* but the magnitudes of the distortions are one-half as great. These variations have been explained in terms of the electronegativities of the substituent groups (35). The angles at C(4) and C(10), mean 118.3°, carrying the boron substituent indicate that this group is weakly electron releasing.

The overall geometry of the molecule suggests

TABLE 10. Selected intra- and intermolecular contacts

Intramolecular		Intermolecular*	
Atoms	Distance (Å)	Atoms	Distance (Å)
O(1)...H(2A)	2.55(7)	C(3)...C(11)[1]	3.393(9)
O(1)...C(2)	3.100(8)	C(3)...C(12)[1]	3.488(10)
O(1)...C(9)	3.137(7)	O(1)...H(3B)[2]	2.24(6)
O(1)...C(15)	3.013(8)	C(1)...H(3B)[2]	2.69(6)
O(2)...H(2A)	2.26(8)	C(4)...H(3C)[3]	2.67(12)
O(2)...H(3A)	2.26(19)	C(7)...H(2B)[3]	2.63(19)
O(2)...H(5)	2.58(5)	C(9)...H(3C)[3]	2.73(13)
O(2)...C(5)	2.916(8)	H(2C)...H(14)[4]	2.46(11)
O(2)...C(11)	2.932(7)	H(5)...H(8)[5]	2.34(7)
C(1)...C(4)	3.117(9)	H(6)...H(8)[5]	2.39(7)

*Superscripts refer to atoms at positions: [1] $1/2 - x, y - 1/2, 1/2 + z$; [2] $x, 1 + y, z$; [3] $1/2 - x, 1/2 + y, z - 1/2$; [4] $1 - x, -y, 1/2 + z$; [5] $x, y - 1, z$.

that the formal charges on B and N in **3** are delocalized in a way such that, formally, the B and O(2) carry partial negative charges while N and O(1) carry partial positive charges. This is in accord with the observed pattern of bond distances, particularly the difference between the two B—O distances.

The mean bond angles in the molecule are as expected. There are a number of significant deviations from the mean values resulting from steric and electronic effects. Interior angles in the rings have already been discussed. The C(4)—B—C(10) angle, 112.4(4)°, is significantly smaller than in ***6a*** and ***6b***, but is generally as expected. Asymmetry in the packing arrangement appears to be responsible for significant differences between corresponding angle pairs O—B—C and C—N—C.

The geometry involving hydrogen atoms is as follows: mean C(ar)—H, 0.99 Å; mean C(sp^3)—H, 1.14 Å; mean C(ar)—C(ar)—H, 119°; mean R—C(sp^3)—H, 107°; and mean H—C(sp^3)—H, 113°. The distances are long for X-ray data, probably as a result of relatively large thermal motion in the sample.

The crystal structure consists of discrete molecules separated by normal van der Waals distances, the shortest of which are listed in Table 10.

We wish to thank Professor H. Nöth, University of Munich, for running the ^{11}B-n.m.r. spectrum; the National Research Council of Canada for financial support; and the University of British Columbia Computing Centre for assistance.

1. G. ZINNER and W. RITTER. Angew. Chem. **74**, 217 (1962).
2. W. RITTER. Ph.D. Thesis. Marburg, 1963.
3. H. WEIDMANN and H. K. ZIMMERMAN. Liebig's Ann. Chem. **619**, 28 (1958).
4. H. WEIDMANN and H. K. ZIMMERMAN. Liebig's Ann. Chem. **620**, 4 (1958).
5. H. C. FU, T. PSARRAS, H. WEIDMANN, and H. K. ZIMMERMAN. Liebig's Ann. Chem. **641**, 116 (1961).
6. G. ZINNER, W. RITTER, and W. KLIEGEL. Pharmazie, **20**, 291 (1965).
7. G. ZINNER and W. KLIEGEL. Arch. Pharm. **299**, 166 (1966).
8. G. ZINNER and W. KLIEGEL. Chem. Ber. **99**, 895 (1966).
9. G. ZINNER and R. MOLL. Chem. Ber. **99**, 1292 (1966).
10. G. ZINNER and E. DUERKOP. Arch. Pharm. **301**, 776 (1968).
11. P. A. S. SMITH. Open-chain nitrogen compounds. Vol. 2. W. A. Benjamin, Inc., New York. 1966. pp. 3 and 22.
12. H. ARNOLD, N. BROCK, and H. J. HOHORST. Arzneimittelforsch. **7**, 735 (1957).
13. S. RETTIG and J. TROTTER. Can. J. Chem., **51**, 1288 (1973).
14. S. RETTIG and J. TROTTER. Acta Cryst. Submitted for publication.
15. H. K. ZIMMERMANN. Adv. Chem. Ser. No. **42**, 23 (1964).
16. W. KLIEGEL. Z. Chem. **9**, 112 (1969).
17. W. KLIEGEL. Z. Chem. **9**, 454 (1969).
18. W. KLIEGEL. Liebig's Ann. Chem. **721**, 231 (1969).
19. W. KLIEGEL. Tetrahedron Lett. 223 (1969).
20. W. KLIEGEL. Angew. Chem. **80**, 614 (1968).
21. J. KARLE and I. L. KARLE. Acta Cryst. **21**, 849 (1966).
22. J. KARLE and H. HAUPTMAN. Acta Cryst. **9**, 635 (1956).
23. M. G. B. DREW. Private communication; M. G. B. DREW, D. H. TEMPLETON, and A. ZALKIN. Acta Cryst. B**25**, 261 (1969).
24. International tables for X-ray crystallography, Vol. III. Kynoch Press, Birmingham. 1962.

Can. J. Chem. Downloaded from www.nrcresearchpress.com by 210.87.254.42 on 09/05/12
For personal use only.

25. R. F. STEWART, E. R. DAVIDSON, and W. T. SIMPSON. J. Chem. Phys. **42**, 3175 (1965).
26. V. SCHOMAKER and K. N. TRUEBLOOD. Acta Cryst. B**24**, 63 (1968).
27. D. W. J. CRUICKSHANK. Acta Cryst. **9**, 747, 754 (1956).
28. D. W. J. CRUICKSHANK. Acta Cryst. **14**, 896 (1961).
29. J. B. HENDRICKSON. J. Am. Chem. Soc. **83**, 4537 (1961); **85**, 4059 (1963).
30. I. A. S. EDWARDS and H. P. STADLER. Acta Cryst. B**26**, 1905 (1970).
31. R. HOFFMANN. Adv. Chem. Ser. **42**, 78 (1964).
32. O. KENNARD, D. G. WATSON, and W. G. TOWN (*Editors*). Molecular structures and dimensions, Vols. 1–4. A. Oosthoek, Utrecht. Vols. 1 and 2, 1970; Vol. 3, 1971; Vol. 4, 1973.
33. Chem. Soc. Special Publ. No. 11, 1958, and No. 18, 1965.
34. R. J. SIME, R. P. DODGE, A. ZALKIN, and D. H. TEMPLETON. Inorg. Chem. **10**, 537 (1971).
35. O. L. CARTER, A. T. MCPHAIL, and G. A. SIM. J. Chem. Soc. A, 822 (1966).

Can. J. Chem. Downloaded from www.nrcresearchpress.com by 210.87.254.42 on 09/05/12
For personal use only.

Inhibition Effects in the Electrochemical Reduction of Hydrogen Peroxide on Sodium Tungsten Bronzes

JEAN-PAUL RANDIN

Hydro-Quebec Institute of Research, Varennes, Quebec J0L 2P0

Received January 29, 1974

JEAN-PAUL RANDIN. Can. J. Chem. **52**, 2542 (1974).

An inhibition effect has been observed during the cathodic reduction of hydrogen peroxide on sodium tungsten bronzes (Na_xWO_3). The effect is explained as competition for available surface sites between hydrogen peroxide and protons. The competing reaction is believed to be the formation of hydrogen bronze ($Na_xH_zWO_3$). The experimental current–potential relationships fit with the theoretical curves calculated under Langmuirian conditions of adsorption to a point 30–40 mV on the cathodic side of the current maximum.

JEAN-PAUL RANDIN. Can. J. Chem. **52**, 2542 (1974).

On a observé un effet d'inhibition durant la réduction cathodique du peroxyde d'hydrogène sur des bronzes de tungstène dont l'élément d'insertion est le sodium (Na_xWO_3). L'effet est expliqué par une compétition pour les sites superficiels disponibles entre le peroxyde d'hydrogène et les protons. La réaction compétitive proposée est la formation de bronzes de tungstène dont l'élément d'insertion est l'hydrogène ($Na_xH_zWO_3$). Les courbes expérimentales courant–potentiel correspondent aux valeurs théoriques calculées dans des conditions d'adsorption de Langmuir jusqu'à un potentiel 30–40 mV cathodique par rapport au courant maximum.

Introduction

Inhibition or passivation effects are observed for most anodic reactions, *e.g.*, organic oxidations, oxidation of hydrogen, metal dissolution, etc. These effects were discussed quantitatively by Gilroy and Conway (1), following earlier suggestions by Bagotskiy and Vasilev (2). Inhibition and passivation arise either as a result of an inhibiting species produced in a competing reaction, or as a self-inhibition from the decomposition of adsorbed radicals. Inhibition effects have rarely been reported, however, for cathodic processes. The purpose of this communication is to discuss the origin of an inhibition process observed during the cathodic reduction of hydrogen peroxide on sodium tungsten bronzes.

Experimental

Sodium tungsten bronzes were prepared by electrolysis of molten mixtures of Na_2WO_4 and WO_3 as described recently (3). Samples with an x-value (in Na_xWO_3) between 0.58 and 0.89 and only a few p.p.m. platinum were investigated. The cell and instruments employed, as well as the details of the electrode mounting, and gas purification were similar to those used in our recent work (4, 5). Solutions were made from sulfuric acid (ULTREX, J. T. Baker Chemical), unstabilized hydrogen peroxide (Fisher Scientific Co., Certified), and conductivity water. The peroxide concentration was determined by titration with potassium permanganate after completion of a set of measurements. The electrode potentials are given with respect to a standard hydrogen electrode. Experiments were carried out at room temperature.

The current–potential measurements were restricted to the potential ranges where there is no interference from the hydrogen evolution reaction, *i.e.* at potentials less cathodic than about -0.3 V. As no detectable spontaneous decomposition of H_2O_2 was observed, the reduction current can be attributed only to the reduction of H_2O_2 and not to that of oxygen.

Results and Discussion

The potentiodynamic profile shown in Fig. 1 exhibits a peak at about $+0.05$ V, whose current density in the maximum region increases slightly with increasing speed of rotation of the electrode. The dependence of the current density on the rotation speed will be examined in relation to the steady-state measurements to be discussed below. The relationships between $1/i$ and $f^{-1/2}$ (f = rotation speed) obtained from the potentiodynamic profiles are similar to those recorded in the steady-state. The analysis of the peak current as a function of scan rate indicates that in the peak region the process is neither under pure diffusion-control (no linear relationship between the peak current *vs.* the square root of the scan rate), nor under pure activation-control (no linear relationship between the peak current *vs.* the scan rate).

Steady-state (point-by-point) current–potential relationships for three typical concentrations of H_2O_2 are given in Fig. 2. The same measurements carried out without H_2O_2 gave current densities lower than 10^{-5} A cm^{-2} over the

Can. J. Chem. Downloaded from www.nrcresearchpress.com by 210.87.254.5 on 09/05/12
For personal use only.

Can. J. Chem. Downloaded from www.nrcresearchpress.com by 210.87.254.5 on 09/05/12
For personal use only.

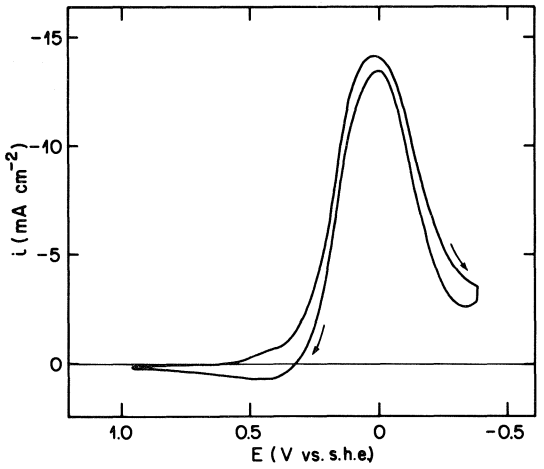

FIG. 1. Potentiodynamic profile for the electroreduction of H_2O_2 on $Na_{0.65}WO_3$ in He-saturated 1 *N* H_2SO_4 + 0.052 *M* H_2O_2 at 4 mV s^{-1} and 900 r.p.m. Direction of sweep indicated by arrows.

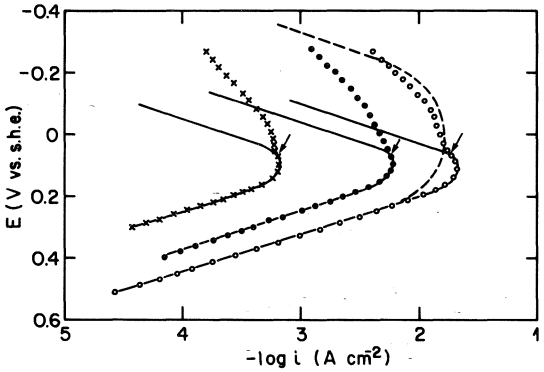

FIG. 2. Steady-state, potentiostatic current–potential relationships on $Na_{0.65}WO_3$ in He-saturated 1 *N* H_2SO_4 at 900 r.p.m. H_2O_2 concentrations: ×, 0.0046 *M*; ●, 0.046 *M*; and ○, 0.18 *M*. Point-by-point measurements, 10 mV steps per 2 min. Solid lines indicate theoretical relationships for inhibition by competing hydride formation reaction under Langmuirian conditions of adsorption, calculated after the treatment of Gilroy and Conway (1). Broken line indicates (in the case of the higher H_2O_2 concentration) best fit of theoretical curve calculate for Temkin conditions of adsorption for $f(\theta) = 10$, after the same authors (1).

entire potential range studied in Fig. 2. This means that the curves in this figure are free of interference from parasitic reactions. In the potential range studied no hysteresis was observed when the scanning potential direction was reversed. The current–potential curves exhibit a Tafel region between 0.5 and 0.2 V (*vs.* standard hydrogen electrode) with a slope close to −120 mV/decade, *i.e.* $2 \times 2.3RT/F$. At potentials more cathodic than about 0.2 V a characteristic inhibition inflexion is observed. The dependence of the current density *vs.* the rotation speed of the electrode (Fig. 3) indicates that, in the inhibition region, the process is first-order with respect to the H_2O_2 concentration (linear dependence of $1/i$ *vs.* $f^{-1/2}$) and is under mixed kinetic and diffusion control (since the extrapolation of the $1/i$ *vs.* $f^{-1/2}$ line intercepts the $1/i$ axis at a value different from zero). In the Tafel region the rotation of the electrode had no significant effect on the current–potential curves.

The kinetic component of the current density in the inhibition inflexion region is found by extrapolation of the $1/i$ *vs.* $f^{-1/2}$ line to $f^{1/2} = 0$ (Fig. 3). The difference between the experimental current density measured at 900 r.p.m. (Fig. 2) and that found from Fig. 3 at infinite rotation speed is negligibly small and would not be significantly different from that plotted in Fig. 2, especially since the current density is given in logarithmic scale. Hence, the relationships in Fig. 2 can be considered as practically free of the diffusion component of the current density.

A plot of the reaction rate as a function of the

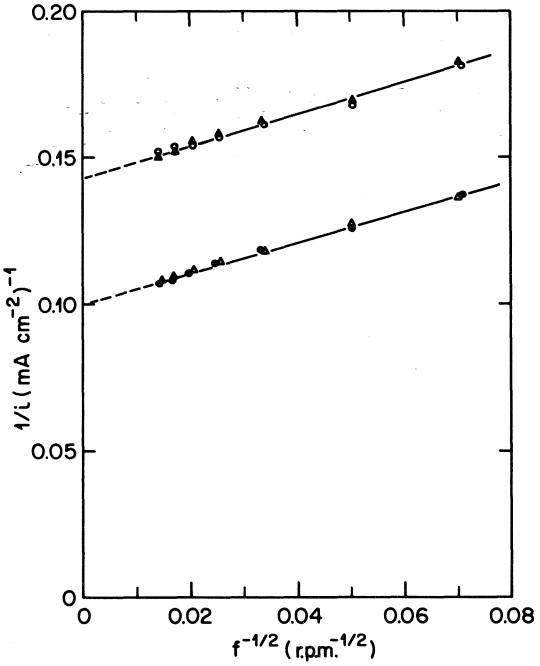

FIG. 3. Inverse of the current density in the inhibition inflexion region *vs.* $f^{-1/2}$ (f = rotation speed of the electrode) for the reduction of H_2O_2 in He-saturated 1 *N* H_2SO_4 + 0.052 *M* H_2O_2 on $Na_{0.65}WO_3$ at *E*: ○, 0.17; ●, 0.07; △, −0.03; and ▲, −0.13 V.

Can. J. Chem. Downloaded from www.nrcresearchpress.com by 210.87.254.5 on 09/05/12
For personal use only.

H_2O_2 concentration indicates that a reaction mechanism first-order with respect to H_2O_2 takes place at constant potential. At low pH values, the reaction order with respect to H^+ is close to zero.

In the following discussion of the origin of the inhibition process it will be assumed that the sodium tungsten bronze electrode plays an important role since this phenomenon has not been observed on other electrodes (*i.e.* mercury (6), platinum (7, 8), and graphite (9)). If a parasitic reaction of the bronze itself were responsible for the negative Tafel slope, this reaction would have a more pronounced effect on the current–potential curve at lower rather than at higher H_2O_2 concentrations. This is not observed since the shape of the current–potential curves does not depend on the concentration of H_2O_2 (Fig. 2).

On the basis of the regular shift of the current–potential curves as the H_2O_2 concentration changes, it may be suggested that for a given potential the same fraction of surface sites are blocked independently of the hydrogen peroxide concentration. The competition for surface sites can arise from the occurrence of a parallel reaction such as the formation of hydrogen bronze

[1] $$Na_xWO_3 + zH^+ + ze^- \rightarrow Na_xH_zWO_3$$

which has been shown to proceed in the same potential range as the beginning of the inhibition region, *i.e.* about 0.2 V (4). If the activity of $Na_xH_zWO_3$ for the reduction of H_2O_2 is much lower than that of Na_xWO_3, the number of active sites decreases with increasingly cathodic potentials, *i.e.*, with the occurrence of reaction 1.

On the basis of previous studies on mercury (6) and on the present study, the reaction mechanism for the reduction of hydrogen peroxide on Na_xWO_3 may be formulated as follows:

[2] $$S + H_2O_2 \rightleftharpoons S(H_2O_2)_{ads}$$

[3] $$S(H_2O_2)_{ads} + e^- \xrightarrow{\text{r.d.s.}} S(OH)_{ads} + OH^-$$

[4] $$S(OH)_{ads} + e^- \rightleftharpoons S + OH^-$$

where S represents an undefined surface adsorption site at the bronze electrode.

In view of the preceding discussion, the inhibition of the cathodic reduction of hydrogen peroxide on Na_xWO_3 may be described as a result of a competition for surface sites between hydrogen peroxide (reaction 2) and protons (reaction 1). The reduction of H_2O_2 is inhibited by the appearance of the reduced form of the bronze electrode, which competes for sites upon the bronze electrode surface. Gilroy and Conway (1) have described numerous cases of anodic oxidations in competition with oxide formation. The present study shows the cathodic analog of the anodic inhibition process, *i.e.*, a cathodic reduction occurring in competition with hydride formation.

The steady-state current–potential relationships in the inhibition region can be examined more quantitatively in terms of the kinetic theory of inhibition effects developed by Gilroy and Conway (1). The inhibition curve predicted for competing reactions of the type

[5] $$S + H^+ + e^- \rightarrow SH$$

and the sequence of reactions 2 to 4 under Langmuirian conditions of adsorption exhibit a symmetrical current–potential curve with an inversion. This means that two Tafel regions arise: (*i*) at low potential values the Tafel line exhibits a $-2RT/F$ slope corresponding to the normal discharge reaction (reaction 3); (*ii*) at potentials greater than that of the inversion phenomenon the Tafel line exhibits a $2RT/F$ slope corresponding to the inhibition reaction 5. The experimental data in Fig. 2 fit these theoretical predictions up to a point marked by the arrow.

Since the experimental current–potential curves in Fig. 2 exhibit quite a broad maximum in the inhibition region, it could appear attractive, at first sight, to suggest that Temkin conditions of adsorption may perhaps apply. The curve calculated for Temkin conditions of adsorption for $f(\theta) = 10$ (θ = electrode coverage) was found to approximate best the broad shape of the experimental points. However, this theoretical curve does not fit the experimental points as exactly as the curve calculated for Langmuirian conditions (Fig. 2).

At potentials more cathodic than the point marked by the arrow in Fig. 2, the experimental current–potential curve departs from the theoretical one (under Langmuirian conditions of adsorption) and results in a slope much greater than the expected $2RT/F$. Such a deviation from the theoretical curve may be associated with the role of the hydride surface compounds in the inhibition process. It is possible that the reduction of H_2O_2 can occur on the layer of

inhibiting hydride after this latter has been formed to an appreciable coverage. This might explain the short, almost constant current region observed after the critical passivation current has been reached and reversal of the direction of the current–potential relation has occurred (Fig. 2). This phenomenon is similar to that reported on platinum in the formate ion discharge or the Kolbe oxidation (1). In this latter case, a current–potential relation exists beyond the passivation region where the Tafel slope can acquire a normal positive sign. Such a region is absent in Fig. 2, however. The shape of the experimental current–potential curves does not permit a more quantitative interpretation of its deviation from the theoretical line.

It may finally be added that the Langmuirian kinetics indicated in Fig. 2 is consistent with the proposed rate-determining step for the hydrogen peroxide reduction reaction (reaction 3).

The author thanks Dr. A. K. Vijh for helpful discussions and Mr. R. Bellemare for his assistance in the experimental work.

1. D. GILROY and B. E. CONWAY. J. Phys. Chem. **69**, 1259 (1965).
2. V. S. BAGOTSKIY and Y. B. VASILEY. Electrochim. Acta, **9**, 869 (1964).
3. J.-P. RANDIN. J. Electrochem. Soc. **120**, 1325 (1973).
4. J.-P. RANDIN, A. K. VIJH, and A. B. CHUGHTAI. J. Electrochem. Soc. **120**, 1174 (1973).
5. J.-P. RANDIN. J. Electrochem. Soc. **120**, 378 (1973).
6. V. S. BAGOTSKIY and I. E. YABLOKOVA. Zh. Fiz. Khim. **27**, 1663 (1953).
7. R. GERISCHER and H. GERISCHER. Z. Phys. Chem. N.F. **6**, 178 (1956).
8. D. WINKELMANN. Z. Elektrochem. **60**, 731 (1956).
9. A. I. ANUROVA, V. S. DANIEL-BEK, and A. L. ROTINYAN. Elektrokhimiya, **4**, 815 (1968).

Can. J. Chem. Downloaded from www.nrcresearchpress.com by 210.87.254.5 on 09/05/12
For personal use only.

The Fluorination of Decachlorocyclopentaphosphonitrile with Potassium Fluorosulfite

NORMAN L. PADDOCK AND JAK SERREQI

Department of Chemistry, University of British Columbia, Vancouver 8, British Columbia

Received February 7, 1974

NORMAN L. PADDOCK and JAK SERREQI. Can. J. Chem. **52**, 2546 (1974).

Decachlorocyclopentaphosphonitrile $N_5P_5Cl_{10}$ is fluorinated by potassium fluorosulfite to give a mixture of chloride–fluorides $N_5P_5Cl_{10-x}F_x$ (x = 1–9), no compound containing more than one PClF group. As for the comparable reactions of $N_3P_3Cl_6$ and $N_4P_4Cl_8$, the dominance of the *geminal* substitution pattern is attributed to the electrostatic or σ-inductive effect of the electronegative fluorine atom. The relative rates of the first two fluorination steps, in comparison with similar information for $N_3P_3Cl_6$ and $N_4P_4Cl_8$, confirm the importance of π-inductive effects in determining the rates of the reactions.

NORMAN L. PADDOCK et JAK SERREQI. Can. J. Chem. **52**, 2546 (1974).

La fluoration du décachlorocyclopentaphosphonitrile, $N_5P_5Cl_{10}$, par le fluorosulfite de potassium conduit à un mélange de chlorure–fluorures de formules $N_5P_5Cl_{10-x}F_x$ (x = 1–9); aucun composé ne contient plus qu'un groupe PClF. Lors de réactions semblables avec le $N_3P_3Cl_6$ et le $N_4P_4Cl_8$ on observe une prédominance de la substitution géminale et ces résultats sont attribués à des effets électrostatiques ou inductifs σ des atomes de fluor électro-affinitaires. Les vitesses relatives des deux premières étapes de la fluoration comparées avec les données semblables obtenues pour $N_3P_3Cl_6$ et $N_4P_4Cl_8$ confirment l'importance des effets inductifs π dans la détermination des vitesses de réactions. [Traduit par le journal]

The reagents used most frequently in the fluorination of phosphonitrilic derivatives are potassium fluorosulfite, first used for the preparation of $N_3P_3F_6$ and $N_4P_4F_8$ (1) and antimony trifluoride, which depends for its action on a primary electrophilic attack on nitrogen, and which gives non-geminally substituted products (2). In an earlier paper (3) it was shown that in the fluorination of $N_3P_3Cl_6$ and $N_4P_4Cl_8$ by potassium fluorosulfite, substitution by a second fluorine atom takes place *geminally*, the third and fourth fluorine atoms entering at the nearest phosphorus atom to the first. All the possible chloride–fluorides based on an N_3P_3 ring have now been obtained, either in this way or in reactions with antimony trifluoride (2). Within the "*geminal–vicinal*" pattern, all the fluoride–chlorides $N_4P_4Cl_{8-x}F_x$ (x = 1–7) have also been prepared by the reaction of KSO_2F with $N_4P_4Cl_8$. Since the entering fluorine atoms are strongly electronegative, it is likely that the *geminal* orientation pattern is an electrostatic or σ-inductive effect, and, as expected, for the two steps $PCl_2 \xrightarrow{k_1} PClF \xrightarrow{k_2} PF_2$, $k_2 > k_1$. The relative rate of the second step is much greater for the tetramer than the trimer, sufficiently so to make different preparative techniques necessary in the two series. The difference was explained (3) in terms of a π-inductive effect modifying the main orientational influences. If the explanation is justified, the same argument would require

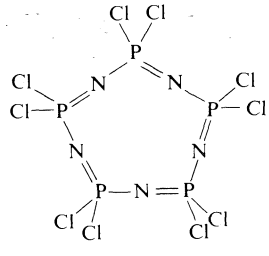

that fluorination of $N_5P_5Cl_{10}$ should also proceed *geminally*, but that the rate of the second step, relative to the first, should be much less than for the reaction of the tetramer. The present work was designed to test these deductions. Broadly speaking, they are confirmed, $N_5P_5Cl_{10}$ behaving more like $N_3P_3Cl_6$ than $N_4P_4Cl_8$ on fluorination, though the details, both qualitative and quantitative, show that a more detailed experimental and theoretical study is desirable.

Experimental

Potassium fluorosulfite was prepared by shaking dry, finely ground potassium fluoride with an excess of sulfur dioxide in an autoclave at room temperature for 80 h.

Can. J. Chem. Downloaded from www.nrcresearchpress.com by 210.87.254.5 on 09/05/12
For personal use only.

Can. J. Chem. Downloaded from www.nrcresearchpress.com by 210.87.254.5 on 09/05/12
For personal use only.

Pentameric phosphonitrilic chloride $N_5P_5Cl_{10}$ was distilled out of a crude mixture of chlorides kindly supplied by Albright and Wilson, Ltd., Birmingham, England, through the courtesy of Dr. A. F. Childs, and purified by distillation and fractional crystallization. Its reaction with potassium fluorosulfite took place readily either dry or in hexane as a solvent, which had no effect on the qualitative composition of the product. In most cases, a solvent was avoided, because it formed an azeotrope with the fluoride $N_5P_5F_{10}$ which was always produced to some extent.

In a typical experiment, decachlorocyclopentaphosphonitrile (50 g, 0.09 mol) was mixed with potassium fluorosulfite (31.6 g, containing 0.2 mol KSO_2F), and heated at 150° for 2 h. A condenser at 0° prevented the escape of the volatile pentameric fluoride in the stream of sulfur dioxide. At the end of the reaction, the more volatile components were distilled out and the remainder extracted with petrol ether (30–60°), the total product weighing 32.5 g. It was fractionally distilled *in vacuo*, and the individual fractions purified by g.l.c., using a stationary phase of 30% silicone gum rubber SE30 supported on Chromosorb W 60/80. The higher boiling components (> 250°) tended to polymerize on the column, which was kept as short as was compatible with a good separation. Longer columns, up to 20 ft, were used in the attempted separation of products known to be mixtures. Boiling points (at 1 mm., except $N_5P_5Cl_2F_8$, $N_5P_5ClF_9$ (760 mm)) and analyses (by Alfred Bernhardt) of the products isolated are as follows:

$N_5P_5Cl_9F$ (b.p. 172–174°)
Anal. Calcd.: P, 27.5; N, 12.4; Cl, 56.7; F, 3.4. Found: P, 27.5; N, 12.5; Cl, 56.5; F, 3.5.

$N_5P_5Cl_8F_2$ (b.p. 146–148°)
Anal. Calcd.: P, 28.3; N, 12.8; Cl, 51.9; F, 7.0. Found: P, 28.1; N, 12.9; Cl, 51.9; F, 7.1.

$N_5P_5Cl_7F_3$ (b.p. 125–126°)
Anal. Calcd.: P, 29.2; N, 13.2; Cl, 46.8; F, 10.8. Found: P, 29.2; N, 13.4; Cl, 46.6; F, 11.0.

$N_5P_5Cl_6F_4$ (b.p. 104–105°)
Anal. Calcd.: P, 30.2; N, 13.6; Cl, 41.4; F, 14.8. Found: P, 30.0; N, 13.9; Cl, 41.3; F, 15.1.

$N_5P_5Cl_5F_5$ (b.p. 83–84°)
Anal. Calcd.: P, 31.2; N, 14.1; Cl, 35.6; F, 19.1. Found: P, 31.0; N, 14.3; Cl, 35.3; F, 19.3.

$N_5P_5Cl_4F_6$ (b.p. 69–70°)
Anal. Calcd.: P, 32.2; N, 14.6; Cl, 29.5; F, 23.7. Found: P, 32.2; N, 14.7; Cl, 29.4; F, 24.2.

$N_5P_5Cl_3F_7$ (b.p. 44–45°)
Anal. Calcd.: P, 33.3; N, 15.1; Cl, 22.9; F, 28.7. Found: P, 33.1; N, 15.1; Cl, 22.6; F, 29.1.

$N_5P_5Cl_2F_8$ (b.p. 168–169°)
Anal. Calcd.: P, 34.6; N, 15.6; Cl, 15.8; F, 34.0. Found: P, 34.4; N, 15.7; Cl, 15.7; F, 34.4.

$N_5P_5ClF_9$ (b.p. 144–145°)
Anal. Calcd.: P, 35.9; N, 16.2; Cl, 8.2; F, 39.7. Found: P, 35.8; N, 16.0; Cl, 8.2; F, 39.9.

As explained later $N_5P_5Cl_xF_{10-x}$, $x = 3$–7, are mixtures of isomers. Mixtures prepared as described sometimes contained unreacted starting material as well as some fully fluorinated pentamer (21% of the fluorinated product in this case). The distribution of chloride–fluorides was typically as shown (Fig. 1). A large proportion of the more highly fluorinated compounds was obtained by using a greater proportion of potassium fluorosulfite, and of those containing less fluorine by using less, or by stopping the reaction at an earlier stage.

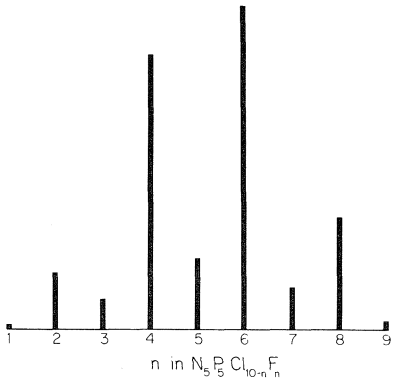

FIG. 1. Relative yields of chlorofluorocyclopentaphosphonitriles in partial fluorination experiment (see text).

The relative rates of the first two fluorination steps were determined as described earlier (3). A thermostated mixture of 2.0 g $N_5P_5Cl_{10}$ and an excess of KSO_2F in 25 ml xylene was stirred magnetically at constant speed. Small samples were taken at 10 min intervals and analyzed by g.l.c., the proportionality constants relating peak area and concentration having been established by separate experiments with $N_5P_5Cl_{10}$ and $N_5P_5Cl_9F$. The decrease in concentration of $N_5P_5Cl_{10}$ with time was approximately first-order, deviations being attributable to change in particle size distribution of the KSO_2F as the reaction proceeded. The concentration of $N_5P_5Cl_9F$ rose to a maximum at 60 min, declining more slowly thereafter. The variations in concentration could be described in terms of two consecutive pseudo-unimolecular reactions, the ratio k_2/k_1 of the rate constants for the successive reactions $PCl_2 \rightarrow PClF \rightarrow PF_2$ being calculated as 7.1 ± 1 at 50 °C.

Results and Discussion

The ^{19}F chemical shifts and coupling constants of the separate products are given in Table 1. Although the spectra are too complicated for a complete analysis (and contain too many phosphorus and fluorine nuclei for the application of decoupling techniques), the PClF and PF_2 regions are clearly separated, and the relative areas of the two sets of bands show that no molecule produced in this series of reactions contains more than one PClF group. Within the scope of this limitation, the possible reaction paths are shown in Fig. 2.

The same spectra help to discriminate the actual paths followed. The PF_2 bands are too complex to be useful, but the PClF bands are more informative, and such assignments as seem

TABLE 1. ^{19}F n.m.r.* and infrared spectra

Product	Identification†	$\delta_F(J_{FP}')$ (PClF groups)	$\delta_F(J_{FP}')$ (PF_2 groups)	ν_{as}(PNP)(cm^{-1})
$N_5P_5Cl_9F$	A	36.4 (968)	—	1345
$N_5P_5Cl_8F_2$	B	—	68.3(921)	1355
$N_5P_5Cl_7F_3$	C	36.3(990), 34.7(959)	68.6(927)	1375
$N_5P_5Cl_6F_4$	D	—	68.5(934), 67.7(914) 67.0(947)	1385
$N_5P_5Cl_5F_5$	E	36.2(980), 35.7(958) 34.9(956)	68.6(908), 68.0(899) 67.1(900)	1400
$N_5P_5Cl_4F_6$	F	—	68.1(903), 66.3(897)	1400
$N_5P_5Cl_3F_7$	G	35.1(969), 33.8(928)	68.1(905), 67.6(888) 66.7(895)	1405
$N_5P_5Cl_2F_8$	H	—	67.4(911), 66.9(894)	1410
$N_5P_5ClF_9$	I	33.6(912)	67.9(897), 67.1(892)	1420

*p.p.m. upfield from $CFCl_3$, internal reference. J(Hz) primed to denote approximation.
†Figure 2.

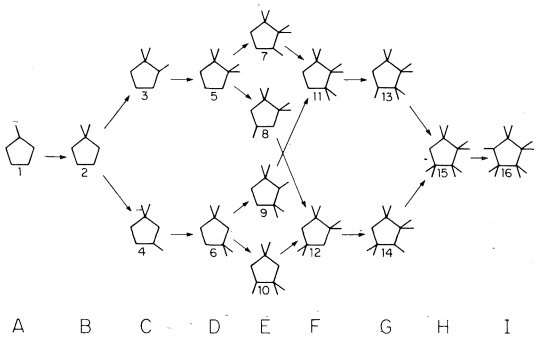

FIG. 2. Orientation patterns found in the reaction of potassium fluorosulfite with cyclodecaphosphonitrile. For clarity the nitrogen and chlorine atoms are omitted.

certain are based on an interpretation of their structure. In addition to the principal coupling constant $^1J_{FP}'$, the spectrum of $N_5P_5Cl_9F$ shows that the spin of the fluorine atom is also coupled to those of the other two pairs of phosphorus nuclei. The nine lines required for a triplet of triplets are indeed observed, but although $^3J_{FP}'$ is clear at 24 Hz, the lines arising from interactions with the remote phosphorus atoms have spacings and intensities which are wrongly predicted by a first-order treatment. Even so, the determination of $^3J_{FP}'$ in this compound is useful in recognizing those other compounds in which a PClF group is flanked by two PCl_2 groups.

The first of these occurs in product C, whose ^{19}F spectrum has two PClF doublets of about equal intensity. Their symmetries indicate that they belong to different environments. The possibility that one doublet might correspond, in spite of the evidence of the areas, to the presence of some non-*geminal* isomers is ruled out, because a mixture of non-*geminal* isomers of the composition $N_5P_5Cl_7F_3$, prepared in another way (9) has a lower shift and higher coupling constant (33.4 p.p.m., 992 Hz). The only two possible *geminal* isomers are 3 and 4; both are evidently present, and their individual shifts and coupling constants can be assigned. Each band of the higher field doublet has a triplet structure ($^3J_{FP}'$ 27 Hz) and is assigned, consistently with its shift, to 4. The environment of the PClF group in 3 is less symmetrical (PCl_2/PF_2) and the fluorine atoms would give additional splitting. The lower field doublet, in agreement, has a large number of lines, many unresolved, and does not approach a triplet structure.

Product E is also a mixture, but the analysis of its ^{19}F spectrum is incomplete. The PClF doublet at highest field again has a triplet structure ($^3J_{FP}'$ 24 Hz) and evidently corresponds to 8. That at lowest field has a diffuse triplet structure, compatible with the symmetry of 9 and secondary splitting by the fluorine pairs; it is much weaker than the other bands. The intermediate bands are reasonably assigned to 7 and 10, with intermediate (PCl_2/PF_2) environments, but there is no certainty that both compounds are present. The PClF region of G is interesting in that the high-field triplet of A, C, and E is not found, presumably because the PClF group has $PCl_2/$

Can. J. Chem. Downloaded from www.nrcresearchpress.com by 210.87.254.5 on 09/05/12
For personal use only.

Can. J. Chem. Downloaded from www.nrcresearchpress.com by 210.87.254.5 on 09/05/12
For personal use only.

PCl_2 neighbors in neither 13 nor 14. The principal doublet has a shift which suggests a PCl_2/PF_2 environment, and is assigned to 13. The low intensity doublet at lower field is similar in appearance to the lowest field doublet in E (assigned to 9) and, more significantly, has a similar shift to the PClF group in 16, in which the two flanking groups must be PF_2/PF_2; it is therefore assigned to 14. As would be expected, the two components of the PClF doublet of 16 are symmetrically related, and show no signs of the additional bands attributed to isomers in the other spectra. Because of the complexity of the PF_2 spectra, no statement can be made about the possible isomers in D or F, though the spectra of B and H are consistent with the unique structures shown.

The orientation pattern so determined, in which a PFCl group is always fluorinated in preference to a PCl_2 group, is similar to that found for the reaction of potassium fluorosulfite with $N_3P_3Cl_6$ and $N_4P_4Cl_8$. It presumably has the same cause, which is that the largest effect of the first fluorine atom is to induce, through its high electronegativity, a partial positive charge at the phosphorus atom to which it is attached, thus encouraging further nucleophilic attack at the same point. The higher reactivity of the PClF group is confirmed by the relative yields illustrated in Fig. 1; they are smaller for those compounds which contain a PFCl group.

There are two differences from the behavior of $N_4P_4Cl_8$. The first is that only one of two possible trifluorides was produced in significant quantities from the tetramer, although small amounts of unidentified compounds may have been formed by the alternative *geminal* route. The pentamer gives both 3 and 4, in approximately equal quantities, and the detection of 8 shows that the use of alternative paths is not confined to the fluorination of the difluoride. There is no obvious explanation in terms of the effect of the substituents on charge density, though fluorination at remote sites is statistically favored more in the ten-membered than in the eight-membered ring.

The second difference relates to the way in which a perturbation of the π-system affects the relative rates of the successive fluorination steps $PCl_2 \rightarrow PClF \rightarrow PF_2$. One of the clearest effects of an electronegative substituent on a phosphonitrilic ring (discussed in more detail elsewhere (4)) is to raise ν_{as}(PNP) by contracting the phosphorus d-orbitals and strengthening the π-bonds. The frequency of this mode, which is degenerate in the end-members $N_5P_5Cl_{10}$ and $N_5P_5F_{10}$, is given in Table 1. The band is very broad (width at half-height $\sim 200\ cm^{-1}$) partly from resolution of the degeneracy and partly because there are other ring vibrations of similar frequency, but the trend of increasing frequency with increasing fluorine content is clear.

The stronger π-bonding concentrates π-electron density on phosphorus, and has a retarding effect on nucleophilic attack, which offsets the direct electrostatic or σ-inductive accelerative effect of fluorine substitution. Such a π-inductive effect on charge density depends on both ring size and the type of π-system, and is measured approximately (5) by the atomic self-polarizabilities $\pi_{P,P} = \partial q_P/\partial \alpha_P$ of the substituted phosphorus atom (Table 2), it being assumed that the substituent affects only the Coulomb parameter of its own phosphorus atom. For the trimer and tetramer it was assumed (3) (as a first approximation) that the reaction rate was controlled primarily by the field and σ-effects, modified by π-electron density changes. The type of π-system is important, as ring size effects will differ for the two cases (Table 2). The alternation of ionization potential with increasing ring size has been interpreted (4, 6) in terms of a homomorphic π-system, and π-electron densities at phosphorus are consequently expected to decrease in the order $(NP)_3 > (NP)_5 > (NP)_4$. The activation energies for the reaction of the cyclic phosphonitrilic chlorides decrease in just this order (7), suggesting that π-electron densities affect reactivity significantly. Table 2 shows that the same applies to *changes* in density caused by a substituent. We expect the second fluorination step to be faster than the first, on the purely electrostatic argument. Its rate is reduced by the induced (negative) π-charge, which again decreases in the order $(NP)_3 > (NP)_5 > (NP)_4$. The acceleration of the second step relative to the first is then expected to be smaller for the trimer and pentamer than for the tetramer. The ratios

TABLE 2. Atomic self-polarizabilities*

System type	N_3P_3	N_4P_4	N_5P_5
Homomorphic	0.309	0.273	0.304
Heteromorphic	0.253	0.273	0.283

*$\pi_{P,P} = \partial q_P/\partial \alpha_P$, calculated (5) from Hückel m.o.'s; units of β^{-1}. $\alpha_N = \alpha_P + \beta$; α,β, Coulomb and resonance parameters.

of rates k_2/k_1 for trimer, tetramer, and pentamer are respectively 8, ~100, 7, confirming the importance of a π-inductive effect to a substitution reaction. In other reactions, it also affects orientation pattern and bond lengths within the ring (8). Strictly, if only the homomorphic system were involved, k_2/k_1 for the pentamer should be greater than 8, not less; a more exact treatment would be required to determine whether this is a result of the simultaneous perturbation of the heteromorphic π-system (6), which could have the observed effect, or a consequence of theoretical or experimental imperfections.

We are grateful to Mr. R. Burton and Dr. D. J. Patmore for spectroscopic and experimental help, and to the National Research Council of Canada for financial support.

1. F. SEEL and J. LANGER. Z. anorg. allgem. Chem. **295**, 316 (1958).
2. P. CLARE, D. B. SOWERBY, and B. GREEN. J. Chem. Soc. (Dalton), 2374 (1972).
3. J. EMSLEY and N. L. PADDOCK. J. Chem. Soc. (A), 2590 (1968).
4. D. P. CRAIG and N. L. PADDOCK. *In* Non-benzenoid aromatics. Vol. 2. Academic Press. 1971. p. 273.
5. C. A. COULSON and H. C. LONGUET-HIGGINS. Proc. Roy. Soc. (London), A**191**, 39 (1947).
6. G. R. BRANTON, C. E. BRION, D. C. FROST, K. A. R. MITCHELL, and N. L. PADDOCK. J. Chem. Soc. (A), 151 (1970).
7. D. B. SOWERBY. J. Chem. Soc. 1396 (1965).
8. T. N. RANGANATHAN, S. M. TODD, and N. L. PADDOCK. Inorg. Chem. **12**, 316 (1973).
9. N. L. PADDOCK and D. J. PATMORE. Unpublished results.

Can. J. Chem. Downloaded from www.nrcresearchpress.com by 210.87.254.5 on 09/05/12
For personal use only.

Erratum: Intrinsic Acidities of α, β, γ Chlorosubstituted Aliphatic Acids from Gas Phase Equilibrian Mesurements

R. YAMDAGNI AND P. KEBARLE
Chemistry Department, University of Alberta, Edmonton, Alberta
Received March 29, 1974

(Ref.: Can. J. Chem. **52**, 861 (1974))

The correct title of this communication should read "Intrinsic Acidities of α, β, γ Chlorosubstituted Aliphatic Acids from Gas Phase Equilibria Measurements".

Can. J. Chem. Downloaded from www.nrcresearchpress.com by 210.87.254.6 on 09/05/12
For personal use only.

Pyridine-catalyzed Halogenation of Aromatic Compounds. I. Bromination

G. E. Dunn and B. J. Blackburn

Department of Chemistry, University of Manitoba, Winnipeg, Manitoba R3T 2N2

Received October 29, 1973

G. E. Dunn and B. J. Blackburn. Can. J. Chem. **52,** 2552 (1974).

The mechanism of catalysis of aromatic bromination by pyridine was investigated by measuring the rates of bromination of mesitylene in acetic acid and in chloroform with and without added pyridinium or other substituted ammonium salts. Most salts increased both the second- and third-order rate constants for bromination, and pyridinium salts were no more effective than others. Bromide salts decreased the rate and sometimes the order of the bromination reaction by complexing bromine as tribromide. The formation constants of pyridinium tribromide and tetra-*n*-butylammonium tribromide in chloroform at 25.0° were found to be 2×10^2 and 9×10^4 M^{-1}, respectively. It is concluded that in dilute solution pyridine catalysis of bromination is simply a salt effect which can be accounted for by the commonly accepted mechanism of bromination.

G. E. Dunn et B. J. Blackburn. Can. J. Chem. **52,** 2552 (1974).

On a étudié le mécanisme des bromurations aromatiques catalysées par la pyridine; pour ce faire on a mesuré les vitesses de bromuration du mésitylène, dans l'acide acétique et dans le chloroforme avec et sans sel de pyridinium ou d'autres sels d'ammonium substitués. La plupart des sels augmentent à la fois les constantes de vitesse du deuxième et du troisième ordres de la bromuration; les sels pyridinium ne sont pas plus efficaces que les autres. L'addition de bromures diminue la vitesse et quelquefois l'ordre de la réaction de bromuration en complexant le brome pour donner du tribromure. On a trouvé que les constantes de formation du tribromure de pyridinium et du tribromure de tétra-*n*-butylammonium dans le chloroforme à 25.0° sont respectivement 2×10^2 et 9×10^4 M^{-1}. On en conclut qu'en solution diluée de pyridine la catalyse de bromuration est simplement un effet de sel qui peut être expliqué par le mécanisme généralement accepté de la bromuration. [Traduit par le journal]

Can. J. Chem. Downloaded from www.nrcresearchpress.com by 210.87.254.40 on 09/05/12
For personal use only.

In 1908 Cross and Cohen reported the use of pyridine as a catalyst for aromatic halogenation (1). The bromination procedure was reproduced in Cohen's widely used laboratory manual (2) and students have learned ever since that pyridine is the catalyst of choice for aromatic bromination. Although pyridine catalysis is still recommended (3) for halogenation, it has never become a common tool in organic synthesis. The most successful of the very few reported uses is de la Mare and Ridd's bromination of *t*-butylbenzene (4).

There are some interesting features of this pyridine catalysis. First, aromatic halogenations are invariably electrophilic substitutions and the usual catalysts are strong electrophiles but it is difficult to formulate pyridine as an electrophile. Various authors (4–6, for example) have speculated that the well-known pyridine–halogen addition complexes serve as sources of positive halogen in the form of *N*-halopyridinium halides but this has never been demonstrated. Second, the halogen halide produced during halogenation will immediately convert the catalytic quantities of pyridine (or pyridine–halogen complex) used in the Cohen, and de la Mare and Ridd procedures to pyridinium halides, which are even more difficult to visualize in the role of electrophiles. Yet they must act as catalysts if the reaction is to proceed beyond the initial stages.

With these ideas in mind, we undertook a study of the influence of pyridine or pyridinium salts on the rate and mechanism of aromatic halogenation. Bromination was examined first because it gave Cohen better results than did chlorination. The latter will be considered in Part III of this series.

Results

Although Cohen, and de la Mare and Ridd all report successful brominations with pyridine, they do not indicate what happens under the same conditions in the absence of pyridine. Consequently, we repeated Cohen's procedure both with and without pyridine. Using bromine and benzene in equimolar quantities at 25° with no solvent, the evolution of hydrogen bromide

Can. J. Chem. Downloaded from www.nrcresearchpress.com by 210.87.254.40 on 09/05/12
For personal use only.

was visibly more rapid in the presence of a trace of pyridine than in its absence. Distillation of the reaction mixtures after 4 h gave 19% bromobenzene in the presence of pyridine and 9% in its absence.

That salts also catalyze the reaction was shown by a similar experiment using *t*-butylbenzene in excess at 35°. After 100 s the consumption of bromine was approximately 3% in the absence of catalyst, 50% in the presence of pyridine, 33% in the presence of either pyridinium bromide or tetra-*n*-butylammonium bromide, and 25% in the presence of pyridinium chloride.

In the experiments at 25°, the reaction mixtures containing pyridine deposited a dark red solid (**1**). When removed from the reaction mixture, **1** could be kept at −20° but at room temperature it rapidly lost bromine, giving first a dark red liquid, then an orange solid (**2**). Compound **2** lost bromine much less readily and could be analyzed. Its n.m.r. spectrum closely resembles that of pyridinium bromide (7) and its analysis fits the formula $3C_5H_5NHBr \cdot 2Br_2$. A compound with similar analyses was prepared by Englert and McElvain (8) by mixing 1 mol of pyridinium bromide with ½ mol of bromine in glacial acetic acid. Repetition of their synthesis produced a compound identical with **2**. Both melted in the range 100–105° individually or in a mixture. Compound **1** contains about 70% reducible bromine, and the most likely composition for it is $C_5H_5NHBr \cdot 2Br_2$. The composition and phase relationships of these bromine – pyridinium bromide complexes will be considered in Part II of this series.

Qualitative experiments of the type described above for pyridine showed that both **1** and **2** catalyze the bromination of benzene under Cohen's conditions. In the process **2** is converted into **1**. However, all the reactions described up to this point are heterogeneous and therefore not suited to kinetic study.

The only reported mechanistic study of pyridine-catalyzed bromination is on the bromination of anisole in carbon tetrachloride by Yeddanapalli and Gnanapragasam (9). However, repetition of some of their experiments showed that their system was also heterogeneous. Bromine – pyridinium bromide complexes precipitated as soon as the reagents were mixed.

Clearly the first requirement for kinetic study is a solvent which does not react with bromine and dissolves not only the reagents but also pyridinium salts. Acetic acid and chloroform were found to be suitable.

Rate Studies

When toluene (0.40 *M*) reacted with bromine (0.075 *M*) in acetic acid at 25° the rate of disappearance of bromine was initially increased by pyridine but it soon dropped back below that of the uncatalyzed reaction. Curiously, more pyridine produced less catalysis. Thus, after 4 h the bromine consumed was 10% in the absence of pyridine, 29% in the presence of 0.06 *M* pyridine, 26% with 0.12 *M* pyridine, and 22% with 0.25 *M* pyridine. When pyridine was replaced by 0.12 *M* pyridinium bromide, no bromine uptake could be detected during 8 h.

The effect of other substituted ammonium salts was then examined. Mesitylene was chosen as the substrate because its bromination has been previously investigated by Keefer *et al.* (10). They showed that this bromination follows the rate law:

$$[1] \quad -d[Br_2]/dt = [\text{Mesitylene}](k_2[Br_2] + k_3[Br_2]^2)$$

and that the only significant product is 2-bromomesitylene. The rate of bromination was followed spectrophotometrically at 400 nm. The results are shown in Table 1. It is seen that not only pyridinium salts but ammonium salts in general increase the rate of bromination in acetic acid. Keefer *et al.* showed that smaller but significant increases in the rate of bromination of mesitylene in acetic acid are produced by alkali metal chlorides, perchlorates, and acetates (10). Therefore the initial increase in the rate of bromination of toluene in acetic acid may reasonably be considered to be a salt effect.

In an attempt to approximate Cohen's conditions (no solvent) more closely, attention was turned to the aprotic solvent chloroform. Results are shown in Fig. 1. Again it is seen that

TABLE 1. Bromination of 0.0480 *M* mesitylene in acetic acid at 25.0 °C

[Bromine] $\times 10^2$ (*M*)	Salt[a] (0.100 *M*)	k_2K_1 (M^{-2} s^{-1})	k_3K_1 (M^{-3} s^{-1})
0.205	None	4.8×10^{-4}	1.2
0.115	PyHCl	2.0×10^{-2}	65
0.110	NEPCl	2.2×10^{-2}	67
0.110	TBACl	1.2×10^{-3}	34

[a]PyHCl = pyridinium chloride, NEPCl = *N*-ethylpiperidinium chloride, TBACl = tetra-*n*-butylammonium chloride.

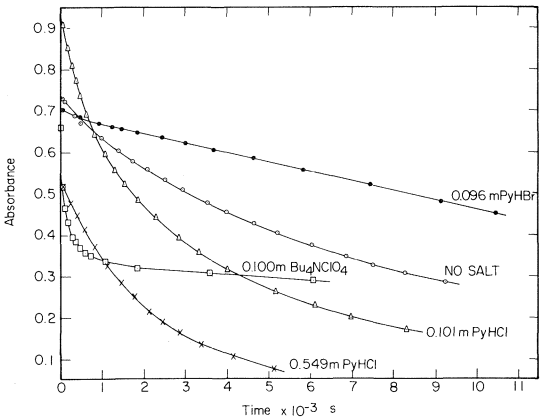

FIG. 1. Bromination of 0.202 *M* mesitylene in chloroform at 25.0° with and without added salts: PyHBr = pyridinium bromide; PyHCl = pyridinium chloride; Bu_4NClO_4 = tetra-*n*-butylammonium perchlorate.

pyridinium chloride increases the rate of bromination but pyridinium bromide decreases it. Tetra-*n*-butylammonium perchlorate is unusual in that it produces an initial large acceleration followed by strong inhibition after about 50% reaction. Tetra-*n*-butylammonium bromide in the same concentration as the other salts nearly stopped the reaction (less than 3% reaction after 3 h).

Equilibrium Constants

To determine the formation constant for pyridinium tribromide in chloroform the spectrophotometric method of Rose and Drago (11) was used in the form of eq. 2.

$$[2] \qquad 1/K = S_0B_0\varepsilon/D - S_0 - B_0 + D/\varepsilon$$

K is the formation constant for the complex, S_0 and B_0 are the initial concentrations of pyridinium bromide and bromine, respectively, $D = A - \varepsilon_s S_0 - \varepsilon_b B_0$, and $\varepsilon = \varepsilon_c - \varepsilon_s - \varepsilon_b$. A is the measured absorbance of the solution, and ε_c, ε_s, and ε_b are the absorptivities of complex, pyridinium bromide, and bromine, respectively. Concentrations were chosen where $D/\varepsilon - B_0$ is negligible so that a plot of S_0 *vs.* S_0B_0/D should give a slope of ε and an intercept of $-1/K$. The results are given in Table 2 and Fig. 2. From a least-squares treatment of the data it was calculated that $K = (2.0 \pm 0.4) \times 10^2\ M^{-1}$ and $\varepsilon = (1.50 \pm 0.04) \times 10^3\ M^{-1}\ cm^{-1}$. Direct measurement on solutions of the components gave $\varepsilon_b = 38.7\ M^{-1}\ cm^{-1}$ and

TABLE 2. Absorbance at 360 nm of pyridinium tribromide solutions in chloroform at 25.0 °C

[Pyridinium bromide] $\times 10^2$ (M)	[Bromine] $\times 10^4$ (M)	Absorbance
0.495	5.98	0.432
1.02	5.33	0.561
1.60	6.08	0.735
2.29	5.04	0.665
3.37	4.92	0.681
4.19	5.33	0.735

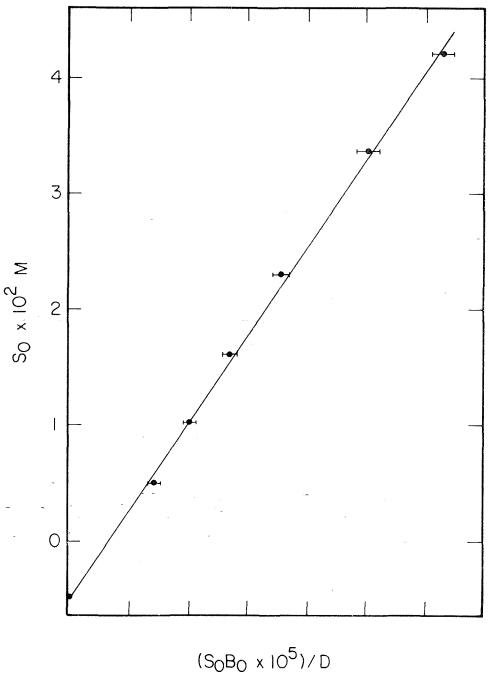

FIG. 2. Determination of the formation constant of pyridinium tribromide from a plot of eq. 2. Symbols are defined in the text.

$\varepsilon_s = 0.3\ M^{-1}\ cm^{-1}$. Hence, the absorptivity of the complex is $(1.54 \pm 0.04) \times 10^3\ M^{-1}\ cm^{-1}$.

Determination of the formation constant for tetra-*n*-butylammonium tribromide was more difficult because the constant is much larger, so that more dilute solutions had to be used. At these high dilutions absorbances tended to drift. With approximately equal quantities of bromine and bromide the drift was less than 3% in 10 min. Readings were taken over 2–10 min and extrapolated back to zero time. The data are reported in Table 3. Under these conditions ε_s is negligible,

Can. J. Chem. Downloaded from www.nrcresearchpress.com by 210.87.254.40 on 09/05/12
For personal use only.

TABLE 3. Absorbance at 360 nm of tetra-*n*-butylammonium bromide solutions in chloroform at 25.0 °C

[Tetra-*n*-butylammonium bromide] $\times 10^4$ (M)	[Bromine] $\times 10^4$ (M)	Absorbance
2.20	2.35	0.277
4.36	5.01	0.613
9.18	9.56	1.283

but $D/\varepsilon - B_0$ is not. The data were substituted into the righthand side of eq. 2 and the three simultaneous equations were solved in all combinations to give $\varepsilon = (1.49 \pm 0.06) \times 10^3\ M^{-1}\ cm^{-1}$. This value was then used to find $K = (9 \pm 1) \times 10^4\ M^{-1}$. ε_c works out to $(1.53 \pm 0.06) \times 10^3\ M^{-1}\ cm^{-1}$, in good agreement with the value found for pyridinium tribromide. Evidently the cation has a much larger effect on the stability of substituted ammonium tribromides than on their absorptivities.

Discussion

Equilibrium Constants

It seems reasonable to attribute the inhibition of bromination by pyridinium and tetra-*n*-butylammonium bromides to attenuation of the bromine concentration by complexation of bromine with bromide ion. Such complexes are well known in the solid state and in aqueous and acetic acid solutions (12). They are generally considered to be polybromides and, in the solid state, tri-, penta-, and heptabromides are known. In solution only tribromides have been identified, although higher complexes may well be formed at high bromine concentrations. Since bromine was followed spectrophotometrically in our rate studies, its concentration was very low and it is probable that only the tribromide would be of importance under these conditions. Popov and co-workers (13) found only tribromide under similar conditions in bromotrichloromethane. Our value of 9×10^4 for the formation constant of tetra-*n*-butylammonium tribromide in chloroform agrees reasonably well with their value of 2×10^4 for the same complex in bromotrichloromethane.

The interesting feature of our formation constant studies is that the formation constant of pyridinium tribromide (2×10^2) is much smaller than that of tetra-*n*-butylammonium tribromide (9×10^4). It is common knowledge that the stabilities of trihalides in the solid state increase with the size and symmetry of the cation (12) but this has not been shown to be true in solution. It seems reasonable, however, that the cation should influence trihalide ion stability in nonpolar organic solvents where ion-pair formation has been found to be extensive (14). Such a conclusion is also required to explain the different influences of different substituted-ammonium salts on the rates of bromination reported above under Results and discussed below.

Formation constants are not known for the mixed trihalides formed when substituted-ammonium chlorides are added to bromination reactions but, by analogy with their stabilities in the solid state (12), they are expected to be much smaller than those of the corresponding tribromides.

Rate Studies

The commonly accepted mechanism (15) for aromatic bromination in the absence of catalyst is summarized in the following scheme.

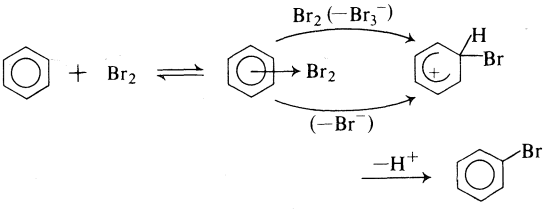

Except for a few very reactive substrates, there is no kinetic hydrogen isotope effect so the second step is usually rate determining. The mixed second- and third-order kinetics commonly encountered (eq. 1) arise from the two routes for heterolysis of the bromine in the arene–bromine π-complex. Since the transition states in both routes are more polar than the initial state, both the second- and third-order terms in the rate expression show positive solvent and salt effects (10, 16).

To facilitate analysis of our results in terms of this mechanism, it will be written in the form of the four equations following.

$$\mathrm{ArH} + \mathrm{Br_2} \overset{K_1}{\rightleftharpoons} \mathrm{ArH \cdot Br_2}$$

$$\mathrm{ArH \cdot Br_2} \overset{k_2}{\rightarrow} \mathrm{ArBr} + \mathrm{HBr}$$

$$\mathrm{ArH \cdot Br_2} + \mathrm{Br_2} \overset{k_3}{\rightarrow} \mathrm{ArBr} + \mathrm{HBr_3}$$

$$\mathrm{HBr} + \mathrm{Br_2} \overset{K_4}{\rightleftharpoons} \mathrm{HBr_3}$$

Can. J. Chem. Downloaded from www.nrcresearchpress.com by 210.87.254.40 on 09/05/12
For personal use only.

Can. J. Chem. Downloaded from www.nrcresearchpress.com by 210.87.254.40 on 09/05/12
For personal use only.

In the presence of pyridine or pyridinium salts, of course, HBr and HBr_3 become pyridinium bromide and pyridinium tribromide, respectively.

The rate expression for this mechanism is given by eq. 3.

$$[3]\quad d[ArBr]/dt = K_1[ArH](k_2[Br_2] + k_3[Br_2]^2)$$

Using the stoichiometric relationship

$$[Br_2] = [Br_2]_0 - [ArBr] - [ArH\cdot Br_2] - [HBr_3]$$

and the equilibrium expressions for K_1 and K_4, the rate expression can be rewritten as eq. 4.

$$[4]\quad \frac{-d[Br_2]}{dt} = \frac{K_1[ArH]}{1 + K_1[ArH] + K_4[HBr]} \times (k_2[Br_2] + k_3[Br_2]^2)$$

In our work the concentrations on the right-hand side of this equation fall in the ranges $[ArH]_0 = 0.05$–0.2 M, $[Br_2]_0 = 0.001$–0.004, and $K_1 = 0.1$–0.25 (10, 16). Hence, $K_1[ArH]$ is negligible in the denominator, and [ArH] is in sufficient excess that $[ArH] \approx [ArH]_0$ in the numerator. Consequently, the rate expression can be integrated in the special case that $K_4[HBr]$ is constant or negligible. Standard tables of integrals yield eq. 5.

$$[5]\quad \ln \frac{(k_2 + k_3[Br_2])[Br_2]_0}{(k_2 + k_3[Br_2]_0)[Br_2]} = \frac{k_2K_1[ArH]_0}{1 + K_4[HBr]}\,t$$

The rate of disappearance of bromine was followed spectrophotometrically. Both $ArH\cdot Br_2$ and HBr_3 absorb at the same wavelengths as Br_2, so the absorbance of the reaction mixture is given by eq. 6.

$$[6]\quad A = \varepsilon_1[Br_2] + \varepsilon_2[ArH\cdot Br_2] + \varepsilon_3[HBr_3]$$

K_1 falls in the range 0.1–0.25, so $[ArH\cdot Br_2]$ is always small compared to $[Br_2]$ and ε_2 is less than ε_1. Hence the second term in eq. 6 can be neglected. Absorbances were measured at the isosbestic point for Br_2 and HBr_3, so $\varepsilon_1 = \varepsilon_3 = \varepsilon$. Therefore the relationship between absorbance and bromine concentration is given by eq. 7.

$$[7]\quad [Br_2] = \frac{A}{\varepsilon(1 + K_4[HBr])}$$

This can be used to convert eq. 5 into eq. 8, in which $q = 1 + K_4[HBr]$.

$$[8]\quad \ln\left(\frac{1}{A} + \frac{k_3}{k_2\varepsilon q}\right) = \frac{k_2K_1}{q}[ArH]_0 t + \ln\left(\frac{1}{A_0} + \frac{k_3}{k_2\varepsilon q}\right)$$

Still considering the special case where $K_4[HBr]$ is constant or negligible compared to 1, a value of $k_3/k_2\varepsilon q$ can be chosen so that the left-hand side of eq. 8 will give a straight-line plot *vs.* t. From this and the slope of the plot, values can be obtained for k_2K_1/q and k_3K_1/q^2.

For the brominations in acetic acid q is expected to be constant and in most cases equal to 1. The maximum possible bromide concentration is that at complete reaction, which is about 0.001 M, and K_4 for tribromide in acetic acid is about 100 (12), so that the maximum value of K_4 is 0.1 and $q \approx 1$. In the presence of chloride salts, the complexing of bromine as $ClBr_2^-$ must be considered. Chloride is in large excess, so q for this complex will be constant. We have assumed $q \approx 1$ because, although there is more chloride present than bromide, K_4 is expected to be much smaller for $ClBr_2^-$ than for Br_3^-. Figure 3*a* shows a plot of eq. 8 for the reaction without added salt, and Table 1 shows the rate and equilibrium constants obtained from the data in acetic acid.

It is seen from Table 1 that pyridinium chloride produces a considerable increase in both the second- and third-order rates of bromination in acetic acid. Because of the crude kinetic treatment, the precision of the constants (about a factor of 2 in k_2 and $\pm 10\%$ in k_3) does not permit a decision as to whether the effect is larger on the second- or third-order terms. Neither is it possible to determine whether the increase is predominantly in the rate constants or in the formation constant of the initial π-complex.

That pyridinium salts are not unique is shown by the fact that *N*-ethylpiperidinium chloride produces a similar rate increase. Tetra-*n*-butylammonium chloride appears to produce a smaller increase but it seems probable that this is caused by a decrease in bromine concentration rather than a smaller increase in rate constants. In chloroform the tetra-*n*-butylammonium cation produces both an increased rate of bromination and an increase in the formation constant of Br_3^-. It may well be, therefore, that K_4 for the formation of $Bu_4N^+ClBr_2^-$ is large enough

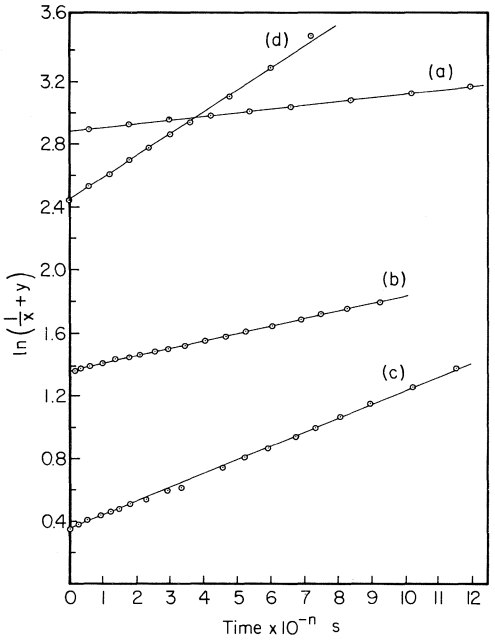

FIG. 3. Bromination of mesitylene at 25.0°. (*a*) 0.0480 *M* solution in acetic acid; $x = A$, $y = 15$, $n = 3$. (*b*) 0.202 *M* solution in chloroform; $x = A$, $y = 2.5$, $n = 3$. (*c*) 0.202 *M* solution in chloroform containing 0.096 *M* pyridinium bromide; $x = A$, $y = 0$, $n = 3.3$. (*d*) 0.202 *M* solution in chloroform containing 0.100 *M* tetra-*n*-butylammonium perchlorate; $x = 2A - A_0$, $y = 10$, $n = 2$.

to make q in eq. 8 greater than 1 in this case, so that the values of k_2K_1 and k_3K_1 shown in Table 1 for this salt are too small.

It appears, then, that pyridinium salts have no special catalytic effect. It is conceivable that pyridinium cation could facilitate bromination by extracting bromide ion from the π-complex, either by complexation with the electron-deficient pyridinium nucleus or by hydrogen bonding with the pyridinium protons. That this is not the case, however, is shown by the fact that the nonaromatic *N*-ethylpiperidinium chloride and the unprotonated tetra-*n*-butylammonium chloride produce rate increases similar to those of pyridinium salts. It appears, therefore, that the rate increase is an ordinary salt effect on either the extent of formation of the π-complex or its rate of decomposition, and pyridinium ion is in no way unique.

In the light of these results, the effect of pyridine on the bromination of toluene in acetic acid can be reasonably explained. Pyridine, as pyridinium acetate, produces an initial increase in rate through its salt effect but, as reaction proceeds, HBr produced in the reaction converts pyridine to pyridinium bromide which ties up bromine as tribromide and thus decreases the rate of reaction. The more pyridine added, the sooner the rate decrease occurs. This latter effect is confirmed by the large inhibition produced by added pyridinium bromide.

In chloroform the results are similar but more complex. In the absence of added salts K_4 is expected to be small so that q is effectively unity and the data should fit eq. 8. Figure 3*b* shows that this is the case, and the values of k_2K_1 and k_3K_1 are given in Table 4. Josephson *et al.* (16) report that the bromination of mesitylene in chloroform gives nuclear substitution and that the reaction is third order. An upward drift in the rate after 50% reaction they attribute to catalysis by the product HBr. However, in view of the inhibition by bromides found in this work, it seems equally reasonable to attribute the deviation from third-order to a second-order term which becomes significant in the latter stages of the reaction.

That a second-order reaction exists in chloroform is evident from the results with added pyridinium bromide which fit simple second-order (pseudo first-order) kinetics as shown in Fig. 3*c*. In this case [HBr] can be taken as equal to the concentration of added pyridinium bromide (0.1 *M*) and therefore effectively constant. K_4 was found to be 200, making $q = 21$, so that the quantity $k_3/k_2\varepsilon q$ becomes negligible *vs.* $1/A$, and eq. 8 becomes that of a pseudo first-order reaction. The second-order rate constants (Table 4) show that pyridinium salts have a positive salt effect in chloroform similar to that in acetic acid. The retardation shown by pyridinium bromide in Fig. 1 is therefore the net result of a rate increase caused by the salt effect

TABLE 4. Bromination of 0.202 *M* mesitylene in chloroform at 25.0 °C

[Bromine] $\times 10^3$ (*M*)	Salt (*M*)	k_2K_1 (M^{-2} s^{-1})	k_3K_1 (M^{-3} s^{-1})
4.21	None	2.4×10^{-4}	0.10
3.93	PyHBr (0.096)	4.9×10^{-3}	—
5.21	PyHCl (0.549)	$1.7q \times 10^{-3}$	$0.11q^2$
4.00	Bu_4NClO_4 (0.100)	1.2×10^{-2}	19

Can. J. Chem. Downloaded from www.nrcresearchpress.com by 210.87.254.40 on 09/05/12
For personal use only.

Can. J. Chem. Downloaded from www.nrcresearchpress.com by 210.87.254.40 on 09/05/12
For personal use only.

which is overwhelmed by a rate decrease due to complexation of bromine as tribromide.

The results in 0.1 M pyridinium chloride do not fit eq. 8 well, probably because the K_4 of pyridinium tribromide is large enough so that q varies during a run, while K_4 of pyridinium dibromochloride is not large enough to swamp it. When the pyridinium chloride concentration is increased to 0.549 M the results fit eq. 8 better, probably because K_4[PyHCl] now exceeds K_4[PyHBr] enough to make q effectively constant. However, since the value of K_4[PyHCl] is not known, the rate constants shown in Table 4 include the unknown value of q.

Because the formation constant of tetra-*n*-butylammonium tribromide in chloroform (9×10^4) is so much larger than that of pyridinium tribromide (2×10^2) the effect of tetra-*n*-butylammonium salts on the rate of bromination in chloroform is much greater than that of pyridinium salts. Thus 0.1 M tetra-*n*-butylammonium bromide practically stops the reaction by complexing nearly all of the bromine. When tetra-*n*-butylammonium perchlorate is used, the perchlorate ion can not complex bromine, but the bromide ion formed during the reaction complexes bromine as tetra-*n*-butylammonium tribromide so effectively that the reaction nearly stops after half the initial bromine is consumed. In other words $[HBr_3] \approx [ArBr]$ so that eqs. 7 and 8 take the form of eqs. 9 and 10.

$$[9] \qquad [Br_2] = (2A - A_0)/\varepsilon$$

$$[10] \qquad \ln\left(\frac{1}{2A - A_0} + \frac{k_3}{k_2\varepsilon}\right) = 2k_2K_1[ArH]_0t + \ln\left(\frac{1}{A_0} + \frac{k_3}{k_2\varepsilon}\right)$$

Figure 3*d* shows a plot of this last equation for the fast part of the bromination with tetra-*n*-butylammonium perchlorate added and the rate constants obtained from it are given in Table 4.

The results in Table 4 show that in chloroform, as in acetic acid, soluble salts produce a sharp increase in the rate of bromination of mesitylene. Furthermore, pyridinium salts are not unique in this respect; in fact, the more highly ionic (less hydrogen bonded) quaternary ammonium perchlorate is more effective than pyridinium salts.

We may conclude that, in dilute solution, no special catalytic effect is required to explain the increased rate of bromination produced by pyridine and pyridinium salts. It can be accounted for by the commonly accepted mechanism for aromatic halogenation, and is essentially a salt effect. It is, of course, impossible to extrapolate from dilute solution to Cohen's preparation of aryl bromides in the absence of solvent. It would appear, however, from the results in chloroform, that the salt effect in nonpolar media might be large enough to account for Cohen's results.

Experimental

Materials

Pyridine (Karl Fischer Reagent), bromine, and *t*-butylbenzene were commercial products used without further purification. Commercial mesitylene was distilled through a 90-plate column collecting the fraction boiling at 164.0–164.2°. Acetic acid was purified by the method of Orton and Bradfield (17). The fraction distilling at 116.9–117.2° and melting at 16.55° was used. Chloroform was purified by the method of Fieser (18). However, when the stabilizing ethanol is removed chloroform rapidly forms decomposition products which absorb in the u.v. and consume bromine. It was found that this could be avoided if the purified chloroform is stored over chromatographic alumina and filtered just before use. Chloroform so stored could be used for a period of several weeks.

Tetra-*n*-butylammonium bromide and tetra-*n*-butylammonium perchlorate were recrystallized from an ether–chloroform mixture. Tetra-*n*-butylammonium chloride (m.p. 74–75°) was prepared from commercial tetra-*n*-butylammonium iodide by the method of Umni *et al.* (19). Pyridinium bromide (m.p. 213–215°) was prepared by the method of Trowbridge and Diehl (20). Pyridinium chloride (m.p. 141–144°) was prepared by passing HCl into an ether solution of pyridine. The precipitated salt was recrystallized twice from 2-propanol. *N*-Ethylpiperidinium chloride (m.p. 231–233°) was prepared similarly and recrystallized from a 3:1 mixture of ligroin and 2-propanol. All hygroscopic salts were stored in a vacuum desiccator over P_2O_5, weighed, and transferred to reaction solutions in a dry box.

Preparation and Analysis of Pyridinium Bromide–Bromine Complexes

Compound **1** precipitated from a solution of 0.5 ml of pyridine and 10 ml of bromine in 15 ml of benzene, and was filtered on sintered glass. Attempts to wash or recrystallize it resulted in decomposition to **2**. A crude analysis for reducible bromine was made by quickly transferring a freshly prepared sample to a tared weighing bottle which was then weighed, immersed in a 1:1 ethanol–water solution containing excess KI, opened, and titrated with sodium thiosulfate.

Anal. Calcd. for $C_5H_5NHBr \cdot 2Br_2$: reducible Br, 66.6. Found: reducible Br, 70.0.

Compound **2** was prepared by the method of Englert and McElvain (8). The orange solid melted at 100–105°. It was analyzed for reducible bromine by the method used for Compound **1**. Total bromine was determined by

dissolving samples in saturated aqueous sulfur dioxide and titrating potentiometrically with silver nitrate. Neutral equivalent was determined by dissolving samples in dimethylformamide, adding excess aqueous potassium iodide (to convert hydrolyzable bromine to less-hydrolyzable iodine), and titrating with standard alkali.

Anal. Calcd. for $3C_5H_5NHBr \cdot 2Br_2$ (neutral equivalent 266.6): reducible Br, 40.0; total Br, 70.0. Found (neutral equivalent 266.7): reducible Br, 40.3; total Br, 70.0.

Rate Measurements

All kinetic experiments were done in a dark room by following the rate of loss of bromine with the aromatic substrate in excess. The data for toluene were obtained by adding aliquots of the reaction mixture to excess arsenious oxide and back titrating with potassium bromate. All other rate measurements were made by following the disappearance of bromine spectrophotometrically. Absorbances were measured at 400 nm in acetic acid and at 440 nm in chloroform. Fast reactions (half life 5 min or less) were followed in the stoppered cuvette of a Beckman DK-1 spectrophotometer thermostatted to 25.0 ± 0.2°. Previously thermostatted solutions of bromine and of substrate plus catalyst were mixed in the cuvette and the absorbance of the mixture was recorded continuously at fixed wavelength. The initial bromine concentration was obtained by titration of the bromine stock solution before mixing. Slower reactions were done in a thermostat and followed with a Beckman DU spectrophotometer with thermostatted cell compartment. All experiments were done in duplicate and rate constants were reproducible to within ±5%.

Formation Constants

Separate chloroform solutions of bromine and bromide were prepared in a dark room, thermostatted, then mixed and immediately transferred to the cell compartment of a Beckman DU spectrophotometer thermostatted at 25.0 ± 0.2°. Concentrations and absorbances are given in Tables 2 and 3.

The authors are grateful to the National Research Council of Canada for financial support.

1. W. E. Cross and J. B. Cohen. Proc. Chem. Soc. 15 (1908).
2. J. B. Cohen. Practical organic chemistry. 3rd Ed. Macmillan, London. 1924. p. 155.
3. A. I. Vogel. Elementary practical organic chemistry. Part I. Small scale preparations. 2nd Ed. Longmans, London. 1965. p. 253.
4. P. B. D. de la Mare and J. H. Ridd. Aromatic substitution. Butterworths Scientific Publications, London, 1959.
5. R. M. Acheson, T. G. Hoult, and K. A. Barnard. J. Chem. Soc. 4142 (1954).
6. J. J. Eisch and B. Jaselskis. J. Org. Chem. **28**, 2865 (1963).
7. G. Kotowycz, T. Schaefer, and E. Bock. Can. J. Chem. **42**, 2541 (1964).
8. S. M. E. Englert and S. M. McElvain. J. Am. Chem. Soc. **51**, 863 (1929).
9. L. M. Yeddanapalli and N. S. Gnanapragasam. J. Ind. Chem. Soc. **36**, 745 (1959).
10. R. M. Keefer, A. Ottenberg, and L. J. Andrews. J. Am. Chem. Soc. **78**, 255 (1956).
11. N. J. Rose and R. S. Drago. J. Am. Chem. Soc. **81**, 6138 (1959).
12. A. I. Popov. *In* Halogen chemistry. Vol. 1. *Edited by* V. Gutman. Academic Press, London. 1967. pp. 251–256.
13. R. E. Buckles, A. I. Popov, W. F. Zelezny, and R. J. Smith. J. Am. Chem. Soc. **73**, 4525 (1951).
14. A. I. Popov and N. E. Skelly. J. Am. Chem. Soc. **76**, 5309 (1954).
15. R. O. C. Norman and R. Taylor. Electrophilic substitution in benzenoid compounds. Elsevier, Amsterdam. 1965. p. 130.
16. R. Josephson, R. M. Keefer, and L. J. Andrews. J. Am. Chem. Soc. **83**, 2128 (1965).
17. K. J. P. Orton and A. E. Bradfield. J. Chem. Soc. 960 (1924).
18. L. F. Fieser. Experiments in organic chemistry. 3rd Ed. revised. D. C. Heath and Co., Boston. 1957.
19. A. K. R. Umni, J. Elias, and H. I. Schiff. J. Phys. Chem. **67**, 1216 (1963).
20. P. F. Trowbridge and O. C. Diehl. J. Am. Chem. Soc. **19**, 558 (1897).

Can. J. Chem. Downloaded from www.nrcresearchpress.com by 210.87.254.40 on 09/05/12
For personal use only.

Pyridine-catalyzed Halogenation of Aromatic Compounds. II. A Study of the Bromine Adducts of Pyridinium Bromide using Differential Scanning Calorimetry and Isothermal Gravimetric Analysis

G. R. TAYLOR,[1] H. D. GESSER, AND G. E. DUNN

Department of Chemistry, University of Manitoba, Winnipeg, Manitoba R3T 2N2

Received October 29, 1973

G. R. TAYLOR, H. D. GESSER, and G. E. DUNN. Can. J. Chem. **52,** 2560 (1974).

The composition and melting points of the bromine adducts of pyridinium bromide have been determined. Differential scanning calorimetry has been found to be particularly well suited to this type of phase study because it uses small, enclosed samples and responds rapidly to small heat changes. The adducts are described in terms of stoichiometric mixtures of pyridinium bromide and pyridinium tribromide, or in terms of a general formula $PyHBr(Br_2)_n$ where n equals 1/3, 1/2, 2/3, 1, 3, 6, 18. When pyridinium bromide is allowed to pick up bromine isothermally in an apparatus for thermogravimetric analysis it does so in a stepwise manner with a plateau for each of the above adducts plus one with n equal to 3/2. This provides valuable confirmation of the compositions of adducts deduced from conventional phase diagrams.

G. R. TAYLOR, H. D. GESSER et G. E. DUNN. Can. J. Chem. **52,** 2560 (1974).

On a déterminé la composition et les points de fusion de produits d'addition du brome sur le bromure de pyridinium. On a trouvé que l'analyse enthalpique différentielle est particulièrement bien adaptée à ce type d'étude de phase parce qu'elle utilise de petits échantillons et qu'elle répond à des petits changements de chaleur. On décrit les produits d'addition en terme de mélanges stoichiométriques de bromure de pyridinium et de tribromure de pyridinium ou en terme d'une formule générale $PyHBr(Br_2)_n$ ou $n = 1/3, 1/2, 2/3, 1, 3, 6$ et 18. Lorsqu'on permet au bromure de pyridinium d'accumuler du brome d'une façon isothermique dans un appareil à analyse thermogravimétrique, la réaction se fait par étapes avec un plateau pour chacun des produits mentionnés plus haut; on observe en plus un autre produit ou n est égal à 3/2. Ces résultats fournissent une confirmation utile de la composition des produits d'addition qui est déduite des diagrammes de phase du type conventionnel. [Traduit par le journal]

Introduction

During an investigation into the pyridine catalyzed bromination of benzene, Part I of this series, it was observed that a dark red solid was precipitated from the reaction mixture (1). An investigation into the composition of this solid showed that it was an adduct of bromine and pyridinium bromide.

Pyridine, pyridinium bromide, and pyridinium chloride have all been reported to give stable crystalline adducts with bromine. Unfortunately these products contained variable proportions of bromine according to the method of preparation (2–4). The reaction between pyridine and bromine in benzene (5) gives an adduct which initially contains 70 mol% bromine but which subsequently decomposes to give an adduct containing 40 mol% bromine (1). The latter adduct was found to be a derivative of pyridinium bromide because the ^1H magnetic resonance spectrum, in methylene chloride, showed that a proton was present on the nitrogen atom (1, 6). The reaction between 1 mol of pyridinium bromide in acetic acid and 1 mol of bromine in acetic acid gives an adduct containing 47 mol% bromine. However, if 0.5 mol of bromine is used then the adduct formed contained only 39.7 mol% bromine (7). Bromine and pyridinium bromide can react in the absence of a solvent to give an adduct whose composition depends on the ratio of the reactants (8). Bromine can also form adducts with a number of tertiary and quaternary ammonium halides (9). Tetramethylammonium bromide has been shown to absorb sufficient bromine to correspond to the adduct $N(CH_3)_4Br_{13}$ (10). However, this adduct is very unstable and decomposes to give the more stable trihalide $N(CH_3)_4Br_3$. Phosphorus trichloride has been shown to form polybromides and there is evidence for the existence of the adduct

[1]Postdoctoral Fellow 1969–1971.

Can. J. Chem. Downloaded from www.nrcresearchpress.com by 210.87.254.42 on 09/05/12
For personal use only.

Can. J. Chem. Downloaded from www.nrcresearchpress.com by 210.87.254.42 on 09/05/12
For personal use only.

PCl_3Br_{18} (11). It has also been reported that an anion exchange resin in the bromide form can absorb bromine corresponding to the formation of Br_7^- ions (12).

The present study was undertaken to determine the exact composition and stability of the adducts of bromine and pyridinium bromide. It was felt that a more comprehensive study of the phase equilibria of the two reactants (8) would serve to identify the adducts. However, there is evidence that the thermal analysis of a similar system, PCl_3–Br_2, had failed to reveal the existence of a compound (13). Therefore the system was studied by isothermal gravimetric analysis in order to confirm the existence and composition of the adducts. It was particularly useful in identifying the composition of compounds with incongruent melting points.

Experimental

Materials

'Baker Analysed' Reagent bromine and aqueous hydrobromic acid (47%) were used without further purification. Pyridine (for Karl Fischer Reagent) was obtained from Matheson Coleman and Bell and was used without further purification. Pyridinium bromide was made by the method of Trowbridge and Diehl (4), m.p. 213–215°, and was stored in a vacuum desiccator. Recrystallization of the product from methanol–acetone did not raise its melting point.

Measurements

Differential Scanning Calorimetry (d.s.c.)

The d.s.c. measurements were made using a Perkin-Elmer Model DSC-1B differential scanning calorimeter. Due to the corrosive nature of bromine, the conventional aluminum or gold sample pans could not be used. A sealed glass ampoule for use with a commercial differential scanning calorimeter was therefore designed (14).

The temperature of the detected phase transitions was assumed to be that temperature at which the first evidence of the change appeared and was taken as the first observable deflection from the baseline. The temperature scale of the apparatus was calibrated at a heating rate of 10° min^{-1} using the phase transitions of ammonium nitrate (15) and the freezing points of water and mercury (16).

Pyridinium bromide was carefully introduced into a weighed glass ampoule so that no crystals were adhering to the sides of the stem and the whole was reweighed. Sufficient sample was introduced so that the total weight of the desired adduct would be approximately 0.20 g. Bromine vapor (at 25°) was carefully added to the pyridinium bromide by means of a 'Pasteur-type' pipette with a fine tip. The bromine immediately reacted exothermally with the pyridinium bromide. The addition of bromine was continued until the final weight of the adduct was 0.20 g. The glass ampoule was then sealed as previously described (14). The glass ampoule and the waste piece of stem were finally weighed to ensure that no sample had been lost in the sealing procedure. Using this method, it was possible to prepare an adduct which contained exactly the desired ratio of bromine and pyridinium bromide.

The quantitative thermal analysis of the adduct was then carried out in the usual way. The adduct was heated at 10° min^{-1} until the temperature was approximately 40° higher than the final detected phase transition. The adduct was then cooled at 10° min^{-1} until the temperature was approximately 40° lower than the first detected phase transition. The cycle was repeated on the same sample and the two sets of endotherms and exotherms were compared and analyzed. At cooling rates slower than 10° min^{-1}, the detection of the phase transitions became less sensitive because of increased uncertainty in locating the onset of the peak. Finally, the bromine content of the adduct was verified by titration using potassium iodide and standard sodium thiosulfate.

The temperatures to which the samples were heated in the course of the d.s.c. measurements were, in some cases, in excess of 200°. Under certain conditions it is possible to brominate the pyridine ring at these high temperatures (7, 17). However, the results obtained for each sample were entirely reproducible and reversible indicating that no side reactions were occurring. Further, the mixtures were analyzed by titration after the d.s.c. measurements and it was found that no bromine had been used in any substitution reaction.

Isothermal Gravimetric Analysis (i.t.g.a.)

The i.t.g.a. measurements were made using a modified version of the automatic recording balance described by Bancroft and Gesser (18). A circular glass pan was used instead of a platinum pan and provision was made so that the cover tube surrounding the glass pan could be immersed in a constant temperature bath. The cover tube was designed so that the glass pan was suspended about 5 cm above the bottom of the tube and an inlet was provided for the introduction of bromine. The balance was calibrated before each measurement with known weights.

Exactly 20 mg of pyridinium bromide was placed in the glass pan and the cover tube was attached. The cover tube was then immersed in a constant temperature bath and left for approximately 30 min to attain the temperature of the bath. During this time no weight loss or weight gain was observed. Approximately 1 g of bromine was then introduced into the cover tube and the bromine vapor, at atmospheric pressure, immediately enveloped the sample in the glass pan. Sufficient bromine was added so that there was always an excess. The uptake of bromine by the pyridinium bromide was continuously monitored until a constant weight was observed. The bromine atmosphere was then removed and the adduct was allowed to lose bromine until a constant weight was again observed. The glass pan was cleaned and the weight calibration repeated.

Results and Discussion

The detection of phase changes involving small heats of transition is difficult by conventional techniques. Figure 1 shows the obvious advantage in the detection and analysis of the phase transitions observed by the d.s.c. technique compared to the usual cooling curve method,

TABLE 1. Data from phase diagrams

Mol% bromine	Temperature (°)	Classification of mixture	Formula of compound[a]
21	95	Eutectic	—
25	107	Compound with congruent m.p.	$(PyH^+Br^-)_2.PyH^+Br_3^-$
29.5	95	Eutectic	—
33	106	Compound with incongruent m.p.	$PyH^+Br^-.PyH^+Br_3^-$
40	121	Compound with incongruent m.p.	$PyH^+Br^-.(PyH^+Br_3^-)_2$
50	155	Compound with congruent m.p.	$PyH^+Br_3^-$
65.5	4	Eutectic	—
75	21	Compound with congruent m.p.	$PyH^+Br_7^-$
81.5	12	Eutectic	—
85.6	17	Compound with congruent m.p.	$PyH^+Br_{13}^-$
89	−14	Eutectic	—
94.7	13	Compound with congruent m.p.	$PyH^+Br_{37}^-$

[a]Py = C_5H_5N.

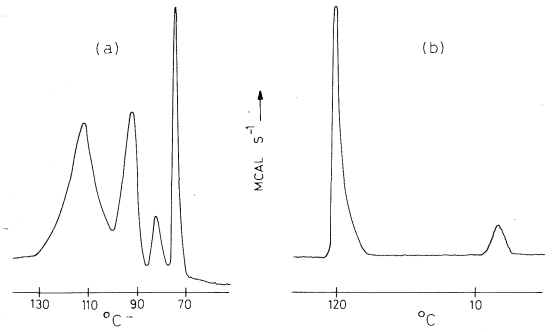

FIG. 1. Typical d.s.c. traces: (*a*) is the trace for the mixture containing 40 mol% bromine; (*b*) is the trace for the mixture containing 59 mol% bromine.

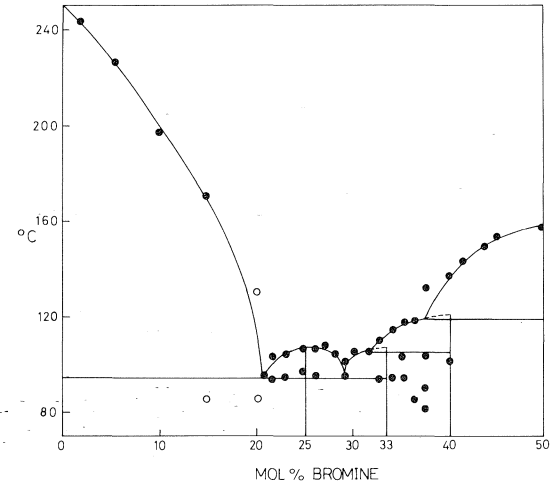

FIG. 2. Phase diagram. The open circles are experimental points which show evidence of supercooling.

especially when it is remembered that only a 200 mg sample is being used.

From an analysis of the d.s.c. measurements the phase diagrams, Figs. 2 and 3, have been constructed. They show the formation of several adducts with the composition and formulae shown in Table 1. The adducts are classified as either having a congruent melting point or an incongruent melting point (19). The formulae of the adducts are described in terms of various pyridine–bromine salts.

It has been proposed that the adduct at 50 mol% bromine has the trihalide formula $PyH^+Br_3^-$, and it has been called pyridine hydrobromide perbromide (20, 21). This adduct is stable at room temperature but after prolonged standing in air it gradually loses bromine. In Table 1, the formulae of the adducts at 25, 33, and 40 mol% bromine are described in terms of a stoichiometric mixture of pyridinium bromide and pyridinium tribromide instead of a non-stoichiometric mixture of pyridinium ion and bromide ion. This would seem more likely since a bromine molecule would diffuse into the crystal lattice of pyridinium bromide and react with a single molecule to form the tribromide. The lattice would be further distorted by the introduction of more bromine molecules until sufficient had reacted to give the more stable adduct $(PyH^+Br^-)_2.PyH^+Br_3^-$. The addition would continue until the adducts $PyH^+Br^-.PyH^+Br_3^-$ and $PyH^+Br^-.(PyH^+Br_3^-)_2$ had been formed. Finally sufficient bromine would react to give the most stable adduct $PyH^+Br_3^-$.

Although the formation of the perbromide has confirmed the results of Lombard and Heywang (8), the occurrence and composition of the intermediate adducts were not reported in their work. They have reported the existence of a sesquibro-

Can. J. Chem. Downloaded from www.nrcresearchpress.com by 210.87.254.42 on 09/05/12
For personal use only.

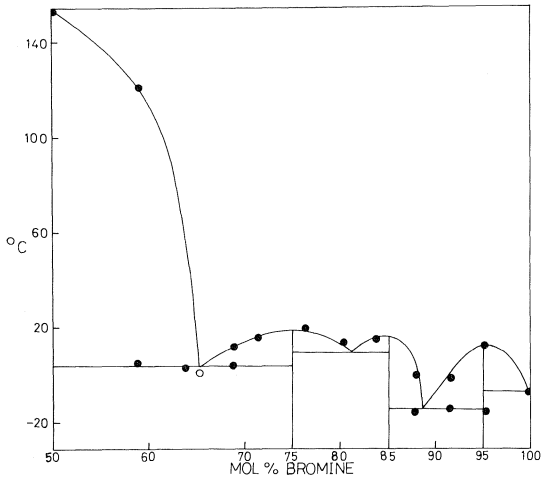

FIG. 3. Phase diagram. The open circle is an experimental point which shows evidence of supercooling.

mide having the formula $(PyHBr)_2Br_3$. Their evidence for the existence of this compound was that the eutectic plateau disappeared at this composition. The temperature of the eutectic that they observed at 93° is in good agreement with the value of 95° obtained in this study. However, since it will be shown in the i.t.g.a. study that an adduct exists at 33 mol% bromine, the eutectic plateau cannot exist beyond this concentration (19). The occurrence of further phase transitions, in their study and in ours, beyond this concentration at approximately the same temperature, must be associated with certain solid–solid phase transitions involving two or more isomorphic crystalline forms. A study of the crystal structure of the adducts in this region was attempted using X-ray powder photography. However, the powder photographs obtained showed only a few diffuse lines and a full analysis was not possible. Further work has to be carried out to confirm the presence of isomorphic crystalline forms.

The presence of an adduct at 40 mol% bromine is indicated by the disappearance of the plateau at 106° (Table 1). The plateau at 121° actually corresponding to the appearance of this compound was not observed. This is probably due to the small heat of transition of this particular phase change and, further, the large peak corresponding to the first appearance of crystals could have masked the phase change since it was very broad and was still present when the phase transition at 121° should have occurred.

The adducts at 50, 75, 85.6, and 94.7 mol% bromine can be described in terms of a general formula $PyH^+Br(Br_2)_n^-$ where n is equal to 1, 3, 6, and 18, respectively. The error in determining the position of the maxima in the phase diagram (Fig. 3) for the adducts containing 85.6 and 94.7 mol% bromine is greater than for the other maxima. However, the adducts $PyH^+Br_{13}^-$ and $PyH^+Br_{37}^-$ would appear to be the most likely compositions (10). The stepwise uptake of bromine by the adducts in this region (Fig. 3) should be analogous to the uptake below 50 mol% bromine. However, there is only evidence for the existence of $PyH^+Br_7^-$, $PyH^+Br_{13}^-$, and $PyH^+Br_{37}^-$. The other adducts of general formula $PyH^+Br(Br_2)_n^-$, where n is equal to 2, 4, 5, 7, etc. would have been expected to exist since they have been found in the analogous tetraalkylammonium perhalide series as far as n equal to 6 (10). Therefore it can be concluded that these other adducts are probably less stable than the three detected adducts.

The results of the i.t.g.a. measurements, at 10°, shown in Fig. 4, confirm the presence of the adducts listed in Table 1. The uptake of bromine by pyridinium bromide shows a series of distinct steps. A similar single step process has been observed in the reaction of chlorine gas with potassium bromide (22). The shape of the curves is similar to a generalised isothermal decomposition curve (23). However, the vast majority of curves, in the literature, involve a single reaction and hence a single step curve results. There are only a few examples of reactions involving more

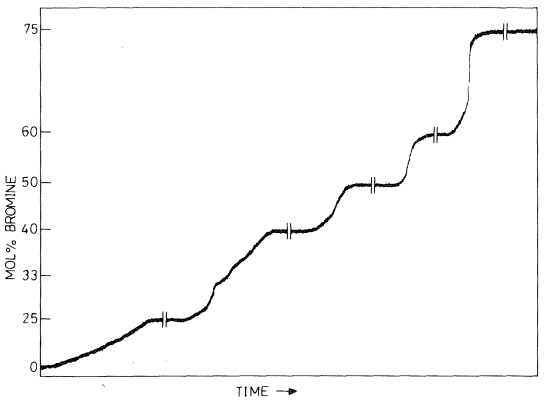

FIG. 4. Isothermal gravimetric analysis of bromine and pyridinium bromide. The length of a plateau varies from run to run, and every plateau does not appear in every run. This is a composite diagram with the sections between discontinuities taken from different runs. Hence the ordinate scale changes between discontinuities.

Can. J. Chem. Downloaded from www.nrcresearchpress.com by 210.87.254.42 on 09/05/12
For personal use only.

Can. J. Chem. Downloaded from www.nrcresearchpress.com by 210.87.254.42 on 09/05/12
For personal use only.

than one step. A review of the isothermal decomposition of copper sulfate pentahydrate (23) indicates that under certain experimental conditions a two step curve is obtained: the first step corresponding to the formation of the trihydrate and the second step corresponding to the formation of the monohydrate.

The crystal shape and size and the presence of impurities in the sample have been shown to affect the shape of the curves which results in nonreproducible diagrams (22, 23). In this study, it was found that although the shape of the step and the length of the plateau (Fig. 4) were not reproducible, the positions of the plateaus were reproducible at the same bromine concentrations. In some cases the stepwise uptake of bromine was not observed, instead there was simply a change in the rate of uptake of bromine which resulted in a change in gradient of the curve for each adduct. The steps in Fig. 4 each correspond to a single process. Initially, bromine reacts slowly with pyridinium bromide, there is then a rapid acceleratory stage, and finally, there is a deceleratory stage (24). Quantitatively each plateau corresponds to the beginning or end of a reaction.

In Fig. 4, the plateaus occur at 25, 33, 40, 50, 60, and 75 mol% bromine. The formation of each adduct occurs in a stepwise manner and the plateaus correspond to the adducts shown in Table 1. The plateau at 33 mol% bromine is very short and indicates the low stability of this adduct compared to the others. In addition, a plateau exists at 60 mol% bromine. This adduct was not observed in the d.s.c. study and this could be due to the large peak corresponding to the first appearance of crystals masking the detection of the phase change. This adduct corresponds to the formula $PyH^+Br_3^-.PyH^+Br_5^-$. By increasing the temperature of the bromine addition to 20° it was possible to observe the formation of the adduct at 85.6 mol% bromine. However, the adduct at 94.7 mol% bromine was not detected since the vapor pressure of this adduct is greater than that of the bromine at the temperature of the experiment. It was not possible to heat the adduct because sublimation was found to occur at high temperatures. Under the conditions of the experiment, the maximum uptake of bromine corresponded to a mixture containing 92 mol% bromine.

When the uptake of bromine reached a constant value, the bromine atmosphere was removed and the mixture was allowed to decompose at atmospheric pressure at 20°. The mixture decomposed rapidly in a stepwise manner (23) until it contained 50 mol% bromine, corresponding to the adduct $PyH^+Br_3^-$. The steps in the decomposition occurred at 75, 60, and 50 mol% bromine again corresponding to the adducts shown in Table 1. The further decomposition of the adduct $PyH^+Br_3^-$ was very slow even under reduced pressure and it showed negligible weight loss after 3 days.

In Part I of this series (1), the dark red solid which was precipitated from a solution of pyridine and bromine in benzene, was found to contain 70.0 mol% bromine. This solid lost bromine rapidly on standing or on washing to give an orange solid containing 40.6 mol% bromine. However, the results in this study would appear to indicate that the dark red solid should decompose to the stable adduct $PyH^+Br_3^-$ containing 50 mol% bromine. The explanation for the failure to do this may be that the presence of any solvent, in this case benzene, would facilitate dissociation of the adduct to give bromine and pyridinium salt (1). In this study, there is no solvent present and hence the results are not comparable.

The melting point of the adduct $PyH^+Br_3^-$, as determined by d.s.c., was found to be 155°. This does not agree with the value of 135° reported by Lombard and Heywang (8) and of 132–135° reported for various commercial samples.[2] The difference in the procedure for determining melting points by d.s.c. and by conventional cooling curve methods is that in the d.s.c. method the sample is encapsulated and hence there is no bromine loss. However, in the latter method, the sample is open to the air and therefore there is the possibility that the mixture does not contain exactly 50 mol% bromine. If the mixture contains less than 50 mol% bromine, then a lower melting point will be observed (Fig. 2). However, the higher melting point observed in the sealed ampoules for this adduct could possibly be due to a lesser extent to the usual effect of pressure on melting point since at elevated temperatures, the pressure inside the ampoule is greater than atmospheric pressure.

The authors are grateful to Dr. E. M. Kartzmark and Dr. A. N. Campbell for their helpful discussion of the

[2]Aldrich Chemical Company Inc., Milwaukee, Wisconsin.

phase diagrams, and to the National Research Council of Canada for financial support.

1. G. E. DUNN and B. J. BLACKBURN. Can. J. Chem. This issue.
2. A. W. HOFMANN. Ber. **12**, 988 (1879).
3. M. E. GRIMAUX. C. R. **95**, 85 (1882).
4. P. F. TROWBRIDGE and O. C. DIEHL. J. Am. Chem. Soc. **19**, 558 (1897).
5. J. B. COHEN. Practical organic chemistry. 3rd Ed. Macmillan and Co., London. 1924. p. 155.
6. G. KOTOWYCZ, T. SCHAEFER, and E. BOCK. Can. J. Chem. **42**, 2541 (1964).
7. S. M. E. ENGLERT and S. M. MCELVAIN. J. Am. Chem. Soc. **51**, 863 (1929).
8. R. LOMBARD and G. HEYWANG. Bull. Soc. Chim. Fr. **331** (1952).
9. Z. E. JOLLES. Bromine and its compounds. Academic Press Inc., New York. 1966. p. 368.
10. F. D. CHATTAWAY and G. HOYLE. J. Chem. Soc. **123**, 654 (1923).
11. Y. A. FIALKOV and A. A. KUZMENKO. Zhur. Obshch. Khim. **21**, 433 (1951).
12. J. AVESTON and D. A. EVEREST. Chem. Ind. 1238 (1957).
13. Y. A. FIALKOV and A. A. KUZMENKO. Zhur. Obshch. Khim. **22**, 1335 (1952).
14. G. R. TAYLOR, G. E. DUNN, and W. B. EASTERBROOK. Anal. Chim. Acta, **53**, 452 (1971).
15. E. S. WATSON, M. J. O'NEILL, J. JUSTIN, and N. BRENNER. Anal. Chem. **36**, 1233 (1964).
16. E. W. WASHBURN (*Editor*). International critical tables. McGraw-Hill, New York. 1929.
17. S. M. MCELVAIN and M. A. GOESE. J. Am. Chem. Soc. **65**, 2227 (1943).
18. G. M. BANCROFT and H. D. GESSER. J. Inorg. Nucl. Chem. **27**, 1537 (1965).
19. A. N. CAMPBELL and N. O. SMITH. A. Findlay, The phase rule. Dover Publications Inc., New York. 1951.
20. L. F. FIESER. J. Chem. Ed. **31**, 291 (1954).
21. A. ALBERT, G. M. BADGER, and C. W. SHOPPEE. Current trends in heterocyclic chemistry. Academic Press Inc., New York. 1958. p. 17–18.
22. J. A. MORRISON and K. NAKAYAMA. Trans. Faraday Soc. **59**, 2560 (1963).
23. D. A. YOUNG. Decomposition of solids. Pergamon Press, Oxford. 1966.
24. A. R. ALLNATT and P. W. M. JACOBS. Can. J. Chem. **46**, 111 (1968).

Can. J. Chem. Downloaded from www.nrcresearchpress.com by 210.87.254.42 on 09/05/12
For personal use only.

Conformational Analysis of *trans-syn-trans*-4,5:9,10-Biscyclohexano-1,3,6,8-tetraoxecane: a Low-energy Pathway for Boat–Chair–Boat (BCB) Interconversion

T. Bruce Grindley[1] and Walter A. Szarek[2]

Department of Chemistry, Queen's University, Kingston, Ontario K7L 3N6

Received December 7, 1973

T. Bruce Grindley and Walter A. Szarek. Can. J. Chem. **52,** 2566 (1974).

Two processes were observed by study of the variable temperature p.m.r. spectra of *trans-syn-trans*-4,5:9,10-biscyclohexano-1,3,6,8-tetraoxecane (**1**), one of which, an equilibrium, was still rapid at $-88°$; the other had an energy of activation ($\Delta G^{\ddagger}$) of 11.7 kcal/mol. These processes are interpreted in terms of interchange in the 10-membered ring between four conformations, namely, two degenerate pairs of diastereomeric boat–chair–boat (BCB) conformations. Possible pathways of conformational interconversion are discussed.

T. Bruce Grindley et Walter A. Szarek. Can. J. Chem. **52,** 2566 (1974).

L'étude, à température variable, du spectre r.m.p. du biscyclohexanotétraoxécane-1,3,6,8 *trans-syn-trans*-4,5:9,10 (**1**) permet d'observer deux processus l'un desquels, un équilibre, est encore rapide à $-88°$; l'autre a une énergie d'activation $\Delta G^{\ddagger}$ de 11.7 kcal/mol. On interprète ces processus en termes d'un cycle à dix s'interchangeant entre quatre conformations à savoir deux paires dégénérées de conformations diastéréoisomère bateau–chaise–bateau (BCB). On discute des chemins possibles pour ces conversions conformationnelles.

[Traduit par le journal]

Introduction

X-Ray crystallography (1) and strain minimization calculations (2, 3) have established that the most stable conformation for virtually all cyclodecane derivatives is the boat–chair–boat[3] (BCB) form. The energies of other conformations have been calculated (2–5) and these are listed in Table 1. Although the most stable form of cyclodecane, namely, the BCB, is well established, little is known about the interconversions of this conformation. Pseudorotation for this form has several unusual features (2). Since a BCB conformation has both an axis through bonds and a plane through atoms, its pseudorotation partner is another BCB conformation. The energy for the process has been calculated to be 24.6 kcal/mol (2) because it must pass through the long-chair (LC) conformation. The magnitude of this value is unique to BCB cyclodecane since pseudorotation for all other conformations of all rings calculated by Hendrickson (2) is of low energy with respect to symmetric interconversions (normally ≤ 2 kcal/mol). Pseudorotation involves slight changes in dihedral angles about every center, whereas symmetric interconversions require major changes about one or two centers. Indirect pseudorotation of a BCB cyclodecane conformation may take place by conversion into another conformational family of relatively low energy, such as the twist-boat–chair (TBC) or twist-boat–chair–chair (TBCC)—boat–chair–chair (BCC), which pseudorotates and then converts back to the pseudorotation partner of the original BCB. Because of the potential complexity, these processes are difficult to study, as are asymmetric interconversions (5). Annelation of other ring systems to cyclodecane can restrict the number of potential conformations and thus allow study of only a portion of the interconversion pathways.

Study of oxygen-containing heterocycles has the advantage that in their p.m.r. spectra separate signals usually appear for protons at different positions on the ring. It suffers from the disadvantage that results obtained from specific heterocyclic systems may not be applicable to other systems. However, it has been found that conformations of five- (6), six- (7), seven- (8), and eight-membered (9) rings containing *O*-methylene groups are qualitatively similar to their carbocyclic analogs.

---

[1]Present address: Department of Chemistry, University of Ottawa, Ottawa, Canada K1N 6N5.

[2]To whom inquiries should be addressed.

[3]The nomenclature used is that devised by Hendrickson (2) for conformations having planes or axes of symmetry.

Can. J. Chem. Downloaded from www.nrcresearchpress.com by 210.87.254.40 on 09/05/12
For personal use only.

TABLE 1. Energies* of cyclodecane conformations

Conformation	Calculated energy (kcal/mol)	Reference
Boat–chair–boat (BCB)	0	2
Twist-boat–chair (TBC)	2.1	4
Twist-boat–chair–chair (TBCC)	3.1	4
Boat–chair–chair (BCC)	3.75 or 4.5	5 or 3
Chair–chair–chair (CCC)	7.5	2
Long-chair (LC)	24.6	2

*Energy of the BCB conformation is set at 0 kcal/mol.

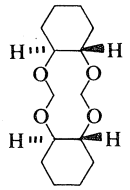

1

The 10-membered ring in *trans-syn-trans*-4,5:9,10-biscyclohexano-1,3,6,8-tetraoxecane (**1**) (10) can exist in two degenerate sets of diastereomeric BCB conformations which are formally neighbors (2, 5) on the BCB pseudorotation itinerary. There is a third type of BCB conformation, in which both cyclohexane rings are axially substituted, which is of considerably higher energy for reasons to be discussed later. The presence of the two fused rings prevents the heterocyclic 10-membered ring from assuming any of the other relatively low energy conformations (TBC, TBCC, or CCB). Two degenerate CCC conformations are also possible, although the energy of the CCC has been calculated to be 7.5 kcal/mol above that of the BCB conformation. Since no low energy alternatives to the BCB are available, discussion of the stable conformations of **1** will be limited to the two pairs of degenerate BCB conformations.

Results

The room temperature spectrum of **1** measured at 100 MHz showed an AB quartet at τ 5.14 (J_{AB} = 7.0 Hz, $\Delta\nu$ = 33.5 Hz) for the *O*-methylene protons, a broad multiplet at τ 6.29 for the protons on the cyclohexane rings geminal to the oxygens (H_α protons), and a complex broad signal between τ 1.12 and 2.04 for the remaining protons.

The ill-defined multiplet for the H_α protons (approximate band widths: 13 Hz at 50° and 60 MHz, and 15 Hz at 40° and 100 MHz) broadened as the temperature was lowered and at −33° at 60 MHz and at −31° at 100 MHz split into two signals which exhibited maximum separations of 41 Hz at −61.5° and 60 MHz, and of 63.5 Hz at −51.5° and 100 MHz. These separations decreased to 39.0 Hz at −88° and 58.5 Hz at −84°, at 60 and 100 MHz, respectively. At these latter temperatures the integrations of the two signals were equal and the apparent band widths were 26 and 27 Hz at 60 MHz and 28 and 31 Hz at 100 MHz. Extrapolation of the chemical shift differences to the coalescence points gave separations of 43 and 67 Hz, respectively. From the separations at the coalescence points, $\Delta G^{\ddagger}$ values were calculated to be 11.7 and 11.6 kcal/mol at 60 and 100 MHz, respectively, using the equation (11) for the collapse of an AB quartet with J_{AB} taken as 9 Hz.[4]

In contrast to the behavior of the signals of the H_α protons, the appearance of the AB quartet for the *O*-methylene changed only gradually as the temperature was lowered. At 50° and 60 MHz the chemical shift difference was 21.3 Hz and the coupling constant was 7.0 Hz. These values slowly altered to 10.8 and 8.4 Hz at −88°, and similar changes were observed at 100 MHz (see Table 2). No extra broadening of these lines, attributable to rate processes, was observed at any temperature. If it is assumed that the observed equilibrium is between two species, then eq. 1 is applicable (13),

$$[1] \qquad K = (P_1 - P_M)/(P_M - P_2)$$

where K is the equilibrium constant and P_1, P_2, and P_M refer to properties of conformations 1, 2, and their mixture, respectively. Reliable values of ΔS° and ΔH° may be obtained using the Eyring equation (eq. 2)

$$[2] \qquad \ln K = \frac{-\Delta H^0}{RT} + \frac{\Delta S^0}{R}$$

[4] $J_{H_1H_2}$ in conformationally stable *trans*-1,2-cyclohexanediol with both hydroxyl groups equatorial is ~9 Hz (12).

Can. J. Chem. Downloaded from www.nrcresearchpress.com by 210.87.254.40 on 09/05/12
For personal use only.

TABLE 2. Proton magnetic resonance spectral parameters for the *O*-methylene groups of compound **1**

Spectrometer frequency	Temperature (°)	J_{AB} (Hz)	$\Delta\nu_{AB}$ (Hz)
60 MHz	50	7.0	21.3
	27	7.1	20.3
	23	7.2	20.6
	3.5	7.4	18.9
	−4	7.4	18.6
	−24.5	7.7	17.4
	−26	7.7	16.9
	−36	7.8	15.6
	−56.5	8.0	14.8
	−61.5	8.2	12.3
	−88	8.4	10.8
100 MHz	40	7.0	33.5
	−5.5	7.3	29.2
	−31.5	7.6	27.3
	−51.5	7.7	23.5
	−81	7.9	18.2
	−84	8.0	18.3

but only if the data and the temperatures have a considerable range and are extremely accurate (13). For this procedure the four most accurate properties were chosen; these were the coupling constants and chemical shift differences at 60 and 100 MHz (Table 2). The approach used was to estimate P_1 and P_2, plot $\ln K$ against $1/T$, and then alter P_1 and P_2 repeatedly to maximize the correlation coefficient; it is assumed that the properties were temperature independent. The use of four different sets of data increased the reliability of the results which are presented in Table 3. The conformation favored above room temperature has the larger enthalpy (average ΔH° 2.1 kcal/mol) and larger entropy (average ΔS° 8.6 e.u.).

Discussion

Interpretation of the Variable Temperature Spectra

Temperature dependence of the p.m.r. spectra of **1** could, in theory, be due to changes in conformation either in the six-membered rings or the ten-membered ring. However, there is a considerable amount of evidence that, in nonpolar solvents, *trans*-1,2-cyclohexanediol (12), and its mono-*O*-acyl (14) and di-*O*-acyl (12) derivatives exist predominantly in the conformation with both substituents in equatorial orientations. The band widths of ~28 Hz observed below −50° for the H_α protons in the spectra of **1** are only consistent with conformational stability with the two H_α protons in each ring axial and anisochronous. At temperatures above coalescence one would expect a band width of approximately 13 Hz for a diequatorially substituted cyclohexane ring and approximately 7 Hz for the diaxial conformation; the observed values (13–15 Hz) indicate that the cyclohexane rings are conformationally stable having diequatorial substitution. The effect of temperature variation on the p.m.r. spectra of **1** will therefore be discussed in terms of changes in the 1,3,6,8-tetraoxecane ring.

Figure 1 shows a BCB conformation in which the three types of carbon atoms are indicated by I, II, and III; this numbering system will be used to indicate positions on a BCB conformation in the following discussion.

The variable temperature p.m.r. spectral properties observed for **1** are consistent with the processes pictured in Fig. 2. Interconversion of the degenerate sets of BCB conformations (BCB1 and BCB2 ⇄ BCB1′ and BCB2′) exchanges enantiotopic positions for the *O*-methylene protons but diastereotopic ones for the H_α protons. Hence slowing of this process ($\Delta G^\ddagger = 11.6$) would be apparent in the signals for the H_α protons but not in those for the *O*-methylene protons. Thus, interconversion of BCB1 and BCB2 is the equilibrium process reflected by changes of the latter signals over the entire temperature range and of the H_α signals below coalescence. The observed changes of the chemical shifts arise chiefly from the fact that the protons occupy disastereotopic positions in the BCB conformations in the equilibrium. The *O*-methylene carbons are of type III in BCB2 and of type II in BCB1; moreover, while one of the H_α protons in each cyclohexane ring retains the axial orientation at a type II carbon in both BCB1 and BCB2, the other proton has the axial orientation at a type I carbon in BCB2 and at a type III carbon in BCB1. A calculation of the maximum energy of activation possible for the equilibrium process was made by assuming that the protons with minimum chemical shift difference are interconverted and that coalescence occurs at a temperature 10° below that of the lowest temperature spectrum, and gave a value for $\Delta G^\ddagger$ of 8.7 kcal/mol. This result is clearly different from that of the process observed in the signals for the H_γ protons.

The variable temperature p.m.r. spectral parameters of the individual conformations are compatible with the equilibrium favoring BCB2 at room temperature and above, and BCB1 at the lower temperatures investigated. Figure 3 shows

Can. J. Chem. Downloaded from www.nrcresearchpress.com by 210.87.254.40 on 09/05/12
For personal use only.

TABLE 3. Parameters obtained for the equilibrium BCB1 ⇄ BCB2

Spectrometer frequency	Property studied	Values calculated for contributors P_1(Hz)	P_2(Hz)	$\Delta H°$ (kcal/mol)	$\Delta S°$ (e.u.)	r*
60 MHz	J_{AB}	8.8	6.4	2.4	9.5	0.993
	$\Delta\nu_{AB}$	7.0	25	2.4	10.2	0.991
100 MHz	J_{AB}	8.5	6.0	1.7	6.1	0.992
	$\Delta\nu_{AB}$	10	42	2.0	8.4	0.997

*The symbol r is the correlation coefficient for the final plot of ln K against $1/T$ using 11 points at 60 MHz and 6 points at 100 MHz.

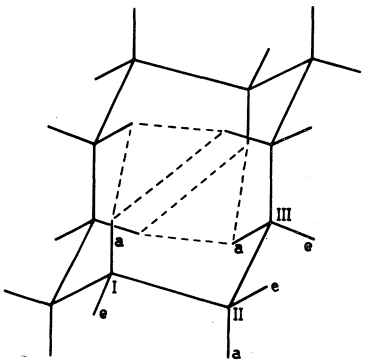

FIG. 1. The BCB conformation of cyclodecane; the numbers I, II, and III indicate the three different types of carbon atoms, and the letters (a) and (e) indicate axial and equatorial orientations. The dotted lines indicate high energy intraannular interactions.

Newman projection formulas depicting bonds from the *O*-methylene carbons in the conformations BCB1 and BCB2 and in two model compounds, namely, 1,3-dioxane and 1,3-dioxolane. In BCB1 each *O*-methylene group has the same relationship to the adjacent oxygens as in 1,3-dioxane but the two protons have opposite relationships when viewed from the two directions (see Fig. 3, formulas a). Hence for the *O*-methylene protons of BCB1, one would expect a small chemical shift difference but a geminal coupling constant decreased algebraically (15) from that in 1,3-dioxane (−6.2 Hz) (15, 16) because of the larger bond angles in the medium ring (15). For BCB2 one of the projection formulas is similar to that of 1,3-dioxane. In the other formula, the O—C—O—C dihedral angle approaches 180°; the effect of this arrangement on the chemical shift difference between the two protons of the *O*-methylene group would be expected to be small. Maciel *et al.* (17) have predicted from INDO calculations on methanol that such an arrangement would represent an effect on the magnitude of the geminal coupling constant approximately intermediate between the effects observed per oxygen atom in 1,3-dioxane and 1,3-dioxolane ($J \sim 0$ Hz) (15, 16). Thus for BCB2 a chemical shift difference approximately half that observed (18) in 1,3-dioxanes (17–40 Hz at 60 MHz) is predicted, namely, ~14 Hz at 60 MHz, while J_{gem} should be decreased algebraically from −4.6 Hz because of the larger bond angles in the medium ring (15). The observed chemical shift differences in BCB1 and BCB2 (see Table 3) are in agreement with these predictions in the relative order of magnitude but are approximately 9 Hz larger. The geminal coupling constants are also consistent with the equilibrium as described if the effects attributed to increase in bond angle were −2.3 to −2.6 Hz on BCB1 and −1.4 to −1.8 Hz on BCB2.

Qualitative evaluation of the thermodynamic parameters also gives support to the proposed scheme. In the most flexible region of the tetraoxecane ring of BCB1, each *O*-methylene group has a *gauche* interaction with each cyclohexane ring, thereby restricting the freedom of motion of the 10-membered ring and hence lowering the entropy. BCB2 has only two such interactions and should have the higher entropy as observed. Enthalpies are more difficult to evaluate. Each of the *gauche* type interactions referred to above can be evaluated as ~0.9 kcal/mol (19); on this basis alone the BCB2 conformation should be preferred by ~1.8 kcal/mol. However, in BCB1, all six of the high energy intraannular H—H interactions (1*c*, 2, 3) have been removed by oxygen substitution, while two remain in BCB2. In BCB1 the $ROCH_2OR$ fragments assume +synclinal, +synclinal (+*sc*, +*sc*) and −*sc*, −*sc* arrangements which have been shown (20) to be present in dimethoxymethane and calculated (21) to be 4.4 kcal/mol more stable than the synclinal, antiperiplanar arrangement in BCB2. From this information it could be predicted that BCB1 would

Can. J. Chem. Downloaded from www.nrcresearchpress.com by 210.87.254.40 on 09/05/12
For personal use only.

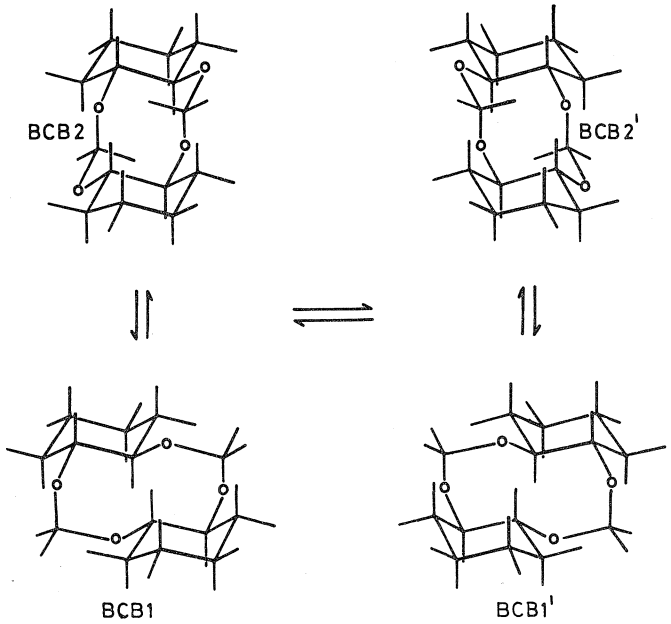

FIG. 2. The stable conformations of *trans-syn-trans*-4,5:9,10-biscyclohexano-1,3,6,8-tetraoxecane (**1**).

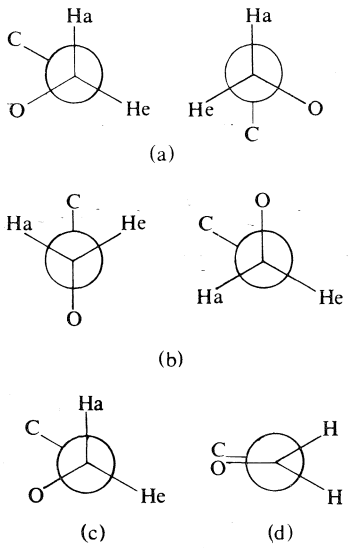

FIG. 3. Newman projection formulas depicting bonds from the *O*-methylene carbons in conformations BCB1 (*a*) and BCB2 (*b*) and in 1,3-dioxane (*c*) and 1,3-dioxolane (*d*).

be considerably more stable than BCB2 than by the 2.1 kcal/mol actually observed. The greater flexibility possible in BCB2 may allow it to distort so as to lower the energy of some of the interactions specified above. All of these points support the model proposed in which an equilibrium between BCB1 and BCB2 changes from favoring BCB2 at room temperature to favoring BCB1 below $-30°$.

Arguments similar to those above may also be applied to the third type of BCB conformation, which has diaxial substitution in both cyclohexane rings. Diaxial substitution in the cyclohexane ring would be of higher energy than diequatorial substitution (12, 14). In this BCB conformation all of the high energy intraannular H—H interactions (1*c*, 2, 3) are retained. In addition, the $ROCH_2OR$ fragments have the $+sc$, $-sc$ arrangement calculated (21) to be 5.5 kcal/mol above the $+sc$, $+sc$ situation present in BCB1. These considerations explain why no experimental evidence was obtained for this conformation.

Pathways of Conformational Interconversion

Fusion of the two cyclohexane rings to the tetraoxecane ring severely limits the number of potential conformational processes for the 10-membered ring. In this system, interconversion of the degenerate sets (see Fig. 2) cannot take place by a process described by Hendrickson (2) for cyclodecane. One way that it can occur is by the following pathway. BCB2 is converted, probably by an asymmetric route, to a CCC conformation (CCC1) which pseudorotates to a TCCC conformation in which the H_α protons become equivalent. Pseudorotation to the degenerate CCC conformation (CCC1′) in which *O*-methylene proton

Can. J. Chem. Downloaded from www.nrcresearchpress.com by 210.87.254.40 on 09/05/12
For personal use only.

Can. J. Chem. Downloaded from www.nrcresearchpress.com by 210.87.254.40 on 09/05/12
For personal use only.

positions are enantiotopic with respect to CCC1 is followed by conversion to BCB2′. The highest barrier for this process would probably be in BCB2 ⇄ CCC1 interconversions. Another possibility is that one of the cyclohexane rings inverts to the diaxial form, a route not inconsistent with the observed barrier of 11.7 kcal/mol. Inversion of a cyclohexane ring provides a number of conformational possibilities, none of which have been described by Hendrickson (2). Inversion of one of the cyclohexane rings, with the tetraoxecane ring in the BCB2 conformation, gives an asymmetric conformation (A1) which can transform into a form having C_2 symmetry with the dihedral angle description (2) of a TBCB conformation $(+\frac{--++}{--++}-)$;[5] in this case there is no plane perpendicular to the axis (compare ref. 2). Also, in this conformation, the H_α protons are equivalent. Transformation to the degenerate conformation (A1′), followed by cyclohexane ring inversion, gives BCB2′. A number of other pathways for interchanging diastereotopic H_α positions are also available, however, after the initial cyclohexane ring inversion. Some involve asymmetric forms, others involve forms having C_2 symmetry. An examination of models suggests that a few of these possibilities may be of similar or lower energy than the above route, but they will not be described in detail.

Hendrickson (2) has shown that the BCB conformations of cyclodecane pseudorotate through the LC conformation; the LC conformation has been calculated to be 24.6 kcal/mol higher in energy than a BCB. The strain energy in the LC conformation of cyclodecane arises chiefly from torsional and nonbonded interactions (2). In the case of compound **1**, the presence of the four oxygen atoms results in the loss of much of the torsional and nonbonded interactions, although electrostatic interactions are added. Thus, the possibility of a LC conformation as an intermediate in the pseudorotation of BCB1 and BCB2 must also be considered for **1**. It is of interest to note that another 10-membered ring, namely, 1,1-difluorocyclodecane, also interconverts BCB conformations by a pathway having a very low energy barrier (5.7 kcal/mol) (5). Noe and Roberts (5) have suggested methods of interconversion of the BCB conformations of this compound which, except for the asymmetric modes and the LC conformation, are not possible for the tetraoxecane BCB conformations.

The LC conformation can be considered to be the mid-point of an S_2 symmetric interconversion of the tetraoxecane BCB conformations (see Fig. 4 for an example of an S_2 symmetric conformation). This interconversion maintains the center of symmetry present in both BCB conformations and hence represents a new type of symmetric interconversion. Symmetric interconversions are normally of high energy because the processes chiefly involve changes in dihedral angles about one or two adjacent centers; however, S_2 symmetric interconversions may be of low energy because changes in dihedral angles occur about a number of centers (compare ref. 2), in the present case six. Symmetric interconversions in which S_n symmetry is maintained are possible for all conformations having this symmetry. For even-membered rings having crown conformations, an S_n symmetric process, when n is the number of atoms in the ring, represents the highest energy pathway, since it passes through a planar conformation. For other systems, this pathway can be of low energy. For example, interconversion of B and BB conformations of cyclooctane maintains S_4 symmetry and the intermediate, namely, the S_4 (2) or twist-boat (23) conformation, is of lower energy (2, 23) than the conformations being interconverted. Anderson *et al.* (23) have discussed

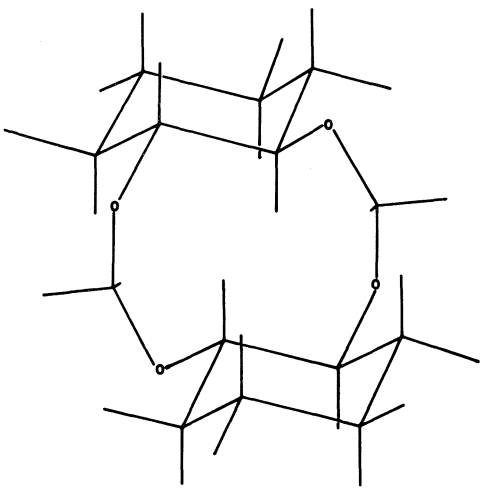

FIG. 4. An S_2 symmetric conformation of tetraoxecane **1**.

[5]Since this shorthand notation is somewhat deceptive in that it does not differentiate between dihedral angles, we prefer to use $a\frac{-b-c\ d\ e}{-b-c\ d\ e}-f$ for this conformation. A more informative, but more unwieldy, description uses the actual sizes of the dihedral angles (22).

this process in detail but not in these terms. Another example of a relatively low energy S_2 symmetric interconversion is the interconversion of CCC conformations of cyclodecane (2); in this case the TCCC is the pseudorotation partner of the CCC but represents the mid-way point on the S_2 interconversion of CCC conformations. It is possible that interconversion of other conformations, such as the D_4 or square conformation of cyclododecane (24, 25), may also occur by S_n pathways.

In the S_2 interconversion of BCB1 and BCB2, two OCOC dihedral angles at opposite ends of the tetraoxecane ring become 0° simultaneously; alternatively it is possible that this process occurs in two separate stages. If the latter is true for compound **1**, then the BCB conformations of 1,1-difluorocyclodecane may interconvert by a similar process.

Experimental

trans-syn-trans-4,5:9,10-Biscyclohexano-1,3,6,8-tetraoxecane (1)

This compound was prepared according to the procedure of Brimacombe *et al.* (26)[6] and had m.p. 164.5–165.5°; (lit. m.p. 166–167.5°).

Proton Magnetic Resonance Spectral Measurements

Proton magnetic resonance spectra were recorded at 60 MHz on a Varian A-60A or Bruker HX-60 spectrometer and at 100 MHz on a Varian HA-100 spectrometer. Measurements were made using 10% (w/v) solutions in chloroform-*d* – carbon disulfide (1:1, v/v) with tetramethylsilane (τ 10.00) as the internal standard on the A-60A or as the locking signal on the HX-60 and the HA-100 spectrometers. Chemical shift calibrations on the latter two machines were provided by an internal counter. Coupling constants and chemical-shift differences were determined at a sweep width of 0.2 Hz/cm. A methanol sample was used to calibrate the sample temperature on the Varian machines (error ±2°) while the probe thermocouple was used for temperature calibration on the Bruker HX-60 (error ±1°).

The authors are grateful to the National Research Council of Canada for its generous financial support of this work. They also wish to thank Professor Morton Raban of Wayne State University for his highly constructive suggestions. The counsel of Dr. J. F. Stoddart is also acknowledged. The 100-MHz spectra were recorded by one of us (T.B.G.) at the School of Chemical Sciences, University of East Anglia.

1. (*a*) J. D. DUNITZ. *In* Perspectives in structural chemistry. Vol. 2. *Edited by* J. D. Dunitz and J. A. Ibers. John Wiley and Sons, Inc., New York. 1968. p. 1; (*b*) G. SAMUEL and R. WEISS. Tetrahedron, **26**, 3005 (1970); (*c*) O. ERMER and J. D. DUNITZ. Chem. Commun. 178 (1971).
2. J. B. HENDRICKSON. J. Am. Chem. Soc. **89**, 7036, 7043, 7047 (1967).
3. M. BIXON and S. LIFSON. Tetrahedron, **23**, 769 (1967).
4. J. D. DUNITZ, H. ESER, M. BIXON, and S. LIFSON. Helv. Chim. Acta, **50**, 1572 (1967).
5. E. A. NOE and J. D. ROBERTS. J. Am. Chem. Soc. **94**, 2020 (1972).
6. W. E. WILLY, G. BINSCH, and E. L. ELIEL. J. Am. Chem. Soc. **92**, 5394 (1970); C. ROMERS, C. ALTONA, H. R. BUYS, and E. HAVINGA. *In* Topics in stereochemistry. Vol. 4. *Edited by* N. L. Allinger and E. L. Eliel. John Wiley and Sons, Inc., New York. 1969. p. 39.
7. E. L. ELIEL. Acc. Chem. Res. **3**, 1 (1970); F. G. RIDDELL. Quart. Rev. (London), **21**, 364 (1967); A. J. DE KOK and C. ROMERS. Rec. Trav. Chim. Pays-Bas, **89**, 313 (1970); K. PIHLAJA and S. LUOMA. Acta Chem. Scand. **22**, 2401 (1968).
8. T. B. GRINDLEY, J. F. STODDART, and W. A. SZAREK. J. Chem. Soc. (B), 172, 623 (1969); T. B. GRINDLEY. Ph.D. Thesis. Queen's University, Kingston, Ontario. 1970; J. F. STODDART and W. A. SZAREK. J. Chem. Soc. (B), 437 (1971).
9. J. DALE, T. EKLAND, and J. KRANE. J. Am. Chem. Soc. **94**, 1389 (1972); F. A. L. ANET and D. J. DEGEN. J. Am. Chem. Soc. **94**, 1390 (1970).
10. T. B. GRINDLEY, J. F. STODDART, and W. A. SZAREK. J. Am. Chem. Soc. **91**, 4722 (1969).
11. R. J. KURLAND, M. B. RUBIN, and W. B. WISE. J. Chem. Phys. **40**, 2426 (1964).
12. J. R. CAMPBELL. Ph.D. Thesis. Queen's University, Kingston, Ontario. 1969.
13. G. GOVIL and H. J. BERNSTEIN. J. Chem. Phys. **47**, 2818 (1967); H. JOSHUA, R. FANS, and K. MISLOW. J. Am. Chem. Soc. **90**, 4884 (1968).
14. R. W. WRIGHT and R. H. MARCHESSAULT. Can. J. Chem. **46**, 2567 (1968).
15. A. A. BOTHNER-BY. Adv. Magn. Res. **1**, 195 (1965); R. C. COOKSON, J. J. FRANKEL, J. HUDEC, and T. A. CRABB. Tetrahedron, Suppl. No. 7, 355 (1966); R. CAHILL, R. C. COOKSON, and T. A. CRABB. Tetrahedron, **25**, 4681, 4711 (1969).
16. M. ANTEUNIS, G. SWAELENS, and J. GELAN. Tetrahedron, **27**, 1917 (1971).
17. G. E. MACIEL, J. W. MCIVER, JR., N. S. OSTLUND, and J. A. POPLE. J. Am. Chem. Soc. **92**, 4151 (1970).
18. K. PIHLAJA and P. AYRAS. Acta Chem. Scand. **24**, 531 (1970).
19. G. MANN. Tetrahedron, **24**, 6495 (1968).
20. E. E. ASTRUP. Acta Chem. Scand. **25**, 1494 (1971).
21. G. A. JEFFREY, J. A. POPLE, and L. RADOM. Carbohydr. Res. **25**, 117 (1972).
22. J. D. DUNITZ. Pure Appl. Chem. **25**, 495 (1971).
23. J. E. ANDERSON, E. S. GLAZER, D. L. GRIFFITH, R. KNORR, and J. D. ROBERTS. J. Am. Chem. Soc. **91**, 1386 (1969).
24. J. D. DUNITZ and H. M. M. SHEARER. Helv. Chim. Acta, **43**, 18 (1960).
25. F. A. L. ANET, A. K. CHENG, and J. J. WAGNER. J. Am. Chem. Soc. **94**, 9250 (1972).
26. J. S. BRIMACOMBE, A. B. FOSTER, B. D. JONES, and J. J. WILLARD. J. Chem. Soc. (C), 2404 (1967).

[6]The *trans-syn-trans* configuration was unequivocally assigned to this compound in a recent study in this laboratory (10).

Can. J. Chem. Downloaded from www.nrcresearchpress.com by 210.87.254.40 on 09/05/12
For personal use only.

The Reaction of Chlorine Monoxide with Cyclohexene. A Molecule Induced Homolysis Reaction[1]

DENNIS D. TANNER, NESTOR NYCHKA, AND TAMEICHI OCHIAI[2]

Department of Chemistry, University of Alberta, Edmonton, Alberta

Received February 22, 1974

DENNIS D. TANNER, NESTOR NYCHKA, and TAMEICHI OCHIAI. Can. J. Chem. **52**, 2573 (1974).

The reaction of chlorine monoxide with cyclohexene at $-20°$ in the dark was found to proceed by an addition reaction to yield *trans*-2-chlorocyclohexyl hypochlorite. Concomitant with the addition, a molecule induced homolysis reaction of the chlorine monoxide occurs with cyclohexene to produce a number of free radical substitution and addition products, as well as products possibly arising from ionic addition reactions. Induced halogenation was found with added cyclohexane.

DENNIS D. TANNER, NESTOR NYCHKA et TAMEICHI OCHIAI. Can. J. Chem. **52**, 2573 (1974).

On a trouvé que la réaction du monoxyde de chlore avec le cyclohexène à $-20°$ dans l'obscurité conduit par une réaction d'addition à l'hypochlorite du chloro-2 cyclohexyl-*trans*. Simultanément à l'addition une réaction homolytique induite par la molécule permet au monoxyde de chlore de réagir avec le cyclohexène pour fournir un certain nombre de produits de substitution radicalaires et d'additions de même que des produits provenant possiblement de réactions d'addition ioniques. En présence de cyclohexane on a trouvé des réactions d'halogénation induites. [Traduit par le journal]

Can. J. Chem. Downloaded from www.nrcresearchpress.com by 210.87.254.42 on 09/05/12
For personal use only.

Introduction

The photoinitiated reaction of carbon tetrachloride solutions of chlorine monoxide with saturated alkanes has been shown to be a free radical chain halogenation having the overall stoichiometry: $2RH + Cl_2O \rightarrow 2RCl + H_2O$. The mechanism of the reaction has been proposed to proceed through a mixed chain (Scheme 1) involving OCl, (*a*), and chlorine and/or hydroxy radicals, (*b*), as the chain-propagating species (1).

(*a*)
$$RH + \cdot OCl \rightarrow R\cdot + HOCl$$
$$R\cdot + Cl_2O \rightarrow RCl + \cdot OCl$$
$$2HOCl \rightleftarrows H_2O + Cl_2O$$

(*b*)
$$RH + Cl\cdot \rightarrow R\cdot + HCl$$
$$HCl + HOCl \rightleftarrows HOH + Cl_2$$
$$R\cdot + Cl_2 \rightarrow RCl + Cl\cdot$$

and/or
$$RH + \cdot OH \rightarrow R\cdot + HOH$$
$$R\cdot + HOCl \rightarrow RCl + \cdot OH$$

SCHEME 1

The reaction was found to be thermally initiated slowly in the dark at 40°.

$$Cl_2O \rightarrow Cl\cdot + \cdot OCl$$

The overall reactivity of the reagent, with saturated alkanes, was found to be similar to that of *t*-butyl hypochlorite (1) and an obvious extension of the investigation of its reactions with organic materials was an investigation of its reactivity with unsaturated hydrocarbons.

Results

The addition of a carbon tetrachloride solution of chlorine monoxide to a large excess of cyclohexene at 40 to $-20°$ resulted in an instantaneous reaction; no color due to chlorine monoxide ever developed in the solutions. The reaction was spontaneous and exothermic at $-20°$ in the absence of light. Addition of atmospheric oxygen did not appear to qualitatively inhibit the rate of the reaction. The titer for active halogen dropped on initial mixing to 31% and after 20 h was still 27% of the titer of the starting chlorine monoxide. Analysis and isolation of the resultant products from the reaction mixtures after titration showed, in addition to water, both addition and substitution products, accounting for all of the chlorine initially added as chlorine monoxide, (see Table 1). Karl–Fischer titration of reactions carried out at ambient temperature showed 0.50 ± 0.03 mol of water were produced for every mole of chlorine monoxide. The minor products (**5–9**) were present in amounts large enough to detect and identify by a comparison

[1]Taken in part from the M.Sc. thesis of Nestor Nychka, University of Alberta, 1969.

[2]University of Alberta Postdoctoral Fellow, 1973–1974.

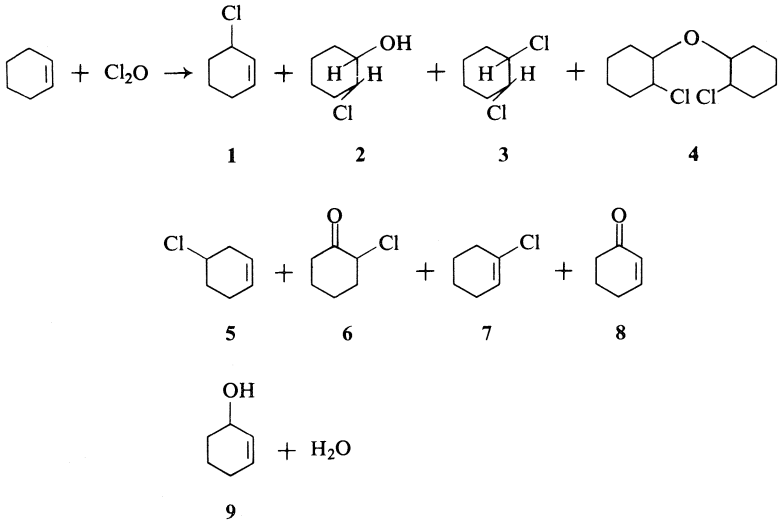

TABLE 1. Products of the dark reaction of cyclohexene with chlorine monoxide in carbon tetrachloride[a]

Products	Yield (mol/mol of Cl_2O[b])
3-Chlorocyclohexene (**1**)	0.79 ±0.01
trans-2-Chlorocyclohexanol (**2**)	0.53 ±0.02
trans-1,2-Dichlorocyclohexane (**3**)	0.082±0.008
2,2′-Dichlorocyclohexyl ether (**4**)	0.115
4-Chlorocyclohexene (**5**)	0.026±0.012
2-Chlorocyclohexanone (**6**)	0.027±0.009
1-Chlorocyclohexene (**7**)	0.01
2-Cyclohexenone (**8**)	0.027±0.007
2-Cyclohexenol (**9**)	0.040±0.009
Unidentified products	0.056
Remaining active halogen[c]	0.272

[a]The reactions of 0.3 *M* chlorine monoxide with cyclohexene (1:10 mol ratio) were carried out at −20°.
[b]Errors reported are deviations from the average values obtained from three or more independent experimental determinations. The product yields are those determined after titration for active halogen.
[c]Since no color for Cl_2O was detectable, the active halogen was presumably in the form of the alkyl hypochlorite (ROCl), **10**.

of their g.l.p.c. retention times (two columns) with those of authentic materials but were present in amounts too small to isolate. One of the minor products, 4-chlorocyclohexene, was not only identified by its g.l.p.c. retention time (three columns) but its mass spectrum was shown to be identical to that of an authentic sample. Compound **6**, 2-chlorocyclohexanone, was found (g.l.p.c.) to react with 2,4-dinitrophenylhydrazine when the reaction mixture was shaken with that reagent. Small amounts of other products, designated as unidentified products in Table 1, were shown by g.l.p.c. to be present in the reaction mixture. Some of these unidentified products decomposed slowly at room temperature to give increasing amounts of products **8** and **9**. No *cis*-1,2-dichlorocyclohexane, *cis*-2-chlorocyclohexanol, cyclohexanol, or cyclohexene oxide were detected as products.

Since the dichlorocyclohexyl ether has four centers of substitution, seven stereoisomers are possible. No stereochemical characterization of the ether products was attempted; it was noted, however, that analysis by g.l.p.c. showed the ether products to be composed of at least three isomers.

Aqueous solutions of hypochlorous acid were used to synthesize authentic samples of *trans*-2-chlorocyclohexanol, **2**. When aqueous hypochlorous acid was allowed to react with carbon tetrachloride solutions of cyclohexene (−20°, dark), not only was the expected major product, **2**, found but lesser amounts of **1**, **3**, **4**, and **5** were also produced.

When cyclohexane was added to the cyclohexene before its reaction with chlorine monoxide, induced halogenation of the saturated material accompanied the reaction of the unsaturated olefin. The yield of cyclohexyl chloride formed in these induced halogenations was diminished by the addition of molecular oxygen (see Table 2).

When the ratio of initially added cyclohexene to chlorine monoxide was varied from 3.5:1 to 35:1 the yield of three of the major products (**2**–**4**) remained relatively constant while the yield of 3-chlorocyclohexene, **1**, increased with increased olefin concentration. The yield of **1**

Can. J. Chem. Downloaded from www.nrcresearchpress.com by 210.87.254.42 on 09/05/12
For personal use only.

Can. J. Chem. Downloaded from www.nrcresearchpress.com by 210.87.254.42 on 09/05/12
For personal use only.

TABLE 2. The production of chlorocyclohexane during the reaction of chlorine monoxide with cyclohexane in the presence of cyclohexene[a]

Concentration (relative amounts)			Yield (mol yield $C_6H_{11}Cl$/mol Cl_2O)	
C_6H_{12}	C_6H_{10}	Cl_2O	Degassed	Not degassed
9.3	2	1.0	0.05±0.005 (0.06)[b]	
9.2	1	1.0	0.059±0.004 (0.14±0.02)[b]	
9.1	0.4	1.0	0.14±0.02	
9.2	0.4	1.0	0.13	0.08
9.3	0.2	1.0	0.10	
9.1	0.017	1.0	0.21±0.06	0.076±0.016
10	—	1.0	0.063±0.018	0.006±0.001

[a]All reactions were quenched immediately after mixing at −20°. Experimental deviations are from two independent experiments.
[b]Values in parenthesis were obtained after 20-h reaction at −20°.

obtained under these conditions was decreased by the addition of molecular oxygen, (see Table 3).

Discussion

The apparently spontaneous reaction of chlorine monoxide with cyclohexene was similar to other chlorination reactions with reagents capable of undergoing both free radical and ionic addition reactions with unsaturated hydrocarbons (2,3). The major product 3-chlorocyclohexene, **1**, has long been recognized as being the product of both ionic addition and free radical substitution (4). The formation of 4-chlorocyclohexene, **5**, however, was indicative of a free radical substitution process, since no ionic pathway to its formation is available (2). Further substantiation of the radical nature of the major portion of the reaction was obtained by observing the effect of molecular oxygen on the relative rates of formation of the four major products (**1**–**4**), see Table 3. The yield of the major product 3-chlorocyclohexene was markedly reduced by the presence of oxygen and it could be inferred that its formation, at least in part, was the result of a free radical chain chlorination which was inhibited by oxygen. A free radical chain chlorination process for the reaction of chlorine monoxide with cyclohexene (−20°) was firmly established by observing the facile induced chlorination of added cyclohexane, a reaction which itself only proceeds slowly by a free radical path with this reagent, see Table 2.

The observation that the rate of free radical substitution of cyclohexane (see Table 2) was dependent upon the concentration of added cyclohexene was indicative of a molecule induced initiation reaction. Molecule induced homolyses have been shown to occur in the liquid phase dark chlorination of olefins with molecular chlorine (2). In the molecular chlorine chlorination of cyclohexene it was demonstrated that the products **1**, **3**, **7**, and **5** were formed by competitive ionic and free radical paths whose relative importance could be modified by molecular oxygen. The addition of cyclohexane, as in the case of chlorine monoxide, led to induced halogenation. The free radical chain chlorination was found to be dependent upon the concentration of the cyclohexene. The dependence of the radical path on the concentration of the olefin was interpreted as being due to an initiation step which had a greater than first order dependence

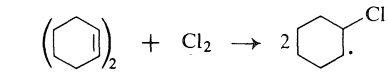

on cyclohexene. A similar type of initiation process has been proposed to explain the spontaneous dark halogenation reactions of *t*-butyl hypochlorite and hypobromite with styrene and 2-butyne (3).

Thermodynamic arguments have been presented to justify the proposal that the formation of radicals directly from the reactants would overcome the activation energy necessary for the homolysis of the halogenation reagent (2,3). By analogy, a dissociation energy, D(Cl—OCl), equal to 21.7–25.1 kcal/mol (5) could be overcome by the interaction of chlorine monoxide with cyclohexene to form radicals in an exo-

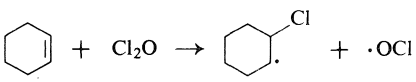

thermic process.[3] A reaction which is bimolecular in olefin would be even more highly exothermic.[4]

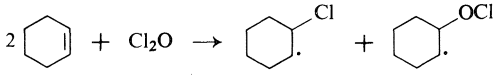

[3]The enthalpy for addition of a chlorine atom to cyclohexene has been estimated by Poutsma (2) to be −26 kcal/mol. The enthalpy for the initiation reaction can be calculated for the reaction of chlorine monoxide and cyclohexene to be exothermic $\Delta H = (D(\text{ClO—Cl}) - 26) = -1$ to -4 kcal/mol.

[4]The enthalpy for the reaction for the addition of OCl· to cyclohexene can be estimated at > 26 kcal/mol since generally D(R—Cl) < D(R—OH). The trimolecular process would be exothermic by > 27 to 31 kcal/mol since two radicals are formed in the process.

TABLE 3. Distribution of major products (>4%) from the reaction between cyclohexene and chlorine monoxide at various olefin concentrations (−20°, dark, CCl_4 solvent)

Mol excess of cyclohexene[a]	Products (mol/mol Cl_2O)[b]			
	1	2	3	4
3.5, degassed	0.59	0.50	0.11	0.194
10, degassed	0.79±0.01	0.53±0.02	0.082±0.008	0.115
10, not degassed	0.38±0.03	0.53±0.02	0.105±0.01	0.124
35, degassed	0.95±0.05	0.50±0.03	0.063±0.006	0.092
35, not degassed	0.66±0.09	0.50±0.03	0.078±0.026	0.105

[a]Mol excess with respect to Cl_2O. Reactions were carried out in degassed ampoules or ampoules containing atmospheric amounts of oxygen (not degassed).
[b]Errors are deviations from the mean of at least three independent experiments.

It can be seen in Table 3 that as the olefin concentration increased the production of **1** was also steadily increased, suggesting that the radical production of **1** involved an initiation step that is higher than first order in olefin.

The observation that the initial titer for active halogen fall to 31% upon mixing and remains relatively constant for 20 h, militates for the formation of a positive halogen species which can coexist under the reaction condition with large amounts of cyclohexene. Since the color of chlorine monoxide immediately fades on mixing and since both molecular chlorine and hypochlorous acid react rapidly with cyclohexene under the reaction conditions; the secondary hypochlorite from the addition of chlorine monoxide to the olefin appears to be a candidate for the active halogen containing compound.

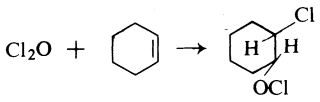

10

Some evidence that the secondary hypochlorite, **10**, is a product of the reaction can be obtained by an examination of the reaction products after titration. The formation of *trans*-2-chlorocyclohexanol, **2**, as a major product found after titration can be rationalized as arising at least in part from the reductive hydrolysis of **10**. The formation of **2** has also been shown to arise from the addition of hypochlorous acid (formed as the product from the homolytic reactions of chlorine monoxide) to cyclohexene and would also be formed from the homolytic halogenation reactions of **10** as well. The amount of **2** arising from **10** after hydrolysis must be at least equal to the titer for active halogen. The ether, **4**, derived from the addition of **10** to cyclohexene, is proposed to arise from the free radical reaction of the reactants since after mixing the titer for active halogen remains even in the presence of a large excess of cyclohexene and therefore precludes a rapid ionic pathway.

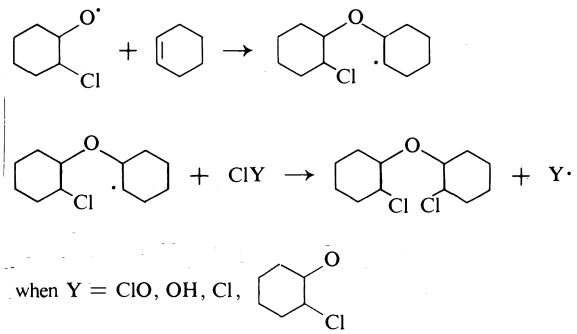

Ether formation from hypochlorite addition to olefins has precedent in the free radical reactions of *t*-butyl hypochlorite, where as high as 17% addition accompanies allylic substitution (6). Chloroethers and 1,2-dichlorides, analogous to 1,2-dichlorocyclohexane, **3**, are also formed in the molecule induced homolytic reaction of *t*-butyl hypochlorite with styrene and disubstituted acetylenes (3).

The formation of 2-chlorocyclohexanone, **6**, is likewise easily rationalized on the basis of intermediate **10**, since carbonyl compounds are the major products from the radical decomposition of primary and secondary alkyl hypochlorites (7–9).

A schematic summary of the reactive pathways described which accounts for >96% of the reaction products is given in Scheme 2.

Can. J. Chem. Downloaded from www.nrcresearchpress.com by 210.87.254.42 on 09/05/12
For personal use only.

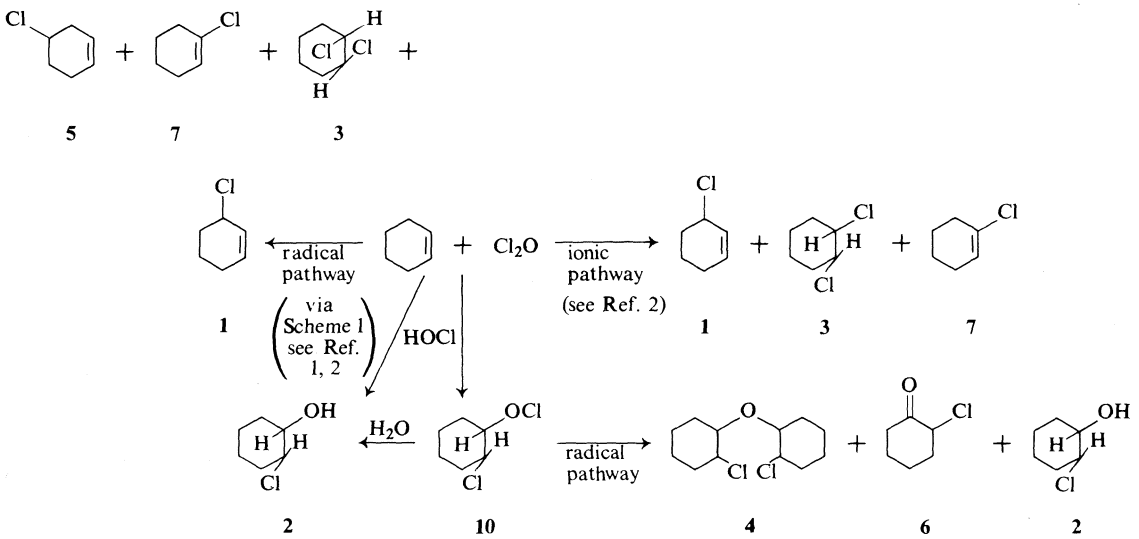

SCHEME 2

Experimental

Materials

Phillips 66 research grade (99.94 mol%) cyclohexene was used without purification; its purity was checked by g.l.p.c. "Freon 112" (tetrachlorodifluoroethane) was distilled through an 18 in. column containing glass helices and the middle fraction collected. Carbon tetrachloride was distilled from phosphorus pentoxide. Cyclohexane was spectroquality reagent grade (Matheson, Coleman, and Bell) and its purity checked by g.l.p.c. before use. Chlorine monoxide was prepared and analyzed as described previously (1). Concentrations of chlorine monoxide from 0.15 to 0.5 *M* were used in the reactions. Aqueous solutions of hypochlorous acid, free of chlorine monoxide and molecular chlorine, were prepared as previously reported (1). All glassware was chromic acid washed, rinsed with ammonia, then water, and dried before use.

Reaction Procedure

In most reactions, 2 ml of a carbon tetrachloride solution of chlorine monoxide (0.3 *M*) were degassed, in the absence of light, in a Pyrex breakseal containing a degassed sample of cyclohexene above the breakseal. The sealed ampoule was then put into a covered −20° bath of glycol–water for at least 15 min and allowed to equilibrate in the dark. The seal was broken with the aid of a teflon covered stirring bar contained within the ampoule and the ampoule inverted to let the chlorine monoxide solution run into the cyclohexene at −20° in the dark. The solution became cloudy and colorless as soon as the chlorine monoxide came in contact with the cyclohexene. The ampoules were kept at −20° prior to analysis. Undegassed ampoules contained atmospheric amounts of oxygen.

Analysis

Analysis of the products from the reaction of chlorine monoxide with cyclohexene was carried out by gas chromatography (g.l.p.c.) on an Aerograph Model 1520-B chromatograph utilizing the flame ionization detector and matrix programmer. All of the products, with the exception of **4**, were analyzed using a 10 ft 0.125 in. polypropylene glycol (PPG) column (40–145°). By use of an internal standard, "Freon 112", the absolute amounts of products **1**–**3** were determined using calibration plots of area ratios *vs.* mol ratio for the standard *vs.* the authentic samples.

The yield of **4** was obtained relative to **3** using a 10 ft 0.125 in. NPGS column (70–200°).

The reaction mixtures containing cyclohexane with added amounts of cyclohexene were frozen with liquid nitrogen, and quenched with acidified potassium iodide solution immediately after mixing at −20° in the dark. Analysis of the reaction mixture was done by g.l.p.c. utilizing a 10 ft 1/4 in. column packed with Apiezon N, 5%, on Chromosorb P. The analysis was carried out using a thermal conductivity detector. The analysis for cyclohexyl chloride was quantitated using an external standard, *o*-dichlorobenzene, and standard calibration curves were used to determine absolute amounts.

Product Identification

Most of the products were identified by comparing their g.l.p.c. retention times with those of authentic samples. The columns used for comparison of retention times were at least one of the columns mentioned previously (PPG and/or NPGS) and a 10 ft 0.125 in. SE-30 (Methyl) column.

Compounds **1**, **3**, and **5** were further identified by comparing their mass spectra with those of commercial samples. Due to their small amounts, the compounds were analyzed by an AEI MS12 mass spectrometer coupled to a Varian Aerograph series 1200 chromatograph fitted with a 10 ft 0.125 in. PPG column.

*trans-2-Chlorocyclohexanol (**2**)*

The compound was isolated from a reaction mixture by distillation through a spinning band column (50° at

Can. J. Chem. Downloaded from www.nrcresearchpress.com by 210.87.254.42 on 09/05/12
For personal use only.

25 mm); the infrared spectrum displayed a strong band at 3400 cm^{-1} and was identical to that of a commercial sample and the same as reported by Stevens and Grummitt (10).

Anal. Calcd. for $C_6H_{11}OCl$: C, 57.37; H, 7.97. Found: C, 57.33; H, 8.01.

2,2'-Dichlorocyclohexyl Ether (4)

A reaction mixture was distilled under vacuum, 60°/20 mm. The residue was subjected to column chromatography on silica gel (chloroform–benzene).

The fraction containing mainly (**4**) was purified by vacuum distillation by collecting the fraction that distilled at 90–91°/0.1 mm. Analysis by g.l.p.c. showed the fraction to contain at least three compounds. The chromatogram showed a major sharp peak followed by a smaller broad peak composed of at least two compounds in the ratio of 7:3, respectively. Since four isomers of the ether are possible, it is reasonable to assume that the purified fraction of compound **4** contains these isomers.

Anal. Calcd. for $C_{12}H_{20}OCl_2$: C, 57.37; H, 7.97. Found: C, 57.24; H, 7.79.

Also consistent with the formula was the mass spectrum. The exact mass by a mass spectrum was 250.0891 (Calcd. 250.0892) and a pattern of three peaks in the ratio of 9:6:1 at the parent peak was indicative of the presence of two atoms of chlorine in the molecule. The infrared spectrum of compound **4** shows a broad ether band at 1095 cm^{-1} and no carbonyl or alcohol bands. The n.m.r. spectrum shows two broad multiplets at 6.3 and 8.2 in the ratio of 1:4, respectively. This is comparable to the n.m.r. spectrum of *trans*-2-chlorocyclohexanol which shows peaks at 5.65, 6.4, and 8.4 in the ratio of 1:2:8, respectively.

2-Chlorocyclohexanone (6)

An authentic sample of the material displayed the same retention times as a sample obtained from the reaction. The material in the reaction mixture was consumed (g.l.p.c. analysis) when the reaction mixture was shaken with an acidified solution of 2,4-dinitrophenylhydrazine. An infrared spectrum of the reaction mixture displayed an absorption band at 1720 cm^{-1}, consistent with that of **6**.

Other products

Two products in the reaction mixture of cyclohexene – chlorine monoxide were identified as 2-cyclohexenone (**8**) and 2-cyclohexenol (**9**) by comparison of retention times with commercial samples. These compounds (**8** and **9**) were always present when the mixture was analyzed, although their areas varied with cyclohexene concentrations. The areas of these two peaks were greatest for undegassed reactions. The peaks also increased if the reaction mixture remained at room temperature for any period of time.

Gas–liquid partition chromatographic retention times of authentic materials were used to establish the absence of *cis*-2-chlorocyclohexanol, cyclohexanol, cyclohexene oxide, *cis*-1,2-dichlorocyclohexane, and chlorocyclohexane.

Hypochlorous Acid Reaction

The reaction of hypochlorous acid with cyclohexene was carried out in a degassed ampoule with a tenfold excess of cyclohexene in carbon tetrachloride and reacted *via* a break seal as described earlier. The ampoules were put in a −20° bath and shaken vigorously during the course of reaction. Vigorous shaking of the mixture prevented the aqueous solution from freezing during reaction. After two minutes, 25% of the hypochlorous acid still remained and after five minutes the reaction was at least 95% complete. After 10 min of shaking at −20° in the dark, the reaction mixture showed less than one percent titer (greater than 99% reaction). Analysis of the mixture by g.l.p.c. showed the presence of a number of the products present in the cyclohexene – chlorine monoxide reaction. The main product was the chlorohydrin (**2**). Compounds **3** and **4** were present in equal amounts (about 25% of **2**) and compounds **1** and **5** were also present; together they made up about 10% of the total. The ratio of **1**:**5** was about 2:1.

The authors wish to thank the National Research Council of Canada and the University of Alberta for their generous support of this work.

1. D. D. Tanner and N. Nychka. J. Am. Chem. Soc. **89**, 121 (1967).
2. M. L. Poutsma. J. Am. Chem. Soc. **87**, 2161 (1965).
3. C. Walling, L. Heaton, and D. D. Tanner. J. Am. Chem. Soc. **87**, 1715 (1965).
4. R. C. Fahey. Topics in Stereochemistry. Vol. 3. Interscience Publishers, New York, N.Y. 1968. pp. 273–274.
5. J. I. Wallace and C. F. Goodeve. Trans. Faraday Soc. **27**, 648 (1931). P. Gunther and K. Wekus. J. Phys. Chem. A, **145**, 193 (1931).
6. C. Walling and W. Thaler. J. Am. Chem. Soc. **83**, 3877 (1961).
7. E. L. Jenner. J. Org. Chem. **27**, 1031 (1962).
8. C. Walling and A. Padwa. J. Am. Chem. Soc. **85**, 1597 (1963).
9. R. Fort and L. Denivelle. Bull. Soc. Chim. Fr. 1109 (1954).
10. H. C. Stevens and O. Grummitt. J. Am. Chem. Soc. **74**, 4876 (1952).

Can. J. Chem. Downloaded from www.nrcresearchpress.com by 210.87.254.42 on 09/05/12
For personal use only.

Radiation-sensitized Thermal Cracking of *n*-Butane. I. Radical Reactions

SHINGO MATSUOKA[1]

Central Research Laboratory, The Furukawa Electric Co., Ltd., 2-9-15, Futaba, Shinagawa-ku, Tokyo, Japan

TAKAAKI TAMURA AND KEICHI OSHIMA

Department of Nuclear Engineering, Faculty of Engineering, University of Tokyo, Bunkyo-ku, Tokyo, Japan

AND

YUNOSUKE OSHIMA

Japan Atomic Energy Research Institute, Takasaki Research Establishment, Watanuki-cho, Takasaki-shi, Gunma-ken, Japan

Received July 4, 1973[2]

SHINGO MATSUOKA, TAKAAKI TAMURA, KEICHI OSHIMA, and YUNOSUKE OSHIMA. Can. J. Chem. **52**, 2579 (1974).

The radiolysis of *n*-butane was investigated at temperatures ranging from 17 to 548 °C in both static and flow systems.

It was concluded that in the radiation-sensitized thermal cracking region the main products, methane, ethane, ethylene, and propylene, were formed by a radical chain mechanism. The conclusion was reached from comparison with the thermal cracking products, the effect of ammonia addition, the dose rate dependence, and in particular the correlation between the temperature change of the type of the main chain-termination reaction and that of the activation energy of propylene formation. The value of the activation energy for propylene formation showed that the main chain-termination reaction at temperatures between 410 and 520 °C was a combination reaction of ethyl radicals. The major part of 1-butene, *trans*-2-butene, and *cis*-2-butene, formed in the chain region, was shown to result from the thermal decomposition of the chain carrying butyl radicals.

Rate parameters for some of the reactions involved were calculated.

SHINGO MATSUOKA, TAKAAKI TAMURA, KEICHI OSHIMA et YUNOSUKE OSHIMA. Can. J. Chem. **52**, 2579 (1974).

On a examiné la radiolyse du butane à des températures allant de 17 à 548 °C dans des systèmes statiques et continus.

On en conclut que les produits principaux obtenus dans la région de craquage thermique sensibilisé par les radiations (méthane, éthane éthylène et propylène), se forment par un mécanisme radicalaire en chaîne. On arrive à cette conclusion par comparaison de ces résultats avec ceux obtenus lors du craquage thermique de même qu'en examinant l'effet de l'addition d'ammoniaque, la dépendance de la vitesse sur la dose de radiation et en particulier par une corrélation entre le type de réaction principale de terminaison de chaîne suivant la température et l'énergie d'activation de formation du propylène. La valeur de l'énergie d'activation pour la formation du propylène montre que la réaction principale de terminaison de chaîne à des températures entre 410 et 520 °C est une réaction de combinaison des radicaux éthyles. On a démontré qu'une proportion importante du butène-1 et butène-2 *trans* et *cis* formés dans la région de la réaction en chaîne, résulte d'une décomposition thermique des radicaux butyles propageant la chaîne.

On a calculé les paramètres de vitesse de quelques unes des réactions impliquées.

[Traduit par le journal]

Introduction

Radiation-sensitized thermal cracking (r.t.c.) of hydrocarbons was first studied by Lucchesi *et al.* (1) and has been followed by many others (2–13) mainly from the point of view of industrial interest.

In these reports, it was shown that in the temperature range of about 350–450 °C, there exists an r.t.c. region giving high *G*-values of decomposition, 10^2–10^6, even though thermal cracking (t.c.) does not proceed at significant rate in this temperature range. However, an unequivocal answer to the question whether r.t.c. results in the same product composition as t.c. or not is not yet obtained. Topchiev (2) observed a marked increase in the olefin content of the C_2–C_4 prod-

[1]Present address: Japan Atomic Energy Research Institute, Takasaki Research Establishment, Watanuki-cho, Takasaki-shi, Gunma-ken, Japan.

[2]Revision received March 26, 1974.

Can. J. Chem. Downloaded from www.nrcresearchpress.com by 210.87.254.105 on 09/05/12
For personal use only.

Can. J. Chem. Downloaded from www.nrcresearchpress.com by 210.87.254.105 on 09/05/12
For personal use only.

ucts from the gas phase r.t.c. of *n*-heptane, compared with that from t.c., but other authors reported no significant difference between r.t.c. and t.c. in product distributions (1, 5, 9).

In order to explain the existence of the r.t.c. region and the similarity of the products from r.t.c. with t.c., Lucchesi *et al.* proposed a radiation-initiated radical chain mechanism similar to the well-known radical chain mechanism for t.c. of paraffins (14). But there seems to exist some ambiguity in their experimental results so that it is not possible to conclude definitely that the distribution of products obtained by r.t.c. is the same as that by t.c. Pereverzev *et al.* (11) also inferred from the effect of nitric oxide additive that the r.t.c. of propane proceeded via a radical chain mechanism, though there is again some ambiguity because it is known that nitric oxide reacts not only with radicals but also with some ions (15). The authors who reported the significant difference in the product composition between r.t.c. and t.c. did not give explanations (2, 3).

Thus there has been no thorough investigation of the reaction mechanism of r.t.c. of hydrocarbons, and the present study was carried out in order to clarify the reaction mechanism of r.t.c. of *n*-butane.

On the other hand, Freeman and co-workers carried out a detailed study of r.t.c. of ethers and alcohols using γ-radiation, and have established the usefulness of the r.t.c. technique to obtain information about the chain reactions that occur in pyrolysis systems in general (16–18).

Experimental

Radiation Source

Irradiations were performed with a 1.5 MeV collimated electron beam from a Hitachi Cockcroft–Walton type accelerator.

Materials

Takachiho GR ethylene was used after being passed through a molecular sieve 3A column to remove traces of water. Gas chromatographic analysis showed that hydrocarbon impurities having higher boiling points than ethylene were less than 1 p.p.m. A mixture of *n*-butane and isobutane, purchased from Suzuki Shokan Co., was passed through concentrated sulfuric acid and aqueous sodium hydroxide solution, and rectified to obtain pure *n*-butane. The *n*-butane was then dried with molecular sieve 4A and degassed. Hydrocarbon impurities in the *n*-butane were below the detection limit of the gas chromatography; that is, isobutane, butenes, and 1,3-butadiene were less than 0.1, 1, and 1 p.p.m., respectively. Takachiho GR propylene was also rectified, dried, and degassed. The propylene after purifications contained 15 p.p.m. propane as impurity. Matheson GR ammonia (99.99%) was used without treatment.

Irradiation Cells and Apparatus

Experiments were carried out in both static and flow systems. In the static experiments, flame baked Pyrex cylindrical cells (16.5 mm i.d. and 105 mm long) with about 0.3 mm thick electron admission windows were filled with hydrocarbon gas and additives, if added, and were sealed, according to the conventional methods. In the flow experiments, a quartz irradiation cell or a copper cell with a 0.04 mm thick stainless steel window was used. The copper cell was treated before use at 410 °C for 2 h with hydrogen gas stream.

Irradiation apparatus is shown in Fig. 1. The temperature of the cell was automatically controlled within ±1 °C for t.c. and ±2 °C for r.t.c., over the whole length of the cell. In the static experiments, the cells were placed in the preheated furnace for 10 min before irradiation. The quartz and the copper cells used in the flow experiments had both sufficiently long pre-heating tubes. Thus the gas attained the desired temperature before reaction. Tube 6 in Fig. 1, packed with magnesium ribbons and heated to 240 °C, was used to remove traces of dissolved oxygen, which was shown to strongly affect the thermal reaction (19). The gas stream line consisted of stainless

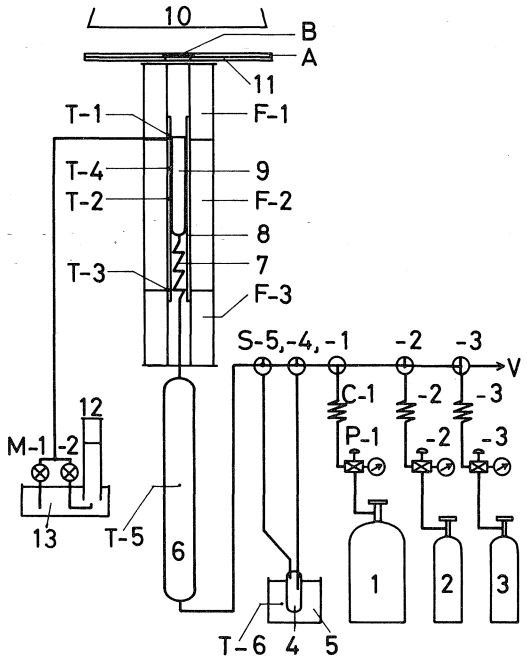

FIG. 1. Apparatus for r.t.c. of *n*-butane in flow system *1*, *n*-butane; *2,3*, additive gases; *4*, liquid additive; *5*, water bath; *6*, heated tube packed with magnesium; *7*, pre-heater; *8*, nickel plated copper sheath; *9*, copper (or quartz) reactor; *10*, accelerator; *11*, asbestos plate; *12*, measuring cylinder; *13*, water solution bath; *A*, aluminum plate; *B*, aluminum foil; *C*-1 to *C*-3, capillary restrictors; *F*-1 to *F*-3, electric furnaces; *M*-1, *M*-2, magnetic valves; *P*-1 to *P*-3, pressure regulators with gauges; *T*-1 to *T*-6, thermocouples; *S*-1 to *S*-5, three-way glass cocks.

TABLE 1. Columns used for gas chromatographic separations

Column	Length (m)	Temperature (°C)	Separated products
Packed column (4 mm i.d.)			
Porapack Q	3	r.t.‡	H_2, (CH_4, C_2H_4)
Capillary column (0.25 mm i.d.)			
DNBM*	50	0	C_3–C_6, (C_7, C_8)
ODPN†–DNBM(63–37 wt%)+DNBM	50+25	25	C_1–C_4, (C_5, C_6)
Squalane	25	25	C_5–C_8

*DNBM = di-*n*-butylmaleate.
†ODPN = β,β′-oxidipropionitrile.
‡r.t. = room temperature.

steel pipe, glassware, and Kovar pipe for connection. For sampling, the effluent gas was collected in a measuring cylinder by replacing sodium chloride saturated water solution. The dissolution phenomena of hydrocarbon gases into the solutions were carefully examined and in our experiments the error caused by dissolution was negligible.

Dosimetry

The absorbed dose rate in *n*-butane, D, was determined from the electron beam current, I, collected by the 4 mm thick aluminum plate A in Fig. 1, according to the following relation.

$$D = f_M k_c I$$

where k_c is a coefficient to convert I to the corresponding absorbed dose rate in ethylene, and f_M is the ratio of the stopping power of *n*-butane to that of ethylene for 1.5 MeV electrons. The coefficient k_c was determined for each cell with ethylene dosimetry since the thickness of window was slightly different from cell to cell. For the static experiments, the absorbed dose in ethylene was calculated based on $G(H_2) = 1.31$(20). For the flow experiments, the acetylene yield of $G(C_2H_2) = 2.45$, which was determined in our static experiments on the basis of $G(H_2) = 1.31$, was used to calculate the absorbed dose in ethylene, though some discrepancies were found in acetylene yields between the reported values (20, 21) and ours. The product yields from the *n*-butane–additive mixtures were calculated on the basis of the energy absorbed only in the *n*-butane.

Analysis

All products were analyzed by gas chromatography; for hydrocarbon measurements flame ionization detectors were used and for hydrogen a thermal conductivity detector. Gas chromatographic columns and their relevant data are listed in Table 1. Products separated by di-*n*-butylmaleate column and by β,β′-oxidipropionitrile-di-*n*-butylmaleate column were identified by use of known compounds, checking relative retentions. Sixty-five pure hydrocarbons between C_1–C_6 were used for identification. Relative retentions on squalane column were obtained from the literature (22, 23).

Accuracy of analysis was better than ±5% with the exception of some minor products.

Results and Discussion

In Fig. 2, the relative dose rate in the cell is plotted as a function of distance from the electron admission window. The dose rate was obtained by measuring the change in transmittance (at 655 nm) of Avisco Blue Cellophane (24).

Static Experiments

The effect of temperature on the radiolysis of *n*-butane (density = 1.35×10^{-3} g/cc) and of *n*-butane with 20 mol% ammonia (density of *n*-butane = 1.1×10^{-3} g/cc) was studied at temperatures from 17 to 421 °C. The dose rate averaged over the length of the cell was 1.17×10^{18} eV/g s. The absorbed dose was varied between 3.10×10^{19} and 3.41×10^{20} eV/g, correspond-

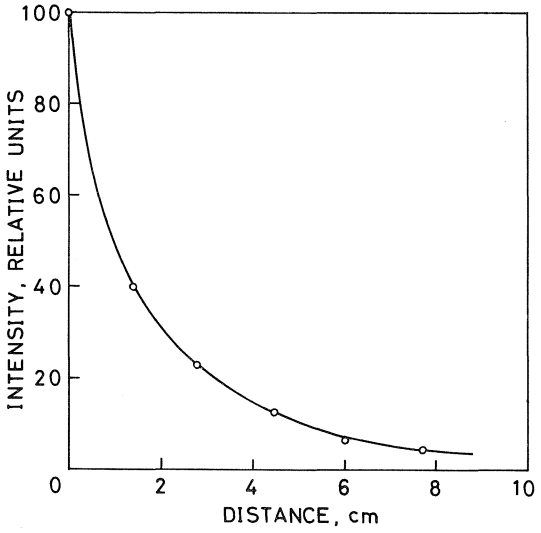

FIG. 2. Relative radiation intensity as a function of distance from the electron admission window.

Can. J. Chem. Downloaded from www.nrcresearchpress.com by 210.87.254.105 on 09/05/12
For personal use only.

Can. J. Chem. Downloaded from www.nrcresearchpress.com by 210.87.254.105 on 09/05/12
For personal use only.

TABLE 2. Comparison of the product distributions obtained by t.c., r.t.c., and r.t.c. with 20 mol% ammonia addition at 421 °C (unit = mol%)

Product	Radiation-thermal cracking	Radiation-thermal cracking (NH_3)	Thermal cracking
H_2	1.48	1.72	0.70
CH_4	36.1	36.9	37.0
C_2H_6	12.1	11.7	12.2
C_2H_4	12.3	12.3	12.8
C_3H_6	35.3	35.7	36.4
1-C_4H_8	0.35	0.37	0.22
trans-2-C_4H_8	0.37	0.31	0.30
cis-2-C_4H_8	0.23	0.19	0.18
The other products	1.73	0.79	0.20

ing to reaction temperature. The conversion was in the range between 0.10 and 2.00%.

Mechanism of Radiation-sensitized Thermal Cracking

The main products formed in the r.t.c. region, where chain reactions proceed, were methane, ethane, ethylene, and propylene, which were in accordance with those formed by the thermal cracking (t.c.). In Table 2, the product distributions obtained by t.c., r.t.c., and r.t.c. with ammonia addition at 421 °C are compared with each other. In the static experiments above 350 °C, some thermal cracking of samples occurred during the time of preheating and the irradiation yields reported were corrected for the contribution of thermal cracking; the maximum correction amounted to 15% at 421 °C. As seen in Table 2, no difference in the main product distributions is observed between t.c. and r.t.c. The addition of 20 mol% ammonia which is well known to scavenge carbonium ions, alters neither the decomposition rate in the r.t.c. of *n*-butane (Fig. 3) nor the distribution of the main products.

In Fig. 3, Arrhenius plots of the yields of propylene from the radiolysis of *n*-butane with and without ammonia are shown. It can be seen that the value of activation energy for propylene formation in the r.t.c. region varies with temperature and is not constant as assumed by previous workers (1, 25). A similar phenomenon was reported by Hölein and Freeman (17) in the r.t.c. of diethylether, and they explained the phenomenon by the change of the type of termination reaction in the radical chain mechanism due to different temperature.

The following radical chain mechanism similar to that of thermal cracking (26) can be proposed for the main product formation in the r.t.c. of *n*-butane.

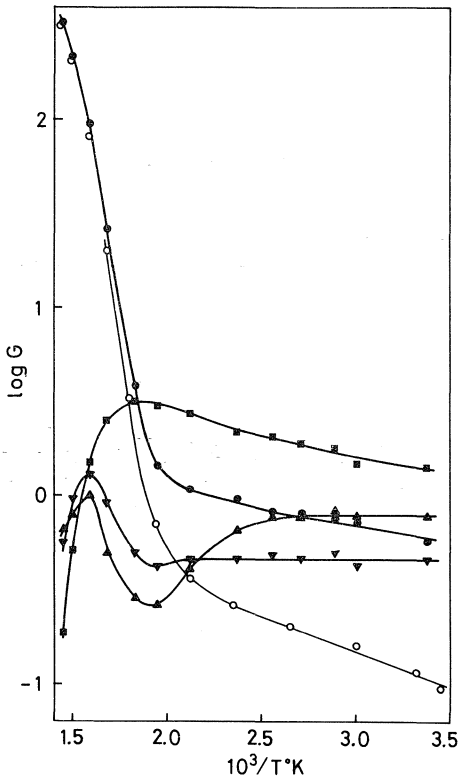

FIG. 3. Arrhenius plots of the yields of (●) propylene, (▲) 2-methylbutane, (▼) 3-methylpentane, and (■) octanes from the radiolysis of *n*-butane with 20 mol% ammonia, and of (○) propylene from the radiolysis of *n*-butane.

Initiation by radiation

[1] $C_4H_{10} \rightsquigarrow H$

[2] $\rightsquigarrow CH_3 \cdot$

[3] $\rightsquigarrow C_2H_5 \cdot$

[4] $\rightsquigarrow C_4H_9 \cdot$

Propagation

[5] $H + C_4H_{10} \rightarrow H_2 + C_4H_9 \cdot$

Can. J. Chem. Downloaded from www.nrcresearchpress.com by 210.87.254.105 on 09/05/12
For personal use only.

[6] $CH_3 \cdot + C_4H_{10} \rightarrow CH_4 + C_4H_9 \cdot$

[7] $C_2H_5 \cdot + C_4H_{10} \rightarrow C_2H_6 + C_4H_9 \cdot$

[8] $C_2H_5 \cdot + C_4H_{10} \rightarrow H + C_2H_4 + C_4H_{10}$

[9] $C_4H_9 \cdot \rightarrow H + C_4H_8$

[10] $C_4H_9 \cdot \rightarrow CH_3 \cdot + C_3H_6$

[10′] $s\text{-}C_4H_9 \cdot \rightarrow CH_3 \cdot + C_3H_6$

[11] $C_4H_9 \cdot \rightarrow C_2H_5 \cdot + C_2H_4$

[11′] $p\text{-}C_4H_9 \cdot \rightarrow C_2H_5 \cdot + C_2H_4$

Termination

[12] $C_4H_9 \cdot + C_4H_9 \cdot \rightarrow$ Products

[13] $C_4H_9 \cdot + C_2H_5 \cdot \rightarrow$ Products

[14] $C_4H_9 \cdot + CH_3 \cdot \rightarrow$ Products

[15] $C_2H_5 \cdot + C_2H_5 \cdot \rightarrow$ Products

[16] $CH_3 \cdot + C_2H_5 \cdot \rightarrow$ Products

[17] $CH_3 \cdot + CH_3 \cdot \rightarrow$ Products

In the radiolysis with ammonia addition, octane, 3-methylpentane, and 2-methylbutane may be formed solely by termination reactions 12, 13, and 14, respectively.[3] Arrhenius plots for these products are also given in Fig. 3. As the overall yield of the termination products does not vary with temperature in the temperature range where thermal initiation does not occur, from Fig. 3 we come to the following conclusions: termination reaction 12 predominates at temperatures below 330 °C; termination reactions 12, 13, and 14, in the neighborhood of 355 °C; and termination reactions 15, 16, and/or 17 above 390 °C. Without ammonia addition, similar temperature dependence curves of the yields of these combination products were obtained.

The rate equations of the chain formation of propylene, which were derived for the individual termination reactions 12–17 on the basis of the proposed mechanism, and their calculated activation energies are given in Table 3. Bodenstein's assumption of stationary state of radical concentrations was used in these derivations and in subsequent calculations. For the rate equations with termination reactions 13–17, the assumption of long chain length was also used. The following activation energies (in kcal/mol) from literature were used for the calculation of overall activation energies in Table 3 and in subsequent discussion: $E_6 = 8.3$ (27), $E_7 = 10.4$ (28), $E_{10} = 32.6$ (29), and $E_{11} = 28.7$ (30). Activation energy of termination reactions is assumed to be zero. The correlation between the type of termination

[3] *n*-Hexane and *n*-pentane were also produced by reactions 13 and 14, respectively. The yields were both 1/4–1/8 of those of the corresponding branched products.

TABLE 3. Rate equations of the radical chain formation of propylene and the calculated activation energies, for the individual termination reactions 12–17

Termination reaction	$v(C_3H_6)$*	E(kcal/mol)
12	$k_{10}\sqrt{\frac{K}{2k_{12}}}$	32.6
13	$k_{10}\sqrt{\frac{(k_7+k_8)KM}{2k_{11}k_{13}}}$	23.4
14	$k_{10}\sqrt{\frac{k_6KM}{2k_{10}k_{14}}}$	20.5
15	$k_{10}\frac{k_7M}{k_{11}}\sqrt{\frac{K}{2k_{15}}}$	14.3
16	$M\sqrt{\frac{k_6(k_7+k_8)k_{10}K}{2k_{11}k_{16}}}$	11.3
17	$k_6M\sqrt{\frac{K}{2k_{17}}}$	8.3

*K is the rate of initiation reaction and M is the density of *n*-butane.

and the value of the activation energy of the chain formation of propylene, which is shown in Table 3, is in good agreement with what is observed in Fig. 3.

In the neighborhood of 281 °C, where termination reaction 12 predominates, the rate for the chain formation of propylene in the irradiation cell is expressed as

$$[18] \quad v(C_3H_6) = \frac{1}{L}\int_0^L k_{10}\sqrt{\frac{K(x)}{2k_{12}}}\,dx$$

where L is the length of the cell, x is a longitudinal position in the cell, and $K(x)$ is the rate of initiation reaction at position x caused by radiation. $v(C_3H_6)$ and $K(x)$ are related to the experimental data as follows,

$$v(C_3H_6) = 10^{-2}\{G(C_3H_6) - G'(C_3H_6)\}\bar{I}MW/N_0$$

$$[19] \quad K(x) = 10^{-2}G(R\cdot)I(x)MW/N_0$$

where $G(C_3H_6)$ is the yield of propylene; $G'(C_3H_6)$ is the non-chain yield which is obtained by extrapolation of low temperature values of $G(C_3H_6)$; $G(R\cdot)$ is the G-value of radicals and is assumed to be 10; $I(x)$ is a dose rate at position x and $\bar{I}$ is the average dose rate, in eV/g s; M is the density of *n*-butane in mol/cc; W is the molecular weight of *n*-butane in g/mol; N_0 is Avogadro's number. $v(C_3H_6)$ and $K(x)$ can be determined from experimental data in Figs. 2 and 3. Substituting these values into eq. 18, one gets

$$k_{10}/\sqrt{k_{12}} = 3.1 \times 10^7 \exp(-32\,000/\mathrm{RT}) \quad \mathrm{mol}^{1/2}\mathrm{cc}^{-1/2}\,\mathrm{s}^{-1/2}$$

Lin and Laidler (29) calculated the similar rate parameter with azomethane-sensitized decomposition of *n*-butane, given by

$$k_{10'}/\sqrt{k_{12\text{-}1}} = 1.31 \times 10^8 \exp(-32\,600/RT) \quad \mathrm{mol}^{1/2}\,\mathrm{cc}^{-1/2}\,\mathrm{s}^{-1/2}$$

where $k_{12\text{-}1}$ is the combination rate constant of *s*-butyl radicals. Since the ratio of $k_{12}/k_{12\text{-}1}$ is 2.1 (31) and $k_{10}/k_{10'}$ is estimated to be 0.81 from Fig. 5, the agreement between our result and that of Lin and Laidler is quite good.

The chain length of r.t.c. can be obtained from Fig. 3, and at 421 °C the length is 42.

Figure 4 shows the dose rate dependence curves of the yields of various products. Dose rate was varied between 0.97–11.5 × 10^{17} eV/g s. The absorbed dose was in the range 1.16–3.46 × 10^{19} eV/g, and the conversion 0.90–1.09%. The yields of the main products depend on dose rate with order of −0.45. It is nearly equal to −0.5 which is derived from the radical chain mechanism (Table 3). The slight difference may be attributed to the insufficient chain length. The insensitivity of the yields of octane, 3-methylpentane, and 2-methylbutane to dose rate supports that they are termination products.

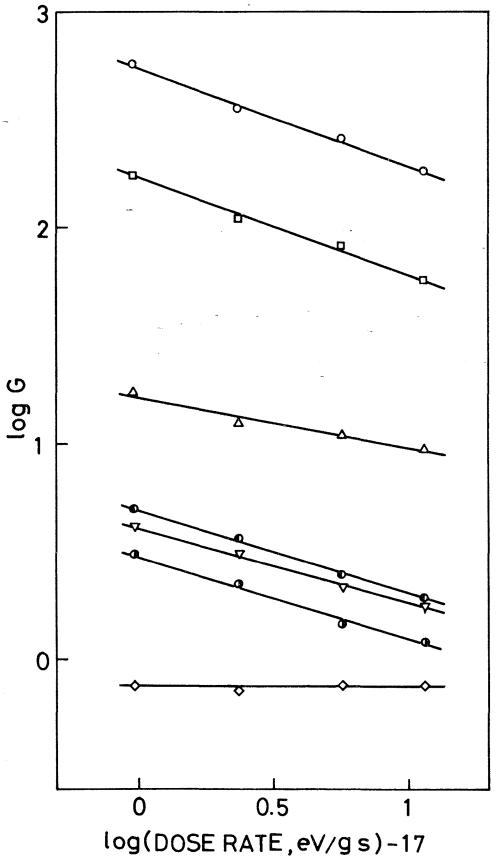

FIG. 4. Dose rate dependences of the yields of (○) methane, (□) ethane, (△) hydrogen, (▽) 1-butene, (◐) *trans*-2-butene, (◑) *cis*-2-butene, and (◇) 3-methylpentane, at 390 °C.

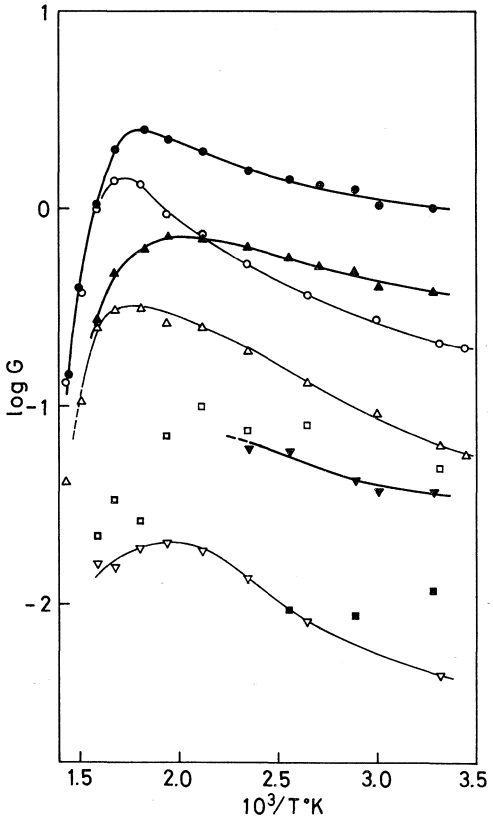

FIG. 5. Temperature dependences of the yields of the individual octanes; (○) 3,4-dimethylhexane, (△) 3-methylheptane, (▽) *n*-octane, and (□) the other octanes. Open and filled marks correspond to the yields in the absence and presence of 20 mol% ammonia, respectively.

Thus, several experimental results confirm that the main products from the r.t.c. of *n*-butane are produced by the radical chain mechanism.

Octane Formation

Lin and Laidler (29) studied the azomethane-sensitized thermal decomposition of *n*-butane at temperatures from 262 to 340 °C. They found 3,4-dimethylhexane and small amounts of hexane and pentane as termination products, but detec-

Can. J. Chem. Downloaded from www.nrcresearchpress.com by 210.87.254.105 on 09/05/12
For personal use only.

Can. J. Chem. Downloaded from www.nrcresearchpress.com by 210.87.254.105 on 09/05/12
For personal use only.

ted no measurable amounts of 3-methylheptane and *n*-octane. Their observations differ from ours. We found 3,4-dimethylhexane (3,4DiMHx), 3-methylheptane (3MHp), *n*-octane (*n*-Oct), and the other octanes as the octane products. The temperature dependences of these octane yields in the absence and the presence of ammonia are represented in Fig. 5. The other octanes are probably formed by ionic processes, since their yields were suppressed by the addition of ammonia. However, 3,4DiMHx, 3MHp, and *n*-Oct result mostly from the following radical combination reactions.

[12-1] $s\text{-}C_4H_9\cdot + s\text{-}C_4H_9\cdot \rightarrow$ 3,4DiMHx

[12-2] $s\text{-}C_4H_9\cdot + p\text{-}C_4H_9\cdot \rightarrow$ 3MHp

[12-3] $p\text{-}C_4H_9\cdot + p\text{-}C_4H_9\cdot \rightarrow n$-Oct

With the assumption that reactions 4, and 5–7 are the only steps leading to butyl radicals, the ratio of G(3,4DiMHx)/G(3MHp), denoted as α, is given by

$$[20]\qquad \alpha = \frac{G(3,4\text{DiMHx})}{G(3\text{MHp})} = \frac{k_{12\text{-}1}[s\text{-}C_4H_9\cdot]}{k_{12\text{-}2}[p\text{-}C_4H_9\cdot]} = \frac{k_{11} + k_T[R\cdot]}{k_{10} + k_T[R\cdot]} \frac{k_{12\text{-}1}\{k_{4s} + (k_{5s}[H] + k_{6s}[CH_3\cdot] + k_{7s}[C_2H_5\cdot])\}[C_4H_{10}]}{k_{12\text{-}2}\{k_{4p} + (k_{5p}[H] + k_{6p}[CH_3\cdot] + k_{7p}[C_2H_5\cdot])\}[C_4H_{10}]}$$

where k_T is the rate constant for radical–radical reaction; $[R\cdot]$ is the overall concentration of radicals; subscripts s and p refer to s- and p-butyl radicals, respectively. The temperature dependence curves of α are given in Fig. 6. The apparent activation energies of α in the absence and the presence of ammonia are found to be -0.38 and -0.16 kcal/mol, respectively, at temperatures below 180 °C where the thermal decomposition of butyl radicals does not occur. These results suggest that the ratio of the s- to p-butyl radical concentration originating from reaction 4 is greater than the ratio from abstraction reactions 5–7, and that these ratios are independent of temperature. Since the contribution of the latter ratio increases with increasing temperature, the negative activation energies are observed. A decrease of the apparent activation energy with the addition of ammonia is ascribed to the increase of the contribution of reaction 5 as follows (32)

$$R^+ + NH_3 \rightarrow P + NH_4^+$$

$$NH_4^+ + e \rightarrow NH_3 + H$$

[5] $$H + C_4H_{10} \rightarrow H_2 + C_4H_9\cdot$$

Jackson *et al.* (33) obtained the activation energy of -1.75 kcal/mol for k_{6s}/k_{6p}, but this conflicts with the observed activation energies for α since considerable part of the octane yields can be ascribed to the formation of butyl radicals by reaction 6 and the subsequent combination reactions, as shown later.

Thus, the second term of the third equality in eq. 20 approaches an asymptotic value of 2.4 above the temperature at which the chain reaction sets in (Fig. 6). Therefore eq. 20 reduces to eq. 20-1 in the chain region.

$$[20\text{-}1]\qquad \alpha = 2.4\frac{k_{11} + k_T[R\cdot]}{k_{10} + k_T[R\cdot]}$$

Substituting into eq. 20-1 the measured values of α at temperatures above 350 °C (Fig. 6), where

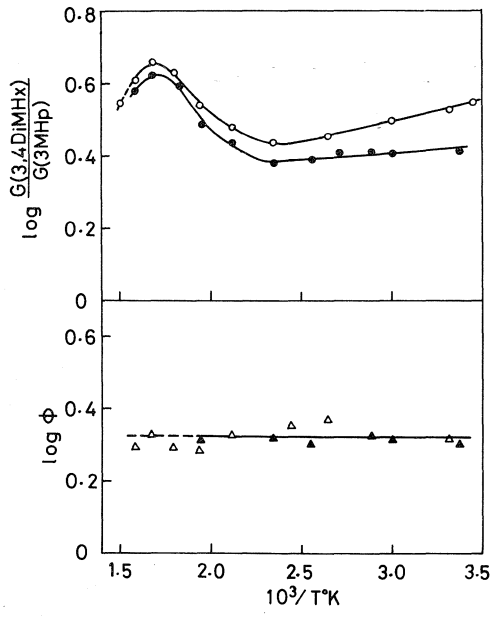

FIG. 6. Temperature dependence curves of G(3,4-DiMHx)/G(3MHp) and of ϕ. Open and filled marks correspond to those obtained in the absence and presence of 20 mol% ammonia, respectively.

$k_{11}, k_{10} \gg k_T[R\cdot]$, and using the literature value of $-E_{11} + E_{10} = 3.9$ kcal/mol, one gets

$$\frac{A_{11}}{A_{10}} = 7.2 \times 10^{-2}$$

This is comparable to the ratio

$$\frac{A_{11}\cdot A_{12\text{-}1}^{1/2}}{A_{10}\cdot A_{12\text{-}3}^{1/2}} = 6.1 \times 10^{-2}$$

which is calculated from literature (29, 30). Here A_i is the frequency factor of reaction i. With these rate parameters, eq. 20-1 explains the convexity of α shown in Fig. 6.

The temperature dependence curves of ϕ, which are defined by

$$\frac{k_{12\text{-}2}}{(k_{12\text{-}1}k_{12\text{-}3})^{1/2}} = \frac{G(3\text{MHp})}{(G(3,4\text{DiMHx})G(n\text{-Oct}))^{1/2}}$$

are also represented in Fig. 6. The value of ϕ is constant at 2.1 in the temperature range of 23–240 °C where it could be determined precisely. This value is close to 2, a value predicted by the simple collision theory of chemical kinetics.

Methane Formation

The effect of temperature on the yield of methane from the radiolysis of *n*-butane with ammonia is given in Fig. 7. In the temperature range between 85 and 220 °C, the methane yield increases with an apparent activation energy of 3.1 kcal/mol. This should be attributed not to the thermal decomposition of $C_4H_{10}^+$ ion (34) but to a hydrogen atom abstraction from *n*-butane molecule by the methyl radical as follows

[2] $\quad C_4H_{10} \quad CH_3\cdot$

[1]–[4] $\quad R\cdot$

[6] $\quad CH_3\cdot + C_4H_{10} \rightarrow CH_4 + C_4H_9\cdot$

[21-1] $\quad CH_3\cdot + R\cdot \rightarrow$ Products

[21-2] $\quad R\cdot + R\cdot \rightarrow$ Products

This mechanism leads to the following expression for the methane yield from reaction 6.

$$[22]\quad G_R(CH_4) = \frac{1}{L\bar{I}} \times \int_0^L \frac{G(CH_3\cdot)I(x)}{1 + \frac{k_{21\text{-}1}}{k_6 M}\sqrt{\frac{10^{-2}G(R\cdot)MWI(x)}{2k_{21\text{-}2}N_0}}}dx$$

Substituting the following values into eq. 22;

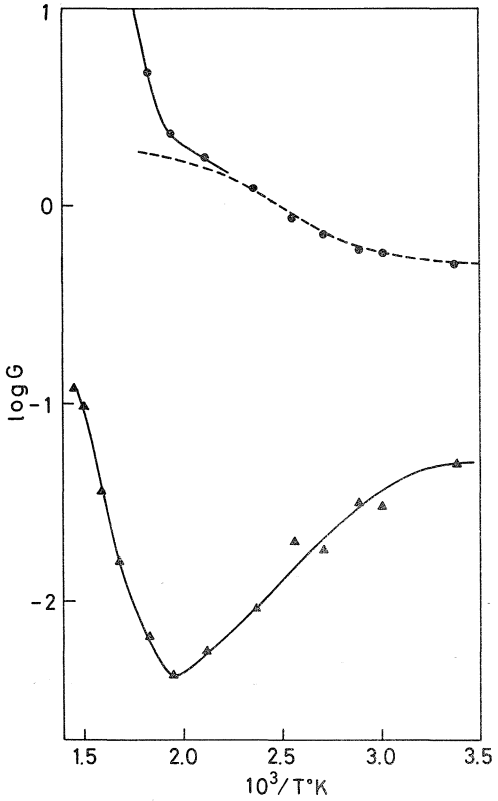

FIG. 7. Temperature dependences of the yields of (●) methane and (▲) isobutane from the radiolysis of *n*-butane with 20 mol% ammonia. Broken line shows a calculated one from eqs. 22 and 23.

$G(CH_3\cdot) = 1.5$ (assumed), $k_{21\text{-}1} = k_{21\text{-}2} = 10^{13}$ cc/mol s (assumed), $G(R\cdot) = 10$ (assumed), $k_6/\sqrt{k_{21\text{-}1}} = 1.56 \times 10^4 \exp(-8300/RT)$ cc$^{-1/2}$ mol$^{1/2}$ s$^{-1/2}$ (27), $M = 1.9 \times 10^{-5}$ mol/cc, $W = 58$ g/mol, $\bar{I} = 1.17 \times 10^{18}$ eV/g s, and $I(x)$ represented in Fig. 2; and integrating, we can calculate $G_R(CH_4)$.

Methane is also formed by reactions other than reaction 6, and this yield, $G_P(CH_4)$, is probably independent of temperature. Though the methane yield from disproportionation reaction 21-1 may show a temperature dependence since the methyl radical concentration decreases with increasing temperature up to about 220 °C, this contribution to $G_P(CH_4)$ is small. $G_P(CH_4)$ is estimated to be 0.5 from the total methane yield at room temperature, where reaction 6 does not proceed. Now we can calculate the total yield of methane at T °K, $G(CH_4)$, by

$$[23]\quad G(CH_4) = G_R(CH_4) + 0.5$$

Can. J. Chem. Downloaded from www.nrcresearchpress.com by 210.87.254.105 on 09/05/12
For personal use only.

TABLE 4. *G*-Values of the chain formation of propylene, and the measured activation energies in the individual temperature ranges (flow experiment)

Temperature (°C)	Thermal cracking $G_{tc}(C_3H_8)$	Radiation-thermal cracking $G_{rtc}(C_3H_8)$	Radiation-thermal cracking E(kcal/mol*)
316		18.2	
			28
356		84	
			23
386		192	
			20
410		326	
			14
445		530	
			14
474	46	770	
			13(12)
497	165	990	
			16(12)
522	560	1380	
			22
548	1520	2140	

*The values of activation energy in parentheses are corrected for the contribution of thermal initiation.

The dashed curve in Fig. 7 shows the results of eq. 23. The agreement between the calculated and the experimental curves is good. The deviation at high temperatures is due to the formation of methyl radicals by the chain reaction 10.

In the radiolysis with ammonia addition, 2-methylbutane and isobutane are formed by the combination of methyl radicals with *s*-butyl radicals and with *s*-propyl radicals, respectively. The yields of these products decrease with increasing temperature up to 220 °C (Fig. 3 and Fig. 7), corresponding to the increase in the methane yield. This confirms the participation of reaction 6 in this temperature range.

In the radiolysis without ammonia addition, the same methane increase was observed.

Flow Experiments

Radiation-sensitized Thermal Cracking at High Temperatures

The flow experiments on t.c. and r.t.c. of *n*-butane were carried out using the copper irradiation cell at temperatures from 316 to 548 °C and at a pressure of 1 atm. The dose rate averaged over the cell was 9.3×10^{17} eV/g s. The contact time was in the range 16.6–21.6 s, and the conversion in the range 0.078–5.0%.

The t.c. reaction of *n*-butane above 400 °C was reported to be 3/2-order with respect to *n*-butane concentration (35). In our experiments, the following 3/2-order rate constant for t.c. was obtained.

$$[24] \quad k_{tc} = 3.4 \times 10^{15} \times \exp(-59\,200/RT)\ \mathrm{cc}^{1/2}\ \mathrm{mol}^{-1/2}\ \mathrm{s}^{-1}$$

Though a small wall effect was observed in the butene formation at temperatures below 500 °C, this rate constant agrees well with that obtained by Sagert and Laidler (36) in a static system, as expressed in the equation

$$k_{tc} = 3.24 \times 10^{15} \times \exp(-59\,900/RT)\ \mathrm{cc}^{1/2}\ \mathrm{mol}^{-1/2}\ \mathrm{s}^{-1}$$

In Table 4, the chain yields of propylene from t.c. and r.t.c., and the activation energies of the propylene formation in r.t.c. in the individual temperature ranges are shown. For convenience, the propylene yield in t.c. is also represented by *G*-value, which was calculated as if the reactant had absorbed the same dose as in r.t.c. The sharp increase of the value of activation energy above 490 °C is due to the contribution of thermal initiation, and the values in parentheses are corrected for this contribution. Above 410 °C, the activation energy is between 14 and 12 kcal/mol. This corresponds to the termination reaction 15 as seen from Table 3; a slight lower value of 12 kcal/mol obtained at high temperatures is probably due to the build-up of the product propy-

Can. J. Chem. Downloaded from www.nrcresearchpress.com by 210.87.254.105 on 09/05/12
For personal use only.

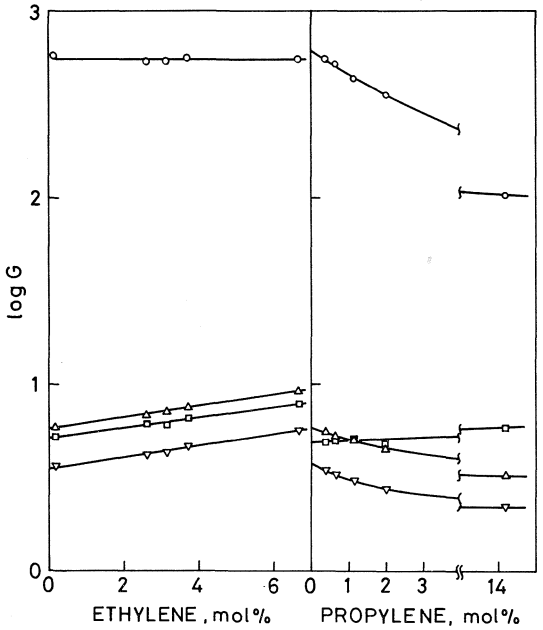

FIG. 8. Effect of the addition of ethylene and of propylene on the yields of (○) methane, (□) 1-butene, (△) *trans*-2-butene, and (▽) *cis*-2-butene at 449 °C.

lene which suppresses the decomposition rate of *n*-butane (Fig. 8).

Purnell and Quinn (26) indicated from the pressure effect on the activation energies for the formation of the major products that reaction 15 was a main chain-ending step in the t.c. of *n*-butane, but Torok and Sandler (35) predicted the predominance of reaction 17 from the calculation of reaction order. Our results give more direct information that the main termination reaction is reaction 15 at temperatures between 410 and 520 °C.

In t.c. and r.t.c., the chain yield of propylene, $G(C_3H_6)$, is proportional to square root of the initiation rate. With a proportionality constant k, $G(C_3H_6)$ is expressed as follows

$$G_{rtc}(C_3H_6) = \frac{1}{L}\int_0^L k\sqrt{K + K'}\,dx$$

$$G_{tc}(C_3H_6) = k\sqrt{K'}$$

where K and K' are the radiation and the thermal initiation rates, respectively. The measured values of $G_{rtc}(C_3H_6)$ and $G_{tc}(C_3H_6)$ at 548 °C (Table 4), together with K given by eq. 19, lead to $K' = 1.2 \times 10^{-10}$ mol/cc s at 548 °C.

The breakdown of *n*-butane into two ethyl radicals

[25] $n\text{-}C_4H_{10} \rightarrow C_2H_5\cdot + C_2H_5\cdot$

would be the most probable thermal initiation. Therefore

$$A_{25}\exp(-E_{25}/RT) = K'/2M = 4.2 \times 10^{-6}\ s^{-1} \text{ at } 548\ °C$$

where A_{25} is the frequency factor of reaction 25 and M is the density of *n*-butane. Using the measured activation energy of 59.2 kcal/mol for the t.c. of *n*-butane, E_{25} is calculated as

$$E_{25} = 2(59.2 + E_{11} - E_7 - E_{10}) = 90 \text{ kcal/mol}$$

Butene Formation

1-Butene, *trans*-2-butene, and *cis*-2-butene are generated as minor products in the t.c. of *n*-butane (26). These butenes were presumed to arise from a dehydrogenation reaction at the wall or from a small molecular component of the reaction (36), or from secondary reactions with the products (26). In the r.t.c. of *n*-butane, these butenes were also formed in nearly the same proportion of the total products as in t.c. (Table 2). Possible processes for the butene formation are as follows: (*a*) direct radiation reactions, (*b*) radical disproportionation reactions, (*c*) secondary reactions with the products, especially with olefins, (*d*) radical chain propagation reactions, (*e*) ionic chain reactions.

Dose rate dependence curves of the yields of hydrogen and of each butene, obtained at 390 °C in the static system, are shown in Fig. 4. If we assume that the *G*-values of hydrogen, 1-butene, *trans*-2-butene, and *cis*-2-butene, produced by the dose rate independent processes (*a*) and (*b*), are 5, 0.5, 0.4, and 0.2, respectively, the remaining yields of these products which can be attributed to the processes (*c*), (*d*), and/or (*e*), depend on dose rate with order of −0.39, −0.45, −0.45, and −0.44, respectively. These orders agree with that of the main products, −0.45. Furthermore, the hydrogen yield increased ($\Delta G(H_2) = 7.8$) by approximately the same amount as the sum of the butene yields increased ($\Delta G(1,2\text{-}C_4H_8) = 7.1$) as the dose rate was decreased from 11.5×10^{17} to 0.97×10^{17} eV/g s. Figure 8 shows the effects of the addition of ethylene and of propylene on the yields of methane and each butene, obtained at 449 °C in the flow system with the quartz reactor. The amount of olefin shown on the abscissa is the sum of the added olefin and the half of the product olefin. Small part of the bu-

Can. J. Chem. Downloaded from www.nrcresearchpress.com by 210.87.254.105 on 09/05/12
For personal use only.

tenes is seen to be formed by reactions with ethylene and propylene. But the yields of the butenes from secondary reactions with the product olefins amount to less than 20% of the total. The addition of ammonia has little effect on the butene formation.

From the facts described above, we may conclude that the major part of the butenes arises from the propagating radicals in the chain reactions as follows

[9] $$C_4H_9 \cdot \rightarrow H + C_4H_8$$

[5] $$H + C_4H_{10} \rightarrow H_2 + C_4H_9 \cdot$$

Thus, in the r.t.c. of *n*-butane at a temperature of 390 °C, a dose rate of 11.5×10^{17} eV/g s, and a conversion rate of 0.90%, 50–70% of the product butenes result from the decomposition of butyl radicals which are generated by the radical chain propagation process. In the t.c. of *n*-butane, reaction 9 may also occupy the major part of the butene formation when a conversion is low.

The authors would like to express their sincere thanks to Prof. Yoneho Tabata of the University of Tokyo for his helpful discussions and encouragement. The authors are also deeply indebted to Mr. Keiichi Yotsumoto and Mr. Hiromi Sunaga of Japan Atomic Energy Research Institute for their valuable assistance.

1. P. J. Lucchesi, B. L. Tarmy, R. B. Long, D. L. Baeder, and J. P. Longwell. Ind. Eng. Chem. **50**, 879 (1958).
2. A. V. Topchiev. Radiolysis of hydrocarbons. Elsevier Pub. Co., 1963. Amsterdam. p. 203.
3. L. S. Polak. Third United Nations International Conference on the Peaceful Uses of Atomic Energy. A/CONF. 28/P/389 USSR. 1964.
4. L. S. Polak, P. Ya. Glazunov, V. Ye. Glushenev, and G. G. Ryabchikova. Neftekhimiya, **5**, 706 (1965).
5. K. P. Lavrovskii, M. M. Florentzev, D. V. Makarov, V. B. Titov, Yu. N. Aleksenko, and Yu. L. Fish. Neftekhimiya, **7**, 580 (1967).
6. A. M. Brodskii, K. P. Lavrovskii, and V. B. Titov. Kinet. Katal. **4**, 337 (1963).
7. A. M. Brodskii, K. P. Lavrovskii, V. B. Titov, and A. Kh. Eglit. Dokl. Akad. Nauk SSSR, **159**, 1319 (1964).
8. A. M. Brodskii, K. P. Lavrovskii, V. B. Titov, and A. Kh. Eglit. Neftekhimiya, **5**, 134 (1966).
9. G. H. Miley and J. J. Martin. Am. Inst. Chem. Eng. J. 7, 593 (1961).
10. E. O. Guernsey, H. Shaw, and W. E. Smith. Am. Inst. Chem. Eng. J. **9**, 744 (1963).
11. A. E. Pereverzev, L. S. Polak, and N. Ya. Chernyak. Neftekhimiya, **8**, 537 (1968).
12. S. A. Gabsatarova and A. M. Kabakchi. Khim. Vys. Energ. **3**, 126 (1969).
13. G. M. Panchenkov and G. I. Zhuravlev. Zh. Fiz. Khim. **46**, 1438 (1972).
14. F. O. Rice and K. F. Herzfeld. J. Am. Chem. Soc. **56**, 284 (1934).
15. P. Ausloos, S. G. Lias, and R. Gorden, Jr. J. Chem. Phys. **29**, 3341 (1963).
16. H. J. van der Linde and G. R. Freeman. J. Am. Chem. Soc. **92**, 4417 (1970).
17. G. Höhlein and G. R. Freeman. J. Am. Chem. Soc. **92**, 6118 (1970).
18. K. M. Bansal and G. R. Freeman. Radiat. Res. Rev. **3**, 209 (1971).
19. I. Engel, A. Combe, M. Letort, and M. Niclause. Rev. Inst. Fr. Pet. **12**, 627 (1964).
20. G. G. Meisels. J. Chem. Phys. **41**, 51 (1964).
21. M. C. Sauer, Jr. and L. F. Dorfman. J. Phys. Chem. **66**, 322 (1962).
22. R. A. Hively and R. E. Hinton. J. Gas Chromatogr. **6**, 203 (1968).
23. D. H. Desty, A. Goldup, and W. T. Swanton. Gas chromatography. *Edited by* N. Brenner, J. E. Callen, and M. D. Weiss. Academic Press, New York. 1962. p. 162.
24. E. J. Henley and D. Richman. Anal. Chem. **28**, 1580 (1956).
25. S. Bywater and E. W. R. Steacie. J. Chem. Phys. **19**, 172 (1951).
26. J. H. Purnell and C. P. Quinn. Proc. R. Soc. Lond. A**270**, 267 (1962).
27. A. F. Trotman-Dickenson, J. R. Birchard, and E. W. R. Steacie. J. Chem. Phys. **19**, 163 (1951).
28. P. J. Boddy and E. W. R. Steacie. Can. J. Chem. **38**, 1576 (1960).
29. M. C. Lin and K. J. Laidler. Can. J. Chem. **45**, 1315 (1967).
30. W. E. Morganroth and J. G. Calvert. J. Am. Chem. Soc. **88**, 5387 (1966).
31. J. T. Gruver and J. G. Calvert. J. Am. Chem. Soc. **78**, 5208 (1956).
32. F. Williams. J. Am. Chem. Soc. **86**, 3954 (1964).
33. W. M. Jackson, J. R. McNesby, and B. deB. Darwent. J. Chem. Phys. **37**, 1610 (1962).
34. T. Miyazaki and S. Shida. Bull. Chem. Soc. Jap. **38**, 716 (1965).
35. J. Torok and S. Sandler. Can. J. Chem. **47**, 2707 (1969).
36. N. H. Sagert and K. J. Laidler, Can. J. Chem. **41**, 838 (1963).

Can. J. Chem. Downloaded from www.nrcresearchpress.com by 210.87.254.105 on 09/05/12
For personal use only.

Champ de force de valence et modes normaux de vibration de la glycylglycine et du monochlorhydrate monohydrate de glycylglycine

CHRISTIAN DESTRADE,[1] ELIANE DUPART, MONIQUE JOUSSOT-DUBIEN ET CHANTAL GARRIGOU-LAGRANGE

Centre de Recherche Paul Pascal, Domaine Universitaire, 33405 Talence, France

Reçu le 28 janvier 1974

CHRISTIAN DESTRADE, ELIANE DUPART, MONIQUE JOUSSOT-DUBIEN et CHANTAL GARRIGOU-LAGRANGE. Can. J. Chem. **52**, 2590 (1974).

Le champ de force de valence et les modes normaux de vibration de la glycylglycine forme α sont calculés à partir des spectres de vibration de dix dérivés isotopiques marqués sélectivement au deutérium ou à l'azote 15. On montre que ce champ de force permet de rendre compte des fréquences du monochlorhydrate de glycylglycine à l'état solide, composé présentant une structure très différente de celle de l'ion bipolaire. L'accord est particulièrement satisfaisant dans le cas des modes de vibration les plus sensibles à la conformation moléculaire. Il est donc possible d'utiliser ce type de calcul pour déterminer la conformation d'un oligopeptide.

CHRISTIAN DESTRADE, ELIANE DUPART, MONIQUE JOUSSOT-DUBIEN, and CHANTAL GARRIGOU-LAGRANGE. Can. J. Chem. **52**, 2590 (1974).

The valence force field and normal modes of vibration of α-glycylglycine have been calculated using the vibrational spectra of ten isotopic derivatives, selectively labeled with deuterium or nitrogen-15. It is shown that this force field permits the determination of the frequencies of glycylglycine-hydrochloride in the solid state, despite a structure very different from that of the zwitterion. The agreement is particularly satisfying for those modes of vibration most sensitive to molecular conformation. It is thus possible to use this type of calculation to determine the conformation of an oligopeptide.

Can. J. Chem. Downloaded from www.nrcresearchpress.com by 210.87.254.42 on 09/05/12
For personal use only.

Nous avons récemment mis au point une méthode permettant, au moyen d'un calcul de modes normaux de vibration, de déterminer avec précision la conformation d'un composé dans un état physique donné, et en particulier en solution aqueuse (1, 2). Nous avons testé cette technique sur un cas relativement simple, la glycine, molécule pour laquelle les modifications conformationnelles observées sont peu importantes ($150° < \psi < 180°$) (3–5). Notre objectif est d'essayer d'appliquer cette méthode à l'analyse structurale d'oligopeptides pour lesquels on sait que les angles dièdres ψ et ϕ peuvent varier de $-180°$ à $+180°$. Dans un premier temps, et c'est l'objet de cet article, il est nécessaire de déterminer de façon précise le champ de force d'un peptide simple, et de vérifier si ce champ de force permet de rendre compte de façon satisfaisante des spectres de vibration de deux composés de formule voisine mais de conformation différente, tels que la glycylglycine et son chlorhydrate.

On sait en effet que si les plans carboxylique et peptidique sont pratiquement confondus dans le cas de la glycylglycine forme cristalline α ($\phi_2 = -156.5°$) (6) ils sont presque perpendiculaires pour son chlorhydrate ($\phi_2 = -79.6°$) (7).

Effectuer un calcul de modes normaux de vibration suppose toujours au départ une excellente interprétation des spectres de vibration. Nous avons pour cela été amenés à synthétiser plusieurs dérivés deutériés sélectivement sur les différents groupements fonctionnels de la glycylglycine, ainsi que le dérivé marqué à l'azote 15 sur l'azote peptidique. La liste des composés que nous avons étudiés et les notations que nous avons utilisées pour les désigner sont données dans le tableau 1.

Méthode de synthèse

La méthode générale de synthèse employée utilise la réaction entre l'ester benzylique de la glycine (gly-OBzl) et le benzyloxycarbonyle de glycine CBz gly. Ces composés ont été préparés respectivement suivant les méthodes de Cipera et Nicholls (8) et de Bergmann et Zernas (9). Le couplage peptidique est réalisé par la *N,N*-dicyclohexyl carbodiimide (10). Le déblocage des fonctions terminales est effectué en une seule étape en utilisant HBr en milieu acétique (11).

Les différents dérivés isotopiques CD_2 de la

[1]A qui la correspondance sera adressée.

Can. J. Chem. Downloaded from www.nrcresearchpress.com by 210.87.254.42 on 09/05/12
For personal use only.

TABLEAU 1. Dérivés isotopiques de la glycylglycine que nous avons étudiés

$H_3\overset{+}{N}—CH_2—CONH—CH_2—COO^-$ (d_0)
$H_3\overset{+}{N}—CH_2—CO^{15}NH—CH_2—COO^-$ (d_0 ^{15}N)
$D_3\overset{+}{N}—CH_2—COND—CH_2—COO^-$ (d_4)
$D_3\overset{+}{N}—CH_2—CO^{15}ND—CH_2—COO^-$ (d_4 ^{15}N)
$H_3\overset{+}{N}—CD_2—CONH—CH_2—COO^-$ ($d_{2\alpha}$)
$H_3\overset{+}{N}—CH_2—CONH—CD_2—COO^-$ ($d_{2\beta}$)
$H_3\overset{+}{N}—CD_2—CONH—CD_2—COO^-$ ($d_{4\alpha\beta}$)
$D_3\overset{+}{N}—CD_2—COND—CH_2—COO^-$ ($d_{6\alpha}$)
$D_3\overset{+}{N}—CH_2—COND—CD_2—COO^-$ ($d_{6\beta}$)
$D_3\overset{+}{N}—CD_2—COND—CD_2—COO^-$ (d_8)

glycylglycine (tableau 1) ont été synthétisés en utilisant suivant le cas gly Bzl et CBz gly hydrogénés ou deutériés sur le carbone. Ces derniers composés ont été obtenus à partir de glycine CD_2 (enrichissement en deutérium de 95%) préparée suivant la méthode de Günther et Bonhoeffer (12). Pour la glycylglycine ^{15}N, nous avons utilisé gly OBzl ^{15}N (13) (enrichissement en ^{15}N de 96%).

(I) Interprétation des spectres de vibration de la glycylglycine et de son chlorhydrate à l'état solide

Les spectres infrarouge des glycylglycines α sont représentés sur la fig. 1, ceux des chlorhydrates sur la fig. 2; ils ont été enregistrés entre 4000 et 200 cm^{-1} à l'aide d'un spectromètre Perkin–Elmer 225 étalonné à l'aide de différents gaz de référence. La précision des lectures est de l'ordre de ± 1 cm^{-1} pour une bande fine. Le spectre Raman de la glycylglycine d_0 (fig. 3) a été réalisé à l'aide d'un spectromètre Raman Coderg type PH1 équipé d'un laser rouge He Ne. Sur les tableaux 2 et 3, nous avons reporté l'interprétation des glycylglycines d_0 et d_4;[2] nous centrerons la discussion sur le seul dérivé d_0.

L'attribution a été faite en utilisant la notion de vibration de groupe; dans le cas particulier du groupement CONH, les notations habituelles amide A et amide I à VII ont été conservées.

Les vibrations de valence ν(XH) n'étant pas influencées par la conformation, nous nous sommes intéressés uniquement à la région 1700–200 cm^{-1}; notons cependant la fréquence de la vibration amide A: 3288 cm^{-1} sur le spectre de la diglycine forme α et 3277 cm^{-1} pour son chlorhydrate.

(A) Analyse vibrationnelle de la glycylglycine forme α

L'attribution de l'ensemble des absorptions comprises entre 1700 et 1400 cm^{-1} se déduit très facilement de la comparaison avec les spectres de la glycine et du *N*-méthylacétamide (NMA); elle est donnée dans le tableau 2.

Région 1400–1200 cm^{-1}

Dans ce domaine doivent apparaître, outre la vibration amide III, les vibrations de groupe $w(CH_2)$ et $t(CH_2)$. Les trois mouvements étant susceptibles d'interagir les uns avec les autres, l'interprétation de cette région nécessite l'analyse préalable des dérivés deutériés sélectivement sur les carbones C_α ou C_β.

Dans le dérivé deutérié sur les carbones C_α et C_β ($d_{4\alpha\beta}$), une seule bande est observée à 1328.5 cm^{-1} (fig. 1); elle correspond sans ambiguité à la vibration amide III.

Le spectre infrarouge du dérivé $H_3\overset{+}{N}CD_2CONHCH_2COO^-$ ($d_{2\alpha}$) présente deux absorptions intenses à 1334 et 1298 cm^{-1} alors que l'on attend trois vibrations (amide III, $w(CH_2)_\beta$ et $t(CH_2)_\beta$). Le mouvement $t(CH_2)$ est en général situé autour de 1260 cm^{-1} (15); une faible absorption existe à cette fréquence, nous lui attribuons $t(CH_2)_\beta$. Dans le spectre du dérivé $D_3\overset{+}{N}CD_2CONDCH_2COO^-$ ($d_{6\alpha}$) n'apparaît qu'une absorption intense à 1313 cm^{-1}, il s'agit donc de $w(CH_2)_\beta$. On peut penser que les deux bandes à 1334 et 1298 cm^{-1} du dérivé $d_{2\alpha}$ sont dues aux mouvements amide III et $w(CH_2)_\beta$ en intéraction.

En ce qui concerne le dérivé $H_3\overset{+}{N}CH_2CONHCD_2COO^-$ ($d_{2\beta}$), on attend dans le domaine de fréquence 1400–1200 cm^{-1} les vibrations $w(CH_2)_\alpha$, $t(CH_2)_\alpha$ et amide III. Effectivement on observe trois absorptions à 1388, 1336 et 1263 cm^{-1} (fig. 1).[3] Dans le cas de la glycine, nous avons montré que les mouvements $t(CH_2)$ et $r_\perp(NH_3)$ sont couplés, ce qui explique l'abaissement de fréquence important de la vibration

[2]Pour l'interprétation des autres dérivés étudiés, *cf.* (14) et le tableau 4.

[3]La faible bande vers 1310 cm^{-1} correspond vraisemblablement à un reste de dérivé hydrogéné.

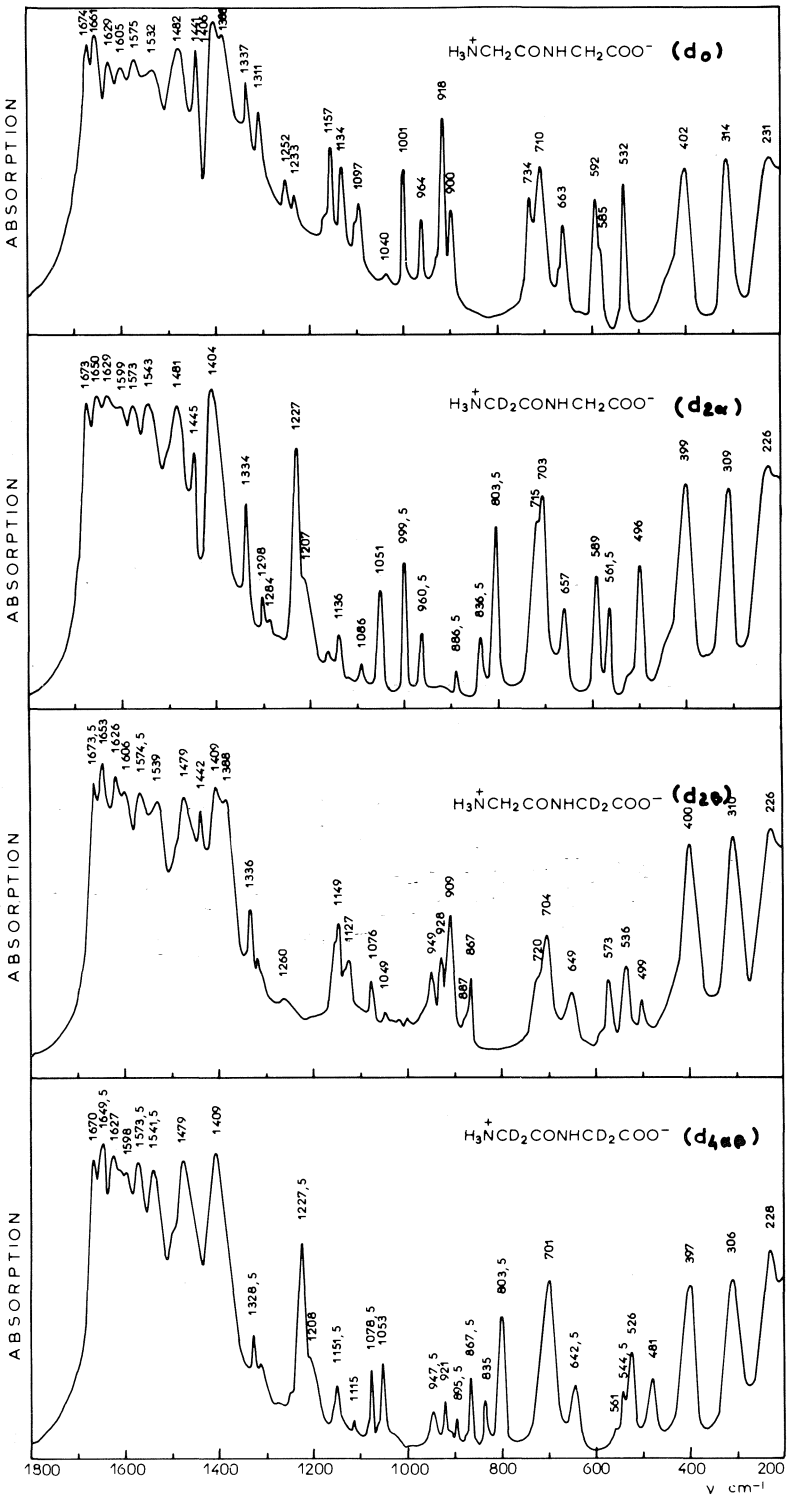

Can. J. Chem. Downloaded from www.nrcresearchpress.com by 210.87.254.42 on 09/05/12
For personal use only.

Can. J. Chem. Downloaded from www.nrcresearchpress.com by 210.87.254.42 on 09/05/12
For personal use only.

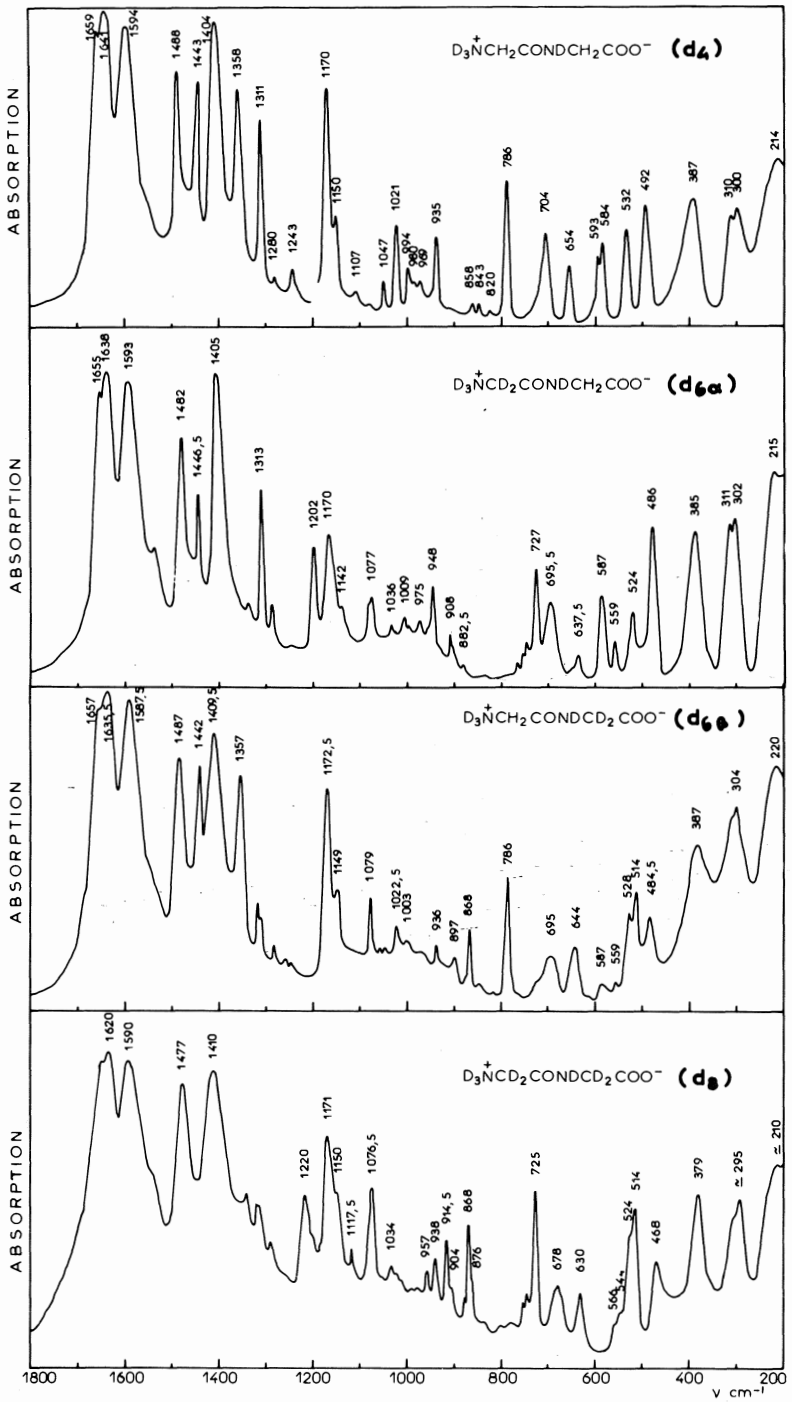

FIG. 1. Spectres infrarouges de 1700 à 200 cm^{-1} des glycylglycines d_0, $d_{2\alpha}$, $d_{2\beta}$, $d_{4\alpha\beta}$, d_4, $d_{6\alpha}$, $d_{6\beta}$ et d_8 dans la forme cristalline α.

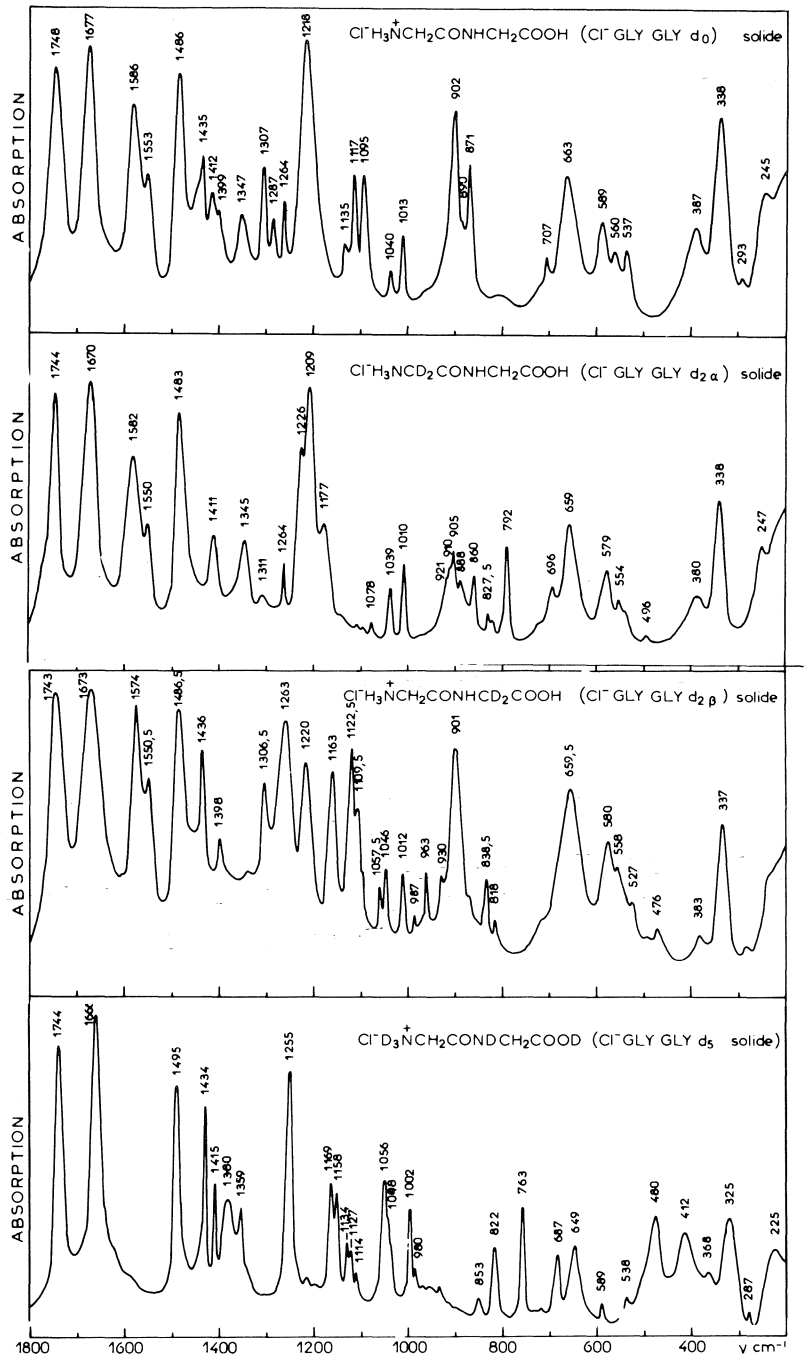

FIG. 2. Spectres infrarouges de 1700 à 200 cm^{-1} des chlorhydrates de glycylglycine d_0, $d_{2\alpha}$, $d_{2\beta}$ et d_5 à l'état solide.

t(CH_2) par deutériation sur l'azote (1). L'absorption à 1336 cm^{-1} du dérivé $d_{2\beta}$ possède bien ces caractéristiques, nous l'attribuons à t$(CH_2)_\alpha$. Par comparaison avec l'acétylglycine *N*-méthylamide (A Gly MA) qui possède, dans sa forme cristalline B, un angle ψ proche de la valeur déterminée pour la forme α (15), on peut penser que les mouvements amide III et w$(CH_2)_\alpha$ sont couplés

Can. J. Chem. Downloaded from www.nrcresearchpress.com by 210.87.254.42 on 09/05/12
For personal use only.

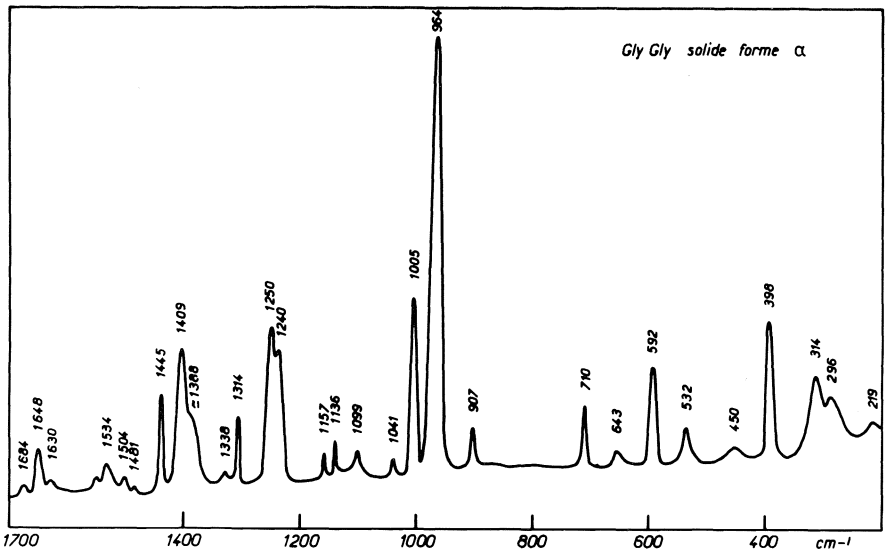

FIG. 3. Spectre Raman de la glycylglycine dans la forme cristalline α.

et situés respectivement à 1388 et 1263 cm^{-1} (tableau 2); en effet dans le composé $D_3\overset{+}{N}CH_2CONDCD_2COO^-$ ($d_{6\beta}$), la vibration $w(CH_2)_\alpha$ est abaissée à 1357 cm^{-1} de la même manière que dans A Gly MA *N*-deutérié (15).

Nous sommes maintenant en mesure d'analyser le spectre de la glycylglycine d_0. Par analogie avec le dérivé $d_{2\beta}$, nous faisons correspondre le mouvement $w(CH_2)_\alpha$ à la bande 1388 cm^{-1}. Deux absorptions sont relevées à 1252 et 1233 cm^{-1}, dues aux deux vibrations amide III et $t(CH_2)_\beta$; la substitution de l'azote peptidique ^{14}N par l'azote ^{15}N les perturbe de la même façon (tableau 2), nous ne pouvons donc pas préciser davantage leur interprétation. Des deux bandes à 1337 et 1311 cm^{-1}, la première, peu intense sur le spectre Raman (fig. 3), se déplace à 1280 cm^{-1} dans le dérivé $D_3\overset{+}{N}CH_2CONDCH_2COO^-$ (d_4), il s'agit donc de $t(CH_2)_\alpha$; l'autre correspond à $w(CH_2)_\beta$. Notons que cette dernière se trouve à la même fréquence que dans le dérivé $d_{6\alpha}$ ce qui traduit, dans ce cas particulier, l'absence de couplage avec la vibration amide III.

Région 1200–1000 cm^{-1}

Quatre absorptions sont observées à 1157, 1134, 1097 et 1040 cm^{-1} et l'on attend, outre les mouvements $r_{\parallel}(NH_3)$ et $r_\perp(NH_3)$, les deux absorptions $\nu(CN)_\alpha$ et $\nu(CN)_\beta$. La vibration à 1097 cm^{-1} présente l'effet isotopique $^{14}N \rightarrow {}^{15}N$ le plus important (tableau 2), elle est due à $\nu(CN)_\beta$ puisque c'est le dérivé substitué à l'azote 15 sur le groupement peptidique que nous avons étudié. Par analogie avec la glycine, nous attribuons les trois autres absorptions dans l'ordre à $r_{\parallel}(NH_3)$, $r_\perp(NH_3)$ et $\nu(CN)_\alpha$ (tableau 2).

Région 1000–800 cm^{-1}

Dans ce domaine doivent apparaître les deux vibrations ν(CC) et les deux vibrations $r(CH_2)$. Effectivement quatre bandes sont observées à 1001, 964, 918 et 900 cm^{-1} (fig. 1).

Les deux premières ne sont pas modifiées par la deutériation sur le carbone C_α; celle à 964 cm^{-1} étant la plus intense en Raman (fig. 2), nous l'attribuons à $\nu(CC)_\beta$; la bande à 1001 cm^{-1} correspond à $r(CH_2)_\beta$.

Des deux absorptions à 918 et 900 cm^{-1}, seule la deuxième est visible sur le spectre Raman, elle est due à $\nu(CC)_\alpha$, l'autre à $r(CH_2)_\alpha$.

Région 800–400 cm^{-1}

Nous avons noté dans le cas de la glycine que la vibration $t(NH_3)$ n'est visible que sur le spectre à froid; il en est de même pour la glycylglycine (tableau 2) et nous localisons cette vibration à 440 cm^{-1}.

Les mouvements δ(COO) et amide V sont attendus autour de 700 cm^{-1}; deux absorptions apparaissent à 734 et 710 cm^{-1} (fig. 1) mais, comme elles présentent toutes deux un effet isotopique $^{14}N \rightarrow {}^{15}N$ voisin, il n'est pas possible de les distinguer.

Les quatre absorptions relevées à 663, 592, 585

Can. J. Chem. Downloaded from www.nrcresearchpress.com by 210.87.254.42 on 09/05/12
For personal use only.

Can. J. Chem. Downloaded from www.nrcresearchpress.com by 210.87.254.42 on 09/05/12
For personal use only.

TABLEAU 2. Fréquences, effets isotopiques et vibrations normales de l'ion $H_3\overset{+}{N}CH_2CONHCH_2COO^-$ dans la forme cristalline α

ν (cm^{-1})		Δ^{15} N*			
Obs.	Calc.	Obs.	Calc.	Distribution d'énergie potentielle (100 $L_{ik}^2 F_{ii}/\lambda_k$)	Attribution
3288	3293.5	7.5	8.7	99 ν(NH)	amide A
1674		0		65 ν(C═O), 10 ν(CN), 15 δ_b	amide I
1661	1668.5	4	2.7		
1629	1626.5	0	0	90 $\delta_s'(NH_3)$	$\delta_d(NH_3)$
1605	1588	0	0	76 $\nu_a(COO)$, 23 $\delta_a(NH_3)$, 10 r(COO)	$\nu_a(COO)$
1575	1588	0	0	64 $\delta_a(NH_3)$, 28 $\nu_a(COO)$	$\delta_d(NH_3)$
1532	1532.5	~12	16.6	43 δ(NH), 40 ν(CN), 11 $\nu(CC)_\alpha$	amide II
1482	1483	0	0.3	83 $\delta_s(NH_3)$, 14 $w(CH_2)_\alpha$	$\delta_s(NH_3)$
1441	1447	0	0	37 $\delta(CH_2)_\beta$, 31 $\delta(CH_2)_\alpha$, 14 $w(CH_2)_\alpha$	$\delta(CH_2)$
1441	1441	0	0.4	38 $\delta(CH_2)_\beta$, 37 $\delta(CH_2)_\alpha$	$\delta(CH_2)$
1406	1403.5	0	0.3	46 $\nu_s(COO)$, 21 $w(CH_2)_\beta$, 27 $\nu(CC)_\beta$, 15 δ(COO), 13 $\delta(CH_2)_\beta$	$\nu_s(COO)$
1388	1382.5	0	0.6	49 $w(CH_2)_\alpha$, 17 $\delta(CH_2)_\alpha$, 12 δ(NH), 10 $\delta_s(NH_3)$	$w(CH_2)_\alpha$, amide III
1337	1335	0.6	0	55 $t(CH_2)_\alpha$, 23 $r_\perp(NH_3)$	$t(CH_2)_\alpha$, $r_\perp NH_3$
1311	1313	0.4	2.4	65 $w(CH_2)_\beta$, 20 $\nu_s(COO)$	$w(CH_2)_\beta$
1252	1246	1.2	2.5	31 δ(NH), 17 ν(CN), 16 $w(CH_2)_\alpha$	
1233	1242	1.9	1.3	90 $t(CH_2)_\beta$	$t(CH_2)_\beta$, amide III, $w(CH_2)_\alpha$
1157	1157.5	0.9	0.4	63 $r_\parallel(NH_3)$	$r_\parallel(NH_3)$
1134	1127.5	4.4	1	38 $r_\perp(NH_3)$, 38 $t(CH_2)_\alpha$, 14 $r(CH_2)_\alpha$	$r_\perp(NH_3)$
1097	1096	8.1	10.1	49 $\nu(CN)_\beta$, 10 $w(CH_2)_\beta$	$\nu(CN)_\beta$
1040	1027.5	3	1.9	64 $\nu(CN)_\alpha$	$\nu(CN)_\alpha$
1001	1006.5	0.9	2.5	51 $r(CH_2)_\beta$, 13 γ(COO)	$r(CH_2)_\beta$
964	964.5	3.2	3	30 $\nu(CC)_\beta$, 11 δ_c, 10 ν(C═O)	$\nu(CC)_\beta$
918	913	1.8	0.3	50 $r(CH_2)_\alpha$, 20 $r_\perp(NH_3)$, 15 γ(C═O)	$r(CH_2)_\alpha$
900	901	2.2	4	18 $\nu(CC)_\alpha$, 15 ν(C═O), 19 $\nu(CC)_\beta$, 12 δ(COO)	$\nu(CC)_\alpha$
734	731.5	2	1.2	29 δ(COO), 13 γ(NH), 10 δ(C═O)	δ(COO)
710	699.5	0.9	2.9	61 γ(NH), 10 t(CN), 14 γ(COO)	amide V
663	664.5	1.2	2.5	22 δ(COO), 21 r(COO), 19 δ(C═O)	r(COO)
592	587.5	3	2.6	47 γ(C═O), 15 $r(CH_2)_\alpha$, 14 r(COO)	amide IV et VI
585	575.5	0.8	0	30 γ(COO), 60 $r(CH_2)_\beta$	γ(COO)
532	532	1.6	1.4	25 δ(C═O), 25 r(COO), 22 γ(C═O), 13 $r(CH_2)_\alpha$	amide IV et VI
440†	437.5	—	0.3	70 $t(NH_3)$, 11 r(COO)	$t(NH_3)$
400	382	—	0.7	28 δ_b, 15 r(COO)	δ squelette
330	323.5	—	0.3	32 δ_a, 19 δ_c	—
232	245	—	0.8	27 δ_a, 23 δ_d	—
—	189	—	1.1	32 t(COO), 23 δ_d, 13 δ_b, 13 δ_c, 11 t(CN)	—
—	118	—	0.7	32 t(COO), 21 t(CN), 21 δ_d, 10 δ_c	—
—	79	—	0.5	35 t(COO), 25 $t(CC)_\alpha$, 16 $t(CN)_\beta$, 16 t(CN)	—
—	55.5	—	0.1	40 $t(CC)_\alpha$, 32 t(CN), 17 $t(CN)_\beta$, 10 t(COO)	—
—	36	—	0.2	65 $t(CN)_\beta$, 33 $t(CC)_\alpha$	—

*Les chiffres donnés sont les abaissements de fréquences.
†À la température de l'azote liquide.

Can. J. Chem. Downloaded from www.nrcresearchpress.com by 210.87.254.42 on 09/05/12
For personal use only.

TABLEAU 3. Fréquences, effets isotopiques et vibrations normales de l'ion $D_3\overset{+}{N}CH_2CONDCH_2COO^-$ dans la forme cristalline α

ν (cm^{-1})		Δ^{15} N*			
Obs.	Calc.	Obs.	Calc.	Distribution d'énergie potentielle 100 $L_{ik}^2 F_{ii}/\lambda_k$	Attribution
2434	2432	14	14.2	96 δ(ND)	amide A
1659		2			
1640	1660	2	2	68 ν(C═O), 15 δ_b, 11 ν(CN)	amide I′
1594	1588	—	0	105 ν_a(COO), 13 r(COO)	ν_a(COO)
1488	1477	14	14.2	49 ν(CN), 26 ν$(CC)_\alpha$, 12 δ(C═O), 10 δ(ND)	amide II′
1443	1446.5	0	0.4	93 δ$(CH_2)_\alpha$	δ$(CH_2)_\alpha$ et $_\beta$
	1443.5		0	79 δ$(CH_2)_\beta$, 13 ν_s(COO)	
1407	1403	0	0	47 ν_s(COO), 27 ν$(CC)_\beta$, 21 w$(CH_2)_\beta$, 15 δ(COO)	ν_s(COO)
1358	1360	4.5	5.3	73 w$(CH_2)_\alpha$	w$(CH_2)_\alpha$
1311	1309	1	1.7	67 w$(CH_2)_\beta$, 20 ν_s(COO)	w$(CH_2)_\beta$
1280	1284	0.25	0.4	83 t$(CH_2)_\alpha$	t$(CH_2)_\alpha$
1243	1242	0.75	0.8	96 t$(CH_2)_\beta$	t$(CH_2)_\beta$
1170	1180	1	0.4	39 $\delta_s$$(ND_3)$, 37 $\delta_s'$$(ND_3)$, 31 ν$(CN)_\alpha$	$\delta_s$$(ND_3)$
	1171.5	0	0	59 $\delta_s'$$(ND_3)$, 29 $\delta_s$$(ND_3)$, 17 ν$(CN)_\alpha$	
1150	1142	0	0	94 $\delta_d$$(ND_3)$	$\delta_d$$(ND_3)$
1107	1094.5	10	9.6	58 ν$(CN)_\beta$, 12 r(COO), 11 δ_c	ν$(CN)_\beta$
1047	1063.5	1	3.1	31 r$(CH_2)_\alpha$, 14 $r_\perp$$(ND_3)$, 12 δ(ND), 10 γ(C═O)	r$(CH_2)_\alpha$
1027	1021	3	1.6	19 r$(CH_2)_\alpha$, 11 $r_\perp$$(ND_3)$, 12 δ(ND), 15 ν$(CC)_\alpha$	—
994	997.5	0.5	0.3	24 $\delta_s$$(ND_3)$, 21 ν$(CN)_\alpha$, 15 $r_\parallel$$(ND_3)$, 10 δ_a	ν$(CN)_\alpha$
989	988.5	3.5	2	55 r$(CH_2)_\beta$, 15 γ(COO)	r$(CH_2)_\beta$
935	935.5	0.6	0.5	35 ν$(CC)_\beta$, 12 δ(COO), 11 ν_s(COO)	ν$(CC)_\beta$
—	902.5	—	1.8	44 δ(ND), 13 ν$(CN)_\alpha$, 11 ν(CN)	—
858.2					
843.5	850	1	3.6	35 $r_\parallel$$(ND_3)$, 10 δ(C═O)	$r_\parallel$$(ND_3)$
786	795	0	1	62 $r_\perp$$(ND_3)$, 15 r$(CH_2)_\alpha$, 12 γ(C═O)	$r_\perp$$(ND_3)$
704	709	0	0.2	39 δ(COO), 10 $r_\parallel$$(ND_3)$	δ(COO)
654	648	1.4	2.3	25 δ(C═O), 20 r(COO), 12 δ(COO)	r(COO)
593	613	1.1	2.8	52 γ(COO), 27 γ(ND), 12 γ(C═O)	amide IV, VI
584	577.2	1.1	1.9	39 γ(C═O), 15 r$(CH_2)_\alpha$, 19 γ(COO), 10 r(COO)	γ(COO)
—	524	2.7	2.4	32 r(COO), 27 δ(C═O), 9 δ_b, 16 γ(C═O), 10 r$(CH_2)_\alpha$	amide IV, VI
492	510	1	2.2	58 γ(ND), 14 r$(CH_2)_\beta$, 10 t(CN)	amide V′
387	395	—	1	33 δ_b, 20 r(COO), 12 t(ND_3)	—
310	314	—	0.5	28 δ_a, 21 δ_c, 14 δ(C═O)	δ squelette
—	305	—	0	76 t(ND_3)	—
225	232.5	—	1	32 δ_a, 25 δ_d	—
—	182	—	1		—
—	113.5	—	1		—
—	76	—	0.5	†	—
—	54.5	—	0		—
—	34	—	0		—

*Les chiffres donnés sont les abaissements de fréquences.
†Distribution d'énergie potentielle très voisine de celle du tableau 2.

TABLEAU 4. Attribution des vibrations de la glycylglycine et de ses dérivés isotopiques

Attribution*	d_0	$d_{2\alpha}$	$d_{2\beta}$	$d_{4\alpha\beta}$	d_4	$d_{6\alpha}$	$d_{6\beta}$	d_8
amide A	3288	3288	3288	3288	2434	2434	2434	2434
amide I	1674 1661	1650	1653	1649.5	1659 1640	1638	1635.5	1620
$\delta_d(NH_3)$	1629	1629	1626	1627	1150	—	1149	1150
$\nu_a(COO)$	1605	1599	1606	1598	1594	1593	1587.5	1590
$\delta_d(NH_3)$	1575	1573	1574.5	1573.5	1150	—	1149	1150
amide II	1532	1541	1539	1541.5	1488	1482	1487	1477
$\delta_s(NH_3)$	1482	1481	1479	1479	1170	1170	1172.5	1171
$\delta(CH_2)_\alpha$	1441	1051	1442	1053	1443	—	—	—
$\delta(CH_2)_\beta$		1445	1049	—		1446.5	1079	1076.5
$\nu_s(COO)$	1406	1404	1409	1409	1407	1405	1409.5	1410
$w(CH_2)_\alpha$	1388	925	1388	921	1358	—	1357	—
$t(CH_2)_\alpha$	1337	910	1336	895.5	1280	—	1282	914.5
$w(CH_2)_\beta$	1311	1334	949	—	1311	1313	—	957
amide III	1252	1298	1263	1328.5	—	—	—	—
$t(CH_2)_\beta$	1233	—	928	—	1243	1245	936	938
$r_{\parallel}(NH_3)$	1157	1207	1157	1208	843.5	—	—	—
$r_{\perp}(NH_3)$	1134	1227	1127	1227.5	786	727	786	725
$\nu(CN)_\beta$	1097	1086	1076	1078.5	1107	—	—	1076.5
$\nu(CN)_\alpha$	1040	1136	1017	1151.5	994	1202	1003	—
$r(CH_2)_\beta$	1001	999.5	—	947	989	975	—	—
$\nu(CC)_\beta$	964	960.5	867	867.5	935	—	868	868
$r(CH_2)_\alpha$	918	803	909	803.5	1047	1036	—	—
$\nu(CC)_\alpha$	900	886	887	878.5	—	—	—	—
$\delta(COO)$	734	715	704	701	704	695.5	695	678
amide V	710	703			492	—	484.5	468
r(COO)	663	657	649	642.5	654	637.5	644	630
amide IV et VI	592	561.5	573	544.5	593	559	587	544
$\gamma(COO)$	585	589	499	526	584	587	—	524
amide IV et VI	532	496	536	481	—	475	514.5	514
$t(NH_3)$	440	430	~430	~430	—	—	—	—
δ squelette	400	399	400	397	387	385	—	379
	320	309	310	306	310	311	—	~295
	232	226	226	228	225	215	—	~210

*Les notations sont données pour le dérivé d_0.

et 532 cm^{-1} correspondent aux vibrations amide IV et VI et aux vibrations de déformation γ(COO) et r(COO). Des deux bandes à 663 et 592 cm^{-1} plus particulièrement sensibles à la deutériation sur le carbone β, c'est la seconde qui subit l'abaissement de fréquence le plus important; nous l'attribuons, comme dans le cas de la glycine, à γ(COO); l'autre est due à r(COO). Les absorptions à 585 et 532 cm^{-1} se déplacent à 561.5 et 496 cm^{-1} dans le dérivé $d_{2\alpha}$, il s'agit des vibrations amide IV et VI. Ces deux bandes présentent pratiquement les mêmes caractéristiques spectroscopiques, une attribution plus fine est donc impossible actuellement.

Région 400–200 cm^{-1}

Il nous reste à situer quatre vibrations de déformation et quatre de torsion. Le domaine spectral que nous avons étudié est limité à 200 cm^{-1}; dans la zone 400–200 cm^{-1}, trois raies intenses sont observées sur les spectres infrarouge et Raman (figs. 1 et 3), elles doivent donc correspondre à trois vibrations de squelette. Les autres modes se trouvent vraisemblablement à une fréquence inférieure à 200 cm^{-1}.

Les attributions de tous les dérivés isotopiques étudiés sont récapitulées sur le tableau 4.

(B) Discussion du spectre de vibration du chlorhydrate de glycylglycine

Par rapport à la glycylglycine forme α, le chlorhydrate cristallisé présente deux différences importantes susceptibles de perturber les spectres de vibration: valeur de l'angle ϕ_2 (fig. 4); liaisons intermoléculaires en raison de la substitution du groupement COO^- par un groupement COOH.

Ces modifications concernent essentiellement la partie $—NHCH_2COOH$ de la molécule. Au contraire, les angles ψ sont très voisins (6, 7);

Can. J. Chem. Downloaded from www.nrcresearchpress.com by 210.87.254.42 on 09/05/12
For personal use only.

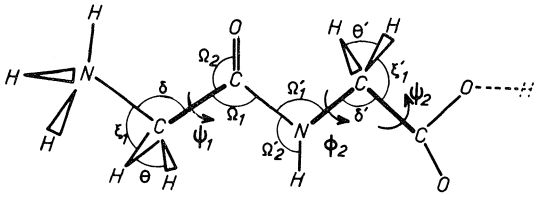

FIG. 4. Conformation de la glycylglycine forme α (*a*) et du chlorhydrate de glycylglycine à l'état solide (*b*) (conventions IUPAC-IUB (18)). (*a*) $\psi_1 = -148.7°$, $\phi_2 = -156.5°$, $\psi_2 = 169.7°$; (*b*) $\psi_1 = -162.1°$, $\phi_2 = -79.6°$, $\psi_2 = 176.8°$.

aussi l'attribution de la plupart des vibrations du groupement $H_3\overset{+}{N}CH_2CO$— se déduit-elle de celle proposée pour la glycylglycine.

Nous discuterons donc principalement des mouvements mettant en jeu la partie —$NHCH_2$-COOH de la molécule à l'exception des vibrations de valence du groupement carboxylique qui sont à des fréquences très proches de celles relevées sur le spectre du chlorhydrate de glycine (16).

Vibrations amide II et III

Les vibrations amide II et amide III sont observées sur le spectre du chlorhydrate à des fréquences beaucoup plus élevées que pour la glycylglycine. On sait que ces modes mettent en jeu les coordonnées ν(CN) peptidiques et δ(NH) (17) qui sont très sensibles à la force des liaisons intermoléculaires; leur fréquence peut aussi varier avec l'angle ϕ_2. Nous ne pouvons pas, à ce stade de notre étude, séparer l'effet respectif de ces deux paramètres sur la position de ces vibrations.

Région 1400–1300 cm^{-1}

En utilisant les mêmes critères d'attribution que pour la diglycine forme α, nous localisons la vibration $w(CH_2)_\beta$ à 1347 cm^{-1}. Nous expliquons la fréquence élevée de ce mode par un couplage avec δ(OH) comparable à celui observé dans le cas du chlorhydrate de glycine (16).

Région 800–400 cm^{-1}

Par analogie avec le chlorhydrate de glycine (16), nous attribuons l'absorption à 707 cm^{-1} à la vibration δ(CC=O). Trois bandes sont encore visibles à 589, 560 et 537 cm^{-1} alors qu'on attend les vibrations amide IV et VI, δ(CC—O) et γ(C=O). Les deux absorptions à 560 et 537 cm^{-1} sont surtout influencées par la deutériation sur le carbone C_α, nous les attribuons donc aux vibrations amide IV et VI. La bande à 589 cm^{-1}, peu déplacée dans les dérivés $d_{2\alpha}$ et $d_{2\beta}$, est vraisemblablement due à δ(CC—O). Enfin la vibration γ(C=O) n'est vue que dans le dérivé $d_{2\alpha}$, à 540 cm^{-1} (fig. 2).

(II) Champ de force de valence de la glycylglycine et de son chlorhydrate

Les coordonnées de groupe utilisées sont celles de la glycine ou de son chlorhydrate pour les groupements $\overset{+}{N}H_3$, CH_2 et COO^- ou COOH, du *N*-méthylacétamide (NMA) pour le groupement CONH; ces dernières sont rappelées dans le tableau 5.

Les longueurs, angles de liaison et angles dièdres ϕ_2, ψ_1 et ψ_2 proviennent de résultats cristallographiques (6, 7). Néanmoins, comme dans le cas de la glycine et du NMA (17), tous les angles autour des atomes C_1, N_1 et C_3 ont été supposés tétraédriques, ceux autour des atomes C_2 et N_2 égaux à 120°.

Nous présenterons tout d'abord la recherche du champ de force de la glycylglycine forme α puis celle de son chlorhydrate.

(A) Recherche du champ de force de la glycylglycine forme α

Nous avons effectué un premier calcul en transférant les champs de force de la glycine (1) et du NMA (17); l'accord entre fréquences calculées et expérimentales est relativement bon (14). Nous avons vérifié également que les répartitions d'énergie potentielle sont souvent en bon accord avec l'interprétation proposée. Néanmoins les effets isotopiques calculés ne sont pas toujours satisfaisants; pour se rapprocher des valeurs expérimentales, il a été nécessaire d'introduire quelques constantes de force d'interaction spécifiques de ce peptide.

Vibrations amide II et II'

D'après les résultats de ce premier calcul, on observe un mélange très important des mouvements amide II et II', $\delta(CH_2)_\alpha$ et $\delta(CH_2)_\beta$ dans les dérivés d_0 et d_4; ceci est en contradiction avec la valeur de l'effet isotopique ^{15}N observé (tableaux 2 et 3). L'introduction des intéractions $f|\nu(CN), \delta(CH_2)_\alpha|$ et $f|\nu(CN), \delta(CH_2)_\beta|$ permet un meilleur accord avec les données expérimentales.

Vibration amide III

L'interprétation des spectres suggère un couplage entre les coordonnées δ(NH), $w(CH_2)_\alpha$ et $w(CH_2)_\beta$, couplage confirmé par le calcul. Néanmoins pour mieux rendre compte des fréquences

Can. J. Chem. Downloaded from www.nrcresearchpress.com by 210.87.254.42 on 09/05/12
For personal use only.

TABLEAU 5. Coordonnées de groupe du groupement CONH et du squelette de la glycylglycine

$\nu(CN)_\alpha = R$	$\delta(N_1C_1C_2) = \delta_a = \frac{1}{\sqrt{30}}(5\delta - \theta - \xi_1 - \xi_2 - \xi_3 - \xi_4)$
$\nu(CN) = P$	$\delta(C_1C_2N_2) = \delta_b = \frac{1}{\sqrt{6}}(2\Omega_1 - \Omega_2 - \Omega_3)$
$\nu(CC)_\alpha = S$	$\delta(C_2N_2C_3) = \delta_c = \frac{1}{\sqrt{6}}(2\Omega_1' - \Omega_2' - \Omega_3')$
$\nu(CC)_\beta = S'$	$\delta(N_2C_3C_4) = \delta_d = \frac{1}{\sqrt{30}}(5\delta' - \theta' - \xi_1' - \xi_2' - \xi_3' - \xi_4')$
$\nu(C{=}O) = s$	
$\nu(NH) = u$	
$\delta(C{=}O) = \frac{1}{\sqrt{2}}(\Omega_2 - \Omega_3)$	$t(CN) = \tau_1$†
$\gamma(C{=}O) = \chi_1$*	$t(CC)_\alpha = \tau_2$
$\delta(NH) = \frac{1}{\sqrt{2}}(\Omega_2' - \Omega_3')$	$t(CC)_\beta = \tau_3$
$\gamma(NH) = \chi_2$*	$t(CN)_\beta = \tau_4$

*χ_1 et χ_2 correspondent respectivement à la sortie hors du plan de l'atome O_1 et H_6.
†τ_1 à τ_4 sont définis comme étant la somme de tous les angles dièdres autour de la liaison considérée.

dans les dérivés substitués par le deutérium, il a été nécessaire de tenir compte des intéractions $f|\delta(NH), w(CH_2)_\alpha|$ et $f|\delta(NH), w(CH_2)_\beta|$.

Vibrations de squelette

Les deux modes mettant principalement en jeu les coordonnées $\nu(CC)_\beta$ et $\nu(CN)_\beta$ sont calculés à des fréquences trop élevées (14); l'examen des répartitions d'énergie potentielle montre qu'y participent également les coordonnées $\delta(C_1C_2N_2)$ et $\delta(C_2N_2C_3)$. L'introduction des intéractions $f|\nu(CC)_\beta, \delta(C_2N_2C_3)|$ et $f|\nu(CN)_\beta, \delta(C_1C_2N_2)|$ permet d'ajuster les fréquences et en même temps d'améliorer les effets isotopiques calculés.

Par raison de symétrie, nous avons également pris en considération l'intéraction $f|\nu(CC)_\alpha, \delta(C_2N_2C_3)|$.

Vibrations amide IV et VI

Nous venons d'attribuer sans les distinguer les vibrations amide IV et VI à 585 cm^{-1} et 532 cm^{-1} dans le dérivé d_0.

Deux types de champ de force ont été essayés, correspondant aux deux interprétations possibles. Si la vibration amide IV est calculée vers 585 cm^{-1}, elle présente un effet isotopique $\Delta\nu(d_0 - d_{2\alpha})$ très faible alors qu'expérimentalement il est de 26 cm^{-1}; de la même manière, l'effet $\Delta\nu$ ^{15}N calculé est trop grand. L'autre solution nécessite l'introduction d'une nouvelle intéraction: $f|\delta(C{=}O), \delta(N_1C_1C_2)|$ mais, comme elle permet de bien rendre compte des effets isotopiques observés, c'est elle que nous avons retenue.

Raffinement

Nous avons raffiné 21 constantes de forces principales et 14 constantes de forces d'intéraction à partir de 190 fréquences expérimentales correspondant aux dérivés d_0, d_4, $d_{2\alpha}$, $d_{2\beta}$, $d_{4\alpha\beta}$, $d_{6\alpha}$ et $d_{6\beta}$. Les valeurs obtenues sont groupées sur le tableau 6. L'écart entre nombres d'ondes calculés et observés est alors de 0.75% en moyenne.

(B) Champ de force du chlorhydrate de glycylglycine

L'étude du chlorhydrate de glycylglycine nécessite la connaissance du champ de force du groupement COOH; celui-ci a été déterminé dans de bonnes conditions dans le cas du chlorhydrate de glycine grâce à l'utilisation de la substitution $^{16}O \rightarrow {}^{18}O$ (14).

Ce champ de force et celui de la glycylglycine forme α ont été appliqués à la géométrie réelle du chlorhydrate de diglycine. Les fréquences calculées sont indiquées sur le tableau 7. D'une façon générale, l'accord avec les fréquences observées est bon sauf en ce qui concerne certaines vibrations impliquées dans des liaisons hydrogènes. Une simple perturbation des constantes de forces principales correspondantes permet de se rapprocher des données expérimentales; cependant pour mieux rendre compte des fréquences des vibrations amide II et III, il a été nécessaire de tenir compte de l'intéraction

Can. J. Chem. Downloaded from www.nrcresearchpress.com by 210.87.254.42 on 09/05/12
For personal use only.

Can. J. Chem. Downloaded from www.nrcresearchpress.com by 210.87.254.42 on 09/05/12
For personal use only.

TABLEAU 6. Champ de force de valence de la glycylglycine forme α†

$F\|\nu(C{=}O)\|$*	8.9; 9.4[a]; 9.18[b]	$F\|\delta(CH_2)_\alpha\|$	0.549; 0.541[b]	$F\|\nu C{-}O)\|$*	9.4
$F\|\nu(CN)\|$*	6.9			$f\|(CO,CO)\|$*	1.1
$F\|\delta(C{=}O)\|$	1.17; 1.20[a]; 1.23[b]	$F\|\delta(CH_2)_\beta\|$	0.545; 0.531[b]	$F\|\delta(COO)\|$*	1.45; 1.30[a]
$F\|\gamma(C{=}O)\|$	0.56	$F\|w(CH_2)_\alpha\|$	0.7	$F\|r(COO)\|$*	1.59; 1.5[a]
$F\|\nu(NH)\|$	5.964; 5.925[b]	$F\|w(CH_2)_\beta\|$	0.692; 0.677[b]	$F\|\gamma(COO)\|$	0.273
$F\|\delta(NH)\|$	0.525, 0.575[a]; 0.605[b]	$F\|t(CH_2)_\alpha\|$	0.696	$F\|t(COO)\|$*	0.0043
$F\|\gamma(NH)\|$	0.205; 0.155[b]	$F\|t(CH_2)_\beta\|$	0.696	$f\|\nu_s(COO), \nu(CC)\|$*	1.1
$F\|\delta(C_1C_2N_2)\|$* $= \delta_b$	1.4	$F\|r(CH_2)_\alpha\|$	0.68	$f\|\nu_s(COO), \delta(COO)\|$*	0.2
$F\|\delta(C_2N_2C_3)\|$* $= \delta_c$	1.3	$F\|r(CH_2)_\beta\|$	0.645; 0.63[b]	$f\|\nu(CC_\beta), \delta(COO)\|$*	−0.4
$F\|t(CN)\|$*	0.008			$f\|\nu_a(COO), r(COO)\|$*	1.1
$f\|\nu(C{=}O), \nu(CN)\|$*	0.6	$F\|\delta(N_1C_1C_2)\|$* $= \delta_a$	1.0	$f\|\delta_d, r(COO)\|$*	0.3
$f\|\nu(CN), \delta(C{=}O)\|$*	−0.45	$F\|\delta(N_2C_3C_4)\|$* $= \delta_d$	1.0	$f\|r(CH_2)_\beta, \gamma(COO)\|$*	0.035
$f\|\nu(CC)_\alpha, \delta(C{=}O)\|$*	0.4	$f\|\nu(CC), \delta(CH_2)\|_\alpha$	−0.162	$f\|w(CH_2)_\beta, \nu_s(COO)\|$*	−0.15
$f\|\nu(CN)_\beta, \delta(NH)\|$	−0.258	$f\|\nu(CC), \delta(CH_2)\|_\beta$	−0.169		
$f\|\nu(CC)_\alpha, \delta_c\|$*	0.17	$f\|\nu(CC), w(CH_2)\|_\alpha$	−0.158		
$f\|\nu(C{=}O), \delta_b\|$	−0.5	$f\|\nu(CC), w(CH_2)\|_\beta$	−0.134		
$f\|\gamma(C{=}O), \gamma(NH)\|$	0.071	$f\|\nu(CN), \delta(CH_2)\|_\alpha$	−0.245		
$f\|\delta(C{=}O), \delta_a\|$*	0.15; 0[a] et [b]	$f\|\nu(CN), \delta(CH_2)\|_\beta$	−0.243		
$f\|\nu(CC)_\beta, \delta_c\|$*	0.14	$f\|\nu(CN), w(CH_2)\|_\alpha$	0.365		
$f\|\nu(CN), \delta(NH)\|$	0; 0.04[a] et [b]	$f\|\nu(CN), w(CH_2)\|_\beta$	0.55		
$F\|\delta_s(NH_3)\|$	0.554	$f\|\delta(NH), w(CH_2)\|_\alpha$	−0.016		
$F\|\delta_s'(NH_3)\|$	0.556	$f\|\delta(NH), w(CH_2)\|_\beta$	−0.014		
$F\|\delta_a(NH_3)\|$	0.526	$f\|\gamma(C{=}O), r(CH_2)\|_\alpha$	−0.055		
$F\|r_{\|\|}(NH_3)\|$	0.723; 0.68[a] et [b]	$f\|\gamma(NH), t(CH_2)\|_\beta$	0.03		
$f\|r_\perp(NH_3)\|$	0.75; 0.68[a] et [b]	$f\|\gamma(C{=}O), t(CC)_\beta\|$*	0.006		
$F\|t(NH_3)\|$*	0.0033; 0.0025[b]	$f\|\gamma(NH), t(CC)\|_\beta$*	0.0115		
$f\|\nu(CN), \delta_s(NH_3)\|$	−0.267	$F\|\nu(CN)_\alpha\|$	4.47		
$f\|r_\perp(NH_3), t(CH_2)\|$	−0.1; −0.09[b]	$F\|\nu(CC)_\beta\|$*	3.9		
$f\|r_\perp(NH_3), r(CH_2)\|$	−0.0045	$F\|\nu(CN)_\beta\|$*	4.6		
$f\|t(NH_3), r(CH_2)\|$*	−0.012	$F\|t(CC)_\alpha\|$*	0.001		
$f\|\gamma(C{=}O), t(NH_3)\|$*	0.0065	$F\|t(CN)_\beta\|$*	0.001		
$f\|\gamma(C{=}O), r(CH_2)_\alpha\|$	−0.055	$f\|\nu(CN)_\beta, \delta_a\|$*	0.35		

*Constantes de forces fixées dans le raffinement.

†Les valeurs correspondant à la solution aqueuse sont notées (*a*), celles du chlorhydrate (*b*) lorsqu'elles diffèrent de l'état solide; le champ de force du groupement COOH est identique à celui du chlorhydrate de glycine (14) à l'exception de: $F|\delta(C{-}O)| = 1.09$; $F|\delta(OH)| = 1.03$; $F|\gamma(OH)| = 0.98$; $F|\gamma(C{=}O)| = 0.592$. Les constantes de forces: des liaisons sont exprimées en mdyne $Å^{-1}$; des angles sont exprimées en mdyne Å rd^{-2}; liaison angle sont exprimées en mdyne rd^{-1}.

TABLEAU 7. Comparaison des fréquences calculées et expérimentales du chlorhydrate de glycine d_0 à l'état solide

Attribution	ν (cm^{-1}) Exp.	Calc.*	Calc.†	Attribution	ν (cm^{-1}) Exp.	Calc.*	Calc.†
amide A	3277	3293.5	3281	$\nu(CN)_\beta$	1095	1097	1096
$\nu(C{=}O)$	1748	1748.5	1753	$\nu(CN)_\alpha$	1040	1037	1039
amide I	1677	1670	1669.5	$r(CH_2)_\beta$	1013	1007	1001
$\delta_s'(NH_3)$		1629	1625	$r(CH_2)_\alpha$	902	924	912
$\delta_a(NH_3)$	1578	1585	1577	$\gamma(OH)$	890	899	897
amide II	1586	1533	1587	$\nu(CC)_\beta$	890	894	885
$\delta_s(NH_3)$	1486	1483	1482.5	$\nu(CC)_\alpha$	871	871.5	868
$\delta(CH_2)_\alpha$	1435	1444.5	1438	$\delta(C{=}O)$	707	756	722
$\delta(CH_2)_\beta$	1412	1433.5	1416.5	amide V	663	703	662.5
$\nu(C{-}O)$	1399	1398.5	1401	$\delta(CC{-}O)$	589	637	603
$w(CH_2)_\alpha$		1382	1392.5	amide IV et VI	560	570	569
$w(CH_2)_\beta$	1347	1322	1328.5	$\gamma(C{=}O)$		543.8	541
$t(CH_2)_\alpha$	1307	1328	1315.5	amide IV et VI	537	520.3	533
amide III	1287	1251	1280.5		387	361	365
$t(CH_2)_\beta$	1264	1263	1257	δ squelette	338	353.5	349
δ(OH)	1218	1208	1219		293	271	262
$r(NH_3)$	1135	1156	1134		245	246	244
$r(NH_3)$	1117	1135	1111.5				

*Fréquences calculées à partir d'un champ de force transféré de la diglycine forme α et du chlorhydrate de glycine.
†Fréquences calculées à partir du champ de force final.

$f|\delta(NH), \nu(CN)|$; comme le montre le tableau 6, cette constante de force est très faible.

Par contre les fréquences calculées des modes sensibles à la conformation moléculaire (15): vibrations de squelette dans la région 1050–850 cm^{-1}, amides IV et V dans la région 750–500 cm^{-1}, sont très proches des fréquences observées. Nous avons vérifié que de la même manière, les effets isotopiques NH → ND ou CH → CD calculés mettant en jeu ces modes sont en bon accord avec les résultats expérimentaux.

Ceci montre donc que les variations de fréquences observées entre deux conformères proviennent essentiellement, pour les vibrations ne mettant pas en jeu de liaison hydrogène, des modifications géométriques (donc de **G**) et qu'en première approximation on peut admettre que **F** est constant quel que soit le domaine angulaire étudié.

1. C. DESTRADE, C. GARRIGOU-LAGRANGE et M. T. FOREL. J. Mol. Struct. **10**, 203 (1971).
2. C. DESTRADE, M. T. FOREL et C. GARRIGOU-LAGRANGE. C. R. Acad. Sci. **273B**, 376 (1971).
3. Y. IITAKA. Acta Cryst. **13**, 35 (1960).
4. Y. IITAKA. Acta Cryst. **14**, 1 (1961).
5. P. G. JÖNSSON et Å. KVICK. Acta Cryst. **B28**, 1827 (1972).
6. H. C. FREEMAN et G. L. PAUL. Acta Cryst. **B26**, 925 (1970).
7. H. KOETZLE et W. C. HAMILTON. Acta Cryst. **B28**, 2083 (1972).
8. J. D. CIPERA et R. V. V. NICHOLLS. Chem. Ind. **16** (1955).
9. M. BERGMANN et L. ZERNAS. Ber. Deutch Chem. Ges. **65**, 1192 (1932).
10. GRAZZ. Chim. Ital. **94**, 322 (1964).
11. D.-BEN-ISHA. Contribution from the Weitzmann Institute of Science (1953).
12. G. GÜNTHER et K. F. BONHOEFFER. Z. Phys. Chem. **A180**, 187, (1937).
13. SALZBERG et SUPNIEWSKI. Org. Synth. **21**, 119 (1941).
14. C. DESTRADE. Thèse Bordeaux. CNRS AO 5482. 1973.
15. Y. KOYAMA et J. SHIMANOUCHI. Biopolymers, **6**, 1037 (1968).
16. B. DUPUY. Thèse Bordeaux. AO 1275. 1967.
17. M. REY-LAFON, C. GARRIGOU-LAGRANGE et M. T. FOREL. Spectrochim. Acta, **29A**, 371 (1973).
18. Commission on biochemical nomenclature IUPAC-IUB. J. Mol. Biol. **52**, 1 (1970).

Can. J. Chem. Downloaded from www.nrcresearchpress.com by 210.87.254.42 on 09/05/12
For personal use only.

Cinétique de l'interaction de l'inosine avec le [Pt(dien)Br]Br

JEAN-YVES SÉGUIN, PI-CHANG KONG ET MIKLOS ZADOR

Département de chimie, Université de Montréal, C.P. 6210, Succursale A, Montréal, Québec H3C 3V1

Reçu le 28 janvier 1974

JEAN-YVES SÉGUIN, PI-CHANG KONG et MIKLOS ZADOR. Can. J. Chem. **52**, 2603 (1974).

La cinétique de la substitution du $[Pt(dien)Br]^+$ par l'inosine dans l'eau a été étudiée. Les ions bromure inhibent fortement la réaction tandis que l'ordre par rapport à l'inosine est plus petit qu'un. Ces résultats sont en accord avec un mécanisme impliquant un complexe intermédiaire du platine, $[Pt(dien)H_2O]^{2+}$, et une contribution relativement faible du mécanisme S_N2. Les paramètres cinétiques correspondants ont été déterminés et sont discutés.

JEAN-YVES SÉGUIN, PI-CHANG KONG, and MIKLOS ZADOR. Can. J. Chem. **52**, 2603 (1974).

Kinetics of substitution of $[Pt(dien)Br]^+$ by inosine in water has been investigated. The reaction is strongly inhibited by bromide ions, while the order with resect to inosine is smaller than one. These results are in agreement with a mechanism via an aquo-intermediate, $[Pt(dien)H_2O]^{2+}$ and also with a relatively small contribution of the S_N2 path. The kinetic parameters have been determined and are discussed.

Can. J. Chem. Downloaded from www.nrcresearchpress.com by 210.87.254.6 on 09/05/12
For personal use only.

La cinétique de substitution de complexes du Pt(II) a fait l'objet de nombreux travaux. Pour les réactions du type $PtA_3X + Y \rightarrow PtA_3Y + X$, on admet généralement le mécanisme de Basolo et Pearson (1), qui en présence d'un excès de ligand conduit à l'expression suivante pour la constante de vitesse expérimentale

$$[1] \qquad k_{exp} = k_S + k_Y[Y]$$

Dans l'éq. 1 k_Y représente la constante de vitesse de la voie réactionnelle S_N2 et k_S est attribué au déplacement de X par le solvant, suivi par une réaction rapide avec Y. Ce mécanisme a été vérifié dans plusieurs cas, avec en général, une contribution prépondérante de la voie S_N2 (2–6), mais avec peu de résultats quantitatifs concernant la voie impliquant le solvant.

L'interaction des sels du Pt(II) avec les nucléosides a fait l'objet récemment de plusieurs travaux (7–9). Ces études ont été initiées par la découverte montrant que le développement des tumeurs cancéreux est inhibé par les sels du Pt(II) (10); une explication possible de ce phénomène serait l'interaction du Pt(II) avec l'ADN.

Dans un effort pour élucider le mécanisme d'interaction du Pt(II) avec les nucléosides, nous avons, dans le présent travail, entrepris l'étude d'un système modèle, soit la substitution de [Pt(dien)Br]Br (ou dien = diéthylène triamine) par l'inosine (In) conduisant à un seul produit $[Pt(dien)In]^{2+}$. Comme dans les systèmes biologiques on est en présence d'ions halogénures, l'influence de l'ion Br^- sur la cinétique a été étudiée quantitativement.

Partie expérimentale

Les réactifs

L'inosine est un produit Raylo Co. Le [Pt(dien)Br]Br a été préparé selon la méthode de Mann (11). Le KBr utilisé provient d'Anachemia (Reagent Grade). Le solvant utilisé est l'eau distillée.

Le produit

L'identification du produit est facilitée par le fait que seul l'ion bromure du complexe est substitué pendant un temps de réaction raisonable (3). Le problème à résoudre concerne le site de coordination de l'inosine.

Malheureusement le produit de la réaction n'a pas pu être isolé; par évaporation du solvant on obtenait les réactifs de départ comme c'était le cas du complexe du [Pt(tripy)Br]Br avec la pyridine (3). Le produit a été obtenu en solution dans le D_2O en mélangeant l'inosine et le [Pt(dien)Br]Br dans un rapport 1:1. L'étude de cette solution par r.m.n. indique la disparition complète des protons de l'inosine libre (H_8, H_2) et l'apparition de deux pics nouveaux. Le proton H_2 subit un léger déplacement (0.17 p.p.m.) vers les champs faibles, tandis que H_8 subit un déplacement beaucoup plus prononcé (0.5 p.p.m.) dans la même direction. Ce dernier proton est couplé en outre au ^{195}Pt, dont l'abondance dans le Pt est de 33%; comme conséquence on obtient un triplet 1:4:1. Par deutération en position H_8, ce triplet disparaît. Ceci suggère fortement que la liaison se fait au voisinage de H_8, soit en position N_7. C'est le cas également des complexes de l'inosine avec le $Pt(NH_3)_2Cl_2$ et le $Pt(en)Cl_2$, qui ont pu être isolés et caractérisés (8).

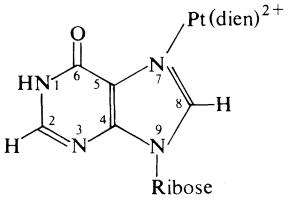

Can. J. Chem. Downloaded from www.nrcresearchpress.com by 210.87.254.6 on 09/05/12
For personal use only.

D'après les résultats qualitatifs de Rosenberg *et al.* (7), obtenus par spectrophotométrie u.v., il semble que l'interaction en position 1 soit aussi possible. Toutefois, ces auteurs ont utilisé un grand excès de *cis* ou de *trans* $Pt(NH_3)_2Cl_2$ par rapport à l'inosine et dans ces conditions on peut avoir coordination à plus d'un site du ligand. Dans notre cas, avec un rapport [Inosine]/[Pt] $\geqq 1$, l'interaction en position 1 n'était pas décelable par r.m.n. Finalement, la position N_9 n'est en général pas complexée par les métaux, dû probablement à l'encombrement stérique du groupe ribose.

Méthode expérimentale

La substitution donne lieu à la libération de Br^- et s'accompagne de l'augmentation de la conductance qui a été enregistrée en fonction du temps. Les réactifs thermostatés ont été mélangés dans la cellule de conductivité (Metrohm EA 645-05) elle-même plongée dans le bain thermostaté; le mélange réactionnel a été agité au moyen d'une barre magnétique. Le conductimètre à lecture directe utilisé est décrit dans la littérature (12); pour les besoins spécifiques de cette étude il a été muni d'un dispositif permettant la compensation de la conductance initiale de la solution, augmentant ainsi la gamme d'utilisation de l'appareil en présence d'un électrolyte tel KBr. En absence d'inosine la variation de conductivité était négligeable.

La constante de vitesse expérimentale, en présence d'un excès d'inosine a été obtenue graphiquement à partir de l'équation intégrée d'ordre un

$$[2] \qquad \ln[(S_\infty - S_0)/(S_t - S_0)] = kt$$

où S_0, S_t et S_∞ représentent le signal enregistré aux temps 0, t et infini respectivement.

Dans certaines expériences où le graphe de l'éq. 2 présentait une courbure, dûe à l'inhibition par l'ion Br^- formé, qui était apparente surtout en absence de KBr ajouté k_{exp} a été obtenu comme la pente initiale.

L'influence de la force ionique est relativement faible aux concentrations étudiées; elle n'atteint qu'un maximum de 12% sur la constante de vitesse aux plus fortes concentrations comme l'indiquent les expériences réalisées en présence de KNO_3. Comme par ailleurs l'erreur expérimentale augmente rapidement en présence de sel inerte dû à la méthode expérimentale utilisée, la force ionique n'a pas été maintenue constante.

Résultats et discussion

La réaction de substitution se fait d'après les éqs. 3 et 4

$$[3] \quad [Pt(dien)Br]Br \xrightarrow{\text{très rapide}} [Pt(dien)Br]^+ + Br^-$$

$$[4] \quad [Pt(dien)Br]^+ + In \rightarrow [Pt(dien)In]^{2+} + Br^-$$

En présence d'un excès d'inosine, *i.e.* [In] $\gg$ [Complexe], on observe un ralentissement de la réaction en fonction du temps par rapport à une cinétique d'ordre un par rapport au complexe de départ; ceci se manifeste par une courbure des droites d'intégration (*c.f.* Partie expérimentale). Le ralentissement a été attribué à l'effet inhibiteur de l'ion bromure libéré et l'hypothèse a été vérifiée en étudiant l'influence de KBr ajouté sur la constante de vitesse expérimentale d'ordre un, k_{exp}; la fig. 1 montre que l'ion Br^- inhibe fortement la réaction. Il faut noter qu'en présence d'un excès de KBr l'ordre un est bien respecté.

L'influence de la concentration en inosine a été étudiée. La fig. 2 montre que la variation de k_{exp} *vs.* [In] ne suit pas l'éq. 1 et qu'il y a une courbure nette impliquant un mécanisme plus complexe que celui observé habituellement (1).

Pour expliquer ce comportement, il faut admettre que la voie réactionnelle, faisant intervenir le déplacement du Br par le solvant devient prépondérante avec les étapes [5] et [6]:

$$[5] \quad [Pt(dien)Br]^+ + H_2O \underset{k_{-1}}{\overset{k_1}{\rightleftharpoons}} [Pt(dien)H_2O]^{2+} + Br^-$$

$$[6] \quad [Pt(dien)H_2O]^{2+} + In \xrightarrow{k_2} [Pt(dien)In]^{2+} + H_2O$$

En appliquant l'état stationnaire pour l'intermédiaire aquo, on obtient l'éq. 7

$$[7] \qquad k_{exp} = \frac{\text{Vitesse de réaction}}{[Pt(dien)Br]^+} = \frac{k_2 k_1 [In]}{k_{-1}[Br^-] + k_2[In]}$$

On peut voir aisément que ce mécanisme

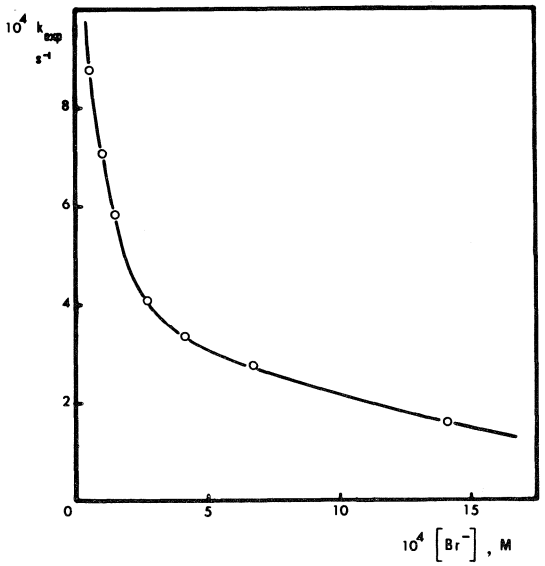

FIG. 1. L'influence de l'ion bromure sur la constante de vitesse expérimentale. $T = 50\,°C$; [Inosine] = 2.5×10^{-3} *M*.

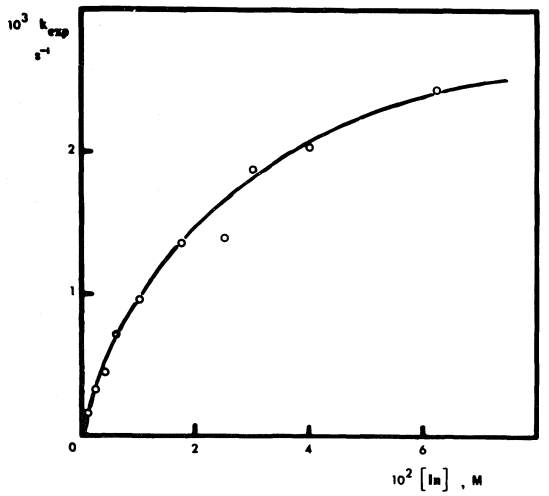

FIG. 2. Influence de l'inosine sur la constante de vitesse expérimentale. $T = 50\,°C$; $[Br^-] = 4.1 \times 10^{-4}$ M.

satisfait qualitativement les résultats en rendant compte de l'inhibition par Br^- et l'ordre inférieur à un par rapport à l'inosine. L'équation 7 prévoit une variation linéaire de $[In]/k_{exp}$ en fonction de $[Br^-]$; la pente de la droite devrait être k_{-1}/k_1k_2 tandis que l'ordonnée à l'origine serait $[In]/k_1$. En essayant l'interprétation graphique de cette manière, on observe, d'une part, une courbure nette des graphes et d'autre part, que l'ordonnée à l'origine n'est pas proportionnelle à la concentration en inosine. Ceci indique qu'il y a un autre terme dont il faut tenir compte; l'hypothèse la plus satisfaisante implique une contribution du mécanisme S_N2, avec la constante de vitesse k_{S_N2}. Ceci est évidemment en accord avec les diverses études ayant conduit à l'éq. 1 (2–6). On obtient alors l'éq. 8.

$$[8] \quad k_{exp} = \frac{k_2k_1[In]}{k_{-1}[Br^-] + k_2[In]} + k_{S_N2}[In]$$

L'équation 8 contient trop de paramètres pour qu'ils puissent être déterminés directement par une méthode graphique. On a dû recourir à une méthode d'itération utilisant une calculatrice électronique programmée. On a choisi en première approximation, une valeur de k_{S_N2} voisine à k_{exp} obtenue à concentration en Br^- élevée. En soustrayant alors le terme $k_{S_N2}[In]$ de k_{exp}, on obtient la contribution du premier terme du membre de droite de l'éq. 8 dont les paramètres peuvent alors être déterminés par voie graphique. Compte tenu de la valeur trop élevée de k_{S_N2}, les valeurs de k_1 et k_{-1}/k_2 obtenues varient d'une série d'expériences à l'autre. En diminuant progressivement la valeur de k_{S_N2}, on arrive à des valeurs de k_1 et k_{-1}/k_2 raisonnablement constantes. L'affinement est alors effectué en recalculant la constante à l'aide de l'éq. 8 et en retenant la valeur des paramètres donnant le meilleur accord entre k_{exp} et k_{calc} sur l'ensemble des données.

A 50 °C on obtient les valeurs suivantes: $k_{S_N2} = 2.5 \times 10^{-2}\ M^{-1}\ s^{-1}$, $k_1 = 1.5 \times 10^{-3}\ s^{-1}$, $k_{-1}/k_2 = 30$. Le tableau 1 résume, pour diverses séries d'expériences, les constantes de vitesse expérimentales et calculées. Comme on peut le constater l'accord est satisfaisant compte tenu de l'erreur expérimentale qui est d'environ 10% en présence de KBr. L'erreur sur k_1 et k_1/k_2 est aussi d'environ 10%; la valeur de k_{S_N2}, à cause de la contribution moindre (de 10% à 40%) du mécanisme S_N2, est évidemment entachée d'une erreur plus grande (~25%).

La variation de ces paramètres avec la température n'a pas été étudiée, par contre l'énergie d'activation globale a été déterminée. Elle est de 17.1 ± 0.5 kcal pour un rapport $[In]/[Br^-] = 24.3$ et 16.9 ± 0.5 kcal pour $[In]/[Br^-] = 60.4$. Bien que les valeurs obtenues n'aient pas de signification univoque, dûe à la complexité de l'éq. 8, il est quand même à noter, qu'elles sont supérieures de 5 à 7 kcal à celles obtenues pour k_Y dans le cas de substitution par SCN^- et I^- (4).

Il est intéressant de comparer les valeurs de nos paramètres avec celles provenant d'études cinétiques indépendantes et concernant des systèmes différents. La valeur de k_1 à 50 °C peut être calculée à partir des données rapportées dans la littérature pour la substitution de $[Pt(dien)Br]^+$ par N_3^- (4) qui répond à l'éq. 1. L'ordonnée à l'origine à faible concentration en Br^-, tend vers k_1, et la valeur pour 50 °C est de 8.77×10^{-2} min^{-1} en bon accord avec notre $k_1 = 9.0 \times 10^{-2}\ min^{-1}$.

Les réactions du complexe aquo $[Pt(dien)H_2O]^{2+}$ ont été étudiées par Gray et Olcott (5). Avec la pyridine on a une constante de vitesse, $k_2 = 1.9 \times 10^{-3}\ s^{-1}$ à 25 °C et à concentration en pyridine de $5 \times 10^{-3}\ M$, tandis que sa réaction avec l'ion Br^- à la même concentration, a une constante correspondant à k_{-1}, de $3.5 \times 10^{-2}\ s^{-1}$. On peut déduire de ces valeurs $k_{-1}/k_2 = 18$ pour la pyridine, relativement proche de notre valeur de 30, compte tenu des différences entre les deux bases azotées et des conditions expérimentales.

Can. J. Chem. Downloaded from www.nrcresearchpress.com by 210.87.254.6 on 09/05/12
For personal use only.

TABLEAU 1. Constantes de vitesse expérimentales et calculées*

[In] $\times 10^2 M$	$[Br^-] = 2.7\ 10^{-4}\ M$†		$[Br^-] = 4.1\ 10^{-4}\ M$‡		$[Br^-] = 6.6\ 10^{-4}\ M$‡		$[Br^-] = 1.4\ 10^{-3}\ M$‡	
	$k_{exp} \times 10^4\ s^{-1}$	$k_{calc} \times 10^4\ s^{-1}$	$k_{exp} \times 10^4\ s^{-1}$	$k_{calc} \times 10^4\ s^{-1}$	$k_{exp} \times 10^4\ s^{-1}$	$k_{calc} \times 10^4\ s^{-1}$	$k_{exp} \times 10^4\ s^{-1}$	$k_{calc} \times 10^4\ s^{-1}$
0.10	2.0	1.87	1.75	1.74	1.1	1.15	—	—
0.25	4.2	4.12	3.4	3.17	2.75	2.69	1.6	1.55
0.40	5.75	5.91	4.6	4.68	4.4	4.05	2.4	2.43
0.50	—	—	—	—	4.8	4.88	3.1	3.0
0.60	9.1	7.84	7.25	6.42	6.2	5.65	3.6	3.55
1.00	11.2	10.80	9.7	9.2	8.3	8.3	4.15	5.6
1.75	16.5	14.26	13.7	12.86	10.3	11.96.	8.2	8.78
2.50	16.8	17.4	14.0	16.3	16.8	15.5	11.1	12.2
3.00	18.8	19.4	18.8	18.2	17.2	17.4	15.2	14.2
4.00	20.3	22.6	20.3	21.6	22.7	21.0	18.3	17.8
6.25	24.3	29.0	24.3	28.3	—	—	20.0	25.18

*$T = 50$ °C; [[Pt(dien)Br]Br] = 2.7×10^{-4} M.
†Concentration en Br^- provenant de la dissociation du [Pt(dien)Br]Br.
‡Concentration totale en Br^- comprenant † et KBr ajouté.

La valeur de k_{S_N2}, soit $2.5 \times 10^{-2}\ M^{-1}\ s^{-1}$ est de loin inférieure aux constantes de vitesse de la plupart d'autres ligands étudiés, d'où naturellement la prépondérance dans notre cas du mécanisme impliquant le solvant.

Il faut souligner qu'une troisième voie réactionnelle, impliquant une réaction d'ordre un du complexe aquo, tel que suggéré par Gray et Olcott (5), peut aussi contribuer faiblement aux résultats, mais dans nos conditions expérimentales elle sera probablement noyée dans l'erreur expérimentale.

Il est intéressant de situer l'équation de vitesse [8] dans l'ensemble des résultats obtenus pour la substitution de $[Pt(dien)Br]^+$. Dans la majorité des cas, l'éq. 1 est vérifiée; par exemple, les résultats obtenus avec des ligands tels que CNS^-, I^-, Cl^-, N_3^-, $SeCN^-$, donnent une relation linéaire, avec une contribution prépondérante du mécanisme S_N2 (4).

Des écarts à la linéarité de l'éq. 1 ont déjà été observés et expliqués qualitativement en faisant intervenir l'intermédiaire aquo dans le cas du ligand NO_2^- (6). Le même travail a mis également en évidence une courbure des équations intégrées attribuée à l'inhibition par le bromure. La substitution par la pyridine a été également inhibée par l'ion bromure (6), bien que les premiers résultats concernant ce système ne montraient aucune inhibition (3), ce qui était probablement dû à la haute concentration en pyridine et surtout à la faible concentration en ion bromure utilisées.

Dans le cas de la substitution du *trans*-Pt-$(NH_3)_2Cl_2$ par la pyridine et l'aniline, Banerjea *et al.* (2) ont constaté une inhibition par le chlorure libéré, et, bien qu'ils n'aient pas effectué une étude détaillée, ont proposé un mécanisme et une équation de vitesse semblables à ceux observés ici. Enfin, dans le cas de complexes de palladium, qui en général réagissent par un mécanisme semblable à l'éq. 1, on a pu supprimer complètement la voie S_N2 en utilisant des ligands encombrés, dans le cas du $Pd(Et_4dien)Br$ (13).

En résumant, l'équation de vitesse [8] indique clairement que la voie réactionnelle impliquant le solvant est loin d'être une réaction d'ordre un simple tel qu'elle apparaît dans l'éq. 1. La raison pour laquelle elle n'a pas été vérifiée quantitativement est probablement dû au fait que dans les conditions expérimentales utilisées par divers auteurs le terme S_N2 est de loin plus important que celui impliquant le solvant.

Conclusion

La cinétique de formation du complexe $[Pt(dien)In]^{2+}$ se fait principalement par une voie réactionnelle impliquant la formation d'un intermédiaire aquo et, par le fait même, cette réaction a pu être étudiée quantitativement. Les paramètres cinétiques cadrent bien avec les valeurs individuelles d'études indépendantes concernant les complexes aquo.

Tous les cas connus qui impliquent des écarts au mécanisme de Basolo et Pearson ont été observés pour les bases azotées. Il est donc très probable que le mécanisme puisse être généralisé

Can. J. Chem. Downloaded from www.nrcresearchpress.com by 210.87.254.6 on 09/05/12
For personal use only.

aux nucléosides, mais dont certains peuvent présenter plusieurs sites de coordination.

Il faut souligner l'importance de l'inhibition par l'ion bromure, étant donné que dans les systèmes biologiques, il y a en général une concentration assez grande d'halogénures.

Les auteurs remercient le Ministère de l'Education du Québec pour la subvention de recherche qui a rendu possible la réalisation de ce travail.

1. F. BASOLO et R. G. PEARSON. Mechanism of inorganic reactions. 2nd ed. John Wiley and Son, New York. 1967. p. 375.
2. D. BANERJEA, F. BASOLO et R. G. PEARSON. J. Am. Chem. Soc. **79**, 4055 (1957).
3. F. BASOLO, H. B. GRAY et R. G. PEARSON. J. Am. Chem. Soc. **82**, 4200 (1960).
4. U. BELLUCO, R. ETTORE, F. BASOLO, R. G. PEARSON et A. TURCO. Inorg. Chem. **5**, 591 (1966).
5. H. B. GRAY and R. J. OLCOTT. Inorg. Chem. **1**, 481 (1962).
6. H. B. GRAY. J. Am. Chem. Soc. **84**, 1548 (1962).
7. S. MANSY, B. ROSENBERG et A. J. THOMSON. J. Am. Chem. Soc. **95**, 1633 (1973).
8. P. C. KONG and T. THEOPHANIDES. Inorg. Chem. Soumis pour publication.
9. P. C. KONG and T. THEOPHANIDES. Inorg. Chem. Soumis pour publication.
10. B. ROSENBERG. Platinum Met. Rev. **15**, 42 (1971); M. J. CLEARE and J. D. HOESCHELE. Platinum Met. Rev. **17**, 2 (1973).
11. F. G. MANN. J. Chem. Soc. 466 (1934).
12. T. CYR, J. PRUD'HOMME et M. ZADOR. J. Chem. Ed. **50**, 572 (1973).
13. W. H. BADDLEY et F. BASOLO. J. Am. Chem. Soc. **88**, 2944 (1966).

Can. J. Chem. Downloaded from www.nrcresearchpress.com by 210.87.254.6 on 09/05/12
For personal use only.

Infrared Chemiluminescence from the Reaction of Oxygen Atoms with Chloroethylenes

S. J. ARNOLD, G. H. KIMBELL, AND D. R. SNELLING

Centre de Recherches pour la Defense, Defence Research Establishment, Valcartier, Québec

Received February 19, 1974

S. J. ARNOLD, G. H. KIMBELL and D. R. SNELLING. Can. J. Chem. **52**, 2608 (1974).

Infrared chemiluminescence from vibrationally excited CO and from vibrationally excited HCl was observed when C_2H_3Cl, 1,1-$C_2H_2Cl_2$, *cis*- and *trans*-1,2-$C_2H_2Cl_2$, or C_2HCl_3 was introduced into a stream of oxygen atoms. The mechanisms describing the reactions of oxygen atoms with these molecules are discussed in detail. The initial step is postulated to involve the formation of an aldehyde and a carbene. The reaction step responsible for the formation of CO† is postulated to be

$$O + CX_1X_2 \rightarrow CO\dagger + X_1 + X_2 \quad (X_1, X_2 = H \text{ or } Cl)$$

and for HCl†

$$H + Cl_2 \rightarrow HCl\dagger + Cl$$

S. J. ARNOLD, G. H. KIMBELL et D. R. SNELLING. Can. J. Chem. **52**, 2608 (1974).

La chimiluminescence infrarouge provenant de molécules de CO et HCl vibrationnellement excitées a été observée lorsque du C_2H_3Cl, $C_2H_2Cl_2$-1,1, $C_2H_2Cl_2$-1,2 *cis* et *trans* ou C_2HCl_3 est introduit dans un débit d'oxygène traité par une décharge à haute fréquence. Les mécanismes décrivant les réactions des atomes d'oxygène avec ces molécules sont discutés. On croit que l'étape initiale produit un aldéhyde et un carbène. La réaction responsable de la formation de CO† serait:

$$O + CX_1X_2 \rightarrow CO\dagger + X_1 + X_2 \quad (X_1, X_2 = H \text{ or } Cl)$$

et de HCl† serait:

$$H + Cl_2 \rightarrow HCl\dagger + Cl$$

Introduction

In a previous paper (1), the infrared chemiluminescence observed in the reactions of oxygen atoms with chloromethanes was discussed. That study has now been extended to include the reactions of oxygen atoms with chloroethylenes, the subject of the present paper.

The reactions of oxygen atoms with fluoroethylenes has been the subject of several studies (2–7). The values of the rate constants for the reactions of $O(^3P)$ atoms with $C_2H_xF_{4-x}$ have been found to lie in the region of 7×10^{-13} cm^3 $molecule^{-1}$ s^{-1} (5–7). The mechanism for $O(^3P)$ atom attack on C_2F_4 has been shown to involve the formation of an aldehyde and a carbene (2, 3)

$$O(^3P) + C_2F_4 \rightarrow CF_2O + CF_2$$

The reactions of oxygen atoms with other haloethylenes, however, have not received much attention. Huie *et al.* (7) have measured the values of the rate constants for the reaction of $O(^3P)$ atoms with C_2H_3Cl and C_2H_3Br obtaining values of 8.7×10^{-13} and 8.2×10^{-13} cm^3 $molecule^{-1}$ s^{-1} respectively and in the case of C_2H_3Cl have observed the aldehydic product, CH_2O.

The present experiments show that intense infrared chemiluminescence is produced when $O(^3P)$ atoms react with C_2H_3Cl, 1,1-$C_2H_2Cl_2$, *cis*- and *trans*-1,2-$C_2H_2Cl_2$, and C_2HCl_3. The chemiluminescence arises from vibrationally excited CO and HCl.

Experimental

The apparatus used in these experiments is identical to that shown in Fig. 1 of ref. 8. The reaction cell consisted of a 1.5 in. glass "tee" equipped with a NaCl window, which was pumped by an Edwards 660 l/min two-stage pump. Oxygen atoms produced by the passage of an oxygen–helium mixture through a 2450 MHz microwave discharge entered the cell through the center tube of the concentric mixer. The chloroethylene in a helium buffer entered through five holes in the outer tube of the concentric mixer. Carbon monoxide, when introduced, was premixed with the chloroethylene–helium mixture.

The spectra were recorded using a McPherson Model 218, 0.3 m monochromator equipped with a 300 line/mm grating, a Dry Ice – acetone-cooled PbS detector, a phase sensitive PAR Model HR-8 amplifier and Hewlett–Packard Model 7100 B strip chart recorder. This assembly

Can. J. Chem. Downloaded from www.nrcresearchpress.com by 210.87.254.40 on 09/05/12
For personal use only.

TABLE 1. Experimental conditions for maximum total emission intensity of CO

Fuel	Fuel:O_2	Temperature	Relative total emission intensity of CO
C_2H_2	0.33:1	150	1.25
C_2H_3Cl	0.15:1		0.20
1,1-$C_2H_2Cl_2$	1.3:1	186	1.00
1,2-$C_2H_2Cl_2$	1.25:1	150	0.59
C_2HCl_3	1.54:1	165	0.70

TABLE 2. Reaction products observed in $C_2H_xCl_{4-x}$–O_2 atomic flames

Chloroethylene	Reaction products						
C_2H_3Cl	Cl_2	CO	CO_2	HCl	CH_2O	1,1,2-$C_2H_3Cl_3$	1,1-$C_2H_2Cl_2$ 1,2-$C_2H_2Cl_2$
1,1-$C_2H_2Cl_2$	Cl_2	CO	CO_2	HCl	CH_2O CCl_2O	1,1,1,2-$C_2H_2Cl_4$	C_2HCl_3 $C_2H_2Cl_2O$
1,2-$C_2H_2Cl_2$	Cl_2	CO	CO_2	HCl		1,1,2,2-$C_2H_2Cl_4$	C_2HCl_3
C_2HCl_3	Cl_2	CO	CO_2	HCl	CCl_2O	C_2HCl_5	C_2Cl_4 C_2HCl_3O

permitted spectral studies in the region 1500 to 4000 nm. The entire optical path was flushed with dry nitrogen to minimize absorption by atmospheric water vapor. A 500 °C black body source was used to provide a relative measurement of the sensitivity of the detection system as a function of wavelength.

Temperatures in the reaction zone were measured with a glass-coated chromel–alumel thermocouple.

Reaction products, trapped at liquid nitrogen temperatures, were analyzed by means of a CEC Model 72-104 mass spectrometer and a Perkin–Elmer Model 900 vapor phase chromatograph.

All gases used were of the highest purity available from Matheson and were used without further purification. The 1,1-$C_2H_2Cl_2$ was supplied by the J. T. Baker Chemical Company, the *cis*-1,2-$C_2H_2Cl_2$ and the *trans*-1,2-$C_2H_2Cl_2$ by Matheson, Coleman and Bell and the C_2HCl_3 by the Fisher Scientific Company. Gas flows were measured using Matheson rotameters.

Results and Discussion

Infrared chemiluminescence attributable to CO† and HCl† was observed from the reactions of oxygen atoms with chloroethylenes: C_2H_3Cl, 1,1-$C_2H_2Cl_2$, *cis*-1,2-$C_2H_2Cl_2$, *trans*-1,2-$C_2H_2Cl_2$, and C_2HCl_3. The experimental conditions for maximum total emission intensity of the first overtone of CO are given in Table 1. The flow rates of the inert buffer, He, and of O_2 were 4.8 mmol/s and 5.4×10^{-2} mmol/s, respectively. The pressure for all experiments was 8.2 ± 0.2 Torr. The most intense HCl emission was from 1,1-$C_2H_2Cl_2$ and the weakest from C_2H_3Cl. In the case of 1,1-$C_2H_2Cl_2$, the HCl emission was strong enough to permit a vibrational analysis of the overtone emission; this indicated vibrational excitation of the HCl up to $v=6$. The results of mass spectrometric and vapor phase chromatographic analysis of the reaction products are given in Table 2.

Only the first 12 vibrational levels of CO† were appreciably populated. Figure 1 shows a plot of the relative vibrational level population, Nv, calculated according to the method of Hancock and Smith (9), against vibrational number, v, for conditions of maximum total emission intensity. Under these conditions the systems did not exhibit complete population inversion. As in the case of the oxygen atom – C_2H_2 and oxygen atom – chloromethane systems when vibrationally "cold" CO was premixed with the fuel–He mixture, a vibrational population inversion was marginally sustained at the 7–6 and 6–5 transitions.

As in the case of chloromethane – oxygen atom systems, the relative vibrational level distribution of CO appears, within experimental error, to be independent of both the amount of fuel added and concentration of oxygen atoms. It thus seems unlikely that vibrational deactivation by fuel molecules or combustion products

Can. J. Chem. Downloaded from www.nrcresearchpress.com by 210.87.254.40 on 09/05/12
For personal use only.

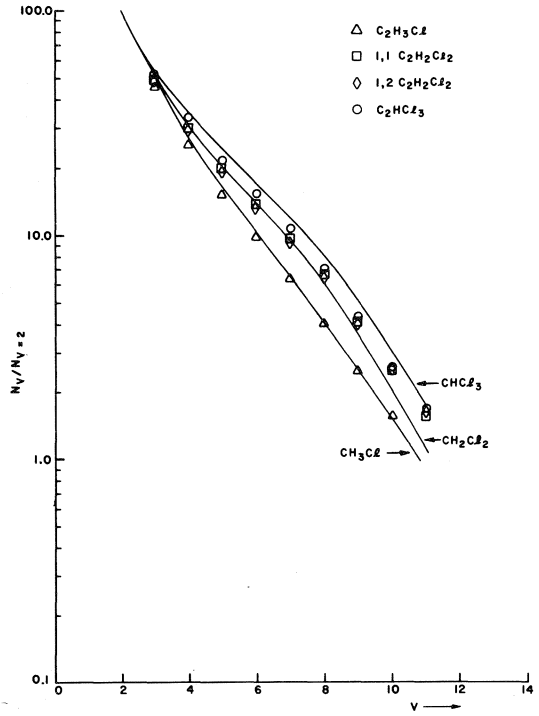

FIG. 1. Relative vibrational level population of CO† produced in $C_2H_xCl_{4-x}/O_2$ ($x = 1, 2, 3$) atomic flames. The data points represent the average value for the following number of experimental determinations $C_2H_3Cl = 5$, 1,1-$C_2H_2Cl_2 = 8$, 1,2-$C_2H_2Cl_2 = 11$, $C_2HCl_3 = 10$. The data for CH_xCl_{4-x}/O_2 ($x = 1, 2, 3$) atomic flames is from ref. 1.

are important in altering the vibrational energy distribution of the product CO. The residence time in the viewed region of 8 ms is of the same order of magnitude as the radiative lifetime of the vibrational levels of CO. Hence, although the relative vibrational level distributions for various fuels can be compared with one another, they represent partially relaxed distributions with the population in the higher vibrational levels reduced with respect to those in the lower vibrational levels.

The reaction of $O(^3P)$ atoms with ethylene has been the subject of numerous studies (10–13). The initial step is thought to involve the formation of an epoxide which would decompose to form a formyl radical and a methyl radical

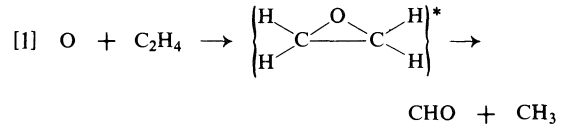

The initial step in the reaction of $O(^3P)$ atoms with C_2F_4, however, is thought to involve the formation of an aldehyde and a carbene (2, 3).

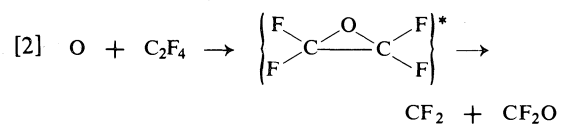

Heicklen and co-workers (2, 3) have shown that the reaction products are CF_2O and cyclo-C_3F_6. The epoxide, C_2F_4O, is observed only in the presence of molecular oxygen and is believed to be formed by a chain process. Mitchell and Simons (4), in their photolytic studies on substituted 1,1-difluoroethylenes indicate that the initial step is analogous to reaction 2.

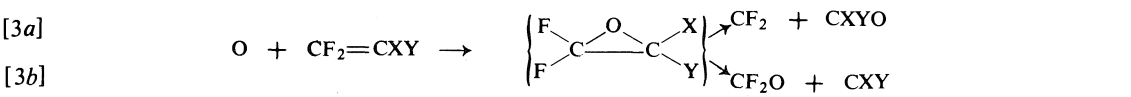

with reaction 3*b* being favored when X,Y = halogen. The mass spectrometric studies of Huie *et al.* (7) on the reactions of $O(^3P)$ atoms with $C_2H_xF_{4-x}$, C_2H_3Cl, and C_2H_3Br also indicate that the initial step involves the formation of an aldehyde and a carbene. Consequently, it appears likely that in the reaction of $O(^3P)$ atoms with $C_2H_xCl_{4-x}$ ($x = 1, 2, 3$) the initial step involves the formation of an aldehyde and a carbene, analogous to reactions 3*a* and *b*, rather than a methyl radical and a formyl radical, analogous to reaction 1.

The possible initial steps in the reactions of $O(^3P)$ atoms with $C_2H_xCl_{4-x}$ ($x = 1, 2, 3$) are given in Table 3. (All rate constants are in units of cm^3 $molecule^{-1}$ s^{-1}.) Except in the case of 1,2-$C_2H_2Cl_2$, two possible aldehydes and two possible carbenes can be formed in each case. The rate constant for the reaction of $O(^3P)$ atoms with C_2H_3Cl has been determined by Huie *et al.*

Can. J. Chem. Downloaded from www.nrcresearchpress.com by 210.87.254.40 on 09/05/12
For personal use only.

TABLE 3. Possible initial steps in the reaction of $O(^3P)$ atoms with $C_2H_xCl_{4-x}$ ($x = 1,2,3$)

Reaction	$k_a + k_b$*
$O + C_2H_3Cl \xrightarrow{a} CHClO + CH_2$ $\xrightarrow{b} CHCl + CH_2O$	8.7×10^{-13}
$O + CCl_2CH_2 \xrightarrow{a} CH_2O + CCl_2$ $\xrightarrow{b} CCl_2O + CH_2$	
$O + CHClCHCl \xrightarrow{a} CHClO + CHCl$	
$O + C_2HCl_3 \xrightarrow{a} CHClO + CCl_2$ $\xrightarrow{b} CCl_2O + CHCl$	$\sim 4.3 \times 10^{-13}$

*All rate constants are in units of cm^3 $molecule^{-1}$ s^{-1}.

(7), $k_{C_2H_3Cl} = 8.7 \times 10^{-13}$ at 307 °K. Their work indicated that the rate constant for $O(^3P) + C_2HCl_3$ was $\simeq 1/2$ this value and for $O(^3P) + C_2Cl_4$, $\simeq 1/5$ (7). Huie *et al.* have shown that in the case of fluoroethylenes, the rate constants for the reactions with $O(^3P)$ atoms lie within a reasonably narrow range (1.05 to 0.43 of that for $O(^3P) + C_2H_4$). For the purposes of the present discussion it is assumed that the effect of successive chlorine atom substitution is not much more pronounced than that of fluorine atom substitution and that the unmeasured rate constants, $O(^3P) + 1,1\text{-}C_2H_2Cl_2$ and $O(^3P) + 1,2\text{-}C_2H_2Cl_2$, will not be greatly different from the value obtained for $O(^3P) + C_2H_3Cl$.

The aldehyde, CHClO, formed in the C_2H_3Cl, $1,2\text{-}C_2H_2Cl_2$, and C_2HCl_3 cases is unstable toward decomposition

[4] $CHClO \rightarrow CO + HCl + 8.5$ kcal/mol

The aldehydes, CH_2O in the case of C_2H_3Cl, CH_2O and CCl_2O in the case of $1,1\text{-}C_2H_2Cl_2$, and CCl_2O in the case of C_2HCl_3 are observed as reaction products.

It has been shown that vibrationally excited CO is formed by the reaction $O(^3P)$ atoms with carbenes (1)

[5*a*] $O + CHCl \rightarrow CO + H + Cl + 85$ kcal/mol

[5*b*] $O + CH_2 \rightarrow CO + 2H + 73.8$ kcal/mol

[5*c*] $O + CCl_2 \rightarrow CO + 2Cl + 85$ kcal/mol

Reaction 5*b* is sufficiently exothermic to populate CO up to $v = 13$ and reactions 5*a* and 5*c* up to $v = 15$.[1]

Thus it would appear probable that these reactions are the source of the vibrationally excited carbon monoxide observed in the present experiments. Indeed the vibrational level distributions observed in the present experiments are remarkably similar to those in the study of the $O(^3P)$ atoms with halomethanes (1). Figure 1 shows a comparison between the halogenated ethylenes and halogenated methanes. As in the case of the chlorinated methanes the carbenes with more halogen atoms yield distributions more highly populated in the upper vibrational levels. Indeed the data points obtained for the chlorinated ethylenes lie very close to lines obtained for the methanes.

Insufficient quantitative information exists to warrant much further discussion of mechanisms for additional product formation or of loss mechanisms for fuel molecules. Nevertheless, sufficient information exists (14) (see Table 4) to show that chlorine atom addition to chloroethylenes is very fast, *i.e.* chlorine atom lifetime is given by

$$\tau_{Cl} = \frac{1}{k[C_2H_xCl_{4-x}]} \leqslant 0.03 \text{ ms}$$

If successive addition of two chlorine atoms occurred and the resultant complex partially decomposed by HCl elimination (15), then both $C_2H_xCl_{6-x}$ Cl_{6-x} and $C_2H_{x-1}Cl_{5-x}$ should be formed as, in fact, they are (Table 2).

Molecular chlorine, an observed reaction product, would appear to be formed by chlorine atom recombination following reactions 5*a* and 5*c* or the fast reaction

[6] $H + HCl \rightarrow H_2 + Cl + 1.1$ kcal/mol

which has a value (16) of

$$k_6 = 3.8 \times 10^{-11} \exp(-3500/RT)$$

Vibrationally excited HCl is thought to be predominately formed by the reaction of hydrogen atoms with molecular chlorine

[7] $H + Cl_2 \rightarrow HCl + Cl + 45.2$ kcal/mol

[1] One of the referees has suggested that the observation of CO† from the C_2Cl_4–O atom system could lead to corroborative evidence for this mechanism. Infrared emission from CO† was observed from this system indicating that reaction 5*c* is operative

Can. J. Chem. Downloaded from www.nrcresearchpress.com by 210.87.254.40 on 09/05/12
For personal use only.

TABLE 4. Reactions of Cl Atoms with $C_2H_xCl_{4-x}$ ($x = 1, 2, 3$)

Reaction	$k_a + k_b$*	Stabilization product	Elimination product
$Cl + C_2H_3Cl \xrightarrow{a} \dot{C}HClCH_2Cl$ $\xrightarrow{b} CHCl_2\dot{C}H_2$	7.3×10^{-11}	$1,1,2\text{-}C_2H_3Cl_3$	$1,2\text{-}C_2H_2Cl_2$ $1,1\text{-}C_2H_2Cl_2$
$Cl + 1,1\text{-}C_2H_2Cl_2 \xrightarrow{a} \dot{C}Cl_2CH_2Cl$ $\xrightarrow{b} CCl_3\dot{C}H_2$	5.3×10^{-11}	$1,1,1,2\text{-}C_2H_2Cl_4$	C_2HCl_3
$Cl + cis\text{-}1,2\text{-}C_2H_2Cl_2 \rightarrow CHCl_2\dot{C}HCl$	1.0×10^{-10}	$1,1,2,2\text{-}C_2H_2Cl_4$	C_2HCl_3
$Cl + trans\text{-}1,2\text{-}C_2H_2Cl_2 \rightarrow CHCl_2\dot{C}HCl$	6.6×10^{-11}	$1,1,2,2\text{-}C_2H_2Cl_4$	C_2HCl_3
$Cl + C_2HCl_3 \xrightarrow{a} \dot{C}HClCCl_3$ $\xrightarrow{b} CHCl_2\dot{C}Cl_2$	5.8×10^{-11}	C_2HCl_5	C_2Cl_4

*All rate constants are in units of cm^3 $molecule^{-1}$ s^{-1}.

which has a value of $k_7 = 1.0 \times 10^{-11}$ (17) which is sufficiently exothermic to produce HCl† in levels up to $v = 6$, the highest level observed to be populated.[2]

The other observed reaction products, the epoxides, $C_2H_2Cl_2O$ in the case of $1,1\text{-}C_2H_2Cl_2$ and C_2HCl_3O in the case of C_2HCl_3, can be formed by stabilization of the epoxide intermediate produced in the initial step.

1. S. J. ARNOLD, G. H. KIMBELL, and D. R. SNELLING. Can. J. Chem. **52**, 271 (1974).
2. D. SAUNDERS and J. HEICKLEN. J. Am. Chem. Soc. **87**, 2088 (1965).

[2]One of the referees has suggested that HCl† may be formed by elimination from the epoxide formed in reaction 3. We consider this process unlikely as all available evidence indicates the epoxide decomposes to form a carbene and an aldehyde.

In systems in which CHCl is formed, the exothermic reactions

$$O + CHCl \rightarrow CO\dagger + HCl + 188 \text{ kcal/mol}$$

$$O_2 + CHCl \rightarrow CO_2 + HCl\dagger + 196 \text{ kcal/mol}$$

may contribute to the formation of HCl†. These reactions are not considered to be as important as reaction 7 because they are not likely to be operative in the O + $1,1\text{-}C_2H_2Cl_2$ system where CHCl can be formed only as a result of a complex rearrangement of the excited epoxide.

3. J. HEICKLEN and V. KNIGHT. J. Phys. Chem. **70**, 3893 (1966).
4. R. C. MITCHELL and J. P. SIMONS. J. Chem. Soc. B, 1005 (1968).
5. S. J. MOSS. Trans. Faraday Soc. **67**, 3505 (1971).
6. W. J. R. TYERMAN. Trans. Faraday Soc. **65**, 163 (1969).
7. R. E. HUIE, J. T. HERRON, and D. D. DAVIS. Int. J. Chem. Kinet. **4**, 521 (1972).
8. S. J. ARNOLD and G. H. KIMBELL. Can. J. Chem. **51**, 451 (1973).
9. G. HANCOCK and I. W. M. SMITH. Chem. Phys. Lett. **3**, 573 (1969).
10. J. M. BROWN and B. A. THRUSH. Trans. Faraday Soc. **63**, 630 (1966).
11. P. N. CLOUGH and B. A. THRUSH. Chem. Commun. **21**, 1351 (1968).
12. H. NIKI, E. E. DABY, and B. WEINSTOCK. Twelfth Symposium (International) on Combustion. University of Poitiers, Poitiers, France. July, 1968. pp. 277–288.
13. D. D. DAVIS, R. E. HUIE, J. T. HERRON, M. J. KURYLO, and W. BROWN. J. Chem. Phys. **56**, 4868 (1972).
14. J. A. KERR and M. H. PARSONAGE. Evaluated kinetic data on gas phase addition reactions. CRC Press, Cleveland, Ohio. 1972. pp. 101–102.
15. J. C. HASSLER, D. W. SETSER, and R. L. JOHNSON. J. Chem. Phys. **45**, 3231 (1966).
16. A. A. WESTENBERG and N. DE HAAS. J. Chem. Phys. **48**, 4405 (1968).
17. F. S. KLEIN and M. WOLFSBERG. J. Chem. Phys. **34**, 1494 (1961).

Can. J. Chem. Downloaded from www.nrcresearchpress.com by 210.87.254.40 on 09/05/12
For personal use only.

Crystal Structure of 1-(Bis-*p*-chlorophenyl)methylene-3-oxo-4,4-dimethyl-1,2-diazetidinium Hydroxide, Inner Salt, $C_{17}H_{14}Cl_2N_2O$

CRISPIN CALVO, PO C. IP, NARASIMHAN KRISHNAMACHARI, AND JOHN WARKENTIN

Department of Chemistry, McMaster University, Hamilton, Ontario, L8S 4M1

Received November 14, 1973

CRISPIN CALVO, PO C. IP, NARASIMHAN KRISHNAMACHARI, and JOHN WARKENTIN. Can. J. Chem. **52**, 2613 (1974).

1(bis-*p*-Chlorophenyl)methylene-3-oxo-4,4-dimethyl-1,2-diazetidinium hydroxide,[1] inner salt, $C_{17}H_{14}Cl_2N_2O$, crystallizes with orthorhombic symmetry, $a = 9.95(1)$ Å, $b = 28.73(2)$ Å, $c = 11.30(1)$ Å, space group *Pbca*, $Z = 8$. The structure of this compound and its isostructural bromine analog were determined. The structure of the chloro-derivative was refined by full-matrix least-squares techniques using 1256 unique reflections to a final R of 0.099. The structure has a short intramolecular C—H...N bond (C...N distance = 2.891(11) Å). One of the phenyl rings is in the same plane as the 4-membered ring whereas the other ring lies in a plane almost perpendicular to this plane. The N—N distance in the heterocyclic ring is 1.415(10) Å, and the N—C distances in the ring are 1.535(11) and 1.377(11) Å. The molecular configuration is stabilized by both the short N...H interaction and delocalization between one of the phenyl groups and the diazetidinium ring.

CRISPIN CALVO, PO C. IP, NARASIMHAN KRISHNAMACHARI, et JOHN WARKENTIN. Can. J. Chem. **52**, 2613 (1974).

Le sel interne, l'hydroxyde du (bis-*p*-chlorophényl) méthylène-1 oxo-3 diméthyl-4,4 diazétidinium-1,2, $C_{17}H_{14}Cl_2N_2O$, cristallise dans le système orthorhombique: $a = 9.95(1)$ Å, $b = 28.73(2)$ Å, $c = 11.30(1)$ Å, groupe d'espace *Pbca*, $Z = 8$. La structure de ce composé et celle de son analogue bromé isostructural ont été déterminées. La structure du dérivé chloré est affinée par la methode des moindres carrés (matrice entière) utilisant 1256 réflexions uniques jusqu'à une valeur finale R de 0.099. La structure a une liaison intramoléculaire C—H...N qui est court (la distance C...N = 2.891(11) Å). Un des noyaux phényles est dans le même plan que le cycle à 4 atomes alors que l'autre cycle se situe dans un plan presque perpendiculaire au cycle à 4 atomes. La distance N—N dans le noyau hétérocyclique est 1.415(10) Å, et les distances N—C dans le noyau sont 1.535(11) et 1.377(11) Å. La configuration moléculaire est stabilisée par une interaction N...H courte et par la délocalisation entre un des groupes phényles et le noyau diazétidinium. [Traduit par le journal]

Introduction

Thermal decomposition of some members of the family of cyclic azo compounds (**1**) involves loss of N_2 to form products for which structures **2–5** were reasonable possibilities. Spectroscopic data served to eliminate **4** from further consideration and to suggest **5** as the most likely structure. However, **2** and **3** could not be excluded rigorously, first because iminooxiranes have not yet been isolated, meaning that there are no models for **2**, and second because good models for **3** (α-lactams with an unsaturated substituent

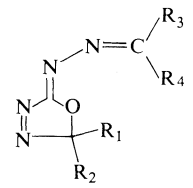

1

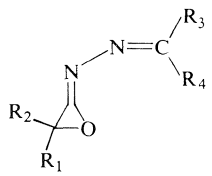

2

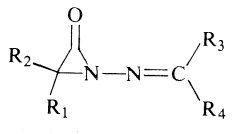

3

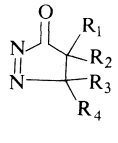

4

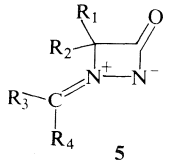

5

[1]The nomenclature is that recommended by Chemical Abstracts. Top priority is given to charged systems; hence the parent name diazetidinium rather than diazetidinone. When there is no obvious anion to go with the cation name the word hydroxide is artificially added and the fact that the system is actually mesoionic is indicated further with the words inner salt.

Can. J. Chem. Downloaded from www.nrcresearchpress.com by 210.87.254.105 on 09/05/12
For personal use only.

Can. J. Chem. Downloaded from www.nrcresearchpress.com by 210.87.254.105 on 09/05/12
For personal use only.

at the ring nitrogen) are also unknown although the simple ring system in known (1).

As the synthesis of any one of the small-ring systems **2**, **3**, or **5** from the readily available **1** (2) could be of considerable value, it seemed important to identify the actual product unambiguously by X-ray crystallography. The fact that the crystal structure of one member of the family **5** ($R_1 = R_2 = H$; $R_3 = C_6H_5$, $R_4 = p\text{-}C_6H_4Br$) had been determined (3) increased our interest for the authors suggested an unusual hydrogen bond between amide nitrogen and ortho hydrogen of R_4; a suggestion that was later challenged on the basis of a study of the infrared spectrum (4). It seemed possible that investigation of our compounds, should they turn out to be **5**, would help to resolve the controversy, for our route has the potential for synthesis of compounds more hindered than, and electronically different from, the few that are known (5).

In this article we report the crystal structure of one of the new members of the series **5**.

Experimental

Synthesis

p,p′-Dichlorobenzophenone-4-aminosemicarbazone

A solution prepared from *p,p′*-dichlorobenzophenone (18.5 g, 0.0735 mol), carbohydrazide (13.2 g, 0.147 mol), acetic acid (1 ml), ethyl alcohol (350 ml), and water (150 ml) was refluxed on a steam bath for 40 h. Cooling caused separation of a white solid which was recrystallized from chloroform to give 10.3 g (43%) of *p,p′*-dichlorobenzophenone-4-aminosemicarbazone (**6**) m.p. 197–198°.

Carbohydrazone from 4,4′-Dichlorobenzophenone and Acetone

A solution of **6** (8.3 g, 0.026 mol) in 600 ml of acetone was refluxed on a steam bath for 8 h. The chalky precipitate of 1-(bis-*p*-chlorophenyl) methylene-5-isopropylidene carbohydrazide (**7**) which had formed weighed 8.7 g (93.5%) and melted sharply at 240°.

2-(bis-p-Chlorophenyl)methylenehydrazono-5,5-dimethyl-Δ^3-1,3,4-oxadiazoline

A solution of **7** (7.0 g, 19.3 mmol) in 70 ml of glacial acetic acid was added during 15 min to an ice-cold solution of lead tetraacetate (45 g, 0.103 mol) in 70 ml of methylene chloride. After 4 h the ice bath was removed and the temperature was gradually raised to 25°. During the following 10 h period at 25°, methylene chloride was added periodically to compensate for losses from evaporation. Water (70 ml) was then added and the resulting mixture was filtered through a cake of Celite. The yellow methylene chloride layer was separated and washed three times with 70 ml portions of water, once with saturated sodium bicarbonate solution, and three times with water before it was dried with anhydrous magnesium sulfate. Evaporation of the solvent left 4.9 g of a yellow solid which was dissolved in 350 ml of petroleum ether (b.p. 30–60°). The solution was gradually concentrated to 80 ml. Cooling gave crystals of 2-(bis-*p*-chlorophenyl)-methylene hydrazono-5,5-dimethyl-Δ^3-1,3,4-oxadiazoline (**8**) (4.0 g, 57.5%), m.p. 143–145°, dec.

*1-(bis-p-Chlorophenyl)methylene-3-oxo-4,4-dimethyl-1,2-diazetidinium Hydroxide, Inner Salt (**5**, $R_1 = R_2 = CH_3$, $R_3 = R_4 = p\text{-}C_6H_4Cl$).*

The above named compound was prepared by thermal decomposition of **8** *in vacuo*. A vertically-mounted Pyrex tube (20 mm diameter), connected to a cold trap by means of a glass connecting tube, served as the reaction vessel. A sample of **8** (0.804 g, 2.22 mmol) was loaded into the vertical tube, the cold trap was fitted, and the system was evacuated. The reaction vessel was then heated at 145° for 4 h with the vacuum pump running. The dark brown residue in the reaction vessel was taken up in acetone–water from which 1-(bis-*p*-chlorophenyl)-methylene-4,4-dimethyl-3-oxo-1,2-diazetidinium hydroxide, inner salt, crystallized, m.p. 200–201°.

Anal. Calcd. for $C_{17}H_{14}Cl_2N_2O$: C, 61.27; H, 4.23; N, 8.41, Cl, 21.27. Found: C, 61.27; H, 4.26; N, 8.46; Cl, 20.98.

X-Ray Structure

A crystal of the chloro-derivative of approximate dimensions 0.04 × 0.02 × 0.02 cm^3 was used. The space group was uniquely *Pbca* (conditions limiting possible reflections: $0kl$, $k = 2n$, $h0l$, $l = 2n$; $hk0$, $h = 2n$).

Crystal Data

$C_{17}H_{14}Cl_2N_2O$ f.w. = 333.23

Orthorhombic, $a = 9.95(1)$, $b = 28.73(2)$, $c = 11.30(1)$ Å, $U = 3230.3$ Å^3, $Z = 8$, $D_x = 1.37$.

$C_{17}H_{14}Br_2N_2O$ f.w. = 422.15

Orthorhombic, $a = 9.90(1)$, $b = 29.81(2)$, $c = 11.38(1)$ Å, $U = 3358.5$ Å^3, $Z = 8$, $D_x = 1.67$.

Both with $\lambda_\alpha = 0.71069$ Å at 21 °C. Accurate parameters were determined by least squares fit to 15 2θ values obtained from diffractometer measurements.

A total of 1256 unique reflections lying in the range $0 < 2\theta \leq 40°$ were measured for the dichloro compound on a Syntex P$\bar{1}$ automatic diffractometer using graphite monochromatized MoKα radiation. Reflections were scanned in the θ–2θ mode at a rate between 2° and 24° per min depending on the peak intensity. Backgrounds were measured at 1° in 2θ from the peak. A smaller data set (878 reflections and 459 with intensities $>3\sigma$) were collected on the bromo analog[2] and used as an aid in locating the heavy atom position in the structure. The data were corrected for Lorentz and polarization effects, but not absorption ($\mu \simeq 4.07$ cm^{-1}). Calculations were carried out using both least-squares refinement programs written by J. S. Stephens and the XRAY-71 package of programs.

A sharpened Patterson function of the bromine derivative revealed the bromine atom positions and successive Fourier and difference Fourier maps led to the positions of all the remaining non-hydrogen atoms. These coordinates were used as a starting model for the chloro compound. All reflections of positive measure were included

[2]The bromo compound was prepared by procedures analogous to those described above for the synthesis of **5**.

TABLE 1. Atomic parameters in 1-[bis-(*p*-chlorophenyl)methylene]-3-oxo-4,4-dimethyl-1,2-diazetidinium hydroxide, inner salt

Atom	*x*	*y*	*z*	*U*(Å²)
N(1)	0.7001(7)	0.6584(2)	0.3240(6)	0.042(2)
N(2)	0.6733(7)	0.6619(2)	0.2013(6)	0.055(2)
C(3)	0.5936(10)	0.7002(3)	0.2221(8)	0.064(3)
C(4)	0.6147(9)	0.7015(3)	0.3531(7)	0.045(2)
O(5)	0.5278(8)	0.7237(2)	0.1504(7)	0.089(2)
C(6)	0.7719(9)	0.6289(3)	0.3829(6)	0.041(2)
C(7)	0.4893(10)	0.6908(3)	0.4274(9)	0.062(3)
C(7′)	0.6949(10)	0.7423(4)	0.3971(9)	0.067(3)
C(8)	0.7652(9)	0.6332(3)	0.5155(7)	0.042(2)
C(9)	0.8512(9)	0.6614(3)	0.5789(8)	0.047(3)
C(10)	0.8414(9)	0.6618(3)	0.7029(8)	0.052(3)
C(11)	0.7483(10)	0.6341(3)	0.7588(7)	0.047(2)
C(12)	0.6607(11)	0.6055(3)	0.6969(8)	0.054(3)
C(13)	0.6699(10)	0.6059(3)	0.5721(8)	0.055(3)
Cl(14)	0.7371(3)	0.63289(9)	0.9120(2)	*
C(15)	0.8520(8)	0.5926(3)	0.3289(7)	0.039(2)
C(16)	0.8448(9)	0.5806(3)	0.2083(8)	0.051(3)
C(17)	0.9269(10)	0.5457(3)	0.1647(9)	0.059(3)
C(18)	0.0182(10)	0.5231(3)	0.2357(8)	0.050(3)
C(19)	0.0265(10)	0.5338(3)	0.3529(8)	0.057(3)
C(20)	0.9433(10)	0.5679(3)	0.4022(8)	0.053(3)
Cl(21)	1.1234(3)	0.48091(9)	0.1761(3)	*
H(9)	0.908(8)	0.6824(25)	0.534(7)	0.05(3)
H(10)	0.903(9)	0.6803(28)	0.743(8)	0.10(3)
H(12)	0.594(12)	0.5817(34)	0.736(10)	0.14(4)
H(13)	0.614(10)	0.5792(31)	0.518(8)	0.13(4)
H(16)	0.769(7)	0.5983(23)	0.169(6)	0.05(2)
H(17)	0.918(8)	0.5403(26)	0.083(7)	0.07(3)
H(19)	0.097(7)	0.5198(22)	0.408(6)	0.04(2)
H(20)	0.963(8)	0.5812(29)	0.482(7)	0.08(3)
H(71)	0.437(9)	0.7205(31)	0.413(8)	0.08(3)
H(72)	0.513(9)	0.6926(32)	0.497(8)	0.08(3)
H(73)	0.457(11)	0.6669(40)	0.407(10)	0.13(4)
H(71′)	0.712(6)	0.7409(20)	0.465(4)	0.02(2)
H(72′)	0.767(6)	0.7449(20)	0.341(6)	0.03(2)
H(73′)	0.645(7)	0.7737(22)	0.392(6)	0.04(2)

Atom	U_{11}(Å²)	U_{22}(Å²)	U_{33}(Å²)	U_{12}(Å²)	U_{13}(Å²)	U_{23}(Å²)
Cl(14)*	0.092(2)	0.075(2)	0.035(1)	0.004(2)	−0.008(1)	−0.001(1)
Cl(21)*	0.083(2)	0.071(2)	0.100(2)	0.009(2)	0.016(2)	−0.024(2)

*The thermal factor is exp $-2\pi^2(U_{11}h^2b_1^2 + \ldots + 2U_{12}hkb_1b_2 + \ldots)$ where the b_i's are reciprocal lattice vectors.

in the refinement. Weights were given by $\omega = [18.46 - 0.4505|F_o| + 0.00409|F_o|^2 + 75o^2/F^2]^{-1}$, with the constants chosen so that $< \omega||F_o| - |F_c||^2 >$ was independent of $|F_o|$. The data were corrected for secondary extinction using the method of Larson (6). Atomic scattering factors were obtained from Cromer and Mann (7).

When convergence had been achieved with this model the hydrogen atoms of the chlorophenyl group were added at C—H lengths equal to 1.084 Å and $U = 0.10$ Å². A difference electron density revealed the positions of the hydrogen atoms of the methyl group and no other significant peaks. Inclusion of all the hydrogen atoms in the refinement resulted in a minimum R of 0.099 and $R_\omega = (\Sigma\omega(|F_o| - |F_c|)^2/\Sigma\omega F_o)^{1/2}$ equal to 0.081. The final atomic parameters are listed in Table 1 and the observed and calculated structure factors are in Table 2.[3] Selected interatomic distances and angles are given in Table 3.

Description of the Structure

A view of the molecule is seen in Fig. 1. The normals to the two chlorophenyl groups subtend an angle of 86.6° while the diazetidinium ring is 10° from coplanarity with the A chlorophenyl ring. Individually the atoms in the chlorophenyl ring and diazetidinium rings are within 0.2 Å of coplanarity as determined by a weighted least-

[3]Photocopies of Table 2 are available for a nominal charge from the Depository of Unpublished Data, National Science Library, National Research Council of Canada, Ottawa, Canada K1A 0S2.

Can. J. Chem. Downloaded from www.nrcresearchpress.com by 210.87.254.105 on 09/05/12
For personal use only.

TABLE 3. Selected bond lengths and angles in 1-(bis-*p*-chlorophenyl) methylene-3-oxo-4,4-dimethyl-1,2-diazetidinium hydroxide, inner salt with standard deviations in parentheses*

Bond	Distance (Å)	Bond	Distance (Å)
Cl(14)—C(11)	1.736(8)	Cl(21)—C(18)	1.737(10)
C(6)—C(15)	1.447(12)	C(6)—C(8)	1.505(10)
N(1)—N(2)	1.415(10)	N(1)—C(6)	1.293(10)
N(2)—C(3)	1.377(11)	C(3)—O(5)	1.240(12)
C(3)—C(4)	1.496(12)	C(4)—C(7)	1.535(13)
C(4)—N(1)	1.535(11)	C(4)—C(7′)	1.503(14)

Bonds	Angle (deg)	Bonds	Angle (deg)
C(4)—N(1)—N(2)	93(1)	N(2)—N(1)—C(6)	131(1)
N(1)—N(2)—C(3)	90(1)	C(4)—N(1)—C(6)	136(1)
N(2)—C(3)—C(4)	96(1)	N(2)—C(3)—O(5)	129(1)
C(3)—C(4)—N(1)	81(1)	C(4)—C(3)—O(5)	135(1)

*The average C—C bond length in the phenyl rings if 1.391 Å and all bond lengths lie within $2\sigma(\sigma = 0.014$ Å) of the mean value except for that of C(19)—C(18) which is within 3σ. The C—C—C bond angles lie within 2σ, $\sigma = 1°$, of 120°.

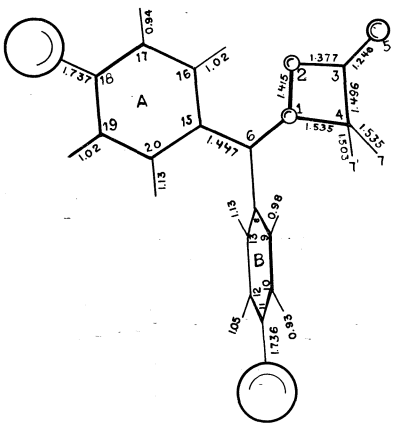

FIG. 1. A schematic view of the molecule of 1-(bis-*p*-chlorophenyl)methylene-3-oxo-4,4-dimethyl-1,2-diazetidinium hydroxide, inner salt. The A and B chlorophenyl groups are designated. The hydrogen atoms of methyl groups are not differentiated. The decimal numbers are distance in Å and the remaining numbers designate the atoms. The average estimated error on the bond lengths involving hydrogen atoms is 0.08 Å.

squares procedure. This planarity favors an interaction between N(2) and H(16) on the C(16) of the A chlorophenyl ring. The N(2)...H(16) distance is found to be 2.09(7) Å. The short C(6)—N(1) bond length (1.293(10) Å) involving the carbon atom shared between the chlorophenyl rings suggests a substantial amount of double bond character, which in turn implies charge separation between the nitrogen atoms. The resulting negative charge on N(2) leads to a stable interaction with H(16) and this together with possible delocalizations in the C(16) C(15) C(6) N(1) N(2) ring leads to coplanar inner salt (3). A similar situation is found in α-1-(*p*-bromophenyl)phenylmethylene-3-oxo-1,2-diazetidinium hydroxide (3). The bond lengths there and those in the present structure agree to within about 2σ except that C(3)—C(4) and C(4)—N(1) appear interchanged.

The B ring is rotated from planarity with the A ring so that the hydrogen atoms of the phenyl rings can avoid interaction. The orientation found leads to interaction between a hydrogen atom on the methyl group, H(71′), and those on the phenyl group, in sufficient excess of the van der Waals contact such that these constraints are not sufficient to cause A and B to be nearly perpendicular.

The molecules pack in layers near planes at $x = \pm 1/4$ with C(7′), N(1), C(6), C(8), C(11), and Cl(14) nearly lying in this plane (see Fig. 2) and the common (molecular) plane of the A ring and the diazetidinium ring is at an angle of 55° to the *a* axis. Translationally equivalent molecules form rows parallel to the *c* axis with adjacent rows generated alternately by the *c* glide plane perpendicular to *b* and the two-fold screw axis at $x = 1/4$ parallel to *c*. The double rows of molecules related by this glide plane form ribbons with the molecular planes on opposite edges of the ribbon but pointing in the same sense along *a*. Adjacent ribbons have this sense reversed but the layers are polar with the components of the N(1)—N(2) vectors along *c* being additive. Adjacent layers are related by the center of symmetries leading to an antiferroelectric arrangement of molecules with the van der Waals contact

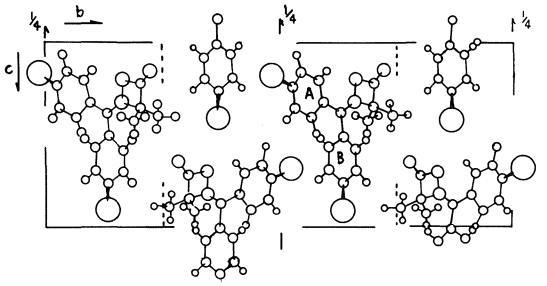

FIG. 2. A view of the structure of 1-(bis-*p*-chlorophenyl)methylene-3-oxo-4,4-dimethyl-1,2-diazetidinium hydroxide, inner salt, near the plane $a = 0.75$.

Can. J. Chem. Downloaded from www.nrcresearchpress.com by 210.87.254.105 on 09/05/12
For personal use only.

between Cl(14) and Cl(21) in these layers defining the *a* axis length.

Discussion

The geometry of the methylene-oxo-diazetidinium moiety in the present compound is very similar to that in α-1-(*p*-bromophenyl)phenylmethylene-3-oxo-1,2-diazetidinium(3). The features of interest are the planarity of the group ($\sigma = 0.010$ Å, but $\sigma = 0.004$ Å excluding the oxygen atom), the contracted N(1)—C(4)—C(3) angle (81°), the double bond character of the C—O and C(6)—N(1) bond and the partial double bond character in the N—N and C(3)—N(2) bonds. The deviation of the angle between the normals to the two chlorophenyl rings from 90° is larger and the A ring is further from coplanarity with the methylene-oxo-diazetidinium grouping in the present case. The ring formed as a result of the intramolecular hydrogen bond is planar ($\sigma = 0.002$ Å) and shows distances very similar to those reported by Fritchie and Wells (3).

There is substantial evidence for π-electron delocalization in that C(6)—C(15) is significantly shorter than C(6)—C(8). The lengths suggest about 15% more double bond character for the former bond. The direction of π-electron polarization can be inferred from the infrared which shows the C=O frequency of **5** at 1775 cm^{-1} and that of N(2)-protonated **5** near 1845 cm^{-1} (8). Substantial amide resonance in **5** is implied; a conclusion incompatible with delocalization from N(2) into ring A. Shortening of C(6)—C(15) most likely arises from π-electron polarization from ring A to N(1), the consequence of which is to decrease electron density at C(16) and to increase the C(16)—H...N(2) interaction. The fact that the latter interaction is short is incontestable. At 134°, the C(16)—H...N(2) angle is not very favorable for hydrogen bonding. On the other hand, the H(16)—C(16)—C(*n*) angles, at 110(3°) and 130(3°) for $n = 15$ and 17 respectively, suggest that the proton has moved toward N(2) to increase interaction with that atom.

Whether the separation between H(16) and N(2) is significantly less than the sum of the van der Waal radii depends to some degree on one's taste concerning corrections to accepted atomic radii for the special environments involved. Negative nitrogen, for example, is undoubtedly larger than neutral nitrogen. Although the magnitude of the interaction in the crystal is not known, it has the qualitative attributes of bonding normally called hydrogen bonding. We suggest that the H(16)...N(2) interaction reinforces the planarity which is imposed primarily by π-electron delocalization rather than that the former is a necessary force for maintaining planarity, as was proposed by Fritchie and Wells (3).

This research was supported through grants from the National Research Council of Canada.

1. (*a*) I. LENGYEL and J. C. SHEEHAN. Angew. Chem. **80**, 27 (1968); Angew. Chem. Int. Ed. Engl. **7**, 25 (1968). (*b*) K. BOTT. Angew. Chem. **79**, 943 (1967); Angew. Chem. Int. Ed. Engl. **6**, 946 (1967). (*c*) J. C. SHEEHAN and J. H. BEESON. J. Am. Chem. Soc. **89**, 362 (1967). (*d*) J. C. SHEEHAN and I. LENGYEL. J. Am. Chem. Soc. **86**, 746 (1964). (*e*) J. C. SHEEHAN and I. LENGYEL. J. Am. Chem. Soc. **86**, 1356 (1964). (*f*) H. E. BAUMGARTEN, J. J. FUERHOLZER, R. D. CLARK, and R. D. THOMPSON. J. Am. Chem. Soc. **85**, 3303 (1963). (*g*) H. E. BAUMGARTEN. J. Am. Chem. Soc. **84**, 4975 (1962).
2. P. R. WEST and J. WARKENTIN. J. Org. Chem. **33**, 2089 (1968).
3. C. J. FRITCHIE, JR. and J. L. WELLS. Chem. Commun. 917 (1968).
4. T. M. GORRIE and N. F. HALEY. Chem. Commun. 1081 (1972).
5. R. B. GREENWALD and E. C. TAYLOR. J. Am. Chem. Soc. **90**, 5272 (1968).
6. A. C. LARSON. Acta Cryst. **23**, 664 (1967).
7. D. T. CROMER and J. B. MANN. Acta Cryst. **A24**, 321 (1968).
8. N. F. HALEY. PH.D. Thesis. Princeton University, 1971. Order No. 72-2712, University Microfilms, Ann Arbor, Michigan.

Can. J. Chem. Downloaded from www.nrcresearchpress.com by 210.87.254.105 on 09/05/12
For personal use only.

Entropy Production in Chemically Reacting Systems

HUW O. PRITCHARD AND NABIL I. LABIB

Centre for Research in Experimental Space Science, York University, Downsview, Ontario M3J 1P3

AND

D. L. SEAN MCELWAIN

Department of Mathematics, University of Newcastle, Newcastle, New South Wales 2308, Australia

Received March 4, 1974

HUW O. PRITCHARD, NABIL I. LABIB, and D. L. SEAN MCELWAIN. Can. J. Chem. **52**, 2618 (1974).

Numerical integration of the gasdynamic equations describing the coupling between vibrational relaxation and dissociation for a hydrogen–helium mixture in a plane shock wave shows that the *total entropy* is a *completely monotonic* function of time; this is found to be the case whether the system is considered to be isolated, or whether there is loss of energy or mass from the flow.

HUW O. PRITCHARD, NABIL I. LABIB, et D. L. SEAN MCELWAIN. Can. J. Chem. **52**, 2618 (1974).

L'intégration numérique des équations de la dynamique des gaz qui décrivent le couplage entre la relaxation vibrationnelle et la dissociation, pour un mélange hydrogène–hélium dans une onde de choc plane, montre que l'entropie totale est une fonction du temps entièrement monotone; il en est ainsi quand le système est considéré isolé, ou bien quand il y a perte d'énergie ou de masse du courant. [Traduit par le journal]

Can. J. Chem. Downloaded from www.nrcresearchpress.com by 210.87.254.40 on 09/05/12
For personal use only.

In 1966, McKean conjectured that successive derivatives with respect to time of the Boltzmann H-function might alternate in sign (1) *i.e.* that for all integral n

$$[1] \qquad (-1)^n \mathrm{d}^n H/\mathrm{d}t^n \geqslant 0$$

Since $S = -kH$, this implies that for entropy production

$$[2] \qquad (-1)^n \mathrm{d}^n S/\mathrm{d}t^n \leqslant 0$$

i.e. the first, third, fifth, etc., derivatives would be $\geqslant 0$ throughout and the second, fourth, sixth, etc., derivatives would be $\leqslant 0$ throughout, with the equality only applying at equilibrium: the mathematical description of such a function is that it is "completely monotonic" (2); conventional thermodynamic reasoning can show only that $\mathrm{d}S/\mathrm{d}t \geqslant 0$ and that, in the linear regime very close to equilibrium, $\mathrm{d}^2S/\mathrm{d}t^2 \leqslant 0$.

McKean's original idea arose from the consideration of the speed of approach to equilibrium of a Maxwellian gas, but no rigorous proof was attempted; such a suggestion however has the kind of elegance which is attractive to mathematical physicists, and there has been in the interim a certain amount of activity to try to establish whether the suggestion has any validity, and if so to delineate the bounds of such validity. The concept was first shown to be valid for a discrete velocity gas (*i.e.* for a rarefied system of particles constrained to move with a constant velocity in a fixed number of directions) by Harris (3) in 1967; the range of validity was extended by Simons to any gas whose behavior could be described by certain simplified forms of the Boltzmann equation (4, 5), and thence to conduction and diffusion in *isolated* systems (6). In addition, several examples have been proved where the H-function is "convex" (*i.e.* eq. 1 is shown to hold for n = 1 and n = 2) (7–11) but Maass on the other hand has shown that this convexity does not extend to spatially inhomogeneous systems (12).

(I) Vibrational Relaxation and Dissociation in an Isolated System

Over the same period of time we had been examining numerically the coupling between vibrational relaxation and dissociation or recombination for H_2 highly diluted in He at shock-wave temperatures, on the assumption that both the relaxation and the kinetics were adequately described by the master equation (13, 14). During the course of these calculations, we noticed that the total entropy of the relaxing and reacting H_2/He mixture was a completely

Can. J. Chem. Downloaded from www.nrcresearchpress.com by 210.87.254.40 on 09/05/12
For personal use only.

monotonic function of time throughout the whole approach to equilibrium, either starting with atoms only, or with ground-state molecules only (14). This calculation was however imperfect in a number of respects, and cannot therefore be accepted as *proof* of the monotonicity principle. The most serious flaw was concerned with the fact that the transition rate coefficients used in the calculation were those corresponding to the final equilibrium temperature of the system and were not allowed to change as the temperature of the relaxing system changed (by about 0.5 °K) during the evolution of the process: thus, the transition rate coefficients only obeyed detailed balancing at equilibrium and were slightly in error at all other times during the trajectory. Other lesser imperfections in the calculation were that it referred to constant energy and constant volume, rather than constant enthalpy which is characteristic of a shock wave, and no allowance was made for the change in shock velocity which accompanies the temperature change in real systems.

We now report the results of a calculation which does not suffer from these deficiencies. We consider a 1000:1 mixture of He and H_2 being heated by a plane shock wave from a low temperature to 2000.5 °K. This heating is envisaged to be instantaneous, and we then integrate the differential equations describing the coupling of the motion of the gas with the vibrational and chemical relaxations. The method of integration is the same as that used to examine the expansion of a dissociated gas through a nozzle which has been described elsewhere (15), basically conventional Runge–Kutta integration in which special attention is paid to the maintenance of detailed balancing and the conservation of particles.[1] Because of the pathological stiffness of these equations (15, 16), very short integration steps were necessary, *viz.* 1×10^{-5} cm at a flow velocity of 4×10^5 cm s^{-1}; thus in a reasonable amount of computer time, it was possible to integrate the system of equations for a reaction time of 2×10^{-7} s. With the transition rates used (16) the vibrational relaxation time is about 2.5×10^{-8} s, so that our integration actually extends well beyond the vibrational relaxation and into the early part of the dissociation regime. During the period the temperature had fallen to 2000.2 °K and the shock velocity had increased to 4.0002×10^5 cm s^{-1} with concomitant changes in the pressure and the density; at the end of the calculation, both the total enthalpy and the number of hydrogenic particles differed from the starting values only in the 14th decimal place.

The results of this calculation were that the first five derivatives of the total entropy per gram of mixture (calculated by standard methods (14)) alternated in sign throughout our range of integration, and a brief summary of these results is shown in Table 1. In addition, the next four derivatives (not shown in Table 1) followed the same alternating pattern, but the 8th and 9th derivatives failed to obey the monotonicity principle at about 1.3×10^{-7} s, and the 6th and 7th derivatives failed near 1.8×10^{-7} and 1.7×10^{-7} s respectively; an analysis of the accumulation of errors in our numerical differentiation in relation to the actual magnitudes of the various derivatives and the step sizes suggests that such failures will occur if the total entropy is incorrect in the 13th decimal place!

(II) Vibrational Relaxation and Dissociation in a Closed System

In this section we show that the same monotonicity principle is obeyed if energy is allowed to escape from our reacting gas. If the principle is going to be valid for any kind of energy loss *e.g.* radiation, conduction, it is clear that the functional form of the energy loss term must be irrelevant, and therefore for computational convenience we chose an energy loss term of $d\varepsilon/dt = 5 \times 10^{10}$ erg s^{-1} per gram of mixture. The gas-dynamic equations were recast to include this loss term and the integration was performed with the same initial conditions for a time period of 1×10^{-7} s; during this time, the temperature fell a little faster, to 1999.3 °K and the velocity rose to 4.0008×10^5 cm s^{-1}. At very early times, the entropy of the *system* (S_i) rose, but after 2×10^{-9} s, it began to fall again because of the cooling caused by the energy loss term: however, the first derivative of the *total* entropy, written as

$$[3] \qquad S^{\mathrm{I}} = \frac{dS_{\mathrm{total}}}{dt} = \frac{dS_i}{dt} + \frac{1}{T}\frac{d\varepsilon}{dt}$$

[1]One minor simplification was made in the present work, in that we used the *theoretical* rather than the experimental equilibrium constant for the dissociation reaction, so that all thermodynamic parameters were automatically consistent without the need for any correction terms.

TABLE 1. Total entropy per gram of a 1000:1 helium–hydrogen mixture and derivatives of the entropy as a function of time*

	Value for time =						
Parameter	5×10^{-9}	10^{-8}	2.5×10^{-8}	5×10^{-8}	7.5×10^{-8}	10^{-7}	2×10^{-7}
$10^5(S - S_0)$	1.32239	1.84797	2.40146	2.55643	2.57396	2.57612	2.57644
S^{I}	1.5×10^{3}	7.6×10^{2}	1.6×10^{2}	1.7×10^{1}	2.1	2.6×10^{-1}	7.5×10^{-4}
S^{II}	-3.0×10^{11}	-9.6×10^{10}	-1.5×10^{10}	-1.5×10^{9}	-1.7×10^{8}	-2.2×10^{7}	-1.4×10^{4}
S^{III}	1.7×10^{20}	1.7×10^{19}	1.6×10^{18}	1.3×10^{17}	1.5×10^{16}	1.8×10^{15}	8.0×10^{11}
S^{IV}	-8.1×10^{28}	-6.0×10^{27}	-1.9×10^{26}	-1.2×10^{25}	-1.3×10^{24}	-1.5×10^{23}	-1.1×10^{20}
S^{V}	1.8×10^{37}	5.5×10^{36}	2.8×10^{34}	1.2×10^{33}	1.1×10^{32}	1.3×10^{31}	1.0×10^{28}

*Time in s and entropies in cal deg^{-1} g^{-1}; S^N denotes d^nS/dt^n (in appropriate derivative units); S_0 = 8.781 cal deg^{-1} g^{-1}; initial density = 2.327×10^{-4} g cc^{-1}.

TABLE 2. Total entropy per gram of the same mixture and its derivatives with an arbitrary energy loss term of $d\varepsilon/dt = 5\times10^{10}$ erg s^{-1} per gram of mixture; see footnotes to Table 1 for additional explanation

	Value for time =				
Parameter	5×10^{-9}	10^{-8}	2.5×10^{-8}	5×10^{-8}	7.5×10^{-8}
$10^5(S_i - S_0)$	0.039	−0.718	−4.181	−10.277	−16.676
S^{I}	1.5×10^{3}	7.6×10^{2}	1.6×10^{2}	1.6×10^{1}	1.0
S^{II}	-3.0×10^{11}	-9.6×10^{10}	-1.5×10^{10}	-1.5×10^{9}	-1.8×10^{8}
S^{III}	1.7×10^{20}	1.7×10^{19}	1.6×10^{18}	1.3×10^{17}	1.5×10^{16}
S^{IV}	-8.1×10^{28}	-6.0×10^{27}	-1.9×10^{26}	-1.2×10^{25}	-1.3×10^{24}
S^{V}	1.8×10^{37}	5.5×10^{36}	2.8×10^{34}	1.2×10^{33}	1.1×10^{32}

rose monotonically up as far as 8×10^{-8} s: beyond this time, the two terms in eq. 3 became almost exactly equal and of opposite sign, so that the net rate of entropy production became inaccurate; nevertheless, in the time range where S^{I} was accurate, the next four derivatives alternated nicely, as shown in Table 2. Thus, the principle of monotonicity clearly extends to systems with an energy loss term: notice that in Tables 1 and 2 the *derivatives* are almost the same; they would have been identical if the transition rate coefficients had not been allowed to change with temperature.

(III) Vibrational Relaxation and Dissociation in an Open System

In this section we show that the principle is also valid if matter is allowed to escape from the system. To simplify the analysis, we assumed that helium leaks out of our imaginary shock tube at the rate of $dm_{He}/dt = 0.3$ g s^{-1} per gram of mixture (causing only changes to the conservation equations with a minor modification to the collision rate in the kinetic equations); furthermore, it was assumed that when the helium escaped from the system, it did so at the current ambient temperature, and took with it also its momentum at the current shock velocity. This mass loss resulted in a rather similar rate of temperature drop and shock acceleration to that found in the preceding section, and after integration over a period of 5×10^{-8} s with the same starting conditions, the temperature had fallen to 1999.9 °K and the velocity (U) had risen to 4.0007×10^{5} cm s^{-1}. As in the energy loss case, the entropy of the residual mixture rose for a short time, roughly 8.5×10^{-9} s, before the reduction due to mass loss overwhelmed the natural increase due to vibrational relaxation. By analogy with eq. 3, we now write for the first derivative of the *total* entropy (per gram of original mixture)

$$[4]\quad S^{I} = \frac{dS_{total}}{dt} = \frac{dS_i}{dt} + S_{He}(T)\frac{dm_{He}}{dt} + \frac{1}{T}\left(\frac{1}{2}\frac{dm_{He}}{dt}U^2\right)$$

where the second term represents the entropy loss associated with the mass loss, and the third term is the (kinetic) energy loss term. Cast in this way, the first derivative of the entropy increased monotonically throughout the range of integration, and the next four derivatives alternated

Can. J. Chem. Downloaded from www.nrcresearchpress.com by 210.87.254.40 on 09/05/12
For personal use only.

TABLE 3. Total entropy per gram of the same mixture and its derivatives with an arbitrary mass loss of $dm_{He}/dt = 0.3$ g s^{-1} per gram of mixture; see footnotes to Table 1 for additional explanation

Parameter	Value for time = 5×10^{-9}	10^{-8}	2.5×10^{-8}	5×10^{-8}
$10^5(S_i - S_0)$	0.872	0.948	0.151	−1.962
S^{I}	1.8×10^{3}	1.1×10^{3}	4.9×10^{2}	3.5×10^{2}
S^{II}	-2.4×10^{11}	-9.1×10^{10}	-1.5×10^{10}	-1.5×10^{9}
S^{III}	6.6×10^{19}	1.4×10^{19}	1.6×10^{18}	4.9×10^{16}
S^{IV}	-5.3×10^{28}	-3.2×10^{27}	-1.8×10^{26}	—
S^{V}	3.3×10^{37}	1.1×10^{36}	2.4×10^{34}	—

nicely in sign, as shown in Table 3 (except that because of cancellation problems, the 3rd and 4th derivatives failed between 4 and 5×10^{-8} s).

Summary

As we noted in the opening paragraphs, the monotonicity of entropy production for certain idealized models has been established in recent years, and the convexity of entropy production has been established for others. The results of our calculation described in Section I above show however that the monotonicity principle must be much more general than has hitherto appeared; in this calculation we have vibrational relaxation and dissociation (both first order in He and in H_2) taking place, as well as recombination (first order in He and second order in H). In addition, our gas changes its properties according to the laws of gasdynamics as they apply to a perfect gas, allowing interchange of thermal energy with flow velocity and with PV terms, through the normal set of conservation relations (15)

$$dE + PdV + VdP + mUdU = 0$$

$$d\rho/\rho + dU/U = 0 \text{ (for constant area)}$$

$$-\rho U dU = dP$$

Thus, in our view, the evidence is virtually conclusive that the monotonicity principle applies to simple internal relaxations and chemical reactions in *isolated* perfect gas systems. Our calculations in Section II and III then show, again in our view conclusively, that this principle extends to cases where energy or mass is being lost from the system; we did not attempt the calculation where both energy and mass were lost, since this must follow automatically and the investment in computer time did not seem necessary. Thus it appears that McKean's concept of monotonicity of entropy production is changing its status from that of a conjecture (which can be shown to be consistent with the Boltzmann equation for certain idealized models) to more nearly the status of a law. We intend to explore further the validity of this concept in chemical kinetic and relaxation regimes, and hope that others concerned with quantitative models in other statistical mechanical hierarchies may be persuaded to make *precise* calculations of the entropy and its time derivatives for their particular systems. Finally, we might add another conjecture: plots of $\ln|S^N|$ against time are markedly curved at early times, but appear to be tending towards linearity later in the evolution of the process; thus, could it be that *in the limit* the total entropy approaches its equilibrium value exponentially for certain classes of systems?

This research was supported by the National Research Council of Canada.

1. H. McKean. Arch. Ratl. Mech. Anal. **21**, 343 (1966).
2. D. V. Widder. The Laplace transform. Princeton University Press, Princeton. 1946. p. 145.
3. S. Harris. J. Math. Phys. **8**, 2407 (1967).
4. S. Simons. J. Phys. **A2**, 12 (1969).
5. S. Simons. J. Phys. **A5**, 1537 (1972).
6. S. Simons. J. Phys. **A4**, 11 (1971).
7. S. Simons. J. Phys. **A4**, L58 (1971).
8. S. Harris. J. Chem. Phys. **48**, 3723 (1968).
9. S. Harris. J. Chem. Phys. **48**, 4012 (1968).
10. D. B. Shear. J. Chem. Phys. **48**, 4144 (1968).
11. S. J. Yao. J. Chem. Phys. **54**, 1237 (1971).
12. W. Maass. J. Phys. **A3**, 331 (1970).
13. V. A. LoDato, D. L. S. McElwain, and H. O. Pritchard. J. Am. Chem. Soc. **91**, 7688 (1969).
14. D. L. S. McElwain and H. O. Pritchard. J. Am. Chem. Soc. **91**, 7693 (1969).
15. N. I. Labib, D. L. S. McElwain, and H. O. Pritchard. Can. J. Chem. **50**, 3832 (1972).
16. D. L. S. McElwain and H. O. Pritchard. Thirteenth Symposium (International) on Combustion. The Combustion Institute, Pittsburgh, Pa., 1971. pp. 37–49.

Can. J. Chem. Downloaded from www.nrcresearchpress.com by 210.87.254.40 on 09/05/12
For personal use only.

Characterization of Monohalogen and Monopseudohalogen Derivatives of Dimethylgermane

GEOFFREY K. BARKER,[1] JOHN E. DRAKE,[2] AND RAYMOND T. HEMMINGS
Department of Chemistry, University of Windsor, Windsor, Ontario N9B 3P4

Received January 21, 1974

GEOFFREY K. BARKER, JOHN E. DRAKE, and RAYMOND T. HEMMINGS. Can. J. Chem. **52**, 2622 (1974).

The high yield syntheses of Me_2GeHX (X = F, Cl, Br, I) and Me_2GeHPs (*Ps* = CN, N_3, NCO, NCS, OAc) are reported. The dimethylgermane derivatives are identified and characterized by various physical methods and by cleavage reactions where appropriate. A normal coordinate analysis based on a modified valence force field provides confirmation of the assignments for all the fundamental frequencies, except the torsional modes, in the vibrational spectra of the monohalogeno(dimethyl)germanes, Me_2GeHX.

GEOFFREY K. BARKER, JOHN E. DRAKE et RAYMOND T. HEMMINGS. Can. J. Chem. **52**, 2622 (1974).

On rapporte les synthèses effectuées avec de bons rendements, des composés du type Me_2GeHX (X = F, Cl, Br, I) et Me_2GeHPs (*Ps* = CN, N_3, NCO, NCS, OAc). On a identifié et caractérisé les dérivés diméthylgermane par diverses méthodes physiques; dans les cas appropriés on a aussi fait appel à des réactions de clivage. Une analyse par coordonnées normales basée sur la théorie du champ des forces de valence modifiée confirme les attributions de toutes les fréquences fondamentales, excepté les modes de torsions des spectres de vibration des monohalogéno diméthylgermane Me_2GeHX. [Traduit par le journal]

Can. J. Chem. Downloaded from www.nrcresearchpress.com by 210.87.254.42 on 09/05/12
For personal use only.

Introduction

Brief reports have appeared in the literature for Me_2GeHCl (1) and Me_2GeHF (2) but the vibrational spectra, although reported in part, were not assigned. We report here the high yield syntheses and spectroscopic analysis of the halogeno- and pseudohalogeno-(dimethyl)germanes, Me_2GeHX (X = F, Cl, Br, I) and Me_2GeHPs (*Ps* = CN, N_3, NCO, NCS, OAc), as an extension to our earlier studies on methylgermanium halides (3, 4) and pseudohalides (5). The various species are identified by ^1H n.m.r., infrared, Raman, and mass spectroscopy with further characterization from vapor pressure measurements, molecular weight determinations, and cleavage reactions where applicable.

Results and Discussion

The preparative reactions used to make the dimethylgermane derivatives are based on those developed earlier (3, 5–7) for the germyl and methylgermyl compounds. A typical series of reactions to produce the halide derivatives is shown in reactions 1–4 with conversion to pseudohalides provided by reactions 5 and 6.

[1] $$6Me_2GeH_2 + 2BCl_3 \rightarrow 6Me_2GeHCl + B_2H_6$$

[2] $$Me_2GeHCl + HX \xrightarrow{X = Br, I} Me_2GeHX + HCl$$

[3] $$Me_2GeH_2 + I_2 \rightarrow Me_2GeHI + HI$$

[4] $$2Me_2GeHI + PbF_2 \rightarrow 2Me_2GeHF + PbI_2$$

[5] $$Me_2GeHI + AgPs \rightarrow Me_2GeHPs + AgI \quad (Ps = CN, NCO, NCS, OAc)$$

[6] $$Me_2GeHF + Me_3SiN_3 \xrightarrow{r.t.} Me_2GeHN_3 + Me_3SiF$$

^1H Nuclear Magnetic Resonance Spectra

The parameters for the new dimethylgermane derivatives are presented in Table 1 along with comparative data for the related Me_2GeX_2 (X = F, Cl, Br, I) and Me_3GePs (*Ps* = CN, N_3, NCO, NCS) species for which apparently no reliable chemical shift and $|J_{CH}|$ measurements have been made.

The spectra of the hydridic species, Me_2GeHX and Me_2GeHPs, are satisfactorily analyzed as first order (AX_6 type) indicating an increased effective symmetry by rapid rotation about the C—Ge bond. For the fully substituted species, Me_2GeX_2 and Me_3GePs, the methyl resonance

[1]Present address: School of Molecular Science, University of Sussex, Brighton, England.
[2]To whom correspondence should be addressed.

TABLE 1. The ^1H n.m.r. parameters of the halogeno- and pseudohalogeno- dimethylgermanes[a]

Compound	δ(Me)	δ(GeH′)	$\lvert J_{HH'}^{vic}\rvert$	$\lvert J_{CH}\rvert$
Me_2GeH_2[b]	0.29	3.73	3.95	128.5
$Me_2GeH'F$[c, d]	0.59	5.79	2.20	128.2
Me_2GeF_2[e]	0.84	—	—	131.4
$Me_2GeH'Cl$	0.80	5.55	2.70	129.8
Me_2GeCl_2	1.14[f, g]	—	—	132.4
$Me_2GeH'Br$	0.94	5.25	2.73	130.1
Me_2GeBr_2	1.44[g]	—	—	132.1
$Me_2GeH'I$	1.08	4.71	2.91	130.8
Me_2GeI_2	1.91[g]	—	—	134.3
$Me_2GeH'CN$	0.64	4.52	3.36	132.0
Me_3GeCN	0.56	—	—	130.2
$Me_2GeH'N_3$	0.84	5.43	2.70	130.5
Me_3GeN_3	0.54	—	—	132.8
$Me_2GeH'NCO$	0.62	5.31	2.78	128.3
Me_3GeNCO	0.48	—	—	128.3
$Me_2GeH'NCS$	0.71	5.45	2.70	129.8
Me_3GeNCS	0.65	—	—	128.2
$Me_2GeHOAc$	0.63[h]	5.62	2.40	127.5

[a]The spectra were recorded at ambient temperature in carbon tetrachloride solutions (*ca.* 5% v/v). Chemical shifts (δ ± 0.02 p.p.m.) are in p.p.m. to low field of tetramethylsilane as internal standard. Deviations for coupling constants are J(HH′) ± 0.05 Hz, $J(^{13}CH)$ ± 0.2 Hz (neat liquid).
[b]Reference 41.
[c]These compare with values measured in cyclohexane, ref. 2.
[d]$\lvert J_{H'F}^{gem}\rvert$, 46.8 Hz and $\lvert J_{HF}^{vic}\rvert$, 7.0 Hz.
[e]$\lvert J_{HF}^{vic}\rvert$, 5.6 Hz.
[f]Reference 40.
[g]Compare with approximate δ values for Me_2GeX_2 (X = Cl, Br, I) of 1.18, 1.46, and 1.90 δ respectively given in ref. 46.
[h]δMe for acetoxy group is 2.00 p.p.m.; $\lvert J_{CH}\rvert$, 128.3 Hz.

is seen as the expected singlet at high field. The expected additional coupling with ^{19}F (100% abundant, $I = \frac{1}{2}$) and ^{13}C (1.1% abundant, $I = \frac{1}{2}$) is observed.

α-Proton Shifts

In the Me_2GeHX series (X = F, Cl, Br, I) the Ge*H* resonance shifts to lower field as the halogen changes from iodine to fluorine. This was also observed in the $MeGeH_2X$ and $MeGeHX_2$ series (3). A comparison of these data with those reported for the parent germanes, GeH_3X and GeH_2X_2 (8), shows that the effect cannot be described by additive substituent parameters with the possible exception of the bromides. The largest deviations from additivity are observed with the fluorides (mean deviations: F, 0.56; Cl, 0.22; Br, 0.07; I, 0.24 p.p.m.) (9). A similar low-field shift in the Ge*H* resonance is observed with increasing methyl substitution; in this case the additivity is good for the monohalides but is poorer when extended to the dihalides (mean deviations: H, 0.04; F, 0.12; Cl, 0.03; Br, 0.11; I, 0.19; CH_3, 0.02 p.p.m.) (9). These results suggest that the more polar or bulkier substituents in polysubstituted germanes give rise to irregular changes in the effective shielding of the germanium proton, which implies that the α-proton shifts are determined only partly by inductive changes in local diamagnetic shielding. Similar effects have been observed for α-substitution in related methylsilyl- (10) and alkyl- (11) derivatives. The linearity of the "α-shift plot" of δ(Si*H*XYZ) *vs.* δ(C*H*XYZ) was interpreted (10) as indicating a common cause of the relative changes in δ(Si*H*) and δ(C*H*), while the slope of 0.4 suggested that Si*H* resonances are less sensitive than C*H* resonances to the nature of substituents. For a large number of pairs of silicon and germanium compounds of the type MHXYZ, where X, Y, and Z represent groups such as H, Me, halogen, Group V, and Group VI elements (9), a plot of δ(Si*H*XYZ) *vs.* δ(GeHXYZ) is also approximately linear but with a slope of *ca.* 0.6. This indicates that the sensitivity of M—*H* resonance to α-substitution decreases in the order CH > GeH > SiH. It is perhaps fortuitous that this order reflects the probable increase in importance of (p → d)π-bonding (12).

β-Proton Shifts

For the substituted methylgermanes $MeGeH_2X$, $MeGeHX_2$, Me_2GeHX, Me_nGeX_{4-n} the CH_3 resonance shifts to lower field as the halogen changes from fluorine to iodine (*i.e.* in the opposite direction from the α-proton shift). The shift increases with increasing halogen substitution but decreases with increasing methyl substitution. Closer examination shows that the β-shifts are approximately additive properties of the α-substituents, the mean deviations (F, 0.04; Cl, 0.06; Br, 0.05; I, 0.02 p.p.m.) being close to the error limits for δ values (9). The sensitivity of the CH_3 resonance to α-substitution in the methylgermanes is now similar to the analogous silicon species (10); both systems showing marked insensitivity compared to the carbon analogs. The linearity of "β-shift plots" such as δCH_3GeH_2X *vs.* δCH_3SiH_2X or δCH_3CH_2X (9) again implies similar factors influence the β-proton resonance changes. Agreement among even semi-quantitative calculations of the relative importance of various second-order phenomena is poor (10, 13–15) although they are expected to act in a direction leading to deshielding of the β-protons.

Carbon–Germanium Bond Shift

Plots of δ(MeGe*H*XY) *vs.* δ(GeH_2XY) show reasonable linearity (9) indicating that the intro-

Can. J. Chem. Downloaded from www.nrcresearchpress.com by 210.87.254.42 on 09/05/12
For personal use only.

TABLE 2. Carbon–germanium bond shift data*

	$GeH_3X \rightarrow MeGeH_2X$		$MeGeH_2X \rightarrow Me_2GeHX$			$GeH_2XY \rightarrow MeGeHXY$	
X	$\Delta_{C-Ge}{}^X$	$\delta MeGeH_2X + \Delta_{C-Ge}{}^X$	$\Delta_{C-Ge}{}^X$	$\delta Me_2GeHX + \Delta_{C-Ge}{}^X$	XY	$\Delta_{C-Ge}{}^{XY}$	$\delta MeGeHXY + \Delta_{C-Ge}{}^{XY}$
H	−0.34	−0.01	−0.24	0.05	F_2	+0.32	1.20
F	−0.09	0.51	−0.02	0.57	Cl_2	−0.27	0.87
Cl	−0.19	0.54	−0.25	0.55	ClBr	−0.36	0.92
Br	−0.38	0.50	−0.37	0.57	Br_2	−0.46	0.98
I	−0.66	0.45	−0.59	0.49	ClI	−0.49	0.99
CH_3	−0.24	0.05	−0.19	0.02	BrI	−0.73	0.91
					I_2	−1.07	0.80

*$\Delta_{C-Ge}{}^X = \delta(GeH_2XY) - \delta(MeGeHXY)$ p.p.m. ^1H n.m.r. parameters for compounds not reported in this study taken from ref. 5, 8, 41, 45. All shifts are corrected to the δ scale (p.p.m. to low field of tetramethylsilane) with no allowance for solvent dependence. For dilute solutions in isotropic solvents this error is expected to be minimal.

duction of the C—Ge bond introduces no drastic perturbations in the shielding of the germanium proton. This effective replacement of a proton in MH_3X (M = C, Si, Ge) by $M'H_3$ (M′ = C, Si, Ge) has been termed the M—M′ bond shift, $\Delta_{M-M'}{}^X$ (10, 15–17). By analogy the observations in the methylgermanes permit the "carbon–germanium bond shift," $\Delta_{C-Ge}{}^X$, to be calculated (Table 2). It has been noted in related systems (10, 15) that the bond effect apparently works to deshield the α- and β-protons equally. Similar effects are observed in the methylgermanes. For the halides, one implication is that when the β-proton shift is corrected for the presence of the C—Ge bond a "constant" shielding and hence electronic environment about the β-proton may be predicted suggesting it is not necessary to invoke second-order effects. However, deviations from this rule have been reported in the dihalogeno(methyl)-silanes (10) so the existence of a general phenomenon is questionable.

Spin–Spin Coupling Constants

The spin interactions between vicinal protons have been studied extensively and an empirical additivity relationship for ethyl (18) and methylsilyl (10) compounds has been proposed. No similar relationship is apparent in the disilanyl series (16). The absolute values of comparable coupling constants generally decrease in the order ethyl > digermanyl > methylsilyl > methylgermyl > disilanyl. If these have the same sign, assumed positive (19), and the changes are primarily due to the changing H—H′ distances as previously suggested (16) the high values of $|J_{HH}{}^{vic}|$ for digermanyl compounds are out of place.

For the related systems (10, 18) a coupling additivity relationship has been expressed:

$$|J_{HH}{}^{vic}| = A(1 - \chi\Delta E)$$

where A is a constant with value approximately that of $|J_{HH}{}^{vic}|$ in the parent hydride, χ is a small arbitrary constant, and $\Delta E = E_x - E_h$, is the difference in Huggins electronegativity (20) of the substituent X and hydrogen.

For the mono- and di-substituted methylsilanes this relationship gave $|J_{HH}{}^{vic}|$ calculated to ±0.3 Hz and ±0.7 Hz respectively. It is clear from plots of $|J_{HH}{}^{vic}|$ *vs.* ΔE (9) that a better description results from treating the mono- and di-substituted derivatives individually. Thus for $MeSiH_2X$, $|J_{HH}{}^{vic}| = 4.11(1 - 0.12\Delta E)$; for MeSiHXY, $|J_{HH}{}^{vic}| = 3.50[1 - 0.18(\Delta E_x + \Delta E_y)]$; for $MeGeH_2X$, $|J_{HH}{}^{vic}| = 3.48(1 - 0.13\Delta E)$; for MeGeHXY, $|J_{HH}{}^{vic}| = 2.82[1 - 0.30(\Delta E_x + \Delta E_y)]$; for Me_2GeHX, $|J_{HH}{}^{vic}| = 3.16(1 - 0.18\Delta E)$; for GeH_3GeH_2X, $|J_{HH}{}^{vic}| = 4.70(1 - 0.13\Delta E)$; for SiH_3SiH_2X, $|J_{HH}{}^{vic}| = 3.1(1 - 0.08\Delta E)$. The average errors of 0.03, 0.05, 0.05, 0.08, 0.02, 0.03, and 0.05 Hz for the values of $|J_{HH}{}^{vic}|$ obtained are close to the error limits quoted for experimental values. In the disubstituted methylgermanes H—H′ coupling for $MeGeH'F_2$ was not observed (3); from the above $|J_{HH}{}^{vic}|$ is calculated to be −0.04 Hz *i.e.* effectively zero within the quoted error limits.

Values for the direct coupling constant $|J_{CH}|$ for the methylgermanes lie in the range 125–138 Hz which is significantly larger than in the methylsilanes (118–127 Hz) but comparable with the data in the methylstannanes and plumbanes (10, 11). It is interesting to note that for methyl derivatives $|J_{CH}|$ is more strongly dependent on the group of the α-substituent and particularly

Can. J. Chem. Downloaded from www.nrcresearchpress.com by 210.87.254.42 on 09/05/12
For personal use only.

TABLE 3. The vibrational spectra (cm^{-1}) of fluoro- and chloro(dimethyl)germane*

Me_2GeHF			Me_2GeHCl			
Infrared (gas)	Raman (liq)	Calcd.	Infrared (gas)	Raman (liq)	Calcd.	Assignment
3004, 2993 m	3001 m,dp	3001.1	3004, 2971 m	3001 w,dp	3001.1	$\nu_1,\nu_2,\nu_{16},\nu_{17}$
2930 wm	2924 s,p	2925.7	2929 m	2922 s,p	2921.8	ν_3,ν_{18}
2097, 2085, 2075 vs	2086 s,p	2086.0	2083 vs	2089 s,p	2089.0	ν_4
1424 m	1423 wm,dp	1421.8	1423 wm, 1417 sh	1416 w,dp	1415.8	$\nu_7,\nu_8,\nu_{20},\nu_{21}$
1265, 1256, 1248 m	1252 m,p	1251.1	1259, 1251 m	1251 m,p	1251.7	ν_9,ν_{22}
	858 sh,dp	854.5	862 sh	862 w,dp	848.2	ν_{23}
845 s,br	845 w,dp	847.7	850, 841, 835 vs	830 w,dp	842.3	ν_{10}
762, 757 m	Not observed	763.3, 756.1	770 m	758 vw,dp	760.1, 755.7	ν_{24},ν_{11}
719, 707, 697 m	715 m,dp	712.7	688 m	690 m,dp	690.0	ν_{25}
*ca.*670	645 ms,dp	637.3	660 w	641 m,dp	641.3	ν_{12}
633 sh, 622 s	Not observed	621.6	628, 618 s	620 sh,dp	619.9	ν_{19}
610 sh	600 vs,p	595.3	600 sh	599 vs,p	598.6	ν_6
*ca.*670 s		676.1	406 s	382 vs,p	382.0	ν_5
	190 s,p	191.0		190 sh	189.1	ν_{13}
	222 s	221.1, 218.7		182 vs	179.2, 176.7	ν_{26} ν_{14}

*The spectra were recorded at room temperature. w = weak, m = medium, s = strong, v = very, sh = shoulder, p = polarized, dp = depolarized, br = broad.

insensitive to changes in electronegativity within each group, *e.g.*, CH_3–Group IV (118–113 Hz); CH_3–Group V (131–140 Hz); CH_3–Group VI (138–148 Hz); CH_3–Group VII (149–152 Hz). Nevertheless, in methylsilicon and methylgermanium compounds, with few exceptions, $|J_{CH}|$ increases markedly with increasing halogen substitution, increases with decreasing halogen electronegativity and decreases with increasing methyl substitution, although it is not possible to describe these effects by simple additive substituent parameters.

Vibrational Spectra

The vibrational spectra of the halogenomethylgermanes Me_nGeX_{4-n} have been interpreted for X = Cl (21), Br (22), and I (23) and we recently concluded studies on the hydridic species $MeGeH_2X$ and $MeGeHX_2$ (X = F, Cl, Br, I) (4). The present study of the Me_2GeHX species completes the spectroscopic characterization of the hydridic halogeno-methylgermanes. Additional interest is focussed on the developing trends in force constants and fundamental frequencies arising from the interchange of halogen and methyl moieties attached to germanium along series such as $GeH_3X \rightarrow MeGeH_2X \rightarrow Me_2GeHX \rightarrow Me_3GeX$. In this context we have carried out a full normal coordinate analysis to obtain compatible sets of harmonic force con-

Can. J. Chem. Downloaded from www.nrcresearchpress.com by 210.87.254.42 on 09/05/12
For personal use only.

TABLE 4. The vibrational spectra (cm^{-1}) of bromo- and iodo(dimethyl)germane*

Me_2GeHBr			Me_2GeHI			
Infrared (gas)	Raman (liq)	Calcd.	Infrared (gas)	Raman (liq)	Calcd.	Assignment
3002 m	2998 wm,dp	2998.1	3003 sh 2992 m	2998 2987 w,dp	2992.2	$\nu_1,\nu_2,\nu_{16},\nu_{17}$
2928 m	2921 s,p	2920.8	2926 m	2916 s,p	2915.7	ν_3,ν_{18}
2083 s	2083 s,p	2083.0	2077 s	2076 s,p	2076.0	ν_4
1422 m	1414 w,dp	1414.4	1418 m	1409 w,dp	1407.3	$\nu_7,\nu_8,\nu_{20},\nu_{21}$
1257 1248 m	1251 m,p	1249.6	1256 1248 m	1247 m,p	1248.1	ν_9,ν_{22}
861 sh	862 w,dp	854.3	867 sh	856 w,dp	841.8	ν_{23}
849 842 836 vs	840 w,p	849.0	843 839 835 vs	824 w,p	836.3	ν_{10}
768 m	770 vw,p	770.5	763 m	756 vw, dp	755.7	ν_{24},ν_{11}
669 s,br	675 m,dp 641 m,dp	674.7 640.9	654 s,br	653 m,dp 637 m,dp	654.1 636.9	ν_{25} ν_{12}
625 617 s	623 m,dp	622.9	615 s	618 m,dp	615.5	ν_{19}
598 sh	596 vs,p	596.6	591 s	589 vs,p	589.9	ν_6
	279 vs,p	279.0		231 vs,p	230.5	ν_5
	187 sh	187.1		187 m	187.3	ν_{13}
	170 ms	169.3		161 ms	160.5	ν_{26}
	154 ms	155.0		142 sh	143.5	ν_{14}

*See footnote to Table 3.

stants, eigenvectors, and potential energy distributions for the Me_2GeHX series (X = F, Cl, Br, I).

The molecules Me_2GeHX are assumed to be in a staggered configuration and to belong to the C_s symmetry group. The expected 27 fundamental modes are then divided into those symmetric (a') or antisymmetric (a'') with respect to the molecular plane of symmetry (Table 5). All bands are i.r. and Raman active. The observed i.r., Raman, and calculated frequencies are collected in Tables 3 and 4 with the assignment of fundamentals. The conventional description of the 27 fundamental vibrations and the potential energy distributions amongst the force constants are given in Table 5. The spectral asssignments are discussed in general terms for all molecules.

Vibrations of the CH_3 Groups

Compared to the related $MeGeH_2X$ and $MeGeHX_2$ series (4) the extra methyl group in the dimethylgermanes increases considerably the complexity of the CH_3 fundamentals and the overlapping band contours do not permit an unambiguous assignment for the individual modes. However, the CH_3 stretching and deformation modes are all readily assigned to band envelopes in the expected regions. Four CH_3 rocks are expected, two of a'-species, ν_{10} and ν_{11}, and two of a''-species, ν_{23}, ν_{24}. Coupling between these modes gives rise to bands in both 830 and 760 cm^{-1} regions and these are only assigned with confidence by means of the normal coordinate analyses. The bands display no definitive i.r. gas contours and are of very low intensity with no clear degrees of polarization in the Raman effect. No assignment of the CH_3 torsions, ν_{15} and ν_{27}, is possible from the available spectra.

Vibrations of the GeH Group

The GeH stretching mode, ν_4, appears at *ca.* 2080 cm^{-1}; its designation as an a'-species being confirmed by the observation of a strongly polarized Raman band. The separation of the two GeH deformation modes, ν_{12} and ν_{25}, decreases with increasing mass of the halogen so that in the gas-phase i.r. spectra of Me_2GeHBr

Can. J. Chem. Downloaded from www.nrcresearchpress.com by 210.87.254.42 on 09/05/12
For personal use only.

Can. J. Chem. Downloaded from www.nrcresearchpress.com by 210.87.254.42 on 09/05/12
For personal use only.

TABLE 5. Description of the fundamental vibrations for Me_2GeHX

Fundamental			Potential energy distribution*			
a'	a''	Description	Me_2GeHF	Me_2GeHCl	Me_2GeHBr	Me_2GeHI
ν_1,ν_2	ν_{16},ν_{17}	CH_3 str. (a)	100(1)	100(1)	100(1)	100(1)
ν_3	ν_{18}	CH_3 str.(s)	100(1)	100(1)	100(1)	100(1)
ν_4		GeH str.	100(3)	100(3)	100(3)	100(3)
ν_5		GeX str.	9(2)+69(4)+7(8)+10(10)	95(4)	87(4)+8(9)	52(4)+22(9)+27(11)
ν_6		GeC_2 str. (s)	81(2)+10(4)	79(2)+5(8)+5(10)	85(2)	86(2)
	ν_{19}	GeC_2 str. (a)	90(2)+6(7)	84(2)+10(8)	78(2)+7(7)+13(8)	60(2)+35(8)
ν_7,ν_8	ν_{20},ν_{21}	CH_3 def. (a)	94(5)	94(5)	93(5)	92(5)
ν_9	ν_{22}	CH_3 def. (s)	7(2)+55(5)+9(6)+37(7)	8(2)+54(5)+9(6)+36(7)	8(2)+54(5)+10(6)+36(7)	8(2)+52(5)+10(6)+36(7)
ν_{10}	ν_{23}	CH_3 rock	87(7)+5(16)	89(7)+5(16)	87(7)+7(16)	90(7)+5(16)
ν_{11}		CH_3 rock	63(6)+26(7)	60(6)+24(7)+5(8)+7(15)	64(6)+26(7)+7(16)	65(6)+24(7)
	ν_{24}	CH_3 rock	5(5)+53(6)+17(7)+16(8)	59(6)+28(7)+7(16)	5(5)+62(6)+20(7)+6(16)	65(6)+29(7)
ν_{12}		HGeX def. (//)	18(4)+33(8)+48(10)	9(2)+36(8)+51(10)	7(2)+34(8)+57(10)	6(2)+32(8)+60(10)
	ν_{25}	HGeX def. ($\perp$)	12(6)+8(7)+77(8)	9(2)+87(8)	10(2)+5(7)+82(8)	29(2)+6(7)+63(8)
ν_{13}		GeC_2 def.	12(8)+9(10)+77(11)	45(9)+51(11)	5(4)+6(8)+80(11)	22(4)+11(8)+7(10)+58(11)
ν_{14}		CGeX bend	11(8)+70(9)+8(10)+5(11)+5(18)	22(8)+27(9)+18(10)+30(11)	7(4)+19(8)+71(9)+12(10)−9(18)	26(4)+14(8)+58(9)+8(10)−6(18)
	ν_{26}	CGeX def.	100(9)	100(9)	87(9)+12(18)	89(9)+9(18)
ν_{15}	ν_{27}	CH_3 torsion	—	—	—	—

*Contributions ≥5%.

TABLE 6. Force constant listings

Force constant		Value in			
Number	Description	Me_2GeHF	Me_2GeHCl	Me_2GeHBr	Me_2GeHI
1	f_{CH}	4.838	4.833	4.826	4.808
2	f_{CGe}	2.946	2.940	2.937	2.929
3	f_{GeH}	2.547	2.555	2.540	2.523
4	f_{GeX}	4.078	2.080	1.692	1.168
5	f_{HCH}	0.501	0.497	0.493	0.481
6	$f_{HCGe(// \text{ to } \sigma_v)}$	0.325	0.322	0.346	0.346
7	$f_{HCGe(\perp \text{ to } \sigma_v)}$	0.460	0.457	0.458	0.454
8	f_{CGeH}	0.454	0.417	0.397	0.367
9	f_{CGeX}	0.618	0.613	0.599	0.606
10	f_{HGeX}	0.324	0.322	0.341	0.350
11	f_{CGeC}	0.481	0.447	0.484	0.545
12	$f_{CH/CH}$	0.046	0.042	0.044	0.044
13	$f_{CGe/CGe}$	0.059	−0.054	−0.015	−0.030
14	$f_{HCH/HCH}$	−0.008	−0.008	−0.010	−0.018
15	$f_{HCGe/HCGe(\parallel, \perp)}$	−0.023	−0.025	−0.023	−0.009
16	$f_{HCGe/HCGe(\perp, \perp)}$	−0.029	−0.027	−0.034	−0.024
17	$f_{CGeH/CGeH}$	0.001	0.003	0.001	0.003
18	$f_{CGeX/CGeX}$	0.047	0.008	−0.080	−0.060
19	$f_{CGe/HCGe}$	0.095	0.024	0.087	0.047
20	$f_{CGe/HCGe}$	−0.003	0.002	−0.028	−0.022

*Units are: mdyn $Å^{-1}$ for stretching, mdyn Å rad^{-2} for bending, mdyn rad^{-1} for stretch bend force constants.

and Me_2GeHI only one broad feature is observed. In the fluoride, the GeF stretch, ν_5, is also expected in this region. However, it is likely to be of extremely low intensity in the Raman effect so that the two fairly intense bands at 715 and 645 cm^{-1} may be attributed to ν_{25} and ν_{12}, respectively. The GeF stretch is then assigned to the intense feature in the i.r. spectrum at 670 cm^{-1}, the band envelope presumably also containing ν_{12}.

Vibrations of the C_2GeX Skeleton

The symmetric GeC_2 stretching mode, ν_6, is an intense, polarized band in the Raman spectrum. In all but Me_2GeHF, the asymmetric stretch, ν_{19}, appears as a depolarized shoulder at higher frequency. In the i.r. spectra ν_{19} has a distinct B-type contour in Me_2GeHCl and Me_2GeHBr. The GeX stretching mode, ν_5, has already been discussed for Me_2GeHF. For the other Me_2GeHX species it is confidently assigned to a Raman polarized band in the typical position. The GeC_2 deformation ν_{13}, is assigned by comparison with the Me_2GeX_2 series in which the corresponding mode appears consistently in the 180 cm^{-1} region (21–23). It is typically unaffected by the nature of the halogen. Only for the fluoride is the band at 190 cm^{-1} clearly polarized. The CGeX deformations, ν_{14} and ν_{26}, are assigned to the remaining features in the low wavenumber region of the Raman spectra. In the lighter chloro- and fluoro-species only one envelope remains. This accidental degeneracy of skeletal modes has been observed in $MeGeCl_3$ and Me_2GeCl_2 (21). However in Me_2GeHBr and Me_2GeHI the envelope is clearly resolved.

As is often the case with such modes, the polarization data are not definitive. The choice of assignment results from the normal coordinate analysis.

The Normal Coordinate Analysis

As was found in the $MeGeH_2X$ and $MeGeHX_2$ (4) series the differences in the corresponding force constants for each mode in all the molecules is small (Table 6). This suggests that we do have a reasonable set of values. The CH_3 stretching modes are seen from the potential energy distributions (Table 5) to be pure modes and there is a gradual stiffening of the C—H bond as reflected by the gradual increase in the corresponding force constant, f_{CH} along the series F > Cl > Br > I. The same is true for the potential energy distributions of the CH_3 asymmetric deformation modes and the force con-

Can. J. Chem. Downloaded from www.nrcresearchpress.com by 210.87.254.42 on 09/05/12
For personal use only.

Can. J. Chem. Downloaded from www.nrcresearchpress.com by 210.87.254.42 on 09/05/12
For personal use only.

stant, f_{HCH}. The CH_3 symmetric deformations are very mixed but show similar potential energy distributions as do the CH_3 rocking modes.

The Ge—H stretch is a pure mode. Some general trends are apparent in both the averaged GeH absorption frequency and force constant: for increasing methyl substitution, *e.g.* GeH_3Cl (24) → $MeGeH_2Cl$ (4) → Me_2GeHCl, both parameters show a marked decrease (*i.e.* ν_{GeH} = 2126, 2105, 2083 cm^{-1}; f_{GeH} = 2.663, 2.594, 2.555 mdyn $Å^{-1}$); for increasing halogen substitution, *e.g.* $MeGeH_3$ (25, 26) → $MeGeH_2Cl$ (4) → $MeGeHCl_2$ (4), the opposite effect is apparent (*i.e.* ν_{GeH} = 2084, 2105, 2125 cm^{-1}; f_{GeH} = 2.544, 2.594, 2.644 mdyn $Å^{-1}$). It is therefore not surprising that for the Me_2GeHX series the combination of the two trends leads to both a low GeH stretching frequency and force constant relative to GeH_3X (24), $MeGeH_2X$ (4), and $MeGeHX_2$ (4). The GeH deformation modes are fairly mixed with the in-plane mode mainly dependent on f_{HGeX} and the out-of-plane mode on f_{HGeC} as would be expected. The GeC_2 stretches show strong dependence on f_{CGe} and the GeC_2 deformation on f_{CGeC}. In the chloride there is an almost equal contribution to the potential energy distribution of the GeC_2 deformation from f_{CGeCl} while in the iodide an important component is f_{GeI} presumably reflecting the proximity of the corresponding modes. Finally, the CGeX out-of-plane deformation has a 100% dependence on f_{CGeX}, X = F or Cl, but for the bromide and iodide there is some contribution to the potential energy distribution from the interaction force constant 18. The in-plane CGeX deformations have very mixed potential energy distributions, although the major component is still f_{CGeX} with contributions from f_{HGeX} and f_{CGeH}.

The pseudohalides, *Me_2GeHPs*, unlike the corresponding $MeGeHPs_2$ species (5), were sufficiently stable towards disproportionation to allow their vibrational spectra as well as their n.m.r. spectra to be recorded. The i.r. and Raman spectra (Table 7) are largely assigned by comparison with the related pseudohalides (5, 9, 27–30) and with the Me_2GeHX series. The replacement of halogen by the polyatomic pseudohalogens introduces additional fundamentals (31) which have distinct group frequencies and it is these modes which best characterize the new species. If the pseudohalide group (represented by N—X—Y for N—C—O, N—C—S, N—N—N) is linear and lies in the molecular plane then at best the hydrides possess C_s symmetry. As a result the Me_2GeH— moiety might be expected to give rise to similar sets of a' and a'' fundamentals as the analogous halides. However, in view of the unknown molecular symmetries we make only tentative assignments to general types of motion.

The pseudohalogen (*Ps*) stretching fundamentals are readily distinguished and appear in typical spectral regions for these species: 2190 cm^{-1} (ν_{CN}); 2106, 1291 cm^{-1} (ν_{NNN}); 2276, 1414 cm^{-1} (ν_{NCO}); 2062, 967 cm^{-1} (ν_{NCS}). The pseudohalogen deformation fundamentals are ill-defined since they appear in spectral regions overlapped by stronger Me_2GeH— fundamentals. By comparison with the related GeH_3— (28–30) Me_3Ge— (28) and $MeGeH_2$— (5) species the following tentative assignments are possible: 674 cm^{-1} (δ_{NNN}); 670 cm^{-1} (δ_{NCO}); 480 cm^{-1} (δ_{NCS}). It should be noted that for triatomic pseudohalides, group theory considerations predict two skeletal N—X—Y deformations, *i.e.* an in-plane and out-of-place component (31). The apparent absence of additional features attributable to the second of these modes both in these and the related molecules may be an indication of a near-degeneracy. The germanium–pseudohalogen stretching modes may be assigned with some confidence to polarized Raman features at 457 cm^{-1} (ν_{Ge-NNN}), 445 cm^{-1} (ν_{Ge-NCO}) 352 cm^{-1} (ν_{Ge-NCS}), and 470 cm^{-1} (ν_{Ge-CN}).

Evidence from ^{14}N n.m.r. spectroscopy (29) and electron diffraction (32) favors the iso-form for the cyanates (*i.e.* Ge—N bonding). There is no direct evidence for similar bonding in the analogous thiocyanates. The pseudosymmetric stretch in organic isothiocyanates (ν_{NCS} at *ca.* 1000 cm^{-1}) occurs at considerably higher frequency than the *normal*-bonded species (ν_{SCN} at *ca.* 600–700 cm^{-1}) (33). This has been taken as good evidence for the iso-form in germanium and silicon compounds which produce spectral features in this region (28, 30, 34). However in this investigation the spectra are ambiguous and it is equally possible to assign a distinct feature at 669 cm^{-1} in the dimethylgermane species to the isomeric $Me_2GeHSCN$ species (ν_{SCN}). This feature also appears in $MeGeH_2NCS$ and $MeGe(NCS)_3$ (5) and may contribute to the observed splitting of the GeH_3 rock (C_{3v} degenerate) in GeH_3NCS (30). It is also noteworthy that the

Can. J. Chem. Downloaded from www.nrcresearchpress.com by 210.87.254.42 on 09/05/12
For personal use only.

TABLE 7. The infrared and Raman spectra (cm^{-1}) of the pseudohalogeno(dimethyl)germanes

Approximate description	Me_2GeHCN		Me_2GeHN_3		$Me_2GeHNCO$		$Me_2GeHNCS$	
	Infrared (gas)	Raman (liq)	Infrared (gas)	Raman (liq)	Infrared (gas)	Raman (liq)	Infrared (liq)	Raman (liq)
CH_3 str. (a)	3003 m	3002 m,dp	2997 m	2996 m,dp	3000 m	2997 m,dp	2996 m	2995 m,dp
CH_3 str. (s)	2931 m	2928 vs,p	2929 m	2923 vs,p	2930 w	2925 vs,p	2924 m	2922 vs,p
Ps str. (a)	2197 m	2189 s,p	2119 vs	2106 s,p	2276 vvs	n.o.	2074 vvs	2062 s,p
GeH str.	2092 s	2108 s,p	2071 s	2073 s,p	2085 s	2090 s,p	(2074)	2105 s,p
CH_3 def. (a)	1427 m	1422 w,dp	1419 wm	1416 w,dp	1398 w*		1415 m	1414 wm,dp
CH_3 def. (s)	1259 m	1256 m,p	1257 m	1252 s,p	1259 m	1253 m,p	1255 m	1252 m,p
Ps str. (s)			1283 s	1291 s,p	1414 w	1404 vs,p	969 vw	967 m,p‡
CH_3 rock (a)	*ca.* 865 sh	864 w,dp	860 sh		860 sh	864 w,dp	*ca.* 860 sh	856 sh,dp
CH_3 rock (s)	849 s		839 s	850 wm,dp	847 s,br	840 w,br	839 s	846 m,p
CH_3 rock (a,s)	780 m	780 vw,dp	766 m	750 vw	770 m		778 m	*ca.* 780 vw,p
GeH def. (bend)	708 s	716 m,dp	709 m	709 m,dp	710 ms	716 m,dp	706 s	710 m,p
GeH def. (twist)	*ca.* 670 w	646 m,dp		640 m,p		642 m,dp		645 m,p
GeC str. (a)	624 s	622 m,dp	622 vs	618 sh	627 ms	624 sh,dp	625 s	626 m,dp
GeC str. (s)	*ca.* 599 sh	599 vs,p	596 sh	596 vs,p	602 s	599 vs,p	600 s	599 vs,p
Ps def.			668	674 m,p	670 m*		488 m	480 w,p
Ge—*Ps* str.	482 m / *ca.* 425 sh	479 w,p / 427 m,p	482 s	457 s,p	477 s†	445 m,p	358 s	352 ms,p
Ge—*Ps* def.		250 vw						
C—Ge—*Ps* defs.		151 sh / 133 s,dp		227 s,p	218 sh*	217 m,dp	*ca.* 232 sh / *ca.* 210 sh	228 sh,dp / 212 s,p
GeC_2 def.		192 m,dp		191 s,dp		192 m,dp		190 s,dp

*Liquid film.
†Appears at 448 cm^{-1} in the liquid.
‡A second band appears at 910 cm^{-1} (m,p).

Can. J. Chem. Downloaded from www.nrcresearchpress.com by 210.87.254.42 on 09/05/12
For personal use only.

Ge—S stretch occurs at 385 cm^{-1} in Me_3GeSMe (35) and 410 cm^{-1} in GeH_3SMe (36) so the fundamental in the 360 cm^{-1} region in germanium thiocyanates may well arise from the *normal*-bonded species *i.e.* —Ge—SCN. We await direct structural evidence with some interest.

Experimental

Manipulations and spectroscopic measurements of all volatile compounds were carried out as described previously (5) except that the Raman data were obtained with laser excitation at 488.0 nm (argon-ion). An IBM S/360-50 series computer was used for the normal coordinate analysis with the programme SOTONVIB, a modified version of GMAT and FPERT as described by Schachtschneider (37). The molecules were assumed to have "all-tetrahedral" angles and the following parameters were assumed from available data on related species: C—H, 1.083 Å; Ge—H, 1.52 Å; Ge—C, 1.945 Å; Ge—F, 1.73 Å; Ge—Cl, 2.15 Å; Ge—Br, 2.30 Å; Ge—I, 2.50 Å (24, 38). Initially a SVFF was set up involving eleven force constants. The fit was improved by iterative adjustment using the conventional least squares method (39) and the best fit between observed and calculated frequencies obtained by introducing stretch–stretch, stretch–angle, and angle–angle interaction terms.

Starting Materials

Dichloro(dimethyl)germane, Me_2GeCl_2, (Alfa Inorganics) was degassed at −45° to remove HCl; the ^1H n.m.r. and i.r. spectra of middle fractions agreed well with those reported (21, 40) Dimethylgermane, Me_2GeH_2, was recovered in yields >95% from the reduction of Me_2GeCl_2 with $LiAlH_4$ in dry *n*-butyl ether; its purity was confirmed by ^1H n.m.r. (41), i.r. (25), and vapor pressure (42) measurements. Hydrogen bromide (Matheson) was fractionated through traps at −78° and degassed by pumping at −196°. Boron trichloride (Matheson) was degassed at −112°; a high degree of purity was indicated from the i.r. spectra and vapor pressures (43) of middle fractions. Iodine (B.D.H.) was resublimed *in vacuo* before use. Reagent grade samples of the heavy metal salts PbF_2, AgCN, AgNCO, AgNCS, and AgOAc were dried in a high vacuum for several days before use. Me_3SiN_3 was obtained from the reaction of Me_3SiCl with NaN_3 in diethyl ether (28).

Preparation of the Halogeno(dimethyl)germanes

Chloro(dimethyl)germane, Me_2GeHCl

Typically, Me_2GeH_2 (3.05 mmol) and BCl_3 (0.76 mmol) were condensed into a reaction vessel (150 ml) held at −196° which was then maintained at −78° (1–2 h). The reaction mixture was then brought to room temperature to complete the reaction and fractionated through cold traps at −23°, −78°, and −196°. The −23° trap contained a trace of Me_2GeCl_2 (identified by its ^1H n.m.r. (40) and i.r. (21) spectra), and Me_2GeHCl (2.1 mmol) was recovered from the −78° trap. (Mol. wt. calcd. for Me_2GeHCl, 139.11; found, 138.8; parent peaks observed in the mass spectrum at *m/e* 135–142 ($H_nC_2GeCl^+$). The vapor pressure relationship for Me_2GeHCl in the range −28° to +29° is given by: $\log p$ (mm) = 7.33 − 1614/*T* which leads to ΔH_{vap}, 7382 cal mol^{-1}, ΔS_{vap}, 20.4 cal deg^{-1} mol^{-1}, and an extrapolated boiling point of 89° (m.p. −74°). The −196° trap was shown to contain a mixture of B_2H_6 (*ca.* 0.35 mmol) and Me_2GeH_2 (*ca.* 0.8 mmol) which could be separated by refractionation at −126°, the latter being involatile at this temperature.

Bromo(dimethyl)germane, Me_2GeHBr

In a typical reaction Me_2GeHCl (1.50 mmol) and HBr (*ca.* 3 mmol) were distilled into a reaction vessel (150 ml) at −196° and allowed to warm to room temperature, occasional quenching with a −78° bath being applied as the reaction became too vigorous. After *ca.* 15 min reaction was complete and fractionation of the volatile products gave Me_2GeHBr (1.45 mmol; mol. wt. calcd. for Me_2GeHBr, 183.57; found, 185; mass spectral parent peaks at *m/e* 176–186 ($H_nC_2GeBr^+$) held in a −78° trap and a mixture of HCl and HBr (total, *ca.* 3 mmol, identified spectroscopically) in a −196° following trap. The vapor pressure relationship for Me_2GeHBr in the range −20 to +23° is given by: $\log p$ (mm) = 6.6 − 1500/*T* which leads to ΔH_{vap}, 6864 cal mol^{-1}, ΔS_{vap}, 17.0 cal deg^{-1} mol^{-1}, and a boiling point (extrapolated) of 131°.

Iodo(dimethyl)germane, Me_2GeHI

Typically, Me_2GeH_2 (3.02 mmol) was distilled into a cooled reaction vessel (*ca.* 20 ml) containing resublimed I_2 (0.52 g, *ca.* 2.1 mmol). The reactants were maintained at −78°; the reaction being accelerated by occasional local warming with the fingers. After *ca.* 1 h a light brown mixture showing no signs of residual I_2 was obtained and after fractionation Me_2GeHI (2.03 mmol; mol. wt. calcd. for Me_2GeHI, 230.57; found, 229; mass spectral parent peaks at *m/e* 227–234 ($H_nC_2GeI^+$) was recovered from a trap held at −78°. A mixture of HI and Me_2GeH_2 (total *ca.* 2.8 mmol, identified spectroscopically) was obtained in a −196° following trap. The vapor pressure relationship for Me_2GeHI in the range −8 to +34° is given by: $\log p$ (mm) = 6.2 − 1509/*T*, which leads to ΔH_{vap}, 6905 cal mol^{-1}, ΔS_{vap}, 15.4 cal deg^{-1} mol^{-1}, and a boiling point (extrapolated) of 175°.

Fluoro(dimethyl)germane, Me_2GeHF

In one experiment Me_2GeHI (1.85 mmol) was passed through a column loosely packed with a mixture of glass wool and lead(II) fluoride (*ca.* 25 g). After five double passes the contents of the column were bright yellow and the ^1H n.m.r. spectrum of the products showed that most of the iodide had been consumed. Distillation of the volatile material through a trap at −45° retained unreacted Me_2GeHI and pure Me_2GeHF (1.52 mmol; mol. wt. calcd. for Me_2GeHF, 122.6; found, 122.1) was collected in a −196° trap. The vapor pressure relationship for Me_2GeHF in the range −21 to +21° is given by: $\log p$ (mm) = 7.98 − 1715/*T* which leads to ΔH_{vap}, 7847 cal mol^{-1}, ΔS_{vap}, 23.3 cal deg^{-1} mol^{-1}, and a boiling point (extrapolated) of 63° (m.p. −31°).

Preparation of Pseudohalogeno(dimethyl)germanes

Azido(dimethyl)germane, Me_2GeHN_3

Typically, Me_2GeHF (1.11 mmol) and Me_3SiN_3 (0.94 mmol) were condensed into a reaction vessel (*ca.* 10 ml) cooled to −196°. The mixture was warmed to room temperature and allowed to react (15 min). Repeated

Can. J. Chem. Downloaded from www.nrcresearchpress.com by 210.87.254.42 on 09/05/12
For personal use only.

fractionation through a trap at −78° gave Me_3SiF (*ca.* 0.9 mmol; identified by its ^1H n.m.r. (10) and i.r. (44) spectra) and unreacted Me_2GeHF (*ca.* 0.2 mmol) in a −196° following trap. Distillation of the products in the −78° trap gave pure Me_2GeHN_3 (0.9 mmol; v.p. *ca.* 13 mm Hg at 10°; parent peaks at *m/e* 142–149 ($H_nC_2GeN_3^+$); mol. wt. calcd., 145.69) condensing in a trap at −45° and traces of Me_2GeHF and Me_3SiN_3 (< 5%) in a −196° following trap.

Cyano-, Isocyanato-, Isothiocyanato-, and Acetoxy-, (dimethyl)germane; Me_2GeHCN, $Me_2GeHNCO$, $Me_2GeHNCS$, $Me_2GeHOAc$

In each case Me_2GeHI (*ca.* 2 mmol) was passed through a column loosely packed with a mixture of glass wool and the appropriate silver(I) pseudohalide, AgCN, AgNCO, AgNCS, or AgOAc (*ca.* 25 g) until ^1H n.m.r. examination showed that all the iodide had been consumed. Complete reaction was usually obtained in three double passes. The yields and physical data for the new series were: Me_2GeHCN (87%; v.p. *ca.* 13 mm Hg at 23°; parent peaks at *m/e* 126–133 ($H_nC_2GeCN^+$); mol. wt. calcd., 129.68); $Me_2GeHNCO$ (78%; v.p. *ca.* 14 mm Hg at 20°; parent peaks at *m/e* 142–148 ($H_nC_2GeNCO^+$); mol. wt. calcd., 145.67); $Me_2GeHNCS$ (93%; v.p. *ca.* 5 mm Hg at 20°; parent peaks at *m/e* 159–163 ($H_nC_2GeNCS^+$); mol. wt. calcd., 161.74); $Me_2GeHOAc$ (83%; v.p. *ca.* 10 mm Hg at 24°; weak parent peaks at *m/e* 147–153 ($H_nC_4GeO_2$); mol. wt. calcd., 150.70).

Prominent features in the liquid phase i.r. and Raman spectra (cm^{-1}) of $Me_2GeHOAc$ assignable to Me_2GeH fundamentals were observed at: 3000 m (3001 m,dp), (2925 m,dp), (2928 s,p), —CH_3 stretch; 2102 s (2097 s,p). —GeH stretch; 1420s (1420 w,dp), (1250 m,p), —CH_3 def.; 841s, 773 m, —CH_3 rocks; (649 w), —GeH def; 628s (627 m,dp), 602s (601 vs,p), —GeC stretch; (555 s,p), —GeO stretch; (205 sh,dp), (194 s,dp), —skeletal modes. Raman values in parentheses.

Cleavage Reactions with Hydrogen Bromide

Known quantities of the pseudohalides were effectively cleaved by reaction with excess gaseous HBr (30 min, r.t.) to give Me_2GeHBr which was identified quantitatively and qualitatively from ^1H n.m.r. and i.r. spectra: Me_2GeHCN (0.95 mmol) gave Me_2GeHBr (0.85 mmol); $Me_2GeHNCO$ (0.72 mmol) gave Me_2GeHBr (0.69 mmol); $Me_2GeHNCS$ (1.02 mmol) gave Me_2GeHBr (0.95 mmol); $Me_2GeHOAc$ (0.85 mmol) gave Me_2GeHBr (0.83 mmol) and AcOH (*ca.* 0.8 mmol). The recovery of near-quantitative amounts of Me_2GeHBr confirms that the Me_2GeH— moiety is present in stoichiometric proportions in monomeric pseudohalide species. The hydrogen pseudohalide species (*i.e.* HCN, HNCO, HNCS) showed a marked tendency to polymerize under the experimental condition so they were identified only on a qualitative basis.

We wish to thank the National Research Council of Canada for financial support.

1. E. Amberger and H. Boeters. Angew. Chem. **73**, 114 (1961).
2. C. H. Van Dyke, J. E. Bulkowski, and N. Viswanathan. Inorg. Nucl. Chem. Lett. **7**, 1057 (1971).
3. J. E. Drake, R. T. Hemmings, and C. Riddle. J. Chem. Soc. A, 3359 (1970).
4. G. K. Barker, J. E. Drake, R. T. Hemmings, and B. Rapp. Spectrochim. Acta, **28A**, 1113 (1972); J. Chem. Soc. A, 3291 (1971).
5. J. E. Drake and R. T. Hemmings. Can. J. Chem. **51**, 302 (1973).
6. C. H. Van Dyke. Prep. Inorg. React. **6**, 157 (1971).
7. S. Cradock and E. A. V. Ebsworth. J. Chem. Soc. A, 1420 (1968).
8. E. A. V. Ebsworth, S. G. Frankiss, and A. G. Robiette. J. Mol. Spectrosc. **12**, 299 (1964).
9. R. T. Hemmings. Ph.D. Thesis, University of Windsor, Windsor, Ontario. 1973.
10. E. A. V. Ebsworth and S. G. Frankiss. Trans. Faraday Soc. **59**, 1518 (1963); **63**, 1574 (1967).
11. J. W. Emsley, J. Feeney, and L. H. Sutcliffe. High resolution nuclear magnetic resonance spectroscopy. Vol. 2. Pergamon Press, Oxford. 1966. Chapt. 10.
12. E. A. V. Ebsworth. Organometallic compounds of the group IV elements. Vol. 1. *Edited by* A. G. MacDiarmid. Dekker, New York, New York. 1968. Part 1.
13. H. Spiesecke and W. G. Schneider. J. Chem. Phys. **35**, 722 (1961); K. M. Mackay and R. Watt. J. Organomet. Chem. **6**, 336 (1966); **12**, 49 (1963).
14. T. Schaefer, W. F. Reynolds, and T. Yonemoto. Can. J. Chem. **41**, 2969 (1963).
15. J. R. Cavanaugh and B. P. Dailey. J. Chem. Phys. **34**, 1099 (1961).
16. C. H. Van Dyke and A. G. MacDiarmid. Inorg. Chem. **3**, 1071 (1964).
17. E. J. Spanier and A. G. MacDiarmid. J. Inorg. Nucl. Chem. **31**, 2976 (1969).
18. C. N. Banwell and N. Sheppard. Disc. Faraday Soc. **34**, 115 (1962).
19. C. Schumann and H. Dreeskamp. J. Magn. Reson. **3**, 204, (1970).
20. M. L. Huggins. J. Am. Chem. Soc. **75**, 4123 (1953).
21. D. F. Van de Vondel and G. P. Van der Kelen. Bull. Soc. Chim. Belg. **74**, 453 (1965); J. E. Griffiths. Spectrochim. Acta, **20**, 1335 (1964); J. R. Durig, K. K. Lau, J. B. Turner, and J. Bragin. J. Mol. Spectrosc. **31**, 419 (1969); J. R. Aronson and J. R. Durig. Spectrochim. Acta, **20**, 219 (1964).
22. D. F. Van de Vondel, G. P. Van der Kelen, and G. Van Hooydonk. J. Organomet. Chem. **23**, 431 (1970).
23. J. W. Anderson, G. K. Barker, J. E. Drake, and R. T. Hemmings. Can. J. Chem. **49**, 3931 (1971); J. R. Durig, C. F. Jumper, and J. N. Willis. J. Mol. Spectrosc. **37**, 260 (1971).
24. D. E. Freeman, K. H. Rhee, and M. K. Wilson. J. Chem. Phys. **39**, 2908 (1963); **43**, 333 (1965).
25. J. E. Griffiths. J. Chem. Phys. **38**, 2879 (1963); D. F. Van de Vondel and G. P. Van der Kelen. Bull. Soc. Chim. Belg. **74**, 467 (1965).
26. G. K. Barker. Ph.D. Thesis. University of Windsor, Windsor, Ontario. 1972.
27. T. D. Goldfarb. J. Chem. Phys. **37**, 642 (1962).
28. J. S. Thayer and D. P. Strommer. J. Organomet. Chem. **5**, 383 (1966); S. Cradock and E. A. V. Ebsworth. J. Chem. Soc. A, 1420 (1968); J. S. Thayer and R. West. Inorg. Chem. **3**, 889 (1964).
29. K. M. Mackay and S. R. Stobart. Spectrochim. Acta. **26A**, 373 (1970); J. E. Griffiths. J. Chem. Phys. **48**, 278 (1968).

30. G. DAVIDSON, L. A. WOODWARD, K. M. MACKAY, and P. ROBINSON. Spectrochim. Acta, **23**A, 2383 (1967).
31. J. S. THAYER. Organomet. Chem. Rev. **1**, 157 (1966).
32. J. D. MURDOCH and D. W. H. RANKIN. Chem. Commun. 748 (1972).
33. N. S. HAM and J. B. WILLIS. Spectrochim. Acta, **16**, 279 (1960); R. P. HIRSCHMANN, R. N. KNISELY, and V. A. FASSEL. Spectrochim. Acta, **21**, 2125 (1965); **23**A, 109 (1967).
34. E. A. V. EBSWORTH, R. MOULD, R. TAYLOR, G. R. WILKINSON, and L. A. WOODWARD. Trans. Faraday. Soc. **58**, 1069 (1962).
35. D. F. VAN DE VONDEL, E. V. VAN DEN BERGHE, and G. P. VAN DER KELEN. J. Organomet. Chem. **23**, 105 (1970).
36. S. CRADOCK. J. Chem. Soc. A, 1426 (1968).
37. I. R. BEATTIE, N. CHEETHAM, M. GARDNER, and D. E. ROGERS. J. Chem. Soc. A, 2240 (1971); J. H. SCHACHTSCHNEIDER. Tech. Rep. No. 57–65, Shell Development Co., Emeryville, California. 1964.
38. J. E. GRIFFITHS. Can. J. Chem. **45**, 2639 (1967); J. E. GRIFFITHS and K. B. MCAFEE. Proc. Chem. Soc. 456 (1961); V. W. LAURIE. J. Chem. Phys. **30**, 1210 (1959).
39. J. E. DRAKE, C. RIDDLE, and D. E. ROGERS. J. Chem. Soc. A, 910 (1969).
40. A. N. EGOROCHKIN, M. L. KHIDEKEL, V. A. PONOMARENKO, G. YA ZUEVA, and G. A. RAZUVAEV. Izv. Akad. Nauk SSSR, 347 (1964).
41. H. SCHMIDBAUR. Chem. Ber. **97**, 1639 (1964).
42. J. E. GRIFFITHS. Inorg. Chem. **2**, 375 (1963).
43. T. WENTINK and V. H. TIENSU. J. Chem. Phys. **28**, 826 (1958); A. STOCK and O. PRIESS. Gesellschaft, **47**, 3113 (1914).
44. M. KRIEGSMAN. Z. Anorg. Allg. Chem. **294**, 113 (1958).
45. G. K. BARKER and J. E. DRAKE. Inorg. Nucl. Chem. Lett. **7**, 39 (1971).
46. K. MOEDRITZER. J. Organomet. Chem. **6**, 282 (1966).

Can. J. Chem. Downloaded from www.nrcresearchpress.com by 210.87.254.42 on 09/05/12
For personal use only.

Infrared and Raman Spectra of Arylazo Complexes: Assignment of ν(N=N) in Some Molybdenum and Tungsten Polypyrazolylborate Compounds of the Type $[RB(pz)_3M(CO)_2(N_2Ar)]$

DEREK SUTTON

Department of Chemistry, Simon Fraser University, Burnaby, British Columbia V5A 1S6

Received January 17, 1974

DEREK SUTTON. Can. J. Chem. **52**, 2634 (1974).

The infrared and Raman spectra have been measured for the series of arylazo complexes $[RB(pz)_3M(CO)_2(N_2Ar)]$, where R = H, pz; M = Mo, W; pz = 1-pyrazolyl, and Ar = C_6H_5, C_6D_5, *p*-C_6H_4F, *m*-C_6H_4F, *p*-$C_6H_4NO_2$, *o*-$C_6H_4CH_3$, and *o*-$C_6H_3(CH_3)_2$. On the basis of spectral shifts (including ^{15}N-substitution) and Raman intensities, a band in the region 1530–1580 cm^{-1} is assigned as ν(NN) and a band at 1600–1630 is tentatively assigned as having a contribution from the antisymmetric —N=N—C stretch.

DEREK SUTTON. Can. J. Chem. **52**, 2634 (1974).

On mesure les spectres infrarouge et Raman d'une série de complexes arylazoïques $[RB(pz)_3M(CO)_2(N_2Ar]$, dans lesquels R = H, pz; M = Mo, W; pz = pyrazolyl-1 et Ar = C_6H_5, C_6D_5, *p*-C_6H_4F, *m*-C_6H_4F, *p*-$C_6H_4NO_2$, *o*-$C_6H_4CH_3$ et *o*-$C_6H_3(CH_3)_2$. En se basant sur les déplacements spectraux (la substitution ^{15}N y comprise) et les intensités Raman, une bande dans la région 1530–1580 cm^{-1} est attribuée à ν(NN) et l'on propose, à titre d'essai qu'une bande à 1600–1630 provient d'une contribution de l'élongation antisymétrique —N=N—C.

[Traduit par le journal]

Introduction

Some years ago, Trofimenko (1) reported the reaction of the anions $[RB(pz)_3M(CO)_3]^-$ with a variety of aryldiazonium salts to yield neutral arylazo complexes $[RB(pz)_3M(CO)_2(N_2Ar)]$, where M = Mo, W; R = H, pz; pz = 1-pyrazolyl. In the infrared spectra of these compounds, a band at ~1620 cm^{-1} was tentatively assigned to vibration of the —N=N— chromophore, or possibly as an aromatic ring mode (1), but no experiments to settle the assignment were undertaken at that time. More recently, the synthesis of a substantial number of transition metal – arylazo complexes has led to the observation that ν(NN) for the coordinated arylazo ligand may extend over a rather wide range of values, at least from 2095 cm^{-1} (2) to 1440 cm^{-1} (3). The range of observed values

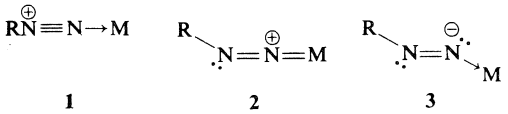

1 **2** **3**

is a reflection of different possible formalisms **1**–**3** for the electronic structure of the metal–arylazo group, and it has recently been suggested that, provided observed ν(NN) values are brought to a common scale, the corrected values ν'(NN) fall into three fairly distinct groups (4). These are (*i*) lower than 1540–1560 cm^{-1}, corresponding to doubly bent geometry **3**, (*ii*) between 1540–1560 and 1700–1740 cm^{-1} corresponding to singly bent geometry **2**, and (*iii*) those greater than 1700–1740 cm^{-1} corresponding to singly bent geometry **2**, but tending to the linear case **1**.

Since the molecular geometry of $[HB(pz)_3Mo(CO)_2N_2C_6H_5]$ has been determined fairly accurately by X-rays (5) and shown to conform closely to type **2**, it seemed worthwhile to use isotopic substitution to settle the actual value of ν(NN) for this compound and its relatives.

Experimental[1]

$[B(pz)_4Mo(CO)_2(^{15}N{=}^{14}NPh)]$ was synthesized from $Mo(CO)_6$, $K[B(pz)_4]$, and $[Ph^{14}N{=}^{15}N]BF_4$ following the published procedure (1). $[Ph^{14}N{=}^{15}N]BF_4$ was synthesized by diazotizing aniline with $Na^{15}NO_2$ (96%) purchased from Isomet Corp. $[B(pz)_4Mo(CO)_2N_2C_6D_5]$ was synthesized using $[C_6D_5N_2]BF_4$ prepared by

[1]Non-isotopically substituted compounds used in this study were kindly supplied by Dr. S. Trofimenko.

Can. J. Chem. Downloaded from www.nrcresearchpress.com by 210.87.254.40 on 09/05/12
For personal use only.

Can. J. Chem. Downloaded from www.nrcresearchpress.com by 210.87.254.40 on 09/05/12
For personal use only.

diazotization of $C_6D_5ND_2$, and the presence of C_6D_5 confirmed by comparison of its n.m.r. and i.r. with that of the C_6H_5 analog.

Infrared spectra were measured as KBr pellets, Nujol mulls, and as solutions in cyclohexane (KBr cell). Significant shifts in band positions for KBr pellets were observed by comparison with solution or mull spectra. Values of ν(CO) for solution spectra were in agreement with published values (1). Spectra were measured on Perkin–Elmer 457 and Beckman IR-12 instruments and are considered reliable to within $\pm 2\ cm^{-1}$. Raman spectra were taken on the pure solids using a Cary Model 81 spectrophotometer equipped with a Spectra-Physics Model 125 He–Ne laser delivering 60 mW. Samples were checked carefully for possible thermal decomposition, and where necessary this was avoided by defocussing. From the relative band positions, the i.r. Nujol mulls correspond most closely with the Raman sampling conditions. Satisfactory solution Raman spectra were not obtained. The Raman spectrometer was calibrated against rare-gas emission lines. Observed Raman shifts are believed to be reliable to $\pm 2\ cm^{-1}$ or better.

Results and Discussion

The compounds under study exhibit no fundamental frequencies other than ν(CO) in the region 2500–1650 cm^{-1}. Attention was focussed on the 1400–1650 cm^{-1} region, where the spectrum was sensitive to the compound and to isotopic substitution. The bands observed in this region (excluding those due to $RB(pz)_3$) are listed in Table 1, and can be seen to fall into four groups: (*i*) a band of medium intensity observed in the region of 1475 cm^{-1} in both Raman and infrared, (*ii*) a band in the region 1530–1580 cm^{-1}, often around 1560 cm^{-1}, present strongly in both Raman and i.r. and of variable position, (*iii*) a band at ~1585 cm^{-1} of much lower intensity, which appears in both Raman and i.r., and (*iv*) a band in the region 1600–1630 cm^{-1} often quite strong in the infrared spectrum but usually weak and difficult to observe in the Raman spectrum. The assignments for these four regions are now discussed.

(i) 1475 cm^{-1} Region

This is the position expected for a ν(C═C) skeletal mode of the aromatic ring of the arylazo ligand derived from the E_{1u} mode of benzene. Splitting into component modes (*e.g.* A_1 and B_1 for C_6H_5X) is sometimes, but not always, distinguishable in such instances (6). Confirmation of the assignment in this case is afforded by the nonexistence of a band in this position in $[B(pz)_4Mo(CO)_2(N_2C_6D_5)]$, together with the appearance of a new band of medium intensity in both Raman and i.r. at 1355 cm^{-1} corresponding to the expected position for the corresponding ν(C═C) mode of the C_6D_5 group (7). The band is virtually insensitive to ^{15}N substitution.

(ii) 1530–1580 cm^{-1} Region

Each compound studied exhibited a band in this region in both the Raman and i.r. spectrum. The band in question usually appeared as a quite well defined single peak in the solution i.r. spectrum. It was not possible to record Raman spectra for the cyclohexane solutions due to limited solubility, and so solid phase i.r. spectra were run for better comparison with the Raman spectra. The solid phase i.r. spectra generally gave much broader peaks in this region (with occasional solid-state splitting) and the positions of the peaks often differed considerably from the solution i.r. positions. There was good agreement between peak positions in the Raman and Nujol–i.r. spectra, and on this basis there seems little doubt that the Raman and i.r. bands in question result from the same normal vibration. There also seems little doubt that this normal vibration is largely ν(NN) since the peak shifts down by about 30 cm^{-1} either on ^{15}N substitution of the coordinated nitrogen atom in $[B(pz)_4Mo(CO)_2(N{=}NC_6H_5)]$ or upon deuteriation of the phenyl group. It is the only strong band in the Raman spectrum between 1500 and 2000 cm^{-1} for any of the compounds measured, with the exception of $\nu(NO_2)$ frequencies of nitro derivatives. As expected, the band for a tungsten compound is invariably at a lower wavenumber than for its molybdenum analog. In most cases, but not all, values appear to be lower when R = H than when R = pz for similar compounds. The shifts induced by a change of substituent are not straightforward; for example in two series substitution by fluorine in a *para* position increases the frequency, whilst substitution *meta* decreases it.

(iii) 1580–1597 cm^{-1} Region

The medium or low intensity band frequently observed in this region in the i.r. and Raman spectra is assigned as the skeletal ν(C═C) mode of the aromatic nucleus derived from the E_{2g} mode of benzene (6). It is unaffected by ^{15}N substitution and appears to shift down by the expected amount upon deuteriation of the phenyl group (7).

TABLE 1. Wavenumbers of observed bands in infrared and Raman spectra of $[RB(pz)_3M(CO)_2(N{=}NAr)]$ in the range 1400–1650 cm^{-1} (excluding $RB(pz)_3$ absorptions)

Compound	Wavenumbers of observed bands (cm^{-1})[h]			
	Infrared			Raman
	KBr pellet	C_6H_{12} solution	Nujol mull	(solid)
$[B(pz)_4Mo(CO)_2(N{=}NPh)]$[a]	~1475m	1483m	1481m	1482m[b]
	(1354m)	(1355m)	(1353m)	(1355m)
	1508m,sh	1505m,sh	1505w	
	(1508m,sh)	(1505m,sh)	(1505w)	
		1540sh	1540sh	
	1550vs	1569vs	1567vs	1569s[b]
	(1537s)	(1539s)	(1542m)	(1536s)
	1580m,sh	1583m	1582m,sp	
	(1555m,sh)	(1552m,sh)	(1555m,sh)	
		1618sh		
	1625vs	1631s	1633vs	
	(1613s)	(1610s)	(1618s)	
$[B(pz)_4Mo(CO)_2(^{15}N{=}^{14}NPh)]$	1470m			
	1485w,sh		1485w,sh	1476m
	1510sh		1510sh	
	1520vs		1523vs,sh	1524m
	1530vs,sh		1537vs	1538m
	1545sh	1553s	1545sh	
	1565w,sh		1565w,sh	
	1580vw		1581sp	1585w
	1610m,b	1612w	1612wm	~1608w
		1622w,sh	1625w,sh	
$[B(pz)_4W(CO)_2(N{=}NPh)]$	1475m		1476s,sh	1476m
	1510sh			
	1525sh			
	1532vs	1540sh	1533vs	1530s
	1545sh	1556s	1555sh	1550w
	1565sh	1565sh		
	1580vw	1580vw	1581w	1580w
	1606m	1610w	1606m	1605w
	1620sh	1620vw,sh	1625w	
$[HB(pz)_3Mo(CO)_2(N{=}NPh)]$	1474m	1485sh	1477s	
			1485w,sh	1478m
		1502sh	1502w	
	1525sh		1525sh	
	1545vs	1540w,sh	1545sh	
	1565sh	1567s	1558vs	1559s
	1580w	1583w	1583w	
	1595sh		1597w	~1590vw[c]
	1613s	1620sh	1613s	
	1625sh	1632m	1626s	
$[HB(pz)_3W(CO)_2(N{=}NPh)]$	1472m		1477m	1477m
	1500sh		1501w	
	1510sh		1525sh	
	1530vs			
	1545sh	~1545s[d]	1550vs	1547s
	1565sh		1565sh	1558vw
	1580vs		1580w	
	1607m		1608m	1608vw
	1625sh		1630w	

Can. J. Chem. Downloaded from www.nrcresearchpress.com by 210.87.254.40 on 09/05/12
For personal use only.

TABLE 1. (*Continued*)

Compound	Wavenumbers of observed bands (cm^{-1})[h]			
	Infrared			Raman (solid)
	KBr pellet	C_6H_{12} solution	Nujol mull	
$[B(pz)_4Mo(CO)_2(N{=}NpC_6H_4F)]$	1475sh			
	1485s	1492s	1490s	1488m
			1505w	
	1545sh		1562sh	
	1565s,b	1574s	1577s	1582m
	1595sh	1595sh	1596m	
	1616s	1622s	1620sh	
			1628s	
$[B(pz)_4W(CO)_2(N{=}NpC_6H_4F)]$	1475sh			
	1487s	1492s	1489s	1488m
	1508w	1505sh	1505w	
	1545sh	1564sh	1560sh	
	1564s	1570s	1569s	1574m
	1595sh		1597w	1590w
	1613s	1619m	1620s	
$[HB(pz)_3Mo(CO)_2(N{=}NpC_6H_4F)]$	1483vs	1492s	1490s	1488s
	1503w		1505w	
	1542sh	1545sh	1540w,sh	
	1560vs	1560sh		
	1575sh	1576s	1569s	1568s
	1595w	1597w	1597w	~1590w
			1617sh	
	1612vs	1623s	1622s	
$[HB(pz)_3W(CO)_2(N{=}NpC_6H_4F)]$	1480vs	1490s	1489s	1485s
	1505w		1504w	
	1515w		1515w,sh	
	1545vs	1561sh		
	1565sh	1568s	1558s	1557s
	1595sh		1595vw	1591m
	1608vs	1617m	1610m	1610w
$[B(pz)_4Mo(CO)_2(N{=}NmC_6H_4F)]$	1475m	1477sh	1478m	1478m
	1510s,sh		1515m	
	~1540vs,b		1545s,sh	1554s
	1565sh	1557s	1556vs	
	1581w,sh	1574w	1578w	1590w
	1617w	1622w	1620m	1621m
$[HB(pz)_3Mo(CO)_2(N{=}NmC_6H_4F)]$	1475s	1475sh	1478s	1475m
	1510s,sh		1505w	
	~1530vs,b	1545sh	1537vs	1538s
	1545s,sh	1557s	1545s,sh	
	1578m,sh	1585w	1582m	
	1613w	1621w	1618w	1618m

Can. J. Chem. Downloaded from www.nrcresearchpress.com by 210.87.254.40 on 09/05/12
For personal use only.

TABLE 1. (*Concluded*)

Compound	Wavenumbers of observed bands (cm^{-1})[h]			
	Infrared			Raman
	KBr pellet	C_6H_{12} solution	Nujol mull	(solid)
$[B(pz)_4Mo(CO)_2(N{=}NpC_6H_4NO_2)]$[e]	1460s,sh			
	1480vs,sh			~1500w,sh
	1508vs,b	1510w,sh		
	1530vs,sh	1525w,sh		1528m
		1538vs		
	1545sh	1544sh		
	1590w	1597w		1592s[f]
	1610w,sh	1616w		1609s
$[HB(pz)_3Mo(CO)_2(N{=}NpC_6H_4NO_2)$[e]	1460s,sh			1449m
	1475vs,sh	1480sh		
	1500vs,b			
	1525vs,sh	1525w,sh		1530m
		1538vs		
	1545sh	1545sh		
	1588m	~1595w		1593[f]
	1610w,sh			
$[HB(pz)_3Mo(CO)_2(N{=}NoC_6H_4CH_3)]$	1479m	1480sh		1482s
	1505sh	1505sh		
	1545s,b	1540w		
	1560sh	1569s		1562s
	1590sh	1594w		
	1610s	1625s		~1600m
$[HB(pz)_3Mo(CO)_2(N{=}NoC_6H_3(CH_3)_2)]$	1500w	1505w,sh		
	1542sh	1535w		
	1560s,sh	1560w,sh		
	1570s	1579s		1579s[g]
	1625vs,b	1624		
		1637		

[a]Values for corresponding peaks in $[B(pz)_4Mo(CO)_2N{=}NC_6D_5]$ in parentheses.
[b]Defocussing necessary; spectrum of low quality.
[c]Probably decomposition product, intensity increased with length of exposure of sample to laser beam.
[d]Not very soluble, weak spectrum.
[e]$\nu_s(NO_2)$ occurs very strongly at 1330 cm^{-1} in the Raman spectrum of these compounds. Solution i.r. is relatively weak due to poor solubility.
[f]Raman enhancement of 1590 cm^{-1} bands possibly due to coupling with $\nu_{as}(NO_2)$. An alternative assignment is $\nu(N{=}N)$ at 1590 (+ phenyl) and $\nu_{as}(NO_2)$ at 1530 (usual position).
[g]Spectrum tentative, sample decomposed in instrument.
[h]vs, very strong; w, weak; s, strong; sh, shoulder; m, medium; b, broad.

(iv) 1600–1630 cm^{-1} Region

The band occurring in this region also shifts with ^{15}N and ^{2}H (phenyl) substitution in $[B(pz)_4Mo(CO)_2(N_2Ph)]$ and must be assigned to a vibration of the azophenyl group to which $\nu(NN)$ makes some contribution. The infrared intensity of this band does not remain reasonably constant from compound to compound (as does the ~1550 band), and in particular decreases substantially in the N^{15}-substituted compound. The Raman intensity is invariably low (in several spectra the band seems to be absent altogether) indicating a very small change in polarizability, and a tentative assignment of this band is that it originates in a vibration involving some contribution from an antisymmetric —N=N—C< stretching mode.

Conclusion

The compounds studied exhibit two bands in the infrared spectrum which shift position with ^{15}N and ^{2}H (phenyl) substitution. The first, in

Can. J. Chem. Downloaded from www.nrcresearchpress.com by 210.87.254.40 on 09/05/12
For personal use only.

the $\sim 1550\ cm^{-1}$ region, appears strongly in the Raman spectrum also, and is assigned as predominantly ν(NN). The second, a band in the $\sim 1620\ cm^{-1}$ region, shows smaller shifts upon isotopic substitution and very low Raman intensity. It is tentatively assigned as due to a vibration involving a contribution from the antisymmetric —N=N—C< stretching mode.

Dr. S. Trofimenko is thanked for kindly making samples available for study, and for his helpful comments. This work was supported by the National Research Council of Canada through operating grants.

1. S. Trofimenko. Inorg. Chem. **8**, 2675 (1969).
2. W. L. Bowden, W. F. Little, and T. J. Meyer, J. Am. Chem. Soc. **95**, 5084 (1973).
3. G. W. Parshall. J. Am. Chem. Soc. **89**, 1822 (1967); **87**, 2133 (1965).
4. A. P. Gaughan, B. L. Haymore, J. A. Ibers, W. H. Myers, T. E. Nappier, and D. W. Meek. J. Am. Chem. Soc. **95,** 6859 (1973).
5. G. Avitabile, P. Ganis, and M. Nemiroff. Acta Cryst. B**27**, 725 (1971).
6. D. H. Whiffen. J. Chem. Soc. 1350 (1956).
7. S. Pinchas and I. Laulicht. Infrared spectra of labelled compounds. Academic Press, N.Y. 1971. p. 103.

Can. J. Chem. Downloaded from www.nrcresearchpress.com by 210.87.254.40 on 09/05/12
For personal use only.

The Hydrolysis of Esters Related to *O*-Hippuryl-2-hydroxybutanoic Acid by Carboxypeptidase A

JOHN W. BUNTING AND JOE MURPHY

Department of Chemistry, University of Toronto, Toronto, Ontario M5S 1A1

Received February 14, 1974

JOHN W. BUNTING and JOE MURPHY. Can. J. Chem. **52**, 2640 (1974).

The hydrolysis of each of the following esters by bovine carboxypeptidase A has been studied at p*H* 7.5, 25°, ionic strength 0.5: *O*-hippuryl-, *O*-phenaceturyl-, *O*-aceturyl-, *O*-(*N*-methylhippuryl)-, and *O*-(*N*-hippurylglycyl)-2-hydroxybutanoic acids, and 2-(3-benzoylpropanoxy)-, 2-benzoxyacetoxy-, and 2-(4-phenylbutanoxy)butanoic acids. Substrate inhibition occurs with only the hippuric and phenaceturic acid esters and in the six other cases simple Michaelis–Menten kinetics are observed. The relatively minor variations in the structures of the acid moieties of these esters lead to quite large variations in K_m, although k_{cat} seems to be relatively independent of the nature of the acid moiety. Binding modes of substrate molecules at both the catalytic and inhibitory sites are discussed in the light of these observations.

JOHN W. BUNTING et JOE MURPHY. Can. J. Chem. **52**, 2640 (1974).

On a étudié l'hydrolyse des esters suivant par la carboxypeptidase A du bovin (p*H* 7.5, 25°, force ionique de 0.5): des acides *O*-hippuryl, *O*-phénacéturyl, *O*-acéturyl, *O*-(*N*-méthylhippuryl) et *O*-(*N*-hippurylglycyl) hydroxy-2 butanoiques et des acides (benzoyl-3 propanoxy)-2, benzoxy-acétoxy-2 et (phényl-4 butanoxy)-2 butanoiques. L'inhibition du substrat n'a lieu seulement avec les esters d'acides hippuriques et phénacéturiques, et dans les six autres cas on observe les cinétiques simples de Michaelis–Menten. Les variations relativement mineures dans les structures des parties acides de ces esters conduisent à des variations assez importantes de K_m, bien que k_{cat} semble être relativement indépendant de la nature de la partie acide. A la lumière de ces observations on discute des modes de liaisons des molécules du substrat aux sites catalytiques et inhibiteurs. [Traduit par le journal]

Can. J. Chem. Downloaded from www.nrcresearchpress.com by 210.87.254.42 on 09/05/12
For personal use only.

The kinetics of the hydrolysis of *N*-protected dipeptides and their ester analogs by bovine carboxypeptidase A are complicated by substrate activation and inhibition effects (1–9). Auld and Vallee (10–12) have shown that these kinetic complications are either absent or displaced to much higher substrate concentrations in analogous tripeptides and the same is also apparently the case for ester depsipeptide subtrates (13).

In a recent communication (9) we presented some of our data on the dependence of substrate inhibition on the structure of the alcohol moiety in the hydrolysis of hippuric acid esters by carboxypeptidase A. In a companion investigation, we are also studying the dependence of this phenomenon on the structure of the acid moiety of the ester substrate for a series of *O*-acyl-2-hydroxybutanoic acids. In the present report, we will discuss the influence of acid moieties closely related to hippuric acid on the kinetics of carboxypeptidase A catalysis. It will be shown that relatively minor variations on the hippuric acid structure can have profound effects on the kinetic parameter, K_m, and also on the occurrence of substrate inhibition. However, k_{cat} is relatively insensitive to these variations in the acid moiety.

Experimental

Materials

Aceturic acid (14), phenaceturic acid (15), *N*-methylhippuric acid (16), and 3-benzoylpropanoic acid (17) were synthesized by the indicated literature routes. Hippuric acid, *N*-hippurylglycine, 4-phenylbutanoic acid, and 2-bromobutanoic acid were commercial products.

Benzoxyacetic Acid

A solution of benzyl chloroacetate (9.7 g) (prepared by the route described below for benzyl 2-bromobutanoate), benzoic acid (6.9 g), and triethylamine (5.3 g) in acetonitrile (150 ml) was heated under reflux for 24 h. After removal of the acetonitrile under vacuum, the residue was taken up in dichloromethane and treated as described below for the synthesis of substrates. After debenzylation, the white solid was recrystallized from benzene – petroleum ether (1:1); yield 86%; m.p. 111–112° (lit. (18) m.p. 112–113°).

Benzyl 2-Bromobutanoate

A solution of 2-bromobutyric acid (0.13 mol) in benzyl alcohol (70 ml) was saturated with dry HCl and allowed to stand overnight. After dilution with ether

Can. J. Chem. Downloaded from www.nrcresearchpress.com by 210.87.254.42 on 09/05/12
For personal use only.

(300 ml) and extraction with saturated aqueous $NaHCO_3$ (500 ml), the ethereal solution was dried over magnesium sulfate and the ether removed at the water pump. The residue was distilled under vacuum with excess benzyl alcohol being collected at 80–90°/3 mm, while the ester was obtained at 135–137°/3 mm; yield 87%.

tert-Butyl 2-Bromobutanoate

To a solution of 2-bromobutyric acid (16.4 g) in dichloromethane (120 ml) was added concentrated H_2SO_4 (0.5 ml) and sufficient tetrahydrofuran to completely dissolve the mineral acid. Isobutene was slowly bubbled through the stirred solution for 4 h, after which the flask was stoppered and stored at room temperature for 3 days. After extraction with saturated aqueous $NaHCO_3$ (2 × 50 ml) and drying over magnesium sulfate, the dichloromethane was removed under vacuum to give the desired ester as a colorless liquid; b.p. 72–76°/12 mm (lit. (19) b.p. 76°/15 mm); yield 90%.

Synthesis of Substrates

All substrates, except 2-(3-benzoylpropanoxy)butanoic acid were synthesized by the following general route.

A mixture of the carboxylic acid (0.055 mol), benzyl 2-bromobutanoate (0.050 mol), triethylamine (0.050 mol), and acetonitrile (100 ml) was heated under reflux for 16–20 h, then cooled. The triethylammonium bromide was filtered off and acetonitrile removed under vacuum. The residue was dissolved in dichloromethane (300 ml) and extracted with 3 *M* HCl (100 ml), then saturated aqueous $NaHCO_3$ (200 ml), and dried over magnesium sulfate. Removal of the dichloromethane under vacuum gave an oil which usually crystallized on standing. A solution of this crude benzyl ester (0.040 mol) in ethyl acetate (400 ml) was hydrogenated at 1 atm and room temperature in the presence of 5% Pd–C (0.5 g) until uptake of hydrogen was complete. Acetone (400 ml) was added and the solution heated to boiling and filtered. Removal of the solvents under vacuum gave the crude 2-acyloxy acid which was purified as indicated in the following individual cases. (Yields are based on 2-bromobutyric acid.)

O-Hippuryl-DL-*2-hydroxybutanoic acid*: recrystallized from 1,2-dichloroethane–acetonitrile (8:1); yield 66%; m.p. 152–153°; p.m.r. (CF_3CO_2H): δ 1.12 (3H, t, J = 7 Hz), 2.08 (2H, m), 4.60 (2H, d, J = 4 Hz),[1] 5.32 (1H, t, J = 6 Hz), 7.73 (6H, m)[1].

Anal. Calcd. for $C_{13}H_{15}NO_5$: C, 58.9; H, 5.70; N, 5.28. Found: C, 58.3; H, 5.73; N, 5.27.

O-Phenaceturyl-DL-*2-hydroxybutanoic acid*: obtained as a noncrystallizable oil. This acid was converted to the solid potassium salt by treating a solution of the oil in 50% aqueous acetone with 1 equiv. of 0.5 *M* potassium hydroxide, removing the solvent under vacuum, and then recrystallizing the residue from acetone containing a few drops of water; yield 50%; m.p. (potassium salt) 161–163°; p.m.r. (CF_3CO_2H): δ 1.13 (3H, t, J = 7 Hz), 2.10 (2H, m), 3.97 (2H, s), 4.41 (2H, d, J = 5 Hz)[1], 5.25 (1H, t, J = 6 Hz), 7.42 (6H, s with broad base)[1].

Anal. Calcd. for $C_{14}H_{16}KNO_5$: C, 53.0; H, 5.08; N, 4.41. Found: C, 53.0; H, 5.29; N, 4.33.

O-Aceturyl-DL-*2-hydroxybutanoic acid*: recrystallized from 1,2-dichloroethane–acetonitrile (8:1); yield 76%; m.p. 111–112°; p.m.r. (CF_3CO_2H): 1.12 (3H, t, J = 7 Hz), 2.10 (2H, m), 2.42 (3H, s), 4.44 (2H, d, J = 5 Hz)[1], 5.27 (1H, t, J = 6 Hz), 8.13 (1H, broad s)[1].

Anal. Calcd. for $C_8H_{13}NO_5$: C, 47.3; H, 6.45; N, 6.90. Found: C, 47.1; H, 6.41; N, 6.90.

O-(N-Methylhippuryl)-DL-*2-hydroxybutanoic acid*: recrystallized from 1,2-dichloroethane–carbon tetrachloride; yield 62%; m.p. 122–123°; p.m.r. (CF_3CO_2H):[2] δ 1.18 (3H, m), 2.12 (2H, m), 3.35 + 3.47 (3H, singlets), 4.47 + 4.72 (2H, singlets), 5.40 (1H, m), 7.63 (5H, broad s).

Anal. Calcd. for $C_{14}H_{17}NO_5$: C, 60.2; H, 6.14; N, 5.01. Found: C, 59.8; H, 6.20; N, 5.00.

DL-*2-(Benzoxyacetoxy)butanoic acid*: recrystallized from hexane–benzene (2:1); yield 61%; m.p. 79–80°; p.m.r. ($CDCl_3$): δ 0.97 (3H, t, J = 7 Hz), 1.90 (2H, m), 4.92 (2H, s), 5.08 (1H, t, J = 6 Hz), 7.43 (3H, m), 8.05 (2H, m), 10.55 (1H, s).

Anal. Calcd. for $C_{13}H_{14}O_6$: C, 58.6; H, 5.30. Found: C, 58.7; H, 5.29.

O-(N-Hippurylglycyl)-DL-*2-hydroxybutanoic acid*: recrystallized from acetonitrile; yield 48%; m.p. 170–172°; p.m.r. (CF_3CO_2H): δ 1.12 (3H, t, J = 7 Hz), 2.10 (2H, m), 4.50 (4H, m), 5.28 (1H, t, J = 6 Hz), 7.75 (6H, m)[1].

Anal. Calcd. for $C_{15}H_{18}N_2O_6$: C, 55.9; H, 5.63; N, 8.69. Found: C, 56.0; H, 5.90; N, 8.75.

DL-*2-(4-Phenylbutanoxy)butanoic acid*: obtained as noncrystallizable oil; converted to potassium salt as described above but this salt also could not be crystallized. After several cycles in which this salt was dissolved in hot chloroform–hexane, and after cooling and decanting off the mother liquor, the glassy salt was dissolved in water, the solution acidified to p*H* 2 with 3 *M* HCl, and extracted with dichloromethane. After drying over magnesium sulfate, the organic solvent was removed under vacuum and the residual pale yellow oil was dried for 24 h at 50°/4 mm over P_2O_5; yield 48%; p.m.r. ($CDCl_3$): δ 1.03 (3H, t, J = 7 Hz), 1.93 (4H, m), 2.32 (2H, t, J = 7 Hz), 2.68 (2H, t, J = 7 Hz), 4.98 (1H, t, J = 6 Hz), 7.22 (5H, s), 10.77 (1H, s).

Anal. Calcd. for $C_{14}H_{18}O_4$: C, 67.2; H, 7.25. Found: C, 66.6; H, 7.27.

DL-*2-(3-Benzoylpropanoxy)butanoic acid*: A solution of *tert*-butyl 2-bromobutanoate (0.040 mol), 3-benzoylpropanoic acid (0.045 mol), and triethylamine (0.040 mol) in nitromethane (80 ml) was heated under reflux for 18–20 h. After cooling, nitromethane was removed under vacuum, and the residue dissolved in dichloromethane (200 ml). This solution was extracted with 3 *M* HCl (200 ml), then with saturated aqueous $NaHCO_3$ (200 ml), and dried over magnesium sulfate. Removal of dichloro-

[1]The signal from the methylene protons of the hippuric acid moiety appears as a poorly resolved doublet, presumably due to splitting by the amide proton which is buried under the aromatic proton signal at δ 7.73. Similar phenomena are observed with the phenaceturic and aceturic acid esters. For a detailed discussion of this phenomenon, see ref. 20.

[2]The complexities in this spectrum are due to the presence of comparable amounts of the *cis* and *trans* amides.

Can. J. Chem. Downloaded from www.nrcresearchpress.com by 210.87.254.42 on 09/05/12
For personal use only.

methane under vacuum gave the *tert*-butyl ester of the required substrate as a brown oil; yield 72%. A mixture of this crude ester (0.030 mol), *p*-toluenesulfonic acid (1 g), and benzene (100 ml) was heated under reflux for 3 h and then cooled. After extraction with p*H* 3 chloroacetate buffer (100 ml) and drying over magnesium sulfate the benzene was removed under vacuum to give the desired acid as a brown oil which solidified on standing and was recrystallized from hexane–benzene (2:1); yield 28%; m.p. 74–75°; p.m.r. ($CDCl_3$): δ 1.05 (3H, t, J = 7 Hz), 1.95 (2H, m), 2.90 (2H, m), 3.38 (2H, m), 5.08 (1H, t, J = 6 Hz), 7.54 (3H, m), 8.02 (2H, m), 11.02 (1H, s).

Anal. Calcd. for $C_{14}H_{16}O_5$: C, 63.6; H, 6.10. Found: C, 63.7; H, 6.33.

Methods

Stock solutions of bovine carboxypeptidase A were prepared by dialysis at 4° of a toluene-preserved suspension of the enzyme (Worthington Biochemical Corp. Code COA) against 1 *M* aqueous sodium chloride in 0.05 *M* tris buffer, p*H* 7.5, containing 10^{-4} *M* zinc nitrate. Enzyme concentrations of these stock solutions were estimated spectrophotometrically at 278 nm ($\varepsilon = 6.42 \times 10^4\ M^{-1}\ cm^{-1}$) (21). All enzyme solutions were stored at 4° and were frequently assayed with *O*-hippuryl-L-3-phenyllactic acid (Fox Chemical Co.) to check for inactivation.

Most of the substrates are relatively insoluble in water as the free acids but quite soluble as salts. Attempted preparation of stock substrate solutions by addition of the carboxylic acid to an aqueous solution of 1 equiv. of base was found to lead to some hydrolysis of the substrate as a result of its relatively slow dissolution. The following typical procedure was therefore adopted. Substrate (0.005 mol) was dissolved in 50 ml of 50% aqueous acetone, warming on the steam bath to promote dissolution if necessary. To this solution was added dropwise, with constant swirling, exactly 10.2 ml 0.500 *M* aqueous KOH (0.0051 mol). After careful concentration on the rotary evaporator to a volume of about 10 ml (effectively removing all the acetone), the resulting solution of the salt of the substrate was transferred to a 50 ml volumetric flask along with several aqueous washings from the original flask. Sodium chloride (1.17 g) was added and the volume adjusted to 50 ml with water. The resultant solution consisted of 0.1 *M* DL-substrate (as the potassium salt), 0.4 *M* sodium chloride, and had p*H* 6–7. By changing the quantities of substrate, aqueous acetone, base, and sodium chloride, this procedure could be modified to allow the preparation of stock DL-substrate solutions with concentrations ranging from 0.01 to 0.5 *M*.

All reaction kinetics were studied at 25°, total ionic strength 0.5 (substrate + NaCl), p*H* 7.5. Hydrolysis of each ester was followed by titration with standard potassium hydroxide solutions on a Radiometer p*H*-stat (22). Initial velocities were estimated directly from the recorder traces. All calculations are based on the assumption that only the L-enantiomers of the racemic esters are hydrolyzed and that the D-esters are neither substrates nor competitive inhibitors. This has been established for several carboxypeptidase A substrates by other workers (3, 5, 23, 24) and was supported by our observations that only 50 ± 2% of each of the present racemic esters had hydrolyzed at equilibrium in those kinetic runs that were allowed to proceed to completion. The influence of the D-enantiomers of two of these substrates as noncompetitive inhibitors is discussed later. Kinetic parameters for those esters not displaying substrate inhibition were estimated using a computer program based on the regression technique of Wilkinson (25).

Results

The dependence of initial velocity (v/E) of enzymic hydrolysis on substrate concentration for the *O*-hippuryl, *O*-aceturyl, and *O*-phenaceturyl derivatives of 2-hydroxybutanoic acid (**1**:R = C_6H_5, CH_3, and $C_6H_5CH_2$, respectively) is shown in Fig. 1. Substrate inhibition is

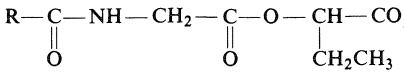

1

apparent for both the hippuric and phenaceturic acid esters, although the additional methylene group in the latter substrate has considerable effect upon the overall curve. Thus, the phenaceturate ester reaches a maximum velocity that is approximately six times greater than that for the corresponding hippurate ester and this increased velocity is also accompanied by displacement of the appearance of substrate inhibition to somewhat higher substrate concentrations.

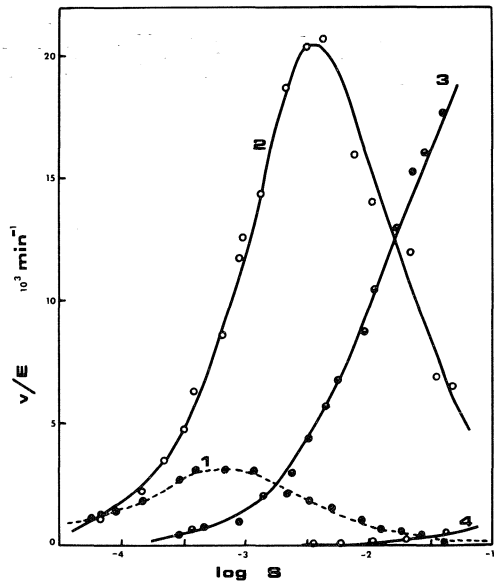

FIG. 1. Ester hydrolysis by carboxypeptidase A at p*H* 7.5, 25°, ionic strength 0.5; (*1*) *O*-hippuryl-L-2-hydroxybutanoic acid; (*2*) *O*-phenaceturyl-L-2-hydroxybutanoic acid; (*3*) *O*-aceturyl-L-2-hydroxybutanoic acid; (*4*) *O*-(*N*-methylhippuryl)-L-2-hydroxybutanoic acid.

Can. J. Chem. Downloaded from www.nrcresearchpress.com by 210.87.254.42 on 09/05/12
For personal use only.

Thus, maximum velocities for **1**: R = C_6H_5 and **1**:R = $C_6H_5CH_2$ occur at substrate concentrations of approximately 8×10^{-4} and 4×10^{-3} *M*, respectively. The aceturic acid ester (**1**:R = CH_3) gives no indication of substrate inhibition over the concentration range examined. A Lineweaver–Burk plot of the data for this ester (Fig. 2) is quite linear and clearly substrate activation is not present, while substrate inhibition is displaced to very high substrate concentrations if it occurs at all.

Data for the hydrolysis of the 2-hydroxybutanoic acid ester of *N*-methylhippuric acid (or *N*-benzoylsarcosine) are also included in Fig. 1. This replacement of the amide hydrogen atom of hippuric acid by a methyl group leads to a drastic reduction in velocity at most substrate concentrations, although at high substrate concentration (>0.05 *M*) the *N*-methyl derivative actually hydrolyzes faster than its hippuric acid analog as a result of the pronounced substrate inhibition of the hydrolysis of this latter ester at these concentrations. A reciprocal plot of the data for the *N*-methylhippuric acid ester is indicated in Fig. 3. While this plot is linear (slope K_m/k_{cat}), it is clear that K_m is very large and cannot be approached under the present experimental conditions (ionic strength 0.5).

Lineweaver–Burk plots (Fig. 4) for the hydrolysis of 2-(3-benzoylpropanoxy)butanoic acid (**2**), 2-(benzoxyacetoxy)butanoic acid (**3**), 2-(4-phenylbutanoxy)butanoic acid (**4**), and *O*-(*N*-hippurylglycyl)-2-hydroxybutanoic acid are all quite linear up to substrate concentrations of the order of 0.1 *M* and so indicate that if substrate

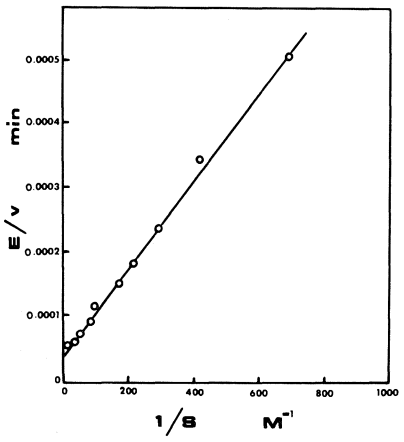

FIG. 2. Lineweaver–Burk plot for the hydrolysis of *O*-aceturyl-L-2-hydroxybutanoic acid.

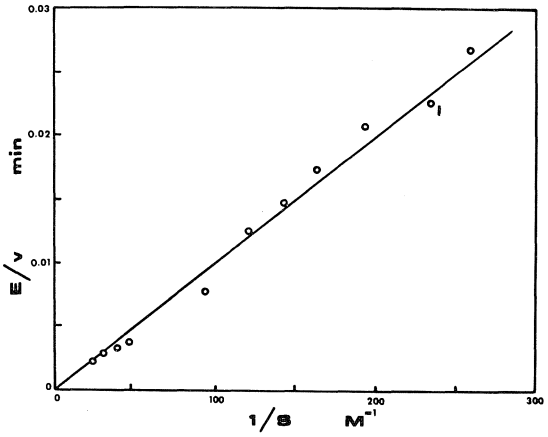

FIG. 3. Lineweaver–Burk plot for the hydrolysis of *O*-(*N*-methylhippuryl)-L-2-hydroxybutanoic acid.

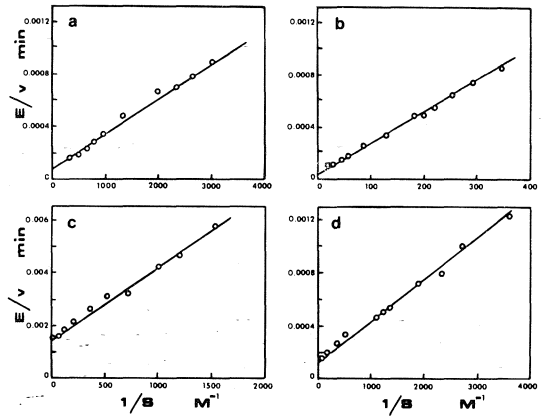

FIG. 4. Lineweaver–Burk plots for the hydrolysis of (*a*) L-2-(3-benzoylpropanoxy)butanoic acid; (*b*) L-2-benzoxyacetoxybutanoic acid; (*c*) L-2-(4-phenylbutanoxy)butanoic acid; (*d*) *O*-(*N*-hippurylglycyl)-L-2-hydroxybutanoic acid.

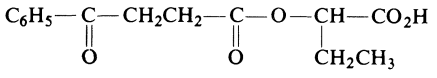

2

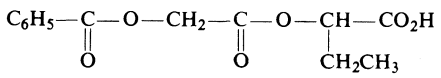

3

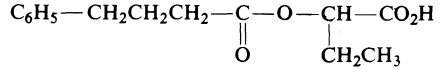

4

TABLE 1. Kinetic parameters for hydrolysis of L-$RCO_2CH(CH_2CH_3)CO_2^-$ by carboxypeptidase A[a]

R	K_S (M)	k_2 (min^{-1})	k_2/K_S	K_{SL} (M)	k_3 (min^{-1})
$C_6H_5CONHCH_2$	3.1×10^{-4}	6.4×10^{3}	2.1×10^{7}	2.4×10^{-3}	200
$C_6H_5CH_2CONHCH_2$	2.9×10^{-3}	5.1×10^{4}	1.8×10^{7}	9.8×10^{-3}	2000
$CH_3CONHCH_2$	1.5×10^{-2}	2.4×10^{4}	1.6×10^{6}	—	—
$C_6H_5COCH_2CH_2$	2.7×10^{-3}	1.2×10^{4}	4.4×10^{6}	—	—
$C_6H_5CON(CH_3)CH_2$	>0.1	>450	9.2×10^{3}	—	—
$C_6H_5CO_2CH_2$	6.0×10^{-2}	2.5×10^{4}	4.2×10^{5}	—	—
$C_6H_5CH_2CH_2CH_2$	1.8×10^{-3}	6.7×10^{2}	3.7×10^{5}	—	—
$C_6H_5CONHCH_2CONHCH_2$	2.7×10^{-3}	8.2×10^{3}	3.0×10^{6}	—	—

[a]At pH 7.5, 25°, ionic strength 0.5, K_m and k_{cat} are assumed equal to K_S and k_2, respectively.

inhibition occurs, it is only important at much higher substrate concentrations than for *O*-hippuryl-2-hydroxybutanoic acid (**1**:R = C_6H_5). Kinetic parameters for these esters from the plots in Figs. 2–4 are collected in Table 1.

We have previously fitted (9) the data for **1**:R = C_6H_5 to eq. 1 where the parameters k_2,

$$[1] \qquad \frac{v}{E} = \frac{k_2S + k_3S^2/K_{ss}}{K_s + S + S^2/K_{ss}}$$

k_3, K_S, and K_{SS} are defined by Scheme 1. More

$$E + S \overset{K_S}{\rightleftharpoons} E\cdot S \overset{k_2}{\rightarrow} E + P_1 + P_2$$

$$E\cdot S + S \overset{K_{SS}}{\rightleftharpoons} E\cdot S_2 \overset{k_3}{\rightarrow} E + S + P_1 + P_2$$

SCHEME 1

recently, in our laboratories[3] and elsewhere (26), it has been found that some D-esters analogous to our substrates do bind to the enzyme, contrary to expectation (3, 5, 23, 24), and act as noncompetitive inhibitors. Thus, Scheme 1 should be modified[4] as in Scheme 2, which generates the dependence of initial velocity on substrate concentration in eq. 2, where S is the concentration of the individual D and L isomers of the racemate.

$$E + S_L \overset{K_s}{\rightleftharpoons} E\cdot S_L \overset{k_2}{\rightarrow} E + P_1 + P_2$$

$$E\cdot S_L + S_L \overset{K_{SL}}{\rightleftharpoons} S_L\cdot E\cdot S_L \overset{k_3}{\rightarrow} E + S_L + P_1 + P_2$$

$$E\cdot S_L + S_D \overset{K_{SD}}{\rightleftharpoons} S_D\cdot E\cdot S_L \overset{k_4}{\rightarrow} E + S_D + P_1 + P_2$$

SCHEME 2

[3]J. Murphy and J. W. Bunting. Unpublished observations.

[4]Both Schemes 1 and 2 are particular cases of a more general scheme involving random binding of substrate molecules to the two enzymic sites. We have previously shown (9) that the data for the hippuric acid ester are consistent with these simpler forms and we continue to use them here for convenience.

This equation is of the same form as equation 1, with $K_{SS} = K_{SL}K_{SD}/(K_{SL} + K_{SD})$. There is evi-

$$[2] \qquad \frac{v}{E} = \frac{k_2S + \left(\frac{k_3}{K_{SL}} + \frac{k_4}{K_{SD}}\right)S^2}{K_S + S + S^2\left(\frac{1}{K_{SL}} + \frac{1}{K_{SD}}\right)}$$

dence[3] (26) that K_{SL} and K_{SD} are similar for those esters previously investigated, and if we assume that $K_{SL} \approx K_{SD}$ and also $k_3 \approx k_4$, then equation 2 becomes the same as equation 1 but with $K_{SS} = K_{SL}/2$. The experimental data for **1**:R = C_6H_5 and **1**:R = $C_6H_5CH_2$ have been fitted (27) to equation 1 making these assumptions. The curves in Fig. 1 for these two esters are based on equation 1 and the parameters in Table 1, and give an acceptable fit to the experimental data (average % errors between calculated and experimental velocities are 5.4 and 6.0% for the hippurate and phenaceturate esters, respectively).

If K_{SS} is very large, the above schemes and equation 1 both reduce to the simple Michaelis–Menten form, and substrate inhibition will not be observed. The linear reciprocal plots observed in Figs. 2–4, also indicate that for these esters, the D-enantiomers do not act as noncompetitive inhibitors.

Discussion

We have previously (9) analyzed the substrate inhibition that is apparent in the carboxypeptidase A catalyzed hydrolysis of various esters (**5**) of hippuric acid in terms of Scheme 1. The

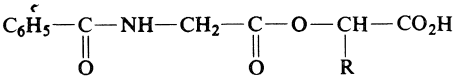

5

dependence of velocity on substrate concentration for six such esters was closely fitted by equation 1 and for each ester the value for K_{SS} was within the range $(1.2 \pm 0.4) \times 10^{-3}$ M.

Can. J. Chem. Downloaded from www.nrcresearchpress.com by 210.87.254.42 on 09/05/12
For personal use only.

Can. J. Chem. Downloaded from www.nrcresearchpress.com by 210.87.254.42 on 09/05/12
For personal use only.

Modification of this analysis as discussed above, changes this value to $K_{SL} = (2.4 \pm 0.8) \times 10^{-3}$ *M*. Since this dissociation constant seems to be independent of the nature of the alcohol moiety (**5**:R = C_2H_5, *n*-C_3H_7, *iso*-C_3H_7, $CH_3(CH_2)_3$, C_6H_5, $C_6H_5CH_2$), it is reasonable to believe that the R group in **5** plays no part in the binding of these esters at the second site of the enzyme in the formation of the $E.S_2$ complex. In this case, it is reasonable to assume that interaction of the substrate (**5**) with the enzyme at this second site is predominantly through the hippuric acid part of the ester molecule. Thus, the dissociation constant K_{SL} should show some sensitivity to the nature of the acid moiety of the ester molecule.

The above hypothesis is supported by the results of the present work, in which we have been able to show, by keeping the alcohol moiety constant and varying the acid moiety, that the occurrence of substrate inhibition is very dependent on the presence of hippuric acid as the acid moiety. Thus, for the eight substrates considered in Table 1, only the phenaceturic and hippuric acid esters show any tendency to pronounced substrate inhibition. Comparison of the structural features of these two esters with the other esters in this table seems to indicate two requirements for significant substrate inhibition:[5] (*i*) the presence of a phenyl ring; and (*ii*) the presence of a —CONH— moiety. Thus, replacement of the phenyl ring of hippuric acid by a methyl group, as in the aceturate ester, does not lead to substrate inhibition, and so indicates that the amide group alone is not sufficient for binding at the second site. Likewise, a phenyl group alone is not sufficient to produce substrate inhibition if an unmodified amide bond is not present (*cf.* $C_6H_5CON(Me)$, $C_6H_5COCH_2$, $C_6H_5CO_2$, $C_6H_5CH_2CH_2$ in Table 1). The quite different behavior of the isoelectronic —CONH— and —CO_2— groups in their ability to promote substrate inhibition strongly suggests that an interaction involving hydrogen-bond donation from this amide bond to an enzymic acceptor atom is involved in the substrate binding to the inhibitory site.

Whereas the formation of an $E.S_2$ complex has fairly rigid specificity requirements for substrate binding at the second site, the values of K_S in Table 1 seem to indicate that a much greater variation in substrate structure is acceptable for binding at the catalytic site to give the active E.S complex. In particular, a comparison of the esters of phenaceturic acid (**1**:R = $C_6H_5CH_2$) and 3-benzoylpropanoic acid (**2**) is of interest. Thus, although these esters have very similar K_S values, the former displays substrate inhibition whereas this phenomenon is not apparent for the latter ester. However, in the comparison of relative K_S values it is important to bear in mind that the experimentally observed value for this parameter may contain contributions from nonproductive binding modes for the substrate (Scheme 3).

$$E + S \overset{K_S}{\rightleftharpoons} E \cdot S \overset{k_2}{\rightarrow} E + P_1 + P_2$$

$$E + S \overset{K_S^{NP}}{\rightleftharpoons} E \cdot S_{NP}$$

SCHEME 3

Kinetic analysis of Scheme 3 gives eq. 3 which

$$\frac{v}{E} = \frac{k_2/(1 + K_S/K_S^{NP})}{1 + \frac{1}{S}\left(\frac{K_S}{1 + K_S/K_S^{NP}}\right)} \qquad [3]$$

has the same form as the classical Michaelis–Menten equation in the absence of nonproductive binding, but with

$$k_{cat} = k_2/\left(1 + \frac{K_S}{K_S^{NP}}\right)$$

and

$$K_m = K_S/\left(1 + \frac{K_S}{K_S^{NP}}\right).$$

This predicts that nonproductive binding according to Scheme 3 gives apparent values for both k_2 and K_S which are less than the true values by the factor $(1 + K_S/K_S^{NP})$, although the ratio k_{cat}/K_m does reflect the true specificity constant k_2/K_S.

We have recently observed (35) that for the ester *O*-benzoyl-2-hydroxybutanoic acid, nonproductive binding modes predominate over catalytically productive binding to this enzyme. Thus it seems unreasonable to arbitrarily rule out the possibility of nonproductive binding for at least some of the esters in Table 1, and this being the case, it is then difficult to draw clear-cut conclusions about the influence of substrate structure upon binding (*i.e.* K_S) and rate of hydrolysis (*i.e.* k_2). It is intriguing to note that although

[5]The observed absence of substrate inhibition in the hydrolysis of esters of acetic (24, 28) and cinnamic acids (6, 29) by carboxypeptidase A is also consistent with this interpretation.

Can. J. Chem. Downloaded from www.nrcresearchpress.com by 210.87.254.42 on 09/05/12
For personal use only.

k_2/K_S is approximately the same for both the hippurate and phenaceturate esters, both k_2 and K_S are approximately a factor of ten lower for the former than for the latter. On the other hand, the aceturate ester is apparently hydrolyzed four times faster than the hippurate ester, although binding of the latter ester is approximately 50-fold stronger. Overall, it is clear from the data in Table 1 that if nonproductive binding does not occur in at least some cases, then there is no correlation between binding affinity and rate of enzymic hydrolysis.

One might suspect that the unusually small value for k_2 for the ester **4** compared with the k_2 values for the other subtrates in Table 1 might indicate unusually strong nonproductive binding in this case. One way in which nonproductive binding could occur would be for the phenyl ring in the acid moiety of **4** to bind in the hydrophobic pocket which is believed to normally accommodate the hydrophobic side chain of the alcohol moiety (30–33). Provided the other parts of the molecule can be reasonably located, one might suspect that the phenylpropyl moiety of **4** might be able to very effectively compete with the relatively small ethyl group for this hydrophobic pocket. It is unlikely that such "wrong-way" bound complexes would be catalytically active. Of all the esters in Table 1, it might be expected that the aceturate ester (**1**:R = CH_3) would show the least tendency to engage in such "wrong-way" binding, and the observed k_2 and K_S values for this ester probably accurately reflect the true rate and binding constants.

Despite the complications from nonproductive binding that are discussed above, some details of the binding of the acid moiety to the catalytic site are discernible from Table 1, since the observed K_S values represent minimum values for the dissociation constants of the catalytically productive E.S complexes. Thus the extremely weak binding of the *N*-methylhippuric acid ester strongly suggests that the —CONH— moiety is involved in an important binding interaction with the enzyme. The difference in binding of the esters of the isoelectronic benzoxyacetic and hippuric acids also may be interpreted tentatively in terms of the —CONH— bond acting as a hydrogen-bond donor towards an enzyme acceptor site in the formation of the productive E.S complex. The extremely poor binding of the *N*-methylhippuric acid ester is consistent with this interpretation, since it not only lacks the required proton for donation to the hydrogen bond, but the presence of the methyl group would also create a very unfavorable steric interaction with the enzyme at separations between enzyme and substrate suitable for hydrogen bond formation.

We have previously commented (9) on the apparent independence of the ratio $k_2/k_3 \approx 26$ on the nature of the alcohol moiety for a number of hippuric acid esters. It is interesting to note that for the phenaceturate ester, the only non-hippurate ester in the current study to display significant substrate inhibition, the ratio k_2/k_3 is also 26 (Table 1).

In view of the many intriguing differences between the peptidase and esterase activities of carboxypeptidase A (8, 34), it is of interest to compare our observed dependences of esterase activity upon the acid moiety of the substrate with the situation in the enzymic peptide hydrolyses. Unfortunately, detailed investigations of the influence of the acid moiety of peptide substrates are not available at present for non-oligopeptide substrates. However, some comparisons can be made. Thus, the reported (10) elimination, or displacement to high substrate concentrations, of substrate activation and inhibition effects in the hydrolysis of N-protected tripeptide substrates parallels our observations on the esters of hippuric acid and hippurylglycine (see also ref. 13). In this regard, it is interesting to note that the most studied peptide substrates with this enzyme have been amides of hippuric acid and carbobenzoxyglycine (*cf.* phenaceturic acid), which one might predict, on the basis of our data for ester subtrates, to be the amide substrates that would be the most susceptible to substrate inhibition effects. Our observation of a drastic decrease in the rate of hydrolysis of an ester of *N*-methylhippuric acid relative to the corresponding hippuric acid ester is also consistent with the observation (23) that (*N*-methylhippuryl)phenylalanine is hydrolyzed much more slowly than hippurylphenylalanine.

We appreciate the continued support of this research by the National Research Council of Canada, and the award of an Ontario Graduate Fellowship to J.M.

1. J. E. SNOKE, G. W. SCHWERT, and H. NEURATH. J. Biol. Chem. **175**, 7 (1948).
2. R. LUMRY, E. L. SMITH, and R. R. GLANTZ. J. Am. Chem. Soc. **73**, 4330 (1951).
3. W. O. MCCLURE, H. NEURATH, and K. A. WALSH. Biochemistry, **3**, 1897 (1964).

4. E. T. KAISER, S. AWAZU, and F.W. CARSON. Biochem. Biophys. Res. Commun. **21**, 444 (1965).
5. J. R. WHITAKER, F. MENGER, and M. L. BENDER. Biochemistry, **5**, 386 (1966).
6. S. AWAZU, F. W. CARSON, P. L. HALL, and E. T. KAISER. J. Am. Chem. Soc. **89**, 3627 (1967).
7. R. C. DAVIES, J. F. RIORDAN, D. S. AULD, and B. L. VALLEE. Biochemistry, **7**, 1090 (1968).
8. B. L. VALLEE, J. F. RIORDAN, J. L. BETHUNE, T. L. COOMBS, D. S. AULD, and M. SOKOLOVSKY. Biochemistry, **7**, 3547 (1968).
9. J. W. BUNTING and J. MURPHY. Biochem. Biophys. Res. Commun. **48**, 1316 (1972).
10. D. S. AULD and B. L. VALLEE. Biochemistry, **9**, 602 (1970).
11. D. S. AULD and B. L. VALLEE. Biochemistry, **9**, 4352 (1970).
12. D. S. AULD and B. L. VALLEE. Biochemistry, **10**, 2892 (1971).
13. D. S. AULD and B. HOLMQUIST. Fed. Proc. **31**, 435 Abstr. (1972).
14. R. M. HERBST and D. SHEMIN. Org. Syn. Coll. Vol. 2, 11.
15. J. H. FORD. J. Am. Chem. Soc. **71**, 3842 (1949).
16. J. L. O'BRIEN and C. NIEMANN. J. Am. Chem. Soc. **79**, 80 (1957).
17. L. F. SOMERVILLE and C. F. H. ALLEN. Org. Syn. Coll. Vol. 2, 81.
18. F. H. CLARKE. J. Org. Chem. **27**, 3251 (1962).
19. F. GAUDEMAR-BARDONE and M. GAUDEMAR. Bull. Soc. Chem. Fr. 2088 (1969).
20. J. MURPHY. Ph.D. Thesis. University of Toronto, Toronto, Ontario. 1974.
21. R. T. SIMPSON, J. F. RIORDAN, and B. L. VALLEE. Biochemistry, **2**, 616 (1963).
22. J. W. BUNTING and C. D. MYERS. Can. J. Chem. **51**, 2639 (1973).
23. J. E. SNOKE and H. NEURATH. J. Biol. Chem. **181**, 789 (1949).
24. E. T. KAISER and F. W. CARSON. J. Am. Chem. Soc. **86**, 2922, (1964).
25. G. N. WILKINSON. Biochem. J. **80**, 324 (1961).
26. L. G. LANGE, D. S. AULD, and J. F. RIORDAN. Fed. Proc. **31**, 435 Abstr. (1972).
27. J. W. BUNTING and J. MURPHY. Can. J. Biochem. **50**, 1369 (1972).
28. F. W. CARSON and E. T. KAISER. J. Am. Chem. Soc. **88**, 1212 (1967).
29. P. L. HALL, B. L. KAISER, and E. T. KAISER. J. Am. Chem. Soc. **91**, 485 (1969).
30. T. A. STEITZ, M. L. LUDWIG, F. A. QUIOCHO, and W. N. LIPSCOMB. J. Biol. Chem. **242**, 4662 (1967).
31. G. N. REEKE, JR., J. A. HARTSUCK, M. L. LUDWIG, F. A. QUIOCHO, T. A. STEITZ, and W. N. LIPSCOMB. Proc. Nat. Acad. Sci. U.S. **58**, 2220 (1967).
32. W. N. LIPSCOMB, G. N. REEKE, JR., J. A. HARTSUCK, F. A. QUIOCHO, P. H. BETHGE, M. L. LUDWIG, T. A. STEITZ, H. MUIRHEAD, and J. C. COPPOLA. Brookhaven Symp. Biol. **21**, 24 (1968).
33. W. N. LIPSCOMB, G. N. REEKE, JR., J. A. HARTSUCK, F. A. QUIOCHO, and P. H. BETHGE. Phil. Trans. R. Soc. London, Ser. B. **257**, 177 (1970).
34. B. L. VALLEE. Ann. N.Y. Acad. Sci. **158**, 377 (1969).
35. J. W. BUNTING, J. MURPHY, C. D. MYERS, and G. G. CROSS. Can. J. Chem. This issue.

Can. J. Chem. Downloaded from www.nrcresearchpress.com by 210.87.254.42 on 09/05/12
For personal use only.

The Hydrolysis of Benzoate Esters by Carboxypeptidase A and the p*H*-Rate Profile for the Hydrolysis of *O*-Hippuryl-L-3-phenyllactic Acid

JOHN W. BUNTING, JOE MURPHY, CHESTER D. MYERS, AND GORDON G. CROSS

Department of Chemistry, University of Toronto, Toronto, Ontario M5S 1A1

Received February 14, 1974

JOHN W. BUNTING, JOE MURPHY, CHESTER D. MYERS, and GORDON G. CROSS. Can. J. Chem. **52**, 2648 (1974).

A series of *para*-substituted *O*-benzoyl-2-hydroxybutanoic acids (but not the unsubstituted ester) are hydrolyzed by bovine carboxypeptidase A (p*H* 7.5, ionic strength 0.5, 25°). For the CH_3O, CH_3, Cl, CN, and NO_2 substituents, there exist linear correlations of k_{cat} and K_m with the Hammett σ constants for these substituents ($\log k_{cat} = 1.17\sigma + 1.17$; $\log K_m = -0.53\sigma - 2.15$), although the *tert*-butyl group shows significant deviations from both correlation lines. The above unsubstituted ester is a reversible inhibitor of the enzymic hydrolysis of *O*-hippuryl-L-3-phenyllactic acid and so the lack of observable hydrolysis of this ester is attributable to nonproductive binding. The p*H*–rate profiles for k_{cat}/K_m and k_{cat} have been determined for the enzymic hydrolysis of *O*-(*p*-nitrobenzoyl)mandelic acid ($pK_{EH_2} = 6.95$, $pK_{EH} = 7.9$ and $pK_{EH_2S} = 7.5$, $pK_{EHS} = 8.3$) and *O*-hippuryl-L-3-phenyllactic acid ($pK_{EH_2} = 5.8$, $pK_{EH} = 9.3$). For the latter ester k_{cat} is p*H* independent in the range p*H* 5–10. The mechanism of ester hydrolysis catalyzed by carboxypeptidase A is discussed in the light of the above observations and the known crystal structure of the enzyme. A definition of specific and nonspecific substrates for this enzyme based on the observed p*H* profiles for k_{cat}/K_m is proposed.

JOHN W. BUNTING, JOE MURPHY, CHESTER D. MYERS et GORDON G. CROSS. Can. J. Chem. **52**, 2648 (1974).

Des séries d'acides *O*-benzoyl hydroxy-2 butanoïques substitués en *para* (mais pas les esters non substitués) sont hydrolysés par la carboxypeptidase A du bovin (p*H* 7.5, 25°, force ionique de 0.5). Il existe des corrélations linéaires entre k_{cat}, K_m et les constances σ de Hammett des substituants CH_3O, CH_3, Cl, CN et NO_2 ($\log k_{cat} = 1.17\sigma + 1.17$; $\log K_m = -0.53\sigma - 2.15$). Toutefois le groupe *tert*-butyle montre des déviations significatives de ces deux droites de corrélations. L'ester non substitué ci-dessus est un inhibiteur réversible de l'hydrolyse enzymatique de l'acide *O*-hippuryl phényl-3 L-lactique, et ainsi on n'observe pas d'hydrolyse de cet ester à cause d'une liaison non-réactive. On détermine la courbe de p*H* pour k_{cat}/K_m et k_{cat} lors de l'hydrolyse enzymatique de l'acide *O*-(*p*-nitrobenzoyl) mandélique ($pK_{EH_2} = 6.95$, $pK_{EH} = 7.9$ et $pK_{EH_2S} = 7.5$, $pK_{EHS} = 8.3$) et de l'acide *O*-hippuryl phényl-3 L-lactique ($pK_{EH_2} = 5.8$, $pK_{EH} = 9.3$). Pour ce dernier ester, k_{cat} reste constant pour une variation du p*H* de 5–10. A la lumière de ces observations et de la structure connue du cristal de l'enzyme, on discute du mécanisme de l'hydrolyse des esters catalysée par la carboxypeptidase A. On propose une définition des substrats spécifiques et non-specifiques pour cette enzyme, basée sur l'observation des courbes de p*H* pour k_{cat}/K_m. [Traduit par le journal]

During the past few years, evidence has accumulated that the γ-carboxyl group of glutamic acid residue 270 plays a role in the mechanism of hydrolyses catalyzed by bovine carboxypeptidase A. Lipscomb and co-workers (1–4), based on their X-ray crystallographic investigation of the structure of this enzyme, originally suggested that this carboxylate ion may be a general-base or nucleophilic catalyst for the hydrolysis of ester and amide substrates. Following upon this suggestion, a number of reagents were observed to irreversibly inhibit both the peptidase and esterase activities of this enzyme by reaction with the glu-270 γ-carboxyl group. Thus, the irreversible inhibition of the enzyme by both *N*-ethyl-5-phenylisoxazolium-3′-sulfonate (Woodward's reagent K) and *N*-bromoacetyl-*N*-methyl-L-phenylalanine has been unambiguously shown (5–8) to be due to modification of glu-270, while 1-cyclohexyl-3-(2-*N*-methylmorpholinioethyl)carbodiimide *p*-toluenesulfonate is also believed (9) to cause inhibition by modification of this same side chain.

Experiments designed to distinguish between a general-base and nucleophilic role for the glu-270 γ-carboxylate ion have not to date provided an unambiguous interpretation. A direct nucleophilic attack by the carboxylate

Can. J. Chem. Downloaded from www.nrcresearchpress.com by 210.87.254.105 on 09/05/12
For personal use only.

Can. J. Chem. Downloaded from www.nrcresearchpress.com by 210.87.254.105 on 09/05/12
For personal use only.

ion on the carbonyl carbon of the hydrolyzable bond of the substrate predicts the formation of a mixed anhydride species as an acyl-enzyme intermediate. Attempts to spectrophotometrically observe such a species (10) or to trap it through transpeptidation or transesterification reactions (11, 12) have been unsuccessful. The lack of positive results in such experiments does not, of course, rule out the existence of an anhydride intermediate, which, if formed, would be expected to be highly reactive towards aqueous solvent. In principle, nucleophilic and general-base mechanistic pathways could also be distinguished by the observation of a relatively large solvent isotope effect in the latter case. Studies in H_2O and D_2O indicate that $k_H/k_D = 1.1–1.2$ for peptide substrates (13–15) and $k_H/k_D \sim 2.0$ for ester substrates (15, 16). This data has been tentatively interpreted as supporting a general-base mechanism for ester hydrolysis; however, the usual complications (17) that obscure the interpretations of isotope effects in enzymic reactions cannot be eliminated and other experimental approaches to this problem are desirable.

In considering this problem, we were attracted by the observation of Hubbard and Kirsch (18) that the Hammett ρ values for nucleophilic attack on substituted benzoate esters show a strong dependence on the charge of the attacking nucleophile (*i.e.* anionic or neutral). Within these two classes of nucleophiles, ρ seems to be relatively independent of the chemical nature of the nucleophile, in both enzymic and nonenzymic systems. Thus, provided a suitable series of benzoate ester substrates can be found, the ρ values for the carboxypeptidase A-catalyzed hydrolysis of such esters may provide an insight into the charge type of the enzymic nucleophile and thus allow a decision on a nucleophilic (anionic nucleophile) or general-base (neutral nucleophile-water molecule) role for glu-270.

In the present work, we have synthesized a series of *para*-substituted *O*-benzoyl-2-hydroxybutanoic acids (**1**) and have shown that, in general, these esters are hydrolyzed by bovine carboxypeptidase A. In addition, we have measured the p*H*–rate profiles for the hydrolysis of *O*-(*p*-nitrobenzoyl)mandelic acid (**2**) and *O*-hippuryl-L-3-phenyllactic acid by this enzyme. Clearly, any mechanistic comparison of the hydrolysis of benzoate and hippurate ester substrates by this enzyme would rely on a similarity in the p*H*–rate profiles for these two

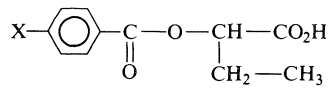

1

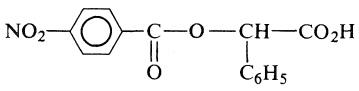

2

classes of substrates. The ester **2** was chosen for a complete p*H* study to allow a more direct comparison with *O*-acetylmandelic acid which has been extensively studied by Carson and Kaiser (41).

Experimental

Substrates

The racemic esters, **1**, were prepared by refluxing the triethylammonium salt of the appropriate *para*-substituted benzoic acid with either *tert*-butyl DL-2-bromobutanoate (X = Cl, CN, NO_2) in nitromethane or benzyl DL-2-bromobutanoate (X = H, CH_3, CH_3O, $(CH_3)_3C$) in acetonitrile followed by removal of the *tert*-butyl (*p*-toluenesulfonic acid in benzene) or benzyl (hydrogenation) protecting groups. The detailed experimental procedures for these preparations closely followed the routes previously described for the synthesis of other ester substrates for this enzyme (19, 20). Melting points, p.m.r. spectra, and elemental analyses of these esters are collected in Table 1.

O-(p-Nitrobenzoyl)-DL-mandelic Acid

A xylene solution (100 ml) of *p*-nitrobenzoyl chloride (9.3 g) was slowly added dropwise to a refluxing solution of mandelic acid (7.6 g) in xylene (30 ml). After refluxing for a further 12 h, the solution was cooled and a small amount of precipitated *p*-nitrobenzoic acid was removed. The solution was concentrated on the rotary evaporator, whereupon the desired ester precipitated. This crude product (m.p. 160–164°) was separated and recrystallized twice from benzene; yield 27%; m.p. 167–169°; p.m.r. (acetone): δ 6.20 (s, 1H), 7.3–7.75 (m, 5H), 8.32 (s, 4H).

Anal. Calcd.: C, 59.9; H, 3.66; N, 4.65. Found: C, 59.5; H, 3.73; N, 4.93.

O-Hippuryl-L-3-phenyllactic acid was a product of Fox Chemical Co., Los Angeles.

Carboxypeptidase A was obtained as a suspension preserved with toluene from Worthington Biochemical Corp. (Code COA). Stock solutions of this enzyme were prepared as previously described (21).

Kinetic Measurements

All hydrolyses were followed on a Radiometer p*H*-Stat in aqueous solution at 25° and p*H* 7.5 unless otherwise indicated. The general experimental technique and estimation of kinetic parameters were as previously described (21). Studies on *O*-hippuryl-L-3-phenyllactic acid and *O*-(*p*-nitrobenzoyl)mandelic acid are at ionic strength 0.2 (NaCl), while the benzoate esters (**1**) were investigated at ionic strength 0.5 (NaCl). It was found

TABLE 1. Characterization of the esters X—$C_6H_4CO_2CH(CH_2CH_3)CO_2H$ (**1**)

X	Melting point (°C)	Proton magnetic resonance (δ in $CDCl_3$)						Analysis (%) Calcd.			Found		
		CH_3[a]	CH_2[b]	CH[c]	Aromatic	OH	Other	C	H	N	C	H	N
H	81	1.12	2.07	5.23	7.43, 8.07[d]	11.57	—	63.5	5.77	—	63.3	5.76	—
CH_3	93	1.10	2.05	5.22	7.22, 7.95[e]	11.10	2.40[f]	64.9	6.31	—	65.5	6.50	—
CH_3O	79	1.08	2.03	5.18	6.88, 8.00[e]	11.00	3.83[f]	60.5	5.88	—	60.3	5.88	—
$(CH_3)_3C$	109–110	1.10	2.05	5.23	7.48, 8.06[e]	9.87	1.35[g]	68.2	7.58	—	68.6	7.70	—
Cl	86–87	1.10	2.03	5.20	7.39, 8.00[e]	10.60	—	54.4	4.57	—	54.4	4.79	—
CN	124–126	1.10	2.07	5.23	7.72, 8.15[e]	11.28	—	61.8	4.75	6.02	61.3	4.66	5.94
NO_2	117–118	1.20	2.17	5.33	8.30[h]	12.62	—	52.2	4.38	5.53	52.1	4.50	5.53

[a]3H,t,J = 7 Hz.
[b]2H,m.
[c]1H,t,J = 6 Hz.
[d]3H and 2H multiplets, respectively.
[e]Both 2H,d,J = 9 Hz.
[f]3H,s.
[g]9H,s.
[h]4H,s.

necessary to work in the presence of 5% dimethyl sulfoxide in order to attain suitable concentrations of **2** since even the sodium salt of this ester proved to be quite insoluble in aqueous solution. Stock solutions of the free acid of **2** were prepared in dimethyl sulfoxide. Suitable aliquots of this solution plus sufficient dimethyl sulfoxide to give a final composition of 5% dimethyl sulfoxide (v/v) in the reaction solution were added to an aqueous solution containing sufficient sodium hydroxide to neutralize the substrate carboxylic acid moiety and sufficient sodium chloride to give a total ionic strength 0.2. Enzyme concentrations for the benzoate ester hydrolyses were in the range 1×10^{-6} to 3×10^{-5} M.

For each of the *para*-substituted benzoate esters only 50 ± 2% of the racemic esters were hydrolyzed at equilibrium. This is consistent with the general observation (22–25) that only the L-enantiomers of substrates of this enzyme are hydrolyzed and all data and calculations are therefore based on the assumption that the D-esters are neither substrates nor competitive inhibitors. In all cases nonenzymic hydrolysis rates were observed to be less than 1% of the enzyme-catalyzed rates.

Results

Each of the esters **1**: X = CH_3, CH_3O, Cl, CN, NO_2, $(CH_3)_3C$ was hydrolyzed by carboxypeptidase A at pH 7.5. Lineweaver–Burk plots for each of these esters are shown in Fig. 1. These plots are clearly linear at low substrate concentrations but positive deviations are observed at high substrate concentrations for X = CH_3O, CH_3, Cl, and $(CH_3)_3C$. This behavior is typical of substrate inhibition and is observed with many ester and peptide substrates of this enzyme (22, 23, 26, 27). In all cases the concentrations at which substrate inhibition becomes important are sufficiently large that reasonably accurate estimates of K_m and k_{cat} can be obtained by fitting the linear portions of these graphs. Values of these two parameters are collected in Table 2.

Surprisingly, no hydrolysis of the unsubstituted ester, **1**: X = H, could be observed under the same conditions as were used for the substituted benzoate esters, or even at enzyme concentrations as great as 10^{-5} M. The ester **1**: X = H, does bind to the enzyme, however, since it reversibly inhibits the enzymic hydrolysis of *O*-hippuryl-L-3-phenyllactic acid (Fig. 2). The inhibition does not appear to take a simple competitive or noncompetitive form, however, and we have been unable to evaluate an inhibition constant for this ester.

From the data in Table 2, it is clear that each of K_m, k_{cat}, and k_{cat}/K_m for the esters, **1**, shows a dependence on the substituent X. Plots of each of these parameters against the Hammett σ substituent constant (28) are indicated in Fig. 3. In each case, there appears to be a linear correlation with σ for five substituents, although the *tert*-butyl group shows a large deviation from each of the correlation lines. Least-squares fitting (ignoring the *tert*-butyl data points) gives the equations:

$$\log k_{cat} = 1.17\sigma + 1.17 \quad (r = 0.985)$$

$$\log K_m = -0.53\sigma - 2.15 \quad (r = 0.943)$$

$$\log (k_{cat}/K_m) = 1.71\sigma + 3.31 \quad (r = 0.998)$$

O-(*p*-Nitrobenzoyl)mandelic acid (**2**) also proved to be a reasonable substrate for bovine carboxypeptidase A. The Lineweaver–Burk plot

Can. J. Chem. Downloaded from www.nrcresearchpress.com by 210.87.254.105 on 09/05/12
For personal use only.

TABLE 2. Hydrolysis of *p*-X—$C_6H_4CO_2CH(CH_2CH_3)CO_2H$ by carboxypeptidase A[a]

X	k_{cat} (min^{-1})	K_m (M)	k_{cat}/K_m (M^{-1} min^{-1})
CH_3O	5.4 ± 0.7	$(8.5 \pm 1.9) \times 10^{-3}$	6.3×10^2
$(CH_3)_3C$	68 ± 3	$(2.4 \pm 0.2) \times 10^{-3}$	2.8×10^4
CH_3	10 ± 2	$(8.4 \pm 2.2) \times 10^{-3}$	1.2×10^3
Cl	37 ± 1	$(7.7 \pm 0.3) \times 10^{-3}$	4.9×10^3
CN	79 ± 2	$(2.8 \pm 0.2) \times 10^{-3}$	2.8×10^4
NO_2	111 ± 3	$(2.5 \pm 0.2) \times 10^{-3}$	4.4×10^4
NO_2[b]	54 ± 9	$(1.3 \pm 0.2) \times 10^{-3}$	4.2×10^4

[a]At p*H* 7.5, 25°, ionic strength 0.5.
[b]5% dimethyl sulfoxide – water, other conditions as above.

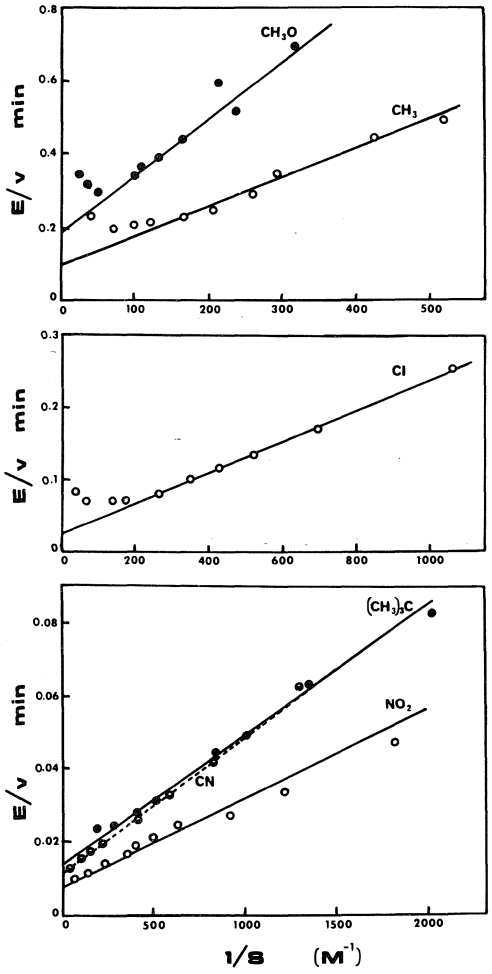

FIG. 1. Hydrolysis of esters **1** by carboxypeptidase A at p*H* 7.5, 25°, ionic strength 0.5; (substituent X is indicated on each line).

for this ester at p*H* 7.5 ($k_{cat} = 167\ min^{-1}$, $K_m = 1.3 \times 10^{-3}\ M$) in Fig. 4 also indicates that substrate inhibition is important at high substrate concentrations in this case. A complete

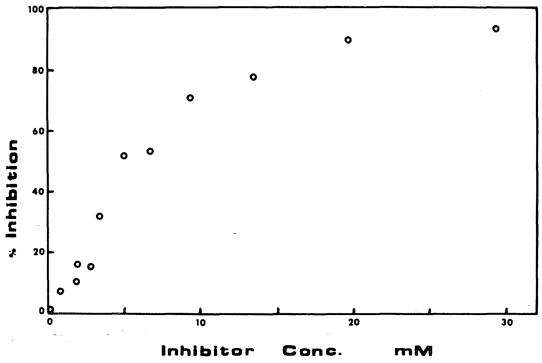

FIG. 2. Inhibition of the hydrolysis of *O*-hippuryl-L-3-phenyllactic acid ($5.5 \times 10^{-5}\ M$) by **1**: X = H.

p*H*–rate profile for this ester was also determined at 25°. The dependences of k_{cat}/K_m and k_{cat} on p*H* are indicated in Fig. 5. Fitting of the data in Fig. 5 to the equations:

$$[1] \qquad k_{cat}/K_m = \frac{k_2/K_S}{1 + [H^+]/K_{EH_2} + K_{EH}/[H^+]}$$

and

$$[2] \qquad k_{cat} = \frac{k_2}{1 + [H^+]/K_{EH_2S} + K_{EHS}/[H^+]}$$

by least-squares analysis according to

$$\frac{K_m}{k_{cat}}[H^+] = \frac{[H^+]^2}{K_{EH_2}}\frac{K_S}{k_2} + [H^+]\frac{K_S}{k_2} + K_{EH}\frac{K_S}{k_2}$$

and

$$\frac{[H^+]}{k_{cat}} = \frac{[H^+]^2}{K_{EH_2S}}\frac{1}{k_2} + \frac{[H^+]}{k_2} + \frac{K_{EHS}}{k_2}$$

gave the curves indicated in Fig. 5, with $pK_{EH_2} = 6.95$, $pK_{EH} = 7.9$, $pK_{EH_2S} = 7.5$, $pK_{EHS} = 8.3$, $k_2 = 260\ min^{-1}$, and $K_S = 3.0 \times 10^{-3}\ M$. The various ionization constants are defined by Scheme 1, which is the simplest general scheme consistent with the observed p*H* dependences.

Can. J. Chem. Downloaded from www.nrcresearchpress.com by 210.87.254.105 on 09/05/12
For personal use only.

Can. J. Chem. Downloaded from www.nrcresearchpress.com by 210.87.254.105 on 09/05/12
For personal use only.

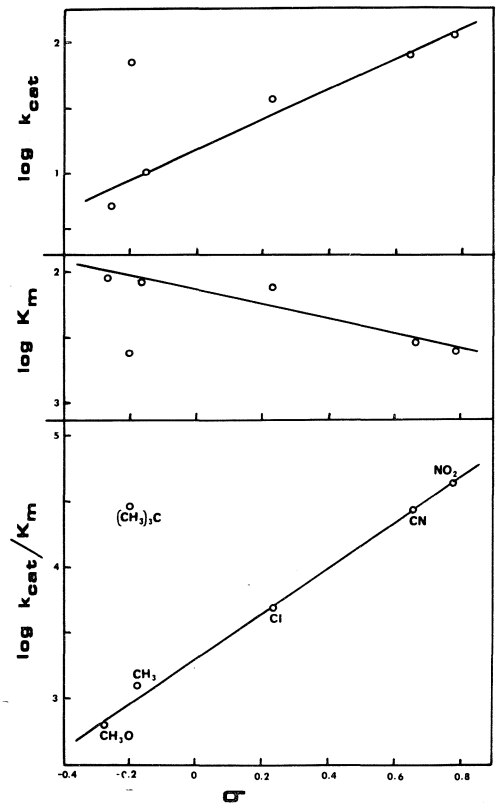

FIG. 3. Dependence of k_{cat}, K_m, and k_{cat}/K_m for the enzymic hydrolysis of **1** on the Hammett σ constant.

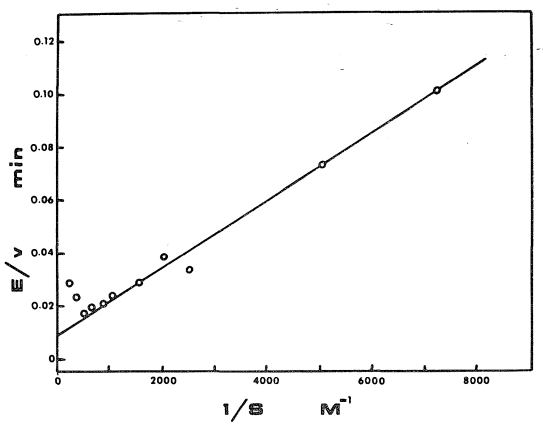

FIG. 4. Hydrolysis of **2** by carboxypeptidase A at p*H* 7.5, 25°, ionic strength 0.2 in 5% dimethyl sulfoxide – water.

The p*H*–rate profile for the carboxypeptidase A-catalyzed hydrolysis of *O*-hippuryl-L-3-phenyllactic acid has also been determined. Typical Lineweaver–Burk plots for the hydrolysis of this ester at a number of p*H* values are indicated in

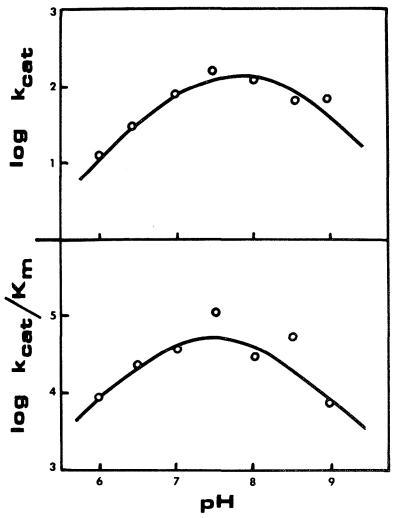

FIG. 5. The p*H* dependence of k_{cat} and k_{cat}/K_m for the hydrolysis of **2** by carboxypeptidase A. Curves are calculated as indicated in the text.

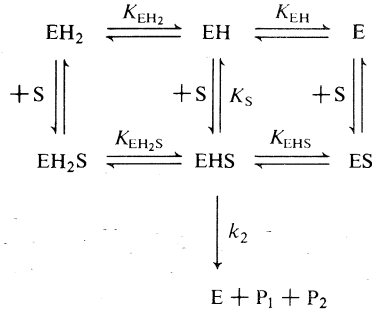

SCHEME 1

Fig. 6. The p*H* profiles for k_{cat} and k_{cat}/K_m for this ester are indicated in Fig. 7. The simplest general scheme applicable to these observed p*H* profiles is outlined in Scheme 2, which is a particular case of Scheme 1 but takes into account the observed p*H* independence of k_{cat} ($= k_2$).[1] Fitting k_{cat}/K_m to eq. 1 by means of the broken lines of slope 1, 0, and −1 in Fig. 7 allows the estimation of $pK_{EH_2} = 5.8$, $pK_{EH} = 9.3$, $k_2 = 3.5 \times 10^4$ min^{-1}, and $K_S = 1.1 \times 10^{-4}$ *M* which have been used to compute the curve in Fig. 7.

Although this ester is by far the most widely studied ester substrate of this enzyme, previous investigators seem to have been dissuaded from

[1]The p*H* independence of k_{cat} could also arise from an alternative, but less likely, modification of Scheme 1, in which EH_2S, EHS, and ES are all catalytically active with identical rate constants, k_2.

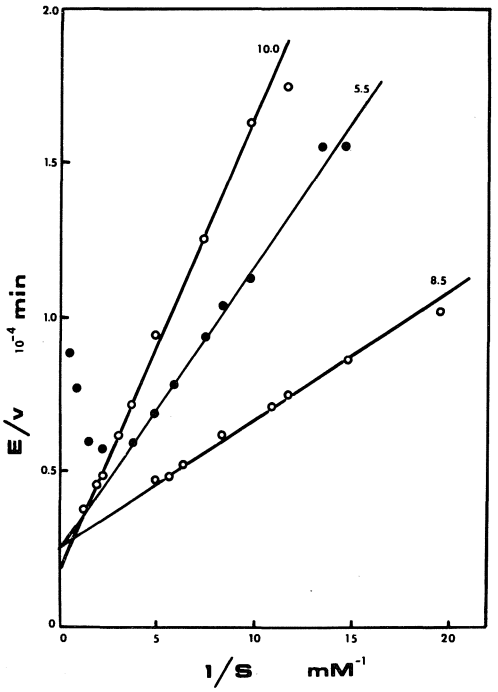

FIG. 6. Hydrolysis of *O*-hippuryl-L-3-phenyllactic acid by carboxypeptidase A at selected p*H* values (25°, ionic strength 0.2).

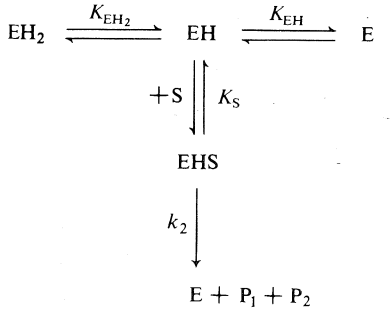

SCHEME 2

attempting a detailed study of the p*H*–rate profile for this ester by the substrate inhibition effects which intrude (22, 23, 26). As a result, relatively uninformative p*H* investigations at only one substrate concentration have previously been attempted (29). Our data indicate that this phenomenon does not, in fact, produce the anticipated limitations on a complete p*H* investigation. Thus, above the optimal p*H* 7.5, the occurrence of substrate inhibition is displaced to higher substrate concentrations, while at p*H* < 7.5, although pronounced substrate inhibition is still present, it does not seriously interfere in the estimation of the catalytic parameters, although at p*H* 4.55 only k_{cat}/K_m could be accurately obtained.

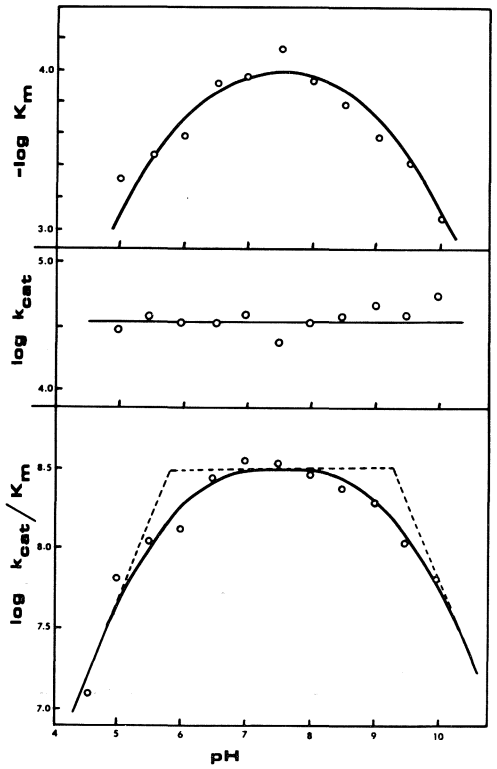

FIG. 7. The p*H* dependence of K_m, k_{cat}, and k_{cat}/K_m for the hydrolysis of *O*-hippuryl-L-3-phenyllactic acid by carboxypeptidase A.

Discussion

The esters **1** and **2** are the first esters of benzoic acid found to be substrates for bovine carboxypeptidase A. All these benzoate esters are relatively poor substrates in terms of both k_{cat} and k_{cat}/K_m compared with this enzyme's most studied ester substrate, *O*-hippuryl-L-3-phenyllactic acid. However, most of these benzoate esters are as good as or better substrates than the extensively studied *O*-acetyl-L-mandelic acid (k_{cat} = 33 min^{-1}, k_{cat}/K_m = 400 M^{-1} min^{-1} (25) at p*H* 7.5, 25°, ionic strength 0.5).

Comparison of the data in Table 1 for **1**: X = NO_2 in water and in 5% dimethyl sulfoxide–water suggests that the presence of this cosolvent tends to decrease both k_{cat} and K_m by a factor of approximately 2, and so has no net effect on k_{cat}/K_m. Thus the ratio k_{cat}/K_m for *O*-(*p*-nitrobenzoyl)mandelic acid should be directly comparable with the specificity constants for other esters in aqueous solution.

Can. J. Chem. Downloaded from www.nrcresearchpress.com by 210.87.254.105 on 09/05/12
For personal use only.

Can. J. Chem. Downloaded from www.nrcresearchpress.com by 210.87.254.105 on 09/05/12
For personal use only.

Significance of the ρ *Parameters*

Figure 3 clearly indicates a close correlation of both k_{cat} and K_m with σ for five substituents X in ester **1** which vary in electronic properties from CH_3O to NO_2. The deviation of X = *tert*-butyl from these correlation lines will be considered later. The value of $\rho(k_{cat}) = 1.17$ for the correlation of k_{cat} with σ is somewhat lower than is observed for correlations of nonenzymic base-catalyzed hydrolyses of benzoate esters: $\rho(k_{OH^-}) = 1.93$ for methyl benzoates in 33% dioxane–water (30); $\rho(k_{OH^-}) = 2.01$ for *p*-nitrophenylbenzoates in 33% acetonitrile–water (31). The value of $\rho(k_{cat})$ is, however, much greater than is typical of nonenzymic acid-catalyzed ester hydrolyses: $\rho(k_{H^+}) = 0.11$ for methyl benzoates in 60% acetone–water (32).

Hubbard and Kirsch (18) have compiled ρ values for nucleophilic attack on acyl-substituted *p*-nitrophenylbenzoates by a series of nucleophiles. The ρ values appear to fall into two groups depending only upon whether the nucleophile is anionic or neutral. Thus for neutral nucleophiles ρ = 1.0–1.4, while for anionic nucleophiles ρ = 1.8–2.0, with each class containing both oxygen and nitrogen nucleophiles of various chemical type. These investigators quite reasonably explain this difference in terms of a greater contribution from electron-withdrawing substituents to the stabilization of anionic transition states for nucleophilic attack relative to the stabilization of analogous neutral transition states. If we assume[2] that a similar relationship also holds for attack by anionic and neutral nucleophiles on alkyl benzoates then the above comparison of $\rho(k_{cat})$ and $\rho(k_{OH^-})$ values in this context clearly suggests that this enzymic reaction involves attack on the carbonyl carbon of the ester substrate by a *neutral* nucleophile.

An alternative interpretation of $\rho(k_{cat}) = 1.17$ is evident, however. If attack by an anionic nucleophile was assisted by general-acid catalysis, one might predict that the observed ρ value would be considerably smaller than normally observed for anionic nucleophiles. Such a prediction would result from the base-weakening effect for protonation of the ester carbonyl group that would be caused by electron-withdrawing substituents in the benzoic acid moiety. Since donation of a proton to the ester oxygen atom via general-acid catalysis will be related to the basicity of the accepting atom, we would therefore have a situation in which ρ will be positive for the nucleophilic attack component but negative for the general-acid proton donation component. The net result will be a reduction in $\rho(k_{cat})$ from the value normally observed for anionic nucleophilic attack and the possibility that this value would fortuitously fall in the range associated with the attack of neutral nucleophiles that are unassisted by general-acid catalysts.[3] The observed p*H* dependence of k_{cat} for both *O*-acetyl- and *O*-(*p*-nitrobenzoyl)mandelic acids on the base form of an enzymic acid ($pK_a \sim 7$) and on the acid form of another acidic group ($pK_a \sim 8$) is also suggestive of this interpretation.

A choice between these two possible interpretations for $\rho(k_{cat}) = 1.17$ can ultimately only be made in the context of the catalytic groups that are available at the active site of the enzyme to play general-acid and general-base nucleophilic roles. Although the amino acid side chains that are present in the vicinity of the active site of this enzyme have been clearly indicated by the X-ray crystallographic investigations of Lipscomb and co-workers (1–4), the mode of binding of substrate molecules in this active-site region is still uncertain. Suggestions (3, 4) have been made from model-building studies that are based on the observed binding to the crystalline enzyme of the very poor substrate, glycyl-L-tyrosine. For both ester and peptide substrates, the favoured modes of binding are such that the side-chain carboxylate group of glu-270 is attractively situated for direct nucleophilic attack on the carbonyl carbon atom of the hydrolyzable bond or for general-base catalysis of the nucleophilic attack by a water molecule on this same bond. Furthermore, in these substrate binding modes, the phenolic OH of tyr-248 is suitably located so that it could donate

[2]The fact that $\rho(k_{OH^-})$ for methyl and *p*-nitrophenylbenzoates are not very different (see above) suggests that the ρ value is not strongly dependent on the nature of the alcohol leaving group (*cf.* $\rho(k_{OH^-}) = 2.2$ for the even more highly activated 2,4-dinitrophenylbenzoates (18)), and therefore this assumption appears quite reasonable.

[3]The extreme case of such general-acid catalysis can be considered to be specific-acid catalysis for which ρ values close to zero (33) are most often observed. In this case the electronic effects of a substituent in the phenyl ring upon susceptibility to nucleophilic attack on the one hand, and basicity on the other, are approximately offsetting.

Can. J. Chem. Downloaded from www.nrcresearchpress.com by 210.87.254.105 on 09/05/12
For personal use only.

a proton as a general-acid catalyst in the transition state for nucleophilic attack. Thus, functional groups would seem to be available to play each of the catalytic roles in the above two suggested interpretations of $\rho(k_{cat}) = 1.17$, provided that the postulated substrate binding modes are correct.

A metal-coordinated water molecule is an alternative possible candidate for a general-acid catalyst role in the above mechanistic interpretation. This would require the assignment of the $pK_a \sim 8.0$ in the E.S complex to the deprotonation of this water molecule. Although in principle the coordinated water molecule may alternatively be able to play the role of a neutral nucleophile, this is unlikely to be the case, since the coordinated hydroxide ion that is produced upon deprotonation should then be a much better nucleophile, and so an enhanced rate of hydrolysis in basic solutions should result. This is not observed in the present cases (Figs. 5 and 7), although a pronounced increase in k_{cat} in basic solutions is observed in the enzymic hydrolysis of *O*-cinnamoyl-L-3-phenyllactic acid (34).

The results of chemical modification studies of this enzyme indicate that modification of tyr-248 in any way, including acetylation of the OH group, destroys peptidase activity but results in activation of the enzyme for hydrolysis of specific ester substrates (23, 26, 29). Much of this activation of esterase activity is due to the relief of substrate inhibition effects. However, for the hydrolysis of *O*-hippuryl-L-3-phenyllactic acid there is a modest increase (two- to three-fold (23, 26)) in k_{cat} for the acetyl-enzyme compared with the native enzyme, and this clearly indicates that a mechanism involving this phenolic group as a general-acid catalyst is unacceptable for the hydrolysis of this ester. Also, K_m for this substrate is increased 30–40-fold upon acetylation (23, 26), and this latter observation is noteworthy in considering the brief report (15) that acetylation of tyr-248 also abolishes the enzymic hydrolysis of the ester substrate, *O*-acetylmandelic acid. Although this indicates an apparent difference in the esterase activity of the acetyl-enzyme towards these two ester substrates, it should be noted that a 40-fold increase in K_m for the latter ester with the acetyl-enzyme over that observed for the native enzyme ($K_m = 0.08\ M$ (25)) would probably lead to undetectable hydrolysis of this poor substrate due to the low concentrations of the relatively unreactive E.S complex that would be present at the usual substrate concentrations.

Thus, we do not feel that the available evidence upon the effects of acetylation of tyr-248 can be used to support a difference in the binding modes of specific and nonspecific ester substrates.[4] On the other hand, the quite different p*H* profiles for k_{cat}/K_m for specific and nonspecific substrates do seem to indicate that the more basic group, at least, that controls substrate binding is different for these two classes of substrates. This must then reflect differences in the binding of specific and nonspecific substrates, and also possibly different catalytic mechanisms for the hydrolysis of these two classes of esters.

The small negative ρ value for K_m clearly indicates that if K_m is a true reflection of the E.S dissociation constant (*i.e.* $K_m = K_S$), then the ester is not bound by coordination of the carbonyl oxygen atom to the zinc ion as has been proposed for specific substrates (3, 4). Such coordination would be expected to be reduced by the presence of electron-withdrawing substituents, and thus lead to a positive value for $\rho(K_m)$, perhaps of the order of $\rho = 1.1$–2.2 as has been observed for the *O*-protonation of benzoic acids (35), benzamides (36), benzaldehydes (37), and acetophenones (38). The only interpretation of $\rho(K_m) = -0.53$ that is immediately apparent is in terms of some weak dipolar interaction. The coordination of the terminal carboxylate group to the metal ion is not ruled out by these observations, however, since this group is sufficiently far removed from the phenyl ring of the benzoic acid moiety, that it is effectively insulated from the electronic effects of substituents in this ring.

Deviations from the σ-Correlations

The above linear free energy correlations of k_{cat}, K_m, and k_{cat}/K_m with σ may be used to predict that $k_{cat} = 15\ min^{-1}$, $K_m = 7 \times 10^{-3}\ M$, and $k_{cat}/K_m = 2 \times 10^3\ M^{-1}\ min^{-1}$ for the unsubstituted benzoic acid ester (**1**: X = H). Clearly, if such parameters are applicable, the failure to observe enzymic hydrolysis of this ester may reflect pronounced substrate inhibition becoming important at much lower substrate concentrations than for any of the *para*-substituted benzoate esters that were investigated.

[4]See later discussion for our definition of "specific" and "nonspecific" substrates for this enzyme.

Such an interpretation would indicate a strong dependence of substrate inhibition on the presence of a *para*-substituent.

On the other hand, the lack of observable hydrolysis of the unsubstituted ester could also be attributed to predominant nonproductive binding of this substrate. If nonproductive binding is represented in terms of the following simple scheme:

$$E + S \underset{}{\overset{K_S}{\rightleftharpoons}} E.S \xrightarrow{k_2} E + P_1 + P_2$$

$$E + S \overset{K_S^{NP}}{\rightleftharpoons} E.S_{NP}$$

then, $k_{cat} = k_2/(1 + K_S/K_S^{NP})$ and $K_m = K_S/(1 + K_S/K_S^{NP})$. Thus, the observed k_{cat} and K_m values are both predicted to be reduced by the presence of nonproductive binding modes for the substrate. For $K_S^{NP} \ll K_S$, k_{cat} may become so small as to be unobservable. An obvious mode of nonproductive binding for this benzoic acid ester would involve "wrong-way" binding, in which the phenyl ring of the acid moiety enters the hydrophobic pocket which is believed (3, 4) to accommodate the alcohol hydrophobic side chain in the productive binding mode.

The linear correlations in Fig. 3 make it unlikely that nonproductive binding modes are important for these *para*-substituted esters, and again a remarkable substituent effect upon nonproductive binding seems to be present. This is in accord, however, with the very pronounced effect from the chlorine substituent in the binding of *O*-hippuryl-*p*-chloromandelic acid to this enzyme relative to the corresponding unsubstituted mandelic acid ester (39). Furthermore, we have also observed[5] that while the benzoate ion is a competitive inhibitor (K_i = 6 m*M* (21)) of esterase activity, the *p*-chloro-, *p*-nitro-, and *p*-methoxybenzoate ions are all noncompetitive inhibitors, and this again indicates a special effect from *para*-substituents in the binding of benzoic acid derivatives.

The complicated biphasic nature of the inhibition of the hydrolysis of *O*-hippuryl-L-3-phenyllactic acid by the unsubstituted benzoate ester is suggestive of the binding of more than one inhibitor species per enzyme molecule. This suggests that the observed lack of hydrolysis of this ester may in fact be due to a combination of the above postulated substrate inhibition (via formation of catalytically less active $E.S_2$ species, etc.) and nonproductive binding.

The *p-tert*-butyl benzoate ester has K_m approximately four-fold smaller than is predicted by the K_m–σ correlation and k_{cat} about seven-fold greater than predicted by the k_{cat}–σ correlation. The deviation of this substituent from the correlation lines cannot be ascribed solely to nonproductive binding, since such schemes predict diminished apparent k_{cat} values rather than the enhanced k_{cat} value observed in this case. If it is assumed that K_m reflects the dissociation constant for the E.S complex, it must be concluded that there is a special interaction of the *tert*-butyl group of this substrate with the enzyme, and that this interaction not only enhances binding but also results in an increased rate of hydrolysis. Similar interpretations have been suggested for other enzymic hydrolyses (*e.g.* chymotrypsin (18), emulsin (40)) in which the data for a *tert*-butyl substituent deviates significantly from linear free energy correlations defined by other substituents in a series of closely related substrates.

Consideration of pH–Rate Profiles

The observed p*H* dependence of k_{cat}/K_m for *O-p*-nitrobenzoylmandelic acid (Fig. 5) is similar to that previously observed for *O*-acetylmandelic acid (41). The estimated pK_a values for the operative enzymic dissociations in Fig. 5 are 6.95 and 7.9 which are comparable with the values observed (6.9 and 7.5) for *O*-acetylmandelic acid. The slightly higher value for the more basic ionization in the present case may be related to the presence of 5% dimethyl sulfoxide in the reaction solution. Although the p*H* dependence of k_{cat}/K_m for the *O*-hippuryl-3-phenyllactic acid (Fig. 7) is nominally of the same shape as for *O-p*-nitrobenzoylmandelic acid, the bell curve is much broader in this case and is best fitted by enzymic ionizations of pK_a = 5.8 and 9.3. These latter ionizations are similar to those reported for *O*-cinnamoyl-L-phenyllactic acid (6.6 and 9.4 (34)), for a series of *N*-protected oligodepsipeptide ester substrates (6.2 and ~9.1 (42)), and also a series of *N*-protected tripeptide substrates (6.1 and 9.1 (43)). Clearly, the ionization of $pK_a \sim 7.5$–7.9 in the *O*-acylmandelic acid substrates cannot be considered to arise from the same moiety as the ionization of $pK_a \sim 9$ that occurs in all the other ester and

[5]J. W. Bunting and C. D. Myers. Unpublished observations.

Can. J. Chem. Downloaded from www.nrcresearchpress.com by 210.87.254.105 on 09/05/12
For personal use only.

Can. J. Chem. Downloaded from www.nrcresearchpress.com by 210.87.254.105 on 09/05/12
For personal use only.

peptide substrates indicated above, and there is also some doubt whether the observed pK_a values ~6.9 and 6.1, respectively, in these two classes of substrates represent the ionization of the same enzymic acid. Furthermore, we feel that the differences between the p*H* dependences of k_{cat}/K_m for these two classes of substrates are sufficiently great that they can be conveniently used to define a distinction between specific (peptides and depsipeptides) and nonspecific (acetate and benzoate esters) substrates for this enzyme. It is interesting that according to this definition, *O*-cinnamoylphenyllactic acid appears to behave as a specific rather than a nonspecific substrate. We feel that this operational definition of specific and nonspecific substrates is more reasonable than the somewhat arbitrary distinctions that have been drawn in the past, and which have led to the classification of *O*-cinnamoyl-L-mandelic acid as a nonspecific substrate and *O*-cinnamoyl-L-3-phenyllactic acid as a specific substrate (44), and yet these two esters differ by only one methylene group.

The acidic groups which are generally considered to be most likely to be responsible for the ionizations discussed above are the phenolic OH of tyr-248, the γ-carboxyl of glu-270, a zinc-coordinated water molecule and possibly the imidazolium ions of his-69 and his-196 which appear to be coordinated to the zinc ion in the crystalline enzyme (3, 4). Auld and Vallee (45) favour the pK_a ~ 9 as being due to tyr-248 since the thermodynamic parameters for this ionization are typical of phenolic ionizations, and furthermore, this pK_a value is the same within experimental error for the Co, Mn, and Zn metalloenzymes which tends to rule out its assignment to the ionization of a metal-coordinated water molecule. However, on the basis of studies with the *O*-acetyltyr-248 enzyme, Kaiser and co-workers (46) have concluded that the pK_a ~ 9 should be assigned to $M(OH)^+$ formation, and have then suggested that the pK_a ~ 7.5 observed with *O*-acetylmandelic acid as substrate is due to tyr-248.

An enzymic pK_a ~ 7.0 is also observed in the modification of glu-270 by two different reagents (5, 7). This presumably reflects the same ionization as the pK_a ~ 6.9 that is observed in the hydrolysis of *O*-*p*-nitrobenzoyl- and *O*-acetylmandelic acids. It is tempting, of course, to assign this ionization to the γ-carboxyl group of glu-270 but there is no direct evidence that this is the case. Certainly, modification of glu-270 abolishes both peptidase and esterase activities towards *specific* substrates (5–8), and suggests an important functional role for this amino acid in the enzymic catalysis, although hindrance to binding through steric effects in the modified enzyme cannot be excluded.

Although it is clear that the same two acidic groups on the enzyme control the overall enzymic activity (k_{cat}/K_m) of the hydrolysis of both *O*-hippuryl-L-3-phenyllactic acid and related peptide substrates, the observed p*H* dependence of k_{cat} for this ester is different from that observed for peptide substrates (43). In fact, k_{cat} for this ester is remarkably p*H* independent over the range p*H* 5–10 (Fig. 7). For peptide substrates, k_{cat} is dependent on a pK_a ~ 6.1 in the acidic portion of this same range, but is not influenced by the group of pK_a ~ 9 (43). Clearly it is not possible to assign the pK_a ~ 6.1 to the γ-carboxyl of glu-270 and still claim a role for the conjugate base of this side chain in the hydrolysis of *both* these peptides and this ester. The p*H* dependence of k_{cat} for *O*-hippuryl-L-3-phenyllactic acid suggests, in fact, that *if* the conjugate base of the glu-270 γ-carboxyl group is involved in the hydrolysis of this ester, it must have a pK_a < 5. In fact, a pK_a ~ 4 for glu-270, typical of a "normal" glutamic acid γ-carboxyl group, is consistent with this assumption.

In the most recently proposed mechanisms for peptide hydrolysis by carboxypeptidase A (15), the phenolic OH of tyr-248 plays the role of a general-acid catalyst in the protonation of the amine leaving group. If such a mechanism is accepted, k_{cat} for peptide hydrolysis should clearly decrease upon deprotonation of tyr-248; therefore, pK_a ~ 9 cannot be assigned to tyr-248 on the basis of the current proposals for the mechanism of peptide hydrolysis, and if tyr-248 does act in this way as a general-acid catalyst, it must have pK_a > 10.

Adoption of the suggestion (46) that the pK_a ~ 9 which controls substrate binding to the free enzyme is due to ionization of the hydrated metal ion seems consistent with the observation that this pK_a does not seem to be present in the catalytically active E.S complex for specific ester and peptide substrates. Coordination of the free carboxylate ion or the carbonyl oxygen of the hydrolyzable bond to the metal ion would be expected to suppress this ionization in the E.S complex.

Can. J. Chem. Downloaded from www.nrcresearchpress.com by 210.87.254.105 on 09/05/12
For personal use only.

It is clear from the above discussion that at present it is not possible to rationalize all of the observed p*H*–rate profiles for ester and amide substrates of carboxypeptidase A in terms of simple catalytic roles for the amino acid side chains which are in the near vicinity of the zinc ion. The differences observed between specific and nonspecific ester substrates even further complicate the situation, and it is fair to say that not one of the ionization constants that have been observed to be catalytically important can be assigned with any certainty at present. The crystallographic investigation of the binding of glycyl-L-tyrosine indicates that the tyr-248 side chain undergoes a major movement upon binding this ligand (2–4). This leads one to wonder whether the binding of good substrates in solution may not involve other major conformational changes in the enzyme, and if such is the case, it is possible that one or more of the observed ionization constants may arise from an acidic group that is somewhat removed from the active site, but which controls an important conformational change.

A change in rate-determining step between formation and breakdown of a tetrahedral intermediate and/or acyl-enzyme is another possible factor which may be responsible for some of the observed p*H*–rate complexities, if this rate-determining step is both p*H* and substrate dependent. If such a factor is operative, an extremely detailed study of systematic substrate structural variations will be necessary before a complete analysis of the observed p*H*–rate profiles will be possible.

This research was supported by an operating grant from the National Research Council of Canada and the award of a Walter C. Sumner Memorial Fellowship to C.D.M.

1. T. A. Steitz, M. L. Ludwig, F. A. Quiocho, and W. N. Lipscomb. J. Biol. Chem. **242**, 4662 (1967).
2. G. N. Reeke, Jr., J. A. Hartsuck, M. L. Ludwig, F. A. Quiocho, T. A. Steitz, and W. N. Lipscomb. Proc. Natl. Acad. Sci. U.S. **58**, 2220 (1967).
3. W. N. Lipscomb, G. N. Reeke, Jr., J. A. Hartsuck, F. A. Quiocho, P. H. Bethge, M. L. Ludwig, T. A. Steitz, H. Muirhead, and J. C. Coppola. Brookhaven Symp. Biol. **21**, 24 (1968).
4. W. N. Lipscomb, G. N. Reeke, Jr., J. A. Hartsuck, F. A. Quiocho, and P. H. Bethge. Phil. Trans. R. Soc. London, Ser. B. **257**, 177 (1970).
5. P. H. Petra. Biochemistry, **10**, 3163 (1971).
6. P. H. Petra and H. Neurath. Biochemistry, **10**, 3171 (1971).
7. G. M. Hass and H. Neurath. Biochemistry, **10**, 3535 (1971).
8. G. M. Hass and H. Neurath. Biochemistry, **10**, 3541 (1971).
9. J. F. Riordan and H. Hayashida. Biochem. Biophys. Res. Commun. **41**, 122 (1970).
10. G. Tomalin, B. L. Kaiser, and E. T. Kaiser. J. Am. Chem. Soc. **92**, 6046 (1970).
11. L. M. Ginodman, N. I. Mal'tsev, and V. N. Orekhovich. Biokhimiya, **31**, 1073 (1966).
12. P. L. Hall and E. T. Kaiser. Biochem. Biophys. Res. Commun. **29**, 205 (1967).
13. R. Lumry, E. L. Smith, and R. R. Glantz. J. Am. Chem. Soc. **73**, 4330 (1951).
14. R. Lumry and E. L. Smith. Discuss. Faraday Soc. **20**, 105 (1955).
15. F. A. Quiocho and W. N. Lipscomb. Adv. Protein Chem. **25**, 1 (1971).
16. B. L. Kaiser and E. T. Kaiser. Proc. Natl. Acad. Sci. U.S. **64**, 36 (1969).
17. W. P. Jencks. Ann. Rev. Biochem. **32**, 657 (1963).
18. C. D. Hubbard and J. F. Kirsch. Biochemistry, **11**, 2483 (1972).
19. J. W. Bunting and J. Murphy. This issue.
20. J. Murphy. Ph.D. Thesis, University of Toronto, Toronto, Ontario. 1974.
21. J. W. Bunting and C. D. Myers. Can. J. Chem. **51**, 2639 (1973).
22. W. O. McClure, H. Neurath, and K. A. Walsh. Biochemistry, **3**, 1897 (1964).
23. J. R. Whitaker, F. Menger, and M. L. Bender. Biochemistry, **5**, 386 (1966).
24. J. E. Snoke and H. Neurath. J. Biol. Chem. **181**, 789 (1949).
25. E. T. Kaiser and F. W. Carson. J. Am. Chem. Soc. **86**, 2922 (1964).
26. R. C. Davies, J. F. Riordan, D. S. Auld, and B. L. Vallee. Biochemistry, **7**, 1090 (1968).
27. J. W. Bunting and J. Murphy. Biochem. Biophys. Res. Commun. **48**, 1316 (1972).
28. L. P. Hammett. Physical organic chemistry. 2nd Ed. McGraw-Hill, New York. 1970. p. 356.
29. J. F. Riordan and B. L. Vallee. Biochemistry, **2**, 1460 (1963).
30. M. L. Bender and R. J. Thomas. J. Am. Chem. Soc. **83**, 4189 (1961).
31. J. F. Kirsch, W. Clewell, and A. Simon. J. Org. Chem. **33**, 127 (1968).
32. E. W. Timm and C. N. Hinshelwood. J. Chem. Soc. 862 (1938).
33. H. H. Jaffe. Chem. Rev. **53**, 191 (1953).
34. P. L. Hall, B. L. Kaiser, and E. T. Kaiser. J. Am. Chem. Soc. **91**, 485 (1969).
35. R. Stewart and K. Yates. J. Am. Chem. Soc. **82**, 4060 (1960).
36. J. T. Edward, H. S. Chang, K. Yates, and R. Stewart. Can. J. Chem. **38**, 1518 (1960).
37. K. Yates and R. Stewart. Can. J. Chem. **37**, 664 (1959).
38. R. Stewart and K. Yates. J. Am. Chem. Soc. **80**, 6335 (1958).

39. J. W. BUNTING and J. MURPHY. Submitted for publication.
40. R. L. NATH and H. N. RYDON. Biochem. J. **57**, 1 (1954).
41. F. W. CARSON and E. T. KAISER. J. Am. Chem. Soc. **88**, 1212 (1966).
42. D. S. AULD and B. HOLMQUIST. Fed. Proc. **31**, 435 Abstr. (1972).
43. D. S. AULD and B. L. VALLEE. Biochemistry, **9**, 4352 (1970).
44. E. T. KAISER and B. L. KAISER. Acc. Chem. Res. **5**, 219 (1972).
45. D. S. AULD and B. L. VALLEE. Biochemistry, **10**, 2892 (1971).
46. J. GLOVSKY, P. L. HALL, and E. T. KAISER. Biochem. Biophys. Res. Commun. **47**, 244 (1972).

Can. J. Chem. Downloaded from www.nrcresearchpress.com by 210.87.254.105 on 09/05/12
For personal use only.

Charge Development and Mechanism in Disrotatory Ring Opening of Cyclopropyl Bromides

JAN HAN ONG[1] AND ROSS ELMORE ROBERTSON

Department of Chemistry, The University of Calgary, Calgary, Alberta T2N 1N4

Received August 29, 1973[2]

JAN HAN ONG and ROSS ELMORE ROBERTSON. Can. J. Chem. **52**, 2660 (1974).

The temperature dependence of the rates of hydrolysis of *cis*- and *trans*-2-vinylcyclopropyl bromides has been determined in water. The temperature coefficient of the enthalpy of activation ($\Delta C_p^{\ddagger}$) for both compounds was unusual (-27 and -35 cal mol^{-1} deg^{-1}). From this fact, it was concluded that the charge development at the transition state was low, in agreement with the conclusions of Clark and Smale (19). The slightly inverse α-deuterium isotope effect ($k_H/k_D = 0.994$) is consistent with that conclusion.

JAN HAN ONG et ROSS ELMORE ROBERTSON. Can. J. Chem. **52**, 2660 (1974).

On a déterminé la variation, en fonction de la température, des vitesses d'hydrolyse dans l'eau des isomères *cis* et *trans* du bromure de vinyl-2 cyclopropyle. La valeur du coefficient de température de l'enthalpie d'activation ($\Delta C_p^{\ddagger}$) pour les deux composés est exceptionnelle (-27 et -35 cal mol^{-1} deg^{-1}). On en conclut qu'à l'état de transition la charge est peu developpée. Ceci est en accord avec les conclusions de Clark et Smale (19). L'effet isotopique légèrement inverse du deutérium-α ($k_H/k_D = 0.994$) est consistant avec cette conclusion.
[Traduit par le journal]

Introduction

In this paper we present evidence bearing on the degree of charge development at the transition state for the hydrolysis of *cis*- and *trans*-2-vinylcyclopropyl bromides and from these observations draw conclusions concerning mechanism.

Solvolytic studies of cyclopropyl derivatives have attracted attention for many years (1–8). Initially there was the question of apparent inertness of such compounds to solvolysis, *e.g.* 170 °C was required to give a specific rate constant of 4.7×10^{-5} s^{-1} (9). Brown attributed this inertness to the unfavorable angle strain, "I-strain" (10, 11). Alternatively, the less than normal internal bond angle (60°) was judged to contribute to excess s-character (12, 13) and hence to stabilize exocyclic bonds of the cyclopropane ring (14). In contrast to these arguments advanced to account for unusual inertness, in 1961, Schleyer and Nicholas (15), noting the even more pronounced stability of 7-norbornyl tosylate toward acetolysis, argued that the cyclopropyl tosylate actually reacted faster than might be predicted from a consideration of the internal bond angles. The authors suggested a kind of anchimeric assistance to provide an extra driving force equivalent to a factor of 10^2 in the rate (15).[3] Further insight into the mechanism of ring opening of cyclopropyl derivatives came with the development of the Woodward–Hoffmann rule governing concerted reactions (16). According to that rule, ring opening of the cyclopropyl cation to allyl cation is allowed in the disrotatory mode.[4] Independently, De Puy and co-workers (18) arrived at the conclusion that the ring opening is governed by the stereochemistry of the leaving group.

Recently Schleyer and co-workers (1, 2) in their extensive studies of the solvolysis of cyclopropyl derivatives in acetic acid proposed that the degree of ring opening at the transition state of the cyclopropyl halides and sulfonates was considerable, "a protoallylic transition state". As a consequence, charge delocalization to the β-positions was extensive. However, Clark and Smale (19) from a consideration of their theoretical calculations and the ρ^+ values obtained by

[1]Postdoctoral Fellow, 1971–1973.

[2]Revision received December 11, 1973.

[3]Schleyer's recent estimate is at least a factor of 10^5; see ref. 2.

[4]Except for deamination reactions (17), allyl derivatives were the only product found for unsubstituted or β-substituted monocyclic systems.

Can. J. Chem. Downloaded from www.nrcresearchpress.com by 210.87.254.5 on 09/05/12
For personal use only.

Can. J. Chem. Downloaded from www.nrcresearchpress.com by 210.87.254.5 on 09/05/12
For personal use only.

De Puy and co-workers (20), suggested that the transition state for the acetolysis of cyclopropyl derivatives was reached at an early stage in the ring-opening and that the angle of rotation could not be over 45°.

While recognizing that studies of solvolysis in water may not resolve the above difference of interpretation, nevertheless it would be useful to investigate charge development at the transition state for the solvolysis of such compounds in water. If the conclusion of Clark and Smale is valid, then the results obtained for hydrolysis in water would have bearing on the interpretation of evidence relative to charge development in other solvents.

The inability of cyclopropyl systems to stabilize positive charge has been fairly well established.[5] As charge increases in the activation process during solvolysis, it is accepted (1, 2, 18, 20, 23) that a concerted back-side overlap of the C_2—C_3 bond on the developing p-orbital of the C_1 carbon (*i.e.* ring opening) provides the necessary stabilization. Therefore charge development and ring opening are co-related. However a different view was suggested by Schleyer and co-workers (1).[6]

A large body of empirical data now exists which provides a basis for estimating the relative degree of charge development at the transition state for ionogenic reactions in water from the temperature coefficient of the enthalpy of activation. This estimation is based on the unique structural properties of water, the nature of solvation of weakly polar solutes in water and the effect of charge development accompanying the activation process (24, 25). In the activation process for ionogenic reactions the requirement for solvent reorganization is a temperature dependent component of $\Delta H^{\ddagger}$ which varies with the extent to which water structure is reorganized or more correctly, disorganized. This disorganization is dependent not only on the degree of charge development but also on the nature of the displaced group, the degree of reorganization for leaving groups having the same charge level being: arenesulfonate = methanesulfonate $\ll$ bromide, chloride, iodide < nitrate.[7] The enthalpy requirement for reorientation of the solvating water molecules decreases as the temperature increases[8] and the extent of this effect is reflected in the rate measurements provided the latter are made with sufficient accuracy. Clearly, this is but one source of a temperature dependency of $\Delta H^{\ddagger}$ (26–29) and care must be exercised to exclude other contributions such as impurities or the possibility of mixed kinetics before drawing conclusions from $(\delta\Delta H^{\ddagger}/\Delta T)_p$ with respect to the extent of solvent reorganization. Where there is reason to believe that the reaction is uncomplicated, values of $(d\Delta H^{\ddagger}/dT)_p = \Delta C_p^{\ddagger}$ for displacement of halides from primary carbon are found to lie in the range -40 to -50 cal deg^{-1} mol^{-1}; from secondary carbons -60 cal deg^{-1} mol^{-1} and from tertiary carbons -80 to -100 cal deg^{-1} mol^{-1} (19). There are exceptions. Thus 4-methylbenzyl chloride gives a value of -79 cal deg.$^{-1}$ mol^{-1}, and cyclopropylcarbinyl chloride (a primary chloride) and cyclobutyl chloride (a secondary halide) which are presumed to undergo rearrangement to nonclassical ions in the activation process give values of $\Delta C_p^{\ddagger}$ of -81 and -107 cal deg^{-1} mol^{-1}, respectively (30). In the absence of water-structure-breaking functional groups near the reaction site (31, 32) compounds showing pronounced anchimeric assistance and hydrogen participation (33) likewise give more negative $\Delta C_p^{\ddagger}$ values than would be expected in the absence of such assistance. This observation is consistent with an approach to a limiting mechanism. Thus normal values of $\Delta C_p^{\ddagger}$ may be taken as evidence that the mechanism of hydrolysis is similar to the class to which the reactant belongs. Values outside of the normal range may be taken as evidence of some alternative mechanistic explanation provided spurious contribution to $\Delta C_p^{\ddagger}$ have been eliminated. Thus the temperature dependence of $\Delta H^{\ddagger}$ for the particular case of hydrolysis in water provides a useful mechanistic probe, even

[5]See ref. 9, 21; however, see ref. 22.

[6]Reference 1, p. 140.

[7]This applies for the nitrate group where the mechanism tends to S_N1.

[8]It is obvious that this is but one of the posssible interpretations since a negative temperature coefficient for $\Delta H^{\ddagger}$ would be found if the solvation of the developing ion increased with an increase in temperature or if the degree of charge development at the transition state increased with temperature or both. These possibilities cannot be excluded on the available evidence. Reasons for believing that the breakdown of the initial state structure is the dominant factor in determining the observed negative temperature coefficient of $\Delta H^{\ddagger}$ have been outlined previously (24).

Can. J. Chem. Downloaded from www.nrcresearchpress.com by 210.87.254.5 on 09/05/12
For personal use only.

though the $\Delta H^{\neq}$ values alone have proven of little analytical value.

From the beginning of this investigation it was recognized that the conclusions based on the values of $\Delta C_p^{\neq}$ obtained for hydrolysis in water need not necessarily apply to transition state characteristics in other solvent. However, as will be shown in the discussion, the particular systems under investigation here may be exceptional in this regard.

Results and Discussion

The rate data were determined conductometrically and are generally good to better than 0.5% for repetitive runs (the *trans* compound gave better reproducibility). The standard error within a particular determination of the specific rate constant was usually better than 0.1%. The discrepancy between cells has been attributed to variations in absorption of the reactants and possibly differential adsorption of ions at the walls, an inherent difficulty at the low concentrations imposed by meagre solubility of the reactants. The use of larger cells would reduce this difficulty but introduces other complications. The methods used were consistent with past practise (24). The rate constants as a function of temperature are fitted to the empirical formula

$$[1] \qquad \log k = A_1 + A_2/T + A_3 \log T$$

assuming $d\Delta C^{\neq}/dT = 0$, an assumption which is imposed by experimental errors and probably is not too serious over the relatively short temperature range available (60–94 °C). The corresponding empirical constants are given in Table 1. The average specific rate constants over a range of temperatures can then be calculated from eq. 1 and Table 1. The method of Clarke and Glew (25, 27, 34) for the treatment of the temperature dependence of equilibrium data was modified to accommodate kinetic rate data and to compute the pseudothermodynamic parameters (Table 2).

TABLE 1. Empirical constants for the three-parameter equation (eq. 1) for the hydrolysis of *cis*- and *trans*-2-vinylcyclopropyl bromides

2-Vinylcyclopropyl bromide	A_1	$-A_2$	$-A_3$	n^*
trans	62.3978	8393.1382	16.4042	34^{91}_{59}
cis	51.5332	8194.3581	12.7857	51^{95}_{70}

*$n_{T_2}{}^{T1}$ = number of rate determination; T_1 and T_2 give the temperature range over which the rates were determined.

The negative values of the $\Delta C_p^{\neq}$ derived from the temperature dependence of the rate of hydrolysis (-35 ± 2 and -27 ± 4 cal deg^{-1} mol^{-1}) are surprisingly low:[9] lower, in fact, than had been found previously for the hydrolysis of any other alkyl halide (24). Careful purification excluded the possibility that the results were spurious as a consequence of impurities.[10] In consequence we were led to the inevitable conclusion that either the transition state was reached at a lower degree of charge development than had been found previously for the hydrolysis of even primary halides, or the results were, in both cases, a consequence of "mixed kinetics" or "partitioning" (26, 27, 29, 35).

A comparison of the values of $\Delta C_p^{\neq}$ obtained in this study with those from the hydrolysis of other allylic halides is useful (Table 3). Allyl chloride and β-methylallyl chloride have values of -50 cal deg^{-1} mol^{-1}. α-Methylallyl chloride, which might be expected to have a transition state resembling that of a S_N1 reaction has a value of -92 cal deg^{-1} mol^{-1}. The latter is consistent with a large degree of charge development at the transition state and provides an obvious contrast to the values of $\Delta C_p^{\neq}$ obtained in this study.

Having excluded impurities as a possible explanation for these less negative values of $\Delta C_p^{\neq}$, we consider three possibilities: (*i*) partitioning, (*ii*) mixed kinetics, and (*iii*) that the low values of $-\Delta C_p^{\neq}$ simply reflect a lower degree of charge development at the transition states than has been observed previously for the displacement of a halide.

The fact that the α-deuterium isotope effect (Table 4) is negligible argues against any important structural change. However, it is doubtful even if the cyclopropyl group opened up to give a fully conjugated allylic cation at the transition state, that a large isotope effect would be observed (36, 37). At best it is consistent with the proposed concerted "internal" S_N2 type reaction. A much stronger argument against the formation of an intimate ion-pair such as implied

[9]Low and high refer to the absolute values of $\Delta C_p^{\neq}$.

[10]Impurities, however, need not always lead to a low negative value of the $\Delta C_p^{\neq}$; see ref. 27.

TABLE 2. Pseudothermodynamic quantities for the hydrolysis of *cis*- and *trans*-2-vinylcyclopropyl bromides in water

2-Vinylcyclopropyl bromide	T (°C)	$\Delta H^{\ddagger}$ (cal mol^{-1})	$\Delta S^{\ddagger}$ (cal deg^{-1} mol^{-1})	$-\Delta C_p^{\ddagger}$ (cal deg^{-1} mol^{-1})
trans	75	26 363 ± 10	1.29 ± 0.03	35 ± 2
cis	75	27 957 ± 28	0.85 ± 0.08	27 ± 4

TABLE 3. Derived thermodynamic parameters for the hydrolysis of allyl chlorides in water*

Compound (chloride)	T (°C)	$\Delta H^{\ddagger}$ (cal mol^{-1})	$\Delta S^{\ddagger}$ (cal deg^{-1} mol^{-1})	$\Delta C_p^{\ddagger}$ (cal deg^{-1} mol^{-1})
Allyl	40	22 495 ± 25	−10.12 ± 0.08	−50
β-Methylallyl	40	21 469 ± 121	−11.69 ± 0.37	−49
α-Methylallyl	40	21 585 ± 85	0.04 ± 0.3	−92
trans-γ-Methylallyl	30	22 712 ± 44	3.36 ± 0.14	−82
cis-γ-Methylallyl	40	21 331 ± 21	−3.68 ± 0.07	−66

*Reference 22.

TABLE 4. Rate constants, α-deuterium isotope effects, and the m values for the hydrolysis of *cis*- and *trans*-2-vinylcyclopropyl bromides

2-Vinylcyclopropyl bromide	T (°C)	k ($\times 10^{-4}$ s^{-1})	m (aqueous alcohol)	k_H/k_D	Reference
cis	95	0.246 (50% EtOH)			4
	95	2.928 (H_2O)	0.59	0.993	This work
trans	95	2.65 (50% EtOH)			4
	95	32.067 (H_2O)	0.59	0.995	This work

by the possibility of partitioning is to be found in the shape of the energy diagram for the opening of the cyclopropyl ring plotted against the angle of rotation as calculated by Clark and Armstrong (38) and by Radom *et al.* (39). These authors show that ring opening in the cyclopropyl system is characterized by a steady steep decrease in energy, hence the existence of a solvent (water) stabilized charge intermediate seems as unlikely as it is unnecessary.

As an alternative mechanism, the unusually low values of $-\Delta C_p^{\ddagger}$ found for these compounds can be attributed to "mixed kinetics", *i.e.* two reactions with different $\Delta H^{\ddagger}$ values occurring in competition. In such a situation the reaction with the higher $\Delta H^{\ddagger}$ value becomes more important as the temperature rises and this results in a positive contribution to $\Delta C_p^{\ddagger}$ combining to reduce the magnitude of the combined normal negative values (28). Such a rationalization is as difficult to prove as to disprove in the present system and the following citations are offered for consideration only. Parham and Yong (40) in attempting to account for the product found in the solvolysis of *cis*- and *trans*-1,1 - dichloro - 2,3 - dipropylcyclopropane, suggested that the ring opening process is accompanied by solvent attack concerted with ionization. Since there are two nonequivalent sites for nucleophilic interaction in our system the above mechanism could provide for the lower negative values of $\Delta C_p^{\ddagger}$. This rationalization would imply two transition states each one occurring at a degree of charge development normal for an S_N2 displacement but with sufficiently different $\Delta H^{\ddagger}$ values to account for the more positive than normal $-\Delta C_p^{\ddagger}$ values. That both *cis* and *trans* isomers should have approximately the same compensating effect is possible but seems unlikely. Product analysis offers no assistance here.

An abnormally low value for $\Delta C_p^{\ddagger}$ for a reaction which might be expected to react by an S_N1-like mechanism is not without precedent. Ko and Robertson have shown recently (41) that the values of $\Delta C_p^{\ddagger}$ for the hydrolysis of a series of sulfamoyl chlorides shift from −76 cal deg^{-1} mol^{-1} for dimethylsulfamoyl chloride to −39

Can. J. Chem. Downloaded from www.nrcresearchpress.com by 210.87.254.5 on 09/05/12
For personal use only.

Can. J. Chem. Downloaded from www.nrcresearchpress.com by 210.87.254.5 on 09/05/12
For personal use only.

cal deg^{-1} mol^{-1} for the diethyl homolog. In the latter, other evidence shows that hydrogen participation occurs and crowding about the sulfur is enhanced. The rate is increased eight-fold over the dimethyl homolog. While charge dispersal may account for some decrease in $\Delta C_p^{\ddagger}$, this could hardly be a sufficient explanation and the possibility that the transition state coincides with the formation of the shared hydrogen bond must be regarded as a distinct possibility.

Thus in the absence of evidence to the contrary, it seems probable that for the hydrolysis of the 2-vinylcyclopropyl bromides, of the several possibilities the simpler hypothesis is sufficient, *i.e.* that the unusually low negative values of $\Delta C_p^{\ddagger}$ obtained in this study give evidence of the transition state having a relatively small charge development on the displaced group and consequently the transition state comes relatively early in the ring opening process. Such a conclusion would be consistent with the conclusion of Clark and Smale (19), the ρ^+ values obtained by DePuy and co-workers (20)[11] for analogous systems (though in a different solvent, acetic acid) and would tend to minimize the differences in $\Delta C_p^{\ddagger}$ between different leaving groups (40). Research on related systems aiming to confirm the generality of this conclusion is now in progress. Even if evidence were uncovered supporting mixed kinetics rather than the simpler hypothesis cited above, the low values of $\Delta C_p^{\ddagger}$ obtained here would still probably imply that the transition state for the ring opening of cyclopropyl halides and hence charge development was at a very early stage, much less advanced than for the corresponding hydrolysis of methyl halides (24).

Experimental

Tri-*n*-butyltin hydride was made in the usual way (43, 44). The physical properties and the n.m.r. spectrum agreed with the literature (45–47).

Tri-*n*-butyltin deuteride was made according to the procedure of Martin and Landgrebe (48, 49) in 60% yield: b.p. 50° (0.02 mm) lit. (48) 78° and up (0.6 mm); the n.m.r. (CCl_4) spectrum showed no signal at τ 5.21.

1,1-Dibromo-2-vinylcyclopropane was prepared by the addition of dibromocarbene to 1,3-butadiene (4, 50–52): b.p. 36–37° (5 mm) (lit. (50, 51) 76–82° (50 mm), (4) 53–56° (10 mm), and (51) 70° (26 mm)); n.m.r. (CCl_4) gave complex multiplet at τ 7.8 and 8.4 (3H, ring protons) and 4.6 (m, 3H, vinyl protons); the mass spectrum gave parent peaks at *m/e* 224, 226, 228 (1:2:1), significant fragments at 66 ($C_5H_6^+$), 65, 39 and 145, 149 (1:1) ($C_5H_6Br^+$), however no complete analysis was possible because the compound was not pure[12] and not so stable[13].

cis- and *trans*-2-Vinylcyclopropyl bromides were made by the reduction of 1,1-dibromo-2-vinylcyclopropane with tri-*n*-butyltin hydride (53) in 60% yield: b.p. 58–62° (80 mm) (lit. (4, 51) 60–74° (90 mm)). The isomers could not be separated by spinning band distillation but were isolated in pure form by passing through the preparative g.c. using a 20 ft × 3/8 in. QF-1 column (90°). The *trans* isomer was eluted first (4): the mass spectrum gave parent peaks at *m/e* 146, 148 (1:1), base peak at 67 ($C_5H_7^+$), and significant fragments at 41 and 39; n.m.r. (CCl_4) gave complex multiplets at τ 4.2–5.16 (3H, vinyl protons), 7.14–7.42 (1H, C*H*Br), 7.9–8.35 (1H, ring proton), and 8.6–9.1 (2H, ring protons). The *cis* isomer gave exactly the same mass spectrum as the *trans* compound, however the n.m.r. (CCl_4) gave complex absorption at τ 4.1–5.05 (3H, vinyl protons), 6.7–7.6 (1H, C*H*Br), 8.1–8.85 (2H, ring protons), and 9.06–9.23 (1H, ring proton). Both isomers were checked again by g.c. using a 20% FFAP on Carbowax W column.

cis- and *trans*-2-Vinylcyclopropyl-1-*d* bromides were made by the reduction of 1,1-dibromo-2-vinylcyclopropane with tri-*n*-butyltin deuteride (53) in 40% yield: b.p. 52–60° (78–74 mm). The pure isomers were obtained as described above. The mass spectrum of the *trans* isomer gave parent peaks at *m/e* 147, 149 (1:1), and significant fragments at 68 ($C_5H_6D^+$, base peak), 42, 41, 40, and 39; n.m.r. (CCl_4) gave complex absorption at τ 4.2–5.15 (3H, vinyl protons), 7.95–8.33 (q, 1H, ring proton), 8.63–8.90 (m, 2H, ring protons). The *cis* isomer again showed exactly the same mass spectrum as the *trans* compound; n.m.r. (CCl_4) gave τ 4.10–5.20 (complex, 3H, vinyl protons), 8.16–8.73 (m, 2H, ring protons), 9.03–9.22 (t, 1H, ring proton). Both isomers showed no C*H*Br signal and the α-deuterium content should be at least 97%.

1. W. F. Sliwinski, T. M. Su, and P. v. R. Schleyer. J. Am. Chem. Soc. **94**, 133 (1972).
2. P. v. R. Schleyer, W. F. Sliwinski, G. W. van Dine, U. Schöllkopf, J. Paust, and K. Fellenberger. J. Am. Chem. Soc. **94**, 125 (1972).
3. U. Schöllkopf. Angew. Chem. Int. Ed. Engl. **7**, 588 (1968).
4. J. A. Landgrebe and L. W. Becker. J. Org. Chem. **33**, 1173 (1968).

[11]The ρ^+ values were found to be -1.75 for the β-substituted and -4.31 for the α-substituted cyclopropyl tosylates (43). Whatever the magnitude these indicate a relatively lower degree of charge development at the β-carbons compared to that at the α-carbon. Therefore at least for the phenyl substituted cyclopropyl derivatives it seems that the cyclopropyl ring does not open up beyond 45° of rotation (19).

[12]The impurities $CHBr_3$, CH_2Br_2 are present. Low intensity but distinct peaks are observable at 196, 198, 200 (1:2:1) corresponding to the loss of C_2H_4, at 184, 186, 188 (1:2:1) corresponding to the loss of C_3H_4 and at 158, 160, 162 (1:2:1) (Br_2^+). However a weak dibromo triplet at 211, 213, 215 (1:2:1) cannot be accounted for.

[13]The freshly distilled dibromo compound is colorless but turns yellow on standing at room temperature.

5. J. W. HAUSER and J. D. UCHIC. J. Org. Chem. **37**, 4087 (1972).
6. W. E. PARHAM and K. S. YONG. J. Org. Chem. **35**, 683 (1970).
7. D. T. CLARK and G. SMALE. Chem. Commun. 868 (1969).
8. M. S. BAIRD and C. B. REESE. Tetrahedron Lett. 4637 (1971).
9. J. D. ROBERTS and V. C. CHAMBERS. J. Am. Chem. Soc. **73**, 5034 (1951).
10. H. C. BROWN, R. S. FLETCHER, and R. B. JOHANNESEN. J. Am. Chem. Soc. **73**, 212 (1951).
11. H. C. BROWN and M. GERSTEIN. J. Am. Chem. Soc. **72**, 2926 (1950).
12. A. STREITWIESER, JR. Chem. Rev. **56**, 571 (1956).
13. D. J. PATEL, M. E. H. HOWDEN, and J. D. ROBERTS. J. Am. Chem. Soc. **85**, 3218 (1963).
14. W. BERNETT. J. Chem. Educ. **44**, 17 (1967).
15. P. V. R. SCHLEYER and R. B. NICHOLAS. J. Am. Chem. Soc. **83**, 182 (1961).
16. R. HOFFMANN and R. B. WOODWARD. Acc. Chem. Res. **1**, 17 (1968).
17. W. KIRMSE and H. SCHÜTTE. J. Am. Chem. Soc. **89**, 1284 (1967).
18. C. H. DE PUY, L. G. SCHNACK, J. W. HAUSER, and W. WIEDEMANN. J. Am. Chem. Soc. **87**, 4006 (1965).
19. D. T. CLARK and G. SMALE. Tetrahedron Lett. **25**, 13 (1969).
20. C. H. DE PUY, L. G. SCHNACK, and J. W. HAUSER. J. Am. Chem. Soc. **88**, 3343 (1966).
21. G. GUSTAVSON. J. Prakt. Chem. **43**, 396 (1891).
22. M. J. S. DEWAR and S. KIRSCHNER. J. Am. Chem. Soc. **93**, 4290 (1971).
23. R. B. WOODWARD and R. HOFFMANN. The conservation of orbital symmetry. Verlag Chemie, GmCH, Weinheim, Germany. 1970. p. 46.
24. R. E. ROBERTSON. Progr. Phys. Org. Chem. **4**, 213 (1967).
25. R. E. ROBERTSON and S. E. SUGAMORI. J. Am. Chem. Soc. **91**, 7254 (1964).
26. J. M. W. SCOTT and R. E. ROBERTSON. Can. J. Chem. **50**, 167 (1972).
27. L. J. BRUBACHER, L. TREINDL, and R. E. ROBERTSON. J. Am. Chem. Soc. **90**, 4611 (1968).
28. G. KOHNSTAM. Advan. Phys. Org. Chem. **5**, 121 (1967).
29. A. QUEEN. Can. J. Chem. **45**, 1619 (1967).
30. C. Y. WU and R. E. ROBERTSON. J. Am. Chem. Soc. **88**, 2666 (1966).
31. M. J. BLANDAMER, H. S. GOLINKIN, and R. E. ROBERTSON. J. Am. Chem. Soc. **91**, 2678 (1969).
32. H. S. GOLINKIN, D. M. PARBHOO, and R. E. ROBERTSON. Can. J. Chem. **48**, 1296 (1970).
33. Y. INOMOTO, R. E. ROBERTSON, and G. SARKIS. Can. J. Chem. **47**, 4599 (1969).
34. E. C. W. CLARKE and D. N. GLEW. Trans. Faraday Soc. **62**, 539 (1966).
35. W. J. ALBERY and B. H. ROBINSON. Trans. Faraday Soc. **85**, 980 (1969).
36. B. CAPON, M. J. PERKINS, and C. W. REES. Organic reaction mechanism. Interscience Publishers, John Wiley & Sons Ltd., London. 1965. p. 63.
37. V. BELANIC-LIPOVAC, S. BORCIC, and D. E. SUNKO. Croat. Chem. Acta, **37**, 61 (1965).
38. D. T. CLARK and D. R. ARMSTRONG. Theor. Chem. Acta, **13**, 365 (1969).
39. L. RADOM, P. C. HARIHARAN, J. A. POPLE and P. V. R. SCHLEYER. J. Am. Chem. Soc. **95**, 6531 (1973).
40. W. E. PARHAM and K. S. YONG. J. Org. Chem. **33**, 3947 (1968).
41. E. C. F. KO and R. E. ROBERTSON. Can. J. Chem. **50**, 946 (1972).
42. K. M. KOSHY and R. E. ROBERTSON, Unpublished work.
43. G. J. M. VAN DER KERK and J. G. A. LUIJTEN. J. Appl. Chem. **6**, 93 (1956).
44. G. J. M. VAN DER KERK, J. G. NOLTES, and J. G. A. LUIJTEN. J. Appl. Chem. **7**, 366 (1957).
45. M. R. KULA, E. AMBERGER, and H. RUPPRECHT. Chem. Ber. **98**, 629 (1965).
46. J. DUFERMONT and J. C. MAIRE. J. Organomet. Chem. **7**, 415 (1967).
47. M. L. MADDOX, N. FLITCROFT, and H. D. KAESZ. J. Organomet. Chem. **4**, 50 (1965).
48. R. A. MARTIN and J. A. LANDGREBE. J. Org. Chem. **37**, 1996 (1972).
49. J. C. LAHOUINERE and J. VALADE. J. Organomet. Chem. **22**, C3 (1970).
50. L. SKATTEBOL. J. Org. Chem. **39**, 2951 (1964).
51. R. L. WOODWORTH and P. S. SKELL. J. Am. Chem. Soc. **79**, 2542 (1957).
52. P. S. SKELL and A. V. GARNER. **78**, 5430 (1956).
53. D. SEYFERTH, H. YAMAZAKI, and D. L. ALLESTON. J. Org. Chem. **28**, 704 (1963).

Can. J. Chem. Downloaded from www.nrcresearchpress.com by 210.87.254.5 on 09/05/12
For personal use only.

Can. J. Chem. Downloaded from www.nrcresearchpress.com by 210.87.254.105 on 09/05/12
For personal use only.

Canadian Journal of Chemistry

Published by
THE NATIONAL RESEARCH COUNCIL OF CANADA

Journal canadien de chimie

Publié par
LE CONSEIL NATIONAL DE RECHERCHES DU CANADA

Volume 52 Number 15 August 1, 1974 Volume 52 numéro 15 1 août 1974

Thallic Ion Oxidation of Styrene: Kinetics of Decomposition of the Oxythallation Adduct C_6H_5—$CH(OCH_3)$—$CH_2Tl(OAc)_2$

LOUISE NADON AND MIKLOS ZADOR

Département de chimie, Université de Montréal, C.P. 6128, Montréal 101, Québec H3C 3V1

Received March 4, 1974

LOUISE NADON and MIKLOS ZADOR. Can. J. Chem. **52,** 2667 (1974).

The kinetics of decomposition of the organo-thallic adduct formed in methanol between styrene and $Tl(OAc)_3$, (C_6H_5—$CH(OCH_3)$—CH_2—$Tl(OAc)_2$) has been studied in a water–methanol solvent. The reaction follows a first order rate law. The organo-thallic compound, $RTl(OAc)_2$, is shown to be dissociated at low concentrations yielding two reactive species, $RTlOH^+$ and RTl^{2+}. The influence of acidity on the rate of decomposition shows that RTl^{2+} is much more reactive than $RTlOH^+$. The kinetic parameters have been determined. The implication of the results on the rate-determining step of Tl(III) oxidation of styrene is discussed.

LOUISE NADON et MIKLOS ZADOR. Can. J. Chem. **52,** 2667 (1974).

La cinétique de décomposition du composé organo-thallique formé dans le méthanol entre le styrène et $Tl(OAc)_3$, (C_6H_5—$CH(OCH_3)$—CH_2—$Tl(OAc)_2$) a été étudiée dans un mélange eau–méthanol. La cinétique de la réaction est du premier ordre. Le composé organo-thallique, $RTl(OAc)_2$, se dissocie à faible concentration et conduit à deux espèces réactives $RTlOH^+$ et RTl^{2+}. L'influence de l'acide sur la vitesse de décomposition montre que RTl^{2+} est beaucoup plus réactif que $RTlOH^+$. Les paramètres cinétiques ont été déterminés. Les conséquences de ces résultats sur l'étape déterminante de l'oxydation thallique du styrène sont discutées.

Several workers have previously described the oxidation of a variety of olefins by thallium (III) salts from a preparative point of view (1–12). However, Henry's first kinetic measurements (13) suggested interesting mechanistic implications and thus prompted several recent kinetic studies (14–19). The kinetics and product distribution for the oxidation of many simple olefins by Tl (III) in aqueous acid solutions have been interpreted by Henry in terms of the following mechanism:

[1] $Tl^{3+} + CH_2{=}CHR + H_2O \xrightarrow{k_1} [TlCH_2CH(R)OH]^{2+} + H^+$

1

[2a] $\mathbf{1} \xrightarrow{k_2} Tl^+ + CH_3{-}\overset{\overset{O}{\|}}{C}{-}R + H^+$

[2b] $\mathbf{1} \xrightarrow{k_2} Tl^+ + CH_2(OH){-}CH(OH){-}R + H^+$

Reaction 1 represents the formation of an organo-thallic intermediate (**1**); it is followed by the decomposition of **1** into the final products reactions (2*a* and 2*b*).

The rate of oxidation of substituted phenylethylenes has been investigated in both methanol (17) and aqueous acetic acid (14) media. In both cases kinetic evidence indicates that the

formation of the organo-thallic intermediate is rate-determining although its rate of decomposition has not been measured experimentally.

Halpern and his co-worker (18) have recently described the oxidation of a series of alkenols by Tl^{3+} in aqueous perchloric acid. In some of the reactions examined, the formation of the oxythallation adduct was found to be rate-determining while in others, the rate of decomposition was definitely much slower.

The present study on the rate of decomposition of the organo-thallic intermediate was prompted by the existence of a stable styrene–Tl(III) adduct (2). Our first kinetic study (17) on the oxidation of styrene by thallic nitrate in methanol led us to propose a second order rate law. Kinetic evidence also suggested that the formation of the organo-thallic intermediate was rate-determining. The rate of decomposition of the intermediate presented in this work can be compared to the previously determined rate of formation in an attempt to characterize completely these reactions.

Experimental

Reactants and Products

The organo–thallic intermediate is prepared by a slightly modified version of Kabbe's method (2). Styrene (J. T. Baker Chemical Co.), 7 g, and $Tl(OAc)_3$ (Alfa Inorganics), 10 g, are dissolved in a minimum of methanol. The solution is allowed to react 1 h at room temperature. The precipitate is then filtered, recrystallized three times from benzene, and dried in a vacuum for 5 h.

The reaction products were identified by g.l.c. retention times in comparison with authentic samples. The g.l.c. analyses were carried out on a F and M 5750 gas chromatograph using two different 6 ft columns, 10% Carbowax 20M on Chromosorb PAW-DMCS at 142 °C and 25% Diglycerol on Chromosorb PAW-DMCS at 125 °C. These analyses identified the reaction products as phenylacetaldehyde (75–85%) and phenylacetaldehyde dimethyl acetal (15–25%), depending on the acidity of the medium.

Kinetic Method

The reactions were studied in a solvent containing 75% (v/v) water and 25% (v/v) methanol. The latter was necessary in order to dissolve the reactant. At high temperatures, the reactant was thermostated in pure methanol to prevent its decomposition prior to the kinetic measurements, and this solution was then mixed with the right amount of water containing all other additives.

The course of the reaction was either followed by monitoring the increase in electrical conductance, or, at high acid concentrations, when accurate conductance measurements were not possible, the reaction was followed by u.v. spectrophotometry at 265–271 and 230 nm depending on the concentrations used.

The fast reactions ($\tau_{\frac{1}{2}} < 60$ s.) were studied by stopped-flow methods on a Durrum–Gibson system using a Jarrel–Ash 0.25 m monochromator. The decrease in absorbance was registered on an oscillograph and the signal was then photographed. In intermediate cases, the stopped-flow system was used with a high-speed recorder.

The temperature in the various reaction cells was maintained constant within 0.1 °C. When necessary, the ionic strength of the solutions was maintained constant by using lithium perchlorate (G. F. Smith Chemical Co.).

Results and Discussion

The decomposition of the organo-thallic adduct of styrene follows the reaction path observed in pure methanol, namely the migration of the phenyl group (17). In our mixed solvent however, containing 75% (v/v) water and 25% (v/v) methanol, one obtains two carbonyl products, resulting from the reactions with H_2O and CH_3OH respectively, according to reactions 3 and 4

[3] $C_6H_5CH(OCH)_3—CH_2Tl(OAc)_2 + H_2O \rightarrow$
$C_6H_5—CH_2—CHO + Tl^+ + OAc^-$
$+ HOAc + CH_3OH$

[4] $C_6H_5CH(OCH_3)—CH_2Tl(OAc)_2 + CH_3OH \rightarrow$
$C_6H_5CH_2—CH(OCH_3)_2 + Tl^+ + OAc^- + HOAc$

Preliminary measurements showed that the conductance of a solution of $RTl(OAc)_2$ increased with time. Furthermore, the high initial conductance of the solution suggested that the intermediate was dissociated to an appreciable extent. A plot of the initial equivalent conductance as a function of the square root of concentration strongly suggests that $RTl(OAc)_2$ is a strong 1:1 electrolyte (with $\Lambda_0 = 114$ at 45 °C) and dissociates according to reaction 5

[5] $RTl(OAc)_2 \rightharpoonup RTlOAc^+ + OAc^-$

Furthermore, the pH of the solution is that of an acetate/acetic acid buffer in which concentrations of acetate ions and acetic acid are equal. This suggests that reaction 5 is followed by a second step

[6] $RTlOAc^+ + H_2O \rightharpoonup RTlOH^+ + HOAc$

The increase of conductance observed during the course of the reaction is solely due to the smaller size and higher ionic conductance of Tl^+ with respect to $RTlOAc^+$ and $RTlOH^+$.

Our first kinetic studies showed a marked catalytic effect of H^+. Hence, it seems reasonable to propose the formation of a more reactive spe-

Can. J. Chem. Downloaded from www.nrcresearchpress.com by 210.87.254.105 on 09/05/12
For personal use only.

Can. J. Chem. Downloaded from www.nrcresearchpress.com by 210.87.254.105 on 09/05/12
For personal use only.

cies, RTl^{2+}

$$[7] \qquad RTlOH^+ + H^+ \overset{K}{\rightleftharpoons} RTl^{2+} + H_2O$$

As the concentration of H^+ increases, the concentration of $RTlOH^+$ decreases in favor of RTl^{2+}. This would explain the observed catalysis by strong acids and acetic acid as well as inhibition by acetate ion.

Kinetics of the Decomposition

The reaction is found to follow a first order rate law in a great variety of experimental conditions

$$[8] \quad R = -\mathrm{d}[RTl(OAc)_2]/\mathrm{d}t = k_{exp}[RTl(OAc)_2]$$

The experimental first order rate constant, k_{exp} depends on experimental conditions such as the concentrations of acetic acid, acetate ions, and strong acid added. However, added styrene has no effect on the rates contrary to the results of Halpern and co-worker (18) who studied the decomposition of the oxythallation adduct of 1-penten-5-ol and observed a catalytic effect of the olefin.

Influence of Acetic Acid and Acetate Ions

As acetic acid and acetate ions are involved in reactions 5 and 6, their effect on the rate has been investigated.

Addition of HOAc and OAc^- in 1:1 ratio at constant pH does not affect the rate constant, at least at low concentrations ($\sim 5 \times 10^{-3}$ M). This observation confirms that equilibria [5] and [6] are well to the right, at least at low HOAc and OAc^- concentrations. If greater amounts of HOAc and OAc^- are added (~ 0.05 M, that is a 50-fold excess with respect to the reactant), there is a significant decrease in k_{exp}. In this case, appreciable amounts of $RTl(OAc)_2$ or $RTlOAc^+$ exist and these species are probably much less reactive than RTlOH and RTl^{2+}.

The experimental results can be interpreted by means of a two-term rate law

$$[8] \qquad R = k_1[RTlOH^+] + k_2[RTl^{2+}]$$

At low acidities, the dominant species is $RTlOH^+$, hence $[RTlOH^+] \gg [RTl^{2+}]$. In this case eq. 8 yields eq. 9 for k_{exp}.

$$[9] \qquad k_{exp} = k_1 + k_2K[H^+]$$

In a buffered medium, the concentration of H^+ can be related to those of acetic acid and acetate.

$$[10] \quad k_{exp} = k_1 + k_2KK_a[HOAc]/[OAc^-]$$

The experimental results seem to agree with eq. 10. Indeed one observes an increase in rate upon addition of HOAc, which is caused by the displacement of equilibrium [7] towards the formation of RTl^{2+} a more reactive species than $RTlOH^+$. On the other hand, addition of OAc^- has a retarding effect as predicted.

Table 1 presents the results obtained at 45 °C at various concentrations of HOAc and OAc^- added to 1.0×10^{-3} M of $RTl(OAc)_2$. The rate constant has been calculated according to eq. 10, using $k_1 = 6.5 \times 10^{-4}$ s^{-1} and $k_2KK_a = 7.8 \times 10^{-4}$ M^{-1} s^{-1}, obtained previously by plotting k_{exp} *vs.* $[HOAc]/[OAc^-]$. The values of [HOAc] and $[OAc^-]$ include the acetate ion liberated in eq. 5 and acetic acid from eq. 6 in concentrations corresponding to that of the organo-thallic intermediate used. As Table 1 indicates, there is a reasonably good agreement between the experimental and calculated rate constants at different HOAc and OAc^- concentrations.

The relatively high value of k_1 indicates that $RTlOH^+$ is a reactive species and, in the absence of additives, its contribution is about 40% of the observed rate. Using the literature value, $K_a = 8.2 \times 10^{-6}$ for our solvent (20), one obtains $k_2K = 95$ at 45 °C.

Influence of Perchloric Acid

Due to the presence of acetate ions resulting from the dissociation of $RTl(OAc)_2$, the perchloric acid added reacts with OAc^- to form HOAc. As long as the quantities of $HClO_4$ are smaller than the initial concentration of $RTl(OAc)_2$, eq. 10 is respected when proper values of [HOAc] and $[OAc^-]$ are used. The results in Table 1 show the agreement between the experimental rate constants and those calculated as above.

When higher perchloric acid concentrations are used, all acetate ions are converted to HOAc and the acidity is no longer that of a buffer system. The equilibrium concentration of H^+ is obtained by substracting the concentration of acetate formed (equalling the initial concentration of the intermediate) from that of $HClO_4$ added. In this case, eq. 9 is followed and the plot of k_{exp} *vs.* $[H^+]$ yields k_1 and k_2K which are in

Can. J. Chem. Downloaded from www.nrcresearchpress.com by 210.87.254.105 on 09/05/12
For personal use only.

TABLE 1. Rate constants of decomposition at 45 °C

[HOAc] (M)	[OAc^-] (M)	[$HClO_4$] (M)	k_{exp} (s^{-1})	k_{calc} (s^{-1})
—	—	—	1.5×10^{-3}	1.43×10^{-3}
1.5×10^{-3}	—	—	2.65×10^{-3}	2.60×10^{-3}
2.25×10^{-3}	—	—	3.4×10^{-3}	3.19×10^{-3}
3×10^{-3}	—	—	4.3×10^{-3}	4.36×10^{-3}
3.75×10^{-3}	—	—	3.8×10^{-3}	3.77×10^{-3}
4×10^{-3}	3×10^{-3}	—	1.85×10^{-3}	1.63×10^{-3}
—	0.5×10^{-3}	—	1.3×10^{-3}	1.17×10^{-3}
—	0.75×10^{-3}	—	1.4×10^{-3}	1.10×10^{-3}
—	1.0×10^{-3}	—	1.3×10^{-3}	1.04×10^{-3}
—	2.0×10^{-3}	—	0.9×10^{-3}	0.91×10^{-3}
—	3.0×10^{-3}	—	0.7×10^{-3}	0.84×10^{-3}
—	5.0×10^{-3}	—	0.7×10^{-3}	0.78×10^{-3}
—	—	0.25×10^{-3}	2.15×10^{-3}	1.95×10^{-3}
—	—	0.5×10^{-3}	3.0×10^{-3}	2.99×10^{-3}
—	—	0.75×10^{-3}	4.3×10^{-3}	6.11×10^{-3}

*[$RTl(OAc)_2$] = 10^{-3} M; solvent: 25% (v/v) methanol, 75% (v/v) water.

good agreement with those determined previously.

When the concentration of perchloric acid is greater than that of the intermediate, the concentration of H^+ becomes much higher than in the buffered system ($> 10^{-3}$ M instead of about 10^{-5} M) and accordingly there is a sharp increase in rate. In these cases the rate parameters can only be determined at lower temperatures because of experimental limitations. The values presented in Table 2 are thus obtained partly using perchloric acid and partly in a HOAc| OAc^- buffer.

In cases where high acid concentrations were used, up to 0.025 M in $HClO_4$, the ionic strength of the solution was maintained constant at 0.5 M by means of lithium perchlorate. This is necessary since preliminary results have shown a marked increase in reaction rate due to an increase in ionic strength. This effect is understandable since the formation of RTl^{2+} in equilibrium [7] is enhanced at high ionic strength as predicted by the Debye–Hückel theory.

At higher acidity, eq. 9 is no longer valid as shown by results in Fig. 1. This is caused by the fact that the concentration of RTl^{2+} is not negligible and one has to take into account the mass balance of the organo–thallic compound.

TABLE 2. Rate parameters at different temperatures*

k_1 (s^{-1})	k_2K (s^{-1} M^{-1})	T (°C)
2.8×10^{-5}	0.36	10
1.5×10^{-4}	6.1	25
6.5×10^{-4}	95	45

*[$RTl(OAc)_2$] 1.0×10^{-3} M; solvent: 25% (v/v) methanol, 75% (v/v) water.

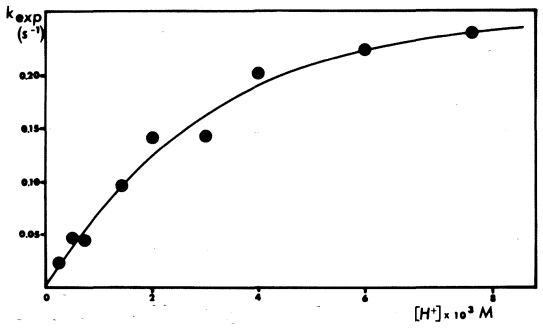

FIG. 1. Influence of perchloric acid at 25 °C, [$RTl(OAc)_2$] = 2.5×10^{-5} M, ionic strength = 0.5 M.

[11] $$[RTl]_{total} = [RTlOH^+] + [RTl^{2+}]$$

Equation 11 leads to a new expression of k_{exp}

[12] $$k_{exp} = \frac{k_1 + k_2K[H^+]}{1 + K[H^+]}$$

Considering that at these acidities k_1 is very small as compared to $k_2K[H^+]$, it can be neglected as a first approximation. The values of k_2 and K have been determined by a weighted least square method on the linear equation $1/k_{exp} = 1/k_2 + 1/k_2K[H^+]$. The values found at 25 °C are $k_2 = 0.36$ s^{-1} and $K = 260$ M^{-1} and the overall agreement is presented in Fig. 1 where the

Can. J. Chem. Downloaded from www.nrcresearchpress.com by 210.87.254.105 on 09/05/12
For personal use only.

experimental points fit reasonably well to the calculated curve using these parameters.

Of course, these rate parameters are much higher than those obtained at ionic strength of about 10^{-3} *M*.

The results also indicate that the reactivity of RTl^{2+} is of about three orders of magnitude greater than that of $RTlOH^{+}$ which shows again the great sensitivity of Tl(III) to coordination effects. The equilibrium constant *K*, is in fact the reciprocal of the hydrolysis constant, which should consequently have a value of 3.8×10^{-3} *M*. The fact that this value is only about one order of magnitude lower than that observed for hydrolysis of free Tl^{3+} (21) indicates that Tl(III) retains its affinity toward hydroxyl ions in the organo–thallic adduct. Therefore, it seems reasonable to expect that other ligands will coordinate RTl^{2+} and thus affect its reactivity. This is also suggested by the decrease in rate observed at high OAc^{-} concentration in a buffered medium.

Activation Parameters

The influence of temperature on k_{exp}, given by eq. 9 or 10 has been studied between 10 and 45 °C. For k_1, the activation parameters are $\Delta H^{\neq} = 15.5 \pm 1$ kcal and $\Delta S^{\neq} = -25 \pm 3$ e.u. For k_2K, values of $\Delta H^{\neq} = 28 \pm 1$ kcal and $\Delta S^{\neq} = 39 \pm 3$ e.u. were obtained. The fact that $\Delta H^{\neq}$ of k_2K is greater than that of k_1 is due to the ΔH^0 value associated with *K* which for Tl^{3+} is known to be 21 kcal (22). This value can be used as an estimate in our case since the hydrolysis constants of Tl^{3+} and RTl^{2+} are similar as pointed our earlier. Hence, the activation energy of k_2 is lower than that of k_1 as is to be expected.

Conclusion

In summary, the present studies show that the organo–thallic adduct, C_6H_5—CH(OCH_3)—CH_2—$Tl(OAc)_2$ is dissociated in 75% water – 25% methanol solvent. The dissociation of $RTl(OAc)_2$ leads to $RTlOH^{+}$ as the dominant species, which, in the presence of strong acid, is converted to RTl^{2+}. The kinetics of decomposition of the organo–thallic intermediate is in agreement with these hypotheses. Furthermore, the results indicate that the most reactive species is RTl^{2+}; however, at low acidities $RTlOH^{+}$ contributes significantly to the reaction rate. The hydrolysis constant of RTl^{2+} obtained from the kinetic data suggests that affinity of RTl^{2+} towards anions is comparable to that of Tl^{3+}.

The information obtained in this work permits the assessment of the rate-determining step of the overall oxidation of styrene by Tl(III) in strong acid media. In most cases, the formation of the organo–thallic adduct has been proposed as the rate-determining step of the Tl(III) oxidation of olefins (13, 14); this was also the case of $Tl(NO_3)_3$ oxidation of styrene in methanol and in methanol–water mixtures (17). It appears however, that at least in this case, the nature of the rate-determining step depends on the concentrations used. Based on the data obtained, it can be estimated that at initial concentrations of 10^{-3} *M*, the formation of the intermediate is about 50 times slower than its decomposition. At higher concentrations, the situation is reversed; at 0.1 *M* the formation becomes twice as fast as the decomposition of the organo–thallic adduct, and thus, there should be a definite accumulation of the intermediate even in strong acid medium, at least for short periods of time.

This implies, of course, that the nature of the rate-determining step largely depends on experimental conditions and this situation is further complicated by the fact that ligands can affect the rates of both reactions.

The financial support given by the National Research Council of Canada is gratefully acknowledged.

1. R. R. Grinstead. J. Org. Chem. **26**, 238 (1961).
2. H. J. Kabbe. Justus Liebigs, Ann. Chem. **656**, 204 (1962).
3. C. B. Anderson and S. Winstein. J. Org. Chem. **28**, 605 (1963).
4. J. B. Lee and M. J. Price. Tetrahedron Lett. 155, (1962); Tetrahedron, **20**, 1017 (1964).
5. E. Taylor and A. McKillop. Acc. Chem. Res. **3**, 338 (1970).
6. A. McKillop, J. D. Hunt, E. C. Taylor, and F. Kienzle. Tetrahedron Lett. **60**, 5275 (1970).
7. A. Kruse and T. M. Bednarski. J. Org. Chem. **36**, 1154 (1971).
8. W. D. Ollis, K. L. Ormand, and I. O. Sutherland. J. Chem. Soc. C, 119 (1970).
9. A. McKillop, B. P. Swann, and E. C. Taylor. Tetrahedron Lett. **60**, 5281 (1970).
10. R. M. Moriarty and H. Gopal. Tetrahedron Lett. 347 (1972).
11. C. Lion and J.-E. Dubois. C. R. Acad. Sci. Paris, 274-C, 1073 (1972).
12. J. R. Lion and A. S. Porter. J. Chem. Soc. Chem. Commun. 618 (1972).
13. P. M. Henry. J. Am. Chem. Soc. **87**, 990 (1965); **87**, 4423 (1965); **88**, 1597 (1966); Adv. Chem. Ser. **70**, 126 (1968).

14. R. J. OUELLETTE, G. KORDOSKY, C. LEVIN, and S. WILLIAMS. J. Org. Chem. **34**, 4104 (1969).
15. R. FAVIER and M. ZADOR. Can. J. Chem. **47**, 3539 (1969); **48**, 2407 (1970).
16. C. FREPPEL, R. FAVIER, J. C. RICHER, and M. ZADOR. Can. J. Chem. **49**, 2586 (1971).
17. L. NADON, M. TARDAT, M. ZADOR, and S. FLISZAR. Can. J. Chem. **51**, 2366 (1973).
18. JAMES E. BYRD and JACK HALPERN. J. Am. Chem. Soc. **95**, 2586 (1973).
19. PETER ABBEY, JAMES E. BYRD, and JACK HALPERN. J. Am. Chem. Soc. **95**, 2591 (1973).
20. T. SHEDLOVSKY and R. L. KAY. J. Phys. Chem. **60**, 151 (1956).
21. G. BIEDERMAN. Rec. Trav. Chim. **75**, 716 (1956).
22. E. M. SAVITSKII, V. V. BARON, and YU V. EFIMOV. Dokl. Akad. Nauk. SSSR, **171**, 331 (1966).

Can. J. Chem. Downloaded from www.nrcresearchpress.com by 210.87.254.105 on 09/05/12
For personal use only.

Determination of $\Delta H_{f298}{}^{0}(C_6F_5I,g)$ from Studies of the Combustion of Iodopentafluorobenzene in Oxygen and Calculation of $D(C_6F_5—X)$ Bond Dissociation Energies

MICHAEL J. KRECH

Department of Chemistry, Wilfrid Laurier University, Waterloo, Ontario N2L 3C4

AND

STANLEY JAMES W. PRICE[1] AND WAYNE F. YARED

Department of Chemistry, University of Windsor, Windsor, Ontario N9B 3P4

Received February 4, 1974

MICHAEL J. KRECH, STANLEY JAMES W. PRICE, and WAYNE F. YARED. Can. J. Chem. **52**, 2673 (1974).

The heat of formation of iodopentafluorobenzene has been determined using the direct combustion method previously developed and used for hexafluorobenzene and octafluorotoluene. The combustion with oxygen yields CO_2, CF_4, F_2, I_2, and IF_5. With a tenfold excess of oxygen the average CO_2 to CF_4 molar ratio is 11.08 ± 0.028. A material balance was obtained for carbon and fluorine. An apparent shortfall of about 30% in iodine has been related to the formation of $IO_2(OH)$ during analysis. The value of $\Delta H_{f298}{}^{0}$ $(C_6F_5I,g) = -133.2 \pm 3.0$ kcal mol^{-1} has been combined with $D(C_6F_5—I)$ and $\Delta H_{f298}{}^{0}(I,g)$ to obtain $\Delta H_{f298}{}^{0}(C_6F_5,g) = -92.6$ kcal mol^{-1}. Using this value and the appropriate values of $\Delta H_{f298}{}^{0}(C_6F_5X,g)$ and $\Delta H_{f298}{}^{0}(X,g)$, values of $D(C_6F_5—X)$ have been calculated for X = OH, H, F, Cl, I, CH_3, and CF_3.

MICHAEL J. KRECH, STANLEY JAMES W. PRICE et WAYNE F. YARED. Can. J. Chem. **52**, 2673 (1974).

La chaleur de formation de l'iodopentafluorobenzène est déterminée par la méthode de combustion directe antérieurement mise au point; elle est utilisée pour l'hexafluorobenzène et l'octafluorotoluène. La combustion dans l'oxygène donne du CO_2, CF_4, F_2, I_2 et IF_5. Avec dix fois plus d'oxygène que nécessaire la moyenne du rapport molaire du CO_2 au CF_4 est 11.08 ± 0.028. On atteint l'équilibre pondéral pour le carbone et le fluor. Un résultat apparamment inférieur d'environ 30% en iode est lié à la formation de $IO_2(OH)$ au cours de l'analyse. La valeur de $\Delta H_{f298}{}^{0}$ $(C_6F_5I,g) = -133.2 \pm 3.0$ kcal mol^{-1} est combinée à celles de $D[C_6F_5—I]$ et $\Delta H_{f298}{}^{0}(I,g)$ et l'on obtient $\Delta H_{f298}{}^{0}$ $(C_6F_5,g) = -92.6$ kcal mol^{-1}. Utilisant ce résultat et les valeurs appropriées de $\Delta H_{f298}{}^{0}$ (C_6F_5X,g) et de $\Delta H_{f298}{}^{0}$ (X,g), on a calculé les valeurs de $D(C_6F_5—X)$ pour X = OH, H, F, Cl, I, CH_3 et CF_3.

[Traduit par le journal]

Introduction

The heats of formation of a variety of compounds containing the pentafluorophenyl group have been reported. Cox *et al.* (1, 2) using combustion of samples contained in either polyester bags or polyethylene capsules have shown that in the presence of water compounds which contain only C, H, O, and F yield CO_2 and aqueous HF along with small quantities of CF_4. When chlorine was present, as in the case of C_6F_5Cl (2), a solution of As_2O_3 was used to reduce all the chlorine to the chloride.

An alternate approach involves open dish combustion under anhydrous conditions and without any auxiliary materials (3). This method has been successfully employed for hexafluorobenzene (3) and octafluorotoluene (4). In both cases complete combustion was obtained and the only products were CO_2, CF_4, and F_2. In the present work this method has been extended to iodopentafluorobenzene.

Experimental

Iodopentafluorobenzene

The iodopentafluorobenzene used was obtained from the Imperial Smelting Corporation. It was subject to fractional distillation with head and tail fractions being discarded. The final product had the following physical properties (values in parentheses are those reported by the manufacturer (5)): b.p. = 165 °C (166 °C), $n_D{}^{25} = 1.4954$ (1.4950). Analysis by gas chromatography (6 ft × 1/8 in. o.d. Silicone Oil DC 710 on 80–100 mesh chromosorb W,

[1]To whom correspondence should be addressed.

Can. J. Chem. Downloaded from www.nrcresearchpress.com by 210.87.254.105 on 09/05/12
For personal use only.

TABLE 1. Combustion data and calculated enthalpy of formation for iodopentafluorobenzene§

Mass C_6F_5I (g)	ΔT_{cor} (°C)	CO_2/CF_4* (by g.c.)	CO_2 collected (g)‡	IF_5 collected (g)	Total F_2 collected (g)†‡	$\Delta H_{298}^0(C_6F_5I,g)$ (kcal/mol)
1.981	0.8804	11.29	1.629 (99.8)			−134.2
2.072	0.9235	11.14	1.704 (99.8)			−132.6
1.531	0.6799	10.90	1.269(100.6)		0.298 (99.7)	−134.7
1.360	0.6047	11.11	1.115 (99.5)			−134.0
1.444	0.6452	11.11	1.187 (99.8)	0.235	0.284(100.7)	−131.2
1.351	0.6017	11.18	1.116(100.3)	0.208	0.268(101.9)	−133.2
1.328	0.5900	11.06	1.111(101.6)	0.213	0.256 (98.8)	−134.5
1.374	0.6130	10.98	1.129 (99.7)	0.231	0.262 (98.0)	−132.6
1.464	0.6518	10.98		0.238	0.290(101.4)	−133.0
1.365	0.6077					−133.2

*Molar ratio.
†From F_2 and IF_5.
‡Values in parentheses are % theoretical yields based on the average CO_2/CF_4 ratio, 11.08, and on the assumption that the only products are CO_2, CF_4, F_2, I_2, and IF_5.
§Additional typical data (see ref. 21 for notation); ΔE,ign/cal = 2.41, E(cal)$(-\Delta t_c)$/cal = −2557.8, $\Delta E_c°/M$ (compound)/cal g^{-1} = −1893.2.

N_2 carrier, 60 cc/min, isothermal at 105 °C, electron capture and flame ionization detection) showed the possible presence of minor impurities which were estimated to represent a maximum of 0.01% of the sample.

Vapor pressure measurements were taken over the range 13–84° using the same modified Ramsay–Young system previously employed for C_6F_6 (3) and $C_6F_5CF_3$ (4). Approximately 50 vapor pressure measurements were made over two separate runs. The conventional log P *vs.* $10^3/T$ plot showed a marked curvature which flattened at the highest temperatures used. When the standard boiling point (166 °C) was included the curve above approximately 60 °C appeared to be nearly linear.

The data from 13–84° are adequately represented by

$$[1] \quad \log_{10} P\,(\text{cm}) = 91.719 - 6685.0/T - 28.334 \log T$$

The resulting heat of vaporization and average heat capacity difference (vapor–liquid) are $\Delta H_{298}^0 = 13.83 \pm 0.05$ kcal mol^{-1} and $\langle \Delta C_p \rangle_{13-84\,°C} = -56.3$ cal deg^{-1} mol^{-1}. The error limits on ΔH are representative of the uncertainty in the precision only.

It appears that over the temperature range studied increasing association in the liquid state is occurring as the temperature decreases. Using ΔH_{298}^0 (vaporization) = 10.6 kcal mol^{-1} (determined from the approximately linear portion of the log P *vs.* $10^3/T$ plot above 60 °C) with an estimated $\langle \Delta C_p \rangle = -12.0$ cal deg^{-1} mol^{-1} (vapor – monomeric liquid) based on related compounds (6) leads to a hypothetical value of $\Delta H_{298}^0 = 11.8$ kcal mol^{-1} for the monomeric species or an apparent enthalpy of association of approximately 3 kcal mol^{-1} at 25 °C.

Sodium Arsenite Solution

Dry arsenic(III) oxide (2.4725 g) was dissolved in 20 ml of 1 *N* sodium hydroxide solution. The resulting solution was neutralized with 1 *N* sulfuric acid and diluted to 500 ml to produce a 0.1 *N* sodium arsenite solution.

CO_2, CF_4, F_2, IF_5

These substances were all obtained from Matheson. CO_2, CF_4, and F_2 were used without further purification. IF_5 was degassed to remove traces of CF_4 and then shaken with mercury under vacuum to remove traces of I_2 which give the IF_5 a deep brown coloration. The resulting clear and nearly colorless (very slight blue tinge) liquid was distilled into a glass trap where it was stored under its own vapor pressure. The vacuum system used had taps equipped with Teflon barrels and Viton O-rings and all joints were greased with KEL-F grease.

Iodine

Reagent grade iodine was used without further purification.

Apparatus and Calorimetric Procedure

The apparatus and procedure used for the main combustion process were identical to those previously used for C_6F_6 (3) and $C_6F_5CF_3$ (4).

The rate of loss of C_6F_5I from the platinum crucible in which it was weighed was 0.0099 mg/s. The time between weighing the crucible containing the C_6F_5I and sealing the bomb was such that less than 0.02% of the total sample was lost by evaporation. The correction for this loss should be accurate to better than ±3%. The error generated by the correction procedure should therefore be less than 0.001%. With the size of sample used (1.3–2.1 g) the accuracy of this correction is not a limiting factor as it exceeds the precision of the balance used (0.05 mg).

Analysis of Reaction Products

The analytical procedures for CO_2, CF_4, and F_2 have been described elsewhere (3, 4). I_2 was either reduced with excess sodium arsenite solution and then determined using an iodine specific ion electrode in conjunction with an Orion 701 digital pH meter or complexed with KI and titrated with standard 0.1 *N* sodium arsenite. Quantitative analysis for IF_5 was based on indirect procedures involving specific ion determinations for F^- and I^- Raman spectra were recorded using a Spectra-Physics model 700 spectrometer equipped with a model 164 Argon ion laser tuned to the 488.0 nm line.

Results and Discussion

The results of the C_6F_5I combustion studies are given in Table 1. The average CO_2/CF_4 ratio is 11.08 with a *probable error* (7) of ±0.028 cor-

Can. J. Chem. Downloaded from www.nrcresearchpress.com by 210.87.254.105 on 09/05/12
For personal use only.

Can. J. Chem. Downloaded from www.nrcresearchpress.com by 210.87.254.105 on 09/05/12
For personal use only.

responding to an uncertainty of ± 0.14 kcal mol^{-1} in $\Delta H_{f298}^0(C_6F_5I,g)$. As previously noted (3) gas chromatographic calibration for CF_4 must be done with CF_4–O_2 mixtures similar to those found in the bomb. Calibration with pure CF_4 leads to an error of 3.2 kcal mol^{-1} in $\Delta H_{f298}^0(C_6F_5I,g)$.

The products formed by the combustion of iodopentafluorobenzene were identified as carbon dioxide, tetrafluoromethane, iodine, fluorine and iodine pentafluoride.

CO_2, CF_4, and F_2 were identified in the same manner as was previously used for the combustions of C_6F_6 and $C_6F_5CF_3$ (3, 4).

Ample evidence was available for the presence of I_2 as a combustion product, as the bottom and sides of the bomb were coated with a layer of crystals having the characteristic purple-grey color of iodine. Titration of a solution formed by the addition of saturated potassium iodide solution to the solid contents of the bomb with a standard solution of 0.1 *N* sodium arsenite and determination of I^- by means of an iodide specific ion electrode further confirmed that I_2 was a combustion product.

In preliminary, non-analytical combustions, the presence of a small amount of a deep red liquid in the platinum crucible and at the bottom of the bomb when it was opened subsequent to a combustion, gave preliminary indication of the possible formation of an interhalogen compound. During these preliminary combustions, a white smoke was given off from the liquid in the bomb when the bomb was opened in the laboratory.

In a subsequent study the liquid present in the bomb after a combustion was isolated from the other combustion products by connecting the outlet of the bomb to two traps in series followed by a vacuum pump. The first trap contained a small amount of mercury in the bottom and was equipped with two high vacuum stopcocks (with Teflon barrels and Viton O-ring seals), one at each end, so that the trap could be removed and sealed. It was important to take careful precautions that this entire system which was connected to the bomb was moisture free. The first trap containing the mercury was set in a cooled acetone bath adjusted to -45 °C. The second trap was placed in a liquid nitrogen bath. The bottom half of the bomb itself was set in an ice–water bath at 0 °C to prevent excessive amounts of iodine from being deposited in the trapping system once pumping on the bomb was started.

After the combustion gases had been emptied from the bomb pumping was continued for approximately 20 min. The first trap was then removed from the trapping system and from its cooled acetone bath and warmed slowly to room temperature.

The contents of the trap were in the form of a deep red liquid. When this liquid was shaken with mercury it decolorized and in a few seconds formed a clear, very slightly blue liquid which rested on the surface of the mercury. This reaction was noted to be similar to that reported by Aynsley (8) for the reaction of IF_5 with mercury. The liquid was distilled, under vacuum, into a Pyrex capillary tube cooled in an acetone bath at -45 °C. The capillary was then sealed under vacuum and removed for subsequent Raman spectrographic analysis. Similar procedures were used to prepare a tube containing an authentic sample of IF_5.

A melting point determination on the liquid sample collected from the combustion bomb gave a value of 9.6 °C in good agreement with the value reported for the melting point of IF_5 of 9.7 °C (5).

The Raman spectrum of IF_5 has been reported by Gillespie and Clase (9), Lord *et al.* (10), and Begun *et al.* (11). These authors reported response in the Raman spectrum of IF_5 at 275, 572, 595, 694, and 705 cm^{-1}. The responses at 694 and 705 cm^{-1} are in the form of a doublet. The Raman spectra of both the liquid removed from the bomb and that of the purified IF_5 were similar producing response at 565, 595, 692, and 706 cm^{-1}.

After the Raman spectra had been run on the pure sample of IF_5 and on the sample obtained from a combustion experiment, the sealed capillaries containing the IF_5 were individually broken under water, reacted with excess sodium arsenite solution, and analyzed for iodide and fluoride using the corresponding specific ion electrodes. In both instances, the yields of iodine and fluorine were in good agreement with that predicted from a knowledge of the original amount of IF_5 present.

Quantitative determination of IF_5 in the combustion studies was based on the residual fluorine content of the bomb (one-fifth the F^- found) plus the I^- found in the aqueous solution con-

tained in the Teflon bubbler through which the bomb gases were passed. Separate tests showed that no detectable I_2 reaches the bubbler when the bomb is maintained at 0 °C during the flushing procedure.

The F_2 material balance shown in Table 1 rules out the formation of significant quantities of IF_7. IF_7 is a highly volatile interhalogen compound (v.p. 2.54 atm at 25 °C) (12) which would be flushed readily from the bomb and would pass through the aqueous solution without reacting (13, 14).

A material balance for iodine could not be obtained, except in an indirect sense. Both titration and specific ion methods consistently gave an apparent 27–32% shortfall. However similar synthetic mixtures of I_2 and IF_5 showed the same shortfall, presumably due to the sequence of reactions (8)

$$[2] \qquad 2I_2 + IF_5 + 5O_2 \xrightarrow[H_2O]{\text{trace}} 5IO_2F$$

$$[3] \qquad IO_2F + H_2O \rightarrow IO_2OH + HF$$

IO_2F is white solid and has been observed as a white smoke when the bomb is opened in room air. No smoke is formed when the bomb is opened in a drybox. This sequence of reactions does not interfere with the fluoride analysis but it has been reported (15) that the IO_2OH can be represented as $(IO_2)^+(OH)^-$, a form in which apparently the iodine is unavailable for analysis by the methods used in this work.

Faced with similar apparent iodide shortfall both in the combustion analyses and test experiments with IF_5 and I_2, and having obtained a material balance for both the total fluoride and total carbon in combustion experiments, it was assumed that all the iodide not found as IF_5 was present as I_2. The CO_2/CF_4 average molar ratio can then be used with the CO_2 and IF_5 yields to give the required combustion equation.

The data for the IF_5 produced shown in Table 1 along with the average CO_2/CF_4 molar ratio were employed to calculate the following reaction which is representative of the combustion of iodopentafluorobenzene.

$$[4] \quad C_6F_5I + 5.504O_2 \rightarrow 5.504CO_2 + 0.496CF_4 + 0.213IF_5 + 0.394I_2 + 0.975F_2$$

In treating a complex mixture of products such as those shown in reaction 4 all interactions between the compounds found must be taken into account. No detectable heat of mixing was observed when F_2, O_2, CF_4, and CO_2 were mixed under anhydrous conditions. However, experiments carried out both in the bomb calorimeter and in various types of auxiliary systems indicated that under conditions similar to those used in the runs a correction to $\Delta H_{f298}{}^0(C_6F_5I,g)$ of -2.2 ± 0.2 kcal mol^{-1} is required to allow for the energy released when I_2 and IF_5 are mixed. An additional and much larger correction of -28.0 ± 1.7 kcal mol^{-1} is required for the interaction of the anhydrous F_2, O_2, CF_4, CO_2 mixture with the mixed I_2 and IF_5.

In carrying out the thermochemical calculations the following heats of formation have been used: $CO_2(g)$, -94.0517 kcal mol^{-1} (16); $CF_4(g)$, -223.0 kcal mol^{-1} (17), and $IF_5(l)$, -210.44 kcal mol^{-1} (18). The enthalpy of vaporization of C_6F_5I was taken from the present work as 13.83 kcal mol^{-1} and a small correction (0.1 kcal mol^{-1}) was made to allow for the C_6F_5I that was in the vapor state at the time of combustion. A correction may also be required for IF_5 in the vapor state in the products. If only IF_5 were present it would have a vapor pressure of 26 mm at 298 K and a correction to $\Delta H_{f298}{}^0(C_6F_5I,g)$ of about 1.0 kcal mol^{-1} would be required. However, the IF_5 exists as an I_2–IF_5 solution which shows marked negative deviations from Raoult's Law. The actual required correction is therefore estimated to be 0–0.2 kcal mol^{-1}.

Based on the preceding data and estimated corrections, reaction 4 leads to $\Delta H_{f298}{}^0(C_6F_5I,g) = -133.3$ kcal mol^{-1}, with a standard deviation of ± 1.10 kcal mol^{-1} and a *probable error* (7) of ± 0.21 kcal mol^{-1}. However, when the uncertainty in the auxiliary experiments is taken into account the overall error limits must be set at about ± 3.0 kcal mol^{-1}.

For the reaction

$$C_6F_5I,g \rightarrow C_6F_5,g + I,g$$

$\Delta H_{298}{}^0 = 66.2$ kcal mol^{-1} (19). Combining this with the present value of $\Delta H_{f298}{}^0(C_6F_5I,g)$ and $\Delta H_f(I,g) = 25.5$ kcal mol^{-1} (18) gives $\Delta H_{f298}{}^0(C_6F_5,g) = -92.6$ kcal mol^{-1}. Defining $D(C_6F_5—X)$ as $\Delta H_{298}{}^0$ for the reaction

$$C_6F_5X,g \rightarrow C_6F_5,g + X,g$$

and using the present value for $\Delta H_{f298}{}^0(C_6F_5,g)$, in conjunction with previous thermochemical data then yields the values of $D(C_6F_5—X)$ shown in Table 2.

Can. J. Chem. Downloaded from www.nrcresearchpress.com by 210.87.254.105 on 09/05/12
For personal use only.

TABLE 2. Calculation of $D(C_6F_5—X)$ and comparison with $D(C_6H_5—X)$‡

X	$\Delta H_{f298}^0(X,g)$ (kcal/mol)	$\Delta H_{f298}^0(C_6F_5X,g)$ (kcal/mol)	$D(C_6F_5—X)$* (kcal/mol)	$D(C_6H_5—X)$ (kcal/mol)
OH	9.3 (16)	−228.8 (2)	145.5	110 (16, 22, 23)
H	52.1 (16)	−192.6 (2)	152.1	110 (22)
F	18.9 (18)	−226.0 (3)	152.3	123 (22, 24)
		−228.5 (2)	154.8	
Cl	29.0 (18)	−193.6 (2)	130.0	94 (22, 24)
I	25.5 (18)	−133.3	66.2†	63 (22, 24)
CH_3	33.2 (16)	−201.6 (2)	142.2	100 (22, 25)
CF_3	−114.0 (16)	−303.2 (4)	96.6	104 (31)

*Based on $\Delta H_{f298}^\circ(C_6F_5,g) = -92.6$ kcal/mol determined from $\Delta H_{f298}^\circ(C_6F_5I,g)$, and the kinetic value of $D(C_6F_5—I)$ (corrected to 298 K).
†Direct kinetic value (corrected to 298 K).
‡Reference numbers in parentheses.

No previous values of $D(C_6F_5—X)$ are available for comparison with the possible exception of $D(C_6F_5—F)$. Based on the appearance potential of $C_6F_5^+$ from C_6F_6 and an estimated value of 10.6 eV for the ionization potential of C_6F_5 an approximate value of 145 kcal was obtained (20).

Also in Table 2 a comparison is made between $D(C_6F_5—X)$ and $D(C_6H_5—X)$. The general pattern seems quite reasonable if it is assumed that the fluorines on the ring tend to *back donate* electrons to the ring. The increased potential overlap (*cf.* bonding of X with C_6H_5) would be expected to have a minimal effect when X = I and to lead to a very strong C—F bond. The value for $D(C_6F_5—Cl)$ is intermediate to C—F and C—I as expected and the similar differences between $D(C_6F_5—X)$ and $D(C_6H_5—X)$ for X = OH, H, and CH_3 seems plausible.

The approximate equivalence between $D(C_6F_5—CF_3)$ and $D(C_6H_5—CH_3)$ seems qualitatively reasonable in terms of a balance between increased potential overlap from C_6F_5 (*cf.* C_6H_5) and a smaller contribution from CF_3 (*cf.* CH_3) due to the electron withdrawing power of F in the CF_3 group.

It is felt that the large difference between $D(C_6F_5—CF_3)$ and $D(C_6F_5—CH_3)$ should be amenable to investigation by vapor phase ESCA studies and work on these compounds along with $C_6H_5CH_3$ and $C_6H_5CF_3$ is planned.

One further point may be worth considering. If the C—H, C—F, and C—C bond energy terms are consistent in aromatic systems then

$$[5]\quad \Delta H_{f298}^0(C_6F_5X,g) = \Delta H_{f298}^0(C_6H_5X,g) + 5\Delta H_{f298}^0(C_6H_5F,g) - 5\Delta H_{f298}^0(C_6H_6,g)$$

The difference between $\Delta H_{f298}^0(C_6F_5X,g)$ obtained from this equation and the experimentally determined value is referred to as ΔH(destabilization) or just the destabilization energy.

Destabilization energies for C_6F_5I and C_6F_5-CF_3 may be calculated using the relevant heats of formation from Table 2 and the following data: $\Delta H_{f298}^0(C_6H_5CF_3,g) = -143.2$ kcal mol^{-1} (26, 27), $\Delta H_{f298}^0(C_6H_5I,g) = 39.1$ kcal mol^{-1} (28), $\Delta H_{f298}^0(C_6H_5F,g) = -27.8$ kcal mol^{-1} (29), and $\Delta H_{f298}^0(C_6H_6,g) = 19.8$ kcal mol^{-1} (30). The resulting values are shown in Table 3 along with values calculated by Cox *et al.* (2) for five related compounds. An alternate value for C_6F_6 is also included.

If only electrostatic considerations are taken into account the destabilization energy of C_6F_5I seems somewhat high. Such considerations have been shown to be useful for $C_6F_5—X$ but possible problems were also pointed out (2). In the case of C_6F_5I then either the simple electrostatic concept is insufficient or significant errors exist in the data used. From considerations of $D(C_6F_5—CF_3)$ it is quite clear that the problem cannot be resolved by assuming a lower value (a larger negative value) for $\Delta H_{f298}^0(C_6F_5I,g)$ than that found in the present work. It would be necessary to assume a value for $\Delta H_{f298}^0(C_6F_5I,g)$ of approximately −160 kcal mol^{-1} to bring the ΔH(destabilization) for C_6F_5I into line. This would imply a value for $D(C_6F_5—CF_3)$ of 70 kcal mol^{-1}. Preliminary experiments on the pyrolysis of $C_6F_5CF_3$ indicate that at 1211 K with a contact time of 0.77 s the rate constant for $C_6F_5—CF_3$ bond rupture is 0.90 s^{-1}. Combining this with a reasonable A factor, $10^{15.5}$ s^{-1} (25), given $E_{1211\,K}$ = 94 kcal mol^{-1} or $\Delta H_{298}^0 \approx 96$ kcal mol^{-1} in excellent agreement with the value given in Table 2.

Can. J. Chem. Downloaded from www.nrcresearchpress.com by 210.87.254.105 on 09/05/12
For personal use only.

TABLE 3. Destabilization energies for C_6F_5X

X	$\Delta H_{f298}^0(C_6F_5X,g)$ Observed	$\Delta H_{f298}^0(C_6F_5X,g)$ Calculated*	ΔH (destabilization)
OH	−228.8†	−261.0†	32
H	−192.6†	−218.1†	26
F	−228.5†	−265.7†	37
F	−226.0‡	−265.7	40
Cl	−193.6†	−225.8†	32
I	−133.3	−198.8	66
CH_3	−201.6†	−226.0†	24
CF_3	−303.2§	−381.1	78

*From eq. 5. All values are expressed in kcal mol^{-1}.
†Reference 2.
‡Reference 3.
§Reference 4.

This agreement suggests that significant systematic errors do not exist in the present determination of $\Delta H_{f298}^0(C_6F_5I,g)$. Since the calculated values in Table 3 all involve $5(\Delta H_{f298}^0(C_6H_5F,g) - \Delta H_{f298}^0(C_6H_6,g))$ only errors in $\Delta H_{f298}^0(C_6H_5X,g)$ are significant in assessing the auxiliary data. The uncertainty from this source is unlikely to exceed about ± 2 kcal mol^{-1}. The relative destabilization energies reported here should therefore all be accurate to within ± 5 kcal mol^{-1}. Obviously caution must be used in trying to put any simple interpretation on ΔH(destabilization) values.

This work has been supported by an operating grant from the National Research Council of Canada.

1. J. D. COX, H. A. GUNDRY, and A. J. HEAD. Trans. Faraday Soc. **60**, 653 (1964).
2. J. D. COX, H. A. GUNDRY, D. HARRUP, and A. J. HEAD. J. Chem. Thermodyn. **1**, 77 (1969).
3. M. KRECH, S. J. W. PRICE, and W. F. YARED. Can. J. Chem. **50**, 2935 (1972).
4. M. J. KRECH, S. J. W. PRICE, and W. F. YARED. Can. J. Chem. **51**, 3662 (1973).
5. Highly fluorinated aromatic and alicyclic compounds. Imperial Smelting Company, St. Andrews Road, Avonmouth, Bristol BS11 9HP, England.
6. Handbook of chemistry and physics. 52nd ed. The Chemical Rubber Co., Cleveland, Ohio. 1971–72. p. D130.
7. Handbook of tables for mathematics. 3rd ed. The Chemical Rubber Co., Cleveland, Ohio. 1967. p. 876.
8. E. E. AYNSLEY, R. NICHOLS, and P. L. ROBINSON. J. Chem. Soc. 623 (1953).
9. R. J. GILLESPIE and H. J. CLASE. J. Chem. Phys. **47**, 1071 (1967).
10. R. C. LORD, M. A. LYNCH, W. C. SCHUMB, and E. J. SLOWINSKI. J. Am. Chem. Soc. **72**, 522 (1950).
11. G. M. BEGUN, W. H. FLETCHER, and D. F. SMITH. J. Chem. Phys. **42**, 2236 (1965).
12. Kirk-Othmer Encyclopedia of Chemical Technology. Vol. 9. Interscience (John Wiley and Sons), New York. 1966. p. 593.
13. N. V. SIDGWICK. The chemical elements and their compounds. Vol. II. Clarendon Press, Oxford. 1950. p. 1158–1160.
14. O. RUFF and R. KEIM. Z. Anorg. Chem. **193**, 176 (1930).
15. M. SCHNEISSER and K. LANG. Angew. Chem. **67**, 156 (1955).
16. Selected values of chemical thermodynamic properties. National Bureau of Standards. U.S. Tech. Notes No. 270-3. 1968.
17. E. GREENBERG and W. N. HUBBARD. J. Phys. Chem. **72** (1), 222 (1968).
18. J. D. COX, J. B. PEDLEY, A. KIRK, S. SEILMAN, and L. G. HEATH. Computer analysis of thermochemical data. National Physical Laboratory, Teddington, U.K. Halogen Compounds. 1972.
19. M. J. KRECH, S. J. W. PRICE, and W. F. YARED. Int. J. Chem. Kinet. **6**, 257 (1974).
20. V. H. DIBELER, R. M. REESE, and F. L. MOHLER. J. Chem. Phys. **26**, 304 (1956).
21. J. COOPS, R. S. JESSUP, and K. VAN NES. *In* Experimental thermochemistry. Vol. 1. *Edited by* F. D. Rossini. Interscience, New York. 1956.
22. G. A. CHAMBERLAIN and E. WHITTLE. Trans. Faraday Soc. **67**, 2077 (1971).
23. R. J. L. ANDON, D. P. BIDDISCOMBE, J. D. COX, R. HANDLEY, D. HARROP, F. E. G. HERINGTON, and J. F. MARTIN. J. Chem. Soc. 5246 (1960).
24. P. SMITH. J. Chem. Phys. **29**, 681 (1958).
25. S. W. BENSON and H. E. O'NEAL. Kinetic data on gas phase unimolecular reactions. NSRDS-NBS 21. Washington, D.C. 1970.
26. D. W. SCOTT, D. R. DOUSLIN, J. F. MESSERLY, S. S. TODD, I. A. HOSSENLOPP, T. C. KINCHELDE, and J. P. MCCULLOUGH. J. Am. Chem. Soc. **81**, 1015 (1959).
27. G. K. JOHNSON, P. W. SMITH, and W. N. HUBARD. J. Chem. Thermodyn. **5**, 793 (1973).
28. J. D. COX and G. PILCHER. Thermochemistry of organic and organometallic compounds. Academic Press, N.Y. 1970.
29. W. GOOD, D. SCOTT, and G. WADDINGTON. J. Phys. Chem. **60**, 1080 (1956).
30. F. D. ROSSINI (*Editor*). American Petroleum Institute, Res. Proj. **44**, Carnegie Press, Pittsburgh, Pa. 1953.
31. I. SZILAGYI and T. BERCES. Int. J. Chem. Kinet. **2**, 199 (1970).

Can. J. Chem. Downloaded from www.nrcresearchpress.com by 210.87.254.105 on 09/05/12
For personal use only.

Rearrangement Studies with ^{14}C. XXXIX. 1,2-Phenyl Shifts in Solvolyses of Triphenylvinyl-2-^{14}C Triflate

CHOI CHUCK LEE, ALLAN J. CESSNA, BRUCE A. DAVIS, AND MITSUO OKA

Department of Chemistry and Chemical Engineering, University of Saskatchewan, Saskatoon, Saskatchewan S7N 0W0

Received February 19, 1974

CHOI CHUCK LEE, ALLAN J. CESSNA, BRUCE A. DAVIS, and MITSUO OKA. Can. J. Chem. **52**, 2679 (1974).

Solvolysis of triphenylvinyl-2-^{14}C triflate was carried out in HOAc, 97% HCOOH, or CF_3COOH. The reaction products showed rearrangements of the ^{14}C-label from C-2 to C-1 averaging about 6.7, 7.7, and 27.0%, respectively, for the acetolysis, formolysis, and trifluoroacetolysis. The presence of the conjugate base of the solvent, added as the sodium salt, did not affect the extent of rearrangement. It is suggested that the 1,2-phenyl shift across the double bond of the triphenylvinyl cation takes place during the ion-pair stage and that the extent of rearrangement is related to the lifetime of the ion-pair and the nucleophilicity of the solvent.

CHOI CHUCK LEE, ALLAN J. CESSNA, BRUCE A. DAVIS et MITSUO OKA. Can. J. Chem. **52**, 2679 (1974).

On effectue la solvolyse du triflate du triphénylvinyl ^{14}C-2 dans AcOH, 97% HCOOH ou CF_3COOH. Les produits de réaction présentent des réarrangements du ^{14}C marqué passant de C-2 à C-1 avec des moyennes respectives de 6.7, 7.7 et 27.0% pour l'acétolyse, la formolyse et la trifluoroacétolyse. La présence de la base conjuguée du solvant, ajoutée à l'état de sel de sodium, n'affecte pas le taux de réarrangement. On suppose que le réarrangement du groupe phényle de 1 vers 2 à travers la double liaison du cation triphénylvinyle se produit durant le stade ion-pairé et que le taux de réarrangement est relié à la durée de vie de l'ion-pairé et la nucléophilie du solvant. [Traduit par le journal]

Can. J. Chem. Downloaded from www.nrcresearchpress.com by 210.87.254.40 on 09/05/12
For personal use only.

The formation and reactions of vinyl cations, including rearrangements, have been the subject of recent extensive reviews (1,2). Much of the reported rearrangements that arose from 1,2-aryl shifts across the double bond of vinyl cations involved conversion of less stable to more stable cations. For example, the decomposition of 1-phenyl-2,2-di-*p*-tolylvinyldiazonium ion generated from the triazene in HOAc gave 20% of the rearranged product, 2-phenyl-1,2-di-*p*-tolylvinyl acetate (3). According to Stang (2), the first example of an aryl migration across the double bond of a vinyl cation generated by solvolysis was reported in 1970 in the reaction of 1-methyl-2,2-diphenylvinyl triflate in 80% EtOH to give almost exclusively the rearranged phenyl 1-phenylethyl ketone (4). Another early example was the 1,2-anisyl migration observed in the acetolysis in the presence of silver acetate of 2,2-dianisyl-1-phenylvinyl bromide quoted by Hanack (5) as a personal communication from Z. Rappoport. Very recently, Rappoport and co-workers (6, 7) have carried out extensive studies on rearrangements arising from 1,2-phenyl or *p*-methoxyphenyl shifts during the solvolyses of a number of 2,2-diaryl-1-phenylvinyl bromides in HOAc–AgOAc (6) or in 60% EtOH or 2,2,2-trifluoroethanol (7). On the basis of stereochemical and kinetic evidence, these workers (6,7) concluded that the initial ionization did not involve β-aryl participation. On the other hand, solvolytic studies on *cis*- and *trans*-1,2-dimethyl-2-phenylvinyl triflates by Stang and Dueber (8,9) have implicated the phenyl-bridged or vinylidene phenonium ion as a reaction intermediate. Since rearrangements involving degenerate cations can be observed only through the use of isotopic tracers, Stang and Dueber utilized D-labeling of one of the methyl groups in order to study the extent of phenyl shifts across the double bond in the 1,2-dimethyl-2-phenylvinyl system. In the present paper, observations are reported on degenerate rearrangements arising from 1,2-phenyl shifts in the triphenylvinyl cation generated from solvolyses of triphenylvinyl-2-^{14}C triflate (**1**-OTf-2-^{14}C).

Phenylacetic acid-1-^{14}C was converted to the ethyl ester and treated with PhMgBr to give 1,1,2-triphenylethanol-1-^{14}C, which on reaction with Br_2 in HOAc gave triphenylvinyl-2-^{14}C

TABLE 1. Data from solvolyses of triphenylvinyl-2-^{14}C triflate (**1**-OTf-2-^{14}C)

Solvent	Specific activity[a] (d.p.m./mmol) × 10^{-5}				Rearrangement from C-2 to C-1, %	
	$(Ph)_2CHCH(Ph)OH$		PhCOPh[b]			
	Run 1	Run 2	Run 1	Run 2	Run 1	Run 2
Dioxane–H_2O–NaOH	18.1	8.52	18.1	8.59	0	0
HOAc–NaOAc	18.1	9.18	16.9	8.54	6.6	7.0
HOAc	4.56	3.06	4.25	2.86	6.8	6.5
HCOOH–HCOONa	18.1	10.5	16.7	9.70	7.7	7.6
HCOOH	6.41	3.74	5.92	3.45	7.6	7.8
CF_3COOH–CF_3COONa	3.63	4.89	2.64	3.49	27.3	28.6
CF_3COOH	6.41	24.8	4.73	18.4	26.2	25.8

[a]Measured by a liquid scintillation counter.
[b]Assayed as the oxime.

bromide (**1**-Br-2-^{14}C), presumably via bromination of triphenylethylene (10). The **1**-Br-2-^{14}C was converted to the Grignard reagent and reacted with I_2 to give **1**-I-2-^{14}C (11), which in turn was treated with AgOTf in a nonpolar solvent, pentane, to give **1**-OTf-2-^{14}C (12). That all the ^{14}C-label was located at the C-2 position was demonstrated by the conversion of **1**-OTf-2-^{14}C to isotopically unrearranged α,α-diphenylacetophenone-α-^{14}C upon reaction with a 60:40 mixture of dioxane and 5% NaOH solution (see Table 1).

The solvolyses were carried out by treating about 5.0 mmol of **1**-OTf-2-^{14}C in 10 ml of HOAc, 97% HCOOH, or CF_3COOH, with or without the presence of a 10% excess of NaOAc, HCOONa, or CF_3COONa, respectively. The acetolysis and formolysis were effected at reflux temperature for 2 h and it was subsequently noted that refluxing the reaction mixture for 24 h did not materially affect the degree of isotopic scrambling in these reactions. The trifluoroacetolysis was carried out at room temperature for 2 h and changing the conditions to heating the reaction mixture at 40° for 24 h also did not significantly change the extent of scrambling. From n.m.r. analyses, the products from reactions in HOAc and CF_3COOH were the expected esters, **1**-OAc and **1**-$OAcF_3$, whereas formolysis in 97% HCOOH gave as product α,α-diphenylacetophenone (**2**) instead of the formate.

All of the products from the active runs were converted to 1,2,2-triphenylethanol (**3**-^{14}C) which, in most cases, was isolated with the aid of added carrier. When the product was **2**-^{14}C, $LiAlH_4$ reduction directly gave **3**-^{14}C, whereas in the case of **1**-OAc-^{14}C or **1**-$OAcF_3$-^{14}C, reduction with $LiAlH_4$ first gave a mixture of **2**-^{14}C and **3**-^{14}C which was treated once more with $LiAlH_4$ to give pure **3**-^{14}C. Each sample of **3**-^{14}C was oxidized with alkaline $KMnO_4$ to benzophenone (**4**-^{14}C) and the difference in specific activity between **3**-^{14}C and **4**-^{14}C gave the extent of scrambling of the isotopic label from C-2 to C-1. The results are summarized in Table 1.

When the formation of products was followed by n.m.r., it was found that at the n.m.r. probe temperature of about 34°, the time required for complete reaction was about 10 h, 5 h, and less than 3 min for acetolysis, formolysis, and trifluoroacetolysis, respectively. The kinetics of acetolysis of a number of triphenylvinyl sulfonates, including the triflate, have been studied by Jones and Maness (13) and it was concluded that the reaction followed an S_N1 mechanism. The reported specific rate constant for the acetolysis of **1**-OTf in the presence of an excess of NaOAc at 25° was 1.12×10^{-5} s^{-1} (13). This was an extrapolated value based on kinetic data determined at higher temperatures by u.v. Because the u.v. absorptions of **1**-OTf and **1**-OAc overlap extensively, we measured the acetolysis rate by titration with NaOAc in HOAc and found a somewhat lower value of 0.78×10^{-5} s^{-1} for the unbuffered acetolysis of **1**-OTf at 24°. The specific rate constant for the formolysis, also at 24°, was determined by u.v. at 310 nm and was found to be 0.86×10^{-5} s^{-1}. These kinetic results, together with the qualitative n.m.r. observations, indicate that the rates of acetolysis, formolysis, and trifluoroacetolysis do parallel the extents of isotopic scrambling as recorded in Table 1.

Can. J. Chem. Downloaded from www.nrcresearchpress.com by 210.87.254.40 on 09/05/12
For personal use only.

Can. J. Chem. Downloaded from www.nrcresearchpress.com by 210.87.254.40 on 09/05/12
For personal use only.

The data in Table 1 definitely demonstrate the occurrence of degenerate rearrangements arising from 1,2-phenyl shifts across the double bond of the triphenylvinyl cation. The extent of isotopic scrambling from C-2 to C-1 averaged about 6.7, 7.7, and 27.0%, respectively, for the acetolysis, formolysis, and trifluoroacetolysis of **1**-OTf-2-^{14}C.[1] Before discussing any possible mechanistic explanations of these rearrangements, it may be of interest to compare the present data with the magnitudes of 1,2-phenyl shifts in similar solvolyses of isotopically labeled 2-phenylethyl tosylate (**5**-OTs). Rearrangements of the ^{14}C- or D-label from C-1 to C-2 amounted to about 6, 45, and 50%, respectively, in solvolyses of **5**-OTs-1-^{14}C or **5**-OTs-1-d_2 in HOAc, HCOOH, and CF_3COOH, buffered by the presence of the conjugate base of the solvent (14, 15). The relative rates for the acetolysis, formolysis, and trifluoroacetolysis, respectively, of **5**-OTs at 75° were 1:137:1118 (15). Thus it appears that both in the extents of rearrangement and in relative rates, a change in solvent did not show parallel effects on the vinyl system, **1**-OTf, and on the saturated system, **5**-OTs. The similarity in the rates of acetolysis and formolysis of **1**-OTf at 24°, with the formolysis being faster than the acetolysis only by a factor of about 1.1, is contrary to expectation on the basis of the higher ionizing power of HCOOH. A full explanation of this anomaly is not apparent from the present work, although a contributing factor may be that in the Grunwald–Winstein mY correlation (16), the m value is reported to be low for solvolyses of triarylvinyl systems (17).

The different extents of rearrangement observed in the different solvents as recorded in Table 1 conceivably could be attributed to different degrees of β-phenyl participation during the solvolysis of **1**-OTf-2-^{14}C in the various solvents. Although strong evidence for phenyl participation has been observed in the 1,2-dimethyl-2-phenylvinyl system (8, 9), kinetic and stereochemical results have indicated that β-aryl participation is not important in solvolyses of triarylvinyl systems (6, 7, 17). It is of interest to note from Table 1 that the presence of the conjugate base of the solvent, added as the sodium salt, did not materially affect the extent of isotopic scrambling. This finding is contrary to the observation that in the decomposition of 1-(triarylvinyl)-3-phenyl-1-triazene in HOAc, the extent of rearrangement was suppressed by the addition of an excess of KOAc (3). This difference may be due to the possibility of ion-pair formation under the conditions of the present experiments, while in the decomposition of triazenes, no counter ion was present to give rise to ion-pairs. It may be suggested that under solvolytic conditions where the presence of the conjugate base does not affect the amount of rearrangement, the rearrangement takes place in the ion-pair stage.[2,3] The longer the lifetime of the ion-pair, the greater will be the extent of rearrangement. It may also be pointed out that the presently observed rearrangements, averaging about 6.7, 7.7, and 27.0%, respectively, for acetolysis, formolysis, and trifluoroacetolysis, appear to be related to the nucleophilicity of the solvents, the nucleophilicity of HOAc and HCOOH being quite similar, and that of CF_3COOH being much lower (18, 19). Such a relationship suggests a competition between rearrangement via 1,2-phenyl shifts in the ion-pair and reaction of the ion-pair with solvent to give the product. Consequently, the highest rearrangement was observed in the solvent of lowest nucleophilicity. When **1**-OTf-2-^{14}C was hydrolyzed in aqueous dioxane in the presence of NaOH, apparently 1,2-phenyl shift could not compete with product formation and no rearrangement was found in the hydrolysis product.

Experimental

1,1,2-Triphenylethanol-1-^{14}C

A solution of 1.64 g (0.01 mol) of ethyl phenylacetate-1-^{14}C (from esterification of phenylacetic acid-1-^{14}C) in 10 ml of ether was added slowly to a solution of PhMgBr (from 0.02 mol of PhBr) in 20 ml of ether. The mixture was gently refluxed for 1 h and then 30 ml of 3 M NH_4Cl was added. The product was recovered by ether extraction and the extract was washed with water and dried over $MgSO_4$. The ether was then removed and the colorless

[1]Quoting from a private communication, Rappoport and Houminer (7) reported that B. M. Benjamin and C. J. Collins have noted a 3.6% degenerate β-phenyl rearrangement during the acetolysis of **1**-OTf.

[2]The ion-pair mechanism was suggested to us by Prof. Z. Rappoport.

[3]In the solvolysis of D-labeled *cis*-1,2-dimethyl-2-phenylvinyl triflate in 60% ethanol, which did not involve phenyl participation, a 34.5% 1,2-phenyl shift was observed and it was suggested that this rearrangement arose from the initial formation of an ion-pair with a classical vinyl cation which subsequently rearranged to the phenyl-bridged vinyl cation (8).

Can. J. Chem. Downloaded from www.nrcresearchpress.com by 210.87.254.40 on 09/05/12
For personal use only.

residue recrystallized from hexane to give 1.8 g (66%) of 1,1,2-triphenylethanol-1-^{14}C, m.p. 88° (lit. (20) m.p. 88–89°).

*Triphenylvinyl-2-^{14}C Bromide (**1**-Br-2-^{14}C)*

A solution of 0.80 g (0.01 mol) of Br_2 in 5.0 ml of HOAc was added dropwise with stirring to a solution of 1.37 g (0.005 mol) of 1,1,2-triphenylethanol-1-^{14}C in 10 ml of HOAc. Stirring was continued for 4 h and during this period a pale yellow solid precipitated. The product was recovered by filtration and washed with water. The filtrate was concentrated and upon cooling yielded more product. The combined product was recrystallized from methanol, giving 1.0 g (60%) of **1**-Br-2-^{14}C, m.p. 115° (lit. (21) m.p. 114–115.5°).

*Triphenylvinyl-2-^{14}C Triflate (**1**-OTf-2-^{14}C)*

1-Br-2-^{14}C was converted to the Grignard reagent and treated with I_2 to give **1**-I-2-^{14}C as described by Morrison (11). **1**-I-2-^{14}C was converted to **1**-OTf-2-^{14}C by reaction with AgOTf using the procedure of Gramstad and Haszeldine (12) for the preparation of ethyl triflate, except that pentane instead of ether was used as solvent. The **1**-OTf-2-^{14}C product, recrystallized from pentane, was obtained in 50% yield, m.p. 83°, dec. (lit. (13) m.p. 83.5-84°, dec.). Its mass spectrum gave the molecular ion with *m/e* at 404. Its n.m.r. spectrum in $CDCl_3$ showed aromatic multiplets at 7.1–7.5 p.p.m., with three main signals at 7.10, 7.36, and 7.46 p.p.m.

Solvolyses

Solvolyses of **1**-OTf or **1**-OTf-2-^{14}C were carried out in a 60:40 mixture of dioxane and 5% NaOH solution, glacial acetic acid, reagent grade 97% HCOOH, and CF_3COOH. Preliminary examination by n.m.r. indicated that the products were the expected α,α-diphenylacetophenone (**2**), **1**-OAc, and **1**-OAcF_3, respectively, from basic hydrolysis, acetolysis, and trifluoroacetolysis. In the formolysis, however, the product was also ketone **2** and not the formate ester. A similar formation of an analogous ketone has also been reported by Rappoport and Apeloig (22) from the reaction of 1,2-dianisyl-2-phenylvinyl bromide with dry HCOOH. All of the products, **2**, **1**-OAc, and **1**-OAcF_3, gave the expected molecular ions in their respective mass spectra. The n.m.r. spectrum of **2**, in $CDCl_3$, was the same as that reported by Rappoport and Houminer (7). The n.m.r. spectrum of **1**-OAc in $CDCl_3$ showed a singlet at 1.98 p.p.m. for the CH_3 protons and three main signals in the aromatic region at 7.15, 7.20, and 7.35 p.p.m. For **1**-OAcF_3, the aromatic protons gave peaks at 7.24, 7.32, and 7.40 p.p.m.

Solvolyses of **1**-OTf-2-^{14}C, with or without the presence of a 10% excess of the conjugate base of the solvent, were carried out in duplicate. A typical run is described below.

A solution of 2.02 g (0.005 mol) of **1**-OTf-2-^{14}C and 0.52 g (0.0055 mol) of NaOAc in 10 ml of HOAc was heated under reflux for 2 h. Most of the solvent was then distilled off and the residue taken up in 100 ml of ether. The ether solution was washed successively with saturated Na_2CO_3 and with water, and then dried over $MgSO_4$. To the resulting ether solution, 2.0 g of $LiAlH_4$ was added in small portions and the reaction mixture was stirred under reflux for 2 h. Water and dilute HCl were added dropwise to decompose the excess hydride. The ether layer was separated and the aqueous layer was extracted with more ether. The combined ether extracts were dried over $MgSO_4$ and the solvent was removed to give a product consisting chiefly of ketone **2**-^{14}C contaminated with a small amount of 1,2,2-triphenylethanol (**3**-^{14}C). This product mixture, together with about 2.0 g of ordinary **2** as carrier, was dissolved in 125 ml of ether and added dropwise to a stirred solution of 3.0 g of $LiAlH_4$ in 250 ml of ether. The reaction mixture was gently refluxed for 4 h and then worked up as before to give **3**-^{14}C which was repeatedly recrystallized from ethanol–water until its specific activity was constant, m.p. 88° (lit. (23*b*) m.p. 88–89°).

*Oxidation of 1,2,2-Triphenylethanol-^{14}C (**3**-^{14}C)*

One gram of the alcohol (**3**-^{14}C) was suspended in 80 ml of water and 5 ml of 10% NaOH. Powdered $KMnO_4$ (4.0 g) was added in small portions and then the mixture was refluxed for 4 h. Shorter reaction times would result in incomplete oxidation and longer reaction times would cause excessive loss of the desired benzophenone through further oxidation to benzoic acid. CH_3OH was added to the reaction mixture to destroy the excess permanganate and the resulting reaction mixture was acidified with dilute H_2SO_4. The MnO_2 was filtered off and washed with acetone. Much of the acetone was distilled off and then the filtrate was repeatedly extracted with ether. The combined ether extract was washed with a saturated $NaHCO_3$ solution to remove the benzoic acid. After drying and removal of the ether, the residual benzophenone was converted to the oxime which was repeatedly crystallized from methanol–water until its specific activity was constant, m.p. 144° (lit. (23*a*) m.p. 144°).

Kinetic Measurements

A 2.5 m*M* solution of **1**-OTf in glacial acetic acid was maintained at 24° and the rate of acetolysis was followed by titration of the liberated sulfonic acid in 5.0-ml aliquots of the reaction mixture with standardized (about 0.001 *N*) NaOAc in HOAc using bromophenol blue as indicator. The mean value of the specific rate constant from triplicate runs was $(0.78 \pm 0.01) \times 10^{-5}$ s^{-1}.

The solubility of **1**-OTf in 97% HCOOH at 24° was low. A saturated solution was prepared by stirring **1**-OTf in 97% HCOOH at 24° for about 10 min and the undissolved **1**-OTf was removed by filtration. The solution was diluted with 97% HCOOH to give an appropriate u.v absorbance reading of about 0.8 at 310 nm and the rate of formolysis was followed by u.v. at 310 nm. The mean value of the specific rate constant from triplicate runs was $(0.86 \pm 0.01) \times 10^{-5}$ s^{-1}.

The financial support given by the National Research Council of Canada and valuable information and comments given by Profs. Z. Rappoport, P. J. Stang, and W. M. Jones are gratefully acknowledged.

1. G. Modena and U. Tonellato. Adv. Phys. Org. Chem. **9**, 185 (1971).
2. P. J. Stang. Progr. Phys. Org. Chem. **10**, 276 (1973).
3. W. M. Jones and F. W. Miller. J. Am. Chem. Soc. **89**, 1960 (1967).
4. M. A. Imhoff, R. H. Summerville, P. v. R. Schleyer,

A. G. MARTINEZ, M. HANACK, T. E. DUEBER, and P. J. STANG. J. Am. Chem. Soc. **92**, 3802 (1970).
5. M. HANACK. Acc. Chem. Res. **7**, 209 (1970).
6. Z. RAPPOPORT, A. GAL, and Y. HOUMINER. Tetrahedron Lett. 641 (1973).
7. Z. RAPPOPORT and Y. HOUMINER. J. Chem. Soc. Perkin II, 1506 (1973).
8. P. J. STANG and T. E. DUEBER. J. Am. Chem. Soc. **95**, 2683 (1973).
9. P. J. STANG and T. E. DUEBER. J. Am. Chem. Soc. **95**, 2686 (1973).
10. S. APELGOT, A. CHEUTIN, S. MARS, and M. R. BERGEN. Bull. Soc. Chim. Fr. 533 (1952).
11. D. C. MORRISON. J. Am. Chem. Soc. **74**, 4459 (1952).
12. T. GRAMSTAD and R. H. HASZELDINE. J. Chem. Soc. 173 (1956).
13. W. M. JONES and D. D. MANESS. J. Am. Chem. Soc. **92**, 5457 (1970).
14. C. C. LEE, G. P. SLATER, and J. W. T. SPINKS. Can. J. Chem. **35**, 1417 (1957).
15. J. E. NORLANDER and W. G. DEADMAN. J. Am. Chem. Soc. **90**, 1590 (1968).
16. E. GRUNWALD and S. WINSTEIN. J. Am. Chem. Soc. **70**, 846 (1948).
17. Z. RAPPOPORT and Y. APELOIG. Tetrahedron Lett. 1817 (1970).
18. P. E. PETERSON and F. J. WALLER. J. Am. Chem. Soc. **94**, 991 (1972).
19. T. W. BENTLEY, F. L. SCHADT, and P. v. R. SCHLEYER. J. Am. Chem. Soc. **94**, 992 (1972).
20. C. J. COLLINS and W. A. BONNER. J. Am. Chem. Soc. **75**, 5379 (1953).
21. C. F. KOELSCH. J. Am. Chem. Soc. **54**, 2045 (1932).
22. Z. RAPPOPORT and Y. APELOIG. J. Am. Chem. Soc. **91**, 6734 (1969).
23. J. R. A. POLLOCK and R. STEVENS (*Editors*). Dictionary of organic compounds. 4th ed. Eyre and Spottiswood, London. 1965. (*a*) p. 348; (*b*) p. 3199.

Can. J. Chem. Downloaded from www.nrcresearchpress.com by 210.87.254.40 on 09/05/12
For personal use only.

Diffusion of Gases in Porous Solids. I. Theoretical Background and Experimental Method

K. R. WELLER[1]

Department of Chemical Engineering, University of Adelaide, Adelaide, Australia

N. S. STENHOUSE[2]

Division of Mathematical Statistics, Commonwealth Scientific and Industrial Research Organization, Adelaide, Australia

AND

HARRY WATTS[3]

Department of Chemical Technology, South Australian Institute of Technology, Adelaide, Australia

Received April 4, 1972[4]

K. R. WELLER, N. S. STENHOUSE, and HARRY WATTS. Can. J. Chem. **52**, 2684 (1974).

In the past, some authors have not defined the diffusion coefficient appropriate to their experimental system, consequently, valuable data have been lost. We discuss the various diffusion coefficients referred to all possible frames of reference in relation to the choice of a suitable experimental system for the determination of gaseous diffusion coefficients in porous media. A modified Ney and Armistead type diffusion cell is described with an improved method of calculation of results from continuously monitored concentration changes in the diffusion cell.

K. R. WELLER, N. S. STENHOUSE et HARRY WATTS. Can. J. Chem. **52**, 2684 (1974).

Quelques auteurs, dans le passé, n'ayant pas défini le coefficient de diffusion approprié à leur système expérimental, il en résulte une perte de données intéressantes. On discute des coefficients de diffusion variés rattachés à toutes les formes de références possibles en relation avec le choix d'un système expérimental convenable pour la détermination de coefficients de diffusion des gaz dans un milieu poreux. On décrit une cellule de diffusion modifiée de type Ney et Armistead ainsi qu'une méthode de calcul des résultats améliorée à cause d'un contrôle continu des changements de concentration dans la cellule de diffusion.

[Traduit par le journal]

Introduction

Three mechanisms have been proposed (1) for the diffusion of a component of a gas mixture which permeates a porous medium: free-gas diffusion, Knudsen diffusion, and surface diffusion. The mechanism at any point in a porous medium depends on the ratio of the mean free path of the gas to the pore dimensions, the neighboring pore structure, and the nature of the gas–solid interactions. Since porous media may contain a wide range of pore sizes, all three types of diffusion could operate simultaneously within the one specimen.

Experimentally, it has not been possible to separate the total diffusion flux into components arising from different diffusion mechanisms, so diffusion rates have been described by an overall effective diffusion coefficient D_{eff}. Many workers have attempted to relate measured values of D_{eff} of free-gas diffusion coefficients by combination of a simple pore structure model with an analytical expression defining the relation between the different diffusion mechanisms. Unfortunately, some authors have not appreciated fully the difference between a diffusion coefficient referred to the apparatus-fixed reference frame and one referred to a different frame of reference, *e.g.* a center-of-mass reference frame. As a result, (*i*) the reference frame cannot be properly defined in some experimental systems, (*ii*) diffusion coefficients measured with respect to the apparatus-fixed frame cannot be compared with those referred to other reference frames because the data necessary to transform

[1]Present address: Division of Chemical Engineering, Commonwealth Scientific and Industrial Research Organization, Melbourne, Australia.

[2]Present address, University of Western Australia, Nedlands, Western Australia.

[3]Present address: Research Department, Dow Chemical of Canada, Ltd., Sarnia, Ontario.

[4]Revision received February 28, 1974.

Can. J. Chem. Downloaded from www.nrcresearchpress.com by 210.87.254.105 on 09/05/12
For personal use only.

Can. J. Chem. Downloaded from www.nrcresearchpress.com by 210.87.254.105 on 09/05/12
For personal use only.

them were not obtained, and (*iii*) methods for developing expressions relating the different diffusion mechanisms have not always been soundly based.

In this paper, diffusion theory is discussed in relation both to the choice of a satisfactory experimental system, and the development of an adequate expression describing the diffusion mechanism. A modified "Ney–Armistead" apparatus which meets the theoretical and experimental requirements, together with an improved method for calculating the diffusion coefficient, is described and compared with previous techniques.

In part II, data obtained with the apparatus are analyzed and are used to formulate a new model for diffusion in porous media.

Theory

Bird and co-workers (2, 3) have discussed consistent definitions of fluxes, driving forces, and diffusion coefficients; we follow his notation. The diffusion coefficient $\mathfrak{D}_{AB}$ is referred to the mean molar velocity, while the diffusion coefficient $\mathfrak{D}_{AB}^{f}$ is referred to an apparatus-fixed reference frame. We note that $\mathfrak{D}_{AB}^{f} \neq \mathfrak{D}_{BA}^{f} \neq \mathfrak{D}_{AB}$ except in the special case of the coincidence of molar and apparatus-fixed references frames when these three diffusion coefficients are equal.

Knudsen diffusion of a single gas species in a capillary has been considered variously as the limit of self diffusion (4) or slip slow (5, 6). We consider it to be the limit of self diffusion. The Knudsen diffusion coefficient D is referred to a fixed reference frame. As the Knudsen number N_{ku} (defined as ratio of gaseous mean free path λ to the capillary diameter d) tends to infinity, a limiting value D_k is reached (7, 8).

For self diffusion, the molar and fixed reference frames coincide, and Pollard and Present (9) showed that D_A tends to the limit D_{kA} at low pressure and to $\mathfrak{D}_{AA}$, the self diffusion coefficient at high pressure. Pollard and Present used mean free path methods, but stated that the same result would follow from the Chapman–Enskog theory (10). However, D_{kA} cannot be regarded physically as a limiting case of $\mathfrak{D}_{AA}$ because D_{kA} is a function of gas–wall collisions only, whereas $\mathfrak{D}_{AA}$ is a function of gas–gas collisions only.

Using the "Random Walk Theory" Bosanquet (11)[5] showed that

$$[1] \qquad D = \bar{v}d/3(1 + d/\lambda)$$

where $\bar{v}$ is the mean thermal velocity of a gas molecule. An alternate form of [1] is

$$[2] \qquad 1/D = 1/D_{kA} + 1/\mathfrak{D}_{AA}$$

The derivation of [1] assumes that gas molecules are diffusely reflected from the surface and that the capillary is long, straight, and circular. The effects of specular reflection and capillary shape and length have been discussed in detail (12).

Wheeler (13) suggested the semi-empirical formulae

$$[3] \qquad D = \bar{v}\lambda[1 - \exp(-d/\lambda)/3]$$

and

$$[4] \qquad D = \mathfrak{D}_{AA}[1 - \exp(-D_k/\mathfrak{D}_{AA})]$$

as alternatives to [1] and [2]. We compare these equations by plotting $d\bar{v}/D$ (Fig. 1) against $1/N_{ku}$ and note that (*i*) if Bosanquet's formula is correct, D_k may be estimated by the extrapolation of high pressure values of D to zero pressure, thus enabling correct values of $\mathfrak{D}_{AA}$ to be determined, but (*ii*) if Wheeler's formula is correct, high pressure values of D are equal to $\mathfrak{D}_{AA}$ and D_k cannot be determined from them with any precision because D_k is the point of inflection on a curve that tends to zero on a $1/D$ plot against pressure. Visner (14) measured self diffusion and flow in capillaries of various lengths at low pressures, but insufficient low pressure diffusion data suitable for testing [1]–[4] are available.

In order to provide a theoretical background for measurements of diffusion in porous media, some authors (15) have assumed that a simple

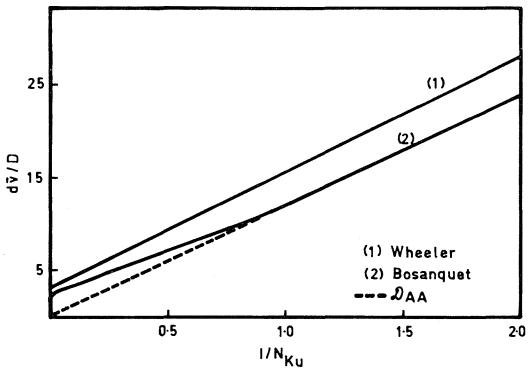

FIG. 1. A comparison of diffusion models.

[5]Cited in ref. 9.

Can. J. Chem. Downloaded from www.nrcresearchpress.com by 210.87.254.105 on 09/05/12
For personal use only.

relation between $\mathfrak{D}_{AB}$ (as distinct from $\mathfrak{D}_{AA}$) and D_{kA} can be derived from the kinetic theory, but no such relation can exist because $\mathfrak{D}_{AB}$ is defined for the molar and D_{kA} the fixed reference frame, and because $\mathfrak{D}_{AB}$ depends only on collisions between molecules of A and B, whereas D_{kA} depends only on collisions between A and a pore wall. Nevertheless, it is true that $\mathfrak{D}_{AB}$, D_{kA}, and D_{kB} do characterize the system in that they collectively account for all intermolecular collisions, hence the overall flux of A, for example, can be described in terms of $\mathfrak{D}_{AB}$ and D_{kA}, but the only type of relation possible between them is an empirical one based on experiment.

One can define an overall coefficient

$$[5] \qquad D_0 = g(\mathfrak{D}_{AB}, D_{kA})$$

referred to the molar reference frame. The form of g may depend not only on the variables that affect $\mathfrak{D}_{AB}$ and D_{kA} individually, but also on the arrangement of a particular experiment (*e.g.* on whether the measurements are transient or steady-state, and on the geometry of the diffusing system).

Scott and Dullien (15) obtained an expression for D_0. They neglected reference frame difficulties and assumed that bulk and Knudsen diffusion resistances acted in series. For a differential change in x_A their expression becomes

$$[6] \qquad D_0 = g(\mathfrak{D}_{AB}, D_{kA}) = 1/[1/\mathfrak{D}_{AB} - 1/D_{kA}(1 - \beta x_A)]$$

where

$$[7] \qquad \beta = 1 + N_B/N_A$$

In fact, [6] and the related integrated expressions (16) arise directly from the correct definition of the diffusion coefficients and the assumption of additive resistances. Nevertheless, [6] is a valid empirical explicit expression for D_0.

We follow prior practice (1, 17) in defining an effective diffusion coefficient D_{eff} referred to the molar frame. When the diffusion flux is measured with respect to a fixed reference frame, as in Knudsen diffusion, the effective diffusion coefficient is D_{eff}^{f}. We emphasize that D_{eff}^{f} must be clearly distinguished from D_{eff}.

Application of Theory to Choice of Experimental System

Dye and Dallevalle (18) used essentially a two-bulb experimental system to measure the interdiffusion of N_2 and CO_2 through cylinders of compressed potassium perchlorate. They calculated D_{eff} from Fick's second law, which is only valid for equimolar counter-diffusion. If equimolar counter-diffusion does not occur, a pressure gradient is quickly set up in opposition to the excess diffusive flow. Pressure gradients have been detected in the usual two-bulb free-gas diffusion experiment (19) but, in the absence of resistance to viscous flow, equimolar counter-diffusion can be safely assumed. The same cannot be said of porous media. Hoogschagen (1) and others (16) observed pressure gradients in transient-state diffusion measurements, and we have detected pressure fluctuations whilst attempting to measure the counter-diffusion rates of CO_2 and N_2 in graphite (12). Dye and Dallevalle (18) did not monitor pressure changes across their specimens, so their values of D_{eff} cannot be accepted with any confidence.

Most other workers have used the steady-state system in which two gas streams flow past opposite faces of a porous sample. Wicke and Kallenbach (20), Weisz (21), and Walker *et al.* (22, 23) measured the concentration change in only one stream and calculated a diffusion coefficient using Fick's first law. However, as later authors have pointed out (17, 24, 25) equimolar counter-diffusion does not occur in steady-state experiments thus, the diffusion coefficient measured was D_{eff}^{f}, not D_{eff}. For this reason their results cannot be compared with later experimental work, nor can they be used immediately in developing diffusion theory for porous media. Some later authors measured the concentration changes in both streams and obtained D_{eff}; their results are discussed in part II.

The steady state method has the advantage of mathematical simplicity but has several serious disadvantages; (*i*) concentration changes are small, therefore analyses must be very accurate in order to minimize errors in calculating D_{eff}, (*ii*) a zero pressure differential across the specimen is difficult to achieve at low pressures, and (*iii*) large quantities of gas are required.

We used the two-bulb method and measured the diffusion of an isotopic trace of one component of a binary gas mixture saturating a porous medium. Thus the molar and fixed reference frames coincide so $D_{eff}^{f} = D_{eff}$; the diffusion approximates equimolar counter-dif-

Can. J. Chem. Downloaded from www.nrcresearchpress.com by 210.87.254.105 on 09/05/12
For personal use only.

fusion so Fick's second law applies, and no correction for composition dependence of D_{eff} is needed in any experiment.

Apparatus and Method

The experiments were performed in a modified Ney and Armistead (26) cell adapted for continuous counting of a radioactive diffusing gas by a Geiger–Muller tube. The apparatus was constructed of glass and evacuated by a three-stage mercury diffusion pump. Most of the components and techniques used were standard for high-vacuum and gas-handling work.

The Diffusion Cell

The cell consisted of two 70 ml compartments, connected by a 15 or 20 mm bore stopcock (Fig. 2); water from a thermostat was circulated through the compartment jackets. Geiger–Muller counters were sealed with epoxy resin to flanges on the ends of the cell. For the measurement of bulk gas diffusion coefficients a length of precision bore capillary tube was sealed into the central stopcock with epoxy resin. For measurements of gas diffusion through graphite, a graphite rod was coated circumferentially with epoxy resin, turned on a lathe to the required diameter and cut into discs. A disc was sealed into an aluminum foil cylinder with epoxy resin and the cylinder was sealed into the bore of the central stopcock. The mounting procedure enabled a graphite disc to be changed without damage to the cell. The cell compartment volumes were equalized by placing a short length of glass rod in one of them.

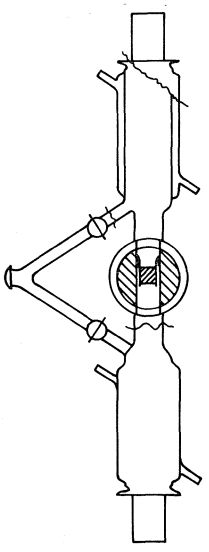

FIG. 2. Diffusion cell partly sectioned to show the water jacket and mounted specimen.

The Counting and Recording System

End window G–M counters (G.E.C. type GM4/LB) with aluminum windows (7 mg/cm^2) were connected to EKCO ratemeters (type N522C) by coaxial cable. As several diffusion cells were used, but only two ratemeters were available, selector switches enabled each ratemeter to be connected to any G–M counter. The output from the two ratemeters was fed to either a Leeds and Northrup Speedomax or a Honeywell–Brown Electronik strip-chart potentiometric recorder. Each ratemeter plus recorder was calibrated against a pulse generator. A linear relationship between input in counts per second and the recorder chart reading was established, thus $n' = CR - G$, where n' is the true count, R the recorder reading, and C and G are constant.

When counting the activity of an isotope, the normal correction for counter dead time and, where appropriate, (*e.g.* with xenon-133), the usual correction for half life, were made. The formula for true count then became

$$[8] \qquad n = \frac{(CR + G)\exp(Ft)}{(1 - \tau(CR - G)) - P}$$

where τ is the dead time of the counter, F the half life correction factor, t the time from the start of the diffusion experiment, and P the background count.

Experimental Procedure

The central stopcock and one cell compartment were filled with the chosen gas mixture at a definite pressure. The other cell compartment was filled to the same pressure with a similar mixture containing a trace of a radioisotope of one component. An experiment was commenced by opening the central stopcock. The recorder trace obtained from an experiment was a curve, asymptotically approaching 90–100% of full scale. The trace showed clearly the normal statistical fluctuations in counting rate which appeared as "noise". The observed counts were obtained from this trace at different times throughout the diffusion process by drawing the best line, by eye, through the "noise".

Can. J. Chem. Downloaded from www.nrcresearchpress.com by 210.87.254.105 on 09/05/12
For personal use only.

Calculation of Diffusion Coefficient

Barnes (27) and Dye and Dallevalle (18) have solved Fick's second law for the two-bulb diffusion cell with equal bulb volumes. Their expression for the instantaneous concentration in one bulb is an exponential series. For values of the various parameters in our experiments, all exponential terms but the first became negligible before 3% of the total time has elapsed. The exact expression reduces to

$$[9] \quad C_i(t) = [C_2(0)/2][1 - \nu/2 + (-1)^i \times (1 - \nu/6) \exp(-2\nu Dt(1 - \nu/6)/L^2)] \qquad i = 1, 2$$

where L is the length of the diffusion path joining the two cell compartments and ν is the ratio of the diffusion path volume to the cell compartment volume. Equation 9 is of the form

$$[10] \quad C_i(t) = A + (-1)^i B \exp(-\alpha t) \qquad i = 1, 2$$

where α is a combination of the diffusion coefficient and a cell geometry factor. The exact solution shows that $A < B$ because ν is always positive. Thus, if the reduced solution is used, $C(t)$ is negative at $t = 0$, a physical impossibility. The effect of the extra exponential terms in the full solution is to bend the curve defined by the reduced solution at small values of t so that it passes through the concentration–time origin.

Ney and Armistead (26) derived the approximate solution by assuming that (*i*) the concentration gradient in the capillary is linear, *i.e.* a quasi-steady state exists, and (*ii*) the volume of the capillary is negligible compared with the volume of the bulbs. This solution gives an equation similar in form to [10] but with the restriction $A = B$, *i.e.* the curve for $i = 1$ passes through the origin. The constants A, B, and α differ slightly from those in the reduced solution, but, if the second approximation is good, this difference is negligible.

$$[11] \quad C_i(t) = [C_2(0)/2] \times [1 + (-1)^i \exp(-2\,Dt/L^2)] \qquad i = 1, 2$$

Ney and Armistead also gave an expression for the end correction on a capillary. Such a correction is meaningless for a porous medium, but we have used it in bulk diffusion work (28, 29).

Calculation of α

To use [10] to find α, and hence D, the constants A and B must be eliminated or separately determined. Most workers calculated $A = C(\infty)$ from the initial concentrations and cell dimensions, then plotted $\ln C(\infty) - C_i(t)$ against time and fitted the best straight line to the data. The slope of this line gives α and the intercept B. Where the least squares line has not been fitted it has sometimes been assumed (30) that the curve passes through the origin. It is clear from the exact solution that the origin and very early points in a run should not be used to fit [10] to experimental data. If three experimental points are chosen at time t_1, t_2, and t_3 where $t_2 = t_1 + \theta$ and $t_3 = t_1 + 2\theta$ then an initial estimate of α is given by

$$[12] \quad \alpha = \ln[(C_2 - C_1)/(C_3 - C_2)]/\theta$$

Between 60 and 90 points were read at equal time intervals from the chart record of each run. Values of α were calculated from [12] for each set of three points and their mean taken as a preliminary estimate of α. We then used the iterative multiple regression procedure developed by Williams (32) to calculate the best values of the coefficients defined by [10] and to estimate their standard errors.

All the calculations were carried out on an I.B.M. 1620 computer. The variance ratio and standard errors in the regression coefficients for all experiments were of the same order of magnitude. Typical values obtained in one experiment are shown in Table 1. Standard errors in the regression coefficients, and the fact that B_2 accounted for a negligible amount of the variability indicated that, for all the runs, the fitted curves represented the experimental data to a high degree of accuracy. In Fig. 3, the fitted curve described by the coefficients in Table 1 is plotted through the data points.

Discussion

Most transient-state gaseous diffusion experiments, whether in the bulk-phase or in porous media, have been performed in cells similar in principle to the two-bulb capillary tube cell described by Ney and Armistead (26). In every two-compartment diffusion cell the mechanism for isolating one compartment from the other must be so constructed that the action of connecting the compartments sets up readily defined boundary conditions.

TABLE 1. Statistical analysis of data plotted in Fig. 3

Regression coefficient		
Parameter	Value	Standard error
B_1*	-330.20	0.277
B_2	6.14×10^{-4}	9.18×10^{-2}
C	6.267×10^{-2}	2.78×10^{-4}
A	329.94	

*The omission of B_2 did not change B_1; A became 329.95.

Analysis of variance				
	d.f.	s.s.	m.s.	v.r.
Regression	2	2.019×10^{5}	1.0099×10^{5}	7.8252×10^{5}
Deviation	75	9.6800	1.2906×10^{-1}	
Total	77	2.020×10^{5}		

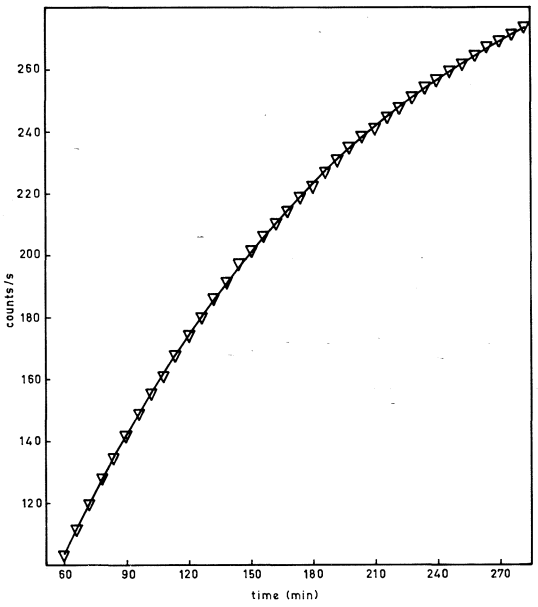

FIG. 3. Experimental points and fitted curve for diffusion of krypton-85 through a mixture of 25% krypton and 75% xenon in a porous graphite at a pressure of 156.3 mm Hg.

However, the action of opening a stopcock, or withdrawing a partition, will introduce a perturbation into a system so that the physical boundary conditions produced may not correspond with the mathematical boundary conditions of the equation used to calculate diffusion coefficients. Our method of calculation eliminates the effect of any discrepancy between physical and mathematical boundary conditions because neither the initial activity nor the first 5–10% of the recorded data were used.

The cells had lengths of capillary or different size graphite for the diffusion paths. Analysis of many results on diffusion both in porous graphite (28) and in bulk gas (29) showed that a significant difference exists between diffusion coefficients measured in different cells. This difference may arise through a difference in cell geometry affecting the diffusion coefficient or, in the case of the capillary tube, the end correction factor being incorrect. More recent work indicates that the effect is due to differences in cell geometry (33). The existence of this difference implies that all measurements of bulk gas diffusion by the two-bulb technique may contain systematic errors up to 2%. Further, any standard error in D estimated from experiments replicated in only one cell would not include errors in the measured cell constant. Unless measurements are made in more than one cell, no estimate of a "cell effect" can be made. The "cell effect" measured in the graphite studies is discussed in detail in part II.

Limitation of the Method

The need to use G–M tubes with thick windows to withstand repeated cell evacuations limits the range of isotopes that can be used with our apparatus. The tubes were entirely satisfactory with the medium to high energy β-radiation of krypton-85 and xenon-133 but would not be suitable for use with carbon-14 labelled gases such as CO_2 or CH_4.

Can. J. Chem. Downloaded from www.nrcresearchpress.com by 210.87.254.105 on 09/05/12
For personal use only.

Can. J. Chem. Downloaded from www.nrcresearchpress.com by 210.87.254.105 on 09/05/12
For personal use only.

Comparison of Methods of Calculation

As shown earlier, the concentration changes in both cell compartments can be described by a simple negative exponential function [10] which may be fitted to the experimental data by least squares procedure provided either A or α can be estimated independently. Previous authors have found A either by direct measurement or by calculation from the cell geometry and the measured initial concentration. In the latter case, the detector on the "active" compartment must be calibrated against the one on the initially inactive compartment. G–M counters age at a variable rate, and ordinarily calibrations would be necessary prior to every run. Our numerical method of curve-fitting eliminates the need for such calibrations and gives a more precise regression than a least squares method using a value of A calculated from the initial conditions.

The most consistent values of α were obtained when $C(t_{max})/C(\infty)$ exceeded 80%. Since some workers using the Ney and Armistead technique followed the course of a run to less than 60% completion (*e.g.* Srivastava and Srivastava (31), values of α quoted by them could be in error, particularly where the line, from which α was calculated, was established with only five or six data points.

The difference of the two equations [11] is

$$[13] \qquad C_2(t) - C_1(t) = 2Be^{-\alpha t}$$

Several authors (34–36) have measured concentration changes in both cell compartments and used [13] to calculate α by a graphical method. This eliminates A but does not necessarily increase accuracy because concentration–time plots must be prepared for both compartments to find corresponding values of C_1 and C_2.

Refinement of our present technique could be made by using scintillation counting with the scintillation phosphor cemented to the diffusion cell in place of the G–M counter. This would eliminate any error from flexing of the counter window with changes in cell gas pressure, and allow the use of gas labelled with low activity emitters such as carbon-14. The most important advantage to be gained, with scintillation counting, that addition of a multi-channel pulse height analyzer would allow the simultaneous diffusion of several gases in a multi-component mixture to be followed.

A further refinement would be to use a scalar equipped with automatic print-out of the total count at predetermined intervals instead of a ratemeter. A sequence of numbers, each being a measure of the area under the exponential concentration time curve would be obtained; this would require modification of our computation method to calculate α from areas under, instead of points on, the curve. This would improve accuracy in two ways, first, the accuracy of a scalar is, in general, higher than that of a ratemeter; second, the errors in reading recorder charts would be eliminated.

We are indebted to the Australian Atomic Energy Commission for the award of a research scholarship to one of us (K.R.W.), and to Mr. W. S. Boundy of the South Australian Institute of Technology for valuable discussions on some theoretical aspects of diffusion in gases.

1. J. Hoogschagen. Ind. Eng. Chem. **47**, 906 (1955).
2. R. B. Bird. Adv. Chem. Eng. **1**, 156 (1956).
3. R. B. Bird, W. E. Stewart, and E. N. Lightfoot. Transport phenomena. Wiley, New York. 1960.
4. L. O. Rutz and K. Kammermeyer. Flow through micro-porous media – theory of flow phenomena. U.S.A.E.C. Report AECU–3921. 1958.
5. D. P. Timofeev. Russ. Chem. Rev. (Engl. Transl.) **29**, 180 (1960).
6. P. C. Carman. Flow of gases through porous media. Butterworths, London. 1956.
7. M. Knudsen. Ann. Phys. **28**, 75 (1909).
8. B. Von Smoluchowski. Ann. Phys. **33**, 1559 (1910).
9. W. G. Pollard and R. D. Present. Phys. Rev. **73**, 762 (1948).
10. S. Chapman and T. G. Cowling. Mathematical theory of non-uniform gases. Cambridge University Press, Cambridge. 1939.
11. C. H. Bosanquet. British TA Report BR-507. 1944.
12. K. R. Weller. Ph.D. Thesis, University of Adelaide, Adelaide, Australia. 1963.
13. A. Wheeler. Adv. Cata. **3**, 249 (1951).
14. S. Visner. Gaseous self diffusion and flow in capillaries at low pressure. U.S.A.E.C. Report K-688. 1951.
15. D. S. Scott and F. A. L. Dullien. Am. Inst. Chem. Eng. J. **8**, 113 (1962).
16. H. A. Kramers and J. Kistemaker. Physica, **10**, 699 (1943).
17. R. B. Evans III, G. M. Watson, and E. A. Mason, J. Chem. Phys. **35**, 2076 (1961).
18. R. F. Dye and J. M. Dallevalle. Ind. Eng. Chem. **50**, 1195 (1958).
19. K. P. McCarthy and E. A. Mason. Phys. Fluids, **3**, 908 (1960).
20. E. Wicke and R. Kallenbach. Kolloid Z. **97**, 135 (1941).
21. P. B. Weisz. Z. Phys. Chem. **11**, 1 (1957).
22. P. L. Walker Jr., F. Rusinko Jr., and E. Raats. Nature, **176**, 1167 (1955).
23. P. L. Walker Jr. and F. Rusinko Jr. J. Phys. Chem. **59**, 241 (1955).

24. D. S. Scott and K. E. Cox. J. Chim. Phys. **57**, 1010 (1960).
25. J. Beek. I. and E. C. Proc. Des. Dev. **1**, 45 (1962).
26. E. P. Ney and F. C. Armistead. Phys. Rev. **71**, 14 (1947).
27. C. Barnes. J. Appl. Phys. **5**, 4 (1934).
28. K. R. Weller, N. S. Stenhouse, and H. Watts. Can. J. Chem. This issue.
29. H. Watts. Trans. Faraday Soc. **60**, 1745 (1964).
30. H. Watts. Can. J. Chem. **43**, 431 (1965).
31. B. N. Srivastava and I. B. Srivastava. J. Chem. Phys. **36**, 2616 (1967).
32. E. J. Williams. Regression analysis. Wiley, New York. 1969. p. 61.
33. H. Watts. Can. J. Chem. **49**, 67 (1971).
34. J. O. Fleming, J. W. Johnson, and H. V. Grubb. Chem. Eng. Prog. **56** (No. 3), 69 (1960).
35. F. Hutchinson. Phys. Rev. **72**, 1256 (1947).
36. C. H. Chou and J. J. Martin. Ind. Eng. Chem. **49**, 758 (1957).

Can. J. Chem. Downloaded from www.nrcresearchpress.com by 210.87.254.105 on 09/05/12
For personal use only.

Diffusion of Gases in Porous Solids. II. Diffusion of an Isotope Trace through Binary Gaseous Mixtures in a Porous Graphite

K. R. WELLER[1]

Department of Chemical Engineering, University of Adelaide, Adelaide, Australia

N. S. STENHOUSE[2]

Division of Mathematical Statistics, Commonwealth Scientific and Industrial Research Organization, Adelaide, Australia

AND

HARRY WATTS[3]

Department of Chemical Technology, South Australian Institute of Technology, Adelaide, Australia

Received April 4, 1972[4]

K. R. WELLER, N. S. STENHOUSE, and HARRY WATTS. Can. J. Chem. **52**, 2692 (1974).

Diffusion coefficients of krypton-85 and xenon-133 through binary mixtures with He, Ne, Ar, Kr, and Xe permeating a porous graphite were measured. The statistical experimental design employing six 5 × 5 Latin squares permitted determination of the effects of gas type, mixture composition, and gas pressure. Five different cells were used and cell effects also determined. A regression equation which adequately correlated the experimental data was derived. This equation also correlated some literature data with better precision than did other model diffusion equations.

K. R. WELLER, N. S. STENHOUSE et HARRY WATTS. Can. J. Chem. **52**, 2692 (1974).

On a mesuré les coefficients de diffusion à travers le graphite poreux, du krypton-85 et du xénon-133 sous forme de mélanges binaires avec du He, Ne, Ar, Kr et Xe. Le dessin expérimental statistique permet, en utilisant six carrés latin 5 × 5, la détermination des effets dûs au genre de gaz, à la composition du mélange et à la pression du gaz. On a utilisé cinq différentes cellules et on a établi leurs effets. On en dérive une équation regressive; elle correspond adéquatement aux données expérimentales. Cette équation correspond aussi à certaines données de la littérature avec une meilleure précision que d'autres équations de modèle de diffusion.

[Traduit par le journal]

In Part I, attention was drawn to deficiencies in diffusion theory as it has been applied to binary diffusion through porous media and to the limitations of the experimental methods described in the literature (1). Most previous workers measured the effective diffusion coefficient, D_{eff} by a steady-state method similar to that of Wicke and Kallenbach (2). They interpreted their results in terms of a simple pore model and a diffusion model developed in full by Scott and Dullien (3), and Evans, *et al.* (4). Their work has been reviewed by Gunn and King (5) and Henry *et al.* (6) who quote various forms of the equations. We note in particular that the ratio of the observed diffusion fluxes in the steady-state system has been theoretically to be

$$[1] \qquad N_A/N_B = (M_B/M_A)^{1/2}$$

(where M is the molecular weight and the subscripts A and B refer to two gaseous species) and that this relationship holds experimentally (7) from the Knudsen to the normal diffusion region in all porous materials tested to date, provided non-adsorbable gases are used. In the extreme limit of Knudsen diffusion, the kinetic theory predicts that the Knudsen diffusion coefficients D_{kA}, D_{kB} are given by

$$[2] \qquad (M_B/M_A)^{1/2} = D_{kA}/D_{kB}$$

Clausing (8) and DeMarcus and Lang (9) have shown theoretically that the effects of capillary shape and length are independent of the gas used, thus [2] should hold for a given capillary of any

[1]Present address: Division of Chemical Engineering, Commonwealth Scientific and Industrial Research Organization, Melbourne, Australia.

[2]Present address: University of Western Australia, Nedlands, Western Australia.

[3]Present address: Research Department, Dow Chemical of Canada Ltd., Sarnia, Ontario.

[4]Revision received March 18, 1974.

Can. J. Chem. Downloaded from www.nrcresearchpress.com by 210.87.254.6 on 09/05/12
For personal use only.

Can. J. Chem. Downloaded from www.nrcresearchpress.com by 210.87.254.6 on 09/05/12
For personal use only.

shape or length and in particular for a porous material. In fact [2] has been found to hold by extrapolating permeability data for non-adsorbed gases to zero pressure (7), but for adsorbed gases, valued of D_{kB} estimated from [2] are lower than experimental ones.

Both Evans *et al.* (4) and Scott and co-worker (3) describe D_{eff} measured at high pressures as $(D_{AB})_{eff}$ and at low pressures as $(D_{kA})_{eff}$ and claim that these measurements completely define the diffusion system (in the absence of surface diffusion) and when taken with $\mathfrak{D}_{AB}$, the binary diffusion coefficient in a bulk gaseous phase characterize the porous medium. Thus

$$[3] \qquad (D_{AB})_{eff}/(\mathfrak{D}_{AB})_{true} = G$$

where G is a property only of the porous medium and is independent of the gas mixture used. However, none of these authors supply any supporting evidence, as they used only one gas mixture per specimen. In the work described below, this limitation was removed by using each gas mixture in all specimens.

Summarizing, three related problems need to be solved for a complete description of the counter-diffusion of a binary mixture through a porous solid: (*1*) the determination of the correct pressure dependence of D_{eff} from very low pressures to pressures high enough for the Knudsen diffusion effect to be negligible, (*2*) the development of a realistic pore model to enable the pressure and gas composition dependence of D_{eff} to be predicted from measurable pore properties and simple gas phase diffusion data, and (*3*) the determination of the effect of adsorption and gas solid interactions, other than diffuse reflections, on the diffusion rate.

Previous workers (3–6, 10) have concentrated on the first two parts of the problem by observing the counter diffusion of a pair of essentially non-adsorbable gases such as He, N_2, Ar, and O_2. We attempted to solve the first part of the problem only. Our approach has been to examine how the measured effective diffusion coefficient varies with pressure and gas composition, to develop a model based on a statistical analysis of the observed variations, to test this model with published data and compare it with models developed by previous workers. No attempt is made to develop a pore structure model.

It is known that the equation

$$[4] \qquad 1/\mathfrak{D}_{A^*M} = x_A/\mathfrak{D}_{AA^*} + x_B/\mathfrak{D}_{BA^*}$$

where the subscript A* refers to a radioisotope of A, gives the effective diffusion coefficient D_{A^*M} of a trace of isotope through a binary mixture in the bulk gaseous phase (11–14), except when xenon-133 is the diffusing isotope (15). It might then be expected that an equation of the form

$$[5] \qquad D_{eff} = g_1(\mathfrak{D}_{AA^*}, \mathfrak{D}_{A^*B}, D_{kA}, x_A, Q, \phi)$$

would give the effective diffusion coefficient for a trace of isotope through a binary mixture in a porous solid. In this equation Q is a function of the pore geometry, ϕ is a term to account for gas–solid interactions, and x is a mole fraction. The immediate aim of the experimental work was to deduce an explicit function for D_{eff} of the form

$$[6] \qquad D_{eff} = g_2(p, M_A, M_B, x_A, Q)$$

where p is the pressure, which then might be used to examine the form of [5].

Experimental

The diffusion cell, its operation and the method of calculation of the results are described (1) in Part I. Five such cells, each equipped with a separate manometer, were attached to the high vacuum gas-handling apparatus enabling five runs using the one gas mixture to be set up at the one time.

The 150 runs comprising the set of measurements reported in this paper were arranged in six 5 × 5 latin squares (16) with the standard pressures, inactive gases, and cells forming the columns, rows, and treatments respectively. The six squares were replicates in pressures, inactive gases, and cell arrangements, but for three squares the active species was krypton-85 and in the remainder it was xenon-133. Also for each active gas, the proportion of inactive species differed between squares as shown in Tables 1 and 2, where the numbers in the squares in Table 1 refer to the cells.[5] Two sets of counting and recording equipment were used; all numbers italicized in Table 1 being run with the one set. This experimental design enabled the total variability within the set to be partitioned into portions ascribable to each of the controlled variates, namely pressure, cells, active gases, inactive gases, gas composition, and instrument sets.

Results

The results given in Table 2 are the quantity α, the quotient of the effective diffusion coefficient and the cell constant F. Values of F are tabulated[5] in Appendix A. The values of α in Table 2 are displayed so as to show the arrangement of the

[5]Tables 1, 4, 5, and 6, Figs. 2, 6, and 12, and Appendices A and B, are available, at a nominal charge, from the Depository of Unpublished Data, National Science Library, National Research Council of Canada, Ottawa, Canada K1A 0S2.

Can. J. Chem. Downloaded from www.nrcresearchpress.com by 210.87.254.6 on 09/05/12
For personal use only.

TABLE 2. Experimental values of α

Active gas	Inactive gas	Series 1* at mean pressure (mm Hg) =					Series 2† at mean pressure (mm Hg) =					Series 3‡ at mean pressure (mm Hg) =				
		0.0	25.0	62.5	156.3	390.6	10.0	25.0	62.5	156.3	390.6	10.0	25.0	62.5	156.3	390.6
Kr	Kr	0.1392	*0.1262*	0.1081	*0.0628*	0.0517	0.1262	*0.1143*	0.0955	*0.0634*	0.0333	0.1536	*0.1139*	0.1057	*0.0602*	0.0378
	Xe	*0.0905*	0.1275	0.1134	*0.0692*	0.0312	*0.0917*	0.1178	0.0999	*0.0787*	*0.0432*	*0.0795*	0.1175	0.1044	*0.0627*	*0.0340*
	A	*0.1386*	0.1214	0.0947	0.0577	*0.0546*	*0.1306*	0.1237	0.0892	0.0608	*0.0513*	*0.1349*	0.1241	0.0953	0.0496	*0.0636*
	Ne	0.1202	*0.0843*	*0.1027*	0.0950	*0.0746*	0.1227	*0.1232*	*0.1124*	0.0699	*0.0569*	0.1125	*0.0832*	*0.1347*	0.0898	*0.0633*
	He	0.1262	*0.1011*	*0.0904*	*0.0848*	0.0622	0.1374	*0.1013*	*0.0598*	*0.0847*	0.0736	0.1347	*0.1091*	*0.0721*	*0.0966*	0.0836
Xe	Kr	*0.1002*	0.0951	*0.0763*	0.0531	*0.0365*	*0.1136*	0.0856	*0.0809*	0.0490	*0.0370*	*0.1276*	0.1076	*0.0898*	0.0549	*0.0119**
	Xe	0.0813	*0.0963*	*0.0326*	0.0496	0.0352	0.0706	*0.1052*	*0.0805*	0.0552	0.0327	0.0713	*0.1124*	*0.0784*	0.0585	0.0340
	Ar	0.1147	*0.0997*	*0.0753*	*0.0523*	0.0386	0.1233	*0.0889*	*0.0854*	*0.0426*	0.0463	0.1207	*0.1062*	*0.0758*	*0.0453*	0.0569
	Ne	*0.0961*	0.1060	0.0942	*0.0716*	0.0485	*0.0962*	0.0693	0.0870	*0.0664*	0.0388	*0.1030*	0.0742	0.1008	*0.0841*	0.0606
	He	*0.1097*	0.0897	0.0660	0.0787	*0.0504*	*0.1121*	0.0988	0.0608	0.0675	*0.0408*	*0.1225*	0.0948	0.0587	0.0863	*0.0680*

*Active gas/inactive gas = 50/50.
†Active gas/inactive gas = 72/25.
‡Active gas/inactive gas = 25/75.

TABLE 3. Symbols for the controlled variates

Controlled variate	Symbol	Levels of variate
Pressure	$P_i(i = 1, 2, ..., 5)$	10, 25, 62.5, 156.3, 390.6 mm Hg
Cell	$c_j(j = 1, 2, ..., 5)$	See Appendix A for geometry of cells.
Active gas	$a_h(h = 1, 2)$	Kr, Xe
Inactive gas	$g_k(k = 1, 2, ..., 5)$	Kr, Xe, Ar, Ne, He
Ratio active/inactive gas (series)	$s_t(t = 1, 2, 3)$	50/50, 75/25, 25/75
Instruments	$I_r(r = 1, 2)$	L and N recorder, H–B recorder

six latin squares. The values italicized were obtained with one set of measuring equipment.

Analysis of Results

An analysis of variance (16) was performed on each latin square L_{ht}, where h and t are defined in table 3. This analysis established the relative significance of the controlled variates. Full details of this analysis are given elsewhere (17). Also, regression analyses (18) were performed using various functional forms of α, in order to linearize the data. We define

$$[7] \qquad \alpha' = \log(100\alpha)$$

and represent α after the removal of cell effects, as described in Appendix B,[5] as α_c. We found that the data could best be linearized by the function

$$[8] \qquad \alpha_c' = A + B\log(p + H)$$

where A, B, and H are constants. The best value of H was 60. Figures 1 and 2 show[5] α_c and α_c' respectively plotted against $\log p$, while Figs. 3–5 show the linearity obtained using [8] for regression of the active gas, inactive gas, and concentration effects. Our analysis gave the model

$$[9] \qquad \alpha' = (\bar{M} + m_{a_h} + m_{g_k} + m_{s_t}) + (B + b_{g_k} + b_{s_t})(\log(p + 60) - P) + e_{hijktr}$$

where

$$[10] \qquad P = \sum_{i=1}^{5} \log(p_i + 60)/5$$

The $\bar{M}$ and B are constants, while the m, b, and p_i depend on the controlled variate, the subscripts having the significance given to them in Table 3. In [9] and [10], the effects were retained only of those variables shown to be significant by the analysis of variance. This analysis of variance is summarized in Table 4.[5] Table 5 gives the numerical values of the terms in [9] and [10].[5] Equation [9], with omission of the error term,

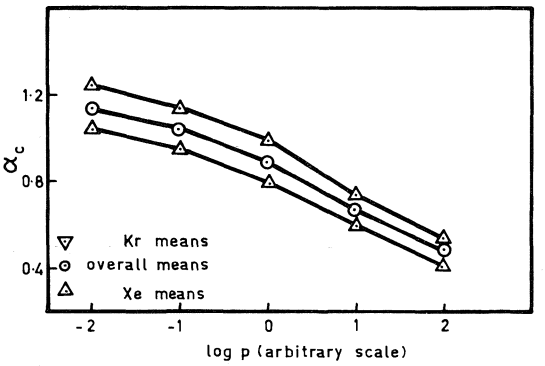

FIG. 1. Plot of α_c against $\log p$ showing mean value for all experiments and the means for experiments with Kr and Xe as diffusing gas separately.

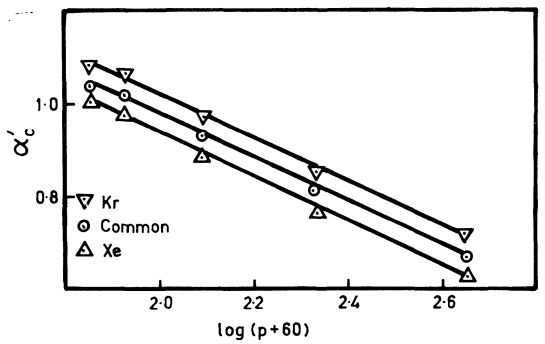

FIG. 3. Plot of α_c' against $\log(p + 60)$ showing the mean value for all experiments and the means for experiments with Kr and Xe separately. The units of p are mm Hg.

Can. J. Chem. Downloaded from www.nrcresearchpress.com by 210.87.254.6 on 09/05/12
For personal use only.

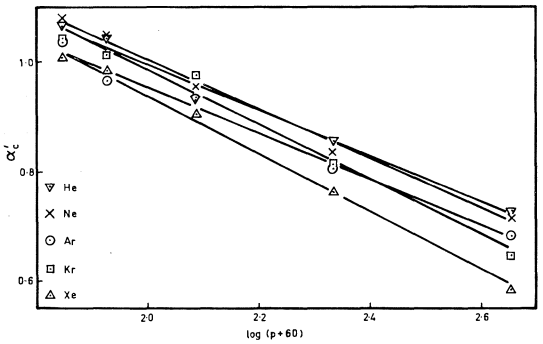

FIG. 4. Plot of α_c' against $\log(p + 60)$ showing g effects. Each line represents all experiments with the same inactive gas. Thus each point is the mean of all experiments in which Kr and Xe diffuse through all mixtures at the same pressure. The units of p are mm Hg.

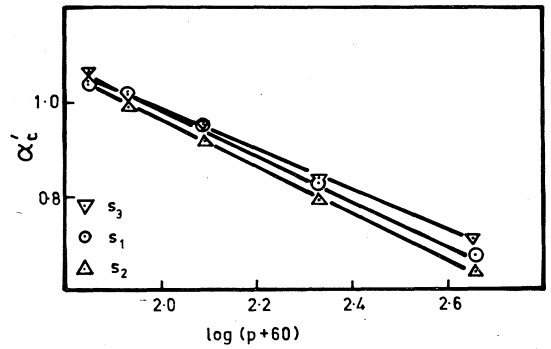

FIG. 5. Plot of α_c' showing series effects. Each point represents the mean of all experiments in which the two gases are present in the same proportion in the mixture. The units of p are mm Hg.

can be used as a prediction equation with a mean square deviation from regression of 0.001759.

Discussion

Comparison of Models

The analysis given above established an equation which adequately correlated the experimental results. Here we discuss the derived regression model [9] and compare it with models suggested by other authors.

The models of Scott and Dullien (3) (S.D.) and Evans *et al.* (4) (E.W.M.) are essentially equivalent. In the present experiments the net diffusion flux is zero, thus any apparent difference between these models is removed. The form of the S.D.–E.W.M. model applicable to our experiments can be derived by specializing the equation for multi-component diffusion (19) for the case where $N_A = -N_{A^*}$, $N_B = 0$, and x_{A^*} is sufficiently small to be neglected in comparison to x_A, and adding a term for Knudsen diffusion, thus

$$[11] \quad N_{A^*} = -(x_A/\mathfrak{D}_{AA^*} + x_B/\mathfrak{D}_{AB} + 1/D_{kA^*})^{-1}\nabla C_A$$

If, following Scott, [3] is assumed to hold for porous media, then

$$[12] \quad G/D_{eff} = (x_A/\mathfrak{D}_{AA^*} + x_B/\mathfrak{D}_{AB} + 1/D_{kA^*})$$

Now D_{kA} is pressure independent and bulk gaseous diffusion coefficients are proportional to $1/p$

$$[13] \quad \mathfrak{D}_{A^*j} = 1/K_{A^*j}p \quad (j = A, B)$$

where K_{AB} is some function of the molecular properties of A and B, so [12] may be put in the form

$$[14] \quad G/D_{eff} = Z(p + H)$$

where

$$[15] \quad Z = x_A K_{AA^*} + (1 - x_A)K_{A^*B}$$

and

$$[16] \quad H = 1/ZD_{kA^*}$$

Using the cell constant F and [7], [14] may be rewritten

$$[17] \quad \alpha' = \log G - \log(100FZ) - \log(p + H)$$

Bearing in mind the physical significance of G and Z, and assuming the properties of A and A* are identical, the log term may be expanded,

$$[18] \quad \alpha' = \text{Constant} + f_1(E,Q,\phi) + f_2(M_A, M_B, \sigma_{AB}, \sigma_{AA}, \varepsilon_{AB}, \varepsilon_{AA}) - \log(p + H)$$

where the σ and ε terms are molecular interaction parameters arising in the Chapman–Enskog kinetic theory, and Q and ϕ have the significance attached to them in [5].

Wheeler's (20) model

$$[19] \quad D_{eff} = \mathfrak{D}_{AA}[1 - \exp(-D_{kA}/\mathfrak{D}_{AA})]$$

similarly transforms to

$$[20] \quad \alpha' = \text{Constant} + f_1(E,Q,\phi) + f_2(M_A, M_B, \sigma_{AB}, \sigma_{AA}, \varepsilon_{AB}, \varepsilon_{AA}) - \log p(1 - \exp(-p/H))$$

The difference between the Wheeler and S.D.–

Can. J. Chem. Downloaded from www.nrcresearchpress.com by 210.87.254.6 on 09/05/12
For personal use only.

Can. J. Chem. Downloaded from www.nrcresearchpress.com by 210.87.254.6 on 09/05/12
For personal use only.

E.W.M. models lies solely in the predicted pressure dependence of α'.

Both the S.D.–E.W.M. model and our regression model are represented by [8], but the S.D.–E.W.M. model predicts that $B = -1$ and is independent of the gases used (strictly, the coefficient of -1 applies only to differential values of D_{eff}, measured at uniform x_a as in our experiments). Previous workers have measured "integral" values of D_{eff} where the appropriate model for the diffusion coefficient must be combined with the correct form of the diffusion equation and integrated). The regression model showed (*i*) the mean value of B for our experiments is -0.47, and (*ii*) B varies from -0.38 when g is He, present as 75% of the mixture, to -0.57 when g is Xe, present as 25% of the mixture. The three models can be expressed in the form

$$[21] \qquad \alpha' = A + Bf(p)$$

In Fig. 7 values of α' calculated from the appropriate function for each model are plotted against $\log(p + 60)$. In each case A in [21] was adjusted to give α' approximately equal to the experimental value of M in [9] at the mean pressure, using $H = 60$ mm Hg. For the regression model B was taken as -0.5, and the plot was limited to the pressure range appropriate to the model. The S.D.–E.W.M. coefficient $B = -1$ does not fit our results well. Wheeler's model gives a nonlinear plot, but if his value of A is adjusted to make his model coincide with the regression model at zero pressure, his model fits our results well up to 100 mm Hg.

The data of Evans *et al.* (21) for the counter diffusion of He and Ar through a fine pored

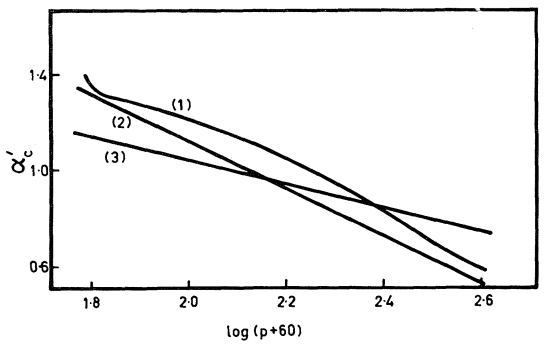

FIG. 7. Plot of α_c' against $\log(p + 60)$, showing a comparison of three different models: (*1*) Wheeler's model; (*2*) S.D.–E.W.M. model; (*3*) regression model. The units of p are mm Hg.

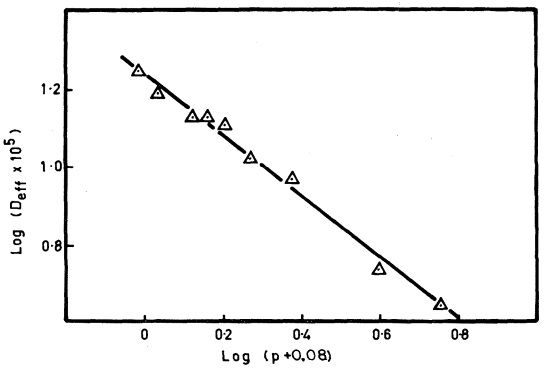

FIG. 8. Data of Evans *et al.* (21). The straight line represents the prediction of the regression model for their data. The units of p are atm.

graphite were treated to yield D_{eff}. Regressions of $\log D_{eff}$ on $\log p$ and $\log(p + H)$ (with $H = 0.08$ atm $= 60$ mm Hg) were fitted to these results. For the regression on $\log p$, $B = -0.77$ and on $\log(p + H)$, $B = -0.79$. The regression on $\log(p + H)$ is plotted, together with the experimental points in Fig. 8. Our model fits their results well.

Scott and Cox (10) measured the counter diffusion of H_2 and N_2 through some catalyst support materials. Unfortunately they plotted D_{eff}^f at low pressures and D_{eff} at high pressures, so there is some doubt as to the actual experimental values. Nevertheless values of B (Table 6)[5] calculated from their Fig. 2 varied from -0.37 for kaolin-2 to -0.90 for celite.

Henry *et al.* (6) measured D_{eff} for the counter-diffusion of He and N_2 through alumina pellets and Vycor glass, and compared their results with the predictions of the S.D.–E.W.M. model and a model proposed by Rothfeld (22). The Rothfeld model combines the S.D.–E.W.M. model with a pore model. Values of D_{eff} predicted from our regression model were compared with predictions of these two other models. A comparison made on the basis of the difference between Henry's experimental values and the predicted values showed that the S.D.–E.W.M. model was badly biased, and even when corrected for bias was still the poorest predictor. There was little difference between the Rothfeld and regression models, but the latter was less biased. As both must be established from diffusion measurements at high and low pressures, our regression model is to be preferred, as it yields equivalent predic-

Can. J. Chem. Downloaded from www.nrcresearchpress.com by 210.87.254.6 on 09/05/12
For personal use only.

tions without the need to incorporate pore size distribution data.

Henry *et al.* (6) plotted the product $D_{eff}p$ against p on a log–log scale, but D_{eff} only decreased eight-fold over a thousand-fold increase in p, so this plot effectively masks the experimental error in D_{eff}. Their data are replotted in Fig. 9 as log $(1000D_{eff})$ against log $(p + 60)$ with the calculated regression lines, and derived values of B are given in Table 6. The experimental scatter is probably no greater than that contained in any one row of five experiments in our experimental plan, but the results in Fig. 9 are to be contrasted with our results in Figs. 3–5 where each point can represent the mean of at least six values of α' in the g regressions and up to 15 values as in the a regressions. The large error reduction achieved by an efficient statistical design is clearly illustrated. Despite the higher error in values of D_{eff} reported by other workers, their results do show that B depends on the pore properties of the solid, a point our results were not designed to show.

Finally, when it is considered that $H = 60$ mm Hg is not necessarily the optimum value for the results of Evans *et al.*, Henry *et al.*, or Scott and co-worker, and that our results show that B depends on the gases used, it can be concluded that all sets of results confirm the form of our regression model, and illustrate its usefulness.

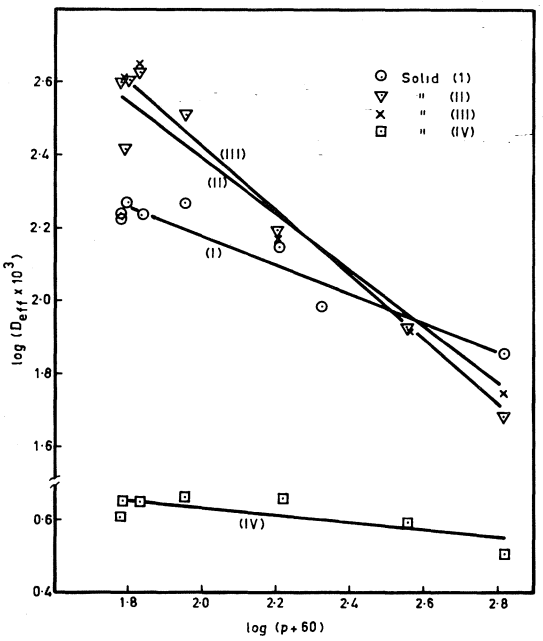

FIG. 9. Data of Henry *et al.* (6) for diffusion through four porous solids. The straight lines represent the predictions of the regression model for their data. The units of p are mm Hg.

The Constant H

For the purpose of the analysis H was regarded merely as a linearizing device. However, the data given in Table 7 show that the ratio H_{Kr}/H_{Xe} approximates to $(M_{Xe}/M_{Kr})^{1/2}$. This should not be taken as establishing a physical relationship because of the high standard error in H. Also, this result does not readily follow from [16] because of the complex nature of Z. Nevertheless the agreement is interesting and merits further investigation.

The Interaction Effects and Means of the Regressions

It was pointed out above that B varied in our experiments, contrasted with the constant value for the S.D.–E.W.M. and Wheeler models. Prior to our experiments no data existed to test this prediction of these last-named models. A plot of the g regression coefficients $B_{g_k}(= B + b_{g_k})$ against log M_k is linear if the value for Kr is neglected (Fig. 10), suggesting that a linear relationship exists. However, the discrepancy with Kr permits no firm conclusion, but it is consistent with the line for Kr being out of sequence in the plots of α_c' against log $(p + 60)$ in Fig. 4. We can offer no explanation of this observation, but the effect invites further investigation.

The g regression lines should all converge to the same value at zero pressure because Knudsen diffusion then occurs and an a molecule does not then collide with any g molecules. The experimental lines do converge at low pressures (Fig. 4), but a lack of a common intercept probably reflects experimental error.

The plot of the g means against log M_B, given in Fig. 11 is of considerable interest. In particular a straight line fits all the points, except the one for He, but the position of the He mean indicates that the true regression on log M_B is curved at the

TABLE 7. Values of H for the a and common regressions

Regression*	H(mm Hg)	Standard error
a_1(Kr)	66.6	25.6
a_2(Xe)	54.0	7.1
Common	60.1	14.2

*$H_{Kr}/H_{Xe} = 1.23$; $(M_{Xe}/M_{Kr})^{1/2} = 1.25$.

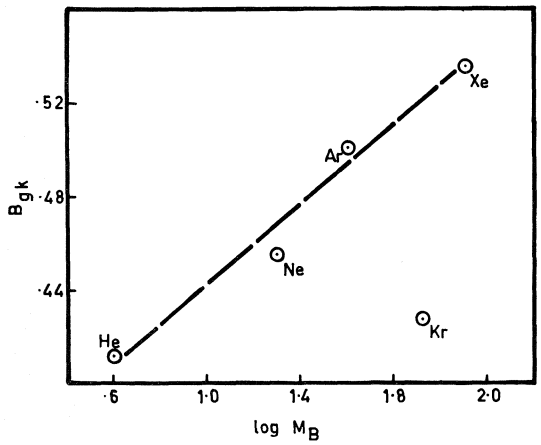

FIG. 10. Plot of the g regression coefficients B_{g_k} against the logarithm of molecular weight of inactive gas.

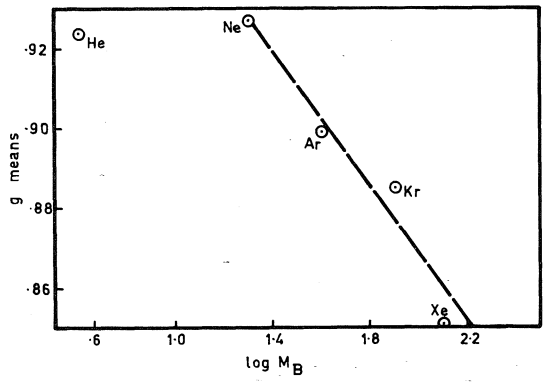

FIG. 11. Plot of g means against the logarithm of molecular weight of the inactive gas.

low molecular weight end. More data are needed before a relation between the g mean and the g molecular weights can be proposed with confidence.

Convergence of the series regressions at low pressure is expected for the same reason as it is expected for the g regressions, and Fig. 5 bears out this expectation. However, insufficient compositions were incorporated in the experimental plan to permit regression of b_{s_t} against mole fraction, but the results do show that α is concentration dependent. Thus one would expect that values of D_{eff} obtained from systems with high concentration gradients would differ from those obtained from systems with low concentration gradients. Nevertheless, the presence of the series term in the regression model means that the model can be used to estimate an "average" D_{eff} for systems in which high concentration gradients are expected, *e.g.* fast gaseous reactions in porous catalysts.

There is no interaction between a and pressure. In particular the expectation that the a regressions would give different intercepts is fulfilled. There are also no significant interactions between the a effects and all the other determining variates. If this result could be shown to be generally true, the prediction of the diffusion rates of other gases would be possible, provided a relation between the a means and a suitable gas property, such as molecular weight, could be established. This result is important since our method for measuring α can only be used with a limited number of suitable radioactive gases.

Cell Effects

The factors likely to contribute to the cell effects may be grouped together as follows: (*1*) the geometry of the diffusion cell, (*2*) the pore structure and surface properties of the specimen, and (*3*) factors associated with the cells such as seals and G–M counters; and the variance due to cell effects may be considered to be made up of parts ascribable to variations in each of these factors.

The normal procedure in experiments such as ours is to use measured cell constants to remove cell effects from the data before analysis. However, if this is done, any errors associated with measured cell constants will be attributed to the data. We therefore performed the analysis without removal of cell effects, and subsequently removed them as outlined[5] in appendix B. The justification of this procedure comes from the following: in Fig. 6 are plotted relative values of cell effects.[5] It is seen that these relative values vary with time, indicating that aging of the cells occurs and at a different rate for each cell. In Fig. 12 is plotted a comparison of α' as measured and as would be calculated from the measured cell constants.[5] This plot only serves as an indication of the contribution of the cell constants to the overall cell effect, because of the variation in cell effect with time (Fig. 6).

Comparison with Diffusion Coefficients in the Bulk Gaseous Phase

A comparison of the present results with our measurements of diffusion coefficients in the bulk gaseous phase of the same systems (14, 15) may be made. If G as defined by [3] is independent of gas type, it follows that

Can. J. Chem. Downloaded from www.nrcresearchpress.com by 210.87.254.6 on 09/05/12
For personal use only.

[22] $$\left(\frac{D_{AC}}{D_{BC}}\right)_{eff} = \left(\frac{\mathfrak{D}_{AC}}{\mathfrak{D}_{BC}}\right)_{true}$$

The mean value of $(D_{AC}/D_{BC})_{eff}$ for all experiments in which Kr and Xe diffuse through their 50% mixture with each other gas (*i.e.* the ratio of the a effects in Table 8) is 1.2. The mean value of $(\mathfrak{D}_{AC}/\mathfrak{D}_{BC})_{true}$, calculated for the same mixtures from the bulk diffusion data (14, 15) is 1.196. Thus [22], and hence [3], is valid.

However, the ratio of the a effects extrapolated to zero pressure gives for the ratio of the Knudsen diffusion coefficients of Kr and Xe a value somewhat different from that predicted by [2] (Table 8). This failure to confirm [2] may mean that there is some surface diffusion occurring in these systems (23). Alternatively it could mean that [2] is not valid for diffusion in a porous solid: previous confirmation of [2] was confined to gas flow measurements in which a net pressure gradient existed across the specimen (7). In a comparison of flow and self diffusion of Xe through this graphite there were indications that gas flow caused by a pressure gradient was not identical to self diffusion under zero pressure gradient in the Knudsen region (24). However, the results were not conclusive, and further work would be required to establish with certainty the reason for failure of [2].

Conclusion

The prime contribution of this paper is in the form of the model derived from our data. This model correlates not only our data, but also those of others, provided that suitable values of the various constants are chosen. There are indications that some of these constants may be related to properties of the diffusing gases, but further work would be required to establish any relationship with certainty. The model is superior to others in the correlation of experimental data. The power of statistical methods of experimental design has been demonstrated. These methods enabled us to establish correlations in systems with many variables from a minimum number of experiments.

TABLE 8. Predictions of the regression model compared with [2]

Pressure (mm Hg)	$(D_{KrKr^*}/D_{XeXe^*})_{eff}$
0	1.176
10	1.196
88[a]	1.297
Ratio of a effects	1.200
$(M_{Xe^*}/M_{Kr^*})^{1/2}$	1.25

[a]The mean pressure on the log $(p + 60)$ scale.

The authors thank the Australian Atomic Energy Commission for the provision of graphite samples, and more particularly for a Postgraduate Research Studentship and equipment grant to one of us (K.R.W.). We also thank Dr. J. D. Blackwood of the C.S.I.R.O. Division of Chemical Engineering for constructive criticisms of the manuscript.

1. K. R. WELLER, N. S. STENHOUSE, and H. WATTS. Can. J. Chem. This issue.
2. E. WICKE and R. KALLENBACH. Kolloid Z. **97**, 135 (1941).
3. D. S. SCOTT and F. A. L. DULLIEN. Am. Inst. Chem. Eng. J. **8**, 113 (1962).
4. R. B. EVANS III, G. M. WATSON, and E. A. MASON, J. Chem. Phys. **35**, 2076 (1961).
5. R. D. GUNN and C. J. KING. Am. Inst. Chem. Eng. J. **15**, 507 (1969).
6. J. P. HENRY, JR., R. S. CUNNINGHAM, and C. J. GEANKOPOLIS. Chem. Eng. Sci. **22**, 11 (1967).
7. R. M. BARRER and D. M. GROVE. Trans. Faraday Soc. **47**, 826 (1951).
8. P. CLAUSING. Physica, **9**, 65 (1929).
9. W. C. DEMARCUS and D. M. LANG. Knudsen flow through a channel with rough walls. U.S.A.E.C. Report K-1435. 1959.
10. D. S. SCOTT and K. E. COX. J. Chim. Phys. **57**, 1010 (1960).
11. L. MILLER and P. C. CARMAN. Trans. Faraday Soc. **57**, 2143 (1961); **60**, 33 (1964).
12. D. N. SRIVASTAVA and R. PAUL. Physica, **28**, 646 (1962).
13. R. PAUL. Indian J. Phys. **36**, 464 (1962).
14. H. WATTS. Trans. Faraday Soc. **60**, 1745 (1964).
15. H. WATTS. Can. J. Chem. **43**, 431 (1965).
16. C. A. BENNETT and N. L. FRANKLIN. Statistical analysis in chemistry and the chemical industry. John Wiley and Sons, Inc., New York. 1954.
17. K. R. WELLER. Ph.D. Thesis. University of Adelaide, Adelaide, Australia. 1963.
18. E. J. WILLIAMS. Regression analysis. John Wiley and Sons, Inc., New York. 1959.
19. R. B. BIRD, W. E. STEWART, and E. N. LIGHTFOOT. Transport phenomena. John Wiley and Sons, Inc., New York. 1960.
20. A. WHEELER. Adv. Catal. **3**, 249 (1951).
21. R. B. EVANS III, G. M. WATSON, and J. TRUITT. J. Appl. Phy. **33**, 2682 (1962).
22. L. B. ROTHFELD. Am. Inst. Chem. Eng. J. **9**, 19 (1963).
23. G. J. FIELD, H. WATTS, and K. R. WELLER. Rev. Pure Appl. Chem. Aust. **13**, 2 (1963).
24. K. R. WELLER and H. WATTS. Carbon, **2**, 337 (1965).

Can. J. Chem. Downloaded from www.nrcresearchpress.com by 210.87.254.6 on 09/05/12
For personal use only.

Crystal Structure of Lead *meta* Vanadate, PbV_2O_6

BYRON D. JORDAN AND CRISPIN CALVO

Department of Physics, McMaster University, Hamilton, Ontario L8S 4M1

Received February 20, 1974

BYRON D. JORDAN and CRISPIN CALVO. Can. J. Chem. **52**, 2701 (1974).

PbV_2O_6 crystallizes in the orthorhombic space group *Pnma* with $a = 9.771(10)$, $b = 3.684(4)$, $c = 12.713(13)$ Å, and $Z = 4$. The structure was determined using 816 reflections measured with an automatic diffractometer and refined by full-matrix least squares to an R value of 0.052. The two unique vanadium ions lie on mirror planes and are each coordinated to five oxygen atoms lying between 1.61 and 2.06 Å. The distorted octahedra are completed by a sixth V–O interaction which is 2.73 Å for V(1) and is 2.57 Å for V(2). The lead ion is coordinated to nine oxygen atoms lying in a spherical shell with inner and outer radii of 2.56 and 2.90 Å. The structure consists of chains of VO_6 octahedra paralleling the b axis.

BYRON D. JORDAN et CRISPIN CALVO. Can. J. Chem. **52**, 2701 (1974).

PbV_2O_6 cristallise dans le système orthorhombique: groupe d'espace *Pnma* avec $a = 9.771(10)$, $b = 3.684(4)$, $c = 12.713(13)$ Å et $Z = 4$. La structure est déterminée à l'aide de 816 réflexions mesurées avec un diffractomètre automatique et affinée par la méthode des moindres carrés à matrice entière jusqu'à une valeur $R = 0.052$. Les deux ions vanadium se trouvent sur des miroirs plans; chacun de ces ions est lié à cinq atomes d'oxygène à des distances variant de 1.61 à 2.06 Å. L'octaèdre déformé est complété par une sixième interaction V—O de longueur 2.73 Å pour V(1) et 2.57 Å pour V(2). L'ion plomb est lié à neuf atomes d'oxygène à des distances variant de 2.56 à 2.90 Å. La structure consiste en chaînes d'octaèdres VO_6 parallèles à l'axe b. [Traduit par le journal]

Introduction

Extensive studies of $n MO \cdot V_2O_5$ systems have established that for $n = 1$ the vanadium ion is coordinated to six oxygen atoms in a highly distorted octahedral environment. For higher integral values of n the vanadium is tetrahedrally coordinated except perhaps in $Mg_2V_2O_7$ (1). The *meta*-vanadates investigated to date, MV_2O_6 with M = Mg, Zn, Cd, Cu, Ca show related structures (2–6) and in addition, polymorphic behavior in some cases. Lead as a metavanadate, with an ionic radius intermediate between that required for an interstial site and that of an oxygen ion, would be expected to crystallize a new structural type. Further, because of the nature of the distorted VO_6 group and the high polarizability of the lead it would be expected to have a high index of refraction. Thus if a non-centrosymmetric phase were obtained, the structure might be of interest in non-linear optics applications.

Experiments

Crystals of PbV_2O_6 were grown from a melt consisting of stoichiometric amounts of PbO and V_2O_5 by slow cooling through the melting point (600 ± 5 °C). The crystals grew predominately as dark brown needles, with the a axis as the needle axis, in a matrix whose composition was not uniform. No independent chemical analysis was performed.

Two crystals were investigated because of difficulties with absorption. One was a needle with dimensions of 0.02 × 0.02 × 0.4 mm and the second was more regularly shaped with dimensions 0.016 × 0.016 × 0.04 mm. The extinctions, $hk0$ with h odd and $0kl$ with $k + l$ odd established the space group as either $Pn2_1a$ or *Pnma*. Unit cell parameters were obtained by least-squares fitting of the calculated angles to 15 2θ ($20 < 2\theta < 25°$) values measured with graphite monochromatized *MoK*α radiation on a Syntex P$\bar{1}$ diffractometer at 21 °C.

Crystal data

PbV_2O_6 f.w. = 405.07

$a = 9.771(10)$, $b = 3.684(4)$, $c = 12.713(13)$ Å, $V = 457.6$ Å^3, $Z = 4$, ρ_m not measured due to inhomogeneous samples, $\rho_{calc} = 5.89$ g/cm, space group *Pnma*.

All the data were collected with a Syntex P$\bar{1}$ automatic diffractometer. Peaks were scanned at a rate dependent upon the peak counting rate and varied between 2 and 24° in 2θ/min. Backgrounds were measured on either side of the peaks. Reflections with intensity measures less than zero were discarded and those with values of less than 3σ were considered unobserved. A data set consisting of 759 unique reflections was collected within a sphere defined by $2\theta \leqslant 50°$ for the needle shaped crystal. These data were corrected for Lorentz, polarization, and absorption effects ($\mu = 400$ cm^{-1}) assuming a cylindrical shape for the crystal.

The structure was solved from the Patterson function

Can. J. Chem. Downloaded from www.nrcresearchpress.com by 210.87.254.105 on 09/05/12
For personal use only.

TABLE 1. Atomic parameters for PbV_2O_6 with estimated standard deviations in parentheses

Atom	x	y	z	U_{11}*	U_{22}	U_{33}	U_{23}
Pb	0.12833(8)	$\frac{1}{4}$	0.11552(6)	0.0184(4)	0.0206(4)	0.0132(3)	0.0009(3)
V(1)	0.0048(3)	$\frac{1}{4}$	0.6242(2)	0.0074(12)	0.0159(11)	0.0122(2)	−0.0002(10)
V(2)	0.2399(3)	$\frac{1}{4}$	0.4100(2)	0.0075(12)	0.0198(16)	0.009(1)	0.0012(10)
O(1)	0.3072(14)	$\frac{1}{4}$	0.9331(11)	0.012(3)			
O(2)	0.0323(15)	$\frac{1}{4}$	0.4103(10)	0.010(3)			
O(3)	0.2808(15)	$\frac{1}{4}$	0.2873(11)	0.015(3)			
O(4)	0.3932(15)	$\frac{1}{4}$	0.4764(12)	0.016(3)			
O(5)	0.9780(15)	$\frac{1}{4}$	0.7521(10)	0.013(3)			
O(6)	0.1736(14)	$\frac{1}{4}$	0.6055(11)	0.014(3)			

*Thermal factor equals $\exp -2\pi^2[b_1^2h^2U_{11} + \ldots + 2b_1b_2hkU_{12} + \ldots]$ and the b_i's are reciprocal lattice vectors. Isotropic U values in Å^2.

using *Pnma* as the space group. Structure factors were calculated using atomic scattering factors from Cromer and Waber (7) for V^{5+} and International tables for X-ray crystallography (8) for O^{2-} and Pb^{3+}. These were corrected for dispersion. Near the end of the refinement the various layer lines along a were given separate scale constants. Significant shifts in these scale values suggested inadequate absorption corrections and thus a second data set was taken primarily to define the scaling between the layers. The second data set consisted of 649 unique reflections although eight quadrants were scanned. Absorption corrections were made using 4 × 4 × 8 grid for the integration network. The two data sets were scaled together and the final refinement used 816 reflections. A least squares program written by J. S. Stephens for the CDC 6400 was used and weights, ω, were chosen so that $\omega\Delta^2$ would be independent of F_o, the observed structure factors. The weighting function was $\omega = [19 - 1.28F_o + 0.0077F_o^2]^{-1}$. A parameter was refined to correct for the effects of secondary extinction. The refinement was terminated when the shift to standard error ratio was less than 0.1. The final R value is 0.052 and the weighted residual $R_\omega = \{\Sigma\omega|F_o - F_c|^2 \Sigma\omega F_o^2\}^{1/2} = 0.058$. The final atomic positional and thermal parameters are in Table 1.[1] No satisfactory solution in the lower symmetry space group could be found.

Description of the Structure

All the atoms lie on mirror planes in PbV_2O_6. There are two types of vanadium atoms in the structure, each bonded to six oxygen atoms in the form of distorted octahedra. Translationally equivalent octahedra share corner oxygen atoms and extend infinitely along the b axis. $V(1)O_6$ and $V(2)O_6$ groups form pairs by sharing an edge coincident with the mirror planes. Such octahedral pairs share edges connecting oxygen atoms on adjacent mirror planes, with double chains related by center of symmetries as shown in Fig. 1.

The lead ions share oxygen atoms with three of these double chains. Eight of the oxygen atoms lie within a spherical shell with inner and outer radii of 2.56 and 2.70 Å with a ninth, O(1), lying over 0.2 Å further removed (Table 3). Three oxygen atoms are coplanar with the lead and the remaining six related in pairs by the mirror plane. The nine form a trigonal prism about the lead ion with the rectangular faces capped.

The structure contains columns of double chains parallel to the b axis centered at the x and z values of $\frac{1}{2}$,0 and 0,$\frac{1}{2}$ as seen in Fig. 2. Adjacent chains are related by the glide plane with Pb ions interspersed. The O–O lengths about the

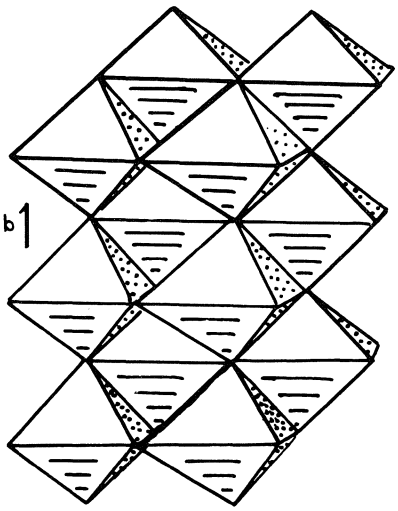

FIG. 1. An idealized view of the edge shared VO_6 chains in PbV_2O_6.

[1]Table 2, containing observed and calculated structure factors, is available at a nominal charge, from the Depository of Unpublished Data, National Science Library, National Research Council of Canada, Ottawa, Canada K1A 0S2.

Can. J. Chem. Downloaded from www.nrcresearchpress.com by 210.87.254.105 on 09/05/12
For personal use only.

TABLE 3. Bond lengths and angles in PbV_2O_6 with standard errors in parenthesis*

Bond	Distance (Å)	Bonds	Angle (deg)	Bonds	Angle (deg)
Pb—O(3)	2.643(14)	O(3)*a*—Pb—O(4)*c*	151.3(5)	O(4)*c*—Pb—O(4)*d*	67.3(4)
—O(4)*c*	2.577(15)	—O(4)*d*	128.1(3)	—O(5)*b*	86.5(4)
—O(4)*d*	2.563(10) (2x)	—O(5)*b*	72.7(4)	—O(6)*d*	128.6(3)
—O(5)*b*	2.703(10) (2x)	—O(6)*d*	68.4(4)	—O(1)*a*	100.1(4)
—O(6)*d*	2.675(10) (2x)	—O(1)*a*	108.7(4)	O(4)*d*—Pb—O(5)*b*	84.7(3)
—O(1)*a*	2.904(14)	O(5)*b*—Pb—O(6)*d*	80.7(3)	—O(6)*d*	62.1(4)
		—O(1)*a*	136.8(2)	—O(1)*a*	59.9(4)
		—O(4)*d*	152.6(5)	—O(4)*d*	91.9(3)
		—O(5)*b*	85.9(3)	—O(6)*d*	121.4(4)
		—O(6)*d*	141.0(4)	O(1)*a*—Pb—O(4)*d*	59.9(4)
		O(6)*d*—Pb—O(1)*a*	61.7(3)	—O(6)*d*	61.7(3)
		—O(6)*d*	87.0(3)		
V(1)—O(2)*a*	2.732(14)	O(2)*a*—V(1)—O(5)*a*	176.5(6)	O(5)*a*—V(1)—O(6)*a*	107.3(7)
—O(5)*a*	1.647(14)	—O(6)*a*	76.2(6)	—O(1)*c*	101.5(7)
—O(6)*a*	1.666(14)	—O(1)*c*	75.0(5)	—O(2)*b*	101.2(4)
—O(1)*c*	2.063(15)	—O(2)*b*	78.0(4)	O(6)*a*—V(1)—O(1)*c*	151.2(6)
—O(2)*b*	1.928(4) (2x)	O(1)*c*—V(1)—O(2)*b*	75.3(6)	—O(2)*b*	98.9(4)
				O(2)*b*—V(1)—O(2)*e*	145.7(6)
V(2)—O(3)*a*	1.611(15)	O(3)*a*—V(2)—O(4)*a*	105.0(7)	O(4)*a*—V(2)—O(1)*d*	97.7(4)
—O(4)*a*	1.719(15)	—O(1)*d*	102.0(6)	—O(2)*a*	150.5(6)
—O(1)*d*	1.921(4) (2x)	—O(2)*a*	104.5(7)	—O(6)*a*	75.2(6)
—O(2)*a*	2.028(14)	—O(6)*a*	179.8(6)	O(1)d—V(2)—O(2)*a*	76.1(4)
—O(6)*a*	2.569(14)	O(2)*a*—V(2)—O(6)*a*	75.3(5)	—O(6)*a*	78.0(4)
				O(1)d—V(2)—O(1)*f*	147.0(6)

*Symmetry transformations: $a = x, y, z$; $b = -x, 1/2 + y, -z$; $c = 1/2 + x, y, 1/2 - z$; $d = 1/2 - x, 1/2 + y, 1/2 + z$; $e = -x, -y, -z$; $f = 1/2 - x, -y, 1/2 + z$.

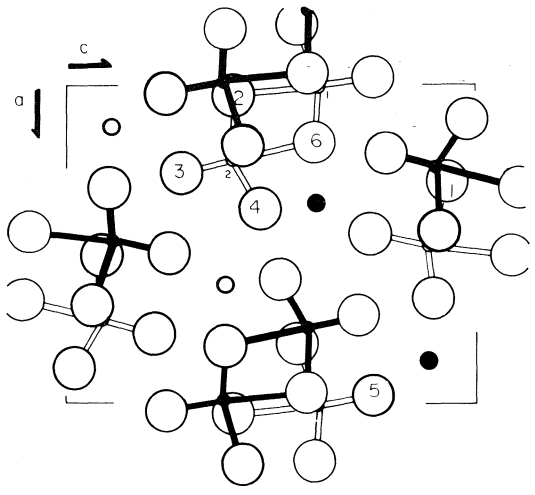

FIG. 2. The structure of PbV_2O_6 projected onto the *ac* plane. The largest circles are oxygen atoms and the smaller ones of V atoms. The leads are shown as immediate sized circles. The filled bonds and open bonds lie in the mirror planes at $b = 3/4$ and $1/4$ respectively. Similarly, the filled circles represent vanadium or lead ions at $b = 3/4$.

vanadium ions are shown in Fig. 3. The O(1)–O(2) edge shared between V(1) and V(2) is short (2.44 Å) and is subtended by V—O bond lengths lying between 1.921 and 2.028 Å. On the other hand, the O(2)–O(6) and O(2)–O(2) shared edges are 2.84 and 3.00 Å long, respectively. These edges are subtended in part by the long V(1)–O(2) and V(2)–O(6) interactions. All the remaining O–O contacts are of intermediate length.

Discussion

The structure of PbV_2O_6 differ from that of other MX_2O_6 systems. All the previous metavanadates investigated have structures based upon the brannerite structure (9) which can be looked upon as a distortion from a close packed array of oxygen atoms. The columbite (10) and trirutile (11) structures also have the MX_2O_6 stoichiometry and are based upon hexagonally close-packed arrays of oxygen atoms. In all these structures the cations lie in octahedrally coordinated sites. It is to be expected that as the

Can. J. Chem. Downloaded from www.nrcresearchpress.com by 210.87.254.105 on 09/05/12
For personal use only.

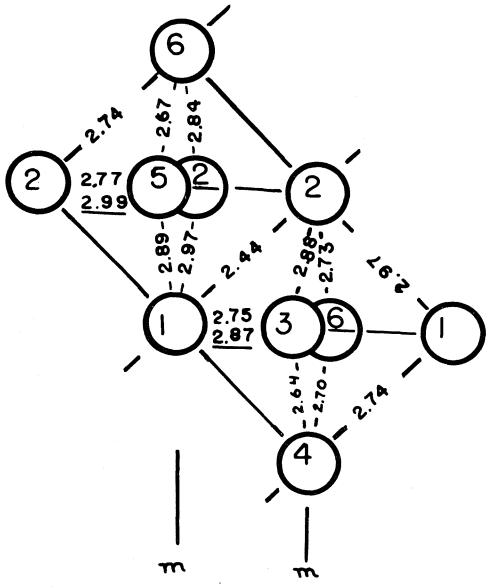

FIG. 3. The O–O contacts around the vanadium ions in PbV_2O_6. The distances are in Å units and the underlined values correspond to interactions involving the oxygen atom below the plane of the figure. The mirror planes are designated by m.

cation radius increases for a fixed X—O bond length that the packing will change because the cations become too large for the interstitial sites.

The PbX_2O_6 series of compounds change from one based upon chains of corner shared tetrahedra when X = P (12) to one based upon octahedra either corner shared, as in $PbNb_2O_6$ (13) or edge shared as in the present case, and in $PbSb_2O_6$ (11). The $PbNb_2O_6$ structure appears to be unacceptable for PbV_2O_6 because it cannot support the *trans* distortion characteristic of the VO_6 grouping. In the VO_6 groups reported to date the shortest V–O, generally near 1.60 Å is *trans* to the longest bond in the grouping. Since both the $PbNb_2O_6$ and PbV_2O_6 have mirror plane through the pentavalent ion, this *trans* distortion must be restricted to the bonds in the mirror plane. The corner octahedral groupings in $PbNb_2O_6$ form rings consisting of 3, 4, and 5 octahedra. In these circumstances it is not possible to arrange the octahedra such that there is only one long–short *trans* pair of V—O bonds per group.

One final point worthy of comment concerns the appearance of crystals of PbV_2O_6 in the present study. Phase diagrams reported by Amadori (14) and Shimohira *et al.* (15) indicate that a eutectic is found between PbO and $Pb_2V_2O_7$ at a composition near $PbO{\cdot}V_2O_5$. Thus it could appear that our crystals are a metastable phase. However, heating crystal PbV_2O_6 and cooling slowly enough to avoid glass formation led to a powder pattern characteristic of the original PbV_2O_6. A DTA study was used to determine the melting temperature and indicated an additional endothermic transition at 545 °C. Thus, further phase studies of the $PbO{\cdot}V_2O_5$ system are indicated.

These studies were supported by a grant from the National Research Council of Canada. We also wish to thank Dr. R. D. Shannon for assistance in the crystal preparation and helpful discussions.

1. R. GOPAL and C. CALVO. Acta Cryst. In press.
2. H. N. NG and C. CALVO. Can. J. Chem. **50**, 3619 (1972).
3. J. ANGENAULT and A. RIMSKY. C. R. Acad. Sci. Paris Ser. C, **267**, 227 (1968).
4. J-C. BOULOUX and J. GALY. Bull. Soc. Chim. Fr. 739 (1969).
5. C. CALVO and D. MANOLESCU. Acta Cryst. **B29**, 1743 (1973).
6. J-C. BOULOUX, G. PEREZ, and J. GALY. Bull. Soc. Fr. Minér. Crist. **95**, 130 (1972).
7. D. T. CROMER and J. WABER. Acta Cryst. **18**, 104 (1965).
8. International tables for X-ray crystallography. Vol. III, Kynoch Press, Birmingham. 1963.
9. R. RUH and A. D. WADSLEY. Acta Cryst. **21**, 974 (1966).
10. E. V. SVESHNIKOVA, A. G. ZHABIN, T. A. YAKOVLEVSKAYA, and V. B. ALEKSANDROV. Tr. Mineral. Muz. Akad. Nauk. SSSR, **16**, 226 (1965).
11. (*a*) A. BYSTRÖM, B. HÖK, and B. MASON. Ark. Kemi Mineral. Geol. **15B**, No. 4 (1941); (*b*) A. MAGNELI. Ark. Kemi Mineral. Geol. **15B**, No. 3 (1941).
12. K. H. JOST. Acta Cryst. **17**, 1539 (1964).
13. P. H. LABBE, M. FREY, and G. ALLAIS. Acta Cryst. **B29**, 2204 (1973).
14. M. AMADORI. Atti. r. ist. Veneto, **76**, 419 (1916–1917).
15. T. SHIMOHIRA, S. IWAI, and H. TAGAI. J. Ceram. Assoc. Jap. **75**, 352 (1967).

Can. J. Chem. Downloaded from www.nrcresearchpress.com by 210.87.254.105 on 09/05/12
For personal use only.

The Hydride Reduction of Hemiaminals of Thiobinupharidine and the Structure of Thionupharoline

T. I. MARTIN AND D. B. MACLEAN
Department of Chemistry, McMaster University, Hamilton, Ontario L8S 4M1
AND
J. T. WRÓBEL, A. IWANOW, AND W. STARZEC
Department of Chemistry, University of Warsaw, Warsaw, Poland
Received January 7, 1974

T. I. MARTIN, D. B. MACLEAN, J. T. WRÓBEL, A. IWANOW, and W. STARZEC. Can. J. Chem. **52**, 2705 (1974).

Thionupharoline has been shown to be identical with 6-hydroxythiobinupharidine. The hydride reduction of hemiaminals of thiobinupharidine has been examined in ethanol solution. The steric course of reduction at C-6 is not nearly as selective as it has been reported to be in solution in methanol.

T. I. MARTIN, D. B. MACLEAN, J. T. WRÓBEL, A. IWANOW et W. STARZEC. Can. J. Chem. **52**, 2705 (1974).

On montre que la thionupharoline est identique à l'hydroxy-6 thiobinupharidine. L'étude de la réduction par un hydrure des hémiaminals de la thiobinupharidine a été effectuée en solution dans l'éthanol. Le développement stérique de la réduction en C-6 n'est pas aussi sélectif que ce qui a été rapporté quand le solvant est le méthanol. [Traduit par le journal]

Can. J. Chem. Downloaded from www.nrcresearchpress.com by 210.87.254.5 on 09/05/12
For personal use only.

In 1970 Wróbel reported the isolation of a new sulfur-containing alkaloid from the yellow water lily (1). He named the new alkaloid thionupharoline ($C_{30}H_{42}N_2O_3S$, **1**) and suggested that it was related structurally to the known isomeric sulfur containing alkaloids of this series, thiobinupharidine **2** and neothiobinupharidine **3**, of composition $C_{30}H_{42}N_2O_2S$, but unlike the others to contain a hydroxyl group. In the same year LaLonde *et al.* (2) reported the isolation from the same species of the isomeric bishemiaminals of composition, $C_{30}H_{42}N_2O_4S$, that were named 6,6′-dihydroxythionuphlutine-A, **4**, and 6,6′-dihydroxythionuphlutine-B, **5**. Later (3) it was shown that thionuphlutine-A was identical with thiobinupharidine and the latter name having precedence in the literature is used for this compound.

The structure of **3** has been known since 1965 (4) but it is only in the last year that the structures of thiobinupharidine (5, 6, 7) and of thionuphlutine-B, **6** (6, 7), have been resolved.

Very recently LaLonde *et al.* (6) reported the isolation and identification of a monohemiaminal, 6-hydroxythiobinupharidine. Here we report the identity of thionupharoline and 6-hydroxythiobinupharidine and describe p.m.r. and reduction studies in this series that differ from those reported (6).

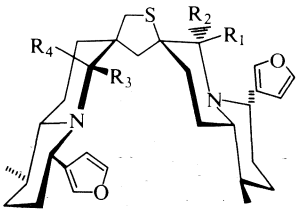

1 $R_1 + R_2 = H + OH$; $R_3 = R_4 = H$
2 $R_1 = R_2 = R_3 = R_4 = H$
4 $R_1 + R_2 = R_3 + R_4 = H + OH$

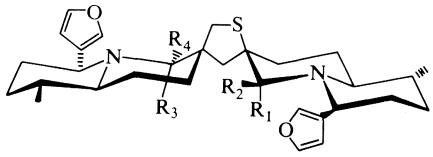

3 $R_1 = R_2 = R_3 = R_4 = H$

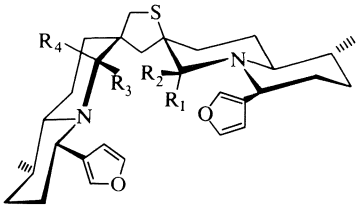

5 $R_1 + R_2 = R_3 + R_4 = H + OH$
6 $R_1 = R_2 = R_3 = R_4 = H$

Can. J. Chem. Downloaded from www.nrcresearchpress.com by 210.87.254.5 on 09/05/12
For personal use only.

Reduction of **1** in sodium borohydride yielded thiobinupharidine. Since hemiaminals but not simple alcohols are known to undergo reduction with this reagent, it was established that **1** was a hemiaminal and that it must be either 6- or 6′-hydroxythiobinupharidine. This conclusion was substantiated by the presence of a singlet in the p.m.r. spectrum of **1** measured in benzene at 4.25 δ assigned to the methine proton adjacent to both oxygen and nitrogen.

We found that the u.v., i.r., p.m.r., and mass spectra of **1** corresponded with those reported by LaLonde *et al.* (6) for 6-hydroxythiobinupharidine.[1] We prepared a monoperchlorate and a diperchlorate of **1** according to the procedure described by LaLonde *et al.* (6) and found them to be identical with the corresponding salts of 6-hydroxythiobinupharidine (6). The diperchlorate of **1** described by Wróbel was reported to melt at 170–172°, nearly 100° lower than that of 6-hydroxythiobinupharidine described by LaLonde. We repeated the preparation according to the original procedure confirming the original result. It is apparent that the diperchlorate is dimorphic or that it crystallizes with a mole of water when prepared by the original procedure of Wróbel. Because of the paucity of **1** we were unable to resolve this problem to our satisfaction.

Before we became aware of the results of LaLonde *et al.* (6) we attempted to resolve the structural problem through p.m.r. studies and mass spectrometry. This led us to examine the p.m.r. spectra of **1** and **2** at 220 MHz and to prepare 6-deuterio- and 6,6′-dideuteriothiobinupharidine for p.m.r. and mass spectrometric studies. The results that we obtained are sufficiently different from those already reported (6) that they merit discussion.

We found that the spectra of **1** and **2** are much better resolved in perdeuteriobenzene than they are in deuteriochloroform. We therefore set about to assign as many of the signals as possible in the spectrum of **2** recorded in benzene solution. Our assignments are based on analogy with those of the corresponding protons of deoxynupharidine **7** and 7-epideoxynupharidine **8**.

The p.m.r. spectrum of **7**, whose structure and absolute configuration are known (8), has been studied in detailed by LaLonde and co-workers (9–11). As a result of their work no ambiguity exists with respect to the assignment of signals of the equatorial methyl group at C-1, the axial methyl group at C-7, and the hydrogens, H-4a, H-6a, H-6e, and H-7e. The majority of the prior work was carried out in $CDCl_3$. We have repeated this work in benzene solution at 220 MHz and have obtained the results shown in Table 1.

7-Epideoxynupharidine was prepared synthetically (12, 13) before it was isolated from nature (14). Its structure and stereochemistry follow from the fact that it is formed along with **7** when $\Delta^{6,7}$-dehydrodeoxynupharidine is treated with hydrogen over a Pd catalyst (10). Its p.m.r. spectrum in deuteriochloroform and in benzene has been examined but only a few resonances have been assigned (14). We have re-examined the spectrum in benzene and through decoupling experiments have made the assignments shown in Table 2.

In the first p.m.r. study of thiobinupharidine (15) the signals of individual protons other than the *C*-methyl and the furan protons were not assigned but in a later study (2) the absorption of the methylene protons adjacent to sulfur were assigned. The latter assignment has been placed on a firm foundation through work on model systems (16). Assignment of the hydrogens at the axial and equatorial positions at C-6 and C-6′ have been made through a study of the deuterated compounds obtained on reduction of 6,6′-dihydroxythiobinupharidine (6). The axial hydrogens at C-4 and C-4′ have also been identified in the spectrum (5, 6). Much of this work has been carried out in $CDCl_3$ where there is much overlap of the signals attributed to the protons at C-4, C-4′, C-6e, and C-6′e (see for example the published spectrum of **2**, (5)) but better separation of the signals is obtained in perdeuteriobenzene (6). The assignments that we have made from 220 MHz studies are shown in Table 3.

Inspection of the three tables shows that the chemical shifts of H-6a and H-6e of **2** differ from one another by approximately the same amount as the corresponding protons of **7**. Similarly the chemical shifts of H-6′a and H-6′e differ from one another by approximately the same amount as the corresponding protons of **8**. The protons at C-4 and C-4′ of **2** absorb in the same region and have virtually the same chemical shift as

[1]We thank Professor LaLonde for disclosing his results to us prior to their publication and for providing spectra and samples of his compounds for comparison.

TABLE 1. Proton magnetic resonance spectrum of deoxynupharidine in C_6D_6

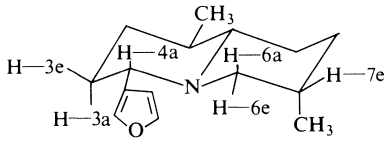

7

Proton	Chemical shift (δ)	Multiplicity	Coupling constants *J* (Hz)
C-1 methyl e	0.81	d	6.0
C-7 methyl a	1.10	d	7.0
H-6a	1.78[a]	q	11.5 (6a-6e) and 3.0 (6a-7e)
H-6e	2.76	q	11.5 (6e-6a) and 2.5 (6e-7e)
H-4a	2.81	q	11.0 (4a-3a) and 3.0 (4a-3e)

[a]Irradiation at 1.78 collapses quartet at 2.76 into broad singlet.

TABLE 2. Proton magnetic resonance spectrum of 7-epideoxynupharidine in C_6D_6

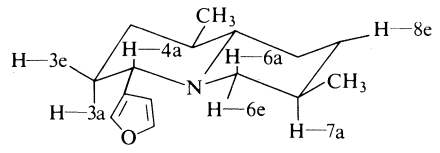

8

Proton	Chemical shift (δ)	Multiplicity	Coupling constants *J* (Hz)
C-7 methyl e	0.68[a]	d	6.5
C-1 methyl e	0.83	d	6.0
H-6a	1.29[e]	t (1:2:1)	11.0 (6a-6e) and 11.0 (6a-7a)
H-7a, H-3e, H-8e	1.64[b]	Complex multiplet	
H-3a	1.77[c]	Multiplet	11.0 (3a-4a) recognizable
H-4a	2.83[d]	q	11.0 (4a-3a) and 3.5 (4a-3e)
H-6e	3.03[f]	d of q	11.0 (6e-6a) and 3.5 (6e-7a) and 2.0 (6e-8e)

[a]Irradiation at 0.68 induced changes in the region 1.64.
[b]Irradiation at 1.64 collapsed doublet at 0.68 into singlet; also collapsed quartet at 2.83 into doublet (J = 11.0 Hz) also collapsed doublet of quartet at 3.03 to doublet (J = 11.0 Hz).
[c]Irradiation at 1.77 collapsed quartet at 2.83 to a doublet (J = 3.5 Hz).
[d]Irradiation at 2.83 collapsed the 11.0 Hz coupling in signal at 1.77.
[e]Irradiation at 1.29 collapsed doublet of quartet at 3.03 to multiplet with couplings 2.0 and 3.5 Hz recognizable.
[f]Irradiation at 3.03 collapsed 1:2:1 triplet at 1.29 to a 1:1 doublet (J = 11.0 Hz).

the protons at C-4 in **7** and **8**. It is apparent that the equatorial alkyl substituent causes a shielding of H-6′a of **2** and H-6a of **8** relative to the corresponding proton of **7**. The protons H-6a and H-6e of **2** are deshielded, presumably by the equatorial sulfur, relative to the corresponding protons of **7**.

When the p.m.r. spectra of **1** and **2** were compared we found it impossible to assign definitively the hydroxy group to C-6 or to C-6′. The presence of the hydroxy function introduced too many changes in the spectrum. We turned therefore to examine the products of the borodeuteride reduction of 6,6′-dihydroxythiobinupharidine **4** and of **1** in the expectation that an examination of these compounds by p.m.r. or mass spectrometry might lead to a resolution of the problem. While our work was in progress it was reported (6) that the reduction of **4** with $NaBD_4$ led to the incorporation of deuterium into the axial position at C-6′ and into an equatorial position at C-6 with complete stereoselectivity. It was also stated that the reduction proceeded with about 70% incorporation of deuterium and 30% incorporation of hydrogen, a result that was surprising.

We reduced **4** with sodium borodeuteride in ethanol and obtained a dideuteriothiobinu-

Can. J. Chem. Downloaded from www.nrcresearchpress.com by 210.87.254.5 on 09/05/12
For personal use only.

TABLE 3. Proton magnetic resonance spectrum of thiobinupharidine in C_6D_6

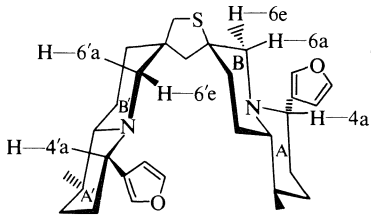

2 Thiobinupharidine ($C_{30}H_{42}N_2O_2S$)

Proton	Chemical shift (δ)	Multiplicity	Coupling constants *J* (Hz)
H-6'a	1.40[a]	d	11.5 (6'a-6'e)
H-6a	1.92[b]	d	11.5 (6a-6e)
H-6e	3.11	q	11.5 (6a-6e); 2.0 (6e-8e)
H-6'e	3.17	q	11.5 (6'a-6'e); 2.5 (6'e-8'e)
H-4a + H-4'a	2.80	q	10.5 (4a-3a); 3.5 (4a-3e)
C-7-CH_2-C-7'	2.18	ABq	J_{AB} = 14.0
-S-CH_2-	2.31	ABq	J_{AB} = 11.5

[a]Irradiation at 1.40 collapses q at 3.17 into broad singlet; q at 3.11 unaffected.
[b]Irradiation at 1.92 collapses q at 3.11 into broad singlet; q at 3.17 unaffected.

pharidine and a monohydroxymonodeuteriothiobinupharidine. Unlike the published result (6) our dideuterio compound was approximately 95% dideuterated material. The 220 MHz spectrum in perdeuteriobenzene showed that one deuterium was incorporated, almost exclusively, into the axial position at C-6′ and that the second deuterium was incorporated to the extent of 40% into the equatorial position and 60% into the axial position at C-6. The signal observed at 1.40 δ (H-6′a) in **2** had virtually disappeared in the spectrum of the dideuterated compound while the signal at 3.16 δ (H-6′e) had collapsed to a poorly resolved doublet, apparently coupled only to H-8′e. The signal at 1.93 δ (H-6a) was now a broad singlet (0.4 H) whereas the signal at 3.10 δ (H-6e) was a poorly resolved doublet (0.6H) coupled to H-8e. Our results are compatible with those of LaLonde *et al.* (6) with respect to reduction at C-6′ but they differ from his with respect to reduction at C-6. We actually observe only 40% introduction of deuterium into the equatorial position at C-6 and not 100% as they observed. They attributed the stereoselectivity to sulfur interaction with an immonium salt intermediate. They proposed that the presence of an equatorial sulfur as in **2** resulted in preferential introduction of deuterium into an equatorial position whereas the presence of an axial sulfur as in thionuphlutine-B led to preferential introduction of deuterium into an axial position (6). Our results show that sulfur in an equatorial position influences the reaction but not to the same extent as it does when the reaction is conducted in methanol solution. Other studies have shown that enamines in the monomeric system are normally attacked on the β face of the molecule to give axial introduction of hydrogen or deuterium at the carbons adjacent to nitrogen (10, 11).

The second product of the borodeuteride reduction proved to be 6′-deuterio-6-hydroxythiobinupharidine with greater than 95% incorporation of deuterium. This compound had a u.v. spectrum identical with **1** in acid and neutral media and formed a diperchlorate of the same melting point as **1**. Its melting point was undepressed in admixture with the diperchlorate of **1**. It differed in its 220 MHz spectrum from that of **1** only in one obvious respect, namely that the quartet present in **1** at 3.18 δ (H-6′e) had collapsed to a poorly resolved doublet integrating for one proton. It is clear that the deuterium has entered axially at C-6′ and that reduction at C-6′ has occurred more rapidly than at C-6. The more rapid attack at C-6′ in this system is predictable on the basis of studies on model compounds (6).

Reduction of **1** with borodeuteride gave 6-deuteriothiobinupharidine with deuterium incorporation in excess of 95%. The 220 MHz spectrum of this compound in benzene showed

Can. J. Chem. Downloaded from www.nrcresearchpress.com by 210.87.254.5 on 09/05/12
For personal use only.

Can. J. Chem. Downloaded from www.nrcresearchpress.com by 210.87.254.5 on 09/05/12
For personal use only.

only minor differences from the spectrum of **2**. The signal at 1.93 δ, formerly a doublet, now appeared as a broad singlet (0.35 H) and the signal at 3.10 δ now appeared as a broadened singlet (0.65 H). Thus deuterium had entered 65% into the axial position and 35% into the equatorial position, a result in clear agreement with the borodeuteride reduction of **4**.

The results of the p.m.r. studies on the borodeuteride reduction products of **1** and **4** are illustrated in Fig. 1. The lower spectrum is that of thiobinupharidine recorded at 220 MHz in C_6D_6 and shows the double irradiation experiments conducted on that compound. The centre spectrum is that of the product of borodeuteride reduction of **1** and the upper spectrum that of the product of complete borodeuteride reduction of **4**. The spectra of the deuterated compounds were recorded with 5–10 mg samples under the same conditions as the spectrum of **2**. The deuterium incorporation at the various sites is indicated.

This work has established the identity of thionupharoline and 6-hydroxythiobinupharidine. It has shown that borohydride reduction in ethanol solution of hemiaminals of thiobinupharidine that carry a hydroxyl group at C-6 does not occur with high stereoselectivity. Our results contrast with those reported before (6) where the reduction was effected in methanol. We found that incorporation of deuterium was nearly complete in the borodeuteride reduction whereas only about 70% incorporation has been observed in an earlier study (6).

Experimental

Apparatus, Methods, and Materials

Infrared spectra were recorded on a Perkin-Elmer 521 spectrometer. Typically, samples of free bases were made up at a concentration of 0.03 *M* in spectroquality carbon tetrachloride or dichloromethane, using cells with KBr windows and a path length of 0.1 mm. Perchlorate salts were made up in KBr discs prepared in the usual manner and the spectra were run against air as the reference side.

Proton magnetic resonance spectra were recorded at 220 MHz on a Varian 220 HR spectrometer using a field sweep mode. All spectra were recorded at ambient temperature. Samples were dissolved in $CDCl_3$ or C_6D_6 as required using added TMS as internal standard. Chemical shifts are reported relative to TMS = 0.0 δ. Typically a sweep width of 2500 Hz was employed but sweep widths of 1000, 500, and 250 Hz facilitated the determination of coupling constants. Symbols s, d, q, m, nw, br, and $W_{1/2}$ refer to singlet, doublet, quartet, multiplet, narrow, broad, and width at half height, respectively. Ultraviolet spectra were recorded on a Cary 14 spectrometer using 1 or 0.1 cm quartz cells as appropriate.

Melting points were determined on a Kofler micro-hot-stage and are uncorrected.

Thin-layer chromatograms were performed under standard conditions using 0.5 mm silica gel coated on glass plates available from Brinkman Instruments, Rexdale, Ontario. Solvent used for development in all cases was hexane–benzene–acetone, 1:5:1. Development was carried out under conditions of tank saturation in a vessel 25 cm × 20 cm × 7 cm. The spray reagent was Dragendorf reagent (17). Column chromatography was performed using neutral alumina, Brockman Activity 1, 80–200 mesh, available from Fischer Scientific, adjusted to give the required activity (18, 19). Sodium borodeuteride-d_4 was purchased from Stohler Isotope Chemicals, and was certified 99% D. It was stored in its container under vacuum over KOH as desiccant.

Mass spectra were determined on a C.E.C. 21-110B double focussing mass spectrometer. Samples were introduced through a direct inlet system. Relative intensity data were obtained from low resolution mass spectra, recorded under identical conditions at an ionization voltage of 70 eV, a trap current of 140 μA, a source temperature of 200 °C (unless otherwise stated), and a source pressure of 2×10^{-6} Torr.

Deuterium contents were determined in the following manner. The molecular ion region from M − 3 to M + 3 of the spectrum was scanned several times using several magnetic sweep velocities. The average peak heights were then determined for the labelled and the unlabelled compounds and the deuterium content calculated by the method of Biemann (20).

Isolation of Thionupharoline from its Perchlorate

A 50 mg sample of thionupharoline diperchlorate, m.p. 172–174° (see below), was treated with 10 ml of 20% ammonia and stirred for 30 min. The resultant oil was extracted with CH_2Cl_2 (5 × 10 ml). The extracts were combined, dried over anhydrous sodium sulfate, and evaporated under reduced pressure to leave a colorless glass on the inside of the vessel. The yield was 34.6 mg of free base which was purified by chromatography from neutral alumina (Activity II, 2 g) using 20% ether in hexane as eluant. The thionupharoline (34 mg) obtained as a glass, showed one spot on t.l.c. R_f 0.36; u.v. (95% EtOH, neutral), end absorption only; u.v. (95% EtOH, acidic) λ_{max_1} 208 nm (*q* 20 000), λ_{max_2} 293 nm (*q* 2540); i.r. (CH_2Cl_2) 2.80 (OH), (weak), 3.59 (Bohlmann band), and unassigned bands at 6.65, 6.90, 7.26, 8.66, 9.08, 9.40, 9.67, 9.74, 11.45 μ; p.m.r. (220 MHz $CDCl_3$): δ 0.88 (d, J = 5 Hz, 6 H, 2 × CHCH_3), 2.20 (ABq, J_{AB} = 12 Hz, 2 H, CH_2—S), 2.26 (OH exchangeable on addition of D_2O), 2.89 (q, J = 5.6 and 8 Hz, 1 H, H-4′), 2.92 (quartet J = 11.5 and 2 Hz, 1 H, H-6′e), 3.70 (q, J = 7.5 and 7 Hz, 1 H, H-4), 3.97 (s, 1 H, H-6, sharpens on addition of D_2O), 6.34 (nw m, $W_{1/2}$ = 7 Hz, 2 H, furan β H), 7.21 (nw m, 1 H, furan α H), 7.30 (nw m, $W_{1/2}$ = 4 Hz, 3 H, furan α H); p.m.r. (220 MHz C_6D_6): δ 0.75 (two superimposed doublets J = 6 Hz, 6 H, 2 × CHCH_3), 2.11 (AB quartet, J_{AB} = 12 Hz, 2 H, CH_2—S), 2.42 (OH, exchangeable with D_2O), 2.79 (q, J = 3 and 11 Hz, 1 H, H-4′), 3.18 (q, J = 2.5 and 12 Hz, 1 H, H-6′e), 3.90 (q, J = 4 and 10 Hz, 1 H, H-4), 4.25 (s, 1 H, H-6), 6.41 (nw m, furan β H), 6.48 (nw m, 2 H, with 6.41 furan β H),

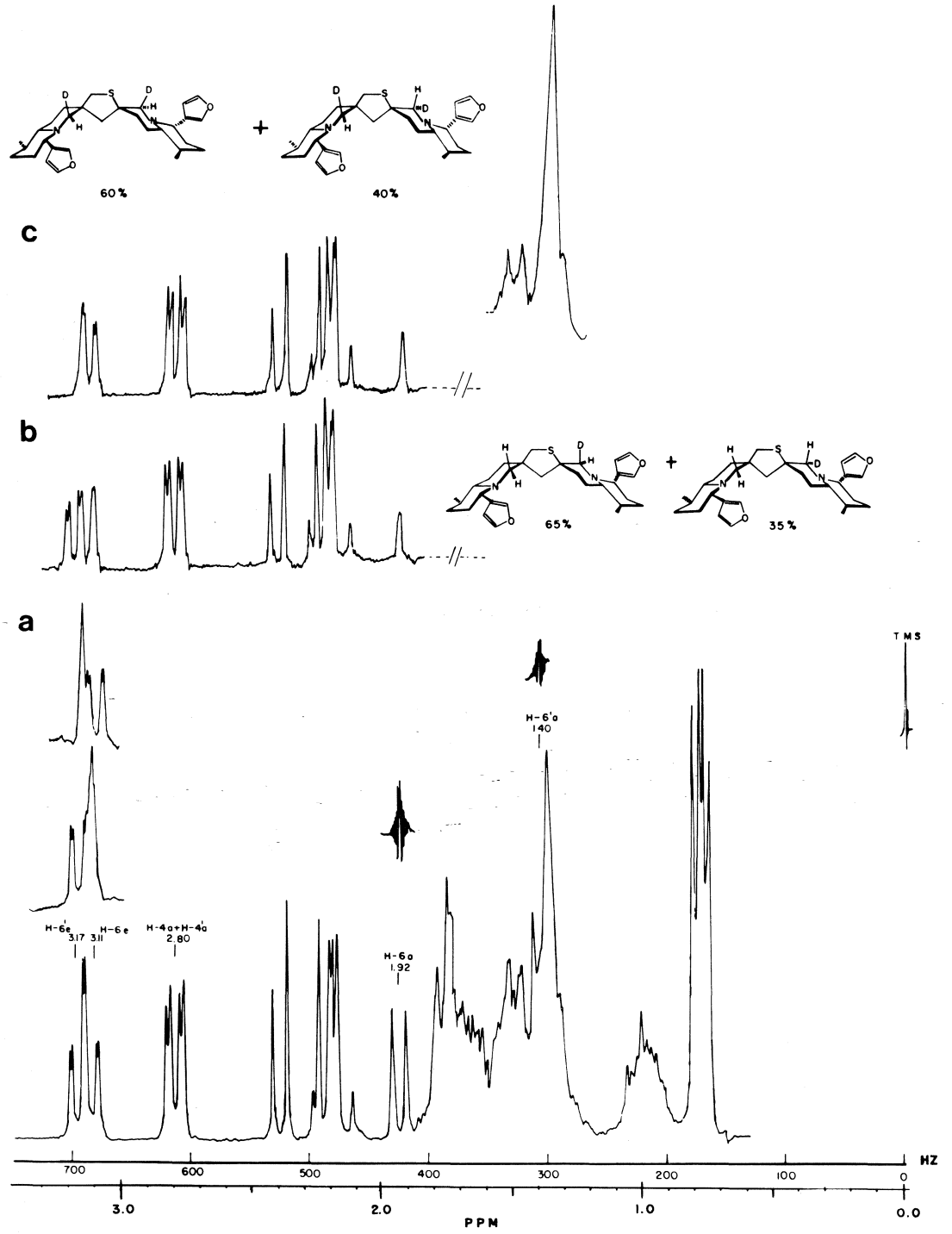

FIG. 1. The 220 MHz spectra in C_6D_6 of thiobinupharidine (a), the product of borodeuteride reduction of **1** (b), and the product of complete borodeuteride reduction of **4** (c).

Can. J. Chem. Downloaded from www.nrcresearchpress.com by 210.87.254.5 on 09/05/12
For personal use only.

Can. J. Chem. Downloaded from www.nrcresearchpress.com by 210.87.254.5 on 09/05/12
For personal use only.

7.16 (nw m, 3 H, furan α H), 7.22 (nw m, 1 H, furan α H); mass spectrum (230°) *m/e* (relative intensity, %) 510 (15) M^+, 494 (19), 493 (31), 492 (72), 481 (1), 477 (2), 475 (0.8), 464 (4), 459 (3), 445 (6), 431 (1.5), 425 (1), 397 (1.5), 383 (1), 375 (8), 359 (2), 357 (2), 304 (4), 262 (5), 246 (5), 244 (4), 231 (24), 230 (100), 229 (28), 228 (45), 215 (9), 178 (24), 176 (54), 136 (12), 107 (26), 94 (50).

Monoperchlorate of Thionupharoline

Thionupharoline (21.6 mg, 0.0424 m*M*) was dissolved in 5 ml MeOH and treated with 2.23 ml of 0.019 *M* $HClO_4$ (0.0424 m*M*). The solution was warmed for a few minutes on a steam bath and the solvent removed under reduced pressure leaving 27 mg of colourless semi-crystalline solid. Recrystallization from ether containing sufficient acetone to effect solution gave 25 mg colourless prismatic needles. Thionupharoline monoperchlorate, m.p. 240–243°; i.r. (KBr disc) 3.62 (weak Bohlmann band), 6.03 and 6.06 (C=N⁺), 6.66 and 11.45 μ (furan).

Treatment of the monoperchlorate with aqueous ammonia led to recovery of the free base, thionupharoline, characterized by its p.m.r. and mass spectra.

Diperchlorate of Thionupharoline

Method 1

Thionupharoline 5.1 mg (0.01 m*M*) was dissolved in 1 ml of anhydrous ethanol and treated with 1 ml 0.02 *M* (0.02 m*M*) perchloric acid. Anhydrous ether (5 ml) was added and the solution was set aside to crystallize. The crystals, well-formed prisms, were filtered and washed several times with anhydrous ether; m.p. 172–174°, i.r. (KBr disc) 6.02 >C=N⁺<, 6.65 and 11.46 (furan). Other unassigned absorptions were present at 6.88, 6.95, 7.06, 7.24, 7.32, 7.52, 7.84, 8.09 μ.

Method 2

Thionupharoline 5.1 mg (0.01 m*M*) was treated directly with 1 ml of 0.02 *M* (0.02 m*M*) perchloric acid and a few milliliters of water were added to ensure that all the glassy base was in contact with the perchloric acid solution. After 30 min the solution was evaporated to dryness under reduced pressure (50 °C bath) and the residue was dissolved in a minimum of boiling anhydrous MeOH. After storage at −5° for 2 days crystallization had occurred. The crystals were washed twice with anhydrous MeOH leaving 4 mg of colourless needles, m.p. 260–263° (softening), 267–269° (main melting), 270° (all liquid), 278° (decomposition).

A mixture m.p. (50:50 mixture) with a sample of the diperchlorate of 6-hydroxythiobinupharidine obtained from Professor R. T. LaLonde (m.p. 258° (softens), 263–266.5° (liquid), 276° (decomposition)), showed no depression in melting point; i.r. (KBr disc) 6.03 and 6.06 (>C=N⁺<), 6.66 and 11.47 (furan), 8.1–10.2 (ClO_4^-), and unassigned absorption at 3.27, 6.85, 6.89, 6.96, 7.08, 7.21, 7.25, 7.47, 7.52, 7.85, 10.38, 10.62, 10.76, 12.35, 13.65 μ. The i.r. spectrum was identical with the i.r. spectrum of the sample of the diperchlorate of 6-hydroxythiobinupharidine.

Reduction of Thionupharoline with Sodium Borohydride

Thionupharoline (10 mg) was dissolved in 2 ml of absolute ethanol and treated with 100 mg of $NaBH_4$. Further portions of 25 mg each of $NaBH_4$ were added four times over the course of 24 h. The slurry thus obtained was stirred occasionally. The mixture was then diluted with water and extracted with CH_2Cl_2 (3 × 10 ml). The extracts were combined, dried over anhydrous sodium sulphate, filtered, and evaporated under reduced pressure. A colourless residue resulted which was adsorbed onto a narrow column of alumina (neutral, Activity II, 1.5 g). The column was then eluted successively with (*i*) 50 ml *n*-hexane and (*ii*) 50 ml 10% anhydrous ether in *n*-hexane. The latter solvent eluted 6 mg of thiobinupharidine from the column, $[\alpha]_D^{22} + 8°$ (CH_3OH); i.r. (CCl_4) 3.59–3.88 (Bohlmann bands), 6.66 and 11.45 (furan), and unassigned absorption at 6.88, 6.91, 6.96, 7.23, 7.26, 7.65, 7.76, 8.63, 8.78, 8.89, 9.05, 9.36, 9.65, 9.74 μ; p.m.r. (220 MHz $CDCl_3$): identical with an authentic sample of **2** (5), δ 0.92 (d, J = 5.6 Hz, 6 H, 2 × CH–CH_3), 1.45 (d, superimposed on envelope, J = 11.5 Hz, H-6′a), 1.72 (d, superimposed on envelope, J = 11.5 Hz, H-6a), 1.90 (ABq, J_{AB} = 14 Hz, 2 H, C-7-CH_2-C-7′), 2.33 (ABq, J_{AB} = 11.5 Hz, 2 H, CH_2-S-), 2.81 (q, J = 11.5 and 2 Hz, 1 H, H-6e), 2.94 (q, superimposed on complex multiplet, J = 11.5 and 2 Hz, H-6′e), 6.39 (nw m, $W_{1/2}$ = 6 Hz, 2 H, furan β H), 7.25 + 7.33 (4 H furan α H), irradiation at 2.94 collapses the doublet at 1.45 into a singlet, irradiation at 1.45 collapses signal at 2.94 into a broad singlet, irradiation at 1.72 collapses signal at 2.81 into a broad singlet, irradiation at 2.81 collapses doublet at 1.72 into a singlet; p.m.r. (220 MHz C_6D_6): δ 0.78 (d, CH-CH_3, J = 5.6 Hz), 0.81 (d, J = 6.0 Hz, $CHCH_3$, with 0.78 = 6 H), 1.40 (d, J = 11.5 Hz, H-6′a), 1.92 (d, J = 11.5 Hz, 1 H, H-6a), 2.18 (ABq, J_{AB} = 14.0 Hz, 2 H, C_7-CH_2-C_7′), 2.31 (ABq, J_{AB} = 11.5 Hz, 2 H, CH_2-S), 2.80 (q, J = 10.5 and 3.5 Hz, 2 H, H-4a + H-4′a), 3.11 (q, J = 11.5 and 2 Hz, 1 H, H-6e), 3.17 (q, J = 11.5 and 2.5 Hz, 1 H, H-6′e), 6.42 (nw m, 2 H, furan β-H), 7.14 (nw m, 4 H, furan α H); irradiation at 1.92 collapsed the quartet at 3.11 into a broad singlet but the quartet at 3.17 was unaffected; irradiation at 1.40 collapsed the quartet at 3.17 into a broad singlet but the quartet at 3.11 was unaffected; mass spectrum *m/e* (relative abundance): 495 (10.3), 494 (30), 493 (5.6), 479 (0.3), 465 (0.75), 461 (2.0), 451 (0.5), 447 (1.6), 427 (1.1), 413 (0.5), 360 (2.0), 359 (8.5), 358 (1.9), 357 (2.1), 264 (1.3), 247 (1.3), 231 (10), 230 (35), 180 (10), 179 (12), 178 (100), 136 (11.5), 107 (23), 94 (40).

Reduction of Thionupharoline with Sodium Borodeuteride

Thionupharoline (20.6 mg) was dissolved in 2 ml of absolute ethanol and treated with 100 mg of sodium borodeuteride. A further 100 mg were added in four portions of 25 mg each over a period of 24 h. The slurry was stirred occasionally and kept at room temperature. After this time the reaction was worked up in the same manner as for the borohydride reduction. The resultant colourless residue was adsorbed onto a narrow column of neutral alumina (Activity II, 3 g). This was eluted with (*i*) 50 ml of *n*-hexane, (*ii*) 50 ml 10% ether in *n*-hexane, (*iii*) 50 ml 20% ether in *n*-hexane, (*iv*) 50 ml 50% ether in *n*-hexane, and (*v*) 50 ml 100% ether.

These eluants were examined by t.l.c. and mass spectrometry.

Eluant (*i*) gave no product, eluant (*ii*) gave pure monodeuteriothiobinupharidine M^+ 495 (R_f 0.51, yield, 8 mg), eluant (*iii*) gave predominantly the monoethyl

Can. J. Chem. Downloaded from www.nrcresearchpress.com by 210.87.254.5 on 09/05/12
For personal use only.

ether of thionupharoline (2 mg), mass spectrum M^+ 538, intense ion at 222 (R_f 0.42, along with traces of slower and faster moving components), eluants (*iv*) and (*v*) gave thionupharoline (8 mg) (R_f 0.36). The thiobinupharidine-6*d*, had 2% d_0, 94% d_1, and 4% d_2 by mass spectrometry; p.m.r. 220 MHz ($CDCl_3$): δ 0.92 (d, J = 5.6 Hz, 6 H, 2 × $CHCH_3$), 1.45 (d, J = 11.5 Hz, H-6′a), 1.70 (br s, superimposed on envelope, H-6a), 1.90 (ABq, J_{AB} = 14 Hz, 2 H, C-7-CH_2-C-7′), 2.33 (ABq, J_{AB} = 11.5 Hz, 2 H, CH_2-S), 2.79 (d, J = 2 Hz, 0.6 H, H-6e), 2.93 (q, J = 11.5 and 2 Hz, H-6′e, superimposed on multiplet assigned to H-4a and H-4′a; 6.39 (nw m, $W_{1/2}$ = 7 Hz, 2 H, furan β H), 7.25 and 7.33 (nw m, 4 H, furan α H). There was a slight deuterium isotope shift in signals at 1.70 and 2.79 δ; p.m.r. 220 MHz (C_6D_6): δ 0.78 (d, J = 5.6 Hz, CH-CH_3), 0.81 (d, J = 6.0 Hz, CH-CH_3, with 0.78, 6 H), 1.40 (d, J = 11.5 Hz, H-6′a), 1.93 (s, 0.35 H, H-6a), 2.18 (ABq, J_{AB} = 14.0 Hz, 2 H, C-7-CH_2-C-7′), 2.31 (ABq, J_{AB} = 11.5 Hz, 2 H, CH_2-S), 2.80 (q, J = 10.5 and 3.5 Hz, 2 H, H-4′a and H-4a), 3.10 (broadened singlet, 0.65 H, H-6e), 3.18 (q, J = 11.5 and 2 Hz, 1 H, H-6′e), 6.42 (nw m, 2 H, furan β H), 7.14 (nw m 4 H, furan α H); mass spectrum *m/e* (relative abundance): 496 (26), 495 (72), 494 (13.5), 480 (0.5), 466 (1.1), 462 (3), 452 (0.7), 448 (2.7), 428 (1.5), 414 (0.7), 361 (5), 360 (17.5), 359 (4.5), 358 (4.5), 265 (1.0), 264 (1.3), 247.5 (2.6), 232 (10), 231 (33), 230 (28), 180 (15), 179 (100), 178 (9.5), 136 (8.5), 107 (18), 94 (28).

6,6′-Dihydroxythiobinupharidine from its Diperchlorate

The diperchlorate of 6,6′-dihydroxythiobinupharidine (35 mg), m.p. 225–227° (2), was stirred with 15 ml of 20% ammonia for 30 min. The resultant oily base was extracted with CH_2Cl_2 (5 × 10 ml). These extracts were combined, dried over anhydrous sodium sulfate, filtered, and evaporated to give 22 mg of glassy residue. This was adsorbed on 4 g of neutral alumina (Activity II) and eluted with 100 ml of 20% ether in benzene to give 17.3 mg of 6,6′-dihydroxythiobinupharidine, R_f 0.18; $[\alpha]_D^{25}$ +80° (*c* 1.73, CH_2Cl_2) (LaLonde *et al.* (2) report +44.5°); u.v. λ_{max} (neutral 95% EtOH) 208 nm, ε 12 000; (acidic 95% EtOH), λ_{max}, 208 nm, ε 16 120; λ_{max_2}, 294 nm, ε 1890; i.r. (CCl_4) 2.75 nw and 2.83 br (OH), no Bohlmann band at 3.59, 6.66, and 11.45 μ (furan); p.m.r. 220 MHz ($CDCl_3$): δ 0.91 (d, J = 6.0 Hz, CH-CH_3), 0.93 (d, J = 6.5 Hz, CH-CH_3, with 0.91, 6 H), 1.85 (ABq, J_{AB} = 14.5 Hz, C-7-CH_2-C-7′), 2.33 (br s, exchangeable with D_2O, OH), 2.44 (ABq, J_{AB} = 12 Hz, 2 H, CH_2-S), 3.58 (q, J = 6 and 8 Hz, 1 H, H-4′a), 3.75 (q, J = 7 and 7.5 Hz, 1 H, H-4a), 3.98 (s, 1 H, H-6), 4.24 (s, 1 H, H-6′), 6.35 (nw m, $W_{1/2}$ = 7 Hz, 2 H, furan β H), 7.25 (nw m, $W_{1/2}$ = 5 Hz, 2 H, furan α H), 7.35 and 7.37 (nw m, $W_{1/2}$ = 3 Hz, 2 H, furan α H); p.m.r. 220 MHz (C_6D_6 + D_2O): δ 0.77 (d, J = 6.0 Hz, $CHCH_3$), 0.80 (d, J = 6.5 Hz, CH-CH_3, with 0.77 = 6 H), 2.11 (ABq, J_{AB} = 14.5 Hz, 2 H, C-7-CH_2-C-7′), 2.46 (ABq, J_{AB} = 12 Hz, 2 H, CH_2-S), 3.41 (q, J = 3.5 and 10.5 Hz, 1 H, H-4′), 3.86 (q, J = 4 and 10 Hz, 1 H, H-4), 4.23 (s, 1 H, H-6), 4.35 (s, 1 H, H-6′), 6.37 (s, $W_{1/2}$ = 3 Hz, 1 H, furan β H), 6.45 (s, $W_{1/2}$ = 3 Hz, 1 H, furan β H), 7.13 (nw m, $W_{1/2}$ = 3 Hz, furan α H), 7.29 (s, $W_{1/2}$ = 3 Hz, furan α H); mass spectrum (230°) *m/e* (relative abundance: 526 (<0.1), 509 (2.5), 508 (7), 507 (2.5), 494 (0.3), 493 (0.3), 492 (0.3), 491 (0.2), 490 (0.2), 480 (0.7), 479 (0.5), 475 (1.5), 461 (0.5), 447 (2.5), 446 (5), 445 (2), 371 (3), 302 (1), 262 (1), 261 (1), 248 (7), 231 (20), 230 (100), 229 (1.5), 228 (1.1), 216 (1.5), 178 (0.7), 176 (1), 136 (1), 107 (5), 94 (7).

Reduction of 6,6′-Dihydroxythiobinupharidine with Sodium Borohydride

6-6′-Dihydroxythiobinupharidine (100 mg) was dissolved in 10 ml methanol and treated with 100 mg sodium borohydride. The slurry was left to stand for 16 h, evaporated to dryness, and 5 ml of water was added. The aqueous solution was extracted with ether. The ethereal extracts were dried over anhydrous potassium carbonate and evaporated to dryness giving 80 mg of crude reduction product. The product was adsorbed onto neutral alumina (5 g Activity IV) and eluted with 100 ml of benzene to give 53 mg of thiobinupharidine identified by comparison of its p.m.r. spectrum and its melting point with an authentic sample of thiobinupharidine.

Reduction of 6,6′-Dihydroxythiobinupharidine with Sodium Borodeuteride

6,6′-Dihydroxythiobinupharidine (17 mg) was dissolved in 2 ml absolute ethanol and treated with 100 mg sodium borodeuteride. A further four portions of 25 mg each of borodeuteride were added over a period of 24 h. The slurry was stirred occasionally at room temperature for this period, then worked up in the usual manner to give 14.5 mg of a colourless glass; t.l.c. showed three spots, R_f 0.50 (intense), 0.27 → 0.42 (intense), and 0.15 (trace), presumed to be starting material. The product was dissolved in *n*-hexane containing the minimum amount of ether to complete dissolution, and was adsorbed onto a narrow column of neutral alumina (Activity II, 1.5 g). The column was eluted with (*i*) 50 ml *n*-hexane, (*ii*) 50 ml 5% ether in hexane, (*iii*) a further 50 ml 5% ether in hexane, (*iv*) 50 ml 25% ether in *n*-hexane, (*v*) 50 ml 50% ether in *n*-hexane. All samples were analysed by t.l.c.

Eluant (*i*) gave 4.5 mg of thiobinupharidine-6,6′-d_2, pure by t.l.c., R_f 0.5. Eluant (*ii*) gave a weak spot (R_f 0.5) and an intense spot with R_f 0.25 → 0.40. Eluants (*iii*) and (*iv*) gave intense spots with R_f 0.26 → 0.42. Eluant (*v*) showed traces of starting material at R_f 0.16. Eluants (*ii*), (*iii*), and (*iv*) were combined to give 9 mg which was adsorbed onto a further 2 g of neutral alumina (Activity II) using hexane as solvent. The column was eluted with 50 ml of *n*-hexane to give 1.5 mg (fraction *vi*), 100 ml of 20% ether in hexane to give 6.6 mg (fraction *vii*), and finally with 50 ml of ether to give less than 1 mg (fraction *viii*). Fraction *vii* showed only one spot on t.l.c., R_f 0.34 (center of spot). This was the sample used for spectroscopic analysis and deduced to be 6-hydroxy-6′-deuteriothiobinupharidine; fractions *vi* and *viii* were not further examined.

Fraction i, Thiobinupharidine-6,6′-d_2

Mass spectrometric analysis gave the following: d_0 = 1%, d_1 = 1%, and d_2 = 98%; p.m.r. 220 MHz ($CDCl_3$): δ 0.92 (J = 5.6 Hz, 6 H, 2 × $CHCH_3$), 1.45 (H-6′a, essentially disappeared), 1.70 (br s, superimposed on envelope, H-6a), 1.90 (ABq, J_{AB} = 14 Hz, 2 H, C-7-CH_2-C-7′), 2.33 (ABq, J_{AB} = 11.5 Hz, 2 H, -CH_2-S), 2.79 (d, J = 2 Hz, ~0.6 H, H-6e), 2.85 → 3.0 (complex m not well resolved, *ca.* 3 protons, H-4a + H-4′a + H-6′e), 6.39 (nw m, $W_{1/2}$ = 7 Hz, 2 H, furan β H), 7.25 + 7.33 (nw m, 4 H, furan α H); p.m.r. 220 MHz (C_6D_6): δ 0.78 (d, J = 5.6 Hz, CH-CH_3), 0.81 (d, J = 6.0 Hz, CH-CH_3, 6 H with 0.78), 1.40 (H-6′a, essentially disappeared), 1.93 (s, 0.4 H, H-6a), 2.18 (ABq, J_{AB} = 14.0 Hz, 2 H, C-7-CH_2-C-7′), 2.31 (ABq, J_{AB} = 11.5 Hz, 2 H, CH_2-S), 2.80 (q, J = 10.5 and 3.5 Hz, 2 H, H-4′a + H-4a),

3.10 (poorly resolved doublet $J \simeq 2$ Hz, 0.6 H, H-6e), 3.16 (poorly resolved doublet, $J \simeq 2$ Hz, 1 H, H-6′e); mass spectrum *m/e* (relative abundance): 497 (17), 496 (47), 495 (9), 481 (0.3), 467 (0.9), 463 (1.9), 453 (0.5), 449 (1.6), 429 (1.1), 415 (0.45), 362 (3), 361 (14), 360 (3), 359 (3), 248 $M^+/2$ (2.5), 232 (10), 231 (32), 230 (16), 181 (10), 180 (13.5), 179 (100), 178 (4.5), 136 (8), 107 (17.5), 94 (24).

Fraction vii, 6-Hydroxythiobinupharidine-6′-d

Mass spectrometric analysis showed 2% d_0 and 98% d_1; u.v. (95% EtOH neutral) end absorption only, (95% acidic EtOH) λ_{max_1} 208 nm, ε 21 000, λ_{max_2} 289 nm, ε 2640. The diperchlorate salt was recrystallized from MeOH at −5 °C; m.p., 260° softens), 266–269° (liquid), 278° (decomposes); p.m.r. 220 MHz ($CDCl_3$): δ 0.88 (d, $J = 5.0$ Hz, 6 H, 2 × $CHCH_3$), 2.21 (ABq, $J_{AB} = 12$ Hz, 2 H, CH_2-S), 2.26 (s, 1 H, exchangeable with D_2O, OH), 2.90 q, $J = 5.6$ and 8 Hz, H-4′a), 2.92 (br s superimposed on q at 2.90, total 2 H, H-6′e), 3.70 (q, $J = 7.5$ and 7 Hz, 1 H, H-4), 3.97 (s, 1 H, H-6), 6.34 (nw m, $W_{1/2} = 7$ Hz, 2 H, furan β H), 7.21 (nw m, 1 H, furan α H), 7.30 (nw m, $W_{1/2} = 4$ Hz, 3 H, furan α H); p.m.r. 220 MHz (C_6D_6): δ 0.75 (two superimposed doublets, $J = 6.0$ Hz, 6 H, 2 × $CHCH_3$), 2.11 (ABq, $J_{AB} = 12$ Hz, 2 H, CH_2-S), 2.42 [br s, 1 H (exchangeable with D_2O), OH] 2.75 (q, $J = 3.5$ and 10.5 Hz, 1 H, H-4′), 3.15 (d, $J = 2.0$ Hz, 1 H, H-6′e), 3.86 (q, $J = 10$ and 4 Hz, 1 H, H-4), 4.24 (s, 1 H, H-6), 6.38 (nw m, $W_{1/2} = 3$ Hz, 1 H, furan β H), 6.44 (nw m, 1 H, $W_{1/2} = 3$ Hz, furan β H), 7.13 (nw m, 3 H, furan α H), 7.25 (nw m, $W_{1/2} = 3$ Hz, 1H, furan α H); mass spectrum (200°) *m/e* (relative abundance): 511 (72), 510 (9), 495 (12), 494 (52), 493 (90), 482 (6), 478 (4), 465 (7), 460 (4), 446 (6), 432 (2), 376 (22), 360 (10), 305 (11), 231 (52), 230 (100), 229 (22), 228 (20), 179 (26), 178 (52), 176 (30), 136 (20), 107 (37), 94 (48).

We thank the National Research Council of Canada for financial support of this work carried out at McMaster University. One of us, T. I. Martin, wishes to acknowledge the award of an NRC postgraduate scholarship for the years 1971–1974. The assistance of Dr. A. Gray and Mrs. V. Robinson of the 220 MHz n.m.r. Centre at Sheridan Park is gratefully acknowledged.

1. J. T. Wróbel. Rocz. Chem. **44**, 457 (1970).
2. R. T. LaLonde, C. F. Wong, and W. P. Cullen. Tetrahedron Lett. 4477 (1970).
3. R. T. LaLonde and C. F. Wong. Phytochemistry, **11**, 3305 (1972).
4. G. I. Birnbaum. Tetrahedron Lett. 4149 (1965).
5. J. T. Wróbel, B. Bobeszko, T. I. Martin, D. B. MacLean, N. Krishnamachari, and C. Calvo. Can. J. Chem. **51**, 2810 (1973).
6. R. T. LaLonde, C. F. Wong, and K. C. Das. J. Am. Chem. Soc. **95**, 6342 (1973).
7. C. F. Wong and R. T. LaLonde. J. Org. Chem. **38**, 3225 (1973).
8. K. Oda and H. Koyama. J. Chem. Soc. B, 1450 (1970).
9. C. F. Wong, E. Auer, and R. T. LaLonde. J. Org. Chem. **35**, 517 (1970).
10. R. T. LaLonde, E. Auer, C. F. Wong, and V. P. Muralidharan. J. Am. Chem. Soc. **93**, 2501 (1971).
11. R. T. LaLonde, J. T. Woolever, E. Auer, and C. F. Wong. Tetrahedron Lett. 1503 (1972).
12. F. Bohlmann, E. Winterfeldt, P. Studt, H. Laurent, G. Boroschewski, and K. Kleine. Chem. Ber. **94**, 202 (1961).
13. I. Kawasaki, S. Matsutani, and T. Kaneko. Bull. Chem. Soc. Japan, **36**, 1474 (1963).
14. C. F. Wong and R. T. LaLonde. Phytochemistry, **9**, 659 (1970).
15. O. Achmatowicz and J. T. Wróbel. Tetrahedron Lett. 129 (1964).
16. R. T. LaLonde, C. F. Wong, and H. G. Howell. J. Org. Chem. **36**, 3703 (1971).
17. M. Murrier. Bull. Soc. Chim. Fr. **33**, 846 (1951).
18. B. L. Loev and M. M. Goodman. Chem. Ind. 2026 (1967).
19. B. L. Loev and K. M. Snader. Chem. Ind. 15 (1965).
20. K. Biemann. Mass spectrometry: organic chemical applications. McGraw-Hill Book Co., Inc., New York. 1962.

Can. J. Chem. Downloaded from www.nrcresearchpress.com by 210.87.254.5 on 09/05/12
For personal use only.

The Stereospecificity of α-Thiohemiaminal Reduction. A 300 MHz Proton Magnetic Resonance Investigation of Deuteride Reduction Products from 6,6′-Dihydroxythiobinupharidine and 6-Hydroxythiobinupharidine[1]

ROBERT T. LALONDE, CHUN F. WONG, AND KALA C. DAS

Department of Chemistry, SUNY College of Environmental Science and Forestry, Syracuse, New York 13210

Received February 4, 1974

ROBERT T. LALONDE, CHUN F. WONG, and KALA C. DAS. Can. J. Chem. **52**, 2714 (1974).

Thiobinupharidine-6-d_1 and thiobinupharidine-6,6′-d_2, products obtained earlier from the sodium borodeuteride reduction of 6-hydroxythiobinupharidine and 6,6′-dihydroxythiobinupharidine, were examined in perdeuteriobenzene solution by 300 MHz p.m.r. Thiobinupharidine-6-d_1 was found to contain 84% equatorial deuterium and 16% axial deuterium at the C-6 position. Thiobinupharidine-6,6′-d_2 was found to contain 82% equatorial deuterium and 18% axial deuterium at C-6.

ROBERT T. LALONDE, CHUN F. WONG et KALA C. DAS. Can. J. Chem. **52**, 2714 (1974).

Thiobinupharidine-6-d_1 et thiobinupharidine-6,6′-d_2, produits obtenus précédemment à partir de la réduction par la borodeutérure de sodium des 6-hydroxythiobinupharidine et 6,6′-dihydroxythiobinupharidine, ont été examinés dans une solution de perdeutériobenzene à 300 MHz r.m.n. Thiobinupharidine-6-d_1, s'est avéré contenir 84% de deutérium équatorial et 16% de deutérium axial en position C-6. Thiobinupharidine-6,6′-d_2 s'est avéré contenir 82% de deutérium équatorial et 18% de deutérium axial en C-6.

Can. J. Chem. Downloaded from www.nrcresearchpress.com by 210.87.254.5 on 09/05/12
For personal use only.

In an earlier publication (1) we reported on the sodium borohydride reduction of several α-thiohemiaminals of the Nuphar alkaloid family. Among these hemiaminals were 6-hydroxythiobinupharidine, **1**, 6,6′-dihydroxythiobinupharidine, **2**, and 6,6′-dihydroxythionuphlutine-B, **3**. We reported that deuteride reduction of **1** and **2** resulted in stereospecific incorporation of equatorial deuterium at C-6 giving **4** and **5** respectively. But incorporation of axial deuterium at the same position was observed in the case of **3**. On the basis of these results, the conformation of the sulfur atom at C-7 in **2** and **3** was assigned and this assignment constituted an important point in our overall assignment of relative stereochemistry to thiobinupharidine **6** and thionuphlutine-B, **7**.

Our earlier determination of the stereochemistry of deuteride reduction at C-6 of the bishemiaminals had rested on 60 MHz p.m.r. spectra determined in deuteriochloroform solution. We employed the chemical shift positions of the p.m.r. of deoxynupharidine as well as decoupling experiments as a basis for locating the positions of the C-6 and -6′ equatorial and

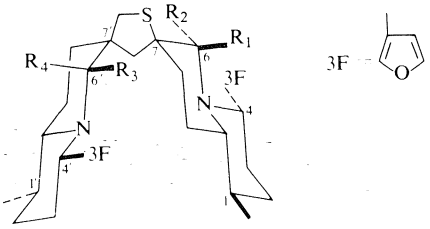

1 $R_1 = R_3 = R_4 = H$; $R_2 = OH$
2 $R_1 = R_3 = H$; $R_2 = R_4 = OH$
4 $R_1 = R_3 = R_4 = H$; $R_2 = D$
5 $R_1 = R_3 = H$; $R_2 = R_4 = D$
6 $R_1 = R_2 = R_3 = R_4 = H$

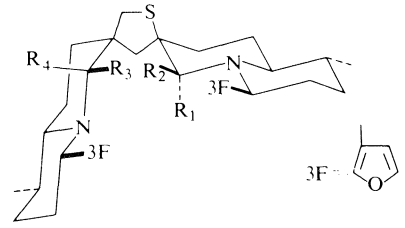

3 $R_1 = R_4 = OH$; $R_2 = R_3 = H$
7 $R_1 = R_2 = R_3 = R_4 = H$

axial protons in the C_{30} thiospiranes **6** and **7**. Thus a comparison of the 60 MHz integration values of the spectral region containing C-4 axial and C-6 equatorial protons against the integration of the higher field region containing all of

[1]Support of this work by the National Institute of Health, U.S. Public Health Service (Grant No. AI 10188) is gratefully acknowledged.

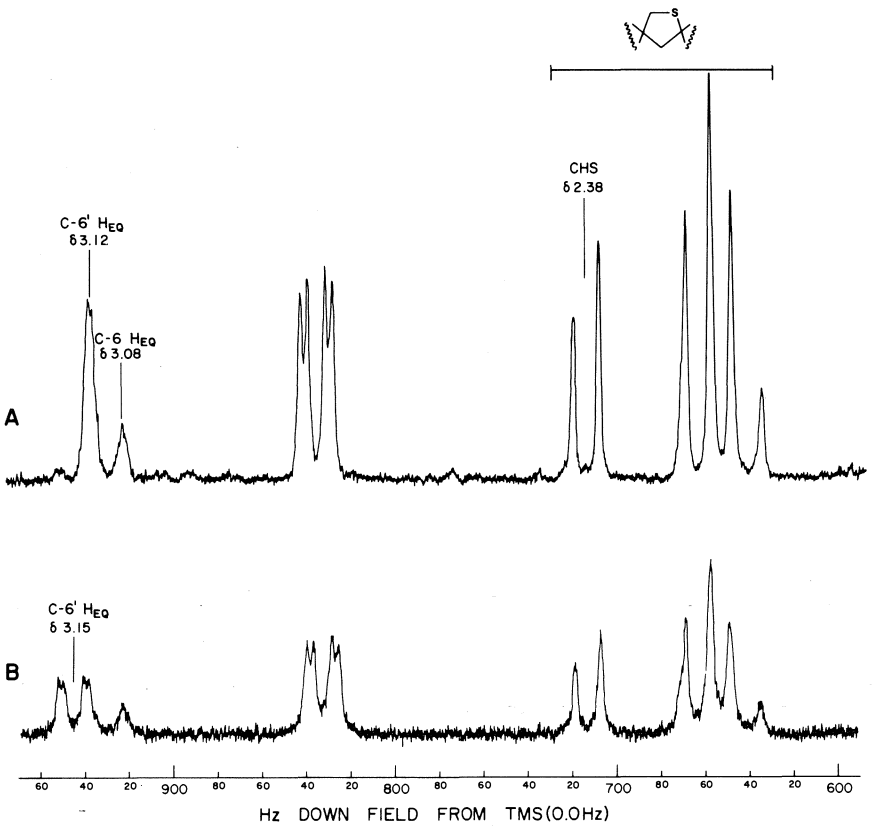

FIG. 1. 300 MHz p.m.r. spectra of: (*A*) thiobinupharidine-6,6′-d_2, **5**; (*B*) thiobinupharidine-6-d_1, **4**.

the remaining protons was done in order to ascertain the loss of C-6 equatorial protons and thus establish the extent to which C-6 equatorial protium had been replaced by deuterium. In the case of the deuteride reduction of the monohemiaminal **1**, a similar analysis was employed although a 100 MHz p.m.r. determination in perdeuteriobenzene solution was used to establish the stereochemistry of deuterium at the C-6 position.

Recently we have learned from Prof. MacLean that, in the hands of his co-workers, the deuteride reduction of the α-thiohemiaminals **1** and **2** are not reduced at C-6 with the same high degree of stereospecificity that we had observed (2).[2] Because our results have been questioned, we have reexamined the p.m.r. spectra of the deuteride reduction products of **1** and **2**.

We had discovered some time ago, in our p.m.r. work with the C_{15} nuphar alkaloids, the effectiveness of the benzene induced shift in ascertaining the stereochemistry of methyl groups substituted on piperidine (3) and quinolizidine (4) rings. Thereafter, we extended the use of this solvent to the more complex p.m.r. of the C_{30} thiospirane alkaloids in order to obtain better separation of resonance signals, as for example in the 100 MHz p.m.r. spectrum of thiobinupharidine-6-d_1, (1). Thus the re-examination of the deuterium labeled thiobinupharidines involved the 300 MHz p.m.r. determined in perdeuteriobenzene solution in order to achieve the best possible separation of resonance signals.[3] The most important region of the spectra is shown in Fig. 1. Using one of the two thiomethylene protons (δ 2.38) as the standard

[2]We wish to thank Prof. D. B. MacLean for sending us a copy of his manuscript which discloses his results which appear in this issue (see ref. 2).

[3]The 300 MHz p.m.r. spectra of thiobinupharidine-6-d_1 and thiobinupharidine-6,6′-d_2 were determined in perdeuteriobenzene solution in 5 mm tubes by E. R. Santee, Jr., NMR Research Center, Institute of Polymer Science, The University of Akron, using a SC 300 NMR spectrometer operating in the sweep mode. Sweep widths of 2500 and 500 Hz were employed. Chemical shifts were determined relative to TMS, δ 0.0.

Can. J. Chem. Downloaded from www.nrcresearchpress.com by 210.87.254.5 on 09/05/12
For personal use only.

for integration, thiobinupharidine-6-d_1, (24% d_0, 76% d_1),[4,5] **4**, contains 1.13 protons in the δ 3.05–3.20 region, the proton in excess of 1.00 being the signal at δ 3.08 which arises in part from the labeled species containing a C-6 equatorial hydrogen and a C-6 axial deuterium. The doublet of a doublet centered at δ 3.15 represents the C-6′ equatorial proton which is coupled in the W-mode to the C-8′ equatorial proton and in the geminal manner to the C-6′ axial proton. Using all the methylene protons of the tetrahydrothiophene ring as the integration standard, the same result is obtained. Employing the same method of analysis for thiobinupharidine-6,6′-d_2 (6% d_0, 24% d_1, and 71% d_2), **5**, we observe 1.14 protons in the δ 3.05–3.20 region. The doublet at δ 3.12 represents the C-6′ equatorial proton coupled only to the C-8 equatorial proton since the C-6′ axial protium is now replaced by deuterium. These analyses give values of 84 and 82%, respectively, for the amount of C-6 equatorial deuterium in **4** and **5** after correction for the amount of C-6-d_0 species.[6] It is noteworthy that duplicate sodium borodeuteride reductions of 6-hydroxythiobinupharidine had been carried out by two of us[7] with the same result.

Both quantitatively and qualitatively, the 300 MHz p.m.r. study reveals that indeed some axial incorporation of deuterium has taken place at C-6 but essentially our earlier results are vindicated and differ from those of MacLean and coworkers. While conditions used by the latter group appear to be the same as we had used there is in fact a subtle difference. The three deuterium samples which we have studied by p.m.r. were obtained by reduction of the hemiaminal in methanol solution (1). No precautions were taken to dry the methanol. MacLean reports (2) that his reductions were carried out in dry ethanol. It is not yet clear why this difference in solvent should change the amount of equatorial deuteration. Regardless, it is remarkable that any equatorial incorporation of deuterium takes place at all since such incorporation must occur by attack of deuteride on the more highly hindered concave α face of the immonium ion. Moreover the occurrence of equatorial incorporation of deuterium at C-6 should be considered along with the near C_2 symmetry of thiobinupharidine and the fact that incorporation of deuterium at C-6′ is completely axial (1, 2).

[4]Singly and doubly labeled samples (**4** and **5**) had been obtained (ref. 1) by reducing the mono- and bishemiaminals with sodium borodeuteride purchased from Merck Sharp and Dohme who indicate that the reducing agent contains a minimum of 98% deuterium.

[5]A referee has requested that we comment on the anomalously low content of deuterium in the singly and doubly labeled thiobinupharidines. The isotopic compositions given were determined by mass spectrometry (ref. 1) which possibly gives low values for d_1 and d_2 because of the inaccuracies associated with comparing peak intensities in labeled and unlabeled samples when large $M^+ - 1$ peaks are observed. Thiobinupharidine does in fact exhibit a large $M^+ - 1$ peak. A second possibility for the low deuterium content may be the greater reactivity of sodium borohydride, relative to sodium borodeuteride, which results from the isotope effect. Typically, 16- to 20-fold excesses of reducing agent were used in deuteride and hydride reductions. Therefore if the sodium borodeuteride contained the minimum amount of deuterium (98%) and if all the sodium borohydride of a 20-fold excess reacted with the hemiaminal before any deuteride reacted, then a minimum of 60% of d_1 species would result from a monohemiaminal. Obviously the hemiaminals are not completely selective for hydride reduction as indicated in this hypothetical case but only partly so. Therefore the d_1 species will exceed 60%.

1. R. T. LaLonde, C. F. Wong, and K. C. Das. J. Am. Chem. Soc. **95**, 6342 (1973).
2. T. I. Martin, D. B. MacLean, J. T. Wróbel, A. Iwanow, and W. Starzec. Can. J. Chem. This issue.
3. C. F. Wong and R. T. LaLonde. Phytochemistry, **9**, 1851 (1970).
4. C. F. Wong and R. T. LaLonde. Phytochemistry, **9**, 659 (1970).

[6]A fraction of the proton signals in the δ 3.05–3.20 region in excess of 1.00 proton results from C-6-d_0 and C-6′-d_0 species. Corrections for the amount of C-6-d_0 and C-6′-d_0 species were made by using the integration value for the residual C-6 axial doublet centered at δ 1.93 and, in the case of **5**, the integration value for the residual C-6′ equatorial doublet of a doublet centered at δ 3.15.

[7]C. F. W. and K. C. D.

Can. J. Chem. Downloaded from www.nrcresearchpress.com by 210.87.254.5 on 09/05/12
For personal use only.

Sorption and Diffusion of *n*-Heptane in 5A Zeolite

I. H. DOETSCH, D. M. RUTHVEN, AND K. F. LOUGHLIN

Department of Chemical Engineering, University of New Brunswick, Fredericton, New Brunswick

Received February 11, 1974

I. H. DOETSCH, D. M. RUTHVEN, and K. F. LOUGHLIN. Can. J. Chem, **52**, 2717 (1974).

Kinetic and equilibrium data for sorption of *n*-heptane in 5A zeolite are presented and discussed in relation to previously reported data for the C_2–C_4 hydrocarbons in the same zeolite.

A satisfactory interpretation of the equilibrium data is obtained on the basis of a simple theoretical model in which it is assumed that there are, within each cavity of the zeolite lattice, two distinct and energetically different adsorption sites. These sites may correspond to the region close to the cavity wall in which adsorption is energetically favorable, giving rise to localized adsorption, and the central region of the cavity in which the sorbate is less strongly bound with greater rotational and translational freedom. The differential diffusivity increases strongly with sorbate concentration and, as with the lighter hydrocarbons, the form of this concentration dependence may be satisfactorily explained by considering the driving force for the transport process to be the gradient of chemical potential. The limiting diffusional activation energy for *n*-heptane is 7.5 kcal and this value is somewhat higher than the activation energy for the lighter paraffins.

I. H. DOETSCH, D. M. RUTHVEN, et K. F. LOUGHLIN. Can. J. Chem. **52**, 2717 (1974).

On établit les données d'équilibre et la cinétique de l'adsorption du *n*-heptane sur la zéolithe 5A. Ces résultats sont discutés en fonction des données déjà publiées pour l'adsorption des hydrocarbures C_2–C_4 sur la même zéolithe.

Une interprétation satisfaisante des données de l'équilibre est établie: elle s'appuie sur un modèle théorique simple pour lequel on suppose qu'il existe deux sites d'adsorption distincts énergiquement différents à l'intérieur de chaque cavité du réseau de la zéolithe. Ces sites peuvent correspondre à une région proche de la paroi de la cavité dans laquelle l'adsorption est énergiquement favorable, donnant lieu à une adsorption localisée, et à la région centrale de la cavité où le produit d'adsorption, qui a une plus grande liberté rotationnelle et translationnelle, est moins fortement lié. La diffusivité différentielle augmente rapidement avec la concentration du produit d'adsorption. Comme pour les hydrocarbures plus légers, la forme de cette variation peut être expliquée d'une manière satisfaisante en considérant que la force nécessaire au procédé de transport est le gradient du potentiel chimique.

L'énergie d'activation de diffusion limite pour le *n*-heptane est 7.5 kcal et cette valeur est légèrement plus élevée que l'énergie d'activation des paraffines plus légères.

[Traduit par le journal]

Recent studies of the sorption and diffusion of light hydrocarbons (C_1–C_4) in type A zeolites have revealed some striking regularities of behavior (1, 2) and it is therefore pertinent to enquire whether or not these features are common to the higher hydrocarbons. For sorption in zeolite T (a synthetic intergrowth of offretite and erionite) it has been shown that the pattern of variation of diffusivity with hydrocarbon chain length may be complex (3). Although the sorption of medium chain hydrocarbons in 5A zeolite has been the subject of several studies (4–9), published experimental data are limited and conflicting conclusions have been drawn. Previous kinetic studies have generally relied on integral measurements of transient uptake curves over comparatively large concentration steps and the results of such measurements can easily conceal the true concentration dependence of the differential diffusivity. The present paper describes the results of a detailed kinetic study of the sorption of *n*-heptane in 5A zeolite, carried out by the differential method (10). The diffusivities so obtained show similar general trends to those observed for the lighter hydrocarbons. Although the study was originally concerned primarily with adsorption kinetics extensive equilibrium data were also obtained and these have been analyzed in terms of simple theoretical models.

Experimental

Equilibrium isotherms and transient sorption curves were measured gravimetrically using a Cahn vacuum microbalance system to follow the change in weight of a

Can. J. Chem. Downloaded from www.nrcresearchpress.com by 210.87.254.5 on 09/05/12
For personal use only.

small sample of 5A zeolite crystals when subjected to a differential step change in heptane pressure. Pressures were measured with a Barocel electronic manometer. The quantity of sorbate adsorbed or desorbed during an experiment was generally less than 2% of the saturation concentration and the volume of the system was sufficiently large so as to ensure that there was no significant change in pressure during the course of a run. The experimental technique and the method by which diffusivities were calculated from the sorption curves have been described elsewhere (10).

The heptane (99% +, Matheson, Coleman and Bell) was vacuum distilled within the system and only the middle fraction was retained. The sample of 5A zeolite was from Linde Lot No. 550043, with a mean cube side (2 μ) of 3.91 μ, as determined by photomicrography (10). Prior to the experimental measurements the zeolite sample was degassed at 400 °C, 10^{-5} Torr for several hours.

Equilibrium Isotherms

Equilibrium isotherms were determined at four temperatures between 409 and 491 °K. The saturation limits obtained by linear extrapolation of a plot of sorbate concentration against the square of the adsorption potential (11) was almost exactly 2 molecules per cavity which is somewhat smaller than the quotient of the cavity volume and the van der Waals co-volume of the sorbate molecule (~2.25 molecules/cavity). The theoretical model isotherm, which has been found to provide a satisfactory interpretation of the equilibrium data for the light hydrocarbons (C_2–C_4) (12), does not provide a satisfactory representation of the heptane isotherms. The data were therefore correlated initially in terms of a general empirical virial expression

$$[1] \qquad \ln(p/c) = A_0 + A_1c + A_2c^2 \ldots$$

as suggested by Barrer and Gibbons (13) and by Kiselev (14). (In this expression p represents sorbate pressure, c is adsorbed phase concentration, and the coefficients A_i are empirical, temperature dependent constants.)

Henry's law equilibrium constants ($K = e^{-A_0}$), calculated from the intercepts of plots of $\log(p/c)$ *vs.* c extrapolated to zero concentration, are given in Table 1 and the corresponding values of K_0 and q_0 ($K = K_0e^{q_0/RT}$) are given in Table 2. The value of q_0 agrees well with the experimental value given by Grossmann *et al.* (15) and is within the range of values estimated from the group contributions and from the linear correlation given by Schirmer (16).

Some information concerning the state of the sorbed molecule may be obtained from the magnitude of the standard entropy of sorption ΔS^0 which, referred to standard states of unit concentration in the gaseous and adsorbed phases, is related to K_0 by the expression

$$[2] \qquad \Delta S^0 = R \ln (K_0kTne)$$

where k is Boltzmann's constant, R is the gas constant, and n is the number of α cavities per unit crystal volume. A lower limit to the magnitude of ΔS^0 may be estimated theoretically from a simple model in which it is assumed that the adsorbed molecules are confined within particular cavities but not adsorbed at specific localized sites within the cavity. It is assumed that the adsorbed molecule has the same rotational and internal vibrational freedom as in the gas phase and that the motion of the center of gravity of the molecule can be represented as three dimensional translation within the free volume of the cavity (ϕ). For such a system

$$[3] \qquad \phi = K_0kTe^2$$

and

$$[4] \qquad \Delta S^0 = R \ln (\phi n/e)$$

For the C_1–C_4 hydrocarbons in both 5A zeolite and in chabazite the values of K_0 (or ΔS^0) calculated from eqs. 3 and 4, using values of ϕ estimated from the free diameter of the cavity and the van der Waals radius of the sorbate, are close to the experimental values, suggesting that the sorbate molecules are essentially freely rotating and non-localized within the cavities (1). Values of K_0 and ΔS^0 calculated in the same way for *n*-heptane are compared with the experimental values in Table 2. It is clear that the experimental value of ΔS^0 derived from the equilibrium data is considerably greater (numerically) than the value estimated from the simple model. This difference suggests either localization of the sorbed molecules with the cavity or loss of rotational freedom. In this respect adsorbed heptane differs significantly from the light hydrocarbons but such differences are perhaps to be expected in view of the increased length and flexibility of the molecule.

Taken in conjunction with the evidence from the entropy data, the precise saturation limit of two molecules per cavity and the lack of variation of this limit with temperature suggest localized sorption with two sites per cavity. We therefore consider four simple theoretical models

Can. J. Chem. Downloaded from www.nrcresearchpress.com by 210.87.254.5 on 09/05/12
For personal use only.

TABLE 1. Henry constants and interaction energies calculated from various model isotherms (values of K are in molecules/cavity-Torr)

	Virial	Equation 6		Equation 7		Equation 8	
T(°K)	K	K	$2w$	K	$2w$	K_1	K_2
409	28.0*	26.5*	—	29.0*	0.51	23*	7.5*
439	7.4	6.9	0.43	7.1	0.48	5.85	1.23
462	2.75	2.4	0.65	2.45	0.68	2.11	0.34
491	0.99	0.87	1.03	0.82	0.95	0.73	0.087

*Determined by extrapolation of the van't Hoff plots since the 409 °K isotherm did not extend to sufficiently low concentrations to allow reliable calculation of the model parameters.

TABLE 2. Values of K_0, q_0, and ΔS^0 for sorption of *n*-heptane in 5A zeolite (K_0 is in molecule/cavity-Torr, q_0 in kcal/mol, and ΔS^0 in cal/mol deg.)

	Experimental values			Theoretical values		
	q_0	$K_0 \times 10^8$	ΔS^0	q_0	$K_0 \times 10^8$	ΔS^0
Equation 6	17.0	2.24	−12.9			
Equation 7	17.9	0.83	−14.8		31.9*	−7.6*
Equation 8: K_1	16.9	2.24	−12.9	15.68†	1.02†	−9.9†
K_2	21.8	0.0018	−20.0	36.8‡	2.6×10^{-9}‡	−53.8‡
Virial	16.7	3.5	−12.0			
Grossmann *et al.* (15)	17.0	—	—			
Schirmer (16)	16.2–18.4	—	—			

*Theoretical values of K_0 and ΔS° calculated according to eqs. 2 and 3 with $\phi = 110$ Å^3, this being the value estimated from the free diameter of the cavity and the van der Waals diameter of the heptane molecule (5.46 Å).
†Values calculated from theoretical entropy and energy for non-localized (volume absorbed) species. (18)
‡Values calculated from theoretical entropy and energy for localized (wall adsorbed) species (18).

representing localized sorption (17):

(*i*) Ideal localized sorption (Langmuir):

$$[5] \qquad \frac{\theta}{p(1-\theta)} = b$$

(*ii*) Localized sorption with weak interaction between molecules on neighboring sites (pair interaction energy = $2w$):

$$[6] \qquad \frac{\theta}{p(1-\theta)} = b \exp\left(-\frac{2w\theta}{RT}\right)$$

(*iii*) Sorption on a system of independent pairs of equivalent sites with interaction energy $2w$ when both sites of a pair are occupied:

$$[7] \qquad c = \frac{Kp + \frac{1}{2}(Kp)^2 \, e^{-2w/RT}}{1 + Kp + \frac{1}{4}(Kp)^2 \, e^{-2w/RT}}$$

(*iv*) Sorption with negligible interaction between adsorbed molecules on a set of independent pairs of nonequivalent sites:

$$[8] \qquad c = \frac{K_1 p}{1 + K_1 p} + \frac{K_2 p}{1 + K_2 p}$$

In these expressions $\theta = c/c_s$, c_s is the saturation limit (two molecules per cavity), b is an equilibrium constant, and $K = bc_s$ is a Henry constant.

The validity of eqs. 5 and 6 may be tested by plotting $\log \theta/p(1-\theta)$ *vs.* θ as shown in Fig. 1. It is evident that the simple Langmuir model is not adequate to describe this system but that eq. 6 does provide a satisfactory representation of the isotherms up to about 70% of saturation. The Henry constants obtained from this model are in satisfactory agreement with the values from the virial extrapolation (see Table 1) and the values derived for w (200–500 cal/mol) suggest a weak repulsive interaction between sorbed molecules which increases with increasing temperature.

The experimental isotherms were fitted directly to eq. 7 using a least squares criterion of best fit to calculate the values of the parameters K and w. The values so obtained (see Table 1) are similar to the values obtained from eq. 6 and it may be seen from Fig. 2 that the model provides

Can. J. Chem. Downloaded from www.nrcresearchpress.com by 210.87.254.5 on 09/05/12
For personal use only.

Can. J. Chem. Downloaded from www.nrcresearchpress.com by 210.87.254.5 on 09/05/12
For personal use only.

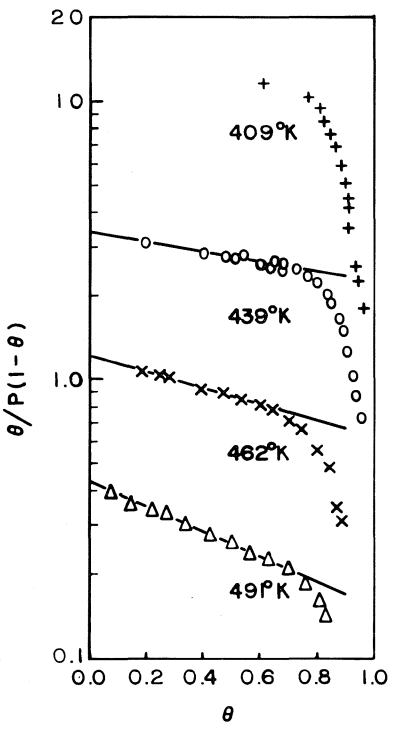

FIG. 1. Variation of log $[\theta/p(1-\theta)]$ with θ for sorption of heptane in 5A zeolite.

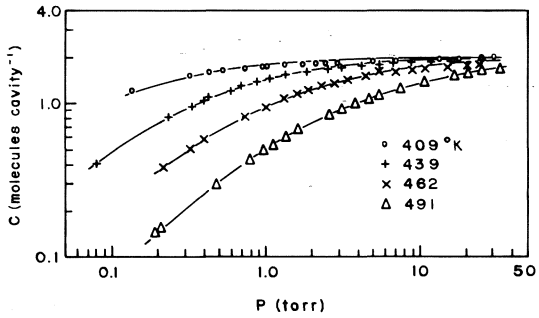

FIG. 2. Equilibrium isotherms for sorption of heptane in 5A zeolite (comparison of experimental points with theoretical curves calculated from eqs. 7 or 8).

an excellent fit of the experimental data over the entire concentration range. The difference between the isotherms given by eqs. 6 and 7 is, however, small and although eq. 7 gives a somewhat better fit in the high concentration region, this improvement is at least partly attributable to the method by which the model parameters were obtained.

Equation 8 may be written as

$$[9] \qquad c = \frac{(K_1 + K_2)p + 2K_1K_2p^2}{1 + (K_1 + K_2)p + K_1K_2p^2}$$

which becomes identical with eq. 7 if $K_1 + K_2 = K$ and $K_1K_2 = \frac{1}{4}K^2 \exp(-2w/RT)$. Thus, with the appropriate values of K_1 and K_2, which are given in Table 1, eqs. 7 and 8 give the same fit of the experimental isotherms (Fig. 2). The van't Hoff plot showing the temperature dependence of K_1 and K_2 is shown in Fig. 3 and the values of K_0 and q_0 ($K_1 = K_{01} \exp(q_1/RT)$; $K_2 = K_{02} \exp(q_2/RT)$) are given in Table 2 together with the corresponding values of ΔS^0 calculated according to eq. 2.

Applied to the present system, eq. 8, which is the sum of two Langmuir terms, implies that each cavity contains one site of each type and that sorbate–sorbate interaction is negligible even when both sites within a given cavity are occupied. In a recent theoretical paper Spangenberg *et al.* (18) have suggested that *n*-paraffins are adsorbed within the type A zeolite lattice in both localized and non-localized forms and that each cavity can accommodate one molecule of each type. The localized molecules are considered as strongly adsorbed in the region of low potential energy near the cavity wall (low energy, low entropy) while the non-localized molecules are assumed to have essentially complete rotational and translational freedom within the

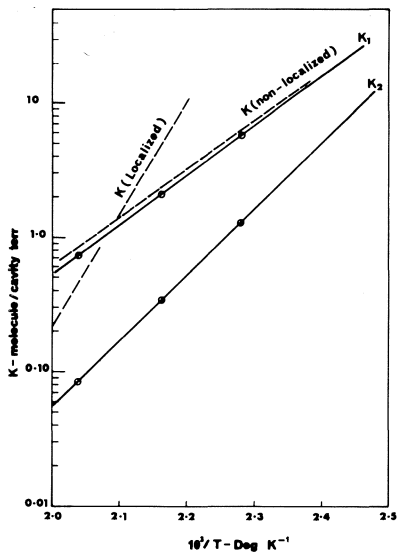

FIG. 3. Van't Hoff plot showing comparison between values of K_1 and K_2 calculated from equilibrium isotherms with theoretical values of K for localized and non-localized adsorbed species.

Can. J. Chem. Downloaded from www.nrcresearchpress.com by 210.87.254.5 on 09/05/12
For personal use only.

central region of the cavity (higher energy and entropy). Using theoretical potential profiles calculated from the Kirkwood–Müller expressions and by making several approximations concerning the internal freedom of the sorbed molecules, values for the entropies and energies of the two forms were estimated (18) (see Table 2). It is clear that the model described by eq. 8 is entirely consistent with Spangenberg's theory if it is assumed that the two different sites refer to the wall and central regions of the cavity. The values of K for both localized and mobile adsorbed species, calculated from the theoretically estimated entropies and energies, are compared in Fig. 3 with the experimental values of K_1 and K_2 obtained by matching the experimental isotherms to eq. 8. There is excellent agreement between K_1 and the theoretical value of K for the non-localized adsorbed species but the agreement between K_2 and the theoretical value for the localized species is less satisfactory. The approximations involved in the theoretical estimation of both the entropy and the energy are however far more severe for the wall adsorbed species than for the non-localized form of adsorbed molecule in the central region of the cavity and the discrepancy is therefore perhaps not surprising.

It appears that over the range of temperatures covered by the present study the mobile form of the adsorbed molecule is dominant (equilibrium constant K_1) except as the saturation limit is approached. However, extrapolation of the van't Hoff plot indicates that at temperatures below 345 °K the wall adsorbed species (equilibrium constant K_2) will become the dominant form. Such a transition can explain the anomalous maximum in the heat capacity – temperature curve for this system and is predicted by the theoretical calculations of Spangenberg *et al.* (18), although at a somewhat higher temperature (400–500 °K).

The variation of isosteric heat (q) with sorbate concentration may be derived, in principle, from eq. 8 but it is not possible to obtain an explicit expression in terms of concentration. An explicit form may however be obtained in terms of pressure:

$$[10] \quad q = RT^2\left(\frac{\partial \ln p}{\partial T}\right)_c = \frac{q_1K_1(1 + K_2p)^2 + q_2K_2(1 + K_1p)^2}{K_1(1 + K_2p)^2 + K_2(1 + K_1p)^2}$$

For the limiting cases this expression gives

$$[11] \quad p \to 0, \; c \to 0, \qquad q \to \frac{q_1K_1 + q_2K_2}{K_1 + K_2}$$

$$[12] \quad p \to \infty, \; c \to 2, \qquad q \to \frac{q_1K_2 + q_2K_1}{K_1 + K_2}$$

Linear isosteres are therefore to be expected only over limited ranges of temperature. If $q_2 > q_1$, the isosteric heat will increase with concentration at temperatures above the temperature at which $K_1 = K_2$ while at lower temperatures the opposite trend is to be expected. At the crossover temperature the isosteric heat should be independent of concentration and equal to $(q_1 + q_2)/2$.

In Fig. 4 isosteric heats calculated from the experimental isosteres are compared with the values calculated according to eq. 10 with the parameters given in Tables 1 and 2 (for the mean temperature of the experimental data). The experimental values are subject to some uncertainty but the trend is quite clear and is correctly predicted by eq. 10. A similar increase in isosteric heat with sorbate concentration has been observed for the lighter paraffins in 5A zeolite (19). Further experimental measurements would be required, at lower temperatures, to establish whether or not the isosteric heat shows the predicted temperature dependence but the low temperature isotherms are so rectangular that accurate data are difficult to obtain.

The simple model represented by eq. 8 thus provides a very satisfactory interpretation of the equilibrium data. Although an equally good correlation of the actual isotherms may be obtained

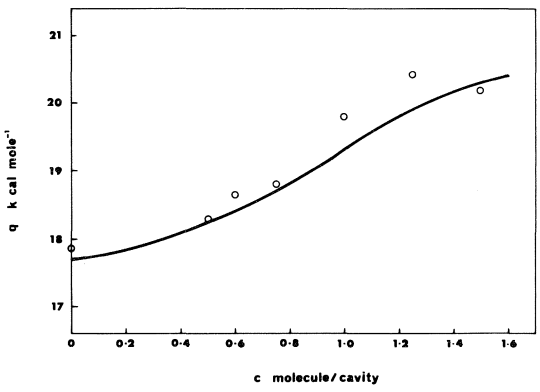

FIG. 4. Variation of isosteric heat of sorption with sorbate concentration (○, experimental points from isosteres; —, theoretical curve from eqs. 8 and 10 for mean temperature of experimental measurements).

from models, such as eqs. 6 or 7, which assume a single set of equivalent sites with interaction between adsorbed molecules, these models are clearly less satisfactory than the two site model since they require additional assumptions concerning the temperature dependence of the molecular interaction energy. Although sorbate–sorbate interaction may be significant in some zeolitic systems it appears to be a second order effect in the present system. The main reason for the deviation of the isotherms from simple Langmuir form seems to be the existence of two distinct types of adsorption site.

Kinetics of Sorption

The kinetic data were correlated in terms of diffusivities calculated by matching the experimental sorption curves to the theoretical uptake curves calculated for a system of cubic particles subject to a step change in surface concentration (10). The diffusivities are shown plotted against sorbate concentration in Fig. 5 from which the strong positive concentration dependence is clearly apparent. There is no significant difference between the diffusivities calculated from adsorption and desorption experiments as may be seen from the data at 439 °K.

If the driving force for the zeolitic transport process is considered to be the gradient of chemical potential, rather than the concentration gradient, the diffusivity D is related to D_0, the limiting diffusivity at low sorbate concentrations, through the expression

$$[13] \qquad D = D_0 \frac{\partial \ln p}{\partial \ln c}$$

where $\partial \ln p/\partial \ln c$ is the activity correction term, calculated from the equilibrium isotherm. Equation 13, with a constant value of D_0, has been found to provide a satisfactory correlation of the diffusivity data for C_1–C_4 hydrocarbons in 5A sieve (1, 2) and it appears to be equally valid for the present system. The curves shown in Fig. 5 were calculated according to eq. 13 using the average value of D_0 from the experimental diffusivities together with values of $\partial \ln p/\partial \ln c$ calculated from the empirical virial equation for the equilibrium isotherm. The curves provide a satisfactory representation of the experimental data points suggesting that, as with the lighter hydrocarbons, the concentration dependence arises entirely from the non-linearity of the relationship between activity and concentration and that the value of D_0 is essentially independent of concentration.

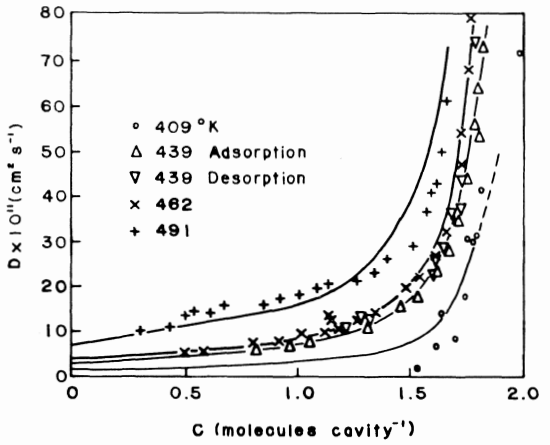

FIG. 5. Variation of diffusivity with sorbate concentration and temperature. (Experimental points; theoretical curves calculated according to eqs. 1 and 13 with average value for D_0.)

It has been shown that, for systems in which the diffusivity increases strongly with concentration, integral diffusivities, calculated from sorption curves measured over a large step change in concentration will be much larger for adsorption than for desorption (20). Such differences have been reported by Eberly (9) for sorption of heptane, and other straight chain hydrocarbons, in 5A zeolite at 366 °K but on the evidence of the present study it seems likely that there is no difference in the intrinsic kinetics of adsorption and desorption and that the difference in the integral diffusivities is due to the effect of the non-linearity of the systems. For such systems integral diffusivities calculated from desorption curves will be only marginally greater than the limiting diffusivity D_0 (20) whereas the integral diffusivity for adsorption will be much larger. The desorption diffusivity, calculated from the value of D/μ^2 reported by Eberly for desorption at 366 °K, assuming the same mean crystal size as in the present sample of 5A zeolite crystals, agrees well with the value of D_0 estimated by extrapolation of the present data to that temperature, as shown in Fig. 6.

The temperature dependence of the limiting diffusivity D_0, which is illustrated in Fig. 6, may be correlated in terms of an Eyring equation

$$[14] \qquad D_0 = D_* \exp(-E/RT)$$

Can. J. Chem. Downloaded from www.nrcresearchpress.com by 210.87.254.5 on 09/05/12
For personal use only.

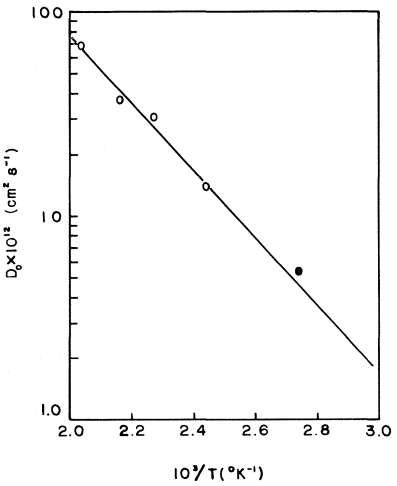

FIG. 6. Temperature dependence of limiting diffusivity D_0. (○, present work; ●, desorption data of Eberly (9)).

with $D_* = 1.5 \times 10^{-7}$ cm^2/s and $E = 7.5$ kcal/mol. According to transition state theory (21) we have

$$[15] \quad D_0 = \frac{\delta^2}{6h} \cdot \frac{1}{K_0} \cdot \frac{f_z^*}{f_g'} \exp\left[-(u' + q_0)/RT\right]$$

where δ^2 is the lattice parameter (12.3 Å), h is Planck's constant, u' is the potential energy of a molecule in the transition state, and f_z^*/f_g' is the ratio of the molecular partition function for the transition state to the partition function per unit volume for a gaseous molecule. For the extreme cases of freely rotating and nonrotating transition states we have

Free rotation

$$[16] \quad \frac{f_z^*}{f_g'} = \frac{f^+}{e}\left[\frac{h^2}{2\pi mkT}\right]^{3/2}$$

No rotation or rocking

$$[17] \quad \frac{f_z^*}{f_g'} = \left[\frac{h^2}{2\pi mkT}\right]^{3/2}\left[\frac{h^2}{8\pi^2 IkT}\right]^{3/2} \frac{\xi f^+}{e\sqrt{\pi}}$$

where m is the mass of a molecule, I is the moment of inertia, ξ is the symmetry number, and f^+ represents the partition function corresponding to motion of the center of gravity of the molecule in the plane of the window. From eqs. 15–17 with $f^+ = 1$ theoretical values of $D_* = 3$–13×10^{-6} cm^2 s^{-1} (free rotation) and $D_* = 9$–40×10^{-11} cm^2 s^{-1} (no rotation or rocking) were obtained.[1] The experimental value (1.5×10^{-7} cm^2 s^{-1}) lies between these two theoretical limits and this result is in agreement with trends previously observed with the lighter hydrocarbons (1, 2). The experimental values of D_* for C_2H_4 and C_2H_6 agreed well with the theoretical values for a non-rotating, non-rocking transition state while, for the C_3 and C_4 molecules, the experimental values were found to lie, as for heptane, between the two extreme limits, thus suggesting an appreciable contribution to f_z^* from restricted rotation or rocking oscillation in the transition state.

Diffusional activation energies for hydrocarbons through C_4 show a good correlation with the critical diameter of the sorbate molecule (1, 2). Although heptane has the same critical diameter as the linear C_3 and C_4 hydrocarbons, its diffusional activation energy is considerably greater (7.5 kcal compared with 3.5–4.0 kcal). Although any speculation as to the origin of this disparity is premature, it presumably must be related to the increase in rocking freedom available to the medium chain hydrocarbon in the transition state.

Conclusion

Equilibrium isotherms for sorption of *n*-heptane in 5A zeolite may be satisfactorily interpreted in terms of a simple model which assumes two adsorption sites per cavity with a significant difference between the energies and entropies of adsorbed molecules on the two types of site. The kinetic data for this system show similar general trends to those previously reported for the light hydrocarbons and the concentration dependence of the diffusivity is satisfactorily accounted for by the Darken equation (eq. 13). This strong positive concentration dependence of the differential diffusivity differs clearly from the pattern of concentration dependence derived by Barrer and Clarke (8) from an analysis of integral diffusivity data for medium chain paraffins in partially ion exchanged type A sieves. For systems in which the diffusivity is strongly concentration dependent it is, however, extremely difficult to derive reliable differential diffusivities from integral data. Furthermore it is evident that, for

[1]The value of I was estimated assuming the linear equilibrium configuration of the heptane molecule. The range of theoretical values of D_* corresponds to the range of K_0 values given in Table 2.

Can. J. Chem. Downloaded from www.nrcresearchpress.com by 210.87.254.5 on 09/05/12
For personal use only.

such systems, the apparent diffusional activation energy will be a function of both temperature and concentration and it is only the activation energy of the limiting diffusivity D_0 which has real physical significance. This activation energy for *n*-heptane is somewhat greater than the comparable quantity for the C_3 and C_4 hydrocarbons.

The continued financial support of the National Research Council of Canada is gratefully acknowledged.

1. D. M. RUTHVEN, K. F. LOUGHLIN, and R. I. DERRAH. Adv. Chem. **121**, 330 (1973).
2. D. M. RUTHVEN, R. I. DERRAH, and K. F. LOUGHLIN. Can. J. Chem. **51**, 3514 (1973).
3. R. L. GORRING. J. Catal. **31**, 13 (1973).
4. W. SCHIRMER. Chem. Tech. **23**, 23 (1971).
5. A. LAURENT and L. BONNETAIN. C. R. Acad. Sci. Ser. C. **275**, 9 (1972).
6. A. QUIG and L. V. C. REES. Third international conference on molecular sieves, Zurich, Sept. 3–7, 1973. Report No. 140.
7. D. J. CLARKE, Ph.D. Thesis, University of London, London, England. 1972.
8. R. M. BARRER and D. J. CLARKE. Faraday Trans. I, **70**, 535. (1974).
9. P. E. EBERLY. Ind. Eng. Chem. Prod. Res. Dev. **8**, 140 (1969).
10. K. F. LOUGHLIN, R. I. DERRAH, and D. M. RUTHVEN. Can. J. Chem. Eng. **49**, 66 (1971).
11. K. F. LOUGHLIN and D. M. RUTHVEN. J. Colloid Sci. **39**, 331 (1972).
12. D. M. RUTHVEN and K. F. LOUGHLIN. Faraday Trans. I, **68**, 696 (1972).
13. R. M. BARRER and R. M. GIBBONS. Faraday Trans. **59**, 2569 (1963).
14. A. V. KISELEV. Proc. 1st Int. Conf. Mol. Sieves. Soc. Chem. Ind. 1968. p. 250.
15. A. GROSSMANN, M. BULOW, and W. SCHIRMER. Chem. Tech. **21**, 167 (1969).
16. W. SCHIRMER. Chem. Tech. **23**, 23, 98 (1971).
17. T. L. HILL. Introduction to statistical thermodynamics. Addison Wesley, Reading, Mass., 1960. p. 131, 252.
18. H. J. SPANGENBERG, K. FIEDLER, H. J. ORTLIEB, and W. SCHIRMER. Z. Phys. Chem. Leipzig, **248**, 49 (1971).
19. W. SCHIRMER, G. FIEDRICH, A. GROSSMANN, and H. STACH. Proc. 1st Int. Conf. Mol. Sieves. Soc. Chem. Ind., London, 1968. p. 276.
20. D. R. GARG and D. M. RUTHVEN. Chem. Eng. Sci. **27**, 417 (1972).
21. D. M. RUTHVEN and R. I. DERRAH. Faraday Trans. I. **68**, 2332 (1972).

Can. J. Chem. Downloaded from www.nrcresearchpress.com by 210.87.254.5 on 09/05/12
For personal use only.

Diverse Reactivity of *N*-Aryl-α-ureidoacetals on Catalysis by Molecular Sieves or Acids

T. P. FORREST, G. A. DAUPHINEE, AND F. M. F. CHEN

Chemistry Department, Dalhousie University, Halifax, Nova Scotia B3H 3J5

Received September 7, 1973[1]

T. P. FORREST, G. A. DAUPHINEE, and F. M. F. CHEN. Can. J. Chem. **52**, 2725 (1974).

The acid-catalyzed cyclocondensation of an *N'*-aryl-α-ureidoacetal (**1**), having a tetrasubstituted urea function, yields a 1,3-benzodiazepin-2-one (**2**), a quinazolinone (**3**), an oxazolidinone (**7**), or an arylaminoalcohol (**6**) depending upon conditions employed. Treatment of **1** with molecular sieves yields the *cis* and *trans* ureidoenolethers **4***a* and **4***b*. The *N'*-aryl-α-ureidoacetal **8** on treatment with molecular sieves undergoes intra- and inter-molecular condensations yielding the imidazolinones **9**, **10**, and **11**. The thioureidoacetal **12** on treatment with molecular sieves yielded the thiazolines **13** and **14**.

T. P. FORREST, G. A. DAUPHINEE et F. M. F. CHEN. Can. J. Chem. **52**, 2725 (1974).

La cyclocondensation acidocatalysé d'un *N'*-aryl-α-uréidoacétal (**1**), possédant une fonction urée tétrasubstituée, conduit, suivant les conditions expérimentales utilisées à une benzodiazépin-1,3-one-2 (**2**), à une quinazolinone (**3**), à une oxazolidinone (**7**) et à un aryl-aminoalcool (**6**). Le traitement de **1** avec des tamis moléculaires fournit les uréidoénoléthers *cis* et *trans* **4***a* et **4***b*. Le *N'*-aryl-α-uréidoacétal **8**, par traitement avec des tamis moléculaires, subit des décondensations intra- et inter-moléculaires conduisant aux imidazolinones **9**, **10** et **11**. Le thiouréidoacétal **12**, par traitement avec des tamis moléculaires, conduit aux thiazolines **13** et **14**.

[Traduit par le journal]

The 1,4-benzodiazepines constitute a class of compounds which has received a great deal of attention in recent years because of the widespread use of some examples as therapeutic agents. The 1,3-benzodiazepines have received much less attention and very few examples of this type are reported. We have employed *N*-aryl-α-ureidoacetals in the synthesis of the 1,3-benzodiazepin-2-one system by a cyclization reaction in which the acetal carbon alkylates the aromatic ring at the ortho position in a reaction similar to a Pomeranz–Fritz reaction (1). The formation of cyclic ureas by cycloalkylations at the urea nitrogen has recently been reviewed (2). We have found that *N*-aryl-α-ureidoacetals undergo a variety of interesting conversions which we wish to report here.

The α-ureidoacetal **1**, obtained by the reaction of 2,2-dimethoxyethyl methyl amine with *N*-methyl-*N*-phenyl carbamoyl chloride, was subjected to acid catalysis under different conditions in attempts to form a 1,3-benzodiazepine ring system. It was found that the 1,3-benzodiazepin-2-one, **2**, could be obtained from **1**, but a variety of other products could also be obtained depending upon the conditions employed in the reaction (See Scheme 1).

On treatment of **1** with relatively strong hydrochloric acid (varying in concentration from 2 to 12 *N*) at room temperature for about 12 h a good yield of **2** was obtained. The progress of the reaction could be easily monitored by carrying out the reaction in an n.m.r. tube using D_2O–DCl as solvent. The acetal **1** quickly hydrolyzes to the hemiacetal, which hydrolyzes more slowly to the hydrated aldehyde which is eventually converted to **2**.

At reflux temperature in 6 *N* HCl the major product from the reaction of **1** is the quinazolinone **3**. In order for **3** to be formed, the carbon α to the acetal group must alkylate the aromatic ring. The cyclization step must occur by means of some intermediate in which this α carbon is converted to a more electrophilic state. A possible mechanism utilizing the vinyl chloride as an intermediate is illustrated in Scheme 2.

An analogous compound, the enol ether **4**, the preparation of which is described later, also undergoes a reaction requiring the intermediacy of an electrophilic α carbon atom. Compound **4** is hydrolyzed at room temperature in 2 *N* HCl to yield *N*,*N'*-dimethyl-*N*-phenylurea **5**. The double bond of the enol ether is activated to protonation at either carbon but it appears that the nitrogen in this case is better able to stabilize the positive charge so that protonation on the

[1]Revision received May 2, 1974.

Can. J. Chem. Downloaded from www.nrcresearchpress.com by 210.87.254.5 on 09/05/12
For personal use only.

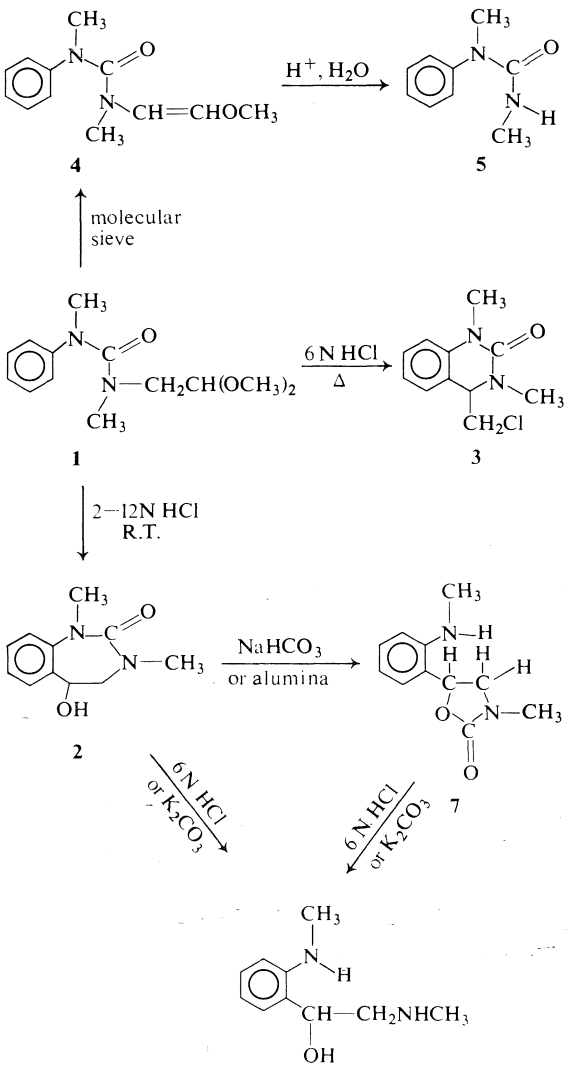

SCHEME 1

oxygen-bearing carbon is preferred. The carbonium ion in this instance, instead of alkylating the aromatic ring, is attacked by water leading to the urea **5**.

The 1,3-benzodiazepinone **2**, which could be formed by treatment of **1** with 6 *N* HCl at room temperature, was found to undergo further reaction on heating at reflux with the same acid. The product was *o*-methylamino-α-methylaminomethyl benzyl alcohol (**6**) formed by hydrolysis of the urea functionality. Hydrolysis of **2** with refluxing aqueous potassium carbonate also yielded **6**. However, under milder basic conditions such as refluxing aqueous sodium bicarbonate, **2** was converted to the oxazolidinone **7**, which could be hydrolyzed in stronger base or in acid to **6**. A good yield of **7** could also be obtained by heating **2** in the presence of alumina in refluxing toluene.

When an *N*-aryl-α-ureidoacetal having a proton on the aryl nitrogen is employed the possibility exists for alkylation to occur at the nitrogen instead of the aromatic ring. In the case of the reaction of **8** with acid, alkylation occurs on the nitrogen yielding 1-phenyl-4-imidazolin-2-one, **9**. The reaction occurs extremely rapidly, being complete in 2 *N* HCl at room temperature within the time required to dissolve the starting material and record the n.m.r. spectrum. This reaction is analogous to that reported for α-ureidoacetaldehyde diethyl acetal (3).

Since it appeared that the alkylation in this case occurred rapidly and exclusively at the nitrogen under acid catalysis an attempt was made to catalyse an aryl alkylation by molecular sieves. Treatment of **8** with molecular sieve 5A in refluxing toluene also gave the *N*-alkylation product **9** as one product. Two other products **10** and **11**, obviously formed from intermolecular reactions, were isolated (Scheme 3).

When the dimethyl analog, **1**, was treated with molecular sieve 5A in the same manner the major products were the *cis* and *trans* enol ethers **4***a* and **4***b*, formed in a ratio of *cis*: *trans* of 3:2. Minor products were *N'*-phenyl-*N*-methylurea and *N*,*N'*-dimethyl-*N'*-phenyl-α-ureidoacetaldehyde, apparently formed by a hydrolysis reaction with residual water in the molecular sieves.

The thioanalogue of **8**, *N'*-phenyl-*N*-(2,2-dimethoxyethyl)thiourea (**12**) gave no aromatic substitution products on treatment with acid. The reaction of **12** with 2 *N* HCl at room temperature yielded the thiazoline **13** as the sole product. This reaction proceeded extremely rapidly as detected by recording the n.m.r. spectrum of **12** dissolved in 2 *N* DCl–D_2O. The formation of thiazolines from *N*-alkyl-α-ureidoacetals on treatment with acid has been reported (4). The reaction of the thioureiodacetal **12** with molecular sieve 5A in refluxing toluene yielded the same thiazoline (**13**) as obtained in the acid catalyzed reaction, as well as a second product the thiourea derivative **14** (Scheme 4).

Experimental

Nuclear magnetic resonance spectra were recorded on a Varian T60 spectrometer using tetramethylsilane as in-

Can. J. Chem. Downloaded from www.nrcresearchpress.com by 210.87.254.5 on 09/05/12
For personal use only.

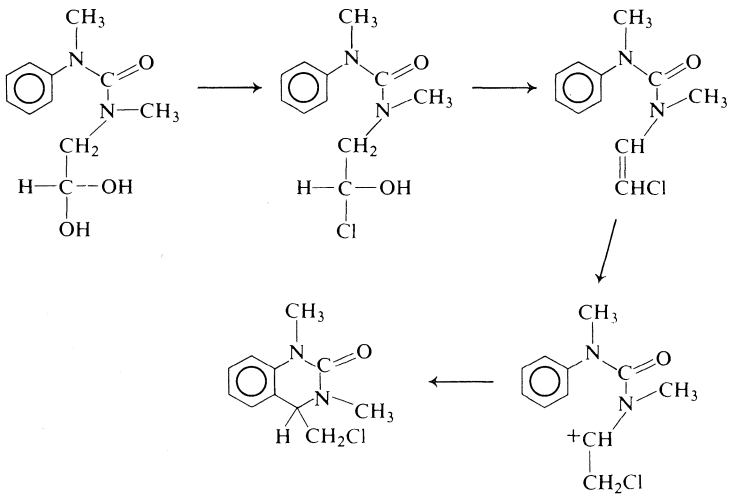

SCHEME 2

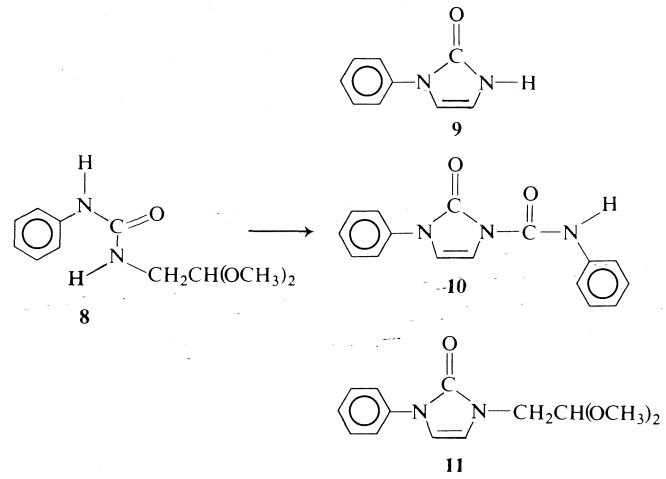

SCHEME 3

ternal standard. Chemical shifts are reported as δ values and absolute values of couplings in Hz with the following abbreviations: s = singlet, d = doublet, t = triplet, b = broad. Infrared spectra were recorded on a Perkin-Elmer 237 B spectrometer. Silica gel (Fisher A-288) was used for chromatography. Mass spectra were determined on a DuPont 21-104 mass spectrometer at 30 eV. Melting points are uncorrected.

*N,N′-Dimethyl-N-phenyl-N′-(2,2-dimethoxyethyl)urea (**1**)*

N-Methyl-*N*-phenylcarbamoyl chloride (5) (16 g, 0.1 mol) in benzene (100 ml) was stirred vigorously for 18 h with 2,2-dimethoxyethyl methylamine (12 g, 0.1 mol) in aqueous sodium carbonate (10%, 600 ml). The benzene layer was then separated, dried (Na_2SO_4), and the solvent removed *in vacuo*; yield 23 g, 92%; b.p. 130–135°/0.4 mm Hg; n.m.r. ($CDCl_3$) δ 2.56 (s, NCH_3), 3.17 (s, NCH_3), 3.35 (d, J = 6 Hz, CH_2), 3.35 (s, OCH_3), 4.42 (t, J = 6 Hz, CH), 6.9–7.4 (b, aromatic H's); i.r. 1660 cm^{-1}.

*1,3-Dimethyl-5-hydroxy-1,3,4,5-tetrahydro-2H-1,3-benzodiazepin-2-one (**2**)*

N,N′-Dimethyl-*N′*-phenyl-*N*-(2,2-dimethoxyethyl)urea (**1**) (6.3 g, 0.025 mol) was added to 2 *N* aqueous hydrochloric acid (200 ml) and stirred at room temperature for 18 h. The solution was then made basic with 2 *N* sodium hydroxide solution and extracted once with ether (30 ml) which removes a small quantity of *N*-methylaniline. The aqueous layer is then extracted several times with benzene. The combined benzene layers are dried (Na_2SO_4) and the solvent removed to yield **2** as a colorless oil; yield 4.5 g, 90%; b.p. 160–162°/0.7 mm Hg; n.m.r. (C_6D_6) δ 2.13 (s, NCH_3), 2.98 (s, NCH_3), 2.62 (B), 2.78, (A), 5.10 (X of ABX, J_{AB} = 16 Hz, J_{AX} = 10 Hz, J_{BX} = 5 Hz), 6.30–7.00 (m, aromatic H's); i.r. 3600, 1700 cm^{-1}; mass

Can. J. Chem. Downloaded from www.nrcresearchpress.com by 210.87.254.5 on 09/05/12
For personal use only.

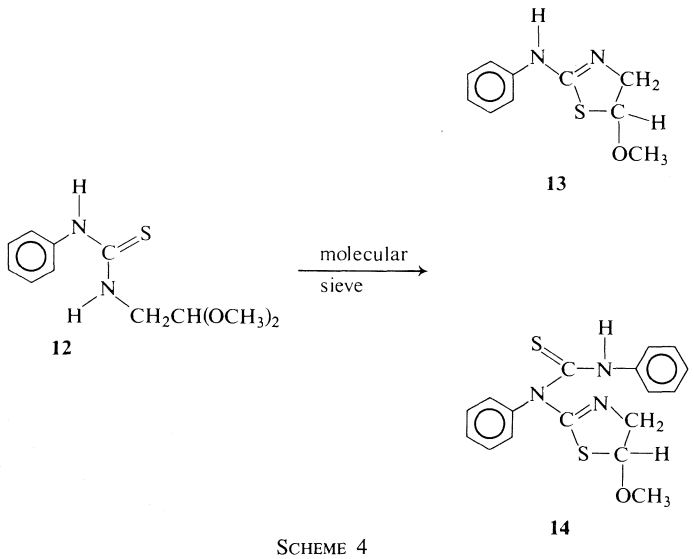

SCHEME 4

spectrum 206(29), 163(8), 162(9), 148(11), 134(14), 132(23), 106(23), 44(100).

4-Chloromethyl-1,3-dimethyl-3,4-dihydro-2(1H)-quinazolinone (3)

N,N'-Dimethyl-*N'*-phenyl-*N*-(2,2-dimethoxyethyl)urea (**1**) (5 g, 0.02 mol) was added to refluxing 6 *N* hydrochloric acid (50 ml) and the solution heated under reflux for 10 min. The solution was then poured into ice cold 2 *N* sodium hydroxide solution (200 ml). The aqueous solution was extracted with ether and after removal of the ether the residue was chromatographed on a silica gel column using chloroform as eluant. The first fraction yielded 4-chloromethyl-1,3-dimethyl-3,4-dihydro-2(1*H*)-quinazolinone (**3**) (yield 2.7 g, 60%) and the second fraction yielded the 1,3-benzodiazepinone (**2**) (yield 0.4 g, 20%). Compound **3** was recrystallized from petroleum ether – benzene (30–60°); m.p. 73°; n.m.r. ($CDCl_3$) 3.13 (s, NCH_3); 3.25 (s, NCH_3), 3.58 (d, J = 5.5 Hz, CH_2), 4.43 (t, J = 5.5 Hz, CH), 6.7–7.4 (m, 4 aromatic H's) mass spectrum 226(1.4), 224(4.1), 175(100), 131(3.2); i.r. 1650 cm^{-1}.

Anal. Calcd. for $C_{11}H_{13}N_2OCl$: C, 58.80; H, 5.83; N, 12.47; Cl, 15.78. Found: C, 58.95; H, 6.07; N, 12.48; Cl, 15.66.

N-N'-Dimethyl-N'-phenyl-N-(2-methoxyvinyl)urea (4)

N,N'-Dimethyl-*N'*-phenyl-*N*-(2,2-dimethoxyethyl)urea (**1**) (5 g, 0.02 mol) was heated under reflux in toluene (100 ml) with molecular sieve 5A (100 g) for 18 h. The solution was filtered and the molecular sieves washed with fresh toluene. The toluene was then removed *in vacuo* and the residue chromatographed on silica being eluted with chloroform. The first fraction contained a mixture of the *cis* and *trans* isomers of (**4**) (2.4 g, 55%), the second fraction contained α-(*N,N'*-dimethyl-*N'*-phenylureido) acetaldehyde (0.2 g, 5%), and the third fraction contained *N,N'*-dimethyl-*N*-phenylurea (0.3 g, 9%). The *cis* and *trans* isomers of **4** which were obtained in a ratio of about *cis*: *trans* 3:2, were separated by chromatography of the mixture on silica using benzene as eluant.

Compound **4***a* (*cis*): n.m.r. ($CDCl_3$) 3.00 (s, NCH_3) 3.25 (s, NCH_3), 3.44 (s, OCH_3), 5.03 (A), 5.07, (B, of AB, J_{AB} = 5 Hz, 2 olefinic H's) 6.8–7.4 (m, 5 aromatic H's); i.r. 1630 cm^{-1}; mass spectrum 220(55), 134(100), 106(40).

Compound **4**b (*trans*): n.m.r. ($CDCl_3$) 2.80 (s, NCH_3), 3.20 (s, NCH_3), 3.26 (s, OCH_3), 6.07 (A), 6.13 (B, of AB, J_{AB} = 12 Hz, 2 olefinic H's); i.r. 1630 cm^{-1}; mass spectrum 220(17), 134(100), 106(64).

o-Methylamino-α-methylaminomethylbenzyl Alcohol 6

1,3-Dimethyl-5-hydroxy-1,3,4,5-tetrahydro-2*H*-1,3-benzodiazepine (**2**) (1 g, 0.005 mol) or 3-methyl-5-(o-methylaminophenyl)-2-oxazolidinone (**7**) (1 g, 0.005 mol) was heated under reflux for 18 h with an aqueous 10% K_2CO_3 solution (10 ml) or 2 *N* HCl (10 ml). The solution was cooled and extracted with benzene (after basification in the HCl case). After evaporation of the benzene, the residue was crystallized from petroleum ether (30–60°); yield 0.75 g, 85%; m.p. 86 °C; n.m.r. ($CDCl_3$) δ 2.37 (s, NCH_3), 2.79 (s, NCH_3), 2.82 (B), 3.05 (A), 4.72 (X of ABX, J_{AB} = 12.5 Hz, J_{AX} = 9.5 Hz, J_{BX} = 4 Hz), 6.50–7.34, (m, aromatic H's); mass spectrum 180(100), 162(18), 137(64), 122(20), 118(55), 136(32).

Anal. Calcd. for $C_{10}H_{16}N_2O$: C, 66.63; H, 8.95; N, 15.55. Found: C, 66.76; H, 9.15; N, 15.36.

3-Methyl-5-(o-methylaminophenyl)-2-oxazolidinone 7

1,3-Dimethyl-5-hydroxy-1,3,4,5-tetrahydro-2*H*-1,3-benzodiazepin-2-one (**2**) (6 g, 0.03 mol) and alumina (Baker Analyzed, p*H* of 10% slurry 8.0, 20 g) in toluene (100 ml) was heated under reflux with stirring for 3 h. The alumina was removed by filtration and washed with an additional 100 ml of toluene. Evaporation of the toluene from the combined filtrates yielded a solid which was recrystallized from petroleum ether (60–80°): yield 5.5 g, 92%; m.p. 88–89°; i.r. 1750 cm^{-1}; n.m.r. (acetone-d_6) δ 282 (bs, NCH_3), 2.84 (s, NCH_3), 3.47 (B), 3.97 (A), 5.60 (X, of ABX, J_{AB} = 8.5 Hz, J_{AX} = 8.5 Hz, J_{BX} = 7.5 Hz), 4.68 (bs, NH), 6.55–7.40 (m, aromatic H's); mass spectrum 206(26), 162(7), 161(6), 132 (85), 131(53), 106(29), 91(23), 77(20), 44(100).

Can. J. Chem. Downloaded from www.nrcresearchpress.com by 210.87.254.5 on 09/05/12
For personal use only.

*N′-Phenyl-N-(2,2-dimethoxyethyl)urea (**8**)*

Phenyl isocyanate (17.9 g, 0.15 mol) was added over a period of 5 min to 2,2-dimethoxyethylamine (15.8 g, 0.15 mol) while cooling in an ice bath. The reaction mixture was allowed to remain at room temperature for 1 h during which time a crystalline mass formed. The solid was washed with petroleum ether (30–60°); yield 32 g, 95%; m.p. 86–87°; i.r. 1700, 1650 cm^{-1}; n.m.r. ($CDCl_3$) δ 3.32 (s, OCH_3's) ≃3.30 (CH_2), 4.35 (t, J = 5 Hz, CH), 6.09 (bt, J = 5.5 Hz, NH), 6.80–7.36 (aromatic H's), 7.95 (bs, NH); mass spectrum 224(3.6), 209(0.5), 193(2.5), 119(2.5), 93(17), 75(100).

*1-Phenyl-4-imidazolin-2-one (**9**)*

N′-Phenyl-*N*-(2,2-dimethoxyethyl)urea (5 g, 0.22 mol) was dissolved in 2 *N* hydrochloric acid (50 ml). After 10 min at room temperature the solution was made basic with 2 *N* sodium hydroxide and extracted with ether. Evaporation of the ether yielded a crystalline solid; yield 3.5 g, 99%; m.p. 123°; i.r. 1690 cm^{-1}; n.m.r. ($CDCl_3$) δ 6.32 (d, J = 3 Hz, H-4), 6.44 (d, J = 3 Hz, H-5), 10.9 (bs, NH), 7.00–7.64 (m, aromatic H's); mass spectrum 160(100), 139(42), 104(36), 77(44), 51(23).

*Molecular Sieve Treatment of N′-Phenyl-N-(2,2-dimethoxyethyl)urea (**8**)*

N′-Phenyl-*N*-(2,2-dimethoxyethyl)urea (1 g, 0.0044 mol) was heated under reflux in toluene (25 ml) in the presence of molecular sieves 5A (10 g) for 16 h. The molecular sieves were removed by filtration and washed with an additional portion (10 ml) of toluene. The combined filtrates were concentrated *in vacuo* yielding an oily residue. Addition of ether caused precipitation of a solid which was recrystallized from ether–hexane to yield 0.16 g, 23% of **9**.

The mother liquor from the recrystallization of **9** was concentrated *in vacuo* and the residue separated by chromatography on silica gel (solvent, hexane–ether 9:1).

The first fraction yielded compound **10**, m.p. 123 °C; yield 0.22 g, 19%; n.m.r. δ 6.61 (d, J = 3 Hz, H-5), 7.20 (d, J = 3 Hz, H-4) 7.20–7.64 (m, aromatic H's); 10.9 (bs, NH); i.r., 1730, 1685 cm^{-1}; mass spectrum 279(12), 160(100), 131(24).

The second fraction yielded compound **11**; m.p. 75°; yield 0.26 g, 24%; n.m.r. δ 3.44 (s, OCH_3's) 3.84 (d, J = 5 Hz, CH_2) 4.54 (t, J = 5 Hz, CH), 6.41 (d, J = 3 Hz, H-4) 6.55 (d, J = 3 Hz, H-5) 7.05–7.70, m, aromatic H's; i.r. 1685 cm^{-1}; mass spectrum 248(30), 217(15), 160(20), 75(100).

When the above reaction was attempted using molecular sieve 4A, the starting material was recovered unreacted and when molecular sieve 10A was used no starting material or products could be recovered.

*N′-Phenyl-N-(2,2-dimethoxyethyl)thiourea (**12**)*

Phenylisothiocyanate (19.2 g, 0.14 mol) was added over a period of 5 min to 2,2-dimethoxyethylamine (15.8 g, 0.15 mol) while cooling in an ice bath. The reaction mixture was allowed to remain at room temperature for 1 h during which time a crystalline mass formed. The solid was washed with petroleum ether (30–60°); yield 34.8 g, 99%; m.p. 56°; n.m.r. ($CDCl_3$) δ 3.35 (s, OCH_3's) 3.75 (t, J = 5 Hz, CH_2), 4.50 (t, J = 5 Hz, CH), 6.45 (bt, J = 5 Hz, NH), 7.10–7.45 (m, aromatic H's) 8.80 (bs, N′H).

*2-Anilino-5-methoxy-2-thiazoline (**13**)*

N′-Phenyl-*N*-(2,2-dimethoxyethyl)thiourea (**12**) (3.8 g, 0.02 mol) was dissolved in 2 *N* hydrochloric acid (50 ml) (6). After 10 min at room temperature the solution was made basic with 2 *N* sodium hydroxide and extracted with ether (2 × 100 ml). Evaporation of the ether yielded a solid residue which was crystallized from ether–petroleum ether (30–60°); yield 3.0 g, 95% (m.p. 140°); i.r. 1650 cm^{-1}; n.m.r. (C_6D_6) δ 2.96 (s, OCH_3), 3.74 (A), 3.91 (B), 4.92 (X or ABX, J_{AB} = 13.5 Hz, J_{AX} = 4.5 Hz, J_{BX} = 1.5 Hz), 6.62 (bs, NH), 6.85–7.40 (m, aromatic H's).

*Molecular Sieve Treatment of N′-Phenyl-N-(2,2-dimethoxyethyl)thiourea (**12**)*

N′-Phenyl-*N*-(2,2-dimethoxyethyl)thiourea (**12**) (1 g, 0.0042 mol) was heated under reflux in toluene (25 ml) in the presence of molecular sieves 5A (10 g) for 16 h. The molecules sieves were removed by filtration and washed with toluene (10 ml). The toluene was removed from the combined filtrates by distillation under reduced pressure (0.5 torr). The solid which formed was washed with ether leaving a crystalline residue of **13**, 0.3 g, 36%. The ether washings were subjected to silica gel column chromatography (eluant, hexane–ether 9:1) yielding compound **14**; 0.26 g, 18%; m.p. 103°; i.r. 1620 cm^{-1}; n.m.r. ($CDCl_3$) δ 3.34 (s, OCH_3), 4.48 (dd, J = 5 Hz, J = 13 Hz, H-4), 5.07 (d, J = 5 Hz, H–5), 5.49 (d, J = 13 Hz, H–4), 6.85–7.64 (aromatic H's); mass spectrum 208(100), 207(83), 177(25), 150(10), 132(50), 104(44).

The financial assistance of the National Research Council of Canada is acknowledged.

1. W. J. GENSLER. *In* Organic reactions. Vol. 6. John Wiley and Son, N.Y. 1951. p. 191.
2. H. PETERSEN. Synthesis, 243 (1973).
3. R. DUSCHINSKY and L. A. DOLAN. J. Am. Chem. Soc. **68**, 2350 (1946).
4. R. BURTLES, F. L. PYMAN, and J. ROYLANCE. J. Chem. Soc. **127**, 581 (1925).
5. O. SCHMIDT. Ber. **36**, 2479 (1903).
6. A. WOHL and W. MARCKWALD. Ber. **22**, 568 (1889).

Can. J. Chem. Downloaded from www.nrcresearchpress.com by 210.87.254.5 on 09/05/12
For personal use only.

Isomeric Mixture Analysis of Some Ring-opening Reactions of Styrene Oxide

M. B. HOCKING

Department of Chemistry, University of Victoria, Victoria, British Columbia V8W 2Y2

Received August 20, 1973[1]

M. B. HOCKING, Can. J. Chem. **52**, 2730 (1974).

Mixtures of ring-opened and other products of reactions of acetic or benzoic acids, or ethanol, or phenol with styrene oxide under various conditions can be qualitatively and quantitatively analyzed without isolation of the components by the use of n.m.r. This method, in the case of the ester products, avoids confusing the initial ring-opening result with the results observed after subsequent acyl migrations which readily occur in this type of system.

M. B. HOCKING. Can. J. Chem. **52**, 2730 (1974).

Le mélange des produits ouverts et des autres produits de réaction de l'acide acétique ou de l'acide benzoïque ou de l'éthanol ou des phénols avec l'oxyde de styrène sous diverses conditions expérimentales peut être analysé quantitativement et qualitativement sans isoler les produits grâce à la r.m.n. Cette méthode dans le cas des esters évite de confondre le résultat de l'ouverture initiale du cycle avec les résultats obtenus après la migration subséquente du groupe acyle qui se produit facilement dans ce type de système. [Traduit par le journal]

Introduction

Synthetic (1, 2) and kinetic (3) studies of the ring-opening reactions of styrene oxide have gone a long way towards elucidation of the mechanism. The difficulty in studies of this type has been the qualitative and quantitative analysis of the often complex product mixtures obtained (4, 5). Isomer mixtures are frequently obtained on the opening of unsymmetrical epoxides (*e.g.* 1, 6) and the first-formed isomer mixture with carboxylic acids may undergo ready acyl migration with heat or even mildly acidic or alkaline conditions, as seen with glyceryl part esters (7). Concomitant epoxide rearrangements in the presence of acid or base give by-products which complicate ring-opened product recovery and analysis (8, 9), and low polymer oils from condensation of two or three units of original epoxide (5, 10) also contribute to the difficulties. Complicating factors such as these confused much of the early work with epoxide ring-opening reactions (4, 5).

We have examined the use of n.m.r. as a tool for qualitative and quantitative use in a study of some ring-opening reactions of styrene oxide. This method appeared to offer simplicity and speed of analysis, and also to make possible the determination of initial product ratios in the presence of extraneous material and prior to possible subsequent rearrangements. Not only would success with this procedure permit analysis in appropriate systems without isolation of the components but it would avoid errors of interpretation caused by chemical changes introduced by the work-up or derivitization techniques themselves.

Experimental

Styrene oxide was purchased from Aldrich Chemical Company and vacuum redistilled (fraction boiling at 74.5–75°/11 mm) immediately prior to use. Preparative details are given in Table 1, with footnoted elemental analyses by A. B. Gygli and Associates, Toronto, for new compounds. Nuclear magnetic resonance spectra were obtained on 10% solutions in deuteriochloroform at room temperature on Varian A-60 and HA-60 instruments. Shifts are reported as centers of the respective multiplets from internal tetramethylsilane (Table 2). Isomer mixtures were identified by n.m.r. and quantified by calculation using integrals of the same groupings of each isomer.

Results and Discussion

Styrene oxide was chosen as a sample substrate for this study because it was an unsymmetrical epoxide expected to give ring-opened products with relatively simple n.m.r. resonance patterns for the aliphatic protons. And styrene oxide is no different from other epoxides in the appearance of conflicting reports on its behavior during ring-opening reactions. With acetic acid, for instance, Hickinbottom and Hogg (10) claim that attack is predominantly at the primary

[1]Revision received May 2, 1974.

Can. J. Chem. Downloaded from www.nrcresearchpress.com by 210.87.254.105 on 09/05/12
For personal use only.

Can. J. Chem. Downloaded from www.nrcresearchpress.com by 210.87.254.105 on 09/05/12
For personal use only.

TABLE 1. Summary of ring-opening reactions of styrene oxide, plus derivative preparations and disproportionations

Product (average yield)	Reagents	Reaction conditions	Isomer ratios (mol%) 2° alcohol, 1° derivative	Isomer ratios (mol%) 1° alcohol, 2° derivative
2-Acetoxy-2-phenylethanol **3***a* (50%)	Acetic acid + styrene oxide	(*a*) Neat, 24 h at 3° + 24 h at 23°; unreacted starting materials:	0	100
		(*i*) removed via cold wash;*	0	100
		(*ii*) distilled off at <32°;	5	95
		(*iii*) product from above distilled (93–98°/0.3 mm)	50	50
		(*b*) Neat, 23° for 7 days	50	50
2-Acetoxy-1-phenylethanol **4***a* (75%)	1-Phenyl-1,2-ethanediol **1**, pyridine, + acetyl chloride	(*a*) In benzene, 1 h at 5–10° + 1 h at 25°;	95	5
		(*i*) above product distilled (112–113°/1 mm);	70	30
		(*ii*) distilled product heated at 117°/8 days	53	47
2-Benzoyloxy-1-phenylethanol **4***b* + 2-Benzoyloxy-2-phenylethanol **4***a* (total = 15%)	Benzoic acid + styrene oxide	(*a*) In ethanol, 1.5 h at 85° + 14 h at 23°, cold wash* work-up	70†	30†
		(*b*) In ethanol, 48 h at 25°;	80†	20†
		(*i*) product distilled (157°/0.1 mm) m.p. 67.5–70° (lit. (1) m.p. 62–64°);	80	20
		(*ii*) evaporated filtrate from crystallization	62	38
		(*c*) Neat, 2.5 h at 100° + product distilled (152–7°/0.1 mm)	70	30
2-Benzoyloxy-1-phenylethanol **4***b* (50%)	**1**, pyridine, + benzoyl chloride	(*a*) In benzene, 2.3 h at 20°	100	0
		(*b*) In benzene, 1 h at 80°	100	0
2-Ethoxy-1-phenylethanol **7***a* + 2-Ethoxy-2-phenylethanol **6***a* (total = 30%)	Ethanol (excess) + styrene oxide	(*a*) Neat, 48 h at 85°, distilled (119–123°/9.5 mm); 20% of styrene oxide polymerized	40	60
2-Ethoxy-2-phenylethanol **6***a* (30%)	Ethanol (excess), styrene oxide (30 g), + benzoic acid (61 g)	(*a*) Neat, 48 h at 23°, with benzoic acid "catalysis"	0	100
		(*b*) Boiled 1.5 h with benzoic acid "catalysis", wash* recovery;	0	100
		product distilled (113–115°/8 mm)‡	0	100

Can. J. Chem. Downloaded from www.nrcresearchpress.com by 210.87.254.105 on 09/05/12
For personal use only.

TABLE 1. (*Concluded*)

Product (average yield)	Reagents	Reaction conditions	Isomer ratios (mol%) 2° alcohol, 1° derivative	Isomer ratios (mol%) 1° alcohol, 2° derivative
2-Ethoxy-2-phenylethyl benzoate (60%)	**6***a*, pyridine, + benzoyl chloride	Boiled 1 h in benzene, isolated by washing,* plus distillation (170–176°/2.3 mm); crystallized, hexane, m.p. 39–40°§	—	—
			0	100
2-Phenyl-2-iodoethanol (50%)	hydriodic acid + styrene oxide	In petroleum ether, 0–5°/1 h, wash purification (11), pale yellow solid, m.p. 60–65° (lit. (11) m.p. 77.5°)	0	100
2-Phenoxy-2-phenylethanol **6***b* (10%)	phenol + styrene oxide	In benzene, 2.5 h at 85°, aqueous carbonate wash + distillation (175°/0.1 mm); recryst. 4×, ether–hexane, m.p. 77–79° (lit. (12) 62–63.5°)‖	0	100
			—	—
2-Phenoxy-2-phenylethyl benzoate (55%)	**6***b*, pyridine, + benzoyl chloride	Boiled 1 h in benzene, isolated by washing,* recryst. 2×, methanol, m.p. 78–80°	—	—
Derivatives of 1-phenyl-1,2-ethanediol **1**¶ -diacetate (80%)	**1**, pyridine, + acetyl chloride	In boiling benzene, wash* work up, distilled (107–107.5°/0.5 mm) (lit. (13) b.p. 107–112°/0.4 mm)	—	—
		As above, b.p. 127–131°/0.05 mm; about 10% crotonic anhydride also obtained	—	—
-dicrotonate (35%)	**1**, pyridine, + crotonoyl chloride			
-dibenzoate (90%)	**1**, pyridine, + benzoyl chloride	As above but crystallized from benzene, m.p. 91.5–93° (lit. (14) m.p. 93.5–95°)	—	—

*Dilution with cold CH_2Cl_2, followed by ice water, cold aqueous $NaHCO_3$, and ice water washes, drying (Na_2SO_4), and solvent removal under reduced pressure.
†About 25% yield ring-opened products, plus prototropic shift to yield observed phenylacetaldehyde.
‡Anal. Calcd. for $C_{10}H_{14}O_2$: C, 72.26; H, 8.49. Found: C, 72.21; H, 8.45. Isomeric assignment confirmed by benzoylation.
§Anal. Calcd. for $C_{17}H_{18}O_3$: C, 79.22; H, 5.70. Found: C, 79.21; H, 5.67.
‖Anal. Calcd. for $C_{14}H_{14}O_2$: C, 78.48; H, 6.59. Found: C, 78.44; H, 6.62.
¶Diacrylate preparations gave insoluble red polymers.

TABLE 2. Nuclear magnetic resonance chemical shifts and calculated shift differences for some 1-phenyl-1,2-ethanediol derivatives*

Compound	Proton shifts p.p.m. (δ)		$\delta_{diester}-\delta_{monoester}$		$\delta_{derivative}-\delta_{diol}$	
	Methine	Methylene	Methine	Methylene	Methine	Methylene
1-Phenyl-1,2-ethanediol	4.67	3.56	—	—	—	—
Acetates						
diacetate	5.97	4.25	—	—	1.30	0.69
sec. mono, **3***a*	5.92	3.88	0.05	0.37	1.25	0.32
prim. mono, **4***a*	4.87	4.18	1.10	0.07	0.20	0.62
Benzoates						
dibenzoate	6.41	4.70	—	—	1.74	1.14
sec. mono, **3***b*	5.97	3.68	0.44	1.02	1.30	0.12
prim. mono, **4***b*	4.97	4.33	1.44	0.37	0.30	0.78
Monoethyl ethers:						
sec., **6***a*	4.39	3.69	—	—	−0.28	0.13
prim., **7***a*	4.77	3.40	—	—	0.10	0.16
sec. ether, prim. benzoate	4.67	4.45	1.74	0.25	—	—
Monophenyl ethers:						
sec., **6***b*	5.13	3.78	—	—	−0.46	−0.22
sec. ether, prim. benzoate	5.56	4.65	0.85	0.05	—	—
2-Phenyl-2-iodoethanol	5.13	3.91	—	—	−0.46	−0.35
Styrene oxide	3.74	2.83				

*Integration of relative peak areas in all cases agreed with the assignments given.

carbon to give 2-acetoxy-1-phenylethanol **4***a*, whereas others (1, 6) claim that the secondary carbon is preferentially attacked giving largely 2-acetoxy-2-phenylethanol **3***a*. The present study finds support for the latter claim and provides a method which may prove helpful in other systems.

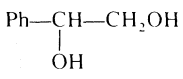

1

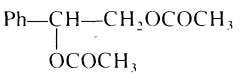

2

Nuclear magnetic resonance chemical shifts were determined for the methine and the methylene protons of, for example, styrene glycol, **1**, and styrene glycol diacetate, **2**. Subtracting the shifts of the methine protons of the diol **1** from the diester **2**, and subtracting the methylene protons in the same way, we obtained shift differences of 1.30 and 0.69, respectively (Table 2).

For a styrene glycol monoacetate of unknown ester orientation, relative integrals establish whether a multiplet is arising from the methine or the methylene group. Noting the respective shifts and carrying out the same type of operation as outlined above but now between the monoester **3***a* and the diester **2**, we obtain shift

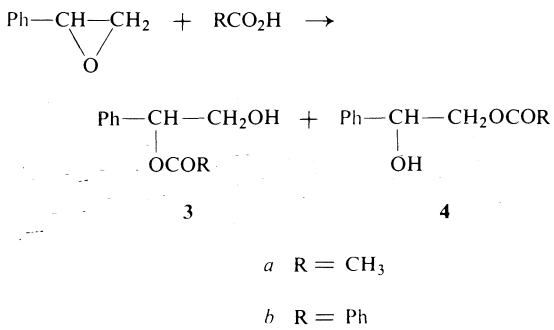

3 **4**

a R = CH_3

b R = Ph

differences for **3***a* of 0.05 and 0.37 for the methine and the methylene groups, respectively. This result immediately suggests that ester attachment is on methine. To confirm this, repeating the procedure, but now between monoester **3***a* and diol **1** we obtained shift differences of 1.25 for the methine proton and 0.32 for the methylene protons, indicating that hydroxyl in **3***a* is on methylene. The evidence that both operations on **3***a* agreed and that duplicating the result on **4***a* gave the opposite ester orientation, strongly supported the use of the method for this purpose. With benzoate esters the method was found to be equally suitable.

With monoethers, where the deshielding effect of an aryl or alkyl group was much less different

Can. J. Chem. Downloaded from www.nrcresearchpress.com by 210.87.254.105 on 09/05/12
For personal use only.

Can. J. Chem. Downloaded from www.nrcresearchpress.com by 210.87.254.105 on 09/05/12
For personal use only.

from hydrogen than the deshielding effect of an acyl group, the distinction was far less marked than with the monoesters. But the method still gave the correct result, demonstrated by esterification of the free hydroxyl and repeating the calculations based on ester differences. Since the ethers obtained by epoxide opening are much less prone to disproportion, even if ester preparation is necessary to distinguish ether orientation in particular case, it does not seriously detract from the usefulness of the method.

The method may be used to simultaneously determine each component (mol%) of mixtures of acetic acid, styrene oxide, and the two monoesters because the respective multiplets are well separated. And in ester systems at least, the side reactions of styrene oxide leading to phenylacetaldehyde or polymeric products **5** can again be separated from the desired results

$$\text{+O—CHPh—CH}_2\text{+}_n\text{O—}$$

5

because the deshielding effects of aldehyde and ether functions differ sufficiently from the compounds of interest.

Reacting styrene oxide with acetic acid at room temperature gave mixtures of the two monoacetates **3***a* and **4***a* (Table 1), in accordance with that found earlier by Berti *et al.* (1) and Cohen *et al.* (6), and not 2-acetoxy-1-phenylethanol (10). At about +3° only 2-acetoxy-2-phenylethanol **1***a* was obtained, the first time this has been demonstrated and vindicating suggestions by others (1, 6).

Reacting 1-phenyl-1,2-ethanediol with acetyl chloride yielded 2-acetoxy-1-phenylethanol contaminated with only about 5% of the other isomer (Table 1). Distillation only decreased the proportion of 2-acetoxy-1-phenylethanol present to 70%, and further heating established that the equilibrium lay at near a 50:50 mixture.

At elevated temperatures, benzoic acid plus styrene oxide gave a mixture (about 70% primary, **2***b*) of monobenzoate esters, not significantly changed by reaction at room temperature (*cf.* 1). Pure 2-benzoyloxy-1-phenylethanol was obtained directly via 1-phenyl-1,2-ethanediol and benzoyl chloride (Table 2) but attempts to obtain 2-benzoyloxy-2-phenylethanol in pure form through silver benzoate plus 2-phenyl-2-iodoethanol or by fractional crystallization of the potassium xanthate salts of the mixed monoesters were unsuccessful.

The monoether 2-ethoxy-2-phenylethanol **6***a*, was isolated pure as a co-product. This finding supports the two earlier reports by Chapman *et al.* (3) and Winstein and Ingraham (15) claiming purely secondary ether formation on strong acid catalyzed ring opening of styrene oxide with methanol and does not correspond with Reeve and Christoffel's (16) finding that mixtures resulted. In the absence of benzoic acid 60% 2-ethoxy-2-phenylethanol **6***a* was formed.

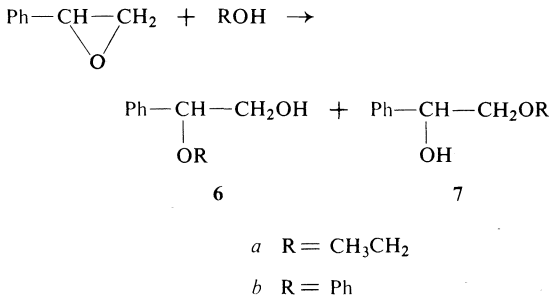

With phenol in boiling benzene 100% attack at the secondary carbon of styrene oxide was obtained, near the 90% **6***b* that was found by Guss (17) for this reaction. The initial product, 2-phenoxy-2-phenylethanol **6***b*, was not prone to rearrangement.

The halogen acid ring-opened styrene oxide, which had been previously characterized (11) as 2-phenyl-2-iodoethanol, was also found to fit the assignment scheme quite well.

The author thanks the National Research Council of Canada for partial financial support.

1. G. Berti, F. Bottari, and B. Macchia. Ann. Chim. (Rome), **52**, 1101 (1962).
2. G. Berti, F. Bottari, P. L. Ferrarini, and B. Macchia. J. Org. Chem. **30**, 4091 (1965).
3. N. B. Chapman, J. Biggs, A. Finch, and V. Wray. J. Chem. Soc. B, 55, (1971).
4. R. E. Parker and N. S. Isaacs. Chem. Rev. **59**, 737 (1959).
5. A. Rosowsky. *In* The Chemistry of heterocyclic compounds. Vol. 19, Part 1. *Edited by* A. Weissberger. Interscience, New York. 1964. pp. 273 and 366.
6. T. Cohen, M. Dughi, V. A. Notaro, and G. Pinkus. J. Org. Chem. **27**, 814 (1962).
7. O. E. Van Lohuizen and P. E. Verkade. Rec. Trav. Chim. **79**, 133 (1960).
8. J. G. Buchanan and H. Z. Sable. *In* Selective organic transformations. Vol. 2. *Edited by* B. S. Thyagaran. Wiley-Interscience, New York. 1972. p. 52.

9. D. N. KIRK. Chem. Ind. (London), No. 3, 109 (1973).
10. W. J. HICKINBOTTOM and D. R. HOGG. J. Chem. Soc. 4200 (1954).
11. C. GOLUMBIC and D. L. COTTLE. J. Am. Chem. Soc. **61**, 996 (1939).
12. P. YATES, D. G. FARNUM, and D. H. STOUT. J. Am. Chem. Soc. **80**, 196 (1958).
13. S. V. ZAVGORODNI and I. A. NASYR. Dokl. Akad. Nauk SSSR, **145**, 1061 (1962); Chem. Abstr. **58**, 1376h (1963).
14. M. J. KUNITSCHECK and W. A. BONNER. J. Org. Chem. **26**, 2194 (1961).
15. S. WINSTEIN and L. L. INGRAHAM. J. Am. Chem. Soc. **77**, 1738 (1955).
16. W. REEVE and I. CHRISTOFFEL. J. Am. Chem. Soc. **72**, 1480 (1950).
17. C. O. GUSS. J. Am. Chem. Soc. **71**, 3460 (1949).

Can. J. Chem. Downloaded from www.nrcresearchpress.com by 210.87.254.105 on 09/05/12
For personal use only.

Synthetic Morphinans and Hasubanans. II.[1] On the Mechanism of Acid-catalyzed Transformations of 17-(*N*-Phenylthioamido)-3-methoxy-$\Delta^{8,14}$-morphinan

MICHEL SAUCIER AND IVO MONKOVIĆ[2]

Bristol Laboratories of Canada, 100 Industrial Blvd., Candiac, Quebec J5R 1J1

Received February 1, 1974

MICHEL SAUCIER and IVO MONKOVIĆ. Can. J. Chem. **52**, 2736 (1974).

The acid-catalyzed rearrangement of 3-methoxy-17-(*N*-phenylthioamido)-$\Delta^{8,14}$-morphinan (**1**) to 3-methoxy-17-(*N*-phenylthioamido)-$\Delta^{9,10}$-hasubanan (**2**), and acid-catalyzed cyclization of **2** to thiazinohasubanan (**3**) are described. Both transformations are discussed in terms of intramolecular *vs.* intermolecular hydride (proton) transfers. The reduction of **3** afforded 3-methoxy-10β-thiohasubanan (**4**), which was further hydrogenolized to 3-methoxy-hasubanan (**5**).

MICHEL SAUCIER et IVO MONKOVIĆ. Can. J. Chem. **52**, 2736 (1974).

On décrit le réarrangement par catalyse acide du méthoxy-3 (*N*-phénylthioamido)-17 $\Delta^{8,14}$-morphinane **1** en méthoxy-3 (*N*-phénylthioamido)-17 $\Delta^{9,10}$-hasubanane **2**, et de la cyclisation par catalyse acide de **2** en thiazinohasubanane **3**. On discute de ces deux transformations en termes de transferts d'hydrure (proton): transfert intramoléculaire comparé à un transfert intermoléculaire. La réduction de **3** conduit au méthoxy-3 thio-10β hasubanane **4** qui donne par hydrogénation le méthoxy-3 hasubanane **5**. [Traduit par le journal]

Introduction

In the course of our studies of long acting and orally effective "pure" narcotic antagonists and nonaddicting analgesics (1), we have attempted the synthesis of 14-thiomorphinan derivative I via acid-catalyzed cyclization of *N*-thioamido-$\Delta^{8,14}$-morphinan II to the corresponding thiazolinomorphinan III (Scheme 1).

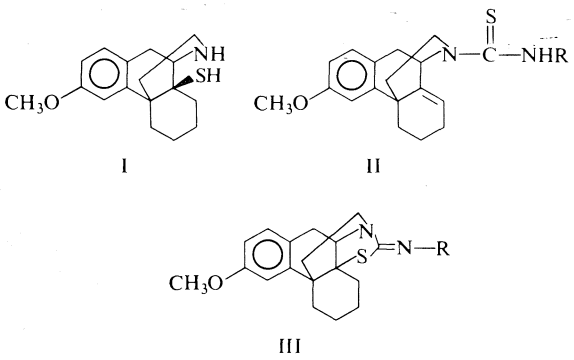

I II III

SCHEME 1

Cyclizations of this type are well documented in the literature; the *N*-allyl- and substituted *N*-allylamides, -urethanes, -ureas, and -thioureas were cyclized in sulfuric acid to the corresponding oxazolines and thiazolines, respectively (2) (Scheme 2). When Z was a carbonium ion stabilizing substituent such as aryl, the alternative six-membered heterocycle was obtained (3). Accordingly, it was expected that the acid-catalyzed cyclization of thioureidomorphinan **1** (Scheme 3) would afford III (Scheme 1, R = Phenyl).

In contrast we obtained thioureidohasubanan **2** and/or corresponding thiazinohasubanan **3** (X = H), which was found to be a convenient starting material for the preparation of hasubanan and 10β-thiohasubanan derivatives (steroid notation), required for structure–activity relationship studies.

Sulfuric acid-d_2-catalyzed rearrangement of **1** to **2** and deuterium chloride-catalyzed transformations of **1** and **2** to **3** enabled us to follow incorporation of deuterium into the hasubanan skeleton and in turn to make interesting mechanistic observations.

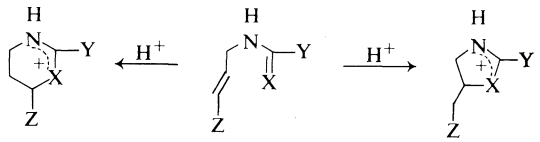

X = O, S; Y = H, Alkyl, *O*-Alkyl, *O*-Aryl, NH_2, NH-Aryl; Z = H, Alkyl, Aryl

SCHEME 2

[1]For Part I see ref. 1.

[2]To whom correspondence regarding this paper should be addressed.

Can. J. Chem. Downloaded from www.nrcresearchpress.com by 210.87.254.105 on 09/05/12
For personal use only.

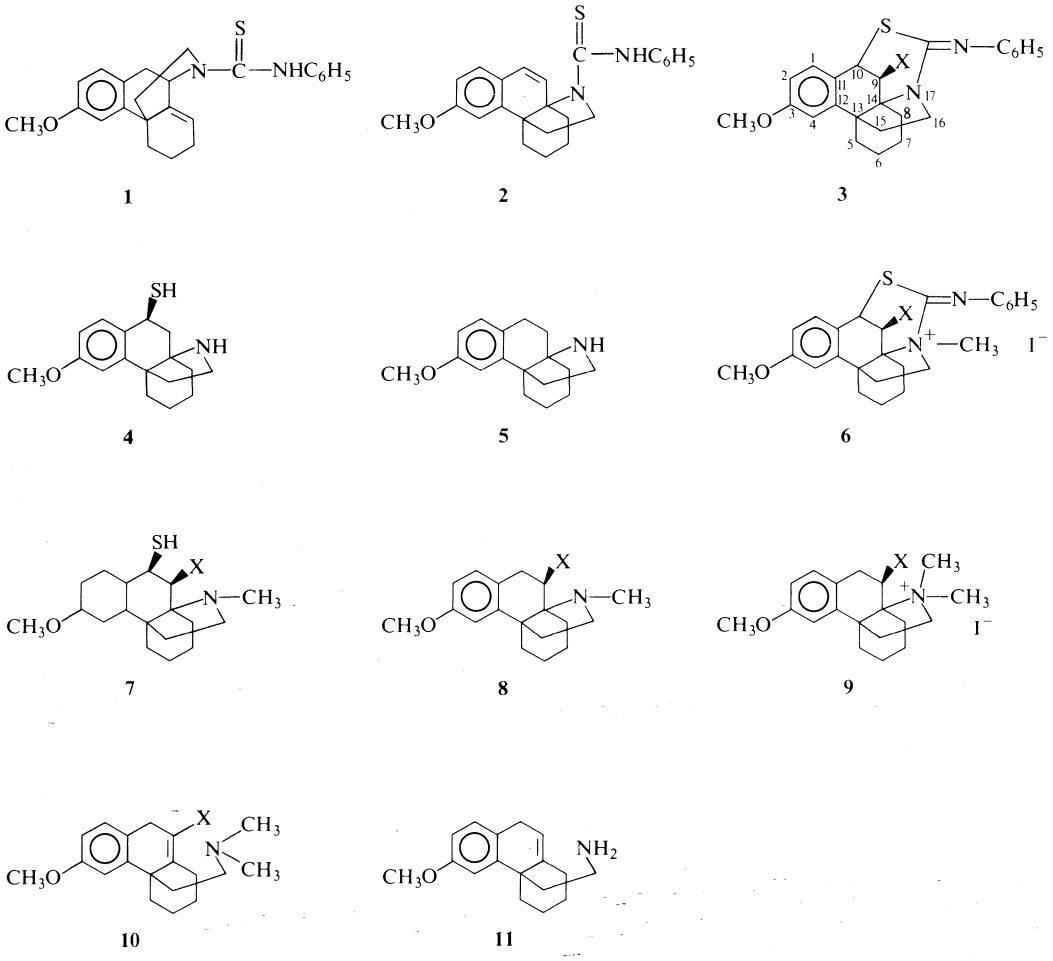

SCHEME 3

Results

The reaction of 3-methoxy-$\Delta^{8,14}$-morphinan (1) with phenyl isothiocyanate afforded the starting material, thioamidomorphinan **1**. Treatment of **1** with concentrated sulfuric acid at room temperature afforded a mixture of thioureidohasubanan **2** (68%) and thiazinohasubanan **3** (8%). The latter was obtained exclusively upon treatment of either **1** or **2** with boiling concentrated hydrochloric acid (67.5 and 69%, respectively), thus establishing intermediacy of **2** in the transformation of **1** to **3**. The thiazinohasubanan **3** was reduced with lithium aluminum hydride to the 10β-thiohasubanan **4**, which in turn was desulfurized by treatment with Raney nickel to afford hasubanan **5**, a suitable intermediate for the synthesis of various *N*-substituted 3-hydroxyhasubanans. The reductive alkylation of **5** (Raney Ni, H_2, CH_2O) afforded the hasubanan **8**.

Alternatively **8** was obtained via the following series of reactions: treatment of **3** with methyl iodide afforded quaternary salt **6**. This was reduced with lithium aluminum hydride to the 10β-thiohasubanan **7**, which in turn was hydrogenolized with Raney nickel to afford **8**. The reaction of **8** with methyl iodide gave quaternary salt **9** and treatment of this with potassium hydroxide in boiling 1-butanol (Hofmann elimination conditions) afforded aminohexahydrophenanthrene **10**, which was identical to the sample obtained by reductive methylation (Raney Ni, H_2, CH_2O) of the aminohexahydrophenanthrene **11** (1).

Can. J. Chem. Downloaded from www.nrcresearchpress.com by 210.87.254.105 on 09/05/12
For personal use only.

Can. J. Chem. Downloaded from www.nrcresearchpress.com by 210.87.254.105 on 09/05/12
For personal use only.

TABLE 1. Nuclear magnetic resonance spectra of thiazinohasubanan **3**

Compound	Aromatic protons	H_A	H_B	H_C	$O—CH_3$	16-H	5–8 and 15-H
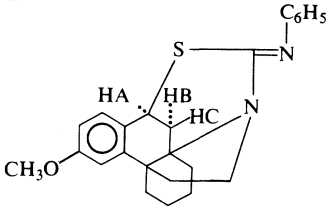	6.7–7.6 (m, 8H)	4.04 (dd, 1H)	2.9 (dd, 1H)	2.25 (d, d, 1H)	3.77 (s, 3H)	3.5–3.9 (m, 2H)	1.3–2.7 (m, 10H)
		J_{AB}=5 Hz, J_{AC}=2 Hz, J_{BC}=13 Hz					
3a*	6.7–7.6 (m, 6H) (2-H and C_6H_5)	4.02 (d, 1H)	2.98 (d, 1H)		3.77 (s, 3H)	3.5–3.9 (m, 2H)	1.3–2.7 (m, 10H)
		J_{AB}=5 Hz					
3b†	6.7–7.6 (m, 6H) (2-H and C_6H_5)	4.02 (d, ≈0.85H)	2.98 (d, ≈0.85H)		3.77 (s, 3H)	3.5–3.9 (m, 2H)	1.3–2.7 (m, ≈9.5H)
		J_{AB}=5 Hz					
		4.01 (s, ≈0.15H)					

*Product obtained by treatment of **2** with DCl.
†Product obtained by treatment of **1** with DCl.

TABLE 2. Nuclear magnetic resonance spectra of hasubanan and phenanthrene systems **9**, **10**, and **12**

Compound	Aromatic protons		$O—CH_3$	$N—CH_3$	16-H	10-H	5–9 and 15-H
9, X = H	7.5 (d, J = 10 Hz, 1H) (1-H)	6.65–7.3 (m, 2H) (2-H and 4-H)	3.85 (s, 3H)	2.3 (s, 3H)	2.7–3.2 (m, 2H)	4.18 (t, J = 6 Hz, 1H)	1.1–2.5 (m, 12H)
9a, X = D	7.5 (s, 1H) (1-H)		3.85 (s, 3H)	2.3 (s, 3H)	2.7–3.2 (m, 2H)	4.12 (d, J = 6 Hz, 1H)	1.1–2.5 (m, 11H)
10, X = H	6.45–6.95 (m, 3H)		3.67 (s, 3H)	2.17 (s, 3H)	2.4–3.0 (m, 4H)		1.1–2.4 (m, 12H)
10a, X = D	6.95 (s, 1H) (1-H)		3.67 (s, 3H)	2.17 (s, 3H)	2.4–3.0 (m, 4H)		1.1–2.4 (m, 11H)
12, X = H	6.6–7.1 (m, 3H)		3.8 (s, 3H)	2.1 (s, 6H)		3.3 (broad s, 2H)*	5.7 (t, J = 3 Hz, 1H) (9-H) 1.2–2.9 (m, 12H)†
12a, X = D	7.05 (s, 1H) (1-H)		3.8 (s, 3H)	2.1 (s, 6H)		3.3 (s, 2H)	1.2–2.9 (m, 12H)†

*The numbering of **12** and ***12a*** is related to the parent hasubanan system for n.m.r. assignment purposes.
†Also included are 16-H_2.

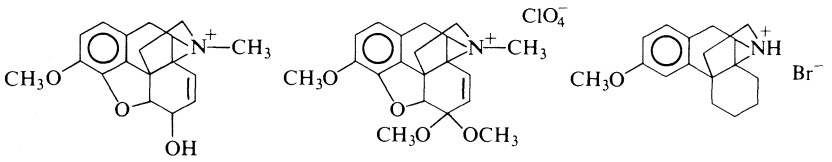

IV V VI

SCHEME 4

The sulfuric acid-d_2-catalyzed rearrangement of **1** to **2** led to the exchange of two aromatic protons as determined by n.m.r. spectroscopy. The extent of incorporation of unexchangeable deuterium was determined by mass spectrometry after cyclization of the above sample of **2** with hydrochloric acid to **3** and it was found to be in average of 0.74 atom/mol. However, 48% of **3** did not have any deuterium incorporated, whereas 13% had two and 1% three deuterium atoms, respectively.

The transformations of **2** to **3** and **1** to **3**, effected with deuterium chloride led, in addition, to the exchange of two aromatic protons to the stereospecific incorporation of one deuterium atom at C-9β site and, in the case of latter, to the additional incorporation of approximately 15% deuterium at C-9α site. The extent and the stereochemistry of incorporated deuterium were determined by n.m.r. spectroscopy and by chemical degradation. The transformation of doublets of doublets at δ 4.04, 2.90, and 2.25 (Table 1, compound **3**) to doublets at δ 4.02 and 2.98 (compound **3***a*), each of which integrates for one proton when cyclization of **2** to **3** was effected with deuterium chloride, shows a specific incorporation of one deuterium atom. A singlet at δ 4.01 in addition to the doublet at δ 4.02 exhibited by the spectrum of compound **3***b* indicates incorporation of some 9α-deuterium (≈ 15%). The fact that the proton with lower chemical shift (δ 2.25) is absent from the spectrum of **3***a* and **3***b* suggests its axial stereochemistry with respect to the dihydrothiazine ring (4). In order to confirm this stereochemical assignment, we have transformed **3** (X = D) via **6**, **7**, **8**, and **9** to **10**, which completely retained the original C-9 deuterium, as shown in Table 2. Although in the last step *cis* elimination under certain conditions could account to some extent for product formation it would not be expected to be the exclusive mode of elimination.[3] Therefore, the combined spectroscopic and chemical evidence can be considered as a sufficient proof for the β-stereochemistry of C-9 deuterium.

Discussion

Solvolytic rearrangements of 14-bromocodeine to 9-substituted indolinocodeine derivatives were postulated to take place via aziridinium intermediate IV (6, 7) (Scheme 4). The analogous intermediate was also postulated in the rearrangement of 9-substituted indolinocodeine series to morphine series (8). The intermediacy of aziridinium ion was proven by the isolation of aziridinium salt V upon silver perchlorate treatment of 7β-iodoneopine dimethyl acetal and 14-bromocodeine dimethyl acetal (9), and by isolation of aziridinium hydrobromide VI as an intermediate in the solvolytic rearrangement of 9α-bromo-3-methoxyhasubanan hydrobromide to the 3-methoxy-$\Delta^{8,14}$-morphinan (1).

Similarly, in the rearrangement of **1** to **2** we considered as possible intermediates aziridium ion **1***c* and carbonium ion **1***d* (Scheme 5) both of which could be derived from cation **1***a*. We assumed that the protonation of **1** to give **1***a* is the first step in the interaction of **1** with acid media on the basis of previous studies (2). Protonation of the thioureido function at the sulfur rather than at one of the nitrogen atoms is expected (10). Thus protonation of **1***a* at C-8 could lead to the dications **1***b* or **1***c* both of which could be subject to a concerted rearrangement to **2**. This process would be expected to lead to the incorporation of at least one deuterium atom at C-8, and possibly in excess of one via the equilibrium between **1***a* and **1***b* or **1***c*, respectively, when rearrangement is effected with sulfuric acid-d_2. The fact that maximum 52% of the **2** could have specifically incorporated one deuterium at C-8 as determined by mass spectrometry indicates existence of alternative pathway or pathways accounting for the remaining 48% of the product. We suggest intramolecular hydride

[3]On this subject see ref. 5.

Can. J. Chem. Downloaded from www.nrcresearchpress.com by 210.87.254.105 on 09/05/12
For personal use only.

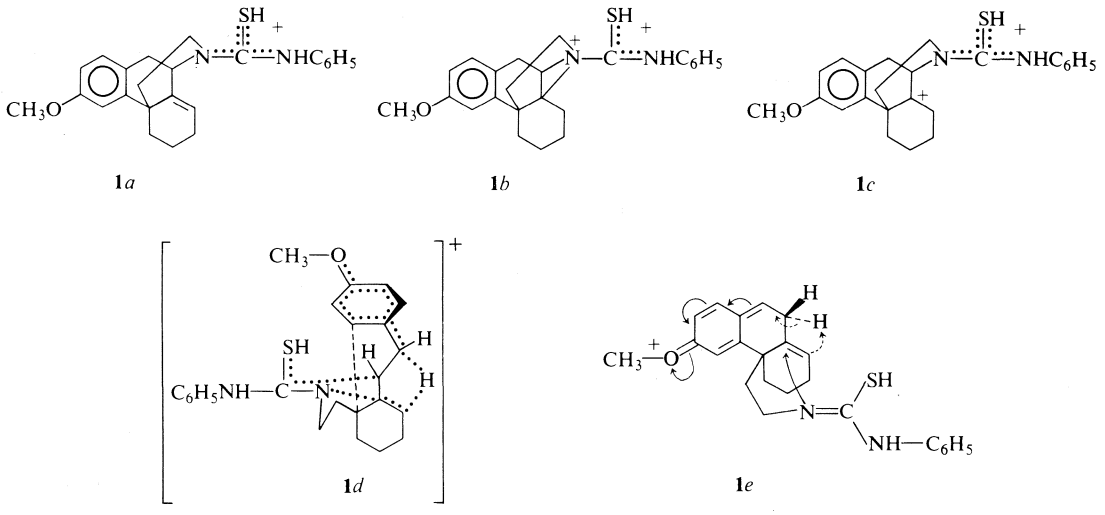

SCHEME 5

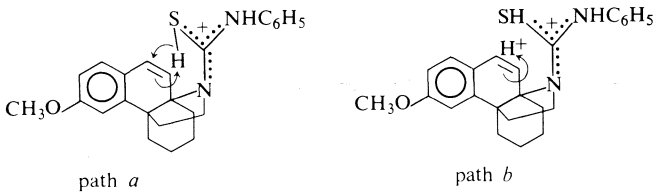

SCHEME 6

shift (11, 12) (C-10α to C-8α) via the transition state **1***d* or 1,2-hydride shift (C-10α to C-9α) followed by 1,3-proton transfer as shown by **1***e*. The initial hydride shift, with considerable C—N bond breaking seems to us more acceptable than initial protonation at C-8, since the former would be assisted by electron-donating *p*-methoxyphenyl function, while the latter would require electron donating participation of positively charged thioureido-function. The incorporation of deuterium at C-8 could occur after initial hydride shift either directly, or indirectly via deprotonation and reprotonation at C-9.

In conclusion, we suggest that rearrangement of **1** to **2** proceeds via two or more competing pathways, involving initial C-10α hydride shift, although initial C-8 protonation at least in part cannot be ruled out.

The stereospecific incorporation of deuterium at C-9β in the course of deuterium chloride-catalyzed cyclization of **2** to **3** could in principle occur either by intramolecular proton transfer (path *a*, Scheme 6) or by external protonation (path *b*). If protonation of the thioureido group is again assumed to be the first step in the interaction of substrate with acid media, then the thiouronium cation can be expected to inhibit external β-protonation (path *b*) both by its charge and by its steric hindrance. On the other hand a concerted addition of the thiouronic acid across the double bond (path *a*) appears to be a reasonable mechanism not only for the cyclization of **2** to **3** but also for cyclization of other substrates such as those studied by McManus and his co-workers (2, 3). In general, protonation of the heteroatomic function is expected to precede that of the double bond and thus if anything to increase the activation energy for the latter process. This accounts for the lack of a neighboring group participation effect, which was observed by McManus *et al.* and on the basis of which they proposed a two-step mechanism involving discrete carbonium ion intermediate (2). In the second step according to our mechanism (path *a*) the protonated species adds across the double bond, as shown by specific incorporation of only one deuterium

Can. J. Chem. Downloaded from www.nrcresearchpress.com by 210.87.254.105 on 09/05/12
For personal use only.

Can. J. Chem. Downloaded from www.nrcresearchpress.com by 210.87.254.105 on 09/05/12
For personal use only.

when deuterium labeling was used. The non-random incorporation of ~15% in excess of one deuterium at C-9 (Table 1, **3***b*), when transformation of **1** to **3** was affected with deuterium chloride is consistent with the already mentioned observation of multi-deuterated species in mass spectrum of **3**.

A significant increase in the reactivity of methylallyl *vs.* allyl derivatives (2) is in harmony with the intramolecular addition mechanism. If intramolecular addition is not favored for steric or electronic reasons, or if other more favorable reaction pathways are available, the rearrangement may take place such as that of **1** to **2** (Scheme 3) or VII to VIII (Scheme 7) (13).

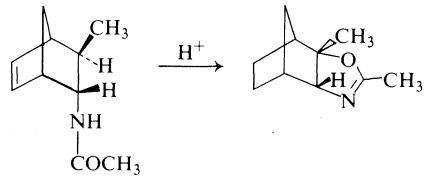

VI VIII

SCHEME 7

In the absence of other pathways the protonation of the double bond may take place under more drastic conditions. It is also conceivable that in some cases the cyclization may take place concurrently with the formation of the dication. If such would be the case, the cyclization would be expected again to take place intramolecularly via the monocation, although incorporation of more than one deuterium should be observed, when catalysis is performed with deuterio acids as shown in Scheme 8.

So far we have discussed the acid-catalyzed cyclizations of protonated *N*-allylamides and related systems in terms of a one-step intramolecular addition processes. However, a two-step process such as proton transfer from one hetero atom to another prior to the cyclization, or participation of the nitrogen to form unstable aziridinium or azetidinium cations which would rearrange under the given reaction conditions to the observed products is also conceivable. If existent, these processes should also involve intramolecular (hetero atom to carbon) proton transfers.

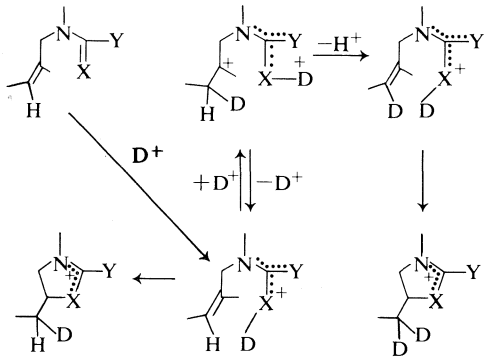

SCHEME 8

Experimental

The melting points were determined in a Gallenkamp melting point apparatus and are not corrected. The i.r. spectra were recorded on a Unicam Sp-200G grating i.r. spectrometer. The n.m.r. spectra were recorded on a Varian A-60A spectrometer using deuteriochloroform as solvent. The chemical shifts are expressed in δ values using tetramethylsilane as internal reference. Mass spectra were determined by the direct sample introduction technique on a LKB 9000 instrument at 20 eV chamber voltage and 100° chamber temperature. Microanalyses were performed by Micro-Tech Laboratories Inc., Skokie, Ill. The acids used were 96–98% reagent grade sulfuric acid, 99% sulfuric acid-d_2, hydrochloric acid, 36.5–38% reagent grade, and deuterium chloride 38% in D_2O (99% D).

17-(N-Phenylthioamido)-3-methoxy-$\Delta^{8,14}$*-morphinan (**1**)*

To a solution of 3-methoxy-$\Delta^{8,14}$-morphinan (**1**) (2 g) in ether (10 ml) was added a solution of phenyl isothiocyanate (0.91 g) in ether (10 ml) and the mixture was heated to reflux for 15 min. Then the ether was evaporated, and the residual solid was recrystallized from methanol to afford thioureidomorphinan **1** (2.9 g, 97%), m.p. 155–157°; n.m.r. δ 5.72 (1H, t, J = 3.5 Hz, 8-H).

Anal. Calcd. for $C_{24}H_{26}N_2OS$: C, 73.80; H, 6.71; N, 7.17. Found: C, 73.94; H, 6.91; N, 7.23.

17-(N-Phenylthioamido)-3-methoxy-$\Delta^{9,10}$*-hasubanan (**2**) and Corresponding Thiazinohasubanan (**3**)*

The thioamidomorphinan **1** (2 g) was added to sulfuric acid (5 ml) under nitrogen atmosphere and stirred for 15 min. Then the deep red solution was poured over ice, carefully neutralized with ammonium hydroxide, and extracted with chloroform. After drying, the solvent was evaporated and the residue was dissolved in boiling benzene, filtered, and upon cooling the solid was removed by filtration to afford thioamidohasubanan **2** (0.96 g), m.p. 165–166°. Another 0.44 g was obtained from mother liquors by chromatography on a silica gel column (20 g; activity V; eluent, dichloromethane) for a total of 1.4 g (68%); n.m.r. δ 6.73 (1H, d, J = 9 Hz, 10-H), 6.2 (1H, d, J = 9 Hz, 9-H) 3.75 (3H, s, O—CH_3), 3.5 (2H, m, 16-H) 1.0–2.0 (8H).

Anal. Calcd. for $C_{24}H_{26}N_2OS$: C, 73.80; H, 6.71; N, 7.17. Found: C, 73.50; H, 6.74; N, 7.02.

Further elution of the column afforded thiazinohasubanan **3** (160 mg, 8%), m.p. 205–207° (from methanol); molecular ions 390 (100%), 391 (28%), 392 (8.6%), and 393 (1.7%).

Can. J. Chem. Downloaded from www.nrcresearchpress.com by 210.87.254.105 on 09/05/12
For personal use only.

Anal. Calcd. for $C_{24}H_{26}N_2OS$: C, 73.80; H, 6.71; N, 7.17. Found: C, 73.73; H, 6.68; N, 7.16.

Alternatively **3** was obtained from **1** in the following manner. A suspension of **1** (7.7 g) in concentrated hydrochloric acid (30 ml) was heated to reflux under a nitrogen atmosphere for 2 h. After cooling, the solution was poured over ice and neutralized with ammonium hydroxide. The crude **3** was extracted with chloroform, dried, and the solvent was evaporated. The residue was recrystallized from hot methanol to afford **3** (5.02 g, 67.5%); m.p. 205–207°.

Similarly **3** was obtained in 69% yield by treatment of thioamidomorphinan **2** with refluxing concentrated hydrochloric acid for 30 min and isolation as described above.

The mass spectrum of **3**, which was obtained by rearrangement of **1** to **2** with sulfuric acid-d_2 and cyclization of this **2** to **3** with hydrochloric acid showed the following distribution of deuterium: d_0, 48, d_1 33, d_2 13, and d_3 1% with total average of 74% atom/mol.

*3-Methoxy-10β-thiohasubanan (**4**)*

To a hot solution of $LiAlH_4$ (500 mg) in dioxane (10 ml) was added dropwise a solution of thiazinohasubanan **3** (1.0 g) in dioxane (10 ml) and the mixture was heated to reflux for 16 h. After cooling, it was diluted with benzene (50 ml) and the excess of hydride was decomposed with saturated aqueous solution of ammonium chloride. The inorganic material was removed by filtration and the filtrate was dried (Na_2SO_4) and concentrated *in vacuo*. The residue was crystallized from ether – petroleum ether to afford thiohasubanan **4** (630 mg, 80%) as a solid, containing 1 mol of water of crystallization; m.p. 96–99°; i.r. ($CHCl_3$) 2500, 3230, 3450 cm^{-1}; n.m.r. δ 7.5 (1H, d, J = 9.5 Hz, 1-H), 6.8–7.0 (2H, m, 2-H and 4-H), 4.4 (1H, t, J = 6 Hz, 10-H), 3.85 (3H, s, O—CH_3), 2.9–3.3 (2H, m) 2.0–2.4 (4H, m), 1.2–2.0 (8H, m).

Anal. Calcd. for $C_{17}H_{23}NOS \cdot H_2O$: C, 66.41; H, 8.19; N, 4.55. Found: C, 66.23; H, 7.93; N, 4.70.

When drying of the analytical sample was performed at above 100°, the water of crystallization was removed as indicated by analysis.

Anal. Calcd. for $C_{17}H_{23}NOS$: C, 70.54; H, 8.00; N, 4.83; S, 11.09. Found: C, 70.29; H, 7.97; N, 4.91; S, 11.15.

*3-Methoxyhasubanan (**5**)*

To a solution of thiohasubanan **4** (180 mg) in methanol (5 ml) was added Raney nickel (≈ 100 mg) and the mixture was heated to reflux for 1 h. The catalyst was then removed by filtration, the filtrate was concentrated *in vacuo*, and the residue (crude **5**, 150 mg, 97%) was purified as hydrochloride salt, by recrystallization from methanol–ether; m.p. 263° (dec.); i.r. (neat) 3340 cm^{-1}; n.m.r. δ 6.5–7.1 (3H, m), 3.73 (3H, s, OCH_3), 2.5–3.7 (3H, m), 1.1–2.3 (12H, m).

Anal. Calcd. for $C_{17}H_{23}NO \cdot HCl$: C, 69.48; H, 8.23; N, 4.76. Found: C, 69.29; H, 8.34; N, 4.50.

*Thiazinohasubanan Methiodide (**6**)*

To a solution of thiazinohasubanan **3** (4.0 g) in acetonitrile–dichloromethane 2:1 mixture (20 ml) was added methyl iodide (3 g) and the mixture was left at room temperature for 20 h. The solvent was then evaporated to afford methiodide **6** (5.0 g, 92%). The analytical sample was recrystallized from dichloromethane–ether; m.p. 214° (dec.).

Anal. Calcd. for $C_{24}H_{26}NOS \cdot CH_3I$: C, 56.38; H, 5.48; N, 5.26. Found: C, 56.24; H, 5.53; N, 5.30.

*3-Methoxy-17-methyl-10β-thiohasubanan (**7**)*

To a suspension of methiodide **6** (2.7 g) in dioxane (30 ml) was added $LiAlH_4$ (0.5 g) and the mixture was heated to reflux for 16 h. After cooling, benzene was added (50 ml) and the excess hydride was decomposed with saturated aqueous solution of ammonium chloride. The inorganic material was removed by filtration and the filtrate was concentrated *in vacuo*. The residue (1.5 g) was chromatographed on alumina (activity III–IV; eluent, dichloromethane) and the second fraction was collected to afford thiohasubanan **7** (0.91 g, 60.5%) as an oil; i.r. (neat) 2490 cm^{-1}.

Anal. Calcd. for $C_{18}H_{25}NOS \cdot HCl$: C, 63.59; H, 7.70; N, 4.12; S, 9.43. Found: C, 63.70; H, 7.90; N, 4.01; S, 9.40.

*3-Methoxy-17-methylhasubanan (**8**)*

To a solution of thiohasubanan **7** (300 mg) in methanol (15 ml) was added Raney nickel (≈ 300 mg) and the mixture was heated to reflux for 1 h. The catalyst was then removed by filtration and the filtrate concentrated *in vacuo* to afford racemic **8** as an oil in a quantitative yield. The **1**-isomer has been prepared from natural sources and reported recently (14). The analytical sample was purified as hydrochloride salt from ethanol; m.p. 258–262° (dec.).

Anal. Calcd. for $C_{18}H_{25}NO \cdot HCl$: C, 70.22; H, 8.51; N, 4.55. Found: C, 70.28; H, 8.60; N, 4.60.

Alternatively **8** was prepared from **5** in the following procedure. A solution of 3-methoxyhasubanan **5** (90 mg) and formaldehyde (40 mg of 35% aqueous solution) in methanol (5 ml) was hydrogenated with Raney nickel as catalyst at 50 p.s.i. for 15 min. The catalyst was removed by filtration and the filtrate was concentrated *in vacuo* to afford **8** (80 mg, 84%).

*3-Methoxy-17-methylhasubanan Methiodide (**9**)*

A solution of 3-methoxy-17-methylhasubanan **8** (0.50 g) and methyl iodide (2.0 g) in acetonitrile (20 ml) was kept at room temperature for 7 days. The solvent was then evaporated, and the residue was crystallized from methanol–ether to afford methiodide **9** (0.676 g, 88%); m.p. 194–195°.

Anal. Calcd. for $C_{18}H_{25}NO \cdot CH_3I$: C, 55.20; H, 6.82; N, 3.38. Found: C, 55.09; H, 6.84; N, 3.34.

*4a-(2-Dimethylaminoethyl)-1,2,3,4,4a,9-hexahydro-6-methoxyphenanthrene (**10**)*

To a suspension of methiodide **9** (0.110 g) in 1-butanol (5 ml) was added potassium hydroxide (0.50 g) and the mixture was heated to reflux for 16 h. After cooling, it was poured into water, extracted with ether, and after drying (K_2CO_3) concentrated *in vacuo* to afford **10** (55 mg, 71.5%) as an oil. The hydrochloride salt was recrystallized from ethanol–ether; m.p. 228–230°.

Anal. Calcd. for $C_{19}H_{27}NO \cdot HCl$: C, 70.89; H, 8.76; N, 4.35. Found: C, 70.50; H, 8.85; N, 4.29.

The same product was obtained in 80% yield by reductive alkylation of 4a-(2-aminoethyl)-1,2,3,4,4a,9-hexahydro-6-methoxyphenanthrene (**11**) (1) in a similar procedure as given for the preparation of **8** from **5**.

Financial support by the National Research Council of Canada with the Industrial postdoctoral fellowship to one of us (M.S.) is gratefully acknowledged. We thank Dr. R. D. Brown, Bristol Laboratories, Syracuse, N.Y. 13201 for mass measurements.

1. I. MONKOVIĆ, T. T. CONWAY, H. WONG, Y. G. PERRON, I. J. PACHTER, and B. BELLEAU. J. Am. Chem. Soc. **95**, 7910 (1973).
2. S. P. MCMANUS, J. T. CARROLL, and C. H. PITTMAN, JR. J. Org. Chem. **35**, 3768 (1970).
3. S. P. MCMANUS, C. H. PITTMAN, JR., and P. E. FANTA. J. Org. Chem. **37**, 2353 (1972).
4. J. A. POPLE, W. G. SCHNEIDER, and H. J. BERNSTEIN. High-resolution nuclear magnetic resonance. McGraw-Hill Book Co., New York. 1959. p. 186.
5. J. SICHER. Angew. Chem. Int. Ed. Engl. **11**, 200 (1972).
6. K. ABE, Y. NAKAMURA, M. ONDA, and S. OKUDA. Tetrahedron, **27**, 4495 (1971).
7. S. OKUDA, K. ABE, and M. ONDA. Chem. Pharm. Bull. (Jap.), **16**, 1124 (1968).
8. K. ABE, Y. NAKAMURA, M. ONDA, and S. OKUDA. Chem. Pharm. Bull. (Jap.), **17**, 1917 (1969).
9. R. M. ALLAN and G. W. KIRBY. J. Chem. Soc. Perkin I, 364 (1973).
10. G. A. OLAH, A. M. WHITE, and D. H. O'BRIAN. Chem. Rev. **70**, 580 (1970).
11. V. PRELOG and J. G. TRAYNHAM. *In* Molecular rearrangements. Vol. 1. *Edited by* P. De Mayo. Interscience Publishers, Inc., New York. 1963.
12. D. M. BROUWER and A. A. KIFFEN. Rec. Trav. Chim. **92**, 906 (1973).
13. S. P. MCMANUS. Chem. Commun. 235 (1969).
14. Y. SAWA. Japan Patent 7121,632 (1971).

Can. J. Chem. Downloaded from www.nrcresearchpress.com by 210.87.254.105 on 09/05/12
For personal use only.

Systèmes aromatiques à 10 électrons π dérivés de l'aza-3a-pentalène. XI. Etude par résonance magnétique nucléaire de l'imidazo [1,2-*b*] pyrazole et du pyrazolo [1,5-*a*] benzimidazole

JOSÉ ELGUERO, ALAIN FRUCHIER, LEIF KNUTSSON[1] ET RENÉ LAZARO

Laboratoire de synthèse et d'étude physicochimique d'hétérocycles azotés, Université des Sciences et Techniques du Languedoc, Place E. Bataillon, 34060 Montpellier Cedex, France

ET

JAN SANDSTRÖM

Division of Organic Chemistry 1, Chemical Center, University of Lund, P.O.B. 740. S-220 07 Lund 7, Sweden

Reçu le 5 avril, 1974

JOSÉ ELGUERO, ALAIN FRUCHIER, LEIF KNUTSSON, RENÉ LAZARO et JAN SANDSTRÖM. Can. J. Chem. **52**, 2744 (1974).

L'étude r.m.n. a permis de déterminer la tautomérie annulaire et l'isomérie de position du dérivé acétylé de deux systèmes hétéroaromatiques [5,5]: dans tous les cas c'est le produit substitué (par H ou $COCH_3$) sur l'atome d'azote imidazolique qui est le plus stable. On a mis également en évidence des couplages peu courants avec le NH dans les produits non substitués sur l'azote et des barrières anormalement élevées dans les azolides, ce qui a conduit à émettre l'hypothèse d'une diminution de l'aromaticité de la partie imidazolique.

JOSÉ ELGUERO, ALAIN FRUCHIER, LEIF KNUTSSON, RENÉ LAZARO, and JAN SANDSTRÖM. Can. J. Chem. **52**, 2744 (1974).

Nuclear magnetic resonance spectroscopy has allowed us to determine the annular tautomerism in two [5,5]-heteroaromatic systems and the position of the acetyl group in their acetyl derivatives. In each case, the more stable compound is the one in which the imidazolic nitrogen atom is bearing H or $COCH_3$. We have also found unusual couplings with the N—H in the *N*-unsubstituted compounds and abnormally high barriers for the azolides. These observations agree well with the hypothesis of a decrease in the aromaticity of the imidazolic part.

Introduction

Le but de ces recherches sur des systèmes à 10 électrons π dérivés de l'aza-3a-pentalène (1, 2) est d'examiner si la jonction de deux cycles pentagonaux plans, avec les tensions que cela entraine, conserve à ces noyaux le caractère aromatique qu'ont les systèmes bicycliques [5,6] et [6,6]. L'étude r.m.n. de deux dérivés de l'imidazo[1,2-*b*]pyrazole, **1** et **2**, et de deux dérivés du pyrazolo[1,5-*a*]benzimidazole, **3** et **4**, a conduit à des résultats concernant des couplages avec le NH, produits **1** et **3**, et des barrières à la rotation, produits **2** et **4**, qui s'interprétent en fonction du caractère peu aromatique de ces bicycles [5,5].

Nous avons adopté pour ces noyaux un système de numérotation non conventionnel afin de rendre la discussion plus claire et leur comparaison plus commode.

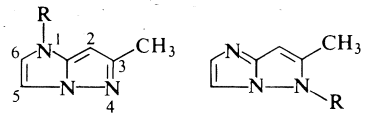

a *b*

1 R = H
2 R = $COCH_3$

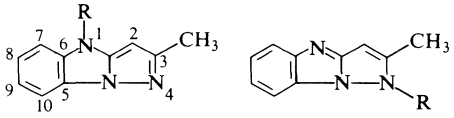

a *b*

3 R = H
4 R = $COCH_3$

Partie expérimentale

Les spectres ont été enregistrés en balayage de fréquence sur des appareils Varian HA-100 (Montpellier) et XL-100 (Lund). Les déplacements chimiques sont exprimés en p.p.m. par rapport au TMS utilisé comme référence interne, et les constantes de couplage en Hz.

Les constantes de vitesse de rotation du groupe acétyle dans **2***a*, **12** et **13** ont été déterminées par comparaison

[1]Adresse actuelle: Department of Organic Chemistry, University of Umeå, Sweden.

Can. J. Chem. Downloaded from www.nrcresearchpress.com by 210.87.254.40 on 09/05/12
For personal use only.

Can. J. Chem. Downloaded from www.nrcresearchpress.com by 210.87.254.40 on 09/05/12
For personal use only.

visuelle entre les spectres expérimentaux des protons $COCH_3$, **12**, ou H_2, **2***a* et **13**, et les spectres calculés au moyen de l'expression de McConnell (3) programmée pour un calculateur Hewlett-Packard 9820-A avec traceur de courbes. Les spectres sont enregistrés à plusieurs températures et les énergies libres d'activation $\Delta G^{\ddagger}$ sont calculées par l'équation d'Eyring et collaborateurs (4). Les valeurs de $\Delta G^{\ddagger}$ ne varient pas systématiquement avec la température et les entropies d'activation $\Delta S^{\ddagger}$ sont probablement proches de zéro.

La température est mesurée par un thermocouple fixé dans la sonde juste au dessus de la bobine. La différence de température entre cette position et celle de l'échantillon a été calibrée au moyen d'un deuxième thermocouple situé dans un tube de r.m.n. à la hauteur de la bobine.

On a utilisé les unités SI pour les données thermodynamiques, ainsi $\Delta G^{\ddagger}$ est donné en kJ mol^{-1}.

Résultats et discussion

A cause de son insolubilité dans le $CDCl_3$, nous avons dû étudier le composé **1** dans le DMSO-d_6. A la concentration de 1 mol l^{-1}, le spectre (fig. 1*a*) est de premier ordre et présente peu de couplages. On y trouve (tableau 1) le signal du NH, celui du méthyle et le système AMX des protons H_2, H_5 et H_6. On note l'existence d'un couplage "cross-ring" J_{25} analogue à celui rencontré dans l'indolizine (5) et plus généralement dans tous les systèmes bicycliques aromatiques. L'absence de couplage mesurable entre H_2 et le groupe méthyle en 3, J_{23}, est en faveur de la structure tautomère **1***a*; en effet dans la série du pyrazole (6) le couplage J_{34} est inobservable dans les méthyl-3 pyrazoles *N*-substitués **5**, tandis que le couplage J_{45} est très net dans les isomères méthyl-5 **6**. Un couplage analogue à ce dernier a été décrit récemment entre le méthyle en 6 et le proton en 5 du méthyl-6 imidazo[2,1-*b*]thiazole **7** (7).

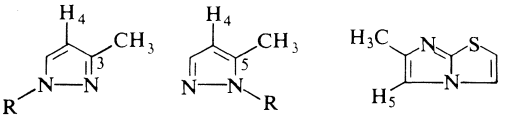

5 **6** **7**

A la concentration de 0.5 mol l^{-1} et dans le même solvant, on voit apparaître des couplages entre les protons H_5 et H_6 d'une part et le proton du N—H d'autre part (fig. 1*b*),[2] ce qui démontre sans ambigüité qu'il s'agit du tautomère **1***a* (1). Seuls le pyrrole (8) et l'indole (9) présentent des couplages analogues; il faut admettre ici, comme pour ces derniers, une vitesse d'échange protonique lente. Ce dernier point est confirmé par le spectre dans l'acide trifluoroacétique (TFA) dans lequel les mêmes couplages avec le N–H en position 1 sont visibles, alors qu'aucun n'apparait avec le second N—H en position 4 dont la vitesse d'échange est normale. Dans ce solvant, le méthyle en 3 est couplé avec le proton H_2; ceci est surprenant car on ne trouve pas de couplage semblable dans les cations pyrazoliums (10). On peut attribuer cette différence de comportement à la présence d'un atome d'azote en position 1 qui permet d'écrire une forme de résonance **8***a*′ ayant une double liaison en position 2–3:

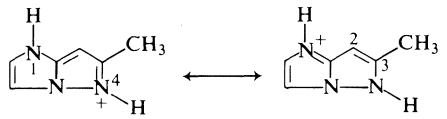

8*a* **8***a*′

Le dérivé acétylé **2** présente dans le DMSO un spectre analogue à celui du composé **1***a* dans le même solvant et à la même concentration de 1 mol l^{-1}. Il apparait seulement, en plus, des

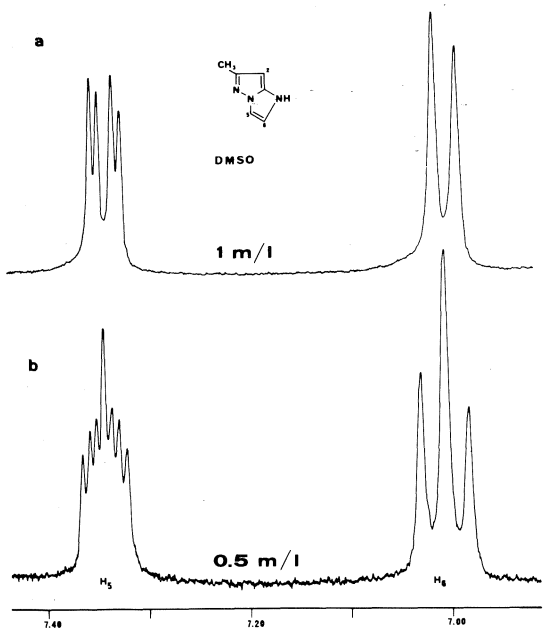

FIG. 1. Le spectre du composé **1** dans le DMSO-d_6: (*a*) à la concentration de 1 mol l^{-1}; (*b*) à la concentration de 0.5 mol l^{-1}.

[2]Cet effet de la concentration met en évidence le caractère intermoléculaire de ces échanges protoniques; vraisemblablement c'est le doublet de l'atome d'azote N_4 qui est l'accepteur du proton.

TABLEAU 1. Déplacements chimiques et constantes de couplage des imidazo[1,2-*b*]pyrazoles. Sauf indication contraire la température est de 300 K et la concentration de 1 mol l^{-1}

	1*a*			**2***a*			
						$CDCl_3$†	
	DMSO-d_6	DMSO-d_6*	TFA	DMSO-d_6	$CDCl_3$	*E*	*Z*
H_1 ou $COCH_3$	10.81	10.60	10.28	2.56	2.56	2.53	2.51
H_2	5.44	5.44	6.20	5.98	5.85§	5.72	6.10
H_3	2.26	2.26	2.57	2.31	2.41	2.39	2.39
H_5	7.35	7.35	7.62	7.72	7.27	7.29	7.26
H_6	7.00	7.00	7.33	7.56	7.27	7.36	6.98
J_{15}	0	1.6	1.5	—	—	—	—
J_{16}	0	2.5	2.5	—	—	—	—
J_{23}	0	0	0.9	0.45	0	0	0
J_{25}	0.8	0.8	0.7	0.6	‡	0.6	0.6
J_{36}	0	0	0	≠0	‡	0	0
J_{56}	2.3	2.3	2.5	2.7	‡	2.6	2.6

*Concentration 0.5 mol l^{-1}.
†Température 253 K.
‡Valeurs non mesurables.
§Signal élargi.

couplages faibles entre le méthyle et les protons H_2 et H_6. Le couplage J_{36}, non mesurable, est prouvé par l'affinement du signal de H_6 lors de l'irradiation de celui du méthyle. Nous avons attribué à ce produit la structure acétyl-1 **2***a* pour justifier le très net déplacement vers les plus hautes fréquences des signaux des protons H_2 et H_6 quand on passe du produit N–H **1***a* au dérivé *N*-acétylé (tableau 1).

Dans le $CDCl_3$ et à la concentration de 1 mol l^{-1}, le produit présente des signaux élargis, en particulier celui de H_2 (température de la sonde: 300 K), qui s'affinent en chauffant: cela est dû à la rotation lente du groupe acétyle (voir plus loin). A 253 K on observe la superposition de deux spectres provenant du mélange de deux rotamères **2***aE* et **2***aZ*: nous avons attribué (11–13) au rotamère **2***aZ* (35%) le proton H_2 le plus déblindé, celui qui résonne à 6.10 p.p.m. Les autres signaux ont été attribués en tenant compte de leur intensité et aussi grâce à des expériences de double résonance. Les déplacements chimiques ont été très peu influencés par la variation de température; en effet, le centre ponderé des signaux à 253 K coincide presque avec l'emplacement des signaux à 300 K.

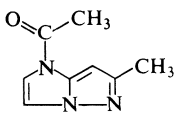

2*aE*

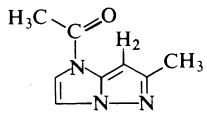

2*aZ*

Le produit **3** présente dans le DMSO un spectre (fig. 2) composé du signal de H_2 et du méthyle, non couplés, d'une partie complexe correspondant aux quatre protons du noyau benzénique et enfin le signal du N—H vers 11.4 p.p.m. Comme dans le cas précédent le fait que J_{23} soit nulle est en faveur du tautomère **3***a* (2). Nous avons effectué, au moyen du programme LAOCN 3 (14), l'analyse du système à quatre spins des protons H_7, H_8, H_9 et H_{10}. Les déplacements chimiques et les constantes de couplage sont donnés dans le tableau 2. L'attribution des signaux a été basée sur le fait que le signal à 7.70 p.p.m. (pouvant être H_7 ou H_{10}) est élargi. Cet élargissement disparait par irradiation du N—H. Comme dans l'indole **9**, Black et Heffernan (9) ont montré que c'est H_4 et non H_7 qui présente un tel couplage, l'attribution du signal à 7.70 p.p.m. au proton H_{10} semble raisonnable. De là découlent naturellement les déplacements chimiques des trois autres protons.

Réciproquement, ce couplage avec le N—H prouve qu'il s'agit du tautomère **3***a*.

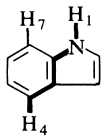

9

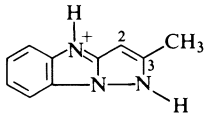

10*a*′

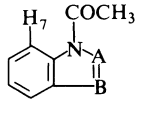

11

A = N; B = CH
A = CH; B = N
A = B = N

Can. J. Chem. Downloaded from www.nrcresearchpress.com by 210.87.254.40 on 09/05/12
For personal use only.

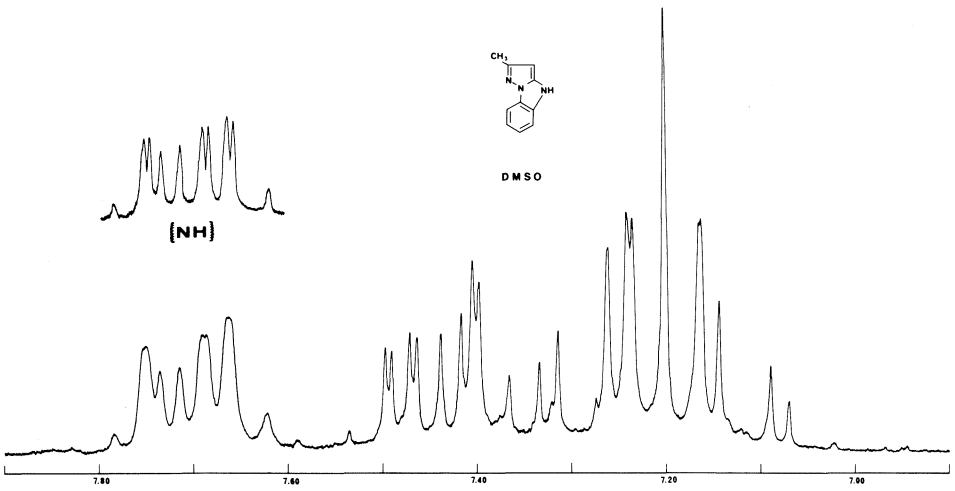

FIG. 2. Le spectre du composé **3** dans le DMSO.

TABLEAU 2. Déplacements chimiques et constantes de couplage des pyrazolo[1,5-*a*]benzimidazoles. Température 300 K et concentration 1 mol l^{-1}

	3*a*		**4***a*
	DMSO-d_6	TFA	$CDCl_3$
H_1 ou CH_3	11.37	10.39	2.56
H_2	5.67	6.28	5.73
H_3	2.37	2.68	2.43
H_7	7.43	†	8.25*
H_8	7.24	†	7.22
H_9	7.17	†	7.29
H_{10}	7.70*	†	7.61
J_{23}	0	0.75	0.4
J_{78}	8.08	†	8.29
J_{79}	1.14	†	1.05
J_{7-10}	0.62	†	0.59
J_{89}	7.43	†	7.55
J_{8-10}	1.26	†	1.15
J_{9-10}	8.02	†	8.11

*Signal élargi.
†Mauvaise résolution ne permettant pas de mesurer les transitions avec précision.

Dans le TFA (cation **10***a*′), une mauvaise résolution n'a pas permis d'effectuer l'analyse du système ABCD. On peut noter cependant, comme dans le cation **8***a*′, la présence d'un couplage J_{23} de 0.75 Hz, absent dans la base.

Dans le $CDCl_3$ (fig. 3), le composé **4** présente le même phénomène de rotation lente du groupe acétyle que son homologue **2***a*. Il est observé ici, non pas sur H_2, mais sur l'un des protons de l'homocycle, celui qui résonne à la fréquence la plus élevée (son élargissement disparait par élévation de la température). Comme il est connu que le groupe acétyle déblinde les protons H_7 des acétyl-1 benzazoles **11** (15, 16), ce signal doit être attribué au proton H_7 du dérivé acétyl-1 **4***a*.

Détermination des barrières à la rotation des dérivés acétylés

Nous avons signalé que les produits **2***a* et **4***a* présentent à 300 K des signaux élargis, conséquence de la rotation lente du groupe acétyle. Comme dans le cas du composé **4***a* le phénomène n'est observable que sur un proton du système ABCD, nous nous sommes limités à faire l'étude quantitative sur le composé **2***a*. Afin de pouvoir discuter du résultat ainsi obtenu nous avons étudié deux autres composés: l'acétyl-1 imidazole, **12**, comme modèle de noyau aromatique, et l'acétyl-1 méthyl-6 dihydro-2,3 imidazo[1,2-*b*]pyrazole, **13** (17), comme modèle de noyau non aromatique.

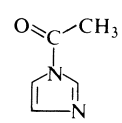
12*E*

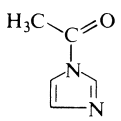
12*Z*

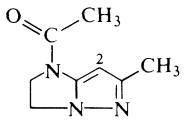
13*E*

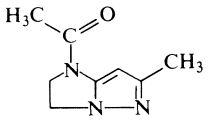
13*Z*

Can. J. Chem. Downloaded from www.nrcresearchpress.com by 210.87.254.40 on 09/05/12
For personal use only.

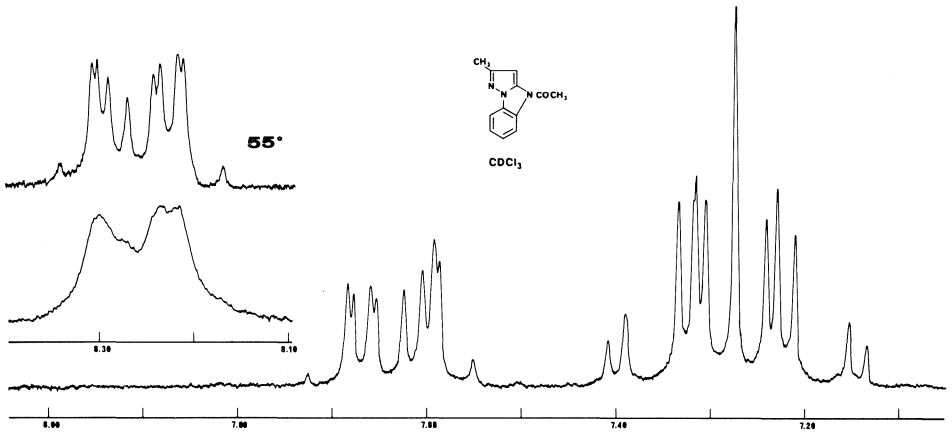

FIG. 3. Le spectre du composé **4** dans le $CDCl_3$.

TABLEAU 3. Barrières à la rotation d'amides et d'azolides ($\Delta G^{\ddagger}$ en kJ mol^{-1})

	Solvant	Population de rotamère E	Signal observé	$\Delta\nu$ (Hz)	$\Delta G^{\ddagger}$ (réf.)
2*a*	$CDCl_3$	0.57*	H_2	36 (100 MHz)	E → Z 62 Z → E 61
12	$CHCl_2F$	0.63†	CH_3CO	6.6 (100 MHz)‡	E → Z 44 ± 5 Z → E 43 ± 0.5§
13	$CDCl_3$	0.85	H_2	41.6 (100 MHz)	E → Z 75 Z → E 71
14	$CDCl_3$	$p_E = p_Z$	H_2	22.8 (60 MHz)	E → Z 52 (19) Z → E 54 (13, 20)‖
15	Sans solvant	—	CH_3	2.7 (60 MHz)	75 (22)
16	$CDCl_3$	0.11	CH_3CO	—	69 (23)
17	$CDCl_3$	0.39	CH_3CO	—	69 (23)

*En solution plus concentrée (tableau 1). $p_E = 0.65$.
†Dans l'acétone, $p_E = 0.25$ (20).
‡23.7 Hz (à 100 MHz) pour H_2.
§Probablement $\Delta S^{\ddagger} \approx 0$.
‖En solution dans le CD_2Cl_2, $\Delta G_{298}^{\ddagger} = 50$ kJ mol^{-1} (21).

Les azolides (18), dérivés *N*-acylés des azoles, ont un comportement très particulier qui les différencie des amides; cela est dû au fait que le doublet de l'atome d'azote en position 1 fait partie du sextet aromatique; on peut donc penser que la hauteur de la barrière à la libre rotation du groupe acétyle donnera une indication sur l'aromaticité de l'hétérocycle.

Le seul azolide à avoir été étudié jusqu'à présent est l'acétyl-1 pyrrole **14** dont la barrière a été déterminée indépendement par trois groupes d'auteurs (19–21) (tableau 3); la valeur trouvée, environ 52 kJ mol^{-1} est beaucoup plus basse que celle des amides; par exemple pour l'acétyl-1 pyrrolidine **15** on trouve $\Delta G^{\ddagger} = 75$ kJ mol^{-1} (22). L'introduction d'un atome d'azote sp^2 en position 3 diminue la barrière d'environ 10 kJ mol^{-1}: comparer les produits **12** et **14**. C'est l'effet normalement attendu si l'on considère qu'un atome d'azote sp^2 a un caractère attracteur d'électrons comparable à un groupe nitro (24) et que les barrières à la rotation de thioamides dérivant du pyrazole suivent l'équation de Hammett (25).

Le produit dihydro, **13**, présente une barrière de ~73 kJ mol^{-1}, clairement plus élevée que

Can. J. Chem. Downloaded from www.nrcresearchpress.com by 210.87.254.40 on 09/05/12
For personal use only.

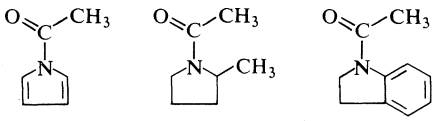

14 **15** (*E*) **16** (*E*)

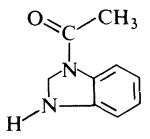

17 (*E*)

celles de l'acétyl-1 indoline, **16** (21),[3] et de l'acétyl-1 benzimidazoline, **17** (23): cela semble indiquer que l'effet de conjugaison du noyau pyrazolique est plus faible que celui du noyau benzénique; il faut cependant tenir compte également que le noyau pentagonal est plus "petit" (comme le montre la proportion plus élevée de rotamère *E*) ce qui doit permettre une plus grande coplanéité et partant, une stabilisation de l'état fondamental.

Enfin, la barrière à la rotation du groupe acétyle du système hétéroaromatique **2***a* est intermédiaire entre celles de l'amide **13** et de l'azolide **12**.

Conclusion

Les quatre résultats essentiels obtenus dans ce travail: prédominance du tautomère avec le proton sur l'atome d'azote imidazolique (ou benzimidazolique); échange lent de ce proton (avec apparition des couplages); stabilité plus grande du dérivé acétylé sur ce même azote, et barrière à la rotation du groupe acétyle intermédiaire entre celles d'un amide et d'un azolide, s'expliquent si l'on admet qu'une réprésentation

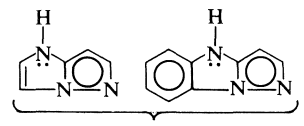

A

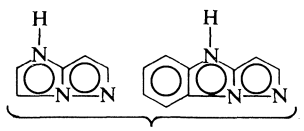

H

du type *A* (aminopyrazole) convient mieux pour ces molécules qu'une représentation du type *H* (hétéroaromatique).

En effet on sait que pour les aminopyrazoles le tautomère amino **18***a* prédomine toujours (27), que l'on observe des couplages NH—CH (28), que l'acylation a lieu sur l'atome d'azote exocyclique (29, 30), et que l'on observe des barrières à la rotation élevées correspondant à leur structure amidique, comme c'est le cas du produit **13**.

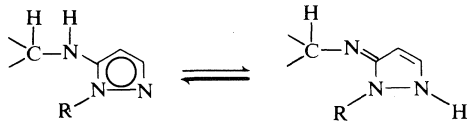

18*a* **18***b*

Toutefois la diminution de la hauteur de la barrière à la libre rotation en passant du produit **13** au produit **2***a* montre une certaine délocalisation du doublet de l'atome d'azote N_1.

1. J. ELGUERO, R. JACQUIER et S. MIGNONAC-MONDON. J. Heterocycl. Chem. **10**, 411 (1973).
2. S. MIGNONAC-MONDON, J. ELGUERO et R. LAZARO. C.R. Acad. Sci. Paris, **276**C, 1533 (1973).
3. H. M. MCCONNELL. J. Chem. Phys. **28**, 430 (1958).
4. S. GLASSTONE, K. J. LAIDLER et H. EYRING. The theory of rate processes. McGraw-Hill, New York. 1941. p. 190.
5. P. J. BLACK, M. L. HEFFERNAN, L. M. JACKMAN, Q. N. PORTER et G. R. UNDERWOOD. Aust. J. Chem. **12**, 1128 (1964).
6. J. ELGUERO et R. JACQUIER. J. Chim. Phys. **63**, 1242 (1966).
7. L. MARCHETTI, L. PENTIMALLI, P. LAZZERETTI, L. SCHENETTI et F. TADDEI. J. Chem. Soc. Perkin Trans. II, 1926 (1973).
8. G. F. KATEKAR et A. G. MORITZ. Aust. J. Chem. **22**, 1199 (1969).
9. P. J. BLACK et M. L. HEFFERNAN. Aust. J. Chem. **18**, 353 (1965).
10. J. ELGUERO, R. JACQUIER et D. TIZANE. Bull. Soc. Chim. Fr. 1687 (1969).
11. K. NAGARAJAN, M. D. NAIR et P. M. PILLAI. Tetrahedron, **23**, 1683 (1967).
12. A. M. MONRO et M. J. SEWELL. Tetrahedron Lett. 595 (1969); J. Chem. Soc. B, 1227 (1971).
13. L. PAPPALARDO, J. ELGUERO et C. MARZIN. C.R. Acad. Sci. Paris, **277**C, 1163 (1973).
14. S. CASTELLANO et A. A. BOTHNER-BY. *In* Computer programs for chemistry. *Edited by* D. F. Detar. Benjamin. 1968.
15. J. ELGUERO, A. FRUCHIER et R. JACQUIER. Bull. Soc. Chim. Fr. 2075 (1966).
16. J. ELGUERO, A. FRUCHIER et L. PAPPALARDO. Résultats non publiés.
17. J. ELGUERO et L. KNUTSSON. Résultats non publiés.

[3]Très récemment (26) on a signalé que dans le spectre r.m.n. du formyl-1 méthyl-3 indole (CCl_4, 304 K) on observe les signaux des deux rotamères.

Can. J. Chem. Downloaded from www.nrcresearchpress.com by 210.87.254.40 on 09/05/12
For personal use only.

18. H. A. STAAB. Angew. Chem. Int. Ed. **1**, 351 (1962).
19. T. MATSUO et H. SHOSENJI. Chem. Commun. 501 (1969).
20. J. ELGUERO, C. MARZIN et L. PAPPALARDO. Bull. Soc. Chim. Fr. Sous presse.
21. K. I. DAHLQUIST et S. FORSEN. J. Phys. Chem. **73**, 4124 (1969).
22. H. PAULSEN et K. TODT. Chem. Ber. **100**, 3385 (1967).
23. G. V. GARNER, O. METH-COHN et H. SUSCHITZKY. J. Chem. Soc. C, 1234 (1971).
24. J. CLARK et D. D. PERRIN. Quart. Rev. **18**, 295 (1964).
25. L-O. CARLSSON. Acta Chem. Scand. **26**, 21 (1972).
26. A. CHATTERJEE et K. M. BISWAS. J. Org. Chem. **38**, 4002 (1973).
27. J. ELGUERO, C. MARZIN, A. R. KATRITZKY et P. LINDA. Heteroaromatic tautomerism. Academic Press, New York. (1974).
28. J. ELGUERO et R. LAZARO. Résultats non publiés.
29. E. L. ANDERSON, J. E. CASEY, L. C. GREENE, J. J. LAFFERTY et H. E. REIF. J. Med. Chem. **7**, 259 (1964).
30. E. ALCALDE, J. DE MENDOZA et J. ELGUERO. Org. Magn. Res. **4**, 733 (1972).

Can. J. Chem. Downloaded from www.nrcresearchpress.com by 210.87.254.40 on 09/05/12
For personal use only.

Kinetics and Mechanism of the Thermal Decomposition of Hexaamminecobalt(III) and Aquopentaamminecobalt(III) Ions in Acidic Aqueous Solution

ANTHONY MARTIN NEWTON AND THOMAS WILSON SWADDLE[1]

Department of Chemistry, The University of Calgary, Calgary, Alberta T2N 1N4

Received March 18, 1974

ANTHONY MARTIN NEWTON and THOMAS WILSON SWADDLE. Can. J. Chem. **52**, 2751 (1974).

The initial step in the thermal decomposition of $Co(NH_3)_6^{3+}$ in acidic aqueous solution is the replacement of NH_3 by H_2O, which occurs by a hydrogen-ion independent path, first order in complex, with rate coefficient $k_1 = 7.9 \times 10^{-5}$ s^{-1} (140.4°), $\Delta H^* = 36.6$ kcal mol^{-1}, and $\Delta S^* = 10.7$ cal deg^{-1} mol^{-1} in 0.1 *M* $HClO_4$. For $Co(NH_3)_5OH_2^{3+}$, there is a similar initial aquation path with $k_1 = 12.6 \times 10^{-5}$ s^{-1} (140.6°), $\Delta H^* = 41.9$ kcal mol^{-1}, and $\Delta S^* = 24$ cal deg^{-1} mol^{-1} and also a path first order in complex but inverse first order in $[H^+]$ with $k_2' = 6.2 \times 10^{-5}$ *M* s^{-1} (140.6°), $\Delta H^* = 43.5$ kcal mol^{-1}, and $\Delta S^* = 26.7$ cal deg^{-1} mol^{-1}, in perchlorate media of ionic strength 1.0 *M*. The effects of electrolyte type and concentration on the rates of these reactions have been examined. Subsequent aquation steps are relatively rapid because of the predominance of inversely $[H^+]$-dependent pathways and are followed by redox to $Co(H_2O)_6^{2+}$, NH_4^+, N_2, N_2O, and a minor amount of O_2. A mechanism involving OH and NH_2 radicals is proposed for the redox step.

ANTHONY MARTIN NEWTON et THOMAS WILSON SWADDLE. Can. J. Chem. **52**, 2751 (1974).

L'étape initiale lors de la décomposition thermique du $Co(NH_3)_6^{3+}$ en solution aqueuse acidifiée est le remplacement d'un NH_3 par une molécule d'eau; cette réaction se produit par une voie n'inpliquant pas d'ions hydrogène, elle est du premier ordre en complexe avec un coefficient de vitesse $k_1 = 7.9 \times 10^{-5}$ s^{-1} (140.4°), $\Delta H^* = 36.6$ kcal mol^{-1} et $\Delta S^* = 10.7$ cal deg^{-1} mol^{-1} dans $HClO_4$ 0.1 *M*. Dans le cas du $Co(NH_3)_5OH_2^{3+}$, il existe une équation similaire pour le chemin initiale et $k_1 = 12.6 \times 10^{-5}$ s^{-1} (140.6°), $\Delta H^* = 41.9$ kcal mol^{-1} et $\Delta S^* = 24$ cal deg^{-1} mol^{-1}; cette réaction est aussi du premier ordre en complexe mais d'un ordre inverse du premier en $[H^+]$ avec $k_2' = 6.2 \times 10^{-5}$ *M* s^{-1} (140.6°), $\Delta H^* = 43.5$ kcal mol^{-1} et $\Delta S^* = 26.7$ cal deg^{-1} mol^{-1} dans un milieu perchlorate ayant une force ionique de 1.0 *M*. On a aussi examiné les effets de type électrolyte et de concentration sur les vitesses de ces réactions, les équations des étapes subséquentes sont relativement rapides à cause de la prédominance d'un chemin dépendant d'une façon inversement proportionnelle à la concentration $[H^+]$, ces étapes sont suivies par une réaction d'oxydo-réduction conduisant à $Co(H_2O)_6^{2+}$, NH_4^+, N_2, N_2O et des quantités mineures de O_2. On propose un mécanisme impliquant des radicaux OH et NH_2 pour l'étape d'oxydo-réduction. [Traduit par le journal]

Introduction

A striking feature of cobalt(III) chemistry is the great decrease in reactivity which occurs on replacing several of the aquo ligands in $Co(H_2O)_6^{3+}$ by NH_3, to the extent that the ammine ligands in $Co(NH_3)_6^{3+}$ and $Co(NH_3)_5X^{(3-n)+}$ (X = halogen, H_2O, oxyanions, etc.) are commonly regarded as substitution inert in acidic aqueous solution. Nevertheless, kinetic studies of the aquations of X^{n-} from $Co(NH_3)_5X^{(3-n)+}$ begin to suffer from the complicating effects of NH_3 loss from either the parent complex or (more usually) from the product $Co(NH_3)_5OH_2^{3+}$ at temperatures above 80° (1). The present study seeks to determine the importance of this complication, as well as to gain insight into the mechanism of decomposition of $Co(NH_3)_6^{3+}$ and $Co(NH_3)_5OH_2^{3+}$ in solution.

Since the completion of our kinetic studies, Garner and his co-workers (2) have published data on the decomposition of $Co(NH_3)_5OH_2^{3+}$ and *cis*-$Co(NH_3)_4(OH_2)_2^{3+}$ in acidic perchlorate media, in addition to their papers on the decomposition of the presumed facial isomer of $Co(NH_3)_3(OH_2)_3^{3+}$ (3) and *cis*-$Co(NH_3)_2(OH_2)_4^{3+}$ (4). It appears that the initial replacement of an ammine ligand by water is the rate-determining step in the decompositions of the penta- and tetra-ammines (2) but that redox decomposition to cobalt(II) predominates in the decomposition of the triammine (3) (however, up to 17% of the observed rate of disappearance

[1]To whom correspondence should be addressed.

Can. J. Chem. Downloaded from www.nrcresearchpress.com by 210.87.254.42 on 09/05/12
For personal use only.

Can. J. Chem. Downloaded from www.nrcresearchpress.com by 210.87.254.42 on 09/05/12
For personal use only.

of the tetraammine could also conceivably be due to redox (2)). *cis*-Diamminetetraaquocobalt(III) decomposes by direct redox to cobalt(II) (4), whereas amminepentaaquocobalt(III) undergoes an extraordinary disproportionation to cobalt(II) and diamminetetraaquocobalt(III) (5).

We shall address ourselves primarily to two salient questions which remain. Firstly, there is no information on the kinetics of decomposition of the hexaammine, and, secondly, the nature of the oxidized reaction products has not been established. The latter has an important bearing on the mechanism of the redox steps. In addition, new information pertaining to electrolyte effects on the reaction rates will be presented, together with improved activation parameters for the decomposition of $Co(NH_3)_5OH_2^{3+}$.

Experimental

Materials

Salts of lithium, $Co(NH_3)_6^{3+}$, and $Co(NH_3)_5OH_2^{3+}$ were made by standard methods (6, 7) and were checked for purity by chemical analysis and by examination of their visible spectra; these and all other spectral measurements were made using a Cary Model 15 spectrophotometer. Baker Analyzed perchloric acid (72%) and Fisher "purified" sodium perchlorate monohydrate and sodium nitrate were used directly. Distilled water was either passed through Barnstead deionizer and organic removal cartridges or else redistilled carefully from alkaline permanganate before use; the kinetic results were the same in either case.

Kinetic Studies

Aliquots of solutions of the appropriate complex in aqueous $NaClO_4$–$HClO_4$ or $LiClO_4$–$HClO_4$ of the required ionic strength I were sealed into Pyrex ampoules, and these were preheated to about 95° (to facilitate thermal equilibration and to dissolve any solid hexaamminecobalt(III) perchlorate) before immersion in an oil-filled Lauda NS-HT thermostat bath (±0.1°). Light levels in the bath were negligible. Timing of the reactions was begun 2 min after immersion of the samples, and ampoules were withdrawn periodically and chilled to room temperature. The samples were then analyzed spectrophotometrically at 427 nm (for the hexaammine) or 344 or 490 nm (for the aquopentaammine). Alternatively, the cobalt(II) content of the samples were determined by making v ml of the aliquot and $(6 - v)$ ml 0.1 M $HClO_4$ up to 25 ml with concentrated HCl, and measuring the optical absorbance of the resulting blue solution at 690 nm (ε 471 M^{-1} cm^{-1} according to a calibration curve established using solutions of pure cobalt(II) nitrate) (8). The cobalt(II) concentrations so measured were also checked in some cases by Kitsen's method (9), with essentially identical results.

Mass Spectra of the Gaseous Decomposition Products

Solution aliquots, made up as for the kinetic experiments, were placed in breakseal ampoules and thoroughly degassed on a vacuum line by repeated freeze–thaw cycles. The ampoules were then sealed and immersed in the thermostat bath at 130.6° for several half-periods of the decomposition reaction. The samples were then frozen at liquid nitrogen temperatures and the gaseous contents of the tubes were released into a Varian/MAT CH-5 mass spectrometer for analysis.

Results

Throughout this article, the molar concentrations cited refer to solutions as at 25°. Uncertainty limits quoted represent standard errors; where these are not stated for an experimental measurement, a single determination is implied.

Decomposition of Aquopentaamminecobalt(III) Ion

The spectrum of the final reaction products (absorption maximum at 505 nm, ε ~ 5 M^{-1} cm^{-1}) identified the Co-containing species as being entirely hexaaquocobalt(II) (10). The absorbance A_t at time t changed in accordance with first order kinetics as the reaction proceeded, except during a short initial "induction period" (Fig. 1); the latter phenomenon was much less marked than that reported (11) for the decomposition of cobalt(III) ammines in molten NH_4HSO_4 and in 97% sulfuric acid. Furthermore, as Garner and co-workers have observed also (2), the visible spectra of partially reacted solutions showed isosbestic points at the early stages of the reaction, but these were not maintained as the reaction proceeded. These facts indicate the presence of a fairly long-lived reaction intermediate in the decomposition.

Because $Co(NH_3)_3(OH_2)_3^{3+}$ is known (3) to decompose rapidly under the conditions of these experiments, the intermediate was presumably a mixture of *cis*- and *trans*-$Co(NH_3)_4(OH_2)_2^{3+}$,

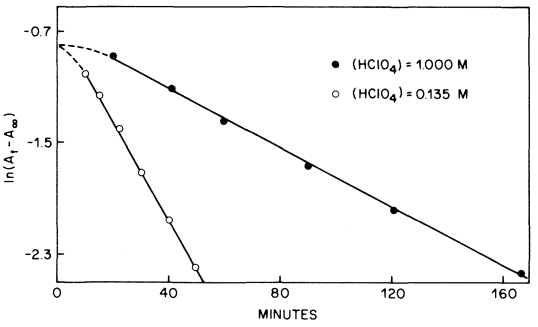

FIG. 1. Time dependence of the optical absorbance A_t (490 nm, 10 mm optical path, 25°) of a solution initially 0.0106 M aquopentaamminecobalt(III) perchlorate in $HClO_4$—$NaClO_4$ (I = 1.0 M) at 140.6°.

Can. J. Chem. Downloaded from www.nrcresearchpress.com by 210.87.254.42 on 09/05/12
For personal use only.

TABLE 1. First-order rate coefficients k_{obs} for the decomposition of $Co(NH_3)_5OH_2^{3+}$ in 0.1 *M* $HClO_4$ [a]

Temperature (°C)	$10^2[NaClO_4]$ (*M*)	$10^2[NaNO_3]$ (*M*)	10^4k_{obs} (s^{-1})
130.6	—	—	4.01±0.01
	—	2.12	4.22
	—	4.25	4.97
	—	6.37	5.46
	—	8.50	6.40
	—	10.62	6.57
	2.12	—	2.85±0.01
	4.25	—	2.61
	6.37	—	2.35±0.01
	10.62	—	2.84±0.16
	21.24	—	2.77
	—	—	5.74±0.01 [b]
120.6	—	—	1.511±0.001 [b]
114.7	—	—	0.744 [b]
110.1	—	—	0.397±0.004 [b]

[a] $[Co]_{total} = 0.0106$ *M*.
[b] Complex present as its nitrate salt; elsewhere, as the perchlorate.

TABLE 2. Hydrogen ion concentration dependence of the first-order rate coefficient k_{obs} for the decomposition of $Co(NH_3)_5OH_2^{3+}$ [a]

Temperature (°C)	$[HClO_4]$ (*M*)	10^4k_{obs} (s^{-1})	10^5k_1 (s^{-1})	$10^5k_2'$ ($M\,s^{-1}$)
140.6	0.100	7.53±0.10	12.6±1.2	6.2±0.2
	0.135	5.80±0.05		
	0.33	3.28±0.01		
	1.00	1.81±0.06		
130.5	0.10	2.01±0.01	3.3±0.3	1.7±0.1
	0.20	1.17±0.02		
	0.30	0.91		
	0.40	0.73±0.06		
120.6	0.10	0.50±0.01	0.9±0.2	0.4±0.1
	0.125	0.43±0.01		
	0.18	0.33±0.01		
	1.00	0.13±0.01		

[a] $I = 1.06$ *M*, adjusted with $NaClO_4$. Initial $[Co(NH_3)_5OH_2^{3+}] = 0.0106$ *M*.

with the former predominating, as Garner and co-workers suggested (2). These decompose more rapidly than their progenitor (2), and so the slopes of the linear portions of the plots of $\log(A_t - A_\infty)$ against t gave the first-order rate coefficient k_{obs} for the rate-controlling reaction

$$[1]\quad Co(NH_3)_5OH_2^{3+} \xrightarrow{H^+} Co(NH_3)_4(OH_2)_2^{3+} + NH_4^+$$

The values of k_{obs} collected in Tables 1 and 2 confirm that parallel acid-independent (rate coefficient k_1) and inversely acid-dependent (k_2) paths operate (2), as per eqs. 2 and 3, and that high concentrations of perchlorate ion have no drastic effect on the reaction rate.

$$[2]\quad Co(NH_3)_5OH_2^{3+} \overset{K_a}{\rightleftharpoons} Co(NH_3)_5OH^{2+} + H^+$$
$$\searrow^{k_1} \qquad \swarrow^{k_2} + H_2O$$
$$Co(NH_3)_4(OH_2)_2^{3+} + NH_3 \xrightarrow{H^+} NH_4^+$$

$$[3]\quad k_{obs} = k_1 + k_2K_a[H^+]^{-1} = k_1 + k_2'[H^+]^{-1}$$

In order to facilitate comparison with the $Co(NH_3)_6^{3+}$ system (in which the low solubility of the perchlorate salt imposes some restrictions on the kinetic experiments), the effect of nitrate ion on the rate was also examined, and this anion was found to cause a modest acceleration

Can. J. Chem. Downloaded from www.nrcresearchpress.com by 210.87.254.42 on 09/05/12
For personal use only.

of the decomposition reaction (Table 1). We attribute this to the fact that nitrate ion has appreciable Brønsted basicity in aqueous solutions at high temperatures (the pK_a of aqueous nitric acid rises from -2 at 0° to $+2$ at 300° (12)) and will therefore decrease the free hydrogen ion concentration and so increase the contribution of the inversely hydrogen-ion dependent pathway.

The reaction product Co^{2+} has been reported to catalyze the radiolytic decomposition of hexaammine- and aquopentaammine-cobalt(III) (13), and to inhibit the reduction of $Co(NH_3)_5OH_2^{3+}$ by $S_2O_8^{2-}/Ag^+$ (14). The effect of added cobalt(II) perchlorate on the rate of the spontaneous decomposition of $Co(NH_3)_5OH_2^{3+}$ in 0.1 *M* $HClO_4$ was therefore studied with reference to control experiments in which Zn^{2+} was added in place of Co^{2+}, as these ions have closely similar ionic radii and therefore similar medium effects. At 130.6°, with an initial aquopentaamminecobalt(III) perchlorate concentration of 0.0106 *M*, and $[M(ClO_4)_2] = 0.0109$ *M*, k_{obs} was $(3.52 \pm 0.13) \times 10^{-4}$ and $(3.49 \pm 0.06) \times 10^{-4}$ s^{-1} for M = Zn and Co, respectively; the corresponding data for $[M(ClO_4)_2] = 0.109$ *M* were $(2.57 \pm 0.02) \times 10^{-4}$ and $(2.61 \pm 0.03) \times 10^{-4}$ s^{-1}, as against $(4.01 \pm 0.01) \times 10^{-4}$ in the absence of added M(II) perchlorates. Thus, divalent metal perchlorates exert a small retarding effect on the reaction (as does $NaClO_4$), but there is no specific effect attributable to cobalt(II). Nevertheless, at high concentrations of added cobalt(II), an unidentified black precipitate formed as the reaction proceeded; this was not observed when Co(II) perchlorate alone was heated in 0.1 *M* perchloric acid at 130° for several days, which suggests that Co(II) in high concentrations can react with one of the decomposition products of $Co(NH_3)_5OH_2^{3+}$ formed after the rate-controlling steps.

Decomposition of Hexaamminecobalt(III) Ion

For this ion, as for the pentaammine, the final cobalt-containing product was $Co(H_2O)_6^{2+}$ but the spectral changes occurring during the decomposition reaction (Fig. 2) make it clear that an intermediate Co(III) complex was again involved, and this is verified by the appearance of the semilog kinetic plots (Fig. 3, *cf.* Fig. 1). Ion exchange chromatography of a solution of partially-decomposed $Co(NH_3)_6^{3+}$ on Dowex 50W-X4 resin with 1.0 *M* $HClO_4$ produced a

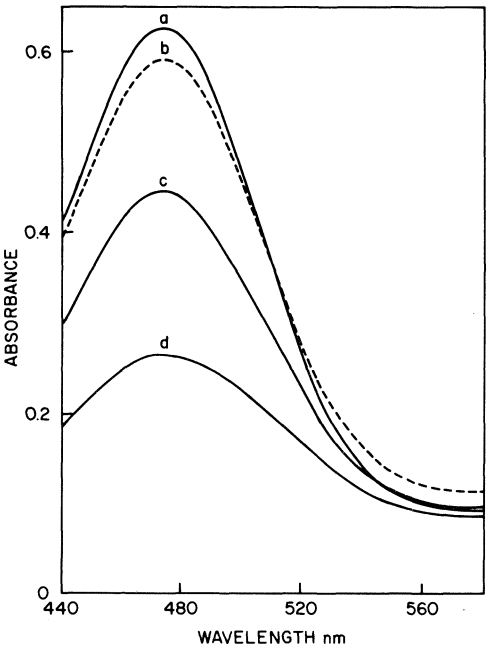

FIG. 2. Spectrum (25°, optical path 10 mm) of a solution originally 0.0106 *M* $Co(NH_3)_6^{3+}$ in 0.1 *M* $HClO_4$, (*a*) initially, and after (*b*) 100, (*c*) 360, and (*d*) 830 min at 130.3°.

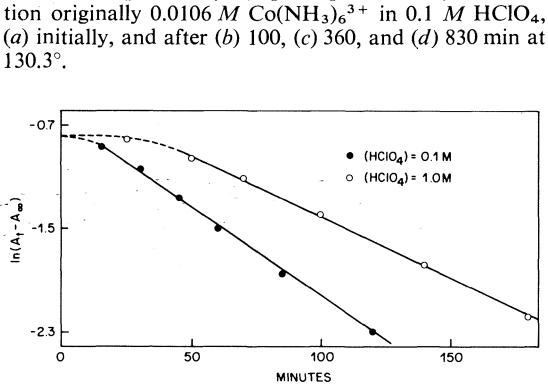

FIG. 3. Decomposition of $Co(NH_3)_6^{3+}$ in $HClO_4$–$NaClO_4$ ($I = 1.0$ *M*) at 149.6°, followed by spectrophotometric determination of cobalt(II) by Kitsen's method (9).

rapidly-moving red band (hexaaquocobalt(II)) and a thin, slow-moving pink band closely followed by an extensive yellow band of $Co(NH_3)_6^{3+}$; the pink band was so small as to render its isolation impracticable, but it almost certainly consisted of $Co(NH_3)_5OH_2^{3+}$, as the more highly aquated ammines would not have survived in detectable quantities under the experimental conditions (2, 3).

The rate coefficients k_{obs} (Table 3) for the decomposition of hexaamminecobalt(III) were obtained from the linear portions of semilog

TABLE 3. First-order rate coefficients k_{obs} for the decomposition of $Co(NH_3)_6^{3+}$ in acidic aqueous solution

Temperature (°C)	$[HClO_4]$ (*M*)	Ionic strength (*M*)	Supporting electrolyte	$10^4 k_{obs}$ (s^{-1})
149.6	0.033	1.0	$NaClO_4$	2.43 ± 0.05 [a]
			$NaClO_4$	2.40 ± 0.06 [b]
			$LiClO_4$	2.44 ± 0.05 [b]
	0.100	1.0	$NaClO_4$	2.24 ± 0.12 [a]
			$NaClO_4$	2.33 ± 0.01 [b]
			$LiClO_4$	2.32 ± 0.04 [b]
	1.00	1.0		1.60 ± 0.05 [a]
				1.59 ± 0.01 [b]
150.1	0.100	0.16		2.35 ± 0.01 [c]
144.8				1.32 [c]
140.4				0.793 ± 0.011 [c]
134.9				0.448 [c]
130.3				0.262 ± 0.003 [c]

[a] $[Co^{2+}]$ measured by HCl method.
[b] $[Co^{2+}]$ measured by Kitsen's method (9).
[c] Direct spectrophotometric determination. $Co(NH_3)_6^{3+}$ present as the nitrate salt (0.0106 *M*); elsewhere, as the perchlorate.

plots such as Fig. 3; this was a valid procedure, since $Co(NH_3)_5OH_2^{3+}$ had been shown to decompose some 20 times faster than its progenitor under the experimental conditions. The effect of $[H^+]$ on the reaction rate in 1.0 *M* perchlorate media was investigated by analyzing for the product Co(II) rather than by attempting to measure the absorbance of the surviving hexaamminecobalt(III) ion, since the perchlorate salt of the latter is insufficiently soluble in these media at room temperature; however, it was established at low perchlorate concentrations that both methods gave the same results.

The data of Table 3 show that the ionic strength effect was independent of the choice of $NaClO_4$ or $LiClO_4$ as the supporting electrolyte and that the hydrogen ion concentration had only a very small effect on the reaction rate. The latter observation contrasts sharply with the case of $Co(NH_3)_5OH_2^{3+}$ but is scarcely surprising, since the pK_a of $Co(NH_3)_6^{3+}$ is about 16 at 25° (15) as against 6.5 for $Co(NH_3)_5OH_2^{3+}$ (16), so that the pathway corresponding to k_2 (eq. 2) is inaccessible for the hexaammine. Hydrogen ion effects have therefore been ignored, *i.e.*, k_{obs} has been set equal to k_1 of eq. 3, in computing the activation parameters for the hexaammine complex (Table 4). The kinetic parameters obtained for the decomposition of the aquopentaammine ion are also listed in Table 4 and are in satisfactory agreement with (and somewhat more precise than) those obtained by Garner and co-workers (2).

Gaseous Reaction Products

The gaseous reaction products of the thermal decompositions of 0.01 *M* $Co(NH_3)_6^{3+}$, $Co(NH_3)_5OH_2^{3+}$, and hydroxylammonium sulfate at 130.6° in 0.1 *M* $HClO_4$ were identified mass spectrometrically as N_2 (*m/e* 28), N_2O (*m/e* 44) and, in the case of the complexes, a minor amount of O_2 (*m/e* 32). The peak heights *R*, relative to that for N_2 being 100, were measured at an electron energy of 70 V. For hexaamminecobalt(III) nitrate, $R = 7$ and 69 for O_2 and N_2O, respectively; for aquopentaamminecobalt(III), the corresponding *R* values were 9 and 35 (for the nitrate salt) and 10 and 51 (for the perchlorate), whereas for $(NH_2OH)_2H_2SO_4$ they were 0 and 29. For a sample of pure N_2O, *R* at 70 eV is 990 for mass 44; thus, virtually all the N_2^+ and O_2^+ detected mass spectrometrically were derived from the N_2 and O_2 in the reaction products and not from the N_2O^+. Furthermore, it was established spectrophotometrically that nitrate ion does not undergo significant decomposition in 0.1 *M* $HClO_4$ at 130°, and in any event it is clear from the mass spectrometric data that the presence of nitrate in place of perchlorate does not affect the relative yields of N_2 and N_2O significantly. It is therefore safe to conclude that the ultimate decomposition products of both

Can. J. Chem. Downloaded from www.nrcresearchpress.com by 210.87.254.42 on 09/05/12
For personal use only.

Can. J. Chem. Downloaded from www.nrcresearchpress.com by 210.87.254.42 on 09/05/12
For personal use only.

TABLE 4. Kinetic parameters for the rate-determining steps in the decomposition of cobalt(III) ammines in 0.1 *M* $HClO_4$ at ionic strength 1.0 *M*

Complex	Nature of rate controlling step	$10^6 k_1$, s^{-1} (109.8°)	ΔH_1^* (kcal mol^{-1})	ΔS_1^* (cal deg^{-1} mol^{-1})	$k_{2'}$, $M\ s^{-1}$ (109.8°)	$\Delta H_{2'}^*$ (kcal mol^{-1})	$\Delta S_{2'}^*$ (cal deg^{-1} mol^{-1})	Ref.
$Co(NH_3)_6^{3+}$ [a]	Aquation to $Co(NH_3)_5OH_2^{3+}$	2.25 [b]	36.6±1.8	10.7± 5.4				This work
$Co(NH_3)_5OH_2^{3+}$	Aquation to $Co(NH_3)_4(OH_2)_2^{3+}$	1.71 [b] 2.05	41.9±1.3 37.9±6.0	24 ± 4 14 ±15	8.1×10^{-7} [a] 8.1×10^{-7}	43.5±1.8 40 ±5	26.7± 5.4 17 ±16	This work 2
cis-$Co(NH_3)_4(OH_2)_2^{3+}$	Aquation to $Co(NH_3)_3(OH_2)_3^{3+}$	~1.1			3.3×10^{-5}	41.8±1.8	29.7± 5.0	2
fac-$Co(NH_3)_3(OH_2)_3^{3+}$	Redox to Co(II)				3.2×10^{-4} [b]	36.8±1.3	21.1± 4.0	3
cis-$Co(NH_3)_2(OH_2)_4^{3+}$	Redox to Co(II)				4.8×10^{-3} [b]	36.7±0.9	26.1± 2.7	4

[a]Ionic strength 0.16 *M*; nitrate salt of complex used.
[b]Calculated for 109.8° from the activation parameters, for comparison with direct measurements made by Garner *et al.* (2) at this temperature.

Can. J. Chem. Downloaded from www.nrcresearchpress.com by 210.87.254.42 on 09/05/12
For personal use only.

$Co(NH_3)_6^{3+}$ and $Co(NH_3)_5OH_2^{3+}$ in dilute perchloric acid are $Co(H_2O)_6^{2+}$, NH_4^+, N_2, N_2O, and a relatively small amount of O_2, and that the yield of N_2O relative to N_2 is roughly the same for both complex ions and close to that expected if NH_2OH were the intermediate giving rise to both these gases.

Discussion

The first step in the thermal decomposition of $Co(NH_3)_6^{3+}$ in acidic aqueous solution is loss of ammonia to yield $Co(NH_3)_5OH_2^{3+}$. The subsequent aquation of this aquo-species and of its successor $Co(NH_3)_4(OH_2)_2^{3+}$ are much more rapid than that of the hexaammine because paths with inverse dependence on the hydrogen-ion concentration become accessible when a coordinated aquo group is present (eq. 2), and these conjugate base pathways are favored over the acid-independent aquation paths at the acidities used in these experiments, as the data of Table 4 will show.

Interestingly, the rate coefficient for the acid independent path (k_1) is essentially the same for $Co(NH_3)_6^{3+}$ and $Co(NH_3)_5OH_2^{3+}$, and if anything somewhat *less* for *cis*-$Co(NH_3)_4(OH_2)_2^{3+}$; this is precisely the pattern found for the stepwise aquations of the corresponding chromium(III) ammines (17). However, whereas the overall decomposition rates of the cobalt(III) complexes are greatly increased by the incursion of conjugate base pathways which increase in importance as the number of aquo groups increases, conjugate base pathways make no significant contribution to the aquation rates of any of the Cr(III) ammines from $Cr(NH_3)_5OH_2^{3+}$ to $Cr(NH_3)(OH_2)_5^{3+}$ in 0.1 *M* $HClO_4$ (17). This is another illustration of the great susceptibility of Co(III) systems to conjugate base hydrolysis mechanisms, relative to their Cr(III) analogs, a phenomenon well documented for hydrolyses in alkaline media (18). The result is that the Cr(III) ammines aquate via a series of ever-slower steps, resulting in complicated rate laws (17), whereas for the hexa-, penta-, and tetra-amminecobalt-(III) ions the overall rates of successive steps become faster and faster, so that spectral changes are very nearly first-order kinetically.

On reaching $Co(NH_3)_3(OH_2)_3^{3+}$, the decomposition of Co(III) ammines proceeds by direct redox to Co(II), N_2, N_2O, and a minor amount of O_2. The gaseous products appear in essentially the same relative amounts whether the starting material be the hexaammine or the pentaammine, which supports the conclusion that the initial step in the decomposition of the former complex is aquation to the latter without redox. A minor redox pathway may conceivably compete with aquation in the case of the tetraammine (2) but even so the important redox step in the sequence is clearly the decomposition of $Co(NH_3)_3(OH_2)_3^{3+}$ (3).

The redox decomposition of $Co(NH_3)_3(OH_2)_3^{3+}$ to cobalt(II) must involve a single-electron transfer at some stage, and oxidation of a water molecule (or aquo ligand) to OH *or* of an ammine ligand to NH_2 afford the only direct one-electron initial redox steps. Since both N_2O and a minor amount of O_2 are ultimately formed, in addition to N_2, an oxygen-containing radical must be involved in the overall redox process. This radical is almost certainly OH, and, because NH_2 is not expected to produce OH by abstraction of H from H_2O (the H—OH bond strength being 119 kcal mol^{-1} as against 103 for H—NH_2 (19)), we may infer that OH is the *first* radical to be formed, as in eq. 4.

$$[4]\quad Co(NH_3)_3(OH_2)_3^{3+} + H_2O \rightleftharpoons Co(NH_3)_3(OH_2)_3^{2+} + OH + H^+$$

It is known (14) that OH does not attack coordinated NH_3 ligands. Thus, as long as the assemblage of species on the right hand side of eq. 4 remains intact within the solvent cage, further reaction (as distinct from recombination) can only occur following dissociation of one of the ammine ligands from $Co(NH_3)_3(OH_2)_3^{2+}$.

$$[5]\quad Co(NH_3)_3(OH_2)_3^{2+} + H_2O \rightarrow Co(NH_3)_2(OH_2)_4^{2+} + NH_3$$

$$[6]\quad NH_3 + OH \rightarrow NH_2 + H_2O$$

The pseudo first-order rate coefficient for reaction 5 is about 6×10^4 s^{-1} at 25° (20), and will be of the order of 10^8 s^{-1} at the temperatures prevailing in the present study. Reaction 5 will therefore be slower by at least three orders of magnitude than the diffusion of H^+ out of the solvent cage, a process which would inevitably be fast by operation of the Grotthus chain mechanism and which in this case will be accelerated and rendered essentially irreversible by the double positive charge on the complex ion. Consequently, as long as OH remains in the solvation cage, reaction 6 (for which the bimolecular

Can. J. Chem. Downloaded from www.nrcresearchpress.com by 210.87.254.42 on 09/05/12
For personal use only.

rate coefficient is $1.0 \times 10^8\ M^{-1}\ s^{-1}$ at 25° (21)) can occur without interference from protonation of the freshly-released NH_3, a significant point, since OH does not attack NH_4^+ (21). Alternatively, NH_2 might be produced by direct oxidation of an NH_3 ligand in $Co(NH_3)_3(OH_2)_3^{3+}$ by Co(III), although, as noted above, coordination deactivates NH_3 toward oxidation (14).

Thus, the free-radical product which emerges from the solvent cage will be OH itself or NH_2, which, being odd-electron species, will survive in bulk solution until meeting another free radical. If the emergent species is NH_2, it will scavenge an OH radical which either has been freshly formed as a Co(II)–OH pair or has escaped from the solvent cage of its parent complex ion. In either case, the product will be hydroxylamine (eq. 7); an encounter between NH_2 and another NH_2 is less likely, as OH may well be the precursor of NH_2 (eq. 6), and reaction 7 is known to be rapid (bimolecular rate coefficient $9.5 \times 10^9\ M^{-1}\ s^{-1}$ at 25° (21)).

[7] $$NH_2 + OH \rightarrow NH_2OH$$

It is well known that hydroxylamine decomposes thermally in acidic aqueous solution to give N_2, N_2O, and NH_4^+ (22), and we have established that the relative amounts of N_2 and N_2O observed for the thermal decompositions of NH_2OH, $Co(NH_3)_6^{3+}$, and $Co(NH_3)_5OH_2^{3+}$ are sufficiently similar to indicate that hydroxylamine (or rather the hydroxylammonium ion) is indeed the first major non-radical oxidation product in the decomposition of the Co(III) ammines to Co(II).

[8] $$4NH_2OH + 2H^+ \rightarrow N_2O + 2NH_4^+ + 3H_2O$$

[9] $$3NH_2OH + H^+ \rightarrow N_2 + NH_4^+ + 3H_2O$$

Alternatively, an OH radical may occasionally escape from the solvent cage before reaction 5 occurs and scavenge another OH radical, similarly formed, rather than NH_2. In this case, hydrogen peroxide will be formed instead of NH_2OH, and will decompose to O_2, which is indeed observed as a minor reaction product.

The stoichiometry of the overall thermal decomposition of $Co(NH_3)_6^{3+}$ may be summarized by eqs. 10–12, in which [11] is most important and [12] least.

[10] $$8Co(NH_3)_6^{3+} + 38H^+ + H_2O = N_2O + 46NH_4^+ + 8Co^{2+}$$

[11] $$6Co(NH_3)_6^{3+} + 28H^+ = N_2 + 34NH_4^+ + 6Co^{2+}$$

[12] $$4Co(NH_3)_6^{3+} + 20H^+ + 2H_2O = O_2 + 4Co^{2+} + 24NH_4^+$$

The kinetics and products of the thermal decompositions of $Co(NH_3)_6^{3+}$ and $Co(NH_3)_5OH_2^{3+}$ in acidic aqueous solution bear a marked resemblance to those of the corresponding decompositions in molten NH_4HSO_4 and in 97% sulfuric acid (11, 23). However, in the latter solvents, the intermediates are inevitably bisulfato rather than aquo complexes, and the gaseous product is exclusively N_2 (apart from trace amounts of NO and SO_2), as might be expected, since there is no obvious source of OH radicals to give rise to N_2O or O_2. The enthalpies of activation associated with the loss of the first NH_3 ligands from the hexaammine, pentaammine, and *cis*-tetraammine in 97% H_2SO_4 are in the range 38–42 kcal mol^{-1}, that is, very close to those for the corresponding processes in water; this suggests that the activation process is independent of the nature of the solvent, *i.e.*, that it is dissociative. In contrast, the initial step in the thermal decomposition of solid salts of Co(III) ammines is evidently redox to Co(II), rather than ligand substitution (24–26).

In the highly acidic solvent H_2SO_4, conjugate base pathways are unlikely to be of any importance, so that the rates of loss of NH_3 from $Co(NH_3)_5HSO_4^{2+}$ and $Co(NH_3)_6^{3+}$ are governed by k_1 alone and are therefore closely similar. Thus, Sutula and Hunt (11) observed substantial accumulations of the pentaammine complex as the hexaammine underwent solvolysis in 97% H_2SO_4, and the kinetics of decompositions in H_2SO_4 were more complicated than those in water, in which the conjugate base pathways facilitate removal of reaction intermediates.

We thank Dr. A. W. Boyd for discussions, and the National Research Council of Canada for financial support.

1. W. E. Jones, L. R. Carey, and T. W. Swaddle. Can. J. Chem. **50**, 2739 (1972).
2. W. D. Stanley, S. Lum, and C. S. Garner. J. Inorg. Nucl. Chem. **35**, 3587 (1973).
3. S. Lum, W. D. Stanley, and C. S. Garner. J. Inorg. Nucl. Chem. **35**, 1293 (1973).
4. W. D. Stanley, T. Davies, T. D. Tullius, and C. S. Garner. J. Inorg. Nucl. Chem. **35**, 3857 (1973).
5. J. D. White, J. C. Sullivan, and H. Taube. J. Am. Chem. Soc. **92**, 4733 (1970).

6. J. BJERRUM and J. P. MCREYNOLDS. Inorg. Synth. **2**, 218 (1946).
7. W. E. JONES and T. W. SWADDLE. Can. J. Chem. **45**, 2647 (1967).
8. R. J. MUREINIK, A. M. FELTHAM, and M. SPIRO. J. Chem. Soc. Dalton, 1981 (1972).
9. R. E. KITSEN. Anal. Chem. **22**, 664 (1950).
10. G. DAVIES and K. O. WATKINS. J. Phys. Chem. **74**, 3388 (1970).
11. R. A. SUTULA and J. B. HUNT. Inorg. Chem. **11**, 1879 (1972).
12. H. C. HELGESON. J. Phys. Chem. **71**, 3121 (1967).
13. D. KATAKIS and A. O. ALLEN. J. Phys. Chem. **68**, 1359 (1964).
14. D. THUSIUS and H. TAUBE. J. Phys. Chem. **71**, 3845 (1967); J. Am. Chem. Soc. **88**, 850 (1966).
15. D. A. BUCKINGHAM, A. M. SARGESON, and L. G. MARZILLI. J. Am. Chem. Soc. **89**, 3428 (1967).
16. L. G. SILLÉN and A. E. MARTELL. Stability constants. Special Publication No. 17. The Chemical Society, London. 1964. p. 55.
17. G. GUASTALLA and T. W. SWADDLE. Inorg. Chem. **13**, 61 (1974).
18. F. BASOLO and R. G. PEARSON. Mechanisms of inorganic reactions. 2nd Ed. J. Wiley and Sons, Inc., New York, N.Y. 1967. p. 188.
19. Handbook of chemistry and physics. 51st Ed. The Chemical Rubber Company, Cleveland, Ohio. 1970. p. F164.
20. M. SIMIC and J. LILIE. J. Am. Chem. Soc. **96**, 291 (1974).
21. P. B. PABSBERG. Risø Report No. 256. Danish Atomic Energy Commission, Risø, Roskilde, Denmark. 1972.
22. K. JONES. *In* Comprehensive inorganic chemistry. Vol. 2. *Edited by* A. F. Trotman-Dickenson. Pergamon Press, London. 1973. p. 272.
23. J. A. DUFFY and W. J. MACDONALD. J. Chem. Soc. (A), 1160 (1971).
24. W. W. WENDLANDT and J. P. SMITH. The thermal properties of transition metal ammine complexes. Elsevier Publishing Co., Amsterdam. 1967.
25. A. V. ABLOV and T. A. MAL'KOVA. Russ. J. Inorg. Chem. **14**, 1594 (1969).
26. E. L. SIMMONS and W. W. WENDLANDT. J. Inorg. Nucl. Chem. **28**, 2187 (1966).

Can. J. Chem. Downloaded from www.nrcresearchpress.com by 210.87.254.42 on 09/05/12
For personal use only.

Etude théorique d'hydrocarbures simples par la méthode PCILO

JACQUES GRIGNON ET SÁNDOR FLISZÁR

Département de chimie, Université de Montréal, Montréal, Québec

Reçu le 10 janvier, 1974

JACQUES GRIGNON et SÁNDOR FLISZÁR. Can. J. Chem. **52**, 2760 (1974).

Les géométries expérimentales d'une série d'alcènes sont dans certains cas assez bien reproduites par les calculs PCILO. Des lacunes apparaissent cependant pour les chaînes linéaires dans le butène-1 et le pentène-1. Dans l'évaluation des angles HCH, les sens de variation expérimentaux sont en général respectés, mais de façon exagérée.

JACQUES GRIGNON and SÁNDOR FLISZÁR. Can. J. Chem. **52**, 2760 (1974).

The experimental geometries of a number of alkyl-substituted ethylenes are satisfactorily reproduced by PCILO calculations. Deficiencies appear, however, with linear substituents, *e.g.*, in 1-butene and 1-pentene. The experimental trends for the HCH angles are in general reflected but over emphasized by the PCILO method.

Can. J. Chem. Downloaded from www.nrcresearchpress.com by 210.87.254.42 on 09/05/12
For personal use only.

En dépit de nombreuses études théoriques sur des oléfines simples tels l'éthylène et le propène (1, 2), ou alors sur des molécules d'un haut degré de complexité (3, 4), aucune étude systématique des oléfines les plus courantes n'a encore été entreprise. Dans le présent travail, les oléfines R—$CHCH_2$, R—$C(CH_3)CH_2$, R—$CHCHCH_3$ (*cis* et *trans*), ainsi que les benzènes monosubstitués R—C_6H_5 (R = alkyle) sont étudiés.

Les conformations les plus stables ont été calculées au moyen de la méthode PCILO (5) qui a déjà donné de bons résultats lors de l'étude conformationnelle de molécules complexes. Ainsi les travaux de Pullman et ses collaborateurs (3, 4) sur des molécules à caractère biologique montrent un excellent accord entre les résultats du calcul et les données d'études cristallographiques. Une brève étude portant sur les molécules $RCHCH_2$, où R = H, CH_3 et CO montre que l'écart entre les angles calculés et expérimentaux est de l'ordre de 2 à 3° (2). Par ailleurs, l'étude des alcanes au moyen de la méthode PCILO a révélé (6) que les distributions de charges sont en accord raisonnable avec "l'intuition chimique" (7, 8), tout en ne possédant pas la qualité des résultats *ab initio* (STO-3G) complètement optimisés (8, 9).

La méthode PCILO ayant été plus particulièrement conçue pour des études conformationnelles, les distances interatomiques n'ont pas été optimisées dans le présent travail.[1] Les distances r_{CC} et r_{CH} utilisées ici (telles qu'extraites de la littérature (10, 11)), sont indiquées au tableau 1.

Le programme[2] utilise un paramètre de polarité δ pour chaque lien de telle sorte que les coefficients c_{i1} et c_{i2} des orbitales liantes sont

$$c_{i1} = [(1 + \delta_i)/2]^{1/2}$$

et

$$c_{i2} = [(1 - \delta_i)/2]^{1/2}$$

Le paramètre δ est optimisé pour l'ensemble des liens de la molécule en mélangeant chaque orbitale liante avec l'orbitale antiliante correspondante jusqu'à la minimisation de l'énergie du déterminant complètement localisé selon un processus itératif. La polarité δ étant en général supposée nulle au départ, il n'y a pas de charge nette dans la fonction d'onde d'ordre zéro. La polarisation résulte à la suite du calcul de perturbation.

Les angles ont été variés jusqu'à l'obtention du minimum de l'énergie totale, ceci en faisant optimiser l'ensemble des paramètres de polarité pour chacune des conformations étudiées. Les calculs ont été effectués à l'aide d'un ordinateur CDC, CYBER 74.

Pour les molécules en C_3 et C_4, les spectres microondes fournissent des résultats expérimentaux qui permettent de vérifier la précision des résultats obtenus par le calcul et, de ce fait, permettent de juger des limites d'application de

[1]Des essais d'optimisation des distances interatomiques ont conduit aux valeurs suivantes: r_{CC}(éthane décalé) = 1.48 Å et r_{CC}(éthylène) = 1.3315 Å, qui illustrent bien que la méthode PCILO ne saurait être utilisée avantageusement pour l'étude des distances interatomiques.

[2]Le calcul PCILO postule la formule chimique comme l'approximation d'ordre zéro et considère la molécule comme un ensemble de liens en interaction, cette interaction étant traitée par la théorie des perturbations. Les hypothèses CNDO/2 sont retenues dans le calcul des intégrales impliquant des orbitales atomiques hybrides.

Can. J. Chem. Downloaded from www.nrcresearchpress.com by 210.87.254.42 on 09/05/12
For personal use only.

TABLEAU 1.
Distances interatomiques

Lien	Distance (Å)
C—C	
sp^3–sp^3	1.54
sp^3–sp^2	1.52
sp^2–sp^2	1.34
Benzène	1.395
C—H benzène	
sp^3_{prim}–H	1.09
sp^3_{sec}–H	1.09
sp^3_{tert}–H	1.108
sp^2–H	1.08

la méthode PCILO. Les géométries obtenus par d'autres méthodes de calcul sont également rapportées pour fin de comparaison.

Résultats

Ethylènes monosubstitués

Le calcul montre que pour le propène tous les atomes, sauf les H du groupement méthyle, sont coplanaires, conformément aux conclusions de l'analyse du spectre de micro-ondes (12). Les paramètres de structure du propène obtenues par la méthode PCILO, ainsi que par d'autres méthodes de calcul, sont comparés aux résultats expérimentaux (tableau 2).

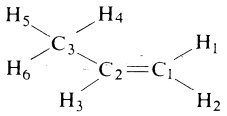

Le butène-1 possède deux isomères de rotation: les formes *cis* et "skew". La forme dite "skew" possède un angle dièdre d'environ 120° à partir de la forme *cis*. Elle est à distinguer de la forme *gauche* usuelle qui forme un angle de

TABLEAU 2. Structure du propène

Angle	Valeur (deg) PCILO	Exp[a]	STO-3G[b]	EHMO[c]
$H_1C_1C_2$	122.5	120.5	122.2	121.5
$H_2C_1C_2$	123.5	121.5	121.9	122.1
$C_1C_2C_3$	123.5	124.3	125.1	124.7
$H_3C_2C_1$	121.0	119.0	119.8	120.7
$C_2C_3H_4$	112.0	111.2	111.1	110.2
$H_4C_3H_5$	106.8	109.0	108.5	108.8
$H_5C_3H_6$	106.8	106.2	107.6	108.8
$H_1C_1H_2$	114.0	118.0	115.9	116.4

[a]Référence 13.
[b]Référence 14.
[c]Référence 15.

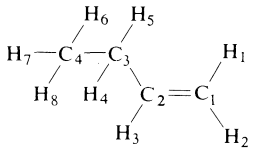

120° à partir de la position *trans*. Le calcul PCILO trouve la forme "skew" comme étant la conformation la plus stable pour le butène-1. La différence d'énergie entre les deux formes est cependent faible (0.28 kcal). Ceci est en accord avec le spectre micro-ondes (16) qui permet de conclure que la forme "skew" est la plus stable, avec une différence d'énergie entre les deux formes de 0.15 ± 0.15 kcal (16). Les paramètres de structure du butène-1 sont exposés au tableau 3.

En ce qui a trait aux homologues supérieurs, leurs spectres micro-ondes ne sont pas disponibles. D'après le calcul, dans le méthyl-3 butène-1, le groupe iso-propyle se place de façon à ce que l'hydrogène tertiaire soit éclipsé par rapport à la double liaison, les méthyles étant situés de part et d'autre du plan de la double liaison. Le diméthyl-3,3 butène-1 adopte la même conformation, c'est-à-dire que deux des méthyles du *tert*-butyle occupent les mêmes positions que ceux de l'isopropyle, alors que le troisième remplace l'hydrogène tertiaire en position *cis* par rapport à la double liaison. Les résultats sont exposés au tableau 4.

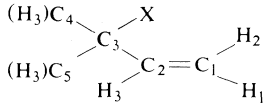

Les résultats exposés aux tableaux 2–4 indiquent que les angles autour de la double liaison sont pratiquement constants tout au long de la série d'oléfines R—$CHCH_2$. Les angles HCH des méthyles sont régulièrement un peu plus

TABLEAU 3. Structure du butène-1

Angle	Valeur (deg) PCILO	Exp.[a]
$C_1C_2C_3$	124.0	125.4
$C_2C_3C_4$	107.5	112.1
Angle dièdre	120.0	119.9
$H_3C_2C_3$	115.0	117.1
$H_{6,7,8}C_4C_3$	112.0	110.3
$H_4C_3H_5$	106.2	105.7
$H_1C_1H_2$	114.0	—

[a]Référence 16.

Can. J. Chem. Downloaded from www.nrcresearchpress.com by 210.87.254.42 on 09/05/12
For personal use only.

TABLEAU 4. Structure du méthyl-3 butène-1 et du diméthyl-3,3 butène-1

	Valeur (deg)	
Angle	X = H	X = CH_3
$H_1C_1H_2$	114.0	114.0
$H_3C_2C_3$	115.0	116.0
$C_1C_2C_3$	123.0	123.0
C_2C_3R	111.0	111.0
$C_2C_3C_{4,5}$	108.0	107.5
HCH (méthyle)	105.7	105.7

fermés pour R = *tert*-C_4H_9 et R = *i*-C_3H_7 que pour R = CH_3 ou C_2H_5. Ces tendances se retrouvent également dans les séries étudiées plus loin. Pour cette raison, les angles ne seront indiqués en détail que pour les membres inférieurs de chaque série, étant donné qu'ils restent pratiquement constants pour les termes supérieurs.

Le substituant néopentyle du diméthyl-4,4 pentène-1 présente une conformation assez particulière. Le groupe C_5H_{11} est situé à 85° du plan de la double liaison alors que l'ensemble des trois méthyles effectue une rotation de 20° par rapport à la position *trans*. Les angles CCC du groupement *tert*-C_4H_9 sont de 109.47°, alors que les autres angles, tels les HCH des méthyles (105.7°) et le HCH de l'éthylène (114°), sont les mêmes que pour les autres molécules de cette série.

Ethylènes gem-disubstitués R—C(CH_3)=CH_2

Pour l'isobutène, le calcul montre que deux atomes d'hydrogène de chaque méthyle sont situés dans le plan des atomes de carbone. Ceci est confirmé par le spectre micro-ondes de l'isobutène (17).

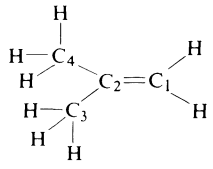

Dans les homologues supérieurs, l'angle HCH de la partie éthylénique reste inchangé; il en est ainsi de l'angle HCH du méthyle en position 2. Les termes suivants (R = C_2H_5, *i*-C_3H_7 et *tert*-C_4H_9) n'étant plus symétriques, l'angle $C_1C_2C_3$ diminue à 121° alors que l'angle entre C_1C_2 et le premier carbone du substituant R augmente à 124–124.5°, quelque soit R. Les substituants occupent la position qu'ils avaient dans la série précédente, c'est-à-dire l'éthyle à 120° de la position *cis* avec un hydrogène éclipsé à la double liaison, l'isopropyle avec l'hydrogène tertiaire *cis* à la double liaison et, enfin, le *tert*-C_4H_9 avec un des carbones en *cis* à la double liaison.

TABLEAU 5. Structure de l'isobutène

	Valeur (deg)		
		Expérimental	
Angle	PCILO	Microonde[a]	Diffraction d'electrons[b]
HCH (méthyle)	106.2	108.0	108.5
HCH (éthyle)	111.0	117.5	115.5
Me—C—Me	114.0	115.9	112.0
$C_1C_2C_3$	123.0	122.0	124.0

[a]Référence 17.
[b]Référence 18.

Ethylènes disubstitués-1,2 R—CHCH—CH_3

Pour les butènes-2 (*cis* et *trans*) le calcul montre que, comme pour l'isobutène, deux atomes d'hydrogène de chaque groupe méthyle se trouvent dans le plan des atomes C, les autres étant situés de part et d'autre de la double liaison. Dans le tableau 6, les résultats du calcul sont comparés aux données de diffraction d'électrons (19).

Ainsi qu'il ressort de cette comparaison, la géométrie du butène-2 *trans* est bien rendue par le calcul. Sauf en ce qui a trait à l'habituelle exagération de la fermeture de l'angle HCH, les autres angles sont (à environ 1° près) ceux fournis par l'expérience. La géométrie de l'isomère *cis*, par contre, est moins bien rendue par le calcul. L'angle $C_3C_2H_1$ est ouvert, alors qu'il devrait être fermé de plusieurs degrés et l'angle $C_1C_2H_1$ est également mal rendu. Encore une fois, les homologues supérieurs présentent les

TABLEAU 6. Structure des butènes-2 *cis* et *trans*

	Valeur (deg)			
	trans		*cis*	
Angle	PCILO	Exp.[a]	PCILO	Exp.[a]
$C_1C_2C_3$	125.0	123.8	124.0	125.4
$C_2C_1H_{3,4,5}$	112.0	109.0	112.0	110.5
$C_3C_2H_1$	121.0	121.5	122.0	114.1
$C_1C_2H_1$	114.0	114.7	114.0	120.5

[a]Référence 19.

TABLEAU 7. Conformations des benzènes substitués

PCILO		STO-3G	
R	Conformation	R	Conformation
CH_3	CCCH *cis*[a]	CH_3	CCCH *cis* ou orthogonal
C_2H_5	CCCC 120°	C_2H_5	CCCC orthogonal
i-C_3H_7	$CCCH_{tert}$*cis*	CHF_2	CCCH *cis*
tert-C_4H_9	CCCC *cis*	CF_3	CCCF *cis*

NOTE: Dans la notation de Pople, CCCH ou CCCC indique un lien C—C du noyau phényle et un lien C—H ou C—C du substituant. La notation *cis* implique que ces deux liens sont *cis* l'un par rapport à l'autre alors que orthogonal signifie qu'ils forment entre eux un angle de 90°.

mêmes angles que les butènes-2 *cis* et *trans*. Les conformations des substituants sont les mêmes que dans les séries étudiées précédemment. Il apparait également que les énergies calculées pour les isomères *trans* sont toujours inférieures à celles calculées pour les isomères *cis*, l'écart étant d'autant plus prononcé que le groupement R est plus volumineux.

Les benzènes monosubstitués

Les benzènes substitués ont été calculés en supposant que le cycle soit planaire avec des longueurs de liens C—C et C—H de 1.395 et 1.08 Å respectivement. Les atomes H du noyau, dans le plan de ce dernier, forment des angles CCH de 120°. Seule la géométrie des substituants a été optimisée. Les résultats sont exposés au tableau 7, en les comparant à des résultats obtenus récemment par Pople et ses collaborateurs (20) par un calcul *ab initio* (STO-3G) en utilisant des angles standards.

Dans le cas des benzènes substitués, il convient de souligner une particularité de la méthode PCILO. Dans la construction de la molécule il est nécessaire de spécifier les quatre liens de chacun des atomes de carbone. Ainsi, dans le cycle benzénique, la position des doubles liaisons est fixée *a priori*. Dès lors, les deux structures de kékulé ne sont pas équivalentes lorsque certains substituants sont rattachés au noyau.

La comparaison des résultats du tableau 7 indique ce qui suit. Pour R = CH_3, la position *cis* est préférée par PCILO, alors que le calcul STO–3G ne différencie pas les positions *cis* et orthogonale. Par analogie avec le cas R = CF_3 où la forme *cis* est préférée par le calcul STO-3G, il semble raisonnable de conclure que la forme *cis* serait également préférée pour R = CH_3. La barrière de rotation étant très faible dans ce cas (14 cal/mol) (21), l'utilisation dans le calcul STO-3G de longueurs et de liens standards n'a peut-être pas permis de mettre en évidence une si petite différence. Les substituants iso-propyle et *tert*-butyle n'ont pas été étudiés par Pople *et al.* (20) mais l'analogie avec CHF_2 et CF_3 semble indiquer que la conformation *cis* calculée par PCILO est probablement correcte. Le cas R = C_2H_5 est plus complexe. Ce substituant forme d'après le calcul un angle de 120° avec la double liaison du cycle. Dès lors, le résultat du calcul dépend de la position assignée à la double liaison du cycle. Un changement de la position des doubles liaisons devient équivalent à faire osciller le groupe C_2H_5 de 60 à 120° si cet angle est mesuré toujours par rapport aux mêmes atomes de carbone. La position moyenne du C_2H_5 est celle correspondant à un angle de 90° (orthogonal, dans la notation de Pople), soit le résultat obtenu par STO-3G avec un noyau benzénique dont les diverses positions des doubles liaisons sont équivalentes.

En conclusion, les conformations obtenues par PCILO sont en accord avec celles calculées par une méthode *ab initio*. En ce qui a trait aux angles entre les divers atomes des substituants, les valeurs obtenues ici sont les mêmes que celles calculées précédemment pour les substituants des diverses séries d'éthylènes substitués.

Moments dipolaires

Les moments dipolaires calculés par la méthode PCILO sont rapportés au tableau 8. Ces résultats y sont comparés aux valeurs expérimentales ainsi qu'aux résultats obtenus par d'autres méthodes de calcul.

Les moments dipolaires calculés sont, en général, plus faibles que les valeurs expérimentales. Deux valeurs PCILO sont en excellent accord, soit celles obtenues pour le butène-1 et l'isobutène. Encore une fois, les sens de variation

Can. J. Chem. Downloaded from www.nrcresearchpress.com by 210.87.254.42 on 09/05/12
For personal use only.

TABLEAU 8. Moment dipolaires

Oléfine	Moment dipolaire (D) PCILO	Exp.[a]	STO-3G[b]	CNDO/2[c]
Propène	0.26	0.364[d]	0.24	0.36
Butène-1	0.36	0.359[e]		
Pentène-1	0.45			
Méthyl-3 butène-1	0.44			
Diméthyl-3,3 butène-1	0.42			
Diméthyl-4,4 pentène-1	0.43			
Isobutène	0.516	0.503[f]		0.65
Méthyl-2 butène-1	0.64	0.54		
Diméthyl-2,3 butène-1	0.72			
Triméthyl-2,3,3 butène-1	0.69			
Méthyl-2 pentène-1	0.64			
Toluène	0.27	0.37	0.25	0.21
Ethyl benzène	0.39	0.58	0.28	
Iso-propyl benzène	0.52	0.65		
tert-Butyl benzène	0.50	0.70		
Butène-2 *trans*	0.0	0.0		
Pentène-2 *trans*	0.15			
Méthyl-4 pentène-2 *trans*	0.21			
Diméthyl-4,4 pentène-2 *trans*	0.18			
Butène-2 *cis*	0.0			
Pentène-2 *cis*	0.15			
Méthyl-4 pentène-2 *cis*	0.09			
Diméthyl-4,4 pentène-2 *cis*	0.10			

[a]Référence 22.
[b]Références 1 et 20.
[c]Référence 11.
[d]Référence 12.
[e]Référence 16.
[f]Référence 17.

sont qualitativement reproduits par le calcul. Dans les quelques cas où la comparaison est possible, les valeurs PCILO s'avèrent être du même ordre ou meilleures que celles calculées par *ab initio* (STO-3G) ou CNDO/2, sauf pour le propène où le calcul CNDO/2 (11) s'avère être nettement meilleur.

Discussion

A la lumière des exemples exposés ici, on constate que d'une manière générale le calcul PCILO conduit à une énergie plus basse pour la conformation *a priori* la plus stable. Ceci confirme que son utilisation pour des études conformationnelles sur des molécules que l'on ne peut traiter commodément avec des méthodes *ab initio* est justifiée. Sa grande rapidité et sa facilité d'utilisation en font un outil très utile pour des molécules comportant jusqu'à environ 120 électrons de valence.

Un examen détaillé des paramètres de structure obtenus par PCILO comparés aux données expérimentales révèle cependant des lacunes assez importantes. Les angles C—C—C sont en général assez bien reproduits (à 1 ou 2° près) et les sens de variation sont bien rendus. Ainsi l'ouverture des angles $C_1C_2C_3$ par rapport à l'angle trigonal de 120° pour le propène (124.3°), le butène (125.4°), l'isobutène (122°) et le butène-2 *trans* (123.8°) est bien reproduite par les valeurs PCILO qui sont, respectivement, 123.5, 124.0, 123.0 et 125.0°. L'angle $C_2C_3C_4$ dans le butène-1 est cependant beaucoup trop faible (107.5°) comparé à une valeur expérimentale de 112.1°. Cette lacune spécifique semble se manifester d'une manière particulièrement prononcée pour une chaîne linéaire; ainsi le terme supérieur, soit le pentène-1, ne donne pas de minimum d'énergie pour des angles $C_2C_3C_4$ et $C_3C_4C_5$ raisonnables. Selon le calcul PCILO, ces deux angles auraient des valeurs inférieures à 103° ce qui impliquerait une déformation beaucoup trop importante. Une autre lacune réside dans l'évaluation des angles HCH. Les sens de variation sont en général respectés, mais de manière exagérée. Ainsi les angles HCH des CH_2 terminaux sont tous inférieurs à 120° ce qui est conforme à l'expérience; pour le propène l'angle expérimen-

Can. J. Chem. Downloaded from www.nrcresearchpress.com by 210.87.254.42 on 09/05/12
For personal use only.

tal est de 118° alors que le calcul conduit à 114°; de manière similaire, pour l'isobutène la valeur calculée pour cet angle est de 111° comparée à la valeur expérimentale de 117.5–115.5°. Le même phénomène se produit pour les HCH des méthyles. Ces angles que l'expérience situe dans le domaine 107–109° sont évalués par le calcul à 106–107°.

En résumé, on peut conclure que les sens de variation sont reproduits mais exagérés dans plusieurs cas. Pour les termes supérieurs qui ont été calculés et pour lesquels les valeurs expérimentales ne sont pas disponibles, les valeurs calculées pour les différents angles sont très voisines de celles calculées pour les premiers termes de chaque série. En raison des écarts entre les valeurs calculées et observées qui ont été constatés dans les comparaisons exposées ci-haut, il y a lieu de soupçonner que les résultats déduits pour les termes supérieurs présentent également des écarts du même ordre par rapport à la réalité tout en étant probablement qualitativement justes.

Nous tenons à remercier le Conseil national de recherches du Canada pour un octroi qui a permis le présent travail.

1. W. J. Hehre et J. A. Pople. J. Am. Chem. Soc. **92**, 2191 (1970).
2. J. Langlet et H. Van der Meer. Theor. Chim. Acta, **21**, 410 (1971).
3. J. Langlet, B. Pullman et H. Berthod. J. Mol. Struct. **6**, 139 (1970); B. Maigret, B. Pullman et J. Caillet. Biochim. Biophys. **40**, 808 (1970).
4. J. Langlet, B. Pullman et H. Berthod. J. Chim. Phys. **67**, 480 (1970).
5. S. Diner, J. P. Malrieu, and P. Claverie. Theor. Chim. Acta (Berl.), **13**, 1 (1969); J. P. Malrieu, P. Claverie, and S. Diner. Theor. Chim. Acta (Berl.), **13**, 18 (1969); S. Diner, J. P. Malrieu, F. Jordan, and M. Gilbert. Theor. Chim. Acta (Berl.), **15**, 100 (1969).
6. S. Fliszár et J. Sygusch. Can. J. Chem. **51**, 991 (1973).
7. S. Fliszár. J. Am. Chem. Soc. **95**, 1068, 7386 (1972).
8. S. Fliszár, G. Kean et R. Macaulay. A paraître.
9. G. Kean et S. Fliszár. A paraître.
10. Table of interatomic distances. Chem. Soc. (London), Special Publication No. 11 (1958).
11. J. A. Pople et M. Gordon. J. Am. Chem. Soc. **89**, 4253 (1967).
12. D. R. Lide et D. E. Mann. J. Chem. Phys. **27**, 868 (1957).
13. D. R. Lide et D. Christensen. J. Chem. Phys. **35**, 1374 (1961).
14. L. Radom, W. A. Lathan, W. J. Hehre et J. A. Pople. J. Am. Chem. Soc. **93**, 5339 (1971).
15. H. Van der Meer. Mol. Phys. **18**, 401 (1970).
16. S. Kondo, E. Hirota et Y. Morino. J. Mol. Spectrosc. **28**, 4718 (1968).
17. V. W. Laurie. J. Chem. Phys. **34**, 1516 (1961).
18. L. S. Bartell et R. A. Bonham. J. Chem. Phys. **32**, 824 (1960).
19. A. Almenningen, I. M. Anfisen et A. Haaland. Acta Chem. Scand. **24**, 43 (1970).
20. W. J. Hehre, L. Radom et J. A. Pople. J. Am. Chem. Soc. **94**, 1496 (1972).
21. H. D. Rudolph, H. Dreizler, A. Jaeschke et P. Windling. Z. Naturforsch. A, **22**, 940 (1967).
22. Table of experimental dipole moments. A. L. McLellan, W. H. Freeman and Co., San Francisco, California, 1963.

Can. J. Chem. Downloaded from www.nrcresearchpress.com by 210.87.254.42 on 09/05/12
For personal use only.

Distributions de charges et effets chimiques. VI. Etude PCILO des répartitions de charges dans les hydrocarbures éthyléniques[1]

JACQUES GRIGNON ET SÁNDOR FLISZÁR
Département de Chimie, Université de Montréal, Montréal, Québec H3C 3V1
Reçu le 18 février, 1974

JACQUES GRIGNON et SÁNDOR FLISZÁR. Can. J. Chem. **52**, 2766 (1974).

Les analyses de population électronique pour des séries d'éthylènes alkyl-substitués reflètent bien le transfert de charge de la part des substituants dans l'ordre inductif habituel. L'accumulation de charge a lieu préférentiellement sur l'atome sp^2 en β par rapport au substituant mais ne suit pas fidèlement l'ordre inductif en raison d'un effet d'alternance de charge qui s'y oppose en partie.

JACQUES GRIGNON and SÁNDOR FLISZÁR. Can. J. Chem. **52**, 2766 (1974).

Analyses of the electron density distribution for some series of alkyl-substituted ethylenes reflects clearly the transfer of charge from the substituents in the normal inductive order. The accumulation of charge occurs preferentially on the sp^2 atom in the β position with respect to the substituent but does not follow exactly the inductive order because of the effect of a charge alternation which opposes in part the inductive effect. [Journal Translation]

Des études récentes (1–4) ayant porté sur les distributions de charges dans les alcanes ont montré que les charges nettes[2] q portées par des atomes H ou des groupes CH_3 dépendent, selon des équations du type Taft, des constantes polaires σ* (5) des groupes alkyles R auxquels ils sont rattachés.

$$[1] \qquad q_H = a\sigma_R^* + b \quad \text{(pour R—H)}$$

$$[2] \qquad q_{(CH_3)} = a\sigma_R^* \quad \text{(pour R—CH}_3\text{)}$$

Il a été vérifié (3,4) que les distributions de charges calculées à partir des éqs. 1 et 2 sont en bon accord avec celles obtenues au moyen de nombreuses méthodes théoriques, voire même en parfait accord avec les résultats *ab initio* (STO-3G, complètement optimisé) (4,6). Il a également été montré que la différence essentielle entre les résultats fournis par les diverses méthodes théoriques réside dans la valeur de a devant être utilisée dans les éqs. 1 et 2 afin de générer les valeurs déduites des calculs théoriques[3]. Finalement, il a été montré que les distributions de charges déduites à partir des divers calculs théoriques, tout en possédant essentiellement un "contenu chimique" (les effets inductifs) ne peuvent généralement pas être utilisées telles quelles pour l'étude des relations: Propriété – distribution électronique (7).[4] Sur cette base, un critère a été développé, en termes d'une reconsidération du mode d'attribution des populations de recouvrement entre les divers centres, en vue de permettre l'étude de propriétés moléculaires qui dépendent des distributions électroniques. Ainsi a-t-il été possible de générer des distributions de charges telles que les déplacements chimiques des carbones (et des protons) des alcanes leur sont linéairement reliés (7).

Il est donc entendu que les charges des éthylènes, calculées par la méthode PCILO (8), qui sont présentées ici ne sauraient être considérées comme étant "vraies" dans un sens absolu. Cependant, la méthode PCILO ayant déjà montré sa capacité de générer des charges respectant "l'intuition chimique" (éqs. 1 et 2) dans le cas des alcanes (3), il paraît raisonnable d'espérer que les distributions de charges PCILO peuvent également être utilisées sur une base relative, pour fin de comparaison, dans le cas des éthylènes. Dans cette hypothèse, il devient notamment intéressant d'examiner à l'aide de cette méthode (*i*) si les effets inductifs rencontrés dans les alcanes se retrouvent également, en termes de distributions de charges, dans les composés in-

[1]Extrait de la thèse (Ph.D.) de J.G., Université de Montréal (1974).

[2]La charge nette de r est définie ici comme étant la charge nucléaire moins la population électronique totale en r.

[3]Cet aspect a été discuté (3,4) en termes d'un paramètre n défini par $a = -10/3n$, dans une échelle d'unités relatives par rapport à $q_C(C_2H_6) = 1$.

[4]Par exemple, en vue d'étudier les déplacements chimiques du ^{13}C en fonction des charges.

Can. J. Chem. Downloaded from www.nrcresearchpress.com by 210.87.254.40 on 09/05/12
For personal use only.

TABLEAU 1. Distribution de charges (me) des éthylènes R—CH(1)=CH$_2$(2)

Molécule (R)	Géométrie*	q_C(R)	$q_{H\text{-}1}$	$q_{C\text{-}1}$	$q_{C\text{-}2}$	$q_{H\text{-}2}{}^{cis}$	$q_{H\text{-}2}{}^{trans}$
CH_3	S	−11.3	8.0	23.7	−69.2	12.6	15.9
	O	−9.2	7.5	25.3	−63.6	13.6	11.8
C_2H_5	S	19.4	8.8	21.5	−77.1	13.6	16.7
	O	18.4	9.0	25.1	−73.8	15.0	12.4
n-C_3H_7	S	13.4	9.2	28.6	−86.6	17.6	14.5
néo-C_5H_{11}	S	6.2	10.5	21.4	−85.5	18.8	15.7
	O	10.5	11.5	22.4	−80.4	17.8	14.9
i-C_3H_7	S	50.9	9.5	19.7	−83.1	17.4	14.3
	O	49.1	10.1	24.8	−81.0	13.3	15.6
tert-C_4H_9	S	74.1	7.8	14.0	−84.0	20.8	13.9
	O	76.6	8.9	18.3	−79.4	17.7	11.3

*S, standard; O, optimisée.

saturés et (*ii*) comment les charges se répartissent entre les carbones sp^2.

Résultats

Les modalités du calcul PCILO (8) ont été exposées antérieurement (9). Les distributions électroniques ont été calculées dans chaque cas en utilisant deux géométries différentes: (*i*) la géométrie optimisée, soit celle correspondant au minimum de l'énergie totale d'ordre 3, et (*ii*) une géométrie "standard", définie par les paramètres exposés antérieurement (9).

Toutes les charges nettes sont exprimées en millièmes d'électron (me). Une charge $q > 0$ indique un défaut d'électron (charge positive) et $q < 0$ indique la présence d'un excès d'électron sur l'atome considéré.

Lors de l'étude de ces distributions de charges, certaines difficultés sont apparues. D'une manière générale, certains caractères géométriques sont quelque peu exagérés par le calcul PCILO, tout en conservant cependant un sens de variation qui est généralement correct. (9) A titre d'exemple, les angles HCH sont régulièrement trop fermés par rapport aux valeurs mesurées expérimentalement. Le cas extrême est représenté par le pentène-1, où le calcul semblerait indiquer que dans le groupement *n*-propyle les angles CCC sont très fermés ($\measuredangle$ CCC < 103°), ce qui est visiblement faux. Ces défauts de géométrie conduisent à des estimations de densités de charges qui sont également entachées d'erreurs. Les erreurs géométriques n'étant pas les mêmes pour les divers groupements considérés, il en résulte une distorsion inégale dans le calcul des charges pour les différentes molécules. Pour cette raison, il a paru avantageux de comparer les effets électroniques en supposant des critères standard pour les géométries des molécules. Par ailleurs, une comparaison des résultats obtenus au moyen des géométries standards avec ceux déduits après optimisation de la géométrie révèle les mêmes tendances générales, aussi bien dans la série des éthylènes monosubstitués (tableau 1) que dans les autres séries.[5]

Pour les raisons énoncées ci-haut, seuls les résultats déduits à partir de géométries standards sont rapportés pour les éthylènes *gem*-disubstitués (tableau 2) et disubstitués-1,2 (tableau 3), ainsi que pour les alkyl benzènes (tableau 4).

Discussion

L'utilité première de résultats tels que ceux exposés aux tableaux 2–5 réside dans "l'information chimique" qui y est contenue. Cette information est extraite à deux points de vue: (*i*) par l'étude du transfert de charge du substituant alkyle vers la partie éthylénique (effet inductif) et (*ii*) par l'étude de la répartition de charge dans la partie insaturée (alternance de charge).

L'Effet inductif

Dans l'interprétation du comportement chimique des molécules organiques, de nombreux et importants arguments sont reliés aux changements de densités électroniques induits par les substituants. Notamment, des interprétations de la réactivité des molécules sont reliées (5) au fait que le pouvoir donneur d'électrons des groupements alkyles peut être chiffré par des constantes (σ* polaires de Taft) dans l'ordre *tert*-C_4H_9 (σ* = −0.300) > *i*-C_3H_7 (−0.190) > néo-

[5]Les résultats détaillés sont indiqués dans la thèse.[1]

Can. J. Chem. Downloaded from www.nrcresearchpress.com by 210.87.254.40 on 09/05/12
For personal use only.

TABLEAU 2. Distribution de charges (me) dans les éthylènes $R_1(CH_3)C^1{=}CH_2^2$

R_1	$q_C(CH_3)$	$q_C(R_1)$	$q_{C\text{-}1}$	$q_{C\text{-}2}$	q_H^{trans}	q_H^{cis}
CH_3	−19.4	−19.4	+70.9	−99.7	+13.3	+13.3
C_2H_5	−21.2	+12.2	+66.9	−105.4	+14.2	+14.2
n-C_3H_7	−22.5	+6.5	+67.4	−107.3	+15.1	+15.1
i-C_3H_7	−22.4	+42.8	+64.3	−106.4	+14.9	+11.3
tert-C_4H_9	−25.1	+67.1	+57.3	−109.6	+14.5	+18.6

TABLEAU 3. Distribution de charges (me) dans les éthylènes $R{-}CH^1{=}CH^2{-}CH_3$

	R	$q_C(R)$	$q_{C\text{-}1}$	$q_{H\text{-}1}$	$q(CH_3)$	$q_{C\text{-}2}$	$q_{H\text{-}2}$
trans	CH_3	−16.0	−13.4	8.5	−16.0	−13.4	8.5
	C_2H_5	15.3	−13.8	9.3	−17.2	−22.8	9.4
	i-C_3H_7	46.2	−13.9	9.8	−18.3	−29.9	10.3
	tert-C_4H_9	69.2	−17.2	8.1	−19.6	−32.5	13.7
cis	CH_3	−19.5	−13.2	6.1	−19.5	−13.2	6.1
	C_2H_5	12.2	−13.7	7.1	−20.9	−22.6	7.2
	i-C_3H_7	51.3	−16.5	7.1	−32.1	−26.7	8.2
	tert-C_4H_9	72.3	−18.3	6.4	−31.7	−29.0	8.6

TABLEAU 4. Distribution de charges dans les alkyl benzènes

R	$q_C(R)$	$q_{C\text{-}1}$	$q_{C\text{-}2}$	$q_{C\text{-}3}$	$q_{C\text{-}4}$
CH_3	−35.3	20.8	−23.9	−15.0	−14.7
C_2H_5	−7.8	25.1	−28.2	−15.9	−14.4
i-C_3H_7	19.2	24.0	−29.3	−17.1	−14.5
tert-C_4H_9	42.2	20.4	−29.8	−17.4	−15.2

$C_5H_{10}(-0.152)(6) > n\text{-}C_3H_7\ (-0.115) > C_2H_5\ (-0.100) > CH_3(0)$. Ainsi s'attend-on à ce que la densité électronique dans la partie insaturée soit plus importante avec un substituant *tert*-butyle qu'avec un méthyle. En fait, l'effet inductif a été implicitement associé à un transfert d'électrons. Une justification théorique de ce point de vue a été présentée récemment (1–4) dans le cas des alcanes.

En vue de reconnaître l'aspect "transfert de charge" dans les éthylènes ici étudiés, nous formons les charges nettes des groupes $CH{=}CH_2$, $CH_3C{=}CH_2$, $CH{=}CHCH_3$ et C_6H_5 (selon la classe de composés considérée) à partir des résultats exposés aux tableaux 1–4.

Par les résultats du tableau 5 il devient possible de relier entre elles d'une manière cohérente les distributions de charges indiquées aux tableaux 1-4. La fig. 1 représente les charges nettes $q(CH{=}CH_2)$ déduites pour les éthylènes monosubstitués en fonction des constantes polaires σ* de Taft (5) des substituants R_1 (géométrie standard).

Il apparaît clairement de cette comparaison que les charges $q(CH{=}CH_2)$ sont en bon accord avec une équation de type Taft (eq. 3).

$$[3] \quad q(CH{=}CH_2) = a\sigma_R^* + \text{constante}$$

Dès lors, il devient raisonnable d'admettre, comme cela avait été fait pour les alcanes (1–4) que l'interprétation usuelle des effets inductifs en termes de transfert d'électrons est adéquate et que les constantes σ* décrivent, comme cela avait été postulé (5), les effets polaires.

L'analyse, en termes de l'éq. 3, des résultats se rapportant aux charges $q(CH_3C{=}CH_2)$ des éthylènes *gem*-disubstitués, $q(CH_3CH{=}CH)$ des éthylènes disubstitués-1,2 (*cis* et *trans*), ainsi qu'aux charges $q(C_6H_5)$ des alkyl-benzènes, conduit à des corrélations en tous points similaires à celle présentée dans la fig. 1. L'accord obtenu avec les géométries optimisées est en général un

Can. J. Chem. Downloaded from www.nrcresearchpress.com by 210.87.254.40 on 09/05/12
For personal use only.

TABLEAU 5. Charges nettes (me) des fragments insaturés des éthylènes R_1 $(R_2)C{=}CHR_3$

Molécule			Fragment considéré	Charge nette* du fragment	
R_1	R_2	R_3			
CH_3	H	H	$CH{=}CH_2$	−9.0	(−5.4)
C_2H_5				−16.5	(−12.3)
n-C_3H_7				−16.7	
néo-C_5H_{11}				−19.1	(−13.8)
i-C_3H_7				−22.2	(−17.2)
tert-C_4H_9				−27.5	(−23.2)
CH_3	CH_3	H	$CH_3C{=}CH_2$	−1.1	(−1.9)
C_2H_5				−9.3	(−1.9)
n-C_3H_7				−8.6	
i-C_3H_7				−15.5	(−15.6)
tert-C_4H_9				−20.5	(−19.6)
CH_3	H	CH_3(*trans*)	$CH{=}CHCH_3$	−5.0	
C_2H_5				−12.6	
i-C_3H_7				−18.3	
tert-C_4H_9				−23.3	
CH_3	H	CH_3(*cis*)	$CH{=}CHCH_3$	−7.5	
C_2H_5				−14.7	
i-C_3H_7				−21.6	
tert-C_4H_9				−24.8	
$CH_3{-}C_6H_5$			C_6H_5	−2.9	(+57)†
$C_2H_5{-}C_6H_5$				−7.5	(+13)†
i-$C_3H_7{-}C_6H_5$				−11.6	(−19)†
tert-$C_4H_9{-}C_6H_5$				−15.3	(−54)†

*Les valeurs indiquées entre parenthèses sont déduites à partir des géométries optimisées, les autres correspondent aux géométries standards.
†Calculé d'après les résultats (10) déduits par une méthode de type SCF.

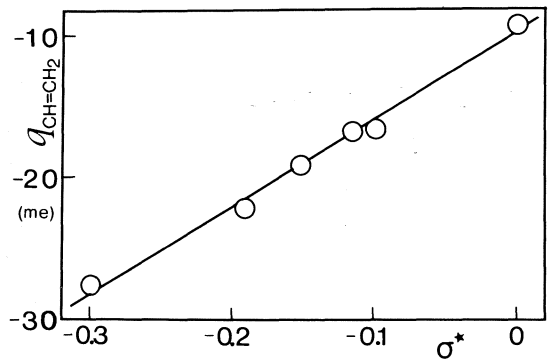

FIG. 1. Vérification de l'éq. 3 pour les éthylènes $RCH{=}CH_2$.

peu moins satisfaisant que celui observé pour les résultats déduits avec les géométries standard, sans pourtant infirmer la validité de l'éq. 3. Notamment, le groupement *n*-propyle, qui donne un résultat satisfaisant lorsqu'on fait appel à la géométrie standard, est complètement hors de la corrélation avec la géométrie optimisée. Ceci n'est cependant pas surprenant étant donné que l'optimisation de la géométrie conduit à une forme moléculaire invraisemblable (9). Notons, finalement, que l'analyse des résultats de Lipscomb et collaborateurs (10) déduits par un calcul du type SCF pour les alkyl-benzènes conduit à une corrélation du type Taft (éq. 3) légèrement supérieure à celle obtenue par PCILO.

Les résultats exposés ci-haut ont trait à la comparaison des groupements alkyles entre eux, en ce qui concerne leur pouvoir donneur d'électrons. En aucun cas il n'a été fait référence à une comparaison entre un groupe alkyle et un atome d'hydrogène. En effet, une telle comparaison ne saurait être valable à la vue seule des densités de charges telles qu'obtenues par la plupart des méthodes théoriques. En effet, une distorsion subsiste dans la plupart des calculs (7) qui prend origine dans le fait que dans le méthane la charge de chaque H est positive (donc $q_C < 0$), ce qui revient à dire que le groupe CH_3 apparaît comme un attracteur d'électrons par rapport à H. Ceci est reflété, par exemple, dans le calcul EHMO (11) qui conduit à $q(C_6H_5) = -21$ me (toluène) et $q(C_6H_5) = -101$ me (benzène), tout aussi bien que dans les calculs *ab initio* (12) ($q(C_6H_5) = -37$ me dans le toluène, -51 me dans le benzène). Cette même distorsion est

Can. J. Chem. Downloaded from www.nrcresearchpress.com by 210.87.254.40 on 09/05/12
For personal use only.

TABLEAU 6. Pentes et ordonnées à l'origine de l'équation $q = a\,\sigma^* + b$ (me)

Oléfines	Géométrie*	a	b	coefficient de corrélation
R—CH=CH_2	S	61.3±2.9	−9.48±0.49	0.993
	O	58.4±3.4	−5.57±0.61	0.991
R—C(CH_3)=CH_2	S	64.8±3.1	−2.04±0.56	0.991
	O	59.9±4.7	−2.72±0.87	0.988
R—CH=CHCH_3 *trans*	S	60.1±3.3	−6.00±0.61	0.994
	O	68.8±6.3	−4.20±1.2	0.984
R—CH=CHCH_3 *cis*	S	59.0±5.8	−8.45±1.1	0.981
	O	58.9±9.0	−6.07±1.7	0.955
C_6H_5—R	S	41.6±0.9	−3.19±0.16	0.997
	O	50.1±3.5	2.44±0.65	0.990

*S, standard; O, optimisé.

en fait retrouvée chaque fois que le calcul théorique conduit à une polarité C^-—H^+ dans le méthane (7). Cet aspect a été discuté en termes d'analyse de populations (7); notamment il a été montré que si le partage des populations de recouvrement $\sum P_{\mu\lambda} S_{\mu\lambda}$ à raison de $\frac{1}{2}$ entre des atomes de carbone liés semble raisonnable, il n'en est plus ainsi pour les liens C—H. Dans ce dernier cas il convient de reconsidérer le départage des populations de recouvrement par une "calibration phénoménologique". C'est à la lumière de ces faits que doit être examiné le cas méthyl-2 propène, par opposition au propène. Les résultats du tableau 5 sembleraient indiquer que le remplacement de l'hydrogène géminé au méthyle dans le propène par un groupe méthyle *diminue* la charge du groupe C=CH_2 de −17.0 me pour le propène à −2.3 me (méthyl-2 propène). Ce résultat est clairement une distorsion du même type que celles rencontrées avec les autres méthodes théoriques conduisant à une polarité C^-—H^+ pour le méthane et ne saurait donc être invoqué en vue d'interprétations de faits expérimentaux. Seuls peuvent être comparés entre eux les résultats de séries de composés ne différant que par la nature, et non pas par le nombre, des groupements alkyles. A titre d'exemple, cet aspect se manifeste dans la comparaison des potentiels d'ionisation avec la somme des charges nettes des deux atomes de carbone éthyléniques (fig. 2): à ce stade, ne peuvent être comparés entre eux que les résultats se rapportant à une même série de composés, dont les membres se distinguent uniquement par la nature des substituants alkyles.

L'alternance de charge

L'examen de la répartitions des charges entre les carbones sp^2 en α et en β par rapport au substituant révèle une accumulation préférentielle en position β des électrons cédés par le substituant. Cependant, la charge nette du carbone en β n'augmente pas régulièrement dans l'ordre inductif CH_3 < .... < *tert*-butyle. Ceci peut être interprété en termes d'alternance de charge (1,2): "un site positif est promu par un entourage négatif." Cette règle (dont le caractère approximatif a déjà été discuté (2)) est représentée par l'éq. 4

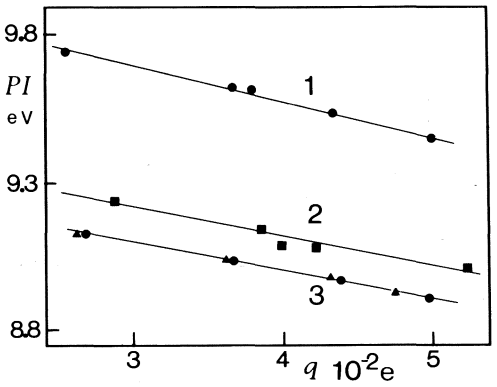

FIG. 2. La comparaison des potentiels d'ionisation (13) avec les charges accumulées dans la partie éthylénique ($q_{C-1} + q_{C-2}$) reflète l'idée (14) que l'arrachement d'un électron est d'autant plus facile que la région moléculaire concernée est plus riche en électrons, ainsi qu'il a été vérifié pour les alcanes (14). La droite *1* (RCH=CH_2) est décalée de 2×10^{-2} électron par rapport á l'échelle. La droite *2* se réfère aux composés R(CH_3)C=CH_2 et la droite *3* aux composés RCH=CHCH_3 *trans* (ronds) et *cis* (triangles).

[4] $$q_i = \sum \alpha_j q_j + \beta$$

reliant la charge nette sur l'atome i à une somme pondérée des charges nettes q_j des voisins j de l'atome i. La fig. 3 représente les charges nettes (q_i) des carbones sp^2 de toutes les molécules

Can. J. Chem. Downloaded from www.nrcresearchpress.com by 210.87.254.40 on 09/05/12
For personal use only.

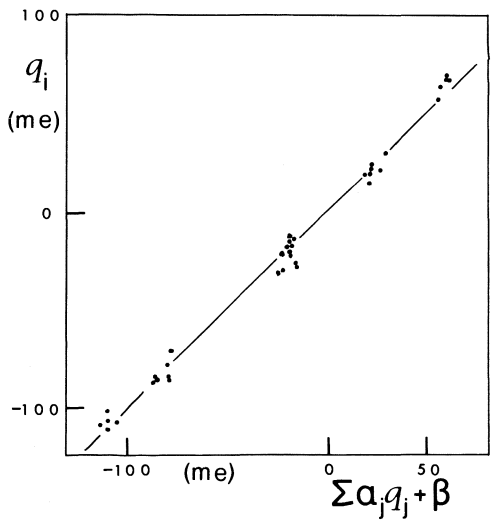

FIG. 3. Alternance de charge. Vérification de l'éq. 4, avec $\alpha_C(sp^3) = -0.1295$, $\alpha_C(sp^2) = -0.7441$, $\alpha_H = -1.4157$, $\beta = -19.86$ me, á partir des résultats des tableaux 1–4.

étudiées ici en fonction de la somme pondérée $\Sigma\alpha_j q_j$ des charges des atomes adjacents à i.

L'alternance de charge permet ainsi d'interpréter d'une façon grossière les tendances observées pour la répartition des charges entre les deux carbones sp^2 de la partie éthylénique. Un substituant CH_3, dont le carbone est "riche" en électrons, "accepte" un voisin sp^2 à caractère positif, d'autant plus que le carbone en β devient lui-même négatif. Avec un substituant *tert*-butyle, l'alternance de charge s'oppose en partie à la transmission de charge sur l'atome sp^2 en β car le carbone central du groupe *tert*-C_4H_9 (entouré de trois CH_3 avec des carbones négatifs) acquière lui-même un caractère positif. Dès lors le carbone sp^2 en α tend à reprendre un caractère moins positif (par rapport au cas du substituant CH_3) par un reflux partiel de la charge négative, au détriment du carbone sp^2 en β. Dès lors, tout en conservant le caractère global de l'effet inductif, *i.e.* le transfert d'électrons en faveur de la partie éthylénique (fig. 1, éq. 3), l'accumulation de charge en β ne suit pas fidèlement l'ordre inductif. Ainsi, si la réactivité d'un éthylénique venait à dépendre de l'accumulation de charge en β par rapport au substituant, un défaut de la réactivité à suivre fidèlement l'ordre inductif ne saurait être imputé à un manque des substituants à céder des électrons dans cet ordre. Notamment, il n'y aurait alors pas lieu d'invoquer un effet tel l'hyperconjugaison, car l'ordre inductif des groupements alkyles, en ce qui touche leur habileté à céder des électrons (éq. 3), est bien réflétée par les populations électroniques.

Nous tenons à remercier le Conseil national de recherches du Canada pour un octroi qui a permis ce travail, ainsi que le Centre de Calcul de l'Université de Montréal pour toutes les facilités dont nous avons bénéficié.

1. S. FLISZÁR. J. Am. Chem. Soc. **94**, 1068 (1972).
2. S. FLISZÁR. J. Am. Chem. Soc. **94**, 7386 (1972).
3. S. FLISZÁR et J. SYGUSCH. Can. J. Chem. **51**, 991 (1973).
4. S. FLISZÁR, G. KEAN et R. MACAULAY. J. Am. Chem. Soc. Sous presse.
5. R. W. TAFT. J. Am. Chem. Soc. **75**, 4231 (1953). R. W. TAFT. *Dans* Steric effects in organic chemistry. *Rédigé par* M. S. NEWMAN. John Wiley and Sons, Inc., New-York, N.Y. 1956.
6. G. KEAN et S. FLISZÁR. Can J. Chem. 2772 (1974).
7. S. FLISZÁR, A. GOURSOT et H. DUGAS. J. Am. Chem. Soc. Sous presse.
8. S. DINER, J. P. MALRIEU et P. CLAVERIE. Theor. Chim. Acta (Berl.) **13**, 1 (1969) J. P. MALRIEU, P. CLAVERIE et S. DINER. Theor. Chim. Acta (Berl.) **13**, 18 (1969). S. DINER, J. P. MALRIEU, F. JORDAN et M. GILBERT. Theor. Chim. Acta (Berl.) **15**, 100 (1969).
9. J. GRIGNON et S. FLISZÁR. Can. J. Chem. 2760 (1974).
10. M. D. NEWTON, F. P. BOER et W. N. LIPSCOMB. J. Am. Chem. Soc. **88**, 2367 (1966).
11. R. HOFFMANN. J. Chem. Phys. **39**, 1397 (1963).
12. W. J. HEHRE et J. A. POPLE. J. Am. Chem. Soc. **92**, 2191 (1970).
13. P. MASCLET, D. GROSJEAN, G. MOUVIER et J. DUBOIS. J. Electron Spectrosc. Related Phenom. **2**, 225 (1973).
14. H. HENRY et S. FLISZÁR. A paraître.

Can. J. Chem. Downloaded from www.nrcresearchpress.com by 210.87.254.40 on 09/05/12
For personal use only.

Charge Distributions and Chemical Effects. VII. *Ab Initio* Population Analyses of Alkanes

GÉRARD KEAN AND SÁNDOR FLISZÁR

Department of Chemistry, University of Montreal, Montreal, Quebec H3C 3V1

Received March 7, 1974

GÉRARD KEAN and SÁNDOR FLISZÁR. Can. J. Chem. **52**, 2772 (1974).

STO-3G calculations are presented for methane, ethane, propane, isobutane, neopentane, ethylene, and benzene. Optimized geometries were used; all K and L shell exponents were optimized for each molecule until stable charge distributions were obtained. The marked influence of full optimization on calculated charges is discussed in comparison both with selected GTO results and with "chemical expectancy."

GÉRARD KEAN et SÁNDOR FLISZÁR. Can. J. Chem. **52**, 2772 (1974).

Les calculs STO-3G sont présentés pour le méthane, l'éthane, le propane, l'isobutane, le néopentane, l'éthylène et le benzène. Les géométries, ainsi que tous les exposants des couches K et L furent optimisés pour chaque molécule jusqu'à l'obtention de distributions de charges stables. L'influence marquée d'une telle optimisation sur les résultats est discutée en termes de comparaisons avec des calculs GTO et avec l' "intuition chimique."

Can. J. Chem. Downloaded from www.nrcresearchpress.com by 210.87.254.105 on 09/05/12
For personal use only.

A good insight into the possibilities offered by, and the problems related to, *ab initio* calculations at various levels of sophistication can be extracted from recent literature (1–3). In STO-*N*G calculations, the replacement of each Slater-type atomic orbital by an atomic orbital which is a sum of N Gaussian-type orbitals yields total molecular energies which converge rapidly towards the full STO result with increasing size of Gaussian expansions (2). These energies are, however, still far from what can be obtained by an improvement of inner-shell description, *e.g.*, at the 6-31G level (3). Any such improvement in total molecular energy does not necessarily mean that all calculated properties are drastically different or, simply, better than what can be obtained from the relatively simple STO-*N*G calculations: equilibrium geometries and (within limits) relative energies are not altered significantly. Two typical examples are presented in Table 1. At the level of extended sets, the obvious drawback is that the gain in flexibility is accompanied by a definite loss of practical feasibility, in comparison with minimal basis set methods, if all variational parameters were to be optimized in the calculation of each molecule of interest.

In STO-*N*G calculations, the study (2) of the ζ exponents when treated as variational parameters indicated that the optimized values (for each type of atom) are largely independent of the size of the Gaussian expansion but vary considerably from one molecule to another. Using standard geometries, optimum exponents were calculated for atoms in selected molecules, and "standard" exponents were defined as averages of optimized ζ values. While the standard set of ζ exponents appeared to be sufficient for the calculation of total or atomization energies, it also became clear that charge distributions are very sensitive to ζ optimization. For example (2), the carbon net charge in methane drops from -255 me (standard ζ's) to -73 me (optimized ζ's).

Clearly, any attempt of calculating charge distributions which may be regarded "accurate" at the level of the method which is used to derive them implies a very careful optimization of the exponents and, to a lesser extent, of the molecular geometry. Hence, if the calculations are to be kept within reasonable limits of feasibility, the "accuracy" which can be attained depends largely upon the size of the Gaussian expansions. We, therefore, choose to perform the calculations using a minimal basis set STO[$1s \rightarrow 3(1s_g) \mid 2s \rightarrow 3(1s_g)$, $2p \rightarrow 3(2p_g)$] in order to obtain with good accuracy the charge distributions corresponding to this level, thus providing a best possible basis for discussing the merits of such a theoretical approach. Relevant additional information is provided by the results of calculations using GTO functions.

Results

The calculations were made by means of a CDC CYBER 74 computer, using the PHAN-

TABLE 1. Total energies, geometries, and net charges calculated by STO-3G and 6-31G methods

Molecule	Property	STO-3G			6-31G	Experimental
		Fixed ζ[a]	Optimum ζ[a]	This work		
CH_4	Total energy (au)	−39.7153	−39.7305	−39.7334	−40.1720	
	r(CH) (Å)			1.083	1.082	1.085
	C net charge (me)	−524	−73	−48.92	−630	
C_2H_4	Total energy (au)	−77.0506	−77.0725	−77.0766	−78.0032	
	r(CH) (Å)			1.080	1.074	1.076
	r(CC) (Å)			1.318	1.322	1.330
	∠HCC (deg)			116.59	116.1	116.6
	C net charge (me)	−276	−156	−135.47		

[a]From ref. 2.

TABLE 2. Optimization of the exponents for the L shell (propane) and the K shell (neopentane)

Molecule	Exponent (shell)		Energy (au)	Atomic net charge (10^{-3} electron unit)		
Propane	1.760(C_pL)	1.760(C_sL)	−116.898948	−24.54(C_{prim})	23.55(C_{sec})	−1.68(H_{sec})
		1.750	−116.898980	−19.64	−3.88	5.65
		1.755	−116.898987	−29.09	9.85	1.98
	1.7590	1.75354	−116.898992	−23.81	5.94	2.20
Neopentane	5.710(C_pK)	5.705(C_qK)	−194.073250	−31.05(C_{prim})	74.84(C_{quat})	
	5.7048	5.705	−194.077771	−28.04	56.65	
		5.700	−194.077632	−27.90	54.04	
		5.728	−194.077781	−28.66	62.92	

NOTE: C_pL, C_sL: L shells of the primary and secondary C atoms; C_pK, C_qK: K shells of the primary and quaternary C atoms.

TOM (4) system of programs. Optimized molecular geometries were used, and all exponents were optimized individually for each molecule, including those of the carbon K shells. Of course, different C and H atoms in the same molecule were optimized separately. Each energy minimization was carried out until a stable charge distribution was obtained, within ~0.01 me.

The importance of this last criterion can be inferred from the example given in Table 2, illustrating the effect of ζ optimization for the L shells in propane. In this case optimization achieves only a small energy improvement whereas the accompanying changes in atomic electron populations are very pronounced, particularly for the secondary C atom. It became therefore necessary to determine accurately the energy minimum from numerous results, involving small steps in the ζ variations. In other cases, however, the changes in electron densities with those of the exponents were not as pronounced as in the example given above. The effect of the optimization of K-shell exponents on carbon net charges is illustrated in Table 2 for neopentane.

The molecular geometries were calculated using Pople's optimized exponents (2) for methane and ethane which had been derived assuming standard geometries (5). The geometries thus obtained (Table 3) can be regarded as sufficiently accurate for our purpose. The reasons are as follows. (*i*) The new set of optimized ζ's which has been calculated using the optimized geometries of Table 3 turns out to be very similar to that derived by Pople *et al.* (2) from standard geometries. Since small changes in the ζ's appear not to affect significantly the geometrical parameters (and vice versa) a *re*optimization of geometry using the optimum ζ parameters derived from the set given in Table 3 would not achieve any significant improvement of the geometrical parameters. Moreover (*ii*), in the process of calculating the optimum geometries it has appeared that minor changes in their parameters (of the order of what could result from their reoptimization using optimum ζ values) have a negligible effect on the charge distributions. Consequently, we feel justified in using the geometries of Table 3 for pursuing the calculations. The set of optimized ζ values derived

Can. J. Chem. Downloaded from www.nrcresearchpress.com by 210.87.254.105 on 09/05/12
For personal use only.

TABLE 3. Equilibrium geometries[a]

Molecule	Symmetry constraint	Coordinate	STO-3G	Experimental[b]
CH_4	T_d	r(CH)	1.083	1.085
C_2H_6	D_{3d}	r(CC)	1.524	1.531
		r(CH)	1.0935	1.096
		∠HCH	107.92	107.8
C_2H_6(eclipsed)	D_{2h}	r(CH)	1.0925	
		r(CC)	1.539	
		∠HCH	107.49	
C_3H_8	C_{2v}	r(CC)	1.530	1.526±0.002
		r(CH) (sec)	1.097	1.096±0.002
		$r(CH_s)$	1.0935	1.089±0.009
		$r(CH_a)$	1.094	1.094
		∠CCC	111.58	112.4±0.2
		∠HCH sec	107.44	106.1
		$\angle H_aCH_a$	108.00	107.3
		$\angle H_aCH_s$	108.22	108.1
		$\angle CCH_s$	110.90	111.8±1.0
		$\angle CCH_a$	110.49	110.6
i-C_4H_{10}	C_{3v}	r(CC)	1.531	1.525
		$r(CH_t)$	1.0983	1.108
		$r(CH_s)$	1.099	1.100
		$r(CH_a)$	1.091	1.092
		∠CCC	111.40	111.15±0.1
		$\angle CCH_s$	111.40	109.40
		$\angle H_aCH_a$	108.45	108.5
		$\angle H_aCH_s$	107.97	107.9
		$\angle CCH_t$	107.8	
neo-C_5H_{12}	T_d	r(CC)	1.535	
		r(CH)	1.0933	
		∠HCH	107.91	
		∠CCC	109.47	
C_2H_4	D_{2h}	r(CC)	1.318	1.330
		r(CH)	1.080	1.076
		∠HCC	116.59	116.6
C_6H_6	D_{6h}	r(CC)	1.395	1.397
		r(CH)	1.090	1.084

[a]Distances in Å, angles in decimal degrees.
[b]CH_4, C_2H_6, and C_2H_4 from ref. 6; i-C_4H_{10} and C_3H_8 from ref. 7; C_6H_6 from ref. 8.

using these optimum geometries is given in Table 4.

These optimum ζ values are, as expected, similar to those calculated by Pople *et al.* (2) for methane and ethane, which were 1.18 (H) and 1.76 (C, L shell). The carbon K-shell exponents are somewhat different from the value (5.67) used by Pople, which is the ζ corresponding to the free atom Slater-type orbital.

Population analyses were carried out following Mulliken's method (9). The results are given in Table 5.

In order to provide data for the forthcoming discussion, the following calculations were also made. (*i*) A "standard" STO-3G calculation using Pople's recipe (2). Standard geometries were assumed with r(CH) = 1.091 Å, r(CC) = 1.540 Å, ∠HCH = ∠CCC = 109.47°, and Pople's (2) optimized scale factors were used. (*ii*) A GTO(6s3p|3s) calculation, using the optimized geometries and exponents given in Tables 3 and 4. (*iii*) A GTO(9s5p|5s) → [5s3p|3s] calculation of methane and ethane, using the geometries of Table 3 and the exponents calculated by Dunning (10).

The net (*i.e.*, the nuclear minus gross) charges which were calculated in the present study are given in Table 6, in 10^{-3} electron units. Selected "inductive" charge distributions (11–13) are included, which shall be discussed in the next section.

The effect of optimization of geometries and scaling factors at the STO-3G level is clearly reflected by the comparison between "standard"

Can. J. Chem. Downloaded from www.nrcresearchpress.com by 210.87.254.105 on 09/05/12
For personal use only.

TABLE 4. Optimum exponents for molecules

Molecule	Atom	ζ_H	$\zeta_{C(s_L,p)}$	$\zeta_{C(s_K)}$
CH_4		1.183	1.770	5.721
C_2H_6 staggered		1.1760	1.7591	5.706
C_2H_6 eclipsed		1.178	1.756	5.701
C_3H_8	C_{prim}		1.7590	5.706
	C_{sec}		1.75354	5.701
	$H_{prim(s)}$	1.1749		
	$H_{prim(a)}$	1.1750		
	H_{sec}	1.1750		
i-C_4H_{10}	C_{prim}		1.7609	5.705
	C_{tert}		1.7598	5.708
	$H_{prim(s)}$	1.176		
	$H_{prim(a)}$	1.176		
	H_{tert}	1.178		
neo-C_5H_{12}	C_{prim}		1.7581	5.7048
	C_{quat}		1.7420	5.728
	H	1.1709		
C_2H_4		1.226	1.709	5.703
C_6H_6		1.207	1.720	5.704

TABLE 5. Population analyses from the optimized STO-3G calculations (electron units)

		Orbital population				
Molecule	Atom	1s	2s	$2p_x$	$2p_y$	$2p_z$
CH_4	C	1.98975	1.13429	0.97496	0.97496	0.97496
C_2H_6	C	1.99026	1.14590	0.96794	0.96794	0.94891
C_3H_8	C_{prim}	1.99032	1.14913	0.96567	0.95815	0.96053
	C_{sec}	1.99062	1.15219	0.96168	0.94130	0.94826
	$H_{prim(a)}$	0.99290				
	$H_{prim(s)}$	0.99421				
	H_{sec}	0.99780				
i-C_4H_{10}	C_{prim}	1.98922	1.15127	0.96396	0.95936	0.96257
	C_{tert}	1.99159	1.15513	0.93715	0.93715	0.94562
	$H_{prim(a)}$	0.99335				
	$H_{prim(s)}$	0.99681				
	H_{tert}	1.00353				
neo-C_5H_{12}	C_{prim}	1.99072	1.15395	0.96309	0.95604	0.96486
	C_{quat}	1.98744	1.16302	0.92887	0.92887	0.92887
C_2H_4	C	1.99217	1.15392	1.00000	1.00185	0.98752
C_6H_6	C	1.99178	1.13281	0.95355	0.96928	1.00000

and "optimized" net charges. The concurrent lowering of total molecular energy is, in each case, relatively small: $\Delta E = 0.0028$ au (CH_4), 0.0033 (C_2H_6), 0.0050 (C_3H_8), 0.0064 (*i*-C_4H_{10}), and 0.0181 au (neo-C_5H_{12}). A substantial lowering of the energies with respect to the optimum STO-3G ones is observed with the GTO(6s3p|3s) results: −39.77333 (*vs.* −39.73336) au for CH_4, −78.39065 (*vs.* −78.31488) for C_2H_6, −117.0097 (*vs.* −116.89899) for C_3H_8, −155.63221 (*vs.* −155.48318) for *i*-C_4H_{10}, and −194.24842 (*vs.* −194.07778) au for neo-C_5H_{12}. The same trends are observed with GTO(9s5p|5s) → [5s3p|3s] results, *i.e.* still larger charge separations and lower molecular energies: $q_C = -705.17$ me ($E = -40.18721$ au) for methane, and $q_C = -506.38$ me ($E = -79.20852$ au) for ethane.

Discussion

The results given in Table 6 indicate that "better" (*i.e.*, improved Gaussian set) *ab initio* calculations yield quite larger and less credible charge separations than those derived using a minimal basis set. This trend is confirmed by the methane-C net charge (in electron units) calculated by André *et al.* (14) ($q_C = -0.79$),

Can. J. Chem. Downloaded from www.nrcresearchpress.com by 210.87.254.105 on 09/05/12
For personal use only.

TABLE 6. Net charges, 10^{-3} electron units

Molecule	Atom	STO-3G Standard	STO-3G Optimized	GTO (6s3p| 3s)	"Inductive" $n = 14.11$
Methane	C	−72	−48.92	−334.8	−331.5
Ethane	C	−26	−20.96	−234.0	−232.5
Propane	C_{prim}	−31	−23.81	−236.5	−235.6
	C_{sec}	19	5.94	−132.9	−134.6
	H_{prim}[a]	7	6.23	75.9	76.7
	H_{sec}	0.3	2.20	75.3	72.6
Isobutane	C_{prim}	−35	−26.39	−238.3	−238.0
	C_{tert}	57	33.36	−27.6	−36.1
	H_{prim}[a]	6	5.50	74.5	75.9
	H_{tert}	−6	−3.53	71.8	66.5
Neopentane	C_{prim}	−39	−28.66	−237.3	−240.4
	C_{quat}	93	62.92	60.1	64.5

[a]Average for nonequivalent H atoms.

Allen and co-workers (15) (−1.072), and that calculated (13) using Pople's 6-31G extended basis set (3) (−0.63 e).

The adequacy of theoretical charge densities for the study of molecular properties involving charges has been discussed recently (12, 13) in terms involving "inductive" charge distributions. The detailed comparison of "inductive" charges $f(n, \beta)$ with their theoretical counterparts from semi-empirical and partially or nonoptimized *ab initio* methods has revealed an overall agreement which is satisfactory. This applies also to the "standard" STO-3G results; the optimized STO-3G results, however, are virtually in perfect agreement with the "inductive" charges. The comparison of the GTO net charges with their "inductive" counterparts is presented in Table 6. With $n = 14.11$ and $\beta = -232.5$ me, the agreement is satisfactory, although not of the quality which has been observed for the fully optimized STO-3G net charges. It must be noted, however, that the present GTO(6s3p|3s) results have been deduced without any reoptimization of the exponents.

It is also noted that the net charge of the neopentane quaternary C atom is nearly independent of the choice of the method used for calculating it: $q(C_{quat}) = 62.92$ me (STO-3G, optimum), 60.1 me [GTO(6s3p|3s)], 54 me (from André's 7s3p|3s results (14)), and 81 me (from Hoyland's BO results (16)). Finally, from the present contracted GTO(9s5p|5s) calculations, $q(C_{quat})$ is estimated at 90 me. The near invariance of the quaternary C net charge and the fact that all other C charges become increasingly (and excessively) negative as the Gaussian expansions are improved both point at the role of an adequate partitioning of the C—H overlap populations, as discussed earlier (13). This further stresses the need for a more general analysis of the problem, *e.g.*, along the lines recently given by Roby (17).

There is one final point concerning the quality of fully optimized STO-3G charge distributions. The "inductive" charge distributions, with $n = -4.4122$, were found to give a virtually perfect linear relationship between C-13 chemical shifts and carbon charges (13). The standard deviation of ±0.3 p.p.m. implies an accuracy of ±0.13% in the evaluation of the net C charges. Subject to this choice of definition of "accurate" charge distributions, the set of optimized STO-3G results obtained in this study qualify as "excellent" since the modified set which is deduced from the original STO-3G results by an appropriate mode of partitioning CH overlap populations also exhibits a virtually perfect correlation with carbon chemical shifts (13). It appears, therefore, that in view of obtaining charge distributions which are accurate in their relative scaling one should prefer to work at the simple STO-3G level and carry out carefully the optimizations discussed in this paper, rather than attempting calculations involving large Gaussian descriptions without optimizing adequately all the variational parameters.

We wish to express our gratitude to R. Macaulay and D. Goutier for assistance and many helpful discussions. The computational facilities offered by the "Centre de

Can. J. Chem. Downloaded from www.nrcresearchpress.com by 210.87.254.105 on 09/05/12
For personal use only.

Calcul de l'Université de Montréal" and the financial aid given by the National Research Council of Canada are gratefully acknowledged.

1. L. RADOM and J. A. POPLE. *In* International Review of Science, Physical Chemistry, Series One, Theoretical Chemistry (V-1). *Edited by* W. Byers Brown. Butterworth and Co. Ltd., London. 1972. p. 71.
2. W. J. HEHRE, R. F. STEWART, and J. A. POPLE. J. Chem. Phys. **51**, 2657 (1969).
3. W. J. HEHRE, R. DITCHFIELD, and J. A. POPLE. J. Chem. Phys. **56**, 2257 (1972).
4. D. GOUTIER, R. MACAULAY, and A. J. DUKE. Program 236, Quantum Chemistry Program Exchange, University of Indiana, Chemistry Department, Bloomington, Indiana 47401.
5. J. A. POPLE and M. GORDON. J. Am. Chem. Soc. **89**, 4253 (1967).
6. (*a*) L. S. BARTELL, K. KUSCHITSU, and R. J. DENUI. J. Chem. Phys. **35**, 1211 (1961). (*b*) D. E. SHAW, D. W. LEPARD, and H. L. WELSH. J. Chem. Phys. **42**, 3736 (1965). (*c*) K. KUCHITSU. J. Chem. Phys. **44**, 906 (1966).
7. D. R. LIDE. J. Chem. Phys. **33**, 1514, 1519 (1960).
8. A. LANGSETH and B. STOICHEFF. Can. J. Phys. **24**, 350 (1956).
9. R. S. MULLIKEN. J. Chem. Phys. **23**, 1833, 1841, 2338, 2343 (1955).
10. T. H. DUNNING. J. Chem. Phys. **53**, 2823 (1970).
11. S. FLISZÁR and J. SYGUSCH. Can. J. Chem. **51**, 991 (1973).
12. S. FLISZÁR, G. KEAN, and R. MACAULAY. J. Am. Chem. Soc. In press.
13. S. FLISZÁR, A. GOURSOT, and H. DUGAS. J. Am. Chem. Soc. In press.
14. J. M. ANDRÉ, P. DEGAND, and G. LEROY. Bull. Soc. Chem. Belges, **80**, 585 (1971).
15. J. E. WILLIAMS, V. BUSS, and L. C. ALLEN. J. Am. Chem. Soc. **93**, 6867 (1971).
16. J. R. HOYLAND. J. Chem. Phys. **50**, 473 (1969).
17. K. R. ROBY. Mol. Phys. **27**, 81 (1974).

Can. J. Chem. Downloaded from www.nrcresearchpress.com by 210.87.254.105 on 09/05/12
For personal use only.

The Effect of Bond Function Polarization on the l.c.a.o.–m.o.–s.c.f. Calculation of Bond Angles and Energy Barriers

JOHN O. JARVIE AND ARVI RAUK
Department of Chemistry, University of Calgary, Calgary, Alberta T2N 1N4
AND
CLYDE EDMISTON
Department of Chemistry, University of Wyoming, Laramie, Wyoming
Received February 27, 1974

JOHN O. JARVIE, ARVI RAUK, and CLYDE EDMISTON. Can. J. Chem. **52**, 2778 (1974).

The effect of including polarization into a flexible s,p basis set by use of bond functions is studied in the systems H_2O, NH_3, H_2O_2, and N_2H_4. In all cases a decrease and subsequent improvement in calculated bond angles is found. Barriers to nitrogen inversion are also significantly improved. Bond function polarization alone does not account for the *anti* rotation barrier in H_2O_2 although it does lead to stabilization of the *gauche* form relative to the *anti* form. The effect on molecular charge distributions is to allow movement of charge into the bonding regions. The results indicate that bond functions are an efficient means of introducing polarization into a basis set and lead to an improved agreement between calculated and experimental geometric and energetic parameters.

JOHN O. JARVIE, ARVI RAUK et CLYDE EDMISTON. Can. J. Chem. **52**, 2778 (1974).

L'inclusion de la polarisation dans un ensemble de base flexible s,p, par le biais de fonctions de liens, a été étudiée dans les systèmes H_2O, NH_3, H_2O_2 et N_2H_4. Il en résulte dans tous les cas une diminution et une amélioration des angles des liaisons calculés. Les barrières d'inversion de l'azote sont améliorées d'une manière significative. La polarisation des fonctions de liens n'explique pas à elle seule la barrière rotationnelle *anti* dans H_2O_2 bien qu'elle conduise à une stabilisation de la forme *gauche* par rapport à la forme *anti*. L'effet sur les distributions de charges se reflète par un accroissement de densité électronique dans les régions de liaisons. Les résultats montrent que les fonctions de liens sont un moyen efficace pour introduire la polarisation dans un ensemble de base, conduisant ainsi à un meilleur accord entre le calcul et l'expérience pour les paramètres géométriques et énergétiques.

[Traduit par le journal]

Introduction

The results of recent near Hartree–Fock l.c.a.o.–m.o.–s.c.f. calculations have indicated that the independent particle model is capable of accurately determining bond angles and lengths in small molecules. The calculated results for CH_4 (1), NH_3 (2), and H_2O (3) differ by only 1–2% from the results of microwave and electron diffraction experiments. Similar results have also been obtained for the calculation of bond lengths in diatomic molecules where neither of the atoms may be hydrogen (see, for example, the table compiled by Wahl and Bertoncini (4)). In most cases accurate results for both bond lengths and bond angles can also be obtained with carefully chosen but substantially smaller basis sets which give energies significantly above estimated Hartree–Fock limit values. Similarly, it has been demonstrated that the independent particle model is capable of quantitatively predicting both inversion and rotation barriers (5, 6) in molecules in which these features exist. It is apparent that potential surfaces obtained by the Hartree–Fock method for intramolecular motions that do not involve significant bond stretching are parallel to the true potential surfaces. When considering motions of this type, it is unnecessary to extend the method to include configuration interaction (c.i.).

However, in order to obtain consistently reliable results, some important observations regarding atom centered basis sets have emerged. For first row atoms (*e.g.* C, N, and O) the s and p basis should be made flexible by having two or more basis functions (after contraction) for each occupied valence atomic orbital (a.o.). In most instances this ensures the calculation of bond lengths to reasonable accuracy. However, the calculation of accurate bond angles, dihedral angles, and energy barriers in many cases requires

Can. J. Chem. Downloaded from www.nrcresearchpress.com by 210.87.254.5 on 09/05/12
For personal use only.

TABLE 1. Exponents and Contraction coefficients for the 7s–3p basis set

Basis function	X = Nitrogen		X = Oxygen	
	Exponent	Contraction coefficient	Exponent	Contraction coefficient
X–1s	615.6398	0.019462	813.0415	0.019384
	92.84316	0.133704	122.6090	0.134252
	20.70341	0.462798	27.37847	0.462186
	5.470375	0.508829	7.25383	0.524773
X–2s	0.853723	0.379053	1.180484	0.358475
	0.347253	0.531409	0.479531	0.529239
X–2s′	0.139873	1.0	0.189589	1.0
X–2p	6.085492	0.116425	8.093693	0.123250
	1.25207	0.470566	1.674014	0.475569
X–2p′	0.289677	1.0	0.372659	1.0
H–1s	6.409584	1.0	6.409584	1.0
	0.974304	5.721	0.974304	5.721
H–1s′	0.217296	1.0	0.217296	1.0
Bond functions	1.4	0.49	1.6	0.72
	0.30	1.0	0.42	1.0

the inclusion of polarization functions[1] (functions with higher order spherical harmonics). The most notorious cases involve molecules which have atoms with nonbonded electron pairs (2, 5, 6).

It has been proposed on the basis of studies of the methane molecule, that the effect of adding polarization functions can to a large extent also be obtained through the use of bond functions (1, 7), s-type Gaussians centered near the mid-points of the various bonds in the molecule. Rothenberg and Schaefer have concluded "Bond functions provide a reasonable alternative to the more conventional polarization functions. In particular, the effect of eight bond functions . . . was not improved on by using fewer than 18 conventional polarization functions . . ." (7). The results of Meyer and Pulay also on methane support this conclusion (1).

Although bond functions have been reported to be very efficient in introducing polarization into methane (1, 7), it is not clear whether the polarization is of the correct type to allow prediction of bond angles and energy barriers in molecules with fluxional structures. Accordingly we have investigated, and report below, the effect of bond function polarization in H_2O, NH_3, H_2O_2, and N_2H_4. Each of these molecules serves as a test for accuracy of bond angle calculation, the last two having a dihedral angle as well. In NH_3 one has the additional problem of calculating the inversion barrier and in H_2O_2, two rotational barriers including the recalcitrant *anti* barrier. Both barrier problems exist in the case of N_2H_4. The results of detailed calculations on the potential surface for N_2H_4, using one of the basis sets involved in this study, are reported elsewhere (8).

[1]For first row hydrides these functions take the form of 3d-type orbitals on the central atom and 2p-type orbitals on hydrogen centers.

Method

Ab initio l.c.a.o.—m.o.—s.c.f. calculations were carried out according to the Roothaan scheme (9) on H_2O, NH_3, H_2O_2, and N_2H_4. The basis sets used were of the Gaussian lobe function (G.l.f.) type, augmented with bond functions. In all cases, the bond lengths were kept fixed at the values, $R_{OH} = 0.96$ Å, $R_{NH} = 1.013$ Å, $R_{NN} = 1.45$ Å, and $R_{OO} = 1.475$ Å.

The exponents for the 7s–3p basis set were taken from Ditchfield *et al.* (10) with minor modifications and are shown in Table 1. The p-exponents were taken directly from their 3p representation. However, the seven s-exponents were composed of four from their 4s Gaussian representation of a 1s atomic orbital (a.o.) and three from their Gaussian representation of a 2s a.o. The latter three exponents are the outer exponents which are used to describe the

Can. J. Chem. Downloaded from www.nrcresearchpress.com by 210.87.254.5 on 09/05/12
For personal use only.

Can. J. Chem. Downloaded from www.nrcresearchpress.com by 210.87.254.5 on 09/05/12
For personal use only.

valence region. The other two Gaussians in the 5s representation enter with a negative coefficient; consequently they are used to form the inner "cusp" of the 2s a.o. It would seem that this cusp could be sufficiently represented by the 1s a.o. Choosing the s-exponents in this fashion allows three Gaussians to be used for describing the valence region whereas an energy optimized 7s basis set allows only two Gaussians to be used to describe the valence region (11).

The three s-exponents for hydrogen are scaled values of those reported by Whitten (12). A scale factor of 1.2 was used,[2] which we have found to be near the optimum value for CH_4.

The Gaussian composition of the basis functions can be conveniently notated as (4,2,1;2,1/2,1), which indicates how the 7s–3p basis set on O and N and the 3s basis set on H are contracted to 3s–2p and 2s, respectively. The contraction coefficients for the p-type Gaussians on N and O (10) and for the s-type on hydrogen (12) have been previously reported. We have optimized the coefficients (Table 1) for the nitrogen s-type Gaussians in a N atom calculation.

A g.l.f. p-type basis function is formed as a linear combination (with equal and opposite sign) of two s-type Gaussians (lobes) displaced equally and oppositely along a line through the nuclear center. The total energy is quite insensitive to the exact location of the p-lobes. A comparison of Gaussian lobe and Cartesian basis sets has been reported (13). In addition a formula for determining the displacement distances has been given (13, 14)

$$d = k/a^{1/2}$$

where a is the p-exponent to be used. A value of 0.03 for k was used here.

We have optimized exponents and coefficients of a two component bond function in the NH and OH systems using a (3,4,2,1;5/2(b.f.)/4,1) basis set. The 10s–5p bases on nitrogen and oxygen are those reported by Whitten (15). The 5s basis on hydrogen is taken from Fink and Allen (16). For NH, after optimization, the exponents are 0.30 and 1.4 with contraction coefficients of 1.0 and 0.49, respectively. For OH,[3] after optimization, the exponents are 0.42 and 1.6 with contraction coefficients of 1.0 and 0.72 respectively.

The exponents and contraction coefficients were optimized with the bond functions at the midpoints of the NH and OH bonds. For OH, optimization of the displacement along the OH axis led to a minimum energy for displacement distances of $0.8R_{OH}$ and $0.6R_{OH}$[4] for the small and large exponent Gaussians respectively. Since the energy corresponding to both bond functions being located at the bond midpoint was only 0.0056 a.u. (0.35 kcal/mol) above the minimum value, this position was used in later calculations for convenience. This restriction makes a difference of less than half a degree in the HOH bond angle in H_2O as calculated with the 10s–5p basis set. In the studies on N_2H_4 and H_2O_2, the bond functions were placed at the midpoints of the N—N and O—O bonds and are identical to the bond functions used for the N—H and OH bonds, respectively.

Results and Discussion

Water and Ammonia

The initial calculations were performed on H_2O and NH_3 using the 10s–5p basis set (3,4,2,1;4,1/4,1). For H_2O, addition of the bond functions to this basis set improved the calculated bond angle from 112.7° to 109.5° (exp = 104.5° (17)). The corresponding minimum energies are −76.0029 and −76.0209 a.u. which are near the estimated Hartree–Fock limit, −76.06 a.u. (18). For NH_3, a more substantial bond angle improvement, from 115.1° to 110.8°, occurred (exp = 106.7° (19)) with a resulting increase in the calculated barrier to pyramidal inversion, from 0.8 to 2.8 kcal/mol (exp = 5.8 kcal/mol (20)). The minimum energies with and without bond functions are −56.1733 and −56.1911 a.u. which are near the Hartree–Fock limit, −56.22 a.u. (for a discussion, see ref. 21).

With the 7s–3p basis set, inclusion of bond functions resulted in the calculated bond angle changing from 108.5° to 106.2° in H_2O and from

[2]Each exponent is multiplied by the square of the scale factor.

[3]In the OH case, the electronic environment was made cylindrically symmetrical to better simulate a molecular environment by doubly occupying the π-like orbitals on oxygen with electrons of charge 3/4e.

[4]The displacements were restricted to the range $0.25R_{OH}$ to $0.9R_{OH}$, as measured from the oxygen atom.

TABLE 2. Comparison of gross electron populations with and without bond functions for near equilibrium geometries.

	H_2O*		N_2H_4†	
	Without b.f.	With b.f.	Without b.f.	With b.f.
N or O				
Total	8.772	8.193	7.631	6.816
1s	1.992	1.990	1.989	1.985
2s	1.391	1.212	1.259	0.962
2s′	0.563	0.442	0.410	0.249
$2p_x + 2p_y + 2p_z$	2.035	1.977	1.694	1.619
$2p_x' + 2p_y' + 2p_z'$	2.791	2.572	2.279	2.001
H‡				
Total	0.615	0.592	0.684	0.643
1s	0.378	0.324	0.389	0.352
1s′	0.237	0.268	0.295	0.291
Bond functions§				
NH or OH	—	0.312	—	0.356
NN	—	—	—	0.372

*7s–3p basis set. HOH = 105°.
†7s–3p basis set. NNH = HNH = 110°; ϕ = 135°.
‡The values for H in N_2H_4 are an average of two nonequivalent hydrogens.
§See the text for a discussion of the effect of bond functions on the electron distribution.

112.2° to 107.7° in NH_3. The corresponding minimum energies are −75.7700 (without b.f.) and −75.7993 a.u. (with b.f.) for H_2O; the values for NH_3 are −56.0068 (without b.f.) and −56.0356 (with b.f.). A significant improvement, from 1.6 to 6.0 kcal/mol, occurred in the calculated inversion barrier of NH_3. These results indicate that calculations using the 7s–3p basis set with bond functions represent quite well the energy surface of NH_3 and H_2O, even though the s.c.f. energies are significantly above the Hartree–Fock limit.

The results of a Mulliken population analysis (22) for H_2O are shown in Table 2. The calculated atomic populations suggest that the effect of the bond functions is to allow movement of charge from the central atom into the bonding region. There is a subsequent decrease in the calculated dipole moment.

Hydrazine

The calculations on N_2H_4 have been carried out with the constraint that the NNH and HNH angles be the same (8). Inclusion of bond functions into the 7s–3p basis set causes the calculated equilibrium bond angle to change from 112.8° to 109.5° which is very near the experimental value of 110°.[5] The calculated barriers to internal rotation with the bond angles fixed at 110° are similar to other reported values (see Table 3) and are quite independent of the basis set used. However, if the bond angles are relaxed, the inclusion of bond functions causes the *anti* barrier to decrease from 3.1 kcal/mol (without b.f.) to 1.6 kcal/mol. As might be expected from the NH_3 study, an increase occurs in the inversion barrier (from 2.2 to 6.1 kcal/mol; exp = 7.5 kcal/mol (29)).

As for NH_3 and H_2O, a population analysis shows a movement of charge from the nitrogen into the bonding regions when the bond functions are added to the basis set (see Table 2). There is again a decrease in the calculated dipole moment.

Hydrogen Peroxide

For H_2O_2, inclusion of bond functions into the 7s–3p basis set resulted in a small equilibrium bond angle change, from 100.3° to 99.6°, in the *anti* conformation. Calculations both with and without bond functions failed to give the elusive (30, 31) *anti* barrier in H_2O_2, even after optimization of the OOH bond angle at the two dihedral angles, ϕ = 120° and ϕ = 180°. However, the calculated values of the OOH bond angles, 99.6° (100.3° without bond functions) for ϕ = 180° and 100.6° (101.3° without bond functions) for ϕ = 120°, agree very well with those obtained by Veillard using a large conventionally polarized basis set (100.2° and 101.3° at ϕ = 180°

[5]This is a weighted average of the values NNH = 112° and HNH = 106° which result from the analysis of microwave experiments (23).

Can. J. Chem. Downloaded from www.nrcresearchpress.com by 210.87.254.5 on 09/05/12
For personal use only.

TABLE 3. Summary of LCAO–MO–SCF calculations of the barriers to internal rotation in N_2H_4*

E_0 (a.u.)	ϕ_0 (deg)	Constant θ		Optimum θ		Reference
		Trans	*Cis*	*Trans*	*Cis*	
−111.0021	100	3.6	12.3			24
−110.6853	94	3.7	9.6			25
−111.0743	~100	3.7	11.9			26
−111.0301	94	4.7	11.5			27
−110.1239	~90	6.2	11.1			28
−110.8180	95	3.6	13.2	3.1	13.7	Present work†
−110.8785	95	4.6	12.4	1.6	12.0	Present work‡

*Barrier heights are in units of kcal/mol.
†Without bond functions.
‡With bond functions.

and $\phi = 120°$ respectively) (30). The experimental value for the OOH bond angle is 94.8° at a dihedral angle of 111° (32).

An attempt was then made to further improve the H_2O_2 basis set by introducing lone pair polarization functions (l.p.–b.f.). Each function is a d_{x^2}-like orbital and consists of two lobes displaced by a distance $\frac{1}{2}R_{OH}$ in opposite directions from the oxygen center. One l.p.–b.f. is directed in the OOH plane bisecting the OOH angle, while the other is directed perpendicular to the OOH plane. The exponents and contraction coefficients of each lobe are the same as those of an OH bond function.

Only two points of the H_2O_2 surface were determined with this basis set since the results on H_2O indicate almost no change in the calculated bond angle as a result of adding the l.p.–b.f.'s. The *anti* conformation is calculated to be 0.05 kcal/mol above the $\phi = 120°$ conformation for a constant OOH angle of 100°. The small value of the barrier is to be compared with the results of Veillard who obtained a value of 0.6 kcal/mol for the *anti* barrier (exp = 1.1 kcal/mol (33)) with a large polarized basis set and with optimization of the OOH angle (30). Dunning and Winter were able to improve on this by a complete geometry optimization and obtained a value of 1.1 kcal/mol (31).

It is difficult to assess the relative importance of bond functions and l.p.–b.f.'s. Comparison of the data in Table 4 indicates that the effect of bond functions alone (toward destabilizing the *anti* form of H_2O_2 relative to the *gauche* ($\phi = 120°$) form) is slightly less than half of the combined effect of bond functions and l.p.–b.f.'s. However, the total population of the four l.p.–b.f.'s, obtained by the usual Mulliken population analysis, is only 0.3 electron whereas the population of the two OH and one OO bond functions amounts to three times this number.

Summary and Conclusions

The calculated results for all of the molecules studied here are summarized in Table 4. It is significant that in all cases, the addition of bond functions to the basis set results in a decrease and subsequent improvement in the predicted bond angles. The effect of the bond functions on the calculated bond angles is fairly constant and largely independent of basis set size. In H_2O, for example, addition of the bond functions to the 7s–3p basis results in a decrease of 2.3° in the bond angle while their addition to the 10s–5p basis set results in a decrease of 3.2°. In NH_3, the respective values are 4.5° and 4.3°. However, for both H_2O and NH_3 the energy lowering in the 7s–3p basis set is nearly twice that obtained in the 10s–5p set.

Previous conclusions (1, 7) concerning bond functions are further substantiated by this work. In addition some new conclusions are indicated: (*1*) the type of polarization required for the calculation of accurate bond angles in nitrogen and oxygen-containing molecules is to a large extent supplied by bond functions; (*2*) the largest effect of bond functions on the charge distribution is a movement of charge from oxygen (or nitrogen) into the bonding regions; (*3*) improved values of calculated inversion barriers at nitrogen are obtained due to polarization by bond functions. Fortuitously, with the

Can. J. Chem. Downloaded from www.nrcresearchpress.com by 210.87.254.5 on 09/05/12
For personal use only.

TABLE 4. Summary of calculated equilibrium geometries and barrier heights[a]

Molecule	Basis set	Parameter[b]	Calculated value s,p	Calculated value b.f.	Calculated value b.f. + lp − b.f.	Experimental value
H_2O	7s–3p	Bond angle	108.5°	106.2°	106.3°	104.5°[c]
	10s–5p	Bond angle	112.7°	109.5°	—	
H_2O_2	7s–3p	Bond angle ($\phi = 180°$)[b]	100.3°	99.6°	—	
	7s–3p	Bond angle ($\phi = 120°$)[b]	101.3°	100.6°	—	94.8°[d]
	7s–3p	*anti* rotation barrier	−1.2	−0.7	+.05	1.1[e]
NH_3	7s–3p	Bond angle	112.2°	107.7°	—	106.7°[f]
	10s–5p	Bond angle	115.1°	110.8°	—	
	7s–3p	Inversion barrier	1.6	6.0		
	10s–5p	Inversion barrier	0.8	2.8		5.8[g]
N_2H_4	7s–3p	Bond angle[h]	112.8°	109.5°	—	110°
	7s–3p	Dihedral angle	95°	95°		90–95°
	7s–3p	*anti* rotation barrier	3.1	1.6	—	—
	7s–3p	*syn* rotation barrier	13.7	12.0	—	—
	7s–3p	Inversion barrier	2.2	6.1	—	7.5

[a]Barriers are expressed in units of kcal/mol.
[b]ϕ is the HOOH dihedral angle.
[c]Reference 17.
[d]Reference 32.
[e]Reference 33.
[f]Reference 19.
[g]Reference 20.
[h]NNH = HNH = 0.

smaller basis set, the results are nearly quantitative for both NH_3 and N_2H_4; (*4*) the present data suggest that polarization due to bond functions alone cannot account for the *anti* barrier in H_2O_2, although it does lead to stabilization of a *gauche* structure relative to the *anti* structure.

The notorious difficulty that has been encountered in obtaining an *anti* barrier for H_2O_2 offsets the equally notorious success that has been obtained for the isoelectronic C_2H_6. The isoelectronic N_2H_4, of course, lies somewhere between these two extremes. A variety of l.c.a.o.–m.o.–s.c.f. calculations, none of which involved bond angle variation or inclusion of polarization functions, have all succeeded in obtaining a substantial *anti* barrier for hydrazine (see Table 3). Our own calculations indicate that relaxation of bond angles and inclusion of polarization (at least by bond functions) serve to lessen this barrier (Table 4). Apparently, a study of the potential energy surface of hydrazine does not require nearly as much basis set sophistication as is needed for a study of H_2O_2.

In conclusion, the results indicate that the bond functions are an efficient means of introducing polarization into a basis set and lead to an improved agreement between calculated and experimentally derived geometric and energetic parameters.

The authors wish to acknowledge the cooperation of the Department of Computer Services, University of Calgary. Receipt of a generous Computing Grant from the University of Calgary and continued financial support by the National Research Council of Canada and the National Science Foundation are also gratefully acknowledged.

1. W. MEYER and P. PULAY. J. Chem. Phys. **56**, 2109 (1972).
2. (*a*) A. RAUK, L. C. ALLEN, and E. CLEMENTI. J. Chem. Phys. **52**, 4133 (1970); (*b*) R. M. STEVENS. J. Chem. Phys. **55**, 1725 (1971).
3. G. H. F. DIERCKSEN and W. P. KRAEMER. Theor. Chim. Acta, **23**, 387 (1972).

Can. J. Chem. Downloaded from www.nrcresearchpress.com by 210.87.254.5 on 09/05/12
For personal use only.

4. A. C. WAHL, P. J. BERTONCINI, G. DAS, and T. L. GILBERT. Int. J. Quantum Chem. **1S**, 123 (1967).
5. H. F. SCHAEFER III. The electronic structure of atoms and molecules. Addison–Wesley, Don Mills, Ontario. 1972. p. 407.
6. L. C. ALLEN and J. ARENTS. J. Chem. Phys. **57**, 1818 (1972).
7. S. ROTHENBERG and H. F. SCHAEFER III. J. Chem. Phys. **54**, 2764 (1971).
8. J. O. JARVIE and A. RAUK. Can. J. Chem. This issue.
9. C. C. J. ROOTHAAN. Rev. Mod. Phys. **32**, 245 (1960).
10. R. DITCHFIELD, W. J. HEHRE, and J. A. POPLE. J. Chem. Phys. **52**, 5001 (1970).
11. D. R. WHITMAN and C. J. HORNBACK. J. Chem. Phys. **51**, 398 (1969).
12. J. L. WHITTEN. J. Chem. Phys. **39**, 349 (1963).
13. S. SHIH, R. BUENKER, S. PEYERIMHOFF, and B. WIRRAM. Theor. Chim. Acta, **18**, 277 (1970).
14. J. PETKE, J. WHITTEN, and A. DOUGLAS. J. Chem. Phys. **51**, 256 (1969).
15. J. L. WHITTEN. J. Chem. Phys. **44**, 359 (1966).
16. W. FINK and L. C. ALLEN. J. Chem. Phys. **46**, 2261 (1967).
17. W. S. BENEDICT, N. GAILAR, and E. K. PLYLER. J. Chem. Phys. **24**, 1139 (1956).
18. C. D. RITCHIE and H. F. KING. J. Chem. Phys. **47**, 564 (1967).
19. W. S. BENEDICT and E. K. PLYLER. Can. J. Phys. **35**, 1235 (1957).
20. J. D. SWALEN and J. A. IBERS. J. Chem. Phys. **36**, 1914 (1962).
21. R. G. BODY, D. S. MCCLURE, and E. CLEMENTI. J. Chem. Phys. **49**, 4916 (1968).
22. R. S. MULLIKEN. J. Chem. Phys. **23**, 1833, 1841, 2338, 2343 (1955).
23. T. KASUYA and T. KAJIMA. Sci. Pap. I.P.C.R. **56**, 1 (1962). Chem. Abstr. **58**, 6206b (1964).
24. L. RADOM, W. J. HEHRE, and J. A. POPLE. J. Am. Chem. Soc. **94**, 2371 (1972).
25. E. L. WAGNER. Theor. Chim. Acta, **23**, 115 (1971).
26. W. H. FINK, D. C. PAN, and L. C. ALLEN. J. Chem. Phys. **47**, 895 (1967).
27. A. VEILLARD. Theor. Chim. Acta. **5**, 413 (1966).
28. L. PEDERSEN and K. MOROKUMA. J. Chem. Phys. **46**, 3941 (1967).
29. Y. HAMADA, A. Y. HIRAKAWA, K. TAMAGAKE, and M. TSUBOI. J. Mol. Spectrosc. **35**, 420 (1970).
30. A. VEILLARD. Theor. Chim. Acta, **18**, 21 (1970).
31. T. H. DUNNING and N. W. WINTER. Chem. Phys. Lett. **11**, 194 (1971).
32. R. L. REDINGTON, W. B. OLSON, and P. C. CROSS. J. Chem. Phys. **36**, 1311 (1962).
33. R. H. HUNT, R. A. LEACOCK, C. W. PETERS, and K. T. HECHT. J. Chem. Phys. **42**, 1931 (1965).

Can. J. Chem. Downloaded from www.nrcresearchpress.com by 210.87.254.5 on 09/05/12
For personal use only.

A Theoretical Study of the Conformational Changes in Hydrazine

JOHN O. JARVIE AND ARVI RAUK

Department of Chemistry, University of Calgary, Calgary, Alberta T2N 1N4

Received February 27, 1974

JOHN O. JARVIE and ARVI RAUK. Can. J. Chem. **52**, 2785 (1974).

Ab initio restricted Hartree–Fock–Roothaan l.c.a.o.–m.o.–s.c.f. calculations using a Gaussian lobe basis with bond functions have been performed to determine the characteristics of the potential surface for nuclear motions in hydrazine. It was found that in its equilibrium conformation the molecule has a dihedral angle of 95°. The barrier to pyramidal inversion at one nitrogen is 6.1 kcal/mol and the *syn* and *anti* rotational barriers are calculated to be 12.0 and 1.6 kcal/mol, respectively. There is a very slight torsional component in the inversion pathway. During rotation over the *anti* barrier the bond angles contract from their average equilibrium value of 109.5° to 105.3°. This contraction appears to be an important feature of the rotational potential curve. Features of the surface are used to rationalize experimental results in cyclic and acyclic substituted hydrazines.

JOHN O. JARVIE et ARVI RAUK. Can. J. Chem. **52**, 2785 (1974).

On a effectué les calculs *ab initio* et par la méthode l.c.a.o.–m.o.–s.c.f. de Hartree–Fock–Roothaan restrictif en s'appuyant sur une base des lobes de Gauss avec des fonctions de liaisons, afin de déterminer les caractéristiques de la surface d'énergie potentielle pour les mouvements nucléaires dans l'hydrazine. On trouve que la molécule possède un angle dièdre de 95° dans sa conformation d'équilibre. L'inversion pyramidale au niveau d'un atome d'azote possède une barrière de potentiel de 6.1 kcal/mol tandis que les barrières aux rotations *syn* et *anti* sont évaluées respectivement à 12.0 et 1.6 kcal/mol. Il existe une faible composante torsionnelle durant le processus d'inversion. Lors de la rotation impliquant la barrière *anti*, les angles de liaisons se referment et passent de leur valeur moyenne d'équilibre de 109.5° à 105.3°. Il semble que cette contraction soit une caractéristique essentielle de la courbe de potentiel de la rotation. On utilise les caractéristiques de la surface pour appliquer les résultats expérimentaux aux hydrazines substituées cycliques et acycliques. [Traduit par le journal]

Can. J. Chem. Downloaded from www.nrcresearchpress.com by 210.87.254.42 on 09/05/12
For personal use only.

Introduction

The hydrazine system **1** has been the subject of extensive study by a variety of experimental

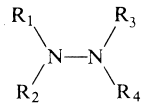

1

techniques and by some molecular orbital calculations. The geometry and bonding is well understood. However, a number of fundamental questions have resisted resolution. Although it is known (1–3) that the parent hydrazine **1** ($R_1 = R_2 = R_3 = R_4 = H$) exists in two enantiomeric interconverting skew conformations **2** in which the dihedral angle is very close to 90°, the detailed mechanism of the interconversion has defied elucidation. Interconversion may take

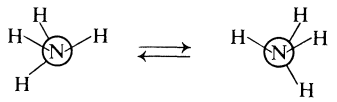

2

place by rotation about the N—N bond or by pyramidal inversion at one of the nitrogen centers. Both processes are complex and, for different reasons, pose difficulties for both the experimental and theoretical chemist.

Rotation may take place through a conformation **3** in which all N—H bonds are eclipsed or through **4** in which all N—H bonds are max-

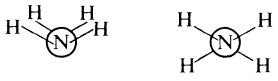

3 **4**

imally staggered. Except by coincidence, the energy barriers hindering the two directions of rotation must have different magnitudes. A variety of theoretical calculations (4, 5) in which the angles at nitrogen were kept constant have yielded values in the range 3.6–6.2 kcal/mol for the *anti* or staggered barrier, E_{anti}, and 9.6–12.3 kcal/mol for the *syn* or eclipsed barrier, E_{syn}. A recent calculation in which the bond angles were varied has yielded the values, 12.4 and 1.6 kcal/mol, respectively, for the two barriers (6).

Can. J. Chem. Downloaded from www.nrcresearchpress.com by 210.87.254.42 on 09/05/12
For personal use only.

A value of 3.1 kcal/mol obtained by microwave spectroscopy (3) is rendered suspect by the assumption that the two barriers are of equal magnitude. As yet there is no accurate experimental value for either rotation barrier of hydrazine.

The magnitude of the inversion barrier in a molecule such as hydrazine is of some theoretical and practical importance also. Barriers to pyramidal inversion at nitrogen atom with hydrogen or alkyl substituents are close to that in ammonia and fall in the range 4–7 kcal/mol (7). It is an empirical observation that substitution by heteroatoms with non-bonded electron pairs generally raises the barrier to pyramidal inversion (7). Whether this is due to a repulsive interaction involving non-bonded electron pairs on the nitrogen and heteroatom, or to the inductive effect of the electronegative heteroatom cannot easily be resolved by experimental measurements since both effects usually occur together. The hydrazine system **1**, however, provides an opportunity for partially separating these effects. One may argue that in the stable skew form **2** of the molecule, one non-bonded lone pair lies approximately in the nodal plane of the other and as a result the repulsive interaction is minimized. In this case the influence of the hetero-

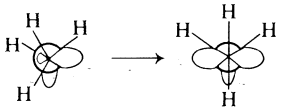

atom (the other nitrogen) on the inversion barrier should be due principally to its inductive effect. Estimates of 7.4 and 6.1 kcal/mol for the inversion barrier of hydrazine have been obtained by CNDO/2 (8) and *ab initio* l.c.a.o.–m.o.–s.c.f. (6) calculations, respectively. Recently, an analysis of the vibrational spectrum of hydrazine was carried out in an attempt to determine the magnitude of the barrier to pyramidal inversion (9). It was found that inversion takes place one nitrogen at a time through an antisymmetric angle bending mode. By assuming that the rotational and vibrational modes are uncoupled (as would be the case if the torsional angle is exactly 90°) a value of 7.5 kcal/mol was found for the barrier to inversion.

From the above considerations it is apparent that a detailed knowledge of the nature of the potential surface for nuclear motions in the hydrazine system is essential for the interpretation of spectroscopic data. We wish to report the results of a theoretical study by restricted Hartree–Fock l.c.a.o.–m.o.–s.c.f. calculations (10) on the potential surface of hydrazine.

Method

Restricted Hartree–Fock–Roothaan l.c.a.o.–m.o.–s.c.f. (10) calculations were performed on N_2H_4. Although the complex multidimensional potential surface may be simplified to some extent without serious loss of information by neglecting bond stretching modes and by restricting angle variation at each nitrogen to be dependent, a minimum of three independent parameters still remain. These are shown in Fig. 1 along with the bond lengths adopted. θ_1 and θ_2 describe the bond angles at N_1 and N_2, respectively, and ϕ describes the torsional angle. The study was conducted in two phases. In the first phase, using a minimal Slater-type orbital basis set as described elsewhere (11), the complete surface was computed over the range of variables $100° \leqslant \theta_1 \leqslant 120°$, $100° \leqslant \theta_2 \leqslant 120°$ and $0°$ (eclipsed geometry) $\leqslant \phi \leqslant 180°$ (staggered geometry). θ_1 and θ_2 were varied in 5° increments and ϕ was varied in 45° increments. The rotational curve with constant bond angles $\theta_1 = \theta_2 = 110°$ agreed well with that obtained in other non-empirical calculations (4, 5), $E_{anti} = 3.1$ kcal/mol and $E_{syn} = 9.6$. However, when θ_1 and θ_2 were varied to their equilibrium values, the *anti* barrier disappeared and the most stable geometry was predicted to be the *anti* conformation, **4**, $\phi = 180°$, $\theta_1 = \theta_2 = 103.9°$, contrary to experimental observations. Variation of the HNH and NNH angles independently gave results which differed negligibly from the average case where $\theta = \frac{1}{3}(2 \times \text{NNH} + \text{HNH})$. Similarly, independent relaxation of the NN and NH bond lengths at selected values of ϕ, θ_1, and θ_2 showed that the computed equilibrium bond

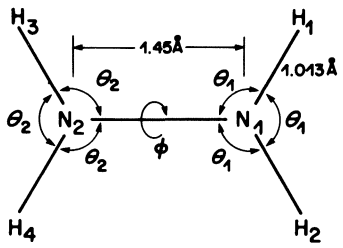

FIG. 1. Bond lengths and variables used to define the potential surface for hydrazine.

Can. J. Chem. Downloaded from www.nrcresearchpress.com by 210.87.254.42 on 09/05/12
For personal use only.

lengths were close to the experimental value (calcd. ($\phi = 90°$, $\theta_1 = \theta_2 = 105°$) NN = 1.461 Å, NH = 1.043 Å; exp ($\phi = 90°$, NNH = 112°, HNH = 106°) NN = 1.45 Å, NH = 1.02 Å) but made a negligible change in the shape of the potential surface. It was found that equilibrium bond lengths are nearly independent of the torsional angle ϕ: for $\phi = 180°$, NN = 1.465 Å, and NH = 1.042 Å ($\theta_1 = \theta_2 = 105°$).

In the second phase of the study a larger, more flexible basis set of Gaussian lobe functions (G.l.f.) (12) was used. Although the basis set has been described in detail elsewhere (6) the salient features are shown in Table 1. Polarization is incorporated into the s,p basis set by the use of bond functions (b.f.)[1] (6). There have been several reports that bond functions are capable of producing an energy lowering in CH_4 which is as substantial as that produced by the addition of 3d orbitals on the carbon atom (13, 14). Specifically, the present basis set has been shown to allow quantitative calculation of the bond angles of H_2O, NH_3, and H_2O_2 and of the inversion barrier in NH_3 (6).

Using this G.l.f. + b.f. basis set (Table 1), key regions of the potential surface for N_2H_4 (as indicated by the first phase of the study) were examined in detail. Important cross-sections of the surface are expressed in analytical form. Previous treatments of spectroscopic data for NH_3 (and other pyramidal species) have indicated that the form of the inversion barrier is represented quite well by a purely parabolic potential energy function, provided that the coordinate is taken to be the change in the HNH bond angle[2] (14) $\Delta\theta = \theta_{min} - \theta$. Thus for N_2H_4 we take the form

$$[1] \quad V(\theta_1, \theta_2) = \tfrac{1}{2}k[(\Delta\theta_1)^2 + (\Delta\theta_2)^2] + V_0$$

where V_0 and k are still functions of ϕ. We comment further on the specific form of [1] in the next section.

In order to express the potential energy $V(\phi)$ hindering internal rotation in analytical form, we have followed the work of Radom *et al.* (4) and assumed a three term Fourier series representation. Thus

$$[2] \quad V(\phi) = \tfrac{1}{2}V_1(1 - \cos\phi) + \tfrac{1}{2}V_2(1 - \cos 2\phi) + \tfrac{1}{2}V_3(1 - \cos 3\phi) + V(0)$$

where $V(0)$ is still a function of θ_1 and θ_2 as are V_1, V_2, and V_3.

[1]Bond functions are s-type Gaussian functions placed at the midpoint of the bonds in the molecule.

[2]The potential function referred to in ref. 14 incorporates some bond length variation which is assumed zero in the present work.

TABLE 1. Parameters for the Gaussian lobe function – bond function basis set*

Basis function	Exponent	Contraction coefficient
N–1s	615.6398	0.019462
	92.84316	0.133704
	20.70341	0.462798
	5.470375	0.508829
N–2s	0.8537230	0.379053
	0.3472534	0.531409
N–2s′	0.1398734	1.0
N–2p	6.085492	0.116425
	1.252070	0.490566
N–2p′	0.289677	1.0
H–1s	6.409584	1.0
	0.974304	5.721
H–1s′	0.217296	1.0
Bond function	0.30	1.0
	1.4	0.49

*Reference 6.

TABLE 2. Self consistent field energies for Gaussian lobe function – bond function basis set

θ_1 (deg)	θ_2 (deg)	ϕ (deg)	E (a.u.)*
100	100	180	−110.869574
105	105	0	−110.856165
105	105	90	−110.874492
105	105	135	−110.875289
105	105	180	−110.876161
105	120	180	−110.850747
110	110	0	−110.858766
110	110	90	−110.878388
110	110	135	−110.874552
110	110	180	−110.871051
110	120	90	−110.868768
115	115	0	−110.849004
115	115	135	−110.863695
120	120	180	−110.826809
120	120	90	−110.858800

*1 a.u. of energy = 627.52 kcal/mol.

Results and Discussion

The total s.c.f. energies calculated using the G.l.f. + b.f. basis set are shown in Table 2. By fitting eq. 1 to points of the same dihedral angle,

Can. J. Chem. Downloaded from www.nrcresearchpress.com by 210.87.254.42 on 09/05/12
For personal use only.

TABLE 3. Calculated Fourier parameters for internal rotation at various bond angles*

θ† (deg)	V_1 (kcal/mol)	V_2 (kcal/mol)	V_3 (kcal/mol)	E_{min} (a.u.)‡§	ϕ_{min} (deg)‡
100	−15.519	−3.803	−2.261	−110.8696	180.0
105	−10.677	−5.226	−1.871	−110.8762	180.0
106	−9.780	−5.728	−1.768	−110.8764	104.8
107	−8.907	−6.302	−1.658	−110.8774	100.5
108	−8.058	−6.949	−1.539	−110.8781	97.8
109	−7.232	−7.668	−1.413	−110.8785	95.9
110	−6.431	−8.459	−1.278	−110.8785	94.6
115	−2.780	−13.501	−.482	−110.8732	91.4
120	0.0	−20.075	0.0	−110.8588	90.0

*The parameters refer to eq. 2.
†$\theta_1 = \theta_2$.
‡Value corresponding to the minimum in the potential curve.
§1 a.u. of energy = 627.52 kcal/mol.

ϕ, and interpolating, we were able to generate a set of Fourier series at various values of the bond angle θ. The results are summarized in Table 3. Additional sets of inversion potential curves (eq. 1) were generated for values of ϕ between 90° and 180° by using the three Fourier series (Table 3) corresponding to bond angles of 105, 110, and 115°. The resulting values for the parameters of eq. 1 are given in Table 4.

Several cross-sections of a part of the potential surface for hydrazine are shown in Fig. 2. The equilibrium geometry corresponds to $\phi = 95°$ and θ_1 and $\theta_2 = 109.5°$. Within the restriction that the HNH and NNH angles are the same (see the previous section), the calculated value of bond angles, 109.5°, agrees well with the experimental value, NNH = 112°, HNH = 106° (15). The experimentally determined torsional angle is 90–95°.

TABLE 4. Calculated parabolic potential parameters for symmetric inversion at various dihedral angles*

ϕ (deg)	k (kcal mol^{-1}deg^{-2})	V_0 (a.u.)†	θ_{min} (deg)†
0	0.1545	−110.8593	108.6
90	0.1146	−110.8784	109.6
100	0.1136	−110.8784	109.4
110	0.1150	−110.8779	108.9
120	0.1186	−110.8772	108.2
130	0.1239	−110.8765	107.5
140	0.1302	−110.8760	106.8
150	0.1366	−110.8759	106.2
160	0.1419	−110.8760	105.7
170	0.1456	−110.8761	105.4
180	0.1468	−110.8762	105.3

*The parameters refer to eq. 1, with $\theta_1 = \theta_2$.
†Values corresponding to the minimum in the potential curve.

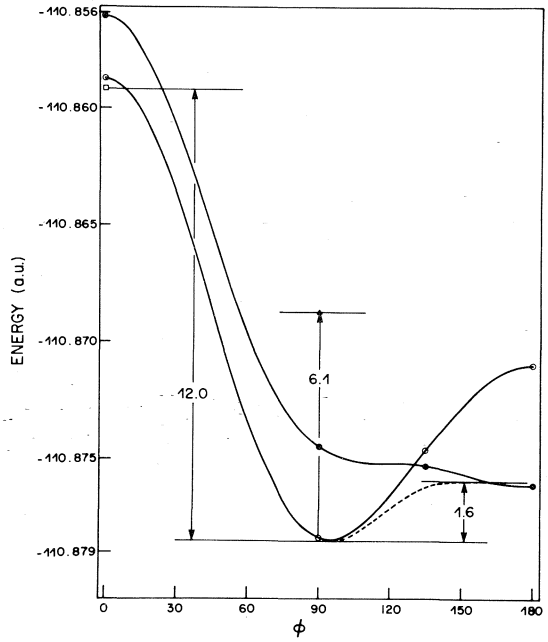

FIG. 2. Representative rotational potential curves $\phi = 0°$ corresponds to **3**; $\phi = 180°$ corresponds to **4**. The barrier heights are in kcal/mol. ●, $\theta_1 = \theta_2 = 110°$; ○, $\theta_1 = \theta_2 = 105°$; □, $\theta_1 = \theta_2 = 108.6°$; △, $\theta_1 = 110°$, $\theta_2 = 120°$. The broken line corresponds to the extrapolated minimum energy path connecting the curves shown with solid lines.

Inversion Barrier

The G.l.f. + b.f. basis set employed in this work allows one to calculate quantitatively the energy barrier to pyramidal inversion in ammonia: calcd. 6.0 kcal/mol (6); exp 5.8 kcal/mol (16). It is of considerable interest, therefore, that the minimum energy required to invert one nitrogen atom of hydrazine, 6.1 kcal/mol, is virtually

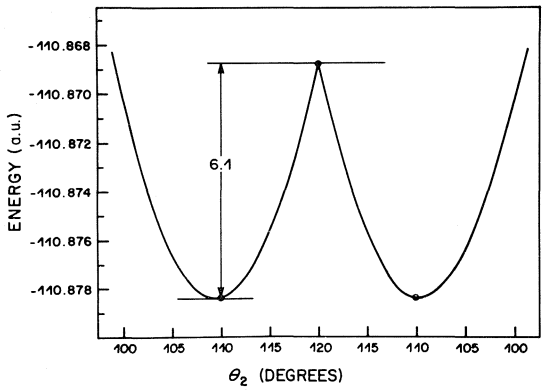

FIG. 3. A cross-section of the potential surface showing the approximate inversion coordinate. $\theta_1 = 110°$, $\phi = 90°$. The barrier height is in kcal/mol.

the same as in ammonia, and that this value is obtained when the torsional angle is 90°. The potential curve for inversion at one nitrogen with $\phi = 90°$ is shown in Fig. 3. It appears that when the lone pair – lone pair interaction is minimized ($\phi = 90°$), the presence of the other nitrogen has little effect on the inversion barrier. That the nitrogen atoms invert independently is dramatized by the observation that the energy required to make both nitrogen atoms planar at $\phi = 90°$ is 12.4 kcal/mol. In fact, the results of the Phase 1 study indicate that to a very good approximation, for any value of ϕ between 90 and 180°, the energy required to make both nitrogens planar is double that required to invert configuration at one nitrogen, hence eq. 1. If the torsional angle ϕ were such as to maximize[3] lone pair – lone pair interactions, $\phi = 180°$, the barrier to pyramidal inversion at one nitrogen is increased to 15.9 kcal/mol. The implications of this torsional dependence of the inversion barrier are discussed after the next subsection.

As mentioned in the introduction, a barrier of 7.5 kcal/mol has been estimated from i.r. spectroscopy (9) with the assumption that the inversion pathway has no ϕ dependence. The present calculations support this approximation in as much as we find that the equilibrium geometry corresponds to $\phi = 95°$, and as a result there is only a very small torsional component in the inversion coordinate (compare Figs. 2 and 3). However, the actual consequences of neglecting this component can only be determined by a detailed vibrational analysis.

[3]By forcing the occupancy of an ethylenic π^*-like molecular orbital.

Rotational Barriers

Observation by dynamic nuclear magnetic resonance (d.n.m.r.) spectroscopy of hindered exchange processes in substituted hydrazines (17, 18), hydroxylamines (19), sulfenamides (20), aminophosphines (21), and aminoarsines (21*a*) have led one to expect substantial barriers to rotation about nitrogen–heteroatom bonds. From our calculated surface (see Fig. 2 and Table 3), the rotational potential curve (eq. 2) is very sensitive to the values of the bond angles at nitrogen. In the equilibrium geometry the dihedral angle is 95° and the bond angles are 109.5°. The bond angles contract slightly to 108.6° in the most stable eclipsed geometry ($\phi = 0°$) and contract significantly to 105.3° in the most stable *anti* geometry ($\phi = 180°$). The *syn* barrier is calculated to be 12.0 kcal/mol, nearly twice the barrier to pyramidal inversion. For the *anti* barrier, a value of 1.6 has been obtained. The rotation coordinate over the *anti* barrier is shown as a broken line in Fig. 2. The values of the bond angles along this coordinate are given in Table 4. The *anti* barrier is very flat in the range $130° < \phi \leqslant 180°$. The interpolated pathway (the broken line in Fig. 2) actually has a very shallow minimum at $\phi = 180°$. Although it is beyond the resolution of the present method to determine whether the minimum at $\phi = 180°$ exists in hydrazine, its presence is consistent with the observation of an *anti* as well as a *gauche* conformer of N_2F_4 (22) and with calculations on the isoelectronic ethylene dicarbanion (23), $[C_2H_4]^{2-}$.

If the geometry at one of the nitrogen atoms is constrained to be planar (as might arise from π conjugation as in an amide or aniline), the *anti* barrier increases significantly. With $\theta_1 = 120°$ and $\theta_2 = 110°$ and assuming a 5° torsional relaxation in θ_2 the *syn* and *anti* barriers to rotation are identical, about 11 kcal/mol. Implications of the θ dependence of the rotational barriers are discussed in the next subsection.

Consequences to Substituted Hydrazines

To the extent that the computed potential surface for hydrazine can be extended to substituted hydrazines, a number of apparently inconsistent experimental results are explained. The inversion barriers found by d.n.m.r. for the alkyl substituted hydrazines **5** and **6** (R = H) are 6.8 kcal/mol (24) and ~8.5 kcal/mol (17), respectively. These values are significantly lower than those found in cyclic and bicyclic hydrazines (7)

Can. J. Chem. Downloaded from www.nrcresearchpress.com by 210.87.254.42 on 09/05/12
For personal use only.

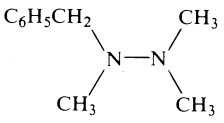

5

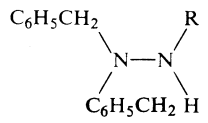

6

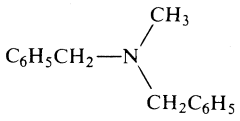

7

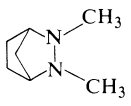

8

where values are typically in the range 11–14 kcal/mol. By extension from the potential surface, one would expect that alkyl substituted hydrazines should have barriers of approximately the same magnitude as alkylamines (an inversion barrier of 6.0 kcal/mol which is similar to that in ammonia was recently found (25) for **7**). Constraints imposed by the ring in cyclic hydrazines render it impossible to attain the optimum torsion angle of $\sim 90°$. For example, inversion in **8** takes place by the route shown in Fig. 4. The corresponding parameters of the surface and interpolated relative energies are given. As deduced from experiment (26), the process is expected to involve a synchronous inversion at the two nitrogens. Although steric and ring relaxation effects are not considered, the value of 14.5 kcal/mol calculated for the synchronous inversion process is in accord with the experimental barrier $\Delta G_c^{\ddagger} = 13$ kcal/mol.[4]

The highly hindered processes observed (17) in **6** (R = 2,4-dinitrophenyl), $\Delta G_c^{\ddagger} = 16.6$, **6** (R = picryl), $\Delta G_c^{\ddagger} = 16.2$, and **6** (R = 2-pyrimidyl), $\Delta G_c^{\ddagger} = 11.5$ must be attributed to hindered rotation.[4] The aryl substituted nitrogen is expected to be nearly planar. By extension from the hydrazine surface, planarity at one nitrogen does not significantly affect the barrier to pyramidal inversion at the other since the optimum dihedral angle, $\phi = 90°$ can be achieved, but does increase the rotational barriers to approximately 11 kcal/mol, neglecting steric effects.

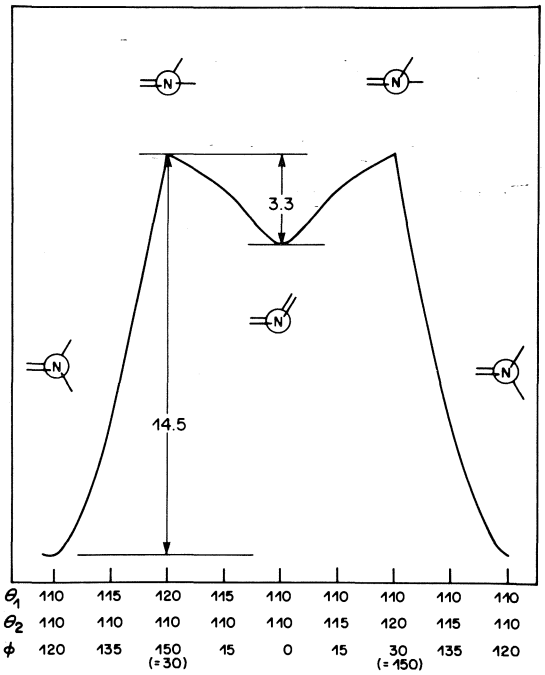

FIG. 4. The extrapolated inversion coordinate for a cyclic hydrazine such as **8**. The barriers are in kcal/mol. The path across the potential surface is traced by the values of θ_1, θ_2, and ϕ in degrees.

The authors wish to acknowledge the cooperation of the Department of Computer Services, University of Calgary. Receipt of a generous Computing Grant from the University of Calgary and continued financial support by the National Research Council of Canada are also gratefully acknowledged.

1. Y. MORINA, T. IIJIMA, and Y. MURATA. Bull. Chem. Soc. Jap. **33**, 46 (1960).
2. A. YAMAGUCHI, I. ICHISHIMA, T. SHIMANOUCHI, and S. MIZUSHIMA. J. Chem. Phys. **31**, 843 (1959).
3. T. KASUYA and T. KOJIMA. J. Phys. Soc. Jap. **18**, 364 (1963).
4. L. RADOM, W. J. HEHRE, and J. A. POPLE. J. Am. Chem. Soc. **94**, 2371 (1972).
5. (*a*) E. L. WAGNER. Theor. Chim. Acta. **23**, 115 (1971); (*b*) W. H. FINK, D. C. PAN, and L. C. ALLEN. J. Chem. Phys. **47**, 895 (1967); (*c*) A. VEILLARD, Theor. Chim. Acta, **5**, 413 (1966); (*d*) L. PEDERSEN and K. MOROKUMA. J. Chem. Phys. **46**, 3941 (1967).
6. J. JARVIE, A. RAUK, and C. K. EDMISTON. Can. J. Chem. This issue.
7. J. M. LEHN. Fortschr. Chem. Forsch. **15**, 311 (1970).
8. A. RAUK, J. D. ANDOSE, W. G. FRICK, R. TANG, and K. MISLOW. J. Am. Chem. Soc. **93**, 6507 (1971).
9. Y. HAMADA, A. Y. HIRAKAWA, K. TAMAGAKE, and M. TSUBOI. J. Mol. Spectrosc. **35**, 420 (1970).
10. C. C. J. ROOTHAAN. Rev. Mod. Phys. **23**, 69 (1951).
11. P. F. ALEWOOD, P. M. KAZMAIER, and A. RAUK. J. Am. Chem. Soc. **95**, 5466 (1973).

[4]For intramolecular processes that do not involve bond dissociation in the transition state, small $\Delta S^{\ddagger}$ are expected (7). Thus $\Delta G^{\ddagger} \simeq \Delta H^{\ddagger}$.

Can. J. Chem. Downloaded from www.nrcresearchpress.com by 210.87.254.42 on 09/05/12
For personal use only.

12. (*a*) H. PREUSS. Z. Naturforsch, **11**, 823 (1956); (*b*) J. L. WHITTEN. J. Chem. Phys. **39**, 349 (1963); (*c*) J. L. WHITTEN, J. Chem. Phys. **44**, 359 (1966); (*d*) J. D. PETKE, J. L. WHITTEN, and A. W. DOUGLAS. J. Chem. Phys. **51**, 256 (1969); (*e*) S. SHIH, R. BUENKER, S. PEYERIMHOFF, and B. WIRRAM. Theor. Chim. Acta, **18**, 277 (1970).
13. (*a*) S. ROTHENBERG and H. F. SCHAEFER III. J. Chem. Phys. **54**, 2764 (1971); (*b*) W. MEYER and P. PULAY. J. Chem. Phys. **56**, 2109 (1972).
14. (*a*) C. C. COSTAIN and G. B. B. M. SUTHERLAND. J. Phys. Chem. **56**, 321 (1952); (*b*) G. W. KOEPPL, D. S. SAGATYS, G. S. KRISHNAMURTHY, and S. I. MILLER. J. Am. Chem. Soc. **89**, 3396 (1967).
15. T. KASUYA and T. KOJIMA. Sci. Pap. Inst. Phys. Chem. Res. Tokyo, **56**, 1 (1962); Chem. Abstr. **58**, 6206b.
16. J. D. SWALEN and J. A. IBERS. J. Chem. Phys. **36**, 1914 (1962).
17. M. J. S. DEWAR and B. JENNINGS. J. Am. Chem. Soc. **91**, 3655 (1969).
18. (*a*) B. H. KORSCH and N. V. RIGGS. Tetrahedron Lett. 5897 (1966); (*b*) G. J. BISHOP, B. J. PRICE, and I. O. SUTHERLAND. Chem. Commun. 672 (1967); (*c*) A. FOUCAND and R. ROUDANT. C. R. Ser. C. **266**, 726 (1968); (*d*) J. R. FLETCHER and I. O. SUTHERLAND. Chem. Commun. 687 (1970).
19. (*a*) B. J. PRICE and I. O. SUTHERLAND. Chem. Commun. 1070 (1967); (*b*) D. L. GRIFFITH and J. D. ROBERTS. J. Am. Chem. Soc. **87**, 4089 (1965).
20. (*a*) H. J. JACOBSEN and A. SENNING. Chem. Commun. 617 (1967); (*b*) M. RABAN, F. B. JONES, Jr., and G. W. J. KENNEY, Jr. Tetrahedron Lett. 5055 (1968); (*c*) J. M. LEHN and J. WAGNER. Chem. Commun. 1298 (1968).
21. (*a*) A. H. COWLEY, M. J. S. DEWAR, and W. R. JACKSON. J. Am. Chem. Soc. **90**, 4185 (1968); (*b*) M. P. SIMONNIN, J. J. BASSELIER, and C. CHARRIER. Bull. Soc. Chim. Fr. 3544 (1967); (*c*) D. IMBERY and H. FRIEBOLIN. Z. Naturforsch, **23**b, 759 (1968).
22. (*a*) C. B. COLBURN, F. A. JOHNSON, and C. HANEY. J. Chem. Phys. **43**, 4526 (1965); (*b*) J. R. DURIG and J. W. CLARK. J. Chem. Phys. **48**, 3216 (1968); (*c*) M. J. CARDILLO and S. H. BAUER. Inorg. Chem. **8**, 2086 (1969).
23. S. WOLFE, L. M. TEL, J. H. LIANG, and I. G. CSIZMADIA. J. Am. Chem. Soc. **94**, 1361 (1972).
24. J. E. ANDERSON, D. L. GRIFFITH, and J. D. ROBERTS. J. Am. Chem. Soc. **91**, 6371 (1969).
25. C. H. BUSHWELLER and J. W. O'NEIL. J. Am. Chem. Soc. **92**, 2159 (1970).
26. J. E. ANDERSON and J. M. LEHN. J. Am. Chem. Soc. **89**, 81 (1967).

Can. J. Chem. Downloaded from www.nrcresearchpress.com by 210.87.254.42 on 09/05/12
For personal use only.

The Structure of Sideritol, a Diterpenoid of the *ent*-Atisane Class

WILLIAM A. AYER AND JO-ANN H. BALL

Department of Chemistry, University of Alberta, Edmonton, Alberta T6G 2E1

AND

BENJAMIN RODRÍGUEZ AND SERAFIN VALVERDE

Instituto de Química Orgánica, CSIC, Juan de la Cierva 3, Madrid 6, Spain

Received March 27, 1974

WILLIAM A. AYER, JO-ANN H. BALL, BENJAMIN RODRÍGUEZ, and SERAFIN VALVERDE. Can. J. Chem. **52**, 2792 (1974).

Sideritol, $C_{20}H_{32}O_3$, diterpenoid isolated from *Sideritis angustifolia* Lag., has been shown to be *ent*-13-atisen-1β,16α,17-triol (**1**). Sideritol is the first reported oxygenated diterpenoid of the *ent*-atisane class which does not contain nitrogen. The transformation of sideritol into *ent*-17-noratisane (**11**), previously prepared from atisine, rigorously defines the skeleton and absolute stereochemistry of sideritol.

WILLIAM A. AYER, JO-ANN H. BALL, BENJAMIN RODRÍGUEZ et SERAFIN VALVERDE. Can. J. Chem. **52**, 2792 (1974).

Le sidéritol, diterpène de formule brute $C_{20}H_{32}O_3$, isolé du *Sideritis angustifolia* Lag., est l'*ent*-antisen-13 triol-1β,16α,17 (**1**). Le sidéritol est le premier diterpène oxygéné ne contenant pas d'azote que l'on mentionne dans la classe de l'*ent*-atisane. On définit rigoureusement le squelette et la stéréochimie absolue du sidéritol par sa transformation en *ent*-nor-17 atisane (**11**) qui a déjà été préparé à partir de l'atisine. [Traduit par le journal]

Although numerous diterpene alkaloids of the atisane-type have been isolated from natural sources (1), only two nitrogen free diterpenoids of this skeleton, atisirene and isoatisirene, have been reported (2). We report herein the structure of the first oxygenated nitrogen-free diterpenoid of the *ent*-atisane type.

Plants of the genus *Sideritis* (family *Labiatae*) have proven to be a rich source of diterpenoids of the kaurene–isokaurene, labdane (3, and refs. therein), rimuene (4), and stachene (5) types. The isolation and separation of the diterpenoids of *Sideritis angustifolia* Lag. have been reported (5). Among the compounds isolated after acetylation of the crude diterpenoid fraction is the oily triacetate of a triol[1] $C_{20}H_{32}O_3$. Saponification of the triacetyl derivative with alcoholic potassium hydroxide yields a nicely crystalline monoacetyl derivative $C_{22}H_{34}O_4$ (monoacetylsideritol) which has been the starting point for our structural studies. In order to facilitate the discussion we will use the structure **1** derived for sideritol throughout.

Inspection of the i.r. and n.m.r. spectra (see Experimental) of sideritol monoacetate (**2**, prepared by saponification of the triacetate), triacetate (**3**), and diacetate (**4**, prepared by acetylation of **2** in the cold) reveals that the oxygen functions of sideritol are present as a primary, a secondary, and a tertiary alcohol and that it is the secondary hydroxyl function which is acetylated in the monoacetate **2**. The spectra also reveal the presence of a disubstituted olefinic linkage. Sideritol is thus a tetracyclic compound. The n.m.r. spectra also show the presence of three quaternary methyl groups.

The mass spectrum of the monoacetyl compound **2** (M^+ 362) was especially informative. A strong metastable ion peak at *m/e* 229 corresponds to the fragmentation of the molecular ion to the intense *m/e* 288 ion (362 − $C_3H_6O_2$, $C_{19}H_{28}O_2$).[2] A metastable peak at 180.5 corresponds to the loss of acetic acid from the *m/e* 288 ion to give the intense 228 ion ($C_{17}H_{24}$).[2] The facile loss of the fragment $C_3H_6O_2$ *in one step* shows that the primary hydroxyl and the tertiary hydroxyl are located on three contiguous carbons. This was confirmed by the finding that **2** readily forms an acetonide (**5**). Periodate cleavage of **2** gave the norketone **6**, absorbing

[1]We have no direct proof that the triol, for which we suggest the name sideritol, does not occur in a partially acetylated form in the plant. Triacetylsideritol is referred to as "the fourth component" in the previously described (5) isolation procedure.

[2]Formulas of fragment ions determined by high resolution mass spectrometry.

Can. J. Chem. Downloaded from www.nrcresearchpress.com by 210.87.254.40 on 09/05/12
For personal use only.

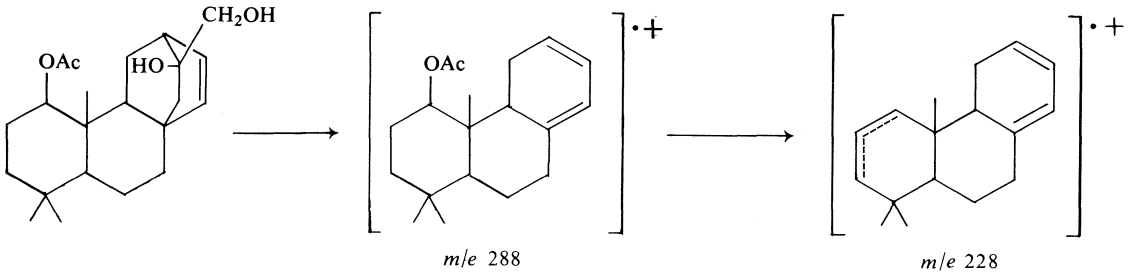

SCHEME 1

at 1720 cm^{-1} in the i.r., showing that **2** is a vicinal diol. The fragmentation may be rationalized in terms of a retro-Diels–Alder cleavage as shown in Scheme 1, and first suggested the presence of the bicyclo[2.2.2]octene system, and thus the atisene skeleton, in sideritol. In bicyclo-[2.2.2]octene systems $J_{olefinic}$ = 8.0–8.8 Hz (6) and $J_{1,2}$ = 6.6 Hz (7). The values found in the sideritol series for $J_{13,14}$ and $J_{12,13}$ agree (see Experimental) with this formulation.

The circular dichroism (c.d.) spectrum of ketone **6** shows a strongly positive Cotton effect at 294 nm ($\Delta\varepsilon$ +4.97) and a negative Cotton effect at 222 nm ($\Delta\varepsilon$ − 3.73), consistent (8) with the absolute stereochemistry of the bicyclo-[2.2.2]octenone system in **6**. However, the c.d. spectrum is also consistent with structure **7** and it was important to determine whether sideritol is an atisane derivative (ketone **7**) or an *ent*-atisane derivative (ketone **6**). It has been shown (9) that in atisene derivatives the presence of a C-13,C-14 double bond causes an abnormal shielding of the C-10 methyl so that it shows a chemical shift in the range δ 0.4–0.6. In none of the sideritol derivatives mentioned thus far is this the case. However, none of the model compounds has an oxygen substituent at C-1. In order to assess the effect of the C-1 substituent the acetonide **5** (highest field methyl at δ 0.79) was transformed to the alcohol **8** (highest field methyl at δ 0.62) by lithium aluminum hydride reduction (the C-1 ester function is extremely difficult to hydrolyze). Alcohol **8** was oxidized to ketone **9** (i.r. 1695 cm^{-1}, highest field methyl

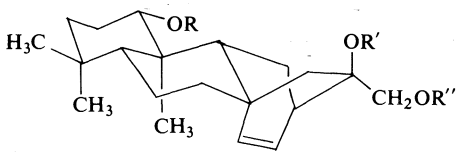

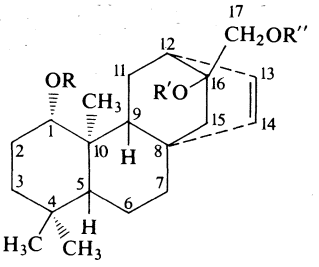

1 R = R′ = R″ = H
2 R = Ac; R′ = R″ = H
3 R = R′ = R″ = Ac
4 R = R″ = AcR′ = H
5 R = Ac; R′ + R″ = $C(CH_3)_2$
8 R = H; R′ = R″ = $C(CH_3)_2$

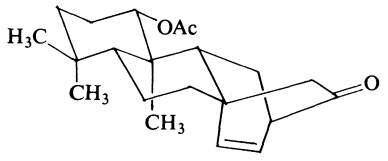

6

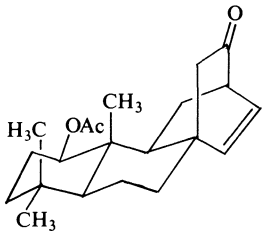

7

Can. J. Chem. Downloaded from www.nrcresearchpress.com by 210.87.254.40 on 09/05/12
For personal use only.

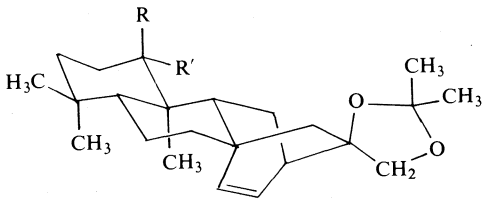

9 R, R′ = Carbonyl
10 R = R′ = H

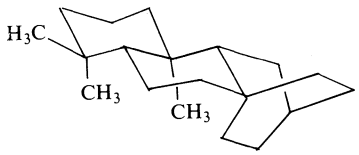

11

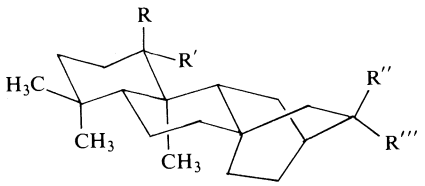

12 R = H; R′ = OAc, R″; R‴ = Carbonyl
13 R = H; R′ = OH; R″ = R‴ = H
14 R, R′ = Carbonyl; R″ = R‴ = H

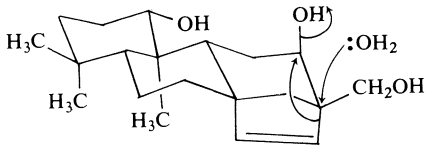

15

δ 0.97) and this was reduced (10) to **10**. The highest field methyl signal in **10** appears at δ 0.57, suggesting that the C-10 methyl *is* shielded by the C-13,C-14 double bond and that sideritol is an *ent*-atisane derivative. Since this argument is subject to some ambiguity the absolute stereochemistry was rigorously established by direct correlation of sideritol with a compound of known absolute stereochemistry.

Both *ent*-17-noratisane (**11**) and its enantiomer 17-noratisane are known compounds of established absolute stereochemistry (11). We have therefore converted sideritol into *ent*-17-noratisane (**11**) in the following manner: catalytic hydrogenation of ketone **6** gave **12** and the latter upon Wolff–Kishner reduction afforded alcohol **13**. As expected (12) ketone **12** shows a negative Cotton effect at 290 nm in its c.d. spectrum. Alcohol **13** was transformed to the ketone **14** by Sarett oxidation and this was reduced (10) to *ent*-17-noratisane (**11**), identical in all respects, including o.r.d. spectrum, with an authentic sample prepared from atisine (11).

There remains to justify the positioning of the secondary hydroxyl group at C-1 and the assignment of stereochemistry at C-16. The latter point will be dealt with first. Catalytic hydrogenation of the olefinic double bond in sideritol derivatives is accompanied by a significant downfield shift of the protons geminal to the primary hydroxy group (δ 3.23 in **2**, 3.75 in dihydro **2**), thus the hydroxymethylene group appears to be *syn* to the olefinic linkage (13).

The location of the secondary hydroxyl group at C-1 is based on the following arguments: the signal for the proton geminal to this oxygen function invariably appears as a doublet of doublets, J = 5 and 10 Hz, indicative of an axial proton flanked by one axial and one equatorial proton. This restricts the location of the hydroxyl to C-1, C-3, or C-7. The extreme resistance to saponification (the monoacetates **2***a*, **5***a*, and **6** are resistant to hydrolysis with hot alcoholic KOH) of an equatorial acetoxyl group is best rationalized if it is located at C-1 (*peri* interaction with C-11). The effect of the functionality on the chemical shift of the C-10 methyl group (*vide supra*) also supports its location at C-1. The c.d. spectra of ketones **9** and **14** both show weakly positive Cotton effects associated with the n → π* transition of the carbonyl group as expected for a C-1 ketone (14). If the carbonyl group were located at C-7 a strongly positive ($\Delta\varepsilon > +2.0$) Cotton effect would be expected in both cases (15).

In conclusion it should be noted that sideritol may be biogenetically related to jativatriol (**15**), a compound occurring in *S. angustifolia* (5). Rearrangement of jativatriol as indicated by the arrows in **15** would lead to sideritol (**1**). A laboratory analogy for the transformation of the *ent*-beyerene skeleton to the *ent*-atisene skeleton

Can. J. Chem. Downloaded from www.nrcresearchpress.com by 210.87.254.40 on 09/05/12
For personal use only.

Can. J. Chem. Downloaded from www.nrcresearchpress.com by 210.87.254.40 on 09/05/12
For personal use only.

has recently been reported (16). Attempts to correlate sideritol with jativatriol utilizing the reported method are in progress.

Experimental

Solutions were dried over anhydrous magnesium sulfate unless otherwise specified.

Melting points were determined on a Fischer-Johns hot-stage melting point apparatus and are uncorrected.

Infrared spectra were recorded on a Unicam SP1000 grating infrared spectrophotometer or a Perkin-Elmer Model 421 dual grating infrared spectrophotometer.

Nuclear magnetic resonance spectra were measured using a Varian Model HR-100 spectrometer with tetramethylsilane as internal standard and are quoted as δ (number of protons, description of signal assignment). Only significant signals are quoted.

Mass spectra including high resolution measurements (h.r.m.s.), were recorded on an A.E.I. Model MS-9 mass spectrometer and are reported as *m/e* (relative intensity). Unless diagnostically significant only peaks over *m/e* 40 and over 20% as intense as the base peak are recorded. Because of the small quantities of pure material available, most of the molecular formulas of transformation products have been determined by h.r.m.s.

Woelm silica gel (less than 0.08 mm) was used for column chromatography.

Isolation of Triacetylsideritol (3)

Triacetylsideritol was isolated as previously described (5). A crystalline sample was prepared by acetylation of purified monoacetylsideritol. The acetylation was accomplished by refluxing a solution of monoacetylsideritol (20 mg), isopropenyl acetate (11 mg), and *p*-toluenesulfonic acid (trace) in benzene (2 ml) for 1 h, then removing the acetone under reduced pressure. The benzene solution (after being washed with saturated $NaHCO_3$ and water, dried, and concentrated) gave triacetylsideritol (13 mg). After crystallization from acetone–ether it melted at 121–124 °C; i.r. (CCl_4) cm^{-1}: 3010 medium (olefinic CH), 2940, 2850 medium (C—H stretching vibrations), 1745 strong, 1730 shoulder, 1715 shoulder (C=O), 1250 strong (C—O of ester); n.m.r. ($CDCl_3$) δ: 5.96 (2H, multiplet, H-13 and H-14), 4.50 (1H, apparent doublet of doublets, H-1α), 4.27 (2H, quartet, —CH_2—OAc), 2.83 (1H, multiplet, $w_{1/2}$ 12 Hz, H-12), 1.97 (3H, singlet, —OCOCH_3), 1.94 (3H, singlet, —OCOCH_3), 1.92 (3H, singlet, —OCOCH_3), 0.82 (3H, singlet, quaternary methyl), 0.78 (3H, singlet, quaternary methyl), 0.72 (3H, singlet, quaternary methyl); mass spectrum *m/e*: 446 (M^+ 3), 386.2457 calcd. for $C_{24}H_{34}O_4$, 386.2461 measured (M^+ − CH_3COOH, 4), 265 (21), 228 (34), 200 (20), 173 (20), 172 (23), 157 (26), 142 (20), 131 (21), 124 (100), 123 (26), 122 (26), 121 (26), 119 (28), 118 (29), 117 (28), 109 (76), 107 (24), 105 (38), 104 (36), 95 (34), 93 (22), 91 (63), 81 (72), 79 (38).

Monoacetylsideritol (2)

Crude triacetylsideritol in ethanol was added to a cooled (0°) solution of KOH in ethanol (2.5%). The solution was allowed to stir at room temperature for 1½ h. It was then acidified (10% HCl) to p*H* 5 and extracted with $CHCl_3$. Column chromatography on silica gel (eluent ethyl acetate) affords monoacetylsideritol **2**, m.p. 181–182 °C (from acetone–pentane); i.r. (Nujol) cm^{-1}: 3400 medium, 3220 broad (OH), 1737 strong (C=O), 1240 (C—O of ester); n.m.r. ($CDCl_3$, 220 MHz) δ: 6.07 (1H, doublet of doublets, $J_{12,13}$ = 6.5 Hz, $J_{13,14}$ = 8 Hz, H-13), 5.82 (1H, doublet, $J_{13,14}$ = 8 Hz, H-14), 4.58 (1H, doublet of doublets, *J* = 6 and 10 Hz, H-1α), 3.23 (2H, quartet *J* = 12 Hz, —CH_2—OH), 2.50 (1H, multiplet $w_{1/2}$ 13 Hz, H-12), 2.00 (3H, singlet, —OCOCH_3), 0.91 (3H, singlet, quaternary methyl), 0.85 (3H, singlet, quaternary methyl), 0.81 (3H, singlet, quaternary methyl); mass spectrum *m/e*: 362 (M^+ 2), 344 (2), 302.2246 calcd. for $C_{20}H_{30}O_2$, 302.2244 measured (3), 288.2089 calcd. for $C_{19}H_{28}O_2$, 288.2097 measured (20), 228.1878 calcd. for $C_{17}H_{24}$, 288.1875 measured (58), 213 (23), 171 (45), 125 (26), 124 (100), 123 (20), 118 (25), 109 (57), 105 (21), 104 (37), 95 (27), 92 (22), 91 (53), 81 (47), 55 (20), 42 (40), 41 (22).

Anal. Calcd. for $C_{22}H_{34}O_4$: C, 72.89; H, 9.46. Found: C, 73.10; H, 9.60.

Monoacetylsideritol (**2**, 100 mg) in ethanol solution was hydrogenated over 10% Pd–C during 8 h; n.m.r. ($CDCl_3$) δ: 4.58 (1H, multiplet, —C*H*OAc), 3.70 (2H, quartet, *J* = 9 Hz, —CH_2—OH), 1.80 (3H, singlet, —OCOCH_3), 1.10 (3H, singlet, quaternary methyl), 0.80 (6H, singlet, 2 quaternary methyls).

Sideritol (1)

To monoacetylsideritol (**2**, 20 mg) in ether (15 ml) was added an excess of a 1 *M* ether solution of $LiAlH_4$. The solution was allowed to stir at room temperature overnight (under nitrogen). Excess $LiAlH_4$ was then destroyed by addition of water and ether extraction gave sideritol (12 mg), m.p. 174–176 °C (from acetone–pentane); i.r. ($CHCl_3$) cm^{-1}: 3590 weak, 3420 broad (—OH), 3015 strong (olefinic C—H), 2930, 2850 strong (C—H stretching vibrations); n.m.r. ($CDCl_3$) δ: 5.95 (2H, multiplet, H-13 and H-14), 3.56 (2H, quartet, *J* = 10 Hz, —CH_2—OH), 3.25 (1H, multiplet, H-1α), 2.52 (1H, multiplet, $w_{1/2}$ 6 Hz, H-12), 0.87 (3H, singlet, quaternary methyl), 0.82 (3H, singlet, quaternary methyl), 0.80 (3H, singlet, quaternary methyl); mass spectrum *m/e*: 302 (M^+ − H_2O, 4), 247 (22), 246 (100), 228 (29), 213 (29), 172 (28), 157 (20), 137 (23), 131 (22), 125 (21), 124 (100), 123 (44), 122 (31), 119 (22), 118 (71), 117 (20), 109 (100), 107 (33), 106 (21), 105 (37), 104 (56), 96 (43), 93 (25), 92 (35), 91 (77), 83 (20), 81 (57), 79 (25), 69 (33), 55 (33), 43 (24), 41 (38).

Diacetylsideritol (4)

A mixture of monoacetylsideritol (20 mg), pyridine (1 ml), and acetic anhydride (0.5 ml), was allowed to stand at 0 °C for 48 h. The reaction mixture was then taken up in benzene (~5 ml) and evaporated under reduced pressure. The residue was taken up in benzene (~2 ml) and washed with one drop of water. The benzene layer was removed and evaporated to afford a crude mixture of the triacetyl and diacetyl derivatives. Chromatography over silica gel (eluent, ethyl acetate) gave diacetylsideritol **4**, (11 mg); i.r. (Nujol) cm^{-1}: 3480 medium (OH), 1740, 1708 strong (C=O's), 1645 very weak (C=C); n.m.r. ($CDCl_3$) δ: 5.95 (2H, multiplet, H-13 and

H-14), 4.52 (1H, doublet of doublets, $J = 6$ and 8 Hz, H-1α) 3.76 (2H, quartet, CH_2—OAc), 2.42 (1H, multiplet, $w_{1/2}$ 7 Hz, H-12), 2.06 (3H, singlet, CH_2—$OCOCH_3$), 1.94 (3H, singlet, CH—$OCOCH_3$), 0.87 (3H, singlet, quaternary methyl), 0.81 (3H, singlet, quaternary methyl), 0.77 (3H, singlet, quaternary methyl); mass spectrum *m/e*: 344 (3), 288 (10), 228 (68), 172 (46), 157 (30), 131 (22), 124 (94), 118 (26), 117 (24), 109 (60), 105 (33), 95 (26), 91 (100), 81 (76), 79 (36), 77 (25), 74 (32).

*ent-1β-Acetoxyatis-13-en-16α,17-acetonide (**5**)*

To a solution of monoacetylsideritol (20 mg) in acetone (2 ml) was added 1 drop of $HClO_4$ (70%). The solution was then allowed to stir at room temperature for 1 h. One drop of pyridine was added and the acetone evaporated under reduced pressure. Water was added to the residue. Extraction with ether gave the acetonide derivative **5** (18 mg), m.p. 152–154 °C, (from acetone–pentane); i.r. ($CHCl_3$) cm^{-1}: 1725 strong (C=O), 1150 medium (C—O—C), 1260 strong (C—O of ester); n.m.r. ($CDCl_3$) δ: 5.98 (2H, multiplet, H-13 and H-14) 4.54 (1H, doublet of doublets, $J = 6$ and 8 Hz, H-1α), 3.57 (2H, quartet, —CH_2—O—), 2.45 (1H, multiplet, $w_{1/2}$ 12 Hz, H-12), 2.00 (3H, singlet, —$OCOCH_3$), 1.40 (3H, singlet —O—C—CH_3), 1.32 (3H, singlet, —O—C—CH_3), 0.90 (3H, singlet, quaternary methyl), 0.85 (3H, singlet, quaternary methyl), 0.79 (3H, singlet, quaternary methyl); mass spectrum *m/e*: 402 (M^+ 4), 288 (6), 228 (14), 124 (16), 91 (26), 79 (23), 43 (100), 41 (32).

The acetonide derivative (**5**, 100 mg) in ethanol solution was hydrogenated over 10% Pd–C during 8 h; n.m.r. ($CDCl_3$) δ: 4.55 (1H, multiplet, —CH—OAc), 3.70 (2H, quartet, $J = 7$ Hz, —CH_2—O), 2.00 (3H, singlet, —$OCOCH_3$), 1.10 (3H, singlet, quaternary methyl), 0.80 (6H, singlet, 2 quaternary methyls).

Mol. wt. Calcd. for $C_{25}H_{38}O_4$: 402.2770. Found (h.r.m.s.): 402.2773.

*ent-1β-Acetoxy-17-noratis-13-en-16-one (**6**)*

Periodic acid (380 mg) in water (4 ml) was added to a solution of monoacetylsideritol (**2**, 170 mg) in methanol (15 ml). The solution was stirred at room temperature for 24 h, diluted with water, and methanol removed under reduced pressure. Extraction with ether and chromatography over silica gel (eluent ethyl acetate) gave the crystalline ketone **6** (88 mg), m.p. 126–127.5 °C (from acetone–pentane); i.r. (Nujol) cm^{-1}: 1735 shoulder, 1720 strong (C=O), 1240 strong (C—O of ester); n.m.r. ($CDCl_3$) δ: 6.12 (2H, apparent doublet, separation 3.5 Hz, H-13 and H-14), 4.60 (1H, doublet of doublets $J = 6$ and 9 Hz, H-1α), 3.02 (1H, multiplet $w_{1/2}$ 8 Hz, H-12), 1.98 (3H, singlet, —$OCOCH_3$), 0.91 (3H, singlet, quaternary methyl), 0.88 (3H, singlet, quaternary methyl), 0.86 (3H, singlet, quaternary methyl); mass spectrum *m/e*: 330 (M^+ 3), 288 (7), 228 (13), 124 (70), 109 (30), 91 (53), 81 (35), 55 (15), 43 (100), 41 (34); circular dichroism (*c* 0.0034 *M*, methanol): $\Delta\varepsilon_{294}$ +4.97, $\Delta\varepsilon_{225}$ −3.73.

Mol. wt. Calcd. for $C_{21}H_{30}O_3$: 330.2195. Found (h.r.m.s.): 330.2200.

*ent-1β-Hydroxyatis-13-en-16α,17-acetonide (**8**)*

The acetonide (**5**, 15 mg) was taken up in ether and treated with $LiAlH_4$ (20 drops of a 1 *M* ether solution) under nitrogen for ½ h. Work-up in the usual manner gave the crystalline alcohol **8** (10 mg), m.p. 129–132 °C (from acetone); i.r. (Nujol) cm^{-1}: 3515 weak, 3400 broad (OH), 1150 medium (C—O—C); n.m.r. ($CDCl_3$) δ: 5.94 (2H, multiplet, H-13 and H-14), 4.00 (2H, quartet, $J = 12$ Hz, —CH_2—O—), 4.23 (1H, multiplet, H-1α), 2.46 (1H, multiplet, H-12), 2.36 (3H, singlet —O—C—CH_3), 2.28 (3H, singlet, O—C—CH_3), 0.62 (3H, singlet, quaternary methyl), 0.74 (3H, singlet, quaternary methyl), 0.81 (3H, singlet, quaternary methyl); mass spectrum *m/e*: 360 (M^+ 4), 246 (42), 228 (8), 124 (100), 118 (36), 109 (65), 105 (20), 104 (30), 95 (20), 92 (20), 91 (64), 81 (42), 79 (20), 69 (32), 57 (30), 55 (50), 43 (74), 41 (65).

Mol. wt. Calcd. for $C_{23}H_{36}O_3$: 360.2665. Found (h.r.m.s.): 360.2677.

*ent-1-Oxoatis-13-en-16α,17-acetonide (**9**)*

To pyridine (18 mg) in methylene chloride was added CrO_3 (30 mg). The resulting dark solution was stirred for 15 min, then alcohol **8** (10 mg) in methylene chloride was added. After 15 min the solution was filtered and evaporated. The residue was distributed between water and ether, and the ether extracts dried and evaporated to give the ketone **9** (7 mg), i.r. (Nujol) cm^{-1}: 1696 strong (C=O), 1145 medium (C—O—C); n.m.r. ($CDCl_3$) δ: 6.00 (2H, multiplet, H_{13} and H_{14}), 3.57 (2H, quartet, $J = 9$ Hz, —CH_2—O), 2.50 (1H, multiplet, H-12), 1.42 (3H, singlet, —O—C—CH_3), 1.35 (3H, singlet, —O—C—CH_3), 1.04 (3H, singlet, quaternary methyl), 0.98 (6H, singlet, quaternary methyls); mass spectrum *m/e*: 358 (M^+ 4), 244 (27), 188 (33), 139 (100), 91 (33), 43 (34), 41 (22); circular dichroism (*c* 0.0028 *M*, methanol) $\Delta\varepsilon_{280}$ −0.09, $\Delta\varepsilon_{310}$ +0.07, $\Delta\varepsilon_{320}$ +0.06.

Mol wt. Calcd. for $C_{23}H_{34}O_3$: 358.2508. Found (h.r.m.s.): 358.2522.

*ent-Atis-13-en-16α,17-acetonide (**10**)*

Anhydrous hydrazine was distilled into a solution of sodium (0.2 g) in diglyme (15 ml) until the solution refluxed freely at 180 °C. The ketone **9** (7 mg) was then added and refluxing continued for 18 h. The temperature was then raised to 210 °C by distilling hydrazine out of the reaction vessel. Refluxing was continued at this temperature for 18 h. The reaction mixture was then cooled and diluted with water. Continuous extraction with pentane (24 h) gave the crystalline compound **10** (3 mg), m.p. 134–136 °C (from acetone); i.r. (CCl_4) cm^{-1}: 2920, 2850 strong (C—H stretching), 1655 very weak ( ), 1385, 1375, 1365 sharp (methyls), 1150 medium (C—O—C); n.m.r. ($CDCl_3$) δ: 0.87 (3H, singlet, quaternary methyl), 0.78 (3H, singlet, quaternary methyl), 0.57 (3H, singlet, quaternary methyl); mass spectrum *m/e*: 344 (M^+ 6), 230 (100), 137 (82), 106 (88), 105 (20), 104 (24), 95 (22), 94 (22), 92 (50), 91 (58), 81 (26), 69 (40), 67 (20), 57 (21), 55 (40), 43 (36), 41 (44).

Mol. wt. Calcd. for $C_{23}H_{36}O_2$: 344.2715. Found (h.r.m.s.): 344.2721.

*ent-1β-Acetoxy-17-noratisan-16-one (**12**)*

Ketone **6** (116 mg) in methanol was hydrogenated, at atmospheric pressure, over 5% Pd–C for ~3 h. The reaction mixture was then filtered and concentrated to give the crystalline ketone **12** (115 mg), m.p. 166–169 °C (from acetone); i.r. (Nujol) cm^{-1}: 1720 strong, 1698 shoulder (C=O), 1240 (C—O of ester); n.m.r. ($CDCl_3$)

Can. J. Chem. Downloaded from www.nrcresearchpress.com by 210.87.254.40 on 09/05/12
For personal use only.

δ: 4.50 (1H, doublet of doublets $J = 6$ and 8 Hz H-1α), 1.92 (3H, singlet, —O—CO—CH_3), 1.14 (3H, singlet, quaternary methyl), 0.82 (6H, singlet, quaternary methyls); mass spectrum *m/e*: 332 (M^+ 6), 272 (25), 230 (50), 106 (30), 93 (20), 81 (25), 79 (20), 55 (30), 53 (31), 43 (100), 41 (40); circular dichroism (*c* 0.0045 *M*, methanol), $\Delta\varepsilon_{290}$ −0.073.

Mol. wt. Calcd. for $C_{21}H_{32}O_3$: 332.2352. Found (h.r.m.s.): 332.2336.

*ent-17-Noratisan-1β-ol (**13**)*

The ketone **12** (115 mg) was reduced as described for the reduction of **9**. Pentane extraction gave the crystalline alcohol **13** (74 mg) purified by sublimation at 88 °C/0.5 mm Hg, m.p. 155.5–156.5 °C; i.r. (Nujol) cm^{-1}: 3370 medium, broad (OH); n.m.r. ($CDCl_3$) δ: 3.32 (1H, doublet of doublets, $J = 6$ and 7 Hz, H-1α), 1.01 (3H, singlet, quaternary methyl), 0.81 (3H, singlet, quaternary methyl), 0.80 (3H, singlet, quaternary methyl); mass spectrum *m/e*: 276 (M^+ 11), 258 (60), 243 (28), 134 (40), 123 (27), 121 (26), 109 (26), 107 (22), 95 (38), 93 (40), 91 (32), 83 (32), 81 (68), 79 (40), 69 (56), 66 (46), 57 (90), 55 (86), 44 (94), 43 (100), 41 (90).

Mol. wt. Calcd. for $C_{19}H_{32}O$: 276.2453. Found (h.r.m.s.): 276.2459.

*ent-17-Noratisan-1-one (**14**)*

The alcohol **13** (65 mg) was oxidized as described above for alcohol **8**, to give the crystalline ketone **14** (40 mg), m.p. 79–81 °C (from methanol – Skelly B); i.r. (CCl_4) cm^{-1}: 1708 strong (C=O); n.m.r. ($CDCl_3$) δ: 2.73 (1H, 8 lines, $J_{2\alpha,2\beta} = 14$ Hz, $J_{2\beta,3\alpha} = 11.5$ Hz, $J_{2\beta,3\beta} = 6$ Hz, H-2β), 1.32 (3H, singlet, quaternary methyl), 1.05 (3H, singlet, quaternary methyl), 0.93 (3H, singlet, quaternary methyl); mass spectrum *m/e*: 274 (M^+ 40), 259 (40), 256 (57), 175 (26), 139 (46), 105 (20), 95 (20), 93 (30), 91 (42), 81 (46), 79 (48), 77 (20), 69 (26), 67 (48), 56 (61), 53 (22), 41 (100); circular dichroism (*c* 0.009 *M*, *iso*-octane) $\Delta\varepsilon_{301}$ +0.11, $\Delta\varepsilon_{311}$ +0.22, $\Delta\varepsilon_{324}$ +0.15; (*c* 0.007 *M*, methanol) $\Delta\varepsilon_{300}$ +0.32.

Mol. wt. Calcd. for $C_{19}H_{30}O$: 274.2297. Found (h.r.m.s.) 274.2293.

*ent-17-Noratisane (**11**)*

The ketone **14** (30 mg) was reduced as described above for **9**. Continuous pentane extraction (2 days) followed by column chromatography of the residue over alumina (eluent pentane) and sublimation (atmospheric pressure, 150 °C) gave the crystalline hydrocarbon **11** (13 mg) m.p. 83–85 °C, identical in i.r., n.m.r., o.r.d., and mass spectra with an authentic sample (11); i.r. (CCl_4) cm^{-1}: 2920, 2855 strong (C—H stretching vibration), 1450 medium (methylene scissoring and asymmetrical methyl bending vibrations), 1380 sharp (—CH_3), 1360 sharp, 1355 shoulder (*gem* dimethyl group); n.m.r. ($CDCl_3$) δ: 1.05 (3H, singlet, quaternary methyl), 0.90 (3H, singlet, quaternary methyl), 0.80 (3H, singlet, quaternary methyl); mass spectrum *m/e*: 261 (M^+ +1, 23), 260 (M^+ 100), 245 (73), 175 (36), 137 (27), 136 (30), 135 (21), 125 (21), 124 (47), 123 (100), 111 (21), 109 (45), 107 (23), 105 (27), 95 (48), 93 (36), 91 (33), 82 (33), 81 (54), 79 (45), 77 (23), 75 (57), 69 (51), 67 (48), 55 (51), 45 (100), 43 (24), 41 (66); optical rotatory dispersion (*c* 0.03, methanol) 25°: $[\alpha]_{240}$ − 370°, $[\alpha]_{260}$ − 270°, $[\alpha]_{280}$ − 200°, $[\alpha]_{300}$ − 130°, $[\alpha]_{350}$ − 100°, $[\alpha]_{400}$ − 80°.

Mol. wt. Calcd. for $C_{19}H_{32}$: 260.2504. Found (h.r.m.s.): 260.2514.

The financial support of the National Research Council of Canada is gratefully acknowledged. We also thank the Canadian 220 MHz NMR Centre, Sheridan Park, Ontario for the 220 MHz spectrum of monoacetylsideritol, Dr. T. Nakashima and his associates for the remaining n.m.r. spectra, Dr. A. Hogg and associates for the mass spectra, and Dr. J. Hudec for a discussion of the c.d. spectra.

1. S. W. Pelletier and L. H. Keith. *In* The chemistry of alkaloids. *Edited by* S. W. Pelletier. van Nostrand-Reinhold. New York. 1970. pp. 503–547.
2. A. H. Kapadi, R. R. Sobti, and Sukh Dev. Tetrahedron Lett. 2729 (1965).
3. B. Rodriguez and S. Valverde. Tetrahedron, **29**, 2837 (1973).
4. F. Martin Panizo, B. Rodriguez, and S. Valverde. Anal. Quim. **70** (2), 164 (1974).
5. C. von Carsten-Lichtenfelde, S. Valverde, and B. Rodriguez. Aust. J. Chem. **27** (3), 517 (1974).
6. K. Tori, Y. Takano, and H. Kitahonoki. Chem. Ber. **97**, 2798 (1964).
7. E. W. Garbisch, Jr. J. Am. Chem. Soc. **86**, 5561 (1964).
8. A. Moscowitz, K. Mislow, M. A. W. Glass, and C. Djerassi. J. Am. Chem. Soc. **84**, 1945 (1962).
9. W. A. Ayer, C. E. McDonald, and J. B. Stothers. Can. J. Chem. **41**, 1113 (1963).
10. D. H. R. Barton, D. A. J. Ives, and B. R. Thomas. J. Chem. Soc. 2056 (1955).
11. W. A. Ayer, C. E. MacDonald, and G. G. Iverach. Tetrahedron Lett. 1095 (1963).
12. P. Crabbé, L. H. Zalkow, and N. N. Girotra J. Org. Chem. **30**, 1678 (1965).
13. R. R. Fraser, Can. J. Chem. **40**, 78 (1962).
14. C. Djerassi, H. Wolf, and E. Bunnenberg. J. Am. Chem. Soc. **84**, 4552 (1962).
15. J. B. Nabors, D. H. Miles, B. Kumor, and L. H. Zalkow. Tetrahedron, **27**, 2385 (1971).
16. K. H. Pegel, L. P. L. Piacenza, L. Phillips, and E. S. Waight. J. Chem. Soc. Chem. Commun. 522 (1973).

Can. J. Chem. Downloaded from www.nrcresearchpress.com by 210.87.254.40 on 09/05/12
For personal use only.

The Synthesis of 1,2-Diazepines from Thiapyrylium Salts[1]

DAVID JOHN HARRIS, GORDON Y.-P. KAN[2], AND VICTOR SNIECKUS[3]
Department of Chemistry, University of Waterloo, Waterloo, Ontario N2L 3G1
AND
E. KLINGSBERG
American Cyanamid Company, Bound Brook, New Jersey
Received January 11, 1974

DAVID JOHN HARRIS, GORDON Y.-P. KAN, VICTOR SNIECKUS, and E. KLINGSBERG. Can. J. Chem. **52**, 2798 (1974).

The reactions of thiapyrylium salts **3***a–c* with hydrazine and methylhydrazine yield the 3,5,7-triphenyl-1,2(4*H*)-diazepines **4***a–c* and 1-methyl-3,5,7-triphenyl-1,2(1*H*)-diazepines **5***a–c* in good to excellent yields. Although numerous 1-acyl-1,2(1*H*)-diazepines are now known, compounds **5***a–c* represent the first examples of 1-alkyl-1,2(1*H*)-diazepine derivatives. With a slight variation in work up conditions, the reaction of thiapyrylium salts **3***a* and **3***c* with methylhydrazine leads to the formation of the pyrazoline derivatives **6***a* and **6***c*, respectively; on the other hand, only pyrazolines **9***a* and **9***b* can be obtained from the corresponding reaction with phenylhydrazine. Pyrolysis of the pyrazolines **6***a*, **6***c*, **9***a*, and **9***b* provides the pyrazoles **7***a*, **7***c*, **10***a*, and **10***b*, respectively. The mechanism of some of these transformations is briefly discussed.

DAVID JOHN HARRIS, GORDON Y.-P. KAN, VICTOR SNIECKUS, et E. KLINGSBERG. Can. J. Chem. **52**, 2798 (1974).

Les sels de thiapyrylium **3***a–c* réagissent avec l'hydrazine et la méthylhydrazine et donnent les triphényl-3,5,7 (4*H*) diazépines-1,2 **4***a–c* et les méthyl-1 triphényl-3,5,7 (1*H*) diazépines-1,2 **5***a–c*; les rendements de ces réactions sont bons à excellents. Bien que plusieurs (1*H*) acyl-1 diazépines-1,2 sont maintenant connues, les composés **5***a–c* représentent les premiers exemples de dérivés de type alkyl-1 (1*H*) diazépine-1,2. Avec une légère variation dans les conditions de réaction, les sels de thiapyrylium **3***a* et **3***c* réagissent avec la méthylhydrazine et donnent les dérivés de la pyrazoline **6***a* et **6***c* respectivement; par ailleurs, la réaction correspondante avec la phénylhydrazine conduit seulement aux pyrazolines **9***a* et **9***b*. La pyrolyse des pyrazolines **6***a*, **6***c*, **9***a* et **9***b* donnent respectivement les pyrazoles **7***a*, **7***c*, **10***a* et **10***b*. Le mécanisme de quelques-unes de ces transformations est brièvement discuté.

[Traduit par le journal]

The reaction of pyrylium salts with nitrogen-containing nucleophiles to yield a variety of pyridine derivatives (3) provides one of the earliest examples of interconversion of aromatic heterocyclic systems in which a one for one interchange of heteroatoms occurs:[4] **1** → **2**, X—Y = $\overset{+}{N}$—Alkyl, $\overset{+}{N}$—CH_2Ar, $\overset{+}{N}$—CH_2CO_2H (4), $\overset{+}{N}$—NHAr, $\overset{+}{N}$—NHCOR: R = NH_2, R = Ph (5), N → O (6). Analogous reactions have been shown to be useful for the conversion of pyrylium salts into sulfur and phosphorus heterocycles (**2**, XY = $\overset{+}{S}$, P) as well as benzene derivatives (**2**, X—Y = C—CO_2R, C—COMe, C—CN, C—NO_2) (3). New transformations of pyrylium salts include the following: reaction with 2-phenyl-Δ^2-oxazolin-5-one to form benzanilides (15); rearangement to 2-amino-3-aroylpyridines with cyanamide (16); ring contraction to isoxazolines with hydroxyl-

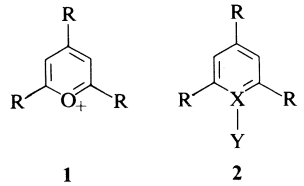

1 **2**

[1]Portions of this work have been presented at conferences (1, 2).

[2]Abstracted in part from the Ph.D. Thesis of G.Y.-P.K. submitted to the University Graduate Council, University of Waterloo, 1971.

[3]To whom correspondence may be addressed.

[4]In recent years the utility of this type of reaction with other π-isoelectronic heteroaromatic systems has been exemplified as follows: 1,2-dithiolium salts → isothiazoles (7); 1,3,5-oxadiazinium salts → aminopyrimidines (8); 1,3,4-oxadiazolium salts → *s*-triazolium salts (9); oxazolium salts → 3-imidazolines and 3-imidazolinium salts (10); 1,2,4-dithiazolium salts → 1,2,4-thiadiazoles (11,12); *N*-(4-Arylmethylene-Δ^2-oxazolin-5-ylidene) ammonium salts → 1,3-diazafulvenes (13); 1,3-oxazinium salts → pyrimidines (14).

Can. J. Chem. Downloaded from www.nrcresearchpress.com by 210.87.254.5 on 09/05/12
For personal use only.

Can. J. Chem. Downloaded from www.nrcresearchpress.com by 210.87.254.5 on 09/05/12
For personal use only.

amine hydrochloride (6, 17), to pyrazolines or pyrazoles (10, 17*b*, 18), and to pyrazolo[2,3-*a*]-quinolines (19); and ring expansion to 1,2-diazepines with hydrazines in a two for one heteroatom exchange reaction (17*a*, 18, 20*a*, 21).[5] Although the mechanism of these transformations are presumably related, evidence is available only in isolated cases (6, 17*b*).

Thiapyrylium salts would be expected to resemble pyrylium salts in their chemistry although it should be noted, perhaps surprisingly, that thiapyrylium salts have by no means received a proportionate amount of attention (3*b*, 28). Herein we report on the reaction of thiapyrylium salts (**3***a–c*) with hydrazine derivatives. When originally announced (1), some of these reactions represented the first preparations of highly unsaturated 1,2-diazepines (**4**, **5**). In the meantime, direct routes to 1,2(4*H*)-diazepines (**4**) (20*a*) and the 1-methyl-1,2(1*H*)-diazepine (**5***a*)[6] (18) from pyrylium salts have been discovered. The structural assignments (1) of **4***a* were partly based on n.m.r. characteristics which have since been extensively discussed by other investigators (20)[7] and therefore are not recapitulated here. The accompanying paper describes the protonation and acid-catalyzed rearrangement studies of these 1,2-diazepine derivatives (30).

Treatment of the triarylthiapyrylium salts **3***a–c* with an excess of hydrazine in ethanol solution gave the 1,2(4*H*)-diazepine derivatives **4***a–c* in 86–90% yield (Scheme 1). Structure assignments were based on n.m.r. spectra as indicated above and on catalytic hydrogenation of **4***a* to the known dihydrodiazepine **8** prepared from hydrazine and 1,3,5-triphenyl-1,5-pentanedione. Pyrylium salts give comparable yields of 1,2(4*H*)-diazepines (20*a*), eliminating a synthetic step, since thiapyrylium salts are prepared from pyrylium salts. Compared to these convenient reactions, thiapyrylium salts provide the 1-methyl-1,2(1*H*)-diazepines only under different and stringently controlled reaction and workup conditions. Addition of the thiapyrylium salt to an excess of neat methylhydrazine at −70° under nitrogen followed by further reaction at 0° gave the crude crystalline 1,2(1*H*)-diazepines (**5***a–c*) in 55–75% yield.[8] Analytical and spectral data (Table 1) are in full support of the proposed structures, in particular the n.m.r. spectrum of **5***a* shows the weakly coupled (J = 1.5 Hz) vinyl hydrogens, C_4- and C_6-H at 2.95 and 4.15 τ, respectively. These chemical shifts and coupling constants may be compared to similar values obtained for the elusive 2,4,6-triphenyl-1,3-oxazepine obtained but not isolated from the photolysis of 2,4,6-triphenylpyridine *N*-oxide (32). The u.v. spectra of the 1,2(1*H*)-diazepines show marked differences from those of the 1,2(4*H*)-diazepine series (20*a*), a fact which was used in support of the original structural assignments (1). Compound **5***a* was also synthesized from the 1,2(4*H*)-diazepine **4***a* and methyl iodide. The invariable production of some 2,4,6-triphenylpyridine in this reaction (see Experimental) speaks for the lability of **5***a* to thermal (18, 33) and acidic (30) conditions.

If, in the reaction of thiapyrylium salts with methylhydrazine, great care is not taken to remove excess methylhydrazine immediately after the reaction (see Experimental), the observed products are pyrazoline derivatives rather than the 1,2(1*H*)-diazepines. For example, pyrazolines **6***a* and **6***c* were obtained under these conditions. Usually the fate of the reaction could be predicted on the basis of whether oily or crystalline material was obtained directly from the reaction mixture. The oily materials obtained were mixtures of diazepine and methylhydrazine and could be shown to produce the pyrazolines upon standing and/or recrystallization (n.m.r. analysis).

The structures of the pyrazolines **6***a*, **6***c* and **9***a*, **9***b* rest on spectral and chemical data. The mass spectrum of compound **6***a* even at low

[5]Related rearrangements and ring contractions have been observed with other heterocycles (nucleophiles): 1,2-dithiolium salts (H_2NNH_2, H_2NNHR, RSH) (7, 22, 26); 1,2,4-dithiazolium salts (KNCO) (12); 1,3,4-oxadiazolium salts (H_2NCN) (9*a*); pyrimidines and pyrimidinium salts (H_2NNH_2, H_2NNHR) (23); oxazolium salts (H_2NNHPh) (24); *N*-phenacylpyridinium ylides ($PhNHN{=}C(Cl)CO_2Et$) (25); 1,3-oxazinium salts (H_2NNH_2, H_2NOH) (14); isothiazolium salts (RNH_2, H_2NNHR, NH_2OH, $H_2N(CH_2)_2SH$, RSH, H_2S) (26); thiazolium salts (RNH_2) (27).

[6]Simple 1,2(1*H*)-diazepines are available by photolysis of *N*-iminopyridinium ylides (29).

[7]This allows unique structural assignment ruling out theoretically possible valence isomers and tautomers. A more highly substituted derivative, 3,7-bis(*p*-iodophenyl)-4,5,6-triphenyl-1,2(4*H*)-diazepine was elucidated by X-ray analysis only after several misassignments based on n.m.r. and u.v. techniques (31).

[8]These reaction conditions have not yet been consistently successful for the preparation of **5***a–c* directly from pyrylium salts; G.Y.-P. Kan and D. J. Harris. In progress.

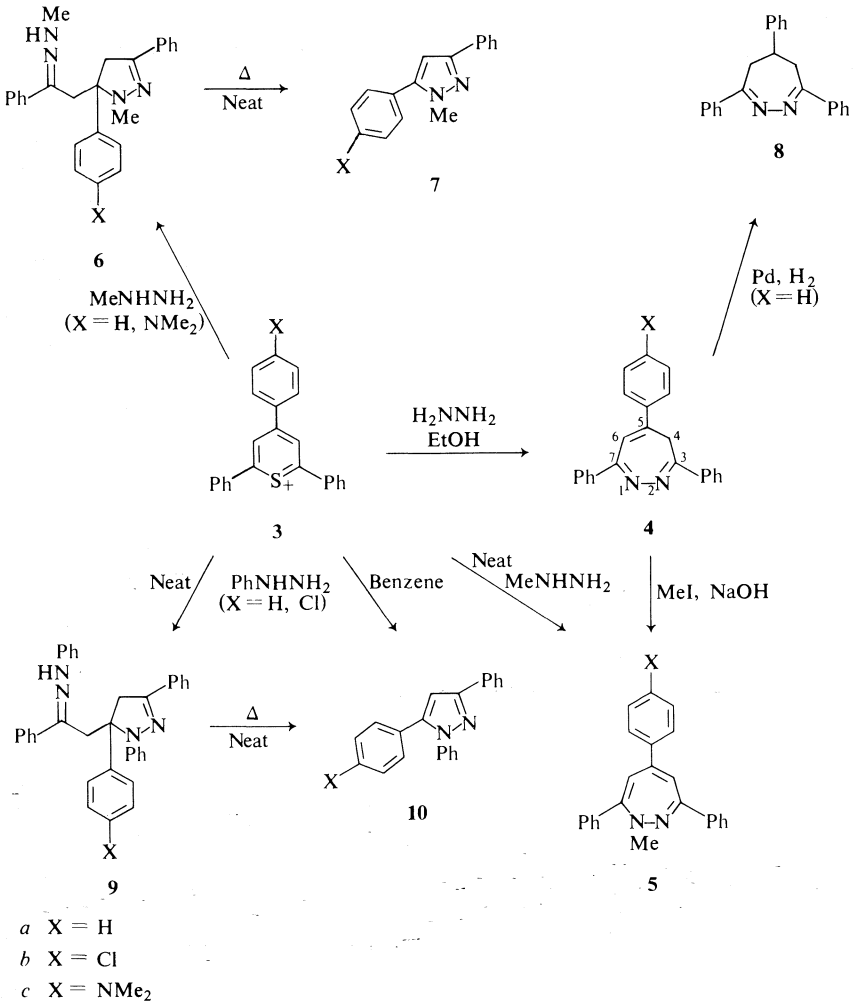

SCHEME 1

voltages did not show a parent peak due to facile loss of acetophenone methylhydrazone to yield the pyrazole **7***a*. The n.m.r. spectrum of **6***a* showed an aliphatic proton pattern (τ 6.6, s, 2H, —CH_2C=N—, 6.5, q, 2H, J = 16 Hz, ring CH_2) which was expected on the basis of that observed for the side chain ketone corresponding to **6***a* whose structure has been established (17*b*, 18). Structures **6***a*, **6***c* and **9***a*, **9***b* were confirmed by thermolysis to the corresponding pyrazoles **7***a*, **7***c*, **10***a*, **10***b*, respectively.

Under the conditions that afforded diazepines **5***a–c*, the reaction of **3***a* and **3***b* with phenylhydrazine unfortunately gave only the pyrazolines **9***a* and **9***b*, nor could the desired 1,3,5,7-tetraphenyl-1,2(1*H*)-diazepine be detected by n.m.r. analysis of the crude reaction product. If this reaction was carried out in benzene suspension, 1,3,5-triphenylpyrazole **10** was obtained as the only major characterizable product.

The mechanism for the formation of the observed products may be discussed by reference to the general comments advanced by Balaban (17*b*) and Buchardt and co-workers (6) for the reaction of pyrylium salts with nucleophiles (Scheme 2). Good precedent and analogy exists for the formation of α-thiapyran (**11**) (3*b*) and open-chain (**12**) (3*b*, 34) intermediates in reactions of pyrylium salts and related heterocycles. In some cases these may be isolated; in the case of thiapyrylium salts they have not been detected

Can. J. Chem. Downloaded from www.nrcresearchpress.com by 210.87.254.5 on 09/05/12
For personal use only.

TABLE 1. Ultraviolet and nuclear magnetic resonance data of 1,2(*1H*)-diazepines (**5**)

Compound	λ_{max}(EtOH) (ε) nm	τ values ($CDCl_3$) NMe[a]	C_4-H[b]	C_6-H[b]	Aromatic	Other
5*a*	407.5 (321) 270 (21 250) 225 (15 100)	7.05	4.15	2.95	2.15–2.8 (m, 15H)	
5*b*	415 (330) 275 (28 200) 222 (20 300)	7.1	4.25	2.9	2.1–2.75 (m, 14H)	
5*c*	357.5 (13 800) 266 (22 100) 222.5 (20 400)	7.05	4.10	2.9	2.0–2.7 (m, 12H)	3.25 (d, 2H, J = 8 Hz, *ortho*-H in $-C_6H_4N(CH_3)_2$), 7.0 (s, 6H, $N(CH_3)_2$).

[a]s, 3H.
[b]d, 1H, J = 1.5 Hz. This coupling was confirmed by decoupling studies.

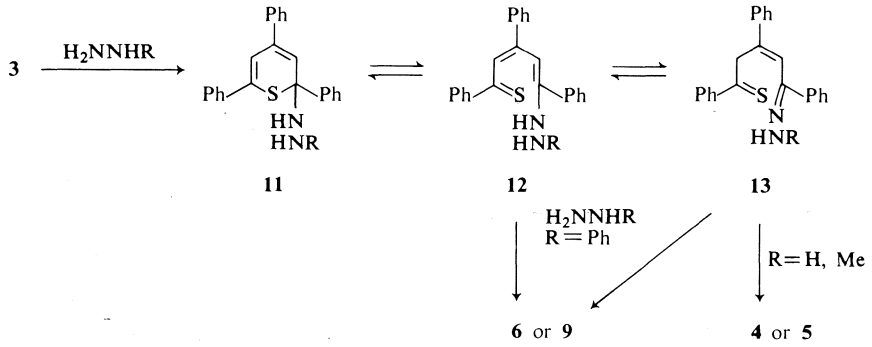

SCHEME 2

and only the 1,2-diazepines (**4**) or pyrazolines (**6** and **9**) have been isolated. Diazepine formation may be favored by equilibration to **13** catalyzed by excess hydrazine. In the case of **13**, R = H and Me, condensation with the thioketone is facilitated by nucleophilic strength and steric factors of the juxtaposed hydrazone. In the intermediate phenylhydrazone **13**, R = Ph, however, nucleophilicity of the attacking nitrogen atom is decreased and unfavorable steric interactions due to the phenyl moiety are introduced. Consequently, a pyrazoline (**6** or **9**) is formed from **13**, R = Ph, or, more likely, from **12**, R = Ph, by an internal Michael addition mechanism. Considering the diversity of results in reactions of pyrylium and thiapyrylium salts with hydrazines (17, 18, 20*a*), it is premature to speculate on the role played by the heteroatom (oxygen *vs.* sulfur) in directing these transformations except to note that thiones are usually much more reactive towards nucleophiles than ketones (35).

Experimental

Melting points were determined on a Fisher-Johns apparatus and are uncorrected. Analysis were performed by Micro-Tech Labs., Inc., Skokie, Ill., A. B. Gygli, Toronto, Ontario, and by J. J. Kobliska, Analytical Laboratories, American Cyanamid Co. The i.r. spectra were recorded on Beckman IR-5A and -10 instruments in chloroform solution unless otherwise noted. The u.v. spectra were measured on a Beckman DB-G spectrophotometer in ethanol solution unless otherwise indicated. The n.m.r. spectra were recorded on Varian T-60 and HA-100 and Perkin-Elmer R-12B spectrometers in deuteriochloroform solution unless otherwise stated using TMS as internal standard. Spectra listed follow the order: chemical shift, multiplicity (s = singlet, d = doublet, t = triplet, q = quartet, and m = multiplet), number of protons, coupling constant (Hz), and assignment. Mass spectra were determined with Hitachi-Perkin Elmer RMU-6E and MS-30 spectrometers. Thin-layer, preparative thick-layer, and column chromatography were performed with silica gel specified for these purposes and obtained from Brinkmann (Canada) Ltd.

Thiapyrylium Salts (3a–c)

These were prepared by the method of Wizinger and Ulrich (36).

Can. J. Chem. Downloaded from www.nrcresearchpress.com by 210.87.254.5 on 09/05/12
For personal use only.

Can. J. Chem. Downloaded from www.nrcresearchpress.com by 210.87.254.5 on 09/05/12
For personal use only.

2,4,6-Triphenylthiapyrylium Fluoroborate (3a).

This was obtained in 80% yield. A sample recrystallized from acetic acid showed m.p. 201–202.5° (lit. (28*c*) m.p. 218°, (40) m.p. 196.5–197.5°).

4-(p-Chlorophenyl)-2,6-diphenylthiapyrylium Fluoroborate (3b).

This was obtained in 72% yield after recrystallization from acetic acid, m.p. 143–146°.

Anal. Calcd. for $C_{23}H_{16}SClBF_4$: C, 61.81; H, 3.58; S, 7.17. Found: C, 61.52; H, 3.42; S, 6.82.

4-(p-Dimethylaminophenyl)-2,6-diphenylthiapyrylium Perchlorate (3c).

This was obtained in 88% yield after recrystallization from acetic acid, m.p. 256–258° (lit. (36), m.p. 247–249°, (37) 256–258°).

1,2(4H)-Diazepines (4a–c)

3,5,7-Triphenyl-1,2(4H)-diazepine (4a)[1]

Two hundred milliliters of 100% hydrazine hydrate (87-fold excess) was stirred at room temperature while 20.0 g (0.048 mol) of 2,4,6-triphenylthiapyrylium perchlorate (36) was sifted in during 1/2 h. Stirring was continued overnight, the product then being filtered, washed with water, and dried. Crystallization from 800 ml of methylcyclohexane (Darco) gave 9.0 g (59%) of pale yellow product, m.p. 186–190°. Recrystallization from acetonitrile gave colorless crystals, m.p. 195–196° (lit. (20*a*) m.p. 191–192°).

When the reaction was carried out under the conditions of Buchardt *et al.* (20*a*), an 89% yield of **4***a* was obtained.

The bright yellow picrate of **4***a* was prepared in butanol and crystallized from alcohol; m.p. 198–200.5°.

Anal. Calcd. for $C_{29}H_{21}N_5O_7$: C, 63.1; H, 3.8; N, 12.7. Found: C, 62.9; H, 3.7; N, 12.8.

Compounds **4***b* and **4***c* were prepared according to the conditions of Buchardt *et al.* (20*a*).

5-(p-Chlorophenyl)-3,7-diphenyl-1,2(4H)-diazepine (4b).

This was obtained in 86% yield. A sample recrystallized from acetonitrile showed m.p. 190–191.5° (lit. (20*a*) m.p. 188–189°).

5-(p-Dimethylaminophenyl)-3,7-diphenyl-1,2(4H)-diazepine (4c).

This was obtained in 90% yield and recrystallized from acetonitrile for analysis, m.p. 216.5–218°.

Anal. Calcd. for $C_{25}H_{23}N_3$: C, 82.2; H, 6.3; N, 11.5. Found: C, 81.9; H, 6.5; N, 11.5.

The picrate of **4***c* was prepared in butanol and crystallized from the same solvent as bronze needles, m.p. 217.5–219.5° (dec.).

Anal. Calcd. for $C_{31}H_{26}N_6O_7$: C, 62.6; H, 4.5; N, 14.1. Found: C, 62.9; H, 4.4; N, 14.3.

Hydrogenation of 4a to 4,5-Dihydro-3,5,7-triphenyl-1,2-(6H)-diazepine (8)

Compound **4***a* (0.141 g, 4.37 mmol) in 35 ml of absolute ethanol was hydrogenated at atmospheric pressure in the presence of *ca.* 70 mg of 5% palladium on charcoal. Hydrogenation was stopped after absorption of approximately 5.25 mmol of hydrogen. The solution was filtered and the filtrate concentrated *in vacuo*. The residue was passed through a column of silica gel to yield 0.091 g (64%) of colorless compound **8**, m.p. 159–161°, identical by mixture m.p. and n.m.r. comparison with an authentic sample prepared according to Amiet and Johns (38).

1,2(1H)-Diazepines (5a–c)

1-Methyl-3,5,7-triphenyl-1,2(1H)-diazepine (5a)

The apparatus consisted of a two-necked flask equipped with a drying tube and an attachment for addition of solid (39). The flask was charged with neat methylhydrazine (10 ml) and the attachment was charged with thiapyrylium salt **3***a* (4.0 g, 10 mmol). After the flask was immersed in a liquid nitrogen bath, compound **3***a* was sifted in over a few minutes. The mixture was allowed to warm to 0° and was stored at this temperature for 13 h. The resulting red crystals (2.55 g, 65%) were collected by filtration and were dried under high vacuum. Careful recrystallization from ethanol or methylcyclohexane at room temperature or below gave burgundy red crystals of **5***a*, m.p. 116.5–118°; mass spectrum (*m/e*, % relative intensity) 336 (M^+, 14), 308(21), 307(48), 306(21), 234(29), 233(100).

Anal. Calcd. for $C_{24}H_{20}N_2$: C, 85.7; H, 6.0; N, 8.3. Found: C, 85.6; H, 6.1; N, 8.2.

Compounds **5***b* and **5***c* were prepared by the above procedure.

1-Methyl-5-(p-chlorophenyl)-3,7-diphenyl-1,2(1H)-diazepine (5b)

This was obtained in 74% yield. Recrystallization from methylcyclohexane and then from ethanol gave an analytical sample, m.p. 132.5–133.5°; mass spectrum (*m/e*, relative intensity) 370.5 (M^+, 18), 369(18), 343(23), 342(23), 341(50), 306(23), 269(36), 268(27), 267(100), 118(45).

Anal. Calcd. for $C_{24}H_{19}N_2Cl$: C, 77.73; H, 5.13; N, 7.56. Found: C, 77.74; H, 4.96; N, 7.63.

1-Methyl-5-(p-dimethylaminophenyl)-3,7-diphenyl-1,2-(1H)-diazepine (5c)

This was obtained in 68% yield. Successive recrystallization from methylcyclohexane and ethanol provided an analytical sample, m.p. 126–127°; mass spectrum (*m/e*, % relative intensity) 379 (M^+, 10), 378(10), 351(30), 350(100), 349(30), 277(23), 276(70), 103(41).

Anal. Calcd. for $C_{26}H_{25}N_3$: C, 82.29; H, 6.64; N, 11.07. Found: C, 82.50; H, 6.75; N, 11.11.

Preparation of 1-Methyl-3,5,7-triphenyl-1,2(1H)-diazepine (5a) from 4a

A mixture of **4***a* (0.190 g, 0.59 mmol), methyl iodide (6 ml), and pulverized sodium hydroxide (0.250 g, 6.25 mmol) was stirred at room temperature for 24 h. The solid was removed by filtration and the filtrate was concentrated to yield a gum (0.229 g) which was subjected to preparative thick-layer chromatography (CH_2Cl_2) to afford 2,4,6-triphenylpyridine (6%) and compound **5***a* (70%) which were shown to be identical to authentic materials by n.m.r., m.p., and mixture m.p. comparison.

Formation of Pyrazoline Derivatives 6a, 6c, and 9a, 9b

The instability of the pyrazoline derivatives described below precluded elemental analysis.

1-Methyl-3,5-diphenyl-5-phenacyl-2-pyrazoline Methylhydrazone (6a)

The apparatus which was described in connection with the preparation of compound **5***a* was used. To methylhydrazine (10 ml) that had been frozen to a glass in liquid nitrogen was added 2,4,6-triphenylthiapyrylium fluoroborate (**3***a*) (2g, 4.85 mmol) under anhydrous conditions. The mixture was allowed to warm to 0°. The resulting red solution was stored at this temperature and deposited,

Can. J. Chem. Downloaded from www.nrcresearchpress.com by 210.87.254.5 on 09/05/12
For personal use only.

over 13 h., a red gum which was collected by filtration. The gum was recrystallized from hot ethanol to give 1.1 g (29%) of **6***a*, m.p. 135° (dec.); n.m.r. τ 2.2–2.9 (m, 15H, aromatics), 3.1 (br s, 1H, NH, exchanged with D_2O), 6.6 (s, 2H, side-chain CH_2), 6.5 (q, 2H, J = 16 Hz, CH_2), 7.05 (s, 3H, side-chain NCH_3), 7.3 (s, 3H, NCH_3); mass spectrum at <10 eV, 80° inlet temperature (*m/e*, % relative intensity) 234 ($M^+ - C_6H_5C(=NNHCH_3)CH_3$, 100), 233(27), 148(50), 147(27), 118(39).

*1-Methyl-3-phenyl-5-(p-dimethylaminophenyl)-5-phenacyl-2-pyrazoline Methylhydrazone (**6c**)*

This compound was obtained under conditions similar to those described for the formation of **6***a*, m.p. 118–120° (dec.); n.m.r. τ 2.2–2.9 (m, 13H, aromatic and NH (exchangeable with D_2O) protons), 3.3 (d, 2H, J = 8 Hz, *ortho*-H of dimethylaminophenyl ring), 6.6 (s, 2H, side-chain CH_2), 6.4 (q, 2H, J = 15 Hz, CH_2), 6.95 (s, 3H, side-chain NCH_3), 7.0 (s, 6H, $N(CH_3)_2$), 7.22 (s, 3H, NCH_3); mass spectrum at <10 eV, 80° inlet temperature (*m/e*, % relative intensity) 277 ($M^+ - C_6H_5C(=N—NHCH_3)CH_3$, 100), 276(20), 148(47), 119(36), 118(55).

*1,3,5-Triphenyl-5-phenacyl-2-pyrazoline Phenylhydrazone (**9a**)*

To phenylhydrazine (2.16 g, 19 mmol) which had been frozen to a glass in liquid nitrogen was added 2,4,6-triphenylthiapyrylium fluoroborate (**3***a*) (4g, 9.6 mmol) and the mixture was set aside at room temperature for one week. The solid was collected by filtration and recrystallized from ethanol to give 1.3 g (26%) of **9***a*, m.p. 101–104°; n.m.r. τ 2.26–3.41 (m, 26H, aromatic and NH (exchangeable with D_2O) protons), 6.14 (s, 2H, side-chain CH_2), 6.65 (q, 2H, J = 18 Hz, CH_2); mass spectrum at <10 eV, 80° inlet temperature (*m/e*, % relative intensity) 296 ($M^+ - C_6H_5C(=NNHC_6H_5)CH_3$, 50), 295(28), 210(36), 105(64), 104(64), 103(100).

*5-p-Chlorophenyl-1,3-diphenyl-5-phenacyl-2-pyrazoline Phenylhydrazone (**9b**)*

This compound was obtained in 20% yield by the method described for the preparation of **9***a*, m.p. 110° (dec.); n.m.r. τ 2.2–3.6 (m, 26H, aromatic and NH (exchangeable with D_2O) protons), 6.1 (s, 2H, side-chain CH_2), 6.65 (q, 2H, J = 17 Hz, CH_2); mass spectrum *m/e*, % relative intensity 330.5 ($M^+ - C_6H_5C(=NNHC_6H_5)CH_3$, 50), 329.5(22), 210(100), 119(57).

*Thermolysis of Pyrazolines **6a**, **6c**, **9a**, and **9b** to Pyrazoles **7a**, **7c**, **10a**, and **10b***

Compound **6***a* (173 mg, 0.45 mmol) was pyrolyzed at its melting point in a sealed tube inserted in an oil bath (135°) for 25 min to give after column chromatography (benzene) 98 mg (91%) of *1-methyl-3,5-diphenylpyrazole* (**7***a*), m.p. 52–54° which was shown to be identical by mixture m.p. determination to an authentic sample prepared by a literature procedure (41).

Under the above conditions, pyrazoline **6***c* gave *1-methyl-3-phenyl-5-(p-dimethylaminophenyl)pyrazole* (**7***c*) in 81% yield, m.p. 98.5–99.5°; n.m.r. τ 2.12 and 2.65 (m, 7H, aromatics), 3.23 (d, 2H, J = 7.5 Hz, *ortho*-H of dimethylaminophenyl ring), 3.46 (s, 1H, pyrazole ring H) 6.09 (s, 3H, NCH_3), 7.02 (s, 6H, $N(CH_3)_2$); mass spectrum (*m/e*, % relative intensity) 277 (M^+, 100), 276(21), 263(32), 167(26), 149(74).

Anal. Calcd. for $C_{18}H_{19}N_3$: C, 77.95; H, 6.90; N, 15.15. Found: C, 77.38; H, 6.99; N, 15.09.

Pyrolysis of **9***a* gave *1,3,5-triphenylpyrazole* (**10***a*) in 68% yield, m.p. 136–140° shown to be identical by mixture m.p. determination to an authentic sample obtained by a literature method (42).

Pyrolysis of **9***b* gave *5-(p-chlorophenyl)-1,3-diphenylpyrazole* (**10***b*) in 60% yield, m.p. 112–114°; lit. (22*c*) m.p. 113–115°; n.m.r. τ 1.8–2.15 and 2.3–2.75 (m, 2H, and 12H, aromatics), 3.15 (s, 1H, pyrazole ring H).

*Direct Formation of 1,3,5-Triphenylpyrazole (**10a**)*

To a suspension of 2,4,6-triphenylthiapyrylium fluoroborate (**3***a*) (2.0 g, 4.8 mmol) in benzene (150 ml) was added phenylhydrazine (1.08 g, 10 mmol) and the mixture was stirred at room temperature overnight. The mixture was evaporated to dryness *in vacuo* and the resulting oil was passed through a short column of silica gel (benzene) to afford 0.97 g (67%) of **10***a* identical to an authentic sample (42) by mixture m.p. determination.

Part of this work was supported by the National Research Council of Canada and Bristol Laboratories. We are grateful to Professor R. Bell and Mr. B. Sayer for 100-MHz n.m.r. spectra and to Professor J. M. Miller for mass spectra. Thanks are due to C. Bender and M. Kaufman (Chem 13 News Award holders, University of Waterloo) for assistance with large scale preparation. We thank J. J. Kobliska, American Cyanamid Co., for carrying out some of the elemental analyses.

1. E. KLINGSBERG, Abstr. Am. Chem. Soc. Meeting, September, 1965. p. 66S.
2. M. T. THOMAS, V. SNIECKUS, and E. KLINGSBERG. Presented in part at the 55th Canadian Chemical Conference of the Chemical Institute of Canada, Quebec, Quebec. June, 1972. p. 8.
3. (*a*) K. DIMROTH and K. H. WOLF. Newer methods of preparative organic chemistry Vol III. *Edited by* W. Foerst. Academic Press, New York. 1964. p. 357; (*b*) H. PERST. Oxonium ions in organic chemistry. Verlag Chemie, Academic Press, New York. 1971. p. 149ff; (*c*) F. BRODY and P. R. RUBY. Pyridine and its derivatives. Part One. *Edited by* E. Klingsberg. Interscience Publishers, Inc., New York. 1960. p. 210ff.
4. M. H. O'LEARY and G. A. SAMBERG. J. Am. Chem. Soc. **93**, 3530 (1971).
5. (*a*) G. N. DOROFEENKO, A. N. NARKEVICH, and YU. A. ZHDANOV. Khim. Geterotsikl. Soedin. 1130 (1967); (*b*) G. N. DOROFEENKO, A. N. NARKEVICH, and YU. A. ZHDANOV. Khim. Geterotsikl. Soedin. Sb.2: Kislorod Soderzh. Geterotsikly. 223 (1970); Chem. Abstr. **76**, 140454v (1972).
6. C. L. PEDERSEN, N. HARRIT, and O. BUCHARDT. Acta Chem. Scand. **24**, 3435 (1970).
7. R. A. OLOFSON, J. M. LANDESBERG, and R. O. BERRY. Tetrahedron, **22**, 2119 (1966).
8. I. SHIBUYA and M. KURABAYASHI. Bull. Chem. Soc. Jap. **42**, 2382 (1969).
9. (*a*) G. V. BOYD and A. J. H. SUMMERS. J. Chem. Soc. C, 409 (1971); (*b*) O. P. SHVAIKA and V. I. FOMENKO. Dokl. Akad. Nauk SSSR. **200**, 134 (1971).
10. G. N. DOROFEENKO, L. V. MEZHERITSKAYA, and V. I. DULENKO. Khim. Geterotsikl. Soedin. Sb.2: Kislorod Soderzh. Geterotsikly. 287 (1970); Chem. Abstr. **76**, 140618b (1972).
11. J. E. OLIVER. J. Org. Chem. **36**, 3465 (1971).

12. J. E. OLIVER, B. A. BIERL, and J. M. RUTH. J. Org. Chem. **37**, 131 (1972).
13. G. V. BOYD and P. H. WRIGHT. J. Chem. Soc. Perkin I, 1140 (1972).
14. R. R. SCHMIDT. Synthesis, 333 (1972).
15. G. V. BOYD and S. R. DANDO. J. Chem. Soc. Perkin I. 1142 (1972).
16. G. V. BOYD and S. R. DANDO. J. Chem. Soc. C, 3873 (1971).
17. (*a*) A. T. BALABAN. Tetrahedron, **24**, 5059 (1968); (*b*) A. T. BALABAN. Tetrahedron, **26**, 739 (1970); (*c*) A. T. BALABAN and W. SILHAN. Tetrahedron, **26**, 743 (1970).
18. V. SNIECKUS and G. KAN. Chem. Commun. 1208 (1970).
19. C. L. PEDERSEN and O. BUCHARDT. Acta Chem. Scand. **24**, 834 (1970).
20. (*a*) O. BUCHARDT, C. L. PEDERSEN, U. SVANHOLM, A. M. DUFFIELD, and A. T. BALABAN. Acta Chem. Scand. **23**, 3125 (1969); (*b*) U. SVANHOLM. Acta. Chem. Scand. **25**, 640 (1971).
21. G. I. ZHUNGIETU, I. V. SHANTSEVOI, and B. P. SUKHANGUK. Zh. Vses. Khim. Obshchest. **16**, 232 (1971); Chem. Abstr. **75**, 5614m (1971).
22. (*a*) E. KLINGSBERG. J. Am. Chem. Soc. **83**, 2934 (1961); (*b*) E. KLINGSBERG. J. Org. Chem. **28**, 529 (1963); (*c*) M.-T. BERGEON, C. METAYER, and H. QUINION. Bull. Soc. Chim. Fr. 917 (1971).
23. M. E. C. BIFFIN, D. J. BROWN, and Q. N. PORTER. Tetrahedron Lett. 2029 (1967); H. C. VAN DER PLAS and H. JONGJAN. Rec. Trav. Chim. **87**, 1065 (1968).
24. I. ADACHI. Chem. Pharm. Bull. (Tokyo). **17**, 2209 (1969).
25. R. FUSCO and P. DALLA CROCE. Gazz. Chim. Ital. **101**, 703 (1971).
26. P. SYKES and H. ULLAH. J. Chem. Soc. Perkin I, 2305 (1972).
27. A. CHINONE, M. MARUYAMA, and M. OHTA. Bull. Chem. Soc. Jap. **45**, 2222 (1972).
28. (*a*) H. SUGIMOTO, Kagaku (Kyoto), **25**, 829 (1970); Chem. Abstr. **74**, 87704g (1971); (*b*) G. A. REYNOLDS and J. A. VAN ALLAN. J. Heterocycl. Chem. **8**, 301 (1971); (*c*) Z. YOSHIDA, S. YONEDA, H. SUGIMOTO, and T. SUGIMOTO. Tetrahedron, **27**, 6083 (1971).
29. J. STREITH, J. P. LUTTRINGER, and M. NASTASI. J. Org. Chem. **36**, 2962 (1971); T. SASAKI, K. KANEMATSU, A. KAHEKI, I. ICHIKAWA, and K. HAYAKAWA. J. Org. Chem. **35**, 426 (1970); A. BALASUBRAMANIAN, J. M. MCINTOSH, and V. SNIECKUS. J. Org. Chem. **35**, 433 (1970).
30. D. J. HARRIS, M. T. THOMAS, V. SNIECKUS, and E. KLINGSBERG. Can. J. Chem. This issue.
31. J. N. BROWN, R. L. TOWNS, and L. M. TREFONAS. J. Am. Chem. Soc. **92**, 7436 (1970).
32. O. BUCHARDT, C. L. PEDERSEN, and N. HARRIT. J. Org. Chem. **37**, 3592 (1972).
33. G. KAN, M. T. THOMAS, and V. SNIECKUS. Chem. Commun. 1023 (1971).
34. G. DAUPHIN, L. DAVID, B. JAMILLOUX, A. KERGOMARD, and H. VESCHAMBRE. Tetrahedron, **28**, 1055 (1972); P. SCHIESS, H. L. CHIA, and P. RINGELE. Tetrahedron Lett. 313 (1972); A. F. KLUGE and C. P. LILLYA. J. Org. Chem. **36**, 1977 (1971); **36**, 1988 (1971).
35. R. MAYER. *In* Organosulfur chemistry. *Edited by* M. J. JANSSEN. Interscience Publ., New York. 1967. p. 226.
36. R. WIZINGER and P. ULRICH. Helv. Chim. Acta. **39**, 207 (1956).
37. A. MISTR, M. VARRA, J. SKOUPY, and R. ZAHRADNIK. Coll. Czech. Chem. Commun. **37**, 1520 (1972).
38. R. G. AMIET and R. B. JOHNS. Aust. J. Chem. **21**, 1279 (1968).
39. R. S. MONSON. Advanced organic synthesis. Academic Press, New York and London, 1971. p. 169.
40. G. SULD and C. C. PRICE. J. Am. Chem. Soc. **84**, 2090 (1962).
41. R. HUISGEN, H. GOTTHARDT, and R. GRASHEY. Chem. Ber. **101**, 536 (1968).
42. K. VON AUWERS and H. STUHLMAN. Chem. Ber. **59**, 1043 (1926).

Can. J. Chem. Downloaded from www.nrcresearchpress.com by 210.87.254.5 on 09/05/12
For personal use only.

Protonation and Acid-catalyzed Rearrangement of 1, 2-Diazepines[1]

DAVID JOHN HARRIS, M. T. THOMAS, AND VICTOR SNIECKUS[2]
Department of Chemistry, University of Waterloo, Waterloo, Ontario N2L 3G1
AND
E. KLINGSBERG
American Cyanamid Company, Bound Brook, New Jersey
Received January 11, 1974

Can. J. Chem. Downloaded from www.nrcresearchpress.com by 210.87.254.105 on 09/05/12
For personal use only.

DAVID JOHN HARRIS, M. T. THOMAS, VICTOR SNIECKUS, and E. KLINGSBERG. Can. J. Chem. **52**, 2805 (1974).

The protonation of the 1,2(4*H*)-diazepines **2***a*, **2***b*, and the 1,2(1*H*)-diazepine **3***a* in various acidic media has been studied by u.v. and n.m.r. spectroscopy. Compounds **2***a* and **3***a* undergo protonation to give **4***a* and **7***a*, respectively, whereas **2***b* provides the monoprotonated species **4***b* in dilute acid and the diprotonated form **4***c* in strongly acidic solution. Spectral characteristics of crystalline 1,2(4*H*)-diazepinium perchlorates **4***a*, **4***d*, **7***a*, and **7***c* correlate well with those observed for the corresponding free bases in acidic solutions; **7***a*-ClO_4 and **7***c*-ClO_4 were obtained either from **2***a* and **2***c* or from **3***a* and **3***c*, respectively. In trifluoroacetic acid-*d* – D_2O, deuterium exchange at C_4 and C_6 of **2***a*, **2***b*, and **3***a* was observed indicating the presence of small equilibrium concentrations of species **1***a*, **1***c* and/or **1***d*, and **1***b* under these conditions. Temperature variable n.m.r. spectroscopy provides evidence for ring inversion phenomena for the protonated forms **4***a* and **7***a*. In the case of **4***a*, the activation energy, $\Delta G_c^{\ddagger} = 10.2 \pm 0.2$ kcal/mol ($T_c = 8 \pm 3°$) has been estimated. The difference in the activation energy between the free base and the protonated form, $\Delta G^{\ddagger}$ (**2***a*) – $\Delta G^{\ddagger}$ (**4***a*) = 6–7 kcal/mol is attributed to strong repulsive N_1—N_2 lone pair interaction in **2***a* in the transition state for the ring inversion process.

Under vigorous acidic conditions, the 1,2(4*H*)-diazepines **2***a–c* give pyrazoles (**10***a–c*), pyridines (**12***a–c*), and acetophenone. Using identical conditions, the 1,2(4*H*)-diazepinium salt, **7***a*-ClO_4 provides pyrazole **11***a* and pyridine **12***a* and, in addition, the 1-methylaminopyridinium salt **13***a*. However, rearrangement also proceeds under very mild conditions (ethanol–water) as shown for **7***a*-ClO_4 and **7***c*-ClO_4 which yield compounds **11***a* and **12***a*, and **11***c*, **12***c*, and **13***c*, respectively. The 1,2(1*H*)-diazepine **3***a* gives **11***a*, **12***a*, and **13***a* in ethanol–water solution and exclusively **13***a* in trifluoroacetic acid. The mechanism of these reactions is discussed in terms of formation of open-chain (**15**) and diaziridine-type (**19**) intermediates. Electrocylic mechanisms are eliminated from consideration on the basis of the absence of products **23**, **24**, and **25** which should have been observed from the reactions of **2***b*, **2***c*, and **7***c*-ClO_4 if these pathways were operative.

DAVID JOHN HARRIS, M. T. THOMAS, VICTOR SNIECKUS et E. KLINGSBERG. Can. J. Chem. **52**, 2805 (1974).

La protonation des 4*H*-diazépines-1,2 **2***a*, **2***b* et de la 1*H*-diazépine-1,2 **3***a* dans des milieux acides variés est étudiée par spectroscopie u.v. et r.m.n. On protone **2***a* et **3***a* pour obtenir respectivement **4***a* et **7***a* tandis qu'avec **2***b* on obtient l'espèce monoprotonée **4***b* en milieu acide dilué et la forme diprotonée **4***c* en solution fortement acide. Les caractéristiques spectrales des perchlorates du 4*H*-diazépinium-1,2 cristallins **4***a*, **4***d*, **7***a* et **7***c* sont en harmonie avec celles qu'on observe pour les bases libres correspondantes en solutions acides; **7***a*-ClO_4 et **7***c*-ClO_4 sont respectivement obtenus soit à partir de **2***a* et **2***c*, soit à partir de **3***a* et **3***c*. Le traitement de **2***a*, **2***b* et **3***a* par un mélange d'acide trifluoroacétique deutérié – D_2O provoque l'introduction de deutérium en C_4 et C_6: ces résultats indiquent la présence, sous ces conditions, de petites concentrations des espèces **1***a*, **1***c* et/ou **1***d*, et **1***b* à l'équilibre. L'étude spectroscopique en r.m.n. à température variable met en évidence les phénomènes d'inversion de noyaux des formes protonées **4***a* et **7***a*. Pour **4***a*, l'énergie d'activation $\Delta G_c^{\ddagger}$ et de 10.2 ± 0.2 kcal/mol ($T_c = 8 \pm 3°$) La différence des énergies d'activation de la forme protonée et de la base libre, $\Delta G^{\ddagger}$ (**2***a*) – $\Delta G^{\ddagger}$ (**4***a*) = 6–7 kcal/mol, est attribuée à l'interaction fortement répulsive des doublets libres de N_1—N_2 dans **2***a* pour l'état de transition amenant l'inversion du noyau.

Dans des conditions fortement acides on obtient les 4*H*-diazépines-1,2 **2***a–c* conduisant aux

[1]A portion of this work has appeared in preliminary form (1) and has been presented at conferences (2, 3).
[2]To whom correspondence may be addressed.

pyrazoles (**10***a–c*), aux pyridines (**12***a–c*) et à l'acétophénone. Dans des conditions identiques, le sel de 4*H*-diazépinium-1,2 le **7***a*-ClO_4, donne du pyrazole **11***a*, de la pyridine **12***a* et en plus du sel de méthylaminopyridinium-1 **13***a*. Pourtant, le réarrangement se produit aussi dans des conditions très douces (éthanol–eau) comme on le montre pour **7***a*-ClO_4 et **7***c*-ClO_4 qui conduisent respectivement, d'une part à **11***a* et **13***a*, et d'autre part à **11***c*, **12***c* et **13***c*. Avec 1*H*-diazépine-1,2 **3***a* en solution éthanol–eau on obtient **11***a*, **12***a* et **13***a* et, en présence d'acide trifluoroacétique seul **13***a* est obtenu. Le mécanisme de ces réactions est discuté en termes de formation d'intermédiaires en chaînes ouvertes (**15**) et d'autres du type diaziridine (**19**). On ne considère par les mécanismes électrocycliques à cause de l'absence des produits **23**, **24** et **25** qu'on aurait observés à partir des réactions de **2***b*, **2***c* et **7***c*-ClO_4 si ces processus intervenaient.
[Traduit par le journal]

Some time ago, the planar structures **1***a*, **1***b*, and **1***c* were suggested for the species resulting from protonation of the 3,5,7-triphenyl-1,2-diazepines **2***a*, **3***a*, and **2***b*, respectively, on the basis of u.v. spectral comparison (2). Likewise, the diprotonated form **1***d* was advanced for compound **2***b* in strongly acidic solution.[3] In connection with the general sysnthesis of 1,2-diazepines from thiapyrylium salts (5), we have re-examined this problem utilizing mainly n.m.r. spectroscopy (1). Herein we report the detailed results of this study together with our observations on the acid-catalyzed rearrangement of the 1,2-diazepine derivatives.[4]

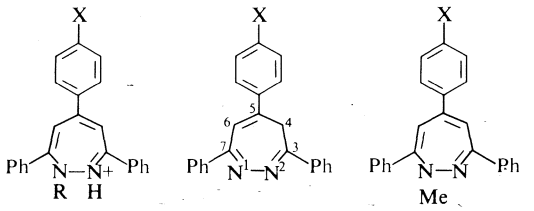

1 **2** **3**

a R = X = H
b R = Me; X = H
c R = H; X = NMe_2
d R = H; X = $\overset{+}{H}NMe_2$

a X = H
b X = NMe_2
c X = Cl

Protonation Studies

Diazepines **2***a* and **3***a* show marked u.v. absorption differences (Fig. 1) which were used for the original structural assignment (2). Both display benzenoid absorption in the 260 nm region but **2***a* shows a second strong band at 293 nm. These spectra are completely changed by acidification and in 5 *N* ethanolic hydrochloric acid the differences between the two compounds almost vanish (Fig. 2, Table 1). To account for this resemblance, and for the bathochromic shift upon protonation, the planar structures **1***a* and **1***b* were suggested for the cations of **2***a* and **3***a*, respectively. Furthermore, the u.v. spectrum of the dimethylamino analog **2***b* (Fig. 1) also undergoes a bathochromic shift in 5 *N* HCl–EtOH solution giving rise to an almost identical spectrum to that displayed by its parent system (**2***a*)

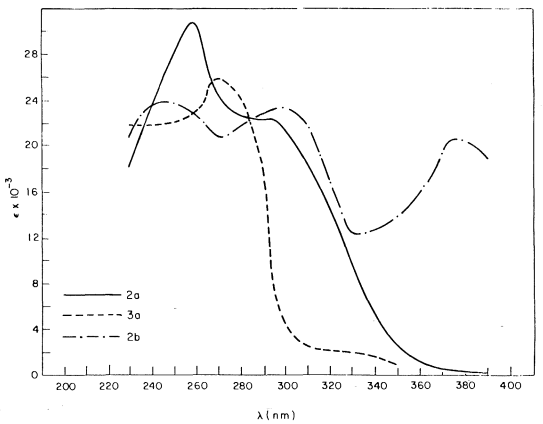

FIG. 1. Ultraviolet spectra of compounds **2***a*, **2***b*, and **3***a* in ethanol solution.

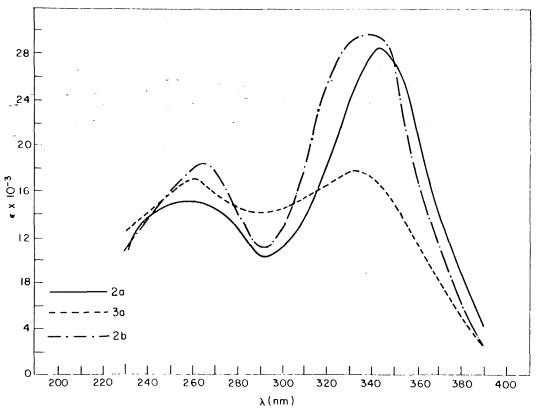

FIG. 2. Ultraviolet spectra of compounds **2***a*, **2***b*, and **3***a* in 5 *N* ethanolic HCl solution.

[3]These interpretations have been quoted in reviews (4).

[4]Prototropic equilibria of 1,2-diazepine derivatives have not been previously studied, whereas these aspects of 1,4-diazepines (4, 6) and 1, 5-benzodiazepines (4) have received considerable attention.

Can. J. Chem. Downloaded from www.nrcresearchpress.com by 210.87.254.105 on 09/05/12
For personal use only.

Can. J. Chem. Downloaded from www.nrcresearchpress.com by 210.87.254.105 on 09/05/12
For personal use only.

TABLE 1. Ultraviolet spectra of 1, 2-diazepines and -diazepinium derivatives

Compound	λ_{max} (EtOH) (ε) nm	λ_{max} ($HCl–CHCl_3$) (ε) nm	λ_{max} (5 *N* HCl – EtOH)[a] (ε) nm	λ_{max} (0.1 *N* HCl – EtOH)[a] (ε) nm	λ_{max} (CF_3CO_2H) (ε) nm	λ_{max} (CH_3CN)[b] (ε) nm
2*a*	293(22 600) 258(30 800)	342(27 600) 266(10 900)	343(28 600) 253(15 100)		343(29 300) 270(13 900)	
4*a*						288(19 300) 255(19 800)
2*b*	376(20 700) 298(23 500) 243(24 000)	484(17 400) 336(20 600) 265(17 400)	340(29 700) 265(18 500)	510(44 900) 325(17 800) 258(16 100)	335(22 900) 262(11 900)	
4*d*						291(21 600) 261(31 700)
3*a*	407.5(320) 270(21 300) 225(15 100)	338(19 500) 257(18 200)	333(18 000) 260(16 600)		475(290) 322(14 000) 288(11 800)	
7*a*-ClO_4			331(21 000) 255(20 800)			329(17 100) 273(13 100) 250(18 700)

[a]These solutions were prepared by dilution (v/v) of concentrated HCl with ethanol.
[b]On the crystalline perchlorate derivatives.

TABLE 2. Nuclear magnetic resonance spectra of 1, 2(4*H*)-diazepinium derivatives[a]

Compound	Solution[b]	τ values (multiplicity) Aromatic	C_4-H_2	C_6-H	Other
4*a*	B	1.8–2.65 (m)	5.5–6.0 (br)		
	C	2.05–2.7 (m)	5.6–6.32 (br)	[c]	
4*b*	A		5.42–5.95 (br)	3.12 (br s)	6.6 (s, 6H, $N(CH_3)_2$)
	B	1.75–2.7 (m)	5.44–6.0 (br)	[c]	6.54 (s, 6H, $N(CH_3)_2$)
	D	1.7–2.68 (m)	5.45–6.45 (br)	2.8 (br s)	6.9 (s, 6H, $N(CH_3)_2$)
4*d*	C	1.9–2.6 (m)	5.7–6.19 (br)	[c]	
7*a*-ClO_4[d]	E	2.0–2.9 (m)	5.15–6.82 (br)	3.15 (br s)	6.0 (s, 3H, NCH_3)

[a]Recorded at ambient temperature.
[b]A = 5 *N* HCl–ethanol-d_6; B = CF_3CO_2D; C = crystalline perchlorate in CD_3CN; D = 0.1 *N* HCl–ethanol-d_6; E = $CDCl_3$.
[c]Masked by aromatic proton absorption.
[d]Essentially identical with the n.m.r. spectrum of **3***a* in HCl–$CDCl_3$ solution.

(Fig. 2). This result was interpreted to mean that the dication **1***d* had been formed from **2***b*, since it is well known that protonation of the normally bathochromic dimethylamino function deprives it of almost all spectral influence. In the case of the cations **1***a* and **1***c*, it was proposed that protonation is accompanied by a 4*H*- to 1*H*-diazepine tautomerization (a [1,5] sigmatropic shift). In 0.1 *N* HCl–EtOH, compounds **2***a* and **3***a* show absorptions very similar to those observed in 5 *N* HCl–EtOH but **2***b* is converted into a red dye (λ_{max} 258, 325, and 510 nm) and this was taken as an indication of the monoprotonated species **1***c*, the color being associated with charge separation due to aromatic resonance as is well known of countless basic dyes (7).

The n.m.r. spectrum of **2***a* in $CDCl_3$ solution containing dry HCl gas shows, however, a broad singlet at τ 6.1, 2H which indicates that the C_4-methylene protons are still present (Table 2). Solutions of **2***a* in trifluoroacetic acid (TFA) and concentrated sulfuric acid and of its crystalline perchlorate salt in acetonitrile-d_3 exhibit essentially the same type of absorption at approximately τ 6.1. In all cases, the starting material was recovered from solution in high yield even after prolonged standing at room temperature. These observations lead to the conclusion that the protonated species of **2***a* is represented by either **4***a* or **5**. The essentially identical u.v. spectra of **2***a* in several acidic solutions (including 5 *N* HCl–EtOH) support this conclusion (Table 1). Of the two forms, **4***a* and **5**, **4***a* is favoured on the basis of the recent X-ray crystallographic analysis of the picrate of **2***a* which shows that it possesses the **4***a* structure (8).[5]

Further work showed that the originally proposed (2) structure **1***a* must obtain in low concentrations upon dissolution of **2***a* in acidic solutions. Prolonged stirring of **2***a* in a TFA-*d* solution containing a few drops of D_2O at room temperature gave a high yield of deuterated **2***a* in which 71% of the deuterium was located at C_4 and 21% at C_6 (n.m.r. analysis). Incorporation of deuterium probably takes place *via* the protonated 1,2(1*H*)-diazepine **1***a* which arises by tautomerization of protonated **2***a*, *i.e.*, **4***a*. An alternative possibility that deuterium exchange occurs *via* the open-chain form **6** is unlikely in view of its much greater thermodynamic instability with respect to **2***a* even in neutral solution (9).

Similar analysis of n.m.r. and u.v. spectral data supports, contrary to our previous tentative conclusions (1), structure **7***a* rather than **8** for the protonated species of the 1-methyl-1,2(1*H*)-diazepine derivative **3***a* in HCl–$CDCl_3$, 5 *N* HCl–EtOH, and TFA solutions (Table 2). In HCl–$CDCl_3$, the n.m.r. spectrum of compound

[5]We warmly thank Dr. Gerdil for this information prior to publication.

Can. J. Chem. Downloaded from www.nrcresearchpress.com by 210.87.254.105 on 09/05/12
For personal use only.

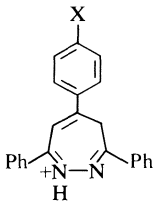

4

a X = H
b X = NMe_2
c X = $\overset{+}{H}NMe_2$
d X = Cl

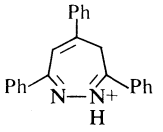

5

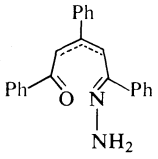

6

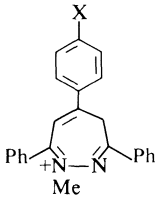

7

a X = H
b X = NMe_2
c X = Cl

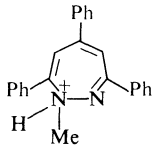

8

3*a* at room temperature shows signals at τ 5.78 (s, 3H, NMe) superimposed on an extremely broad envelope[6] at τ 4.5–6.7 (2H, C_4-CH_2) in addition to a slightly broadened singlet at τ 3.1 (1H, C_6-H) and a complex multiplet at τ 2.04–2.75 (15H, aromatics). The large downfield shifts for the NMe and C_6-H signals in **7***a* (Δ p.p.m. = 1.24 and 1.01, respectively) compared to those of the free base **3***a* (5) are expected and may be compared to similar shifts observed in 1,4-diazepine derivatives (10). The similarity of the u.v. spectra of **3***a* in HCl–$CDCl_3$, 5 *N* HCl–EtOH, and TFA solutions indicate the presence of the same protonated form; what is more significant is the similarity of spectra of **3***a* and **2***a* in these acidic solutions (Table 1). That no transformations of the somewhat sensitive (5) diazepine **3***a* has taken place was shown by recovery of starting material from the acidic solutions used in u.v. and n.m.r. measurements. Deuterium incorporation at C_6 in **3***a* took place in TFA-*d*–D_2O solution but not at room temperature as in the case of **2***a*. Nuclear magnetic resonance analysis indicated 50% C_6-H exchange but the problem was complicated by our inability to determine the extent of C_4-deuteration due to overlapping aromatic and C_4-H signals and competitive rearrangement under the acidic conditions of the experiment (see below).

Chemical support for structure **7***a* as representing the protonated form of **3***a* was obtained as follows (Scheme 1). Treatment of **3***a* with perchloric acid gave a crystalline perchlorate (**7***a*-ClO_4) the n.m.r. spectrum of which was essentially identical to that observed for a $CDCl_3$–HCl solution of **3***a* (Table 2). The same compound (**7***a*-ClO_4) was obtained by successive treatment of **2***a* with methyl fluorosulfonate (Magic Methyl) and perchloric acid.

Once it was established that structures **4***a* and **7***a* represent the species of diazepines **2***a* and **3***a*, respectively, which obtain in acidic solution, the remaining question regarding the protonation of the dimethylamino derivative **2***b* was examined. The n.m.r. spectrum (Table 2) of **2***b* in 5 *N* HCl–ethanol-d_6 showed a broad signal centered at τ 5.7 (2H) characteristic of C_4-methylene protons thus implicating the N_1-protonated 1,2(4*H*)-diazepine structure as already observed for the parent compound (**4***a*). In addition, the dimethylamino singlet which appeared at τ 6.9 in the spectrum of the free base in $CDCl_3$ was observed downfield at τ 6.6 under these acidic conditions. The downfield shift could not be attributed to a solvent effect since compound **2***b* showed essentially the same spectra in HCl–$CDCl_3$ and in TFA-*d* as that observed in 5 *N* HCl–ethanol-d_6 (Table 2). The magnitude (Δ p.p.m. = 0.32) and direction of the chemical shift in acidic solution is strong evidence for the presence of a protonated NMe_2 function as documented for numerous benzenoid (11) and heteroaromatic (12) systems. This information together with the strong similarity in the u.v. spectra of **2***b* in HCl–$CHCl_3$, 5 *N* HCl–ethanol, and TFA (Table 1) indicates the presence of the diprotonated species **4***c* under these acidic conditions. The near identity of the u.v. spectra of **2***b* and **2***a* in strongly acidic solution is therefore easily explained. That tautomerism between **4***c* and low concentrations of **1***c* and/or **1***d* occurs could be demonstrated by deuterium exchange studies in TFA-*d*–D_2O solution as already discussed for the case of **4***a* (see Experimental).

In 0.1 *N* HCl-ethanol-d_6, compound **2***b* exhibits an n.m.r. spectrum consistent with the presence of the monoprotonated species **4***b* (Table 2). The NMe_2 singlet appears at the same chemical shift (τ 5.9) as is observed for the free base in $CDCl_3$ solution. Repeated attempts to

[6]This led to our initial misassignment of structure **8** for the protonated species. Temperature variable n.m.r. data clearly supports **7***a* (see following section).

Can. J. Chem. Downloaded from www.nrcresearchpress.com by 210.87.254.105 on 09/05/12
For personal use only.

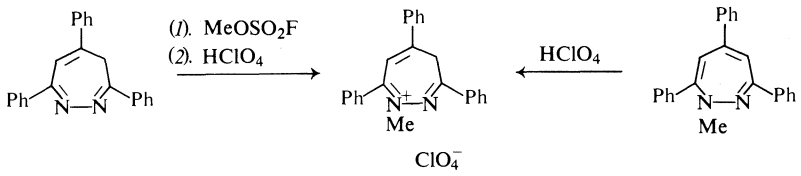

2*a* 7*a*-ClO_4 3*a*

SCHEME 1

prepare crystalline diazepinium salts **4***b* and **7***b*-ClO_4 for u.v. and n.m.r. spectral comparison purposes were unsuccessful.

In summary, the available evidence supports structures **4***a*, **4***c*, and **7***a* for the protonated forms of **2***a*, **2***b*, and **3***a*, respectively, in several strongly acidic solutions and **4***b* for the protonated species of **2***b* in dilute acid. The original u.v. spectra data (2) and the new n.m.r. and chemical information are now fully compatible with these assignments.

Temperature Variable Nuclear Magnetic Resonance Spectra of ***4a*** *and* ***7a***

The temperature variable n.m.r. spectra of **2***a* and a variety of its phenyl substituted derivatives show reversible line-broadening effects as a function of temperature due to the AB exchange of the C_2-methylene protons caused by a ring inversion process (13). Using line shape analysis, the energy of activation ($\Delta G_c^{\ddagger}$) has been determined in several solvents: $\Delta G_c^{\ddagger} = 17.1$ kcal/mol has been recorded for the parent system **2***a* in $CDBr_3$ solution (13*a*).

In comparison to the room temperature n.m.r. spectrum of **2***a* which shows a sharply-defined set of AB quartets at τ 5.58 and 7.37 for the C_2-methylene protons (13*a*), its spectrum in acidic solution exhibits broad absorption at τ 6.1 suggesting a lower $\Delta G_c^{\ddagger}$ for the ring inversion process in the protonated form (**4***a*). This was confirmed by a temperature variable study in HCl–$CDCl_3$.[7] At +60°, the broad absorption coalesces into a sharp spike as expected for rapid exchange. On cooling, first an exchange-broadened doublet is observed (−24°) which then resolves into two distinct AB doublets ($J_{AB} = 10$ Hz) at a separation of 276 cycles representing the low temperature limit spectrum (−40°). The free energy of activation, $\Delta G_c^{\ddagger} = 10.2 \pm 0.2$ kcal/mol, at the coalescence temperature ($T_c = 8 \pm 3°$) is estimated from the well-known approximation equation. Raban has recently demonstrated that activation energies obtained by this equation for coalescing AB quartets are in good agreement with those of complete line shape analysis if the condition $\Delta\nu/J > 3$ is met (14). Our case approximately satisfies this criterion. An estimate of $\Delta G_c^{\ddagger} = 12$ kcal/mol for the ring inversion process in TFA has been previously reported (13*a*) and compares favorably with our value in HCl–$CDCl_3$ solution. We have shown above that the monoprotonated form **4***a* is present in both solvent systems.

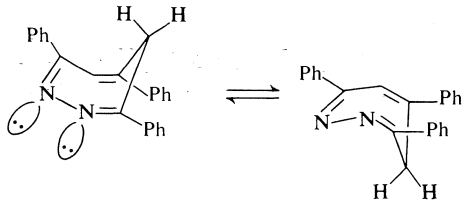

9*a* 9*b*

The difference in activation energy for ring inversion between the free base and the protonated form, $\Delta G^{\ddagger}(2a) - \Delta G^{\ddagger}(4a) = 6$–7 kcal/mol, merits brief comment.[8] In the free diazepine (**2***a*), the ring inversion **9***a* ⇄ **9***b* must pass through a planar transition state in which strong repulsive interaction between the skewed N_1 and and N_2 lone pairs would be expected, *i.e.*, a partial N—N double bond would develop. We propose (1) that monoprotonation at N_1 sub-

[7]The perchlorate of **2***a* could not be studied owing to solubility problems.

[8]A detailed temperature variable n.m.r. study of the protonated species **4**, X = Cl, NO_2, OMe, NMe_2 as well as **7***a*-ClO_4 is in progress in order to gain more insight into this problem. D. J. Harris, T. E. Gough, and V. Snieckus. To be submitted.

Can. J. Chem. Downloaded from www.nrcresearchpress.com by 210.87.254.105 on 09/05/12
For personal use only.

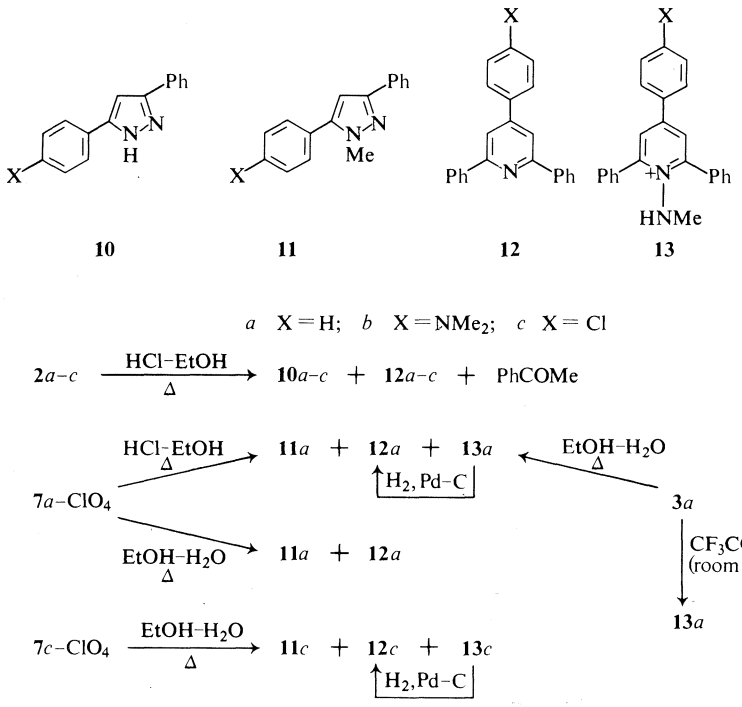

SCHEME 2

stantially diminishes this interaction with the effect that the barrier to ring inversion in **4***a* is decreased thus accounting for the lower observed activation energy. Since only the X-ray crystallographic picture of the 1,2(4*H*)-diazepinium picrate (**4***a*) and not of the conjugate base (**2***a*) has been reported (8), insight into their potential conformational differences in the solid state is not available at the present time.

Temperature variable n.m.r. measurements of **3***a* in $CDCl_3$–HCl and of **7***a*-ClO_4 in $CDCl_3$ also strongly support the existence of the 1,2(4*H*)-diazepinium species in solution. Upon cooling the solution of **3***a* in $CDCl_3$–HCl, the broad absorption for the C_4-hydrogens at $\tau \sim$ 4.5–6.7 observed at +35° gradually splits into two distinct doublets. At −30° (not low temperature limit), these are observed at τ 4.72 and 6.50 (J_{AB} = 10 Hz). Very similar spectral changes were observed for the 1,2(4*H*)-diazepinium salt **7***a*-ClO_4 in $CDCl_3$ solution.[8]

Acid-catalyzed Rearrangements

Upon reflux in 5 *N* ethanolic HCl solution for prolonged periods of time, the 1,2(4*H*)diazepines **2***a–c* underwent rearrangement to pyrazole (**10***a–c*) and pyridine (**12***a–c*) derivatives (Scheme 2). In the case of **2***a*, it was shown that acetophenone was produced in a yield closely corresponding to that of the pyrazole **10***a*. The less satisfactory material balance of products obtained from **2***b* is due to extensive decomposition observed during the course of the reaction. The same products in similar distribution were obtained from the reaction of **2***a* and **2***b* in 1:1 H_2O–TFA mixture at reflux (Table 3). Control runs showed that both types of products result from an acid-catalyzed process. Furthermore, 1-methyl-1,2(4*H*)-diazepinium salt **7***a*-ClO_4 in refluxing ethanolic HCl gave 67% of the *N*-methylpyrazole **11***a*, 13% of **12***a*, and a trace amount of the *N*-methylamino-2,4,6-triphenylpyridinium salt **13***a*. However, compound **7***a* in refluxing ethanol–water ($\sim$ 1:1) solution also provided **11***a* and **12***a* in comparable amounts thus showing the negligible effect of acid on the rearrangement processes. The absence of the pyridinium salt **13***a* is most likely the result of its instability with respect to **12***a* under these conditions as shown by separate control experi-

Can. J. Chem. Downloaded from www.nrcresearchpress.com by 210.87.254.105 on 09/05/12
For personal use only.

TABLE 3. Rearrangement of 1, 2-diazepines and -diazepinium salts

Compound	Condition[a]	Products (% yield)		
2*a*	A	**10***a*(81)	**12***a*(14)	
	B	(83)	(trace)	
2*b*	A	**10***b*(37)	**12***b*(24)	
	B	(35)	(22)	
2*c*	A	**10***c*(81)	**12***c*(14)	
3*a*	A	**11***a*(68)	**12***a*(18)	**13***a*(14)
	C	(12)	(86)	
	D			(100)[b]
	E		(92)	
7*a*-ClO_4	A	**11***a*(67)	**12***a*(13)	**13***a*(trace)[c]
	C	(60)	(5)	
	E	(trace)[c]		(90)
7*c*-ClO_4	C	**11***c*(64)	**12***c*(8)	**13***c*(5)

[a]A = 5 *N* HCl–EtOH, reflux; B = CF_3CO_2H–H_2O, 1:1, reflux; C = EtOH–H_2O, 1:1, reflux; D = CF_3CO_2H, room temperature; E = EtOH.
[b]By n.m.r. analysis.
[c]By t.l.c. analysis.

ments. The effect of exclusion of water and slightly lower reaction temperature was observed when **7***a*-ClO_4 was thermolyzed in ethanol solution. In this reaction, *N*-methylpyrazole (**11***a*) and pyridine (**12***a*) formation was essentially totally supressed and production of **13***a* was enhanced to a 90% yield. Identification of **13***a* was achieved by n.m.r. spectroscopy and by catalytic hydrogenation to 2,4,6-triphenylpyridine (**12***a*). The rearrangement of **7***c*-ClO_4 in ethanol–water provided the analogous products **11***c*, **12***c*, and **13***c* (see Experimental).

The reaction of 1-methyl-1,2(1*H*)-diazepine derivative **3***a* in 5 *N* HCl–EtOH gave the *N*-methylpyrazole **11***a* as the major product and compounds **12***a* and **13***a* in comparable and low yields. The effect of acid on this reaction was demonstrated in the control run (ethanol–water, 1:1) which gave only 12% of **11***a* and 86% of **12***a*. A similar yield of **12***a* was obtained from the thermolysis of **3***a* in ethanol. Clearly compound **12***a* is produced by a purely thermal rearrangement process. Under the nonhydrolytic and relatively milder conditions of TFA at room temperature, compound **3***a* gave the pyridinium salt **13***a* in quantitative yield (n.m.r. analysis).

A common mechanistic rationale for the acid-catalyzed rearrangement of 1,2-diazepines **2**, **3**, and **7** is given in Scheme 3. The 1,2(4*H*)-diazepinium cation **14** could, by hydrolytic ring opening, provide the intermediate **15**. The latter type of compound is known to produce pyrazolines (**16**) in refluxing ethanol solution (15)[9] and *N*-aminopyridinium salts (**20**) under acidic conditions (17). Furthermore, the acid-catalyzed reverse aldol reaction of pyrazolines (**16**) to pyrazoles (**17**) is known (15) and the partial thermal instability of **20**, R = Me, X = H with respect to the pyridine **12**, X = H, has been demonstrated (*vide supra*). Thus all the observed products (pyrazoles, pyridines, and *N*-aminopyridinium salts) may be explained by invoking the common intermediate **15**. However, since in the absence of water and yet under acidic conditions both **3***a* and **7***a* perchlorates provide the pyridinium salt **13***a* in high yield to the almost complete exclusion of pyrazole **11***a*, the alternate pathway for the formation of **13** ≡ **20**, **14** → **18** → **19** → **20**, appears to be more likely. Moreover, literature precedent exists for similar rear-

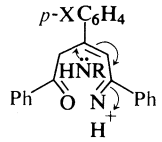

i

[9]Isomerization of **15** to **i** and electrocyclic ring closure of the latter (arrows) could also lead to the pyrazoline **16**. This type of cyclization has been proposed to occur in reactions of α, β-unsaturated ketones with hydrazines (16). However, evidence presented by Balaban (15) makes it unlikely that **i** would be an intermediate leading to the formation of **16**.

Can. J. Chem. Downloaded from www.nrcresearchpress.com by 210.87.254.105 on 09/05/12
For personal use only.

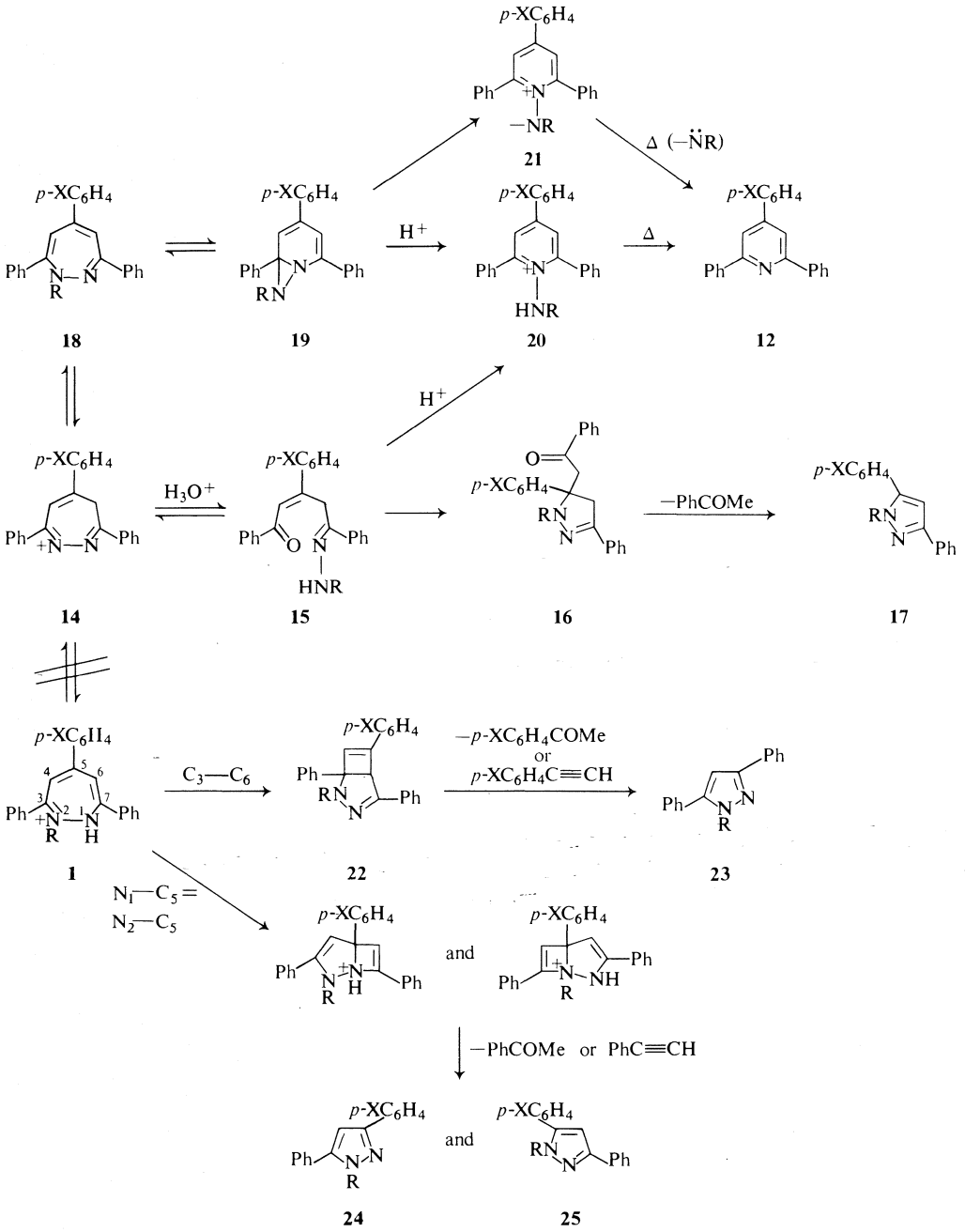

SCHEME 3

rangements in related systems (4a, 18–21).[10] Evidence for a diaziridine-type intermediate (**19**) in the proposed acid-catalyzed rearrangement is available in the single example reported by Pleiss and Moore (22).

In the absence of acid catalysis, the equilibrium **18** ⇄ **14** is not established and thus it is

[10]A series of derivatives **18** (R = COMe and other acyl functions) give compounds **21** and **12** in refluxing acetic acid. V. Snieckus. Unpublished results.

Can. J. Chem. Downloaded from www.nrcresearchpress.com by 210.87.254.105 on 09/05/12
For personal use only.

found that the 1,2(1*H*)-diazepine **3***a*≡**18** gives exclusively **12**, X = H, in protic (*vide supra*) and aprotic (23) solvents. These are then essentially thermolysis reactions and probably proceed *via* an electrocyclic process to the diaziridine **19** which loses a nitrene species[11] either directly or by way of the ylide **21** to give **12**, X = H.

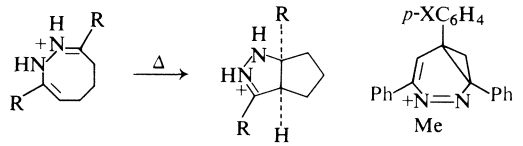

26 **27** **28**

It is of interest to consider an alternate mechanistic pathway for the formation of pyrazoles (**17**) from the 1,2(4*H*)-diazepinium salts (**14**) (Scheme 3) in light of recent categorization of cyclizations of quaternized azines [—CH(R)—CH=N—$\overset{+}{N}$(R)=CH—CH(R)—] (16*a*, 24) and the tautomeric bis-ene-hydrazines [—(R)C=CH—NH—NR—CH=C(R)—] (25) according to the Woodward–Hoffmann rules (16*a*). For example, it has been pointed out that cyclization **26** → **27** may be viewed in terms of a thermal disrotatory process (16*a*). The diazepinium salt **1**, formed by prototropy from **14**, is simply an extended conjugation analog of **26** and some other cases discussed (16*a*, 23, and 24). Clearly, however, this conjugation plays a critical role in the observed acid-catalyzed rearrangements as may be seen by reference to Scheme 3. Disrotatory ring closure of **1**, X = Cl, R = H or Me, involving C_3—C_6 and N_1—C_5 bond formations is predicted to lead to pyrazole **23**, R = H or Me, and an equal mixture of pyrazoles **24** and **25**, X = Cl, R = H or Me, respectively. The experiments carried out with compounds **2***b* and **2***c*, on the one hand, and compound **7***c*-ClO_4, on the other, clearly eliminate both pathways from consideration. Related 2,3-diazabicyclo[3.2.0]heptane derivatives (**22**) have been recently shown to undergo thermal fragmentation to pyrazoles (26).

Finally, it may be noted that products from the electrocyclic pathway **7** → **28** were not observed presumably due to the substantial energy disadvantage in going to an N—N double bond arrangement (27).

[11]Attempts to trap methyl nitrene in the thermolysis of **3***a* have been unsuccessful, ref. 23 and D. J. Harris, work in progress.

Experimental

For general experimental procedures, see the accompanying paper (5). Trifluoroacetic acid-*d* and ethanol-d_6 were obtained from Stohler Isotope Chemicals, Montreal. Methyl fluorosulfonate (Magic Methyl) was purchased from Aldrich Chemical Co.

Preparation of 1,2(4H)-Diazepinium Perchlorates **4***a*, **4***d*, **7***a*, *and* **7***c*

*3,5,7-Triphenyl-1,2(4H)-diazepinium Perchlorate (***4***a)*

Compound **2***a* (5) (0.32 g, 1 mmol) in 100 ml of ethanol was heated on a steam bath until most of the material dissolved. A small amount of solid was removed by filtration and the filtrate was treated with 1 ml of 70% perchloric acid solution. The solution was evaporated to dryness *in vacuo* and the residue was triturated with 5 ml of a chloroform–ether mixture (1:3 v/v) to give crystalline material which was collected by filtration and washed with copious quantities of ether. There was obtained 0.379 g (90%) of **4***a* which, after recrystallization from methylene chloride – petroleum ether (30–60°), showed m.p. 227–229°.

Anal. Calcd. for $C_{23}H_{19}N_2ClO_4$: C, 65.50; H, 4.50; N, 6.62. Found: C, 65.10; H, 4.52; N, 6.47.

*5-(p-Chlorophenyl)-3,7-diphenyl-1,2(4H)-diazepinium Perchlorate (***4***d)*

This compound was similarly prepared in 94.5% yield from **2***c* (5). Recrystallization from methylene chloride–petroleum ether (30–60°) gave an analytical sample, m.p. 226–228°.

Anal. Calcd. for $C_{23}H_{18}N_2Cl_2O_4$: C, 60.39; H, 3.94; N, 6.13. Found: C, 60.56; H, 4.06; N, 5.89.

*1-Methyl-3,5,7-triphenyl-1,2(4H)-diazepinium Perchlorate (***7***a*-ClO_4*)*

(*a*) *From 3,5,7-Triphenyl-1,2(4H)-diazepine (***2***a)*. Compound **2***a* (1.0 g, 3.1 mmol) in 40 ml of methylene chloride solution was cooled to 0° and treated with 3.5 ml of methyl fluorosulfonate also cooled to 0°. The mixture was stirred at 0° for 1 h and evaporated to dryness to yield an oil. The oil was dissolved in methanol and treated with 5 ml of 70% perchloric acid and sufficient water to induce precipitation. After 5 h at 0°, the precipitate was collected by filtration and washed with water and then ether to give 1.2 g (87%) of **7***a*-ClO_4, m.p. 158–160°.

Anal. Calcd. for $C_{24}H_{21}N_2ClO_4$: C, 65.98; H, 4.81; N, 6.41. Found: C, 65.92; H, 4.71; N, 5.79.

*(b) From 1-Methyl-3,5,7-triphenyl-1,2(1H)-diazepine (***3***a)*. Compound **3***a* (0.123 g, 0.75 mmol) in 30 ml of methanol was treated with 2 ml of 70% perchloric acid and then with sufficient water to cause cloudiness. After 1.5 h at 0°, the resulting precipitate was collected by filtration and washed thoroughly with water. There was obtained 0.160 g (90%) of **7***a*-ClO_4 which was shown to be identical with the compound prepared by method (*a*) above by m.p. and mixture m.p. determination.

*1-Methyl-3,7-diphenyl-5-(p-chlorophenyl)-1,2(4H)-diazepinium Perchlorate (***7***c*-ClO_4*)*

This compound was prepared from **2***c* and **3***c* (5) in quantitative and 74% yields, respectively, according to

Can. J. Chem. Downloaded from www.nrcresearchpress.com by 210.87.254.105 on 09/05/12
For personal use only.

Can. J. Chem. Downloaded from www.nrcresearchpress.com by 210.87.254.105 on 09/05/12
For personal use only.

methods (*a*) and (*b*) used for the synthesis of **7***a*-ClO_4. Recrystallization from ethanol–chloroform gave an analytical sample, m.p. 295–297°; n.m.r. τ 1.9–2.9 (m, 14H, aromatics), 3.1 (s, 1H, C_6-H) 5.98 (s, CH_3) superimposed on br envelope, 5.1–6.37 (CH_2), 5H.

Anal. Calcd. for $C_{24}H_{20}N_2Cl_2O_4$: C, 61.15; H, 4.25; N, 5.95. Found: C, 60.84; H, 4.01; N, 5.99.

Deuterium Exchange Studies in CF_3CO_2D–D_2O

Compound 2a

Compound **2***a* (100 mg, 0.31 mmol) was dissolved in TFA-*d* (2 ml), 4 drops of D_2O were added, and the solution was stirred at room temperature for 16.5 days. The solution was diluted with D_2O and extracted with methylene chloride. The organic extract was treated with anhydrous sodium bicarbonate and then dried (Na_2SO_4). Evaporation yielded 91 mg of deuterated **2***a*, m.p. 194.5–195.5°; *d*-content by relative integrated intensities of n.m.r. absorptions: C_4-H (71%), C_6-H (21%); from mass spectrum:[12] d_0 = 14%, d_1 = 32%, d_2 = 37%, d_3 = 12%, d_4 = 4%.

Compound 2b

Compound **2***b* (5) (30 mg, 0.08 mmol) was dissolved in TFA-*d* (1 ml) containing three drops of D_2O and the solution was allowed to stand at room temperature for 72 days. Work-up as for compound **2***a* gave 20 mg of deuterated **2***b*, m.p. 214–216°; *d*-content by integrated intensity of n.m.r. absorptions: C_4-H (100%) (overlap of C_6-H with aromatic proton absorption precluded estimation of exchange at C_6); from mass spectrum: d_0 = 9%, d_1 = 21%, d_2 = 34%, d_3 = 28%, d_4 = 7%.

When the reaction was carried out for 16 days, only 30% exchange at C_4 was observed by n.m.r. analysis.

Compound 3a

Compound **3***a* (5) (100 mg, 0.30 mmol) was dissolved in TFA-*d* (2 ml), 10 drops of D_2O were added, and the solution was heated on a steam bath for 20 min. Work-up as for compound **2***a* gave 84 mg of deuterated **3***a*, m.p. 116–118°; *d*-content by integrated intensity of n.m.r. absorption *immediately* after isolation: C_6-H (50%) (overlap of C_4-H with aromatic proton absorption precluded estimation of exchange at C_4); from mass spectrum: d_0 = 43%, d_1 = 39%, d_2 = 17%, d_3 = 5%, d_4 = 3%.

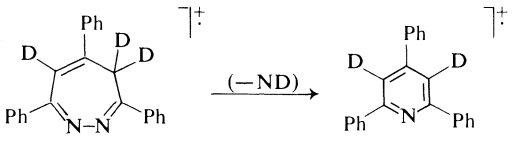

m/e 324 *m/e* 308

[12]Comparison of the mass spectra of **2***a* and deuterated **2***a* [*m/e*, % relative intensity: 324 (M^+, 33), 308 (17), 296 (11), 221 (100), 219 (33), 205 (11), 118 (33), 116 (29), 103 (53)] provides evidence for a minor fragmentation pathway proceeding by ND expulsion (*m/e* 324 → 308) (probably *via* the proposed mechanism for the thermolysis **18** → **19** → **21**, Scheme 3) rather than by loss of the C_4-methylene and a 3-phenyl hydrogen in concert as previously proposed (13*a*).

Rearrangement of Compounds 2a–c, 3a, 7a, and 7c (Scheme 2)

(a) In 5 N Ethanolic HCl and in EtOH–H_2O Solutions

Compound 2a. Compound **2***a* (387 mg, 1.2 mmol) was refluxed in 20 ml of 5 *N* ethanolic HCl solution for 48 h. The mixture was cooled and neutralized with cold concentrated ammonium hydroxide solution. The mixture was extracted with ether and the ether extract was dried (Na_2SO_4) and evaporated to dryness. Chromatography over silica gel (benzene) gave, in order of elution, acetophenone (characterized as its 2,4-dinitrophenylhydrazone by m.p. and mixture m.p. comparison with an authentic sample); 3,5-diphenylpyrazole (**10***a*), m.p. 201.5–204° (lit. (28) m.p. 198–200°); and 2,4,6-triphenylpyridine (**12***a*), m.p. 133.5–135.5° (lit. (29) m.p. 137–138°) in amounts indicated in Table 3. Compounds **10***a* and **12***a* were found to be identical with authentic samples by mixture m.p. and n.m.r. spectral determinations.

In a control experiment, refluxing **2***a* in ethanol–water (57:43 v/v) for 48 h resulted in quantitative recovery of starting material.

The above experiments were carried out on compounds **2***b* and **2***c* to give products and yields indicated in Table 3.

Compound 3a. Compound **3***a* (220 mg, 0.66 mmol) was refluxed in 20 ml of 5 *N* ethanolic HCl solution for 24 h. Work-up and chromatography as in the case of **2***a* gave the pyrazole **11***a*, the pyridine **12***a*, and 1-methylamino-2,4,6-triphenylpyridinium salt **13***a* in yields indicated in Table 3. The characterization of **13***a* is given in a later section.

The control experiment was executed on 355 mg (1.1 mmol) of **3***a* in 40 ml of an ethanol–water (57:43 v/v) mixture for 24 h. Isolation of products as above gave the results shown in Table 3.

Compound 7a-ClO_4. Compound **7***a*-ClO_4 (330 mg, 0.76 mmol) was refluxed in 20 ml of 5 *N* ethanolic HCl solution for 24 h. Processing the reaction mixture in the manner described for **2***a* gave 1-methyl-3,5-diphenylpyrazole (**11***a*), m.p. 54–57° (lit. (30) m.p. 59–60°); 2,4,6-triphenylpyridine (**12***a*); and the pyridinium salt **13***a* in yields indicated in Table 3. Compounds **11***a* and **12***a* were found to be identical with authentic samples by m.p. and n.m.r. spectral determinations.

In the control experiment, compound **7***a*-ClO_4 (300 mg) was refluxed in 40 ml of an ethanol–water (57:43 v/v) solution to give results shown in Table 3.

Compound 7c-ClO_4. Compound **7***c*-ClO_4 (340 mg) was refluxed in 40 ml of an ethanol–water (57:43 v/v) solution as described for **7***a*-ClO_4 to give results indicated in Table 3.

(b) In CF_3CO_2H–H_2O Solution

Compound **2***a* (322 mg, 1.0 mmol) was refluxed in 40 ml of TFA–H_2O solution (1:1) for 24 h. Work-up as in the case of procedure (*a*) above gave the products in yields shown in Table 3.

Compound **2***b* was similarly treated to give the results indicated in Table 3.

Characterization of Pyrazoles 10b, 10c, and 11c

5-(p-Dimethylaminophenyl)-3-phenylpyrazole (10b)

This was prepared in 57% yield by the method of Hauser and co-workers (28). Recrystallization from ethanol gave an analytical sample, m.p. 192.5–193.5°;

n.m.r. (CF_3CO_2H) τ 1.7–2.5 (m, 10H, aromatics), 2.6 (s, 1H, pyrazole ring H), 6.5 (s, 6H, $N(CH_3)_2$); mass spectrum (*m/e*, % relative intensity) 263 (M^+, 100), 262 (39), 131 (21).

Anal. Calcd. for $C_{17}H_{17}N_3$: C, 77.54; H, 6.51; N, 15.96. Found: C, 77.74; H, 6.61; N, 16.34.

*5-(p-Chlorophenyl)3-phenylpyrazole (**10c**)*

This was prepared by the method of Widman (31), m.p. 217–218° (lit. (31) m.p. 216–217°).

*1-Methyl-5-(p-chlorophenyl)-3-phenylpyrazole (**11c**)*

This was first obtained crystalline from the reaction of the 1-methyl-1,2(4*H*)-diazepinium salt **7***c*-ClO_4. Two recrystallizations from hexane gave an analytical sample, m.p. 59–60°; n.m.r. τ 2.0–2.25 (m, 2H) and 2.35–2.75 (m, 7H), aromatics, 3.35 (s, 1H, pyrazole ring H), 6.1 (s, 3H, NCH_3); mass spectrum (m/e, % relative intensity) 270 [$M^+(^{37}Cl)$, 30], 268 [$M^+(^{35}Cl)$ 100], 267(13), 167(< 1), 165(< 1). Fragmentation by loss of PhCN (270 → 167, 268 → 165) is indicated.

Anal. Calcd. for $C_{16}H_{13}N_2Cl$: C, 71.52; H, 4.84; N, 10.43. Found: C, 71.36; H, 5.04; N, 10.51.

*Preparation of Pyridines **12b** and **12c***

*4-(p-Dimethylaminophenyl)-2,6-diphenylpyridine (**12b**)*

This was prepared by adoption of a literature method (29), m.p. 132–134° (lit. (32) m.p. 137°).

*4-(p-Chlorophenyl)-2,6-diphenylpyridine (**12c**)*

This was prepared by adoption of a literature method (29), m.p. 128–130° (lit. (33) m.p. 129–130°).

*Characterization of Pyridinium Salts **13a** and **13c***

*1-Methylamino-2,4,6-triphenylpyridinium Perchlorate (**13a**)*

This compound was best obtained by refluxing **7***a*-ClO_4 (300 mg, 0.72 mmol) in dry acetonitrile (30 ml) for 24 h. Evaporation of the solution to dryness *in vacuo* gave a glass which upon trituration with petroleum ether (30–60°) gave 250 mg (82%) of **13***a* as a powdery solid. Two recrystallizations from ethanol–chloroform (9:1) gave an analytical sample, m.p. 188–189°; n.m.r. τ 2.15 (s, pyridine ring β-H) and 1.90–2.75 (m, aromatics), 17H, 3.9 (q, 1H, J = 6 Hz, NH, exchangeable with D_2O), 7.7 (d, 3H, NCH_3, J = 6 Hz, collapses into singlet upon D_2O exchange).

Anal. Calcd. for $C_{24}H_{21}N_2ClO_4$: C, 65.98; H, 4.81; N, 6.42. Found: C, 65.56; H, 4.91; N, 6.32.

Compound **13***a* (165 mg, 0.378 mmol) was dissolved in 60 ml of absolute ethanol and hydrogenated at atmospheric pressure in the presence of 5% palladium on charcoal (20 mg) (34). The reaction was stopped after 3 h and the solution was processed in the normal manner. Preparative t.l.c. (silica gel) gave 80 mg (69%) of 2,4,6-triphenylpyridine (**12***a*) identified by m.p. and mixture m.p. comparison with an authentic sample.

*1-Methylamino-4-(p-chlorophenyl)-2,6-diphenylpyridinium Perchlorate (**13c**)*

Compound **7***c*-ClO_4 (300 mg, 0.64 mmol) was refluxed in acetonitrile solution as described for **7***a*-ClO_4 to give, after work-up, 280 mg (93%) of **13***c* as a yellow powder. Recrystallization from $CHCl_3$ – EtOH – petroleum ether (30–60°) provided an analytical sample, m.p. 164–165°; n.m.r. τ 2.15 (s, pyridine ring β-H) and 1.9–2.6 (m, aromatics), 16H, 3.9 (q, 1H, J = 6 Hz, NH, exchangeable with D_2O), 7.74 (d, 3H, NCH_3, collapses into singlet upon D_2O exchange).

Anal. Calcd. for $C_{24}H_{20}N_2Cl_2O_4$: C, 61.15; H, 4.25; N, 5.95. Found: C, 61.00; H, 4.28; N, 5.78.

Compound **13***c* (140 mg, 0.30 mmol) was hydrogenated according to the conditions described for **13***a* above to give, after preparative t.l.c., 52 mg (91% based on recovered starting material) of 4-(*p*-chlorophenyl)-2,6-diphenylpyridine (**12***c*) which was found to be identical with an authentic sample by m.p. and mixture m.p. determination.

*Stability of Compound **13a** in Ethanol–Water Solution*

A solution of **13***a* (168 mg) in 35 ml of EtOH–H_2O (57:43 v/v) was refluxed for 24 h. Separation by preparative t.l.c. gave 17 mg (18%) of 2,4,6-triphenylpyridine (**12***a*) identified by m.p. and mixture m.p. comparison with an authentic sample. The remainder of the material balance was recovered **13***a* (n.m.r. analysis).

We thank the National Research Council of Canada and Bristol Laboratories for continued support. We are grateful to Professor L. W. Reeves and Dr. R. Hobson (Waterloo) and Professor R. Bell and Mr. B. Sayer (McMaster University) for the 100-MHz temperature variable n.m.r. spectra. Mass spectra were most efficiently provided by Professor J. M. Miller, Brock University. (We thank our department for financial assistance in this connection). Dr. G. Y.-P. Kan carried out some preliminary experiments and C. Bender and M. Kaufman (Chem 13 News Award holders, University of Waterloo) helped with large scale preparations. We thank J. J. Kobliska, American Cyanamid Co., for carrying out some of the elemental analyses.

1. M. T. Thomas, V. Snieckus, and E. Klingsberg. Chem. Commun. 504 (1972).
2. E. Klingsberg, Abstr. Am. Chem. Soc. Meeting, September, 1965. p. 66S.
3. M. T. Thomas, V. Snieckus, and E. Klingsberg. 55th Canadian Chemical Conference of the Chemical Institute of Canada, Quebec, Quebec. June, 1972. Abstr. p. 8.
4. (*a*) J. A. Moore and E. Mitchell. *In* Heterocyclic compounds. Vol. 9. *Edited by* R. C. Elderfield. Wiley, New York. 1967. p. 224; (*b*) F. D. Popp and A. C. Noble. Advan. Heterocycl. Chem. **8**, 21 (1967).
5. D. J. Harris, G. Y.-P. Kan, V. Snieckus, and E. Klingsberg. Can. J. Chem. This issue.
6. A. R. Butler, D. Lloyd, and D. R. Marshall. J. Chem. Soc. B, 795 (1971).
7. K. Venkataraman. The chemistry of synthetic dyes. Academic Press, Inc. New York. 1963, Chapts. XXIII–XXV and XXXVIII.
8. R. Gerdil. Helv. Chim. Acta, **55**, 2159 (1972).
9. A. T. Balaban. Tetrahedron, **26**, 739 (1970).
10. A. M. Gorringe, D. Lloyd, and D. R. Marshall. J. Chem. Soc. C, 1081 (1969).
11. J. C. N. Ma and E. W. Warnhoff. Can. J. Chem. **43**, 1849 (1965).
12. P. Forsythe, R. Frampton, C. D. Johnson, and A. R. Katritzky. J. Chem. Soc. Perkin 2, 671 (1972).
13. (*a*) O. Buchardt, C. L. Pedersen, U. Svanholm, A. M. Duffield, and A. T. Balaban. Acta Chem.

Can. J. Chem. Downloaded from www.nrcresearchpress.com by 210.87.254.105 on 09/05/12
For personal use only.

Scand. **23**, 3125 (1969); (*b*) U. SVANHOLM. Acta Chem. Scand. **25**, 640 (1971).
14. D. KOST, E. H. CARLSON, and M. RABAN. Chem. Commun. 656 (1971).
15. A. T. BALABAN. Tetrahedron, **26**, 739 (1970).
16. (*a*) J. ELGUERO. Bull. Soc. Chim. Fr. 1925 (1971); (*b*) G. COISPEAU, J. ELGUERO, R. JACQUIER, and D. TIZANE. Bull. Soc. Chim. Fr. 1581 (1970) and H. FERRES, M. S. HAMDAM, and W. R. JACKSON. J. Chem. Soc. Perkin 2, 936 (1973).
17. C. L. PEDERSEN, N. HARRIT, and O. BUCHARDT. Acta Chem. Scand. **24**, 3435 (1970); *cf.* also ref. 4*a*.
18. J. STREITH and J.-M. CASSAL. Bull. Soc. Chim. Fr. 2175 (1969).
19. G. KAN, M. T. THOMAS, and V. SNIECKUS. Chem. Commun. 1022 (1971).
20. J. A. MOORE, E. J. VOLKER, and C. M. KOPAY. J. Org. Chem. **36**, 2676 (1971).
21. I. SATATY. Tetrahedron, **28**, 2307 (1972).
22. M. G. PLEISS and J. A. MOORE. J. Am. Chem. Soc. **90**, 4738 (1968).
23. V. SNIECKUS and G. KAN. Chem. Commun. 1208 (1970).
24. L. ZIRNGIBL and S. W. TAM. Helv. Chim. Acta. **53**, 1927 (1970).
25. H. FRITZ and P. UHRHAN. Ann. **744**, 81 (1971).
26. J. A. MOORE, W. J. FREEMAN, K. KURITA, and M. G. PLEISS. J. Org. Chem. **38**, 2939 (1973).
27. A. STEIGEL, J. SAUER, D. A. KLEIER, and G. BINSCH. J. Am. Chem. Soc. **94**, 2770 (1972).
28. C. F. BEAM, R. S. FOOTE, and C. R. HAUSER. J. Chem. Soc. C, 1658 (1971).
29. K. DIMROTH and K. H. WOLF. *In* Newer methods of preparative organic chemistry. Vol. III. *Edited by* W. Foerst. Academic Press, Inc. New York and London. 1964. p. 413.
30. R. HUISGEN, H. GOTTHARDT, and R. GRASHEY. Chem. Ber. **101**, 536 (1968).
31. O. WIDMAN. Chem. Ber. **49**, 477 (1916).
32. A. TREIBS and H. BADER. Chem. Ber. **90**, 789 (1957).
33. R. L. FRANK and R. P. SEVEN. J. Am. Chem. Soc. **71**, 2629 (1949).
34. T. OKAMOTO, S. HAYASHI, H. HORIKIRI, and M. HIROBE. J. Pharm. Soc. Japan. **91**, 210 (1971).

Can. J. Chem. Downloaded from www.nrcresearchpress.com by 210.87.254.105 on 09/05/12
For personal use only.

Biosynthesis of Corydaline and of Ochotensimine[1]

H. L. Holland, M. Castillo, D. B. MacLean, and Ian D. Spenser
Department of Chemistry, McMaster University, Hamilton, Ontario L8S 4M1

Received February 19, 1974

H. L. Holland, M. Castillo, D. B. MacLean, and Ian D. Spenser. Can. J. Chem. **52**, 2818 (1974).

Radioactivity from [3-^{14}C]tyrosine and from [*methyl*-^{14}C]methionine is incorporated non-randomly into predicted positions of corydaline and ochotensimine in *Corydalis solida* and *C. ochotensis*, respectively. The methyl group of methionine supplies the *C*-methyl group of corydaline and the exocyclic methylene group of ochotensimine, as well as the "bridge" carbon atom and the exocyclic *O*- and *N*-attached one-carbon units of each alkaloid. Maintenance of the $^{3}H/^{14}C$ ratio of [*methyl*-^{3}H,^{14}C]methionine within these units of corydaline is consistent with incorporation of intact CH_3 groups.

Partial loss of ^{3}H relative to ^{14}C is observed in the course of a Schmidt reaction of [2-^{3}H,2-^{14}C] acetate.

H. L. Holland, M. Castillo, D. B. MacLean et Ian D. Spenser. Can. J. Chem. **52**, 2818 (1974).

La radioactivité due à la [^{14}C-3] tyrosine et à la [^{14}C-méthyl]méthionine est respectivement introduite, d'une façon ordonnée, dans des positions prévues de la corydaline et d'ochotensimine dans la *Corydalis solida* et la *C. ochotensis*. Le groupe méthyle de la méthionine alimente le groupe *C*-méthyl de la corydaline, le méthylène exocyclique de l'ochotensimine ainsi que l'atome de carbone de pont et les groupements exocycliques à un atome de carbone relié à *O* ou *N* de chaque alcaloïde. La conservation du rapport $^{3}H/^{14}C$ de la [^{3}H-, ^{14}C-méthyl] méthionine à l'intérieur de ces unités de corydaline est en accord avec l'hypothèse que les groupes CH_3 sont introduits d'une façon intacte. On observe une perte partielle de ^{3}H relative à ^{14}C durant la réaction de Schmidt effectuée sur de l'acétate [^{3}H-2, ^{14}C-2].

[Traduit par le journal]

Introduction

Chemical models which have been proposed (1) for the biogenesis of ochotensine (**1**) and ochotensimine (**2**), spirobenzylisoquinoline alkaloids which contain an exocyclic methylene group (2,3), envisage a skeletal rearrangement of a suitably functionalized protoberberine precursor in which a preformed *C*-methyl group is already present at the corresponding position, C-13, and is converted into the exocyclic methylene group in the course of the rearrangement (Scheme 1). Such a C-13 methylated protoberberine precursor would be closely related to the alkaloid corydaline (**5**). The simultaneous occurrence of corydaline and ochotensine in *Corydalis solida*[2] may then be more than coincidental.

The origin of the *C*-methyl group of corydaline has not been determined. The suggestion has been made (5) that this group arises from a one-carbon unit which is introduced into C-13 of a preformed protoberberine system (Scheme 2). An analogous chemical synthesis of the corydaline skeleton, by reaction of formaldehyde (6) or of methyl iodide (7) with a dihydroprotoberberine, has been accomplished.

An alternative proposal (8) for the biogenesis of corydaline (Scheme 3) does not invoke an intermediate containing a preformed protoberberine system, but envisages that the corydaline skeleton is generated by *de novo* combination of amino acid fragments. In particular, the segment of corydaline containing the *C*-methyl group is thought to be derived from a branched chain C_6—C_3 unit (*e.g.*, **6**), analogous in structure to tropic acid (**13**).

It was the aim of the present study to establish the origin of the *C*-methyl group of corydaline and the exocyclic methylene group of ochotensimine. The evidence to be presented demon-

[1]This paper is dedicated to Professor Otto Hoffmann-Ostenhof, Professor of Biochemistry, Institute of General Biochemistry, University of Vienna, Austria, on the occasion of his 60th birthday, October 18, 1974.

[2]C. K. Yu, H. L. Holland, D. B. MacLean, R. H. F. Manske, and R. Rodrigo. Unpublished observation (1972).

Can. J. Chem. Downloaded from www.nrcresearchpress.com by 210.87.254.6 on 09/05/12
For personal use only.

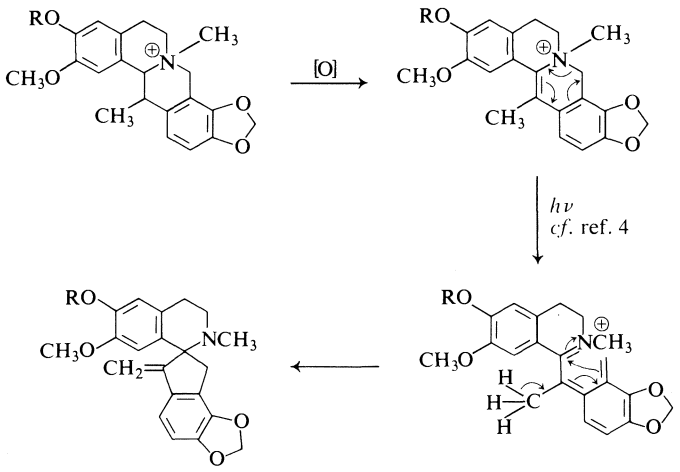

1 R = H (Ochotensine)
2 R = CH_3 (Ochotensimine)

SCHEME 1 Biogenesis of ochotensimine. One of several possible routes (*cf.*, refs. 1, 4) for the transformation of the protoberberine into the spirobenzylisoquinoline skeleton

strates unequivocally that in each case a one-carbon unit serves as the precursor. The findings lend support to the view that the spirobenzylisoquinoline and the 13-methylprotoberberine systems are further structural variants among the alkaloids related to norlaudanosoline (**3**), as had been widely assumed.

Methods and Results

In six tracer experiments, specifically labelled samples of methionine, tyrosine, and phenylalanine were administered by the wick method to intact plants of *Corydalis solida* (L.) Swartz (Expts. *S*1, *S*2, *S*3) and of *Corydalis ochotensis* Turcz. (Expts. *O*1, *O*2, *O*3). Samples of corydaline and of ochotensine and ochotensimine, respectively, were isolated from these plants. Corydaline was purified to constant radioactivity by repeated crystallization and sublimation at reduced pressure. Ochotensine was purified by crystallization. Ochotensimine was converted into the methiodide which was crystallized to constant radioactivity. The details of these experiments are recorded in Tables 1 and 2.

The alkaloids from the feeding experiments with methionine and tyrosine were highly radioactive (Expts. *S*1, *S*2, *S*3, *O*1, *O*3). Label from phenylalanine was not incorporated to a significant extent into the alkaloids of *C. ochotensis* (Expt. *O*2).

The labelled samples of corydaline and of ochotensimine, obtained from individual feeding experiments, were diluted with inactive carrier and degraded by reactions, described in the Experimental section, into the degradation products shown in Schemes 4 and 5. The specific activities of the degradation products are listed in Tables 3 and 4 (indicated limits are standard deviation of the mean).

The samples of corydaline and of ochotensimine, derived from the experiments with [3-^{14}C]tyrosine (Expts. *S*3 and *O*3) yielded acetic acid containing one-half of the activity of the intact alkaloid (Tables 3 and 4). Since the methylamine obtained by further degradation of the acetic acid was devoid of activity in each case, it was the carboxyl group of the acetate, and hence the ring carbon of corydaline and of ochotensimine to which the *C*-methyl and the *C*-methylene group, respectively, is attached, which contained one-half of the activity of each alkaloid molecule.

The sample of ochotensimine, derived from the experiment with [*methyl*-^{14}C]methionine

Can. J. Chem. Downloaded from www.nrcresearchpress.com by 210.87.254.6 on 09/05/12
For personal use only.

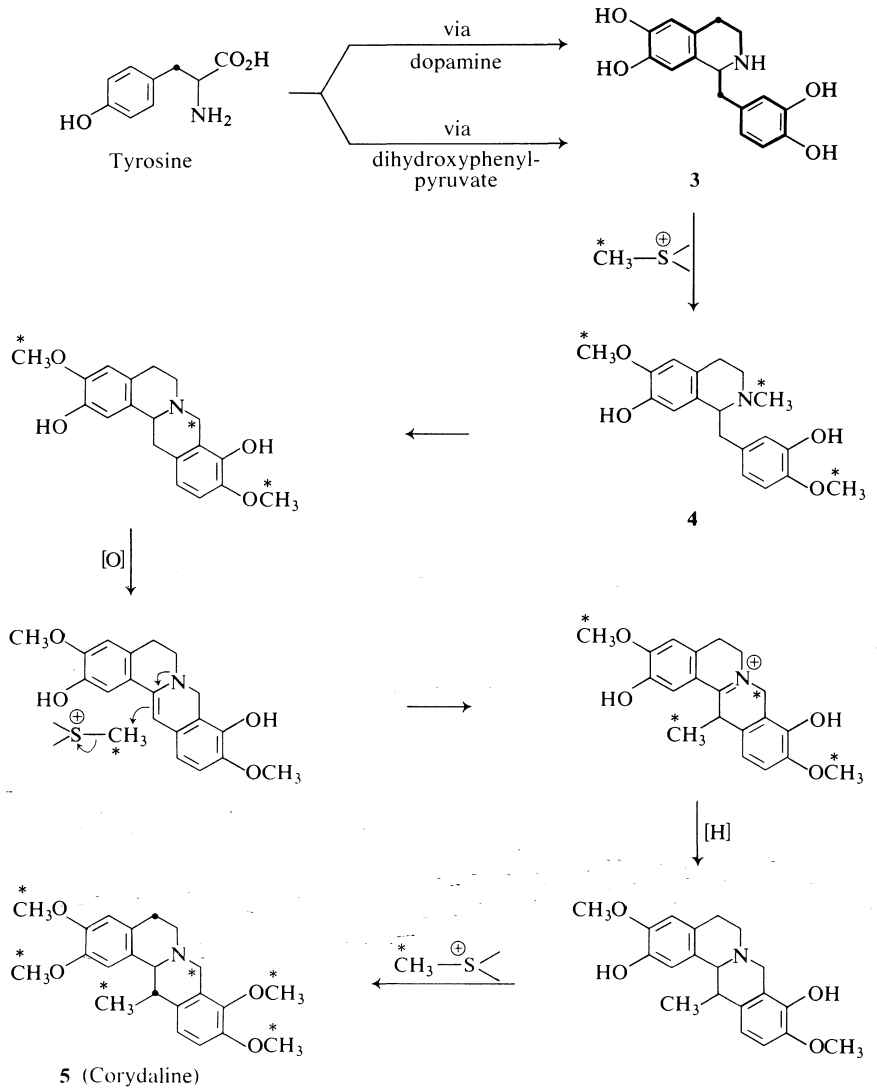

SCHEME 2. Protoberberine route to corydaline

(Expt. *O*1) contained approximately one-sixth of its activity within the exocyclic methylene group (Schmidt methylamine), and one-sixth within the methylenedioxy group (formaldehyde). The phthalic acid derivative (**11**) obtained from rings C and D contained one third of the total activity. Half of this activity, *i.e.* one-sixth of the total, is accounted for by the methylenedioxy group (Table 4).

The corydaline derived from [*methyl*-^{14}C]methionine (Expt. *S*1 and Expt. *S*2, ^{14}C activity) contained one fifth of its ^{14}C-activity at the *C*-methyl group (Schmidt methylamine) and one fifth at the berberine bridge (C-8) (benzoic acid). Des-*O*-methylcorydaline (**7**) accounts for two fifths of the ^{14}C-activity of corydaline. The relative specific activity of tetramethylammonium chloride, representing the average ^{14}C activity of four *O*-methyl groups, was one sixth that of the intact alkaloid. The four *O*-methyl groups thus

Can. J. Chem. Downloaded from www.nrcresearchpress.com by 210.87.254.6 on 09/05/12
For personal use only.

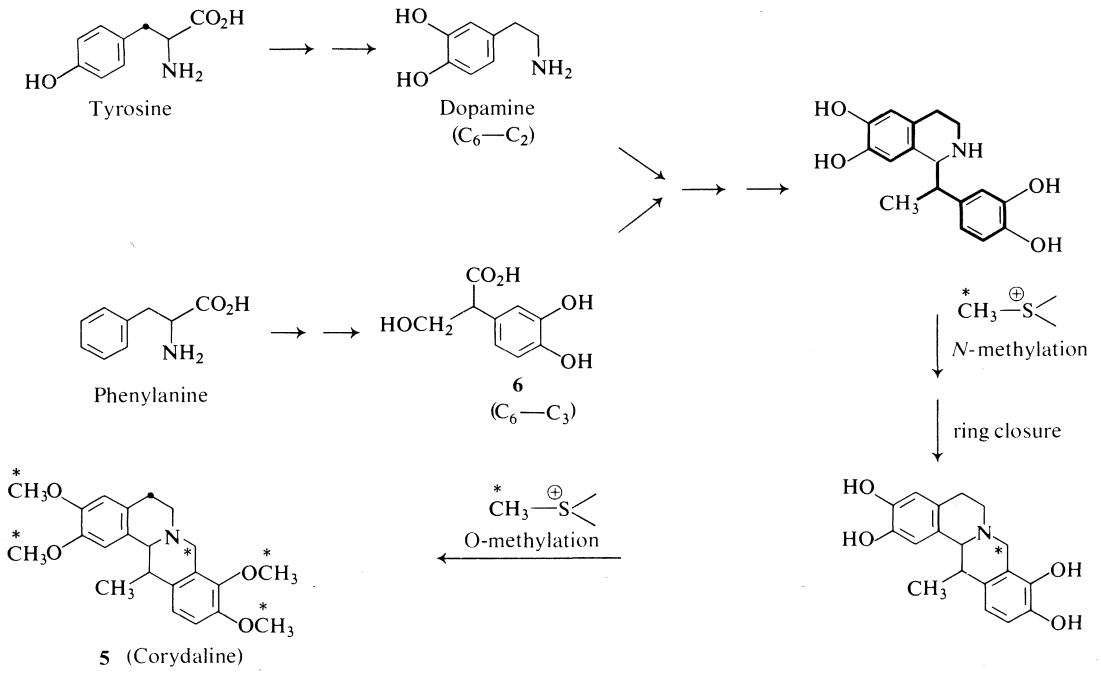

SCHEME 3. Biogenesis of corydaline. Route from a branched C_6—C_3 precursor (now disproved)

account for two thirds of the ^{14}C activity of the alkaloid (Table 3).

The $^{3}H/^{14}C$ ratio found within the corydaline derived from [*methyl*-^{3}H,^{14}C]methionine (Expt. *S*2) is compared with the $^{3}H/^{14}C$ ratio of the precursor and with that observed within the degradation products of corydaline (Table 5). Some loss of ^{3}H, relative to ^{14}C (10–20%) in corydaline and in all but one of its degradation products is observed, compared to the $^{3}H/^{14}C$ ratio of the doubly labelled methionine.

Schmidt degradation of [2-^{3}H,2-^{14}C]acetate under three different experimental conditions (sulfuric acid (98 and 85% w/v) and phosphoric acid (85%)) leads to [^{3}H,^{14}C]-methylamine whose $^{3}H/^{14}C$ ratio is approximately 5% lower than that of the acetate from which it is derived (Table 6).

Discussion

Several tests can be applied to invalidate one or the other of the two hypotheses which have been advanced to account for the origin of corydaline.

The simplest of these tests is a tracer experiment with a one-carbon donor such as [*methyl*-^{14}C]methionine. The protoberberine route (5) to corydaline demands that the *C*-methyl group is derived from such a precursor. The branched chain route (8) demands that it is not. In the case of the protoberberine route (9), and probably also in the other case, five other sites within the molecule, namely the "berberine bridge" (C-8) and four *O*-methyl functions, will incorporate the tracer if corydaline formation occurs at the time of the experiment, and this serves as internal evidence of active biosynthesis (Scheme 6).

Tyrosine would serve as a precursor of the two C_6—C_2 units which complete the skeleton of the molecule, if corydaline originated via the protoberberine route (10). In the case of the other postulated route to corydaline only one tyrosine derived C_6—C_2 unit is likely to be involved. The other fragment required to complete the corydaline skeleton by this route, a phenolic branched chain C_6—C_3 unit, might be derived from phenylalanine or tyrosine by rearrangement of the carbon chain. Such a rearrangement might be analogous to that which leads, by a carboxyl migration of unknown mechanism, from phenylalanine (**12**) to tropic acid (**13**) (11) or it might be similar to that which leads from phenylalanine, by phenyl migration, to the branched chain phenylpropanoid moiety of the isoflavones (*e.g.*,

Can. J. Chem. Downloaded from www.nrcresearchpress.com by 210.87.254.6 on 09/05/12
For personal use only.

Can. J. Chem. Downloaded from www.nrcresearchpress.com by 210.87.254.6 on 09/05/12
For personal use only.

TABLE 1. Experiments with *Corydalis solida*

Expt. No.	Substrate	Nominal activity: Specific (mCi/mmol)	Nominal activity: Total (mCi)	No. of plants	Date	Product, corydaline (**4**): (mg)	Product, corydaline (**4**): Specific activity (^{14}C) (d.p.m./mmol)
*S*1	L-[*methyl*-^{14}C]Methionine[a]	60	0.1	25	April 1970	10	2.5×10^7
*S*2	L-[*methyl*-^{14}C]Methionine[a] L-[*methyl*-^{3}H]Methionine[a]	56 5000	0.1 1.0	16	May 1972	9	5.5×10^7
*S*3	DL-[3-^{14}C]Tyrosine[b]	11	0.1	16	May 1972	12.5	4.1×10^7

[a]Amersham/Searle.
[b]New England Nuclear.

TABLE 2. Experiments with *Corydalis ochotensis*

Expt. No.	Substrate	Nominal activity: Specific (mCi/mmol)	Nominal activity: Total (mCi)	No. of plants	Date	Products: Ochotensimine (**6**): Yield (mg)	Products: Ochotensimine (**6**): SA (d.p.m./mmol)	Products: Ochotensine (**5**): Yield (mg)	Products: Ochotensine (**5**): SA (d.p.m./mmol)
*O*1	L-[*methyl*-^{14}C]Methionine[a]	56	0.1	4	July 1972	95	7.6×10^6	16	5.8×10^4
*O*2	DL-[3-^{14}C]Phenylalanine[b]	50	0.1	5	July 1971	62	5.8×10^3	20	2.5×10^3
*O*3	DL-[3-^{14}C]Tyrosine[b]	50	0.1	8	August 1972	272	2.3×10^5	24	1.1×10^6

[a]Amersham/Searle.
[b]Commissariat à l'Énergie Atomique, France.

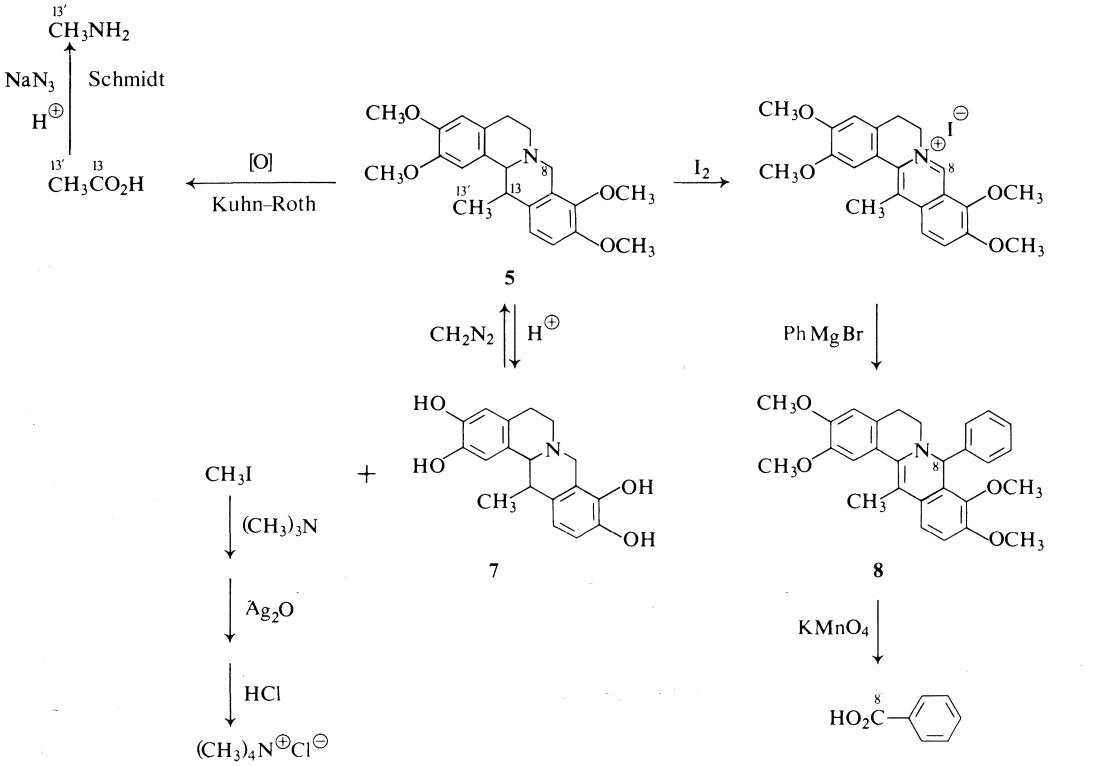

SCHEME 4. Degradation of corydaline

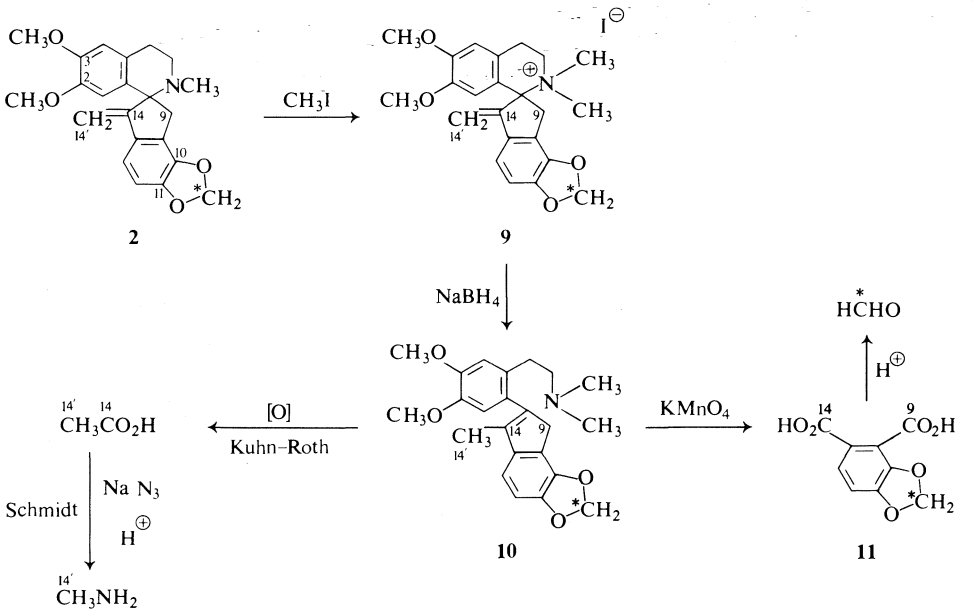

SCHEME 5. Degradation of ochotensimine

Can. J. Chem. Downloaded from www.nrcresearchpress.com by 210.87.254.6 on 09/05/12
For personal use only.

Can. J. Chem. Downloaded from www.nrcresearchpress.com by 210.87.254.6 on 09/05/12
For personal use only.

TABLE 3. Distribution of label within corydaline

Products	Carbon atoms of corydaline	Substrates: L-[*methyl*-^{14}C]Methionine Expt. *S*1 SA[a]	RSA[b]	L-[*methyl*-^{14}C]Methionine Expt. *S*2 SA[ac]	RSA[b]	DL-[3-^{14}C]Tyrosine Expt. *S*3 SA[a]	RSA[b]
Corydaline (diluted) (**4**)	All	10.11 ± 0.22[d]	100 ± 2	90.43 ± 0.87[d]	100 ± 1	15.64 ± 0.19[d]	100 ± 1
Kuhn–Roth acetate (as α-naphthylamide)	C-13,13′	1.91 ± 0.05	19 ± 1	18.61 ± 0.25	21 ± 1	7.84 ± 0.16	50 ± 1
Schmidt methylamine (as β-naphthoyl derivative)	C-13′			17.30 ± 0.16	19 ± 1	0.01 ± 0.02	0
Corydaline (diluted) (**4**)	All	10.11 ± 0.22[d]	100 ± 2	76.20 ± 0.53[d]	100 ± 1		
Methyl iodide (as tetramethylammonium chloride)	Average of four OCH_3 groups	1.67 ± 0.04	17 ± 1	11.96 ± 0.52	16 ± 1		
Corydaline (diluted) (**4**)	All			98.01 ± 0.94[d]	100 ± 1		
Benzoic acid	C-8			17.37 ± 0.48	18 ± 1		
Corydaline (diluted) (**4**)	All			72.85 ± 0.30[d]	100 ± 1		
Des-*O*-methylcorydaline(**7**)	All except four OCH_3 groups			28.10 ± 0.81	39 ± 1		

[a]SA = specific activity (d.p.m. per mmol) × 10^{-4}.
[b]RSA = relative specific activity (%) (intact corydaline = 100).
[c]Specific activity due to ^{14}C only.
[d]Obtained from the original labelled corydaline (Table 1) by dilution with inactive corydaline.

TABLE 4. Distribution of label within ochotensimine

Product	Carbon atoms of ochotensimine	Substrates: Expt. *O*1 L-[*methyl*-^{14}C]Methionine SA[a]	Expt. *O*1 RSA[b]	Expt. *O*3 DL-[3-^{14}C]Tyrosine SA[a]	Expt. *O*3 RSA[b]
Reduction product (**10**) of ochotensimine methiodide[c]	All	64.01±0.57	100±1	9.24±0.11	100±1
Kuhn–Roth acetate (as α-naphthylamide)	C-14,14′	10.30±0.19	16±1	4.53±0.08	49±1
Schmidt methylamine (as β-naphthoyl derivative)	C-14′	10.42±0.16	16±1	0.05±0.03	1±1
3,4-Methylenedioxyphthalic acid (**11**) (as *N*-ethylimide)	C-9 to 14, —OCH_2O—	21.36±0.26	33±1		
Formaldehyde (as dimedone derivative)	—OCH_2O—	10.47±0.11	16±1		

[a]SA specific activity (d.p.m. per mmol) × 10^{-4}.
[b]RSA = relative specific activity (%) (reduction product of ochotensimine methiodide = 100).
[c]Obtained from the original labelled ochotensimine (Table 2) by dilution with inactive ochotensimine, followed by methylation and borohydride reduction.

TABLE 5. The $^3H/^{14}C$ ratio at the one-carbon sites of corydaline derived from L-[*methyl*-^{3}H,^{14}C]methionine (Expt. *S*2)

		$^3H/^{14}C$ ratio	% retention of ^3H, relative to ^{14}C: Observed	Calculated
Precursor L-[*methyl*-^{3}H,^{14}C]methionine		10.4±0.1	100±1	
Products	One-carbon units			
Corydaline (**4**)	All six	9.6±0.1	92±1	17/18 = 94.4
Des-*O*-methylcorydaline (**7**)	C-8 plus C-13′	8.6±0.1	82±1	5/6 = 83.3
Methyl iodide (as tetramethylammonium chloride)	Average of four OCH_3	10.7±0.1	103±1	3/3 = 100
Kuhn–Roth acetate (as α-naphthylamide)	C-13′	9.8±0.1	93±1	3/3 = 100
Corrected[a]		10.5±0.2	101±2	
Schmidt methylamine (as β-naphthoyl derivative)	C-13′	9.1±0.1	87±1	3/3 = 100

[a]See text.

TABLE 6. Schmidt reaction of [2-^{3}H,2-^{14}C]acetate

Solvent	$^3H/^{14}C$ ratio of acetate (as α-naphthylamide)	$^3H/^{14}C$ ratio of methylamine (as β-naphthoyl derivative)	Tritium loss (%)
Sulfuric acid (98% w/v)	21.0±0.1	20.1±0.1	4.3
Sulfuric acid (85% w/v)	21.0±0.1	19.5±0.1	7.2
Phosphoric acid (85%)	21.0±0.1	20.3±0.1	3.4

Can. J. Chem. Downloaded from www.nrcresearchpress.com by 210.87.254.6 on 09/05/12
For personal use only.

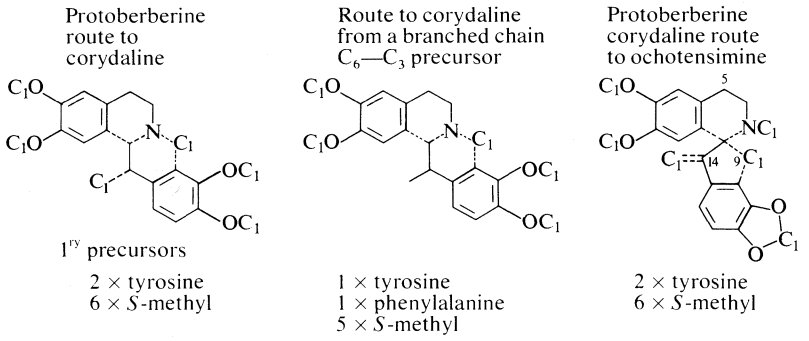

SCHEME 6. Construction of the skeletons of corydaline and ochotensimine from precursor fragments

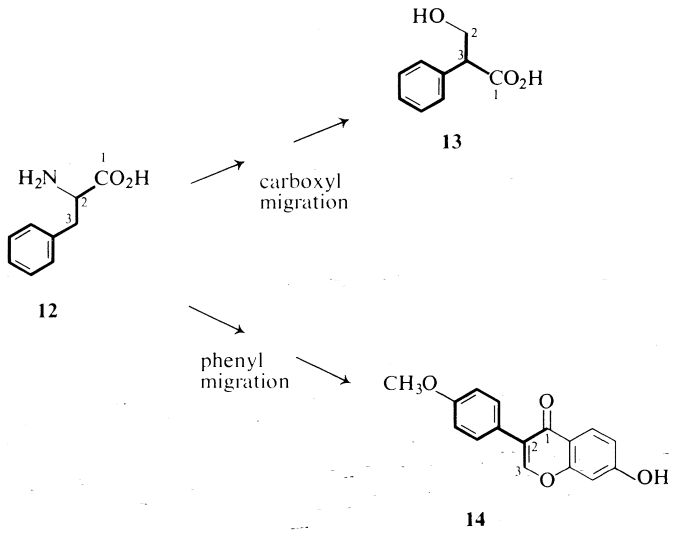

SCHEME 7. Rearrangement of phenylalanine to tropic acid and to the branched phenylpropanoid unit of the isoflavones (numbers refer to C-atoms of phenylalanine)

formononetin (**14**)) (12) and rotenoids (13) (Scheme 7).

Since phenolic C_6—C_3 units which participate in alkaloid biosynthesis appear to be derived from phenylalanine (*e.g.*, colchicine (14), decodine, and decinine (15)), whereas tyrosine supplies phenolic C_6—C_2 units, phenylalanine would be a more likely precursor than tyrosine. In most higher plants phenylalanine is not convertible into tyrosine (16).

In the event, the *C*-methyl group (C-13′) of corydaline was found to originate from the *S*-methyl group of methionine (Table 3, Expts. *S*1 and *S*2). The Kuhn–Roth acetate (C-13′, -13) obtained from [*methyl*-^{14}C]methionine-derived corydaline contained 20% of the total activity of the molecule, all of which, within experimental error, was shown to reside in the *C*-methyl group (C-13′) recovered as methylamine in a Schmidt reaction. The berberine bridge (C-8), recovered as benzoic acid, contained 18% of the total label. That no carbon atom within the carbon skeleton of corydaline, other than C-8 and C-13′, contained radioactivity is shown by the observation that des-*O*-methylcorydaline (**7**) contained 39 ± 1% of the total activity of the alkaloid. The label within des-*O*-methylcorydaline (**7**) is fully accounted for, within experimental error, by C-8 plus C-13′ ((19 ± 1) + (18 ± 1) = 37 ± 1%). The four *O*-methyl groups contain the rest of the activity (4 × (16 ± 1) = 64 ± 4%).

Can. J. Chem. Downloaded from www.nrcresearchpress.com by 210.87.254.6 on 09/05/12
For personal use only.

Can. J. Chem. Downloaded from www.nrcresearchpress.com by 210.87.254.6 on 09/05/12
For personal use only.

It is noteworthy that the six one-carbon units do not each contain exactly one sixth of the activity of the alkaloid. This is to be expected, since, even though the six units arise from the same precursor, they are introduced into the product at different stages of biosynthesis. However, even though it might be tempting to do so, it is not possible on the basis of the observed data to draw conclusions regarding the sequence in which the units enter the product.

The distribution of activity within corydaline, derived from [3-^{14}C]tyrosine, is in accord with prediction and consistent with the protoberberine route of biosynthesis. Half of the activity within the molecule resides at C-13, the benzylic carbon of one of the C_6—C_2 units of the protoberberine system (Kuhn–Roth acetate (C-13′, -13) minus Schmidt methylamine (C-13′)) (Expt. *S*3, Table 3). The other half of the activity was not extruded, but can be predicted to be localized at C-5, the benzylic carbon of the other C_6—C_2 unit (*cf.* ref. 10).

The distribution of activity within corydaline derived from [*methyl*-^{14}C]methionine and [3-^{14}C]tyrosine is clearly consistent with the protoberberine route (Scheme 2) and inconsistent with the route from a branched chain C_6—C_3 precursor (Scheme 3).

A similar conclusion was arrived at on the basis of the incorporation into corydaline of label from [*N-methyl*-^{14}C]reticuline (**4**) (17). Since the site of activity (presumably C-8) within the corydaline was not determined the experiment was indicative rather than conclusive.

If the spirobenzylisoquinoline system of ochotensimine were indeed derived by rearrangement of a corydaline-type skeleton (Scheme 1), whose *C*-methyl group yields the exocyclic methylene group of the product, label from [*methyl*-^{14}C] methionine and [3-^{14}C]tyrosine must enter sites within the ochotensimine skeleton which correspond to those now established for corydaline. The results of the tracer experiments with ochotensimine, summarized in Table 4, agree with this prediction.

One half of the activity of ochotensimine derived from [3-^{14}C]tyrosine resides at C-14 (Kuhn–Roth acetate (49 $\pm$ 1) minus Schmidt methylamine (1 $\pm$ 1) = 48 $\pm$ 1) (Expt. *O*3). The other half of the label, which was not isolated, is presumably located at C-5.

Ochotensimine, derived from [*methyl*-^{14}C] methionine, contains one-sixth of its activity at the exocyclic methylene (Schmidt methylamine) and one-sixth at the methylenedioxy group (formaldehyde). C-14, the C-atom to which the exocyclic methylene group is attached, is free of activity (Kuhn–Roth acetate (16 $\pm$ 1) minus Schmidt methylamine (16 $\pm$ 1) = 0 $\pm$ 1%). Since the 3,4-methylenedioxyphthalic acid derivative (**11**) contained two-sixths of the total activity, half of which resides in the methylenedioxy group, and since one of its two carboxyl groups (that derived from C-14 of ochotensimine) is devoid of label, and since the nucleus is part of a tyrosine-derived C_6—C_2 unit, the remaining sixth of the total activity must be located at the other carboxyl group, derived from C-9, which thus corresponds to the "berberine bridge". Half of the total label of the alkaloid is thus accounted for in terms of three sites, namely the exocyclic methylene group, C-9, and the methylenedioxy group. The other half of the activity, presumably located at the *N*-methyl and the two *O*-methyl groups, was not separated. Label from [3-^{14}C] phenylalanine, a putative precursor of the branched chain C_6—C_3 unit (*vide supra*) was not incorporated significantly into ochotensine or ochotensimine (Expt. *O*2).

The tracer evidence is thus entirely consistent with the view that the skeleton of spirobenzylisoquinolines such as ochotensimine arises by rearrangement of a C-13 methylated protoberberine skeleton of the corydaline type, which, in turn, originates from a preformed protoberberine intermediate by introduction of a one-carbon unit.

That this one-carbon unit originates from a CH_3-group, presumably the *S*-methyl group of methionine, and that this group is incorporated intact, without C—H bond cleavage, is made likely by the results, presented in Table 5, of an experiment (Expt. *S*2) with L-[*methyl*-^{3}H,*methyl*-^{14}C]methionine.

Corydaline contains six one-carbon sites (Table 3). Five of these, the *C*-methyl group (C-13′) and the four *O*-methyl groups are each associated with three H atoms. The sixth, the berberine bridge (C-8), originates by oxidative cyclization of an *N*-methyl group (18), a reaction in the course of which one of the H atoms must be extruded.

Thus, if *S*-methyl groups supplied all six one-carbon sites as well as the H atoms which are

Can. J. Chem. Downloaded from www.nrcresearchpress.com by 210.87.254.6 on 09/05/12
For personal use only.

attached to them, a maximum of 17 of the original 18 H atoms associated with the precursor methyl groups could be retained within corydaline. A maximum of 94.4% (17/18) of the tritium, relative to ^{14}C, of the doubly [*methyl*-^{3}H,^{14}C]-labelled precursor would then be recovered within the alkaloid in the absence of an isotope effect. The observed value (92 ± 1%) (Table 5) agrees with this prediction. That the *O*-methyl groups represent intact precursor-methyls is shown by the quantitative retention of tritium, relative to ^{14}C, within the tetramethylammonium chloride obtained as the degradation product representing these groups. The des-*O*-methylcorydaline (**7**), which retains the remaining two one-carbon sites, the *C*-methyl group (C-13′) (3 H) and the bridge (C-8) (2 H), retains 82% ^{3}H, relative to ^{14}C. The predicted value for retention of five of six H atoms is 83.3%.

The observed $^{3}H/^{14}C$ ratios are entirely consistent with and therefore support the view that the *O*-methyl and *C*-methyl groups of corydaline represent precursor CH_3-groups whose H atoms are entirely retained, and that in the formation of the berberine bridge two of the original three H atoms of the methyl precursor are preserved.

At first sight, the 7% loss, rather than quantitative retention of tritium, relative to ^{14}C, within the Kuhn–Roth acetate, representing the one-carbon unit, C-13′, of corydaline together with the ring carbon to which it is attached (Table 5), appears to be inconsistent with the other results. However, not all the ^{14}C within this acetate resides within the methyl group. It is evident from Table 3 (Expt. *S*2) that of (18.61 ± 0.25) × 10^4 d.p.m. per mmol (specific activity of Kuhn–Roth acetate) only (17.30 ± 0.16) × 10^4 d.p.m. per mmol (specific activity of Schmidt methylamine), *i.e.* 93 ± 2% of the total activity of the acetate, resides within its methyl group. If the observed $^{3}H/^{14}C$ ratio of the Kuhn–Roth acetate (9.8 ± 0.1) is corrected to allow for this scatter of label

$$\left((9.8 \pm 0.1)\Big/\frac{(17.30 \pm 0.16) \times 10^4}{(18.61 \pm 0.25) \times 10^4} = 10.5 \pm 0.2\right)$$

retention of tritium, relative to ^{14}C, within the methyl group of acetate, *i.e.*, within the *C*-methyl group of corydaline, is indicated, in conformity with the other results.[3]

Schmidt degradation of the Kuhn–Roth acetate ($^{3}H/^{14}C$ ratio observed 9.8 ± 0.1, corrected 10.5 ± 0.2) yielded methylamine whose $^{3}H/^{14}C$ ratio (9.1 ± 0.1) was significantly lower than that of the acetate. This apparent tritium loss under the conditions used in the Schmidt reaction (concentrated H_2SO_4) is presumably due to exchange. That the loss is indeed inherent in the Schmidt reaction of the doubly labelled acetate is indicated by the results of a series of experiments in which [2-^{3}H,2-^{14}C]acetate of known $^{3}H/^{14}C$ ratio was subjected to this reaction under different experimental conditions (Table 6). In each case a small but significant loss of tritium, relative to ^{14}C, was observed. It may well be that, by a more extensive search, conditions for quantitative tritium retention in the course of this reaction can be found. Until such a search is successful, however, the present results serve to indicate that caution is advisable in the interpretation of $^{3}H/^{14}C$ ratios obtained in the products of a Schmidt reaction.

Experimental

Administration of Labelled Compounds to Corydalis solida (L.) Swartz and to Corydalis ochotensis Turcz

Plants

Corydalis solida, a perennial, and *Corydalis ochotensis*, a biennial, were propagated out of doors. *Corydalis solida* was potted and transferred to the greenhouse in April, and kept at a temperature not exceeding 18 °C. The experiments were carried out in May. *Corydalis ochotensis* was potted and transferred to the greenhouse in May. The feeding experiments were carried out 2 months later. Voucher specimens of both species are deposited in the herbarium of the Royal Botanical Gardens, Hamilton.

Administration of Labelled Compounds

The labelled compounds were administered to the plants by infusion into the stem, using the cotton wick technique described elsewhere (10). The plants were kept in contact with the radioactive tracers for 3–4 days. The details of the individual feeding experiments are summarized in Tables 1 and 2.

Extraction of the Alkaloids

Corydaline

After exposure to the radioactive amino acid for 4

[3]Correction for scatter of label of the $^{3}H/^{14}C$ ratios of corydaline and des-*O*-methylcorydaline does not affect the ratios significantly, since the amount of ^{14}C, at centers other than those derived from one-carbon units, represents a much smaller fraction of the total ^{14}C than in the case of the Kuhn–Roth acetate. Such correction would increase the ratios and bring them closer to the calculated values.

Can. J. Chem. Downloaded from www.nrcresearchpress.com by 210.87.254.6 on 09/05/12
For personal use only.

days, the plant material from 16 plants (aerial parts and corms, fresh weight, typically 80 and 40 g, respectively), of *Corydalis solida* (L.) Swartz was dried at 40° for 72 h. In a typical feeding, the yield of dry plant material was 20 g. The corydaline was extracted by a method similar to that used by Manske (19); the finely ground plant material was extracted with methanol in a Soxhlet apparatus for 48 h. After this time, the solution was evaporated and the residue dissolved in hydrochloric acid (5%, 50 ml), the solution filtered, and the filtrate extracted with chloroform. The chloroform extract was dried over Na_2SO_4, evaporated, and the residue redissolved in 5% hydrochloric acid (30 ml). The acidic solution was then washed with ether, basified with 10% KOH and then thoroughly re-extracted with ether. The ethereal extract was dried and evaporated to give a residue (Manske fraction BC, typically 200 mg) which was redissolved in the minimum quantity (*ca.* 5 ml) of methanol.

A sample of the methanolic solution was examined by t.l.c. (Merck silica gel F-254; 2% methanol in chloroform). Five components, at R_f 0.1, 0.2, 0.3, 0.5, and 0.65, were detected under u.v. light. Most of the radioactivity of the fraction was shown by radioscanning (Radiochromatogram Scanner, Model 7201 Packard Instrument Company) to be associated with the major component, corydaline, at R_f 0.5. Inactive corydaline (typically 200–400 mg) was added to the methanol solution and the total corydaline allowed to crystallize from this solution. Recrystallization from methanol gave corydaline (typically 200–400 mg) melting at 135–136° (lit. (19) m.p. 135°), which was sublimed at 100–110° and 5×10^{-3} mm to give the sample used in the degradation experiments.

Ochotensine and Ochotensimine

The plant material (aerial parts and roots, fresh weight, typically 160 and 30 g, respectively) from five plants of *Corydalis ochotensis* Turcz used in each radioactive feeding was dried and ground to a fine powder (typically 20 g) which was extracted as outlined above to give fraction BC of the Manske extraction procedure (20). Radioscanning of a thin-layer chromatogram (Merck silica gel F-254; 2% methanol in chloroform) of the material isolated from the methionine and tyrosine feedings showed most of the activity to be associated with ochotensimine at R_f 0.4. A similar scan of the crude product obtained from the phenylalanine feeding experiment failed to detect significant activity on the thin-layer plate. The crude fraction BC was dissolved in a small quantity of benzene and applied to a silica gel column (Woelm activity 1, 100 g). A 5% stepwise elution from benzene to chloroform afforded ochotensimine as a pale yellow oil. Further elution of the column with 5% methanol in chloroform gave ochotensine, which on crystallization from chloroform melted at 247–250° (lit. (20) m.p. 252°). Radioactive ochotensimine was diluted with inactive material before degradation.

*Degradation of Corydaline (**5**) (Scheme 4)*

Carbon-13 and the C-Methyl Group as Acetic Acid

Chromium trioxide (4 g) was added to a solution of corydaline (200 mg) in sulfuric acid (4 *M*, 20 ml) and the mixture subjected to the Kuhn–Roth oxidation procedure (21). The acetic acid formed was converted to sodium acetate by titration with 0.1 *M* sodium hydroxide and the solution divided into two equal portions. One portion was evaporated to give sodium acetate (8 mg) which was redissolved in water (1 ml) and reacted with α-naphthylamine hydrochloride (15 mg) as described (22) to give *N*-acetyl-α-naphthylamine (3 mg), m.p. 158–160° after sublimation at 80–90° and 1×10^{-3} mm (lit. (22) m.p. 159–160°).

The C-Methyl Group as Methylamine

The second portion of the sodium acetate solution from the Kuhn–Roth oxidation (see above) was evaporated to dryness to give sodium acetate (8 mg), which was reacted with sodium azide (50 mg) and concentrated sulfuric acid (1 ml) as described (21). The methylamine evolved upon basification of the reaction mixture was trapped by passage through three traps each containing 1 ml of 0.1 *M* HCl and the resulting solution evaporated at 90° to give methylamine hydrochloride (4 mg). This was dissolved in dry dimethylsulfoxide (0.5 ml) and added to a solution of β-naphthoyl chloride (40 mg) in pyridine (1 ml). The solution was kept at room temperature for 12 h and was then poured onto water (4 ml) and extracted with ether (3×5 ml). The ethereal extract was washed with aqueous sodium bicarbonate (2 *M*, 3×5 ml) and with water (3×5 ml), was dried over sodium sulfate, and evaporated to give a residue which was crystallized from benzene and sublimed at 75–80° and 5×10^{-3}mm. The resulting *N*-methyl-β-naphthoamide (3 mg) melted at 107–109° (sealed capillary) (lit. (23) m.p. 108–109.5°).

Carbon-8 as Benzoic Acid

The procedure used followed the published method (9) for the isolation of C-8 of berberine as benzoic acid. Iodine (380 mg) was added to a solution of corydaline (280 mg) in anhydrous ethanol (50 ml) and the solution was stirred at room temperature for 12 h. The solvent was then removed and the resulting dehydrocorydaline iodide dried *in vacuo* for 12 h at room temperature and 5×10^{-3} mm. The salt was then suspended in dry ether (50 ml) and the stirred suspension treated with a solution of phenylmagnesium bromide (0.05 mol) in ether (50 ml). After 2 h at reflux temperature, the solution was cooled and excess phenylmagnesium bromide decomposed by the careful addition of ice (100 g). The resulting solution was extracted with ether, and the ethereal extract re-extracted with 5% hydrochloric acid. The acid extract was then basified with 10% aqueous ammonia and extracted with ether. The ether extract was washed with water, dried (Na_2SO_4), and evaporated to give crude 8-phenyl-13,14-didehydrocorydaline (**8**) (200 mg) which was used in the next stage without further purification.

Potassium permanganate (1.5 g) was added at room temperature over a period of 72 h to a stirred suspension of 8-phenyl-13,14-didehydrocorydaline (**8**) (200 mg) in water containing potassium carbonate (1.5 g). Work-up of the reaction by the procedure outlined (9) gave benzoic acid (6 mg, 10.5%), which after sublimation at 80–90° and 1×10^{-2}mm, and recrystallization from water, melted at 119–120°.

The O-methyl Groups as Tetramethylammonium Chloride

Corydaline (200 mg) was reacted with freshly distilled hydriodic acid (*d* 1.7, 10 ml) and the evolved methyl iodide converted to tetramethylammonium iodide (0.13 g) by the described procedure (9). The product was recrystallized from methanol and converted into tetramethylammonium chloride as follows. Freshly precipita-

Can. J. Chem. Downloaded from www.nrcresearchpress.com by 210.87.254.6 on 09/05/12
For personal use only.

ted silver oxide (250 mg) was added to a solution of the iodide (100 mg) in water (10 ml), and the resulting suspension was stirred at room temperature for 20 h. The suspension was filtered and the filtrate neutralized with 0.1 *M* HCl. The neutral solution was evaporated to dryness at 80° and the residue was crystallized from methanol yielding tetramethylammonium chloride (44 mg).

Des-O-methylcorydaline (7) and its Treatment with Diazomethane

A solution of corydaline (50 mg) in freshly distilled hydrobromic acid (5 ml, 48%) was heated under reflux for 7 h, the methyl bromide produced being swept away in a slow stream of nitrogen. After this period, the solution was cooled, basified with ammonia, and extracted with ether. The ethereal extract was washed with sodium metabisulfite solution (5% w/v, 10 ml) and with water, dried (Na_2SO_4) and evaporated. The residue (37 mg) was dissolved in methanol (5 ml), and the solution mixed with a large excess of diazomethane dissolved in ether (100 ml) and the mixture allowed to stand at room temperature for 48 h.

Evaporation of the ether gave a solid residue which, on purification by preparative layer chromatography (Merck silica gel F-254, 2% methanol in chloroform), afforded corydaline which was sublimed at 100–110° and 5×10^{-3} mm (1.2 mg), m.p. 135–136° (lit. (19) m.p. 135°).

Degradation of Ochotensimine (2) (Scheme 5)

Ochotensimine Methiodide (9)

A solution of iodomethane (0.3 ml) in ether (3 ml) was added to ochotensimine (365 mg) dissolved in methanol (3 ml). After 48 h at room temperature the deposited crystals were filtered off and dried *in vacuo* to give a pure sample of methiodide (470 mg, 84%), melting with decomposition at 225–228° (lit. (20) m.p. 225°).

1-Methyl-2[2′-(2′′-dimethylaminoethyl)-4′,5′-dimethoxyphenyl]-4,5-methylenedioxy-1-indene (10)

Sodium borohydride (370 mg) was added to a stirred suspension of ochotensimine methiodide (510 mg) in 2-propanol (30 ml) and the resulting mixture stirred at room temperature for 24 h. Water (200 ml) was then added and the solution extracted with chloroform. The extract was dried and evaporated to give a residue which, on recrystallization from hexane, afforded the title compound (**10**) (250 mg, 66%), melting at 87–89° (lit. (3) m.p. 91–92°). For degradation purposes, the compound was sublimed at 70–75° and 5×10^{-3}mm to give a sample melting at 87–89°.

The C-Methyl Group and Carbon-1 of (10) as Acetic Acid

1-Methyl-2[2′-(2′′-dimethylaminoethyl(-4′,5′-dimethoxyphenyl]-4,5-methylenedioxy-1-indene (**10**) (200 mg) was subjected to Kuhn–Roth oxidation as outlined above for corydaline. A portion of the sodium acetate (7 mg) from this reaction was converted to *N*-acetyl-α-naphthylamine (3.8 mg, m.p. 158–160°) as described above.

The C-Methyl Group of (10) as Methylamine

Another portion (7 mg) of the sodium acetate obtained from the Kuhn–Roth oxidation described above was converted to methylamine by the Schmidt degradation procedure and the methylamine was characterized as *N*-methyl-β-naphthoamide (2 mg) by the procedure described above.

Rings C and D of Ochotensimine as the N-Ethylimide of 3,4-Methylenedioxyphthalic Acid (11)

Potassium permanganate solution (50 ml, 2% w/v) was added over a period of 1 h to a suspension of 1-methyl-2[2′-(2′′-dimethylaminoethyl)-4′,5′-dimethoxyphenyl]-4,5-methylenedioxy-1-indene (**10**) (120 mg) in water (5 ml) containing potassium carbonate (1.0 g) at 60°. When addition was complete, the solution was acidified (5% HCl), decolorized with sodium bisulfite and extracted with ether. The ethereal extract was re-extracted with 2 *M* sodium bicarbonate solution and the basic extract acidified (concentrated HCl) and extracted with ether. This extract was dried and evaporated to give a residue (220 mg) to which an excess of a solution of ethylamine in ethanol (5 ml, *ca.* 30% w/v) was added. The resulting solution was evaporated, and the residue reacted twice more with ethanolic ethylamine. The final residue (310 mg) was sublimed at 90° and 0.4 mm to give *N*-ethyl-3,4-methylenedioxyphthalimide (15 mg) melting at 126–128° after recrystallization from ether (lit. (24) m.p. 127–130°).

The Methylenedioxy Group of Ochotensimine as Formaldehyde (Dimedone Derivative)

A suspension of *N*-ethyl-3,4-methylenedioxyphthalimide (10 mg) and dimedone (5,5-dimethylcyclohexan-1,3-dione) (30 mg) in dilute sulfuric acid (3 ml, 33% v/v) was refluxed for 24 h. The mixture was cooled, water (5 ml) added, and the solution extracted with ether. The extract was washed with water, dried, and evaporated to give a residue which on crystallization from aqueous methanol and sublimation at 75–80° and 3×10^{-1}mm afforded the dimedone derivative of formaldehyde (3 mg, 20%) melting at 188–190°.

Conversion of [2-^{3}H,2-^{14}C]Acetic Acid into [^{3}H,^{14}C]Methylamine by the Schmidt Reaction

A solution of sodium [2-^{3}H,2-^{14}C]acetate was prepared by mixing samples of sodium [2-^{14}C]acetate (nominal total activity 5 μCi, nominal specific activity 2 mCi per mmol, New England Nuclear), sodium [2-^{3}H]acetate (nominal total activity see footnote 4, nominal specific activity, 1.3 Ci per mmol, New England Nuclear), and inactive sodium acetate (100 mg). The mixture was dissolved and the volume of the solution adjusted to 10 ml.[4]

[4]In a preliminary experiment solutions containing sodium [2-^{3}H]acetate and [2-^{14}C]acetate were mixed in proportions calculated to yield a ^{3}H/^{14}C ratio of 12.0. A sample of the solution of the resulting sodium[^{3}H,^{14}C] acetate did indeed show a ^{3}H/^{14}C ratio close to this predicted value. However, when the α-naphthylamide derivative of this [^{3}H,^{14}C]acetate was prepared, the ^{3}H/^{14}C ratio of the derivative was found to be much lower (~4) than that given by the solution of the sodium acetate from which it had been obtained. That this discrepancy was due to the presence of exchangeable tritium in the sample of sodium [^{3}H]-acetate (presumably as tritiated water of crystallization) was confirmed as follows.

A sample of known total activity of the original solution of sodium [2-^{3}H]acetate, to which a weighed amount of carrier sodium acetate had been added, was repeatedly evaporated and redissolved in distilled water. Sodium [^{3}H]acetate was ultimately obtained whose specific activity was less than 30% of that calculated for the original sample.

For each of the following experiments a 2-ml portion of the solution, containing approximately 20 mg sodium acetate, was used.

Determination of the $^3H/^{14}C$ Ratio of the Doubly Labelled Acetate

A portion of the sodium[2-^{3}H,2-^{14}C]acetate (approximately 20 mg) was converted into *N*-acetyl-α-naphthylamine (22), which was purified by sublimation at 5×10^{-3}mm.

This purified derivative was used for the determination of the $^3H/^{14}C$ ratio[4] of the sodium acetate which was to be converted to methylamine by the Schmidt reaction.

Methylamine by the Schmidt Reaction

In each of three separate experiments a sample (20 mg) of sodium [2-^{3}H,2-^{14}C]acetate, obtained by evaporation of 2 ml of the stock solution at 80°, was dissolved in the appropriate solvent (2 ml) (Table 6). Sodium azide (100 mg) was added and the Schmidt reaction performed in the usual manner (21). The methylamine formed in the reaction was converted into *N*-methyl-β-naphthoamide (typically 10 mg) which was purified as described above (see section on the C-methyl group as methylamine).

Determination of Radioactivity

Radioactivity was assayed by liquid scintillation counting (Mark 1 liquid scintillation computer, Model 6860, Nuclear Chicago). Activity due to ^{3}H and ^{14}C was determined simultaneously, by external standardization counting with ^{133}Ba. Samples were dissolved in methanol or water and the solution dispersed in a solution of Aquasol (New England Nuclear). Triplicate samples of each compound were counted under comparable conditions of quenching. For highly quenched samples the confidence limits of the quench correction curves were ±5%. Confidence limits shown in the tables are standard deviation of the mean.

We are greatly indebted to Dr. R. H. Manske, University of Waterloo, for providing generous samples of the alkaloids and of dried plant material, as well as live plants of *Corydalis solida* and *Corydalis ochotensis* from his private garden in Guelph, Ontario. His co-operation and advice made this investigation possible. This work was supported by the National Research Council of Canada.

1. M. Shamma and C. D. Jones. J. Am. Chem. Soc. **91**, 4009 (1969); **92**, 4943 (1970); M. Shamma and J. F. Nugent. Tetrahedron Lett. 2625 (1970); Chem. Commun. 1642 (1971); Tetrahedron, **29**, 1265 (1973).
2. S. McLean and M-S. Lin. Tetrahedron Lett. 3819 (1964).
3. S. McLean, M-S. Lin, and R. H. F. Manske. Can. J. Chem. **44**, 2449 (1966).
4. B. Nalliah, R. H. F. Manske, R. Rodrigo, and D. B. MacLean. Tetrahedron Lett. 2795 (1973).
5. R. Robinson. The structural relations of natural products. Clarendon Press, Oxford. 1955. pp. 87, 104.
6. H. W. Bersch. Arch. Pharm. **283**, 192 (1950).
7. M. Freund and K. Fleischer. Ann. **409**, 188 (1915); F. von Bruchhausen. Arch. Pharm. **261**, 28 (1923).
8. R. H. F. Manske. The Alkaloids, **4**, 1 (1954).
9. R. N. Gupta and I. D. Spenser. Can. J. Chem. **43**, 133 (1965).
10. J. R. Gear and I. D. Spenser. Can. J. Chem. **41**, 783 (1963).
11. E. Leete. Biosynthesis, **2**, 115 (1973).
12. H. Grisebach. Z. Naturforsch. **14B**, 802 (1959); H. Grisebach and N. Doerr. Z. Naturforsch. **15B**, 284 (1960).
13. L. Crombie and M. B. Thomas. J. Chem. Soc. (C) 1796 (1967); L. Crombie, C. L. Green, and D. A. Whiting. J. Chem. Soc. (C) 3029 (1968).
14. E. Leete. J. Am. Chem. Soc. **85**, 3666 (1963); A. R. Battersby, R. Binks, J. J. Reynolds, and D. A. Yeowell. J. Chem. Soc. 4527 (1964).
15. S. H. Koo, F. Comer, and I. D. Spenser. Chem. Commun, 897 (1970).
16. I. D. Spenser. Compr. Biochem. **20**, 291 (1968).
17. G. Blaschke. Arch. Pharm. **301**, 439 (1968).
18. D. H. R. Barton, R. H. Hesse, and G. W. Kirby. Chem. Commun. 267 (1963); A. R. Battersby, R. J. Francis, M. Hirst, and J. Staunton. Chem. Commun. 268 (1963).
19. R. H. F. Manske. Can. J. Chem. **34**, 1 (1956).
20. R. H. F. Manske. Can. J. Res. **18B**, 75 (1940).
21. R. E. Hill, F. J. Rowell, R. N. Gupta, and I. D. Spenser. J. Biol. Chem. **247**, 1869 (1972).
22. E. Leete, H. Gregory, and E. G. Gros. J. Am. Chem. Soc. **87**, 3475 (1965).
23. W. E. Bachmann and M. X. Barton. J. Org. Chem. **3**, 300 (1938).
24. F. Šantavý, J. L. Kaul, L. Hruban, L. Dolejš, V. Hanuš, K. Bláha, and A. D. Cross. Coll. Czech. Chem. Commun. **30**, 3479 (1965).

Can. J. Chem. Downloaded from www.nrcresearchpress.com by 210.87.254.6 on 09/05/12
For personal use only.

Solid-Phase Synthesis of Selectively Protected Peptides: Use of Thallous Alkoxide as Catalyst in the Transesterification Step[1]

J. Y. Savoie[2] and Moira A. Barton[3]

Department of Immunology, University of Alberta, Edmonton, Alberta T6G 2E1

Received March 5, 1974

J. Y. Savoie and Moira A. Barton. Can. J. Chem. **52**, 2832 (1974).

Transesterification with 2-dimethylaminoethanol, in the presence of thallous alkoxide, was found to provide a useful method for the cleavage of protected peptides from the Merrifield resin after solid-phase synthesis. The extent of racemization, at the C-terminal residue, was low (< 1%) in the case of peptides containing C-terminal alanine or valine residues. The method was also found to provide good yields of the protected peptide derivative even in the case of the severely sterically hindered C-terminal valine peptides. A study of the $\alpha \rightarrow \beta$ aspartyl transpeptidation, showed that the extent of this side reaction was low (< 1% β-isomer) in the case of the labile α-aspartylglycine sequence, when a short transesterification time was employed. The *t*-butyl ester group was shown to be stable under the conditions of transesterification and this group is recommended for the protection of carboxylic acid side chains. Hydrolysis of the 2-dimethylaminoethyl esters was accomplished by treatment with water or dilute base, to yield the selectively protected peptide acids, suitable for use as building units in the synthesis of large molecules by solid-phase or solution techniques.

J. Y. Savoie et Moira A. Barton. Can. J. Chem. **52**, 2832 (1974).

On a constaté que la transestérification avec le diméthyl-2 aminoéthanol, en présence d'alcoolate thalleux était une méthode très utile pour le clivage de peptides protégés de la résine de Merrifield après la synthèse en phase solide. Le taux de racémisation, au niveau du résidu C-terminal, est faible (< 1%) dans le cas de peptides contenant comme résidu C-terminal l'alanine ou la valine. La méthode conduit au peptide protégé avec de bons rendements même dans le cas de peptides contenant la valine, dont le C-terminal est très encombré stériquement. Une étude de la transpeptidation $\alpha \rightarrow \beta$ aspartyl montre le peu d'importance de cette réaction secondaire (isomère β < 1%) dans le cas de la séquence labile α-aspartyl-glycine, lorsque l'on utilise un temps court pour la transestérification. Le groupe ester de *t*-butyle est stable sous les conditions de transestérification et ce groupe est recommendé pour la protection des fonctions carboxyliques portées par les chaînes latérales. Les esters de diméthyl-2 aminoéthyle sont hydrolysés par l'eau ou les bases diluées, pour donner sélectivement les acides de peptides protégés. Ces derniers sont appropriés pour la synthèse par séquences de grandes molécules par voie solide ou liquide. [Traduit par le journal]

Introduction

The solid-phase method of peptide synthesis (1) provides a useful route for the rapid synthesis of unprotected peptides. The method is applicable for the synthesis of peptides in the size range of 10–20 amino acids, provided that effective purification procedures are available for the separation of the final product. The application of the method for the synthesis of large molecules, including enzymes, has proved to be of more limited value, as a result of the escalation in the magnitude of the purification difficulties with increasing size of the target molecule (2). These problems are well documented in a recent account of the attempted solid-phase synthesis of lysozyme (3).

It is evident that some of the major difficulties of the solid-phase method will be avoided if purification steps are introduced at intermediate points in the course of the synthesis. For this reason there has been some interest in the development of routes for the preparation of protected peptides by solid-phase methods (4–10). After purification these peptides would be useful as building blocks for the preparation of large

[1]Presented in part by J. Y. Savoie and Moira A. Barton at the 16th Annual Meeting of the Canadian Federation of Biological Societies, Saskatoon, June 26–29, 1973. Abstract No. 90.

[2]Postdoctoral Fellow supported by the Banting Research Foundation, 1972–1973. Present address: Centre de Toxicologie, Centre Hospitalier de l'Université Laval, Québec.

[3]Address correspondence to: Dr. M. A. Barton, Department of Immunology, 345 Medical Sciences Building, University of Alberta, Edmonton, Alberta T6G 2E1.

Can. J. Chem. Downloaded from www.nrcresearchpress.com by 210.87.254.5 on 09/05/12
For personal use only.

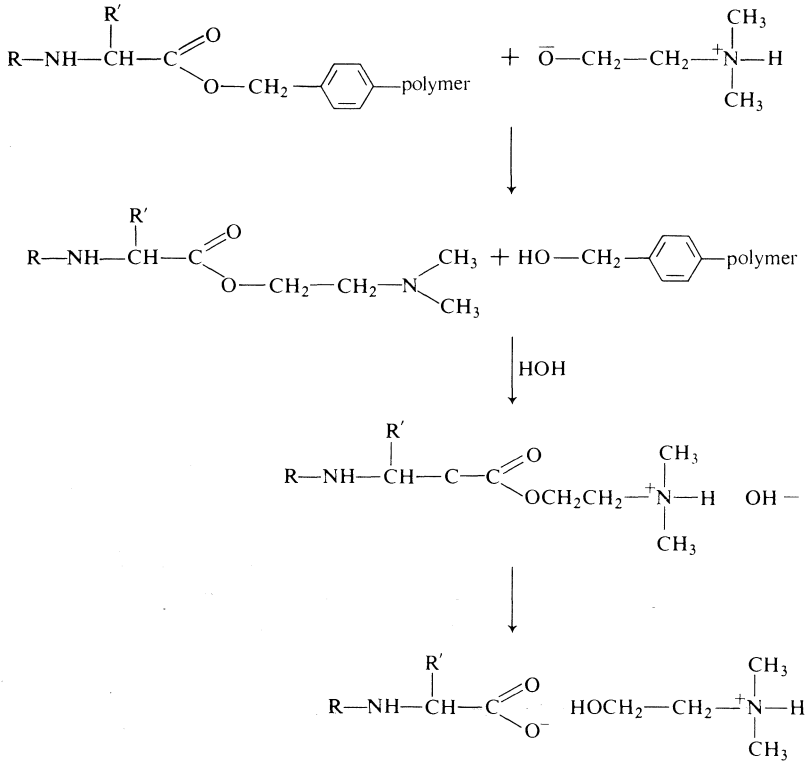

SCHEME 1

molecules by solid-phase fragment condensation techniques (11–15) or by solution methods.

We recently described a method for the solid-phase synthesis of selectively protected peptides bearing a free terminal carboxylic acid group (15). This procedure employed a self-catalyzed transesterification step, using 2-dimethylaminoethanol, with formation of the water-labile 2-dimethylaminoethyl ester of the protected peptide. Since the rate of transesterification with 2-dimethylaminoethanol was slow this method was limited, in practice, to peptides containing a nonsterically hindered C-terminal amino acid. In the present paper we describe the use of thallous alkoxide as a catalyst in the transesterification step. This catalyst gives a considerable increase in the reaction rate, which allows a more general application of the transesterification route.

Results and Discussion

Transesterification with 2-dimethylaminoethanol (15) was developed as a method for the release of protected peptides from the solid support, after solid-phase synthesis on the conventional Merrifield resin. In the Merrifield solid-phase method the peptide is linked to the solid support by means of a benzyl ester bond *via* the C-terminal carboxylic acid group. This bond was found to be susceptible to transesterification with 2-dimethylaminoethanol with accompanying release into solution of the 2-dimethylaminoethyl ester of the protected peptide, according to Scheme 1. The ester was obtained by evaporation of the solution after filtration from the resin. On treatment with water the 2-dimethylaminoethyl group was removed to yield the selectively protected peptide containing a free terminal carboxylic acid group. Preliminary results (15) indicated that the addition of a catalytic amount of thallous 2-dimethylaminoethoxide caused a significant increase in the rate of transesterification. The thallium derivative was found to be a more effective catalyst than the corresponding sodium compound. To evaluate the general utility of thallous alkoxide as a transesterification catalyst in this reaction, we have now studied the transesterifi-

Can. J. Chem. Downloaded from www.nrcresearchpress.com by 210.87.254.5 on 09/05/12
For personal use only.

TABLE 1. Elution conditions and operational color values of dipeptides*

Dipeptide	Eluent p*H*	Sodium citrate (*N*)	Peak position (ml)	Operational color value†
L-Leu-L-Ala	4.32	0.20	125.0	1.06
L-Leu-D-Ala	4.32	0.20	106.0	0.85
L-Leu-L-Ala	6.00	0.35	36.5	1.29
L-Leu-D-Ala	6.00	0.35	44.0	1.15
L-Ala-L-Phe	6.00	0.35	50.0	1.09
L-Ala-D-Phe	6.00	0.35	59.5	0.87
L-Leu-L-Val	6.00	0.35	36.0	1.42
L-Leu-D-Val	6.00	0.35	49.5	1.20
β-L-Aspgly	3.25	0.20	48.0‡	0.67
α-L-Aspgly	3.25	0.20	105.0‡	1.34

*Chromatography of the dipeptides on a column, 0.9 × 59 cm, packed with Beckman UR-30 resin; flow rate 58 ml/h; temperature 57°. Samples applied at p*H* 2.2.
†Relative to glycine 1.00.
‡Flow rate 68 ml/h.

cation of a series of model dipeptides which enabled the calculation of both reaction yields and the extent of racemization at the C-terminal amino acid residue. The dipeptides chosen for study were BOC-L-leucyl-L-alanine,[4] BOC-L-alanyl-L-phenylalanine, and BOC-L-leucyl-D-valine. These dipeptides each form pairs of diastereoisomers which are easily separable by ion-exchange chromatography using the amino acid analyzer (16). The transesterification of β-*t*-butyl benzyloxycarbonyl-L-aspartylglycine was also studied in order to determine the stability of the β-*t*-butyl group under the transesterification conditions and to determine the extent of α → β aspartyl transpeptidation occurring during the transesterification. The elution conditions and operational color values of the dipeptides are reported in Table 1.

Enhancement of the Rate of Transesterification by the Addition of Thallous Alkoxide

The rate of transesterification with 2-dimethylaminoethanol was studied using the polymer-linked dipeptide BOC-L-ala-L-phe-*O*-polymer, in both the presence and absence of thallous alkoxide. As shown in Fig. 1 the addition of the catalyst brought about a significant increase in the reaction rate, close to quantitative reaction being obtained in a 5 h reaction time. A similar increase in rate in the transesterification of BOC-L-leu-L-ala-*O*-polymer was obtained on addition of the catalyst, as shown in Table 2. In the case of the severely sterically hindered dipeptide BOC-L-leu-D-val-*O*-polymer,

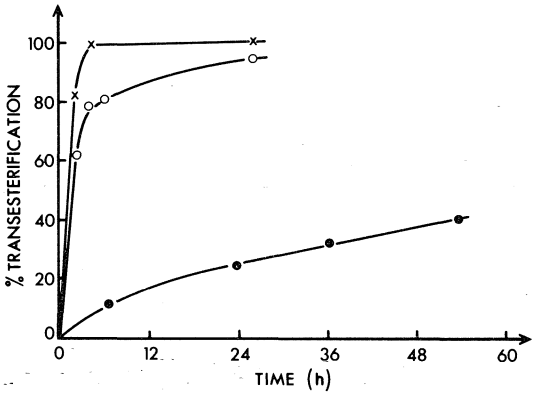

FIG. 1. Transesterification of BOC-L-ala-L-phe-*O*-polymer (2 g; 1.1 mmol peptide) in 2-dimethylaminoethanol–dimethylformamide solution (15 ml; 1:1 v/v); –●–, no catalyst; –○–, 0.1 equiv. thallous 2-dimethylaminoethoxide; –×–, 0.2 equiv. thallous 2-dimethylaminoethoxide.

where no significant transesterification was observed in the absence of catalyst, addition of 0.25 equiv. of thallous alkoxide gave a transesterification yield of 85% in a reaction time of 16 h. Similarly the hindered proline derivative BOC-L-pro-*O*-polymer gave little transesterification in the absence of catalyst but addition of 0.1 equiv. of thallous alkoxide gave a transesterification yield of 96% in a 21 h reaction time.

Extent of Racemization of the C-Terminal Amino Acid during Transesterification with 2-Dimethylaminoethanol in the Presence of Thallous Alkoxide

For measurement of the racemization occurring in the transesterification, the 2-dimethyl-

[4]BOC indicates *t*-butyloxycarbonyl.

Can. J. Chem. Downloaded from www.nrcresearchpress.com by 210.87.254.5 on 09/05/12
For personal use only.

TABLE 2. Transesterification with 2-dimethylaminoethanol in the presence of thallous alkoxide*

Protected peptide–resin	Thallous alkoxide (equiv.)	Time (h)	Transesterification yield (%)	Racemization† (%)
BOC-L-Leu-L-Ala-*O*-polymer	None	72	65±5	0.5±0.1
	0.1	5	100	0.6
BOC-L-Ala-L-Phe-*O*-polymer	None	43	37	2.8
	0.1	5	80	4.5
BOC-L-Leu-D-Val-*O*-polymer	0.15	2.5	70	0.6
	0.1	16	66	0.8
	0.25	16	85	0.8
BOC-L-Pro-*O*-polymer	None	96	5	—
	0.1	21	96	—

*See Experimental for detailed procedure.
†Racemization (for L,L-peptides) = [D,L/(D,L + L,L)] × 100%.

aminoethyl ester group was removed from the transesterification product, by treatment with water or dilute base. Acidolytic cleavage of the BOC group then yielded the fully deprotected dipeptide. The product was applied to the column of the amino acid analyzer, without purification, and the diastereoisomers were quantitated by the method of Manning and Moore (16). As shown in Table 2, the extent of racemization in the catalyzed reactions generally fell below 1%.[5] Thus the product of transesterification of BOC-L-leu-L-ala-*O*-polymer showed 0.6% racemization after a 5 h reaction, at which time the transesterification was complete. Similarly BOC-L-leu-D-val-*O*-polymer showed 0.6% racemization in a 2.5 h reaction, increasing to 0.8% after 16 h. Thus the extent of racemization occurring in the transesterification of these two peptides fell within reasonable limits for a practical use of the method, being similar in magnitude to that obtained in the saponification of the dipeptide methyl esters in solution (17). As expected, the dipeptide BOC-L-ala-L-phe-*O*-polymer showed a much greater extent of racemization. In the absence of catalyst the racemization of this dipeptide was 2.8% in a 43 h reaction, where the transesterification yield was 37%. In the presence of 0.1 equiv. of thallous alkoxide the extent of racemization was 4.5% in a 5 h reaction with a transesterification yield of 80%. Thus it appears that this transesterification procedure will not be applicable in the case of peptides containing a C-terminal aromatic amino acid as these are particularly susceptible to racemization by direct α-hydrogen abstraction. The use of the amino acids cysteine, serine, threonine, and aspartic acid at the C-terminal position, will also be precluded as these amino acids are known to be labile to racemization by the same mechanism.

As shown in Table 3, it was found that the extent of racemization was minimised if the isolation of the product from the reaction mixture was performed at a number of intermediate points during the course of the reaction. Thus the lowest level of racemization was obtained by the batchwise method of operation, whereby the transesterification solution was filtered off and worked up at regular intervals during the course of the reaction, the transesterification of the peptide resin then being continued by the addition of a fresh batch of solvent and catalyst. In practice, the batchwise procedure also provided a convenient method for monitoring the course of the reaction, the procedure being repeated until no further yield of product was obtained. This method was utilised in preparative scale experiments for the isolation of BOC-L-leucyl-L-alanine and BOC-L-leucyl-D-valine.

Transesterification of Peptides Containing Acidic Amino Acids

If the transesterification procedure is to be utilised for the preparation of protected peptides containing acidic amino acids, it is evident that a transesterification-resistant protecting group will be required for the protection of the carboxylic acid side chains. For this reason an investigation of the stability of the *t*-butyl ester group, was carried out using the dipeptide β-*t*-butyl benzyl-

[5]The treatment of solvents with alumina, as described in the experimental section, was essential to obtain a low level of racemization.

Can. J. Chem. Downloaded from www.nrcresearchpress.com by 210.87.254.5 on 09/05/12
For personal use only.

TABLE 3. Yields and racemization in the batchwise transesterification procedure using 2-dimethylaminoethanol*

Protected peptide–resin	Batch	Batch reaction time (h)	Total reaction time (h)	Yield in each batch (%)	Total yield (%)	Racemization in each batch§ (%)
BOC-Leu-Ala-*O*-polymer†	A	0.5	0.5	10	10	0.4±0.1
	B	0.5	1	12	22	0.4
	C	1	2	22	44	0.4
	D	1	3	23	67	0.5
	E	2	5	24	91	0.6
	F	7	12	9	100	0.8
BOC-Leu-Val-*O*-polymer‡	A	2.5	2.5	70	70	0.6
	B	2.5	5	27	97	0.7
	C	4	9	2	99	0.9

*See Experimental for detailed procedure.
†0.02 equiv. thallous alkoxide.
‡0.15 equiv. thallous alkoxide.
§Racemization (for L,L peptides) = [D,L/(D,L + L,L)] × 100%.

TABLE 4. Extent of α → β transpeptidation during cleavage of β-*t*-butyl benzyloxycarbonyl-L-aspartylglycine–resin*

Reagent	Thallous alkoxide (equiv.)	Time (h)	Yield (%)	β-Isomer (%)
Hydrogen bromide – trifluoroacetic acid	—	0.5	95	0.5
2-Dimethylaminoethanol	None	24	40	9.2
2-Dimethylaminoethanol†	0.1	1	55	1.0
		2	21	2.3

*See Experimental for detailed procedure.
†Batchwise transesterification procedure (total reaction time, 2 h, total yield, 76%, preparative scale reaction).

oxycarbonyl-L-aspartylglycine. Transesterification of the polymer-linked β-*t*-butyl benzyloxycarbonyl-L-aspartylglycine in 2-dimethylaminoethanol containing 0.1 equiv. of thallous alkoxide, yielded 76% of the protected dipeptide ester, after two 1 h reaction periods. Examination of the product by n.m.r. spectroscopy confirmed that the *t*-butyl ester group remained intact under these conditions. The dimethylaminoethyl ester function was selectively removed by treatment with aqueous dimethylformamide and the product, β-*t*-butyl benzyloxycarbonyl-L-aspartylglycine, was characterised by conversion to the crystalline dicyclohexylammonium salt.

The protected aspartylglycine dipeptide was also utilised to determine the extent of α → β transpeptidation, occurring at the aspartyl residue, under the transesterification conditions. This side reaction generally presents a serious problem when aspartyl peptides are exposed to alkali (18) and the reaction has also been found to occur in anhydrous hydrogen fluoride (19) under the conditions which are used routinely for the cleavage of the peptide from the resin in conventional solid-phase synthesis. The aspartylglycine dipeptide was chosen for the present work because this peptide is known to be unusually prone to transpeptidation (20) and thus provided a severe test of the transesterification conditions. Quantitation of the α- and β-isomers was accomplished by ion exchange chromatography of the deprotected peptide, using the Beckman 120C amino acid analyzer. In the absence of catalyst the transesterification was accompanied by considerable transpeptidation as shown in Table 4, the amount of β-isomer being 9.2% in a 24 h reaction. When the reaction was performed with the addition of 0.1 equiv. of thallous alkoxide, the amount of β-isomer was

Can. J. Chem. Downloaded from www.nrcresearchpress.com by 210.87.254.5 on 09/05/12
For personal use only.

Can. J. Chem. Downloaded from www.nrcresearchpress.com by 210.87.254.5 on 09/05/12
For personal use only.

1.0% in a 1 h reaction, with a total yield of 55%. When this reaction was continued for a further 1 h period, by addition of fresh solvent and catalyst, an additional 20% yield of product was obtained, containing 2.3% β-isomer. A control cleavage reaction using hydrogen bromide in trifluoroacetic acid gave a product containing 0.5% β-isomer; therefore it was assumed that this amount of β-isomer existed in the synthetic peptide before cleavage from the resin. Thus the net extent of transpeptidation occurring during the transesterification was 0.5% in the 1 h reaction with thallous alkoxide catalysis.

From the above results we conclude that transesterification with 2-dimethylaminoethanol in the presence of thallous alkoxide, provides a convenient method for the removal of protected peptides from the solid support, after solid-phase synthesis by conventional methods. The reaction is applicable to peptides containing both hindered or nonhindered C-terminal residues, however the route is not recommended for use in the case of peptides containing the C-terminal amino acids phenylalanine, cysteine, serine, threonine, or aspartic acid, where the risk of racemization is greatly increased. In the case of peptides containing an acidic amino acid, the *t*-butyl ester grouping is recommended for the protection of the carboxylic acid side chain. This protecting group is compatible with the use of the biphenylisopropoxycarbonyl group for the temporary protection of α-amino functions. Catalysis of the transesterification, with thallous alkoxide, is required in the case of peptides containing acidic amino acids, in order to keep the risk of transpeptidation to a minimum.

Selective removal of the 2-dimethylaminoethyl ester group from the transesterification product, is readily accomplished by treatment with aqueous dimethylformamide, to yield the partially protected peptide containing a free terminal carboxylic acid group. After purification by conventional techniques, the selectively protected peptide is available for use as a building unit in the synthesis of larger molecules by either solid phase or solution methods.

Experimental

2-Dimethylaminoethanol, obtained from Eastman Organic Chemicals, was dried by distillation with two volumes of dry benzene. The fraction boiling at 133–135° (760 mm) was collected and kept over molecular sieve (Type 4A) and was filtered through a column of alumina (B. D. H., Brockman activity II) immediately before use. Dimethylformamide was purified by distillation (25 mm) over phosphorus pentoxide, stored over Linde molecular sieve (Type 4A), and filtered through a column of alumina immediately before use. Peroxide-free dioxane was prepared and tested as described by Stewart and Young (21). BOC amino acids were obtained from Cyclo Chemical Corp. or were synthesized by the method of Schnabel (22). β-*t*-Butyl benzyloxycarbonyl-L-aspartic acid dicyclohexylamine salt was obtained from Schwartz Bioresearch Inc. DL-Leucyl-DL-alanine, L-leucyl-L-valine, α-L-aspartylglycine, and β-L-aspartylglycine were obtained from Fox Chemical Co., Inc. L-Alanyl-L-phenylalanine and L-alanyl-D-phenylalanine were prepared as described by Lemieux and Barton (23). Chloromethylated copolystyrene, 2% divinylbenzene, containing 1.8–2.2 mequiv. chlorine per gram, was obtained from Schwartz Bioresearch Inc.

Synthesis of resin-linked peptides was performed by the conventional solid-phase method (1) using a 2% cross-linked resin, except for the case of BOC-L-leu-D-val-*O*-polymer where a 1% cross-linked resin was employed. The progress of these syntheses was monitored by amino acid analysis of hydrolysates of samples of the peptide–resin. Acid hydrolysis of peptide–resin and peptide samples was performed using 6 *N* hydrochloric acid – propionic acid (1:1 v/v) *in vacuo* at 130° for 3 h (24). Amino acid analyses were performed using a Beckman amino acid analyzer, Model 120C.

Thallous ethoxide was obtained from Aldrich Chemical Co., Inc. Thallous 2-dimethylaminoethanol solution was prepared by mixing thallous ethoxide (1.4 mmol) with 2-dimethylaminoethanol (25 ml). An aliquot of this standard solution was added to each reaction mixture. Precautions were taken to ensure that skin contact, and contamination of work areas, with thallium derivatives, was scrupulously avoided (25).

Thin-layer chromatography was performed using silica gel G (Brinkman Instruments, (Canada) Ltd.). The following solvent systems were used: TLC-1, 1-butanol – acetic acid – water (2:1:1 v/v); TLC-2, chloroform–methanol–water (40:25:5 v/v); TLC-3, dimethylformamide–chloroform (2:3 v/v); TLC-4, chloroform – methanol – acetic acid (85:15:5 v/v). The plates were sprayed with ninhydrin and with the chlorine peptide spray (26).

Nuclear magnetic resonance spectra were obtained using a Varian A-60 instrument. Optical rotations were measured using a Perkin-Elmer polarimeter (Model 141) with a 10 cm tube.

Transesterification Procedure with Thallous Alkoxide Catalysis. Measurement of Yields and Racemization

The peptide–resin was stirred in 2-dimethylaminoethanol–dimethylformamide (1:1, 10 ml/g resin) containing thallous alkoxide catalyst, as described in Tables 2 and 3. At the end of the reaction time the resin was filtered off and the filtrate (the transesterification solution) was passed through a column of Amberlite IRC-50 in order to remove the thallium salt. The resin was washed with dimethylformamide and the washings were passed through the ion-exchange column as above. The filtrates were evaporated *in vacuo* at 30° and reevaporated twice with dimethylformamide to yield the protected peptide

Can. J. Chem. Downloaded from www.nrcresearchpress.com by 210.87.254.5 on 09/05/12
For personal use only.

2-dimethylaminoethyl ester. When the batchwise transesterification method was employed, as in Table 3, the above procedure was repeated a number of times, with the same sample of peptide–resin, until the removal of the peptide from the resin was complete.

For cleavage of the 2-dimethylaminoethyl ester group the protected peptide ester was dissolved in 50% aqueous dimethylformamide and the mixture was kept overnight at room temperature. In the case of peptides containing a C-terminal valine residue, the solution was kept at p*H* 10.5 by titration with 0.2 *N* NaOH for 8 h using a p*H* stat. The reaction mixture was evaporated *in vacuo*. The BOC group was then removed by treatment with 1 *N* HCl in acetic acid for 15 min at room temperature. After evaporation of the solution *in vacuo*, the peptide diastereoisomers were quantitated by the method of Manning and Moore (16), using a Beckman amino acid analyzer, Model 120C(59 × 0.9 cm column packed with Beckman UR-30 resin, flow rate 58 ml/h, 57°). Peak positions and operational color values of the diastereoisomers are reported in Table 1.

Determination of the Extent of α → β Aspartyl Transpeptidation during the Preparation of β-t-Butyl Benzyloxycarbonyl-L-Aspartylglycine via the Transesterification Route

β-*t*-Butyl benzyloxycarbonyl-L-aspartylglycine-polymer (30 mg; 10 μmol dipeptide) was stirred in the transesterification solution as described above, for the reaction times shown in Table 4. The crude protected aspartylglycine dipeptide solutions were treated with aqueous dimethylformamide as described above, to bring about the cleavage of the 2-dimethylaminoethyl ester group. The solution was evaporated *in vacuo*, the product was dissolved in trifluoroacetic acid (10 ml), and hydrogen bromide gas was passed into the solution for 30 min at room temperature to bring about the removal of the benzyloxycarbonyl and *t*-butyl ester groups. The solution was evaporated *in vacuo* and reevaporated twice with aqueous acetic acid (3:1, 10 ml). Quantitation of the α- and β-isomers was accomplished by ion-exchange chromatography using a Beckman amino acid analyzer, Model 120C (59 × 0.9 cm column packed with Beckman UR-30 resin, flow rate 58 ml/h, 57°). Peak positions and operational color values, given in Table 1, were determined using commerical samples of α-L-aspartylglycine and β-L-aspartylglycine. Direct cleavage of the protected dipeptide from the resin, using hydrogen bromide in trifluoroacetic acid (ref. 21, p. 40), was performed to determine the amount of β-isomer occurring in the synthetic peptide before transesterification.

Preparation of BOC-L-leucyl-L-alanine via the Transesterification Route

BOC-L-leucyl-L-alanine-resin (400 mg; 0.23 mmol dipeptide) was transesterified in the presence of thallous alkoxide catalyst (0.02 equiv.; 5 μmol) for 0.5 h as in the transesterification procedure described above. The filtrates were evaporated *in vacuo* to yield the first batch of product (Batch A, Table 3). The transesterification was continued by addition of fresh solvent and catalyst to the same sample of peptide-resin to give the further yields of product (B–F), as described in Table 3. The first five batches of product (A–E) were pooled. Thin-layer chromatography showed one major spot having the following R_f values: TLC-1, 0.65; TLC-2, 0.76. The protected peptide 2-dimethylaminoethyl ester was hydrolyzed in aqueous dimethylformamide for 24 h and, after evaporation of the solvent, the residual oil was taken up in ethyl acetate, washed with 10% citric acid solution and saturated sodium chloride solution, dried ($MgSO_4$) and evaporated *in vacuo* at 30° to yield BOC-L-leucyl-L-alanine (60 mg; oil) which crystallized from ether–hexane (52 mg, 76%); m.p. 133–134°; $[\alpha]_D^{25}$ −33.8° (*c*, 1 in methanol) (lit. (16) m.p. 132–133°; $[\alpha]_D^{25}$ −32.6° (*c*, 1.01 in methanol)). The product showed a single spot by thin-layer chromatography, having the following R_f values: TLC-1, 0.90; TLC-2, 0.50; TLC-4, 0.68.

Anal. Calcd. for $C_{14}H_{26}O_5N_2$: C, 55.62; H, 8.66; N, 9.26. Found: C, 55.54; H, 8.47; N, 9.33.

Preparation of BOC-L-leucyl-D-valine via the Transesterification Route

BOC-L-leu-D-val-*O*-polymer (5 g; 2.16 mmol dipeptide, 1% cross-linked resin) was transesterified in the presence of thallous alkoxide catalyst (0.15 equiv.; 0.33 mmol) for 2.5 h, as in the transesterification procedure described above. The filtrates were evaporated *in vacuo* to yield the first batch of product (Batch A, Table 3). The transesterification procedure was repeated to give further batches of product (B and C) as described in Table 3. Batches A and B were pooled, dissolved in ethyl acetate, washed with 1 *M* ammonium carbonate, followed by saturated sodium chloride, dried ($MgSO_4$), and evaporated *in vacuo* at 30° to yield the protected dipeptide ester (830 mg, oil). Thin-layer chromatography showed a single spot having the following R_f values: TLC-1, 0.68; TLC-2, 0.80. A portion of the product (600 mg; 1.5 mmol) was dissolved in dimethylformamide (20 ml), 0.1 *N* sodium hydroxide (20 ml) was added, and the solution was stirred overnight. Acetic acid (0.5 ml) was added and the solution was evaporated *in vacuo* at 30°. The residue was taken up in ethyl acetate, washed with 10% citric acid and saturated sodium chloride, dried ($MgSO_4$), and evaporated to give an oil which precipitated from ether on addition of *n*-hexane (490 mg; 96%). The product, BOC-L-leucyl-L-valine, was recrystallized twice from *n*-hexane–ether (435 mg; 85%); m.p. 106–107°; $[\alpha]_D^{25}$ −34° (*c*, 1 in methanol). Thin-layer chromatography showed a single spot having the following R_f values: TLC-1, 0.90; TLC-4, 0.70.

Anal. Calcd. for $C_{16}H_{29}O_5N_2$: C, 58.38; H, 8.87; N, 8.50. Found. C, 58.32; H, 9.06; N, 8.28.

Preparation of β-t-Butyl Benzyloxycarbonyl-L-Aspartylglycine via the Transesterification Route

β-*t*-Butyl benzyloxycarbonyl-L-aspartylglycine-polymer (2 g; 0.71 mmol dipeptide) was transesterified in the presence of thallous alkoxide catalyst (0.1 equiv; 0.07 mmol) for 1 h as in the transesterification procedure described above. The filtrates were evaporated *in vacuo* to yield the first batch of product (0.39 mmol; 55%). Quantitation of α- and β-isomers, as described above showed the presence of 1% (0.004 mmol) β-isomer. The transesterification procedure was repeated for a further 1 h period to give an additional yield of product (0.15 mmol, 20%) which was found to contain 2.3% β-isomer. The two batches of the protected peptide 2-dimethyl-

aminoethyl ester were combined. Thin-layer chromatography showed one major spot having the following R_f values: TLC-1, 0.60 with traces at 0.50 and 0.70 (protected dipeptide acid); TLC-3, 0.80 with traces at 0.70 and at the origin (protected dipeptide acid). The n.m.r. spectrum ($CDCl_3$, 60 MHz, TMS internal) showed peaks at τ 9.60 (s, 9H (CH_3)$_3$C), 7.72 (s, 6H, (CH_3)$_2$N), 7.43 (t, OCH_2CH_2N), 7.25 (m, $CHCH_2CO$, 4H with 7.43 peak), 5.98 (d, 2H $NHCH_2CO$), 5.78 (t, 2H, OCH_2CH_2N), 5.38 (m, 1H, $NHCHCO$), 4.90 (s, 2H, $C_6H_5CH_2O$), 2.67 (s, 5H, $C_6H_5CH_2$), plus two broad doublets at 3.00 and 3.90 ($CONHCH$).

A portion of the protected dipeptide ester (0.43 mmol) was treated with aqueous dimethylformamide for 24 h. The solvent was evaporated *in vacuo* to yield β-*t*-butyl benzyloxycarbonyl-L-aspartylglycine (220 mg; oil) which was converted to the dicyclohexylammonium salt (27) and recrystallized from *n*-hexane–benzene (210 mg, 87%); m.p. 138–139°; $[\alpha]_D^{25}$ −10.7° (*c*, 1 in methanol). Thin-layer chromatography showed a single spot for the free acid, R_f values: TLC-1, 0.70; TLC-4, 0.65.

Anal. Calcd. for $C_{30}H_{47}O_7N_3$: C, 64.15; H, 8.43; N, 7.48. Found. C, 63.99; H, 8.30; N, 7.62.

The authors express their appreciation to Ester Fraga for valuable technical assistance. This work was supported by the Medical Research Council of Canada (grant number MA-4638) and by the Banting Research Foundation.

1. R. B. MERRIFIELD. J. Am. Chem. Soc. **85**, 2149 (1963); R. B. MERRIFIELD. Advan. Enzymol. **32**, 221 (1969).
2. J. H. JONES and B. RIDGE. Amino acids, peptides and proteins. Vol. 4. The Chemical Society, London. 1972. p. 375.
3. J. J. SHARP, A. B. ROBINSON, and M. D. KAMEN. J. Am. Chem. Soc. **95**, 6097 (1973).
4. S. WANG and R. B. MERRIFIELD. J. Am. Chem. Soc. **91**, 6488 (1969).
5. S. WANG and R. B. MERRIFIELD. Int. J. Protein Res. **1**, 235 (1969).
6. D. L. MARSHALL and I. E. LIENER. J. Org. Chem. **35**, 867 (1970).
7. G. W. KENNER, J. R. MCDERMOTT, and R. C. SHEPPARD. J. Chem. Soc. D, 636 (1971).
8. B. HALPERN, L. CHEW, V. CLOSE, and W. PATTON. Tetrahedron Lett. 5163 (1968).
9. W. PEREIRA, V. CLOSE, W. PATTON, and B. HALPERN. J. Org. Chem. **34**, 2032 (1969).
10. H. C. BEYERMAN, H. HINDRICKS, and E. W. B. DE LEER. Chem. Commun. 1668 (1968).
11. H. YAJIMA, H. KAWATANI, and H. WATANABE. Chem. Pharm. Bull. **18**, 1333 (1970).
12. S. SAKAKIBARA, Y. KISHIDA, Y. KIKUCHI, R. SAKAI, and K. KAKACHI. Bull. Chem. Soc. Jap. **41**, 1273 (1968).
13. G. OMENN and C. B. ANFINSEN. J. Am. Chem. Soc. **90**, 6571 (1968).
14. H. YAJIMA and H. KAWATANI. Chem. Pharm. Bull. **19**, 1905 (1971).
15. M. A. BARTON, R. U. LEMIEUX, and J. Y. SAVOIE. J. Am. Chem. Soc. **95**, 4501 (1973).
16. J. M. MANNING and S. MOORE. J. Biol. Chem. **243**, 5591 (1968).
17. G. W. KENNER and J. H. SEELY. J. Am. Chem. Soc. **94**, 3259 (1972).
18. B. RINIKER and R. SCHWYZER. Helv. Chim. Acta, **47**, 2357 (1964).
19. T. BABA, H. SUGIYAMA, and S. SETO. Chem. Pharm. Bull. **21**, 207 (1973).
20. M. A. ONDETTI, A. DEER, J. T. SHEEHAN, J. PLUSCEC, and O. KOCY. Biochemistry, 7, 4069 (1968).
21. J. M. STEWART and J. T. YOUNG. Solid-phase peptide synthesis. W. H. Freeman, San Francisco, California. 1969, p. 27.
22. E. SCHNABEL. Ann. **702**, 188 (1967).
23. R. U. LEMIEUX and M. A. BARTON. Can. J. Chem. **49**, 767 (1971).
24. J. SCOTCHLER, R. LOZIER, and A. B. ROBINSON. J. Org. Chem. **35**, 3151 (1965).
25. E. C. TAYLOR and A. MCKILLOP. Acc. Chem. Res. **3**, 338 (1970).
26. R. H. MAZURE, B. W. ELLIS, and F. S. CAMMARATA. J. Biol. Chem. **237**, 1619 (1962).
27. E. KLIEGER, E. SCHRODER, and H. GIBIAN. Ann. **640**, 157 (1961).

Can. J. Chem. Downloaded from www.nrcresearchpress.com by 210.87.254.5 on 09/05/12
For personal use only.

COMMUNICATIONS

Structure and Reactivity of Methyl Radical — Cyanide Ion Pairs in Crystal I and Crystal II of Acetonitrile[1]

ESTEL DEAN SPRAGUE,[2] KEIJI TAKEDA,[3] JIH TZONG WANG,[4] AND FFRANCON WILLIAMS[5]

Department of Chemistry, University of Tennessee, Knoxville, Tennessee 37916

Received May 13, 1974

ESTEL DEAN SPRAGUE, KEIJI TAKEDA, JIH TZONG WANG, and FFRANCON WILLIAMS. Can. J. Chem. **52**, 2840 (1974).

The extent of interaction between methyl radicals and cyanide ions produced in pairs by dissociative electron capture in the two solid phases of acetonitrile has been studied by e.s.r. using CD_3 ^{13}CN. Although no interaction is observed when the radical–anion pairs are generated by photobleaching the acetonitrile dimer radical anion in Crystal I, a very weak interaction as evidenced by an isotropic ^{13}C hyperfine splitting of 3.4 G is found for the corresponding species produced from the acetonitrile monomer radical anion in Crystal II. The rate of hydrogen atom abstraction by the methyl radical in Crystal I is at least a factor of 10 greater than in Crystal II at the same temperature over the range 77–113 K. These results show that the weak perturbation of the methyl radical by the cyanide ion does not enhance methyl radical reactivity in hydrogen atom abstraction. Evidence from ^{13}C hyperfine splitting measurements on $^{13}CD_3 \cdot\text{---}CN^-$ and $^{13}CH_3 \cdot\text{---}Br^-$ indicates that the configuration of the methyl radical is planar in these radical–anion pairs. It is emphasized that quantum mechanical tunneling provides a satisfactory explanation for the low apparent activation energies, the curved Arrhenius plots, and the abnormally large deuterium isotope effects which characterize hydrogen atom abstraction reactions by methyl radicals in glassy and crystalline solids at low temperatures. Moreover, since the tunneling rate is extremely sensitive to the width of the barrier, methyl radical reactivity is expected to show a very strong dependence on the precise geometry of the reacting partners in the solid state.

ESTEL DEAN SPRAGUE, KEIJI TAKEDA, JIH TZONG WANG et FFRANCON WILLIAMS. Can. J. Chem. **52**, 2840 (1974).

On a étudié grâce à la r.p.e. et en faisant appel à du CD_3 ^{13}CN, le taux d'interaction entre les radicaux méthyles et les ions cyanures produits sous forme de paires par la capture d'électrons produisant des dissociations; on a effectué ces études dans deux phases solides de l'acétonitrile. Quoique l'on observe aucune interaction quand les paires de radicaux anions sont générées par photodécoloration du radical–anion dimère avec l'acétonitrile dans le crystal I, on trouve grâce à un h.f.s. isotopique ^{13}C de 3.4 G une très faible interaction dans les espèces correspondantes produites à partir du radical–anion monomère avec l'acétonitrile dans le crystal II. Le taux d'abstraction des atomes d'hydrogène par le radical méthyle dans le crystal I est au moins 10 fois plus grand que dans le crystal II à la même température entre 77–113 K. Ces résultats montrent que la faible perturbation du radical méthyle par l'ion cyanure n'augmente pas la réactivité du radical méthyle lors de l'enlèvement d'atomes d'hydrogène. Les résultats obtenus lors de la mesure de h.f.s. ^{13}C pour $^{13}CD\cdot\text{---}CN^-$ et $^{13}CH_3\cdot\text{---}Br^-$ montre que la configuration du radical méthyle est plane dans ces paires de radicaux anions. On met en évidence que l'effet tunnel de la mécanique quantique fourni une explication satisfaisante pour les énergies d'activation apparamment basses, pour les courbes d'Arrhénius courbées et pour les effets isotopiques du deutérium qui sont anormalement grandes et qui caractérisent les réactions d'abstraction d'atomes d'hydrogène par des radicaux méthyles dans des matériaux vitreux ou cristallins à basse température. De plus puisque le taux d'effet tunnel est extrêmement sensible à la largeur de la barrière, on s'attend à ce que la réactivité des radicaux méthyles montre une très grande dépendence sur la géométrie exacte des partenaires réactifs dans l'état solide.

[Traduit par le journal]

[1]This work was supported by the U.S. Atomic Energy Commission (Document No. ORO-2968-87).

[2]Department of Chemistry, University of Cincinatti, Cincinatti, Ohio 45221.

[3]Fuji Photo Film Co. Ltd., Research Laboratories Tokyo, Asaka, Saitama, Japan 351.

[4]Institute of Nuclear Energy Research, Atomic Energy Council, P.O. Box 3, Lung-Tan, Taiwan, Republic of China.

[5]John Simon Guggenheim Memorial Foundation Fellow, 1972–1973; author to whom correspondence should be addressed.

Can. J. Chem. Downloaded from www.nrcresearchpress.com by 210.87.254.42 on 09/05/12
For personal use only.

Can. J. Chem. Downloaded from www.nrcresearchpress.com by 210.87.254.42 on 09/05/12
For personal use only.

A recent Communication (1) has suggested an alternative explanation to quantum mechanical tunneling (2, 3) for the unusually low value of the apparent activation energy ($E_a < 2$ kcal mol^{-1}) for hydrogen atom abstraction by methyl radicals in γ-irradiated crystalline acetonitrile at 77–87 K. According to these authors (1), the proximity of the cyanide ion to the methyl radical produces a perturbation which distorts the methyl radical from planarity and lowers the energy requirements for the reaction. Before commenting on the evidence presented in support of this proposal (1), we wish to report new e.s.r. results which bear directly on this question.

Earlier work from this laboratory (4–11) has established that the photobleachable product of electron capture in γ-irradiated acetonitrile at 77 K differs according to the nature of the crystalline phase. Thus in Crystal I metastabilized at 77 K by rapid cooling from above the solid–solid phase transition at 217 K (12), the radiation-induced color center ($\lambda_{max} = 510$ nm) is the dimer radical anion $(MeCN)_2^-$, whereas in Crystal II the corresponding light-sensitive species ($\lambda_{max} = 430$ nm) is the monomer radical anion $MeCN^-$. Since both of these radical anions give rise to a methyl radical and a cyanide anion on photobleaching with visible light as depicted formally in reactions 1*a* and *b*,

$$[1a] \qquad (MeCN)_2^- \underset{\Delta}{\overset{h\nu}{\rightleftarrows}} Me\cdot + CN^- + MeCN$$

$$[1b] \qquad MeCN^- \underset{\Delta}{\overset{h\nu}{\rightleftarrows}} Me\cdot + CN^-$$

a comparison of the results for these two systems might well be expected to shed some light on whether or not the extent of interaction between the radical and the anion is related to the reactivity of the methyl radical in the irreversible hydrogen atom abstraction [2],

$$[4] \qquad Me\cdot + CH_3CN \rightarrow MeH + \cdot CH_2CN$$

as postulated by Sargent *et al.* (1).

It has been shown that the photochemical dissociation products in reactions 1*a* and *b* undergo a thermal reaction to regenerate the acetonitrile radical anions (4, 6). Each of these recovery reactions competes with [2] in CH_3CN (2, 13–15) but in CD_3CN the radical anions are regenerated with close to 100% efficiency, this difference in behavior corresponding to a primary kinetic isotope effect k_2^H/k_2^D greater than 2×10^3 for the abstraction reaction in Crystal I at 77 K. For this reason and to avoid the broadening effect of unresolved ^1H hyperfine coupling in the e.s.r. spectra of the radical anions (11), most of our structural e.s.r. studies have been carried out on the deuterated compounds $CD_3C^{14}N$, $CD_3C^{15}N$, $^{13}CD_3C^{14}N$, and $CD_3{}^{13}C^{14}N$. However, it should be emphasized that the unusually large hydrogen isotope effects in these two systems are entirely kinetic, not structural.

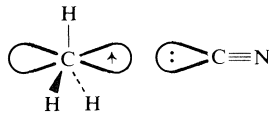

FIG. 1. Geometrical arrangement of a methyl radical – cyanide anion pair showing the possibility of interaction between the unpaired electron in the carbon 2p orbital of the methyl radical and the lone pair in the carbon sp orbital of the cyanide anion.

In this report we focus on the results obtained with $CD_3{}^{13}CN$ since any interaction between the $CD_3\cdot$ radical and the $^{13}CN^-$ anion should be revealed most clearly by a weak hyperfine coupling to the ^{13}C nucleus. As depicted in Fig. 1, the likely disposition of the dissociation products results in a favorable geometry for possible overlap between the lone-pair sp orbital on the carbon of the cyanide ion and the carbon 2p orbital containing the unpaired electron in the methyl radical; indeed, were the C_{3v} symmetry of the neutral CD_3CN molecule to be retained in the dissociation products, the major axes of these two orbitals would coincide exactly. In addition to this orientation factor, the extent of interaction will be governed by the $CD_3\cdot$---CN^- recoil distance. The possibility therefore exists for the formation of a weak three-electron (σ^2,σ^{*1}) bond resulting in a partial delocalization of the unpaired electron into the sp hybrid orbital of the cyanide carbon. It is readily calculated from the magnetic resonance parameters for atomic orbitals (16) that a spin density ρ distributed equally between the s and p orbitals of the lone pair should result in an isotropic ^{13}C hyperfine splitting (G) of 565ρ and an anisotropic ^{13}C hyperfine splitting (G) tensor of [33ρ, −16.5ρ, −16.5ρ]. In the case where ρ is of the order of 0.01, the ^{13}C coupling will

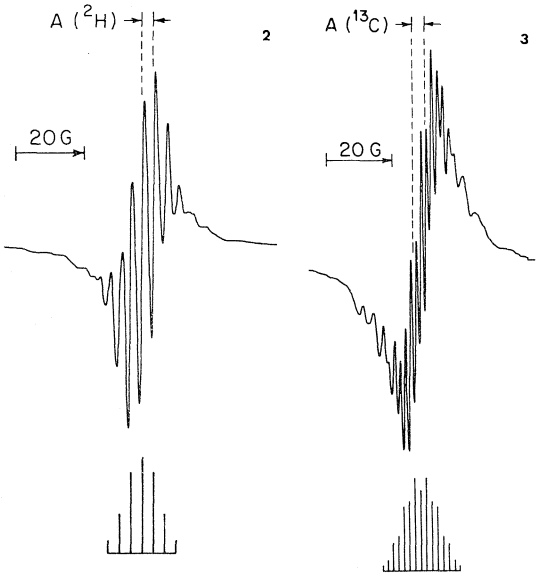

FIG. 2. The e.s.r. spectrum of γ-irradiated Crystal I of acetonitrile-d_3 containing 55% $CD_3{}^{13}CN$ after photobleaching with visible light at 77 K. The stick diagram represents the spectrum of the $CD_3\cdot$ radical.

FIG. 3. The e.s.r. spectrum of γ-irradiated Crystal II of acetonitrile-d_3 containing 55% $CD_3{}^{13}CN$ after photobleaching with visible light at 77 K. For an explanation of the stick diagram, see text.

appear to be isotropic since the total anisotropy is less than the linewidth. Therefore, we have available an extremely sensitive magnetic probe to determine if there is a methyl radical – cyanide anion interaction in these two systems.

The e.s.r. spectrum shown in Fig. 2 was obtained on photobleaching the dimer radical anion of CD_3CN in a sample of Crystal I enriched to 55% $CD_3{}^{13}CN$. The simple septet pattern with the intensity ratios 1:3:6:7:6:3:1 and the ^{2}H hyperfine splitting of 3.35 G is clearly that of $CD_3\cdot$, the spectrum being indistinguishable from that obtained on photobleaching the dimer radical anion of $CD_3{}^{12}CN$. In contrast, Fig. 3 shows that the spectrum obtained after photobleaching the monomer radical anion derived from the same enriched $CD_3{}^{13}CN$ material in Crystal II is not a simple septet, the pattern consisting of 11 prominent components with a constant spacing of *ca.* 1.7 G. These components are extremely narrow and well resolved for a polycrystalline spectrum, suggesting immediately that the additional lines originate from an isotropic ^{13}C hyperfine splitting, as envisaged earlier. Since the spectrum of the products from the photobleaching of the $CD_3{}^{12}CN$ monomer radical anion is the usual $CD_3\cdot$ septet (6), this proves beyond a doubt that the superhyperfine structure in the spectrum of Fig. 3 originates from a ^{13}C interaction. Below the spectrum is a stick diagram calculated for a ^{13}C doublet of ^{2}H septets superimposed on a ^{2}H septet according to the coupling constants $A_{iso}(^{13}C) = A_{iso}(^2H) = 3.4$ G, the intensities of the two contributing spectra being in the $^{13}C/^{12}C$ ratio of 0.55 to 0.45. This plot consists of 15 lines with an even spacing of 1.7 G and intensity ratios (for half the spectrum) of 1.1:1.8:4.4:5.4:9.9:10.8:14.3:12.6, in satisfactory agreement with the observed spectrum consisting of 11 major components. The uniqueness of the fit is readily established since the spacing excludes ^{13}C hyperfine splitting values other than $3.4n$ G, where n is an odd integer, and the intensity distribution is consistent only with $n = 1$.

Additional studies on authentic single crystals of the enriched $CD_3{}^{13}CN$ material showed that the e.s.r. spectrum of the photodissociation products from the monomer radical anion in Crystal II exhibited no orientation dependence, the pattern being identical with that obtained in the polycrystalline spectrum of Fig. 3. These experiments verify that the ^{13}C superhyperfine coupling is isotropic, the splitting of 3.4 G representing a spin density of 0.003 in the 2s orbital of the cyanide carbon. Since no anisotropy was observed in the single crystal spectrum, the spin density in the 2p orbital of the cyanide carbon cannot be reliably estimated. However, an upper limit of 0.01 is set by the fact that the total anisotropy ($3B$) cannot be greater than the linewidth of *ca.* 1 G. Thus, the results in Crystal II are completely consistent with an extremely weak σ interaction between the unpaired electron in the p orbital of the methyl radical and the lone pair of electrons in the sp hybrid orbital of the cyanide ion.

A brief comment is needed here on the implications of the negative ^{13}C results in Crystal I. At the very least this shows a negligible σ interaction since the isotropic hyperfine splitting is an extremely sensitive measure of this perturbation. However, even if a π interaction were to apply such that spin density is transmitted exclusively to the 2pπ orbitals of the cyanide ion,

Can. J. Chem. Downloaded from www.nrcresearchpress.com by 210.87.254.42 on 09/05/12
For personal use only.

Can. J. Chem. Downloaded from www.nrcresearchpress.com by 210.87.254.42 on 09/05/12
For personal use only.

the failure to observe ^{13}C splittings in the spectra obtained from single crystals points again to a spin density of less than 0.01 in the p orbitals of the cyanide carbon. The suggestion that the ^{13}C lines may be too broad to detect can be rejected since small anisotropic ^{13}C splittings were resolved in the spectra of the dimer radical anion (10) obtained from the same samples of Crystal I. It should also be added that a π interaction would require almost a 90° reorientation of the C_{3v} axis of the methyl radical after photodissociation of the almost linear MeCN fragment in the dimer radical anion (10). Moreover, this geometry would obviously be much less favorable than that of Fig. 1 for the thermal recombination of the methyl radical and the cyanide ion. In our view the most reasonable explanation for the difference in the ^{13}C hyperfine splitting results is that the $Me\cdot\text{---}CN^-$ recoil distance is greater in Crystal I than it is in Crystal II.

Having established the occurrence of a methyl radical – cyanide ion interaction in the products formed in Crystal II but not in Crystal I, we now turn our attention to the question of methyl radical reactivity in reaction 2. From comprehensive kinetic studies of the parallel reactions −1 and 2 using both e.s.r. and optical methods of detection, we have found (2, 3, 14, 15) that the pseudo first-order rate constants k_2 for hydrogen atom abstraction in Crystal I and Crystal II of CH_3CN at 77 K are 2.5×10^{-2} min^{-1} and 1.4×10^{-3} min^{-1}, respectively, the former result being in essential agreement with the value of 2.2×10^{-2} min^{-1} reported by Sargent *et al.* (1).[6] Moreover, in the entire range between 77 and 113 K for which comparative measurements are available (15), the value of k_2 in Crystal I is at least a factor of 10 greater than in Crystal II at the same temperature. Evidently, as far as reaction 2 is concerned, the reactivity of the methyl radical produced from the monomer radical anion in Crystal II is lower than that of the methyl radical produced from the dimer radical anion in Crystal I, contrary to the postulate (1) that the reactivity is enhanced by a perturbation from the cyanide ion. This observation should certainly not be construed to mean that the reactivity of the methyl radical is actually depressed by the weak perturbation observed in Crystal II. It is our view that such weak interactions have little or no effect on the reactivity of the methyl radical and that other considerations are paramount (see below).

We now turn to information from e.s.r. studies about the geometry of the methyl radical in these systems. Sargent *et al.* (1) suggest that the cyanide ion interaction causes the configuration of the methyl radical in the radical–ion pair to become intermediate between sp^2 and sp^3 and that the sp^3 character lowers the activation energy for abstraction. In support of this idea, the authors attach particular significance to small apparent differences of *ca.* 1 G in ^1H splittings for methyl radicals and say that values slightly below 23 G are indicative of pyramidal deformation from the planar state. However, a much more sensitive and precise indicator of pyramidal deformation is the isotropic component of the ^{13}C hyperfine splitting tensor which responds directly to the percentage s character in the orbital of the unpaired electron. Along these lines, Rogers and Kispert (17) have shown that the ^{13}C hyperfine splitting tensor for the methyl radical in γ-irradiated single crystals of sodium acetate trihydrate is definitely characteristic of a planar radical although the isotropic ^1H hyperfine splitting of 22.3 ± 0.5 G is again lower than the value of 23.02 G obtained for the radical in solution (18). In addition, unpublished work carried out in our group has shown from the ^{13}C splitting ($A_{||} = 83.3$ G) that the configuration of the methyl radical in the $CH_3\cdot\text{---}Br^-$ radical–anion pair (8) is planar despite the fact that the ^1H isotropic splitting is only 20.8 G, the reduction in the ^1H hyperfine splitting arising in this case from transfer of spin density to the bromine. Finally and most directly, the ^{13}C splittings derived from single crystal spectra of the dissociation products derived from the two radical anions of $^{13}CD_3CN$ indicate a contribution of less than 4% from the 2s orbital of the methyl carbon to the orbital

[6]The similarity between our kinetic data for hydrogen atom abstraction in Crystal I (2, 3, 14, 15) and the results obtained by Sargent *et al.* (1) at 77 K appears to establish that the latter experiments were also carried out on samples of Crystal I. Consistent with this conclusion, we have observed that Crystal I is the phase invariably formed when samples of pure liquid acetonitrile are shock cooled in liquid nitrogen. It might also be noted here that Sargent's results (1) are apparently uncorrected for any contribution due to the simultaneous regeneration of the dimer radical anion. Although this correction is relatively small at 77 K, it becomes significant at higher temperatures when the experiments are not carried out under continuous photobleaching conditions.

occupied by the unpaired electron. This is of the correct magnitude for spin polarization (18) and so there is no spectroscopic evidence to suggest that the methyl radical is nonplanar in the systems under investigation.

In conclusion, we comment on the general question of reactivity differences between methyl radicals generated in different ways within a particular crystalline solid. Actually, such effects are to be expected if tunneling applies since the tunneling rate is calculated to be extremely sensitive to the barrier width as well as to the barrier height (3, 15). Consequently, we do not view the results of Sargent *et al.* (1) as inconsistent with the tunneling hypothesis which has been shown to provide a satisfactory description of the low apparent activation energies, the curvature in the Arrhenius plots, and the large deuterium isotope effects for a variety of hydrogen atom abstraction reactions in the solid state (2, 3, 14, 15, 19–21).

We thank Dr. F. P. Sargent for sending us a preprint of his paper and the Editor of the Canadian Journal of Chemistry for inviting us to comment on this previous article.

1. F. P. SARGENT, M. G. BAILEY, and E. M. GARDY. Can. J. Chem. **52**, 2171 (1974).
2. E. D. SPRAGUE and F. WILLIAMS. J. Am. Chem. Soc. **93**, 787 (1971).
3. R. J. LE ROY, E. D. SPRAGUE, and F. WILLIAMS. J. Phys. Chem. **76**, 546 (1972).
4. M. A. BONIN, K. TSUJI, and F. WILLIAMS. Nature, **218**, 946 (1968).
5. M. A. BONIN, K. TAKEDA, and F. WILLIAMS. J. Chem. Phys. **50**, 5423 (1969).
6. K. TAKEDA and F. WILLIAMS. Mol. Phys. **17**, 677 (1969).
7. L. HOLLOMAN, E. D. SPRAGUE, and F. WILLIAMS. J. Am. Chem. Soc. **92**, 429 (1970).
8. E. D. SPRAGUE and F. WILLIAMS. J. Chem. Phys. **54**, 5425 (1971).
9. E. D. SPRAGUE, K. TAKEDA, and F. WILLIAMS. Chem. Phys. Lett. **10**, 299 (1971).
10. M. A. BONIN, Y. J. CHUNG, E. D. SPRAGUE, K. TAKEDA, J. T. WANG, and F. WILLIAMS. Nobel Symposium, **22**, 103 (1973).
11. T. GILLBRO and F. WILLIAMS. J. Chem. Soc. Faraday Trans II, **70**, 465 (1974).
12. W. E. PUTNAM, D. M. MCEACHERN, JR., and J. E. KILPATRICK. J. Chem. Phys. **42**, 749 (1965).
13. K. TAKEDA and F. WILLIAMS. J. Phys. Chem. **74**, 4007 (1970).
14. E. D. SPRAGUE. Ph.D. Thesis, University of Tennessee, 1971.
15. J. T. WANG. Ph.D. Thesis, University of Tennessee, 1972.
16. P. W. ATKINS and M. C. R. SYMONS. Structure of inorganic radicals. Elsevier, Amsterdam. 1967. p. 21.
17. M. T. ROGERS and L. D. KISPERT. J. Chem. Phys. **46**, 221 (1967).
18. R. W. FESSENDEN. J. Phys. Chem. **71**, 74 (1967).
19. J. T. WANG and F. WILLIAMS. J. Am. Chem. Soc. **94**, 2930 (1972).
20. A. CAMPION and F. WILLIAMS. J. Am. Chem. Soc. **94**, 7633 (1972).
21. E. D. SPRAGUE. J. Phys. Chem. **77**, 2066 (1973).

Can. J. Chem. Downloaded from www.nrcresearchpress.com by 210.87.254.42 on 09/05/12
For personal use only.

Can. J. Chem. Downloaded from www.nrcresearchpress.com by 210.87.254.42 on 09/05/12
For personal use only.

Canadian Journal of Chemistry

Published by
THE NATIONAL RESEARCH COUNCIL OF CANADA

Journal canadien de chimie

Publié par
LE CONSEIL NATIONAL DE RECHERCHES DU CANADA

Volume 52 Number 16 August 15, 1974

Volume 52 numéro 16 15 août 1974

Study of the Reactions of Chromium(III) Halides and Heterocyclic Ligands Containing Group VA and VIA Donor Atoms

C. PRETI AND G. TOSI

Istituto di Chimica Generale ed Inorganica, University of Modena, 41100 Modena, Italy

Received March 12, 1974

C. PRETI and G. TOSI. Can. J. Chem. **52**, 2845 (1974).

Complexes of thiomorpholin-3-one, thiomorpholin-3-thione, thiazolidine-2-thione, and thiazolidine-2-selenone with $CrX_3 \cdot nH_2O$ (X = Cl, Br, I) were prepared and characterized. On the basis of vibrational (conventional and far infrared) and electronic spectroscopy, magnetism and conductivity measurements, the structures of these complexes were identified. The bonding occurs through the oxygen in the complexes of thiomorpholin-3-one and through the nitrogen in all the remaining complexes. The complexes CrL_3X_3 involve unidentate ligands, are neutral, monomeric, and hexacoordinate. Spectroscopic parameters for the complexes have been calculated and compared with similar chromophores containing CrN_3X_3, CrO_3X_3, and CrS_3X_3 chromophores.

C. PRETI et G. TOSI. Can. J. Chem. **52**, 2845 (1974).

On a préparé et caractérisé les complexes du $CrX_3 \cdot nH_2O$ (X = Cl, Br, I) avec la thiomorpholinone-3, la thiomorpholinethione-3, la thiazolidinethione-2 et de la thiazolidïnesélénone-2. On a identifié la structure de ces complexes en utilisant les spectroscopies de vibration (conventionnelle et infrarouge lointain) et électronique de même que des mesures de magnétisme et de conductivité. La liaison se rait par l'oxygène dans les complexes de la thiomorpholinone-3 et par l'azote dans tous les autres complexes. Les complexes CrL_3X_3 impliquent des ligands monovalents; ces complexes sont neutres, sous forme de monomères et hexacoordonnés. On a calculé les paramètres spectroscopiques des complexes et ces calculs ont été comparés avec ceux obtenus pour des chromophores semblables contenant des chromophores CrN_3X_3, CrO_3X_3 et CrS_3X_3. [Traduit par le journal]

In order to study the competition between group VA and VIA donor atoms in heterocyclic ligands in the coordination to the metals, we have reported in our previous papers (1–3) the characterization of several complexes of thiomorpholin-3-one

(tm = O=C—NH—CH_2—CH_2—S—CH_2),

thiomorpholin-3-thione

(ts = S=C—NH—CH_2—CH_2—S—CH_2),

thiazolidine-2-thione

(ttz = S=C—NH—CH_2—CH_2—S),

and thiazolidine-2-selenone

(tzse = Se=C—NH—CH_2—CH_2—S).

These ligands behave as a soft or a hard base depending on the metal class.

In this paper we have studied the complexation behavior of tm, ts, ttz, and tzse with chromium(III), a metal classified as typically hard, in order to further our present knowledge and to fill in some of the gaps in the knowledge of the behavior of chromium(III) with this class of ligands.

By reaction of $CrX_3 \cdot nH_2O$ (X = Cl, Br, I) with the ligands, according to the methods described in the experimental section, we have obtained complexes of the general formula CrL_3X_3 (L = tm, ts, ttz, tzse; X = Cl, Br, I). The com-

TABLE 1. Analytical data

Compound	Color	Found (%)			Calculated (%)			Decomposition temperature (°C)	μ (B.M.)	Λ DMF
		M	C	H	M	C	H			
$[Crtm_3Cl_3]$	Dark-green	10.0	27.4	4.1	10.2	28.2	4.2	155	3.9	44.0
$[Crtm_3Br_3]\cdot 2H_2O$	Dark-green	7.8	21.6	3.9	7.7	21.2	3.7	95–100	3.9	dec.
$[Crtm_3I_3]$	Dark-green	—	18.1	2.9	6.6	18.4	2.7	160	4.2	39.2
$[Crts_3Cl_3]$	Dark-green	9.8	25.3	3.4	9.4	25.8	3.7	230	4.2	16.5
$[Crts_3Br_3]$	Dark-violet	7.7	20.7	2.9	7.5	20.8	3.0	220	4.0	32.1
$[Crts_3I_3]$	Dark-violet	6.1	17.2	3.1	6.2	17.3	2.5	170	3.9	31.4
$[Crttz_3Cl_3]$	Violet	10.3	20.1	2.6	10.1	20.7	2.9	196–197	4.2	24.8
$[Crttz_3Br_3]\cdot 2H_2O$	Violet	8.0	15.9	3.2	7.6	15.8	2.8	178–179	3.9	dec.
$[Crttz_3I_3]$	Dark-violet	6.5	13.1	2.1	6.6	13.7	1.9	205	4.0	22.0
$[Crtzse_3Cl_3]\cdot 2H_2O$	Green	7.4	15.5	3.0	7.5	15.6	2.8	190–192	3.8	20.1
$[Crtzse_3Br_3]$	Green	6.7	13.6	1.8	6.6	13.7	1.9	180–182	3.7	18.2
$[Crtzse_3I_3]$	Dark-violet	6.0	11.4	1.4	5.6	11.6	1.6	180–185	3.7	19.1

pounds are microcrystalline and high-spin; they are sparingly soluble in most solvents; only in coordinating solvents such as dimethylsulfoxide, acetonitrile, and acetone is the solubility relatively high, but then the dissolution is accompanied by extensive solvolysis. This behavior prevents recrystallization of the products; purification can be accomplished by means of repeated washing with a noncoordinating solvent.

The metal complexes obtained, their analytical data and room-temperature magnetic moments, and other physical properties are listed in Table 1. The most important i.r. data are shown in Tables 2 and 3, and the solid state electronic spectra are reported in Table 4. These derivatives are nonelectrolytes, Λ lying in the range 16.5–44.0 ohm^{-1} cm^2 mol^{-1} in *N,N'*-dimethylformamide. The Λ values, even for 1:1 electrolytes, are 65–90 ohm^{-1} cm^2 mol^{-1} in *N,N*-dimethylformamide (4).

With chromium halides, complexes of essentially octahedral geometry are formed. Their magnetic moments and solid state electronic spectra are in accord with those expected for this stereochemistry. The μ values in the range 3.7–4.2 B.M. are as expected for three unpaired electrons and these magnetic moments are given by the spin-only term (5).

As for the infrared spectra, passing from the tm free ligand spectrum to those of the complexes, we observe that ν(NH) falls at 3250–3270 cm^{-1} against the value of 3400 cm^{-1} for ν(NH) for the free ligand in chloroform solution. The ν(C=O) vibration occurs at 1660 cm^{-1} in the spectrum of the free ligand and is shifted towards lower frequencies, 1610–1620 cm^{-1}, in the spectra of the complexes. The stretching vibrations due to the prevailing contribution of ν(CS) symmetric and asymmetric occur at the same wave number or show small positive shifts.

Passing on thiomorpholin-3-thione derivatives we observe that the band I and II of the —N—C=S group, according to the nomenclature of Rao and co-worker (6), are at the same wave numbers while band III is moderately shifted toward lower energies. The ν(NH) in the ts-complexes is shifted towards lower wave numbers of about 250 cm^{-1} using as reference the value of 3380 cm^{-1} for ν(NH) for the free ligand in chloroform solution. The bands due to the symmetric and asymmetric ν(CS) show positive shifts.

In the complexes of thiazolidine-2-thione, the ν(NH) appears as a sharp band and shows a shift of *ca.* 300 cm^{-1}, having as reference the ν(NH) solution value for the ligand. The thioamide I band, the band at 1288 cm^{-1}, attributed to ν(C=S) + δ(NCS) and those due to symmetric and asymmetric ν(CS) show positive shifts.

The same behavior is observed in the derivatives of thiazolidine-2-selenone. The ν(NH) shows a negative shift of *ca.* 250 cm^{-1} having as reference the value of 3400 cm^{-1} for the free ligand in chloroform solution. The selenoamide I band (7) and the band at 1285 cm^{-1} attributed to ν(C=Se) + δ(NCSe) show positive shifts while the bands due to the prevailing contribu-

Can. J. Chem. Downloaded from www.nrcresearchpress.com by 210.87.254.42 on 09/05/12
For personal use only.

Can. J. Chem. Downloaded from www.nrcresearchpress.com by 210.87.254.42 on 09/05/12
For personal use only.

TABLE 2. Most important i.r. bands (4000–200 cm^{-1}) for tm and ts complexes

	ν(N—H)	ν(C═O)	ν(C—S) sym. and asym.	ν(M—X)	ν(M—L)
tm solid	3220s	1620s	692m, 643m	—	—
$CHCl_3$ solution	3400s	1660vs	690m, 650m	—	—
$[Crtm_3Cl_3]$	3270vs	1620vs	700m, 650m	380m, 350m, 320vs	340m
$[Crtm_3Br_3]\cdot 2H_2O$	3250s	1610vs	700m, 650m	325m, 290ms	335ms
$[Crtm_3I_3]$	3270s	1615vs	715mw, 655m	—	345m

		—N—C═S					
	ν(N—H)	I	II	III	ν(C—S) sym. and asym.	ν(M—X)	ν(M—L)
ts solid	3225s	1590vs, 1560vs	1345vs	1100vs	700w, 620w	—	—
$CHCl_3$ solution	3380s	1580vs, 1570vs	1335vs	1100vs	—	—	—
CS_2 solution	3380s	—	1338vs, 1325vs	1108vs	690w, 670w	—	—
$[Crts_3Cl_3]$	3100s	1590s, 1570vs	1350s	1085vs	710w, 680w	370m, 330ms 300s	245m
$[Crts_3Br_3]$	3160s	1590s, 1560vs	1350s	1080vs	720w, 670w	310m, 265s	234m
$[Crts_3I_3]$	3150vs	1600ms, 1565vs	1340s	1090s	— 685mw	—	230m

TABLE 3. Most important i.r. bands (4000–200 cm^{-1}) for ttz and tzse complexes

	ν(N—H)	Thioamide I	ν(C═S)+ δ(NCS)	ν(C—S) sym. and asym.	ν(M—X)	ν(M—L)
ttz $CHCl_3$ solution	3400s	1490s	1288vs	690s, 650vs	—	—
$[Crttz_3Cl_3]$	3100s	1550vs	1310s	690m, 660m	350s, 339vs 305s	238m
$[Crttz_3Br_3]\cdot 2H_2O$	3100s	1530vs	1310s	700m, 660m	320m, 280s	225m
$[Crttz_3I_3]$	3130s	1515s	1305ms	700m, 655m	—	229m
	ν(N—H)	Seleno-amide I	ν(C═Se)+ δ(NCSe)	ν(C—S) sym. and asym.	ν(M—X)	ν(M—L)
tzse $CHCl_3$ solution	3400vs	1515vs	1285vs	705ms, 655ms	—	—
$[Crtzse_3Cl_3]\cdot 2H_2O$	3200s	1560s	1340s	705m, 655m	350m, 330ms 300m	230m
$[Crtzse_3Br_3]$	3150s	1530s	1320s	700m, 660m	320m, 285ms	225m
$[Crtzse_3I_3]$	3160s	1550m	1300ms	705w, 655w	—	230m

TABLE 4. Electronic spectra and crystal field parameters

Compound	$^4A_{2g}(F) \rightarrow {}^4T_{2g}(F)$	$^4A_{2g}(F) \rightarrow {}^4T_{1g}(F)$	ν_3*	Dq	B'	β
$[Crtm_3Cl_3]$	15 875	22 220	34 925	1590	648	0.71
$[Crtm_3Br_3]\cdot 2H_2O$	15 200	21 280	33 440	1520	620	0.68
$[Crtm_3I_3]$	14 700	21 050	32 340	1470	600	0.65
$[Crts_3Cl_3]$	14 700	20 000	32 340	1470	600	0.65
$[Crts_3Br_3]$	14 250	18 870	31 350	1425	582	0.63
$[Crts_3I_3]$	14 100	18 520	31 020	1410	576	0.63
$[Crttz_3Cl_3]$	14 300	18 870	31 460	1430	584	0.64
$[Crttz_3Br_3]\cdot 2H_2O$	13 900	18 520	30 580	1390	567	0.62
$[Crttz_3I_3]$	13 500	18 020	29 700	1350	551	0.60
$[Crtzse_3Cl_3]\cdot 2H_2O$	15 625	20 400	34 375	1560	638	0.69
$[Crtzse_3Br_3]$	15 000	19 850	33 000	1500	612	0.67
$[Crtzse_3I_3]$	14 600	18 520	32 120	1460	596	0.65

*Calculated values; B is taken as 918 cm^{-1} for the chromium(III) ion.

tion of ν(CS) are unchanged at the same wave numbers as in the free ligand.

From these facts we can suppose that the coordination center is the oxygen atom in the tm-derivatives; in fact the carbonyl stretching frequency is lowered (*ca.* 40 cm^{-1}) whenever the oxygen atom is bonded to the metal (8). The nitrogen atom clearly is the donor atom in the ts-, ttz-, and tzse-derivatives, because when a ligand is *N*-bonded, as in complexes of morpholine, thiazolidine-2-thione, thiomorpholin-3-thione, and thiazolidine-2-selenone, the ν(NH) occurs as a sharp band near 3100 cm^{-1} with a shift of *ca.* 300 cm^{-1} (1, 2, 9–13). The positive shifts of stretching vibrations due to bonds involving sulfur and selenium atoms suggest that these atoms are not involved in the coordination to the metal.

The small negative shifts of ν(NH) in the tm-derivatives spectra could arise from intermolecular hydrogen bonding.

The above conclusions, that the tm compounds are bonded through oxygen while all those of ts, ttz, and tzse are nitrogen bonded, are in keeping with most of the previous observations on the complexes previously studied and reported. The electronic spectra below provide some further evidence to this point.

Some strong bands are present in the i.r. spectra of the complexes in the range 400–200 cm^{-1} (Tables 2 and 3), at 380m, 350m, 320vs cm^{-1} for $[Crtm_3Cl_3]$, at 325m, 290ms for $[Crtm_3Br_3]$, at 370m, 330ms, 300s for $[Crts_3Cl_3]$, at 310m, 265s for $[Crts_3Br_3]$, at 350s, 339vs, 305s for $[Crttz_3Cl_3]$, at 320m, 280s for $[Crttz_3Br_3]$, at 350m, 330ms, 300m for $[Crtzse_3Cl_3]$, and at

Can. J. Chem. Downloaded from www.nrcresearchpress.com by 210.87.254.42 on 09/05/12
For personal use only.

Can. J. Chem. Downloaded from www.nrcresearchpress.com by 210.87.254.42 on 09/05/12
For personal use only.

320m, 285ms for $[Crtzse_3Br_3]$. They may be attributed to metal–halogen stretching by comparison with the spectra of similar chromium(III) complexes (14, 15).

The medium absorption bands present in the range 3490–3450 cm^{-1}, ν(OH) and 1650–1620 cm^{-1}, δ(HOH) in $[Crtm_3Br_3]\cdot 2H_2O$, $[Crttz_3Br_3]\cdot 2H_2O$, and $[Crtzse_3Cl_3]\cdot 2H_2O$ confirm the presence of water of crystallization. This water is purely lattice water since it is lost near 100 °C. In addition the wagging, the twisting, and the rocking vibrational modes of coordinated water are not present in the expected ranges (16).

Analysis of the electronic spectra of the complexes allows us to determine the mode of bonding. Three spin allowed transitions are predicted for chromium(III) in an octahedral field; these are in order of energy.

$$\nu_1\ {}^4A_{2g}(F) \rightarrow {}^4T_{2g}(F)$$
$$\nu_2\ {}^4A_{2g}(F) \rightarrow {}^4T_{1g}(F)$$
$$\nu_3\ {}^4A_{2g}(F) \rightarrow {}^4T_{1g}(P)$$

The ν_3 transition, expected to appear at about 31 000 cm^{-1}, usually is not observed due to intense charge-transfer bands in the ultraviolet region.

The chromium-tm spectra exhibit two major bands in the range 14 700–16 000 and 21 000–22 300 cm^{-1} (Table 4). The bands positions are similar to those reported with other oxygen coordinating ligands (17, 18). The bands can be assigned to the ν_1 and ν_2 transitions.

The spectra of the complexes yield, by the standard treatment, values for the ligand field parameters, *Dq*, *B'*, and β (19). These parameters and the ν_3 calculated values are reported in Table 4. Data for other complexes of the type $[CrL_3Cl_3]$ have been compared (14, 20–25). The parameter *Dq* lies in the order, with respect to the donor atoms, of P > O > As > N > S > Cl. The phosphorus-, arsenic- and sulfur-donor ligands have uniformly low values for β (0.50–0.44) in comparison with those for oxygen- and nitrogen-donor ligands (0.70–0.60).

The *Dq* values decrease in the order Cl > Br > I and this is consistent with the generally accepted sequence in the spectrochemical series. As for the different ligands, *Dq* values are in the order tm > tzse > ts > ttz. The *B'* values are of the order of 60–70% of the free ion value (918 cm^{-1}) suggesting that there is a considerable orbital overlap. The nephelauxetic parameter β shows an order ts ≃ ttz < tzse < tm.

The β values in our complexes are in the range 0.60–0.71. Since selenium has the same soft character as sulfur, we can conclude in good agreement with the infrared results that the sulfur and selenium atoms are not involved in coordination bonds.

By comparison of *Dq* and *B'* values reported for CrL_3X_3 complexes and for CrL_6^{3+} cations and CrX_6^{3-} anions (26, 27) we can distinguish between *N*- or *O*-bonded complexes. For CrO_6^{3+} chromophores, *Dq* lies in the range 1480–1650 cm^{-1} and *B'* in the range 605–670 cm^{-1}. The corresponding ranges for CrN_6^{3+} chromophores are 1300–1470 cm^{-1} and 530–600 cm^{-1}, respectively. The *Dq* and *B'* values for CrL_3X_3 complexes may be calculated by taking averages of *Dq* and *B'* values of CrL_6^{3+} and CrX_6^{3-} ions, using the "law of average environment" (26, 27). Table 4 shows that *Dq* and *B'* values of the complexes are in very good agreement with the literature data for CrL_3X_3 derivatives containing chromium–oxygen bonds in the tm-derivatives and chromium–nitrogen bonds in all the other complexes. The *Dq* and *B'* values for the tzse-derivatives are at the upper limit for the CrN_3X_3 chromophores, and near the lower limit for the CrO_3X_3 chromophores, but this ligand contains sulfur, selenium, and nitrogen donor atoms only.

From these results, the halogen independent bands at 340 cm^{-1}, 335 cm^{-1}, and 345 cm^{-1} present in the i.r. spectra of chloro-, bromo-, and iodo-derivatives of tm, and absent in the spectra of the other complexes, can be attributed to the ν(Cr—O) vibrations according to the literature data (28–33). Medium strong bands appear in the infrared spectra of the complexes of ts, ttz, and tzse in the range 225–245 cm^{-1} (Table 2, 3) that may be attributed to a metal–nitrogen stretching mode (34).

This type of coordination is coherent with the behavior of chromium(III), classified as typically hard acid.

Experimental

Preparation of the Ligands

Thiomorpholin-3-one: tm supplied by Aldrich was purified by extraction with ethyl ether in soxlet apparatus (m.p. 93 °C, lit. 93 °C) (35).

Thiomorpholin-3-thione: ts was prepared by treating thiomorpholin-3-one with an excess of P_4S_{10} slurry in

refluxing benzene as previously described (1) (m.p. 141–141.5 °C).

Thiazolidine-2-thione: ttz supplied by Fluka, was twice recrystallized from water (m.p. 106–107 °C, lit. (36) 106–107 °C).

Thiazolidine-2-selenone: tzse was prepared as previously described (3).

Preparation of Complexes

All compounds were obtained by reaction of $CrX_3 \cdot nH_2O$ (X = Cl, Br, I) in the molar ratio 1:3 in refluxing chloroform or chlorobenzene solution of the ligands for 6–10 h. The iodo-derivatives have been better obtained by reaction of the chromium halides in molten ligands. The complexes have been purified by means of repeated washing with chloroform or chlorobenzene.

Infrared Measurements

The i.r. spectra have been recorded in the range 4000–200 cm^{-1} with Perkin–Elmer 457 and 225 spectrophotometers as KBr discs. The far i.r. spectra have been recorded as Nujol mulls between polyethylene sheets.

Ultraviolet–visible Spectra

Solid state electronic spectra have been recorded with a Shimadzu MPS-50L spectrophotometer by the method of Venanzi and co-workers (37).

Magnetic Susceptibility Measurements

These were carried out by Gouy's method. Molecular susceptibilities were corrected for diamagnetism of the component atoms by use of the Pascal's constants.

Conductivity Measurements

These measurements were carried out with a WTW, LBR type conductivity bridge for 10^{-3} *M* *N,N'*-dimethylformamide solutions at 25 ± 0.1 °C. In order to avoid solvolytic effects every measurement has been made immediately after the dissolution of the complex.

We thank Dr. V. Braidi for his experimental work and the National Research Council (C.N.R.) of Italy for financial support.

1. D. De Filippo, A. Lai, C. Preti, E. F. Trogu and G. Verani. J. Inorg. Nucl. Chem. **36**, 73 (1974) and literature therein quoted.
2. C. Preti, G. Tosi, D. De Filippo and G. Verani. J. Inorg. Nuclear Chem. In press.
3. C. Preti, G. Tosi, D. De Filippo, and G. Verani. Can. J. Chem. In press.
4. W. J. Geary. Coord. Chem. Rev. **7**, 81 (1971).
5. B. N. Figgis and J. Lewis. Prog. Inorg. Chem. **6**, 102 (1964).
6. C. N. R. Rao and R. Venkataraghavan. Spectrochim. Acta, **18**, 541 (1962).
7. K. Jensen and P. H. Nielsen. Acta Chem. Scand. **20**, 597 (1966).
8. S. C. Jain and R. Rivest. J. Inorg. Nucl. Chem. **29**, 2787 (1967).
9. I. S. Ahuja. J. Inorg. Nuclear Chem. **29**, 2091 (1967).
10. I. S. Ahuja and P. Rastogi. Inorg. Nucl. Chem. Lett. **5**, 255 (1969).
11. D. De Filippo, F. Devillanova, C. Preti and G. Verani. J. Chem. Soc. A, 1465 (1971).
12. D. De Filippo, F. Devillanova, C. Preti, E. F. Trogu, G. Verani, and P. Viglino. Can. J. Chem. **51**, 1172 (1973).
13. P. P. Singh and R. Rivest. Can. J. Chem. **46**, 2361 (1968).
14. R. J. H. Clark and G. Natile. Inorg. Chim. Acta, **4**, 533 (1970).
15. D. M. Adams. Metal–ligand and related vibrations. E. Arnold, London. 1967.
16. K. Nakamoto. Infrared spectra of inorganic and coordination compounds. Wiley, New York. 1963.
17. B. C. Stonestreet, W. E. Bull, and R. J. Williams. J. Inorg. Nucl. Chem. **28**, 1895 (1956).
18. T. Bates. Modern aspects of the vitreous state. Vol. 2. *Edited by* J. D. Mackenzie. Butterworths, London. 1961.
19. C. J. Ballhausen. Z. Phys. Chem. Frankfurt, **11**, 205 (1957).
20. I. V. Howell, L. M. Venanzi, and D. C. Goodall. J. Chem. Soc. A, 395 (1967).
21. R. J. H. Clark and M. L. Greenfield. J. Chem. Soc. A, 409 (1967).
22. E. König and H. L. Schläfer. Z. Phys. Chem. Frankfurt, **26**, 371 (1960).
23. A. D. J. Goodwin. Ph.D. Thesis. London, England. 1969.
24. E. Cervone, P. Cancellieri, and C. Furlani. J. Inorg. Nucl. Chem. **30**, 2431 (1968).
25. W. E. Hatfield, R. C. Fay, C. E. Pfluger, and T. S. Piper. J. Am. Chem. Soc. **85**, 265 (1963).
26. A. B. P. Lever. Inorganic electronic spectroscopy. Elsevier, Amsterdam. 1968.
27. Pakinam Askalani and R. A. Bailey. Can. J. Chem. **47**, 2275 (1969).
28. R. G. Garvey, J. H. Nelson, and R. O. Ragsdale. Coord. Chem. Rev. **3**, 375 (1968).
29. M. Orchin and P. J. Schmidt. Coord. Chem. Rev. **3**, 345 (1968).
30. J. H. Nelson, L. C. Nathan, and R. O. Ragsdale. Inorg. Chem. **7**, 1840 (1968).
31. L. C. Nathan and R. O. Ragsdale. Inorg. Chim. Acta, **3**, 473 (1969).
32. R. Whyman, W. H. Hatfield, and J. S. Paschal. Inorg. Chim. Acta, **1**, 113 (1967).
33. N. M. Karayannis, C. M. Mikulski, M. J. Strocko, L. L. Pytlewski, and M. M. Labes. J. Inorg. Nucl. Chem. **33**, 3185 (1971).
34. R. J. H. Clark and C. S. Williams. Inorg. Chem. **5**, 350 (1964).
35. A. H. Sommers and B. W. Horrom. J. Am. Chem. Soc. **76**, 1187 (1954).
36. R. C. Weast (*Editor*). Handbook of Chemistry and Physics, 49th ed. Published by the Chemical Rubber Co., Cleveland, Ohio. 1968–1969. p. C565.
37. G. Dyer, J. G. Hartley, and L. M. Venanzi. J. Chem. Soc. A, 1293 (1965).

Can. J. Chem. Downloaded from www.nrcresearchpress.com by 210.87.254.42 on 09/05/12
For personal use only.

Resonance Raman Spectra of Cu-tetrapyridinoporphyrazine[1]

S. SUNDER[2] AND H. J. BERNSTEIN

Division of Chemistry, National Research Council of Canada, Ottawa, Canada K1A 0R6

Received March 4, 1974

S. SUNDER and H. J. BERNSTEIN. Can. J. Chem. **52**, 2851 (1974).

Resonance Raman spectra of dilute aqueous solutions of Cu-tetrapyridinoporphyrazine have been obtained using a tunable dye and Ar^+ lasers. Six bands in the spectra have anomalous depolarization ratios. This is the first observation of anomalous polarization in a molecule of C_{4h} point group symmetry. Intensities and depolarization ratio, ρ_l, of the observed bands are measured as a function of the wavelength of the exciting radiation. Bands are assigned to different symmetry species on the basis of the dispersion of their ρ_l values.

S. SUNDER et H. J. BERNSTEIN. Can. J. Chem. **52**, 2851 (1974).

Les spectres de résonance Raman de solutions aqueuses diluées de tétrapyridinoporphyrazine de cuivre sont obtenus par des lasers à colorants accordables et d'ions Ar^+. Six bandes de ces spectres ont des rapports anormaux de dépolarisation. C'est la première observation de polarisation anormale dans une molécule dont la symétrie du groupe ponctuel est C_{4h}. Les intensités et les rapports de dépolarisation ρ_l des bandes observées sont mesurées en fonction de la longueur d'onde de la radiation d'excitation. Les bandes sont attribuées à des espèces de différente symétrie en se basant sur la dispersion de leur valeur ρ_l.

[Traduit par le journal]

Can. J. Chem. Downloaded from www.nrcresearchpress.com by 210.87.254.42 on 09/05/12
For personal use only.

Introduction

Resonance Raman scattering occurs when the frequency of the exciting radiation falls within an electron absorption band of the scattering molecule (1, 2). The main feature which distinguishes the resonance Raman scattering from conventional Raman scattering is the preferentially strong enhancement in the intensity of the vibrations coupling the electronic transitions (1, 2). Another interesting feature of the resonance Raman scattering is that the depolarization ratio is a function of the exciting radiation frequency and some of the modes can show anomalous values (1–9) for ρ_l greater than $\frac{3}{4}$.

The phenomenon of resonance Raman scattering was treated theoretically by Placzek (3) in his classic paper on Raman scattering. Interest in this field has significantly increased since the observation of "anomalously polarized (ap) bands" by Spiro and Strekas in ferrocytochrome C and oxyhemoglobin (4). So far all reports of the ap bands in molecules have been limited to asymmetrically substituted porphins (4–9) whose rigorous symmetry is no more than C_1. Here we report the resonance Raman spectra of Cu-tetrapyridinoporphyrazine-methosulfate, CuPP, called quinolinic phthalocyanin in ref. 10. The resonance Raman spectrum arises from the tetravalent cation, Fig. 1*A*, which is essentially of symmetry C_{4h}. The cation can have C_{4h} symmetry either with the methyl groups in suitable configuration or behave like free rotors. Its resonance Raman spectrum is of biological interest as CuPP is a model compound for phthalocyanines and for the dyes used for staining in biological studies (10–13).

Experimental

A crystalline sample of CuPP was obtained from Dr. J. E. Scott (10) of Medical Research Council of U.K. by Dr. R. Williams of National Research Council of Canada who supplied us with a small sample. The Raman spectra of the dilute aqueous solutions of CuPP were obtained using a Jarrell–Ash model 25-102, double monochromator, a photomultiplier tube (RCA-C31034), and photon counting electronics. The exciting radiation was obtained from an Ar^+ laser (Spectra Physics model 164) and a tunable dye laser (Spectraphysics model 370, with model 371 dye circulator) using a solution of rhodamine 6G dye in methanol–water mixture. The laser power at the sample was about 150 mW for the region between 5700 to 6250 Å. The Raman samples were contained in a spinning cell to avoid local heating and the focussed laser beam was kept very close to the cell walls to minimize reabsorption of the scattered light (14). A 90° scattering geometry was used. The depolarization ratios of the bands in the Raman spectra were measured by analyzing the scattered light, keeping a scrambler in front of the entrance slit. The intensities of the bands were approximated by

[1]NRCC contribution No. 14023.

[2]NRCC Postdoctorate Fellow, 1973–present.

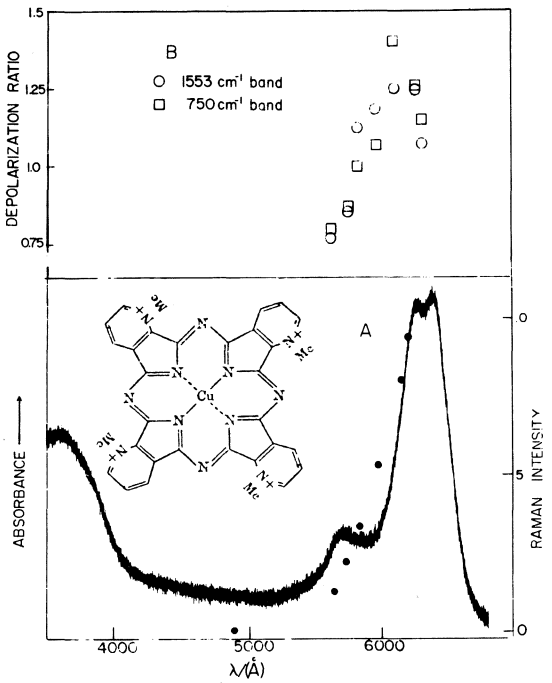

FIG. 1. (*A*) Absorption spectra of aqueous solution of CuPP —; relative Raman intensity of 1553 cm^{-1} band with different exciting radiation, ●. (*B*) Depolarization ratio of 1553 and 750 cm^{-1} bands with different exciting radiation.

their peak heights and corrected for the instrument and photomultiplier response. The band due to the O—H stretch of the solvent (H_2O) was used as the internal reference to study the intensity of the Raman bands as a function of the wavelength of the exciting radiation. The visible and u.v. absorption spectra were recorded with a Cary 14 spectrophotometer.

Results

The aqueous solution of CuPP is deep blue in color. Its absorption spectrum for the region 6700 to 3500 Å is shown in Fig. 1*A*. In the visible region, there is a strong doublet with maxima at about 6230 and 6370 Å having a shoulder at about 5675 Å.

The resonance Raman spectra of a dilute aqueous solution of CuPP shown in Fig. 2 were obtained with 4 different exciting radiations of wavelength 5615, 5974, 6032, and 6241 Å. These spectra were recorded at ~4 cm^{-1} resolution and different gain settings were used for different exciting radiation. The relative intensity of the 1553 cm^{-1} band is plotted as a function of wavelength of the exciting radiation in Fig. 1*A*. Thus Figs. 1*A* and 2 show that the intensity of the features seen in the resonance Raman spectra increases as the exciting radiation approaches the region of higher absorption. But the increase is more marked for some of the low frequency bands, particularly the one at 750 cm^{-1}. The frequencies of the different features seen in the spectra are given in Table 1 and are accurate to ±2 cm^{-1}. These frequencies remain constant within the limits of the experimental error, for different exciting radiations. Qualitative relative intensities of the different lines, obtained with the 6241 Å exciting radiation, Fig. 2, are listed in Table 1, to help in correlating the features in Table 1 and Fig. 2, as the Jarell–Ash spectrometer used here is linear in wavelength and not in wavenumbers. The Raman spectra showed a weak fluorescence background which reaches a maximum around 6500 Å (Fig. 2). However, the interference from the background was not very strong and did not require the use of zero suppression to record the spectra.

The depolarization ratios for the observed bands in the Raman spectra are given in Table 1 for five different exciting radiations and are accurate to ±0.1 unless stated otherwise. The six bands at 680, 750, 992, 1171, 1209, and 1553 cm^{-1} show anomalous polarization in the region of strong absorption. Here it may be mentioned that this is the first observation of anomalously polarized bands in a molecule of "rigorous C_{4h} symmetry". The depolarization ratios of two strong bands at 750 and 1553 cm^{-1} are plotted as a function of the exciting radiation wavelength in Fig. 1*B*. Both appear to pass through a maximum in the region of the visible absorption band. Similar results have been reported for other related systems (6).

Discussion

The CuPP tetravalent cation contains the same number of π electrons as Cu-phthalocyanine (CuPc) and is also square planar, with a similar structure, Fig. 1*A*. It has been suggested that in CuPc, as well as in Cu-benzoporphin, Cu-azoporphin, and Cu-porphin, the visible and near u.v. absorption spectra arise from π–π* transitions (ref. 15 and references cited therein). The similarity of the absorption spectra of CuPP and CuPc (16–17) suggests that the absorption spectrum of CuPP probably also arises from π–π* transitions.

Can. J. Chem. Downloaded from www.nrcresearchpress.com by 210.87.254.42 on 09/05/12
For personal use only.

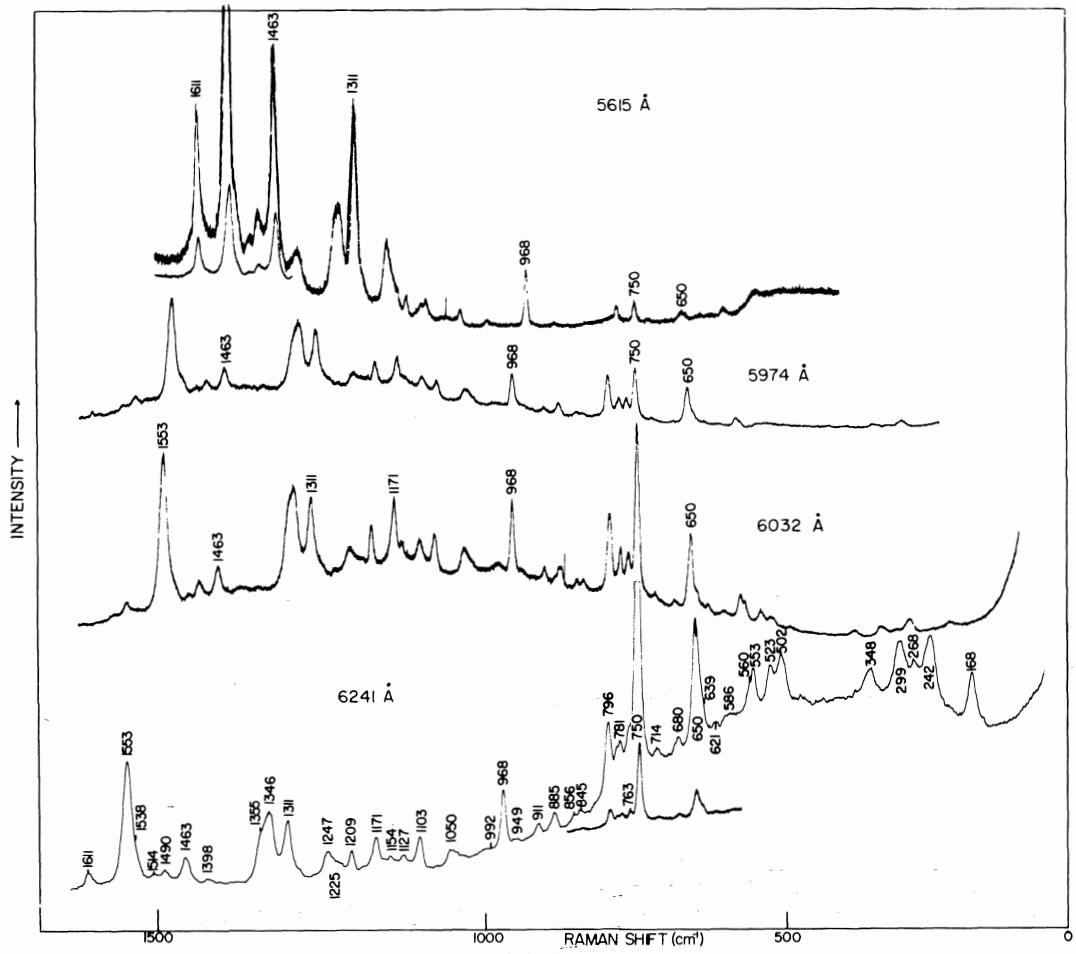

FIG. 2. Resonance Raman spectra of 4×10^{-5} M aqueous solution of CuPP, slit $\sim 4\ cm^{-1}$. The frequency scale at the bottom is for the spectrum with 6241 Å excitation, monochromator used was linear in wavelength.

CuPP, molecular formula $C_{32}H_{24}N_{12}Cu$, Fig. 1*A*, has 32 A_g + 33 B_g + 17 E_g modes active in its Raman spectrum (18) under the molecular point group C_{4h}. Of these 5 A_g + 5 B_g + 1 E_g are C—H stretching modes which were not observed under the experimental conditions used here. It is not possible to describe the observed Raman bands in terms of the internal coordinates with the present data. But it is possible to identify the symmetry of the vibration on the basis of the dispersion in the ρ_l values obtained in this work.

In conventional Raman spectroscopy (18) B_g and E_g modes are expected to be depolarized $\rho_l = \frac{3}{4}$, while A_g modes should be polarized, *i.e.* $\rho_l < \frac{3}{4}$. Under the conditions of resonance Raman scattering the above relations are modified and the depolarization ratio is given by (3, 4).

$$\rho_l = \frac{I_\perp}{I_{||}} = \frac{3g^s + 5g^a}{10g^0 + 4g^s}$$

where

$$g^0 = 3\bar{\alpha}^2 = \tfrac{1}{3}(\alpha_{xx} + \alpha_{yy} + \alpha_{zz})^2$$

$$g^s = \tfrac{1}{3}[(\alpha_{xx} - \alpha_{yy})^2 + (\alpha_{yy} - \alpha_{zz})^2 + (\alpha_{zz} - \alpha_{xx})^2] + \tfrac{1}{2}[(\alpha_{xy} + \alpha_{yx})^2 + (\alpha_{xz} + \alpha_{zx})^2 + (\alpha_{yz} + \alpha_{zy})^2]$$

and

$$g^a = \tfrac{1}{2}[(\alpha_{xy} - \alpha_{yx})^2 + (\alpha_{yz} - \alpha_{zy})^2 + (\alpha_{zx} - \alpha_{xz})^2]$$

Can. J. Chem. Downloaded from www.nrcresearchpress.com by 210.87.254.42 on 09/05/12
For personal use only.

Can. J. Chem. Downloaded from www.nrcresearchpress.com by 210.87.254.42 on 09/05/12
For personal use only.

TABLE 1. Resonance Raman spectra of 4×10^{-5} *M* aqueous solution of CuPP

Δν (cm^{-1})	Intensity* for 6241 Å	Depolarization ratio† for exciting radiation =					Symmetry assignment	Possible combination
		5636 Å	5761 Å	5838 Å	6104 Å	6275 Å		
1611	w	0.5	0.45	p	p	p	A_g	$299a_g + 1311a_g = 1610A_g$
1553	vs	0.77	0.85	1.12	1.25	1.25	A_g	
1538	sh	p	p	p	p	p	A_g	
1514	vvw		dp	dp	dp	dp	B_g	
1490	vw		dp	dp	dp	dp	B_g	$268a_g + 1225b_g = 1493B_g$
1463	m	0.55	0.50	0.55	0.65	0.6	A_g	
1398	vvw, b					—		$650a_g + 750a_g \times 1400A_g$
1355	sh	dp				dp	B_g	
1346	s	0.45	0.45	0.55	p	0.7	A_g	
1311	s	0.5	0.4	0.38	p	0.6	A_g	
1247	w	p	0.5	0.4	p	p	A_g	$299a_g + 299a_g + 650a_g = 1248A_g$
1225	sh		dp				B_g	
1209	w	0.77	0.78	1.0	1.45	1.75	A_g	
1171	m		0.8	0.85	1.5	1.7	A_g	
1154	vvw			dp	dp		B_g	
1127	vw			p	p		A_g	$242a_g + 299a_g + 586a_g = 1127A_g$
1103	m			0.4	0.55	0.5	A_g	
1050	w, b			p	p		A_g	$299a_g + 750a_g = 1049A_g$
992	vvw, b				1.6 ± 0.3	1.5 ± 0.5	A_g	$242a_g + 750a_g = 992A_g$
968	s		0.38	0.4	0.55	0.6	A_g	
949	vvw, b			p			A_g	$299a_g + 650a_g = 949A_g$
911	w	p	p	p	p	p	A_g	

Can. J. Chem. Downloaded from www.nrcresearchpress.com by 210.87.254.42 on 09/05/12
For personal use only.

TABLE 1 (*Concluded*)

Δν (cm^{-1})	Intensity* for 6241 Å	Depolarization ratio† for exciting radiation =					Symmetry assignment	Possible combination
		5636 Å	5761 Å	5838 Å	6104 Å	6275 Å		
885	vw		p	p	p		A_g	$299a_g + 586 = 885$
856	vvw						—	$299a_g + 553a_g = 852A_g$
845	vw			p	p		A_g	$168a_g + 680a_g = 848A_g$
796	s		0.21	0.23	0.3		A_g	
781	m			p	p		A_g	
763	m			p	p		A_g	
750	strongest	0.8	0.87	1.0	1.4	1.26	A_g	
714	w		p	p	p		A_g	
680	w				1.6 ± 0.3	1.6 ± 0.3	A_g	
650	vs		0.2	0.2	0.4	0.3	A_g	
639	sh						—	
621	vw						—	
586	vw, b						—	
560	sh			p	p		A_g	
553	m			p	p		A_g	
523	w			p	p		A_g	
502	m				p		A_g	
348	w				p	p	A_g	
299	m				p	p	A_g	
268	w				p	p	A_g	
242	s				p	p	A_g	
168	m				p	p	A_g	

*vw = very weak, w = weak, m = medium, s = strong, sh = shoulder, b = broad.
†p = polarized, $\rho_l < 0.65$, dp = polarized, $0.65 \leq \rho_l < 0.85$.

Can. J. Chem. Downloaded from www.nrcresearchpress.com by 210.87.254.42 on 09/05/12
For personal use only.

The three quantities g^0, g^s, and g^a are the isotropic, the quadrupole, and the magnetic dipole components of the scattering tensor (3, 4). For non-resonance Raman scattering, the scattering tensor is symmetric and, hence, $g^a = 0$. As g^0 is zero for nontotally symmetric modes one obtains the value of $\frac{3}{4}$ for ρ_l for B_g and E_g modes in non-resonance Raman scattering.

The range of possible values of ρ_l for the vibrations of different symmetry species can be determined by reference to the tables which are available in the literature (19–20) giving the form of the scattering tensor. For A_g modes of C_{4h} $\alpha_{xx} = \alpha_{yy}$, $\alpha_{xy} = -\alpha_{yx}$, and all other elements except α_{zz} are zero; for B_g modes $\alpha_{xx} = -\alpha_{yy}$ and $\alpha_{xy} = \alpha_{yx}$, all other elements are zero; and for E_g modes $\alpha_{xz} = -i\alpha_{yz}$ and $\alpha_{zx} = -i\alpha_{zy}$, other elements are zero. Using these values in the above relations it turns out that for A_g modes $\rho_l > 0$, for E_g modes $\rho_l > \frac{3}{4}$ and for B_g modes $\rho_l = \frac{3}{4}$. From the observed depolarization ratios given in Table 1 it is clear that 28 modes are polarized (p), $\rho_l < \frac{3}{4}$, and of A_g symmetry while 5 modes are depolarized (dp), $\rho_l = \frac{3}{4}$, and of B_g symmetry. The six bands showing ap character can in principle be either A_g or E_g modes. All of the E_g modes arise from out-of-plane deformations so none of them can have a value as high as 1553 cm^{-1}. Hence the band at 1553 cm^{-1} must be assigned to an A_g mode.[3] The direct product of the representations of the allowed electronic transitions (E_u, A_u) indicates that E_g and B_g modes can borrow intensity in the event that appropriate transitions can interact vibronically. In other porphyrin-like molecules only the intensity of the in-plane modes have been vibronically enhanced (4–9). Thus the out-of-plane E_g modes are expected to be weak and probably absent in the resonance Raman spectra. The remaining five a.p. bands are also likely then to be A_g modes.[3] This increases the number of observed A_g modes to 34 from the 27 predicted by theory for the spectral region considered here. Hence at least seven of the features assigned as A_g mode must correspond to overtones or combinations. An analysis of the frequency values does indicate that more than seven of the weak features can be assigned as combination bands as shown in Table 1. Although the B_g modes can in principle gain intensity because of vibronic coupling, the fact that only 5 out of 28 were observed and with weak intensity, and no intensity enhancement with frequency, strongly indicates that the B_g modes have not been intensity enhanced in this spectrum. Thus only the A_g modes account for most of the observed intensity in the resonance Raman spectra of this molecule.

[3]We thank the referee for drawing our attention to this point.

We thank Dr. Ross Williams for supplying us with a sample of CuPP and Dr. W. F. Murphy for help in setting up the dye laser.

1. J. Behringer. Raman spectroscopy, Vol. I. *Edited by* H. A. Szymanski. Plenum Press, New York. 1967. pp. 168–220.
2. H. J. Bernstein. Advances in Raman spectroscopy, Vol. I, Heyden and Son Ltd., London. 1972. p. 305.
3. A. Placzek. Handbuch der radiologie, Vol. VI, part 2. *Edited by* Erich Marx, Akademische Verlagsgezellschaft, Leipzig. 1934. pp. 209–374.
4. T. G. Spiro and T. C. Strekas. Proc. Natl. Acad. Sci. **69**, 2622 (1972).
5. L. A. Nafie, M. Pézolet, and W. L. Peticolas. Chem. Phys. Lett. **20**, 563 (1973).
6. D. W. Collins, D. B. Fitchen, and A. Lewis. J. Chem. Phys. **59**, 5714 (1973).
7. J. Nestor and T. G. Spiro. J. Raman Spectrosc. **1**, 539 (1973).
8. M. Pézolet, L. A. Nafie, and W. L. Peticolas. J. Raman Spectrosc. **1**, 455 (1973).
9. A. L. Verma and H. J. Bernstein. J. Raman Spectrosc. In press.
10. J. E. Scott. Histochemie, **21**, 277 (1970); **30**, 215 (1972).
11. J. E. Scott and H. Guilford. J. Histochem. Cytochem. **26**, 387 (1972).
12. J. E. Scott. Histochemie, **32**, 191 (1972).
13. J. E. Scott. Biochem. Soc. Trans. 7, 787 (1973).
14. W. Kiefer and H. J. Bernstein. Appl. Spectrosc. **25**, 500 (1971).
15. A. M. Schaffer, M. Gouterman, and E. R. Davidson. Theor. Chim. Acta. **30**, 9 (1973).
16. L. Edwards and M. Gouterman. J. Mol. Spectrosc. **33**, 292 (1970).
17. D. Eastwood, L. Edwards, M. Gouterman, and J. Steinfeld. J. Mol. Spectrosc. **20**, 381 (1966).
18. E. B. Wilson, Jr., J. C. Decius, and P. C. Cross. Molecular vibrations, McGraw-Hill Book Co. Inc., New York. 1955.
19. L. N. Ovander. Opt. Spectrosc. **9**, 302 (1960).
20. W. M. McClain. J. Chem. Phys. **55**, 2789 (1971).

Isomerization of 1-Olefins by Dihalogenobis(nitrile)palladium Complexes $[PdX_2(RCN)_2]$

SHIGEYOSHI SAKAKI, HIROYOSHI KANAI, AND KIMIO TARAMA

Department of Hydrocarbon Chemistry, Faculty of Engineering, Kyoto University, Sakyo-ku, Kyoto, Japan

Received December 19, 1973

SHIGEYOSHI SAKAKI, HIROYOSHI KANAI, and KIMIO TARAMA. Can. J. Chem. **52**, 2857 (1974).

Isomerizations of 1-olefins were carried out with dihalogenobis(nitrile)palladium(II). The activity of palladium complexes decreased in the order $PdCl_2(C_6H_5CN)_2 > PdCl_2(CH_3CN)_2 \gg PdBr_2(C_6H_5CN)_2 > PdBr_2(CH_3CN)_2$. The ratio of *cis*-2-olefin to *trans*-2-olefin, which exceeded the thermal equilibrium ratio, decreased in the order Cl > Br > I, while nitriles did not influence this ratio. The reactivity of olefins decreased in the order 1-hexene > 1-pentene ≫ 1-butene. The isomerization of 1-butene was accelerated by the presence of other olefins. Addition of lithium borohydride also accelerated the isomerization of olefins. The nature of active species and the effects of ligands on activity are discussed.

SHIGEYOSHI SAKAKI, HIROYOSHI KANAI et KIMIO TARAMA. Can. J. Chem. **52**, 2857 (1974).

Les isomérisations des oléfines-1 sont effectuées avec le dihalogéno-bis (nitrile) palladium(II). L'activité des complexes de palladium décroit dans l'ordre $PdCl_2(C_6H_5CN)_2 > PdCl_2(CH_3CN)_2 \gg PdBr_2(C_6H_5CN)_2 > PdBr_2(CH_3CN)_2$. Le rapport *cis* oléfine-2/*trans* oléfine-2 qui excède le rapport d'équilibre thermique, décroit dans l'ordre Cl > Br > I, tandis que les nitriles sont sans effet sur rapport. La réactivité des oléfines décroit dans l'ordre hexène-1 > pentène-1 ≫ butène-1. On accélère l'isomérisation du butène-1 par la présence d'autres oléfines. L'addition de borohydrure de lithium accélère aussi l'isomérisation des oléfines. On discute de la nature des espèces actives et des effets des ligands sur l'activité des oléfines.

[Traduit par le journal]

Introduction

Much work has been carried out on the catalysis of reactions of olefins by palladium(II) complexes (1). Such a study is the isomerization of olefins, which is the simplest and most convenient reaction for studies on the interaction between palladium and olefins. Many studies have been carried out to clarify the mechanism of isomerization (2–5). However, the isomerization by palladium bromide complexes has not been studied extensively (5) and ligand effects on catalytic activity have received little attention.

To ascertain what determines the catalytic activity, we have carried out the isomerization of 1-butene, 1-pentene, and 1-hexene with $PdX_2(RCN)_2$ (X = Cl or Br, R = CH_3 or C_6H_5) and have obtained the kinetic parameters of these reactions. Explanations of the difference in the catalytic activities between palladium chloride and palladium bromide complexes are also presented.

Experimental

Materials

Dihalogenobis(nitrile)palladium, $PdX_2(RCN)_2$, was prepared by Kharash's method (6). Palladium chloride was extra pure grade from Nakarai Chemical Co. Palladium bromide was prepared from palladium metal and a mixture of concentrated hydrobromic acid and concentrated nitric acid (7). Palladium iodide was prepared by addition of aqueous potassium iodide to aqueous palladium chloride (8). However, $PdI_2(RCN)_2$ could not be obtained. Commercially available 1-butene (Takachiho Chemical grade), 1-pentene, and 1-hexene (Nakarai Chemical grade) were purified by distillation.

Reaction Procedure and Analysis

Isomerizations of 1-pentene and 1-hexene were carried out homogeneously in three-necked 50-ml flasks under stirring by a magnetic stirrer in toluene at 40–90 °C. The mol ratio of olefin to palladium was 800–900:1 and the concentration of catalyst was 0.5–0.6 mmol/l. Samples were syringed from the stirred solution at regular time intervals and analyzed by gas chromatography ($AgNO_3$ – benzyl cyanide column (3 m), carrier gas hydrogen). Since $PdI_2(RCN)_2$ could not be prepared, the saturated solution of PdI_2 in toluene was used.

Isomerization of 1-butene, on a scale one-third of that used for 1-pentene and 1-hexene, was carried out in sealed glass tubes. Products were analyzed by gas chromatography (dimethylsulfolane column (3.5 m), carrier gas hydrogen).

Palladium complexes were used with and without lithium borohydride in tetrahydrofuran as cocatalyst.

Results and Discussion

The isomerization of 1-pentene was pseudo first order in 1-pentene (4). Reaction rate constants per unit concentration of catalyst, k

Can. J. Chem. Downloaded from www.nrcresearchpress.com by 210.87.254.40 on 09/05/12
For personal use only.

TABLE 1. Kinetic parameters of isomerization of 1-pentene with $PdX_2(RCN)_2$

Catalyst	k (l/mol s)[a]	E (kcal/mol)[b]	ln A (1/mol s)[c]
$PdCl_2(C_6H_5CN)_2$	0.888	18.8±0.02	27.3±0.3
$PdCl_2(CH_3CN)_2$	0.753	17.2±0.76	25.3±1.1
$PdBr_2(C_6H_5CN)_2$	0.0237	17.8±0.01	22.6±0.2
$PdBr_2(CH_3CN)_2$	0.0137	15.1±0.01	17.9±0.2

[a]The first-order rate constant per unit concentration of catalyst (mol/l) at 70 °C
[b]The activation energy.
[c]The frequency factor.

(1/mol s), activation energies, E (kcal/mol), and frequency factors, A (1/mol s), are given in Table 1. The reaction rates at 70 °C decrease in the order $PdCl_2(C_6H_5CN)_2 > PdCl_2(CH_3CN)_2 \gg PdBr_2(C_6H_5CN)_2 > PdBr_2(CH_3CN)_2$. The ligand effects on catalytic activity are Cl ≫ Br and $C_6H_5CN > CH_3CN$. The frequency factors of chloro systems are much larger than those of bromo systems, while the activation energies of these catalytic systems are nearly equal.[1] The activity of catalysts seems to depend mainly on the frequency factors. The larger frequency factors of chloro systems are considered to be due to the higher concentration of active species than those of bromo systems; this is also supported by the acceleration due to $LiBH_4$ as described below.

While the isomerization of 1-butene by $PdCl_2(RCN)_2$ and those of 1-butene, 1-pentene, and 1-hexene by $PdBr_2(RCN)_2$ were very slow,[2] the addition of $LiBH_4$ accelerated these reactions, as shown in Fig. 1. The hydride anion (H^-) generally reacts with transition metal halogen complexes to form hydride complexes or low valent metal complexes (9). In our experiments, the acceleration depended almost linearly on the concentration of $LiBH_4$, although too high a concentration of $LiBH_4$ decreased the activity and deposited palladium metal. Thus, the acceleration by $LiBH_4$ is simply explained by the formation of palladium hydride complexes and by the fact that at too high concentration of $LiBH_4$ these palladium complexes would be reduced via low valent palladium complexes thus decreasing the activities. This explanation agrees with our previous discussion on the low activities of palladium complexes; *i.e.*, their low activities are due to the low concentration of active species; however once the active species are formed, they are expected to have high activities.[3] The quantity of $LiBH_4$

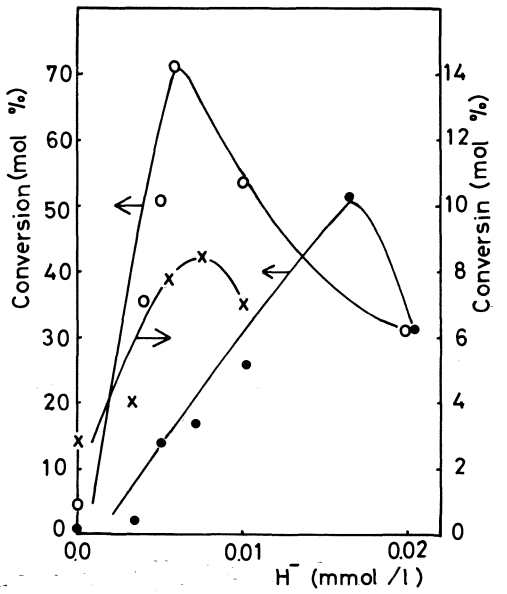

FIG. 1. Effect of the addition of $LiBH_4$; 70 °C, 0.5 h. ○; $PdBr_2(C_6H_5CN)_2$ – 1-pentene, ●; $PdBr_2(C_6H_5CN)_2$ – 1-butene, ×; $PdCl_2(C_6H_5CN)_2$ – 1-butene.

[1]The authors do not present a discussion on the small difference of frequency factors between benzonitrile and acetonitrile, since the kinetic parameters obtained in this work include thermodynamic parameters of equilibrium 1

[1] $2\,PdX_2(RCN)_2 + 2\,RCH{=}CH_2 \rightleftarrows [PdX_2(RCH{=}CH_2)]_2 + 4\,RCN$

However, the large difference in frequency factors between chloro and bromo systems is discussed, for this discussion is supported by another experimental result; see the results of acceleration by $LiBH_4$ and the discussion of the results.

[2]In the case of $PdBr_2(C_6H_5CN)_2$ system, the isomerization of 1-butene was not observed at 70 °C, the values of k (1/mol s) for the isomerization of 1-pentene and 1-hexane are 0.23 and 0.70, respectively.

[3]The active species in the system without $LiBH_4$ seem to be the same in the system with $LiBH_4$ as described below.

Can. J. Chem. Downloaded from www.nrcresearchpress.com by 210.87.254.40 on 09/05/12
For personal use only.

TABLE 2. Isomerization of 1-butene with presence of other olefins[a]

Conversion of 1-butene (%)	Conversion of 1-pentene (%)	Conversion of 1-hexene (%)
2.9[b]	49.2[b]	55.5[b]
4.6[c]		
9.4[d]	8.6	
18.3[e]		18.6

[a]Catalyst is $PdCl_2(C_6H_5CN)_2$, 70 °C 0.5 h, a mixture of olefin–Pd, 800–900 (in mol ratio), 1-butene – other olefin, 1.0 (mol ratio).
[b]Without other olefin.
[c]In presence of propene.
[d]In presence of 1-pentene.
[e]In presence of 1-hexene.

Can. J. Chem. Downloaded from www.nrcresearchpress.com by 210.87.254.40 on 09/05/12
For personal use only.

which gave the maximum catalytic activity depends on the natures of the halogens and the olefins. This result suggests that halogen anion and olefin coordinate to palladium hydride complexes. Generally speaking, complexes coordinated by strong electron donor ligands such as hydride and alkyl groups are stabilized by ligands which can accept nonbonding d electrons of the metal ion through π-backbonding (9). Since an olefin has an accessible π-antibonding orbital, palladium hydride complexes are presumably stabilized by the coordination of olefins.

The addition of $LiBH_4$ scarcely changed the stereoselectivity, which suggests that the active species are the same as in these reaction systems whether or not $LiBH_4$ is added. Harrod *et al.* (3*a*) also proposed that the palladium hydride complexes were the active species in the isomerization reaction and that their hydrogen source was olefin. Thus, palladium complexes would react with olefin giving active species: palladium hydride complexes.

The reactivities of 1-olefins are compared in Table 2. It is noted that 1-butene was isomerized very slowly and that its isomerization was accelerated by the presence of propene, 1-pentene, or 1-hexene. This acceleration is similar to that of the isomerization of 2-pentene by the presence of 1-pentene (4). The hydrogen atoms of 1-butene are considered to be much less effective as a hydride source than those of 1-pentene, 1-hexene, and propene. This consideration is supported by the fact that the 1-butene isomerization was accelerated by the addition of $LiBH_4$; *i.e.*, the slow isomerization of 1-butene is not due to its low reactivity but to the low ability for forming the active species. A hydrogen–deuterium exchange reaction occurs at the γ position of 1-olefins catalyzed by Pt(II) complexes (10), suggesting the hydrogen atom at the γ position interacts preferably with the platinum atom relative to other hydrogens. Since 1-pentene and 1-hexene have hydrogen atoms at the γ position but 1-butene does not, they seem to be more effective hydride sources than is the latter. However, there remains a problem why the propene accelerated the isomerization of 1-butene.

Two mechanisms were proposed by Assinger *et al.* (2) and Bond and Hellier (4), which are (*i*) the hydride addition and elimination mechanism and (*ii*) the π-allyl mechanism, respectively. The π-allyl mechanism is based on the high activation energy (25 kcal/mol) for 1-pentene isomerization in the range of 40–70 °C (4). In our results, the activation energy was about 18 kcal/mol for the same reaction system. An activation energy of 23.9 kcal/mol was reported for 1-pentene isomerization with $RhH(CO)[PPh_3]_3$ via the hydride addition and elimination mechanism (11). Therefore, a high activation energy is not a requirement for the π-allyl mechanism. While we do not have decisive evidence to distinguish between the two mechanisms, it is difficult to explain the acceleration of the isomerization of 1-butene by the presence of 1-pentene, 1-hexene, and propene.[4] Our results are not in conflict with the hydride addition and elimination mechanism.

The stereoselectivity of the reaction (*i.e.*, the mole ratio of *cis*-2-olefin to *trans*-2-olefin) depends not on nitrile but on halogen ligands. *cis*-2-Olefin is formed to a greater extent than

[4]In the π-allyl mechanism, a catalyst abstracts a hydrogen atom as a proton from one carbon atom of the olefin, forming a π-allyl complex, and then adds it to another carbon atom of the π-allyl group, forming the isomerized olefin. The presence of other olefins cannot be expected to accelerate these steps.

TABLE 3. Stereoselectivities in the isomerization of 1-olefins

	Cl[a]	Br	I
1-Butene	0.95	0.67	—
1-Pentene	0.64	0.56	0.54
1-Hexene	0.43	0.34	0.30

[a]The stereoselectivity does not depend on nitrile ligands.

the thermodynamic equilibrium value. While *cis*-selectivity in the 1-butene isomerization with Ni(II)– or Co(II)–phosphine complexes increases in the order Cl < Br < I, *i.e.*, their coordination bond radii (12), the *cis*-selectivity in this work, decreases in the order Cl > Br > I, as shown in Table 3. In the former case the selectivity has been considered to arise from the steric effect of the halogen ligands in the intermediate σ-alkyl complexes (12) but in the latter case it is unreasonable for the selectivity to arise from steric effects because of the absence of large ligand groups such as tertiary phosphine and because of the decrease in *cis*-selectivity with the increase in the coordination bond radii of halogen ligands.

The formation constant of the palladium-*cis*-2-butene complex is larger than that of *trans*-2-butene complexes in eq. 2 (13, 14). A reasonable hypothesis is therefore that *cis*-selectivity arises from the stability difference of the palladium olefin complexes. Its stability difference should be influenced by the electronic character of halogen ligands.

[2] $PdCl_4^{-2} + C_nH_{2n} \rightleftarrows [PdCl_3(C_nH_{2n})]^- + Cl^-$

1. P. M. MAITLIS. The organic chemistry of palladium. Academic Press, New York and London. 1971.
2. F. ASSINGER, B. FELL, and P. KRINGS. Tetrahedron Lett. 633 (1966).
3. J. F. HARROD and A. J. CHALK. (*a*) J. Am. Chem. Soc. **86**, 1766 (1964); (*b*) J. Am. Chem. Soc. **88**, 3491 (1966).
4. G. C. BOND and M. HELLIER. J. Catal. **4**, 1 (1965).
5. M. B. SPARKE, L. TURNER, and A. J. M. WENHAM. J. Catal. **4**, 332 (1965).
6. M. A. KHARASH, R. C. SEYLER, and F. R. MAYOR. J. Am. Chem. Soc. **60**, 882 (1935).
7. J. W. MELLOR. A comprehensive treatise on inorganic and theoretical chemistry. Vol. XV. Longmans, Green and Co., London. 1936. p. 675.
8. F. A. COTTON and G. WILKINSON. Advanced inorganic chemistry, a comprehensive text. John Wiley and Sons, Inc., New York, 1962. p. 851.
9. J. P. CANDLIN, K. A. TAYLOR, and D. T. THOMPSON. Reactions of transition metal complexes. Elsevier Publ. Co., Amsterdam. 1968. p. 327.
10. C. MASTER. Chem. Commun. 1258 (1972).
11. M. YAGUPSKY and G. WILKINSON. J. Chem. Soc. (A), 941 (1970).
12. H. KANAI, S. SAKAKI, and K. TARAMA. To be published.
13. P. M. HENRY. J. Am. Chem. Soc. **88**, 1595 (1966).
14. G. F. PREGAGLIA, F. CONTI, B. MINASSO, and R. UGO. J. Organomet. Chem. **47**, 165 (1973).

Can. J. Chem. Downloaded from www.nrcresearchpress.com by 210.87.254.40 on 09/05/12
For personal use only.

Mass Spectra of C-Amino- and C-Azido-1,2,4-triazoles

BRUCE T. HEITKE AND C. GORDON MCCARTY

Department of Chemistry, West Virginia University, Morgantown, West Virginia 26506

Received January 22, 1974

BRUCE T. HEITKE and C. GORDON MCCARTY. Can. J. Chem. **52**, 2861 (1974).

A study of low resolution mass spectra of 1,2,4-triazoles shows that fragmentations of *C*-amino-1,2,4-triazole nuclei are analogous to the three fragmentation modes reported for pyrrole. The extent to which these fragmentations account for the peaks in the mass spectra depends on the substituents of the 1,2,4-triazoles. Mass spectra of *C*-azido-1,2,4-triazoles cannot be interpreted by the three modes found for pyrrole. Without exception, their mass spectra contain a base peak which is shown, with the aid of deuterium labeling, to represent an ion formed by the loss of four nitrogen atoms plus the substituent on the endocyclic nitrogen atom.

BRUCE T. HEITKE et C. GORDON MCCARTY. Can. J. Chem. **52**, 2861 (1974).

Une étude des spectres de masse à basse résolution des triazoles-1,2,4 montre que les fragmentations des noyaux *C*-aminotriazole-1,2,4 sont semblables aux trois modes de fragmentations déjà observés dans le cas du pyrrole. Les quantités relatives de ces fragmentations dépendent des substituants des triazoles-1,2,4. Les spectres de masse des *C*-azidotriazoles-1,2,4 ne peuvent pas être interprétés par les trois modes trouvés dans le cas du pyrrole. Leurs spectres de masse contiennent sans exception un pic de base qui a été identifié grâce au marquage par du deutérium comme étant un ion formé par perte de quatre atomes d'azote en plus du substituant sur l'atome d'azote endocyclique. [Traduit par le journal]

Can. J. Chem. Downloaded from www.nrcresearchpress.com by 210.87.254.42 on 09/05/12
For personal use only.

Recently, there have appeared a number of reports of the mass spectra of 1,2,4-triazoles (1–10); however, only one (4) sets forth a general fragmentation pattern for 1,2,4-triazole nuclei. This paper reports our analyses of low resolution mass spectra (only one of which has been previously reported) of some 1,2,4-triazoles (Tables 1 and 2). We conclude that the fragmentations of compounds in Table 1 are analogous to those of pyrrole (11). Although the general fragmentation scheme cited above (4) predicts many of the fragment ions that are accounted for by our interpretation, the proposed processes by which these fragments are obtained are different; furthermore, the inclusion of metastable transitions in the other general fragmentation scheme seems unwarranted in view of the paucity of pertinent metastable data reported.

Results and Discussion

C-Amino-1,2,4-triazoles

The three modes of fragmentation for pyrrole are shown in Scheme 1. The complete fragmentation mechanisms were reported by Budzikiewicz *et al.* (11).

The possible application of fragmentation modes of pyrrole (*a*, *b*, *c*) to 1,2,4-triazole nuclei is complicated when hydrogen is bonded to one of

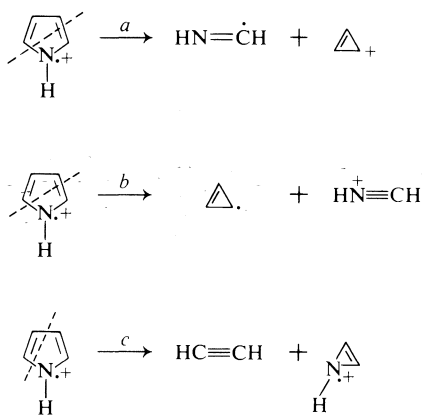

SCHEME 1

the ring nitrogens because of the possible tautomerism (1 ⇌ 2 ⇌ 3). There is evidence that such 1,2,4-triazoles exist in the gas phase as a mixture of primarily unsymmetrical tautomers 1 and 2 (7, 12), which may then give rise to isomeric molecular ions (7).

Using the same mechanistic approach of charge localization in the molecular ion prior to its fragmentation, the modes of fragmentation in Scheme 1 were applied to the interpretation of the mass spectrum of 1,2,4-triazoles listed in

TABLE 1. Fragmentation modes of 1,2,4-triazoles analogous to those of pyrrole

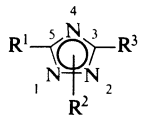

Compound	R^1	R^2 (position on ring)	R^3	Transition	Fragmentation mode
1	CH_3	H	NH_2	98 → 42	1*b*
				98 → 57	*1*c*
				98 → 56	1*c*
2	CH_3	CH_3 (1)	NH_2	112 → 43	1*b*
				112 → 71	*1*c*
3	CH_3	CH_3 (2)	NH_2	112 → 69	2*a*
				112 → 43	2*b*
				112 → 70	2*c*
4	CH_3	CH_3 (2)	H	97 → 42	2*b*
				97 → 70	2*c*
5	$(CH_3)_2N$	H	NH_2	127 → 98	*1*a*
				127 → 56	1*a*
				127 → 71	1*b*
				127 → 85	*1*c*
				127 → 43	2*b*
6	CH_3O	H	NH_2	114 → 85	*1*a*
				114 → 58	1*b*
				114 → 57	*1*c*
				114 → 43	2*b*
7	CH_3S	H	NH_2	130 → 74	1*b*
				130 → 57	1*c*
				130 → 43	2*b*
8	CH_3S	H	Cl	149 → 74	1*b*
				149 → 76	1*c*
9	CH_3S	CH_3 (2)	NH_2	144 → 87	2*a*
				144 → 43	2*b*

TABLE 2. Expelled fragments which account for the base peaks in the mass spectra of the C-azido-1,2,4-triazoles

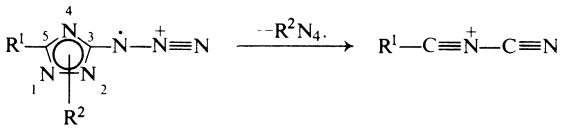

Compound	R^1	R^2 (position on ring)	Transition	Fragment expelled
11*a*	CH_3	H	124 → 67	HN_4
11*b*	CH_3	D	125 → 67	DN_4
12	CH_3	CH_3 (2)	138 → 67	CH_3N_4
13*a*	$(CH_3)_2N$	H	153 → 96	HN_4
13*b*	$(CH_3)_2N$	D	154 → 96	DN_4
14*a*	CH_3O	H	140 → 83	HN_4
14*b*	CH_3O	D	141 → 83	DN_4
15*a*	CH_3S	H	156 → 99	HN_4
15*b*	CH_3S	D	157 → 99	DN_4
16	CH_3S	CH_3 (2)	170 → 99	CH_3N_4

Can. J. Chem. Downloaded from www.nrcresearchpress.com by 210.87.254.42 on 09/05/12
For personal use only.

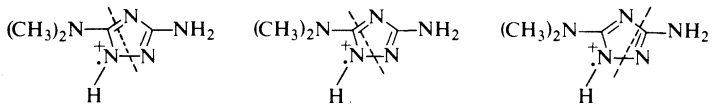

1*a* 1*b* 1*c**

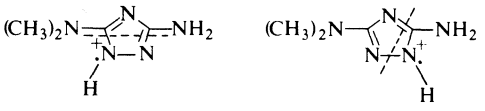

1*a** 2*b*

SCHEME 2

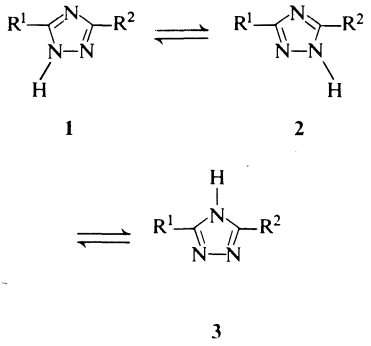

1 2 3

Table 1. As an example, Scheme 2 accounts for five major peaks in the mass spectrum of 3-amino-5-dimethylamino-1,2,4-triazole (**5**, Fig. 2). Fragmentations labeled 1*a*, 1*b*, and 1*c* correspond to the cleavage of tautomer 1 by each of the three modes indicated in Scheme 1, and fragmentation 2*b* corresponds to the cleavage of tautomer 2 by mode *b*. In contrast to unsubstituted pyrrole, a 1,2,4-triazole nucleus can fragment by a particular mode in two different ways (*e.g.* 1*a* and 1*a**) giving rise to two different ions. A comparison of the *m/e* ratios of the resulting ions listed in Table 1 with the mass spectra of compounds **1**–**9** (*e.g.*, Figs. 1–3) indicates the extent to which this interpretation is successful.[1]

As might be expected, when the methyl groups are separated from the triazole nucleus by a heteroatom (**5**–**9**), ions appear in the mass spectra which are unexplained by the interpretation described above. The existence of M − 1 peaks in the spectra of compounds **5**–**9**, however, is probably not due to the fact that a heteroatom separates the methyl group from the ring, but rather that

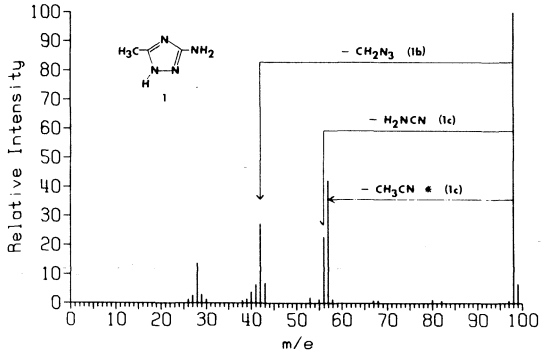

FIG. 1. The mass spectrum of 3-amino-5-methyl-1,2,4-triazole (**1**).

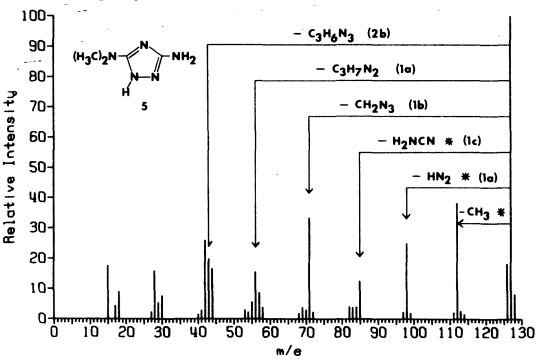

FIG. 2. The mass spectrum of 3-amino-5-dimethylamino-1,2,4-triazole (**5**).

[1]Spectra of compounds listed in Tables 1 and 2 which are not contained in this paper and a table of all metastable data are available, at a nominal charge, from the Depository of Unpublished Data, National Science Library, National Research Council of Canada, Ottawa, Canada K1A 0S2; they are also included in the Ph.D. dissertation of B.T.H., West Virginia University, August, 1973.

Can. J. Chem. Downloaded from www.nrcresearchpress.com by 210.87.254.42 on 09/05/12
For personal use only.

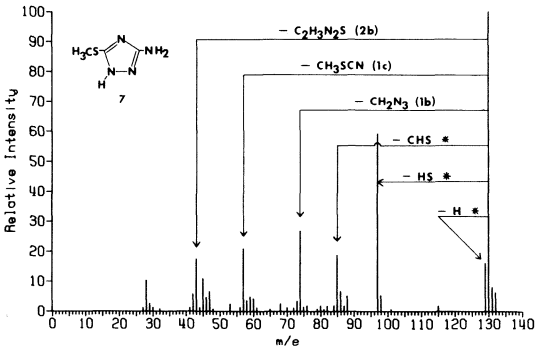

FIG. 3. The mass spectrum of 3-amino-5-methylthio-1,2,4-triazole (**7**).

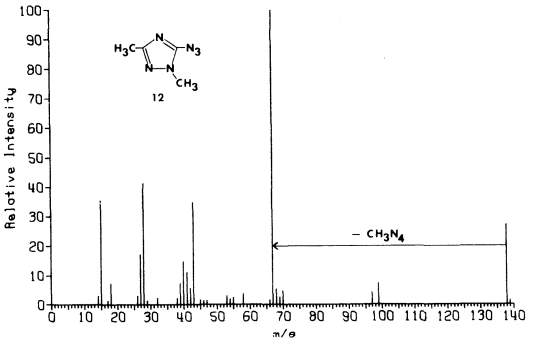

FIG. 4. The mass spectrum of 5-azido-1,3-dimethyl-1,2,4-triazole (**12**).

the hydrogen atoms are β, instead of α, to the ring (9).

Mass spectra of compounds **7**–**9**, in which the methyl group is separated from the triazole nucleus by a sulfur atom, reveal other deviations. All three display metastable peaks which indicate the loss of CHS and HS from the molecular ions. Metastable peaks for these transitions have been observed in the mass spectrum of 3-methylthio-1,2,4-triazole and the daughter ion of the process in which CHS is lost is regarded as protonated 1,2,4-triazole (4). Daughter ions of the transitions in which HS is lost may be represented as **10**. Metastable peaks indicating loss of HS

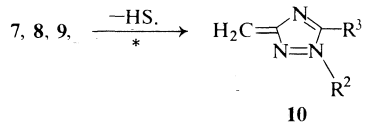

10

have been observed in the mass spectra of a number of 2-alkylthio-5-aminothiazolo[5,4-*d*]pyrimidines and a fragmentation mechanism leading to an ion analogous to **10** has been proposed (13).

C-Azido-1,2,4-triazoles

The loss of nitrogen in the decomposition of azides by electron impact is common (14–18) and, in the case of aryl azides, the base peak usually corresponds to the remaining ion (16, 18). However, in the cases of triarylmethyl azides (14), sulfonyl azides (17), and benzoyl azides (18), the base peak represents the ion formed when the azide group is lost. In these last three cases, the driving force is probably the formation of a stable cation. We have obtained and examined the low resolution mass spectra of *C*-azido-1,2,4-triazoles and their deuterated analogs (Table 2) for the first time and propose that the fragmentations of these compounds lead, primarily, to stable nitrilium ions.

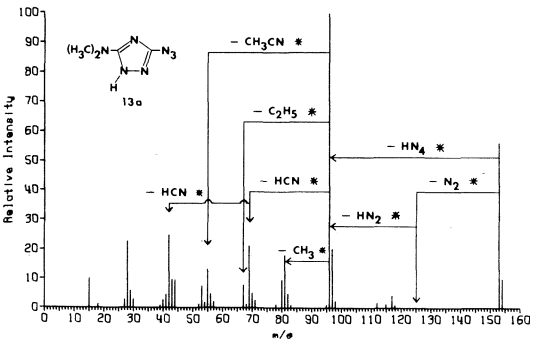

FIG. 5. The mass spectrum of 3-azido-5-dimethylamino-1,2,4-triazole (**13***a*).

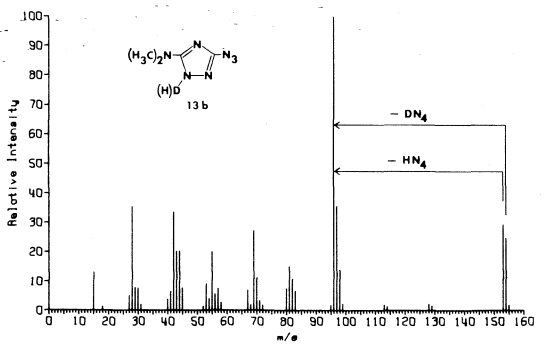

FIG. 6. The mass spectrum of 3-azido-1-deuterio-5-dimethylamino-1,2,4-triazole (**13***b*).

The mass spectra of the *C*-azido-1,2,4-triazoles (*e.g.*, Figs. 4–6) are characterized by a strong peak corresponding to the molecular ion and the base peak which together account for 28 to 48% of the total ionization at 70 eV. The mass spectrum of 3-azido-5-dimethylamino-1,2,4-triazole

Can. J. Chem. Downloaded from www.nrcresearchpress.com by 210.87.254.42 on 09/05/12
For personal use only.

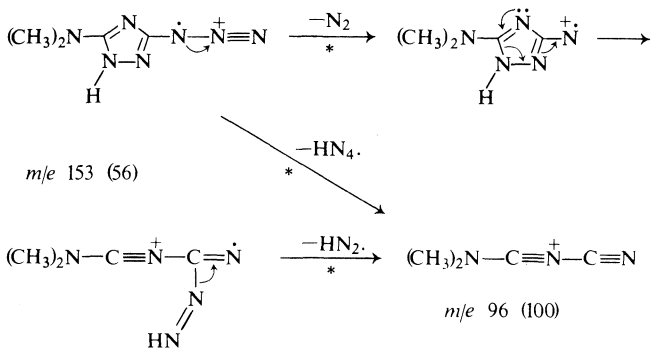

SCHEME 3

(**13***a*) contains metastable peaks which illuminate the transitions leading to its base peak. These transitions, which are shown in Scheme 3, can be rationalized by charge localization in the molecular ion on the azide group. Even though the peak representing the $M-N_2$ species is not present in the spectrum (Fig. 5), a metastable peak indicates the loss of nitrogen typical of azides. The additional loss of HN_2 forms a species corresponding to the base peak, which can be represented by the stable nitrilium ion.

Table 2 indicates that the formation of a nitrilium ion is likely for all the *C*-azido-1,2,4-triazoles, since, in every case, the base peak corresponds to the loss of a molecule of nitrogen plus 1-N, 2-N, and any group attached to them. The mass spectra of compounds **11**, **13**, **14**, and **15** in which approximately 50% of the exchangeable hydrogen was replaced with deuterium are essentially unchanged from those of the undeuterated compounds, except for the peaks representing the molecular ions.

The original mass spectra bar graphs from which Figs. 1–6 were obtained were plotted by a CalComp plotter. The computer program which generates the plots requires the input of the *m/e* value and height of each peak and allows the lengths of the units along the abscissa and ordinate to be varied independently. The program is available on request.

Experimental

The mass spectra were determined with a Nuclide 12-90-G single focusing instrument operating at 70 eV. Both the solids and liquids were introduced via the direct inlet at the lowest temperature at which a spectrum could be obtained.

The *C*-azido-1,2,4-triazoles were deuterated prior to determining their mass spectra by a general method (19). The syntheses of the various 1,2,4-triazoles will be published elsewhere (20).

1. A. L. JENNINGS, JR. and J. E. BOGGS. J. Org. Chem. **29**, 2065 (1964).
2. P. R. BRIGGS, W. L. PARKER, and T. W. SHANNON. Chem. Commun. 727 (1968).
3. H. G. O. BECKER, D. BEYER, and H.-J. TIMPE. J. Prakt. Chem. **312**, 869 (1970).
4. K. T. POTTS, R. ARMBRUSTER, and E. HOUGHTON. J. Heterocycl. Chem. **8**, 773 (1971).
5. Y. KATO and I. HIRAO. Bull. Chem. Soc. Jap. **45**, 1876 (1972).
6. J. L. COTTER. Org. Mass Spectrom. **6**, 1071 (1972).
7. A. MAQUESTIAU, Y. VAN HAVERBEKE, and R. FLAMMANG. Org. Mass. Spectrom. **6**, 1139 (1972).
8. A. J. BLACKMAN and J. H. BOWIE. Aust. J. Chem. **25**, 1335 (1972).
9. A. J. BLACKMAN and J. H. BOWIE. Org. Mass Spectrom. **7**, 57 (1973).
10. J.-L. BARASCUT, R.-M. CLARAMUNT, and J. ELGUERO. Bull. Soc. Chim. Fr. 1849 (1973).
11. H. BUDZIKIEWICZ, C. DJERASSI, and D. H. WILLIAMS. Interpretation of mass spectra of organic compounds. Holden-Day, San Francisco 1964.
12. K. BOLTON, R. D. BROWN, F. R. BURDEN, and A. MISHRA. Chem. Commun. 873 (1971).
13. A. TATEMATSU, S. SUGIURA, S. INOUE, and T. GOTO. Org. Mass. Spectrom. **1**, 205 (1968).
14. R. M. MORIARTY and A. M. KIRKIEN-KONASIEWICZ. Tetrahedron Lett. 4123 (1966).
15. C. WENTRUP. Tetrahedron, **26**, 4969 (1970).
16. R. A. ABRAMOVITCH, E. P. KYBA, and E. F. V. SCRIVEN. J. Org. Chem. **36**, 3796 (1971).
17. M. M. CAMPBELL and A. D. DUNN. Org. Mass Spectrom. **6**, 599 (1972).
18. R. T. M. FRASER, N. C. PAUL, and M. J. BAGLEY, Org. Mass. Spectrom. **7**, 83 (1973).
19. A. V. IOGANSEN and M. Sh. ROZENBERG. Zh. Prikl. Spektrosk. **9**, 1027 (1968); Chem. Abstr. **70**, 71602d (1969).
20. B. T. HEITKE and C. G. MCCARTY. J. Org. Chem. **39**, 1522 (1974).

Can. J. Chem. Downloaded from www.nrcresearchpress.com by 210.87.254.42 on 09/05/12
For personal use only.

The Halogen-scrambling Mechanism Leading to Formation of the Mixed Boron Trihalide Adducts of Trimethylamine[1]

BARRIE W. BENTON[2] AND JACK M. MILLER[3]

Department of Chemistry, Brock University, St. Catharines, Ontario L2S 3A1

Received February 5, 1974

BARRIE W. BENTON and JACK M. MILLER. Can. J. Chem. **52**, 2866 (1974).

Trimethylamine adducts of the boron trihalides, $Me_3N{\cdot}BX_3$ are shown to react in solution with free boron trihalides BY_3 to yield mixed halide adducts such as $Me_3N{\cdot}BX_2Y$. Isotope labelling shows that the B—N bond remains intact and that the reaction proceeds in either direction, *i.e.* either X or Y may be the heavier halogen. A bridged transition state involving five-coordinate boron is postulated. Only in the case of $Me_3N{\cdot}BI_3$ is an ionic predissociation of a B—X bond indicated by reaction with ionic species. Two adducts do not react in solution without the presence of excess Lewis acid, again indicative of a lack of predissociation. In the gas phase two adducts will scramble their halogens even in the absence of excess acid but these reactions occur via B—N bond cleavage.

BARRIE W. BENTON et JACK M. MILLER. Can. J. Chem. **52**, 2866 (1974).

Les produits d'addition des trihalogénures de bore sur la triméthylamine, $Me_3N{\cdot}BX_3$, réagissent en solution avec des trihalogénures de bore libres BY_3 pour donner des produits d'addition d'halogénures mixtes tels que $Me_3N{\cdot}BX_2Y$. Le marquage avec des isotopes montre que le lien B—N reste intact et que la réaction se produit dans un sens ou dans l'autre: c'est à dire que X ou Y peut être l'halogène le plus lourd. On admet un état de transition ponté impliquant du bore pentacoordonné. Seul le cas de $Me_3N{\cdot}BI_3$ présente une prédissociation ionique du lien B—X marquée par une réaction avec des espèces ioniques. Deux produits d'addition ne réagissent en solution qu'en présence d'acide de Lewis en excès; ces résultats montrent à nouveau un manque de prédissociation. En phase gazeuse, deux produits d'addition mêlent leurs halogènes même en l'absence d'excès d'acide, ces réactions se produisent toutefois par la rupture du lien B—N. [Traduit par le journal]

Introduction

The formation of mixed boron trihalide complexes of dimethyl ether (1, 2), trimethylamine, and other amines (3–7), esters (8), ureas (9), dimethyl sulfide (10), and phosphines (11, 12) have been studied by n.m.r. while $Me_3N{\cdot}BF_2Br$ and $Me_3N{\cdot}BFBr_2$ have been isolated (4) and studied by mass spectrometry (13). Unlike the more labile oxygen and sulfur donor adducts, the amine adducts tend to be stable at room temperature, halogen exchange in solution occurring while the B—N bond remains intact (14, 15), thus making these ideal systems for the study of the halogen exchange mechanism leading to mixed adduct formation. We now report our results on the trimethylamine system (15) and compare mechanisms which differ in part from those reported by others for similar systems, (6, 16).

Experimental

Materials

Trimethylamine and the boron trihalides were purified as described elsewhere (2). The pure unmixed adducts were similarly prepared and purified (17, 4). Boron-10 trifluoride (isotopic purity, 96%) was prepared by the action of heat on the stable calcium fluoride – boron trifluoride adduct (Oak Ridge National Laboratories). Typically 0.02 mol of $CaF_2{}^{10}BF_3$ were placed in a stainless steel tube which was evacuated. The temperature was raised slowly to 300 °C using heating tape; the BF_3 evolved was trapped at —196 °C and then distilled prior to use. $Me_3N{\cdot}{}^{10}BCl_3$ and $Me_3N{\cdot}{}^{10}BBr_3$ were prepared by adding unlabelled natural abundance BCl_3 or BBr_3 to a solution of about 0.01 mol of $Me_3N{\cdot}{}^{10}BF_3$ in methylene chloride. A large excess of free trihalide was used and the reaction allowed to stand overnight or until all traces of $Me_3N{\cdot}{}^{10}BFX_2$ were absent from the n.m.r. spectrum. Solvent was removed under vacuum and the labelled adduct sublimed. $Me_3N{\cdot}{}^{10}BI_3$ was prepared in a similar fashion at 0 °C although some decomposition occurred. The ^1H n.m.r. spectrum was consistent with 96% labelling, the same as that of the $^{10}BF_3$. Bu_4N^+Br, $Et_4N^+F^-$ (Pfatz + Bauer), $Bu_4N^+I^-$, and $Et_4N^+Cl^-$ (Eastman

[1]Abstracted in part from the M.Sc. Thesis of B. W. Benton-Jones, Brock University.

[2]Present address: Department of Chemistry, Vanier College, Montreal, P.Q.

[3]Address correspondence to this author.

Can. J. Chem. Downloaded from www.nrcresearchpress.com by 210.87.254.6 on 09/05/12
For personal use only.

Kodak) were used without further purification. $R_4N^+BX_4^-$ salts (X = F, Cl, Br) were prepared using the method of Schrobilgen (18), the tetrabutyl salts being preferred to the tetraethyl since they were more soluble in methylene chloride, although the butyl group caused more interference in the n.m.r.

Reagent grade methylene chloride (BDH) was fractionated before use and stored over Linde 4A molecular sieves. Hydrogen halides (X = Cl, Br, I) and arsenic trichloride were purified by vacuum distillation. Aluminum chloride, silicon tetrachloride, phosphorus trichloride, and pentachlorides were used without further purification.

Sample Preparation

Samples were prepared in 5 mm o.d. diameter n.m.r. tubes on a standard vacuum system. Solids were weighed out into the tubes which were then evacuated and known amounts of solvent, free trihalide, or other reagent were condensed in at −196, after which the tube was sealed. Adduct concentrations of both 0.1 and 0.2 *M* were used, while Lewis acid – adduct ratios of 0.5:1 through 10:1 were examined. Moisture sensitive solids were transferred in a nitrogen filled dry box. When the reaction had reached equilibrium the contents of most of the tube (the iodides excepted) then remained unchanged with respect to their n.m.r. spectra over a period of many months, although, as a precaution, they were stored at −196 °C.

Gas phase dissociation reactions were carried out in 25-cm long heavy walled glass tubes. Weighed amounts of two adducts were sealed in the evacuated tubes and heated to +160 °C. If necessary, boron trihalide was also added. At the completion of the reaction the tube was opened, excess halide removed, and the resulting solid dissolved for n.m.r. study. The n.m.r. instrumentation for ^{11}B noise decoupling with a Varian A-60 ^1H n.m.r. spectrometer has been described previously (4).

Results[4]

Forward Reactions in Solution

Reactions in the forward direction, *i.e.* those leading to formation of adducts of heavier halides, for example, $Me_3N{\cdot}^{10}BF_3 + BCl_3 \rightleftarrows Me_3N{\cdot}^{10}BF_2Cl + BCl_2F$ were carried out using labelled boron to ascertain whether the B—N bond remained intact. Boron-10 with a spin of 3 gives a characteristic septet in the ^1H n.m.r. of the adducts compared to the ^{11}B quartet that dominates the spectra of adducts prepared with natural abundance boron. A solution of $Me_3N{\cdot}^{10}BF_3$ gave rise to a broad envelope due to overlapping of fluorine and boron splittings. Boron-11 decoupling gave a small peak on the top of the broad resonance, due to the 4% isotopic contamination of the starting material with ^{11}B. Addition of natural abundance BCl_3 to the solution rapidly gave rise to three new multiplets corresponding to $Me_3N{\cdot}^{10}BF_2Cl$, $Me_3N{\cdot}^{10}BFCl_2$, and $Me_3N{\cdot}^{10}BCl_3$, the latter two clearly showing ^{10}B septets (Fig. 1) which did not change appreciably on turning on the ^{11}B decoupler, indicating that the Me_3N was still bonded to the original labelled ^{10}B. Similar results were observed for all the possible halide combinations for the forward reaction. The septets had coupling constants about 1/3 those originally reported for the ^{11}B couplings (4) as would be expected from the relative gyromagnetic ratio of the two boron isotopes. There was some quadrupole broadening which could be reduced by heating the adducts to about 70 °C sharpening the lines considerably.

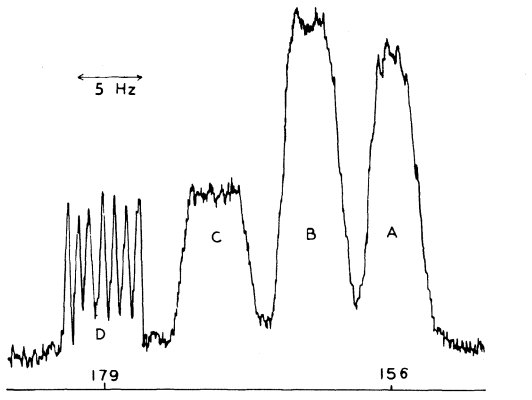

FIG. 1. $Me_3N{\cdot}^{10}BF_3$–BCl_3 system: (*A*) $Me_3N{\cdot}^{10}BF_3$; (*B*) $Me_3N{\cdot}^{10}BF_2Cl$; (*C*) $Me_3N{\cdot}^{10}BFCl_2$; (*D*) $Me_3N{\cdot}^{10}BCl_3$.

Reverse Reactions in Solutions

Reactions in the reverse direction involve the adduct with a free trihalide containing a halogen of lower atomic weight, such as $Me_3N{\cdot}BBr_3 + BCl_3 \rightleftarrows Me_3N{\cdot}BBr_2Cl + BCl_2Br$. These reactions were undertaken in an effort to determine whether the relative strengths of the free and complexed Lewis acid were an important criterion in the halogen exchange mechanism and also as a test of the hypothesis that an ionic pre-dissociation step occurred for the heavier halide adducts.

$Me_3N{\cdot}BI_3$ reacted almost immediately with BBr_3 at ambient temperatures, the n.m.r. showing the presence of all four possible adducts (Fig. 2). Reaction with BCl_3 was slower re-

[4]Detailed n.m.r. shifts and coupling constants are not given in this paper as they have been reported previously (4).

Can. J. Chem. Downloaded from www.nrcresearchpress.com by 210.87.254.6 on 09/05/12
For personal use only.

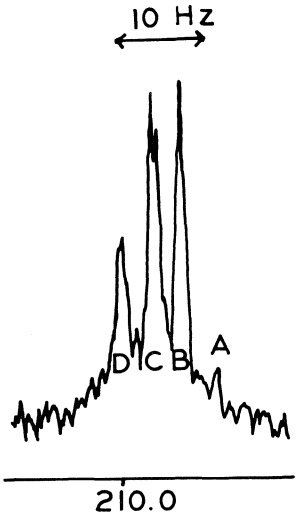

FIG. 2. $Me_3N{\cdot}BI_3$–BBr_3 system, ^{11}B decoupled: (*A*) $Me_3N{\cdot}BBr_3$; (*B*) $Me_3N{\cdot}BBr_2I$; (*C*) $Me_3N{\cdot}BBrI_2$; (*D*) $Me_3N{\cdot}BI_3$.

quiring 24 h before all four adducts could be observed whereas BF_3 reacted only slightly in several days, not surprising in view of the unfavorable equilibrium constants for mixed fluoride iodide complexes (4). $Me_3N{\cdot}BBr_3$ reacted at a moderate rate with BCl_3 but neither $Me_3N{\cdot}BBr_3$ or $Me_3N{\cdot}BCl_3$ was found to react to any extent with BF_3 when the adduct – acid ratio was about 1:1. A report by Krishnamurthy and Lappert (6) suggested that, contrary to our results, the $Me_3N{\cdot}BBr_3$ would react with BF_3 when the solution was 0.2 *M* in each. If however, the BF_3 concentration was increased so that the adduct – acid ratio was 1:10 then mixed adducts involving B—F bonds were observed for both the BBr_3 and BCl_3 adducts, the latter not having been reported by Krishnamurthy and Lappert (6). These reactions were more rapid at 50 °C but proceeded slowly at ambient temperature. In an attempt to ascertain if Krishnamurthy had some impurity to catalyze his reactions we prepared a series of tubes 0.2 *M* in both BF_3 and either $Me_3N{\cdot}BBr_3$ or $Me_3N{\cdot}BCl_3$. Each of these in addition contained potential catalysts such as small quantities of water, ethanol, BBr_4^-, BCl_4^-, BF_4^-, and HBr. In none of these systems was significant reaction observed even after several days at 50 °C. Using ^{10}B labelling for the reverse reactions we again find the ^{10}B label retained attached to nitrogen, *i.e.* no B—N bond breaking is observed just as for the forward reaction. This applies as well to the BI_3 adduct whose reactions were somewhat anomalous.

Gas Phase Reactions

As we had previous evidence of donor–acceptor bond breaking (4, 14) in particular for the more labile oxygen donors, and for comparison with our solution results, a series of gas phase reactions were attempted using adduct – free acid ratios of 5:2 in sealed tubes at 160°. The reactions were carried out in both forward and reverse directions for all combinations of adduct and free halide, the adducts being ^{10}B labelled while the free halide contained natural abundance boron isotopes ($\simeq$ 80% ^{11}B, 20% ^{10}B). Mixed adducts were obtained in all cases, but unlike the solution reactions at lower temperatures, in this case isotopic equilibration had occurred.

Reactions in Solution with Anhydrous Metal Halides

In reactions analogous to the forward and reverse solution reactions, aluminum chloride was added to methylene chloride solutions of $Me_3N{\cdot}BF_3$, $Me_3N{\cdot}BBr_3$, and $Me_3N{\cdot}BI_3$ and in each case mixed adducts and $Me_3N{\cdot}BCl_3$ were formed rapidly at 25 °C. With silicon tetrachloride, however, only small amounts of product were formed in reaction with $Me_3N{\cdot}BF_3$ for several days at 50 °C, while no reaction occurred with $Me_3N{\cdot}BBr_3$. However, $Me_3N{\cdot}BI_3$ was again the exception, $Me_3N{\cdot}BClI_2$ and $Me_3N{\cdot}BCl_3$ being produced but no BCl_2I adduct.

Arsenic trichloride did not react with the BF_3 or BBr_3 adduct but again $Me_3N{\cdot}BI_3$ reacted differently. A thick white crystalline precipitate formed and Me_3NH^+Cl (characteristic doublet $J = 5.0$ Hz) was detected in solution, and some iodine was liberated. The n.m.r. showed that $Me_3N{\cdot}BI_3$ had decreased and $Me_3N{\cdot}BClI_2$ and $Me_3N{\cdot}BCl_3$ were formed, the BCl_2I adduct barely being detected. The reaction proceeded until only $Me_3N{\cdot}BCl_3$ adduct was present. Phosphorus trichloride showed no halogen exchange with any of the adducts even after 24 h at 50 °C. Phosphorus pentachloride reacted slowly with $Me_3N{\cdot}BF_3$ in solution at 50 °C until after 24 h all four adducts were detectable but mostly the BCl_3 adduct was formed. No reaction was observed with

Can. J. Chem. Downloaded from www.nrcresearchpress.com by 210.87.254.6 on 09/05/12
For personal use only.

Can. J. Chem. Downloaded from www.nrcresearchpress.com by 210.87.254.6 on 09/05/12
For personal use only.

$Me_3N{\cdot}BBr_3$ but the iodide was again different, rapidly yielding large quantities of $Me_3N{\cdot}BCl_3$ with only traces of mixed adducts.

Reaction of Adducts with Adducts in Solution

Equimolar amounts of pairs of different adducts were dissolved and heated in various solvents for 6 h (50 °C in CH_2Cl_2, 70 °C in $CHCl_3$, and 100 °C in C_6H_5Cl). No formation of mixed adducts was detected, nor after further periods of days at 25 °C. As halogen exchange in the presence of excess base has been documented (1, 2) excess trimethylamine was also added to samples in the series, again without observable results. Some decomposition was observed in all the samples heated to the higher temperatures but no mixed adducts were detected. The one common decomposition product observed appeared to be Me_3NH^+. $Me_3N{\cdot}BF_3$ showed the greatest degree of decomposition as evidenced by the decrease in intensity of the adduct resonance. Sealed samples kept in solution at room temperature, showed no appreciable decomposition after 2 years.

Reaction of Adducts with Adducts in the Gas Phase

Since the gas phase reaction of adduct and BX_3 leading to formation of mixed adducts were conducted at a high enough temperature for B—N bond rupture as shown by the isotope labelling study, an analogous series of adduct–adduct reactions without excess acid was attempted. Typically 0.5 mmol each of a pair of $Me_3N{\cdot}BX_3$ adducts were sealed in a tube at 160 °C and allowed to react for several hours. At this temperature the pair adducts did not show decomposition products when examined by n.m.r. after opening the tubes. The n.m.r. spectra of the product from the binary mixtures showed that halogen scrambling leading to mixed adduct formation had occurred. Using one adduct labelled with ^{10}B, it was shown that complete equilibration of both boron isotopes occurred.[5] Traces of decomposition product detected included Me_3NH^+ and MeX (X = Br and I).

Reactions of Adducts with Hydrogen Halides in Solution

Methylene chloride solutions 0.2 *M* in adduct and both 0.2 and 2 *M* in anhydrous HX (X = Cl, Br, I) were prepared for all adducts. With the exception of $Me_3N{\cdot}BI_3$ none of the other adducts showed the formation of any mixed halide species. For those systems which had not reacted, a new series was prepared to which water was added, to encourage ionization if this was an important mechanism. No mixed adducts were observed but some $Me_3NH^+Cl^-$ was detected. $Me_3N{\cdot}BI_3$ reacted very slowly with hydrogen bromide when both components were 0.2 *M* in an anhydrous solution. $Me_3N{\cdot}BBrI_2$ was detected by n.m.r. In the sample 2 *M* in HBr all four adducts were identifiable after 24 h at 50 °C. In an analogous system under the same conditions but with added water, halogen exchange had occurred to a greater extent, in agreement with previously postulated ionic mechanisms for the $Me_3N{\cdot}BI_3$ system (15).

Reactions of Adducts with Ionic Species in Solution

Methylene chloride solutions were prepared of all possible combinations of $Me_3N{\cdot}BX_3$ (X = F, Cl, Br, I) with the following tetraalkylammonium salts: $Et_4N^+A^-$ (A = F^-, Cl^-, BF_4^-, BCl_4^-, OAc^-, NO_3^-, BH_4^-) and $Bu_4^nN^+B^-$ (B = Br^-, I^-, and BBr_4^-). Some systems had free trimethylamine added but, with the exception of the production of some $Me_3N{\cdot}BCl_3$ from solutions of $Et_4N^+BCl_4^-$, the free base had no effect. Nothing assignable to mixed adducts was observed when X was F, Cl, or Br, although the BF_3 adduct in particular partially decomposed in the presence of OAc^-.

However, with $Me_3N{\cdot}BI_3$ halogen exchange was observed. After maintaining a sample of the adduct with $Et_4N^+BCl_4^-$ at 50° for 48 h, $Me_3N{\cdot}BCl_3$ and Me_3NBClI_2 could clearly be identified. Identical results were obtained for the sample with $Et_4N^+Cl^-$. In the presence of $Bu_4^nN^+Br^-$ it was possible to detect $Me_3N{\cdot}BBrI_2$ but results were inconclusive with the BBr_4^- ion. No mixed adduct was detected when F^- was allowed to react but BF_4^- led to the formation of some $Me_3N{\cdot}BF_3$. No mixed F—I adduct was detected.

A labelling experiment involving $Me_3N{\cdot}^{10}BI_3$ in reaction with $Et_4N^+BCl_4^-$ gave further evidence for an ionic B—I predissociation as an important mechanism, the B—N bond remaining intact, since after several days at 50 °C a very clear-cut $Me_3N{\cdot}^{10}BCl_3$ septet was observed.

[5]See for example Fig. 3 in ref. 15.

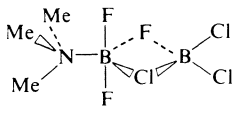

FIG. 3. Transition state.

Discussion

The Mechanism of Halogen Exchange

Possible mechanisms of substituent redistribution in three- and four-coordinate boron have been discussed by Lockhart (19), Massey (20), and Hartman and Schrobilgen (18). Exchange may occur in three-coordinate compounds via a bridged four-coordinate transition state, B_2X_6. Four-coordinate compounds such as BX_4^- probably require a preliminary dissociation to BX_3 and X^- as a first step (18), followed by reaction with either Y^- or BY_4^-, the latter giving an intermediate analogous to $B_2F_7^-$ (21, 22), or $Al_2X_7^-$ (23), or DB_2F_6 (24).

In the trimethylamine adduct system, an initial examination reveals that there are three classes of mechanism worthy of consideration. The first, a bimolecular reaction, involves only halogen exchange without rupture of the B—N bond. This could resemble a typical S_N2 substitution at carbon, *i.e.*;

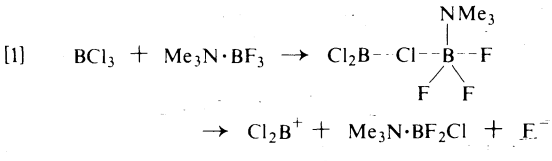

or a doubly bridged intermediate (I, eq. 2) whose geometry is shown in Fig. 3.

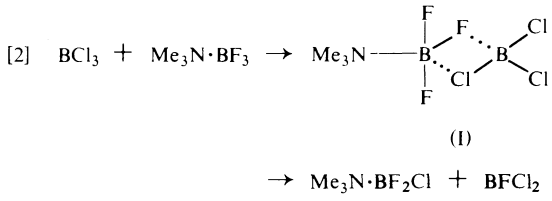

Secondly, the mechanism may be first order, with an initial pre-ionization step (6) in which a halide ion is lost:

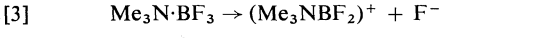

The third mechanism would involve breaking the B—N bond, followed by halogen scrambling among the free boron trihalides, followed by recombination with the base.

It is evident from the results above that adducts react rapidly in solution with free boron trihalides, particularly when the free acceptor is a stronger Lewis acid than that complexed. The growth of seven-line resonances corresponding to $Me_3N{\cdot}^{10}BX_3$ (X = Cl, Br, I) during the appropriate reactions is consistent with halogen exchange occurring without the donor–acceptor bond being broken. Similar conclusions are drawn when an adduct was reacted with a weaker boron trihalide Lewis acid. These reactions were generally slower but nonetheless indicated that halogen scrambling occurred without exchange of boron and, therefore, without rupture of the B—N bond, eliminating the third mechanism from consideration for solution reactions.

Although the halogen exchange can probably be explained by one of the first two basic mechanisms suggested above, we feel that we have eliminated the first order mechanism except in the case of $Me_3N{\cdot}BI_3$. Krishnamurthy and Lappert (6) had advanced a pre-ionization process to explain the reaction of $Me_3N{\cdot}BBr_3$ with BF_3 in methylene chloride. They found that when the concentration of each reactant was 0.2 *M*, mixed adducts and $Me_3N{\cdot}BF_3$ formed after several days. Their argument was that pre-ionization,

is to be expected in this system in which the ligand–boron bond is strong while the boron–halogen bond may be relatively easily heterolyzed. Heaton and Riley (25) proposed a similar mechanism to explain the kinetics of solvolysis of amine–boron trihalide complexes. However, it was also suggested (6) that the BF_3 and BCl_3 trimethylamine adducts would only undergo halogen exchange if a stronger Lewis acid was present. We could not duplicate their results; only traces of mixed F—Br adducts could be detected after several weeks when the initial concentrations were 0.2 *M* in each component. Reproducible results were, however, obtained when the $Me_3N{\cdot}BBr_3:BF_3$ mol ratio was 1:10. Under identical conditions it was also found that $Me_3N{\cdot}BCl_3$ would react with BF_3. Thus the boron trichloride complex does react with a weaker Lewis acid and an equilibrium is established.

The fast forward reaction and the slow

Can. J. Chem. Downloaded from www.nrcresearchpress.com by 210.87.254.6 on 09/05/12
For personal use only.

Can. J. Chem. Downloaded from www.nrcresearchpress.com by 210.87.254.6 on 09/05/12
For personal use only.

reverse reactions are readily explained, steric factors being important about the five-coordinate boron in either the typical S_N2 or doubly bridged (Fig. 3) transition state. It is far more difficult for the fluorine of BF_3 to attack a boron surrounded by a Me_3N and three bromines of $Me_3N{\cdot}BBr_3$, than for the bromine of BBr_3 to attack a boron surrounded by Me_3N and the three fluorines of $Me_3N{\cdot}BF_3$.

To examine more closely the possibility of pre-ionization playing a predominant role in halogen exchange, samples of adducts in an ionic environment were prepared. Both hydrogen halides and tetraalkylammonium salts were used for this purpose. The results almost universally showed that no reaction occurred. This is taken as good evidence against a facile rupture of the boron–halogen bond and that the most probable mechanism for halogen exchange must be bimolecular. The notable exception was $Me_3N{\cdot}BI_3$. This adduct reacted fairly readily with BF_4^-, BCl_4^-, Cl^-, and Br^- to form mixed adducts, except in the F—I system. Halogen exchange occurred even more readily when $Me_3N{\cdot}BI_3$ was mixed with HBr in the presence of a trace of water, compared with an anhydrous system. Water therefore seems to play an important role in the exchange reaction with HBr, presumably by encouraging its ionization.

The mechanism of acid and alkali catalyzed hydrolysis of $Me_3N{\cdot}BF_3$ (26) and $Me_3N{\cdot}BCl_3$ (25, 27) has been studied. For the former, an S_N1 dissociation of the coordinate bond is the rate determining step, whereas for the latter, S_N2 attack of water and rupture of the B—Cl bond probably controls the rate. Blackborrow (16) has recently reported complete line shape analyses of the BCl_3 adducts of *N*,*N*-dimethylaniline and *p*-chloro-*N*,*N*-dimethylaniline over a range of temperatures, the spectra being complicated at low temperatures by quadrupole collapse of the methyl proton ^{11}B quartet and at higher temperatures by collapse due to halogen exchange. These data for exchange were analyzed in terms of a unimolecular ionization process. Our spectra, over the temperature range used by Blackborrow, continued to sharpen with increasing temperatures, *i.e.* quadrupole broadening was reduced but dissociation had not begun. Since in addition, our exchange reactions were carried out at temperatures corresponding to Blackborrow's "absence of exchange," this is further evidence for our proposed bimolecular mechanism in the presence of excess Lewis acid. If, for our system, the Blackborrow, or other pre-ionization mechanisms were operative, we would have observed scrambling and mixed adduct formation when two adducts were heated together in solution.

It is noteworthy that one of the mixed adducts, namely $Me_3N{\cdot}BX_2I$, was normally discriminated against. Its concentration was considerably lower than other adducts in the equilibrium reaction mixtures. The ability of iodine to behave as a leaving group may be enhanced in the monoiododihalogenoborane complexes. This also supports, for the iodide systems, the first order, ionic, dissociative mechanism of Krishnamurthy and Lappert (6), as shown in eqs. 5 and 6, particularly since isotopic labelling again showed that the dative bond remained intact.

$$[5] \qquad Me_3N{\cdot}BI_3 \rightarrow (Me_3NBI_2)^+ + I^-$$

$$[6] \qquad Cl^- + (Me_3NBI_2)^+ \rightarrow Me_3N{\cdot}BI_2Cl$$

Solution reactions of adducts with adducts also ruled out the possibility of either B—N or B—X bond cleavage under mild conditions, no halogen exchange being observed, even after several months at 50 °C. This supports our previous work (3) in which a solution of $Me_3N{\cdot}BF_3$ and $Me_3N{\cdot}BCl_3$ was heated to 180° in an unsuccessful attempt to prepare mixed adducts. In sharp contrast is the dimethyl ether – BX_3 system (1, 2), for which halogen exchange occurs, apparently because the weaker B—O bond is constantly breaking and reforming; thus producing trigonal boron trihalides in solution, capable of exchange.

For nitrogen donors, at higher temperatures and in the absence of a solvent, dissociation of the coordinate bond does become an important factor in halogen exchange reactions. Coyle (14) showed that $Et_3N{\cdot}BF_3$ reacted with BCl_3 via B—N bond breaking at 60° and via some halogen exchange pathway with the B—N bond maintained at 0 °C. Our results substantiate his findings. Reaction between two adducts in the gas phase did not provide any meaningful data even when one adduct was ^{10}B enriched. If however, an adduct containing only ^{10}B was allowed to react with a free boron trihalide containing natural abundance boron, the mecha-

nism would be established if the mixed adducts contained isotopically equilibrated ^{11}B, as our work clearly showed, thus establishing dissociation of the B—N bond as the operative mechanism in the gas phase. The free boron trihalides would undergo halogen scrambling and recombine with Me_3N.

The results of the reactions of the trihalide adducts with the anhydrous metal chlorides are difficult to interpret. Aluminum chloride behaves as a Lewis acid but is normally a dimer, there being little evidence for monomers in relatively non-polar solvents such as methylene chloride. If the monomer were the reacting species, bridging exchange mechanisms similar to those mentioned above (eqs. 1 and 2) could be suggested. This may be the case since considerable steric hindrance would be expected in any transition state involving the dimer. The possibility of B—N bond rupture is ruled out since no $Me_3N{\cdot}AlCl_3$ was detected. The iodide adduct presumably reacts as usual via the ionic mechanism.

The reaction of adducts with PCl_5 supplies some interesting data. $Me_3N{\cdot}BF_3$ and $Me_3N{\cdot}BI_3$ were observed to undergo halogen exchange, while $Me_3N{\cdot}BBr_3$ did not react. An S_N1 mechanism involving B—N bond rupture has already been ruled out under mild conditions. If a bimolecular reaction of the S_N2 variety controlled the reaction we would expect a very crowded transition state. The reaction may proceed via a polar mechanism in which PCl_5 would abstract a fluorine from the adduct to form the hexacoordinate PCl_5F^-. Formation of a boron–chlorine bond during further interaction of the PCl_5F^- with the $(Me_3NBF_2)^+$ species would yield a neutral chlorinated adduct. This polar mechanism could also explain why $Me_3N{\cdot}BBr_3$ does not react with PCl_5. The bulky bromine atom may prevent the formation of PCl_5Br^-, even though B—Br bonds in the adducts are more easily broken than B—F bonds. This suggestion could be tested by mixing $Me_3N{\cdot}BF_2Br$ or $Me_3N{\cdot}BFBr_2$ with PCl_5. If the mechanism is valid, formation of $Me_3N{\cdot}BCl_2Br$ and $Me_3N{\cdot}BClBr_2$, respectively, would be expected. The tertiary mixed adduct, $Me_3N{\cdot}BFClBr$ may also be formed. Again, for $Me_3N{\cdot}BI_3$, a mechanism involving pre-ionization of the B—I bond may be the best explanation, particularly since the mixed adducts are discriminated against.

The authors wish to thank the National Research Council of Canada for financial support, and Professors J. S. Hartman and J. E. Drake for helpful discussions.

1. D. E. Hamilton, J. S. Hartman, and J. M. Miller. Chem. Commun. 1417 (1969).
2. M. J. Bula, D. E. Hamilton, and J. S. Hartman. J. Chem. Soc. Dalton, 1405 (1972).
3. J. S. Hartman and J. M. Miller. Inorg. Nucl. Chem. Lett. **5**, 831 (1969).
4. B. Benton-Jones, M. E. A. Davidson, J. S. Hartman, J. J. Klassen, and J. M. Miller. J. Chem. Soc. Dalton, 2603 (1972).
5. G. E. Ryschkewitsch and W. J. Rademaker. J. Magn. Res. **1**, 584 (1969).
6. S. S. Krishnamurthy and M. F. Lappert. Inorg. Nucl. Chem. Lett. **7**, 919 (1971).
7. B. W. Ashcroft and A. K. Holliday. J. Chem. Soc. A, 2581 (1971).
8. M. J. Bula, J. S. Hartman, and C. V. Raman. J. Chem. Soc. Dalton, 725 (1974).
9. J. S. Hartman and G. J. Schrobilgen. In preparation.
10. M. J. Bula and J. S. Hartman. J. Chem. Soc. Dalton, 1047 (1973).
11. J. E. Drake and B. Rapp. J. Chem. Soc. Dalton, 2341 (1972).
12. G. Jugie, J. P. Laussac, and J. P. Laurent. Bull. Soc. Chim. Fr. 2542, 4238 (1970).
13. G. F. Lanthier and J. M. Miller. J. Chem. Soc. A 346 (1971).
14. T. D. Coyle. Proc. Chem. Soc. 172 (1964).
15. B. Benton-Jones and J. M. Miller. Inorg. Nucl. Chem. Lett. **8**, 485 (1972).
16. J. R. Blackborrow. J. Chem. Soc. Dalton, 2139 (1973).
17. J. M. Miller and M. Onyszchuk. Can. J. Chem. **41**, 2898 (1963).
18. J. S. Hartman and G. J. Schrobilgen. Inorg. Chem. **11**, 940 (1972).
19. (*a*) J. C. Lockhart. Redistribution reactions. Academic Press, N.Y. 1970. (*b*) J. C. Lockhart. Chem. Rev. **65**, 131 (1965).
20. A. G. Massey. Adv. Inorg. Chem. Radiochem. **10**, 1 (1967).
21. J. J. Harris. Inorg. Chem. **5**, 1627 (1966).
22. S. Brownstein and J. Paasivirta. Can. J. Chem. **43**, 1645 (1965).
23. C. M. Begun, C. R. Boston, G. Torsi, and G. Mamantov. Inorg. Chem. **10**, 886 (1971).
24. R. J. Gillespie and J. S. Hartman. Can. J. Chem. **46**, 2147 (1968).
25. G. S. Heaton and P. N. K. Riley. J. Chem. Soc. A, 952 (1966).
26. I. G. Ryss and S. L. Idel. Russ. J. Inorg. Chem. **5**, 852, 855 (1960).
27. I. G. Ryss and U. D. Mahonin. Ukrainski Khimicheskii Zhurnal, **37**, 9, 863 (1971).

Can. J. Chem. Downloaded from www.nrcresearchpress.com by 210.87.254.6 on 09/05/12
For personal use only.

Studies on Theoretical Psychotogens. Synthesis of *O*-Methylated Analogs of Catecholamine Neurotransmitters and Metabolic Precursors

J. R. BUTTERICK AND A. M. UNRAU

Department of Chemistry, Simon Fraser University, Burnaby, British Columbia V5A 1S6

Received February 4, 1974

J. R. BUTTERICK and A. M. UNRAU. Can. J. Chem. **52**, 2873 (1974).

The catecholamine analogs (±)-1-(3,4-dimethoxyphenyl)-2-alanine (**1**), β-(3,4-dimethoxyphenyl)ethylamine (**2**), (±)-1-(3,4-dimethoxyphenyl)-2-amino propane (**3**), (±)-*erythro*,*threo*-α-aminomethyl-3,4-dimethoxybenzyl alcohol (**4**), and (±)-*erythro*, *threo*-α-methylaminomethyl-3,4-dimethoxybenzyl alcohol (**5**) have been synthesized and optimized yields are reported. The availability of certain carbon-14 compounds has dictated logical starting points in the synthesis of ^{14}C-tagged analogs. These syntheses were designed for metabolic and disposition work in connection with a pilot project concerned with the aetiology of schizophrenia with particular reference to the Osmond–Smythies – Harley-Mason hypothesis (2) of 1952.

J. R. BUTTERICK et A. M. UNRAU. Can. J. Chem. **52**, 2873 (1974).

Les analogues de la catécholamine (±)-(diméthoxy-3,4 phényl)-1 alanine-2 (**1**), β-(diméthoxy-3,4 phényl) éthylamine (**2**), (±)-(diméthoxy-3,4 phényl)-1 amino-2 propane (**3**) l'alcool (±)-*érythro*, *thréo*-α-aminométhyl diméthoxy-3,4 benzylique (**4**) et l'alcool (±)-*érythro*, *thréo*-α-méthylaminométhyl diméthoxy-3,4 benzylique (**5**) sont synthétisés et les meilleurs rendements sont rapportés. La disponibilité de certains composés du carbone-14 a imposé des points de départ logiques dans la synthèse d'analogues marqués au ^{14}C. Ces synthèses sont destinées à un travail sur le métabolisme en relation avec un projet pilote concernant l'étiologie de la schizophrénie plus particulièrement en rapport avec les hypothèse de Osmond–Smythies – Harley-Mason (1952).

[Traduit par le journal]

Can. J. Chem. Downloaded from www.nrcresearchpress.com by 210.87.254.42 on 09/05/12
For personal use only.

Introduction

The aetiology of the diffusive clinical syndrome "schizophrenia" remains unresolved to date despite the fact that an estimated 600 papers on the subject appear each year (1). Osmond and Smythies in 1952 (2) put forward their hypothesis for an "M-substance model psychosis" couched in terms of what was the best understanding of catecholamine metabolism at the time. In consultation with Harley-Mason, Osmond and Smythies postulated an aberration in transmethylation of noradrenalin to *O*-methylated derivatives, such as α-aminomethyl-3,4-dimethoxybenzyl alcohol (**4**) and α-aminomethyl-3-hydroxy-4-methoxybenzyl alcohol (**6**). These authors were struck by the similarities of the psychiatric syndrome and mescaline (**7**) intoxication, and postulated a metabolic transformation from normal body metabolites to compounds which structurally resembled mescaline.

Osmond and Smythies (2) noted in passing that β-(3,4-dimethoxyphenyl)ethylamine (**2**), a "catatonic" in animals, (3) required fairly high doses for its effect (> one mescaline unit (4)). In the ensuing years, a considerable amount of research has accumulated (5). Of historical significance, Friedhoff and Van Winkle in 1962 (6) isolated a ninhydrin positive "compound" from the urine of schizophrenics (by means of a paper chromatographic system) which they claimed to be isographic with β-(3,4-dimethoxyphenyl)-ethylamine. Also notable were the subsequent refutations and confirmations that appeared over the next 10 years (7). In 1969, Shulgin *et al.* (4) in a study of mescaline analogs in humans suggested examination of α-aminomethyl-3,4-dimethoxybenzyl alcohol (**4**), the compound Harley-Mason had suggested originally. In 1969 we embarked on synthesis of *O*-methylated derivatives of the dopamine–noradrenergic metabolic pathway with the future objective toward pharmacological testing, ease of carbon-14 incorporation, and subsequent metabolic and distribution studies.

Results and Discussion

Published syntheses (8, 9) of (±)-1-(3,4-dimethoxyphenyl)-2-alanine (**1**) proved to be sensitive to side reactions. In the course of our work, we substituted a facile synthesis based on an

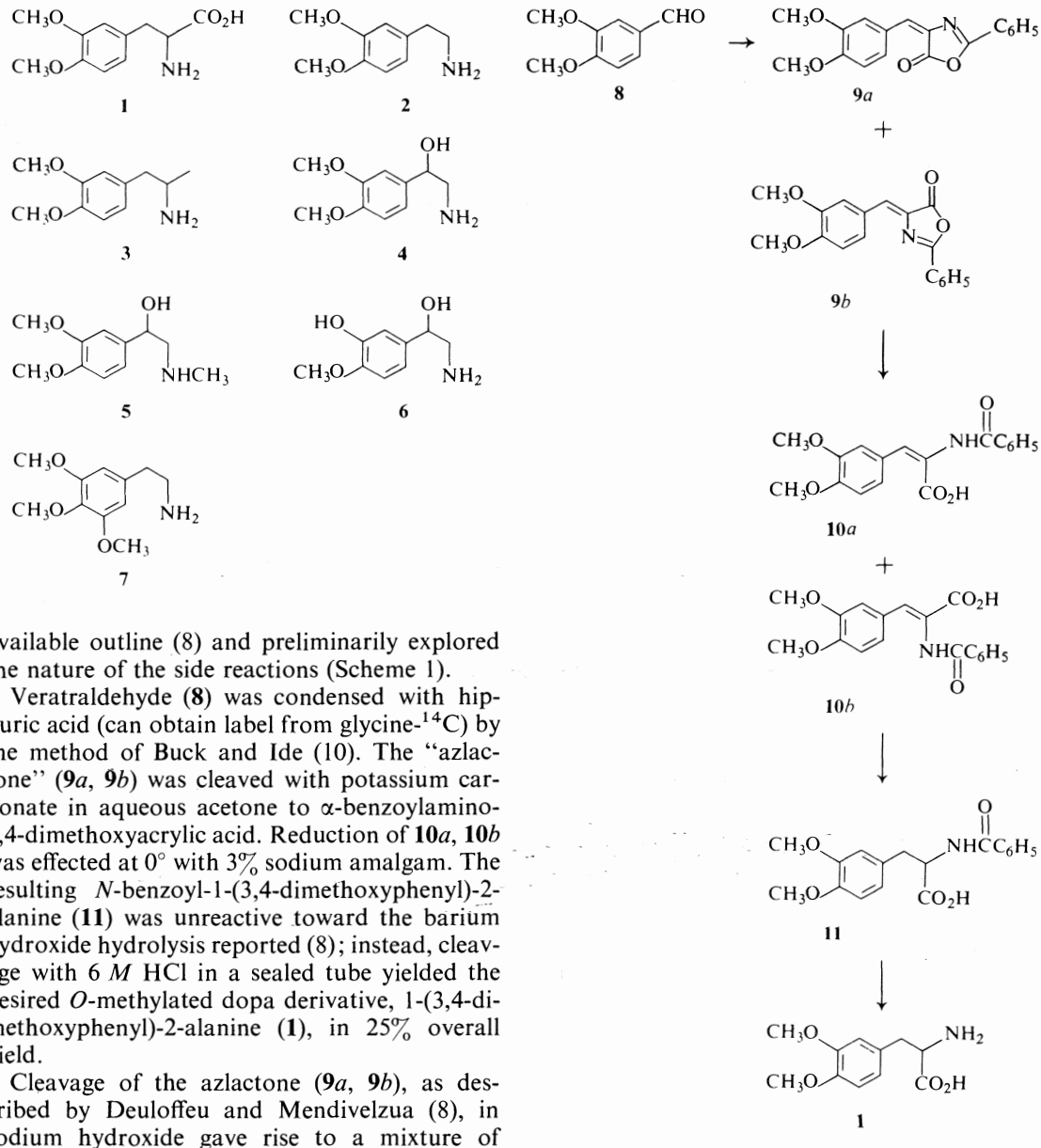

SCHEME 1

available outline (8) and preliminarily explored the nature of the side reactions (Scheme 1).

Veratraldehyde (**8**) was condensed with hippuric acid (can obtain label from glycine-^{14}C) by the method of Buck and Ide (10). The "azlactone" (**9***a*, **9***b*) was cleaved with potassium carbonate in aqueous acetone to α-benzoylamino-3,4-dimethoxyacrylic acid. Reduction of **10***a*, **10***b* was effected at 0° with 3% sodium amalgam. The resulting *N*-benzoyl-1-(3,4-dimethoxyphenyl)-2-alanine (**11**) was unreactive toward the barium hydroxide hydrolysis reported (8); instead, cleavage with 6 *M* HCl in a sealed tube yielded the desired *O*-methylated dopa derivative, 1-(3,4-dimethoxyphenyl)-2-alanine (**1**), in 25% overall yield.

Cleavage of the azlactone (**9***a*, **9***b*), as described by Deuloffeu and Mendivelzua (8), in sodium hydroxide gave rise to a mixture of α-benzoylamino-3,4-dimethoxyacrylic acid (**10***a*, **10***b*) and *N*-benzoyl-1-(3,4-dimethoxyphenyl)-1-hydroxy-2-alanine (**12**). Such a hydrolytic cleavage to **12** has been exploited recently in the syntheses of substituted phenylpyruvates (**14**) via the intermediacy of **12** or **13** (11, 12) (Scheme 2).

Reduction of the azlactone (**9***a*, **9***b*) with a specially prepared Raney nickel catalyst utilized as described by Badshah *et al.* (13) gave rise to 4-(3,4-dimethoxy benzyl)-4-methoxy-2-phenyl-5-oxazolone (**15**) in addition to the cited *N'*-benzoyl-1-(3,4-dimethoxyphenyl)-2-alanine amide (**16**) (Scheme 3). The fact that the authors neglected to mention the requisite washes associated with Raney nickel generation afforded us the opportunity of observing an ambient temperature reaction of ethoxide with the azlactone (**9***a*, **9***b*).

β-(3,4-Dimethoxyphenyl)ethylamine (**2**) and 1-(3,4-dimethoxyphenyl)-2-aminopropane (**3**)

Can. J. Chem. Downloaded from www.nrcresearchpress.com by 210.87.254.42 on 09/05/12
For personal use only.

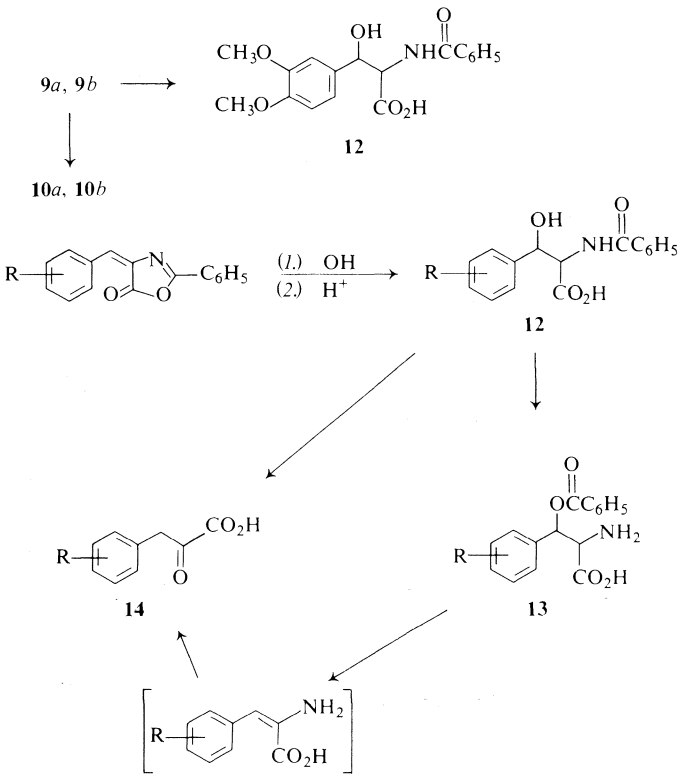

SCHEME 2

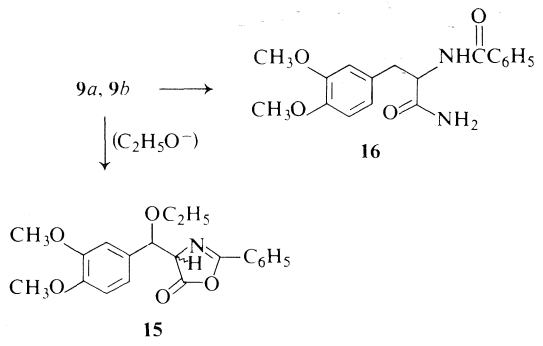

SCHEME 3

were prepared by methods of Raiford and Fox (14) and Ramirez and Burger (15). In addition, **3** was prepared by a modified procedure (16). Commercial ^{14}C-nitromethane and accessibility of ^{14}C-nitroethane via a Victor Meyer displacement (17) of ^{14}C-ethyliodide renders this route especially attractive for labelling purposes. Overall yields were 68% for **2** and 35% and 60% for **3**.

Of three published accounts for the synthesis of α-aminomethyl-3,4-dimethoxybenzyl alcohol (**4**), two were unattractive because of low yields due to side reactions (18, 19) and one was published without details (20). The synthetic route most attractive to us involved the use of potassium cyanide (can be obtained radioactively labelled). In a modified method of Hahn and Rumpf (21) 3,4-dimethoxybenzaldehyde cyanohydrin (**16**), was obtained from commercially available veratraldehyde (**8**). Lithium aluminum hydride reduction (19) of the cyanohydrin gave rise to α-aminomethyl-3,4-dimethoxybenzyl alcohol (**4**) in 94% overall yield.

A serious side reaction in the procedure of Hahn and Rumpf (21) is the formation of 3,3′,4,4′-tetramethoxybenzoin (**17**).

α-Methylaminomethyl-3,4-dimethoxybenzyl alcohol (**5**) was not obtainable by the method of Adityachaudhury and Chatterjee (19) for reasons mentioned below. The method of choice appears to be that of Friedman *et al.* (22). 1-(3,4-Di-

Can. J. Chem. Downloaded from www.nrcresearchpress.com by 210.87.254.42 on 09/05/12
For personal use only.

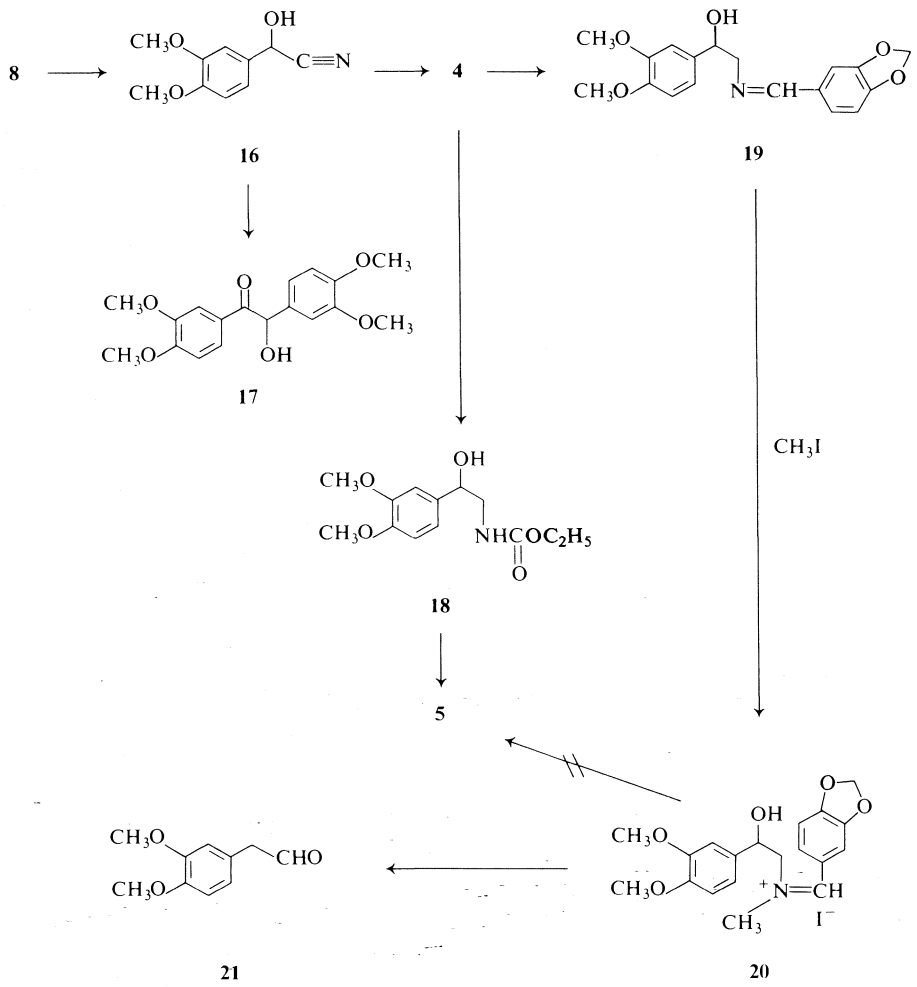

SCHEME 4

methoxyphenyl)-2-ethanolamine (**4**) was condensed with ethyl chloroformate and the resulting urethane (**18**) was reduced with lithium aluminum hydride to yield the desired *N*-methyl compound (**5**) in 22% overall yield (starting with veratraldehyde (**8**)). The method of Adityachaudhury and Chatterjee (19) was explored. α-Aminomethyl-3,4-dimethoxybenzyl alcohol (**4**) formed a Schiff's base with piperonal (**19**) and a methiodide adduct (**20**) with methyliodide. However, cleavage with hydrochloric acid resulted in 1-(3,4-dimethoxy)acetaldehyde (**21**) instead of the reported α-methylaminomethyl-3,4-dimethoxybenzylamine (**5**) (Scheme 4). The reaction of 1-aryl-2-amino alcohols with strong acid had been known for some time (23–25) and mechanism studies have recently been reported (26).

Experimental

Melting points were measured on a Fischer-Johns apparatus and are uncorrected. Ultraviolet spectra were measured on a Unicam SP 800 with ethanol as solvent. Infrared spectra were measured on a Perkin-Elmer 457 spectrometer. Nuclear magnetic resonance spectra were recorded using a Varian A56/60 and the requisite data are reported as δ *vs.* an internal TMS standard. Mass spectra were obtained on a Perkin-Elmer Hitachi RMU-7 instrument using an ionization voltage of 80 eV. Gas–liquid partition chromatographic analyses were performed on a Bendix Chroma-Lab series 2200 equipped with a T.C. detector.

*4-(3,4-Dimethoxybenzal)-2-phenyl-5-oxazolones (**9a, 9b**)*

The procedure by Buck and Ide (10) was found to be satisfactory (65% yield); m.p. 151–152°, (lit. (10) m.p. 151–152°); n.m.r. ($CDCl_3$): 3.90 (*m*-OCH_3, s, 6), 4.00 (*p*-OCH_3, s, 6), 6.75–7.25 (olefinic H, 2s, 2), 7.40–8.20 (Ar-H, m, 16); ν_{max} (KBr): 1745, 1760 cm^{-1} (carbonyls,

Can. J. Chem. Downloaded from www.nrcresearchpress.com by 210.87.254.42 on 09/05/12
For personal use only.

Can. J. Chem. Downloaded from www.nrcresearchpress.com by 210.87.254.42 on 09/05/12
For personal use only.

1625 cm^{-1} (C=N); λ_{max} (EtOH): 298 (ε 10 500), 350 nm (ε 5000).

Anal. Calcd. for $C_{18}H_{15}NO_4$ (mol. wt. 309): C, 69.89; H, 4.89; N, 4.52. Found (M^+, 309): C, 69.46; H, 4.85; N, 4.49.

*α-Benzoylamino-3,4-dimethoxyacrylic Acid (**10a**, **10b**)*

The azlactones (**9a**, **9b**) (81 g, 0.262 mol) were refluxed (12 h) in a 1 l 10% K_2CO_3 solution – 200 ml acetone. The reaction mixture was poured over 1 l 10% HCl – 500 g ice. The product was collected, recrystallized from acetic acid – water, 78.0 g (92.0% yield); m.p. 196–198°; n.m.r. (DMSO-d_6): 3.60 (*m*-OCH_3, s, 6), 3.75 (*p*-OCH_3, s, 6), 6.80–8.10 (Ar-H, olefinic, —$NHCOC_6H_5$, m, 20), 9.85 (CO_2H, s, 1) (D_2O exchange, 4.00–4.70, broad s); ν_{max} (KBr): 3200 ($NHCOC_6H_5$), 2500 (CO_2H), 1600–1690 cm^{-1} (C=C, C=O); λ_{max} (EtOH): 295 nm (ε 12 500).

Anal. Calcd. for $C_{18}H_{17}NO_5$ (mol. wt. 327): C, 66.04; H, 5.24; N, 4.28. Found (M^+, 327): C, 66.01; H, 5.21; N, 4.30.

*N-Benzoyl-3-(3,4-dimethoxyphenyl)-2-amino Proprionic Acid (**11**)*

The acrylic acid (**10a**, **10b**), (1 g, 3.06 mmol) was suspended in deionized water (10 ml), cooled, and stirred in an ice bath (0 °C). Powdered 3% sodium amalgam (3 g) was added in three portions at 15 min intervals; 15 min after the last addition, the solution was stirred at room temperature (25 °C) for 30 min, Hg was filtered through a gravity funnel with two thicknesses of filter paper, and washed with 10 ml deionized water. The filtrate was cooled in an ice bath, acidified (20% HCl), stored in a refrigerator overnight, and the precipitate subsequently dried. The compound after recrystallization from acetic acid – water, 620 mg (1.89 mmol, 57.5% yield) had m.p. 182–184°; n.m.r. (DMSO-d_6): 3.20 (CH_2, m, 2), 3.70 (OCH_3, s, 6), 4.6 (CH, m, 1), 6.80–7.00 (Ar-H, m, 3), 7.4–8.0 (Ar-H, m, 5), 8.50 ($NHCOC_6H_5$, s, 1), 9.00 (CO_2H, s, 1) D_2O exchange, 4.00–4.70 (broad s, 1); ν_{max} (KBr): 3300 ($NHCOC_6H_5$), 2500 (CO_2H), 1690–1670 cm^{-1} (C=O's).

Anal. Calcd. for $C_{18}H_{19}NO_5$ (mol. wt. 329): C, 65.64; H, 5.81; N, 4.25. Found (M^+, 329): C, 65.64; H, 5.87; N, 4.44.

*(±)-3-(3,4-Dimethoxyphenyl)-2-alanine (**1**)*

The *N*-benzoyl amino acid (**11**) (130.3 mg, 0.396 mmol) dissolved in 6 *M* HCl (5 ml) was hydrolysed for 1 h in a sealed tube (97°). The solution was cooled in an ice bath, extracted immediately with 5 ml ether to remove benzoic acid and the aqueous acidic layer evaporated on a vacuum pump (1 mm) at room temperature. The crude material (111.7 mg) was taken up in water and eluted with the same from a silica gel column and the effluent was evaporated on a vacuum pump. The residue was dried *in vacuo* over P_2O_5, 62.9 mg (0.280 mmol, 70.8% yield); m.p. 249–250°; t.l.c. (silica gel GF-254): $CHCl_3$:CH_3OH:NH_4OH(concentrated) 80:20:1; R_f 0.20; g.l.p.c. of the trifluoroacetic acid – *n*-butyl ester (27) (1.5% GE-XF1105 on Chromosorb W) (160°) showed a single component; n.m.r. (D_2O): 3.30 (CH_2, m, 2), 3.92 (OCH_3, s, 6), 4.60 (CH, m, 1), 4.75 (NH_2, CO_2H exchanged, s, 3), 6.98 (Ar-H, m, 3); ν_{max} (KBr): 3000 (NH_2), 2100 cm^{-1} (CO_2H).

Anal. Calcd. for $C_{11}H_{15}O_4N$ (mol. wt. 225): C, 58.65; H, 6.71; N, 6.22. Found (M^+, 225): C, 58.64; H, 6.70; N, 6.22.

*Hydrolysis of Azlactone (**9a**, **9b**) (8)*

The azlactones (**9a**, **9b**) (5 g, 16 mmol) were refluxed in 2% NaOH solution (500 ml) for 10 h. On cooling in ice, the mixture was acidified with dilute HCl and the crude product collected; t.l.c. (silica gel GF-254) acetone – water (1:1, v/v) revealed two major components. The α-benzoyl-3,4-dimethoxyacrylic acid (**10a**, **10b**) (20%) which chromatographed as one component was characterized by mass spectrum and m.p. as described previously. The other compound, *N*-benzoyl-1-(3,4-dimethoxyphenyl)-1-hydroxy-2-alanine (**12**), (65% yield) had m.p. 211–212°; n.m.r. (DMSO-d_6): 3.70 (OCH_3, s, 6), 4.60–5.20 (CH's OH, m, 3), 7.40–8.00 (Ar-H, m, 8), 8.50 ($NHCOC_6H_5$, s, 1), 9.00 (CO_2H, s, 1), D_2O exchange, 4.00–4.50 (broad s, 2).

Anal. Calcd. for $C_{18}H_{19}NO_6$ (mol. wt. 345): C, 62.60; H, 5.54; N, 4.06. Found (*m/e*, 345): C, 62.58; H, 5.52; N, 4.02.

*4-(3,4-Dimethoxybenzyl)-4-ethoxy-2-phenyl-5-oxazolone (**15**)*

The azlactones (**9a**, **9b**) (3.86 g, 12.5 mmol) in 100 ml 95% EtOH, were hydrogenated with a mixture of 4.25 g NH_3 (anhydrous) and 1.5 g catalyst (prepared as described by Badshah *et al.* (13)) at 42 p.s.i. H_2 for 14 h using a Parr shaker. The catalyst was filtered, washed with hot ethanol, and the filtrate evaporated. The product (92% yield) had m.p. 215–217°; n.m.r. (DMSO-d_6): 2.10 (CH_3, t, 3), 4.55 (CH_2, quartet, 2), 3.70 (OCH_3, s, 6), 4.60–5.00 (CH's, m, 2), 6.75–8.20 (Ar-H, m, 8).

Anal. Calcd. for $C_{20}H_{21}NO_5$ (mol. wt. 355): C, 67.59; H, 5.96; N, 3.94. Found (M^+, 355): C, 67.55; H, 5.94; N, 3.90.

*β-(3,4-Dimethoxyphenyl)ethylamine (**2**)*

Condensation of veratraldehyde (**8**) with nitromethane and ammonium acetate in acetic acid (14) gave the known nitrostyrene; m.p. 140–141° (lit. (14) m.p. 140–141°); n.m.r. ($CDCl_3$): 2.9 (OCH_3, s, 6), 6.85–7.45 (Ar-H, m, 3), 7.71 (CH=CH, dd, 2, J = 15 Hz); ν_{max} (KBr): 1570 cm^{-1} (CH=CH); λ_{max} (EtOH): 290 nm (ε 10 000); M^+ 209. Lithium aluminum hydride reduction of the nitro styrene in ether (15) gave **2**, (68% yield), m.p. (HCl salt) 156–157° (lit. (28) m.p. 156–157°); n.m.r. (DMSO-d_6): 2.70–3.00 (CH_2CH_2, m, 4), 3.80 (OCH_3, s, 6), 6.8–7.0 (Ar-H, m, 3), 8.40 (NH_3, s, 3); ν_{max} 3400 cm^{-1} (NH_2); t.l.c. (silica gel GF-254) $CHCl_3$:CH_3OH:NH_4OH(concentrated) 80:20:1 showed a single compound, R_f 0.30, as did g.l.p.c. on 3% OV-17 – Gas Chrom Q (220°).

*(+)-1-(3,4-Dimethoxyphenyl)-2-aminopropane (**3**)*

Condensation of veratraldehyde (**8**) with nitro ethane and ammonium acetate in acetic acid (14) as well as with nitroethane (neat) (16), gave the nitropropenyl derivative, 35 and 60% yield, respectively; m.p. 145–146°; n.m.r. ($CDCl_3$): 2.50 (CH_3-C=C, s, 3), 3.95 (OCH_3, s, 6), 6.9–7.0 (Ar-H, m, 3), 8.0 (CH=C, broad s, 1); ν_{max}: 1590 cm^{-1} (CH=C); λ_{max} (EtOH): 296 nm (ε 11 000).

Mol. Wt. Calcd.: 223. Found (*m/e*): 223.

Lithium aluminum hydride reduction of the β-nitropropene in anhydrous THF (15) gave **3** (74% yield); m.p. (HCl salt) 147–148° (lit. (29) m.p. 147.5–148°); n.m.r. ($CDCl_3$): 1.05 (CH_3, d, 3), 2.5–3.0 (CH_2CH, m, 3), 3.80 (OCH_3, s, 6), 6.80–7.00 (Ar-H, m, 3); ν_{max} (KBr): 3400 cm^{-1} (NH_2) t.l.c. (silica gel GF-254) $CHCl_3$:CH_3OH:NH_4OH-(concentrated) 80:20:1, R_f 0.35; g.l.p.c.

on 3% OV-17 – Gas Chrom Q (220°) both showed a single component.

Mol. Wt. Calcd.: 195. Found (*m/e*): 195.

*3,4-Dimethoxybenzaldehyde Cyanohydrin (**16**) (21)*

Freshly distilled veratraldehyde (**8**) (0.1 mol) was ground in a mortar and slurried with 0.172 mol KCN dissolved in 23 ml water. Hydrochloric acid (17 ml) was added dropwise with rapid stirring until the temperature of the mixture reached 45–50° and maintained at this level by cooling with ice. The mixture was allowed to come to room temperature, cooled in ice, the solid removed by filtration and washed with cold water (5 × 50 cc), and dried *in vacuo* (m.p. 59–69°). The crude material was stirred in 100 ml cold anhydrous benzene (twice), filtered, and dried *in vacuo*; 18.7 g (0.097 mol, 97.2% yield); m.p. 87–90°; n.m.r. ($CDCl_3$): 3.40 (OH, s, 1), 4.05 (OCH_3, s, 6), 5.65 (CH, s, 1), 6.90–7.60 (Ar-H, m, 3). ν_{max} (KBr): 3430 (OH), 2000 cm^{-1} (C≡N); λ_{max} (EtOH): 295 nm (ε 10 000).

Anal. Calcd. for $C_{10}H_{11}NO_3$ (mol. wt. 193): C, 62.16; H, 5.74; N, 7.25. Found (M^+, 193): C, 62.17; H, 5.70; N, 7.12.

*α-Aminomethyl-3,4-dimethoxybenzyl Alcohol (**4**)*

The cyanohydrin (**16**) (12.3 g, 64 mmol), dissolved in anhydrous THF, was added dropwise to an ice-cooled slurry of $LiAlH_4$ (12 g, 318.5 mmol) in dry THF (250 ml). The mixture was stirred at room temperature (15 min), refluxed thereafter for 5 h followed by hydrolysis with H_2O under cooling until the salts that formed coagulated. The mixture was filtered and the filtrate dried and evaporated *in vacuo*, leaving a high boiling liquid. Vacuum distillation afforded a fraction collected at 160–164° (0.7 mm), 11.5 g (0.058 mol, 97%) which had as the solid HCl salt m.p. 163–165° (lit. (19) m.p. 163°); n.m.r. (DMSO-d_6): 2.70–3.00 (CH_2-NH_2, m, 2), 3.50 (OH, NH_2, broad s, 4), 3.75 (OCH_3, 2s, 6), 4.60–4.80 (C*H*(OH)CH_2, m, 1) 6.8–7.0 (Ar-H, m, 3); ν_{max} 3400–3500 cm^{-1} (NH_2, OH); t.l.c. (Silica Gel GF 254): $CHCl_3$:CH_3OH:NH_4OH-(concentrated) 80:20:1, R_f, 0.33; g.l.p.c. on 5% SE 30 – Chromasorb W DMCS A/W, 60–80, 160°, showed a single peak for the Trisil–BSA derivative.

Anal. Calcd. for $C_{10}H_{15}NO_3$ (mol. wt. 197): C, 60.90; H, 7.67; N, 7.10. Found (M+, 197): C, 60.85; H, 7.50; N, 7.05.

*N-(1-(3,4-Dimethoxyphenyl)-2-ethanol) Carbamate (**18**)*

The ethanolamine **4** (0.349 g, 2 mmol), slurried in water (10 ml) and 2 g chopped ice, was treated with ethylchloroformate by the method of Friedman *et al.* (22) to yield **18**, (0.349 g, 65%); m.p. 63–65°; n.m.r. (DMSO-d_6): 1.30 (CH_3, t, 3), 2.80–3.30 (CH_2NH, m, 2), 3.50 (OH, NH_2, s, 2), 3.75 (OCH_3, s, 6), 4.50 (CH_2, q, 2), 4.60–4.80 (C*H*(OH)NH, m, 1), 6.80–7.00 (Ar-H, m, 3); ν_{max} 1750 (C=O), 3430–3500 cm^{-1} (NH, OH).

Anal. Calcd. for $C_{13}H_{19}NO_5$ (mol. wt. 269): C, 57.98; H, 7.11; N, 5.20. Found (M+, 269): C, 57.96; H, 7.10; N, 5.16.

*(±)-erythro,threo-α-Methylaminomethyl-3,4-dimethoxybenzyl Alcohol (**5**)*

The carbamate (**18**) (0.345 g, 1.31 mmol), dissolved in anhydrous THF, was added with stirring to a slurry of 266 mg (7.0 mmol) $LiAlH_4$ in anhydrous THF (10 ml) at room temperature. The mixture was refluxed for 80 h, then hydrolyzed with water, and precipitated salts removed. The filtrate was dried ($MgSO_4$) and evaporated yielding the crude amino alcohol which was purified by elution with ether from a silica gel column. The combined ether fractions were dried over $MgSO_4$ and evaporated to a small volume followed by saturation with anhydrous HCl. The ethanolamine hydrochloride (**5**) was collected and dried, 97 mg (0.46 mmol, 35%); m.p. 132–133°; n.m.r. (DMSO-d_6): 2.44 (CH_3NH, s, 3), 2.7–3.0 (CH_2NH$_2$, m, 2), 3.70–3.80 (OCH_3, 2s, 6), 4.6–5.0 (C*H*OH, s, 1), 6.8–7.0 (Ar-H, m, 3); ν_{max}: 3400–3500 cm^{-1} (NH, OH) t.l.c. (silica gel GF 254): C_6H_6:$CHCl_3$:CH_3OH:NH_4OH-(concentrated) 8:6:5:1; and g.l.p.c. of the Trisil–BSA derivative on 5% SE-30 as above (160°) showed one compound.

Anal. Calcd. for $C_{11}H_{17}NO_3$ (mol. wt. 211): C, 62.53; H, 8.11; N, 6.63. Found (M+, 211); C, 62.50; H, 8.09; N, 6.61.

*Conversion of (**4**) to 1-(3,4-Dimethoxyphenyl)-acetaldehyde (**21**) (19)*

1-(3,4-Dimethoxyphenyl)-2-ethanolamine (**4**) formed, as has been reported (19), the Schiff's base (**19**) with piperonal; n.m.r. ($CDCl_3$): 3.50 (OH, s, 1) 3.7–3.8. (OCH_3, s, 6), 4.6–5.0 ($CHCH_2$, m, 3), 6.0 (OCH_2O, s, 2), 6.8–7.0 (Ar-H, m, 6), 7.20 (CH, s, 1).

Anal. Calcd. for (mol. wt. 329): C, 65.64; H, 5.81; N, 4.25. Found (*m/e*, 329): C, 65.62; H, 5.75; N, 4.15.

The Schiff's base (**19**) was reacted with CH_3I (19) to form the adduct (**20**); n.m.r.: 2.30 (=N—CH_3, s, 3), 2.70–3.00 (CH_2-N, m, 2), 3.50 (OH, s, 1), 3.75 (OCH_3, 2s, 6), 4.60–4.80 (C*H*(OH)CH_2, m, 1), 5.50 (CH, s, 1), 6.00 (O-CH_2-O, s, 2), 6.80–7.50 (Ar-H, m, 6).

Anal. Calcd. for $C_{19}H_{22}NO_5I$ (mol. wt. 471): C, 48.42; N, 4.70; N, 2.97; Found (M^+, 471): C, 48.35; H, 4.69; N, 2.95.

The adduct **20** (2.4 g, 0.535 mol) was refluxed in a mixture of water (25 ml) and HCl (2.5 ml, 12 *M*) for 2 h. The solution was extracted with ether and the aqueous solution treated with 30% NaOH. The alkaline solution was extracted with $CHCl_3$, the $CHCl_3$ layer dried ($MgSO_4$), and evaporated leaving an oil which was distilled *in vacuo*; b.p. 125° (1.5 mm); n.m.r. ($CDCl_3$): 3.50 (CH_2, d, 1), 4.75 (OCH_3, s, 6), 6.8–7.0 (Ar-H, m, 3), 9.0 (CHO, s, 1); ν_{max} (NaCl plate): 1725 cm^{-1}.

Mol. Wt. Calcd.: 180. Found (M^+): 180.

1. D. Bannister. Brit. J. Psych. **114**, 181 (1968).
2. H. Osmond and J. Smythies. J. Ment. Sci. **98**, 309 (1952).
3. A. M. Ernst. Psychopharmacologia, **7**, 383 (1965).
4. A. T. Shulgin, T. Sargent, and C. Naranjo. Nature, **221**, 537 (1969)
5. A. P. Ridges. Orthomolecular psychiatry. *Edited by* D. Hawkins and L. Pauling. W. H. Freeman and Co. San Francisco. 1973. p. 120.
6. A. J. Friedhoff and E. Van Winkle. Nature, **194**, 897 (1962).
7. H. Weil-Malherbe and S. Szara. The biochemistry of functional and experimental psychoses. Charles C. Thomas, Springfield, Ill. 1971.

Can. J. Chem. Downloaded from www.nrcresearchpress.com by 210.87.254.42 on 09/05/12
For personal use only.

8. V. DEULOFFEU and G. MENDIVELZUA. Hoppe-Seylers Z. Physiol. Chem. **219**, 233 (1933).
9. A. BADSHAH, N. H. KHAN, and A. R. KIDWAI. J. Org. Chem. **37**, 2916 (1972).
10. J. S. BUCK and W. S. IDE. Org. Syn. Coll. Vol. 2, 55 (1943).
11. B. T. HO, L. W. TANSEY, and J. T. HUANG. J. Med. Chem. **14**, 1132 (1971).
12. A. PAPADAKI, V. GUIOCA, and G. TSATSAS. Chim. Ther. **8**, 308 (1973).
13. A. BADSHAH, N. H. KHAN, and A. R. KIDWAI. J. Org. Chem. **37**, 2916 (1972).
14. L. C. RAIFORD and D. E. FOX. J. Org. Chem. **9**, 170 (1944).
15. F. A. RAMIREZ and A. BURGER. J. Am. Chem. Soc. **72**, 2781 (1950).
16. J. R. BUTTERICK and A. M. UNRAU. Chem. Commun. **8**, 307 (1974).
17. V. MEYER and O. STUBER. Ber. **5**, 203 (1872).
18. K. KINDLER, W. PESCHKE, and E. BRANDT. Ber. **68B**, 2241 (1935).
19. N. ADITYACHAUDHURY and A. CHATTERJEE. J. Indian Chem. Soc. **36**, 586 (1959).
20. J. L. MCLAUGHLIN and W. J. KERRED. J. Pharm. Sci. **61**, 147 (1972).
21. G. HAHN and F. RUMPF. Ber. **71B**, 2141 (1938).
22. O. M. FRIEDMAN, K. N. PARAMESWARAN, and S. BURSTEIN. J. Med. Chem. **6**, 227 (1963).
23. F. KROHNKE and A. SCHULZE. Chem. Ber. **75**, 1154 (1942).
24. H. AUTERHOFF and H. J. ROTH. Arch. Pharm. **289**, 470 (1956).
25. P. T. SOU. Bull. Fac. Sci. Univ. Fr-Chin. Peiping. **5**, 1 (1935); Chem. Abstr. **30**, 4463 (1936).
26. S. A. FINE, R. F. FREESE, and M. G. GREENE. J. Org. Chem. **38**, 2089 (1973).
27. K. IMAI, N. ARIZUMI, M. WANG, S. TOSHIUE, and Z. TAMUKA. Chem. Pharm. Bull. Tokyo. **20**, 2436 (1972).
28. K. D. CHARALAMPOUS and L. W. TANSEY. J. Pharm. Exp. Ther. **155**, 318 (1966).
29. B. T. HO, W. M. MCISAAC, R. AN, L. W. TANSEY, K. E. WALKER, L. F. ENGLERT, JR., and M. B. NOEL. J. Med. Chem. **13**, 26 (1970).

Can. J. Chem. Downloaded from www.nrcresearchpress.com by 210.87.254.42 on 09/05/12
For personal use only.

Some Metal Halide – Phosphorus Halide – Alkyl Halide Complexes. Part III. The μ-Trihalohexahalodimetallate Ions of Titanium and Zirconium

JOSEPH I. BULLOCK

The Joseph Kenyon Laboratory, Department of Chemistry, The University of Surrey, England

AND

FREDERICK W. PARRETT AND NICHOLAS J. TAYLOR[1]

Chemistry Department, Royal Military College of Canada, Kingston, Ontario K7M 2W3

Received January 9, 1974

JOSEPH I. BULLOCK, FREDERICK W. PARRETT, and NICHOLAS J. TAYLOR. Can. J. Chem. **52**, 2880 (1974).

Titanium tetrachloride reacts rapidly with trichloro-, tribromo- and methyldichlorophosphine in the presence of *t*-butyl chloride to give compounds containing a phosphonium cation $R^1R^2PX_2^+$ (R^1 = *t*-butyl, R^2 = chloride, bromide, or methyl, X = chloride or bromide) and the principal metal-containing anion, $Ti_2Cl_9^-$. For tribromophosphine and *t*-butyl chloride a stoichiometric product, $[Bu^tPBr_3][Ti_2Cl_9]$ was obtained which was characterized using vibrational spectroscopy. The other reactions gave non-stoichiometric materials, the sublimates of which may contain higher polymeric anions whilst the residues contained $TiCl_5^-$ along with the parent dimeric anion.

Zirconium tetrachloride and titanium tetrabromide reacted in a similar way to give the new ions $Zr_2Cl_9^-$ and $Ti_2Br_9^-$ in stoichiometric reactions.

JOSEPH I. BULLOCK, FREDERICK W. PARRETT et NICHOLAS J. TAYLOR. Can. J. Chem. **52**, 2880 (1974).

Le tétrachlorure de titane réagit rapidement avec les trichloro-, tribromo- et méthyldichlorophosphines en présence de chlorure de *t*-butyle pour donner des composés contenant un cation phosphonium $R^1R^2PX_2^+$ (R^1 = *t*-butyle, R^2 = chlorure, bromure ou méthyle, X = chlorure ou bromure) et le principal anion contenant un métal $Ti_2Cl_9^-$. Pour la tribromophosphine et le chlorure du *t*-butyle, on obtient un produit stoechiométrique $[Bu^tPBr_3][Ti_2Cl_9]$ qui est caractérisé par spectroscopie vibrationnelle. Les autres réactions donnent des substances non-stoechiométriques dont les produits de sublimation peuvent contenir des anions d'un degré de polymérisation plus élevé tandis que les résidus contiennent $TiCl_5^-$ avec l'anion dimère apparenté.

Le tétrachlorure de zirconium et le tétrabromure de titane réagissent d'une façon similaire pour donner des ions nouveaux $Zr_2Cl_9^-$ et $Ti_2Br_9^-$ dans des réactions stoechiométriques.

[Traduit par le journal]

Introduction

The anions (1, 2)[2] BCl_4^-, $AlCl_4^-$, $SnCl_5^-$, $NbCl_6^-$, $TaCl_6^-$, and WCl_6^- have been synthesized from the chlorides BCl_3, $AlCl_3$, $SnCl_4$, $NbCl_5$, $TaCl_5$, and WCl_6 by reaction with *t*-butyl chloride and a phosphorus(III) halide. The analogous reactions for titanium(IV) and zirconium(IV) chlorides are now presented in which μ-trichlorohexachlorodimetallate ions, $M_2Cl_9^-$, are formed. The titanium bromo-ion, $Ti_2Br_9^-$, is also reported. Previously (3), the phosphorane complex, $(C_6H_5)_2PCl_3$, $TiCl_4$, which may be $[(C_6H_5)_2PCl_2][TiCl_5]$, was prepared by refluxing a diphenyl phosphinodithionic acid, $(C_6H_5)_2P(S)SH$ and $TiCl_4$, in either chloroform or carbon tetrachloride. The anions $TiCl_5^-$, $TiCl_6^{2-}$, $Ti_2Cl_9^-$, and $Ti_2Br_9^-$ have been reported (4, 5) in the reactions of titanium (IV) halides with tetraethylammonium halide at the required molar ratios and $ZrCl_6^{2-}$ is known for zirconium (6).

Experimental

Purification of Reagents

Titanium tetrachloride, phosphorus tribromide, phosphorus trichloride, methyldichlorophosphine, *t*-butyl chloride, and *t*-butyl bromide were purified by fractional distillation in a stream of dry nitrogen. Carbon disulfide and isopentane were shaken with phosphorus pentoxide

[1]Present address: Chemistry Department, The University of Waterloo, Waterloo, Ontario.

[2]Reference 1 is part II of the series.

before distillation. Titanium tetrabromide and zirconium tetrachloride (99%) were used as supplied.

Preparations

The compounds were water sensitive so vacuum-line and glove-box techniques were employed for all preparations and manipulations.

The reactions with titanium tetrahalides were rapid and exothermic resulting in poor mixing of the reagents and localized reaction. Titanium tetrahalides were diluted with isopentane prior to adding slight excesses of the phosphorus halide and then the *t*-butyl halide. Precipitates formed quickly.

The compounds could not be recrystallized but sublimation significantly altered the composition of the titanium compounds. Samples for sublimation were heated in an evacuated all-glass apparatus and the sublimates collected in a cooled part of the system.

The use of large excesses of *t*-butyl chloride and phosphorus halide did not significantly suppress the formation of polymeric anions. For aluminum trichloride (2), a 10-fold excess of phosphorus trichloride was found necessary to prevent formation of such species as $Al_2Cl_7^-$ and yield a product containing only $AlCl_4^-$.

Zirconium tetrachloride was suspended in carbon disulfide.

All products were stored in sealed glass tubes.

Analyses

Experimental and theoretical results of analyses are set in table form as follows:

(*a*) Experimental results of product analyses

Component 1	Component 2	Results				Comments
		% M	% P	% Cl(Br)	M:P:Cl(Br)	
PCl_3	$TiCl_4$	16.7	4.7	68.5	2.3:1:12.8	
	$TiCl_4$	17.55	4.05	70.8	2.8:1:15.2	Sublimate
	$ZrCl_4$	26.45	4.5	61.4	2.0:1:11.95	
CH_3PCl_2	$TiCl_4$	16.6	5.1	66.5	2.1:1:11.4	
	$TiCl_4$	17.2	4.75	67.0	2.35:1:12.3	Sublimate
	$TiCl_4$	14.5	6.3	64.7	1.5:1:9.0	Residue
PBr_3	$TiCl_4$	12.95	4.15	43.0	2.0:1:9.0(3.0)	Br = 32.4%
	$TiBr_4$	8.25	2.7	83.4	2.0:1:12.0	

(*b*) Theoretical results of product analyses

Complex	Analysis				
	M	Amount (%)	Amount of P (%)	X	Amount (%)
$C_4H_9PTi_2Cl_{12}$	Ti	15.7	5.3	Cl	69.8
$C_4H_9PZr_2Cl_{12}$	Zr	26.2	4.45	Cl	61.15
$C_5H_{12}PTi_2Cl_{11}$	Ti	16.3	5.25	Cl	66.2
$C_4H_9PTi_2Cl_9Br_3$	Ti	12.9	4.15	Cl	42.95
				Br	32.2
$C_4H_9PTi_2Br_{12}$	Ti	8.35	2.7	Br	83.9

Spectroscopy

Raman spectra of the compounds in sealed capillary tubes were obtained using a Spex 1401 spectrometer with helium–neon excitation. The compounds were more stable than the corresponding tetraethylammonium salts (5) in the laser beam. Infrared spectra of Nujol mulls between potassium bromide or polythene plates were obtained using the Grubb Parsons Spectromaster (1000–400 cm^{-1}) and the R.I.I.C. FS-720 Interferometer (400–30 cm^{-1}).

The reactions did not yield single crystals and the products dissolved only in reactive solvents so that polarized Raman spectra could not be obtained.

Results and Discussion

The Cation Spectra

The C_{3v}, $Bu^tPCl_3^+$ cation with $\Gamma_{vib} = 3A_1$ (i.r., Raman) + $3E$ (i.r., Raman) and the C_s, $Bu^tMePCl_2^+$ cation with $\Gamma_{vib} = 6A'$ (i.r., Raman) + $3A''$ (i.r., Raman) were identified in similar reactions (1, 2) with other metal halides (the internal modes of the *t*-butyl group were ignored in assigning symmetry groups).

For BCl_3, $AlCl_3$, $SnCl_4$, $NbCl_5$, $TaCl_5$, and

WCl_6 the six modes for the $Bu^tPCl_3^+$ cation occurred in the following ranges.

Symmetry	Assignment	Frequency (cm^{-1})
A_1	νP—C	778–783
	νP—Cl sym	481–486
	δP—Cl_3	229–235
E	νP—Cl asym	632–648
	δBu^t—P—Cl	208–214
	δCl—P—Cl	154–159

The above values are self-consistent and correlate well with the results (7) for $MePCl_3^+$.

For $Bu^tMePCl_2^+$, strong anion vibrations usually obscured two of the deformation modes but the remaining seven and an *overtone* were consistently observed for $SnCl_4$, $NbCl_5$, $TaCl_5$, and WCl_6 complexes

Symmetry	Assignment	Frequency (cm^{-1})
A'	νP—C(Me)	796–803
	νP—C(Bu^t)	774–781
	δP—Cl(sym)	505–510
	δPCl_2	208–218
	δPCl_2 twisting } δBu^t—P—Me }	obscured
A''	νP—Cl asym	610–614
	δMe—P—Cl	248–260
	δBu^t—P—Cl	223–232
3x	δPCl_2 ?	620–635

Because of these observations, we felt justified in subtracting these vibrations from the observed spectra of the titanium and zirconium complexes and assigning the remainder to anion vibrations (Table 1).

TABLE 1. Vibrational *† assignments for $Bu^tPCl_3^+$ and $Bu^tMePCl_2^+$

(*i*) $Bu^tPCl_3^+$

$[Bu^tPCl_3][Ti_{2.3}Cl_{9.8}]$		$[Bu^tPCl_3][Zr_2Cl_9]$			
Raman	Infrared	Raman	Infrared	Mode	Assignments
	780vw		781vw	A_1	νP—C
485w	483mw	484m	482m		νP—Cl
235mw	233mw‡	232m	230sh		νP—Cl_3
	639s		639s	E	νP—Cl
212w	210w	212w	212wbr		δBu^t—P—Cl
	§		156wsh?		δCl—P—Cl

(*ii*) $Bu^tMePCl_2^+$

$[Bu^tMePCl_2][Ti_{2.1}Cl_{9.4}]$			
Raman	Infrared	Mode	Assignments
	796m	A'	νP—C(Me)
	774ms		νP—C(Bu^t)
	629ms		Overtone?‖
	610s	A''	νP—Cl
505w	506s	A'	νP—Cl
	250wsh	Deformations	
	228sh		
208w	212w		

*Anion vibrations omitted.
†R, i.r. results (cm^{-1}).
‡May be an anion vibration.
§Obscured by an anion vibration.
‖May also be a very mixed vibration although the observed intensity is variable.

For $Bu^tPBr_3^+$ it was necessary to compare our spectra with those of PBr_4^+ (8, 9). The T_d PBr_4^+ has four vibrational frequencies at 227 cm^{-1} (ν_1), 72 cm^{-1} (ν_2), 474 cm^{-1} (ν_3), and 140 cm^{-1} (ν_4). By analogy with $Bu^tPCl_3^+$ we would expect 6 vibrational frequencies for $Bu^tPBr_3^+$ which we have assigned as follows:

Mode	Assignment	Frequency (cm^{-1}) $[Bu^tPBr_3][Ti_2Cl_9]$	Frequency (cm^{-1}) $[Bu^tPBr_3][Ti_2Br_9]$
ν_1	A_1 νP—C	772w	769w
ν_2	νP—Br sym	260sh	260sh
ν_3	δPBr_3	168w	166w
ν_4	νP—Br asym	524vs	526ssh
			518s
ν_5	δBu^t—P—Br	144vw?	146w
ν_6	δBr—P—Br	—	123w

Thus ν_1, ν_2, ν_3, and ν_4 (PBr_4^+) correspond to ν_1, ν_6, ν_4, and ν_3 ($Bu^tPBr_3^+$) respectively but there was some doubt as to the assignment of ν_6 because of possible anion vibrations in that region. The νP—C vibrations of $Bu^tPX_3^+$ (X = Cl or Br) may well be similar and δBu^t—P—Br should be at a lower frequency than δBu^t—P—Cl. The last splits at low temperature in the i.r. spectrum eliminating the possibility that this might be the non-degenerable ν_3.

A number of combination bands based upon this cation are included in Table 2 for $[Bu^tPBr_3][Ti_2Br_9]$. These are symmetry allowed and confirm the assignments made for the cation fundamentals. These assignments have been verified (18) by the vibrational spectra of other complexes containing $Bu^tPBr_3^+$.

Anion Spectra

$[Bu^tPBr_3][Ti_2Cl_9]$

This was stoichiometric and the i.r. and Raman spectra (Tables 1 and 3) were assignable in terms of these ions only.

The i.r. spectrum (4) of the anion as the tetraethylammonium salt has absorptions at 416 vs, 379 vs, 268 m, 230 w, 188 w, 171 w, 74 w, and 57 cm^{-1}. There are no Raman spectra (4, 5). The ion has near D_{3h} symmetry (10) with the following i.r. and Raman active vibrations expected, $4A_1'(R) + 3A_2''$ (i.r.) $+ 5E'$ (i.r., R) $+ 4E''(R)$. These are subdivided to give: 4 terminal Ti—Cl stretches, $A_1' + A_2'' + E' + E''$; 4 bridge Ti—Cl stretches, $A_1' + A_2'' + E' + E''$; 6 terminal Ti—Cl deformations, $A_1' + A_2'' + 2E' + 2E''$; and 2 bridge Ti—Cl deformations, $A_1' + E'$.

Beattie *et al.* (11) have characterized the spectra of the D_{3h}, $Tl_2Cl_9^{3-}$ as the caesium salt using single crystal Raman, infrared, and normal coordinate analytic techniques. Both experimental and calculated results gave the order, $A_1'(R) > A_2''$(i.r.) $> E''(R) > E'$(i.r., R) for the terminal Tl—Cl stretching modes. These four were closely grouped (264–288 cm^{-1}) and it was pointed out that for such bridged species related Raman- and i.r.-active vibrations are likely to occur at closely similar frequencies without being true coincidences.

In the present case it was not possible to obtain polarized Raman spectra (see Experimental).

We observed three strong i.r.- and two strong and one weak Raman-active vibrations in the region expected for the Ti—Cl stretching modes. There were alternative assignments for these.

First, the highest frequency i.r. band (419 cm^{-1}) could be assigned to A_2'' apparently coincident with A_1' in the Raman spectrum (416 cm^{-1}). The other two i.r. bands (409 and 382 cm^{-1}) could be components of E', split by lowering of the crystal symmetry, with the corresponding E' Raman-active mode at 390 cm^{-1}. The weak Raman shift at 342 cm^{-1} could then be assigned E''. These assignments follow the pattern for $Tl_2Cl_9^{3-}$ although in our case the order of the E modes was reversed and the A modes were accidentally coincident.

Secondly, the i.r. bands at 419 and 409 cm^{-1} could be components of E' with the corresponding E' Raman shift at 416 cm^{-1}. The third i.r. absorption would then be assigned A_2'' and the remaining Raman bands to A_1' (390 cm^{-1}) and E'' (342 cm^{-1}). The splitting of the E' mode in the i.r. would be smaller in this case.

It was fairly clear that the highest Ti—Cl bridge stretching frequency was A_1' (R, 314 cm^{-1}) and the E' mode (i.r., 240 cm^{-1}) the lowest (Table 3) although there was some doubt as to the assignment of the other bridge stretching modes. A cation vibration may interfere.

For $Zr_2Cl_9^-$ we have assigned the highest frequency bands to A_1' and A_2'' terminal stretching modes (see below). This suggested

TABLE 2. (*i*) Vibrational spectrum for $[Ti_2Br_9^-]$*

Frequency (cm^{-1})			
Infrared	Raman	Assignments	
321vs	320vs		
316sh		$A_1' + A_2'' + E' + E''$	vTi—Br terminal
297m	294m	(see text)	
278wsh	280w		
244w	247wbr	E'(i.r., R)	
237w	—	A_2'' (i.r.)	vTi—Br bridging
—	224w	E''(R)	(see text)
—	198ms	A_1'(R)	
187m	—	A_2'' (i.r.)	
—	170w	A_1' (R)	
110w	110w	E' (i.r., R)	δTi—Br terminal
—	101w	E'' (R)	
94w	93w	E'(i.r., R)	
—	83s	E'' (R)	
—	71s	A_1' (R)	δTi—Br bridging
46w	48wsh	E' (i.r., R)	

*Cation vibrations omitted.

(*ii*) Infrared combination bands from $[Bu^tPBr_3^+]$*

Frequency (cm^{-1})	Combination mode	Note
893wbr	$\nu_1 + \nu_6$	(769 + 123 = 892)
812wbr	$\nu_3 + \nu_4 + \nu_6$	(166 + 522 + 123 = 811)
597mw	$\nu_1 - \nu_3$	(769 − 166 = 603)
476wsh	$2\nu_3 + \nu_5$	(2 × 166 + 146 = 478)
412mw	$\nu_2 + \nu_5$	(260 + 146 = 406)
390vw	$\nu_3 PBr_3$?	
380vw	$\nu_2 + \nu_6$	(260 + 123 = 383)
350vw	$\nu_4 - \nu_3$	(522 − 166 = 352)

that the preferred interpretation of the bands in $Ti_2Cl_9^-$ was that based upon the $Tl_2Cl_9^{3-}$ model. However, in the octahedral MCl_6^{2-} (M = Ti, Zr) the $\nu_1(A_{1g})$ and $\nu_3(T_{1u})$ modes of O_h are accidentally coincident for titanium but ν_1 clearly has the higher frequency for zirconium (6).

The remaining absorptions of $[Bu^tPBr_3][Ti_2Cl_9]$ were assigned as shown in Table 3.

The vibrational spectra were not interpretable in terms of the alternative product $[Bu^tPBr_2Cl][Ti_2Cl_8Br]$ which suggested that the mechanism of reaction involves the simple transfer of the components of the alkyl halide (12) rather than dissociation of the phosphorus halide (13) or a pre-equilibrium (14) involving the alkyl and phosphorus halides.

$[Bu^tPCl_3][Zr_2Cl_9]$

This new anion has been assigned the vibrational modes shown in Table 4. The spectra were much as expected for the D_{3h} model based upon the known structures of $Ti_2Cl_9^-$ and $Ti_2Cl_9^{3-}$ except that the assignments of the Zr—Cl terminal stretching E modes were reversed as was the case for the $Ti_2Cl_9^-$ ion. Weak shoulders in the i.r. spectra may correspond to the Raman allowed transitions. Splitting of the degenerate E modes was again observed in the i.r. spectra.

For the bridge stretching modes, A_1' and E' were at the highest and lowest frequencies, respectively. In this case, a cation band did not interfere and so we placed E'' at a higher frequency than A_2'' because of the clear coincidence which confirmed that the same may be true for $Ti_2Cl_9^-$ (Table 4).

$[Bu^tPBr_3][Ti_2Br_9]$

No μ-tribromohexabromodimetallate has been fully characterized using vibrational techniques. The stretching frequencies for the tetrahedral $TiBr_4$ are (15) 384 cm^{-1} (T_2) and 230 cm^{-1} (A_1). The totally symmetric stretching frequency (6) of $TiBr_6^{2-}$ is 190 cm^{-1}. For $Ti_2Cl_9^-$ the

TABLE 3. The vibrational spectrum of $(Bu^tPBr_3)(Ti_2Cl_9)$ (cm^{-1})

Infrared frequency			
Room temperature	Low temperature	Raman	Assignments
772vw		774vw	ν_1
631vwbr			$\nu_1 - \nu_5$
598mw		594vw	$\nu_1 - \nu_3$?
524vs		523vw	ν_4
330wbr			$2\nu_3$? } $Bu^tPBr_3^+$
260sh	261m	259m	ν_2
168w	167vwsh	164m	ν_3
144vw	144vw		ν_5
		124m	ν_6 ?
419vs	424vs	416vs	$A_1' + A_2'' + E' + E''$
409vs	412s		
		390m	νTi—Cl terminal (see text)
382s	384ms		
		342wsh	
		314m	A_1' (R)
296vwsh	294wsh	296sh	E'' (R) } νTi—Cl bridging
275m	281m		A_2''(i.r.) } (see text)
240sw	241wbr	234w	E'(i.r., R)
234wsh			
188mw	189w	187vw	E'(i.r., R)
179w	180wsh		A_2'' (i.r.)
		140s	A_1' (R) } δTi—Cl terminal
		124	E'' (R) ?
109vw	112vw	108m	E' (i.r., R)
		81wsh	E'' (R)
		77w	A_1' (R)
69vw		68w	E' (i.r., R) } δTi—Cl bridging
		64mw	
210vwbr	214w	207vw	?
	207wsh		
54w	56w		?

TABLE 4. The vibrational spectra of $(Zr_2Cl_9^-)$ (cm^{-1})*

Infrared frequency			
Room temperature	Low temperature	Raman	Assignments
387msh	387wsh	386vs	A_1'(R)
	378msh		} Zr—Cl terminal
375vs	370s		A_2''(i.r.) } (see text)
366vs	362ssh	366mbr	E' (i.r., R)
359vs	356msh		
—	—	350m	E''(R)
315w	—	315ms	A_1'(R)
—	—	268mw	E''(R) } Zr—Cl bridging
257ms	259ms	—	A_2''(i.r.)
247msh	250msh	246mbr	E'(i.r., R)
240wsh	240wsh		
—	—	177ms	A_1'(R)
160m	160m	160mw	E' (i.r., R)
144m	144m	—	A_2''(i.r.) } Zr—Cl terminal
121w	121w	120s	E'(i.r., R)
—	—	109w	E'' (R)
—	—	76mbr	E'' (R)
—	—	87s	A_1'(R) } Zr—Cl bridging
54vw	54vw	40mbr	E' (i.r., R)

*Cation vibrations omitted.

TABLE 5. Vibrational spectra of the unsublimed titanium complexes (cm^{-1})*

Frequency (cm^{-1})						
$[Bu^tPCl_3][Ti_{2.3}Cl_{9.8}]$			$[Bu^tMePCl_2][Ti_{2.1}Cl_{9.4}]$			
Infrared			Infrared			
Room temperature	Low temperature	Raman	Room temperature	Low temperature	Raman	Assignment
417vs	425s	422vs	426vs	424vs	418vs	$A_1' + A_2'' + E' + E''$ vTi—Cl terminal (see text)
	410s		412vs	406vs		
—	—	394m	—	392s	392m	
378vs	386s	—	380vs	382vs	—	
—	358sh	353w	360wsh	360vw	358vw	
—	—	322m	315vw	314vw	317m	A_1' (R)
—	—	302wsh	—	—	296wsh	E'' (R)
276s	278s	—	274vs	278vs	—	A_2''(i.r.)
233mw	252mw	255wsh	250wsh	250wsh	246wsh	E'(i.r., R) vTi—Cl bridging
	242mw	235mw	240mbr	241mbr	235mw	
188w	187wbr	191wsh	186m	186mbr	192vw	E'(i.r., R)
179w	178w	—	180wsh	180wsh	—	A_2''(i.r.)
—	144vw	145s	144vw	144vw	140s	A_1'(R)
—	—	129m	—	121vw	124w	E''(R) δTi—Cl terminal
—	108vw	—	—	109vw	110w	E'(i.r., R)
—	—	—	—	100vw	101w	
—	—	—	—	92vw	92w	E''(R)
					87w	
—	76vw	79w	—	—	75w	A_1' (R) δTi—Cl bridging
64w	64wbr	—	68vw	63wbr	—	E'(i.r., R)

*Cation vibrations omitted.

terminal stretching modes were at lower frequencies than the asymmetric stretching frequency (16) of $TiCl_4$ (499 cm^{-1}) but at higher frequencies than the totally symmetric stretching frequencies of $TiCl_6^{2-}$ (320 cm^{-1}, ref. 6) and $TiCl_4$ (388 cm^{-1}, ref. 16). Much the same is true for the zirconium chloride system: $ZrCl_4$, 421 and 388 cm^{-1} (17); $ZrCl_6^{2-}$, 321 cm^{-1} (6); $Zr_2Cl_9^-$ 350–387 cm^{-1} (see above). Assuming that similar relationships hold for $Ti_2Br_9^-$ we may expect the terminal stretching modes to occur near 300 cm^{-1}. The only previous report of spectra for the $Ti_2Br_9^-$ ion is an i.r. spectrum of $[Et_4N][Ti_2Br_9]$ where strong bands at 325 and 278 cm^{-1} were assigned to Ti—Br terminal stretching (5). Our tentative assignments of these bands in our compound are discussed from considering our Raman data.

For $Ti_2Br_9^-$ we again encountered the difficulties found for $Ti_2Cl_9^-$ in that the terminal Ti—Br stretching frequencies (Table 2) occur at closely similar positions. A Raman-active mode A_1' should possibly be at the highest frequency. Two bands in the i.r. (321 cm^{-1}, vs) and the Raman (320 cm^{-1}, vs) spectra appeared to be coincident and it was tempting to assign these to the E' mode. Following this, an absorption at 279 cm^{-1} (m) in the i.r. spectrum may correspond to the observed Raman shift at 294 cm^{-1}. In D_{3h} symmetry this (A_1') is i.r.-forbidden. We would then obtain the order: E' (i.r., Raman) 321 and 316(sh) cm^{-1}, 320 $cm^{-1} > A_2''$ (i.r.) 288 $cm^{-1} > A_1'$ (Raman) 294 cm^{-1} (allowed in i.r. at 297 cm^{-1} by breakdown of D_{3h}) $> E''$ (Raman) 280 cm^{-1} (weak shoulder in i.r. at 278 cm^{-1}).

Alternatively, using the $Tl_2Cl_9^{3-}$ pattern the assignments would be: A_1' (Raman) 320 $cm^{-1} \simeq A_2''$ (i.r.) 321 cm^{-1}, (sh, 316 cm^{-1}) $> E'$ (i.r., Raman) 297 and 288 cm^{-1}, 294 $cm^{-1} > E''$ (Raman) 280 cm^{-1}.

These possibilities cannot be distinguished in the absence of polarized Raman results.

Similar problems occurred in the assignment of the Ti—Br bridges stretching modes in that the strongest band in the Raman spectrum (198 cm^{-1}) was not the highest frequency transition observed in the likely bridge stretching region. Again, it is possible that the E modes are at higher energy than the A (Table 2).

Possible assignments for the bending modes are also given in Table 2.

The Non-stoichiometric Chloro-complexes

It was not possible to obtain a stoichiometric product using *t*-butyl chloride, phosphorus trichloride (or methyldichlorophosphine), and titanium tetrachloride (see Experimental).

The spectra of the unsublimed materials were very similar to those of $[Bu^tPBr_3][Ti_2Cl_9]$ and so we allocated the absorptions shown in Table 5. The assignments of the terminal and bridge stretching modes were ambiguous (see above).

The chemical analyses of the parent compounds and their sublimates suggested that more than two titanium atoms per phosphorus atom were present. If small amounts of trimeric or higher polymeric anions were present they would not be detected necessarily by vibrational spectroscopy, since the vibrational frequencies would be very close to those of $Ti_2Cl_9^-$. The titanium-to-phosphorus ratio increased in the sublimates but no difference in the spectra was observed except for an absorption at 495 cm^{-1} which appeared in the i.r. spectrum. This could be ν_3, $TiCl_4$. For the tin compounds some decomposition to give $SnCl_4$ was noted (2) in the laser beam and a similar process may have occurred here. Some vibrational bands of residues are due to $Ti_2Cl_9^-$ but they have medium intensity absorption at 388 and 348 cm^{-1} in the i.r. spectra with a Raman-active coincidence at 348 cm^{-1}. The i.r. spectrum (4) of $[(C_2H_5)_4N][TiCl_5]$ has strong bands at 385 cm^{-1} and 346 cm^{-1} which were assigned to ν_5, E'(i.r., R) and ν_3, A_2'' (i.r.) modes respectively of the trigonal bipyramidal $TiCl_5^-$. We suggest our residues contained $TiCl_5^-$ and the assignments were reversed because of the Raman-active coincidence. The analytical results require a titanium to phosphorus ratio of less than 2 so that a monomeric titanium species is likely to occur.

The unsublimed materials contained $Ti_2Cl_9^-$ as the major anion although excesses of the organic reagents were used. The ready formation of $Ti_2Cl_{10}^{2-}$, $Ti_2Cl_9^-$, $TiCl_5^-$, and $TiCl_6^{2-}$ was reported (4, 5, 10) for reactions with titanium (IV) chloride and quaternary chlorides at the required molar ratios. Our reactions generated products which were chlorine deficient with respect to the highest reported chloro-species. Thus, there was no evidence for $TiCl_6^{2-}$ or $Ti_2Cl_{10}^{2-}$ and $TiCl_5^-$ was only synthesized as a minor component of a thermolysis reaction. A similar result was found (2) for $SnCl_4$.

This work was supported in part by grants from the Science Research Council and the Defence Research Board of Canada (Grant No. 9530–102).

1. J. I. BULLOCK, F. W. PARRETT, and N. J. TAYLOR. J. Chem. Soc. Dalton, 522 (1973).
2. J. I. BULLOCK, F. W. PARRETT, and N. J. TAYLOR. J. Chem. Soc. Dalton, 1843 (1972).
3. W. E. BACON. French patent 1451986, Sept. 1966.
4. J. A. CREIGHTON and J. H. S. GREEN. J. Chem. Soc. A, 808 (1968).
5. R. J. H. CLARK and M. A. COLES. J. Chem. Soc. Dalton, 2454 (1972).
6. W. VAN BRONSWYK, R. J. H. CLARK, and L. MARESCA Inorg. Chem. **8**, 1395 (1969).
7. I. R. BEATTIE, K. LIVINGSTON, and T. R. GILSON. J. Chem. Soc. A, 1, (1968).
8. A. MULLER and A. FADINI. Z. Anorg. Chem. **349**, 164 (1967).
9. H. GERDING and P. C. NOBEL. Rec. Trav. Chim. **77**, 472 (1958).
10. T. J. KISTENMACHER and G. D. STUCKY. Inorg. Chem. **10**, 122 (1971).
11. I. R. BEATTIE, T. R. GILSON, and G. A. OZIN. J. Chem. Soc. A, 2765 (1968).
12. J. A. CADE. Tetrahedron, **2**, 322 (1958).
13. G. LINDER and P. O. GRANBOM. Acta Chem. Scand. **20**, 432 (1966).
14. J. P. CLAY. J. Org. Chem. **16**, 892 (1951).
15. F. A. MILLER and G. L. CARLSON. Spectrochim. Acta. **16**, 6 (1960).
16. N. J. HAWKINS and D. R. CARPENTER. J. Chem. Phys. **23**, 1700 (1955).
17. J. K. WILMSHURST. J. Mol. Spectrosc. **5**, 343 (1960).
18. N. J. TAYLOR. Unpublished results.

On the Mechanism of Quenching by Amines: A New Method for Investigation of Interactions with Triplet States[1]

ROBERT H. YOUNG,[2] D. BREWER, R. KAYSER, R. MARTIN, AND D. FERIOZI
Chemistry Department, Georgetown University, Washington, D.C.
AND
RICHARD A. KELLER
National Bureau of Standards, Gaithersburg, Maryland 20234
Received January 8, 1974

ROBERT H. YOUNG, D. BREWER, R. KAYSER, R. MARTIN, D. FERIOZI, and RICHARD A. KELLER. Can. J. Chem. **52**, 2889 (1974).

Rate constants for the quenching of singlet oxygen by a series of substituted *N,N*-dimethylanilines were obtained by a direct method employing a dye-laser. The Hammett ρ value obtained from the data (−1.71) suggests that a (partial) charge-transfer complex may be responsible for the quenching action. This rate data was combined with that obtained for the total quenching action on the sensitized photooxidation of 1,3-diphenylfuran. The quenching action on the photooxidation reaction is due to both the quenching of singlet oxygen and the quenching of the triplet state of the sensitizer (rose bengal or methylene blue). The combination of the data from each series of experiments resulted in rate constants of quenching of the triplet states of the sensitizers. A number of the *N,N*-dimethylanilines quenched the triplet states at the diffusion limit. Hammett ρ values (−1.86 for rose bengal and −4.19 for methylene blue) indicate that charge-transfer intermediates are probably responsible for the quenching action. This was confirmed by the observation of a transient intermediate assigned to the charge-transfer radical of methylene blue. The technique used here represents a novel approach to the investigation of triplet states.

ROBERT H. YOUNG, D. BREWER, R. KAYSER, R. MARTIN, D. FERIOZI, et RICHARD A. KELLER. Can. J. Chem. **52**, 2889 (1974).

Utilisant une méthode directe faisant appel à un laser à colorant, on a obtenu les constantes de vitesse de piégeage de l'oxygène à l'état singulet par une série de *N,N*-diméthylanilines. La valeur de −1.71, évaluée à partir de ces résultats comme constante rho d'Hammett, suggère que le piégeage est causé par un complexe de transfert (partiel) de charge. On a combiné les valeurs obtenues pour ces vitesses de réaction avec celles obtenues pour le piégeage total de la photooxydation sensibilisée du diphényl-1,3 furanne. Le piégeage de la réaction de photooxydation est dû à l'effet combiné de piégeage de l'oxygène à l'état singulet et de l'état triplet du sensibilisateur (rose de Bengale ou bleu de méthylène). La combinaison des résultats obtenus dans chaque série d'expériences conduit aux constantes de vitesse de piégeage des états triplets des sensibilisateurs. Un certain nombre de *N,N*-diméthylanilines piègent les états triplets à la limite de diffusion. Les valeurs des constantes rho d'Hammett (−1.86 pour le rose de Bengale et −4.19 pour le bleu de méthylène) indiquent que les intermédiaires du transfert de charge sont probablement responsables pour l'effet de piégeage. Cette conclusion est confirmée par l'observation d'un intermédiaire de courte durée de vie attribué au radical de transfert de charge du bleu de méthylène. La technique utilisée ici représente une nouvelle approche pour l'étude des états triplets. [Traduit par le journal]

Introduction

The number of review articles on singlet oxygen chemistry over the past few years (1) aptly illustrates the increase in the understanding of the interactions between excited states and oxygen. Recently, Kearns and co-worker (2) and Wilkinson and co-worker (3) independently developed a flash technique for the determination of the lifetime of singlet oxygen in solution. We have modified this method to obtain the lifetime of singlet oxygen in a number of solvents (4) and have applied it to the determination of abso-

[1]Presented in part at the 55th C.I.C. Conference, Quebec, P.Q. Canada, June 1972 and at the W. A. Noyes, Jr., Symposium, Austin, Texas, November 1972.

[2]To whom correspondence should be addressed. Present address: Union Carbide Chemicals and Plastics, 1 River Road, P.O. Box 670, Bound Brook, New Jersey 08805.

Can. J. Chem. Downloaded from www.nrcresearchpress.com by 210.87.254.40 on 09/05/12
For personal use only.

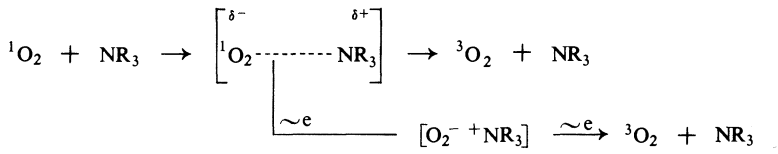

lute rate constants of quenching of singlet oxygen by various acceptors and quenchers, including a series of *N*,*N*-dimethylanilines. This method involves the measurement of the effect of an added quencher on the lifetime of singlet oxygen. The results are not affected by possible interactions between the quencher and the sensitizer excited states, a problem previously encountered (5).

We have rationalized that a comparison of these data with the rate of quenching of a photooxidation reaction (dependent on the quenching of both singlet oxygen and excited state(s) of the sensitizer) should yield rate constants for the quenching of the sensitizer excited state(s). This would be the triplet state, provided there was no significant interaction by the anilines used with the singlet state of the sensitizer. This was shown to be true as there was little fluorescence quenching of the singlet state of rose bengal (5).

This comparative technique is unique in that rate constants can be obtained for triplet state quenching by measuring the combined effective quenching of the triplet state and singlet oxygen and comparing the results with singlet oxygen quenching only. Other methods, including stationary and flash photolytic techniques, have been used to explore interactions between various compounds and triplet states. These methods do not have general applicability and at times require extensive instrumentation. Perhaps the best method is measurement of the decay of triplet–triplet absorption as a function of quencher concentration. However, not all triplets have easily discernible triplet–triplet absorption bands and in some cases the photolytic products obscure the absorption band(s). This was particularly true for the investigation of the interaction between methylene blue (and similar dyes) and amines. For this reason the present technique was developed to overcome these difficulties. It represents a simple method for investigation of triplet state – quencher interactions. In addition, the results obtained in this study provide confirmation for some previous work which involved the use of a much less sophisticated technique (5, 6).

Discussion

Quenching of Singlet Oxygen

Evidence is increasing to indicate that the mechanism for the quenching of singlet oxygen by amines involves a charge-transfer (7) or partial charge-transfer intermediate (8). The best evidence for this is through the correlation of the log of the rate constant for quenching of singlet oxygen by various amines and the ionization potential for the amines in both the gas phase (7*b*) and in solution (8).

In addition, there is some evidence (9) that the mechanism of the quenching of singlet oxygen by amines is similar to the amine quenching of other excited singlet states which have also been postulated to proceed by charge-transfer intermediates (10).

We have previously obtained a Hammett substituent effect for the quenching of the first excited singlet state of a series of substituted naphthalenes by diazobicyclooctane (DABCO) ($\rho = -2.24 \pm 0.11$) and other amines (9). This Hammett ρ indicates a moderate charge-transfer as measured by the acceptor species. In order to further investigate the interaction between

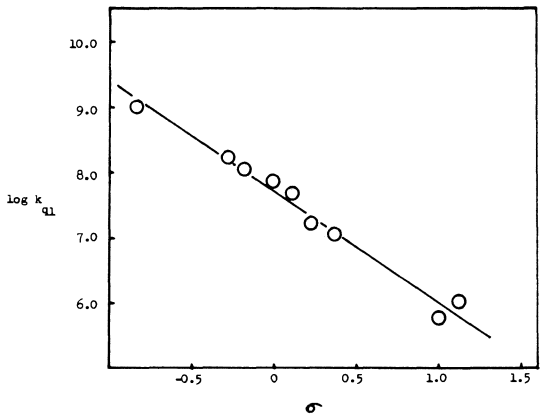

FIG. 1. Hammett plot for the quenching of singlet oxygen by substituted *N*,*N*-dimethylanilines.

Can. J. Chem. Downloaded from www.nrcresearchpress.com by 210.87.254.40 on 09/05/12
For personal use only.

amines and excited states, rate constants were obtained for quenching of singlet oxygen by a series of *N,N*-dimethylanilines. These results were obtained by the direct determination (see ref. 4 for method) of the effect of each substituted *N,N*-dimethylaniline on the lifetime of singlet oxygen in methanol and agree very well with those obtained by a less direct method (5).

A Hammett substituent plot of $\log k_q$ *vs.* σ (σ^- for *p*-CHO and *p*-CN) is given in Fig. 1. σ^- values were used for the last two anilines and indicate the extensive ground state stabilization of the amine by these two substituents. The slope of the Hammett plot was found to be -1.71 ± 0.22 (previous result -1.4 by less direct method) (5). This is a moderate slope and indicates a partial charge-transfer complex may be involved in the quenching of singlet oxygen. This confirms previous suggestions that the complex responsible for quenching of singlet oxygen is charge-transfer in nature (8). The contribution of such a state would perturb the singlet state

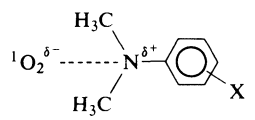

so as to cause increased singlet–triplet interaction and hence enhance intersystem crossing. The extent of the charge-transfer contribution is reflected in the rate constants for quenching and is affected by changes in the substituents of the *N,N*-dimethylanilines.

Quenching of Triplet States by N,N-Dimethylanilines

The mechanism of the quenching of the photooxidation reaction of 1,3-diphenylisobenzofuran, DPBF, is illustrated in the following scheme:

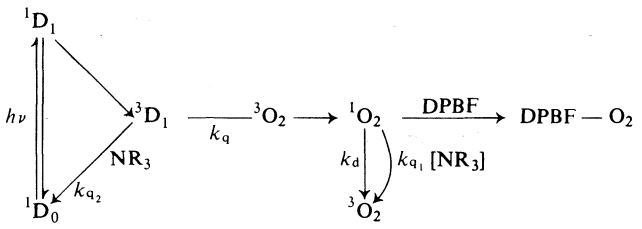

where D is the sensitizer (rose bengal or methylene blue).

A combination of the results from the quenching of singlet oxygen by the *N,N*-dimethylanilines with the effect of these anilines on both the triplet state of the sensitizer *and* singlet oxygen, in a sensitized photooxidation reaction of 1,3-diphenylisobenzofuran, yields the rate constant for quenching of the triplet state (Table 1). As can be seen from these results, the quenching action of the triplet states of rose bengal and methylene blue is very rapid by most *N,N*-dimethylanilines. In fact, for a number of anilines the rate constant probably approximates the rate of diffusion. This is especially noticed when Hammett plots are made by plotting the log of the rate constants of quenching *vs.* the appropriate σ constants (see Fig. 2). Although the rate constants of quenching of the triplet state of rose bengal and methylene blue approach the rate constant of diffusion for a number of the anilines, those that remain were used to calculate Hammett ρ values (-1.86 for rose bengal and -4.19 for methylene blue). These values indicate, especially for methylene blue, that a charge-transfer intermediate may be responsible for the quenching action of the triplet states by the *N,N*-dimethylanilines.

These results are substantiated by the evidence presented by Cohen and co-worker (11). They found that the triplet state of fluorenone was quenched by a series of substituted *N,N*-dimethylanilines. They suggested that this quenching action was a result of a charge-transfer intermediate between the anilines and the triplet excited state. Their results gave a Hammett ρ value of -1.83 (using σ^+) or -2.6 (using σ). The results of Cohen and co-worker can be compared to those obtained by ourselves and it appears that there is a higher charge-transfer interaction between methylene blue and the *N,N*-dimethylanilines than for either rose bengal or fluorenone. This is indicated by the higher Hammett ρ value obtained with methylene blue. The higher rate constants obtained for the quenching of the methylene blue triplet suggests that the rate of quenching is proportional to the degree of charge-transfer in the intermediate. This has

Can. J. Chem. Downloaded from www.nrcresearchpress.com by 210.87.254.40 on 09/05/12
For personal use only.

TABLE 1. Rate constants for the quenching of singlet oxygen and the triplet states of rose bengal and methylene blue by anilines X—C$_6$H$_4$—N(CH$_3$)$_2$

X	σ*	Singlet oxygen $k_q \times 10^{-8}$(s^{-1} M^{-1})†	Triplet states: Rose bengal $k_{q_2} \times 10^{-8}$(s^{-1} M^{-1})	Triplet states: Methylene blue $k_{q_2} \times 10^{-8}$(s^{-1} M^{-1})
p-N(CH$_3$)$_2$	−0.83	10 ±2	26	37
p-OCH$_3$	−0.27	1.8 ±0.4	28	110
p-CH$_3$	−0.17	1.2 ±0.4	23	88
H	0.00	0.73 ±0.08	7.5	86
m-OCH$_3$	0.12	0.48 ±0.04	3.9	82
p-Br	0.23	0.17 ±0.04	2.8	32
m-Cl	0.37	0.11 ±0.01	1.2	4.2
p-CN	1.00 (σ$^-$)	0.0057±0.001	0.22	0.13
p-CHO	1.13 (σ$^-$)	0.012 ±0.006	—	—

*Reference 14.
†Errors expressed to a 95% confidence level.

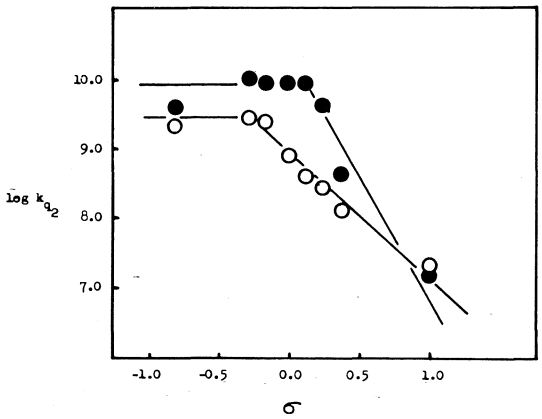

FIG. 2. Hammett plots for the quenching of triplet states of rose bengal (○) and methylene blue (●) by substituted *N*,*N*-dimethylanilines.

been substantiated by ourselves and others (12) by the observation of a transient charge-transfer species, $\lambda_{abs} \sim 420$ nm, from the methylene blue triplet. This absorption band is assigned to the semiradical form of methylene blue. We are investigating these results further.

Conclusions

This paper illustrates a novel and useful technique for investigation of triplet states with specific triplet state quenchers. The method was applied to two dyes, rose bengal and methylene blue, although it should be applicable to any other compound which acts as a singlet oxygen ($^1\Delta_g$) sensitizer. The rate constants of interaction between singlet oxygen and a series of *N*,*N*-dimethylanilines gave results which were comparable to those obtained by a less direct method (Hammett $\rho = -1.7$ *vs.* -1.4). In addition, the method was used to obtain improved rate constants for the quenching of the triplet state of rose bengal by the *N*,*N*-dimethylanilines and to obtain the rate constants of interaction with the triplet state of methylene blue which was not previously possible (5). Comparison of the results of these triplet state interactions show significant differences which are probably due to the differences in reduction potentials of the triplet states.

Experimental

N,*N*-Dimethylaniline and *p*-bromo-*N*,*N*-dimethylaniline were obtained commercially (Fisher). All other *N*,*N*-dimethylanilines were prepared, as outlined by Vogel (13), from the appropriately substituted aniline. All compounds were purified by one or more distillations and checked by n.m.r.

The method used to obtain the rate constants for the quenching of singlet oxygen by the *N*,*N*-dimethylanilines is given in detail in ref. 4. The method used to measure the effect of each *N*,*N*-dimethylaniline on the quenching of the photooxidation reaction of 1,3-diphenylisobenzofuran was similar to that given in detail in ref. 6.

The following equation was used to calculate the rate constants (K_{q_2}) of triplet state interaction (see ref. 5):

$$\frac{S_0}{S_{NR_3}} \times \frac{1}{\left(1 + \frac{k_{q_1}}{k_d}[NR_3]\right)} = 1 + \frac{k_{q_2}[NR_3]}{k_q[^3O_2]}$$

where S_0 is the slope of the first order decay plot for the photooxidation reaction of DPBF, and S_{NR_3} is the slope of the first order reaction plot for the photooxidation

Can. J. Chem. Downloaded from www.nrcresearchpress.com by 210.87.254.40 on 09/05/12
For personal use only.

reaction of DPBF with different concentrations of amine (NR_3). The rate constant of decay of singlet oxygen in the methanol solvent has been obtained previously ($k_d = 9.0 \times 10^4\ s^{-1}$).[4]

The rate constants of quenching of the triplet states of the sensitizers (rose bengal or methylene blue) by oxygen were measured by observing the pseudo-first order decay of the triplet–triplet absorption band (λ_{abs} 390 nm for rose bengal and λ_{abs} 400 nm for methylene blue triplets) in a solution of known oxygen concentration. The triplet states of the sensitizers were generated and monitored using the flash system described in ref. 4. The oxygen concentration of the solutions was varied by shaking the solutions with nitrogen–oxygen mixtures containing known pressures of oxygen. The rate constants which were obtained are the averages of three or more measurements ($k_q = 1.36 \times 10^9\ s^{-1}\ M^{-1}$ for rose bengal and $k_q = 2.70 \times 10^9\ s^{-1}\ M^{-1}$ for methylene blue).

1. (*a*) K. Golnick. Adv. Photochem. *Edited by* Noyes, Hammond, and Pitts, Interscience, New York. 1969. p. 1; (*b*) C. S. Foote. Acc. Chem. Res. **1**, 104 (1968); (*c*) D. R. Kearns. Chem. Rev. **71**, 395 (1971); (*d*) Ann. N.Y. Acad. Sci. **171**, 1–302 (numerous papers) (1970).
2. P. B. Merkel and D. R. Kearns. Chem. Phys. Lett. **12**, 120 (1971).
3. D. R. Adams and F. Wilkinson. J. Chem. Soc. Faraday Trans. II, 586 (1972).
4. R. H. Young, D. Brewer, and R. A. Keller. J. Am. Chem. Soc. **95**, 375 (1973).
5. R. H. Young, R. L. Martin, D. Feriozi, D. Brewer, and R. Kayser. Photochem. Photobiol. **17**, 233 (1973).
6. R. H. Young, K. Wehrly, and R. L. Martin. J. Am. Chem. Soc. **93**, 5774 (1971).
7. (*a*) C. Ouannes and T. Wilson. J. Am. Chem. Soc. **90**, 6527 (1968); (*b*) E. A. Ogryzlo and C. W. Tang. J. Am. Chem. Soc. **92**, 5034 (1970); (*c*) C. S. Foote, R. W. Denny, L. Weaver, Y. Chang, and J. Peters. Ann. N.Y. Acad. Sci., **171**, 139 (1970).
8. R. H. Young, R. L. Martin, K. Wehrly, and D. Feriozi. Symposium on Singlet Oxygen, 162nd A.C.S. Meeting, Washington, D.C., Pet. Paper #31, 1972.
9. R. H. Young and R. L. Martin. J. Am. Chem. Soc. **94**, 5183 (1972).
10. (*a*) T. R. Evans. J. Am. Chem. Soc. **93**, 2081 (1971); (*b*) A. Nakajima and H. Akamatu. Bull. Chem. Soc. Jap. **41**, 1961 (1968); (*c*) A. Nakajima and H. Akamatu. Bull. Chem. Soc. Jap. **42**, 3030 (1969).
11. S. G. Cohen and G. Parsons. J. Am. Chem. Soc. **92**, 7603 (1970).
12. H. E. A. Kramer and A. Maute. Photochem. Photobiol. **15**, 7 (1972).
13. A. I. Vogel. Practical organic chemistry. 3rd ed. Wiley, New York, 1956. p. 572.
14. J. March. Advanced organic chemistry. McGraw-Hill, New York. 1968. p. 241.

Can. J. Chem. Downloaded from www.nrcresearchpress.com by 210.87.254.40 on 09/05/12
For personal use only.

Nouvelle voie d'accès aux β-cétophosphonates γ,δ-éthyléniques

GILBERT PEIFFER

Institut Universitaire de Technologie de Marseille, Rue des Géraniums – 13337 Marseille Cedex 3, France

ET

PIERRE COURBIS

Ecole Supérieure de Chimie de Marseille, Traverse de la Barasse – 13013 Marseille, France

Reçu le 25 février, 1974

GILBERT PEIFFER et PIERRE COURBIS. Can. J. Chem. **52**, 2894 (1974).

L'addition d'alcools aux phosphonates ényniques $(RO)_2—P(=O)—C\equiv C—C(R_1)=CH—R_2$ en présence de trifluorure de bore, conduit avec des rendements pouvant atteindre 70% à une nouvelle famille de cétophosphonates éthyléniques, les β-cétophosphonates γ,δ-éthyléniques.

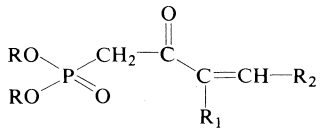

Que l'on parte des isomères *Z* ou *E* des dérivés ényniques, on obtient dans tous les cas étudiés le cétophosphonate *E*. Les moments dipolaires de ces deux familles de composés ont été mesurés.

GILBERT PEIFFER and PIERRE COURBIS. Can. J. Chem. **52**, 2894 (1974).

The addition of enynic phosphonates $(RO)_2—P(=O)—C\equiv C—C(R_1)=CH—R_2$ to alcohols in the presence of boron trifluoride, leads to γ,δ-ethylenic β-ketophosphonates.

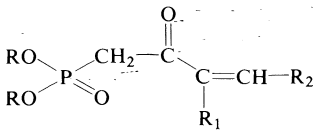

Yields of 70% have been obtained. Whether *Z* or *E* enynic derivates are starting materials the *E* ketophosphonate is obtained in both cases. The dipole moments of both families of compounds have been measured.

L'étude de la réactivité de l'enchaînement énynique conjugué a fait l'objet de nombreux travaux. En ce qui concerne l'addition des alcools, en présence de trifluorure de bore, les résultats ne sont pas toujours concordants. Ainsi Favorskaya et ses collaborateurs (1–3) isolent dans la plupart des cas des dérivés de di- et de triaddition **1** et **2**

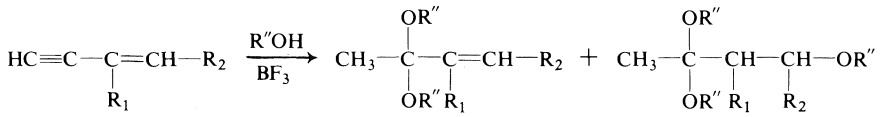

1 **2**

Reprenant une telle étude, l'un d'entre nous (4) a montré qu'il se formait à côté de ces composés, des dérivés de la bicyclo[2,2,2]-octanone-2 **3**, avec des rendements voisins de 80%. Compte tenu de ces résultats, nous pensions pouvoir accéder aux composés **4**

Can. J. Chem. Downloaded from www.nrcresearchpress.com by 210.87.254.5 on 09/05/12
For personal use only.

TABLEAU 1. Constantes physiques des phosphonates énynes $(RO)_2P(=O)-C\equiv C-C(R_1)=CHR_2$

Nature des groupements				Point d'ébullition			
R	R_1	R_2	Isomère	(°C/mmHg)	n_d^t	d_4^t	Rendement (%)
CH_3	CH_3	H		71/0.1	1.4760/21	1.130/21	52
C_2H_5	CH_3	H		110/2	1.4670/23	1.063/23	32
CH_3	C_2H_5	H		80/0.2	1.4818/24	1.121/24	54
C_2H_5	C_2H_5	H		82/0.1	1.4702/25	1.042/25	60
CH_3	CH_3	CH_3	*Z*	81/0.1	1.4855/24	1.100/24	30
C_2H_5	CH_3	CH_3	*Z*	86/0.1	1.4753/23	1.043/23	58
CH_3	CH_3	CH_3	*E*	92/0.2	1.5093/23	1.196/23	52
C_2H_5	CH_3	CH_3	*E*	102/0.2	1.4810/20	1.069/20	52
C_2H_5				147/0.05	1.5030/23	1.106/23	77

par condensation d'éthanol sur des phosphonates ényniques:

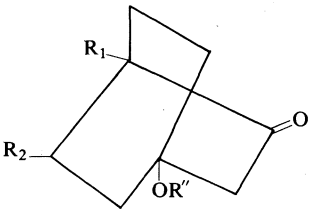

3

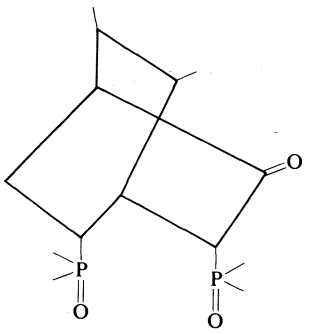

4

En fait la réaction évolue différemment et conduit avec un rendement pouvant atteindre 70% à une nouvelle famille de cétophosphonates éthyléniques, les β-cétophosphonates γ,δ-éthyléniques **5**:

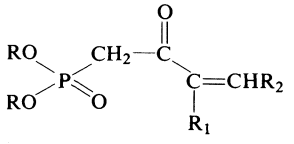

5

Ce résultat présente un certain intérêt, d'autant plus que, comme l'a montré Sturtz *et al.* (5), l'oxydation des phosphonates ényniques en présence d'ions mercuriques ne conduit pas au produit normalement attendu. Il est à noter cependant que l'utilisation de l'éthylèneglycol conduit non pas à un cétophosphonate mais à l'acétal correspondant **6**

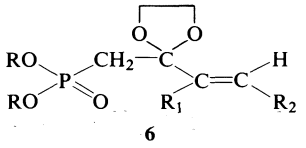

6

Les travaux de Bertrand et Monti (6, 7) relatifs à la préparation de dérivés cyclopropaniques par addition d'éthylèneglycol aux énynes conjugués suivi d'une réaction de Simmons Smith (11, 12), nous ont permis de déterminer la configuration des produits obtenus. Que l'on parte des énynes *Z* ou *E*, on obtient toujours l'isomère *E*. L'acétal intermédiaire étant également de forme *E*. Par comparaison avec les travaux de McGreer *et al.* (8) sur l'étude r.m.n. des isomères *Z* et *E* de la méthyl-3 pentène-3 one-2, nous avons pu préciser sans équivoque la structure *E* pour tous nos cétophosphonates obtenus:

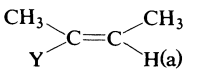

En particulier, le proton (a) sort sous forme d'une quadruplet dans tous les cas, avec un déplacement chimique égal à 6.84 p.p.m., et

Can. J. Chem. Downloaded from www.nrcresearchpress.com by 210.87.254.5 on 09/05/12
For personal use only.

Can. J. Chem. Downloaded from www.nrcresearchpress.com by 210.87.254.5 on 09/05/12
For personal use only.

TABLEAU 2. Déplacements chimiques et constantes de couplage des phosphonates énynes

Phosphonates	Déplacements chimiques (p.p.m.) Protons (a) Ex	(a) Th	(b) Ex	(b) Th	(c) Ex	(c) Th	(d) Ex	(d) Th	(e) Ex	(e) Th	Phosphore	Constantes de couplage (Hz) J_{P-Hc}	J_{c-d}	J_{e-b}
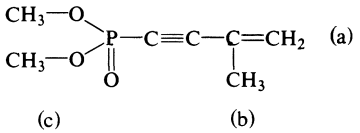 (a) (c) (b)	m		t		d							12		
	5.60		1.98		3.72									
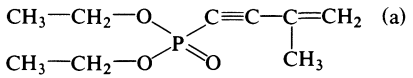 (a) (d) (c) (b)	m	d	t	t	m		t					9	7	
	5.58	5.50	1.97	1.95	4.10		1.35							
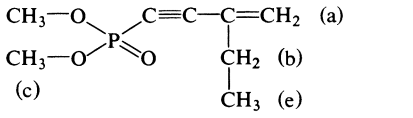 (a) (b) (c) (e)	d	d	m	q	d				t	t				
	5.52	5.80	2.18	2.23	3.74				1.14	1.14		12		7.5
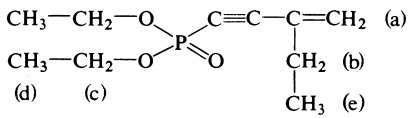 (a) (b) (d) (c) (e)	d	d	m	q	m		t		t	t				
	5.52	5.50	2.16	2.22	4.08		1.38		1.15	1.12		9	7	7.5
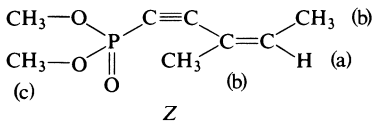 (b) (a) (c) (b) *Z*	m		m		d									
	5.97		1.90		3.72						3.7	12		
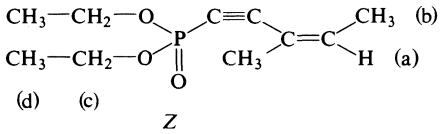 (b) (a) (d) (c) *Z*	m		m		m		t							
	6.05		1.90		4.09		1.36				6.8	9	7	

Can. J. Chem. Downloaded from www.nrcresearchpress.com by 210.87.254.5 on 09/05/12
For personal use only.

TABLEAU 2. (*Concluded*)

Phosphonates	Déplacements chimiques (p.p.m.) Protons (a) Ex	(a) Th	(b) Ex	(b) Th	(c) Ex	(c) Th	(d) Ex	(d) Th	(e) Ex	(e) Th	Phosphore	Constantes de couplage (Hz) J_{P-Hc}	J_{c-d}	J_{e-b}
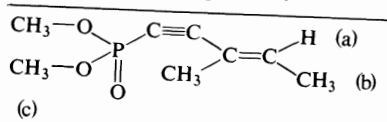 (a) (b) (c)	q 6.22		m 1.87		d 3.63						3.26	12		
E 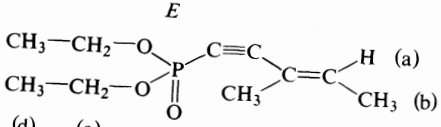 (a) (b) (d) (c) (e)	q 6.15	q 6.15	m 1.78	t 1.70	m 3.96		t 1.30		s 1.72	s 1.74	6.6	9	7	
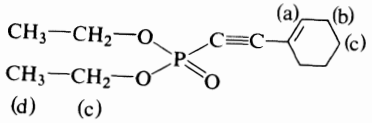 (a) (b) (c) (d) (c)	s 6.41		m 2.17		m 4.06		t 1.35		m 1.65			9	7	

NOTE: m, massif; s, singulet; d, doublet; q, quadruplet; t, triplet.

TABLEAU 3. Constantes physiques des cétophosphonates

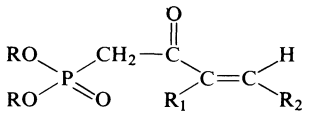

Nature des groupements				Point d'ébullition			
R	R_1	R_2	Isomère	(°C/mmHg)	n_d^t	d_4^t	Rendement (%)
C_2H_5	CH_3	CH_3	*E*	128/0.15	1.4668/24	1.095/24	70
C_2H_5	CH_3	H		92/0.15	1.4468/23	1.104/23	25
C_2H_5	C_2H_5	H		110/0.2	1.4603/23	1.090/23	30
CH_3	CH_3	CH_3	*E*	102/0.3	1.4738/24	1.092/24	49

ceci que l'on parte des isomères *Z* ou *E* des phosphonates ényniques.

Nous avons déterminé également les moments dipolaires expérimentaux des phosphonates ényniques (tableau 5) et des β-cétophosphonates (tableau 6).

En ce qui concerne les premiers le comportement des isomères *Z* et *E* est totalement différent. Les isomères *Z* ayant un moment dipolaire supérieur à celui des isomères *E*. Ainsi dans le cas des isomères *Z* et *E* du (méthyl-3 pentène-3 yne-1) yl phosphonate de diméthyle, on trouve 2.82 D pour le composé *E* et 3.57 D pour le dérivé *Z*. Les cétophosphonates quant à eux ayant une structure *E*, ont des moments dipolaires très voisins, de l'ordre de 3.15 D.

Etude Expérimentale

Synthèse des phosphonates ényniques

Ils sont obtenus par action des trialcoylphosphites sur les halogénures ényniques selon un mode opératoire décrit précédemment (9, 10).

Les constantes physiques des produits obtenus se trouvent rassemblées tableau 1. Nous avons par ailleurs regroupé dans le tableau 2 les déplacements chimiques des différents types de protons et du phosphore ainsi que les constantes de couplage J_{HH} et J_{PH}. Les déplacements chimiques des protons sont donnés par rapport au tétraméthylsilane pris comme référence interne, alors que nous avons utilisé PO_4H_5 à 85% comme référence interne pour le phosphore. Nous avons calculé dans certains cas les déplacements chimiques des protons à l'aide du programme LAOCOON III (13).

Synthèse des cétophosphonates

Dans un ballon de 250 cm³ muni d'un système d'agitation, d'une ampoule à brome et d'un réfrigérant, on place un mélange de 1.5 g d'oxyde mercurique, 0.2 g d'acide monochloracétique, 0.5 g d'éthérate de trifluorure de bore et 1.5 cm³ d'alcool (méthanol ou éthanol). On chauffe ce mélange jusqu'à obtention d'une boue homogène. Le catalyseur étant ainsi préparé, on ajoute en une seule fois 70 cm³ d'éthanol absolu et on agite en chauffant doucement. Le mélange prend une coloration jaune orangée. On additionne alors goutte à goutte un mélange composé de 30 cm³ d'alcool et de 0.25 mol de phosphonate ényne en chauffant à très léger reflux. L'addition dure 1 h environ. Le mélange réactionnel devient gris. On maintient le reflux 5 h. On termine alors en ajoutant 0.5 g d'éthylate de sodium afin de neutraliser l'acide monochloracétique. L'excès d'alcool est chassé sous pression atmosphérique. Une rectification sous vide permet d'obtenir les β-cétophosphonates γ,δ-éthyléniques dont les constantes physiques se trouvent rassemblées tableau 3. Les déplacements chimiques des différents types de protons et les constantes de couplage se trouvent rassemblés tableau 4.

Synthèse du (méthyl-3 éthylène cétal-2 pentène-3) yl phosphonate de diéthyle

On utilise le même mode opératoire que celui employé précédemment pour la synthèse des β-cétophosphonates γ,δ-éthyléniques. On additionne au méthyl-3 pentényne (*Z* ou *E*) l'éthylèneglycol. Après les traitements habituels on isole le *E* (méthyl-3 éthylène cétal-2 pentène-3) yl phosphonate de diéthyle:

p.éb. °C/mm, 112/0.1; n_d^{23}, 1.4614; d_4^{23}, 1.109; Rendement, 40%. Spectre r.m.n.: les déplacements chimiques des différents protons sont les suivants:

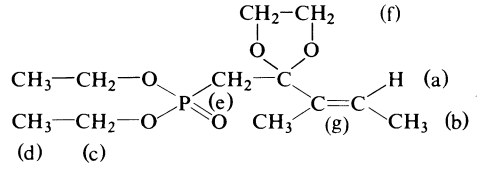

(a) quadruplet centré à 5.66 10^{-6}; (b) massif centré à 1.57 10^{-6}; (g) massif centré à 1.52 10^{-6}; (c) massif centré à 3.94 10^{-6}; (d) triplet centré à 1.22 10^{-6}; (e) doublet centré à 2.18 10^{-6}; (f) massif centré à 3.72 10^{-6}; constantes de couplage: J_{P-He} 9 Hz; J_{P-He} 18 Hz.

Détermination des moments dipolaires

Nous avons déterminé les moments dipolaires des phosphonates ényniques et des β-cétophosphonates, en solution diluée en utilisant la théorie fondamentale de Debye–Clausius–Mosotti et le procédé de calcul proposé par Hedestrand (14), et Gaydou (15). Les mesures ont été faites en utilisant soit le tétrachlorure de carbone (ε_1 = 2.2363 à 25 °C) soit le cyclohexane (ε_1 = 2.0148 à

Can. J. Chem. Downloaded from www.nrcresearchpress.com by 210.87.254.5 on 09/05/12
For personal use only.

Can. J. Chem. Downloaded from www.nrcresearchpress.com by 210.87.254.5 on 09/05/12
For personal use only.

TABLEAU 4. Déplacements chimiques et constantes de couplage des cétophosphonates

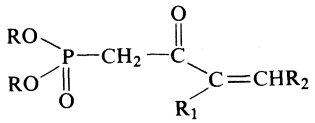

Cétophosphonates	Déplacement chimique des protons (p.p.m.)												Constantes de couplage (Hz)		
	(a)		(b)		(b′)		(c)		(d)		(e)				
	Ex	Th	Ex	Th	Ex	Th	Ex	Th	Ex	Th	Ex	Th	J_{P-He}	J_{a-b}	J_{P-He}
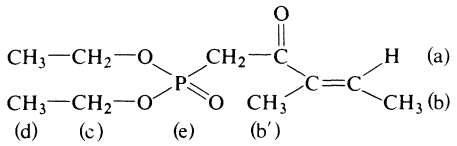	q	q	d	d	s	m	m		t		d				
	6.84	6.83	1.89	1.84	1.74	1.70	3.96		1.22		3.22		9	7	22
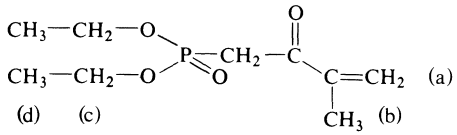	d	d	s	m			m		t		d				
	5.97	5.96	1.83	1.82			4.02		1.26		3.29		9		22
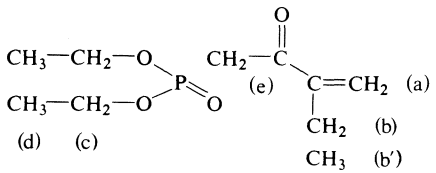	d	d	q	q	t	t	m		t		d				
	5.98	5.95	2.22	2.18	0.99	0.99	4.00		1.25		3.29		9	1.4	22
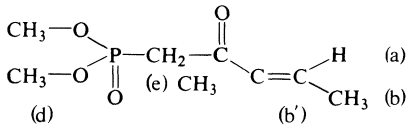	q	q	d	d	s	m			d		d				
	6.92	6.84	1.90	1.86	1.76	1.70			3.70		3.22		12	7	22

TABLEAU 5. Détermination des moments dipolaires des phosphonates énynes

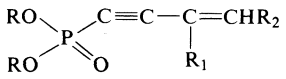

Composés							
R	R_1	R_2	Isomère	Solvant	ε_1	d_1^t	γ (D)
C_2H_5	CH_3	CH_3	*Z*	C_6H_6	2.0148	0.7738/25	3.68
C_2H_5	CH_3	CH_3	*Z*	C_6H_6	2.0148	0.7738/25	3.44
CH_3	CH_3	CH_3	*Z*	C_6H_6	2.0148	0.7738/25	3.57
CH_3	CH_3	CH_3	*E*	C_6H_6	2.0148	0.7738/25	2.82
CH_3	C_2H_5	H		CCl_4	2.2363	1.5843/25	3.45
C_2H_5	CH_3	H		CCl_4	2.2363	1.5843/25	3.28

TABLEAU 6. Détermination des moments dipolaires des β-cétophosphonates

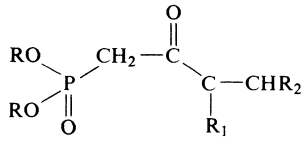

Composés							
R	R_1	R_2	Isomère	Solvant	ε_1	d_1^t	γ (D)
C_2H_5	CH_3	CH_3	*E*	C_6H_6	2.0148	0.7738/25	3.12
CH_3	CH_3	CH_3	*E*	CCl_4	2.2363	1.5843/25	3.18
C_2H_5	C_2H_5	H		C_6H_6	2.0148	0.7738/25	3.09
C_2H_5	CH_3	H		CCl_4	2.2363	1.5843/25	3.15

25 °C) comme solvants à l'aide d'un dipolmètre WTW type DM 01 comportant des cellules du type DFL2. Les résultats obtenus se trouvent rassemblés dans les tableaux 5 et 6.

1. I. A. FAVORSKAYA et L. V. FEDEROVA. Zh. Obshch. Khim. **23**, 47 (1953).
2. I. A. FAVORSKAYA et L. V. FEDEROVA. Zh. Obshch. Khim. **24**, 242 (1954).
3. I. A. FAVORSKAYA et E. AUVINEN. Zh. Org. Khim. 484, (1965).
4. G. PEIFFER, R. FREZE et A. GUILLEMONAT. Bull. Soc. Chim. 4117 (1969).
5. G. STURTZ, C. CHARRIER et H. NORMANT. Bull. Soc. Chim. 1707 (1966).
6. M. BERTRAND et H. MONTI. Tetrahedron Lett. **9**, 1069 (1968).
7. H. MONTI. C.R. **265**, 522 (1967).
8. D. E. MCGREER, N. W. K. CHIU et M. G. VINJE. Can. J. Chem. **43**, 1398 (1965).
9. G. PEIFFER et M. FAURE. C.R. **268**, 358 (1969).
10. M. FAURE. Thèse, Docteur engénieur. Marseille, n° CNRS A.O. 7878 (1973).
11. P. ARNAUD, R. PERRAUD et Y. ARMAND. Bull. Soc. Chim. 1893 (1965).
12. L. V. QUANG et P. CADIOT. Bull. Soc. Chim. 1525 (1965).
13. E. GAYDOU, J. LLINAS, G. PEIFFER et A. GUILLEMONAT. Ann. Fac. Sci. Marseille, **43**A, 83 (1970).
14. G. HEDESTRAND. Z. Phys. Chem. **2** (B), 428 (1939).
15. E. M. GAYDOU. J. Chim. Phys. **69**, 1733 (1972).

Can. J. Chem. Downloaded from www.nrcresearchpress.com by 210.87.254.5 on 09/05/12
For personal use only.

An Electron Spin Resonance Study of the Arylsilyl Adducts of Phenyl *tert*-Butyl Nitrone and Their Decomposition Kinetics

BABATUNDE B. ADELEKE, SAU-KING WONG, AND JEFFREY K. S. WAN

Department of Chemistry, Queen's University, Kingston, Ontario K7L 3N6

Received October 26, 1973[1]

BABATUNDE B. ADELEKE, SAU-KING WONG, and JEFFREY K. S. WAN. Can. J. Chem. **52**, 2901 (1974).

The formation and the stability of some arylsilyl adducts of phenyl *tert*-butyl nitrone were studied in a photochemical system using di-*tert*-butyl peroxide as solvent. The β-proton splittings of all the arylsilyl adducts, ranging from 5.6 to 8.3 G, are relatively larger than their carbon analogs, which are usually less than 4 G. The arylsilyl adducts are found to decompose in di-*tert*-butyl peroxide solvent by a first-order kinetics. The activation energy involved in the decomposition of a series of arylsilyl adducts varies from about 14 to about 9 kcal/mol, as the size of the silyl group increases. In all cases, very low values of the *A* factors (between 10^6 and 10^{10}) were observed.

BABATUNDE B. ADELEKE, SAU-KING WONG et JEFFREY K. S. WAN. Can. J. Chem. **52**, 2901 (1974).

On a étudié la formation et al stabilité de quelques produits d'addition arylsilylés de la phényl *tert*-butyl nitrone dans un système photochimique utilisant le peroxyde de di-*tert*-butyle comme solvant. Les couplages des protons β de tous les produits d'addition arylsilylés qui s'étalent entre 5.6 et 8.3 G sont relativement plus larges que ceux de leurs dérivés carbonés analogues qui sont généralement de l'ordre de 4 G. On a trouvé que les produits addition arylsilylés se décomposent dans un solvant comme le peroxyde de di-*tert*-butyle par une cinétique du premier ordre. L'énergie d'activation impliqué dans la décomposition d'une série de produits d'addition arylsilylés varie de 14 à 9 kcal/mol au fur et à mesure que la grosseur du groupe silylé augmente. Dans tous les cas ou observe des valeurs très basses (entre 10^6 et 10^{10}) pour les facteurs *A*.

[Traduit par le journal]

Can. J. Chem. Downloaded from www.nrcresearchpress.com by 210.87.254.42 on 09/05/12
For personal use only.

Introduction

The technique of spin trapping (1) has been increasingly popular in mechanistic studies involving elusive free radical intermediates. The persistent failure of observing the e.s.r. spectrum of the triphenylsilyl radical in liquid solution in our laboratory has led us to consider the application of spin trapping methods. Thus in a related study we have shown that the presence of triphenylsilyl radicals can be detected by using benzophenone as the spin trap at high temperatures (2). Because the phenyl *tert*-butyl nitrone (PBN) has been widely used as a spin trap, we chose PBN in this study as traps to react with various arylsilyl radicals produced in a conventional photochemical system using *tert*-butyl peroxide as the solvent. Quantitative kinetic studies on the subsequent decomposition of these arylsilyl adducts were carried out. The results suggest that under the same experimental conditions, various arylsilyl radicals give spin adducts of different stability, hence different steady-state concentrations of the resulting adducts. The conclusion illustrates the point that for quantitative studies of the relative reactivity of free radicals in solution using the spin trapping techniques, steady-state intensities of the e.s.r. spectra of the various spin adducts are not reliable indications of the relative reactivity.

Experimental

Triphenylsilane (Alfa), diphenylsilane (K & K), phenylsilane (Alfa), phenyl *tert*-butyl nitrone (Eastman), and di-*tert*-butyl peroxide (K & K) were used as received. Use of zone-refined triphenylsilane gave identical results.

About 0.05 *M* solution of each of the nitrone and the silane was prepared in liquid di-*tert*-butyl peroxide (BOOB). Attempts have been made to use BOOB in a variety of common solvents, including benzene, cyclohexane, and carbon tetrachloride. The best results were obtained with BOOB as solvent.

In a typical experiment, the sample solution in a Pyrex tube was degassed thoroughly under 10^{-5} Torr vacuum. The sample tube was sealed and placed in an optical microwave cavity equipped with a variable temperature controller. The sample was irradiated *in situ* using a 200 W high pressure mercury lamp with Pyrex optics. The

[1]Revision received May 13, 1974.

TABLE 1. Experimental e.s.r. parameters of the arylsilyl and $B\dot{O}$ adducts of phenyl *tert*-butyl nitrone in *tert*-butyl peroxide

Radical adduct	a_N (G)	a_β^H (G)	g value
$Ph_3\dot{Si}$	14.5±0.1	5.6±0.1	2.0056±0.0002
$Ph_2\dot{Si}H$	14.5±0.1	7.5±0.1	2.0057±0.0002
$Ph\dot{Si}H_2$	14.8±0.1	8.3±0.1	2.0056±0.0002
$(CH_3)_3\dot{Si}$	14.5±0.1	6.0±0.1	2.0057±0.0002
$(CH_3)_3C\dot{O}$	14.0±0.1*	1.6±0.1	2.0056±0.0002

*Somewhat larger values of a_N (14.22 G) and a_β^H (1.95 G) observed in benzene solvent have been given by Janzen and Evans (3).

decay of the e.s.r. spectra between −20 and 30 °C was followed using a Hewlett Packard fast speed recorder with a response time better than 0.5 s. The decay curve of the e.s.r. signal monitored at the maximum of one of the outermost hyperfine lines was obtained after the light beam was cut off.

Electron spin resonance spectra were recorded with a Varian X-band spectrometer with 100 kHz modulation. The magnetic field was calibrated with a Varian F-8A fluxmeter and the g-value measurements were made with DPPH as a standard at 2.0036. Calibration of the absolute concentration of the radicals studied was found to be unnecessary, since they decay by first-order kinetics.

Results

Photolysis of BOOB in the Presence of Phenyl tert-Butyl Nitrone

At room temperature and without specific irradiation, the solution of phenyl *tert*-butyl nitrone in BOOB exhibits a weak e.s.r. signal. The intensity and resolution of the signal increased greatly upon irradiation. This spectrum has parameters similar to those of the butoxy radical adduct (3) (**1**) formed in the following reactions

[1] $$BOOB + h\nu \rightarrow 2B\dot{O}$$

[2] 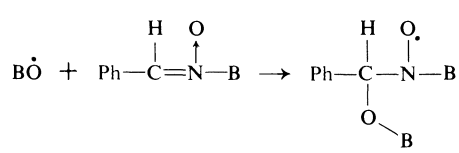

1

The experimental hyperfine coupling constant for adduct **1** is listed in Table 1. Upon further irradiation, the doublet fine structure of the main triplet spectrum disappeared, leaving only a three-line spectrum with a splitting of 13.6 g. This is consistent with the following reaction scheme:

[3] 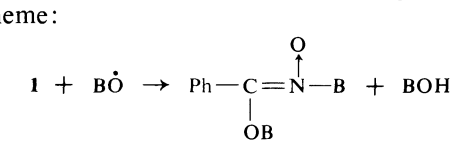

[4] 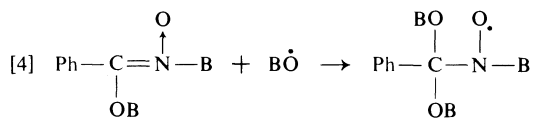

2

It is reasonable to expect the radical adduct (**2**) to give a simple triplet spectrum with a nitrogen splitting in the order of 13 G. Further experiments show that in the presence of a better hydrogen donor such as silane, the triplet spectrum was not observed.

Photolysis of BOOB in the Presence of Triphenylsilane and Phenyl tert-Butyl Nitrone

Photolysis of this solution led to the observation of an e.s.r. spectrum shown in Fig. 1. This spectrum is analyzed into three component radicals; two of them are readily recognized by their hyperfine splittings as the $BN(\dot{O})OB$ radical (4) and the butoxy adduct (**1**). The third radical has a triplet splitting of 14.5 G and a smaller doublet splitting of 5.6 G. Both the $BN(\dot{O})OB$ radical and the third radical are found to be unstable in the dark. Considering analogous reactions (5) we *tentatively* assign the third radical to be the triphenylsilyl adduct, $PhCH(SiPh_3)N(\dot{O})B$. To support this assignment, we have made a thorough search for the ^{29}Si splitting. All attempts were unsuccessful and we suspect that the ^{29}Si splitting may be too small to be resolved, since the Si is in the γ-position (6). Nevertheless, in the absence of observable ^{29}Si splitting, the identification of this radical must remain tentative.

It is noted here that all reported spin adducts of the phenyl *tert*-butyl nitrone and either hydrocarbon radicals[2] or oxygen radicals have β-proton splittings less than 4 G and nitrogen splittings between 12 and 16 G (7). Only the

[2]One of the referees had pointed out to us that the trifluoroacetyl spin adduct of PBN (see E. G. Janzen *et al.* (13)) is reported to have a β-proton splitting of 5.4 G.

Can. J. Chem. Downloaded from www.nrcresearchpress.com by 210.87.254.42 on 09/05/12
For personal use only.

Can. J. Chem. Downloaded from www.nrcresearchpress.com by 210.87.254.42 on 09/05/12
For personal use only.

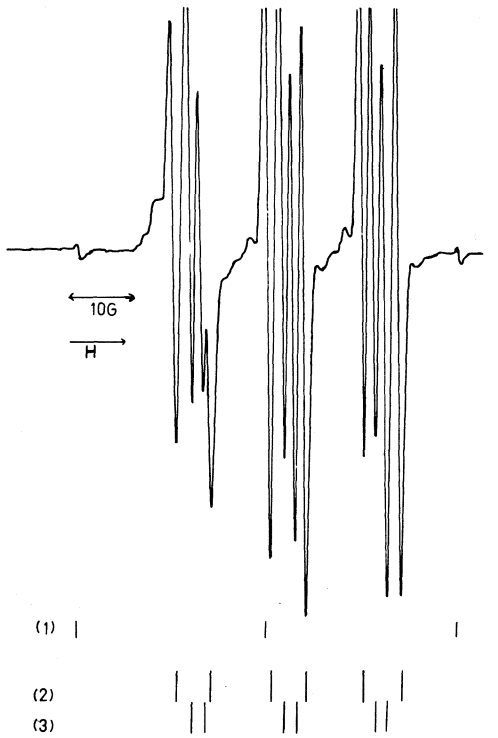

FIG. 1. Electron spin resonance spectrum obtained upon photolysis of BOOB in the presence of phenyl *tert*-butyl nitrone and triphenylsilane: (*1*) BN(Ȯ)OB; (*2*) the triphenylsilyl adduct; and (*3*) the butoxy adduct.

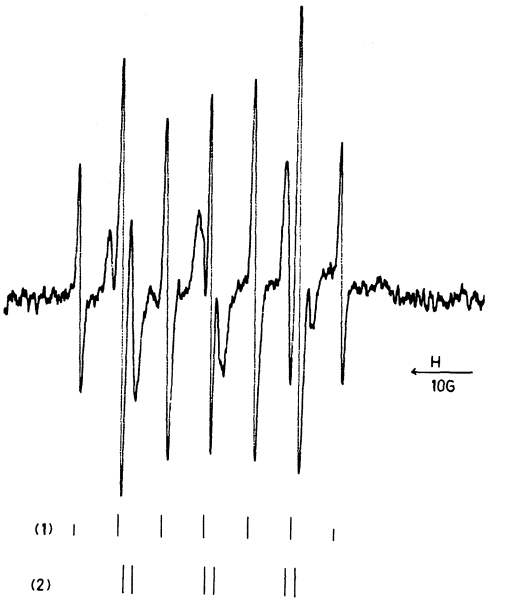

FIG. 2. Electron spin resonance spectrum obtained upon mixing at room temperature BOOB and diphenylsilane in the presence of phenyl *tert*-butyl nitrone: (*1*) $PhCH_2N(\dot{O})B$; (*2*) the butoxy adduct.

hydrogen adduct, $PhCH_2N(\dot{O})B$, has a larger β-proton splitting of 7.13 G (7). It is thus interesting to observe that the radical adducts in the arylsilane systems all have β-proton splittings substantially greater than 4 G (see Table 1).

Photolysis of BOOB in the Presence of Diphenylsilane and Phenyl tert-Butyl Nitrone

At room temperature and without irradiation, a liquid mixture of phenyl *tert*-butyl nitrone and diphenylsilane undergoes a thermal reaction producing the hydrogen adduct $PhCH_2N(\dot{O})B$. In the presence of BOOB, both the hydrogen adduct and the butoxy adduct (**1**) were observed without irradiation (Fig. 2). Upon photolysis of the solution, the hydrogen adduct disappeared and two other radicals were produced (Fig. 3): one is the $BN(\dot{O})NB$ radical and the other radical has a triplet splitting of 14.5 G and a smaller doublet splitting of 7.5 G. This radical is *tentatively* assigned to the diphenylsilyl adduct $PhCH(SiHPh_2)N(\dot{O})B$.

The disappearance of the hydrogen adduct upon photolysis is probably due to the reaction with the photo generated BȮ radicals.

Photolysis of BOOB in the Presence of Phenylsilane and Phenyl tert-Butyl Nitrone

Photolysis of this solution led to the observation of an e.s.r. spectrum which can be tentatively assigned to two component radicals: the butoxy adduct (**1**) and the corresponding phenylsilyl adduct $PhCH(SiH_2Ph)N(\dot{O})B$. The parameters of the latter radical having a large doublet splitting of 8.3 G, are given in Table 1.

Photolysis of BOOB in the Presence of Trimethylsilane and Phenyl tert-Butyl Nitrone

Photolysis of this solution gave an e.s.r. spectrum which is tentatively assigned to the trimethylsilyl adduct $PhCH(Si[CH_3]_3)N(\dot{O})B$. The experimental parameters are given in Table 1. Unlike the arylsilyl adducts, the trimethylsilyl adduct was found to be very stable in the dark.

Decay of the Arylsilyl Adducts

The decay of arylsilyl adducts in the dark was found to follow the first-order kinetics. Figure 4 shows a typical first-order plot obtained from the decay curves of the diphenylsilyl adduct. The decay rate constants at various temperatures and the Arrhenius parameters are summarized in Table 2 for the three arylsilyl adducts studied.

TABLE 2. Kinetic parameters for the decay of arylsilyl adducts

Adduct	Temperature (°K)	First-order rate constants $k \times 10^2$ (s^{-1})	Activation energy (kcal/mol)	log A
Phenylsilyl	265	13 ± 1	13.7±0.3	10.6±0.2
	273	36 ± 1		
	282	69 ± 2		
	291	139 ±10		
	300	212 ±12		
Diphenylsilyl	247	4.5± 0.3	11.7±0.3	9.0±0.3
	255	8.1± 0.7		
	265	22 ± 1		
	273	47 ± 3		
	282	69 ± 2		
Triphenylsilyl	264	2.4± 0.2	9.3±0.3	6.1±0.3
	273	4.7± 0.5		
	282	7.1± 0.5		
	291	15 ± 4		
	319	50 ± 4		

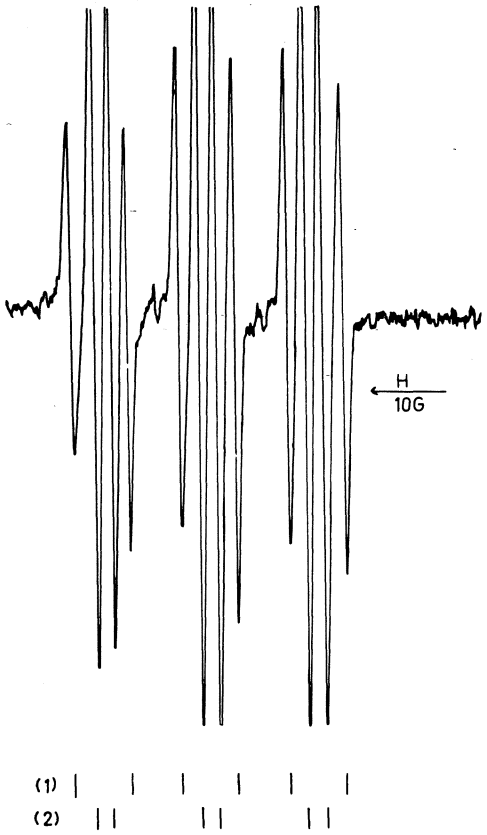

FIG. 3. Electron spin resonance spectrum obtained upon photolysis of BOOB solution of diphenylsilane and phenyl *tert*-butyl nitrone: (*1*) the diphenylsilyl adduct; and (*2*) the butoxy adduct.

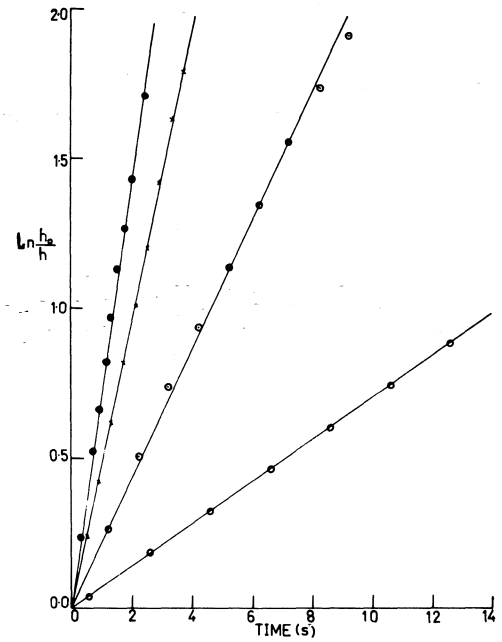

FIG. 4. A first-order plot for the decay of the diphenylsilyl adduct; h_0/h is the relative e.s.r. signal heights at initial time t_0 and time t.

Discussion

In all three arylsilanes systems studied, the adduct radical spectra consistently exhibit a relatively large doublet splittings *presumably* due to the β-proton of the adduct radical. This is a rather interesting observation. In the case of spin

Can. J. Chem. Downloaded from www.nrcresearchpress.com by 210.87.254.42 on 09/05/12
For personal use only.

Can. J. Chem. Downloaded from www.nrcresearchpress.com by 210.87.254.42 on 09/05/12
For personal use only.

adducts of hydrocarbon and oxygen radicals, the variation in the β-proton splittings of the nitroxide seems to be related to the size of the carbon or oxygen radical group. For example, the β-proton splitting in $CH_3N(\dot{O})B$ is 12.7 G (8). Upon replacing one of the methyl protons with a phenyl group, the β-proton splitting of the resultant nitroxide drops to 7.13 G (7). In this respect, we observe (Table 1) the similar trend in the arylsilyl adducts; the phenylsilyl adduct has a larger β-proton splitting than that of the diphenyl and triphenyl substituted silyl adducts. However, on the basis of group size alone, it would be expected that the arylsilyl adducts should have smaller β-proton splittings than their carbon analogs. In a solid state pulse n.m r. study, it has been determined (9) that the activation energy for the C_3 rotation in the solid state of the methyl group in $(CH_3)_3SiCl$ and in CH_3SiCl_3 is substantially lower than the values for their carbon analogs $(CH_3)_3CCl$ and CH_3CCl_3. Perhaps despite the larger size of the arylsilyl group there is less steric strain in these arylsilyl adducts as compared to their carbon analogs.

While the triphenylmethyl radicals do not seem to add to the phenyl *tert*-butyl nitrone (7), arylsilyl radicals including the triphenylsilyl radical appear to add readily to the nitrone and their resultant adducts can be observed by e.s.r. during irradiation. These arylsilyl adducts are unstable in the dark and they decompose with various first-order rate constants. In all three systems studied, the $BN(\dot{O})OB$ radicals were also observed. These observations are consistent with the following reaction scheme:

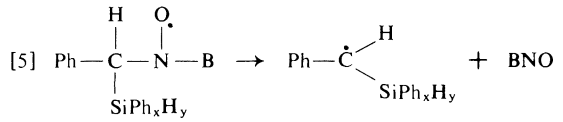

[6] $$BNO + B\dot{O} \rightarrow BN(\dot{O})OB$$

Similar schemes of reactions of carbon analogs have been proposed by Maender and Janzen (10).

The fate of the silyl substituted benzyl radical formed in reaction 5 is not known.

The present experiments show that among the three arysilyl adducts the activation energy of their decomposition decreases with the increasing size of the arylsilyl group. This is also consistent with the observation of Maender and Janzen (10) for carbon adducts. It should be emphasized that the present experiments were carried out in BOOB solvent. However, the use of BOOB as solvent does not seem to interfere with the decomposition of the adducts. For example, we had used liquid diphenylsilane itself as solvent and the decay of the diphenylsilyl adduct was virtually the same as in BOOB. Indeed, the use of BOOB as solvent for radical studies is relatively common in recent years.

Finally the low values of the *A* factor determined and given in Table 2 cannot be satisfactorily explained at the present time. While there have been a few other low values of *A* factors reported for unimolecular reactions (11, 12), further systematic studies of unimolecular decomposition of free radicals are required before this can be explained.

This research is supported by the National Research Council of Canada. B.B.A. also wishes to acknowledge the award of a Canadian Commonwealth Postgraduate Scholarship.

1. E. G. JANZEN. Acc. Chem. Res. **4**, 31 (1971).
2. A. R. MCINTOSH and J. K. S. WAN. Mol. Phys. **22**, 183 (1971); Can. J. Chem. **49**, 812 (1971).
3. E. G. JANZEN and C. A. EVANS. J. Am. Chem. Soc. **95**, 8205 (1973).
4. M. J. PERKINS and P. WARD. J. Chem. Soc. B, 395 (1970).
5. S. W. BENNETT, C. EABORN, A. HUDSON, and H. A. HUSSAIN. J. Organomet. Chem. **16**, P36 (1969).
6. P. J. KRUSIC and J. K. KOCHI. J. Am. Chem. Soc. **93**, 846 (1971).
7. E. G. JANZEN and B. J. BLACKBURN. J. Am. Chem. Soc. **91**, 4481 (1969).
8. A. R. FORRESTER, J. M. HAY, and R. H. THOMSON. Organic chemistry of stable radicals. Academic Press, London. 1970. p. 195.
9. S. CHANDRA. Ph.D. Thesis. Queen's University, Kingston, Ontario. 1973.
10. O. W. MAENDER and E. G. JANZEN. J. Org. Chem. **34**, 4072 (1969).
11. B. G. GOWENLOCK. Q. Rev. **14**, 133 (1960).
12. M. DAVIES and F. P. EVANS. Trans. Faraday Soc. **51**, 1506 (1955).
13. E. G. JANZEN, I. G. LOPP, and T. V. MORGAN. J. Phys. Chem. **77**, 139 (1973).

Thermodynamics of Ionization of Benzoic Acid and Substituted Benzoic Acids in Relation to the Hammett Equation

TAKEKI MATSUI, HON CHUNG KO, AND LOREN G. HEPLER
Department of Chemistry, University of Lethbridge, Lethbridge, Alberta T1K 3M4

Received February 4, 1974

TAKEKI MATSUI, HON CHUNG KO, and LOREN G. HEPLER. Can. J. Chem. **52**, 2906 (1974).

We have made both ampoule and titration calorimetric measurements leading to ΔH^0 of ionization of aqueous benzoic acid at 298 K, and have considered our results in relation to those from several earlier investigations in an effort to select the "best" value for this important quantity. We have also made calorimetric measurements leading to ΔH^0 values for ionization of several substituted benzoic acids, and have selected "best" ΔH^0 values for 15 *meta*- and *para*-substituted benzoic acids. It is found that there are good linear relationships between ΔG^0, ΔH^0, and ΔS^0 values for most of these substituted benzoic acids. It is also found that the Hammett equation accounts well for ionization constants over the temperature range 278–318 K for all of these acids and accounts very well for ionization constants of those acids with positive σ substituent parameters.

TAKEKI MATSUI, HON CHUNG KO et LOREN G. HEPLER. Can. J. Chem. **52**, 2906 (1974).

Des mesures par ampoule et par titrage calorimétrique, on obtient la valeur de ΔH^0 d'ionisation de l'acide benzoïque aqueux à 298 K; on considère ces résultats en rapport avec ceux de plusieurs études antérieures pour choisir la "meilleure" valeur de cette importante quantité. On fait aussi des mesures calorimétriques qui mènent aux valeurs de ΔH^0 d'ionisation de plusieurs acides benzoïques substitués, et l'on choisit les "meilleures" valeurs de ΔH^0 pour 15 acides benzoïques substitués en *méta* et *para*. On trouve une bonne relation linéaire entre les valeurs de ΔG^0, ΔH^0 et ΔS^0 pour la plupart de ces acides benzoïques substitués. L'équation de Hammett explique bien les constantes d'ionisation dans l'intervalle de températures de 278–318 K de tous ces acides, et elle explique très bien les constantes d'ionisation de ceux qui ont les paramètres de substituants σ positifs. [Traduit par le journal]

Introduction

Ionization constants for benzoic acid and substituted benzoic acids in aqueous solution at 298 K were the basis for Hammett's original assignment of σ substituent parameters (1). Although applications of the Hammett equation and other linear free energy equations have been extended far beyond Hammett's early applications to equilibria and rates of reactions involving *meta*- and *para*-substituted benzene derivatives, the ionization constants and corresponding standard free energies of ionization of benzoic acid and substituted benzoic acids are still of fundamental importance in relation to substituent effects.

For many years there has been considerable interest in the temperature dependence of ionization constants and of related substituent effects. This interest has been based partly on the practical desire to apply the Hammett equation at temperatures other than 298 K and partly on a desire to gain more understanding of the theoretical basis and consequences of the Hammett equation. All of these concerns can be expressed in terms of ΔH^0 and ΔS^0 values for the various acid ionization reactions, as discussed in several previous publications (2–8).

In spite of a considerable number of experimental investigations of the thermodynamics of ionization of benzoic acid and substituted benzoic acids (cited later in this paper), there are still substantial disagreements between the results of different investigators. We have therefore undertaken the calorimetric measurements and thermodynamic calculations that are described in this paper.

Experimental

All calorimetric measurements were made with an LKB Precision Calorimetry System. Many of our measurements were made with "standard" glass ampoules from LKB. Small corrections to allow for heat effects associated with ampoule-breaking were based on results of blank determinations. For titration calorimetry measurements the titrant was supplied by a Metrohm Dosimat automatic titrator. Heats of dilution of titrant solutions were determined separately. All of our results refer to (298.15 ± 0.05) K and are reported in terms of the defined calorie (1 cal = 4.1840 J).

Sodium benzoate (BDH) was recrystallized three or

Can. J. Chem. Downloaded from www.nrcresearchpress.com by 210.87.254.105 on 09/05/12
For personal use only.

Can. J. Chem. Downloaded from www.nrcresearchpress.com by 210.87.254.105 on 09/05/12
For personal use only.

more times from aqueous ethanol and then dried in vacuum for 24 h at 120 °C.

Sodium *m*-nitrobenzoate was prepared by reaction of NaOH in 95% ethanol with *m*-nitrobenzoic acid (J. T. Baker) that had been previously recrystallized from aqueous ethanol. The sodium *m*-nitrobenzoate was recrystallized three times from aqueous ethanol and then dried in vacuum for 24 h at 120 °C.

Sodium salts of *m*-fluorobenzoic acid (Aldrich), *m*-methylbenzoic acid (Eastman and BDH), and *m*-methoxybenzoic acid (Eastman) were prepared by reaction of the acid, previously recrystallized from water, with NaOH in 95% ethanol. The salts were recrystallized three times from aqueous ethanol and then dried in vacuum for 24 h at 120 °C.

For every compound we made duplicate measurements on at least two different samples prepared and purified at different times.

Results and Discussion

We have measured heats of solution of sodium benzoate and sodium *m*-fluorobenzoate in 0.001 *M* NaOH (to repress hydrolysis) as represented generally by

[1] $\mathrm{NaBz(c) = Na^+(aq) + Bz^-(aq)} \quad \Delta H_1^0$

Results of seven determinations of heats of solution of sodium benzoate (concentrations from 0.01 to 0.03 *M*) have been extrapolated *vs.* the square root of concentration to infinite dilution to yield $\Delta H_1^0 = -581$ cal mol^{-1}. Similar treatment of similar results for sodium *m*-fluorobenzoate has led to $\Delta H_1^0 = 260$ cal mol^{-1}.

We have also measured heats of solution of sodium benzoate and sodium *m*-fluorobenzoate in 0.024 *M* HCl solution, as represented generally by

[2] $\mathrm{NaBz(c) + H^+(aq) = HBz(aq) + Na^+(aq)} \quad \Delta H_2^0$

Again, results of seven determinations (concentrations of HBz formed ranging from 0.005 to 0.018 *M*) have been extrapolated to infinite dilution to yield $\Delta H_2^0 = -687$ cal mol^{-1} for sodium benzoate and $\Delta H_2^0 = 40$ cal mol^{-1} for sodium *m*-fluorobenzoate.

Our estimates of *total* uncertainties (calorimetric, chemical, and extrapolation) are about ± 25 cal mol^{-1} in ΔH_1^0 and ΔH_2^0 values for sodium benzoate. For sodium *m*-fluorobenzoate the total uncertainties in ΔH_1^0 and ΔH_2^0 are about ± 40 cal mol^{-1} and ± 50 cal mol^{-1}, respectively.

Combination of ΔH_1^0 and ΔH_2^0 values leads to the desired enthalpies of ionization as follows:

[3] $$\Delta H_i^0 = \Delta H_1^0 - \Delta H_2^0$$

[4] $\mathrm{HBz(aq) = H^+(aq) + Bz^-(aq)} \quad \Delta H_i^0$

In this way we obtain $\Delta H_i^0 = 106 \pm 35$ cal mol^{-1} for ionization of benzoic acid and $\Delta H_i^0 = 220 \pm 65$ cal mol^{-1} for ionization of *m*-fluorobenzoic acid.

We have also carried out titration calorimetry measurements in which perchloric acid solution was added to a solution of a sodium salt in the calorimeter. Combination of these results with separately evaluated heats of dilution has led to the following standard enthalpies of ionization: $\Delta H_i^0 = 114 \pm 25$ cal mol^{-1} for benzoic acid, $\Delta H_i^0 = 381 \pm 30$ cal mol^{-1} for *m*-nitrobenzoic acid, $\Delta H_i^0 = 49 \pm 35$ cal mol^{-1} for *m*-methoxybenzoic acid, $\Delta H_i^0 = 70 \pm 30$ cal mol^{-1} for *m*-methylbenzoic acid. All of the $\pm$ values listed here are estimates of the *total* uncertainty, as described above.

In Table 1 we list our two calorimetric ΔH^0 values for ionization of aqueous benzoic acid at 298 K, along with results reported by earlier investigators. The considerable range (-420 to $+169$ cal mol^{-1}) in these values must be due to substantial systematic errors in some of the cited investigations. Because of these systematic errors and because different authors attach different meanings to quoted $\pm$ values, it is impossible to carry out any weighted averaging pro-

TABLE 1. ΔH^0 values for ionization of aqueous benzoic acid at 298 K[a]

ΔH^0 (cal mol^{-1})	Reference
+40 (T)	9
+110 ± 60 (C)[b]	10
−420 (T)	11
+104 ± 150 (T)	12
+105 ± 50 (C)	13
+90 (C)[c]	14, 15
+169 (T)	16
+1 (T)	17
+150 ± 24 (T)	18
+150 ± 50 (C)	19
+100 (C)	20
+118 (C)	21
−67 ± 19 (T)	7
+110 (C)	22
+106 ± 35 (C)	This work, ampoule calorimetry
+114 ± 25 (C)	This work, titration calorimetry

[a](T) indicates that the quoted ΔH^0 value was derived from equilibrium constants at several temperatures. (C) indicates that the quoted ΔH^0 value was derived from calorimetric measurements. All ± values are those quoted by the original authors.

[b]Calorimetric measurements were made at 10, 20, and 30 °C. The value listed is based on our interpolation of the published results.

[c]The authors originally reported $\Delta H^0 = +90$ cal mol^{-1}, based on their ΔH^0 for ionization of water. Recalculation of their results, using the "best" ΔH^0 of ionization of water (3), now leads to $\Delta H^0 = -70$ cal mol^{-1} for ionization of benzoic acid. Because of probable cancellation of errors, it is likely that the original +90 cal mol^{-1} is "better" than the recalculated −70 cal mol^{-1}.

Can. J. Chem. Downloaded from www.nrcresearchpress.com by 210.87.254.105 on 09/05/12
For personal use only.

cedure to obtain the "best" ΔH^0 value. We therefore proceed as follows.

An average of *all* the ΔH^0 values listed in Table 1 leads to $\Delta H^0 = +61$ cal mol^{-1}. An average of all ΔH^0 values except that (−420) from ref. 11 leads to $\Delta H^0 = +93$ cal mol^{-1}. An average of all positive ΔH^0 values leads to $\Delta H^0 = +105$ cal mol^{-1}. An average of all positive ΔH^0 values derived from equilibrium constants at several temperatures is $\Delta H^0 = +93$ cal mol^{-1}. An average of all calorimetric values gives $\Delta H^0 = +111$ cal mol^{-1}. On the basis of these averages and our opinions about the various reported values, we select $\Delta H^0 = +110$ cal mol^{-1} as the "best" standard enthalpy of ionization of aqueous benzoic acid at 298 K. We estimate that the total uncertainty in this value is no more than $\pm$ 20 cal mol^{-1}.

Equilibrium results reported in refs. 7, 9, 12, and 16–18 and reviewed in ref. 3 lead us to select the following "best" values for ionization of aqueous benzoic acid at 298 K: $K = 6.25 \times 10^{-5}$, pK = 4.204, $\Delta G^0 = 573_5$ cal mol^{-1}. The total uncertainty in this ΔG^0 appears to be less than ± 10 cal mol^{-1}.

Combination of the "best" ΔG^0 and ΔH^0 values above leads to $\Delta S^0 = -18.87$ cal K^{-1} mol^{-1} for the standard entropy of ionization of aqueous benzoic acid at 298 K. All of these ΔG^0, ΔH^0, and ΔS^0 values for benzoic acid (and those given later for substituted benzoic acids) are based on the "infinite dilution" or "hypothetical 1.0 molal" solute standard state.

In Table 2 we list our ΔH^0 values for ionization of substituted benzoic acids, along with values reported by earlier investigators for several acids. We first consider the accuracy and reliability of the various reported ΔH^0 values and then turn to consideration of these values in relation to other thermodynamic quantities.

On the basis of a previous review (3) and comparison of ΔH^0 values in Tables 1 and 2, we suggest that the ΔH^0 values based on the work of Briegleb and Bieber (11) are too uncertain to warrant further discussion.

Everett and Wynne-Jones (9) used old (1898) equilibrium data from Schaller and Euler to calculate ΔH^0 values for ionization of benzoic acid and several substituted benzoic acids. Generally reasonable agreement between their ΔH^0 values and those reported subsequently suggests that we can accept (most of) their results with confidence.

TABLE 2. ΔH^0 values for ionization of substituted benzoic acids at 298 K[a]

Acid	ΔH^0 (cal mol^{-1})	Reference
m-Fluorobenzoic	+220 ± 60 (C)	This work
m-Chlorobenzoic	+20 (T)	11
	+233 ± 46 (T)	18
	+178 ± 17 (T)	7
m-Bromobenzoic	−60 (T)	11
	+168 ± 16 (T)	18
	+197 ± 17 (T)	7
m-Iodobenzoic	+190 (T)	9
m-Hydroxybenzoic	+150 (C)[c]	10
	+170 (T)	9
m-Methoxybenzoic	+60 (C)[b]	15
	+22 ± 12 (T)	7
	+49 ± 35 (C)	This work
m-Methylbenzoic	+70 (T)	9
	+70 (C)[b]	15
	+1201 ± 93 (T)	18
	−91 ± 13 (T)	7
	+70 ± 30 (C)	This work
m-Nitrobenzoic	+320 (T)	9
	+421 ± 25 (T)	7
	+381 ± 30 (C)	This work
p-Chlorobenzoic	+230 (T)	11
	+388 ± 15 (T)	18
	+100 ± 26 (T)	7
p-Bromobenzoic	+110 (T)	11
	+191 ± 24 (T)	18
	+107 ± 28 (T)	7
p-Iodobenzoic	78 ± 15 (T)	7
p-Hydroxybenzoic	+360 (C)[c]	10
	+540 (T)	11
	+386 ± 34 (T)	18
p-Methoxybenzoic	+800 (T)	9
	+570 (C)[b]	15
	+258 ± 26 (T)	7
p-Methylbenzoic	+300 (T)	9
	+240 (C)[b]	15
	+1101 ± 82 (T)	18
	−134 ± 9 (T)	7
p-Nitrobenzoic	+70 (T)	11
	+432 ± 36 (T)	7

[a](T) indicates that the quoted ΔH^0 value was derived from equilibrium constants at several temperatures. (C) indicates that the quoted ΔH^0 value was derived from calorimetric measurements. All ± values are those quoted by the original authors.

[b]Values quoted are those reported by the authors, based on their ΔH^0 for ionization of water. Because of probable cancellation of errors, it is likely that these values are "better" than those that can be obtained by recalculation with the "best" ΔH^0 for ionization of water.

[c]Calorimetric measurements were made at 10, 20, and 30 °C. The value listed is based on our interpolation of the published results.

Comparison of calorimetric results reported by Cottrell *et al.* (10) and by Zawidski *et al.* (15) with independent results listed in Tables 1 and 2 suggests that the values attributed to these workers can generally be accepted as reliable.

Wilson *et al.* (18) have measured equilibrium constants for ionization of benzoic acid and several substituted benzoic acids at several tem-

TABLE 3. "Best" ΔG^0, ΔH^0, and ΔS^0 values for ionization of aqueous benzoic acids at 298 K

Acid		ΔG^0 (cal mol^{-1})	ΔH^0 (cal mol^{-1})	ΔS^0 (cal K^{-1} mol^{-1})	σ
Benzoic	(1)	5735	110	−18.87	0
m-Fluorobenzoic	(2)	5272	220	−16.94	0.339
m-Chlorobenzoic	(3)	5230	200	−16.87	0.370
m-Bromobenzoic	(4)	5198	180	−16.83	0.394
m-Iodobenzoic	(5)	5260	190	−17.00	0.348
m-Hydroxybenzoic	(6)	5561	160	−18.12	0.128
m-Methoxybenzoic	(7)	5583	49	−18.56	0.111
m-Methylbenzoic	(8)	5800	70	−19.22	−0.048
m-Nitrobenzoic	(9)	4720	380	−14.56	0.744
p-Chlorobenzoic	(10)	5437	240?	−17.43?	0.218
p-Bromobenzoic	(11)	5430	150	−17.71	0.224
p-Iodobenzoic	(12)	5450	78	−18.02	0.209
p-Hydroxybenzoic	(13)	6250	370	−19.72	−0.378
p-Methoxybenzoic	(14)	6120	600?	−18.51?	−0.282
p-Methylbenzoic	(15)	5950	250?	−19.12?	−0.158
p-Nitrobenzoic	(16)	4671	432	−14.22	0.780

peratures and calculated corresponding ΔH^0 values as listed in Tables 1 and 2 for several acids, with still others being listed in their original paper. Comparison of their results with others listed in Tables 1 and 2 suggests that several of their quoted $\pm$ values are optimistic and that there are probably large systematic errors in their results for *m*-methylbenzoic acid and *p*-methylbenzoic acid.

The most recent extensive investigation of ionization of benzoic acids is that of Bolton *et al.* (7), who measured equilibrium constants at several temperatures and calculated corresponding ΔH^0 values. Comparison of their $\Delta H^0 = -67 \pm 19$ cal mol^{-1} for benzoic acid with other values listed in Table 1 suggests that the reported value is either in error by about 180 cal mol^{-1} or that the uncertainty is much larger than that given in the original publication. For *m*-methylbenzoic acid we have $\Delta H^0 = +70$ cal mol^{-1} from three independent investigations, $\Delta H^0 = -91 \pm 13$ cal mol^{-1} from Bolton *et al.* (7), and $\Delta H^0 = +1201 \pm 93$ cal mol^{-1} from Wilson *et al.* (18). Again we suggest that the result from Bolton *et al.* (7) is in error or that the uncertainty is much larger than the quoted estimate. It appears that there is a large systematic error in the work of Wilson *et al.* (18) on this compound. Similar comments apply to results for *p*-methylbenzoic acid.

In spite of uncertainties and possible errors of 100–200 cal mol^{-1} in some of the results from Bolton *et al.* (7), we believe that their ΔH^0 for *p*-nitrobenzoic acid is to be preferred to that from another investigation (11). Several other ΔH^0 values from Bolton *et al.* (7) are in satisfactory agreement with results of other investigations.

Our selection of "best" values for ΔH^0, ΔG^0, and ΔS^0 of ionization of benzoic acid and substituted acids is given in Table 3. All ΔH^0 values are based on our assessments of the ΔH^0 values listed separately in Tables 1 and 2. The ΔG^0 of ionization of *m*-fluorobenzoic acid is taken from Dippy and Lewis (23). All other ΔG^0 values are taken from investigations (7, 9, 18) cited in Tables 1 and 2. Some ΔH^0 and ΔS^0 values in Table 3 (followed by ? mark) are based on our uncertain selection from among conflicting values reported by different investigators.

Bolton *et al.* (7) have noted that their published results lead to linear relationships between ΔG^0 and ΔS^0, between ΔG^0 and ΔH^0, and between ΔH^0 and ΔS^0. Similar graphs of values reported by Wilson *et al.* (18) for some of the same acids (and others) exhibit considerable scatter about any single line. Because of substantial uncertainties or errors in several of the ΔH^0 and ΔS^0 values reported by these investigators (18), neither the presence nor absence of these linear relationships can be taken as proven on the basis of their results.

We have used the "best" ΔG^0, ΔH^0, and ΔS^0 values in Table 3 for construction of graphs of each of these thermodynamic functions against the other two, as previously done by Bolton *et al.* (7). Although there are differences between our graphs and theirs (due to some substantial differences between our "best" values and their

Can. J. Chem. Downloaded from www.nrcresearchpress.com by 210.87.254.105 on 09/05/12
For personal use only.

values), we also find that most of the points fall reasonably close to a straight line in each graph.

For consideration of the thermodynamics of substituent effects, it is most convenient to work with the thermodynamic functions for reactions of type

[5] $HBzX(aq) + Bz^-(aq) = BzX^-(aq) + HBz(aq)$

in which HBz represents benzoic acid and HBzX represents a substituted benzoic acid The standard free energy change for reaction 5 is obtained as $\delta\Delta G^0 = \Delta G^0_{HBzX} - \Delta G^0_{HBz}$; $\delta\Delta H^0$ and $\delta\Delta S^0$ values are obtained similarly. These $\delta\Delta G^0$, $\delta\Delta H^0$, and $\delta\Delta S^0$ values are direct measures of substituent effects.

A graph of $\delta\Delta H^0$ *vs.* $\delta\Delta S^0$ is shown in Fig. 1. If we exclude points 13, 14, and 15 from consideration, we see that there is a good linear correlation of $\delta\Delta H^0$ with $\delta\Delta S^0$. Because there are substantial differences in the uncertainties to be associated with the various thermodynamic quantities listed in Table 3, there is no reliable statistical method for determining the "best" straight line. We can, however, say that the slope of the "best" straight line is about 80°. A graph of $\delta\Delta G^0$ *vs.* $\delta\Delta S^0$ also shows points 13, 14, and 15 significantly above a straight line drawn through the other points. In this case, the slope of the "best" line is about −220°. It may be shown by way of $\delta\Delta G^0 = \delta\Delta H^0 - T\delta\Delta S^0$ that the slope in Fig. 1 minus the slope of $\delta\Delta G^0$ *vs.* $\delta\Delta S^0$ must equal T, as they do here.

Points 13, 14, and 15 (*p*-hydroxy-, *p*-methoxy-, and *p*-methylbenzoic acids) are distinctly above any reasonable straight line through the other points in a graph of $\delta\Delta G^0$ versus $\delta\Delta S^0$. Although there are larger than usual uncertainties in the thermodynamics of ionization of two of these acids, any reasonable selection of "best" values leads to points above the lines. It therefore appears that we must regard these substituents as "abnormal" in some sense.

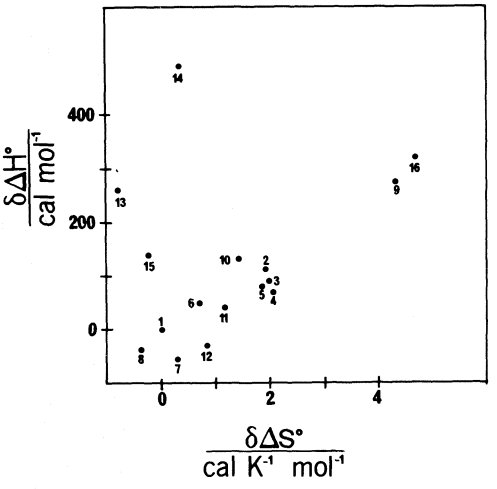

FIG. 1. Correlation of enthalpies and entropies for the "Hammett reaction" represented by eq. 5.

The Hammett equation may be written in terms of the equilibrium constant for reaction 5 as

[6] $$\log K_5 = \rho\sigma$$

and thence

[7] $$\delta\Delta G^0 = -2.303RT\rho\sigma$$

in which ρ is a temperature and solvent dependent "reaction" parameter and σ is a substituent parameter. Taking $\rho \equiv 1$ at 298 K, we have used $\delta\Delta G^0$ values to calculate the "best" σ parameters that are listed in Table 3.

Now we note that the three points that fall above the line drawn through "normal" points in Fig. 1 represent the three acids that have reasonably large negative σ values. It therefore seems reasonable to conclude that substituents with negative σ values exhibit "abnormal" enthalpy–entropy relationships in this reaction series.

Rigorous thermodynamic analysis (4) of the Hammett equation has shown that eq. 6 can be *exactly* valid over a range of temperature only if there are linear relationships between the thermodynamic quantities $\delta\Delta G^0$, $\delta\Delta H^0$, and $\delta\Delta S^0$. It has also been shown (4) how "compensation" of $\delta\Delta H^0$ and $\delta\Delta S^0$ may lead to an approximate linear free energy relationship such as eqs. 6 or 7 even when there is no linear relationship between $\delta\Delta H^0$ and $\delta\Delta S^0$. Thus we can anticipate from Fig. 1 that eqs. 6 and 7 will apply very well to most substituted benzoic acids over a range of temperature, and may even apply reasonably well to the "abnormal" acids with negative σ values over this same temperature range.

It has been shown (4) that the reaction parameter ρ can be expressed as

[8] $$\rho = \rho_\infty(1 - \beta_i/T)$$

in which β_i is the slope of $\delta\Delta H^0$ versus $\delta\Delta S^0$ and ρ_∞ is a constant of integration. Thus we may use $\beta_i = 80$ K and $\rho \equiv 1$ at 298 K to evaluate ρ_∞

Can. J. Chem. Downloaded from www.nrcresearchpress.com by 210.87.254.105 on 09/05/12
For personal use only.

and thence obtain values of ρ at various temperatures. In this way we have calculated ρ at 278 and 318 K. Then, using eq. 6, we have calculated values of K_5 at 278 and 318 K for all of the acids listed in Table 3. We denote these K_5 values calculated from the Hammett equation by K_H.

We have also used the ΔH^0 and ΔS^0 values in Table 3 to calculate K_5 values for all of these same acids at 278 and 318 K. These K_5 values, which can be regarded as reliable experimental quantities based only on thermodynamic quantities, are designated K_T.

If the Hammett equation were exactly valid over the range of temperature 278–318 K, each K_H value at each temperature would be identical with each corresponding K_T value. On the basis of previous work (4) as summarized in the paragraph above eq. 8, we should expect very good agreement between K_H and K_T values for all "normal" benzoic acids, with at least some chance of good agreement for other acids.

The average $|\log K_T - \log K_H|$ for *all* acids listed in Table 3 is 0.007 at 278 K and 0.006 at 318 K. The largest difference between $\log K_H$ and $\log K_T$ is 0.031 for *p*-methoxybenzoic acid. The standard deviation of the difference between $\log K_H$ and $\log K_T$ for all acids is 0.003 at both temperatures. We can therefore see that the Hammett equation "works" well for this whole group of substituted acids over the range of temperature 278–318 K.

If we now eliminate from consideration those acids for which σ is negative, we find that the average $|\log K_T - \log K_H|$ is 0.004 at 278 K and 0.003 at 318 K, with the largest difference being 0.007. The standard deviation of the difference between $\log K_T$ and $\log K_H$ is 0.001. Thus we see that the Hammett equation "works" *very* well for this group of "normal" acids over this temperature range.

We are grateful to the Research Corporation for their support of preliminary measurements that led to the work reported here, which was supported by the National Research Council of Canada. We also thank Dr. W. F. O'Hara for sending us the results of his measurements that are cited in Table 1. Dr. F. M. Hall has kindly discussed with us his earlier work (7).

1. L. P. HAMMETT. Physical organic chemistry. 2nd ed. McGraw-Hill, New York. 1970.
2. P. R. WELLS. Chem. Rev. **63**, 174 (1963).
3. J. W. LARSON and L. G. HEPLER. *In* Solute-solvent interactions. *Edited by* J. F. Coetzee and C. D. Ritchie. Marcel Dekker, Inc., New York. 1969.
4. L. G. HEPLER. Can. J. Chem. **49**, 2803 (1971).
5. P. D. BOLTON and L. G. HEPLER. Quart. Rev. **25**, 521 (1971).
6. L. D. HANSEN and L. G. HEPLER. Can. J. Chem. **50**, 1030 (1972).
7. P. D. BOLTON, K. A. FLEMING, and F. M. HALL. J. Am. Chem. Soc. **94**, 1033 (1972).
8. L. G. HEPLER and E. M. WOOLLEY. *In* Water: a comprehensive treatise. Vol. 3. *Edited by* F. Franks. Plenum Press, New York. 1973.
9. D. H. EVERETT and W. F. K. WYNNE-JONES. Trans. Faraday Soc. **35**, 1380 (1939). The quoted ΔH^0 values are based on equilibrium (conductivity) data from Schaller (1898), except for *m*-hydroxybenzoic acid, which is based on data from Euler (1898).
10. T. L. COTTRELL, G. W. DRAKE, D. L. LEVI, K. J. TULLY, and J. H. WOLFENDEN. J. Chem. Soc. 1016 (1948).
11. G. BRIEGLEB and A. BIEBER. Z. Electrochem. **55**, 250 (1951).
12. A. V. JONES and H. N. PARTON. Trans. Faraday Soc. **48**, 8 (1952).
13. L. P. FERNANDEZ and L. G. HEPLER. J. Phys. Chem. **63**, 110 (1959).
14. W. J. CANADY, H. M. PAPEE, and K. J. LAIDLER. Trans. Faraday Soc. **54**, 502 (1958).
15. T. W. ZAWIDSKI, H. M. PAPEE, and K. J. LAIDLER. Trans. Faraday Soc. **55**, 1743 (1959).
16. A. J. ELLIS. J. Chem. Soc. 2299 (1963).
17. B. S. SMOLYAKOV and M. P. PRIMANCHUK. Russ. J. Phys. Chem. **40**, 331 (1966).
18. J. M. WILSON, N. E. GORE, J. E. SAWBRIDGE, and F. CARDENAS-CRUZ. J. Chem. Soc. (B), 852 (1967).
19. J. J. CHRISTENSEN, R. M. IZATT, and L. D. HANSEN. J. Am. Chem. Soc. **89**, 213 (1967).
20. L. AVEDIKIAN and N. DOLLET. Bull Soc. Chim. Fr. 4551 (1967).
21. C. S. LEUNG and E. GRUNWALD. J. Phys. Chem. **74**, 687 (1970).
22. W. F. O'HARA. Personal communication. December, 1973.
23. J. F. J. DIPPY and R. J. LEWIS. J. Chem. Soc. 644 (1936).

Can. J. Chem. Downloaded from www.nrcresearchpress.com by 210.87.254.105 on 09/05/12
For personal use only.

Calorimetric Heats of Ionization of Aqueous Benzoic Acid from 5–100 °C and Derived Thermodynamic Quantities

TAKEKI MATSUI, HON CHUNG KO, AND LOREN G. HEPLER
Department of Chemistry, University of Lethbridge, Lethbridge, Alberta T1K 3M4
Received February 22, 1974

TAKEKI MATSUI, HON CHUNG KO, and LOREN G. HEPLER. Can. J. Chem. **52**, 2912 (1974).
We have made calorimetric measurements at 5.0, 12.5, 25.0, 40.0, 50.0, 65.0, 75.0, 85.0, and 100 °C that lead to values of ΔH^0 of ionization of aqueous benzoic acid at each of these temperatures. These ΔH^0 values have been used with pK = 4.204 at 25.0 °C for calculation of pK values from 5 to 100 °C and also ΔC_p^0 of ionization values over this range. Usefulness of various extrapolation functions for ΔH^0, ΔC_p^0, and pK up to 225 °C has been investigated.

TAKEKI MATSUI, HON CHUNG KO et LOREN G. HEPLER. Can. J. Chem. **52**, 2912 (1974).
Des mesures calorimétriques à 5.0, 12.5, 25.0, 40.0, 50.0, 65.0, 75.0, 85.0 et 100 °C permettent d'évaluer les ΔH^0 d'ionisation de l'acide benzoïque aqueux à chacune de ces températures. A l'aide de ces valeurs de ΔH^0 et le pK de 4.204 à 25.0 °C, on calcule les pK entre 5 et 100 °C et les ΔC_p^0 d'ionisation dans ce même intervalle de températures. On examine l'utilité de l'extrapolation des fonctions ΔH^0, ΔC_p^0 et pK jusqu'à 225 °C. [Traduit par le journal]

Introduction

There have been many investigations of the thermodynamics of ionization of aqueous benzoic acid, as reviewed in another paper (1) from this laboratory. Results of many of these investigations are in poor agreement with each other. For example, reported values for ΔH^0 of ionization at 298 K range from -420 to $+169$ cal mol^{-1}. Although it now appears (1) that $\Delta H^0 = +110$ cal mol^{-1} is reliably established as the "best" value at 298 K, there are still substantial uncertainties in the thermodynamics of ionization at other temperatures.

Three previous calorimetric investigations (2–4) have led to ΔH^0 and ΔC_p^0 values for ionization of aqueous benzoic acid from 5 to 55 °C. Disagreements between reported results are sufficient to justify further calorimetric measurements. Further, it is desirable to extend calorimetric measurements on aqueous benzoic acid to substantially higher temperatures.

The most recent investigation of the ionization constant of aqueous benzoic acid over a range of temperatures (5–60 °C) was that of Bolton *et al.* (5), who used a spectrophotometric method. Earlier conductance measurements from 25 to 90 °C by Smolyakov and Primanchuk (6) and from 25 to 225 °C by Ellis (7) have also led to ionization constants for aqueous benzoic acid over the designated temperature ranges. Still other investigations over smaller temperature ranges as reviewed previously (1) have also led to ionization constants at several temperatures. There are modest differences in reported K values and very large differences in such derived quantities as ΔH^0 and ΔC_p^0 of ionization at various temperatures. These differences can only be resolved by results of further measurements at temperatures both above and below 25 °C.

Feates and Ives (8), Ives and Marsden (9), and Leung and Grunwald (4) have all discussed the relationship between solute–solvent interactions and ΔC_p^0 of ionization, with particular emphasis on the temperature dependence of ΔC_p^0. Evaluation of ΔC_p^0 from pK values at different temperatures requires two differentiations with respect to temperature and inevitably leads to magnification of experimental errors in the original measurements and subsequent data treatment. Evaluation of ΔC_p^0 from calorimetric ΔH^0 values at different temperatures requires only one differentiation with respect to temperature and may therefore be preferable. In either case, it is important to have reliable experimental results of the best attainable accuracy that cover the widest possible range of temperature.

In this paper we report the results of our calorimetric determinations of the ΔH^0 of

Can. J. Chem. Downloaded from www.nrcresearchpress.com by 210.87.254.6 on 09/05/12
For personal use only.

Can. J. Chem. Downloaded from www.nrcresearchpress.com by 210.87.254.6 on 09/05/12
For personal use only.

ionization of aqueous benzoic acid from 5 to 100 °C, along with results of our thermodynamic calculations.

Experimental

All calorimetric measurements were made with an LKB Precision Calorimetry System. Measurements at 5.0, 12.5, 25.0, 40.0, and 50.0 °C were made with the standard 100 ml LKB glass reaction calorimeter, using glass ampoules to contain the solid sample to be dissolved in the calorimetric solution. Measurements at 25 °C were also made with the LKB glass titration calorimeter, with the titrant solution being supplied by a Metrohm Dosimat automatic titrator (1). Measurements at 50.0, 65.0, 75.0, 85.0, and 100.0 °C were made with a stainless steel bomb calorimeter identical to that described by Olofsson *et al.* (10). Heat effects associated with ampoule breaking and titrant dilution were determined by means of separate experiments. All ΔH^0 values, reported in terms of the defined calorie (1 cal = 4.1840 J), refer to the stated temperature to within ±0.05 °C.

Preparation of sodium benzoate has been described previously (1). Acid and base solutions were prepared and standardized by traditional methods.

Results

We have measured heats of solution of sodium benzoate in 0.001 *M* NaOH (to repress hydrolysis) as represented by

[1] $$NaBz(c) = Na^+(aq) + Bz^-(aq) \qquad \Delta H_1^0$$

At each temperature (5, 12.5, 25, 40, 50, 65, 75, 85, and 100 °C) we have made at least seven determinations, with final concentrations of dissolved sodium benzoate ranging from 0.005 to 0.035 *M*. The results at each temperature have been extrapolated *vs.* the square root of concentration to infinite dilution to obtain the corresponding value of ΔH_1^0, as listed in Table 1.

We have also measured heats of solution of sodium benzoate in dilute hydrochloric acid (0.024 and 0.049 *M*) as represented by

[2] $$NaBz(c) + H^+(aq) = HBz(aq) + Na^+(aq) \qquad \Delta H_2^0$$

At each of the temperatures listed above we have made at least seven determinations, with final concentration of dissolved benzoic acid ranging from 0.003 to 0.030 *M*, and have again extrapolated to infinite dilution to obtain the ΔH_2^0 values listed in Table 1.

Combination of ΔH_1^0 and ΔH_2^0 values leads to the desired enthalpies of ionization as follows:

[3] $$\Delta H_i^0 = \Delta H_1^0 - \Delta H_2^0$$

[4] $$HBz(aq) = H^+(aq) + Bz^-(aq) \qquad \Delta H_i^0$$

Our ΔH_i^0 values are listed in Table 1.

If we had any adequate theory for partial molal heat capacities of aqueous solutes, we could start with an equation for ΔC_p^0 of the "right" functional form and by integration obtain the corresponding equation for ΔH_i^0 as a function of temperature. Then the parameters of this equation could be adjusted to fit our experimental ΔH_i^0 values. Finally, an equation of this sort could be used for reliable extrapolation outside the temperature range of the original experimental ΔH_i^0 values.

In the absence of any semi-adequate theory for $\bar{C}_p^0$ of aqueous solutes, we must make use of arbitrarily selected algebraic expressions, such as polynomials in temperature *T*. We have been unable to find any two or three parameter equations that fit all of our ΔH_i^0 values satisfactorily and have therefore turned to four parameter equations:

[5] $$\Delta H_i^0 = A + BT + CT^2 + DT^3$$

[6] $$\Delta H_i^0 = A + BT^2 + CT^3 + DT^4$$

[7] $$\Delta H_i^0 = A + BT + CT^2 + D \ln T$$

[8] $$\Delta H_i^0 = A + BT + CT^2 + DT^{-1}$$

Equations 5–8 have been fitted to our ΔH_i^0

TABLE 1. ΔH^0 values for solution of sodium benzoate in base and in acid and for ionization of aqueous benzoic acid[a]

t (°C)	ΔH_1^0 (cal mol^{-1})	ΔH_2^0 (cal mol^{-1})	ΔH_i^0 (cal mol^{-1})
5.0	−908 ± 20	−1867 ± 30	+959 ± 35
12.5	−799 ± 20	−1400 ± 30	+601 ± 35
25.0	−581 ± 20	−687 ± 30	+106 ± 35[b]
40.0	−281 ± 20	+174 ± 30	−455 ± 35
50.0	−75 ± 25[c]	+712 ± 30[c]	−787 ± 40[c]
65.0	+308 ± 40	+1453 ± 40	−1145 ± 55
75.0	+521 ± 40	+1943 ± 50	−1422 ± 65
85.0	+612 ± 40	+2325 ± 50	−1713 ± 65
100.0	+950 ± 60	+3122 ± 60	−2170 ± 85

[a]All ± values indicate our estimates of *total* uncertainties (calorimetric, chemical, and extrapolation).

[b]We have also used titration calorimetry (1) to obtain ΔH_i^0 = +114 cal mol^{-1}. On the basis of our work and ΔH_i^0 values from earlier workers, we selected (1) ΔH_i^0 = +110 cal mol^{-1} as the "best" value. In this paper we use ΔH_i^0 = 106 cal mol^{-1} because we are partly concerned with $d\Delta H_i^0/dT$ and consider that this quantity is best obtained from ΔH_i^0 values that have all been obtained in the same way.

[c]At 50 °C we have made measurements with both of our calorimeter vessels (same electrical circuitry used throughout) to ensure that there is no systematic difference. Results obtained with different vessels were the same, and values reported here are based on all measurements made with both calorimeters.

TABLE 2. Values of parameters in equations for ΔH_i^0 as function of temperature[a]

Parameter	Value			
	Eq. 5	Eq. 6	Eq. 7	Eq. 8
A	86051.7	29520.9	833046.8	−170505.8
B	−712.02	−1.33990	1086.775	496.629
C	2.00298	4.9818×10^{-3}	−0.815246	−0.513144
D	−0.0019521	-5.3619×10^{-6}	−190346.7	0.203167×10^{8}

[a]All ΔH_i^0 values are expressed in terms of cal mol^{-1} and all temperatures in Kelvins.

TABLE 3. Comparison of ΔH_i^0 values[a] for aqueous benzoic acid

t (°C)	ΔH_i^0						$\frac{d \ln K}{dT}$
	Eq. 5	Eq. 6	Eq. 7	Eq. 8	Our calorimetry	Earlier calorimetry	
5.0	+961	+969	+958	+973	+959	+736[b]	
10.0	+716	+724	+713	+726		+622[c], +785[d]	+362[e]
12.5	+600	+607	+597	+610	+601		
15.0	+488	+494	+486	+499		+460[b]	+243[e], +974[f]
20.0	+276	+279	+276	+288		+295[c]	+123[e], +562[f], +338[g]
25.0	+78	+79	+80	+91	+110	See ref. 1	See ref. 1
30.0	−107	−110	−103	−92		−68[c]	−262[f], −143[g]
35.0	−280	−286	−275	−265		−272[b]	−250[e], −674[f], −390[g]
40.0	−444	−452	−437	−429	−455	−465[d]	−1087[f]
45.0	−599	−609	−592	−585		−657[b]	
50.0	−747	−757	−740	−735	−787		−642[e], −677[h]
55.0	−890	−899	−844	−881		−1029[b]	
60.0	−1028	−1037	−1024	−1024			−914[e]
65.0	−1164	−1170	−1162	−1165	−1145		
75.0	−1434	−1434	−1437	−1446	−1422		−1337[e], −1541[h]
85.0	−1711	−1706	−1717	−1733	−1713		
90.0	−1856	−1849	−1863	−1882			−1779[e]
100.0	−2166	−2161	−2168	−2193	−2170		−2084[e], −2424[h]
125.0	−3126	−3195	−3062	−3091			−2882[e], −3325[h]
150.0	−4496	−4845	−4224	−4226			−3772[e], −4245[h]
175.0	−6461	−7469	−5739	−5666			−5183[h]
200.0	−9202	−11477	−7679	−7465			−6140[h]
225.0	−12903	−17327	−10107	−9665			−7116[h]

[a]All ΔH_i^0 values are expressed in cal mol^{-1}.
[b]Leung and Grunwald, ref. 4.
[c]Cottrell *et al.*, ref. 2.
[d]Fernandez and Hepler, ref. 3.
[e]Smolyakov and Primanchuk, ref. 6, based on experimental K values over the range 25–90 °C.
[f]Wilson *et al.*, ref. 11.
[g]Jones and Parton, ref. 12.
[h]Ellis, ref. 7; based on experimental K values over the range 25–225 °C.

values over the range 5–100 °C (278–373 K). Values of the A, B, C, and D parameters for each equation are listed in Table 2. Standard deviations of these equations are ±19.5, ±18.5, ±21.7, and ±26.8 cal mol^{-1}, respectively. Although these equations are all about the same in terms of representation of our experimental ΔH_i^0 values, they may well be significantly different in other respects that are discussed in detail later.

Our experimental and calculated ΔH_i^0 values are summarized in Table 3, along with results from several other investigations. The earlier calorimetric ΔH_i^0 values (2–4), which were determined from 5 to 55 °C, are in reasonable agreement with our results except at 5 and 55 °C. This limited disagreement is of considerable importance in connection with evaluation of ΔC_p^0 and extrapolation of thermodynamic functions to higher temperatures.

We also have ΔH_i^0 values calculated from $d \ln K/dT$. It has been suggested previously (1)

Can. J. Chem. Downloaded from www.nrcresearchpress.com by 210.87.254.6 on 09/05/12
For personal use only.

TABLE 4. Comparison of ΔC_p^0 values[a] for ionization of aqueous benzoic acid

t (°C)	ΔC_p^0 Eq. 5′	Eq. 6′	Eq. 7′	Eq. 8′	Ref. 4[b]	Ref. 6[c]	Ref. 7[d]
10	−47.2	−47.5	−47.1	−47.4	−27.6	−23.5	
15	−43.9	−44.4	−43.6	−43.8		−23.9	
20	−40.9	−41.5	−40.5	−40.6	−34.2	−24.3	
25[e]	−38.2	−38.8	−37.7	−37.9		−24.7	−29.1
30	−35.8	−36.4	−35.4	−35.6	−39.0		
35	−33.7	−34.2	−33.3	−33.6		−25.5	
40	−31.8	−32.2	−31.6	−31.9	−38.5		
50	−29.0	−29.1	−29.1	−29.6	−37.2	−26.8	−29.4
60	−27.4	−27.1	−27.8	−28.3		−27.6	
75	−27.2	−26.6	−27.6	−28.3		−28.8	−29.8
90	−29.6	−29.4	−29.5	−30.1		−30.1	
100	−32.6	−33.4	−31.7	−32.2		−30.9	−30.2
125	−45.4	−51.5	−40.5	−40.2		−33.0	−30.6
150	−65.5	−83.0	−52.9	−51.1		−35.0	−30.9
175	−92.9	−129.8	−68.6	−64.5			−31.3
200	−127.6	−194.0	−87.0	−79.7			−31.7
225	−169.7	−277.5	−107.5	−96.5			−32.1

[a]All ΔC_p^0 values are expressed in cal K^{-1} mol^{-1}.
[b]Based on calorimetric measurements from 5–55 °C.
[c]Based on K values from 25–90 °C.
[d]Based on K values from 25–225 °C.
[e]Bolton *et al.* (5) report $\Delta C_p^0 = -42 \pm 3$ cal K^{-1} mol^{-1} at 25 °C, based on K values from 5–60 °C.

that some of the results of Wilson *et al.* (11) contain substantial errors. We now see that their ΔH_i^0 values are mostly in poor agreement with our results and also with other results listed in Table 3. Our ΔH_i^0 values are in reasonable agreement with those of Jones and Parton (12) near 25 °C. Smolyakov and Primanchuk (6) have calculated ΔH_i^0 values for temperatures from 10–150 °C. Agreement between their results and ours is reasonably good for 25–100 °C but is generally poor outside this temperature range. Here it should be noted that all of their values for $t > 90$ °C and also our values for $t > 100$ °C are based on extrapolations and that their values for $t < 25$ °C are based on extrapolations. We have used the equation given by Ellis (7) for log K over the range 25–225 °C to calculate ΔH_i^0 values at 25° intervals with results that are in fair agreement with our ΔH_i^0 values at the lower temperatures and poorer agreement at the higher temperatures.

Differentiation of our eqs. 5–8 with respect to temperature leads us to related equations for ΔC_p^0 of ionization:

$$[5'] \qquad \Delta C_p^0 = B + 2CT + 3DT^2$$

$$[6'] \qquad \Delta C_p^0 = 2BT + 3CT^2 + 4DT^3$$

$$[7'] \qquad \Delta C_p^0 = B + 2CT + DT^{-1}$$

$$[8'] \qquad \Delta C_p^0 = B + 2CT - DT^{-2}$$

Numerical values of ΔC_p^0 at various temperatures calculated from these equations are listed in Table 4, along with ΔC_p^0 values from earlier investigations.

Our ΔC_p^0 values based on eqs. 5′–8′ are in generally good agreement with one another over the temperature range 5–100 °C, which is also the range covered by our experimental ΔH_i^0 values. We estimate the uncertainty in ΔC_p^0 to be about ± 2 cal K^{-1} mol^{-1} in this temperature range. A graph of our ΔC_p^0 values against temperature clearly has a *maximum* of $\Delta C_p^0 \cong -27$ cal K^{-1} mol^{-1} at $t \cong 70$ °C. The ΔC_p^0 values reported by Leung and Grunwald (4) exhibit a distinctly different temperature dependence over a smaller temperature range. Their ΔC_p^0 values pass through a minimum of ~ -39 cal K^{-1} mol^{-1} at $t \cong 35$ °C. Because their ΔH_i^0 values extend only to 55 °C, it is impossible to use their results to conclude anything about a possible maximum (such as we find) at $t \cong 70$ °C. Smolyakov and Primanchuk (6) and also Ellis (7) were able to fit their pK values to functions of T that lead to ΔC_p^0 expressed as linear functions of T. Thus neither of these latter investigations (6, 7) by themselves can tell us anything about a possible minimum

Can. J. Chem. Downloaded from www.nrcresearchpress.com by 210.87.254.6 on 09/05/12
For personal use only.

TABLE 5. Comparison of pK values[a] for ionization of aqueous benzoic acid

t (°C)	pK						
	Eq. 5″	Eq. 6″	Eq. 7″	Eq. 8″	Graphical	Ref. 6[b]	Ref. 7[c]
5	4.227	4.231	4.225	4.231	4.231		
10	4.217	4.219	4.215	4.220	4.220	4.211	
15	4.209	4.211	4.209	4.212	4.211	4.208	
20	4.204	4.206	4.205	4.206	4.206	4.206	
25	4.204	4.204	4.204	4.204	4.204	4.205	4.214
35	4.205	4.206	4.209	4.206	4.206	4.207	
50	4.226	4.224	4.229	4.223	4.223	4.222	4.228
60	4.243	4.242	4.249	4.240	4.242	4.238	
75	4.280	4.277	4.286	4.275	4.277	4.269	4.281
90	4.324	4.319	4.331	4.318	4.319	4.310	
100	4.358	4.351	4.365	4.351	4.352	4.341	4.364
125	4.456	4.448	4.464	4.447		4.432	4.470
150	4.579	4.576	4.584	4.565		4.538	4.592
175	4.733	4.750	4.729	4.706			4.728
200	4.933	4.989	4.902	4.874			4.873
225	5.189	5.318	5.109	5.071			5.027

[a]All pK = −log K values are on the molal scale.
[b]Quoted values are based on the authors' equation, which was fitted to experimental pK values over the range 25–90 °C and extrapolated outside this range.
[c]Quoted values are based on the authors' equation, which was fitted to experimental pK values over the range 25–225 °C.

or maximum in a graph of ΔC_p^0 against temperature.

There are, however, results from other investigations that give us some ideas about "normal" variation of ΔC_p^0 of ionization with respect to temperature.

A recent analysis (13) of all available thermodynamic data for the ionization of water shows that there is a maximum in ΔC_p^0 for this reaction at about 70 °C, similar to our results here for benzoic acid. Because the results of Leung and Grunwald (4) for ionization of water lead to a maximum in ΔC_p^0 at about 30 °C (rather than 70 °C) and because their ΔC_p^0 values for ionization of benzoic acid appear to exhibit an "abnormal" temperature dependence, we suggest that there are *small* temperature dependent systematic errors in their calorimetric results. It should be recognized that *small* temperature dependent errors can lead to substantial errors in quantities such as ΔC_p^0 that are obtained by differentiation.

We also note that calorimetric measurements by Ackermann and Schreiner (14) lead to maxima (at 70–80 °C) in graphs of ΔC_p^0 of ionization of formic acid, acetic acid, and propionic acid against temperature.

Our experimental values of ΔH_i^0 can be used with a pK value at any temperature within the range 5–100 °C to calculate pK values at any other temperature within this range. One way to do these calculations begins with the thermodynamic equation $\mathrm{d}(\Delta G^0/T)/\mathrm{d}T = -\Delta H^0/T^2$. Integration of this equation and combination with $\Delta G^0 = -RT \ln K$ leads to

$$[9] \quad \mathrm{p}K_T = \mathrm{p}K_{298} - \frac{1}{2.303R} \int_{T=298}^{T} \frac{\Delta H^0}{T^2} \mathrm{d}T$$

We take $\mathrm{p}K_{298} = 4.204$ from our previous analysis (1) of several determinations of the ionization constant at 25 °C. Then, using our ΔH_i^0 values for ionization of aqueous benzoic acid, we evaluate the integral in eq. 9 from a large scale graph of $\Delta H^0/T^2$ against T and calculate values of pK at various temperatures T, with results listed in Table 5. The uncertainty in the calculated pK at 100 °C due to uncertainties in our ΔH_i^0 values is estimated to be no more than ±0.01, with still smaller uncertainties at temperatures closer to 25 °C.

Another way to calculate pK values at various temperatures is to integrate the van't Hoff equation $\mathrm{d} \ln K/\mathrm{d}T = \Delta H^0/RT^2$ using our eqs. 5–8 for ΔH^0 as functions of temperature and the "best" $\mathrm{p}K_{298} = 4.204$. The resulting equations are the following:

$$[5''] \quad \mathrm{p}K_T = 18\,802.9/T + 358.303 \log T - 0.437665T + 2.13269 \times 10^{-4}T^2 - 833.929$$

Can. J. Chem. Downloaded from www.nrcresearchpress.com by 210.87.254.6 on 09/05/12
For personal use only.

$$[6''] \quad pK_T = 6450.51/T + 0.292777T - 5.44281 \times 10^{-4}T^2 + 3.90540 \times 10^{-7}T^3 - 66.690$$

$$[7''] \quad pK_T = 140\,434/T + 0.178137T - 546.888 \log T - 95\,786.4 \log T/T + 1628.271$$

$$[8''] \quad pK_T = -37\,256.6/T + 0.112125T - 249.869 \log T + 2\,219\,663/T^2 + 689.047$$

The pK values we have calculated with these equations are listed in Table 5.

All of the pK values calculated graphically and from eqs. 5''–8'' (listed in Table 5) are in good agreement with one another from 5–100 °C, the *largest* difference between calculated pK values at a single temperature being 0.014 at 100 °C. This excellent agreement of the various pK values is expected because all calculations are based on the same experimental data and the same principles of thermodynamics.

We also see that our calculated pK values from 25–90 °C are in good agreement with the experimental values reported by Smolyakov and Primanchuk (6), the *largest* difference between any of our values and theirs being 0.021 at 90 °C. Similarly, our pK values at temperatures from 25–100 °C are in excellent agreement with those from Ellis, the *largest* difference between any of our values and his being 0.010 at 25 °C.

It is both well known and often forgotten that algebraic expressions of distinctly different forms can be used to fit experimental results about equally well. If one is interested only in concise representation of a large number of results or in interpolation between closely spaced points, one equation may very well be as "good" as another equation of drastically different functional form. But if one is interested in differentiation or extrapolation beyond the range of original fit, then one equation may be much better than another. As stated earlier, our eqs. 5–8 for ΔH_i^0 as functions of temperature all fit the experimental results about equally well. We now consider extrapolations and derivatives of these equations.

We have used our eqs. 5–8 for calculating ΔH_i^0 values at 25° intervals from 125–225 °C, well above the range (5–100 °C) of our original measurements and fits of experimental results to the equations. Although the ΔH_i^0 values calculated with these equations are in good agreement with one another and with our experimental ΔH_i^0 value at 100 °C, differences between values calculated with different equations are more than 600 cal mol^{-1} at 150 °C and more than 7000 cal mol^{-1} at 225 °C. It is therefore obvious that these equations must be used cautiously for extrapolation outside the range of original measurements and fit of equations to experimental results.

Because eqs. 5–8 all fit our ΔH_i^0 results quite well over our entire range of experimental temperatures, it might be hoped that eqs. 5'–8' obtained by differentiation will yield ΔC_p^0 values in good agreement with one another over this same temperature range. Calculated ΔC_p^0 values listed in Table 4 support this hope. But calculated ΔC_p^0 values obtained from the different equations are drastically different from one another at temperatures above 100 °C, thus forcing us once again to be cautious about extrapolation.

Analysis (13) of the thermodynamics of ionization of water over the temperature range 5–300 °C *suggests* that eq. 8' is likely better than eqs. 5'–7' for extrapolation above 100 °C and that eq. 6' is likely worse than the other equations for similar extrapolation. Evidence for or against these suggestions cannot be obtained from the ΔC_p^0 values calculated by Smolyakov and Primanchuk (6) because their values are based on extrapolation above 90 °C. Although the ΔC_p^0 values we have calculated by two differentiations of the $\log K = f(T)$ equation given by Ellis (7) are based on experimental data obtained above 100 °C, the accuracy of these ΔC_p^0 values is too low to permit us to choose between eqs. 5'–8'. However, the ΔH_i^0 values we have calculated by one differentiation of the $\log K = f(T)$ equation from Ellis (7) are of sufficient accuracy to suggest that eq. 8 is better than eqs. 5–7 for extrapolation to high temperatures and that eq. 6 is worse than the others for this purpose. Thus we do have indirect evidence that eq. 8' is best and eq. 6' is worst for extrapolation above 100 °C.

Because very accurate pK values over a wide range of temperature are needed to yield reliable information about ΔC_p^0 by way of two differentiations with respect to temperature, it follows that relatively inaccurate ΔC_p^0 values

Can. J. Chem. Downloaded from www.nrcresearchpress.com by 210.87.254.6 on 09/05/12
For personal use only.

will suffice for calculation of pK values over a wide range of temperature. This point is illustrated by our calculated pK values (Table 5) for temperatures above 100 °C. Although our calculated ΔC_p^0 values are considerably different from one equation to another, calculated pK values differ from one another by relatively small amounts. For example, the *largest* difference between our highest and lowest calculated pK values at any temperature is 0.247 at 225 °C. At 150 °C (a 50° extrapolation) our highest and lowest calculated pK values differ from each other by only 0.019, in spite of substantial differences in calculated ΔC_p^0 values at this temperature.

Comparison of our calculated pK values with those from Ellis (7) provides further support for the suggestion that eq. 8′ (also 8 and 8″) is best for extrapolation. The *worst* discrepancy between our pK values calculated from eq. 8″ and values from Ellis is 0.044 at 225 °C. Thus we see that eq. 8 leads to a very good extrapolation formula (eq. 8″) for pK of aqueous benzoic acid. Even the worst extrapolation formula (eq. 6″) leads to pK values in fair agreement with the experimental values.

As a matter of principle, it should be noted that our calculated pK values at temperatures above 100 °C are all for hypothetical solutions maintained at a constant pressure of exactly 1 atm, while the experimental pK values from Ellis (7) are for solutions at the saturation pressure at each particular temperature. With $P_{\text{sat'd}} \cong 20$ atm at $t \cong 225$ °C and an estimated (13) ΔV^0 for ionization at this temperature, we can calculate pK (1 atm) − pK (20 atm) and find that the difference is too small to worry about in connection with this investigation. At $t = 300°$ where $-\Delta V^0$ and $P_{\text{sat'd}}$ are both larger than at 225 °C, this effect is too large to be ignored.

The work reported here has shown that it is possible to use calorimetric ΔH^0 values over a range of temperature for calculation of accurate and reliable equilibrium constants over a considerably wider range of temperatures. These ΔH^0 values also permit calculation of ΔC_p^0 values over a range of temperatures by way of only one differentiation rather than two as required to obtain ΔC_p^0 from pK values at different temperatures. These ΔC_p^0 values are of considerable potential value (4, 8, 9) for gaining understanding of solute–solvent interactions.

We are grateful to the National Research Council of Canada for support of this research and to Dr. Gerd Olofsson for her helpful advice on all aspects of this research.

1. T. Matsui, H. C. Ko, and L. G. Hepler. Can. J. Chem. This issue.
2. T. L. Cottrell, G. W. Drake, D. L. Levi, K. J. Tully, and J. H. Wolfenden. J. Chem. Soc. 1016 (1948).
3. L. P. Fernandez and L. G. Hepler. J. Phys. Chem. **63**, 110 (1959).
4. C. S. Leung and E. Grunwald. J. Phys. Chem. **74**, 687 (1970).
5. P. D. Bolton, K. A. Fleming, and F. M. Hall. J. Am. Chem. Soc. **94**, 1033 (1972).
6. B. Smolyakov and M. P. Primanchuk. Russ. J. Phys. Chem. **40**, 331 (1966).
7. A. J. Ellis. J. Chem. Soc. 2299 (1963).
8. F. S. Feates and D. J. G. Ives. J. Chem. Soc. 2798 (1956).
9. D. J. G. Ives and P. D. Marsden. J. Chem. Soc. 649 (1965).
10. G. Olofsson, S. Sunner, M. Efimov, and J. Laynez. J. Chem. Thermodynamics, **5**, 199 (1973).
11. J. M. Wilson, N. E. Gore, J. E. Sawbridge, and F. Cardenas-Cruz. J. Chem. Soc. (B), 852 (1967).
12. A. V. Jones and H. N. Parton. Trans. Faraday Soc. **48**, 8 (1952).
13. G. Olofsson and L. G. Hepler, manuscript in preparation.
14. T. Ackermann and F. Schreiner. Zeit. Electrochem. **62**, 1143 (1958).

Can. J. Chem. Downloaded from www.nrcresearchpress.com by 210.87.254.6 on 09/05/12
For personal use only.

Electron Spin Resonance Studies in Aqueous Solution: Titanium(III) in the p*H* Region 1.0–3.5

PAVLE ILIJA PREMOVIĆ AND PAUL RONALD WEST
Department of Chemistry, University of Victoria, Victoria, British Columbia V8W 2Y2

Received February 14, 1974

PAVLE ILIJA PREMOVIĆ and PAUL RONALD WEST. Can. J. Chem. **52**, 2919 (1974).

In aqueous solutions of titanium(III) between p*H* 1.0 and 3.5 a single line e.s.r. signal is recorded with $g = 1.9408 \pm 0.001$ and linewidth 95 ± 3 G. Evidence is presented in support of a hydrolyzed metal ion complex $[Ti(OH)_2(H_2O)_4]^+$ as the likely active species.

PAVLE ILIJA PREMOVIĆ et PAUL RONALD WEST. Can. J. Chem. **52**, 2919 (1974).

En solutions aqueuses de titane(III), entre des p*H* variant de 1.0 à 3.5, on enregistre un signal d'une seule raie r.p.e. avec $g = 1.9408 \pm 0.001$ et de largeur 95 ± 3 G. On fournit des données indiquant que l'ion métallique complexe hydrolysé $[Ti(OH)_2(H_2O)_4]^+$ est l'espèce active probable. [Traduit par le journal]

Can. J. Chem. Downloaded from www.nrcresearchpress.com by 210.87.254.6 on 09/05/12
For personal use only.

Introduction

The titanium(III) ion ($3d^1$) exists in acidic aqueous solution as the hexaaquo ion $Ti(H_2O)_6^{3+}$. In spite of the unpaired electron that is present, no e.s.r. signal is observed for this species. Such an observation is fully consistent with the octahedral crystal field symmetry of the ion. In the orbitally degenerate ground state, $^2T_{2g}$, the spin angular momentum is cancelled by the residual orbital angular momentum, leading to the expectation that $g \approx 0$ (1, 2). Although small axial or rhombic distortions can partially quench the orbital angular momentum, spin–lattice relaxation time is too short to detect the e.s.r. signal. Reduction of the symmetry of the ion to tetragonal or lower leaves essentially only the spin angular momentum, and hence a signal with g close to the free electron (2.0023) and with a narrow linewidth expected. The complexes $Ti(CH_3O)^{2+}$ and TiF_2^+ in methanol solutions have such a distortion of the octahedral field, and exhibit e.s.r. signals (3). Other examples of e.s.r. spectra from titanium(III) complexes have been published (4–8).

We now wish to report the observation of an e.s.r. spectrum from aqueous solutions of $TiCl_3$, $Ti_2(SO_4)_3$, and TiI_3 in the p*H* interval 1.0–3.5. Our experiments indicate that the signal arises from one of the equilibrium forms of the partially hydrolyzed titanous ion $Ti(OH)^{2+}$, most reasonably either the species $[TiO(H_2O)_5]^+$ or $[Ti(OH)_2(H_2O)_4]^+$.

Experimental

All spectra were recorded on a Varian E-6S X band e.s.r. spectrometer operating at 100 kHz modulation. Samples were contained in standard Varian E-248 aqueous solution cells.

The titanium(III) solutions were prepared by dissolving the metallic sponge (Fisher) with gentle heating in approximately 1 *N* HCl or H_2SO_4 respectively. In all cases a nitrogen atmosphere was employed to minimize oxidation of the titanous species. Alternatively Fisher reagent titanium(III) chloride solution (20%) was used directly as received without qualitative change in any results. Titanium(III) iodide was prepared in methanol by the procedure of Giggenbach and Brubaker (9). Methanol was eliminated by several evaporations to dryness employing water as the solvent in the second and subsequent cycles.

The g factors are quoted relative to DPPH, $g = 2.0036$. Relative spin concentrations were estimated from the product of the peak-to-peak height of the first derivative signal and the square of the maximum slopewidth. Absolute concentrations were estimated by comparison with standard aqueous manganous chloride. The u.v./visible spectra were recorded on a Cary Model 17 instrument.

Results and Discussion

Detailed examinations of the behavior of dilute aqueous titanium(III) solutions in the p*H* region between 0.0 and 3.5 indicate that $Ti(H_2O)_6^+$ and $Ti(OH)^{2+}$ are the dominant species with insignificant amounts of further hydrolyzed ions present below p*H* 3.5 (10–12). Applying e.s.r. spectroscopy we observe the existence of a paramagnetic signal from dilute titanous ion in aqueous solutions of p*H* 1.0–3.5. The e.s.r.

TABLE 1. Electron spin resonance data for complex ions

Proposed complex ion*	g factor ±0.001	ΔH_{PP} ±2 G†	Total unpaired spins (%)
$[TiO(H_2O)_5]^+$ or $[Ti(OH)_2(H_2O)_4]^+$	1.9408	95‡	~2
$[TiO(D_2O)_5]^+$ or $[Ti(OD)_2(D_2O)_4]^+$	1.9411	72	~2

*Total concentration of Ti^{3+} was between 0.001 to 0.500 M in the pH region between 1.5 to 3.5.
†ΔH_{PP} is the peak-to-peak linewidth.
‡Room temperature. Value decreases to 84 ± 3 G at 0 °C.

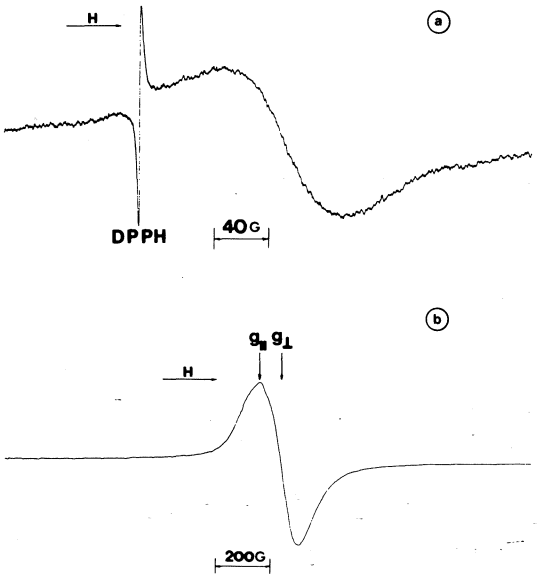

FIG. 1. (*a*) $TiCl_3$, 0.016 M, 25 °C; pH 2.7. (*b*) $TiCl_3$, 0.018 M, 77 °K (frozen solution); Solution pH 2.2 D_2O; $g_\perp = 1.925 \pm 0.001$, $g_\parallel = 1.961 + 0.001$.

spectrum is shown in Fig. 1*a* and the spectral data are tabulated in Table 1. By approximate calculation, employing graphical integration of the derivative absorption curve, we estimate the maximum concentration of spins contributing to the signal to be *ca.* 2% of the total Ti^{3+} concentration.

Assignment of the basic structural feature of the *complex providing the signal* is based on the close agreement of its pH dependence with that of the hydrolyzed ion $Ti(OH)^{2+}$. In Fig. 2 the relative concentration of $Ti(OH)^{2+}$ both based on the absorption maximum at 465 nm, and based on the titrimetric data of Pecsok and coworker (10) is compared with the e.s.r. signal. The close correspondence of the relative intensity of the e.s.r. signal with the titrimetric $Ti(OH)^{2+}$ concentration in particular, is clearly apparent. Note that precipitation brings a halt to spectrally estimated concentrations at about pH 3.5.

Examination of the effect of the anions Cl^-, SO_4^{2-}, and I^- on the e.s.r. signal sheds further light on the nature of the paramagnetic species. First, the variation of the relative signal intensity with pH is nearly the same for the three species, Fig. 2. Second, the linewidth of the signal is in-

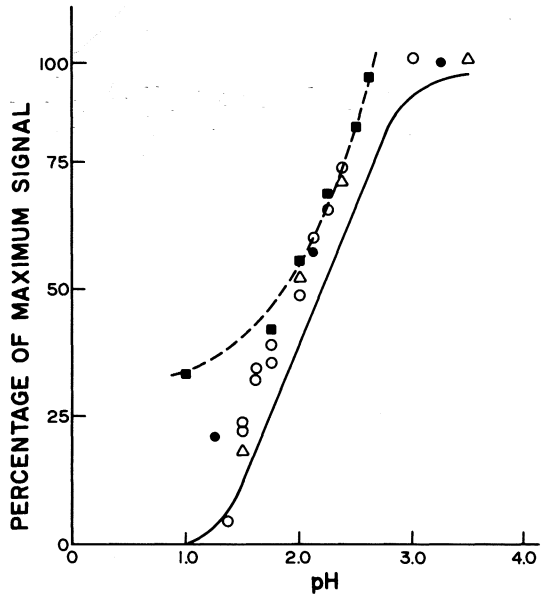

FIG. 2. The pH dependence of $Ti(OH)^{2+}$ concentration and of relative e.s.r. signal intensity for aqueous solutions of titanium (III). ●, TiI_3, 0.016 M, e.s.r. signal; ○, $TiCl_3$, 0.008 M, e.s.r. signal; △, $Ti_2(SO_4)_3$ 0.005 M, e.s.r. signal; - - - ■, $Ti(OH)^{2+}$, λ_{max} 465 nm, absorbance; — $Ti(OH)^{2+}$, titrimetric, calculated as per ref. 10.

Can. J. Chem. Downloaded from www.nrcresearchpress.com by 210.87.254.6 on 09/05/12
For personal use only.

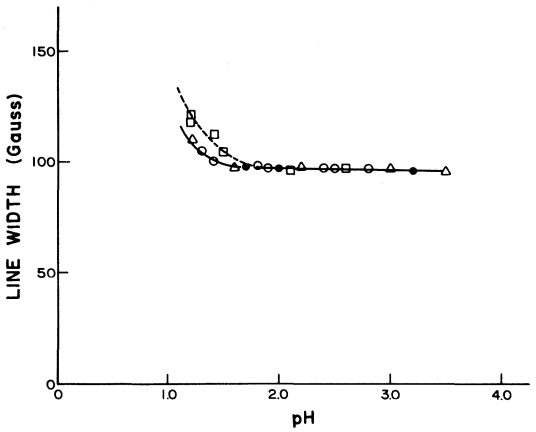

FIG. 3. Electron spin resonance signal linewidth for aqueous titanium(III) solutions, 25 °C. ●, TiI_3, 0.016 *M*; ○, $TiCl_3$, 0.008 *M*; △, $Ti_2(SO_4)_3$, 0.005 *M*; □, $TiCl_3$, 0.080 *M*.

dependent of anion above p*H* 1.6 as shown in Fig. 3. Finally, the intensity of the signals in the case of the chloride and iodide do not change on increasing the anion concentrations to 2.0 *M* in samples of 0.001 *M* titanous ion, in keeping with their low complexation constants (10–12). In contrast, increased sulfate (2.0 *M*) *destroyed* the signals in chloride, iodide, or sulfate samples. We ascribe the effect to complexation of the e.s.r. "active" species by added sulfate. In summary, the anion is not required in the primary coordination sphere, indeed in the case of sulfate it diminishes signal intensity. Moreover since we see no change in *g* value or linewidth, Fig. 3, even though crystal field effects of the anions should be significantly different, we conclude that the anion is not present in the e.s.r. active complex.

The possibility that the species was a dimeric or polymeric oxygen bridged form of Ti(III) and Ti(IV), **3** and **4** were considered.

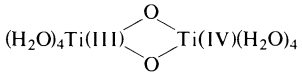

3

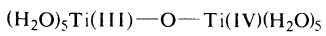

4

However no increase in signal intensity was achieved by either deliberate addition of excess Ti(IV) ions or purposeful partial oxygenation of a $TiCl_3$ test solution at p*H* 2.5. We note that the internuclear separation of the metal ions in a bridged species precludes a Ti(III)—Ti(III) dimer in view of the expected rapid spin–spin relaxation processes. Likewise spin exchange with Ti(IV) might be expected to broaden any signal from species **3** and **4** making them unlikely candidates for the e.s.r. active species. Moreover, at concentrations from 0.01 to 0.500 *M*, a direct variation in signal intensity with increasing titanium(III) was observed.

Clearly the structural possibilities reduce to aquated and hydrolyzed titanium(III) ions **1**, **2**, and **5**, as produced in reactions 1–3.

$$[1]\quad Ti(H_2O)_6^{3+} + H_2O \rightleftharpoons \underset{\mathbf{5}}{TiOH(H_2O)_5^{2+}} + H_3O^+$$

$$[2]\quad TiOH(H_2O)_5^{2+} + H_2O \rightleftharpoons \underset{\mathbf{1}}{TiO(H_2O)_5^{+}} + H_3O^+$$

$$[3]\quad [Ti(OH)(H_2O)_5]^{2+} + H_2O \rightleftharpoons \underset{\mathbf{2}}{[Ti(OH)_2(H_2O)_4]^{+}} + H_3O^+$$

Since **5** is the predominant form of titanium in these solutions, it cannot be the e.s.r. "active" species that is present at only 2% of the nominal metal concentration. The complex ion **1** is more attractive since it will be present in low concentration but linearly related to titanium concentration and independent of anion.

Moreover in analogy to VO^{2+}, we can expect a much stronger axial perturbation by the oxide ligand in $[TiO(H_2O)_5]^+$ than by OH^- in the dominant complex **5**. However, in the particular case of VO^{2+}, e.s.r. and spectroscopic studies (13–15) have convincingly demonstrated that the local point symmetry of vanadium in $[VO(H_2O)_5]^+$ is C_{4v} and that the unpaired electron lies in the d_{xy} orbital ($^2B_{2g}$). Hence axial π bonding is possible, effectively giving rise to a triple bond between the vanadium and the unique oxygen atom. Therefore the axial component to the ligand field will lead to a high deviation from O_h symmetry. The isotropic *g* factor for the complex $[VO(H_2O)_5]^{2+}$ is 1.964 (13–15) and indicates a strong axial field and a relatively small anisotropy in the *g* value. In contrast, the active titanium species described here has a lower *g* value (1.9408), and moreover, a rather large linewidth (see Discussion below). Accordingly, although not recognized in the solution studies (9–11) we feel that the complex **2** $[Ti(OH)_2(H_2O)_4]^+$, is a more likely candidate than the $[TiO(H_2O)_5]^+$. The dihydroxy species

Can. J. Chem. Downloaded from www.nrcresearchpress.com by 210.87.254.6 on 09/05/12
For personal use only.

Can. J. Chem. Downloaded from www.nrcresearchpress.com by 210.87.254.6 on 09/05/12
For personal use only.

will have the necessary axial perturbation, but much less than the alternative TiO^+ species.

To test further the nature of the e.s.r. active species we have prepared T,Cl_3 in D_2O at pH 2.2, observing a decrease in linewidth at 0.008 M from 96 to 72 G. The change is assigned to replacement of the hydrogens of water ligands by deuterium, narrowing the resonance line by removing the larger hyperfine interaction with the protons.[1] For example, Johnson *et al.* (8) have reported a splitting of 1.8 G for each proton in four water ligands of a titanium(III) complex with *t*-butyl alcohol. If the present complex **2** has four water ligands and two OH groups, as formulated, we can project a total contribution of *ca.* 20 G from this source. A slight change in coupling constant would clearly accommodate the whole of the line narrowing that is observed. Clearly the comparable proton hyperfine coupling in our complex and that of Johnson *et al.* (8) is consistent with a similar degree of delocalization of the d electron onto the water ligand in both instances.

Linewidth Effects

The spectrum of the frozen solution in D_2O at 77 °K provides evidence for the axial symmetry expected for complexes **1** and **2** (Fig. 1*b*). From the values of $g_\perp = 1.9250 \pm 0.001$ and $g_\parallel = 1.9606 \pm 0.001$, one calculates $g_o = \frac{1}{3}(g_\parallel + 2g_\perp) = 1.9368 + 0.002$ which compares favorably with the value recorded in solution 1.9411 ± 0.001. The possibility of species such as $Ti(OH)_3$ and the unsymmetrical bridged species **3** and **4** are ruled out by this observation. Finally, we observe no resonance lines indicative of dimeric titanium(III) species with triplet character. One is struck by the relatively narrow line (*ca.* 115 G) observed in the randomly oriented frozen sample. Consideration of the linewidth at room temperature 72 ± 3 G would indicate that the basic resonance linewidth has actually decreased.

There are several sources that contribute to the relaxation of the e.s.r. signal. Electric quadrupole effects are negligible in magnitude. Anisotropic processes and intermolecular interactions are eliminated by the nature of the temperature dependence of the linewidth and by the lack of effect of the anion or metal ion concentration. Over the range 0.001 to 0.500 M of titanium(III) concentration no change in linewidth is observed (Fig. 3). Accordingly, we can conclude that the linewidth is determined mainly by the relaxation processes within the coordination shell of the ion.

It seems plausible that vibrational spin–orbit processes are responsible for the linewidth, and that there is a near degeneracy of the electronic levels. Observation of significant narrowing on going from room temperature to 0 °C (see Table 1) and the relatively narrow linewidth of the randomly oriented sample at 77 °K in D_2O (see Fig. 1*a* and *b*), is consistent with excitation energies of the order kT.

[1]The broad resonance line obscures resolution of both proton and ^{47}Ti or ^{49}Ti coupling with the electron spin.

The generous support from the National Research Council of Canada and the University of Victoria in operating funds for this project is gratefully acknowledged.

1. C. J. Ballhausen. Introduction to ligand field theory. McGraw Hill, New York, N.Y. 1962. Chapt. 6.
2. A. Carington and A. D. McLachland. Introduction to magnetic resonance with applications to chemistry and chemical physics. Harper and Row, New York. 1967. Chapt. 10.
3. E. L. Waters and A. H. Maki. Phys. Rev. **125**, 233 (1962).
4. (*a*) V. I. Avvakumov, N. S. Garif'yanov, and E. I. Semenova. Sov. Phys. Jetp, **12**, 847 (1961); (*b*) N. S. Garif'yanov, A. V. Danilova, and R. R. Shagidullen. Opt. Spectrosk. **13**, 212 (1962); Opt. Spectrosc. (USSR), **13**, 116 (1962).
5. S. Fujiwara and M. Codell. Bull. Chem. Soc. Jap. **37**, 79 (1964).
6. S. Fujiwara, K. Nagashima, and M. Codell. Bull. Chem. Soc. Jap. **37**, 773 (1964).
7. I. B. Goldberg and W. F. Goedpinger. Inorg. Chem. **11**, 3129 (1972).
8. R. Johnson, P. W. Murchison, J. R. Bolton. J. Am. Chem. Soc. **92**, 6357 (1970).
9. W. Giggenbach and C. H. Brubaker, Jr. Inorg, Chem. **8**, 1157 (1969).
10. R. L. Pecsok and A. N. Fletcher. Inorg. Chem. **1**, 155 (1962).
11. F. R. Dure and P. R. Quinney. J. Am. Chem. Soc. **76**, 3800 (1954).
12. H. J. Gardner. Aust. J. Chem. **20**, 2357 (1967).
13. C. J. Ballhausen and H. B. Gray. Inorg. Chem. **1**, 111 (1962).
14. D. Kivelson and S. V. Lee. J. Chem. Phys. **41**, 1896 (1964).
15. C. J. Ballhausen and H. B. Gray. Inorg. Chem. **2**, 426 (1963).

Structure cristalline et moléculaire du *cis*-dithiocyanatobis(phénanthroline-1,10)mercure(II), $Hg(SCN)_2(C_{12}H_8N_2)_2$

ANDRÉ L. BEAUCHAMP, BERNARD SAPERAS ET ROLAND RIVEST

Département de Chimie, Université de Montréal, Case Postale 6210, Montréal 101, Québec H3C 3V1

Reçu le 13 juin 1973[1]

ANDRÉ L. BEAUCHAMP, BERNARD SAPERAS et ROLAND RIVEST. Can. J. Chem. **52**, 2923 (1974).

Le complexe *cis*-$Hg(SCN)_2(Phen)_2$ cristallise dans le système triclinique, groupe spatial $P\bar{1}$, $a = 13.252(5)$, $b = 11.077(4)$, $c = 8.443(3)$ Å, $\alpha = 105.20(3)$, $\beta = 83.25(3)$, $\gamma = 90.92(3)°$ et $Z = 2$. La structure a été résolue par la méthode de l'atome lourd et affinée jusqu'à $R = 0.069$ au moyen de 1718 réflexions indépendantes. Le cristal est constitué de molécules individuelles dans lesquelles le mercure est hexacoordonné. L'environnement du mercure correspond à un octaèdre déformé. Les liaisons Hg—N avec les molécules de phénanthroline varient de 2.42(2) à 2.52(2) Å, alors que les liaisons Hg—S avec les groupes thiocyanates sont égales à 2.622(8) et 2.582(8) Å. Les molécules de complexe sont empilées de manière à former des couches parallèles aux plans (110), entre lesquelles il n'existe que des contacts normaux de van der Waals. A l'intérieur des couches, la disposition parallèle des phénanthrolines à une distance de ~3.4 Å assure une grande surface de contact entre ligands appartenant à des molécules voisines. L'azote terminal des groupes thiocyanates n'est pas coordonné.

ANDRÉ L. BEAUCHAMP, BERNARD SAPERAS, and ROLAND RIVEST. Can. J. Chem. **52**, 2923 (1974).

The compound *cis*-$Hg(SCN)_2(Phen)_2$ belongs to the triclinic space group $P\bar{1}$, with $a = 13.252(5)$, $b = 11.077(4)$, $c = 8.443(3)$ Å, $\alpha = 105.20(3)$, $\beta = 83.25$ (3), $\gamma = 90.92(3)°$, and $Z = 2$. The structure was solved by the heavy atom method and refined on 1718 independent reflections to an R factor of 0.069. The crystal contains discrete molecules, in which mercury is coordinated to four nitrogen atoms from two phenanthroline molecules and to two sulfur atoms from thiocyanate groups. These donor atoms define a distorted octahedral geometry around mercury. The Hg—N bond lengths are in the range 2.42(2)–2.52(2) Å, whereas the Hg—S bonds are equal to 2.622(8) and 2.582(8) Å. The molecules are packed in layers parallel to the (110) planes and the layers are held together by normal van der Waals interactions. Within the layers, the packing of the complex is characterized by parallel stacking of phenanthroline ligands at distances of ~3.4 Å. The terminal nitrogen atoms of the thiocyanate groups are uncoordinated.

Le composé d'addition $Hg(SCN)_2 \cdot 2Phen$ (où Phen = phénanthroline-1,10) a été préparé par Jain et Rivest (1). Son spectre infrarouge a été interprété en fonction d'une espèce monomère dans laquelle le mercure est hexacoordonné. L'étude cristallographique de ce composé a été entreprise dans le but de vérifier la coordination octaédrique du mercure, d'une part, et de déterminer duquel des isomères *cis* ou *trans* il s'agit. Ce travail a fait l'objet d'une communication préliminaire (2).

Partie expérimentale

Paramètres cristallographiques

Formule: $C_{26}H_{16}N_6S_2Hg$ Masse moléculaire = 677.17 Maille triclinique, groupe spatial $P\bar{1}$ (confirmé par l'absence d'effet piézoélectrique), $a = 13.252(5)$, $b = 11.077(4)$, $c = 8.443(3)$ Å, $\alpha = 105.20(3)$, $\beta = 83.25(3)$, $\gamma = 90.92(3)°$, $V = 1187$ Å^3, $D_m = 1.95$ g cm^{-3} (pycnométrie), $Z = 2$, $D_c = 1.99$ g cm^{-3}, $t = 23$ °C. λCuKα = 1.5418 Å, λCuKβ = 1.3922 Å, μCuK$\bar{\alpha}$ = 152 cm^{-1}.

La structure est décrite en fonction du système d'axes non-conventionnel ci-dessus. La maille réduite (type I) (3) aurait les paramètres suivants: $a_r = 8.443$, $b_r = 11.077$, $c_r = 13.252$ Å, $\alpha_r = 89.08$, $\beta_r = 83.25$ et $\gamma_r = 74.80°$. Les axes de la maille réduite seraient reliés aux autres par les transformations $a_r = c$, $b_r = -b$ et $c_r = a$.

Mesures cristallographiques

Les cristaux ont été obtenus par recristallisation dans la diméthylformamide. Ils ne sont aucunement altérés par l'air. Les paramètres de maille ont été obtenus par affinement (4) des angles 2θ, ω et χ de douze pics CuKβ ($28° < 2\theta < 42°$) centrés automatiquement sur le diffractomètre Picker FACS-1.

Pour recueillir les intensités, un cristal de dimensions $0.06 \times 0.09 \times 0.13$ mm^3 a été monté sur le diffractomètre. Les mesures ont été faites avec la radiation CuK$\bar{\alpha}$ filtrée au nickel, selon la technique du balayage $\theta/2\theta$, à raison de 1° (2θ) par min. Le balayage s'étalait sur un intervalle 2θ initialement fixé à 1.6° et graduellement élargi en fonction de 2θ. On procédait au comptage du fond continu durant 20 s au début, puis à la fin de l'intervalle de balayage. Les réflexions témoins 400, 42$\bar{2}$ et 123, dont l'intensité a été déterminée à toutes les 30 mesures, ont manifesté des fluctuations de l'ordre de ±5% pendant la durée de travail.

[1]Revision reçue le 2 mai 1974.

Can. J. Chem. Downloaded from www.nrcresearchpress.com by 210.87.254.40 on 09/05/12
For personal use only.

Can. J. Chem. Downloaded from www.nrcresearchpress.com by 210.87.254.40 on 09/05/12
For personal use only.

Parmi les 3620 mesures effectuées (*hkl*, $h\bar{k}l$, $hk\bar{l}$ et $h\bar{k}\bar{l}$, $2\theta \leqslant 120°$), seules celles qui satisfaisaient au critère $I \geqslant 3\sigma_I$ ont été jugées statistiquement significatives. Ces critères ont conduit au rejet de ~1700 réflexions. Après avoir pris la moyenne, dans le cas de réflexions mesurées plus d'une fois, on disposait d'un ensemble de 1769 réflexions non-équivalentes statistiquement significatives, auxquelles les corrections habituelles pour la polarisation et l'effet de Lorentz ont été appliquées.

Détermination et affinement de la structure

La structure a été déterminée par la méthode de l'atome lourd et les paramètres atomiques ont été affinés par moindres carrés en inversant la totalité de la matrice. Après un affinement isotrope portant sur les paramètres de tous les atomes, sauf les hydrogènes, le facteur résiduel $R = \Sigma||F_o| - |F_c||/\Sigma|F_o|$ valait 0.116.

Une correction d'absorption a ensuite été calculée pour chaque réflexion, d'après le coefficient d'absorption $\mu = 152\ cm^{-1}$ et les équations des faces du cristal (Programme NRC-3, Ahmed et Singh). L'affinement isotrope sur les données corrigées a réduit le facteur R à 0.089. Les atomes d'hydrogènes ont alors été placés aux positions prévues par calcul[2] (distance C—H de 1.08 Å) et leurs facteurs thermiques isotropes ont été fixés à 5 Å^2. Par la suite, les paramètres des atomes d'hydrogène n'ont pas été affinés, mais les déplacements subis par les carbones ont également été appliqués aux atomes d'hydrogène correspondants.

Vers la fin de l'affinement isotrope, il persistait des écarts anormalement grands entre $|F_o|$ et $|F_c|$ pour une cinquantaine de réflexions situées à $\sin\theta/\lambda = 0.33$ ou 0.44. Un examen attentif des données brutes a révélé, d'une part, que les mesures en question avaient des fonds continus avant et arrière inégaux et, d'autre part, que dans le domaine $0.33 \leqslant \sin\theta/\lambda \leqslant 0.44$, le fond continu était généralement plus élevé qu'ailleurs, ce qui entraînait une proportion plus élevée de réflexions jugées statistiquement inacceptables. Par la suite, les réflexions pour lesquelles $||F_o| - |F_c|| > 7$ ont été exclues des calculs de moindres carrées. De la sorte, toutes les réflexions présentant un fond continu asymétrique ont été éliminées, ainsi que quatre réflexions très intenses aux petits angles (022, 111, $11\bar{1}$ et $1\bar{1}\bar{1}$), qui semblent affectées par l'extinction.

L'affinement a été complété au moyen des 1718 réflexions restantes. Comme ce nombre de mesures ne permet pas un affinement anisotropic complet, nous avons procédé à des affinements partiels sur quelques atomes à la fois. Nous avons alors noté que l'anisotropie, peu marquée pour les molécules rigides de phénanthroline, était plus importante pour les groupes SCN. Des facteurs thermiques anisotropes ont donc été attribués au mercure et aux atomes des groupes SCN, tandis que les atomes des molécules de phénanthroline conservaient leurs facteurs thermiques isotropes. Des poids individuels, basés sur les statistiques de comptage $\sqrt{w} = 1/\sigma_F$ (5) ont été appliqués lors des derniers cycles d'affinement. Après stabilisation, le facteur R était 0.069, alors que le facteur résiduel pondéré $R_w = \Sigma w||F_o| - |F_c||^2/\Sigma w|F_o|^2$ valait 0.077. Sur la carte différence de Fourier calculée avec les paramètres affinés, le fond continu restait inférieur à ± 0.8 e/Å^3, sauf au voisinage du mercure, où se trouvent quatre pics de ± 1.7 e/Å^3.

Les facteurs de diffusion utilisés sont ceux de Cromer et Waber et on a tenu compte des facteurs de dispersion $\Delta f'$ et $\Delta f''$ du mercure et du soufre (6). Les paramètres atomiques affinés sont réunis au tableau 1.[2]

Les calculs ont été effectués sur un ordinateur CDC 6400. Les versions localement modifiées des programmes suivants ont été utilisées: Ahmed et Huber, NRC-2 (traitement préliminaire des données); Ahmed et Singh, NRC-3 (correction pour l'absorption); Prewitt, SFLS5 (moindres carrés, matrice entière); Zalkin, FORDAP (cartes de Patterson et Fourier); Shiono et Chu, BONDLA (distances interatomiques et angles de liaisons); Pippy et Ahmed, NRC-22 (plans moyens et angles dièdres); Johnson, ORTEP (traçage des figures).

Description de la structure et discussion

Le cristal renferme des molécules monomères $Hg(SCN)_2(Phen)_2$ dans lesquelles le mercure est hexacoordonné (fig. 1). L'environnement immédiat du mercure peut être décrit comme un octaèdre déformé dont deux sommets *cis* sont occupés par les atomes de soufre des groupes thiocyanates. Ce type de chélates donne lieu à l'isomérie optique, mais le cristal étudié est un racémique.

L'environnement octaédrique du mercure est très irrégulier (tableau 2). Les angles N—Hg—N à l'intérieur des cycles sont particulièrement petits (~67°) à cause de la taille du mercure, qui exige une liaison Hg—N longue, d'une part, et de la rigidité du ligand, qui fixe l'écartement des atomes d'azote, d'autre part. Dans un complexe du thallium (7), on a observé un angle N—Tl—N de 63° comparable à ceux-ci. Notons qu'un angle N—M—N de ~60° permet d'obtenir des angles M—N—C voisins de la valeur normale de 120°, ce qui pourrait contribuer à la stabilisation de chélates de métaux volumineux, en dépit des angles N—M—N très petits qu'exige la phénanthroline.

Les groupes SCN présentent les caractéristiques habituelles (8–10): coordination au mercure par l'intermédiaire du soufre, angles Hg—S—C voisins de 100°, segments S—C—N à peu près linéaires, liaisons S—C (1.64, 1.67 Å) et C—N (1.14, 1.16 Å) de longueur normale. Les liaisons Hg—S (2.62 et 2.58 Å) sont plus longues que celles qu'on a observées dans diverses espèces Hg—SCN tétraédriques (2.54–2.56 Å) (8, 10).

[2]Le tableau des facteurs de structure et les coordonnées des hydrogènes sont déposés en archives. Les photocopies des documents archivés peuvent être obtenues du Dépôt des documents non publies, Bibliothèque scientifique nationale, Conseil national de recherches du Canada, Ottawa, Canada K1A 0S2.

TABLEAU 1. (*a*) Coordonnées ($\times 10^3$) et facteurs thermiques anisotropes* ($\times 10^3$) du mercure et des atomes des groupes thiocyanates

Atome	x	y	z	β_{11}	β_{22}	β_{33}	β_{12}	β_{13}	β_{23}
Hg	264.0(1)	274.3(1)	22.0(1)	5.5(1)	6.6(1)	16.6(2)	−1.8(1)	−1.8(1)	2.1(1)
S(1)	358.8(6)	450.9(7)	−88.3(11)	9.2(7)	10.9(8)	29.8(20)	−4.2(6)	−4.1(10)	6.5(11)
S(2)	221.7(7)	145.3(8)	−263.9(9)	11.7(8)	14.5(9)	14.3(13)	−1.3(7)	−4.0(8)	−0.6(9)
C(1)	404(2)	371(3)	−278(5)	6(2)	17(4)	26(8)	1(2)	5(3)	7(5)
C(2)	165(2)	25(3)	−215(3)	6(2)	15(4)	20(6)	1(2)	−1(3)	−6(4)
N(1)	434(3)	325(3)	−413(4)	23(4)	25(5)	24(7)	1(4)	15(5)	11(5)
N(2)	126(2)	−63(2)	−188(3)	6(2)	13(3)	34(7)	−4(2)	−7(3)	−1(4)

*f.t. = exp $\{-(\beta_{11}h^2 + \beta_{22}k^2 + \beta_{33}l^2 + 2\beta_{12}hk + 2\beta_{13}hl + 2\beta_{23}kl)\}$.

TABLEAU 1. (*b*) Coordonnées fractionnaires ($\times 10^3$) et facteur thermique isotrope des atomes des molécules de phénanthroline

Atome	x	y	z	B
N(101)	85(1)	358(2)	110(2)	3.9(4)
C(102)	5(2)	311(2)	35(3)	4.7(6)
C(103)	−87(2)	374(2)	70(3)	5.1(6)
C(104)	−101(2)	484(3)	195(3)	5.7(6)
C(105)	−30(2)	647(3)	404(3)	5.6(6)
C(106)	54(2)	686(2)	494(3)	4.5(5)
C(107)	232(2)	660(2)	543(3)	5.4(6)
C(108)	324(2)	592(2)	496(3)	4.8(6)
C(109)	326(2)	485(2)	367(3)	4.0(5)
N(110)	245(2)	447(2)	286(3)	5.2(5)
C(111)	158(2)	513(2)	324(3)	3.9(5)
C(112)	73(2)	464(2)	234(3)	3.5(4)
C(113)	−19(2)	533(3)	281(3)	5.0(6)
C(114)	149(2)	625(2)	454(3)	4.0(5)
N(201)	417(1)	200(1)	102(2)	2.8(3)
C(202)	510(2)	248(2)	72(3)	4.3(5)
C(203)	593(2)	196(2)	122(3)	4.7(5)
C(204)	581(2)	98(2)	201(3)	5.4(6)
C(205)	476(2)	−45(2)	301(3)	5.2(6)
C(206)	376(2)	−92(2)	332(3)	5.2(6)
C(207)	191(2)	−74(2)	334(3)	5.2(6)
C(208)	113(2)	−19(3)	281(4)	6.2(7)
C(209)	127(2)	82(2)	208(3)	4.4(5)
N(210)	228(2)	116(2)	173(2)	4.1(4)
C(211)	302(2)	61(2)	220(3)	4.2(5)
C(212)	400(2)	110(2)	187(3)	3.5(4)
C(213)	487(2)	56(2)	226(3)	3.7(5)
C(214)	288(2)	−34(2)	298(3)	4.1(5)

La longueur des liaisons entre le mercure et les azotes de la phénanthroline se situe entre 2.42 et 2.52 Å. Pour le complexe mercureux $[Hg_2Phen](NO_3)_2$(11), l'une des liaisons Hg—N (2.48 Å) s'apparente aux nôtres, mais l'autre est beaucoup plus courte (2.30 Å). Les structures de deux complexes du mercure avec des pyridines sont connues, mais toute comparaison s'avère difficile parce que les longueurs des liaisons Hg—N (2.18 Å pour $HgCl_2$·Collidine (12) et 2.60 Å pour $HgCl_2$·2Pyridine (8)) diffèrent considérablement en dépit de la grande similitude des ligands.

Les angles dans la molécule de phénanthroline sont compris entre 117(2) et 123(2)° (moyenne 120°). Les liaisons C—N, 1.33(3)–1.39(3) Å (moyenne 1.35 Å) sont plus courtes que les liaisons C—C, 1.35(3)–1.45(3) Å (moyenne 1.40 Å). Les molécules de phénanthroline sont planes aux erreurs expérimentales près. L'atome de mercure devrait normalement occuper ces plans. Il se trouve à ~0.2 Å du plan passant par le ligand 2, écart comparable à ceux qu'on a rapportés (0.1–0.3 Å) pour des chélates de la phénanthroline avec d'autres métaux (13). Toutefois, dans le cas du ligand 1, la distance est de 0.45 Å, ce qui correspond à un angle de ~10° entre le plan du ligand et le plan Hg—N(101)—N(110). L'empilement moléculaire permet d'expliquer cet angle relativement grand.

Les molécules $Hg(SCN)_2(Phen)_2$ s'empilent en couches parallèles aux plans réticulaires (110) (fig. 2). Les atomes d'azote des groupes SCN ne sont pas coordonnés, comme le laissait prévoir la position des bandes $\nu_{C\equiv N}$ et ν_{C-S} du spectre infrarouge (1). Chaque couche renferme un nombre égal des deux isomères optiques et les molécules sont disposées de manière à assurer une grande surface de contact entre les ligands phénanthrolines. Deux ligands adjacents sont à peu près parallèles, à ~3.4 Å l'un de l'autre, et le contact implique principalement deux cycles de chaque ligand. Les ligands de type 2 (azotes blancs, fig. 2) interagissent deux à deux et on dénombre 5 contacts plus courts que 3.6 Å entre la molécule (x, y, z) et la molécule $(1 - x, \bar{y}, \bar{z})$. Chaque paire est en retrait par rapport à la suivante et il y a peu de contact d'une paire à l'autre. Par ailleurs, chaque ligand de type 1 (azotes noirs, fig. 2) est pris "en sandwich" entre deux autres. Ainsi, la molécule (x, y, z) possède 12 contacts plus courts

Can. J. Chem. Downloaded from www.nrcresearchpress.com by 210.87.254.40 on 09/05/12
For personal use only.

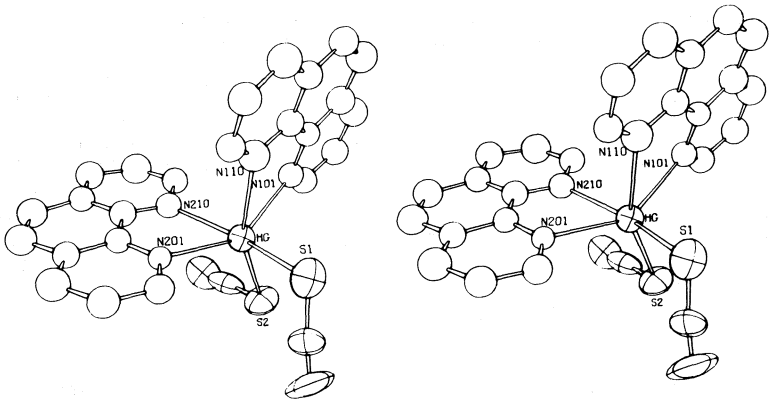

FIG. 1. Projection stéréoscopique de la molécule *cis*-$Hg(SCN)_2(Phen)_2$. Les enveloppes des atomes correspondent à une probabilité de 50%.

TABLEAU 2. Distances interatomiques et angles de liaisons

Liaisons	Distance (Å)	Liaisons*	Angle (deg)	Liaisons	Angle (deg)
Hg—S(1)	2.622(8)	N(101)—Hg—N(110)	66.3(7)	S(1)—Hg—S(2)	95.2(3)
Hg—S(2)	2.582(8)	N(201)—Hg—N(210)	68.0(6)	N(110)—Hg—N(210)	91.4(7)
Hg—N(101)	2.52(2)			N(101)—Hg—N(201)	147.3(6)
Hg—N(110)	2.52(2)	N(101)—Hg—N(210)	89.5(6)	Hg—S(1)—C(1)	100.6(12)
Hg—N(201)	2.42(2)	N(110)—Hg—N(201)	89.9(6)	Hg—S(2)—C(2)	100.7(11)
Hg—N(210)	2.43(2)			S(1)—C(1)—N(1)	174(3)
S(1)—C(1)	1.67(4)	S(1)—Hg—N(201)	93.6(4)	S(2)—C(2)—N(2)	177(3)
S(2)—C(2)	1.64(3)	S(2)—Hg—N(101)	93.1(5)	Hg—N(101)—C(112)	116(2)
C(1)—N(1)	1.14(5)			Hg—N(101)—C(102)	124(2)
C(2)—N(2)	1.16(4)	S(1)—Hg—N(110)	81.4(5)	Hg—N(110)—C(109)	120(2)
		S(2)—Hg—N(210)	98.3(5)	Hg—N(110)—C(111)	117(2)
				Hg—N(201)—C(212)	114(2)
		S(1)—Hg—N(101)	104.0(5)	Hg—N(201)—C(202)	123(2)
		S(2)—Hg—N(201)	112.8(4)	Hg—N(210)—C(209)	120(2)
				Hg—N(210)—C(211)	119(2)
		S(1)—Hg—N(210)	160.3(5)		
		S(2)—Hg—N(110)	157.2(5)		

*Dans cette colonne, les angles d'une même paire devraient être équivalents si le squelette HgS_2N_4 possédait l'axe binaire prévu pour un chelate du type *cis*-$MX_2(L—L)_2$.

que 3.6 Å avec la molécule ($\bar{x}$, $1 - y$, $1 - z$) et 12 autres avec la molécule ($\bar{x}$, $1 - y$, $\bar{z}$). C'est sans doute pour favoriser cet emboîtement que le plan du ligand de type 1 fait un angle avec le plan Hg—N(101)—N(110), tel que mentionné précédemment.

Le tableau 3 renferme les contacts courts entre atomes non-liés. Trois d'entre eux seulement sont intramoléculaires et le contact H(209)...C(102) (2.8 Å) est le seul qui pourrait dénoter quelque tension à l'intérieur de la molécule. On a invoqué cette absence de tension pour expliquer la préférence que manifestent les complexes MX_2-$(Phen)_2$ pour la configuration *cis*. Dans l'isomère *trans*, au contraire, il existerait des répulsions importantes (H(102)...H(202) et H(109)...H(209)) entre deux molécules de phénanthroline forcées d'occuper un même plan (14). Compte tenu des valeurs extrêmes (2.42 et 2.52 Å) observées pour les liaisons Hg—N dans le chélate *cis*-$Hg(SCN)_2$-$(Phen)_2$, on peut aisément calculer que dans l'isomère *trans*, la distance H...H se situerait entre 2.2 et 2.4 Å. Comme le rayon de van der Waals de l'hydrogène est 1.2 Å (15), il y aurait une certaine répulsion H...H, mais beaucoup moindre que dans le cas de complexes d'éléments plus légers. Par conséquent, bien que l'isomère *cis* du complexe mercurique soit favorisé, il n'est pas inconcevable qu'on puisse isoler un chélate *trans*, dans lequel les répulsions H...H déjà faibles soient éliminées en laissant les ligands pivoter quelque peu l'un par rapport à l'autre autour de

Can. J. Chem. Downloaded from www.nrcresearchpress.com by 210.87.254.40 on 09/05/12
For personal use only.

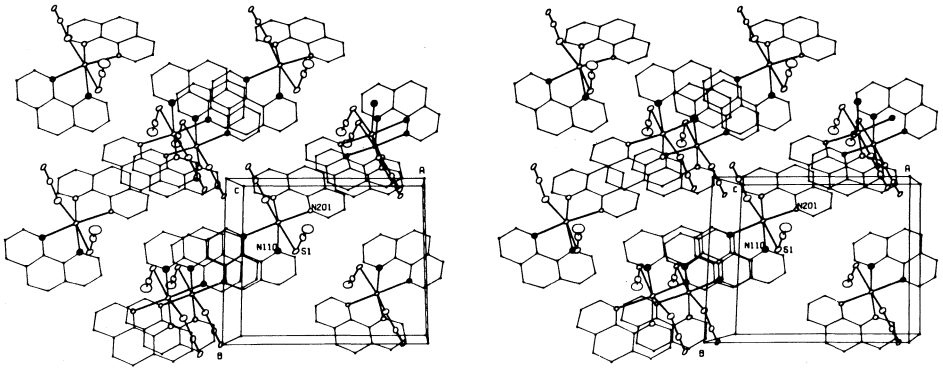

FIG. 2. Projection stéréoscopique de l'empilement dans le cristal *cis*-$Hg(SCN)_2(Phen)_2$. Les molécules de phénanthroline peuvent être distinguées d'après leurs atomes d'azote (sphères noires pour les ligands de type 1 et sphères blanches pour les ligands de type 2). Sur la diagonale de la figure, on remarque les couches des molécules orientées selon les plans réticulaires (110). La disposition parallèle des phénanthrolines est un facteur important qui gouverne l'empilement à l'intérieur de la couche.

TABLEAU 3. Choix de distances entre atomes non-liés

Atomes	Transformation*	Distance (Å)
Dans la molécule		
S(1)–H(202)		2.93(3)
C(102)–H(209)		2.81(4)
C(202)–H(109)		2.94(4)
A l'intérieur d'une couche		
S(1)–H(104)	$\bar{x}, 1-y, \bar{z}$	2.91(3)
S(2)–H(204)	$1-x, \bar{y}, \bar{z}$	2.95(3)
C(2)–H(204)	$1-x, \bar{y}, \bar{z}$	2.61(4)
Entre couches		
C(106)–H(207)	$x, 1+y, z$	2.71(4)
C(114)–H(207)	$x, 1+y, z$	2.74(4)
S(1)–H(202)	$1-x, 1-y, \bar{z}$	2.96(3)
N(2)–H(106)	$x, -1+y, -1+z$	2.60(4)
N(2)–H(107)	$x, -1+y, -1+z$	2.60(4)
N(2)–H(209)	$\bar{x}, \bar{y}, \bar{z}$	2.64(4)

*Appliquée au second atome, le premier étant à (x, y, z).

leurs axes binaires respectifs, comme c'est apparemment le cas pour l'ion $(Pd(Phen)_2]^{2+}$ dans le perchlorate (16).

Nous remercions le Dr. A. Terzis qui a effectué une partie des calculs nécessaires au présent travail. Nous remercions également le Conseil national de recherches du Canada pour des subventions de recherches.

1. S. C. JAIN et R. RIVEST. Inorg. Chim. Acta, **4**, 291 (1970).
2. A. L. BEAUCHAMP, B. SAPERAS et R. RIVEST. Can. J. Chem. **49**, 3579 (1971).
3. International tables for X-ray crystallography. Vol. I. Kynoch Press, Birmingham. 1969. p. 531.
4. W. R. BUSING et H. A. LEVY. Acta Cryst. **22**, 457 (1967).
5. G. H. STOUT et L. H. JENSEN. X-Ray structure determination. Macmillan Co., New York. 1968. p. 457.
6. D. T. CROMER et J. T. WABER. Acta Cryst. **18**, 104 (1965); D. T. CROMER. Acta Cryst. **18**, 17 (1965).
7. T. L. BLUNDELL et H. M. POWELL. Chem. Commun. 54 (1967).
8. D. GRDENIC. Q. Rev. **19**, 303 (1965).
9. A. L. BEAUCHAMP et D. GOUTIER. Can. J. Chem. **50**, 977 (1972).
10. R. C. MAKHIJA, A. L. BEAUCHAMP et R. RIVEST. J. Chem. Soc. Dalton Trans. 2447 (1973).
11. R. C. ELDER, J. HALPERN et J. S. POND. J. Am. Chem. Soc. **89**, 6877 (1967).
12. S. KULPE. Z. Anorg. Allg. Chem. **349**, 314 (1967).
13. K. R. BUTLER et M. R. SNOW. J. Chem. Soc. A, 565 (1971). C. W. REIMANN, S. BLOCK et A. PERLOFF. Inorg. Chem. **5**, 1185 (1966). A. J. GRAHAM et R. H. FENN. J. Organomet. Chem. **25**, 173 (1970). O. P. ANDERSON. J. Chem. Soc. Dalton Trans. 1237 (1973).
14. W. R. MCWHINNIE et J. D. MILLER. Adv. Inorg. Chem. Radiochem. **15**, 135 (1969).
15. F. A. COTTON et G. WILKINSON. Advanced inorganic chemistry. Interscience, New York, N.Y. 1966. p. 115.
16. J. V. RUND. Inorg. Chem. **7**, 24 (1968).

Can. J. Chem. Downloaded from www.nrcresearchpress.com by 210.87.254.40 on 09/05/12
For personal use only.

Infrared Spectra of Water in Crystalline Hydrates: $KSnCl_3 \cdot H_2O$, an Untypical Monohydrate[1]

MICHAEL FALK AND CHUNG-HSI HUANG

Atlantic Regional Laboratory, National Research Council of Canada, Halifax, Nova Scotia B3H 3Z1

AND

OSVALD KNOP

Department of Chemistry, Dalhousie University, Halifax, Nova Scotia B3H 3J5

Received March 19, 1974

MICHAEL FALK, CHUNG-HSI HUANG and OSVALD KNOP. Can. J. Chem. **52**, 2928 (1974).

Infrared spectra of polycrystalline $KSnCl_3 \cdot H_2O$ were recorded between 4000 and 300 cm^{-1} at different degrees of deuteration and at temperatures between 30 and -160 °C. At low temperatures the spectra show a complexity indicative of the presence of several crystallographically distinct water molecules. These molecules occupy sites with nearly identical environments and at room temperature are spectroscopically indistinguishable. The environment of each of these molecules is asymmetric. Hydrogen bonds are very weak and probably highly bent. The water molecules are less separated from one another than in $K_2SnCl_4 \cdot H_2O$ and may share their potassium neighbors.

MICHAEL FALK, CHUNG-HSI HUANG et OSVALD KNOP. Can. J. Chem. **52**, 2928 (1974).

On a enregistré les spectres infrarouges de $KSnCl_3 \cdot H_2O$ polycristallin entre 4000 et 300 cm^{-1} à différentes températures et degrés de deutération. La complexité des spectres à basse température indique que plusieurs types distincts de molécules d'eau existent dans la structure. Ces molécules, situées sur des sites aux entourages asymétriques presque identiques, ne peuvent pas être distinguées, à température ambiante, par les spectres infrarouges. Les liaisons hydrogène sont très faibles et probablement coudées. Les séparations intermoléculaires H_2O–H_2O sont moins grandes dans $KSnCl_3 \cdot H_2O$ que dans $K_2SnCl_4 \cdot H_2O$.

Recently good crystals of $KSnCl_3 \cdot H_2O$ (**I**) were obtained as a byproduct in the preparation of $K_2SnCl_4 \cdot H_2O$ (**II**) (1). No crystallographic work appears to have been reported on **I**, and the only spectroscopic work is that by Davies and Tench (2) on the Raman spectrum below about 325 cm^{-1}. We have taken advantage of the availability of analyzed and authenticated $KSnCl_3 \cdot H_2O$ to see how much information about the water molecule could be extracted from the i.r. spectra of partially deuterated polycrystalline samples of a hydrate in the complete absence of crystal-structure data.

The preparation of samples for i.r. spectra has been described in ref. 1.

Results

The room-temperature survey spectra of undeuterated **I** and **II** (Fig. 3 of ref. 1) differ mainly in the frequencies of the OH stretching bands. These are higher in **I**, indicating that hydrogen bonding in **I** is weaker than in **II**. Since the spectrum of **I** looks even simpler than that of **II** and both compounds contain only one H_2O per formula unit, a single type of water molecule was expected to exist in the structure; the room-temperature spectra of partially deuterated **I** (discussed in the following) reinforced this impression. The appearance of additional peaks in the spectra of undeuterated **I** on lowering the temperature (Figs. 1 and 2, Table 1) came therefore as a surprise. It left no doubt about the considerably greater complexity of the structural situation in $KSnCl_3 \cdot H_2O$ than had been anticipated.

The bending fundamentals of isotopically dilute D_2O (Fig. 2) and H_2O (not shown) were singlets at room temperature, like in **II**, which is normally evidence of only one crystallographically distinct type of water molecule (3). Below about -60 °C these singlets gradually resolved into close doublets, with peak separation (at -160 °C) of 4.8 cm^{-1} for H_2O and 3.3 cm^{-1} for D_2O. These doublets require the existence of two or more types of water molecules in the structure. The gradual coalescence of the doublets with in-

[1]NRCC No. 14046.

Can. J. Chem. Downloaded from www.nrcresearchpress.com by 210.87.254.5 on 09/05/12
For personal use only.

TABLE 1. Vibrational assignments for water in $KSnCl_3 \cdot H_2O$*

Description	HOH		HOD		DOD	
	30 °C	−160 °C	30 °C	−160 °C	30 °C	−160 °C
OH stretch	3618 3538	3632† ~3558 3550	~3596 ~3554	3616† 3577 3565		
OD stretch			2653 2621	2666† 2638 2630	2690 2595	2700† ~2610 2604
Bend (isotopically pure)	1615	1616 1612 1602				
Bend (isotopically dilute)	1610	~1609 1608 1603	1422 1411	1419 1412 1405†	1186	1184 1181
Libration	430	427				

*Frequencies are in cm^{-1}.
†Shows signs of being an unresolved multiplet.

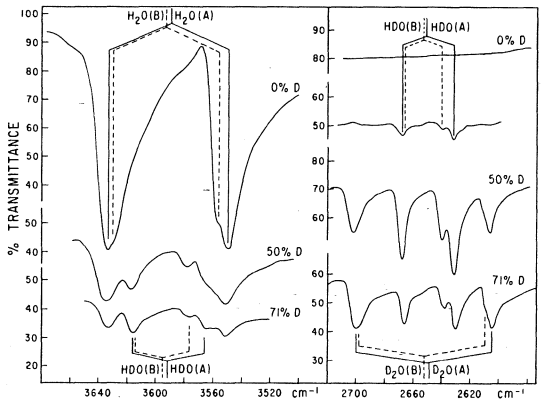

FIG. 1. Spectra of $KSnCl_3 \cdot H_2O$ (Nujol mulls) at −160 °C in the OH and OD stretching regions at different deuterium contents. *A* and *B* indicate two of the component doublets resulting from non-equivalent water molecules.

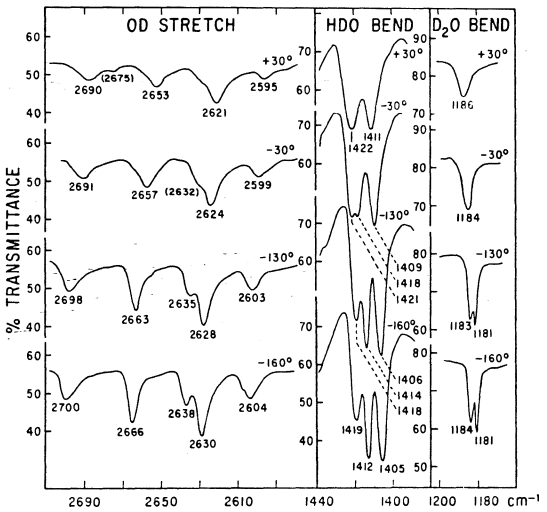

FIG. 2. Spectra of $KSnCl_3 \cdot H_2O$ (Nujol mulls) at different temperatures. OD stretching region, 50% D; HDO bending region, 30% D; D_2O bending region, 30% D.

creasing temperature corresponds to structural changes which make the molecular environment of the different types of H_2O more similar.

At room temperature the bending fundamental of isotopically dilute HDO was a doublet, but those of D_2O and H_2O were singlets (Fig. 2; the H_2O spectrum is not shown). This would indicate the presence of a single type of asymmetric water molecule (3). However, at lower temperatures the HDO doublet split further, giving rise to three bands of unequal intensity at 1405, 1412, and 1419 cm^{-1}. The most intense band of the three, at 1405 cm^{-1}, showed some evidence of further structure compatible with an incompletely resolved quartet. The HDO bending region can thus be interpreted as arising from at least two very similar types of asymmetric water molecules.

The spectra of the OH and OD stretching regions (Figs. 1 and 2, Table 1) support this analysis. At room temperature, the doubling of the HDO fundamentals is consistent with one type of water molecule in an asymmetric environment. Emergence of structure on temperature lowering points, however, to the presence of at least two

Can. J. Chem. Downloaded from www.nrcresearchpress.com by 210.87.254.5 on 09/05/12
For personal use only.

Can. J. Chem. Downloaded from www.nrcresearchpress.com by 210.87.254.5 on 09/05/12
For personal use only.

distinct types of asymmetric water molecules in the crystal. The asymmetry must be appreciable, to judge by the large splitting of the room-temperature doublet. The non-equivalent water molecules must be chemically very similar, for the low-temperature doublets nearly coincide and remain only partially resolved even at −160 °C. The spectra of the stretching fundamentals of H_2O and D_2O showed features analogous to those observed in the HDO stretching region. This again is consistent with the existence of at least two distinct types of water molecules.

Consideration of the relative intensities of the spectral features shows that the situation is even more complex. Assuming that the structure of the low-temperature bands can be interpreted as the result of superposition of two discrete sets of bands, each corresponding to one type of water molecule, the band-intensity ratio estimated from the HDO stretching bands (Fig. 1) is approximately 3:1 but only 1:1 when estimated from the isolated D_2O bending fundamental (Fig. 2).[2] This apparent discrepancy can be explained only on the assumption that more than two types of water molecules are present in the crystal. Three types with an abundance ratio of 2:1:1 would, in certain circumstances, be compatible with the estimated band-area ratios (see Discussion).

The stretching frequencies in partially deuterated **I** confirm the conclusion from the room-temperature spectrum of the undeuterated compound, namely, that hydrogen bonding in **I** must be considerably weaker than in **II**. More specifically, the stronger bonds in **I** are somewhat weaker than the bifurcated bond involving H(2) in **II**, while the weaker bonds in **I** are weaker than either bond in **II** and may correspond to a non-hydrogen-bonded situation. The only stretching frequency for water in crystalline hydrates that is of comparably high value has been reported for H(2) in sodium nitroprusside dihydrate (5): this hydrogen is known to participate in a H-bond which is at best borderline. The properties of borderline and non-bonded water hydrogens have not yet been adequately investigated (4).

All of the stretching frequencies exhibit appreciable negative values of $d\nu/dT$, which implies, as for OH(2) of **II**, that all the H-bonds in **I** are highly bent and possibly bifurcated or nearly bifurcated.

At higher isotopic concentrations the band shapes in the stretching region are not appreciably modified. Those in the bending region, on the other hand, become more complex and an incompletely resolved multiplet is observed for H_2O in undeuterated samples and for D_2O in highly deuterated ones. This shows that, in contrast to **II**, dynamic coupling of bending vibrations (though not of stretching vibrations) of water molecules is appreciable in **I**. The magnitude of the frequency splitting is comparable to that in sodium nitroprusside dihydrate, in which structure the water molecules share their sodium neighbors (5). One may thus infer that water molecules in **I** are less well isolated from one another than the water molecules in **II**.

Conclusions

The following information has been extracted from the i.r. spectra of $KSnCl_3 \cdot H_2O$, in spite of the unexpected complications encountered in their analysis:

(*1*) The unit cell contains several crystallographically distinct sets of water molecules. These molecules occupy sites with nearly identical environments, whose similarity increases with temperature.

(*2*) The water molecules are asymmetric. Barring orientational disorder in the structure, this requires the oxygen atoms of the water molecules to be located at sites of symmetry C_s (both H atoms in the mirror plane) or C_1.

(*3*) Hydrogen bonding is very weak and the bonds are highly bent, possibly bifurcated. In each type of water molecule one of the H atoms may be borderline- or non-bonded.

(*4*) The water molecules are less well isolated from one another than in **II** and may share their potassium neighbors.

Discussion

Stoichiometric crystalline monohydrates containing more than one type of water molecule are rare. A survey of 146 monohydrates whose crystal structures have been reported has uncovered only two such cases. Both are listed in Wyckoff's compilation (6): $BaS_4 \cdot H_2O$ (D_2^3, $Z = 4$, two types of H_2O of symmetry C_2) and $CaC_2O_4 \cdot H_2O$ (whewellite, $P2_1/c$, $Z = 8$, two types of H_2O of symmetry C_1).

[2]These are the two bands studied with most care.

A preliminary examination of single crystals of **I** by X-ray diffraction (8) gave a diffraction symmetry *mmm* and approximate unit-cell dimensions of 8.55, 8.76, and 18.24 Å. Combining these values with the density reported for **I** in ref. 7, 2.78 g/cm^3, leads to 8[$KSnCl_3 \cdot H_2O$] per unit cell. If these crystallographic data are confirmed, and assuming further that **I** is a stoichiometric hydrate with an ordered structure, the population ratio of the non-equivalent water molecules must correspond to a non-trivial partition of 8 and the partition must be compatible with the site multiplicities 1, 2, or 4 admissible in orthorhombic space groups. The above tentative estimates of the band-area ratios as 3:1 and 1:1 are consistent with the ternary partition 4:2:2: and the band-area groupings (4+2):2 = 3:1 and 4:(2+2) = 1:1. A monohydrate structure containing *three* types of water molecules would be most unusual but conceivable. For example, if **I** has a layer-like structure with the H_2O molecules between $SnCl_3^-$ layers, certain stacking arrangements might produce environments of the water molecules that would differ only slightly.

We thank Dr. Peter S. White for obtaining the unit-cell dimensions of $KSnCl_3 \cdot H_2O$, and to Mr. P. F. Seto for technical help.

1. M. Falk, C.-H. Huang, and O. Knop. Can. J. Chem. **52**, 2380 (1974).
2. J. E. D. Davies and I. R. Tench. Inorg. Nucl. Chem. Lett. **7**, 491 (1971).
3. V. Seidl, O. Knop, and M. Falk. Can. J. Chem. **47**, 1361 (1969).
4. M. Falk and O. Knop. Water: a comprehensive treatise, Vol. 2. *Edited by* F. Franks. Plenum Press, New York. 1973. Chapt. 2.
5. M. Holzbecher, O. Knop, and M. Falk. Can. J. Chem. **49**, 1413 (1971).
6. R. W. G. Wyckoff. Crystal structures. 2nd ed. Vols. 1–5. Interscience, New York. 1963–1966.
7. H. Brasseur and A. De Rassenfosse. Z. Krist. **101**A, 389 (1939).
8. P. S. White. Unpublished results.

Can. J. Chem. Downloaded from www.nrcresearchpress.com by 210.87.254.5 on 09/05/12
For personal use only.

On the Reaction of *p*-Cresol with 4-Aminoantipyrine[1]

VINOD DAVE, J. B. STOTHERS, AND E. W. WARNHOFF
Department of Chemistry, University of Western Ontario, London, Ontario N6A 3K7

Received February 19, 1974

VINOD DAVE, J. B. STOTHERS, and E. W. WARNHOFF. Can. J. Chem. **52**, 2932 (1974).

The structure of the yellow product from the ferricyanide oxidation of *p*-cresol and 4-aminoantipyrine is shown to be **1** and not **3**. Borohydride reduction of the imine **1** gave **2** which underwent elimination to **5***a*. Ferricyanide oxidation of **5***a* regenerated **1**.

VINOD DAVE, J. B. STOTHERS et E. W. WARNHOFF. Can. J. Chem. **52**, 2932 (1974).

On démontre que le produit jaune, obtenu lors de l'oxydation au ferricyanure du *p*-crésol et de l'amino-4 antipyrine, possède la structure **1** et non la structure **3**. La réduction de l'imine **1** par le borohydrure conduit à **2** qui subit une élimination pour fournir **5***a*. L'oxydation au ferricyanure du produit **5** regénère le produit **1**. [Traduit par le journal]

Can. J. Chem. Downloaded from www.nrcresearchpress.com by 210.87.254.5 on 09/05/12
For personal use only.

In a recent publication in this journal structure **3** was proposed for the yellow compound, m.p. 150°, formed on ferricyanide oxidation of a mixture of *p*-cresol and 4-aminoantipyrine (1). One experimental fact, the position of the methyl signal at δ 1.52 in the ^{1}Hm.r. spectrum of the compound, was not in keeping with formula **3**, and the authors attributed this discrepancy to strong shielding of the 5-methyl group of the antipyrine moiety by the adjacent *o*-quinoneimide. However, the "unusually high field position" of this methyl group could more plausibly be explained by its being on an sp^3 carbon instead of an sp^2 carbon. Moreover, **3** would be expected to undergo fast electrocyclic ring closure to **1** which does place this methyl group on an sp^3 carbon. In the following is presented evidence that the structure of the yellow compound is indeed **1** and not **3**.

The ^{13}Cm.r. spectrum of the yellow compound (Table 1) had signals from four sp^3 carbon atoms, three from methyl carbon (19.7, 20.3, and 39.7 p.p.m.) and one from carbon not bearing hydrogen (87.4 p.p.m.), in agreement with **1** but not with **3**. When the yellow compound in methanol–tetrahydrofuran was treated with sodium borohydride at −10°, the yellow color was discharged within 2½ min. There was isolated a colorless crystalline solid **2**, m.p. 155–175° (dec.), whose i.r. spectrum contained an NH peak at 3350 cm^{-1}. Its ^{1}Hm.r. spectrum contained, in addition to three methyl singlets, a one-proton (non-exchangeable) singlet at δ 4.27 which is required by structure **2**. The ^{13}Cm.r. spectrum of the reduction product now contained five sp^3 carbons: three methyl (19.4, 20.8, and 38.1 p.p.m.), one quaternary (90.4 p.p.m.), and a new methine carbon (57.6 p.p.m.) in agreement with **2**. On standing, the borohydride reduction product underwent elimination of the phenol oxygen part of the carbinolamine ether and tautomerization to **5***a*, m.p. 205°. Its ^{13}C, ^{1}H, and u.v. (Fig. 1) spectra agree with this formulation. In addition, acetylation produced an *O*,*N*-diacetate **5***b*,

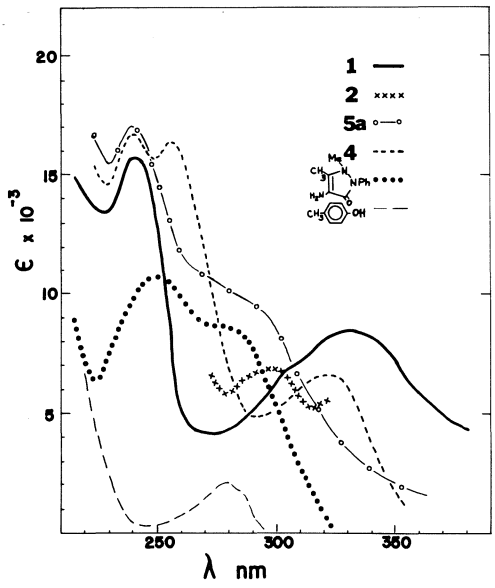

FIG. 1. Ultraviolet spectra of *p*-cresol – 4-aminoantipyrine transformation products.

[1]Part 41 of ^{13}Cm.r. Studies; for Part 40, ref. 5.

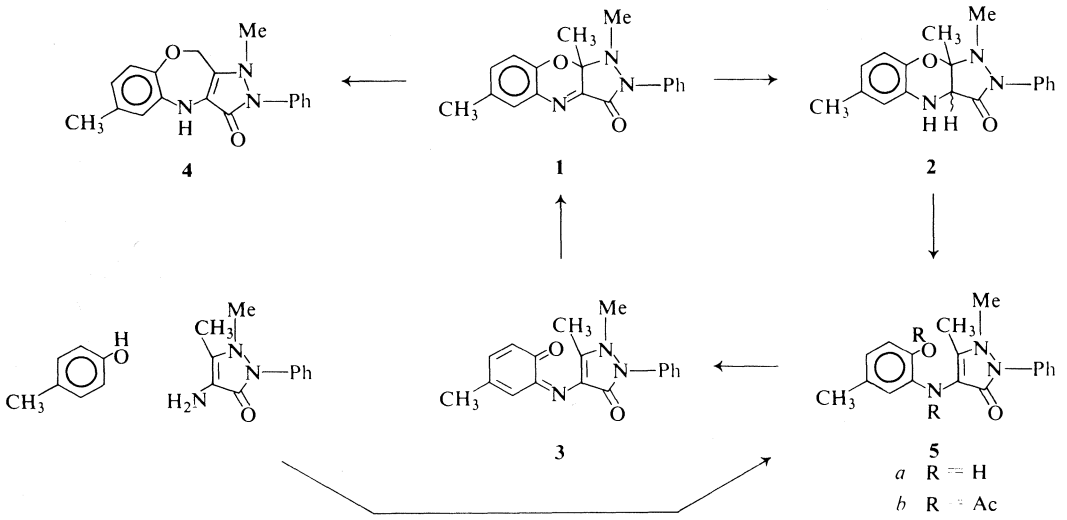

m.p. 151°, which was hydrolyzed in aqueous hydrochloric acid back to **5***a*. Since aminophenol **5***a* would be expected to be the first-stage intermediate in the two-stage oxidation of *p*-cresol and 4-aminoantipyrine to **1**, it is not surprising that treatment of **5***a* with ferricyanide gave **1** in very high yield.

With the revised structure **1**, the formation of compound **4**, whose structure was correctly assigned (1), can be regarded in a more familiar alternative way than the [1,7] sigmatropic shift suggested in ref. 1. Thus, the carbinolamine ether of **1** opens to the imonium ion **3′** (merely a canonical form of **3**) which, after proton loss from the methyl group, can undergo readdition of the phenol to the conjugated imine **6** to produce **4**. This interpretation accommodates both the thermal reaction and the catalysis by hydroxylic solvents. The suggested base catalysis (1) could well be just the effect of the greater polarity of pyridine (*vs.* $CDCl_3$) on formation of the polar resonance hybrid **3** ↔ **3′**. A further point of interest is that the ring closure of **6** to **4** is reversible. When **4** was heated at 105° in ethanol-*O*-*d*, the recovered **4** had partially exchanged the protons of the —OCH_2— group for deuterium, a result which is only possible if the reaction sequence **4** → **6** → **3′** occurs. Although compound **6** can cyclize either to a 6-membered ring (**1**) or to a 7-membered ring (**4**), the unusual result is that the 7-membered ring is strongly favored at equilibrium.

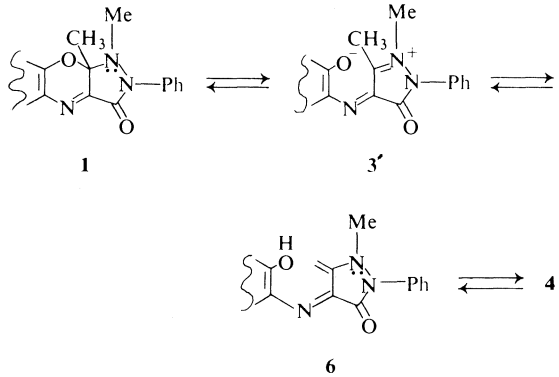

The very low-field position (δ 8.00–8.22) for two of the aromatic protons of the cresyl ring of **1** is not exceptional; quinoxaline and quinoline derivatives also have such low-field protons (2). Nor is the yellow color of **1** surprising when it is noted that **1** has more extended conjugation than 4-aminoantipyrine which is yellow.

Therefore, although **3** is probably an intermediate in the formation of **1**, it remains undetected as yet.

Experimental

General

Procedures and apparatus were the same as in ref. 3 except for the following. Infrared spectra were recorded on Beckman IR-5A and IR-20A instruments. Aromatic protons in the ^{1}Hm.r. spectra are not reported. ^{13}Cm.r. spectra were obtained with a Varian XL-100-15 system operating in the Fourier transform mode with proton decoupling. The nature of specific carbons (*i.e.* quaternary, methyl, etc.) was determined by off-resonance decoupling with and without noise modulation. Samples of ~20 mg/0.3 ml were examined in the solvents noted (Table 1). Merck aluminum oxide PF-254 (type E) was used for some thick-layer chromatography. Thin layer

Can. J. Chem. Downloaded from www.nrcresearchpress.com by 210.87.254.5 on 09/05/12
For personal use only.

TABLE 1. ^{13}Cm.r. absorption data relative to TMS standard

Compound (solvent)	Antipyrine ring					*N*-Phenyl				Cresol ring[a]		
	C-5	C-4	C-3	N-Me	C-Me	C-1	C-2	C-3	C-4	CH	C	Me
4-NH_2 antipyrine ($CDCl_3$)	137.9	119.1	162.1	37.9	10.1	135.5	122.8	129.0	125.8	—	—	—
1 (C_6D_6)	87.4	159.3	161.1	39.7	19.7	133.4	118.9	129.3	125.7	116.7 (C-6) 130.2 131.7	133.2 (C-4) 138.3 (C-2) 141.6 (C-1)	20.3
2 (Ac-d_6)	90.4	57.6		38.1	19.4	131.7	120.1	129.5	125.3	115.5 117.5 119.6	120.4 (C-4) 129.8 (C-2) 138.9 (C-1)	20.8
5*a* ($CDCl_3$)	144.2	113.8	163.9	36.4	11.1	134.7	124.5	129.3	127.1	114.0 114.9 119.7	128.5 (C-4) 134.4 (C-2) 150.8 (C-1)	21.1
4 ($CDCl_3$)	137.5	119.2	159.6	39.2	68.5[b]	135.1	123.1	129.2	126.4	119.4 (C-6) 122.3 123.4	134.8 135.1 146.1 (C-1)	20.7

[a]The assignments indicated for the aryl carbons were made by comparison with those observed for benzoxazole (4), *p*-cresol, and *o*-aminophenol.
[b]—CH_2O— signal.

chromatography plates were sprayed with a 4:1 mixture of concentrated H_2SO_4 – concentrated HNO_3.

Reaction of p-Cresol with 4-Aminoantipyrine

The reaction was performed as described by Jones and Johnson (1) with *p*-cresol (175 mg, B.D.H.), 4-aminoantipyrine (550 mg, Matheson), $K_3Fe(CN)_6$ (10.5 g), and p*H* 10 phosphate buffer (Coleman) solution (125 ml). The filtered material was dried under reduced pressure to give a yellowish-brown solid (420 mg, 85%), m.p. 130–134°. The ^{1}Hm.r. spectrum of the crude material showed methyl peaks corresponding only to the yellow oxidation product **1**, and it could be used without further purification (*vide infra*). For spectroscopy, the compound was purified by recrystallization from *n*-pentane or by preparative t.l.c. on alumina with benzene–ether (75:25) eluent. The yellow band at R_f 0.65 yielded bright yellow granules of **1**, m.p. 146–148°, after recrystallization from ether; ν_{max} ($CHCl_3$) 1689 (amide C=O) and 1658 (weak)[2] cm^{-1}, λ_{max} (MeOH) 242 (15 800) and 330 nm (8600); δ ($CDCl_3$) 1.54 (3H, s, CH_3), 2.40 (3H, s, $ArCH_3$), and 2.76 p.p.m. (3H, s, NCH_3).

[2]The absorption peak at 1658 cm^{-1} has only about one sixth of the intensity of the 1689 cm^{-1} peak (amide C=O) and therefore cannot be due to a carbonyl group.

Borohydride Reduction of 1

To a stirred (magnetic bar) solution of **1** (25 mg) in a mixture of methanol (1.0 ml) and tetrahydrofuran (1.0 ml) at −10° was added $NaBH_4$ (25 mg). Within 2.5 min the yellow color was discharged. After stirring at −10° for another 0.5 min, the reaction mixture was diluted with cold ether, washed with ice-cold water, dried, and concentrated at room temperature to give an almost colorless crystalline solid. Three recrystallizations from acetone – petroleum ether (b.p. 30–60°) gave colorless granules (7 mg) of essentially one stereoisomer of **2**, m.p. 155–175° (dec.);[3] ν_{max} ($CHCl_3$) 3350 (NH) and 1725 cm^{-1} (amide C=O); λ_{max} (MeOH) 245 (16 000) and 295 nm (~7000); δ ($CDCl_3$) 1.63 (3H, s, CH_3), 2.13 (3H, s, $ArCH_3$), 2.73 (3H, s, NCH_3), and 4.27 p.p.m. (1H, s, N—CH—C=O); *m/e* 309 (molecular ion).

Anal. Calcd. for $C_{18}H_{19}N_3O_2$ (309.4): C, 69.88; H, 6.19. Found: C, 69.57; H, 6.03.

[3]The clean ^{1}Hm.r. spectrum is the best indication that a single stereoisomer of **2** is present. The wide m.p. is probably caused by some elimination to **5***a* which is apparent from t.l.c. of the melt. It is also possible that the *cis* and *trans* stereoisomers of **2** are being interconverted via **3** ↔ **3**′ during t.l.c. or melting.

Can. J. Chem. Downloaded from www.nrcresearchpress.com by 210.87.254.5 on 09/05/12
For personal use only.

Can. J. Chem. Downloaded from www.nrcresearchpress.com by 210.87.254.5 on 09/05/12
For personal use only.

Thin-layer chromatography on silica gel in ether–benzene (75:25) showed two overlapping spots more polar than **1** but less polar than **5***a*.[3]

Elimination Product 5a

(*a*) The ^{1}Hm.r. solution of **2** in $CDCl_3$ was allowed to stand overnight, whereupon the three methyl signals due to **2** had disappeared and three new methyl signals had appeared. Recrystallization from chloroform – petroleum ether (b.p. 60–80°) gave colorless microcrystals of **5***a*, m.p. 199–205° (dec.); ν_{max} ($CHCl_3$) 3100–3500 (broad, OH, NH) and 1675 cm^{-1} (amide C=O); λ_{max} (MeOH) 240 (17 000) and λ_{inf} (MeOH) ~280 nm (10 000); δ ($CDCl_3$) 2.14 (3H, s, CH_3), 2.18 (3H, s, CH_3), and 3.09 p.p.m. (3H, s, NCH_3); *m/e* 309 (molecular ion). This sample was identical with that prepared in *b*.

(*b*) To a stirred (magnetic bar) solution of crude **1** (100 mg) in a mixture of methanol (1.0 ml) and tetrahydrofuran (1.5 ml) at room temperature was added $NaBH_4$ (100 mg). After being stirred for 0.5 h, the mixture was diluted with ether, washed with water, dried, and evaporated to leave an oily solid (102 mg). The crude solid dissolved in acetone (5 ml) was treated with 0.1 *N* aqueous HCl (1 ml) for 1 h. Work-up and two recrystallizations from chloroform – petroleum ether (b.p. 60–80°) gave colorless crystals of **5***a* (40 mg), m.p. 199–205° (dec.).

Anal. Calcd. for $C_{18}H_{19}N_3O_2$ (309.4): C, 69.88; H, 6.19. Found: C, 69.42; H, 6.40.

Diacetate 5b

A solution of aminophenol **5***a* (100 mg), pyridine (1.0 ml), and acetic anhydride (1.5 ml) was stirred (magnetic bar) under nitrogen at 100° for 2.5 days. After distillation of the pyridine and excess anhydride at reduced pressure, the residual mass was taken into chloroform, washed with 5% aqueous $NaHCO_3$ and water, dried, and concentrated to an amber oil. Thin-layer chromatography on 20 g of silica gel with ether–methanol (85:15) gave under u.v. a band at R_f 0.43 which was extracted several times with ether to yield 60 mg of solid. Recrystallization of 40 mg from acetone – petroleum ether (b.p. 30–60°) gave colorless granules of **5***b* (30 mg), m.p. 150–151°; ν_{max} ($CHCl_3$) 1760 (acetate C=O) and 1675 cm^{-1} (2 amide C=O); λ_{max} (MeOH) 275 nm (12 670); δ ($CDCl_3$) 2.08 (3H, broad hump, CH_3 of acetate, sharpened at 80° to a singlet), 2.18 (3H, s, CH_3), 2.27 (3H, s, CH_3), 2.33 (3H, s, CH_3), and 3.10 p.p.m. (3H, s, NCH_3); *m/e* 393 (molecular ion).

Anal. Calcd. for $C_{22}H_{23}N_3O_4$ (393.4): C, 67.16; H, 5.89; N, 10.68. Found: C, 67.85; H, 6.05; N, 10.21.[4]

Acid hydrolysis of **5***b* (10 mg) with 10% aqueous HCl (0.8 ml) in a sealed glass tube at 100° for 2.5 h gave 4 mg of oily solid. Four recrystallizations from chloroform – petroleum ether (b.p. 60–80°) gave colorless **5***a* (1.3 mg) identical (m.p., mixture m.p., t.l.c.) with an authentic sample.

Ferricyanide Oxidation of 5a

To a stirred (magnetic bar) solution of **5***a* (2.0 mg) in tetrahydrofuran (0.1 ml) and p*H* 10 buffer solution (0.5 ml) was added 20 mg of $K_3Fe(CN)_6$. A yellow solid precipitated immediately. After 0.5 h the solid was filtered, washed thoroughly with water, and dried to yield 0.5 mg of bright yellow granules of **1** identical with an authentic sample (m.p., mixture m.p., and t.l.c.). Extraction of the filtrate with ether gave 1.5 mg more of yellow oily solid which t.l.c. showed to be essentially pure **1**.

Deuterium Exchange with 4

A solution of **4** (10 mg) in ethanol-*O*-*d* (1 ml) was heated in a sealed tube at 105° for 2 days. Two recrystallizations of the product from ethanol to remove ND gave 7.3 mg of colorless **4**, m.p. 215–218°. Deuterium analysis by mass spectroscopy gave 52% d_0, 32% d_1, and 16% d_2. The ^{1}Hm.r. spectrum of the recovered **4** revealed a considerable decrease (~40%) in the intensity of the —OCH_2— peak at δ 5.07.

We thank the National Research Council of Canada for financial support.

1. P. F. Jones and K. E. Johnson. Can. J. Chem. **51**, 3733 (1973).
2. Varian NMR Spectra Catalog, Vol. 2, spectra 494 and 578. Varian Associates. 1963.
3. V. Dave and E. W. Warnhoff. Can. J. Chem. **49**, 1911 (1971).
4. L. F. Johnson and W. C. Jankowski. Carbon-13 NMR spectra. Wiley-Interscience, New York. 1972.
5. G. I. Birnbaum, A. Stoessl, S. H. Grover, and J. B. Stothers. Can. J. Chem. **52**, 993 (1974).

[4]Three analyses of the same sample of **5***b* gave carbon values varying by 1.8%. However, the sharp melting point, single t.l.c. spot, molecular ion at *m/e* 393, and the absence of extraneous absorption in the ^{1}Hm.r. spectrum are convincing evidence of its formula and purity.

A Salamander Alkaloid Synthesis

MICHAEL BENN AND ROGER SHAW[1]

Department of Chemistry, The University of Calgary, Alberta T2N 1N4

Received February 28, 1974

MICHAEL BENN and ROGER SHAW. Can. J. Chem. **52**, 2936 (1974).

Lithium–ethylamine reduction of 17β-acetoxy-1α-hydroxy-2a-aza-*A*-homo-5β-androstan-3-one, obtained by a Schmidt reaction on 17β-acetoxy-1α-hydroxy-5β-androstan-3-one, yielded an alkaloid isolated from *Cryptobranchus maximus* Stanley and provided access to other salamander alkaloids.

MICHAEL BENN et ROGER SHAW. Can. J. Chem. **52**, 2936 (1974).

La réaction de Schmidt sur l'acétoxy-17β hydroxy-1α androstane-5β one-3 conduit à l'acétoxy-17β hydroxy-1α aza-2a *A*-homo-androstane-5β one-3 qui par réduction avec du lithium en présence d'éthylamine conduit à un alkaloide isolé du *Crystobranchus maximus* Stanley; cette méthode permet aussi d'obtenir d'autres alkaloides de la Salamandre.

Apart from toxicities, to which they presumably owe their role as predator-repellants, the salamander alkaloids possess some interesting and potentially useful physiological properties; thus samandarine (**1**) has been reported to be a potent local anesthetic (1). As supplies of the alkaloids from natural sources are limited and difficult to obtain their synthesis therefore has some practical importance.

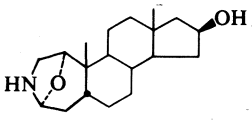

1

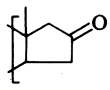

2

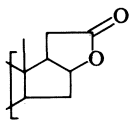

3

The characteristic skeleton of the alkaloids is that of a 2a-aza-*A*-homo-5β-steroid and, as exemplified by samandarine, samandarone (**2**), and samandaridine (**3**), there is usually a 1α,3α-oxide bridge and further oxygenation at C-16. The visualization of the alkaloids as steroid metabolites has some experimental substantiation in the observation that cholesterol can function as their precursor (2). Intrigued by this transformation we decided to construct our synthetic approach to the alkaloids by attempting to mimic reactions which might occur *in vivo*.

The formation of **2** from a simple sterol can be considered as involving two operations: the synthesis of a 16-oxoandrostane (3); and formation of the expanded and oxygen-bridged ring *A*. We concentrate our discussion here on the second of these operations, selecting as our target the alkaloid **4** isolated from *Cryptobranchus maximus* Stanley (4).

The most obvious routes for construction of the desired *A*-ring system proceed either by way of 2,3-seco intermediates, involving **5** or its equivalent, or else employ ring expansion followed by bridging *e.g.* **7** → **8** → **10** → **4**. Both the first two successful syntheses of salamander alkaloids (5, 6) employed seco steroid routes.

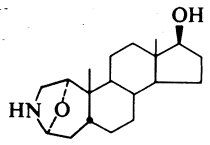

4

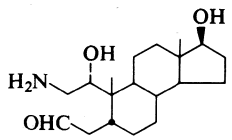

5

We preferred the alternative approach, and planned our synthesis as shown in Scheme 1.

Experiments by Pelc and Hodková (7) have revealed that hydrogenation of 1α,2α-epoxy-3-oxoandrosta-4,6-dienes, prepared by alkaline hydrogen peroxide epoxidation (8*a*) of the corresponding 1,4,6-trien-3-one (8*b*) yielded 1α-hydroxy-3-oxo-5β-androstanes. Application of their procedure to **6** gave reasonable yields of the desired 1α-hydroxy compound **7**. The stereochemistry at C-5 was established unequivocally by the following methods: the half-band width of the C-19 protons was within the range suggested for 5β-steroids (9); the mass-spectral cleavage of combined C-3 and C-4 units (42

[1]Work completed at the Department of Biochemistry, Rice University, Houston, Texas 77001; present address: Department of Biochemistry, St. Louis University Medical School, St. Louis, Missouri.

Can. J. Chem. Downloaded from www.nrcresearchpress.com by 210.87.254.42 on 09/05/12
For personal use only.

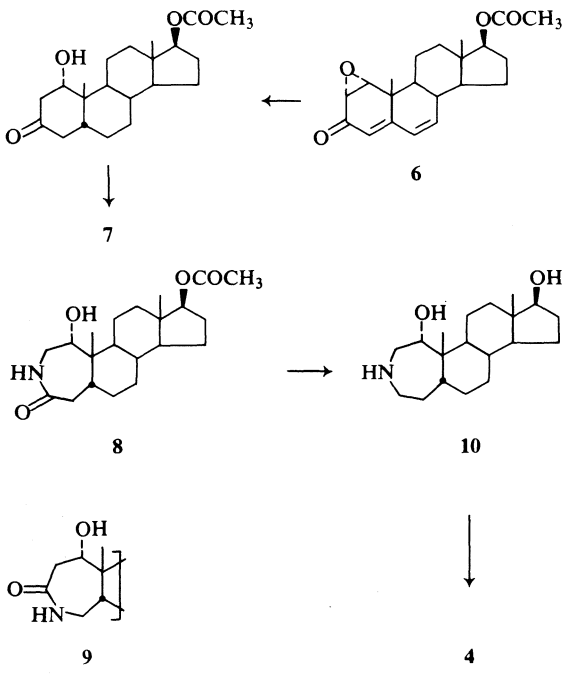

SCHEME 1

a.m.u.) from the molecular ion or the dehydrated molecular ion was weak, in accordance with the findings of Egger (10); and finally, a weakly negative Cotton effect was observed, analogous to 5β-cholestanone (11).

Our original plan was to prepare the mixed *E*- and *Z*-oximes of 17β-acetoxy-1α-hydroxy-5β-androstan-3-one (**7**), separate them (12) and identify them by p.m.r. (13). Stereospecific Beckmann rearrangement (14) of the *Z*-oxime should then afford the lactam **8** with the correct skeleton and functionalization for conversion to **4**. An attractive feature of this approach is that the "wrong" *E*-oxime might be isomerized to provide more of the "right" *Z*-oxime. In the event, preliminary experiments with 1α-hydroxy-5β-cholestan-3-one persuaded us that it would probably be less time consuming to convert **7** to a mixture of **8** and **9** by a Schmidt reaction, and then to separate the mixed lactams, and this we did. The conversion of **7** to **8** and **9** was good. Separation of the mixed lactams ultimately proved to be the most difficult step in the entire synthesis and was achieved by careful preparative thin-layer chromatography.

The assignment of structures **8** and **9** to the two lactams was made on the basis of spectroscopic evidence, including the relatively facile formation of an αβ-unsaturated lactam when (**9**), was heated briefly with acetic anhydride in the presence of pyridine. Final proof of the correctness of the assignments was provided by the successful conversion of the lactam **8** to the *Cryptobranchus* alkaloid.

Lithium aluminum hydride reduction of **8** gave satisfactory yields of 1α,17β-dihydroxy-2α-aza-*A*-homo-5β-androstane (**10**) but partial back-oxidation with a variety of agents including silver(II) picolinate (15), gave complex mixtures in which, however, the presence of **4** was evidenced by g.l.c.–m.s.

Another approach to the ring-*A* transformation involves a direct partial reduction of the lactam to the intermediate iminol **11** which should spontaneously cyclize to the more stable oxazolidine structure.

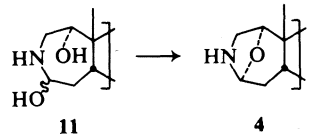

Benkeser *et al.* (16) have shown that such a partial reduction can be accomplished electrolytically. Using an analogous, but technically simpler approach, dissolving lithium in a solution of **8** in ethyl amine containing 2-methyl-2-propanol, we were indeed able to convert lactam **8** to the *Cryptobranchus* alkaloid in a reasonable yield.

Since **4** has been converted into **1** (*5a*), and this into **2** and **3** (*1*), in a formal sense our synthesis also provides access to these other salamander alkaloids.

Experimental

Melting points were uncorrected. Thin-layer chromatography was carried out on silica gel G plates. Proton magnetic resonance spectra were measured on a Varian A60 or HA100 spectrometer. Mass spectra were recorded on AEI-MS9 and Varian-M-18-CH5 spectrometers and g.l.c.–m.s. were carried out on a Varian CH7 spectrometer coupled with a Varian G2700 gas chromatograph fitted with a 6 ft column containing 3% OV1 on Chromosorb Q (oven 210°; He 50 ml/min). Optical rotary dispersion and c.d. curves were determined on a Durrum-Jasco ORD-UV/5 spectropolarimeter with 20 c.d. modification, at 31°, in chloroform–ethanol. The estimated $[\alpha]_D$ error was ±2°.

Preparation of 17β-Acetoxy-1,4,6-androstatrien-3-one

17β-Acetoxyandrostan-1,4-dien-3-one (18.246 g; 55.6 mmol) (Sigma Chemical Co.) was dissolved in distilled, anhydrous, oxygen-free (scrubbed with nitrogen) carbon tetrachloride (200 ml). To this solution was added *N*-bromosuccinimide (10.00 g; 56.2 mmol) and benzoyl

Can. J. Chem. Downloaded from www.nrcresearchpress.com by 210.87.254.42 on 09/05/12
For personal use only.

Can. J. Chem. Downloaded from www.nrcresearchpress.com by 210.87.254.42 on 09/05/12
For personal use only.

peroxide (0.63 g) and the mixture was refluxed in the dark for 5 h, with continuous stirring, in a slow current of nitrogen with rigorous exclusion of moisture. The resulting red-brown suspension was allowed to cool to room temperature in the dark under a nitrogen atmosphere. It was then filtered and the solid which had separated was collected and washed well with carbon tetrachloride. The filtrate and washings were combined, and evaporated to dryness at room temperature under reduced pressure.

The product, a red-brown gum (31 g) was dissolved in anhydrous, freshly distilled dimethylformamide (300 ml) containing suspended powdered calcium carbonate (10 g), and the reaction mixture was stirred and refluxed, under an atmosphere of nitrogen, for 1 h. It was then cooled, acidified with 2 *N* hydrochloric acid, and extracted with ethyl acetate. The ethyl acetate extracts were combined, washed with saturated aqueous sodium bicarbonate solution, and water, dried ($MgSO_4$), filtered, and finally evaporated to dryness under reduced pressure. The residual red-brown gum (20 g) was chromatographed on a column of Florisil from which ether–benzene (1:8) eluted 17β-acetoxy-1,4,6-androstatrien-3-one as a yellow solid (16.7 g, 92.5%). This substance, which was more than 90% pure on t.l.c. (R_f 0.19; EtOAc–C_6H_6, 1:2), was recrystallized from aqueous ethanol and then carbon tetrachloride – hexane to yield yellowish prisms, m.p. 151–152° (lit. (8*b*) m.p. 151–153°); t.l.c. homogeneous (R_f 0.32; Et_2O–C_6H_6, 1:2); ν_{max} (KBr) 3030, 1735, 1650, 1610, and 1580 cm^{-1}; λ_{max} 220 (ε 18 120), 258.5 (ε 11 100), and 305 nm (ε 16 160) [*cf.* lit. (17) 222 (11 100), 257 (9500), and 299 nm (12 800)]; δ 0.88 (S)(3H), 1.18 (S) (*ca.* 3H), 1.97 (S) (*ca.* 3H), 4.37–4.75 (m) (1H), 5.70–6.37 (m) (4H), and 6.94 p.p.m. (d; J = 10 Hz) (1 H).

The Epoxidation of 17β-Acetoxy-1,4,6-androstatrien-3-one: Preparation of 1α,2α-Epoxy-17β-acetoxy-4,6-androstadien-3-one (6)

The trienone (16.8 g; 51 mmol) was dissolved in a 2:1 mixture of methanol–dichloromethane (660 ml). After the addition of 10% aqueous sodium hydroxide (11 ml), the mixture was kept at room temperature for ¾ h and 30% hydrogen peroxide (66 ml) was then added, after which the reaction mixture was kept at 0° for 12 h. At the end of this time the solvents were removed under reduced pressure, at room temperature, with the simultaneous addition of small amounts (*ca.* 10 ml) of water until the total volume was about 100 ml. The solid (11 g) which separated was collected and washed with water until the washings were neutral. The mother liquors were diluted with more water and extracted with ethyl acetate. The organic extracts were combined, washed with water, dried ($MgSO_4$), filtered, and evaporated to dryness under reduced pressure to yield a gum (1.18 g).

The solid and gum products were combined and acetylated with acetic anhydride (30 ml) and pyridine (15 ml), at room temperature, overnight. The reaction mixture was then diluted with ice water and extracted with chloroform. The combined chloroform extracts were washed successively with 2 *N* sulfuric acid, water, saturated aqueous sodium bicarbonate, water, and then dried ($MgSO_4$), filtered, and evaporated to dryness.

The crude product from the acetylation was purified by p.l.c. (Et_2O–C_6H_6, 1:2) with low loadings, giving three components: R_f 0.17 (0.8 g), 0.28 (0.15 g), and 0.41 (11 g; 62%).

The component with R_f 0.41, 1α,2α-epoxy-17β-acetoxy-4,6-androstadien-3-one (**6**) was recrystallized from acetone–hexane to yield colourless needles m.p. 187–203°, not raised by further recrystallization, (*cf.* lit. (8*a*) 205–206°); ν_{max} ($CHCl_3$) 1735, 1675, 1630, 1595, and 1260 cm^{-1} (lit. 1725, 1665, 1620, 1590, and 1250 cm^{-1}); λ_{max} 293 nm (ε 35 870) (lit. (8*a*) 292 nm (34 300)); δ 0.94 (S) (3H); 1.21 (S) (*ca.* 3H), 2.05 (S) (*ca.* 3H), 3.41 (q; J = 2 and 4 Hz) (1 H), 3.57 (d; J = 4 Hz) (1 H), 4.63 (m) (1 H), 5.61 (d; J = 2 Hz) (1 H), and 6.04 p.p.m.(m) (2 H), (*cf.* lit.(7) δ 0.92 (S), 1.19 (S), 2.04 (S), 3.41 (q; J = 2.4 Hz), 3.54 (d; J = 4 Hz), 4.62 (b), 5.62 (d; J = 2 Hz), and 6.05 p.p.m. (m)); *m/e* 342 ($M^{+\bullet}$) (30), 300 (40), 282 (30), and 43 a.m.u. (100).

The component with R_f 0.28, 1ξ,2ξ-6ξ,7ξ-diepoxy-17β-acetoxy-4-androsten-3-one, was recrystallized from acetone–hexane as yellow rods m.p. 230–250°, unchanged by further recrystallization; g.l.c. showed it to be almost pure (R_T 23.2 min; 90% of total area); ν_{max} ($CHCl_3$) 1735, 1685, and 1635 cm^{-1}; λ_{max} 243 nm (ε 11 250); δ 0.92 (S) (3H), 1.19 (S) (*ca.* 3H), 2.08 (S) (*ca.* 3H), 3.28–3.99 (m) (*ca.* 4H), 4.54–4.90 (m) (1 H), and 6.12 (S) (1H); *m/e* 358 ($M^{+\bullet}$) (12), 342 (3), 326 (30), 316 (8), 300 (10), 284 (40), and 43 a.m.u. (100).

The component with R_f 0.17, 1α-methoxy-17β-acetoxy-4,6-androstadien-3-one was recrystallized repeatedly from acetone–hexane to give colorless rods, m.p. 202.5–207.5°; $[\alpha]_D$ +159; ν_{max} ($CHCl_3$) 1735, 1670, 1630, and 1600 cm^{-1}; λ_{max} 290 nm (ε 16 900); δ 0.90 (S) (3H), 1.14 (S) (*ca.* 3H), 2.06 (S) (*ca.* 3H), 2.64 (q; J = 3 and 17 Hz) (1 H), 2.84 (q; J = 3 and 17 Hz) (1 H), 3.31 (S) (3 H), 3.63 (t; J = 3 Hz) (1 H) 4.67 (t; J = 7 Hz) (1 H), 5.74 (S) (1 H), and 6.12 p.p.m. (S) (2 H); *m/e* 358.2135 ($M^{+\bullet}$ Calcd. for $C_{22}H_{30}O_4$: 358.2144) (10), 326 (30), 298 (5), 284 (60), 266 (10), 251 (10), and 28 a.m.u. (100).

The Hydrogenation of 1α,2α-Epoxy-17β-acetoxy-4,6-androstadien-3-one: Preparation of 17β-Acetoxy-1α-hydroxy-5β-androstan-3-one (7)

Various solvent systems were investigated for the room-temperature, atmospheric-pressure hydrogenation of **6**, over 5% palladium on calcium carbonate. The most satisfactory conditions which we discovered used 2-propanol as solvent and a typical experiment is described below.

A solution of the epoxide **6** (0.393 g; 1.15 mmol) in 2-propanol (40 ml) was added to a mixture of prereduced 5% palladium on calcium carbonate (0.200 g) and 2-propanol (10 ml). The hydrogenation was carried out at room temperature and atmospheric pressure. The uptake of hydrogen gas was constant at 85.2 ml (*cf.* calculated hydrogen uptake 95.4 ml) after 42 min.

The reaction mixture was filtered through Celite and then evaporated to dryness at room temperature under reduced pressure. The colorless gum (0.442 g) so obtained was separated by p.l.c. with low loadings (Et_2O–C_6H_6 1:2; developed twice), whereby one major fraction (R_f 0.34), and three minor fractions (R_f values 0.13, 0.60, and 0.75) were isolated.

The major fraction, corresponding to 17β-acetoxy-1α-hydroxy-5β-androstan-3-one (**7**), (0.198 g; 49% yield) was recrystallized from acetone–hexane as colorless rods, m.p. 185–188°, ν_{max} ($CHCl_3$) 3520, 1735, and 1700 cm^{-1}; $[\alpha]_D \approx 0$; $[\theta]_{294}$ −522; δ 0.92 (S) (3 H), 1.22 (S) (*ca.* 3H), 2.04 (S) (*ca.* 3H), 3.64 (t; J = 8 Hz) (1 H), and 4.45–4.83

Can. J. Chem. Downloaded from www.nrcresearchpress.com by 210.87.254.42 on 09/05/12
For personal use only.

p.p.m. (m) (1 H); the difference in the half band-widths of the C-19 methyl and TMS absorptions = 0.1 Hz (15% w/v steroid in $CDCl_3$; 2% TMS) (*cf.* ≤ 0.36 Hz for 5β-steroids (9)); *m/e* 348 ($M^{+\bullet}$) (8), 330 (6), 262 (40), 202 (40), and 28 a.m.u. (100).

The Schmidt Reaction of 17β-Acetoxy-1α-hydroxy-5β-androstan-3-one (7)

A solution of 17β-acetoxy-1α-hydroxy-5β-androstan-3-one (2 g; 5.75 mmol) in anhydrous chloroform (300 ml) was treated with a freshly prepared and standardized 0.89 *M* solution of hydrazoic acid in chloroform (7.1 ml; 6.32 mmol). The mixture was cooled in an ice bath under anhydrous conditions, and to it was added, dropwise, concentrated sulfuric acid (2 ml) at such a rate that the temperature of the mixture was maintained below 5°. The reaction mixture was stirred throughout the addition, and was stirred for a further 20 min at 0° after the addition had been completed. Excess ice water was then added and the mixture was left in the refrigerator overnight.

The reaction mixture was brought to p*H ca.* 6 with 2 *N* sodium hydroxide, and then extracted exhaustively with chloroform. The combined chloroform extracts were washed with saturated aqueous sodium bicarbonate and then water, dried ($MgSO_4$), filtered, and evaporated to dryness *in vacuo*. The greenish foam (2.22 g) thus isolated was separated by p.l.c. ($MeOH–CHCl_3–Et_2O$ 1:3:3) into three components; R_f 0.41 (0.101 g; u.v. active), R_f 0.24 (0.377 g; barely visible on the p.l.c. plates under u.v. light), and R_f 0.20 (0.793 g; barely visible on the p.l.c. plates under u.v. light). The last two components had to be eluted with 20% methanol–chloroform as neither was soluble in pure chloroform; they were purified by crystallization.

The major component, R_f 0.20, 17β-acetoxy-1α-hydroxy-2a-aza-*A*-homo-5β-androstan-3-one (**8**) (38% yield), separated from acetone as a gel, but this gradually turned into colorless plates when air dried, m.p. 223–228.5°; $[\alpha]_D$ +128; ν_{max} (KBr) 3400, 1735, and 1630 cm^{-1}; λ_{max} (CE) 210 nm (ε 15 130), $\delta^{CF_3CO_2D}$ 0.97 (S) (3 H), 1.24 (S) (*ca.* 3H), 2.20 (S) (*ca.* 3H), 2.78–3.00 (m) (2 H), 4.76 (t; *J* = 8 Hz) (1 H), and 4.94 p.p.m. (q; *J* = 3 and 10 Hz) (1 H); *m/e* 363.2426 ($M^{+\bullet}$, Calcd. for $C_{21}H_{33}NO_4$: 336.2410) (12), 348 (1), 346 (1), 334 (20), 320 (2), 304 (3), 303 (3), 291 (6), 273 (10), 262 (8), 260 (10), 243 (10), and 30 a.m.u. (100); microanalysis: Calcd.: *N*, 3.85. Found: *N*, 3.62.

The pure 2a-aza-lactam (0.050 g) was acetylated by allowing it to stand overnight, at room temperature, in a mixture of pyridine (5 ml) and acetic anhydride (10 ml). The solution so obtained was diluted with ice water and then extracted repeatedly with chloroform. The chloroform extracts were combined, washed successively with saturated aqueous sodium bicarbonate solution and water, then dried ($MgSO_4$), filtered, and evaporated to dryness *in vacuo*. The colorless crystalline residue (0.048 g) of 1α,17β-diacetoxy-2a-aza-*A*-homo-5β-androstan-3-one was recrystallized once from acetone–hexane and obtained as colorless needles, m.p. 222–224.5°; $[\alpha]_D$ −64; ν_{max} 3460, 3100, 1735, and 1680 cm^{-1}; δ 0.79 (S) (3 H), 1.12 (S) (*ca.* 3H), 1.98 (S) and 2.03 (S) (*ca.* 6H), 2.55 (d; *J* = 9 Hz) (2 H), 2.98 (heptet; *J* = 3.5, 10.5, and 14 Hz) (1 H), 3.99 (octet; *J* = 2, 8, and 14 Hz) (1 H), 4.30 (q; *J* = 2 and 10.5 Hz) (1 H), and 4.56 p.p.m. (q; *J* = 7 and 9 Hz) (1 H); *m/e* 405.2532 ($M^{+\bullet}$ Calcd. for $C_{23}H_{35}NO_5$: 405.2515) (20), 346 (10), 333 (35), 291 (40), 286 (15), and 273 a.m.u. (90), and 43 a.m.u. (100).

The other major product of the Schmidt reaction, R_f 0.24, 17β-acetoxy-1α-hydroxy-3a-aza-*A*-homo-5β-androstan-3-one (**9**) (18% yield), crystallized from methanol–chloroform as colorless microcrystals, m.p. 322–325° (dec.); $[\alpha]_D$ −16; ν_{max} (KBr) 3455, 3235, 3090, 1735, and 1675 cm^{-1}; λ_{max} (CE) 209 nm (ε 13 360); $\delta^{CF_3CO_2D}$ 0.96 (S) (3 H), 1.13 (S) (*ca.* 3H), 2.17 (S) (*ca.* 3 H), 3.00–3.40 (m) (3 H), 4.05–4.47 (m) (2 H), and 4.55–4.85 p.p.m. (m) (1 H); *m/e* 363.2426 ($M^{+\bullet}$, Calcd. for $C_{21}H_{33}NO_4$: 363.2410) (20), 345 (5), 335 (25), 320 (15), 303 (8), 290 (8), 276 (20), 216 (60), and 101 a.m.u. (100).

Lactam **9** (0.05 g) was allowed to stand overnight at room temperature, in a mixture of pyridine (51 ml) and acetic anhydride (10 ml). This lactam, however, did not dissolve. The mixture was therefore refluxed for 10 min, cooled, and the homogeneous solution so obtained diluted with ice water. The mixture was extracted well with chloroform and the chloroform extracts were combined, washed successively with 2 *N* sulfuric acid, water, saturated aqueous sodium bicarbonate, and water, then dried ($MgSO_4$), filtered, and evaporated to dryness *in vacuo*. A slightly yellowish gum (0.053 g), a mixture of 1α,17β-dihydroxy-3a-aza-*A*-homo-5β-androstan-3-one triacetate and 17β-hydroxy-3a-aza-*A*-homo-5β-androst-1-en-3-one diacetate obtained, which could not be induced to crystallize. The gum had ν_{max} (film) 1735, 1695, 1675, and 1630 cm^{-1}; λ_{max} 225 nm (ε 5875); δ 0.81 (S) (3 H), 1.04 (S) and 1.12 (S) (*ca.* 3 H), 2.03 (S) (*ca.* 4 H), 2.45 (S) and 2.52 (S) (*ca.* 3H), 3.13–3.71 (m) (1.5–2 H), 4.10–4.93 (m) (2.5–3 H), 5.85 (d; *J* = 13 Hz) (0.5 H), and 6.28 p.p.m. (d; *J* = 13 Hz) (*ca.* 0.5 H).

The minor product apparently 17β-acetoxy-3a-aza-*A*-homo-5β-androst-1-en-3-one, R_f 0.41 (5.5% yield), was repeatedly recrystallized from acetone–hexane from which it separated as light yellow rods, m.p. 323–333°; g.l.c. (C) suggested that it was more than 90% pure, R_T 25.2 min; ν_{max} (KBr) 3030, 1735, 1675, and 1630 cm^{-1}; δ 0.82 (S) (3 H), 1.14 (S) (*ca.* 3H), 2.03 (S) (*ca.* 3H), 3.49–3.82 (m) (2 H), 4.60 (t; *J* = 7 Hz) (1 H), 5.73 (d; *J* = 13 Hz) (1 H), 6.20 (d; *J* = 13 Hz) (1 H), and 6.80–7.04 p.p.m. (m) (1 H); *m/e* 345.2318 ($M^{+\bullet}$, Calcd. for $C_{21}H_{31}NO_3$: 345.2304) (50), 330 (40), 316 (15), 302 (10), 285 (8), 270 (15), and 43 a.m.u (100).

The Reduction of 17β-Acetoxy-1α-hydroxy-2a-aza-A-homo-5β-androstan-3-one 17-Acetate (8)

The reduction with lithium aluminum hydride could not be carried out in ether because the compound was insufficiently soluble.

The lactam (0.119 g; 0.33 mmol) was added to a suspension of lithium aluminum hydride (0.6; 15.2 mmol) in freshly double-distilled tetrahydrofuran (100 ml) and the mixture was refluxed for 29 h. Ice was added slowly to the cold, well-stirred reaction mixture until the evolution of gas became mild; then water was added until the solids turned almost completely white. The mixture was filtered and the filter cake washed well with chloroform. The mother liquor and the washings were combined, dried ($MgSO_4$), filtered, and evaporated to dryness under reduced pressure. The colorless solid, **10**, so obtained (0.096 g; 80.3%) m.p. 235–240° and 250–260° (dec.), was sublimed (193°; 0.003 mm Hg), giving almost quantitative

amounts of colorless microcrystals, m.p. 247.5–248.5°; ν_{max} (KBr) 3370–3400, 3320 cm^{-1}; *m/e* 307.2499 ($M^{+\bullet}$, Calcd. for $C_{19}H_{33}NO_2$: 307.2511) 292 (10), 278 (45), 274 (10), 234 (5), and 44 a.m.u. (100).

A solution of the amine **10** (0.082 g; 0.267 mmol) in anhydrous, freshly distilled dimethyl sulfoxide (30 ml) was stirred with argentic picolinate (0.188 g; 0.534 mmol) at room temperature for 45 min after which time the color had turned from red to colorless. The mixture was filtered and then diluted with water (70 ml), followed by the addition of concentrated ammonia until the p*H* became 11 to 11.5 (indicator paper). The brown solution was exhaustively extracted with ether; and the extracts were combined, washed with water, dried ($MgSO_4$), filtered, and evaporated to dryness under water-pump vacuum, and finally under high vacuum, overnight at room temperature.

The crude product so obtained (0.058 g) was compared with a genuine sample of **4** by both t.l.c. and g.l.c. The t.l.c. suggested that the reaction product was a mixture of seven components, three of them major R_f 0.00, 0.16, and 0.25; two medium, R_f 0.36 and 0.50, and two minor R_f 0.10 and 0.60. The spot at R_f 0.25 was coincident, and cochromatographed with **4**. Gas–liquid chromatography analysis revealed only four components but the second of these cochromatographed with **4**, and upon g.l.c.–m.s. the fragmentation pattern of this component was identical to that of the *Cryptobranchus* alkaloid: *m/e* 305 (7) (M^+), 287 (4), 277 (8), 262 (4), 260 (5), 246 (8), 218 (5), 201 (5), 187 (7), 176 (4), and 85 a.m.u. (100). An attempt was made to isolate this component by preparative t.l.c. (MeOH–$CHCl_3$–Et_2O 1:3:3; detected by iodine vapor) but we were unable to recover the compounds from the silica gel, even when 50% methanol–chloroform was used as eluant.

Preparation of the Cryptobranchus Alkaloid by a Modified Birch Reduction of ***8***

Anhydrous ethylamine (Eastman; *ca.* 7 ml) was distilled into a cold mixture of 17β-acetoxy-1α-hydroxy-5β-androstan-3-one (14 mg; 38.6 μmol) and 2-methylpropan-2-ol (MCB; 0.5 ml) under anhydrous conditions. The reaction mixture was allowed to warm up to the room temperature and small pieces of freshly-cut lithium metal were added in two portions of *ca.* 50 mg ½ h apart. The reaction mixture was allowed to stir vigorously at room temperature. After a total reaction time of 1½ h, the light blue suspension was treated with dropwise addition of saturated aqueous ammonium chloride until excess lithium was destroyed. After removal of most of the ethylamine on a rotary evaporator, the mixture was diluted with water and then extracted extensively with ether. The combined ether extract was washed with water, then extracted with dilute hydrochloric acid. The combined acid extracts were washed with ether, cooled, and finally basified with solid sodium hydroxide. The colorless solid which separated was extracted with ether. The combined ether extracts were washed with water, dried, and evaporated to dryness, giving a colorless gum (6.4 mg) which was crystallized from acetone–hexane as colorless needles (5.8 mg; 49.3%); m.p. 186–188°; m.p. of supplied sample[2] 186–188°; mixed m.p. 186–188° (lit.(*5a*) m.p. 191–193°). Gas-liquid chromatography (3% OV 1, 6 ft; 230°; 60 ml/min) revealed a single component which cochromatographed with a genuine sample; t.l.c. (methanol–chloroform–ether 1:3:3) also showed identical mobility and the i.r. (in KBr) was superimposable upon that of the authentic alkaloid.

1. G. Habermehl. *In* The Alkaloids. Vol. 9. *Edited by* R. H. F. Manske. Academic Press, New York, N.Y. 1967. p. 427.
2. G. Habermehl and A. Haaf. Chem. Ber. **101**, 198 (1968).
3. M. H. Benn and R. Shaw. Chem. Commun. 327 (1970).
4. S. Hara and M. Oka. Japan Patent No. 70 18, 663; Chem. Abstr. **73**, 56316g (1970).
5. (*a*) S. Hara and K. Oka. J. Am. Chem. Soc. **89**, 1041 (1967). (*b*) K. Oka and S. Hara. Tetrahedron Lett. 1987 (1969).
6. Y. Shimizu. Tetrahedron Lett. 2919 (1972).
7. B. Pelc and J. Hodková. Collect. Czech. Chem. Commun. **32**, 410 (1967).
8. (*a*) J. Pfister, C. Lehmann, and H. Wehrli. Helv. Chim. Acta. **51**, 1505 (1968). (*b*) C. Djerassi, G. Rosenkranz, J. Romo, St. Kaufmann, and J. Pataki. J. Am. Chem. Soc. **72**, 4531 (1950); **72**, 4534 (1950).
9. K. L. Williamson, T. Howell, and T. A. Spencer. J. Am. Chem. Soc. **88**, 325 (1966).
10. H. Egger. Monatsh. Chem. **97**, 1290 (1966).
11. P. Crabbe. ORD and CD in organic chemistry. Holden-Day, Inc., San Francisco. 1965. p. 103.
12. S. Hara, K. Oka, and Y. Ike. Chem. Ind. 832 (1967).
13. K. Oka and S. Hara. Chem. Ind. 911 (1968).
14. K. Oka and S. Hara. Chem. Ind. 168 (1969).
15. R. G. R. Bacon and W. J. W. Hanna. J. Chem. Soc. 4962 (1965).
16. R. A. Benkeser, H. Watanabe, S. J. Mels, and M. A. Sabol. J. Org Chem. **35**, 1210 (1970).
17. W. Neudert and H. Ropke. Atlas of steroid spectra. *Translated by* J. B. Leane. Springer-Verlag, New York, Inc., New York. 1965.

[2]Kindly supplied by Dr. S. Hara.

Can. J. Chem. Downloaded from www.nrcresearchpress.com by 210.87.254.42 on 09/05/12
For personal use only.

Regiospecific Syntheses of Modified Steroid Hormones. Part VI.[1] α-, α′-, and β-Mode Reactions of Hydrogen Halides with 1,2-Epoxy- and 4,5-Epoxy-3-oxo-androstanes and -estranes

M. NEEMAN AND J. S. O'GRODNICK

Roswell Park Memorial Institute and Graduate Program in Chemistry, Faculty of Institutes and Centers, State University of New York at Buffalo, New York 14203

Received January 11, 1974

M. NEEMAN and J. S. O'GRODNICK. Can. J. Chem. **52**, 2941 (1974).

The reaction of **A/B** *cis*-4β,5β-epoxy-17β-hydroxyandrostan-3-one acetate **1***b* with hydrogen fluoride in chloroform gave 5α-fluoro-4α,17β-dihydroxyandrostan-3-one acetate **10***b* by β-mode oxirane opening to **10***a*, followed by epimerization at C-4. Reactions of **A/B** *cis*-α,β-epoxyketones **1***a* and **1***c* in acetone containing aqueous hydrogen chloride resulted in α-mode regiospecific oxirane opening, followed by β-dehydration to 4-chloro-4-en-3-ones **4***a* and **4***c*. Reaction of hydrogen chloride in "10%" ethanol–chloroform with 4β,5β-epoxy-17β-hydroxyandrostan-3-one **1***a* gave non-regioselectively **3***a* and **4***a* (α:α′, 1:1), whereas the reactions with 4α,5α-epoxy-17β-hydroxyandrostan-3-one acetate **2**, 1α,2α-epoxy-17β-hydroxy-5α-androstan-3-one **6***a*, and 1β,2β-epoxy-17β-hydroxy-5α-androstan-3-one acetate **5** were α-mode regiospecific. Epoxyketone **5** was readily converted to the *trans*-diequatorial 2α-chloro-1β,17β-dihydroxy-5α-androstan-3-one acetate **7**. The reactions of hydrogen fluoride with 4β,5β-epoxy-17β-hydroxy androstan-3-one **1***a* in "10%" ethanol–chloroform or in *N,N*-dimethylformamide, and with 1α,2α-epoxy-17β-hydroxy-5α-androstan-3-one **6***a* in *N,N*-dimethylformamide were α′-regioselective. Mechanisms are proposed for the observed α-, β-, and α′-mode reactions of hydrogen halides with steroidal α,β-epoxyketones **1**, **2**, **5**, and **6**.

M. NEEMAN et J. S. O'GRODNICK. Can. J. Chem. **52**, 2941 (1974).

La réaction de l'acétate de l'époxy-4β,5β hydroxy-17β androstanone-3 **A/B** *cis* (**1***b*) avec l'acide fluorhydrique dans le chloroforme conduit à l'acétate du fluoro-5α dihydroxy-4α,17β androstanone-3 (**10***b*); cette transformation s'effectue par une ouverture du type β de l'oxiranne conduisant au produit (**10***a*) qui s'épimérise ensuite en position C-4. La réaction des époxy-α,β cétones **A/B** *cis* **1***a* et **1***c* dans l'acétone contenant de l'acide chlorhydrique aqueux conduit à des ouvertures régiospécifiques de l'oxiranne par un mode α; ces ouvertures sont suivies par une déshydration-β fournissant les chloro-4 èn-4 one-3 **4***a* et **4***c*. L'acide chlorhydrique dans un mélange éthanol–chloroforme à 10% réagit avec l'époxy-4β,5β hydroxy-17β androstanone-3 (**1***a*) et conduit d'une façon non-régiosélective aux produits **3***a* et **4***a* (α:α′, 1:1) alors que les réactions de l'acétate de l'époxy-4α,5α hydroxy-17β androstanone-3 (**2**), de l'époxy-1α,2α hydroxy-17β androstane-5α one-3 (**6***a*) et de l'acétate de l'époxy-1β,2β hydroxy-17β androstane-5α one-3 se produisent d'une façon régiospécifique avec un mode α. L'époxycétone **5** se transforme rapidement en produit *trans* diéquatorial, acétate de chloro-2α dihydroxy-1β,17β androstane-5α one-3 (**7**). Les réactions de l'acide fluorhydrique avec l'époxy-4β,5β hydroxy-17β androstanone-3 (**1***a*) dans un mélange d'éthanol–chloroforme à 10% ou dans la *N,N*-diméthylformamide et avec l'époxy-1α,2α hydroxy-17β androstane-5α one-3 (**6***a*) dans la *N,N*-diméthylformamide sont régiosélectives α′. On propose des mécanismes pour les modes de réaction α,β et α′ observés lors des réactions des halogénures d'hydrogène avec les cétones stéroïdales α,β époxydées **1**, **2**, **5** et **6**.

[Traduit par le journal]

Introduction

Recently we reported reactions of hydrogen halides with steroidal 4,5-epoxy-3-ones (1). These studies have led to revision of several erroneous structure assignments based on mechanistic misconceptions (1*a*, 2) and the development of regiospecific routes, via 19-norsteroid intermediates, to 2-fluoro and 4-bromo- ring-A-aromatic steroids (3*a* and *b*). The present paper gives a full account of these reactions and extends the study to 1α,2α- and 1β,2β-epoxy-5α-androstan-3-ones. The α,β-epoxyketones **1**, **2**, **5**, and **6**, (Schemes 1 and 3) were selected as model compounds in which stereoelectronically normal *trans*-diaxial oxirane cleavage could occur either by α-mode, or by β-mode reactions. These conformational determinants did, however, not account for all the observed reactions: several "abnormal" re-

[1]Part V, see ref. 3*c*.

Can. J. Chem. Downloaded from www.nrcresearchpress.com by 210.87.254.40 on 09/05/12
For personal use only.

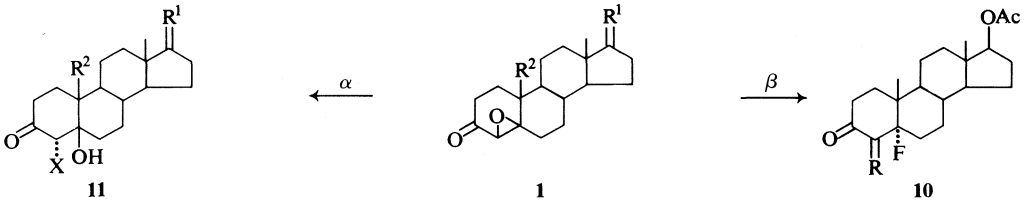

11

a R^1 = α-H, β-OH; R^2 = Me; X = Cl
b R^1 = α-H, β-OH; R^2 = H; X = Cl
c R^1 = α-H, β-OH; R^2 = H; X = Br

1

a R^1 = α-H, β-OH; R^2 = Me
b R^1 = α-H, β-OAc; R^2 = Me
c R^1 = α-H, β-OH; R^2 = H
d R^1 = α-H, β-OH; R^2 = OH
e R^1 = O; R^2 = OH

10

a R = α-H, β-OH
b R = α-OH, β-H
c R = α-OD, β-H
d R = α-OAc, β-H

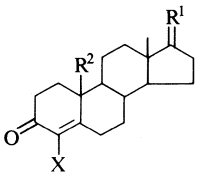

4

a R^1 = α-H, β-OH; R^2 = Me; X = Cl
b R^1 = α-H, β-OAc; R^2 = Me; X = Cl
c R^1 = α-H, β-OH; R^2 = H; X = Cl
d R^1 = α-H, β-OH; R^2 = H; X = Br
e R^1 = α-H, β-OH; R^2 = OH; X = Br
f R^1 = O; R^2 = OH; X = Br

SCHEME 1

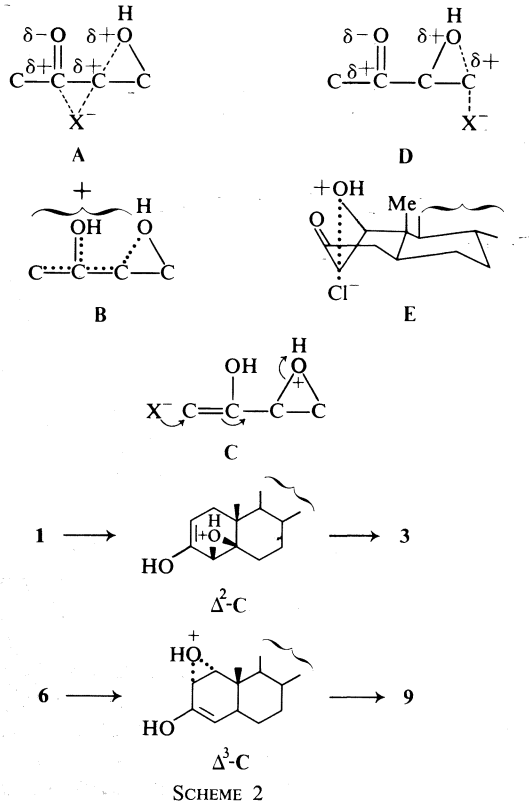

SCHEME 2

actions occurred, such as facile *trans*-diequatorial α-mode oxirane cleavage by chloride; and α′-mode *cine*-halogenations by chloride (non-regioselective) and by fluoride (regioselective). The present study is addressed to mechanistic interpretations of these reactions with regard to halide polarizabilities and steric requirements, as well as the interaction of neighboring orbitals in nucleophilic oxirane cleavage (Scheme 2).

Results and Discussion

Reaction of **A**/**B** *cis*-4β,5β-epoxy-17β-hydroxyandrostan-3-one acetate **1***b* with hydrogen fluoride in neat chloroform proceeded by β-mode (Scheme 1) and gave, as the only isolable product, the 5α,4α-fluorohydrin **10***b*, ν_{max} (KBr) 3462, 3510 (OH), 1731 (17-ester C=O), 1715 cm^{-1} (C(3)=O); δ($CDCl_3$) 4.71(1H, t, J = 7.5 Hz, 17α-H), 4.64 (1H, q, J_{H_a,F_a} = 33 Hz (4), J_{HH} = 6.5 Hz, 4-H), 3.45 (1H, d, J_{HH} = 6.5 Hz, 4-OH), 1.13 (3H, s, 19-H_3), 0.89 (3H, s, 18-H_3). The 6.5 Hz coupling between the 4-H and the 4-OH proton was removed by spin decoupling; as well as by conversion of **10***b* to the diacetate **10***d*, or by exchange of the hydroxyl proton of **10***b* for deuterium in **10***c*, ν_{max} (KBr) 2580, 2405 cm^{-1}

Can. J. Chem. Downloaded from www.nrcresearchpress.com by 210.87.254.40 on 09/05/12
For personal use only.

Can. J. Chem. Downloaded from www.nrcresearchpress.com by 210.87.254.40 on 09/05/12
For personal use only.

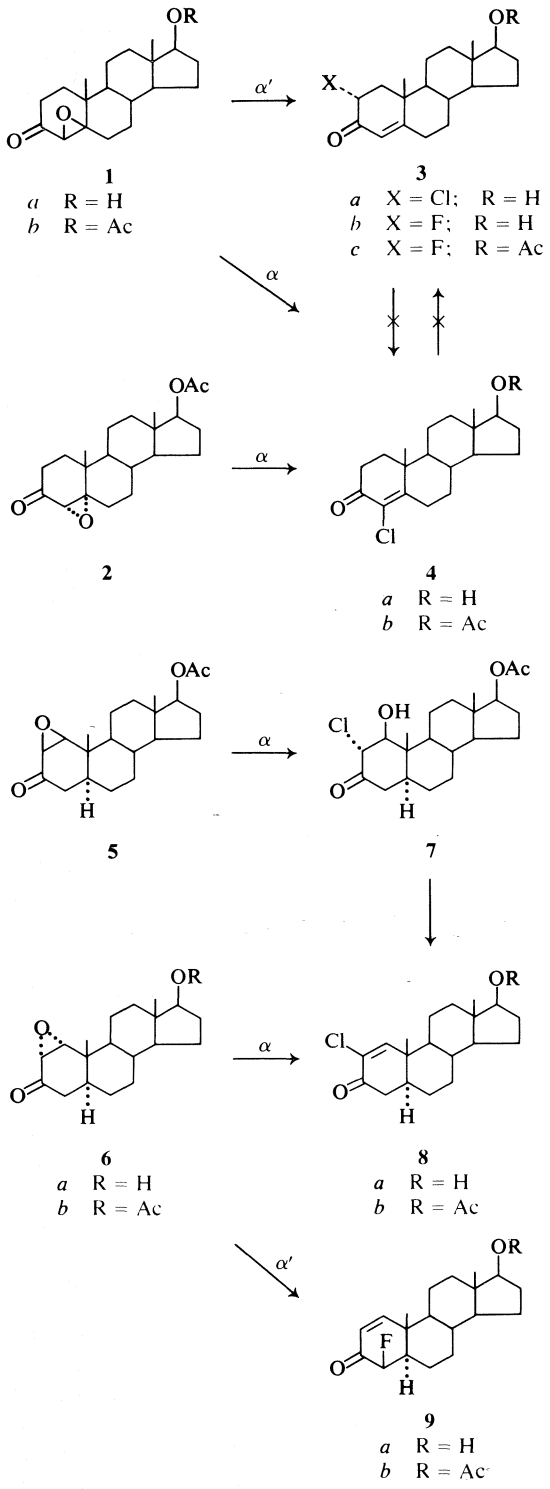

SCHEME 3

(associated OD (5)). The OH stretching band at 3510 cm^{-1} of the 5α,4α-fluorohydrin **10***b* was concentration independent in the range 0.005–0.015 *M* in carbon tetrachloride solution, as was the C=O stretching band at 1715 cm^{-1}. These data are interpreted as supporting an OH···F hydrogen bonded structure for the *cis*-fluorohydrin **10***b*. The β-mode reaction is envisaged to produce initially the *trans*-diaxial fluorohydrin **10***a*, via a transition state **D** (Scheme 2) of the protonated oxirane bearing a partial positive charge at C-5, where it can be more readily accommodated than at C-4, adjacent to the positive end of the carbonyl dipole. A fractional positive charge at C-5 in **D** could, in part, be the consequence of the positive charge on the leaving group, the protonated oxirane oxygen (6*a*). The nature of the transition state **D** is akin to that proposed by Diggle and co-workers (6*b*) for acid catalyzed ring opening of steroidal 5α,6α-epoxides in largely non-aqueous medium (butanone containing 0.05 *N* perchloric acid); bond-breaking at C-6 in the protonated oxirane was considered more advanced than bond-making, with a partial positive charge developing at C-6 in the transition state. A similar mechanism would allow a close approach to C-5 of the small nucleophile of low polarizability F^- (or its equivalent HF_2^-) from the steroid's hindered α-side. The *cis*-5α,4α-fluorohydrin **10***b* is regarded as the end product of facile acid-catalyzed epimerization at C-4 of the primary reaction product, the *trans*-diaxial 5α,4β-fluorohydrin **10***a*.[2] In contrast to the β-mode regioselectivity of the hydrogen fluoride reaction with epoxyketone **1***a*, hydrogen chloride in chloroform reacted α-mode regiospecifically with **1***a*, giving 4-chlorotestosterone **4***a*.

Attempted reaction of hydrogen fluoride with **A**/**B** *cis*-epoxyketone **1***c* in the presence of a small amount of water (acetone containing aqueous 30% hydrofluoric acid; 1.8 *N* in HF) led to re-

[2]The reaction of boron trifluoride etherate in benzene with 4β,5β-epoxycholestan-6-one and 5β,6β-epoxycholestan-4-one afforded respectively the *trans*-diaxial fluorohydrin 4β-fluoro-5β-hydroxycholestan-6-one and the *trans*-diequatorial fluorohydrin 6α-fluoro-5β-hydroxycholestan-4-one (7). In contrast to the predictable instability of the axial C-4 carbinol in **10***a*, the configurations of the tertiary C-5 carbinols in the heteroannular cholestanone β,α-fluorohydrins are stable. These β-regiospecific *trans*-oxirane cleavages are thus akin to the *trans*-oxirane opening of **1***a* to **10***a* via **D**.

Can. J. Chem. Downloaded from www.nrcresearchpress.com by 210.87.254.40 on 09/05/12
For personal use only.

covery of **1***c*, reflecting the expected lowered nucleophilicity of fluoride on hydration (8). Hydrogen chloride, however, reacted under similar conditions (acetone containing aqueous 10 *N* hydrochloric acid; 1.0 *N* in HCl) with the **A**/**B** *cis*-epoxyketone **1***a* α-mode regiospecifically, affording 4-chlorotestosterone **4***a*. That this reaction proceeds through the intermediate *trans*-diaxial 4α,5β-chlorohydrin **11***a* is evidenced by the isolation of the corresponding 4α,5β-chlorohydrin **11***b* after reaction of **A**/**B** *cis*-19-norepoxyketone **1***c* with hydrochloric acid in acetone (0°, 15 min). The analogous 19-nor-4α,5β-bromohydrin **11***c* was obtained by reaction of **1***c* with hydrogen bromide in acetone at 20° for 15 min, whereas reaction at 57° for 1 h of either the α,β-epoxyketone **1***c* or the β,α-bromohydrin **11***c* afforded 4-bromo-19-nortestosterone **4***d*. The α-mode regiospecific oxirane cleavage of the **A**/**B** *cis*-10β-hydroxyepoxyketones **1***d* and **1***e* with hydrogen bromide was utilized in the regiospecific syntheses of 4-bromo-17β-estradiol and -estrone via 19-norsteroid intermediates **4***e* and **4***f* (3*b*). The regiospecific α-mode oxirane opening of the **A**/**B** *cis*-epoxyketones **1***a*, **1***c*, **1***d*, and **1***e* was envisaged to pass through a transition state **A** stabilized by orbital overlap with carbonyl, and the observed difference in α vs. β regioselectivity between hydrogen chloride and hydrogen fluoride (in chloroform) was viewed as a reflection of the polarizability of chloride, in contrast to fluoride (1*b*).

Reaction of **A**/**B** *cis*-4β,5β-epoxy-17β-hydroxyandrostan-3-one **1***a* in "10%" ethanol–chloroform with hydrogen chloride (3 min, 23°) was non-regioselective, affording a 1:1 mixture of the α-mode product 4-chlorotestosterone **4***a* and the α′-mode product 2α-chlorotestosterone **3***a* (Scheme 3).[3] This finding could suggest as an intermediate a delocalized allylic cation **B**, which is attacked by nucleophile at α and α′ (9), however, such a rationalization of the non-regioselectivity would involve the unwarranted presumption that the charge distribution in **B** would not be rendered unsymmetrical by overlap with the C-5β oxygen. The observed non-regioselectivity may reflect competing reactions: α-mode oxirane opening **A** at C-4α of the 4β,5β-epoxyketone **1***a* by chloride assisted by neighboring orbital overlap with carbonyl (10), and concurrent α′-mode reaction of chloride at C-2α of the Δ^2-enol **C** of **1***a* concomitant with opening of the protonated 4β,5β-oxirane and fast β-elimination in the resulting 5β-hydroxy-Δ^3-enol.

The plausibility of these mechanisms, **A** and **C**, for the concurrent α- and α′-mode reactions of the **A**/**B** *cis*-epoxyketone **1***a* with hydrogen chloride is supported by the finding that hydrogen fluoride, in contrast to hydrogen chloride, reacted α′-mode regioselectively with **1***a* in "10%" ethanol–chloroform (3.5 min, 43°), or in *N*,*N*-dimethylformamide (22 *N*, 3 h, 23°) affording 2α-fluorotestosterone **3***b* as the sole isolable product. In contrast to the polarizable nucleophile Cl^- with a relatively large bonding orbital, the small and non-polarizable F^- would not be capable of orbital overlap (as in **A**) and thus oxirane cleavage adjacent to carbonyl by fluoride would be precluded. In the presence of protic solvent, solvated fluoride would not be sufficiently nucleophilic to effect β-mode oxirane opening **D** and due to its solvent shell it would encounter hindrance in the approach to C-5α in the **A**/**B** *cis*-epoxyketone **1***a*. The α′-mode *cine*-fluorination was exploited in the regiospecific synthesis of 2α-fluoro-10β-hydroxyestr-4-ene-3,17-dione from 4β,5β-epoxy-10β-hydroxyestr-4-ene-3,17-dione **1***e*, the key intermediate in the synthesis of 2-fluoroestrone via 19-norsteroid intermediates (1*a*, 3*a*).

The **A**/**B** *trans*-1α,2α-epoxy-3-one **6***a* gave the α′-mode reaction product **9***a* with 22 *N* hydrogen fluoride in *N*,*N*-dimethylformamide. The mechanism of the α′-mode fluorination of **6***b* to **9***b*, proposed by Kerb and co-workers (11) (rearrangement involving fluoride migration) is implausible and contradicted by available experimental evidence (1*a*). Plausible reactive intermediates in the α′-mode reactions of epoxyketones **1** and **6** are the respective enols Δ^2-**C** and Δ^3-**C** protonated on oxirane oxygen (Scheme 2), which give rise to the halogen configurations observed in the products **3** and **6** on nucleophilic displacement by halide entering *trans* to the oxonium leaving group. Precedents for *trans* S_N2' type reactions are the displacement by hy-

[3]The two products **3***a* and **4***a* were shown not to be interconvertible by migration of chloride. The α-mode chlorohydrin 4α-chloro-5β,17β-dihydroxyestran-3-one **11***b* gave 4-chloro-19-nortestosterone **4***c* on reaction with hydrogen chloride in "10%" ethanol–chloroform, which rules out α,β-chlorohydrins **11** as intermediates in the α′-mode reaction.

Can. J. Chem. Downloaded from www.nrcresearchpress.com by 210.87.254.40 on 09/05/12
For personal use only.

dride in diastereomeric 1,3-*t*-butylpropargyl sulfonates (12*a*) and acylolyzes of steroidal α-bromoketones (12*b*).[4]

In contrast to the α′-mode reaction of hydrogen fluoride with **A/B** *trans*-1α,2α-epoxy-3-one **6***a*, its reaction with hydrogen chloride in "10%" ethanol–chloroform proceeded regiospecifically by α-mode, as did the same reaction with **A/B** *trans*-4α,5α-epoxy-3-one **2**. These α-mode regiospecific reactions of **6***a* and **2**, as contrasted with the non-regioselective reaction of the **A/B** *cis*-4β,5β-epoxy-3-one **1***a* with hydrogen chloride, may reflect a relatively more hindered approach of solvated chloride to C-4α in the **A/B** *cis*-epoxyketone **1***a* than to C-2β and C-4β in the **A/B** *trans*-epoxyketones **6***a* and **2**. Consequently, the α′-mode reaction can successfully compete with the normally favored α-mode reaction, when the latter is sterically impeded, as in **1***a*, provided the reaction milieu is favorable to enolization.

In contrast to the **A/B** *trans*-epoxyketones **2** and **6***a*, in which α-mode oxirane opening by hydrogen chloride leads to the stereoelectronically normal *trans*-diaxial product, the **A/B** *trans*-1β,2β-epoxy-3-one **5** would give the diaxial chlorohydrin if it reacted by β-mode, which was not realized. In fact, the reaction of **5** with hydrogen chloride in "10%" ethanol–chloroform was fast (1 min, 23°) and α-mode regiospecific, affording the *trans*-diequatorial chlorohydrin **7** together with its dehydration product, the 2-chloro-enone **8**.

An α-mode oxirane opening in epoxyketone **5** via a transition state with ring **A** in a half-boat conformation **E**, followed by conformational change to the diequatorial chlorohydrin **7**, would have to overcome severe non-bonded interactions in the near-eclipsed conformation of the incipient chlorohydrin hydroxyl and the C-19 methyl, as well as the hindrance by H-5α to the approach of chloride in forming the "flagpole" bond at C-2α. This mechanism would therefore not be conducive to a fast reaction.

[4]Bordwell (13*a*–*c*) has questioned whether the concerted S_N2' mechanism can be realized. He favored alternative step-wise carbonium-type mechanisms involving reversible formation of ion-pair intermediates, pointing out the difficulty of distinguishing experimentally between these mechanisms. The C=C bonds in the enols **Δ²-C** and **Δ³-C** are not akin to the unactivated C=C bonds discussed by Bordwell, and the C-halogen bond-making may well assist significantly in the bond-breaking of the protonated oxirane.

The facile diequatorial α-mode oxirane opening of epoxide **5** can be envisaged to pass through a transition state **A** sufficiently stabilized to compensate for the oxirane conformation in **5**, which is stereoelectronically unfavorable for α-mode ring opening. Transition state **A** reflects the mechanistic concepts of Dewar (10*a*) or Streitwieser (13*b*). This reaction is stereochemically akin to the accelerated S_N2 reaction of the conformationally fixed axial α-chloroketone *trans*-2-chloro-4-*t*-butyl-cyclohexanone, in which both $\Delta H^{\ddagger}$ and $\Delta S^{\ddagger}$ were found to be lowered relative to these parameters in *trans*-3-*t*-butylchlorocyclohexane (10*d*). The expected lower activation energy due to delocalized bonding in transition state **A**, although partly offset by entropic loss reflecting the geometric requirements of the three-center reaction, would account for the observed fast diequatorial oxirane opening of epoxyketone **5** to chlorohydrin **7**.

Experimental

Melting points were determined with a Thomas microstage and are corrected. The u.v. spectra were recorded with a Cary 14 spectrophotometer and the i.r. spectra with a Beckman IR-9 spectrophotometer, n.m.r. spectra were determined at 60 MHz with a Varian A60A spectrometer, with tetramethylsilane as internal standard; o.r.d. and c.d. measurements were made with a Jasco ORD/UV 5 spectropolarimeter with c.d. attachment. Microanalyses were performed by Huffman Laboratories, Wheatridge, Colorado. Mass spectral analyses were performed by Morgan Schaffer Corporation, Montreal. Nylon tubing used for dry columns was obtained from Walter Coles and Co., 47/49 Tanner Street, London, England. Dry column adsorbent was Woelm silica gel, obtained from Waters Associates, Framingham, Massachusetts, preequilibrated with 10% by weight of benzene – ethyl acetate – ethanol (80:20:1); t.l.c. was performed on Eastman "Chromagram" silica gel with benzene – ethyl acetate – ethanol (80:20:1) as the developing solvent, unless otherwise specified.

4β,5β-Epoxy-17β-hydroxyandrostan-3-one (**1***a*)

Melting point 155–158° (lit. (14) 157–158°, (17) 156–157°); δ ($CDCl_3$) 3.00 (1H, s, 4α-H), 3.72 (1H, t, J = 7.5 Hz, 17α-H), 1.07 (3H, s, 19-H_3), and 0.69 (3H, s, 18-H_3); o.r.d. (*c* 0117, chloroform) $[\Phi]_{700}$ + 260°, $[\Phi]_{589}$ + 417°, $[\Phi]_{334}$ + 9750°, $[\Phi]_{310}$ 0°, $[\Phi]_{290}$ −7580°; $[\alpha]_D^{23}$ + 137° (lit. (14) + 136°, (17) + 145°); c.d. (0.00158 *M* in methanol) $\Delta\varepsilon_{313}$ + 3.80; t.l.c. R_f 0.58; mass spectrum *m/e* 304 (M^+).

4β,5β-Epoxy-17β-hydroxyandrostan-3-one Acetate (**1***b*)

ν_{max} (CCl_4) 1735 (17-ester C=O), 1715 (C(3)=O), and 1245 cm^{-1} (17-ester C—O); δ ($CDCl_3$) 4.67 (1H, t, J = 7.5 Hz, 17α-H), 3.00 (1H, s, 4α-H), 2.03 (3H, s, 17-OAc), 1.15 (3H, s, 19-H_3), and 0.82 (3H, s, 18-H_3); o.r.d. (*c* 0.052, chloroform) $[\Phi]_{700}$ +261°, $[\Phi]_{589}$ +460°, $[\Phi]_{329}$ +

Can. J. Chem. Downloaded from www.nrcresearchpress.com by 210.87.254.40 on 09/05/12
For personal use only.

11 000°, $[\Phi]_{309}$ 0°, $[\Phi]_{284}$ −10 600°; $[\alpha]_D^{23}$ +134° (lit. (17) +130°); c.d. (0.00134 *M* in chloroform) $\Delta\varepsilon_{310}$ +4.30 (lit. (15) +4.2); t.l.c. R_f 0.82.

*4α,5α-Epoxy-17β-hydroxyandrostan-3-one Acetate (**2**)*

Melting point 171–172° (lit. (17) 172–173°); ν_{max} ($CHCl_3$) broad 1722 cm^{-1} (C(3)=O and 17 ester C=O); δ ($CDCl_3$) 4.70 (1H, t, J = 7.5 Hz, 17α-H), 3.05 (1H, s, 4β-H), 2.04 (3H, s, 17-OAc), 1.07 (3H, s, 19-H_3), and 0.82 (3H, s, 18-H_3); o.r.d. (*c* 0.178, dioxane) $[\Phi]_{700}$ −135°, $[\Phi]_{589}$ −194°, $[\Phi]_{342}$ −8400°, $[\Phi]_{332}$ −8760°, $[\Phi]_{312}$ 0°, $[\Phi]_{287}$ +10 000°; c.d. (0.00515 *M* in dioxane) $\Delta\varepsilon_{311}$ −3.50, shoulder at 320 nm; t.l.c. R_f 0.82.

*1β,2β-Epoxy-17β-hydroxy-5α-androstan-3-one Acetate (**5**)*

Melting point 178–179° (lit. (18) 179–180°); ν_{max} (KBr) 1730 (C(3)=O and 17 ester C=O) and 1245 cm^{-1} (17 ester C—O); δ ($CDCl_3$) 4.68 (1H, t, J = 7.5 Hz, 17α-H), 3.50 (1H, d, J = 3.5 Hz, 1-H), 3.12 (1H, d, J = 3.5 Hz, 2-H, $w_{1/2}$ 3 Hz), 2.07 (3H, s, 17-OAc), 1.09 (3H, s, 19-H_3), and 0.86 (3H, s, 18-H_3); c.d. (0.00527 *M* in dioxane) $\Delta\varepsilon_{302}$ −0.23; $[\alpha]_D^{23}$ +43.7° (lit. (18) +38.5°); t.l.c. R_f 0.83; mass spectrum *m/e* 347 (M^+).

*1α,2α-Epoxy-17β-hydroxy-5α-androstan-3-one (**6a**)*

Melting point 159–161° (lit. (20) 161–162°); ν_{max} (KBr) 1712 cm^{-1} (C(3)=O); δ ($CDCl_3$) 3.72 (1H, t, J = 7.5 Hz, 17α-H), 3.58 (1H, d, J = 3.5 Hz, 1-H), 3.27 (1H, d, J = 3.5 Hz, 2-H) 0.93 (3H, s, 19-H_3), and 0.78 (3H, s, 18-H_3); o.r.d. (*c* 0.08, dioxane) $[\Phi]_{589}$ +178°, $[\Phi]_{328}$ +6030°, $[\Phi]_{310}$ 0°, $[\Phi]_{278}$ −5800°; c.d. (0.00277 *M* in dioxane) $\Delta\varepsilon_{310}$ +2.08; $[\alpha]_D^{23}$ +58.7°; t.l.c. R_f 0.50; mass spectrum *m/e* 304 (M^+).

*1α,2α-Epoxy-17β-hydroxy-5α-androstan-3-one Acetate (**6b**)*

Melting point 160–161° (lit. (20) 160–161°); δ ($CDCl_3$) 3.73 (1H, t, J = 7.5 H, 17α-H), 3.57 (1H, d, J = 3.5 Hz, 1-H), 3.25 (1H, d, J = 3.5 Hz, 2-H), 0.90 (3H, s, 19-H_3), and 0.77 (3H, s, 18-H_3); t.l.c. R_f 0.78.

*5α-Fluoro-4α,17β-dihydroxyandrostan-3-one 17-Acetate (**10b**)*

Anhydrous hydrogen fluoride was bubbled into chloroform (50 ml, ethanol-free) for 7 min. A solution of 4β,5β-epoxy-17β-hydroxyandrostan-3-one acetate **1***b* (1.365 g) in chloroform (15 ml, ethanol-free) was added to the hydrogen fluoride solution at 25°. After 2 h a portion (47 ml) was poured into sodium hydroxide (2.0 *N*, 200 ml, 0°), extracted with chloroform, washed with water, dried (Na_2SO_4), and evaporated. The residue was placed on a column (2 × 77 in.) of dry column adsorbent (1020 g) (21). The column was developed with benzene–ethyl acetate–ethanol (80:20:1). The fraction R_f 0.18 to 0.44 was rechromatographed on a column (1 × 65 in.) of dry column adsorbent (290 g) and gave **10***b* (22%), needles of m.p. 186–189° (from ethyl acetate–ligroin); o.r.d. (*c* 0.236, dioxane) $[\Phi]_{700}$ 0°, $[\Phi]_{589}$ +9°, $[\Phi]_{298}$ −575°, $[\Phi]_{282}$ 0°, $[\Phi]_{254}$ +770°; c.d. (0.00646 *M* in dioxane) $\Delta\varepsilon_{284}$ −0.88; t.l.c. R_f 0.57.

Anal. Calcd. for $C_{21}H_{31}FO_4$: C, 68.82; H, 8.53; F, 5.19. Found: C, 68.66; H, 8.08; F, 5.04.

The diacetate **10***d* was prepared in the usual manner, m.p. 189–193° (from methanol–water); ν_{max} ($CHCl_3$) 1751 (4 ester C=O), 1733 (17 ester C=O), 1255 cm^{-1} (ester C—O); δ ($CDCl_3$) 5.75 (1H, d, $^3J_{H_a,F_a}$ = 33 Hz, 4-H), 4.68 (1H, t, J = 7.5 Hz, 17α-H), 2.25 (3H, s, 4-OAc), 2.05 (3H, s, 17-OAc), 1.10 (3H, s, 19-H_3), and 0.82 (3H, s, 18-H_3); c.d. (0.00823 *M* in dioxane) $\Delta\varepsilon_{302}$ +0.098, shoulder at 308 nm, $\Delta\varepsilon_{272}$ −0.088; t.l.c. R_f 0.72.

*4-Chlorotestosterone (**4a**)*

(*a*) Hydrogen chloride was bubbled into chloroform (ethanol-free) for 15 min (0.6 *N* HCl). To the stirred hydrogen chloride solution (19.0 ml) was added 4β,5β-epoxy-17β-hydroxyandrostan-3-one **1***a* (1.008 g) in chloroform (15.0 ml, ethanol-free) at 0°. After 10 min at 0°, a 3.5-ml portion of the mixture was poured into aqueous sodium hydroxide (2.0 *N*, 0°), extracted with chloroform, washed with water, dried (Na_2SO_4), and evaporated. The residue contained starting material **1***a* and 4-chlorotestosterone **4***a* (33% by u.v.). After 35 min at 0°, a 3.5-ml portion was worked up and yielded 4-chlorotestosterone **4***a* (67% by u.v.), m.p. 188–189° (from acetone–ligroin) (lit. (14, 16) 188–189°); λ_{max} (EtOH) 256 nm (ε 14 700); t.l.c. R_f 0.43.

(*b*) To a stirred solution of **1***a* (0.350 g) in acetone (8.6 ml) at 23° was added hydrochloric acid (10 *N*, 0.86 ml). After 40 min at 23°, the reaction mixture was worked up as in *a*, yielding **4***a* (99% by u.v.) identical (t.l.c., i.r., u.v., m.p.) with **4***a* from *a*.

*4α-Chloro-5β,17β-dihydroxyestran-3-one (**11b**)*

To a stirred solution of 4β,5β-epoxy-17β-hydroxyestran-3-one **1***c* (19) (0.604 g) in acetone (2.0 ml) at 0° was added aqueous hydrochloric acid (10 *N*, 0.43 ml). After 10 min at 0°, the crystalline precipitate formed was filtered and washed with acetone, yielding **11***b* (30%), m.p. 189–190°; ν_{max} (KBr) 3480 and 3270 (OH) and 1735 cm^{-1} (C(3)=O); δ (DMSO) 4.10 (1H, s, 4β-H), and 0.67 (3H, s, 18-H_3); o.r.d. (*c* 0.120, methanol) $[\Phi]_{700}$ +127°, $[\Phi]_{589}$ +127°, $[\Phi]_{315}$ +3720°, $[\Phi]_{294}$ 0°, $[\Phi]_{272}$ −3370°; c.d. (0.00352 *M* in methanol) $\Delta\varepsilon_{303}$ +1.42; m.p. 198–200°.

Anal. Calcd. for $C_{18}H_{27}ClO_3$: C, 66.14; H, 8.34; Cl, 10.85. Found: C, 65.61; H, 8.60; Cl, 10.51.

A second crop of crystals (15%) was identical (i.r.) with the first crop of **11***b*. The filtrate was worked up yielding a material (0.265 g) which showed the 4-chloro-4-en-3-one chromophore λ_{max} (EtOH) 256 nm (ε 6800).

*4α-Bromo-5β,17β-dihydroxyestran-3-one (**11c**)*

To a stirred solution of 4β,5β-epoxy-17β-hydroxyestran-3-one **1***c* (19) (0.6804 g) in acetone (10 ml) at 20° was added aqueous hydrobromic acid (30%, 1.2 ml). After 15 min at 20°, the crystalline precipitate formed was filtered and washed with acetone, yielding **11***c* (45%), m.p. 128–129°; ν_{max} (KBr) 3487 and 3270 (OH) and 1714 cm^{-1} (C(3)=O); δ (DMSO) 4.13 (1H, s, 4β-H) and 0.68 (3H, s, 18-H_3); o.r.d. (*c* 0.034, methanol) $[\Phi]_{700}$ +260°, $[\Phi]_{589}$ +260°, $[\Phi]_{332}$ +5600, $[\Phi]_{287}$ −8860°, $[\Phi]_{278}$ −9300°; c.d. (0.00108 *M* in dioxane) $\Delta\varepsilon_{308}$ +3.52, $\Delta\varepsilon_{311}$ +3.06 (inflection), $\Delta\varepsilon_{313}$ +3.46 (inflection). A second crop of crystals (24%) was identical (i.r., o.r.d.) with the first crop of **11***c*.

Anal. Calcd. for $C_{18}H_{27}BrO_3$; C, 58.22; H, 7.33; Br. 21.52. Found: C, 58.43; H, 7.35; Br, 21.22.

*4-Bromo-19-nortestosterone (**4d**)*

(*a*) To a solution of 4α-bromo-5β,17β-dihydroxy estran-3-one **11***c* (0.145 g) in acetone (12.0 ml) was added aqueous hydrobromic acid (30%, 2.0 ml) and the mixture heated to 60° for 75 min. After cooling to 23°, the crystal-

Can. J. Chem. Downloaded from www.nrcresearchpress.com by 210.87.254.40 on 09/05/12
For personal use only.

line **4***d* was filtered (41% by u.v.). The product was placed on a column of Fluorisil (6.0 g). Elution with heptane–acetone (19:1) gave **4***d*, m.p. 149–152° (lit. (22) 125–128°); λ_{max} (EtOH) 262 nm (ε 11 800) (lit. (22) 262 nm (ε 8000)); ν_{max} (KBr) 1677 (conjugated C=O) and 1576 cm^{-1} (conjugated C=C); δ ($CDCl_3$) 0.77 (3H, s, 18-H_3); t.l.c. (Eastman "Chromagram" alumina sheets, benzene – ethyl acetate, 4:1) R_f 0.49.

(*b*) To a solution of 4β,5β-epoxy-17β-hydroxyestran-3-one **1***c* (0.540 g) in acetone (4.0 ml) was added aqueous hydrobromic acid (30%, 1.0 ml). The mixture was warmed to 60° for 1 h, and water was added to turbidity. The product **4***d* which crystallized was identical (t.l.c., u.v., i.r., n.m.r.) with **4***d* described in *a*.

*Attempted α-Mode Reaction of 4β,5β-Epoxy-17β-hydroxyestran-3-one (**1***c*) with Hydrogen Fluoride*

To a stirred solution of **1***c* (0.830 g) in acetone (3.0 ml) at 0° was added aqueous hydrofluoric acid (30%, 0.40 ml). After 3 h at 0°, the mixture was poured into sodium hydroxide (2.0 *N*, 0°), extracted with chloroform, washed with water, dried (Na_2SO_4), and evaporated, yielding starting material **1***c*.

*4-Chlorotestosterone (**4***a*) and 2α-Chlorotestosterone (**3***a*) from 4β,5β-Epoxy-17β-hydroxyandrostan-3-one (**1***a*)*

To a stirred solution of 1.9 *N* hydrogen chloride in "10%" ethanol–chloroform (2.0 ml) was added at 23° **1***a* (0.063 g) in "10%" ethanol–chloroform (1.0 ml). After 1 min at 23°, the reaction mixture was poured into aqueous sodium hydroxide (2.0 *N*, 0°), extracted with chloroform, washed with water, dried (Na_2SO_4), and evaporated, leaving a 1:1 mixture[5] of 4-chlorotestosterone **4***a* and 2α-chlorotestosterone **3***a* (by n.m.r.) which was placed on a column (1 × 22 in.) of dry column adsorbent (140 g) (21). The column was developed with benzene – ethyl acetate – ethanol (80:20:1). The fraction R_f 0.13 to 0.18 yielded **4***a*, m.p. 188–189°; λ_{max} (EtOH) 256 nm (ε 14 700); ν_{max} ($CHCl_3$) 3620 and 3450 (OH), 1688 (conjugated C=O), and 1582 cm^{-1} (conjugated C=C); δ ($CDCl_3$) 1.26 (3H, s, 19-H_3) and 0.80 (3H, s, 18-H_3); t.l.c. R_f 0.51. The fraction R_f 0.25 to 0.54 yielded **3***a*; λ_{max} (EtOH) 244 nm (ε 14 800) (from ether) (lit. (23) 243 nm (ε 14 500)); ν_{max} (KBr) 3500–3400 (OH), 1695 (conjugated C=O), 1618 (conjugated C=C) cm^{-1}, δ ($CDCl_3$) 5.90 (1H, broad s, 4-H), 4.70 (1H, q, J_{ae} = 5.5 Hz, J_{aa} = 14 Hz, 2β-H), 1.31 (3H, s, 19-H_3), and 0.79 (3H, s, 18-H_3); t.l.c. R_f 0.59.

*4-Chlorotestosterone Acetate (**3***c*) from 4α,5α-Epoxy-17β-hydroxyandrostan-3-one Acetate (**2**)*

To a stirred solution of 1.9 *N* hydrogen chloride in "10%" ethanol–chloroform (9.0 ml) was added at 23° **2** (0.300 g) in "10%" ethanol–chloroform (3.0 ml). After 1 min at 23°, a 4.0 ml portion of the mixture was worked up as usual, affording a mixture of **3***c* (66% by u.v.) and unreacted starting material **2** (25% by n.m.r.). Dry column chromatography gave **3***c*, m.p. 225–227° (from methanol–water) (lit. (16) 228–230°); λ_{max} (EtOH) 255 nm (ε 12 900) (lit. (16) 255 nm (ε 13 300)).

*2-Chloro-17β-hydroxy-5α-androst-1-en-3-one (**8***a*) from 1α,2α-Epoxy-17β-hydroxy-5α-androstan-3-one (**6***a*)*

To a stirred solution of 1.9 *N* hydrogen chloride in "10%" ethanol–chloroform (2.0 ml) was added at 23° **6***a* (0.063 g) in "10%" ethanol–chloroform (1.0 ml). After 1 min at 23° the reaction mixture was worked up as usual, affording **8***a* (82% by u.v.). This material was placed on a column (1 × 21 in.) of dry column adsorbent (140 g). This column was developed with benzene – ethyl acetate – ethanol (80:20:1) and yielded (R_f 0.25–0.81) **8***a*, m.p. 224–225° (from methanol) (lit. (24) 224–226°); λ_{max} (EtOH) 248 nm (ε 11 400); ν_{max} (KBr) 3510 (OH), 1693 (conjugated C=O), 1600 cm^{-1} (conjugated C=C); δ ($CDCl_3$) 7.41 (1H, s, 1-H), 3.73 (1H, t, *J* = 7.5 Hz, 17α-H), 1.10 (3H, s, 19-H_3), 0.80 (3H, s, 18-H_3); t.l.c. R_f 0.56.

*2-Chloro-17β-hydroxy-5α-androst-1-en-3-one Acetate (**8***b*) and 2α-Chloro-1β,17β-dihydroxy-5α-androstan-3-one 17-Acetate (**7**) from 1β,2β-Epoxy-17β-hydroxy-5α-androstan-3-one Acetate (**5**)*

To a stirred solution of 1.9 *N* hydrogen chloride in "10%" ethanol–chloroform (2.0 ml) was added **5** (0.700 g) in "10%" ethanol–chloroform (1.0 ml). After 1 min at 23°, the reaction mixture was worked up as usual, yielding a mixture of **8***b* (48% by u.v.) and **7** (50% by n.m.r.). The mixture was placed on a column (1 × 2 in.) of dry column adsorbent (140 g) and developed with benzene – ethyl acetate – ethanol (80:20:1). The fraction R_f 0.68 to 0.86 yielded **8***b*, m.p. 155–157° (from methanol) (lit. (24) 155.5–156.5°); λ_{max} (EtOH) 247 nm (ε 11 200); ν_{max} ($CHCl_3$) 3460 (OH), 1735 (17 ester C=O), and 1717 cm^{-1} (conjugated C=O); δ ($CDCl_3$) 7.40 (1H, s, 1-H), 4.63 (1H, t, *J* = 7.5 Hz, 17α-H), 2.06 (3H, s, 17-OAc), 1.10 (3H, s, 19-H_3), and 0.83 (3H, s, 19-H_3); t.l.c. R_f 0.89. The fraction from R_f 0.41 to 0.59 yielded **7** (52%), m.p. 220–222° (from diethyl ether); ν_{max} ($CHCl_3$) 3580 (OH), 1733 (17 ester C=O), and 1727 cm^{-1} (C(3)=O); δ ($CDCl_3$) 4.68 (1H, t, *J* = 7.5 Hz, 17α-H) 4.61 (1H, d, $J_{1\alpha,2\beta}$ = 9.5 Hz, 2-H), 3.60 (1H, d, $J_{1\alpha,2\beta}$ = 9.5 Hz, 1-H), 2.08 (3H, s, 17-OAc), 1.22 (3H, s, 19-H_3), and 0.80 (3H, s, 18-H_3); o.r.d. (*c* 0.032, methanol) $[\Phi]_{700}$ +97.3°, $[\Phi]_{589}$ +194°, $[\Phi]_{310}$ +3180°, $[\Phi]_{281}$ 0°, $[\Phi]_{262}$ −3300°; t.l.c. R_f 0.75; mass spectrum *m/e* 382 (M^+).

*2-Chloro-17β-hydroxy-5α-androst-1-en-3-one Acetate (**8***b*) from 2α-Chloro-1β,17β-dihydroxy-5α-androstan-3-one 17-Acetate (**7**)*

To a stirred solution of 1.9 *N* hydrogen chloride in "10%" ethanol–chloroform (2.0 ml) was added at 23° the 2α,1β-chlorohydrin **7** (0.015 g) in "10%" ethanol–chloroform (1.0 ml). After 2 min at 23° the reaction mixture was worked up as usual, affording a mixture of the 2-chloro-1-en-3-one **8***b* and starting material **7** in a 2:1 ratio (by u.v. and n.m.r.).

*Attempted Rearrangement of 4-Chlorotestosterone (**4***a*)*

To a stirred solution of 2.46 *N* hydrogen chloride in "10%" ethanol–chloroform (6.6 ml) was added 4-chlorotestosterone **4***a* (0.150 g) at 23°. After 7 min at 23° the reaction mixture was poured into sodium hydroxide (2.0 *N*, 0°), extracted with chloroform, washed with water, dried, and evaporated, yielding unchanged **4***a* (t.l.c., u.v., i.r., n.m.r.).

*4-Chloro-19-nortestosterone (**4***c*) from 4α-Chloro-5β,17β-dihydroxyestran-3-one (**11***b*)*

A solution of the chlorohydrin **11***b* (0.100 g) in "10%" ethanol–chloroform (11.0 ml) was added to a solution of

[5]The ratio α:α′ was 3:2 after 3 min reaction at 0° and 7:3 after 0.5 min reaction at 40°.

Can. J. Chem. Downloaded from www.nrcresearchpress.com by 210.87.254.40 on 09/05/12
For personal use only.

1.15 *N* hydrogen chloride in "10%" ethanol–chloroform (4.4 ml). The mixture was stirred at 21° for 7 min, poured into sodium hydroxide (2.0 *N*, 0°), extracted with chloroform, washed with water, dried, and evaporated, yielding **4***c* (25) (70% by u.v.), m.p. 220–222° (from methanol–water) (lit. (25) 220–223°); λ_{max} (EtOH) 255 nm (ε 13 500).

*Attempted Interconversion of 2α-Chlorotestosterone (**3a**) and 4-Chlorotestosterone (**4a**)*

To a stirred solution of 7.63 *N* hydrogen chloride in tetrahydrofuran (7.0 ml) was added a 1:1 mixture of **3***a* and **4***a* (0.358 g) in tetrahydrofuran (7.0 ml) at 0°. After 10 min at 0° the reaction mixture was poured into sodium hydroxide (2.0 *N*, 0°), extracted with chloroform, washed with water, dried, and evaporated, giving unchanged starting mixture (1:1) of **3***a* and **4***a*; δ ($CDCl_3$) 5.89 (0.50 H, s, 4-H) 4.20 (0.50 H, q, J_{ae} = 5.5 Hz, J_{aa} = 14 Hz, 2β-H), 1.3 (1.5 H, s, 19-H_3 of **3***a*), and 1.26 (1.5 H, s, 19-H_3 of **4***a*).

*2α-Fluorotestosterone (**3b**)*

(*a*) Anhydrous hydrogen fluoride was bubbled into "10%" ethanol–chloroform (68.2 ml) for 7 min, while the temperature rose to 43°. Two phases separated: the concentration of hydrogen fluoride was 44 *N* in the upper phase and 0.7 *N* in the lower phase. Powdered 4β,5β-epoxy-17β-hydroxyandrostan-3-one **1***a* (1.562 g) was added in one batch. A portion (17.0 ml) was removed after 1 min, poured into sodium hydroxide (2.0 *N*, 0°), extracted with chloroform, washed with water, dried, and evaporated. The product was placed on a column ($1\frac{1}{2}$ × 32 in.) of neutral alumina ("Woelm"), pre-equilibrated with water (6% by weight). The column was developed with benzene – ethyl acetate – ethanol (80:20:1) and gave (R_f 0.18 to 0.45) **3***b* (44%), m.p. 152–153° (lit. (26) 150–151°); λ_{max} (EtOH) 240 nm (ε 16 100); ν_{max} (KBr) 1698 (conjugated C=O), 1664 cm^{-1} (conjugated C=C); δ ($CDCl_3$) 5.79 (1H, d, $^4J_{HF}$ = 5 Hz, 4-H), 5.04 (1H, octet, $^2J_{HF}$ = 49 Hz, J_{aa} = 5.5 Hz, J_{ae} = 13 Hz, 2β-H), 3.67 (1H, t, *J* = 7.5 Hz, 17α-H), 1.30 (3H, s, 19-H_3), and 0.78 (3H, s, 18-H_3); o.r.d. (*c* 0.04, dioxane) $[\Phi]_{700}$ +480°, $[\Phi]_{589}$ +815°, $[\Phi]_{360}$ −2540°, $[\Phi]_{300}$ +13 700°; c.d. (0.00131 *M* in dioxane) $\Delta\varepsilon_{335}$ −2.60; t.l.c. R_f 0.47. This specimen of **3***b*, R=H) was identical (i.r., u.v., o.r.d., t.l.c., m.p.) with an authentic sample of 2α-fluorotestosterone **3***b* synthesized by an independent route (26).

(*b*) To a stirred solution of 22 *N* hydrogen fluoride in *N*,*N*-dimethylformamide, was added **1***a* (0.340 g). After 1 h at 23° the reaction mixture contained **3***b* (42% by n.m.r.) and starting material **1***a* (50% by n.m.r.). After 3 h at 23°, the reaction mixture was worked up yielding **3***b* (80% by n.m.r.), which was placed on a column (1 × 12 in.) of dry column adsorbent (84 g). The column was developed with benzene – ethyl acetate – enol (80:20:1), yielding **3***b* (65%), identical (i.r., u.v., o.r.d., t.l.c., m.p.) with the specimen from reaction *a*.

*2α-Fluorotestosterone Acetate (**3c**)*

Hydrogen fluoride was bubbled through a solution of 4β,5β-epoxy-17β-hydroxyandrostan-3-one acetate **1***a* (1.913 g, 5.56 mmol) in "10%" ethanol–chloroform (83.6 ml). Portions (8.8 ml) were removed at 1 min intervals, poured into sodium hydroxide (2.0 *N*, 0°), extracted with chloroform, washed with water, dried, and evaporated. The portions from 1 to 5 min gave unreacted **1***a* (as determined by n.m.r.). The 7-min portion yielded **3***c* (76% by n.m.r.), m.p. 179–181° (from methanol) (lit. (26) 180–182°); λ_{max} (EtOH) 240 nm (ε 14 800); ν_{max} (KBr) 1738 (17 ester C=O), 1704 (conjugated C=O), and 1618 cm^{-1} (conjugated C=C); t.l.c. R_f 0.69.

*4β-Fluoro-17β-hydroxy-5α-androst-1-en-3-one (**9a**)*

To a stirred solution of 22 *N* hydrogen fluoride in *N*,*N*-dimethylformamide (9.0 ml) at 23° was added 1α,2α-epoxy-17β-hydroxy-5α-androstan-3-one **6***a* (0.150 g). After 3 h at 23°, the reaction mixture was worked up in the usual manner, yielding **10***d* (83% by n.m.r.), which was placed on a column (1 × 14 in.) of dry column adsorbent (100 g). The column was developed with benzene – ethyl acetate – ethanol (80:20:1) yielding (R_f 0.14 to 0.78) **9***a*, m.p. 156–158° (from acetone–water); λ_{max} (EtOH) 234 nm (ε 10 400); δ ($CDCl_3$) 7.44 (1H, d, *J* = 10 Hz, H-1), 6.08 (1H, d, *J* = 10 Hz, 2-H), 4.53 (1H, q, $^2J_{HF}$ = 49 Hz, J_{ae} = 3 Hz, 4α-H), 1.20 (3H, d, $^5J_{HF}$ = 2 Hz, 19-H_3), and 0.80 (3H, s, 18-H_3); t.l.c. R_f 0.47; mass spectrum *m*/*e* 306 (M^+).

One of us (J.S.O.) thanks the National Institutes of Health for a pre-doctoral traineeship and the State of New York Health Department for a pre-doctoral fellowship.

1. (*a*) M. Neeman and J. S. O'Grodnick. Tetrahedron Lett. **50**, 4847 (1971); 1996 (1972). (*b*) M. Neeman and J. S. O'Grodnick. Tetrahedron Lett. **9**, 783 (1972).
2. M. Neeman, Y. Osawa, and T. Mukai. J. Chem. Soc. Perkin I, 2297 (1972).
3. (*a*) M. Neeman, T. Mukai, J. S. O'Grodnick, and A. L. Rendall. J. Chem. Soc. Perkin I, 2300 (1972); (*b*) M. Neeman, J. S. O'Grodnick, and K. Morgan. J. Chem. Soc. Perkin I, 2302 (1972). (*c*) M. Neeman, Y. Osawa, and T. Mukai. J. Chem. Soc. Perkin I, 1462 (1973).
4. J. Levisalles and M. Rudler-Chauvin. Bull. Soc. Chim. Fr. 3947 (1969).
5. A. V. Stuart and G. B. B. M. Sutherland. J. Chem. Phys. **24**, 559 (1956).
6. (*a*) R. A. Wohl. Chimia, 28, (1974); (*b*) J. M. Diggle, M. D. Halliday, A. Kasal, G. D. Meakins, and M. S. Saltmarsh. J. Chem. Soc. (C), 2325 (1970).
7. J. R. Bull. Tetrahedron Lett. 5959 (1968).
8. A. J. Parker. Q. Rev. **16**, 163 (1962).
9. (*a*) G. Richard. Bull. Soc. Chim. Fr. **5**, 286 (1938); (*b*) F. G. Bordwell and R. G. Scamehorn. J. Am. Chem. Soc. **90**, 6751 (1968).
10. (*a*) M. J. S. Dewar. The electronic theory of organic chemistry. Clarendon Press, Oxford. 1949. p. 73; (*b*) A. Streitwieser, Jr. Solvolytic displacement reactions. McGraw-Hill, New York. 1962. pp. 25–29; (*c*) A. J. Sisti and S. Lowell. Can. J. Chem. **42**, 1896 (1964); (*d*) J. W. Thorpe and J. Warkentin. Can. J. Chem. **51**, 927 (1973).
11. U. Kerb, G. Schulz, and R. Wiechert. Angew. Chem. Int. Eng. Ed. **7**, 893 (1968).
12. (*a*) W. T. Borden and E. J. Corey. Tetrahedron Lett. 313 (1969); (*b*) J. Y. Satoh and T. T. Takahashi. Chem. Commun. 1714 (1970).
13. (*a*) F. G. Bordwell. Acc. Chem. Res. **3**, 281 (1970);

(*b*) F. G. BORDWELL and T. G. MECCA. J. Am. Chem. Soc. **94**, 5825 (1972); (*c*) F. G. BORDWELL and T. G. MECCA. J. Am. Chem. Soc. **94**, 5829 (1972).
14. H. J. RINGOLD, E. BATRES, O. MANCERA, and G. ROSENKRANZ. J. Org. Chem. **21**, 1432 (1956).
15. M. LEGRAND, R. VIENNET, and J. COUMARTIN. C.R. **253**, 2378 (1961).
16. B. CAMERINO, B. PATELLI, A. VERCELLONE, and F. MEDA. II Farmaco Ed. Sci. **11**, 586 (1956).
17. B. CAMERINO, B. PATELLI, and A. VERCELLONE. J. Am. Chem. Soc. **78**, 3540 (1956).
18. R. E. COUNSELL and P. D. KLIMSTRA. J. Med. Pharm. Chem. **5**, 477 (1962).
19. J. S. O'GRODNICK. Ph.D. dissertation, State Univ. of New York at Buffalo (1973). Dissert. Abstr. 2527b (1973).
20. W. M. HOEHN. J. Org. Chem. **23**, 929 (1958).
21. B. LOEV and K. M. SNADER. Chem. Ind. 15 (1965); B. LOEV and M. M. GOODMAN. Chem. Ind. 2026 (1967).
22. P. L. JULIAN and H. C. PRINTY. U.S. Pat. 2,933,510. Chem. Abstr. **54**, P 17482i (1960).
23. K. YASUDA. Chem. Pharm. Bull. Jap. **12**, 1217 (1964).
24. P. D. KLIMSTRA and R. E. COUNSELL. J. Med. Pharm. Chem. **5**, 1216 (1962).
25. Y. NOMURA, B. TAKEGAWA, and I. CHUMA. Jap. Pat. 8232 (1960). Chem. Abstr. **55**, P 9478 (1961).
26. A. H. NATHAN, J. C. BABCOCK, and J. A. HOGG. J. Am. Chem. Soc. **82**, 1436 (1960).

Can. J. Chem. Downloaded from www.nrcresearchpress.com by 210.87.254.40 on 09/05/12
For personal use only.

Five-membered Heterocyclic Thiones. Part V.[1] The Sulfurization of 5-Lithioisothiazoles

DONALD E. HORNING AND JOSEPH M. MUCHOWSKI[2]
Bristol Laboratories of Canada, Candiac, Quebec

Received March 4, 1974

DONALD E. HORNING and JOSEPH M. MUCHOWSKI. Can. J. Chem. **52**, 2950 (1974).

5-Lithioisothiazoles reacted with sulfur at −70° to produce the corresponding unstable (in air) lithium isothiazole-5-thiolates. The salts could be utilized *in situ* to prepare 5-alkylthioisothiazoles or they could be transformed in low yield into stable mercuric thiolates.

DONALD E. HORNING et M. MUCHOWSKI. Can. J. Chem. **52**, 2950 (1974).

Les lithioisothiazole-5 réagissent avec le soufre à −70° pour donner les lithium isothiazole thiolate-5 correspondants instables (à l'air). Ces sels peuvent être utilisés in situ pour préparer les alkylthioisothiazole-5 ou bien ils peuvent être transformés, avec un faible rendement, en thiolates mercuriques stables. [Traduit par le journal]

Can. J. Chem. Downloaded from www.nrcresearchpress.com by 210.87.254.5 on 09/05/12
For personal use only.

Isothiazole-5-thiols and thiolates have heretofore been prepared by total synthesis (2–6) or by displacement of halide ion from electronegatively substituted 5-halo isothiazoles (3, 7). Inasmuch as C-5-unsubstituted isothiazoles are known to undergo metalation at that position (8), it occurred to us that the sulfurization reaction, which has been especially successful in the thiophene series (9, 10), might also be applicable to the synthesis of lithium isothiazole-5-thiolates. Accordingly, metalation of 4-methylisothiazole (**1***a*) with butyl lithium at −70°, followed by the addition of sulfur, gave a solution of the lithium salt **2***a*. When ethyl bromoacetate was added to this solution, a mixture was produced which was judged to contain about 80% of the ester **3***a* by n.m.r. spectroscopy. Saponification of the crude ester gave a crystalline carboxylic acid **3***b* in 51% yield from the isothiazole. Similarly, 3-methylisothiazole (**1***b*) gave the acid **3***d* in approximately 40% overall yield. The thiols corresponding to **2** had limited stability in air since acidification of the solution containing **2** failed to give any material which was soluble in dilute alkali. If, however, the thiolate solutions were added to an excess of aqueous mercuric acetate, mixtures, from which could be isolated the mercuric salts **4**[3] and **5**, were produced (Scheme 1). The structures of these salts were supported by spectroscopic and analytical data (Table 1). The mercuric salts could be transformed into the corresponding sodium salts with sodium sulfide, and these were converted into the thioacetic acid derivatives **4***b* and **4***d* identical to those derived from the lithium salts.

The experiments described herein promise to have wide applicability for the synthesis of simple substituted isothiazol-5-yl alkyl sulfides, most of which have heretofore been relatively inaccessible. Indeed, the methodology described in this paper has already been utilized to attach various isothiazol-5-thio moieties to certain water soluble alkylating agents.[4]

Experimental

The isothiazoles were purchased from Raylo Chemicals Ltd., Edmonton, Alta., Canada. The melting points were determined in a Mel Temp or a Gallenkamp melting point apparatus and are not corrected.

Sulfurization of 5-Lithioisothiazoles

The sulfurization of 4-methyl-5-lithioisothiazole was typical. A solution of the lithium compound, prepared in the usual way (11) from 4-methylisothiazole (4.76 g, 48 mmol) in dry tetrahydrofuran (125 ml) and *n*-butyllithium in hexane (30 ml of a 15.05% solution (48 mmol)), was treated all at once with sulfur (1.68 g, 52.5 mmol) at −60 to −70°. The stirred solution was left to come to room temperature (1.25 h) and then cooled to 0°. Ethyl bromoacetate (8.78 g, 53 mmol) was added in a dropwise manner, the solution was allowed to reach room temperature, and then heated at reflux temperature for 1 h. The cooled mixture was evaporated *in vacuo*, water was added to the residue, and the product was extracted into ether. The dried extract was evaporated *in vacuo* and the

[1]For Part IV see ref. 1.

[2]To whom enquiries should be addressed at, Syntex, S.A., Division de Investigacion, Apartado Postal 10-820, Mexico 10, D.F.

[3]This compound had a strong infrared absorption at 1575 cm^{-1}. The data at hand are also consistent with a 1:1 complex of mercuric acetate and the diarylthio mercuric salt analogous to **5**.

[4]Unpublished observations of the Antibiotic Chemistry Department, Bristol Laboratories, Syracuse, New York.

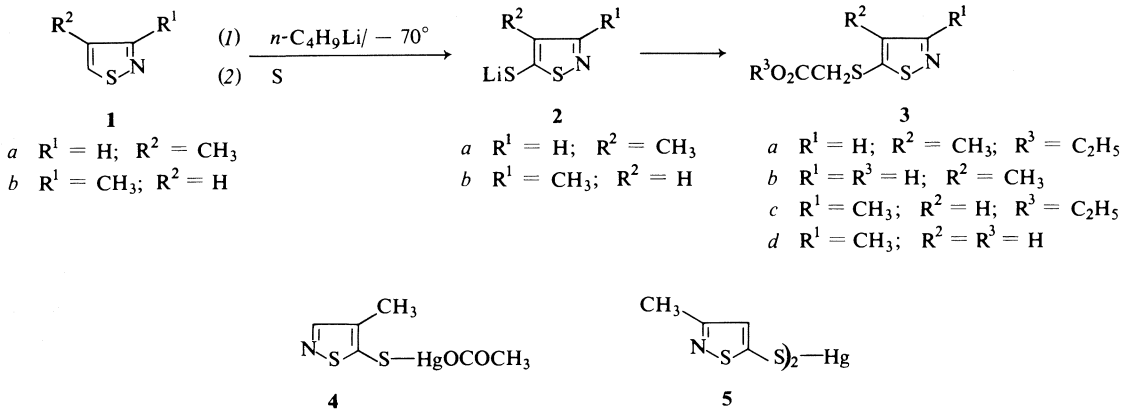

1

a $R^1 = H$; $R^2 = CH_3$
b $R^1 = CH_3$; $R^2 = H$

2

a $R^1 = H$; $R^2 = CH_3$
b $R^1 = CH_3$; $R^2 = H$

3

a $R^1 = H$; $R^2 = CH_3$; $R^3 = C_2H_5$
b $R^1 = R^3 = H$; $R^2 = CH_3$
c $R^1 = CH_3$; $R^2 = H$; $R^3 = C_2H_5$
d $R^1 = CH_3$; $R^2 = R^3 = H$

4 **5**

SCHEME 1

TABLE 1. Spectral properties of some 5-substituted isothiazoles

Compound	Infrared[a] (cm^{-1})	Ultraviolet[b] λ_{max} (nm)(log ε)	Nuclear magnetic resonance[c] δ (p.p.m.)
3*a*	1739		1.28(t, 3H, J = 7.4), 2.53(s, 3H), 3.65(s, 2H), 4.27(q, 2H, J = 7.4), 8.45(s, 1H)
3*b*	3400–2350 1723	277 (3.66) 262 (3.70) 225 (3.60)	2.27(s, 3H),[d] 3.80(s, 2H), 4.92(s, 1H, W_H = 34 Hz), 8.37(s, 1H)
3*c*	1732		1.30(t, 3H, J = 7.2), 2.47(s, 3H), 3.74(s, 2H), 4.25(q, 2H, J = 7.2), 6.84(s, 1H).
3*d*	3500–2400[e] 1736	270 (3.48) 256 (3.79) 221 (3.76)	2.37(s, 3H)[d], 3.93(s, 2H), 5.67 (s, 1H, W_H = 70 Hz), 7.16(s, 1H)

[a]Recorded as chloroform solutions with a Unicam SP-200G i.r. spectrophotometer or a Perkin-Elmer 267 Grating i.r. spectrophotometer.
[b]Measured in methanol with a Perkin-Elmer 402 u.v. spectrophotometer.
[c]Recorded in $CDCl_3$ (unless otherwise indicated) with a Varian A-60A spectrometer or a Varian T-60 spectrometer; q = quartet, s = singlet, t = triplet; J values in Hz.
[d]Recorded in DMSO-d_6.
[e]Measured in dioxan solution.

residual oil was distilled to give a fraction b.p. 105–112°/0.3 mm (7.05 g). This material had a purity of *ca.* 80% as deduced from its n.m.r. spectrum.

The crude ester (3.26 g, 15 mmol) in 50% aqueous methanol (30 ml) which was 1 *N* in sodium hydroxide, was boiled under reflux for 2.5 h. The solution was diluted with water and extracted with benzene (discarded). The aqueous phase was made acidic with hydrochloric acid and the solid which precipitated was collected by filtration. The crude acid was crystallized from 50% aqueous ethanol to give the product (2.12 g, 51% based on 4-methylisothiazole) m.p. 111–113° in three crops. Two further crystallizations gave material with m.p. 112–113°.

Anal. Calcd. for $C_6H_7NO_2S_2$: C, 38.06; H, 3.73; N, 7.40. Found: C, 37.88; H, 3.74; N, 7.44.

In the same way 3-methyl-5-carboxymethylthioisothiazole (**3***d*) was prepared in 36% yield overall from 3-methylisothiazole. After crystallization from aqueous ethanol (1:1) the carboxylic acid had m.p. 166–168°.

Anal. Calcd. for $C_6H_7NO_2S_2$: C, 38.06; H, 3.73; N, 7.40. Found: C, 37.89; H, 3.72; N, 7.56.

Preparation of the Mercuric Salts

The lithium thiolate solution (20 mmol), prepared by the sulfurization of the 5-lithioisothiazole (as described above), was added in a dropwise manner to a stirred solution of mercuric acetate (8.28 g, 26 mmol) in water (120 ml) containing acetic acid (1.2 ml). After ½ h the white solid was collected by filtration, washed first with water, and then with tetrahydrofuran, and finally dried *in vacuo*.

In this way mercuric-3-methylisothiazole-5-thiolate (**5**) was obtained in a crude yield of 96%. A sample, after crystallization from a large volume of acetone gave a small amount (15% recovery) of material with m.p. 199–200°; u.v. 258 nm (log ε = 4.40).

Anal. Calcd. for $C_8H_8N_2S_4Hg$: C, 20.85; H, 1.75; N, 6.08. Found: C, 20.59; H, 1.80; N, 6.32.

Can. J. Chem. Downloaded from www.nrcresearchpress.com by 210.87.254.5 on 09/05/12
For personal use only.

In the same manner, the hemiacetate **4** was obtained in 100% yield (crude). It is not understood why the hemiacetate was obtained in preference to the normal mercuric salt. After crystallization from a large volume of methanol, a low yield of the salt, which had m.p. 210–212° dec., was obtained.

Anal. Calcd. for $C_4H_4NS_2$: $HgC_2H_3O_2$: C, 18.62; H, 1.81; N, 3.62. Found: C, 18.46; H, 1.75; N, 4.00.

The compound was not sufficiently soluble in methanol to measure the u.v. spectrum.

Generation of the Carboxymethylthio Derivatives from the Mercuric Salts

The method described by Soderback (12) was used. The crude mercuric salt (10 mmol) was added at 0° to a stirred solution of sodium sulfide nonahydrate (9 mmol) in water (150 ml). The mixture was stirred in a nitrogen atmosphere at 0° for $\frac{1}{2}$ h, ethyl bromoacetate (20 mmol) was added, and stirring at room temperature was then maintained for 20–24 h. Ether was added, the mixture was filtered through celite, the organic phase was separated, dried, and evaporated *in vacuo*. The excess ethyl bromoacetate was removed at 80°/15 mm and the oil which remained (crude yields *ca.* 20%) was hydrolysed to the corresponding acid in the normal manner. The carboxylic acids obtained in this way were identical in all respects to those (**3***a*, **3***d*) obtained from the corresponding lithium salts (**2***a*, **2***b*).

The authors gratefully acknowledge the proficient assistance of M. C. Doria.

1. G. Lacasse and J. M. Muchowski. Can. J. Chem. **51**, 2353 (1973).
2. E. Soderback. Acta Chem. Scand. **17**, 362 (1963); **19**, 549 (1965); **24**, 228 (1970).
3. W. R. Hatchard. J. Org. Chem. **29**, 665 (1964).
4. M. Pianka. J. Sci. Food Agr. **19**, 507 (1968).
5. K. Gewald. J. Prakt. Chem. **31**, 214 (1966).
6. M. Davis, G. Snowling, and R. W. Winch. J. Chem. Soc. C, 124 (1967).
7. W. R. Hatchard. J. Org. Chem. **29**, 660 (1964).
8. K. R. H. Wooldridge. *In* Advances in heterocyclic chemistry. Vol. 14. *Edited by* A. R. Katritzky and A. J. Boulton. Academic Press, Inc. New York, N.Y. 1972. pp. 18–20.
9. S. Gronowitz. *In* Advances in heterocyclic chemistry. Vol. I. *Edited by* A. R. Katritzky. Academic Press, Inc. New York, N.Y. 1963. p. 86.
10. E. Jones and I. M. Moodie. Organic syntheses. Vol. 50. John Wiley and Sons, Inc., New York. 1970. pp. 103–106.
11. R. G. Micetich. Can. J. Chem. **48**, 2006 (1970).
12. E. Soderback. Ann. **465**, 184 (1928).

Can. J. Chem. Downloaded from www.nrcresearchpress.com by 210.87.254.5 on 09/05/12
For personal use only.

The Synthesis and Reactions of Chiral Sulfonium Ylids

STEWART J. CAMPBELL[1] AND D. DARWISH[2]

Department of Chemistry, University of Alberta, Edmonton, Alberta

Received February 6, 1974

STEWART J. CAMPBELL and D. DARWISH. Can. J. Chem. **52**, 2953 (1974).

Treatment of (−)-ethylmethylsulfonium phenacylid, (−)-**1**, in THF at room temperature with 15 equiv. of benzoic anhydride, acetic anhydride or 1 equiv. phenyl isocyanate produces the corresponding (−)-ethylmethylsulfonium diacylmethylids, (−)-**5**, (−)-**6**, and (−)-**8**. Treatment of (−)-**1** with dimethyl sulfate in acetone gives (*Z*)-(+)-ethylmethyl-α-methoxy-β-styrylsulfonium methyl sulfate, (+)-**10**. Resolution of (±)-**10** via its DBT salt and conversion to perchlorate gives the corresponding vinyl perchlorates (+)- and (−)-**13**. Under the resolution conditions the ketal perchlorates, (−)- and (+)-ethylmethyl-2,2-dimethoxy-2-phenylethylsulfonium perchlorate, (−)- and (+)-**14**, are also obtained. The rates of racemization at 50° in benzene of **1**, **5**, **6**, and **8** are 39.7, 55.5, 106, and 79.1 × 10^{-5} s^{-1}, respectively. The rates of racemization at 50° in methanol of **10**, **13**, and **14** are 1.93, 2.08, and 5.64 × 10^{-5} s^{-1}. Racemization is proposed to proceed via pyramidal inversion. The synthetic potential of chiral sulfonium ylids is discussed with respect to their ease of racemization.

STEWART J. CAMPBELL et D. DARWISH. Can. J. Chem. **52**, 2953 (1974).

Le traitement du phénacylure de (−)-éthylméthylsulfonium, (−)-**1**, à température de la pièce dans le THF, par 15 équiv. d'anhydride benzoïque, d'anhydride acétique ou 1 équiv. d'isocyanate de phényle conduit aux diacylméthylures correspondants, (−)-**5**, (−)-**6** et (−)-**8**. Le traitement de (−)-**1** avec du sulfate de diméthyle dans l'acétone donne le méthylsulfate de (*Z*)-(+)-éthylméthyl α-méthoxy β-styrylsulfonium, (+)-**10**. La résolution du (±)-**10** par son sel de DBT et sa conversion en perchlorate donne les perchlorates de vinyle correspondants (+)- et (−)-**13**. Dans les conditions de résolution on obtient aussi les perchlorates de l'acétal et les perchlorates des (−)- et (+)-éthylméthyldiméthoxy-2,2 phényl-2 éthylsulfonium, (−)- et (+)-**14**. Les taux de racémisation à 50° dans le benzène de **1**, **5**, **6** et **8** sont respectivement de 39.7, 55.5, 106 et 79.1 × 10^{-5} s^{-1}. Les taux de racémisation de **10**, **13** et **14** dans le méthanol à 50 °C sont respectivement de 1.93, 2.08 et 5.64 × 10^{-5} s^{-1}. On suppose que la racémisation s'effectue par une inversion pyramidale. On discute des possibilités de synthèse qu'offrent des ylures chiraux de sulfonium par rapport à leur facilité de racémisation.

[Traduit par le journal]

The first sulfonium ylid, dimethylsulfonium fluorenylid, was prepared by Ingold and Jessop (1) in 1930 by the reaction of its conjugate acid bromide with base. A number of stable sulfonium ylids has been prepared since 1930, the chemical properties of which have been extensively studied and reviewed (2). Although chiral sulfonium salts have been known since 1900 (3), failures in obtaining chiral sulfonium ylids were reported as late as 1966. Nozaki *et al.* (4), for example, obtained racemic methylphenylsulfonium *p*-iodophenacylid upon basic treatment of (−)-*p*-iodophenacylmethylphenylsulfonium picrate. The pyramidal configuration of the sulfur atom in sulfonium ylids, however, had been confirmed by n.m.r. spectroscopy (5–7) and X-ray crystallography studies (8, 9). In 1968, Darwish and Tomilson (10) reported the isolation and facile racemization via pyramidal inversion of (−)-ethylmethylsulfonium phenacylid, (−)-**1**.

Because of the general utility of ylids as synthetic intermediates, it has been desirable to investigate the synthetic potential of chiral sulfonium ylids as asymmetric transfer agents. In testing the carbonyl and conjugate addition reactions of a chiral sulfonium methylid and the [2,3] sigmatropic rearrangement of a chiral allyl sulfonium salt, Trost and Hammen (11) observed an efficient transfer of asymmetry for the [2,3] sigmatropic rearrangement only. By comparison, several chiral oxosulfonium methylids are efficient asymmetric transfer agents (12). Several factors including temperature and steric effects (13–17), and angular constraint of the

[1]National Research Council of Canada Scholarship holder, 1972–1973. Current address: Oilseeds Research, Agriculture Canada Research Station, Saskatoon, Saskatchewan.

[2]Deceased April 15, 1973.

Can. J. Chem. Downloaded from www.nrcresearchpress.com by 210.87.254.5 on 09/05/12
For personal use only.

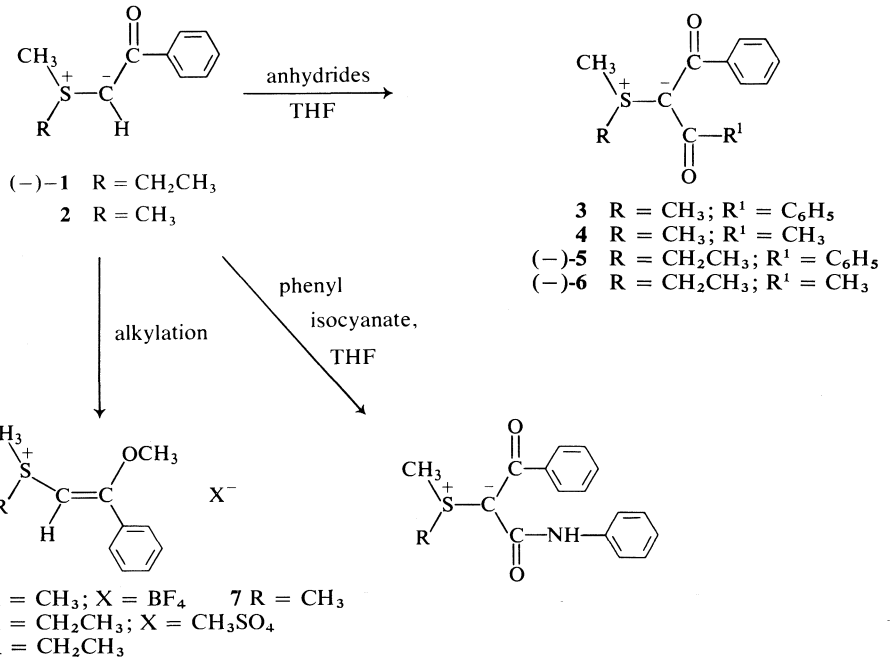

(−)-**1** R = CH_2CH_3
2 R = CH_3

3 R = CH_3; R^1 = C_6H_5
4 R = CH_3; R^1 = CH_3
(−)-**5** R = CH_2CH_3; R^1 = C_6H_5
(−)-**6** R = CH_2CH_3; R^1 = CH_3

9 R = CH_3; X = BF_4 **7** R = CH_3
(+)-**10** R = CH_2CH_3; X = CH_3SO_4
(−)-**8** R = CH_2CH_3

SCHEME 1

sulfonium center (18) affect the rates of pyramidal inversion of sulfonium salts. Presumably, similar factors affect the pyramidal inversion of sulfonium ylids.

In this article, we describe several reactions of the ylid (−)-**1** in which the stereochemistry of the pyramidal sulfur is largely maintained during the course of each reaction. Kinetic studies of the racemization of the novel sulfonium ylids and salts prepared are reported. From these and a study of a conjugate addition reaction of (−)-**1**, the synthetic potential of chiral sulfonium ylids is discussed in relation to the racemization phenomena.

Synthesis and Reactions

The treatments of the achiral analog of (−)-**1**, dimethylsulfonium phenacylid, **2**, with acylating and alkylating agents have afforded various sulfonium compounds as depicted in Scheme 1 (19–21). The synthesis of (−)-**5** and (−)-**6** from (−)-**1** illustrates one solution to the problem associated with racemization of starting material. (−)-**1** racemizes with $t_{\frac{1}{2}}$ *ca.* $5\frac{1}{2}$ h at 25° in CH_2Cl_2 (10). Benzoylation of **2** with equimolar benzoic anhydride is reported to require a reaction time of 43 h (21). Even if (−)-**5** were to racemize at the same rate as (−)-**1**, it would have been impossible to isolate (−)-**5** in the reaction time reported. However, a kinetic study of the loss of optical activity of a THF solution of (−)-**1** containing 15 equiv. of benzoic anhydride at 25° indicated the benzoylation reaction time could be reduced to *ca.* 50 min. The rate of loss of optical activity did not become first order until after 50 min which suggested that before this time (−)-**1** was reacting to give a product of different optical rotatory power than itself. Therefore, by quenching the acylation reactions after 1 h, the chiral ylids (−)-**5** and (−)-**6** were obtained. The synthesis of (−)-**8** required no such modification as the reaction of (−)-**1** with equimolar phenyl isocyanate is complete within 15 min.

Alkylation of (−)-**1** with excess dimethyl sulfate in acetone for 30 min at room temperature afforded (*Z*)-(+)-ethylmethyl-α-methoxy-β-styrylsulfonium methyl sulfate, (+)-**10**. The alkylation of **2** with trimethyloxonium tetrafluoroborate has been reported to yield a *Z*:*E* isomeric mixture of the vinyl sulfonium salt **9** in a ratio of 94:6 (22). The assignment of the *Z* configuration to (+)-**10** is based on analogy to that of the major product of this alkylation reaction.

Because considerable quantities of (+)-**10** were required for racemization studies, a more

Can. J. Chem. Downloaded from www.nrcresearchpress.com by 210.87.254.5 on 09/05/12
For personal use only.

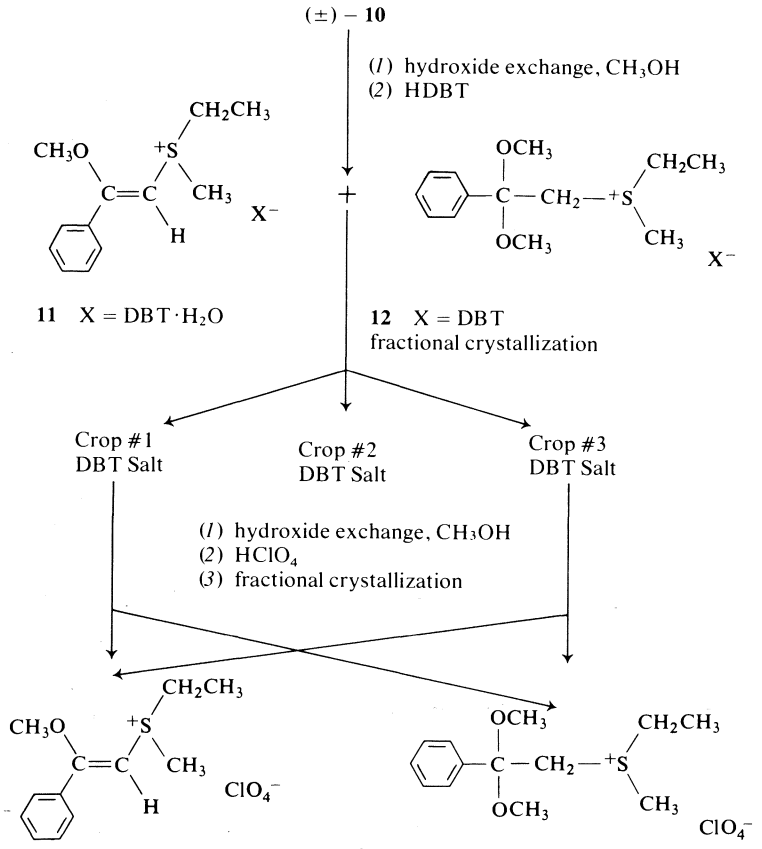

SCHEME 2

efficient synthesis was attempted by direct resolution. Upon elution of a methanolic solution of (±)-**10** through a Dowex 1-X8 hydroxide exchange column and neutralization of the eluate with (2*R*,3*R*)-2,3-dibenzoyltartaric acid monohydrate (HDBT), a diastereomeric salt mixture of the corresponding DBT·H_2O salt, **11**, was obtained. In addition to **11**, variable amounts of the ketal sulfonium salt, ethylmethyl-2,2-dimethoxy-2-phenylethylsulfonium hydrogen (2*R*,3*R*)-2,3-dibenzoyltartrate **12**, were also obtained. The complex mixtures of vinyl and ketal sulfonium DBT salts were resolved by fractional crystallization and conversion to the corresponding perchlorate salts, **13** and **14**, as outlined in Scheme 2. Unfortunately, the experimental conditions could not be established such that either DBT salt could be obtained predictably. Recently, Stirling and co-workers (23) have reported the base-catalyzed addition of methanol across the double bonds of analogous vinyl sulfonium salts.

Carbonyl stabilized sulfonium ylids are considerably less nucleophilic than simple alkylids. Thus, **1** decomposed to phenacylmethyl sulfide (10) rather than undergoing the carbonyl addition reaction with cyclohexanone or benzaldehyde. Treatment of **1** with equimolar chalcone in benzene for 17 h at 25° yielded the expected *dl*- and *meso*-cyclopropanes (19). Under the same conditions, (–)-**1** also provided the *dl*- and *meso*-cyclopropanes. The enantiomeric purity of this reacting ylid would have been considerably reduced prior to the cyclopropanation. Therefore, we diverted our attention to studies of more reactive chiral sulfonium ylids. In this

Can. J. Chem. Downloaded from www.nrcresearchpress.com by 210.87.254.5 on 09/05/12
For personal use only.

TABLE 1. Rates of racemization of some sulfonium ylids[a]

Compound	[Ylid]	Temperature (°C)	$10^5 k_{rac}$ (s^{-1})	ΔH^* (kcal/mol)	ΔS^* (e.u.)
(−)-**5**	0.0463	50	55.5 ±1.3	23.9±0.5	0.4±1.5
	0.0232	50	57.7 ±1.1		
	0.0463[b]	25	2.27±0.07		
(−)-**6**	0.0325	50	106 ±2	23.7±0.3	0.1±0.9
	0.066	50	107 ±2		
	0.0325	25	4.40±0.07		
(−)-**8**	0.0232	50	79.1 ±0.3	23.9±0.2	1.1±0.6
	0.0232	25	3.20±0.04		
(−)-**1**[c]	0.018	50	39.7 ±0.2	23.6±0.2	−1.1±0.5
	0.021	25	1.67±0.01		

[a]546 nm; Method I unless otherwise specified; benzene.
[b]546 nm; Method II; benzene.
[c]References 10 and 27.

connection, our observations with chiral benzyl sulfonium salts[3] parallel those recently reported by Trost and Hammen for chiral allyl sulfonium salts.

Kinetic Studies

The rates of loss of optical activity, k_α, of the chiral sulfonium ylids and salts prepared were studied by following the disappearance of optical activity with time. A Perkin-Elmer Model 141 Polarimeter was used with incident light of wavelength 546 and 365 nm as required. Reaction solutions were heated either in thermostated polarimeter cells (Method I) or in sealed ampoules immersed in constant temperature oil baths (Method II). Rotations were obtained directly from the digital readout of the instrument with infinity measurements taken after 10 half-lives of reaction. Reactions were usually followed to *ca.* 85% completion. As the n.m.r. spectra of the evaporation residues obtained after 10 half-lives of loss of optical activity were superimposable upon those for racemic materials, k_{dec} for these ylids and salts were estimated to be very much smaller than k_α. Therefore, to an excellent approximation, $k_{rac} = k_\alpha$.

Table 1 summarizes the racemization rate constants for the sulfonium ylids and Table 2, those for the salts. The values for (−)-**1** and (−)-ethylmethylphenacylsulfonium perchlorate, (−)-**15**, are included for comparison. The estimation of errors in the enthalpy and entropy of activation was calculated from the average deviation of the rate constants using the method described by Wiberg (24). Though the average deviations for the salts are high, it was not practical to endeavour to reduce them because of the low specific rotations of the salts and the difficulties in the resolutions.

Discussion

In 1967, Nozaki *et al.* (7) reported an n.m.r. spectral study of dimethylsulfonium diacetylmethylid. This compound exhibited magnetic equivalence of the two *C*-methyl groups at room temperature. At −60°, the *C*-methyl signal split into a 1:1 doublet with the coalescence temperature being *ca.* −25°. However, no change was observed for the *S*-methyl signal. Nozaki also observed that the *C*-methyl signal of **4** was broadened on cooling to −60°. Of the processes postulated to account for these observations, hindered rotation around the ylid bond and inversion of configuration at the sulfur atom, both of which would be slowed down upon cooling, were considered most likely. In favoring the latter interpretation, these authors calculated the half-life of pyramidal inversion to be *ca.* 0.02 s at −25°. We have recorded a broadening of the *C*-methyl signal of (−)-**6** identical to that reported for the related ylid **4**. In view of the isolation and kinetic study of the related optically active diacylmethylids, the kinetic process observed in the temperature dependent n.m.r. appears related to hindered rotation about the ylid bond. Furthermore, the steric and electronic effects of a diacylmethylid substituent *vs.* those of a phenacylid are not so great as would be

[3]Asymmetric induction in the Sommelet rearrangement of chiral sulfonium salts. Stewart J. Campbell and D. Darwish. In preparation.

Can. J. Chem. Downloaded from www.nrcresearchpress.com by 210.87.254.5 on 09/05/12
For personal use only.

TABLE 2. Rates of racemization of some ethylmethylsulfonium salts*

Compound	[Salt]	Temperature (°C)	$10^5 k_{rac}$ (s^{-1})	$\Delta H^{\ddagger}$ (kcal/mol)	$\Delta S^{\ddagger}$ (e.u.)
(+)-**10**	0.127†	70	29.7 ±1.5†	29.5±0.5	11 ±1.6
	0.163	50	1.93 ±0.06		
(+)-**13**	0.078†	70	32.8 ±2.0†	29.8±1.8	12 ±5.7
	0.072	50	2.08 ±0.17		
(+)-**14**	0.111	50	5.61 ±0.14		
	0.077	50	5.64 ±0.02	25.5±0.5	0.8±2.6
	0.074†	25	0.187±0.010		
(−)-**15**‡	0.020†	70	5.58 ±0.18	29.0±0.5	4.4±0.6
	0.020†	50	0.373±0.006		

*365 nm; Method I unless otherwise specified; methanol.
†365 nm; Method II; methanol.
‡References 13 and 27.

implied from the earlier results of Nozaki *et al.* and Darwish and Tomilson.

Pyramidal inversion of sulfonium salts has been shown to be subject to steric acceleration. For example, substitution of a phenyl for an ethyl substituent in several aryl sulfonium salts results in *ca.* 10-fold increases in the rates of racemization (16). A rate acceleration from substitution of a phenyl for an ethyl substituent probably accounts for the failure to obtain chiral methylphenylsulfonium *p*-iodophenacylid (4).

The slower rate of racemization of (+)-**10** compared with that for (−)-**1** is expected from changes in the electronegativities of the sulfur substituents (25). To explain the fact that the salt (−)-**15** racemized 200 times slower than the ylid (−)-**1** in methanol, it was assumed the greater electronegativity of the phenacyl substituent relative to that of the phenacylid favored a less planar ground state in the salt (10). Thus, a higher activation energy for the racemization of the salt was expected. Similarly, the β-styryl substituent of **10** would be more electronegative than the phenacylid substituent of **1** and (+)-**10** would racemize slower than (−)-**1**. The 15-fold rate enhancement upon ketalization of the phenacyl substituent of (−)-**15** may be due to the reduced electronegativity of the ketal substituent relative to that of the phenacyl substituent and to the increased steric size of the ketal substituent.

The ease racemization and reduced reactivity of the ylid (−)-**1** contributed to the failure to observe significant optical activity in the product of the conjugate addition reaction. As shown by Trost and Hammen (11), extensive racemization may be avoided by operating at low temperatures, however the chemical reactivity of the ylid must be considered. Enantiomeric stability of an ylid may be improved by minimizing steric interactions of the sulfonium substituents. Nevertheless, chiral sulfonium ylids will serve as useful asymmetric transfer agents only if significant free energy differences between diastereomeric transition states exist.

Experimental

All melting points (uncorrected) were obtained using a Hershberg-type melting point apparatus with a set of Anschutz thermometers. Nuclear magnetic resonance spectra were recorded on Varian Analytical n.m.r. Spectrometers, Models A-60 and A-56-60. Chemical shifts are reported in δ units from internal TMS. Infrared spectra were recorded on a Perkin-Elmer Grating Infrared Spectrometer, Model 421. Optical rotations were obtained using a Perkin-Elmer Polarimeter, Model 141. Synthetic procedures and physical constants, except specific rotation, were identical for racemic and chiral compounds.

*(—)-Ethylmethylsulfonium Phenacylid ((—)-**1**)*

(±)-**1** was obtained by treatment with 5% NaOH of the crude product from reaction of phenacyl bromide with ethyl methyl sulfide in acetone and extraction of the mixture with $CHCl_3$. The racemic ylid was treated with equimolar HDBT (26) in methanol to provide the corresponding crude diastereomeric tartrates after evaporation of the solvent. (—)-Ethylmethylphenacylsulfonium hydrogen (2*R*,3*R*)-2,3-dibenzoyltartrate, $[\alpha]_{589}^{r.t.}$ −90.2° (*c* 0.56, methanol) (reported $[\alpha]_{589}^{r.t.}$ −88.2° (*c* 0.44, methanol) (27) was obtained after three to five fractional crystallizations at 5° of the crude dissolved in minimum amounts of methanol at room temperature. (−)-**1**, $[\alpha]_{589}^{r.t.}$ −216° (*c* 0.42, benzene) (lit. (10) $[\alpha]_{589}^{r.t.}$ −137° (*c* 0.49, benzene)) was prepared directly from the resolved tartrate by treatment with 5% NaOH at 0°. Extraction of the crude ylid with cold $CHCl_3$, a rapid and efficient evaporation of the solvent, and recrystallization of the residual oil from benzene – Skellysolve B at −10° provided ylid of high specific rotation. In synthetic experiments, (−)-**1**, with $[\alpha]_{589}^{r.t.}$ *ca.* −180° was used as the

Can. J. Chem. Downloaded from www.nrcresearchpress.com by 210.87.254.5 on 09/05/12
For personal use only.

final recrystallizations of the resolution were extremely tedious. Other physical data for (−)-**1** were identical with those reported elsewhere (10).

The precautions indicated in isolating (−)-**1** with high optical rotation were rigorously followed in isolating the new diacylmethylids.

*(−)-Ethylmethylsulfonium Dibenzoylmethylid ((−)-**5**)*

Benzoic anhydride (20.3 g, 91 mmol) and (−)-**1** (1.16 g, 5.97 mmol) were dissolved in 15 ml THF. The solution was stirred for 1 h at room temperature, diluted with chloroform, and extracted with dilute NaOH several times. The combined aqueous layers were extracted with $CHCl_3$. The organic layers were washed with water, dried over $MgSO_4$ and concentrated. The residual oil was recrystallized from $CHCl_3$ – Skellysolve B to yield (−)-**5** (1.132 g, 3.80 mmol, 63.4%), m.p. 153–154°; $[\alpha]_{546}^{r.t.}$ −31.9° (*c* 1.38, benzene); n.m.r. ($CDCl_3$), δ 7.02 (m, 10H), 3.92 (m, 1H), 3.24 (m, 1H), 2.95 (s, 3H), 1.34 (t, J = 7.0 Hz, 3H); i.r. (Nujol), 1570, 1545, 1015, 955 cm^{-1}.

Anal. Calcd. for $C_{18}H_{18}O_2S$: C, 72.45; H, 6.08; S, 10.74. Found: C, 72.26, 72.48; H, 6.23, 5.89; S, 10.85, 10.67.

*(−)-Ethylmethylsulfonium Acetylbenzoylmethylid ((−)-**6**)*

Acetic anhydride (10 ml, 106 mmol) and (−)-**1** (1.26 g, 6.47 mmol) were dissolved in 10 ml THF. The solution was stirred for 45 min at room temperature diluted with 100 ml 10% NaOH and the resulting mixture stirred for 20 min at 0°. Extraction of the mixture with CH_2Cl_2, drying and concentration of the extracts and crystallization of the residual oil from benzene – Skellysolve B provided (−)-**6** (1.31 g, 5.55 mmol, 85%), m.p. 98–99°; $[\alpha]_{546}^{r.t.}$ −30.8° (*c* 0.77, benzene); n.m.r. ($CDCl_3$), δ 7.33 (s, 5H), 3.81 (m, 1H), 3.06 (m, 1H), 2.86 (s, 3H), 2.14 (s, 3H), 1.24 (t, J = 7.0 Hz, 3H); i.r. (Nujol), 1605, 1560, 1020, 960, 710 cm^{-1}.

Anal. Calcd. for $C_{13}H_{16}O_2S$: C, 66.07; H, 6.82; S, 13.57. Found: C, 65.69, 66.10; H, 6.83, 6.76; S, 13.50, 13.44.

*(−)-Ethylmethylsulfonium Benzoyl-(N-phenylcarbamoylmethylid) ((−)-**8**)*

Phenyl isocyanate (1.3 g, 10.9 mmol) and (−)-**1** (2.09 g, 10.8 mmol) were dissolved in 25 ml THF, and the solution stirred for 15 min at room temperature. The solvent was removed and the residual oil crystallized from $CHCl_3$ – Skellysolve B to yield (−)-**8** (3.03 g, 9.67 mmol, 89.6%), m.p. 171–172°; $[\alpha]_{546}^{r.t.}$ −39.9° (*c* 0.73, benzene); n.m.r. ($CDCl_3$), δ 12.32 (s, 1H), 7.34 (m, 10H), 3.97 (m, 1H), 3.09 (m, 1H), 2.89 (s, 3H), 1.20 (t, J = 7.0 Hz, 3H); i.r. (Nujol), 2200–4000, 1635, 1595, 1520, 1055 cm^{-1}.

Anal. Calcd. for $C_{18}H_{19}NO_2S$: C, 68.98; H, 6.11; N, 4.47; S, 10.23. Found: C, 68.79, 69.11; H, 6.37, 6.20; N, 4.42, 4.45; S, 10.49, 10.38.

*(Z)-(+)-Ethylmethyl-α-methoxy-β-styrylsulfonium Methyl Sulfate ((+)-**10**)*

Dimethyl sulfate (2.2 g, 17.5 mmol) and (−)-**1** (2.2 g, 11.3 mmol) were dissolved in 30 ml acetone, and the solution stirred for 30 min at room temperature. Ether was added to the cloud point and the mixture cooled at −5° to yield (+)-**10**, m.p. 103°; $[\alpha]_{365}^{r.t.}$ +3.94° (*c* 5.2, methanol); n.m.r. ($CDCl_3$), δ 7.51 (s, 5H), 6.00 (s, 1H), 3.74 (s, 1H), 3.62 (s, 3H), 3.62 (q, J = 7.0 Hz, 2H), 3.13 (s, 3H), 1.42 (t, J = 7.0 Hz, 3H); i.r. ($CHCl_3$), 2990, 1608, 1572, 1490, 1452, 1210, 610, 575 cm^{-1}.

Anal. Calcd. for $C_{13}H_{20}O_5S_2$: C, 48.73; H, 6.29; S, 20.01. Found: C, 48.60, 48.95; H, 6.18, 6.23; S, 20.26, 20.28.

*Resolution of (±)-**10***

The difficulties encountered in this resolution are illustrated by the nonreproducibility of the following three experiments.

Experiment 1: (±)-**10** (2.75 g, 8.58 mmol) was dissolved in a minimum amount of CH_3OH, and the solution eluted through a Dowex 1–X8 hydroxide exchange column into a flask containing HDBT (3.15 g, 8.48 mmol). The solution was concentrated to *ca.* 50 ml, ether added to the cloud point and the mixture cooled at 5° to yield **11** (1.39 g, 2.46 mmol), m.p. 114°; $[\alpha]_{589}^{r.t.}$ −78.2° (*c* 0.60, methanol); n.m.r. (DMSO-d_6), δ 8.00–7.10 (m, 15H), 6.08 (s, 1H), 5.70 (s, 2H), 3.76 (s, 3H), 3.43 (q, J = 7.0 Hz, 2H), 3.03 (s, 3H), 1.30 (t, J = 7.0 Hz, 3H); i.r. (Nujol), 3500, 1715, 1645, 1625, 1600, 1255, 1110, 715 cm^{-1}.

Anal. Calcd. for $C_{30}H_{32}O_{10}S$: C, 61.63; H, 5.52; S, 5.48. Found: C, 61.75, 61.40; H, 5.51, 5.54; S, 5.54, 5.74.

Experiment 2: (±)-**10** (5.50 g, 17.2 mmol) was treated in a similar manner with equimolar HDBT to yield **12** (6.6 g, 11.0 mmol), m.p. 129°; $[\alpha]_{589}^{r.t.}$ −75.6° (*c* 0.45, methanol); n.m.r. (DMSO-d_6), δ 8.08–7.17 (m, 15H), 5.64 (s, 2H), 4.05 (s, 2H), 3.26 (q, J = 7.0 Hz, 2H), 3.20 (s, 6H), 2.73 (s, 3H), 1.22 (t, J = 7.0 Hz, 3H); i.r. (Nujol), 1728, 1670, 1600, 1585, 1260, 710 cm^{-1}.

Anal. Calcd. for $C_{31}H_{34}O_{10}S$: C, 62.20; H, 5.72; S, 5.36. Found: C, 62.51, 62.41; H, 5.74, 5.63; S, 5.35, 5.57.

Experiment 3: (±)-**10** (4.68 g, 14.6 mmol) was treated in a similar manner with equimolar HDBT to yield 2.67 g of a 3:2 mixture (by n.m.r.) of **11**:**12**, m.p. 114–120°.

In each of the above three experiments, a second crop of material was obtained by the addition of more ether and the cooling of the resulting mixture at 5°. After filtering the second crop, the mother liquor was concentrated to near dryness and excess ether added. After cooling, the supernatant was decanted leaving a tacky white semi-solid which solidified to a hard cake under reduced pressure.

Conversion of DBT Salts to Perchlorate Salts

A methanolic solution of 2.67 g of a 3:2 mixture of **11**:**12** (first crop) was eluted through an hydroxide exchange column into a flask containing 70% $HClO_4$ (0.72 g, 5.04 mmol). The resulting solution was neutralized by the addition of dilute sodium methoxide, reduced in volume and ether added to the cloud point. The mixture was cooled at 5° to precipitate (−)-**13** (0.361 g, 1.17 mmol), m.p. 115°; $[\alpha]_{365}^{r.t.}$ −8.80° (*c* 0.72, methanol); n.m.r. (DMSO-d_6), δ 7.56 (s, 5H), 6.02 (s, 1H), 3.79 (s, 3H), 3.43 (q, J = 7.0 Hz, 2H), 3.04 (s, 3H), 1.36 (t, J = 7.0 Hz, 3H); i.r. ($CHCl_3$), 1610, 1570, 1490, 1080, 1000, 970 cm^{-1}. Excess ether was added to the mother liquor to precipitate after cooling (+)-**14** (0.621 g, 1.82 mmol), m.p. 65°; $[\alpha]_{365}^{r.t.}$ +4.75° (*c* 0.64, methanol); n.m.r. (DMSO-d_6), δ 7.55 (s, 5H), 4.03 (s, 2H), 3.24 (q, J = 7.0 Hz, 2H), 3.28 (s, 6H), 2.72 (s, 3H), 1.73 (t, J = 7.0 Hz, 3H); i.r. ($CHCl_3$), 2840, 1490, 1450, 1420, 1285, 1090, 703,

Can. J. Chem. Downloaded from www.nrcresearchpress.com by 210.87.254.5 on 09/05/12
For personal use only.

622 cm^{-1}. The conversion of a sample of pure **11** (first crop) to its perchlorate gave only (+)-**14**.

In a similar manner, a 1.77 g quantity of a 2:1 mixture of **11**:**12** (third crop) was converted to the less soluble (+)-**13**, m.p. 114°; $[\alpha]_{365}^{r.t.}$ +8.84° (*c* 0.84, methanol) and the more soluble (−)-**14**, m.p. 55°; $[\alpha]_{365}^{r.t.}$ −5.16° (*c* 1.14, methanol).

Conjugate Addition Reaction of (−)-1

(−)-**1** (1.16 g, 6 mmol) and chalcone (1.25 g, 6 mmole) were stirred in 20 ml benzene for 17 h at room temperature. The solvent was removed and the residual oil crystallized from benzene–pentane. The precipitate was collected and recrystallized from cyclohexane to yield 0.14 g (1.26 mmol, 21%) of the *meso*-cyclopropane, m.p. 149° (19). The original mother liquor was concentrated and the residual oil crystallized from cyclohexane to yield 0.49 g (1.5 mmole, 25%) of the *dl*-cyclopropane, m.p. 114°, $[\alpha]_{589}^{25} \sim 0$.

1. C. K. Ingold and J. A. Jessop. J. Chem. Soc. 713 (1930).
2. A. W. Johnson. Ylid chemistry. Academic Press, New York, N.Y. 1966.
3. W. J. Pope and S. J. Peachey. J. Chem. Soc. 1072 (1900).
4. H. Nozaki, M. Takaku, and K. Kondo. Tetrahedron. **22**, 2145 (1966).
5. K. W. Ratts. Tetrahedron Lett. 4707 (1966).
6. A. Hochrainer and W. Silan. Monatsh. Chem. **97**, 1477 (1966).
7. H. Nozaki, D. Tunemoto, K. Nakamura, K. Watanabe, M. Takaku, and K. Kondo. Tetrahedron. **23**, 4279 (1967).
8. A. F. Cook and J. C. Moffat. J. Am. Chem. Soc. **90**, 740 (1968).
9. J. P. Schaefer and L. L. Reed. J. Am. Chem. Soc. **94**, 908 (1972).
10. D. Darwish and R. L. Tomilson. J. Am. Chem. Soc. **90**, 5938 (1968).
11. B. M. Trost and R. F. Hammen. J. Am. Chem. Soc. **95**, 962 (1973).
12. C. R. Johnson and C. W. Schroeck. J. Am. Chem. Soc. **95**, 7418 (1973).
13. D. Darwish and G. Tourigny. J. Am. Chem. Soc. **88**, 4303 (1966).
14. D. Darwish, S. H. Hui, and R. Tomilson. J. Am. Chem. Soc. **90**, 5631 (1968).
15. D. Darwish. Mech. Reactions Sulfur Compd. **3**, 33 (1968).
16. D. Darwish and C. E. Scott. Can. J. Chem. **51**, 3647 (1973).
17. B. C. Menon and D. Darwish. Tetrahedron Lett. 4119 (1973).
18. B. M. Trost, W. L. Schinski, and I. B. Mantz. J. Am. Chem. Soc. **91**, 4320 (1969).
19. B. M. Trost. J. Am. Chem. Soc. **89**, 138 (1967).
20. K. W. Ratts and A. N. Yao. J. Org. Chem. **31**, 1185 (1966).
21. A. W. Johnson and R. T. Amel. J. Org. Chem. **34**, 1240 (1969).
22. S. H. Smallcombe, R. J. Holland, R. H. Fish, and M. C. Caserio. Tetrahedron Lett. 5987 (1968).
23. J. W. Batty, P. D. Howes, and C. J. M. Stirling. J. Chem. Soc. Perkin I, 59 (1973).
24. K. B. Wiberg. Physical organic chemistry. Wiley, New York. 1964. p. 378.
25. A. Rauk, L. C. Allen, and K. Mislow. Angew. Chem. Int. Ed., **9**, 400 (1970).
26. C. L. Butler and L. H. Cretcher. J. Am. Chem. Soc. **55**, 2605 (1933).
27. R. L. Tomilson. Master's Thesis. University of Alberta, Edmonton, Alberta. 1968.

Can. J. Chem. Downloaded from www.nrcresearchpress.com by 210.87.254.5 on 09/05/12
For personal use only.

Hydrogen – Water Deuterium Exchange over Unsupported Group VIII Noble Metals[1,2]

NORMAN H. SAGERT AND RITA M. L. POUTEAU

Research Chemistry Branch, Atomic Energy of Canada Limited, Whiteshell Nuclear Research Establishment, Pinawa, Manitoba R0E 1L0

Received March 4, 1974

NORMAN H. SAGERT and RITA M. L. POUTEAU. Can. J. Chem. **52**, 2960 (1974).

Specific activities of unsupported powders of all six Group VIII noble metals have been determined for hydrogen – water deuterium isotope exchange. The metal surface areas, which are required to calculate the specific activities were measured by hydrogen chemisorption and were checked by electron microscopy. Specific activities were measured as a function of temperature in the range 353 to 573 K and also as a function of the partial pressure of hydrogen and water at suitable temperatures and over a tenfold range of partial pressures.

The variation in the specific activities was Pd < Ir ≤ Ru < Rh < Os < Pt, and these specific activities varied over a range of about 1000. The observed orders with respect to hydrogen and water are shown to be consistent with a mechanism in which chemisorbed hydrogen atoms exchange with physically adsorbed water.

From the orders and the apparent activation energies, the chemical activation energies (E_0) were calculated. These varied randomly within the range 61 ± 6 kJ mol^{-1} for all the metals studied. Previously we showed that there was a correlation of E_0 with the work function of the metal when metals were supported on a highly graphitized carbon black, and suggested that electron donation from the carbon to the metal was responsible for the correlation. This suggestion is supported by the present results which show that E_0 is relatively constant for all six metals in the absence of a support.

NORMAN H. SAGERT et RITA M. L. POUTEAU. Can. J. Chem. **52**, 2960 (1974).

On a déterminé les activités spécifiques des six métaux nobles du groupe VIII pour l'échange de deutérium hydrogène – eau. La superficie de la surface métallique, qui est nécessaire pour calculer les activités spécifiques a été évaluée par chemisorption de l'hydrogène et vérifiée par microscopie électronique. On a mesuré les activités spécifiques en fonction de la température dans l'intervalle de 353 à 573 K et aussi en fonction de la pression partielle d'hydrogène et d'eau aux températures appropriées et sous dix intervalles de pressions partielles.

Les activités spécifiques varient dans l'ordre Pd < Ir ≤ Ru < Rh < Os < Pt, dans un intervalle environ de 1000. Les ordres que l'on observe par rapport à l'hydrogène et l'eau sont en accord avec le mécanisme dans lequel des atomes d'hydrogènes chemisorbés s'échangent avec l'eau adsorbée de manière physique.

On calcule les énergies d'activation (E_0) à partir des ordres et des énergies apparentes d'activation. Les valeurs obtenues varient d'une façon désordonnée dans l'intervalle de 61 ± 6 kJ mol^{-1} pour tous les métaux étudiés. Précédemment nous avions montré qu'il y avait une corrélation de E_0 avec la fonction de travail du métal lorsque ce dernier était fixé sur du noir de charbon graphitisé et nous avions suggéré que cette corrélation était due au transfert d'électrons du carbone au métal. Les présents résultats, qui montrent que E_0 est relativement constant pour les six métaux en l'absence d'un support, viennent à l'appui de cette suggestion.

[Traduit par le journal]

Introduction

Two recent studies from this laboratory concerned the effect of the support on the hydrogen – water deuterium exchange reaction over supported noble metal catalysts (1, 2). Such studies have become possible with the development of methods for determining metal surface areas in the presence of a support (3). The hydrogen – water deuterium exchange reaction was selected for study because it is a simple reaction and is not complicated by varying selectivities, high heats of reaction, and self-poisoning. It is sterically simple and so allows us to examine the "chemical" or "electronic" effects of a change in the support without the complication of "geometric" effects which may arise in reactions requiring very special sites (4). In addi-

[1]AECL No. 4794.

[2]Presented in part at the Third North American Meeting of the Catalysis Society, San Francisco, California, February 1974.

Can. J. Chem. Downloaded from www.nrcresearchpress.com by 210.87.254.105 on 09/05/12
For personal use only.

TABLE 1. Properties of the metal powders

Metal	Source of metal	Calculated site area (10^{-20} m^2)	Metal surface area (10^3 m^2 kg^{-1})
Pd	$(NH_4)_2PdCl_6$	8.8	17.8
Rh	$RhCl_3$	8.4	15.4
Ru	$RuCl_3.1$–$3H_2O$	11.0	27.0
Pt	H_2PtCl_6	8.9	2.7_2
Ir	H_2IrCl_6	8.6	8.3_2
Os	H_2OsCl_6	11.7	10.6

tion, the reaction is of interest as a method of producing heavy water commercially.

We previously noted that the reaction was faster and proceeded with a lower activation energy over platinum supported on highly graphitized carbon than over unsupported platinum (1) or over platinum supported on silica (5). This led us to propose that graphite donated electrons to the platinum, giving rise to a platinum–hydrogen bond polarized in the sense $Pt^{\delta+}$—$H^{\delta-}$. It was thought that such a polarization should lead to a lower activation energy. In order to test this hypothesis, we then studied the exchange over the six Group VIII noble metals supported on Graphon, a highly graphitized carbon black (2). An inverse correlation was obtained between the surface chemical activation energy and the thermionic work function of the metal. This correlation was taken as evidence that electronic interactions between the metal and the support could be important. However, it was realized that this correlation could be a function of the metal itself. Therefore we have now examined the hydrogen–water exchange over unsupported Group VIII noble metal powders, where no metal–support interactions are possible.

Experimental

Rates were measured in a flow system at a total pressure of 101 kN m^{-2} using techniques previously described (1, 2). The HD concentrations were measured with a Consolidated 21-621 mass spectrometer fitted with a continuous inlet. Its calibration has been described (5). Catalysts were evacuated at 423 K for 2 h and were then reduced *in situ* in flowing hydrogen at 573 K for 18 h. They were then cooled to reaction temperature in flowing hydrogen. Their activity became constant after about 30 min conditioning in a water–hydrogen stream, and remained constant (± 5%) for several weeks provided that they were kept in flowing hydrogen at ~400 K when runs were not being made.

Metal surface areas were measured by hydrogen chemisorption as previously described (5). The catalyst structure was examined by electron microscopy. Samples were prepared in the dry state (6) and were examined on a Hitachi HU-11A electron microscope.

The sources and means of purifying water, D_2O, hydrogen, and argon have been described (5). The metal powders were prepared by reduction of appropriate compounds (Table 1) with sodium borohydride. About 2 g of the metal salts was dissolved in 50 ml of water, the solution was cooled in an ice bath, and 50 ml of a 5% solution (w/w) of sodium borohydride was added slowly. The precipitates were allowed to age for several days at room temperature and then were filtered and washed carefully using a 50 μm millipore filter. Finally the washed powders were air dried at 383 K.

Results

Metal surface areas were calculated from the amount of hydrogen chemisorbed, assuming that one H atom covers one metal atom (7). The area of an exposed platinum atom was taken as 8.9×10^{-20} m^2 (7) and the relative areas of the other metal atoms were estimated by averaging the site areas of crystal faces with high densities of atoms (8). The areas of the other metals were then calculated from the area of a platinum atom and the relative areas of the other metals. The resulting surface areas are shown in Table 1. Figure 1 shows an electron micrograph of the platinum black. The size of the particle is about 0.1 μm which is in rough agreement with the size of 0.086 μm calculated from hydrogen chemisorption data.

The reaction rate coefficient, k, in moles of HD per kg of catalyst per s is given by eq. 1. This equation is valid for deuterium concentrations of less than 5% (5, 9).

$$[1] \qquad k = \frac{F}{(\alpha + \gamma)W} \ln\left(\frac{n_e - n_0}{n_e - n}\right)$$

In eq. 1, F is the hydrogen flow rate in mol s^{-1}, W is the catalyst weight in kg, α is the reciprocal of the equilibrium constant for reaction 2, and γ is the ratio of hydrogen partial pressure to

Can. J. Chem. Downloaded from www.nrcresearchpress.com by 210.87.254.105 on 09/05/12
For personal use only.

Can. J. Chem. Downloaded from www.nrcresearchpress.com by 210.87.254.105 on 09/05/12
For personal use only.

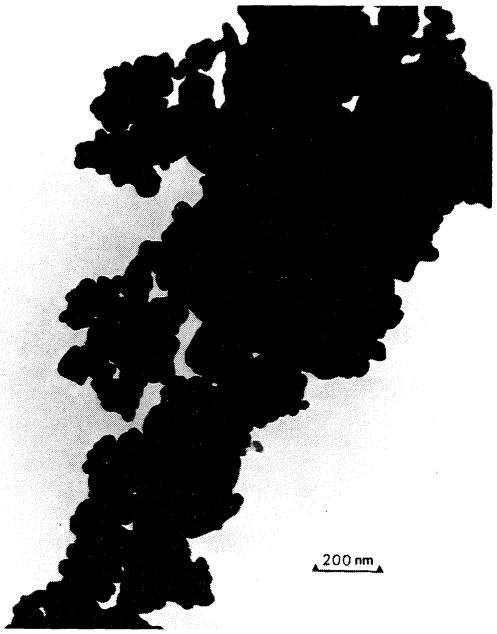

FIG. 1. Electron micrograph of the catalyst after the standard reduction procedure, and use for 100 h for hydrogen–water exchange. Particle size ~0.1 μm.

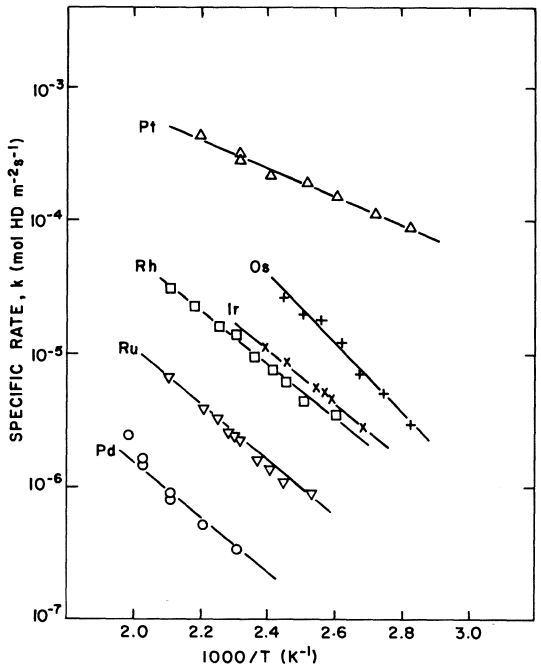

FIG. 2. Arrhenius plots of specific rates. P_{H_2} = 78.0 kN m^{-2} and P_{H_2O} = 23.7 kN m^{-2}.

water partial pressure. The HD concentration at

[2] $$HDO + H_2 \rightleftarrows H_2O + HD$$

equilibrium is given by n_e, the HD concentration in the incoming hydrogen by n_0, and that at the reactor exit by n. The rate coefficient, k, can be shown to be the initial rate of reaction 2 in the forward direction if static experiments could be done using pure HDO and H_2 as reactants. We have previously shown that our results were not affected by internal or external diffusion for Graphon supported catalysts with particle diameters up to 0.35 mm (1). The metal particle diameters used in this work were of the order of 0.1 μm, with agglomerates of particles up to 0.1 mm, so no effects of diffusion are expected.

Specific rates were calculated by dividing the rate coefficient, k, by the metal surface area per kilogram of catalyst. These specific rates are shown in Fig. 2 as a function of temperature. All points were calculated from experiments done at a number of flow rates by taking initial slopes to plots of $\ln (n_e - n_0)/(n_e - n)$ against W/F. The hydrogen pressure was 78.0 kN m^{-2} and the water pressure was 23.7 kN m^{-2} in all cases. The experimental kinetic parameters are listed in Table 2. The apparent activation energies, E_{app}, were taken directly from the slopes of the lines in Fig. 2, and the orders were taken from double logarithmic plots of k against hydrogen or water pressure. The pressures were varied over about an order of magnitude. Straight lines were generally obtained so that the rate expression could be written as

[3] $$k = k' P_{H_2O}{}^a P_{H_2}{}^b$$

For the hydrogen pressure variation on osmium and iridium curved lines were obtained which had a zero slope at high pressures and a slope approaching 0.5 at low pressures. The value of b used, *i.e.* zero, was taken from the slope at a pressure of 78 kN m^{-2} which was the pressure used in determining the activation energies.

It has previously been shown (1, 10, 11) that the true surface activation energy (E_0) is related to the apparent activation energy by eq. 4. where

[4] $$E_0 = E_{app} + b\lambda_{H_2} + a\lambda_{H_2O}$$

λ_{H_2} and λ_{H_2O} are the heats of desorption of hydrogen and water, respectively. It has also been shown (1, 10, 11) that a equals $(1 - \theta_{H_2O})$ and $2b$ equals $(1 - \theta_H)$ where θ_{H_2O} and θ_H are the water and hydrogen atom coverages expressed as fractions of a monolayer. The heat

TABLE 2. Experimental kinetic parameters

Metal	Specific rate at 433.2 K (mol HD m^{-2} s^{-1})	Order in water a	Order in hydrogen b	Temperature where orders obtained (K)	E_{app} (kJ mol^{-1})
Pd	3.3×10^{-7}	0.5	0.0	473.2	41.6
Rh	1.25×10^{-5}	0.4	0.0	433.2	41.5
Ru	2.6×10^{-6}	0.4_3	0.0	433.2	38.8
Os	7.6×10^{-5}	0.0	0.0	373.2	60.9
Ir	1.6×10^{-5}	0.2_8	0.0	433.2	40.5
Pt	3.3×10^{-4}	0.9_7	0.0	373.2	16.2

of desorption of water was required and this was taken as 50 kJ mol^{-1} (12). Table 3 gives the values of E_0 as well as the absolute surface concentration of hydrogen atoms, C_H, and water, C_{H_2O}, and the frequency factors A_0' as defined by eq. 14. For comparison, E_0 and A_0' are also shown from our previous results on Graphon-supported noble metals (2).

Figure 3 shows specific rates at 433.2 K and E_0's plotted against periodic group number. For the third triad metals, a minimum in specific rate is observed for iridium, and for the second triad metals a maximum in specific rate is observed for rhodium. The E_0's are constant within experimental error, the values being 60.6 ± 6.1 (2σ) kJ mol^{-1}.

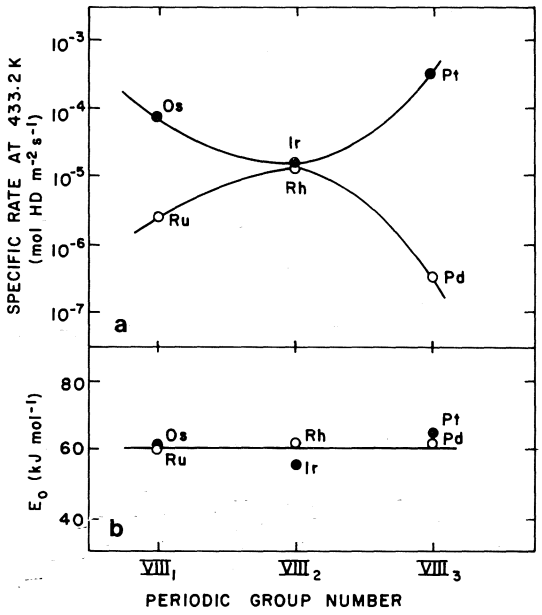

FIG. 3. Correlations of specific rate at 433.2 K (Fig. 3*a*) and surface activation energy E_0 (Fig. 3*b*) with periodic group number.

Discussion

The results will be discussed in terms of the mechanism previously proposed for hydrogen – water deuterium exchange over platinum supported on alumina (13) and on Graphon (1, 2). The mechanism is summarized below and involves adsorption of hydrogen and water vapor

[5] $H_2(g) + 2(I) \rightleftarrows 2H_{ads}$

[6] $HDO(v) + (II) \rightleftarrows HDO_{ads}$

[7] $H_{ads} + HDO_{ads} \rightleftarrows H_2O_{ads} + D_{ads}$

[8] $H_{ads} + D_{ads} \rightleftarrows HD(g) + 2(I)$

[9] $H_2O_{ads} \rightleftarrows H_2O(v) + (II)$

on different sites I and II. If reaction 7 is taken to be rate limiting, the following rate expression is obtained (1, 13):

[10] $$k = k_7 K_6 K_9 \theta_{H_2O} \theta_H$$

where small k's refer to rate constants and large K's to equilibrium constants. If the water is in equilibrium with the surface then K_6K_9 will simply be the isotope effect for the adsorption of HDO, and will be close to unity. Thus the final rate expression is

[11] $$k = k_7 \theta_{H_2O} \theta_H$$

As previously discussed, reaction 7 may consist of a number of steps (2). We have also shown that taking reaction 8 or 9 as rate limiting does not lead to the proper form for the rate expression (2). If k_7 may be expressed as a frequency factor and an exponential term, we obtain

[12] $$k = \theta_{H_2O} \theta_H A_7 e^{-E_7/RT}$$

It is easily shown that if a Freundlich isotherm is assumed (11, 12), eq. 3 can be written as

[13] $$k = k_0 \theta_{H_2O} \theta_H$$

Can. J. Chem. Downloaded from www.nrcresearchpress.com by 210.87.254.105 on 09/05/12
For personal use only.

Can. J. Chem. Downloaded from www.nrcresearchpress.com by 210.87.254.105 on 09/05/12
For personal use only.

TABLE 3. Derived kinetic parameters

	Powders				Graphon supported (2)			
Metal	C_{H_2O} (10^{-5} mol m^{-2})	C_H (10^{-5} mol m^{-2})	E_0 (kJ mol^{-1})	A_0' (m^2 mol^{-1} s^{-1})	C_{H_2O} (10^{-5} mol m^{-2})	C_H (10^{-5} mol m^{-2})	E_0 (kJ mol^{-1})	A_0' (m^2 mol^{-1} s^{-1})
Pd	0.78_4	1.89	61.8	6.29×10^{10}	1.56	1.89	80	2.05×10^{14}
Rh	0.94_0	1.98	61.5	1.76×10^{12}	0.15_6	1.98	89	1.88×10^{17}
Ru	0.89_3	1.51	60.3	3.62×10^{11}	0.94_0	0.604	103	3.19×10^{18}
Os	1.58	1.42	60.9	7.59×10^{12}	0.627	0.28	102	5.17×10^{18}
Ir	1.12	1.93	54.5	2.77×10^{11}	0.470	1.93	57	1.21×10^{13}
Pt	0.04_7	1.8_7	64.7	2.40×10^{15}	0.705	1.87	36	$6.5_6 \times 10^{10}$

Can. J. Chem. Downloaded from www.nrcresearchpress.com by 210.87.254.105 on 09/05/12
For personal use only.

Thus the experimental k_0 can be identified with k_7, and A_0 and E_0 with A_7 and E_7. Since θ is expressed as a fraction of a monolayer coverage, it is convenient to use θ together with the measured surface areas to calculate the surface concentrations of water and hydrogen atoms, C_{H_2O} and C_H, in mol m^{-2} and to insert these in eq. 12 to give eq. 14.

$$[14] \qquad k = C_H C_{H_2O} A_7' e^{-E_7/RT} = C_H C_{H_2O} A_0' e^{-E_0/RT}$$

The values obtained for C_H, C_{H_2O}, A_0', and E_0 are listed in Table 3.

A comparison of activity as a function of position of the metal in the periodic table is of some interest (Fig. 3*a*). For the third triad metals, osmium, iridium, and platinum, the specific activity shows a minimum at iridium. On the other hand, for the second triad metals, ruthenium, rhodium, and palladium, a maximum is noted at rhodium. This pattern is somewhat similar to that observed for the hydrogenation of cyclopropane (14) except for the position of iridium. All the rates fall within a spread of 3.5 orders of magnitude, indicating that the reaction is facile in the sense used by Boudart *et al.* (3, 15). For a really demanding reaction, such as the hydrogenolysis of ethane, rates vary by as much as eight orders of magnitude (14, 16). The relative insensitivity of the rates and activation energies to the metal suggests that the reaction may not require dissociative chemisorption of water, as previously discussed (2), and thus is in accord with our suggestions for a mechanism.

The E_0's are relatively constant at 61 ± 6 kJ mol^{-1}. This is a reasonable number for the true surface exchange (reaction 7) when compared to the gas phase equivalent for reaction 7 which has an activation energy of 85 kJ mol^{-1} (17). Over Graphon-supported metals, however, E_0 varied from 103 kJ mol^{-1} for ruthenium to 36 kJ mol^{-1} for platinum and a good correlation of E_0 was obtained with the thermionic work functions selected by Bouwman and Sachtler (18).

We previously suggested (1, 2) that the Graphon could lower E_0 by donating electrons to the platinum, giving rise to platinum–hydrogen bonds polarized in the form $Pt^{\delta+}$—$H^{\delta-}$ which should give a lower value of E_0. This general picture is supported by the present results which show that, in the absence of any support,

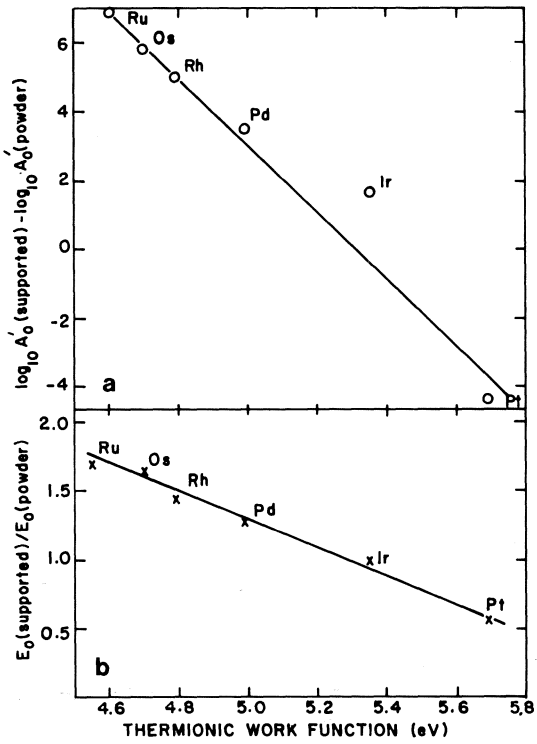

FIG. 4. Ratio of the chemical activation energies over powders to those of Graphon-supported catalysts (*b*) and ratio of frequency factors over powders to those over Graphon-supported catalysts (*a*) as a function of thermionic work function.

E_0 is relatively constant. However, E_0 over the powders is lower than the highest value obtained over the supported metals. In Fig. 4*b* we show the ratio of E_0 over supported metal divided by the E_0 over the powder as a function of the thermionic work functions selected by Bouwman and Sachtler (18). A good correlation is obtained, and it is noted that the ratio of activation energies is equal to unity at a work function of about 5.3 eV. This suggests that the work function of the Graphon is effectively about 5.3 eV, which is somewhat higher than the 4.6 eV previously assumed (1, 2). It appears that although E_0 is lowered relative to the powder for Graphon supported platinum, it is actually increased for Graphon supported ruthenium, osmium, rhodium, and palladium and is little affected for Graphon supported iridium. Thus the Graphon support may cause the metal–hydrogen bonds to be polarized in the form $M^{\delta+}$—$H^{\delta-}$ for platinum, relatively unchanged for iridium, and polarized in the form $M^{\delta-}$—$H^{\delta+}$ for palladium,

Can. J. Chem. Downloaded from www.nrcresearchpress.com by 210.87.254.105 on 09/05/12
For personal use only.

ruthenium, osmium, and rhodium. Evidence from the infrared spectra of hydrido-platinum complexes suggests that the former polarization gives a weaker metal–hydrogen bond, and that the latter polarization gives a stronger one (19). If a weaker metal–hydrogen bond leads to a lower activation energy for exchange, as seems probable, our interpretation is justified.

The model presented is also supported in a general way by the variation of frequency factor with the thermionic work function of the metal. Some caution should be noted here as the data listed in Table 3 for the Graphon-supported catalysts show that there is a linear relationship between A_0' and E_0. Such correlation can be observed as a result of small errors in measuring activation energies for rates that are similar (20). On the other hand, E_0's are relatively constant over the powders while the A_0's vary. Figure 4*a* shows the logarithm of the ratio of frequency factors over Graphon-supported and -unsupported catalysts as a function of the thermionic work function of the metal (18). The relative frequency factor for platinum is less than one. This suggests that there are relatively fewer active sites produced by electron transfer to the metal than were present in the absence of this effect. Similarly the relative frequency factor for ruthenium, osmium, and rhodium is much greater than unity suggesting that more of the surface participates in the reaction. The implication is that electrons are withdrawn from some of the more active sites leaving a much more uniform surface for reaction. It should also be noted that the ratio of frequency factors is unity for a work function of about 5.4 eV, suggesting that the effective work function of Graphon is about this value. The relative frequency factor for iridium seems anomalously high. This may be the result of experimental error since the E_0 for unsupported iridium is the lowest of the six E_0's measured.

For unsupported platinum, the reaction is almost exactly first order in water pressure and zero order in hydrogen pressure. Robertson (21, 22) has stated that, for catalytic reactions involving two reactants when the order with respect to any reactant is first, the rate of reaction of that reactant can be expressed in terms of the probability, P, that a reactant will react at a collision with the surface. The situation is similar to a first order reaction involving one reactant, and P is given by eq. 15.

$$P = Be^{-E_{app}/RT} \qquad [15]$$

The rate of production of HD is equal to the rate of disappearance of HDO. Now the rate coefficient is the initial rate of reaction 2 in the forward direction if pure HDO could be used as a reactant, so that we wish to calculate the collision rate for HDO with the surface under these hypothetical conditions. Under such conditions all the water would be HDO, so under our actual conditions we can calculate the collision rate using the total water pressure. Since P_{HDO} is small compared to P_{H_2O}, the total number of collisions of water molecules with the surface per m^2 s is $P_{H_2O}(2\pi m_{HDO}kT)^{-1/2}$. Thus the reaction probability P is 2.9×10^{-7} at 433.2 K for a water pressure of 23.7 kN m^{-2}, so B equals 2.6×10^{-5}. Such a value of B, being several orders of magnitude less than unity, suggests a rather immobile transition state (21). This is in accord with our postulate of a definite adsorption site (site II) for water adsorption. These sites appear to be present on the metal itself, and probably exist in addition to the water adsorption sites located at the edges of metal particles deposited on hydrophilic surfaces as postulated by Rolston and Goodale (13). It would be instructive to obtain a similar analysis for the other metals, supported and unsupported. However, the calculation is not possible, as the orders of reaction are not zero and one for these catalysts.

At the standard pressures used (78 kN/m^2) the orders with respect to hydrogen were zero for all the metal powders (Table 2). This implies that a full coverage of hydrogen is maintained. However, as mentioned above, the orders with respect to hydrogen approach 0.5 over osmium and iridium at lower pressures. Since $2b$ equals $(1 - \theta_H)$, hydrogen coverages approach zero under these conditions. Thus at low pressures a full hydrogen coverage is maintained with the second triad metals, but for the third triad metals hydrogen coverage increases with atomic number. Water coverages are all about 0.5 over the second triad metals, but decrease with increasing atomic number for the third triad metals.

In summary, the pattern of specific activities for hydrogen – water deuterium exchange is similar to that for cyclopropane hydrogenation (14). Thus the reaction is probably facile. Surface activation energies are constant for all six metals,

which confirms the conclusion that the reaction is facile. The previously noted (2) correlation of activation energies with metal work function for Graphon supported metals is thus peculiar to that system. We propose that the metal support interaction which is responsible for that effect is electron transfer, just as the promotion of various ammonia synthesis catalysts by alkali metals is thought to involve electron transfer from an alkali metal to a transition metal (23, 24).

We would like to thank E. E. Sexton of the Materials Science Branch, WNRE, for taking the electron micrographs. Useful discussions with G. G. Strathdee and H.-C. Chen are gratefully acknowledged.

1. N. H. SAGERT and R. M. L. POUTEAU. Can. J. Chem. **50**, 3686 (1972).
2. N. H. SAGERT and R. M. L. POUTEAU. Can. J. Chem. **51**, 4031 (1973).
3. M. BOUDART. Adv. Catal. Relat. Subj. **20**, 153 (1969).
4. M. BOUDART, A. W. ALDAG, L. D. PTAK, and J. E. BENSON. J. Catal. **11**, 35 (1968).
5. N. H. SAGERT and R. M. L. POUTEAU. Can. J. Chem. **49**, 3411 (1971).
6. T. BAIRD, Z. PAAL, and S. J. THOMSON. J. Chem. Soc. Faraday I, **69**, 50 (1973).
7. T. A. DORLING, C. J. BURLACE, and R. L. MOSS. J. Catal. **12**, 207 (1968).
8. J. H. ROLSTON. Private communication.
9. P. MARGINEANU and A. OLARIU. J. Catal. **8**, 359 (1967).
10. Y. L. SANDLER. J. Chem. Phys. **21**, 2243 (1953).
11. D. D. ELEY. Nature, **194**, 1076 (1962).
12. H. D. F. COLE. Ph.D. Thesis. The University of Texas, Austin, Texas. 1964.
13. J. H. ROLSTON and J. W. GOODALE. Can. J. Chem. **50**, 1900 (1972).
14. R. A. DALLA BETTA, J. A. CUSUMANO, and J. H. SINFELT. J. Catal. **19**, 343 (1970).
15. M. BOUDART, A. ALDAG, J. E. BENSON, N. A. DOUGHARTY, and C. G. HARKINS. J. Catal. **6**, 92 (1966).
16. J. H. SINFELT. Adv. Catal. Relat. Subj. **23**, 91 (1973).
17. N. E. BIBLER and R. F. FIRESTONE. J. Phys. Chem. **76**, 612 (1972); J. Phys. Chem. **76**, 4041 (1972).
18. R. BOUWMAN and W. M. H. SACHTLER. Surf. Sci. **24**, 140 (1971).
19. A. P. GINSBERG. *In* Transition metal chemistry, Vol. I. *Edited by* R. L. Carlin. Marcel Dekker, New York, 1965. p. 214.
20. P. G. ASHMORE. Catalysis and inhibition of chemical reactions. Butterworths, London. 1963. pp. 185–188.
21. A. J. B. ROBERTSON. Catalysis of gas reactions by metals. Logos Press, London. 1970. pp. 133–140.
22. D. J. FABIAN and A. J. B. ROBERTSON. Proc. R. Soc. Lond. Ser. A**237**, 1 (1956).
23. K. I. AIKA, H. HORI, and A. OZAKI. J. Catal. **27**, 424 (1972).
24. L. A. RUDNITSKY, M. G. BERENGARTEN, and A. M. ALEKSEJEV. J. Catal. **30**, 444 (1973).

Can. J. Chem. Downloaded from www.nrcresearchpress.com by 210.87.254.105 on 09/05/12
For personal use only.

Additivity Parameters for Organotin ^{13}C Chemical Shifts

D. E. AXELSON, S. A. KANDIL, AND C. E. HOLLOWAY

Department of Chemistry, York University, 4700 Keele Street, Downsview, Ontario M3J 1P3

Received March 18, 1974

D. E. AXELSON, S. A. KANDIL, and C. E. HOLLOWAY. Can. J. Chem. **52**, 2968 (1974).

Twenty-four four-coordinate organotin derivatives have been examined by ^{13}C n.m.r. and a set of 11 additive parameters computed to determine shielding effects of substituents. The chemical shift coefficients obtained are compared to their organic analogs.

D. E. AXELSON, S. A. KANDIL et C. E. HOLLOWAY. Can. J. Chem. **52**, 2968 (1974).

On a examiné, par r.m.n. du ^{13}C, 24 dérivés organiques de l'étain possédant une coordinance de quatre. On a obtenu un groupe de 11 paramètres additifs permettant d'évaluer les effets de blindage causés par les substitutions au sein de ces dérivés. On a comparé les coefficients ainsi déterminés avec leurs analogues organiques. [Traduit par le journal]

Can. J. Chem. Downloaded from www.nrcresearchpress.com by 210.87.254.105 on 09/05/12
For personal use only.

Introduction

Although a body of ^{13}C n.m.r. data is now available for organometallic derivatives, there are often insufficiently different related derivatives to warrant an analysis of the shifts for additivity relationships. In many cases the appropriate parameters available for organic compounds (1–7) can be applied quite successfully. In this study we have taken 90 ^{13}C chemical shifts from 24 tetrasubstituted organotin compounds and obtained additivity parameters to compare with those derived for analogous carbon systems. Modifications introduced by the presence of the tin atom are then observable as differences in the parameters obtained for the tin and the corresponding organic compounds.

The multiple regression analysis employed (8) searches for the best least-squares fit to the equation

$$\delta_C(k) = B + \sum_l A_l n_{kl}$$

where $\delta_{C(k)}$ is the chemical shift of the k'th carbon, B is a constant, n_{kl} is the number of like substituents in the l'th position relative to the k'th carbon, and A_l are additive chemical shift parameters assigned to the l'th substituent. Input data to the computer programme consists of all the observed shifts (dependent variables) and a population matrix representing the presence or absence of a particular substituent and the number of like substituents in a particular position. Positions are denoted by α, β, γ, etc. depending on whether the substituent is at the k'th carbon (α), or one atom removed (β), and so on. For substitutions at the β position or further, it is necessary to specify the intervening atoms. This has been done by denoting any non-carbon atoms in the parameter subscript, similar to the way in which coupling constants across hetero atoms are denoted. Thus β_{SnC} refers to the shift on substituting a carbon atom for a hydrogen at a position β to the k'th carbon (the one being calculated), when the intervening atom is tin. Similarly a β_{Ph} would imply substitution at the β position by a phenyl group where the intervening atom is carbon. Ambiguity can arise with γ_{SnX} parameters since the k'th carbon can be either α or β to the tin atom. We have ignored this problem in the results presented because the observed γ effects are all very small and the number of relevant cases are insufficient to establish a statistically significant difference. Dimerization, with formation of a tin–tin bond, introduces a β_{SnSn} term which describes a shift at all the carbons directly attached to each tin atom. Finally, a special parameter ξ has been designated to account for the shift of the neophyl tertiary carbon atom. Removal of this parameter, together with the neophyl tertiary carbon shift data, leaves the regression analysis virtually unchanged. The parameter thus has no direct relevance to the presence or absence of the tin atom but is effectively an upfield correction for the positional constraint associated with the neophyl group, for which there is other n.m.r. evidence (9).

The best fit with the least number of parameters was aimed for and this was accomplished with the 11 substituent effects discussed below.

TABLE 1. ^{13}C Substituent effects

Substituent effect[a]	Coefficient	No. of observations	Organoalkane coefficient[b]
α_C	11.4±0.2[c]	79	9.1
β_C	9.0±0.15	51	9.4
α_{Ph}	25.6±1.45	26	23 (estimate)
β_{Ph}	7.5±1.2	35	9.5
α_{Sn}	−5.2±0.65	39	—
β_{Sn}	4.0±1.6	31	—
γ_{Sn}	−0.3±0.15	21	(γ_C −2.5)
$\beta_{Sn\ Ph}$	1.1±0.05	39	—
β_{SnSn}	2.2±0.1	6	—
ξ(neophyl)	−22.7±4.7	15	(See text)
β_{SnI}	9.5±2.0	5	(β_I 11.3)[d]
Constant term	−3.2	90	−2.5
Correlation coefficient	0.995		
	Estimated parameters[e]		
β_{SnCl}	9.2±0.25[f]	7	β_{Cl} 10.5[d]
β_{SnBr}	9.1±0.8	11	β_{Br} 10.6[d]
$\beta_{Sn(OR)}$	5.4±0.6	6	β_O 10(approx)[d]
$\beta_{Sn(NR_2)}$	2.6±0.85	4	β_N 11(approx)[d]

[a]In p.p.m. from TMS, positive downfield.
[b]Reference 3.
[c]Standard deviation, see ref. 8.
[d]From data in ref. 7.
[e]For β_{SnC} and γ_{SnX} see text.
[f]Standard deviation.

Experimental

The organotin compounds were prepared by published methods (10) and contain phenyl, benzyl, neophyl, methyl, isopropyl, *t*-butyl, and *t*-amyl groups in various combinations. Halo tin derivatives were also included but because few in number the halogen substituent effects were deduced independently of the regression analysis. Chemical shift data were obtained in $CDCl_3$ solution at approximately 20% w/v concentration and relative to internal TMS, using a Varian NV-14-FT spectrometer. Some spectra obtained at higher concentrations and also in CCl_4 indicated that solvent effects are negligible. Comparison of our data with some recently published data (11) in which some identical compounds were examined almost in the pure state also confirms the relative unimportance of the solvent shift. The largest variations, about 0.5 p.p.m., occurred with halo tin derivatives such as trialkyltin chlorides.

Results and Discussion

The additivity parameters derived as above are shown in Table 1. In correlations of this type it must be assumed that the parameters are actually independent. This is not strictly true since deletion of the smaller parameters does cause changes in the values of the others. The choice of 11 parameters was made on the basis that inclusion of more less important effects gave no overall improvement in terms of statistical tests. In addition, the 11-parameter set gave values which are compatible with the corresponding shift parameters observed in organic compounds.

The constant term *B* may be considered largely as a correction from methane to TMS as reference and might therefore be expected to approach the methane ^{13}C chemical shift of −2.1 p.p.m. The value obtained is reasonably close and this was also taken into account in the selection of a parameter set. The large ξ parameter, although it has the air of an arbitrary correction factor, also has its correspondence with related branched organic derivatives. For example the quaternary carbon shifts in compounds such as 3-ethyl-3-methylpentane (34.8 p.p.m.) and in dineophyl itself (39.5 p.p.m.) can be reproduced using a similar parameter together with the coefficients for simple alkanes. It represents a summation of branching parameters which constitute an overall upfield shift. Such effects have been discussed at length in the literature. The development of a more extensive set of branching corrections, such as those of Lindeman and Adams (6), is not warranted since only the neophyl group appears to be affected in our series of compounds. The isobutyl group (see below, Table 3) also seems to

Can. J. Chem. Downloaded from www.nrcresearchpress.com by 210.87.254.105 on 09/05/12
For personal use only.

TABLE 2. ^{13}C shifts with low predictability[a]

Compound	$\delta_{(calcd)} - \delta_{(obs)}$ (p.p.m.)				
	Methyl or other	Neophyl		Benzyl	*tert*-Butyl
		CH_2	*tert*-C	CH_2	CH_3
(φNeoBzMe)Sn	3.2	−1.3	0.1	−1.9	—
(NeoBzMe)SnI	3.3	−1.7	−0.7	0.1	—
(φNeoBzPr^i)Sn	(0.0)[b]	0.0	0.3	1.2	—
(Bu^{t}NeoBzPr^i)Sn	(−0.4)[b]	1.3	1.4	−0.1	0.5
(φNeoBu^t)SnI	(−1.4)[c]	0.9	0.0	—	1.3
(φNeoBu^t)SnBr	(−1.0)[c]	0.1	−0.3	—	1.3
(φNeoBu^{t}Sn)$_2$	(−0.8)[c]	2.1	0.1	—	−0.5
(φ$_2$BzAm^t)Sn	(1.2)[d]	—	—	−0.1	—
(φBzBu^{t}Am^t)Sn[e]	(−2.5)[c]	—	—	0.2	−1.1

[a]Worse than ±1 p.p.m.
[b]Isopropyl secondary carbon.
[c]*tert*-Butyl tertiary carbon.
[d]*tert*-Pentyl tertiary carbon.
[e](φBzBu^t)Sn

	— C —	— $(CH_3)_2$ —	— CH_2 —	— CH_3	
Organotin coefficients	−0.3	−0.6	+4.0	+3.4	(with γ_C included)
Organoalkane coefficients	—	—	+1.7	+1.1	

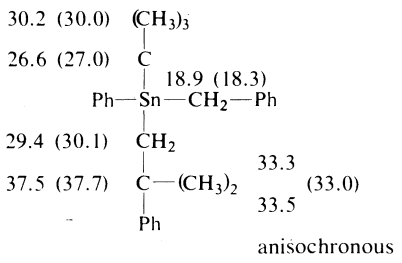

FIG. 1. Typical fit of ^{13}C data, observed (calculated).

require a smaller upfield correction at the tertiary carbon atom.

A typical fit is shown for *tert*-butylphenylneophylbenzyltin in Fig. 1, the predicted shifts being shown in parenthesis. Most of the shifts were reproducible to within ±1 p.p.m. and those that were not are shown in Table 2. In the case of the *tert*-pentyl derivatives (designated Am^t), the poorer predictions can be improved by using the coefficients for organo alkanes (Table 1). The carbon atom particularly affected is two atoms removed from the tin and it is reasonable to expect that it reverts to an essentially unperturbed organic situation. A similar argument should apply to the neophyl methyl groups. However, here the differences between organotin and organoalkane parameters cancel out (see α_C and β_{Ph}, Table 1). This raises an important problem with interpretation of additive effects such as these, since coefficients which cancel on a one to one basis are virtually impossible to detect. This is particularly relevant to the discussion of β and γ effects in our system.

Since the main value of parameters such as these is in their predictive ability, it is of interest to examine shifts which were not used in the analysis. Some recent data (11) on simpler organotin derivatives have been used to test our coefficients and the results are shown in Table 3. The relatively poor fit for ethyl and *n*-propyl derivatives in particular attests to the presence of other, possibly long range or conformational, effects which we have not been able to take into account. In the *n*-butyl examples a better fit is observed, in general, if organo alkane parameters are used for C_3 and C_4. This applies both to calculations of their own shifts and their contributions to the other shifts. The summation of halogen effects across tin appears to deviate from the simple additivity relationship to a much less extent than in corresponding halo alkanes (12, 13). We suggest that the larger size of the tin atom serves to mitigate interactions leading to pairwise additivity corrections and this also appears to play a role in the attenuation of β effects across tin in general. A brief assessment of the individual effects is now given.

α *Effects*

The negative value of the α_{Sn} effect is consistent with the electronegativity difference between tin and carbon. The dependence of α_X on the electronegativity of X has been indicated previously (14). A valence-bond calculation by Cheney and Grant (15), based on simple electron transfer arguments relating to electronegativity differences, gave an α_C effect of 9.9 p.p.m. com-

Can. J. Chem. Downloaded from www.nrcresearchpress.com by 210.87.254.105 on 09/05/12
For personal use only.

TABLE 3. Predictions of ^{13}C shifts

Compound	$\delta_{(calcd)} - \delta_{(obs)}$ (p.p.m.)			
	C_1	C_2	C_3	C_4
Me_4Sn	(1.2[a] or 0.7[b])	—	—	—
Me_3SnCl	(0.8[a] or 1.3[b])	—	—	—
Et_4Sn	3.0	1.1	—	—
Et_3SnCl[a]	2.9	2.3	—	—
Et_3SnCl_2[b]	2.7	3.1	—	—
Pr_4Sn[a]	−0.3	2.7(0.4)[c]	−2.3(−3.5)	—
Pr_3SnBr[a]	0.9	3.8(1.5)	−1.4(−2.6)	—
Pr_2SnBr_2[a]	0.3	3.5(1.2)	−0.4(−1.7)	—
Bu_4Sn[a]	0.4	3.0(1.2)	0.7(−0.6)	1.0(−0.1)
$(Bu_3Sn)_2$[a]	1.4	1.6(−0.2)	0.5(−0.8)	1.0(−0.1)
Bu_3SnBr[a]	1.4	4.1(2.3)	1.4(0.1)	1.1(0.0)
Bu_2SnCl_2[a]	0.9	5.6(3.8)	2.0(0.7)	1.2(0.1)
i-Bu_2SnCl_2[a]	0.9	9.1(4.5)	0.2(−0.4)	—

[a]Data from ref. 11.
[b]Our data.
[c]Bracketed data uses organic parameters for C_3 and C_4.

pared to the experimental value of 9.1 p.p.m. Thus charge density variations causing changes in the paramagnetic shielding term, σ_p, would appear to be the dominant mechanism of the α effect. It was therefore surprising to note a 25% increase in α_C for the organotin compounds (Table 1). Using the simplified expression (16)

$$\sigma_p = -(e^2h^2/2m^2c^2)\,(\Delta E)^{-1}\,\langle r^{-3}\rangle_{2p}\Sigma Q_{AB}$$

changes in ΔE (the average excitation energy) and ΣQ_{AB} (bond-order charge density terms) can occur but seem unlikely to be as large as 25%. The electronegativity difference of tin and carbon suggests that any changes in the average radius of the carbon 2p orbital, $\langle r\rangle_{2p}$, will lead to a decrease in σ_p if anything. It is not altogether impossible that the α_C effect includes another smaller parameter which has not been delineated, a possible candidate being the β_{SnC} effect. In such a case, however, one might expect a larger scatter for the coefficient concerned since the number of carbons β across tin to the k'th carbon does not vary systematically with its degree of substitution. Similar studies on related organometallics such as silicon and germanium derivatives would be of considerable interest.

β *and* γ *Effects*

Perhaps the most striking difference between tin and carbon is the general attenuation of β effects across tin. The apparent absence of a β effect through some hetero atoms has been noted earlier (17) and it was interesting to see the same unfold from this analysis. Using the ^{13}C data of Mitchell (11), an *a priori* estimation of a β_{SnC} effect can be obtained. Looking at the carbon α to the tin, a direct comparison of the trialkyltin hydride and tetraalkyltin shifts indicates possible β_{SnC} effects of 2.2 p.p.m, (methyl), 0.3 p.p.m. (ethyl), and 0.8 p.p.m. (*n*-butyl). Thus substitution of carbon for hydrogen on tin moves the other directly attached carbons downfield.

The big change in the apparent β_{SnC} from methyl to ethyl may indicate a comparable, but negative, γ_{SnC} effect operative in the ethyl and *n*-butyl derivatives. This cancellation of β and γ effects would not be detectable in our compounds since, except for methyl groups, each alkyl group would contribute both effects. This is rather different to the situation with the α_C plus β_{SnC} possibility mentioned above. Nevertheless, the β_{SnC} effect is obviously quite small, being around one-fifth of its corresponding β_C effect. The β_{SnPh} effect is similarly reduced in magnitude. Comparing the β_{SnSn} effect with the β_{Sn} effect also reveals the attenuating effect of the intervening tin atom but now only to a factor of one-half. Since steric interactions are believed to play a role in β effect (18), these observations are all consistent with the interposing of a larger atom between sterically interacting fragments. An *a priori* β_{SnSn} effect can also be obtained from Mitchell's study (11) by subtracting trialkyltin hydride shifts from the corresponding hexaalkylditin shifts. The values so obtained are 1.6 (methyl), 2.1 (ethyl), and 2.0 (*n*-butyl) which compare favorably with our value of 2.2. Dimerization thus leads to a downfield shift, *provided* that comparisons are made from the tin hydride. In all known cases, except the methyl,

Can. J. Chem. Downloaded from www.nrcresearchpress.com by 210.87.254.105 on 09/05/12
For personal use only.

TABLE 4. Average ^{13}C shifts for aryl groups

Group	δ ring (p.p.m.) C_1	C_2	C_3	C_4	No. of observations
Phenyl	139.9(5.1)[a]	136.5(2.0)	127.5(2.8)	128.0(2.2)	19
Benzyl	141.6(3.5)	126.9(3.1)	127.5(2.7)	123.2(3.1)	15
Neophyl	150.4(4.2)	124.8(5.5)	125.3(1.4)	124.8(1.9)	8
Benzene		128.7			

[a]Range from highest to lowest shift observed.

there is also a downfield ^{13}C shift on going from the tetraalkyltin to the trialkyltin dimer. The anomaly in the methyl case is almost certainly due to the concomitant loss of the β_{SnC} effect.

Halide β effects are only slightly attenuated across tin, relative to carbon, which may indicate the greater importance of an inductive route for this effect (15). Again, comparison between organometallic series would be of interest here.

The γ effects are equally elusive in these compounds, but those obtained are negative as expected. There is some evidence for a negative γ-halogen effect of 1–2 p.p.m. Thus the *tert*-butyl methyl shift is overestimated by 1.3 p.p.m. for both an iodotin and bromotin derivative. From the simple alkyl derivatives (11) a similar γ-halogen effect can be estimated for chloride and bromide but in triethyltin iodide the effects appear to be small and positive. Evidence for a δ effect of the same order of magnitude and negative can be inferred from the *n*-butyltin series.

In a recent paper (22) the γ effect of a trimethyltin moiety has been discussed in *exo* and *endo* norbornyl derivatives. However, the carbon atoms under consideration are γ to a tin atom and also δ to the three methyl groups on the tin. Distortions in the norbornyl skeleton, particularly in the *endo* derivative, can also introduce small changes in the α and β effects. Estimation of a γ effect is therefore difficult to justify under the circumstances. A more convincing demonstration of a γ effect across tin can be obtained from data in the same paper by comparison of the ^{13}C shifts of the common trimethyltin moiety. The shift of this group hovers around −9 to −11 in most alkyltin derivatives but moves upfield to −13 p.p.m. in the 2-adamantyl derivative. In the adamantyl group there are three carbon atoms γ to the methyl carbons on tin, and each has two C—H bonds in fixed orientations favorable for operation of a negative γ-effect. Thus the upfield shift can be explained by a γ effect of around −2 p.p.m. In general (23) γ effects are not additive or necessarily reciprocal. Thus the relevant adamantyl carbons (at 38.2 p.p.m. in the parent hydrocarbon) are shifted by the β_{Sn} effect to 42.2 p.p.m., which is where they are observed. However, if the enhanced α_C effect *vide supra* is taken into account the predicted shift becomes 44.5 p.p.m., which then requires a γ effect of about −2 p.p.m. to reproduce the observed shift.

The Aryl Carbons

No attempt was made to correlate the aryl carbon shifts, primarily because systematic shifts were not apparent for the derivatives studied. Table 4 lists average ^{13}C shifts for each type of aryl group with the range from highest to lowest noted in brackets. The neophyl and benzyl aryl carbon shifts are as expected from shifts in comparable organic compounds. The phenyl group shows a large shift from benzene at C_1, to which the tin is attached, but unlike its behavior in the alkyl derivatives, the tin deshields the attached carbon by about 10 p.p.m. A similar effect is noted with $C_6H_5Si(CH_3)_3$ (7) where the phenyl C_1 carbon is deshielded by some 13 p.p.m. Electron spin resonance studies of substituted benzene anions (19), show the groups $-Si(CH_3)_3$ and $-Ge(CH_3)_3$ are electron withdrawing, while $-C(CH_3)_3$ is electron releasing. This has been explained in terms of π electron drift onto the metalloid atom, and the same effect might be expected with $-SnR_3$, leading to a comparable ^{13}C shift at the phenyl C_1 carbon. Substituents with −I and +M effects, such as halides, also show large changes in directly bonded ^{13}C substituent effects from alkyl to aryl derivatives (7), but in the opposite sense to those noted above. Changes at the *para* carbon in all these cases are relatively small. Assignments were made from J_{SnC} measurements, using published data (24) as a guide.

Can. J. Chem. Downloaded from www.nrcresearchpress.com by 210.87.254.105 on 09/05/12
For personal use only.

To summarize, a consistent set of additive parameters can be derived for the ^{13}C shifts of a fairly wide range of organotin derivatives. The effect of the tin atom appears to be a damping out of long range effects operating through or across itself, and a general relaxing of steric interactions due to branching of the alkyl chain. An attempt to remove the ξ parameter by applying a correction for the diamagnetic contribution to the shifts was unsuccessful. This correction using the formula of Flygare and Goodisman (20) for neighbor diamagnetic contributions has been applied by Mason (21) to branched alkanes and alkyl halides, but does not seem to be effective in removing ambiguities in the present case.

In conclusion, organometallic derivatives represent perturbed organic moieties where ^{13}C chemical shift data may provide extra insight into the origins of the additivity effects which have proved so useful in ^{13}C spectroscopy.

One of us (D.E.A.) thanks the province of Ontario for a Graduate Fellowship. We also acknowledge support from the National Research Council of Canada and the loan of an NV-14 FT NMR from Varian Associates.

1. R. A. Friedal and H. L. Retcofsky. J. Am. Chem. Soc. **85**, 1300 (1963).
2. G. E. Savitsky and K. Namikawa. J. Phys. Chem. **68**, 1956 (1964).
3. D. M. Grant and E. G. Paul. J. Am. Chem. Soc. **86**, 2984 (1964).
4. E. R. Malinowski, T. Vladimiroff, and R. F. Tavares. J. Phys. Chem. **70**, 2046 (1966).
5. J. B. Grutzner, M. Jautelat, J. B. Dence, R. A. Smith, and J. D. Roberts. J. Am. Chem. Soc. **92**, 7107 (1970).
6. I. P. Lindeman and J. Q. Adams. Anal. Chem. **43**, 1245 (1971).
7. J. B. Stothers. Carbon-13 NMR spectroscopy. Academic Press, N.Y. 1972. Chapt. 3–7.
8. P. R. Bevington. Data reduction and error analysis for the physical sciences. McGraw-Hill, N.Y. 1969.
9. C. E. Holloway, S. A. Kandil, and I. M. Walker. J. Am. Chem. Soc. **94**, 4027 (1972).
10. S. A. Kandil and C. E. Holloway. J. Chem. Soc. Dalton, 1421 (1973).
11. T. N. Mitchell. J. Organomet. Chem. **59**, 189 (1973).
12. P. C. Lauterbur. Ann. N.Y. Acad. Sci. **70**, 841 (1958).
13. G. Miyazima, Y. Utsumi, and K. Takahashi. J. Phys. Chem. **73**, 1370 (1969).
14. P. Bucci. J. Am. Chem. Soc. **90**, 252 (1968).
15. B. V. Cheney and D. M. Grant. J. Am. Chem. Soc. **89**, 5319 (1967).
16. M. Karplus and J. A. Pople. J. Chem. Phys. **38**, 2803 (1963).
17. F. J. Weigert, M. Winokur, and J. D. Rcberts. J. Am. Chem. Soc. **90**, 1566 (1968).
18. D. M. Grant and B. V. Cheney. J. Am. Chem. Soc. **89**, 5315 (1967).
19. J. A. Bedford, J. R. Bolton, A. Carrington, and R. H. Prince. Trans. Faraday Soc. **59**, 53 (1963).
20. W. H. Flygare and J. Goodisman. J. Chem. Phys. **49**, 3122 (1968).
21. J. Mason. J. Chem. Soc. (A), 1038 (1971).
22. D. Doddrell, I. Burfitt, W. Kitching, M. Bullpitt, R. J. Mynott, J. L. Considine, H. G. Kuivila, and R. H. Sarma. J. Am. Chem. Soc. **96**, 1640 (1974).
23. E. Lippmaa, T. Pehk, and J. Paasivirta. Org. Magn. Res. **5**, 277 (1973).
24. D. Doddrell, M. L. Bullpit, C. J. Moore, C. W. Fong, W. Kitching, W. Adcock, and B. D. Gupta. Tetrahedron Lett. **9**, 665 (1973).

Can. J. Chem. Downloaded from www.nrcresearchpress.com by 210.87.254.105 on 09/05/12
For personal use only.

Erratum: ^{13}C Nuclear Magnetic Resonance Studies. 32. The ^{13}C Spectra of Several Norbornyl Derivatives

J. B. STOTHERS, C. T. TAN, AND K. C. TEO
Department of Chemistry, University of Western Ontario, London, Ontario N6A 3K7

Received June 3, 1974
(Ref.: Can. J. Chem. **51**, 2893 (1973))

In Table 4, page 2897, the chemical shifts of protons 1 and 4 should read 2.80 and 3.075 p.p.m., respectively.

Can. J. Chem. Downloaded from www.nrcresearchpress.com by 210.87.254.5 on 09/05/12
For personal use only.

Studies on Trifluoromethanesulfonic Acid. Part I. Trifluoromethanesulfonic Acid as a Weak Acid of the Sulfuric Acid Solvent System

DAVID GRAHAM RUSSELL AND JOHN BRIAN SENIOR[1]

Department of Chemistry and Chemical Engineering, University of Saskatchewan, Saskatoon, Saskatchewan S7N 0W0

Received January 31, 1974

DAVID GRAHAM RUSSELL and JOHN BRIAN SENIOR. Can. J. Chem. **52**, 2975 (1974).

Trifluoromethanesulfonic acid ionizes as a weak acid in anyhdrous sulfuric acid. Conductance measurements and conductimetric titrations with the base potassium hydrogensulfate, lead to a K_a value of 8×10^{-4} mol kg^{-1} at 25 °C. Trifluoromethanesulfonic acid is thus a weaker acid in this solvent than is fluorosulfuric acid and is similar in strength to chlorosulfuric acid.

DAVID GRAHAM RUSSELL et JOHN BRIAN SENIOR. Can. J. Chem. **52**, 2975 (1974).

L'acide trifluorométhanesulfonique s'ionise comme acide faible dans l'acide sulfurique anhydre. Des mesures de conductibilité et des titrages conductimétriques avec la base hydrogénosulfate de potassium donnent une valeur K_a de 8×10^{-4} mol kg^{-1} à 25 °C. L'acide trifluorométhanesulfonique est donc un acide plus faible dans ce solvant que n'est l'acide fluorosulfurique; sa force est comparable à celle de l'acide chlorosulfurique.

Introduction

Shortly after it was first prepared, the claim was made, based on measurements of the electrical conductivities and Hammett acidity functions of solutions in glacial acetic acid, that trifluoromethanesulfonic acid is the strongest simple monoprotic acid known (1). More recently Engelbrecht and Rode (2), on the basic of conductimetric studies in anhydrous acetic acid, have obtained the following order of acid strengths in that solvent: $CF_3SO_3H > HClO_4 > HBr > HI > FSO_3H > H_2SO_4 > HCl$. In sulfuric acid, on the other hand, the order of acid strengths $FSO_3H > ClSO_3H > HClO_4$ has been reported (3), the first two species behaving as weak acids, whereas perchloric acid, though described as a very weak acid, is effectively a nonelectrolyte. The behavior of trifluoromethanesulfonic acid in sulfuric acid has not been studied previously, although it has been suggested (4) that it should be intermediate in strength between fluorosulfuric and chlorosulfuric acids.

We are currently studying the behavior of trifluoromethanesulfonic acid as an ionizing solvent and it was thus of interest to compare its acid strength with that of other acids in the sulfuric acid system, in which the dissociation of a considerable number of simple and complex acids has been studied (3).

[1]To whom correspondence should be addressed.

Results and Discussion

We have measured the specific conductances at 25 °C of solutions of trifluoromethanesulfonic acid in anhydrous sulfuric acid. Experimental data are presented in Table 1. Trifluoromethanesulfonic acid behaves as a very weak electrolyte, with specific conductances at any given concentration very slightly less than the values reported for chlorosulfuric acid (3), although the differences are probably within experimental error. The solutions can be titrated to a conductivity minimum with the strong base potassium hydrogensulfate, showing that trifluoromethanesulfonic acid does indeed behave as a weak acid, ionizing according to eq. 1.

$$[1] \quad CF_3SO_3H + H_2SO_4 \rightleftharpoons H_3SO_4^+ + CF_3SO_3^-$$

It may be assumed, to a good approximation, that solutions of different acids in sulfuric acid having the same conductivity contain the same concentration of the $H_3SO_4^+$ ion (3). By comparison of the conductivities of solutions of trifluoromethanesulfonic acid with published data for disulfuric acid (5), whose dissociation behavior is known, the acid dissociation constant, $K_a = [H_3SO_4^+][CF_3SO_3^-]/[CF_3SO_3H]$ may be determined. Table 2 shows the results of such calculations. Columns 1 and 2 list the stoichiometric molalities $[H_2S_2O_7]^s$ and $[CF_3SO_3H]^s$ of solutions of the two acids having the same conductivities. Columns 3 and 4 give the cor-

Can. J. Chem. Downloaded from www.nrcresearchpress.com by 210.87.254.40 on 09/05/12
For personal use only.

Can. J. Chem. Downloaded from www.nrcresearchpress.com by 210.87.254.40 on 09/05/12
For personal use only.

TABLE 1. Conductivities of solutions of trifluoromethanesulfonic acid in sulfuric acid

Molality (mol kg^{-1})	$\kappa \times 10^{-2}$ ($ohm^{-1}cm^{-1}$)	Molality (mol kg^{-1})	$\kappa \times 10^{-2}$ ($ohm^{-1}cm^{-1}$)
0.0120	1.0455	0.1548	1.0881
0.0160	1.0470	0.1613	1.0889
0.0480	1.0523	0.2409	1.1153
0.0628	1.0582	0.3603	1.1589
0.0962	1.0688	0.3609	1.1534
0.0971	1.0684	0.3684	1.1515
0.1040	1.0713	0.6984	1.2442
0.1357	1.0816		

TABLE 2. Dissociation constant from conductivities

$[H_2S_2O_7]^s$ (mol kg^{-1})	$[CF_3SO_3H]^s$ (mol kg^{-1})	$[H_3SO_4^+]$ (mol kg^{-1})	$[CF_3SO_3^-]$ (mol kg^{-1})	$[CF_3SO_3H]$ (mol kg^{-1})	$K_a \times 10^4$ (mol kg^{-1})
0.020	0.206	0.0189	0.0116	0.194	11.3
0.030	0.362	0.0213	0.0159	0.346	9.8
0.040	0.534	0.0236	0.0195	0.515	9.0
0.050	0.727	0.0256	0.0229	0.704	8.3
					Ave. 9.6

responding concentrations of $H_3SO_4^+$ and $CF_3SO_3^-$, derived from Tables 4 and 2, respectively, of ref. 6. Column 5 shows the concentrations of undissociated CF_3SO_3H derived from the material balance relation $[CF_3SO_3H] = [CF_3SO_3H]^s - [CF_3SO_3^-]$. Column 6 gives the calculated values of K_a.

It has been shown (7) that in the titration of a weak acid HA with the strong base $MHSO_4$ in sulfuric acid, the conductivity minimum occurs at the molar ratio $r_{min} = n_{MHSO_4}/n_{HA}$ given by eq. 2, where K_a is the dissociation constant of HA and a is the initial stoichiometric molality of HA.

$$[2] \quad r_{min} = (1 + 0.013/K_a)^{-1} + 0.0007/a$$

The results of four conductimetric titrations of trifluoromethanesulfonic acid with potassium hydrogensulfate and the derived values of K_a are given in Table 3.

The values of K_a obtained by the two methods are in reasonably good agreement, considering that approximations are involved in both methods. There seems to be no compelling reason to prefer the results of one method over those of the other, and we therefore adopt the average value, $K_a = 8 \times 10^{-4}$ mol kg^{-1}, as the best value for this quantity. Trifluoromethanesulfonic acid is thus a significantly weaker acid in sulfuric acid than is fluorosulfuric acid ($K_a = 2.3 \times 10^{-3}$) and is very close in acid strength to chlorosulfuric acid ($K_a = 9 \times 10^{-4}$). This is consistent with the similar group electronegativities (8) of the CF_3 (3.35) and Cl (3.16) moieties, which would be expected to exert similar inductive effects on acid strengths, although trifluoromethanesulfonic acid might indeed have been expected to be slightly stronger than chlorosulfuric acid. Fluorosulfuric acid is appreciably stronger than either, consistent with the much greater electronegativity of F. Although the order of acid strengths $FSO_3H > CF_3SO_3H > HClO_4$ in sulfuric acid is very different from that found in acetic acid, the two series are not strictly comparable. In a solvent of low dielectric constant, such as acetic acid, ionization of an acid HX occurs by proton transfer to give ion-pairs, H_2OAc^+,X^-, which are dissociated only to a very slight extent to give free ions. The over-all acid dissociation constant K_a, as determined from conductimetric measurements, is given by eq. 3.

$$[3] \quad K_a = \frac{[H_2OAc^+][X^-]}{[HX] + [H_2OAc^+, X^-]} = \frac{K_I K_D}{1 + K_I}$$

where K_I is the ionization constant, $K_I = [H_2OAc^+, X^-]/[HX]$ and K_D is the ion-pair dissociation constant, $K_D = [H_2OAc^+][X^-]/$

TABLE 3. Dissociation constant from conductimetric titrations

a (mol kg^{-1})	r_{min}	$K_a \times 10^4$ (mol kg^{-1})
0.155	0.050	6.2
0.361	0.051	6.7
0.368	0.050	6.6
0.698	0.051	6.8
	Ave.	6.6

$[H_2OAc^+, X^-]$. Engelbrecht and Rode (2) make the assumption that for strong mineral acids in acetic acid, $K_I \gg 1$ so that $K_a = K_D$. In fact the only separately determined value in the literature is $K_I = 0.8$–1.0 for perchloric acid (9). It is likely that fluorosulfuric and trifluoromethanesulfonic acids would also have K_I values of this order of magnitude and would thus be "strong" acids in acetic acid, arbitrarily defined as those acids with $K_I \geqslant 1$ (9). For such acids, the value of K_a is mainly determined by K_D and is rather insensitive even to quite large changes in K_I. Thus K_a is not a good measure of acid strength in the sense of proton-donor ability toward the solvent, which would be properly measured by K_I. In sulfuric acid on the other hand, ion-pair formation is negligible and K_a gives a direct measure of the ability of an acid to donate a proton to the solvent.

While it is becoming increasingly obvious that no unique order of protonic acid strengths, independent of solvent, can be obtained (see, *e.g.*, the inversion in the acid strengths of FSO_3H and $H_2S_2O_7$ on going from sulfolane (10) to propylene carbonate (11) as solvent), it is probable that the order found in sulfuric acid will also be valid in other solvents of the same general type, *i.e.* strong, highly associated protonic oxo acids of high dielectric constant. At least in such solvents, trifluoromethanesulfonic acid is not the strongest simple acid known. Although no necessary relationship exists between the relative strengths of acids in dilute solution, and the acidities of the corresponding bulk acids, which are modified by intermolecular association through hydrogen bonding, it is of interest to mention our finding (to be published in detail in a later paper) that a number of weak organic bases are all ionized to a lesser extent in trifluoromethanesulfonic acid than in fluorosulfonic acid, showing that the latter is also the stronger acid in the bulk state.

Experimental

Conductance measurements were made at 25 ± 0.002 °C. Details of the equipment used have been given elsewhere (12). Trifluoromethanesulfonic acid (3M Co.) was distilled twice under an atmosphere of dry nitrogen (b.p. 162 °C). Conductimetric titrations were carried out as described (3).

This work was supported in part by an operating grant from the National Research Council of Canada.

1. T. GRAMSTAD. Tidsskr. Kjemi, Bergvesen Met. **19**, 62 (1959).
2. A. ENGELBRECHT and B. M. RODE. Monatsh. Chem. **103**, 1315 (1972).
3. J. BARR, R. J. GILLESPIE, and E. A. ROBINSON. Can. J. Chem. **39**, 1266 (1961).
4. E. A. ROBINSON. Can. J. Chem. **39**, 247 (1961).
5. S. J. BASS, R. H. FLOWERS, R. J. GILLESPIE, E. A. ROBINSON, and C. SOLOMONS. J. Chem. Soc. 4315 (1960).
6. R. H. FLOWERS, R. J. GILLESPIE, E. A. ROBINSON, and C. SOLOMONS. J. Chem. Soc. 4327 (1960).
7. R. H. FLOWERS, R. J. GILLESPIE, and E. A. ROBINSON. Can. J. Chem. **38**, 1363 (1960).
8. P. R. WELLS. Progr. Phys. Org. Chem. **6**, 111 (1968).
9. I. M. KOLTHOFF and S. BRUCKENSTEIN. J. Am. Chem. Soc. **78**, 1 (1956).
10. R. L. BENOIT, C. BUISSON, and G. CHOUX. Can. J. Chem. **48**, 2353 (1970).
11. M. L'HER and J. COURTOT-COUPEZ. J. Electroanal. Chem. **48**, 265 (1973).
12. J. B. SENIOR and J. L. GROVER. Can. J. Chem. **49**, 2688 (1971).

Can. J. Chem. Downloaded from www.nrcresearchpress.com by 210.87.254.40 on 09/05/12
For personal use only.

Photo-CIDNP Studies of 2-Butanone and 3-Pentanone in Solution

SHIV P. VAISH, ROBERT D. MCALPINE,[1] AND MICHAEL COCIVERA
Department of Chemistry, University of Guelph, Guelph, Ontario N1G 2W1
Received March 12, 1974

SHIV P. VAISH, ROBERT D. MCALPINE, and MICHAEL COCIVERA. Can. J. Chem. **52**, 2978 (1974).

The results of photolysis of 2-butanone and 3-pentanone as studied by chemically induced dynamic nuclear polarization (CIDNP) and electron spin resonance spectroscopy (e.s.r.) are reported. In aqueous solutions and *t*-butanol only the ethyl radical is detected by means of e.s.r., indicating α cleavage to be a major path involving excited states. This observation is further supported by the n.m.r. spectra which are obtained during irradiation of these ketones in D_2O and a mixture of CD_3CN–D_2O (1:1 by volume) containing carbon tetrachloride. Several compounds are detected with their protons spin polarized. A mechanism involving radical reactions is proposed which is consistent with the experimental results.

SHIV P. VAISH, ROBERT D. MCALPINE et MICHAEL COCIVERA. Can. J. Chem. **52**, 2978 (1974).

On rapporte les résultats de la photolyse de la butanone-2 et de la pentanone-3 tels qu'étudiés par polarisation nucléaire dynamique induite chimiquement (CIDNP) et par spectroscopie de résonance paramagnétique électronique (r.p.e.). En solution aqueuse et dans le *tert*-butanol on ne détecte par r.p.e. que des radicaux éthyles indiquant que le clivage α est une route importante pour les états excités. Cette observation est corroborée par des données de r.m.n. obtenues durant l'irradiation de ces cétones dans D_2O et dans un mélange de CD_3CN–D_2O (1:1 par volume) contenant du tétrachlorure de carbone. On détecte plusieurs composés ayant des protons avec des spins polarisés. On propose un mécanisme impliquant des réactions radicalaires; ce mécanisme est en accord avec les données expérimentales.

[Traduit par le journal]

Introduction

In our earlier paper (1) we reported the results of photolysis of acetone as studied by chemically induced dynamic nuclear polarization (CIDNP). In this case, α cleavage and intermolecular hydrogen abstraction involving the triplet state of acetone were the main photochemical reactions responsible for the CIDNP effects. The present study is an extension of our earlier work to other ketones, namely 2-butanone and 3-pentanone, to ascertain if α cleavage and hydrogen abstraction steps occur for these systems also. In this paper, we report CIDNP evidence which supports the occurrence of the α-cleavage step. We obtained no evidence in support of hydrogen-abstraction step.

Experimental

Nuclear Magnetic Resonance

The proton n.m.r. spectra at 100 MHz were obtained at 15 °C using a Varian HA-100-15 spectrometer, which was modified to operate on a time-sharing mode. This enabled us to use a quartz probe built in our laboratory (2) and take the n.m.r. spectrum while the sample was being irradiated. The radiation source was a 1000 W Hanovia mercury–xenon arc lamp. Filtering the light to transmit radiation having wavelengths greater than 310 nm reduced the intensity of polarization without altering any details.

Electron Spin Resonance

The e.s.r. spectra were obtained at 9.6 GHz (X band) using Varian E-12 and Bruker BE-414 spectrometers. These spectra were obtained during irradiation with the full spectrum of a 1000 W mercury–xenon lamp at room temperature. The solutions were flowed at a rate of about 1 ml per s.

Chemicals

2-Butanone (Aldrich) and 3-pentanone (Aldrich) were fractionally distilled and the purity was checked using g.l.c. and n.m.r. Deuterioacetonitrile and D_2O were obtained from Stohler Isotope Chemicals, and carbon tetrachloride (spectroquality) from Matheson, Coleman and Bell. These solvents were used as received. Other solvents used were also reagent grade.

Results

Electron Spin Resonance

The e.s.r. spectrum obtained during irradiation of 8% 2-butanone in water is given in Fig. 1. The spectrum is assigned to the ethyl radical on the basis that the hyperfine splittings 27.0 G for CH_3 and 22.1 G for CH_2 protons are similar to those reported in the literature (A_β = 26.9 G and A_α = 22.4 G) at −180 °C (3).

When *t*-butanol was used as a solvent, no new

[1]Present address: Atomic Energy of Canada Ltd., Chalk River, Ontario.

Can. J. Chem. Downloaded from www.nrcresearchpress.com by 210.87.254.105 on 09/05/12
For personal use only.

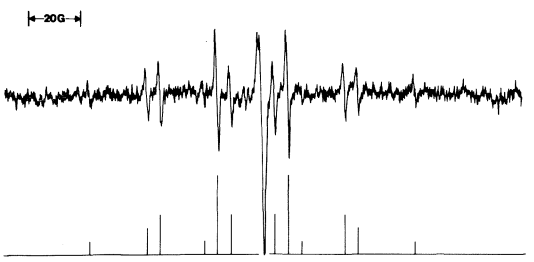

FIG. 1. Electron spin resonance of 8% 2-butanone in water at room temperature obtained during irradiation with the full spectrum of a mercury–xenon lamp. The large line in the center is a cell signal. The theoretical reconstruction is given below the experimental spectrum as a stick figure.

lines were observed, however the intensity of ethyl radical spectrum was improved. When 3-pentanone was photolyzed in the cavity of the e.s.r. spectrometer in *t*-butanol, only the spectrum of ethyl radical was again observed although the intensity of the spectrum was stronger than when 2-butanone was used. Ethyl radicals can be generated by the following reactions:

$$C_2H_5COCH_3 \xrightarrow{h\nu} C_2H_5^{\cdot} + \cdot COCH_3$$

$$C_2H_5COC_2H_5 \xrightarrow{h\nu} C_2H_5^{\cdot} + \cdot COC_2H_5$$

Since we were not able to observe any signal corresponding to $CH_3CO\cdot$ or $C_2H_5CO\cdot$ radicals, these radicals are probably too short lived to be detected under our experimental conditions. Furthermore, the observation of only the ethyl radical (resulting from α cleavage) suggests that the hydrogen abstraction involving excited triplet or singlet states may be less important for these ketones. The n.m.r. results are consistent with this observation.

Nuclear Magnetic Resonance

The n.m.r. spectra obtained during irradiation of an air-saturated solution of 0.11 *M* 2-butanone and 0.10 *M* 3-pentanone in D_2O are shown in Fig. 2. These spectra were obtained using the full spectrum of a 1000 W mercury–xenon arc lamp. When irradiation is stopped after exposing the samples for a few minutes, the spectrum of each ketone is observed without enhancement and all other signals disappear. The temperature in the n.m.r. probe was maintained at 15 °C although the irradiated portion of sample was hotter.

As is evident in these spectra, a number of compounds are formed during irradiation. The

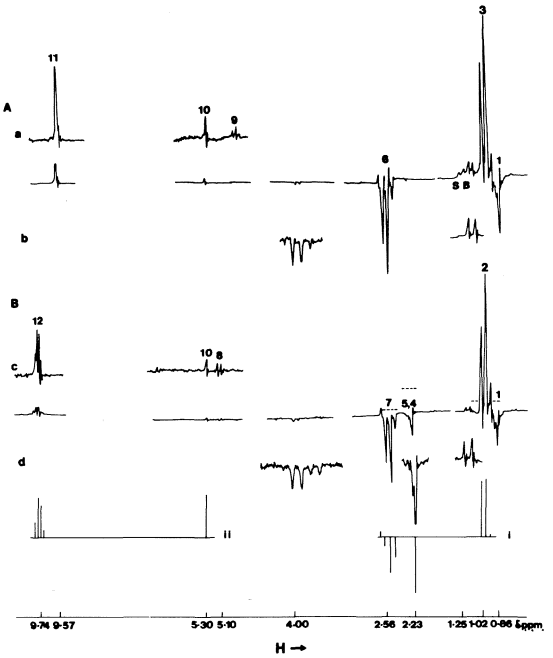

FIG. 2. Proton nuclear magnetic resonance spectra obtained at 100 MHz for an air-saturated solution during irradiation of: (*A*) 0.10 *M* 3-pentanone in D_2O at 1000 Hz sweep-width. Spectrum *a* at increased sensitivity and at 1000 Hz sweep-width: spectrum *b* at 500 Hz sweep-width and at different higher gains. (*B*) 0.11 *M* 2-butanone in D_2O at 1000 Hz sweep-width. Spectrum *c* at increased sensitivity and at 1000 Hz sweep-width; spectrum *d* at 500 Hz sweep-width and at different higher gains. Dashed lines indicate the intensity of larger signal of the multiplet after irradiation. The stick diagram refers to calculated relative intensities on the basis of radical pair $[CH_3CH_2\cdot \cdot COCH_3]^{T,F}$ where *i* denotes recombination and *ii* denotes disproportionation. Numbers on the top of the signals refer to assignments given in Table 1.

spectrum 2*A* was obtained for 3-pentanone and the spectrum 2*B* for 2-butanone. As is clear from the figure, both compounds show very similar spectra and exhibit either enhanced absorption or emission indicating non-Boltzmann nuclear spin polarization. Assignment of these lines is given in Table 1. Compounds were identified either by adding them to the solution or by their literature chemical shifts. The lines at 1.25 and at 4.00 p.p.m. in Fig. 2 were not identified. The calculated spectra based on the theory given elsewhere (4) are also shown as stick diagrams for 2-butanone in Fig. 2.

In the presence of nitric oxide no polarizations were observed. The rates for triplet quenching of ketones by nitric oxide in the gas phase are estimated to be diffusion controlled (5). Additional

Can. J. Chem. Downloaded from www.nrcresearchpress.com by 210.87.254.105 on 09/05/12
For personal use only.

TABLE 1. Assignment of n.m.r. lines observed during irradiation of 2-butanone and 3-pentanone in D_2O or CD_3CN–D_2O (1:1 by volume)

Resonance	Position [a]		CIDNP[b]		Compound[d]
	2-Butanone	3-Pentanone		CCl_4[c]	
1	0.86	0.86	E	—	CH_3CH_3
2	1.02		A(A/E)	A(A/E)	$CH_3CH_2COCH_3$
3		1.02	A(A/E)	A(A/E)	$CH_3CH_2COCH_2CH_3$
4	2.23		E	E	$CH_3CH_2COCH_3$
5	2.28		E	—	CH_3CHO
6		2.52	E(A/E)	E(A/E)	$CH_3CH_2COCH_2CH_3$
7	2.56		E(A/E)	E(A/E)	$CH_3COCH_2CH_3$
8	5.10		A	—	$CH_3CH(OH)_2$(hydrate)
9		4.96	A	—	$CH_3CH_2CH(OH)_2$(hydrate)
10	5.30	5.36	A	E	CH_2CH_2
11		9.57	A	A[e]	CH_3CH_2CHO
12	9.74		A	A[e]	CH_3CHO
13	1.30	1.31		E	$CH_3CH_2CCl_3$
14	1.50	1.50		E(E/A)	CH_3CH_2Cl
15	2.06			A	CH_3COOH
16	2.80	2.82		A	$CH_3CH_2CCl_3$
17	3.72	3.66		E(E/A)	CH_3CH_2Cl
18	7.64	7.67		E	$CHCl_3$

[a]In p.p.m. relative to TMS as external standard.
[b]Absorption A, emission E, and multiplet A/E and E/A with A and E, respectively, at lower field.
[c]In CD_3CN–D_2O mixture.
[d]Position refers to italicized groups.
[e]Very weak.

information about the photoreactions of these ketones was obtained by trapping experiments using carbon tetrachloride which acts as a free-radical scavenger. Since carbon tetrachloride does not dissolve appreciably in D_2O, a mixture of equal volumes of deuterioacetonitrile and D_2O was used as a solvent. The spectra in this solvent, in the presence of 0.07 *M* carbon tetrachloride, are given in Fig. 3. The spectrum without CCl_4 differs only slightly from that obtained in pure D_2O. The difference is that the hydrates of the corresponding aldehydes were not observed in the mixed solvent, probably due to lower intensities. Also some more lines appeared at 0.9 and 1.3 p.p.m. which are presently not conclusively identified although their chemical shifts fall in the same region as those for butane. As is evident from Fig. 3, new polarized products are observed. Both 2-butanone and 3-pentanone again show very similar spectra. When irradiation is stopped after exposing the samples for a few minutes, the spectrum of each ketone is observed without enhancement, and all other signals disappear. The assignments of the resonances are listed in Table 1. Except for 1,1,1-trichloropropane, all assignments were confirmed by adding the compound to the solution.

As indicated in Table 1, acetic acid is formed when CCl_4 is present. We suggest that it results from the hydrolysis of acetyl chloride which is a radical trapping product during photolysis of 2-butanone. One would expect to observe propionic acid in the same way from the hydrolysis of C_2H_5COCl formed by the trapping of propionyl radical generated during photolysis of 3-pentanone in presence of CCl_4. However we were not able to observe any lines due to the acid or the acid chloride. 1,1,1-Trichloropropane ($CH_3CH_2CCl_3$) (triplet at 1.3 p.p.m. and quartet at 2.8 p.p.m.) could not be obtained commercially and we were not able to obtain literature values of the chemical shifts for this compound. However, we report its presence on the grounds discussed later. The signals (absorption) at 3.97 p.p.m. and the singlet (emission) at 6.6 p.p.m. could not be identified. The calculated spectra are given as stick diagrams in the case of the 2-butanone system but not for the 3-pentanone system because the results are very similar for both cases.

Discussion

The spectra obtained in Fig. 2 can be explained according to following scheme in terms of reactions involving radical-pairs. The photoreactions in the case of 3-pentanone could be explained in

Can. J. Chem. Downloaded from www.nrcresearchpress.com by 210.87.254.105 on 09/05/12
For personal use only.

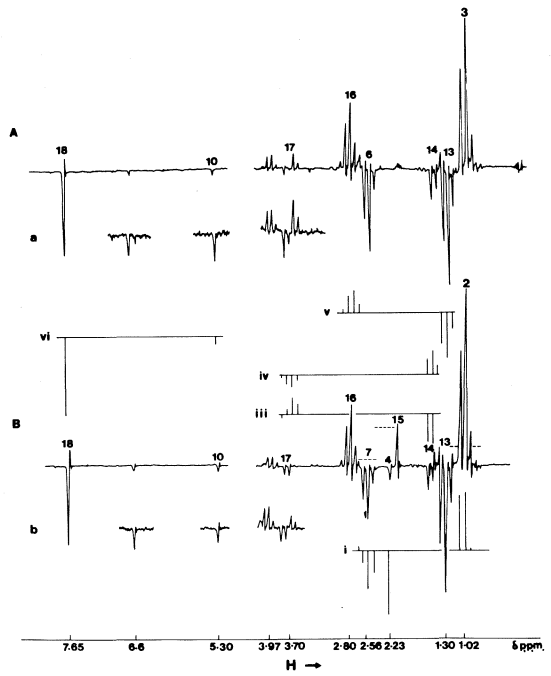

FIG. 3. Proton nuclear magnetic resonance spectra obtained at 100 MHz for an air-saturated solution during irradiation of: (*A*) 0.1 *M* 3-pentanone in CD_3CN–D_2O (1:1 by volume) solutions in presence of 0.07 *M* CCl_4. Spectrum *a* was taken at higher gain. Sweep-width 1000 Hz. (*B*) 0.11 *M* 2-butanone in CD_3CN–D_2O (1:1 by volume) solutions in the presence of 0.07 *M* CCl_4. Spectrum *b* was taken at higher gain. Dashed lines indicate the larger signal of the multiplet after the irradiation is stopped. Stick diagrams refer to calculated relative intensities on the basis of radical pairs *i* to *vi*, where *i* denotes $[CH_3CO\cdot\cdot CH_2CH_3]^T$, recombination; *iii* $[CH_3CO\cdot\cdot CH_2CH_3]^T$, trapped; *iv* $[CH_3CH_2\cdot\cdot CCl_3]^F$, trapped; *v* $[CH_3CH_2\cdot\cdot CCl_3]^F$, recombination; *vi* $[CH_3CH_2\cdot\cdot CCl_3]^F$, disproportionation. Figures 3*A* and 3*B* were recorded at about twice the gain used for Figs. 2*A* and 2*B*.

a similar fashion. In this scheme, the brackets indicate a radical pair and the superscripts indicate that the radical pair has a triplet T and/or free-radical F, precursor. The signs beneath the products indicate the calculated signs for the n.m.r. signals for the proton, (+) for enhanced adsorption, and (−) for emission.

According to Scheme 1, a molecule of 2-butanone is excited into a singlet state, which goes to a triplet state via intersystem crossing. The radical pair formed in eq. 2 via the triplet state of the ketone could have three pathways. It could recombine to give the parent molecule in the ground state (eq. 3) or it could disproportionate to give acetaldehyde and ethylene (eq. 4). For the third path, the radical pair could dissociate and the free radicals could undergo other reactions such as eq. 6 (discussed below) or reassociate. Comparison of the observed signs in Table 1 with the calculated signs for the products indicates that this scheme is consistent with our experimental results. The calculations were based on a model in which non-Boltzmann nuclear spin polarization occurs as a result of reaction via a radical pair (6). Details of the theory given in earlier publications (4), will not be repeated here.

For calculations, literature values for the isotropic *g* factors and electron–nuclear hyperfine coupling constants were used (3), and positive values were used for the indirect nulcear–nuclear coupling constants for vicinal protons of the products. Since some of the parameters used in the calculation are somewhat arbitrary, only the relative values of intensities are meaningful. Consequently for a compound exhibiting only one n.m.r. line, the calculated relative intensities have not been illustrated, unless a comparison with another line is possible. As a result in Fig. 2, the calculated relative intensities are illustrated only for acetaldehyde, ethylene, and 2-butanone. When comparing the calculated and experimental spectra for 2-butanone, one must take into account the fact that the experimental spectrum is a superposition of spectra due to some molecules having Boltzmann polarization and others having non-Boltzmann polarization. The intensity due to Boltzmann polarization during irradiation could be approximated as equal to the intensity of the spectrum after irradiation (indicated by dashed lines in Fig. 2). When this intensity is subtracted from the spectrum obtained during irradiation, agreement between calculated and experimental intensities is obtained for the 2-butanone molecule.

According to eq. 4, acetaldehyde and ethylene are formed via a disproportionation step involving $[CH_3CO\cdot\cdot CH_2CH_3]^{T,F}$. While the calculation based on this radical pair gives the proper signs for the polarization of acetaldehyde carbonyl hydrogen *vs.* the ethylene hydrogen, the relative intensities do not agree as well as might be expected. That is, relative to the acetaldehyde carbonyl hydrogen, the experimental value for ethylene appears smaller than the calculated value. This lower than expected value for the ethylene intensity might be explained by the fact

Can. J. Chem. Downloaded from www.nrcresearchpress.com by 210.87.254.105 on 09/05/12
For personal use only.

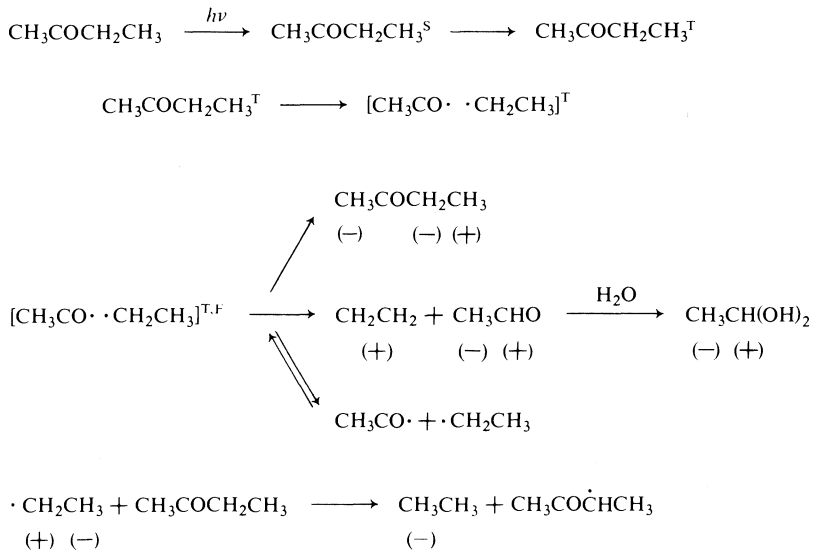

SCHEME 1

that we observed the evolution of gas from the n.m.r. sample during irradiation. On the other hand, we cannot rule out the possibility that the difference between calculated and observed relative intensity may be due in part to different relaxation times and/or some additional contribution to the polarization from other steps. The possibility of an additional step also is suggested by radical trapping experiments discussed below.

The polarization observed for ethane may be accounted for by eqs. 5 and 6. According to this mechanism, dissociation of $[CH_3CO\cdot\ \cdot CH_2CH_3]^{T,F}$ results in free radicals whose nuclei are initially polarized. If these radicals react to form diamagnetic products at rates which are competitive with nuclear spin – lattice relaxation rates, the polarization is carried over into the products. Thus, we suggest that the rate for eq. 6 is competitive with relaxation rates. Other steps are possible but either do not account for the polarization or are not consistent with other facts. For example, disproportionation in $[CH_3CO\cdot\ \cdot CH_2CH_3]^{T,F}$ results in positive rather than negative polarization for ethane and would require the formation of ketone (or acetic acid, its hydrolysis product) which is not observed. Disproportionation in $[CH_3CO\cdot\ \cdot CH_2CH_3]^S$ gives the correct sign for ethane polarization but is not consistent with the CCl_4 trapping results discussed below. Thus we conclude that eqs. 5 and 6 provide the main contribution to the ethane polarization.

n-Butane formed by a coupling reaction via $[C_2H_5\cdot\ C_2H_5]^F$ will have net zero polarization but would exhibit a multiplet effect. In CD_3CN–D_2O there are some lines where butane spectrum is expected; however its presence is not conclusively proved.

In the case of 2-butanone in D_2O, spin-polarized acetaldehyde hydrate (methine proton quartet at 5.1 p.p.m.) is observed and similarly for 3-pentanone in D_2O, spin-polarized propionaldehyde hydrate (methine proton, triplet at 4.96 p.p.m.) is observed. Since the rates of hydration of these aldehydes are known to be competitive (7, 8) with the spin–lattice relaxation rates, the polarization for the methine hydrogen of each hydrate may be explained by a process in which the polarization of the carbonyl hydrogen in the aldehyde (eq. 4) is carried into the hydrate as a result of the hydration process.

In the presence of carbon tetrachloride, the following scheme is suggested when 2-butanone is photolyzed in CD_3CN–D_2O solutions. A similar mechanism should hold for 3-pentanone. According to this scheme in eq. 2, 2-butanone forms a radical pair via its excited triplet state. The radical pair could either combine as in eq. 3 or could dissociate (eq. 5). After dissociation, acetyl and ethyl radicals cannot recombine be-

Can. J. Chem. Downloaded from www.nrcresearchpress.com by 210.87.254.105 on 09/05/12
For personal use only.

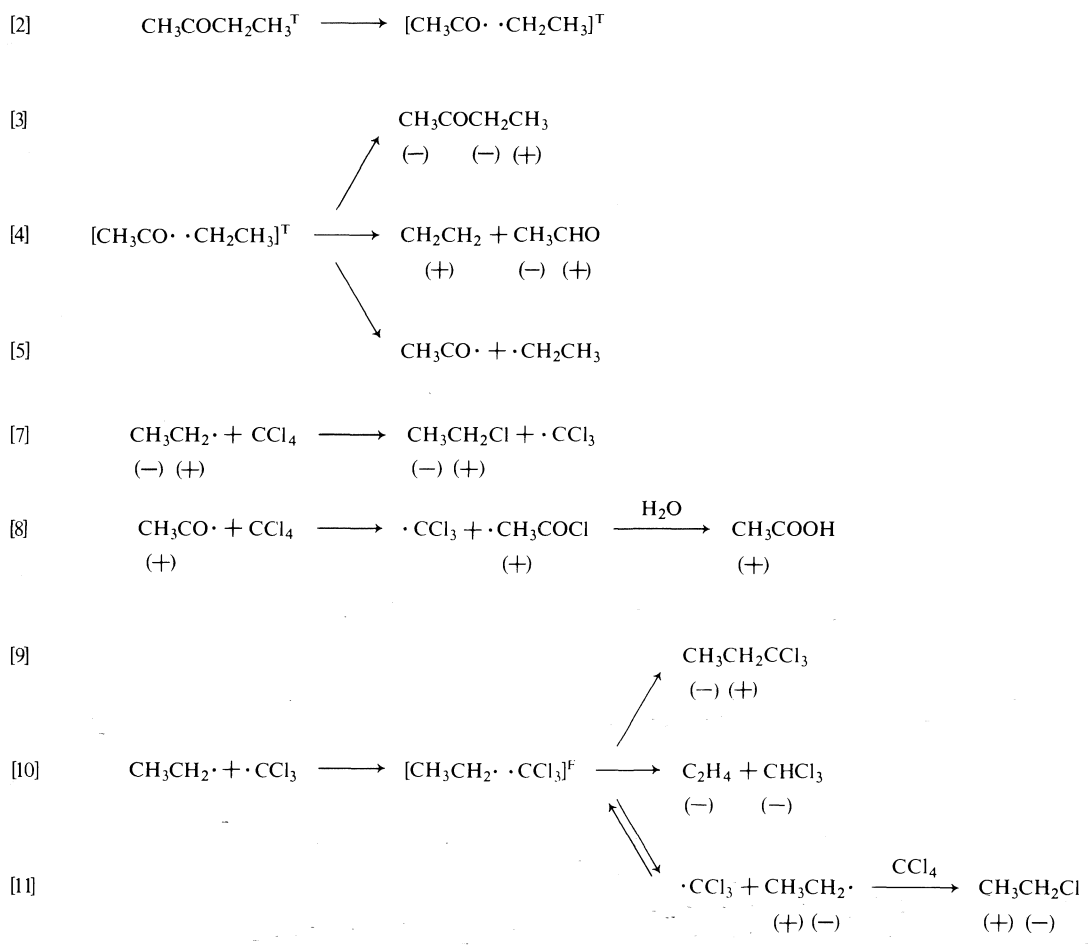

SCHEME 2

cause carbon tetrachloride traps these radicals to give products: acetyl chloride (eq. 8), ethyl chloride (eq. 7), and CCl_3 radical. The acetyl chloride signal is not observed because it is rapidly hydrolyzed in aqueous solution to spin-polarized acetic acid whose enhanced absorption signal is observed. For 3-pentanone, neither spin-polarized propionyl chloride nor propionic acid is observed, indicating either that nuclear spin-polarized propionyl radical is not trapped by 0.07 *M* CCl_4 or that the polarization is weak because the hyperfine coupling constant for the CH_2 proton of this radical is small (9). According to eqs. 9, 10, and 11, $[CH_3\dot{C}H_2\ \dot{C}Cl_3]^F$ can combine to form $CH_3CH_2CCl_3$, disproportionate to form ethylene and $CHCl_3$, and dissociate with the subsequent formation of ethyl chloride by a trapping step with CCl_4. Except for ethyl chloride, the agreement between calculated and observed signs of polarization can be seen by comparing Table 1 with the signs given in Scheme 2. In addition, this scheme is consistent with the fact that the signal due to ethane is not observed when CCl_4 is present (Fig. 3). When carbon tetrachloride is added for radical trapping experiments, the polarization in the parent compound is reduced. The reduction is evident by comparing Fig. 2 with Fig. 3 which was obtained at twice the gain used in Fig. 2. This reduction cannot be considered to be conclusive evidence for polarization due to $[CH_3\dot{C}O\ \dot{C}H_2\text{-}CH_3]^F$ since CCl_4 might also be acting as a triplet quencher. For the aldehydes, the polarization for the carbonyl hydrogen is reduced much more than that for the parent ketone. Although this reduction indicates that the aldehyde polarization results from F as well as T pairs, it seems unlikely that the F type polarization comes

Can. J. Chem. Downloaded from www.nrcresearchpress.com by 210.87.254.105 on 09/05/12
For personal use only.

Can. J. Chem. Downloaded from www.nrcresearchpress.com by 210.87.254.105 on 09/05/12
For personal use only.

solely from $[CH_3\dot{C}O\ \dot{C}H_2CH_3]^F$ since the reduction is not the same for both the aldehyde and the ketone. Consequently an additional free radical reaction is probably responsible for at least part of the polarization observed for the aldehydes in the absence of carbon tetrachloride. This additional path may also be indicated by the discrepancy between calculated and observed polarizations for acetaldehyde and ethylene discussed above. The nature of this path is not obvious to us. It is difficult to use this evidence as an indication of a hydrogen abstraction mechanism as observed for acetone (1) because additional products would be expected and we have not detected them. If this process occurs, it does not appear to make a major contribution to the observed polarization.

For comparison, the calculated relative intensities are shown in Fig. 3 to illustrate the agreement between calculated and observed values. The only exception is ethyl chloride whose observed relative intensities do not conform to the calculated values based on either eq. 7 or eq. 11 (indicated in Fig. 3 as *iii* and *iv*, respectively). However, good agreement is obtained for both the CH_3 and CH_2 resonances if the calculated values based on eq. 7 are added to those based on eq. 11. For this reason we suggest that eqs. 7 and 11 make comparable contributions to the polarization observed for ethyl chloride. Alternative mechanisms such as contributions from singlet and triplet pairs do not give the proper relative intensities.

The assignment of the quartet at 2.80 p.p.m. and the triplet at 1.3 p.p.m. to 1,1,1-trichloropropane cannot be considered conclusive since we have not added the compound to the solution and have been unable to find a report of its spectrum. We base this assignment on indirect evidence. For example, compounds such as ethyl chloride, propionyl chloride, and propionic acid have been ruled out because their chemical shifts differ substantially from 2.80 and 1.3 p.p.m. Other compounds have been ruled out on the basis of multiplicity in addition to chemical shift. Second, the chemical shifts for the protons of trichloroisobutane are CH_3, 1.30 p.p.m. and CH, 2.73 p.p.m. (10). and the chemical shift for 1,1,1-trichloroethane is 2.80 p.p.m. (1). Finally, as can be seen in Table 1 and in Fig. 3, the identical spectrum (including relative intensities) is observed when 3-pentanone replaces 2-butanone. Since α cleavage of both compounds can provide ethyl radicals, 1,1,1-trichloropropane would be expected in both cases. The calculated relative intensities based on $[CH_3CH_2\cdot\ \cdot CCl_3]^F$ are given in Fig. 3 (denoted *v*) to illustrate the agreement with observed values.

At CCl_4 concentrations which are substantially higher than 0.07 *M*, CIDNP evidence has been obtained (10, 11) for the reaction of excited singlet state ketones with CCl_4. Furthermore, for more highly branched di-*t*-butyl ketone, quenching data indicate reaction occurs via excited singlet and triplet states (12). In the case of 2-butanone and 3-pentanone, the maximum concentration attainable for CCl_4 in the mixed solvent is not large enough to provide the opportunity to detect the singlet mechanism. At any rate, our results do not preclude the possibility that both the singlet and triplet mechanism occur. Our results indicate only that Schemes 1 and 2 provide the main contribution to the CIDNP effects observed for 2-butanone and 3-pentanone in D_2O and D_2O–CD_3CN.

We are grateful to Prof. Hanns Fischer for providing a preprint of his work and a copy of H. Paul's Thesis. This work has been supported in part by the donors of the Petroleum Research Fund and by the National Research Council of Canada.

1. Shiv P. Vaish, Robert D. McAlpine, and Michael Cocivera. J. Am. Chem. Soc. **96**, 1683 (1974).
2. M. Cocivera, M. Tomkiewicz, and A. Groen. J. Am. Chem. Soc. **94**, 6598 (1972).
3. (*a*) R. Fessenden and R. Schuler. J. Chem. Phys. **39**, 2147 (1963); (*b*) H. Fischer. J. Phys. Chem. **73**, 3834 (1969).
4. M. Tomkiewicz, A. Groen, and M. Cocivera. J. Chem. Phys. **56**, 5850 (1972).
5. J. M. Edwards and M. I. Christie. Chem. Commun. 789 (1967).
6. R. Lawler. Acc. Chem. Res. **5**, 25 (1972).
7. R. P. Bell, M. H. Rand, and K. M. A. Wynne-Jones. Trans. Faraday Soc. **52**, 1093 (1956).
8. L. C. Gruen and P. T. McTigue. J. Chem. Soc. 5217 (1963).
9. H. Paul. Ph.D. Dissertation. University of Zurich, Zurich. 1973.
10. J. den Hollander, R. Kaptein, and P. Brand. Chem. Phys. Lett. **10**, 430 (1971).
11. B. Blank, A. Henne, and H. Fischer. Helv. Chim. Acta. In press.
12. N. Yang, E. Feit, M. Hui, N. Turro, and J. Dalton. J. Am. Chem. Soc. **92**, 6974 (1970).

Can. J. Chem. Downloaded from www.nrcresearchpress.com by 210.87.254.42 on 09/05/12
For personal use only.

Canadian Journal of Chemistry

Published by
THE NATIONAL RESEARCH COUNCIL OF CANADA

Journal canadien de chimie

Publié par
LE CONSEIL NATIONAL DE RECHERCHES DU CANADA

Volume 52 Number 17 September 1, 1974

Volume 52 numéro 17 1 septembre 1974

Crystal and Molecular Structure of Benzylidenimine Disulfide

JAMES C. BARRICK, CRISPIN CALVO, AND FREDRIC P. OLSEN

Department of Chemistry, McMaster University, Hamilton, Ontario L8S 4M1

Received December 21, 1973

JAMES C. BARRICK, CRISPIN CALVO, and FREDRIC P. OLSEN. Can. J. Chem. **52**, 2985 (1974).

The crystal and molecular structure of benzylidenimine disulfide has been determined. Crystals are monoclinic with space group $P2_1/c$, $Z = 4$, $a = 12.93(2)$, $b = 5.554(9)$, $c = 20.46(3)$ Å, and $\beta = 112.5(2)°$. A full matrix least squares refinement on 2304 unique reflections of positive intensity measure collected on a $P\bar{1}$ Automatic diffractometer produced a conventional R of 0.029. The molecular geometry is very similar to that in the corresponding tetra- and trisulfides with a fairly short sulfur–sulfur bond length of 2.033(2) Å and a fairly long sulfur–nitrogen bond length of 1.690(3) Å.

JAMES C. BARRICK, CRISPIN CALVO et FREDRIC P. OLSEN. Can. J. Chem. **52**, 2985 (1974).

On détermine la structure cristalline et moléculaire du disulfure de la benzylidènimine. Les cristaux sont monocliniques, groupe d'espace $P2_1/c$, $Z = 4$, $a = 12.93(2)$, $b = 5.554(9)$, $c = 20.46(3)$ Å et $\beta = 112.5(2)°$. Les données sont collectées sur un diffractomètre automatique $P\bar{1}$; un affinement par la méthode des moindre carrés (matrice complète) sur 2304 réflexions non-équivalentes d'intensité positive mène à un facteur conventionnel R de 0.029. La géométrie moléculaire est très similaire à celles des tétra- et trisulfures correspondants; la longueur de liaison soufre–soufre, 2.033(2) Å, est toutefois assez courte alors que la longueur de liaison soufre–azote, 1.690(3) Å, est assez longue. [Traduit par le journal]

Benzylidenimine tetrasulfide (1) and a number of other tetrasulfide chains (2–5) show alternation in sulfur–sulfur bond lengths. In seeking an explanation for this effect, comparative data on very similar compounds with differing numbers of sulfur atoms in the sulfur chain would be highly desirable. A preceding paper (6) discussed the structure of the odd membered chain, benzylidenimine trisulfide. This paper reports the crystal and molecular structure of the comparable compound with an even membered sulfur chain, benzylidenimine disulfide.

Experimental

Crystal Data

$C_{14}H_{12}N_2S_2$ f.w. 272.4

Monoclinic, $a = 12.93(2)$, $b = 5.554(9)$, $c = 20.46(3)$ Å, $\beta = 112.5(2)°$, $V = 1357.5$ Å^3, $\rho_c = 1.33$ g/cm^3, $Z = 4$, MoKα, $\lambda = 0.71069$ Å.

The compound was prepared from the reaction of sulfur with benzylamine in the presence of lead oxide at the 5:2 sulfur:benzylamine ratio expected (7) to optimize the yield of the disulfide. The product was isolated as previously described (6, 7) and recrystallized from benzene to give white needles melting at 100–100.5 °C (lit. (7) 100–100.5 °C). $h0l$ and $h1l$ Weissenberg photographs with systematic absences of the type $l = 2n + 1$ on the $h0l$ layer and $k = 2n + 1$ along the $0k0$ axis established the space group as $P2_1/c$. Unit cell parameters were determined at room temperature by least squares adjustment to the 2θ values of 38 well centered reflections measured on a Syntex $P\bar{1}$ Diffractometer. The crystal used for intensity measurements had dimensions of 0.6 mm × 0.6 mm × 0.35 mm. The maximum variation in transmission factor was less than 4.5%, and no absorption corrections were applied. Intensity data were collected on the above diffractometer using graphite monochromated radiation with a monochromater angle of 12°. Intensities were measured using a variable scan time in the θ–2θ technique with stationary counts on each side of the peak for 1/2 of the scan time to establish background. Thus, the peak intensity, $N_{Pk} = N_T -$

$N_{Bg1} - N_{Bg2}$ where N_T is the total peak count and N_{Bg1} and N_{Bg2} are the background counts. σ_I's were derived from

$$\sqrt{\sigma_{Pk}^2 + (0.01|F_o|^2)^2}$$

where

$$\sigma_{Pk} = \sqrt{N_T + N_{Bg1} + N_{Bg2}}$$

A total of 2304 symmetry independent nonzero reflections resulted of which 1807 had $I > 3$ and were considered as "observed". After correction for Lorentz and polarization effects using the XRAY 67 program DATRDN, these gave the structure factors used for comparison with model structures.[1]

Solution of the Structure

Application of direct methods yielded an E-map from which the position of two sulfur atoms, a nitrogen, and two carbon atoms were obtained. Successive refinement (CUDLS)[2] and electron density and difference Fourrier synthesis (SYMFOU)[2] then led to the gradual location of the remaining non-hydrogen atoms. Hydrogens were added in their calculated positions assuming sp^2 hydridization at carbon and a C—H bond distance of 0.97 Å (most hydrogens were also visible in an electron density difference map). Positional and isotropic temperature factors were then refined for hydrogen along with other atoms by full matrix least squares methods. The function minimized in the least squares refinement was $\Sigma w(|F_o| - |F_c|)^2$. A total of 212 parameters, including those for scale and extinction corrections (9, 10), were refined. The weighting scheme used took the form

$$w = 1/[0.07 + 0.0015F_o + 0.00045F_o^2 + 22.5(\sigma_F/F_o)^2]$$

where the σ_F's were derived from counting statistics. In the final cycle of refinement the maximum shift/error was 0.28 and the average value was 0.052. The final unweighted *R*-factor (all reflections) was 0.029 and the weighted value (all reflections) was 0.036 where

$$R = \frac{\sum ||F_o| - |F_c||}{|F_o|}$$

and

$$R_w = \sqrt{\frac{\sum w(|F_o| - |F_c|)^2}{\sum w|F_o|^2}}$$

The final calculated and observed structure factors are compared in Table 1,[3] and the final values for atomic positions and thermal parameters[4] are listed in Table 2. Table 3 lists bond lengths and angles with their estimated standard deviations.

Results and Discussion

Figure 1 shows a perspective view of the molecule and gives the system of atom labels used. In this view, in which the two nitrogens are approximately superimposed, the aromatic rings are rotated well away from each other on one side and the two sulfur atoms are on the other side.

Phenyl Rings

The ring carbon atoms are planar with maximum and average deviations of 0.013 Å (C_9) and 0.007 Å, respectively. The ring hydrogen atoms refined to give average and maximum deviations of 0.02 Å and 0.05 Å (H_{10}) from the planes established by the carbon atoms. The average carbon–carbon distance in the two rings of 1.381 Å (ring A) and 1.383 Å (ring B) are in good agreement with values of 1.381 Å and 1.372 Å in the tri- and tetrasulfide and with those of 1.392(4) Å reported (11) for crystalline benzene considering that translational and librational corrections have not been applied.

The average C—C—C angle in both rings is 120° with maximum and average deviations of 1.6 and 0.5°. The average carbon–hydrogen bond length as refined was 0.94 Å with maximum and average deviations of 0.06 and 0.03 Å, respectively. A riding correction (12), if applied, would increase the average value to 0.97 Å. The corresponding value without corrections was 0.92 Å in the trisulfide.

The C—Phenyl and C=N Bonds

The aliphatic carbon–carbon bonds average[5] 1.468(3) Å compared to values of 1.464(4) Å in the trisulfide and 1.460(8) Å in the tetrasulfide. The C—C—N angles at 121.2(3)° are nearly identical to the values of 121.9(4)° and 121.6(7)° in the tri- and tetrasulfides. The carbon–nitrogen bonds at 1.268(3) Å are also in excellent agreement with values of 1.269(3) and 1.271(8) Å found in the tri- and tetrasulfides, respectively. As observed in the tri- and tetrasulfides, the nitrogen atoms lie very near the planes of the aromatic rings. Deviations from these planes are 0.02 Å for N_1 and 0.11 Å for N_2 (*i.e.* dihedral angles around the phenyl–C bonds of 2.5° and 4.0°, respectively). The

[1]Atomic scattering factors were taken from ref. 8.

[2]Computer programs CUDLS and SYMFOU were written locally by J. Stephens and J. Rutherford, respectively.

[3]Table 1 is available, at a nominal charge, from the Depository of Unpublished Data, National Science Library, National Research Council of Canada, Ottawa, Canada K1A 0S2.

[4]Thermal factors are in Å^2 and were obtained from $U_{ij} = \beta_{ij}/2\pi^2 a_i^* a_j^*$ where the β_{ij}'s appear as the effect of temperature through $\exp[-\beta_{11}h^2 + 2\beta_{12}hk \ldots]$ in the structure factor expression and the a_i^*'s are the reciprocal lattice vectors. These units are chosen so that U = mean square thermal displacement directly.

[5]Where $\sigma_{ave} = 1/\Sigma(1/\sigma_i^2)$.

Can. J. Chem. Downloaded from www.nrcresearchpress.com by 210.87.254.42 on 09/05/12
For personal use only.

TABLE 2. Positional and thermal parameters* for benzylidenimine disulfide

Atom	x/a	y/b	z/c	U_{11}	U_{22}	U_{33}	U_{12}	U_{13}	U_{23}
S1	0.29594(4)	0.99957(10)	0.63918(2)	578(3)	760(4)	550(3)	101(3)	254(2)	10(2)
S2	0.28072(4)	0.22889(9)	0.55856(3)	554(3)	580(3)	647(3)	−24(2)	168(2)	−5(2)
N1	0.3942(1)	0.7866(3)	0.64809(8)	537(9)	680(10)	503(8)	49(8)	177(7)	−13(7)
N2	0.1820(1)	0.1329(3)	0.48183(8)	519(9)	558(9)	598(9)	11(7)	181(7)	40(7)
C1	0.4512(1)	0.7754(3)	0.60985(9)	539(10)	599(11)	461(9)	−22(9)	170(8)	−27(9)
C2	0.5370(1)	0.5891(3)	0.62149(9)	471(9)	558(10)	461(9)	−35(8)	129(7)	−65(8)
C3	0.6015(2)	0.5931(4)	0.58084(11)	756(13)	637(12)	653(12)	91(11)	353(10)	77(10)
C4	0.6813(2)	0.4165(4)	0.58948(13)	785(15)	944(14)	852(15)	149(12)	467(12)	58(12)
C5	0.6974(2)	0.2370(4)	0.63810(12)	618(13)	631(13)	798(14)	94(11)	234(11)	−10(11)
C6	0.6348(2)	0.2340(4)	0.67983(11)	601(12)	655(13)	635(12)	37(10)	138(9)	90(10)
C7	0.5553(2)	0.4090(4)	0.67155(10)	512(11)	676(12)	496(10)	−26(9)	152(8)	−3(9)
C8	0.1272(2)	0.9380(3)	0.47399(10)	550(10)	512(11)	609(11)	77(8)	272(9)	51(9)
C9	0.0393(1)	0.8736(3)	0.40572(9)	478(10)	483(10)	619(10)	50(8)	251(8)	−20(8)
C10	0.9781(2)	0.6632(4)	0.39841(12)	701(13)	522(11)	789(14)	9(10)	335(11)	34(11)
C11	0.8920(2)	0.6066(4)	0.33457(13)	680(13)	586(12)	951(17)	−109(11)	341(12)	−217(12)
C12	0.8677(2)	0.7574(4)	0.27765(12)	583(12)	741(14)	721(13)	4(11)	230(11)	−185(12)
C13	0.9298(2)	0.9635(4)	0.28339(11)	607(12)	705(14)	630(12)	72(10)	218(9)	−3(11)
C14	0.0149(2)	0.0224(4)	0.34674(10)	533(10)	529(11)	648(11)	23(9)	238(9)	21(9)

Atom	x/a	y/b	z/c	U_{iso}	Atom	x/a	y/b	z/c	U_{iso}
H1	0.437(1)	0.882(3)	0.571(1)	30(5)	H8	0.140(2)	0.829(4)	0.513(1)	31(5)
H3	0.588(2)	0.711(4)	0.548(1)	38(6)	H10	0.999(2)	0.566(4)	0.437(1)	39(6)
H4	0.725(2)	0.425(4)	0.559(1)	52(6)	H11	0.853(2)	0.469(4)	0.330(1)	55(7)
H5	0.752(2)	0.118(4)	0.646(1)	48(6)	H12	0.810(2)	0.720(4)	0.235(1)	58(7)
H6	0.648(2)	0.112(4)	0.714(1)	45(6)	H13	0.913(2)	0.069(4)	0.244(1)	46(6)
H7	0.512(2)	0.412(4)	0.698(1)	36(5)	H14	0.058(2)	0.171(4)	0.352(1)	33(5)

*All U's $\times 10^4$ except $U_{iso} \times 10^3$.

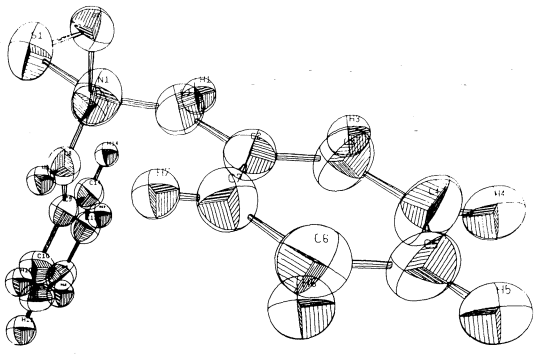

FIG. 1. Perspective view of benzylidenimine disulfide.

C—N—S angles at 124.5(2)° are quite reasonable compared to 126.0(2)° and 124.0(4)° in the tri- and tetrasulfides. The C—C—N/C—N—S dihedral angles are quite small at 1.5° and 2.5°, respectively, for C_1—N_1 and C_8—N_2. These compare with values of 1.5° in the trisulfide and 1.1° and 3.0° in the tetrasulfide.

The Sulfur–Nitrogen Bonds

The two crystallographically independent sulfur–nitrogen bond lengths at 1.694(3) and 1.687(3) Å are quite consistent, and the average value is 1.690 Å. This is somewhat longer than expected compared with values of 1.655(5) Å in the tetrasulfide and 1.661(3) Å in the trisulfide. Comparing the disulfide to the trisulfide gives Δ and σ_Δ of 0.029 and 0.004 Å while comparing it to the tetrasulfide gives Δ and σ_Δ of 0.035 and 0.006 Å, where $\sigma_\Delta = \sqrt{\sigma_1^2 + \sigma_2^2}$. These differences of 7 and 6 σ_Δ, respectively, are difficult to ignore in view of the excellent agreement in the phenyl and C—N parts of the structure and appear to be "significant". The N—S—S angles average 111.2(3)° and compare well with values of 111.4(2)° and 111.5(3)° in the tri- and tetrasulfides. In the latter two compounds quite small C—N—S—S dihedral angles (3° in both structures) were observed leading to planarity in the full C_6H_5-$CHNS_2$ units. This structural feature is retained in the disulfide where the two C—N—S—S dihedral angles are 1.0° and 3.0° for N_1—S_1 and N_2—S_2, respectively. Thus, S_1 and S_2 lie 0.02 and 0.11 Å, respectively, from the plane of ring A and 0.37 and 0.23 Å from the plane

Can. J. Chem. Downloaded from www.nrcresearchpress.com by 210.87.254.42 on 09/05/12
For personal use only.

TABLE 3. Bond lengths* and angles in benzylidenimine disulfide

Bond	Distance (Å)	Bond	Distance (Å)	Bond	Distance (Å)
S_1—S_2	2.033(2)	C_7—C_2	1.386(3)	C_4—H_4	1.00(3)
S_1—N_1	1.694(3)	C_8—C_9	1.468(4)	C_5—H_5	0.93(2)
S_2—N_2	1.687(4)	C_9—C_{10}	1.387(3)	C_6—H_6	0.95(2)
N_1—C_1	1.265(4)	C_{10}—C_{11}	1.390(5)	C_7—H_7	0.91(3)
N_2—C_8	1.270(3)	C_{11}—C_{12}	1.370(4)	C_8—H_8	0.96(2)
C_1—C_2	1.468(3)	C_{12}—C_{13}	1.377(4)	C_{10}—H_{10}	0.90(2)
C_2—C_3	1.386(4)	C_{13}—C_{14}	1.381(4)	C_{11}—H_{11}	0.90(3)
C_3—C_4	1.385(4)	C_{14}—C_9	1.396(3)	C_{12}—H_{12}	0.93(2)
C_4—C_5	1.367(4)	C_1—H_1	0.96(2)	C_{13}—H_{13}	0.95(2)
C_5—C_6	1.384(4)	C_3—H_3	0.91(2)	C_{14}—H_{14}	0.98(2)
C_6—C_7	1.377(3)				

Bonds	Angle (deg)	Bonds	Angle (deg)	Bonds	Angle (deg)
S_1—S_2—N_2	111.1(3)	C_{10}—C_{11}—C_{12}	120.1(5)	C_7—C_6—H_6	121(1)
S_2—S_1—N_1	111.2(4)	C_{11}—C_{12}—C_{13}	120.0(4)	C_6—C_7—H_7	122(1)
S_1—N_1—C_1	124.0(3)	C_{12}—C_{13}—C_{14}	120.4(5)	C_2—C_7—H_7	117(1)
S_2—N_2—C_8	125.0(3)	C_{13}—C_{14}—C_9	120.5(6)	N_2—C_8—H_8	121(1)
N_1—C_1—C_2	121.1(3)	C_{14}—C_9—C_{10}	118.4(4)	C_9—C_8—H_8	117(1)
N_2—C_8—C_9	121.3(5)	C_{14}—C_9—C_8	121.0(4)	C_9—C_{10}—H_{10}	116(1)
C_1—C_2—C_3	118.9(4)	N_1—C_1—H_1	121(1)	C_{11}—C_{10}—H_{10}	123(1)
C_2—C_3—C_4	120.2(4)	C_2—C_1—H_1	118(1)	C_{10}—C_{11}—H_{11}	121(1)
C_3—C_4—C_5	120.5(4)	C_2—C_3—H_3	118(1)	C_{12}—C_{11}—H_{11}	119(1)
C_4—C_5—C_6	119.7(4)	C_4—C_3—H_3	121(1)	C_{11}—C_{12}—H_{12}	120(1)
C_5—C_6—C_7	120.1(4)	C_3—C_4—H_4	117(1)	C_{13}—C_{12}—H_{12}	120(1)
C_6—C_7—C_2	120.6(4)	C_5—C_4—H_4	122(1)	C_{12}—C_{13}—H_{13}	120(1)
C_7—C_2—C_3	118.9(4)	C_4—C_5—H_5	123(1)	C_{14}—C_{13}—H_{13}	120(1)
C_7—C_2—C_1	122.2(4)	C_6—C_5—H_5	118(1)	C_9—C_{14}—H_{14}	118(1)
C_8—C_9—C_{10}	120.7(4)	C_5—C_6—H_6	119(1)	C_{13}—C_{14}—H_{14}	121(1)
C_9—C_{10}—C_{11}	120.7(4)				

*Errors are estimated standard deviations and include uncertainty in both the least squares adjustments from Table 1 and the errors in cell parameters.

of ring B. Planes fit to the full $C_6H_5CHNS_2$ unit (excluding hydrogens) have maximum and average deviations of just 0.024 and 0.047 Å (S_2) for ring A, and 0.046 and 0.087 Å (S_1) for ring B. Thus, where the tetrasulfide consisted of two coplanar units joined by an S—S bond, the trisulfide had these same two units sharing a sulfur atom, and in the disulfide the same two coplanar units share two sulfur atoms.

The Sulfur–Sulfur Bond

The sulfur–sulfur bond has a length of 2.033(2) Å. In the trisulfide the value for the sulfur–sulfur bond was 2.051(1) Å. With Δ and σ_Δ of 0.018 and 0.002 Å, these two bonds differ by $9\sigma_\Delta$, an amount taken as "significant". The long S—S bond of the tetrasulfide at 2.085(4) Å is also significantly different from that in the disulfide with Δ and σ_Δ of 0.052 and 0.005 Å, a difference of more than $10\sigma_\Delta$. The short bond of the tetrasulfide at 2.026(3) Å, however, differs by only 0.007 Å with a σ_Δ of 0.004 Å, and is apparently equivalent.

The N—S—S—N dihedral angle at 91.2° is quite similar to the outer (N—S—S—S) dihedral angles of 89.4° and 94.3° in the tetrasulfide and somewhat larger than the N—S—S—S dihedral angle of 78.2° in the trisulfide.

Packing

Unlike the tri- and tetrasulfides where the packing along the short axis was determined primarily by sulfur–sulfur and sulfur–nitrogen Van der Waals contacts, the short axis distance in the disulfide depends on ring–ring contact. The cants of the rings with respect to the short (*b*) axis are 56° and 60° and account for the thickness of the unit cell relative to the thinnest dimension of a benzene ring (3.4 Å).

The closest intermolecular contact distance is H_5–H_{12} at 2.52 Å (Van der Waals contact: 2.4 Å); the closest non-hydrogen distance is C_1–C_o at 3.4 Å (Van der Waals contact: 3.4 Å);

Can. J. Chem. Downloaded from www.nrcresearchpress.com by 210.87.254.42 on 09/05/12
For personal use only.

and the closest involving sulfur are S_1–C_{11} and S_1–C_{12}, both at 3.46 Å (Van der Waals contact: 3.55 Å). Thus, there are no unusual intermolecular non-bonding interactions. As in the tri- and tetrasulfide, however, the S_2–C_1 and S_1–C_8 intramolecular distances at 3.25 and 3.26 Å are rather short.

This work was supported under a grant from the National Research Council of Canada.

1. J. Barrick, C. Calvo, and F. P. Olsen. J. Chem Soc. D, 1043 (1971); Can. J. Chem. **51,** 3691 (1973).
2. J. C. Ricci Jr. and I. Bernal. J. Chem. Soc. B, 1928 (1971).
3. B. R. Davis and I. Bernal. Proc. Natl. Acad. Sci. U.S.A. **70**, 279 (1973).
4. B. R. Davis, I. Bernal, and A. V. Schmidt. Angew. Chem. Int. Ed., **11**, 632 (1972).
5. B. R. Davis and I. Bernal. J. Cryst. Mol. Struct. **2**, 135 (1972).
6. J. Barrick, C. Calvo, and F. P. Olsen. Can. J. Chem. **51,** 3697 (1973).
7. Y. Sasaki and F. P. Olsen. Can. J. Chem. **49**, 283 (1971).
8. International tables for X-ray crystallographers. Vol. 3. Kynoch Press, Birmingham, England. 1962. p. 202.
9. J. S. Stephens and D. W. J. Cruickshank. Acta. Cryst. B**26**, 223 (1970).
10. W. H. Zachariasen. Acta Cryst. **16**, 1142 (1963).
11. E. G. Cox, D. W. J. Cruickshank, and J. A. S. Smith. Proc. R. Soc. A**247**, 1 (1958).
12. W. R. Busing and H. A. Levy. Acta Cryst. **17**, 142 (1964).

Can. J. Chem. Downloaded from www.nrcresearchpress.com by 210.87.254.42 on 09/05/12
For personal use only.

Reactions of Sodium Tetrahydroborate and Cyanotrihydroborate With Divalent Co, Ni, Cu, Pd, and Pt Chlorides In the Presence of Tertiary Phosphines

DAVID G. HOLAH, ALAN N. HUGHES, BENJAMIN C. HUI, AND KEN WRIGHT

Department of Chemistry, Lakehead University, Thunder Bay, Ontario P7B 5E1

Received February 8, 1974

DAVID G. HOLAH, ALAN N. HUGHES, BENJAMIN C. HUI, and KEN WRIGHT. Can. J. Chem. **52**, 2990 (1974).

The reactions of divalent Co, Ni, Cu, Pd, and Pt chlorides with $NaBH_4$ and $NaBH_3CN$ in the presence of tertiary phosphines under inert atmosphere conditions have been examined. The nature of the product varies enormously depending upon reaction conditions, and compounds obtained include complexes involving coordinated BH_4^- and BH_3CN^- of the type ML_n, MBL_n, and $MHBL_n$ (L = phosphine, B = BH_4^- or BH_3CN^-, n = 2, 3, or 4). The first univalent nickel and cobalt BH_4 complexes are reported. Platinum abstracts the CN group from BH_3CN^- to form the species $PtH(CN)L_2$. Infrared spectral data are reported and appear to indicate two types of bonding (M—N and M—H) between BH_3CN^- and metals. Some electronic reflectance spectra and magnetic properties are also reported, including those of Co(I) and Ni(I) species. Attempts are made to rationalize the data in terms of a suggested mechanism for the reduction of metal halides by $NaBH_4$.

DAVID G. HOLAH, ALAN N. HUGHES, BENJAMIN C. HUI et KEN WRIGHT. Can. J. Chem. **52**, 2990 (1974).

On examine les réactions des chlorures de Co, Ni, Cu, Pd et Pt bivalents avec $NaBH_4$ et $NaBH_3CN$ en présence de phosphines tertiaires dans des conditions d'atmosphère inerte. La nature du produit varie énormément selon les conditions de la réaction et les composés obtenus comprennent des complexes du type ML_n, MBL_n et $MHBL_n$ (L = phosphine, B = BH_4^- ou BH_3CN^-, n = 2, 3 ou 4). On rapporte les premiers complexes de BH_4 avec du nickel et du cobalt monovalents. La platine enlève le groupe CN de BH_3CN^- pour former les espèces $PtH(CN)L_2$. On rapporte les spectres infrarouges de ces complexes qui semblent indiquer deux genres de liaisons (M—N et M—H) entre BH_3CN^- et les métaux. On rapporte aussi quelques spectres de réflexion électronique et des propriétés magnétiques, y compris ceux des espèces de Co(I) et Ni(I). On essaie de rationaliser les données en termes d'un mécanisme suggéré pour la réduction d'halogénures métalliques par $NaBH_4$. [Traduit par le journal]

Introduction

As well as being a powerful reducing agent and an excellent source of hydride ion in the synthesis of metal hydrides, the BH_4^- group will coordinate to a variety of metals to form covalent complexes such as $M(BH_4)_n$ (for an excellent review of metal tetrahydroborate derivatives see ref. 1 and references therein) *e.g.* $Zr(BH_4)_4$. While the use of the octahydrotriborate ($B_3H_8^-$) (2–4) and the cyanotrihydroborate (BH_3CN^-) anions (5–7) as coordinating species has been demonstrated, much less is known about their coordinating abilities.

In the case of divalent Co, Ni, Cu, Pd, and Pt, the metal ions of interest in this study, no simple compounds with BH_4 or BH_3CN are known, although it is well established that transition metal complexes of BH_4 can be stabilized by, for example, tertiary phosphines (2, 8, 9), cyclopentadiene (10), and various other ligands. Thus, nickel complexes of BH_4 and BH_3CN stabilized by nitrogen containing bases have been characterized (11, 12) and complexes formulated as *trans*-$(R_3P)_2MH(BH_4)$ (M = Ni, Pd, but not Pt; R = Pr^i or cyclohexyl) have been prepared and briefly investigated as reducing agents (13–15). Copper forms numerous complexes containing these groups and various phosphines, examples being $L_2Cu(BH_4)$ (2, 8) or, for chelating phosphines, $LCu(BH_4)$ (8) as well as $L_3Cu(BH_3CN)$ (L = PPh_3, $AsPh_3$, $SbPh_3$), and $[L_2Cu(BH_3CN)]_2$ (L = PPh_3) (6, 12).

This paper reports in detail (16) the results of our studies on the very carefully controlled reactions between some transition metal chlorides and both $NaBH_4$ and $NaBH_3CN$ in the presence of various phosphines and related ligands. We were particularly interested in studying the conditions under which BH_4^- and

Can. J. Chem. Downloaded from www.nrcresearchpress.com by 210.87.254.40 on 09/05/12
For personal use only.

Can. J. Chem. Downloaded from www.nrcresearchpress.com by 210.87.254.40 on 09/05/12
For personal use only.

BH_3CN^- will either (*a*) fully reduce the above mentioned metal ions to metal(0) compounds, (*b*) coordinate to divalent metal ions or to reduced species, or (*c*) produce metal hydrides or even mixed hydride – BH_4 type complexes. These compounds of type (*c*) are of interest to us as part of our homogeneous catalysis work (17), particularly since they may be important intermediates in hydrogenation and hydrogen transfer reactions. A later paper will deal with Rh, Ru, and Ir systems.

Results and Discussion

Copper Complexes

While tertiary phosphines themselves reduce Cu(II) to Cu(I) in ethanol solutions, addition of $NaBH_4$ to the reaction mixture *in situ* produces complexes such as $Cu(BH_4)(PPh_3)_2$ (2) and $Cu(BH_4)(DBP)_2$ (16).[1] Analytical data are recorded in Table 1 while i.r. spectroscopic data appear in Table 2. The former complex has also been made previously by the reaction between $CuClL_3$ (L = PPh_3 or other substituted phosphines) and $NaBH_4$ (8). Studies on hydroborate complexes (18, 19) indicate that the BH_4 group is bonded via a double hydrogen bridged structure shown below

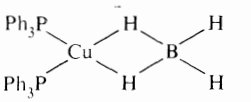

(ref. 18)

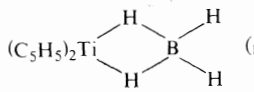

(ref. 19)

and on this basis the i.r. spectrum of $Cu(BH_4)(PPh_3)_2$ has been satisfactorily explained (2). Thus the band which occurs in the i.r. spectrum at 1100 cm^{-1} is assigned to the B—H deformation mode, the 1900–2000 cm^{-1} band to the chelating BH_2 grouping, while the terminal B—H stretching mode appears at between 2300 and 2400 cm^{-1}. Even though these Cu(I) hydroborate complexes are more stable than similar Co and Ni complexes (*vide infra*) we were, as were previous workers (2*a*), unable to form $AsPh_3$ and $SbPh_3$ adducts. Nitrogen donors also are not generally effective in stabilizing the BH_4 complexes although $Cu(BH_4)(PPh_3)$(*o*-phen) has been reported (8).

Similar reactions to those reported above using $NaBH_3CN$ result in the formation of complexes of the type $Cu(BH_3CN)L_3$ (L = PPh_3, DBP, $PEtPh_2$) and $Cu(BH_3CN)(Diphos)_{1.5}$ (Diphos = 1,2-bis(diphenylphosphino)ethane). A complex with the stoichiometry $Cu(BH_3CN)(PPh_3)_3$ different from that mentioned above has been previously reported by Lippard and co-worker (6) who obtained it from the reaction of $NaBH_3CN$ and $CuCl(PPh_3)_3$ in an ethanol–chloroform solvent and both complexes with this stoichiometry are further discussed below. Cyanotrihydroborate complexes of Rh(I) and Ir(I) (20) have also been synthesized and these complexes, together with Lippard's complex $Cu(BH_3CN)(PPh_3)_3$ (6), are believed to contain *N*-bonded BH_3CN groups which invariably show an increase of up to 20 cm^{-1} in the CN stretching frequencies (from 2180 cm^{-1} in $NaBH_3CN$), although the shifts are generally smaller than for most coordinated nitriles (21).

While the complex $Cu(BH_3CN)(PPh_3)_3$ synthesized by us (complex A, m.p. 159–162°) and that synthesized by a different procedure by Lippard and co-worker (6) and also duplicated by us (complex B, m.p. 157–158°) have the same empirical formula, they differ, sometimes considerably, in a number of respects. For example, although the i.r. spectrum of A is almost identical to that of B (Table 2) it has an extra band at 2122 cm^{-1}. At room temperature B is soluble in chloroform and insoluble in benzene, although it does slowly dissolve at higher temperatures. Addition of *n*-hexane to this benzene solution precipitates $[Cu(BH_3CN)(PPh_3)_2]_2$ (6). On the other hand, A is soluble in benzene from which it can be recovered unchanged by addition of *n*-hexane. A solution of A in chloroform has the same i.r. spectrum as does a mull of the solid, but addition of ethanol to the chloroform solution precipitates a mixture of A and $[Cu(BH_3CN)(PPh_3)_2]_2$.

The relatively minor differences between the i.r. spectra of the two complexes A and B together with their different solubilities in various solvents might suggest that they are merely different crystalline forms of the same compound. However, the differences in behavior of A and B in solution mentioned above

[1]DBP is the cyclic phosphine, 5-phenyl-5*H*-dibenzophosphole.

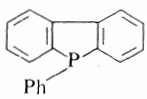

Can. J. Chem. Downloaded from www.nrcresearchpress.com by 210.87.254.40 on 09/05/12
For personal use only.

TABLE 1. Analytical data

Complex	Color	Analyses C Calcd.	C Found	H Calcd.	H Found	N Calcd.	N Found	M Calcd.	M Found	Magnetic moment (B.M.)
$Cu(BH_4)(DBP)_2 \cdot C_6H_6$	White	74.5	75.0	5.4	5.3					
$Cu(BH_3CN)(PPh_3)_3$	White	74.2	74.5	5.4	5.9	1.6	1.5			
$Cu(BH_3CN)(DBP)_3$	White	74.7	74.9	4.8	5.0	1.6	1.7			
$Cu(BH_3CN)(PEtPh_2)_3$	White	69.2	68.9	6.5	6.4	1.9	1.8			
$Cu(BH_3CN)(Diphos)_{1.5}$	White	68.5	67.7	5.6	5.6	2.0	1.8			
$Co(BH_4)(PPh_3)_3$	Yellow	75.4	74.2	5.7	5.6			6.9	6.7	2.71
$Co(BH_3CN)(DBP)_4$	Yellow-green	76.9	77.0	4.9	4.8	1.2	1.1			3.02
$Co(BH_3CN)(Diphos)_2$	Yellow-green	71.1	71.2	5.7	6.3	1.6	1.6			Diamagnetic
$Ni(BH_4)(PPh_3)_3$	Yellow-brown	75.4	75.6	5.7	5.7	10.8*	10.9	6.8	6.2	Diamagnetic
$Ni(BH_3CN)(PPh_3)_2$	Yellow	71.3	71.1	5.3	5.5	2.3	1.9			1.88
$NiH(BH_3CN)(PPh_3)_2$	Orange	71.2	71.2	5.5	5.3	2.2	1.8			Diamagnetic
$NiH(BH_3CN)(DBP)_3$	Brown	75.0	74.9	4.9	4.9	1.6	1.7	6.7	6.3	Diamagnetic
$NiCl(BH_3CN)(Diphos)$	Orange	60.9	61.0	5.1	5.0	2.6	2.1	11.0	11.0	Diamagnetic
$Co(DBP)_2$	Purple-brown	74.6	74.6	4.5	4.7			10.2	9.7	$\chi_g = 3.33 \times 10^{-6}$
$Co(DBP)_4$	Red-brown	78.6	78.1	4.8	5.1			5.4	5.1	Diamagnetic
$CoCl(DBP)_3$	Yellow-brown	74.1	73.5	4.5	4.6			6.7	6.7	3.25
$Ni(DBP)_2$	Dark-brown	74.7	73.7	4.5	4.7			10.1	10.0	Diamagnetic
$Ni(DBP)_4 \cdot C_6H_6$	Brick-red	79.5	79.8	5.0	5.2			5.0	4.9	
$NiCl(DBP)_3$	Orange-yellow	74.1	73.3	4.5	4.5			6.7	6.6	1.95
$Pd(DBP)_4$	Yellow	75.4	75.7	4.6	4.9					
$Pt(DBP)_4 \cdot C_6H_6$	Yellow	71.3	71.1	4.5	4.6					
$PtH(CN)(PPh_3)_2 \cdot 0.5C_6H_6$	White	61.2	61.3	4.4	4.5	1.8	2.1			
$PtH(CN)(DBP)_2 \cdot 0.5C_6H_6$	Pale-yellow	61.5	61.3	3.9	3.9	1.8	2.1			

*% P.

TABLE 2. Infrared spectral data*

BH_4 complexes	Infrared (cm^{-1}) Deformation δ_{B-H}	Chelating ν_{MH_2B}	Terminal ν_{B-H}
$Cu(BH_4)(DBP)_2C_6H_6$	1065s	2030m	2340s
$Co(BH_4)(PPh_3)_3$	1105m		2340sh 2390s
$Ni(BH_4)(PPh_3)_3$	1120m		2350sh 2388s

BH_3CN (B) complexes	Infrared (cm^{-1}) Deformation δ_{B-H}	ν_{M-B-H}	$\nu_{C\equiv N}$	Terminal ν_{B-H}	Other
$CuB(PPh_3)_3$†	1153 1125sh		2192s	2330s 2358sh	
$CuB(PPh_3)_3$	1115s	2122m	2185s	2280sh 2340s	
$CuB(DBP)_3$	1119s		2188s	2290sh 2350b	
$CuB(PEtPh_2)_3$	1112s		2190s	2336s	
$CuB(Diphos)_{1.5}$	1116s	2106w	2188s	2340sb	
$CoB(DBP)_4$	1112s		2188s	2360sb	
$CoB(Diphos)_2$	1112s		2190s	2336s	
$NiB(PPh_3)_2$	1118s	2070w	2185s	2340sb	
$NiHB(PPh_3)_2$	1120s	2140m	2200s	2336s	722s(Ni—H?)
$NiHB(DBP)_3$	1133m	2138m	2201s	2334s	
NiClB(Diphos)	1103s		2192s	2340sb	343m(Ni—Cl)
NaB	1130s		2180s	2325s 2350sh	

Pt complexes	Infrared (cm^{-1}) δ_{Pt-H}	ν_{Pt-H}	ν_{CN}
$PtH(CN)(PPh_3)_2$	822w	2074w	2146s
$PtH(CN)(DBP)_2$	817m	2068w	2141s

*s = strong, m = medium, w = weak, b = broad.
†Lippard's complex, ref. 6.

together with the fact that the additional band at 2122 cm^{-1} in the i.r. spectrum of A is retained in chloroform solution strongly suggests that they are indeed different compounds. Since both compounds are almost certainly normal tetrahedral Cu(I) complexes, it follows that the differences probably arise from a different mode of attachment of one or more of the ligands. It is difficult to see how the three PPh_3 ligands could bond through anything but the phosphorus atoms but the unidentate BH_3CN grouping could bond through either the B—H link or the nitrile group.

Lippard and co-worker (6) have produced considerable chemical and i.r. spectroscopic evidence for the Cu—$NCBH_3$ linkage in B. Therefore it seems likely that in A the mode of attachment is through the B—H link and the available evidence is consistent with this suggestion.Thus, the additional band at 2122 cm^{-1} in the i.r. spectrum of A is consistent with the Cu—H—B vibration and Lippard and co-worker (6) have also attributed bands in this region of the i.r. spectrum of the related compound $[(PPh_3)_2Cu(BH_3CN)]_2$ to Cu—H—B bonding where the presence of such linkages, as well as groupings of the type Cu—NCB, has been shown by X-ray crystallographic studies.

Similar bands occur at ~2100 cm^{-1} in the i.r. spectra of several other cyanotrihydroborate complexes of Cu (*e.g.* $Cu(BH_3CN)(Diphos)_{1.5}$) and Ni (see Table 2) and the implication is that M—H—B bonding is also present in these compounds. However, there is little difference in the CN stretching frequency between those compounds which show the extra 2100 cm^{-1} band and those which do not and some doubt must therefore remain regarding the detailed method of BH_3CN bonding in these compounds although it should be borne in mind that at

Can. J. Chem. Downloaded from www.nrcresearchpress.com by 210.87.254.40 on 09/05/12
For personal use only.

Can. J. Chem. Downloaded from www.nrcresearchpress.com by 210.87.254.40 on 09/05/12
For personal use only.

least in some cases both types of bonding (with the BH_3CN group acting as a bridging ligand) may be present as in the case of $[(PPh_3)_2Cu(BH_3CN)]_2$ (6).

In the case of the complexes A and B, where comparison of the CN stretching frequencies may be expected to yield some positive information because of the very closely related nature of the two complexes, it is worth noting that in the i.r. spectrum of A, where Cu—H—B bonding is postulated, the CN stretching vibration is at 2185 cm^{-1} which is only marginally higher than in uncoordinated BH_3CN^- (2180 cm^{-1}). On the other hand, in the i.r. spectrum of B where Cu—NCB bonding is postulated (6) the band occurs at the significantly higher value of 2192 cm^{-1}.

Exactly what determines why either or both of two different modes of bonding occur in the BH_3CN complexes is not clear although it appears to be related to both steric and electronic factors. Thus, the rigid and flattened DBP, which has very similar donor character to PPh_3, apparently forms a less sterically hindered situation when the BH_3CN is *N*-bonded to give $(DBP)_3Cu—NCBH_3$. All attempts to form the corresponding Cu—H—B bonded isomer were unsuccessful. This *N*-bonding is also apparently adopted by the Cu—BH_3CN complex of the more basic $PEtPh_2$, possibly to enable more effective back donation of metal electron density.

Cobalt Complexes

Addition of triphenylphosphine (6 *M* excess) to an ethanol solution of hydrated cobalt(II) halides followed by addition of $NaBH_4$ at room temperature under nitrogen results in the precipitation of the known (22) complexes $CoX(PPh_3)_3$ (X = Cl, Br, or I) which, on addition of more $NaBH_4$ yield a paramagnetic solid $Co(BH_4)(PPh_3)_3$ with a magnetic moment of 2.71 B.M. Its electronic spectrum (Fig. 1) is typical of a tetrahedral d^8 system and is extremely similar to the spectra of $CoX(PPh_3)_3$ (22). The BH_4 group must therefore be bonded to the metal through one hydrogen atom, consistent with the absence of the ring breathing mode in the i.r. spectrum (Table 2). Recrystallization of $Co(BH_4)(PPh_3)_3$ from nitrogen-saturated benzene and *n*-hexane produces a yellow-brown complex which approximates to $Co(N_2)(BH_4)(PPh_3)_3$, although elemental analysis invariably indicated that less than 1 mol of nitrogen had been taken up. The dinitrogen gives rise to two intense bands in the infrared region at 2089 and 2098 cm^{-1} while the bands due to the BH_4 group are essentially unchanged. The analogous dinitrogen complex $CoH(N_2)(PPh_3)_3$ has been prepared by (*a*) the reduction of bis(acetylacetonato) cobalt(II) with dialkylaluminum alkoxide in the presence of N_2 (23) or by (*b*) the displacement of H_2 from $CoH_3(PPh_3)_3$ by N_2 (24). It is interesting that in the synthesis of $CoH_3(PPh_3)_3$ involving a mixture of $CoCl_2$–PPh_3–$NaBH_4$ in ethanol, an intermediate red solid (Co(I) halide or BH_4 complex?) was observed which subsequently decomposed to the Co(III) hydride.

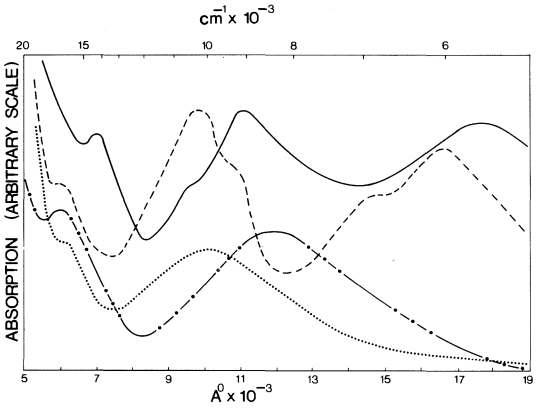

FIG. 1. Reflectance spectra of Co compounds: —, $Co(BH_4)(PPh_3)_3$; ---, $CoCl(DBP)_3$; -·-·-·, $Co(BH_3CN)(DBP)_4$; ···, $Co(BH_3CN)(Diphos)_2$.

Similar reactions of Co(II) with $NaBH_4$ in the presence of $AsPh_3$, $SbPh_3$, or *o*-phen result in the precipitation of a small amount of a black solid, presumably cobalt metal, while a reaction in the presence of Diphos produces $CoH(Diphos)_2$ (25*a*).

The first stage of the reaction between Co(II) chloride and $NaBH_4$ (1:1) in the presence of the bulky DBP is similar to the case of PPh_3 in that the analogous yellow brown, paramagnetic ($\mu = 3.25$ B.M.) $CoCl(DBP)_3$ is produced (ν_{Co-Cl} at 315 cm^{-1}). Its electronic spectrum (Fig. 1) is basically similar to that of $CoCl(PPh_3)_3$ suggesting a tetrahedral Co(I) system. Addition of an excess of $NaBH_4$ to $CoCl(DBP)_3$ *in situ* does not give the expected tetrahydroborate complex, and when the reaction is left for ~60 h, $Co(DBP)_4$ is the only product. However, a brown solid isolated after ~20 h has an intense Co—H stretching frequency in the i.r. spectrum at 1840 cm^{-1} and a Co—Cl stretching frequency at

Can. J. Chem. Downloaded from www.nrcresearchpress.com by 210.87.254.40 on 09/05/12
For personal use only.

315 cm^{-1}. Its reflectance spectrum shows bands due to $CoCl(DBP)_3$ (although of lower intensity than when the latter is pure) and the solid appears to be a mixture of the unreacted $CoCl(DBP)_3$ and possibly a Co(I) hydride – DBP intermediate complex which decomposes readily to the diamagnetic $Co(DBP)_4$. This last complex can also be made by the addition of $NaBH_4$ to Co(II) chloride and a 6-fold excess of DBP in boiling ethanol. There is no evidence in the i.r. spectrum of this compound of a Co—H band, and only a charge transfer transition at ~14000 cm^{-1} is visible in its reflectance spectrum. Probably the diamagnetism is accounted for by dimerization, although molecular weights were low and clearly indicative of extensive dissociation in benzene. The complex is somewhat analogous to the weakly paramagnetic, monomeric $Co(Diphos)_2$ (*25b*).

A similar reaction of Co(II) and $NaBH_4$ with a 3-fold excess of DBP produces the paramagnetic ($\chi_g = 3.33 \times 10^{-6}$ c.g.s) $Co(DBP)_2$. Again no metal hydride could be detected by i.r. or n.m.r. and molecular weight data were complicated by dissociation and air sensitivity.

We have been unable to identify a specific product from the $CoCl_3$–PPh_3–$NaBH_3CN$ reaction in ethanol, contrary to what we reported in our previous communication (16). However, with DBP under similar conditions the complex $Co(BH_3CN)(DBP)_4$ is obtained. This complex is high spin with a magnetic moment of 3.02 B.M. and has a reflectance spectrum (Fig. 1) showing two bands at 8350 and 16700 cm^{-1} which could correspond to the $^3A_{2g} \rightarrow {}^3T_{2g}$ and $^3A_{2g} \rightarrow {}^3T_{1g}(F)$ transitions in an octahedral d^8 system, implying that the BH_3CN group occupies two of the coordination sites on the Co. Varying amounts of dinitrogen ($\nu_{N_2} = 2104$ cm^{-1}) are incorporated into this compound after recrystallization from solvents saturated with nitrogen.

Finally, reactions of Co(II) with $NaBH_3CN$ in the presence of Diphos produce the diamagnetic compound $Co(BH_3CN)(Diphos)_2$. Unlike some Co complexes mentioned above, recrystallization of this does not result in N_2 uptake and the difference may be associated with greater lability of the monodentate phosphine ligands in $Co(BH_3CN)(DBP)_4$ compared to the chelating Diphos, and the readiness of $Co(BH_4)(PPh_3)_3$ to expand its coordination shell. The Diphos complex has a band in its reflectance spectrum (Fig. 1) at 10000 cm^{-1} with a shoulder at 16000 cm^{-1}, and is very similar to the spectra of some other complexes (*e.g.* $CoX(C_2H_4PPh_2)_2$) (26). These spectra are considered typical of low spin, d^8 trigonal bipyramidal (C_{3v}) structures.

Nickel Complexes

Hydrated nickel(II) halides react in the presence of an excess of PPh_3 with $NaBH_4$ at room temperature ($Ni:BH_4$ molar ratio 1:1) under nitrogen to produce the complexes $NiXL_3$ (X = Cl, Br, I; L = PPh_3). These paramagnetic compounds (μ = 2.1–2.3 B.M.) were previously made by "a curious process in which [(h^3-allyl)NiX]$_2$ is treated with an excess of PPh_3 in the presence of norbornene" (27). Their electronic reflectance spectra (Fig. 2) show what appears to be a spin-forbidden band at 11100 cm^{-1} and a broad strong band centered at ~6000 cm^{-1}, not inconsistent with the $^2T_2 \rightarrow {}^2E$ transition in a tetrahedral d^9 system.

As in the case of cobalt, addition of more $NaBH_4$ (6–10 *M* excess) to the above Ni(I) halide complexes produce the same (regardless of the halide used) yellow-brown complex $Ni(BH_4)(PPh_3)_3$. In a preliminary communication (16), we reported this complex as $NiH(BH_4)(PPh_3)_3$, but we now feel it to be a Ni(I) compound on the following grounds:

(*1*) It is made from a Ni(I) complex in the presence of the reducing $NaBH_4$ in a manner entirely analogous to that used for $Co(BH_4)(PPh_3)_3$.

(*2*) It would be unusual for a Ni(II) compound

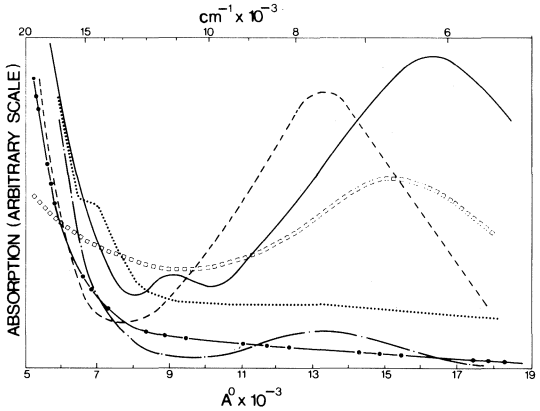

FIG. 2. Reflectance spectra of Ni compounds: —, $NiX(PPh_3)_3$; ---, $NiCl(DBP)_3$; □□□, $Ni(BH_3CN)(PPh_3)_2$; ···, $NiH(BH_3CN)(PPh_3)_2$ and $NiCl(BH_3CN)$(Diphos); -·-·-·, $NiH(BH_3CN)(DBP)_3$; and -●-●-●, $Ni(BH_4)(PPh_3)_3$.

Can. J. Chem. Downloaded from www.nrcresearchpress.com by 210.87.254.40 on 09/05/12
For personal use only.

to show the extreme air-sensitivity of this compound in both the solid state (pyrophoric) and in solution, in which it is too unstable to allow n.m.r. and molecular weight determinations.

(*3*) A diamagnetic, presumably 5-coordinate Ni(II) compound, would probably have bands in the reflectance spectrum below where the charge transfer transition starts, at $\sim$16000 cm^{-1}.

(*4*) The absence of a Ni—H band in the i.r. spectrum. Bands at 1120 and 2388 cm^{-1} in the i.r. spectrum (Table 2) are due to the BH_4 group and it seems likely therefore that, unlike $Co(BH_4)(PPh_3)_3$, the species is dimeric with bridging BH_4 groups and with spin interaction between the Ni atoms. Further reactions of this compound are under investigation.

The only other known hydroborate–phosphine complexes of nickel are the Ni(II) compounds $NiH(BH_4)L_2$ (13) (L = tricyclohexylphosphine or triisopropylphosphine) which were prepared by the reaction of $NaBH_4$ on the corresponding $NiHClL_2$ complexes. A double hydrogen-bridged structure has also been suggested for these compounds which have been used effectively as reducing agents. However, other Ni—BH_4 complexes appear to exist and, in this connection, reports (28, 29) on the uses of a soluble nickel hydrogenation catalyst prepared by adding $NaBH_4$ to $NiCl_2$ in DMF at 25° have appeared. It is likely that the active species is a hydroborate complex *e.g.* $NiH(BH_4)(DMF)_x$ or $Ni(BH_4)(DMF)_x$. Finally, the Ni(II) complexes $NiA(BH_4)ClO_4$ and $NiA(BH_4)_2$, where A is a nitrogen donor (cyclic tetramine or a noncyclic tetradentate Schiff base) have been reported (11) although in this present study we have been unable to stabilize Ni—BH_4 compounds using *o*-phenanthroline.

As in the case of cobalt, the product of the reaction between Ni(II) chloride and $NaBH_4$ in the presence of DBP depends on the amount of DBP present and the reaction temperature. With a Ni:DBP molar ratio of 1:3 in boiling ethanol, the dark brown diamagnetic Ni(0) complex $Ni(DBP)_2$ is formed, while a 1:6 ratio produces the red $Ni(DBP)_4$. No Ni—H bands were found in the i.r. spectra of these complexes and their reflectance spectra show only charge transfer transitions. Molecular weight data indicated extensive dissociation in benzene. These compounds are not isostructural with the analogous Co–DBP complexes, although $Ni(DBP)_4$ is presumably similar to $Ni(PPh_3)_4$ (30). However, if the above (1:6) reaction is carried out at room temperature an orange-yellow colored, paramagnetic ($\mu = 1.95$ B.M.) complex $NiCl(DBP)_3$ is formed even when an excess of $NaBH_4$ is used. Its reflectance spectrum (Fig. 2) is similar to that of $NiCl(PPh_3)_3$ with the broad band centered at $\sim$7600 cm^{-1}, and the Ni—Cl stretching frequency occurs at 272 cm^{-1} in the i.r. spectrum. Addition of more $NaBH_4$ and prolonged stirring produces $Ni(DBP)_4$ with no tetrahydroborate complex found in this case. Thus it would seem that the sterically bulky DBP prevents the substitution of chloride by the BH_4^- ion in both $CoCl(DBP)_3$ and $NiCl(DBP)_3$, although DBP appears to have a similar donor strength to PPh_3.

Unlike Co(II), $NiCl_2$ is not reduced to the metal in the presence of $AsPh_3$ or $SbPh_3$ by $NaBH_4$. In both cases the NiL_4 (30) complexes are formed. Similarly, Diphos forms $Ni(Diphos)_2$ (31).

We now turn to reactions between $NiCl_2.6H_2O$ and $NaBH_3CN$ in ethanol in the presence of phosphines. So far these reactions have yielded only Ni(II) compounds such as $NiH(BH_3CN)(PPh_3)_2$, $NiH(BH_3CN)(DBP)_3$, and $NiCl(BH_3CN)(Diphos)$ (Table 1). However, the paramagnetic ($\mu = 1.88$ B.M.) Ni(I) complex $Ni(BH_3CN)L_2$ (L = PPh_3) is formed from the reaction between $NiClL_3$ and $NaBH_3CN$ in ethanol. Its electronic reflectance spectrum (Fig. 2) is similar to that of $NiX(PPh_3)_3$, except that the weak higher energy band is not seen, while the i.r. spectrum (Table 2) shows a weak Ni—H—B band at 2070 cm^{-1} and very little shift of the CN stretching frequency (2185 cm^{-1}) compared to that of uncoordinated BH_3CN^- (2180 cm^{-1}). These data are consistent with a monomeric structure involving tetrahedral Ni(I)

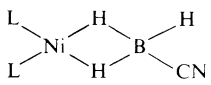

as shown. The nature of the ligand is once again extremely important in determining the product formed. Thus we were unable to isolate an analogous Ni(I)–BH_3CN–DBP complex from the reaction between $NiCl(DBP)_3$ and $NaBH_3CN$, which yielded $Ni(DBP)_2$.

Can. J. Chem. Downloaded from www.nrcresearchpress.com by 210.87.254.40 on 09/05/12
For personal use only.

The diamagnetic Ni(II) complexes $NiCl(BH_3CN)$(Diphos) and $NiH(BH_3CN)(PPh_3)_2$ have electronic spectra (Fig. 2) very characteristic of 4-coordinate, square planar d^8 systems. The i.r. spectra (Table 2) of the two compounds are different in that the former shows no Ni—H—B vibration while the latter has a band at 2140 cm^{-1}. This implies a different mode of attachment of BH_3CN in the two cases. Alternatively, the 2140 cm^{-1} band (and the 2138 cm^{-1} band in $NiH(BH_3CN)(DBP)_3$, see below) may be due to Ni—H vibrations at unusually high energy, although we were unable to find a hydride in the n.m.r. spectrum of $NiH(BH_3CN)(PPh_3)_2$, and the DBP compound is not sufficiently soluble for n.m.r. studies.

Most of the visible region of the electronic spectrum of the diamagnetic $NiH(BH_3CN)(DBP)_3$ is obscured by a charge transfer transition, but a very weak absorption occurs at $\sim$7600 cm^{-1}. While this is in the same position as the intense band in the spectrum of $NiCl(DBP)_3$ (Fig. 2), we have found no other evidence for reduction of Ni(II) by $NaBH_3CN$ and therefore the presence of a trace amount of this complex in $NiH(BH_3CN)(DBP)_3$ is not likely. Hence the weak absorption is probably an unusually low energy transition associated with the low spin d^8 system (32).

Palladium and Platinum Complexes

Tetrahydroborate and cyanotrihydroborate complexes of palladium and platinum could not be isolated even under the mildest reaction conditions employed in this study. For example, the room temperature reaction of *trans*-$PdCl_2(PPh_3)_2$ and *cis*-$PtCl_2(PPh_3)_2$ with $NaBH_4$ in ethanol in the presence of a large excess of ligand results in the deposition of the yellow complexes $M(PPh_3)_4$ (M = Pd or Pt) which have been prepared before in a number of different ways (30, 33). Similar reactions between the $PdCl_2L_2$ (L = PPh_3 or DBP) species and $NaBH_3CN$ also yield the PdL_4 complexes. The ML_4 (M = Pd or Pt, L = PPh_3 or DBP) derivatives may also be isolated from the reaction between $NaBH_4$, the metal(II) chloride, and a six-fold excess of ligand under reflux in ethanol.

The room temperature reaction of $PtCl_2L_2$ (L = PPh_3 or DBP) with $NaBH_3CN$ in ethanol in the presence of an excess of ligand leads to the unexpected formation of the platinum(II) cyanohydrido complexes $PtH(CN)L_2 \cdot 0.5C_6H_6$ (L = PPh_3 or DBP). This reaction does not appear to be general and its synthetic value is uncertain at present. The i.r. spectra (Table 2) of these complexes contain bands associated with Pt—H stretching and bending modes and also to a C≡N stretching mode. The complex $PtH(CN)(PPh_3)_2$ has been previously reported (34, 35) but the methods of preparation differ considerably from that used here.

Conclusions

In this study, reactions between $NaBH_4$ or $NaBH_3CN$ and Cr(III), Mn(II), Fe(II), Fe(III), Pd(II), or Pt(II) halides in the presence of various ligands have not yielded complexes containing coordinated BH_4 or BH_3CN groups. In the Co, Ni, and Cu cases, it appears that the nature of the product depends essentially on three factors:

(*1*) *Ease of reduction of the metal.* For example the stability of the $M(BH_4)(PPh_3)_3$ complexes is clearly in the order Cu > Co > Ni ≫ Pd and Pt. The less powerful reducing properties of $NaBH_3CN$ are probably responsible for the absence of the direct formation of Ni(I)–BH_3CN complexes while Co(I) and Cu(I) are readily formed under similar conditions.

(*2*) *Nature of the ligand.* In this work, it was found that only PPh_3 stabilized the Co(I) and Ni(I)–BH_4 complexes, the more bulky, rigid DBP and Diphos leading generally to the formation of hydrido species of Co(I) (*e.g.* CoH(Diphos)$_2$ (25*a*)), or zero valent complexes such as $Ni(DBP)_4$ or $Ni(Diphos)_2$ (31), while $AsPh_3$ and $SbPh_3$ resulted in reduction (even of Cu(I)) to the metals, except in the case of nickel. Nitrogen bases do not generally stabilize these lower oxidation states.

(*3*) *Experimental conditions.* It is well established (30) that divalent metal halides can be reduced by $NaBH_4$ under refluxing conditions producing, generally, metal(0) complexes *e.g.* $M(PPh_3)_4$ M = Ni, Pd, Pt), although whether this is a stepwise reduction M(II) → M(I) → M(0), or whether reduction occurs through a dihydride intermediate is not known. By carefully controlling reaction conditions of temperature, time, and mole ratios of reactants, we have identified intermediate products and therefore suggest the following stepwise mechanism for the reduction process for divalent metal halides:

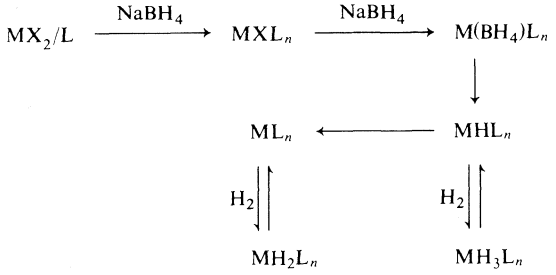

(L = phosphines or possibly N_2 or CO, n = 2, 3, or 4)

The final product then will depend on a combination of factors outlined in points *1*, *2*, and *3*. For example, $Cu(BH_4)L_n$ species are particularly stable while in the Ni, Pd, and Pt series, only the unstable $Ni(BH_4)L_n$ complex has been isolated (with difficulty) and therefore reactions involving these metal halides readily result in the ML_n species. Reduction to the M(0) state is therefore likely to go through a M(I) hydride complex, such as, for example, $NiH(N_2)(PEt_3)_2$ (36), prepared by the reaction of triisobutylaluminum and bis(acetylacetonato) nickel(II). $Co(BH_4)L_n$ forms readily and $CoHL_n$ complexes have been reported. (25). Oxidative addition of H_2 to MHL_n or ML_n probably accounts for the formation of CoH_3L_3 (24) and $FeH_2(Diphos)_2$ (37).

This mechanism is probably not restricted to divalent metal halides and hydrido complexes such as RuH_2L_4, $RuHL_4$, and IrH_3L_3, prepared (38) by $NaBH_4$ reduction of the metal chlorides in ethanol under reflux are probably the decomposition products of the intermediate tetrahydroborate complexes. Indeed $RuH(BH_4)L_3$ and $IrH_2(BH_4)L_3$ have been isolated in our laboratories and are being investigated.

Experimental

Materials

DBP was prepared by the method of Hoffmann (39). All other reagents were used without further purification. All solvents were purified in the usual way, degassed, and stored over molecular sieves (4A).

Physical Measurements

Room temperature magnetic moments were measured in the standard way using a double ended Gouy tube suspended from a semimicro balance between the poles of a Varian magnet. All other physical measurements were carried out as previously described (40). Infrared spectra were calibrated using polyethene.

Syntheses

All reactions were carried out under nitrogen atmospheres in glove boxes. The complexes were prepared by dissolving the metal halide in ethanol followed by the addition of the phosphine at room temperature. $NaBH_4$ or $NaBH_3CN$, suspended in ethanol, was then added dropwise and the mixture stirred by a magnetic stirrer for periods which varied between 2 and 20 h depending on the reaction. The product was separated, washed with ethanol, ethanol/water, ethanol, and *n*-hexane and recrystallized either from benzene/*n*-hexane or chloroform/*n*-hexane if necessary. Yields were generally high. Unless otherwise specified, the amount of $NaBH_4$ or $NaBH_3CN$ used in the reactions amounted to a 6–10 *M* excess over the metal concentrations. Analytical data are recorded in Table 1.

Copper Complexes

$CuCl_2 \cdot 2H_2O$ (0.15 g) was dissolved in ethanol (15 ml) and the phosphine (6 *M* excess) added. A white precipitate formed on stirring the mixture. A saturated solution of $NaBH_4$ or $NaBH_3CN$ in ethanol (10 ml) was then added to the mixture which was stirred at room temperature for $\sim\frac{1}{2}$ h before isolation of the product.

$Co(BH_4)(PPh_3)_3$

$CoCl_2 \cdot 6H_2O$ (0.21 g) was mixed with PPh_3 (1.41 g) in ethanol (20 ml). Dropwise addition of sufficient of a saturated solution of $NaBH_4$ in ethanol to give a Co:BH_4 mole ratio of 1:1 immediately produced $CoCl(PPh_3)_3$. Further addition of $NaBH_4$ (at least a 10 *M* excess) was made and the reaction mixture stirred for 3 h before isolation of the complex. $CoBr_2$ and CoI_2 hydrates gave the same complex.

Recrystallization of $Co(BH_4)(PPh_3)_3$ from nitrogen saturated benzene and *n*-hexane resulted in the uptake of varying amounts of dinitrogen and the formation of presumably $Co(N_2)(BH_4)(PPh_3)_3$.

$CoCl(DBP)_3$

$CoCl(DBP)_3$ was prepared in a similar way to $CoCl(PPh_3)_3$. Addition of more $NaBH_4$ to the chloride complex *in situ* with stirring for ~60 h resulted in the formation of $Co(DBP)_4$.

$Co(BH_3CN)(DBP)_4$ and $Co(BH_3CN)(Diphos)_2$

These complexes were prepared in a way analogous to that used for $Co(BH_4)(PPh_3)_3$. Varying amounts of nitrogen can be incorporated into $Co(BH_3CN)(DBP)_4$ by recrystallization in a nitrogen atmosphere.

$NiXL_3$ ($L = PPh_3$, $X = Cl$, Br, or I; $L = DBP$, $X = Cl$)

PPh_3 or DBP (0.7 g) was added to NiX_2 hydrates (6:1 molar ratio) in ethanol followed by a 1 molar ratio of $NaBH_4$, suspended in ethanol. The mixture was stirred for ~3 h when the solid products had precipitated as orange red to brown solids. Prolonged stirring (20–40 h) of $NiCl(DBP)_3$ in an excess of $NaBH_4$ produced $Ni(DBP)_4$.

$Ni(BH_4)(PPh_3)_3$ and $Ni(BH_3CN)(PPh_3)_2$

$NaBH_4$ (6–10 *M* excess) was added to $NiX(PPh_3)_3$ (X = Cl, Br, I) *in situ* and the mixture stirred for 18–20 h. In each case the yellow-brown $Ni(BH_4)(PPh_3)_3$ was produced.

$Ni(BH_3CN)(PPh_3)_2$ was prepared by suspending $NiCl(PPh_3)_3$ in ethanol and adding an excess of $NaBH_3CN$. The reaction mixture was stirred for 20 h.

Can. J. Chem. Downloaded from www.nrcresearchpress.com by 210.87.254.40 on 09/05/12
For personal use only.

$NiH(BH_3CN)(PPh_3)_2$, $NiH(BH_3CN)(DBP)_3$, or $NiCl(BH_3CN)$(Diphos)

$NiCl_2 \cdot 6H_2O$ (0.2 g) and either a 2 *M* excess of Diphos or a 6 *M* excess of the other phosphines were mixed in ethanol (20 ml) followed by the addition of an excess of $NaBH_3CN$. The mixture was stirred for 4–5 h before isolation of the product.

$M(DBP)_2$(M = Co, Ni):$M(DBP)_4$(M = Co, Ni, Pd, Pt)

These complexes were precipitated by heating under reflux in ethanol, mixtures of the metal halide, DBP (1:3 mole ratio for the former adduct, 1:6 for the latter), and an excess of $NaBH_4$. $Pd(DBP)_4$ was obtained even when the reaction was carried out at room temperature. Also, reaction of Pt and Pd(II) chlorides with $NaBH_4$ in the presence of PPh_3 at room temperature resulted in the $M(PPh_3)_4$ complexes.

$PtH(CN)L_2 \cdot 0.5C_6H_6$ (L = PPh_3 or DBP)

$PtCl_2$ and ligand (PPh_3 or DBP, 1.4 molar ratio) were heated under reflux in ethanol (20 ml) for 20 h. An excess of solid $NaBH_3CN$ was slowly added with stirring to the cooled solution which was then allowed to stand for 24 h. The solvent was removed under vacuum and the product was recrystallized twice from benzene/*n*-hexane and washed with *n*-hexane.

We thank the National Research Council of Canada for generous financial support of this work and one of us (A.N.H.) thanks the Faculty of Science, Mahidol University, Bangkok 4, Thailand for facilities provided during sabbatical leave. We also acknowledge discussions with Dr. I. M. Hoodless.

1. B. D. James and M. G. H. Wallbridge. Prog. Inorg. Chem. **11**, 99 (1970).
2. (*a*) S. J. Lippard and D. A. Ucko. Inorg. Chem. **7**, 1051 (1968); (*b*) J. M. Davidson. Chem. Ind. 2021 (1964).
3. F. Klanberg, E. L. Muetterties, and L. J. Guggenberger. Inorg. Chem. **7**, 2272 (1968).
4. E. L. Muetterties, W. G. Peet, P. A. Wegner, and C. W. Alegranti. Inorg. Chem. **9**, 2447 (1970).
5. R. C. Wade, E. A. Sullivan, J. R. Bershied, and K. F. Purcell. Inorg. Chem. **9**, 2146 (1970).
6. S. J. Lippard and P. S. Welcker. Inorg. Chem. **11**, 6 (1972).
7. P. C. Ford. Chem. Commun. 7 (1971).
8. F. Cariati and L. Naldini. Gazz. Chim. Ital. **95**, 3 (1965).
9. F. Cariati and L. Naldini. J. Inorg. Nucl. Chem. **28**, 2243 (1966).
10. D. F. Shriver. J. Am. Chem. Soc. **85**, 1405 (1963).
11. N. F. Curtis. J. Chem. Soc. 924 (1965).
12. S. J. Lippard and P. S. Welcker. Chem. Commun. 515 (1970).
13. M. L. H. Green, H. Munakata, and T. Saito. J. Chem. Soc. A, 469 (1971).
14. M. L. H. Green and H. Munakata. Chem. Commun. 1287 (1969).
15. H. Munakata and M. L. H. Green. Chem. Commun. 881 (1970).
16. D. G. Holah, A. N. Hughes, B. C. Hui, and K. Wright. Inorg. Nucl. Chem. Lett. **9**, 835 (1973); **10**, 427 (1974).
17. D. Budd, D. G. Holah, A. N. Hughes, and B. C. Hui. Can. J. Chem. **52**, 775 (1974).
18. S. J. Lippard and K. M. Melmed. J. Am. Chem. Soc. **89**, 3929 (1967).
19. K. M. Melmed, D. Coucouvanis, and S. J. Lippard. Inorg. Chem. **12**, 232 (1973).
20. L. Vaska, W. V. Miller, and B. R. Flynn. Chem. Commun. 1615 (1971).
21. R. A. Walton. Q. Rev. Chem. Soc. **19**, 126 (1965).
22. M. Aresta, M. Rossi, and A. Sacco. Inorg. Chim. Acta, **3**, 227 (1969).
23. A. Yamamoto, S. Kitazume, L. S. Pu, and S. Ikeda. J. Am. Chem. Soc. **93**, 371 (1971).
24. A. Sacco and M. Rossi. Inorg. Chim. Acta, **2**, 127 (1968).
25. (*a*) J. Lorberth, H. Nöth, and P. V. Rinze. J. Organomet. Chem. **16**, P1 (1969). (*b*) J. Chatt, F. A. Hart, and D. T. Rosevear. J. Chem. Soc. 5504 (1961).
26. C. F. Nobile, M. Rossi, and A. Sacco. Inorg. Chim. Acta, **5**, 698 (1971).
27. F. A. Cotton and G. Wilkinson. Advanced inorganic chemistry. 3rd ed. Interscience, New York. 1972. p. 903; L. Porri, M. C. Gallazzi, and G. Vitulli. Chem. Commun. 228 (1967).
28. P. Abley and F. J. McQuillin. J. Catal. **24**, 536 (1972).
29. A. G. Hinze and D. J. Frost. J. Catal. **24**, 541 (1972).
30. P. M. Maitlis. The organic chemistry of palladium. Vol. I, Metal complexes. Academic Press, New York. 1971. pp. 9–26 and references therein.
31. J. Chatt, F. A. Hart, and H. R. Watson. J. Chem. Soc. 2537 (1962).
32. M. Ciampolini. Struct. Bonding, **6**, 52 (1969).
33. R. Ugo. Coord. Chem. Rev. **3**, 319 (1968).
34. F. Cariati, R. Ugo, and F. Bonati. Inorg. Chem. **5**, 1128 (1966).
35. J. C. Bailar, Jr. and H. Itatani. J. Am. Chem. Soc. **89**, 1592 (1967).
36. S. C. Srivastava and M. Bigorgne. J. Organomet. Chem. **18**, P30 (1969).
37. M. Arresta, P. Giannoccaro, M. Rossi, and A. Sacco. Inorg. Chim. Acta, **5**, 115 (1971).
38. J. J. Levison and S. D. Robinson. J. Chem. Soc. A. 2947 (1970).
39. H. Hoffmann. Chem. Ber. **95**, 2563 (1962).
40. P. R. Heckley, D. G. Holah, and D. Brown. Can. J. Chem. **49**, 1151 (1971).

Can. J. Chem. Downloaded from www.nrcresearchpress.com by 210.87.254.40 on 09/05/12
For personal use only.

The Synthesis and Application of Anchored Catalysts in Hydrogen Isotope Exchange Systems. D_2 – Protic Solvent Exchange[1]

GRAEME STRATHDEE AND RUSSELL GIVEN

Research Chemistry Branch, Atomic Energy of Canada Limited, Whiteshell Nuclear Research Establishment, Pinawa, Manitoba R0E 1L0

Received March 7, 1974

GRAEME STRATHDEE and RUSSELL GIVEN. Can. J. Chem. **52**, 3000 (1974).

A number of polymer-attached, or anchored, catalysts of rhodium and ruthenium have been synthesized, and their activities for D_2 exchange with ethanol have been measured. Among the rhodium anchored catalysts, three exhibited specific activity comparable to Wilkinson's catalyst, $RhCl(PPh_3)_3$. No polymer-attached ruthenium species had specific activities close to that of the active homogeneous catalyst $RuCl_2(PPh_3)_3$. Conditions for the synthesis and optimum loading of complexing resins are discussed. Structural and kinetic comparisons are made between anchored catalysts and their homogeneous analogs.

GRAEME STRATHDEE et RUSSELL GIVEN. Can. J. Chem. **52**, 3000 (1974).

On a synthétisé un certain nombre de catalyseurs polymériques sur lesquels se trouvent fixés le rhodium et le ruthénium et mesuré leur activité pour l'échange de D_2 avec l'éthanol. Trois des catalyseurs sur lesquels le rhodium se trouve fixé, présentent une activité spécifique comparable au catalyseur de Wilkinson, $RhCl(PPh_3)_3$. Aucun catalyseur sur lequel le ruthénium se trouve fixé ne présente d'activité spécifique comparable au catalyseur homogène actif $RuCl_2(PPh_3)_3$. On discute des conditions pour la synthèse des résines complexantes, et de la façon d'obtenir une fixation optimale sur ces dernières. Des comparaisons structurales et cinétiques sont faites entre les catalyseurs ancrés et leurs analogues homogènes. [Traduit par le journal]

Introduction

Deuterium enrichment for production of heavy water is a topic of particular importance to us, since D_2O is an essential material for CANDU reactors. Several processes for concentration of deuterium make use of the variation of the equilibrium constants for hydrogen isotope exchange reactions with temperature. For example, the exchange of deuterium between hydrogen and water has been employed in a two-phase counter-current contactor (1):

[1] $$HDO + H_2 \rightleftarrows H_2O + HD$$

The exchange of HD with other protic solvents, particularly ammonia or amines, is also important.

Catalysts are required to promote rapid exchange of deuterium between hydrogen and water, or other protic solvents. Conventional metal catalysts, for example, of the supported or promoted Group VIII type, have been used but the specific activity is generally reduced significantly upon immersion in the liquid phase unless a protective hydrophobic coating is employed. Some soluble transition metal complexes promote H–D exchange but the maximum overall rate is often determined by the solubility limit of the complex. A third class of catalyst has received considerable attention recently: the polymer-supported transition metal complex catalyst, or anchored catalyst.

We have employed this nomenclature to signify that the metal atom essentially retains the properties of a homogeneous catalyst while being covalently bonded to a solid substrate with appropriate functional groups. Since the immobilized species is an analog of a homogeneous catalyst, it is useful to regard the active metal complex as fixed or anchored, in this case, to a polymer support. This terminology also avoids the imprecise use of the terms "homogeneous" or "heterogeneous" to describe these compounds. The synthesis and applications of these materials have been reviewed recently in considerable detail (2).

The following topics have been of importance to us and are considered in the text: (*i*) the synthesis of high capacity complexing resins; (*ii*) the synthesis of highly loaded anchored catalysts; (*iii*) the activities of anchored species relative to their homogeneous analogs; (*iv*) the process of complex formation on the resin.

[1]AECL No. 4796.

Can. J. Chem. Downloaded from www.nrcresearchpress.com by 210.87.254.6 on 09/05/12
For personal use only.

Can. J. Chem. Downloaded from www.nrcresearchpress.com by 210.87.254.6 on 09/05/12
For personal use only.

This work has dealt mainly with anchored rhodium(I) complexes.

Experimental

Preparations

All preparations were conducted in a nitrogen filled glove box purged with N_2 containing less than 10 p.p.m. oxygen. All solvents were slowly percolated through Linde 4A molecular sieves before distillation under flowing N_2.

Complexing Resins

A chloromethylated macroporous crosslinked polystyrene (Rohm and Haas, GRA-806) containing 5.74 mequiv. Cl per gram of dry resin was washed with water, ethanol, and THF and vacuum-dried. The resin was ground to a fine powder and was employed for all resin syntheses. Diphenylphosphinolithium was prepared quantitatively in one of two ways: (*i*) by reaction of 3.5 g (0.5 mol) Li metal in anhydrous THF distilled from $LiAlH_4$ with 25 ml (0.1 mol) chlorodiphenylphosphine and, (*ii*) by dilution of 5.35 g (28.6 mmol) diphenylphosphine (Alpha Inorganics) with 10 ml THF and slow addition of an equimolar amount of *n*-butyl lithium as 2.2 *M* solution in hexane. An excess of either Ph_2PLi solution was stirred with a portion of resin for 20 h at room temperature, then was filtered and washed with THF and ethanol to remove LiCl and any unreacted Ph_2PLi. A typical product contained 2.9 ± 0.1 mequiv. —PPh_2 and about 0.5 mequiv. Cl per gram of dry resin. This apparent reduction in capacity was due to the introduction of the high mass —PPh_2 group. A typical analysis was:

Anal. Calcd. for $C_{24}H_{23}Cl_{0.13}P$: C, 83.0; H, 6.6; Cl, 1.3; P, 8.9. Found: C, 81.7; H, 6.4; Cl, 1.3; P, 8.7.

The calculated formula may be regarded as that for a polymer composed of these monomers: 74% diphenyl-*p*-vinylbenzyl phosphine, 7% α-chloro-4-vinyltoluene, 4% divinylbenzene, and 15% styrene.

Metal Complexes

Literature methods were used to prepare the following compounds: μ-dichlorotetraethylenedirhodium(I) (3) (this complex remained stable if stored at 263 K under a positive pressure of C_2H_4); bis(ethylene)rhodium acetylacetonate (4); μ-dichlorodicyclopentadienerhodium(I) (5); dichlorotetrakis(dimethylsulfoxide)ruthenium(II) (6), dichlorobis(dimethylsulfoxide)(triphenylphosphine)-ruthenium(II) (6). Melting points and u.v. or infrared spectra agreed with those reported for these compounds.

Anchored Rhodium Complexes

(*I*) To a suspension of $(C_2H_4)_4Rh_2Cl_2$ (444 mg, 1.14 mmol dimer) in 10 ml of C_6H_6 was added 662 mg (1.92 mmol) —PPh_2 substituted resin. Ethylene was evolved. The mixture was stirred overnight at room temperature and filtered to yield a clear filtrate and a brown solid which was then vacuum dried. Chemical analysis yielded Rh:P = 0.56, therefore high loading had been achieved.

(*II*) $(C_2H_4)_2$Rhacac (0.5 g, 1.94 mmol) was dissolved in 10 ml C_6H_6 and added to 1.1 g of the resin with stirring. Rapid reaction occurred with evolution of C_2H_4. After 3 h the bright yellow resin was filtered and washed with C_6H_6, and 50 mg unreacted starting complex was recovered. Thus, 0.55 mol Rh reacted per mole —PPh_2. Chemical analysis showed Rh:P was 0.54. The ν_8 and ν_1 acetylacetonate bands (7) had intense maxima at 1580 and 1510 cm^{-1} respectively in the i.r. spectrum (KBr disk) as expected.

(*III*) An excess of $(C_{10}H_{12})_2Cl_2Rh_2$ (46 mg, 85 μmol) in 5.0 ml C_6H_6 was added to 58 mg of the resin (168 μmol P) and stirred until no further decrease in concentration of the complex was detectable by u.v.–visible spectrometry. Unreacted complex was washed from the resin with C_6H_6. The resin absorbed 0.25 mequiv. Rh per mequiv. —PPh_2.

(*IV*) Evolution of CO occurred during rapid quantitative reaction of about 50 mg $[Rh(CO)_2Cl]_2$ (Strem Chemicals) with excess resin in C_6H_6. The product had two carbonyl bands in the i.r. spectrum (KBr disk): 2085 m, 1950 s br cm^{-1}.

Anchored Ruthenium Complexes

(*V*) About 0.2 mmol of the cluster anion $Ru_5Cl_{12}^{2-}$,[2] prepared by H_2 reduction of hydrated $RuCl_3$ in CH_3OH over platinum black (8), was reacted with 2 g resin (5.8 mmol —PPh_2) for 3 days at room temperature. The pale green product was filtered, washed with CH_3OH, and vacuum dried.

(*VI*) One gram (1.04 mmol) of $RuCl_2(PPh_3)_3$ (Strem Chemicals) was dissolved in 50 ml $CHCl_3$ and 100 mg resin (0.29 mmol) was added. The suspension was stirred for 2 weeks under N_2, then the product was filtered, washed, and analyzed.

Anal. Calcd. for $C_{429}H_{491}Cl_7P_{19}Ru$: C, 78.3; H, 7.5; Cl, 3.8; P, 9.0; Ru, 1.5. Found: C, 75.4; H, 7.2; Cl, 3.7; P, 8.8; Ru, 1.5.

(*VII*) An excess of $RuCl_2[(CH_3)_2SO]_4$ (0.5 g, 1.03 mmol) and 0.15 g resin (0.43 mequiv. P) were suspended in toluene and heated at 353 K for 2 h. The light brown product was filtered and washed with toluene and ethanol. A low frequency shoulder at 1090 cm^{-1} on the ν(S═O) band in the i.r. spectrum suggested that unreacted starting material was present (6). Extraction with ethanol under N_2 in a Soxhlet apparatus was continued for several hours until the extract was colorless for several cycles. From the total weight of unreacted $RuCl_2(Me_2SO)_4$ (0.35 g, 0.723 mmol) the ratio of Ru to —PPh_2 in the product was calculated to be 0.71. The i.r. spectrum had ν(S═O) at 1132 s, 1115 s, and 1100 s cm^{-1}.

(*VIII*) $Fe_3(CO)_{12}$ (9) (0.27 g, 0.69 mmol) was dissolved in 25 ml anhydrous THF and filtered. The solution was added to 0.30 g resin (0.87 mequiv. P) and the suspension was stirred overnight at 353 K. The grey colored resin was filtered and washed with THF until the filtrate was clear. The carbonyl region of the i.r. spectrum (KBr disk) had intense bands at 2060 s, 1975 s, 1940 s br, 1897 m, 1875 m cm^{-1}.

D_2 Exchange Experiments

The procedure used to measure and calculate the rates of D_2 exchange with H_2O or C_2H_5OH as the protic solvent was similar to that previously described for

[2]Mercer and Dumas (27) have shown that the formulation of this cluster ion may be incorrect. This notation is used here for convenience.

experiments with $RhCl(PPh_3)_3$ (10). Dilute suspensions (about 0.10 g) in 20.0 ml of the solvent were generally used in a glass reactor of volume 95 ml. All rate data below are quoted as initial rates of exchange of D_2, calculated with the expression

$$[2] \qquad -d[D_2]/dt = \ln [(n_0 - n_e)/(n_t - n_e)]A/t$$

where n_0 and n_t = gas phase mol% D_2 at $t = 0$ and $t = t$ s, and n_e was the value at equilibrium. The gas:liquid ratio A = initial D_2 (mol) ÷ liquid volume (liters).

Generally the decay of D_2 was accurately first-order during the periods of observation which were up to 5 h. There was never any loss of catalytic activity with time, but in some experiments the exchange rates increased with time to upper limiting values. These cases are identified in the text.

Hydrogenation of Butene-1

A suspension of 80 mg of the catalyst in C_2H_5OH was equilibrated with 88 kPa of H_2 for 15 minutes in a reaction flask of 0.120 l total volume. Hydrogenation commenced with injection of 5.0 ml butene-1. Gas phase samples were taken with a gas sampling valve and were fractionated on 2.0 m *n*-octane Durapak at 25 °C.

Results

Resin Syntheses

Preparation of Ph_2PLi by reaction 3 was more rapid and convenient than by reaction 4

$$[3] \qquad n\text{-}C_4H_9Li + Ph_2PH \rightarrow n\text{-}C_4H_{10} + Ph_2PLi$$

$$[4] \qquad Ph_2PCl + 2Li \rightarrow Ph_2PLi + LiCl$$

About 90% of the chlorine in the chloromethylated divinylbenzene-crosslinked polystyrene was replaced by reaction with Ph_2PLi. The specific volume of the dry resin had approximately doubled after this substitution reaction due to introduction of the large Ph_2P group. Probably reaction of the residual Cl was prevented by the large volume requirement of the diphenylphosphine group.

Anchored Catalyst Syntheses

With Rh Complexes

Rapid, quantitative attachment of a metal complex to the resin was achieved if the initial reagent complex (*i*) was very soluble in the solvent used, and (*ii*) possessed a small, volatile ligand easily displaced by the Ph_2P function. For example, $Rh(C_2H_4)_2acac$ reacted readily with the resin with evolution of C_2H_4, whereas the precursor dimer $[Rh(C_2H_4)_2Cl]_2$ which was relatively insoluble in C_6H_6, reacted more slowly. The bulky dimer $[(C_{10}H_{12})_2RhCl]_2$, although more soluble in benzene than $[(C_2H_4)_2RhCl]_2$, also was absorbed slowly, probably because of the greater steric requirements of the large dicyclopentadiene ligand.

Volatile carbon monoxide was readily displaced from the soluble dimer $[Rh(CO)_2Cl]_2$ by the PPh_2 group of the resin. The analogous homogeneous reaction with PPh_3 is complex, giving several carbonyl-containing dimers and *trans*-$Rh(CO)Cl(PPh_3)_2$ (11, 12). The presence of the broad, intense i.r. band at 1950 cm^{-1} suggested that most of the Rh(I) had been anchored as *trans*-$Rh(CO)Cl(Ph_2P—)_2$. However, the moderately intense band at 2085 cm^{-1} indicated that some Rh(I) was present as a dimer, perhaps as

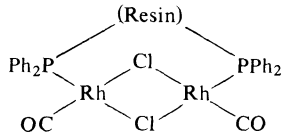

Presumably, the second ν(C≡O) band expected from this species was hidden under the broad 1950 cm^{-1} peak (11). Because it has been demonstrated in the homogeneous case that intermediates of this type do form (11, 12) this carbonyl displacement reaction cannot be employed to demonstrate that coordination of PPh_2 to a metal center in this anchored catalyst is unique and stereospecific.

With Ru Complexes

It was desirable to anchor an analog of the extremely active homogeneous catalyst $RuCl_2(PPh_3)_3$ (13). Since no suitable Ru(II) complexes existed which would enable resin attachment to be achieved by ligand displacement, two different approaches (*V* and *VI*) were tried. The slow reaction of "$Ru_5Cl_{12}^{2-}$" with the resin gave a green product, probably a Ru(III) species. In view of the low catalytic activity of this material, the identity of the complex was not investigated. In contrast, PPh_3 reacts readily with "$Ru_5Cl_{12}^{2-}$" in solution to yield $RuCl_2(PPh_3)_3$ (14). This suggests that either the fixed PPh_2 groups on the resin cannot participate in the complex cleavage of the cluster anion or the large "$Ru_5Cl_{12}^{2-}$" anion cannot penetrate the resin matrix for steric reasons.

Reaction of a large excess of $RuCl_2(PPh_3)_3$ with the complexing resin anchored only 1.5 weight percent Ru. This ligand exchange procedure (—PPh_2 for PPh_3) is extremely slow both in this Ru(II) case and in Rh(I) system

Can. J. Chem. Downloaded from www.nrcresearchpress.com by 210.87.254.6 on 09/05/12
For personal use only.

studied by Grubbs *et al.* (15). Since the yield of anchored Ru(II) was so low, we did not determine if the magnitude of the equilibrium constant for the ligand exchange reaction

[5] $RuCl_2(PPh_3)_3 + n(Ph_2P—) \rightleftarrows RuCl_2(PPh_3)_{3-n}(Ph_2P—)_n + (3 - n)PPh_3$

or the component rate constants were limiting.

The infrared spectrum of the anchored complex obtained by reaction of $RuCl_2[(CH_3)_2SO]_4$ with the resin (preparation *VII*) differed from that of $RuCl_2[(CH_3)_2SO]_2PPh_3$ prepared by the method of Evans *et al.* (6). All three Ru complexes had two intense S-bonded ν(S=O) bands centered at 1120 and 1090 cm^{-1}. In addition, the anchored complex had a strong shoulder at 1135 cm^{-1}. Since the S=O stretch occurs at 1055 cm^{-1} in neat $(CH_3)_2SO$ and at 928 cm^{-1} for O-bonded $(CH_3)_2SO$ in $RuCl_2[(CH_3)_2SO]_4$ (6), the 1135 cm^{-1} band may be due to the presence of an isomeric analog of $RuCl_2[(CH_3)_2SO]_2PPh_3$ on the resin. It is also possible that the resin functioned to some extent as a tridentate ligand towards Ru(II). Evans *et al.* (6) found that triphenylphosphite, $(PhO)_3P$, a less sterically demanding ligand than PPh_3, yielded the complex $RuCl_2[(PhO)_3P]_3[(CH_3)_2SO]$. Molecular models showed that the phosphorous atom is somewhat less hindered in the resin than in PPh_3.

With Fe Complexes

The reaction of PPh_3 with Fe(0) carbonyls yields a mixture of $Fe(CO)_4(PPh_3)$ and $Fe(CO)_3(PPh_3)_2$. Each compound possesses a distinct infrared spectrum and detection of each in a mixture is a simple matter. It was of interest to determine if the complexing resin acted as a mono- or bi-dentate ligand towards Fe(0).

Triiron dodecacarbonyl was reacted with the resin (preparation *VIII*) to yield a product with an infrared spectrum in the carbonyl region identical to that for $Fe(CO)_4PPh_3$, except for a weak shoulder at 1875 cm^{-1}. This peak may have been due to the formation of a trace of an analog of $Fe(CO)_3(PPh_3)_2$. These data are summarized in Table 1.

These data show that the complexing resin functioned mainly as a monodentate ligand towards carbonyl stabilized Fe(0). The product distribution may have been affected by the use of $Fe_3(CO)_{12}$ instead of $Fe(CO)_5$, for example by the size of the molecular triiron complex, the mechanism of the cleavage process, or the rigidity of the $—PPh_2$ functional group in the resin matrix. However, in the fully homogeneous case with PPh_3, the product distribution is independent of the iron carbonyl complex used (9, 16).

TABLE 1. Comparison of infrared spectra in the carbonyl region for Fe(0) complexes

Complex	Infrared bands (cm^{-1})
$Fe(CO)_4PPh_3$	2055 s, 1977 s, 1935 s br, 1895 m
$Fe(CO)_3(PPh_3)_2$	1875 s br
Reaction product Resin + $Fe_3(CO)_{12}$	2055 s, 1975 s, 1930 s br, 1895 m, 1875 m

Catalytic Activity

D_2–C_2H_5OH Exchange

As noted in the experimental section, the decay of D_2 was usually accurately first-order. This is illustrated in Fig. 1 for catalyst *II* prepared from $(C_2H_4)_2$ Rh acac and the complexing resin. The effect of addition of concentrated HCl is clearly shown. Other catalysts caused D_2 to exchange on approximately the same time-scale. The catalyst activities have been compared on the basis of initial rates,

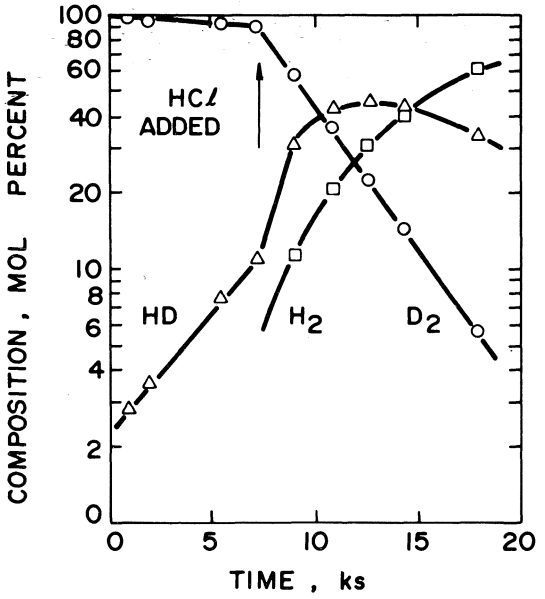

FIG. 1. D_2–C_2H_5OH exchange catalyzed by Rh-catalyst *II*. Addition of 200 μl concentrated HCl was made at 7.3 ks.

Can. J. Chem. Downloaded from www.nrcresearchpress.com by 210.87.254.6 on 09/05/12
For personal use only.

TABLE 2. Anchored catalyst activity for D_2 exchange with H_2O and C_2H_5OH*

Starting metal complex	Preparation number	Initial rate of D_2 exchange ($\times 10^6$) (Mol D_2/gram catalyst second) in H_2O	in C_2H_5OH
$[(C_2H_4)_2RhCl]_2$	*I*	76	1.9
$(C_2H_4)_2Rh$ acac†	*II*	8.3	6.9
$[(C_{10}H_{12})RhCl]_2$	*III*	105	25.0
$Ru_5Cl_{12}^{2-}$	*V*	—	0.4‡
$RuCl_2(PPh_3)_3$	*VI*	—	1.8
$RuCl_2[(CH_3)_2SO]_4$	*VII*	—	0.5

*T, 298 K; P, 88 kPa D_2.
†In 0.1 M HCl.
‡Rate ($\times 10^6$) was 19 mol D_2 g^{-1} s^{-1} with excess $TiCl_3$ added to suspension.

calculated from the slopes of these log D_2 *vs.* time plots and the gas:liquid ratios (*c.f.* eq. 2).

Initial rates per gram for D_2–H_2O and D_2–C_2H_5OH exchange in the presence of some of the anchored catalysts noted above are summarized in Table 2. Those not listed were inactive for this D_2 exchange application. The catalysts will be referred to below by preparation number.

Rhodium Catalysts

(*I*) and (*II*) These anchored species are considered similar. Little catalytic activity for D_2 exchange was exhibited by *II* until the acetylacetonate ligand was displaced by addition of 200 μl of concentrated HCl to the ethanolic suspension. Table 3 contains a comparison of the rates of D_2–C_2H_5OH exchange per equivalent of rhodium for *I* and *II* together with that for the homogeneous analog $RhCl(PPh_3)_3$ in 1:1 $CHCl_3$–C_2H_5OH (19). The specific rates for *I*, *II*, and $RhCl(PPh_3)_3$ are similar, suggesting that the catalytically active species are closely related. The higher specific rate obtained with *II* may indicate that the Rh(I) metal center was stabilized by just two PPh_2 groups of the resin, that is, it was coordinatively unsaturated. Montelatici *et al.* (20) have shown that maximum activity for olefin hydrogenation occurs in the $RhClL_n$ class of homogeneous catalysts when $n = 2$. Alternatively, it is possible that the excess HCl added to activate *II* acted as a co-catalyst for D_2 exchange. We have observed this behavior with $RhCl(PPh_3)_3$ (19).

TABLE 3. Comparison of anchored and homogeneous rhodium and ruthenium catalysts for D_2–C_2H_5OH exchange[a]

Catalyst	Initial rate ($\times 10^3$) (mol D_2/mol metal second)
I	1.4
II[b]	6.5
$RhCl(PPh_3)_3$[c]	6.3
VI	12.3
$RuCl_2(PPh_3)_3$[d]	113.0
VII	0.30
$RuCl_2[(CH_3)_2SO]_4$[e]	0.21
$RuCl_2[(CH_3)_2SO]_2PPh_3$[f]	1.19

[a]T, 298 K; P, 88 kPa D_2.
[b]In 0.1 M HCl.
[c]1.1 mM in 1:1 $CHCl_3$–C_2H_5OH.
[d]5.6 mM in 1:1 C_6H_6–C_2H_5OH.
[e]3.1 mM in 1:1 C_6H_6–C_2H_5OH.
[f]2.9 mM in 1:1 C_6H_6–C_2H_5OH.

Care must be taken in the synthesis of *I* to avoid the formation of metallic rhodium, an extremely effective D_2 exchange and hydrogenation catalyst (17). Some preparations of *I* possessed catalytic activities more than 1000 times that shown in Table 3. Electron microscopy on the powdered resin samples showed that particles in the range 500–1000 Å were in the matrix. X-Ray diffraction analysis proved that rhodium was present. This metal may have been formed by (*i*) reduction of unreacted starting material absorbed on, but not complexed by, the resin, (*ii*) by reduction of partially PPh_2-stabilized Rh(I), or (*iii*) because Rh particles were present in the $[(C_2H_4)_2RhCl]_2$. Data reported in Table 3 are for anchored catalysts which did not promote hydrogenation of benzene. This is a sensitive test for the presence of Rh or Ru metal in these materials.

We attribute the exchange rate increase observed with *I* in H_2O to reduction of some Rh(I) to the metal. The solubility of D_2 is less in H_2O than in C_2H_5OH, thus the enhanced

Can. J. Chem. Downloaded from www.nrcresearchpress.com by 210.87.254.6 on 09/05/12
For personal use only.

Can. J. Chem. Downloaded from www.nrcresearchpress.com by 210.87.254.6 on 09/05/12
For personal use only.

activity cannot be explained by this factor (18). A similar effect is not noted with *II* which also required activation by HCl in H_2O suspension.

(*III*) The exchange rate quoted in Table 2 was calculated from the upper limiting value of the experimental rate constant reached after 2 h of exchange. This anchored complex had approximately the same specific activity per mol Rh as did *I* and *II*: 2.6×10^{-3} mol D_2/mol Rh s. This may be compared with 1.5×10^{-3} mol D_2/mol Rh s obtained for the homogeneous catalyst prepared by reacting 3:1 PPh_3 and $(C_{10}H_{12})_2Rh_2Cl_2$ in 1:1 $CHCl_3$–C_2H_5OH at 298 K and 88 kPa D_2. The higher activity per gram of *III* over *I* and *II* was not due to the presence of Rh metal.

Ruthenium Catalysts

(*V*) and (*VI*) It was expected that these anchored complexes would be analogs of the extremely efficient homogeneous catalyst $RuCl_2(PPh_3)_3$. Reaction of "$Ru_5Cl_{12}^{2-}$" with excess PPh_3 readily yields this Ru(II) complex (14), and n.m.r. ligand exchange studies (21) have indicated that the phosphines in $RuCl_2(PPh_3)_3$ are labile, so that exchange of the resin with excess $RuCl_2(PPh_3)_3$ should have yielded a related anchored complex. Data in Table 3 illustrate that the anchored Ru species *VI* had little D_2 exchange activity compared to $RuCl_2(PPh_3)_3$. Perhaps this is because the anchored species were Ru(III) rather than Ru(II) complexes, since addition of the reducing agent $TiCl_3$, which converts Ru(III) to Ru(II), enhanced the exchange rate with *V* by a factor of 47 (*c.f.* Table 2).

(*VII*) This anchored catalyst and the precursor dimethylsulfoxide complexes $RuCl_2[(CH_3)_2SO]_4$ and $[RuCl_2[(CH_3)_2SO]_2PPh_3$ were all comparatively inactive for D_2–ethanol exchange. Our infrared spectroscopic study indicated that the anchored species was essentially equivalent to the PPh_3 derivative. The rate data in Table 3 show that the anchored species was about four times less active per mol of Ru than was $RuCl_2[(CH_3)_2SO]_2PPh_3$. The low activity of the common starting complex confirmed that the exchange in the presence of the anchored catalyst was not due to physically adsorbed $RuCl_2[(CH_3)_2SO]_4$ on the resin. Thus, a reduction in specific catalytic activity was evident upon resin attachment.

TABLE 4. Hydrogenation of butene-1*

Catalyst	Initial rate of hydrogenation ($\times 10^3$) (mol butene-1/mol Rh s)
II	1.76
II + 5 m*M* HCl	11.7
$RhCl(PPh_3)_3$†	55.5

*T, 298 K; P, 88 kPa.
†4.3 m*M* in 1:1 C_6H_6–C_2H_5OH.

Hydrogenation of Butene-1

The activity of catalyst *II* for hydrogenation of butene-1 was assessed. Table 4 shows that the rate obtained with *II* was increased more than six times if a 10:1 excess of HCl:anchored rhodium was added. The datum for the homogeneous catalyst $RhCl(PPh_3)_3$ taken under similar conditions was somewhat higher, but was within a factor of 5 of that for *II*. This difference may arise with solvent or mass transport effects in the resin.

Discussion

High Capacity Complexing Resins

The preparation of anchored catalysts with high activity per gram requires a resin with the maximum number of complexing functional groups per unit weight. It is also desirable to employ cross-linked resins of the porous or macroreticular type to minimize effects of reagent diffusion.

The diphenylphosphino group was readily attached to the chloromethylated polystyrene substrate in about 90% yield based on Cl by using diphenylphosphinolithium as the coupling agent. Other methods may be employed such as the polymerization of vinyldiphenylphosphine (22), diphenyl-*p*-strylphosphine (22, 23), or by lithiating the halogen substituted resin followed by reaction with Ph_2PCl (24, 25). Different supporting polymers such as polyvinyl chloride have also been used (26). However, we favor the route discussed above because of its facility, convenience (*c.f.* ref. 14) and the fact that the copolymer structure is uniform.

Synthesis of Highly Loaded Anchored Catalysts

To obtain high overall conversion rates for a given reaction it is necessary that the quantity of catalyst per unit reactor volume be as large as possible. It is therefore desirable that the catalyst itself have a high activity or loading

Can. J. Chem. Downloaded from www.nrcresearchpress.com by 210.87.254.6 on 09/05/12
For personal use only.

factor per unit volume. For the case of anchored catalysts, the number of functional groups required to stabilize and activate a metal atom should be kept to a minimum.

Our results show that these criteria are best met by using soluble starting metal complexes which have small volatile ligands easily displaced by the functional group of the complexing resin. For example, the Rh(I) complexes $(C_2H_4)_2$Rhacac and $[Rh(CO)_2Cl]_2$ reacted rapidly and quantitatively with the diphenylphosphino-substituted resin. The less soluble $[(C_2H_4)_2RhCl]_2$ and the larger $[C_{10}H_{12}RhCl]_2$ required longer reaction times. The levels of rhodium present in the catalysts prepared by these ligand substitution methods were higher than those obtained by simple PPh_3 ligand exchange of $RhCl(PPh_3)_3$ with the PPh_2 groups of the resin (15).

From a synthetic point of view, it should not be assumed that metal species attached to resins by these techniques will be exact analogs of active homogeneous catalysts such as $RhCl(PPh_3)_3$ or $RuCl_2(PPh_3)_3$. The chemical evidence of Collman *et al.* (25) and our construction of molecular models show that PPh_2-substituted styrene-divinylbenzene polymers can behave either as mono- or bidentate ligands. The steric requirements of the aromatic groups which surround the P(III) centers, and the restricted rotation of these ligand units about the polymer backbone make tridentate coordination by three adjacent PPh_2 units essentially impossible. In the limiting case, it may be shown with molecular models that either two adjacent or two alternate PPh_2 groups on the same polymer chain may bond to a metal atom. A third PPh_2 in close proximity, but from a neighboring chain, may participate to provide the equivalent of tridentate coordination. It is also possible that PPh_2 groups from different polymer chains may complex the metal atom.

The infrared spectrometric data suggest that some anchored species are similar to their homogeneous analogs. For example the spectrum of *IV* resembles that of $RhCl(CO)(PPh_3)_2$, that of *VII* is like that of $RuCl_2[(CH_3)_2SO]_2PPh_3$, and that of *VIII* is similar to that of $Fe(CO)_4$-PPh_3. Unfortunately, the spectra of those catalysts which possessed the highest activities for D_2 exchange were not suitable for this type of comparison.

A Comparison of the Catalytic Activities of Anchored Species Relative to Their Homogeneous Analogs

The activity of rhodium catalysts *I* and *II* was equivalent to that of $RhCl(PPh_3)_3$ for D_2–C_2H_5OH exchange (*c.f.* Table 3). Catalyst *II* promoted butene-1 hydrogenation at a specific rate five times lower than that obtained with $RhCl(PPh_3)_3$ (*c.f.* Table 4). Collman *et al.* (25) have found that a similar polymer-attached Rh(I) catalyst, prepared using $RhCl(C_2H_4)$-$(PPh_3)_2$ and a PPh_2-substituted resin, had similar activity to Wilkinson's catalyst for olefin reduction. In contrast, Grubbs *et al.* found that the anchored Rh(I) catalyst obtained by ligand exchange of $RhCl(PPh_3)_3$ with the same type of resin gave a product which was about 16 times less active per mole of Rh (15). We have found no evidence that the specific catalytic activity of either Rh or Ru is enhanced upon anchoring, compared to that of their homogeneous analogs.

Such comparisons must be made with caution in view of the effects of olefin size and solvent polarity which Grubbs *et al.* (15) have discussed. Undoubtedly, the active coordination site of the homogeneous catalyst will be generally more accessible to incoming substrate molecules compared to the anchored species in the matrix of a cross-linked polymer. We suggest that comparison of the rates of hydrogen isotope exchange reactions involving small molecules may be a better test for the relative activities of related anchored and homogeneous catalysts than the comparison of the rates of olefin hydrogenation reactions.

Anchored Complex Formation

The feasibility of preparation of a particular anchored catalyst must depend on the chemistry of the anchoring reaction. In this work, the same complexing resin has functioned as a monodentate ligand in the reactions with $Fe_3(CO)_{12}$ and $RuCl_2[(CH_3)_2SO]_4$. By analogy with the work of Collman *et al.* (25), it is probably also monodentate with $[(C_{10}H_{12})$-$RhCl]_2$. The resin behaved at least as a bidentate ligand in the Rh(I) compounds *I* and *II*.

The Fe(0) example is particularly important, because in the homogeneous case $Fe_3(CO)_{12}$ reacted with excess PPh_3 to yield about equal quantities of mono- and disubstituted products

$Fe(CO)_4PPh_3$ and $Fe(CO)_3(PPh_3)_2$ (9). Under similar conditions, the reaction with the resin gave only the monosubstituted complex, perhaps because the PPh_2 ligand sites were insufficiently free to displace a second mole of CO. Thus, steric control of anchored species must be anticipated in some systems.

The reaction between $RuCl_2[(CH_3)_2SO]_4$ and PPh_3 is facile in the homogeneous case and yields the monosubstituted $RuCl_2[(CH_3)_2SO]_2$-PPh_3. The group $RuCl_2[(CH_3)_2SO]_2$ appeared to be the dominant one attached to the resin, but our infrared and catalytic evidence suggested that the two cases were not identical. The possibility that isomeric modifications of species present in solution might become attached to the resin must be considered.

Conclusions

In the Rh(I) case, a comparison of specific activities has shown that an anchored analog of the efficient homogeneous catalyst $RhCl(PPh_3)_3$ may be synthesized by several methods. We have been unable to fix a Ru(II) species, with activity comparable to the homogeneous catalyst $RuCl_2(PPh_3)_3$, to the complexing resin.

Since D_2 exchange or olefin conversion reactions over an anchored catalyst or its homogeneous analog may proceed at similar rates per mole of metal, the use of dense anchored catalyst slurries will enable the reaction rates at the solubility limit of the homogeneous catalyst to be exceeded. Problems associated with precipitation, dimerization, or side-reaction of soluble catalysts may thus be avoided.

The authors wish to thank M. Tomlinson and Dr. N. H. Sagert for useful discussions, and D. Bell and his assistants for the deuterium analyses.

1. S. Walter, E. Nitschke, C. Bode, E. W. Becker, R. P. Hübener, R. W. Kessler, and U. Schindewolf. Angew. Chem. Int. Ed. Engl. **1**, 21 (1962).
2. N. Kohler and F. Dawans. Rev. Inst. Fr. Pét. **27**, 105 (1972).
3. R. Cramer. Inorg. Chem. **1**, 722 (1962).
4. R. Cramer. J. Am. Chem. Soc. **86**, 217 (1964).
5. J. Chatt and L. M. Venanzi. J. Chem. Soc. 4735 (1957).
6. J. P. Evans, A. Spencer, and G. Wilkinson. J. Chem. Soc. Dalton, 204 (1973).
7. K. Nakamoto. Infrared spectra of inorganic and coordination compounds. Wiley, New York. 1963. p. 216.
8. D. Rose and G. Wilkinson. J. Chem. Soc. A, 1791 (1970).
9. A. F. Clifford and A. K. Mukherjee. Inorg. Synth. **8**, 185 (1965).
10. G. G. Strathdee and R. M. Given. Can. J. Chem. **52**, 2216 (1974).
11. D. F. Steele and T. A. Stephenson. J. Chem. Soc. Dalton, 2161 (1972).
12. J. Gallay, D. de Montauzon, and R. Poilblanc. J. Organomet. Chem. **38**, 179 (1972).
13. P. S. Hallman, B. R. McGarvey, and G. Wilkinson. J. Chem. Soc. A, 3143 (1968).
14. J. D. Gilbert, D. Rose, and G. Wilkinson. J. Chem. Soc. A, 2765 (1970).
15. R. H. Grubbs, L. C. Kroll, and E. M. Sweet. J. Macromol. Sci. Chem. A**7**, 1047 (1973).
16. A. Reckziegel and M. Bigorgne. J. Organomet. Chem. **3**, 341 (1965).
17. P. N. Rylander. Catalytic hydrogenation over platinum metals. Academic Press, New York. 1967. p. 309.
18. W. F. Linke. Solubilities of inorganic and metal organic compounds. Am. Chem. Soc. 1958.
19. G. G. Strathdee and R. M. Given. Can. J. Chem. **52**, 2226 (1974).
20. S. Montelatici, A. van der Ent, J. A. Osborn, and G. Wilkinson. J. Chem. Soc. A, 1054 (1968).
21. G. G. Strathdee and R. M. Given. Unpublished results.
22. R. Rabinowitz, R. Marcus, and J. Pellon. J. Polym. Sci. A**2**, 1233 (1964); 1241 (1964).
23. D. Braun, H. Daimon, and G. Becker. Makromol. Chem. **62**, 183 (1963).
24. D. Braun. Makromol. Chem. **30**, 85 (1959).
25. J. P. Collman, L. S. Hegedus, M. P. Cooke, J. R. Norton, G. Dolcetti, and D. N. Marquardt. J. Am. Chem. Soc. **94**, 1789 (1972).
26. K. G. Allum, R. D. Hancock, and P. J. Robinson. Canadian Patent No. 902846.
27. E. E. Mercer and P. E. Dumas. Inorg. Chem. **10**, 2755 (1971).

Can. J. Chem. Downloaded from www.nrcresearchpress.com by 210.87.254.6 on 09/05/12
For personal use only.

Determination of Trace Cadmium in Biological Materials by Neutron and Photon Activation Analyses

ROBERT E. JERVIS, BELLA TIEFENBACH, AND AMARES CHATTOPADHYAY

Department of Chemical Engineering and Applied Chemistry, and Institute for Environmental Studies, University of Toronto, Toronto, Ontario M5S 1A4

Received February 13, 1974

ROBERT E. JERVIS, BELLA TIEFENBACH, and AMARES CHATTOPADHYAY. Can. J. Chem. **52**, 3008 (1974).

Two nuclear activation techniques have been applied for the determination of trace cadmium residues in a variety of Canadian foodstuffs, soils, and other biological materials. A neutron activation procedure based on radiochemical isolation of ^{115}Cd has been used for p.p.b. concentrations in foods, vegetables, and scalp hair whereas an instrumental photon activation method employing assay of ^{111m}Cd with a solid state Ge(Li) detector has been useful for soil, fertilizer, and a few vegetation samples at p.p.m. levels. For the latter technique, bombardment at either 15 or 35 MeV has been used, the higher energy bombardment gave a slightly higher sensitivity. However, in samples containing appreciable amounts of indium and tin, interference is minimized by irradiating at the lower energy.

The cadmium content of most Canadian foods ranged from 2–70 p.p.b.; agricultural soils studied contained 0.5–2 p.p.m., some of which could be attributed to fertilizers containing up to 5 p.p.m. of cadmium, whereas vegetable crops grown on such soils generally contained 0.1–0.2 p.p.m. For scalp hair, cadmium concentrations ranged from 0.25–2.7 p.p.m.

The accuracy of the nuclear activation techniques was assessed with standard reference materials and by comparison with atomic absorption and the agreement was generally in the range of 2–7%.

ROBERT E. JERVIS, BELLA TIEFENBACH et AMARES CHATTOPADHYAY. Can. J. Chem. **52**, 3008 (1974).

On a utilisé deux techniques d'activation nucléaire pour déterminer les traces de cadmium contenues dans les résidus d'un grand nombre d'aliments, de sols et d'autres substances biologiques trouvés au Canada. Pour déterminer des concentrations en p.p.b. de cet élément contenu dans les aliments, les légumes et les cheveux, on a fait appel a un procédé d'activation de neutrons basé sur l'isolement du cadmium ^{115}Cd; au niveau des p.p.m. dans les sols, les fertilisants et quelques échantillons de végétation, une méthode instrumentale d'activation de photon faisant appel à la détermination du ^{111m}Cd avec un détecteur Ge(Li) à l'état solide s'est avérée utile. Pour cette dernière technique, l'on a utilisé des bombardements soit à 15 ou 35 MeV; le bombardement à l'énergie la plus élevée donne une sensibilité quelque peu améliorée. Toutefois dans les échantillons contenant des quantités appréciables d'indium ou d'étain, l'interférence est minimisée en irradiant à l'énergie la plus basse.

Les quantités de cadmium contenues dans la plupart des aliments canadiens varient entre 2–70 p.p.b.; les sols étudiés contiennent entre 0.5–2 p.p.m. et une certaine quantité de ce cadmium peut provenir des fertilisants qui contiennent jusqu'à 5 p.p.m. de cet élément alors que les aliments qui poussent dans ces sols en contiennent en général 0.1–0.2 p.p.m. Les concentrations de cadmium dans les cheveux s'étalent entre 0.25–2.7 p.p.m.

On a évalué la précision des techniques d'activation nucléaire a l'aide de matériaux de références internes et par comparaison avec l'absorption atomique; la correspondance entre les deux méthodes est généralement de l'ordre de 2 à 7%. [Traduit par le journal]

Cadmium and its compounds are known to be very toxic to living species (1). Cadmium has been classified as the second most toxic heavy metal for numerous aquatic organisms, mercury being considered the most toxic (2). The toxicity of cadmium to human beings is perhaps dramatized most clearly in the reported deaths of about 150 women affected by the "itai-itai" disease in the Jintsu River Valley of Japan. The "itai-itai" disease caused by acute cadmium poisoning (3, 4) is again second only in heavy metal intoxication of human populations to the fatal mercury poisoning and subsequent death of several hundred people in Iraq (5, 6) and Japan. In Canada, several cases of industrial poisoning due to the inhalation of vapors containing cadmium have been reported (7).

Environmental cadmium has been of concern

Can. J. Chem. Downloaded from www.nrcresearchpress.com by 210.87.254.42 on 09/05/12
For personal use only.

Can. J. Chem. Downloaded from www.nrcresearchpress.com by 210.87.254.42 on 09/05/12
For personal use only.

in air, industrial effluent, sediment, soil, crops, fish, meat, and tobacco, among numerous other materials (8, 9). Moreover, traces of cadmium in the biosphere can be strongly enriched from a negligibly small level to a potentially hazardous concentration through the food chains. In order to follow these pathways, to reveal sources of cadmium intake, and to understand the mechanism of accumulation of cadmium in man, it is necessary to have available very sensitive and highly specific techniques for rapid and accurate determination of trace quantities of cadmium bound in varying degrees to complex sample matrices. At present, there is a considerable effort directed to developing methods for the measurement of trace cadmium as evidenced in a recently compiled bibliography (10). The nuclear activation technique "is one of the four most popular techniques for trace element analysis" (11). Not long ago, activation analysis was found very useful for the accurate determination of mercury. The same technique has been used in this study to measure cadmium. Two types of nuclear activation, one in which radioactivity is induced by thermal neutrons and the other by 15- and 35-MeV photons, are compared for this purpose and reported here.

Thermal neutron activation analysis (NAA) of cadmium in biological materials has been reported by a number of other investigators (12–15). Although it is theoretically possible to determine submicrogram (*viz.* 10^{-7}–10^{-9} g) quantities of cadmium present in a suitable matrix by instrumental neutron activation analysis (INAA) (9*a*), in practice, the analysis is almost always carried out by separating radiocadmium from any activated matrix using suitable radiochemical methods. We, also, have observed a large radioactivity due to numerous nuclides present in neutron activated biological materials and have appreciated the necessity therefore of developing a radiochemical separation method for accurate and reproducible measurements of low level cadmium. When neutron activation is followed by radiochemical separation (RNAA), the 336-keV γ-ray of ^{115m}In (in equilibrium with ^{115}Cd; half-life, 53.5 h) has been assayed with a NaI(Tl) detector for the determination of cadmium concentrations.

Alternatively, radioactivity can be induced in cadmium isotopes by irradiating the samples in a bremsstrahlung beam, a technique otherwise known as photon activation analysis (PAA). In PAA, an entirely different spectrum of nuclides is formed by (γ, γ′), (γ, n), (γ, p), and other complex photonuclear reactions compared to NAA. The main advantage of PAA over NAA of biological materials is the virtual absence of matrix activity in photon activated samples. Moreover, many interfering competing reactions in PAA can often be eliminated by a suitable choice of the energy of irradiation (E_{irr}). It is also possible in practice to determine cadmium in biological materials without a need for chemical separation using instrumental photon activation analysis (IPAA) and by selecting an interference-free nuclide and γ-ray. Photon activation of cadmium has been reported by the authors of this paper (16, 17) as well as by others (18–21). In this study, the samples have been irradiated at 15- and 35-MeV maximum electron energies and the 247-keV γ-ray of ^{111m}Cd (half-life, 49 min) has been followed using a high resolution Ge(Li) detector for the measurement of cadmium.

In the work reported here, both RNAA and IPAA have been used to determine cadmium in seeds, fertilizers, soils, vegetation, fish, meat, and a number of other consumable materials. Human scalp hair has been analyzed to estimate cadmium concentration in the body. The cadmium content of soil has also been measured after chemical separation by atomic absorption spectrophotometry (AAS) for comparison purposes. The coal and fly ash standards circulated to analytical laboratories for intercomparison purposes by the U.S. Environmental Protection Agency (EPA) and the National Bureau of Standards (NBS), the multielement gelatin standard (TEG-50-A) supplied by the U.S. Eastman Kodak Co., and NBS Orchard Leaves Standard Reference Material (1571) have all been analyzed for the cadmium content to check the accuracy of the methods developed here. The precision of measurement has also been discussed. The advantages of each of the activation methods used in this study in analyzing specific samples are also described here.

Experimental

Samples

Various types of food were obtained from most provinces across Canada for the determination of several toxic metals with the assistance of the Food and Drug Laboratories, Department of National Health and Welfare. Some tissue samples were received in frozen condition and were stored in a refrigerator. Prior to the neutron activation, samples were freeze-dried for 24 h and known

Can. J. Chem. Downloaded from www.nrcresearchpress.com by 210.87.254.42 on 09/05/12
For personal use only.

quantities of them were placed in cylindrical quartz tubes (length, 4.5 cm; internal diameter, 0.4 cm) which were subsequently heat sealed. Other foodstuffs were received in their normal dry condition. Since these samples were analyzed in our laboratory for a number of toxic metals including mercury, and since mercury can be lost from the samples (especially from fish) in polyethylene containers during neutron activation (22, 23), all food samples were irradiated in the quartz tubes to eliminate any such loss.

Soils, fertilizers, seeds, and vegetation were collected from a market gardening tract known as the Holland Marsh in south central Ontario and were analyzed by RNAA for cadmium content. Very little pre-irradiation treatment was given to these samples. For example, soils, fertilizers, and seeds were dried in air at room temperature. However, vegetation specimens had been washed and dried previously at 65 °C in an oven by the Botany Department, and were used as such. Human scalp hair samples collected from the residents of the Holland Marsh area were carefully washed with ether to remove oily layers with externally attached dust particles and were dried in air.

Cultivated soils with a high organic matter content, fertilizers, and vegetation, collected from the Holland Marsh were also analyzed by IPAA. For this purpose, the dried samples were packed in polyethylene bags and heat sealed. A typical sample package size was 2 cm × 1.2 cm. The polyethylene bags were placed in cylindrical polyethylene irradiation capsules for IPAA.

Standards

To serve as comparator standards for RNAA, microliter quantities of pure cadmium nitrate solution (containing known microgram quantities of cadmium) were weighed into clean quartz tubes.

A synthetic soil matrix was prepared as a support material for trace amounts of cadmium by mixing starch powder (46.1%), diammonium hydrogen phosphate (42.8%), calcium oxide (2.1%), ferric trioxide (2.2%), and silicon dioxide (6.8%). Microgram quantities of pure cadmium oxide were added to the synthetic soil matrix and mixed thoroughly. A known amount of this mixture was placed in a clean polyethylene bag, sealed, and used as the cadmium standard for IPAA of soil. For IPAA of other materials, known amounts of pure cadmium oxide sealed in polyethylene bags were used as the standard reference material.

Irradiations

Two different nuclear reactors were used for the RNAA reported here. At the McMaster University Nuclear Reactor, Hamilton, Ontario, a flux of 2×10^{13} and 5×10^{13} neutrons/cm^2 s were available for the neutron activation work. The samples, standards, and a blank quartz tube or polyethylene bag, as the case might be, were put in an aluminum irradiation capsule and were normally irradiated for 20–60 h. About 50 to 80 mg portions of each food sample were used and as many as 10 different samples plus standards were irradiated simultaneously in each capsule.

However, it was possible to irradiate a larger amount, *viz.* about 1 g, of each sample in a flux of 2.5×10^{11} neutrons/cm^2 s at a Safe Low Power Critical Experiment (SLOWPOKE) Nuclear Reactor of the University of Toronto. A few samples were irradiated at a higher neutron flux, namely at 1×10^{12} neutrons/cm^2 s, at the above reactor whenever the higher flux was available. For certain types of sample, especially soils, a 1-g portion was considered to be more representative than a 100-mg portion of the soil analyzed such as was used in the high flux irradiations. Therefore, many soils with suspected elevated levels of cadmium were irradiated in the SLOWPOKE Reactor for RNAA determination. Soil samples along with the cadmium standard, an empty quartz tube, and a polyethylene bag were placed in a SLOWPOKE 7-cc polyethylene irradiation capsule and were irradiated for a maximum period of 16 h.

A Vickers 45-MeV electron linear accelerator (Linac) at the University of Toronto was used as the bremsstrahlung source for IPAA. The maximum current output at a given electron energy was obtained in this Linac by using pulses of 2.1 μs width at the repetition rate of 240 pulses per second. The bremsstrahlung was produced by allowing the electron beam to impinge on a 3-mm-thick water-cooled tungsten converter placed 3 cm away from the face of the beam exit window of the Linac. The beam currents were measured on the tungsten converter by a current monitor and typical average electron currents were found to be 80 μA at 15 MeV and 225 μA at 35 MeV. An energy precision of about ±0.5 MeV and a current spread of ±5 μA from the selected values were observed during this work. The average flux of photons was of the order of 1 to 2×10^{13} photons/cm^2 s. A detailed description of this Linac and the various facilities for IPAA have been discussed elsewhere (24). Soil samples (normally 1 g) along with the cadmium standard and a blank polyethylene bag were irradiated at 15 MeV for 1 h. All other samples were irradiated at 35 MeV, also for 1 h. Irradiations were carried out by placing the polyethylene irradiation capsules on a specially designed rotating sample holder which has been described in a previous paper (16). This sample holder was used to achieve the same mean irradiation exposure to samples and standard even though there was a considerable spatial bremsstrahlung flux variation at the sample position.

Postirradiation Treatment of Neutron Activated Samples

Following neutron activation, the samples were "cooled" for 1–2 days to minimize radiation standards before chemical processing. Then the external surface of the quartz tubes containing samples and standards were cleaned by boiling in aqua regia, rinsed several times with distilled water, and dried. For RNAA, samples were dissolved by the method described below.

About 20 ml of liquid nitrogen were placed in a beaker containing 5 ml of concentrated HNO_3. The acid was thus solidified. This was designed to protect the beaker from breaking during subsequent crushing of the sample quartz tube. The quartz tube was placed in the beaker and more liquid nitrogen was added to make the quartz tube fragile and also to eliminate loss of any volatile material that might have been formed during irradiation. The quartz tube was crushed with a stainless steel plate which was washed with concentrated HNO_3 and the washings added to the beaker. Cadmium carrier solution (normally 10 mg) was added to the solution and the beaker was left covered in an ice bath for about 16 h to allow cold digestion of the mixture overnight.

The resulting solution was evaporated almost to dryness to eliminate nitric oxide fumes and then concentrated HCl was added dropwise while boiling gently. In the case

Can. J. Chem. Downloaded from www.nrcresearchpress.com by 210.87.254.42 on 09/05/12
For personal use only.

of samples which were difficult to dissolve, approximately 2 ml of 30% H_2O_2 were added slowly into the solution to destroy any residual organic matter in samples. A detailed method for the dissolution of soils was reported earlier (15). The final solution was made 10 *N* with respect to HCl. The anionic chloro complexes of cadmium thus formed were separated from those of other elements using an anion exchange resin column.

Several tracer experiments involving arsenic, cadmium, mercury, selenium, and zinc nuclides were carried out to determine the most suitable conditions for ion exchange separation of cadmium. From the results of these experiments, a strongly basic anion exchange resin (4602, CGA-549, 100–200 mesh) in a column of 10 cm height and 1.2 cm internal diameter was selected. The flow rate was adjusted to 2 ml/m.

The 10 *N* HCl solution containing the chloro complexes of several elements including cadmium was transferred onto the ion exchange column. Arsenic, selenium, and zinc were first eluted by washing the column with varying strengths of HCl down to 0.01 *N* concentration. Cadmium was eluted with 1 *N* H_2SO_4. The first 30 ml of the eluate were found to contain very little cadmium and thus were discarded. The next 55 ml of the eluate contained most of the cadmium and were collected in a beaker for further treatment.

Tracer experiments revealed the presence of a small amount of zinc in the cadmium eluate. A precipitation method (25, 26) using Reinecke salt for the separation of zinc from cadmium was found to be excellent for our purpose and thus was used.

To the cadmium eluate, 10 ml of 5% thiourea solution (w/v) were added. Then 4 ml of a freshly prepared 4% solution on Reinecke salt in 1% thiourea were added after cooling with constant stirring. The mixture was left on an ice bath for 30 min with frequent stirring. The $[Cd(thiourea)_2][Cr(SCN)_4(NH_3)_2]_2$ precipitate was centrifuged and the supernatant was discarded. The precipitate was washed with 15 ml of 1% thiourea solution, centrifuged, and the supernatant was discarded again. The precipitate was washed with 10 ml of chilled absolute ethanol and was transferred to a tared circle of Whatman filter paper No. 41. It was washed with an additional 5 ml of chilled absolute ethanol on the filter paper.

The precipitate containing cadmium was dried at 110 °C for 30 min and cooled in the desiccator for an equal length of time. A chemical recovery of 80–95% of the added cadmium carrier was typical. The radiochemically separated cadmium was found to be absolutely free from zinc. The total time for the radiochemical separation of nanogram traces of cadmium was approximately 8 h for a batch of six samples.

The nuclide ^{115m}In (half-life, 4.5 h), daughter product of ^{115}Cd (half-life, 53.5 h), was allowed to grow into the radiochemically pure cadmium precipitate and to reach equilibrium after 20 h from the final precipitation of cadmium. The activity due to the 336-keV γ-ray of ^{115m}In was then assayed with a 7.5 cm × 7.5 cm NaI(Tl) detector in conjunction with a 1024 channel model 601 Northern Scientific Inc., pulse height analyzer. Background subtractions, chemical yield, and decay corrections were made in estimating the net activity due to the sample. The integrated net peak area method (corrected for background) was used in determining the concentration of cadmium in the sample.

Instrumental Analysis of Photon Activated Samples

Following photon activation, the samples, standard, and the blank polyethylene bag were transferred to clean glass counting vials and were given identical geometrical shape. After a "cooling period" of about 2 h from the end of irradiation, samples and standards were counted with two high resolution Ge(Li) detectors (described below). Background subtractions and decay corrections were made as usual. The number of events detected in the 247-keV γ-ray of ^{111m}Cd (half-life, 49 min) were calculated by using the net peak area method.

Two solid-state detectors were used: either a 60- or 40-cm^{3}Ge(Li) detector coupled, one to a 4096-channel Canberra and one to a Kicksort pulse height analyzer was used in various experiments for the instrumental analysis of cadmium. The full-width at half-maximum of the photopeak produced by the 1332-keV γ-ray of ^{60}Co was 1.9 and 2.5 keV for these two detectors, respectively. The peak-to-Compton ratios were 30:1 and 18:1, respectively. The efficiencies for these two detectors were, respectively, 6.7 and 4.0% with respect to a standard NaI(Tl) detector.

Results and Discussion

Photon Activation of Cadmium Isotopes

In 1941, Feldmeier and Collins (27) have reported the formation of ^{111m}Cd by photoexcitation of cadmium isotopes. However, not much work was done until 1964 when Lukens *et al.* (28) studied the possible applications of such nuclear inelastic scattering reactions to trace element analysis. Since then a few investigators (21, 29, 30) have measured cross sections, half-lives, γ-ray energies, detection limits, and some have used them to determine cadmium in samples.

With the advent of high resolution Ge(Li) detectors, the possibility of instrumental analysis of cadmium employing metastable isomers has increased considerably in recent years. Moreover, no studies of the photon activation of cadmium isotopes and their interferences have been reported so far. For these reasons, we have irradiated pure cadmium standards at 8, 10, 12, 14, 15, 20, 22, 25, 30, 35, and 40 MeV maximum bremsstrahlung energies and have identified the nuclides produced, determined their half-lives and γ-ray energies. We have compared these nuclear data with those published in recent literature and found them to be very consistent. We have also studied the interferences that may be encountered for the kind of environmental samples analyzed in this work. Some of the nuclear data relating to the present analysis are shown in Table 1.

Hislop and Williams (18) suggested the use of the 336 keV γ-ray of ^{115m}In for the determination of cadmium in air particulates. In an attempt to

Can. J. Chem. Downloaded from www.nrcresearchpress.com by 210.87.254.42 on 09/05/12
For personal use only.

TABLE 1. Data for photon activation of cadmium isotopes and their interferences

Nuclides produced					Interfering γ-rays				Competing reactions	
Activation reaction	Target isotopic abundance (%)	E_{sep} (MeV)	Half-life of nuclide	Major γ-rays keV (% intensity)	Major γ-rays keV (% intensity)	Method of production	E_{sep} (MeV)	Half-life of nuclide	Activation reaction	E_{sep} (MeV)
$^{106}Cd(\gamma, n)^{105}Cd$	1.22	10.9	56 min	347.1(84)	347.1	Unknown		~3.2 days	—	—
				433.0(67)	430.0(12.4)	$^{107}Ag(\gamma, n)^{106m}Ag$	9.6	8.4 days		
				961.1(100)	962.0(7.2)	$^{64}Zn(\gamma, n)^{63}Zn$	11.9	38 min		
$^{106}Cd(\gamma, 2n)^{104}Cd$	1.22	19.3	57 min	83.8(100)	—	—	—	—	—	—
				555.5(70)	558.3(3.5)	$^{115}In(\gamma, n)^{114m}In$	9.0	50 days		
$^{106}Cd(\gamma, p)^{105}Ag$	1.22	7.3	40 days	279.9(32)	279.1(77)	$^{204}Hg(\gamma, n)^{203}Hg$	7.5	47 days	$^{107}Ag(\gamma, 2n)^{105}Ag$	17.4
$^{108}Cd(\gamma, t)^{105}Ag$	0.88	17.1			279.6(20)	$^{76}Se(\gamma, n)^{75}Se$	11.2	120.4 days		
$^{108}Cd(\gamma, n)^{107}Cd$	0.88	10.3	6.5 h	93.1(99.6)	90.6(30)	$^{50}Cr(\gamma, n)^{49}Cr$	12.9	42 min	$^{112}Sn(\gamma, n\alpha)^{107}Cd$	12.1
					96.7(3.6)	$^{76}Se(\gamma, n)^{75}Se$		120.4 days		
$^{111}Cd(\gamma, \gamma')^{111m}Cd$	12.75		49 min	150.6(30)	149.6(14)	$^{86}Sr(\gamma, n)^{85m}Sr$	11.5	70 min	$^{115}Sn(\gamma, \alpha)^{111m}Cd$	3.2
$^{112}Cd(\gamma, n)^{111m}Cd$	24.07	9.4			152.8(14)	$^{50}Cr(\gamma, n)^{49}Cr$	12.9	42 min	$^{116}Sn(\gamma, n\alpha)^{111m}Cd$	12.8
$^{113}Cd(\gamma, 2n)^{111m}Cd$	12.26	15.9		246.8(94)	—	—	—	—	$^{113}In(\gamma, np)^{111m}Cd$	15.5
									$^{114}Sn(\gamma, {}^3He)^{111m}Cd$	16.2
$^{111}Cd(\gamma, p)^{110m}Ag$	12.75	9.1	253 days	657.6(95.6)	657.4(6)	$^{77}Se(\gamma, p)^{76}As$	9.6	26.5 h	$^{115}In(\gamma, n\alpha)^{110m}Ag$	12.6
$^{112}Cd(\gamma, np)^{110m}Ag$	24.07	18.5		884.5(72.4)	888.4(100)	$^{47}Ti(\gamma, p)^{46}Sc$	10.4	84 days	$^{113}In(\gamma, {}^3He)^{110m}Ag$	16.8
$^{113}Cd(\gamma, t)^{110m}Ag$	12.26	16.5		937.4(31)	—	—	—	—		
$^{112}Cd(\gamma, p)^{111}Ag$	24.07	9.6	7.5 days	342.1(8)	—	—	—	—	$^{115}In(\gamma, \alpha)^{111}Ag$	3.8
$^{113}Cd(\gamma, np)^{111}Ag$	12.26	16.2							$^{113}In(\gamma, 2p)^{111}Ag$	15.7
$^{114}Cd(\gamma, t)^{111}Ag$	28.86	16.7								
$^{113}Cd(\gamma, p)^{112}Ag$	12.26	9.8	3.2 h	617.1(40)	617.2(81)	$^{44}Ca(\gamma, p)^{43}K$	12.2	22 h		
$^{114}Cd(\gamma, np)^{112}Ag$	28.86	18.8								
$^{114}Cd(\gamma, p)^{113}Ag$	28.86	10.3	5.3 h	300.0(100)	303.8(3.6)	$^{76}Se(\gamma, n)^{75}Se$	11.2	120.4 days	$^{115}In(\gamma, 2p)^{113}Ag$	17.1
$^{116}Cd(\gamma, t)^{113}Ag$	7.58	16.6			296.8(1%)	$^{68}Zn(\gamma, p)^{67}Cu$	10.0	61.6 h		
$^{116}Cd(\gamma, n)^{115}Cd$–$^{115m}Cd$	7.58	8.7	53.5 h–43 days	492.2(9.5)	489.5(5)	$^{48}Ca(\gamma, n)^{47}Ca$	10.0	4.53 days	$^{119}Sn(\gamma, \alpha)^{115}Cd^{115m}Cd$	4.4
				527.8(30.3)	—	—	—	—	$^{120}Sn(\gamma, n\alpha)^{115}Cd$–$^{115m}Cd$	13.5
				935.0(1.9)	—	—	—	—	$^{117}Sn(\gamma, 2p)^{115}Cd$–$^{115m}Cd$	16.9
									$^{118}Sn(\gamma, {}^3He)^{115}Cd$–$^{115m}Cd$	18.5
$^{116}Cd(\gamma, n)\beta^{-115m}In$	7.58	8.7	4.5 h	336.1(45)	333.1(25)	$^{197}Au(\gamma, n)^{196}Au$	8.1	6.2 days	$^{115}In(\gamma, \gamma')^{115m}In$	
									$^{117}Sn(\gamma, np)^{115m}In$	16.2
									$^{118}Sn(\gamma, t)^{115m}In$	17.1
									$^{116}Sn(\gamma, p)^{115m}In$	18.3

Can. J. Chem. Downloaded from www.nrcresearchpress.com by 210.87.254.42 on 09/05/12
For personal use only.

use ^{115m}In for the same purpose in soil analyses, we have experienced interferences from a number of competing reactions, particularly that of indium and tin isotopes (Table 1). Interference from the reaction ^{115}In(γ, γ')^{115m}In seems unavoidable in soil analyses even at 15 MeV irradiation energy. The nuclide ^{115}Cd suggested by Sulin (19) could not be used for the determination of cadmium in soil because of similar interferences from the competing reactions of a number of tin isotopes (Table 1). Moreover, the sensitivities of IPAA determination of cadmium using ^{115}Cd reported by Kato (31) and Sulin (19) of 15 and 5 p.p.m., respectively, are not low enough for trace cadmium analysis.

The 300 keV γ-ray of ^{113}Ag has been interfered with by the 303.8 keV γ-ray of ^{75}Se as well as by a competing reaction shown in Table 1. On the other hand, although ^{112}Ag has not apparently been produced by any interfering photonuclear reaction, its most abundant γ-ray of 617.1 keV has been seriously interfered with. Kato (31) has reported a sensitivity of cadmium determination of 104 p.p.m. using the 617.1 keV line of ^{112}Ag. Several interferences and the unfavorable long half-lives of both ^{105}Ag and ^{110m}Ag (Table 1) have restricted the use of these nuclides for the rapid determination of cadmium. γ-Rays emitted by relatively short-lived ^{105}Cd and ^{107}Cd were also interfered with. The full energy peak of 83.8 keV of ^{104}Cd cannot be measured efficiently with the high volume Ge(Li) detectors used in this study.

The nuclide ^{111m}Cd, which was finally selected for use in this work, can be produced by three different reactions from cadmium isotopes as shown in Table 1 along with the interfering reactions. At an E_{irr} of 15 MeV, the reaction ^{115}Sn(γ, α)^{111m}Cd (E_{sep}, 3.2 MeV) can interfere. However, considering the low isotopic abundance of ^{115}Sn(0.34%), any such interference has been estimated to be negligible. The other reaction ^{116}Sn(γ, nα)^{111m}Cd has an E_{sep} of 12.8 MeV and is not expected to interfere seriously at energies only a couple of MeV above that. For these reasons, soil samples have been irradiated at 15 MeV for the determination of cadmium. The main photon reactions at 15 MeV producing this nuclide are: ^{111}Cd(γ, γ')^{111m}Cd and ^{112}Cd(γ, n)^{111m}Cd.

The 246.8 keV γ-ray of ^{111m}Cd which is quite abundant (94%) and relatively free from interference, was used in this study. Baciu *et al.* (32) have mentioned γ-rays such as the 246 keV of ^{39}Cl (from ^{40}Ar), 247.9 keV of ^{84m}Rb, and 249.8 keV of ^{135}Xe as the possible sources of interference. However, we have not observed any detectable quantities of these nuclides in irradiated soils. Aras *et al.* (33) have detected the 249.7 keV γ-ray of ^{77}Br produced by the reaction ^{79}Br(γ, 2n)^{77}Br in photon-activated air particulate samples. To reveal any interference from ^{77}Br, a search for other abundant γ-rays such as the 238.9 and 521.0 keV of ^{77}Br was made in the gross γ-ray spectra of soils recorded at different time intervals. No such γ-rays were identified. It was concluded therefore that no detectable amount of bromine is present in soils analyzed. Moreover, the half-life of the 247 keV γ-ray was found to be 48 $\pm$ 2 min which is in excellent agreement with the reported half-life of 49 min of ^{111m}Cd. Thus any interference from the above nuclides has been considered negligible.

When significant amounts of indium and tin were not present, as we have observed for fertilizers, seeds, and vegetation, the samples were irradiated at 35 MeV, and the maximum obtainable beam current was used to induce maximum possible activity and improve detection levels for cadmium. Under such circumstances, a number of nuclides can be used for the determination of cadmium. Advantage can be taken of the longer 53.5 h half-life of ^{115}Cd (in equilibrium with ^{115m}In) for routine cadmium analysis provided appreciable gold is also absent from the sample (Table 1). However, a better detection limit can still be achieved by using the ^{111m}Cd nuclide. This is due to the fact that ^{111m}Cd is simultaneously produced by three different photonuclear reactions at the higher energy of 35 MeV as shown in Table 1.

Cadmium in Food

The cadmium residues detected by RNAA in the various specimens of a variety of typical food items are summarized in Table 2. The cadmium concentrations of all food items are expressed as ranges in parts per million (p.p.m.) by weight, based on the fresh weight of the sample. To be specific, the levels of cantaloup, fish, meat, oyster, etc. are expressed with their respective normal water content (*i.e.*, wet weight) while those for coffee, flour, tea, etc. are based on the normal dry condition in which they are available in the market (*i.e.*, dry weight). In giving the approximate ranges of cadmium content in food,

Can. J. Chem. Downloaded from www.nrcresearchpress.com by 210.87.254.42 on 09/05/12
For personal use only.

TABLE 2. Cadmium content of food by RNAA

Sample	Range (p.p.m., as received, weight basis)
Buck wheat	0.094
Cantaloup	0.007
Coffee	0.007, 0.017
Cream of wheat	0.032
Egg	0.004, 0.005
Fish	0.004–0.008 (0.10, 0.014, 0.015)
Flour (wheat)	0.028
Meat	
beef	0.002–0.021 (0.061, 0.097, 0.115)*
chicken	0.002–0.003 (0.063, 0.068)*
lamb	0.003–0.016 (0.253)*
pork liver	0.033–0.069
Oats	0.026
Oyster	0.445, 0.796
Rice	0.015–0.023
Tea	0.004, 0.015
Wheat	0.29

*High cadmium contents beyond the range quoted are shown in the parentheses and are mostly for organs such as liver and kidneys.

care is taken to exclude the scattered high values which are separately shown in the parentheses. The cadmium concentrations of individual items are shown in a few cases where enough samples have not been analyzed to give a range but for most foods analyzed the individual concentrations are too numerous to be listed separately.

Different cuts of various types of meat have been analyzed. In general, the muscle mass of these meats show a very low cadmium content. However, kidney and liver have been observed to concentrate more cadmium (up to 10 times more). The cadmium concentrations of these organs in beef, chicken, and lamb are considerably higher and are shown in the parentheses of Table 2. Similar enrichment of cadmium in the organs has also been described by Yamagata and Shigematsu (3). Das and de Vries (34) reported less than 2 parts per billion (p.p.b.) of cadmium in commercially available canned beef for infants. On the other hand, Ishizaki *et al.* (35) and Rautu and Sporn (36) found 0.054 and 0.060 p.p.m. of cadmium in beef, respectively. Schroeder *et al.* (37) originally estimated 0.89 p.p.m. of cadmium in beef. Although this value could be reduced to half of the original amount after making necessary corrections for the interferences observed in their analytical technique used for the determination of cadmium (8*a*, 9*b*), even then it appears to be almost four times as high as the highest value found in this study. Essing *et al.* (38) homogenized four beef samples of different origin and found a 0.017 p.p.m. cadmium content. We have observed a range of 0.003 to 0.20 p.p.m. and Ishizaki *et al.* (35) detected 0.027 p.p.m. of cadmium in chicken whereas Schroeder *et al.* (37) reported 0.31 and 2.00 p.p.m. for chicken wing and leg, respectively. The range of cadmium content in pork liver is shown in Table 2. For comparison, the normal concentration of cadmium in Japanese pork liver has been reported as 0.080 p.p.m. (3).

In general, the cadmium concentration of the axial muscle of freshwater fish is of the order of a few p.p.b. irrespective of the species as observed in this study. This is in contrast to the food-chain accumulation in predatious fish found for mercury. Similar low values have been reported from Japan (35) and West Germany (38). In the U.S., cadmium content of 0.036 in fish has been quoted (9*c*). The cadmium concentrations in the muscle of pike from southeast Sweden (13) have been found to be $\leqslant$20 p.p.b. in general with a few scattered high values up to $\leqslant$100 p.p.b. Jaakkola *et al.* (2) have analyzed pikes from both non-polluted and polluted waters in Finland and have observed an enrichment of cadmium from muscle to liver and kidney. They observed the lowest cadmium residue in the clean water fish muscle ranging from 2 to 3 p.p.b. and approximately five times more in the contaminated water fish muscle. For clean water fish, they reported a cadmium enrichment of about 10 times in liver and 50 times in kidney compared to that in the muscle.

Oysters are reported to concentrate cadmium from sea water. The cadmium contents of oysters observed in this study, *viz.* 0.4 and 0.8 p.p.m. (Table 2), are comparable to those of 0.62 (35) and 0.85 p.p.m. (3) found in Japan.

Eggs have been found to contain about 5 p.p.b. of cadmium (Table 2). Slightly higher values of 15 (35) and 21 p.p.b. (36) have also been reported. However, even after correcting for interference as mentioned above the 90 p.p.b. result observed by Schroeder *et al.* (37) appears unusually high.

The cadmium content of rice found in this study (Table 2) is considerably lower than that of 0.07 p.p.m. found normally in Japan (3). A wheat sample has been found to contain 0.29 p.p.m. of cadmium in this study. Recently, Huffman and Hodgson (39) reported an average of 0.20 p.p.m. of cadmium in wheat from 19 states east of the Rocky Mountains. The cadmium resi-

Can. J. Chem. Downloaded from www.nrcresearchpress.com by 210.87.254.42 on 09/05/12
For personal use only.

dues of 0.047 and 0.07 p.p.m. in wheat flour reported by Essing *et al.* (38) and Schroeder and Balassa (40), respectively, are considerably higher than that of 0.028 p.p.m. found in this work (Table 2) which, in turn, agrees with concentrations of 0.02 and 0.025 p.p.m. of cadmium reported by others (41, 35).

The cadmium residues of three types of edible vegetation from the Holland Marsh area have also been analyzed by RNAA and are listed in Table 3. Seeds, in general, contain very low cadmium except some onion seeds which had a level of 0.066 p.p.m. There is not any satisfactory explanation at this stage for high cadmium content found in onion seeds. The cadmium concentrations of the various portions of the vegetables were calculated on the dry weight basis (often after drying at 65 °C for 48 h). The cadmium content in the edible portion of the vegetables on the wet weight basis are estimated from the dry weight results as: 0.024 p.p.m. in carrot (root), 0.036 p.p.m. in lettuce (leaf), and 0.013 p.p.m. in onion (bulb). We have also obtained similar vegetation samples from the open market in Toronto, analyzed them by RNAA, and calculated the cadmium content on both the wet weight and dry weight basis. The similarities in the cadmium residues of these vegetables from two different sources is generally quite close.

By comparison, Ishizaki *et al.* (35) and Yamagata and Shigematsu (3) have detected 0.041 and 0.050 p.p.m. (wet weight) cadmium residues, respectively, in normal carrots. Essing *et al.* (38) have reported 0.032 p.p.m. cadmium in carrot which agrees with our findings. They have also reported 0.042 p.p.m. of cadmium in lettuce. Somers (42) has reported cadmium contents up to 0.69 p.p.m. in carrots and 2.4 p.p.m. in lettuce grown within 2–3 miles of a smelter in Trail, British Columbia. Onions have been analyzed by a number of investigators in many countries. The cadmium concentrations in onions range from 0.0077 p.p.m. (36) in Rumania, 0.003 (3) and 0.012 p.p.m. (35) in Japan, 0.01 p.p.m. (37) in the U.S., to 0.017 p.p.m. (38) in West Germany. Yamagata and Shigematsu (3) have noticed a difference in the cadmium content of two types of onion described as onion (0.003 p.p.m.) and long onion (0.018 p.p.m.). Although both species were collected from two nonpolluted areas they were not grown on the same soil area so any comparison in the accumulation of cadmium between the two different onion species cannot be made.

TABLE 3. Cadmium content of fertilizers and vegetables* by RNAA

Sample	Content (p.p.m., dry weight basis)
Muriated potash (60% KCl)	1.25
Ammonium nitrate (33%)	0.302
Carrot	
seed	0.003
leaf	0.105
root	0.250
Lettuce	
seed	0.008
leaf	0.429
root	0.506
Onion	
seed	0.066
leaf	0.346
root	0.941
bulb	0.160

*Samples of fertilizers and crop vegetables from Holland Marsh.

Celery has also been analyzed by the IPAA technique. The cadmium content of celery leaf has been found to be 0.63 p.p.m. (dry weight) corresponding to 0.085 p.p.m. (wet weight) on the average (Table 5). Essing *et al.* (38) have reported a mean concentration of 0.085 p.p.m. (wet weight) cadmium in celery leaf by analyzing a homogeneous mixture obtained from four different sources.

Cadmium in Soils and Fertilizers

Cultivated soils collected from the Holland Marsh at various depths have been analyzed in replicate by RNAA, IPAA, and AAS after chemical separation. The concentrations of cadmium in these soils are presented in Table 4. The approximate range of cadmium in soils found in this study was 0.50–1.72 p.p.m. (air-dry basis).

The concentration of cadmium in soils has been reported by many other workers. Bowen (43) has summarized the range of cadmium in typical soil as 0.01–0.7 p.p.m. with an average of 0.06 p.p.m. Yamagata and Shigematsu (3) reported less than 1 p.p.m. of cadmium in nonpolluted Japanese soils. In general, a high cadmium content has been observed throughout the entire depth profile (Table 4) of the Holland Marsh muck soils. This is not surprising in view of the fact that the Holland Marsh soils have a high organic matter content (85–90%) and that both cadmium and zinc tend to concentrate in the organic matter of soils. Moreover, cadmium

Can. J. Chem. Downloaded from www.nrcresearchpress.com by 210.87.254.42 on 09/05/12
For personal use only.

TABLE 4. Cadmium content of cultivated soils by RNAA, IPAA, and AAS methods (p.p.m., dry weight basis)

Depth in cm	Destructive NAA	Instrumental PAA	AAS
Surface-1	1.42	1.40	1.45
Surface-2	1.37	1.40	1.35
0.0– 7.5	1.72	1.65	1.69
7.5–15.0	0.95	0.99	1.05
15.0–22.5	0.83	0.81	0.82
22.5–30,0	1.02	1.09	1.15
30.0–37.5	1.25	1.28	1.36
37.5–45.0	0.55	0.50	0.62

TABLE 5. Precision of cadmium determination by RNAA and IPAA

		Number of measurements and contents (p.p.m., dry weight basis)		
	Sample	First	Second	Third
RNAA	Surface-1 soil	1.42	1.40	1.41
	0.0– 7.5 cm soil	1.72	1.72	1.71
	7.5–15.0 cm soil	0.950	0.942	0.929
IPAA	Surface-1 soil	1.40	1.38	1.42
	5-10-15 Fertilizer	4.48	4.50	4.51
	Celery			
	leaf	0.629	0.636	0.631
	root	0.562	0.564	0.560

and zinc are known to occur together in nature and also cadmium is present in numerous phosphate fertilizers in appreciable concentrations (*9d*, 37). To check the latter, three widely used fertilizers were analyzed for trace cadmium (Table 3 and Table 5). The 5-10-15 fertilizer was found to contain the maximum amount of cadmium (about 4.5 p.p.m.). Recently, Hammer *et al.* (44) reported 15 p.p.m. of cadmium in the 18% superphosphate fertilizer from a U.S. source. Since muck soils in the Holland Marsh were originally found to be rather deficient in zinc and phosphates, large amounts of these nutrients have been applied through the years to improve vegetable cultivation. This can very well explain the relatively high cadmium concentrations (*viz.* 1–2 p.p.m.) observed in the surface soil layers which are normal recipients of fertilizers and nutrients. We have also observed a high zinc content in these soils as reported in our earlier study (15). Zinc to cadmium ratio in these soils has been found to vary between 250 and 850 compared to a value of 445:1 in the earth's crust (1).

Cadmium in Hair

Hair has been well recognized as an important human tissue in the forensic individualisation studies. In the past, it has been mostly used in criminalistics with some success (45). On the other hand, in this laboratory numerous hair samples from various sources have been analyzed for about a decade to monitor human ingestion of different toxic metals. Consequently, data on the normal concentrations of many metals are available from more than 1000 hair samples. By comparing these background hair metal levels with those measured in hair from a person exposed to abnormal environmental metal concentrations, it is possible to determine whether pollution sources have caused increased ingestion into that individual's body. This method has been particularly valuable in assessing cases of mercury poisoning in Japan and also in Iraq (6). Moreover, a relationship between blood concentration and hair mercury content has been established. At present, there is a growing interest in the use of hair as a "practical dosimeter" for a number of environmental contaminants such as arsenic, cadmium, and lead (46, 47).

Sixty-two scalp hair samples were collected from the residents of the Holland Marsh community (who regularly consume vegetable produce from the area) and analyzed for the cadmium content by RNAA. The results are shown in the form of a histogram in Fig. 1. The range observed in this study is 0.25–2.7 p.p.m. for all the samples analyzed.

The cadmium content of hair has also been reported by a number of other investigators. For example, Schroeder and Nason (48) have reported 0.48–2.8 p.p.m. for male and 0.24–1.8 p.p.m. for female hair cadmium concentrations. They have also observed a difference in cadmium content according to the color of hair and the age of the subject. Hammer *et al.* (46) pretreated their hair samples with EDTA before analysis and reported a mean hair cadmium content of four groups of people between 0.9 and 2.0 p.p.m. They also reported a mean cadmium content in hair of 45 10-year-old boys from five different areas having varying degrees of cadmium contamination, as 3.5 p.p.m. Recently, Lagerwerff *et al.* (49) found 0.9 p.p.m. cadmium on average in hair collected from low exposure areas. Cad-

TABLE 6. Cadmium content of interlaboratory intercomparison standards (p.p.m., dry weight basis)

Sample (agency)	RNAA	IPAA	Information value
Coal (NBS-EPA)	0.20±0.02	0.20±0.02	0.23± 0.03
Fly ash (NBS-EPA)	1.06±0.16	1.52±0.15	1.45± 0.06
Gelatin (Kodak)	50.4 ±1.0	—	40–60
Orchard leaves (NBS)	0.11±0.013	0.11±0.01	0.11± 0.02*

*Certified value.

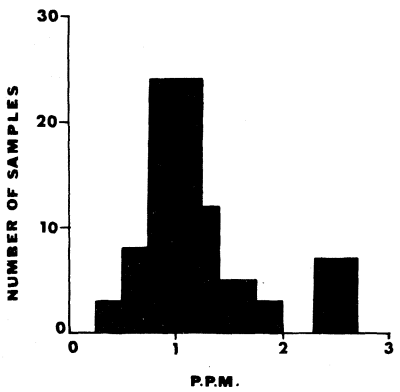

FIG. 1. Frequency distribution of cadmium in human head hair.

mium contents of 0.24–1.3 p.p.m. have been reported for Swedish hair and 0.20–1.5 p.p.m. in hair collected in rural areas of Yugoslavia (8*b*). It should be noted that all these hair samples were cleaned with detergents. Das and de Vries (34) found 0.04 p.p.m. cadmium in normal hair and reported a range of 2.2–27 p.p.m. cadmium for hair samples that were possibly contaminated. Ishizaki *et al.* (35*a*) reported 0.4 and 0.7 p.p.m. cadmium in hair for men and women above 55 years of age, respectively.

Precision and Accuracy of Measurements

The reproducibility of both the RNAA and IPAA techniques for the determination of cadmium reported here have been evaluated by analyzing replicate samples. The results are shown in Table 5 and it is quite clear that the reproducibility of both techniques is very good (*viz.* within ±2 to 10%) and is of a degree that is expected of a reliable micro-analytical technique.

It has already been mentioned that the cadmium concentrations in muck soils have been determined by a relative method, *i.e.*, by reference to the cadmium standard supported on a synthetic soil mixture. In order to check the accuracy of the cadmium content obtained using this synthetic mixture in IPAA, the same samples were analyzed by a third (nonactivation) standard analytical technique, namely atomic absorption. For this purpose a few selected soils were dissolved by following a standard dissolution method described in an earlier paper (15). Cadmium was then extracted from an alkaline solution with dithizone. The cadmium content was determined using a Jarrell Ash Dial Atom Mark II atomic absorption spectrophotometer. The results are shown in Table 4. The agreement in the cadmium content obtained by three different methods, namely RNAA, IPAA, and AAS, is quite acceptable (*viz.* ±2 to 7%) as can be seen from the table.

As an additional check on the accuracy of both the RNAA and IPAA techniques, NBS Orchard Leaves Standard Reference Material (1571) was analyzed for cadmium by the procedures described above. It can be seen from Table 6 that the agreement between the NBS certified value and the results obtained in this study is excellent, *i.e.* within the limits of reference value.

The coal and fly ash trace element standards circulated for inter-laboratory comparison purposes by the U.S. EPA and NBS have been analyzed and the results are shown in Table 6 along with the information values supplied by NBS. The agreement in the cadmium content of coal between RNAA and IPAA is excellent again. In the case of fly ash, the cadmium residue obtained by IPAA is higher than that by RNAA. It should be pointed out here that although the sample dissolution method described earlier has been satisfactory for other materials analyzed in this study, it apparently did not completely dissolve the fly ash sample. Under such conditions, the cadmium content of 1.06 p.p.m. should be considered as the acid extractable cadmium of fly ash only.

A multielement gelatin standard (TEG-50-A)

Can. J. Chem. Downloaded from www.nrcresearchpress.com by 210.87.254.42 on 09/05/12
For personal use only.

Can. J. Chem. Downloaded from www.nrcresearchpress.com by 210.87.254.42 on 09/05/12
For personal use only.

supplied by the U.S. Eastman Kodak Co. was also analyzed. The cadmium content of the gelatin powder was measured only by RNAA and the mean value of five such measurements is also shown in Table 6. The analysis of gelatin by IPAA presents some difficulty because of the considerable radiation damage caused by the high intensity photons, and for this reason, gelatin was not analyzed by IPAA.

Errors in Analyses

Activation analysis, like other analytical techniques, is also not entirely free from error. Since it is a highly sensitive method of analysis, the possibility of external contamination is always present. This has been considerably reduced in this study by minimal pre-irradiation treatment of all samples. Moreover, with the availability of nuclear reactors, such as the SLOWPOKE at the University of Toronto, in which samples can be irradiated without any pre-irradiation drying, the loss of volatile elements or their compounds from the samples during drying can be eliminated. There can be a number of other systematic errors in RNAA. However, with proper precautions as have been taken in this study, the total error in RNAA can be limited to about $\pm 10\%$.

The general errors involved in IPAA have already been discussed in earlier publications (16, 24, 50). With a careful choice of E_{irr}, the main interfering photonuclear reactions can be eliminated and such errors can be kept to a minimum. The total error in cadmium analysis by IPAA is about $\pm 7\%$ at the 0.5 p.p.m. level. However, it increases to more than $\pm 10\%$ near the detection limit.

Limits of Detection

The limits of detection for cadmium by RNAA have been described by many investigators (12–14) including the present authors (15). Depending on the flux of neutrons and the length of irradiation, different sensitivity limits can be obtained. The results of such evaluations are shown in Table 7. A maximum sensitivity of 0.08 ng for the determination of cadmium can be obtained by following the method described here. The various parameters for achieving this limit are listed at the bottom of Table 7. The sensitivity limit of 0.08 ng was found to be more than sufficient for the detection of trace cadmium in all samples analyzed in this study.

Limits of detection for the measurement of cadmium by IPAA vary widely with the activation parameters. The energy and length of irradiation, the beam current intensity, and presence of interfering elements in the matrix are the most important factors determining the detection limits. The sensitivities obtained at two different irradiation energies and for three different irradiation times are shown in Table 8. It can be seen from this table that optimal sensitivity for the determination of cadmium by IPAA can be achieved by irradiating samples at 35 MeV for 60 min. The various criteria used in calculating these limits are given at the bottom of Table 8. It should be pointed out here that no interference was assumed in estimating these limits. Other investigators (18–21) have reported slightly higher detection limits for the determination of cadmium by IPAA in a number of matrices.

TABLE 7. Detection limits of cadmium by RNAA

Length of irradiation (h)	Neutron flux (n/cm^2 s)	Detection limit (ng)*
16	2.5×10^{11}	50
30	2×10^{13}	0.5
30	5×10^{13}	0.3
60	2×10^{13}	0.1
60	5×10^{13}	0.08

*Criteria: $t_d \simeq 20$ h from chemical separation of cadmium; counting of 336-keV γ-ray of ^{115m}In with a 7.5 cm × 7.5 cm NaI(Tl) detector, and minimum detectable radioactivity of 1000 d.p.m.

TABLE 8. Detection limits of cadmium by IPAA

Length of irradiation (min)	Energy of irradiation (MeV)	Detection limit (ng)*
10	15	900
30	15	400
60	15	100
10	35	750
30	35	300
60	35	80

*Criteria: beam currents of 80 μA at 15 MeV and 225 μA at 35 MeV measured on the converter; $t_d \simeq 2$ half-lives; counting of 247-keV γ-ray of ^{111m}Cd with a 60-cc Ge(Li) detector; and weight approximation 3 σ detector background.

Comparison between RNAA and IPAA

Irradiation facilities in a nuclear reactor are readily available for the thermal neutron activation of cadmium isotopes. On the other hand, at present, access by analytical chemists to an electron Linac or betatron for photon irradiations is rather limited. However, if both the facilities are equally available for use in cadmium analysis, the neutron activation technique involving the radiochemical separation of cadmium is a fairly

Can. J. Chem. Downloaded from www.nrcresearchpress.com by 210.87.254.42 on 09/05/12
For personal use only.

lengthy procedure. Since IPAA as developed here is a purely nondestructive method, and provided the cadmium concentration is not less than 80 ng, a sample can be analyzed in a much shorter time for example, about 3 h. With respect to the limits of sensitivity it is obvious from the above that RNAA is 1000 times more sensitive than IPAA.

In RNAA, both the cadmium standard and the sample are irradiated in precisely the same flux of neutrons. On the other hand appreciable errors can be introduced in IPAA due to fluctuation in the photon flux. However, such errors can be kept to a minimum by designing a special irradiation assembly such as the one used in this study.

In conclusion, neutron activation followed by radiochemical separation (RNAA) has been found to be an invaluable technique for the determination of cadmium in food and other materials in which very low p.p.b. concentrations are often present. We have not observed any distinct pattern of the cadmium residues in various specimens of food items from different geographical locations of the various provinces in Canada. For this reason, we have not specified the origins of the foods individually. Moreover, the cadmium content of the foods analyzed are very similar to those reported by other investigators in several countries (*viz.* a range of approximately 2–70 p.p.b. with higher contents for a few specific items). It should be stressed at this point that a number of additional food items need to be analyzed before any general conclusion regarding the cadmium residues in food can be drawn. At present, we are analyzing various foods for cadmium content on a routine basis using the RNAA method as developed here.

Samples such as the fly ash which are very difficult to dissolve by the available methods, can be easily analyzed by instrumental photon activation analysis (IPAA). Since the contaminated materials such as soils and fertilizers are suspected to have high concentrations of cadmium, they can be rapidly analyzed by IPAA. This is also an inexpensive method for measuring cadmium in a large batch of samples. The real art of IPAA, however, lies in the fairly simple multielement determinations (24). This method is now being extended to determine cadmium in this laboratory in air particulates, human organs, tissues, urine, blood, and bone for monitoring purposes.

The assistance of the group of Prof. T. C. Hutchinson, Department of Botany of the University of Toronto in obtaining soil and vegetable samples is greatly appreciated. Financial assistance to this project under a Public Health Research Grant, Project No. 605–7–664, Department of National Health and Welfare is also acknowledged, as well as an NRCC research operating grant.

1. R. Nilsson. Aspects on the toxicity of cadmium and its compounds. Ecol. Res. Comm. Bull. No. 7. Swedish Natural Science Research Council, Stockholm. 1970. p. 2.
2. T. Jaakkola, H. Takahashi, R. Soininen, K. Rissanen, and J. K. Miettinen. Proc. Symp. Radiotracer Stud. Chem. Residues Food Agric. IAEA, Vienna. 69 (1972); Environmental quality and safety, global aspects of chemistry, toxicology and technology as applied to the environment. Vol. II. *Edited by* F. Coulston and F. Korte. Academic Press, N.Y. (1973). p. 230.
3. N. Yamagata and I. Shigematsu. Bull. Inst. Pub. Health, **19**, 1 (1970).
4. K. Nomiyama. Proc. Int. Conf. Heavy Met. Aquat. Environ. Vanderbilt University, Tenn. 1973. In press.
5. F. Bakir, S. F. Damluji, L. Amin Zaki, M. Murtadha, A. Khalidi, N. Y. Al Rawi, S. Tikriti, H. I. Dhahir, T. W. Clarkson, J. C. Smith, and R. A. Doherty. Science, **181**, 230 (1973).
6. T. W. Clarkson. Proc. Int. Conf. Heavy Met. Aquat. Environ. Vanderbilt University, Tenn. 1973. In press.
7. Ontario Ministry of Health Memo. Citation of Dr. E. Mastromatteo, Environmental Health Section. 1972.
8. L. Friberg, M. Piscator, and G. Nordberg. Cadmium in the environment. CRC Press, Ohio. 1971. (*a*) pp. 17, 23, (*b*) p. 59.
9. W. Fulkerson and H. E. Goeller (*Editors*). Cadmium—the dissipated element. ORNL-NSF-EP-21. Oak Ridge, Tenn. 1973. (*a*) p. 437, (*b*) p. 226, (*c*) p. 227, (*d*) p. 72.
10. E. D. Copenhaver, G. U. Ulrikson, L. T. Newman, and W. Fulkerson. Cadmium in the environment—an annotated bibliography. ORNL-EIS-73-17. Oak Ridge, Tenn. 1973.
11. H. J. M. Bowen. Proc. Symp. Nucl. Act. Tech. Life Sci. IAEA, Vienna. 393 (1972).
12. K. W. Lieberman and H. H. Kramer. Anal. Chem. **42**, 266 (1970).
13. K. Ljunggren, B. Sjostrand, A. G. Johnels, M. Olsson, G. Otterlind, and T. Westermark. Proc. Symp. Nucl. Techn. Environ. Pollut. IAEA, Vienna. 373 (1971).
14. H. A. Das and H. A. van der Sloot. Proc. Symp. Nucl. Act. Techn. Life Sci. IAEA, Vienna. 309 (1972).
15. A. Chattopadhyay, L. G. I. Bennett, and R. E. Jervis. Can. J. Chem. Eng. **50**, 189 (1972).
16. A. Chattopadhyay and R. E. Jervis. Radiochem. Radioanal. Lett. **11**, 331 (1972).
17. A. Chattopadhyay and R. E. Jervis. Proc. Int. Conf. Photonucl. React. Appl. *Edited by* B. L. Berman. Lawrence Livermore Lab., Calif. Vol. **2**, 1009 (1973).

18. J. S. HISLOP and D. R. WILLIAMS. Proc. Int. Conf. Modern Trends Act. Anal. Saclay, France. 1972. Paper No. M67. In press.
19. V. V. SULIN. Colloque Int. CNRS. Saclay, France. 1972. Paper No. C29. In press.
20. E. RICCI. Colloque Int. du CNRS. Saclay, France. 1972. Paper No. C46; Anal. Chem. In press.
21. C. ENGELMANN. Advances in activation analysis. *Edited by* J. M. A. Lenihan, S. J. Thomson, and V. P. Guinn. Academic Press, N.Y. Vol. 2, 3 (1972).
22. R. E. JERVIS and B. TIEFENBACH. Proc. ANS Topic. Meet. Nucl. Methods Environ. Res. *Edited by* J. R. Vogt, T. F. Parkinson, and R. L. Carter. University of Missouri, Columbia. 188 (1971).
23. L. C. BATE. Proc. ANS Topical Meet. Nucl. Methods Environ. Res. *Edited by* J. R. Vogt, T. F. Parkinson, and R. L. Carter. University of Missouri, Columbia. 197 (1971); Radiochem. Radioanal. Lett. **6**, 139 (1971).
24. A. CHATTOPADHYAY and R. E. JERVIS. Anal. Chem. In press.
25. J. R. DEVOE. The radiochemistry of cadmium. NAS-NS-3001. U.S. Bureau of Commerce, Washington, D.C. 1960. p. 31.
26. C. L. RULFS, E. P. PRZYBYLOWICZ, and C. E. SKINNER. Anal. Chem. **26**, 408 (1954).
27. J. R. FELDMEIER and G. B. COLLINS. Phys. Rev. **59**, 937 (1941).
28. H. R. LUKENS, JR., J. W. OTVOS, and C. D. WAGNER. Int. J. Appl. Rad. Isot. **11**, 30 (1961).
29. J. LAW and F. A. IDDINGS. J. Radioanal. Chem. **3**, 53 (1969).
30. G. H. ANDERSEN, F. M. GRABER, V. P. GUINN, H. R. LUKENS, and D. M. SETTLE. Proc. Symp. Nucl. Act. Techn. Life Sci. IAEA, Vienna, 99 (1967).
31. T. KATO. Res. Rep. Lab. Nucl. Sci. Tohoku University, Japan, **5**(2), 137 (1972).
32. G. BACIU, V. GALATANU, and M. GRECESCU. Proc. 5th. Int. Betatron Symp. Bucharest, Rumania, 319 (1971).
33. N. K. ARAS, W. H. ZOLLER, G. E. GORDON, and G. J. LUTZ. Anal. Chem. **45**, 1481 (1973).
34. H. A. DAS and H. H. DE VRIES. React. Centrum Nedeland Rep. 136. Petten, Netherlands. 1971.
35. A. ISHIZAKI, M. FUKUSHIMA, and M. SAKAMOTO. Jap. J. Hyg. **25**, 207 (1970); (*a*) Jap. J. Hyg. **24**, 375 (1969).
36. R. RAUTU and A. SPORN. Nahrung. **14**, 25 (1970).
37. H. A. SCHROEDER, A. P. NASON, I. H. TIPTON, and J. J. BALASSA. J. Chron. Dis. **20**, 179 (1967).
38. H. G. ESSING, K. H. SCHALLER, D. SZADKOWSKI, and G. LEHNERT. Arch. Hyg. Bakteriol. **153**, 490 (1969).
39. E. W. D. HUFFMAN and J. F. HODGSON. J. Environ. Qual. **2**, 289 (1973).
40. H. A. SCHROEDER and J. J. BALASSA. J. Chron. Dis. **14**, 236 (1961).
41. J. LENER and B. BIBR. Vitalstoffe Zivilisationskrankheiten, **15**, 139 (1970).
42. E. SOMERS. Proc. Symp. Identification Meas. Environ. Poll. NRCC, Ottawa, 199 (1971).
43. H. J. M. BOWEN. Trace elements in biochemistry. Academic Press, London. 1966. p. 39.
44. D. I. HAMMER, J. F. FINKLEA, J. P. CREASON, S. H. SANDIFER, J. E. KEIL, L. E. PRIESTER, and J. F. STARA. Proc. 6th. Symp. Trace Subst. Environ. Health. *Edited by* D. D. Hemphill. University of Missouri, Columbia, **6**, 269 (1972).
45. R. E. JERVIS. Proc. Symp. Nucl. Act. Techn. Life Sci. IAEA, Vienna. 645 (1967); Radioisotopes, **17**, 26 (1968).
46. D. I. HAMMER, J. F. FINKLEA, R. H. HENDRICKS, and C. M. SHY. Am. J. Epidem. **93**, 84 (1971).
47. A. A. GORDUS. Proc. 2nd. Int. Conf. Forensic Act. Anal. Glasgow, Scotland. 1972. Paper No. 23; Environ. Aspects Trace Met. Human Hair. University of Michigan, Ann Arbor. 1973. Rep. No. 2.
48. H. A. SCHROEDER and A. P. NASON. J. Invest. Derm. **53**, 71 (1969).
49. J. V. LAGERWERFF, R. M. DICKERSON, and D. L. BROWER. Proc. 7th Symp. Trace Subst. Environ. Health. *Edited by* D. D. Hemphill. University of Missouri, Columbia. In press.
50. R. E. JERVIS, A. CHATTOPADHYAY, E. CSILLAG, and B. TIEFENBACH. Proc. Symp. Water Qual. Parameters—Sel. Meas. Monit. CIC-CCIW, Ontario. 1973. In press.

Can. J. Chem. Downloaded from www.nrcresearchpress.com by 210.87.254.42 on 09/05/12
For personal use only.

The Oxidation of Heterocyclic Thiones

JAMES L. CHARLTON, SHEENA M. LOOSMORE, AND DAVID M. MCKINNON
Department of Chemistry, University of Manitoba, Winnipeg, Manitoba R3T 2N2

Received February 7, 1974

JAMES L. CHARLTON, SHEENA M. LOOSMORE, and DAVID M. MCKINNON. Can. J. Chem. **52**, 3021 (1974).

The treatment of a variety of heterocyclic thiones with hydrogen peroxide in acetic acid produces either heteroaromatic cations or the corresponding "oxo" compound. The results may be correlated with structural and electronic features. Benzo substitution or the presence of strongly electron withdrawing groups in the molecule favors the latter product, whereas the presence of a σ trivalent nitrogen atom in the molecule favors the former.

JAMES L. CHARLTON, SHEENA M. LOOSMORE et DAVID M. MCKINNON. Can. J. Chem. **52**, 3021 (1974).

La réaction d'un grand nombre de thiones hétérocycliques avec le peroxyde hydrogène dans l'acide acétique produit soit des cations hétéroaromatiques ou les composés oxo correspondants. Les résultats peuvent être reliés avec des caractéristiques structurales et électroniques. La substitution par des groupements benzéniques ou la présence de groupes fortement électro-affinitaires dans la molécule favorise la formation des dérivés oxo alors que la présence d'un atome d'azote trivalent favorise la formation des cations. [Traduit par le journal]

Can. J. Chem. Downloaded from www.nrcresearchpress.com by 210.87.254.105 on 09/05/12
For personal use only.

A useful reaction in heterocyclic chemistry is the treatment of heterocyclic thiones with peracetic acid to form heteroaromatic cations. While the reaction actually involves reduction of the ring system, the exocyclic sulfur atom is oxidized and eliminated as sulfate. Although the reaction was originally applied to 1,2-dithiole-3-thiones **1** (1, 2) and has since been applied to a variety of other systems indicated below, it is by no means general and fails in other apparently related or isoelectronic systems. In these cases, the exocyclic sulfur atom is replaced by oxygen. This has been observed for 1,2,4-dithiazole-3-thiones (3), pyran-2- and -4-thiones, and thiopyran-4-thiones (4). Even in certain cases in systems which usually give cationic products, certain other products are obtained. These will also be indicated below.

To clear this confusion and to establish the conditions and structural features which would lead to either of these types of products, we have investigated the reaction of a number of heterocyclic thiones with 3 equiv. of hydrogen peroxide in acetic acid, which behaves analogously to peracetic acid (5). To maintain uniformity of experimental parameters, we have used this as a standard reaction condition.

In view of our interest in sulfur chemistry, we have confined our studies mainly to simple systems containing only sulfur atoms, *e.g.* dithiolethiones and thiopyranthiones or to sulfur and nitrogen containing compounds which have similar structural and electronic features to these. A large amount of work is reported on the oxidation of nitrogen containing thiones, *e.g.*, pyrazolethiones (6, 7), 1,2,4-triazoline-3-thiones (8, 9). thiazolinethiones, and imidazolethiones (10–12) but in these cases, while products are more diverse, no cationic material formed by loss of sulfur is found. Oxidation of 1,2-dithiole-3-thiones with alkaline hydrogen peroxide is also reported (13) but the treatment affords acyclic products.

For this study, we used a number of selected heterocyclic thiones, some of which are new or prepared by different methods to established literature procedures. These are indicated below. For convenience we will refer to cationic products as "salt" and to the other type of product as "oxo." These products included thiolactones, lactams, and, in some cases, ketones. For the 5,6-benzothiopyran-2-thiones (dithiocoumarins) **4**, the usual method of preparation has been by the sulfurization of *o*-methoxyallylbenzenes (14) but we have found a more convenient procedure to be the sulfurization of benzodihydrothiopyrans, in the form of their crude mixtures with benzodihydrothiophenes, obtained by thio-Claisen rearrangement of allyl phenyl sulfides (15).

To examine the effect of two benzo rings on the reaction of thiopyran-2-thiones we synthesized 3,4:5,6-dibenzothiopyran-2-thione (**4***m*).

Can. J. Chem. Downloaded from www.nrcresearchpress.com by 210.87.254.105 on 09/05/12
For personal use only.

TABLE 1. Oxidation products of heterocyclic thiones

Compound	Source (ref.)	Product	Melting point (°C)	Yield (%)	Formula	Analysis (%) C Calcd.	C Found	H Calcd.	H Found	N Calcd.	N Found	S Calcd.	S Found	Cl Calcd.	Cl Found
1*a*	(32)	**1***b*	58 (lit. (33) 58)	62											
1*c*	(34)	**1***d*	60 (lit. (34) 60)	80											
1*c*	(34)	**7**	145–146	9	$C_9H_{11}S_2ClO_5$	36.18	36.30	3.69	3.89			21.44	21.69	11.89	11.63
2*a*	(35)	**3***a*	182, dec.	73	$C_{17}H_{13}SClO_4$	58.53	58.87	3.73	3.80			9.18	9.45	10.19	10.27
2*b*	(36)	**2***c*	93 (lit. (36) 93)	60											
2*j*	(47)	**3***b*	X = I, 116 (lit. (50) 116)	69											
2*d*	*	**2***e*	77 (lit. (39) 77)	72											
2*f*	*	**2***g*	175 (lit. (40) 175)	65											
2*h*	(36)	**2***i*	90 (lit. (36) 90)	82											
4*a*	*	**4***b*	80–80.5 (lit. (37) 80–80.5)	81											
4*c*	*	**4***d*	80 (lit. (48) 80)	76											
4*c*	*	**5**	128–132	15	$C_{10}H_9SClO_4$	46.07	45.94	3.45	3.41			12.28	12.28	13.63	13.40
4*e*	(14)	**4***f*	84–86	76	$C_{11}H_{10}SO$	69.47	69.43	5.26	5.30			16.84	16.76		
4*g*	*	**4***h*	129 (lit. (49) 129–130)												
4*i*	(14)	**4***j*	176	81	$C_{13}H_8SO$	73.58	73.41	3.77	3.78			15.09	15.21		
4*k*	(14)	**4***l*	145	80	$C_{13}H_8SO$	73.58	73.82	3.77	3.65			15.09	15.01		
4*m*	*	**4***n*	130–131	95	$C_{13}H_8SO$	73.58	73.40	3.77	3.57			15.09	14.92		
8*a*	(41)	**8***b*	§	60											
8*c*	(21)	**8***d*	217–128 (lit. (21) 217–218)	68											
8*e*	(42)	**8***f*	§	90											
9*a*	*	**11***c*	194–196 (lit. (45) 194–196)	95											
9*b*	*	**11***f*	†	70											
10*a*	(22)	**11***a*	102 (lit. (23) 102)	86											
10*b*	(22)	**11***b*	†	80											
10*c*	(43)	**11***d*	209–210	91	$C_{13}H_{10}NSClO_4$	50.08	49.73	3.21	3.35	4.49	4.34	10.27	10.16	11.40	11.38
10*d*	(43)	**11***e*	X = I, 178 (lit. (44) 178)	63											
12*a*	*	**13***a*	145	65	$C_{10}H_{10}HSClO_4$	43.55	43.29	3.63	3.78	5.08	4.88	11.62	11.37	12.89	12.92
12*b*	‡	**13***b*	145–146 (lit. (51) 145–146)	81											
14*a*	(46)	**14***b*	§	79											

*This work.
†Product could not be obtained crystalline, even by alteration of anion.
‡Aldrich Chemical Company Inc.
§Product was an oil and was not analyzed. Mass spectrum was satisfactory.

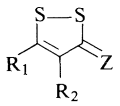

1

a R_1 = Ph; R_2 = CO_2Et; Z = S
b R_1 = Ph; R_2 = CO_2Et; Z = O
c R_1, R_2 = $CO{\cdot}CH_2{\cdot}CMe_2{\cdot}CH_2$; Z = S
d R_1, R_2 = $CO{\cdot}CH_2{\cdot}CMe_2{\cdot}CH_2$; Z = O

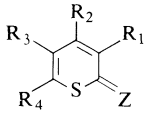

2

a R_1 = R_3 = Ph; R_2 = R_4 = H; Z = S
b R_1, R_2 = $(CH{=}CH)_2$; R_3 = H; R_4 = Ph; Z = S
c R_1, R_2 = $(CH{=}CH)_2$; R_3 = H; R_4 = Ph; Z = O
d R_1 = CO_2Et; R_2 = R_4 = Ph; R_3 = H; Z = S
e R_1 = CO_2Et; R_2 = R_4 = Ph; R_3 = H; Z = O
f R_1 = CN; R_2 = R_4 = Ph; R_3 = H; Z = S
g R_1 = CN; R_2 = R_4 = Ph; R_3 = H; Z = O
h R_1, R_2 = $(CH{=}CH)_2$; R_3 = H; R_4 = Ph; S = O; Z = S
i R_1, R_2 = $(CH{=}CH)_2$; R_3 = H; R_4 = Ph; S = Z = O
j R_1 = R_2 = R_3 = R_4 = H; S = NMe; Z = S

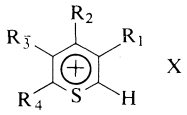

3

a R_1 = R_3 = Ph; R_2 = R_4 = H; X = ClO_4
b R_1 = R_2 = R_3 = R_4 = H; S = NMe; X = I

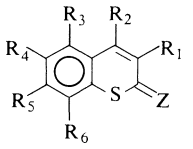

4

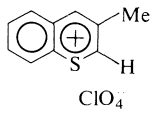

5

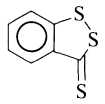

6

a R_1 = R_2 = R_3 = R_4 = R_5 = R_6 = H; Z = S
b R_1 = R_2 = R_3 = R_4 = R_5 = R_6 = H; Z = O
c R_1 = Me; R_2 = R_3 = R_4 = R_5 = R_6 = H; Z = S
d R_1 = Me; R_2 = R_3 = R_4 = R_5 = R_6 = H; Z = O
e R_1 = R_6 = Me; R_2 = R_3 = R_4 = R_5 = H; Z = S
f R_1 = R_6 = Me; R_2 = R_3 = R_4 = R_5 = H; Z = O
g R_1 = R_2 = R_3 = R_5 = R_6 = H; R_4 = OMe; Z = S
h R_1 = R_2 = R_3 = R_5 = R_6 = H; R_4 = OMe; Z = O
i R_1 = R_2 = R_3 = R_4 = H; R_5, R_6 = $(CH{=}CH)_2$; Z = S
j R_1 = R_2 = R_3 = R_4 = H; R_5, R_6 = $(CH{=}CH)_2$; Z = O
k R_1 = R_2 = R_5 = R_6 = H; R_3, R_4 = $(CH{=}CH)_2$; Z = S
l R_1 = R_2 = R_5 = R_6 = H; R_3, R_4 = $(CH{=}CH)_2$; Z = O
m R_3 = R_4 = R_5 = R_6 = H; R_1, R_2 = $(CH{=}CH)_2$; Z = S
n R_3 = R_4 = R_5 = R_6 = H; R_1, R_2 = $(CH{=}CH)_2$; Z = O

Diazotized 2-aminodiphenyl was converted to 2-mercaptodiphenyl via the xanthate and treatment of this with thiophosgene in base gave 2-diphenylyl dithiochloroformate, which cyclized on treatment in carbon disulfide with anhydrous aluminum chloride to give the desired product (**4***m*). This latter reaction is analogous to a preparation of dithiobenzoates from aryl dithiochloroformates and aromatic compounds (16).

To obtain some results on the effect of electron withdrawing groups on the course of the reaction of monocyclic thiopyran-2-thiones, the ester **2***d* and the nitrile **2***f* were synthesized by thionation of the corresponding thiopyran-2-ones **2***e* and *g*, respectively.

2-Methyl-4,5-diphenylisothiazoline-3-thione (**9***b*) was prepared by treatment of 3-methylthio-4,5-benzo-1,2-dithiolium iodide with methylamine. This convenient method is analogous to the preparation of *N*-alkylisothiazoline-3-thiones from monocyclic 3-alkylthio-1,2-dithiolium salts and primary aliphatic amines (17).

The results of the oxidative studies are presented in Table 1. The oxidation of 3,5-diphenylthiopyran-2-thione gave the salt **3***a*. This is consistent with other thiopyranthione oxidations reported (4) and demonstrates that it is a general reaction. On the other hand, two monocyclic thiopyran-2-thiones containing strongly electron attracting groups, *i.e.* the ester **2***d* and the nitrile **2***f*, the 4,5-benzothiopyran-2-thiones (**4***a*, *c*, *e*, and *g*), the 3,4-benzothiopyran-2-thione, (**2***b*), and the naphthothiopyran-2-thiones (**4***i* and *k*) and 3,4:5,6-dibenzothiopyran-2-thione (**4***m*) all gave "oxo" products on reaction. Only in one case, **4***c*, were we able to isolate a small amount of "salt", whose analysis corresponded to 3-methylbenzothiopyrylium perchlorate (**5**).

The 3,4-benzopyran-2-thione (**2***h*) also gave "oxo" product **2***i* on oxidation. This result is comparable to reactions of monocyclic pyran-2-thiones and 5,6-benzopyran-2-thiones (4).

For simple 1,2-dithiole-3-thiones (**1**) the reaction is an established method of conversion to 1,2-dithiolium salts (2, 5). Although 1,2-dithiole-3-thiones containing strongly electron withdrawing groups have been little studied, 3-thio-

Can. J. Chem. Downloaded from www.nrcresearchpress.com by 210.87.254.105 on 09/05/12
For personal use only.

Can. J. Chem. Downloaded from www.nrcresearchpress.com by 210.87.254.105 on 09/05/12
For personal use only.

1,2-dithiole-5-carboxylic acid gave the unsubstituted 1,2-dithiolium cation on treatment with peracetic acid (1). Whether the decarboxylation was prior or subsequent to the formation of cation was not established. The reaction performed on the ester **1***a* gave only "oxo" product **1***b* and on the ketone **1***c* gave predominantly "oxo" product **1***d*. Only a small amount of salt **7***a* was obtained. The effect of benzo substituents on the oxidation of 1,2-dithiole-3-thiones has been established. "Poorly defined oxidation products which were not salt-like" (18, 19) were generally obtained but one naphtho derivative was unusual in that it did give a small amount of a naphtho-1,2-dithiolium salt (18).

Generally, the reaction applied to 1,3-dithiole-2-thiones (**8**) affords 1,3-dithiolium salts in good yields (5, 20). When we applied it to the ester **8***a*, the dicarboxamide **8***c*, and 5-methylbenzo-1,3-dithiole-2-thione (**8***e*) the corresponding "oxo" products (**8***b*, *d*, and *f*, respectively) were obtained. Peracetate oxidation of 2-thio-1,3-dithiole-4-carbonitrile is reported to produce a sulfine, whereas 2-thio-1,3-dithiole-4,5-dicarboxylic acid and 2-thio-1,3-dithiole-4-carboxylic acids give unidentifiable products (21).

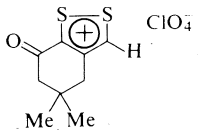

7

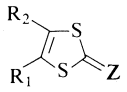

8

a $R_1 = R_2 = CO_2Me$; Z = S
b $R_1 = R_2 = CO_2Me$; Z = O
c $R_1 = R_2 = CONH_2$; Z = S
d $R_1 = R_2 = CONH_2$; Z = O
e $R_1, R_2 = (CH{=}CMe{-}CH{=}CH)$; Z = S
f $R_1, R_2 = (CH{=}CMe{-}CH{=}CH)$; Z = O

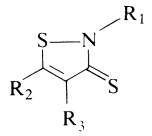

9

a $R_1 = R_2 = Ph$; $R_3 = H$
b $R_1 = Me$; $R_2, R_3 = (CH{=}CH)_2$

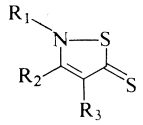

10

a $R_1 = CH_3$; $R_2 = H$; $R_3 = Ph$
b $R_1 = Ph{\cdot}CH_2$; $R_2 = H$; $R_3 = Ph$
c $R_1 = Ph$; $R_2, R_3 = (CH{=}CH)_2$
d $R_1 = Me$; $R_2, R_3 = (CH{=}CH)_2$

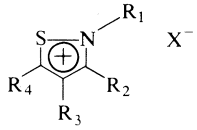

11

a $R_1 = Me$; $R_2 = R_4 = H$; $R_3 = Ph$; X = ClO_4
b $R_1 = Ph{\cdot}CH_2$; $R_2 = R_4 = H$; $R_3 = Ph$;
c $R_1 = R_4 = Ph$; $R_2 = R_3 = H$; X = ClO_4
d $R_1 = Ph$; $R_3, R_4 = (CH{=}CH)_2$; $R_2 = H$; X = ClO_4
e $R_1 = Me$; $R_3, R_4 = (CH{=}CH)_2$; $R_2 = H$; X = I
f $R_1 = Me$; $R_2, R_3 = (CH{=}CH)_2$; $R_4 = H$

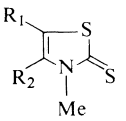

12

a $R_1 = H$; $R_2 = Ph$
b $R_1, R_2 = (CH{=}CH)_2$

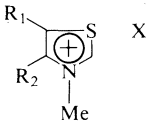

13

a $R_1 = H$; $R_2 = Ph$; X = ClO_4
b $R_1 = R_2 = (CH{=}CH)_2$; X = ClO_4

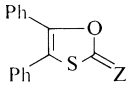

14

a Z = S
b X = O

Among mixed sulfur nitrogen systems, the recently available (22) *N*-alkylisothiazoline-5-thiones (**10***a* and *b*), the *N*-arylisothiazoline-3-thione (**9***a*), and the benzisothiazoline-5-thiones (**10***c* and *d*) were converted to the corresponding isothiazolium salts (**11***a* and *e*, respectively). These results correspond to earlier studies of

Can. J. Chem. Downloaded from www.nrcresearchpress.com by 210.87.254.105 on 09/05/12
For personal use only.

isothiazolinethiones (23, 24). Oxidations of thiazoline-2-thiones appear to have been little studied. We have found that 3-methyl-4-phenylthiazoline-2-thione (**12***a*) and 3-methylbenzothiazoline-2-thione (**12***b*) gave salts **13***a* and *b* on reaction. It is known (10, 25) that 2-mercaptothiazoles, which on the basis of related structures probably exist as the thione tautomers (26), are converted into 2-unsubstituted thiazoles by loss of the sulfhydryl group.

From these results and from the literature certain features become evident. It appears that treatment of monocyclic compounds containing

the —S—C— group will lead to formation of "salt" where such would have aromatic character. If the ring is fused or if it has an electron withdrawing substituent or group, the preferred product of the reaction is the "oxo" compound. In the five-membered rings these principles hold and replacement of a sulfur atom in dithiolethiones

by an —N—R group, giving thiazoline- or isothiazolinethiones, also favors "salt" formation. The effect in the benzo series of these compounds is also to favor "salt" formation. The benzisothiazoles and benzothiazoles should be contrasted with the isoelectronic benzothiopyrans and benzodithioles, where the formation of "oxo" products is usually favored. The difference is likely due to the electron releasing ability of the nitrogen atom. Replacement of a sulfur atom by an oxygen in the 1,3-dithiole system appears, in the one example we studied, to have an opposite effect to nitrogen. We found that reaction of 4,5-diphenyl-1,3-thioxole-2-thione (**14***a*) gave the "oxo" compound (**14***b*). This may be related to the reactions of pyran-2-thiones, which in contrast to thiopyran-2-thiones, give "oxo" products on oxidation (4). There are insufficient data to assess the effect of carboxyl groups on the oxidation products but it seems likely that if decarboxylation could occur, "salt" would be obtained. Phenyl substituents appear to be too weakly electron withdrawing (27) to be important in determining the course of the reaction.

It should also be noted that these results are only applicable to thiones which have potentially aromatic character. It is known (28) that the oxidation of certain cyclic trithiocarbonates which do not have potentially aromatic character gives an array of products.

Finally, in an attempt to assess the structural features necessary in compounds without ring sulfur atoms, the reaction performed on *N*-methylpyridine-2-thione (**2***e*) yielded the *N*-methylpyridinium cation (**3***b*). This result differs from studies reported on pyridine-4-thiones (29), although a peroxide oxidation of 4-mercaptopyridines, which exist predominantly in the thione forms (30), gave 4-unsubstituted pyridines (31). Such variety of products is also reported for pyran-2- and -4-thiones and may be due to similar causes.

Experimental

Mass spectra of compounds prepared were obtained on a Finnegan 1015 quadrupole mass spectrometer. Thin-layer chromatography, where necessary, was performed on "Camag" silica gel D.S.F.5 and column chromatography on Alumina 506-C-1 Brockman Activity 1, both supplied by Mondray Ltd. Development of both, unless otherwise stated, was by benzene. Melting points were obtained on a precalibrated Kofler Micro hot-stage apparatus.

Treatment of Heterocyclic Thiones with Hydrogen Peroxide in Acetic Acid

Fairly standard conditions were used. The thiones (0.1–0.5 g) in glacial acetic acid (~10 ml) were treated with 3 equiv. of 30% aqueous hydrogen peroxide. In most cases the solutions warmed somewhat, accompanied by intensification of color. After 5–10 min there was gradual decolorization. After 30 min the solutions were treated with 70% perchloric acid (0.1–0.5 ml) and diluted with ether. Salts usually precipitated as crystalline solids, especially on scratching, but in a few cases they were hygroscopic and precipitated as oils. Any salts were removed by filtration or decantation and the filtrate was diluted with water. The ether extracts were washed, dried, and evaporated to yield the "oxo" compounds which were purified by recrystallization from appropriate solvents, usually ethanol. Where perchlorate salts were noncrystalline they were freed of hydrogen peroxide by reprecipitation from acetic acid and converted to their iodides by treatment with saturated aqueous potassium iodide solution. Unless otherwise stated, salts were obtained as perchlorates ($X = ClO_4$). The results are presented in Table 1.

*Preparation of 5,6-Benzothiopyran-2-thione (**4a**)*

Allyl phenyl sulfide (30 g, 0.2 mol) was converted into a mixture of benzodihydrothiopyran and methylbenzodihydrothiophene according to the procedure of Kwart *et al.* (15). The crude mixture was added to sulfur (25 g) in refluxing ethyl benzoate and the mixture heated 1½ h. The cooled mixture was diluted with ether, let stand 4 h, and filtered to remove excess sulfur. Treatment with saturated mercuric chloride solution in methanol (50 ml) afforded a dark precipitate which was collected and decomposed with aqueous sodium sulfide. Extraction of the mixture with ether gave on evaporation a red solid which was purified by chromatography and crystallized from ethanol–benzene, 1:1 mixture, as red needles m.p. 109° (lit. (37) 109°, 6% from allyl phenyl sulfide).

Can. J. Chem. Downloaded from www.nrcresearchpress.com by 210.87.254.105 on 09/05/12
For personal use only.

*Preparations of Other 5,6-Benzothiopyran-2-thiones (**4**c and g)*

This was done by analogous methods to above using suitably substituted alkyl phenyl sulfides. Melting points of compounds obtained were identical with those reported (14) by alternate synthesis.

*Preparation of Ethyl 2-Thio-4,6-diphenylthiopyran-3-carboxylate (**2**d)*

Ethyl 2-oxo-4,6-diphenylthiopyran-3-carboxylate (336 mg, 1 mmol) (39) and phosphorus pentasulfide (0.7 g) were refluxed in benzene (10 ml) for 1 h. The mixture was treated with sodium carbonate solution and the benzene extract washed and dried. A deep red solid was obtained which was recrystallized from ethanol as dark red prisms, m.p. 79–80°.

Anal. Calcd. for $C_{20}H_{16}S_2O_2$: C, 68.18; H, 4.54; S, 18.18. Found: C, 67.89; H, 4.54; S, 18.04.

The mass spectrum M^+ 352, calcd. 352.

*Preparation of 2-Thio-4,6-diphenylthiopyran-3-carbonitrile (**2**f)*

This was prepared as above from 2-oxo-4,6-diphenylthiopyran-3-carbonitrile (40); red prisms, m.p. 196° (lit. (40) 196°) were obtained (82%).

*Preparation of 3-Methyl-4-Phenylthiazoline-2-thione (**12**a)*

3-Methyl-4-phenylthiazoline-2-one was thionated as above. Work-up yielded pale yellow prisms, m.p. 126–128° (58%).

Anal. Calcd. for $C_{10}H_9NS_2$: C, 57.97; H, 4.35; N, 6.76; S, 30.92. Found: C, 58.08; H, 4.41; N, 6.62; S, 30.69.

The mass spectrum M^+ 207, calcd. 207.

Preparation of 2-Mercaptodiphenyl

2-Aminodiphenyl (84.5 g, 0.5 mol) was added to a mixture of concentrated hydrochloric acid (100 ml) and crushed ice (100 g). The mixture was diazotized by addition of saturated sodium nitrite (37 g) solution in water. The diazotized solution was added over 1½ h to a solution of potassium ethyl xanthate (93 g, 0.58 mol) in water (250 ml) at 45°. The oil which separated was hydrolyzed in boiling alcoholic potassium hydroxide (20 g in 100 ml) for 6 h and the mixture diluted with water. Any oily material which separated was rejected and the cooled alkaline solution was acidified and extracted with ether. Further purification was effected by back extraction into aqueous sodium hydroxide solution and re-acidification. The dried ether extract on evaporation gave a pale yellow oil which crystallized on standing. The product was recrystallized from petroleum ether as colorless needles, m.p. 36° (62%).

Anal. Calcd. for $C_{12}H_{10}S$: C, 77.41; H, 5.38; S, 17.21. Found: C, 77.35; H, 5.56; S, 16.99.

The mass spectrum M^+ 186, calcd. 186.

Preparation of 2-Diphenylyl Chlorodithioformate

2-Mercaptodiphenyl (18.6 g, 0.1 mol) was treated with a solution of sodium hydroxide (4 g, 0.1 mol) in water (6 ml). A slurry was formed which was slowly added to a stirred solution of thiophosgene (12.65 g, 0.11 mol) in benzene (30 ml). Temperature was maintained at 10–15° during the addition. The mixture was left 16 h, then the benzene layer was separated, dried, and evaporated to give a yellow oil (79%). This was not purified but was used directly in the next reaction.

*Preparation of 3,4;5,6-Dibenzothiopyran-2-thione (**4**m)*

The crude diphenylyl chlorodithioformate from above (13.27 g, 0.05 mol) in carbon disulfide (50 ml) at 0° was treated with anhydrous aluminum chloride (6.5 g, 0.05 mol). The mixture became virtually solid and hydrogen chloride was evolved. After standing 16 h, the mixture was decomposed by addition of water and dilute hydrochloric acid. The carbon disulfide layer was separated, dried, and evaporated to give a pasty solid. Recrystallization from benzene afforded red fibrous needles, m.p. 113–114° (85%).

Anal. Calcd. for $C_{13}H_8S_2$: C, 68.62; H, 3.51; S, 28.07. Found: C, 68.44; H, 3.50; S, 27.88.

The mass spectrum M^+ 228, calcd. 228.

*Preparation of 2-Methyl-4,5-benzisothiazoline-3-thione (**9**b)*

3-Methylthio-4,5-benzodithiolium iodide (3.24 g, 10 mmol) in ethanol (10 ml) was treated with 25% methylamine solution in ethanol (25%) with stirring. The mixture rapidly turned yellow and was stirred until homogeneous. After 1 h the solution was diluted with saturated sodium chloride solution in water and ether extracted. The dried extract gave on evaporation a crystalline yellow solid which was recrystallized from methanol as yellow needles, m.p. 137° (lit. (38) 137°) (62%).

The authors are very grateful to the National Research Council of Canada for financial support of this research. We also wish to thank Mr. M. Arneson and Mr. R. Dickinson for the preparation of spectra.

1. E. KLINGSBERG. Chem. and Ind. 1568 (1960).
2. E. KLINGSBERG and A. SCHREIBER. J. Am. Chem. Soc. **83**, 2934 (1961).
3. M. AHMED and D. M. MCKINNON. Can. J. Chem. **48**, 2142 (1970).
4. D. M. MCKINNON. Can. J. Chem. **48**, 3388 (1970).
5. D. LEAVER, W. A. H. ROBERTSON, and D. M. MCKINNON. J. Chem. Soc. 5104 (1962).
6. R. KITAMURA and G. SUNAGAWA. J. Pharm. Soc. Jap. **61**, 26 (1941).
7. R. KITAMURA. J. Pharm. Soc. Jap. **58**, 447 (1938).
8. A. J. BLACKMAN and J. B. POLYA. J. Chem. Soc. [C], 2403 (1970).
9. W. DYMEK, M. DZIEWONSKA, and M. POLONSKA. Diss. Pharm. **16**, 495 (1964).
10. E. R. BUCHMAN, A. O. REIMS, and H. SARGENT. J. Org. Chem. **6**, 764 (1941).
11. I. E. BALABAN and H. KING. J. Chem. Soc. 1858 (1927).
12. T. O. NORRIS and R. L. MCKEE. J. Am. Chem. Soc. **77**, 1056 (1955).
13. B. BOTTCHER and A. LUTTRINGHAUS. Ann. **557**, 89 (1947).
14. Y. MOLLIER and N. LOZAC'H. Bull. Soc. Chim. Fr. 651 (1958).
15. H. KWART and E. R. EVANS. J. Org. Chem. **31**, 413 (1966).
16. H. VIOLA, S. SCHEITHAUER, and R. MAYER. Ber. **101**, 3526 (1968).
17. G. LE COUSTUMER and Y. MOLLIER. Bull. Soc. Chim. Fr. 3076 (1970).
18. E. KLINGSBERG. J. Org. Chem. **37**, 3226 (1972).

19. E. KLINGSBERG and A. SCHREIBER. J. Am. Chem. Soc. **84**, 2941 (1962).
20. E. KLINGSBERG. J. Am. Chem. Soc. **84**, 3410 (1962).
21. E. KLINGSBERG. J. Am. Chem. Soc. **86**, 5290 (1964).
22. M. H. CHAUHAN, M. E. HASSAN, and D. M. MCKINNON. Can. J. Chem. 1738 (1974).
23. G. E. BACHERS, D. M. MCKINNON, and J. M. BUCHSHRIBER. Can. J. Chem. **50**, 2568 (1972).
24. M. E. HASSAN and D. M. MCKINNON. Can. J. Chem. **51**, 3081 (1973).
25. G. VERNIN and J. METZGER. Bull. Soc. Chim. Fr. 2498 (1963).
26. A. R. KATRITZKY and J. M. LAGOWSKI. Adv. Heterocycl. Chem. **2**, 27 (1963).
27. J. HINE. Physical organic chemistry. McGraw-Hill, New York. 1962.
28. T. J. ADLEY, A. K. ANISUZZAMAN, and L. N. OWEN. J. Chem. Soc. [C], 807 (1967).
29. M. A. F. ELKASCHEF, M. H. NOSSEIR, and A. ABDEL-KADER. J. Chem. Soc. 4647 (1963).
30. A. R. KATRITZKY and J. M. LAGOWSKI. Adv. Heterocycl. Chem. **1**, 339 (1963).
31. M. DOHRN and P. DIEDRICH. Ann. **494**, 284 (1932).
33. P. RAOUL and J. VIALLE. Bull. Soc. Chim. Fr. 213 (1960).
33. C. TREBAUL and J. TESTE. Bull. Soc. Chim. Fr. 2456 (1969).
34. M. EBEL, L. LEGRAND, and N. LOZAC'H. Bull. Soc. Chim. Fr. 1961 (1963).
35. R. MAYER, G. LABAN, and M. WIRTH. Ann. **703**, 140 (1967).
36. L. LEGRAND and N. LOZAC'H. Bull. Soc. Chim. Fr. 1787 (1964).
37. G. PFISTER-GUILLOUZO and N. LOZAC'H. Bull. Soc. Chim. Fr. 1624 (1962).
38. H. BOSHAGEN, H. FELTKAMP, and W. GEIGER. Ber. **100**, 2435 (1967).
39. D. LEAVER, D. M. MCKINNON, and W. A. H. ROBERTSON. J. Chem. Soc. 32 (1965).
40. R. PINEL, N. K. SON, and Y. MOLLIER. C.R. Acad. Sci. Paris Ser. C, 955 (1970).
41. D. B. J. EASTON and D. LEAVER. Chem. Commun. 585 (1965).
42. I. L. SODER and R. WIZINGER. Helv. Chim. Acta, **42**, 1733 (1959).
43. L. LEGRAND and N. LOZAC'H. Bull. Soc. Chim. Fr. 1170, 1173 (1969).
44. M. DAVIS, E. HOMFIELD, and K. S. L. SRIVASTAVA. J. Chem. Soc. Perkin Trans. I, 1863 (1973).
45. D. M. MCKINNON and E. A. ROBAK. Can. J. Chem. **46**, 1855 (1968).
46. J. M. BUCHSHRIBER. Ph.D. Thesis, University of Manitoba, Winnipeg, Manitoba, 1971.
47. J. RENAULT. Bull. Soc. Chim. Fr. 1000 (1953).
48. A. RUWET and M. RENSON. Bull. Soc. Chim. Belg. **77**, 465 (1968).
49. I. DEGANI, R. FOCHI, and G. SPUNTA. Boll. Sci. Fac. Chim. Ind. Bologna, **26**, 31 (1968).
50. A. HANTZSCH. Ber. **42**, 68 (1909).
51. H. QUAST and S. HUNIG. Ber. **99**, 2017 (1966).

Can. J. Chem. Downloaded from www.nrcresearchpress.com by 210.87.254.105 on 09/05/12
For personal use only.

The Barrier to Rotation About the N—N Bond in *N*-Nitrosamines as Determined by Nuclear Magnetic Resonance Total Line Shape Analysis[1,2]

J. D. COONEY AND S. K. BROWNSTEIN

Division of Chemistry, National Research Council of Canada, Ottawa, Canada K1A 0R9

AND

J. W. APSIMON

Department of Chemistry, Carleton University, Ottawa, Canada K1S 5B6

Received March 4, 1974

J. D. COONEY, S. K. BROWNSTEIN, and J. W. APSIMON. Can. J. Chem. **52**, 3028 (1974).

The energy barrier to internal N—N bond rotation in five cyclic and two bicyclic *N*-nitrosamines ($>$N—N=O) has been determined using high temperature 100 MHz n.m.r. spectroscopy. A substantial contribution from the ionic resonance structure of $>$N—N=O (**1**) produces considerable double bond character in the nitrogen–nitrogen bond and a concomitant increase in the rotational barrier about the N—N bond. The molecules were examined in the

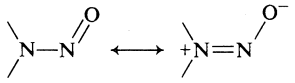

1

liquid state and had ring sizes varying from five to nine atoms. The Arrhenius and Eyring activation parameters for the energy barrier were determined using total line shape analysis and the intensity ratio approximation method. The energy barrier to N—N bond rotation was found to range from 23–29 kcal/mol depending on the molecular structure and the solvent.

J. D. COONEY, S. K. BROWNSTEIN et J. W. APSIMON. Can. J. Chem. **52**, 3028 (1974).

On a déterminé la barrière d'énergie pour la rotation interne autour du lien N—N dans cinq *N*-nitrosamines ($>$N—N=O) cycliques et deux bicycliques; les résultats ont été obtenus en faisant appel à la spectroscopie r.m.n. à 100 MHz à haute température. Une contribution importante de la structure de résonance ionique de $>$N—N=O (**1**) induit un caractère de double liaison important dans le lien azote–azote et augmente par le fait même la barrière à la rotation autour du lien N—N.

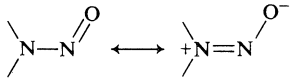

1

On a examiné les molécules à l'état liquide et elles possédaient des cycles contenant cinq à neuf atomes. On a déterminé les paramètres d'activation d'Arrhenius et d'Eyring pour les barrières d'énergie en faisant appel à l'analyse de la forme globale des bandes et à la méthode d'approximation des rapports d'intensité. On a trouvé que la barrière d'énergie pour la rotation autour du lien N—N est de 23–29 kcal/mol suivant la structure moléculaire et le solvant.

Contribution from the 1,3-dipolar resonance structure **1** of the *N*-nitrosamino group produces a planar $C_\alpha C_{\alpha'}NNO$ structure with double bond character between the two nitrogen atoms resulting in hindered rotation about the N—N bond.

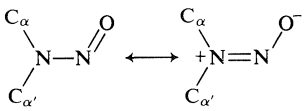

1

[1]Issued as NRCC No. 14079.

[2]Portions of this work were first reported in the M.Sc. Thesis of J.D.C., Carleton University, April, 1970, and second at the 56th Canadian Chemical Conference of the Chemical Institute of Canada, Montreal, June, 1973.

Can. J. Chem. Downloaded from www.nrcresearchpress.com by 210.87.254.42 on 09/05/12
For personal use only.

TABLE 1. Energy barrier to nitrosamine N—N bond rotation

Compounds	Solvent	E_a (kcal/mol)	ΔG_c^* (kcal/mol)	Ref.
N-Nitrosodimethylamine	Neat	23[a]	23	5
N-Nitrosodimethylamine	Neat	25±5[b]	25	6
N-Nitrosodimethylamine	Neat	21.9±1.6[c]	—	7
N-Nitrosodimethylamine	Neat	22.9±1.7[d]	—	7
N-Nitrosodimethylamine	Gas	—	21.1±0.1	8
N-Nitrosodimethylamine	Chloronaphthalene or phenyl cyanide	23		6
N-Nitrosodimethylamine	Ethylene glycol	18–38[e]		6
N-Nitrosoazetidine	Neat	—	20.5[f]	9
N-Nitroso-*N*-methylaniline	Neat	—	<6	5
N-Nitroso-*cis*-2,6-dimethylpiperidine	*o*-DCB	—	19.4	10
N-Nitroso-7-azabicyclo[2.2.1]heptane	CS_2	—	16.5	11
N-Nitrosohexafluorodimethylamine	Neat	—	~5	12

[a]Peak separation method.
[b]Intensity ratio method.
[c]Spin-echo, on resonance.
[d]Spin-echo, off resonance.
[e]Concentration dependent.
[f]Calculated from literature data.

This statement is supported by i.r. spectroscopy (1), a large dipole moment, 4.01 D (2), electron diffraction studies (3), molecular orbital theory (4), and a large barrier to N—N bond rotation (5–13) determined by various means. The energy barrier to N—N bond rotation has been estimated from n.m.r. spectra in several ways: (*a*) The free energy of activation, ΔG_c^* (14) calculated from the "slow exchange" peak separation ($\Delta\nu$) and the coalescence temperature (T_c). (*b*) The Arrhenius activation energy, E_a, calculated from: (*i*) peak separation approximation method (15); (*ii*) intensity ratio approximation method (16); (*iii*) spin-echo method (7). Literature values obtained from these calculations are listed in Table 1. Measurements of ΔG_c^* and E_a by all these methods have been obtained for *N*-nitrosodimethylamine and the energy barrier ranges from 18 to 38 kcal/mol depending on the environment of the molecule, *i.e.* neat liquid, in the presence of a solvent, or in the gas phase and also depending on the method of calculation. The most acceptable value appears to be 23.0 kcal/mol for the neat liquid (5).

At present, the total n.m.r. line shape fitting methods and the spin-echo Carr–Purcell measurements are the preferred techniques of obtaining activation energies but it must be noted that the spin-echo method has been reported (17) to generate values that are approximately 10–15% too low.

This paper outlines the first use of total line shape analysis, to determine a nitrosamine's barrier to N—N bond rotation. We used the variable high temperature 100 MHz n.m.r. spectra of some cyclic and bicyclic nitrosamines to determine the activation parameters for hindered N—N bond rotation. Data obtained from the intensity ratio approximation method and the calculation of ΔG_c^* have also been included for comparison.

The n.m.r. spectra of nitrosamines can be interpreted in terms of the NNO shielding cones and deshielding zones (18). The *trans*-α-hydrogens[3] will therefore resonate further downfield than the *cis*-α-hydrogens[4] for the cyclic and [3.2.2]bicyclic nitrosamines described in this paper.

Experimental

The nitrosamines were prepared by nitrosation of the parent amine with HNO_2 prepared *in situ* (19) and showed all the requisite spectral and analytical properties for the structures quoted (20).

Proton resonance spectra were recorded at 100 MHz on a Varian Associates HA-100 spectrometer using TMS as an internal standard. The sample temperature was regulated by a Varian V-4343 temperature controller, calibrated against ethylene glycol (21), and should be accurate within 1 °C. All n.m.r. spectra were of neat liquids unless a solvent is quoted. The theoretical and experimental spectra were compared visually and τ was varied until the best fit and an indication of the error was obtained.

The data were correlated by least-squares analysis and the errors in Table 2 are quoted as standard deviations.

[3]*Trans* to the oxygen atom.
[4]*Cis* to the oxygen atom.

Can. J. Chem. Downloaded from www.nrcresearchpress.com by 210.87.254.42 on 09/05/12
For personal use only.

Can. J. Chem. Downloaded from www.nrcresearchpress.com by 210.87.254.42 on 09/05/12
For personal use only.

Results

N-Nitrosopyrrolidine

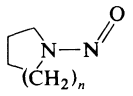

n=1–5

2

The *cis*- and *trans*-α-methylene resonances of *N*-nitrosopyrrolidine **2**, $n = 1$, Fig. 1, appear as complicated multiplets because of coupling with the β-methylenes in a small ring system. The multiplet at δ 3.41 represents the *cis*-α-methylene resonance while the multiplet at δ 4.17 is the *trans*-α-methylene resonance. The "slow exchange", 23 °C, *cis*- and *trans*-α-methylene resonance separation is 76.4 Hz. Each multiplet in the "slow exchange" experimental spectrum, the bottom left of Fig. 1, has a central multiplet with a width at half-height approximately twice that of the flanking multiplets. This suggests AB coupling with the adjacent β-hydrogens. Neglecting further splitting, this would indicate an eight-line input for total line shape analysis (t.l.s.) in the region of interest using a stochastic approach, *i.e.* the Johnson method (22, eq. 5). The populations and positions of each line were varied but this failed to give a reasonable fit, so a simpler six-line input was employed. Since it was difficult to duplicate the 23 °C spectrum, we varied the parameters to obtain a satisfactory fit at 140 °C as shown in Fig. 1. The mean lifetime, τ (s), of the exchange process is included with each theoretical spectrum. Figure 2 shows some

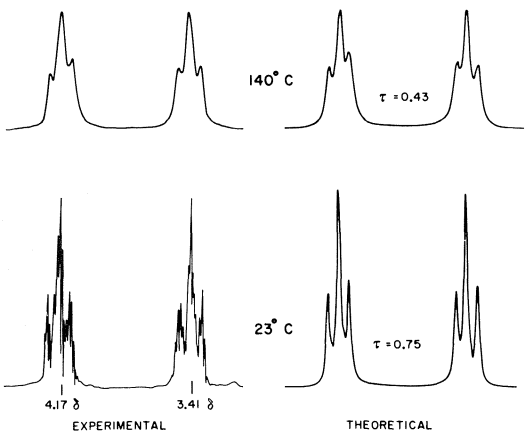

FIG. 1. Temperature dependence of the experimental and theoretical *N*-α-methylene n.m.r. resonances of *N*-nitrosopyrrolidine.

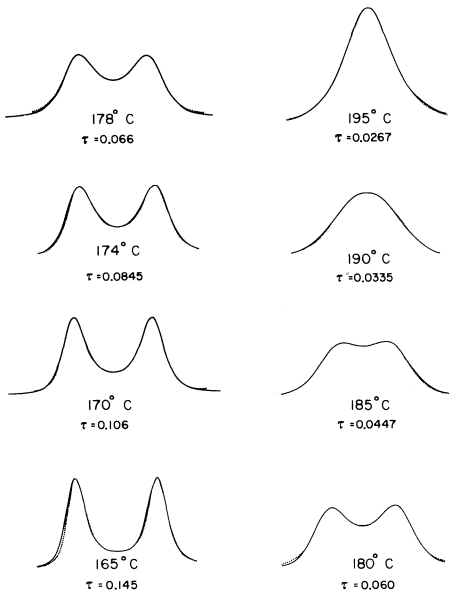

FIG. 2. Temperature dependence of the experimental (——) and theoretical (·····) *N*-α-methylene n.m.r. resonances of *N*-nitrosopyrrolidine.

experimental α-methylene resonances above 140 °C with deviations in the fit of the theoretical curves indicated by dots. Coalescence occurs at 190 °C. An Arrhenius plot [log $1/\tau$ *vs.* $10^3/T$ °K] produced the thermodynamic activation parameters listed in Table 2.

N-Nitrosopiperidine

The multiplet at δ 3.68 in the n.m.r. spectrum of *N*-nitrosopiperidine **2**, $n = 2$, represents the *cis*-α-methylene resonance while the multiplet at δ 4.12 is the *trans*-α-methylene resonance. The "slow exchange" *cis*- and *trans*-α-methylene resonance separation is 43.9 Hz at 23 °C but this increases to 47.8 Hz at 140 °C. Above 140 °C the exchange rate is fast enough that the peaks are starting to broaden and come together. At 23 °C, the *trans* multiplet at δ 4.12 was too complicated to duplicate by t.l.s. while the *cis* multiplet at δ 3.68 was much simpler to approximate. The *cis* multiplet suggests a four-line program because the central peak has a width at half-height that is double that of the flanking peaks, as well as a shoulder indicating the presence of two resonance lines. An eight-line input was used for t.l.s. analysis in the region of interest, again using the Johnson method (22, eqn. 5). The computer program included four lines for the *cis*- and four lines for the *trans*-α-methylene resonances with

TABLE 2. Arrhenius and Eyring activation parameters for nitrosamine hindered N—N bond rotation

Compound	Method	E_a (kcal/mol)	Log A	ΔH^*_{298} (kcal/mol)	ΔS^*_{298} (e.u.)	ΔG^*_{298} (kcal/mol)	ΔG_c^* (kcal/mol)
2, $n = 1$	t.l.s.	23.4±0.5	12.5±0.2	22.8±0.5	−3.3±1.1	23.8±0.8	22.8±0.1
2, $n = 1$	I_{max}/I_{min}[a]	20.3±0.4	11.8±0.2	19.7±0.4	−6.3±1.0	21.6±0.7	
2, $n = 2$	t.l.s.	24.0±0.4	12.8±0.2	23.4±0.4	−1.8±0.9	24.0±0.7	22.7±0.1
2, $n = 2$	I_{max}/I_{min}	19.4±0.4	11.4±0.2	18.8±0.4	−8.5±0.9	21.3±0.7	
3 in *o*-DCB	t.l.s.	29.0±0.8	15.0±0.4	28.4±0.8	+8.3±1.8	25.9±1.3	>23.6
3 in DPE	t.l.s.	26.5±0.5	13.8±0.2	25.9±0.5	+2.8±1.0	25.1±0.8	>23.9
4 in DPE	t.l.s.	25.1±0.4	13.3±0.2	24.5±0.4	+0.2±0.9	24.5±0.6	~24.5
4 in *o*-DCB	—	—	—	—	—	—	~23.9

[a] I_{max}/I_{min} ≡ intensity ratio method.

the line positions being determined from a straight line plot of the "slow exchange" Δν *vs.* temperature for 23–140 °C and extrapolation to 195 °C. The experimental and theoretical 23 and 150 °C α-methylene resonances are shown in Fig. 3 and a fair fit was obtained for the 150 °C spectrum. Some experimental spectra at higher temperatures are shown in Fig. 4 with the theoretical spectra superimposed and deviations in fit shown as dots. A fair fit of the experimental and theoretical spectra was obtained and coalescence occurs at 180 °C. The calculated activation parameters are listed in Table 2.

N-Nitrosoazacycloheptane

N-Nitrosoazacycloheptane **2**, $n = 3$, has a *cis*-α-methylene resonance multiplet at δ 3.56 and a *trans*-α-methylene resonance multiplet at δ 4.29 (Fig. 5) giving a "slow exchange" Δν of 73 Hz. The collapse of the triplets, slight peak broadening, and valley filling of the resonances at 200 °C suggests a very slow rate of N—N bond rotation even at this high temperature. A $T_c > 200$ °C indicates a $\Delta G_c^* > 23.3$ kcal/mol.

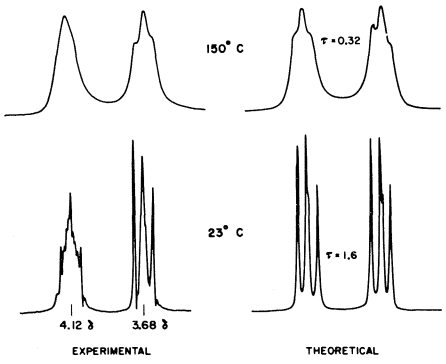

FIG. 3. Temperature dependence of the experimental and theoretical *N*-α-methylene n.m.r. resonances of *N*-nitrosopiperidine.

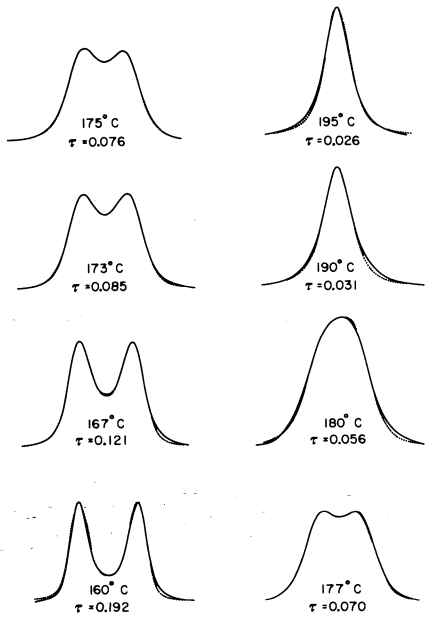

FIG. 4. Temperature dependence of the experimental (——) and theoretical (·····) *N*-α-methylene n.m.r. resonances of *N*-nitrosopiperidine.

N-Nitrosoazacyclooctane

N-Nitrosoazacyclooctane **2**, $n = 4$, has a *cis*-α-methylene resonance multiplet at δ 3.62 and a *trans*-α-methylene resonance multiplet at δ 4.20 giving a "slow exchange" Δν of 58 Hz. A slow rate of N—N bond rotation is calculated from the collapse of the triplets, slight peak broadening, and valley filling of the resonances even at 200 °C. The rate constant is only 4.0 s^{-1} at 200 °C as determined by the crude six line t.l.s. (22) shown in Fig. 6. A $T_c > 200$ °C indicates a $\Delta G_c^* > 23.5$ kcal/mol.

N-Nitrosoazacyclononane

N-Nitrosoazacyclononane **2**, $n = 5$, has a *cis*-

Can. J. Chem. Downloaded from www.nrcresearchpress.com by 210.87.254.42 on 09/05/12
For personal use only.

Can. J. Chem. Downloaded from www.nrcresearchpress.com by 210.87.254.42 on 09/05/12
For personal use only.

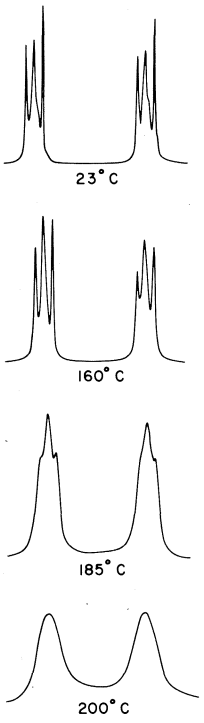

FIG. 5. Temperature dependence of the experimental *N*-α-methylene n.m.r. resonances of *N*-nitrosoazacycloheptane.

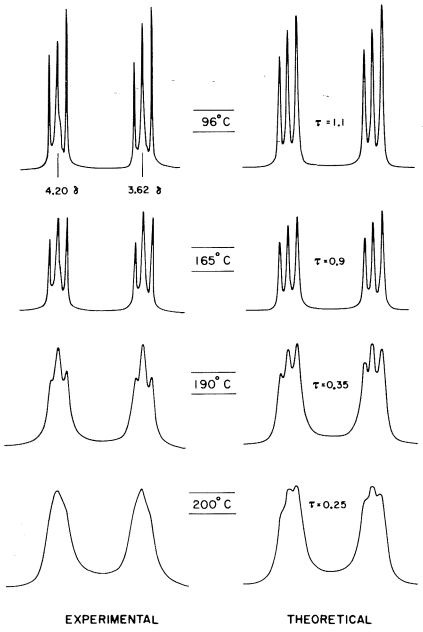

FIG. 6. Temperature dependence of the experimental and theoretical *N*-α-methylene n.m.r. resonances of *N*-nitrosoazacyclooctane.

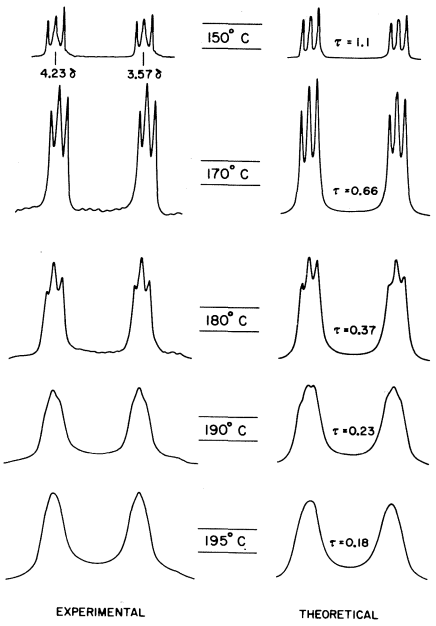

FIG. 7. Temperature dependence of the experimental and theoretical *N*-α-methylene n.m.r. resonances of *N*-nitrosoazacyclononane.

α-methylene resonance multiplet at δ 3.57 and a *trans*-α-methylene resonance multiplet at δ 4.23 giving a "slow exchange" Δν of 66 Hz. Applying the t.l.s. Johnson method (22) in the region of interest, with an eight-line program gave the theoretical spectra shown in Fig. 7. The rate of N—N bond rotation was still slow at 195 °C (k = 5.6 s^{-1}) and this did not give sufficient information to calculate a realistic E_a value. Even so, the $\Delta G^*_{298} = 24.2 \pm 1.0$ kcal/mol is quite close to the expected value. A $T_c > 195$ °C gives a $\Delta G_c^* > 23.4$ kcal/mol which supports the ΔG^*_{298} value. ΔG_c^* values have been reported to be less sensitive to systematic errors (23). An indication of the magnitude of ΔG^*_{298} was obtained from $\Delta H^*_{298} - T\Delta S^*_{298}$, where ΔH^* and ΔS^* were calculated from data in the Arrhenius plot.

N-Nitroso-3-azabicyclo[3.2.2]nonane

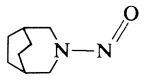

3

N-Nitroso-3-azabicyclo[3.2.2]nonane (**3**) in *o*-dichlorobenzene (*o*-DCB) solution has a "slow exchange", 23 °C, *cis*-α-methylene doublet resonance at δ 3.75 (J = 3.9 Hz) and a *trans*-α-methylene doublet resonance at δ 4.26 (J = 3.9

Can. J. Chem. Downloaded from www.nrcresearchpress.com by 210.87.254.42 on 09/05/12
For personal use only.

Hz). This splitting arises from coupling with the β-methines. The peak separation, Δν, between the α-methylene resonances is 50.7 Hz at 23 °C but increases to 56.0 Hz at 175 °C. A t.l.s. Binsch DNMR3 $AB_2 \rightleftharpoons CD_2$ program (24) with a transverse relaxation time, $T_2 = 0.34$ s, and variable "slow exchange" chemical shifts were used to generate the theoretical spectra shown on the right in Fig. 8. The rate constant, k, is quite small (0.1–8.5 s^{-1}) for the temperatures studied and therefore we would expect less accurate results, see Table 2.

N-Nitroso-3-azabicyclo[3.2.2]nonane (**3**) dissolved in diphenyl ether (DPE) has a "slow exchange", 23 °C, *cis*-α-methylene doublet resonance at δ 3.50 ($J = 3.9$ Hz) and a *trans*-α-methylene doublet resonance at δ 3.92 ($J = 3.9$ Hz). This splitting again arises from coupling with the β-methines. The *cis*- and *trans*-α-methylene peak separation is 42.3 Hz at 23 °C but increases to 51.0 Hz at 185 °C then decreases at higher temperatures as the peaks broaden and start moving together. A t.l.s. Binsch DNMR3 program with a transverse relaxation time, $T_2 = 0.265$ s and variable "slow exchange" chemical shifts were used to generate the theoretical curves

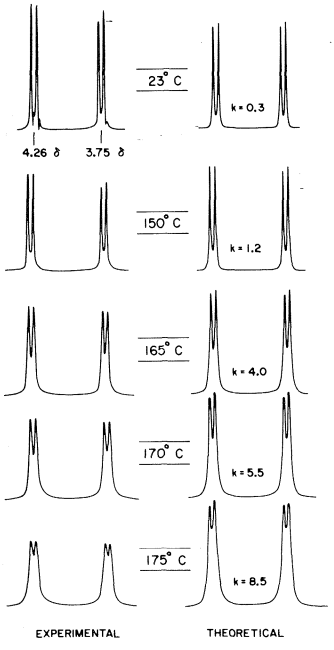

FIG. 8. Temperature dependence of the experimental and theoretical *N*-α-methylene n.m.r. resonances of *N*-nitroso-3-azabicyclo[3.2.2]nonane in *o*-dichlorobenzene solution.

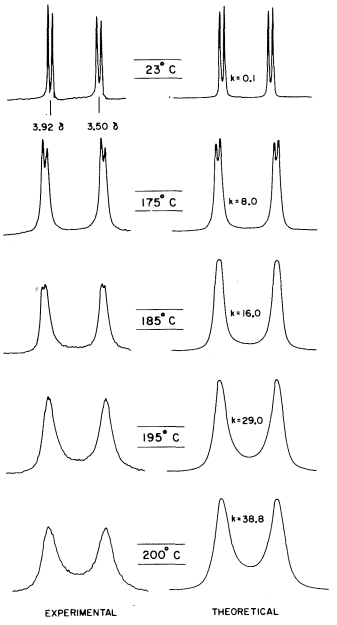

FIG. 9. Temperature dependence of the experimental and theoretical *N*-α-methylene n.m.r. resonances of *N*-nitroso-3-azabicyclo[3.2.2]nonane in diphenyl ether solution.

shown on the right in Fig. 9. The rate constant, k, varies from 0.1–38.8 s^{-1} and is expected to give quite accurate activation parameters, since it is quite large at 185, 195, and 200 °C, see Table 2.

N-Nitrosocamphidine

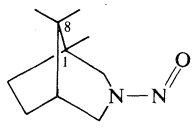

4

N-Nitrosocamphidine (**4**) (*N*-nitroso-1,8,8-trimethyl-3-azabicyclo[3.2.1]octane) exists as a 1:1 mixture of *syn* and *anti* isomers (25) showing four methyl resonances in its n.m.r. spectrum. A single resonance is observed for each of the two 8-methyls and two resonances for the 1-methyl, *i.e.* one for *syn* isomer and one for the *anti* isomer. The four methyl peaks, shown for the 100 °C, "slow exchange" spectrum in Fig. 10, resonate at δ 0.886, 0.821, 0.799, and 0.733 in DPE solution. Designating the resonances, from left to right, δ 0.886 represents the *cis*-8-methyl[5] of the *syn* and *anti* isomer, δ 0.821 represents the 1-methyl in the *anti* isomer, δ 0.799 represents the

[5]8-Methyl closest to the ring nitrogen.

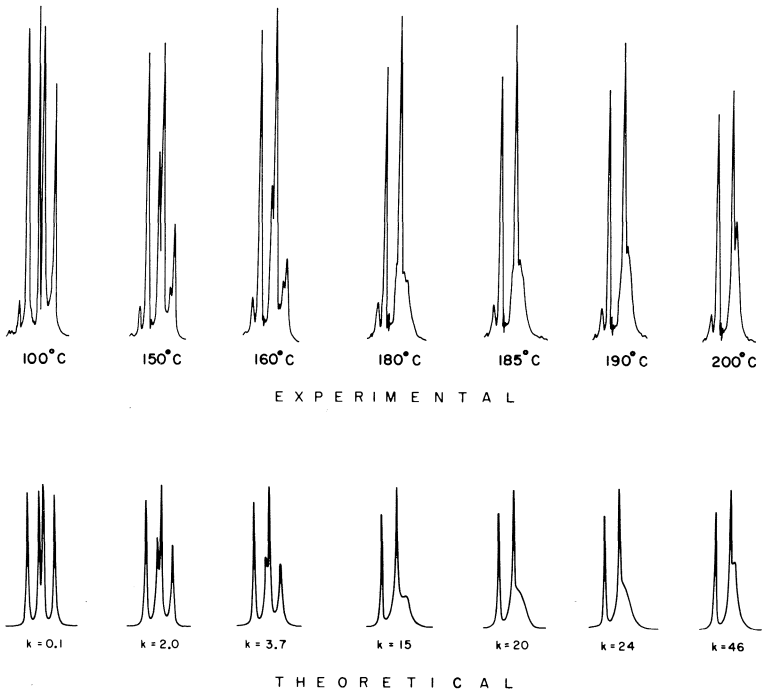

FIG. 10. Temperature dependence of the experimental and theoretical methyl n.m.r. resonances of *N*-nitrosocamphidine in diphenyl ether solution.

trans-8-methyl[6] of the *syn* and *anti* isomer, and δ 0.733 represents the 1-methyl in the *syn* isomer. On heating, the 1-methyl resonances, *i.e.* the second and fourth peaks from the left, decrease in height, coalesce at 185 °C, then eventually appear as a single resonance at 200 °C. A density matrix approach to total line shape analysis, Binsch DNMR3 and an ABC $\rightleftharpoons$ ADC system was used to duplicate this event. A transverse relaxation time, $T_2 = 0.3$ s was used along with variable methyl chemical shifts (determined by linear plots of "slow exchange" peak positions *vs.* temperature and extrapolation of the lines where necessary). The theoretical spectra are shown at the bottom of Fig. 10 and agree quite well with experimental spectra considering the close proximity of the methyl resonances. The calculated activation parameters are listed in Table 2.

A similar total line shape analysis of **4** in *o*-DCB solution did not yield enough data to produce a reliable Arrhenius plot since the maximum temperature was 175 °C and this just produced coalescence. We needed spectra above the coalescence temperature as obtained in diphenyl ether solution.

[6]8-Methyl furthest from the ring nitrogen.

Discussion

In examining the data in Table 2 the thermodynamic parameters obtained by the intensity ratio method and ΔG_c^* should only be looked on as an approximation of the value to be expected from t.l.s. analysis. The intensity ratio method is inaccurate in the region where the most information is available, that is the region where the spectral shape is changing most rapidly (near T_c) while this is just the region where t.l.s. is most accurate. The activation parameters listed for t.l.s. are therefore considered to be the most reliable. The ΔG_c^* values are based on only two measurements, the chemical shift and coalescence temperature, and do not compare the total spectral shape at several temperatures as is done with t.l.s. Therefore, ΔG_c^* is only a rough estimate of the actual free energy of activation.

The Arrhenius activation energy, E_a, derived from t.l.s. analysis was found to vary from 23–29 kcal/mol, for the nitrosamines examined in this paper, depending on the ring structure and solvent. It was hoped to observe a ring size effect on

Can. J. Chem. Downloaded from www.nrcresearchpress.com by 210.87.254.42 on 09/05/12
For personal use only.

TABLE 3. α-Methylene nuclear magnetic resonances of nitrosamines in CCl_4 solution[a]

Nitrosamine	α-Methylene resonances (δ) *Trans*	*Cis*	Average α-methylene resonance (δ)
N-Nitroso-			
pyrrolidine	4.204	3.415	3.81
piperidine	4.131	3.642	3.89
azacycloheptane	4.279	3.526	3.90
azacyclooctane	4.180	3.539	3.86
azacyclononane	4.208	3.500	3.85
camphidine	4.097	3.501	3.80
3-azabicyclo[3.2.2]nonane	4.366	3.755	4.06

[a]Internal standard is 0.000.

the energy barrier to rotation with the five- and six-membered rings having the smallest energy barriers because of the strain induced in attempting to have a double bond exocyclic to small rings but insufficient data was obtained on the seven-, eight-, and nine-membered ring systems to substantiate this statement.

Chemical shifts of the α-methylene resonances also indicate the extent of N—N double bond character. The α-methylene resonances of *N*-nitroso-3-azabicyclo[3.2.2]nonane were observed to be further downfield than those of any other nitrosamine examined (26) and this is confirmed by examining the average α-methylene resonances listed in Table 3. This suggests that *N*-nitroso-3-azabicyclo[3.2.2]nonane will have more N—N double bond character and therefore a larger energy barrier to N—N bond rotation. This is precisely as observed in Table 2. The E_a's (29.0 and 26.5 kcal/mol) of *N*-nitroso-3-azabicyclo-[3.2.2]nonane in *o*-DCB and DPE solutions indicate the substantial role the solvent can play in determining the N—N double bond character. The more polar *o*-DCB, $\mu = 2.27$ D (27), stabilizes the 1,3-dipolar NNO resonance structure **1** more than DPE, $\mu = 1.1$ D (27), and therefore encourages the formation of more N—N double bond character and a larger E_a.

Error analysis of the Arrhenius equation (28) utilizes the error in temperature (σ_T), the tem-

$$\left(\frac{\sigma E_a}{E_a}\right)^2 \simeq \frac{2T^2}{(\Delta T)^2}\left(\frac{\sigma_T}{T}\right)^2 + 2\left(\frac{1}{\Delta(\ln k)}\right)^2\left(\frac{\sigma_k}{k}\right)^2$$

perature range of study (ΔT) and the error in the rate constant (σ_k) and points out the importance of a large temperature range of study. This error analysis is more indicative of the actual errors in E_a than is the standard deviation obtained by least-squares analysis. Arrhenius equation error analysis of our t.l.s. data gave the following errors in E_a.

Compound	*n*	Solvent	Average error in *k* (%)[a]	ΔT (°K)	E_a (kcal/mol)
2	1	Neat	2.0	30	23.4 ± 1.2
2	2	Neat	2.3	34.5	24.0 ± 1.1
3		*o*-DCB	6.3	25	29.0 ± 2.1
3		DPE	4.2	25	26.5 ± 1.8
4		DPE	6.7	20	25.1 ± 2.8

[a]$\sigma_T = 1$ °K.

The errors in *k* were determined by varying *k* until the t.l.s. curve definitely did not correspond to the experimental curve at a particular temperature.

The Arrhenius activation energies to N—N bond rotation of the nitrosamines (23–29 kcal/mol) are definitely larger than observed for total n.m.r. line shape analysis of *N*,*N*-dimethylformamide 20.8 ± 0.6 (17) and 20.5 ± 0.2 kcal/mol (29).

The frequency factor, log *A*, (Table 2) is expected to be 13 for a unimolecular process such as we are observing here with simple hindered two-fold barriers and the entropy of activation ΔS^* would be expected to be approximately zero. These criteria are observed for all compounds except **3** dissolved in *o*-DCB which had large log $A = 15$ and $\Delta S^* = +8.3$ e.u. but still a very realistic $\Delta G^*_{298} = 25.9$ kcal/mol (ΔG^* is predominantly determined by intramolecular interactions). This large positive ΔS^*_{298} for **3** indicates loss of solvent involvement in going from the ground state to the transition state for N—N bond rotation (ΔH^* and ΔS^* are sensitive to intermolecular interactions (30)).

Can. J. Chem. Downloaded from www.nrcresearchpress.com by 210.87.254.42 on 09/05/12
For personal use only.

We wish to thank Mr. Jacques Bornais for recording all spectra. We thank the NRCC for generous financial assistance for the work performed at Carleton University.

1. R. N. Haszeldine and J. Jander. J. Chem. Soc. 691 (1954); R. L. Williams, R. J. Pace, and G. J. Jeacocke. Spectrochim. Acta, **20**, 225 (1964); J. W. Linnett and R. M. Rosenburg. Tetrahedron, **20**, 53 (1964).
2. E. G. Cowley and J. R. Partington. J. Chem. Soc. 1255 (1933).
3. P. Rademacher and R. Stølevik. Acta Chem. Scand. **23**, 660 (1969); P. Rademacher, R. Stølevik, and W. Lüttke. Angew. Chem. Int. Ed. Engl. **7**, 806 (1968).
4. P. Rademacher and R. Stølevik. Acta Chem. Scand. **23**, 660 (1969); J. Tanaka. J. Chem. Soc. Jap. **78**, 1647 (1957); W. D. Phillips. Ann. N.Y. Acad. Sci. **70**, 817 (1958).
5. C. E. Looney, W. D. Phillips, and E. L. Reilly. J. Am. Chem. Soc. **79**, 6136 (1957).
6. D. J. Blears. J. Chem. Soc. 6256 (1964).
7. K. H. Abramson, P. T. Inglefield, E. Krakower, and L. W. Reeves. Can. J. Chem. **44**, 1685 (1966).
8. R. K. Harris and R. A. Spragg. Chem. Commun. 362 (1967).
9. C. L. Bumgardner, K. S. McCallum, and J. P. Freeman. J. Am. Chem. Soc. **83**, 4417 (1961).
10. Y. L. Chow, C. J. Colón, and J. N. S. Tam. Can. J. Chem. **46**, 2821 (1968).
11. R. R. Fraser and R. B. Swingle. Can. J. Chem. **48**, 2065 (1970).
12. S. Andreades. J. Org. Chem. **27**, 4163 (1962).
13. A. Mannschreck, H. Münsch, and A. Mattheus. Angew. Chem. Int. Ed. Engl. **5**, 728 (1966); A. Mannschreck and H. Münsch. Angew. Chem. Int. Ed. Engl. **6**, 984 (1967); A. Mannschreck and H. Münsch. Tetrahedron Lett. 3227 (1968).
14. J. A. Pople, W. G. Schneider, and H. J. Bernstein. High-resolution nuclear magnetic resonance. McGraw-Hill Book Co., Inc., New York. 1959. p. 223.
15. H. S. Gutowsky and C. H. Holm. J. Chem. Phys. **25**, 1228 (1956).
16. M. T. Rogers and J. C. Woodbrey. J. Phys. Chem. **66**, 540 (1962).
17. P. T. Inglefield, E. Krakower, L. W. Reeves, and R. Stewart. Mol. Phys. **15**, 65 (1968).
18. R. K. Harris and R. A. Spragg. J. Mol. Spectrosc. **23**, 158 (1967); Y. L. Chow and C. J. Colón. Can. J. Chem. **46**, 2827 (1968); Y. L. Chow. Angew. Chem. Int. Ed. Engl. **6**, 75 (1967).
19. H. H. Hart. Organic Synthesis Coll. Vol. II. John Wiley and Sons, Inc., New York, N.Y. 1943. p. 211; S. Marburg. J. Org, Chem. **30**, 2834 (1965).
20. J. D. Cooney. M.Sc. Thesis, Carleton University, Ottawa, Canada, 1970.
21. A. L. Van Geet. Anal. Chem. **40**, 2227 (1968).
22. C. S. Johnson and C. G. Moreland. J. Chem. Ed. **50**, 477 (1973).
23. A. Allerhand, H. S. Gutowsky, J. Jonas, and R. A. Meinzer. J. Am. Chem. Soc. **88**, 3185 (1966); H. Kessler. Angew. Chem. Int. Ed. Engl. **9**, 219 (1970).
24. D. A. Kleier and G. Binsch. DNMR3: a computer program for the calculation of complex exchange-broadened NMR spectra. Modified version for spin systems exhibiting magnetic equivalence or symmetry. Program 165, Quantum Chemistry Program Exchange, Indiana, 1970.
25. J. W. ApSimon and J. D. Cooney. Can. J. Chem. **49**, 2377 (1971).
26. J. G. Traynham and M. T. Yang. Tetrahedron Lett. 575 (1965).
27. A. L. McClellan. Tables of experimental dipole moments. W. H. Freeman and Co., San Francisco. 1963. pp. 166, 411.
28. A. Steigel, J. Sauer, D. A. Kleier, and G. Binsch. J. Am. Chem. Soc. **94**, 2770 (1972).
29. M. Rabinovitz and A. Pines. J. Am. Chem. Soc. **91**, 1585 (1969).
30. K. N. Shaw and L. W. Reeves. Chem. Phys. Lett. **10**, 89 (1971).

Can. J. Chem. Downloaded from www.nrcresearchpress.com by 210.87.254.42 on 09/05/12
For personal use only.

Proton Magnetic Resonance Study of Intramolecular Hydrogen Bonding in Halophenols

J. Brian Rowbotham[1] and T. Schaefer

Department of Chemistry, University of Manitoba, Winnipeg, Manitoba R3T 2N2

Received April 29, 1974

J. Brian Rowbotham and T. Schaefer. Can. J. Chem. **52**, 3037 (1974).

The long-range spin–spin coupling constants over five bonds between the hydroxyl proton and the ring protons in a series of trihalophenols imply that the intramolecular hydrogen bond strength (negative enthalpy) to fluorine is greater than that to iodine by 75 ± 20 cal/mol, whereas the strengths to chlorine and bromine are 460 ± 60 cal/mol greater than to iodine. If a distinction can be made between chlorine and bromine, then chlorine–hydrogen bonds more strongly by only a few tens of calories per mol. The measurements were made mainly on dilute solutions in carbon tetrachloride at 32 °C.

J. Brian Rowbotham et T. Schaefer. Can. J. Chem. **52**, 3037 (1974).

Les valeurs des constantes de couplage spin–spin à longue distance sur cinq liens entre le proton de l'hydroxyle et les protons du cycle ont été mesurées pour une série de phénols trihalogénés; ces valeurs impliquent que la force du lien hydrogène intramoléculaire (enthalpie négative) vers le fluor est plus grande que celle vers l'iode par 75 ± 20 cal/mol alors que les forces des liens hydrogènes intramoléculaires vers le chlore et le brome sont plus grandes que celle de l'iode par 460 ± 60 cal/mol. Si l'on peut faire une distinction entre le chlore et le brome on note alors que les atomes de chlore font des liens qui sont plus forts; la différence n'est que quelques dizaines de calories par mol. On a fait les mesures principalement sur des solutions diluées dans le tétrachlorure de carbone à 32 °C. [Traduit par le journal]

Introduction

The strengths and relative strengths of the intramolecular hydrogen bonds in *o*-halophenols have been investigated extensively but with conflicting results (1–3). The most common approach has involved the temperature dependence of the intensities of the hydroxyl stretching frequencies (4–6). Competitive hydrogen bonding with added ether (7), dipole moments (8), and hydroxyl proton chemical shifts (9) have also been studied. It has been pointed out (3, 10) that all of these techniques suffer from weak assumptions and/or rather large uncertainties in the derived thermodynamic parameters.

More recently, the frequencies of the hydroxyl torsion bands in the far i.r. were employed in the gas phase and in cyclohexane solution to find the strengths of the intramolecular hydrogen bonds (3, 11). Contrary to some of the earlier work, it was shown that all four halogens form a hydrogen bond with the hydroxyl group in both phases. In cyclohexane solution, the relative strengths were Cl > Br > I > F but the quoted errors of 120 cal/mol allow an inversion of the relative stabilities.

[1]Research Associate, 1973–1974.

Now, it is known (10, 12) that strong intramolecular hydrogen bonds exist in the salicylaldehydes and *o*-nitrophenols.[2] In these compounds a stereospecific coupling over five bonds between the hydroxyl proton and the ring proton occurs over the all-*trans* or zigzag bond path. Such a stereospecific coupling of α protons in the side chain to *meta* protons in aromatic systems is also observed in halogenated toluenes (13), benzaldehydes (14, 15), anilines (16, 17), styrenes (18), and in bicyclic systems (19, 20). It is predicted theoretically in toluenes (21), benzaldehydes (15), and styrenes (18, 22).

In principle, this stereospecificity can be used to find the preferred conformation, **A** or **B**, of a

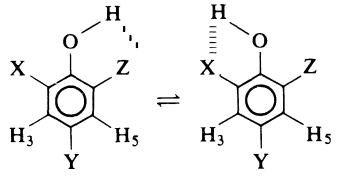

A **B**

[2]The free energy of activation for intermolecular hydroxyl proton exchange in a 5 mol% solution of 3,5-dichlorosalicylaldehyde in CCl_4 is at least 22 kcal/mol at 350 °K (10).

Can. J. Chem. Downloaded from www.nrcresearchpress.com by 210.87.254.105 on 09/05/12
For personal use only.

TABLE 1. Hydroxyl proton coupling constants in Hz and free energy differences in cal/mol in 2-X-4-Y-6-Z-halophenols

Compound	X	Y	Z	mol %*	J_3	J_5	$J_3 + J_5$	ΔG^0
1	F	Br	H	4.9	0.00	0.435	0.435	—
2	Cl	Cl	H	6.3	0.00	0.456	0.456	—
3	Br	Br	H	1.6	0.00	0.481	0.481	—
4	Cl	Cl	Cl	0.4†	0.307	0.307	0.614	—
5	Cl	Br	Cl	3.9	0.300	0.300	0.600	—
6	Br	Br	Br	2.0	0.290	0.290	0.580	—
7	I	I	I	0.6‡	0.290	0.290	0.580	—
8	F	Cl	Cl	3.4	0.403	0.204	0.607	412§
9	F	Br	Br	2.8‖	0.379	0.197	0.576	397
10	F	I	I	2.2	0.251	0.283	0.534	−73
11	Cl	Cl	Br	3.2	0.268	0.288	0.556	−44
12	Cl	Cl	I	1.5‡	0.182	0.378	0.560	−443
13	Br	Br	I	1.9	0.167	0.367	0.534	−477

*In CCl_4, unless otherwise noted, to an accuracy of 10%.
†In toluene-d_8.
‡In chloroform-*d*.
§The conformer with the hydroxy proton *trans* to substituent X is the more stable at 32 °C when ΔG^0 is positive.
‖At 1.1 mol% J_3 and J_5 are 0.390 and 0.196 Hz, respectively, at 5.7 mol% they are 0.380 and 0.193 Hz.

phenol derivative, and will give the energy difference between **A** and **B** if both conformations are significantly populated.

When the ring substituents are halogen atoms only, no coupling to ring protons has been reported, presumably because of intermolecular exchange of the hydroxyl protons. If this exchange can be slowed sufficiently, **A** and **B** (X, Y, Z = halogens) become candidates for a p.m.r. study of the relative stabilities of the intramolecular hydroxyl–halogen hydrogen bonds; because both **A** and **B** are substantially populated near room temperature and because the presence of two halogen atoms in the *ortho* position will discourage competitive hydrogen bonding between hydroxyl groups in different molecules.

In this paper the results of such a study are reported.

Experimental

The halophenols were commercial materials or were prepared by standard methods, namely, addition of chlorine gas to a cold aqueous alkaline solution of a phenol; addition of bromine to a cold carbon disulfide solution of a phenol; addition of an aqueous iodine – potassium iodide solution to an aqueous alkaline solution of a phenol.

Nuclear magnetic resonance sample tubes were dried at 120 °C for several days. Solutions were left over molecular sieve for at least a day and were then transferred to the tubes in a dry atmosphere. Several pieces of molecular sieve were added and the tubes were degassed by the freeze–pump–thaw technique.

Proton magnetic resonance spectra were repeatedly calibrated on an HA100D spectrometer at sweep widths of 1 Hz/cm and sweep rates of 0.02 Hz/s. Tickling experiments were carried out in the usual manner. The sample temperature was 32 °C.

Because many compounds were insufficiently soluble in inert solvents such as cyclohexane, most of them were studied in carbon tetrachloride solution. Deuteriochloroform was needed for triiodophenol, while toluene-d_8 was used for trichlorophenol to indicate that the couplings of interest were not appreciably solvent dependent. Concentrations were not constant but were held below 6 mol% to discourage intermolecular hydrogen bonding. At this concentration a solution of phenol in benzene is 85% monomeric (23*a*) but a 3.4 mol% solution in CCl_4 is 57% associated (23*b*). However, appreciable intermolecular hydrogen bonding in solutions of *o*-halophenols would be manifested as a concentration dependence of the five-bond couplings. Such was not the case, see Table 1.

Results and Discussion

Analysis of Spectra

Although most spectra were almost first order in character, all were fully analyzed by the program LAME (24) coupled to a plotting routine (25). All peaks were assigned to calculated transitions, chemical shifts were assigned on the basis of known halogen atom substituent effects (26, 27), and the signs of the five-bond couplings were determined by double irradiations (28).

Linewidths, including those from the hydroxyl protons varied from 0.12 to 0.15 Hz, and comparison of simulated with the relatively simple observed spectra convinced us that $^5J^{H,OH}$ is known to an accuracy of ± 0.01 Hz, the probable errors being a factor of four or five smaller than this. The couplings are listed in Table 1.

In Fig. 1 a representative p.m.r. spectrum is displayed. Note the sharpness of the hydroxyl proton resonance peaks, normally appearing as rather broad in the literature.

Can. J. Chem. Downloaded from www.nrcresearchpress.com by 210.87.254.105 on 09/05/12
For personal use only.

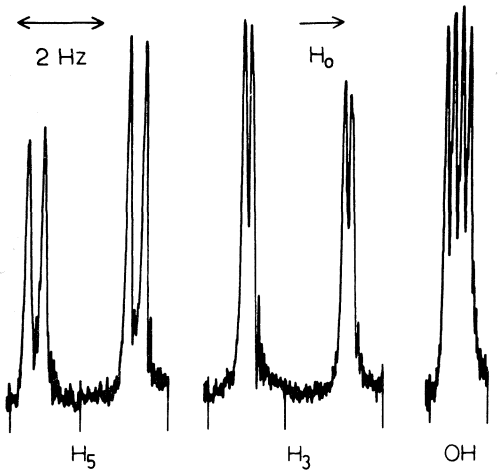

FIG. 1. The p.m.r. spectrum at 100 MHz of a 1.5 mol% solution of 2,4-dichloro-6-iodo-phenol in $CDCl_3$ under anhydrous conditions. Note that the linewidth of the hydroxyl proton peaks is the same as that of the ring proton peaks.

The 2,4-Dihalophenols

In phenol the barrier to rotation of the hydroxyl group from one planar (29, 30) form to the other is 3.56 kcal/mol in cyclohexane solution (30). Therefore only planar conformations are significantly populated at room temperature. We shall assume that planar hydroxyl conformations **A** and **B** exist in all the halophenols in Table 1.

Substantial contributions from conformations in which the hydroxyl group lies sufficiently far from the ring plane would lead to observable coupling to H_3 in **C**.

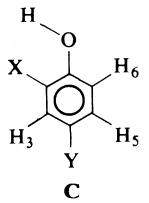

C

$$J_5 = J_{trans} = {}^5J_m^{H_5,OH}$$
$$J_3 = J_{cis} = {}^5J_m^{H_3,OH}$$

Nematic phase n.m.r. measurements on salicylaldehyde suggest that the hydroxyl and aldehyde groups are twisted out of the ring plane by 10 to 15° (31), consistent with an unobserved but deduced anti-zigzag coupling (J_{cis}) over five bonds from the hydroxyl proton to H_6 of 0.13 ± 0.05 Hz in 3-methoxysalicylaldehyde (32).

However, in the halophenols the formation of the weak hydrogen bond completes a five-membered ring and there is no obvious reason why nonplanar conformations should be preferred. Small deviations from coplanarity will not significantly alter the later conclusions.

In **C** a hydrogen bond to the halogen, X, implies an observable coupling, ${}^5J_m^{H_5,OH} \equiv J_5$, and is observed (compounds **1** to **3** in Table 1), whereas J_3 is unobservably small. This result indicates that the hydrogen bonded form is favored by at least 1.5 kcal/mol at ambient temperatures, previous work placing it between 1.0 and 3.5 kcal/mol for the *o*-halophenols (3, 6–9).

J_5 is substituent dependent, increasing from 0.43_5 Hz for X = F to 0.48_1 for X = Br. One might argue that for X = F the C—O—H angle is smaller than for X = Cl, Br because the hydrogen atom is drawn towards the smaller fluorine atom, thereby decreasing the zigzag nature of the coupling path and causing a decrease in J_5, relative to X = Br. Another possibility involves the formation of planar *cis–trans* dimers, as suggested by Allan and Reeves (9) on the basis of proton chemical shifts, which would be most highly populated for X = F. Such dimers imply an observable J_3 as large as 0.05 Hz, which we did not observe.

Jaffé (33) points out that the entropy change on intramolecular hydrogen bond formation in these compounds is practically negligible and ΔH and ΔG are essentially equal. Therefore the weak intramolecular bond can form in preference to the stronger intermolecular bonds, where the entropy change is as much as −20 cal/mol deg. (23). When both *ortho* positions in phenol are occupied by halogen atoms the probability of intermolecular hydrogen bonding decreases further, so that the discussion of the other compounds in Table 1 can safely ignore intermolecular bonds.

In any event, J_5 for X = F indicates hydrogen bonding to fluorine, contrary to hydroxyl proton chemical shift (9) and i.r. data (34), only one hydroxyl stretching band being present for *o*-fluorophenol, but in agreement with far i.r. work (3).

Symmetrical 2,4,6-Trihalophenols (X = Z)

Rapid interconversion of the isoenergetic forms **A** and **B** occurs at ambient temperatures. If J_{cis} is still zero, then $J_{trans} = J_3 + J_5$ and is rather larger than in the 2,4-dihalophenols. The increase in J_{trans} apparently depends mainly on the degree of substitution and not much on, for example, the electronegativity of the substituents,

Can. J. Chem. Downloaded from www.nrcresearchpress.com by 210.87.254.105 on 09/05/12
For personal use only.

Can. J. Chem. Downloaded from www.nrcresearchpress.com by 210.87.254.105 on 09/05/12
For personal use only.

J_{trans} varying between 0.58_0 and 0.61_4 Hz for compounds **4**–**7** in Table 1.

It may be that the symmetrical substitution pattern causes a similar distortion of the benzene skeleton in each of the four compounds, leading to essentially the same geometry for the coupling path over five bonds. In that event an asymmetrical 2,4,6-trisubstitution pattern implies a greater variation in J_{trans}, as observed in the next set of compounds.

Asymmetrical 2,4,6-Trihalophenols ($X \neq Z$)

On the assumption that J_{trans} is the same for **A** and **B** for a given X, Y, Z, the relative free energies (and enthalpies, ΔS being essentially zero) of the two conformers are calculated from eq. 1. At 32 °C the ΔG^0 values are entered in Table 1 for compounds **8**–**13**.

$$[1] \quad \Delta G^0 = G_1{}^0 - G_2{}^0 = -RT \ln (J_5/J_3)$$

From these numbers for compounds **8**–**11** and **13** in Table 1, one then has the relative hydrogen bond strengths as Cl > Br > F > I, in agreement with the qualitative deductions for similar trihalophenols based on hydroxyl stretching band intensities (35). In cyclohexane solution (3), the torsion band frequencies yield Cl > Br > I > F for the *o*-halophenols, the enthalpies being −1.62, −1.57, −1.45, −1.44 kcal/mol, respectively, all with an estimated error of 0.12 kcal/mol.

The order of hydrogen bond strengths in the *o*-halophenols need not be the same as in the 2,4,6-trihalophenols. On the basis of hydroxyl deformation frequencies, it is argued that in 2-nitro-6-X-phenols a large substituent X enhances the strength of the hydrogen bond by bending the hydroxyl group closer to the nitro group (36). A similar buttressing effect in the trihalophenols may account for their somewhat greater difference in relative hydrogen bond strengths than is observed for the *o*-halophenols.

The result for compound **12** implies that chlorine forms a weaker hydrogen bond than bromine, in that comparison of **8** with **10** suggests $\Delta G^0 = -485$ cal/mol for **12** instead of the observed −443 cal/mol, while comparison with **11** and **13** suggests −521 cal/mol for **12**. Compound **12** is, therefore, an exception, all others indicating chlorine as the strongest hydrogen bond acceptor in this series.

This exception may be a consequence of the assumption of invariance in the two values of J_{trans} for a given compound. A safer conclusion is that in these compounds the hydrogen bond strengths are Cl ~ Br > F > I and that, *relative to iodine*, they are 75 ± 20 cal/mol for fluorine and 460 ± 60 cal/mol for chlorine and bromine; the errors reflecting the 14% range of $J_3 + J_5$ (from 0.53_4 to 0.60_7 Hz) in the asymmetrical 2,4,6-trihalophenols.

Finally, if J_{cis} were slightly greater than zero the relative energies would be a few tens of calories larger than stated.

We are grateful to the National Research Council of Canada for financial support.

1. M. Maclean Davis. Acid-base behaviour in aprotic organic solvents. NBS Monograph 105. Washington, D.C. 1968.
2. S. N. Vinogradov and R. H. Linnell. Hydrogen Bonding. Van Nostrand Reinhold Company. New York. 1971.
3. G. L. Carlson, W. G. Fateley, A. S. Manocha, and F. F. Bentley. J. Phys. Chem. **76**, 1553 (1972).
4. O. R. Wulf and U. Liddel. J. Am. Chem. Soc. **57**, 1464 (1935).
5. L. Pauling. J. Am. Chem. Soc. **58**, 94 (1936).
6. A. W. Baker and A. T. Shulgin. Can. J. Chem. **43**, 650 (1965).
7. H. Bourassa-Bataille, P. Sauvageau, and C. Sandorfy. Can. J. Chem. **41**, 2240 (1963).
8. J. H. Richards and S. Walker. Trans. Faraday Soc. **57**, 412 (1961).
9. E. A. Allan and L. W. Reeves. J. Phys. Chem. **66**, 613 (1962); **67**, 591 (1963).
10. T. Schaefer and G. Kotowycz. Can. J. Chem. **46**, 2865 (1968).
11. G. L. Carlson and W. G. Fateley. J. Phys. Chem. **77**, 1157 (1973).
12. S. Forsén and B. Åkermark. Acta Chem. Scand. **17**, 1712 (1963).
13. T. Schaefer, R. Schwenk, C. J. Macdonald, and W. F. Reynolds. Can. J. Chem. **46**, 2187 (1968).
14. V. J. Kowalewski and D. G. de Kowalewski. J. Chem. Phys. **36**, 266 (1962).
15. R. Wasylishen and T. Schaefer. Can. J. Chem. **49**, 3216 (1971).
16. T. Schaefer and R. Wasylishen. Can. J. Chem. **48**, 1343 (1970).
17. R. Wasylishen, J. B. Rowbotham, L. Ernst, and T. Schaefer. Can. J. Chem. **50**, 2575 (1972).
18. M. Barfield, C. J. Macdonald, I. R. Peat, and W. F. Reynolds. J. Am. Chem. Soc. **93**, 4195 (1971).
19. J. B. Rowbotham and T. Schaefer. Can. J. Chem. **51**, 953 (1973).
20. R. W. Crecely and J. H. Goldstein. Org. Magn. Res. **2**, 613 (1970).
21. R. Wasylishen and T. Schaefer. Can. J. Chem. **50**, 1852 (1972).
22. J. B. Rowbotham and T. Schaefer. Can. J. Chem. **52**, 136 (1974).
23. (*a*) E. M. Woolley and L. G. Hepler. J. Phys. Chem.

76, 3058 (1972); (*b*) V. VON KEUSSLER. Z. Elektrochem. **58**, 136 (1954).
24. C. W. HAIGH and J. M. WILLIAMS. J. Mol. Spectrosc. **32**, 398 (1969).
25. J. B. ROWBOTHAM and T. SCHAEFER. Can. J. Chem. **50**, 2344 (1972).
26. B. RICHARDSON and T. SCHAEFER. Can. J. Chem. **46**, 2195 (1968).
27. J. L. ROARK and W. B. SMITH. J. Phys. Chem. **73**, 1043 (1969).
28. R. FREEMAN and W. A. ANDERSON. J. Chem. Phys. **37**, 2053 (1962).
29. T. KOJIMA. J. Phys. Soc. Jap. **15**, 284 (1960).
30. L. RADOM, W. J. HEHRE, J. A. POPLE, G. L. CARLSON, and W. G. FATELEY, J. Chem. Soc. Chem. Commun. 308 (1972).
31. P. DIEHL and P. M. HENRICHS. J. Magn. Res. **5**, 134 (1971).
32. S. FORSÉN and R. A. HOFFMAN. J. Mol. Spectrosc. **20**, 168 (1966).
33. H. H. JAFFÉ. J. Am. Chem. Soc. **79**, 2373 (1957).
34. TIEN-SUNG LIN and E. FISHMAN. Spectrochim. Acta A, **23**, 491 (1967).
35. A. W. BAKER and W. F. KAEDING. J. Am. Chem. Soc. **81**, 5904 (1959).
36. R. NYQUIST. Spectrochim. Acta, **19**, 1655 (1963).

Can. J. Chem. Downloaded from www.nrcresearchpress.com by 210.87.254.105 on 09/05/12
For personal use only.

Thyroid Hormone Stereochemistry. II. Molecular Structure of Thyronine · HCl Ethyl Ester Monohydrate[1]

ARTHUR CAMERMAN

Departments of Medicine (Neurology) and Pharmacology, University of Washington School of Medicine, Seattle, Washington

AND

NORMAN CAMERMAN

Department of Biochemistry, University of Toronto, Toronto, Ontario M5S 1A8

Received January 16, 1974

ARTHUR CAMERMAN and NORMAN CAMERMAN. Can. J. Chem. **52**, 3042 (1974).

The three-dimensional structure of L-thyronine, the non-iodinated physiologically inactive analog of thyroxine, has been determined by single crystal X-ray diffraction and compared to the active thyroid hormones. The compound crystallized as the monohydrate of thyronine hydrochloride ethyl ester in the monoclinic space group $P2_1$ with cell dimensions $a = 10.502$, $b = 5.165$, $c = 17.940$ Å, $\beta = 109.74°$. The structure was solved by Patterson methods to find the chloride ion and iterative Fourier maps to locate the rest of the atoms. Refinement was by anisotropic full-matrix least squares to convergence at $R = 0.048$.

The two phenyl rings adopt a twisted orientation with respect to each other with angles of $-37°$ and $-67°$ between the plane of the inter-ring ether linkage and the planes of the α- and β-rings, respectively. This orientation differs considerably from that found in the iodinated thyronines. The conformation of the alanine side chain is remarkably similar to that of the alanine in the iodinated thyronines.

ARTHUR CAMERMAN et NORMAN CAMERMAN. Can. J. Chem. **52**, 3042 (1974).

Faisant la diffraction par rayons-X d'un cristal unique, on détermine la structure tridimensionnelle de la L-thyronine, l'analogue non-iodé et physiologiquement inactif de la thyroxine et on la compare aux hormones actives de la thyroide. Le composé cristallise sous forme de chlorhydrate de l'ester d'éthyle de la thyronine monohydraté dans le système monoclinique, groupe d'espace $P2_1$, avec les dimensions de la maille $a = 10.502$, $b = 5.165$, $c = 17.940$ Å, $\beta = 109.74°$. La structure est résolue par la méthode de Patterson pour localiser le chlore et avec des cartes répétées de Fourier, on localise le reste des atomes. On affine par la méthode des moindres carrés (matrice entière) jusqu'à une convergence à $R = 0.048$.

Les deux noyaux phényles adoptent une orientation croisée l'un par rapport à l'autre avec des angles de $-37°$ et $-67°$ respectivement entre le plan de la liaison éther reliant les noyaux et les plans des noyaux α et β. Cette orientation diffère considérablement de celle trouvée pour les thyronines iodées. La conformation de la chaîne latérale d'alanine est remarquablement similaire à celle de l'alanine dans les thyronines iodées. [Traduit par le journal]

Introduction

One of the features deemed necessary to confer biological activity upon a thyronine derivative is substitution of iodines or other bulky groups at the 3, 5, and 3′ positions of the α- and β-rings (1) (see fig. 2 for ring nomenclature). Thyronine, which has no substitution at any of these positions, is physiologically inactive as a thyroid hormone.

A comparison of the three-dimensional structure of this inactive compound with those of the active hormones L-thyroxine and 3,5,3′-triiodo-L-thyronine will show the effects that iodination has upon the molecular conformation of this type of molecule. Of particular interest is the effect of iodine substitution on the orientation of the α- and β-rings with respect to one another, and on the conformation of the alanine side chain. Kier and Hoyland (2) have concluded from theoretical calculations that the most stable orientation for the two phenyl rings in thyronine would be an eclipsing arrangement. We consider such a conformation to be highly unlikely and deem a crystallographic investigation appropriate to settle this question.

For the above reasons and as part of our investigations of the stereochemistry of thyroid hormones and analogs we have determined the

[1]For Part I of this series see ref. 3.

Can. J. Chem. Downloaded from www.nrcresearchpress.com by 210.87.254.105 on 09/05/12
For personal use only.

Can. J. Chem. Downloaded from www.nrcresearchpress.com by 210.87.254.105 on 09/05/12
For personal use only.

crystal and molecular structure of L-thyronine hydrochloride ethyl ester·H_2O.

Experimental

L-Thyronine (T_0) was dissolved by heating in a mixture of ethanol and HCl and slow solvent evaporation yielded small needle-shaped crystals. Structure determination subsequently showed that thyronine had reacted with ethanol to form the ethyl ester and had crystallized as thyronine ethyl ester hydrochloride with one water molecule of crystallization per molecule of thyronine. The unit cell dimensions were determined from diffractometer measurements and these and other crystal data are listed in Table 1. X-Ray intensities were measured on an automated four-circle diffractometer (Ni-filtered Cu radiation) in shells of 2θ: (*i*) $2\theta \leqslant 55°$, (*ii*) $55° \leqslant 2\theta \leqslant 90°$, (*iii*) $90° \leqslant 2\theta \leqslant 100°$. Reflections in all three shells were scanned over a 2° interval in 2θ; for the first two groups we used a scan rate of 1° per min with 20-s background counts on either side of the peak, while the third group was collected at a scan rate of ½° per min with 40-s background counts. The three layers were scaled together using the "standard" reflections which had been measured multiple times in each data collection shell as monitors of crystal deterioration. There was no appreciable intensity fall-off of the standards during data collection. Of the 1082 measured reflections, 916 had intensity greater than twice the standard deviation of their net counts and were used in the structure refinement. Absorption of X-rays by the crystal was examined by measuring the intensity of the 020 reflection at $\chi = 90°$ for different values of φ. Total intensity change was only ±2.5% and no absorption corrections were calculated. Structure amplitudes were obtained from the intensities in the usual fashion.

Structure Determination and Refinement

Because both thyroxine and triiodothyronine had crystallized as the hydrochlorides we assumed that thyronine would do the same. Thus, we interpreted a sharpened, origin-removed three-dimensional Patterson function for the chloride ion position. A Fourier map phased with the chloride ion alone, although containing a false plane of symmetry, allowed the positions of two more atoms to be determined. The rest of the molecule was iteratively located from further successive three-dimensional Fourier maps. The electron-density plots revealed that thyronine had crystallized as the ethyl ester and also revealed the presence of one water molecule per molecule of T_0.

TABLE 1. Thyronine ethyl ester crystal data

Formula	$C_{17}H_{19}NO_4 \cdot HCl \cdot H_2O$
Mol. wt.	355.86
Crystal system	Monoclinic
a, Å	10.502±0.005
b, Å	5.165±0.002
c, Å	17.940±0.007
β, deg	109.74 ±0.04
D_x g cm^{-3} ($z = 2$)	1.29
Space group	$P2_1$
μ (for Cu$K\alpha$) cm^{-1}	20.8
Crystal size, mm	0.1×0.2×0.2

Atomic coordinates and anisotropic thermal parameters of all the atoms were refined by full-matrix least squares to a discrepancy index *R* of 0.070. The weighting scheme used was the same as for triiodothyropropionic acid (7). During refinement we verified that we had correctly chosen the L-configuration for the molecule.

At this stage, we computed a ΔF map which revealed the positions of 15 hydrogen atoms. The other 7 hydrogens were located from a second ΔF map phased on the refined positions of all non-hydrogen atoms plus the initially found 15 hydrogens. After final least-squares refinement with the hydrogens assigned isotropic thermal parameters and the rest of the atoms anisotropic, the discrepancy factor $R = 0.048$, and the weighted discrepancy factor $wR = 0.026$. Fractional coordinates and thermal parameters are listed in Table 2 (non-hydrogen atoms) and Table 3 (hydrogens). The anisotropic thermal parameters are coefficients in the expression $\exp[-2\pi^2(h^2U_{11}a^{*2} + \ldots + 2klU_{23}b^*c^*)]$. Atomic scattering factors used were the same as for L-thyroxine (3). The table of final observed and calculated structure factors may be found in the Depository of Unpublished Data.[2]

Discussion

A stereoscopic drawing of thyronine hydrochloride ethyl ester is presented in Fig. 1. The conformation of the amino acid portion of the molecule can be described by five torsion angles; angles labelled ψ refer to rotation about the carboxyl carbon – C(α) bond, χ_1 refers to rotation about the C(α)—C(β) bond, and χ_2 indicates rotations about the C(β)—C(γ) bond. Thus for thyronine ψ_1 and ψ_2 are the angles which the O(3)—C(9)—C(8) and O(4)—C(9)—C(8) planes, respectively, make with the C(9)—C(8)—N plane; *i.e.*, ψ_1 and ψ_2 are the torsion angles N—C(8)—C(9)—O(3) and N—C(8)—C(9)—O(4), respectively, where the term A—B—C—D means the angle between the plane A—B—C and the plane B—C—D. (See Fig. 2 for atom numbering scheme.) Similarly, χ_{11} is the torsion angle N—C(8)—C(7)—C(1), χ_{21} is the angle C(8)—C(7)—C(1)—C(2), and χ_{22} is the angle C(8)—C(7)—C(1)—C(6). The values of these five torsion angles for L-thyronine are listed in Table 4 and compared with the same angles found in the crystal structures of L-thyroxine, triiodo-L-thyronine, diiodo-L-thyronine, and tyrosine. In accordance with the rules adopted by the IUPAC–IUB Commission on

[2]Tables of final observed and calculated structure factors for T_0 are available, at a nominal charge, from the Depository of Unpublished Data, National Science Library, National Research Council of Canada, Ottawa, Canada K1A 0S2.

TABLE 2. Fractional atomic coordinates and anisotropic thermal parameters ($\times 10^4$) for the non-hydrogen atoms

Atom	x	y	z	U_{11}	U_{22}	U_{33}	U_{12}	U_{13}	U_{23}
O(1)	−0.5666	0.5274	0.3389	563	688	567	24	−75	29
O(2)	−0.0685	0.5785	0.5754	635	560	453	−134	−56	130
O(3)	0.2576	0.2949	0.9282	736	393	861	−32	240	−85
O(4)	0.3747	−0.0294	0.8964	537	479	783	−104	172	−100
N	0.0464	−0.0061	0.9147	654	503	323	−45	120	−51
C(1′)	−0.1984	0.5585	0.5163	543	387	425	−150	104	17
C(2′)	−0.2177	0.3606	0.4621	518	586	558	80	163	−85
C(3′)	−0.3437	0.3482	0.4009	537	583	538	47	75	−206
C(4′)	−0.4416	0.5280	0.3984	472	599	358	−42	27	40
C(5′)	−0.4209	0.7238	0.4543	721	500	536	63	132	−32
C(6′)	−0.2945	0.7372	0.5143	836	446	454	25	174	−109
C(1)	0.0582	−0.0010	0.7461	517	388	345	−84	70	−153
C(2)	0.1485	0.1159	0.7138	549	715	337	8	145	−2
C(3)	0.1030	0.3134	0.6575	438	750	496	−202	61	160
C(4)	−0.0304	0.3852	0.6311	606	483	245	−98	0	−77
C(5)	−0.1200	0.2679	0.6622	411	676	396	−7	22	62
C(6)	−0.0766	0.0771	0.7184	463	710	429	−170	109	−4
C(7)	0.1052	−0.2140	0.8071	691	471	413	−6	147	−83
C(8)	0.1571	−0.1219	0.8926	558	304	402	55	170	27
C(9)	0.2679	0.0772	0.9089	640	455	330	105	47	99
C(10)	0.4886	0.1546	0.9055	1045	1343	1007	−146	414	−274
C(11)	0.5851	0.0104	0.8781	1030	1699	1757	77	919	166
Cl^-	−0.1367	−0.5000	0.8988	479	525	398	−48	59	13
O(W)	−0.6161	0.0549	0.2650	1035	652	805	−129	−186	−23
			Approximate standard deviations						
Cl^-	0.0001	—	0.0001	10	12	10	12	7	11
O	0.0004	0.0009	0.0002	28	36	28	30	23	30
O(water)	0.0009	0.0015	0.0004	52	52	42	41	36	37
C and N	0.0006	0.0014	0.0003	45	52	39	45	36	41
C(ethyl)	0.0008	0.0025	0.0006	68	102	85	85	69	98

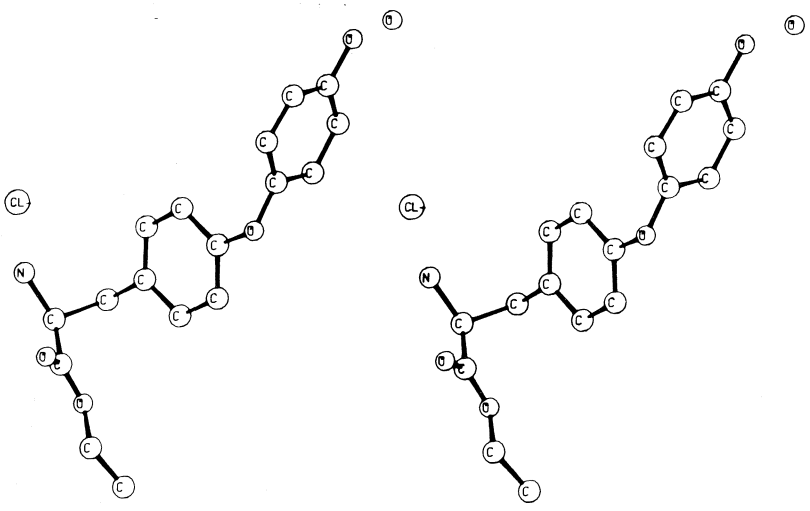

FIG. 1. Stereoscopic drawing of thyronine hydrochloride ethyl ester illustrating the molecular conformation in the crystal. The water molecule of crystallization is included in the drawing.

Can. J. Chem. Downloaded from www.nrcresearchpress.com by 210.87.254.105 on 09/05/12
For personal use only.

Can. J. Chem. Downloaded from www.nrcresearchpress.com by 210.87.254.105 on 09/05/12
For personal use only.

TABLE 3. Fractional atomic coordinates and isotropic thermal parameters (Å²) for the hydrogen atoms

Atom	x	y	z	B
H(O1)	−0.590	0.359	0.312	3.2
H(2)	0.255	0.045	0.730	6.9
H(3)	0.174	0.379	0.643	1.6
H(5)	−0.219	0.313	0.641	1.8
H(6)	−0.144	0.007	0.737	7.0
H(2′)	−0.149	0.247	0.450	5.7
H(3′)	−0.356	0.188	0.358	5.4
H(5′)	−0.517	0.889	0.448	11.1
H(6′)	−0.276	0.861	0.558	8.5
H(N1)	0.075	0.020	0.962	3.2
H(N2)	−0.025	0.130	0.883	15.5
H(N3)	−0.005	−0.107	0.901	2.0
H(7.1)	0.163	−0.306	0.790	2.8
H(7.2)	0.030	−0.366	0.803	5.1
H(8)	0.189	−0.242	0.934	3.3
H(10.1)	0.523	0.209	0.961	6.1
H(10.2)	0.467	0.328	0.867	13.5
H(11.1)	0.639	0.131	0.858	12.5
H(11.2)	0.655	−0.232	0.928	26.8
H(11.3)	0.510	−0.095	0.804	17.2
H(W1)	−0.677	−0.012	0.245	15.4
H(W2)	−0.587	−0.049	0.267	9.2
Approximate standard deviations				
H	0.004	0.011	0.003	2.1
H(ethyl)	0.009	0.024	0.006	5.0
H(water)	0.008	0.020	0.005	5.7

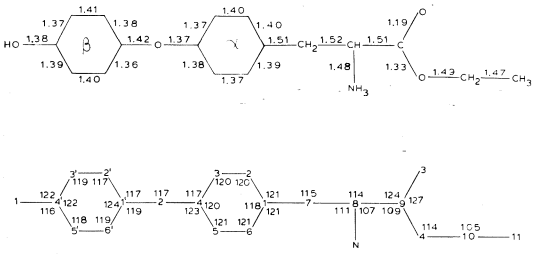

FIG. 2. Bond lengths (Å) and angles (deg) in thyronine hydrochloride ethyl ester.

Biochemical Nomenclature (4) each angle is measured in the range from −180 to +180°. As can be seen in Table 4, there is relatively little difference in the conformations of the amino acid parts of the various molecules compared. In particular, a comparison of thyronine, which is physiologically inactive, with the active thyroid hormones T_3 and T_4, shows that differences in the torsion angles are slight. These results suggest that this is the preferred conformation for this type of aromatic amino acid. However, they also show that *in itself alone* this alanine conformation is not sufficient to confer physiological activity.

The orientation of the two phenyl rings in thyronine type compounds can also be described by the values of relevant torsion angles. The planes A—B—C and B—C—D which give the most accurate conformation description for this part of the molecule are the two phenyl ring planes and the ether-linkage plane, C(4), O(2), C(1′). In thyronine, the orientation of the two phenyl rings is very different from that found for the iodinated compounds. Whereas the α-ring ether-linkage interplanar (or torsion) angle is approximately +85 to +100° for the iodinated diphenyl ethers, for thyronine this angle is −37°. The angle between the β-ring and ether-linkage plane in thyronine is −67°, again very different from that found in the iodinated compounds. Table 5 compares the phenyl ring orientations of thyronine with those found in other compounds in this series. It is obvious from this table that iodination of the 3 and 5 positions of the α-ring in these compounds greatly affects the orientation of the α- and β-rings with respect to each other.

Kier and Hoyland (2), using molecular orbital calculations, predicted that the most stable conformation for thyronine would be with the two phenyl rings eclipsed, *i.e.* with both phenyl rings perpendicular to the ether-linkage plane. The crystal structure results suggest that this prediction is entirely incorrect; as is apparent in Fig. 1 and from the phenyl ring ether-linkage torsion angles quoted above the orientation of the two phenyl rings is far from an eclipsing conformation. One of Kier and Hoyland's major errors is that they considered only rotations of the β-ring about its ether bond in their calculations and did not consider the possibility of concurrent rotations of the α ring about its ether bond. Thus their calculations omitted most of the possible conformations that the thyronine molecule can adopt, including the observed crystal structure conformation which is of lower energy (5) than the eclipsed arrangement which they predicted.

Bond lengths and angles in thyronine ethyl ester are shown in Fig. 2. The standard deviations, estimated from the shifts in the final least-squares cycle, are less than 0.01 Å for the bond lengths and approximately 0.6° for the angles (0.017 Å and 0.9° for bonds and angles

TABLE 4. Torsion angles (deg) in the alanine side chain of thyronine (T_0), triiodothyronine (T_3), thyroxine (T_4), diiodothyronine (T_2), and tyrosine

	ψ_1	ψ_2	χ_{11}	χ_{21}	χ_{22}
Thyronine (T_0)	−7	+174	+66	+90	−90
Triiodothyronine (T_3) (3)	+8	−175	+56	+98	−89
Thyroxine (T_4) (3)	−9	+172	+66	+98	−84
Diiodothyronine (T_2) (6)	+18	−165	+60	+120	−55
Tyrosine (8)	−18	+164	+72	+96	−83

TABLE 5. Dihedral angles (deg) between phenyl ring planes and ether linkage plane and deviation of atom C(4) from plane 1 and atom C(1′) from plane 2 in thyronine and iodinated compounds

Compound	C—O—C α-ring	C—O—C β-ring	Deviation (Å) of atom C(4) from the plane containing the β-ring, phenolic oxygen, and ether oxygen	Deviation (Å) of atom C(1′) from the plane containing the α-ring and ether oxygen
L-Thyronine (T_0)	−37	−67	1.05±0.02	0.75±0.01
3,5,3′-Triiodo-L-thyronine (T_3) (3)	+86	−13	0.29±0.05	1.08±0.03
L-Thyroxine (T_4) (3)	+101	−34	0.73±0.07	1.28±0.10
3,5-Diiodo-L-thyronine (T_2) (6)	+84	+19	0.39±0.01	1.10±0.04
3,5,3′-Triiodothyropropionic acid (7)	±88	∓10	0.17±0.01	1.17±0.02

in the ethyl group). The values of the bond distances and angles are normal and require little comment. The angle at the inter-ring ether linkage is 117°, similiar to the values for the other molecules of this series. The C(10)—C(11) bond in the ester part of the molecule appears shorter than it should be and this is undoubtedly due to the large thermal motion of these atoms (thermal parameters are listed in Table 2).

As was the case for T_3 also (3), the chloride ion in this structure makes close contacts (hydrogen bonds) with the nitrogen atoms of three symmetry-related thyronine molecules and with one of the water molecule hydrogens. There is hydrogen bonding also between the water molecule and the phenolic hydroxyl group of the β ring. All short intermolecular distances are listed in Table 6.

As a possible model for thyromimetic and thyro-antagonistic action Jorgensen (1) has postulated that the bulky 3 and 5 substituents of thyroxine-like analogs sterically prevent resonance interaction between the ether oxygen and the α-ring. His hypothesis is that "coplanarity of the phenolic hydroxyl oxygen, β-ring, ether oxygen and C(4) of the α-ring may permit the β-ring to act as a hydroquinone with facilitated release of electrons to a substrate via the 4′-hydroxyl oxygen. Analogs lacking a 3 or 5 bulky substituent could undergo phenyl ring rotation about the C(4)—O bond and assume a coplanar orientation for the α-ring, ether oxygen, and C(1′) of the β-ring. The α-ring could then compete with the β-ring in its resonance interaction with the ether oxygen. This could provide an extended π bond character for the α-ring and might enhance α-ring receptor binding. At the same time, this resonance competition would reduce the electron-donating ability of the β-ring. If such electron donation is associated with the functional role of the hormone, thyroxine-like activity of such ana-

TABLE 6. Short intermolecular distances

Atom (molecule 1)	to	Atom	in	Molecule*	d (Å)
Cl^-		N		*1*	3.15
Cl^-		H(N3)		*1*	2.45
Cl^-		N		*2*	3.20
Cl^-		H(N2)		*2*	2.31
Cl^-		N		*3*	3.15
Cl^-		H(N1)		*3*	2.37
Cl^-		H(W1)		*4*	2.65
O(W)		O(1)		*1*	2.74
O(W)		H(O1)		*1*	1.77

*Molecule *1* at x, y, z; molecule *2* at $x, y-1, z$; molecule *3* at $-x, y-\frac{1}{2}, 2-z$; molecule *4* at $-1-x, -\frac{1}{2}+y, 1-z$.

Can. J. Chem. Downloaded from www.nrcresearchpress.com by 210.87.254.105 on 09/05/12
For personal use only.

logues would decrease and antagonistic activity could result."

Although this hypothesis does not adequately explain why replacement of iodine with other bulky groups at the 3 and 5 positions results in decrease of hormonal activity, it may illustrate a partial role for the 3 and 5 iodines. To examine this hypothesis in the light of the crystal structure results we have so far obtained, we have calculated the deviations of C(4) of the α-ring from the best plane through the β-ring including the phenolic and ether oxygens, and the deviations of C(1′) of the β-ring from the best plane through the atoms of the α-ring and ether oxygen, for L-thyroxine, 3,5,3′-triiodo-L-thyronine, L-thyronine, 3,5,3′-triiodothyropropionic acid, and 3,5-diiodo-L-thyronine. The results are shown in Table 5.

Four of the five compounds have iodines at the 3 and 5 positions; these four should, according to the above hypothesis, show very little deviation of atom C(4) from the plane of the phenolic β-ring plus ether oxygen (plane 1) and large deviation of atom C(1′) from the plane of the α-ring plus ether oxygen (plane 2). Thyronine, which contains no iodine on either ring, has no steric restrictions to rotation about the phenyl–oxygen bonds and could adopt either of the conformations postulated for thyromimetic action or thyro-antagonism. The values in Table 5 show that for the four molecules containing 3 and 5 iodines deviations of C(4) from plane 1 are much less than deviations of C(1′) from plane 2 which is certainly consistent with the hypothesis. However, the deviations of atom C(4) from plane 1 are all relatively large and it is doubtful whether the crystal structure results for these four molecules provide an experimental foundation to the above hypothesis for thyroid hormone activity. In the crystal thyronine displays neither of the two hypothesized conformations but is closer to that suggested to be thyro-antagonistic.

It should be noted that these results do not disprove Jorgensen's hypothesis. It is certainly possible that at the active site there may be sufficient rotation about the phenyl–oxygen bonds such that C(4) could become more coplanar with plane 1 and hydroquinone-like activity ensue. A better test of this hypothesis would be comparison of the corresponding deviation-from-the-plane values for a known thyroid antagonist such as 3,3′5′-triiodo-L-thyronine (reverse T_3). X-Ray investigation of this molecule is in progress in these laboratories.

Support was from the Medical Research Council of Canada grant MA-4695 and from the general research support grant of the University of Washington School of Medicine, supplied by USPHS grant RR 05432 from the National Institutes of Health.

1. E. C. JORGENSEN. Mayo Clinic Proc. **39**, 560 (1964).
2. L. B. KIER and J. R. HOYLAND. J. Med. Chem. **13**, 1182 (1970).
3. A. CAMERMAN and N. CAMERMAN. Acta Cryst. In press.
4. IUPAC-IUB Commission on Biochemical Nomenclature, Biochem. J. **121**, 577 (1971).
5. N. CAMERMAN and A. CAMERMAN. In preparation.
6. V. CODY, W. L. DUAX, and D. A. NORTON. Acta Cryst. B**28**, 2244 (1972).
7. N. CAMERMAN and A. CAMERMAN. Can. J. Chem. This issue.
8. D. C. FRIES and M. SUNDARALINGAM. Acta Cryst. B**27**, 401 (1971).

Can. J. Chem. Downloaded from www.nrcresearchpress.com by 210.87.254.105 on 09/05/12
For personal use only.

Thyroid Hormone Stereochemistry. III. Molecular Structure of Triiodothyropropionic Acid Ethyl Ester[1]

NORMAN CAMERMAN

Department of Biochemistry, University of Toronto, Toronto, Ontario M5S 1A8

AND

ARTHUR CAMERMAN

Departments of Medicine (Neurology) and Pharmacology, University of Washington School of Medicine, Seattle, Washington

Received January 16, 1974

NORMAN CAMERMAN and ARTHUR CAMERMAN. Can. J. Chem. **52**, 3048 (1974).

The three-dimensional structure of triiodothyropropionic acid ethyl ester has been determined as part of an investigation of the stereochemistry of the thyroid hormones. The compound crystallizes in the monoclinic space group $P2_1/c$, with cell dimensions $a = 14.60$, $b = 8.843$, $c = 16.70$ Å, $\beta = 111°27'$; $Z =$ four molecules per cell. The structure was determined by direct centrosymmetric phasing procedures to locate the iodine atoms and phasing on the iodines to find the light atoms. Refinement was by anisotropic full-matrix least squares to a final discrepancy value $R = 0.038$.

The two phenyl rings in the molecule are skewed with respect to each other and are not far from being mutually perpendicular, with angles of 88 and 10° between the plane of the inter-ring ether linkage and the planes of the diiodo-ring and the monoiodo-ring, respectively. The conformation is such that the 3′-iodine atom is *proximal* to the diiodo-ring, similar to the molecular conformation found in the crystal structure of triiodo-L-thyronine hydrochloride.

NORMAN CAMERMAN et ARTHUR CAMERMAN. Can. J. Chem. **52**, 3048 (1974).

On détermine la structure tridimensionnelle de l'ester éthylique de l'acide triiodothyropropionique comme une partie de l'étude stéréochimique des hormones thyroides. Le composé cristallise dans le système monoclinique, groupe d'espace $P2_1/c$ avec les dimensions de la maille $a = 14.60$, $b = 8.843$, $c = 16.70$ Å, $\beta = 111°27'$; $Z = 4$ molécules par maille. On détermine la structure par des procédés directs de phasage centrosymétrique pour localiser les atomes d'iode; on phase les iodes pour trouver les atomes légers. On affine par moindres carrés à matrice entière anisotrope à une valeur finale de $R = 0.038$.

Les deux noyaux phényles dans la molécule sont gauches l'un par rapport à l'autre, et ne sont pas loin d'être perpendiculaires avec les angles de 88 et 10° entre d'une part le plan de lien éther entre les noyaux et, d'autre part, les plans respectifs du noyau diiodé et du noyau monoiodé. La conformation est telle que l'atome iodo-3′ est le plus proche du noyau diiodé: elle est similaire à la conformation moléculaire trouvée dans la structure cristalline du hydrochlorure triiodo L-thyronine. [Traduit par le journal]

Introduction

Triiodothyropropionic acid (T_3P) (β-[4-(3′-iodo-4′-hydroxyphenoxy)-3,5-diiodophenyl]propionic acid) is chemically very similar to triiodothyronine (T_3), the most potent naturally-occurring thyroid hormone; the two molecules differ in chemical structure only in that T_3P lacks an α-amino group. In various tests of thyromimetic action T_3P exhibits from 2–20% of the hormonal potency of T_3 and from 10–60% of the activity of thyroxine, depending on the biological function being measured (1). Indeed, in one test, the determination of the minimal dose of a compound which would promote metamorphosis of the tadpole (*Rana pipiens*), T_3P was 60 times as active as T_3 and 300 times more active than thyroxine (1). It has also been found (1) that T_3P administered to myxedematous patients mimicked T_3 in lowering serum cholesterol levels but had little effect on the basal metabolism rate; these results indicate that certain physiologic effects of thyroid hormones can be dissociated by alteration of molecular structure. The thyromimetic action of T_3P has led to its marketing in Europe as a thyroid supplement and cholesteropenic agent.

We have recently determined the three-dimensional structure of triiodo-L-thyronine (2) and

[1]For Part II of this series see ref. 8.

Can. J. Chem. Downloaded from www.nrcresearchpress.com by 210.87.254.40 on 09/05/12
For personal use only.

Can. J. Chem. Downloaded from www.nrcresearchpress.com by 210.87.254.40 on 09/05/12
For personal use only.

found that the molecular conformation is such that the β-ring 3′-iodine is situated *proximal* to the diiodotyrosyl (α) ring, rather than *distal* as was concluded from chemical structure – biological activity tests (3). Though molecular orbital calculations (2) gave additional support for the greater stability of the 3′-iodine *proximal* conformation than the *distal* possibility in T_3, it is highly desirable to seek other structural data of T_3 analogs to clarify this conformational question. The close chemical similarity of T_3P to T_3 and the fact that it also possesses some degree of thyromimetic activity make it the obvious and ideal choice for structural elucidation and conformational comparison with T_3. Thus we have determined the three-dimensional molecular structure of triiodothyropropionic acid ethyl ester in order to see if the 3′-iodine *proximal* conformation found for T_3 is the generally favored one for this type of thyromimetic agents and to see if differing stereochemical features can be invoked to clarify the differing spectra of biological actions of these two hormones.

Experimental

Triiodothyropropionic acid (whitish powder) was dissolved in an ethanol–HCl solution and thin colorless diamond shaped plates (later shown by the structure determination to be the ethyl ester of T_3P) were obtained by solvent evaporation. The unit cell dimensions were determined from diffractometer measurements and crystal data are as follows: ethyl triiodothyropropionate, $C_{17}H_{15}I_3O_4$, mol. wt. 664.02, monoclinic, $a = 14.60 \pm 0.01$, $b = 8.843 \pm 0.005$, $c = 16.70 \pm 0.01$ Å, $\beta = 111° 27' \pm 10'$, space group $P2_1/c$. The density, calculated on the basis of four molecules per unit cell is 2.199 g cm^{-3}. Absorption coefficient, μ (for Mo Kα radiation) is 47.5 cm^{-1}.

Intensity data were collected on an automated four-circle diffractometer (Zr-filtered Mo radiation) and all independent reflections with 2θ (MoKα) < 48° (corresponding to a minimum interplanar spacing of 0.87 Å) were measured. The moving crystal – moving counter technique was employed (2θ scan) with stationary counts for background radiation on each side of the reflection. A total of 3152 reflections was measured, of which 2488 had intensity greater than $2\sigma_c$, where $\sigma_c = (N_{B1} + N_{PK} + N_{B2})^{1/2}$, N_{B1} and N_{B2} are the background counts, and N_{PK} is the scan count. Those reflections with intensities less than $2\sigma_c$ were classified "unobserved" and were not used in structure refinement. The crystal used for data collection had dimensions approximately 0.1 × 0.2 × 0.9 mm, and absorption corrections were applied using a modified version of a computer program by Coppens *et al.* (4). Lorentz and polarization factors were applied and structure amplitudes $|F|$ and normalized structure amplitudes $|E|$ were derived.

Structure Determination

The symbolic addition procedure was used to determine the phases of the reflections. Three reflections were assigned phases of 0°, three more were assigned symbolic phases, and the Σ2 formula was iteratively applied. Phases were ultimately determined for 391 reflections with $|E| \geq 1.4$ and these were used to calculate a three-dimensional E map. It had been noted early in the structure determination that almost all of the planes with high $|E|$ values had indices of the form l = even (only 2 of 86 planes with $|E| \geq 2.2$ had l = odd and similarly only 22 of 184 planes with $|E| \geq 1.9$), which indicates that the iodines in the molecule of T_3P (ethyl ester) are situated at rather special positions in the cell with respect to their y coordinates. This was confirmed by the E map: there were four major peaks on the map and all had y coordinates close to 0, 1/2, or 3/4. In addition, one of the peaks was at $x = 0.25$ and two of the others were related to each other by a pseudo mirror plane at $x = 0.25$. One of these mirror-related peaks was chosen along with the other two independent peaks as the positions of the three iodines, structure factors were calculated and a difference-Fourier map was computed. All of the carbon and oxygen atoms of the T_3P molecule were clearly revealed and additional density in the map showed that the compound was the ethyl ester of triiodothyropropionic acid, esterification apparently having taken place during crystallization from HCl–ethanol.

Structure Refinement

The atomic coordinates and thermal parameters were refined by full-matrix least squares. The function minimized was $\Sigma w (|F_o| - |F_c|)^2$ with weights $w = (1/\sigma_F)^2$ and the atomic scattering factors were taken from the International Tables for X-Ray Crystallography (5).[2] Two cycles of refinement with isotropic thermal parameters resulted in a discrepancy index $R = 0.099$ and two anisotropic cycles lowered R to 0.044. The hydrogen atoms were located from difference Fourier maps and three cycles of refinement, allowing everything to vary except the hydrogen thermal parameters (held fixed at the values of the atoms to which the hydrogens are bonded) resulted in a final R of 0.038. The atomic fractional coordinates and thermal parameters are given in Table 1, in which the U_{ij} are coefficients in the expression exp $[-2\pi^2 (h^2U_{11}a^{*2} + ... + 2klU_{23}b^*c^*)]$. The table of final observed and calculated structure factors may be found in the Depository of Unpublished Data.[3] Coordinates for the hydrogen atoms are given in Table 2.

Discussion

A stereoscopic drawing of ethyl triiodothyropropionate illustrating both the molecular conformation and the relative magnitudes and

[2]The scattering curve for iodine was not corrected for anomalous dispersion.

[3]Tables of final observed and calculated structure factors for T_3P are available, at a nominal charge, from the Depository of Unpublished Data, National Science Library, National Research Council of Canada, Ottawa, Canada, K1A 0S2.

TABLE 1. Fractional atomic coordinates and anisotropic thermal parameters ($\times 10^5$)

Atom	x	y	z	U_{11}	U_{22}	U_{33}	U_{12}	U_{13}	U_{23}
I(3′)	0.2491	0.0864	0.3744	726	570	719	8	332	104
I(5)	0.4454	0.7547	0.4804	634	628	646	87	323	−30
I(3)	0.3369	0.5108	0.1205	756	775	576	−41	204	−1
O(1)	0.0576	0.2650	0.3520	564	845	1181	−43	520	−88
O(2)	0.3167	0.6604	0.2884	455	473	716	160	229	139
O(3)	0.9091	0.3960	0.3930	593	1186	1119	275	533	320
O(4)	0.9063	0.2894	0.5127	649	949	758	258	272	61
C(1′)	0.2538	0.5573	0.3064	400	500	442	78	178	−29
C(2′)	0.2813	0.4079	0.3292	373	569	502	95	162	28
C(3′)	0.2123	0.3144	0.3436	417	468	452	29	153	−24
C(4′)	0.1209	0.3661	0.3358	402	606	522	5	241	−66
C(5′)	0.0976	0.5129	0.3152	393	454	762	29	336	−117
C(6′)	0.1660	0.6094	0.3003	524	794	683	125	227	−26
C(1)	0.6112	0.5526	0.3390	549	675	781	105	340	150
C(2)	0.5384	0.5214	0.2589	600	608	611	105	288	44
C(3)	0.4431	0.5550	0.2434	392	476	549	9	175	66
C(4)	0.4138	0.6204	0.3060	425	430	705	82	366	94
C(5)	0.4846	0.6495	0.3856	539	320	594	13	268	23
C(6)	0.5820	0.6155	0.4006	542	583	499	88	207	52
C(7)	0.7178	0.5148	0.3552	542	960	906	145	456	126
C(8)	0.7698	0.4371	0.4362	543	969	716	124	336	88
C(9)	0.8689	0.3750	0.4426	473	672	802	86	324	29
C(10)	1.0029	0.2248	0.5282	806	976	1102	348	332	141
C(11)	1.0352	0.1486	0.6117	1207	1482	934	668	282	233
				Standard deviations					
I	0.0001	0.0001	0.0000	4	5	4	3	3	3
O	0.0005	0.0009	0.0006	43	59	62	40	43	42
C (ring)	0.0007	0.0011	0.0007	56	55	55	43	43	42
C (7–10)	0.0009	0.0017	0.0008	61	85	73	61	59	63
C (11)	0.0025	0.0025	0.0018	138	163	95	140	93	116

TABLE 2. Hydrogen atom fractional coordinates

Atom	x	y	z	Atom	x	y	z
H(O)	0.019	0.296	0.360	H(8)	0.723	0.310	0.451
H(2′)	0.339	0.392	0.335	H(8*a*)	0.766	0.486	0.476
H(5′)	0.028	0.538	0.316	H(10)	0.988	0.124	0.493
H(6′)	0.159	0.689	0.295	H(10*a*)	1.052	0.258	0.517
H(2)	0.559	0.503	0.226	H(11)	0.962	0.023	0.561
H(6)	0.624	0.629	0.453	H(11*a*)	1.091	0.084	0.613
H(7)	0.728	0.434	0.325	H(11*b*)	1.002	0.100	0.627
H(7*a*)	0.760	0.617	0.345	Standard deviations	0.007–013	0.010–020	0.006–010

shapes of the atomic thermal ellipsoids is shown in Fig. 1. The conformation of the molecule is such that the 3′-iodine atom is *proximal* to the α-diiodo ring and the uniodinated 5′ position is *distal*, identical to the conformation observed in the crystal structure of triiodo-L-thyronine (2). The aromatic rings are planar (Table 3) and are close to being completely skewed with respect to each other and mutually perpendicular. The angles between normals to the plane of the inter-ring ether linkage and the planes of the α-diiodo and β-monoiodo rings are ± 88 and $\mp 10°$, respectively; these values compare closely with the values of $+86$ and $-13°$ for the related angles in triiodo-L-thyronine and are also similar to angles $+86$ and $+19°$ found in 3,5-diiodo-L-thyronine when it is complexed with *N*-methylacetamide (6). A plus value of the angle indicates rotation of the phenyl ring away from coplanarity with the plane of the inter-ring ether linkage in an anticlockwise direction when viewed along the (phenyl)C—O(ether) bond in the direction from

Can. J. Chem. Downloaded from www.nrcresearchpress.com by 210.87.254.40 on 09/05/12
For personal use only.

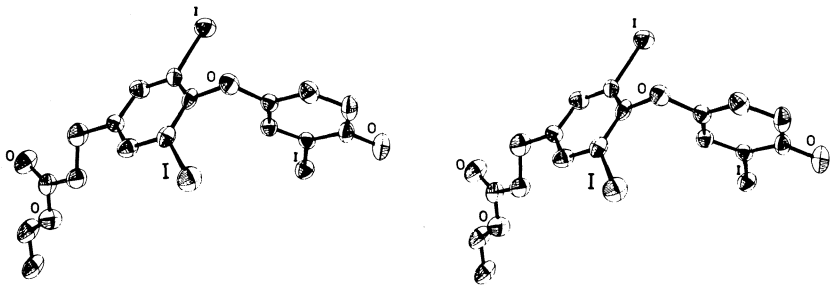

FIG. 1. Stereoscopic drawing of ethyl triiodothyropropionate showing the molecular conformation and the relative sizes and shapes of the thermal motion ellipsoids.

TABLE 3. Deviations of atoms from least-square planes

Plane 1		*Plane 2*		*Plane 3*	
Atom	Δ (Å)	Atom	Δ (Å)	Atom	Δ (Å)
C(1)	0.007	C(1′)	0.008	O(3)	0.002
C(2)	−0.006	C(2′)	−0.004	O(4)	0.001
C(3)	0.000	C(3′)	−0.006	C(8)	0.001
C(4)	0.006	C(4′)	0.011	C(9)	−0.004
C(5)	−0.004	C(5′)	−0.006	C(7)[a]	0.189
C(6)	−0.002	C(6′)	−0.003	C(10)[a]	−0.010
C(7)[a]	0.003	O(1)[a]	0.000	C(11)[a]	−0.258
O(2)[a]	0.072	O(2)[a]	0.045		
I(3)[a]	0.035	I(3′)[a]	0.035		
I(5)[a]	0.077				

[a]These atoms not used in calculating the plane.

C to O. The angles for T_3P have dual signs because the $P2_1/c$ space group contains a glide plane which means that both conformers must exist in the crystal. Thus the conformation of the diphenyl ether parts of these three molecules are remarkably similar. The conformation of this part of the L-thyroxine molecule (7) differs somewhat from these, with greater deviations of the two rings from being perpendicular to and coplanar with the inter-ring ether plane (angles of +101 and −34°).

The conformation of the propionic acid chain in T_3P differs markedly from that of the alanine chains in L-thyroxine, triiodo-L-thyronine, and L-thyronine (8). In these latter three molecules the alanine conformations are virtually identical, whereas in T_3P, in which the propionic acid chain differs from alanine only in that it lacks the α-amino group of alanine, the conformation about the C(α)—C(β) bond is different from that occurring in the thyronine derivatives; the side chain in T_3P is more extended and lies slightly more in a direction "proximal" to the β-ring, rather than "distal" to it as is the case with the alanine chains (see Fig. 1 and related figures for the thyronine derivatives in refs. 2, 7, and 8). The atoms comprising the carboxyl grouping lie on a plane (Table 3).

Bond lengths and angles in the T_3P molecule are shown in Fig. 2. Because the iodine atoms dominate the X-ray scattering the estimated standard deviations for light atom bond distances and angles are rather high (0.015–0.022 Å, except for C(10)—C(11) which is 0.035 Å, and 0.7–1.8°) but the values are all near normal and require no special comment. The iodine–carbon bond lengths average 2.10 Å, in good agreement with average values of 2.11 Å in triiodo-L-thyronine and L-thyroxine, and 2.10 Å in 3,5-diiodo-L-thyronine. This is longer than the normal carbon (aromatic) – iodine distance of 2.05 Å and may explain why the iodinated thyronine-type compounds often exhibit tendencies toward decomposition when irradiated with X-rays, with apparent liberation of iodine. The angle at the inter-ring ether linkage is 119°, similar to what has been found for other diphenyl ether compounds. Bond distances and angles involving

Can. J. Chem. Downloaded from www.nrcresearchpress.com by 210.87.254.40 on 09/05/12
For personal use only.

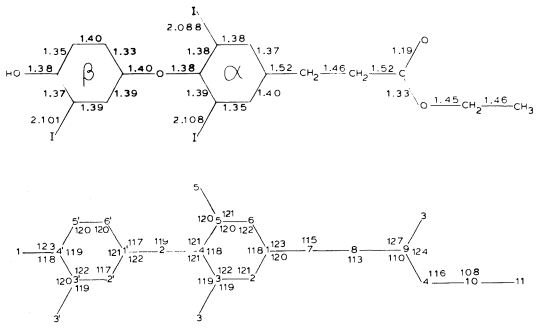

FIG. 2. Bond lengths (Å) and angles (°) in ethyl triiodothyropropionate.

hydrogen atoms are omitted from Fig. 2: the inaccuracies in their values are too large to merit their inclusion.

The hydroxyl group is the only hydrogen donor in the molecule for hydrogen bonding and it takes part in an intermolecular contact with the carbonyl oxygen in the molecule one unit cell away in the x direction; the hydrogen...carbonyl oxygen distance is 2.1 Å (oxygen–oxygen distance = 2.76 Å) and the O—H...O angle is 176°. There is also a network of short intermolecular iodine...iodine distances: every I(3′) at (x,y,z) has an intermolecular contact of 4.03 Å with an I(5) in a related molecule at $(x, 1/2-y, 1/2+z)$, and one of 3.93 Å with an I(3) in a molecule at $(x, y-1, z)$, and these latter two atoms are separated by 3.78 Å. These intermolecular separations are significantly shorter than the normal I...I van der Waals separation of 4.30 Å given by Pauling (9) (though only slightly shorter than the 4.08 Å value of Bondi (10)) and indicate some degree of charge transfer bonding may be taking place among the iodines, aiding in stabilizing the crystal structure.

The elucidation of the crystal and molecular structures of ethyl 3,5,3′-triiodothyropropionate has shown that the molecular conformation is such that the 3′-iodine is situated *proximal* to the α-ring, identical to the results found in the structure determination of triiodo-L-thyronine. Thus the structural evidence obtained so far consistently indicates this conformation to be an energetically favored one, whereas the indications of Jorgenson *et al.* (3), from biological activity studies of thyroid hormone analogs, are that the 3′-iodine *distal* conformation is biologically more active. Further clarification of these contradictory results must await structural studies of other thyromimetic agents and of the analogs used in the biological activity studies; such investigations are now in progress in these laboratories.[4,5]

The conformation of the propionate chain of T_3P is quite different from the alanine conformation found in L-thyroxine, triiodo-L-thyronine, and L-thyronine ethyl ester; and since the diphenyl ether parts of T_3P and triiodo-L-thyronine are conformationally virtually identical, the differences in biological potency of the two hormones undoubtedly result from these differing side chain structures. The essential differences are (*a*) absence of the amine functional group in T_3P and (*b*) the change in conformation about the β-carbon atom of the chain.

We thank Dr. Robert Meltzer of Warner-Lambert Research Institute for supplying the triiodothyropropionic acid. Support was from the Medical Research Council of Canada grant MA-4695, and from the general research support grant of the University of Washington School of Medicine, supplied by USPHS grant RR 05432 from the National Institutes of Health.

1. R. W. RAWSON. Mayo Clinic Proc. **39**, 637 (1964).
2. N. CAMERMAN and A. CAMERMAN. Science, **175**, 764 (1972).
3. E. C. JORGENSEN, P. A. LEHMAN, C. GREENBERG, and N. ZENKER. J. Biol. Chem. **237**, 3832 (1962); E. C. JORGENSEN, N. ZENKER, and C. GREENBERG. J. Biol. Chem. **235**, 1732 (1960).

[4]Since preparation of this work for publication a note has appeared (see ref. 11) describing the crystal structure of 3,5,3′-triiodothyroacetic acid *N*-diethanolamine (1:1) complex, in which the 3′-iodine was found to be oriented distal to the α-ring. The authors also refer to unpublished data for other structures having distal orientations for 3′-iodines. At the same time we have described the results of a structural investigation of 3′-isopropyl-3,5-diiodo-L-thyronine, the most potent known thyromimetic agent (see ref. 12) in which the conformation is such that the 3′-isopropyl group is proximal to the α-ring. Our crystals were prepared from acidic alcoholic solutions, while Cody and Duax (11) appear to have had large excesses of organic reagents present in their crystallization media. These results indicate that crystallization conditions may play a significant role in influencing the conformation of these asymmetric thyronine derivatives, and will undoubtedly provoke much interesting work on structural and biological aspects of thyroid hormones and analogs under different environmental conditions.

[5]We have recently performed high-resolution n.m.r. studies of T_3P in solutions similar in composition to those trom which the crystalline proximally- and distally-orienfed T_3- and T_3-like analogs were obtained. The spectra are consistent with there being two resolvable conformers in acidic media, the proximal conformer dominating, and only one conformer (or, more probably, a time-averaged conformation) in neutral solution (see ref. 13).

Can. J. Chem. Downloaded from www.nrcresearchpress.com by 210.87.254.40 on 09/05/12
For personal use only.

4. P. COPPENS, L. LEISEROWITZ, and D. RABINOWITZ. Acta Cryst. **18**, 1035 (1965).
5. International tables for X-ray crystallography. Vol III. The Kynoch Press, Birmingham, England. 1962.
6. V. CODY, W. L. DUAX, and D. A. NORTON. Acta Cryst. B**28**, 2244 (1972).
7. N. CAMERMAN and A. CAMERMAN. Proc. Nat. Acad. Sci. **69**, 2130 (1972).
8. A. CAMERMAN and N. CAMERMAN. Can. J. Chem. This issue.
9. L. PAULING. The nature of the chemical bond. Cornell University Press, Ithaca, N.Y. 1960.
10. A. BONDI. J. Phys. Chem. **68**, 441 (1964).
11. V. CODY and W. L. DUAX. Biochem. Biophys. Res. Commun. **52**, 430 (1973).
12. J. K. FAWCETT, N. CAMERMAN and A. CAMERMAN. Biochem. Biophys. Res. Commun. **52**, 407 (1973).
13. N. CAMERMAN, A. CAMERMAN, and J. K. FAWCETT. *In* Molecular and quantum pharmacology. *Edited by* E. D. Bergman and B. Pullman. Reidel Publishing Co., Dordrecht, Holland, 1974.

Can. J. Chem. Downloaded from www.nrcresearchpress.com by 210.87.254.40 on 09/05/12
For personal use only.

A Synthesis of Specifically Substituted Pyrenes: 2,7-Dimethylpyrene

REGINALD H. MITCHELL[1] AND ROBERT J. CARRUTHERS

Department of Chemistry, University of Victoria, Victoria, British Columbia V8W 2Y2

Received April 3, 1974

REGINALD H. MITCHELL and ROBERT J. CARRUTHERS. Can. J. Chem. **52**, 3054 (1974).

The synthesis of 2,7-dimethylpyrene (**1***a*) from mesitylene is described as an example of a general synthesis applicable to many substituted pyrenes. Intermediates in the synthesis are 2,11-dithia[3,3]metacyclophanes (**4**) and [2,2]metacyclophane-1,9-dienes (**6**).

REGINALD H. MITCHELL et ROBERT J. CARRUTHERS. Can. J. Chem. **52**, 3054 (1974).

A titre d'exemple d'une synthèse générale pouvant s'appliquer à plusieurs pyrènes substitués, on décrit la synthèse du diméthyl-2,7 pyrène (**1***a*) à partir du mésitylène. Les intermédiaires dans la synthèse sont les dithia-2,11 [3,3]métacyclophanes (**4**) et les [2,2]métacyclophadiènes-1,9 (**6**). [Traduit par le journal]

Introduction

It came to our notice recently when we required substantial quantities of 2,7-dimethylpyrene[2] that most syntheses (1) of the pyrene ring system are not readily adaptable for specifically substituted pyrenes. This would not be so important if it were not for the fact that it is difficult to control electrophilic substitution of pyrene itself (1, 2). A controlled synthesis, in which the positions of substituents can be predecided is thus desirable. We would now like to report such a synthesis using the now readily accessible metacyclophane-1,9-dienes recently reported by one of us (R.H.M.) and Boekelheide (3, 4).

Results and Discussion

Our synthesis of generally substituted pyrenes is depicted in Scheme 1. The metacyclophane-1,9-dienes (**6**) can be prepared readily in good overall yield from benzylic halides by way of the dithiametacyclophanes (**4**) (3, 4). Conversion of **6** to the pyrene (**1**) is then achieved in essentially quantitative yield by irradiation with light of wavelength 2537 Å to the 15,16-dihydropyrene (**7**) and then either continued irradiation to **1** or exposure of **7** to oxygen gas. Since the sequence can be carried out in the presence of a variety of substituent groups (*e.g.* R = Me, F, Cl, Br, CN, CO_2Et) a versatile and fairly general synthesis is thus in hand (see Experimental).

Convincing evidence for the need and utility of such a synthesis is apparent for the case in point, 2,7-dimethylpyrene (**1***a*) (*a* refers to $R_2 = R_5 = Me$; $R_1 = R_3 = R_4 = R_6 = H$). Although **1***a* has been referred to several times in the literature (5–9), it has been synthesized only in very poor yield. Originally **1***a* was isolated from various lignites in milligram amounts (5) and has subsequently been synthesized by pyrolysis of bimesityl in $\ll 1\%$ yield (6) and from 1,4,5,8-naphthalene tetracarboxylic dianhydride in $< 5\%$ yield (7), none of which seemed particularly suitable to prepare gram amounts of **1***a*. Application of our synthesis however readily yielded **1***a* in overall yield of up to 35% from 3,5-bis(bromomethyl)toluene (**2***a*) as is detailed in the Experimental below.

Experimental

All melting points were determined on a Kofler hot stage and are uncorrected. The p.m.r. spectra were determined on a Perkin–Elmer R12A spectrometer using tetramethyl silane as internal standard. The mass spectra were recorded on a Hitachi–Perkin–Elmer RMU-7 mass spectrometer at 70 eV. Microanalyses were performed by Dr. D. McGillivray.

*3,5-Bis(bromomethyl)toluene (**2a**)*

This compound could be prepared in markedly improved yield (60–80%) over that of the literature (10) by treating mesitylene dissolved in refluxing carbon tetrachloride (1 g per 25 ml) with 2.0 molar equiv. of *N*-bromosuccinimide (added in four batches) in the presence of benzoyl peroxide catalyst. The product was obtained (after removal of succinimide) by direct recrystallization of the crude reaction mixture from ethanol and showed physical properties in agreement with those reported (11).

*3,5-Bis(mercaptomethyl)toluene (**3a**)*

The bisbromide (**2***a*) could be converted to the bismercaptan **3***a* in essentially quantitative yield by the thiourea method (12). The crude light yellow oil so

[1]To whom correspondence should be addressed.

[2]Previously called 4,9-dimethylpyrene.

Can. J. Chem. Downloaded from www.nrcresearchpress.com by 210.87.254.5 on 09/05/12
For personal use only.

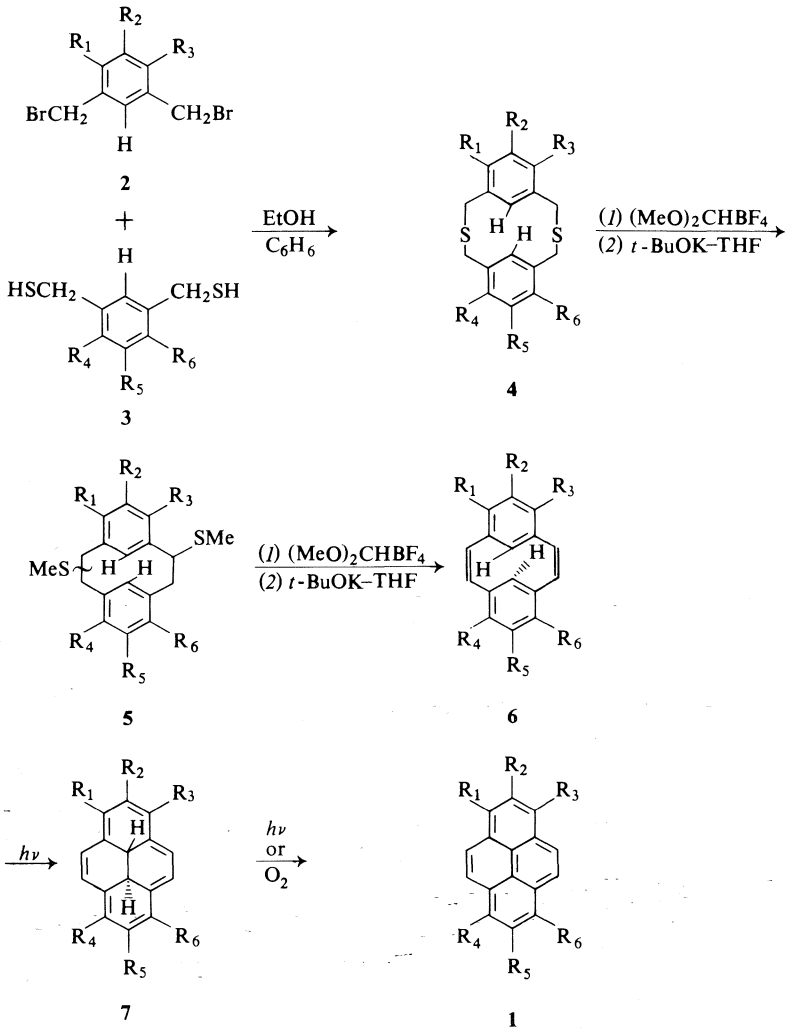

SCHEME 1

obtained was shown by n.m.r. to be sufficiently pure to use directly in the cyclization step that follows.

6,15-Dimethyl-2,11-dithia[3.3]metacyclophane (4a)

A filtered solution of the bisbromide (**2a**) (24 g, 0.086 mol) and the crude bisthiol (**3a**) (16 g, 0.086 mol) in benzene (2 l) was added dropwise at room temperature under nitrogen over about 48 h to a well stirred solution of KOH (12 g, 0.2 mol) in 95% ethanol (3 l). After evaporation of the solvent, the residue was washed several times with water and extracted with hot benzene. After cooling the benzene deposited some crystals of product, the remainder being obtained by evaporation of the solvent and chromatography of the crystalline residue on silica gel using benzene – petroleum ether (25 : 75) as eluant.

Crystallization from cyclohexane gave colorless crystals of **4a** in 40–80% yield, m.p. 104–105.5°; p.m.r., $CDCl_3$ (τ) 3.34 (4H, bs, ArH), 3.42 (2H, bs, internal ArH), 6.38 (8H, s, $—CH_2—$), and 7.87 (6H, s, $—CH_3$); mass spectrum *m/e* (relative intensity), M^+ = 300 (100), 151 (52), 150 (42), 149 (27), 120 (80), 119 (68).

Anal. Calcd. for $C_{18}H_{20}S_2$: C, 71.95; H, 6.71; Found: C, 72.05; H, 6.99.

Conversion of 4a to the Mixed Isomers of 5a

A solution of **4a** (4.0 g, 13.3 mmol) in CH_2Cl_2 (50 ml) was added over 15 min to a stirred suspension of dimethoxy carbonium fluoroborate (13) (36 mmol) in CH_2Cl_2 (20 ml) at −30° under N_2. After stirring for 4 h without further cooling, ethyl acetate (75 ml) was added and stirring continued for a further 30 min. The bissulphonium salt was collected, washed well with ethyl acetate and dried under vacuum to give 6,15-dimethyl-2,11-dithia[3,3]metacyclophane bismethylsulphonium fluoroborate in near quantitative yield, as a white powder, m.p. 200° dec.

Anal. Calcd. for $C_{20}H_{26}S_2B_2F_8$: C, 47.65; H, 5.20. Found: C, 47.55; H, 5.24.

Potassium *t*-butoxide (3.14 g, 28 mmol) was added to

Can. J. Chem. Downloaded from www.nrcresearchpress.com by 210.87.254.5 on 09/05/12
For personal use only.

a suspension of the above sulphonium salt (6.41 g, 12.7 mmol) in dry THF at room temperature under N_2. After stirring for 5–10 min, aqueous HCl, H_2O, and CH_2Cl_2 were added. The organic layer was washed, dried, and evaporated to give a better than 95% yield of **5***a*, as a mixture of isomers (by p.m.r.) which was used directly without further purification.

*anti-5,13-Dimethyl[2,2]metacyclophane-1,9-diene (**6***a*)

A solution of the mixed isomers of **5***a* (8.2 g, 25 mmol) in CH_2Cl_2 (80 ml) was added to a stirred suspension of dimethoxy carbonium fluoroborate (70 mmol) in CH_2Cl_2 (20 ml) and the mixture of bissulphonium salt isomers was isolated in *ca.* 90% yield as described above.

This salt was suspended in dry THF (400 ml) under N_2 at room temperature and potassium *t*-butoxide (17 g, 0.15 mol) was added. The mixture was allowed to stir at room temperature for 3 h, after which time benzene was added and the mixture was acidified carefully with aqueous HCl. The organic layer was separated, washed with water, dried, and evaporated at reduced pressure below 30°. The pale greenish residue was chromatographed on silica gel using petroleum ether as eluant to give **6***a* in 40–50% yield. Careful recrystallization of a sample of **6***a* from petroleum ether below 40° gave pale yellow crystals, m.p. 150–151° (dec.)[3] which rapidly turn green on their surface; p.m.r., CCl_4, (τ) 2.39 (2H, s, internal ArH), 3.57 (4H, s, ArH), 3.80 (4H, s, —CH=CH—), and 7.79 (6H, s, $—CH_3$); mass spectrum, *m/e*, M^+ 232.

Anal. Calcd. for $C_{18}H_{16}$: C, 93.06; H, 6.94. Found: C, 93.18; H, 7.01.

The Hofmann elimination to give **6***a* could also be affected by KOH–H_2O, KOH–EtOH, *t*-BuOK–DMSO with varying amounts of **6***a* and **1***a* being produced.

*2,7-Dimethylpyrene (**1***a*)

A solution of **6***a* dissolved in degassed cyclohexane (1 g/200 ml) under vacuum, was irradiated with light of wavelength 2537 Å from a 6 W source (Ultraviolet Products PCOX1). Examination of the resultant bright green solution by n.m.r. indicated the presence of *trans*-15,16-dihydro-2,7-dimethylpyrene (internal protons at τ 15.31). Continued irradiation until the green colour was totally destroyed or exposure of the green solution to the atmosphere or O_2 gave, after filtration through silica gel, an essentially quantitative yield of **1***a*, m.p. 235–236° (lit. (6,7) m.p. 238°) identical to an authentic sample (9).

Other Pyrenes

Whilst we have not deliberately carried out the above scheme to achieve the synthesis of other substituted pyrenes, it has been noticed (14) that the sequence does in fact work for a variety of substituent groups. The experimental technique used was identical to that described above, and although not optimized, overall yields of 10–40% can be expected.

We thank the National Research Council and the University of Victoria for the support of this investigation.

[3]Sample put on at 135°, turns dark green at once and resolidifies after melting, *cf.* ref. 4.

1. E. CLAR. Polycyclic hydrocarbons. Vol. 2. Academic Press, London. 1964. Chapt. 31.
2. H. VOLLMANN, H. BECKER, M. CORELL, and H. STREECK. Liebigs Ann. Chem. **531**, 1 (1937).
3. R. H. MITCHELL and V. BOEKELHEIDE. J. Am. Chem. Soc. **92**, 3510 (1970).
4. R. H. MITCHELL and V. BOEKELHEIDE. J. Am. Chem. Soc. **96**, 1547 (1974).
5. E. O. WOOLFOLK, M. ORCHIN, and H. H. STORCH. Fuel, **26**, 78 (1947); F. RUNGE, J. FREYTAG, and J. KOLBE. Chem. Ber. **87**, 873 (1954).
6. M. ORCHIN, L. REGGEL, and R. A. FRIEDEL. J. Am. Chem. Soc. **74**, 1094 (1952).
7. F. RUNGE and A. MECKELBURG. Chem. Ber. **86**, 373 (1953).
8. E. CLAR, B. A. MCANDREW, and M. ZANDER. Tetrahedron, **23**, 985 (1967); E. CLAR, B. A. MCANDREW, and U. SANIGOK. Tetrahedron, **26**, 2099 (1970).
9. V. BOEKELHEIDE and R. A. HOLLINS. J. Am. Chem. Soc. **95**, 3201 (1973).
10. V. BOEKELHEIDE and R. W. GRIFFIN. J. Org. Chem. **34**, 1960 (1969).
11. J. VON BRAUN and O. ENGEL. Chem. Ber. **58**, 283 (1919).
12. A. J. SPEZIALE. Org. Synth. **4**, 401 (1963).
13. R. F. BORCH. J. Am. Chem. Soc. **90**, 5303 (1968); J. Org. Chem. **34**, 627 (1969).
14. R. H. MITCHELL, V. BOEKELHEIDE, and co-workers. Unpublished results.

Can. J. Chem. Downloaded from www.nrcresearchpress.com by 210.87.254.5 on 09/05/12
For personal use only.

The Vibrational Spectra of Methyl Cyanoacetate and Methyl Cyanoacetate-d_3[1]

DEEPALI SINHA AND J. E. KATON

Department of Chemistry, Miami University, Oxford, Ohio 45056

Received March 12, 1974

DEEPALI SINHA and J. E. KATON. Can. J. Chem. **52**, 3057 (1974).

The i.r. spectra of methyl cyanoacetate in both liquid and solid phases and of methyl cyanoacetate-d_3 in the liquid phase have been recorded in the region 4000–250 cm^{-1}. The Raman spectra of both the compounds in the liquid phase have also been recorded. A tentative vibrational assignment has been made both for the light and the heavy ester. Evidence is presented for the existence of conformational isomers in the liquid phase.

DEEPALI SINHA et J. E. KATON. Can. J. Chem. **52**, 3057 (1974).

On a enregistré le spectre i.r. du cyanoacétate de méthyle en phases liquide et solide et celui du cyanoacétate de méthyl-d_3 en phase liquide dans la région 4000–250 cm^{-1}. On a aussi enregistré les spectres Raman de chacun de ces composés en phase liquide. Des attributions vibrationnelles non définitives sont faites pour les esters légers et lourds. On présente des données qui impliquent l'existence d'isomères conformationnels dans la phase liquide.

[Traduit par le journal]

Introduction

Although a number of workers have concerned themselves with the vibrational spectra of organic esters, very few detailed spectral studies have been reported. Vapor and liquid spectra of methyl formate and methyl acetate, together with a partial assignment of the spectral bands have been reported by Wilmshurst (1) and Susi and Zell (2) but spectra of these compounds in the solid state have not been studied. The vibrational spectra and structure of two isomeric esters, methyl acrylate and vinyl acetate, have been discussed by Feairheller and Katon (3). Recently a detailed and thorough study of methyl chloroformate has been reported (4) from this laboratory.

This paper reports the i.r. and Raman spectra of methyl cyanoacetate and methyl cyanoacetate-d_3 in the liquid phase. In addition, the i.r. spectrum of methyl cyanoacetate in the crystalline state has also been recorded. A tentative vibrational assignment has been made based on these spectra and comparison with the assignments of cyanoacetic acid (5), methyl acetate, and methyl acrylate. Evidence is presented for the existence of a conformational equilibrium of methyl cyanoacetate in the liquid state but the detailed structures of the conformers cannot be determined from the data available.

[1]Supported in part by the U.S. Air Force under contracts F33615-72-C-1040 and F33615-73-C-5013.

Experimental

Methyl cyanoacetate (Eastman Organic Chemical) was purified by distillation under reduced pressure. $CH_2CNCO_2CD_3$ was prepared by refluxing CD_3OD with CH_2CNCO_2H in ether and then separating the ester by fractional distillation. Infrared spectra in the 4000–250 cm^{-1} region were recorded as capillary films between CsBr windows on a Perkin-Elmer Model 180 infrared spectrophotometer. Infrared spectra in the region 300–75 cm^{-1} were recorded on the pure liquid on a Perkin-Elmer Model 301 Far Infrared spectrophotometer. A crystal film of methyl cyanoacetate was obtained with difficulty by keeping a capillary film near the temperature of liquid nitrogen for about 3 h. Under usual conditions of cooling only a glass could be obtained. A crystal film of the deuterated compound could not be obtained even under similar conditions. All attempts to induce crystallization of this compound failed and only a glass was obtained.

Raman spectra of both compounds were recorded on a Cary Model 81 Raman spectrometer utilizing an argon ion laser source. The i.r. spectra of a capillary film and crystal film of $CH_2CNCO_2CH_3$ and that of a capillary film of $CH_2CNCO_2CD_3$ are shown in Figs. 1–3. Typical Raman spectra of the light and the heavy esters are shown in Figs. 4 and 5. The vibrational absorption bands with their proposed assignments are listed in Table 1.

Vibrational Assignments

The assignment of the vibrational spectra of methyl cyanoacetate is aided by the fact that several of the vibrations of this molecule are well-known group frequencies. In addition, the published assignments of methyl acetate, methyl acrylate, and cyanoacetic acid provide useful guides to some of the assignments. The lack of symmetry and the relatively large number of

Can. J. Chem. Downloaded from www.nrcresearchpress.com by 210.87.254.6 on 09/05/12
For personal use only.

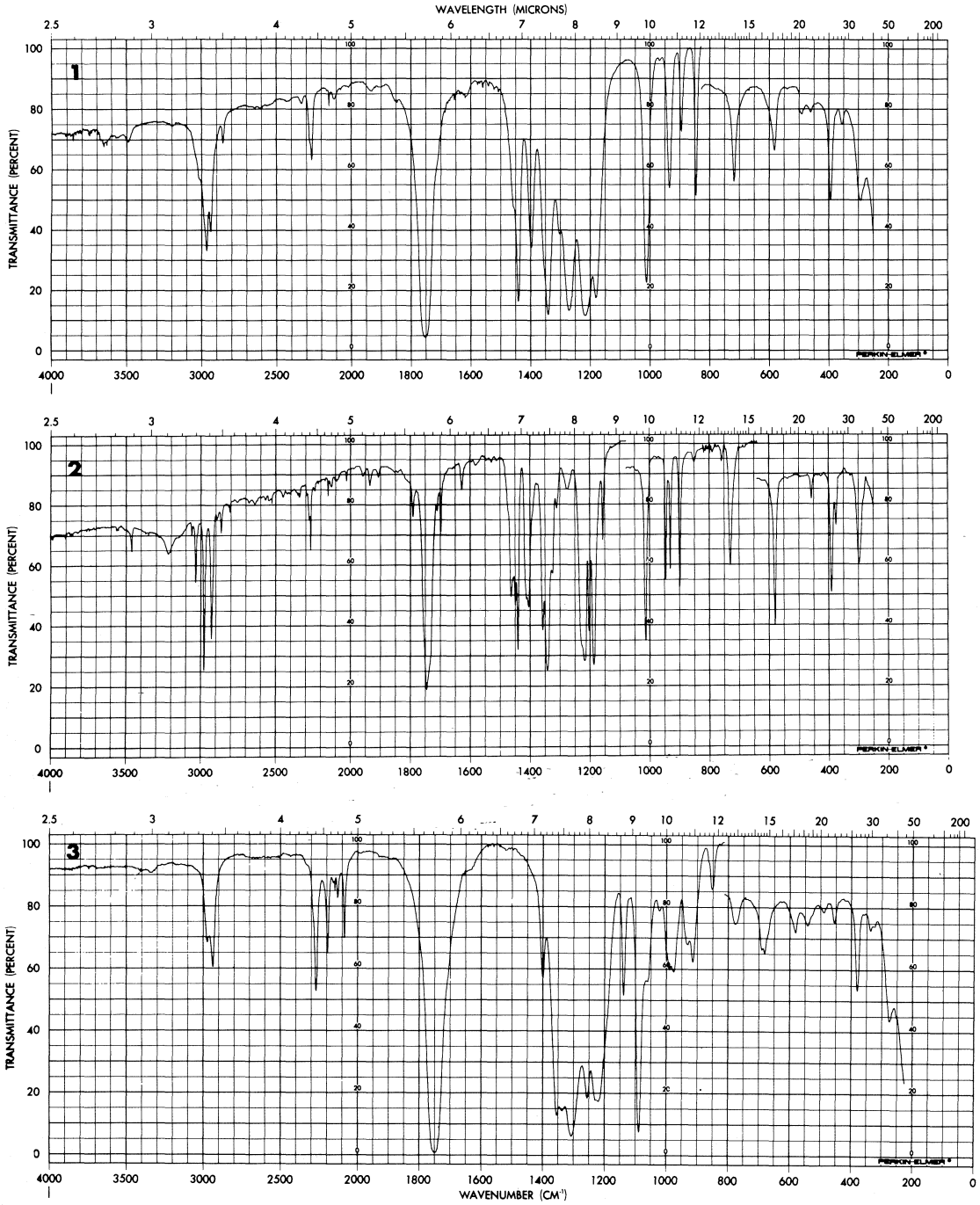

FIG. 1. The i.r. spectrum of liquid methyl cyanoacetate.
FIG. 2. The i.r. spectrum of crystalline methyl cyanoacetate.
FIG. 3. The i.r. spectrum of liquid methyl cyanoacetate-d_3.

Can. J. Chem. Downloaded from www.nrcresearchpress.com by 210.87.254.6 on 09/05/12
For personal use only.

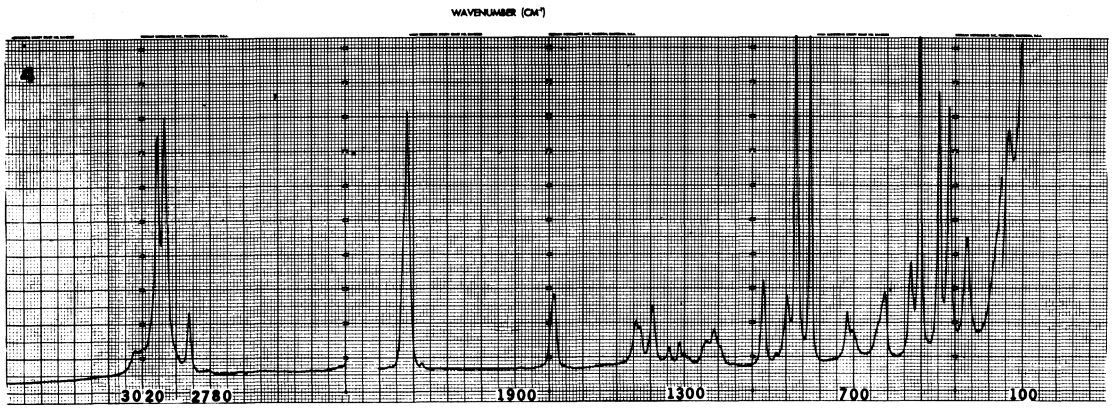

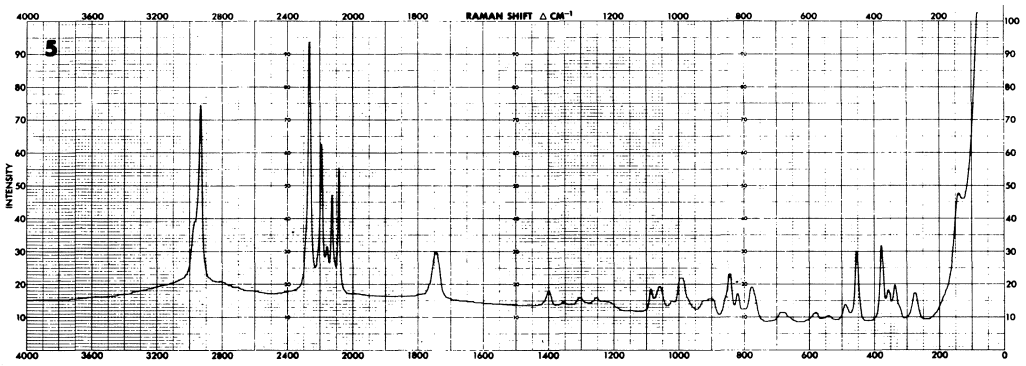

FIG. 4. The Raman spectrum of liquid methyl cyanoacetate.
FIG. 5. The Raman spectrum of liquid methyl cyanoacetate-d_3.

fundamental vibrations, however, prevent a completely unambiguous assignment of the molecule at the present time.

Methyl cyanoacetate has five C—H stretching modes, consisting of two antisymmetric and one symmetric for the CH_3 group and one symmetric and one antisymmetric for the CH_2 group, and they are relatively easily located by comparison of the spectra of the light and heavy isotopically substituted molecules. The two strong Raman bands at 2966 and 2938 cm^{-1} must represent the two symmetric modes. The relatively strong intensity of the lower frequency band in the Raman spectrum of the d_3 compound leads to the assignment of this band as the νCH_2 symmetric mode, the 2966 cm^{-1} then represents the νCH_3 symmetric mode. The antisymmetric νCH_3 mode at 3025 cm^{-1} is close to the 3035 cm^{-1} band in methyl acetate. The other CH_3 antisymmetric mode has been assigned to the very weak i.r. band at 3057 cm^{-1} in the spectrum of the solid compound. These two antisymmetric modes occur at 2189 and 2124 cm^{-1} in the -d_3 compound. The remaining C—H stretching mode to be assigned is the νCH_2 antisymmetric mode. In cyanoacetic acid this mode occurs at 2972 cm^{-1} and we feel that this vibration in methyl cyanoacetate must occur near 2970 cm^{-1} and is therefore assigned as being accidentally degenerate with the νCH_3 symmetric mode. The occurrence of a band at 2966 cm^{-1} in the d_3 compound and its relatively low intensity in the Raman spectrum further confirms this assignment. The band at 2860 cm^{-1} which appears as a reasonably strong band in the Raman is believed to be the overtone of the symmetric CH_3 bending mode in Fermi resonance with the νCH_3 symmetric stretching mode.

The assignment of $\nu C{\equiv}N$ and $\nu C{=}O$ modes is obvious as they are good group frequencies.

In the 1500–1380 cm^{-1} region there are only three observed bands in the liquid phase and four in the solid phase spectra. This is the region expected for the three CH_3 bending modes and the

Can. J. Chem. Downloaded from www.nrcresearchpress.com by 210.87.254.6 on 09/05/12
For personal use only.

TABLE 1. Observed vibrational frequencies of methyl cyanoacetate and methyl cyanoacetate-d_3 and their proposed assignment (in cm^{-1})

$CH_2CNCO_2CH_3$			$CH_2CNCO_2CD_3$		
Infrared		Raman	Infrared	Raman	
Liquid	Solid	liquid	liquid	liquid	Assignment
	3460 vw				2262+1202 = 3464
	3057 vw	3048 w			νCH_3 (antisym)
3025 sh	3029 w–m	3018 w, sh			νCH_3 (antisym)
2963 m	2973 m	2966 s	2970 w–m	2970 sh	νCH_3 (sym), νCH_2 (antisym)
2936 m	2925 m	2938 s	2936 w–m	2936 s	νCH_2 (sym)
2860 w	2860 w	2860 m			2×1440 = 2880
2270 sh	2278 sh				1342+931 = 2273
2258 w	2262 w	2263 s	2263 w–m	2265 s	νCN
			2189 w–m	2190 m–s	νCD_3 (antisym)
			2124 vw	2125 w	νCD_3 (antisym)
				2155 w	2×1060 = 2120
			2083 w–m	2085 m–s	νCD_3 (sym)
	1790 w				2×894 = 1788
1749 vs	1745 s	1753 m, b	1746 vs	1746 m, b	$\nu C{=}O$
	1699 w				1405+297 = 1702
	1626 w				894+728 = 1622
1455 sh	1463 m–s	1460 w–m, b			δCH_3 (antisym)
1439 s	1449 m–s, 1440 m–s	1443 sh			δCH_3 (antisym), δCH_3 (sym)
1396 m	1415 sh, 1405 m–s	1400 w–m	1396 m	1400 w	δCH_2 (scissors)
	1357 m–s				894+460 = 1354
1341 s	1342 s	1347 vw	1349 m–s	1350 vw, b	δCH_2 (wag)
	1324 sh				931+391 = 1322
1303 sh	1310 sh	1310 w			1010+295 = 1305
			1302 s	1305 vw, b	926+377 = 1303
1269 s	1269 vw		1252 s	1255 vw	νCOC (antisym) Isomer
1216 s, b	1216 s	1215 w, b	1218 s, b		νCOC (antisym), δCH_2 (twist)
	1202 m–s				δCH_2 (twist)
1181 m–s	1185 s	1190 w, b			δCH_3 (rock)
	1156 w–m	1174 vw			δCH_3 (rock)
			1135 m		687+453 = 1140
			1085 s	1086 w	δCD_3 (antisym)
			1053 sh	1060 w	δCD_3 (sym)
1010 s	1010 s	1015 w–m	986 w–m	990 m, b	νCOC (sym)
			971 w–m		δCD_3 (rock) Isomer
		967 vw			δCH_2 (rock)
	947 m				
			926 m	930—	δCD_3 (rock)
933 m	931 m	930 w	912 w–m		$\nu C{-}CN$
894 w–m	894 m	898 s		900 m, b	$\nu C{-}C$
845 m	849 vw	849 s	848 w–m	845 m, 820 w–m	Isomer
			770 w	777 w–m	
716 m	728 m	720 w–m			δCO_2 (scissors) Isomer
		705 w			
			687 w	680 vw, b	δCO_2 (scissors) Isomer
			677 w		

Can. J. Chem. Downloaded from www.nrcresearchpress.com by 210.87.254.6 on 09/05/12
For personal use only.

TABLE 1. (*Concluded*)

$CH_2CNCO_2CH_3$			$CH_2CNCO_2CD_3$		
Infrared		Raman	Infrared	Raman	
Liquid	Solid	liquid	liquid	liquid	Assignment
~600 vw, sh		608 vw, sh			Isomer
581 w–m	580 m	590 w	577 vw	580 vw	δCCC
			539 w	540 vw	Isomer
495 vw		493 m	487 vw	490 w	Isomer
465 vw	460 w	463 s	453 vw	455 m	δCO_2 (rock)
392 m	391 m	393 s	377 m	380 m	δCCN
354 w	374 w	360 s		360 w	δCOC
			338 w	338 w	Isomer
295 m	297 m	300 m	271 m	275 w–m	γCCN
		150 w		140 w	γCO_2 (wag)

CH_2 scissors mode. The lowest frequency band at 1396 cm^{-1} appears both in the light and the heavy ester and is obviously the δCH_2 scissors. The high frequency bands disappear in the spectrum of the deuterated compound with the concomitant appearance of two new bands in the 1100–1000 cm^{-1} region and have been assigned as the CH_3 bending modes.

It is interesting to note that two reasonably strong bands at 1269 and 845 cm^{-1} essentially disappear in the spectrum of the solid phase indicating the presence of rotational isomers in the liquid phase. The antisymmetric νCOC stretching mode is expected near 1200 cm^{-1}. The two bands at 1269 and 1216 cm^{-1} seem reasonable for this mode. Only the 1216 cm^{-1} remains in the low temperature spectrum, however, and has therefore been assigned as the νCOC antisymmetric mode for the stable form while the 1269 cm^{-1} band is probably due to the same mode of the less stable conformer. The band at 1341 cm^{-1} seems to be unusually high for any of the fundamentals expected in the 1350–800 cm^{-1} region. This has been assigned as the CH_2 wagging mode and must certainly be highly mixed with other CH_2 bending modes as well as perhaps skeletal modes. The 1180 cm^{-1} band that disappears in the heavy ester has been assigned as the remaining CH_3 deformation mode, namely CH_3 rock; the other CH_3 rocking mode is found only in the solid phase spectrum. The CH_2 twisting mode assigned at 1202 cm^{-1} is hidden under the νCOC antisymmetric mode in the liquid phase spectra. The frequencies assigned to the CH_2 twist, CH_2 rock, νC—CN and νC—C are very close to those assigned in cyanoacetic acid.The medium band at 845 cm^{-1} that disappears in the solid phase spectrum has been assigned as the νC—C for the less stable conformer. The remaining band at 1010 cm^{-1} has been assigned as νCOC symmetric stretch. The skeletal bending vibrations expected below 800 cm^{-1} are certainly highly coupled and hence their descriptions are very approximate. The assignments made are reasonably close to those observed in methyl acetate, methyl acrylate, and cyanoacetic acid. One of the major uncertainties is probably the assignment of the 1010 and 894 cm^{-1} bands, and these possibly could be reversed. Both νCOC (sym) and νC—C are expected to be strong in the Raman spectrum but only the 894 cm^{-1} is actually strong. Since deuteration of the CH_3 group would be expected to affect νCOC (sym) more than νC—C, we have chosen the higher frequency band as this mode.

Another area of uncertainty is a number of bands below 900 cm^{-1}. The Raman spectra of both the light and heavy compounds contain a larger number of bands than can be explained in terms of fundamentals of one isomer. The corresponding frequencies in the infrared are either very weak or absent. Since skeletal bending modes are expected in this region and such normal modes are nearly always much stronger in the Raman than in the i.r., these are assigned as fundamentals of a second isomer rather than as overtones or combinations. Unfortunately the lack of low temperature Raman data prevents rigorous assignment in terms of the fundamental modes of one isomer.

Can. J. Chem. Downloaded from www.nrcresearchpress.com by 210.87.254.6 on 09/05/12
For personal use only.

Can. J. Chem. Downloaded from www.nrcresearchpress.com by 210.87.254.6 on 09/05/12
For personal use only.

Discussion

When the liquid and solid state infrared spectra (Figs. 1 and 2) of methyl cyanoacetate are compared, two features are immediately apparent. First, the spectrum of the solid is much better defined than that of the liquid. Most of the bands in the spectrum of the liquid are broad and unresolved whereas those obtained in the solid state are sharp and well resolved. Secondly, two reasonably strong bands (1269 and 845 cm^{-1}) essentially disappear on crystallization, a typical effect when a substance exists as a mixture of conformational isomers in the liquid state, but as only one conformer in the solid. Further, the Raman spectra of both the light and heavy compounds contain far more bands than can be explained on the basis of one conformer only. Evidence for the existence of a conformational equilibrium brought about by rotation about the carbonyl carbon – ether oxygen bond in esters has been sought by many workers. These efforts have been recently reviewed by Jones and Owen (6). Only very recently has such an equilibrium mixture been reported for a methyl ester (7), and all indications are that the *cis* ester structure is considerably more stable than the *trans* in all esters other than possibly those in which a tertiary butyl structure is bonded to the oxygen atom. On the other hand, conformational equilibria resulting from rotation about the carbon–carbon single bond adjacent to a carbonyl group is well known. Mizushima (8) summarizes the early work with such compounds as chloroacetyl chloride and chloroacetone and shows that the stable forms are those in which a substituent on the alpha carbon atom eclipses the carbonyl oxygen atom, or nearly so, leading to *trans* and *gauche* isomers. Such structures of the conformers have been more recently proposed for acyl halides (9), substituted ethyl acetates (6, 10), chloro- and bromoacetaldehydes (11, 12) and bromo-, fluoro- and iodoacetone (13, 14). In all cases, the more stable conformer is that one with the bulky group *trans* to the second carbonyl substituent (*cis* to the carbonyl oxygen atom).

The liquid phase of methyl cyanoacetate therefore is probably a complex equilibrium between four conformers, two differing by rotation about the carbon–carbon bond and two differing by rotation about the carbon–oxygen bond. By analogy with other molecules possessing these structural features, we would certainly expect that the most stable structure, and that possessed by crystalline methyl cyanoacetate, is that in which the CN group eclipses the carbonyl oxygen (*trans* carbon–carbon structure), as does the methyl group (*cis* ester structure).

We wish to thank Dr. G. L. Carlson of Carnegie-Mellon University for the use of his Raman spectrometer.

1. J. K. Wilmshurst. J. Mol. Spectrosc. **1**, 201 (1957).
2. J. Susi and T. Zell. Spectrochim. Acta, **19**, 1933 (1963).
3. W. R. Feairheller, Jr. and J. E. Katon. J. Mol. Struct. **1**, 239 (1967–68).
4. J. E. Katon and M. G. Griffin. J. Chem. Phys. **59**, 5868 (1973).
5. Deepali Sinha and J. E. Katon. Appl. Spectrosc. **26**, 599 (1972).
6. G. I. L. Jones and N. L. Owen. J. Mol. Struct. **18**, 1 (1973).
7. J. E. Katon and M. D. Cohen. Can. J. Chem. **52**, 1994 (1974).
8. S. Mizushima. Structure of molecules and internal rotation. Academic Press, Inc., New York. 1954.
9. J. E. Katon and W. R. Feairheller Jr. J. Chem. Phys. **44**, 144 (1966).
10. T. L. Brown. Spectrochim. Acta, **18**, 1615 (1962).
11. G. J. Karabatsos and D. J. Fenoglio. J. Am. Chem. Soc. **91**, 1124 (1969).
12. G. Lucazeau and A. Novak. J. Chim. Phys. **67**, 1614 (1970).
13. G. A. Crowder and B. R. Cook. J. Chem. Phys. **47**, 367 (1967).
14. B. R. Cook and G. A. Crowder. J. Chem. Phys. **47**, 1700 (1967).

The Kinetics of the Water–Gas Shift Reaction on Nickel(II) Oxide Catalysts in the Néel Temperature Region

BORDAN WALTER KRUPAY AND ROBERT ANDERSON ROSS

Department of Chemistry, Lakehead University, Thunder Bay "P", Ontario P7B 5E1

Received February 25, 1974

Can. J. Chem. Downloaded from www.nrcresearchpress.com by 210.87.254.42 on 09/05/12
For personal use only.

BORDAN WALTER KRUPAY and ROBERT ANDERSON ROSS. Can. J. Chem. **52**, 3063 (1974).

The water–gas shift reaction has been studied from 200 to 300 °C at atmospheric pressure on both black and green forms of nickel(II) oxide which contrast in their magnetic properties and stoichiometry. Whereas black oxide samples, prepared in various ways, exhibited activation energies of 23 ± 1 kcal mol^{-1} throughout the temperature interval, the green oxides were characterized by a change in activation energy from 20 ± 1 kcal mol^{-1} above 250 °C to between 10 and 15 kcal mol^{-1} below this temperature. These values were obtained with a standard water–gas mixture of 40 Torr carbon monoxide and 40 Torr water vapor. With a carbon monoxide partial pressure of 80 Torr the green oxide gave a monotonic value of 21 ± 1 kcal mol^{-1}.

Rate order data suggest that the rate-limiting process does not change on the black oxides in this temperature interval, whereas on the green oxides rate control is probably associated with the surface reactivity of carbon monoxide above 250 °C and water vapor below this temperature. These effects may be related to different forms of active surface oxygen species that are present on the green oxide samples above and below the Néel temperature region.

BORDAN WALTER KRUPAY et ROBERT ANDERSON ROSS. Can. J. Chem. **52**, 3063 (1974).

On étudie la réaction d'équilibre du système eau–gaz de 200 à 300 °C à pression atmosphérique sur les deux formes noire et verte de l'oxyde de nickel(II) qui contrastent dans leurs propriétés magnétiques et stoechiométriques. Tandis que des échantillons d'oxyde noir, préparés par différents procédés, présentent des énergies d'activation de 23 ± 1 kcal mol^{-1} sur tout l'intervalle de température; par ailleurs les oxydes verts sont caractérisés par un changement de l'énergie d'activation qui varie de 20 ± 1 kcal mol^{-1} au-dessus de 250 °C à entre 10 et 15 kcal mol^{-1} au-dessous de cette température. On obtient ces valeurs en utilisant un mélange standard contenant 40 Torr de monoxyde de carbone et 40 Torr de vapeur d'eau. Avec une pression partielle de 80 Torr de monoxyde de carbone, l'oxyde vert donne une valeur constante de 21 ± 1 kcal mol^{-1}.

On suggère d'après les données de l'ordre de la réaction que l'étape déterminante de la réaction ne change pas pour les oxydes noirs dans cet intervalle de températures, tandis que, pour les oxydes verts, le contrôle de la vitesse est probablement lié à la réactivité superficielle du monoxyde de carbone au-dessus de 250 °C et à la vapeur d'eau au-dessous de cette température. Ces influences peuvent être reliées aux différentes formes des espèces d'oxygène sur la surface active qui sont présentes sur les échantillons d'oxyde vert au-dessus et au-dessous de la région de températures de Néel. [Traduit par le journal]

Introduction

In a recent study (1) of the kinetics and mechanism of the water–gas shift reaction on manganese(II) oxide, a change in the activation energy of the reaction was observed around 340 °C, which corresponds closely to the Curie temperature of the oxide, and it was proposed that the change was associated with the type of surface oxygen species most active during the different stages of the temperature cycle. Previously, variations of catalytic activity have been reported in the temperature region of magnetic transitions (2–6) especially for nickel oxides (2, 5–9). Studies of hydrogen oxidation (6), carbon monoxide oxidation (3, 10), and oxygen adsorption rates (11) have also been made. These variations have been related to the magnetic properties of the oxides. Hence it was felt that nickel(II) oxide catalysts presented a suitable model system to use in a study of the kinetics of the water–gas shift reaction, especially since the oxide can be prepared in both green and black forms which have associated differences in their stoichiometry as well as their magnetic properties.

This paper reports the results of a study of the water–gas shift reaction between 200 and 300 °C using a range of nickel(II) oxide catalyst

preparations with attention given to the possible relationships between catalytic activities and the surface condition and established magnetic properties of the oxides.

Experimental

Apparatus and Procedure

The all-glass flow system and quartz reactor were described previously (12, 13). High-purity helium was used as the carrier gas at atmospheric pressure in the flow system and in the Beckman GC-5 gas chromatograph. Carbon monoxide, water, and carbon dioxide were analyzed by a thermal conductivity bridge using stainless-steel columns, 120 × 0.125 in., o.d., packed with Poropak Q, 100–120 mesh, at 100 °C.

Surface areas were determined by low temperature krypton adsorption (B.E.T.; −196 °C; $\sigma = 21.5$ Å^2).

Experimental conditions were established in the usual manner (12) such that the reaction was studied in the regime of chemical kinetics. Measurements were conducted at a total gas flow rate of 350 ml min^{-1} normal temperature and pressure (n.t.p.) which was equivalent to a range of space velocities from 12.9 to 15.6 (cc gas) (cc catalyst)$^{-1}$ s^{-1} between 200 and 300 °C.

All reaction rate measurements were made after the steady catalyst activity levels were attained and experimental rates were determined from the rates of carbon dioxide production.

Materials

The black and green forms of nickel(II) oxide were prepared by calcining nickel(I) carbonate (Baker; >99.9% pure) in air at 400 °C for 3 h and 800 °C for 5 h, respectively. Complete decomposition of the carbonate was confirmed by thermogravimetric analysis in air using a Stanton–Redcroft Thermobalance Model HT5A. The maximum rate of decomposition was observed at 360 °C. The black and green forms had surface areas of 96 and 7 m^2 g^{-1}, respectively.

In all experiments, 0.5 g of the black or 7.0 g of the green oxide was used after pretreatments at 200 °C in the standard water–gas stream of 350 ml min^{-1} (n.t.p.) helium containing 40 Torr carbon monoxide and 40 Torr water vapor. From the results of nickel analysis by atomic absorption spectroscopy, the black catalyst samples contained excess oxygen to a maximum level of 3 g-atom %.

Carbon monoxide (C.P.; 99.5% minimum) and helium (high purity; 99.995%) were supplied by Matheson of Canada Ltd. The water in the gas saturators was deionized and boiled prior to use.

Results

From a previous publication (14) on the water–gas shift reaction on various first-row transition metal oxides and their chromites, it was noted that cobalt and nickel oxides were reduced to the metals by carbon monoxide. Hence preliminary experiments were conducted to establish if such bulk reduction could be avoided. Thus, the reaction of the standard water–gas mixture on black nickel(II) oxide was studied at temperatures below 300 °C when conversions were less than 3% and no metallic phase could be detected by either X-ray powder diffraction or X-ray diffractometry. In all cases, the physical appearance and the surface area of the samples were the same before and after catalysis.

The Effect of Water–Gas Components on Catalyst Activity

The effects of components of the water–gas mixture were studied at 250 °C on black oxide samples which had been equilibrated in the standard water–gas mixture. Exposing these subsequently to a mixture of 120 Torr carbon monoxide and 40 Torr water vapor for 0.5 h followed by the standard water–gas mixture showed a 36% increase in the rate of reaction 15 min later which then remained at a constant level. Such reduced samples were oxidized more slowly by water vapor, 215 min, than by air, 60 min, as shown by the return of the shift reaction rate to its original level prior to reduction. These experiments indicated that the catalyst activity was influenced by changes in the surface stoichiometry which was affected by the amount of excess carbon monoxide in the reacting gas mixture and that such changes in surface composition were reversible.

Equilibrated catalyst samples exposed to 120 Torr carbon monoxide and 40 Torr water vapor for 60 min at 250 °C showed a 38% increase in steady activity after 15 min when followed by the standard water–gas mixture. By cycling the temperature of the reduced sample to 300 °C for 0.5 h and then to 250 °C, the rate of reaction was found to have increased to 55% above the initial activity level. X-Ray diffractometry did not show the presence of any metallic phase in any of these catalyst samples. Also, the increased rate of reaction after thermal cycling returned to the initial catalytic activity of the equilibrated surface if the samples were exposed to either water vapor for 5 h or air for 0.5 h at 250 °C. Thus, the surface stoichiometry was sensitive to temperature as well as the reacting-gas composition.

Kinetic Experiments

(1) Black Nickel(II) Oxide

Catalysts Equilibrated in the Standard Water–Gas Mixture:—Black oxide samples, designated

Can. J. Chem. Downloaded from www.nrcresearchpress.com by 210.87.254.42 on 09/05/12
For personal use only.

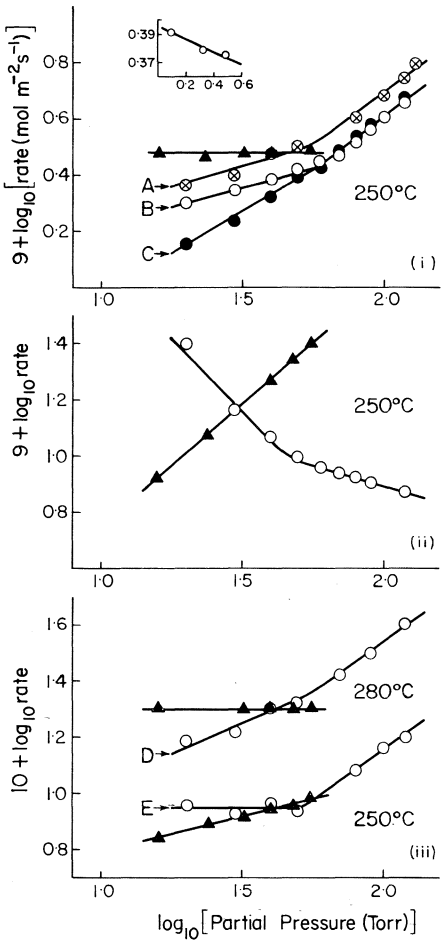

FIG. 1. Reaction rate dependency on variations in the partial pressures of carbon monoxide: (*i*) black nickel(II) oxide at 250 °C; A, NiO(ES1) (⊗); B, NiO(ES2) (○); C, NiO(FS) (●); inset: effect of carbon dioxide on reaction rate; (*ii*) NiO(RS) (○); (*iii*) green nickel(II) oxide at 280 (D) and 250 °C (E); and water-vapor (▲) partial pressure in (*i*), (*ii*), and (*iii*). (For experimental details, see text.)

NiO(ES1), were equilibrated for 2 h at 250 °C in the standard gas mixture and the rate order for water vapor was then determined from 16 to 56 Torr while the carbon monoxide partial pressure was maintained at a constant 40 Torr. Figure 1(*i*), curve A, shows that the water-vapor rate order was zero in this partial pressure range.

The rate order with respect to carbon dioxide partial pressure was studied in a narrow partial pressure range corresponding to the limit of 5% set on the experimental conversion percentage while maintaining both carbon monoxide and water-vapor partial pressures constant at 40 Torr. In the partial pressure range 1 to 3 Torr, rate inhibition by carbon dioxide was indicated by an order of −0.4 (inset of Fig. 1(*i*)).

The carbon monoxide rate order was determined from 20 to 130 Torr carbon monoxide partial pressure while maintaining the water-vapor partial pressure constant at 40 Torr (Table 1). A change in the order with respect to carbon monoxide was observed at 60 Torr. In the partial pressure range 20 to 60 Torr the order was 0.4, which changed to 0.8 between 60 and 130 Torr (Fig. 1(*i*)).

Fresh Catalysts:—Carbon monoxide rate orders were determined at 250 °C on fresh samples of black nickel(II) oxide which had not been pretreated in the standard water–gas mixture. The samples, designated NiO(FS), were initially exposed to a gas mixture consisting of 20 Torr carbon monoxide and 40 Torr water vapor until the steady catalyst activity level was attained. The carbon monoxide partial pressure was then increased stepwise from 20 to 120 Torr while the water-vapor partial pressure was held constant at 40 Torr. The results are shown in Fig. 1(*i*) and Table 1.

The same catalyst samples, designated as NiO(ES2), were then pretreated in the standard water–gas mixture until the onset of steady catalytic activity and the rate order for carbon monoxide was again determined from 20 to 120 Torr at 250 °C (Fig. 1(*i*)).

In separate experiments, NiO(ES1) and NiO(ES2) samples were exposed to 100 ml min^{-1} (n.t.p.) air at 250 °C for 3 h to determine if the behavior of NiO(FS) would be re-established. In both cases, the carbon monoxide rate orders, determined in the same manner as on NiO(FS), were identical to those for NiO(ES1) and NiO(ES2).

Reduced Catalysts:—Carbon monoxide rate orders were determined at 250 °C on the reduced catalyst samples, NiO(RS) (Fig. 1(*ii*) and Table 1).

(2) Green Nickel(II) Oxide

Rate orders were determined at 280 and 250 °C after catalysts had been stabilized at each of these temperatures in the standard mixture for 90 min. The variations in rate orders shown by the black oxide samples were not exhibited in these experiments (Fig. 1(*iii*) and Table 1). Since the maximum conversion was 1.6%,

Can. J. Chem. Downloaded from www.nrcresearchpress.com by 210.87.254.42 on 09/05/12
For personal use only.

TABLE 1. Reaction rate order results for the water–gas shift reaction on nickel(II) oxides: rate of reaction, r (mol m^{-2} s^{-1}) = $kp_{CO}{}^{x}p_{H_2O}{}^{y}p_{CO_2}{}^{z}$

Component	Catalyst	Temperature (°C)	Pressure range (Torr)	x	y	z
Carbon monoxide (p_{H_2O} = 40 Torr)	Green NiO	280	20–50	0.5	—	—
			50–120	0.7	—	—
	Green NiO	250	20–50	0.0	—	—
			50–120	0.7	—	—
	NiO(ES1, ES2)	250	20–60	0.4	—	—
			60–130	0.8	—	—
	NiO(FS)	250	20–60	0.6	—	—
			60–120	0.8	—	—
	NiO(RS)	250	20–50	−0.8	—	—
			50–120	−0.3	—	—
Water (p_{CO} = 40 Torr)	Green NiO	280	16–56	—	0.0	—
	Green NiO	250	16–56	—	0.3	—
	NiO(ES1, ES2)	250	16–56	—	0.0	—
	NiO(RS)	250	16–56	—	0.9	—
(p_{CO} = 80 Torr)	Green NiO	250	16–56	—	0.0	—
Carbon dioxide (p_{CO} = p_{H_2O} = 40 Torr)	NiO(ES1, ES2)	250	1–3	—	—	−0.4

accurate rate orders with respect to carbon dioxide could not be obtained. However, it was assumed that the desorption of carbon dioxide would readily occur as the ability of nickel(II) oxides to desorb carbon dioxide increases progressively from the black to the green forms (17, 18).

The reaction rate, r (mol m^{-2} s^{-1}), can be represented for catalysis on all nickel(II) oxide samples as

$$[1] \qquad r = kp_{CO}{}^{x}p_{H_2O}{}^{y}p_{CO_2}{}^{z}$$

The values of the exponents x, y, and z are shown in Table 1.

The Effect of Temperature on the Reaction Rate

Rate measurements were recorded after the catalysts had been equilibrated at 200 °C in the standard water–gas mixture for 120 min. Steady activity levels were established after 60 min exposure. These levels were verified at several fixed temperatures in separate tests when the variation of reaction rate was within 0.5% after exposure for several hours.

The reaction rate was determined at various temperatures from 200 to 300 °C, 300 to 200 °C, and again from 200 to 300 °C in stepwise increments between 4 and 10 °C.

Rate constants were computed from eq. 1 with component concentrations in mol l^{-1}. The Arrhenius plots are shown in Fig. 2. Black nickel(II) oxides gave an activation energy value of 23 ± 1 kcal mol^{-1} throughout the temperature range while green nickel(II) oxides were characterized by a change in activation energy from 20 ± 1 kcal mol^{-1} above about 250 °C to

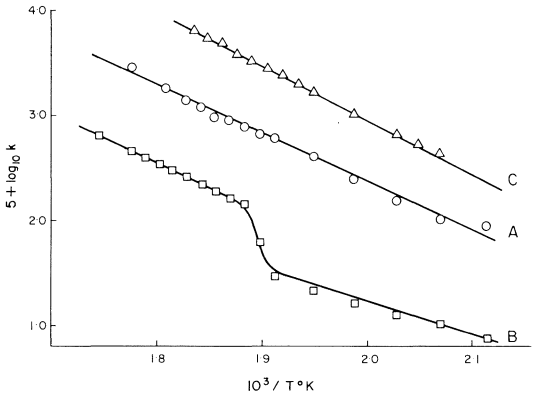

FIG. 2. Arrhenius plots of the rate constants of the water–gas shift reaction on nickel(II) oxides: A, black nickel(II) oxide; B, green nickel(II) oxide (A and B determined with the standard gas mixture); C, green nickel(II) oxide with 80 Torr carbon monoxide and 40 Torr water vapor.

Can. J. Chem. Downloaded from www.nrcresearchpress.com by 210.87.254.42 on 09/05/12
For personal use only.

Can. J. Chem. Downloaded from www.nrcresearchpress.com by 210.87.254.42 on 09/05/12
For personal use only.

between 10 and 15 kcal mol^{-1} below this temperature.

In separate experiments, samples of green oxide were exposed to 80 Torr carbon monoxide and 40 Torr water vapor and a monotonic activation energy of 21 ± 1 kcal mol^{-1} was determined throughout the temperature interval (Fig. 2). The reaction rate was found to be independent of water-vapor partial pressure at 250 °C in contrast to the results obtained using the standard water–gas mixture.

Discussion

Studies of the water–gas shift reaction have tended to focus mainly on technological aspects concerned with iron oxide based catalysts (19). On pure iron(III) oxide a mechanism involving respective reaction of components with oxidized and reduced sites (20) has been proposed and interpreted to proceed via a two-step alternating oxidation–reduction scheme on an iron(III) oxide catalyst promoted with chromium oxide (20) and via a concerted redox process on iron – chromium oxide (21) and copper chromite (22). At the same time variations of kinetic expressions and mechanisms for the water–gas shift reaction on industrial iron oxide based catalysts have been attributed to factors such as changing surface composition, the presence of H_2S impurities, nonisothermal conditions, and surface diffusion (19).

On manganese(II) oxide, a Langmuir–Hinshelwood mechanism was proposed (1) for the shift reaction and the surface process was interpreted to proceed via alternating oxidation and reduction of the reactants on specific sites.

The present kinetic data were analyzed by application of the Langmuir, Freundlich, and Temkin adsorption isotherms (15, 16). For the Freundlich case, the relationship between the reaction rate and the surface coverage of carbon monoxide, θ_{CO}, can be expressed (16) in terms of the carbon monoxide rate order data, in which all other components are maintained at fixed concentration, as

$$[2] \qquad r = k^1\theta_{CO}$$

or

$$[3] \qquad \frac{1}{\ln (r/k^1)} = \frac{1}{\ln c} - \frac{a}{\ln c} \ln p_{CO}$$

where $a = RT/\Delta H_a$, and $-\Delta H_a$ is the heat of adsorption at surface coverage, θ. Thus a plot of $1/\log_{10} (r/k^1)$ *vs.* $\log_{10} p_{CO}$ should be linear over the entire carbon monoxide partial pressure range studied.

The results for fresh and equilibrated samples of black nickel(II) oxide, NiO(FS), NiO(ES1), and NiO(ES2), conformed to this relationship (Fig. 3). It may be noted also that plots of $1/\log_{10} r$ *vs.* $\log_{10} p_{CO}$ were also linear and this procedure provided a useful and rapid test of the results. Equations, similar to eq. 3, were derived from the Langmuir (1) and Temkin adsorption isotherms (15, 16) but the results did not give a linear relationship for any of these samples. The applicability of the Freundlich adsorption isotherm suggests that reaction occurs on surface sites of a heterogeneous character, which is consistent with conclusions derived from oxygen isotopic exchange studies and calorimetric measurements (23, 24). With equilibrated black nickel(II) oxide samples the reversibility in reduction by carbon monoxide and the oxidation by either water vapor or air

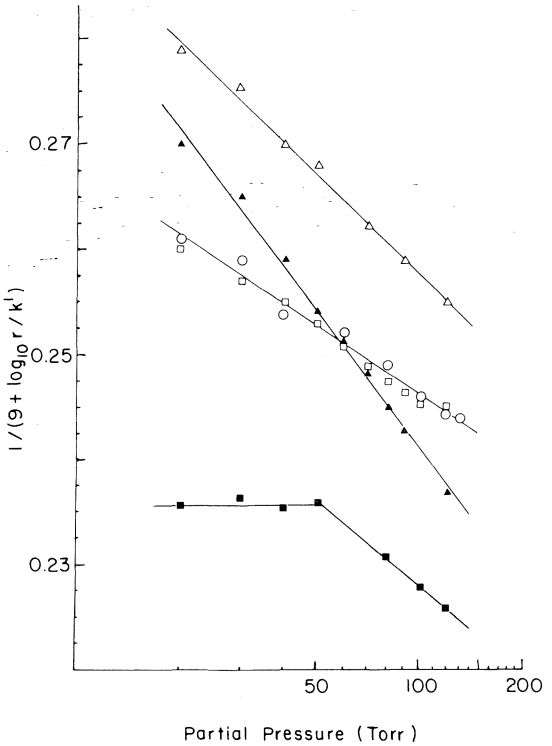

FIG. 3. Plots of carbon monoxide rate order data according to eq. 3. Black nickel(II) oxide at 250 °C. (○), NiO(ES1); (□), NiO(ES2); and (▲), NiO(FS). Green nickel(II) oxide at 280 °C (△) and 250 °C (■).

suggests that reaction occurs by a redox process

[4] $CO(ads) + [O] \rightarrow CO_2(ads)$

[5] $CO_2(ads) \rightarrow CO_2(g) + [\ ]$

[6] $H_2O(ads) + [\ ] \rightarrow H_2(g) + [O]$

consistent with rate inhibition by carbon dioxide (inset of Fig. 1(*i*)).

On NiO(RS), pretreatment with carbon monoxide rich gas mixtures would be expected to deplete much of the excess surface oxygen (25) creating a surface of homogeneous character which is consistent with the linear relationship established between the reaction rate and surface coverage assuming Langmuirian behavior (Fig. 4). Lattice oxygen would then become the predominant adsorption site for carbon monoxide and if water vapor interacts dissociatively with the catalyst surface, that is by the formation of surface hydroxyl groups (26) involving a lattice anion, then competitive adsorption with carbon monoxide might be anticipated (Fig. 1(*ii*)). Carbon monoxide could effectively block these sites to water dissocation which would be consistent with the observed rate order values.

The catalytic behavior of black nickel(II) oxide samples (Figs. 1, 3, and 4) shows trends similar to those observed in the oxidation of hydrogen (25) where surface stoichiometry had a critical influence on the results.

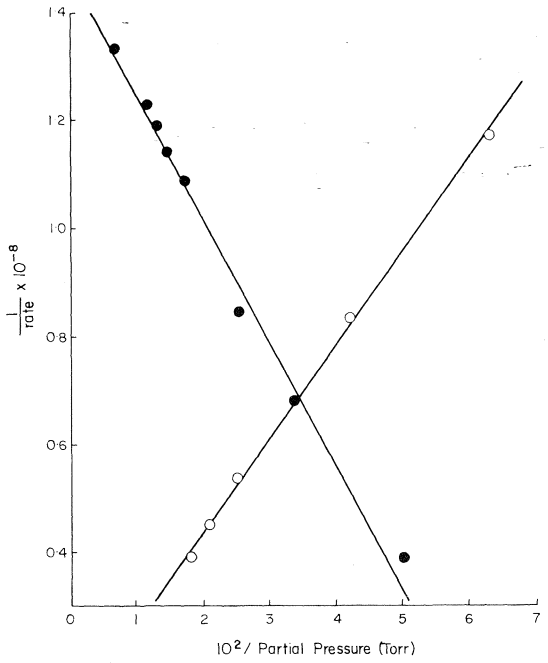

FIG. 4. Relationship between reaction rate and the partial pressures of carbon monoxide (●) and water vapor (○) according to the Langmuir isotherm at 250 °C on NiO(RS).

Correlations between the reaction rate and carbon monoxide surface coverage for catalysis on the green oxides were obtained using eq. 3 (Fig. 3), while the rate order data suggest that a change in the rate-determining step may occur at about 250 °C (Table 1). Further, the activation energy for catalysis on green nickel(II) oxide samples exposed to the standard gas mixture also changes at about this temperature which lies in the Néel temperature range of the oxide (27) where the transition from antiferro- to paramagnetism occurs. This transition has been reported (27) to take place between 220 and 260 °C for green oxides while particle size affects the value for black oxide samples such that temperatures near 200 °K have been observed with fine powders (28).

Variations in the catalytic and chemisorptive properties of nickel oxide (2, 5–11) have been observed at the Néel temperature, as well as changes in crystallographic and magnetic properties (29). In particular, the magnetic state of nickel oxide has been correlated with the nature of the adsorption forms of the surface oxygen (11) in studies of carbon monoxide oxidation and these correlations used to explain differences in catalytic behavior which have also been observed in the oxidation of hydrogen (5, 6). The present results are in good agreement with these previous studies (Fig. 2).

The different values for the rate orders observed with the green oxides above and below about 250 °C (Fig. 1(*iii*) and Table 1) are believed to be connected with a switch in rate control from a step associated with the surface adsorptivity and reactivity of carbon monoxide to one connected with water vapor. This phenomenon probably has its source in the change which occurs in metal-to-oxygen bond strength in the oxide (2, 11, 30) at the Néel temperature which has consequences on the nature and reactivity of the surface oxygen species. Further, rates measured on green oxide samples exposed to a reaction mixture containing excess carbon monoxide gave a monotonic Arrhenius plot (Fig. 2, curve C) which is in agreement with the latter proposal since at and below 250 °C the reaction rate was independent of water-vapor partial pressure. This feature may be the con-

Can. J. Chem. Downloaded from www.nrcresearchpress.com by 210.87.254.42 on 09/05/12
For personal use only.

sequence of the depletion of much of the reactive surface oxygen (25) species by the carbon monoxide, thus altering the surface stoichiometry as observed previously in calorimetric studies on this system (24).

We thank Dr. D. G. Klissurski and Dr. D. Dollimore for helpful suggestions and Mr. S. Spivak for drafting assistance.

1. B. W. KRUPAY and R. A. ROSS. Can. J. Chem. **51**, 3520 (1973).
2. A. CIMINO, E. MOLINARI, and G. ROMEO. Z. Phys. Chem. N. F. **16**, S101 (1958).
3. G. PARRAVANO. (*a*) J. Chem. Phys. **20**, 342 (1952); (*b*) J. Am. Chem. Soc. **15**, 1448, 1497 (1953).
4. G. M. SCHWAB and M. GOETZELER. Z. Phys. Chem. N. F. **2**, 1 (1954); **4**, 148 (1955).
5. D. MEHANDJEV and G. BLIZNAKOV. Proc. 3rd Int. Congr. Catal. Amsterdam, 1964. Elsevier Publishing Co. Amsterdam. 1965. p. 781.
6. D. McC. JAMIESON, D. G. KLISSURSKI, and R. A. ROSS. Z. Anorg. Allg. Chem. In press.
7. B. DELMON and A. ROMAIN. J. Chem. Soc. Faraday Trans. 1, **69**, 941 (1973).
8. F. S. STONE. Adv. Catal. **13**, 1 (1962).
9. P. GRAVELLE and S. J. TEICHNER. Adv. Catal. **20**, 167 (1969).
10. G. K. BORESKOV, V. I. MARSHNEVA, and V. D. SOKOLOVSKII. Kinet. Catal. **13**, 1086 (1972); M. E. DRY and F. S. STONE. Discuss. Faraday Soc. **28**, 192 (1959); E. R. S. WINTER. Discuss. Faraday Soc. **28**, 216 (1959).
11. E. R. S. WINTER. J. Catal. **6**, 35 (1966).
12. R. A. ROSS and B. G. WALSH. J. Appl. Chem. **11**, 469 (1961).
13. A. B. HART, J. MCFADYEN, and R. A. ROSS. Trans. Faraday Soc. **59**, 1458 (1963).
14. G. K. BORESKOV, V. A. CHIRGINA, L. S. EGOROVA, V. V. POPOVSKII, and T. M. YUR'EVA. Kinet. Catal. **12**, 116 (1971).
15. G. HALSEY and H. S. TAYLOR. J. Chem. Phys. **15**, 624 (1947); G. HALSEY. Adv. Catal. **4**, 259 (1952).
16. G. C. BOND. Catalysis by metals. Academic Press, New York and London. 1962. pp. 65–103; A. CLARK. The theory of adsorption and catalysis. Academic Press, New York and London. 1970. pp. 239–271.
17. G. K. BORESKOV, YU. D. PANKRAT'EV, and V. V. POPOVSKII. Kinet. Catal. **13**, 1101 (1972).
18. J. KONDO, T. UCHIJIMA, and Y. YONEDA. Bull. Chem. Soc. Jap. **40**, (Part 1), 1040 (1967).
19. H. BOHLBRO. An investigation on the kinetics of the conversion of carbon monoxide with water vapour over iron oxide based catalysts. Gjellerup, Copenhagen. 1969.
20. N. V. KULKOVA and M. I. TEMKIN. Zhur. Fiz. Khim. **23**, 695 (1949).
21. G. K. BORESKOV, A. S. SERGEEVA, and T. M. YUR'EVA. Kinet. Catal. **11**, 1476 (1970).
22. G. K. BORESKOV, V. SH. GRUVER, and T. M. YUR'EVA. Kinet. Catal. **10**, 862 (1969).
23. W. M. H. SACHTLER and J. H. DE BOER. Proc. 3rd Int. Congr. Catal., Amsterdam, 1964. Vol. 1. Elsevier Publishing Co. Amsterdam. 1965. p. 252.
24. YU. D. PANKRAT'EV, N. P. KEIER, V. I. SOLOV'EV, and G. V. GRIDASOVA. Kinet. Catal. **11**, 1061 (1970).
25. G. K. BORESKOV, E. A. MAMEDOV, and V. V. POPOVSKII. Kinet. Catal. **13**, 125 (1972); Dokl. Akad. Nauk S.S.S.R. Phys. Chem. **197**, 243 (1971).
26. E. R. S. WINTER. J. Chem. Soc. A, 2889 (1968).
27. Y. SHIMOMURA and I. TSUBOKAWA. J. Phys. Soc. Jap. **9**, 19 (1954).
28. J. T. RICHARDSON and W. O. MILLIGAN. Phys. Rev. **102**, 1289 (1956).
29. G. A. SLACK. J. Appl. Phys. **31**, 1571 (1960); A. P. CRACKNELL and S. J. JOSHUA. Proc. Cambridge Phil. Soc. **66**, 493 (1969).
30. G. BLIZNAKOV, D. MEKHANDZHIEV, and B. D'YAKOVA. Kinet. Catal. **9**, 269 (1968).

Can. J. Chem. Downloaded from www.nrcresearchpress.com by 210.87.254.42 on 09/05/12
For personal use only.

Structure of a Phosphonomannan, as Determined by the Effect of Lanthanide Ions on Its Carbon-13 Magnetic Resonance Spectrum[1]

PHILIP A. J. GORIN AND MYTOSK MAZUREK

Prairie Regional Laboratory, National Research Council of Canada, Saskatoon, Saskatchewan S7N 0W9

Received December 17, 1973

PHILIP A. J. GORIN and MYTOSK MAZUREK. Can. J. Chem. **52**, 3070 (1974).

The carbon-13 magnetic resonance spectrum of phosphonomannan **2** in deuterium oxide expands on addition of europium and praseodymium chlorides. With the aid of a parallel study on structurally related α-D-mannose-1-phosphate and α-D-mannose-6-phosphate the signal displacements were interpreted in terms of chemical structure. Both ions cause predominantly contact shifts, and in general addition of praseodymium ion produces a downfield shift of the ^{13}C.m.r. signal of the esterified ^{13}C nucleus, which is accompanied by a smaller downfield shift of that of the adjacent carbon. Europium ion produces smaller and approximately equal shifts of signals of the corresponding α-^{13}C and β-^{13}C nuclei, but in the opposite direction and with less broadening. Displacements produced by neodymium chloride were comparable in size and downfield. Other lanthanide chlorides, namely those of ytterbium, holmium, neodymium, and gadolinium, broadened the signal of the ^{13}C nucleus attached to the phosphodiester group without displacement. Changes produced in proton nuclear magnetic resonance spectra of the phosphates and phosphodiester **2** are more difficult to interpret in terms of structure.

PHILIP A. J. GORIN et MYTOSK MAZUREK. Can. J. Chem. **52**, 3070 (1974).

Le spectre de résonance magnétique du carbone 13 du phosphonomannane **2** en solution dans le D_2O est étalé lorsqu'on y ajoute des chlorures d'europium et de praséodymium. A l'aide d'une étude parallèle sur l'α-D-mannose phosphate-1 et l'α-D-mannose phosphate-6 qui lui sont reliés au point de vue structure, on a pu interpréter les déplacements de signaux en terme de structure chimique. Les deux ions causent principalement des déplacements par contact et d'une façon générale l'addition d'ions praséodymes produit un déplacement vers les bas champs des signaux r.m.n. du C^{13} du carbone estérifié qui est accompagné par un déplacement plus petit vers les bas champs du carbone qui lui est adjacent. L'ion europium produit des déplacements plus petits et approximativement égaux de signaux correspondants des carbones α et β du noyau; les déplacements sont toutefois dans des directions opposées et se font avec moins d'élargissement des bandes. Les déplacements produits par le chlorure de néodyme étaient ous les bas champs et à pen près de la même grandeur. D'autres chlorures de lanthanide, à savoir ceux de l'itterbium, de l'holmium, de néodymium et de gadolinium, élargissent les signaux du carbone 13 attaché au groupe phosphodiester et ceci sans déplacement. Les changements produits dans le spectre de résonance magnétique nucléaire du proton des phosphates et du phosphodiester **2** sont plus difficiles à interpréter en termes de structure.

The yeast *Hansenula capsulata* produces an exocellular phosphonomannan which was originally assigned structure **1** (Fig. 1). The position of the phosphodiester link was based on the production of formaldehyde on periodate oxidation of the mannobiose phosphate obtained by acidic cleavage of the C-6-orthophosphate linkage (1). On the other hand, carbon-13 magnetic resonance (^{13}c.m.r.) studies on the mannobiose phosphate favored structure **2** (Fig. 1), which has repeating units of 2-*O*-β-D-mannopyranosyl-α-D-mannopyranose joined by (1→6)-linked phosphodiester (2). The present study concerns the expansion of the ^{13}c.m.r. spectrum of the polymer that is observed on addition of chlorides of europium and praseodymium and the interpretation of the signal displacements that leads to a confirmation of structure **2**.

Recently, Birdsall *et al.* (3) observed that the ^{13}c.m.r. spectrum of aqueous α,β-D-ribose-5-phosphate contains signals that change their relative positions on addition of europium ion. Presumably this is due to two effects, one caused by complexing with the phosphate group and the other caused by complexing with OH-1, OH-2, and OH-3 of the α-anomer. Phosphate–Eu^{3+} interactions have also been demonstrated by Barry *et al.* (4) since addition of europium ion to a solution of 9-β-D-ribofuranosyladenine-5′-phosphate in deuterium oxide resulted in a strong upfield shift of the H-5′ signal in the proton spectrum. Strong interactions by lanthanide ions

[1]NRCC No. 14078.

Can. J. Chem. Downloaded from www.nrcresearchpress.com by 210.87.254.40 on 09/05/12
For personal use only.

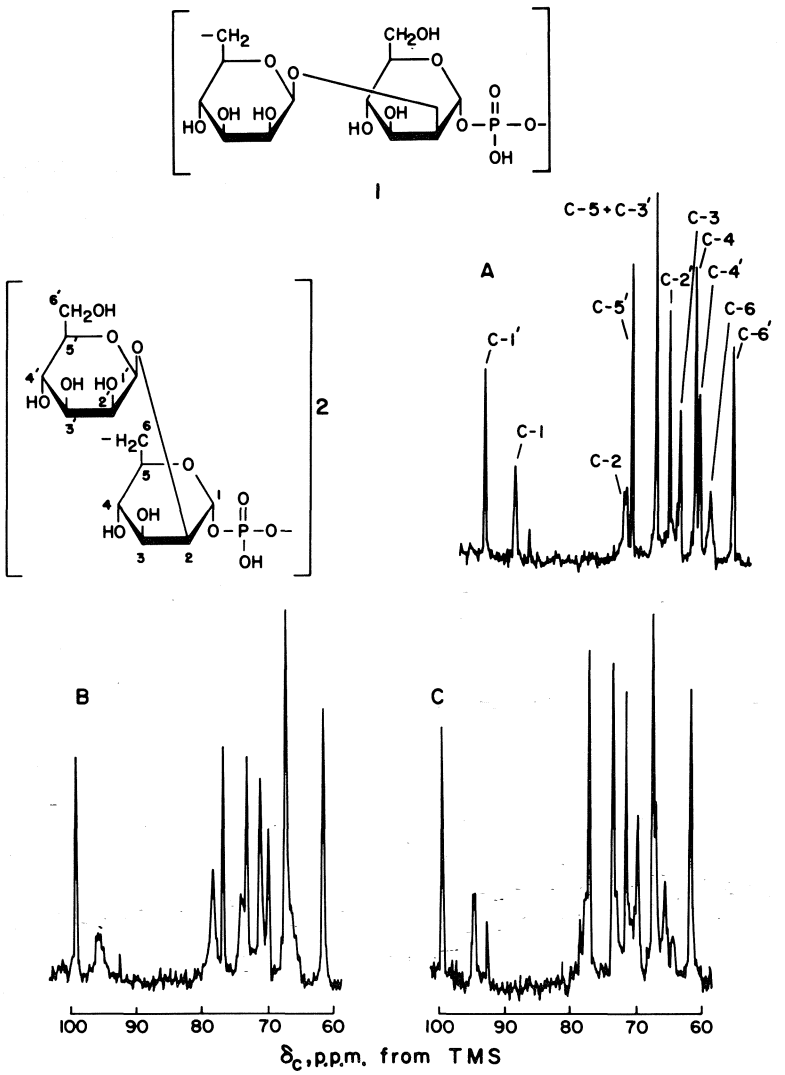

FIG. 1. Structure of phosphonomannan from *Hansenula capsulata* **2** and its ^{13}c.m.r. spectra, before and after addition of lanthanide ion. Spectrum A: **2** (80 mg) in D_2O (2 ml). Spectrum B: after addition of $PrCl_3 \cdot 6H_2O$ (7 mg). Spectrum C: after addition of $EuCl_3 \cdot 6H_2O$ (14 mg).

and hydroxyl groups occur since improved and modified proton spectra have been obtained from methyl-β-D-hammamelopyranoside on addition of praseodymium chloride or europium nitrate (5). However, this type of complexing would not be expected to take place in the unesterified mannopyranose series since the stereochemistry appears unsuitable.

The exocellular phosphonomannan of *H. capsulata* forms a very viscous aqueous solution (6) and it was necessary to partially degrade it with hot aqueous 1% potassium hydroxide prior to spectral examination. Since the ^{13}c.m.r. spectrum of the derived free acid contained 11 signals (Fig. 1, Spectrum A) instead of the expected 12, tests were carried out on a number of lanthanide salts that might expand the spectrum. According to Barry *et al.* (4), Eu^{3+} and Nd^{3+} should cause signal displacement in proton spectra with little line broadening, whereas broadening should be greater with Ho^{3+}, and greatest with Gd^{3+}. A summary compiled by Mayo (7) shows that broadening of proton signals relative to their displacement is smallest in shift reagents containing praseodymium and europium, and larger with those of samarium, holmium, and ytter-

Can. J. Chem. Downloaded from www.nrcresearchpress.com by 210.87.254.40 on 09/05/12
For personal use only.

TABLE 1. Chemical shifts and assignments of ^{13}c.m.r. signals of mannose and related phosphates

Compound	Downfield difference of chemical shifts of signals from that external TMS, contained in a coaxial capillary in p.p.m. (δ_c)
α-D-Mannose (2)	94.5 (C-1), 72.9 (C-5), 71.2 (C-2), 70.8 (C-3), 67.5 (C-4), 61.6 (C-6)
β-D-Mannose (2)	94.1 (C-1), 76.7 (C-5), 73.6 (C-3), 71.8 (C-2), 67.1 (C-4), 61.6 (C-6)
α-D-Mannose-6-phosphate	95.20 (C-1), 72.38; *J* 8 Hz (C-5), 71.75 (C-2), 71.19 (C-3), 67.50 (C-4), 65.71; *J* 5 Hz (C-6)
β-D-Mannose-6-phosphate	94.84 (C-1), 75.95; *J* 8 Hz (C-5), 73.97 (C-3), 72.22 (C-2), 67.26 (C-4), 65.71; *J* 5 Hz (C-6)
α-D-Mannose-1-phosphate	97.10; *J* 5 Hz (C-1), 74.76 (C-5), 71.51; *J* 8 Hz (C-2), 70.99 (C-3), 67.58 (C-6)
Phosphonomannan	99.72 (C-1′), 95.29 (C-1), 78.29 (C-2), 77.38 (C-5′), 73.81 (C-5, C-3′), 71.83 (C-2′), 70.24 (C-3), 67.86 (C-4), 67.26 (C-4′), 65.60 (C-6), 62.22 (C-6′)

bium. In the present study, considerable downfield shifts were produced on addition of praseodymium chloride (Fig. 1, Spectrum B) and smaller ones with neodymium chloride. Europium chloride, on the other hand, produced upfield shifts (Fig. 1, Spectrum C).[2] Chlorides of holmium, ytterbium, and gadolinium caused considerable broadening of signals of the two esterified ^{13}C nuclei (for assignments see Fig. 1 and below), without displacement to higher or lower field. Samarium chloride did not displace or broaden signals when added in relatively large amounts. (In these studies the acid form of the phosphonomannan was used rather than the K salt, whose ^{13}C spectrum was less susceptible to modification.) Using the preferred salts, the chlorides of praseodymium and europium, 4 signals were affected and the direction of the displacement, which is opposite to that produced by a pseudocontact interaction, indicates a contact interaction (8).[3] These results suggest that both the signals of the esterified ^{13}C nucleus and the adjacent ^{13}C nucleus are displaced. To aid interpretation of the displacements, parallel results from structurally related α-D-mannose-1-phosphate and β-D-mannose-6-phosphate were obtained.

The signals of the ^{13}c.m.r. spectra of the 1- and 6-phosphate are assignable since most of them are close in shift to those of α,β-D-mannose (2). The only differences are that the ^{13}C—O—^{31}P signal is displaced downfield (3–4 p.p.m.) with coupling (5 Hz) and that the ^{13}C—C—O—^{31}P signal is coupled and without displacement (9, 10) (8 Hz; see Table 1). Addition of Pr^{3+} (17 mg) causes a downfield shift of the signals of the phosphorylated ^{13}C nuclei and a smaller downfield shift of those of the adjacent nuclei (Tables 1 and 2). C-6 and C-5 signals of α-D-mannose-6-phosphate underwent shifts of +1.9 and +0.6 p.p.m. respectively. The C-1 and C-2 shifts of α-D-mannose-1-phosphate were +1.4 and +0.6 p.p.m., respectively, and were accompanied by a shift of −0.6 p.p.m. of the C-6 resonance. On addition of Eu^{3+} (19 mg) to the mannose phosphates the shifts of the phosphorylated ^{13}C nuclei were smaller and upfield (Table 2; −0.6 to −0.7 p.p.m.). Their magnitude was almost matched by the shifts of the adjacent nuclei (−0.5 to −0.6 p.p.m.). A downfield shift, +0.3 p.p.m., of the C-6 signal of α-D-mannose-1-phosphate was also observed (Table 2).

As stated above, 4 signals in Spectrum A of the phosphonomannan are displaced on addition of Pr^{3+} or Eu^{3+} (compare with Spectra B and C, Fig. 1). Based on the nomenclature presented in Fig. 1, three of the signals are respectively from C-2 (δ_c 78.69), C-5 (δ_c 73.81) which is superimposed on the C-3′ signal, and phosphorylated C-6 (δ_c 65.67). These assignments are made since the resonances are close respectively to those of the following: C-2 of 2-*O*-β-D-mannopyranosyl-α-D-mannose (2; δ_c 78.6), C-5 of α-D-mannose (2; δ_c 72.9), and C-6 of α-D-mannose-6-phosphate (δ_c 65.71). The displacement of the C-5 signal is particularly significant since it supports structure **2**, rather than structure **1**, which would require a displacement of a signal in the region of C-5 of β-D-mannose (2; δ_c 76.7), that is the one at δ_c 77.38. Displacement of the signal at δ_c 95.29 on addition of the salts indicates its ^{13}C nucleus is attached to a phosphate group and must be C-1. This signal, and the three others, do not show two- or three-bond coupling with ^{31}P (9) because they are too broad.

Comparison of the 4 signal displacements ob-

[2]Under similar conditions the ^{13}c.m.r. signals of α,β-D-mannose, α-D-Manp$\underline{1,2}$α-D-Manp$\underline{1,2}$D-Man and a polysaccharide containing alternating (1 → 4)- and (1 → 3)-linked β-D-mannopyranose units were shifted less than 0.04 p.p.m.

[3]No diamagnetic effect, due to the charge of the cation, was observed since no shift was observed with lanthanum nitrate.

Can. J. Chem. Downloaded from www.nrcresearchpress.com by 210.87.254.40 on 09/05/12
For personal use only.

Can. J. Chem. Downloaded from www.nrcresearchpress.com by 210.87.254.40 on 09/05/12
For personal use only.

TABLE 2. Signal displacements observed in ^{13}c.m.r. spectra on addition of lanthanide ion to solutions of mannose phosphates and phosphonomannan in the acid forms (33°)

Compound	Shift reagent	Shift of ^{13}C signal (p.p.m.)					
		C-1	C-2	C-3	C-4	C-5	C-6
α-D-Mannose-6-phosphate	$PrCl_3 \cdot 6H_2O$ (8 mg)	+0.04	+0.08	0	+0.16	+0.40	+1.19
(65 mg) in D_2O (0.8 ml)	$PrCl_3 \cdot 6H_2O$ (17 mg)	+0.04	+0.08	−0.04	+0.20	+0.63	+1.90
	$EuCl_3 \cdot 6H_2O$ (9 mg)	−0.04	−0.08	−0.04	−0.08	−0.28	−0.32
	$EuCl_3 \cdot 6H_2O$ (19 mg)	−0.12	−0.08	−0.04	−0.12	−0.56	−0.67
β-D-Mannose-6-phosphate	$PrCl_3 \cdot 6H_2O$ (8 mg)	−0.16	−0.08	−0.12	+0.16	+0.40	+1.19
(65 mg) in D_2O (0.8 ml)	$PrCl_3 \cdot 6H_2O$ (17 mg)	−0.24	−0.16	−0.12	+0.24	+0.60	+1.90
	$EuCl_3 \cdot 6H_2O$ (9 mg)	0	0	−0.12	−0.08	−0.28	−0.32
	$EuCl_3 \cdot 6H_2O$ (18 mg)	0	0	−0.12	−0.16	−0.56	−0.67
α-D-Mannose-1-phosphate	$PrCl_3 \cdot 6H_2O$ (8 mg)	+0.79	+0.32	+0.16	+0.04	0	−0.28
(65 mg) in D_2O (0.8 ml)	$PrCl_3 \cdot 6H_2O$ (17 mg)	+1.43	+0.56	+0.28	+0.12	+0.04	−0.63
	$EuCl_3 \cdot 6H_2O$ (9 mg)	−0.28	−0.28	−0.08	−0.12	0	+0.12
	$EuCl_3 \cdot 6H_2O$ (18 mg)	−0.56	−0.48	−0.20	−0.20	−0.04	+0.28
Phosphonomannan	$PrCl_3 \cdot 6H_2O$ (3 mg)	+0.60	+0.26			+0.42	+0.72* or +0.01
(80 mg) in D_2O (2 ml)	$PrCl_3 \cdot 6H_2O$ (7 mg)	+1.11	+0.48			+0.60	+1.4 or more
	$EuCl_3 \cdot 6H_2O$ (7 mg)	−0.20	−0.12			−0.12	+0.28 or −0.30*
	$EuCl_3 \cdot 6H_2O$ (14 mg)	−0.40	−0.32			−0.12	+0.48 or −0.50*
	$NdCl_3 \cdot 6H_2O$ (14 mg)	+0.20	+0.28			—	+0.80

*Assigned on the basis of shifts observed with signals of α-D-mannose-1-phosphate and α-D-mannose-6-phosphate.

served in the phosphonomannan spectra with those of α-D-mannose-1,6-diphosphate would be ideal, but unfortunately this compound was not readily available. Instead estimates of the displacements were made by addition of the values observed for given ^{13}C nuclei in α-D-mannose-1-phosphate and α-D-mannose-6-phosphate. The additive values (in p.p.m.) are as follows: Pr^{3+}: C-1, +1.47; C-2, +0.62; C-5, +0.67; C-6, +1.27 and Eu^{3+}: C-1, −0.68; C-2, −0.56; C-5, −0.60; C-6, −0.39. It can be seen from comparison of these values to those in Table 2 that they are of the same direction as those of the phosphonomannan and are of aid in assigning C-6 signals in the expanded spectra. This assignment was doubtful since the signal assigned to C-6 resolved into 2 signals on addition of salt.

The other eight ^{13}C nuclei can be assigned to signals in Spectrum A, since the signals in the phosphorylated mannose unit should have resonances similar to those of α-D-mannopyranose (2). Those of the other unit should correspond to β-D-mannopyranose (2) with the exception of the C-1′ signal, which should be at δ_c 99.72 by a process of elimination. On this basis the following assignments were made, values being in δ_c: 77.38 (C-5′), 73.81 (C-3′ and C-5), 71.83 (C-2′), 70.24 (C-3), 67.86 (C-4), 67.26 (C-4′), and 62.22 (C-6′).

Since the signals of α-^{13}C and β-^{13}C nuclei of the above phosphorylated compounds can be detected by addition of Pr^{3+} and Eu^{3+}, it follows that similar spectral studies can be extended to other phosphonomannans and phosphonogalactans (11).

The proton nuclear magnetic resonance spectrum of the potassium salt[4] of the phosphonomannan (Fig. 2, Spectrum D) was expanded downfield on addition of praseodymium chloride (Fig. 2, Spectrum E), but the changes are far more difficult to interpret in terms of chemical structure: europium chloride caused upfield shifts resulting in crowded spectra that cannot be interpreted. At lower concentrations of Pr^{3+}, the coupled H-1 signal at δ6.45 shifted downfield and as the concentration increased stepwise (see inserts a and b in Spectrum D, Fig. 2, and Table 3) further shifts to δ8.26 took place which were accompanied by broadening. In addition, two

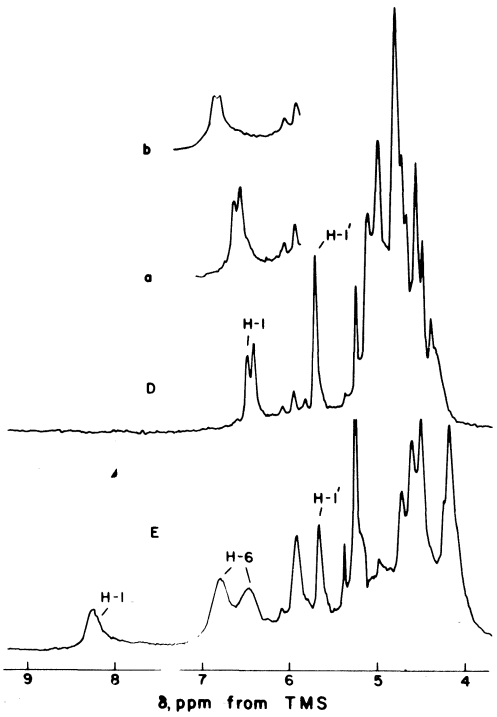

FIG. 2. Proton spectra of the potassium salt of the phosphonomannan (40 mg) in D_2O (2 ml), before (D) and after addition of 9 mg of $PrCl_3 \cdot 6H_2O$ (E). Inserts a and b are the H-1 portions of spectra after addition of 0.9 mg and 1.8 mg of salt, respectively.

new broad single proton signals appeared at δ6.46 and δ6.78 (Fig. 2, Spectrum E), which are attributable to the two nonequivalent H-6's. On reduction of the temperature to 27°, a new signal appeared, which was formerly obscured by the DOH signal.

The proposed downfield shifts of the H-1 signals occurred in the proton nuclear magnetic resonance spectrum of the disodium salts of α-D-mannose-1-phosphate. The investigation was hindered somewhat since a precipitate frequently formed on addition of Pr^{3+} and the spectra were poorly resolved (improved resolution occurred on going to the free acidic forms). Similar experiments carried out with the 6-phosphate could not be interpreted properly because the H-6 signal could not be assigned.

The p.m.r. shifts observed on addition of lanthanide ion to solutions of the mannose phosphates are due almost entirely to the presence of the phosphate group. When α,β-D-mannose, α-D-Manp^{1,2}α-D-Manp^{1,2}D-Man, and a polysaccharide containing alternate (1→3)- and (1→4)-

[4]When the acidic form of the polymer was used the ratio of signal broadening to signal displacement was very large.

Can. J. Chem. Downloaded from www.nrcresearchpress.com by 210.87.254.40 on 09/05/12
For personal use only.

TABLE 3. Signal displacements observed in proton spectra on addition of lanthanide ion to solutions of mannose phosphates and phosphonomannan in the salt and acid forms (27° and 70°)

	Shift reagent	Temperature (°C)	Observed signal*	Shift of signal (p.p.m.)
Disodium salt of α-D-mannose-1-phosphate (20 mg) in D_2O (2 ml)	—	70	H-1 (δ 5.90)	+0
	$PrCl_3 \cdot 6H_2O$ (1.8 mg)	70	H-1	+0.33
	$PrCl_3 \cdot 6H_2O$ (3.6 mg)	70	H-1	+0.56
	$EuCl_3 \cdot 6H_2O$ (1.8 mg)	70	H-1	−0.15
	$EuCl_3 \cdot 6H_2O$ (3.6 mg)	70	H-1	−0.31
Disodium salt of α,β-D-mannose-6-phosphate (20 mg) in D_2O (2 ml)	—	70	H-6 (δ∼4.56)	0
	$PrCl_3 \cdot 6H_2O$ (0.9 mg)	70	H-6	∼+0.2
	$PrCl_3 \cdot 6H_2O$ (1.8 mg)	70	H-6	∼+0.4
Potassium salt of phosphonomannan (40 mg) in D_2O (2 ml)	—	70	H-1 (δ 6.44)	0
	$PrCl_3 \cdot 6H_2O$ (0.9 mg)	70	H-1	+0.18
	$PrCl_3 \cdot 6H_2O$ (1.8 mg)	70	H-1	+0.38
	$PrCl_3 \cdot 6H_2O$ (9 mg)	70	H-1	+1.82
	$PrCl_3 \cdot 6H_2O$ (9 mg)	70	H-6's	+1.5 to 1.8
Acid form of α-D-mannose-1-phosphate (17 mg) in D_2O (2 ml)	—	27	H-1 (δ 5.57),s	0
	$PrCl_3 \cdot 6H_2O$ (0.9 mg)	27	H-1, b	+0.14
	$EuCl_3 \cdot 6H_2O$ (1.8 mg)	27	H-1, b	−0.09
	—	70	H-1 (δ 5.95),s	0
	$PrCl_3 \cdot 6H_2O$ (0.9 mg)	70	H-1, b	+0.25
	$EuCl_3 \cdot 6H_2O$ (1.8 mg)	70	H-1, s	−0.11
Acid form of α,β-D-mannose-6-phosphate (17 mg) in D_2O (2 ml)	—	27	H-6 (δ 4.26), s	0
	$PrCl_3 \cdot 6H_2O$ (0.9 mg)	27	H-6, b	+0.20
	$EuCl_3 \cdot 6H_2O$ (1.8 mg)	27	H-6, b	−0.17
	—	70	H-6 (δ 4.62), b	+0.36
	$PrCl_3 \cdot 6H_2O$ (0.9 mg)	70	H-6, s	+0.36
	$EuCl_3 \cdot 6H_2O$ (1.8 mg)	70	H-6, s	−0.24

*s = sharp with a half-height line width of 1 Hz; b = relatively broad with a half-height line width of 2–3 Hz.

linked β-D-mannopyranose units (12) were subjected to the same conditions only very small spectral shifts were induced.

Experimental

The disodium salt of D-mannose-6-phosphate and disodium salt of α-D-mannose-1-phosphate were obtained from the Sigma Chemical Co., St. Louis, Missouri, and were converted to their free acidic forms by shaking in water with Amberlite IR120 (H^+ form) and lyophilizing. Hexahydrates of holmium chloride, ytterbium chloride, samarium chloride, praseodymium chloride, neodymium chloride, and europium chloride were supplied by Alfa Inorganics, Beverley, Mass. Hydrated gadolinium chloride was from Apache Chemicals, Rockford, Ill. The phosphonomannan from *Hansenula capsulata* NRRL Y-1842 was kindly supplied by Dr. M. E. Slodki of the Northern Utilization Research and Development Division, U.S. Dept. of Agriculture, Peoria, Ill. A portion (1 g) was degraded with 1% aqueous potassium hydroxide (200 ml) at 100° for 30 min. The solution was neutralized (AcOH), evaporated to 25 ml, and excess ethanol added. The precipitate of the potassium salt which formed was collected on a filter, washed with ethanol, and dried. The acid form was prepared by the same method as used above for the mannose phosphates.

Carbon-13 Magnetic Resonance Spectroscopy

Carbon-13 magnetic resonance spectra were obtained using a Varian XL-100-15 spectrometer with Fourier transform. The phosphonomannan (as its acidic form and potassium salt; 80 mg) was dissolved in D_2O (2 ml) and examined at 33° in a 12 mm diameter × 8 in. n.m.r. tube fitted with a Teflon vortex-plug. The spectral width used was 5000 Hz, the acquisition time 0.4 s, the pulse width 50 μs which represents a 43° pulse width, and the number of transients 100 000. Chemical shifts are expressed as δ_c in p.p.m., based on the downfield difference of the signal resonance and that of external TMS. Six runs were carried out, one addition of neodymium chloride (14 mg), two successive additions of praseodymium (3.5 mg each) and europium chloride hexahydrates (7 mg each), each being added to the acid form of the phosphonomannan. (Likewise, similar additions were made to a solution of the K salt.) Additions of ytterbium chloride or holmium chloride (3 mg amounts) or gadolinium chloride (1 mg) resulted in broadening of the C-1 and C-6 signals. Com-

Can. J. Chem. Downloaded from www.nrcresearchpress.com by 210.87.254.40 on 09/05/12
For personal use only.

paratively, high levels of samarium chloride (28 mg) and lanthanum nitrate (14 mg) did not affect the spectrum.

The ^{13}c.m.r. spectra of α,β-D-mannose-6-phosphate and α-D-mannose-1-phosphate were obtained from samples (65 mg) in D_2O (0.8 ml) contained in a coaxial cylinder within a 12 mm diameter × 8 in. tube containing D_2O (4 ml). The temperature used was 33°, the spectral width 2500 Hz, the acquisition time 0.8 s, the pulse width 65 μs, representing a 55° pulse, and the number of transients was 4000. Two runs were carried out with each phosphate, two successive additions of praseodymium chloride (8.5 mg each) and europium chloride (9 mg each) being made.

Proton Nuclear Magnetic Resonance Spectroscopy

Proton spectra were obtained using the spectrometer described above. The acidic form and the potassium salt of the phosphonomannan (40 mg) were each dissolved in 99.7% D_2O, which was evaporated and the process repeated. Finally, the polymer was examined in 99.97% D_2O (2 ml) at 70° or 27° in a 12 mm diameter × 8 in. n.m.r. tube containing a Teflon vortex-plug. The spectral width was 1000 Hz, the acquisition time 2.0 s, the pulse width 65 μs, and the number of transients 200. The chemical shifts are based on the downfield difference of the signals' resonance and that of external TMS in a coaxial capillary and are expressed as δ in p.p.m. The downfield difference of the resonance of dioxan and external TMS is 4.18 p.p.m. at 27° and 4.29 p.p.m. at 70°. In the determination of spectral shifts, on addition of lanthanide ion, dioxan was used as an internal reference. Two successive additions of praseodymium chloride (0.9 mg each, that had previously been equilibrated with D_2O) were made followed by a larger one (7.2 mg). Similar additions of europium chloride were made following replacement of the water of crystallization with D_2O. When a quantitative estimation of proton size was needed a continuous wave mode was used.

The conditions used for proton studies on α-D-mannose-1-phosphate and α,β-D-mannose-6-phosphate are summarized in Table 3.

The authors wish to thank Mr. R. J. Magus for technical assistance.

1. M. E. SLODKI. Biochim. Biophys. Acta, **69**, 96 (1963).
2. P. A. J. GORIN. Can. J. Chem. **51**, 2105 (1973).
3. B. BIRDSALL, J. FEENEY, J. A. GLASEL, R. J. P. WILLIAMS, and A. V. XAVIER. Chem. Commun. 1473 (1971).
4. C. D. BARRY, A. C. T. NORTH, J. A. GLASEL, R. J. P. WILLIAMS, and A. V. XAVIER. Nature, **232**, 236 (1971).
5. S. J. ANGYAL. Carbohydr. Res. **26**, 271 (1973).
6. M. E. SLODKI, L. J. WICKERHAM, and M. C. CADMUS. J. Bacteriol. **82**, 269 (1961).
7. B. C. MAYO. Chem. Soc. Rev. **2**, 49 (1973).
8. W. B. LEWIS, J. A. JACKSON, J. F. LEMONS, and H. TAUBE. J. Chem. Phys. **36**, 694 (1962).
9. H. H. MANTSCH and I. C. P. SMITH. Biochem. Biophys. Res. Commun. **46**, 808 (1972).
10. D. E. DORMAN and J. D. ROBERTS. Proc. Natl. Acad. Sci. U.S. **65**, 19 (1970).
11. P. A. J. GORIN and J. F. T. SPENCER. Adv. Carbohydr. Chem. **23**, 367 (1968).
12. P. A. J. GORIN, K. HORITSU, and J. F. T. SPENCER. Can. J. Chem. **43**, 950 (1965).

Can. J. Chem. Downloaded from www.nrcresearchpress.com by 210.87.254.40 on 09/05/12
For personal use only.

Erratum: The Electron Pair in Chemistry

R. DAUDEL
Centre de Mécanique Ondulatoire Appliquée de C.N.R.S., Paris, France
AND
R. F. W. BADER, M. E. STEPHENS, AND D. S. BORRETT
Department of Chemistry, McMaster University, Hamilton, Ontario

Received June 20, 1974
(Ref.: Can. J. Chem. **52**, 1310 (1974))

A computational error was made in this laboratory[1] for *one* of the three-loge partitionings of BeH_2. Specifically, the simple partitioning which yields a spherical core loge and two bond loges all with average populations of 2.0 is found to yield the best partitioning of BeH_2 in terms of maximizing the probability of the event (2,2,2) and minimizing the missing information function $I(P,\Omega)$. The correct data for this case, replacing that in Table 5(*a*) is given below. The discussion given on p. 1318 of the original article stating that in BeH_2 an "extended" core yields a better partitioning of BeH_2 is incorrect. The new Table 5(*a*) together with the data in Tables 5(*b*) and 5(*c*) indicate that $I(P,\Omega)$ undergoes a continuous decrease as the volume of the "core" loge is decreased to that of the traditional tight two-electron core. The data given in the original Table 5(*a*) actually refer to the symmetrical partitioning of the BeH_2 (with the exception of the core loge) by a σ_v symmetry plane, rather than by a σ_h symmetry plane as was implied. A comparison of the original and the new results for Table 5(*a*) shows that the important requirement for the minimization of $I(P,\Omega)$ is the maximization of $P_2(\Omega)$ rather than simply obtaining loges with average populations of 2.00. This result is in agreement with the same comparison given in the paper for the isoelectronic system BH.

[1]This refers to the laboratory at McMaster University, Hamilton, Ontario.

The corrected result for BeH_2 reinforces the conclusion reached in the paper, that for the molecules considered in this investigation, the most probable partitioning is one which localizes pairs of electrons in well-defined spatial regions or loges.

TABLE 5. Three-loge partitioning in BeH_2 ($X^1\Sigma_g^+$)
(*a*) Symmetrical partitioning*

(*i*) Probability of events (n_c,n_b,$n_{b'}$)

n_c \ n_b	1	2	3
1	0.0012	0.0309	0.0309
2	0.0340	0.8028	0.0340
3	0.0301	0.0301	0.0006

(*ii*) Leading events for two-loge partitioning and $I(P,\Omega)$ values

	Core	Bonded
$P_2(\Omega)$	0.8715	0.8644
$I(P,\Omega)$	0.4862	0.5061

*r_c = 0.93 a.u., $\alpha = 90°$, $\bar{N}(\Omega_c) = 1.998$, $\bar{N}(\Omega_b) = 2.001$, $\bar{N}(\Omega_{b'}) = 2.001$, $I(P,\Omega_c,\Omega_b) = 0.8847$.

Can. J. Chem. Downloaded from www.nrcresearchpress.com by 210.87.254.105 on 09/05/12
For personal use only.

Partition Function Ratios of the Methyl Halides Differing Only in Isotopic Substitution

JAN BRON

Department of Chemistry, University of Natal, Durban, South Africa

Received February 27, 1974

JAN BRON. Can. J. Chem. **52**, 3078 (1974).

By using the best available spectroscopic data for the force fields and geometries of the methyl halides, partition function ratios for these species are evaluated as a function of temperature. These ratios are of the type $q(AXYZB)/q(^{12}CH_3B)$ in which q is the partition function; A is ^{12}C, ^{13}C, or ^{14}C; X, Y, and Z are either ^1H, ^2H, or ^3H; and B stands for either F, Cl, Br, or I. To the logarithm of these functions at the various temperatures (200–500 K) a curve is fitted with the equation $\ln(q_2/q_1) = p_1 \ln(T/500) + \sum_{n=2} p_n(T/500)^{n-3}$. All ratios are determined with respect to the unsubstituted $^{12}CH_3B$ molecule. Examples of the utility of the partition function ratios are given.

JAN BRON. Can. J. Chem. **52**, 3078 (1974).

Faisant appel aux meilleures données spectroscopiques disponibles pour les champs de force et les géométries des halogénures de méthyle, on évalue les rapports de la fonction de partition de ces composés en fonction de la température. Ces rapports sont du type $q(AXYZB)/q(^{12}CH_3B)$ où q est la fonction de partition, A est ^{12}C, ^{13}C ou ^{14}C, X, Y, et Z sont ^1H, ^2H ou ^3H et B représente F, Cl, Br ou I. Avec le logarithme de ces fonctions à diverses températures (200–500 K), on trace une courbe dont l'équation est $\ln(q_2/q_1) = p_1 \ln(T/500) + \sum_{n=2} p_n(T/500)^{n-3}$. Tous les rapports sont déterminés par rapport à la molécule $^{12}CH_3B$ non substituée. On donne des exemples de l'utilité des rapports de la fonction de partition. [Traduit par le journal]

Introduction

Methyl halides are frequently used as models to study the mechanistic aspects of a particular type of chemical reaction. Kinetic isotope effects are frequently used to gain this mechanistic insight, since isotopic substitution creates the smallest possible structural perturbation of a molecule (1). Examples may be proton transfer and nucleophilic substitution reactions (2, 3).

By using transition state theory and statistical mechanics the bonding and geometry of the activated complex can be deduced (2, 4). The theoretical expression for the kinetic isotope effect involves beside the partition function ratio (p.f.r.) of the transition states also p.f.r.'s of the reactant molecules (4). In order to evaluate the p.f.r.'s of molecular species, which may be either stable or transient, the geometry and force field should be known (5). The geometry and force field of the transient species or transition state depend upon the reaction conditions (6) contrary to the reactant molecules.

It is, therefore, useful to know the p.f.r.'s of the methyl halides as a function of temperature since it eliminates the necessity of recomputation if these quantities are needed. The p.f.r.'s can also be used for calculating the *equilibrium* constants (7) of isotope exchange reactions involving methyl halides. The ratios evaluated are of the type $q(AXYZB)/q(^{12}C^1H_3B)$ in which q is the partition function; A is ^{12}C, ^{13}C, or ^{14}C; X, Y, and Z are either ^1H, ^2H, or ^3H; and B stands for either F, Cl, Br, or I.

The expression for the p.f.r. (8) is

$$[1]\quad \frac{q_2}{q_1} = \left(\frac{M_2}{M_1}\right)^{3/2}\left(\frac{I_2^{(x)}I_2^{(y)}I_2^{(z)}}{I_1^{(x)}I_1^{(y)}I_1^{(z)}}\right)^{1/2} \times \prod_{i=1}^{3N-6}\frac{\sinh(\frac{1}{2}u_{1i})}{\sinh(\frac{1}{2}u_{2i})}$$

where M_i is the molecular mass, $I_i^{(x)}$ the principal moment of inertia, and u_i is equal to $(hc\omega_i/kT)$. The vibrational frequency of normal mode i is ω_i. Application of the Teller–Redlich product rule (9) reduces eq. 1 to a ratio involving vibrational frequencies and atomic masses (m_{ij}) only (4). The result is

$$[2]\quad \frac{q_2}{q_1} = \prod_{i=1}^{N}\left(\frac{m_{2i}}{m_{1i}}\right)^{3/2}\prod_{j=1}^{3N-6}\frac{u_{2j}\sinh(\frac{1}{2}u_{1j})}{u_{1j}\sinh(\frac{1}{2}u_{2j})}$$

In eqs. 1 and 2 symmetry numbers have been ignored.

Can. J. Chem. Downloaded from www.nrcresearchpress.com by 210.87.254.5 on 09/05/12
For personal use only.

Can. J. Chem. Downloaded from www.nrcresearchpress.com by 210.87.254.5 on 09/05/12
For personal use only.

Calculations

The normal frequencies of vibration of a molecule can be calculated from a detailed knowledge of the geometry and force field of the molecule. In this case the frequencies have been determined by the Wilson's **FG** matrix method (10). The internal (symmetry) coordinates for the halides (11, 12) are presented in Table 1. The coordinate S_2 is a function of the geometry of the molecule and hence depends upon the identity of the halide atom. Although the coordinates in Table 1 are *symmetry* coordinates (10) for the species CX_3Y only, they have been used, for reasons of convenience, for all methyl halides regardless of the symmetry of the molecule.

The equilibrium geometries of methyl fluorides, chlorides, bromides, and iodides are listed in Table 2. The quadratic force constants in the coordinates used (Table 1) are given in Table 3. All force constants have the units of mdyn/Å. In order to obtain the proper units for the stretching–bending and bending force constants they should be multiplied by the C—H bond distance and the square of this distance respectively (12).

Results and Discussion

The p.f.r.'s have been calculated by using eq. 1

TABLE 1. Symmetry coordinates for the methyl halide molecules

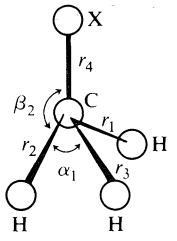

$S_1 = (\Delta r_1 + \Delta r_2 + \Delta r_3)/\sqrt{3}$
$S_2 = PS_{2a} - QS_{2b}$
$S_3 = \Delta r_4$
$S_4 = (2\Delta r_1 - \Delta r_2 - \Delta r_3)/\sqrt{6}$
$S_5 = (\Delta r_2 - \Delta r_3)/\sqrt{2}$
$S_6 = (2\Delta\alpha_1 - \Delta\alpha_2 - \Delta\alpha_3)/\sqrt{6}$
$S_7 = (\Delta\alpha_2 - \Delta\alpha_3)/\sqrt{2}$
$S_8 = (2\Delta\beta_1 - \Delta\beta_2 - \Delta\beta_3)/\sqrt{6}$
$S_9 = (\Delta\beta_2 - \Delta\beta_3)/\sqrt{2}$
$S_{2a} = (\Delta\alpha_1 + \Delta\alpha_2 + \Delta\alpha_3 - \Delta\beta_1 - \Delta\beta_2 - \Delta\beta_3)/\sqrt{6}$
$S_{2b} = (\Delta\alpha_1 + \Delta\alpha_2 + \Delta\alpha_3 + \Delta\beta_1 + \Delta\beta_2 + \Delta\beta_3)/\sqrt{6}$
$P = (1 + K)/(2 + 2K^2)^{1/2}$
$Q = (1 - K)/(2 + 2K^2)^{1/2}$
$K = -3 \sin\beta \cos\beta/\sin\alpha$

in the temperature range of 200 to 500 °K, using steps of 25 °K. This range of 300 °K has been chosen since it represents the temperature region of main chemical interest. In order to avoid the usual listings (13–15) of the p.f.r.'s at the various equally spaced (25 °K) temperatures a curve with the equation (16, 17)

$$[3] \quad \ln (q_2/q_1) = p_1 \ln (T/500) + \sum_{n=2}^{5} p_n (T/500)^{n-3}$$

has been fitted to the values of $\ln (q_2/q_1)$ at the various temperatures by using the method of least squares. Table 4 lists the value of p_n in eq. 3 for the various p.f.r.'s together with the errors. The error, mean % deviation, is defined as

$$[4] \quad \frac{100}{13} \sum_{i=1}^{13} \left[\left(\frac{q_2}{q_1}\right)_{T_i}^{(e)} - \left(\frac{q_2}{q_1}\right)_{T_i}^{(s)} \right] \Big/ \left(\frac{q_2}{q_1}\right)_{T_i}^{(e)}$$

The quantity $(q_2/q_1)_{T_i}^{(e)}$ is the value of the p.f.r. as evaluated by eq. 1 or 2 at temperature T_i, while $(q_2/q_1)_{T_i}^{(s)}$ is the value of the p.f.r. recomputed from eq. 3 at the same temperature. As can be seen in the table the error does not exceed 0.005%. It is important to attach no theoretical significance to the values for p_n, since they may depend upon the computer and program used.

The utility of the series method may be demonstrated by some examples. The deuterium isotope effect for the reactions

$$[5] \quad \begin{aligned} CH_3X + B &\leftrightharpoons BCH_3X^* \rightarrow P_1 \\ CD_3X + B &\leftrightharpoons BCD_3X^* \rightarrow P_2 \end{aligned}$$

in which BCY_3X^* is the transition state, is simply within the framework of the transition state theory (4)

$$[6] \quad \left(\frac{k_H}{k_D}\right)_T = \exp\left[\Delta p_1 \ln \left(\frac{T}{500}\right) + \sum_{n=2}^{5} \Delta p_n \left(\frac{T}{500}\right)^{n-3} \right] \times \frac{q(BCH_3X^*)}{q(BCD_3X^*)}$$

where Δp_i is equal to $[p_i(CD_3X) - p_i(CH_3X)]$. The p.f.r.'s of the non-linear transition state can be calculated by means of eq. 1, but the product in this equation involves then only $3N - 7$ frequencies since the zero or imaginary frequency, which corresponds to the reaction coordinate, should be left out (8).

Another example may be the exchange equilibrium

TABLE 2. Equilibrium geometries of methyl halides*

Compound	r_e(CX) (Å)	r_e(CH) (Å)	∠HCH (α) (deg)	∠HCX (β) (deg)
CH_3F	1.398	1.109	110.0	108.93
CH_3Cl	1.780	1.085	110.83	108.07
CH_3Br	1.938	1.085	111.33	107.54
CH_3I	2.139	1.085	111.67	107.18

*The geometries of molecules differing only in isotopic substitution are the same.

TABLE 3. Harmonic force fields* of methyl halides (mdyn/Å)

Force constants	Value			
	CH_3F	CH_3Cl	CH_3Br	CH_3I
F_{11}	5.354	5.492	5.534	5.530
F_{12}	0.0	0.026	0.070	0.119
F_{13}	0.0	0.173	0.121	0.065
F_{22}	0.616	0.541	0.512	0.479
F_{23}	−0.588	−0.489	−0.436	−0.383
F_{33}	5.803	3.499	2.938	2.393
F_{44},F_{55}	5.382	5.364	5.436	5.450
F_{46},F_{57}	−0.121	−0.121	−0.135	−0.131
F_{48},F_{59}	0.121	0.056	0.074	0.118
F_{66},F_{77}	0.498	0.461	0.454	0.447
F_{68},F_{79}	−0.057	−0.071	−0.016	−0.009
F_{88},F_{99}	0.756	0.610	0.545	0.474

*The force fields of molecules only differing in isotopic substitution are the same.

[7] $CH_3Cl + CD_3Br \rightleftharpoons CH_3Br + CD_3Cl$

In terms of p.f.r.'s the equilibrium constant for this reaction is

$$[8] \qquad K(T) = \frac{q(CD_3Cl)/q(CH_3Cl)}{q(CD_3Br)/q(CH_3Br)}$$

Written in terms of the coefficients p_i the equilibrium constant becomes

$$[9] \qquad K(T) = \exp\left[\Delta p_1 \ln\left(\frac{T}{500}\right) + \sum_{n=2}^{5} \Delta p_n \left(\frac{T}{500}\right)^{n-3}\right]$$

The quantity Δp_i is now defined as

$$[10] \qquad \Delta p_i = p_i(CD_3Cl) - p_i(CH_3Cl) - p_i(CD_3Br) + p_i(CH_3Br)$$

By substituting the values for p_i from Table 4 $K(T)$ becomes 1.104, 1.065, 1.042 and 1.028 at 200, 300, 400, and 500 °K respectively. Since in the p.f.r.'s as listed in Table 4 symmetry numbers have been ignored they should be inserted if the need arises. Other p.f.r.'s, like $q(CD_3X)/q(CHD_2X)$, which are not directly obtainable from Table 4 may be determined by simple division or multiplication. In this case, for example

$$[11] \qquad q(CD_3X)/q(CHD_2X) = [q(CD_3X)/q(CH_3X)]/[q(CHD_2X)/q(CH_3X)]$$

Differences in thermodynamic quantities between the isotopic species can be obtained as a series from the p.f.r.'s by using the standard statistical mechanical relationships (8).

The p.f.r.'s have been calculated within the, so-called, harmonic approximation (4). To correct for, say, anharmonicity would require a knowledge of the cubic and quartic force constants. At the moment these data are lacking. Other corrections (7) can also be applied but, again, the necessary data are not available. However, even if the detailed force fields of the methyl halides were known, the amount of computer time required to calculate all possible corrections would be prohibitive.

Over the last 25 years (18–21) much work has been done in expanding eq. 2 in terms of a power series of u_i. This essentially involves expansion of the function $(\frac{1}{2}u_i)^{-1}\sinh(\frac{1}{2}u_i)$, which leads to a power series involving only even powers of u_i. By use of the sum rule (10) the sum of even powers of u_i can then be expressed in terms of the **FG** matrix elements. So rather than calcu-

Can. J. Chem. Downloaded from www.nrcresearchpress.com by 210.87.254.5 on 09/05/12
For personal use only.

TABLE 4. Coefficients* p_n for $\ln(q_A/q_B) = p_1 \ln(T/500) + \sum_{n=2}^{5} p_n(T/500)^{n-3}$

A	B	$p_1 \times 10^4$	$p_2 \times 10^2$	$p_3 \times 10^2$	$p_4 \times 10^2$	$p_5 \times 10^3$	Mean % deviation
CH_2DF	CH_3F	−4074.59402	194.616112	−18.3582183	66.4074682	−93.5466778	0.001
CHD_2F		−8732.47523	390.891094	−46.5324248	143.800632	−211.108292	0.001
CD_3F		−13932.6776	588.568171	−83.2875308	230.807442	−348.861015	0.002
CH_2TF		−6012.18332	276.286631	−23.1275012	105.192765	−157.631351	0.001
CHT_2F		−13177.4878	557.159889	−69.5447470	235.965255	−375.811497	0.001
CT_3F		−21413.4801	841.825228	−135.966240	388.745848	−644.007733	0.001
$^{13}CH_3F$		−433.470426	10.2524690	2.23961978	7.30977893	−12.5244827	0.000
$^{14}CH_3F$		−825.989812	19.1275259	4.51168841	14.0431716	−24.3606883	0.000
CH_2DCl	CH_3Cl	−3851.31288	193.539367	−23.0947966	72.0401594	−118.127811	0.000
CHD_2Cl		−8255.23485	388.710589	−55.4906433	154.410465	−258.595901	0.001
CD_3Cl		−13221.6687	585.127145	−96.2859981	246.302926	−418.558960	0.001
CH_2TCl		−4945.54589	276.521922	−23.7601769	103.583989	−173.494569	0.001
CHT_2Cl		−10964.1419	557.563835	−69.4662915	231.027317	−403.111282	0.002
CT_3Cl		−18169.2545	841.863984	−135.289054	381.161257	−683.038076	0.004
$^{13}CH_3Cl$		−219.984970	9.54709108	2.97473766	6.35743692	−13.8192839	0.000
$^{14}CH_3Cl$		−391.537507	17.8833672	6.18613707	11.8030777	−25.8671586	0.000
CH_2DBr	CH_3Br	−3389.81135	193.742870	−21.6998192	69.6302937	−119.295585	0.001
CHD_2Br		−7359.82506	389.048989	−52.9104904	149.945871	−261.688889	0.001
CD_3Br		−11885.1464	585.592240	−92.3608124	239.557766	−422.826055	0.002
CH_2TBr		−3906.98073	277.586058	−18.1329872	94.6386704	−163.204966	0.001
CHT_2Br		−8906.90951	559.624275	−58.2813678	213.289178	−382.656242	0.003
CT_3Br		−15208.1510	844.615359	−119.395836	356.113060	−655.679989	0.005
$^{13}CH_3Br$		1.29688777	9.76354448	4.48553707	3.95378301	−9.66212858	0.000
$^{14}CH_3Br$		38.3689022	18.3222145	9.15653248	7.08096839	−17.5923933	0.000
CH_2DI	CH_3I	−2734.32687	193.045415	−17.3996858	63.6539123	−112.081981	0.001
CHD_2I		−6069.94103	387.605235	−44.4338303	138.194647	−247.507898	0.002
CD_3I		−10038.5940	583.234109	−80.3566088	223.083048	−403.977645	0.002
CH_2TI		−2714.80653	276.954339	−8.91028710	81.7408583	−142.560114	0.001
CHT_2I		−6600.60835	558.186593	−40.4343789	188.473014	−343.353640	0.003
CT_3I		−11858.9826	842.204010	−93.4089488	320.172000	−599.051559	0.005
$^{13}CH_3I$		156.184987	9.57238537	6.03819433	1.89538207	−5.62719236	0.000
$^{14}CH_3I$		329.958603	17.9589180	12.1117573	3.17152050	−9.8784224	0.000

*Symmetry numbers have been ignored.

lating the normal frequencies ω_i, which requires the diagonalization of two symmetric matrices (22), the equality $\sum u_i^2 = CT^{-2}\sum\sum F_{ij}G_{ij}$ is used. In this equality C is a constant. The double sum requires that the **F** and **G** matrix elements for each molecule must be calculated or taken from tables. Closely related methods to *estimate* p.f.r.'s have been developed by Bigeleisen *et al.* (20).

The quadratic terms in u_i are usually referred to as the first quantum correction. To be more specific for the equilibrium constant of the exchange equilibrium $H_2O + D_2O = 2HDO$ the classical value plus the first quantum correction is

$$[12] \quad \tfrac{1}{4}K(T) = 1 + (1/24)\sum_{i=1}^{3}[u_i^2(H_2O) + u_i^2(D_2O) - 2u_i^2(HDO)]$$

In this case the first quantum correction is zero at all temperatures by virtue of the rule of the mean (10). Since the experimental value for K is 3.76 at 25 °C (23) the first quantum correction is obviously inadequate and higher corrections should be considered. Application of eq. 1 or 2 gives results very close to the experimental value (24). For the same reasons the first quantum correction for the equilibrium constant of the reaction 7 is zero, quite different from the results obtained by eq. 1 or 2.

To consider higher quantum corrections defeats the purpose of the method and in general cannot be carried out without the aid of a computer. The methods to calculate normal frequencies are well known (10, 22, 25) and are readily programmed. By means of eq. 1 or 2 p.f.r.'s as a function of temperature can then be

Can. J. Chem. Downloaded from www.nrcresearchpress.com by 210.87.254.5 on 09/05/12
For personal use only.

calculated at the various temperatures. As pointed out before a least squares fit results in a very small error. Therefore, it follows that these p.f.r.'s, for example, which are the key to differences in thermodynamic quantities and which are listed by means of five constants only, result in much more accurate predictions than the first quantum correction.

Over the years the expansion of eq. 2 has increased in sophistication but not in simplicity (18–21) and the results are certainly not better than the simple series method proposed in this paper. However, it should be realized that the first purpose of the series method is to eliminate long listings of thermodynamic quantities at various equally spaced temperatures. Furthermore, an accurate knowledge of p.f.r.'s in isotope effect calculations eliminates at least one of the many uncertainties inherent in these computations (6, 26).

The author would like to thank the South African Council for Scientific and Industrial Research and the Atomic Energy Board for financial assistance.

1. M. J. GOLDSTEIN. Science, **154**, 1616 (1966).
2. H. S. JOHNSTON. Gas phase reaction rate theory. The Ronald Press Company, New York. 1966.
3. A. V. WILLI. Z. Phys. Chem. Neue Folge, **66**, 317 (1969).
4. M. WOLFSBERG and M. J. STERN. Pure Appl. Chem. **8**, 225 (1964).
5. P. C. VOGEL and M. J. STERN. J. Chem. Phys. **54**, 779 (1971).
6. J. BRON. Can. J. Chem. **52**, 903 (1974).
7. J. BRON and M. WOLFSBERG. J. Chem. Phys. **57**, 2862 (1972).
8. T. L. HILL. An introduction to statistical thermodynamics. Addison Wesley Publishing Company, London. 1960.
9. G. HERZBERG. Infrared and Raman spectra. Van Nostrand Reinhold Company, New York. 1945.
10. E. B. WILSON, J. C. DECIUS, and P. C. CROSS. Molecular vibrations. McGraw–Hill Book Company, Toronto. 1955.
11. J. ALDOUS and I. M. MILLS. Spectrochim. Acta, **16**, 889 (1960).
12. J. W. RUSSELL, C. D. NEEDHAM, and J. OVEREND. J. Chem. Phys. **45**, 3383 (1966).
13. H. C. UREY. J. Chem. Soc. 562 (1947).
14. A. S. FRIEDMAN and L. HAAR. J. Chem. Phys. **22**, 2051 (1954).
15. L. HAAR, A. S. FRIEDMAN, and C. W. BECKET. Ideal gas thermodynamic functions and isotope exchange functions for the diatomic hydrides, deuterides and tritides. National Bureau of Standards Monograph 20. 1961.
16. G. M. MURPHY. J. Chem. Phys. **5**, 637, (1937).
17. G. N. LEWIS and M. RANDALL. Thermodynamics. McGraw–Hill, New York. 1961.
18. J. BIGELEISEN and M. WOLFSBERG. Adv. Chem. Phys. **1**, 15 (1958).
19. M. WOLFSBERG. Ann. Rev. Phys. Chem. **20**, 449 (1969).
20. J. BIGELEISEN, T. ISHIDA, and W. SPINDEL. J. Chem. Phys. **55**, 5021 (1971).
21. J. BIGELEISEN and T. ISHIDA. J. Am. Chem. Soc. **95**, 6155 (1973).
22. J. H. SCHACHTSCHNEIDER and R. G. SNYDER. Spectrochim. Acta, **19**, 117 (1963).
23. L. FRIEDMAN and V. J. SHINER, JR. J. Chem. Phys. **44**, 4639 (1966).
24. M. WOLFSBERG, A. A. MASSA, and J. W. PYPER. J. Chem. Phys. **53**, 3138 (1970).
25. M. A. PARISEAU, I. SUZUKI, and J. OVEREND. J. Chem. Phys. **42**, 2335 (1965).
26. J. BRON and M. WOLFSBERG. J. Chem. Phys. **57**, 2862 (1972).

Can. J. Chem. Downloaded from www.nrcresearchpress.com by 210.87.254.5 on 05/05/12
For personal use only.

Redox Interchange Reactions of Halogenoplatinum(IV) Complexes. p*H* Dependence of the Hexabromoplatinate(IV)–Iodide Reactions

DAVID W. JOHNSON AND ANTHONY POË[1]

Erindale College and the Chemistry Department, University of Toronto, Mississauga, Ontario L5L 1C6

Received April 9, 1974

DAVID W. JOHNSON and ANTHONY POË. Can. J. Chem. **52**, 3083 (1974).

Successive stages in the reaction of the complex $[PtBr_6]^{2-}$ with iodide have been reexamined with particular attention to their p*H* dependence. A reassignment of two of the three stages is necessary although the intimate mechanism remains unchanged. Reoxidation of $[PtBr_4]^{2-}$ produced by the slow reduction of $[PtBr_6]^{2-}$ with iodide leads to a mixture of *trans*-$[PtBr_4I(OH_2)]^-$ and *trans*-$[PtBr_4I(OH)]^{2-}$. Rate constants for reaction of iodide with the aquo- and hydroxy-complexes have been determined, as well as a value of 3.7 for the pK_a of the aquo complex.

DAVID W. JOHNSON et ANTHONY POË. Can. J. Chem. **52**, 3083 (1974).

On réexamine les étapes successives de la réaction du complexe $[PtBr_6]^{2-}$ avec l'iodure en portant une attention particulière à leur dépendance du pH. Une revision de deux des trois étapes est nécessaire; le mécanisme intime reste toutefois inchangé. La réoxydation de $[PtBr_4]^{2-}$ produite par la réduction lente de $[PtBr_6]^{2-}$ avec l'iodure conduit à un mélange de *trans*-$[PtBr_4I(OH_2)]^-$ et de *trans*-$[PtBr_4I(OH)]^{2-}$. On détermine les constantes de vitesse des réactions de l'iodure avec le complexe aqueux et l'hydroxy-complexe de même que la valeur de pK_a de 3.7 pour le complexe aqueux. [Traduit par le journal]

Can. J. Chem. Downloaded from www.nrcresearchpress.com by 210.87.254.40 on 09/05/12
For personal use only.

Reaction mechanisms of platinum(IV) complexes have recently been reviewed (1, 2). One that is of particular importance for halide interchange reactions of anionic complexes is reductive elimination followed by oxidative addition (r.e.o.a.). Proposed originally by Grinberg and co-worker (3) it has recently been confirmed and elaborated (4). This mechanism is believed to operate in the reaction of $[PtBr_6]^{2-}$ with iodide to form $[PtI_6]^{2-}$ (5), a reaction that proceeds in three kinetically distinct stages, each of which was proposed to be of the form shown in reaction 1 where the four ligands in the plane perpendicular to the page (omitted for simplicity) were Br_4, *trans*-Br_2I_2, and I_4 in the first, second, and third stages, respectively. This conclusion was based in part on the observation that the second and third stages were also detected after the very rapid oxidation of $[PtBr_4]^{2-}$ by I_3^-–I^- mixtures. However, a study of the p*H* dependence of the reactions has shown that Stages II and III are more complicated than this, each consisting of at least two parallel reactions, but that no change is necessary in the basic type of mechanism proposed.

$$[1]\quad I^- + Br\text{—}Pt(IV)\text{—}Br \xrightarrow[\text{slow}]{} I\text{—}Br + Pt(II) + Br^- \xrightarrow[\text{very fast}]{I^-} Br^- + I\text{—}Pt(IV)\text{—}I$$

Experimental and Results

Sodium hexabromoplatinate(IV) hexahydrate, sodium hexachloroiridate(IV), and potassium tetrabromoplatinate(II) (Johnson, Mathey and Mallory, Ltd.) were used as received. The kinetics were followed in the same way as before (5), reacting solutions being contained in tightly stoppered cells in the thermostatted cell holder of a Perkin–Elmer 402 or Cary 16K recording spectrophotometer and the changing absorbance at a fixed wavelength being followed automatically. The temperatures of the solutions were measured directly with a calibrated thermistor and Wheatstone Bridge, and were constant to within ± 0.05 °C throughout the period of the reactions. The ionic strengths of the solutions were controlled by addition of sodium perchlorate and their p*H* values were adjusted with standard perchloric acid solutions, the values being measured with an Instrumental Laboratory, Model 205, p*H* meter.

Stage I

The kinetics were followed in the presence of a pseudo-first-order excess of iodide by observing the growth in absorbance at 430 nm which is close to an isosbestic point for Stage II. Isos-

[1]To whom all correspondence should be addressed.

Can. J. Chem. Downloaded from www.nrcresearchpress.com by 210.87.254.40 on 09/05/12
For personal use only.

TABLE 1. Rate constants for Stage I of the $[PtBr_6]^{2-}$–I^- reaction[a]

Temperature (°C)	$10^3\ \mu$[b] (M)	pH	k_2 (l mol^{-1} s^{-1})
20.0	1.00	3.90	2.08, 2.06
20.0	1.00	3.90	2.02, 2.10[c]
20.0	1.00	3.90	1.83, 1.95[d]
20.0	1.00	3.40	2.26, 2.48
20.0	1.00	4.40	1.99, 2.16
20.0	1.00	5.40	2.18, 2.30
20.0	1.00	6.90	2.08, 2.12
20.0	0.50	6.90	1.99, —
20.0	2.00	2.85	1.99, 2.03
20.0	2.50	6.90	2.10, —
20.0	10.0	2.30	2.70, 2.74
20.0	10.5	6.90	2.64, —
20.0	50.5	6.90	4.34, —
20.0	100	6.90	4.86, —
15.0	5.50	6.90	1.87, 1.69
20.0	5.50	6.90	2.36, 2.40
25.0	5.50	6.90	3.44, 3.75
30.0	5.50	6.90	6.02, 6.10
35.0	5.50	6.90	8.02, 8.45

$\Delta H^{\ddagger} = 56.6 \pm 2.9$ kJ mol^{-1} $\Delta S^{\ddagger} = -44.2 \pm 9.7$ J mol^{-1} K^{-1}

$\sigma_{k_2} = \pm 9.0\%$

[a] $[PtBr_6^{2-}] = 9.1 \times 10^{-5}\ M$, $[I^-] = 5.0 \times 10^{-4}\ M$, $k_2 = k_{obs}/[I^-]$.
[b] μ = ionic strength.
[c] $[IrCl_6^{2-}] = 8 \times 10^{-6}\ M$.
[d] $[IrCl_6^{2-}] = 1 \times 10^{-4}\ M$.

bestic points were observed at 279, 334, 371, and 393 nm during Stage I at pH = 6.9 in quite good agreement with those observed before (5). However, the isosbestic point at 279 nm shifted to 283 nm at pH = 2.3 and the growth of a shoulder at *ca.* 490 nm was much more pronounced at the lower pH, suggesting a possible pH-dependence of the nature of the product. The observed pseudo-first-order rate constants were divided by $[I^-]$ (the reaction having already been shown to be first-order in iodide (5)) and the resulting values of the second-order rate constant for Stage I are reported in Table 1. The activation parameters were obtained by a least-squares analysis of data at ionic strength $5.5 \times 10^{-3}\ M$ in which each value of k_2 was assumed to have the same percentage uncertainty. The quoted uncertainties are standard deviations that have been adjusted according to the number of degrees of freedom so that 95% confidence limits can be obtained by doubling them.

Stage II

This was followed at 470 nm (an isosbestic point for the subsequent stage (5)) with a pseudo-first-order excess of iodide and the observed pseudo-first-order rate constants were divided by $[I^-]$ to give values of k_2 for Stage II (Table 2).

TABLE 2. Rate constants for Stage II of the $[PtBr_6]^{2-}$–I^- reaction[a]

Temperature (°C)	$10^3\ \mu$ (M)	pH	$10^2\ k_2$ (l mol^{-1} s^{-1})
17.1	50.0	6.90	15.2[b]
17.1	50.0	6.90	14.0[b,c]
17.1	50.0	6.90	15.5[b,d]
20.0	10.0	5.40	25.2, 27.6
20.0	10.0	5.16	28.0
20.0	10.0	5.02	29.1
20.0	10.0	4.70	29.6, 30.4
20.0	10.0	4.62	29.9
20.0	10.0	4.40	32.0
20.0	10.0	4.10	33.9
20.0	10.0	3.86	41.8, 43.4
20.0	10.0	3.00	52.8, 55.4
20.0	10.0	2.70	57.6, 58.5

[a] $[PtBr_6^{2-}] = 9.1 \times 10^{-5}\ M$, $[I^-] = 5.0 \times 10^{-3}\ M$, $k_2 = k_{obs}/[I^-]$.
[b] $[I^-] = 5.0 \times 10^{-2}\ M$.
[c] $[IrCl_6^{2-}] = 8.0 \times 10^{-6}\ M$.
[d] $[IrCl_6^{2-}] = 2 \times 10^{-5}\ M$.

The rate constants at 17.1 °C interpolate quite well into the rather scattered data in ref. 5 but Fig. 1 shows that the rates are dependent on the pH of the solutions.

Discussion

Data in Table 1 are in good agreement with earlier ones (5) and show, in addition, that the

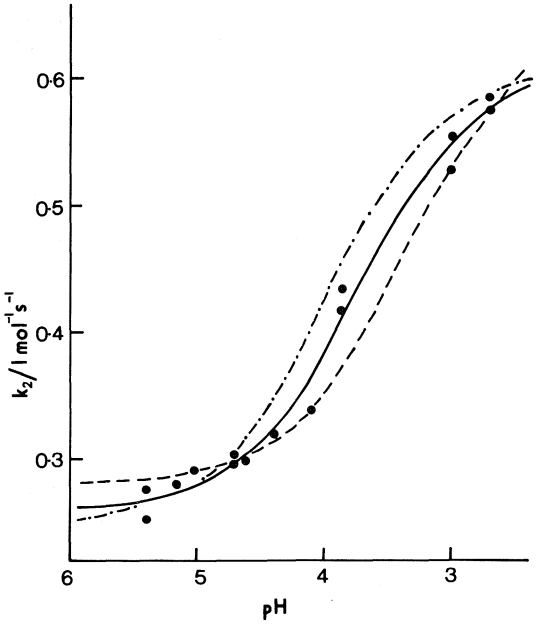

FIG. 1. pH dependence of k_2 for Stage II. Curves are calculated according to parameters quoted in the text.

rates are independent of pH from 3.4 to 6.9. Values of log k_2 increase linearly with $\mu^{1/2}$ up to $\mu = 0.05\ M$. A least-squares analysis shows the gradient to be $1.75 \pm 0.20\ M^{-1/2}$, each individual measurement of the rate constant having a standard deviation of $\pm 4.5\%$. This compares with values $\pm 9.0\%$ and $\pm 8.4\%$ obtained from the temperature dependence (Table 1) and from the data at 20 °C and $\mu = 1.0\ M$, respectively. The gradient is in accord with that expected (6) for a bimolecular reaction between uni- and di-valent anions in solution. Hexachloro-iridate(IV) has no effect on the rates and this confirms the absence of complications due to platinum(III) intermediates (5, 7). The suggestion that there is an acid–base equilibrium involving the products of Stage I is confirmed by the pronounced pH-dependence of the rates of Stage II (Fig. 1). This can most reasonably be explained if Stage I is as shown in reaction 2 so

$$[2a] \quad [PtBr_6]^{2-} \xrightarrow[\text{slow}]{I^-} IBr + [PtBr_4]^{2-} + Br^-$$

$$[2b] \quad [PtBr_4]^{2-} \xrightarrow[\text{fast}]{IBr} \textit{trans}\text{-}[PtBr_4I(OH_2)]^- \text{ and } \textit{trans}\text{-}[PtBr_4I(OH)]^{2-}$$

that the product is an equilibrium mixture of *trans*-iodoaquo- and *trans*-iodohydroxy-complexes. This implies that even in the presence of iodide, admittedly at rather low concentrations, solvent usually competes successfully with iodide for the active site *trans* to the site of oxidation by halogen.

This competition was previously assumed (5) to be in favor of the iodide ion. However, oxidation of $[Pt(CN)_4]^{2-}$ with bromine in the presence of bromide has been shown to occur extremely rapidly to form *trans*-bromoaquo and *trans*-bromohydroxy products at low $[Br^-]$ (8, 9) and even up to $[Br^-] = 0.02\ M$ (12) so the phenomenon is probably quite general. The relatively slow reaction following the rapid oxidation is anation of the aquo complex by bromide to form *trans*-$[Pt(CN)_4Br_2]^{2-}$ and data for this reaction are also in accord with the r.e.o.a. mechanism (12), the slowness being due to the small proportion of oxidation processes that lead directly to the product with two *trans* bromide ligands. The reaction scheme, somewhat simplified, is therefore as shown in reactions 3*a*–3*c*

$$[3a] \quad Br_2 + Pt(CN)_4^{2-} \xrightarrow[\text{fast}]{\text{very}} Br^- + \textit{trans}\text{-}[Pt(CN)_4Br(OH_2)]^- \text{ and } \textit{trans}\text{-}[Pt(CN)_4Br(OH)]^{2-}$$

$$[3b] \quad \textit{trans}\text{-}[Pt(CN)_4Br(OH_2)]^- + Br^- \xrightarrow[\text{slow}]{} Br_2 + Pt(CN)_4^{2-}$$

$$[3c] \quad Br_2 + Pt(CN)_4^{2-} + Br^- \xrightarrow[\text{fast}]{} Br^- + \textit{trans}\text{-}[Pt(CN)_4Br_2]^{2-}$$

the initial "kinetic" products being a mixture of aquo and hydroxy complexes, the final, thermodynamically most stable product being formed by the r.e.o.a. anation of *trans*-$[Pt(CN)_4Br(OH_2)]^-$. (Although the intermediates Br_2 and $Pt(CN)_4^{2-}$ are shown as separate, independent species there is good evidence that they are probably associated with each other to some extent (8*a*, 12).)

The data for Stage II can be analyzed according to the rate equation in [4] characteristic of parallel second order reductions of the aquo

$$[4] \quad k_2 = k_{obs}/[I^-] = \{k_{OH_2} + k_{OH}K_a/[H^+]\}/\{1 + K_a/[H^+]\}$$

and hydroxy complexes. K_a is the acid dissociation constant of the aquo complex, and k_{OH_2} and

Can. J. Chem. Downloaded from www.nrcresearchpress.com by 210.87.254.40 on 09/05/12
For personal use only.

Can. J. Chem. Downloaded from www.nrcresearchpress.com by 210.87.254.40 on 09/05/12
For personal use only.

k_{OH} are the second-order rate constants for the slow reduction of the aquo and hydroxy complexes, respectively. Equation 4 can be rearranged to give [5]. Above p*H* *ca.* 5 the second-order rate constants are essentially independent

$$[5] \quad (k_2 - k_{OH})/[H^+] = k_{OH_2}/K_a - k_2/K_a$$

of p*H* with a value of *ca.* 0.26 l mol^{-1} s^{-1}. This value is therefore assignable to k_{OH}, and a plot of $(k_2 - k_{OH})/[H^+]$ against k_2 is linear as expected. The extreme curves in Fig. 1 correspond to the values $k_{OH} = 0.28$ l mol^{-1} s^{-1}, $k_{OH_2} = 0.63$ l mol^{-1} s^{-1}, and $K_a = 3.8 \times 10^{-4}$ mol l^{-1} (- - -), and $k_{OH} = 0.24$ l mol^{-1} s^{-1}, $k_{OH_2} = 0.60$ l mol^{-1} s^{-1}, and $K_a = 1 \times 10^{-4}$ mol l^{-1} (·····), so that the values of k_{OH} and k_{OH_2} are quite well defined and pK_a must certainly fall within the limits 3.7 ± 0.3. The solid line corresponds to $k_{OH} = 0.26$ l mol^{-1} s^{-1}, $k_{OH_2} = 0.60$ l mol^{-1} s^{-1}, and $K_a = 1.7 \times 10^{-4}$ mol l^{-1} with a standard deviation of k_2 (obs) from k_2 (calcd) of $\pm 4.3\%$.

The p*H* dependence of the rates of anation of mixtures of *trans*-$[Pt(CN)_4Br(OH_2)]^-$ and *trans*-$[Pt(CN)_4Br(OH)]^{2-}$ shows that the hydroxy complex is reduced by bromide at a rate that is quite negligible compared with that of the aquo complex whereas *trans*-$[PtBr_4I(OH)]^{2-}$ is reduced by iodide less than 3 times more slowly than the corresponding aquo complex. This suggests that the site of reduction of the hydroxy complex in Stage II is probably a bromide ligand *trans* to another bromide rather than one *trans* to hydroxide. It is also possible that a similar site is attacked in the aquo complex (so that the small difference between k_{OH} and k_{OH_2} represents a relative *cis* effect of OH^- and OH_2 ligands) although attack at the iodide *trans* to the OH_2 ligand cannot be ruled out. The products of Stage II may therefore be quite complex mixtures of aquo- and hydroxy-iodobromo complexes and this makes any consideration of Stage III premature at this stage. The original study of Stage II (5) involved solutions equilibrated with the atmosphere and the activation parameters obtained then are, therefore, appropriate to the r.e.o.a. reaction of the hydroxy complex.

The value of $pK_a = 3.7$ for *trans*-$[PtBr_4I(OH_2)]^-$ compares with 4.4 for $[PtBr_5(OH_2)]^-$ (10), where only the ligand *trans* to the aquo group is changed, and a value of 8.6 for $[PtI_5(OH_2)]^-$ (11), where the four *cis* ligands have been changed. The *cis* effect of four iodides relative to four bromides decreases the acidity by about 5 units of pK_a whereas a *trans* iodide increases the acidity by *ca.* 0.7 units compared with bromide. The pK_a value of *ca.* 1.6 for *trans*-$[Pt(CN)_4Br(OH_2)]^-$ (8, 9) shows that four *cis* cyanides strengthen the acidity by *ca.* 3 pK_a units compared with four bromides. A *cis* acid-strengthening effect CN > Br > I, and a *trans* acid-strengthening effect I > Br are, therefore, defined. The magnitudes of the inequalities are not too dissimilar when the *cis* effect is adjusted to take account of the number of ligands involved. Further data obtained under more closely comparable conditions are required before a detailed explanation can be offered but one might remark here that the *trans* effect is not in accord with the relative Pt—OH_2 bond strengths expected from the σ inductive effects of iodide and bromide but could be explained in terms of greater repulsive π effects in the Br—Pt—OH system compared with that in I—Pt—OH. The *cis* effect order seems to require a normal inductive effect for bromide and iodide but an overriding π-acceptor effect of CN which allows for a smaller repulsive π effect in the Pt—OH bond.

The authors are grateful to the National Research Council of Canada and Erindale College for support of this work.

1. A. Peloso. Coord. Chem. Rev. **10**, 121 (1973).
2. W. R. Mason. Coord. Chem. Rev. **7**, 241 (1972).
3. A. A. Grinberg and G. A. Shagisultanova. Bull. Acad. Sci. USSR, 895 (1955).
4. A. J. Poë and D. J. Vaughan. J. Am. Chem. Soc. **92**, 7537 (1970) and references therein.
5. E. J. Bounsall, D. J. Hewkin, D. Hopgood, and A. J. Poë. Inorg. Chim. Acta, **1**, 281 (1967).
6. A. A. Frost and R. G. Pearson. Kinetics and mechanism. 2nd ed. Wiley, New York. 1961. p. 150.
7. R. L. Rich and H. Taube. J. Am. Chem. Soc. **76**, 2608 (1954).
8. (*a*) C. E. Skinner and M. M. Jones. J. Am. Chem. Soc. **91**, 4405 (1969); (*b*) M. M. Jones and K. A. Morgan. J. Inorg. Nucl. Chem. **34**, 259 (1972).
9. W. R. Mason. Inorg. Chem. **10**, 1914 (1971).
10. C. M. Davidson and R. F. Jameson. Trans. Faraday Soc. **61**, 2462 (1965).
11. B. Corain and A. J. Poë. J. Chem. Soc. A, 1633 (1967).
12. A. J. Poë and C. P. J. Vuik. Unpublished results.

Etude cinétique des interactions électrostatiques entre la phosphatase alcaline intestinale de veau et ses substrats[1]

MARIUS JULIEN[2] ET LUDOVIC OUELLET

Département de Chimie, Université Laval, Québec 10, Québec G1K 7P4

Reçu le 15 février 1974

MARIUS JULIEN et LUDOVIC OUELLET. Can. J. Chem. **52**, 3087 (1974).

Le rôle de la charge de la molécule d'enzyme dans la cinétique de la réaction catalysée par diverses phosphatases alcalines a été étudié. Les données expérimentales obtenues en utilisant le phosphate de *p*-nitrophényle (charge nette -2) comme substrat montrent que la répulsion entre le molécule d'enzyme, de charge négative, et la molécule de substrat peut tenir compte, quantitativement, de la variation de la constante de Michaelis du système avec le p*H* entre p*H* 8.5 et p*H* 10.5. Toutefois les résultats obtenus en utilisant le phosphate d'éthanolamine (charge nette, -1) et de *p*- ou *o*-carboxyphényle (charge nette -3) montrent soit que la partie organique de la molécule de substrat ne joue aucun rôle dans la formation du complexe enzyme–substrat, ou que la charge de la molécule d'enzyme ne joue pas le rôle suggéré par les résultats obtenus avec le phosphate de *p*-nitrophényle.

Une étude plus poussée de cette dernière réaction en variant la force ionique et la constante diélectrique du milieu suggère que le centre actif de la molécule d'enzyme soit porteur d'une charge positive, et soit hydrophobe.

MARIUS JULIEN and LUDOVIC OUELLET. Can. J. Chem. **52**, 3087 (1974).

The role played by the ionic charge of the enzyme in the kinetics of the reactions catalyzed by alkaline phosphatases has been investigated. Data obtained from the hydrolysis of *p*-nitrophenyl phosphate (net charge -2) indicate that the repulsion between the negatively charged enzyme molecule and the substrate molecule is sufficient to take into account, quantitatively, the variation of the Michaelis constant with the p*H* of the system between p*H* 8.5 and 10.5. However, the results obtained with ethanolamine phosphate (net charge -1) and *p*- or *o*-carboxyphenyl phosphate (net charge -3) show that either the organic part of the substrate molecule is not involved in the formation of the enzyme substrate intermediate or the charge of the enzyme does not have the role suggested from the work with *p*-nitrophenyl phosphate.

Further investigation of this reaction in solutions of various ionic strength and dielectric constants suggests that the active center of the enzyme molecule is positively charged, but that hydrophobic effects are important.

Introduction

La phosphatase alcaline intestinale de veau (EC 3.1.3.1.) a déjà fait l'objet de plusiers études cinétiques. Lazdunski et Ouellet ont étudié son action catalytique sur l'hydrolyse du phosphate de *p*-nitrophényle (1), sa sensibilité à certains inhibiteurs (2), et, en collaboration avec Brouillard, sa sensibilité aux variations de force ionique et de constante diélectrique (3). Fernley et Walker ont examiné sa phosphorylation par quelques substrats (4), sa spécificité (5), et sa catalyse de l'hydrolyse du phosphate de méthyl-4 umbellyphéryle (6). Quant à Fernley et Bisaz, ils ont étudié sa phosphorylation par l'acide pyrophosphorique (7).

Jusqu'à présent, Lazdunski *et al.* (3) semblent les seuls à avoir accordé une importance prépondérante aux effets des variations de charge de la phosphatase intestinale sur son action catalytique. Or, il est difficile de penser que les effets de p*H* en particulier ne sont pas liés à ceux de la charge de la molécule de phosphatase. En effet, de p*H* 7.5 à p*H* 10.5, domaine couvrant la majorité des études cinétiques, la charge de cette molécule varie considérablement et comme tous les substrats sont également porteurs de charges, les interactions entre ces charges et celle de l'enzyme ne sont peut-être pas à négliger.

Malheureusement, une étude quantitative de ces interactions est pratiquement impossible pour l'instant, parce que la phosphatase alcaline intestinale de veau n'a pas encore été titrée à l'état pur. Les données de Lazdunski *et al.* à ce sujet (3) furent en effet obtenues à partir de

[1]Extrait de la thèse de doctorat de Marius Julien, Université Laval, Québec 10, Québec, 1970.

[2]Adresse actuelle: Petit Séminaire de Québec, 1, rue de la Fabrique, Québec 4, Québec.

Can. J. Chem. Downloaded from www.nrcresearchpress.com by 210.87.254.42 on 09/05/12
For personal use only.

préparations dont le contenu en phosphatase était de beaucoup plus faible qu'ils ne le croyaient et ne peuvent donc être retenues telles quelles. On peut, malgré tout, avoir une idée de la charge nette de cet enzyme en sachant, d'une part, qu'elle diminue lorsque le p*H* augmente et en la comparant, d'autre part, avec celle d'une molécule apparentée: la phosphatase alcaline d'*Escherichia coli*. Quelques électrophorèses sur papier nous ont en effet permis d'observer que le point isoélectrique de la phosphatase intestinale est aux environs de p*H* 6.5 à 25 °C. Le titrage de la phosphatase bactérienne, réalisé par Reynolds et Schlesinger (8), établit par ailleurs que le point isoionique de cet enzyme est à p*H* 6.3 à 6 °C. Sachant ainsi que les deux phosphatases ont à peu près le même point isoionique et que la masse moléculaire de la phosphatase intestinale est légèrement supérieure à celle de la phosphatase de *E. coli* (100 000 (9) dans le premier cas contre 86 000 (10) dans le second) on peut admettre en première approximation que les charges sont dans le même rapport que les masses moléculaires. Ces données doivent nous suffire pour préciser l'influence de la charge de la phosphatase intestinale sur son activité catalytique.

Théorie et modèle

L'hydrolyse enzymatique des monoesters phosphoriques, catalysée par la phosphatase alcaline intestinale de veau, se fait au minimum en trois étapes qu'on peut schématiser comme suit:

$$[1]\quad E + S \underset{k_{-1}}{\overset{k_1}{\rightleftharpoons}} ES \xrightarrow{k_2} EP_i \xrightarrow{k_3} E + P_i$$
$$\qquad\qquad\qquad\qquad\qquad\qquad\quad P$$

où, E représente l'enzyme, S le substrat, ES le complexe de Michaelis, EP_i la phosphorylphosphatase, P le radical organique du substrat et P_i l'acide phosphorique.

Aux conditions rapportées dans ce travail, la vitesse initiale d'hydrolyse est donnée par la loi de Michaelis–Menten (11).[3]

$$[2]\qquad v = \frac{V_m[S]}{K_m + [S]}$$

où, d'après Hearon (12)

$$[3]\qquad V_m = \frac{[E]_0}{1/k_2 + 1/k_3}$$

et

$$[4]\qquad K_m = \frac{(k_{-1} + k_2)k_3}{k_1(k_2 + k_3)}$$

Or, d'après les résultats de Fernley et Walker (4), la formation de la phosphorylphosphatase est l'étape déterminante de la réaction en milieu alcalin; on peut donc admettre que la constante k_2 de l'éq. 1 est bien inférieure à la constante k_3. Cette conclusion est d'ailleurs confirmée par les résultats de la fig. 7 qui montrent des vitesses maxima différentes selon les substrats. Si la déphosphorylation (k_3) était déterminante, on devrait avoir des courbes identiques et superposées pour les trois cas qui y sont montrés, ce qui n'est manifestement pas le cas. L'éq. 3 devient alors:

$$[5]\qquad V_m = k_2[E]_0$$

Par ailleurs, on peut considérer, en première approximation, que la formation du complexe de Michaelis est une réaction d'équilibre véritable. Cela implique que la constante k_2 est également inférieure à la constante k_{-1}, de telle sorte que l'éq. 4 devient:

$$[6]\qquad K_m = k_{-1}/k_1$$

Si l'on veut maintenant considérer les effets que peuvent avoir les interactions électrostatiques entre la charge de la phosphatase et celles de ses substrats, on peut se référer aux modèles de la fig. 1. La formation du complexe de

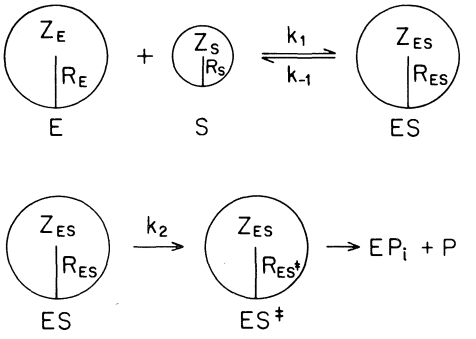

FIG. 1. Modèle cinétique décrivant les interactions électrostatiques entre la phosphatase alcaline et ses substrats (voir le texte pour la signification des symboles).

[3]A p*H* inférieur à 9 et à force ionique faible (0.01), la réaction d'hydrolyse présente un effet certain d'activation par excès de substrat, lequel disparaît progressivement lorsque le p*H* et/ou la force ionique s'élève. Il est évidemment invisible à toutes conditions lorsque la concentration de substrat est faible (26).

Can. J. Chem. Downloaded from www.nrcresearchpress.com by 210.87.254.42 on 09/05/12
For personal use only.

Can. J. Chem. Downloaded from www.nrcresearchpress.com by 210.87.254.42 on 09/05/12
For personal use only.

Michaelis y est représentée comme l'association de deux ions sphériques, E et S, de charges respectives Z_E et Z_S et de rayons R_E et R_S, laquelle association donne un ion également sphérique ES, de charge Z_{ES} supposée égale à $Z_E + Z_S$ et de rayon R_{ES}. En admettant, comme l'explicite la relation 6, que K_m est une constante d'équilibre, on peut alors écrire:

$$[7] \qquad -kT \ln K_m = \Delta G_{n.e.s.} + \Delta G_{e.s.}$$

où, $\Delta G_{n.e.s.}$ et $\Delta G_{e.s.}$ représentent respectivement les variations d'énergie libre standard non électrostatique et électrostatique relatives à la dissociation du complexe ES, k est la constante de Boltzman et T la température absolue.

Or, d'après Tanford (13), l'énergie libre électrostatique G_i d'un ion sphérique i, de rayon R_i et charge Z_i, plongé dans un milieu de constante diélectrique D et de force ionique μ, est donnée par la relation suivante:

$$[8] \qquad G_i = \frac{Z_i^2 e^2}{2DR_i}\left(1 - \frac{\kappa R_i}{1 + \kappa a_i}\right)$$

où

$$[9] \qquad \kappa = \left(\frac{8\pi e^2 N\mu}{1000DkT}\right)^{1/2}$$

Dans ces relations 8 et 9, e est la charge de l'électron, N le nombre d'Avogadro et a_i le rayon d'exclusion de l'ion i. Ainsi, en admettant que Z_{ES} soit égale à $Z_E + Z_S$, et en combinant les relations 7 et 8, on obtient:

$$[10] \quad -\ln K_m = \Delta G_{n.e.s.}/kT + Z_E^2(w_E - w_{ES}) + Z_S^2(w_S - w_{ES}) - 2Z_E Z_S w_{ES}$$

où, w_i le facteur électrostatique de l'espèce i est donné par

$$[11] \qquad w_i = \frac{e^2}{2DkT}\left(\frac{1}{R_i} - \frac{\kappa}{1 + \kappa a_i}\right)$$

Si l'on admet de plus, que le facteur w_{ES} est à peu près égal au facteur w_E, ce que permet la similitude des rayons des espèces ES et E, et que le terme en Z_S^2 est une constante et probablement négligeable devant le terme en $Z_E Z_S$, on obtient finalement

$$[12] \qquad pK_m = pK_m' - 0.87\, Z_E Z_S w_E$$

où, pK_m' est une constante qui dépend la nature du substrat. De là, on tire ensuite les relations 13 et 14, qui rendent compte des effets de constante diélectrique et de force ionique sur pK_m.

$$[13] \qquad \frac{dpK_m}{d(1/D)} = \frac{0.435e^2 Z_E Z_S}{kTR_E}$$

$$[14] \qquad \frac{dpK_m}{d\mu^{1/2}} = \frac{0.435\kappa e^2 Z_E Z_S}{DT\mu^{1/2}(1 + \kappa a_E)^2}$$

La relation 13 suppose que le facteur de Debye–Hückel κ est une constante. Ceci tient si le rapport μ/DT est constant (voir résultats et discussion).

Quant à la formation de la phosphorylphosphatase, la fig. 1 montre que, d'un point de vue électrostatique, la formation du complexe activé correspondant devrait apparaître comme le changement de volume d'un ion sphérique de charge Z_{ES} dont le rayon passerait d'une valeur R_{ES} à une valeur $R_{ES}^{\ddagger}$. Ce modèle a déjà permis à Lazdunski *et al.* (3) d'interpréter certains de leurs résultats, lesquels ne tenaient toutefois pas compte de l'effet d'activation par excès de substrat auquel fait allusion la note 3.

En combinant les relations 5, 8, 11 et 15,

$$[15] \qquad \ln k_2 = \ln k_2^0 - \Delta G^{\ddagger}/kT$$

on obtient

$$[16] \quad \log V_m = \log V_m' - 0.435Z_{ES}^2(w_{ES}^{\ddagger} - w_{ES})$$

où V_m' est une constante. Les effets de constante diélectrique et de force ionique sur $\log V_m$ sont alors donnés par les relations 17 et 18

$$[17] \qquad \frac{d \log V_m}{d(1/D)} = -\frac{Z_{ES}^2 e^2}{4.6kT}\left(\frac{1}{R_{ES}^{\ddagger}} - \frac{1}{R_{ES}}\right)$$

$$[18] \qquad \frac{d \log V_m}{d\mu^{1/2}} = -\frac{Z_{ES}^2 e^2 A(a_{ES}^{\ddagger} - a_{ES})}{4.6DkT}$$

La relation 17 est obtenue en supposant que le facteur $\kappa/(1 + \kappa a_i)$ est le même pour chacun des complexes ES et $ES^{\ddagger}$. Le symbole A de l'éq. 18 représente une fonction positive de la force ionique.[4]

Partie expérimentale

Les réactifs

La phosphatase alcaline intestinale de veau provient de Mann Research Laboratories (No 4806). L'activité spécifique de cette préparation n'étant que d'environ 2.2×10^2 unités Roche *et al.* (14), elle fut portée à 4.5×10^4 unités Roche grâce à une chromatographie sur DEAE-cellulose, suivie d'une filtration sur gel de séphadex de type G-200. Dans chacun des cas, la préparation

[4] $A = (2\kappa^2 + \kappa^3 a_{ES}^{\ddagger} + \kappa^3 a_{ES})/\sqrt{\mu}(1 + \kappa a_{ES}^{\ddagger})^2(1 + \kappa a_{ES})^2$.

Can. J. Chem. Downloaded from www.nrcresearchpress.com by 210.87.254.42 on 09/05/12
For personal use only.

des colonnes (2.5 × 100 cm) et l'élution furent réalisées avec un tampon trishydroxyméthylaminométhane–HCl 0.01 *M* à p*H* 8.5, contenant du $MgCl_2$ 10^{-5} *M* et du KCl en quantité adéquate pour donner une force ionique de 0.01. Pour la chromatographie toutefois, la force ionique fut augmentée linéairement de 0.01 à 0.1 avec les 600 premiers ml élués, et gardée constante par la suite. Toutes les opérations furent effectuées à 15 °C.

La phosphatase alcaline d'*Escherichia coli* provient de Sigma Chemical Corp. (Alkaline Phosphatase from *E. coli*, type III). Son degré de pureté étant supérieur à 95%, elle fut utilisée directement après dilution dans des tampons appropriés.

La phosphate de *p*-nitrophényle vient de Sigma Chemical Corp. (Sigma 104, Phosphatase Substrate). Les phosphates d'éthanolamine et d'*o*-carboxyphényle sont de Mann Research Laboratories (No 2264 et 2029). Le phosphate de *p*-carboxyphényle fut préparé selon les indications de Chanley et Feageson (15).

Comme tampons, le trishydroxyméthylaminométhane (Fisher Chemical Corp.; No T-370) servit aux p*H* inférieurs à 8.6, l'éthanolamine (Eastman Organic Chemical; No 1597) de p*H* 8.6 à p*H* 10.0 et la triéthylamine (Matheson, Coleman et Bell; No 5325) aux p*H* supérieurs à 10.0. Ils furent utilisés à une concentration de 0.004 *M* et amenés aux p*H* choisis par addition de HCl 1.0 *N*.

Le dioxanne (Fisher Scientific Co.; No D-111) fut purifié selon la méthode rapportée par Fieser (16). Cette purification est particulièrement importante, parce que les impuretés présentes dans le dioxanne affectent le p*H* des mélanges eau–dioxanne.

Toutes les solutions furent préparées dans l'eau distillée dans un appareil en verre.

Les mesures

Toutes les mesures, sauf celles dont les résultats sont donnés dans la fig. 2, furent effectuées à une température de 25.3 ± 0.1 °C.

La force ionique μ toujours controlée rigoureusement, fut généralement maintenue à une valeur de 0.01, par des additions adéquates de KCl. Lors de ces additions, il fut tenu compte des constantes d'ionisation des substrats et des tampons.

Le dioxanne servit de modificateur de constante diélectrique, *D*. Les valeurs de *D* des mélanges eau–dioxanne furent calculées à partir des données de Akerlöf et Short (17).

La mesure du p*H* se fit avec un p*H*-mètre Radiometer TTTl-b, muni d'une électrode de calomel K-401. Les tampons standard Harleco (Canlab; No 43-907/1, /2 et /3) servirent à l'étalonnage. Le p*H* des solutions contenant du dioxanne fut déterminé par la méthode de Inagami et Sturtevant (18), telle que décrite par Lazdunski *et al.* (3).

Les vitesses initiales d'hydrolyse des substrats furent déterminées comme suit: 39 ml d'une solution contenant du tampon, du substrat et d'autres réactifs (KCl, dioxanne) sont incubés à 25.3 °C pendant 15 min, en même temps que 1 ml d'une solution diluée d'enzyme. La réaction est mise en marche par le mélange rapide des deux solutions. Une portion du mélange est aussitôt versée dans une cellule de 1 cm, de 5 cm ou de 10 cm de trajet optique et placée dans un spectrophotomètre Beckman DU. La réaction est suivie par la mesure de la variation d'absorbance d'un des produits, à une longueur d'onde appropriée. L'absorbance est enregistrée pendant une période de 5 à 15 min suivant les grandeurs des variations observées. La concentration initiale d'enzyme est réglée de façon à ce que le pourcentage de transformation du substrat n'excède pas 10% pendant la durée de l'observation. De cette façon, la vitesse mesurée peut être considérée égale à la vitesse initiale d'hydrolyse. Elle est exprimée en unité arbitraire proportionnelle à la variation d'absorbance en fonction du temps.

L'hydrolyse du phosphate de *p*-nitrophényle est suivie à 407 nm, celle du phosphate d'*o*-carboxyphényle à 310 nm et celle du phosphate de *p*-carboxyphényle à 280 nm. Le phosphate d'éthanolamine ne fut utilisé que comme inhibiteur. Les coefficients d'extinction molaire furent déterminés de la façon habituelle par mesure des variations d'absorbance en fonction de la concentration. A 25.3 °C et à une force ionique de 0.01 les valeurs obtenues pour le *p*-nitrophénol, l'acide salicylique et l'acide *p*-hydroxybenzoïque sont respectivement de 17 880 (407 nm), de 1912 (310 nm) et de 16 480 (280 nm) lorsque ces substances sont totalement ionisées. Dans le cas du *p*-nitrophénol et de l'acide *p*-hydroxybenzoïque, une variation du p*H* s'accompagne d'une variation apparente du coefficient d'extinction qui est due au changement de concentration de l'espèce ionique observée. On tient compte de cette variation en faisant intervenir dans les calculs le facteur de correction $(1 + 10^{pK-pH})$ où *K* est la constante de dissociation qui règle l'ionisation du produit observé. L'hydrolyse des phosphates de *p*-nitrophényle et de *p*-carbonyphényle fut également étudiée en présence de dioxanne. Nous avons vérifié que l'extinction de l'ion *p*-nitrophénolate n'est pas affectée par la présence de dioxanne aux p*H* utilisés dans nos travaux. Par contre, il y a un effet considérable pour l'ion *p*-carboxyphénolate à cause surtout du voisinage du p*H* d'étude et du p*K* d'ionisation de la fonction phénolique (p*H* 9.6, p*K* 9.21). Cet effet étant dû à plusieurs facteurs, nous avons déterminé empiriquement la correction nécessaire à la normalisation des vitesses d'hydrolyse. Nous avons constaté que le logarithme du coefficient d'extinction molaire de l'ion *p*-carboxyphénolate varie linéairement avec l'inverse de la constante diélectrique, à p*H* 9.6, à 25.3 °C et à μ/DT égale à 5.13×10^{-7}. Il diminue de 4.07 à 3.55 lorsque la concentration en volume de dioxanne passe de 0 à 25%.

Quant à la mesure es constantes cinétiques V_m et K_m, elle s'est faite graphiquement, au moyen de la représentation de Lineweaver–Burk (19) de la loi de Michaelis–Menten (éq. 2).

Résultats et discussions

Les données sur la phosphatase alcaline intestinale de veau ne permettant pas une vérification quantitative rigoureuse du modèle proposé dans la fig. 1, nous avons choisi d'en faire tout d'abord une vérification partielle, en l'appliquant à des données obtenues avec la phosphatase alcaline de *E. Coli*. En effet, le titrage de cet enzyme réalisé par Reynolds et Schlesinger (8) permet une telle vérification.

La fig. 2 montre les variations de pK_m pour le

Can. J. Chem. Downloaded from www.nrcresearchpress.com by 210.87.254.42 on 09/05/12
For personal use only.

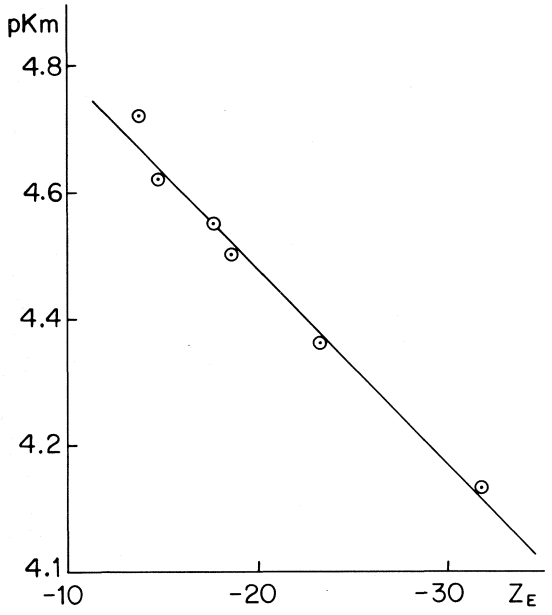

FIG. 2. Variation de pK_m avec la charge de l'enzyme pour le système phosphatase alcaline de *E. coli* – phosphate de *p*-nitrophényle, à 6 °C et à une force ionique de 0.1.

système phosphatase alcaline de *E. Coli*, phosphate de *p*-nitrophényle en fonction de la charge Z_E de la molécule de phosphatase. Les données cinétiques furent obtenues aux mêmes conditions de température et de force ionique que le titrage de l'enzyme, soit à 6 °C et à une force ionique de 0.1. Comme le prévoit l'éq. 12, pK_m varie linéairement avec la charge de la molécule de phosphatase. Le facteur électrostatique w_E calculé à partir de la pente de la courbe de la fig. 2 est, à l'erreur près, égal à celui rapporté par Reynolds et Schlesinger (8) lors du titrage de la phosphatase de *E. coli*. Il est de 0.018 dans le premier cas et de 0.019 dans le second.

La fig. 3, quant à elle, montre l'influence du p*H*, et indirectement celle de la charge de la molécule de phosphatase alcaline intestinale de veau, sur les constantes de Michaelis des phosphates de *p*-carboxyphényle, d'*o*-carboxyphényle, de *p*-nitrophényle et d'éthanolamine. Les charges des substrats sont respectivement de -3, -3, -2 et -1 (-2). Etant donné que la variation de Z_E avec le p*H* est indépendante du substrat, tout comme l'est le facteur w_E, la relation 12 prévoit que les pentes des courbes pK_m–p*H* doivent être proportionnelles aux charges des substrats. Il est évident à l'examen de cette figure que ce n'est pas le cas. Il semble même n'y avoir aucun rapport entre les pentes et les charges des substrats puisque les 4 courbes sont rigoureusement parallèles; la pente étant dans tous les cas de -1.58. Elles sont par surcroît non entières, contrairement à ce qu'exigerait une interprétation classique des effets de p*H* (20). On doit donc admettre que les interactions électrostatiques enzyme–substrat, si elles existent dans ces cas, n'obéissent pas à l'éq. 12.

La fig. 4 montre la variation de pK_m avec l'inverse de la constante diélectrique, à p*H* 9.6 et μ/DT égale à 5.13×10^{-7} (κ constant), dans le cas des phosphates de *p*-carboxyphényle et de *p*-nitrophényle. De façon à maintenir le facteur μ/DT constant, la force ionique varie de 0.0120 à 0.0085 lorsque la constante diélectrique passe de 78.35 à 55.48, ce qui donne une valeur moyenne de μ d'environ 0.01. L'examen de cette figure mène au résultat assez étonnant que les pentes des courbes pK_m–$(1/D)$, tout comme le prévoit l'éq. 13, sont exactement dans le rapport des charges des substrats (-3 à -2), mais qu'elles sont positives. En effet les valeurs de ces

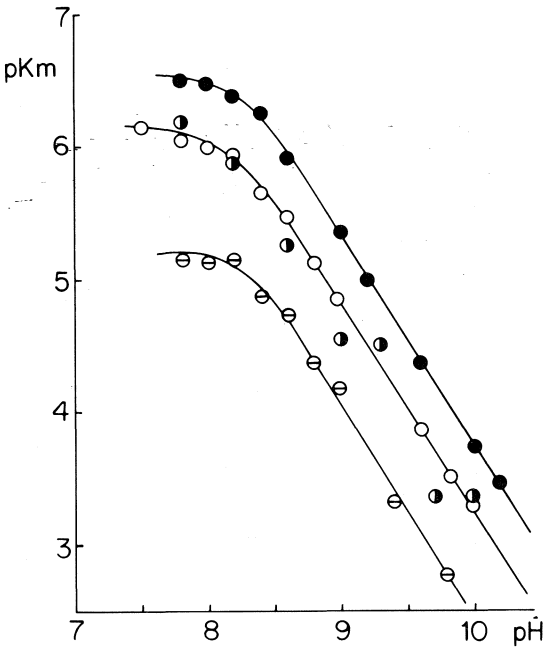

FIG. 3. Variation de pK_m avec le p*H* pour différents systèmes phosphatase alcaline intestinale de veau – substrat à 25.3 °C et à une force ionique de 0.01. Les substrats sont les phosphates de *p*-carboxyphényle (●), d'*o*-carboxyphényle (◑), de *p*-nitrophényle (○), et d'éthanolamine (⊖).

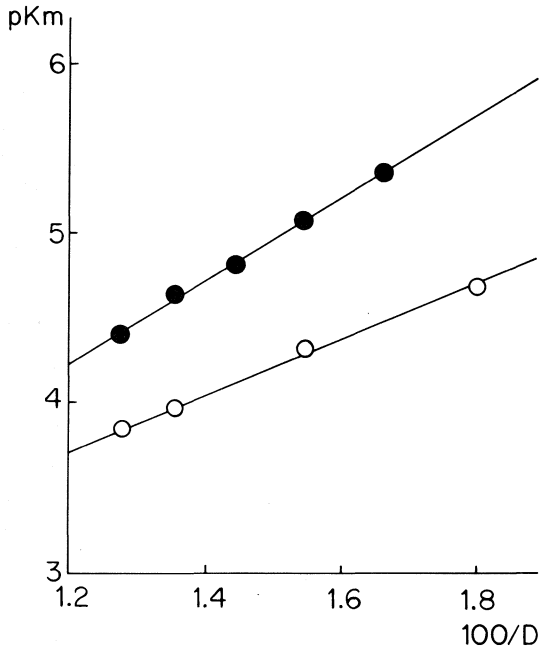

FIG. 4. Variation de pK_m avec l'inverse de la constante diélectrique à 25.3 °C, à pH 9.6 et à μ/DT égal à 5.13×10^{-7} (voir texte) pour les systèmes phosphatase alcaline intestinale de veau – phosphates de *p*-carboxyphényle (●) et de *p*-nitrophényle (○).

pentes sont de 242 et de 161, donnant ainsi un rapport de 1.50.

La plus simple hypothèse permettant d'expliquer ce résultat à la lumière de la relation 13, est de supposer que le centre actif de la molécule de phosphatase porte une charge positive dont les effets sont plus importants que ceux de la charge globale de la molécule. On peut alors prévoir qu'à un pH inférieur à 9.6, les pentes seront encore dans le rapport 3 à 2 mais plus grandes. En effet, on peut considérer ces pentes comme une différence de deux termes dont le plus grand est proportionnel à la charge positive du centre actif et l'autre à la charge négative de la molécule d'enzyme. Si une diminution du pH affecte ces charges, elle ne peut qu'augmenter la charge du centre actif et diminuer celle de l'enzyme dont le point isoionique est en bas de pH 7.

La fig. 5 montre les résultats obtenus à pH 9.0. Cette fois les valeurs des pentes, encore positives, sont de 113 et de 89, donnant ainsi un rapport de 1.27. Aucune des prédictions formulées dans le paragraphe précédent n'est donc vérifiée. D'une part, pour chacun des substrats, les pentes sont plus faibles à pH 9.0 qu'à pH 9.6. D'autre part, le rapport des pentes à pH 9.0 (1.27) est différent du rapport à pH 9.6 (1.50).

L'effet de force ionique sur la constante de Michaelis peut au moins confirmer les hypothèses déjà avancées quant au signe du potentiel électrostatique du centre actif. Comme le montre la fig. 6, obtenue avec le phosphate de *p*-nitrophényle à pH 9.6, pK_m diminue avec la force ionique. Ce résultat, interprété à la lumière de l'éq. 14, mène à la même conclusion que l'examen des figs. 4 et 5: le centre actif est porteur d'une charge positive dont l'influence est plus grande que celle de la charge globale de la molécule de phosphatase.

Ainsi donc, d'après les effets de pH (fig. 2), la charge nette du substrat n'a aucune importance sur les variations de pK_m puisque les courbes pK_m–pH de substrats différemment chargés sont parallèles. Si l'on se rapporte au modèle de la fig. 1, il faut admettre pour expliquer ce parallélisme que les répulsions enzyme–substrat sont limitées au seul groupement phosphorique du substrat. On peut justifier une telle restriction en tenant compte des dimensions relatives de l'atmosphère ionique (environ 30 Å à une force ionique de 0.01) et de la molécule de phosphatase

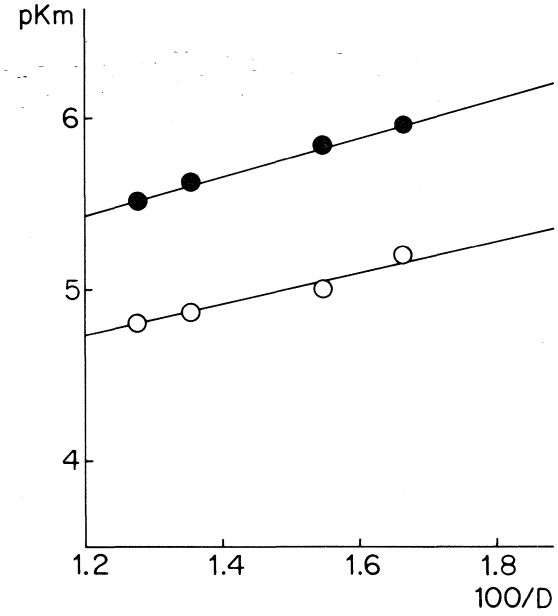

FIG. 5. Variation de pK_m avec l'inverse de la constante diélectrique, à 25.3 °C, à pH 9.0 et à μ/DT égal à 5.13×10^{-7} pour les systèmes phosphatase alcaline intestinale de veau – phosphates de *p*-carboxyphényle (●) et de *p*-nitrophényle (○).

Can. J. Chem. Downloaded from www.nrcresearchpress.com by 210.87.254.42 on 09/05/12
For personal use only.

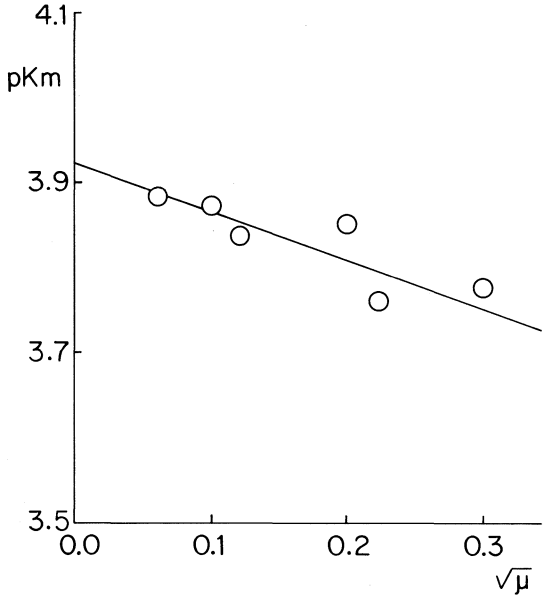

FIG. 6. Influence de la racine carrée de la force ionique sur pK_m pour le système phosphatase alcaline intestinale de veau – phosphate de *p*-nitrophényle, à 25.3 °C et à p*H* 9.6.

(environ 30 Å également). Il est possible en effet que seule la charge du groupement phosphorique du substrat soit en relation étroite avec la charge globale de l'enzyme, les autres se trouvant alors en dehors de l'atmosphère ionique. Cette explication permet de rendre compte des effets de p*H* sur pK_m au moyen de l'éq. 12. Par contre, il faut de nouveau considérer la charge globale du substrat et restreindre celle de l'enzyme à une charge positive située au centre actif, pour expliquer les effets de constante diélectrique et de force ionique sur pK_m.

Plutôt que de tenter de concilier des hypothèses aussi contradictoires, il nous semble préférable de faire intervenir d'autres facteurs, et de considérer, par exemple, la formation du complexe de Michaelis comme un quelconque procédé d'extraction. Une telle hypothèse a déjà permis de rendre compte de certaines propriétés de l'α-chymotrypsine (21, 22), de la déshydrogénase malique (23) et de l'hémoglobine bovine (24). La constante de Michaelis, qui devient en quelque sorte un coefficient de partage, serait alors proportionnelle à la solubilité du substrat dans la phase aqueuse (le solvant) et inversement proportionnelle à sa solubilité dans la phase enzymatique (le centre actif).

Comme tous les substrats de la phosphatase intestinale sont porteurs de charges et fortement polaire, leur solubilité dépend à la fois de leur charge, de leur moment dipolaire et de la polarité du milieu. La région du centre actif, surtout si elle s'étend sous la surface de la molécule d'enzyme, est probablement très hydrophobe et caractérisée par une constante diélectrique très faible. De telles caractéristiques se retrouvent en particulier au centre actif de cette autre hydrolase qu'est la chymotrypsine (25). Posons donc, en tenant compte de la spécificité de groupe de la phosphatase intestinale, que la fixation du substrat à l'enzyme se fait surtout en surface et que seul le groupement phosphorique interfère étroitement avec le centre actif. La faible constante diélectrique de la région située sous la surface pourrait justifier l'importance accordée aux attractions entre la charge positive du centre actif, dont les résultats des figs. 4 et 5 indiquent l'existence, et la charge négative du groupement phosphorique. D'un autre côté, si la charge du centre actif est due à la présence à cet endroit du zinc que contient la phosphatase (9), on pourrait aller jusqu'à concevoir la formation du complexe de Michaelis comme la formation d'un phosphate de zinc. L'extraction du substrat serait alors une association d'ions où, encore une fois, les interactions entre la charge du centre actif et celle du groupement phosphorique auraient beaucoup d'importance.

Quoi qu'il en soit, on peut expliquer les variations de pK_m en admettant que tous les facteurs qui augmentent la solubilité du substrat dans la phase aqueuse ou diminuent sa solubilité au centre actif provoquent une diminution de pK_m. Par exemple, la diminution de pK_m avec l'augmentation du p*H* pourrait s'expliquer par une diminution de la polarité du centre actif, causée par la neutralisation progressive de la charge positive du centre actif par la charge négative de la matrice protéique. Puisque seul le groupement phosphorique interfère étroitement avec le centre actif, cette variation de polarité serait ressentie également par tous les substrats, ce qui expliquerait le parallélisme des courbes pK_m–p*H* de la fig. 3. L'addition d'un solvant non-polaire comme le dioxanne, en diminuant la constante diélectrique du milieu, aurait pour effet de diminuer la solubilité des substrats dans la phase aqueuse et d'augmenter les pK_m. De même, une augmentation de la force ionique, en augmentant cette solubilité, provoquerait une diminution des

Can. J. Chem. Downloaded from www.nrcresearchpress.com by 210.87.254.42 on 09/05/12
For personal use only.

Can. J. Chem. Downloaded from www.nrcresearchpress.com by 210.87.254.42 on 09/05/12
For personal use only.

pK_m. En se concentrant dans la région hydrophobe du centre actif, les solvants organiques aménerait des effets différents selon le pH. Ainsi, à haut pH où le centre actif est pratiquement neutralisé et peu polaire, la solubilité du substrat dans l'enzyme est peu influencée par l'addition d'un solvant comme le dioxanne. A plus bas pH, où la polarité du centre actif s'exerce davantage, une telle addition cause une diminution de la solubilité du substrat dans la phase enzymatique, laquelle compense la diminution produite dans la phase aqueuse. Ceci rendrait compte du fait que les pentes des courbes pK_m–$(1/D)$ sont plus faibles à pH 9.0 qu'à pH 9.6.

Bien que qualitative et incomplète, cette explication des variations des constantes de Michaelis est corroborée par la suite qu'on peut lui donner en interprétant les effets de constante diélectrique et de force ionique sur les vitesses maximums. En effet, il ressort de ce qui précède que la molécule de substrat reste relativement loin de la molécule d'enzyme dans le complexe de Michaelis, le groupement phosphorique étant la seule partie du substrat unie étroitement au centre actif. Si cette hypothèse est correcte, la formation de la phosphorylphosphatase à partir du complexe de Michaelis devrait conduire à un contact beaucoup plus intime entre l'enzyme et le substrat. D'où, le modèle présenté dans la fig. 1, où cette étape de la réaction (k_2) est décrite comme une variation de rayon d'un ion sphérique. Les effets électrostatiques de charge, de constante diélectrique et de force ionique sur V_m sont alors donnés par les relations 16, 17 et 18.

La fig. 7 montre les variations de log V_m avec le pH pour les phosphates d'*o*-carboxyphényle, de *p*-nitrophényle et de *p*-carboxyphényle. Les pentes des segments linéaires des courbes sont respectivement de 0.95, de 0.68 et de 0.49. Les unités de V_m sont arbitraires mais semblables dans les 3 cas. Les positions relatives des courbes sont donc significatives.

L'interprétation de ces résultats à la lumière de la relation 16 n'est pas simple. En effet, d'après cette relation et les variations des charges Z_{ES} en fonction du pH, les pentes des courbes obtenues avec les 2 phosphates de carboxyphényle devraient être identiques et différer assez peu de celle obtenue avec le phosphate de *p*-nitrophényle. Or, les résultats sont tout autres. Il semble donc que la variation de rayon du

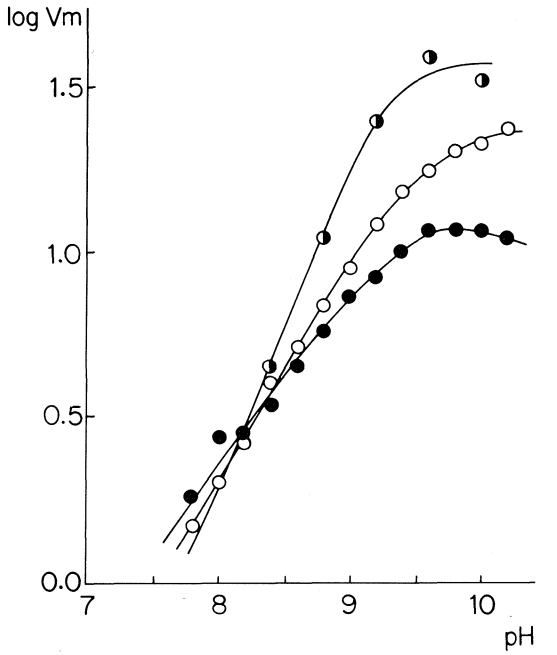

FIG. 7. Variation de log V_m avec le pH pour différents systèmes phosphatase alcaline intestinale de veau – substrat à 25.3 °C et à une force ionique de 0.01. Les substrats sont les phosphates d'*o*-carboxyphényle (◑), de *p*-nitrophényle (○), et de *p*-carboxyphényle (●).

complexe ES, dont tient compte la différence $w_{ES}^{\ddagger} - w_{ES}$ de la relation 16, soit plus importante que la variation de charge de ce même complexe.

La fig. 8 montre la variation des pentes d log V_m/d$(1/D)$ en fonction du pH; le phosphate de *p*-nitrophényle étant le substrat. Chacun des points fut obtenue en mesurant la variation de vitesse en fonction de la constante diélectrique à concentration de substrat élevée et constante. L'extrapolation de chacune des vitesses à concentration infinie de substrat aurait pour effet de diminuer légèrement la valeur absolue des pentes. D'après les résultats des figs. 4 et 5, cette diminution serait moindre que 10% aux pH inférieurs à 9.6 et plus grande que 10% aux pH supérieurs.

En bas de pH 10.6, les pentes d log V_m/d$(1/D)$ sont négatives. Ainsi, d'après l'éq. 17, le rayon $R_{ES}^{\ddagger}$ est plus petit que le rayon R_{ES}. Le passage du complexe de Michaelis à l'état activé, conduisant à la formation du phosphate d'enzyme, implique donc une contraction de l'espèce ES. A pH 10.6, le passage de l'état initial à l'état

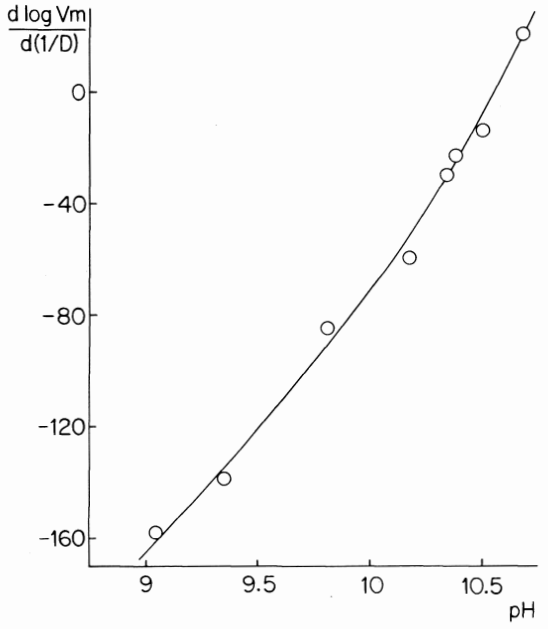

FIG. 8. Influence du pH sur les pentes des courbes log $V_m - (1/D)$ pour le système phosphatase alcaline intestinale de veau – phosphate de p-nitrophényle à 25.3 °C et à une force ionique de 0.01.

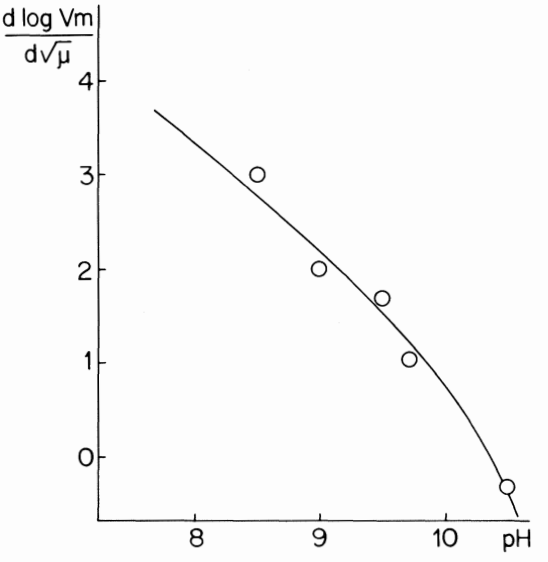

FIG. 9. Influence du pH sur les pentes des courbes log $V_m - \sqrt{\mu}$ pour le système phosphatase alcaline intestinale de veau – phosphate de p-nitrophényle à 25.3 °C.

activé se ferait sans variation de rayon et au-dessus de pH 10.6 avec augmentation de rayon.

Ces résultats sont confirmés par ceux obtenus en étudiant les variations de la vitesse maximum avec la force ionique (éq. 18). La fig. 9 montre les variations des pentes d log V_m/d $\mu^{1/2}$ en fonction du pH, toujours avec le phosphate de p-nitrophényle. Cette fois-ci, la pente est nulle à pH 10.4. Cela implique, d'après l'éq. 18, que la variation du rayon d'exclusion de l'espèce ES, lors de son passage à l'état activité, est nulle à ce pH de 10.4. Aux pH inférieurs, il y aurait une diminution de rayon et aux pH supérieurs, une augmentation.

La vérification la plus intéressante du modèle proposé à la fig. 1 est probablement celle que permettent les données de la fig. 10 à partir desquelles on peut comparer les pentes d log V_m /d(1/D) à pH 9.60 pour les phosphates de p-nitrophényle et de p-carboxyphényle. Les points furent obtenus en tenant compte des variations de pK_m avec la constante diélectrique et en gardant le facteur κ constant ($\mu/DT = 5.13 \times 10^{-7}$). Si on suppose que le produit $R_{ES}R_{ES}^{\ddagger}$ est égal à R_{ES}^2 et que la différence $R_{ES} - R_{ES}^{\ddagger}$ est la même pour chacun des substrats, l'éq. 17 permet d'écrire la relation 19,

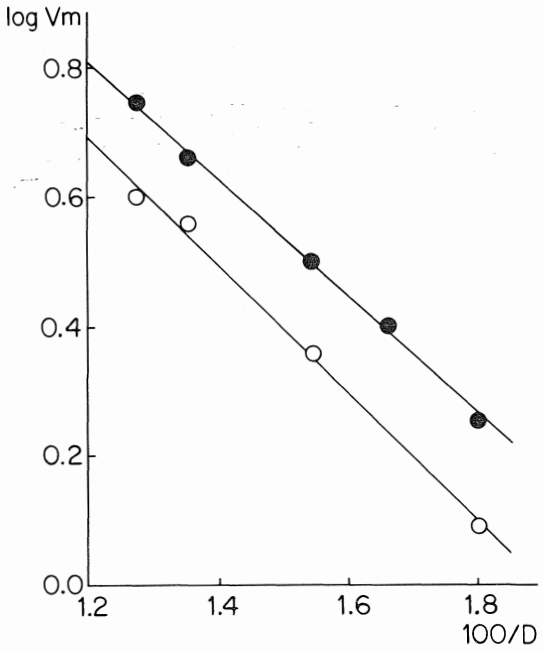

FIG. 10. Variation de log V_m avec l'inverse de la constante diélectrique, à 25.3 °C, à pH 9.6 et à μ/DT égal à 5.13×10^{-7} (κ constant), pour les systèmes phosphatase alcaline intestinale de veau – phosphates de p-carboxyphényle (●) et de p-nitrophényle (○).

Can. J. Chem. Downloaded from www.nrcresearchpress.com by 210.87.254.42 on 09/05/12
For personal use only.

où les symboles N et C réfèrent aux phosphates de *p*-nitrophényle et de *p*-carboxyphényle respectivement.

$$[19] \quad \frac{(\mathrm{d} \log V_m/\mathrm{d}(1/D))_N}{(\mathrm{d} \log V_m/\mathrm{d}(1/D))_C} = \frac{(Z_{ES}^2/R_{ES}^2)_N}{(Z_{ES}^2/R_{ES}^2)_C}$$

D'après les données que l'on possède sur la phosphatase alcaline intestinale de veau, on peut estimer que Z_{ES} est égal à $-27-2$ dans le cas du phosphate de *p*-nitrophényle et à $-27-3$ dans l'autre cas. De même, d'après la conformation des substrats et celle proposée plus haut des complexes de Michaelis correspondants, la charge du groupement carboxyle du phosphate de *p*-carboxyphényle est probablement située à environ 10 Å de la surface de la phosphatase. Ceci devrait donner une sphère équivalente au complexe enzyme–substrat dont le rayon est de 2 (ou 3) Å supérieur à celui du complexe phosphatase–phosphate de *p*-nitrophényle. Approximativement, on aurait R_{ES} égal à 32 Å dans le premier cas et à 30 Å dans le second. D'après ces données, le rapport des pentes (éq. 19) serait de 1.12. Celui des courbes de la fig. 10 est de 1.09 ($-98/-90$). Avec une différence de rayon de 3 Å au lieu de 2 Å, le rapport des pentes serait de 1.14; avec une différence de 4 Å, il serait de 1.21.

L'accord entre les valeurs calculées et expérimentales est assez satisfaisant pour corroborer le modèle de la fig. 1, où la formation de la phosphorylphosphatase à partir du complexe de Michaelis apparaît, d'un point de vue électrostatique, comme une variation de rayon d'un ion sphérique. Par ailleurs, on peut attribuer cette variation à une réorganisation du complex enzyme–substrat au cours de laquelle la molécule de substrat, d'abord fixée par son groupement phosphorique à la charge positive du centre actif, glisserait sur cette charge pour pénétrer plus profondément dans le centre actif. On peut alors spéculer sur les grandeurs relatives des pentes d log V_m/d pH (fig. 7). En effet, la neutralisation progressive de la charge positive du centre actif par l'augmentation de la charge négative de la matrice protéique avec le pH, serait ressentie différemment par les substrats lors d'un tel déplacement. Elle le serait davantage par le phosphate d'*o*-carboxyphényle, dont les 3 charges sont rapprochées, que par le phosphate de *p*-nitrophényle qui n'en porte que 2. De même, elle le serait davantage par le phosphate de *p*-nitrophényle que par le phosphate de *p*-carboxyphényle dont la troisième charge serait placée de façon à faciliter le glissement de la molécule au-dessus de la charge du centre actif.

Ce même modèle, relatif aux vitesses maxima, confirme à posteriori, celui proposé à l'interprétation des constantes de Michaelis, à savoir une fixation du substrat à la surface de l'enzyme. En effet une telle association doit normalement être suivie d'une pénétration du substrat au coeur même du centre actif. L'image de la formation du complexe de Michaelis et celle de sa transformation en phosphorylphosphatase forme ainsi un ensemble cohérent.

Nous adressons des remerciments au Conseil national de recherches du Canada pour l'octroi des subventions ayant permis la réalisation de ce travail et des bourses accordées à l'un de nous (M.J.); de même qu'au Dr. A. Lebrun et à M. C. Langevin dont la collaboration fut très appréciée.

1. M. Lazdunski et L. Ouellet. Can. J. Chem. **39**, 1298 (1961).
2. M. Lazdunski et L. Ouellet. Can. J. Biochem. Physiol. **40**, 1619 (1962).
3. M. Lazdunski, J. Brouillard et L. Ouellet. Can. J. Chem. **43**, 2222 (1965).
4. H. N. Fernley et P. G. Walker. Biochem. J. **102**, 48P (1967).
5. H. N. Fernley et P. G. Walker. Biochem. J. **99**, 39P (1966).
6. H. N. Fernley et P. G. Walker. Biochem. J. **97**, 95 (1965).
7. H. N. Fernley et S. Bisaz. Bichem. J. **107**, 279 (1968).
8. J. A. Reynolds et M. J. Schlesinger. Biochemistry, **7**, 2080 (1968).
9. L. Engström. Biochem. Biophys. Acta, **52**, 36 (1961).
10. R. T. Simpson, B. L. Vallée et G. H. Tait. Biochemistry, **7**, 4336 (1968).
11. L. Michaelis et M. L. Menten. Biochem. Z. **49**, 333 (1913).
12. J. Z. Hearon. Phys. Rev. **32**, 499 (1952).
13. C. Tanford. Physical chemistry of macromolecules. John Wiley and Sons, Inc., New York. 1961. p. 465.
14. J. Roche, S. Bouchilloux et M. Roger. Bull. Soc. Chim. Biol. **32**, 30 (1950).
15. J. D. Chanley et E. Feageson. J. Am. Chem. Soc. **77**, 4002 (1955).
16. L. F. Fieser. Experiments in organic chemistry. D. C. Health and Co., Boston. 3e éd. rev. 1957. p. 284.
17. G. Akerlöf et O. A. Short. J. Am. Chem. Soc. **58**, 1241 (1936).
18. T. Inagami et J. M. Sturtevant. Biochim. Biophys. Acta, **38**, 64 (1960).
19. H. Lineweaver et D. Burk. J. Am. Chem. Soc. **56**, 658 (1934).

Can. J. Chem. Downloaded from www.nrcresearchpress.com by 210.87.254.42 on 09/05/12
For personal use only.

20. K. J. LAIDLER. The chemical kinetics of enzyme action. Oxford University Press, London. 1958. Chap. V.
21. R. WILDNAUER et W. J. CANADY. Biochemistry, **5**, 2885 (1966).
22. I. V. BEREZIN, A. V. LEVASHOV et K. MARTINEK. Eur. J. Biochem. **16**, 472 (1970).
23. R. T. WEDDING, C. HANSCH et T. R. FUKUTO. Arch. Biochem. Biophys. **121**, 9 (1967).
24. K. KIEHS, C. HANSCH et L. MOORE. Biochemistry, **5**, 2602 (1966).
25. J. KALLOS et K. AVATIS. Biochemistry, **5**, 1979 (1966).
26. M. JULIEN. Thèse de doctorat. Université Laval, Québec 10, Quebéc. 1970.

Can. J. Chem. Downloaded from www.nrcresearchpress.com by 210.87.254.42 on 09/05/12
For personal use only.

Photolyse du chlorure d'éthyle gazeux en-dessous et au-dessus du potentiel d'ionisation

LIONEL CREMIEUX ET JAN A. HERMAN

Département de chimie et Centre de Recherche sur les Atomes et les Molécules, Université Laval, Québec, Québec G1K 7P4

Reçu le 16 avril 1974

LIONEL CREMIEUX et JAN A. HERMAN. Can. J. Chem. **52**, 3098 (1974).

La photolyse du chlorure d'éthyle gazeux est effectuée à $\lambda = 123.6$ et 106.7–104.8 nm. A 123.6 nm il n'y a pas ionisation de la molécule, tandis qu'à 106.7–104.8 nm 40% de photons absorbés conduisent à la formation d'ions. Les produits de photolyse identifiés sont: H_2, CH_4, C_2H_2, C_2H_4, C_2H_6, C_3H_6, C_3H_8, C_4H_{10}, CH_3Cl, C_2H_3Cl, 2-C_4H_9Cl, 2,3-$C_4H_8Cl_2$ et 1,3-$C_4H_8Cl_2$. La formation des produits est étudiée en présence de capteurs de radicaux et d'électrons. Les réactions de neutralisation des charges augmentent sensiblement les rendements en H_2, C_2H_2 et C_2H_4.

LIONEL CREMIEUX and JAN A. HERMAN. Can. J. Chem. **52**, 3098 (1974).

Photolysis of gaseous ethyl chloride was performed at $\lambda = 123.6$ and 106.7–104.8 nm. There is no ionisation at 123.6 nm, while at 106.7–104.8 nm 40% of the absorbed light lead to ions. The identified products are the following: H_2, CH_4, C_2H_2, C_2H_4, C_2H_6, C_3H_6, C_3H_8, C_4H_{10}, CH_3Cl, C_2H_3Cl, 2-C_4H_9Cl, 2,3-$C_4H_8Cl_2$, and 1,3-$C_4H_8Cl_2$. The effect of radical and electron scavengers on the product formation was studied. Charge neutralization reactions increase yields of H_2, C_2H_2, and C_2H_4.

Introduction

Les études de photochimie dans l'ultraviolet à vide ($\lambda < 180$ nm) des hydrocarbures substitués par des atomes d'halogène sont jusqu'à présent peu nombreuses. En particulier l'influence des substituants halogénés sur les processus primaires photolytiques n'a pas reçue l'attention qu'elle mérite. Dans le cas du chlorure d'éthyle il existe une étude photolytique à $\lambda = 123.6$ nm de Tiernan et Hughes (1), mais l'accent est mis sur les processus ioniques en regard des phénomènes radiolytiques. Wijnen et ses coll. (2) ont étudié la photochimie des chloro-alcanes à $\lambda > 200$ nm. Signalons enfin le travail de Schindler (3) sur la radiolyse du chlorure d'éthyle gazeux par des électrons de 2.8 MeV. Nous avons repris l'étude de ce système en vue d'apporter des précisions supplémentaires sur les mécanismes impliqués lors de l'absorption des énergies inférieures et supérieures au seuil d'ionisation.

Procedure expérimentale

Les sources de lumière ultraviolette sont des lampes au krypton $\lambda = 123.6$ (~85%), 116.5 nm (~15%), et argon $\lambda = 106.7$ (~70%), 104.8 nm (~30%), construites suivant la description de Ausloos et coll. (4). Ces lampes sont munies de fenêtres en fluorure de lithium. Elles sont fixées par un joint étanche à des cellules d'irradiation d'environ 300 ml.

L'actinométrie est réalisée par la mesure du courant d'ionisation dans les cellules d'irradiation. A cet effet, elles sont munies d'électrodes circulaires parallèles en nickel (4). Pour le rayonnement de résonance de l'argon et du krypton on utilise l'oxyde nitrique et l'isobutylène comme gaz actinométriques pour lesquels les rendements quantiques de photoionisation sont connus (5–7).

Les produits de photolyse sont analysés par chromatographie en phase gazeuse (c.p.g.) dans des instruments équipés de détecteurs à ionisation de flamme. Les produits sont séparés sur les colonnes suivantes: les hydrocarbures C_1 à C_5 sur du squalane, les chloro- et dichlorobutanes sur l'huile de silicone GE SF96. Dans certains cas les produits ont été piégés à la sortie du c.p.g. et analysés par spectrométrie de masse. Toutes les irradiations sont faites à la température ambiante, soit 23 °C ± 3.

Le chlorure d'éthyle ainsi que les autres gaz proviennent de Matheson Co. Tous ces gaz sont purifiés avant leur emploi par chromatographie à gaz préparative. Le chlorure d'éthyle perdeutéré (-d_5) provient de Merck, Sharp et Dohme. Il contient 10.8% d'impureté isotopique, C_2D_4HCl; les résultats sont corrigés pour la présence de ce dernier.

Résultats

Le potentiel d'ionisation du C_2H_5Cl étant 11.0 eV (8), seul le rayonnement de résonance de l'argon (11.6–11.8 eV) est suffisant pour ioniser cette molécule. Dans ce cas, le rendement photochimique peut être représenté par le rendement ionique, $M(X)/N_i$, qui exprime le nombre de molécules M d'espèce X produit par paire d'ions,

Can. J. Chem. Downloaded from www.nrcresearchpress.com by 210.87.254.105 on 09/05/12
For personal use only.

Can. J. Chem. Downloaded from www.nrcresearchpress.com by 210.87.254.105 on 09/05/12
For personal use only.

N_i. Si par extension, $M(X)/N_{ex}$ représente le nombre de molécules M d'espèce X produit par molécule neutre excitée ne s'autoionisant pas, ni ne se dissociant pas en paire d'ions, alors $M(X)/N_{ex}$ est identique au rendement quantique, Φ, au-dessous du potentiel d'ionisation de la molécule irradiée. Par contre la relation qui lie $M(X)/N_i$ avec $M(X)/N_{ex}$ au-dessus du potentiel d'ionisation est

$$M(X)/N_{ex} = [M(X)/N_i]\frac{\eta}{1-\eta}$$

où η est le rendement quantique d'ionisation. Dans le cas du chlorure d'éthyle ce rendement de photoionisation à $\lambda = 106.7$–104.8 nm est 0.405, tel que mesuré par rapport à NO pris comme référence.

Dans le tableau 1 sont présentés les rendements $M(X)/N_{ex}$ des produits de photolyse pour les 2 lampes à raies de résonance des gaz nobles. Pour obtenir les rendements ioniques, $M(X)/N_i$, des irradiations à 106.7–104.8 nm il suffit de multiplier par 1.46 les valeurs des rendements $M(X)/N_{ex}$ correspondant. Les concentrations des additifs varient, en général, entre 0.1 et 6%. Les rendements pour ces mélanges présentés au tableau 1 correspondent aux valeurs du palier où l'influence de la concentration de l'additif ne se faisait plus sentir.

Malgré de nombreux essais, le chlorure d'hydrogène, HCl, qui est un produit majeur de la photolyse, n'a pu être analysé en raison des difficultés analytiques. En effet, la méthode par voie humide a une sensibilité qui est à la limite des quantités de HCl formé, et de plus on ne peut l'employer en raison du matériel des fenêtres des lampes d'irradiation. D'autres essais par voie sèche n'ont pas donné les résultats escomptés. Néanmoins, on peut estimer la valeur supérieure du rendement en HCl à partir du bilan C:H:Cl des produits. Pour l'irradiation à 123.6 nm on trouve un rapport expérimental lequel comparé au rapport théorique montre un déficit de 0.42 pour l'hydrogène et 0.54 pour le chlore. Si l'hydrogène manquant se trouvait uniquement sous forme du chlorure d'hydrogène, on a alors un rendement quantique en HCl $\leqslant 0.42$. Mais il en manque aussi du carbone, indiquant ainsi qu'il y a encore des produits non identifiés et du coup le rendement en HCl doit être encore plus bas. Le même bilan pour l'irradiation à 106.7–104.8 nm ne permet pas l'évaluation du rendement en HCl, car cette fois l'hydrogène et le chlore ne concordent plus. Cela suggère que des produits polyhalogenés sont formés en quantités non négligeables dans des processus ioniques ou de recombinaison de charges, lesquels n'ont pas été identifiés et détectés par c.p.g. dans les conditions de nos expériences.

Le chlorure de propyle a été identifié, mais pas mesuré.

Effets de dose et de pression

Il y a un faible effet de dose (fig. 1) au moins jusqu'à conversion de 0.05% du C_2H_5Cl, sauf en ce qui concerne l'hydrogène. Les rendements en éthylène et acétylène fléchissent légèrement au fur et à mesure de l'accumulation de ces produits. Pour le méthane et l'éthane il y a un faible effet d'accumulation. L'effet de pression pour les produits les plus importants est montré dans la fig. 2 pour les rayonnements de résonance du krypton et de l'argon. Pour les irradiations à 123.6 nm les courbes montrent une légère décroissance des rendements lorsque la pression augmente, sauf pour le chlorure de vinyle qui subit l'effet inverse. Dans le cas des irradiations à 106.7–104.8 nm l'effet de pression se traduit par une décroissance des rendements en fonction de l'augmentation de la pression, sauf pour C_2H_4 et C_2H_3Cl qui ne sont pas affectés.

Effets des additifs

Les résultats montrent (tableau 1) que pour les énergies en-dessous du potentiel d'ionisation l'oxygène entraîne la disparition de CH_4, C_2H_6, C_3H_8, CH_3Cl, n-C_4H_{10}, 2-C_4H_9Cl, 2,3-$C_4H_8Cl_2$ et 1,3-$C_4H_8Cl_2$, diminue les rendements en C_2H_4, et C_2H_3Cl, mais affecte peu les rendements en C_2H_2 et H_2. Pour le rayonnement d'énergie supérieure au potentiel d'ionisation

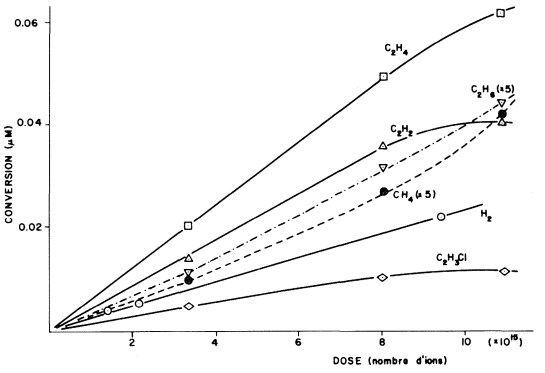

FIG. 1. Effet de dose pour l'irradiation à 106.7–104.8 nm. Pression 10 Torr.

Can. J. Chem. Downloaded from www.nrcresearchpress.com by 210.87.254.105 on 09/05/12
For personal use only.

TABLEAU 1. Rendements $M(X)/N_{ex}$ de la photolyse du chlorure d'éthyle à 5 Torr

λ (nm)	Additif	H_2	CH_4	C_2H_2	C_2H_4	C_2H_6	C_3H_6	C_3H_8	CH_3Cl	C_2H_3Cl	C_4H_{10}	2-C_4H_9Cl	2,3-$C_4H_8Cl_2$	1,3-$C_4H_8Cl_2$
123.6	—	0.21	0.03	0.11_0	0.31_8	0.03	0.02	0.004	0.01	0.07	0.01	0.03	0.03	0.01
	1–5% NO	0.19	0.0	0.09_2	0.26_3	0.0	0.0	0.0	0.0	0.05	0.0	0.0	0.0	0.0
	1–5% O_2	0.19	0.0	0.10_3	0.26_6	0.0	0.0	0.0	0.0	0.04	0.0	0.0	0.0	0.0
	5% SF_6	—	—	0.11_4	0.30_3	—	0.02	0.004	—	—	—	0.03	0.04	0.01
106.7–104.8	—	0.98	0.03	0.18_7	0.26_6	0.03	0.01	0.006	0.04	0.04	0.005	0.02	0.03	0.005
	5% NO	0.33	—	0.17_0	0.20_6	0.02	0.0	0.0	—	0.04	0.0	0.0	0.0	0.0
	5% O_2	0.35	0.01	0.18_3	0.18_4	0.02	0.0	0.0	0.02	0.02	0.0	0.0	0.0	0.0
	5% CCl_4	—	—	0.14_0	0.16	—	—	—	—	—	—	—	—	—
	5% SF_6	0.39	—	0.15_0	0.16_3	0.02	—	—	—	—	—	0.01	0.03	0.01
	5% O_2 + 5% SF_6	0.29	—	0.15_6	0.15_6	0.02	—	—	0.01	—	—	0.0	0.0	0.0

TABLEAU 2. Composition isotopique de l'éthylène et du chlorure de vinyle*†

Produits	λ (nm)	$-d_0$	$-d_1$	$-d_2$	$-d_3$	$-d_4$
Ethylènes	123.6	61.6	4.3	0	2.8	31.3
	106.7–104.8	63.0	7.7	0	3.4	25.9
Chlorures de vinyle	123.6	52.6	5.5	2.5	39.4	
	106.7–104.8	12.8	0.1	0	87.6	

*$C_2H_5Cl:C_2D_5Cl:O_2$ = 50:50:5.
†Pression totale: 10 Torr.

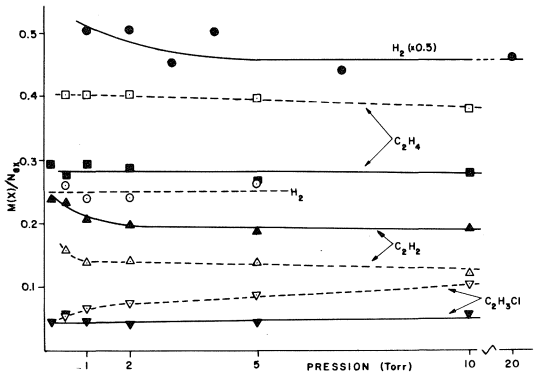

FIG. 2. Rendements $M(X)/N_{ex}$ en ethylène, acetylène, chlorure de vinyle et hydrogène en fonction de la pression. Symboles blancs; irradiations à 123.6 nm, symboles noires: irradiations à 104.8–106.7 nm.

l'oxygène a un effet différent de celui rencontré pour la lampe précédente. Si le C_2H_2 n'est pas affecté, le C_2H_4 connait une chute de 30% de sa valeur sans additif. Le CH_4 et le C_2H_6 sont encore ici présents, tandis que les autres composés disparaissent. Le C_2H_3Cl est affecté de façon similaire à celle observée lors des irradiations à 123.6 nm. On observe aussi une diminution importante de l'hydrogène. L'oxyde nitrique a, d'une manière générale, un effet semblable à celui de l'oxygène.

Le SF_6 ajouté au système semble n'avoir aucune action marquée sur les rendements dans les limites des erreurs expérimentales pour les irradiations aux énergies inférieures au potentiel d'ionisation. Par contre dans le cas d'irradiation à λ = 106.7–104.8 nm, le SF_6 ajouté au système provoque une diminution des rendements du C_2H_2 (~30%), du C_2H_4 (~40%) et de l'hydrogène d'environ de moitié. On peut remarquer que l'addition simultanée de SF_6 et O_2 n'entraîne pas un effet cumulatif de chacun de ces deux additifs pris séparément.

L'addition de l'ammoniac au système ne donne aucun résultat significatif en raison d'une diminution rapide de la transparence de la fenêtre en LiF due à la formation d'un dépôt, probablement du NH_4Cl.

Expériences isotopiques

Les analyses isotopiques de l'éthylène et du chlorure de vinyle sont données au tableau 2. Ces produits proviennent de l'irradiation du mélange $C_2H_5Cl:C_2D_5Cl:O_2$ = (50:50:5) aux deux radiations de résonance. Toutefois, la durée de ces expériences étant très longue, il est possible que l'oxygène ait été consommé et qu'une partie de ces produits soit formée par voie radicalaire.

Discussion

La nature de l'excitation suggère que l'on distingue deux cas: (*a*) celui où les photons ont une énergie inférieure au potentiel d'ionisation du chlorure d'éthyle, et (*b*) celui où leur énergie est supérieure à ce potentiel. Dans le premier cas la molécule est portée dans un état électronique excité

[1] $$C_2H_5Cl + h\nu \rightarrow C_2H_5Cl^{**}$$

Dans le second on doit ajouter à ce processus un autre qui décrit l'ionisation de la molécule

[2] $$C_2H_5Cl + h\nu \rightarrow C_2H_5Cl^+ + e^-$$

[2*a*] $$\rightarrow C_2H_5Cl^{**} \rightarrow C_2H_5Cl^+ + e^-$$

les ions pouvant provenir soit par l'ionisation directe, soit de l'autoionisation de la molécule superexcitée.

(a) Irradiation à 123.6 nm

Le tableau 1 montre que même en présence d'intercepteurs de radicaux les composés principaux sont C_2H_4, C_2H_2, C_2H_3Cl et H_2, ce qui laisse supposer que les processus primaires de décomposition de la molécule excitée sont

Can. J. Chem. Downloaded from www.nrcresearchpress.com by 210.87.254.105 on 09/05/12
For personal use only.

Can. J. Chem. Downloaded from www.nrcresearchpress.com by 210.87.254.105 on 09/05/12
For personal use only.

[3] $C_2H_5Cl^{**} \rightarrow C_2H_4 + HCl$ $\Delta H_3 = 16.7$ kcal/mol

[4] $\rightarrow C_2H_4 + H + Cl$ $\Delta H_4 = 120.2$ kcal/mol

[5] $\rightarrow C_2H_3Cl + H_2$ $\Delta H_5 = 34.8$ kcal/mol

[6] $\rightarrow C_2H_3Cl + H + H$ $\Delta H_6 = 139$ kcal/mol

[7] $\rightarrow C_2H_3^{\cdot} + HCl + H$ $\Delta H_7 = 116$ kcal/mol

[8] $\rightarrow C_2H_3^{\cdot} + H + Cl$ $\Delta H_8 = 115$ kcal/mol

Ces processus sont confirmés par l'analyse par spectrométrie de masse de l'éthylène et du chlorure de vinyle où les espèces perhydrogenées et perdeuterées représentent plus de 85% du total (tableau 2). On remarquera sur le tableau 2 que le détachement subit un effet isotopique marqué, du probablement à une différence de coefficients d'extinction des chlorures d'éthyle perhydrogène et perdeuteré. Même en présence d'oxygène environ 15% de l'éthylène est $-d_1$ et $-d_3$. Cela s'explique par la réaction

[9] $C_2H_3^{\cdot} + C_2D_5Cl \rightarrow C_2H_3D + C_2D_4Cl^{\cdot}$...etc

car les radicaux vinyles produits en [7] et [8] ne sont pas tous interceptés par l'oxygène et réagissent avec le monomère.

En prenant comme énergie excitatrice 231 kcal, celle délivrée par la lampe au krypton, on peut calculer grossièrement l'énergie disponible pour l'éthylène formé par la réaction 3 et dont $\Delta H_3 = 16.7$ kcal/mol (9). En supposant une répartition statistique de l'énergie suivant les degrés de libertés internes de la molécule on déduit que l'énergie emportée par C_2H_4 sera 145 kcal environ, où on a pris 57 kcal/mol (10, 11) comme énergie d'activation du processus 3. Cette valeur est suffisante pour entraîner la décomposition de l'éthylène suivant le processus 10:

[10] $C_2H_4^* \rightarrow C_2H_2 + H_2$ $\Delta H_{10} = 41.4$ kcal/mol

Il y a cependant une autre voie possible, proposée par Schindler (3), consistant à la décomposition simultanée du $C_2H_5Cl^{**}$ en C_2H_2, HCl et H_2:

[11] $C_2H_5Cl^{**} \rightarrow C_2H_2 + H_2 + HCl$ $\Delta H_{11} = 58.9$ kcal/mol

L'endothermicité de la réaction 11 est compatible avec l'énergie des photons incidents. Il n'est guère facile de distinguer l'importance relative de cette décomposition 11 par rapport au processus 3 suivi de la réaction 10, puisque l'effet de pression ne permet pas de trancher entre ces deux voies, celui-ci étant sensiblement le même dans un cas comme dans l'autre. Il y a cependant un effet de pression sur la formation de l'éthylène et de l'acétylène comme en témoigne la variation du rapport C_2H_2/C_2H_4 en fonction de la pression (fig. 3) et il semble être de même importance pour les irradiations à 123.6 et 106.7–104.8 nm. Les processus 10 et/ou 11 sont justifiés par l'augmentation du rapport C_2H_2/C_2H_4 en fonction de l'énergie excitatrice. Celui-ci passe pour les irradiations faites en présence de O_2 ou NO de 0.39 à 0.99 quand l'énergie passe de 10.0 à 11.6–11.4 eV.

Outre les processus 5, 8, 10 et 11 qui ne peuvent rendre compte de l'apparition de tout l'hydrogène, les réactions suivantes peuvent être suggérées pour répondre au bilan du composé

[12] $C_2H_5Cl^* \rightarrow C_2H_4Cl + H^{\cdot}$

[13] $H^{\cdot} + C_2H_5Cl \rightarrow H_2 + C_2H_4Cl$

[14] $\rightarrow HCl + C_2H_5^{\cdot}$

L'énergie de rupture de la liaison C_2H_5—Cl étant de 81.5 kcal/mol (12), alors que celle de la liaison C_2H_4Cl—H est estimée à 98 kcal/mol (13), la réaction 14 doit être plus importante que la réaction 13. Ce fait est confirmé par l'étude des vitesses de réaction de l'atome d'hydrogène avec divers hydrocarbures chlorés où l'on trouve $k_{13}/k_{14} = 0.68$ (14).

Les quantités des intercepteurs ajoutés au système sont trop faibles pour affecter de manière importante le rendement en hydrogène provenant par voie radicalaire, [13]. D'autre part on peut s'attendre qu'une partie des atomes d'hy-

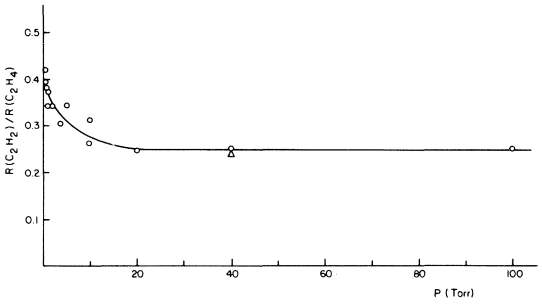

FIG. 3. Rapport des rendements en acetylène et ethylène en fonction de la pression pour l'irradiation à 123.6 nm. (Δ) valeur de la réf. 1.

Can. J. Chem. Downloaded from www.nrcresearchpress.com by 210.87.254.105 on 09/05/12
For personal use only.

drogène soit constituée d'atomes chauds, car les énergies disponibles après fragmentation de la molécule parent excitée sont suffisantes pour qu'elles se retrouvent sous forme translationnelle dans les fragments atomiques. Les atomes chauds échappant aussi à l'action des capteurs de radicaux, on prévoit au total une faible diminution du rendement en hydrogène pour les irradiations en présence d'intercepteurs et cela est confirmé par les données du tableau 1.

Environ 18% de l'éthylène formé à 123.6 nm l'est par voie radicalaire. Une partie de celui-ci provient de la réaction de dismutation des radicaux éthyl et chloréthyl

[15] $C_2H_5^{\cdot} + C_2H_4Cl^{\cdot} \rightarrow C_2H_4 + C_2H_5Cl$

[16] $\rightarrow C_4H_9Cl$

Le rapport $k_{15}/k_{16} = 0.22$ calculé à partir des données de Schindler (3) et Roquitte et coll. (15), pourrait justifier qu'une partie du C_2H_4 disparaisse en présence d'oxygène ou d'oxyde nitrique. Il faut cependant tenir compte du fait que les réactions 15 et 16 sont en compétition avec

[17] $C_2H_5^{\cdot} + C_2H_5^{\cdot} \rightarrow C_4H_{10}$

[18] $C_2H_4Cl^{\cdot} + C_2H_4Cl^{\cdot} \rightarrow C_4H_8Cl_2$

A partir des données du tableau 1 on calcul que le rendement en C_2H_4 formé par la réaction 15 compte pour 0.015. Il faut donc admettre que la contribution de la réaction 9 au $\Phi(C_2H_4)$ est d'environ 0.04.

Le chlorure de vinyle provient à 60% environ de la décomposition monomoléculaire [5] et [6]. Le restant a pour origine un (des) précurseur(s) susceptible(s) de réagir avec des capteurs de radicaux. Les processus suivants

[19] $C_2H_3^{\cdot} + C_2H_5Cl \rightarrow C_2H_3Cl + C_2H_5^{\cdot}$

[20] $C_2H_2 + Cl^{\cdot} \rightarrow C_2H_2Cl^{\cdot}$

[21] $C_2H_2Cl^{\cdot} + HCl \rightarrow C_2H_3Cl + Cl^{\cdot}$

pourraient contribuer au rendement du C_2H_3Cl radicalaire. L'addition du C_2H_2 entraîne une augmentation du chlorure de vinyle (3) et dans notre cas l'effet de dose corrobore l'hypothèse des réactions 20 et 21, par contre nous n'avons pas décelé ni du chlorobutène, ni du dichlorobutène qui pourraient être formés par recombinaison du $C_2H_2Cl^{\cdot}$ avec des radicaux éthyl et chloroéthyl.

L'origine du CH_4, C_2H_6, CH_3Cl, C_3H_6, C_3H_8, C_4H_9Cl, C_4H_{10} et les dichlorobutanes est radicalaire comme l'indique leur disparition en présence d'oxygène et de l'oxyde nitrique (tableau 1). Les réactions suivantes

[22] $C_2H_5Cl^{**} \rightarrow CH_3^{\cdot} + CH_2Cl^{\cdot}$

[23] $CH_3^{\cdot} + HCl \rightarrow CH_4 + Cl^{\cdot}$

[24] $C_2H_5^{\cdot} + HCl \rightarrow C_2H_6 + Cl^{\cdot}$

et les recombinaisons et dismutations entre les divers radicaux: $CH_3^{\cdot}$, $C_2H_5^{\cdot}$, $CH_2Cl^{\cdot}$ et $C_2H_4Cl^{\cdot}$, rendent compte de ces produits. Nous ne détaillerons pas toutes ces réactions.

L'augmentation des concentrations du CH_4 et du C_2H_6 avec la dose tend à montrer que les réactions 23 (dont l'énergie d'activation est estimée à 2–5 kcal/mol (16)) et 24 ont bien lieu. D'autre part l'abstraction de l'hydrogène à la molécule parent par les radicaux méthyl et éthyl thermalisés devrait être insignifiante, vue les énergies d'activation élevées de réactions similaires (17). De même l'abstraction d'un atome de chlore à la molécule parent par le radical méthyl n'est pas favorisée, car elle est largement préférentielle pour l'atome d'hydrogène (18). La formation du CH_3Cl, C_4H_{10}, C_4H_9Cl et des $C_4H_8Cl_2$ a été déjà discuté dans d'autres travaux (1, 3).

Irradiations à 106.7–104.8 nm

L'ionisation ne porte que sur 40% des molécules ayant absorbé le rayonnement incident. Les autres molécules excitées vont se décomposer comme dans le cas précédent, avec cependant la différence due à l'énergie qui est de 27 kcal supérieure à ce qu'elle était dans le cas des photons émis par la lampe de krypton. En conséquence cela changera les proportions relatives des différents produits de décomposition. Ceci est mis en évidence par l'effet des additifs (tableau 1).

L'hydrogène a une valeur élevée, mais en présence de O_2 et du NO on ne retrouve plus que 40% environ de l'hydrogène total. Par ailleurs la présence de 1% de SF_6 a le même effet sur la formation de l'hydrogène que l'oxygène ou l'oxyde nitrique. Pourtant le SF_6 n'est pas reconnu comme intercepteur efficace de radicaux. Cela nous amène à envisager une autre explication de la baisse de rendement en hydrogène en présence de ces additifs.

L'ion $C_2H_5Cl^+$ est la seule espèce ionique primaire possible produite par photolyse du chlorure d'éthyle à 106.7–104.8 nm (19). Cette

Can. J. Chem. Downloaded from www.nrcresearchpress.com by 210.87.254.105 on 09/05/12
For personal use only.

présence d'ions positifs et d'électrons peut conduire: (*a*) l'attachement dissociatif d'électrons sur la molécule, (*b*) aux réactions ion–molécule d'ions positifs aussi bien que négatifs, (*c*) à la neutralisation des charges.

L'attachement dissociatif

$$C_2H_5Cl + e^- \rightarrow C_2H_5^{\cdot} + Cl^-$$

est certainement sans grande importance pour le chlorure d'éthyle, car sa section efficace est faible, $\sigma = 7 \times 10^{-20}$ cm^2 et de plus ce processus exige des électrons de 0.4 eV (20). A partir de ces données et des dimensions de la cellule d'irradiation nous estimons que dans nos conditions la probabilité de ce processus est inférieure à 0.01, donc négligeable. Les réactions ion–molécule de l'ion parent, $C_2H_5Cl^+$, ont été étudiées par spectrométrie de masse par Tiernan et Hughes (1) et par Wincel et Luczynski (21). Selon Tiernan et coll. (1) les seules réactions de l'ion parent observées dans leurs conditions de mesure (~250 °C) sont

[25] $C_2H_5Cl^+ + C_2H_5Cl \rightarrow C_2H_6Cl^+ + C_2H_4Cl$

[26] $\rightarrow C_2H_3Cl^+ +$ produits neutres

suivie de

[27] $C_2H_6Cl^+ + C_2H_5Cl \rightarrow C_4H_{10}Cl^+ + HCl$

et l'ion vinyle ne réagissant pas avec le chlorure d'éthyle. Wincel et Luczynski (21) ont montré qu'à température plus base (~120 °C) et aux vitesses thermiques la réaction prépondérante aux pressions 0.1–0.2 Torr est

[28] $C_2H_5Cl^+ + C_2H_5Cl \rightarrow C_2H_6Cl_2^+ +$ produits neutres

Dans nos conditions d'irradiation à 25 °C on peut penser que nous aurons aux pressions utilisées, l'espèce $C_2H_6Cl_2^+$ ou même des ions plus lourds provenant de la condensation sur l'ion parent. Par conséquent seul la neutralisation semble jouer un rôle inportant

[29] $C_2H_6Cl_2^+ + e^-, (R^-) \rightarrow$ produits

sauf en ce qui concerne le HCl, dont une partie peut parvenir par réaction ion–molécule.

S'il en est ainsi l'addition du SF_6 ou du CCl_4, qui ont des sections efficaces d'attachement d'électron élevée, respectivement 5.7 et 1.3×10^{-16} cm^2 (22), va avoir une influence sur le rendement de divers produits de la décomposition résultant de la neutralisation [29]. Un calcul sommaire indique que dans nos conditions 1% en SF_6 (ou CCl_4) suffit pour attacher tous les électrons. Il est difficile de savoir sur quelles espèces ioniques la neutralisation va avoir lieu. Par exemple, il est possible que l'anion chlore, Cl^-, soit formé dans un processus d'attachement dissociatif d'électron sur des produits polyhalogénés, $C_xH_yCl_z$ où $z \geqslant 2$. Cependant, en admettant que la vitesse de neutralisation ion positif – électron est environ 10^{-6} cm^3 molécule^{-1} s^{-1}, alors que celle d'une neutralisation ion positif – ion négatif est supposée être un ordre de grandeur plus faible (23), et que la constante de vitesse de la réaction ion–molécule du genre [28] est d'environ 10^{-9} cm^3 molécule^{-1} s^{-1}, on arrive à la conclusion que dans nos conditions de concentration en électrons dans le volume irradié la neutralisation de l'ion parent, $C_2H_5Cl^+$, par l'électron a peu de chance de se réaliser. Il résulte donc que la neutralisation s'effectuera sur l'espèce ionique prépondérante aux pressions utilisées. Les résultats obtenus en présence du SF_6 et du CCl_4 montrent une diminution des rendements en H_2, C_2H_2 et C_2H_4 principalement. On peut donc penser que la neutralisation conduit à la formation de ces produits via un processus radicalaire sensible aux capteurs de radicaux. Par ailleurs, on a signalé que l'addition simultanée de SF_6 et O_2 n'entraîne pas un effet cumulatif de chacun de ces additifs pris séparément. Ceci semble montrer que les mécanismes ionique et radicalaire sont consécutifs.

Remarques finales

Il est à remarquer que la somme des rendements primaires de décomposition du $C_2H_5Cl^{**}$ en C_2H_4, C_2H_2 et C_2H_3Cl (réactions 3–6, 10) est constante, soit 0.41, pour les deux rayonnements de résonance. Seul change le rapport C_2H_2/C_2H_4 qui augmente au fur et à mesure que les photons absorbés transportent de plus en plus d'énergie. Il resterait alors à expliquer les contributions des autres processus primaires de décomposition comptant pour la différence:

$$1.00 - \left[\frac{M(C_2H_4) + M(C_2H_2) + M(C_2H_3Cl)}{N_{ex}}\right]_{primaire} = 0.59$$

Les processus mis en jeu sont, selon toute vraisemblance, [7, 8, 12, 22] et

[30] $C_2H_5Cl^* \rightarrow C_2H_5^{\cdot} + Cl^{\cdot}$

La contribution du processus 22 est partiellement visualisée par les rendements en méthane et chlorure de méthyle. Par contre, l'estimation relative des ruptures C—H et C—Cl suivant les processus 12 et 30 s'avère très difficile, sinon impossible, sans la connaissance du rendement en HCl.

Nous remercions le Dr H. Wincel pour avoir mis aimablement à notre disposition les résultats non publiés sur les réactions ion–molécule dans le chlorure d'éthyle. Ce travail a pu être accompli grâce aux subventions du Conseil National de Recherche du Canada et du Ministère d'Education du Québec.

1. T. O. Tiernan et B. M. Hughes. Adv. Chem. Ser. **82**, 412 (1968).
2. W. H. S. Yu et M. H. J. Wijnen. J. Chem. Phys. **52**, 4166 (1970); T. Fujimoto et M. H. J. Wijnen. J. Chem. Phys. **56**, 4032 (1972).
3. R. N. Schindler. Radiochem. Acta, **2**, 62 (1963).
4. R. Gorden Jr., R. E. Rebbert et P. Ausloos. NBS Techn. Note #496. 1969.
5. K. Watanabe, F. M. Matsunaga et H. Sakai. J. Appl. Opt. **6**, 391 (1967).
6. J. A. Herman, K. Herman et P. Ausloos. J. Chem. Phys. **52**, 28 (1970).
7. A. A. Siddiqi, C. T. Chen, G. G. Meisels et R. Gorden Jr. J. Chem. Phys. **57**, 4506 (1972).
8. S. Tsuda et W. H. Hamill. J. Chem. Phys. **41**, 2713 (1964).
9. S. W. Benson et H. E. O'Neal. Kinetic data on gas phase unimolecular reactions. NSRDS, NBS 21, 1970.
10. H. Hartman, H. G. Bosche et H. Heydtmann. Zeit. Phys. Chim. N.F. **42**, 329 (1964).
11. K. A. Holbrook et A. R. Marsh. Trans. Faraday Soc. **63**, 643 (1967).
12. S. W. Benson. Thermochemical kinetics. Ed. John Wiley & Sons, New York. 1968, p. 215.
13. J. L. Franklin et G. Huybrechts. Int. J. Chim. Kinet. **1**, 3 (1969).
14. T. J. Hardwick. J. Phys. Chem. **66**, 2246 (1966).
15. B. C. Roquitte et M. H. J. Wijnen. J. Am. Chem. Soc. **85**, 2053 (1963).
16. T. G. Majury et E. W. R. Steacie. Discuss. Faraday Soc. **14**, 45 (1953).
17. A. F. Trotman-Dickenson. Q. Rev. Lond. **7**, 198 (1953).
18. M. S. Kharash et G. Buchi. J. Am. Chem. Soc. **73**, 632 (1951).
19. M. J. Akop'ian, F. J. Vilesov et J. L. Siergiejev. Teor.i Exper. Khimia, **7**, 271 (1971).
20. L. G. Christoforou, R. N. Compton, G. S. Hurst et P. W. Reinhardt. J. Chem. Phys. **45**, 536 (1966).
21. H. Wincel et Z. Luczynski. Résultats non publiés.
22. N. S. Buchelnikova. Zh. Eksper. Teor. Fiz. **35**, 1119 (1958).
23. G. H. Mahan et J. C. Person. J. Chem. Phys. **40**, 392 (1964).

Can. J. Chem. Downloaded from www.nrcresearchpress.com by 210.87.254.105 on 09/05/12
For personal use only.

Sur la réduction de polyméthyldihydro-2,3 phénalènones-1 par l'hydrure de lithium et d'aluminium

E. COSTAKIS[1], P. CANONNE ET R. ST-JEAN[2]

Département de chimie, Université Laval, Québec, Québec G1K 7P4

Reçu le 4 avril, 1974

E. COSTAKIS, P. CANONNE et R. ST-JEAN. Can. J. Chem. **52**, (3106) 1974.

La réduction de quelques polyméthyldihydro-2,3 phénalènones-1 par l'hydrure de lithium et d'aluminium fournit un mélange d'isomères *cis* et *trans* et le pourcentage de chaque isomère dépend considérablement de leur structure. En effet, pour certaines, l'isomère *trans* reste prépondérant tandis que pour d'autres l'isomère *cis* est obtenu jusqu'à 88%. Par ailleurs, dans le cas particulier où l'isomère *trans* se forme en faibles quantités, sa conformation privilégiée est *trans* diaxiale.

Nous discutons à l'aide des données spectroscopiques des alcools obtenus, les contraintes stériques qui défavorisent certains états de transition lors de l'attaque de l'hydrure.

E. COSTAKIS, P. CANONNE and R. ST-JEAN. Can. J. Chem. **52**, (3106) 1974.

The reduction of some polymethyl-2,3-dihydro phenalen-1-ones by lithium aluminum hydride yields a mixture of *cis* and *trans* isomers; the percentage of each isomer depends to a considerable extent on its structure. Indeed, for some, the *trans* isomer predominates while for others the *cis* isomer is obtained in up to 88% yields. Moreover, in the particular case in which the *trans* isomer is formed in low yields, its preferred conformation is *trans* diaxial.

The steric constraints which render certain transition states unfavourable during the attack of the hydride are discussed with the aid of spectroscopic data on the alcohols obtained.

[Journal translation]

Introduction

Dans le cadre général de nos recherches sur la synthèse d'hydrocarbures aromatiques polycycliques (1, 2, 3) nous avons entrepris, en relation avec un travail déjà publié par l'un de nous (4), la préparation de polyméthylphénalènes.

Selon l'approche prévue, nous devons obtenir les phénalènes par réduction de polyméthyldihydro-2,3 phénalènones suivis d'une déshydratation des polyméthyldihydrophénalènols-1. Les différences entre le pourcentage des isomères *cis* et *trans* obtenus ainsi que la conformation inattendue des isomères *trans* dans le cas de cétones encombrés nous ont paru mériter l'intérêt du présent travail. En effet, les théories actuelles sur la stéréochimie de la réduction des cétones reposaient sur l'étude de certains types de cétones alors que nous travaillions sur des types différents et que nous désirions leur étendre l'application de ces théories (5–8). Nous avons donc fait une étude systématique de cette réduction dans le but de dégager la relation entre la position des substituants dans les composés de départ et les produits obtenus.

Méthode de synthèse

La synthèse des polyméthyldihydrophénalènols-1 repose essentiellement sur la série des réactions données au schéma 1. Les polyméthylnaphtalènes préparés selon les méthodes décrites (9, 10) ont été chlorométhylés avec de meilleurs rendements en suivant deux modes opératoires différents (3) tenant compte de la réactivité des naphtalènes et de la tendance à la polymérisation des chlorométhylnaphtalènes **1**–**4** obtenus.

La synthèse malonique appliquée sur ces substrats en utilisant comme solvant le benzène fournit les esters maloniques substitués **5**–**8**.

L'hydrolyse des esters maloniques est effectuée par une solution hydroalcoolique d'hydroxyde de potassium (3 *M*) et le rendement de cette opération varie entre 80 et 90%. Les acides maloniques sont décarboxylés par chauffage aux environs de 180 °C et fournissent, avec un rendement presque quantitatif, les acides β-naphtylpropioniques correspondants **9**–**12** lesquels sont cyclisés en présence d'acide fluorhydrique.

Les polyméthyldihydro-2,3 phénalènones obtenues sont réduites par $LiAlH_4$ de façon

[1]Adresse actuelle: Laboratoire de Chimie Pharmaceutique, Université d'Athènes, 104, rue Solonos, Athènes, Grèce.

[2]Services de Protection de l'Environnement, Québec, P.Q.

Can. J. Chem. Downloaded from www.nrcresearchpress.com by 210.87.254.6 on 09/05/12
For personal use only.

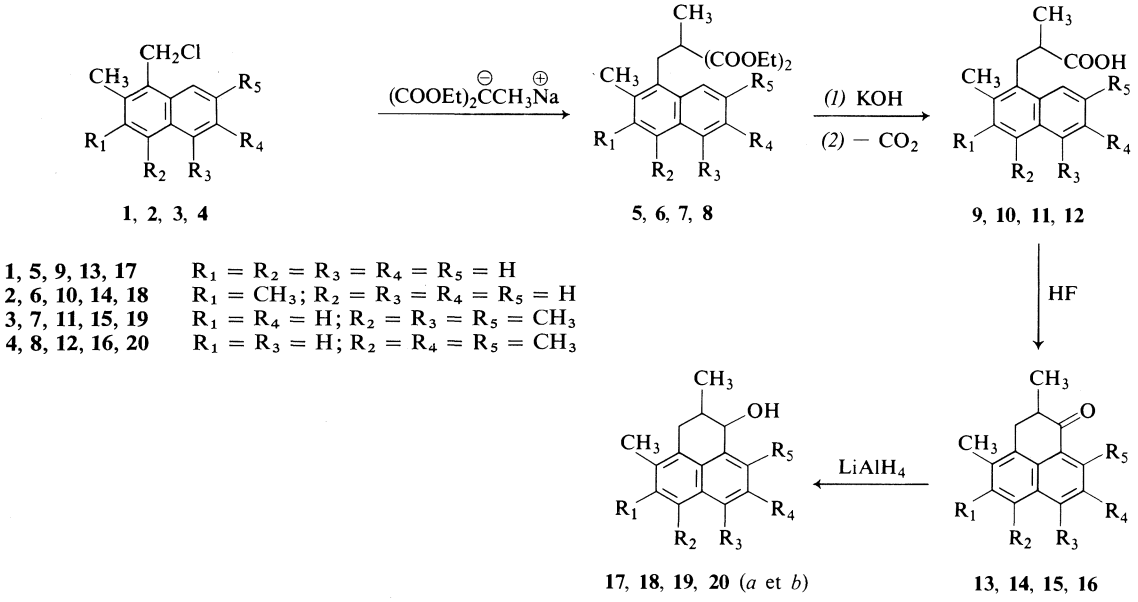

1, 5, 9, 13, 17 $R_1 = R_2 = R_3 = R_4 = R_5 = H$
2, 6, 10, 14, 18 $R_1 = CH_3$; $R_2 = R_3 = R_4 = R_5 = H$
3, 7, 11, 15, 19 $R_1 = R_4 = H$; $R_2 = R_3 = R_5 = CH_3$
4, 8, 12, 16, 20 $R_1 = R_3 = H$; $R_2 = R_4 = R_5 = CH_3$

SCHÉMA 1

TABLEAU 1. Caractéristiques spectrales, i.r. et r.m.n., des polyméthyldihydro-2,3 phénalènols-1

		Résonance magnétique nucléaire ($CDCl_3$)					
		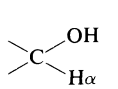		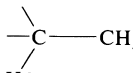		Infrarouge (CS_2) ν (CO) (cm^{-1})	
Polyméthyldihydro-2,3 phénalènols-1		δ (p.p.m.)	*J* (Hz)	δ (p.p.m.)	*J* (Hz)	Axial	Equatorial
17	*a* (*cis*) 35%	4.86	2	1.25	6.5	1020(m)*	1050(f)
	b (*trans*) 65%	4.55	7.5	1.06	6.5	1010(tf)	1050(f)
18	*a* (*cis*) 36%	4.75	2	1.21	6.5	1020(m)	1050(f)
	b (*trans*) 64%	4.48	8	1.05	6.5	1010(tf)	1050(f)
19	*a* (*cis*) 88%	4.93	2	1.26	6.5	1015(m)	1050(m)
	b (*trans*) 12%	4.72	3	0.66	7	1015(f)	—
20	*a* (*cis*) 87%	5.02	2	1.28	6.5	1015(m)	1050(m)
	b (*trans*) 13%	4.87	3	0.73	7	1015(f)	—

*f = fort, m = moyen, tf = très faible.

habituelle en les mettant en solution dans le benzène. Après hydrolyse, les alcools **17**–**20** sont extraits et le dosage des stéréoisomères est effectué par r.m.n. et vérifié après séparation chromatographique.

Résultats

L'examen des résultats rassemblés au tableau 1, montre que les pourcentages d'alcools isomères *a* et *b* sont totalement différents selon les cétones étudiées, et dans le cas des cétones fortement encombrées (**15** et **16**) où l'isomère *a* prédomine, la réduction fait apparaître une plus grande stéréosélectivité. Les cétones peu encombrées au voisinage du carbonyle (**13** et **14**) montrent une stéréosélectivité moins marquée et l'isomère *b* prédomine légèrement.

Stéréochimie des alcools peu encombrés 17 et 18

Pour déterminer la configuration et les conformations des alcools isomères **17**, **18** (*a* et *b*), nous nous basons sur les spectres de r.m.n. et tout particulièrement sur les déplacements chimiques et les constantes de couplages des

Can. J. Chem. Downloaded from www.nrcresearchpress.com by 210.87.254.6 on 09/05/12
For personal use only.

protons rapportés au tableau 1. Le signal du proton lié au carbone portant la fonction hydroxyle (Hα) se manifeste à δ 4.86 et 4.75 p.p.m. pour les isomères **17***a* et **18***a* tandis qu'on le retrouve à δ 4.55 et 4.48 p.p.m. pour les isomères **17***b* et **18***b*. Les valeurs des constantes de couplage de (Hα) avec le proton adjacent (Hβ) sont respectivement de $J = 2$ Hz pour les alcools *a* et de $J = 8$ Hz pour les alcools *b*. Ces valeurs permettent de déterminer, sans ambiguïté, la configuration de chaque couple d'isomères car le déplacement chimique le plus déblindé ne peut être attribué qu'à un proton équatorial et il a la constante de couplage la plus faible.

On attribue alors à l'isomère *b* la configuration *trans* dans laquelle le méthyle se trouve en position équatoriale et l'hydroxyle en position pseudo-équatoriale (forme **E**, schéma 2). La conformation et la configuration de ces alcools *trans* "diéquatoriaux" ont été également confirmées par spectroscopie i.r. En effet, on observe pour ces alcools que la bande caractéristique de la liaison C—O des hydroxyles équatoriaux à 1050 cm^{-1}.

En ce qui concerne les alcools *cis* (**17***a* et **18***a*), les résultats spectroscopiques suggèrent que nous sommes en présence d'un équilibre rapide entre les deux conformations possibles pour ces isomères. (formes **C** et **D**, schéma 2).

Premièrement, les spectres i.r. montrent la présence des deux bandes (1050 et 1020 cm^{-1}) caractéristiques dans la région d'absorption des liaisons C—O des hydroxyles.

Deuxièmement, les spectres de r.m.n. confirment la présence des deux conformères en équilibre rapide car le signal du méthylène se retrouve simplifié en un doublet alors qu'il se manifeste sous une forme plus complexe dans le cas des isomères *b*.

Stéréochimie des alcools encombrés ***19***, ***20*** (*a et b*)

Pour déterminer la configuration et les conformations des isomères *a* et *b*, nous nous basons aussi sur leurs spectres i.r. et de r.m.n. En examinant les spectres de r.m.n. (tableau 1) on constate que la valeur des constantes de couplage du proton Hα nous permet d'exclure la présence de la conformation diéquatoriale pour l'isomère *trans* des alcools **19** et **20**.

Nous attribuons la configuration *trans* à l'isomère *b* des alcools **19** et **20** en nous basant sur le spectre i.r. lequel montre pour l'isomère *b* une seule bande à 1015 cm^{-1} correspondant à une

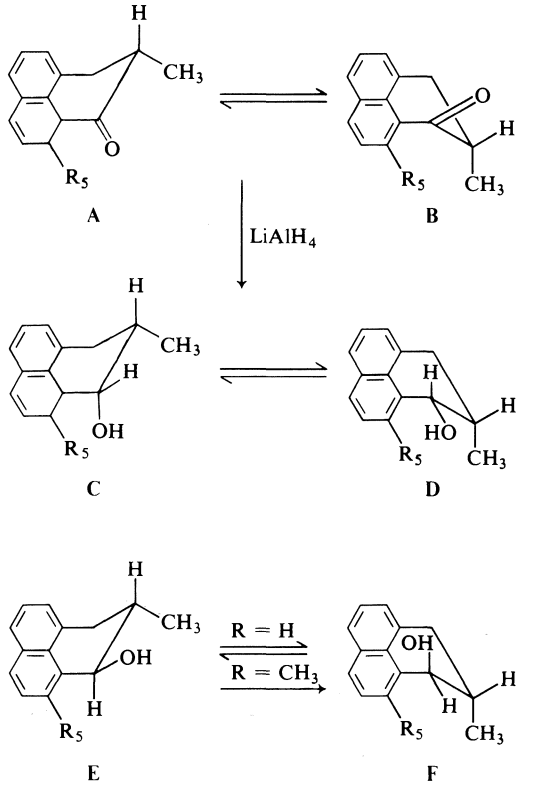

SCHÉMA 2

absorption d'un hydroxyle axial. Par ailleurs, les données de r.m.n. concernant les constantes de couplage du proton Hα(3 Hz) et le signal du méthyle cyclanique fortement blindé nous permettent d'assigner sans ambiguïté cette configuration *trans*.

A l'isomère *a* des alcools **19** et **20** nous attribuons la configuration *cis* en nous basant également sur leurs spectres i.r. En effet, leurs spectres présentent deux bandes à 1015 et 1050 cm^{-1} correspondant à ν (C—O) axial et ν (C—O) équatorial.

En suivant le même raisonnement que pour les isomères **17***a* et **18***a*, nous pouvons déduire que les isomères **19***a* et **20***a* ont la configuration *cis* sous forme d'un équilibre conformationnel (formes **C** et **D**, schéma 2). Cependant nous pensons qu'en solution la conformation **C** est favorisée à cause de l'intéraction avec le méthyle.

Discussion

Les résultats obtenus lors de la présente étude montrent une diminution du pourcentage de l'isomère *trans* des dihydrophénalènols par

Can. J. Chem. Downloaded from www.nrcresearchpress.com by 210.87.254.6 on 09/05/12
For personal use only.

Can. J. Chem. Downloaded from www.nrcresearchpress.com by 210.87.254.6 on 09/05/12
For personal use only.

rapport à celui obtenu dans le cas de la méthyl-2 cyclohexanone. Cette diminution est particulièrement forte dans le cas des dihydrophénalènols très encombrés par le méthyle aromatique et l'isomère *cis* prédomine, tandis que l'isomère *trans* qui se trouve en plus faible proportion (12%) a la conformation diaxiale.

Pour tenter d'expliquer ces constatations il nous a semblé nécessaire de reconsidérer les hypothèses émises récemment sur la stéréochimie de la réduction des cyclohexanones substituées (5–8). Elles envisagent d'une part les contraintes stériques des substituants en position 3 et 5 lors de l'entrée axiale de l'hydrure sur le carbone sp^2, et d'autre part les tensions de torsion avec les substituants en position 2 et 6, lors de l'entrée équatoriale.

Nous avons représenté au schéma 3 les états de transition possibles et indiqué par "A" l'attaque axiale qui conduit à l'hydroxyle pseudo-équatorial et par "E" l'attaque équatoriale qui conduit à l'hydroxyle pseudo-axial.

Le fait que l'hydroxyle préfère la position axiale dans le cas des alcools **19***b* et **20***b* (*trans* aa) montre qu'une intéraction stérique déstabilisante existe entre l'oxygène et le groupe méthyle aromatique qui empêche la formation de l'isomère *trans* ee. Lorsque l'on examine les différents états de transition, on constate que cette intéraction est importante dans CA et encore davantage dans TA dans laquelle trois groupes tendent à s'éclipser. Au contraire, les états de transition CE et TE permettent d'éviter une telle intéraction déstabilisante avec les méthyles. Par ailleurs, l'état de transition TE est moins favorisé que CE car le réactif est éclipsé par le méthyle cyclanique en position axiale. On peut ainsi expliquer la configuration *trans* aa des alcools fortement encombrés et leur formation en faibles quantités dans le mélange réactionnel.

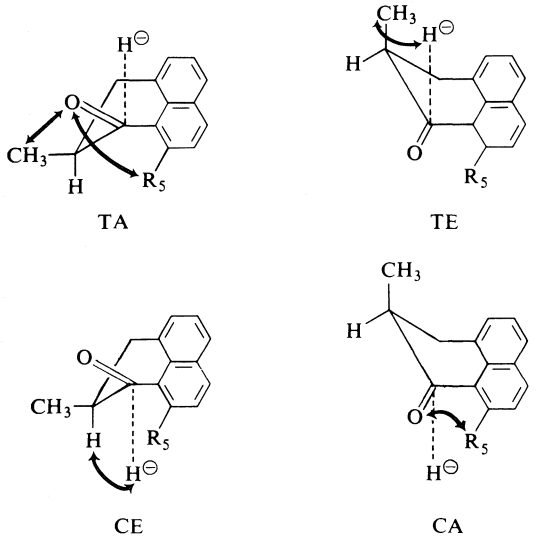

SCHÉMA 3

On peut supposer encore que l'état de transition CE, fournissant l'isomère *cis* prépondérant (88%), est le plus favorisé car non seulement il permet d'éviter des intéractions entre le méthyle aromatique et l'oxygène mais il facilite aussi l'entrée de l'hydrure. En effet, les tensions de torsion sont moins importantes du fait qu'un seul hydrogène en position 2 éclipse le réactif attaquant.

Nous ne pouvons néanmoins exclure la participation de l'état de transition CA pour l'obtention de l'isomère **D** (schéma 2) étant donné l'existence de deux hydroxyles dans l'isomère *cis*, sauf si nous tenons compte de la faible différence d'énergie mise en cause entre les deux conformations possibles (**C** et **D** schéma 2).

Les hypothèses émises ci-dessus sont appuyées également par les pourcentages d'isomères obtenus dans le cas des dihydrophénalènones non encombrées **13** et **14** et surtout par la stéréochimie des alcools **17** et **18**.

L'obtention de l'alcool *trans* diéquatorial prépondérant (65%) indique que l'état de transition TA est favorisé comme dans le cas de la méthyl-2 cyclohexanone et l'on impute ce résultat à l'absence du méthyle aromatique au voisinage du carbonyle.

De même l'isomère *cis* (35%) peut provenir de l'état de transition CE que nous retenons comme étant plus favorisé que CA. Cependant on ne peut exclure la participation de CA puisque les données spectroscopiques i.r. montrent deux bandes correspondant aux positions axiale et équatoriale de l'hydroxyle. Toutefois il faut également tenir compte de la structure plane des phénalènones qui fait disparaître les interactions habituelles **3**, **5** avec le méthyle en position axiale.

Partie expérimentale

Les points de fusion sont rapportés non corrigés et ont été déterminés sur un appareil Thomas–Hoover. Les spectres i.r. ont été enregistrés sur un spectrophotomètre Perkin–Elmer 457 en solution dans CCl_4 et CS_2 (solvants pour spectroscopie préalablement séchés). Les analyses élémentaires ont été effectuées sur un appareil F et M

Can. J. Chem. Downloaded from www.nrcresearchpress.com by 210.87.254.6 on 09/05/12
For personal use only.

modèle 181. Les spectres i.r. ont été pris à chaque étape; en raison de la grande similitude entre les composés des quatre séries, nous avons remarqué dans tous les cas les absorptions suivantes: ν (C=O) (ester malonique) ~1740 cm^{-1}, ν (C=O) (acide malonique) ~1720 cm^{-1}, (acide β-naphthylpropionique) ~1710 cm^{-1}, ν (C=O) (cétone) ~1680 cm^{-1}. Les spectres de r.m.n. sont mesurés sur un spectromètre Varian A-60 en utilisant le $CDCl_3$ comme solvant et le TMS comme référence interne. Pour la chromatographie sur colonne nous avons utilisé de l'alumine Woëlm p*H* 7.0–7.5 et pour la chromatographie en couche mince du gel de silice GF 254 (Merck).

Préparation du chlorométhyl-1 méthyl-2 naphtalène ***1*** *(3)*

Dans un ballon, on chauffe à 60 °C, 35.5 g (0.25 mol) de méthyl-2 naphtalène, 13.75 g (0.45 mol) de paraformaldéhyde, 32.5 ml d'acide acétique pur, 45 ml d'acide chlorhydrique concentré et 21 ml d'acide phosphorique à 85%. On arrête la réaction en ajoutant 250 ml d'eau glacée et le mélange est extrait par l'éther de pétrole et l'éther diéthylique (50:50). On lave au bicarbonate de soude et à l'eau, sèche sur $MgSO_4$ et évapore le solvant sous pression réduite. Par cristallisation fractionnée dans l'éther de pétrole, on recueille 36.0 g (86%) de chlorométhyl-1 méthyl-2 naphtalène, p.f. 65 °C.

Anal. calc. pour $C_{12}H_{11}Cl$: C, 75.58; H, 5.81. Trouvé: C, 75.72; H, 5.89.

Préparation du chlorométhyl-1 diméthyl-2,3 naphtalène ***2***

On suit le mode opératoire précédent en utilisant 39.0 g de diméthyl-2,3 naphtalène et on obtient 22 g (43%) de chlorométhyl-1 diméthyl-2,3 naphtalène, p.f. 86–87 °C (litt (11) p.f. 88 °C).

Préparation du chlorométhyl-1 tétraméthyl-2,4,5,7 naphtalène ***3***

Dans un flacon, on met 8.0 g (0.2 mol) de paraformaldéhyde en suspension dans 750 ml d'acide acétique pur et on y fait barboter un courant de gaz chlorhydrique, préalablement séché sur H_2SO_4, jusqu'à dissolution du paraformaldéhyde. Après addition de 23.0 g (0.125 mol) de tétraméthyl-1,3,6,8 naphtalène, on ferme le flacon qui est abandonné, pour 2 h, à 25 °C. La réaction est arrêtée par l'addition de 150 ml d'eau glacée et on extrait par un mélange éther – éther de pétrole. La phase organique est lavée au carbonate de sodium à 5%, à l'eau, puis séchée sur sulfate de magnésium. Après évaporation du solvant et recristallisation dans l'éther de pétrole on recueille 6% de bis(polyméthylnaphthyl) méthane et 26.7 g (92%) de chlorométhyl-1 tétraméthyl-2,4,5,7 naphtalène, p.f. 123 °C.

Anal. calc. pour $C_{15}H_{17}Cl$: C, 77.42; H, 7.31. Trouvé: C, 77.52; H, 7.35.

Préparation du chlorométhyl-1 tétraméthyl-2,4,6,7 naphtalène ***4***

On suit le mode opératoire précédent en utilisant 23.0 g (0.125 mol) de tétraméthyl-1,3,6,7 naphtalène et on obtient 26.1 g (90%) de chlorométhyl-1 tétraméthyl-2,4,6,7 naphtalène, p.f. 144 °C.

Anal. calc. pour $C_{15}H_{17}Cl$: C, 77.42; H, 7.31. Trouvé: C, 77.71; H, 7.34.

Préparation de l'éthoxycarbonyl-2 méthyl-2 [(méthyl-2 naphtyl-1)]-3 propionate d'éthyle ***5***

En utilisant le mode opératoire déjà développé dans notre laboratoire (1, 2), on introduit 1.72 g (0.075 at.-g) de sodium dans 150 ml de benzène anhydre, puis 13.0 g (0.075 mol) de méthylmalonate d'éthyle et porte à reflux. Après attaque complète du sodium, on ajoute goutte à goutte, une solution de 14.3 g (0.075 mol) de chlorométhyl-1 méthyl-2 naphtalène dissous dans le minimum de benzène anhydre. Après introduction complète, on porte à reflux une nuit, verse dans l'eau glacée, décante, extrait la phase aqueuse à l'éther, sèche la phase organique sur sulfate de sodium anhydre, filtre et évapore le solvant.

On redissous dans le pentane et chromatographie sur colonne en éluant au pentane. On obtient 22.6 g (92%) d'une huile incolore.

Anal. calc. pour $C_{20}H_{24}O_4$: C, 73.14; H, 7.37. Trouvé: C, 73.25; H, 7.52.

Préparation de l'éthoxycarbonyl-2 méthyl-2 [(diméthyl-2,3 naphtyl)-1]-3 propionate d'éthyle ***6***

On suit le mode opératoire précédent en utilisant 15.3 g (0.075 mol) de chlorométhyl-1 diméthyl-2,3 naphtalène pour obtenir, après chromatographie selon le mode décrit précédemment, 22.9 g (89%) d'une huile incolore.

Anal calc. pour $C_{21}H_{26}O_4$: C, 73.66; H, 7.66. Trouvé: C, 73.42; H, 7.83.

Préparation de l'éthoxycarbonyl-2 méthyl-2 [(tétraméthyl-2,4,5,7 naphtyl)-1]-3 propionate d'éthyle ***7***

On suit le mode opératoire général en opérant sur 17.4 g (0.075 mol) de chlorométhyl-1 tétraméthyl-2,4,5,7 naphtalène pour obtenir, après chromatographie, 23.6 g (86%) d'une huile incolore (n_D^{23} 1.5749).

Anal. calc. pour $C_{23}H_{30}O_4$: C, 74.56; H, 8.16. Trouvé: C, 74.59; H, 7.94.

Préparation de l'éthoxycarbonyl-2 méthyl-2 [(tétraméthyl-2,4,6,7 naphtyl)-1]-3 propionate d'éthyle ***8***

On suit le mode opératoire général en utilisant 17.4 g (0.075 mol) de chlorométhyl-1 tétraméthyl-2,4,6,7 naphtalène pour obtenir, après chromatographie, 25.2 g (91%) d'une huile incolore (n_D^{23} 1.5779).

Anal. calc. pour $C_{23}H_{30}O_4$: C, 74.56; H, 8.16. Trouvé: C, 74.49; H, 8.24.

Préparation de l'acide méthyl-2 [(méthyl-2 naphtyl)-1]-3 propionique ***9***

On met en présence 9.84 g (0.03 mol) d'ester malonique **5** dissout dans 30 ml d'éthanol à 99% et une solution de 10.1 g (0.18 mol) de KOH dans 30 ml d'eau. On porte à reflux une nuit puis on distille pour éliminer l'alcool. On refroidit le résidu, on lave à l'éther pour éliminer les composés neutres, puis on acidifie la phase aqueuse pour obtenir l'acide malonique. Le diacide est décarboxylé par chauffage sous atmosphère d'azote à 180 °C jusqu'à cessation du dégagement de CO_2. Après refroidissement, le solide recueilli est recristallisé dans un mélange pentane–benzène et l'on obtient 6.50 g (95%) de l'acide propionique substitué 9, p.f. 98–99 °C.

Anal. calc. pour $C_{15}H_{16}O_2$: C, 78.92; H, 7.06. Trouvé: C, 79.14; H, 7.10.

Préparation de l'acide méthyl-2 [(diméthyl-2,3 naphtyl)-1]-3 propionique ***10***

En procédant selon le mode opératoire précédent et sur 8.55 g (0.025 mol) d'ester malonique **6** on obtient après hydrolyse et décarbonylation, 5.7 g (94%) de cristaux incolores de l'acide 10, p.f. 123–124 °C.

Can. J. Chem. Downloaded from www.nrcresearchpress.com by 210.87.254.6 on 09/05/12
For personal use only.

Anal. calc. pour $C_{16}H_{18}O_2$: C, 79.31; H, 7.49. Trouvé: C, 79.33; H, 7.63.

Préparation de l'acide méthyl-2 [(tétraméthyl-2,4,5,7 naphtyl-1)]-3 propionique ***11***

Après hydrolyse de 9.25 g (0.025 mol) d'éther malonique **7** suivit d'une décarboxylation on obtient 6.5 g (96%) de l'acide attendu **11**, p.f. 143 °C.

Anal. calc. pour $C_{18}H_{22}O_2$: C, 79.96; H, 8.20. Trouvé: C, 79.81; H, 8.34.

Préparation de l'acide méthyl-2 [(tétraméthyl-2,4,6,7 naphtyl-1)]-3 propionique ***12***

Selon le mode opératoire précédent on traite 9.25 g (0.025 mol) d'ester malonique **8**, on obtient après hydrolyse et décarboxylation, 6.3 g (93%) de cristaux incolores: de l'acide **12**, p.f. 125–5 °C.

Anal. calc. pour $C_{18}H_{22}O_2$: C, 79.96; H, 8.20. Trouvé: C, 80.18; H, 8.37.

Préparation de la dimethyl-2,4 dihydro-2,3 phénalénone-1 ***13***

On ajoute, par petites portions, 4.56 g (0.02 mol) d'acide naphtylpropionique **9** dans un récipient en polyéthylène contenant 60 ml d'acide fluorhydrique, puis on agite doucement jusqu'à dissolution complète de l'acide **9**. On abandonne dix min pour compléter la cyclisation puis on hydrolyse en versant le mélange réactionnel sur de la glace et on extrait la cétone **13** au benzène. Cette phase organique est lavée par une solution de NaOH (5%) puis à l'eau et est séchée sur sulfate de sodium anhydre. Après évaporation du solvant, on obtient 3.95 g (94%) de la cétone **13** qui est recristalisé dans l'éther de pétrole, p.f. 83 °C.

Anal. calc. pour $C_{15}H_{14}O$: C, 85.68; H, 6.71. Trouvé: C, 85.74; H, 6.93.

Préparation de la triméthyl-2,4,5 dihydro-2,3 phénalènone-1 ***14***

On suit le mode opératoire précédent en utilisant 4.84 g (0.02 mol) d'acide naphtylpropionique **10** et on obtient après recristallisation dans l'éther de pétrole, 4.30 g (96%) de cristaux incolores, p.f. 102 °C que l'on identifie par spectroscopie comme étant la phénalènone **14**.

Anal. calc. pour $C_{16}H_{16}O$: C, 85.68; H, 7.19. Trouvé: C, 85.78; H, 7.08.

Préparation de la pentaméthyl-2,4,6,7,9 dihydro-2,3 phénalènone-1 ***15***

On suit le même mode opératoire et sur 5.40 g (0.02 mol) d'acide naphtylpropionique **11** on obtient après recristallisation dans l'éther de pétrole, 4.74 g (94%) de fins cristaux blanc, p.f. 103 °C.

Anal. calc. pour $C_{18}H_{20}O$: C, 85.67; H, 7.99. Trouvé: C, 85.58; H, 7.86.

Préparation de la pentaméthyl-2,4,6,8,9 dihydro-2,3 phénalènone-1 ***16***

On suit le mode opératoire général et en opérant sur 5.40 g (0.02 mol) d'acide naphtylpropionique **12** on obtient après recristallisation dans l'éther de pétrole, 4.89 g (97%) de fins cristaux blancs, p.f. 136–5 °C.

Anal. calc. pour $C_{18}H_{20}O$: C, 85.67; H, 7.99. Trouvé: C, 85.55; H, 7.99.

Préparation du diméthyl-2,4 dihydro-2,3 phénalènol-1 ***17***

A une suspension de 190 mg (0.005 mol) d'hydrure de lithium et d'aluminium dans 60 ml d'éther anhydre, on ajoute une solution de 2.10 g (0.01 mol) de cétone **13** dissoute dans 30 ml de benzène anhydre, de façon à maintenir une douce ébullition. Après $1\frac{1}{2}$ h de reflux, on refroidit puis hydrolyse de la façon habituelle. On extrait plusieurs fois la phase aqueuse au benzène, on réunit les phases organiques qu'on lave à l'eau et sèche sur sulfate de sodium anhydre. Par évaporation du solvant, on recueille un solide, qui d'après ses spectres i.r. et de r.m.n. et l'analyse chromatographique sur couche mince, est un mélange d'isomère *cis* et *trans* (rendement 93%).

Les alcools isomères sont séparés par chromatographie sur alumine en éluant par un mélange éther – éther de pétrole et nous obtenons: une première fraction (**17***a*) de 0.69 g (35%), p.f. 119 °C; i.r. (solution 0.1 *M* dans CS_2) ν (C—O) équatorial fort à 1050 cm^{-1} et ν (C—O) axial moyen à 1020 cm^{-1}; i.r. (KBr) ν (C—O) équatorial fort à 1050 cm^{-1} et ν (C—O) axial absent à 1020 cm^{-1}; r.m.n. ($CDCl_3$) δ 1.25 (d, J = 7 Hz, méthyl-2), 2.44 (s, méthyl-4), 4.86 (d, J = 2 Hz, C*H*—OH).

Une seconde fraction (**17***b*) de 1.28 g (65%), p.f. 140 °C; i.r. (solution 0.1 *M* dans CS_2) ν (C—O) équatorial fort à 1050 cm^{-1} et ν (C—O) axial très faible à 1010 cm^{-1}; i.r. (KBr) ν (C—O) équatorial fort à 1050 cm^{-1} et ν (C—O) axial absent à 1010 ou 1020 cm^{-1}; r.m.n. ($CDCl_3$) δ 1.09 (d, J = 6.5 Hz, méthyl-2) 2.43 (s, méthyl-4), 4.63 (d, J = 8 Hz, C*H*—OH).

Anal. calc. pour $C_{15}H_{16}O$: C, 84.87; H, 7.60. Trouvé: (**17***a*) C, 84.69; H, 7.82. Trouvé (**17***b*): C, 84.78; H, 7.51.

Préparation du triméthyl-2,4,5 dihydro-2,3 phénalènol-1 ***18***

Selon le mode opératoire précédent on utilise 2.24 g (0.01 mol) de cétone **14** et on obtient par chromatographie sur alumine, pour un rendement global de 93%.

Une première fraction (**18***a*) de 0.76 g (36%), p.f. 144 °C; i.r. (solution 0.1 *M* dans CS_2) ν (C—O) équatorial fort à 1050 cm^{-1}, ν (C—O) axial moyen à 1020 cm^{-1}; i.r. (KBr) ν (C—O) équatorial fort à 1050 cm^{-1} et ν (C—O) axial absent à 1020 cm^{-1}; r.m.n. ($CDCl_3$) δ1.21 (d, J = 6.5 Hz, méthyl-2) 2.33 et 2.41 (s, s, méthyles aromatiques), 4.75 (d, J = 2 Hz, C*H*—OH).

Une seconde fraction (**18***b*) de 1.345 g (64%), p.f. 164 °C; i.r. (solution 0.1 *M* dans CS_2) ν (C—O) équatorial fort à 1050 cm^{-1} et ν (C—O) axial très faible à 1010 cm^{-1}; i.r. (KBr) ν (C—O) équatorial fort à 1050 cm^{-1} et ν (C—O) axial absent à 1010 ou 1020 cm^{-1}; r.m.n. ($CDCl_3$) δ 1.05 (d, J = 6.5 Hz, méthyle-2) 2.33 et 2.41 (s, s, méthyles aromatiques), 4.48 (d, J = 8 Hz, C*H*—OH).

Anal. calc. pour $C_{16}H_{18}O$: C, 84.91; H, 8.02. Trouvé (**18***a*): C, 84.82; H, 8.17. Trouvé (**18***b*): C, 84.99; H, 8.21.

Préparation du pentaméthyl-2,4,6,7,9 dihydro-2,3 phénalènol-1 ***19***

En suivant le même mode opératoire que précédemment, on utilise 2.52 g (0.01 mol) de cétone **15** et on obtient par chromatographie sur alumine, pour un rendement global de 95%.

Une première fraction (**19***a*) de 2.16 g (88%), p.f. 136 °C; i.r. (solution 0.2 *M* dans CS_2) ν (OH) libre à 3610 cm^{-1}, ν (OH) polymère absent à 3310 cm^{-1}, ν (C—O) équatorial moyen à 1050 cm^{-1}, ν (C—O) axial moyen à 1015 et 1000 cm^{-1}; r.m.n. ($CDCl_3$) δ1.26 (d, J = 6.5 Hz, méthyl-2); 2.33, 2.48 et 2.81 (singulets, méthyles aromatiques), 4.93 (d, J = 2 Hz, C*H*—OH).

Une seconde fraction (**19***b*) de 0.29 g (12%), p.f. 150 °C; i.r. (solution 0.2 *M* dans CS_2) ν (OH) libre à 3610 cm^{-1},

ν (OH) polymère à 3310 cm^{-1}, ν (C—O) équatorial absent à 1050 cm^{-1}, ν (C—O) axial à 1015 et 1000 cm^{-1}; r.m.n. ($CDCl_3$) δ 0.66 (d, $J = 7$ Hz, méthyle-2) 2.33, 2.48 et 2.81 (singulet, méthyles aromatiques), 4.82 (d, $J = 3$ Hz, C*H*—OH).

Anal. calc. pour $C_{18}H_{22}O$: C, 85.00; H, 871. Trouvé (**19***a*): C, 84.88; H, 8.77. Trouvé (**19***b*): C, 84.86; H, 8.68.

Préparation du pentaméthyl-2,4,6,8,9 dihydro-2,3 phénalènol-1 ***20***

En opérant sur 2.52 g (0.01 mol) de cétone **16** selon le mode opératoire précédent de réduction on obtient l'alcool **20** avec un rendement global de 97%.

Une première fraction (**20***a*) de 2.12 g (87%), p.f. 107 °C; i.r. (solution 0.2 *M* dans CS_2) ν (OH) libre à 3610 cm^{-1}, ν (OH) polymère absent à 3310 cm^{-1}, ν (C—O) équatorial moyen à 1050 cm^{-1}, ν (C—O) axial moyen à 1015 et 1000 cm^{-1}; r.m.n. ($CDCl_3$) δ1.19 (d, $J = 6.5$ Hz, méthyle-2) 2.33, 2.42 et 2.55 (singulets, méthyles aromatiques), 5.02 (d, $J = 2$ Hz, C*H*—OH).

Une seconde fraction de 0.32 g (13%), p.f. 157 °C; i.r. (solution 0.2 *M* dans CS_2) ν (OH) libres à 3610 cm^{-1}, ν (OH) polymère à 3310 cm^{-1}, ν (C—O) équatorial absent à 1050 cm^{-1}, ν (C—O) axial à 1015 et 1000 cm^{-1}; r.m.n. ($CDCl_3$) δ 0.67 (d, $J = 7$ Hz, méthyl-2), 2.33, 2.42 et 2.55 (singulets, méthyles aromatiques), 4.95 (d, $J = 3$ Hz, C*H*—OH).

Anal. calc. pour $C_{18}H_{22}O$: C, 85.00; H, 8.71. Trouvé (**20***a*): C, 85.08; H, 8.67. Trouvé (**20***b*): C, 84.92; H, 8.69.

Nous remercions le Conseil National de Recherches et le Ministère de l'Education du Québec pour l'aide financière apportée ainsi que le Dr. H. Felkin pour les fructueuses discussions.

1. A. Regnault et P. Canonne. Tetrahedron, **25**, 2349 (1969).
2. P. Canonne et A. Regnault. Can. J. Chem. **47**, 2837 (1969).
3. R. St-Jean et P. Canonne. Bull. Soc. Chim. Fr., 3330 (1971).
4. P. Canonne et L. C. Leitch. Tetrahedron Lett. 1757 (1967).
5. M. Cherest, H. Felkin et N. Prudent. Tetrahedron Lett. 2199 (1968).
6. M. Cherest et H. Felkin. Tetrahedron Lett. 2205 (1968).
7. M. Cherest et H. Felkin. Tetrahedron Lett. 383 (1971).
8. E. L. Eliel et Y. Senda. Tetrahedron, **26**, 2411 (1970).
9. P. Canonne et A. Regnault. Can. J. Chem., **45**, 1267 (1969).
10. P. Canonne, P. Holm et L. C. Leitch. Can. J. Chem., **45**, 2151 (1967).
11. G. Darzens et A. Levy. C. R., **202**, 73 (1936).

Can. J. Chem. Downloaded from www.nrcresearchpress.com by 210.87.254.6 on 09/05/12
For personal use only.

A Study of d-Orbital Effects in Esters of Trifluorothiolacetic Acid. A Comparison of Evidence from Dipole Moment and Kinetic Data

E. Bock, A. Queen, S. Brownlee,[1,2]
T. A. Nour,[3] and M. N. Paddon-Row[4]

Parker Chemistry Laboratory, University of Manitoba, Winnipeg, Manitoba R3T 2N2

Received February 14, 1972[5]

E. Bock, A. Queen, S. Brownlee, T. A. Nour, and M. N. Paddon-Row. Can. J. Chem. **52**, 3113 (1974).

The dipole moments of a series of esters of trifluoroacetic acid and trifluorothiolacetic acid have been determined in benzene solution at 25 °C. The results are consistent with conjugative and hyperconjugative electron release by the hydrocarbon groups to the d-orbitals of sulfur. This conclusion is supported by data for the hydrolysis of these compounds in water or aqueous acetone.

E. Bock, A. Queen, S. Brownlee, T. A. Nour et M. N. Paddon-Row. Can. J. Chem. **52**, 3113 (1974).

On a déterminé les moments dipolaires d'une série d'esters des acides trifluoroacétique et trifluorothiolacétique dans des solutions benzéniques à 25 °C. Les résultats sont en accord avec le concept que les groupes hydrocarbonés repoussent vers les orbitales d du soufre des électrons par conjugaison et hyperconjugaison. Cette conclusion est confirmée par les données sur l'hydrolyse de ces composés dans l'eau et dans des solutions aqueuses d'acétone.

[Traduit par le journal]

Introduction

The dipole moments of thiolesters and similar compounds are usually greater than those of their oxygen analogs and the differences are particularly large for aryl compounds. We have recently demonstrated that this also applies to chloroformate (**1**; X = Cl) and chlorothiolformate esters (**2**; X = Cl) (1) and also that the differences decrease as the hydrocarbon groups change from phenyl to secondary alkyl. For this reason, we have proposed that the observed differences between sulfur and oxygen compounds mainly reflect conjugative or hyperconjugative electron release to the d-orbitals of sulfur in the thio compounds. Under appropriate conditions such effects might manifest themselves in kinetic phenomena. Unfortunately, we have found that chloroformates react bimolecularly with water (mechanism 1) (2) whereas the corresponding chlorothiolformates react unimolecularly (mechanism 2) (3, 4). Consequently, a comparison of the reactivities of these compounds towards water would hardly constitute a test of d-orbital effects in the thiolesters. However, esters of trifluoroacetic acid and trifluorothiolacetic acid react bimolecularly with water (mechanisms 4 and 5) (5–7) at convenient rates for systematic study. It therefore seemed that a comparison of the evidence obtainable from dipole moment and kinetic data would be a useful way in which to test the importance of d-orbital effects in sulfur compounds. Moreover, since dipole moments have not been previously reported for any of these compounds, their determination seemed to be a worthwhile piece of work in its own right. We have therefore measured these quantities for seven esters of trifluoroacetic acid (**1**; X = CF_3) and the corresponding derivatives of trifluorothiolacetic acid (**2**; X = CF_3) in dilute benzene solutions. The hydrocarbon groups were varied so as to provide a wide variation in their abilities to donate electrons by conjugation or hyperconjugation to the d-orbitals of sulfur. The rates of hydrolysis of some of the thiol esters and phenyl trifluoroacetate in water or aqueous acetone

[1]Summer student 1968.
[2]Deceased 1971.
[3]University of Manitoba post-doctorate fellow, 1967–1969.
[4]University of Manitoba post-doctorate fellow, 1968–1970.
[5]Revision received May 2, 1974.

Can. J. Chem. Downloaded from www.nrcresearchpress.com by 210.87.254.6 on 09/05/12
For personal use only.

Can. J. Chem. Downloaded from www.nrcresearchpress.com by 210.87.254.6 on 09/05/12
For personal use only.

TABLE 2. Boiling points of esters of trifluoroacetic acid and trifluorothiolacetic acid*

R	Y	Boiling point (°C)			Calculated (%)				Found (%)			
		This work	Literature	Reference	C	H	F	S	C	H	F	S
CH_3	O	44	43	16								
C_2H_5	O	62	61.5	16								
—C_3H_7	O	82.5	82	16								
—C_3H_7	O	73.5	73	17								
—C_4H_9	O	104	104	16								
—C_4H_9	O	87	85–86	18								
C_6H_5	O	66/38 mm	67/40 mm	17								
CH_3	S	71–72			25.0	2.1	39.6	22.2	25.0	2.1	39.0	21.8
C_2H_5	S	90.5	90.5	19								
—C_3H_7	S	112			34.9	4.1	33.1	18.6	34.7	4.0	32.8	18.9
—C_3H_7	S	104			34.9	4.1	33.1	18.6	34.7	4.3	33.4	18.5
—C_4H_9	S	135										
—C_4H_9	S	113			38.7	4.8	30.6	17.2	38.4	4.6	31.0	17.0
C_6H_5	S	109/70 mm	140–150	20								

*General formula, R—Y—(CO)—CF_3.

TABLE 3. Dipole moments for halo-esters in benzene solution at 25 °C*

R	μ (D)			μ (D)		
	RO—(CO)—Cl‖	RS—(CO)—Cl‖	Δμ(S—O)†	RO—(CO)—CF_3§	RS—(CO)—CF_3§	Δμ(S—O)‡
C_6H_5	2.39	2.86	0.47	2.68	2.95	0.27
CH_3	2.38	2.69	0.31	2.71	2.84	0.13
C_2H_5	2.66	2.84	0.18	3.00	3.07	0.07
C_3H_7	2.70	2.88	0.18	3.02	3.10	0.08
$n-C_4H_9$	2.71	2.93	0.21	3.10	3.16	0.06
$i-C_3H_7$	2.86	2.96	0.10	3.08	3.15	0.07
$t-C_4H_9$	—	3.20	—	3.30	3.37	0.07

*Given in Debye unit D.
†Δμ(S—O) = μ(RS—CO—Cl) − μ(RO—CO—Cl).
‡Δμ(S—O) = μ(RS—CO—CF_3) − μ(RO—CO—CF_3).
§This work.
‖Reference 1.

have also been measured, corresponding data for the oxygen analogs being already available in the literature (5).

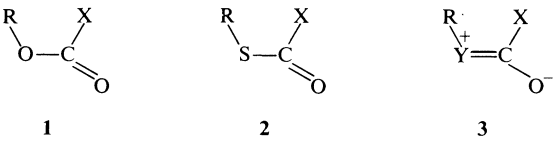

1 2 3

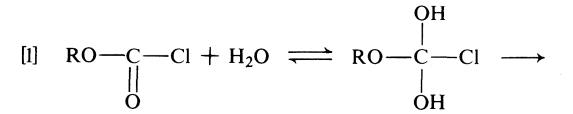

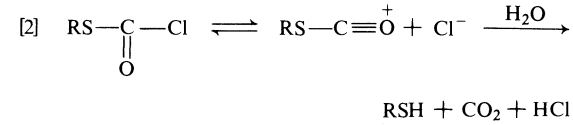

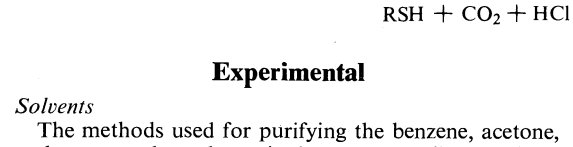

Experimental

Solvents

The methods used for purifying the benzene, acetone, and water used as solvents in the present studies have been previously described (1–4). Some physical properties of benzene solutions are listed in Table I lodged with the Depository of Unpublished Data.[6]

Materials

The esters were prepared by reacting the corresponding alcohols and thiols with trifluoroacetic anhydride and were purified by distillation before use. Physical properties are recorded in Table 2.

Procedures

These have been previously described (1–4).

Products of Hydrolysis

Experiments were carried out with methyl and isopropyl trifluorothiolacetates as previously described for the corresponding chlorothiolformate esters (3). The thiols produced were characterized by conversion to the corresponding 2,4-dinitrophenyl alkyl sulfides which were then shown to be identical with authentic samples.

Results

Table 1 summarizes the experimental data from which the solution dipole moments (Table 3) have been calculated by Smith's method (8) using eq. 3

$$[3] \qquad \mu = \frac{27kT}{4N} \frac{M_2}{d_1(\varepsilon_1 - 2)^2}(a - \nu)$$

[6]Complete set of data may be obtained, at a nominal charge, from the Depository of Unpublished Data, National Science Library, National Research Council of Canada, Ottawa, Canada K1A 0S2.

The symbols have the same meanings as those used in our earlier papers (1). In order to facilitate comparisons, Table 3 also includes previously reported values of the dipole moments of the corresponding chloroformate (9) and chlorothiolformate esters (1).

Table 4 lists rate constants for the hydrolysis of four esters of trifluorothiolacetic acid (**2**; X = CF_3, R = C_6H_5, C_2H_5, i-C_3H_7) and the corresponding esters of trifluoroacetic acid (**1**; X = CF_3), the solvent being water in the cases of the alkyl esters and 70% aqueous acetone for the phenyl compounds which react very rapidly with water. The values for the alkyl trifluoroacetates have been calculated from the data of Winter and Scott (5). These workers have shown that *t*-butyl trifluoroacetate hydrolyses, at least partly, by an S_N1 mechanism and we have therefore excluded tertiary esters from our studies. In the case of isopropyl trifluorothiolacetate, complete hydrolysis of 0.002 mol of the ester in 100 ml of water gave only 94.7% of the calculated amount of acid. Nevertheless, the compound appeared to be quite pure since only a single peak was produced when it was examined by vapor phase chromatography. Isopropyl mercaptan was identified as a product of hydrolysis and there was no evidence that isopropyl alcohol was formed, indicating that the possibility of alkyl–sulfur bond fission may be ignored. In individual runs at concentrations of approximately 0.001 *M*, good first order kinetics were obtained but agreement between the values obtained in different experiments were rather poor. However, by working at lower concentrations of the ester (approximately 0.00005 *M*), satisfactory agreement between separate runs was achieved. These problems were probably associated with supersaturation in the more concentrated solutions. Despite these difficulties, it is considered that the rate constants for the hydrolysis of isopropyl trifluorothiolacetate are sufficiently reliable for the purposes of the present studies. No similar problems arose with the other compounds which gave excellent, reproducible rate constants and at least 99% of the theoretical amount of acid on hydrolysis.

Discussion

Dipole Moments

The results in Table 3 show three features to which we have previously drawn attention (1).

Can. J. Chem. Downloaded from www.nrcresearchpress.com by 210.87.254.6 on 09/05/12
For personal use only.

TABLE 4. Rates of hydrolysis of esters of trifluoroacetic acid and trifluorothiolacetic acid in water or 70% aqueous acetone at 6.09 °C

Solvent	R	k ($\times 10^4$ s^{-1}) RO—(CO)—CF_3	RS—(CO)—CF_3*	k_{obs}^{o}/k_{obs}^{s}
70% aqueous acetone	C_6H_5	82.54*	15.90	0.1926
Water	CH_3	25.72†	19.55	0.7601
Water	C_2H_5	9.642†	14.08	1.460
Water	$i-C_3H_7$	2.702†	9.753	3.610

*Values obtained in this work.
†Reference 5.

First of all, the dipole moments of the sulfur compounds are larger than those of their oxygen analogs. Then, the monotonous decrease in the values for the oxygen compounds, as the inductive effect of the group R decreases ($t-C_4H_9 > i-C_3H_7 > C_2H_5 > CH_3 > C_6H_5$), is not exactly mirrored in the thiol esters. In particular, the dipole moments of the phenyl thiolesters are greater than those of the methyl thiolesters, a reversal of the situations for the oxygen compounds. Thirdly, the values of $\Delta\mu$(S—O) decrease as the ability of the group R to donate electrons conjugatively or hyperconjugatively falls off. It is admitted that the trend is less marked for the present fluorinated esters than for the chlorothiolformates, an apparently constant difference of about 0.07 D being reached at the ethyl compounds. However, this small difference may be less than the combined experiment errors[7] in the quantities subtracted and may not be really constant. Since we have previously presented our interpretation of these trends in some detail (1) it seems unnecessary to repeat them at this time. However, on the basis of earlier conclusions, the results are consistent with the proposal that conjugative and hyperconjugative electron release to the d-orbitals of sulfur are the main reasons for the larger dipole moments of the sulfur compounds. Other explanations are, of course, quite possible. For example, the different sizes of oxygen and sulfur atoms and different steric effects associated with the hydrocarbon groups (R) could markedly alter bond angles and spacial orientations of the "lone-pair" electrons. However, in this case it would be reasonable to expect that the largest groups (R = C_6H_5 and $t-C_4H_9$) would generate the most closely related values of $\Delta\mu$(S—O), which is not the case. Moreover, the relationships $\mu(C_6H_5O—CO—CF_3) < \mu(CH_3O—CO—CF_3)$ and $\mu(C_6H_5S—CO—CF_3) > \mu(CH_3O—CO—CF_3)$ would still remain unexplained. In the absence of a knowledge of such differences, further speculation would seem to be pointless and a more profitable approach is to consider evidence of a different kind.

Rates of Hydrolysis

Esters of trifluoroacetic acid react with water at low acid concentrations by the uncatalyzed process shown in [4]. The observed pseudo first-order rate constant (k_{obs}^{o}) is given by eq. 5.

[4] $$RO—\underset{\underset{O}{\|}}{C}—CF_3 + H_2O \underset{k_2}{\overset{k_1}{\rightleftharpoons}} RO—\underset{\underset{O^-}{|}}{\overset{\overset{OH}{|}}{C}}—CF_3 \xrightarrow{k_3} ROH + CF_3COOH$$

4

[5] $$k_{obs}^{o} = \frac{k_1}{1 + k_2/k_3}$$

Esters of trifluorothiolacetic acid react by a slightly different mechanism [6] in which step 2 is subject to acid catalysis. The rate constant is given by eq. 7 which, at the low acid concentrations generated in the present studies (less than 10^{-3} M) reduces to eq. 8

[7]The calculation of the standard errors in the dipole moments from the measured quantities is a very complicated procedure. However, one of us has previously demonstrated (10) that the dipole moments calculated from measurements made with our equipment are probably good to ±0.1 D on an absolute scale and to better than this on a relative scale since standardized conditions and procedures were used for all the experiments.

Can. J. Chem. Downloaded from www.nrcresearchpress.com by 210.87.254.6 on 09/05/12
For personal use only.

[6] $$RS-\underset{\underset{O}{\|}}{C}-CF_3 + H_2O \underset{k_2'[H^+]}{\overset{k_1'}{\rightleftharpoons}}$$

$$RS-\underset{\underset{O^-}{|}}{\overset{\overset{OH}{|}}{C}}-CF \xrightarrow{k_3'} RSH + CF_3COOH$$

5

[7] $$k_{obs}^{s} = \frac{k_1'}{1 + (k_2'/k_3')H^+}$$

[8] $$k_{obs}^{s} = k_1' \text{ at low } [H^+]$$

These differences have been discussed in detail by Johnson (6).

Esters, including the present trifluoroacetates (**1** and **2**, X = CF_3), and similar compounds are stabilized by conjugation (**3**; Y = O or S) involving the carbonyl group and the "lone-pair" electrons on the hetero-atom (Y). Similar conjugation is not possible for the tetrahedral intermediates (**4** and **5**) formed in step 1 of the two reactions. It would therefore be expected that the rates of these steps would largely reflect the differences in initial state conjugation for the oxygen and sulfur compounds. Since sulfur shows less tendency than oxygen to use its "lone-pair" electrons for π-bond formation (11), it follows that the oxygen esters should be more stabilized than the thio-analogs with $k_1 < k_1'$. Equation 5 shows that k_1 is the upper limit for k_{obs}^{o}, the rate constant for hydrolysis of the oxygen esters, while eq. 8 gives $k_1' = k_{obs}^{s}$. It would therefore be expected that the oxygen esters would hydrolyze more slowly than the thiolesters. On the other hand, the replacement of oxygen by sulfur should alter the inductive effects of the substituent groups (R) by roughly similar amounts, if at all, so that the relative orders of reactivities within each series should be rather similar. While the first of these expectations is realized for the ethyl and isopropyl compounds (Table 4), the second one is not realized at all. Moreover, methyl and phenyl trifluoroacetates hydrolyze more rapidly than the corresponding trifluorothiolacetates, the difference being particularly large for the aromatic compounds. The departures from expectation are particularly well shown by a comparison of the changes of relative reactivities (k_{obs}^{s}/k_{obs}^{o}) as the substituent (R) changes from phenyl to isopropyl. Clearly, some effect or effects other than those described above must be operating in at least one of these two series of compounds. Moreover, these effects must decrease as the group R changes from phenyl to isopropyl. But, this is just the trend that would be expected if conjugative or hyperconjugative electron release to the d-orbitals of sulfur occurs in the initial states for the hydrolysis of the present compounds. This is reasonable, since the partial positive charge on sulfur (resonance form **3**; Y = S) should facilitate electron release towards this center.

A referee has suggested that for the phenyl compounds the results might be explained in terms of electron withdrawal due to π overlap, which would be more important for oxygen than sulfur. The phenyl trifluorothiolacetate then reacts more slowly than the oxygen analog due to decreased initial-state stability of the latter compound, rather than increased stability of the sulfur compound due to d-orbital participation as we have suggested. However, this explanation cannot apply to the methyl compounds, where the R group is not only electron donating but cannot participate in electron withdrawing π overlap, despite which the oxygen ester is the more reactive. Moreover, this explanation ignores the dipole moment data which indicates that charge separation is greater in $C_6H_5SCOCF_3$ than in CH_3SCOCF_3, despite the fact that the phenyl group should withdraw electrons inductively.

No doubt other explanations involving transition state differences could be advanced. However, it is significant that the kinetic data do support the conclusions drawn from comparisons of dipole moments, which must reflect ground-state properties. While previous studies by Bordwell *et al.* (12) have failed to demonstrate that d-orbital effects influence chemical reactivity, Tarbell and co-workers (13) have previously argued that such electron donation to sulfur could account for the inversion of the ratio k_{obs}^{s}/k_{obs}^{o} in the basic hydrolysis of alkyl acetates and thiolacetates.

Lee (14, 15) has recently carried out INDO and CNDO/2 calculations for methyl chloroformate (**1**; R = CH_3, X = Cl) and its various thio-analogs and compared the results with our experimental dipole moment and kinetic data. He concludes that d-orbital effects account for at least some of the differences between the oxygen

Can. J. Chem. Downloaded from www.nrcresearchpress.com by 210.87.254.6 on 09/05/12
For personal use only.

and sulfur compounds. We are presently carrying out similar calculations for the trifluoroacetates.

The authors gratefully acknowledge financial support for this work by the National Research Council of Canada and by the Research Board of the University of Manitoba.

1. A. Queen, T. A. Nour, and E. Bock. Can. J. Chem. **47**, 343, (1969).
2. A. Queen. Can. J. Chem. **45**, 1619 (1967).
3. A. Queen, T. A. Nour, M. N. Paddon-Row, and K. Preston. Can. J. Chem. **48**, 522 (1970).
4. D. M. McKinnon and A. Queen. Can. J. Chem. **50**, 1401 (1972).
5. J. Winter and J. M. W. Scott. Can. J. Chem. **46**, 2887 (1968).
6. L. R. Fedor and T. C. Bruice. J. Am. Chem. Soc. **87**, 4138 (1965).
7. S. L. Johnson. Advances in physical-organic chemistry. **5**, 237 (1967).
8. J. W. Smith. Trans. Faraday Soc. **46**, 394 (1950).
9. E. Bock and D. Iwacha. Can. J. Chem. **45**, 3177 (1967).
10. E. Bock and E. F. Dojack. Can. J. Chem. **45**, 1097 (1967).
11. H. Bohme, H. Fisher, and R. Frank. Ann. **563**, 54 (1949).
12. F. G. Bordwell, G. D. Cooper, and H. Morita. J. Am. Chem. Soc. **79**, 376 (1957).
13. P. N. Rylander and D. S. Tarbell. J. Am. Chem. Soc. **72**, 3021 (1950).
14. I. Lee. J. Korean Chem. Soc. **16**, 334 (1972).
15. I. Lee. J. Korean Nucl. Soc. **4**, 294 (1972).
16. A. Moffat and H. Hunt. J. Am. Chem. Soc. **79**, 54 (1957).
17. A. Moffat and H. Hunt. J. Am. Chem. Soc. **80**, 2985 (1958).
18. A. Moffat and H. Hunt. J. Am. Chem. Soc. **81**, 2082 (1959).
19. M. Hauptschein, C. S. Stokes, and E. A. Nodiff. J. Am. Chem. Soc. **74**, 4005 (1952).
20. S. Sakakibara and N. Inukai. Bull. Chem. Soc. Jap. **38**, 1979 (1965).

Can. J. Chem. Downloaded from www.nrcresearchpress.com by 210.87.254.6 on 09/05/12
For personal use only.

Composition and Stability of Iron and Copper Citrate Complexes in Aqueous Solution

TERRENCE B. FIELD, JANET L. MCCOURT, AND W. A. E. MCBRYDE
Department of Chemistry, University of Waterloo, Waterloo, Ontario N2L 3G1

Received March 7, 1974

TERRENCE B. FIELD, JANET L. MCCOURT, and W. A. E. MCBRYDE. Can. J. Chem. **52**, 3119 (1974).

The acidity constants of citric acid and the stability constants of the citrate complexes of copper(II), iron(II), and iron(III) have been measured at 25 °C in 0.1 *M* KNO_3 background. The measurements were based on mass balances on hydrogen ions, supplemented in the case of Cu(II) and Fe(III) complexes by measurements of free metal concentration with a solid-state copper-ion-sensitive electrode and a redox electrode respectively. The data required the assumption of a binuclear copper complex, but all complexes characterized were of 1:1 stoichiometry.

TERRENCE B. FIELD, JANET L. MCCOURT et W. A. E. MCBRYDE. Can. J. Chem. **52**, 3119 (1974).

On a mesuré, à 25 °C et en présence de KNO_3 0.1 *M*, les constantes d'acidité de l'acide citrique et les constantes de stabilité des complexes de citrate avec le cuivre(II), le fer(II) et le fer(III). Ces mesures sont basées sur les balances des masses des ions hydrogène auxquels s'ajoute dans le cas des complexes du cuivre(II) et du fer(III) des mesures de concentration d'ions métalliques libres en utilisant respectivement une électrode sensible aux ions cuivre et une électrode redox. Les données recueillies nécessitent que l'on fasse l'hypothèse que les complexes de cuivre sont binucléaires mais que tous les complexes sont caractérisés par une stoichiométrie 1:1. [Traduit par le journal]

Introduction

Citrates have been traditionally used as masking agents for various metal ions and as eluting agents in ion exchange chromatography. Recently citrate has been considered as a possible substitute for polyphosphates added to solid detergents. These applications are based on formation of stable complexes with metal ions, but examination of the literature discloses some uncertainty regarding the composition and stability of some of these, especially those of copper(II) and iron(III). This investigation was undertaken to try to clarify this situation for the last-named complexes. Two facilities, novel for the study of citrate complexes, were applied: first, a solid-state electrode was able to furnish data on the concentration of copper ion in equilibrium with complexes; second, the experimental data were interpreted by the computer program SCOGS (1), which is of particular value when, as in this case, protonated, deprotonated, or polynuclear species are involved.

Experimental

All solutions were prepared from reagent grade chemicals and standardized by conventional methods. Sodium or potassium hydroxide solutions were stored and used under nitrogen to limit contamination by carbon dioxide. Volumetric glassware for preparation, dilution, or transfer of solutions was Class A grade. Small amounts of acid or alkaline solutions were delivered from an Agla syringe equipped with micrometer drive, the delivery of which was calibrated by direct weighing.

The cell used for titrations, measurements of p*H*, etc., consisted of a jacketed upper and lower compartment through which water thermostatted at 25.0 ± 0.1 °C was circulated (2). Measurements of p*H* or cell e.m.f. were made with an Orion Model 801 meter. All p*H* readings were converted to hydrogen ion concentrations by the use of an empirical factor measured in the appropriate salt background (3, 4). A solid-state copper(II) ion sensitive electrode (Orion #94-29) was used in conjunction with a reference electrode (Orion #90-01-00) for measurements of copper(II) ion concentration. This electrode was calibrated for this purpose with solutions of known concentrations of copper(II). A platinum electrode, used to measure redox potential, was similarly calibrated with solutions containing known concentrations of iron(II) and iron(III) in the background electrolyte used.

Spectrophotometric measurements were made on a Cary Model 14 spectrophotometer with carefully matched 1 cm cells. In view of the known sensitivity of iron citrate solutions toward light (5), these were prepared and titrated in wrapped glass vessels. Also, in view of the marked sensitivity of the copper ion electrode to illumination, all measurements with it were made in a shrouded titration vessel.

Can. J. Chem. Downloaded from www.nrcresearchpress.com by 210.87.254.42 on 09/05/12
For personal use only.

Can. J. Chem. Downloaded from www.nrcresearchpress.com by 210.87.254.42 on 09/05/12
For personal use only.

Treatment of Data

Acidity constants were calculated as protonation constants, β_i^0, and used as concentration quotients applicable to the particular medium in which measurements were consistently made, namely 0.1 *M* potassium nitrate solution. It is worth calling attention to the fact that conventional thermodynamic acidity constants, particularly for citric acid, differ from these conditional constants owing to the appreciable effect of multiple ionic charges on the activity coefficients.

The data from p*H* titrations (except those which included simultaneous measurement of copper-ion concentration in some cases) were submitted to processing by the powerful computer program SCOGS (1), which finds best fit values of acidity constants or metal–complex stability constants. In using this, one postulates a set of plausible species to describe the composition of the solution throughout the range of the p*H* titration; tentative stability constants are assigned to these, and the computer adjusts these until a minimum is found in the standard deviation of titre (s.d.t.). The most probable of several alternative sets of postulated constituents is that yielding the smallest s.d.t., though it is wise to recognize that this criterion cannot be regarded as proof for the preferred selection of species. The program will also reject a particular constituent by failing to give convergence in the refinement of a constant for it, so that the inappropriateness of certain species or groups of species is thus signalled.

Spectrophotometric Competitive Method

Within the p*H* range 1.5 to 2.5 iron(III) will react with sulfosalicylic acid (H_2A) or with citric acid (H_3L), or will undergo some hydrolysis. The sulfosalicylate complex under these conditions is MA and has an intense purple color. In the presence of citric and sulfosalicylic acids together the intensity of this purple color is diminished. Apart from a uniform reduction in absorbance the visible spectral characteristics of these solutions are in no way altered from those of MA, and so it may be assumed that no mixed complex has been formed by the two ligands together.

The mass balances and other relationships applying in these solutions are given by the following equations.

$$[1] \qquad F = 1 + \beta_1^0[\mathrm{H}] + \beta_2^0[\mathrm{H}]^2 + \ldots$$

The symbols F^0 and F^1 will be used respectively to apply to citric acid and to sulfosalicylic acid.

$$[2] \qquad C_\mathrm{A} = [\mathrm{A}]F^1 + [\mathrm{MA}]$$

In the absence of citrate

$$[3] \qquad C_\mathrm{M} = [\mathrm{M}](1 + K_\mathrm{h}/[\mathrm{H}]) + [\mathrm{MA}]$$

This contains the quantity K_h, the first-stage hydrolysis constant of iron(III); at the p*H* and prevailing concentrations in these experiments this adequately compensates for hydrolysis; the value of K_h used (6) was 2.5×10^{-3}.

It had been established from p*H* and potentiometric titrations subsequently to be described that the citrate complexes apparently present were MHL, ML, and MOHL. Therefore with citrate and sulfosalicylate present together

$$[4] \qquad C_\mathrm{M} = [\mathrm{M}](1 + K_\mathrm{h}/[\mathrm{H}]) + [\mathrm{MA}] + [\mathrm{MHL}] + [\mathrm{ML}] + [\mathrm{MOHL}]$$

$$[5] \qquad C_\mathrm{L} = [\mathrm{L}]F^0 + [\mathrm{MHL}] + [\mathrm{ML}] + [\mathrm{MOHL}]$$

The concentrations of the citrate complexes may be expressed in terms of their stability constants designated β_{pqr} for $\mathrm{M}_p\mathrm{H}_q\mathrm{L}_r$.

$$[6] \qquad [\mathrm{MHL}] + [\mathrm{ML}] + [\mathrm{MOHL}] = x = [\mathrm{M}][\mathrm{H}][\mathrm{L}]\,(\beta_{111} + \beta_{101}[\mathrm{H}]^{-1} + \beta_{1\text{-}11}[\mathrm{H}]^{-2})$$

There is a reliable method for evaluating ε_1, the molar absorptivity for MA (7), so from the measured absorbance [MA] can be determined. There is sufficient information in eqs. 2 and 3 to enable β_1 for MA to be evaluated under these experimental conditions. With this information x, the concentration of iron(III) in citrate complexes could be found in any solution by means of eq. 4, and hence [L] from eq. 5. It is seen from eq. 6 that x is p*H*-dependent. However, if values of $x/[\mathrm{M}][\mathrm{H}][\mathrm{L}]$ were plotted against $1/[\mathrm{H}]$, all data fell on a smooth curve (Fig. 1). Either by standard curve-fitting routines or by solutions of equations in x, values of the required β's could be obtained.

Results

Most investigations published in the past twenty years have shown 1:1 stoichiometry in the reactions of copper(II) and iron(III) with citric acid, and this has been confirmed by the results in this study. Also in agreement with several previous studies, it was observed that up

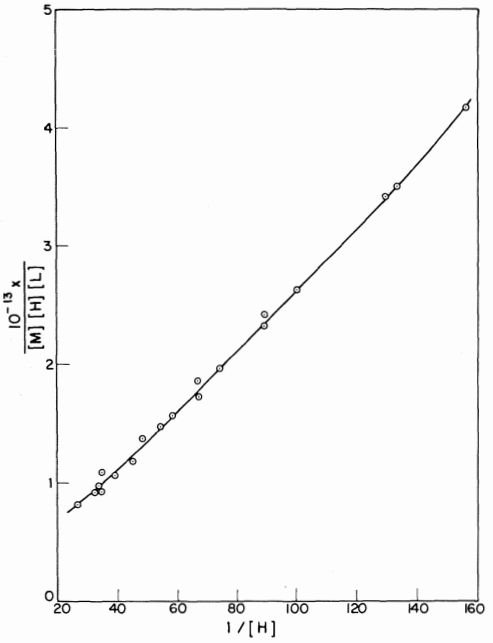

FIG. 1. Variation of $x/[M][H][L]$ with $1/[H]$ for iron(III) citrate complexes; x is the total concentration of iron(III) present as citrate complexes.

to four protons were displaced through complex formation per metal ion or per molecule of citric acid reacting. It is not yet proven whether the fourth proton is displaced from the carbinol group of the citric acid or from the remaining coordinated water molecules associated with the central metal ion. It is also clear that the proton balance observed in formation of these complexes indicates the presence of two or more species differing in degree of protonation. Thus if citric acid is represented as H_3L, mononuclear metal complexes may form from among the series MH_2L, MHL, ML, and MOHL.

It is advisable to point out that systems of this sort stretch the capabilities of the Calvin–Bjerrum p*H*-titration method of establishing the formation of metal complexes because the proton balance, which is normally the basis of calculating the concentration of free ligand, must additionally define the extent of protonation of the series of metal complexes. This is demonstrated by the relationship

$$[7]\quad C_H - [H] + [OH] = \Sigma q\beta_{pqr}[M]^p[H]^q[L]^r + \Sigma j\beta_j{}^0[H]^j[L]$$

in which C_H is the total net concentration of ionizable hydrogen at any point. If $q = 0$ throughout, [L] is immediately available provided the $\beta_j{}^0$ are known; but if $q \neq 0$, this relationship is alone insufficient to define [L] and must be combined with other conservation equations to secure information on [M] and [L]. The solution of the necessary equations containing experimental quantities is less precise and can also lead to a number of possible sets of p, q, and r values (*i.e.*, alternative sets of possible complex species) which satisfy the data roughly as well. It is undoubtedly for this reason that somewhat different assignments of compositions and stabilities have been made in the case of the metal citrates by various investigators.

Acidity Constants

From p*H* titrations at 25 °C in a background solution of 0.1 *M* potassium nitrate the following conditional proton-association constants were obtained: $\log \beta_1{}^0 = 5.70 \pm 0.02$; $\log \beta_2{}^0 = 10.06 \pm 0.02$; $\log \beta_3{}^0 = 12.87 \pm 0.08$.

Copper Complexes

When p*H* titrations were carried out with copper(II) present at various ligand:metal ratios, the results could be fitted reasonably well by the assumption that the complex species present were MHL, ML, and MOHL. A second set of titrations was then performed in which point-by-point the copper ion concentration was measured as well as the p*H*. The p*H* titration data were analyzed by SCOGS according to the above choice of constituents, with print-out of the theoretically related concentrations of free metal ion. The latter were then compared with the measured copper ion concentrations. The comparison revealed a significant discrepancy between these values in the range of occurrence of the species ML, the difference increasing and decreasing in much the same way as the concentration of this species. A marked improvement in fit to the data was obtained by assuming that the species present were MHL, M_2L_2, and MOHL, and allowing the computer to seek the best values for the corresponding formation constants. There were thus two criteria for best fit of the data to assumed species and derived equilibrium constants: the standard deviation in titre (volume of base), and minimum deviation between calculated and observed metal ion concentration. For these two criteria together the above choice of species gave the optimum fit to the data.

A number of other combinations of species were tried out, particularly those suggested by

Can. J. Chem. Downloaded from www.nrcresearchpress.com by 210.87.254.42 on 09/05/12
For personal use only.

Can. J. Chem. Downloaded from www.nrcresearchpress.com by 210.87.254.42 on 09/05/12
For personal use only.

TABLE 1. Stability constants of metal citrates 0.1 *M* KNO_3 background 25 °C

Metal	Method	Average values of log $\beta \pm \sigma$ β_{111}	β_{101}	β_{202}	β_{1-11}	Number of measurements
Copper(II)	p*H* and p*M* titration					
	SCOGS	9.31 ± 0.08		14.72 ± 0.10	1.61 ± 0.04	5
	CLLSQ	9.27 ± 0.09		15.03 ± 0.02	1.64 ± 0.07	
Iron(II)	p*H* titration					
	SCOGS	8.62 ± 0.47	4.80 ± 0.31			27
Iron(III)	p*H* and p*M* titration					
	CLLSQ	12.38 ± 0.34	11.21 ± 0.10		8.60 ± 0.64	12
	spectrophotometric	12.37 ± 0.18	11.16 ± 0.07		8.38 ± 0.64	20

TABLE 2. Stability constants of metal citrates (from other investigations), values of log β_{pqr}

β_{111}	β_{101}	β_{1-11}	β_{202}	β_{2-22}	Other β	Temperature (°C)	Medium *M*	Reference
Cu(II)								
—	5.2	—	12.8	6.0	—	20	1 $NaClO_4$	9
—	—	—	13.2	5.1	—	25	1 KNO_3	10
9.8	5.9	1.6	—	—	β_{201} 8.1 β_{2-11} 5.0	20	0.1 $NaClO_4$	11
—	6.5	2.15	—	—	β_{121} 12.5	30	0.1 $NaNO_3$	12
9.4	—	—	—	—	—	25	0.05	13
—	3.09	—	—	—	—	—	0.2 $NaNO_3$	14
—	3.95							
9.7	6.3	1.8	—	—	—	32	0.25 KNO_3	15
—	6.03	—	—	—	β_{102} 10.43	25	0.1 $NaClO_4$	21
Fe(II)								
8.2	3.1	—	—	—	—	25	1 $NaClO_4$	16
8.3	4.4	—	—	—	—	20	0.1 $NaClO_4$	17
Fe(III)								
—	11.40	—	—	—	β_{2-22} 21.17	20	0.1 $NaClO_4$	17
	11.56							
11.45	—	—	—	—	—	25	1 $NaNO_3$	18
11.44	11.85	9.40	—	—	—	25	1 $NaClO_4$	16
—	11.38	9.46	—	—	—	24	0.1 $NaNO_3$	12
—	11.7	—	—	—	—	—	0.1	19
	12.5							

Can. J. Chem. Downloaded from www.nrcresearchpress.com by 210.87.254.42 on 09/05/12
For personal use only.

the work of other investigators (see Table 2), but in all cases these either yielded stability constants that failed to give convergence in the computer treatment, or they did not give as good agreement with observations on the basis of the two criteria mentioned. For instance, the species $M_2(OH)_2L_2$ has been identified in similar solutions by other workers, but assumption of its presence made worse the fit to the observed concentrations of metal ions.

Calculation of stability constants from our data could be done in either of the two ways: (*i*) the values and their standard deviations determined by the SCOGS program; (*ii*) values obtained by the solution of simultaneous linear equations. Conservation equations such as [7], or others based on C_M–[M], can be set up with simultaneous values of [M], [H], and [L], and solved for the appropriate values of β_{pqr}. For this particular choice of constituents only

$$[8] \qquad [L] = (C_L - C_M + [M](F^\circ)^{-1}$$

An IBM computer subroutine CLLSQ conveniently handles the solution of the equations, yielding values of the β_{pqr} and standard deviation of these. The results of five titrations of this sort gave the values shown in Table 1. The lack of agreement between two estimates of $\beta_{M_2L_2}$ based on the same data illustrates the difficulty in fixing values of equilibrium constants unambiguously, especially for polynuclear species.

Iron Complexes

The direct determination of formation constants for the iron(III) citrate complexes proved to be unsatisfactory. The complexes are so stable that at all hydrogen ion concentrations which can be measured precisely with a p*H* meter [M] or [L], according to which reactant is not in excess, cannot be fixed precisely by the experimental data (8). The difficulty can be overcome in the presence of excess ligand if an independent probe is available to measure [M]. For this purpose the authors employed Fe^{3+}/Fe^{2+} redox electrode in the presence of a fixed concentration of iron(II).

It was first necessary to determine the formation constants of the iron(II) citrate complexes. This was done by a direct p*H* titration carried out in triplicate at each of nine different metal and ligand concentrations. The results obtained are included in Table 1. Their magnitude is such that under the conditions of low p*H* applying to the study of the iron(III) complexes very little formation of iron(II) complexes occurs. The actual extent of such complex formation can, however, be calculated.

Iron(III) complexes were studied by titrations with p*H* and redox electrodes enabling the determination of [H] and [M], point by point. Corresponding values of [L] could be deduced as before, though allowance had to be made for hydrolysis of free iron(III) as mentioned previously. The experimental results were processed by solution of linear conservation equations based on C_M–[M], as in the second method for copper(II) complexes mentioned previously. The values of stability constants obtained in this way are given in Table 1. In order to have a cross check on the foregoing work, the spectrophotometric competitive procedure described earlier was applied. These results are also included in Table 1.

Discussion

A comparison of the results in Table 1 for copper(II) citrates with a selection of other published results shown in Table 2 reveals that the values for MHL and MOHL are in reasonable agreement with those obtained by other workers who have postulated these species. The variety of different assumptions apparent in Table 2 concerning which complexes are or are not present illustrates the difficulty mentioned previously concerning interpretation of p*H* measurements. For instance, our data when fitted to the complexes MHL, ML, and MOHL gave log $\beta_{111} = 9.1$, log $\beta_{101} = 5.8$, and log $\beta_{1\text{-}11} = 1.6$. But, taking into account the measured values of [M], we were led to replace ML by the dimer and to assign the relatively high value of log β_{202} shown in Table 1. This value is appreciably larger than those for the same species proposed by Lefebvre (9) and by Rajan and Martell (10).

The formation of a dimeric complex of copper(II) is consistent with the e.s.r. spectra and magnetic susceptibility measurements of Dunhill *et al.* (20). These authors have deduced that in solutions at low and high p*H* copper citrate exists as a chelate monomer, whilst over an intermediate range of p*H* a dimeric species is formed. This is qualitatively in agreement with our findings, though these authors worked with ranges of concentration very different from ours, and did not evaluate any equilibrium constants; they regarded their dimeric species as deprotonated, *e.g.*, $M_2(OH)_2L_2$. This matter clearly requires further study.

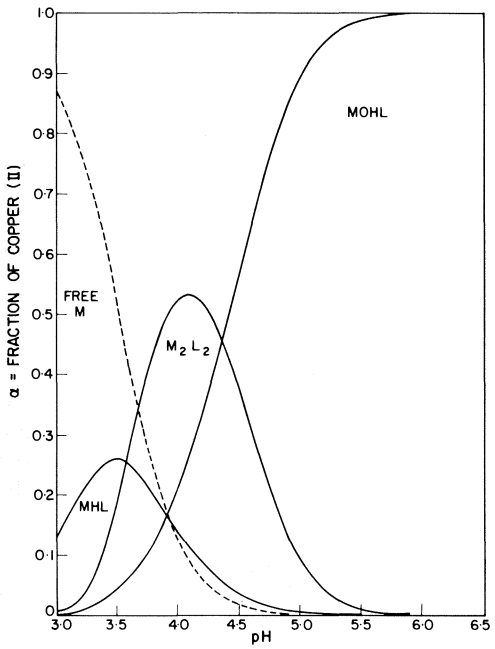

FIG. 2. Distribution of copper(II) among citrate complexes according to stability constants reported in this paper. $C_{Cu} = 1.0 \times 10^{-3}$ *M*, $C_{H_3L} = 2.0 \times 10^{-3}$ *M*.

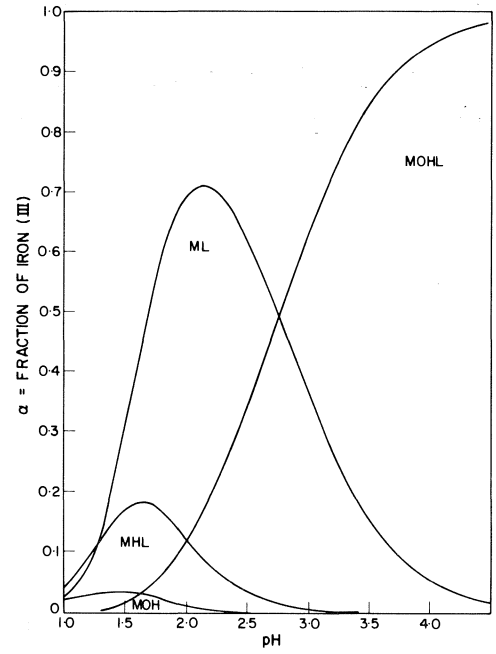

FIG. 3. Distribution of iron(III) among citrate complexes according to stability constants reported in this paper. $C_{Fe} = 1.0 \times 10^{-3}$ *M*, $C_{H_3L} = 2.0 \times 10^{-3}$ *M*.

The data for iron(III) citrate complexes in Table 1 are in fair agreement with those of other workers for ML (see Table 2). The formation along with this of a protonated species of p$K \sim 1.2$ is revealed by the experiments conducted at fairly low p*H*. Formation of the deprotonated species MOHL has been reported previously; nothing in our observations, which included measurements of [M], suggested formation of a dimer as reported by Timberlake (17), but this may simply be a consequence of working in more dilute solutions.

Species distribution diagrams for copper(II) and iron(III) citrates, calculated with the constants of Table 1, are shown in Figs. 2 and 3.

The authors are obliged to Dr. V. Cheam, Canada Centre for Inland Waters, Burlington, Ontario, for providing facilities for and assistance with the measurements with the copper-ion-sensitive electrode; also to W. J. Reynolds for preliminary experiments with the spectrophotometric method described. The work was assisted by a grant from the Inland Waters Directorate, Department of the Environment, Government of Canada.

1. I. G. SAYCE. Talanta, **15**, 1397 (1968).
2. D. D. PERRIN and I. G. SAYCE. Chem. Ind. 661 (1966).
3. W. A. E. MCBRYDE. Analyst, **94**, 337 (1969); **96**, 739 (1971).
4. H. M. IRVING, M. G. MILES, and L. D. PETTIT. Anal. Chim. Acta, **38**, 475 (1967).
5. G. G. RAO and G. ARAVAMUDIN. Anal. Chim. Acta, **13**, 328 (1955).
6. N. BJERRUM. Kgl. danske Videnskab Selskab Skriftes, Nat.-mad. Afd. **4**, 1 (1906).
7. W. A. E. MCBRYDE, JANET L. ROHR, J. S. PENCINER, and J. A. PAGE. Can. J. Chem. **48**, 2574 (1970).
8. G. SCHWARZENBACH and E. FREITAG. Helv. Chim. Acta, **34**, 1492 (1951).
9. J. LEFEBVRE. J. Chim. Phys. **54**, 581 (1957).
10. K. S. RAJAN and A. E. MARTELL. J. Inorg. Nucl. Chem. **29**, 463 (1967).
11. E. CAMPI, G. OSTACOLI, M. MEIRONE, and G. SAINI. J. Inorg. Nucl. Chem. **26**, 553 (1964).
12. R. C. WARNER and I. WEBER. J. Am. Chem. Soc. **75**, 5086 (1953).
13. S. SUZUKI. Sci. Rep. Tohoku Univ. **4**, 464 (1952).
14. C. HEITNER and I. ELIEZER. Bull. Soc. Chim. Fr. 574 (1956).
15. R. DAS, R. K. PATNAIK, and S. PANIT. J. Indian Chem. Soc. **37**, 59 (1960).
16. R. E. HAMM, C. M. SHULL, JR., and D. M. GRANT. J. Am. Chem. Soc. **76**, 2111 (1954).
17. C. F. TIMBERLAKE. J. Chem. Soc. 5078 (1964).
18. O. E. LANFORD and J. R. QUINAN. J. Am. Chem. Soc. **70**, 2900 (1948).
19. C. BERTIN-BATSCH. Ann. Chim. Fr. **7**, 481 (1952).
20. R. H. DUNHILL, J. R. PILBROW, and T. D. SMITH. J. Chem. Phys. **45**, 1474 (1966).
21. S. RAMAMOORTHY, P. G. MANNING, and C. GUARNASCHELLI. J. Inorg. Nucl. Chem. **34**, 3443 (1972).

Can. J. Chem. Downloaded from www.nrcresearchpress.com by 210.87.254.42 on 09/05/12
For personal use only.

The Crystal and Molecular Structure of Diazido-2,2′-bipyridinecopper(II)

GORDON W. BUSHNELL AND MASOOD A. KHAN

Department of Chemistry, University of Victoria, Victoria, British Columbia V8W 2Y2

Received March 27, 1974

GORDON W. BUSHNELL and MASOOD A. KHAN. Can. J. Chem. **52**, 3125 (1974).

The crystal and molecular structure of diazido-2,2′-bipyridinecopper(II), $C_{10}H_8N_2(N_3)_2Cu$, is determined by single crystal X-ray diffraction, and refined to an *R* value of 0.067. The cell dimensions are $a = 664.9(2)$, $b = 843.3(1)$, $c = 1082.0(2)$ pm, $\alpha = 86.99(2)°$, $\beta = 87.77(3)°$, $\gamma = 78.59(2)°$. The space group is $P\bar{1}$ (No. 2) with 2 molecules per unit cell and the measured density is 1.71(2) g cm^{-3}. The copper coordination is square planar with two additional longer bonds. The coordinate bond lengths in pm to the bipyridine ligand are: Cu—N(1), 201.6(6); Cu—N(2), 201.9(6). The coordinate bonds to the azido ligands are: Cu—N(3), 194.9(6); Cu—N(6), 196.6(6). The longer bonds are: Cu—N(3)′′, 268.0(8), Cu—N(6)′, 268.2(8). The N—N bond lengths within each azido ligand are unequal: N(3)—N(4), 118.2(10); N(4)—N(5), 115.4(11); N(6)—N(7), 119.2(9); N(7)—N(8), 114.8(9). The angles at N(3) and N(6) are both 130° and at N(4) and N(7) the angles are both 175(1)°. Each azide takes part in asymmetric bridging through a single nitrogen atom. The results are compared with other structural studies on azido complexes and to a nitrate complex of Ag(II) which is structurally similar.

GORDON W. BUSHNELL et MASWOOD A. KHAN. Can. J. Chem. **52**, 3125 (1974).

On a étudié la structure cristalline et moléculaire du diazido bipyridyl-2,2′ cuivrique ($C_{10}H_8N_2(N_3)_2Cu$) par diffraction des rayons-x sur crystal unique, et affiné cette structure jusqu'à un facteur d'accord de 0.067. Les dimensions de la maille sont: $a = 664.9(2)$, $b = 843.3(1)$, $c = 1082.0(2)$ pm, $\alpha = 86.99(2)°$, $\beta = 87.77(3)°$, $\gamma = 78.59(2)°$. Groupe spatial $P\bar{1}$ (No. 2) avec deux molécules par maille et la densité mesurée est de 1.71(2) g cm^{-3}. La coordination du cuivre est plan carré avec deux autres liaisons plus longues. Les liaisons entre le cuivre et les azotes de la bipyridine mesurent: Cu—N(1) = 201.6(6) et Cu—N(2) = 201.9(6) pm. Quant aux liaisons entre le cuivre et les coordinats azido, elles sont de: Cu—N(3) = 194.9(6) et Cu—N(6) = 196.6(6) pm. Les liaisons plus longues sont Cu—N(3)′′ = 268.0(8), Cu—N(6)′ = 268.2(8) pm. Les longueurs de liaisons N—N à l'intérieur de chaque coordinat azido sont: N(3)—N(4) = 118.2(10); N(4)—N(5) = 115.4(11); N(6)—N(7) = 119.2(9); N(7)—N(8) = 114.8(9) pm. Les angles aux N(3) et N(6) sont tous deux de 130° tandis qu'aux N(4) et N(7) ils sont de 175(1)°. Chaque groupe azide participe au pontage asymétrique par un seul atome d'azote. On compare ces résultats avec ceux d'autres études structurales effectuées sur les azido-complexes ainsi qu'avec un complexe de nitrate d'argent, qui possède une structure semblable.

[Traduit par le journal]

Introduction

In the last few years numerous crystal structures involving the copper(II) ion have appeared in the literature. The $3d^9$ electronic configuration lacks cubic symmetry, and causes distortions from regular cubic structures (1, 2). A similar electronic system, the silver(II) ion ($4d^9$) also shows similar distortions and it would be interesting to study the two ions in similar surroundings. Last year we reported (3) the crystal structure of dinitratobipysilver(II).[1] After some exploratory preparative work, we decided to investigate the crystal structure of diazidobipycopper(II). The choice of azido ligand for the copper(II) complex made a wide range of results possible. It has been shown (4–7) that the azide group may coordinate to a metal atom in a number of ways, the simplest being as a terminal group (T). Bridging (B) may occur in the short (S) or long (L) modes.

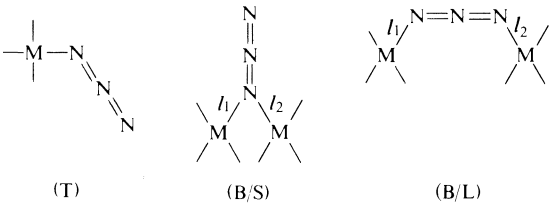

The bridging may be symmetric (I) or asymmetric (II) with respect to the metal nitrogen bond lengths. For type I, $l_1 = l_2$ and for type II, $l_1 \neq l_2$. The structures observed contain combinations of the above elements. A related but separate topic is the comparison of the two

[1] bipy = 2,2′-bipyridine.

Can. J. Chem. Downloaded from www.nrcresearchpress.com by 210.87.254.5 on 09/05/12
For personal use only.

Can. J. Chem. Downloaded from www.nrcresearchpress.com by 210.87.254.5 on 09/05/12
For personal use only.

N—N bond lengths in each ligand, for which an accurate structure determination is necessary. We anticipated an interesting comparison of the structural aspects of the coordinated azide in our complex with data already existing.

Experimental

Diazidobipycopper(II) was prepared according to the method of Dutta and De (8). Long needle shaped green crystals were obtained by evaporating a solution of complex in dimethylsulfoxide at room temperature.

Anal. Calcd. for $Cu(C_{10}H_8N_2)(N_3)_2$: Cu, 20.92; C, 39.54; H, 2.65; N, 36.89. Found: Cu, 20.80; C, 39.05; H, 3.06; N, 35.21.[2]

Crystallographic Measurements

Microscopic examination of crystals indicated the possibility of twinning. Preliminary photographic work showed that the crystals were rotationally twinned with a two fold twin axis along *a*. The cell parameters were obtained by using the method of double offset reported previously (3). It was also possible to obtain single crystals by cutting the twinned crystals into two halves along the needle axis. The cell parameters were confirmed by obtaining the precession photographs (*hk*0 and *h*0*l* layers) of a single crystal. A single crystal used for the diffractometer measurement had dimensions 0.60 × 0.08 × 0.06 mm. The crystal was mounted on a Picker 4-circle diffractometer along reciprocal axis *a**. A set of 64 2θ measurements were obtained at 22 °C and the cell parameters were refined by the method of least squares. The crystal data are given in Table 1. Confirmation of space group $P\bar{1}$ was based solely on structure refinement. The density of the crystals was measured by flotation method using a solution of carbon tetrachloride and bromoform. The set of independent intensity data was collected at room temperature on a manual Picker four-circle diffractometer using $MoK_{\bar{\alpha}}$ radiation (λ = 71.069 pm) and a Zr filter. A θ/2θ scan for 1 min at a rate of 2°/min in 2θ was used. The scan range was from −1.0° to 1.0° of the calculated 2θ value. The instrument was operated in the bisecting position with ω = 0. Background counts were measured for 30 s at each end of the scan. The positions of a set of three reflections were measured twice a day for orientation checking and one of the three reflections was used as an intensity standard and examined after every batch of 30 reflections. The intensities of a total of 1550 independent reflections (2θ ≤ 45°) were measured. 1396 of these reflections were given "observed" status using the criterion that the net count must be $>\sigma$, where σ is the standard deviation of the background count. The intensities were corrected for the usual Lorentz and polarization effects but no absorption correction was applied owing to the smallness of the absorption coefficient (μt = 0.15 and 0.11) and the uniformity of the two relevant crystal dimensions (0.08, 0.06 mm).

Structure Determination

The structure was solved by the usual heavy atom method. The atomic scattering factor curve for copper was obtained from the work of Cromer and Waber (9). Atomic scattering factor curves for C and N were obtained from the International tables for X-ray crystallography (10). All atoms were assumed to be uncharged and a correction for the anomalous dispersion of copper was made (11). The calculations were done using a set of programs supplied by Penfold (12). The coordinates of the copper atom and the four closest nitrogens were obtained from a three dimensional Patterson map. A subsequent Fourier synthesis phased on these 5 atoms revealed the coordinates of 15 atoms. A refinement for the minimization of $\Sigma w(|F_o| - |F_c|)^2$ using full matrix least squares was applied at this stage. The weights were derived from counting statistics and an experimentally determined instrument instability factor of 0.04 using the formula given by Stout and Jensen (13). The unobserved reflections were included in the structure factor calculations but excluded from the least squares sums. The first cycle of refinement with 15 atoms with isotropic temperature factors gave R = 0.249. The second Fourier synthesis phased on the coordinates of 15 atoms revealed all the nonhydrogen atoms. For the second cycle of refinement all the atoms were allowed to vibrate anisotropically and the R value dropped to 0.115. The refinement was continued with anisotropic temperature factors till the maximum shift/error ratio was 0.05. The final R value was 0.067, and including the "unobserved" reflections it was 0.074. Defining the weighted R factor as $(\Sigma w\Delta^2/wF_o^2)^{1/2}$, the final values for the "observed" set only and for all reflections were 0.087 and 0.091 respectively. A final difference synthesis did not show any peak higher than 9.35×10^{-7} e pm^{-3} whereas the typical electron density value for a C atom was 7.13×10^{-6} e pm^{-3}. The estimated standard deviations of the parameters were calculated using the full variance–covariance matrix. The structure factor table is in the Depository of Unpublished Data.[3]

TABLE 1. Crystal data for diazido-2,2′-bipyridine copper(II)

System	Triclinic
Space group	$P\bar{1}$ (No. 2)
Molecular weight	303.77
Cell dimensions	a = 664.9 ± 0.2 pm
	b = 843.3 ± 0.1 pm
	c = 1082.0 ± 0.2 pm
	α = 86.99 ± 0.02°
	β = 87.77 ± 0.03°
	γ = 78.59 ± 0.02°
Cell volume	593.6(2) × 10^{-24} cm^3
Density (measured)	1.71 ± 0.02 g cm^{-3}
Molecules per cell (calculated)	2.01
Absorption coefficient ($MoK_{\bar{\alpha}}$)	19.11 cm^{-1}
Density (calculated)	1.70 g cm^{-3}

Results

The fractional atomic coordinates and the anisotropic temperature parameters are given in

[2]The discrepancies in the analytical results are attributed to the explosive nature of the diazidobipycopper(II).

[3]Copies may be obtained, at a nominal charge, from the Depository of Unpublished Data, National Science Library, National Research Council of Canada, Ottawa, Canada K1A 0S2.

Can. J. Chem. Downloaded from www.nrcresearchpress.com by 210.87.254.5 on 09/05/12
For personal use only.

TABLE 2. Fractional atomic coordinates*

Atom	x	y	z
Cu	0.2461(1)	0.0056(1)	0.0508(1)
N(1)	0.3215(9)	−0.1074(8)	0.2162(5)
N(2)	0.1307(10)	0.1851(7)	0.1653(5)
N(3)	0.4347(11)	−0.1568(9)	−0.0407(7)
N(4)	0.4138(11)	−0.2151(9)	−0.1353(7)
N(5)	0.4058(16)	−0.2709(15)	−0.2297(10)
N(6)	0.0932(11)	0.1189(8)	−0.0904(6)
N(7)	0.1411(10)	0.1218(7)	−0.1976(6)
N(8)	0.1715(13)	0.1284(11)	−0.3028(7)
C(1)	0.4082(13)	−0.2671(10)	0.2335(8)
C(2)	0.4420(14)	−0.3391(10)	0.3494(8)
C(3)	0.3874(15)	−0.2474(12)	0.4529(9)
C(4)	0.2956(13)	−0.0833(11)	0.4380(7)
C(5)	0.2665(11)	−0.0172(9)	0.3160(6)
C(6)	0.1649(11)	0.1504(9)	0.2869(6)
C(7)	0.1120(14)	0.2681(11)	0.3772(7)
C(8)	0.0205(15)	0.4226(11)	0.3346(8)
C(9)	—0.0142(17)	0.4593(11)	0.2109(8)
C(10)	0.0416(14)	0.3365(10)	0.1275(7)

*Estimated standard deviations in parentheses.

TABLE 3. Anisotropic temperature parameters*

Atom	β_{11}	β_{22}	β_{33}	β_{12}	β_{13}	β_{23}
Cu	245(3)	78(2)	28(1)	5(1)	5(1)	−11(1)
N(1)	172(17)	97(11)	30(5)	−9(10)	4(7)	−9(6)
N(2)	230(18)	64(10)	31(6)	2(11)	5(8)	−8(6)
N(3)	268(22)	138(13)	54(7)	31(13)	16(9)	−42(8)
N(4)	260(22)	127(13)	83(9)	−37(13)	37(10)	−48(9)
N(5)	409(33)	353(28)	124(12)	−90(23)	26(15)	−158(16)
N(6)	296(21)	93(11)	31(7)	20(12)	−21(9)	−5(6)
N(7)	237(19)	79(11)	35(7)	−34(11)	4(8)	−10(6)
N(8)	381(28)	225(19)	33(7)	−80(17)	27(10)	−9(8)
C(1)	250(24)	66(13)	68(9)	11(13)	−17(11)	4(8)
C(2)	318(28)	94(14)	64(9)	−32(15)	2(12)	4(9)
C(3)	289(27)	130(16)	80(9)	−17(16)	−17(12)	46(10)
C(4)	247(25)	133(16)	49(8)	−34(15)	−12(11)	14(9)
C(5)	150(18)	102(13)	26(6)	−18(12)	−2(8)	−9(7)
C(6)	214(21)	89(13)	23(6)	−30(13)	8(9)	−16(7)
C(7)	300(26)	113(15)	40(7)	−4(15)	10(10)	−25(8)
C(8)	364(30)	103(15)	63(9)	−3(16)	6(12)	−38(9)
C(9)	438(35)	98(15)	59(9)	12(18)	28(13)	−16(9)
C(10)	329(28)	104(15)	44(7)	14(16)	−0(11)	−11(8)

*$T = \exp[-(h^2\beta_{11} + k^2\beta_{22} + l^2\beta_{33} + 2hk\beta_{12} + 2hl\beta_{13} + 2kl\beta_{23})]$. The parameters have been multiplied by 10^4. Estimated standard deviations are given in parentheses.

Tables 2 and 3. Figure 1 gives the atom labels and the intramolecular bond lengths. The copper coordination is tetragonally distorted octahedral, the two longer coordinate bonds being considered intermolecular for convenience only. Figure 2 gives a perspective view of several units cells and shows the longer coordinate bonds. Selected edge to edge intermolecular contacts are indicated by dashed lines. The thermal ellipsoids are based on 50% probability. Considering Cu—N_3'' and Cu—N_6' the crystal structure is polymeric in the x-direction (the primes are defined below Table 6).

The bond lengths in Fig. 1 are largely symmetrical about a central vertical line. The magnitudes of the bond angles visible on this figure show similar symmetry (see Table 4). Cu—N (azide), mean 195.8(4), is significantly shorter than Cu—N(bipy), mean 201.8(4), indicating strong covalent bonds between Cu and the azide

TABLE 4. Bond angles*

(*a*) Copper atom octahedron

Bonds	Angle (deg)	Bonds	Angle (deg)	Bonds	Angle (deg)
N(1)—Cu—N(6)	163.7(3)	N(2)—Cu—N(3)	162.7(3)	N(3)″—Cu—N(6)′	171.4(2)
N(1)—Cu—N(2)	79.6(2)	N(1)—Cu—N(3)″	93.7(2)	N(2)—Cu—N(3)″	81.6(2)
N(2)—Cu—N(6)	92.6(3)	N(3)″—Cu—N(6)	99.4(3)	N(3)″—Cu—N(3)	83.2(3)
N(6)—Cu—N(3)	98.0(3)	N(6)—Cu—N(6)′	83.0(3)	N(3)—Cu—N(6)′	104.8(3)
N(3)—Cu—N(1)	93.2(3)	N(6)′—Cu—N(1)	82.7(2)	N(6)′—Cu—N(2)	90.0(2)

(*b*) Azido ligands

Bonds	Angle (deg)	Bonds	Angle (deg)
N(3)—N(4)—N(5)	175.7(10)	N(6)—N(7)—N(8)	174.7(8)
N(4)—N(3)—Cu	130.1(6)	N(7)—N(6)—Cu	129.6(6)

(*c*) 2,2′-Bipyridine ligand

Bonds	Angle (deg)	Bonds	Angle (deg)	Bonds	Angle (deg)
N(1)—C(1)—C(2)	121.9(7)	N(2)—C(10)—C(9)	121.5(7)	N(1)—C(5)—C(6)	114.5(6)
C(1)—C(2)—C(3)	119.5(8)	C(10)—C(9)—C(8)	118.6(8)	N(2)—C(6)—C(5)	114.3(6)
C(2)—C(3)—C(4)	119.8(8)	C(9)—C(8)—C(7)	121.6(7)	C(1)—N(1)—Cu	124.9(5)
C(3)—C(4)—C(5)	117.5(8)	C(8)—C(7)—C(6)	116.4(7)	C(10)—N(2)—Cu	124.6(5)
C(4)—C(5)—N(1)	122.0(7)	C(7)—C(6)—N(2)	122.4(7)	C(5)—N(1)—Cu	115.7(5)
C(1)—N(1)—C(5)	119.2(6)	C(10)—N(2)—C(6)	119.4(6)		
C(4)—C(5)—C(6)	123.3(6)	C(7)—C(6)—C(5)	123.3(7)	C(6)—N(2)—Cu	115.7(5)

*Estimated standard deviations are given in parentheses.

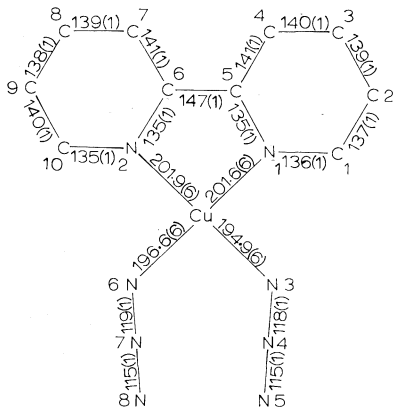

FIG. 1. The diazido-2,2′-bipyridinecopper(II) molecule with atom labels and bond lengths shown.

groups. Within the azide groups the N—N bonds closer to the Cu atom are longer than the other more distant N—N bonds. Treating each ligand individually, the differences in the bonds were 2.8(15) and 4.4(13) pm. Averaging over both ligands, the difference between the mean N—N length nearer to the Cu atom and that further from the Cu atom is 3.6(9). The significance of such small differences can be judged by standard statistical methods. The bond lengths within the bipyridine ligand are in accordance with the reported values for monobipy complexes of Cu(II) and Ag(II) (3, 14, 15) and the free bipy molecule (16).

Table 4(*a*) gives the bond angles for the Cu coordination. The first row gives the angles for the *trans* ligands (ideally 180°). The remaining four rows list the angles (ideally 90°) within the three mutually perpendicular planes of the octahedron. The copper atom coordination is significantly distorted. Table 4(*b*) contains bond angles involving the azido ligand. The angles around the central N atoms are slightly less than 180°, a feature which has already been observed in several azido complexes (6, 7, 17). The angles subtended by the coordinated nitrogens N(3) and N(6) indicate trigonal hybridization. Table 4(*c*) contains the bond angles of the bipyridine ligand. The angles of the 6 membered rings deviate $\leq 3.6°$ from 120°, whereas the other angles are generally less regular, as might be expected. The bond angles involving the bipy ligand are comparable with the reported values in the literature (3, 14–16).

Some selected least squares planes are pre-

Can. J. Chem. Downloaded from www.nrcresearchpress.com by 210.87.254.5 on 09/05/12
For personal use only.

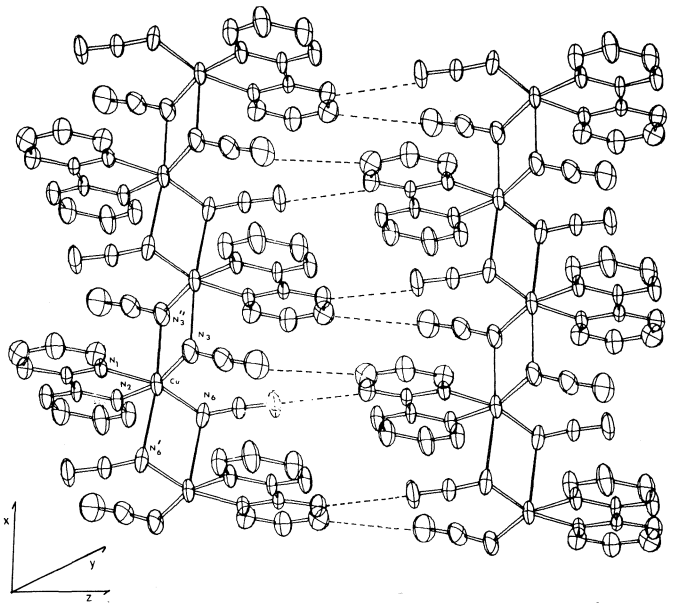

FIG. 2. A packing diagram of diazido-2,2′-bipyridine copper(II) illustrating the explanation of the crystal twinning.

sented in Table 5. The orthogonal axis system used has x along a, y in the (a,b) plane, and z along c^*. The quantity minimized was $R = \sum_i w_i P_i^2$, where the weight w_i for atom i is given by $3/[\sigma^2(x_i) + \sigma^2(y_i) + \sigma^2(z_i)]$ and P_i is the perpendicular distance of atom i from the plane. The quantity $\chi^2 = \sum_i P_i^2/\sigma^2(P_i)$, is calculated as an index of the planarity of the group. The perpendicular distance of the copper atom from the planes is denoted P_{Cu}. Planes 1–6 are calculated to show the distortion of the octahedral configuration around Cu. Planes 1 and 2 indicate that the 4 strongly coordinated nitrogens are not planar and that the Cu atom lies almost in these least squares planes. Two reasonably good planes (4 and 6) are found involving the atoms N(3)′′ and N(6)′, but the Cu atom lies 11 and 17 pm respectively from these planes. Planes 7, 8, and 9 show that individually each pyridyl ring is planar but that the complete bipyridyl ligand is non-planar. The departure from planarity can be described as a rotation about C(5)—C(6), and this phenomenon is commonly observed in coordinated bipyridine compounds (3, 14, 15).

The intermolecular contacts given in Table 6 resemble closely those found in dinitratobipy-Ag(II) which have been described in terms of a slipping stack of coins (3). The crystal axis a is almost perpendicular to the coin faces and the contacts are head-to-head and tail-to-tail alternately. Table 6(*a*) presents important face-to-face contacts and the two coordinate bond distances in the first row are obviously most important. Such weak coordination is quite common in copper(II) complexes and these bonds are called semicoordinate bonds by Hathaway and Billing (1). The semicoordination occurs along the x-axis and this direction coincides with the needle axis of the crystals. Crystal growth is presumably facilitated by this bonding. Table 6(*b*) gives the very weak edge-to-edge contacts.

Discussion

The crystal structure of diazidobipyridylcopper(II) is very similar to that of dinitratobipyridylsilver(II) (3), both being based on tetragonally distorted octahedral coordination geometry, having bridging groups, and belonging to the same space group. There is an approximate similarity in unit cell lengths and the way in which the x, y, and z crystallographic directions have been chosen in relation to the molecules. In the copper compound the metal to bipyridyl nitrogen bond lengths are equal, whereas inequality of the corresponding Ag—N bonds was found and attributed to the limited span of the bipyridyl ligand and the size of the silver atom (3). The bridging of the molecules through semicoordinate bonding in the x-direction is done in slightly different ways: in the diazidocopper compound both azides are similarly involved but in the dinitratosilver compound one

Can. J. Chem. Downloaded from www.nrcresearchpress.com by 210.87.254.5 on 09/05/12
For personal use only.

Can. J. Chem. Downloaded from www.nrcresearchpress.com by 210.87.254.5 on 09/05/12
For personal use only.

TABLE 5. Least squares planes $k_1x + k_2y + k_3z = k_4$ *

Number	Plane	k_1	k_2	k_3	k_4	χ^2	P_{Cu}(pm)
1	Cu,N(1),N(2),N(3),N(6)	0.8822	0.4615	−0.0937	1.4520	5072	+0.01
2	N(1),N(2),N(3),N(6)	0.8822	0.4614	−0.0938	1.4507	5071	+0.13
3	Cu,N(2),N(3),N(3)″,N(6)′	−0.3166	+0.4922	−0.8109	−0.9437	1080	+0.61
4	N(2),N(3),N(3)″,N(6)′	−0.3126	0.4803	−0.8195	−1.0432	159.2	+11
5	Cu,N(1),N(6),N(3)″,N(6)′	0.3032	−0.7996	−0.5184	0.1535	2405	+1.0
6	N(1),N(6),N(3)″,(N6)′	0.3105	−0.7893	−0.5297	−0.0010	29.39	+17
7	N(1),C(1)–C(5)	0.9718	0.2353	−0.0175	1.7658	1.095	−14
8	N(2),C(6)–C(10)	0.9645	0.2332	−0.1241	1.3559	0.5174	+20
9	N(1),N(2),C(1)–C(10)	0.9655	0.2498	−0.0735	1.5376	540.6	+4.9

*Angles between normals of planes: 2,4 = 88.7°; 2,6 = 92.3°; 2,9 = 13.1°; 4,6 = 92.4°; 7,8 = 6.1°.

TABLE 6. Intermolecular contacts*

(*a*) Face-to-face

Contact	Length (pm)	Contact	Length (pm)
Cu–N(3)″	268.0(8)	Cu–N(6)′	268.2(8)
N(1)–N(7)′	311.7(9)	N(2)–N(4)″	309.2(10)
N(1)–N(6)′	314.3(9)	N(2)–N(3)″	311.2(9)
N(3)–N(3)″	312.1(16)	N(6)–N(6)′	312.6(14)
N(5)–C(6)″	324.1(13)	N(8)–C(5)′	324.1(11)
N(5)–C(10)′	327.3(14)		

(*b*) Edge-to-edge

Contact	Length (pm)	Contact	Length (pm)
N(5)–C(3)^{I}	343.5(14)	N(8)–C(4)^{I}	339.0(12)
N(7)–C(9)^{II}	346.3(11)		

*Estimated standard deviations are given in parentheses. Superscripts on the atoms correspond to the atoms with coordinates as follows: ′ = $-x, -y, -z$; ″ = $1-x, -y, -z$; I = $x, y, -1+z$; II = $-x, 1-y, -z$.

nitrate group deals with both bridges, one on each side of the plane of closest coordination. These two bridges differ being of the one atom and three atom types AgOAg and AgONOAg respectively. The shape of the nitrate ion causes a predominantly unidentate nitrato ligand to have some bidentate character (3), and in dinitratodipyridylsilver(II) both of the nitrato ligands apply this effect on the same side of the plane of closest coordination. Presumably as a consequence of these effects the Ag atom lies 19.9(2) pm from the least squares plane through the four closely coordinated atoms, in contrast to the Cu atom in diazidobipyridylcopper(II) which lies very close to such a plane. An interesting feature of the two structures is the occurrence of twinned crystals. Both complexes show similar crystal habits, and crystallize as triclinic twins. The formation of twinned crystals is probably caused by the occasional reorientation of the polymeric units. Such reorientation can be visualized in Fig. 2. If one strand is fixed and the other allowed to rotate by 180° about the *x*-axis, the resulting setup would have considerable nonbonding repulsions owing to the closely approaching bipy ligands. But by translating the rotated unit $a/2$ along x, unfavorable interactions can be minimized and the result has very similar intermolecular contacts to the original single crystal.

Table 7 contains structural information related to the coordinated azide ligand (1 × T indicates one terminal, 2 × B indicates two bridging azido groups, etc.). Since each coordinate bond involves a metal atom and a ligand, the sum of the coordination numbers (N_i) for the metal atoms present (i) must equal the sum over all ligands (j) of the number of bonds formed by each ligand (n_j).

$$[1] \qquad \Sigma_i N_i = \Sigma_j n_j$$

A ligand may form one bond thus being terminal or it may form more than one bond in two ways: (*i*) to the same metal atom (polydentate behavior), (*ii*) to different metal atoms (bridging behavior). The azide ligand is never polydentate and though often terminal it also displays great versatility in bridging. When the bridging involves three metal atoms the nomenclature (S.I, L.II, L.II), for example, signifies

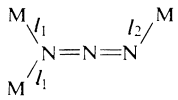

Equation 1 can be applied to the crystal structure analysis results of Table 7, but does not have any predictive powers. Within Table 7 this difficulty lies more with the various modes of azide coordination than with (*a*) the behavior of other ligands, or (*b*) metal atom stereochemistry. Accordingly, some attention may well be directed towards understanding the behavior of the azide ligand.

In copper azide the complicated bridging is necessary to attain the coordination number of 6 for Cu(II), and the (S, S, S) type of bridge is probably only feasible in the absence of large

Can. J. Chem. Downloaded from www.nrcresearchpress.com by 210.87.254.5 on 09/05/12
For personal use only.

TABLE 7. Mode of azide coordination*

Compound	Stereochemistry	N	Steric interaction	Mode of azide coordination	Reference
$Cu(N_3)_2$	Distorted octahedral	6	Low	1 × B (S.I, L.II, L.II) 1 × B (S.I, S.II, S.II)	4
$Cu(N_3)_2(NH_3)_2$	Distorted octahedral	6	Low	1 × T 1 × B (S.II, L.II, L.II)	18
$Cu(N_3)_2(C_5H_5N)_2$	Distorted octahedral	6	Low	1 × T 1 × B (S.II, L.II, L.II)	19
$Cu(N_3)_2(C_{10}H_8N_2)$	Distorted octahedral	6	Moderate	2 × B (S.II)	This work
$[Cu(N_3)\{P(C_6H_5)_3\}_2]_2$	Distorted tetrahedral	4	High	2 × B (L.I)	6
$[Co(N_3)(NH_3)_5](N_3)_2$	Octahedral	6	Low	1 × T	20
$(Ph_4As^+)_2[Fe(N_3)_5]^{2-}$	Trigonal bipyramidal	5	Low	5 × T	5
$Et_4N^+[Mn_2(CO)_6(N_3)_3]^-$	Octahedral	6	Low	3 × B (S.I)	21
$(Ph_4As^+)_2[Pd_2(N_3)_6]^{2-}$	Square-planar	4	Low	4 × T 2 × B (S.I)	7
$[Ru(N_3)(N_2)(en)_2]^+PF_6^-$	Octahedral	6	Moderate	1 × T	22
$Zn(N_3)_2(NH_3)_2$	Distorted tetrahedral	4	Low	2 × T	23
$Zn(N_3)_2(C_5H_5N)_2$	Distorted tetrahedral	4	Low	2 × T	24
$Cd(N_3)_2(C_5H_5N)_2$	Octahedral	6	Moderate	2 × B (L.I)	25

*T = Terminal, B = Bridging, S = Short, L = Long, I = symmetric, II = asymmetric.

TABLE 8. Bond lengths in azides

Compound	N_A—N_B*	N_B—N_C*	Comment	Reference
CH_3N_3	124(1)	112(1)	Covalent	26
HN_3	124.0(3)	113.4(3)	Covalent	27
NaN_3	115.0(16)	115.0(16)	Ionic	28
$Cd(N_3)_2(C_5H_5N)_2$	116.7(20)	114.1(21)	L.I bridged	21
$Cu(N_3)_2(NH_3)_2$	118.6(11)	113.9(13)	Terminal	18
	117.4(11)	114.2(12)	Bridging	
$Cu(N_3)_2(C_5H_5N)_2$	114(4)	108(4)	Terminal	19
	123(3)	119(4)	Bridging	
$Cu(N_3)_2(C_{10}H_8N_2)$	118.2(10)	115.4(11)	—	This work
	119.2(9)	114.8(9)	—	This work
$[Co(N_3)(NH_3)_5](N_3)_2$	117.2(7)	115.8(7)	Ionic	20
	120.8(7)	114.5(7)	Coordinated	

*Where coordinated azide is represented as $M—N_A=N_B=N_C$.

ligands. We see also in Table 7 that $M(N_3)_2(NH_3)_2$ resembles $M(N_3)_2(C_5H_5N)_2$ in mode of azide coordination where M = Cu or Zn. On the other hand the mode of azide coordination in diazidobipyridine copper(II) differs from that in diazidobis(pyridine)copper(II) and the difference arises from the *cis* and *trans* structures respectively of these complexes in their crystals.

The occurrence of short and long bridging can be rationalized in terms of the steric interactions present in a complex. $(Cu(N_3)\{P(C_6H_5)_3\}_2)_2$ is a good example of a double L.I type bridge providing relief from the overcrowding which would occur in the analogous double S.I bridged structure.

Asymmetric bridging occurs in Table 7 for the Cu(II) complexes only and is therefore best explained in terms of the d^9 configuration of the cupric state.

In Table 8 we present some N—N bond lengths in various azides. In hydrazoic acid and the alkyl azides there is no doubt that a significant difference exists between the two N—N bond lengths. Equal N—N lengths occur in ionic

Can. J. Chem. Downloaded from www.nrcresearchpress.com by 210.87.254.5 on 09/05/12
For personal use only.

azides and L.I bridged complexes. The majority of cases found in coordination chemistry would be expected to give intermediate results with the difference between the two N—N lengths being dependent on the polarising power of the metal atom(s) present and their positions. Unfortunately, the difference between the N—N bond lengths is often small and the error in the same quantity appreciable. Thermal motion analysis for the azido ligand (29) has been applied only infrequently. The application of this correction usually diminishes the difference between the bond lengths. It is interesting that one of the best examples of an asymmetric azido ligand does occur in a Co(III) complex where the oxidation number is high and the group is terminal. The topic of N—N lengths in azido complexes has been discussed (17), our results are relevant, but more accurate structure determinations will be needed to fully explore the factors involved.

The authors acknowledge grants from the University of Victoria and the National Research Council of Canada. Computing facilities were provided by the University of Victoria and the paper was prepared at the Chemical Crystallography Laboratory, Oxford.

1. B. J. HATHAWAY and D. E. BILLING. Coord. Chem. Rev. **5**, 143 (1970).
2. B. J. HATHAWAY. Essays Chem. **2**, 61 (1971).
3. G. W. BUSHNELL and M. A. KHAN. Can. J. Chem. **50**, 315 (1972).
4. I. AGRELL and S. LAMNEVIK. Acta Chem. Scand. **22**, 2038 (1968).
5. J. DRUMMOND and J. S. WOOD. Chem. Commun. 1373 (1969).
6. R. F. ZIOLO, A. P. GAUGHAN, Z. DORI, C. G. PIERPONT, and R. EISENBERG. Inorg. Chem. **10**, 1289 (1971).
7. W. P. FEHLHAMMER and L. F. DAHL. J. Am. Chem. Soc. **94**, 3377 (1972).
8. R. L. DUTTA and D. DE. J. Indian Chem. Soc. **46**, 1 (1969).
9. D. T. CROMER and J. T. WABER. Acta Cryst. **18**, 104 (1965).
10. J. A. IBERS. International tables for X-ray crystallography. Vol. III. Kynoch Press, Birmingham. 1962. Table 3.3.1A, p. 201.
11. D. T. CROMER. Acta Cryst. **18**, 17 (1965).
12. B. R. PENFOLD. University of Canterbury Crystallographic Programs, Christchurch, New Zealand.
13. G. H. STOUT and L. H. JENSEN. X-ray structure determination. Macmillan, New York. 1968. p. 456.
14. F. S. STEPHENS. J. Chem. Soc. A, 2081 (1969).
15. R. J. MAJESTE and E. A. MEYERS. J. Phys. Chem. **74**, 3497 (1970).
16. L. L. MERRITT and E. D. SCHROEDER. Acta Cryst. **9**, 801 (1956).
17. R. F. ZIOLO, M. ALLEN, D. D. TITUS, H. B. GRAY, and Z. DORI. Inorg. Chem. **11**, 3044 (1972).
18. I. AGRELL. Acta Chem. Scand. **20**, 1281 (1966).
19. I. AGRELL. Acta Chem. Scand. **23**, 1667 (1969).
20. G. J. PALENIK. Acta Cryst. **17**, 360 (1964).
21. R. MASON, G. A. RUSHOLME, W. BECK, H. ENGLEMANN, K. JOOS, B. LINDENBERG, and H. S. SMEDAL. Chem. Commun. 496 (1971).
22. B. R. DAVIS and J. A. IBERS. Inorg. Chem. **9**, 2768 (1970).
23. I. AGRELL and N. G. VANNERBERG. Acta Chem. Scand. **25**, 1630 (1971).
24. I. AGRELL. Acta Chem. Scand. **24**, 1247 (1970).
25. I. AGRELL. Acta Chem. Scand. **24**, 3575 (1970).
26. R. L. LIVINGSTON and C. N. RAMACHANDRA RAO. J. Phys. Chem. **64**, 756 (1960).
27. E. AMBLE and B. P. DAILEY. J. Chem. Phys. **18**, 1422 (1950).
28. L. K. FREVEL. J. Am. Chem. Soc. **58**, 779 (1936).
29. R. SÖDERQUIST. Acta Cryst. B**24**, 450 (1968).

Can. J. Chem. Downloaded from www.nrcresearchpress.com by 210.87.254.5 on 09/05/12
For personal use only.

Concertedness in the Thermolysis of Some 1-Pyrazolines

ROBERT J. CRAWFORD AND MASATOMI OHNO

Department of Chemistry, University of Alberta, Edmonton, Alberta T6G 2G2

Received March 13, 1974

ROBERT J. CRAWFORD and MASATOMI OHNO. Can. J. Chem. **52**, 3134 (1974).

A mixture of *cis*- and *trans*-3,5-divinyl-1-pyrazoline was synthesized and isolated at 0° by the cycloaddition of vinyldiazomethane to butadiene. The kinetics of the thermolysis in diphenyl ether at 35–65° were studied by measuring the rate of nitrogen evolution. The *cis* isomer gave $\log (k_1/s^{-1}) = (12.28 \pm 0.9) - (22.8 \pm 0.4)/\theta$ where $\theta = 2.303RT$ in kcal mol^{-1}, for the *trans* isomer $\log (k_2/s^{-1}) = (13.9 \pm 0.9) - (25.7 \pm 0.4)/\theta$ was obtained. These data when compared with those of 1-pyrazoline and 3-vinyl-1-pyrazoline lead to the conclusion that both carbon–nitrogen bonds are being broken in the rate determining step. Thus the alkyl-1-pyrazolines are concerted whereas the azoalkanes are not.

ROBERT J. CRAWFORD et MASATOMI OHNO. Can. J. Chem. **52**, 3134 (1974).

Un mélange de divinyl-3,5 pyrazoline-1, *cis* et *trans* a été préparé et isolé à 0° par cycloaddition du vinyldiazométhane sur le butadiène. La cinétique de la thermolyse dans l'éther diphénylique à 35.0–65° a été étudiée en mesurant la vitesse du dégagement d'azote. L'isomère *cis* a donné un $\log (k_1/s^{-1}) = (12.28 \pm 0.9) - (22.8 \pm 0.4)/\theta$ où $\theta = 2.303RT$ en kcal mol^{-1}, pour l'isomère *trans* on a obtenu un $\log (k_2/s^{-1}) = (13.9 \pm 0.9) - (25.7 \pm 0.4)/\theta$ où $\theta = 2.303RT$ en kcal mol^{-1}. Ces résultats, comparés à ceux de la pyrazoline-1 et de la vinyl-3 pyrazoline-1 nous amènent à conclure que les deux liaisons carbone–azote sont rompues dans l'étape lente. Ainsi les alkyl pyrazolines-1 ont une rupture concertée au contraire des azoalkanes.

Introduction

The question of whether both carbon–nitrogen bonds are breaking in the rate determining step during the thermolysis of 1-pyrazoline is central to the possibility of trimethylene diradicals being produced from such a source (1). In an earlier publication we suggested that the concerted cleavage of both carbon to nitrogen bonds was indeed operative (2). This was based upon the observed decrease in activation energy, 1.2 kcal mol^{-1}, for each methyl introduced α to the azo link in the 1-pyrazoline system. The kinetic and product data for 4-methyl-1-pyrazoline and 4-methyl-1-pyrazoline-4-d_1 demonstrated that there was an intermediate after the rate determining transition state. It was, at that time, generally accepted that symmetrical azoalkanes undergo thermolysis by the concerted cleavage of both carbon–nitrogen bonds (3). Carter and Bergman (4) have questioned the size of the α-methyl substituent effect, 1.2 kcal mol^{-1}, and suggested, on the basis of hydrocarbon data, that a value in excess of 2 kcal mol^{-1} should have been observed. This has lead to the suggestion that the mechanism proposed by Roth and Martin (5) can be used for the methylated 1-pyrazolines (6). More recently it has been observed that the thermolysis of several azoalkanes occur by a step-wise mechanism (7, 8) and thus some of our earlier suggestions as to concertedness in the pyrazoline thermolysis require closer examination.

The allyl group with its large resonance stabilization of allylic radicals (9) presents an ideal group for probing concertedness in thermolysis reactions and this fact was taken advantage of in the study of azoalkene thermolyses (7). An additional advantage of the allyl system is that the influence of possible steric factors can be minimized by comparing the vinyl and ethyl groups in the compounds under investigation. We wish to report herein the thermolysis of *cis*- and *trans*-3,5-divinyl-1-pyrazoline (**1** and **2**). If the rate determining transition state in pyrazoline thermolysis is concerted with respect to the breaking of two carbon–nitrogen bonds then we expect a significant decrease in activation energy upon the introduction of each vinyl group on going from **3** to **5** to **1** and **2**. The size of this decrease in activation energy should be clearly greater than that expected from steric factors, the largest of which appear to be around 2–3 kcal mol^{-1} (10).

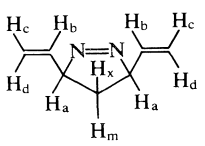

1

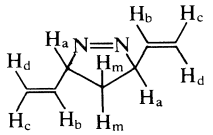

2

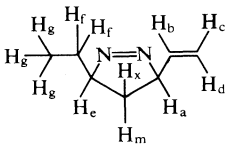

5-*cis*

3

4

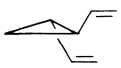

6

7

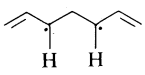

8

Results

Synthesis

The synthesis of a 40:60 mixture of *cis*- and *trans*-3,5-divinyl-1-pyrazoline (**1** and **2**) was achieved by adding a concentrated solution of vinyldiazomethane (11) in diethyl ether, purified by distillation, to a large excess of 1,3-butadiene maintained as a liquid in a pressure bottle at 5 °C. The intermolecular 1,3-cycloaddition of the diazoalkane proceeded more rapidly than the intramolecular cyclization to pyrazole (12). While we were not able to separate **1** and **2** we were able to obtain different mixtures of isomers, because of the greater reactivity of **1**, and thus analyze the n.m.r. spectrum of the mixture and make the assignments given in Table 1. Because of the thermal lability of **1** and **2** all purifications etc. had to be carried out at less than 5 °C. For comparison we have also synthesized *cis*- and *trans*-3-ethyl-5-vinyl-1-pyrazoline (**5**) by the cycloaddition of 1-diazopropane to 1,3-butadiene.

Kinetics

The rate of evolution of nitrogen from a diphenyl ether solution of **1** and **2** was measured volumetrically at four temperatures. Attempts to plot log $(V_\infty - V_t/V_\infty)$ *vs.* t resulted in curvature due to the isomers reacting at different rates. The rates in Table 2 were obtained by computer fitting of the equation for two simultaneous first-order reactions giving a common product; *e.g.*

$$[1] \quad y = (V_\infty - V_t)/V_\infty = A_0 e^{-k_1 t} + B_0 e^{-k_2 t}$$

where V_t and V_∞ are the volume of nitrogen evolved at times t and infinity. The rate constants k_1 and k_2 are assigned to **1** and **2**, respectively, and A_0 and B_0 are the mole fractions of **1** and **2** present in isomer mixture at $t = 0$. The eq. 1 was rearranged to give 2 and an estimated value of the slower isomer, k_2, was estimated from the

$$[2] \quad k_1 = -1/t \ln (1/A_0)(y - B_0 e^{-k_2 t})$$

rate of evolution of nitrogen between 70 and 80% completion. From n.m.r. studies it was observed that the *cis* isomer **1** was the faster and values of A_0 and B_0 for each sample were measured from the n.m.r. spectrum immediately before each rate measurement. The mean value of k_1 and its standard deviation σ_1 for the 40 data points was then computed. The value of k_2 was then decreased by 1% and a new σ_1 was calculated. This was repeated until σ_1 was minimized and the corresponding mean value of k_1 was adopted. The value of σ_2 for each k_2 was obtained in a complementary fashion and the errors listed in Table 2 were calculated from the standard deviations. The success of this method was confirmed by the isolation of a small sample of the pure *trans* isomer and measuring its rate at 50.5°. This was found to be $(3.38 \pm 0.02) \times 10^{-4}\ s^{-1}$ and compares favorably with the value computed $(3.40 \pm 0.06) \times 10^{-4}\ s^{-1}$ from the data obtained from the mixture of isomers.

The rate data for the thermolysis of *cis*- and *trans*-**5** produced a good straight line with no detectable curvature when log $(V_\infty - V_t/V_\infty)$ was plotted *vs.* t. The computer treatment of the data indicated that the rate constants for the pair of isomers must be essentially equal. The activation parameters for **5** are those indicated in Table 3.

Experimental

Vinyldiazomethane

A solution of *N*-nitrosoallylurea (11) (10.3 g, 81 mmol) in ether (70 ml) was added slowly to a stirred, cooled (salt-ice bath), solution of potassium hydroxide (4.5 g, 81 mmol) in methanol (12 ml). Upon completion of

TABLE 1. The proton magnetic resonance spectra for some 1-pyrazolines (chemical shift δ in p.p.m., solvent C_6D_6 at 5 °C)

Compound	Proton (intensity)	Shift	Coupling (Hz)
1 (*cis*)	H_x (1)	0.70	$J_{mx} = 12.6, J_{ax} = 9.9$
	H_m (1)	1.54	$J_{mx} = 12.6, J_{am} = 8.1$
	H_a (2)	4.28	$J_{ax} = 9.9, J_{am} = 8.1, J_{ab} = 7.1$
	H_c, H_d (4)	4.9∼5.3[a]	Complex multiplet
	H_b (2)	5.4∼6.1[a]	Complex multiplet
2 (*trans*)	H_m (2)	1.13	$J_{am} = 7.1$
	H_a (2)	4.75	$J_{ab} = J_{am} = 7.1$
	H_c, H_d (4)	4.9∼5.3[a]	Complex multiplet
	H_b (2)	5.4∼6.1[a]	Complex multiplet
3 (*cis*)	H_x (1)	0.42	$J_{mx} = 12.2, J_{am} = J_{em} = 9.5$
	H_f, H_g, H_m (6)	0.7∼2.1[a]	Complex multiplet
	H_e (1)	3.66	Approximate quintet
	H_a (1)	4.24	Approximate quartet[b]
	H_c, H_d (2)	4.9∼5.3[a]	Complex multiplet
	H_b (1)	5.5∼6.2[a]	Complex multiplet
3 (*trans*)	H_f, H_g, H_m, H_x (7)	0.7∼2.1[a]	Complex multiplet
	H_e (1)	4.12	Approximate quintet[b]
	H_a (1)	4.74	Approximate quartet
	H_c, H_d (2)	4.9∼5.3[a]	Complex multiplet
	H_b (1)	5.5∼6.2[a]	Complex multiplet

[a]Assigned by analogy with **4** in ref. 17.
[b]*cis*-H_a and *trans*-H_e overlapped each other.

TABLE 2. Thermolysis rate constants for **1** and **2** from isomer mixture

Temperature (°C)	$10^4 k$ (slow isomer) (s^{-1})	$10^4 k$ (fast isomer) (s^{-1})
34.98±0.04	0.418±0.024	1.28±0.01
40.44±0.04	0.940±0.009	2.32±0.11
50.45±0.03	3.40 ±0.06[a]	6.98±0.37
65.00±0.04	18.2 ±0.4	34.8 ±0.8
E_a (kcal mol^{-1})	25.7 ±0.2	22.8 ±0.4
log A	13.90	12.28

[a]A sample of essentially pure **2** gave a rate constant of (3.38 ± 0.02) × 10^{-4} s^{-1} at this temperature.

TABLE 3. Thermolysis rate constants for **3**

Temperature (°C)	$10^4 k$ (s^{-1})	
100.33±0.02	0.033±0.008	E_a 31.3±0.3 kcal mol^{-1}
110.18±0.03	2.72 ±0.03	log A 14.29
120.16±0.03	7.82 ±0.08	

addition the stirring was maintained for 1 h before ice-cold water (50 ml) was added to the reaction mixture. The ether layer was then separated, washed with ice-cold water (3 × 50 ml), and dried over anhydrous sodium sulfate. Thin-layer chromatography (t.l.c.) indicated that the wine-colored vinyldiazomethane had an impurity so the ethereal solution was transferred in a stream of nitrogen to a flask cooled with Dry Ice. The yield was 30–40% as measured by the amount of nitrogen evolved upon treating an aliquot with *p*-nitrobenzoic acid. This solution showed no impurity by t.l.c. and was used directly for the preparation of 3,5-divinyl-1-pyrazoline.

*Synthesis of cis- and trans-3,5-Divinyl-1-pyrazoline (**1** and **2**)*

The freshly prepared ethereal solution of vinyldiazomethane (see above) was divided into equal portions and each was added to butadiene (40 ml) in a 100-ml pressure

bottle maintained at −80°. The reaction mixture was allowed to stand at 5 °C until the wine color had faded (3–4 days). The excess butadiene and ether were removed at 0° and aspirator pressure. The residual oil was taken up in pentane (50 ml) and the solution was washed with ice water to remove any pyrazole (3 × 50 ml), dried over anhydrous sodium sulfate, and never allowed to warm above 0°. The solvent was removed at 0° (20 Torr) and the residual colorless oil was vacuum transferred (0.02 Torr) to a trap cooled to −35°; yield, 300–400 mg of 3,5-divinyl-1-pyrazoline (60% *trans*, 40% *cis*), 10% based on vinyldiazomethane; i.r. (neat) 3090, 1637, 988, 922 cm^{-1} (CH=CH_2), 1546 cm^{-1} (—N=N—); mass spectrum exact mass (25°, 70 e.V.) calcd. for $C_7H_{10}N_2$: 122.0844; found: 122.0846; u.v. (cyclohexane) 334 nm, log ε 2.56 for mixture of 60% *trans* and 40% *cis*. The n.m.r. spectra of *cis* and *trans* are described in Table 1.

Synthesis of cis- and trans-3-Ethyl-5-vinyl-1-pyrazoline (5)

A solution of 1-diazopropane (6.3 g, 90 mmol) in ether (100 ml) was prepared from *N*-nitroso-*N*-*n*-propylurea (16 g, 0.122 mmol) and purified by flask-to-flask transfer by vigorously passing a stream of nitrogen through the system (13). The ethereal diazopropane solution was added to four 100-ml pressure bottles containing butadiene (*ca.* 160 ml) at Dry Ice temperature. The mixture was then allowed to warm to room temperature and after the color had completely disappeared (approx. 1 h) the excess butadiene and ether were removed by evaporation under slightly reduced pressure. The residual oil was subjected to trap-to-trap distillation (25 °C, 0.05 Torr) to afford 7.69 g (69% based on diazopropane) of a colorless oil. The n.m.r. spectrum indicated a 1:1 mixture of *cis*- and *trans*-3-ethyl-5-vinyl-1-pyrazoline (see Table 1); mass spectrum (25°, 14 e.V.) calcd. for $C_7H_{12}N_2$: 124.1000; found: 124.1004; i.r. (neat) 3080, 1638, 985, and 920 cm^{-1} (—$CH=CH_2$), 1548 cm^{-1} (—N=N—); $u.v._{max}$ (cyclohexane) 332 nm (log ε 2.56).

A sample enriched in the *trans* isomer was prepared by subjecting a 50:50 *cis*:*trans* sample to silica gel column chromatography (Mallinkrodt 100 mesh silicic acid using a 15:85 ether:*n*-pentane as the eluent). One of the early fractions, followed by vacuum distillation, afforded a sample of **5** which had a *cis* to *trans* ratio of 18:82.

Product Proportions from the Thermolysis of cis- and trans-5

A solution of *cis*- and *trans*-**5** (20 mg; 18% *cis*, 82% *trans*, n.m.r.) in diphenylether (2 ml) was heated at 120° for 2 h. The product proportions were determined by g.c. to be 57% *cis*-1-ethyl-2-vinylcyclopropane and 43% *trans*. The *cis* isomer was identified by its thermal isomerization at 220° to 2,5-heptadiene and from its n.m.r. spectrum.

Preparation of a Sample of trans-3,5-Divinyl-1-pyrazoline (2)

A sample of essentially pure (n.m.r.) **2** was obtained by allowing a sample of **1** and **2** (40:60 mixture, 800 mg) to stand for 2 weeks at 6 °C and then 1 week at −10 °C. During this period all of the *cis* isomer and approximately half of the *trans* isomer decomposed. The remaining pyrazoline was subjected to trap-to-trap distillation under reduced pressure (2 Torr/0 °C) and after complete evaporation of the cycloheptadiene and divinylcyclopropane the sample was distilled (0.02 Torr/0°) to afford *trans*-3,5-divinyl-1-pyrazoline (<95% pure by n.m.r.; 75 mg).

Product Proportions from the Thermolysis of 1 and 2

A solution of **1** and **2** (50 mg; 39.5% *cis* and 60.5% *trans*, n.m.r.) in C_6D_6 (0.5 ml) was placed in an n.m.r. tube. The upper portion of the tube was fitted with an extension such that Dry Ice could be packed around it to prevent the removal of any volatile products. The lower part of the tube was then immersed in an oil-bath heated at 40.9° for 18 h. The n.m.r. spectrum of the resulting solution corresponded to a mixture (63:37) of 1,4-cycloheptadiene (**4**) and *trans*-1,2-divinylcyclopropane (**5**). A sample of 50 mg of pure **2** treated in the same manner gave a 60:40 mixture of **4** and **5**.

Kinetic Method

The reactions were followed by measuring manometrically the volume of nitrogen evolved. The apparatus used was essentially that described by Petersen *et al.* (14). The cell containing diphenyl ether (10 ml) was first saturated with nitrogen while immersed in the constant temperature bath. A solution of 3,5-divinyl-1-pyrazoline (*ca.* 2 mmol) in diphenyl ether (1 ml) was injected into the solvent and the measurements started immediately. Each reaction was carried to an estimated 10 half-lives before the V_∞ was recorded. Barometric corrections were made as required. The yield of nitrogen in each run was greater than 90% of that calculated on the basis of sample size.

A sample run for a mixture of 38.3% **1** and 61.7% **2**, at 34.98°, gave the following data: t in s × 10^{-4}, $(V_\infty - V_t)/V_\infty$; 0.3290, 0.7955; 0.3466, 0.7840; 0.3874, 0.7619; 0.4102, 0.7495; 0.4637, 0.7215; 0.4988, 0.7052; 0.5225, 0.6941; 0.5596, 0.6773; 0.5948, 0.6600; 0.6329, 0.6430; 0.6943, 0.6178; 0.7458, 0.5982; 0.7909, 0.5807; 0.8374; 0.5644; 0.8855, 0.5472; 0.9317, 0.5319; 0.9770, 0.5177; 1.0155, 0.5065; 1.0708, 0.4889; 1.1486, 0.4671; 1.1969, 0.4541; 1.2894, 0.4310; 1.3232, 0.4231; 1.3798, 0.4099; 1.4265, 0.3995; 1.5010, 0.3830; 1.5562, 0.3749; 1.6066, 0.3619; 1.7311, 0.3369; 1.7896, 0.3280; 1.8514, 0.3184, 1.9258, 0.3070; 1.9884, 0.2996; 2.1474, 0.2767; 2.2233, 0.2656; 2.3101, 0.2554; 2.4076, 0.2427; 2.6214, 0.2198; 2.7414, 0.2074.

Discussion

The activation enthalpies, entropies, and relative rates at 50° for the thermolysis of a series of azoalkanes and 1-pyrazolines are given in Table 4. In the azoalkane series the introduction of a double bond, such that the carbon–nitrogen bond becomes allylic, affects a rate enhancement of 10^7 for the first double bond but less than six for the second (7). This is in contrast to the pyrazoline series wherein the introduction of the first vinyl group increases the rate constant by 10^5 and the second increases the rate constant by an additional factor of 10^3! The rate constants for **1** and **2** were measured in diphenyl ether solution and while the change

TABLE 4. Activation enthalpies, entropies, and relative rates of thermolysis, at 50°, for several azo compounds[a]

	$\Delta H^{\neq}$	Log A	$\Delta S^{\neq}$	Relative rate (kcal mol^{-1})
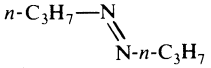	45.1±0.5(15)	14.6	+6±2	1.0
	39.7±0.3(2)	15.4	10.6±0.5	1.0
	39.6±0.3	15.7	11.0±0.5	1.0
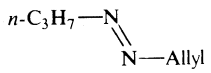	35.0±0.3(7)	14.8	+7±1	10^7
5-*cis*	30.7±0.3	14.3	+4.7±2	10^5
5-*trans*	30.7±0.2	14.3	+4.7±2	10^5
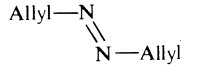	33.5±0.5(16)	14.5	+6±2	5.6×10^7
1	22.2±0.4	12.3	−4.4±2.0	5.2×10^8
2	25.1±0.2	13.9	+2.9±1.0	10^8

[a]Compounds **1**, **2**, and **5** were measured in diphenyl ether solution, all others in the gas phase.

from the gas phase to solution is not readily assessed, it is known from the work of Masters (17) that **4** undergoes thermolysis in *n*-butyl phthalate solution at 128° at one half the rate that it reacts in the gas phase. Masters found $\Delta H^{\neq}$ of 33.4 kcal mol^{-1} and $\Delta S^{\neq}$ of +8.7 e.u. in solution (17) in comparison with $\Delta H^{\neq}$ of 31.4 kcal mol^{-1} and $\Delta S^{\neq}$ of +4.7 in the gas phase (18), thus if anything the rate constants for **1** and **2** would be larger if they could be measured in the gas phase. There is a 9.0 kcal mol^{-1} decrease in $\Delta H^{\neq}$ on introducing the first vinyl group in the pyrazoline system, and an additional decrease of 8.5 kcal mol^{-1} on introducing the second vinyl group in the *cis* series, but only 5.6 in the *trans* series. There can be no doubt that for both **1** and **2** that both vinyl groups are contributing to the decrease in activation enthalpy. The possibility that steric factors are contributing is minimized by comparing **1** and **2** with **5**, and with *cis*- and *trans*-3,5-dimethyl-1-pyrazoline, rather than with **3** and **4**.

Evidence for concertedness has previously been provided in cyclic azo compounds by the observation of enhanced rates of thermolysis and high stereospecificity (19, 20). In the case of **1** and **2** the product distribution is given in Table 5 along with that implied from studies on the implied diradical, **8**, as produced during the racemization of (−)-**6** (21). The recent work of Brown *et al.* (22) makes it clear that any *cis*-1,2-divinylcyclopropane produced, under the conditions of thermolysis of **1** and **2**, will be observed as **7** but it is not necessary that all of the **7** produced has been generated via *cis*-1,2-divinylcyclopropane since the diradical **8** may close directly to **7**. It is evident from the work of Hamelin and Carrie (23) and McGreer *et al.*

TABLE 5. Product proportions for the thermolysis of **1**, **2**, (−)-**6** and *cis*- and *trans*-**5**

Reactant	Product ratio **6**:**7**
1	34:66
2	40:60
(−)-**6**	43:57[a]
cis-**5**	44:56[b]
trans-**5**	60:40[b]

[a]Obtained by extrapolation of k_1, the rate constant for the interconversion of enantiomers, and k_2, the formation of **7** from (−)-**6** (21).
[b]Ratio of *cis*-1-ethyl-2-vinylcyclopropane to *trans*-1-ethyl-2-vinylcyclopropane.

(24) that other mechanisms prevail for the thermolysis of 1-pyrazolines wherein electron withdrawing groups, such as nitrile or carbethoxy, are located on the α-carbons but support for a concerted cleavage to a diradical is found in thermolysis of *trans*-3,5-diphenyl-1-pyrazoline (25).

We suggest, on the basis of the evidence presented herein and upon the observation of secondary deuterium kinetic isotope effects from 1-pyrazoline-3,3-d_2, 1-pyrazoline-3,3,5,5-d_4 (2), and 3-vinyl-1-pyrazoline-5,5-d_2 (18), that the transition state for alkylpyrazolines is best represented as an extension of the normal mode vibration, *i.e.* the symmetric C—N stretching frequency, 880 cm^{-1}, observed by Durig and Harris (26) in the i.r. spectrum of **3**. In the case of **1** and **2** the similarity of the product mixture suggests that nitrogen does not influence the ratio of **6** and **7**. The fact that *cis*- and *trans*-**5** show the now familiar cross-over supports the suggestion of Roth and Martin (5) that even though kinetic evidence is available to suggest cleavage of the primary carbon–nitrogen bond, in systems such as **4**, that a sufficient amount of bonding remains to influence the stereochemical distribution of the products and that inversion will dominate but not overwhelm the product distribution.

The authors gratefully acknowledge the award of a Killam Postdoctoral fellowship to M.O. and the support of the National Research Council of Canada for experimental facilities. We also wish to acknowledge some preliminary experiments by Dr. Burkhardt Strehlke.

1. R. G. Bergman. *In* Free radicals. Vol. 1. *Edited by* J. Kochi. Wiley-Interscience Publishers, New York, N.Y. 1973. p. 191.
2. R. J. Crawford and A. Mishra. J. Am. Chem. Soc. **88**, 3963 (1966); B. H. Al-Sader and R. J. Crawford. Can. J. Chem. **46**, 3302 (1968).
3. S. Seltzer. J. Am. Chem. Soc. **83**, 2625 (1961); S. Seltzer and E. Hamilton, Jr. J. Am. Chem. Soc. **88**, 3775 (1966); C. G. Overberger and A. V. Digulio. J. Am. Chem. Soc. **81**, 2154 (1959).
4. W. L. Carter and R. G. Bergman. J. Am. Chem. Soc. **90**, 7344 (1968).
5. W. R. Roth and M. Martin. Ann. **702**, 1 (1967).
6. H. E. O'Neal and S. W. Benson. NSRDS-NBS Monograph No. 21, 1970. pp. 30–34; P. Condit and R. G. Bergman. Chem. Commun. 4 (1971).
7. R. J. Crawford and K. Takagi. J. Am. Chem. Soc. **94**, 7406 (1972).
8. R. A. Johnson and S. Seltzer. J. Am. Chem. Soc. **95**, 938 (1973); S. Seltzer and F. T. Dunne. J. Am. Chem. Soc. **87**, 2628 (1965); S. Seltzer and S. Mylonakis. J. Am. Chem. Soc. **89**, 6584 (1967); N. A. Porter, M. E. Landis, and L. J. Marnett. J. Am. Chem. Soc. **93**, 795 (1971).
9. D. M. Golden, N. A. Gac, and S. W. Benson. J. Am. Chem. Soc. **91**, 2136 (1969).
10. S. G. Cohen, S. J. Groszos, and D. B. Sparrow. J. Am. Chem. Soc. **72**, 2078 (1950); S. E. Scheppele and S. Seltzer. J. Am. Chem. Soc. **90**, 358 (1968); C. G. Overberger, W. H. Hale, M. B. Berenbaum, and A. Finestone. J. Am. Chem. Soc. **76**, 6185 (1954); M. Prochazka, O. Ryba, and D. Lim. Coll. Czech. Chem. Commun. **36**, 2640 (1971).
11. J. Hooz and H. Kono. Org. Prep. Proc. Int. **3**, 47 (1971).
12. J. L. Brewbaker and H. Hart. J. Am. Chem. Soc. **91**, 711 (1969).
13. J. R. Dyer, R. B. Randall Jr., and H. M. Deutsch. J. Org. Chem. **29**, 3423 (1964).
14. R. C. Petersen, J. H. Markgraf, and S. D. Ross. J. Am. Chem. Soc. **83**, 3819 (1961).
15. G. Geisler and J. Hoffmann. Zeit. Phys. Chem. **57**, 318 (1968).
16. B. H. Al-Sader and R. J. Crawford. Can. J. Chem. **48**, 2745 (1970); T. Boddington, P. Gray, and B. J. Taylor. Int. J. Chem. Kinet. In press.
17. I. M. E. Masters. Ph.D. Thesis, University of British Columbia, February 1969. p. 67.
18. R. J. Crawford and D. M. Cameron. Can. J. Chem. **45**, 691 (1967).
19. J. A. Berson, E. W. Petrillo, Jr., and P. Brickart. J. Am. Chem. Soc. **96**, 636 (1974); J. A. Berson and S. S. Olin. J. Am. Chem. Soc. **91**, 777 (1969).
20. E. L. Allred and K. J. Voorhees. J. Am. Chem. Soc. **95**, 620 (1973); E. L. Allred, J. C. Hinshaw, and A. L. Johnson. J. Am. Chem. Soc. **91**, 3382 (1969).
21. M. Arai and R. J. Crawford. Can. J. Chem. **50**, 2158 (1972).
22. J. M. Brown, B. T. Golding, and J. J. Stofko. Chem. Commun. 319 (1973).
23. J. Hamelin and R. Carrie. Bull. Soc. Chim. Fr. 2162, 2513, 2521 (1968).
24. D. E. McGreer and J. W. McKinley. Can. J. Chem. **49**, 105 (1971) and earlier papers in this series.
25. J. W. Timberlake and B. K. Bandlish. Tetrahedron Lett. 1393 (1971).
26. J. R. Durig and W. C. Harris. J. Chem. Phys. **52**, 6096 (1970).

Water-soluble Lysine-containing Polypeptides. I. The Synthesis and Characterization of Several Sequential Lysine–Glycine Polypeptides Including a Preliminary Study of their Interaction with DNA[1]

JOHN BROWN,[2] JEAN R. LANGLOIS,[3] DENIS R. LAUREN,[4] BARBARA K. STOOCHNOFF,[5] AND ROSS E. WILLIAMS[6]

Division of Biological Sciences, National Research Council of Canada, Ottawa, Canada K1A 0R6

Received May 24, 1974

JOHN BROWN, JEAN R. LANGLOIS, DENIS R. LAUREN, BARBARA K. STOOCHNOFF, and ROSS E. WILLIAMS. Can. J. Chem. **52**, 3140 (1974).

The preparation and characterization of several sequential lysine–glycine polypeptides is described. A preliminary study of their interaction with DNA is also presented.

JOHN BROWN, JEAN R. LANGLOIS, DENIS R. LAUREN, BARBARA K. STOOCHNOFF et ROSS E. WILLIAMS. Can. J. Chem. **52**, 3140 (1974).

La préparation et caractérisation de plusieurs lysine–glycine polypeptides d'une sequence régulière est décrite. De plus, une étude préliminaire sur leur association avec ADN est presentée.

Introduction

Chromosomal proteins, of which the basic amino acid containing histones constitute by far the largest class, play an important role in the determination of the morphology and metabolism of the eukaryotic cell (1, 2). The associations between these basic proteins and the cellular DNA (deoxyribonucleic acid) have been postulated to play an important role in the maintenance of the chromosomal architecture and may offer some degree of regulation during the various stages of cell development (2).

The formation and stability of these protein–DNA complexes is governed primarily by long and short range interactions. The longer range electrostatic interactions form the basis of histone–DNA association and are of prime importance in formation of histone–DNA complexes.

A firmer understanding of the various ways in which electrostatic interactions between the histones and DNA could regulate cell architecture and metabolism could be gained from experiments using models of the natural proteins. As models, synthetic polypeptides containing significant quantities of either of the basic amino acids, lysine or arginine, could be used. The homopolymers, poly-(L-lysine) and poly-(L-arginine), have been used as models in the study of DNA – basic protein (polypeptide) interactions (3, 4). A natural extension to these studies would be to use synthetic copolymers containing one or more of the common aliphatic amino acids as well as a basic amino acid. Incorporation of the amino acids in a sequential or known manner would facilitate the interpretation of experiments designed to investigate the interaction of these polypeptides with DNA. This should give some insight into the effect of chain sequence and solution conformation on the interaction of proteins with DNA.

We have synthesized several polypeptides having the amino acids lysine and glycine in a defined sequence. In this paper we wish to describe the synthesis of the monomer blocks used for the preparation of the polymers, the polymerization conditions used, and the spectroscopic characterization of the final polypeptide products. Preliminary results on the interaction of the polypeptides with DNA are also presented.

Methods and Materials

Experimental

All chemicals were of reagent grade and were used as received unless otherwise stated.

[1]NRCC No. 14077.

[2]National Research Council Postdoctoral Fellow, 1969–1971. Present address: I.C.I. Pharmaceuticals, Macclesfield, U.K.

[3]Present address: Canadian Department of Agriculture, Ste. Foy, P.Q., Canada.

[4]National Research Council Fellow, 1971–1973. Present address: Ruakura Agricultural Research Centre, Hamilton, New Zealand.

[5]Present address: Canadian Department of Consumer and Corporate Affairs, Ottawa, Canada.

[6]To whom correspondence should be directed.

Can. J. Chem. Downloaded from www.nrcresearchpress.com by 210.87.254.42 on 09/05/12
For personal use only.

TABLE 1. Molecular weights of lysine–glycine polypeptides

Polymer[a]	End-group analysis[b]	Gel filtration[c]
Poly-(L-lys)	10 250	—
Poly-(L-lys)	20 540	—
Poly-(L-lys-gly)	19 000	19 000 ± 2000
Poly-(L-lys-gly-gly)	12 500	12 000 ± 3000
Poly-(gly-L-lys-gly-gly)	7 410	7 000 ± 1000

[a]Final polypeptide product isolated as the hydrobromide salt.
[b]Measured on fully blocked polypeptide, perchloric acid procedure, ref. 9. All values given are ± 5% given value.
[c]Measured on unblocked polypeptide: Sephadex G-100, 0.002 *M* sodium phosphate, p*H* 7.0, refs. 10, 11. Distribution limits are given. Ribonuclease, chymotrypsinogen, and ovalbulmin were used as standards.

Can. J. Chem. Downloaded from www.nrcresearchpress.com by 210.87.254.42 on 09/05/12
For personal use only.

Optical rotations were measured on a Perkin-Elmer polarimeter, model 141 in a 1 dm microcell. Dilute hydrochloric acid (HCl), acetic acid (HOAc), or methanol (MeOH) were used as solvents as noted. Melting points were taken on a Fisher-Johns melting point apparatus (heated block) and are uncorrected. Combustion analyses were determined on a Perkin-Elmer C, H, and N analyzer, model 240. Amino acid analyses were done on a Beckman automatic analyzer, model 120 C. Amino acid hydrolyses were carried out at 110 °C for 16 h.

N^{ϵ}-Benzyloxycarbonyl(Cbz)-L-lysine m.p. 235–237 °C, $[\alpha]_D$ +14.1° (*c* 1.0, 0.1 *N* HCl) (lit. (5) m.p. 235 °C, $[\alpha]_D$ +14.0 (*c*, 2.6 dilute HCl)), *N*-hydroxysuccinimide (HOSu), dicyclohexylcarbodiimide (DCC), and glycylglycine were purchased from Fluka AG, Buchs, Switzerland. Triethylamine (TEA) (B.D.H. reagent grade) was used only if taken from a freshly opened bottle. For polymerizations it was purified by distillation from *p*-toluenesulfonyl chloride and stored under nitrogen atmosphere (6). Dimethylformamide (DMF) was purified by treatment with barium oxide, filtration, and distillation under reduced pressure (6). Dimethoxyethane (DME) was purified by distillation from lithium aluminum hydride (6).

N^{α}-*t*-Butyloxycarbonyl(Boc)-glycine, m.p. 85–86 °C, was prepard in 94% yield according to the procedure of Schnabel (7) from glycine and *t*-butyloxycarbonyl azide (Pierce Chemicals, Rockford, Illinois); reaction conditions: pH_{obs} 10.0, in water. N^{α}-*t*-Boc-N^{ϵ}-Cbz-L-lysine was prepared similarly (isolated in 92% yield as N^{α}-*t*-Boc-N^{ϵ}-Cbz-L-lysine·DCHA salt, m.p. 113 °C, $[\alpha]_D$ −9.3° (*c* 1.0, HOAC)); reaction conditions: pH_{obs} 10.2, in dioxane–water, 2:1, v/v, 50 g per 700 ml of solution, vigorous stirring.

Highly polymerized deoxyribonucleic acid (DNA) was obtained from Worthington Biochemicals (Freehold, N.J.). Stock solutions (approximately 1 mg/l) were prepared by suspension of the solid in cacodylate buffer, 0.01 *M*, p*H* 7.0, and dialysis overnight (4 °C) against this buffer. The solution was centrifuged before being diluted to the desired concentration. DNA-phosphate concentration was estimated from the absorbance at 260 nm (ε phosphate 6600(8)).

Polymer molecular weights were estimated on the blocked polypeptides by end-group titration (perchlorate procedure) (9) and on the unblocked polymers by thin-layer gel filtration on Sephadex G-100 (sodium phosphate, 0.002 *M*; sodium chloride, 0.05 *M*; p*H* 7.0) using ribonuclease, chymotrypsinogen, and ovalbumin. as standards (10, 11). Detection was by trinitrobenzenesulfonic acid treatment of a paper replica (12). The molecular weights are given in Table 1.

Circular dichroic spectra were taken on a Cary spectropolarimeter, model 61, in quartz cells (path length 0.1 cm). Reported ellipticities are based upon the lysine concentration (as determined by amino acid analysis). The ellipticities measured at 225 nm are given in Table 2.

Poly-(N^{ϵ}-Cbz-L-lysine) (13) of differing molecular weights was prepared by polymerizing N^{ϵ}-Cbz-L-lysine *N*-carboxyanhydride, m.p. 97–98 °C (lit. (14) m.p. 100 °C dec.) in DMF solution using diethylamine as initiator. The polymer was precipitated with acidified water (2.3 drops concentrated HCl per liter), washed with methanol–ether (2:1 v/v) to remove small molecular weight impurities, and dried under high vacuum.

Monomer Preparation

The monomers used for the preparation of the polypeptides were prepared according to the procedures outlined in Scheme 1. The physical constants and elemental analyses are given in Table 3. The general procedure for the preparation may be exemplified by the preparation of N^{α}-*t*-Boc-N^{ϵ}-Cbz-L-lysylglycylglycine·DCHA salt. N^{α}-*t*-Boc-N^{ϵ}-Cbz-L-lysine (73.9 g, 0.195 *M*) and *N*-hydroxysuccinimide (22.4 g, 0.195 *M*) were dissolved in purified dimethoxyethane (750 ml). The solution was cooled to melting ice temperature and dicyclohexylcarbodiimide (DCC) (40.6 g, 0.205 *M*) was added. After stirring overnight, during which time the temperature was allowed to rise to ambient, the solution was filtered to remove the precipitated dicyclohexylurea. The filtrate was evaporated (93 g) and was taken up in 150 ml dimethoxyethane. This solution was added directly to a stirred solution containing the following: glycylglycine (27.1 g), sodium bicarbonate (65.5 g), and water (225 ml). Reaction was allowed to proceed with stirring for 20 h at room temperature. Water (2000 ml) was added and the solution carefully acidified with saturated citric acid solution to p*H* 3. The product was extracted into ethyl acetate, the organic phase was dried over sodium sulfate, and evaporated to dryness under reduced pressure (oil, 96 g). This oily product was taken up in ether (260 ml) and purified dicyclohexylamine (38.2 g, 0.211 *M*) was added. The solution was refluxed on a steam bath for 2 h during which time the salt precipitated. The solution was then allowed

TABLE 2. Circular dichroic ellipticities

	$\varepsilon_L - \varepsilon_R$ (225 nm)[a]			
	0.14 *M* NaF		1.0 *M* NaF	
	p*H* 7	p*H* 12	p*H* 7	p*H* 12
N^{α}-Acetyl-L-lysine amide[b]	−0.32	−0.18	—	—
Poly-(L-lys)[c]	+0.47	−6.36	+0.49	−6.54
Poly-(L-lys-gly)	−0.44	−0.39	−0.36	−0.36
Poly-(L-lys-gly-gly)	−0.34	−0.24	−0.43	−0.48
Poly-(gly-L-lys-gly-gly)	−0.24	−0.24	−0.21	−0.13

[a]All values of $\Delta\varepsilon$ ($\varepsilon_L - \varepsilon_R$) are ±5%. The calculations are based upon the number of moles of lysine in solution (approximately 5–10 × 10^{-4} *M*/l) as determined by hydrolysis and amino acid analysis. Spectra were first taken at p*H* 7 in Tris–HCl buffer, 0.01 *M*, at the salt concentrations noted. The solutions were then adjusted to p*H* 12 with concentrated sodium hydroxide (1 *N*) and the spectra measured. All compounds were as their hydrobromide salts.
[b]Prepared by HBr removal of the Cbz blocking group from *N*-α-acetyl-N^{ε}-Cbz-L-lysine amide (21).
[c]Molecular weight, 10 250 (end group titration). The lower $\Delta\varepsilon$ observed for this polymer may be related to effects of the lower molecular weight upon the dichroic properties (22, 23).

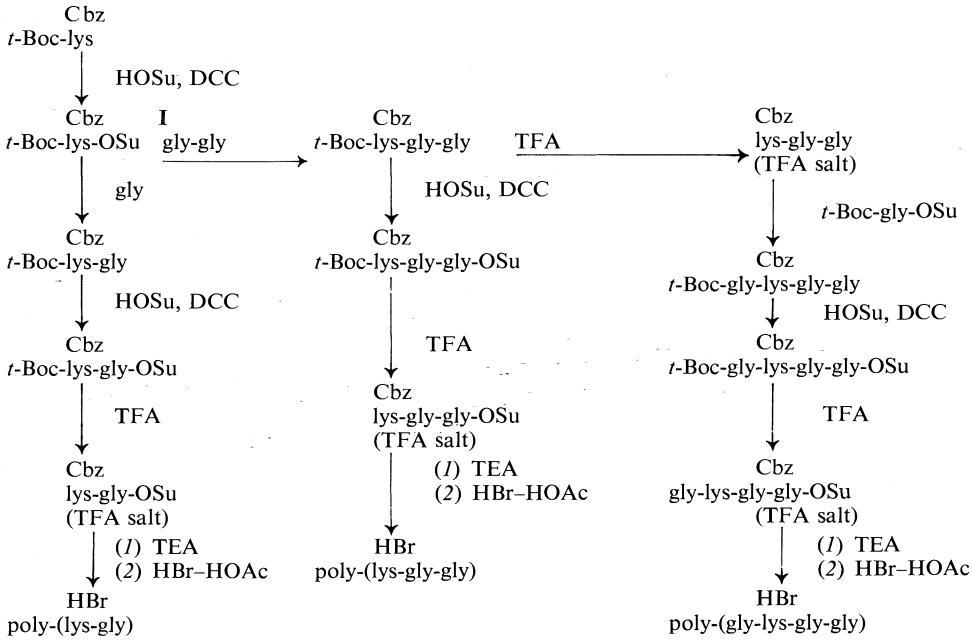

SCHEME 1

to cool overnight to room temperature. The salt was collected by filtration and crystallized from ethyl acetate (EtOAc) – petrol (30–60°) (107.5 g).

N^{α}-*t*-Boc-N^{ε}-Cbz-L-lysylglycine·DCHA salt was prepared in a similar manner from N^{α}-*t*-Boc-N^{ε}-Cbz-L-lysine succinimide ester and glycine.

N^{α}-*t*-Boc-glycyl-*N*-Cbz-L-lysylcylglycine was prepared as the free acid by coupling *t*-Boc-glycine *N*-hydroxysuccinimide ester (15) with N^{ε}-Cbz-L-lysylglycylglycine in aqueous sodium bicarbonate and working up as described above. The unblocked tripeptide used was prepared from N^{α}-*t*-Boc-N^{ε}-Cbz-L-lysylglycylglycine by deblocking with 1:1 (v/v) trifluoroacetic acid (TFA) – methylene chloride (0.5 h, room temperature) (16) and precipitating with ether.

Activation and Polymerization of the Monomer Blocks

N-Hydroxysuccinimide esters of the blocked peptides were prepared by coupling the free acid (liberated from its DCHA salt where necessary) with *N*-hydroxysuccinide using DCC. The coupling was done in ice cold dimethoxyethane–pyridine (95:5, v/v). After reaction (usually 6 h) the urea was filtered off and the solution evaporated. The oily residue was triturated several times with ether to remove excess pyridine. The washed residue was then thoroughly dried and treated with an excess of trifluoro-

Can. J. Chem. Downloaded from www.nrcresearchpress.com by 210.87.254.42 on 09/05/12
For personal use only.

Can. J. Chem. Downloaded from www.nrcresearchpress.com by 210.87.254.42 on 09/05/12
For personal use only.

acetic acid and methylene chloride (1:1, v/v) at room temperature (20 min). The TFA salt was precipitated by addition of 10–20 volumes of ether and then washed several times with ether by decantation.

The TFA-succinimide ester salt (approximately 1 g) was suspended in amine-free, purified DMF in a centrifuge tube (50 ml) to make the solution 1 *M* in monomer. A chain terminator (HCl·N^{ε}-Cbz-L-lysine methyl ester) (17) was added to give a monomer:terminator ratio of 50–100:1, depending on the molecular weight desired. Purified triethylamine (2–3 mol equiv. per mol of monomer) was added and the mixture rapidly stirred with a glass rod. No attempt was made to remove the heat of reaction. The polymerization was allowed to proceed overnight at ambient temperature. The gel or viscous solution which had formed was then diluted with purified DMF to give a monomer concentration of approximately 0.2 *M*. The polymerization was allowed to proceed for a further 2 or 3 days. The polymeric material was isolated by addition of the DMF solution to approximately 10 volumes of acidified water (1 drop concentrated HCl per liter). The resulting solid was collected by centrifugation and dried under vacuum. Small molecular weight fragments and cyclic materials were removed by washing the solid with methanol three times (15–25 ml/g). The insoluble residue was washed with ether and dried under vacuum. The blocked polymers could be generally prepared in 60–80% overall yield based upon the amount of monomer acid used to prepare the succinimide ester.

Blocking Group Removal

Benzyloxycarbonyl (Cbz) blocking groups were removed from all polymers with saturated HBr – acetic acid (18). The hydrobromide salt was isolated by precipitation with ether. The HBr – acetic treatment acid was repeated in order to ensure complete removal of all blocking groups. The ether insoluble salt was then washed with isopropanol (three times) (10 ml/g) and with ether and then thoroughly dried under high vacuum over KOH pellets. The extent of blocking group removal after two treatments with HBr – acetic acid was estimated from the residual benzyloxycarbonyl (Cbz) absorption at 254 nm (aqueous solution, approximately 2 mg/ml (ε_{254} 200 (19)). In all cases greater than 99.5% of all blocking groups were estimated to have been removed.

Precipitation Experiments

DNA precipitation experiments were performed by a method similar to that described by Leng and Felsenfeld (20). To prepare samples with equal lysine:DNA-phosphate ratios, 20 μl aliquots of a buffered stock solution of the polypeptide (cacodylate, 0.01 *M*, p*H* 7.0; polypeptide 1.0–2.5 mg per ml; lysine concentration approximately 4×10^{-4} *M*) were added sequentially to 3.0 ml of a buffered salt solution containing DNA (50 ± 5 μg per ml, phosphate concentration approximately 1.5×10^{-5} *M*). Each aliquot was added as the solution was vigorously mixed (Vortex mixer). After the final addition to obtain the desired ratio (5 × 20 μl), the solution was thoroughly mixed and allowed to equilibrate for 30 min at room temperature. At the end of the equilibrium period the solutions were again mixed. The tubes (15 ml Corex) were then centrifuged at 10 000 r.p.m. (Sorval, rotor SS-34, 12 000 g) at 4 °C for 20 min. The u.v. absorption at 260 nm (1 cm pathlength) of the top portion of the supernatant (approximately 1.5 ml) was then read to estimate the amount of DNA remaining in solution. A solution of DNA in the same buffered salt solution without added polypeptide was used as a control (100% soluble). It was thoroughly mixed to simulate conditions of addition, incubated, spun and read as above. The % DNA precipitated by each of the polymers under these standardized conditions is presented in Table 4.

Results

Synthesis of Monomers and Polypeptides

The synthetic scheme for preparation of the monomers and their polymerization is given in Scheme 1. All monomers were prepared from the common *N*-hydroxysuccinimide active ester **I** via a backing-off procedure (15) and led directly without racemization (24, 25) to the desired acid products. They were either purified and characterized directly or converted to their dicyclohexylamine (DCHA) salts for characterization (Table 1). For polymerization the acids were converted to their respective *N*-hydroxysuccinimide esters since it has been previously demonstrated that good yields of polymeric materials could be obtained using these esters (26–30). The *t*-Boc blocking group was removed and the resulting active ester trifluoroacetate (TFA) salt used for polymerization in DMF solution. During polymerization monomer concentration was kept high (approximately 1 *M*) in order to reduce the formation of cyclic and low molecular weight material and molecular weights were controlled by use of a chain terminator. The polymers were isolated by precipitation in acidified water and extracted with methanol to remove cyclic and low molecular weight material. The fully blocked polymers were generally isolated in 60–80% yield based upon the amount of free acid used to prepare the monomer active ester. Two treatments with HBr – acetic acid were then used to ensure complete removal of all the benzyloxycarbonyl blocking groups. The resulting hydrobromide salts were washed with isopropanol, rinsed with ether, and dried under high vacuum.

Polypeptide Molecular Weights

Molecular weight determinations of the polymers (Table 1) were performed on the fully blocked material by end-group titration using perchloric acid titration in acetic acid (9). After unblocking the molecular weights were again checked by gel filtration on Sephadex G-100 (10, 11). This latter determination allowed us to determine molecular weight distribution (Table 2)

Can. J. Chem. Downloaded from www.nrcresearchpress.com by 210.87.254.42 on 09/05/12
For personal use only.

TABLE 3. Physical constants and elemental analyses of lysine–glycine monomers

Compound	M.p. (°C) (crystallization solvent)	$[\alpha]_D$ (deg.)	Elemental analysis (%)					
			Calculated			Found		
			C	H	N	C	H	N
Cbz | *t*-Boc-lys-gly·DCHA	146–151 (EtOAc–petrol)	−3.39 (*c* 2.42, HOAc)	64.05	8.79	9.05	64.09	8.85	8.94
Cbz | *t*-Boc-lys-gly-gly·DCHA	128–130 (EtOAc–petrol)	−3.52 (*c* 2.21, HOAc) −2.52 (*c* 1.03, MeOH)	62.20	8.50	10.36	62.06	8.67	10.09
Cbz | *t*-Boc-gly-lys-gly-gly	73–75 (EtOAc–petrol)	−10.2 (*c* 1.00, HOAc)	54.43	6.76	12.70	54.30	6.85	12.52

TABLE 4. Amount (%) DNA precipitated by lysine–glycine polymers[a]

Polymer	Salt concentration (M)[b]				
	0.15	0.30	0.40	0.60	1.0
Poly-(L-lys)[c]	99	91	92	95	35(45[d])
Poly-(L-lys-gly)	63	32	12	0	0
Poly-(L-lys-gly-gly)	80	27	0	0	0
Poly-(gly-L-lys-gly-gly)	73	5	0	0	0

[a]Percentage precipitated was estimated at lysine – DNA phosphate ratio, 1.0 ± 0.05. All polypeptides were as their hydrobromide salts. All values are an average of three determinations. Estimated error in each value is ± 5%.
[b]Sodium chloride concentration in cacodylate buffer, 0.01 M, pH 7.0.
[c]Titrated molecular weight, 10 250.
[d]Titrated molecular weight, 20 540.

Can. J. Chem. Downloaded from www.nrcresearchpress.com by 210.87.254.42 on 09/05/12
For personal use only.

and determine if any degradation had occurred during the deblocking. As indicated the distributions were quite narrow and little degradation seemed to have occurred.

From the gel filtration results, one thing may be noted. At pH 7 all lysine–glycine polymers seemed to behave hydrodynamically very much like globular proteins, because the end-group titrated molecular weights and those determined by gel filtration analysis (when globular proteins were used as standards) were identical. This would indicate that the polypeptides were not adopting a rod shaped conformation but were completely disorganized in solution. This is in accord with following the circular dichroism results.

Circular Dichroic Spectra

Circular dichroic spectra have been used to investigate the conformation of polypeptides and proteins (31). Circular dichroic spectra of polypeptides in the various standard conformations are available (32, 33) and comparison of these with the circular dichroic spectra of the lysine–glycine polypeptides would indicate which, if any, of the standard conformations the synthetic polypeptides adopt.

Circular dichroic spectra under differing conditions of pH (7 and 12) and salt concentrations (0.14 and 1.0 M) have been taken of each of the polypeptides. The ellipticities at 225 nm, presented in Table 2, are based upon the concentration of lysine in solution. The ellipticity observed at 225 nm has been used to compare each of the polymers with poly-(L-lysine) in random and α-helical conformations (pH 7 and 12, respectively) and with N^{α}-acetyl-L-lysine amide under the same experimental conditions. The 225 nm band is sensitive to changes in environment (changes in salt concentration) and conformation (changes in pH) as is readily seen in the results obtained with poly-(L-lysine), molecular weight 10 250.

In general, as evidenced by the weak negative ellipticity at 225 nm, each one of the lysine–glycine polymers exhibited CD spectra at pH 7 (0.14 M NaF) which were apparently those of a random coil conformation. This may be contrasted with the poly-(L-lysine) spectrum which is that of an extended or disordered conformation under these conditions (34–36). When the pH of the solution was changed to 12 in order to neutralize the side-chain charges, the poly-(L-lysine) conformation shifted to that of the α-helix with the concomitant production of an intense negative band at 225 nm. With the lysine–glycine polymers, on the other hand, changing the salt concentration (0.14 to 1.0 M) or altering the charge on the side chains (pH 7 to 12) caused only slight changes in the shapes or intensity of the spectra, thus indicating that the insertion of one or more glycines into alternating positions along the lysine chain had hindered the formation of helical structure. In fact, the observed intensities of the n–π^* band at 225 nm were found to resemble those of N^{α}-actyl-L-lysine amide, again indicating that the lysine residues were behaving more or less independently and were not being influenced by their nearest neighbors. These observations on the influence of the glycine residue on helix formation are in accord with recent *ab initio* calculations made by Scheraga and co-workers (37).

In conclusion, circular dichroic spectra indicated that all lysine–glycine polymers were very flexible chains, lacking, for the most part, the rigidity observed in the polypeptide poly-(L-lysine).

Can. J. Chem. Downloaded from www.nrcresearchpress.com by 210.87.254.42 on 09/05/12
For personal use only.

DNA-Polypeptide Interactions

The ability of each of the lysine–glycine polymers to precipitate DNA from solution was determined in a manner similar to that used by Leng and Felsenfeld (20). Poly-(L-lysine) of two different molecular weights was used to allow comparison of our results (Table 4) with those previously reported. As can be seen, at a lysine: DNA-phosphate ratio of 1.0, poly-(L-lysine) was very effective in precipitating DNA from solution at salt concentrations below 1 *M*. In salt concentrations at or above 1 *M*, poly-(L-lysine) became decreasingly effective, as had previously been reported (20). At salt concentrations above 0.8 *M* the amount of DNA precipitated increased linearly with lysine – DNA-phosphate ratio. The amount precipitated also appeared to be dependent upon the molecular weight of the sample (see 1 *M* salt results).

Three things are immediately obvious when comparison is made of the abilities of the lysine-glycine polypeptides to precipitate DNA at lysine:DNA-phosphate ratios of 1.0: (*a*) all polymers are ineffective at precipitating DNA above sodium chloride concentrations of 0.40 *M*; (*b*) in 0.30 *M* salt solutions, their precipitating ability is apparently inversely proportional to either charge density or molecular weight; (*c*) the most striking difference among the polymers is seen under physiological conditions (*i.e.* p*H* 7.0, 0.15 *M* sodium chloride). Of all polymers, poly-(L-lysylglycine) precipitated the least at 0.15 *M* salt even though it has the highest molecular weight and charge density. Poly-(L-lysylglycylglycine) is almost as effective as poly-(L-lysine) under these conditions while poly-(glycyl-L-lysylglycylglycine), on the other hand, did not completely precipitate the DNA.

The differing abilities of the lysine–glycine polymers to precipitate DNA under the physiological conditions do not appear to be caused simply by changes in charge density along the peptide chain. It is unlikely to be a reflection of the initial conformational differences since the c.d. data indicates that each has roughly the same conformation. Rather, the differences seem to arise from the changing lysine–lysine spacings in the polymers.

Discussion

As can be seen from the c.d. spectra the lysine–glycine polymers exist in a random conformation. The insertion of an amino acid containing no side chain between the lysines seems to have caused a complete loss of the disordered or extended conformation of poly-(L-lysine) (34–36). These results seem to be in accord with recent *ab initio* calculations made on the conformational stabilities of polypeptides containing glycine residues (37) and support the fact that whenever one glycine residue, and most certainly whenever two are found in sequence, the surrounding polypeptide chain conformation will be broken.

The precipitation experiments show that considerable difference exists in the ability of the lysine–glycine polymers to precipitate DNA from solution, especially at physiological salt concentrations (0.15 *M*). These differences must reflect changes in primary sequence only and not changes in initial conformational states, since the c.d. spectra indicate that each has essentially the same conformation. The differences are not a reflection of changes in molecular weight since poly-(L-lysylglycine) with a molecular weight of 19 000 precipitated less DNA than poly-(L-lysylglycylglycine) with a molecular weight of 12 500. The cause of the differences must reside then in the changing lysine–lysine spacings which would lead to alterations in the degree of coincidence of lysines and DNA-phosphates in the complex.

The differences amongst the polymers can be satisfactorily explained by a modified version of a previous proposal (38). The distance between phosphate groups spacings along the sugar phosphate backbone in one strand of DNA (β-conformation) is 7.1 Å (39). In poly-(L-lysine) inter-lysine side chain distances depend upon helix geometry, but are approximately 3.5 Å in the disordered or zig-zag form (46). Thus, in poly-(L-lysine)-DNA complexes, every other lysine residue is out of phase with the phosphates, and thus is available to make not only inter-strand bonds which would cause helix disruption and lead to DNA aggregation but also bonds between two DNA helices and so crosslink the helices. This network would be more easily centrifuged from solution. In poly-(L-lysylglycine), the inter-lysine spacings are about 7 Å apart, depending again on the helix geometry. The random form, indicated by the c.d. results, could easily adopt a zig-zag form, and this would put the two side chains very nearly 7.2 Å apart (40). This distance would allow each lysine residue to be coincident with a DNA-phosphate within the same strand. The result would lead to little or no helix disruption and/or crosslinking

Can. J. Chem. Downloaded from www.nrcresearchpress.com by 210.87.254.42 on 09/05/12
For personal use only.

of the complex, and thus, a greater solubility. Similar arguments would explain the results obtained for the two other polypeptides; poly-(L-lysylglycylglycine) would have every second lysine out of phase, while each lysine in poly-(glycyl-L-lysylglycylglycine) could coincide with a DNA phosphate. The increased amount of cross-linking seen in going from poly-(L-lysylglycine) to poly-(glycyl-L-lysylglycylglycine) may be explained by a diminished cooperative factor by which one lysine is able to position the subsequent lysine for the making of the next lysine–phosphate bond.

The results we have obtained through the precipitation experiments may have relevance to the interaction of proteins, especially of lysine-rich histones, with DNA (41). Our observations on the interactions of the polypeptides with DNA indicate a similarity in behavior between the lysine-rich histone F1 and the polypeptides described here, since little or no complex formation was observed above 0.4 *M* salt. Histones F1 can be dissociated from the calf thymus chromatin complex quite readily with salt concentrations around 0.5 *M* (41). These observations might lead one to conclude that the electrostatic bonds between DNA and histone F1 are either very accessible to dissociation and the number of charged amino acid groups are spread along the chains. Examination of the primary sequence of several F1 fractions indicates that only two short blocks of basic amino acids exist in the molecule whereas the remainder of the basic groups are spread throughout the chain (42). This distribution of charges would make it more easily dissociated from complexes with DNA.

Experiments, now in progress, are aimed at examining the physicochemical nature of complexes formed between these lysine–glycine polypeptides and DNA's of various base compositions.

The authors wish to thank M. Hector Seguin for the elemental analyses and for determining the polymer molecular weights by titration. Preliminary experiments on the synthesis of monomer blocks were carried out by Mr. Eric Wiseman, NRCC summer student, 1969–1970. Large-scale syntheses of several of the intermediates were done by Mr. Eric M. Grovestine, NRCC summer student, 1971–1972.

1. L. S. HNILICA. The structure and biological functions of histones. CRC Press, Cleveland, Ohio 1972.
2. R. J. DELANGE and E. L. SMITH. Ann. Rev. Biochem. **40**, 279 (1971).
3. D. E. OLINS, A. L. OLINS, and P. H. VON HIPPEL. J. Mol. Biol. **24**, 157 (1967).
4. M. TSUBOI. *In* Conformation of biopolymers. Vol. 2. *Edited by* G. N. Ramachandran. Academic Press, N.Y. 1967. p. 689.
5. A. A. COSTOPANAGIOTIS, J. PRESTON, and B. WEINSTEIN. J. Org. Chem. **31**, 3398 (1968).
6. D. D. PERRIN, W. L. F. ARMAREGO, and D. R. PERRIN. Purification of laboratory chemicals. Pergamon Press, N.Y. 1966.
7. E. SCHNABEL. Ann. Chem. **702**, 188 (1967).
8. H. R. MAHLER, B. KLINE, and B. D. MOHROTRA. J. Mol. Biol. **9**, 801 (1964).
9. M. SELA and A. BERGER. J. Am. Chem. Soc. **77**, 1893 (1955).
10. B. RADOLA. J. Chromatogr. **38**, 61 (1968).
11. B. G. JOHANSSON. *In* New techniques in amino acids peptide and protein analysis. *Edited by* A. Niederwieser and G. Pataki. Ann Arbor Science Publishers, Ann Arbor, Mich. 1971. p. 249.
12. C. WILSON, R. F. KIBLER, and R. SHAPIRA. Anal. Biochem. **35**, 371 (1970).
13. E. KATCHALSKI. *In* Methods in enzymology. Vol. 3. *Edited by* S. P. Colowick and N. O. Kaplan. Academic Press, N.Y. 1957. p. 540.
14. J. P. GREENSTEIN and M. WINITZ. Chemistry of the amino acids. J. Wiley, N.Y. 1961. p. 865.
15. G. W. ANDERSON, J. E. ZIMMERMAN, and F. M. CALLAHAN. J. Am. Chem. Soc. **86**, 1839 (1964).
16. B. GUTTE and R. B. MERRIFIELD. J. Biol. Chem. **246**, 1922 (1971).
17. R. A. BOISSONNAS, S. GUTTMANN, R. L. HUGUENIN, P.-A. JAQUENOD, and E. SANDRIN. Helv. Chem. Acta, **41**, 1867 (1958).
18. J. P. GREENSTEIN and M. WINITZ. Chemistry of the amino acids. J. Wiley, N.Y. 1961. p. 1245.
19. M. FRIDKIN, A. PATCHORNIK, and E. KATCHALSKI. J. Am. Chem. Soc. **90**, 2953 (1968).
20. M. LENG and G. FELSENFELD. Proc. Natl. Acad. Sci. U.S. **56**, 1325 (1966).
21. K. DAIGO, W. T. BRADY, and L. J. REED. J. Am. Chem. Soc. **84**, 622 (1962).
22. J. M. VOURNAKIS, J. F. YAN, and H. A. SCHERAGA. Biopolymers, **6**, 1531 (1968).
23. I. TINOCO, R. M. WOODY, and D. F. BRADLEY. J. Chem. Phys. **38**, 1317 (1963).
24. J. E. ZIMMERMAN and G. W. ANDERSON. J. Am. Chem. Soc. **89**, 7151 (1967).
25. N. IZUMIYA, M. MURAKO, and H. AOYAGI. Bull. Chem. Soc. Jap. **44**, 3391 (1971).
26. B. B. DOYLE, W. TRAUB, G. P. LORENZI, F. R. BROWN, III, and E. R. BLOUT. J. Mol. Biol. **51**, 47 (1970).
27. G. P. LORENZI, B. B. DOYLE, and E. R. BLOUT. Biochemistry, **10**, 3046 (1971).
28. M. FRIDKIN, A. FRENKEL, and S. ARIELY. Biopolymers, **8**, 661 (1969).
29. G. RAMACHANDRAN, A. BERGER, and E. KATCHALSKI. Biopolymers, **10**, 1829 (1971).
30. V. A. SHIBNEV, T. P. CHUVAEVA, K. T. POROSHIN. Izv. Akad. Nauk. SSR Ser. Khim. 121 (1970).
31. (*a*) I. TINOCO, JR. and C. R. CANTOR. *In* Methods of biochemical analysis. *Edited by* D. Glick. Wiley-Interscience, New York. 1970. p. 81; (*b*) S. BEYCOCK. *In* Poly α-amino acids. *Edited by* G. D. Fasman. M. Dekker, New York. 1967. p. 293.
32. G. HOLZWORTH and P. DOTY. J. Am. Chem. Soc. **87**, 218 (1965).

33. G. D. FASMAN and J. POTTER. Biochem. Biophys. Res. Commun. **27**, 209 (1967).
34. D. G. DEARBORN and D. B. WETLAUFER. Biochem. Biophys. Res. Commun. **39**, 314 (1970).
35. M. L. TIFFANY and S. KRIMM. Biopolymers, **6**, 1379 (1968).
36. M. L. TIFFANY and S. KRIMM. Biopolymers, **8**, 347 (1969).
37. V. S. ANANTHANARAYNAN, R. H. ANDREATTA, D. POLAND, and H. A. SCHERAGA. Macromolecules, **4**, 417 (1971).
38. M. H. F. WILKINS. Cold Spring Harbour Symp. Quart. Biol. **21**, 75 (1956).
39. R. E. FRANKLIN and R. G. GOSLING. Nature, **171**, 740 (1953).
40. R. B. COREY and L. PAULING. Proc. Roy. Soc. Lond. Ser. B **141**, 10 (1963).
41. J. D. WATSON and F. H. C. CRICK. Nature, **171**, 964 (1953).
42. L. S. HNILICA. The structure and biological functions of histones. CRC Press, Cleveland, Ohio. 1972. p. 16ff.

Can. J. Chem. Downloaded from www.nrcresearchpress.com by 210.87.254.42 on 09/05/12
For personal use only.

Can. J. Chem. Downloaded from www.nrcresearchpress.com by 210.87.254.42 on 09/05/12
For personal use only.

Canadian Journal of Chemistry

Published by
THE NATIONAL RESEARCH COUNCIL OF CANADA

Journal canadien de chimie

Publié par
LE CONSEIL NATIONAL DE RECHERCHES DU CANADA

Volume 52 Number 18 September 15, 1974

Volume 52 numéro 18 15 septembre 1974

The Infrared and Raman Spectra of Trifluoronitrosomethane

HERBERT F. SHURVELL, SHIV C. DASS, AND ROBERT D. GORDON

Department of Chemistry, Queen's University, Kingston, Ontario K7L 3N6

Received June 26, 1972[1]

HERBERT F. SHURVELL, SHIV C. DASS, and ROBERT D. GORDON. Can. J. Chem. **52**, 3149 (1974).

The infrared spectrum of gaseous CF_3NO has been studied in the region 4000–35 cm^{-1}. The infrared spectrum of the condensed phase has also been recorded and a complete vibrational assignment is proposed. Attempts to record the Raman spectrum have been hampered by photolysis. A frequency of 50 cm^{-1} for the CF_3 torsional mode has been estimated from combination and hot bands. This corresponds to a barrier to internal rotation of approximately 425 cal/mol (150 cm^{-1}). A normal coordinate analysis has been carried out and potential energy distributions, and valence and symmetry force constants are reported.

HERBERT F. SHURVELL, SHIV C. DASS et ROBERT D. GORDON. Can. J. Chem. **52**, 3149 (1974).

On a étudié le spectre infrarouge du CF_3NO à l'état gazeux dans la région de 4000–35 cm^{-1}. On a aussi enregistré le spectre infrarouge à l'état condensé et on propose des attributions vibrationnelles pour toutes les bandes. Des essais en vue de déterminer le spectre Raman ont été faits; la photolyse du produit a empêché d'obtenir des spectres convenables. On estime que le mode torsionnel de CF_3 a une fréquence de 50 cm^{-1}; cette évaluation est dérivée des bandes de combinaisons et des bandes chaudes. Ceci correspond à une barrière à la rotation interne d'environ 425 cal/mol (150 cm^{-1}). On a effectué une analyse de coordonnée normale et l'on rapporte les distribution d'énergie potentielle et constante de force de valence et de symétrie.
[Traduit par le journal]

Introduction

The present study of CF_3NO is an extension of previous work in this laboratory on the symmetric top molecule CF_3CN (1, 2). CF_3NO belongs to point group C_s, but is very nearly an accidentally symmetric top (prolate). Splittings are expected for those CF_3 vibrations which are degenerate in CF_3CN and other C_{3v} molecules containing the CF_3 group. It was also hoped to learn something about the barrier to internal rotation. These aspects have all been studied here and previous assignments (3, 4) of the fundamentals have been revised.

Nitroso compounds are employed in the nitroso rubber field, and can be used as blowing agents to produce foamed thermoplastics and rubbers. CF_3NO and CF_3NO–C_2F_4 polymers have recently been produced at NASA (5). Thus, a spectroscopic study of CF_3NO, one of the simplest nitroso compounds, could be of some practical interest.

Infrared spectra of CF_3NO recorded under low resolution between 4000 and 400 cm^{-1} were reported several years ago (3, 4). An assignment was made in which two absorption bands were each attributed to two (accidentally degenerate) fundamentals. The estimate of the CF_3 torsional frequency was very high (200 cm^{-1}). The extended range and higher resolution of our instrument has enabled us to record many pre-

[1]Revision received May 6, 1974.

Can. J. Chem. Downloaded from www.nrcresearchpress.com by 210.87.254.42 on 09/05/12
For personal use only.

viously unobserved absorptions and to assign individual bands to 11 of the 12 fundamentals of CF_3NO. Also, from combination and hot bands and from the Raman spectrum, a more reasonable estimate of the CF_3 torsional frequency has been made.

Normal coordinate calculations using both valence and symmetry force constants have been carried out in support of the new assignment reported here.

Trifluoronitrosomethane is a deep blue gas at room temperature. The color changes through green to yellow on exposure to visible light and fluorine magnetic resonance studies (6) confirm that complex photochemical reactions occur in both the gas phase and in solution in CCl_4, $CHCl_3$, and $CFCl_3$. This has made the observation of the Raman spectrum very difficult.

Boggs *et al.* (7) have measured the dipole moment of CF_3NO and found it to be much lower (0.31 ± 0.03 D) than the value (1.5 to 1.9 D) predicted by addition of bond moments. Their attempt to study the microwave spectrum was not successful and an ionic structure $CF_3^-(N{\equiv}O)^+$ was suggested, indicating a withdrawal of electron density by the "pseudo-halogen" CF_3 group. It was hoped that the vibrational spectrum might provide some evidence for or against this structure.

The vibrational spectra of several molecules containing a CF_3 group have been published recently. Berney *et al.* studied the compounds CF_3COZ (Z = Cl, H, F) (8–10) and $CF_3C{\equiv}CH$, $CF_3C{\equiv}CD$, and $CF_3C{\equiv}CCF_3$ (11). More recently, studies on trifluoroacetate esters (12), trifluoroacetic acid (13), and methyl trifluoroacetate (14) have appeared in the literature.

Experimental

The compound CF_3NO was obtained from Penninsular Chemresearch Inc. High purity of the samples was indicated by gas chromatography and mass spectra, and no impurity could be identified in the infrared spectrum. The compound is a blue gas which slowly photolyses irreversibly on the absorption of visible light. Therefore, precautions were taken to protect the sample from room light. Gas phase infrared spectra were run on a Perkin–Elmer model 180 spectrometer. A 15 cm variable temperature gas cell (15) with CsI windows and a metal cell with polyethylene windows were used to record the spectra at various temperatures and pressures.

When sprayed onto a CsI window cooled to 77 K by liquid nitrogen, a viscous liquid film is formed. The compound does not appear to crystallize. Both a conventional glass Dewar and an Air Products and Chemicals Inc. Cryotip refrigerator were used for the condensed phase work. Spectra were recorded using Perkin–Elmer models 180 and E 14 spectrometers. The instruments were calibrated using standard reference spectra of methane, carbon dioxide, ammonia, and water vapor, and the frequencies reported in Tables 1 and 2 are believed to be accurate to within ± 1.0 cm^{-1}. The resolution varied from 0.5 to 4.0 cm^{-1}, depending on the band studied.

Raman spectra were recorded of the gas at 2 atm pressure, a solution in CCl_4 under 1–2 atm of gas in a sealed tube, the liquid at 110 K, and condensed films deposited at 4 and 77 K. Instruments used were Jarrell–Ash 25-100 and Spex 1400 monochromators with photon counting systems in the laboratory of Bernstein at the National Research Council of Canada in Ottawa and a Cary 82 spectrometer in the laboratory of James and Hall at the University of Queensland. Several lasers provided numerous exciting lines which were used at powers ranging from 30 to 200 mW. A conventional type of low temperature cell, described in ref. 2, and an Oxford Instruments CF 100 cryostat were used for the condensed film studies. A Raman spectrum of a solution in CCl_4 was also recorded by Cook of Cary Instruments using a Cary 83 spectrometer and a spectrum of the liquid at 110 °K was obtained by Sipos of Dupont of Canada, using a Spex Ramalab instrument.

Molecular Structure

An electron diffraction study (16) gave the following structural parameters. C—F = 1.321 ± 0.004 Å; C—N = 1.555 ± 0.015 Å; N—O = 1.171 ± 0.008 Å; F—C—F = $111.9 \pm 0.4°$; C—N—O = $121.0 \pm 1.6°$. The N=O group was found to be eclipsed with one of the C—F bonds so that the molecule has C_s symmetry. Figure 1 shows the resulting structure of CF_3NO relative to the principal axes of inertia. The atoms C, N, and O and one of the F atoms lie on the symmetry plane and the other fluorine atoms are above and below this plane.

Rotational constants calculated from the data above indicate an asymmetry parameter ≈ -0.99, so that the molecule is very nearly an accidentally symmetric top (prolate).

Results and Discussion

A survey spectrum of the infrared absorption of CF_3NO in the gas phase is shown in Fig. 2, from which the relative intensities of the bands can be seen. Figure 3 illustrates the shapes of the gas phase bands recorded under higher resolution and at different temperatures. The infrared spectrum of the condensed phase is shown in Fig. 4. Observed wavenumbers and assignments are listed in Tables 1 and 2.

The assignments of the fundamentals are based on group frequencies, normal coordinate

TABLE 1. Observed frequencies (cm^{-1}) in the infrared and Raman spectra of CF_3NO in the regions of the fundamentals*

Infrared				
Gas phase		Condensed phase	Raman† (various phases)	Assignment‡
1602 1597 1594 1590	vs	1593.5 vs	1596 w	$\nu_1(A')$ NO stretch
1292 1283 1276	vs	1280 vvs	1286 w	$\nu_2(A')$ CF stretch $\nu_5 + \nu_6$ (1282)
1249 1240 1233	vs	1220 vvs	1236 m	$\nu_4 + \nu_7$ (1237) $\nu_3(A')$ CF stretch $\nu_2 - \nu_{12}$(~1230)
1189 1181 1176 1173	vs	1165.5 vvs	1172 w	$\nu_4 + \nu_{11}$ (1183) $\nu_9(A'')$ CF stretch $\nu_7 + 2\nu_{11}$(1173)
817 810 798	s	809 vs	811 w	$\nu_4(A')$ CN stretch
741 731 723	s	729 vs	731 m	$\nu_5(A')$ CF_3 def.
551	s	551 vs	551 m	$\nu_6(A')$ CF_3 def.
541 533		533.5 vs	529 m	$\nu_{10}(A'')$ CF_3 def.
436 427 418	m	421.5 s	423 m	$\nu_7(A')$ skeletal bend
382 373 362	w	370 m	379 ms	$\nu_{11}(A'')$ CF_3 rock
303 296 292 287	w	296 m	300 vw	$\nu_8(A')$ CF_3 rock
—		—	~50 sh	$\nu_{12}(A'')$ torsion

*v = very, s = strong, m = medium, w = weak, sh = shoulder.
†These are the frequencies believed to be due to monomer, see text.
‡Some possible combination bands which might contribute to the complicated structure in the 1300–1100 cm^{-1} region are included.

calculations discussed below, and comparisons of the observed frequencies and band shapes with those reported for a series of similar molecules CF_3COZ (Z = Cl, H, F) studied by Berney (8–10). In all these molecules the arrangement of the atoms with respect to the principal axes shown in Fig. 1 is approximately the same as in CF_3NO so that similar band shapes might be expected. The similarity of CF_3NO to CF_3CHO (9) is particularly marked. These molecules are isoelectronic and have closely similar atomic arrangements, moments of inertia, vibrational frequencies, and band shapes.

Most of the bands contain multiple peaks, the relative intensities of which do not change with temperature. The wavenumber of the strongest feature in the region of each fundamental was taken to coincide with the frequency of the fundamental.

The bands in the infrared spectrum of the con-

Can. J. Chem. Downloaded from www.nrcresearchpress.com by 210.87.254.42 on 09/05/12
For personal use only.

TABLE 2. Observed frequencies (cm^{-1}) of overtone and combination bands in the infrared spectrum of CF_3NO

Infrared frequency*		
Gas phase	Condensed phase	Assignment†
3160 mw	3165 m	$2\nu_1$ (3188)
2770 w	2774, 2748 w	$\nu_1 + \nu_9$ (2775)
2520 w	—	$\nu_2 + \nu_3$ (2523)
2430 mw	2436 w	$3\nu_4$ (2430)
2400 mw	2397 w	$\nu_1 + \nu_4$ (2404)
2080 vw	2088 w	$\nu_2 + \nu_4$ (2095)
2020	2021 vw	$\nu_3 + \nu_4$ (2050)
1970 w	1969 w	$\nu_3 + \nu_5$ (1971)
1905 vw	1896 w	$\nu_5 + \nu_9$ (1912)
—	1716 vw	$\nu_6 + \nu_9$ (1716.5)
—	1698 vvw	$\nu_9 + \nu_{10}$ (1699)
1619 ssh	1617 s	$2\nu_4$ (1620)
1586 sh	1567, 1560.5 w	$\nu_5 + 2\nu_7$ (1585)
—	1537 w	$\nu_4 + \nu_5$ (1538)
1460 vw	1460.5 w	$2\nu_5$ (1462)
—	1358 sh	$\nu_4 + \nu_6$ (1360)
—	1340 m	$\nu_4 + \nu_{10}$ (1342.5)
1254 s	1261 sh	$\nu_5 + \nu_{10}$ (1264)
—	1152 sh	$\nu_5 + \nu_7$ (1150.5)
—	1134.5 sh	$2\nu_7 + \nu_8$ (1139)
—	1100 m	$\nu_4 + \nu_8$ (1105), $2\nu_6$ (1102), $\nu_5 + \nu_{11}$ (1099)
968 vw	966.5 vw	$\nu_6 + \nu_7$ (972)
952 vw	954 w	$\nu_7 + \nu_{10}$ (960)
—	864 vw	$\nu_4 + \nu_{12}$ (~860)
—	843.5 m	$\nu_6 + \nu_8$ (847)
—	768 vvw	$\nu_5 + \nu_{12}$ (~779)
—	662 w	$\nu_8 + \nu_{11}$ (666)
—	615 vw, 585 sh	$2\nu_8$ (592)
318 variable‡	Not observed	$\nu_{11} - \nu_{12}$ (323)

*s = strong, m = medium, v = very, w = weak, sh = shoulder.
†Wavenumbers of combinations and overtones are based on gas phase fundamentals, except where the band is only observed in the condensed phase.
‡The intensity of this band varied with temperature (see text).

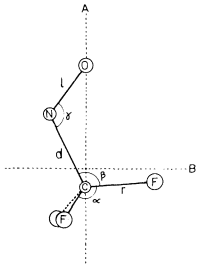

FIG. 1. The structure and principal axes of CF_3NO. One of the fluorine atoms lies on the symmetry plane. The accuracy of the calculated moments of inertia is such that the *B* and *C* axes could be interchanged.

densed phase were generally sharper than in the gas phase and the absence of rotational structure simplified the spectrum. This spectrum was particularly useful in the interpretation of the complex absorption in the 1300–1100 and 540 cm^{-1} regions. Only the CF_3 stretching fundamentals were significantly shifted in going from gas to condensed phase.

Raman Spectra

Many attempts have been made to record the Raman spectrum of CF_3NO in gas, solution, and condensed phases. Five Raman spectrometers and many exciting lines from various lasers have been used in these attempts, which have involved three independent groups of workers. Spectra have been observed, but in no case has it been possible to obtain the spectrum of the pure monomer. Almost instantaneous photolysis appears to occur where the laser beam meets the sample. This can be monitored by the appearance of a line at 1515 cm^{-1} which soon becomes very strong. A transient peak can be observed at 1596 cm^{-1} which rapidly disappears.

Table 1 includes the wavenumbers of Raman lines observed in most spectra which correspond with infrared bands assigned to fundamentals. Many other lines were observed in the Raman spectra but these are due most likely to the dimer or other photolysis products.

Normal Coordinate Calculations

The twelve fundamental vibrations of CF_3NO comprise eight A' and four A'' modes. A normal coordinate calculation was carried out in the hope of obtaining a reasonable description of the normal modes in terms of a potential energy distribution (p.e.d.), and a set of force constants.

The vibrational problem was set up in internal valence coordinates, using the Wilson **FG** matrix method (17). The internal coordinates are shown in Fig. 1 and the symmetry coordinates based on the C_s point group are given in Table 3. The **G** matrices were calculated using the structural parameters given above. Computer programs written by Schachtschneider (18) and modified by Brooks (19) were used for the calculations.

Initial values of some force constants were taken from work on related molecules (20). After making several changes to the original assignment (3), we were able to obtain a reasonable fit between our observed and calculated frequencies.

Can. J. Chem. Downloaded from www.nrcresearchpress.com by 210.87.254.42 on 09/05/12
For personal use only.

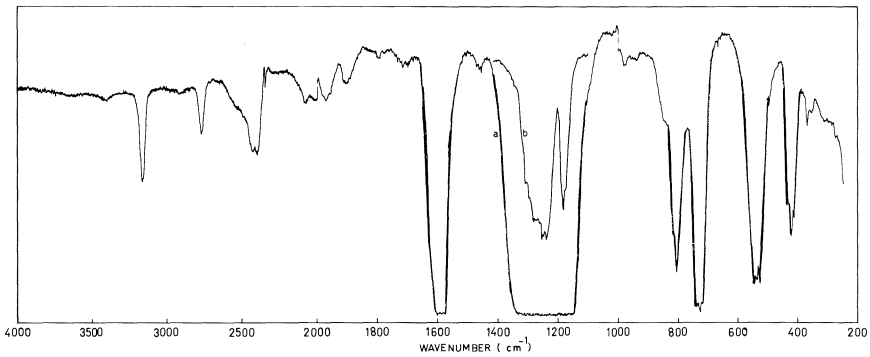

FIG. 2. A survey spectrum of CF_3NO gas (15 cm cell): (*a*) pressure = 100 Torr; (*b*) pressure = 3 Torr.

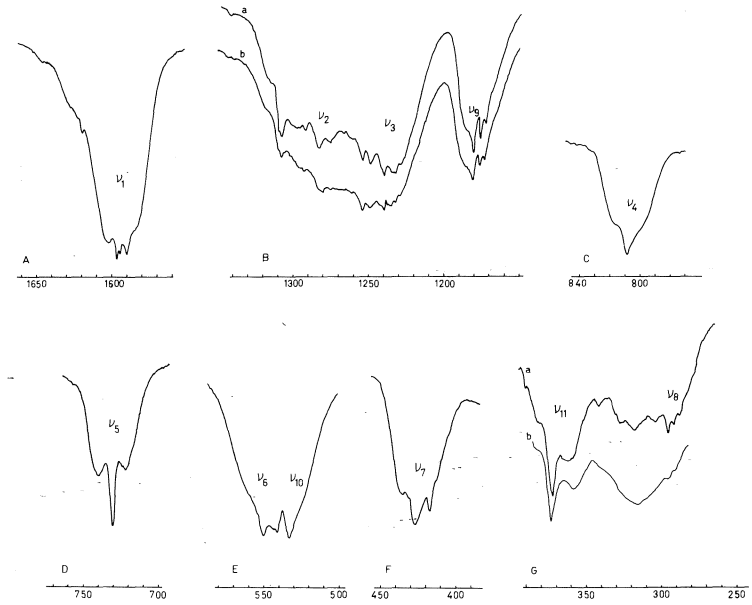

FIG. 3. Infrared band contours of CF_3NO gas (15 cm cell): (*A*) ν_1 at 35 °C and 20 Torr pressure; (*B*) The ν_2, ν_3, and ν_9 regions at 3 Torr pressure, (*a*) at −60 °C, (*b*) at +35 °C; (*C*) ν_4 at 35 °C and 100 Torr pressure; (*D*) ν_5 at 35 °C and 20 Torr pressure; (*E*) ν_6 and ν_{10} at 35 °C and 63 Torr pressure; (*F*) ν_7 at 35 °C and 100 Torr pressure; (*G*) ν_8 and ν_{11} at 500 Torr pressure using a five fold ordinate expansion, (*a*) at −70 °C, (*b*) at +90 °C.

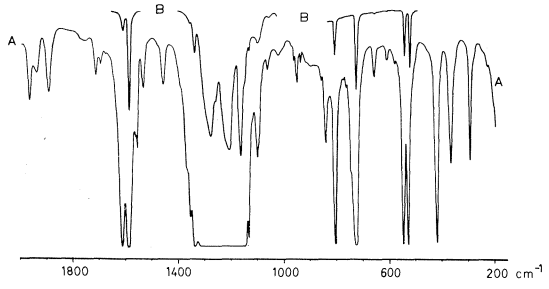

FIG. 4. The infrared spectrum of CF_3NO at 77 K: (*A*) thick film; (*B*) a very thin film.

The resulting valence force constants are listed in Table 4. A set of symmetry force constants was obtained by the method of Brunvoll and Cyvin (21). These are listed in Table 5. The frequencies calculated using the force constants of Table 5 are all within 3.5 cm^{-1} of the observed values. Table 6 summarizes the results, including the major contributions to the p.e.d.

The approximate descriptions given for the normal modes correspond to those used for similar molecules (8–10). For seven of the twelve normal modes (ν_1, ν_6, ν_8, and ν_{9-12}), it can be

Can. J. Chem. Downloaded from www.nrcresearchpress.com by 210.87.254.42 on 09/05/12
For personal use only.

TABLE 3. Symmetry coordinates of CF_3NO*

Symmetry coordinate	Description
Species A'	
$S_1 = l_{N=O}$	N=O stretch
$S_2 = 3^{-1/2}(r_1 + r_2 + r_3)$	CF_3 stretch
$S_3 = 6^{-1/2}(2r_1 - r_2 - r_3)$	FCF_2 stretch
$S_4 = d_{C-N}$	C—N stretch
$S_5 = 6^{-1/2}(\alpha_1 + \alpha_2 + \alpha_3 - \beta_1 - \beta_2 - \beta_3)$	CF_3 def.
$S_6 = 6^{-1/2}(-\alpha_1 + 2\alpha_2 - \alpha_3)$	FCF_2 def.
$S_7 = 6^{-1/2}(2\beta_1 - \beta_2 - \beta_3)$	CF_3 rock
$S_8 = \gamma_{C-N=O}$	C—N=O bend
$S_R = 6^{-1/2}(\alpha_1 + \alpha_2 + \alpha_3 + \beta_1 + \beta_2 + \beta_3)$	Redundancy
Species A''	
$S_9 = 2^{-1/2}(r_2 - r_3)$	FCF stretch
$S_{10} = 2^{-1/2}(\alpha_1 - \alpha_3)$	FCF def.
$S_{11} = 2^{-1/2}(\beta_2 - \beta_3)$	CF_3 rock
$S_{12} = \tau$ FCNO	Torsion

*The internal coordinates are shown in Fig. 1.

TABLE 4. Valence force constants (in mdyn/Å) for CF_3NO

Diagonal constant		Interaction constant	
Value	Assignment	Value	Assignment
4.900	C—F str.	1.053	CF—CF
3.626	C—N str.	0.233	CF—FCF
10.101	N=O str.	0.316	CN—CNO
1.034	FCF bend	0.015	FCF—FCF
0.504	FCN bend	−0.002	FCF—FCN
1.290	CNO bend	0.063	FCF—CNO
0.004	FCNO torsion	0.055	FCN—FCN

seen from the chief contribution to the p.e.d. that the description is quite meaningful. The other five modes (ν_{2-5}, ν_7) involve extensive mixing of the symmetry coordinates, and the descriptions, which are given in parentheses, have no precise significance.

Assignments

The strong band centered at 1594 cm^{-1} is clearly the N=O stretch, ν_1. Mixing with other vibrations is negligible. There is almost no shift of this band on going to the condensed phase.

A very strong and complex absorption system is observed in the gas phase between 1320 and 1160 cm^{-1}. In the condensed phase, only three very strong bands are observed at 1280, 1220, and 1165.5 cm^{-1}. These are assigned to the three CF stretching modes. The gas phase absorption is so complicated by hot bands and overtones and combinations that no definite assignments can be made. The peaks are sharpened a little at −60 °C (Fig. 3*B*, trace *a*) and the frequencies reported in Table 1 for the gas phase were taken from this spectrum. The most prominent peaks, located at 1283, 1240, and 1181 cm^{-1} are assigned to the fundamentals.

There is a very prominent feature at 1308 cm^{-1} in the gas phase spectrum. This band is absent in the low temperature condensed phase spectrum and is probably due to hot bands such as $\nu_1 - \nu_{11}$ (1308) or $\nu_4 + \nu_6 - \nu_{12}$ (~1310). Another strong feature at 1254 in the gas phase spectrum only appears as a shoulder on the low frequency side of the 1280 cm^{-1} band at 77 K. This is probably a combination band, whose intensity is enhanced by hot bands in the gas phase spectrum.

The order of assignment of the CF stretching frequencies has given rise to some discussion in the literature. Mason and Dunderdale (3) assigned the highest frequency CF_3 band in CF_3NO to the A'' stretching vibration ν_9, and

Can. J. Chem. Downloaded from www.nrcresearchpress.com by 210.87.254.42 on 09/05/12
For personal use only.

TABLE 5. Symmetry force constants in mdyn/Å for CF_3NO

(*a*) Species A'

	S_1	S_2	S_3	S_4	S_5	S_6	S_7	S_8
S_1	10.101	—	−0.084	—	—	0.158	—	—
S_2		7.006	—	—	0.414	—	—	—
S_3			3.847	—	—	−0.182	—	—
S_4				3.626	—	—	—	0.216
S_5					0.843	—	—	0.080
S_6						1.019	0.237	0.1359
S_7							0.592	0.011
S_8								1.290

(*b*) Species A''

	S_9	S_{10}	S_{11}	S_{12}
S_9	3.847	0.242	−0.011	−0.010
S_{10}		0.979	0.020	—
S_{11}			0.449	−0.007
S_{12}				0.004

TABLE 6. Approximate description of the normal modes and potential energy distributions of CF_3NO in terms of symmetry coordinates S_i*

(*a*) Species A'

Mode	Frequency (cm^{-1})	Assignment	Potential energy distribution							
			S_1	S_2	S_3	S_4	S_5	S_6	S_7	S_8
ν_1	1594	N═O stretch	84	—	—	—	—	—	—	—
ν_2	1283	(CF_3 stretch)	—	20	16	31	24	—	—	14
ν_3	1240	(FCF_2 stretch)	—	13	38	—	15	16	—	—
ν_4	810	(C—N stretch)	—	29	19	20	—	—	—	38
ν_5	731	(CF_3 def.)	—	38	—	—	24	—	—	14
ν_6	551	FCF_2 def.	—	—	11	—	—	71	—	—
ν_7	427	(skeletal bend)	—	—	—	34	33	—	17	—
ν_8	296	CF_3 rock	—	—	—	—	—	15	75	18

(*b*) Species A''

Mode	Frequency (cm^{-1})	Assignment	Potential energy distribution			
			S_9	S_{10}	S_{11}	S_{12}
ν_9	1181	FCF stretch	71	27	10	—
ν_{10}	533	FCF def.	21	69	—	—
ν_{11}	373	CF_3 rock	—	—	92	—
ν_{12}	(50)	torsion	—	—	—	102

*Potential energy distribution terms smaller than 10 are omitted.

bands at 1250 and 1181 cm^{-1} to the A' modes ν_2 and ν_3. Berney (8) has suggested that when a CF_3 group is attached to a hydrogen or halogen atom, the degenerate[2] stretch has the higher frequency, but when the CF_3 group is bonded to another polyatomic group, it is the non-degenerate[2] stretch whose frequency is higher. This assignment has been adopted for several other molecules containing the CF_3 group (8–14). Thus, for CF_3NO we assign the highest frequency, 1283 cm^{-1}, as the CF_3 symmetric stretch, ν_2, while the 1240 and 1181 cm^{-1} bands

[2]These are the mode(s) which would be degenerate or non-degenerate in a C_{3v} molecule containing a CF_3 group.

Can. J. Chem. Downloaded from www.nrcresearchpress.com by 210.87.254.42 on 09/05/12
For personal use only.

Can. J. Chem. Downloaded from www.nrcresearchpress.com by 210.87.254.42 on 09/05/12
For personal use only.

are attributed to $\nu_3(A')$ and $\nu_9(A'')$ respectively (these correspond to the degenerate stretching modes of a free CF_3 group).

The band at 810 cm^{-1} is assigned as the C—N stretch, ν_4. Its PQR band contour resembles that of the C—C stretching band contours in the CF_3COZ series (8–10).

A PQR structure was observed for the band at 731 cm^{-1} and this can be assigned to ν_5, the symmetric deformation of the CF_3 group. The contour and location is in agreement with that found for similar molecules.

Mason and Dunderdale (3) assigned a single band at 542 cm^{-1} to both CF_3 deformation modes, $\nu_6(A')$ and $\nu_{10}(A'')$. They were assumed to be accidentally degenerate at this frequency. Under our higher resolution this band shows three peaks (Fig. 3*E*). The two peaks at 551 and 533 cm^{-1} are assigned (arbitrarily) to ν_6 and ν_{10} respectively. A very strong sharp doublet was observed at 551 and 533.5 cm^{-1} in the solid state spectrum (Fig. 4).

The 427 cm^{-1} band is assigned as the skeletal bending mode ν_7. The corresponding solid state frequency is 421.5 cm^{-1}. Two previously unobserved fundamentals were found below 400 cm^{-1}. The band at 373 cm^{-1}, which has a PQR contour, is assigned to ν_{11}, the CF_3 rocking mode of A'' symmetry. A less well resolved feature at 296 cm^{-1} is assigned to the A' CF_3 rocking mode ν_8. Corresponding sharp bands of medium intensity were observed in the solid at 370 and 296 cm^{-1} respectively. The order of these frequencies is the same as in CF_3COH (9) and the p.e.d. is in agreement with the assignment.

A broad absorption was observed in the gas phase spectrum centered at 318 cm^{-1}. This band is almost as strong as the 296 cm^{-1} fundamental at room temperature, but is absent from the spectrum of the solid at 77 °K. The region between 400 to 250 cm^{-1} was studied at various temperatures, ranging from −70 to +80 °C (see Fig. 3*G*). The band near 318 cm^{-1} becomes stronger at higher temperatures. This, together with its absence from the spectrum of the solid, indicates that it is a hot band. The lower level of the transition giving rise to this band is most probably the CF_3 torsion. If we assume that the torsional frequency is approximately 50 cm^{-1}, then the band at 318 can be assigned as $\nu_{11} - \nu_{12}$ (373 − 50 = 323 cm^{-1}).

The far infrared region was scanned to 35 cm^{-1} on a Perkin–Elmer model 180 spectrometer in the laboratory of Jones at the National Research Council of Canada, Ottawa, in an attempt to observe the torsional mode directly. However, no real evidence of any absorption was found with up to 500 Torr pressure of CF_3NO gas in a 10 cm cell.

The Barrier to Internal Rotation

An estimate of 50 cm^{-1} has been made for the torsional mode (ν_{12}) from the hot band at 318 cm^{-1}, from a shoulder on the exciting line in the Raman spectrum of a liquid film, and from several combination bands in the infrared spectrum.

A torsional frequency of 50 cm^{-1} corresponds to a barrier to internal rotation of the order of 150 cm^{-1} (425 cal mol^{-1}), as calculated by the method given in refs. 22, 24, and 25. This torsional frequency must be considered tentative pending confirmation by a thorough investigation of the far infrared region.

The interactions leading to internal rotation barriers are not well understood, but similar molecules are often found to have barriers of the same order of magnitude. Barrier heights in some closely related molecules are listed below.

Molecule	Barrier V_3 (cm^{-1})	Reference
CH_3CHO	408	22
CH_3NO	398	23
CF_3CHO	190	9
CF_3NO	150 (approx.)	This work

It has already been pointed out that CF_3NO and CF_3CHO are very similar in many ways, and they might also be expected to have similar barriers to internal rotation. In going from CH_3CHO to CH_3NO the barrier decreases slightly. If the same is true for the pair CF_3CHO and CF_3NO, then CF_3NO should have a barrier somewhat less than 190 cm^{-1}, in agreement with our findings.

Conclusions

The gas phase infrared spectrum of CF_3NO has been reinvestigated under higher resolution over an extended range and all 12 fundamentals of the molecule have been located. A completely revised assignment based on C_s symmetry has been made. This assignment is supported by a

normal coordinate analysis, infrared spectra of the solid at 77 °K, and Raman spectra.

The barrier to internal rotation has been calculated as 425 cal/mol (150 cm^{-1}), which fits well into a pattern established for related molecules. The valence force field calculated for CF_3NO includes a low value for the C—N stretching constant. This may be an indication of a contribution from an ionic structure such as $CF_3^-NO^+$, as suggested by Boggs *et al.* (7). The frequency of the NO stretching vibration lies midway between that observed in the negative ions NO_2^- and NO_3^- on the one hand and the neutral molecules NO and XNO (where X is a halogen atom) on the other.

Studies of the dimer and other photochemical products of CF_3NO are in progress using infrared and fluorine n.m.r. techniques (6). An attempt to obtain a microwave spectrum is being made (26), and the visible absorption spectrum is being reinvestigated by the present authors.

The authors gratefully acknowledge the financial support of the National Research Council of Canada. We are grateful to S. J. Daunt for helpful discussions and to P. Sipos of Dupont of Canada and R. Cook of Cary Instruments for some Raman spectra. We are also grateful to Dr. H. J. Bernstein and N.R.C.C. Ottawa and Drs. D. W. James and J. R. Hall of the University of Queensland, for the use of their Raman instruments.

1. J. A. Faniran and H. F. Shurvell. Spectrochim. Acta, **26**A, 1459 (1970); **27**A, 1945 (1971).
2. H. F. Shurvell and J. A. Faniran. J. Mol. Spectrosc. **33**, 436 (1970).
3. J. Mason and J. Dunderdale. J. Chem. Soc. 754 (1956).
4. J. Jander and R. N. Haszeldine. J. Chem. Soc. 912 (1954).
5. J. Green. NASA Accession No. 65-33416, Rept. No. AD461044, 1964. 26 pp.
6. B. K. Hunter. Private communication.
7. J. E. Boggs, D. Coffey, Jr., and J. C. Davis, Jr. J. Phys. Chem. **68**, 2383 (1964).
8. C. V. Berney. Spectrochim. Acta, **20**, 1437 (1964).
9. C. V. Berney. Spectrochim. Acta, **25**A, 793 (1969).
10. C. V. Berney. Spectrochim. Acta, **27**A, 663 (1971).
11. C. V. Berney, L. R. Cousins, and F. A. Miller. Spectrochim. Acta, **19**, 2019 (1963).
12. G. A. Crowder. J. Fluorine Chem. **1**, 219 (1971/72).
13. R. L. Redington and K. C. Lin. Spectrochim. Acta, **27**A, 2445 (1971).
14. G. A. Crowder and D. Jackson. Spectrochim. Acta, **27**A, 1873 (1971).
15. H. F. Shurvell and J. A. Faniran. Can. Spectrosc. **13**, 109 (1968).
16. M. I. Davis, J. E. Boggs, and D. Coffey, Jr. J. Phys. Chem. **69**, 3727 (1965).
17. E. B. Wilson, Jr., J. C. Decius, and P. C. Cross. Molecular vibrations. McGraw-Hill, New York. 1955.
18. J. H. Schachtschneider. Tech. Rept. No. 57-65, Shell Development Co. 1965.
19. W. V. F. Brooks. Private communication.
20. A. Castelli, A. Palm, and C. Alexander, Jr. J. Chem. Phys. **44**, 1577 (1966).
21. J. Brunvoll and S. J. Cyvin. J. Mol. Struct. **6**, 289 (1970).
22. D. R. Herschbach. J. Chem. Phys. **31**, 91 (1959).
23. D. Coffey, Jr., C. O. Britt, and J. E. Boggs. J. Chem. Phys. **49**, 591 (1968).
24. D. Steele. The theory of vibrational spectroscopy. W. B. Saunders Company, Philadelphia. 1971.
25. K. D. Möller and W. G. Rothschild. Far infrared spectroscopy. Wiley–Interscience, New York. 1971.
26. D. H. Whiffen. Private communication.

Can. J. Chem. Downloaded from www.nrcresearchpress.com by 210.87.254.42 on 09/05/12
For personal use only.

Kinetics of the Thermal Decomposition of β-Trifluoroethylsilanes and Hot Molecule Kinetics of ($CF_3CH_2SiF_3$)*[1]

T. N. BELL, R. BERKLEY, A. E. PLATT, AND A. G. SHERWOOD

Department of Chemistry, Simon Fraser University, Burnaby 2, British Columbia V5A 1S6

Received March 19, 1974

T. N. BELL, R. BERKLEY, A. E. PLATT, and A. G. SHERWOOD. Can. J. Chem. **52**, 3158 (1974).

The thermal decomposition of β-trifluoroethylsilanes ($CF_3CH_2SiF_x(CH_3)_{3-x}$ where $x = 0$–3) is described by the reaction

$$CF_3CH_2SiF_x(CH_3)_{3-x} \rightarrow CF_2CH_2 + FSiF_x(CH_3)_{3-x}$$

The Arrhenius parameters for the series of silanes studied are as follows:

$CF_3CH_2Si(CH_3)_3$	$\log A = 12.38$	$E = 47.24$ kcal mol^{-1}
$CF_3CH_2SiF(CH_3)_2$	$\log A = 12.59$	$E = 41.35$ kcal mol^{-1}
$CF_3CH_2SiF_2CH_3$	$\log A = 12.59$	$E = 39.57$ kcal mol^{-1}
$CF_3CH_2SiF_3$	$\log A = 11.7$	$E = 37.27$ kcal mol^{-1}
preferred value	$\log A = 12.5$	$E = 37.01$ kcal mol^{-1}

Some results for the decomposition of the hot molecule $CF_3CH_2SiF_3$* are reported.

$$CF_3CH_2SiF_3^* \rightarrow SiF_4 + CF_2CH_2$$

T. N. BELL, R. BERKLEY, A. E. PLATT et A. G. SHERWOOD. Can. J. Chem. **52**, 3158 (1974).

La décomposition thermique de β-trifluoroéthylsilane ($CF_3CH_2SiF_x(CH_3)_{3-x}$ ou $x = 0$–3) est décrite par l'équation

$$CF_3CH_2SiF_x(CH_3)_{3-x} \rightarrow CF_2CH_2 + FSiF_x(CH_3)_{3-x}$$

Les paramètres d'Arrhénius pour la série de silanes étudies sont les suivants

$CF_3CH_2Si(CH_3)_3$	$\log A = 12.38$	$E = 47.24$ kcal mol^{-1}
$CF_3CH_2SiF(CH_3)_2$	$\log A = 12.59$	$E = 41.35$ kcal mol^{-1}
$CF_3CH_2SiF_2CH_3$	$\log A = 12.59$	$E = 39.57$ kcal mol^{-1}
$CF_3CH_2SiF_3$	$\log A = 11.7$	$E = 37.27$ kcal mol^{-1}
la valeur préférée	$\log A = 12.5$	$E = 37.01$ kcal mol^{-1}

On rapporte aussi quelques résultats pour la décomposition de la molécule "chaude" $CF_3CH_2SiF_3$*

$$CF_3CH_2SiF_3^* \rightarrow SiF_4 + CF_2CH_2$$

[Traduit par le journal]

Introduction

In recent work involving hydrogen abstraction from alkyl silanes and Group IV organometallics (1–3), we obtained β-fluoro compounds $CF_3CH_2MX_3$ through radical combination.

$$CF_3 + CH_2Si\langle \rightarrow CF_3CH_2Si\langle$$

As initially formed, these molecules are vibrationally "hot" due to the energy released in the formation of the new C—C bond.

The hot molecule may undergo a β-fluoro rearrangement elimination reaction

$$CF_3CH_2MX_3^* \rightarrow CF_2{=}CH_2 + FMX_3$$

or be stabilized by collision (1–3). In order to treat the kinetic data for the hot molecule by unimolecular theory, knowledge of the Arrhenius parameters for the corresponding thermal decomposition is required. The present work was designed to measure these parameters for the series of compounds $CF_3CH_2SiF_xMe_{3-x}$ where x varies from 0 to 3. In addition some results were obtained for the decomposition of the hot molecule $CF_3CH_2SiF_3$*.

Experimental

Materials

Hexafluoroacetone (Allied Chemical), tetramethylsilane (Alfa Inorganics NMR Grade), trimethylfluorosilane, dimethyldifluorosilane, and methyltrifluorosilane (Peninsular), were degassed and purified by low temperature distillation. 1,1-Difluoroethylene and silicon tetrafluoride (Matheson), which were used for calibration, were purified by preparative gas chromatography.

[1]*denotes hot molecule.

Can. J. Chem. Downloaded from www.nrcresearchpress.com by 210.87.254.6 on 09/05/12
For personal use only.

Can. J. Chem. Downloaded from www.nrcresearchpress.com by 210.87.254.6 on 09/05/12
For personal use only.

The β-trifluoroethylsilanes required for the present study were prepared through the radical combination reaction

$$CF_3 + CH_2SiF_xMe_{3-x} \rightarrow CF_3CH_2SiF_xMe_{3-x}$$

which occurs during the photolysis of hexafluoroacetone in the presence of the appropriate silane. Isolation and purification was through preparative gas chromatography.

2,2,2-Trifluoroethyltrifluorosilane ($CF_3CH_2SiF_3$) was difficult to isolate in quantity in the above way, and most of the pyrolysis experiments were carried out on this compound unisolated from the starting materials (hexafluoroacetone + methyltrifluorosilane) (3).

Apparatus

Pyrolyses were carried out in a Pyrex cell of 117 ml volume having a small cold finger as an appendage. Before first use, the cell walls were conditioned by overnight photolysis of a HFA–silane mixture at about 200 °C. The cell was heated by a tubular aluminium block furnace, and was connected to a vacuum line through a series of distillation traps. The furnace temperature was regulated to ±0.5° by a Sirect MK 2 Proportional Temperature Controller, and the temperature was measured with a copper–constantan thermocouple.

Procedure

Pyrolyses were carried out by freezing a known quantity of the β-trifluoroethylsilane compound into the cold finger of the cell, closing off the cell from the vacuum line, and abruptly warming the cold finger with hot water. Pressures in all pyrolyses were between 10 and 50 Torr. At various pyrolysis times the reaction was quenched by freezing, and the CF_2CH_2 formed was separated by fractionation, following which, the remaining reactant was returned to the cell for another period of pyrolysis. Thus the formation of CF_2CH_2 was monitored as a function of time. Reaction times were sufficiently long that the interruptive procedure led to negligible error in the time parameter. The total CF_2CH_2 formed after complete pyrolysis of a given sample of starting material correlated 1:1 with the amount of starting material. Hence the CF_2CH_2 formed at time t_∞ (see below) was used as a measure of the initial amount of silane. The terminal pyrolyses, corresponding to a time of t_∞ were achieved by raising the cell temperature to approximately 300°, and maintaining the reaction mixture at that temperature until no more CF_2CH_2 was formed. Blank experiments showed that the products of reaction, $FSiF_x(CH_3)_{3-x}$ and CF_2CH_2, were stable under the pyrolysis conditions used. The CF_2CH_2 formed was measured by a gas burette and gas chromatography (2 ft × 1/4 in. alumina column).

For the *in situ* pyrolysis of $CF_3CH_2SiF_3$, the amount of $CF_3CH_2SiF_3$ was determined solely from the total amount of CF_2CH_2 produced at t_∞ (3).

Results

Pyrolysis of β-Fluorosilanes

The photolysis of hexafluoroacetone leads to the formation of CF_3 radicals, which results in the following reactions which are relevant to the present work.

[1] $CF_3 + CH_3SiF_x(CH_3)_{3-x} \rightarrow CF_3H + CH_2SiF_x(CH_3)_{3-x}$

[2] $CF_3 + CH_2SiF_x(CH_3)_{3-x} \rightarrow (CF_3CH_2SiF_x(CH_3)_{3-x})^*$

[3] $(CF_3CH_2SiF_x(CH_3)_{3-x})^* + M \rightarrow CF_3CH_2SiF_x(CH_3)_{3-x} + M$

The β-fluoro compounds produced in reaction 3 were purified as described above, and used in the present work.

Stoichiometry

The pyrolysis of β-fluorosilanes has been shown (4) to proceed cleanly via the β-fluoro transfer reaction 4, with a 1:1 ratio of products, and a stoichiometry corresponding to 1 mol of each product from 1 mol of reactant.

[4] $CF_3CH_2Si\langle \rightarrow CF_2CH_2 + FSi\langle$

The remarkable cleanness of this reaction has been confirmed in the present work.

Rate Equation

Haszeldine and co-workers (4, 5) demonstrated the first order dependence of the pyrolysis reaction in the case of several 2:2 difluoroethylsilanes. Bell and Zucker (3) showed the decomposition of $CF_3CH_2SiF_3$ fitted a first order kinetic analysis for an *in situ* pyrolysis.

In the present work, we have clearly demonstrated the pyrolysis is first order with respect to the β-trifluoroethylsilanes for, (*a*) the *in situ* pyrolysis ($CF_3CH_2SiF_3$), and (*b*) the pyrolysis of the pure samples of the other β-fluoro silanes, (pressures used >10 Torr). First order plots corresponding to log $(a_0/a_0 - x)$ *vs.* time, are shown in Figs. 1 and 2.

Thus the rate of reaction of [4] is adequately described by

$$-\mathrm{d(Silane)}/\mathrm{d}t = k[\mathrm{Silane}]^1$$

Rate Data

Rate constants were derived for each of the pyrolyses at various temperatures by applying the integrated first order rate equation, log $(a_0/a_0 - x) = kt$ to the experimental data.

The results from the pyrolyses of the isolated compounds are given in Table 1, and Arrhenius plots shown in Fig. 3.

Because of the difficulty in purifying CF_3CH_2-

Can. J. Chem. Downloaded from www.nrcresearchpress.com by 210.87.254.6 on 09/05/12
For personal use only.

TABLE 1. Pyrolysis of isolated β-trifluoroethylsilanes*

$CF_3CH_2Si(CH_3)_3$				$CF_3CH_2SiF(CH_3)_2$				$CF_3CH_2SiF_2CH_3$				$CF_3CH_2SiF_3$			
Temp. (°C)	Time (min)	$[CF_2CH_2]$ (μmol)	$k \times 10^6$ (s^{-1})	Temp. (°C)	Time (min)	$[CF_2CH_2]$ (μmol)	$k \times 10^6$ (s^{-1})	Temp. (°C)	Time (min)	$[CF_2CH_2]$ (μmol)	$k \times 10^6$ (s^{-1})	Temp. (°C)	Time (min)	$[CF_2CH_2]$ (μmol)	$k \times 10^6$ (s^{-1})
301	60	1.12	2.449	250	120	15.32	20.17	220	270	14.60	11.32	219	45	26.40	109.2
301	1150	13.04		250	120	13.15		210	205	4.26	4.922	219	30	13.86	
301	1600	14.03		250	120	11.66		198	565	3.86	1.716	219	27	10.12	
301	1080	7.71		250	120	10.08		189	1520	4.34	0.7645	219	25	7.81	
301	1130	6.79		250	120	8.63		179	2745	2.82	0.2916	219	25	6.60	
395	∞	39.03		250	121	7.55		169	6015	2.13	0.1050	219	25	5.85	
	Total	81.72		327	∞	47.74		335	∞	55.14		301	∞	32.46	
					Total	114.13			Total	87.15			Total	103.10	
311	60	1.62	5.122												
311	1035	21.17		260	70	17.77	43.14	230	85	12.56	25.77	200	95	12.10	25.29
321	70	2.30	10.19	270	55	22.33	87.00	230	140	17.47		200	105	10.45	
321	505	14.50		280	30	18.42	178.2	230	70	7.43		200	90	7.48	
331	60	2.87	20.83	290	30	22.87	352.1	230	95	9.03		300	∞	54.21	
331	295	11.45		320	∞	25.86		230	140	11.04			Total	84.24	
395	∞	25.66			Total	107.25		230	295	16.62					
	Total	79.57						304	∞	28.77					
									Total	102.92					
341	60	7.92	39.26	240	69	5.19	10.06								
341	120	12.75		230	190	6.00	4.422								
351	60	8.88	71.52	221	360	4.90	1.998	240	60	17.94	54.22				
395	∞	30.28		208	1225	5.69	0.5990	250	46	22.83	116.1				
	Total	59.83		200	3965	7.66	0.3169	260	30	20.83	234.9				
				190	4221	2.92	0.1198	270	20	16.62	453.8				
				335	∞	94.88		300	∞	22.97					
291	1300	7.82	1.074		Total	127.24			Total	101.19					
281	1375	3.92	0.5429												
271	2450	3.05	0.2472												
261	4180	2.27	0.1113												
251	5520	1.52	0.05773												
395	∞	78.81													
	Total	97.39													

*Times are those between analyses and amounts of CF_2CH_2 are those corresponding to each individual analysis.

Can. J. Chem. Downloaded from www.nrcresearchpress.com by 210.87.254.6 on 09/05/12
For personal use only.

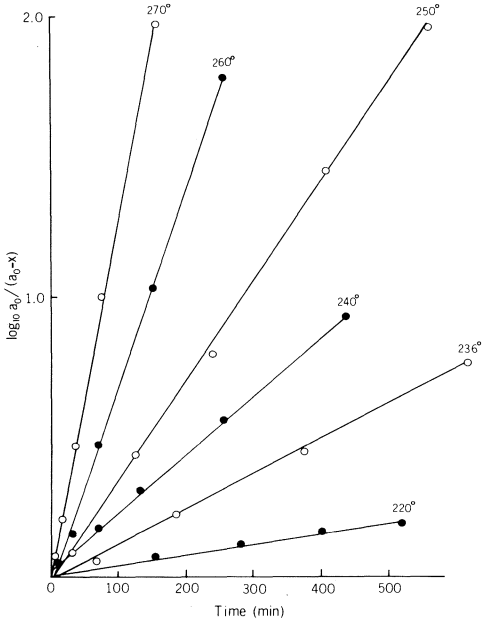

FIG. 1. First order dependence of log $a_0/(a_0 - x)$ *vs.* time for the pyrolysis of $CF_3CH_2SiF_3$ (*in situ*).

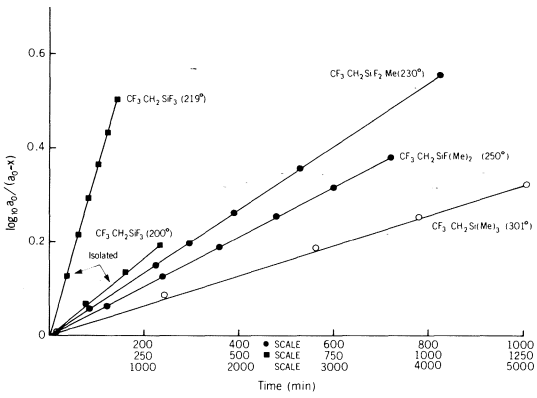

FIG. 2. First order dependence of log $a_0/(a_0 - x)$ *vs.* time for the pyrolysis of isolated β-trifluoroethylsilanes. ●, 1000 min scale; ■, 1250 min scale; ○, 5000 min scale.

SiF_3 only two pyrolyses were made on the purified compound (results in Table 1). The *in situ* pyrolysis results are given in Table 2.

Least squares treatment of the data plotted in Fig. 2, yielded the rate constants which are graphed in Arrhenius form in Fig. 3. It is to be noted that the results by the *in situ* and isolated methods do differ, and this is commented on below.

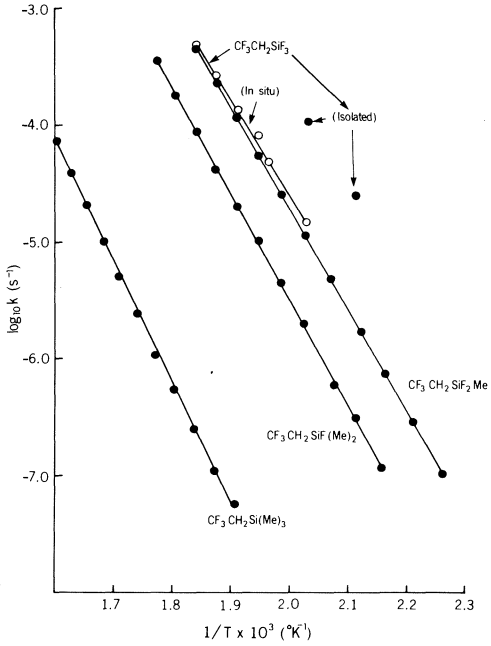

FIG. 3. Arrhenius plots of $\log_{10} k$ *vs.* $1/T$ for the pyrolysis of β-trifluoroethylsilanes.

The Arrhenius parameters derived from the above data are collected in Table 3.

Hot Molecules

When initially formed (reaction 2) the molecule $CF_3CH_2Si\langle$ is hot, several studies (1–3), have shown that this hot molecule gives rise to CF_2CH_2 through a molecular elimination, reaction 5.

$$[5] \qquad (CF_3CH_2Si\langle)^* \rightarrow CF_2CH_2 + FSi\langle$$

The rate of the hot molecule decomposition is considerably faster than the normal pyrolysis process, and occurs during the photolysis of hexafluoroacetone with the parent silane. Thus, by measuring the CF_2CH_2 formed during the period of photolysis, and subsequently measuring the total CF_2CH_2 produced from the complete *in situ* pyrolysis of the stabilized trifluoroethylsilane, a measure of the stabilization/decomposition ratios may be determined.

The *in situ* pyrolysis of $CF_3CH_2SiF_3$ was treated this way, by measuring both the CF_2CH_2 formed during the photolysis of HFA + CH_3SiF_3, and the total CF_2CH_2 formed at t_∞ (corresponding to the amount of β-fluorosilane stabilized).

Can. J. Chem. Downloaded from www.nrcresearchpress.com by 210.87.254.6 on 09/05/12
For personal use only.

TABLE 2. Pyrolysis of 1,1,1-trifluoroethyltrifluorosilane ($CF_3CH_2SiF_3$) *in situ*

Temperature (°C)	Time (min)	$[CF_2CH_2]$ (mol × 10^9)	$k \times 10^6$ (s^{-1})
220	155	7.82	14.63
	125	3.67	
	120	3.99	
	120	2.50	
	∞	30.94	
	Total	48.92	
236	65	4.38	47.88
	120	9.93	
	190	8.60	
	240	6.46	
	∞	6.17	
	Total	35.54	
240	70	6.79	81.16
	60	3.57	
	125	4.48	
	180	3.21	
	∞	2.40	
	Total	20.45	
250	32	4.22	135.8
	93.5	10.88	
	113	4.90	
	170	2.95	
	152	0.58	
	∞	0.26	
	Total	23.79	
260	10	2.73	267.4
	20	5.29	
	40	9.61	
	83	6.46	
	105	2.01	
	∞	0.44	
	Total	26.54	
270	5	3.41	488.3
	10	4.27	
	20	6.01	
	40	5.23	
	80	1.92	
	∞	0.23	
	Total	21.54	

TABLE 3. Arrhenius parameters for the pyrolysis of β-trifluoroethylsilanes

Compound	log A	E (kcal/mol)
$CF_3CH_2SiMe_3$	12.38 ± 0.16	47.24 ± 0.42
$CF_3CH_2SiFMe_2$	12.59 ± 0.07	41.35 ± 0.16
$CF_3CH_2SiF_2Me$	12.59 ± 0.03	39.57 ± 0.06
$CF_3CH_2SiF_3$ (isolated pyrolysis)	12.5 (assumed)	37.01 (calcd.)
$CF_3CH_2SiF_3$ (*in situ* pyrolysis)	11.70 ± 0.53	37.27 ± 1.26

$$[6] \quad (CF_3CH_2SiF_3)^* \xrightarrow{M} CF_3CH_2SiF_3$$

$$[7] \quad (CF_3CH_2SiF_3)^* \rightarrow CF_2CH_2 + SiF_4$$

$$\frac{R_{stab}}{R_{decomp}} = \frac{k_6[M]}{k_7}$$

The results are given in Table 4.

As expected the ratio R_{stab}/R_{decomp} decreases with temperature, and the pressure dependence of this ratio has been well demonstrated in this and similar systems (2, 3). Because of the higher activation energies associated with the thermal

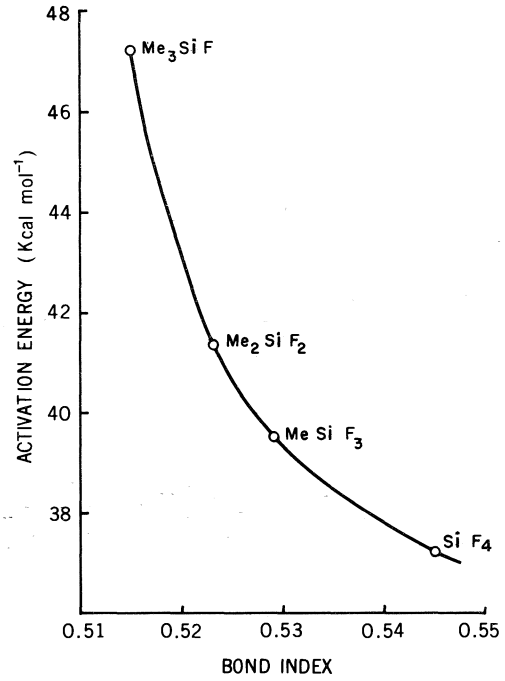

FIG. 4. Plot of activation energy for decomposition *vs.* Si—F bond index of bonds being formed.

TABLE 4. Stabilization/decomposition ratios for the hot molecule $CF_3CH_2SiF_3$*[a]

Temperature (°C)	$[CF_2CH_2]$ (mol × 10^9) From pyrolysis	From photolysis	R_{stab}/R_{decomp}
220	48.92	117.7	0.416
236	35.54	103.1	0.345
240	20.45	63.4	0.322
250	23.79	90.38	0.263
260	26.54	109.1	0.243
270	21.54	113.8	0.189

[a]Experiments carried out in the presence of 30 Torr HFA and 60 Torr CH_3SiF_3.

Can. J. Chem. Downloaded from www.nrcresearchpress.com by 210.87.254.6 on 09/05/12
For personal use only.

decomposition of substituted ethanes compared with the β-fluoroethylsilanes, the hot silanes will likely have a much greater excess energy (~50 kcal) above the critical energy than with the ethane systems (~30 kcal). It is reasonable therefore to suggest that a multi-step cascade deactivation process is likely with the silane systems. The data is insufficient at this stage for a satisfactory R.R.K. calculation to be made to test this proposal.

Discussion

Pyrolysis of β-Fluorosilanes

Experimentally the thermal decomposition is first order with the kinetics being adequately described by the equation

$$-\mathrm{d}(CF_3CH_2Si\equiv)/\mathrm{d}t = k[CF_3CH_2Si\equiv]$$

Mechanistically we consider the reaction

$$CF_3CH_2Si\equiv \rightarrow CF_2CH_2 + FSi\equiv$$

to be unimolecular involving a four center transition state.

$$\begin{array}{ccc} CF_2 & \cdots & CH_2 \\ \cdot & & \cdot \\ \cdot & & \cdot \\ \cdot & & \cdot \\ F & \cdots & Si \end{array}$$

The A factors in the present work are in three cases $\sim 10^{12.5}$ and, for the *in situ* pyrolysis, $10^{11.7}$. A review of the tabulated data of Benson and O'Neal (6) for molecular elimination processes involving four center transition states shows that while many are in the range $10^{13-13.5}$ there are a number of preferred values somewhat smaller.

Of particular relevance here is the data on β-fluorine transfer. Thus in the case of $CF_2HCH_2SiF_3$ $A = 10^{12.27}$; $CHF_2CH_2SiMeF_2$, $A = 10^{13}$ (5).

Thus we consider our values $\sim 10^{12.5}$ to fall within the expected range. The value of $10^{11.66}$ for $CF_3CH_2SiF_3$ must be considered low in comparison, and possibly due to additional factors occurring in the *in situ* pyrolysis. Such factors include problems of analysis of CF_2CH_2 in the presence of large amounts of HFA + silane, and the possibility of minor secondary reactions of CF_2CH_2 with the reactants over the long periods of the pyrolysis. Even if minor, such secondary reactions could lead to significant loss of CF_2CH_2 in the content of the small quantities being formed overall.

Two experiments were carried out on small amounts of purified $CF_3CH_2SiF_3$ yielding values of k (Fig. 3), an order of magnitude higher than for the *in situ* situation. These two values are certainly more in line with the results for the rest of the series of compounds. Assigning an average experimental value of log $A = 12.5$ to the two isolated pyrolysis results for $CF_3CH_2SiF_3$ leads to an estimate of $E = 37.01$ kcal for each k value. This compares with the value of 37.27 determined from the *in situ* pyrolyses. We prefer these estimates for the Arrhenius parameters to the *in situ* values.

The entropy changes associated with the processes under consideration ~30 gibbs/mol, correlate with the A factors determined.

The activation energies decrease with increasing fluorine substitution on the silicon atom (Table 3), thus, in those cases where the silane is fluorosubstituted, addition of an additional fluorine atom results in a decrease in the activation energy ~2 kcal. A large difference, ~6 kcal, is observed between the non-fluoro-substituted compound $(CF_3CH_2Si(CH_3)_3$ and the mono-fluoro system $CF_3CH_2SiF(CH_3)_2$.

A similar trend has been observed (5) in β-difluoro systems $CHF_2CH_2SiF_3$ ($E = 32.7$), $CHF_2CH_2SiMeF_2$ ($E = 36$), $CHF_2CF_2Si(Me)_3$ ($E = 46.9$).

The enthalpy of reaction is given by the sum of the bond, breaking and forming terms. For each of the pyrolyses we can assume $D_{C\pi C}$ and D_{C-F} will be unchanged. D_{Si-C} is not likely to have an extensive π bond contribution and to a first approximation may be considered unchanged. The most likely change will be associated with D_{Si-F}. If E_{act} is a function of ΔH the experimental results would conform with the Si—F bond increasing in strength with an increasing degree of fluorine substitution, thus, D_{Si-F} values are expected to be in the order $F_3Si—F > F_2CH_3Si—F > F(CH_3)_2Si—F \gg (CH_3)_3Si—F$.

The lower activation energies for β-fluoro transfer from the β-difluoroethylsilanes would indicate that the C—F bond strength is greater in the βCF_3 group compared to the βCF_2H group assuming again E_{act} is a function of ΔH.

In all cases the reaction should be endothermic. The least endothermic case ($CF_3CH_2SiF_3$) taking, (7), $D_{C-F} \sim 115$, $D_{C\pi C} \sim 45$, $D_{Si-C} \sim$

Can. J. Chem. Downloaded from www.nrcresearchpress.com by 210.87.254.6 on 09/05/12
For personal use only.

76, D_{Si-F} (In SiF_4) ~ 135 yields an endothermicity $\Delta H = +11$ kcal. The measured activation energies are not unreasonable for such endothermicities associated with a molecular elimination process. For a free radical process having some bond breaking step as the rate determining step, the measured activation energies would be unreasonably low.

The β-fluoro transfer process is the reverse of molecular addition to a double bond and is forbidden by the application of symmetry rules to chemical reactions (8). It would be expected that an increase in the polarity of the Si—F bond would decrease the "degree of forbiddeness", and enhance the probability of reaction as reflected in the relative reactivities.

The relative reactivities are in line with this argument assuming the F_3Si—F bond is more polar than the $\rangle$Si—F bond. Of course, as pointed out above, relative bond energies are of critical importance in defining the energy of activation, and differences observed are not necessarily a simple function of bond polarity.

Professor P. Perkins (University of Strathclyde, Glasgow, Scotland) has very kindly calculated bond polarities and bond indices relevant to our systems, the results of which confirm the above predictions. Professor Perkins' calculated values and conclusions are below.

Si—F bond polarities (units fraction of an electron charge)

Molecule	Charge at Si	Charge at F
SiF_4	+1.704	−0.426
$MeSiF_3$	+1.283	−0.420
Me_2SiF_2	+0.908	−0.407
Me_3SiF	+0.524	−0.377

This is in accord with the polarity of the $Si^{\delta+}$ $F^{\delta-}$ in the order $SiF_4 > \ldots . Me_3Si$—F.

Bond Indices of the Si—F Bond

The bond index is a measure of the overall bond order of the Si—F bond and the experimental activation energies suggest an order of bond energies $D_{F_3Si-F} > D_{F_2MeSi-F} > D_{FMe_2Si-F} > D_{Me_3Si-F}$.

Bond indices calculated as sums of elements from the rotationally invariant density matrix (overlap weighted) are: SiF_4 = 0.545; $MeSiF_3$ = 0.529; Me_2SiF_2 = 0.523; Me_3SiF = 0.515. Hence, the bond indices follow the same trend as the polarities and the dissociation energies.

A plot, Fig. 4, of the measured activation energy *vs.* the bond index of the newly formed Si—F bond of the product of the β-fluoro transfer reaction, shows an excellent correlation.

dπ–pπ bonding in the Si—F bond might be expected to markedly influence the bond polarity. Calculated values of the dπ–pπ bond orders (abstracted from the rotationally invariant density matrix) are: SiF_4 = 0.030, $MeSiF_3$ = 0.032, Me_2SiF_2 = 0.039, Me_3SiF = 0.044, showing the greatest extent of dπ–pπ bonding with the least degree of fluorine substitutions. However the extent of dπ–pπ bonding is insignificant compared to the σ and pπ–pπ interactions reflected in the total bond index measurements. Thus dπ–pπ interactions have little effect on the polarity and strength of the Si—F bond, which is greatest for F_3Si—F and least for Me_3Si—F.

We are most grateful to Professor P. Perkins for his contribution to the analysis of the results, and to the National Research Council of Canada for financial support.

1. T. N. Bell and U. F. Zucker. J. Phys. Chem. **74**, 979 (1970).
2. T. N. Bell and A. E. Platt. Int. J. Chem. Kinet. **11**, 299 (1970).
3. T. N. Bell and U. F. Zucker. Can. J. Chem. **47**, 1701 (1969).
4. R. N. Haszeldine, P. J. Robinson, and R. F. Simmons. J. Chem. Soc. 1890 (1964).
5. G. Fishwick, R. N. Haszeldine, C. Parkinson, P. J. Robinson, and R. F. Simmons. Chem. Commun. 383 (1965).
6. S. W. Benson and H. E. O'Neal. NSRDS-NBS 21. 1970.
7. T. L. Cottrell. The strengths of chemical bonds. 2nd ed. Butterworths, London. 1958.
8. R. G. Pearson. Acc. Chem. Res. **4**, 152 (1971).

The Effects of Adsorbed Ions on Simple Electrode Reactions. II. The Reduction of Chromium(III) Ion in the Presence of Toluene *p*-Sulfonate Anions

KAMARUZZAMAN ALIAS AND W. RONALD FAWCETT

Department of Chemistry, University of Guelph, Guelph, Ontario N1G 2W1

Received March 26, 1974

KAMARUZZAMAN ALIAS and W. RONALD FAWCETT. Can. J. Chem. **52**, 3165 (1974).

The kinetics of electroreduction of Cr^{3+} ion have been studied at a mercury electrode both in the absence and in the presence of chemisorbed toluene *p*-sulfonate ions. The rate of the reaction was considerably accelerated in the presence of the chemisorbed anions. Analysis of the data has shown that the reaction acceleration can be accounted for on the basis of Frumkin's theory for double layer effects suggesting that the reaction site is at the outer Helmholtz plane or close to it in the diffuse layer.

KAMARUZZAMAN ALIAS et W. RONALD FAWCETT. Can. J. Chem. **52**, 3165 (1974).

On a étudié la cinétique de l'électroréduction de l'ion Cr^{3+} à une électrode de mercure en présence et en l'absence d'ions *p*-toluene-sulphonates absorbés chimiquement. Le taux de réaction est accéléré considérablement en présence de ces ions adsorbés. L'analyse des données montre que l'accélération de la réaction peut être attribuée sur la base de la théorie de Frumkin sur les effets des doubles couches suggérant que le site de la réaction est au plan de Helmholtz le plus éloigné ou près de celui-ci dans la couche diffuse. [Traduit par le journal]

Can. J. Chem. Downloaded from www.nrcresearchpress.com by 210.87.254.42 on 09/05/12
For personal use only.

Introduction

In recent years considerable effort has been directed to examining the catalytic effect of adsorbed anions on the kinetics of simple redox reactions involving cations (1). The systems studied have included the Cr(III)/Cr(II) (2–5), Eu(III)/Eu(II) (6–8), and V(III)/V(II) couples (9). However, unambiguous analysis of the kinetic data is often difficult because the nature of the species reacting at the electrode is not always clearly defined, and because the electron transfer process is sometimes accompanied by ligand exchange. The first problem has been discussed recently by Rodgers and Anson (8) with respect to their study of the accelerating effect of adsorbed thiocyanate ions on the rate of reduction of Eu(III). They concluded that the kinetic data must be analyzed in terms of the parallel reduction of Eu^{3+} and $EuNCS^{2+}$ ions and thereby demonstrated serious shortcomings in the work of Sluyters and co-workers (6, 7). The second problem arises when the adsorbed anion is also a good Lewis base and is involved as a ligand bridge in the transition state complex. Thus, in the electrooxidation of Cr(II), Anson and coworkers (4, 5) have demonstrated that adsorbed halide and thiocyanate ions are incorporated to varying extents in the reaction product at the electrode.

In order to avoid the problems of ligand exchange reactions in the bulk of the solution and at the electrode it was decided to study the kinetics of the electroreduction of Cr^{3+} ion in the presence of a strongly adsorbed anion which is also a good Lewis acid. In this regard, it is well known that sulfonate ions are not good ligands for transition metal ions. In addition, from their interfacial impedence measurements, Parry and Parsons (10, 11) showed that benzene disulfonate and toluene *p*-sulfonate ions are strongly chemisorbed at the mercury/aqueous solution interface. The latter ion was chosen for the present study since it is monovalent and thus will exhibit less tendency to ion pair in solutions containing polyvalent cations. The Cr(III)/Cr(II) redox couple was chosen since its standard potential (−0.65 V against a saturated calomel electrode) is the most negative of the three systems discussed above. Thus, its kinetics could also be determined in the presence of the non-complexing perchlorate anion in a potential region where adsorption of this ion at the electrode is very small (12).

Experimental

Current–potential curves for the reduction of chromium(III) cation were measured at a dropping mercury electrode in solutions of constant ionic strength (0.51 *M*) containing varying concentrations of sodium toluene *p*-

sulfonate (TPS) and sodium perchlorate, and a constant concentration of perchloric acid (0.01 *M*). The acid was added to establish a p*H* of 2 and thereby eliminate hydrolysis of the Cr^{3+} ion (5). The data were obtained using a Radiometer PO4 polarograph modified with an operational amplifier in order to achieve potentiostatic control of the working electrode, and with an external linear voltage ramp generator (Chemical Electronics, Newcastle, England) which supplied a voltage ramp of 30 mV min^{-1} to the working electrode. Other details of the apparatus, experimental procedure, and general methods of reagent purification were given previously (13).

The necessary equilibrium double layer data were obtained by measuring the differential capacity of the mercury/solution interface as a function of electrode potential in the same solutions. The details of the experimental procedure and results are presented elsewhere (14).

Sodium perchlorate was recrystallized twice from doubly distilled water and dried at 100 °C. Sodium TPS was prepared by neutralizing the acid (Eastman) with sodium hydroxide and purified by double recrystallization. The water of crystallization as determined by Karl Fischer titration was one-third mole of water per mole of NaTPS. The depolariser, $Cr(ClO_4)_3.6H_2O$ was recrystallized from 0.5 *M* perchloric acid and dried *in vacuo* at room temperature. The water content of the product was verified by Karl Fischer titration.

All experiments were carried out at 25.0 ± 0.1 °C. The potential of the working electrode was measured with respect to a saturated calomel electrode (s.c.e.).

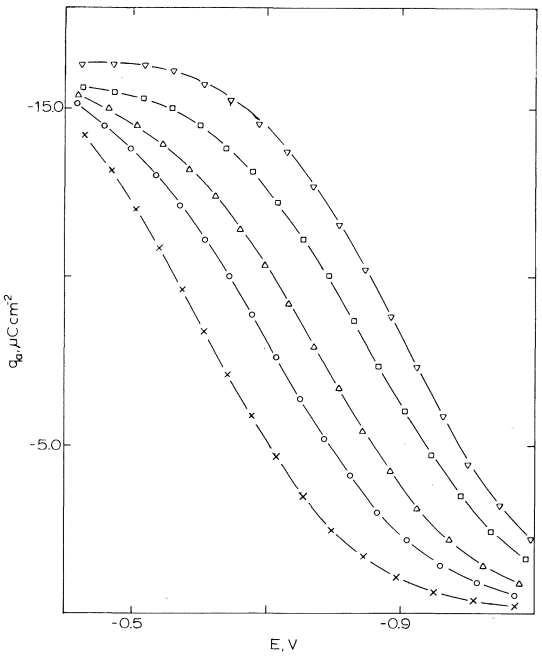

FIG. 1. The adsorbed charge density due to toluene *p*-sulfonate anions, q_a plotted against electrode potential, *E* (*vs.* s.c.e.) for various bulk concentrations of the adsorbing anion: ×, 0.01; ○, 0.025; Δ, 0.05; □, 0.10; and ▽, 0.16 *M*.

Results and Discussion

Capacity–potential curves were measured for ten solutions of composition *x M* NaTPS + (0.51 − *x*) *M* $NaClO_4$ where *x* had the values 0, 0.005, 0.01, 0.016, 0.025, 0.05, 0.1, 0.16, 0.25, and 0.4. Analysis of the data to obtain the charge density due to adsorbed TPS ions as a function of electrode potential was based on the Parsons–Hurwitz method and has been described in detail in Part I (14). From the data obtained (Fig. 1), it is apparent that adsorption of TPS is strong in the potential region where Cr^{3+} is reduced.

Current–potential curves for the electroreduction of Cr^{3+} ion were recorded in solutions of the same ionic strength for seven different TPS concentrations (*x* = 0, 0.01, 0.016, 0.025, 0.05, 0.1, and 0.16 *M*); the concentration of Cr^{3+} was 5×10^{-4} *M* and the p*H* maintained at 2.0 by addition of $HClO_4$. The diffusion coefficient of Cr^{3+} as determined from the diffusion limited current using Koutecký's equation was 4.1×10^{-6} cm^2 s^{-1} in the absence of TPS. It was observed that the limiting current decreased by 5% with increase in TPS concentration from 0 to 0.16 *M* for constant depolariser concentration, mercury flow rate, and drop time. A similar observation was made with data obtained for the electroreduction of periodate ion in the presence of TPS (14). The decrease is attributed to a decrease in the diffusion coefficient of the depolariser with increase in the viscosity of the solution which results when perchlorate ion is substituted by TPS ion (15). In this regard, it should be noted that the decrease cannot be attributed to a decrease in available electrode area due to adsorption of TPS (16). This follows from the fact that the diffusion controlled current is unaffected by nonuniformity of the reaction kinetics at the surface when the thickness of the diffusion layer is large compared with the thickness of the inner layer (17).

Values of current were read from the recorded current–potential curves at 15 mV intervals in the range −0.600 to −0.945 V. The standard potential for the reaction was confirmed to be −0.65 V against the s.c.e. using the method of Hale and Parsons (18) for the data obtained in the absence of TPS. The current readings were corrected for the back reaction as described by Anson *et al.* (5). The rate constant at each potential was then calculated using Koutecký's theory with correction for electrode sphericity (13).

Can. J. Chem. Downloaded from www.nrcresearchpress.com by 210.87.254.42 on 09/05/12
For personal use only.

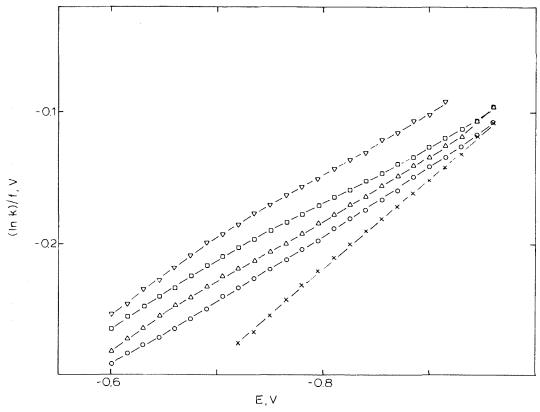

FIG. 2. Rate constant data ($(\ln k)/f$ where $f = F/RT$) for the electroreduction of chromium ion plotted against electrode potential E for various bulk concentrations of adsorbing toluene p-sulfonate ions: ×, 0; ○, 0.01; Δ, 0.025; □, 0.05; and ▽, 0.16 M.

The rate constant data are shown as a function of electrode potential for various TPS concentrations in Fig. 2. The accelerating effect of the adsorbed anions is apparent and amounts to as much as a forty-fold increase in reaction rate for the highest TPS concentration studied.

Corrected Tafel plots (c.t.p.) were constructed assuming that the reaction plane coincides with the outer Helmholtz plane (o.h.p.), the average potential on the o.h.p., ϕ_2 being calculated according to Gouy–Chapman theory. The latter calculation was based on the equation

$$[1] \quad (q_m + q_a)^2 = \frac{\varepsilon RT}{2\pi} \sum_i c_i(e^{-z_i f \phi_2} - 1)$$

where q_m is the charge density on the electrode, q_a, that due to adsorbed TPS ions, c_i, the concentration of ion i having charge z_i in the bulk, and ε, the dielectric constant of the pure solvent. The calculation took into consideration the presence of Cr^{3+} in the bulk, and thus, is the diffuse layer but was much less complicated than that described by Sluyters and co-workers (6); the simplification resulted from the facts that a significant concentration of the reaction product, Cr^{2+} was absent from the system and complex ion formation equilibria did not have to be considered.[1] It was also assumed that specific adsorption of ClO_4^- ion was negligible in the potential region where kinetic data were obtained; thus, the only contribution to q_a was that due to adsorbed TPS ions.

[1]For a discussion of the approximations involved in calculating ϕ_2 as described see ref. 8.

The resulting c.t.p. are remarkably simple in the present case, being both linear and coincident within experimental error (Fig. 3). This result differs from that obtained for periodate reduction where the c.t.p. are not coincident in potential regions where TPS adsorption is significant (14). Thus, it can be concluded that the reaction plane for Cr^{3+} is sufficiently far away from the adsorption plane for TPS ions that lateral interaction and coverage effects can be neglected. The reaction plane is therefore very close to the o.h.p. or slightly beyond it in the diffuse layer.

It is interesting to note that no effects of adsorbate reorientation are apparent from the data presented in Fig. 3. From the work of Parry and Parsons (11) it is postulated that the TPS ion lies flat with the delocalized electron density of the benzene ring interacting with the mercury electrode at low coverages. Under these circumstances, the traditional model which envisages the inner layer as the region adjacent to the electrode accessible to chemisorbed species and solvent but not to nonadsorbed species is probably valid. At higher coverages it is proposed that the TPS ion reorientates so that the benzene ring is perpendicular to the surface and the polar sulfonate group is directed to the aqueous phase. Considering the size of the TPS ion, it is quite probable that on reorientation the plane containing the charge centers of the sulfonate groups is further from the electrode than the o.h.p. which is chiefly occupied by solvated Na^+ ions. Then, the usual model of the double layer is not valid and one would expect marked deviations of

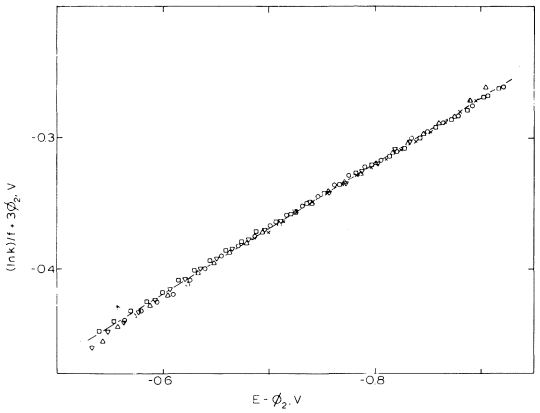

FIG. 3. Corrected Tafel plots of kinetic data for the electroreduction of chromium ion for various bulk concentrations of the adsorbing toluene p-sulfonate ions: ×, 0; ○, 0.01; Δ, 0.025; □, 0.05; and ▽, 0.16 M.

Can. J. Chem. Downloaded from www.nrcresearchpress.com by 210.87.254.42 on 09/05/12
For personal use only.

Can. J. Chem. Downloaded from www.nrcresearchpress.com by 210.87.254.42 on 09/05/12
For personal use only.

the c.t.p. from the simple behavior found here. Thus, it is concluded that for the range of potential and bulk concentration used, the TPS is chiefly adsorbed in the flat configuration.

The value of the transfer coefficient, α determined from the c.t.p. is 0.50 ± 0.01. This value is slightly higher than that obtained by Anson *et al.* (5) in acidified 0.5 *M* $NaClO_4$ ($\alpha = 0.46$). The discrepancy could be due to the use by these authors of a model to correct for mass transfer polarisation which does not account for the effects of electrode curvature (19). The value of α obtained by Parsons and Passeron (20) in the same overpotential range is also lower but it seems clear that these authors worked under conditions in which complications due to Cr^{3+} hydrolysis were present (5). It is interesting that the transfer coefficient obtained here is exactly that predicted by Marcus' theory of heterogenous electron transfer for slow reactions when the Frumkin correction for double layer effects is valid (21, 22). The corrected rate constant at the standard potential ($E - \phi_2 = 0.624$ V) is 1.3×10^{-7} cm s^{-1} ($\ln k + 3f\phi_2 = -15.85$). This value is close to those reported by other authors (5, 20), differences being due to extrapolation errors and other variations in calculation procedures.

An alternative technique for investigating double layer effects in electrode kinetics is to study the dependence of the reaction rate on ionic strength at constant overpotential. Unfortunately, for the present system these experiments are limited to systems of high ionic strength because of the development of polarographic maxima when lower base electrolyte concentrations are employed (5). Anson *et al.* (5) observed a negligible decrease in reaction rate at constant potential (-0.65 V *vs.* the s.c.e.) when the electrolyte was changed from 0.5 *M* $NaClO_4$ to 1.0 *M* $NaClO_4$. However, more recent experiments by Zielinska-Ignaciuk and Galus (23) have clearly shown that an increase in $NaClO_4$ concentration in the range 1 to 5 *M* results in a shift in the standard potential of the reaction from -0.655 to -0.614 V *vs.* s.c.e. Thus, the decrease in rate expected due to the drop in o.h.p. potential with increase in electrolyte concentration is apparently compensated by the increase in overpotential at constant potential for the two systems considered by Anson *et al.* (5). Careful investigation of double layer effects as a function of ionic strength in concentrated solutions would require information regarding the variation of the standard potential and activity coefficients, and regarding the limitations of Gouy–Chapman theory. For these reasons, the present investigation was limited to one ionic strength.

It is interesting to note that no complications due to ClO_4^- adsorption are apparent in the data as analyzed. From Payne's interfacial impedance data for the systems x *M* $NH_4ClO_4 + (1 - x)$ *M* NH_4F (12), it might be construed that this anion is significantly adsorbed in the region of the standard potential of the Cr(III)/Cr(II) couple for a bulk $NaClO_4$ concentration of 0.5 *M*. However it must be emphasized that the Hurwitz–Parsons analysis used to obtain the surface excess data in Payne's study contains a non-thermodynamic assumption, namely, that the planes of closest approach for the adsorbing ion (ClO_4^-) and nonadsorbing ion (F^-) are coincident (24). It is reasonable that the weakly solvated ClO_4^- ion can actually move closer to the electrode than the strongly solvated F^- ion. Then, the calculated surface excess will be high and contain a contribution from the diffuse layer distribution of the ClO_4^- ion. The fact that linear c.t.p. are obtained over the whole potential region suggests that adsorption of ClO_4^- is indeed negligible for the present conditions.

It is interesting to speculate on the significance of the present results with respect to discreteness-of-charge effects in heterogenous electron transfer kinetics. It has recently been shown (25, 26) that significant discreteness-of-charge effects are expected when the reaction plane is in the inner part of the double layer. Indeed the anomalously large double layer effects observed for the electroreduction of H^+ ions and some oxyanions can be explained if such an assumption is made (25). One contribution to discreteness effects is the variation in self-atmosphere potentials of the reactant and product with electrode potential due to changing imaging conditions in the electrode and diffuse layer (26). The self-atmosphere potential is always attractive at the metal/solution interface, its significance being such that the ionic concentrations on a given plane are underestimated if they are calculated on the basis of the average potential on that plane. Imaging forces decrease rapidly with distance from the interface due to the screening effect of other ions in the reaction plane. The simple character of the present results suggests that discreteness-of-

charge effects are minimal. Hale (27) has shown this to be the case when the reaction site is in the diffuse layer away from the vicinity of the o.h.p. However, no estimate of these effects based on a reasonable model has been made at the o.h.p. This problem certainly merits more intensive investigation.

The financial assistance of the National Research Council of Canada and of the Governments of Canada and Malaysia through award of a Commonwealth Scholarship to K.A. are gratefully acknowledged.

1. R. deLevie. J. Electrochem. Soc. **118**, 185C (1971).
2. D. A. Aikens and J. W. Ross. J. Phys. Chem. **65**, 1213 (1961).
3. J. J. Jones and F. C. Anson. Inorg. Chem. **8**, 195 (1969).
4. D. J. Barclay, E. Passeron, and F. C. Anson. Inorg. Chem. **9**, 1024 (1970).
5. F. C. Anson, N. Rathjen, and R. D. Frisbee. J. Electrochem. Soc. **117**, 477 (1970).
6. C. W. de Kreuk, M. Sluyters-Rehbach, and J. H. Sluyters. J. Electroanal. Chem. **28**, 391 (1970).
7. C. W. de Kreuk, M. Sluyters-Rehbach, and J. H. Sluyters. J. Electroanal. Chem. **33**, 267 (1971).
8. R. S. Rodgers and F. G. Anson. J. Electroanal. Chem. **42**, 381 (1973).
9. F. C. Anson and J. Caja. J. Electrochem. Soc. **117**, 306 (1970).
10. J. M. Parry and R. Parsons. Trans. Faraday Soc. **59**, 241 (1963).
11. J. M. Parry and R. Parsons. J. Electrochem. Soc. **113**, 992 (1966).
12. R. Payne. J. Phys. Chem. **70**, 204 (1966).
13. W. R. Fawcett and Y. C. Kuo Lee. Can. J. Chem. **49**, 2657 (1971).
14. K. Alias, W. R. Fawcett, and R. Parsons. J. Chem. Soc. Faraday I, **70**, 1046 (1974).
15. D. M. Brasher and F. R. Jones. Trans Faraday. Soc. **42**, 775 (1946).
16. T. Biegler and H. A. Laitinen. J. Electrochem. Soc. **113**, 852 (1966).
17. K. J. Vetter. Z. Phys. Chem. **199**, 300 (1952).
18. J. M. Hale and R. Parsons. Coll. Czech. Chem. Commun. **27**, 2444 (1962).
19. K. B. Oldham and E. P. Parry. Anal. Chem. **40**, 65 (1968).
20. R. Parsons and E. Passeron. J. Electroanal. Chem. **12**, 524 (1966).
21. R. A. Marcus. J. Chem. Phys. **43**, 679 (1965).
22. D. M. Mohilner. J. Phys. Chem. **73**, 2652 (1969).
23. M. Zielinska-Ignaciuk and Z. Galus. J. Electroanal. Chem. **50**, 41 (1974).
24. W. R. Fawcett. J. Electroanal. Chem. **39**, 474 (1972).
25. W. R. Fawcett and S. Levine. J. Electroanal. Chem. **43**, 175 (1973).
26. S. Levine, K. Robinson, and W. R. Fawcett. J. Electroanal. Chem. In press.
27. J. M. Hale. *In* Reactions of molecules at electrodes. *Edited by* N. S. Hush. Wiley–Interscience, New York, 1971. p. 229.

Can. J. Chem. Downloaded from www.nrcresearchpress.com by 210.87.254.42 on 09/05/12
For personal use only.

Effect of Molecular Weight on Glass Transition by Differential Scanning Calorimetry[1]

LOUIS-PHILIPPE BLANCHARD, JEAN HESSE,[2] AND SHADI LAL MALHOTRA

Département de Génie chimique, Faculté des Sciences, Université Laval, Québec, Québec G1K 7P4

Received April 16, 1974

LOUIS-PHILIPPE BLANCHARD, JEAN HESSE, and SHADI LAL MALHOTRA. Can. J. Chem. **52**, 3170 (1974).

The influence of molecular weight (900 to 1.8×10^6) on the glass transition temperature of low polydispersity polystyrene (anionically prepared) has been studied by differential scanning calorimetry at heating rates of 5 to 80 °C min^{-1}. Over the range of molecular weight studied, and at an extrapolated heating rate of 1 °C min^{-1}, $T_{ge}(°C) = 106 - 2.1 \times 10^5/\overline{M}_n$. A thermally prepared polystyrene sample ($\overline{M}_n = 1.35 \times 10^5$ and $Pd = 3.2$) showed a T_{ge} value of 93 °C, some 10° below the value predicted by the above equation. Low molecular weight species in the highly polydisperse sample are believed to be responsible for the discrepancy. The changes in heat capacity brought about by the glass transitions are accompanied in all cases on heating by an endothermic peak and this regardless of the heating rate (even extrapolated to 1 °C min^{-1}) or the molecular weight of the sample, suggesting that the glass transition phenomenon encountered with polystyrene is a process involving a positive heat effect.

LOUIS-PHILIPPE BLANCHARD, JEAN HESSE et SHADI LAL MALHOTRA. Can. J. Chem. **52**, 3170 (1974).

L'influence de la masse moléculaire (900 à 1.8×10^6) sur la température de transition vitreuse d'échantillons de polystyrène de faible polydispersité (préparé par voie anionique) a été étudiée par la technique d'analyses enthalpiques différentielles à des vitesses de chauffage allant de 5 à 80 °C min^{-1}. Dans la gamme des masses moléculaires étudiées et à un taux de chauffage extrapolé à 1 °C min^{-1}, $T_{ge}(°C) = 106 - 2.1 \times 10^5/\overline{M}_n$. Un échantillon de polystyrène ($\overline{M}_n = 1.35 \times 10^5$ et $Pd = 3.2$) préparé par voie thermique a montré une valeur de T_{ge} de 93 °C soit quelques 10° en-dessous de la valeur prédite par l'équation ci-haut. Les espèces de faible masse moléculaire dans cet échantillon de grande polydispersité seraient vraisemblablement responsables de cette divergence. Les variations de chaleur spécifique que provoquent les transitions vitreuses sont accompagnées dans tous les cas d'un pic endothermique au moment du chauffage et ceci sans égard au taux de chauffage même extrapolé à 1 °C min^{-1} ou à la masse moléculaire de l'échantillon. Cette observation laisse croire que le phénomène de transition vitreuse dans le cas du polystyrene est un processus accompagné d'un effet thermique réel.

Introduction

The temperature at which an amorphous polymer in the liquid state passes, upon cooling, to the solid state without undergoing a crystallization process is generally referred to as its glass transition temperature T_g. A number of years ago Flory and his co-worker (1) defined the glass transition process as being "a second order transition which is not an equilibrium transition in the thermodynamic sense but that originating from kinetic limitations on the rates of internal adjustments occasioned by changes in temperature".

The literature today abounds with papers promoting varying opinions on the subject, many centered on a kinetic phenomenon approach (1–4), and numerous others on a thermodynamic equilibrium approach (5, 6); the controversy between the two schools of thought is far from being settled. This paper which deals primarily with the effects of molecular weight on glass transition nevertheless touches upon some aspects of the controversy though making no pretense at settling the difficult issue.

In literature (1–4) the expression relating the glass transition temperature to the molecular weight is generally accepted to be the following

$$[1] \qquad T_g = T_{g\infty} - K/\overline{M}_n$$

[1]Paper presented at the 56th annual Conference of the CIC, Montreal, Quebec, June 4 to 6, 1973. The work described here is part of the general research program of the "Groupe de Recherche en Science Macromoléculaire" at Laval University.

[2]Present address: Villa Société Nationale des Pétroles Aquitaines 6, 64370 Arthez-de-Béarn, France.

Can. J. Chem. Downloaded from www.nrcresearchpress.com by 210.87.254.6 on 09/05/12
For personal use only.

TABLE 1. Influence of heating rate* and molecular weight on T_g

	T_g (°C)					T_{ge}(°C)
$\overline{M}_n$	$q = 80$	$q = 40$	$q = 20$	$q = 10$	$q = 5$	$(q = 1)$†
1.8×10^6	115.5	114.0	113.0	—	—	107.3
8.6×10^5	114.0	113.0	110.5	109.5	106.5	107.1
5.0×10^5	113.5	112.5	110.5	110.0	—	106.2
4.1×10^5	115.5	110.5	109.8	109.0	108.0	105.9
1.6×10^5	—	109.5	109.0	108.5	—	105.2
5.1×10^4	111.0	109.0	108.0	106.0	100.0	100.1
1.98×10^4	—	104.0	102.0	100.5	—	93.0
1.03×10^4	—	97.0	95.0	93.5	—	86.6
4.08×10^3	78.0	74.0	71.0	69.0	—	59.8
2.03×10^3	—	57.0	55.5	54.0	—	49.6
0.90×10^3	—	36.0	34.0	32.0	31.0	27.0
(Hoechst PS) 1.35×10^5	—	111.0	107.0	101.5	—	93.0

*Unit of q = °C min^{-1}.
†Extrapolated value.

in which T_g is the glass transition temperature (in °K) observed with a polymer of molecular weight $\overline{M}_n$, $T_{g\infty}$ is the glass transition temperature when the polymer molecular weight goes off to infinity, and K is a constant whose units are °K mol g^{-1}.

Most if not all of the earlier studies reported are based on results obtained by dilatometry or differential thermal analysis. Recently differential scanning calorimetry has been used to investigate glass transitions (7). In this laboratory it has been used to study the effect of molecular weight and polydispersity on T_g of polystyrene as well as other associated heat effects.

Experimental

Polymer Samples

Anionically prepared polystyrene (PS) standards having molecular weights ranging from 900 to 1.8×10^6 were obtained from the Pressure Chemical Company in the U.S.A. A thermally prepared polystyrene sample, provided by Farbwerke Hoechst A.G. in Germany, was also included in the study. Its viscosity-average ($\overline{M}_v = 4.47 \times 10^5$) and number average ($\overline{M}_n = 1.40 \times 10^5$) molecular weights were found to agree reasonably well with molecular weight values obtained by GPC ($\overline{M}_w = 4.35 \times 10^5$ and $\overline{M}_n = 1.35 \times 10^5$) using a calibration curve prepared with the polystyrene standard samples. These were used as such, without further purification, for the DSC runs when preliminary tests with purified (by precipitation) and nonpurified samples yielded the same results.

Experimental Procedure

Following the method suggested by Ellerstein (7), polymer samples weighing approximately 2 to 5 mg each were pressed between 100 mesh stainless steel screens placed in standard DSC aluminum sample pans. Both pans and screens were weighed together before and after the addition of polymer. Similar screens were placed in the reference pan but it contained no polymer. The pans were closed with aluminum covers bearing tiny holes to allow the free movement of trapped gases. The use of identical aluminum covers reduced differential radiant energy losses in the DSC. The pans were then placed in the DSC instrument which was continuously flushed with a gentle stream of pure dry nitrogen flowing through the heating area. To condition the polymer samples prior to making the initial T_g measurements, each sample was heated for 30 min to a temperature approximately 30° above the estimated T_g value (first heating) after which it was cooled through the glass transition region at a rate of 1.25 °C min^{-1} as suggested in the literature (8–10). After cooling, T_g was determined by subsequent heatings of the sample at several different heating rates. (See Table 1 for a summary of the principal experimental results.)

Results

In Fig. 1(*a*) and (*b*) are shown typical DSC thermograms (1(*a*), after first heating and 1(*b*), on subsequent heatings) obtained with a polystyrene standard ($\overline{M}_n = 5.1 \times 10^4$) heated at a rate of 40 °C min^{-1}. In this case, as in all others studied in this work, ΔC_p, the change in heat capacity with glass transitions, is accompanied by an endothermic peak and this regardless of the heating rate or the molecular weight of the sample. The glass transition temperature itself was estimated in all cases at the half-height of the observed ΔC_p. The presence of such a peak, analogous to that obtained during the fusion of any crystalline substance in the same apparatus, indicates that the phenomenon observed at the glass transition in the case of polystyrene carries with it (over and above the baseline shift caused by the change in C_p) a positive heat effect even though polystyrene is well known to be noncrystalline in nature from X-ray analyses.

Can. J. Chem. Downloaded from www.nrcresearchpress.com by 210.87.254.6 on 09/05/12
For personal use only.

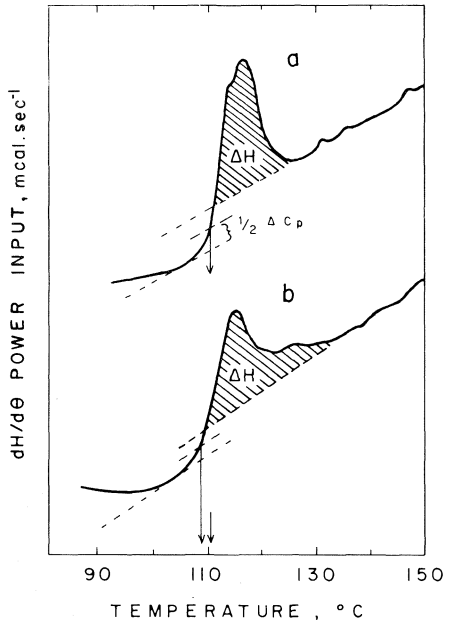

FIG. 1. Typical DSC thermograms obtained in the glass transition range at a heating rate of 40 °C min^{-1}. Sample: PS, 51 000; (*a*) first heating; (*b*) subsequent heatings.

Wunderlich and co-worker (11) encountered a similar endothermic peak in their DTA studies on the glass transition temperature of polystyrene. They explained their observation in terms of the "hole theory" which suggests that, on fast heating, the equilibrium number of holes N_h is overshot in the absence of sufficient time to reach equilibrium. As the temperature continues to rise, the glass eventually reaches equilibrium conditions but via a temperature path (in DTA) which gives every indication of being endothermic. This explanation may be plausible in the light of the fact that Wunderlich and co-worker (11) made use of substantial quantities (0.5 g) of polymer which produced, by overshooting, the apparently endothermic peak. When they heated their samples at much lower rates no endothermic peak was found.

In the present study the quantity of polymer involved during a run was never more than 5 mg. The possibility of overshooting equilibrium conditions, though present, cannot alone explain the area observed under the peak. Reducing the heating rate to 5 °C min^{-1} did not eliminate or reduce proportionately the area observed at higher heating rates. It is difficult under these circumstances to discard the notion of a heat effect associated with the glass transition of PS. This will be discussed further later on.

In DSC, the rate of heating q was found to have an influence on the value of T_g. These can be related in the following fashion (11)

$$[2] \qquad \log q = A - B/T_g$$

Values of T_g obtained with several polystyrene standards, at different heating rates, are summarized in Table 1. It is clear that T_g increases with heating rate. To compare DSC data with values obtained by other methods (dilatometry and DTA), a standard procedure was adopted whereby T_g values were determined at several heating rates after which an extrapolated value T_{ge} was determined at a heating rate of 1 °C min^{-1} from the line representing the variation of $\log q$ with $1/T_g$. The T_{ge} values for the polystyrene standards available were plotted and are shown in Fig. 2. T_{ge} increases up to a point beyond which it remains essentially constant. The critical value of the molecular weight is located in the vicinity of 1.6×10^5, keeping in mind the fact that the maximum error in these measurements does not exceed ± 0.5 °C. This agrees well with the idea put forth by Fox and Loshaek (3) according to which the structure of low molecular weight polystyrene differs somewhat from that of the higher molecular weight species.

T_{ge} values of polymers having molecular weights ranging from 4.08×10^3 to 1.8×10^6 have also been plotted as a function of $1/\bar{M}_n$ (Fig. 3). T_{ge} is found to vary as follows:

$$[3] \qquad T_{ge}\ (\text{in °C}) = 106.0 - 2.1 \times 10^5/\bar{M}_n$$

The glass transition temperature $T_{g\infty}$ (106 °C)

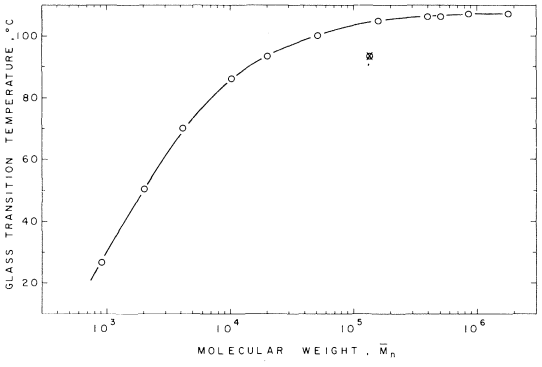

FIG. 2. Glass transition temperature (extrapolated values at a rate of 1 °C min^{-1}) as a function of $\bar{M}_n$. ⊗, Hoechst polystyrene.

Can. J. Chem. Downloaded from www.nrcresearchpress.com by 210.87.254.6 on 09/05/12
For personal use only.

TABLE 2. Components used to simulate the GPC size distribution of the Hoechst polystyrene and the contribution of each to the lowering of T_g*

Component	$\overline{M}_w$	$\overline{M}_n$	Pd	T_{ge} (°C)	Weight fraction (%)	Contribution towards lowering of T_g
A	1.80×10^6	1.10×10^6	1.66	107.0	6.0	0.0
B	3.17×10^5	2.17×10^5	1.46	106.0	40.5	0.0
C	1.66×10^5	1.38×10^5	1.2	104.0	38.5	0.8
D	5.00×10^4	3.66×10^4	1.37	97.0	15.0	1.0

*Total $T_{g\infty} - T_g = 1.8$, $T_g = 104.2$.

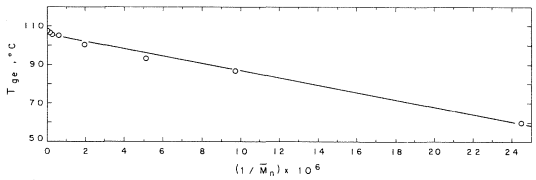

FIG. 3. Glass transition temperature as a function of $1/\overline{M}_n$.

and the value of K (2.1×10^5) obtained in this work are higher than some values reported in the literature (1, 12) (100 °C for $T_{g\infty}$ and (1.0 to 1.2) $\times 10^5$ for K), but close to the value reported by Jenckel and co-worker (13) (105 °C).

As a consequence of the higher value of $T_{g\infty}$, the T_g data in this work are found to be higher than that obtained by others using polystyrenes prepared by free-radical reactions. With this in mind, the free-radically prepared Hoechst polystyrene sample ($\overline{M}_n = 1.35 \times 10^5$) was brought forth in order to determine its T_{ge} by DSC. As was expected, the T_{ge} value of this sample was about 10 °C lower than that of an anionically prepared polystyrene standard of nearly the same molecular weight. In order to elucidate structure differences between the two polymers, these were subjected to an n.m.r. study in the 220 MHz instrument at Sheridan Park in Toronto. The spectra obtained were superimposable, indicating that both samples had similar stereoregularity in their structures. Furthermore, the ratios of —CH and $—CH_2$ protons to those of benzene in the two polymers were identical, indicating that there is little or no detectable chain branching in these samples. The absence of branching in the thermally prepared polymer was further supported by viscosity measurements which were of comparable magnitudes regardless of the polymer origins. The only noteworthy difference observed between the two samples resided in their polydispersities, that of the thermally prepared polystyrene being 3 times that of the anionic polystyrene. Could the higher polydispersity be the factor responsible for the lowering of its T_{ge} value?

In order to verify the effect of polydispersity on glass transition temperatures, the GPC size distribution of the Hoechst polystyrene sample ($Pd = 3.2$) was reconstructed with the help of low polydispersity polystyrene components (A, B, C, and D) as shown in Fig. 4. Polystyrene standards with $M_w = 1.8 \times 10^6$ and 1.6×10^5 are represented by the distribution of components A and C, respectively. The other two distributions denoted by B and D, have been fitted in such a way that the sum of the combined areas of four components is equal to that of the GPC distribution of the Hoechst polystyrene. Table 2 shows the weight percent proportions of each of the components along with their respective molecular weights and their corresponding contribution towards the lowering of the T_g values.

Computation of the contribution of com-

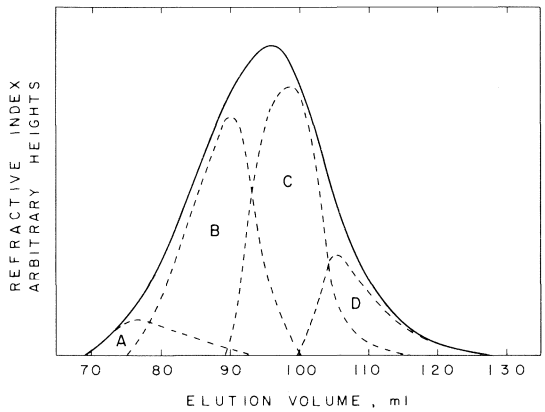

FIG. 4. GPC size distribution of the Hoechst polystyrene sample reconstituted with four low dispersity components (A, B, C, and D).

Can. J. Chem. Downloaded from www.nrcresearchpress.com by 210.87.254.6 on 09/05/12
For personal use only.

TABLE 3. Influence of heating rate and molecular weight on ΔH

$\bar{M}_n$	ΔH (cal g^{-1}) $q = 80$	$q = 40$	$q = 20$	$q = 10$	$q = 5$	ΔH_e ($q = 1$)*
8.6×10^5	1.23	0.87	0.85	0.80	—	0.73
5.0×10^5	1.21	1.01	0.67	—	—	0.83
4.1×10^5	1.21	1.04	0.99	1.16	—	0.92
1.6×10^5	—	0.82	0.68	0.60	—	0.60
5.1×10^4	0.92	0.75	0.68	0.60	—	0.60
1.98×10^4	—	0.73	0.60	0.50	—	0.55
1.03×10^4	—	0.78	0.67	0.60		0.56
4.08×10^3	—	0.78	0.75	0.70	—	0.70
2.03×10^3	—	0.89	0.72	0.60		0.55
0.90×10^3	—	1.38	1.00	0 77	0.83	0.66

*Extrapolated value.

ponents towards the lowering of T_g values is based on eq. 1 rewritten in the following form

$$[4] \qquad 1/M_n = (T_{g\infty} - T_g)/K$$

Furthermore, for a highly polydisperse sample, made up of known weight percentages (N_1, N_2, N_3, and N_4) of four low polydisperse components (A, B, C, and D) each having a known number-average molecular weight (M_1, M_2, M_3, and M_4), its number-average molecular weight $\bar{M}_n$ is related to these components as follows:

$$[5] \qquad \frac{N_1}{M_1} + \frac{N_2}{M_2} + \frac{N_3}{M_3} + \frac{N_4}{M_4} = \frac{100}{\bar{M}_n}$$

Combining eqs. 4 and 5, one obtains

$$[6] \qquad \frac{N_1(T_{g\infty} - T_{g1})}{K} + \frac{N_2(T_{g\infty} - T_{g2})}{K} + \frac{N_3(T_{g\infty} - T_{g3})}{K} + \frac{N_4(T_{g\infty} - T_{g4})}{K} = \frac{100(T_{g\infty} - T_g)}{K}$$

from which the T_g value of a highly polydisperse sample can be easily computed when T_g of each component has been established by one or other of the well established techniques. The value 104.2 °C computed with eq. 6 for a mixture simulating the Hoechst thermally prepared polystyrene sample, is high when compared to 93 °C, the experimental value. One is led to conclude that other factors, over and above polydispersity and stereoregularity must contribute more significantly to the discrepancy.

An analysis of the results given in Table 2 shows that 15 wt% of the species in the Hoechst polystyrene have an $\bar{M}_n$ value of the order of 3.66×10^4 with a T_{ge} of 97 °C (Fig. 3). It would seem, therefore, that the glass transition temperature (93 °C) obtained with the Hoechst polystyrene sample is in reality that of its lowest molecular weight species. The presence of other higher molecular weight species would seem to change but the shape of the remainder of the endothermic peak in the DSC thermogram without influencing unduly the initial value of the glass transition temperature; hence, the lower T_{ge} value observed.

It was mentioned earlier in the text that the glass transition of polystyrene carries with it a positive heat effect. In differential scanning calorimetry such heat effects can readily be determined by comparing endothermic areas in the DSC thermograms (Fig. 1) with corresponding areas obtained for the fusion of indium whose enthalpy of fusion per unit weight is very well known. The ΔH values (in cal g^{-1}), obtained at the heating rates used in this study with the various polystyrene samples, are listed in Table 3. It is clear from the values reported that increasing the heating rate increases the ΔH values. This is what one would expect if thermal lag associated with overshooting of equilibrium conditions were the sole element responsible for this area, but plots of ΔH values as a function of the heating rate q prepared (but not shown here) for each of the polystyrene standards studied revealed that ΔH obeys a law of the form $y = a + bx$ and not $y = bx$. This indicates that, if overshooting from thermal lag contributes to the areas under the thermogram, it is not the sole factor involved since ΔH retains a substantial value ΔH_e when the data is extrapolated to zero heating rate. In practice and

Can. J. Chem. Downloaded from www.nrcresearchpress.com by 210.87.254.6 on 09/05/12
For personal use only.

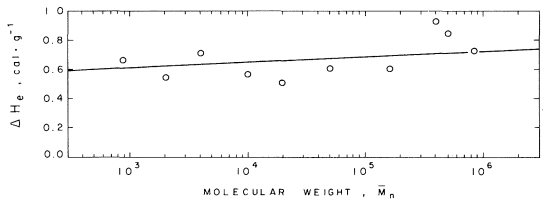

FIG. 5. Extrapolated value (zero heating rate) of ΔH as a function of molecular weight.

for comparison purposes only, extrapolated values are given in Table 3 for a heating rate of 1 °C min^{-1}. Any discrepancy introduced in ΔH_e, the heat effect associated with the glass transition process, is negligible. Figure 5 shows a plot of ΔH_e (in cal g^{-1}) as a function of the molecular weight $\bar{M}_n$. Though no definite trend can be detected from this plot other than the fact that ΔH_e has a positive value from 0.5 to 0.9 cal g^{-1} over the whole range of molecular weights studied, these values, averaging around 0.65, are not too far removed from the experimental enthalpic value (0.92 cal g^{-1}) reported by Lambert (10). Gee (14) in a separate study involving the effects of pressure on the glass transition of polystyrene came forth in his thermodynamic study with a residual enthalpic value of 0.8 cal g^{-1} for his process. He did not assign this value to any one step in his study and it is difficult to say that it belongs particularly to the glass transition itself. Strangely enough the value reported by Gee is comparable to that observed experimentally in the present work and which the authors have associated with the glass transition process itself.

The authors are grateful to the National Research Council of Canada for financial assistance in support of this work. One of the authors (J.H.) acknowledges receipt of a post-graduate bursary from the Canada Council.

1. T. G. Fox and P. J. Flory. J. Appl. Phys. **21**, 581 (1950).
2. T. G. Fox and P. J. Flory. J. Polym. Sci. **14**, 315 (1954).
3. T. G. Fox and S. Loshaek. J. Polym. Sci. **15**, 371 (1955).
4. F. Bueche. J. Chem. Phys. **21**, 1850 (1953); **24**, 418 (1956).
5. J. H. Gibbs and E. A. DiMarzio. J. Chem. Phys. **28**, 373 (1958); J. Polym. Sci. **1A**, 1417 (1963).
6. E. A. DiMarzio. J. Res. Natl. Bur. Stand. **68A**, 611 (1964).
7. S. M. Ellerstein. Appl. Polym. Symp., *No. 2*, 111 (1966); R. S. Porter and J. F. Johnson (*Editors*). Analytical calorimetry. Proc. Am. Chem. Soc. Symp. (155th). Plenum Press, N.Y. 1968. p. 279.
8. A. M. Kovacs. Fortschr. Hochpolym.-Farsch. **3**, 394 (1963).
9. B. Wunderlich, D. M. Bodily, and M. H. Kaplan. J. Appl. Phys. **35**, 95 (1964).
10. A. Lambert. Polymer, **10**, 319 (1969).
11. B. Wunderlich and D. M. Bodily. J. Polym. Sci. C**6**, 137 (1964).
12. I. Uematsu, K. Takagi, T. Moriguch, H. Sukejima, and T. Fukazawa. Asahi Garasu Kogyo Shorukai Kenkgu, **15**, 593 (1969).
13. E. Jenckel and K. Ueberreiter. Z. Phys. Chem. Leipzig A, **182**, 361 (1938).
14. G. Gee. Polymer, **7**, 177 (1966).

Can. J. Chem. Downloaded from www.nrcresearchpress.com by 210.87.254.6 on 09/05/12
For personal use only.

Dielectric Behavior of the Aniline–Cyclohexane System in the Consolute Region

I. LUBEZKY[1] AND R. MCINTOSH

Department of Chemistry, Queen's University, Kingston, Ontario K7L 3N6

Received March 25, 1974

I. LUBEZKY and R. MCINTOSH. Can. J. Chem. **52**, 3176 (1974).

Measurements of ε' and ε'' at 5 kHz are reported for the system aniline–cyclohexane in the region of the consolute temperature. No anomalously large values of ε' and ε'' were found in the region of concentration where the binodal curve is essentially flat. Traces of water increase the temperature for phase separation. An explanation in terms of the formation of molecular clusters is offered for the difference of behavior of this system and that of nitrobenzene – trimethyl pentane.

I. LUBEZKY et R. MCINTOSH. Can. J. Chem. **52**, 3176 (1974).

On rapporte des mesures de ε' et de ε'' à 5 kHz pour le système aniline–cyclohexane dans la région de température de miscibilité. On ne trouve pas de valeurs anormalement élevées pour ε' et ε'' dans la région de concentration où la courbe binodale est essentiellement aplatie. Des traces d'eau augmentent la température pour la séparation de phase. On présente une explication faisant appel à la formation d'amas moléculaires pour la différence de comportement entre ce système et celui du nitrobenzène–triméthyl pentane.

[Traduit par le journal]

Can. J. Chem. Downloaded from www.nrcresearchpress.com by 210.87.254.42 on 09/05/12
For personal use only.

Introduction

Although Gibbs' treatment predicts generally a sharp and indefinitely large increase of ε', the real part of the dielectric constant, at the temperature of transition from a one phase to a two phase system (1), experimental evidence is meager and is frequently contradictory. Thus, for partially miscible two component liquid systems near the consolute temperature, Piekara (2) noted a sharp increase of ε', while Arkhangelskii and Semenchenko (3) reported maxima in ε' and ε'' at a slightly higher temperature than that of the break in the curve obtained by Piekara. A study of the nitrobenzene – 2,2,4-trimethyl pentane system using a frequency of 3300 MHz (4) revealed maxima in the dielectric constant and loss tangent at a temperature 1.5 °C above the separation temperature. In this system the maxima were sharpest near the consolute temperature and concentration, but increased in magnitude with increasing concentration of nitrobenzene. Quinn and Smyth (5) examined the same system at a single concentration of nitrobenzene, namely 25% by weight, at frequencies of 0.5, 3.0×10^3, 9.3×10^3, and 2.4×10^4 MHz. A pronounced maximum was found in ε' at a temperature about 2 °C above the consolute temperature. Dispersion was characterized by a single relaxation time over much of the temperature range in the microwave region of frequencies. More recently (6) the same chemical system, when studied using a frequency of 60 kHz, showed maxima in ε' for compositions from 22.3 to 35% nitrobenzene by weight, but an abrupt change in the value of $d\varepsilon'/dT$ between that concentration and 75% nitrobenzene by weight. At this high concentration $d\varepsilon'/dT$ appears to be continuous. There is therefore a measure of agreement both with Piekara's results and those of Arkhangelskii and Semenchenko. One difference in the nature of the studies is that audio and low radio frequencies were employed by Piekara (2) and Semenchenko (3), microwave frequencies in ref. 4 and by Quinn and Smyth (5). However, the study reported in ref. 6 employed low frequencies and shows agreement with both refs. 2 and 3 for particular concentration ranges.

Snider (7, 8) has discussed the dielectric parameters of such systems theoretically using the concept of density fluctuations in submicroscopic regions. Losses were attributed to diffusion as the critical systems respond to the applied field. Large contributions to ε' were considered to arise because of correlation effects between dipoles. Snider's work predicted losses at a frequency of about 0.5 MHz and contributions to the dielectric parameters which would be greatest at the critical or consolute composition, and

[1]Postdoctoral Fellow, 1972–1973. Present address: Physical Chemistry Laboratory, South Parks Road, Oxford University, Oxford, England.

Can. J. Chem. Downloaded from www.nrcresearchpress.com by 210.87.254.42 on 09/05/12
For personal use only.

which would shift to low frequency at the consolute point.

In addition to predicted anomalies in ε' at the consolute temperature, viscosity and specific heat are known (9, 10) to show maxima at a temperature closely above the transition temperature. Arcovito *et al.* (11) have reported the viscosity anomaly for the system aniline–cyclohexane, while Rowden and Rice (12) have established that a substantial part of the coexistence curve is flat at the consolute temperature. In a one component system Harrison and Mayer (13) have depicted a region above the critical temperature in which a denser phase exists with no surface tension and gives rise to a flat coexistence curve near the critical temperature. Such a conception, extended to binary systems, is consistent with the assumption of submicroscopic regions of differing composition and density. On these grounds it seemed advantageous to determine the dielectric parameters of the system aniline–cyclohexane over the compositional range which the very careful earlier work of Rowden and Rice established as a flat portion of the coexistence curve.

Experimental

Dielectric constants and losses were measured at a frequency of 5 kHz. The measuring circuit, dielectric cell, and experimental arrangements were described in an earlier work (6). The impurity of the chemicals, especially the presence of water, had a pronounced influence on the critical temperature and the behavior of the dielectric quantities. Therefore, special attention was paid to purification of the chemicals prior to measurements.

Aniline, 99.9+% from Aldrich Chemical Company, was twice refluxed for 4 h in the presence of CaH_2, followed by a vacuum distillation each time. Further treatment did not alter the values of the critical transitions.

Cyclohexane, spectrophotometric grade from Aldrich Chemical Company, was refluxed for 4 h over CaH_2 and distilled.

Purified aniline and cyclohexane were kept in sealed vessels, covered with aluminum foil, and stored in a vacuum dessicator. Upon exposure to the laboratory atmosphere, aniline absorbed, in minutes, an amount of water which increased the consolute temperature almost 0.5 °C.

Results

In Fig. 1*a* the dielectric constants (ε') are represented as a function of temperature in the consolute regions for different concentrations. It seems that within experimental error, ε' is linear with temperature until break points in the curves which occur at phase separation. Between the concentrations 0.417 mole fraction and 0.459 mole fraction of aniline these points possess a constant temperature, 29.61 ± 0.01 °C, which agrees with the data of Rowden and Rice (12), though it appears slightly higher than the value 29.587 °C reported by Atack and Rice (14). This difference could be attributed to better purification of the components, or due to a different thermometer calibration in the latter case.

The point of separation into two phases was observed as a distinct cloudiness followed by the appearance of the meniscus. Clearly, there is no sign of anomalous behavior in ε' over the entire concentration range of interest.

The same behavior is indicated by the losses (ε'') which are represented over the same concentration and temperature range in Fig. 1*b*. Despite the greater scattering in loss measurements, the same trend of linearity in the curves, down to the critical temperature, and the same delineation of the flat portion of the coexistence curve result.

In Fig. 2 *a* and *b* a few curves are depicted for ε' and ε'' in the same concentration range, where the system contains traces of water as a result of a short exposure to the laboratory atmosphere. Besides a shift in the critical temperatures toward higher values, by about 0.3 °C, the separation into two phases is no longer accompanied by a sharp break in the curves. The transitions in ε' and ε'' are now gradual and deviation from linearity begins 0.3 to 0.5° above the critical temperature.

In this audio frequency range the reaction of aniline or cyclohexane to an electric field perturbation is fast enough to allow the polarization to reach its equilibrium value. Therefore the losses of the system at temperatures far from the critical temperature could be due to d.c. conductivity, dielectric relaxation of particles greater than 100 Å (15) in diameter, or a combination of these. To examine the extent of the d.c. contribution one should employ lower frequencies for measurements. However, this frequency range was beyond the capabilities of the present apparatus.

The behavior of the dielectric parameters could be interpreted despite the uncertainty in the origin of the losses. As previously mentioned, measurements of the solution viscosity did show an anomalous behavior before the critical temperature (11), and despite the Debye correlation between viscosity and dielectric properties, no

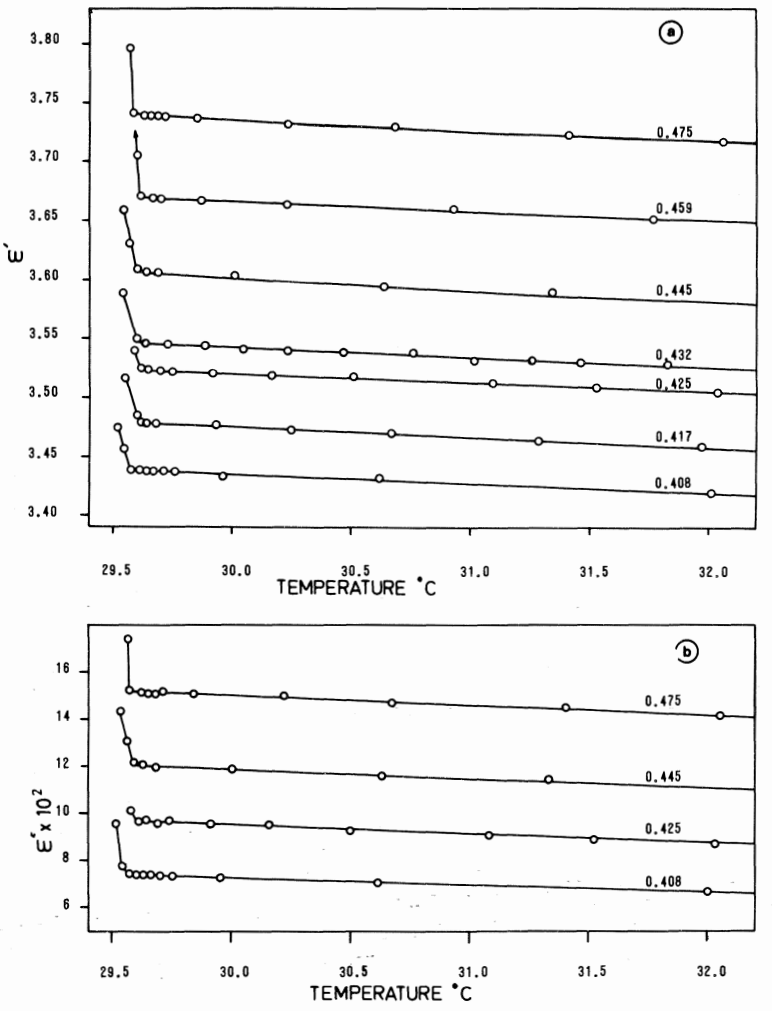

FIG. 1. (*a*) ε′ 5 kHz as a function of temperature and composition.Composition is expressed as mole fraction of aniline. (*b*) ε′′ at 5 kHz as a function of temperature and composition. Composition is expressed as mole fraction of aniline.

such behavior has been observed here, until phase separation occurs.

Discussion

At temperatures far from the critical region, local density fluctuations occur, but the time intervals are usually smaller than 10^{-12} s (16). Thus, as far as dielectric processes are concerned, the liquid is homogeneous. As the system approaches the critical region, the fluctuations become longer in duration and extend over longer spatial regions (17). Quinn and Smyth (5) therefore expect such a solution to reach a point of heterogeneity, due to fluctuations in the molecular environment, where the dielectric parameters would be affected suddenly. More specifically, according to Snider (7, 8), losses would be attributed in this case to diffusion of molecules towards their new equilibrium positions as the system is subjected to the applied alternate electric field perturbation. The correlation effects among the dipoles will cause the anomalous behavior of the dielectric parameters. The correlation effects will be the result of a rapid increase of molecular clusters in the liquid as the system approaches the phase separation point.

Such a model would in general explain the anomalous dielectric behavior which has been found in the different frequency ranges as described in the introduction. However, the question

Can. J. Chem. Downloaded from www.nrcresearchpress.com by 210.87.254.42 on 09/05/12
For personal use only.

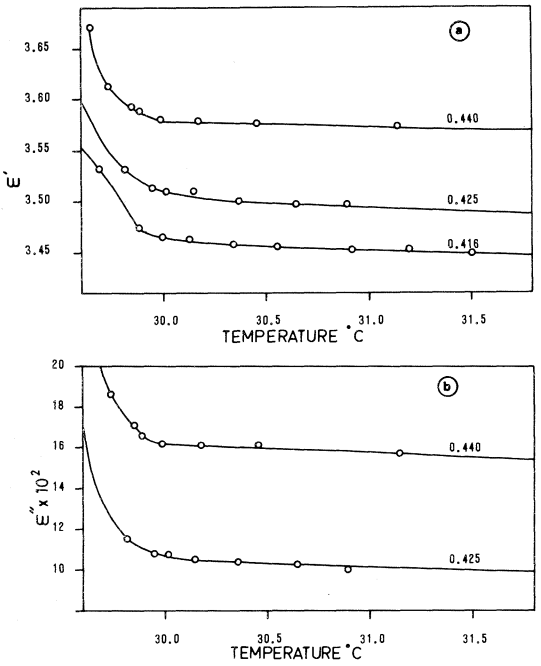

FIG. 2. (*a*) ε′ at 5 kHz as a function of temperature and composition. Composition is expressed as mole fraction of aniline. Moisture has been admitted to the dried system. (*b*) ε″ at 5 kHz as a function of temperature and composition. Composition is expressed as mole fraction of aniline. Moisture has been admitted to the dried system.

remains why the dielectric phenomena have not been observed for the aniline–cyclohexane system down to the separation point.

A feasible explanation would be that for the given concentration range of the system, the components are divided between two types of microregions even at temperatures far above the critical temperature. Each of the microregions contains an excess of one component, namely, aniline or cyclohexane. These microregions are separated by density gradients, and while the temperature decreases, the microregions increase in size and change slightly in concentration. During this process, the density gradients become sharper, until finally the molecular aggregates reach their maximum size and concentration and phase separation occurs. As in such a system there is no sudden increase of clusters above the critical temperature, no anomaly in the dielectric parameters is expected to the point of phase separation. In such a case the dielectric constant and energy losses will be continuous function of temperature down to the phase transition.

The same conclusion, that in the present system there is no sudden buildup of molecular clusters (multimers) above the critical temperature, is developed by the results of Sen and Ghosh (18) on different grounds. Also, according to Harrison and Mayer (13), in a one component system, a wide region exists, above the critical temperature, where the denser phase exists with no surface tension. Such a model, extended to a binary solution, fits into the present concept of the microregions.

In such a system, traces of water are likely to adsorb on the surfaces of the aniline aggregates. The hydrogen bonds among the different surfaces will result in increasing the temperature at which the surface tension of the aggregates is created and phase separation occurs. As the aggregates increase in size, for geometrical reasons the water content on the surfaces will increase too. This can explain the deviation from linearity of the dielectric curves in the region preceding the phase separation when water traces are present (Fig. 2 *a* and *b*).

The anomalous effects reported in the various systems (see Introduction) occur in the same temperature interval where the curves in the present study begin to deviate from linearity in the presence of water. One should therefore carefully verify that any anomalous dielectric effects obtained in this region are not connected with the presence of impurities in the system.

Conclusion

The jump in the dielectric parameters at phase separation of a pure binary solution was found to be a convenient and sensitive tool for the determination of the critical temperature. The results obtained here support (within the experimental accuracy) the observations by Rice and collaborators of a flat portion in the coexistence curve of the aniline–cyclohexane system. It is suggested that the approach of the system to phase separation involves only density fluctuations and gradual changes of the concentration of aggregates already existing far from the critical region. No evidence was found for the sudden formation of molecular clusters upon approaching the critical point of the system.

This work was made possible by support from the National Research Council of Canada through an operating grant to R. McIntosh.

Can. J. Chem. Downloaded from www.nrcresearchpress.com by 210.87.254.42 on 09/05/12
For personal use only.

1. J. A. V. BUTLER. *In* Commentary of the scientific writings of J. Willard Gibbs. Vol. 1. Yale University Press, New Haven, Connecticut. 1936. p. 146 *et seq.*
2. A. PIEKARA. Phys. Rev. **42**, 448 (1932).
3. K. V. ARKHANGELSKII and V. K. SEMENCHENKO. Russ. J. Phys. Chem. **41**, 692 (1967).
4. B. D. RIPLEY and R. MCINTOSH. Can. J. Chem. **39**, 526 (1961).
5. R. G. QUINN and C. P. SMYTH. J. Chem. Phys. **39**, 3285 (1963).
6. I. LUBEZKY and R. MCINTOSH. Can. J. Chem. **51**, 545 (1973).
7. N. S. SNIDER. J. Chem. Phys. **55**, 3994 (1971).
8. N. S. SNIDER. J. Chem. Phys. **56**, 233 (1972).
9. V. K. SEMENCHENKO and E. L. ZORINA. Dokl. Akad. Nauk. SSSR, **80**, 903 (1951): National Research Council Technical Translation TT298.
10. V. K. SEMENCHENKO and V. P. SKRIPOV. Zhur. Fiz. Khim. **25**, 362 (1951): National Research Council Technical Translation TT243.
11. G. ARCOVITO, C. FALOCI, M. ROBERTI, and L. MISTURA. Phys. Rev. Lett. **22**, 1040 (1969).
12. R. W. ROWDEN and O. K. RICE. J. Chem. Phys. **19**, 1423 (1951).
13. S. F. HARRISON and J. E. MAYER. J. Chem. Phys. **6**, 101 (1938).
14. D. ATACK and O. K. RICE. Disc. Faraday Soc. **15**, 270 (1953).
15. P. DEBYE. Polar molecules. Chemical Catalog Co., New York. 1929. p. 83 *et seq.*
16. D. C. DOUGLASS, J. Chem. Phys. **35**, 81 (1961).
17. M. FIXMAN. J. Chem. Phys. **36**, 310 (1962).
18. S. N. SEN and R. GHOSH. J. Phys. Soc. Jap. **33**, 838 (1972).

Can. J. Chem. Downloaded from www.nrcresearchpress.com by 210.87.254.42 on 09/05/12
For personal use only.

The Effect of Pressure on the Solubility of $CaCO_3$, CaF_2, and $SrSO_4$ in Water

ROBIE W. MACDONALD[1] AND NEIL A. NORTH
Department of Oceanography, Dalhousie University, Halifax, Nova Scotia
Received October 1, 1973[2]

ROBIE W. MACDONALD and NEIL A. NORTH. Can. J. Chem. **52**, 3181 (1974).

The effect of pressure on the solubility of $CaCO_3$(calcite), CaF_2, and $SrSO_4$ in water was investigated for temperatures between 0 and 35 °C for pressures up to 1000 atm. It was found that for $SrSO_4$ at 0 °C, and at 22 °C above 500 atm, and $CaCO_3$ the high pressure solubility products were appreciably lower than those expected from calculations based on the anhydrous salts. It is postulated that this effect may be due to the formation of a bulk or surface hydrate. Consequently, care must be taken in assigning the solid phase when predicting the pressure dependence of the solubility of a sparingly soluble salt.

ROBIE W. MACDONALD et NEIL A. NORTH. Can. J. Chem. **52**, 3181 (1974).

On a examiné l'effet de la pression sur la solubilité du $CaCO_3$(calcite), CaF_2 et $SrSO_4$ dans l'eau à des températures variant entre 0 et 35 °C pour des pressions allant jusqu'à 1000 atm. On a trouvé que les produits de solubilité à haute pression du $CaCO_3$ et du $SrSO_4$ à 0 et à 22 °C au-dessus de 500 atm sont beaucoup plus bas que ceux attendus en se basant sur des calculs extrapolés de données pour des sels anhydres. On fait l'hypothèse que cet effet peut être dû à la formation d'un hydrate à la surface. Par conséquent l'on doit prendre garde en attribuant des phases solides lorsque l'on prédit la dépendance sur la pression de la solubilité d'un sel très peu soluble. [Traduit par le journal]

Introduction

The pressure dependence of the thermodynamic equilibrium constants is described by the equation

$$[1] \qquad \frac{\partial}{\partial P}(\ln K_p) = \frac{-\Delta V}{RT}$$

where ΔV is the difference between the partial molal volumes of the product and reactant species. For homogeneous reactions in aqueous solutions, it has been demonstrated both in theory and by experiment that the ΔV calculated from the pressure dependence of equilibrium constants are in good agreement with the ΔV determined from the partial molal volumes of the product and reactant species. The same agreement should also be found with heterogeneous equilibrium constants, in particular for the solubility products of sparingly soluble salts.

Some recent determinations of the pressure dependence of $SrSO_4$ solubilities (11) produced an experimental ΔV that was approximately 11.0 $cm^3\ mol^{-1}$ more positive than the theoretical value calculated from the partial molal volumes of Sr^{2+}, SO_4^{2-}, and anhydrous $SrSO_4$. This discrepancy was tentatively attributed to the formation of a layer of hydrated $SrSO_4$ on the surface of the anhydrous crystals.

In this paper are reported the solubility products of three sparingly soluble group II salts: $CaCO_3$, CaF_2, and $SrSO_4$, for pressures of up to 1000 atm and at various temperatures between 0 and 35 °C. The experimental ΔV calculated from these measurements are compared to the theoretical ΔV calculated from the partial molal volumes, assuming the equilibrating solid phases to be the anhydrous salts. From these comparisons the authors were able to show that the previously reported behavior of $SrSO_4$ is also found, to a lesser extent, with $CaCO_3$ and, in both cases, this behavior appears to arise from the formation of crystalline hydrates.

Method

The solubility products of CaF_2, $CaCO_3$, and $SrSO_4$ in distilled water were measured at pressures between 1 and 1000 atm and at various temperatures between 0 and 35 °C. The distilled water used in these measurements was de-ionized water which was boiled vigorously prior to use to expell any dissolved CO_2. The pH of the water,

[1]Present address: 211 Harbour Road, Victoria, British Columbia V9A 3S2.

[2]Revision received May 3, 1974.

Can. J. Chem. Downloaded from www.nrcresearchpress.com by 210.87.254.6 on 09/05/12
For personal use only.

Can. J. Chem. Downloaded from www.nrcresearchpress.com by 210.87.254.6 on 09/05/12
For personal use only.

before the addition of the salts, was between 6.5 and 7.0.

The $SrSO_4$ solid was a powder, of Laboratory Reagent purity, supplied by B.D.H. The $CaCO_3$ was in the form of small natural calcite crystals from Mexico. An analysis of the calcite showed that it contained less than 0.1 mol% magnesium. The CaF_2 were small handpicked crystals from a geological laboratory specimen of unknown origin.

The solubilities were determined using the apparatus shown diagrammatically in Fig. 1. The solutions were saturated by allowing the water to percolate, at a known rate, through the reaction column which was packed with the dissolving solid. This method produces a large surface area to liquid volume ratio and so allows a relatively rapid attainment of equilibrium. After percolation through the column, the liquid was collected in flasks and diluted with acidified NaCl solution. The resulting solution was analyzed for either Ca or Sr by atomic absorption, where all determinations had better than $\pm 2\%$ accuracy. Saturation was considered to be attained when an increase in the contact time between the percolating solution and the solid produced no increase in the metal ion concentration in the solution.

The thermodynamic solubility products for each of the salts were calculated from the concentrations of the respective metal ions in the saturated solution. For $SrSO_4$ and CaF_2 the solubility products are

$$[2] \quad K(\mathrm{d,SrSO_4}) = [Sr^{2+}]\,[SO_4^{2-}]\,\gamma_{\pm}^{2}(SrSO_4)$$

$$[3] \quad K(\mathrm{d,CaF_2}) = [Ca^{2+}]\,[F^-]^2\,\gamma_{\pm}^{3}(CaF_2)$$

As the pK_a's of HSO_4^- and HF are 1.92 and 3.45 respectively (1), the concentration of these species in the saturated solutions are negligible. A simple calculation will show that the HF in the present solutions is over 99% dissociated. Consequently, the anion concentrations are given by

$$[4] \quad [SO_4^{2-}] = [Sr^{2+}]$$

and

$$[5] \quad [F^-] = 2[Ca^{2+}]$$

The mean activity coefficients for the dissolved solutes ($\gamma_{\pm}$) were calculated from the extended Debye–Hückel equation, following the same procedure used by Fisher (2). This gives $\gamma_{\pm}$ as a function of pressure. The method is well documented by Fisher, and a repetition here would be superfluous.

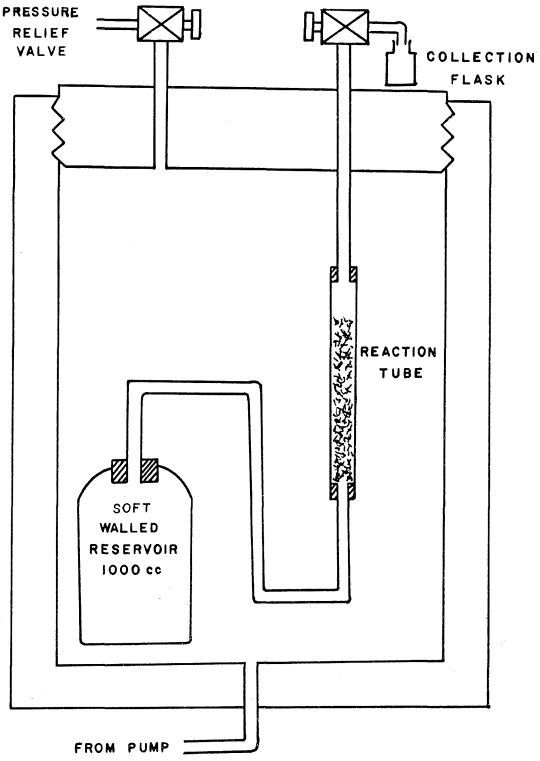

FIG. 1. Schematic diagram of the apparatus.

In calculating the $CaCO_3$ solubility products, allowance was made for the carbonate equilibria. In the closed system, with no CO_2 gas dissolved in the water, the concentration of $H_2CO_{3\,aq}$ was found to be negligible compared with CO_3^{2-} and HCO_3^-. In fact it was found that it contributed less than 0.1% to the total carbonate present. As a result, only a correction for the formation of HCO_3^- was necessary. In order to do this a temperature and a pressure correction were required. The temperature correction was applied first by using the data of Harned and Hamer (3) for K_w and the values given by Horne (4) for K_2, where

$$[6] \quad K_w = [H^+]\,[OH]$$

$$[7] \quad K_2 = [H^+]\,[CO_3^{2-}]/[HCO_3^-]$$

Thus it was possible to obtain K_w and K_2 at 1 atm and at any temperature between 0 and 25 °C.

Can. J. Chem. Downloaded from www.nrcresearchpress.com by 210.87.254.6 on 09/05/12
For personal use only.

The further correction for pressure was made by using the equation of Lown *et al.* (5). This procedure has been shown to work well for pressures below 2000 atm. The ΔV values were obtained from Millero (6) and were adjusted for temperature by assuming that ΔV varied linearly with temperature between 0 and 25 °C. The ΔK value for water was taken from North (7), while ΔK pertaining to K_2 was obtained from Owen and Brinkley (8). It was assumed that ΔK did not vary appreciably with temperature. Following the above method, $K_w(P,T)$ and $K_2(P,T)$ were found. From these and the measured concentration of Ca^{2+}, the concentration of other species present were calculated. By applying the extended Debye–Hückel equation, and the values for $\mathring{a}$, the ion size parameter for individual ions given by Berner (9), the equilibrium was recalculated in terms of activity. The Debye–Hückel equation was reapplied to the second set of equilibrium values, but owing to rapid conversion, significant changes in concentrations were not found.

The thermodynamic solubility products were then calculated in the same manner as those for CaF_2 and $SrSO_4$ yielding

$$[8]\quad K(\mathrm{d,CaCO_3}) = [Ca^{2+}][CO_3^{2-}]\gamma_{\pm}^2(CaCO_3)$$

In eq. 8 the measured value of Ca and the calculated value of CO_3^{2-} were used. The extended Debye–Hückel equation was applied in the same procedure as that used by Fisher (2) to give $\gamma_{\pm}$ as a function of pressure.

The calculated thermodynamic solubility products are collected in Table 1, and some of these are shown graphically in Figs. 2 and 3. The values of ΔV^0 were determined by using a least squares fit of the data. Both parabolic and linear representations were examined. From the standard error it was found that the parabolic fit was an improvement over the linear fit in the case of $SrSO_4$, and to a lesser extent for CaF_2. $CaCO_3$, however, was better represented by a linear fit. The calculated ΔV^0 at one atm are reported in Table 2. The parabolic fit is equivalent to the equation given by Lown *et al.* (5) and therefore takes into account the compressibility. Particular note should be made of the $SrSO_4$ curve for 22 °C found in Fig. 3. Unlike the curves at 35 and 2 °C, the 22 °C curve has a definite break. ΔV for $P \leqslant 500$ atm and $P \geqslant 500$ atm are reported in Table 2.

Taking $SrSO_4$ as an example, the dissolution

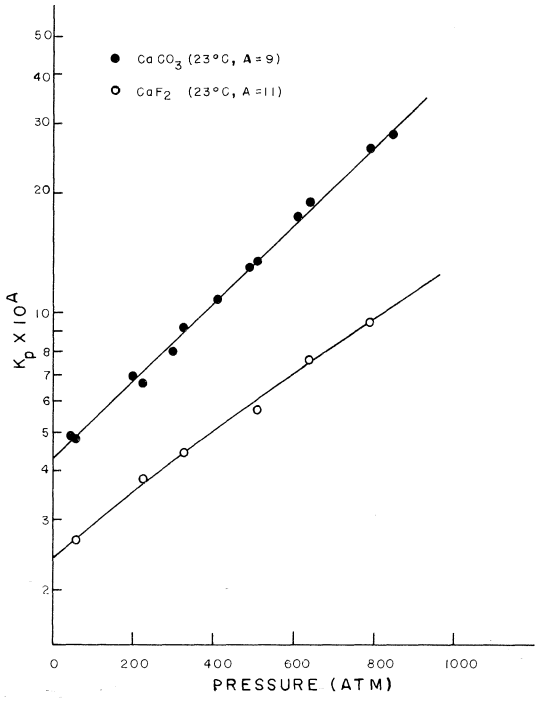

FIG. 2. A semi-log plot of K_p *vs.* pressure (in atm) for $CaCO_3$ and CaF_2.

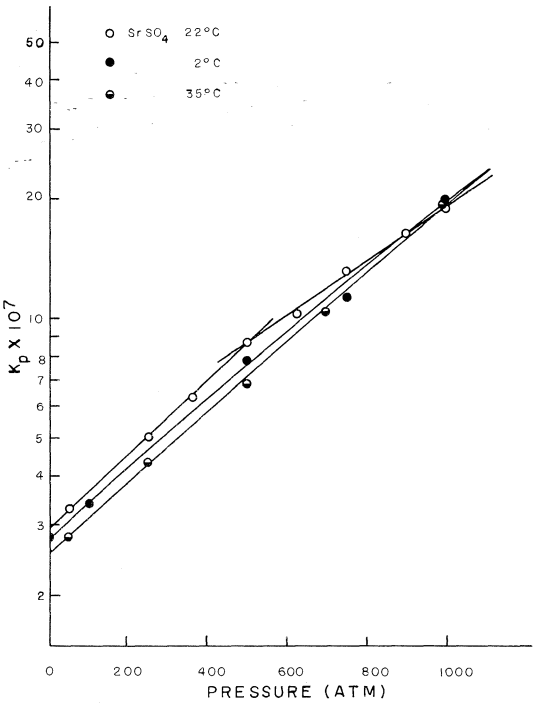

FIG. 3. A semi-log plot of K_p *vs.* pressure (in atm) for $SrSO_4$.

Can. J. Chem. Downloaded from www.nrcresearchpress.com by 210.87.254.6 on 09/05/12
For personal use only.

TABLE 1. Concentration of M^{2+} in saturated solutions and thermodynamic solubility products (pressures in atm, M^{2+} in μg/g)

$SrSO_4$				CaF_2				$CaCO_3$			
T (°C)	P	M^{2+}	$K_p \times 10^7$	T (°C)	P	M^{2+}	$K_p \times 10^{11}$	T (°C)	P	M^{2+}	$K_p \times 10^9$
2	1	55.0	2.77	25	25	7.22	2.19	1	95	4.62	6.51
	100	62.0	3.36		410	9.09	4.34		260	5.67	10.44
	500	97.8	7.76		518	9.86	5.52		390	6.42	13.85
	750	126.2	12.3		690	10.27	6.24		590	8.04	22.95
	1000	161.5	19.8		950	12.31	10.67		685	9.10	30.14
									795	10.22	39.01
22	50	61.0	3.26	23	55	7.73	2.86		875	11.33	48.66
	250	76.4	4.96		225	8.70	3.81				
	360	86.6	6.26		330	9.16	4.44	25	25	4.90	4.11
	500	102.6	8.57		510	9.96	5.69		250	5.91	6.74
	625	113.1	10.1		640	10.97	7.60		410	6.88	9.94
	750	130.0	13.0		790	11.82	9.45		518	7.75	13.41
	900	145.9	16.2						690	8.58	20.74
	1000	154.7	18.9						950	11.50	35.23
35	50	55.8	2.76					8	35	4.60	5.53
	250	75.4	4.23						185	5.46	8.37
	500	90.8	6.78						350	6.65	13.29
	700	114.3	10.4						505	7.69	17.27
	1000	154.7	18.0						640	8.91	25.99
									815	10.72	39.52
								23	45	5.28	4.93
									55	5.22	4.77
									200	6.02	6.96
									225	5.92	6.69
									300	6.43	8.03
									330	6.69	9.24
									405	7.13	10.77
									495	7.64	12.90
									510	7.80	13.50
									605	8.64	17.42
									640	8.92	18.91
									790	10.13	25.86
									845	10.45	27.96

TABLE 2. Volume change of dissolution

Solute	Temperature (°C)	V^0 (experimental, cc/mol)	Confidence intervals (95%)	V^0 (theoretical, anhydrous salt cc/mol)
$SrSO_4$	2	−48.1	±6.2	−56.1
$SrSO_4$	22 ($P \leqslant 500$)	−51.8	±2.7	−50.8
$SrSO_4$	22 ($P \geqslant 500$)	−39.0	±4.2	−50.8
$SrSO_4$	35	−53.2	±11.2	−49.5
$CaCO_3$	25	−58.0	±3.9	−59.1
$CaCO_3$	23	−54.9	±2.2	−59.5
$CaCO_3$	8	−57.5	±5.0	−62.3
$CaCO_3$	1	−57.1	±1.8	−63.7
CaF_2	25	−43.4	±7.8	−44.7
CaF_2	23	−44.3	±4.0	−44.9

reaction for the anhydrous salts is

[9] $$SrSO_{4(s)} \rightleftharpoons Sr^{2+} + SO_4^{2-}$$

and ΔV^0 for this reaction is

[10] $$\Delta V^0 = V^0(Sr^{2+},SO_4^{2-}) - V(SrSO_4)$$

where $V^0(Sr^{2+},SO_4^{2-})$ is the partial molal volume at atmospheric pressure of $SrSO_4$ dissolved in water at the same temperature at which the solubility products were determined. $V(SrSO_4)$ is the molal volume of anhydrous $SrSO_4$. The partial molal volumes of ions in distilled water at 0, 25, and 50 °C have been tabulated by Millero (6). Using these tables it is found that

[11] $$\Delta V^0(d,SrSO_4) = -50.6 \mp 0.097(T-25)$$

[12] $$\Delta V^0(d,CaCO_3) = -59.1 \mp 0.188(T-25)$$

[13] $$\Delta V^0(d,CaF_4) = -44.7 \mp 0.164(T-25)$$

where T is in °C.

Discussion

A comparison of the experimental and theoretical ΔV^0 for the dissolution of these three solids shows that only in the cases of $SrSO_4$, in the high temperature – low pressure region, and CaF_2 are the solubility pressure dependences in agreement with those predicted for the anhydrous salt. For $SrSO_4$, in the low temperature – high pressure region, the difference between the experimental and theoretical values is approximately 11 $cm^3\ mol^{-1}$.

This discrepancy between the experimental and theoretical ΔV^0 for $CaCO_3$ and $SrSO_4$ can be resolved if the equilibrating solid phases are considered to contain water(s) of crystallization. Using $SrSO_4$ as an example, the dissolution reaction for a hydrated solid is

[14] $$SrSO_4 \cdot nH_2O \rightleftharpoons Sr^{2+} + SO_4^{2-} + nH_2O$$

and the molal volume change for this reaction is

[15] $$\Delta V^0(d,SrSO_4 \cdot nH_2O) = V^0(Sr^{2+},SO_4^{2-}) + nV_W - V(SrSO_4 \cdot nH_2O)$$

where V_W and $V(SrSO_4 \cdot nH_2O)$ are the molal volumes of pure water and of the hydrated $SrSO_4$ solid respectively. To calculate a value for ΔV^0 from eq. 15, it is necessary to know the molal volume of the hydrated salt. Whilst the molal volumes of hydrated forms of $SrSO_4$ and $CaCO_3$ are not known, it is possible to estimate these from the measured molal volumes of other salts which occur in the anhydrous and hydrated forms. A comparison of the molal volumes of the corresponding hydrated and anhydrous forms of a number of group II salts shows that these volumes are related by the approximate expression

[16] $$V(SrSO_4 \cdot nH_2O) = V(SrSO_4) + n\overline{V}_W(cryst.)$$

where $\overline{V}_W(cryst.)$, the mean partial molal volume of the water of crystallization, is approximately 14.6 $cm^3\ mol^{-1}$ (1). By combining eqs. 10, 15, and 16 with 18.1 $cm^3\ mol^{-1}$ as the molal volume of water, it is seen that

[17] $$\Delta V^0(d,SrSO_4 \cdot nH_2O) = \Delta V^0(d,SrSO_4) + 3.5n$$

There are two significant features of eq. 17 which should be noted. Firstly, the volume change for the dissolution of a hydrated salt must always be more positive than that for the corresponding anhydrous salt. Secondly, the difference between the ΔV^0 for the corresponding

Can. J. Chem. Downloaded from www.nrcresearchpress.com by 210.87.254.6 on 09/05/12
For personal use only.

anhydrous and hydrated salts should be approximately 3.5 $cm^3\ mol^{-1}$ for each water of crystallization.

These two features are observed in the pressure of the solubilities of $CaCO_3$ and $SrSO_4$ (low temperature – high pressure region). The differences between the experimental and the theoretical, anhydrous, ΔV^0 for these two salts suggests that the hydrated solid phases are $CaCO_3 \cdot H_2O$ and $SrSO_4 \cdot 3H_2O$ respectively. From eq. 15 it follows that the molal volume of $CaCO_3 \cdot H_2O$ is 52.6 $cm^3\ mol^{-1}$, and that of $SrSO_4 \cdot 3H_2O$ is 89.7 $cm^3\ mol^{-1}$.

The $SrSO_4$ solubility measurements indicate the presence of two $SrSO_4$ solid phases: anhydrous $SrSO_4$, and $SrSO_4 \cdot 3H_2O$. The anhydrous salt forms the equilibrating solid phase at 35 °C, up to at least 1000 atm, and at 22 °C for pressures up to 500 atm. The hydrated salt forms the equilibrating solid phase at 2 and at 22 °C for pressures greater than 500 atm. In both cases the equilibrating solid phase is that form which has the lower solubility in water under the experimental conditions.

With $SrSO_4$, the phase transformation reaction is

$$[18] \quad SrSO_{4(s)} + 3H_2O \rightleftharpoons SrSO_4 \cdot 3H_2O_{(s)}$$

For this reaction ΔV^0 is $-11.0\ cm^3\ mol^{-1}$. From the value of ΔV^0 it is seen that, in accordance with the experimental observations, increasing the pressure will favor the formation of the hydrated solid from the anhydrous salt. The increased stability of anhydrous $SrSO_4$ with respect to $SrSO_4 \cdot 3H_2O$ at higher temperatures is a feature frequently observed with the hydrateable group II salts. For example, $MgSO_4 \cdot 7H_2O$ converts to anhydrous $MgSO_4$ at 200 °C (1).

In this paper the authors have postulated the existence of two hydrated salts: $CaCO_3 \cdot H_2O$, and $SrSO_4 \cdot 3H_2O$. The former has previously been reported (10) as the precipitant from solutions slightly over-saturated with Ca^{2+} and Co_3^{2-} ions. There have been no previous reports of any hydrated form of $SrSO_4$. However, the experimental conditions which were used in this work, namely a suspension of the solid in a large excess of water at low temperatures and high pressures, should be close to the ideal conditions for the formation of hydrated solids. Consequently, the hydrated solids formed under these conditions may not be sufficiently stable to be characterized by the more usual procedures: *i.e.*, at room temperature, atmospheric pressure, and isolation from the liquid. Conversely, when a normally anhydrous salt is placed in water, a hydrated phase may form on the surface of the solid. The presence of such a phase may not have a significant effect on solubility measurements carried out at constant pressure, but if the pressure dependency of the solubility of the salt is predicted on the assumption that the solid phase is anhydrous, the calculated high pressure solubility products will be appreciably greater than the true values.

Conclusion

The thermodynamic solubility products for CaF_2, $CaCO_3$, and $SrSO_4$ were determined at various temperatures between 0 and 35 °C for pressures of up to 1000 atm. The pressure dependence of the solubilities of $SrSO_4$, at 22 °C up to 500 atm and at 35 °C up to 1000 atm, and CaF_2 were in agreement with those calculated for the respective anhydrous salts. For $SrSO_4$, at 0 and at 22 °C above 500 atm, and $CaCO_3$ the high pressure solubility products were appreciably lower than those expected for the anhydrous salts. It was shown that these lower solubility products could be reasonably attributed to the formation of hydrated solids in equilibrium with the liquid. Such hydrate formation may occur with other salts which are normally only found in the anhydrous form. Consequently, any prediction of the pressure dependence of the solubility of a sparingly soluble salt should be treated with caution unless there is experimental evidence to justify the choice for the equilibrating solid phase.

1. The handbook of chemistry and physics, 51st ed. Chemical Rubber Company, 1971.
2. F. H. Fisher. J. Phys. Chem. **66**, 1607 (1962).
3. H. S. Harned and W. J. Hamer. J. Am. Chem. Soc. **55**, 2194 (1933).
4. R. A. Horne. Marine chemistry. Wiley–Interscience, New York. 1969. p. 207.
5. D. A. Lown, H. R. Thirsk, and Lord Wynne-Jones. Trans. Faraday Soc. **64**, 2073 (1968).
6. F. J. Millero. Water in aqueous solutions. *Edited by* R. A. Horne. J. Wiley and Sons, New York. 1972. Chapt. 13.
7. N. A. North. J. Phys. Chem. **77**, 931 (1973).
8. B. B. Owen and S. R. Brinkley. Chem. Rev. **29**, 461 (1941).
9. R. A. Berner. Principles of chemical sedimentology. McGraw–Hill, New York. 1971. p. 217.
10. I. W. Duedall and D. E. Buckley. Nature, Phys. Sci. **234**, 39 (1971).
11. N. A. North. Geochim. Cosmochim. Acta. To be published.

Can. J. Chem. Downloaded from www.nrcresearchpress.com by 210.87.254.6 on 09/05/12
For personal use only.

Alkali Tin Paraperiodates ($MSnIO_6$): Thermal Analyses, Electrical Conductivity, Infrared, and X-Ray Diffraction Studies

MAHADEVA NATARAJAN, PALEPU RAMAMURTHY, AND ETALO A. SECCO[1]

Department of Chemistry, St. Francis Xavier University, Antigonish, Nova Scotia

Received March 25, 1974

MAHADEVA NATARAJAN, PALEPU RAMAMURTHY, and ETALO A. SECCO. Can. J. Chem. **52**, 3187 (1974).

Crystalline sodium tin paraperiodate has been prepared; the X-ray powder diffraction data are indexed to the hexagonal system.

The thermal analyses, TG and DTA of $MSnIO_6$, where M = NH_4, Na, K, Rb, Cs, reveal that the initial mode of decomposition is via partial evolution of I_2 and O_2.

The infrared spectra of these compounds exhibit six well-defined absorption bands. These bands are located within the frequency region characteristic of I—O vibrational modes suggesting a lowering of the normal O_h symmetry for the $[IO_6]^{5-}$ species.

The electrical conductivity *vs.* temperature behavior for $CsSnIO_6$ is reported.

MAHADEVA NATARAJAN, PALEPU RAMAMURTHY et ETALO A. SECCO. Can. J. Chem. **52**, 3187 (1974).

On a préparé du periodato-stannate de sodium cristallin et déterminé sa structure à l'aide d'un diagramme de poudre. Les résultats permettent de l'identifier comme étant un système hexagonal.

Les analyses thermiques du composé $MSnIO_6$, dans lequel M est successivement NH_4, Na, K, Rb, Cs montrent que le mode initial de décomposition passe par une évolution partielle de I_2 et O_2.

Les spectres infrarouges de ces composés montrent six bandes d'absorption bien définies. Celles-ci sont situées dans la région de fréquences, caractéristique des modes vibrationnels I—O, et laissent supposer une diminution de la symétrie normale O_h pour le type $[I0_6]^{5-}$. On traite aussi du comportement de la conductivité électrique en fonction de la température du $CsSnIO_6$. [Traduit par le journal]

Introduction

Mixed metal paraperiodates (hereafter referred to simply as periodates) of the type $M^{I}M^{IV}IO_6$ have been known for some time (1, 2) but hitherto no detailed work on the physico-chemical aspects and mode of decomposition of this type of compound has been reported in the literature.

Recently, the alkali tin periodates, $MSnIO_6$ where M is NH_4, K, Rb, or Cs were prepared by Frydrych (3). The reported X-ray powder diffraction data were fitted to the hexagonal system; $NaSnIO_6$ was not obtained in the crystalline form.

The purpose of this paper is to report on the preparation of sodium tin periodate, the X-ray powder diffraction data of $NaSnIO_6$, the mode of decomposition, and infrared spectra of all the known alkali tin periodates along with some electrical conductivity measurements.

Experimental

All the periodate compounds used in this study were prepared according to Frydrych (3) with a slight modification in the procedure where $SnCl_4$ solution was added dropwise under constant stirring. The precipitates were aged at room temperature up to six weeks. (A trend in ageing time required for crystallization was observed: for Cs and Rb less than two weeks, for NH_4, K, and Na about six weeks.) The aged precipitates were washed in 30% acetic acid, ethanol, and ether, and finally dried at ~110 °C. The identity of each compound was ascertained from its known X-ray diffraction data and/or the results of thermogravimetry.

The X-ray diffraction patterns for $NaSnIO_6$, confirmed in four different preparations, were recorded on a Norelco diffractometer unit previously described (4).

Thermoanalytical results were obtained on a DuPont Thermal Analyzer, DTA-900 and TGA-950, and DuPont 1200 °C DTA cell, at constant heating rate of 20° min^{-1} as previously described (5). The solid products of decomposition were identified by their X-ray powder diffraction patterns.

The infrared spectra were recorded on a Perkin–Elmer Model-180 spectrometer using the standard KCl pellet technique.

Conductivity measurements were made on compressed polycrystalline powder discs (2 mm thickness and 12 mm diameter) in a stainless steel conductivity cell whose construction (6*a*) and conditions of operation (6*b*) have already been described.

[1]To whom correspondence should be addressed.

Can. J. Chem. Downloaded from www.nrcresearchpress.com by 210.87.254.42 on 09/05/12
For personal use only.

TABLE 1. Powder diffraction X-ray data on $NaSnIO_6$*

Line number	d (Å) Observed	d (Å) Calculated	hkl	Uncorrected I/I_0
1	5.198	5.198	002	85
2	4.555	4.555	100	70
3	3.423	3.423	102	100
4	2.626	2.627	110	70
5	2.591	2.590	004	10
6	2.347	2.345	112	70
7	2.253	2.257	104	15
8	2.081	2.081	202	35
9	1.849	1.848	114	50
10	1.720	1.720	120	10
11	1.711	1.712	204	13
12	1.631	1.633	122	20
13	1.539	1.541	123	30
14	1.448	1.447	116	10
15	1.436	1.434	124	8

*Cell constants: $a_0 = 5.278$ Å; $c_0 = 10.398$ Å.

Results and Discussion

X-Ray Diffraction Analysis

Our X-ray powder diffraction data agree very well with those data previously reported by Frydrych (3). The data for $NaSnIO_6$ were indexed (7) to the hexagonal system with the cell constants calculated to be $a_0 = 5.28$ Å and $c_0 = 10.40$ Å. The sodium analog is therefore isomorphous with the other members of this series. The observed and calculated d spacings (Table 1) along with their relative intensities and hkl values are placed with the Depository of Unpublished Data.[2]

An examination of the d spacings for the $MSnIO_6$ compounds reveals that those d values identified with crystallographic planes (hkl) incorporating the cell edge c_0 vary in the series whereas the cell edge a_0 remains unaffected. Assuming the c_0 to be a function of the crystal radius of the alkali metal ion r (8), the c_0/a_0 ratio was plotted against the ionic radius r, Fig. 1. The quasi-linear dependence of c_0/a_0 with r indicates a contraction of the hexagonal unit cell in going from $CsSnIO_6$ to $NaSnIO_6$. The unfilled dotted circle represents the extrapolated $c_0/a_0 \sim 1.63$ for the expected Li analog with $r(Li^+) = 0.60$ Å; this value is the theoretical limit of c_0/a_0 assumed for the closest packed hexagonal system. The above relation could explain our repeated failure to obtain crystalline $LiSnIO_6$.

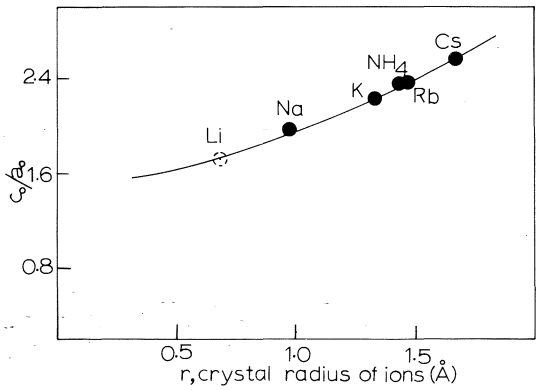

FIG. 1. The c_0/a_0 ratio of the hexagonal unit cell of $MSnIO_6$ (M = Na, K, Rb, Cs, or NH_4) as a function of r, the ionic crystal radius of the ions, M^+.

Thermal Analyses

The thermal decomposition of these periodates were studied by both differential thermal analysis (DTA) and thermogravimetry (TG). On the basis of thermal analysis behavior, the compounds are discussed under two groups.

$MSnIO_6$ (M = Na, K, Rb, or Cs)

Typical DTA and TG recorded traces represented by $NaSnIO_6$ and $CsSnIO_6$ are presented in Fig. 2 *a* and *b* where solid and broken lines in Fig. 2*a* represent heating and cooling modes, respectively. Similar recorded curves were obtained for $KSnIO_6$ and $RbSnIO_6$. The peak

[2]Complete set of data may be obtained, at a nominal charge, from the Depository of Unpublished Data, National Science Library, National Research Council of Canada, Ottawa, Canada K1A 0S2.

Can. J. Chem. Downloaded from www.nrcresearchpress.com by 210.87.254.42 on 09/05/12
For personal use only.

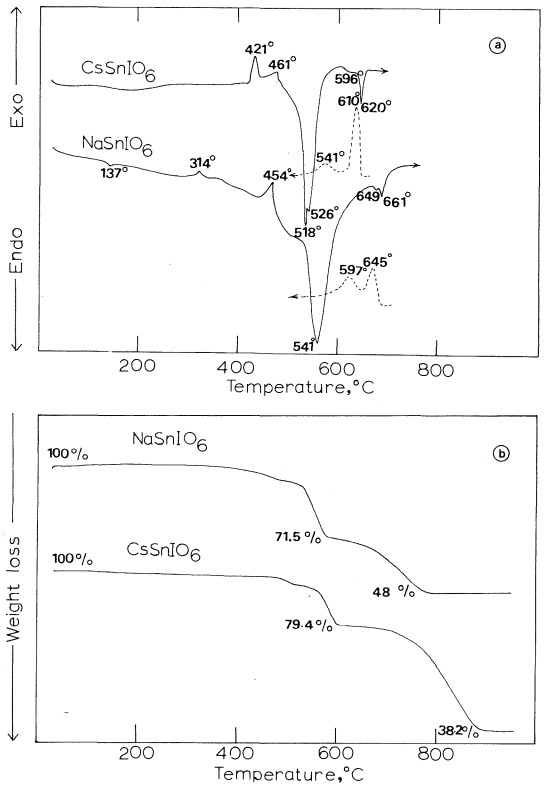

FIG. 2. (*a*) Differential thermal analyses traces of $CsSnIO_6$ and $NaSnIO_6$. Solid lines refer to heating mode, broken lines refer to cooling mode. (*b*) Thermogravimetrical analyses curves for $NaSnIO_6$ and $CsSnIO_6$. The weight ordinate in arbitrary units.

temperatures for the observed thermal effects and the thermogravimetric data are given in Table 2.

Since these compounds were in a highly crystalline state, the two weak exothermic effects preceding the intense decomposition endotherm cannot be ascribed to crystallization. The TG trace shows a very slight weight loss in the temperature interval of these two weak exotherms which suggests a predissociation of metastable imperfections (occlusions and/or surface growth) prior to the major bulk decomposition step. The TG data for the main decomposition step can be fitted to the general equation

$$[1]\quad 3MSnIO_6 \rightarrow 2MI + \tfrac{1}{2}M_2O_2 + 3SnO_2 + \tfrac{11}{2}O_2\uparrow + \tfrac{1}{2}I_2\uparrow$$

The visual evolution of elemental iodine fumes during this stage supports this mode of decomposition and is consistent with the earlier observation (2). A shoulder precedes the major endotherm for the Rb, K, and Na compounds, becoming most prominent in $NaSnIO_6$, suggesting that the decomposition involves two overlapping steps. The decreasing peak temperature for the decomposition endotherm in going from Na to Cs, Table 2, parallels the trend reported by Balek and Julek (9) on some group IIA periodates.

Two additional endotherms appear on the DTA heating curve after the bulk decomposition reaction, that is, in the residue from [1]. The first weaker endotherm is assigned to M_2O_2 melting and the second endotherm is identified with MI fusion (both effects appear as exotherms on cooling). These two latter endotherms were confirmed by DTA on a Na_2O_2–NaI–SnO_2 mixture in a 1:4:6 mole ratio. However, X-ray diffraction of the solid residue from [1] revealed lines characteristic of only SnO_2 and NaI. The second major weight loss in the TG curve was confirmed using a stoichiometric mixture as above, to be due to (*i*) volatilization of I_2 in the case of Na salt, (*ii*) volatilization of MI in the case of K and Rb salts, and (*iii*) volatilization of CsI and Cs_2O_2 leaving a final residue of SnO_2 in the case of $CsSnIO_6$. The final residue from Na, K, and Rb periodates gave a strong alkaline test in water whereas the final residue from $CsSnIO_6$ was non-alkaline.

NH_4SnIO_6

Differential thermal analysis and TG heating traces are presented in Figs. 3*a* and *b*.

The TG data for NH_4SnIO_6 (*A*) are fitted to the decomposition pattern of $CsSnIO_6$ as shown in Table 2. In contrast with this result, the TG curve for NH_4SnIO_6 (*B*), that is the original NH_4SnIO_6 precipitate stored for two months in a dessicator, reveals a sharp one step process amounting to 83% weight loss. This feature suggests a rapid disintegration process with a concomitant volatilization and splattering of the reaction products.

The DTA heating trace for NH_4SnIO_6 illustrates the fundamental distinct features relative to the heavier members of this series, *viz.* the decomposition step occurs at much lower temperatures with an exothermic effect and no evidence of MI or M_2O_2 fusion endotherms. The presence of NH_4I and $(NH_4)_2O_2$ are thought to

Can. J. Chem. Downloaded from www.nrcresearchpress.com by 210.87.254.42 on 09/05/12
For personal use only.

Can. J. Chem. Downloaded from www.nrcresearchpress.com by 210.87.254.42 on 09/05/12
For personal use only.

TABLE 2. DTA and TGA data of $MSnIO_6$

	DTA			TGA				
						% of total weight lost		
M	Peak No.	Peak temperature (°C)	Reaction*	Step No.	Temperature (°C)	Observed	Calculated	Reaction*
Na	1	314	[D]	1	350–380	28.5	27.6	[1]
	2	454						
	3†	541	[1]	2	630–860	52.0	51.0	[A]
	4†	649	Na_2O_2 fusion					
	5†	661	NaI fusion					
K	1	436	[D]	1	510–620	26.5	26.5	[1]
	2	464						
	3†	513	[1]	2	685–960	57.5	56.0	[B]
	4†	527						
	5†	626	K_2O_2 fusion					
	6†	669	KI fusion					
Rb	1	424	[D]	1	440–600	22.8	23.5	[1]
	2	457						
	3†	525	[1]	2	630–930	59.0	57.5	[B]
	4†	534						
	5†	605	Rb_2O_2 fusion					
	6†	630	RbI fusion					
Cs	1	421	[D]	1	480–595	20.6	21.3	[1]
	2	461						
	3†	518	[1]	2	660–910	61.6	61.3	[C]
	4†	526						
	5†	596	Cs_2O_2 fusion					
	6†	620	CsI fusion					
NH_4	1	296	[1]	1	200–350	26.2	27.9	[1]
	2†	435		2	410–630	56.5	58.2	[C]

*[A], loss of I_2; [B], loss of 2MI; [C], loss of 2MI, $\frac{1}{2}M_2O_2$; [D], metastable micro effects.
†Endotherm.

Can. J. Chem. Downloaded from www.nrcresearchpress.com by 210.87.254.42 on 09/05/12
For personal use only.

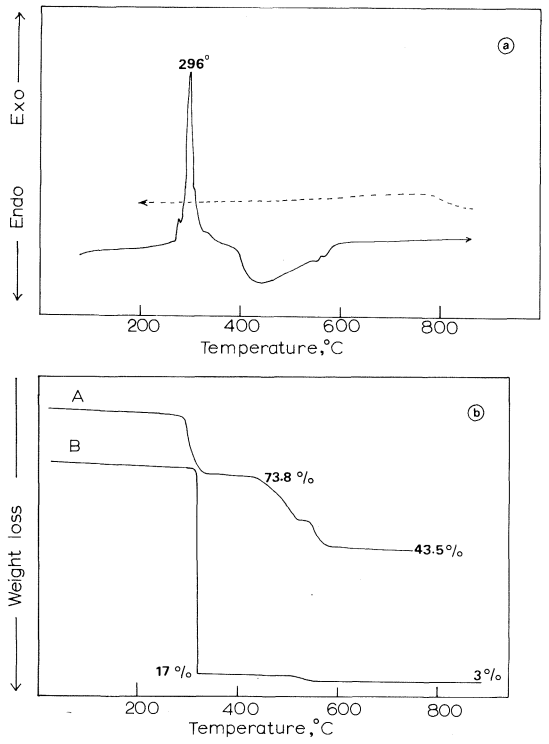

FIG. 3. (*a*) Differential thermal analyses curve (solid and broken lines refer to heating and cooling modes respectively) of NH_4SnIO_6 (*A*). (*b*) Thermogravimetric analyses curves for fresh NH_4SnIO_6 (*A*) and stored NH_4SnIO_6 (*B*).

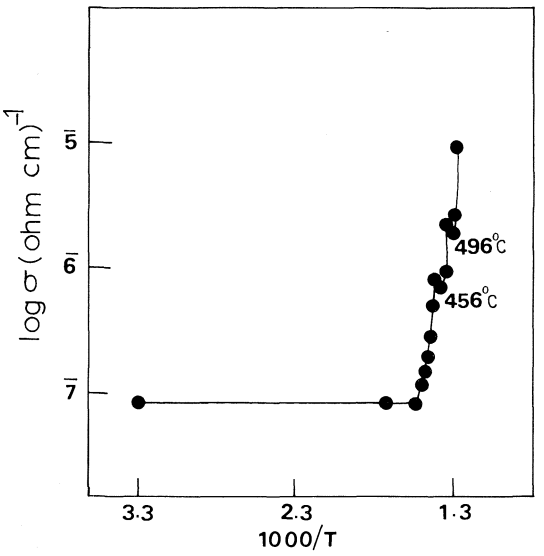

FIG. 4. Logarithm of electrical conductivity, σ versus reciprocal of absolute temperature, *T* for $CsSnIO_6$.

be tied up with SnO_2 as $NH_4I.(NH_4)_2SnO_4$ which subsequently dissociates at >410 °C to give a residue of SnO_2 identified by X-ray diffraction.

Electrical Conductivity

The results of conductivity measurements on $CnSnIO_6$ powder specimen is shown in Fig. 4 where the logarithm of conductivity, σ, is plotted *vs.* reciprocal temperature, *T*. The conductivity of $CsSnIO_6$ remains constant from room temperature to 380 °C. The rapid rise in conductivity above 380 °C and the two anomalies at 456 and 496 °C can be correlated with the two weak exothermic effects ascribed to the predissociation of metastable imperfections. Above 500 °C the conductivity increases sharply with the onset of decomposition.

Infrared Spectra

The infrared spectral data of all compounds are presented in Table 3. All compounds gave six well-defined absorption bands typified by $RbSnIO_6$ in Fig. 5.

To our knowledge no infrared spectrum has been reported and no vibrational analysis is available for tin paraperiodates, $MSnIO_6$. Since each of the six bands show essentially a constant

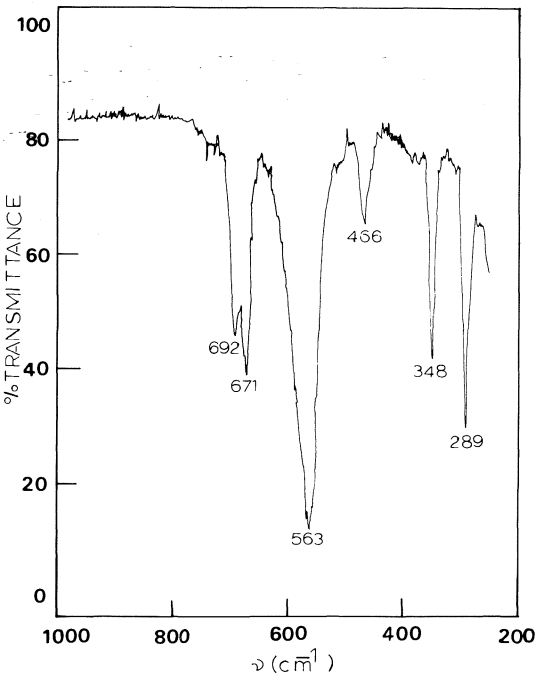

FIG. 5. Infrared absorption spectrum of $RbSnIO_6$ in KCl pellet matrix.

TABLE 3. Infrared absorption band frequencies of $MSnIO_6$*

	Frequency (cm^{-1}) for M =				
Band	Na	K	Rb	Cs	NH_4
1	695(s)	690(s)	692(s)	687(s)	693(s)
2	674(s)	674(s)	671(s)	670(s)	675(s)
3	570(s,br)	563(s,br)	563(s,br)	560(s,br)	560(s,br)
4	478(m)	470(m)	466(m)	462(m)	467(m)
5	353(s)	349(s)	348(s)	349(s)	347(s)
6	293(s)	290(s)	289(s)	288(s)	287(s)

*s = strong, m = medium, w = weak, br = broad, vbr = very broad.

frequency, within 10 cm^{-1}, it is unlikely that any mode intimately involves the alkali metal M. Furthermore, these bands are located within the frequency region characteristic of iodine–oxygen vibrational modes observed in iodates (10, 11), periodates, and paraperiodates (12).

The paraperiodate ion $[IO_6]^{5-}$ was fitted to an octahedral arrangement of six oxygens about the central iodine (13). Of the six normal modes of vibration for O_h symmetry, only two (ν_3, ν_4) are predicted to be infrared active. The appearance of six infrared bands in the I—O vibrations region strongly suggests a reduction of the $[IO_6]^{5-}$ O_h symmetry. Two structural effects can account for this lowering of symmetry, (*i*) monodentate (C_{4v}) IO_6 group and (*ii*) crystal field. It is virtually impossible to distinguish between these two effects in the absence of single crystal structural data on $MSnIO_6$ compounds.

In addition to the IO_6 group, the presence of the SnO_6 group in crystalline state of the $MSnIO_6$ compounds is a distinct possibility. We have observed stannates to exhibit absorption bands in the region 300–700 cm^{-1} as well and it has been suggested (14) that of the six observed bands in this region some bands might originate with SnO_6 vibrational modes (ν_3 and ν_4).

Grateful acknowledgement is made to the National Research Council of Canada and the University Council for Research for financial support of this research program.

1. P. RAY and B. SHARMA. J. Indian Chem. Soc. **25**, 205 (1948).
2. I. REIMER and M. W. LISTER. Can. J. Chem. **39**, 2431 (1961).
3. R. FRYDRYCH. Chem. Ber. **103**, 327 (1970).
4. E. A. SECCO. Can. J. Chem. **42**, 2144 (1964).
5. O. K. SRIVASTAVA and E. A. SECCO. Can. J. Chem. **45**, 579 (1967).
6. (*a*) P. N. MEHROTRA. Ph.D. Thesis, Indian Institute of Technology, Kanpur, India. 1968; (*b*) M. NATARAJAN and E. A. SECCO. Can. J. Chem. **52**, 712 (1974).
7. B. D. CULLITY. Elements of X-ray diffraction. 2nd ed. Addison–Wesley, Mass. 1959. p. 312.
8. L. PAULING. Nature of chemical bond. 3rd Ed. Cornell University Press, Ithaca, New York. 1960. p. 514.
9. V. BALEK and J. JULEK. J. Thermal Anal. **4**(3), 293 (1972).
10. W. E. DASENT and T. C. WADDINGTON. J. Chem. Soc. 2429 (1966).
11. C. ROCCHICCIOLI. C. R. **242**, 2922 (1956); **249**, 236 (1959); **250**, 1232 (1960).
12. H. SIEBERT. Z. Anorg. Allg. Chem. **273**, 22 (1953); **303**, 162 (1960).
13. L. HELMHOLZ. J. Am. Chem. Soc. **59**, 2036 (1937).
14. G. BLASSE. Private communication. J. TH. W. DEHAIR, A. F. CORSMIT, and G. BLASSE. J. Inorg. Nucl. Chem. **36**, 313 (1974).

Can. J. Chem. Downloaded from www.nrcresearchpress.com by 210.87.254.42 on 09/05/12
For personal use only.

Isoxazole Hydrate

S. R. GOUGH, S. K. GARG, J. A. RIPMEESTER, AND D. W. DAVIDSON
Division of Chemistry, National Research Council of Canada, Ottawa, Canada K1A 0R9

Received April 22, 1974

S. R. GOUGH, S. K. GARG, J. A. RIPMEESTER, and D. W. DAVIDSON. Can. J. Chem. **52**, 3193 (1974).

X-Ray, n.m.r., and dielectric studies show that the hydrate of isoxazole is a typical type II clathrate hydrate in structure, in reorientation rates of host and guest molecules, and in composition.

S. R. GOUGH, S. K. GARG, J. A. RIPMEESTER et D. W. DAVIDSON. Can. J. Chem. **52**, 3193 (1974).

Des études de rayon-X, de r.m.n. et de relaxation diélectriques montrent que l'hydrate d'isoxazole est un hydrate de clathrate de type II typique tant au point de vue de sa structure, des taux de réorientation des molécules réticulaires et encagées, et de sa composition.
[Traduit par le journal]

A hydrate of isoxazole (CH=CHCH=NO) with a decomposition temperature of 271 K was recently found by Kaloustian *et al.* (1) from thermal analysis. It was reported to give (2) the same X-ray powder diffraction pattern as the well-known structure II (3) clathrate hydrate of tetrahydrofuran (4) but to contain (1) 34 mol of water per mol of isoxazole, in contrast to the ~17:1 water/guest mole ratio which characterizes tetrahydrofuran and other structure II hydrates (5).

We summarize here the results of X-ray, continuous wave n.m.r., and dielectric studies of isoxazole hydrate.

The X-ray powder diffraction pattern (6) of a sample of composition $C_3H_3NO{\cdot}14.7H_2O$, conditioned for 36 h at 259 K, was that characteristic of the structure II hydrate lattice, $Fd3m$, a = 17.17 ± 0.09 Å at ~120 K, where the error is the standard deviation of measurement of 16 lines. Several weak lines due to ice I*h* were also observed.

Derivatives of the proton magnetic resonance lines of a sample of composition $C_3H_3NO{\cdot}19.9D_2O$, conditioned for more than a week at 261 K, were recorded at temperatures between 4.2 and 212 K and a frequency of ~16 MHz with a marginal oscillator (7). Spectra obtained below about 15 K and above about 85 K showed some saturation even at the lowest level of oscillation, but not to the extent necessary to significantly affect the line widths (separation of derivative *extrema*)

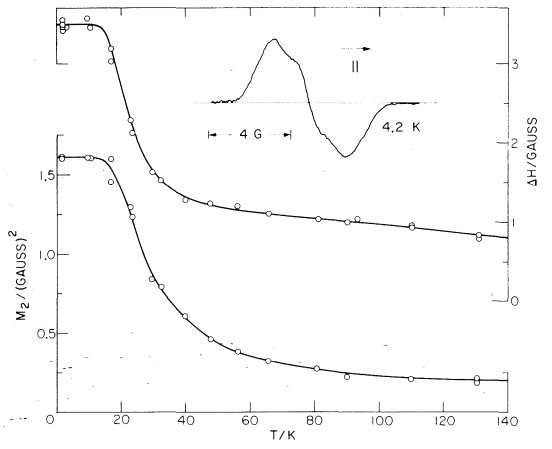

FIG. 1. Line width and second moment of the p.m.r. of the deuteriohydrate of isoxazole. The rigid-lattice derivative line shape is also shown.

and second moments (corrected for audio-frequency modulation) plotted in Fig. 1.

The rigid-lattice line shape reached at the lowest temperatures has no well-defined fine structure; the corresponding second moment (1.6_1 G^2) is much smaller than that of a Gaussian line of the experimental width (3.5 G). The experimental rigid-lattice second moment agrees well with the value of 1.6 G^2 calculated for the model (8) in which the isoxazole molecule is fixed in random orientations with the center of mass located at the center of the 16-hedral cage and the C_3H_3 group is assumed to have the same geometry as the corresponding group in furan (9). The second moment then includes an intra-

[1]NRCC No. 14133.

Can. J. Chem. Downloaded from www.nrcresearchpress.com by 210.87.254.42 on 09/05/12
For personal use only.

isoxazole contribution of 1.3_8 G^2, an inter-isoxazole contribution of 0.09 G^2, and a contribution of 0.13 G^2 from D_2O.

The second moment (Fig. 1) begins to fall at about 15 K, reaches 0.80 G^2 at 32 K and 0.20 G^2 at 125 K, and at 211 K attains a value ($\sim$0.14 G^2) not much greater than the 0.10 G^2 that corresponds (8) to isotropic rotation of both isoxazole and D_2O molecules. A similar decrease of second moment over a wide temperature range is found in structure II deuteriohydrates of other polar guest molecules; the shape of the second moment curve of Fig. 1 resembles especially that shown by tetrahydrofuran (10).

Dielectric relaxation of both water and isoxazole molecules was measured (11) at frequencies between 0.1 Hz and 1 MHz and temperatures between 1.8 and 262 K. A suspension of composition $C_3H_3NO{\cdot}17.0H_2O$ was frozen in the dielectric cell and conditioned at 261 K for a week.

The complex permittivity plot at relatively high temperatures showed the locus characteristic of the relaxation of the water molecules of the structure II lattice (11), overlapped on the low-frequency side by a dispersion–absorption region ascribable to ice. Since the maximum absorption by ice occurred at a frequency which was lower by a factor of more than 30 than the frequency of the maximum of the dominant absorption by the hydrate, the latter was not appreciably affected by the presence of ice. The Arrhenius plot of this frequency (Fig. 2) gives an activation energy of 7.1 kcal/mol for reorientation of the water molecules in isoxazole hydrate above 180 K (*cf.* 7.4 kcal/mol in tetrahydrofuran hydrate (11)). The curvature which occurs at lower temperatures is also present in the rate plots of all structure II hydrates previously studied (8, 11).

Figure 3 shows the variation with temperature of the permittivity measured on the high frequency side of the water dispersion region. This is shown as ε_{02}, the static permittivity with respect to reorientation of isoxazole molecules. Its dependence on temperature may be explained in the same way as for other structure II hydrates of polar molecules (II), the relatively large values of ε_{02} (*eg.*, almost 14 near 40 K) being a consequence of the reorientational freedom and large dipole moment (2.9 D (12)) of isoxazole. Dispersion of the permittivity occurs at low temperatures as the reorientation rates become comparable to the measuring frequencies. The corresponding absorption is illustrated in the inset of Fig. 3. In terms of frequency, the dispersion and absorption are very broad and as before (11) squat and asymmetric Cole–Cole plots result. The Arrhenius plot (Fig. 2) of the rather ill-defined frequency of maximum absorption yields an "activation energy" of 1.25 kcal/mol for reorientation of encaged isoxazole between 17 and 30 K. Values of 0.91 and 1.02 kcal/mol were previously found (11) for reorientation of

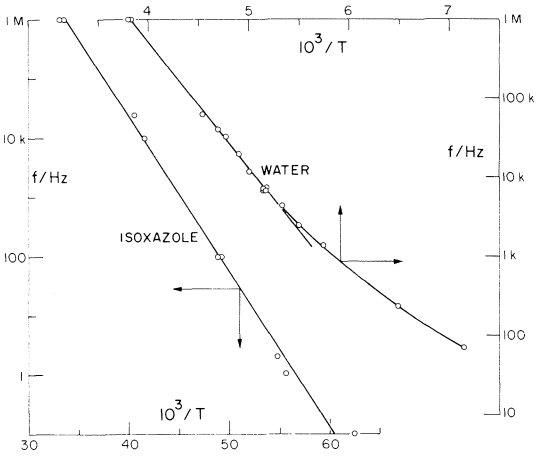

FIG. 2. Arrhenius plots of frequencies of maximum dielectric absorption by host and guest molecules of isoxazole hydrate.

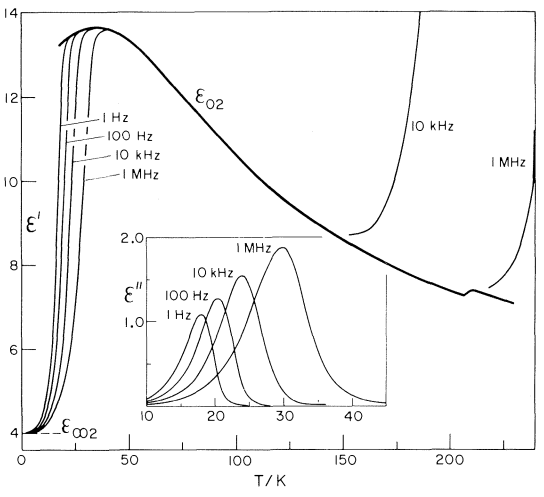

FIG. 3. Temperature dependence of measured ε_{02} of isoxazole hydrate. Dispersion associated with reorientation of isoxazole and water molecules is shown at low and high temperatures, respectively. Dielectric absorption by isoxazole is shown in the inset.

Can. J. Chem. Downloaded from www.nrcresearchpress.com by 210.87.254.42 on 09/05/12
For personal use only.

tetrahydrofuran and acetone in the isostructural hydrates.

At the lowest temperatures the permittivity measured is $\varepsilon_{\infty 2}$, a value which includes no relaxational contribution. When allowance is made for the presence of ice, the experimental value of 4.0 is raised to 4.2. This high value, like the values of 3.5 and 4.0 previously reported (11) for tetrahydrofuran and acetone hydrates, must include a substantial contribution from rotational oscillations of the guest molecules.

Previous examination (5) of the composition data for structure II hydrates of a large number of guest species M failed to show an experimentally significant departure from the ideal composition of $M{\cdot}17H_2O$. Likewise, the present dielectric and n.m.r. results are not consistent with any substantial departure from this stoichiometry. For example, the experimental value of ε_{02} is 8.1 at 168 K, a temperature where the n.m.r. results show the isoxazole molecules to be undergoing very nearly isotropic reorientation. As a result of some incomplete "reaction", the dielectric sample contained not only ice but also some unhydrated isoxazole, as may be seen from the small break in the ε_{02} curve (Fig. 3) at 206 K, the eutectic temperature. Allowance for the ice and solid isoxazole present raises ε_{02} at 168 K to about 9.4, a value which lies on the line relating ε_{02} to the square of the guest-molecule dipole moment for structure II hydrates of normal composition. (See Fig. 2 of ref. 13.) A value of no more than 6.2 would be expected for the composition $C_3H_3NO{\cdot}34H_2O$ previously proposed (1) to result from occupancy of only half of the 16-hedral cages.

We conclude that isoxazole hydrate differs in no essential way from other structure II hydrates. Isoxazole molecules of maximum van der Waals diameter $\sim$5.9 Å easily occupy, and have considerable reorientational freedom within, the 16-hedral cages of free diameter 6.6 Å.

Concurrent permittivity measurements of solid isoxazole gave values between 2.9 and 3.0 at temperatures down to 77 K and therefore showed no evidence of the presence of a rotator phase such as is found for furan (14, 15).

We are indebted to Mrs. F. Lee for the diffraction photographs.

1. J. KALOUSTIAN, J. C. ROSSO, and L. CARBONNEL. C.R. Acad. Sci. Paris, Ser. C. **275**, 249 (1972).
2. L. CARBONNEL, J. C. ROSSO, and C. CARONI. C.R. Acad. Sci. Paris, Ser. C. **276**, 619 (1973).
3. M. VON STACKELBERG and H. R. MÜLLER. Z. Elektrochem. **58**, 25 (1954).
4. M. VON STACKELBERG and B. MEUTHEN. Z. Elektrochem. **62**, 130 (1958).
5. S. R. GOUGH and D. W. DAVIDSON. Can. J. Chem. **49**, 2691 (1971).
6. D. F. SARGENT and L. D. CALVERT. J. Phys. Chem. **70**, 2689 (1966).
7. S. K. GARG and D. W. DAVIDSON. J. Chem. Phys. **58**, 1898 (1973).
8. D. W. DAVIDSON. *In* Water, a comprehensive treatise. Vol. 2. *Edited by* F. Franks. Plenum Press, New York. 1973. p. 115.
9. B. BAK, L. HANSEN, and J. RASTRUP-ANDERSEN. Discuss. Faraday Soc. **19**, 30 (1955).
10. J. A. RIPMEESTER, S. K. GARG, and D. W. DAVIDSON. J. Magn. Reson. To be published.
11. S. R. GOUGH, R. E. HAWKINS, B. MORRIS, and D. W. DAVIDSON. J. Phys. Chem. **77**, 2969 (1973).
12. W. C. MACKRODT, P. A. CURNUCK, A. WARDLEY, N. L. OWEN, and J. J. SHERIDAN. Chem. Commun. **19**, 692 (1966).
13. S. R. GOUGH and D. W. DAVIDSON. *In* Physics and chemistry of ice. *Edited by* E. Whalley, S. J. Jones, and L. W. Gold. R. Soc. Can. Ottawa, Canada. 1973.
14. F. FRIED and B. J. LASSIER. J. Chim. Phys. **63**, 1 (1966).
15. J. A. RIPMEESTER and B. A. DUNELL. Can. J. Chem. **52**, 192 (1974).

Can. J. Chem. Downloaded from www.nrcresearchpress.com by 210.87.254.42 on 09/05/12
For personal use only.

Carbon-13 Nuclear Magnetic Resonance Studies of Some Methyl Substituted Diphenylmethanes

GERALD W. BUCHANAN[1]

Department of Chemistry, Carleton University, Ottawa, Canada K1S 5B6

AND

GIORGIO MONTAUDO AND PAOLO FINOCCHIARO

Institute of Industrial Chemistry of the University of Catania, Catania, Italy 95125

GERALD W. BUCHANAN, GIORGIO MONTAUDO, and PAOLO FINOCCHIARO. Can. J. Chem. **52**, 3196 (1974).

Carbon-13 n.m.r. chemical shifts are reported for diphenylmethane and nine methylated derivatives. Results are compared with those for related methylbenzenes. In the case of tri-*ortho*-substituted materials the predominance of a perpendicular conformation is suggested. Ring current calculations show that in contrast to the ^1H chemical shift interpretations, the ^{13}C shielding trends cannot originate primarily from anisotropic effects.

GERALD W. BUCHANAN, GIORGIO MONTAUDO et PAOLO FINOCCHIARO. Can. J. Chem. **52**, 3196 (1974).

On rapporte les déplacements chimiques du carbon 13 en r.m.n. pour le diphénylméthane et neuf dérivés méthylés. On compare les résultats avec ceux obtenus pour des méthylbenzènes similaires. Dans le cas des composés tri-*ortho* substitués, les résultats suggèrent la prépondérance d'une conformation perpendiculaire. Des calculs de courant de cycle montrent que contrairement aux interprétations de déplacement chimique des protons, les tendances dans les constantes d'écran des carbon 13 ne peuvent pas avoir leur origine dans des effets anisotropiques.
[Traduit par le journal]

Introduction

Previous reports from these laboratories have dealt with ^{13}C n.m.r. chemical shifts for a series of *ortho*-substituted diphenyl ketones (1) and diphenyl ethers (2). In particular, the ^{13}C shieldings were correlated with molecular conformations via a measure of the steric interference to conjugation between the bridged carbonyl group or oxygen atom and the phenyl rings.

For diphenylmethanes, conjugation through the bridging methylene group is expected to be minimal. From ^1H n.m.r. data (3, 4), preferred conformations can be deduced only for tri- and tetra-*ortho*-substituted diphenylmethanes. Among the possible conformers in the tri-substituted materials, only those with the *ortho* hydrogen inside the π-cloud of the adjacent phenyl moiety were judged to be populated appreciably.

No conformational conclusions regarding mono- and di-*ortho*-substituted diphenylmethanes were possible based on ^1H n.m.r. data. Since it is known (5) that ^{13}C shieldings can be an order of magnitude more sensitive to structural change than ^1H shifts, we now have investigated the application of ^{13}C n.m.r. to this problem. Furthermore, supporting evidence for the previous conclusions regarding the solution geometry of triply substituted materials is desirable.

Results and Discussion

To facilitate comparison, previously reported (6) carbon shifts for some pertinent methylbenzenes are presented in Table 1. Aryl carbon shieldings for the diphenylmethanes are shown in Table 2 while the shifts for the methyl and methylene groups are tabulated in Table 3. Values in parentheses indicated possible ambiguities in the assignments.

Standard procedures were employed for resonance assignments. Carbons bearing no directly bonded protons were identified by their retention of singlet structure in off-resonance decoupling. From the previous ^1H n.m.r. work (3) it is known that diphenylmethanes having at least one *ortho* methyl group in each ring exhibit shielding effects for the remaining *ortho* proton, thus permitting designation of *ortho* carbon resonance from specific decoupling. In symmetrical compounds, relative peak intensities were valuable as an aid,

[1]To whom correspondence should be addressed.

TABLE 1. ^{13}C chemical shifts for some methylbenzenes (δ_C from TMS ± 0.1)*

Compound	Methyl position	C-1	C-2	C-3	C-4	C-5	C-6	1-CH_3	2-CH_3	3-CH_3	4-CH_3	5-CH_3
1	1	137.8	129.3	128.5	125.6	128.5	129.3	21.3				
2	1,2	136.4	136.4	129.9	126.1	126.1	129.9	19.6	19.6			
3	1,4	134.5	129.1	129.1	134.5	129.1	129.1	20.9			20.9	
4	1,2,4	133.4	136.3	130.5	135.2	126.7	129.8	19.1	19.5		20.9	
5	1,2,3,5	136.0	131.6	136.0	128.9	134.3	128.9	20.3	14.6	20.3		20.9
6	1,2,3,4,5	133.0	132.1	134.5	132.1	133.0	131.5	20.7	15.8	16.1	15.8	20.7

*0.5 *M* solutions in $CDCl_3$.

since care was taken to minimize differential nuclear Overhauser enhancements.

It is interesting to compare the ring carbon chemical shifts of diphenylmethane **7** with toluene **1**. With the exception of C-1 of **7** which is deshielded by a β substituent effect (5) relative to C-1 of **1**, the aryl carbon shieldings are remarkably similar, suggesting minimal conjugative interaction between the aromatic functions of **7**.

For the 2-methyl derivative **8**, the aryl shieldings for the substituted ring correspond closely to those for *o*-xylene **2**. Chemical shifts for carbons in the non-methylated ring are nearly identical to those for **7**, indicating that a single *ortho* methyl function induces little or no conformational preference in diphenylmethanes which is detectable by ^1H or ^{13}C chemical shifts. A clear consequence of *ortho*-methyl substitution, however, is the shielding effect of 2.5 p.p.m. exhibited by the methylene carbon of **8** relative to **7**. This is a manifestation of the 'γ' steric shift (5) for which a theoretical model based on a concept of sterically induced charge polarization (7) has been advanced.

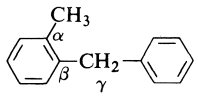

Results for the 4-methyldiphenylmethane **9** can be compared with those for *p*-xylene **3** and a striking similarity is evident for the methylated ring. As might be expected, there is no pronounced influence of the 4-CH_3 group on either the CH_2 or the remote ring carbons relative to **7**.

In the tetramethyl derivative **10**, again the remote ring carbon shieldings are within 1 p.p.m. of those of **7**, suggesting that no conformational preferences can be detected by ^{13}C n.m.r. for di-*ortho*-methylated diphenylmethanes. The ^1H spectra (3) are similarly insensitive. Methyl carbon shieldings are similar to those of pentamethylbenzene **6**. Upfield shifts for the 2,6-CH_3 groups of **10** are a consequence of the additional γ interaction (6) with 3- and 5-CH_3 functions, respectively. The methylene carbon resonance undergoes a shielding of 3.9 p.p.m. relative to **8**, indicating that the γ effects of successive *ortho*-methyl substitution are not strictly additive (*cf.* **7** *vs.* **8**).

Employing results for **9** and **10** as a basis, carbon shifts for **11** are consistent with the above trends. For **13** and **14**, previous findings for pseudocumene **4** can be used for comparison and no unusual features seem evident for these diphenylmethanes.

In the tri-*ortho*-methyl derivatives **12** and **16**, the preferred conformations on the basis of ^1H n.m.r. (3) are suggested to be the perpendicular forms in which the one *ortho* H is inside the π-cloud of the adjacent phenyl ring. Accordingly the upfield *ortho*-proton shift has been attributed

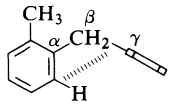

to the shielding influence of the ring current (9) in the remote phenyl moiety. Most interestingly, specific ^1H decoupling indicates that C-6′ of **12** is shielded by *ca.* 3 p.p.m. relative to C-6′ of **8** in which the adjacent phenyl ring lacks *ortho* substituents. Also C-6′ of **16** is shielded by more than 3 p.p.m. compared to C-6′ of **14**. If the perpendicular conformation is preferred, C-6′ and C-1 will be *cis*-coplanar and the shielding γ effect will be maximal at C-6′ of **12** and **16**. The magnitudes of these γ steric shifts are nearly identical to those in related systems such as triphenylene and phenanthrene (13), where the geometries are essentially planar. Examination of molecular models shows that in the perpendicular form, C-6′ does not lie directly in the

TABLE 2. Aryl carbon shifts for diphenylmethanes (δ_C from TMS ± 0.1)*

Compound	Methyl position	C-1	C-2	C-3	C-4	C-5	C-6	C-1′	C-2′	C-3′	C-4′	C-5′	C-6′
7	—	140.8	(128.7)	(128.3)	125.7	(128.3)	(128.7)						
8	2	138.5	136.1	129.6	126.1	127.0	130.0	140.0	(128.4)	(128.1)	125.6	(128.1)	(128.4)
9	4	137.8	(128.8)	(128.6)	134.5	(128.6)	(128.8)	141.2	(128.4)	(128.1)	125.6	(128.1)	(128.4)
10	2,3,5,6	136.2	132.7	133.3	129.8	133.3	132.7	140.0	(128.0)	(127.6)	125.3	(127.6)	(128.0)
11	2,3,5,6,4′	136.5	132.7	133.3	129.7	133.3	132.7	137.0	(128.7)	(127.5)	134.6	(127.5)	(128.7)
12	2,3,5,6,2′	136.1	132.9	133.3	129.7	133.3	132.9	137.8	135.6	129.4	125.7	126.4	125.4
13	2,5	138.3	133.1	129.9	126.8	134.9	130.5	140.3	(128.4)	(128.0)	125.5	(128.0)	(128.4)
14	2,5,2′,5′	138.0	133.0	(129.8)	126.6	135.0	(129.7)						
15	2,4,6,2′,4′,6′	134.6	136.3	129.0	134.5	129.0	136.3						
16	2,4,6,2′,5′	135.0	136.7	128.6	134.9	128.6	136.7	137.4	133.4	129.2	126.5	133.6	126.0

*0.5 *M* in $CDCl_3$.

TABLE 3. Methyl and methylene carbon shifts for diphenylmethanes (δ_C from TMS ± 0.1)*

Compound	Methyl position	2-CH_3	3-CH_3	4-CH_3	5-CH_3	6-CH_3	2′-CH_3	4′-CH_3	5′-CH_3	6′-CH_3	CH_2
7	—										42.0
8	2	19.6									39.5
9	4		21.0								41.6
10	2,3,5,6	15.8	20.6		20.6	15.8					35.6
11	2,3,5,6,4′	15.8	20.6		20.6	15.8		20.9			35.3
12	2,3,5,6,2′	15.7	20.5		20.5	15.7	19.2				33.3
13	2,5	19.2			21.0						39.5
14	2,5,2′,5′	19.2			21.2		19.2		21.2		36.6
15	2,4,6,2′,4′,6′	20.9		20.9		20.9	20.9	20.9		20.9	31.2
16	2,4,6,2′,5′	20.2		21.1		20.2	19.3		21.2		32.1

*0.5 *M* in $CDCl_3$.

shielding 'cone' of the adjacent phenyl ring, in contrast to its directly bonded proton. Thus, anisotropic effects cannot be invoked to rationalize the upfield shifts at the *ortho* carbon position.

In order to quantify this argument somewhat, the anisotropic shielding influence of the adjacent phenyl ring on the C-6′ and H-6′ resonances of a triply-*ortho*-substituted diphenylmethane have been calculated and the results are depicted in Fig. 1. Clearly, the 6′-proton is subject to a much greater shielding anisotropic effect than C-6′. Theoretical values for the ring current contributions were taken from the Johnson and Bovey tables (9). The C-1—CH_2—C-1′ angle was taken as 116° and the CH_2—C-Ar bond lengths as 1.525 Å using the X-ray data for 4-bromo-2,3,5,6-tetramethyl-2′-chlorodiphenylmethane as a model (10).

For the tetra-*ortho*-methylated material **15**, the methylene carbon resonance is the most shielded of all the compounds studied due to the four γ steric interactions with the *ortho* CH_3 groups. In general the chemical shifts for **15** and **16** are in close agreement with the corresponding methylbenzenes **4** and **5**, although a small deshielding effect (*ca.* 0.6 p.p.m.) is evident for the *ortho* CH_3's of **15** relative to the C-2,6 methyls of **16** and the C-1,3 methyls of **5**. This may originate from a deshielding 'δ' steric interaction (11) with C-1 of the adjacent ring. X-Ray data on 4,4′-dihydroxydidurylmethane (12) indicate that this compound adopts a helical conformation in which the two aryl rings are equally twisted ($\phi = \theta = 43°$) and a similar solution geometry has been suggested for **15** (3) shown below.

Averaging between the equivalent conformations of **15** will render the *ortho* CH_3 groups alternately in the shielding and deshielding regions of the adjacent phenyl ring. Accordingly the anisotropic influence on the methyl resonances would be expected to average to a near zero value.

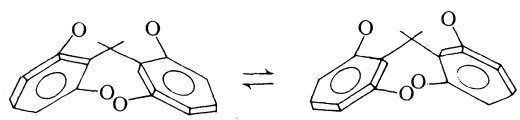

To summarize, it is clear that ^{13}C n.m.r. constitutes a useful addition to the existing methods of studying diphenylmethane geometry only for tri-*ortho*-methylated materials in which supporting evidence for perpendicular conformations has been obtained. No conformational conclusions can be drawn for mono- and di-*ortho*-alkylated materials from either ^1H or ^{13}C magnetic resonance chemical shifts.

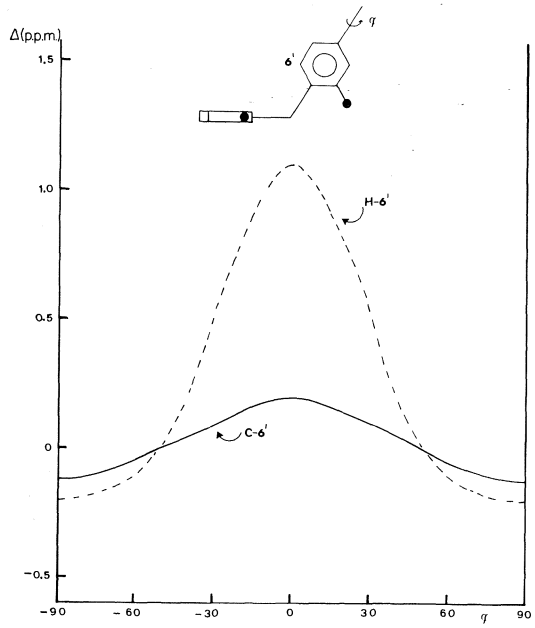

FIG. 1. Calculated anisotropic contributions to the ^{13}C and ^1H chemical shifts for the 6′ position of 2,6,2′-trimethyl substituted diphenylmethanes. For the conformation depicted, $\phi = 0°$.

Experimental

Materials

Synthetic procedures for the diphenylmethanes have been described previously (8).

Spectra

The carbon-13 spectra were obtained at 25.2 MHz using a Varian XL-100-12 NMR spectrometer, most commonly under conditions of complete proton noise decoupling. Spectral accumulations were accomplished with a Varian C-1024 time-averaging computer. Samples were contained in 8 mm tubes and were examined as 0.5 *M* solutions in $CDCl_3$ containing 2% TMS as an internal standard. Off-resonance decoupling experiments were carried out with the proton frequency offset approximately 500 Hz from the center of the proton spectral region.

We thank the North Atlantic Treaty Organization and the National Research Council of Canada for their generous financial aid.

1. G. W. BUCHANAN, G. MONTAUDO, and P. FINOCCHIARO. Can. J. Chem. **51**, 1053 (1973).
2. G. W. BUCHANAN, G. MONTAUDO, and P. FINOCCHIARO. Can. J. Chem. **52**, 767 (1974).

3. G. MONTAUDO, S. CACCAMESE, and P. FINOCCHIARO. J. Am. Chem. Soc. **93**, 4202 (1971).
4. G. MONTAUDO and P. FINOCCHIARO. J. Mol. Struct. **14**, 53 (1972).
5. J. B. STOTHERS. Carbon-13 NMR Spectroscopy. Academic Press, New York, N.Y. 1972.
6. W. R. WOOLFENDEN and D. M. GRANT. J. Am. Chem. Soc. **88**, 1496 (1966).
7. D. M. GRANT and B. V. CHENEY. J. Am. Chem. Soc. **89**, 5315 (1967).
8. G. MONTAUDO, P. FINOCCHIARO, S. CACCAMESE, and F. BOTTINO. J. Chem. Eng. Data, **16**, 249 (1971).
9. C. E. JOHNSON and F. A. BOVEY. J. Chem. Phys. **29**, 1012 (1958).
10. P. FINOCCHIARO, K. MISLOW, and J. F. BLOUNT. Unpublished observations.
11. S. H. GROVER, J. P. GUTHRIE, J. B. STOTHERS, and C. T. TAN. J. Mag. Res. **10**, 227 (1973).
12. B. CHANDHURI and A. HARGREAVES. Acta Cryst. **9**, 793 (1956).
13. R. S. OZUBKO, G. W. BUCHANAN, and I. C. P. SMITH. Can. J. Chem. **52**, 2493 (1974).

Oxydation du cyclohexène par le nitrate cérique d'ammonium[1]

CLAUDE BRIGUET,[2] CHRISTIAN FREPPEL, JEAN-CLAUDE RICHER ET MIKLOS ZADOR

Université de Montréal, Département de Chimie, C.P. 6210, Montréal, Québec H3C 3V1

Reçu le 28 mars, 1974

CLAUDE BRIGUET, CHRISTIAN FREPPEL, JEAN-CLAUDE RICHER et MIKLOS ZADOR. Can. J. Chem. **52**, 3201 (1974).

On étudie l'oxydation du cyclohexène par le CAN. Dans le DMSO anhydre, la réaction conduit au nitrato-3 cyclohexène tandis que dans l'acétonitrile, il y a formation de *N*-(cyclohexène-2 yl) acétamide. En présence d'eau, il y a formation des produits hydroxylés. Les résultats obtenus s'expliquent en faisant appel à la formation d'un intermédiaire provenant de l'addition du radical $NO_3^{\cdot}$ sur la double liaison de l'oléfine.

CLAUDE BRIGUET, CHRISTIAN FREPPEL, JEAN-CLAUDE RICHER, and MIKLOS ZADOR. Can. J. Chem. **52**, 3201 (1974).

The oxidation of cyclohexene by ceric ammonium nitrate has been studied. In anhydrous DMSO the reaction leads to cyclohexene-3-nitrate, while in acetonitrile *N*-(cyclohexene-2-yl) acetamide is formed. Hydroxylated products are formed in the presence of water. The results obtained are explained in terms of the formation of an intermediate arising from the addition of the radical $NO_3^{\cdot}$ to the olefinic double bond. [Journal translation]

Introduction

L'oxydation des produits organiques par le cérium(IV) a fait l'objet de nombreuses études tant au point de vue synthèse qu'au point de vue du mécanisme (1–5). Le réactif le plus fréquemment utilisé, à cause de sa solubilité dans les solvants organiques ou mixtes contenant de l'eau, est le nitrate cérique d'ammonium (CAN); il a été rapporté que ce réactif conduit quelquefois à des nitrates organiques comme produits de réaction (3–5).

Un travail préliminaire sur le styrène ayant indiqué que l'oxydation de doubles liaisons par le CAN conduit, dans certains cas, à des dinitrates, nous avons porté notre attention vers l'étude de l'oxydation du cyclohexène (**1***a*) afin de déterminer si des cyclohexanes 1,2-disubstitués peuvent se former dans cette réaction; les résultats obtenus au cours de ce travail font l'objet de la présente communication.

Résultats et discussion

Des études préliminaires nous ont permis de déterminer que le diméthylsulfoxyde (DMSO) et l'acétonitrile sont des solvants efficaces pour le CAN et de plus qu'ils sont relativement résistants à l'oxydation par ce réactif; nos travaux ont donc été effectués dans ces solvants.

L'oxydation du cyclohexène (**1***a*) par le CAN, dans le DMSO anhydre et sous atmosphère d'azote, conduit au nitrato-3 cyclohexène (**1***b*) souillé par environ 10% d'un produit dont la nature n'a pas été déterminée. Cette réaction s'avère une méthode utile pour obtenir en une seule étape ce nitrate (**1***b*) à partir du cyclohexène. En utilisant un excès de cyclohexène, on obtient un rendement de 40% par rapport au Ce(IV) utilisé, ce qui est assez élevé si l'on tient compte du fait que le Ce(IV) attaque la plupart des solvants organiques. Le nitrato-3 cyclohexène était inconnu jusqu'à ce jour, et sa synthèse univoque a été réalisée par réaction du bromo-3 cyclohexène (**1***c*) avec le nitrate d'argent (6). Il est à noter que l'oxydation, réalisée dans du DMSO commercial ou con-

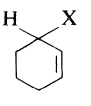

1

a X = H
b X = ONO_2
c X = Br
d X = OH
e X = $NHCOCH_3$
f X = N_3
g X = NH_2

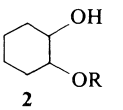

2

a R = H
b R = NO_2

[1]Présenté au 56ème Congrès de l'Institut de Chimie du Canada, Montréal, Québec, 4–6 juin, 1973.

[2]Les résultats rapportés dans ce travail font partie du mémoire de Maîtrise en chimie soumis par M. Claude Briguet à la Faculté des Etudes Supérieures de l'Université de Montréal (septembre 1973).

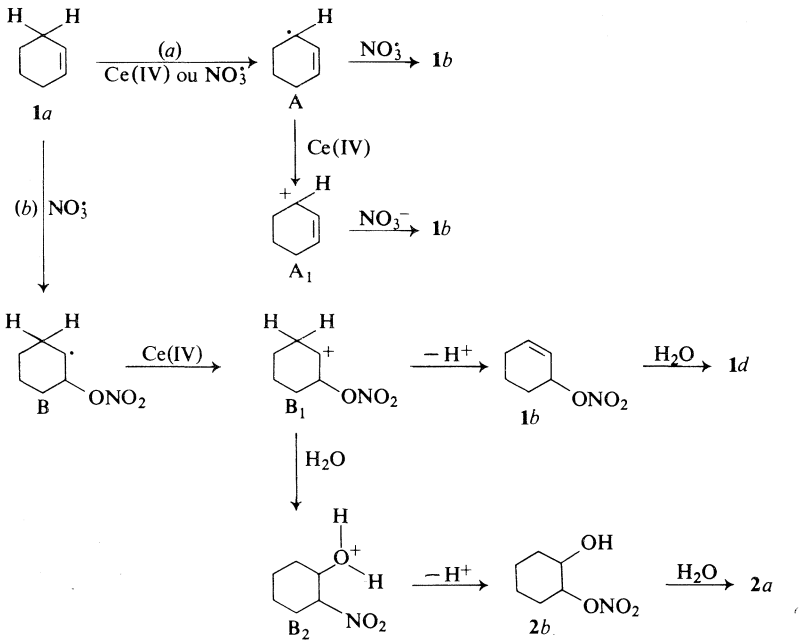

SCHÉMA 1

tenant des quantités progressivement plus grandes d'eau, conduit alors à du cyclohexène-2 ol [(**1***d*) jusqu'à 75%] et du cyclohexanediol-1,2 [(**2***a*) jusqu'à 25%].

Par ailleurs, l'oxydation du cyclohexène (**1***a*) par le CAN dans l'acétonitrile contenant 1% d'eau conduit à un seul produit soluble en milieu acide 3 *N*; ce produit est le *N*-(cyclohexène-2 yl) acétamide (**1***e*). Cette oxydation conduit donc encore une fois à la formation en une seule étape d'un dérivé d'amine de nature allylique. Au moment où ce travail a été réalisé, ce dérivé n'était pas connu et une synthèse univoque en a été faite par l'intermédiaire du bromo-3 cyclohexène (**1***c*), de l'azido-3 cyclohexène (**1***f*) et de l'amino-3 cyclohexène (**1***g*). Depuis Shono et Ikeda (7) ont obtenu le même dérivé par oxydation électrochimique du cyclohexène dans l'acétonitrile.

Comme en milieu DMSO, l'addition de quantités de plus en plus grande d'eau lors de l'oxydation par le CAN dans l'acétonitrile entraîne une augmentation progressive des rendements en cyclohexène-2 ol (**1***d*) et en cyclohexanediol-1,2 (**2***a*) au détriment de l'amide (**1***e*).

Mécanisme

Les résultats obtenus lors de l'oxydation du cyclohexène par le CAN dans le DMSO sont compatibles avec les voies réactionnelles présentées dans le schéma 1.

Les conclusions obtenues par Roček et collaborateurs (8) lors de l'oxydation du cycloheptatriène par le CAN nous inciteraient à considérer la voie *b* comme la plus probable. Les résultats qualitatifs obtenus dans nos laboratoires lors de l'oxydation du diméthyl-1,2 cyclohexène, montrant que celui-ci réagit beaucoup plus rapidement que le cyclohexène, supportent aussi cette hypothèse. Lors de l'oxydation réalisée sous l'influence de la lumière (conditions dans lesquelles la formation de radicaux nitrates a été bien démontrée (9)), on a noté qualitativement que les vitesses d'oxydation sont augmentées par un facteur d'au moins 10. Cette observation nous suggère donc que des radicaux $NO_3^{\bullet}$ sont impliqués dans la réaction et, suivant la voie *b* par addition sur la liaison double, conduisent à un radical intermédiaire B similaire à celui préconisé par Roček et collaborateurs (8) lors de l'oxydation du cycloheptatriène par le CAN.

Notre préférence pour l'addition d'un radical libre plutôt qu'un transfert de ligand tel que suggéré par Roček est basé d'une part sur nos résultats photochimiques et d'autre part sur les résultats de Martin *et al.* (9) qui ont mis en

évidence la formation de radicaux $NO_3^{\bullet}$ par la réaction thermique:

$$Ce(IV)^{\cdot}NO_3^{-} \rightleftarrows Ce(III) + NO_3^{\bullet}$$

Bien que cet équilibre, en absence d'alcène soit déplacé vers la gauche, l'introduction d'oléfine dans le milieu favoriserait son déplacement vers la droite à cause de la réaction des radicaux $NO_3^{\bullet}$ avec le substrat. Mise à part cette différence, le mécanisme proposé est en accord avec celui proposé par Roček et collaborateurs (8) mais pour le confirmer d'une manière univoque une étude plus approfondie serait nécessaire.

Considérant que nous avons observé que le nitrato-3 cyclohexène (**1***b*) se transforme en *N*-(cyclohexène-2 yl) acétamide (**1***e*) dans les conditions d'oxydation, on peut donc proposer que les résultats obtenus en milieu acétonitrile peuvent s'expliquer par la formation intermédiaire de **1***b* par le mécanisme décrit plus haut. Il est à noter toutefois que l'intermédiaire A_1 pourrait donner lieu, en présence d'acétonitrile et d'eau, à une réaction de Ritter conduisant directement à l'amide.

Il est bien connu que les nitrates s'hydrolysent lentement en alcools lorsque mis en présence d'eau (10). La formation des produits hydroxylés (**1***d* et **2***a*) obtenus en milieu DMSO ou acétonitrile aqueux peuvent donc être rationalisés d'après les mécanismes décrits plus haut. Le cyclohexène-2 ol (**1***d*) se formerait lentement par l'hydrolyse de **1***b*. La formation de cyclohexanediol-1,2 (**2***a*) impliquerait que l'eau attaque l'intermédiaire $\mathbf{B}_1$ pour conduire au produit **2***b* (que l'on à jamais isolé) qui s'hydrolyserait lentement dans le milieu. On observe que les produits hydroxylés (**1***d* et **2***a*) susceptibles d'être oxydés par le Ce(IV), sont retrouvés intacts; ce résultat s'explique d'une part par le fait que l'hydrolyse des nitrates est relativement lente (10) et d'autre part par le fait que l'oxydation ultérieure des produits hydroxylés par le CAN est aussi une réaction qui n'est pas rapide. En effet des alcools ont été isolés par Trahanovsky lors de l'oxydation de diaryléthanes par le CAN à 80 °C (5).

On peut donc conclure que le CAN réagit, dans le DMSO anhydre ou dans l'acétonitrile contenant 1% d'eau, avec le cyclohexène pour conduire, en une seule étape respectivement au nitrato-3 cyclohexène et au *N*-(cyclohexène-2 yl) acétamide. Les résultats obtenus au cours de ce travail suggèrent que l'étape initiale de la réaction implique la formation du radical B provenant de l'addition d'un groupe nitrate sur la double liaison.

Partie expérimentale

Les spectres de masse ont été pris sur un spectromètre de masse "Hitachi Perkin Elmer" modèle RMU 6-D et l'énergie du faisceau ionisant est de 70 eV. Les spectres infrarouges ont été pris sur un spectromètre "Beckman" modèle IR-8 à double faisceau entre deux plaques de chlorure de sodium. Les spectres r.m.n. ont été déterminés sur un spectromètre "Jeol" modèle C-60H pour le nitrato-3 cyclohexène et le *N*-(cyclohexène-2 yl) acétamide et sur un spectromètre "Jeol" modèle JNM-4H100 pour la détermination des couplages du *N*-(cyclohexène-2 yl) acétamide. Les spectres ont été déterminés dans le tétrachlorure de carbone et le tétraméthylsilane est utilisé comme référence interne. Les indices de réfraction ont été déterminés à l'aide d'un réfractomètre type "Abbe". Les analyses en phase gazeuse par chromatographie ont été effectuées à l'aide d'un chromatographe à ionisation de flamme "F et M" modèle 700. Le cyclohexène-2 ol (**1***d*), et le cyclohexanediol-1,2 (**2***a*) ont été identifiés par leur temps de rétention sur deux colonnes différentes: *1*, colonne en acier d'une longueur de 6 pd. sur $\frac{1}{8}$ po. de diamètre remplie de Diatoport 80-100S supportant 10% d'huile de silicone UCW98; *2*, colonne en cuivre d'une longueur de 10 pd. sur $\frac{1}{8}$ po. de diamètre remplie de Chromosorb W supportant 15% de Carbowax 1000. Sauf indications contraires la température de l'injecteur et du détecteur est de 225 °C, celle de la colonne de 80 °C. Le gaz porteur utilisé est l'azote et son débit est de 40 ml/min.

(1) Oxydation du cyclohexène dans le DMSO

(a) En milieu anhydre

Dans un ballon de 300 ml contenant 150 ml de DMSO fraichement distillé sur de l'hydrure de calcium, on introduit, sous vive agitation 33 g (0.06 mol) de nitrate cérique d'ammonium et 7.32 g (0.09 mol) de cyclohexène (**1***a*). Le milieu réactionnel est maintenu sous atmosphère d'azote pendant 3 jours c'est-à-dire jusqu'à la disparition complète des ions cériques tels que détectée par la décoloration de la solution. On ajoute alors 100 ml d'éther à la solution et 100 ml d'eau distillée saturée en chlorure de sodium. La phase éthérée est lavée quatre fois avec 25 ml d'eau saturée en chlorure de sodium et séchée sur carbonate de sodium. Après évaporation sous vide (la température du bain est maintenue en bas de 40 °C) on obtient 1.90 g d'un liquide jaune. Le rendement en nitrato-3 cyclohexène (**1***b*) (1.72 g soit 40% par rapport à la quantité de cérium utilisable) est déterminé par chromatographie en phase gazeuse en utilisant le bromo-3 cyclohexène (**1***c*) comme référence interne. Le nitrato-3 cyclohexène se décomposant sur les colonnes de cuivre et d'aluminium, une colonne d'acier a été utilisée. Pour la même raison l'injection s'est faite directement dans la colonne en supprimant l'injecteur. Les meilleurs résultats ont été obtenus sur une colonne d'acier d'une longueur de 6 pd. sur $\frac{1}{8}$ po. de diamètre remplie de Diatoport 80-100S supportant 10% d'huile de silicone UCW98. La tempéra-

ture du détecteur est de 175 °C et celle de la colonne de 100 °C.

(b) Réaction dans le DMSO contenant 10% d'eau

La réaction rapportée précédemment a été répétée en ajoutant volontairement 10% d'eau au milieu réactionnel. On obtient alors 1.12 g d'un liquide; la chromatographie en phase gazeuse nous indique qu'il s'agit du cyclohexène-2 ol (**1***d*) (75%) et du cyclohexanediol-1,2 (**2***a*) (25%).

*(c) Synthèse univoque du nitrato-3 cyclohexène (**1***b*)*

Dans un ballon à col rodé contenant 50 ml de DMSO, on introduit 4.05 g (0.025 mol) de bromo-3 cyclohexène (**1***c*). En maintenant une vive agitation, on y ajoute goutte à goutte une solution contenant 5.5 g (0.032 mol) de nitrate d'argent dissous dans 50 ml de DMSO. Après filtration du bromure d'argent, on ajoute 100 ml d'éther et 50 ml d'eau saturée en nitrate de sodium au milieu réactionnel. La phase éthérée est recueillie et lavée quatre fois par 50 ml d'eau saturée en nitrate de sodium. Après séchage sur du carbonate de sodium et évaporation sous vide, on obtient 2.1 g (60% de rendement) de nitrato-3 cyclohexène (**1***b*) présentant les caractéristiques physiques suivantes: i.r.: bandes à 1650 (C=C) et à 1280 cm^{-1} (O—N); r.m.n.: 5.9 sous forme de multiplet (2 protons oléfiniques) et 5.35 p.p.m. (proton allylique); spectre de masse: 97 ($M^+ - 46$), caractéristique du groupe nitrate.

*(2) Oxydation du cyclohexène (**1***a*) dans l'acétonitrile*

(a) Oxydation dans l'acétonitrile contenant 1% d'eau

Dans un ballon de 500 ml contenant 250 ml d'acétonitrile fraichement distillé et 2.5 ml d'eau distillée, on ajoute sous vive agitation 33 g (0.06 mol) de nitrate cérique d'ammonium. Lorsque la solution est homogène, on introduit 7.38 g (0.09 mol) de cyclohexène (**1***a*). Le mélange réactionnel est alors abandonné à la température de la pièce. A mesure que la réaction progresse, la solution tend vers la couleur jaune pâle et une suspension de sels céreux peu solubles dans l'acétonitrile apparaît. Après 8 jours, le milieu réactionnel devient effectivement jaune pâle indiquant ainsi la fin de la réaction. La solution est alors concentrée sous vide jusqu'à un volume de 50 ml. Les produits organiques sont alors solubilisés dans 100 ml d'éther et l'amide extraite par lavage avec de l'acide chlorhydrique 3 *N*, (1 × 100 ml et 2 × 50 ml); les trois fractions aqueuses sont réunies et de la soude environ 5 *N* y est alors ajoutée jusqu'à l'obtention d'un p*H* de 9. Le *N*-(cyclohexène-2 yl) acétamide (**1***e*) est extrait de la phase aqueuse par de l'éther (3 × 100 ml). Après séchage de la solution étherée sur carbonate de calcium et évaporation du solvant sous vide, on obtient 2.15 g de produit cristallisé. Après purification par sublimation, l'on recueille 1.98 g (rendement de 50% par rapport à la quantité de cérium utilisable) de *N*-(cyclohexène-2 yl) acétamide (**1***e*) possédant les caractéristiques suivantes: p.f.: 77 °C [litt. (7) 78 °C]; r.m.n.: pic à 7.6 (doublet correspondant au proton NH), 5.5 (deux protons sur la double liaison), 4.2 (proton allylique) et 1.98 p.p.m. (3 protons du $COCH_3$); spectre de masse: pics caractéristiques à 139, 111, 97, 96, 60 et 43.

(b) Oxydation dans l'acétonitrile contenant 10% d'eau

La réaction qui vient d'être rapportée a été répétée en ajoutant volontairement 10% d'eau au milieu réactionnel. On n'obtient alors que du cyclohexène-2 ol (**1***d*) et du cylohexanediol-1,2 (**2***a*).

*(c) Synthèse univoque du N-(cyclohexène-2 yl) acétamide (**1***e*)*

A 1.33 g (0.01 mol) de chlorhydrate de l'amino-3 cyclohexène (**1***g*) préparé selon les indications de Boyer (11), on ajoute 20 ml de méthanol, 2 g d'acétate d'argent et 2 ml d'anhydride acétique. La solution est agitée à 0 °C durant 1 journée, 5 h à la température de la pièce puis portée quelques min à ébullition. Après refroidissement l'amide est extrait en introduisant dans le milieu 50 ml d'éther et 25 ml de soude 0.1 *N*. La phase éthérée est lavée deux fois avec 25 ml d'eau saturée en carbonate de sodium et séchée sur le même carbonate. Après évaporation du solvant sous vide et sublimation du produit, on obtient 0.980 g (70% de rendement) de *N*-(cyclohexène-2 yl) acétamide (**1***e*) dont les caractéristiques sont identiques à celles décrites dans le paragraphe *2a*.

(3) Influence de la lumière sur la réaction

Afin d'évaluer l'influence de la lumière sur la réaction d'oxydation, on a irradié par de la lumière émise par une lampe Hanovia High Pressure Quartz Mercury-Vapor A 6373 une cellule en quartz contenant une solution 4×10^{-2} *M* en nitrate cérique d'ammonium et 6×10^{-2} *M* en cyclohexène dans l'acétonitrile. Les filtres Hanovia numéros 6544–001 et 6540–001, donnant une bande passante à 360 nm, nous assuraient une absorption uniquement par le cérium. Dans ces conditions la réaction était complétée en 55 min alors qu'à la lumière ambiante la même réaction prenait 10 h pour se réaliser.

*(4) Substitution du groupe nitrate allylique de (**1***b*) dans l'acétonitrile*

(*a*) Dans un ballon à col rodé de 250 ml contenant 100 ml d'acétonitrile et 1 ml d'eau, on introduit 1.43 g (0.01 mol) de nitrato-3 cyclohexène (**1***b*). Le mélange est abandonnée sous agitation à la température ambiante pour une journée. Après extraction par la méthode décrite au paragraphe **2***a*, on obtient 0.76 g (0.055 mol, soit un rendement de 55%) de *N*-(cyclohexène-2 yl) acétamide (**1***e*).

(*b*) Afin d'examiner si le nitrate cérique d'ammonium avait une influence sur cette réaction de substitution, une réaction semblable a été effectuée en présence de nitrate cérique d'ammonium et le rendement en *N*-(cyclohexène-2 yl) acétamide est alors de 73%.

Les auteurs remercient vivement le Conseil national de recherches du Canada et le Conseil des Arts du Canada pour l'aide financière apportée sous forme d'octrois de recherches (CNR A-1295 et CNR A-2862) et de bourses d'étude (C.B.).

1. W. H. Richardson. *Dans* Oxidation in organic chemistry. Chap. IV. *Rédigé par* K. B. Wiberg. Academic Press, New York. 1965.
2. (*a*) W. S. Trahanovsky et L. B. Young. J. Chem. Soc. 5777 (1965). (*b*) W. S. Trahanovsky, L. H. Young et M. H. Bierman. J. Org. Chem. **34**, 869 (1969). (*c*) J. W. Bird et D. G. M. Diaper. Can. J. Chem. **47**, 145 (1969). (*d*) W. S. Trahanovsky, L. B. Young et M. D. Robbins. J. Am. Chem. Soc. **91**, 7084 (1969). (*e*) W. S. Trahanovsky et J. Cramer. J. Org. Chem. **36**, 1890 (1971). (*f*) T. Ho, H. C. Ho et C. M. Wong. Chem. Commun. **13**,

791 (1972). (*g*) W. S. TRAHANOVSKY, J. R. GILMOR et P. C. HEATON. J. Org. Chem. **38**, 760 (1973).
3. L. A. DUST et E. W. GILL. J. Chem. Soc. (C), 1630 (1970).
4. (*a*) P. DESLONGCHAMPS, P. SOUCY et T. HO. Can. J. Chem. **50**, 2047 (1972). (*b*) K. MEYER et J. ROČEK. J. Am. Chem. Soc. **94**, 1209 (1972).
5. W. S. TRAHANOVSKY et D. W. BRIXIUS. J. Am. Chem. Soc. **95**, 6778 (1973).
6. A. F. FERRIS, K. W. MCLEAN, I. D. MARKS et W. D. EMMONS. J. Am. Chem. Soc. **75**, 4078 (1953).
7. T. SHONO et A. IKEDA. J. Am. Chem. Soc. **94**, 7892 (1972).
8. P. MÜLLER, E. KATTEN et J. ROČEK. J. Am. Chem. Soc. **93**, 7114 (1971).
9. (*a*) T. W. MARTIN, A. HENSHALL et R. C. GROSS. J. Am. Chem. Soc. **85**, 113 (1963). (*b*) T. W. MARTIN, R. E. RUMMEL et R. C. GROSS. J. Am. Chem. Soc. **86**, 2595 (1964).
10. J. W. BAKER et D. M. EASTY. J. Chem. Soc. 1193 (1952).
11. J. H. BOYER. J. Am. Chem. Soc. **73**, 5865 (1951).

Dimetallation of β-Lactams. Introduction of 3-Substituents in *N*-Unsubstituted β-Lactams

T. DURST, R. VAN DEN ELZEN, AND R. LEGAULT
Department of Chemistry, University of Ottawa, Ottawa, Canada K1N 6N5

Received February 20, 1974

T. DURST, R. VAN DEN ELZEN, and R. LEGAULT. Can. J. Chem. **52**, 3206 (1974).

β-Lactams, unsubstituted in the 1 and 3 position react with 2 equiv. of *n*-butyllithium in THF at 0° within 1 h to form 1,3-dilithio salts. The dilithio salts react with various electrophiles (ketones, alkyl halides, I_2) to give β-lactams substituted in the 3 position.

T. DURST, R. VAN DEN ELZEN et R. LEGAULT. Can. J. Chem. **52**, 3206 (1974).

Les β-lactams, non-substitués dans leurs position 1 et 3, réagissent en moins d'une heure avec deux équivalents de *n*-butyllithium dans le THF à 0° pour former les sels dilithiés en position 1 et 3. Les sels dilithiés réagissent avec divers électrophiles (les cétones, les halogénures d'alkyle et I_2) pour fournir des β-lactams substitués en position 3. [Traduit par le journal]

Recently we reported on the metallation of *N*-substituted β-lactams at the 3 position upon treatment of lactams such as **1** (R = Alkyl or Aryl) with lithium diisopropylamide and on the synthetic utility of the metallated species **2** for the introduction of substituents into the 3 position into such lactams (see eq. 1) (1*a*). Closely related to the above has been the considerable use over the past few years of carbanionic intermediates at position 6 in penicillins (1*b*) and 7 in cephalosporins (1*b*) for the introduction of a variety of substituents into these positions (eq. 2).

[1]

1

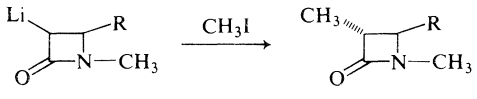

2 **3**

[2] 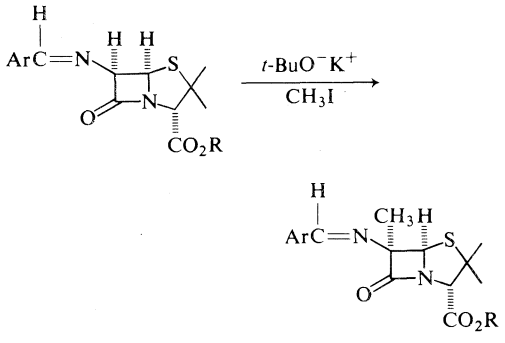

We would now like to report an extension of the above results to the formation of *N*,*C*-3-dimetallated β-lactams such as **5**. Addition of various electrophiles such as alkyl halides, carbonyl compounds, and iodine results, as expected, in reaction only at C-3 and thus provides a relatively simple method for the introduction of substituents at that position in simple *N*-unsubstituted β-lactams.

[3] 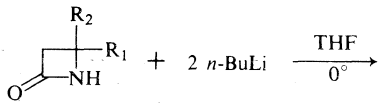

4

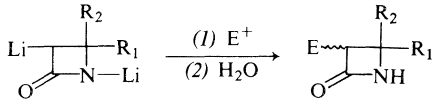

5 **6**

a R_1 = Ph; R_2 = H
b R_1 = Vinyl; R_2 = H
c R_1 = Vinyl; R_2 = CH_3
d R_1 = CH_2CH_3; R_2 = H

The expectation that β-lactams might form stable dianions was based on the observation by Hauser and co-workers (2) that acetanilide undergoes dimetallation on reaction with *n*-butyllithium in tetrahydrofuran at 0°. When the β-lactams **4***a–d* were reacted with 2 equiv. of *n*-BuLi in THF at 0° for 30–60 min, dimetallation occurred in up to 90% yield as shown by subsequent trapping experiments (see Table 1).

Can. J. Chem. Downloaded from www.nrcresearchpress.com by 210.87.254.6 on 09/05/12
For personal use only.

TABLE 1. Introduction of substituents into position 3 of β-lactams

β-Lactam	Electrophile	Yield (%) of 3-substituted product
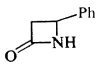 **4a**	Acetone	55
	Methyl iodide	53
	n-Butyl bromide	66
	Iodine	16
4b	Benzophenone	88
	Cyclohexanone	55
	n-Butyl bromide	77
	Isopropyl bromide	45
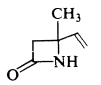 **4c**	Benzophenone	57
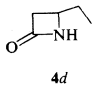 **4d**	Benzophenone	65
	n-Butyl bromide	65

The structures of the products followed from spectroscopic and analytic data. The i.r. spectrum of each product showed bands in the regions 3300–3400 and 1730–1760 cm^{-1} thus confirming that the *N*-unsubstituted β-lactam structure had been retained. In contrast to the reaction of the monoanion **2** with electrophiles which produced only *trans*-3,4-substituted β-lactams (1), the reaction of the dianions **5** with the same electrophiles usually produced mixtures, the *trans–cis* ratio varying from about 3:1 to 10:1. The formation of the two isomers from **4***a*, *b*, *d* was confirmed by the n.m.r. spectra of the crude products. Inspection of the signal due to the C-4 proton revealed two areas of absorption, one showing a coupling constant of ~2 Hz, the other a J = 4–5 Hz with the remaining proton on C-3. These were assigned to the *trans* and *cis* isomers, respectively (3). For the products obtained from **5***c* the isomeric mixture was evident from the appearance of two singlets due to the remaining proton at C-3.

Dimetallation of the 3-alkylated β-lactam **7** under conditions which resulted in metallation of **4** was not successful and the starting material was recovered. This result was not altogether unexpected in view of the well-known decrease in acidity in going from a secondary to a tertiary hydrogen.

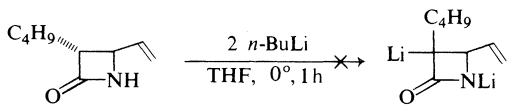

7

Experimental

Melting points were taken on a Thomas Hoover apparatus and are uncorrected. Infrared spectra were obtained as films for liquids and in $CHCl_3$ solution for solids on a Beckman IR-20A Spectrophotometer; n.m.r. spectra were obtained using Varian HA-100 and T-60 Spectrometers; peak positions are reported in δ units. All reactions involving alkyllithiums were carried out using freshly distilled tetrahydrofuran (THF) and under N_2. Usual work-up refers to quenching the reaction with excess H_2O, extraction with CH_2Cl_2, drying the organic extracts over $MgSO_4$, and evaporation of the solvents under reduced pressure. For the sake of clarity the azetidin-2-one nomenclature will be used throughout this section.

Formation of the Dilithio Salts

General Procedure

The appropriate 2-azetidinone (approx. 0.5 g) was dissolved in THF (30 ml) at 0° and reacted with 2 equiv. of *n*-BuLi (1.9 *M* in hexane, Alfa Inorganics Inc.) The reaction mixture was stirred at 0° for 30–60 min. The appropriate electrophile was then added and the reaction mixture was stirred for an additional 5–10 min. The usual work-up gave the crude product which was purified by recrystallization or column chromatography over silica.

The azetidinones used in this study were prepared by cycloaddition of chlorosulfonyl isocyanate with the appropriate olefins (4) followed by reduction of the chlorosulfonyl group with Na_2SO_3 (5).

Reactions of 1,3-Dilithio-4-phenylazetidin-2-one (5a)

n-Butyl Bromide

To 4-phenylazetidin-2-one (400 mg) dissolved in 30 ml of THF at 0° was added 3.0 ml of *n*-BuLi solution. The reaction mixture was stirred for 1 h during which time the solution darkened considerably. *n*-Butyl bromide (400 mg) was added and the solution was allowed to stir for a further 20 min. The crude product obtained upon usual work-up was chromatographed (silica gel). Elution with ether yielded 330 mg (60%) of the *trans* isomer; n.m.r.: 0.8–2.1 (m, 9H), 2.95 (d of t, J = 2.0 and 7.0 Hz, 1H), 4.25 (d, J = 2.0 Hz, 1H), 7.0 (broad s, 1H), and 7.30 (s, 5H); i.r. peaks at 3270 and1753 cm^{-1}. Further elution with ether furnished 30 mg (6%) of the *cis* isomer; n.m.r.: 0.8–2.1 (m, 9H), 3.3 (m, 1H), 4.79 d(J = 5.5 Hz, 1H), 6.0 (broad s, 1H), and 7.2 (s, 5H). The N—H and C=O peaks of the *cis* isomer occurred at 3250 and 1745 cm^{-1} respectively.

Anal. Calcd. for $C_{13}H_{17}NO$ (the *trans* isomer): C, 76.83; H, 8.42. Found: C, 76.78; H, 8.40.

Methyl Iodide

To a solution of the dianion **5***a* prepared from 500 mg of **4***a* was added 0.26 ml (1 equiv.) of methyl iodide. Work-up, followed by careful chromatography gave 310 mg of a 4:1 *trans–cis* mixture of methylated products. Several recrystallizations from ether–pentane gave a

Can. J. Chem. Downloaded from www.nrcresearchpress.com by 210.87.254.6 on 09/05/12
For personal use only.

Can. J. Chem. Downloaded from www.nrcresearchpress.com by 210.87.254.6 on 09/05/12
For personal use only.

sample of the pure *trans* isomer, m.p. 95–96° (lit. (6) m.p. 99–100°). The n.m.r. of the *trans* isomer showed peaks at 1.30 (d, J = 7.5 Hz, 3H), 2.95 (d of q, J = 7.5 and 2.5 Hz, 1H), 4.21 (d, J = 2.5 Hz, 1H), 6.2 (s, 1H), and 7.26 (s, 5H).

Iodine

The solution of the dianion **5***a* prepared from 500 mg of **4***a* was added 864 mg of solid I_2. The reaction mixture was stirred at 0° for 30 min, then worked up. The crude product was purified by preparative t.l.c. The yield of *trans*-3-iodo-4-phenylazetidin-2-one was 150 mg (16%), m.p. 118–119°; n.m.r.: 4.67 (d, J = 2.1 Hz, 1H), 4.88 (d, J = 2.1 Hz, 1H), 6.9 (s, 1H), and 7.4 (s, 5H); i.r. 3420 and 1770 cm^{-1}.

Anal. Calcd. for C_9H_8INO: C, 39.58; H, 2.95; I, 46.47. Found: C, 39.83; H, 2.95; I, 46.29.

Acetone

Acetone (1 ml) was added to a solution of the dianion **5***a* prepared from 400 mg of **4***a*. Work-up gave 0.6 g of crude product whose n.m.r. indicated it to be mainly a mixture of the *trans* and *cis* adducts (5:1 ratio). Preparative t.l.c. yielded 380 mg 55% of crystalline material, m.p. 121–129°. The *trans* isomer showed the methyl groups as two singlets at 1.30 and 1.40, the C-3 H at 3.02 (d, J = 2.0 Hz), and C-4 H at 4.72 (J = 2.0 Hz). The corresponding peaks for the *cis* isomer occurred at 0.95 (s), 1.13 (s), 3.60 (d, J = 5.5 Hz), and 4.97 (d, J = 5.5 Hz).

Anal. Calcd. for $C_{12}H_{15}NO_2$: C, 70.22; H, 7.37. Found: C, 70.08, H, 7.34.

*Reactions of 1,3-Dilithio-4-vinylazetidin-2-one (**5***b*)

Benzophenone

Dianion **5***b* was generated at 0° from 500 mg of **4***b* and allowed to react with 910 mg of benzophenone. The crude product (1.48 g) was recrystallized from CH_2Cl_2–pentane. Yield, 1.24 g (88%), m.p. 186–190°. The n.m.r. spectrum was very complex but in general agreement with the expected product; i.r. peaks: 3600, 3420, 1750, 983, and 922 cm^{-1}.

Anal. Calcd. for $C_{18}H_{17}NO_2$: C, 77.39; H, 6.13. Found: C, 77.33; H, 6.16.

n-Butyl Bromide

n-Butyllithium (21 mmol) was added to a solution of 970 mg (10 mmol) of 4-vinylazetidin-2-one in 40 ml of THF. The reaction mixture was stirred for 1 h and 1.37 g (10 mmol) of *n*-butyl bromide was added. The crude reaction product was purified by chromatography on silica gel. Elution with 1:2 ethyl acetate – petroleum ether (35–60°) gave 1.19 g of *trans*-3-*n*-butyl-4-vinylazetidin-2-one; n.m.r.: 1.7–2.2 (m, 9H), 2.8–3.0 (m, 1H), 3.73 (d of d, J = 2.0 and 6.0 Hz, 1H) 5.6–6.4 (m, 3H), and 7.7 (s, 1H); i.r.: 3260, 3090, 1748, 1642, 985, and 920 cm^{-1}.

Anal. Calcd. for $C_9H_{15}NO$: C, 70.55; H, 9.87. Found: C, 70.75; H, 9.79.

Isopropyl Bromide

To the dianion **5***b* generated from 500 mg of **4***b* was added 630 mg of isopropyl bromide. The reaction mixture was stirred for 15 min then worked up. The crude product was chromatographed (ether) to yield 315 mg (45%) of *trans*-3-isopropyl-4-vinylazetidin-2-one. The n.m.r. spectrum showed peaks at 0.98 (d, J = 6.0 Hz, 3H), 1.05 (d, J = 6.0 Hz, 3H), 1.65–2.35 (m, 1H), 2.62 (d of d, J = 2.2 and 7.5 Hz, 1H), 3.60 (d of d, J = 2.2 and 6.5 Hz, 1H), 5.0–6.3 (m, 3H), and 7.3–7.8 (s, 1H); i.r. peaks occurred at 3270, 3090, 1750, 1646, 985, and 920 cm^{-1}.

Anal. Calcd. for $C_8H_{13}NO$: C, 69.03; H, 9.42. Found: C, 69.49; H, 9.73.

Cyclohexanone

The crude product obtained from 500 mg of **4***b*, 12.0 mmol of *n*-BuLi and 490 mg of cyclohexanone was purified by preparative t.l.c. (ether–pentane 4:1). The colorless oil (480 mg, 55%) thus obtained had n.m.r. peaks at 1.0–2.0 (m, 10H) 1.7 (s, OH), 1.80 (d, J = 2.2 Hz, 1H), 4.02 (d of d, J = 2.2 and 6.0 Hz, 1H), 5.0–6.5 (m, 3H), and 6.8 (s, NH); i.r. peaks occurred at 3470, 3400, 1750, 978, and 930 cm^{-1}.

Anal. Calcd. for $C_{11}H_{17}NO_2$: C, 67.66; H, 8.78. Found: C, 67.41; H, 8.63.

Reaction of 1,3-Dilithio-4-methyl-4-vinylazetidin-2-one with Benzophenone

Azetidin-2-one (**4***c*, 250 mg, 2.3 mmol) in 40 ml of THF at 0° was reacted with 5.0 mmol of *n*-BuLi for 0.5 h and then condensed with 420 mg of benzophenone. The crude product was recrystallized from ether–pentane to give 380 mg (57%) of adduct. Several further crystallizations gave one isomer as colorless crystals, m.p. 201–202°.

Anal. Calcd. for $C_{19}H_{19}NO_2$: C, 77.79; H, 6.53. Found: C, 77.84; H, 6.27.

Reactions of 1,3-Dilithio-4-ethylazetidin-2-one

n-Butyl Bromide

The crude product produced in the usual manner from 500 mg of 4-ethylazetidin-2-one and 685 mg of *n*-butyl bromide was chromatographed on silica gel. Elution with ether gave 506 mg (65%) of *trans*-3-*n*-butyl-4-ethylazetidin-2-one; n.m.r. 0.7–2.3 (m, 14 H), 2.6–3.0 (m, 1H), 3.50 (d of t, J = 1.8 and 6.0 Hz, 1H), and 7.7 (s, NH); i.r. peaks 3270 and 1755 cm^{-1}.

Benzophenone

The adduct was obtained in 65% yield. Recrystallization from ether–hexane gave colorless needles, m.p. 148–155°. The n.m.r. was in agreement with the expected structure.

Anal. Calcd. for $C_{18}H_{19}NO_2$: C, 76.84; H, 6.81. Found: C, 76.93; H, 7.06.

Financial Assistance by Bristol Laboratories, Syracuse, N.Y., and by the National Research Council of Canada is gratefully acknowledged.

1. (*a*) T. DURST and M. J. LEBELLE. Can. J. Chem. **50**, 3196 (1972); (*b*) E. W. H. BOHME, H. E. APPLEGATE, J. B. EWING, P. T. FUNKE, M. S. PUAR, and J. E. DOLFINI. J. Org. Chem. **38**, 230 (1973).
2. R. L. GAY, S. BOATMAN, and C. R. HAUSER. Chem. Ind. (Lond.), 1789 (1965).
3. D. A. JOHNSON and D. MANIA. Tetrahedron Lett. 267 (1969).
4. (*a*) R. GRAF. Ann. **661**, 111 (1963); (*b*) E. J. MORICONI and W. C. MEYER. Tetrahedron Lett. 3823 (1968).
5. T. DURST and M. J. O'SULLIVAN. J. Org. Chem. **35**, 2043 (1970).
6. E. J. MORICONI and J. F. KELLY. Tetrahedron Lett. 1435 (1968).

Etude de l'oxydation des éthylènes $RCH{=}CH_2$ et $R_1(R_2)C{=}CH_2$ par le $Tl(NO_3)_3$ dans le méthanol

J. GRIGNON ET S. FLISZÁR

Département de Chimie, Université de Montréal, Montréal, Québec H3C 3V1

Received January 28, 1974

J. GRIGNON et S. FLISZÁR. Can. J. Chem. **52**, 3209 (1974).

La distribution des produits engendrés par l'oxydation des oléfines $R{-}CH{=}CH_2$ et $R_1(R_2)C{=}CH_2$ dans le méthanol par le $Tl(NO_3)_3$ a été étudiée. Les éthylènes monosubstitués (R = alkyle) engendrent un diéther $RCH(OCH_3){-}CH_2OCH_3$ et une cétone $RC(O)CH_3$, cette dernière dans une proportion de 40–55%; avec R = CH_2Cl, seulement le diéther est formé. Avec les éthylènes $R_1(R_2)C{=}CH_2$, le rapport des constantes de vitesse de formation des cétones isomères k_1 (impliquant la migration de R_1) et k_2 (impliquant la migration de R_2) est relié aux constantes polaires de Taft par l'équation $\log (k_2/k_1) = \rho^*(\sigma_2^* - \sigma_1^*)$ avec $\rho^* = -4$, ce qui indique que la migration du meilleur donneur d'électrons se fait de façon préférentielle. En plus du mélange de cétones (~10–15%), ~75–80% de diéther et ~10–20% d'aldéhyde sont formés.

J. GRIGNON and S. FLISZÁR. Can. J. Chem. **52**, 3209 (1974).

The distribution of products formed in the oxidation by $Tl(NO_3)_3$ of the olefins $RCH{=}CH_2$ and $R_1R_2C{=}CH_2$ in methanol has been studied. The monosubstituted ethylenes (R = alkyl) lead to a diether $RCH(OCH_3){-}CH_2OCH_3$ and to a ketone $RC(O)CH_3$, the latter being formed in an amount of 40–55%; when R = CH_2Cl only the diether is formed. With the disubstituted ethylenes $R_1R_2C{=}CH_2$, the ratio of the rate constants for the formation of the isomeric ketones k_1 (implying the migration of R_1) and k_2 (implying the migration of R_2) is related to the polar Taft constants by the equation $\log (k_2/k_1) = \rho^*(\sigma_2^* - \sigma_1^*)$ with $\rho^* = -4$. This indicates that the migration of the better electron donor occurs preferentially. In addition to the ketone mixture (~10–15%), ~75–80% of the diether and ~10–20% of the aldehyde are formed. [Journal translation]

Can. J. Chem. Downloaded from www.nrcresearchpress.com by 210.87.254.42 on 09/05/12
For personal use only.

Le grand intérêt présenté par les réactions du thallium(III) avec les composés organiques au point de vue synthétique a incité divers auteurs à étudier leurs mécanismes; l'approche étant alors celle de l'étude systématique des effets de substituant, de solvant, de température et de la participation d'ions étrangers sur les vitesses de réaction et sur la distribution des produits. En ce qui a plus particulièrement trait à l'oxydation des oléfines aliphatiques, les études sont, cependant, relativement peu nombreuses (1–5). C'est dans le but d'évaluer les effets des groupements alkyles sur la distribution des produits que la présente étude de l'oxydation des oléfines aliphatiques par le nitrate thallique dans le méthanol a été effectuée; elle porte sur (*i*) les éthylènes $RCH{=}CH_2$ et (*ii*) sur les éthylènes *gem*-disubstituées $R_1(R_2)C{=}CH_2$.

Résultats

Dans la présente étude, le nitrate thallique a été choisi comme agent oxydant à cause de sa grande réactivité ainsi que pour sa solubilité dans le méthanol. Le nitrate thalleux qui se forme au cours de la réaction est insoluble dans ce solvant, ce qui permet une appréciation visuelle de l'avancement de la réaction. Le méthanol s'est avéré être un solvant très sélectif lors de l'oxydation des oléfines aromatiques (6), ce qui a motivé son choix pour la présente étude. Son utilisation permet d'effectuer facilement les dosages des divers produits de réaction en chromatographie en phase gazeuse. A moins de spécifications contraires, les expériences ont été effectuées à 25 ± 0.1 °C.

Oxydation des éthylènes RCH=CH₂

Identification des produits de réaction

L'oxydation des éthylènes monosubstitués engendre la formation de deux produits de réaction. Ceux-ci ont été identifiés comme étant le diméthoxy-1,2 éthane (**1**) correspondant à l'oléfine utilisée et la cétone (**2**) résultant de la migration de l'hydrogène du carbone-2.

$$R{-}CH{=}CH_2 \xrightarrow[MeOH]{Tl(NO_3)_3} \begin{cases} R\,CH(OCH_3){-}CH_2OCH_3 \quad \textbf{1} \\ R\,C(O){-}CH_3 \quad \textbf{2} \end{cases}$$

TABLEAU 1. Bilan de l'oxydation du méthyl-3 butène-1 à 25 ± 0.1 °C

Oléfine consommée (mmol)	Produits formés (mmol)		
	Cétone	Diéther	Total
0.273	0.102	0.170	0.272
0.450	0.151	0.275	0.426
0.456	0.151	0.299	0.450
0.768	0.241	0.483	0.724
1.335	0.439	0.838	1.277

L'identification des produits de réaction a été effectuée au moyen de diverses méthodes analytiques. En ce qui a trait aux diéthers (**1**), dans deux cas (ceux du diméthoxy-1,2 chloro-3 propane et du diméthoxy-1,2 méthyl-3 butane) les diéthers attendus ont également été synthétisés par une autre voie en vue d'une comparaison avec les produits isolés des mélanges réactionnels. La comparaison des spectres r.m.n., des points d'ébullition, ainsi que des temps de rétention en chromatographie en phase gazeuse des substances de référence avec ceux des produits de réaction ont confirmé l'identité de ces derniers. De plus, dans quelques cas, les microanalyses confirment la formule des produits de réaction isolés. Les cétones (**2**) ont été identifiées par la comparaison de leurs temps de rétention en chromatographie en phase gazeuse avec ceux d'échantillons authentiques. Ces comparaisons des temps de rétention ont été effectuées sur trois colonnes différentes. Dans un cas, celui de l'oxydation de l'hexène-1 qui engendre l'hexanone-2, la cétone a été isolée du mélange réactionnel. Son point d'ébullition, le point de fusion de la semicarbazone correspondante, ainsi que son spectre r.m.n. confirment qu'il s'agit bien de l'hexanone-2.

Dans chaque cas, le seul produit carbonylé obtenu résulte de la migration de l'hydrogène porté par l'atome C-2. La migration du groupe alkyle porté par ce même carbone entraînerait la formation d'un aldéhyde. Or, l'absence d'un tel aldéhyde et de son acétal parmi les produits de réaction a été vérifiée dans tous les cas. Ceci implique qu'il n'y a pas de migration appréciable du groupement alkyle dans nos conditions expérimentales.

Reproductibilité des résultats

La reproductibilité est satisfaisante. Ainsi, par exemple, l'oxydation du méthyl-3 butène-1 à 25 ± 0.1 °C a conduit à une fraction molaire en méthyl-3 butanone-2 de 0.345 ± 0.007 (par rapport aux produits formés, *i.e.* cétone et diéther); ce résultat étant indiqué avec une limite de confiance de 95%, à partir de huit expériences indépendantes, pour des concentrations initiales en oléfine comprises entre 0.087 et 0.24 *M*.

Il a été vérifié dans tous les cas que la réaction est pratiquement quantitative après 10–20 min à 25 °C: les rendements sont alors de l'ordre de 95–100%, ainsi que l'illustre l'exemple rapporté au tableau 1.

Le tableau 2 rapporte la distribution des produits de réaction observée lors de l'oxydation des éthylènes monosubstitués à 25 ± 0.1 °C. Chaque série d'expériences a été répétée au moins cinq fois et les résultats sont indiqués avec une limite de confiance de 95%.

Ces résultats indiquent une tendance générale d'une migration préférentielle d'un hydrogène voisin d'un groupement donneur d'électrons par rapport à celui qui est voisin d'un attracteur, ce qui se traduit par une proportion de cétone engendrée plus grande avec R = *tert*-butyle qu'avec R = CH_2Cl. Il n'est cependant pas possible d'établir une corrélation précise en termes d'effets polaires.

Effet de température

Lors de la décomposition de l'intermédiaire organothallique il y a compétition entre le clivage du lien C—Tl par le solvant pour donner le diéther et la migration de l'hydrogène en C-2 pour engendrer la cétone. Ces deux processus étant différents, on peut s'attendre à ce que les proportions relatives des deux voies de réactions (conduisant à **1** et à **2**) dépendent de la température. Cette dépendance est indiquée par les résultats rapportés au tableau 3.

Dans l'hypothèse que les deux réactions soient du même ordre *par rapport à l'intermédiaire*, le rapport des deux vitesses de réaction k_c

Can. J. Chem. Downloaded from www.nrcresearchpress.com by 210.87.254.42 on 09/05/12
For personal use only.

TABLEAU 2. Produits obtenus lors de l'oxydation des éthylènes $RCH{=}CH_2$ à 25 ± 0.1 °C

Oléfine (R)	Cétone	Fractions molaires	
		Cétone	Diéther
tert-C_4H_9	Pinacolone	0.539 ± 0.007	0.461
iso-C_3H_7	Méthyl-3 butanone-2	0.345 ± 0.007	0.655
n-C_4H_9	Hexanone-2	0.396 ± 0.012	0.604
n-C_3H_7	Pentanone-2	0.385 ± 0.012	0.615
C_2H_5	Butanone-2	0.395 ± 0.013	0.605
CH_2Cl	Chloro-3 propanone	0.00	1.00

TABLEAU 3. Proportions des produits obtenus à partir des éthylènes $RCH{=}CH_2$, en fonction de la température

Oléfine (R)	Température (°C)	Fractions molaires	
		Cétone	Diéther
n-C_3H_7	0	0.326	0.674
	15	0.359	0.641
	25	0.385	0.611
	30	0.400	0.600
	35	0.413	0.587
n-C_4H_9	−11	0.313	0.687
	0	0.345	0.655
	15	0.374	0.626
	22	0.384	0.616
	30	0.411	0.589
	35	0.420	0.580
iso-C_3H_7	0	0.308	0.692
	11	0.323	0.677
	21	0.338	0.662
	25	0.345	0.655
	30	0.358	0.642
tert-C_4H_9	0	0.570	0.430
	12	0.556	0.444
	25	0 539	0.461
	31	0.513	0.487
	39	0.450	0.550

(conduisant à la cétone) et k_d (conduisant au diéther) est égal au rapport des fractions molaires X_c (de la cétone) X_d (du diéther) des produits formés. En termes de la théorie du complexe activé (7), *i.e.*, dans la notation habituelle

$$[1] \qquad k = (KT/h) \exp(-\Delta G^{\ddagger}/RT)$$

il s'ensuit que

$$[2] \quad \ln(X_c/X_d) = \ln(k_c/k_d) = -\Delta\Delta G^{\ddagger}/RT$$

avec $\Delta\Delta G^{\ddagger} = \Delta G_c^{\ddagger} - \Delta G_d^{\ddagger}$, où $\Delta G_c^{\ddagger}$ et $\Delta G_d^{\ddagger}$ se réfèrent, respectivement, à la formation de cétone et de diéther.

Ainsi que le montre la fig. 1, le logarithme du

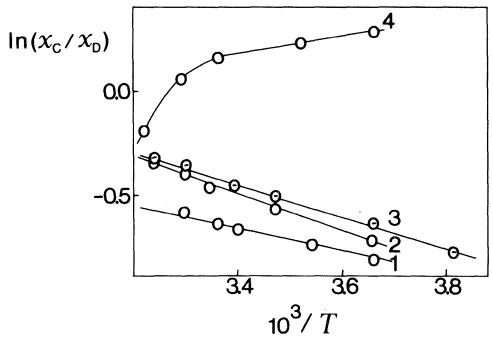

FIG. 1. Proportions des produits d'oxydation à différentes températures pour le méthyl-3 butène-1 (1), le pentène-1 (2), l'hexène-1 (3) et le diméthyl-3,3 butène-1 (4).

Can. J. Chem. Downloaded from www.nrcresearchpress.com by 210.87.254.42 on 09/05/12
For personal use only.

Can. J. Chem. Downloaded from www.nrcresearchpress.com by 210.87.254.42 on 09/05/12
For personal use only.

TABLEAU 4. Valeurs de $\Delta\Delta H^{\neq}$ et $\Delta\Delta S^{\neq}$ pour l'oxydation des éthylènes R—CH=CH_2

Oléfine (R)	$\Delta\Delta H^{\neq}$ (kcal)	$\Delta\Delta S^{\neq}$ (u.e.)
n-C_3H_7	1.80 ± 0.06	5.13 ± 0.03
n-C_4H_9	1.57 ± 0.06	4.44 ± 0.05
iso-C_3H_7	1.19 ± 0.07	2.74 ± 0.03
tert-C_4H_9*	−0.83 ± 0.01	−2.47 ± 0.03

*Calculé à partir de la partie linéaire, *i.e.*, pour T ≤ 25 °C.

rapport des fractions molaires X_c/X_d est relié linéairement à l'inverse de la température dans tous les cas, sauf celui du diméthyl-3,3 butène-1. La chute brusque de la proportion de pinacolone observée aux températures supérieures à 25 °C peut être possiblement attribuée à une décomposition partielle de cette cétone dans le milieu réactionnel.

L'équation $\partial(\Delta\Delta G^{\neq}/T)/\partial(1/T) = \Delta\Delta H^{\neq}$ permet le calcul de $\Delta\Delta H^{\neq} = \Delta H_c^{\neq} - \Delta H_d^{\neq}$ à partir des pentes (fig. 1) de ln (X_c/X_d) *vs.* 1/T (eq. 2). Le tableau 4 rapporte les valeurs de $\Delta\Delta H^{\neq}$ et $\Delta\Delta S^{\neq}$ calculées au moyen de la méthode des moindres carrés à partir des résultats du tableau 3.

Oxydation des éthylènes gem-disubstitués

Identification des produits de réaction

L'oxydation des éthylènes *gem*-disubstitués entraîne la formation de plusieurs produits. Ceux-ci comprennent (*i*) un diéther (**3**) analogue à celui formé lors de l'oxydation des éthylènes monosubstitués, (*ii*) deux cétones isomères (**4** et **5**) résultant de la migration de l'un ou de l'autre des groupes alkyles et (*iii*) un aldéhyde (**6**) et son acétal méthylique (**7**) provenant de la participation du groupe méthoxyle de l'intermédiaire organothallique.

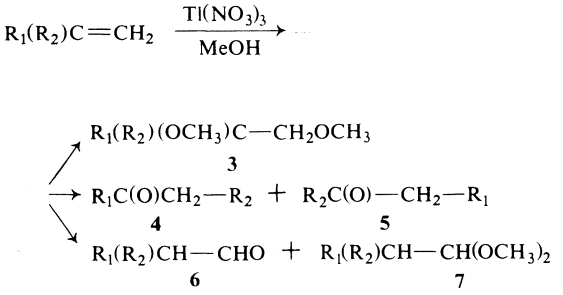

Malgré la complexité des mélanges réactionnels obtenus, l'intérêt présenté par l'étude de cette série d'oléfines réside dans le fait qu'elle permet de comparer entre elles les aptitudes migratrices des divers groupes alkyles. De plus, cette étude permet également de suivre la migration concurrente du groupe méthoxyle de l'intermédiaire.

Les diéthers **3** ont été identifiés comme cela avait été fait lors des expériences avec les éthylènes monosubstitués surtout à l'aide de leurs spectres r.m.n., semblables à ceux des diéthers issus des éthylènes RCH=CH_2. Un diéther, le diméthoxy-1,2 éthyl-2 hexane, a également été synthétisé par une autre voie et a été reconnu identique à un des produits d'oxydation de l'éthyl-2 hexène-1. De plus, les analyses élémentaires des produits isolés à partir des mélanges réactionnels ont bien confirmé les formules postulées. Les aldéhydes, les cétones et les acétals ont été identifiés par la comparaison de leurs temps de rétention en chromatographie en phase gazeuse par rapport à des échantillons authentiques obtenus de source commerciale ou synthétisés par des méthodes standards. Cette comparaison des temps de rétention a été effectuée dans tous les cas à l'aide d'au moins deux colonnes différentes. De plus, il a été vérifié qu'en présence d'acide le pic chromatographique attribué à l'acétal disparaît, alors que celui attribué à l'aldéhyde augmente.

Distribution des produits formés

Il a été vérifié dans tous les cas étudiés que les rendements en produits engendrés sont de l'ordre de 90–100% par rapport à l'oléfine consommée. Un bilan typique est présenté dans le tableau 5, qui se rapporte à l'oxydation du diméthyl-2,3 butène-1.

Dans les tableaux 5 et 6 le terme cétone dénote la somme des deux cétones isomères formées lors de la réaction alors que le terme aldéhyde se réfère à la somme de l'aldéhyde et de son acétal méthylique qui est présent en proportion appréciable dans le milieu réactionnel. Les proportions des différents produits sont exprimées par rapport au total des produits formés. La reproductibilité des résultats est illustrée par l'exemple de l'éthyl-2 hexène-1 à 25 ± 0.1 °C. Les fractions molaires en produits observées lors de cinq oxydations indépendantes étaient alors: 0.173 ± 0.09 (cétones), 0.043 ± 0.008 (aldéhyde) et 0.782 ± 0.007 (diéther), ces résultats étant indiqués avec une limite de confiance de 95%.

L'ensemble des résultats concernant la distribution des produits issus de l'oxydation des éthylènes *gem*-disubstitués est rapporté au tableau 6. Ces données représentent dans

TABLEAU 5. Bilan de l'oxydation du diméthyl-2,3 butène-1, à 25 ± 0.1 °C

Oléfine consommée (mmol)	Produits formés (mmol)			
	Cétones	Aldéhyde	Diéther	Total
0.899	0.0848	0.285	0.494	0.863
0.899	0.110	0.248	0.498	0.856
0.788	0.0849	0.207	0.477	0.769
0.789	0.0765	0.239	0.443	0.758
0.839	0.0960	0.246	0.486	0.828

TABLEAU 6. Distribution des produits d'oxydation des éthylènes $R_1(R_2)C{=}CH_2$ à 25 ± 0.1 °C

R_1	R_2	Fractions molaires		
		Cétones	Aldéhyde	Diéther
CH_3	C_2H_5	0.085 ± 0.004	0.140 ± 0.011	0.775 ± 0.009
CH_3	n-C_3H_7	0.113 ± 0.001	0.125 ± 0.019	0.762 ± 0.020
CH_3	n-C_4H_9	0.148 ± 0.002	0.120 ± 0.005	0.732 ± 0.010
CH_3	iso-C_3H_7	0.108 ± 0.014	0.314 ± 0.024	0.582 ± 0.015
CH_3	CH_2Cl	0.00	0.200 ± 0.018	0.800 ± 0.021
C_2H_5	n-C_4H_9	0.173 ± 0.009	0.043 ± 0.008	0.782 ± 0.007

chaque cas les résultats d'au moins cinq déterminations indépendantes et sont indiquées avec une limite de confiance de 95%.

Les résultats du tableau 6 permettent d'évaluer (*i*) l'importance de la migration des groupements alkyles, telle qu'elle est reflétée par la quantité totale de cétone formée, (*ii*) la migration du groupe méthoxyle indiquée par la proportion d'aldéhyde engendré et (*iii*) la proportion de diéther formé. On constate que, tout comme pour la série des éthylènes monosubstitués, la quantité de diéther formé diminue d'autant plus que (à R_1 égal) le substituant R_2 est un meilleur donneur d'électrons.

Influence de la température

En raison de la complexité des mélanges réactionnels, la dépendance de la distribution des produits en fonction de la température n'a pas été étudiée de façon systématique. Il a cependant été vérifié que le rapport des deux cétones isomères formées est indépendant de la température dans le domaine 0 à 40 °C étudié ici. Ceci est illustré par les résultats de l'oxydation de l'éthyl-2 hexène-1, où le rapport octanone-3–octanone-4 est 1.17 ± 0.01 entre 0 et 40 °C. Il a également été vérifié que ce rapport ne varie pas lorsque la solution est laissée au repos durant plusieurs heures.

Aptitude migratrice des groupes alkyles

Lors de l'étude de l'oxydation des oléfines monosubstituées il a été montré que seuls les atomes H migrent. Dès lors, les aptitudes migratrices relatives des groupements alkyles ne pouvaient être déterminées. Par contre, ceci devient possible par l'étude des éthylènes *gem*-disubstitués. Le rapport des quantités des deux cétones isomères engendrées est une mesure de l'habilité relative de migration des groupes R_1 et R_2. Les aptitudes migratrices sont exprimées par la suite en termes de k_2/k_1, où k_1 et k_2 dénotent, respectivement, les constantes de vitesse de réaction impliquant la migration de R_1 et de R_2. Ces aptitudes migratrices sont exposées au tableau 7, avec une limite de confiance de 95%.

En postulant pour k_1 et k_2 la validité de l'éq. 1 et en faisant appel à la relation linéaire d'enthalpie libre (7) $\Delta G^{\ddagger} = \Delta G_0{}^{\ddagger} - 2.3RT\rho^*\sigma^*$, il en découle une équation du type Taft (8)

$$\log (k_2/k_1) = \rho^*(\sigma_2{}^* - \sigma_1{}^*)$$

qui est bien vérifiée, ainsi que le montre la fig. 2, pour les deux séries, *i.e.*, avec $R_1 = CH_3$ et $R_1 = C_2H_5$.

Les deux droites parallèles correspondent à une pente $\rho^* = -4.0$. Ces résultats indiquent

Can. J. Chem. Downloaded from www.nrcresearchpress.com by 210.87.254.42 on 09/05/12
For personal use only.

Can. J. Chem. Downloaded from www.nrcresearchpress.com by 210.87.254.42 on 09/05/12
For personal use only.

TABLEAU 7. Proportions relatives des produits de migration lors de l'oxydation des éthylènes $R_1(R_2)C{=}CH_2$

R_1	R_2	k_2/k_1
CH_3	CH_3	1.00
CH_3	C_2H_5	2.64 ± 0.09
CH_3	n-C_3H_7	2.85 ± 0.10
CH_3	n-C_4H_9	3.00 ± 0.18
CH_3	iso-C_3H_7	4.41 ± 0.09
C_2H_5	CH_3	0.38 ± 0.01
C_2H_5	C_2H_5	1.00
C_2H_5	n-C_4H_9	1.18 ± 0.02

donc clairement que la migration du meilleur donneur d'électrons se fait de façon préférentielle. Ceci est en parfait accord avec les résultats obtenus par Ouellette *et al.* (9) pour l'oxydation des styrènes substitués (dans l'acide acétique), où $\rho^+ = -1.7$, ainsi qu'avec les résultats observés lors de l'oxydation des diphényl-1,1 éthylènes dans le méthanol (6), avec $\rho^+ = -2.27$.

Discussion

Les présents résultats suggèrent que, lors de la migration, il y a un important développement de charge positive. La formation d'un ion carbonium, tel que postulé précédemment (9) résulterait d'une rupture préalable du lien C—Tl. Il semble plus satisfaisant de supposer, comme cela avait été fait pour les phényléthylènes (6), que le groupement alkyle migre vers un carbone possédant une charge positive partielle due à la forte électronégativité du Tl(III) auquel il est attaché. La rupture du lien C—Tl et la migration de l'alkyle seraient alors concertées. Ceci est en accord avec l'étude stéréochimique de l'oxydation de cyclohexènes rigides qui conclut que la décomposition de l'organothallique intermédiaire n'est pas initiée par la rupture de la liaison C—Tl (10).

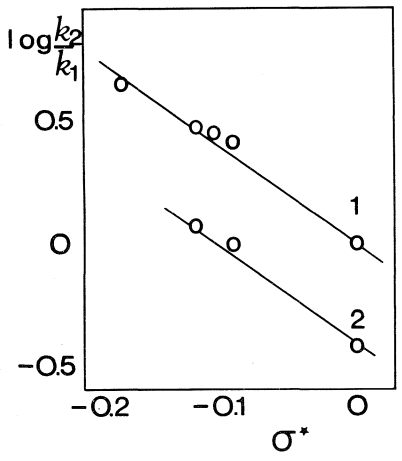

FIG. 2. Vérification de l'éq. log $(k_2/k_1) = \rho^*(\sigma_2^* - \sigma_1^*)$ pour les produits de migration des éthylènes $R_1(R_2)C{=}CH_2$, avec $R_1{=}CH_3$ (1) et $R_1{=}C_2H_5$ (2).

Contrairement aux oléfines aromatiques qui conduisent, avec le $Tl(NO_3)_3$ dans le méthanol, à un seul produit carbonylé résultant de la migration du groupe aryle (6), les oléfines aliphatiques étudiées dans ce travail conduisent à plusieurs produits. Les éthylènes monosubstitués engendrent un diéther et un produit carbonylé résultant d'une migration d'hydrogène, tandis que les éthylènes disubstitués conduisent à la formation de cinq produits: un diéther, deux cétones isomères, ainsi qu'un aldéhyde et son acétal. L'ensemble de ces résultats peuvent être rationalisés par le schéma réactionnel 1 suivant, à partir de l'intermédiaire organothallique $R_1(R_2)C(OCH_3){-}CH_2TlX_2$ (**8**).

La voie *C* (contrairement à *B*) implique également une migration d'hydrure, en plus de celle du groupe CH_3O. Il est difficile, à ce stade, de définir la chronologie des événements ainsi que le moment précis de la rupture du lien C—Tl. De plus, les présentes données ne permettent pas d'établir si un défaut de réaction doit être attribué en premier lieu à un manque d'habilité migratrice du groupe CH_3O ou, par contre, de l'hydrure. La formation d'un ion $R(OCH_3)(CH_3)C^+$ ne semble, cependant, pas pouvoir être invoquée facilement, d'après les résultats de Zador et coll. (10).

La formation de l'intermédiaire organothallique (**8**) ayant été prouvée pour les oléfines aromatiques (1, 6) et certaines oléfines aliphatiques (12) l'attention est maintenant portée sur sa décomposition.

Seule la voie *A* implique la migration d'un des substituants R du carbone 2. La voie B implique le clivage du lien C—Tl avec ou sans participation du groupe méthoxyle rattaché au carbone 2 alors que la voie *C* implique la migration du groupe méthoxyle et d'hydrure.

Le groupe méthoxyle n'étant pas un bon groupement participant (13), la migration du groupe aryle est de beaucoup plus importante qu'une quelconque participation du groupe méthoxyle et seule la voie *A* est suivie dans le cas des oléfines aromatiques. Ceci explique la formation d'un seul composé carbonylé dans ce cas.

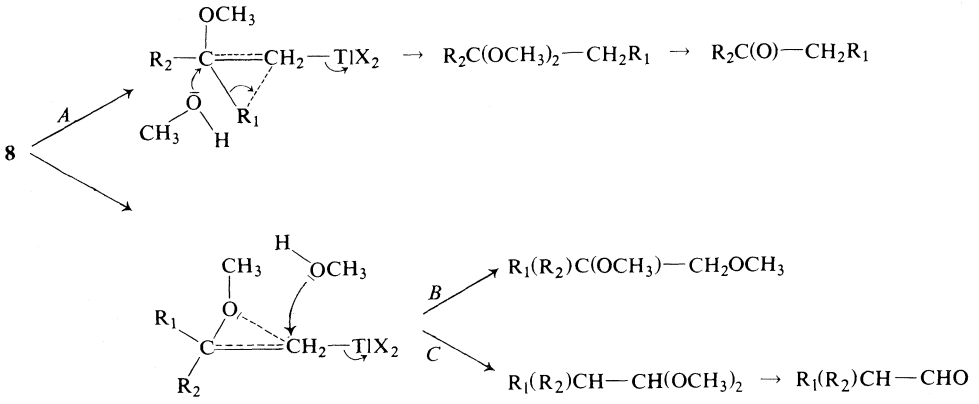

SCHÉMA 1

En effet, le phényle migre beaucoup mieux que l'hydrogène puisque les styrènes substitués conduisent quantitativement aux diméthylacétals des aryléthanals correspondants (6).

Pour les éthylènes monosubstitués nous avons en présence un alkyle, un hydrogène et le groupe méthoxyle. La migration de l'hydrogène l'emporte d'emblée sur celle de l'alkyle ou sur la participation du méthoxyle ce qui fait qu'un seul composé carbonylé est observé; mais, cette migration étant quand même appréciablement plus lente que celle du phényle, le clivage du lien C—Tl devient appréciable. Il y a donc compétition entre les voies *A* et *B*. Il se forme en moyenne environ 40% de cétone et 60% de diéther.

Pour les éthylènes *gem*-disubstitués la situation est encore plus complexe. En effet, il y a alors compétition entre deux groupes alkyles (voie *A*) et le groupement méthoxyle. De plus, le clivage du lien C—Tl par le solvant devient prédominant, les groupes alkyles migrant encore moins que l'hydrogène. Les deux groupes alkyles ayant des aptitudes migratrices voisines, les deux migrent et deux cétones isomères sont formées (voie *A*). De plus la participation du groupe méthoxyle est maintenant compétitive à celle des alkyles entraînant également la formation d'un aldéhyde et de son acétal. Il se forme dans cette série environ 10 à 15% de cétone, 75 à 80% de diéther et 10 à 20% d'aldéhyde ou de son acétal.

Le choix entre les voies *B* d'une part, et *A* ou *C* d'autre part dépend du solvant, lequel détermine la nature du groupe OR de l'intermédiaire. Alors que le méthanol est un mauvais participant, l'acide acétique favoriserait la formation de diacétate car OAc est un très bon groupement participant (13). Pour un solvant donné, les aptitudes de migration des groupements R déterminent les proportions de cétone et de diéther qui seront formés. Plus R migre facilement, plus il y aura de cétone formée.

L'aldéhyde résultant de la migration du groupe OR dépendra de l'abondance de l'intermédiaire ponté (**9**) qui est en fait une forme hybride résultant des structures **9** (14).

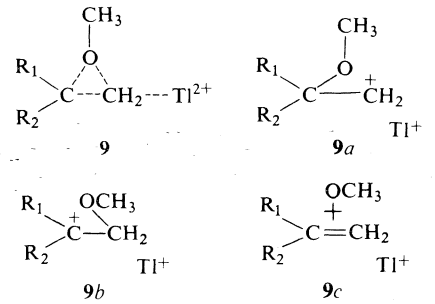

La facilité de migration de OR est liée à l'abondance relative de la structure **9***b* qui augmente avec la capacité des groupements R_1 et R_2 à stabiliser une charge positive sur le carbone adjacent. Le fait que l'aldéhyde n'est formé qu'à partir des éthylènes disubstitués peut alors être attribué à la stabilisation accrue d'une charge positive sur un carbone tertiaire par rapport à celle sur un carbone secondaire.

Partie expérimentale

Réactifs et produits de référence

La préparation du nitrate thallique, la stabilité de sa solution dans le méthanol, ainsi que son dosage iodométrique ont été décrits précédemment (6).

Les oléfines, de source commerciale (Eastman et K & K), ont été redistillées et leur pureté a été vérifiée par chromatographie en phase gazeuse (c.p.g.).

Les diéthers de référence ont été préparés selon des

Can. J. Chem. Downloaded from www.nrcresearchpress.com by 210.87.254.42 on 09/05/12
For personal use only.

Can. J. Chem. Downloaded from www.nrcresearchpress.com by 210.87.254.42 on 09/05/12
For personal use only.

méthodes standards. Pour la préparation du diméthoxy-1,2 méthyl-3 butane, l'oléfine a été convertie en diol selon (15*a*). La méthylation du diol au moyen de sulfate de méthyle a été effectuée selon (15*b*). Après trois distillations, le diéther (p.éb. 68–70 °C/15 mm Hg) pur présente le spectre r.m.n. (dans le CCl_4, par rapport au TMS): un singulet à 3.33 p.p.m. (OCH_3 et OCH_2), un multiplet large à 1.70 p.p.m. (H tertiaire du iso-C_3H_7) et un doublet à 0.93 p.p.m., dû aux deux groupes méthyles. Le proton voisin des OCH_3 semble sortir sous le singulet à 3.33 p.p.m. L'intégration des signaux est compatible avec cette attribution (9:1:6).

Le chloro-3 diméthoxy-1,2 propane a été obtenu à partir du diol correspondant (Baker) par méthylation au moyen de sulfate de méthyle et purifié par distillation (p.éb. 60 °C/15 mm Hg; 150 °C à 1 atm). Le spectre r.m.n. présente un massif vers 3.4–3.6 p.p.m., par rapport au TMS, en solution dans le CCl_4.

Le diméthoxy-1,2 éthyl-2 hexane a été obtenu par oxydation de l'oléfine par H_2O_2 (15*c*) pour former le diol qui a été méthylé par CH_3I en présence d'oxyde d'argent (16) dans le DMF. Le diéther purifié (p.éb. 80–82 °C/15 mm Hg) présente le spectre r.m.n. suivant (dans le CCl_4, par rapport au TMS): 2 singulets à 3.17 et 3.20 p.p.m. (OCH_3 et OCH_2), un multiplet à 1.33 (CH_2), ainsi qu'un multiplet vers 0.9 p.p.m. (CH_3). Les intégrations relatives sont dans le rapport 8:8:6.

La chloro-4 butanone-2 a été préparée selon (17); p.éb. 56–58 °C/15 mm Hg; (litt. (18) p.éb. 57–60 °C/15 mm Hg). Le spectre r.m.n. (dans le CCl_4, relatif au TMS) montre un triplet à 3.87 p.p.m. (CH_2Cl), un triplet à 3.03 p.p.m. (CH_2) et un singulet à 2.33 p.p.m. (CH_3CO). L'intégration conduit au rapport 2:2:3.

La chloro-1 butanone-2 a été préparée en générant la chlorhydrine (19) à partir du butène-1, qui a été oxydée par le mélange chromique (15*d*) pour engendrer la cétone, p.éb. 136–138 °C (litt. (19) p.éb. 135–137 °C). Le spectre r.m.n. (dans le CCl_4, relatif au TMS) montre un singulet à 3.8 p.p.m. (CH_2Cl), un multiplet large à 2.0 p.p.m. (CH_2) et un triplet à 1.2 p.p.m. (CH_3) avec un rapport d'intégration de 2:2:3.

Les acétals $RCH(CH_3)—CH(OCH_3)_2$ avec R = C_2H_5, *n*-C_3H_7 et *n*-C_4H_9 ont été préparés par synthèse magnésienne à partir des iodo- ou bromo-2 alcanes correspondants (15*e*). Les acétals du diméthyl-2,3 butanal, de l'éthyl-2 hexanal, du valéraldéhyde et de l'isovaléraldéhyde ont été préparés par acétalisation de ces aldéhydes. Le diméthyl-2,3 butanal a été préparé selon (20). Les autres aldéhydes de référence ont été obtenus par hydrolyse de l'acétal en présence de H_2SO_4 à 20%. L'iodo-2 hexane requis pour la préparation de l'acétal méthylique du méthyl-2 hexanal a été synthétisé selon (15*f*).

Méthode d'oxydation

L'oléfine est mise en solution dans 2 ml de méthanol, à une concentration de 0.1–0.25 *M*. Une quantité égale d'une solution méthanolique de $Tl(NO_3)_3$ de concentration légèrement inférieure à celle de l'oléfine est préparée séparément, puis ajoutée à la solution d'oléfine. Il a été vérifié que les résultats sont les mêmes lorsque le $Tl(NO_3)$ est ajouté sous sa forme solide à la solution d'oléfine. Toutes les solutions ont été thermostatées avant leur usage. Le nitrate thalleux précipite en général après une trentaine de secondes. Au bout de 15–20 min la réaction est complète et le mélange est analysé.

Méthodes analytiques

Les analyses ont été effectuées par chromatographie en phase gazeuse au moyen d'un appareil Hewlett-Packard F & M 5750 équipé d'un détecteur à flamme, en utilisant l'hélium comme gaz vecteur. La quantité injectée a toujours été de 5 ml. Les spectres r.m.n. ont été enregistrés à une fréquence de 60 Mc, en solution dans le CCl_4 en utilisant le tétraméthylsilane comme référence interne, au moyen de spectromètres Jeolco C-60H et Varian T-60.

Pour les dosages, les solutions ont été injectées dans le chromatographe sans aucun traitement préalable, le premier dosage ayant été effectué après un temps de réaction de 20 min. Chaque mélange a été analysé plusieurs fois, ce qui a permis de s'assurer que la réaction était terminée. Chaque résultat final repose sur cinq ou six réactions conduites de manière indépendante.

Les surfaces des différents pics chromatographiques obtenus sont ensuite mesurées à l'aide d'un planimètre. La surface de chacun des pics est mesurée au moins quatre fois puis comparée à l'aire d'un pic de référence obtenu en injectant une solution de concentration connue de la même substance. La distribution des produits de la réaction s'obtient en procédant de la même façon pour chacun des pics d'un mélange réactionnel donné. Il est possible de cette façon de calculer le rendement de la réaction et les proportions relatives en chacun des produits. L'ensemble des résultats obtenus pour les divers mélanges réactionnels est ensuite soumis à une analyse statistique et les résultats finaux sont exprimés avec une limite de confiance de 95%.

Pour l'identification des diéthers, les réactions ont été effectuées sur une plus grande échelle: soit ~7–10 g d'oléfine dans le CH_3OH et 15–20 g d'oxyde thallique dans l'acide nitrique. Lorsque le test au KI confirme que l'ion thallique est entièrement disparu, la solution est concentrée, reprise par environ 200 ml d'eau puis extraite à l'éther. La phase éthérée est lavée avec une solution à 5% de carbonate de sodium, puis à l'eau jusqu'à neutralité. Après séchage et évaporation du solvant, le diéther est ensuite distillé sous pression réduite. Lors de l'oxydation des éthylènes disubstitués, l'acétal qui se forme simultanément a un point d'ébullition très voisin de celui du diéther ce qui fait qu'il faut répéter la distillation deux ou trois fois. Lorsqu'une petite quantité de diéther suffit, la meilleure technique consiste à distiller grossièrement une première fois et à purifier cette solution contenant de 80 à 90% de diéther par chromatographie préparative. L'appareil utilisé à cette fin est un chromatographe Hewlett-Packard F & M 5750 équippé d'un détecteur à conductivité thermique et d'un dispositif de chromatographie préparative F & M 5797-8. Les colonnes utilisées avaient un diamètre de $\frac{1}{4}$ po. et une longueur de 15 pi. Il s'agissait d'une colonne à 20% de β,β′-oxydipropionitrile ou à 20% de nitrile–silicone gum XE-60. Les analyses élémentaires, effectuées par Dr. C. Daesslé, Organic Microanalyses, Montréal, ainsi que les spectres r.m.n. ont dans tous les cas bien confirmé la nature de ces produits, qui ont également été comparés aux produits de synthèse.

L'identification des produits carbonylés a été faite par

la comparaison de leurs temps de rétention en c.p.q. sur deux ou trois colonnes différentes avec ceux observés pour des échantillons authentiques.

Nous tenons à remercier le Conseil national de recherches du Canada pour un octroi qui a permis ce travail.

1. A. McKillop, J. D. Hunt, E. C. Taylor et F. Kienzle. Tetrahedron Lett. **60**, 5275 (1970).
2. A. McKillop, J. D. Hunt, F. Kienzle, E. Bigham et E. C. Taylor. J. Am. Chem. Soc. **95**, 3635 (1973).
3. J. E. Dubois et C. Lion. C.R. Sér. C, **274**, 1073 (1972).
4. P. M. Henry. J. Am. Chem. Soc. **87**, 990 (1965).
5. P. M. Henry. J. Am. Chem. Soc. **87**, 4423 (1965); **88**, 1597 (1966).
6. L. Nadon, M. Tardat, M. Zador et S. Fliszár. Can. J. Chem. **51**, 2366 (1973).
7. K. J. Laidler. Chemical kinetics. McGraw-Hill Book Co., New York. 1965.
8. R. W. Taft. *Dans* Steric effects in organic chemistry. *Edité par* M. Newman. John Wiley and Sons, Inc., New York, N.Y. 1956.
9. R. J. Ouellette, G. Kordosky, C. Levin et S. William. J. Org. Chem. **34**, 4104 (1969).
10. C. Freppel, R. Favier, J. C. Richer et M. Zador. Can. J. Chem. **49**, 2586 (1971).
11. R. Criegee. Angew. Chem. **70**, 173 (1958).
12. W. Kruse et T. M. Bednarski. J. Org. Chem. **36**, 1154 (1971).
13. A. Streitwieser Jr. Solvolytic displacement reactions. McGraw-Hill Book Co. Inc., New York, N.Y. 1962; M. J. Strauss, L. J. Andrews et R. M. Keefer, J. Am. Chem. Soc. **90**, 3473 (1968).
14. J. A. Berson et S. Suzuki. J. Am. Chem. Soc. **81**, 4088 (1959).
15. (*a*) A. H. Blatt (*Editeur*). Organic synthesis. Vol II. John Wiley, New York. 1943. p. 307. (*b*) E. C. Horning (*Editeur*). Organic synthesis. Vol. III. John Wiley, New York, 1955. p. 800. (*c*) E. C. Horning (*Editeur*). Organic synthesis. Vol. III. John Wiley, New York, 1955. p. 217. (*d*) H. Gilman (*Editeur*). Organic synthesis. Vol. I. John Wiley, New York, 1932. p. 340. (*e*) A. H. Blatt (*Editeur*). Organic synthesis. Vol. II. John Wiley, New York. 1943. p. 323. (*f*) N. Rabjohn (*Editeur*). Organic synthesis. Vol. IV. John Wiley, New York. 1963. p. 543.
16. H. G. Walker Jr., M. Gee et R. M. McCready. J. Org. Chem. **27**, 2100 (1962).
17. L. I. Smith et J. A. Sprung. J. Am. Chem. Soc. **65**, 1279 (1953).
18. F. G. Bordwell et W. T. Brannen Jr. J. Am. Chem. Soc. **86**, 4645 (1964).
19. M. Montmollin et P. Matile. Helv. Chim. Acta, **7**, 107 (1924).
20. R. A. Barnes et W. M. Budde. J. Am. Chem. Soc. **68**, 2339 (1946).

Can. J. Chem. Downloaded from www.nrcresearchpress.com by 210.87.254.42 on 09/05/12
For personal use only.

Coordinating Properties of the Fluorosulfate Ion. Tetrakis(pyridine) Complexes of Zinc(II), Copper(II), and Nickel(II) Fluorosulfates

CARL S. ALLEYNE AND ROBERT C. THOMPSON

Department of Chemistry, The University of British Columbia, Vancouver, British Columbia V6T 1W5

Received May 24, 1974

CARL S. ALLEYNE and ROBERT C. THOMPSON. Can. J. Chem. **52**, 3218 (1974).

Complexes of the type $M(py)_4(SO_3F)_2$ (py = pyridine, M = Ni, Cu, Zn) have been prepared and characterized. Infrared spectra of all three complexes, electronic spectra and magnetic susceptibility studies of the copper and nickel complexes, and e.p.r. studies of the copper complex are reported. The complexes have tetragonally distorted octahedral structures with fluorosulfate groups coordinated to metal ions as unidentate ligands. To facilitate comparison of the coordinating action of the fluorosulfate ion with other polyatomic anions the complexes, $Cu(py)_4X_2$ (X = ClO_4^-, BF_4^-, NO_3^-, p-$CH_3C_6H_4SO_3^-$, $CF_3CO_2^-$) have been prepared and their electronic properties examined. The studies indicate that the coordinating strength of SO_3F^- towards metals is greater than ClO_4^-, BF_4^-, and NO_3^- but less than p-$CH_3C_6H_4SO_3^-$ and $CF_3CO_2^-$. Electrical conductivity studies on solutions in acetonitrile indicate a correlation between the relative coordinating strength of the anion in a given complex and the extent to which the complex undergoes ionic dissociation in this solvent.

CARL S. ALLEYNE et ROBERT C. THOMPSON. Can. J. Chem. **52**, 3218 (1974).

On a préparé et caractérisé des complexes de type $M(py)_4(SO_3F)_2$ (py = pyridine, M = Ni, Cu, Zn). On rapporte aussi les spectres infrarouges des trois complexes, les spectres électroniques et les études de susceptibilité magnétique des complexes de cuivre et de nickel ainsi que les études r.p.e. des complexes de cuivre. Les complexes ont des structures octaédriques déformées tétragonalement et elles contiennent les groupes fluorosulfates coordonnés aux ions métalliques sous forme de ligands univalents. Afin de faciliter la comparaison de l'action coordinante de l'ion fluorosulfate avec celle d'autres anions polyatomiques, on a préparé les complexes $Cu(py)_4X_2$ (X = ClO_4^-, BF_4^-, NO_3^-, p-$CH_3C_6H_4SO_3^-$, $CF_3CO_2^-$) et on a examiné leurs propriétés électroniques. Ces études montrent que la force de coordination de SO_3F^- vis à vis les métaux est plus grande que celle de ClO_4^-, BF_4^- et NO_3^- mais plus faible que celle de p-$CH_3C_6H_4SO_3^-$ et CH_3CO_2. Des études de conductivités électriques sur des solutions dans l'acétonitrile montrent une corrélation entre les forces relatives de coordination des anions dans un complexe donné et le taux de dissociation ionique que subit ce complexe dans ce solvant. [Traduit par le journal]

Introduction

As the anion of a very strong acid, the fluorosulfate ion might be expected to coordinate only weakly to metal ions in complex compounds; relatively little is known, however, about the coordinating properties of this anion. Lange (1) and Wilke-Dörfurt *et al.* (2) appear to have been the first to study such complexes while, more recently, reports have appeared on ammonia complexes of copper(II) and nickel(II) fluorosulfates (3), pyridine and substituted pyridine complexes of copper(II) fluorosulfate (4), and methyl cyanide complexes of zinc(II), copper(I), and copper(II) fluorosulfates (5).

We describe here the preparation and characterization of three complex compounds of the type $M(py)_4(SO_3F)_2$ (py = pyridine, M = Ni, Cu, Zn). To facilitate comparisons of the coordinating properties of the fluorosulfate ion and other anions we have also prepared and studied tetrakis(pyridine) complexes of copper(II) perchlorate, tetrafluoroborate, *p*-tolysulfate, nitrate, and trifluoroacetate.

Experimental

Materials

Fluorosulfuric acid was purified by double distillation as described previously (6). Diethyl ether, pyridine, and acetonitrile were reagent grade and were dried by refluxing over calcium hydride followed by distillation. The acetonitrile used in conductivity measurements was purified by the method of Forcier and Olver (7) and had a specific conductance of $3\text{–}5 \times 10^{-8}$ ohm^{-1} cm^{-1}. Dichloromethane was allowed to stand over Linde 4A molecular sieves for several days and then was distilled. This treatment gave dichloromethane with a specific conductance of 4×10^{-11} ohm^{-1} cm^{-1}.

Preparations

Previously reported procedures for the preparation of pyridine complexes of metal fluorosulfates have involved

Can. J. Chem. Downloaded from www.nrcresearchpress.com by 210.87.254.5 on 09/05/12
For personal use only.

Can. J. Chem. Downloaded from www.nrcresearchpress.com by 210.87.254.5 on 09/05/12
For personal use only.

reactions in aqueous solutions (1). It has been claimed recently that such methods applied to the preparation of ammonia complexes result in hydrolysis and the formation of sulfates rather than fluorosulfates (3). To avoid the possibility of product contamination by sulfate impurity we have employed anhydrous conditions throughout this work. Whenever possible, manipulations involving metal fluorosulfates and their pyridine complexes were performed in a dry box. Anhydrous metal fluorosulfates were prepared as described previously (8). Pyridine complexes were prepared by reacting acetonitrile solutions of the appropriate metal fluorosulfate with excess pyridine. Detailed descriptions of individual preparations follow.

Anhydrous zinc(II) fluorosulfate (0.004 mol) was dissolved in 8 ml of boiling methyl cyanide and an excess (0.050 mol) of hot pyridine was added. On cooling to room temperature colorless crystals separated out of solution. The yield of product was increased by cooling in an ice–water bath. The crystals of $Zn(py)_4(SO_3F)_2$ were filtered, washed with dry ether, and dried under vacuum.

Anal. Calcd. for $ZnC_{20}H_{20}N_4S_2O_6F_2$: C, 41.43; H, 3.48; N, 9.66; Zn, 11.27. Found: C, 41.0; H, 3.70; N, 9.72; Zn, 11.3.

Anhydrous copper(II) fluorosulfate (0.004 mol) was dissolved in 18 ml of boiling methyl cyanide and an excess (0.045 mol) of hot pyridine was added. When the solution cooled a solid product separated out. Analysis of this material showed that it contained pyridine in excess of the required 4:1 mole ratio of pyridine to copper. The solution was filtered and on addition of ether to the filtrate a quantity of a purple solid precipitated. This material was filtered from the solution, washed with ether, and dried under vacuum. Analysis showed it to be the complex $Cu(py)_4(SO_3F)_2$.

Anal. Calcd. for $CuC_{20}H_{20}N_4S_2O_6F_2$: C, 41.56; H, 3.49; N, 9.69; Cu, 10.99. Found: C, 41.2; H, 3.27; N, 9.56; Cu, 11.0.

Anhydrous nickel(II) fluorosulfate (0.004 mol) was dissolved in 10 ml of boiling methyl cyanide and an excess (0.81 mol) of hot pyridine was added. The solution was then cooled to room temperature. On addition of dry ether a pale blue product precipitated from solution. The complex, $Ni(py)_4(SO_3F)_2$, was filtered, washed with ether, and dried under vacuum.

Anal. Calcd. for $NiC_{20}H_{20}N_4S_2O_6F_2$: C, 41.91; H, 3.52; N, 9.77; Ni, 10.24. Found: C, 41.8; H, 3.50; N, 9.50; Ni, 10.5.

The tetrakis(pyridine) complex of copper(II) *p*-tolylsulfate was prepared as follows. Copper(II) chloride and silver *p*-tolysulfate were reacted in stoichiometric amounts in aqueous solution. Precipitated silver chloride was removed by filtration and on concentration the filtrate yielded pale blue hydrated copper(II) *p*-tolysulfate. About 3 g of this copper salt was dissolved in 20 ml of warm methanol and 8 ml of pyridine was added. The complex $Cu(py)_4(p\text{-}CH_3C_6H_4SO_3)_2$, was precipitated from solution with ether, filtered under vacuum, washed with ether, and dried under vacuum.

Anal. Calcd. for $CuC_{34}H_{34}N_4S_2O_6$: C, 56.53; H, 4.74; N, 7.76. Found: C, 56.2; H, 4.94; N, 7.54.

The following were prepared by literature methods: $Cu(py)_4(ClO_4)_2$ (9), $Cu(py)_4(BF_4)_2$ (9), $Cu(py)_4(NO_3)_2$ (10), $Cu(py)_4(CF_3CO_2)_2$ (11). All gave satisfactory analyses for C, H, and N.

Elemental analyses for carbon, hydrogen, and nitrogen were done in the microanalytical laboratory in this department. Metal analyses were performed by EDTA titration.

Physical Methods

Infrared spectra were recorded on a Perkin–Elmer 457 spectrophotometer over the frequency range 4000–250 cm^{-1}. Samples were contained as Nujol and hexachlorobutadiene mulls between KRS-5 (Harshaw Chemical Co.) plates. Spectra were calibrated using polystyrene film and frequencies are considered accurate to $\pm 4\ cm^{-1}$.

A Cary 14 recording spectrophotometer was used to obtain electronic spectra in the range 5–33 kK. Solution spectra were run on 10^{-2} to 10^{-3} *M* solutions contained in matched silica glass cells with 1 or 10 cm path lengths. Solid state mull spectra were obtained on samples using Nujol, hexachlorobutadiene, or Kel-F mulls pressed between silica windows. The background due to light scattering from the sample was subtracted from the spectra of the copper complexes as described previously (12). Light scattering was compensated for in the spectra of the nickel complex by placing a Nujol-soaked filter paper in the reference beam. Diffuse reflectance spectra were recorded over the range 13.5–28.5 kK on a Bausch and Lomb Spectronic 600 spectrophotometer equipped with a visible reflectance attachment. Magnesium carbonate was used as the reflectance standard.

Magnetic susceptibilities were measured using the Gouy apparatus and calibration procedure described previously (12). For all of the compounds studied, the room temperature magnetic susceptibilities were determined from at least three separate packings of the Gouy tube and magnetic moments are considered accurate to ± 0.02 B.M. Measurements at magnetic fields of approximately 4500 and 7000 G gave no evidence for dependence of magnetic susceptibilities on field strength. The molar magnetic susceptibilities were corrected for the diamagnetic contributions of the ligands and metal ions. The diamagnetic susceptibility values, obtained from published sources (12–14) are: -13×10^{-6} for nickel and copper, -49×10^{-6} for pyridine, -40×10^{-6} for SO_3F^-, -32×10^{-6} for ClO_4^-, -39×10^{-6} for BF_4^-, and -97×10^{-6} for $p\text{-}CH_3C_6H_4SO_3^-$ (all values in c.g.s.u.).

Electron paramagnetic resonance spectra were recorded on a Varian E-3 spectrometer using 100 kHz field modulation. The X-band microwave frequency was monitored on a Hewlett–Packard 5245L electronic counter equipped with a 8–18 GHz frequency converter. The solutions, which generally had a concentration of about 5×10^{-4} *M*, were contained in 3 mm i.d. quartz tubes.

Electrical conductivities were obtained at 25.00 ± 0.01 °C using equipment and techniques described previously (15). Molar conductance values, corrected for solvent conductivity, are considered accurate to ± 1 $ohm^{-1}\ cm^2\ mol^{-1}$.

Results and Discussion

Infrared Spectra

The infrared spectra of $M(py)_4(SO_3F)_2$ (M = Ni, Cu, Zn) provide good evidence that the

TABLE 1. Infrared data for pyridine complexes of metal fluorosulfates[a]

Complex	Infrared frequency (cm^{-1})							
	SO_3F vibrations[b]					Pyridine ring vibrations[b]		
	$\nu_4(E)$	$\nu_1(A_1)$	$\nu_2(A_1)$	$\nu_5(E)$	$\nu_3(A_1)$	8*a*	6*a*	16*b*
$Ni(py)_4(SO_3F)_2$	1333 s 1259 s	1082 s	743 s	590 s 573 s	557 m	1609 1605 } s	631 m	432 m
$Zn(py)_4(SO_3F)_2$	1331 s 1259 s	1080 s	737 s	588 s 574 s	557 m	1609 1604 } s	634 629 } m	422 m
$Cu(py)_4(SO_3F)_2$	1316 s 1266 s	1072 s	732 724 } s	581 sh 578 s	558 m	1610 1608 } s	643 639 } m	433 428 } m

[a]s = strong, m = medium, sh = shoulder.
[b]See text for description of vibrations.

fluorosulfate ions are coordinated to the metal ions in all three complexes. By comparing the spectra with those of pyridine and previously studied pyridine complexes (16) they are readily resolved into bands arising from vibrations of the fluorosulfate groups and those arising from vibrations of coordinated pyridine molecules. Bands assigned to vibrations of the SO_3F group are given in Table 1. The free fluorosulfate ion has C_{3v} symmetry and is expected (8, 17) to show six infrared active bands ($3E$ and $3A_1$). The anion symmetry is clearly lower than C_{3v} in all three complexes as the spectra show splittings of the doubly degenerate $\nu_4(E)$ and $\nu_5(E)$ modes. We did not observe the $\nu_6(E)$ modes for these complexes, possibly because they are weak or, more likely, because they are obscured by pyridine bands at 420–430 cm^{-1}. The remaining bands in the spectra of each of the complexes are assignable to coordinated pyridine; three of these bands are given for each complex in Table 1. In liquid pyridine the 16*b* vibration (an out-of-plane ring deformation) is at 403 cm^{-1} while the 6*a* and 8*a* vibrations (in-plane ring deformations) are at 601 and 1578 cm^{-1} respectively (16). As expected from previous studies, the three bands show significant shifts to higher frequencies on coordination of pyridine to the metal (16, 18). The doubling of some of the pyridine bands probably arises (18) from interactions between different pyridine molecules.

The infrared spectra of the nickel and copper complexes show that all pyridine molecules are coordinated to metal ions. This, together with evidence (to be presented later) from electronic spectral and magnetic studies that the metal ions are hexacoordinated, suggests a molecular structure in which the fluorosulfate ions are coordinated as unidentate ligands. Since $Zn(py)_4(SO_3F)_2$ has an infrared spectrum virtually identical to the spectra of the nickel and copper complexes, it probably has a similar structure. By comparison, the perchlorate ions in $Zn(py)_4(ClO_4)_2$ are apparently uncoordinated and the coordination about zinc is tetrahedral in this complex (9).

The magnitude of the fluorosulfate E mode splitting and the position of ν_2 (SF stretch) in these complexes suggests a "semi-coordination" of the fluorosulfate groups. This term has been used (19, 20) to describe anions which are involved in coordination of sufficient strength to produce slight distortions of the anion, but not of sufficient strength to produce the gross distortion and full symmetry lowering which occurs when the anions are involved as "fully coordinated" groups. The ν_2 band frequencies of 724–743 cm^{-1} are low indicating relatively weak interactions between the fluorosulfate ion and the metal (8, 17). This, together with a ν_4 band splitting of only 50–74 cm^{-1}, suggests a much weaker fluorosulfate coordination than is present, for example, in CH_3SO_3F (21) and $KBr(SO_3F)_4$ (22) where ν_4 band splittings of the order of 230 and 180 cm^{-1} and ν_2 band frequencies of 840 and 834 cm^{-1}, respectively, are observed.

Electronic Spectra

The electronic spectrum of $Ni(py)_4(SO_3F)_2$ is that expected for a tetragonally distorted octahedral complex and is given in Table 2 together with the spectrum of the perchlorate complex (23) with assignments according to Peeters (24). Expressions relating transition energies in tetragonal nickel(II) complexes to the crystal field

Can. J. Chem. Downloaded from www.nrcresearchpress.com by 210.87.254.5 on 09/05/12
For personal use only.

TABLE 2. Electronic spectra of nickel complexes

Energies of band maxima (kK)		
$Ni(py)_4(SO_3F)_2$[a]	$Ni(py)_4(ClO_4)_2$[b]	Assignment[c]
8.48	7.18	$^3B_{1g} \rightarrow {}^3E_g(^3F)$
11.8	12.5	$\rightarrow {}^3B_{2g}(^3F)$
13.6	13.4	$\rightarrow \begin{cases} {}^1A_{1g}, {}^1B_{1g} \\ {}^3A_{2g}(^3F) \end{cases}$
16.4	16.7	$\rightarrow {}^3E_g(^3F)$
27.2[d]	26.8	$\rightarrow \begin{cases} {}^3A_{2g}(^3P) \\ {}^3E_g(^3P) \end{cases}$

[a]Kel-F mull spectrum.
[b]Data from ref. 23.
[c]Assignments from ref. 24.
[d]A shoulder on the low energy side of this band (~25 kK) is observable in the diffuse reflectance spectrum of this complex giving evidence for band splitting.

TABLE 3. Electronic spectra of copper complexes

	Energies of band maxima (kK)			
Complex	Diffuse reflectance	Mull	CH_2Cl_2 solution[a]	CH_2Cl_2/C_5H_5N solution[b]
$Cu(py)_4(NO_3)_2$	18.1	18.3	14.2(81)	16.6(55)
$Cu(py)_4(ClO_4)_2$	17.8	—	17.8(60)	17.8(61)
$Cu(py)_4(BF_4)_2$	17.7	18.0	18.0(53)	18.0(53)
$Cu(py)_4(SO_3F)_2$	17.0	17.2	17.3(52)	17.1(56)
$Cu(py)_4(p\text{-}CH_3C_6H_4SO_3)_2$	16.5	16.9	14.0(76)	16.6(52)
$Cu(py)_4(CF_3CO_2)_2$	15.5	15.7	15.0(74)	14.7(91)

[a]Molar absorptivities, ε, in parentheses.
[b]Solutions are 10% pyridine by volume. Numbers in parentheses are molar absorptivities.

parameters Ds, Dt, Dq_{xy}, and Dq_z have been given (25) and of particular interest here is the radial parameter Dt. This parameter, which to a first order approximation is 4/35 of the separation between the two lowest energy transitions, is a direct measure of the degree of tetragonality ($Dt = (4/7)(Dq_{xy} - Dq_z)$ assuming the absence of configurational interaction between E states). Using data obtained from room temperature spectra the degree of tetragonality in the fluorosulfate complex ($Dt = 380$ cm^{-1}) is less than that in the perchlorate complex ($Dt = 600$ cm^{-1}) greater than that in the analogous chloride complex ($Dt = 250$ cm^{-1} (26)) and similar to that in the analogous bromide and iodide complexes ($Dt = 340$ and 400 cm^{-1}, respectively (26)).

The complex ion $[Ni(py)_6]^{2+}$ was first identified (23) in solutions of $Ni(py)_4(ClO_4)_2$ and $Ni(py)_4(BF_4)_2$ in nitromethane containing excess pyridine. It appears that the fluorosulfate complex, $Ni(py)_4(SO_3F)_2$, gives the same complex ion when dissolved in dichloromethane containing excess pyridine. The spectrum of this complex in a solution containing 20% pyridine by volume consists of three bands at 9.57, 16.2, and 26.3 kK, with molar absorptivities of the band maxima of 5, 9, and 18 respectively, in good agreement with the spectrum previously reported for $[Ni(py)_6]^{2+}$.

The diffuse reflectance and mull spectra of the copper(II) complexes studied here have asymmetrical bands which span the entire visible region. Energies of band maxima are recorded in Table 3. Solid state spectra have been reported previously for the perchlorate (9, 27, 28), tetrafluoroborate (9), nitrate (10), and trifluoroacetate (29, 30) complexes and there is good agreement with the earlier results although we were unable to observe the band splitting previously reported in the spectrum of the trifluoroacetate complex. Although the molecular structures of these copper complexes are not known with cer-

Can. J. Chem. Downloaded from www.nrcresearchpress.com by 210.87.254.5 on 09/05/12
For personal use only.

Can. J. Chem. Downloaded from www.nrcresearchpress.com by 210.87.254.5 on 09/05/12
For personal use only.

TABLE 4. Magnetic moment data for $Cu(py)_4X_2$ complexes and $Ni(py)_4(SO_3F)_2$

$Ni(py)_4(SO_3F)_2$ (t.i.p.) = 246 × 10^{-6})[b]		$Cu(py)_4(SO_3F)_2$ (t.i.p. = 61 × 10^{-6})[b]		$Cu(py)_4(ClO_4)_2$ (t.i.p. = 59 × 10^{-6})[b]		$Cu(py)_4(BF_4)_2$ (t.i.p. = 59 × 10^{-6})[b]		$Cu(py)_4(p\text{-}CH_3C_6H_4SO_3)_2$ (t.i.p. = 63 × 10^{-6})[b]	
T(°K)	μ_{eff}[a]	T(°K)	μ_{eff}[a]	T(°K)	μ_{eff}[a]	T(°K)	μ_{eff}[a]	T(°K)	μ_{eff}[a]
313	3.13	314	1.82	309	1.83	316	1.83	312	1.81
293	3.14	293	1.82	292	1.82	295	1.84	293	1.82
274	3.14	276	1.81	273	1.83	274	1.83	268	1.82
244	3.13	244	1.82	245	1.82	244	1.84	244	1.81
216	3.13	212	1.82	215	1.82	216	1.86	216	1.81
185	3.11	184	1.80	186	1.82	184	1.85	185	1.81
165	3.11	164	1.82	157	1.82	165	1.84		
145	3.11	145	1.80	132	1.82	143	1.84		
125	3.10	125	1.80	98	1.84	124	1.83		
		103	1.79						
		91	1.82						

[a] $\mu_{eff} = 2.828\sqrt{\chi_M - (\text{t.i.p.})T}$ where χ_M is the molar magnetic susceptibility corrected for the diamagnetism of all atoms and t.i.p. is the temperature independent paramagnetism.

[b] t.i.p. = $\alpha N\beta^2/10Dq$ where α is 4 for the Cu complexes and 8 for the Ni complex (39). The ligand field $10Dq$ parameters were estimated from the electronic spectra. t.i.p. values are in c.g.s.u.

Can. J. Chem. Downloaded from www.nrcresearchpress.com by 210.87.254.5 on 09/05/12
For personal use only.

tainty, the earlier work indicated tetragonal structures in which four pyridine molecules form a square plane about the central copper ion with anions coordinated in axial positions. Tetragonal structures of this type are well established for the related bis(ethylenediamine) copper(II) complexes (20). Three electronic transitions, $^2B_{1g} \rightarrow {}^2A_{1g}$, $^2B_{1g} \rightarrow {}^2B_{2g}$, and $^2B_{1g} \rightarrow {}^2E_g$, are expected for such complexes. The observation of a single broad and asymmetrical band which presumably contains all three transitions, unresolved, is not uncommon particularly where spectra were obtained as in the present work, on polycrystalline samples at room temperature. The relative intensities of the different components of the visible band could change on going from diffuse reflectance to mull and this may account for the small differences observed in the reflectance spectra compared to the mull spectra (Table 3).

From studies of a large number of complexes, Lever and Mantovani (31) showed that in bis(ethylenediamine) complexes of copper(II) the position of the visible band provides a useful indication of the degree of tetragonal distortion, the band shifting to higher energies with increasing tetragonal distortion. Hathaway *et al.* (32) have shown, from polarized single-crystal electronic spectral studies, that the highest energy component in the visible band of these complexes arises from the $^2B_{1g} \rightarrow {}^2E_g$ transition and it is largely the shift of this transition to higher energies on increasing tetragonal distortion that accounts for the overall shift of the visible band. The data in Table 3 suggest that the energy of the visible band maximum provides a measure of the degree of tetragonal distortion in tetrakis(pyridine) copper(II) complexes also. Highest energies are observed for complexes containing the weakly coordinating NO_3^-, ClO_4^-, and BF_4^- ions. The degree of tetragonal distortion in the fluorosulfate complex appears to be less than that in the perchlorate complex (the same relative order of degree of tetragonal distortion in the analogous nickel complexes was demonstrated above) but greater than that in the *p*-tolylsulfate or trifluoroacetate complex. Similar arguments were used before (33) to show that the degree of tetragonal distortion in $Cu(py)_4(PF_6)_2$ (where the room temperature mull spectrum shows a main band at 19.1 and a shoulder at 16.2 kK) is greater than that in the perchlorate or tetrafluoroborate complex.

For the electron paramagnetic resonance studies, to be discussed below, we required a solvent that would dissolve the copper complexes without significantly changing their molecular structures. The solution electronic spectral data, recorded in Table 3, indicate that dichloromethane containing 10% by volume of pyridine is a suitable solvent for the perchlorate, tetrafluoroborate, fluorosulfate, and *p*-tolylsulfate complexes. The spectra of the first three remain essentially unchanged when the complexes are dissolved in dichloromethane or in dichloromethane containing 10% pyridine, indicating that the tetragonal $Cu(py)_4X_2$ molecular structures present in the solid state are retained in these solutions. The spectrum of $Cu(py)_4(p\text{-}CH_3C_6H_4SO_3)_2$ changes significantly when the complex is dissolved in dichloromethane. This change is apparently caused by the dissociation of pyridine from the complex since in the dichloromethane–pyridine solvent, where the excess pyridine would suppress such dissociation, the spectrum is essentially that observed in the solid state. The spectra of the nitrate and trifluoroacetate complexes show shifts in their visible bands to lower energies on dissolution in dichloromethane. Similar band shifts accompanying dissolution of these complexes in chloroform were reported previously (10, 29) and were ascribed to the dissociation of pyridine. The data in Table 3 show that even in solutions containing 10% pyridine the dissociation of pyridine is not completely suppressed for these complexes. The trifluoroacetate complex, dissolved in pure pyridine, gives a visible spectrum consisting of a single broad line with the band maximum at 15.4 kK and $\varepsilon = 64$. It appears that the undissociated $Cu(py)_4(CF_3CO_2)_2$ complex species is present in these solutions. The low solubility of the nitrate complex in pyridine precluded a similar investigation of that complex.

Magnetic Properties

The magnetic moment of $Ni(py)_4(SO_3F)_2$ has been determined from bulk magnetic susceptibility measurements over the temperature range 313–125 °K and the results are given in Table 4. The room temperature magnetic moment of 3.14 B.M. is comparable to the values reported elsewhere for the analogous trifluoroacetate (34), trichloroacetate (35), cyanate, thiocyanate, and selenocyanate (36), chloride, bromide, and iodide (37), perrhenate (38), perchlorate, and tetra-

Can. J. Chem. Downloaded from www.nrcresearchpress.com by 210.87.254.5 on 09/05/12
For personal use only.

fluoroborate complexes (9, 23). The magnetic moments observed for these complexes are in the range normally observed for six-coordinate Ni(II) complexes. The increase in magnetic moment over the spin-only value of 2.83 B.M. has been ascribed to an orbital contribution arising from spin–orbit coupling between the ground state and excited states (39, 40). Variable temperature magnetic susceptibility data on $Ni(py)_4X_2$ complexes are available only for the fluorosulfate derivative studied here. For regular octahedral nickel(II) complexes the magnetic moment should be independent of temperature. The data obtained for the fluorosulfate complex gives evidence for a small decrease in magnetic moment with decreasing temperature. The origin of this temperature dependence may be the departure of this complex from regular octahedral symmetry (39); unfortunately, the effect is too small to permit further analysis.

Magnetic susceptibility data were obtained over the temperature range 316–90 °K for the tetrakis(pyridine) copper(II) complexes, $Cu(py)_4X_2$ ($X = SO_3F^-, ClO_4^-, BF_4^-, p\text{-}CH_3C_6H_4SO_3^-$). Data, at room temperature, have been reported previously for the perchlorate (9, 27) and tetrafluoroborate (9) complexes. The magnetic moments, given in Table 4, are of a magnitude usually observed for copper(II) complexes (39) and are independent of temperature. The moments do not vary significantly from one complex to another; the bulk magnetic susceptibility measurements used to obtain these moments are not sufficiently sensitive to detect variations in the electronic properties of the complexes arising from differences in the coordinating properties of the anions.

Electron paramagnetic resonance, e.p.r., techniques provide another method of investigating the magnetic properties of copper(II) complexes. We obtained e.p.r. spectra, at room temperature and liquid nitrogen temperature, of solutions of $Cu(py)_4X_2$ complexes in dichloromethane containing 10% pyridine by volume. Results are given here for the perchlorate, tetrafluoroborate, fluorosulfate, and *p*-tolylsulfate complexes; we are reasonably certain, from the electronic spectral studies described above, that these complexes dissolve in this solvent without appreciable change in molecular structure. Figures 1 and 2 show spectra obtained for $Cu(py)_4(SO_3F)_2$; the general features of the spectra of all four complexes were the same. The

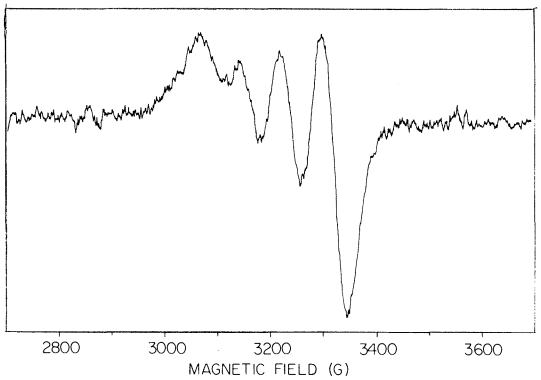

FIG. 1. Tetrakis(pyridine) copper(II) fluorosulfate in 90% dichloromethane – 10% pyridine. Electron paramagnetic resonance spectrum at room temperature.

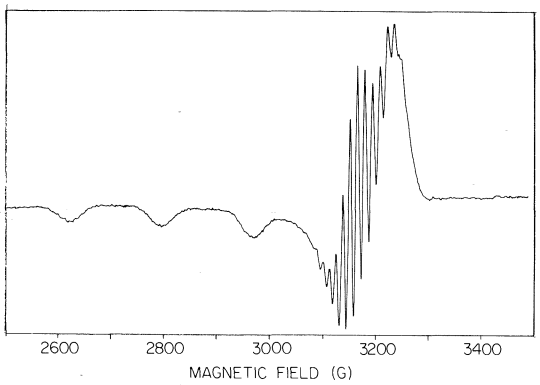

FIG. 2. Tetrakis(pyridine) copper(II) fluorosulfate in 90% dichloromethane – 10% pyridine. Electron paramagnetic resonance spectrum at liquid nitrogen temperature.

room temperature spectrum shows four lines arising from copper nuclear hyperfine interaction. The spectrum obtained at liquid nitrogen temperature indicates a tetragonal copper(II) environment with two regions of absorption centered at $g_{\|}$ and $g_{\perp}$. The splitting of the $g_{\|}$ peak by copper nuclear hyperfine interaction is observed where three of the four components are clearly resolved; the fourth is hidden by the $g_{\perp}$ peak which overlaps it. The splitting on the $g_{\perp}$ peak is not resolved because of the smaller magnitude of $A_{\perp}$ compared to $A_{\|}$ and because of superimposed nitrogen superhyperfine splitting. The complex pattern of lines appearing at $g_{\perp}$ has not been analyzed in this work.

The e.p.r. parameters, calculated employing equations which include magnetic hyperfine coupling to second order (41) are listed in Table 5. The isotropic g_0 and A_0 values were calculated

TABLE 5. Electron paramagnetic resonance parameters of copper complexes in CH_2Cl_2/C_5H_5N solution [a]

Complex	$g_\parallel$	$g_\perp$	g_0	$A_\parallel \times 10^4$ (cm^{-1})	$A_\perp \times 10^4$ (cm^{-1})	$A_0 \times 10^4$ (cm^{-1})
$Cu(py)_4(ClO_4)_2$	2.263	2.040	2.114	204	13	77
$Cu(py)_4(BF_4)_2$	2.256	2.043	2.114	207	14	78
$Cu(py)_4(SO_3F)_2$	2.253	2.054	2.121	209	5	73
$Cu(py)_4(p\text{-}CH_3C_6H_4SO_3)_2$ [b]	2.260	2.062	2.128	207	6	65

[a] The signs of the hyperfine parameters are not determined. Values reported are absolute magnitude.
[b] The values of $A_\parallel$ and $A_\perp$ have opposite signs in this complex.

from the room temperature spectra and the $g_\parallel$ and $A_\parallel$ values were obtained from the low temperature spectra. It is not possible to measure $A_\perp$ and $g_\perp$ directly from the spectrum of the frozen solution and these values have been calculated, instead, from the equations $g_0 = \frac{1}{3}(g_\parallel + 2g_\perp)$ and $A_0 = \frac{1}{3}(A_\parallel + A_\perp)$ (42). The complexes each exhibit a two g-value spectrum in which the lowest g-value is equal to or greater than 2.04. According to Hathaway and Billings (43), this is consistent with an elongated tetragonal octahedral environment about copper in which the unpaired electron occupies the $d_{x^2-y^2}$ orbital in the ground electronic state.

The effect of varying axial interactions on e.p.r. parameters of copper(II) complexes has been examined in some detail by other workers. Antosik *et al.* (42) investigated weak complexes of a number of copper(II) β-ketoenolates with chloroform and they predicted and observed greater values of $g_\parallel$ and numerically smaller values of $A_\parallel$ for the chloroform complexes compared to the isolated copper(II) chelates. In a study of the e.p.r. spectra of copper(II) acetylacetonate in a variety of solvents Adato and Eliezer (44) found $A_\perp$ to be the parameter most sensitive to changes in solvent, decreasing in magnitude as the coordinaiting strength of the solvent increases.

Although variations on the e.p.r. parameters of the tetrakis(pyridine) complexes studied here are small (Table 5) trends are readily apparent. Assuming increasing values of g_0 and decreasing values of A_0 accompany increasing axial interaction, the relative coordinating strengths of the anions is $ClO_4^- \sim BF_4^- < SO_3F^- < p\text{-}CH_3C_6H_4SO_3^-$, the same order as determined above from electronic spectral results. Adato and Eliezer (44) pointed out that the perpendicular components of the e.p.r. parameters are expected to be strongly influenced by variations in axial ligand coordination. In spite of the possibility of relatively large errors in the absolute magnitudes of $g_\perp$ and $A_\perp$ values, arising from the fact that the values were calculated, as described above, from measurements at two different temperatures (42), a comparison of the value obtained for one compound relative to another is probably valid. In particular we note that the variations in the perpendicular components of the parameters correlate well with variations in the isotropic components. The sensitivity of $g_\perp$ to variations in axial ligand coordination is easily understood. The expression for $g_\perp$ for a copper(II) ion in D_{4h} symmetry with a $^2B_{1g}$ ground state is (20)

$$g_\perp = 2 - \frac{2K_\perp{}^2\lambda}{E(^2B_{1g} \rightarrow {}^2E_g)}$$

where $K_\perp$ and λ are the orbital reduction factor and spin–orbit coupling constant respectively. Hathaway *et al.* have shown that decreasing tetragonal distortion, *i.e.* increasing axial coordination, leads to a shift in the $^2B_{1g} \rightarrow {}^2E_g$ transition to lower energies (32). In the absence of a relatively larger decrease in the magnitude of $K_\perp{}^2\lambda$ (λ is negative for copper(II)) this would result in an increase in $g_\perp$. This appears to be the case for the pyridine complexes studied in the present work. Taking the position of the visible band in the electronic spectrum as a measure of the relative energy of the $^2B_{1g} \rightarrow {}^2E_g$ transition (see previous discussion), as this energy decreases on going from the perchlorate and tetrafluoroborate to the fluorosulfate to the *p*-tolylsulfate complex, the value of $g_\perp$ increases.

The room temperature magnetic moments of the four copper(II) complexes in solution may be calculated from the expression

$$\mu_{eff} = g_0\sqrt{S(S+1)}$$

using g_0 values obtained from the e.p.r. spectra. The values so calculated are 1.83 B.M. for the perchlorate and tetrafluoroborate complexes and

Can. J. Chem. Downloaded from www.nrcresearchpress.com by 210.87.254.5 on 09/05/12
For personal use only.

Can. J. Chem. Downloaded from www.nrcresearchpress.com by 210.87.254.5 on 09/05/12
For personal use only.

1.84 B.M. for the fluorosulfate and *p*-tolylsulfate complexes. Within experimental error, the values are in agreement with those obtained from bulk magnetic susceptibility measurements on the powdered samples. This supports our assumption that these complexes dissolve in the dichloromethane–pyridine solvent without appreciable change in molecular structure.

Electrical Conductivities

The extent to which a complex compound undergoes dissociation into ions in coordinating solvents depends on factors such as solvent coordinating strength and dielectric constant, the solvation energies of the neutral complex and of the ions produced, and the coordinating strength of the anion towards the metal ion. Acetonitrile is a good coordinating solvent with a sufficiently large dielectric constant to support ionic dissociation of complex compounds (45). We have measured electrical conductivities of acetonitrile solutions of the complexes prepared in the present work in an effort to determine the extent to which they undergo ionic dissociation in this solvent and to look for possible correlations with anion coordinating strength. Molar conductivities of 1×10^{-3} *M* solutions of the complexes and of tetrabutylammonium bromide are given in Table 6. The bromide salt was studied to give an indication of values expected for strong 1:1 electrolytes.

The molar conductivities of the fluorosulfates, the perchlorate, and the tetrafluoroborate are all high indicating that these complexes are extensively dissociated into complex cations, probably in the form of $[M(py)_4L_2]^{2+}$ (where L is a solvent molecule), and coordinately non-bonded anions. Some replacement of pyridine by solvent molecules in the complex cation is possible. The differences which are observed in the molar conductivities of these five complexes arise from variations in the degree of ion association present in the different solutions and variations in ion mobilities. Of these two effects the latter is probably the least important. The lack of significant variations in mobilities of large complex cations has been demonstrated previously for a number of hexakis(acetonitrile) complexes (46). In addition, it has been shown that the perchlorate and fluorosulfate ions have similar mobilities in different solvents (15). The smaller molar conductivity of $Cu(py)_4(SO_3F)_2$ on the one hand compared to $Cu(py)_4(BF_4)_2$ and $Cu(py)_4(ClO_4)_2$ on the other suggests a slightly higher degree of ion association in the fluorosulfate complex. In a study of electrical conductivities of solutions of tetrakis(acetonitrile) complexes of copper(II) and zinc(II) fluorosulfates Milne (5) also found that the fluorosulfates were less conducting than corresponding perchlorates; however, in Milne's study the fluorosulfates were found to be less conducting even than 1:1 electrolytes making the difference between perchlorates and fluorosulfates considerably greater than that observed here.

For one complex, tetrakis(pyridine) copper(II) fluorosulfate, electrical conductivities were measured over a range of concentrations and data are recorded as molar conductivities in Table 7. Of relevance to the present study is the work of Libuś and Strzelecki (46) involving conductometric studies on solutions of bivalent metal perchlorates in acetonitrile. The authors found that the manganese, cobalt, cadmium, nickel, copper, and zinc perchlorates have conductivi-

TABLE 6. Molar conductances, Λ_M, of 1×10^{-3} *M* solutions of complexes in acetonitrile at 25 °C

Complex	Λ_M (ohm^{-1} mol^{-1} cm^2)
$Cu(py)_4(ClO_4)_2$	317
$Cu(py)_4(BF_4)_2$	321
$Cu(py)_4(SO_3F)_2$	285
$Zn(py)_4(SO_3F)_2$	259
$Ni(py)_4(SO_3F)_2$	224
$Cu(py)_4(p\text{-}CH_3C_6H_4SO_3)_2$	76
$Cu(py)_4(NO_3)_2$	58
$Cu(py)_4(CF_3CO_2)_2$	11
Bu_4NBr	150

TABLE 7. Molar conductance data for solutions of $Cu(py)_4(SO_3F)_2$ in acetonitrile at 25 °C

Concentration (10^3 *M*)	Λ_M (ohm^{-1} cm^2 mol^{-1})
11.871	185.9
9.947	193.4
4.974	223.2
3.974	234.4
2.519	250.5
1.259	276.5
0.969	285.9
0.818	297.1
0.806	302.0
0.630	313.5
0.599	312.6
0.403	319.0
0.315	326.7
0.242	331.2
0.114	349.6

Can. J. Chem. Downloaded from www.nrcresearchpress.com by 210.87.254.5 on 09/05/12
For personal use only.

ties which are very similar at any given concentration (range 0.001–0.085 *M*) and concluded that the salts undergo ionic dissociation to give exclusively $[ML_6]^{2+}$ complex cations (where L is acetonitrile) and coordinatively non-bonded perchlorate anions. The equivalent conductivity values we obtained for solutions of tetrakis(pyridine) copper(II) fluorosulfate at different concentrations over the range 0.001–0.01 *M* are about 15% lower, but otherwise parallel, those reported for solutions of copper(II) perchlorate. This result supports the conclusion drawn above that the fluorosulfate complex undergoes rather extensive ionic dissociation in acetonitrile solutions.

The equivalent conductivity at infinite dilution of $Cu(py)_4(SO_3F)_2$, obtained by extrapolation of a plot of equivalent conductivity *vs.* the square-root of the molar concentration, is 188 ohm^{-1} cm^2 $equiv^{-1}$, compared to the value 198.5 ohm^{-1} cm^2 $equiv^{-1}$ reported for $Cu(ClO_4)_2$. The difference between these two values, which reflects differences in ionic mobilities, is not sufficiently large to account for the differences in molar conductivities at finite concentrations. It is probable that although both compounds are extensively dissociated into ions in solution there is some ion association present, the extent of which is slightly higher in the solutions of the fluorosulfate complex. It is not known whether this ion association involves the formation of a complex ion in which the anion coordinates directly to the metal or whether it involves an ion-pair in which the anion does not penetrate the first coordination sphere of the metal.

The molar conductance data (Table 6) for the tetrakis(pyridine) complexes of copper(II) *p*-tolylsulfate, nitrate, and trifluoroacetate show them to be less conducting even than 1:1 electrolytes. They are significantly less dissociated in solution than the perchlorate and fluorosulfate compounds and it seems likely that the primary mode of ionic dissociation for these complexes involves the formation of complex ions such as $[Cu(py)_4X]^+$ (where X is the appropriate anion) and coordinately non-bonded anions. The differences in the molar conductance values probably reflect differences in relative degrees of dissociation.

Ordering the anions according to decreasing molar conductivity of the appropriate tetrakis(pyridine) copper(II) complex gives, $ClO_4^- \sim BF_4^- > SO_3F^- > CH_3C_6H_4SO_3^- > NO_3^- > CF_3CO_2^-$. This order correlates well with the relative coordinating strengths of the anions as determined by the electronic spectral and magnetic studies described above. The more weakly coordinating anions have a greater tendency to dissociate in acetonitrile solution giving more highly conducting solutions. The NO_3^- ion is an exception. The electronic spectral data suggest it is a weakly coordinating anion yet the copper complex is not extensively dissociated in acetonitrile solution. The SO_3F^- ion is again found to occupy a position intermediate between the weakly coordinating ClO_4^- and BF_4^- ions and the more strongly coordinating *p*-$CH_3C_6H_4SO_3^-$ ion.

We thank Dr. F. G. Herring and Dr. R. L. Tapping for help in the interpretation of the e.p.r. spectra. The financial support of the National Research Council of Canada is gratefully acknowledged.

1. W. Lange. Ber. **60**, 962 (1927).
2. E. Wilke-Dörfurt, G. Balz, and A. Weinhardt. Z. Anorg. Allg. Chem. **185**, 417 (1929).
3. D. A. Edwards, M. J. Stiff, and A. A. Woolf. Inorg. Nucl. Chem. Lett. **3**, 427 (1967).
4. H. G. Mayfield, Jr. Ph.D. Thesis. University of Tennessee, Knoxville, Tennessee. 1970.
5. J. B. Milne. Can. J. Chem. **48**, 75 (1970).
6. J. Barr, R. J. Gillespie, and R. C. Thompson. Inorg. Chem. **3**, 1149 (1964).
7. G. A. Forcier and J. W. Olver. Anal. Chem. **37**, 1447 (1965).
8. C. S. Alleyne, K. O'Sullivan Mailer, and R. C. Thompson. Can. J. Chem. **52**, 336 (1974).
9. D. H. Brown, R. H. Nuttall, J. McAvoy, and D. W. A. Sharp. J. Chem. Soc. A, 892 (1966).
10. R. V. Biagetti, W. G. Bottjer, and H. M. Haendler. Inorg. Chem. **5**, 379 (1966).
11. A. B. P. Lever and D. Ogden. J. Chem. Soc. A, 2041 (1967).
12. J. M. Taylor and R. C. Thompson. Can. J. Chem. **49**, 511 (1971).
13. A. Earnshaw. Introduction to magnetochemistry. Academic Press, London. 1968.
14. E. König. *In* Landolt-Börnstein, numerical data and functional relationships in science and technology. New Series II/2. *Edited by* K.-H. Hellwege and A. M. Hellwege. Springer–Verlag, Berlin. 1966.
15. W. Reed, D. W. Secret, R. C. Thompson, and P. A. Yeats. Can. J. Chem. **47**, 4275 (1969).
16. N. S. Gill, R. H. Nuttall, D. E. Scarfe, and D. W. A. Sharp. J. Inorg. Nucl. Chem. **18**, 79 (1961).
17. J. Goubeau and J. B. Milne. Can. J. Chem. **45**, 2321 (1967).
18. R. J. H. Clark and C. S. Williams. Inorg. Chem. **4**, 350 (1965).
19. D. S. Brown, J. D. Lee, B. G. A. Melson, B. J. Hathaway, I. M. Procter, and A. A. G. Tomlinson. Chem. Commun. 369 (1967).

20. I. M. PROCTER, B. J. HATHAWAY, and P. NICHOLLS. J. Chem. Soc. A, 1678 (1968).
21. F. B. DUDLEY, G. H. CADY, and D. F. EGGER, JR. J. Am. Chem. Soc. **78**, 290 (1956).
22. H. A. CARTER, S. P. L. JONES, and F. AUBKE. Inorg. Chem. **9**, 2485 (1970).
23. M. R. ROSENTHAL and R. S. DRAGO. Inorg. Chem. **4**, 840 (1965).
24. J. PEETERS. Bull. Soc. Chim. Belges. **81**, 333 (1972).
25. A. B. P. LEVER. Coord. Chem. Rev. **3**, 119 (1968).
26. D. M. L. GOODGAME, M. GOODGAME, M. A. HITCHMAN, and M. J. WEEKS. J. Chem. Soc. A, 1769 (1966).
27. W. C. JONES and W. E. BULL. J. Chem. Soc. A, 1849 (1968).
28. S. A. BELL, J. C. LANCASTER, and W. R. MCWHINNIE. Inorg. Nucl. Chem. Lett. **7**, 405 (1971).
29. S. F. A. KETTLE and A. J. P. PIOLI. J. Chem. Soc. A, 1243 (1968).
30. C. A. AGAMBAR and K. G. ORRELL. J. Chem. Soc. A, 897 (1969).
31. A. B. P. LEVER and E. MANTOVANI. Inorg. Chem. **10**, 817 (1971).
32. B. J. HATHAWAY, D. E. BILLINGS, P. NICHOLLS, and I. M. PROCTER. J. Chem. Soc. A, 319 (1969).
33. H. G. MAYFIELD, JR. and W. E. BULL. J. Chem. Soc. A, 2279 (1971).
34. S. AMASA, D. H. BROWN, and D. W. A. SHARP. J. Chem. Soc. A, 2892 (1969).
35. F. MAGGIO, R. BOSCO, R. CEFALÙ, and V. ROMANO. Inorg. Nucl. Chem. Lett. **5**, 59 (1969).
36. S. M. NELSON and T. M. SHEPHERD. Inorg. Chem. **4**, 813 (1965).
37. S. M. NELSON and T. M. SHEPHERD. J. Chem. Soc. 3276 (1965).
38. H. G. MAYFIELD, JR. and W. E. BULL. Inorg. Chim. Acta, **3**, 676 (1969).
39. B. N. FIGGIS and J. LEWIS. *In* Progress in inorganic chemistry. Vol. 6. *Edited by* F. A. Cotton. Interscience. New York. 1965. p. 37.
40. L. SACCONI. *In* Transition metal chemistry. Vol. 4. *Edited by* R. L. Carlin. Dekker. New York. 1968. p. 199.
41. B. BLEANEY. Phil. Mag. **42**, 441 (1951).
42. S. ANTOSIK, N. M. D. BROWN, A. A. MCCONNELL, and A. L. PORTE. J. Chem. Soc. A, 545 (1969).
43. B. J. HATHAWAY and D. E. BILLINGS. Coord. Chem. Rev. **5**, 143 (1970).
44. I. ADATO and I. ELIEZER. J. Chem. Phys. **54**, 1472 (1971).
45. R. S. DRAGO and K. F. PURCELL. *In* Non-aqueous solvent systems. *Edited by* T. C. Waddington. Academic Press. London. 1965. p. 211.
46. W. LIBUŚ and H. STRZELECKI. Electrochim. Acta, **15**, 703 (1970); **16**, 1749 (1971).

Can. J. Chem. Downloaded from www.nrcresearchpress.com by 210.87.254.5 on 09/05/12
For personal use only.

Dielectric Studies. Part XXXV. Relaxation Studies of Benzaldehyde and Four *para*-Substituted Aldehydes

P. F. MOUNTAIN AND S. WALKER
Lakehead University, Thunder Bay, Ontario P7B 5E1

Received March 11, 1974

P. F. MOUNTAIN and S. WALKER. Can. J. Chem. **52**, 3229 (1974).

The dielectric absorption has been determined for benzaldehyde, *p*-fluoro-, *p*-chloro-, *p*-bromo-, and *p*-nitro-benzaldehyde in *p*-xylene solution at mainly five or six frequencies in the 6.70 to 70.1 GHz region. For all three *p*-halo- substituents the mean relaxation time values indicate that some mechanism faster than molecular relaxation occurs whereas none was apparent in benzaldehyde itself. A detailed study has been made of *p*-chlorobenzaldehyde in *p*-xylene solution at five temperatures, and the data have been analyzed into contributions from a molecular relaxation process and a shorter relaxation time τ_2. In the *p*-xylene solutions of benzaldehyde the relaxation data indicate weak intermolecular hydrogen bonding between the solute and the solvent which is probably of the type C—H...Π.

P. F. MOUNTAIN et S. WALKER. Can. J. Chem. **52**, 3229 (1974).

On a déterminé l'absorption diélectrique du benzaldéhyde et des *p*-fluoro, *p*-chloro, *p*-bromo et *p*-nitro benzaldéhydes en solution dans le xylène; on a effectué ces mesures principalement à 5 ou 6 fréquences entre 6.70 et 70.1 GHz. Dans le cas des trois dérivés substitués par des halogènes en position para, la valeur moyenne des temps de relaxation indique qu'un mécanisme plus rapide que la relaxation moléculaire se produit alors qu'il n'y en a pas d'apparent dans le benzaldéhyde lui-même. On a fait une étude détaillée du *p*-chlorobenzaldéhyde dans le *p*-xylène à 5 températures différentes et on a analysé les données afin de déterminer les contributions provenant d'un processus de relaxation moléculaire et d'un processus de relaxation τ_2 plus court. En solution dans le *p*-xylène les données de relaxation pour le benzaldéhyde montrent que des ponts hydrogène intermoléculaires faibles existent entre le soluté et le solvant et que ceux-ci sont probablement du type C—H...Π. [Traduit par le journal]

Introduction

Fischer (1) examined the dielectric absorption of benzaldehyde in solution and was unable to detect the relaxation of the aldehyde group. Even if aldehyde group relaxation cannot be detected for benzaldehyde by dielectric absorption in the microwave region, this does not rule out such a possibility in the *p*-halo and *p*-nitro benzaldehydes. In the *p*-halo case withdrawal of electrons from the Π-electron system by an inductive (−1) effect occurs with respect to the halogen substituent while a release of electrons into the ring also takes place by a mesomeric (+M) effect (2). Thus, the two effects are opposed although the inductive outweighs the mesomeric effect, and the net effect is electron withdrawal from the ring. If electron withdrawal from the conjugated C_6H_4—CO system results from the introduction of a *p*-halo substituent in benzaldehyde, then the electron density in the $C_{aromatic}$—$C_{aliphatic}$ bond may well be reduced as could be the energy barrier for rotation of the aldehyde group. It is interesting to note that from far-infrared studies in benzaldehyde, *p*-fluoro-, *p*-chloro-, and *p*-bromobenzaldehyde the energy barriers evaluated for the vapors are 19.5, 15.0, 11.8, and 9.8 kJ mol^{-1} while for the pure liquids they are 28.0, 21.9, 19.2, and 15.6 kJ mol^{-1} respectively (3). *p*-Chlorobenzaldehyde has also been examined in Nujol solution, and its energy barrier (4) is 20.4 kJ mol^{-1}. Both the vapor and liquid phase values bear out the fall in the energy barrier in passing from benzaldehyde to the *p*-halogenated aldehyde. However, as Miller *et al.* (3) have indicated the energy barrier values quoted for the condensed states are not to be trusted if they are deduced from torsional frequency data. Thus, of the values given above, only the values for the vapors may be regarded as reliable.

From the actual energy barrier values themselves it would be difficult to predict whether re-

Can. J. Chem. Downloaded from www.nrcresearchpress.com by 210.87.254.105 on 09/05/12
For personal use only.

Can. J. Chem. Downloaded from www.nrcresearchpress.com by 210.87.254.105 on 09/05/12
For personal use only.

TABLE 1. Relaxation times (in ps), distribution parameter (α), static dielectric constant (ε_0), dielectric constant at very high frequency (ε_∞), and dipole moment (μ in Debye units) for solutions at weight fractions (w_2) at temperature t (°C) for benzaldehyde and some *para*-substituents

Solute	Solvent	t (°C)	w_2	τ_0	τ_1	τ_2	C_1	α	ε_0	ε_∞	μ
Benzaldehyde	*p*-Xylene	15	0.018	13.3				0.05	2.449	2.290	2.90
		25	0.018	11.8				0.04	2.447	2.279	2.90
		40	0.018	9.6				0	2.407	2.253	2.90
		60	0.018	7.7				0	2.355	2.214	2.90
	Cyclohexane	15	0.0199	9.0				0.04	2.192	2.048	2.95
		25	0.0199	8.3				0.02	2.167	2.028	2.95
		40	0.0199	6.5				0.01	2.132	2.003	2.95
p-Fluorobenzaldehyde	*p*-Xylene	15	0.03904	15.9	28	11.5	0.4	0.05	2.433	2.296	1.98
		40	0.03904	11.2	18	8.2	0.4	0.04	2.371	2.254	1.95
p-Chlorobenzaldehyde	*p*-Xylene	15	0.0571	18.5	36	13.0	0.4	0.07	2.480	2.309	1.94
		25	0.0571	15.8	33	10.8	0.4	0.08	2.455	2.294	1.93
		40	0.0571	12.0	18	9.0	0.4	0.03	2.355	2.234	1.88
		50	0.0571	11.1	17	8.3	0.4	0.03	2.332	2.238	1.88
		60	0.0571	9.9	14	7.9	0.4	0.02	2.309	2.222	1.86
p-Bromobenzaldehyde	*p*-Xylene	15	0.042	19.2	37	13.3	0.4	0.06	2.392	2.296	1.96
		40	0.042	13.6	20	10.8	0.4	0.02	2.335	2.253	1.92
p-Nitrobenzaldehyde	*p*-Xylene	40	0.025	15.8	24	8.6	0.6	0.07	2.337	2.248	2.33

Can. J. Chem. Downloaded from www.nrcresearchpress.com by 210.87.254.105 on 09/05/12
For personal use only.

laxation of the aldehyde group could be detected by dielectric absorption measurements on dilute solutions in the microwave region which are best applied to energy barriers less than ~ 15 kJ mol^{-1}. The most favorable case for detection would appear to be that of *p*-bromobenzaldehyde which has the lowest energy barrier in the vapor phase. Potentially, solely from an I and M effect point of view, the chances of detecting relaxation of the aldehyde group in the microwave region should increase in the sequence benzaldehyde < *p*-halobenzaldehyde < *p*-nitrobenzaldehyde.

Experimental Methods

The apparatus and techniques employed have been described previously (5, 6) and the errors assessed (7). The dielectric constant (ε') and loss factor (ε'')[1] were determined by a bridge method at some of the following frequencies 70.1, 35.11, 23.98, 9.313, 16.20, and 6.70 GHz. The static dielectric constant (ε_0) was measured with a heterodyne beat apparatus at 2 MHz.

Purification of Materials

The materials were obtained from commercial sources. The *p*-fluorobenzaldehyde and benzaldehyde were first dried, then purified by distillation under reduced pressure by using a (30 theoretical plates) spinning band column, and a small center fraction was collected and then stored over a suitable drying agent in darkened glassware. The *p*-chlorobenzaldehyde was fractionally distilled and then recrystallized, while the *p*-nitrobenzaldehyde was recrystallized. The observed boiling and melting points compared well with literature values, and gas-liquid chromatography could not then detect impurities in these compounds.

Results

The evaluation of the high frequency dielectric constant (ε_∞), distribution coefficient (α), mean relaxation time (τ_0), discrete relaxation times (τ_1 and τ_2), weight factors (C_1 and C_2), and dipole moment (μ) has been described previously (8), and these results are presented in Table 1.

The use of Debye distributions to analyze the dielectric data of dilute solutions can be defended empirically and theoretically (9) and has been confirmed by experiment (7). If the dielectric data are analyzed into contributions from two relaxation times, τ_1 and τ_2, then the values of the dielectric constant (ε'_{calc}) and the loss (ε''_{calc}) calculated from the τ_1, τ_2, and C_1 values have to correspond with the measured values within the limits of the appropriate experimental error.

The weight factors for the molecular and group relaxation, C_1 and C_2 respectively, may be estimated from dipole moment data. The weight factors C_1 and C_2 in benzaldehyde depend on the angle, θ, that the molecular dipole moment subtends with the long axis of the molecule (between the carbon-1–carbon-4 axis in the benzene ring). If μ is the dipole moment of the molecule, then $\mu_1 = \mu \cos\theta$ and $\mu_2 = \mu \sin\theta$ while $C_1/C_2 = (\mu_1/\mu_2)^2$ and $C_1 + C_2 = 1$ (10). This value of θ may be taken as equal to that in benzaldehyde if there is only a little mesomeric interaction between the aldehyde group and the *para*-substituent.

Fischer (1) deduced θ to be 30°, and from this and the above equations the corresponding C_1 values are 0.75, 0.37, 0.30, 0.29, and 0.49 for benzaldehyde, *p*-fluoro-, *p*-chloro-, *p*-bromo, and *p*-nitrobenzaldehyde, respectively. From analyses of the dielectric data according to the Budó equations the accuracy of C_1 is not normally better than ± 0.1. Thus, the C_2 values for the *p*-halobenzaldehydes are very similar.

The errors in the Budó analysis may be appreciable, and Grubb and Smyth (10) have quoted an accuracy of $\pm 20\%$ for τ_1 and τ_2 values. A recent study by Crossley *et al.* (11) revealed that such analyses have limitations when applied to a wide variety of cases. A case which is favorable for analysis for τ_2 values is when $C_2 > C_1$ and $\tau_2 > 6 \times 10^{-12}$ s while $\tau_1 > \tau_2$. The average calculated value of C_2 from group moments for the *p*-halobenzaldehydes is 0.68 and agrees with the one from the Budó analysis within the range of error (11) (± 0.1) for such an analysis. A comparison of the τ_0 values for the *p*-halobenzaldehydes at a given temperature supports C_2 being greater than C_1. The resulting τ_2 values for the *p*-halobenzaldehydes at the various temperatures range between 8 to 12×10^{-12} s. Thus, these cases would seem potentially satisfactory for a successful analysis (11) for τ_2. Points in support of the analyses are (*i*) that they all can be analyzed for a C_2 value of the correct magnitude, (*ii*) the C_2 value does not vary with temperature (this is a severe test in the case of *p*-chlorobenzaldehyde where five temperatures are employed), (*iii*) the values of ε' and ε'' calculated from τ_1, τ_2, and C_1 agree with the measured values within experimental error. This did not prove to be the case

[1]The ε' and ε'' data for all the systems may be obtained, at a nominal charge, from the Depository of Unpublished Data, National Science Library, National Research Council of Canada, Ottawa, Canada K1A 0S2.

for benzaldehyde, (*iv*) the plot of log $\tau_2 T$ *vs.* $1/T$ for *p*-chlorobenzaldehyde is a good linear one.

The error in the τ_1 values may well be appreciable and could well be of the order of $\pm 20\%$ or greater (11). However, such an error in the τ_1 values in Table 1 permits an acceptable sequence of τ_1 values for the *p*-halobenzaldehydes for a particular temperature if it is borne in mind that the error in the values may be $\pm 20\%$ or greater.

Discussion

Hassell and Walker (12) found that for a number of monosubstituted benzenes the molecular relaxation time has a linear dependence on the volume of the molecule as estimated from Courtauld models. From measurements on these models the sequence of molecular relaxation times would be expected to increase as follows, chlorobenzene > benzaldehyde > bromobenzene, where the benzaldehyde value would be closer to the chlorobenzene than the bromobenzene value. This is, in fact, the sequence of the observed relaxation times which in cyclohexane solution at 25 °C are 7.1, 8.3, and 11.6 $\times 10^{-12}$ s respectively. At 40 and 60 °C for benzaldehyde in *p*-xylene solution the distribution parameter is zero while at 40 °C in cyclohexane the $\alpha = 0.01$ may not be significant. The near zero α at 15 and 25 °C in cyclohexane and *p*-xylene solutions could be accounted for by local association which becomes negligible at higher temperatures. In addition, no satisfactory Budó analyses could be obtained where the value of C_1 remained constant at different temperatures and for both solvents. Thus, a detailed study of benzaldehyde bears out that the microwave dielectric data can best be accounted for in terms of molecular relaxation and that it does not appear feasible to detect relaxation of the aldehyde group from such data.

On a comparison of the observed relaxation times of benzaldehyde in cyclohexane and *p*-xylene solution it will be noted that in the latter solvent, the relaxation time increases by about 45% at each of the three temperatures. This is an exceptional increase between the two solvents which normally would be about 10% (13); such an increment is indicative of some form of interaction between the solute and solvent. Interaction of pyrrole with the solvent *p*-xylene of the type N—H...N has been noted previously by Tucker and Walker (14).

In *p*-xylene solution at 15 °C the observed relaxation times of chlorobenzene, benzaldehyde, and bromobenzene are 10.2, 13.3, and 14 $\times 10^{-12}$ s respectively (that is, the bromobenzene and benzaldehyde are now of the same order and appreciably longer than that of chlorobenzene which is to be contrasted with the behavior in cyclohexane solution). At 60 °C in *p*-xylene solution the relaxation times of bromobenzene and benzaldehyde are virtually identical, being 7.6 and 7.7 $\times 10^{-12}$ s respectively. Thus, it would seem likely that some form of interaction occurs between the benzaldehyde and the *p*-xylene which lengthens the relaxation time. An estimation of the interaction may be made by an equation employed to study the interaction of halogenated ethanes (15, 16) with various solvents. Thus, if $\tau_{p\text{-X}}$ is the relaxation time of the solute in *p*-xylene solution and τ_{cyc} the corresponding relaxation time in the inert solvent, cyclohexane, then application of the equation to this system gives:

$$[1]\quad \frac{\tau_{p\text{-X}}}{\tau_{cyc}} = \exp\left(\frac{\Delta G^{\ddagger}_{p\text{-X}} - \Delta G^{\ddagger}_{cyc}}{RT}\right) = \exp\left(\frac{\Delta\Delta G^{\ddagger}}{RT}\right) = \exp\left(\frac{\Delta S^{\ddagger}_{cyc} - \Delta S^{\ddagger}_{p\text{-X}}}{R}\right) \exp\left(\frac{\Delta H^{\ddagger}_{p\text{-X}} - \Delta H^{\ddagger}_{cyc}}{RT}\right)$$

The most probable form of interaction would be where the H in the aldehyde group acts as an electron acceptor and a hydrogen bond of the type C—H...Π is formed with the Π-electrons of

TABLE 2. $\Delta\Delta G^{\ddagger}$ data (in kJ mol^{-1}) for benzaldehyde based on relaxation time data in the inert solvent cyclohexane and the interacting solvent *p*-xylene. The relaxation time are quoted in ps

Solvent	*t* (°C)	τ	$\Delta\Delta G^{\ddagger}$
cyc	15	9.0	0.92
p-X	15	13.3	
cyc	25	8.3	0.88
p-X	25	11.8	
cyc	40	6.5	1.17
p-X	40	9.6	

Can. J. Chem. Downloaded from www.nrcresearchpress.com by 210.87.254.105 on 09/05/12
For personal use only.

Can. J. Chem. Downloaded from www.nrcresearchpress.com by 210.87.254.105 on 09/05/12
For personal use only.

p-xylene which act as the donor. This would be a very weak form of interaction and no stable complex would be anticipated but just a viscous drag on the re-orienting molecule which would lengthen the molecular relaxation time. For such a case of weak interaction the use of eq. 1 is permissible and has previously been employed in studies of weak interaction (15, 16). However, for strong molecular interaction a pre-exponential factor might be necessary in eq. 1 probably involving an inertia term which might change in passing from an unassociated to a strongly associated system.

If $\tau_{p\text{-X}} > \tau_{cyc}$, then $\Delta\Delta G^{\ddagger}$ may be regarded as the increased free energy of activation for molecular relaxation in *p*-xylene as opposed to cyclohexane solution. Further, if $\Delta S^{\ddagger}_{p\text{-X}} \sim \Delta S^{\ddagger}_{cyc}$, then $\Delta\Delta G^{\ddagger}$ may be looked upon as reflecting the larger enthalpy of activation ($\Delta H^{\ddagger}_{p\text{-X}} > \Delta H^{\ddagger}_{cyc}$) required when interaction takes place between the solute and *p*-xylene when weak attachment leads to the hindering of rotation of the solute molecule. Since inductive effects of the polar solute molecule may influence the value of $\Delta H^{\ddagger}_{p\text{-X}}$, then some similar reference molecules are required to gain an estimation of this effect. The dipole moments of benzotrichloride and benzonitrile are 2.06 and 4.03 D respectively, while that for benzaldehyde is 2.92 D. The $\Delta\Delta G^{\ddagger}$ values for benzotrichloride and benzonitrile are 0.23 and 0.53 kJ mol^{-1}, respectively. Since the moment of benzaldehyde lies between that of benzotrichloride and benzonitrile, then, if only inductive effects operate between the benzaldehyde and the *p*-xylene, its $\Delta\Delta G^{\ddagger}$ might be expected to lie between 0.34 and 0.53 kJ mol^{-1}. In fact, its average value for the three temperatures is 0.93 kJ mol^{-1} which is slightly more than double the mean of these two values.

The $\Delta\Delta G^{\ddagger}$ of benzophenone based on the $\tau_{benzene}/\tau_{cyc}$ ratio is only 0.33 kJ mol^{-1}. Benzophenone has a similar dipole moment (2.98 D) to benzaldehyde, and the moments of both these compounds are largely determined by the keto grouping. Thus, it would seem that the appreciably larger $\Delta\Delta G^{\ddagger}$ value of benzaldehyde requires an additional form of interaction with the solvent to account for its magnitude; the most likely type is —C—H...Π. Pimentel and McClellan (17) have already indicated that there remains uncertainty concerning hydrogen bonding by the aldehyde C—H bond. Hence the detection of C—H...X, where X is a weak electron donor (such as *p*-xylene), by most physical methods can be difficult and uncertain. Thus, this dielectric approach employing eq. 1 would seem useful to indicate such weak interaction.

For solubility reasons the *p*-halo- and *p*-nitrobenzenes had to be examined in *p*-xylene solution rather than in the inert solvent, cyclohexane. As indicated earlier the observed relaxation times of benzaldehyde in *p*-xylene are very similar to those for bromobenzene in the same solvent at the same temperature, and, in addition, Courtauld models indicate that the methyl and chloro groups are of similar size, and therefore it follows that a reasonable comparison for the molecular relaxation time of *p*-chlorobenzaldehyde would be that of *p*-bromotoluene. The relaxation times of *p*-bromotoluene are 22.3×10^{-12} s at 25 °C and 18.8×10^{-12} s at 40 °C, while the τ_0 values for *p*-chlorobenzaldehyde are 15.8 and 12×10^{-12} s respectively. Such a big difference between the two values at each temperature suggests some additional relaxation process in the case of *p*-chlorobenzaldehyde which makes the observed relaxation time shorter than that of the molecular relaxation time. This is borne out by comparison of (*i*) and (*ii*) below:

(*i*) the molecular relaxation times of *p*-chloro- and *p*-bromotoluene in *p*-xylene at 15 °C are 19.3 and 27.2×10^{-12} s respectively; that is on substitution of Br for Cl the relaxation time increases by ~40%.

(*ii*) the observed relaxation times of *p*-chloro and *p*-bromobenzaldehyde are 18.5 and 19.2×10^{-12} s at 15 °C;

that is, they are virtually identical.

The variation of the observed relaxation times of *p*-fluoro-, *p*-chloro, and *p*-bromobenzaldehyde in *p*-xylene at 40 °C are comparatively very small, their values being 11.2, 12, and 13.6×10^{-12} s respectively. This is to be contrasted with the variations in the molecular relaxation times for fluoro-, chloro-, bromo-, and iodobenzene which in *p*-xylene at 15 °C are 6.8, 10, 14, and 18×10^{-12} s respectively; thus, as the halogens increase in size (their van der Waals' radii being 1.35, 1.80, 1.95, and 2.15 Å respectively) the relaxation time exhibits an appreciable increase altering by more than 100% from the fluoro to the iodine derivative. Hence, variation in the size in the *p*-halobenzaldehydes on their passing from the fluoro to the bromo derivative should produce a much greater alteration in the molecular relaxation times than the variation seen in the

observed relaxation times. There can be little doubt from the near constancy of the observed relaxation times for fluoro-, chloro-, bromobenzaldehydes in *p*-xylene at 40 °C that the contribution to the dielectric absorption is not the major absorption process; that is $C_1 < C_2$. This bears out the C_1 values for the *p*-halobenzaldehydes (as estimated from group moments) which are ~ 0.3. The Budó analyses for τ_2 and C_2 (see Table 1) *p*-halobenzaldehydes, on the whole, appear to be reasonable and in line with the C_2 value calculated from group moments since the value from the Budó analysis would not be more accurate than ± 0.1. Since the weight factor for C_1 is small, then the error in τ_1 could well be appreciable (11). The enthalpy of activation ($\Delta H_2^{\neq}$) for the *p*-chlorobenzaldehyde τ_2 process is 6.7 kJ mol^{-1} from transition state theory while from the Arrhenius equation the value is 9.2 kJ mol^{-1} where the accuracy would not be greater than $\pm$ 2 kJ mol^{-1}. Thus, the $\Delta H_2^{\neq}$ value is of a similar order to the value (11.8 kJ mol^{-1}) obtained for aldehyde group rotation in the gaseous phase. In view of the criticism (3) levelled at values derived from far-infrared data in condensed phases, it would seem unwise to compare our value with those in the pure liquid state (3) and Nujol solution (4).

Although the molecular time of *p*-bromo- and *p*-nitrobenzaldehyde ought to be fairly similar, since the molecular relaxation times of bromo- and nitrobenzene in *p*-xylene at 15 °C are within experimental error the same, their observed relaxation times differ, being 13.6 and 15.8 $\times$ 10^{-12} s respectively in *p*-xylene at 40 °C. However, this could be accounted for since the calculated C_1 value for the *p*-nitro derivative is appreciably greater than that for the *p*-bromo.

Conclusions

All the three *p*-halo substituents and probably the *p*-nitro compound have a contribution from some mechanism characterized by the relaxation time τ_2 which is faster than molecular relaxation whereas none was apparent in benzaldehyde itself. The vapor phase energy barrier value for aldehyde rotation in benzaldehyde is about 65% higher than that in *p*-chlorobenzaldehyde. Thus, it would be understandable if in solution measurements within our frequency range, we detected aldehyde relaxation in *p*-chlorobenzaldehyde but not in benzaldehyde itself. The difference in behavior between these *p*-substituted aldehydes and benzaldehyde itself could then be related to the electron-withdrawing characteristics of the *p*-halo and *p*-nitro groups. However, little is known as to how the energy barrier would vary on passing from the gaseous phase to solution, and perhaps, at this stage no definite conclusions should be drawn until more data become available as to how energy barriers for group rotation vary with the medium. It would appear that in the *p*-xylene solutions of benzaldehyde weak intermolecular hydrogen bonding of the type —C—H...Π solvent occurs.

1. E. Fischer. Z. Naturforsch. **4***a*, 707 (1949).
2. J. W. Smith. Electric dipole moments. Butterworths, London. 1955.
3. F. A. Miller, W. G. Fateley, and R. E. Witkowski. Spectrochim. Acta, **23**A, 891 (1967).
4. H. C. Silver and J. L. Wood. Trans. Faraday Soc. **60**, 5 (1964).
5. W. F. Hassell, M. D. Magee, S. W. Tucker, and S. Walker. Tetrahedron, **20**, 2137 (1964).
6. D. B. Farmer and S. Walker. Tetrahedron, **22**, 111 (1966).
7. M. D. Magee and S. Walker. Trans. Faraday Soc. **62**, 3093 (1966).
8. M. D. Magee and S. Walker. J. Chem. Phys. **50**, 2580 (1969).
9. C. J. F. Böttcher. Theory of electric polarization. Elsevier, Amsterdam. 1962. p. 374.
10. E. L. Grubb and C. P. Smyth. J. Am. Chem. Soc. **83**, 4873 (1961).
11. J. Crossley, S. Walker, and S. P. Tay. Adv. Mol. Relaxation Proc. **6**, 79 (1974).
12. W. F. Hassell and S. Walker. Trans. Faraday Soc. **62**, 2695 (1966).
13. J. Crossley and S. Walker. Can. J. Chem. **46**, 2369 (1968).
14. S. W. Tucker and S. Walker. Trans. Faraday Soc. **62**, 2690 (1966).
15. K. Chitoku and K. Higasi. Bull. Chem. Soc. Jap. **40**, 773 (1967).
16. J. Crossley and C. P. Smyth. J. Am. Chem. Soc. **91**, 2482 (1969).
17. G. C. Pimentel and A. L. McClellan. The hydrogen bond. W. H. Freeman and Co., San Francisco, 1960.

Can. J. Chem. Downloaded from www.nrcresearchpress.com by 210.87.254.105 on 09/05/12
For personal use only.

Occurrence of Strontium–Iron Oxide $SrFe_{12}O_{19}$ in the Fe_2O_3–Na_2O–$SrSO_4$ System

R. J. ROUTIL[1] AND D. BARHAM

Department of Chemical Engineering and Applied Chemistry, University of Toronto, Toronto, Ontario M5S 1A4

Received May 15, 1973[2]

R. J. ROUTIL and D. BARHAM. Can. J. Chem. **52**, 3235 (1974).

The formation of $SrFe_{12}O_{19}$ in the Fe_2O_3–Na_2CO_3–$SrSO_4$ system was found to proceed through three stages, first an endothermic reaction between Fe_2O_3 and Na_2CO_3 to form $Na_2Fe_2O_4$ and CO_2, second an exothermic reaction of $Na_2Fe_2O_4$ with $SrSO_4$ to produce Na_2SO_4, $Sr_7Fe_{10}O_{22}$, and $SrFe_{12}O_{19}$, third an exothermic reaction between $Sr_7Fe_{10}O_{22}$ and Fe_2O_3 towards more $SrFe_{12}O_{19}$. The yield of $SrFe_{12}O_{19}$ depended on the molar ratio of the reactants and on temperature. Below 700 °C the formation did not proceed beyond the second stage. Samples prefired at 900–1200 °C contained $SrFe_{12}O_{19}$ in all cases when the original relative molar concentrations xFe_2O_3, yNa_2CO_3, and $zSrSO_4$ satisfied the condition $(x - y + z)/z > 5/7$ or $x/y > 5/7 \geqslant x/z$. Substitution of Na_2CO_3 in the reaction mixtures with equivalent amounts of NaOH or other precursors of Na_2O did not affect the second and the third stage of the reaction and the final yield of $SrFe_{12}O_{19}$. On the ternary diagram of the Fe_2O_3–Na_2O–$SrSO_4$ system the $SrFe_{12}O_{19}$ region was represented by the area of a quadrilateral with the corner points located at the composition points 98-1-1, 1-1-98, 26-36-38, and 50-49-1 mole percent. The highest yields were obtained from the mixtures represented by the molar ratio $6Fe_2O_3$:$1Na_2O$:$1SrSO_4$. The hexagonal lattice parameters of $SrFe_{12}O_{19}$ were determined as $a_0 = 5.885$ Å and $c_0 = 23.047$ Å. X-Ray diffraction reflections of $SrFe_{12}O_{19}$ were indexed and reassignment of several indices in ASTM 7-276 for $BaFe_{12}O_{19}$ was suggested.

R. J. ROUTIL et D. BARHAM. Can. J. Chem. **52**, 3235 (1974).

La formation de $SrF_{12}O_{19}$ dans le système Fe_2O_3–Na_2CO_3–$SrSO_4$ passe par trois étapes: la première, une réaction endothermique entre Fe_2O_3 et Na_2CO_3 qui donne $Na_2Fe_2O_4$ et CO_2; la seconde, une réaction exothermique de $Na_2Fe_2O_4$ avec $SrSO_4$ qui produit Na_2SO_4, $Sr_7Fe_{10}O_{22}$ et $SrFe_{12}O_{19}$; la troisième, une réaction exothermique entre $Sr_7Fe_{10}O_{22}$ et Fe_2O_3 qui donne d'autre $SrFe_{12}O_{19}$. Le rendement de $SrF_{12}O_{19}$ dépend du rapport molaire des réactifs et de la température. A des températures plus basses que 700 °C la formation s'arrête à la deuxième étape. Des échantillons précuits à 900–1200 °C contiennent du $SrFe_{12}O_{19}$ dans tous les cas quand les concentrations molaires relatives originales xFe_2O_3, yNa_2CO_3 et $zSrSO_4$ satisfont la condition $(x - y + z)/z > 5/7$ ou $x/y > 5/7 \geqslant x/z$. La substitution de Na_2CO_3 dans les mélanges réactionnels avec des quantités équivalentes de NaOH ou d'autres précurseurs de Na_2O n'affecte pas la seconde ou la troisième étape de la réaction ni le rendement final de $SrFe_{12}O_{19}$. Sur le diagramme ternaire du système Fe_2O_3–Na_2O–$SrSO_4$, la région de $SrFe_{12}O_{19}$ est représentée par un quadrilatère dont les sommets sont localisés aux pourcentages de composition 98-1-1, 1-1-98, 26-36-38 et 50-49-1 mole. Les rendements les plus élevés sont obtenus à partir des mélanges dont le rapport molaire est: $6Fe_2O_3$:$1Na_2O$; $1SrSO_4$. On détermine les paramètres de la maille hexagonale de $SrFe_{12}O_{19}$: $a_0 = 5.885$ et $c_0 = 23.047$ Å. On indexe les réflexions de la diffraction des rayons-X de $SrF_{12}O_{19}$, et l'on suggère une attribution de plusieurs indices de l'ASTM 7-276 pour $BaFe_{12}O_{19}$. [Traduit par le journal]

Introduction

Preparation of ferrimagnetic oxides $BaFe_{12}O_{19}$ and $SrFe_{12}O_{19}$ according to the overall reaction

$$[1]\quad (Ba,Sr)SO_4 + 6Fe_2O_3 + Na_2CO_3 \rightarrow (Ba,Sr)Fe_{12}O_{19} + Na_2SO_4 + CO_2$$

was originally reported in ref. 1. The possibility of using barium and strontium in their most common natural form, sulfates, and other potential advantages of this method over the traditional methods requiring carbonates or other non-sulfate forms of barium and strontium was outlined in ref. 2. The study of the Fe_2O_3–Na_2O–$SrSO_4$ system with respect to the occurrence of $SrFe_{12}O_{19}$ was stimulated by the recognition of $SrFe_{12}O_{19}$ as superior to other hexagonal ferrite materials for manufacturing permanent magnets (3) and by the discovery of large deposits of $SrSO_4$ ores in Cape Breton.

Experimental Strategy

The area of $SrFe_{12}O_{19}$ in the Fe_2O_3–Na_2O–$SrSO_4$ system was established by investigating Fe_2O_3–Na_2CO_3–$SrSO_4$ mixtures prefired to 600–

[1]Present address: Atlantic Industrial Research Institute, Nova Scotia Technical College, Halifax, Nova Scotia.

[2]Revision received May 6, 1974.

Can. J. Chem. Downloaded from www.nrcresearchpress.com by 210.87.254.105 on 09/05/12
For personal use only.

Can. J. Chem. Downloaded from www.nrcresearchpress.com by 210.87.254.105 on 09/05/12
For personal use only.

1400 °C. Na_2CO_3 was chosen as the most convenient source of Na_2O. As noted in ref. 1 the use of NaOH, $NaNO_3$, or other Na_2O precursors would not affect the final yield of $SrFe_{12}O_{19}$, but it would be less practical both experimentally and from the point of view of prospective industrial application. The whole concentration range of the system was subdivided into smaller regions represented by the nineteen evenly spaced concentration points derived by substituting (1,1,1) and all permutations of (5,5,2), (2,1,1), (7,4,1), (4,1,1), and (10,1,1) for (x,y,z) with x, y, and z indicating relative molar ratios of Fe_2O_3, Na_2O, and $SrSO_4$ respectively. Depending on the $SrFe_{12}O_{19}$ yields from these nineteen concentration points, a series of additional concentration points was investigated to determine the boundaries of the $SrFe_{12}O_{19}$ region.

Small quantities of $SrFe_{12}O_{19}$ were found in all samples fired to 700 °C. After firing to higher temperatures the concentration of $SrFe_{12}O_{19}$ increased in samples with $x \geqslant y$ and decreased in those representing the Na_2O-rich corner of the system. Heating temperatures below 850 °C appeared insufficient for the completion of the $SrFe_{12}O_{19}$ formation. Heating to temperatures above 1250 °C was associated with a decrease of weight which was attributed to losses of sodium and oxygen.

Variations of the heating rate did not have any appreciable effects on the samples, provided that the heating rate was slow enough to prevent spattering of sodium carbonate. The effects of the cooling rate were apparent only on the samples which were preheated to, or above, their liquidus temperatures; the grain size of the $SrFe_{12}O_{19}$ particles was then inversely proportional to the cooling rate.

The heating time affected the yield of $SrFe_{12}O_{19}$ from the samples heated below 900 °C. The effects of repeated heating to the same temperature were cumulative with respect to the total heating time.

For homogenized samples heated above 1000 °C for 10 min or longer heating time had no effect. The effects of heating time on the grain growth of $SrFe_{12}O_{19}$ particles became apparent only when the temperature exceeded 1100 °C. No differences were observed between the samples heated intermittently at gradually increasing temperatures and the samples heated only once to the maximum temperature.

The effects of the homogeneity of the samples on the yield of $SrFe_{12}O_{19}$ were studied on a series of samples subjected to repeated heating and intermediate crushing to either 10, 60, 100, or 200 mesh. The homogeneity of the samples was important to the formation of $SrFe_{12}O_{19}$ up to 900 °C. Above 900 °C the inadequacies in the homogeneity could be compensated for by prolonged heating. The homogeneity was less important above 1000 °C and after heating to 1200 °C for 1 h no differences were observed between the samples homogenized by a single screen through a 20-mesh sieve and those screened twice through a 200-mesh sieve.

Heating to 1200 °C for 1 h was selected arbitrarily as the standard heat treatment of the Fe_2O_3–Na_2CO_3–$SrSO_4$ mixtures preceding the separation of the $SrFe_{12}O_{19}$ phases for the purpose of comparative evaluation of the yield, chemical composition, and lattice parameters of the $SrFe_{12}O_{19}$ phase with respect to the relative molar ratios of the original components. This was considered a suitable compromise between the use of a high temperature to ensure the completion of the $SrFe_{12}O_{19}$ formation in a relatively short time and to minimize potential effects of any inhomogeneities, and the necessity of keeping the temperature below 1250 °C reported to cause appreciable evaporation of Na_2O (4). The total weight losses observed in the samples fired at 1200 °C for 1 h were in good agreement with the theoretical loss of carbon dioxide. The 1 h period of heating was fully adequate as no further changes in the appearance and in the weight of the samples were observed after the first 20 min at 1200 °C. A relatively slow heating rate, about 10 °C per minute, which was necessary to prevent spattering of the samples containing large amounts of sodium carbonate, was adopted for all samples in order to standardize the heat treatment.

Experimental Results

Preparation of Samples

Certified grade ferric oxide and anhydrous sodium carbonate from Fisher Scientific Co. and reagent grade strontium sulfate from British Drug Houses Ltd. were used. The reagents were stored at 110 °C to prevent the intake of moisture.

The total weight of individual samples before firing was maintained at about 20 g. Each sample was homogenized in an agate mortar and then it was tightly packed into a 20 ml platinum crucible and covered with a platinum lid. The samples were heated in a muffle furnace and on completion of

Can. J. Chem. Downloaded from www.nrcresearchpress.com by 210.87.254.105 on 09/05/12
For personal use only.

the 1 h period at 1200 °C the furnace was switched off and the samples were allowed to cool in the furnace.

Separation of Ferrimagnetic Phases

The reacted samples, cooled to room temperature, contained two or more solid phases. To separate the $SrFe_{12}O_{19}$ phase the sample was first leached with warm water in order to remove water soluble phases such a sodium sulfate. This treatment was sufficient to isolate high purity $SrFe_{12}O_{19}$ from the samples based on the molar ratio 6:1:1. The samples based on other molar ratios were then leached with slowly boiling 10% nitric acid to dissolve the phases insoluble in water and soluble in nitric acid, *e.g.* $Na_2Fe_2O_4$ and $Sr_7Fe_{10}O_{22}$. The acid leaching was completed when the whole sample disintegrated to small particles and when no appreciable change in the color of fresh leaching acid was observed for at least 1 h of leaching. The leaching acid was then decanted and the sample was washed with water. After drying, the samples were tested for non-magnetic particles. The samples containing non-magnetic particles, such as strontium sulfate or hematite, were ground to 100 mesh and then subjected to magnetic separation. Although the magnetic separation improved the purity of the ferrimagnetic phase, the separation was not quantitative.

Preparation of Standard $SrFe_{12}O_{19}$

The method devised by Gambino and Leonhard (4) for growing single crystals of $BaFe_{12}O_{19}$ from sodium ferrate flux was adapted for the preparation of a $SrFe_{12}O_{19}$ standard.

A mixture containing 28.7 g Fe_2O_3, 7.95 g Na_2CO_3, and 4.43 g $SrCO_3$ was prefired at 900 °C for 1 h and after cooling it was ground to pass 40 mesh. The powder was heated in a closed platinum crucible up to 1200 °C and after 15 h at 1200 °C it was cooled at the rate of about 10 °C per hour to 1100 °C; then the furnace was turned off and the sample was allowed to cool inside. After cooling to room temperature the crucible containing the solidified melt was immersed in 10% nitric acid in a 250 ml beaker and was heated to slow boiling. The leaching acid was changed every 4 h until the major part of the solidified melt disintegrated. The separated $SrFe_{12}O_{19}$ crystals were leached with boiling 5% nitric acid for 2 h. After washing with water the crystals were dried at 110 °C. The total yield of $SrFe_{12}O_{19}$ crystals was 17.85 g.

The crystals were sorted according to their size by screening, the fraction 0.15-0.25 mm was selected as a standard.

Chemical Analysis

Samples of the separated ferrimagnetic phases were dissolved in hot hydrochloric acid; excess hydrochloric acid was evaporated; the remaining solution was diluted with 50% ethanol, and if any strontium sulfate was present it was separated by filtration. In the filtrate iron was determined by titration with 0.01 F EDTA at p*H* 2 using salicylic acid as indicator (5) and strontium was determined by precipitation of strontium sulfate in 50% ethanol (6). Only those samples which apparently did not contain any foreign phases other than strontium sulfate were analyzed. The attempts to analyze the samples containing hematite or other iron oxides as foreign phases were abandoned because of the difficulties in distinguishing the iron introduced by the foreign phases from the iron of the $SrFe_{12}O_{19}$ phase.

The strontium hexaferrite phase formed within that area of the Fe_2O_3–Na_2O–$SrSO_4$ system represented by the samples listed in Table 1 was stoichiometric strontium–iron oxide $SrFe_{12}O_{19}$. The deviations of the analytical results from the theoretical value were attributed to some minute amounts of undetected foreign phases and to analytical errors rather than to real variations in the composition of the hexaferrite phase. This assumption was confirmed as valid for the whole strontium hexaferrite region of the system on basis of the lattice parameter determination.

X-Ray Diffraction Analysis

The ferrimagnetic phases separated from the samples were identified by the Debye–Scherrer technique. The photographs were taken in a Straumanis-type 114.6 mm powder diffraction camera using manganese filtered iron K radiation. The wavelengths $\lambda_{\alpha_1} = 1.936042$ Å and $\lambda_{\alpha_2} = 1.939980$ Å were used for the calculation of the *d*-values from the fully resolved α-doublets, and the weighted average wavelength $\bar{\lambda}_\alpha = 1.937354$ Å, based on $(2\lambda_{\alpha_1} + \lambda_{\alpha_2})/3$, was used in the cases of unresolved doublets.

An exposure of about 15 h (10 mA, 30 kV) was found necessary to obtain good quality lines in the high angle region and to detect the strongest lines of the foreign phases present in minor quantities.

The X-ray diffraction pattern of the strontium hexaferrite standard sample appeared identical

TABLE 1. Composition of the strontium hexaferrite phase separated from various samples fired at 1200 °C for 1 h

Original molar ratio			% Fe_2O_3 in the $SrFe_{12}O_{19}$ phase	Standard error	Value of n in $SrO.nFe_2O_3$	Standard error
$\equiv Fe_2O_3$	Na_2CO_3	$SrSO_4$				
6	1	1	90.229	0.058	5.999	0.004
13	3	3	90.325	0.066	6.006	0.004
4	1	1	90.267	0.120	6.002	0.008
7	2	2	90.133	0.066	5.993	0.004
2	1	1	90.246	0.105	6.000	0.007
1	1	1	90.063	0.178	5.988	0.012
1	1	2	90.029	0.125	5.986	0.008
5	5	2	90.000	0.051	5.984	0.003
5	2	5	90.289	0.248	6.003	0.017
7	4	1	90.210	0.066	5.998	0.004
7	1	4	90.450	0.167	6.014	0.011
4	1	7	90.296	0.114	6.004	0.008
Standard sample			90.210	0.066	5.998	0.004
Theory			90.241	—	6.000	—

with the patterns of several samples isolated from the Fe_2O_3–Na_2O–$SrSO_4$ system. The corresponding d-values of all these samples differed by less than 1% in the low angle region and by less than 0.002% in the high angle region. With respect to the relative intensities of the observed reflections, evaluated visually, no discernible differences were found among the patterns of these samples.

As strontium hexaferrite has not been included in the Powder Diffraction File 1968 and the available data on the isostructural magnetoplumbite, barium hexaferrite, and lead hexaferrite (ASTM 4-0704, ASTM 7-276, ASTM 15-623, and ASTM 17-660) contained considerable discrepancies in the indices assigned to corresponding reflection of the three patterns, it was necessary to recalculate relative intensities of all possible reflections for the d-values between 5 and 0.968 Å using the structure factors calculated from observed reflections of single crystal barium hexaferrite as given in ref. 7.[3] The results revealed a number of indices in ASTM 7-276 as incorrect (Table 2). Similar recalculations for magnetoplumbite and for lead hexaferrite showed that the indices in ASTM 4-0704 were basically correct and the indices in ASTM 15-623 and ASTM 17-660 contained only a few errors.

The indices assigned to the X-ray diffraction pattern of strontium hexaferrite (Table 3) were considered correct as a good agreement was found between the experimental d-values and the theoretical d-values calculated from the lattice parameters.

Lattice Parameters of $SrFe_{12}O_{19}$

As shown in Table 3, the number of either $hk0$ or $00l$ lines in the high angle region of the FeK_α diffraction pattern was not sufficient to determine the lattice parameters by the Nelson–Riley extrapolation method. Under these circumstances the Cohen's least-squares method was employed as the most suitable alternative. Of the relatively large number of good quality lines in the region of $\theta > 60°$, the following 19 were selected: the α_1-reflections 410, 10.21 and 21.18, and the α_1–α_2 doublets of 327, 22.14, 414, 40.11, 30.18, 40.14, 330, and 507.

Using the error term

$$\delta_i = 10 \sin^2 2\theta_i \left(\frac{1}{\sin \theta_i} + \frac{1}{\theta_i}\right)$$

the system of three linear algebraic equations, devised by Cohen for finding the "most probable lattice parameters" in the hexagonal system, was transformed into an augmented matrix which, as it contained the coefficient matrix in the form of a symmetric positive definite matrix, could be con-

[3]The observed and the calculated structure factors for the reflections 00.14, 20.11, and 220, omitted in ref. 7 were obtained from the principal author W. D. Townes via private communication:

h	k	l	F_o	F_c
0	0	14	3515	3762
2	0	11	3687	4058
2	2	0	5192	6418

Can. J. Chem. Downloaded from www.nrcresearchpress.com by 210.87.254.105 on 09/05/12
For personal use only.

Can. J. Chem. Downloaded from www.nrcresearchpress.com by 210.87.254.105 on 09/05/12
For personal use only.

TABLE 2. ASTM 7-276 compared with the values calculated form the lattice parameters and structure factors given for $BaFe_{12}O_{19}$ in ref. 7

ASTM 7-276					Calculated				
d (Å)	I/I_1	h	k	l	d (Å)	I/I_1	h	k	l
4.94	10	1	0	1	4.98	12	1	0	1
4.65	13	1	0	2	4.67	21	1	0	2
3.86	15	0	0	6	3.87	11	0	0	6
					3.83	5	1	0	4
					3.08	9	1	0	6
2.94	40	1	1	0	2.95	56	1	1	0
2.89	13	0	0	8	2.90	17	0	0	8
2.85	10	1	1	2	2.86	11	1	1	2
2.77	100	1	0	7	2.78	100	1	0	7
2.62	100	1	1	4	2.63	88	1	1	4
2.55	8	2	0	0	2.55	10	2	0	0
					2.54	7	2	0	1
2.52	8	1	0	8	2.52	7	1	0	8
2.42	40	2	0	3	2.42	45	2	0	3
					2.34	5	1	1	6
2.23	40	2	0	5	2.24	31	2	0	5
2.13	25	2	0	6	2.13	25	2	0	6
1.945	10	1	0	11	1.949	7	1	0	11
					1.823	4	1	1	10
1.814	15	1	1	10*	1.813	9	2	0	9
1.715	5	2	1	0*	1.716	4	2	0	10
1.699	10	2	1	6*	1.701	8	3	0	0
1.666	40	2	1	7	1.667	43	2	1	7
					1.657	7	0	0	14
					1.632	25	3	0	4
1.625	50	3	0	4*	1.625	46	2	0	11
					1.616	6	1	1	12
1.606	5	2	1	8	1.606	8	2	1	8
1.530	10	2	1	9*	1.542	5	2	1	9
							2	0	12
1.473	40	2	2	0	1.473	37	2	2	0
					1.423	6	2	1	11
1.389	15	3	1	0*	1.390	14	2	0	14
					1.318	1	1	0	17
1.313	8	1	0	17*	1.313	11	2	2	8
1.302	20	1	1	16*	1.302	22	3	1	7
					1.301	5	1	1	16

*To be corrected.

veniently solved by the method of conjugate gradients (8) in three iterations using double precision intermediate values.

The lattice parameters of the strontium hexaferrite standard sample and samples prepared from mixtures of nineteen different Fe_2O_3:Na_2CO_3:$SrSO_4$ molar ratios varied within a very limited range of 5.8843–5.8848 Å for a_0, 23.044–23.051 Å for c_0, and 3.9160–3.9173 for c/a. The overall average values and their standard deviations were calculated: $a_0 = 5.8845 \pm 0.0002$ Å, $c_0 = 23.047 \pm 0.002$ Å, and $c/a = 3.9165 \pm 0.0003$. The limited range of the variations from the average values and the lack of any discernible correlation between the lattice parameters and the chemical composition, together with the obvious independence of the lattice parameters on the original Fe_2O_3:Na_2CO_3:$SrSO_4$ molar ratios, confirmed the assumption that the strontium hexaferrite phase separated from the Fe_2O_3–Na_2CO_3–$SrSO_4$ systems after a one-hour heating to 1200 °C was stoichiometric strontium–iron oxide $SrFe_{12}O_{19}$, and that this phase did not differ, either chemically or crystallographically, from the strontium hexaferrite phases separated from the hexaferrite regions of the Fe_2O_3–$SrCO_3$ or Fe_2O_3–$SrCO_3$–Na_2CO_3 systems.

The values of the strontium hexaferrite lattice parameters determined in this work differ from those published earlier, *e.g.* $a_0 = 5.86$ Å and $c_0 = 23.00$ Å (9), $a_0 = 5.864$ Å and $c_0 = 23.03$ Å (10), $a_0 = 5.876$ Å and $c_0 = 23.08$ Å (11). These variations could be explained by the different methods of the lattice parameter determination used by individual authors, by the differences in the wavelength values used in the calculations, and, possibly, in some cases by the incorrect indexing of reflections mentioned earlier. The results presented in this work, based on the Cohen's least squares method applied to nineteen reflections in the range $60 < \theta < 85°$, should be considered more reliable.

Differential Thermal Analysis

Differential thermal analysis was employed to obtain general information on the temperatures at which reactions in the Fe_2O_3–Na_2CO_3–$SrSO_4$ system start and on the exo- or endothermic character of these reactions. The DTA samples included pure Fe_2O_3 and the stoichiometric mixtures ($6Fe_2O_3 + Na_2CO_3$), ($6Fe_2O_3 + SrSO_4$), ($Na_2CO_3 + SrSO_4$), ($6Fe_2O_3 + Na_2CO_3 + SrSO_4$), ($Na_2Fe_2O_4 + SrSO_4$), ($5Fe_2O_3 + Na_2Fe_2O_4 + SrSO_4$), and ($SrFe_{12}O_{19} + Na_2SO_4$). α-Alumina was used as a standard with all samples and in supplementary tests the mixtures ($6Fe_2O_3 + SrSO_4$) and ($5Fe_2O_3 + Na_2Fe_2O_4$) were used as standards against the samples ($6Fe_2O_3 + Na_2CO_3 + SrSO_4$) and ($6Fe_2O_3 + Na_2CO_3$). The non-standard DTA equipment used in the tests required a relatively high heating rate of 40 °C per minute, the observations of pertinent temperatures were nevertheless made with an accuracy of ±5 °C as confirmed by tests on inorganic standards with well defined melting points.

The DTA curve of ($6Fe_2O_3 + Na_2CO_3$) in Fig.

TABLE 3. X-Ray diffraction pattern of $SrFe_{12}O_{19}$*

d (Å)	I/I_1	h k l	d (Å)	I/I_1	h k l	d (Å)	I/I_1	h k l
4.66	10	1 0 2	1.806	5	2 0 9	1.209	5	4 0 6
4.25	2	1 0 3	1.709	2	2 0 10	1.174	10	1 1 18
3.84	10	0 0 6	1.699	10	3 0 0	1.172	5	3 1 11
3.07	2	1 0 6	1.663	50	2 1 7	1.112	10	4 1 0
2.94	50	1 1 0	1.646	10	0 0 14	1.1017	20	3 2 7
2.88	15	0 0 8	1.629	30	3 0 4	1.0969	20	2 2 14
2.85	8	1 1 2	1.618	50	2 0 11	1.0919	25	4 1 4
2.765	90	1 0 7	1.601	10	2 1 8	1.0886	30	4 0 11
2.620	100	1 1 4	1.534	5	2 0 12	1.0729	10	1 0 21
2.548	10	2 0 0	1.471	70	220 10 15	1.0663	15	2 1 18
2.533	10	2 0 1	1.455	5	2 0 13	1.0476	5	0 0 22
2.508	10	1 0 8	1.418	5	2 1 11	1.0402	5	3 1 15
2.418	50	2 0 3	1.383	20	2 0 14	1.0346	5	4 0 13
2.336	10	1 1 6	1.310	10	228 10 17	1.0292	5	2 2 16
2.288	2	1 0 9	1.299	15	3 1 7	1.0225	20	3 0 18
2.230	40	2 0 5	1.294	5	1 1 16	1.0076	20	4 0 14
2.123	30	2 0 6	1.272	2	30 12 401	1.0016	5	4 1 10
2.015	2	2 0 7	1.257	5	4 0 3	0.9889	2	2 1 20
1.938	5	1 0 11	1.242	2	1 0 18	0.9808	20	3 3 0
1.814	5	1 1 10	1.228	5	4 0 5	0.9736	50	5 0 7

Additional weak lines were not recorded

*Radiation FeK_α; $\lambda = 1.936042$; filter, Mn; I/I, visual; Straumanis camera 114.6 mm. Not corrected for absorption. System, hexagonal; space group $D_{6h}^4 - P6_3/MMC$. $a_0 = 5.884_5$, $C_0 = 23.047$, unit cell = 2 ($SrFe_{12}O_{19}$).

1 showed a small endothermic peak at 685 °C characteristic for the Néel point of hematite (18). The start of an endothermic reaction was indicated at 760 °C by a slight deviation which changed to strongly endothermic at 850 °C and reached a peak at 890 °C. The reaction (formation of sodium ferrate $Na_2Fe_2O_4$) was completed at 940 °C.

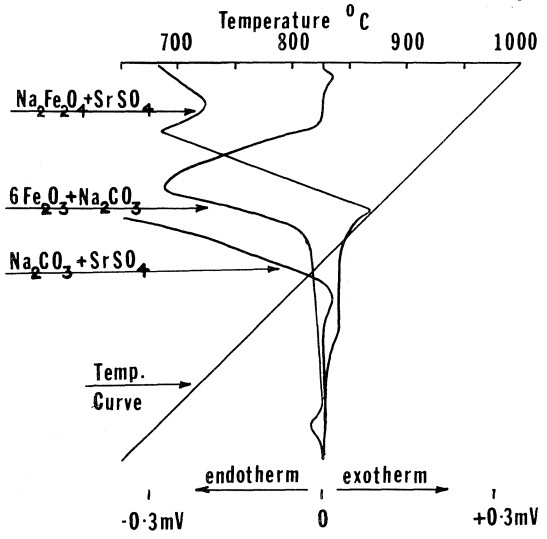

FIG. 1. DTA curves of $Na_2Fe_2O_4 + SrSO_4$, $Na_2CO_3 + SrSO_4$, and $6Fe_2O_3 + Na_2CO_3$.

A small exothermic peak occurred at 980 °C. Because no counterpart to this peak was observed on cooling and because a similar peak appeared also with prefired ($5Fe_2O_3 + Na_2Fe_2O_4$) used as a standard, the possibility of a reversible phase transformation had to be excluded. A feasible explanation for this peak would be the formation of sodium–iron oxide $Na_{10}Fe_{16}O_{29}$ (19).

In the sample ($Na_2CO_3 + SrSO_4$) (Fig. 1), a slightly exothermic reaction started at 740 °C and reached a small flat peak at 780 °C. At 800 °C the reaction became strongly endothermic.

The DTA curve of the ($Na_2Fe_2O_4 + SrSO_4$) sample (Fig. 1) showed the start of an exothermic reaction at 700 °C with a further exothermic deviation at 765 °C. A sharp exothermic peak and a sudden change to endothermic occurred at 870 °C followed by a sharp endothermic peak at 940 °C with a change of direction to exothermic. Around 965 °C the direction gradually changed back to endothermic again.

These results indicated that the reaction between sodium ferrate and strontium sulfate started at 700 °C and was completed below 965 °C. The rate of the reaction increased at 765 °C and again at about 850 °C. The endothermic trend between 870 and 940 °C was explained as melting of the sodium sulfate generated by the reaction and by dissolution of unreacted strontium sulfate

Can. J. Chem. Downloaded from www.nrcresearchpress.com by 210.87.254.105 on 09/05/12
For personal use only.

Can. J. Chem. Downloaded from www.nrcresearchpress.com by 210.87.254.105 on 09/05/12
For personal use only.

in the sodium sulfate melt. A part of the strontium–iron oxides produced by the reaction started dissolving in sodium sulfate above 965 °C.

The curve of the ($6Fe_2O_3 + Na_2CO_3 + SrSO_4$) sample (Fig. 2) showed a slightly endothermic reaction immediately after the Néel point of hematite. The reaction became distinctly endothermic at 800 °C and an endothermic peak was reached at 840 °C. Between 870 and 890 °C the trend of the curve gradually changed from endothermic to exothermic and a sharp exothermic peak followed at 910 °C.

With the exception of the Néel point peak of hematite the DTA curve of the sample ($5Fe_2O_3 + Na_2Fe_2O_4 + SrSO_4$) (Fig. 2) did not show any trend up to 885 °C, then at this temperature an exothermic reaction started. The exothermic peak which followed at 910 °C was considerably lower and flatter than the peak of the ($6Fe_2O_3 + Na_2CO_3 + SrSO_4$) sample. This could be explained by endothermic formation of a sodium carbonate – sodium sulfate – strontium sulfate liquid phase which was hidden in the endothermic part of the ($6Fe_2O_3 + Na_2CO_3 + SrSO_4$) curve below 870 °C and before the exothermic reaction started, whereas in the sample ($5Fe_2O_3 + Na_2Fe_2O_4 + SrSO_4$) the endothermic formation of a sodium sulfate – strontium sulfate liquid phase could not start before the melting point of sodium sulfate was reached. The endothermic formation of the liquid phase then partly overshadowed the exothermic reaction proceeding simultaneously.

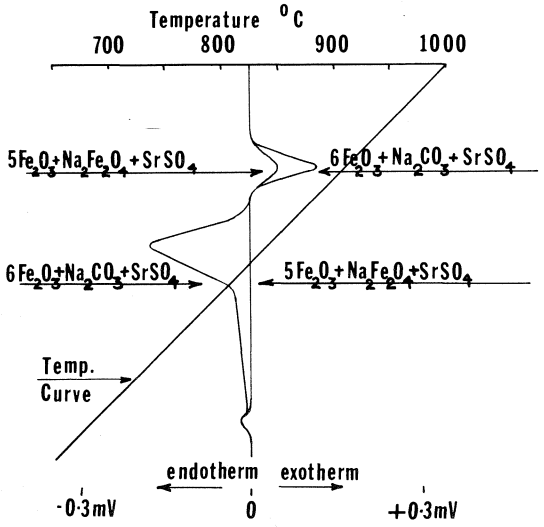

FIG. 2. DTA curves of $6Fe_2O_3 + Na_2CO_3 + SrSO_4$ and $5Fe_2O_3 + Na_2Fe_2O_4 + SrSO_4$.

The DTA curve of the ($6Fe_2O_3 + SrSO_4$) sample did not show any definite trend between the Néel point of hematite and 1050 °C. The only distinct feature on the DTA curve of the sample ($SrFe_{12}O_{19} + Na_2SO_4$) between 700 and 1100 °C was the melting of sodium sulfate indicated by a sharp endothermic peak at 885 °C.

After completion of the DTA tests the X-ray diffraction patterns of the samples ($6Fe_2O_3 + Na_2CO_3 + SrSO_4$), ($5Fe_2O_3 + Na_2Fe_2O_4 + SrSO_4$), and ($SrFe_{12}O_{19} + Na_2SO_4$) were identical.

The results of the DTA tests showed that the formation of $SrFe_{12}O_{19}$ proceeded through two or more distinct stages rather than being a one-step reaction of all three starting components. Among the three hypothetical possibilities of the first stage, *i.e.* the reactions of any two of the three starting components

[2] $Fe_2O_3 + Na_2CO_3 \rightarrow Na_2Fe_2O_4 + CO_2$

[3] $Na_2CO_3 + SrSO_4 \rightarrow SrCO_3 + Na_2SO_4$

[4] $xFe_2O_3 + 3SrSO_4 \rightarrow 3SrO{:}(x-2)Fe_2O_3 + Fe_2(SO_4)_3$

the reaction between ferric oxide and sodium carbonate [2] appeared to represent the actual reaction mechanism better than [3] or [4].

Thermo-gravimetric Analysis

The main purpose of the TGA tests was to determine the effects of temperature and composition on the rate of disappearance of sodium carbonate or strontium carbonate from the stoichiometric mixtures ($6Fe_2O_3 + Na_2CO_3 + SrSO_4$), ($6Fe_2O_3 + SrCO_3 + Na_2SO_4$), ($6Fe_2O_3 + Na_2CO_3$), and ($6Fe_2O_3 + SrCO_3$). Under the experimental conditions of the tests the disappearance of the carbonates was equivalent to the formation of carbon dioxide which in turn was represented by the decrease of weight of the samples.

The loss of carbon dioxide expressed in percentage of the total amount of the carbon dioxide present in ($6Fe_2O_3 + Na_2CO_3 + SrSO_4$) is represented graphically in Fig. 3. Two distinct types of the loss *vs.* time curves are obvious. In one group the curves at the temperatures 950, 900, and 850 °C have a similar S-shape while in the other group the curves for 800, 750, 700, and 650 °C appear almost linear. Particularly interesting are the relatively small differences in the slopes of the curves within one group in comparison with the large gap between the two groups of curves.

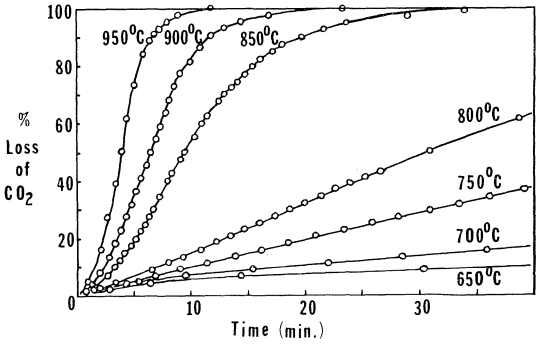

FIG. 3. Loss of CO_2 from $6Fe_2O_3 + Na_2CO_3 + SrSO_4$ *vs.* time at various temperatures.

The sudden increase in the rate of disappearance of sodium carbonate around the melting point of sodium carbonate when the solid–solid reaction changed to solid–liquid reaction was interpreted as an indication that the activation energy of reaction 2 decreased between 800 and 850 °C.

The results of the TGA tests on the samples ($6Fe_2O_3 + Na_2CO_3$), ($6Fe_2O_3 + Na_2CO_3 + SrSO_4$), ($6Fe_2O_3 + SrCO_3$), and ($6Fe_2O_3 + SrCO_3 + Na_2SO_4$) at 700 and 900 °C are shown in Fig. 4. The reaction of strontium carbonate with hematite in the ($6Fe_2O_3 + SrCO_3$) samples proceeded at a considerably slower rate than the reactions in all the other samples tested at the same temperature. This together with the similarity between the reaction rates observed in ($6Fe_2O_3 + Na_2CO_3$) and ($6Fe_2O_3 + Na_2CO_3 + SrSO_4$) was considered an additional proof that the initial stage of reaction 1 was reaction 2.

The formation of strontium hexaferrite in the ($6Fe_2O_3 + SrCO_3 + Na_2SO_4$) sample apparently proceeded first through a stage during which

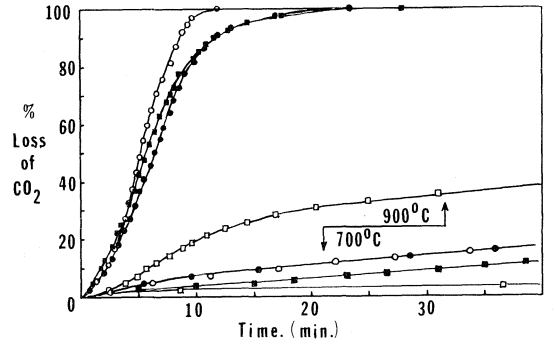

FIG. 4. Loss of CO_2 from samples ○, ●, □, and ■ *vs.* time at 700 and 900 °C. ○, $6Fe_2O_3 + Na_2CO_3$; ●, $6Fe_2O_3 + Na_2CO_3 + SrSO_4$; □, $6Fe_2O_3 + SrCO_3 + Na_2SO_4$.

small amounts of strontium sulfate and sodium carbonate were produced by the reversible reaction.

[5] $Na_2CO_3 + SrSO_4 \rightleftharpoons Na_2SO_4 + SrCO_3$

This reaction could not reach equilibrium as sodium carbonate and strontium sulfate were continuously removed from the system by the reaction 1.

The difference between the rates of the reactions in the ($6Fe_2O_3 + SrCO_3 + Na_2SO_4$) and ($6Fe_2O_3 + Na_2CO_3 + SrSO_4$) samples at 700 °C was explained by a presumed difference between the rates of the reactions 2 and 5. At 900 °C, above the melting point of sodium sulfate, the rate of reaction 5 increased sufficiently to become approximately equal to the rate of [2] and the difference between the reaction rates observed on the two samples practically disappeared.

Identification of Intermediate Phases

The samples from TGA were used for qualitative identification of intermediate phases by X-ray diffractometry and for quantitative chemical analysis. The effect of heating time on the disappearance of hematite and appearance of strontium hexaferrite in the ($6Fe_2O_3 + Na_2CO_3 + SrSO_4$) samples fired to 850 °C or higher became evident from the change in the relative intensities of the hematite and hexaferrite reflections of the X-ray diffraction patterns. The samples fired to lower temperatures showed little change in their diffraction patterns even after prolonged heating. The weight loss of a sample fired at 700 °C for 100 h was equal to the stoichiometric amount of carbon dioxide generated by reaction 1 and the amount of sodium sulfate separated from the sample by leaching with water was also in agreement with the stoichiometry. The sample was slightly ferrimagnetic, but its X-ray diffraction pattern showed mainly hematite lines, with intensities similar to those of an unfired sample and only a few weak reflections indicative of the hypothetical '$SrFe_2O_4$' (ASTM 1-1027).

An assumption that the second stage of reaction 1 is

[6] $Na_2Fe_2O_4 + SrSO_4 \rightarrow$ '$SrFe_2O_4$' $+ Na_2SO_4$

was supported by a remarkable similarity between the X-ray diffraction patterns of the ($6Fe_2O_3 + Na_2CO_3 + SrSO_4$) sample fired at 700 °C for 100 h and leached with water and the pattern of a mixture prepared from a ($Fe_2O_3 + Na_2CO_3 +$

Can. J. Chem. Downloaded from www.nrcresearchpress.com by 210.87.254.105 on 09/05/12
For personal use only.

Can. J. Chem. Downloaded from www.nrcresearchpress.com by 210.87.254.105 on 09/05/12
For personal use only.

$SrSO_4$) sample, prefired at 950 °C for 30 min and leached with water, and an equivalent of ($5Fe_2O_3$) added in the form of Fe_2O_3 precalcined at 700 °C. Similar X-ray diffraction pattern was obtained from a mixture of ($5Fe_2O_3$) and '$SrFe_2O_4$', the '$SrFe_2O_4$' prepared by heating an equimolar mixture of $SrCO_3$ and Fe_2O_3 at 900 °C for 60 h with intermittent homogenization every 12 h. Thus '$SrFe_2O_4$' appeared to be the intermediate phase in the formation of $SrFe_{12}O_{19}$.

In ASTM 1-1027 '$SrFe_2O_4$' was classified as hexagonal, in ref. 12 as orthorhombic. Although claims of preparing '$SrFe_2O_4$' and identifying it as a single phase were made occasionally, *e.g.* by Beretka and Brown (13), the existence of '$SrFe_2O_4$' as a single phase has not been acknowledged by most researchers in the Sr–Fe–O system. For the phase between $SrFeO_{2.5+x}$ and $SrFe_{12}O_{19}$, Kanamaru and Kiriyama (14) and Goto and Takahashi (15) proposed the composition approximately '$Sr_3Fe_4O_9$' (Sr/Fe ratio 0.75); this was later denied by Kanamaru *et al.* (16), who suggested that '$Sr_3Fe_4O_9$' is a mixture of $SrFeO_{2.5+x}$ and '$Sr_4Fe_6O_{13}$' (Sr/Fe ratio 0.67), whereas earlier Batti (17), probably unknown to the former, suggested the formula $Sr_7Fe_{10}O_{22}$ (Sr/Fe ratio 0.7) and identified both '$Sr_4Fe_6O_{13}$' and '$SrFe_2O_4$' as mixtures of $Sr_7Fe_{10}O_{22}$ and $SrFe_{12}O_{19}$.

To clarify this matter a series of samples was prepared by mixing $SrCO_3$ and Fe_2O_3 in the ratios corresponding to Sr/Fe = 0.50, 0.60, 0.67, and 0.70. The samples were fired at 900 °C for 12 h, homogenized by crushing to pass 200 mesh, then the firing and homogenization were repeated until the X-ray diffractograms of the samples did not show any further changes. Another series was processed similarly at 1000 °C and a third series at 1200 °C. After the initial firing the X-ray diffractograms of all samples were very similar, after the final firing all samples had the same basic pattern of the (Sr/Fe = 0.7) sample corresponding to the pattern assigned to '$Sr_4Fe_6O_{13}$' in ref. 16. Besides this pattern, the samples (Sr/Fe = 0.5, 0.6, and 0.67) showed similar foreign reflections with intensities decreasing inversely to the Sr/Fe ratio. The diffractograms of the (Sr/Fe = 0.5) samples corresponded roughly to ASTM 1-1027, but numerous splittings were obvious (*e.g.* the strongest reflection in ASTM 1-1027, d = 2.75 Å, split into three separate reflection d = 2.782, 2.765, and 2.734 Å; this was explained by the relatively short molybdenum radiation on which the data in ASTM 1-1027 were based).

Finally each sample was subjected to leaching in hot 10% nitric acid with magnetic stirring for 30 min. The undissolved particles from all samples appeared strongly ferrimagnetic, their amounts were barely visible in the (Sr/Fe = 0.7) samples but those from the other samples were sufficient for mass balance calculation and for X-ray diffraction analysis which in all cases showed the pattern of $SrFe_{12}O_{19}$. The leaching acids were analyzed for strontium and iron, the Sr/Fe ratio in all cases was close to 0.7. The results of mass balance calculations were in good agreement with the assumption that the samples were mixtures of two phases, the $SrFe_{12}O_{19}$ phase which is only slightly soluble in nitric acid, and a second phase soluble in nitric acid. This second phase is better represented by the formula $Sr_7Fe_{10}O_{22}$ (17) than by the formula $Sr_4Fe_6O_{13}$ (16). The intermediate product '$SrFe_2O_4$' was thus identified as a stoichiometric mixture ((5/37)$Sr_7Fe_{10}O_{22}$ + (2/37)-$SrFe_{12}O_{19}$).

The Effect of Sodium Sulfate

The effect of sodium sulfate on completion of the reaction

$$[7]\quad 5Fe_2O_3 + (5/37)Sr_7Fe_{10}O_{22} + (2/37)SrFe_{12}O_{19} \rightarrow SrFe_{12}O_{19}$$

was studied on the stoichiometric mixtures ($5Fe_2O_3$ + (5/37)$Sr_7Fe_{10}O_{22}$ + (2/37)$SrFe_{12}O_{10}$) and ($5Fe_2O_3$ + (5/37)$Sr_7Fe_{10}O_{22}$ + (2/37)-$SrFe_{12}O_{10}$ + Na_2SO_4) prepared by mixing equimolar ($SrCO_3$ + Fe_2O_3) samples, prefired to 1200 °C, with additional ferric oxide or with ferric oxide and sodium sulfate in proper molar ratios, and in parallel experiments on samples prepared from prefired (Fe_2O_3 + Na_2CO_3 + $SrSO_4$) mixtures and additional ferric oxide. These samples were fired to 850, 900, or 950 °C for various periods of time and then examined by X-ray diffractometry. The intensities of hematite reflections decreased and the intensities of hexaferrite reflections increased at a considerably faster rate in the samples containing sodium sulfate than in the samples without sodium sulfate. This was particularly apparent on the samples fired above the melting point of sodium sulfate.

This was explained by the action of molten sodium sulfate as a transfer agent for $SrSO_4$, Na_2O, and SrO generated by the presumed reactions

[8] $Sr_7Fe_{10}O_{22} + 7Na_2SO_4 \rightleftharpoons 7SrSO_4 + 5Na_2Fe_2O_4 + 2Na_2O$

and

[9] $SrSO_4 + Na_2O \rightleftharpoons Na_2SO_4 + SrO$

The Na_2SO_4–$SrSO_4$–Na_2O–SrO liquid phase thus formed diffused into the neighboring unreacted ferric oxide with which it reacted according to

[10] $Na_2O + Fe_2O_3 \rightarrow Na_2Fe_2O_4$

and [6]. The chain of reactions 8, 9, 10, and 6 continued until completion of [7]. This assumption was confirmed by analysis of the molten phase poured off a ($Fe_2O_3 + Na_2CO_3 + SrSO_4$) sample heated to 1200 °C for 1 h. The composition of the phase was approximately $27Na_2SO_4$:$3SrSO_4$:$1(Sr,Na_2)O$, which is substantially below the solubility of strontium sulfate in sodium sulfate at 1200 °C, approximately represented by the ratio $10Na_2SO_4$:$11SrSO_4$. The absence of iron in the molten phase poured off the ($Fe_2O_3 + Na_2CO_3 + SrSO_4$) sample was in agreement with the conclusion that the diffusion controlled reactions in the Fe_2O_3–Na_2O–$SrSO_4$ system were based on diffusion of strontium and sodium ions rather than on diffusion of iron ions.

Proposed Reaction Mechanism

The formation of $SrFe_{12}O_{19}$ in the $6Fe_2O_3$–Na_2CO_3–$SrSO_4$ system above 650 °C according to the overall reaction 1 proceeds in three major stages, the first of which is the endothermic reaction 2, the formation of carbon dioxide and sodium ferrate from equimolar amounts of ferric oxide and sodium carbonate, the second stage, simultaneous with the first stage is the exothermic reaction 6 during which equimolar amounts of sodium ferrate and strontium sulfate form sodium sulfate and the strontium–iron oxides $Sr_7Fe_{10}O_{22}$ and $SrFe_{12}O_{19}$, followed by the third stage, a complex chain of reactions formally summarized as the exothermic reaction 7. The chain of reactions expressed summarily as [7] include the reaction 8, the products of which in part react according to [6] while the remaining strontium sulfate and sodium oxide dissolve in sodium sulfate and by diffusion to unreacted ferric oxide react according to [10] and [6].

The first stage starts at about 650 °C and proceeds very slowly at the temperatures below the melting point of sodium carbonate (851 °C). Around 850 °C the reaction rate increases substantially. In the second stage, the rate of the reaction 6, *per se* faster than the rate of the first stage reaction 2, is controlled by the rate of [2]. In the third stage the rate is controlled by the diffusion of sodium oxide and strontium sulfate towards the unreacted ferric oxide. The diffusion is facilitated by the formation of a Na_2SO_4–$SrSO_4$–Na_2O–SrO liquid phase at temperatures near the melting point of sodium sulfate (884 °C).

The completion of the overall reaction 1 depends on temperature, homogeneity, and grain size of the components. At 700 °C the reaction does not proceed beyond the second stage, at 850 °C it progresses into the third stage without reaching completion, and at 900 °C the completion requires 30 min to several hours depending on homogeneity and grain size. The effect of homogeneity and grain size on the completion of the reaction decreases gradually as the firing temperature exceeds 1000 °C.

Region of $SrFe_{12}O_{19}$ in the Fe_2O_3–Na_2O–$SrSO_4$ System

The proposed reaction mechanism and the actual yields of $SrFe_{12}O_{19}$ from the ($xFe_2O_3 + yNa_2CO_3 + zSrSO_4$) mixtures discussed earlier were applied to formulation of mathematical models simulating the formation of $SrFe_{12}O_{19}$ from any x:y:z ratio. The experimental yields of $SrFe_{12}O_{19}$ from the samples subjected to the standard 1 h firing at 1200 °C were found in good agreement with the yields computed by the model represented in flow-chart form in Fig. 5. Substitution of Na_2CO_3 with equivalent amounts of NaOH or other Na_2O precursors did not affect the yield of $SrFe_{12}O_{19}$.

The best agreement between the theoretical and the experimental yield was found with the 6:1:1 molar ratio where no acid leaching was required and consequently no strontium hexaferrite was lost by dissolution. The effect of the leaching with acid was demonstrated on the x:1:1 molar ratios where the amount of the acid necessary for the decomposition of $Sr_7Fe_{10}O_{22}$ increased with the decreasing value of x, *e.g.* the molar ratios 4:1:1, 2:1:1, and 1:1:1.

Very good agreement between the theoretical and the experimental yields, around 95%, was observed on the ratios 7:4:1, 6:3:1, and 7:3:1. The samples based on these ratios melted during the firing and the strontium hexaferrite phase separated from these samples was in the form of

Can. J. Chem. Downloaded from www.nrcresearchpress.com by 210.87.254.105 on 09/05/12
For personal use only.

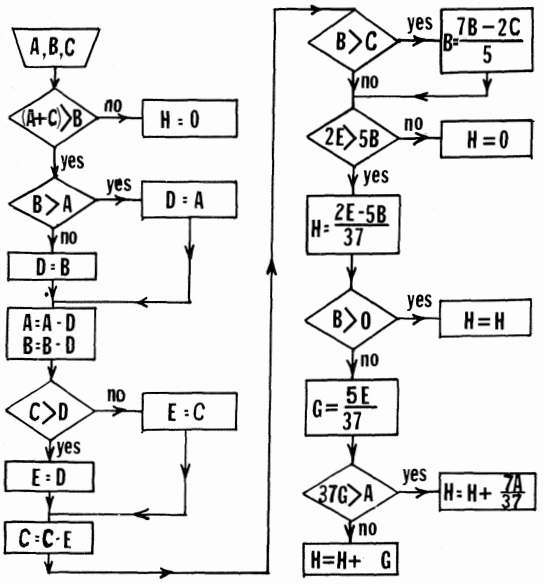

FIG. 5. Flow chart for computation of the yield of $SrFe_{12}O_{19}$ symbols representing molar fractions of reactants and products: *A*, Fe_2O_3; *B*, Na_2CO_3; *C*, $SrSO_4$; *D*, $Na_2Fe_2O_4$; *E*, '$SrFe_2O_4$'; *G*, $Sr_7Fe_{10}O_{22}$; and *H*, $SrFe_{12}O_{19}$.

relatively large crystals resistent to the leaching acid. The samples based on the molar ratios with $x/y \approx 2$ and $x/z > 7$ melted during the firing and the hexaferrite phase was crystalline, but the yields were generally lower, mostly in the 80–90% range, because more extensive acid leaching was necessary during the separation process. This was well demonstrated on the molar ratios $(6 + x):(1 + x):1$.

Strontium hexaferrite in the form of fine powder was separated from the $x:x:z$ molar ratios. The yields were in the range 72–78% of the theory, for z/x ranging from 0.4 to 10. The yields decreased with the increasing value of z, this was caused by the more difficult separation from the larger excesses of strontium sulfite, as was observed on the molar ratios 5:5:2, 1:1:1, 1:1:2, 1:1:4, and 1:1:10.

The combined effect of fine grain size and extensive leaching with acid was apparent on the series of the molar ratios $6:(1 + y):1$. The strontium hexaferrite phase changed with the value of y, from a crystalline powder (ratio 6:1.5:1) to large crystals (ratio 6:3:1) to very fine powder (ratio 6:6:1). The extent of the acid leaching necessary for separation increased proportionally with the value of y. The very low yield from the ratio 6:6:1 was explained by the effect of large amounts of the acid, needed to dissolve sodium ferrate, on the very fine strontium hexaferrite phase distributed evenly in the sample.

Although the main emphasis of the investigation was on the samples fired at 1200 °C, several experiments at lower firing temperatures were included in the evaluation of the strontium hexaferrite yields. The yields from the samples based on the molar ratios close to 6:1:1 and fired at 900–1000 °C were approximately the same as from the samples fired at 1200 °C.

The firing temperature had a considerable effect on the yields from the samples based on the 1:1:1 molar ratio. The yields from the samples fired at 900 °C were about 100% of the theory, compared with the 78% yields from the samples fired at 1200 °C. This difference was explained by the separation of the strontium sulfate rich liquid phase at 1200 °C which on cooling could not penetrate the compact iron-rich phase at the bottom of the crucible. Under such conditions the formation of strontium hexaferrite could not be completed. The separation of the liquid phase did not occur at lower temperatures and the conditions necessary for the formation of strontium hexaferrite were thus maintained.

On the ternary diagram of the Fe_2O_3–Na_2O–$SrSO_4$ system (Fig. 6) the region of strontium hexaferrite was represented by the area of a quadrilateral with the corner points located at the composition points 98-1-1, 1-1-98, 26-36-38, and 50-49-1 in mol% Fe_2O_3–Na_2O–$SrSO_4$.

In the terms of the relative concentrations of the original components expressed as molar ratio $xFe_2O_3:yNa_2CO_3:zSrSO_4$, the region of

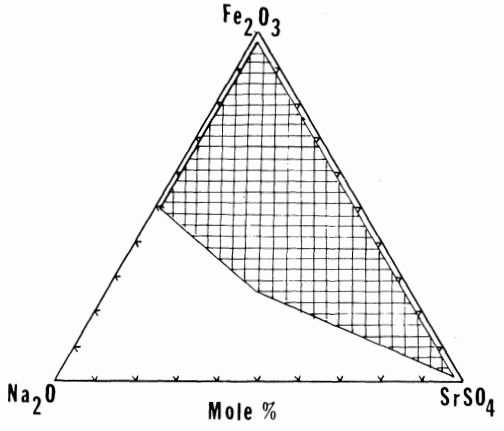

FIG. 6. Region of $SrFe_{12}O_{19}$ (squared area) in the $Fe_2O_3 + Na_2O + SrSO_4$ system.

Can. J. Chem. Downloaded from www.nrcresearchpress.com by 210.87.254.105 on 09/05/12
For personal use only.

$SrFe_{12}O_{19}$ included that area where either $x - y + z)/z \geqslant 5/7$ or where $x/y > 5/7 \geqslant x/z$.

Conclusions

Strontium–iron oxide, $SrFe_{12}O_{19}$, was found to form a stable phase within a wide concentration range of the Fe_2O_3–Na_2O–$SrSO_4$ ternary system at temperatures above 700 °C. The region of $SrFe_{12}O_{19}$ in the system after heating to 900–1200 °C was determined. Within the region of $SrFe_{12}O_{19}$ (M-type) none of the other hypothetical ferrimagnetic hexagonal oxides, namely $SrFe_{18}O_{27}$ (W-type), $Sr_2Fe_{14}O_{22}$ (Y-type), and $Sr_3Fe_{26}O_{41}$ (Z-type) were found.

The reaction mechanism of the $SrFe_{12}O_{19}$ formation was proposed and a method for calculating theoretical yields of $SrFe_{12}O_{19}$ from the molar ratios of original reactants was developed.

The X-ray diffraction pattern of $SrFe_{12}O_{19}$ was indexed and the lattice parameters were determined.

1. R. J. Routil and D. Barham. Can. J. Chem. **47**, 3919 (1969).
2. R. J. Routil and D. Barham. J. Can. Ceram. Soc. **40**, 1 (1971).
3. A. Cochardt. J. Appl. Phys. **37**, 1112 (1966).
4. R. J. Gambino and F. Leonhard. J. Am. Ceram. Soc. **44**, 221 (1961).
5. T. S. West and A. S. Sykes. Analytical applications of diamino-ethane-tetraacetic acid. British Drug Houses Ltd., Poole, England. 1956.
6. W. F. Hillebrand and G. E. F. Lundell. Applied inorganic analysis. J. Wiley and Sons, Inc., New York. 1955.
7. W. D. Townes, J. H. Fang, and A. J. Perrotta. Z. Kristallogr. **125**, 437 (1967).
8. A. Ralston and H. S. Wilf. Mathematical methods for digital computers. John Wiley and Sons, Inc., New York. 1960.
9. L. H. Brixner. J. Am. Chem. Soc. **81**, 3841 (1959).
10. V. Adelsköld. Ark. Kem. Mineral. Geol. **12A**, 1 (1938).
11. R. W. G. Wyckoff. Crystal structures. Vol. 3. 2nd Ed., J. Wiley and Sons, New York. 1965. p. 497.
12. M. Hill, H. S. Peiser, and J. R. Rait. Acta Cryst. **9**, 981 (1956).
13. J. Beretka and T. Brown. Aust. J. Chem. **24**, 237 (1971).
14. F. Kanamaru and R. Kiriyama. J. Chem. Soc. Jap. (Pure Chem. Sect.) **85**, 458 (1964).
15. Y. Goto and K. Takahashi. J. Jap. Soc. Powder Powder Metall. **17**, 193 (1971).
16. K. Kanamaru, M. Shimada, and M. Koizumi. J. Phys. Chem. Solids, **33**, 1169 (1972).
17. P. Batti. Ann. Chim. Rome, **52**, 941 (1962).
18. W. S. Bowman, Sutarno, N. F. H. Bright, and J. L. Horwood. J. Can. Ceram. Soc. **38**, 1 (1969).
19. J. Thery. Ann. Chim. Paris, **7**, 215 (1962).

Can. J. Chem. Downloaded from www.nrcresearchpress.com by 210.87.254.105 on 09/05/12
For personal use only.

The Carbon-13 Magnetic Resonance Spectrum of Propane

RODERICK E. WASYLISHEN[1]

National Institute of Arthritis, Metabolism, and Digestive Diseases, National Institutes of Health, Bethesda, Maryland 20014

AND

TED SCHAEFER

Department of Chemistry, University of Manitoba, Winnipeg, Manitoba R3T 2N2

Received April 10, 1974

RODERICK E. WASYLISHEN and TED SCHAEFER. Can. J. Chem. **52**, 3247 (1974).

The carbon-13 magnetic resonance spectra of propane and of propane-2,2-d_2 are analyzed to give $^1J(^{13}C_1,H) = 124.3_5$, $^1J(^{13}C_2,H) = 125.3_5$, $^2J(^{13}C_1,H) = -4.2_5$, $^2J(^{13}C_2,H) = -4.3_9$, $^3J(^{13}C,H) = 5.8_0$, $^3J(H,H) = 7.37_5$, $^4J(H,H) < \pm 0.18$ Hz. The deuterium isotope shift at C_2 is 0.72 ± 0.10 p.p.m. to high field.

RODERICK E. WASYLISHEN et TED SCHAEFER. Can. J. Chem. **52**, 3247 (1974).

On a analysé les spectres de résonance magnétique nucléaire du carbon-13 du propane et du propane [d_2-2,2] et l'on peut en tirer les valeurs suivantes: $^1J(^{13}C_1H) = 124.3_5$, $^1J(^{13}C_2,H) = 125.3_5$, $^2J(^{13}C_1,H) = -4.2_5$, $^2J(^{13}C_2,H = -4.3_9$, $^3J(^{13}C,H) = 5.8_0$, $^3J(H,H) = 7.37_5$, $^4J(H,H) < \pm 0.18$ Hz. L'effet isotopique du deutérium sur le déplacement chimique en position C_2 est de 0.72 ± 0.10 p.p.m. vers les hauts champs. [Traduit par le journal]

Introduction

Analysis of the carbon-13 magnetic resonance spectrum of propane yields one-, two-, and three-bond coupling constants between ^{13}C nuclei and protons. These data serve as reference values in the experimental (1, 2) and theoretical (3, 4) study of substituent effects. Combined with spectral data on propane-2,2-d_2, information is obtained about proton–proton coupling data over four bonds and about the deuterium isotope shift at carbon-2($^{13}C_2$).

Experimental

The ^{13}C resonance spectrum of propane-2,2-d_2 from Merck, Sharpe and Dohme was recorded on a 220 MHz spectrometer in the FT mode (1200 pulses, 4 points/Hz, unfiltered) on a sample consisting of ~50:50 v/v% solution in cyclohexane-d_{12}. The ^{13}C spectrum of neat propane was similarly recorded (2000 pulses at 55.32512 MHz). In order to estimate the optimum pulse delay times, the spin–lattice relaxation times of $^{13}C_1$ and $^{13}C_2$ were measured as 14.5 ± 2 and 12.3 ± 2 s, respectively. The ^{13}C spectra obtained on different occasions agreed very well and had line widths at half-height of about 0.8 Hz.

In addition, the p.m.r. spectrum of propane was measured at 220 MHz and that of propane-2,2-d_2 was recorded under conditions of deuterium decoupling.

Calculations of the coupling constants were carried out by the CNDO/2 and INDO–MO–FPT methods (3, 5) using convergence criteria described previously (4).

[1]NRCC Postdoctorate Fellow, 1972–1973.

Results and Discussion

Spectral Analysis

The ^{13}C spectrum of propane was analyzed as a composite of $A_3A_3{}^1B_2X$ and A_6B_2X spectra for C_1 and C_2, respectively, by means of the computer program LAME (6). For the $^{13}C_1(^{13}C_2)$ spectrum, 93(86) of the strongest of the 145(143) calculated transitions with a reasonable intensity were assigned, the r.m.s. deviation between calculated and observed peaks being 0.084(0.078) Hz. Correlation numbers for parameters were less than 0.08(0.20). Values of 7.37_5 Hz for $^3J(H,H)$ and 0.0 Hz for $^4J(H,H)$ were assumed in the iterations. These couplings were obtained from the p.m.r. spectra. No reasonable fit between observed and calculated spectra was obtained for a positive $^2J(^{13}C,H)$. The standard deviations of the final parameters are given in Table 1 and should be increased by a factor of 5 to obtain a realistic error limit (7). Figure 1 displays the spectrum.

A first-order analysis of the $^{13}C_1$ spectrum of propane-2,2-d_2 gave $^1J(^{13}C,H) = 124.1_5 \pm 0.2$ Hz and $^3J(^{13}C,H) = 5.7_5 \pm 0.2$ Hz. Under conditions of deuterium decoupling, the line widths in the p.m.r. spectrum of the $^{13}CH_3$ group showed that $^4J(H,H) < \pm 0.18$ Hz.

The Coupling Constants

The values of $124.3_5 + 0.1_5$ Hz for $^1J(^{13}C_1,H)$

Can. J. Chem. Downloaded from www.nrcresearchpress.com by 210.87.254.105 on 09/05/12
For personal use only.

Can. J. Chem. Downloaded from www.nrcresearchpress.com by 210.87.254.105 on 09/05/12
For personal use only.

TABLE 1. Chemical shifts and coupling constants* for $^{13}C_1$ and ^{1}H in propane† and propane-2,2-d_2

	$\nu(^{13}C_2)-\nu(^{13}C_1)$	$\nu(CH_3)-\nu(CH_2)$	$^{1}J(^{13}C_1, H)$	$^{1}J(^{13}C_2, H)$	$^{2}J(^{13}C_1, H)$	$^{2}J(^{13}C_2, H)$	$^{3}J(^{13}C, H)$	$^{3}J(H,H)$	$^{4}J(H,H)$
Propane	0.518 p.p.m. $28.6_6 \pm 0.1$ Hz	−0.435 p.p.m. 95.68 ± 0.04 Hz	124.349 (0.010)	125.352 (0.014)	−4.254 (0.014)	(−4.389) (0.007)	5.864 (0.012)	$7.37_5 \pm 0.03$	0.0 ± 0.2
Propane-2,2-d_2	-0.21 ± 0.05 p.p.m.		124.15 ± 0.2				5.75 ± 0.2		$< \pm 0.18$

*In Hz.
†Propane was measured as a neat sample while propane-2,2-d_2 was a 50 v/v% solution in cyclohexane-d_{12}.

Can. J. Chem. Downloaded from www.nrcresearchpress.com by 210.87.254.105 on 09/05/12
For personal use only.

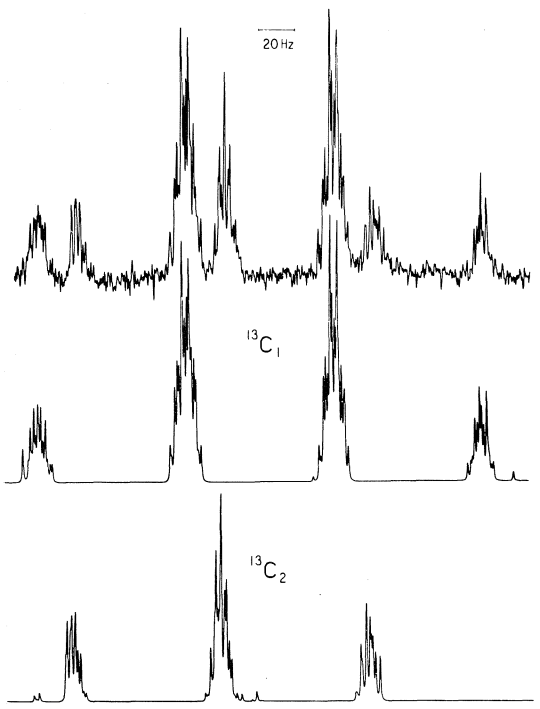

The carbon-13 magnetic resonance spectrum of neat propane at 55.325 MHz is shown together with the spectra of C_1 and C_2 calculated from the parameters in Table 1. The calculated spectra assumed as linewidth of 0.8 Hz. The analysis was performed on spectra expanded to 2 Hz/cm.

and of $125.3_5 \pm 0.1_5$ Hz for $^1J(^{13}C_2,H)$ may be compared with 125.0 ± 0.2 Hz in ethane (8, 9). $^3J(^{13}C,H)$ is $5.8_0 \pm 0.1_5$ Hz, whereas the numbers calculated by INDO are 4.26 Hz (4) for the standard, all-staggered, geometry (10) and 4.47 Hz for the microwave (11) geometry. Substituent effects have been calculated (4). The observed value may be compared with the measured values of 5.7 ± 0.1, -1.8 ± 0.1, -1.4 ± 0.2 Hz in dimethylether (12), dimethylmercury (12), and dimethylcadmium (13), respectively.

$^2J(^{13}C_1,H)$ is -4.25 ± 0.07 Hz while $^2J(^{13}C_2,H)$ is -4.39 ± 0.04 Hz in propane, indicating a similar magnitude of the substituent effects of the methyl group on $^2J(^{13}C,H)$ in the two sites symbolized by $^{13}C_1$—C—H(CH_3) and H—C—$^{13}C_2$(CH_3). In ethane, $^2J(^{13}C,H)$ is -4.8 ± 0.2 Hz (8, 9) but is $+1.1$ Hz in *sym*-tetrabromoethane (14). Taken together, these data suggest that the $^{13}C,H$ couplings observed (2) in a number of isopropyl derivatives are $^3J(^{13}C,H)$ and not $^2J(^{13}C,H)$. As these are lower in magnitude than $^3J(^{13}C,H)$ in propane itself, there exists qualitative agreement with the predicted (4) changes in $^3J(^{13}C,H)$ caused by an electronegative substituent at C_2.

The $7.37_5 \pm 0.04$ Hz for $^3J(H,H)$ lies near the values of 7.35 ± 0.02 (15) and of 7.45 ± 0.10 Hz (16) measured at 60 MHz. The CNDO/2 value is 7.48 Hz for the microwave geometry. $^4J(H,H)$ has a magnitude of less than 0.18 Hz. No negative values are known for protons in geminal methyl groups bonded to an sp^3 carbon atom (17, 18). For the microwave geometry, the CNDO/2 value is 0.02 Hz while INDO yields -0.33 Hz. For a series of *n*-propyl derivatives (19) $^4J^{H,H}$ varies between -0.05 ± 0.03 and -0.12 ± 0.03 Hz.

The Chemical Shifts

In neat propane at 220 MHz the internal proton chemical shift is 0.435 p.p.m., compared with 0.439 p.p.m. at 60 MHz (16). The $^{13}C_2$ resonance lies 0.518 p.p.m. to low field of the $^{13}C_1$ resonance in neat propane (Table 1), in good agreement with the 0.5 p.p.m. reported for a proton-decoupled ^{13}C spectrum (20). In propane-2,2-d_2, the $^{13}C_2$ shift is 0.21 p.p.m. to high field of $^{13}C_1$. Hence the deuterium isotope shift of $^{13}C_2$ is 0.72 ± 0.1 p.p.m., within the range recently reported for some hydrocarbon derivatives (21).

We are grateful to the National Research Council of Canada for financial assistance.

1. J. B. Stothers. Carbon-13 NMR spectroscopy. Academic Press, New York. 1972. Chapt. 10.
2. G. Schrumpf. Tetrahedron Lett. 3421 (1972).
3. J. A. Pople and D. L. Beveridge. Approximate molecular orbital theory. McGraw-Hill Book Co., New York, 1970.
4. R. Wasylishen and T. Schaefer. Can. J. Chem. **51**, 961 (1973).
5. J. A. Pople, J. W. McIver, Jr., and N. S. Ostlund. J. Chem. Phys. **49**, 2965 (1968).
6. C. W. Haigh and J. M. Williams. J. Mol. Spectrosc. **32**, 398 (1969).
7. S. Castellano, C. Sun, and R. Kostelnik. Tetrahedron Lett. 5205 (1967).
8. D. M. Graham and C. E. Holloway. Can. J. Chem. **41**, 2114 (1963).
9. R. M. Lynden-Bell and N. Sheppard. Proc. Roy. Soc. A**269**, 385 (1962).
10. J. A. Pople and M. Gordon. J. Am. Chem. Soc. **89**, 4254 (1967).
11. D. R. Lide, Jr. J. Chem. Phys. **33**, 1514 (1960).
12. H. Dreeskamp and K. Hildenbrand, and G. Pfisterer. Mol. Phys. **17**, 429 (1969).

13. H. DREESKAMP and K. HILDENBRAND. Z. Naturforsch **23**a, 940 (1968).
14. R. FREEMAN and W. A. ANDERSON. J. Chem. Phys. **39**, 806 (1963).
15. R. C. FERGUSON and D. W. MARQUARDT. J. Chem. Phys. **41**, 2087 (1964).
16. P. L. CORIO and L. C. HIRST. J. Chem. Educ. **46**, 345 (1969).
17. H. DREESKAMP. Z. Phys. Chem. (Frankfurt), **59**, 321 (1968).
18. D. J. SARDELLA. J. Mol. Spectrosc. **31**, 70 (1969); J. Am. Chem. Soc. **94**, 5206 (1973).
19. G. SCHRUMPF. J. Magn. Resonance, **6**, 243 (1972).
20. D. M. GRANT and E. G. PAUL. J. Am. Chem. Soc. **86**, 2984 (1964).
21. G. C. LEVY and J. D. CARGIOLI. J. Magn. Resonance, **6**, 143 (1972).

Can. J. Chem. Downloaded from www.nrcresearchpress.com by 210.87.254.105 on 09/05/12
For personal use only.

The Methyl Ethers of 2-Amino-2,6-dideoxy-D-galactopyranose (D-Fucosamine)[1]

MALCOLM B. PERRY AND VIRGINIA DAOUST

Division of Biological Sciences, National Research Council of Canada, Ottawa, Canada K1A 0R6

Received June 12, 1974

MALCOLM B. PERRY and VIRGINIA DAOUST. Can. J. Chem. **52**, 3251 (1974).

The 3-, 4-, and 3,4-dimethyl ethers of 2-amino-2,6-dideoxy-D-galactose (D-fucosamine) have been synthesized. 2-Amino-2,6-dideoxy-3,4-di-*O*-methyl-D-galactose was made by the methylation of methyl 2-acetamido-2,6-dideoxy-α-D-galactopyranoside to its 3,4-di-*O*-methyl derivative which was hydrolyzed to yield pure 2-amino-2,6-dideoxy-3,4-di-*O*-methyl-D-galactose hydrochloride. 2-Amino-2,6-dideoxy-3-*O*-methyl-D-galactose was made from methyl 2-acetamido-2-deoxy-3-*O*-methyl-α-D-galactopyranoside by conversion of its 6-sulfonate to the 6-deoxy-6-iodo derivative, followed by reduction to the 6-deoxy derivative which, on hydrolysis, gave 2-amino-2,6-dideoxy-3-*O*-methyl-D-galactose hydrochloride. 2-Amino-2,6-dideoxy-4-*O*-methyl-D-galactose was made from methyl 2-acetamido-2-deoxy-3,6-di-*O*-(*p*-tolylsulfonyl)-α-D-galactopyranoside which was methylated to yield the 4-*O*-methyl derivative and subsequent conversion of the latter compound to its 6-deoxy derivative, via its 6-deoxy-6-iodo derivative, followed by detosylation, gave methyl 2-acetamido-2,6-dideoxy-4-*O*-methyl-α-D-galactopyranoside convertible by acid hydrolysis to 2-amino-2,6-dideoxy-4-*O*-methyl-D-galactose hydrochloride.

MALCOLM B. PERRY et VIRGINIA DAOUST. Can. J. Chem. **52**, 3251 (1974).

On a synthétisé les éthers méthyl-3 et -4 ainsi que diméthyl-3,4 de l'amino-2 didéoxy-2,6 D-galactose (D-fucosamine). On a préparé l'amino-2 didéoxy-2,6 di-*O*-méthyl-3,4 D-galactose par méthylation de l'acétamido-2 didéoxy-2,6 α-D-galactopyrannoside de méthyle qui fournit le dérivé di-*O*-méthylé en positions 3 et 4; l'hydrolyse de ce dernier conduit au chlorhydrate de l'amino-2 didéoxy-2,6 di-*O*-méthyl-3,4 D-galactose. On a préparé l'amino-2 didéoxy-2,6 *O*-méthyl-3 D-galactose à partir de l'acétamido-2 déoxy-2 *O*-méthyl-3 α-galactopyrannoside de méthyle sous forme de sulfonate en position 6 qui permet d'obtenir le dérivé déoxy-6 iodo-6; une réduction de ce dernier dérivé forme le déoxy-6 qui par hydrolyse donne le chlorhydrate de l'amino-2 didéoxy-2,6 *O*-méthyl-3 D-galactose. On a préparé l'amino-2 didéoxy-2,6 *O*-méthyl-4 D-galactose à partir de l'acétamido-2 déoxy-2 di-*O*-(*p*-tolylesulfonyl)-3,6 α-D-galactopyrannoside de méthyle qui par méthylation conduit au dérivé *O*-méthyl-4; la transformation subséquente de ce dernier composé fournit successivement le dérivé déoxy-6 iodo-6 puis le dérivé déoxy-6 et finalement par détosylation l'acétamido-2 didéoxy-2,6 *O*-méthyl-4 α-D-galactopyrannoside de méthyle qui peut être transformé par hydrolyse en chlorhydrate de l'amino-2 didéoxy-2,6 *O*-méthyl-4 D-galactose. [Traduit par le journal]

Both 2-amino-2,6-dideoxy-D-galactose (D-fucosamine) (1–6) and 2-amino-2,6-dideoxy-L-galactose (L-fucosamine) (7–9) are components of some bacterial polysaccharides. The methyl ethers of 2-amino-2,6-dideoxy-D-galactopyranose were prepared in this laboratory for use as reference compounds in the identification of these compounds which have been isolated from the hydrolysis products of methylated polysaccharides currently under study.

2-Amino-2,6-dideoxy-3-*O*-methyl-D-galactose was synthesized from methyl 2-acetamido-2-deoxy-3-*O*-methyl-α-D-galactopyranoside (10). Monotosylation of the latter compound afforded methyl 2-acetamido-2-deoxy-3-*O*-methyl-6-*O*-(*p*-tolylsulfonyl)-α-D-galactopyranoside which on acetylation afforded methyl 2-acetamido-4-*O*-acetyl-2-deoxy-3-*O*-methyl-6-*O*-(*p*-tolylsulfonyl)-α-D-galactopyranoside. On heating this compound with sodium iodide in acetone solution it was converted to methyl 2-acetamido-4-*O*-acetyl-2,6-dideoxy-6-iodo-3-*O*-methyl-α-D-galactopyranoside which, on catalytic reduction gave crystalline methyl 2-acetamido-4-*O*-acetyl-2,6-dideoxy-3-*O*-methyl-α-D-galactopyranoside. 2-Amino-2,6-dideoxy-3-*O*-methyl-D-galactose hydrochloride was obtained in chromatographically pure form by the hydrolysis of the methyl 2-acetamido-4-*O*-acetyl-2,6-dideoxy-3-*O*-methyl-α-D-galactopyranoside with hot dilute hydrochloric acid.

2-Amino-2,6-dideoxy-4-*O*-methyl-D-galactose

[1]NRCC No. 14168.

Can. J. Chem. Downloaded from www.nrcresearchpress.com by 210.87.254.5 on 09/05/12
For personal use only.

Can. J. Chem. Downloaded from www.nrcresearchpress.com by 210.87.254.5 on 09/05/12
For personal use only.

was made from methyl 2-acetamido-2-deoxy-3-*O*-(*p*-tolylsulfonyl)-α-D-galactopyranoside (11). Monotosylation of this latter compound afforded methyl 2-acetamido-2-deoxy-3,6-di-*O*-(*p*-tolylsulfonyl)-α-D-galactopyranoside which on treatment with methyl iodide and silver oxide gave methyl 2-acetamido-2-deoxy-4-*O*-methyl-3,6-di-*O*-(*p*-tolylsulfonyl)-α-D-galactopyranoside. On heating this compound with sodium iodide in acetone solution it was converted to methyl 2-acetamido-2,6-dideoxy-6-iodo-4-*O*-methyl-3-*O*-(*p*-tolylsulfonyl)-α-D-galactopyranoside which on catalytic reduction gave methyl 2-acetamido-2,6-dideoxy-4-*O*-methyl-3-*O*-(*p*-tolylsulfonyl)-α-D-galactopyranoside which could be subsequently reduced in aqueous methanol by sodium amalgam to yield crystalline methyl 2-acetamido-2,6-dideoxy-4-*O*-methyl-α-D-galactopyranoside. The methyl 2-acetamido-2,6-dideoxy-4-*O*-methyl-α-D-galactopyranoside was hydrolyzed with hot dilute hydrochloric acid to yield chromatographically pure 2-amino-2,6-dideoxy-4-*O*-methyl-D-galactose hydrochloride.

2-Amino-2,6-dideoxy-3,4-di-*O*-methyl-D-galactose hydrochloride was prepared directly from 2-acetamido-2,6-dideoxy-D-galactose (12). 2-Acetamido-2,6-dideoxy-D-galactose with boiling methanolic hydrogen chloride gave crystalline methyl 2-acetamido-2,6-dideoxy-α-D-galactopyranoside which on treatment with methyl iodide and silver oxide was converted to methyl 2-acetamido-2,6-dideoxy-3,4-di-*O*-methyl-α-D-galactopyranoside. Hydrolysis of this latter compound with hot dilute hydrochloric acid gave 2-amino-2,6-dideoxy-3,4-di-*O*-methyl-D-galactose hydrochloride.

The chromatographic properties of the 3-, 4-, and 3,4-dimethyl ethers of 2-amino-2,6-dideoxy-D-galactopyranose hydrochloride and their corresponding *N*-acetyl derivatives are recorded together with the gas chromatographic relative retention times of the corresponding acetylated 2-acetamido-2,6-dideoxygalactitol methyl ethers prepared by borohydride reduction and acetylation of the parent glycoses (13, 14).

Experimental

Paper chromatography was performed by the descending method (15) on Whatman No. 1 filter paper using either (A) pyridine – ethyl acetate – water (2:5:5 v/v, top layer) or (B) 1-butanol – ethanol – water (4:1:5 v/v, top layer) as the mobile phase. Glycoses were detected with either (*a*) 2% silver nitrate in acetone followed by 3% sodium hydroxide in ethanol (16), (*b*) 2% *p*-anisidine hydrochloride in ethanol (17), or (*c*) 2% ninhydrin in acetone. The rates of movement of the glycoses are quoted relative to L-rhamnose (R_{Rh}) or to 2-amino-2-deoxy-D-glucose hydrochloride (R_{GN}).

Thin-layer chromatography (t.l.c.) was done on silica gel G coated plates using benzene–methanol (5:1 v/v) and compounds located by heating developed plates, sprayed with 10% sulfuric acid in ethanol, at 130 °C for 20–30 min; mobilities are quoted relative to the solvent front (R_f).

Gas–liquid partition chromatography (g.l.p.c.) was carried out using a Hewlett-Packard model 402 chromatograph with a hydrogen flame detector and fitted with glass U-tubes (4 ft × 6 mm × 3 mm internal diameter) packed with either (A) 10% (w/w) neopentylglycol sebacate polyester on 80–100 mesh acid washed Chromosorb W or (B) 3% (w/w) ECNSS-M on 100–120 mesh Gas-Chrom Q (Applied Science Labs., State College, Pa.) Retention times are quoted relative to 2-acetamido-2-deoxy-1,3,4,5,6-penta-*O*-(trimethylsilyl)-D-glucitol (T_{GN}) or to penta-*O*-acetyl-L-arabinitol (T_A).

Melting points were determined on a Fisher-Johns apparatus and are corrected. Solutions were concentrated under reduced pressure and below 40 °C. Optical rotations were determined at 20 °C using a Perkin-Elmer 141 polarimeter.

(1) 2-Amino-2,6-dideoxy-3-O-methyl-D-galactose hydrochloride

(a) Methyl 2-Acetamido-4-O-acetyl-2-deoxy-3-O-methyl-6-O-(p-tolylsulfonyl)-α-D-galactopyranoside

To a solution of methyl 2-acetamido-2-deoxy-3-*O*-methyl-α-D-galactopyranoside (10) (1.24 g) in dry pyridine (18 ml) was added a solution of *p*-toluenesulfonyl chloride (1.86 g) in dry pyridine (12 ml), both solutions having been previously cooled to −15 °C. The stirred mixture was kept at 2 °C for 18 h and at 20 °C for 12 h. The excess chloride was destroyed by the addition of ice (2–3 g) and, after 1 h, the solution was poured into ice water (100 ml) containing acetic acid (15 ml). The reaction product was extracted with chloroform (3 × 70 ml) and the extract after successive washings with cold *N* hydrochloric acid, saturated sodium bicarbonate solution, and water, was dried (anhydrous Na_2SO_4) and the chloroform solution was concentrated to a syrup (2.5 g). The syrup (2.5 g), which failed to crystallize from methanol solution, was dissolved in dry pyridine (6 ml) and, following the addition of acetic anhydride (3.4 ml), the mixture was kept at 75 °C for 1 h. The cooled reaction mixture was poured into ice water (100 ml) containing acetic acid (10 ml) and, after 1 h, the product was extracted with chloroform (2 × 50 ml). The chloroform solution was washed successively with water, *N* sulfuric acid, sodium bicarbonate solution, and water and the dried (anhydrous Na_2SO_4) chloroform solution was concentrated to a syrup (2.7 g). The product was dissolved in a minimum amount of hot methanol and on keeping this solution at 2 °C it afforded crystalline methyl 2-acetamido-4-*O*-acetyl-2-deoxy-3-*O*-methyl-6-*O*-(*p*-tolylsulfonyl)-α-D-galactopyranoside (2.2 g) which had m.p. 147–148 °C and $[\alpha]_D$ +103° (*c*, 0.25 in chloroform) and on t.l.c. gave a single spot with R_f 0.41.

Anal. Calcd. for $C_{19}H_{27}NO_9S$: C, 51.22; H, 6.11; N, 3.14; S, 7.19. Found: C, 51.40; H, 6.21; N, 3.28; S, 7.31.

Can. J. Chem. Downloaded from www.nrcresearchpress.com by 210.87.254.5 on 09/05/12
For personal use only.

(b) Methyl 2-Acetamido-4-O-acetyl-2,6-dideoxy-6-iodo-3-O-methyl-α-D-galactopyranoside

Methyl 2-acetamido-4-*O*-acetyl-2-deoxy-3-*O*-methyl-6-*O*-(*p*-tolylsulfonyl)-α-D-galactopyranoside (2 g) and sodium iodide (2 g) in dry acetone (35 ml) were heated in a sealed glass tube at 100 °C for 5 h. The crystalline sodium *p*-toluenesulfonate was filtered off from the cooled reaction mixture and the filtrate, after dilution with chloroform (150 ml), was washed with 3% sodium thiosulfate solution (15 ml), with water (20 ml), and the dried (anhydrous Na_2SO_4) solution was concentrated to a syrup (1.70 g). The product was dissolved in hot methanol (*ca.* 4 ml) and, on keeping the solution at 0 °C, it gave crystalline methyl 2-acetamido-4-*O*-acetyl-2,6-dideoxy-6-iodo-3-*O*-methyl-α-D-galactopyranoside (1.46 g) which had m.p. 81–82 °C and $[\alpha]_D$ +150° (*c*, 0.35 in chloroform) and gave a single spot on t.l.c. with R_f 0.43.

Anal. Calcd. for $C_{12}H_{20}INO_6$: C, 35.92; H, 5.02; N, 3.49; I, 31.63. Found: C, 36.03; H, 5.23; N, 3.35; I, 31.45.

(c) Methyl 2-Acetamido-4-O-acetyl-2,6-dideoxy-3-O-methyl-α-D-galactopyranoside

Methyl 2-acetamido-4-*O*-acetyl-2,6-dideoxy-6-iodo-3-*O*-methyl-α-D-galactopyranoside (1.3 g) was dissolved in methanol (28 ml) containing triethylamine (0.4 ml) and, following the addition of fresh Raney nickel (3 g), the mixture was shaken vigorously for 5 h under a hydrogen atmosphere of 50 p.s.i. pressure. The filtered reaction mixture was concentrated to a syrup which was dissolved in a methanol–ether mixture. On keeping the solution at 2 °C, crystalline methyl 2-acetamido-4-*O*-acetyl-2,6-dideoxy-3-*O*-methyl-α-D-galactopyranoside (0.71 g) was obtained which had m.p. 147–148 °C, $[\alpha]_D$ +104.2° (*c*, 0.92 in chloroform), and gave a single spot on t.l.c. with R_f 0.42.

Anal. Calcd. for $C_{12}H_{21}NO_6$: C, 52.35; H, 7.69; N, 5.09; OMe, 22.55. Found: C, 52.30; H, 7.70; N, 5.08; OMe, 21.99.

(d) 2-Amino-2,6-dideoxy-3-O-methyl-D-galactose Hydrochloride

Methyl 2-acetamido-4-*O*-acetyl-2,6-dideoxy-3-*O*-methyl-α-D-galactopyranoside (0.5 g) was hydrolyzed with 3 *N* hydrochloric acid (10 ml) at 100 °C for 3 h and the solution was concentrated to dryness. The residue was dissolved in warm methanol, decolorized with a little charcoal, filtered, and on concentration afforded 2-amino-2,6-dideoxy-3-*O*-methyl-D-galactose hydrochloride (0.27 g) as a syrup which had $[\alpha]_D$ +85.3° (*c*, 1.1 in water) and on paper chromatography (solvent B) it gave a single ninhydrin positive spot with R_{GN} 1.69.

Anal. Calcd. for $C_7H_{16}ClNO_4$: C, 39.35; H, 7.55; Cl, 16.59; N, 6.56; OMe, 14.52. Found: C, 39.25; H, 7.50; Cl, 16.70; N, 6.66; OMe, 14.37.

(2) 2-Amino-2,6-dideoxy-4-O-methyl-D-galactose Hydrochloride

(a) Methyl 2-Acetamido-2-deoxy-3,6-di-O-(p-tolylsulfonyl)-α-D-galactopyranoside

To a solution of methyl 2-acetamido-2-deoxy-3-*O*-(*p*-tolylsulfonyl)-α-D-galactopyranoside (11) (2.4 g) in dry pyridine (8 ml) was added a solution of *p*-toluenesulfonyl chloride (1.36 g) in pyridine (14 ml), both solutions having been previously cooled to −15 °C. The mixture was kept at 0 °C for 18 h and at room temperature for 24 h. Ice (3 g) was added to the mixture to destroy excess chloride and, after 2 h, the mixture was poured into ice water (100 ml) containing acetic acid (20 ml). The water solution was extracted with chloroform (3 × 80 ml) and the combined extracts were washed successively with *N* sulfuric acid, sodium bicarbonate solution, and water and the dried (anhydrous Na_2SO_4) solution was concentrated to a syrup (3.24 g). The product gave a single spot on t.l.c. with R_f 0.63 (t.l.c. starting product had R_f 0.41) and had $[\alpha]_D$ +87° (*c*, 0.1 in chloroform).

Anal. Calcd. for $C_{23}H_{29}NO_{10}S_2$: C, 50.81; H, 5.38; N, 2.58; S, 11.80. Found: C, 50.88; H, 5.30; N, 2.51; S, 11.77.

(b) Methyl 2-Acetamido-2-deoxy-4-O-methyl-3,6-di-O-(p-tolylsulfonyl)-α-D-galactopyranoside

Methyl 2-acetamido-2-deoxy-3,6-di-*O*-(*p*-tolylsulfonyl)-α-D-galactopyransoside (3 g) dissolved in methyl iodide (60 ml) was heated under gentle reflux while freshly prepared silver oxide (10 g) was added in 2-g portions over 12 h. The mixture was filtered and the residue was washed with warm acetone. The filtrate and washings were concentrated to a semicrystalline mass (3.2 g) which on t.l.c. showed a major new spot with R_f 0.82 and a trace of starting material (R_f 0.63). The methyl 2-acetamido-2-deoxy-4-*O*-methyl-3,6-di-*O*-(*p*-tolylsulfonyl)-α-D-galactopyranoside had $[\alpha]_D$ +79° (*c*, 1.2 in chloroform).

Anal. Calcd. for $C_{24}H_{31}NO_{10}S_2$: C, 51.69; H, 5.60; N, 2.51; S, 11.50; OMe, 11.13. Found: C, 51.63; H, 5.68; N, 2.48; S, 11.39; OMe, 11.30.

(c) Methyl 2-Acetamido-2,6-dideoxy-6-iodo-4-O-methyl-3-O-(p-tolylsulfonyl)-α-D-galactopyranoside

A solution of methyl 2-acetamido-2-deoxy-4-*O*-methyl-3,6-di-*O*-(*p*-tolylsulfonyl)-α-D-galactopyranoside (2 g) and sodium iodide (2 g) in dry acetone (50 ml) contained in a sealed glass tube was heated at 100 °C for 6 h. The cooled reaction mixture was filtered to remove crystalline sodium *p*-toluenesulfonate and the filtrate was diluted with chloroform (200 ml). The chloroform solution was washed with 2% sodium thiosulfate solution (20 ml) and with water (20 ml), and the dried (anhydrous Na_2SO_4) solution was concentrated to yield methyl 2-acetamido-2,6-dideoxy-6-iodo-4-*O*-methyl-3-*O*-(*p*-tolylsulfonyl)-α-D-galactopyranoside (1.72 g) as a syrup having $[\alpha]_D$ +71° (*c*, 0.7 in chloroform) and giving a single spot on t.l.c. with R_f 0.85.

Anal. Calcd. for $C_{17}H_{24}INO_7S$: C, 39.77; H, 4.71; I, 24.72; N, 2.73; S, 6.25; OMe, 12.09. Found: C, 39.80; H, 4.62; I, 23.47; N, 2.58; S, 6.20; OMe, 12.00.

(d) Methyl 2-Acetamido-2,6-dideoxy-4-O-methyl-3-O-(p-tolylsulfonyl)-α-D-galactopyranoside

To a solution of methyl 2-acetamido-2,6-dideoxy-6-iodo-4-*O*-methyl-3-*O*-(*p*-tolylsulfonyl)-α-D-galactopyranoside (1.5 g) in dry methanol (45 ml) containing triethylamine (0.3 ml) was added fresh Raney nickel (4 g) and the mixture was shaken vigorously under a hydrogen atmosphere of 50 p.s.i. pressure over 6 h. The filtered solution was concentrated to a syrup (1.5 g) which was fractionated on a column of silica gel (3 × 35 cm) (100–200 mesh) using benzene–methanol (10:1 v/v) as the mobile phase to yield pure methyl 2-acetamido-2,6-dideoxy-4-*O*-methyl-3-*O*-(*p*-tolylsulfonyl)-α-D-galactopyranoside (1.1 g) as a syrup having $[\alpha]_D$ +102.5° (*c*, 2 in chloroform) and giving a single spot on t.l.c. with R_f 0.81.

Can. J. Chem. Downloaded from www.nrcresearchpress.com by 210.87.254.5 on 09/05/12
For personal use only.

Anal. Calcd. for $C_{17}H_{25}NO_7S$: C, 52.70; H, 6.50; N, 3.62; S, 8.28. Found: C, 52.50; H, 6.45; N, 3.80; S, 8.30.

(e) Methyl 2-Acetamido-2,6-dideoxy-4-O-methyl-α-D-galactopyranoside

A solution of methyl 2-acetamido-2,6-dideoxy-4-*O*-methyl-3-*O*-(*p*-tolylsulfonyl)-α-D-galactopyranoside (0.9 g) in 90% aqueous methanol (80 ml) was treated with 2% sodium amalgam (15 g) and the mixture was stirred vigorously at room temperature over 18 h. The methanol solution was filtered, the filtrate was saturated with carbon dioxide and was then concentrated to dryness. The residue was extracted with acetone and the concentrated extract was then taken up in a small amount of warm methanol. On cooling, the methanol solution gave crystalline methyl 2-acetamido-2,6-dideoxy-4-*O*-methyl-α-D-galactopyranoside (0.54 g) which had m.p. 220–221 °C, $[\alpha]_D$ +125° (*c*, 0.12 in chloroform), and gave a single spot on t.l.c. with R_f 0.52.

Anal. Calcd. for $C_{10}H_{19}NO_5$: C, 51.49; H, 8.21; N, 6.01. Found: C, 51.29; H, 8.37; N, 6.07.

(f) 2-Amino-2,6-dideoxy-4-O-methyl-D-galactose Hydrochloride

Methyl 2-acetamido-2,6-dideoxy-4-*O*-methyl-α-D-galactopyranoside (0.5 g) was hydrolyzed with 3 *N* hydrochloric acid (15 ml) at 100 °C for 2 h and the solution was concentrated to dryness. The residue was taken up in hot methanol, decolorized with a little charcoal, filtered, and the concentrated filtrate was diluted with acetone. On keeping the solution at 2 °C it gave crystalline 2-amino-2,6-dideoxy-4-*O*-methyl-D-galactose hydrochloride (0.38 g) which had m.p. 192–195 °C (dec.), $[\alpha]_D$ +122 → +97° (*c*, 0.14 in water), and on paper chromatography (solvent B) it gave a single ninhydrin positive spot with R_{GN} 1.92.

Anal. Calcd. for $C_7H_{16}ClNO_4$: C, 39.35; H, 7.55; Cl, 16.59; N, 6.56; OMe, 14.52. Found: C, 39.32; H, 7.40; Cl, 16.70; N, 6.55; OMe, 14.48.

(3) 2-Amino-2,6-dideoxy-3,4-di-O-methyl-D-galactose Hydrochloride

(a) Methyl 2-Acetamido-2,6-dideoxy-D-galactopyranoside

2-Acetamido-2,6-dideoxy-D-galactose (12) (0.5 g) dissolved in 2% (w/v) methanolic hydrogen chloride (50 ml) was boiled under reflux for 3 h and the cooled solution was neutralized with silver carbonate and filtered. The filtrate was passed down a column of methanol washed mixture of Duolite A4 (OH^-) (4 ml) and Rexyn 101(H^+) (4 ml) ion-exchange resins and the eluate was concentrated to a crystalline solid (0.51 g) which on crystallization from ethanol gave pure methyl 2-acetamido-2,6-dideoxy-α-D-galactopyranoside (0.43 g) which had m.p. 227–228 °C and $[\alpha]_D$ +179° (*c*, 0.11 in methanol).

Anal. Calcd. for $C_9H_{17}NO_5$: C, 49.30; H, 7.82; N, 6.39. Found: C, 49.44; H, 7.90; N, 6.37.

Gas–liquid partition chromatography of the trimethylsilylated methyl 2-acetamido-2,6-dideoxy-α-D-galactopyranoside (column A, 200 °C) gave a single peak with T_{GN} 1.28.

(b) Methyl 2-Acetamido-2,6-dideoxy-3,4-di-O-methyl-α-D-galactopyranoside

Methyl 2-acetamido-2,6-dideoxy-α-D-galactopyranoside (0.4 g) was dissolved in methyl iodide (20 ml) and fresh silver oxide (4 g) was added. The mixture was refluxed gently for 5 h and, following the addition of chloroform (60 ml), the mixture was filtered and the concentrated filtrate was remethylated by the same reagents under the same conditions. Gas–liquid partition chromatographic examination of the product (column A, 200 °C) showed a single peak having T_{GN} 1.86 corresponding to authentic methyl 2-acetamido-2,6-dideoxy-3,4-di-*O*-methyl-α-D-galactopyranoside (prepared in a separate experiment via the sequence methyl 2-benzamido-2-deoxy-6-*O*-(*p*-tolylsulfonyl)-α-D-galactopyranoside (18) → methyl 2-benzamido-2-deoxy-3,4-di-*O*-methyl-6-*O*-(*p*-tolylsulfonyl)-α-D-galactopyranoside → methyl 2-benzamido-2,6-dideoxy-6-iodo-3,4-di-*O*-methyl-α-D-galactopyranoside → methyl 2-benzamido-2,6-dideoxy-3,4-di-*O*-methyl-α-D-galactopyranoside → methyl 2-acetamido-2,6-dideoxy-3,4-di-*O*-methyl-α-D-galactopyranoside (low overall yield, *ca.* 8%)). The methyl 2-acetamido-2,6-dideoxy-3,4-di-*O*-methyl-α-D-galactopyranoside (0.28 g) obtained from methanol solution had m.p. 199–200 °C and $[\alpha]_D$ +134° (*c*, 0.5 in chloroform).

Anal. Calcd. for $C_{11}H_{21}NO_5$: C, 53.42; H, 8.56; N, 5.66; OMe, 37.65. Found; C, 53.40; H, 8.54; N, 5.55; OMe, 37.80.

(c) 2-Amino-2,6-dideoxy-3,4-di-O-methyl-D-galactose Hydrochloride

Methyl 2-acetamido-2,6-dideoxy-3,4-di-*O*-methyl-α-D-galactopyranoside (0.22 g) was hydrolyzed with 3 *N* hydrochloric acid (25 ml) at 100 °C for 2.5 h and following the concentration of the solution and removal of excess acid by distillation with toluene, the residue was dissolved in methanol, decolorized with charcoal, filtered, and the filtrate was concentrated to a syrup (0.20 g). The syrup was thinned with a little methanol and, on keeping at 2 °C it afforded crystalline 2-amino-2,6-dideoxy-3,4-di-*O*-methyl-D-galactose hydrochloride which had m.p. 198–200 °C (dec.), $[\alpha]_D$ +61° (*c*, 0.5 in water), and on paper chromatography it gave a single ninhydrin positive spot with R_{GN} 2.63 (solvent B).

Anal. Calcd. for $C_8H_{18}ClNO_4$: C, 42.20; H, 7.97; Cl, 15.57; N, 6.15; OMe, 27.26. Found: C, 42.14; H, 7.80; Cl, 15.76; N, 6.11; OMe, 27.00.

(4) Chromatographic Analysis of the Methyl Ethers of 2-Amino-2,6-dideoxy-D-galactopyranose

(a) Methyl Ethers of 2-Acetamido-2,6-dideoxy-D-galactopyranose

Samples of the 3-, 4-, and 3,4-dimethyl ethers of 2-amino-2,6-dideoxy-D-galactose hydrochloride (*ca.* 3 mg) were converted to their corresponding *N*-acetyl derivatives by treatment with aqueous acetic anhydride in the presence of basic ion-exchange resin (19) and the single product obtained from each glycose, on paper chromatography (solvent A), gave the following relative retention values: 2-acetamido-2,6-dideoxy-D-galactose, R_{Rh} 0.97; 2-acetamido-2,6-dideoxy-3-*O*-methyl-D-galactose, R_{Rh} 1.19; 2-acetamido-2,6-dideoxy-4-*O*-methyl-D-galactose, R_{Rh} 1.29; 2-acetamido-2,6-dideoxy-3,4-di-*O*-methyl-D-galactose, R_{Rh} 1.56.

(b) Gas–Liquid Partition Chromatography of the Acetate Derivatives of the 3-, 4-, and 3,4-Dimethyl Ethers of 2-Acetamido-2,6-dideoxy-D-galactitol

Samples (*ca.* 2 mg) of the 3-, 4-, and 3,4-dimethyl ethers of 2-acetamido-2,6-dideoxy-D-galactose (from

Experimental, 4*a*) in water (1 ml) were reduced by the addition of sodium borohydride (4 mg) and, after 12 h the excess borohydride was destroyed by acidification with acetic acid. The mixtures were concentrated to dryness and the residues were repeatedly evaporated with methanol (5 × 10 ml). The residues were treated with acetic anhydride (0.6 ml) and kept at 130 °C for 2 h. Samples (1–5 μl) of the solutions were taken for direct injection on column B at 200 °C. Each derivative gave a single peak and had the relative retention values recorded: 2-acetamido-1,3,4,5-tetra-*O*-acetyl-2,6-dideoxy-D-galactitol, T_A 5.43; 2-acetamido-1,3,5-tri-*O*-acetyl-2,6-dideoxy-4-*O*-methyl-D-galactitol, T_A 3.92; 2-acetamido-1,4,5-tri-*O*-acetyl-2,6-dideoxy-3-*O*-methyl-D-galactitol, T_A 2.85; and 2-acetamido-1,5-di-*O*-acetyl-2,6-dideoxy-3,4-di-*O*-methyl-D-galactitol, T_A 1.85.

1. M. J. CRUMPTON and D. A. L. DAVIES. Biochem. J. **70**, 729 (1958).
2. R. WHEAT, E. L. ROLLINS, and J. LEATHERWOOD. Nature, **202**, 492 (1958).
3. R. W. WHEAT, E. L. ROLLINS, and J. M. LEATHERWOOD. J. Biol. Chem. **238**, 26 (1963).
4. J. D. HIGGINBOTHAM and M. HEIDELBERGER. Carbohydr. Res. **23**, 165 (1972).
5. N. SHARON, I. SHIF, and U. ZEHAVI. Biochem. J. **93**, 210 (1964).
6. U. ZEHAVI and N. SHARRON. J. Org. Chem. **29**, 3654 (1964).
7. G. T. BARRY and E. ROARK. Nature, **202**, 493 (1964).
8. S. A. BARKER, J. S. BRIMACOMBE, M. J. HOW, and M. STACEY. Nature, **189**, 303 (1961).
9. J. A. CIFONELLI, J. A. REBERS, M. B. PERRY, and J. K. N. JONES. Biochemistry, **5**, 3066 (1966).
10. P. J. STOFFYN and R. W. JEANLOZ. J. Am. Chem. Soc. **76**, 561 (1954).
11. P. J. STOFFYN and R. W. JEANLOZ. J. Am. Chem. Soc. **76**, 563 (1954).
12. M. B. PERRY and V. DAOUST. Can. J. Chem. **51**, 974 (1973).
13. M. B. PERRY and A. C. WEBB. Can. J. Chem. **47**, 4091 (1969).
14. M. B. PERRY and V. DAOUST. Can. J. Biochem. **51**, 1335 (1973).
15. S. M. PARTRIDGE. Biochem. J. **42**, 238 (1948).
16. W. E. TREVELYAN, D. P. PROCTOR, and J. S. HARRISON. Nature, **166**, 444 (1950).
17. L. HOUGH, J. K. N. JONES, and W. H. WADMAN. J. Chem. Soc. 1702 (1950).
18. R. KAHN and L. HOUGH. Carbohydr. Res. **24**, 147 (1972).
19. S. ROSEMAN and J. LUDOWIEG. J. Am. Chem. Soc. **76**, 301 (1954).

Can. J. Chem. Downloaded from www.nrcresearchpress.com by 210.87.254.5 on 09/05/12
For personal use only.

Erratum: Reactions of Aralkyl and Unsaturated Chloramines: the Nitrenium Ion Question

O. E. EDWARDS, G. BERNATH, J. DIXON, J. M. PATON, AND D. VOCELLE
Division of Biological Sciences, National Research Council of Canada, Ottawa, Canada K1A 0R6

Received August 1, 1974
(Ref.: Can. J. Chem. **52**, 2123 (1974))

Reference 24 should read Chemistry Letters, 393 (1972).

Downloaded from www.nrcresearchpress.com by 210.87.254.40 on 09/05/12
For personal use only.

Methyl 5-Bromolevulinate[1]

S. F. MacDonald

Division of Biological Sciences, National Research Council of Canada, Ottawa, Canada K1A 0R6

Received March 12, 1974

S. F. MacDonald. Can. J. Chem. **52**, 3257 (1974).

Methyl 5-bromolevulinate (30%) is obtained directly by brominating levulinic acid in methanol. The synthesis of 5-aminolevulinic acid over the 5-phthalimido ester thus becomes a three-step one.

S. F. MacDonald. Can. J. Chem. **52**, 3257 (1974).

La bromuration de l'acide lévulinique dans le méthanol conduit directement au bromo-5 lévulinate de méthyle avec un rendement de 30%. La préparation de l'acide amino-5 lévulinique par l'intermédiaire de l'ester phtalimido en position 5 devient donc une synthèse en trois étapes.

[Traduit par le journal]

Can. J. Chem. Downloaded from www.nrcresearchpress.com by 210.87.254.5 on 09/05/12
For personal use only.

Of the numerous routes to 5-aminolevulinic acid (ALA), *cf.* ref. 1, the five-step synthesis (2) from hippuric acid and succinic anhydride over 5-phenyl-2-oxazolone (3) and β-carbomethoxypropionyl chloride is apparently preferred (4).

5-Chloro- and 5-bromolevulinic esters are converted into ALA via the 5-phthalimido derivatives (>70%) *cf.* ref. 5. However, the halogenation of levulinic acid or its esters has led almost exclusively to 3- rather than to 5-halo derivatives. The latter were usually obtained from β-carbalkoxypropionyl chlorides with diazomethane followed by HCl or HBr (5, 6). Alternatively, diethyl acetylsuccinate was brominated, the initial product was rearranged to diethyl bromacetylsuccinate, and the latter hydrolyzed, partially decarboxylated, and re-esterified (1).

We have obtained methyl 5-bromolevulinate (30%) directly by brominating levulinic acid in methanol, conditions under which the methyl groups of methyl ketones are brominated preferentially (7). Fractional distillation readily separated methyl 5-bromolevulinate and the by-products: the 3-bromo ester and smaller amounts of methyl levulinate and its 3,5-dibromo derivative. However, as the boiling points wandered, the fractionation was followed by gas–liquid chromatography (g.l.c.); inconsistencies in the reported boiling points had been noted (8).

Unfortunately, further work on the bromination was impracticable because the writer became sensitive to the products. Presumably the bromine should be added more rapidly (7) and the product could be separated more efficiently. Methyl 3-bromolevulinate has also been converted to ALA (9, 10), and both the 3-bromo acid and the 3,5-dibromo acid have been converted to 5-bromolevulinic acid (the "α" acid of ref. 11), see refs. 8 and 11. We found no definite evidence that the bromo esters were interconverted during their purification or that the 3- was converted into the 5-bromo ester when heated with methanolic HBr.

[1]NRCC 14111.

Experimental

The products were identified by their p.m.r. spectra (*cf.* ref. 8). The composition of the fractions as determined by g.l.c. are given as (% methyl levulinate, % 3-bromo, % 5-bromo, % 3,5-dibromo ester).

Bromination of Levulinic Acid

A solution of levulinic acid (58 g,) in methanol (500 ml, dried with magnesium) was stirred in a 20° bath of water while bromine (80 g) was added at a rate which maintained the temperature of the solution at 30°. After 2½ h the KI–starch test was negative and the solution was refluxed for 1 h. After removing the methanol (rotary, finally at 0.5 mm), the residue was stirred with ether (500 ml) and water (100 ml) while excess sodium bicarbonate was added. The ether layer was washed with aqueous bicarbonate, dried (Na_2SO_4), and the ether was distilled off. The residue was distilled to 95° at 0.2 mm. Yield: 94 g (90%) (8, 31, 56, 5) or 50% of the 5-bromo ester.

Levulinic acid (29 g), methanol (500 ml reagent grade), and bromine (40 g) by the same method gave 45 g (86%) (8, 28, 61, 3) or 52% of the 5-bromo ester.

Methyl 5-Bromolevulinate

The crude product (396 g) (8,28,56,8) was distilled through a 12 in. vacuum jacketed Vigreux column at *ca.* 0.1 mm, collecting seven fractions between 40 and 85°: *1*: 116 g (35,62,3,0): *2*: 44 g (1,88,11,0); *3*: 18 g (0,6,92,2); *4*: 89 g (0,0,96,4); *5*: 78 g (0,0,93,7); *6*: (0,0,72,28); *7*: (0,0,5,95); residue (0,0,3,97).

The fractions *4* and *5* were combined and fractionated again in the same way to give successively 8 g (< 1, < 1, 99, 0), 103 g (0,0,99,1), 35 g (0,0,97,3), 16 g (0,0,80,20) etc. The first three distillates came over at 55–64° and were combined as the product (146 g (0,0,98,2)), a stable (sic) colorless oil; n.m.r. ($CDCl_3$): τ 6.00 (s, 2H, CH_2Br), 6.33 (s, 3H, OCH_3), 7.19 p.p.m. (m, 4H, CH_2CH_2); yield from levulinic acid 30%.

Anal. Calcd. for $C_6H_9O_3Br$: C, 34.48; H, 4.43; Br, 38.23. Found: C, 34.22; H, 4.19; Br, 38.41.

The methyl β-(2-amino-4-thiazolyl) propionate from it had m.p. 97–98.5° (corr.) (lit. (8) 96–97.5°).

5-Bromolevulinic Acid

The above ester was stirred to solution in 10 parts of 20% hydrobromic acid at 20°. The acid was extracted into ether, the ether was removed, and the residue was recrystallized from benzene–hexane as colorless plates, m.p. 79–80° (corr.) (lit. (11) 79–80°).

Anal. Calcd. for $C_5H_7O_3Br$: C, 30,80; H, 3.62; Br, 40.99. Found: C, 30.92; H, 3.63; Br, 40.81.

1. S. Lartillot and C. Baron. Bull. Soc. Chim. Fr. 3798 (1966).
2. U. R. Hearn and M. E. Wildfeuer. Anal. Biochem. **2**, 140 (1961).
3. P. T. Frangopol, A. T. Balaban, L. Barladeanu, and E. Gioranescu. Tetrahedron, **16**, 59 (1961).
4. D. Gurne and D. Shemin. Science, **180**, 1188 (1973).
5. L. Pichat, M. Hucleux, and M. Herbert. Bull. Soc. Chim. Fr. 1750 (1956).
6. D. Shemin. *In* Methods in Enzymology. *Vol.* 4. *Edited by* S. P. Colowick and N. O. Kaplan. Academic Press, New York. 1957. p. 648.
7. M. Gaudy and A. Marquet. Tetrahedron, **26**, 5611 (1970).
8. C. Rappe. Ark. Kemi, **13**, 425 (1959); **14**, 467 (1959); **20**, 51 (1963).
9. H. Pauly, R. Gilmour, and G. Will. Ann. Chem. **403**, 119 (1914).
10. R. W. Wynn and A. H. Corwin. J. Org. Chem. **15**, 203 (1950).
11. L. Wolff. Ann. Chem. **264**, 229 (1891).

Can. J. Chem. Downloaded from www.nrcresearchpress.com by 210.87.254.5 on 09/05/12
For personal use only.

Pulse Radiolytic Formation of Solvated Electrons, Ion-pairs, and Alkali Metal Anions in Tetrahydrofuran[1]

G. A. SALMON,[2] W. A. SEDDON, AND J. W. FLETCHER

Physical Chemistry Branch, Atomic Energy of Canada Limited, Chalk River Nuclear Laboratories, Chalk River, Ontario K0J 1J0

Received March 25, 1974

G. A. SALMON, W. A. SEDDON, and J. W. FLETCHER. Can. J. Chem. **52**, 3259 (1974).

Pulse radiolysis of solutions of alkali metal cations in tetrahydrofuran (THF) demonstrates the formation of solvated electrons e_s^-, alkali metal cation – ion pairs (M^+, e_s^-), and alkali metal anions M^-. This paper describes the spectra, extinction coefficients, and radiolytic yields of e_s^-, lithium, sodium, potassium, and cesium species in THF. The reaction kinetics are complex but largely involve reactions A and B

[A] $$e_s^- + M^+ \rightleftharpoons (M^+, e_s^-)$$

[B] $$(M^+, e_s^-) + e_s^- \rightarrow M^-$$

with the concomitant disappearance of all three species by reaction with radiolytically produced radicals. Rate constants and ion-pair dissociation constants for e_s^- and the sodium and potassium species are presented and compared with data established from studies of blue solutions of alkali metals dissolved in THF.

G. A. SALMON, W. A. SEDDON, et J. W. FLETCHER. Can. J. Chem. **52**, 3259 (1974).

La radiolyse pulsée de solutions de cations de métaux alcalins dans le tétrahydrofuranne (THF) décèle la formation d'électrons solvatés e_s^-, de paires d'ion métaux alcalins (M^+, e_s^-) et d'anions de métaux alcalins (M^-). Cette étude décrit les spectres, les coefficients d'extinction et les rendements radiolytiques de e_s^-, et de paires d'ions et anions de lithium, de sodium, de potassium et de césium dans le THF. La cinétique de la réaction est complexe mais fait essentiellement intervenir les réactions A et B

[A] $$e_s^- + M^+ \rightleftharpoons (M^+, e_s^-)$$

[B] $$(M^+, e_s^-) + e_s^- \rightarrow M^-$$

avec une disparition simultanée de toutes les trois espèces par une réaction avec les radicaux produits d'une façon radiolytique. On établit les constantes de vitesse et les constantes de dissociations des paires d'ions pour e_s^- et les espèces de sodium et de potassium, et on les compare avec des données déjà connues par les études faites sur des solutions bleues de métaux alcalins dissous dans le THF. [Traduit par le journal]

Introduction

Numerous investigations of solutions of alkali metals in amines and ethers have shown that three species coexist in equilibrium (1–3). These species are considered to be the solvated electron (e_s^-), the alkali metal cation – ion pair (M^+, e_s^-), and the alkali metal anion M^-.

Pulse radiolysis and flash photolysis experiments in ethylamine (4, 5), tetrahydrofuran (THF) (6–9), 2-methyl THF (10), diglyme (11), and dimethoxyethane (DME) (12) have demonstrated that each species has a distinct optical absorption spectrum and the conversion of e_s^- to (M^+, e_s^-) and ultimately M^- can be readily observed. This paper expands our preliminary account (7) and describes the spectra and kinetics of formation and decay of e_s^-, lithium, sodium, potassium, and cesium species in THF.

Experimental

Detailed accounts of the pulse radiolysis facilities and techniques have been described elsewhere (5, 13). Solutions were irradiated in 0.5 to 2.0 cm quartz cells with 0.3 to 1 μs pulses of electrons from a 2.5 MeV Van de Graaff accelerator and optical absorptions were monitored using fast infrared detectors (14). THF was purified and distilled from blue solutions prepared and stored over Na/K alloy as described earlier (7, 15).

Solutions of alkali metal ions were prepared by dissolving either (*a*) the pure mirrored metal (potassium only), (*b*) Na/K alloy, (*c*) the tetraphenylboron salts (Na^+, K^+, Cs^+), or (*d*) the aluminum hydride salts

[1]AECL No. 4851.

[2]This work was carried out while G.A.S. held the post of visiting scientist CRNL, June–September 1973. Present address: Cookridge Radiation Research Centre, The University of Leeds, Cookridge Hospital, Leeds LS16 6QB.

Can. J. Chem. Downloaded from www.nrcresearchpress.com by 210.87.254.42 on 09/05/12
For personal use only.

Can. J. Chem. Downloaded from www.nrcresearchpress.com by 210.87.254.42 on 09/05/12
For personal use only.

(Li^+, Na^+). Sodium tetraphenylboron ($NaB\varphi_4$), Fisher Chemicals, was used as received. The corresponding potassium and cesium salts were prepared and purified as described previously (16). Sodium aluminum hydride (K & K Laboratories Inc.) and lithium aluminum hydride (J. T. Baker Chemical Co.) were "purified" under vacuum by dissolving in THF, filtering the residue, and then evaporating to dryness. Both salts were stored in a drybox and appropriate quantities transferred under vacuum to the flow system (17).

Results and Discussion

Pure THF

Figure 1 (open circles) shows the spectrum of e_s^- observed immediately after an $\sim$1 krad pulse. This is in good agreement with the normalized spectrum (solid line) obtained previously by Dorfman *et al.* (18, 19). Correcting for decay during the pulse ($\sim 10\%$) and taking $G_{e_s^-} = 0.39$ (6, 19), we obtain $\varepsilon(e_s^-) = 5 \pm 0.5 \times 10^4\ M^{-1}\ cm^{-1}$ at 2000 nm. This is to be compared with $\varepsilon(e_s^-)_{2100\ nm} = 4 \pm 0.8 \times 10^4\ M^{-1}\ cm^{-1}$ (19) obtained by measuring $G\varepsilon$ at 1000 nm, extrapolating to zero pulse length, and then normalizing to the maximum at 2100 nm. Although the agreement is within experimental error it is significant that in our work using a 300 ns pulse $G\varepsilon$ remains constant over a dose range of 200 to 1250 rads and is about twice that measured previously (19) for a corresponding pulse length.

The doses/pulse used in the latter work were not stated explicitly but the beam currents used indicate that the doses delivered by the 400 ns pulse were probably about 10 krad. Extrapolation of our data on the decay of e_s^- (see below) to this dose indicates that the difference can be accounted for by the decay, in (19), of e_s^- during the pulse.

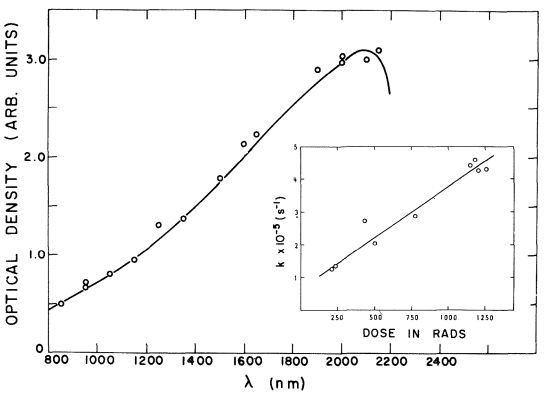

FIG. 1. Transient absorption spectrum of e_s^- observed immediately after the pulse in pure THF. Open circles, this work; solid line, normalized spectrum obtained previously (18, 19). The inset shows the observed (uncorrected) first order rate constant for the decay of e_s^- as a function of dose/pulse (see text).

At the doses used in our study (200 to 1250 rads) the decay of e_s^- was essentially first order, but the quality of the first-order plots was somewhat better at the smallest doses. The observed first-order rate constant increased from 1.25×10^5 to $4.5 \times 10^5\ s^{-1}$ (see inset to Fig. 1) over the range of doses studied. Jou and Dorfman (19) using either shorter pulses or larger doses/pulse observed a significant second-order component to the decay of e_s^- and concluded that $k_1 = 2 \times 10^{12}\ M^{-1}\ s^{-1}$, where k_1 is the rate constant for the homogeneous reaction between free e_s^- and cations derived from THF.

[1] $\quad e_s^- + THF(H)^+ \rightarrow Product$

We therefore assume that this reaction is occurring but at the doses employed in this work significant deviations in the linearity of the first order plots are not discernible.

The decay of a light absorbing species by a mixed order process is given by eq. C (20)

$$[C]\quad A_t = \left[\left(1/A' + \frac{k_{II}}{k_I \varepsilon l}\right)\exp\{k_I(t - t')\} - \frac{k_{II}}{k_I \varepsilon l}\right]^{-1}$$

where A_t is the absorbance at time t, A' the absorbance at $t = t'$, k_I and k_{II} first and second order rate constants, ε the extinction coefficient of the light absorbing species, and l the optical path length of the cell. We therefore treated our data using eq. C, and the method of least squares refinements (21) in order to obtain the best fit values of k_I when substituting $k_{II} = k_I = 2 \times 10^{12}\ M^{-1}\ s^{-1}$ (see above).

This treatment produced fits of our data on the decay of e_s^-, as judged by $\sum(\text{deviations})^2$, which were significantly better at the higher doses than were obtained on the basis of a simple first-order decay. The values of k_I obtained were proportional to dose (see Fig. 2) and we assign this decay process to the reaction between e_s^- and radiolytically produced radicals (reaction 2).

[2] $\quad e_s^- + R\cdot \rightarrow Product$

Since $G(e_s^-) = 0.39$ (6, 19) and $G(R\cdot) \simeq 6.0$ (22) this process is expected to obey a first-order law as observed. On this basis we deduce $k_2 = dk_I/d[R\cdot] = k_I/[R] = 3.0 \times 10^{10}\ M^{-1}\ s^{-1}$.

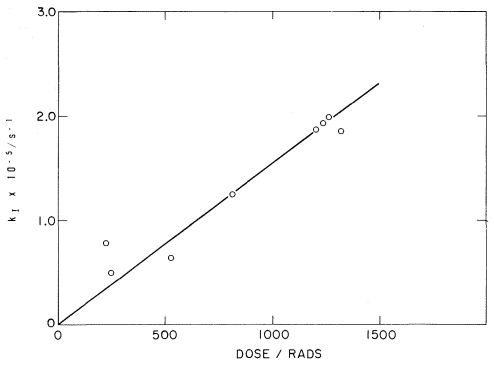

FIG. 2. Corrected pseudo first order rate constant for the reaction of e_s^- with radiolytically produced radicals. The results were deduced from the original data using eq. C and the method of least squares refinements (see text).

THF Containing Salts of Tetraphenylboron, Optical Absorption Spectra

Figure 3 shows the transient absorption spectra obtained in solutions containing 10^{-2} *M* $NaB\varphi_4$ and saturated solutions ($\leq 7 \times 10^{-4}$ *M*) of $KB\varphi_4$ and $CsB\varphi_4$ respectively. The actual concentrations of the latter two salts were not established in view of their limited solubility in THF.

The spectrum obtained in $NaB\varphi_4$ solutions has been assigned to the sodium cation – electron pair (Na^+, e_s^-) formed in reaction 3. The line drawn through our experimental points (open circles) represents the normalized spectrum presented by Bockrath and Dorfman (6).

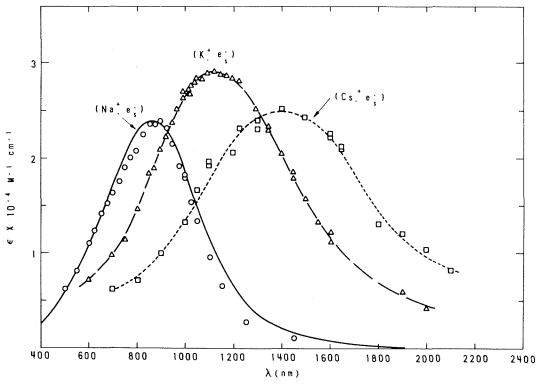

FIG. 3. Ion-pair absorption spectra observed in solutions containing 10^{-2} *M* $NaB\varphi_4$ and saturated solutions ($\leq 7 \times 10^{-4}$ *M*) of $KB\varphi_4$ and $CsB\varphi_4$ respectively: ○, (Na^+, e_s^-); Δ, (K^+, e_s^-); and □, (Cs^+, e_s^-). The solid line drawn through our data (open circles) represents the spectrum of (Na^+, e_s^-) presented by Bockrath and Dorfman (6).

[3] $\quad Na^+ + e_s^- \rightarrow (Na^+, e_s^-)$

As in the case of Na^+ the precursors of the transient species obtained in $KB\varphi_4$ and $CsB\varphi_4$ were found to be e_s^- and the corresponding cations K^+ and Cs^+, respectively. Therefore we assign the absorption bands with maxima at 1125 and 1400 nm to the corresponding ion-pairs (K^+, e_s^-) and (Cs^+, e_s^-). Hitherto complete spectra for the latter species have not been obtained but a flash photolysis study of (tetracene^{2-}, $2K^+$) in 2-methyl THF (10) gave a broad absorption with a maximum at 1100 nm attributed to (K^+, e_s^-).

Reaction Kinetics and Molar Extinction Coefficients

Rate constants for the formation of (Na^+, e_s^-) and (K^+, e_s^-) were determined by observing the pseudo first order decay of e_s^- at either 1650 or 2000 nm. The concentrations of Na^+ and K^+ were deduced using the known dissociation constants of 8.22×10^{-5} and 3.22×10^{-5} *M* for $NaB\varphi_4$ and $KB\varphi_4$ respectively (16). Salt concentrations (4 to 7×10^{-6} *M*) were adjusted to give a halflife for reaction 3 of about 150 ns, *i.e.* ~10 times shorter than the decay of e_s^- in pure THF using doses ≤1 krad/pulse. At these low concentrations the salts are almost completely dissociated and hence possible reactions with the undissociated form were ignored. However, unlike the situation in pure THF the absorption of e_s^- does not decay completely in solutions containing μ*M* concentrations of Na^+ but reaches a constant value (see below) some 2 μs after the pulse. Rate constants were therefore deduced from linear plots of $-\log (OD_t - OD_\infty)$ *vs.* time where OD_∞ represents the optical density after ~2 μs. The average value found for Na^+, $k_3 = 7.8 \pm 0.7 \times 10^{11}$ M^{-1} s^{-1} is in excellent agreement with the earlier determination of $7.9 \pm 0.7 \times 10^{11}$ M^{-1} s^{-1} obtained by monitoring the formation of (Na^+, e_s^-) (6). For K^+ the reaction is slower with $k_4 = 4.6 \pm 0.6 \times 10^{11}$ M^{-1} s^{-1}.

[4] $\quad e_s^- + K^+ \rightarrow (K^+, e_s^-)$

Experiments with Cs^+ were not attempted because of the significant spectral overlap of the e_s^- and (Cs^+, e_s^-) absorptions. However the corresponding rate constant must be of similar magnitude since the formation of (Cs^+, e_s^-) is complete in ~500 ns in solutions containing 1.15×10^{-4} *M* $CsB\varphi_4$ ($K_{diss} = 1.87 \times 10^{-6}$ *M* and therefore $Cs^+ = 1.37 \times 10^{-5}$ *M* (16)).

The molar extinction coefficients $\varepsilon_{(Na^+, e_s^-)}$,

Can. J. Chem. Downloaded from www.nrcresearchpress.com by 210.87.254.42 on 09/05/12
For personal use only.

Can. J. Chem. Downloaded from www.nrcresearchpress.com by 210.87.254.42 on 09/05/12
For personal use only.

$\varepsilon_{(K^+, e_s^-)}$, and $\varepsilon_{(Cs^+, e_s^-)}$ were determined by comparison of the optical densities obtained at 900, 1125, and 1400 nm, respectively, with that of the biphenylide ion-pair (M^+, B^-) produced in reaction 5, (6).

[5] $(M^+, e_s^-) + B \rightarrow (M^+, B^-)$

Taking $\varepsilon_{(M^+, B-)}$ at 407.5 nm $= 4 \times 10^4$ M^{-1} cm^{-1} (23), extinction coefficients were calculated in each case from linear optical density plots obtained over the dose range of 200–1250 rads/pulse in the presence and absence of $\sim 10^{-4}$ M biphenyl. Any small contribution to the overall yield of e_s^- from the addition of biphenyl was neglected.

The values obtained for the extinction coefficients were (2.4 ± 0.2), (2.9 ± 0.2), and (2.5 ± 0.2) $\times 10^4$ M^{-1} cm^{-1} for (Na^+, e_s^-), (K^+, e_s^-), and (Cs^+, e_s^-) respectively. Bockrath and Dorfman (6) also obtained $\varepsilon_{(Na^+, e_s^-)} = 2.4 \times 10^4$ M^{-1} cm^{-1} and on this basis determined an oscillator strength, $f = 1.0$, by integration of the entire absorption band. We have not attempted a similar analysis for (K^+, e_s^-) and (Cs^+, e_s^-) since it is clear from the above extinction coefficients and a comparison of the spectral widths (plotted on an energy scale) at half height that the oscillator strengths are close to unity and hence consistent with the assignment of the optical bands to (K^+, e_s^-) and (Cs^+, e_s^-).

With increasing concentrations of $NaB\varphi_4$ (4.0×10^{-6} to 10^{-2} M) $G(Na^+, e_s^-)$ increased from 0.4 to 1.8 in a manner similar to that observed previously (6). It is apparent that this enhanced yield is due to the scavenging of e_s^- which otherwise undergo fast geminate or spur recombination processes. Also, either the reactivity of the THF counter ion is lower with (Na^+, e_s^-) than with e_s^- (reaction 6), or the $B\varphi_4^-$ ion reacts with the counter ion (reaction 7) to yield a species, possibly $B\varphi_4$, which is less reactive towards (Na^+, e_s^-) (reaction 8).

[6] $(Na^+, e_s^-) + THF^+(H) \rightarrow Na^+ + THF(+H)$

[7] $B\varphi_4^- + THF(H)^+ \rightarrow B\varphi_4 + THF(+H)$

[8] $(Na^+, e_s^-) + B\varphi_4 \rightarrow Na^+ + B\varphi_4^-$

Dissociation Constants for (Na^+, e_s^-) and (K^+, e_s^-)

From studies on the flash photolysis of sodium pyrenide in THF, Fisher *et al.* (8, 9) have estimated that the dissociation constant $K_9 = 3 \times 10^{-8}$ M.

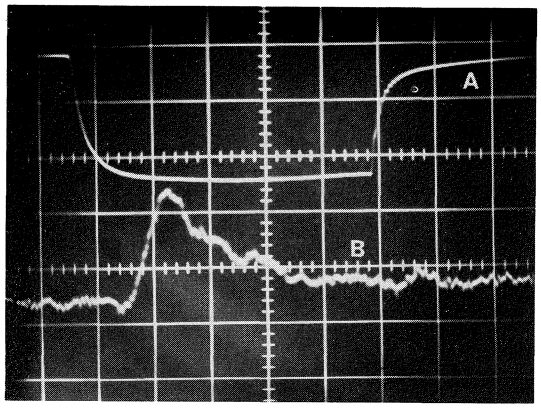

FIG. 4. Oscilloscope trace (curve B) showing the formation and decay of e_s^- at 2000 nm in solutions containing 4×10^{-6} M $NaB\varphi_4$; cell length 1.0 cm, ordinate, 1.65% absorption/division, abscissa 500 ns/division, dose/pulse 5.9×10^{19} eV/l. Trace A shows the profile of the analyzing light at lower gain and a sweep speed of 500 μs/division.

[9] $(Na^+, e_s^-) \rightleftharpoons Na^+ + e_s^-$

Furthermore they concluded that following the production of e_s^- the equilibrium was established within 50 μs in solutions containing about 2×10^{-6} M Na^+.

Figure 4 shows an oscilloscope trace showing the decay of e_s^- observed at 2000 nm in a solution containing 4×10^{-6} M $NaB\varphi_4$ (3.85×10^{-6} M Na^+). As mentioned above the decay is incomplete on a μs time scale. Since the contribution to the optical absorption from (Na^+, e_s^-) is negligible at 2000 nm we suggest the residual absorption (~0.6%), which corresponds to approximately 20% of the initial e_s^- absorption and represents the equilibrium concentration of e_s^-. Both (Na^+, e_s^-) and e_s^- eventually decay on a longer time scale by reaction with radiation produced radicals (see later) but by measuring their relative concentrations ~2 μs after the pulse in solutions containing 3.85 to 9.8×10^{-6} M Na^+ we estimate $K_9 = 1$ to 3×10^{-7} M. Since $k_3 \equiv k_{-9} = 7.8 \times 10^{11}$ M^{-1} s^{-1} then $k_9 = 7.8 \times 10^4$ s^{-1} to 2.3×10^5 s^{-1}.

Similar measurements in $KB\varphi_4$ solutions were subject to larger errors in view of the greater spectral overlap of the e_s^- and (K^+, e_s^-) absorptions. However we estimate the corresponding dissociation constant to be of similar magnitude with $K_{10} = 4 \pm 2 \times 10^{-7}$ M

[10] $(K^+, e_s^-) \rightleftharpoons K^+ + e_s^-$

Can. J. Chem. Downloaded from www.nrcresearchpress.com by 210.87.254.42 on 09/05/12
For personal use only.

This can be compared with $K_{10} = 1 \times 10^{-6}$ M deduced from e.s.r. data presented by Catterall *et al.* (24) and since $k_4 \equiv k_{-10} = 4.6 \times 10^{11}$ M^{-1} s^{-1} then $k_{10} = 9 \times 10^4$ s^{-1} to 4.6×10^5 s^{-1}.

Decay Kinetics of (M^+, e_s^-)

The ion-pair decay kinetics have not been investigated in detail, but whereas at low concentrations ($\leqslant 10^{-5}$ M) of the tetraphenylboron salts we find the kinetics to be first order as stated previously (6), at higher salt concentrations (10^{-2} M) and larger doses (up to 1.5 krads) mixed order decays were observed. Unlike previous pulse radiolysis studies in ethylamine (4, 5) or flash photolysis in DME (12) the ion-pair decay is not associated with the concomitant formation of M^-, except in solutions also containing sodium aluminum hydride (see below).

In the absence of aluminum hydride ion the reactions probably involved in the decay of (M^+, e_s^-) are [6], [8], and [11].

[11] $(M^+, e_s^-) + R\cdot \rightarrow M^+ + \text{Product}$

For low concentrations of M^+, $G(M^+, e_s^-) \simeq 0.4$ and since $G(R) \simeq 6.0$ (22) the decay of (M^+, e_s^-) will be approximately first order as observed. Our data at low salt concentrations and low doses indicate that the values of k_{11} for (Na^+, e_s^-), (K^+, e_s^-), and (Cs^+, e_s^-) are approximately 9.5×10^9, 5×10^{10}, and 4×10^{10} M^{-1} s^{-1} respectively, but the latter two values are upper limits only since some second-order component probably remains.

THF Solutions Containing K^- and Na^-

Blue solutions of alkali metals in ethers were first reported by Down *et al.* (25, 26). Since that time solutions of potassium in THF and DME have been studied by electrical conductance (27), optical absorption (15, 24, 27, 28), and e.s.r. (12, 24). Sodium alone is insoluble in THF (and DME) but is carried into solution in the presence of potassium. Optical spectra of potassium solutions prepared in quartz cells (28), or in the presence of crown compounds (3), show a maximum at 900 ± 10 nm. However, in Pyrex cells (24), solutions of Na/K alloy (26), or solutions containing sodium plus crown compounds (3), the maximum is shifted to 715 ± 10 nm. It is now accepted that these spectra correspond to species of stoichiometry M^- and are generally considered to be the alkali metal anions K^- and Na^-, respectively (1, 2, 28).

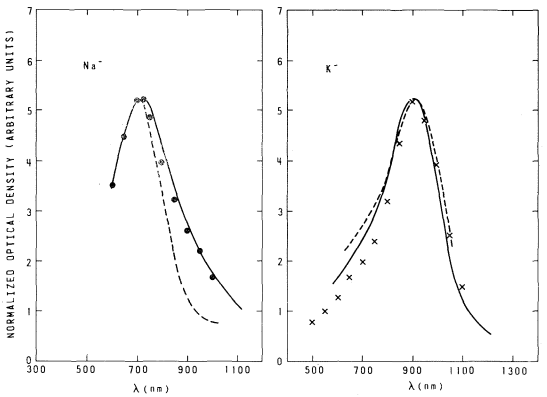

FIG. 5. Optical spectra of Na^- and K^- observed in THF. Solid line, this work, spectrum obtained in Na/K alloy solutions, solubility ~2–3 μM; dotted line represents the spectrum of Na^- observed by ourselves in solutions containing $NaAlH_4$ (see text and (7)). The solid circles represent the calculated spectrum corresponding to 75% Na^- and 25% K^- assuming identical extinction coefficients for both species. K^-, all spectra observed in potassium solutions: solid line, this work, solubility ~2 μM; dotted line, Eloranta and Linschitz (15); ×, Hurley *et al.* (28).

In Fig. 5 our spectra are compared with those obtained previously. The agreement for K^- is good but it is noticeable that the spectrum obtained with Na/K alloy is broader toward longer wavelengths than that due to Na^- obtained by pulse radiolysis (7) and in the presence of crown compound (3) (see Fig. 8). This difference suggests the Na/K alloy spectrum contains both Na^- and K^- with the latter present to about 25%.

Flash photolysis studies of K^- in DME (12) have been explained in terms of the production of e_s^-, the intermediate formation of (K^+, e_s^-), and the ultimate regeneration of K^- via a second order process involving e_s^- and (K^+, e_s^-).

[12] $e_s^- + K^+ \rightleftharpoons (K^+, e_s^-)$

[13] $(K^+, e_s^-) + e_s^- \rightarrow K^-$

Similar studies made earlier in THF and DME (15) were interpreted as resulting from photodissociation of doubly trapped electrons (e_2^{2-}) followed by recombination to an intermediate triplet state of e_2^{2-} and finally recovery back to the original singlet. Current knowledge suggests that this earlier work should be re-interpreted in terms of the species K^- and (K^+, e_s^-). These results suggested to us that a similar process ought to occur with radiolytically produced e_s^-.

Figure 6 shows oscilloscope traces monitored

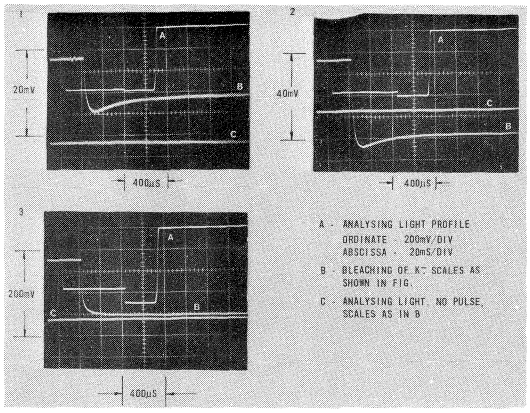

FIG. 6. Bleaching of K^- observed at 900 nm in THF. Scale factors refer to trace B, cell length, 0.5 cm. Picture 1, dose/pulse = 2.7×10^{18} eV/l^{-1}; picture 2, dose/pulse = 1.2×10^{19} eV/l^{-1}; picture 3, dose/pulse = 6.7×10^{19} eV/l^{-1}.

at 900 nm for THF solutions saturated with potassium at room temperature and subject to doses ranging from ~ 50 to 1000 rads per pulse. Taking $\varepsilon_{900} = 1 \times 10^5\ M^{-1}\ cm^{-1}$ (5) the initial optical density corresponds to a K^- concentration of $2 \times 10^{-6}\ M$. The traces show an initial rapid bleaching of K^- followed by a much slower partial recovery of the original absorption. The extent of recovery is markedly dose dependent and is not observed at doses of ~ 1000 rads/pulse. The yield of bleaching measured after ~ 100 μs decreases significantly with increasing dose but for doses $\leqslant 100$ rads/pulse is reasonably constant giving $G(-K^-) = 4 \pm 0.4$. This value does not represent the maximum yield since some 25% of K^- is being reformed in a period of 2.8 ms (Fig. 6). Nevertheless this yield indicates that the bleaching is not simply due to a reaction of K^- with, for example, cations

[14] $$THF(H)^+ + K^- \rightarrow (K^+, e_s^-) + THF + H$$

since $G(THF(H)^+) = G_{e_s^-} = 0.39$ (6). We therefore suggest the only reasonable alternative must involve the oxidation of K^- by radiolytically produced radicals (R). Cherniak *et al.* (22) estimated $G(R) \sim 6$ from the reduction of $FeCl_3$ in the γ-radiolysis of THF. Our results show $G(R) > 4$ and hence K^- to be a stronger reducing agent than R in THF.

At very low doses ($\leqslant 100$ rads/pulse) the rate of disappearance of K^- is approximately first order. Assuming $[K^-] = 2 \times 10^{-6}\ M$ we then estimate $k_{15} \sim 2.5 \times 10^{10}\ M^{-1}\ s^{-1}$.

[15] $$K^- + R \rightarrow (K^+, e_s^-) + \text{Products}$$

We propose that the reaction scheme for bleaching of the K^- solutions includes reactions 12 and 13 proposed by Glarum and Marshall (12), reactions 2 and 14, and the radical reactions 11, 15, and 16.

[16] $$R + R \rightarrow R_2$$

Using this mechanism we have utilized the computer program WR 20 (29) to calculate the concentrations of all the species taking part in the simultaneous first and second order reactions occurring during and after the pulse. The programs require for input data a list of the species taking part in the chemical reactions, the reaction rate constants, radiation yields of the

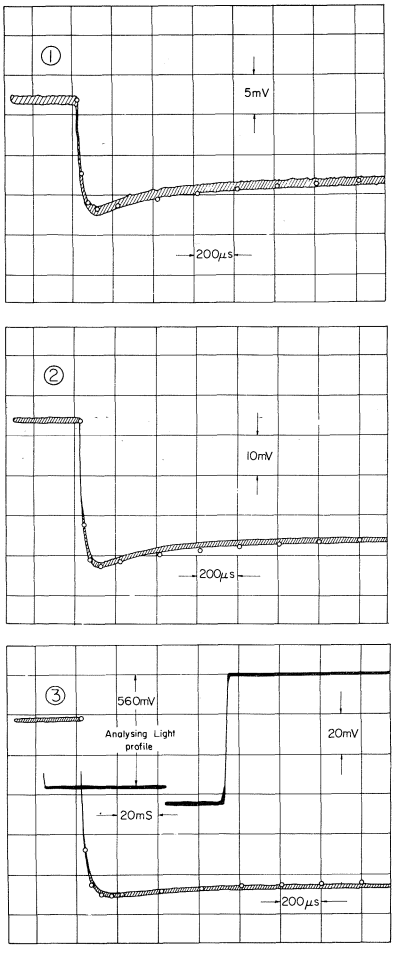

FIG. 7. Reproduction of oscilloscope traces showing the bleaching of K^- in THF. The open circles represent the computed values based on the mechanism and parameters described in the text and Table 1; (*1*) dose/pulse = 3.2×10^{18} eV/l^{-1}, (*2*) dose/pulse 1.0×10^{19} eV/l^{-1}, (*3*) 3.2×10^{19} eV/l^{-1}; cell length, 0.5 cm.

Can. J. Chem. Downloaded from www.nrcresearchpress.com by 210.87.254.42 on 09/05/12
For personal use only.

TABLE 1. Reactions and rate constants used in the computer simulation of the K^- bleaching experiments.

	Reaction	Rate constant*
[4], [−10]	$e_s^- + K^+ \rightarrow (K^+, e_s^-)$	$4.6 \times 10^{11}\ M^{-1}\ s^{-1}$ (4.6×10^{11})
[14]	$THF^+ + K^- \rightarrow (K^+, e_s^-) + THF$	$1.0 \times 10^{11}\ M^{-1}\ s^{-1}$
[10]	$(K^+, e_s^-) \rightarrow e_s^- + K^+$	$1.6 \times 10^5\ s^{-1}$ (0.9 to 4.6×10^5)
[13]	$(K^+, e_s^-) + e_s^- \rightarrow K^-$	$1.0 \times 10^{10}\ M^{-1}\ s^{-1}$
[2]	$e^- + R \rightarrow$ Products	$6 \times 10^{10}\ M^{-1}\ s^{-1}$ (3×10^{10})
[15]	$R + K^- \rightarrow (K^+, e_s^-) +$ Products	$2.0 \times 10^{10}\ M^{-1}\ s^{-1}$ ($\sim 2.5 \times 10^{10}$)
[11]	$R + (K^+, e_s^-) \rightarrow K^+ +$ Products	$2.0 \times 10^{10}\ M^{-1}\ s^{-1}$ ($\leq 5 \times 10^{10}$)
[16]	$R + R \rightarrow$ Products	$5.0 \times 10^9\ M^{-1}\ s^{-1}$

*The values in parentheses correspond to those presented, measured, or estimated in this work.

primary radiolysis products, the initial concentration of species, extinction coefficients of the absorbing species, and the dose per pulse. We have therefore sought to check the validity of the above reaction sequence by comparing the computed result with the experimental observations. Figure 7 curves *1* to *3* show reproductions of the experimentally observed transient signals as a function of dose per pulse. The computed points (open circles) superimposed on the traces were calculated using $G_{e_s^-} = G_{THF(H^+)} = 0.5$, $G_R = 5.5$, $\varepsilon^{K^-}_{900\ nm} = 1 \times 10^5$, $\varepsilon^{(K^+, e_s^-)}_{900\ nm} = 2.0 \times 10^4$, and $\varepsilon^{e_s^-}_{900\ nm} = 1.0 \times 10^4\ M^{-1}\ cm^{-1}$, respectively. Initial concentrations of e_s^- and (K^+, e_s^-) were taken as 4.3×10^{-8} and 8.6×10^{-8} M (24), and K^- as 2×10^{-6} M. Reactions and rate constants are summarized in Table 1. The inclusion of reaction 17

[17] $(K^+, e_s^-) + (K^+, e_s^-) \rightarrow K^- + K^+$

requires unreasonably low values of k_{13} ($< 10^9\ M^{-1}\ s^{-1}$). This suggests, as noted previously (12), that reaction 17 is not a significant process in the recovery of K^-.

Although the agreement between experiment and calculation is good we do not claim that this represents a unique solution. However, we believe it illustrates the importance of radical reactions and their high reactivity with e_s^- and alkali metal species in the radiolytic system.

Solutions of THF Containing $NaAlH_4$

Figure 8 shows the absorption spectra observed in saturated solutions (~ 1 M) both immediately after the pulse and 750 μs after the pulse. Apart from the slight shoulder at ~720 nm the spectrum observed at the end of the pulse is very similar to that observed in $NaB\varphi_4$ solutions (Fig. 3) and hence is attributed to (Na^+, e_s^-). The species remaining after ⩾750 μs has a

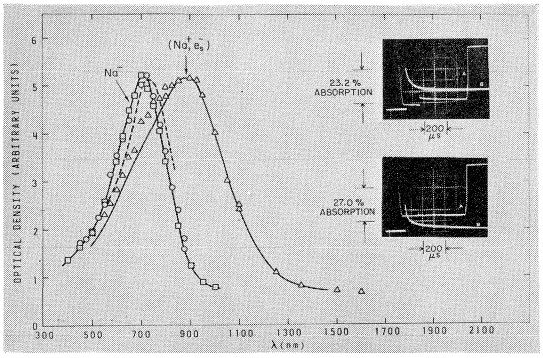

FIG. 8. Absorption spectra observed in ~1 M solutions of $NaAlH_4$ in THF. Δ, immediately after the pulse; □, ○ different experiments, 750 μs after the pulse. The solid line drawn through the triangles represents the normalized spectrum (our data) of (Na^+, e_s^-) from Fig. 3. The dotted line represents the spectrum of Na^- obtained by Lok *et al.* (3). The upper inset (trace B) shows a transient signal observed at 725 nm, dose/pulse 1.27×10^{20} eV/l^{-1}, and the lower inset a corresponding signal at 1050 nm, dose/pulse 1.27×10^{20} eV/l^{-1}. Cell length in both cases, 2.0 cm. In both cases trace A shows the profile of the analyzing light (with the transient signal superimposed at lower gain) at a sweep speed of 100 ms/division.

spectrum corresponding to that of Na^- (see earlier discussion and Fig. 5). The shoulder on the initial (Na^+, e_s^-) spectrum is therefore attributed to a small contribution from Na^-. Also shown as insets in Fig. 8 are oscilloscope traces of signals observed at 725 and 1050 nm. At the latter wavelength where the absorption is predominantly due to (Na^+, e_s^-) the decay is complete in ~1 ms, but that part of the signal at 725 nm due to Na^- is very long lived (>1 s).

As with $LiAlH_4$ (30) the yield of e_s^-, monitored in our case as (Na^+, e_s^-), increases with increasing concentrations of $NaAlH_4$ to a maximum $G(e_s^-) = 2.0 \pm 0.1$ in saturated solutions (Fig. 9). However, in ~0.4 M $LiAlH_4$ solutions $G(e_s^-) = 2.6$ (30). Assuming e_s^- does not react

Can. J. Chem. Downloaded from www.nrcresearchpress.com by 210.87.254.42 on 09/05/12
For personal use only.

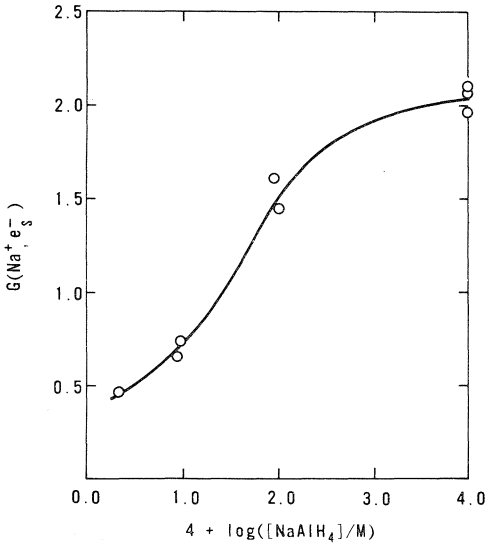

FIG. 9. Yield of (Na^+, e_s^-) as a function of $NaAlH_4$ concentration in THF.

with the undissociated salts this suggests that $NaAlH_4$ is less dissociated that $LiAlH_4$ in THF. Since k_3 ($e_s^- + Na^+$) is known the concentration of Na^+ can be deduced from the e_s^- half lives in solutions containing different initial concentrations of $NaAlH_4$. Using this technique we estimate $K_{18} = 1 \pm 0.2 \times 10^{-7}$ M.

[18] $$NaAlH_4 \rightleftharpoons Na^+ + AlH_4^-$$

From the data in (30) and assuming $k(e_s^- + Li^+) \sim k(e_s^- + Na^+)$ then one can deduce $K_{19} \geqslant 1 \times 10^{-6}$ M.

[19] $$LiAlH_4 \rightleftharpoons Li^+ + AlH_4^-$$

In the preliminary work (7) it was suggested that the difference between $NaAlH_4$ and $NaB\varphi_4$ hinged on the capacity of the former to (*a*) increase $G(e_s^-)$ and hence $G(Na^+, e_s^-)$, (*b*) to extend the lifetime of (Na^+, e_s^-) by eliminating its reaction with $THF(H)^+$, and (*c*) to reduce the yield of radicals formed by the geminate recombination reaction 20

[20] $$e_s^- + THF^+ \rightarrow R$$

These suggestions were apparently supported by our finding (7) that in ~ 1 M $NaAlH_4$ solutions only about 25% of the (Na^+, e_s^-) decays to produce Na^- whereas a careful examination of 10^{-2} M $NaB\varphi_4$ solutions showed the corresponding conversion to be $\leqslant 1\%$. However in 10^{-2} M $NaB\varphi_4$ solution we observe $G(Na^+, e_s^-) = 1.8$ indicating that both $NaAlH_4$ and $NaB\varphi_4$ cause an increase in the yield $G(Na^+, e_s^-)$ by reducing the rate of geminate recombination processes with the THF positive ions.

It seems likely, therefore, that the major difference between these solutes lies in the nature of the products of reactions 7 and 21.

[21] $$THF(H)^+ + AlH_4^- \rightarrow AlH_3 + THF + H_2$$

It may be that whereas reaction 21 yields products which are unreactive towards (Na^+, e_s^-) and which do not yield radicals by reaction with THF^+, reaction 7 may yield $B\varphi_4$ radicals, which probably react by reaction 8, and H atoms, which would react with the solvent to generate free radicals.

Using the computer program WR 20 (29) and taking $G(e_s^-) = 2.0$, $G(R) = 2.5$, and assuming $THF(H)^+$ is removed rapidly by reaction 21 we have attempted to fit by computer calculations the experimental traces observed at 725 and 900 nm. Figure 10 shows the computed points (crosses) superimposed on reproductions of the experimental traces. Table 2 summarizes the reactions, rate constants, and extinction coefficients used in the calculations.

It is significant that if reaction 22 is omitted it is impossible to predict the correct yield of Na^- unless $K_9 \sim 10^{-4}$ M, a value which is incompatible with our estimate of $\sim 10^{-7}$ M (see earlier) or that of Fisher *et al.* (3×10^{-8} M) (8, 9).

[22] $$(Na^+, e_s^-) + (Na^+, e_s^-) \rightarrow Na^+ + Na^-$$

The significance of reaction 22 as distinct from the analogous, but apparently much slower, reaction 17 in potassium solutions (see above), may well be important in the predominant formation of Na^- in solutions containing mixtures of Na^+ and K^+ ions (28, 31, 32).

Reaction 23 representing the collapse of sodium ion-pairs into sodium atoms, Na^0, was proposed by Fisher *et al.* (8, 9)

[23] $$(Na^+, e_s^-) \rightarrow Na^0$$

If we exclude this process the computed yield of Na^- continues to increase slightly rather than level off with time as depicted in Fig. 10. Using $k_{23} = 4 \times 10^3$ s^{-1} (8, 9) causes Na^- to continuously decrease. Reactions 24 and 25 assume that Na^0 would react in an analogous manner to (Na^+, e_s^-). Further experiments are

Can. J. Chem. Downloaded from www.nrcresearchpress.com by 210.87.254.42 on 09/05/12
For personal use only.

TABLE 2. Reactions, rate constants, and extinction coefficients used in the computer simulation of the pulse radiolysis of $NaAlH_4$ solutions in THF

Reaction	Rate constant*
[3] $e_s^- + Na^+ \rightarrow (Na^+, e_s^-)$	$8 \times 10^{11}\ M^{-1}\ s^{-1}$ (7.8×10^{11})
[9] $(Na^+, e_s^-) \rightarrow e_s^- + Na^+$	$8 \times 10^4\ s^{-1}$ (0.8 to 2.3×10^5)
$(Na^+, e_s^-) + e_s^- \rightarrow Na$	$1 \times 10^{10}\ M^{-1}\ s^{-1}$
[22] $(Na^+, e_s^-) + (Na^+, e_s^-) \rightarrow Na^- + Na^+$	$3 \times 10^9\ M^{-1}\ s^{-1}$
[2] $e_s^- + R \rightarrow$ Product	$6 \times 10^{10}\ M^{-1}\ s^{-1}$ (3×10^{10})
$R + Na^- \rightarrow (Na^+, e_s^-)$ + Product	$2.0 \times 10^{10}\ M^{-1}\ s^{-1}$
[11] $R + (Na^+, e_s^-) \rightarrow Na^+$ + Product	$1.3 \times 10^{10}\ M^{-1}\ s^{-1}$ ($\sim 9.5 \times 10^9$)
[16] $R + R \rightarrow$ Product	$5 \times 10^9\ M^{-1}\ s^{-1}$
[23] $(Na^+, e_s^-) \rightarrow Na^0$	$1.5 \times 10^3\ s^{-1}$ (4×10^3)†
[24] $Na^0 + e_s^- \rightarrow Na^-$	$1 \times 10^{10}\ M^{-1}\ s^{-1}$
[25] $Na^0 + R \rightarrow Na^+$ + Product	$1 \times 10^{10}\ M^{-1}\ s^{-1}$

Species	$\varepsilon\ (M^{-1}\ cm^{-1})$ 725 nm	900 nm
e_s^-	6×10^3	1×10^4
(Na^+, e_s^-)	1.8×10^4	2.4×10^4
Na^-	1×10^5	2.5×10^4

*The values in parentheses correspond to those presented, measured, or estimated in this work.
†Reference 9.

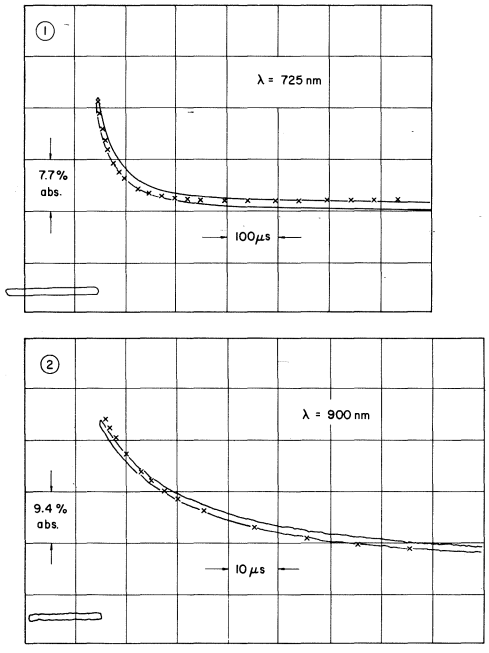

FIG. 10. Reproductions of oscilloscope traces showing the formation and decay of (Na^+, e_s^-) and Na^- in ~1 M solutions of $NaAlH_4$ in THF. The crosses represent the computed values based on the mechanism and parameters given in the text and Table 2. (*1*) Formation and decay monitored at 900 nm (λ_{max} for (Na^+, e_s^-)); (*2*) formation and decay monitored at 725 nm (λ_{max} for Na^-). Dose/pulse 1.27×10^{20} eV/l, cell length, 2.0 cm.

[24] $Na^0 + e_s^- \rightarrow Na^-$

[25] $Na^0 + R \rightarrow Na^+ + Product$

necessary to substantiate the significance, if any, of this result.

As in the case of K^- experiments we do not claim that computer simulation yields a unique solution, but again the calculated curves are self-consistent with the rate constants, equilibrium constant, and extinction coefficients deduced in this paper.

Solutions Containing $LiAlH_4$ or LiCl

THF solutions containing $LiAlH_4$ were not investigated in detail but are worthy of mention since unlike previous claims (30) it was found that the absorption maximum of e_s^- does not shift towards shorter wavelengths in the presence of $LiAlH_4$. Similar spectra were obtained with either $LiAlH_4$ or LiCl as solute, but in both cases the spectrum was indistinguishable from that of e_s^- in pure THF, although $G\varepsilon$ at 2000 nm depended on the solute concentration. The observation by Baxendale *et al.* (30) of a peak at 900 nm in $LiAlH_4$ solutions strongly suggests that their solutions were contaminated by Na^+ ions.

In a saturated $LiAlH_4$ solution containing $5.4 \times 10^{-4}\ M$ $NaB\varphi_4$, $G\varepsilon_{2000\ nm} \sim 2.0 \times 10^4$ at the end of 0.3 μs pulse. If K_{diss} for $NaB\varphi_4$ is

Can. J. Chem. Downloaded from www.nrcresearchpress.com by 210.87.254.42 on 09/05/12
For personal use only.

unaffected by the presence of $LiAlH_4$, $t_{\frac{1}{2}} \sim 4.5 \times 10^{-8}$ s for reaction 3 at this concentration of $NaB\varphi_4$ and therefore little absorption due to e_s^- should be observed at the end of the pulse. This suggests that, like the situation in ethylamine (5), (Li^+, e_s^-) ion pairs are formed, the absorption spectrum of which is indistinguishable from that of e_s^-. Again further experimentation is required to verify this suggestion.

The authors gratefully acknowledge the technical assistance given by Mr. F. C. Sopchyshyn, Mr. E. B. Selkirk, and Mr. J. J. Jevcak.

1. J. J. Lagowski and M. J. Sienko (*Editors*). Metal-ammonia solutions. Colloque Weyl II, Int. Union Pure and Appl. Chem., Butterworth and Co., London. 1970.
2. J. L. Dye. Electrons in fluids. *Edited by* J. Jortner and L. R. Kestner. Springer–Verlag, West Berlin. 1973. p. 77.
3. M. T. Lok, F. J. Tehan, and J. L. Dye. J. Phys. Chem. **76**, 2975 (1972).
4. J. W. Fletcher, W. A. Seddon, J. Jevcak, and F. C. Sopchyshyn. Chem. Phys. Lett. **18**, 592 (1973).
5. J. W. Fletcher, W. A. Seddon, and F. C. Sopchyshyn. Can. J. Chem. **51**, 2975 (1973).
6. B. Bockrath and L. M. Dorfman. J. Phys. Chem. **77**, 1002 (1973).
7. G. A. Salmon and W. A. Seddon. Chem. Phys. Lett. **24**, 366 (1974).
8. M. Fisher, G. Rämme, S. Claesson, and M. Szwarc. Chem. Phys. Lett. **9**, 309 (1971).
9. M. Fisher, G. Rämme, S. Claesson, and M. Szwarc. Proc. R. Soc. Lond. A**327**, 481 (1972).
10. L. J. Giling, J. G. Kloosterboer, R. P. H. Rettschnick, and J. D. W. van Voorst. Chem. Phys. Lett. **8**, 457 (1971).
11. J. G. Kloosterboer, L. J. Giling, R. P. H. Rettschnick, and J. D. W. van Voorst. Chem. Phys. Lett. **8**, 462 (1971).
12. S. H. Glarum and J. H. Marshall. J. Chem. Phys. **52**, 5555 (1970).
13. W. A. Seddon, C. Willis, M. J. Young, and E. B. Selkirk. Atomic Energy of Canada Limited, Report AECL-3853.
14. W. A. Seddon, E. B. Selkirk, and J. W. Fletcher. Int. J. Radiat. Phys. Chem. **5**, 323 (1973).
15. J. Eloranta and H. Linschitz. J. Chem. Phys. **38**, 2214 (1963).
16. D. N. Bhattacharyya, C. L. Lee, J. Smid, and M. Szwarc. J. Phys. Chem. **69**, 608 (1965).
17. W. A. Seddon, J. W. Fletcher, J. Jevcak, and F. C. Sopchyshyn. Can. J. Chem. **51**, 3653 (1973).
18. L. M. Dorfman, F. Y. Jou, and R. Wageman. Ber. Bunsen. Physik Chem. **75**, 681 (1971).
19. F. Y. Jou and L. M. Dorfman. J. Chem. Phys. **58**, 4715 (1973).
20. F. S. Dainton, T. Morrow, G. A. Salmon, and G. F. Thompson. Proc. R. Soc. Lond. A**328**, 457 (1972).
21. F. S. Dainton, R. May, T. Morrow, G. A. Salmon, and G. F. Thompson. Proc. R. Soc. Lond. A**328**, 497 (1972).
22. E. A. Cherniak, E. Collinson, F. S. Dainton, and G. M. Meaburn. Proc. Chem. Soc. 54 (1958).
23. J. Jagur-Grodzinski, M. Feld, S. L. Yang, and M. Szwarc. J. Phys. Chem. **69**, 628 (1965).
24. R. Catterall, J. Slater, and M. C. R. Symons. Metal–ammonia solutions, Colloque Weyl II, Int. Union Pure Appl. Chem. *Edited by* J. J. Lagowski and M. J. Sienko. Butterworth and Co., London. 1970. p. 329.
25. J. L. Down, J. Lewis, B. Moore, and G. Wilkinson. Proc. Chem. Soc. 209 (1957).
26. J. L. Down, J. Lewis, B. Moore, and G. Wilkinson. J. Chem. Soc. 3767 (1959).
27. F. Cafasso and B. R. Sundheim. J. Chem. Phys. **31**, 809 (1959).
28. I. Hurley, T. R. Tuttle, Jr., and S. Golden. Metal–ammonia solutions, Colloque Weyl II, Int. Union Pure Appl. Chem. *Edited by* J. J. Lagowski and M. J. Sienko. Butterworth and Co., London. 1970. p. 449.
29. K. H. Schmidt. Argonne National Laboratory report, ANL 7693.
30. J. H. Baxendale, D. Beaumond, and M. A. J. Rodgers. Trans. Faraday Soc. **66**, 1996 (1970).
31. I. Hurley, T. R. Tuttle, Jr., and S. Golden. J. Chem. Phys. **48**, 2818 (1968).
32. M. G. DeBacker and J. L. Dye. J. Phys. Chem. **75**, 3092 (1971).

Can. J. Chem. Downloaded from www.nrcresearchpress.com by 210.87.254.42 on 09/05/12
For personal use only.

Pulse Radiolysis of Liquid Methylamine, Ethylamine, and Ammonia: The Yield of Solvated Electrons[1]

WILLIAM ARTHUR SEDDON, JOHN WALLACE FLETCHER, FRED CHARLES SOPCHYSHYN, AND JOHN JEVCAK

Physical Chemistry Branch, Atomic Energy of Canada Limited, Chalk River Nuclear Laboratories, Chalk River, Ontario K0J 1J0

Received March 25, 1974

WILLIAM ARTHUR SEDDON, JOHN WALLACE FLETCHER, FRED CHARLES SOPCHYSHYN, and JOHN JEVCAK. Can. J. Chem. **52**, 3269 (1974).

Yields of solvated electrons, $G_{e_s^-}$, have been measured in both the pure and basic solvents using biphenyl and pyrene as electron scavengers. In pure methylamine and ethylamine $G_{e_s^-} = 2.2 \pm 0.1$ and $1.8_4 \pm 0.1$, respectively. However in basic solution these yields more than double giving $G_{e_s^-} = 4.75 \pm 0.2$. In liquid NH_3 and ND_3 at -15 °C, $G_{e_s^-} = 3.1_7 \pm 0.15$ and 3.6 ± 0.2, respectively. The latter yields seem independent of base and temperature from -15 to -50 °C. Comparisons with previous work are discussed.

WILLIAM ARTHUR SEDDON, JOHN WALLACE FLETCHER, FRED CHARLES SOPCHYSHYN et JOHN JEVCAK. Can. J. Chem. **52**, 3269 (1974).

On mesure les rendements d'électrons solvatés, $G_{e_s^-}$, dans des solvants purs et basiques en utilisant le biphényle et le pyrène comme pièges d'électrons. Dans la méthylamine et l'éthylamine pures, on obtient respectivement $G_{e_s^-} = 2.2 \pm 0.1$ et $1.8_4 \pm 0.1$. Pourtant, dans une solution basique, la valeur de ces rendements est plus que doublée $G_{e_s^-} = 4.75 \pm 0.2$. Dans du NH_3 et ND_3 liquide à -15 °C, on obtient respectivement $G_{e_s^-} = 3.1_7 \pm 0.15$ et 3.6 ± 0.2. Ces derniers rendements ne dépendent pas de la base et de la température entre -15 et -50 °C. On discute ces résultats par comparaison avec ceux obtenus au cours d'études antérieures.

[Traduit par le journal]

Introduction

Pulse radiolysis studies in liquid amines and ammonia (1, 2) have illustrated that significant discrepancies exist in the literature concerning the radiolytic yield of solvated electrons in these solvents. With the exception of our earlier work in liquid ammonia (1) little attempt has been made to measure these yields directly. In the nondeuterated solvents the solvated electron, e_s^-, has a broad absorption band with a maximum at ≥ 1800 nm at room temperature (2–4). However, yield measurements at the peak wavelength are difficult due to solvent absorption and uncertainties in the extinction coefficients. In this paper we have determined the yields $G_{e_s^-}$ (mol/100 eV), using the well known electron scavengers biphenyl (B) and pyrene (P) which form the corresponding radical anions B^- and P^- with known extinction coefficients.

Experimental

Detailed descriptions of the experimental procedures and solvent preparation have been given elsewhere (1, 2, 5, 6). Solutions were irradiated with 2.25 MeV electrons using 0.3 μs pulses and doses $\leq 6 \times 10^{19}$ eV l^{-1} as determined by comparison with the thiocyanate dosimeter (6). Dosimetry corrections based on stopping powers per gram for 2.2 MeV electrons in H_2O, NH_3, ND_3, CH_3NH_2, and $C_2H_5NH_2$ (7) were within 1% of electron density corrections using $\rho(NH_3)$ (-15 °C) = 0.659 g cm^{-3} and the ratio $\rho(ND_3)/\rho(NH_3) = 1.184$ (8), $\rho(CH_3NH_2) = 0.662$ and $\rho(C_2H_5NH_2) = 0.683$ g cm^{-3} at 20 °C (9). At -30 and -50 °C $\rho(NH_3) = 0.678$ and 0.703 g cm^{-3}, respectively (10). Zone refined (Aldrich Chem. Co., Inc.) biphenyl and pyrene were used as received.

Results and Discussion

The aromatic radical anions B^- or P^- are formed by attachment of the solvated electron, e_s^-, to the aromatic compound in solution (11, 12).

[1] $$e_s^- + B \rightarrow B^-$$

[2] $$e_s^- + P \rightarrow P^-$$

Such reactions are known to be fast and rate constants range from $k_1 = 4.3 \times 10^9$ in ethanol (12) to k_1 and $k_2 = 1.2 \pm 0.2 \times 10^{11}$ M^{-1} s^{-1} in tetrahydrofuran (THF) (13, 14). Since extinction coefficients for B^- and P^- are known in THF (15), and assuming these are solvent independent (16), values for $G_{e_s^-}$ are deduced from

[1]AECL No. 4852.

Can. J. Chem. Downloaded from www.nrcresearchpress.com by 210.87.254.5 on 09/05/12
For personal use only.

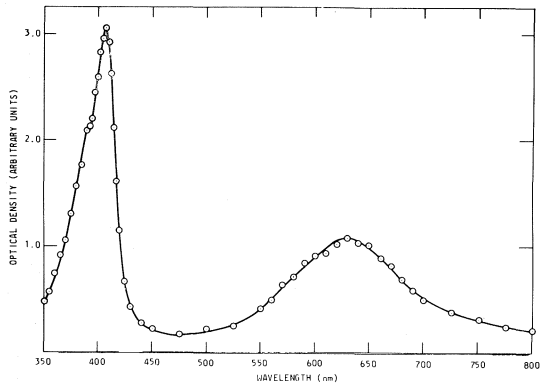

FIG. 1. Spectrum of the biphenylide anion observed immediately after the pulse in 10^{-2} *M* solutions of biphenyl in ethylamine.

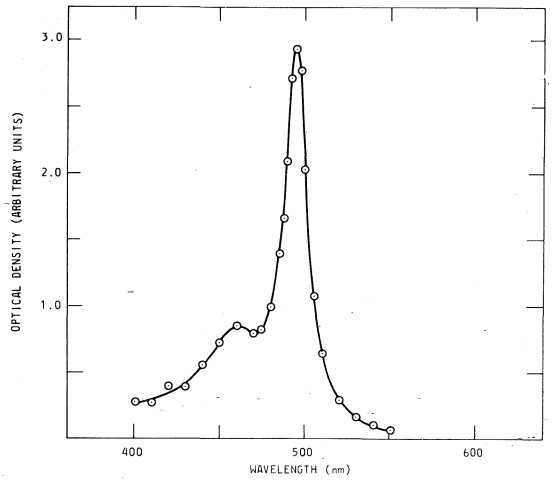

FIG. 2. Spectrum of the pyrenide anion observed immediately after the pulse in 10^{-2} *M* solutions of pyrene in methylamine.

measurements of $G\varepsilon$ (anion) as a function of biphenyl or pyrene concentration.

Figures 1 and 2 show examples of the spectra due to B^- and P^- as observed immediately after the pulse for solutions containing 10^{-2} *M* pyrene in methylamine and 10^{-2} biphenyl in ethylamine. Identical spectra were observed in liquid NH_3 or ND_3 and all are in good agreement with previous work in alcohols and ethers (12, 17–19). Yields in each case were calculated from linear plots of optical density against dose for B^- at 407.5 nm and P^- at 495 nm taking $\varepsilon_{B^-} = 4 \times 10^4$ and $\varepsilon_{P^-} = 5 \times 10^4 M^{-1} cm^{-1}$ (15).

Liquid Ammonia (NH_3) at −15 °C

Since pyrene was found to be less soluble than biphenyl ($\leq 5 \times 10^{-4}$ *M* compared to $\sim 10^{-2}$ *M*, respectively) most experiments were done using biphenyl. Figure 3 shows examples of the optical density of B^- (observed immediately after the pulse) as a function of dose per pulse, biphenyl and sodium amide concentration. Similar plots were obtained in solutions ranging from 10^{-3} to 10^{-2} *M* biphenyl and mixtures containing 10^{-3} biphenyl and 10^{-4} *M* $NaNH_2$ to 10^{-2} *M* in both solutes. The result of eight separate experiments gave $G_{e_s^-} = 3.1_7 \pm 0.15$. The value obtained in 10^{-2} biphenyl and 10^{-2} *M* $NaNH_2$ was somewhat higher giving $G_{e_s^-} = 3.4 \pm 0.1_7$.

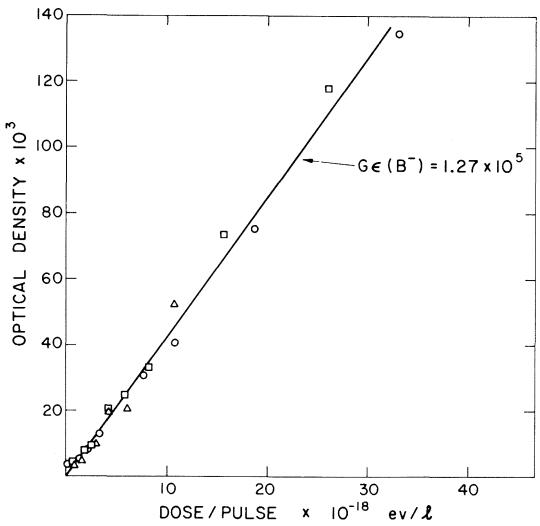

FIG. 3. Optical density of the biphenylide ion observed immediately after the pulse in liquid NH_3 at −15 °C; cell length, 2.0 cm; △, 9.9×10^{-3} *M* biphenyl (B); ○, 9.5×10^{-3} *M* B, 1×10^{-3} *M* $NaNH_2$; □, 1×10^{-3} *M* B, 1×10^{-3} *M* $NaNH_2$.

A single dose study in a solution containing $\leq 5 \times 10^{-4}$ *M* pyrene and 5×10^{-5} *M* $NaNH_2$ gave $G_{e_s^-} = 2.7$.

Liquid ND_3 at −15 °C

Similar experiments to those above were made in solutions containing 1×10^{-4} $NaND_2$ and biphenyl concentrations from 1×10^{-4} to 1.2×10^{-2} *M*. The results gave $G_{e_s^-} = 3.6 \pm 0.2$.

Liquid ND_3, −15 to −50 °C

Figure 4 shows results obtained as a function of temperature and dose per pulse in solutions containing $\sim 10^{-4}$ *M* $NaND_2$ and $\sim 10^{-2}$ *M* biphenyl. From the slope we calculate $G_{e_s^-} = 3.7_5 \pm 0.2$.

The results in NH_3 and ND_3 confirm our earlier indication (1) of a significant isotope

Can. J. Chem. Downloaded from www.nrcresearchpress.com by 210.87.254.5 on 09/05/12
For personal use only.

Can. J. Chem. Downloaded from www.nrcresearchpress.com by 210.87.254.5 on 09/05/12
For personal use only.

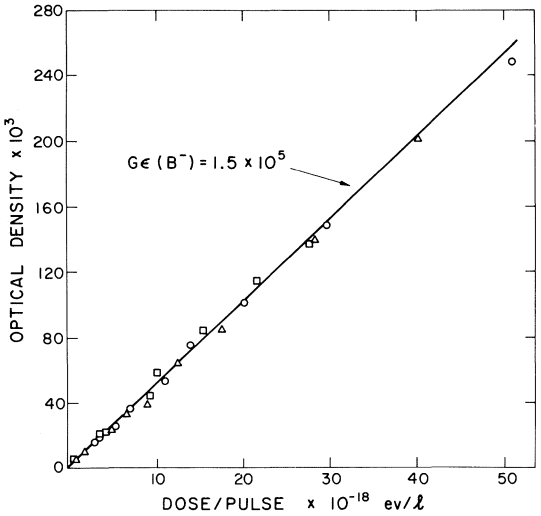

FIG. 4. Optical density of the biphenylide ion observed immediately after the pulse in liquid ND_3 containing $\sim 10^{-2}$ M B and $\sim 10^{-4}$ M $NaND_2$; cell length, 2.0 cm; △, −15 °C; ○, −30 °C; □, −50 °C.

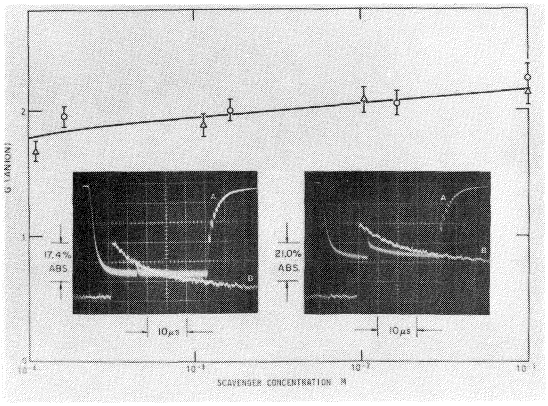

FIG. 5. Anion yields observed immediately after the pulse in methylamine; △, (biphenyl⁻); ○, (pyrene⁻). Insets show transient signals observed in a 1.0 cm cell, lower left trace B, formation and decay of (biphenyl⁻); dose/pulse 8.2×10^{19} eV l^{-1}; lower right trace B, formation and decay of (pyrene⁻), dose/pulse 1.2×10^{20} eV l^{-1}. In both cases trace A shows the analyzing light profile and transient signal at lower gain, abscissa, 500 μs/div.

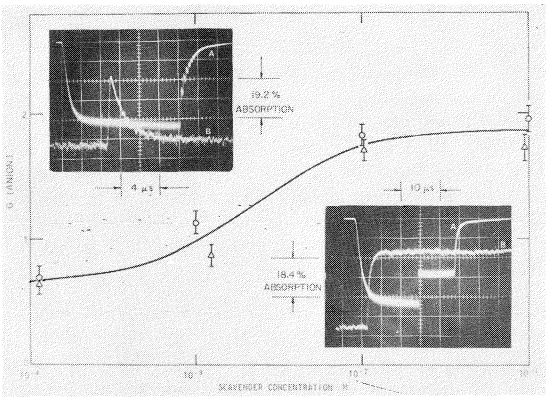

FIG. 6. Anion yields observed immediately after the pulse in ethylamine: △, (biphenyl⁻); ○, (pyrene⁻). Insets show transient signals observed in a 1.0 cm cell, upper left trace B, formation and decay of (biphenyl⁻), dose/pulse 1.6×10^{20} eV l^{-1}; lower right trace B, formation of (biphenyl⁻) in solutions containing $\sim 10^{-2}$ M biphenyl and 1.6×10^{-3} M CH_3CH_2NHK (see text); dose/pulse 2.1×10^{19} eV l^{-1}. In both cases trace A shows the analyzing light profile and transient signal at lower gain, abscissa, 500 μs/div.

effect for $G_{e_s^-}$ in the ammonia system. A comparable effect has been established in the analogous aqueous system where $G_{e_s^-} = 2.6$ in H_2O and 2.9 in D_2O (20–22). The effect of temperature on $G_{e_s^-}$ in ammonia is, however, within experimental error at −15 and −50 °C.

Considerable discrepancy exists in the literature concerning $G_{e_s^-}$ in liquid ammonia. Values range from ~0.35 (23, 24), 0.75 (25), 1.2 (26), ~3 (27) to our preliminary measurements (1) of 3.3 ± 0.3 (NH_3) and 3.6 ± 0.4 (ND_3). After the present paper was submitted for publication Farhataziz *et al.* (28) also reported $G_{e^-(am)} = 3.1 \pm 0.4$. Thus the most recent results all confirm the validity of the higher values.

Methylamine and Ethylamine

Figures 5 and 6 show the initial anion yields observed in methylamine and ethylamine as a function of biphenyl and pyrene concentration. The insets illustrate typical transient signals. Although the effect of scavenger concentration is more pronounced in ethylamine the end of pulse yield, $G(\text{anion})_0$, in both cases approaches a plateau at $\geq 10^{-2}$ M giving $G(\text{anion})_0 = G_{e_s^-} = 2.2 \pm 0.1$ and $1.8_4 \pm 0.1$ for methylamine and ethylamine, respectively. However, the addition of base in the form of the corresponding alkyl amide, CH_3NHM or CH_3CH_2NHM where M = alkali metal (2), results in an additional growth and stabilization of the anion absorption. This effect is shown by the oscilloscope traces in Fig. 6.

Quantitative studies of this effect were done only in ethylamine. It was shown that in solutions containing 10^{-2} M biphenyl $G(B^-)_0 = 1.8_4 \pm 0.2$, remains independent of base concentration from 6×10^{-5} to 10^{-2} M. However the long time scale yield, $G(B^-)_t$, is a function of

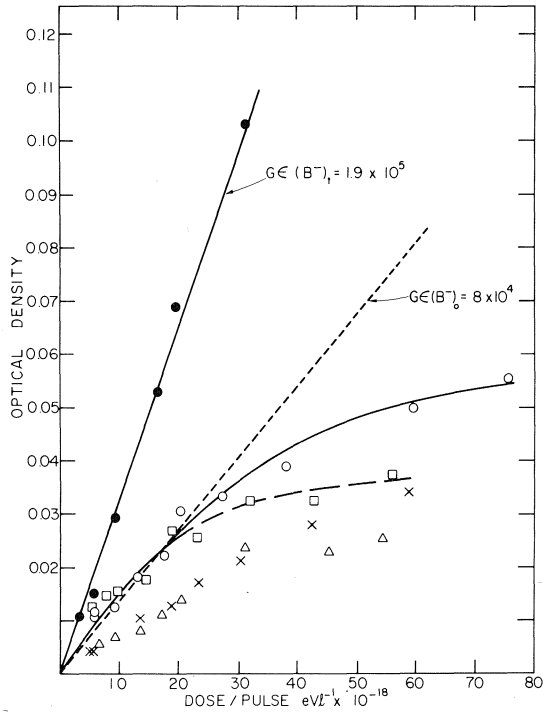

FIG. 7. Optical density of B_t^- observed in a 1.0 cm cell in the presence of various concentrations of potassium ethylamide: ●, 1.6×10^{-3} *M*; ○, 8.4×10^{-4} *M*; □, 7.6×10^{-4} *M*, △, 6.7×10^{-4} *M*, ×, 6.2×10^{-4} *M*. The optical densities △ and × were monitored 40 μs after the pulse (owing to faster decay of B^-) and the remainder 400 μs after the pulse. The dotted line represents the slope corresponding to the yield of B^- observed immediately after the pulse, $G(B^-)_0 = 2.0$.

base concentration. This is illustrated in Fig. 7 which shows that the optical density of B_t^-, measured 40–400 μs after the pulse, is markedly dose dependent at potassium ethylamide concentrations $<10^{-3}$ *M*. At 1.6×10^{-3} *M* and dose/pulse $\leq 4 \times 10^{19}$ eV l^{-1} $G(B^-)_t = 4.7_5 \pm 0.2$ (mean of 51 separate measurements) and is independent of biphenyl concentration from 10^{-4} to 10^{-1} *M*.

We suggest that $G(B^-)_t = G(e_s^-) = 4.8$ represents the ion yield due to scavenging of geminate and solvated electrons while $G(B^-)_0 = G_{e_s^-} \sim 2.0$ is the free ion or homogeneous yield of solvated electrons (29, 30). However $G(B^-)_t$ is not observed instantaneously indicating that the conversion of geminate electrons to B_t^- is more complex than simple scavenging in the spur. Since aromatic radical anions are readily protonated (12, 18, 31) it is possible that B^- produced in the spur could first recombine with the geminate positive ion (RH^+)

[3] $$B^- + RH^+ \rightarrow BH\cdot + R$$

followed by a slower regeneration step involving the solvent base (RNH^-)

[4] $$BH\cdot + RNH^- \rightarrow B^- + RNH_2$$

Although this process is speculative a weak absorption ($G\varepsilon \sim 2 \times 10^4$ M^{-1} cm^{-1}) with a maximum at ~310 nm is observed 1–2 μs after the pulse and may be due to BH· (12, 32). Furthermore in solutions containing 10^{-2} *M* biphenyl and 8×10^{-4} *M* potassium ethylamide this absorption decays at a rate corresponding to the concomitant formation of B_t^-.

The marked dose dependence is probably due to a second order disappearance of BH·, B^-, or their precursors e_s^-, (M^+, e_s^-), or M^-, with positive ions or solvent radicals, R, produced during the pulse (33). Increasing concentrations of base may inhibit such processes by removing the positive ion and/or converting R into a less reactive basic form as in ethanol (34).

We have not attempted any detailed kinetic study but note that in ethylamine the rate of formation of B_t^- is (*a*) first order, (*b*) increases with base concentration, and (*c*) is independent of biphenyl concentration. In 10^{-4} base the first order rate constant $k(B_t^-)_{obs} = 3 \times 10^5$ s^{-1}.

From other work in ethylenediamine (35) it has been proposed that the solvent base reacts with radiolytically produced radicals to form a radical ion which in turn subsequently rearranges to produce e_s^-. Alkali metal cations can also scavenge e_s^- to produce ion-pairs (M^+, e_s^-), which in turn can react with biphenyl to produce B^- (2, 13, 33). With these additional complications and the lack of information concerning the dissociation constants of alkali metal alkylamides in liquid amines (2), we feel that further speculation on the overall mechanism is outside the scope of this paper.

Comparisons with Previous Work

Steady state data obtained from the γ radiolysis of liquid methylamine (36) and ethylamine (37), give $G_{e_s^-} = 3.2 \pm 0.2$ and 2.1 ± 0.1, respectively. In both amines $G(H_2) = 5.5 \pm 0.1$ and $G_{e_s^-}$ was deduced by observing the decrease in $G(H_2)$ in the presence of electron scavengers. Experiments were not extended to basic solution although the addition of acid did enhance the yield of hydrogen by a further 0.6. This increase was attributed to the scavenging of geminate electrons which otherwise would not form hydrogen.

Can. J. Chem. Downloaded from www.nrcresearchpress.com by 210.87.254.5 on 09/05/12
For personal use only.

Can. J. Chem. Downloaded from www.nrcresearchpress.com by 210.87.254.5 on 09/05/12
For personal use only.

Our results clearly demonstrate that additional e_s^- can be scavenged, and apparently more easily, in basic amine solutions. Furthermore a value of $G_{e_s^-} \geq 4$ is self consistent with our earlier work concerning the yield and extinction coefficient of Na^- ($G\varepsilon \sim 2 \times 10^5$) in the pulse radiolysis of ethylamine (2). Assuming $G_{e_s^-} = 4.8$ then $G_{Na^-} = 2.4$ and $\varepsilon_{Na^-} \sim 8$ to $10 \times 10^4\ M^{-1}\ cm^{-1}$ which is in good agreement with previous measurements (2, 38).

By comparison in pure water $G_{e_s^-} = 2.8$ at 120 ns and 3.6 at 7.5 ns after a 5 ns pulse and increases to ≤ 5 in the presence of 1 *M* OH^- and 1 *M* CH_3OH (39). This time and concentration dependence was explained in terms of the diffusion model and competing spur processes for e_s^-. Since lower solute concentrations are required in amines our results suggest that the time scale for spur processes must be longer than those observed in water. In liquid ammonia Farhataziz *et al.* (28), comment that $G_{e_s^-}$ is exceptionally large and, compared to water, indicates some difference in the nature of the spur processes. Further theoretical studies are required to explain this apparent anomaly.

Decay Kinetics of B^- and P^-

No attempt was made to study the decay mechanisms of B^- or P^- since these are quite clearly complex and of mixed order. A few points are however worth noting. In a given solvent P^- decays more slowly than B^-. Both anions have longer "half lives" in methylamine (and NH_3) than in ethylamine. An indication of these differences can be seen by reference to the oscilloscope traces in Figs. 5 and 6. The second order component (*i.e.* dose dependence) of the decay is more significant in methylamine than in ethylamine.

1. W. A. Seddon, J. W. Fletcher, J. Jevcak, and F. C. Sopchyshyn. Can. J. Chem. **51**, 3653 (1973).
2. J. W. Fletcher, W. A. Seddon, and F. C. Sopchyshyn. Can. J. Chem. **51**, 2975 (1973).
3. J. Belloni and J. F. De La Renaudiére. Nature Phys. Sci. **232**, 173 (1971).
4. J. Corset and G. Lepoutre. Metal-ammonia solutions. *Edited by* G. Lepoutre and M. J. Sienko. W. A. Benjamin Inc., New York. 1964. p. 187.
5. W. A. Seddon, C. Willis, M. J. Young, and E. B. Selkirk. Atomic Energy of Canada Limited report No. AECL-3853.
6. W. A. Seddon, J. W. Fletcher, and F. C. Sopchyshyn. Can. J. Chem. **51**, 1123 (1973).
7. M. J. Berger and S. M. Seltzer. Tables of energy losses and ranges of electrons and positrons, NASA report No. SP-3012. 1964.
8. C. A. Hutchison, Jr. and D. E. O'Reilly. J. Chem. Phys. **34**, 163 (1961).
9. Matheson gas data book. The Matheson Co. Inc. Matheson of Canada Limited, Whitby, Ontario. 1961. pp. 311, 305.
10. E. W. Washburn (*Editor-in-chief*). International critical tables, Vol. III. McGraw Hill Book Co., Inc., New York and London. 1928. p. 23.
11. I. A. Taub, D. A. Harter, M. C. Sauer, Jr., and L. M. Dorfman. J. Chem. Phys. **41**, 979 (1964).
12. S. Arai and L. M. Dorfman. J. Chem. Phys. **41**, 2190 (1964).
13. B. Bockrath and L. M. Dorfman. J. Phys. Chem. **77**, 1002 (1973).
14. F. Y. Jou and L. M. Dorfman. J. Chem. Phys. **58**, 4715 (1973).
15. J. Jagur-Grodzinski, M. Feld, S. L. Yang, and M. Szwarc. J. Phys. Chem. **69**, 628 (1965).
16. E. Hayon. J. Chem. Phys. **53**, 2353 (1970).
17. P. Balk, G. J. Hoijtink, and J. W. Schreurs. Rec. Trav. Chim. **76**, 813 (1957).
18. S. Arai, D. A. Grev, and L. M. Dorfman. J. Chem. Phys. **46**, 2572 (1967).
19. J. H. Baxendale, D. Beaumond, and M. A. J. Rodgers. Trans. Faraday Soc. **66**, 1996 (1970).
20. E. M. Fielden and E. J. Hart. Radiat. Res. **33**, 426 (1968).
21. E. M. Fielden and E. J. Hart. Radiat. Res. **32**, 564 (1967).
22. K. D. Asmus and J. H. Fendler. J. Phys. Chem. **73**, 1583 (1969).
23. D. M. J. Compton, J. F. Bryant, R. A. Cesena, and B. L. Gehman. Pulse radiolysis. Academic Press, New York. 1965. p. 43.
24. F. S. Dainton, T. Skwarski, D. Smithies, and E. Wezranowski. Trans. Faraday Soc. **60**, 1068 (1964).
25. J. Belloni and J. F. De La Renaudiére. Int. J. Radiat. Phys. Chem. **5**, 22 (1973); **5**, 31 (1973).
26. G. I. Khaikin, V. A. Zhigunov, and P. I. Dolin. High Energy Chem. Engl. Trans. **5**, 44 (1971).
27. B. Ward. Adv. Chem. Ser. **81**, 601 (1968).
28. Farhataziz, L. M. Perkey, and R. R. Hentz. J. Chem. Phys. **60**, 717 (1974).
29. J. M. Warman, K.-D. Asmus, and R. H. Schuler. Adv. Chem. Ser. **82**, 25 (1968).
30. S. J. Rzad, P. P. Infelta, J. M. Warman, and R. H. Schuler. J. Chem. Phys. **52**, 3971 (1970).
31. S. Arai, E. L. Tremba, J. R. Brandon, and L. M. Dorfman. Can. J. Chem. **45**, 1119 (1967).
32. F. S. Dainton, G. A. Salmon, and U. F. Zucker. Proc. R. Soc. Lond. A**325**, 23 (1971).
33. G. A. Salmon, W. A. Seddon, and J. W. Fletcher. Can. J. Chem. This issue.
34. J. W. Fletcher, P. J. Richards, and W. A. Seddon. Can. J. Chem. **48**, 3765 (1970).
35. J. L. Dye, M. G. DeBacker, J. A. Eyre, and L. M. Dorfman. J. Phys. Chem. **76**, 839 (1972).
36. D. Smithies and A. J. Whitworth. J. Chem. Soc. A, 1987 (1969).
37. A. Habersbergerová, I. Janovský, and J. Teply. Chem. Commun. 1678 (1970).
38. M. G. DeBacker and J. L. Dye. J. Phys. Chem. **75**, 3092 (1971).
39. G. V. Buxton. Proc. R. Soc. Lond. A**328**, 9 (1972).

Hydrates des halogenures de gallium. II[1] Spectroscopie de vibration des complexes coordinés $GaX_3 \cdot H_2O$ (X = Cl ou Br)

JACQUES ROZIERE,[2] MARIE-THÉRÈSE ROZIERE-BORIES, ALAIN MANTEGHETTI ET ANTOINE POTIER

Laboratoire des Acides Minéraux, associé au CNRS nº 79, Université des Sciences et Techniques du Languedoc 34060 Montpellier, France

Reçu 5 mars 1974

JACQUES ROZIERE, MARIE-THÉRÈSE ROZIERE-BORIES, ALAIN MANTEGHETTI et ANTOINE POTIER. Can. J. Chem. **52**, 3274 (1974).

$GaX_3.H_2O$ (X = Cl, Br) est un complexe tetracoordiné du gallium. Les attributions sont faites à partir des hydrates, deutériates et deutériates partiels dans l'état solide. Les modèles de base sont $OGaX_3$ (C_{3v}) et H_2O (C_{2v}), la symétrie maximale du complexe peut être C_s mais elle est en réalité C_1 car les deux liaisons O—H de l'eau ne sont pas équivalentes. Les fréquences de vibration "Ga—O" sont identifiées et le champ de force calculé. La liaison de coordination est forte et les liaisons Ga—X sont plus courtes que dans les ions GaX_4^-.

JACQUES ROZIERE, MARIE-THÉRÈSE ROZIERE-BORIES, ALAIN MANTEGHETTI, and ANTOINE POTIER. Can. J. Chem. **52**, 3274 (1974).

$GaX_3.H_2O$ (X = Cl, Br) is a tetrahedrally coordinated adduct of gallium. From vibrational spectra of hydrates, deuteriates, and mixed crystals, bands assignments are made. Spectra are consistent with $OGaX_3$ (C_{3v}) and H_2O (C_{2v}) groups but the maximum symmetry of the whole complex (C_s) is lowered to C_1 owing to the nonequivalence of the two O—H of the water molecule. The "Ga—O" stretching modes are located and the valence force field of $OGaX_3$ skeleton is computed. The coordination bond is strong and the halogen–metal bonds are shorter than in the tetrahalogenogallate ions.

Introduction

Si l'on connaît de nombreux composés d'addition 1:1 entre les halogénures de bore, d'aluminum et de gallium et un ligand, peu d'entre eux ont fait l'objet de déterminations structurales. Parmi les plus récentes, on citera:

$C_6H_5COCl: \rightarrow AlCl_3$ (réf. 1)

$H_2S: \rightarrow AlBr_3$ (réf. 2)

$Me_2O: \rightarrow BF_3$ (réf. 3)

$H_3N: \rightarrow BF_3$ (réf. 4)

Dans tous les cas, le groupement $L—MX_3$ est pyramidal, l'atome métallique occupant le centre d'un tétraèdre pratiquement régulier formé par les trois halogènes et l'atome donneur d'électrons.

Il est normal d'accepter la même structure pour les monohydrates considérés ici; d'ailleurs, une étude rapide permet d'éliminer d'autres structures admissibles qui pourraient être: ($Ga_2X_6.2H_2O$), ($Ga_2X_6OH^-.H_3O^+$), ($GaX_4^-.GaX_2(H_2O)_2^+$) soit du fait de la relative pauvreté des spectres, soit pour des raisons plus spécifiques (absence de ponts Ga—X—Ga, Ga—O—Ga, etc..).

Resultats experimentaux

Sur la fig. 1, on a reporté les spectres infrarouges à −180 °C du monohydrate de $GaBr_3$ fortement deutérié (95% D_2O, 5% H_2O) et

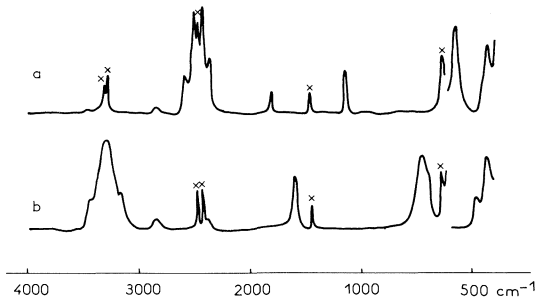

FIG. 1. Spectres infrarouges du monohydrate du tribromure de gallium: (*a*) fortement deutérié (95% D_2O, 5% H_2O); (*b*) faiblement deutérié (5% D_2O, 95% H_2O). Les bandes marquées d'une croix sont dues aux molécules isotopiques HOD.

[1]La première partie de cette étude: Hydrates successifs du tribromure de gallium – Equilibres liquide–solide doit paraître au Bulletin de la Société Chimique de France.

[2]À qui toute correspondance doit être adressée.

Can. J. Chem. Downloaded from www.nrcresearchpress.com by 210.87.254.42 on 09/05/12
For personal use only.

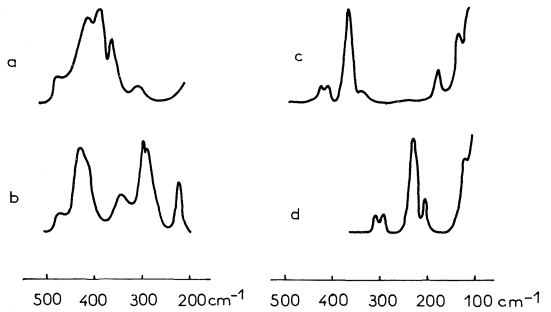

FIG. 2. Spectres infrarouges et Raman des monohydrates $GaX_3.H_2O$ au dessous de 500 cm^{-1}: (*a*) spectre infrarouge de $GaCl_3.H_2O$ (*b*) spectre infrarouge de $GaBr_3.H_2O$ (*c*) spectre Raman de $GaCl_3.H_2O$ (*d*) spectre Raman de $GaBr_3.H_2O$.

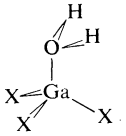

FIG 3. Géométrie du complexe $GaX_3.H_2O$. Les angles autour des atomes de gallium et d'oxygène sont supposés tétraédriques.

faiblement deutérié (5% D_2O, 95% H_2O) entre 400 et 4000 cm^{-1}. Sur la fig. 2, sont représentés les spectres infrarouges entre 200 et 500 cm^{-1} et Raman entre 100 et 500 cm^{-1} de $GaCl_3.H_2O$ et $GaBr_3.H_2O$ à température ambiante. Les fréquences observées font l'objet des tableaux 2 et 3.

Modele de base et denombrement

On considère que $H_2O: \rightarrow GaX_3$ est un complexe de coordination très classique où le gallium est à la coordinence 4. Le modèle le plus simple est le motif représenté ci-dessous (fig. 3).

Les modes de vibration peuvent être décrits, en première approximation, dans l'hypothèse des vibrations de groupe. Il y a alors à considérer les vibrations du groupe H_2O et celles du groupe OMX_3, puis celles résultant de l'association de ces deux groupes. La symétrie maximale de l'ensemble est C_s lorsqu'un plan de symétrie du groupe OMX_3 coïncide avec le plan de symétrie du groupe H_2O.

On doit attendre six vibrations fondamentales pour le squelette $OGaX_3$, toutes actives à la fois en infrarouge et Raman: deux modes de vibration de valence ν_s et $\nu_{deg}(GaX_3)$, deux modes de vibration de déformation δ_s et $\delta_{deg}(GaX_3)$, un mode de vibration de balancement $\rho_{deg}(GaX_3)$ et un mode de vibration de valence $\nu(GaO)$. Du fait de la plus basse symétrie du complexe, les mouvements dégénérés du groupe $OGaX_3$ peuvent éclater en deux composantes.

Outre les vibrations caractéristiques de la molécule d'eau: $\nu_s(H_2O)$, $\nu_{as}(H_2O)$ et $\delta(H_2O)$, il existe trois vibrations provenant des mouvements de rotation de cette même molécule: R_z, R_y, R_x qui sont respectivement la torsion $\tau(H_2O)$, la rotation plane $\rho(H_2O)$ et le balancement $\omega(H_2O)$.

Etude générale

On étudiera séparément les vibrations propres aux complexes qui sont entremêlées dans le domaine 100–1000 cm^{-1} et les vibrations internes des molécules H_2O, HDO, D_2O, seules présentes entre 1000 et 4000 cm^{-1}.

(I) Vibrations du squelette et librations de l'eau

(a) Méthode d'attribution

Discutant des résultats obtenus en termes de vibrations ou de fréquences de groupe, on utilisera les trois critères principaux suivants: (*i*) l'effet isotopique du deuterium qui doit permettre de différencier les librations de l'eau des vibrations du squelette, (*ii*) la substitution d'halogène qui a pour effet principal de différencier les vibrations de valence métal–halogène de la vibration de valence $\nu(GaO)$, (*iii*) enfin, la comparaison avec les spectres de vibration de composés voisins, en particulier, les complexes d'addition GaX_3–éther.

(b) Discussion

Librations de l'eau

La bande intense en infrarouge vers 770 cm^{-1} et l'épaulement vers 480 cm^{-1} dans le spectre de $GaCl_3.H_2O$ se retrouvent peu déplacés dans le spectre de $GaBr_3.H_2O$ mais disparaissent dans le spectre de $GaCl_3.D_2O$. Seul, l'équivalent de la bande la plus intense est observé vers 585 cm^{-1}; nous pensons que l'autre bande est masquée par l'absorption $\nu_s(GaCl_3)$ à 360 cm^{-1}. Le rapport des fréquences ν_H/ν_D peut être comparé aux valeurs attendues pour les vibrations de rotation d'une molécule H_2O isolée: ν_H/ν_D (torsion) $\simeq$ 1.41, ν_H/ν_D(balancement) $\simeq$ 1.34, ν_H/ν_D(rotation plane) $\simeq$ 1.39.

Nous pensons que le rapport isotopique observé de 1.32 et l'intensité de l'absorption à 770 cm^{-1} permettent d'attribuer cette bande au balancement $\omega(H_2O)$. L'épaulement à 480

Can. J. Chem. Downloaded from www.nrcresearchpress.com by 210.87.254.42 on 09/05/12
For personal use only.

TABLEAU 1. Fréquences infrarouge et Raman du squelette O—GaX_3*

(*a*) $GaCl_3$

Infrarouge Et_2O–$GaCl_3$	Infrarouge THF–$GaCl_3$	H_2O–$GaCl_3$ Infrarouge	H_2O–$GaCl_3$ Raman	Attributions
412	415	410 F 390 F	418 f 404 f	$\nu_{deg}(GaCl_3)$ et ν(GaO)
361	360	360 ép 320 f	364 F 320 f	ν_s ($GaCl_3$) 2 $\rho_{deg}(GaCl_3)$
155			169 f	$\rho_{deg}(GaCl_3)$
140				

(*b*) $GaBr_3$

Infrarouge Et_2O–$GaBr_3$ Réf. 5	Réf. 6	H_2O–$GaBr_3$ Infrarouge	Raman	Attributions
	450†	440 F 345 f		ν(GaO) ν_s ($GaBr_3$) + $\rho_{deg}(GaBr_3)$
308	304	305 F 295 F	310 f 290 f	$\nu_{deg}(GaBr_3)$
230	224	230 ép	225 F 204 M	ν_s ($GaBr_3$) $\rho_{deg}(GaBr_3)$ + $\delta_s(GaBr_3)$
112			120 f	$\rho_{deg}(GaBr_3)$
85				δ_s ($GaBr_3$)

*Intensités relatives des bandes: F, fort; M, moyen; f, faible; ép, épaulement.
†Observé mais non attribué par (2).

cm^{-1} provient plutôt de la rotation plane $\rho(H_2O)$.

Vibrations métal–halogène

Au dessous de 500 cm^{-1}, plusieurs bandes infrarouges et Raman ne sont pas sensibles à la substitution isotopique mais sont fortement déplacées par changement d'halogène. Les absorptions intenses du composé chloré à 410 et 390 cm^{-1} se retrouvent à 305 et 295 cm^{-1} dans le spectre infrarouge de $GaBr_3.H_2O$. La raie de diffusion intense à 364 cm^{-1} dans le spectre Raman de $GaCl_3.H_2O$ se retrouve à 230 cm^{-1} dans celui du composé bromé. Ces fréquences doivent donc correspondre aux vibrations de valence métal–halogène. La comparaison des intensités relatives de ces bandes en infrarouge et Raman, la comparaison avec de nombreux composés L—GaX_3 où L est un ligand organique (5, 6), nous permettent d'attribuer les bandes de plus hautes fréquences (intenses en infrarouge) aux vibrations provenant de la levée de dégénérescence de $\nu_{deg}(GaX_3)$, celle de plus basse fréquence (intense en Raman) à la vibration $\nu_s(GaX_3)$. Dans le tableau suivant, ces fréquences peuvent être comparées à celles obtenues par différents auteurs pour des complexes L—GaX_3 (5, 6). (Tableau 1).

Ceci confirme la structure proposée comme hypothèse de départ: l'atome de gallium est dans un environnement tétraédrique constitué par trois atomes d'halogène et l'atome d'oxygène provenant de la molécule d'eau.

Les bandes observées en diffusion à des fréquences inférieures à 200 cm^{-1} ne sont pas attribuables avec précision; elles correspondent certainement aux vibrations de déformation du squelette: $\rho_{deg}(GaX_3)$, δ_s et $\delta_{as}(GaX_3)$.

Il faut toutefois remarquer que l'éclatement des vibrations $\nu_{deg}(GaX_3)$ théoriquement prévu n'est pas observé pour les complexes Et_2OGaX_3 ou $THFGaX_3$ par Greenwood *et al.* (5) ou Lewis *et al.* (6). Les spectres de ces complexes ont été obtenus dans l'état liquide ou en solution et on peut être tenté d'attribuer l'éclatement observé pour $GaX_3.H_2O$ à un effet de cristal: coulage

Can. J. Chem. Downloaded from www.nrcresearchpress.com by 210.87.254.42 on 09/05/12
For personal use only.

TABLEAU 2. Fréquences infrarouge des complexes entre 4000 et 400 cm^{-1}*

Fréquence				
$GaCl_3.H_2O$	$GaBr_3.H_2O$	$GaCl_3.D_2O$	$GaBr_3.D_2O$	Attributions
	3420 ép	2620 ép	2600 ép	
3290 TF	3290 TF	2460 TF	2460 TF	ν_s et $\nu_{as}(H_2O)$
3180 ép	3180 ép	2350 ép	2350 ép	$2\delta(H_2O)$
2380 M	2350 M	1800 f	1770 f	$\delta(H_2O) + \omega(H_2O)$
1615 M	1605 M	1185 M	1175 M	$\delta(H_2O)$
770 F	750 F	585 F	570 F	$\omega(H_2O)$
480 ép	475 ép			$\rho(H_2O)$
	440 TF		418 TF	ν(GaO)
410 TF		410 TF		$\nu_{deg}(GaCl_3) + \nu$(GaO)

*Intensités relatives des bandes: TF, très fort; F, fort; M, moyen; f, faible; ép, épaulement.

TABLEAU 3. Bandes provenant de HDO en dilution isotopique

$GaBr_3.HDO$	$GaCl_3.HDO$	Attributions
3305	3315	ν(OH)
3270	3275	
2800	2840	2 ∂(HDO)
2465	2470	ν(OD)
2435	2440	
2070	2100	∂(HDO) + ω(HDO)
1420	1445	∂(HDO)
640	655	ω(HDO)

intermoléculaire ou effet de site. Etant donné l'écart assez important pour les deux composantes (17 cm^{-1} en moyenne pour $GaCl_3.H_2O$, 15 cm^{-1} pour $GaBr_3.H_2O$), on peut penser plutôt à un effet de site accompagné d'une distorsion appréciable des groupes terminaux GaX_3.[3]

Localisation de la vibration (GaO)

Il existe peu de données dans la bibliographie. Carty *et al.* (7), dans l'ion $[Ga(Me_2SO)_6]^{3+}$, la situent entre 400 et 500 cm^{-1}. Ici, on peut utiliser les deux critères suivants: absence de déplacement par substitution d'halogène et déplacement isotopique puisque cette vibration peut être considérée comme une des trois translations de l'eau.

Dans le spectre infrarouge de $GaBr_3.H_2O$, une bande très intense, dont le maximum se situe vers 440 cm^{-1}, glisse vers 418 cm^{-1} dans le spectre de $GaBr_3.D_2O$; le rapport des fréquences ($\rho \simeq 1.05$) est tout à fait compatible avec celui attendu pour une des translations de l'eau. Il est plus difficile de localiser la vibration ν(GaO) dans le spectre de $GaCl_3.H_2O$. Dans le spectre infrarouge, ce domaine est obscurci par la vibration $\nu_{deg}(GaCl_3)$ particulièrement intense et il est probable que la vibration métal–oxygène est ici masquée par cette bande dont le maximum se situe vers 410 cm^{-1}. On peut remarquer que l'intensité de cette bande doit être particulièrement faible en diffusion puisque rien n'apparaît entre 420 et 500 cm^{-1} dans le spectre Raman de ces complexes.

(II) Vibrations internes de l'eau

(a) Méthode d'attribution

Dans le domaine entre 4000 et 1000 cm^{-1}, on n'attend que les vibrations internes de la molécule d'eau.

TABLEAU 4. Champ de force de valence des motifs $OGaX_3$*

	$OGaCl_3$	$OGaBr_3$
Constantes de forces principales		
k(GaO)	1.43	1.48
$F(\nu_s(GaX_3))$	2.25	2.05
$F(\nu_{deg}(GaX_3))$	2.14	1.90
$F(\partial_s(GaX_3))$	0.55	0.50
$F(\partial_{deg}(GaX_3))$	0.50	0.43
$F(\rho_{deg}(GaX_3))$	0.50	0.43
Constantes d'interactions		
ν(GaO) ↔ $\nu_s(GaX_3)$	0.20	0.30
$\nu_s(GaX_3)$ ↔ $\delta_s(GaX_3)$	0.30	0.20
ν(GaO) ↔ $\delta_s(GaX_3)$	−0.20	−0.35
$\nu_{deg}(GaX_3)$ ↔ $\delta_{deg}(GaX_3)$	−0.29	−0.28
$\nu_{deg}(GaX_3)$ ↔ $\rho_{deg}(GaX_3)$	0.29	0.28
$\delta_{deg}(GaX_3)$ ↔ $\rho_{deg}(GaX_3)$		0.02

*Les constantes de forces correspondant aux différentes vibrations de groupes sont données en: 10^{-5} dyn/cm pour les vibrations de valence, 10^{-11} dyn cm/rad^2 pour les vibrations de déformation, 10^{-3} dyn/rad pour les interactions valence-déformation.

Les constantes de forces de liaisons et d'angles peuvent être obtenues à partir des valeurs de ce tableau par des relations simples telles que: $k(GaX) = [F(\nu_s(GaX_3) + 2F(\nu_{deg}(GaX_3))]/3$.

[3]Les auteurs tiennent à remercier l'un des rapporteurs pour avoir attiré leur attention sur ce point.

Can. J. Chem. Downloaded from www.nrcresearchpress.com by 210.87.254.42 on 09/05/12
For personal use only.

Can. J. Chem. Downloaded from www.nrcresearchpress.com by 210.87.254.42 on 09/05/12
For personal use only.

Plusieurs facteurs sont susceptibles de modifier le spectre de l'eau dans un sel hydraté: liaison hydrogène, effet de coordination de l'atome d'oxygène sur le métal, multiplicité des bandes due, soit à l'interaction entre molécules d'une même maille (effet de corrélation), soit à l'existence de molécules d'eau non équivalentes à l'intérieur de la maille cristalline. La méthode des cristaux mixtes (obtenus par dilution isotopique) déjà décrite par Falk et coll. (8) permet de supprimer le couplage intermoléculaire et de mettre en évidence l'existence (ou la non existence) de molécules d'eau non équivalentes. Cette méthode a, de plus, l'avantage de préciser la géometrie de la molécule d'eau et de différencier les vibrateurs OH (ou OD), deux vibrateurs différents donnant naissance à deux bandes ν(OH) (ou ν(OD)).

(b) Discussion

Spectres des composés hydrogénés

Dans les spectres infrarouges des deux hydrates, les bandes, qui apparaissent à 3290 et 1615 cm^{-1} (1605 cm^{-1} pour $GaBr_3.H_2O$), sont dues aux vibrations de valence et de déformation. Aucune de ces deux bandes ne semble dédoublée, même à basse température (−180 °C). Il apparaît seulement un épaulement à la première vers 3180 cm^{-1} qui semble correspondre à l'harmonique 2 $\delta(H_2O)$. Une bande additionnelle de faible intensité est observée vers 2360 cm^{-1} et peut être attribuée à une combinaison $\delta(H_2O) + \omega(H_2O)$. L'abaissement de température ne cause aucune modification importante du spectre, ni augmentation d'intensité, ni déplacement en fréquence (excepté pour la combinaison qui devient plus intense), contrairement à ce qui aurait pu être attendu dans le cas d'interactions fortes par liaison hydrogène. Toutes ces bandes subissent le déplacement isotopique habituel après deutériation.

Théoriquement, on doit attendre dans la région 4000–3000 cm^{-1} les deux vibrations de valence de la molécule d'eau: ν_s et $\nu_{as}(H_2O)$. Il est probable que ces deux vibrations se situent ici à des fréquences voisines et que chacune peut donner lieu à différentes composantes provenant du couplage des mouvements de molécules voisines. Ceci doit conduire à l'existence d'une bande unique dont le maximum se situe à 3290 cm^{-1}.

Ce point particulier peut être éclairci par la dilution isotopique et la deutériation partielle de la molécule d'eau.

Bandes de HDO, H_2O et D_2O en dilution isotopique, environnement et symétrie de la molécule d'eau

A faible concentration de deuterium ou d'hydrogène (5% H_2O, 95% D_2O et 5% D_2O, 95% H_2O), les trois vibrations fondamentales des molécules HDO: ν(OH), ν(OD) et δ donnent des bandes simples à température ambiante. A la température de l'air liquide, les vibrations de valence ν(OH) et ν(OD) éclatent en deux composantes (3305 cm^{-1}, 3270 cm^{-1} pour ν(OH) et 2455, 2435 cm^{-1} pour ν(OD) dans le bromure). Les rapports isotopiques pour les deux fréquences sont très voisins (1.342 ± 0.001 et 1.347 ± 0.001). Ce phénomène est dû à l'existence de *deux groupes OH distincts dans le cristal.* L'application de la règle de Badger (9) conduit à une différence de distance O—H de l'ordre de 5×10^{-3} Å. Ces deux groupes distincts peuvent provenir, soit de l'existence de deux espèces de molécules d'eau différentes mais symétriques, soit d'une seule espèce de molécule d'eau asymétrique.

Pour des concentrations plus élevées de deuterium ou d'hydrogène, l'apparition d'un seul pic pour la déformation d'une molécule H_2O ou D_2O isotopiquement isolée prouve l'existence d'*un seul type de molécule distordue* dans un environnement dissymétrique. La distorsion est plus importante à basse température puisqu'à température ambiante, les deux groupes OH sont indiscernables spectroscopiquement. Dans ces domaines de concentration, on peut voir apparaître de part et d'autre des bandes ν(OH) des molécules HDO les bandes $\nu_s(H_2O)$ et $\nu_{as}(H_2O)$ de la molécule d'eau en dilution isotopique ($\nu_{as}(H_2O)$ à 3350 cm^{-1}, $\nu_{as}(D_2O)$ à 2490 cm^{-1} et $\nu_s(H_2O)$ à 3250 cm^{-1}, $\nu_s(D_2O)$ à 2405 cm^{-1} pour le bromure).

Pour des concentrations supérieures à 50%, les bandes ν(OH) et ν(OD) sont plus structurées; en particulier, cette structure est due à l'apparition de l'harmonique 2 $\delta(H_2O)$ et en partie aux composantes provenant du couplage intermoléculaire. Cependant, deux épaulements sur la branche haute fréquence peuvent être attribués à des combinaisons des vibrations ν(OH) avec des modes de basse fréquence. En effet, les différences (ν(combinaison) − ν(OH) $\simeq 160 \pm 10$ cm^{-1} pour $GaCl_3.H_2O$, 130 ± 10 cm^{-1} pour $GaBr_3.H_2O$) semblent présenter une légère dépendance à l'égard de la substitution d'halogène mais, par contre, ne sont pas apparemment

Can. J. Chem. Downloaded from www.nrcresearchpress.com by 210.87.254.42 on 09/05/12
For personal use only.

très sensibles à la substitution isotopique. Or, en Raman, des bandes à 169 cm^{-1} pour le composé chloré, 120 cm^{-1} pour le composé bromé, ont été déjà décrites comme des vibrations de déformation du squelette. Certains de ces modes pouvant posséder un caractère de translation de la molécule d'eau, il n'est pas exclu qu'ils puissent participer à ces combinaisons.

Effet de la coordination: constantes de forces des complexes

(I) Sur la molécule d'eau

On doit remarquer tout d'abord que la substitution d'halogène n'a que très peu d'effet sur les fréquences ν(OH), ce qui laisse supposer que les interactions du groupe H_2O avec le reste du complexe et avec les molécules voisines sont du même ordre pour le composé chloré et le composé bromé.

Les fréquences ν_s et $\nu_{as}(H_2O)$ sont très inférieures à celles de la molécule isolée. Les constantes de forces des vibrateurs OH pour le composé bromé ($k_1 \simeq 6.04$ et $k_2 \simeq 5.94$ mdyn/Å) sont environ 20% plus faibles que celle de la molécule d'eau diluée dans un solvant inerte tel que CCl_4 (9). Cet affaiblissement de la liaison O—H est du même ordre que celui obtenu par la formation de liaisons hydrogène de force moyenne. Par exemple, les constantes de forces sont tout à fait comparables à celles obtenues pour le perchlorate de di-oxonium (10) où les molécules d'eau sont engagées dans des liaisons hydrogène de 2.78 et 2.79 Å (11). Cependant, bien que les bandes ν(OH) et ν(OD) de $GaX_3.H_2O$ et $GaX_3.D_2O$ soient relativement larges, les bandes ν(OH) et ν(OD) dans les cristaux mixtes sont étroites: la faible demi-largeur des bandes (inférieure à 10 cm^{-1}, par exemple, pour les bandes ν(OD)) n'est donc compatible qu'avec une liaison hydrogène faible. Les principales causes d'élargissement sont donc le couplage intermoléculaire et la présence de combinaisons et harmoniques dans le domaine des vibrations ν_s et $\nu_{as}(H_2O)$ et non la formation de liaisons hydrogène et nous pensons que *l'abaissement des fréquences ν(OH) est due en grande partie à l'affaiblissement des liaisons O—H par coordination de l'atome d'oxygène sur le gallium.*

(II) Sur le squelette $OGaX_3$

Il semble, après l'examen des vibrations du squelette $OGaX_3$, que la liaison GaO soit de force comparable dans le complexe bromé et le complexe chloré. La légère différence de fréquence observée peut provenir d'un couplage possible avec $\nu_s(GaX_3)$ résultant de la levée de dégénérescence de $\nu_{deg}(GaX_3)$ qui, dans le cas du chlorure, doit se situer à une fréquence voisine de ν(GaO).

Les attributions proposées pour les fréquences correspondant aux vibrations ν(GaO), $\nu_{deg}(GaX_3)$, $\nu_s(GaX_3)$ doivent permettre une estimation des constantes de forces metal–ligand à partir d'un modèle simplifié $OGaX_3$ de symétrie C_{3v}. De plus, le calcul des fréquences de vibrations de déformation à partir d'un champ de force dérivé de celui de l'anion tétraédrique GaX_4^- doit permettre de préciser les différentes attributions dans le domaine des vibrations de déformation du squelette. Les résultats sont rassemblés dans le tableau 4. La quasi transférabilité des constantes de force de l'anion GaX_4^- au squelette $OGaX_3$ constitue une bonne confirmation des attributions proposées. En particulier, se trouve justifiée l'attribution des vibrations de balancement $\rho_{deg}(GaX_3)$ à des fréquences supérieures à celles des vibrations de déformation $\delta_s(GaX_3)$. Les constantes de forces obtenues ici pour les liaisons Ga—O ($k \simeq 1.48$ mdyn/Å pour le bromure et $k \simeq 1.43$ mdyn/Å pour le chlorure) sont sensiblement plus faibles que celles obtenues par Derouault (13) pour les liaisons Al—O dans les complexes $(CH_3)_2O$—AlX_3 ($k \simeq 1.96$ pour le bromure et $k \simeq 1.91$ pour le chlorure). La liaison gallium–oxygène semble donc plus faible que la liaison aluminium–oxygène et ceci est en accord avec les forces relatives des deux acides de Lewis GaX_3 et AlX_3.

On peut remarquer que des conclusions différentes (la liaison Ga—O est plus forte que la liaison Al—O) ont été obtenues dans une étude récente des hexahydroxodialuminate et digallate de potassium ($KAl_2O(OH)_6$ et $KGa_2O(OH)_6$) (13) mais il faut penser que, dans ce dernier cas, ce sont plutôt les acidités relatives des atomes Ga et Al que l'on doit comparer. Les constantes de force k(Ga—O) sont très voisines dans les deux composés, bromé et chloré, ce qui indique que les acidités des deux halogénures sont très voisines. Greenwood *et al.* (5) font une remarque analogue pour les complexes 1–1 de $GaCl_3$ et $GaBr_3$ avec des ligands contenant le soufre ou l'azote comme atome donneur.

Les constantes de forces obtenues pour les

liaisons métal–halogène ($k \simeq 2.17$ pour le chlorure, $k \simeq 1.95$ pour le bromure) sont environ 6% plus élevées pour le chlorure et 12% plus forte pour le bromure que les constantes métal halogène des anions tétraédriques MX_4^- (14). Ce renforcement des liaisons peut être relié à un raccourcissement appréciable des distances gallium–halogène lorsqu'on passe de l'anion GaX_4^- à H_2O—GaX_3. Cet effet semble cependant moins important que lors du passage de $GaCl_4^-$ à $Ga_2Cl_7^-$ où un accroissement de plus de 15% de la constante de force (14) traduit un raccourcissement de 3×10^{-2} Å de la longueur moyenne des liaisons terminales Ga—Cl (15).

Conclusion

Le composé $GaX_3.H_2O$ est un des plus simples complexes de coordination. Cette simplicité a permis de donner une attribution complète du spectre de vibration et d'analyser les effets de la coordination sur le donneur et l'accepteur.

La liaison de coordination est forte (la vibration ν(GaO) est localisée entre 440 et 410 cm^{-1}) et les perturbations qu'elle apporte sont surtout sensibles sur les liaisons OH de la molécule d'eau. Le reste du squelette est affecté par la coordination et on a pu montrer que les distances métal–halogène étaient plus courtes que celles des anions tétraédriques MX_4^-.

L'analyse des spectres a permis de préciser la géométrie du complexe dans le cristal. L'atome de gallium est au centre d'un tétraèdre distordu formé par les trois atomes d'halogène et l'atome d'oxygène. La molécule d'eau est elle-même asymétrique. La symétrie du site du complexe ne peut donc être supérieure à C_1.

Techniques expérimentales et appareils

Les hydrates sont préparés directement par action de l'eau sur l'halogénure selon une technique déjà décrite (16–18).

Les spectres infrarouges entre 4000 et 200 cm^{-1} sont obtenus à partir de films polycristallins préparés par fusion et recristallisation du composé entre deux faces de fluorine, d'iodure de cesium ou de silicium suivant le domaine étudié.

Les spectromètres utilisés sont des appareils Perkin–Elmer 225 entre 200 et 400 cm^{-1} et 337 entre 400 et 4000 cm^{-1}. L'erreur sur les fréquences est de ± 5 cm^{-1} pour les bandes larges dans le domaine 4000 à 1000 cm^{-1} et de ± 1 cm^{-1} au dessous. Les spectres ont été enregistrés à température ambiante et à la température de l'air liquide dans des cellules de type conventionnel.

Les spectres Raman entre 500 et 100 cm^{-1} ont été obtenus à température ambiante pour des échantillons contenus dans des tubes scellés de Pyrex de 2 mm de diamètre. L'appareil utilisé est un spectromètre PH1 Coderg équipé d'un laser He–Ne Spectraphysics (70 mW sur la raie à 6328 Å).

1. S. C. Rasmussen et N. C. Broch. Acta Chem. Scand. **20**, 1351 (1966).
2. A. Weiss et R. Plass. Z. Anorg. Chem. **283**, 390 (1956).
3. S. H. Bauer, G. R. Finlay et A. W. Laubengayer. J. Am. Chem. Soc. **67**, 339 (1965).
4. J. L. Hoard, S. Geller et W. M. Cashin. Acta Cryst. **4**, 396 (1951).
5. N. N. Greenwood, T. S. Srivastava et B. P. Straughan. J. Chem. Soc. 699 (1966).
6. J. Lewis, J. R. Miller, R. L. Richard et A. Thompson. J. Chem. Soc. 5850 (1965).
7. A. J. Carty, H. A. Patel et P. M. Boorman. Can. J. Chem. **48**, 492 (1970).
8. V. Seild, O. Knop et M. Falk. Can. J. Chem. **47**, 1361 (1969).
9. R. Badger. J. Chem. Phys. **3**, 710 (1935).
10. P. Saumagne. Thèse d'Etat. Université de Bordeaux, Bordeaux, France. 1961.
11. J. Roziere. Thèse d'Etat. Université des Sciences et Techniques du Languedoc, Montpellier, France n° CNRS: AO 8634, 1973.
12. I. Olovsson. J. Chem. Phys. **49**, 1063 (1968).
13. J. Derouault. Thèse d'Etat. Université de Bordeaux, Bordeaux, France. n° CNRS: AO 2220. 1971.
14. J. Haladjian et J. Roziere. J. Inorg. Nucl. Chem. **35**, 3821 (1973).
15. A. Manteghetti. Thèse 3me Cycle. Université des Sciences et Techniques du Languedoc. Montpellier, France. 1973.
16. P. Vitse, B. Granier et A. Potier. Publication à paraître.
17. M. T. Bories. Thèse 3me Cycle. Université des Sciences et Techniques du Languedoc, Montpellier, France. 1970.
18. M. T. Bories, J. Roziere et A. Potier. J Chem. Soc. Chem. Commun. 213 (1971).

Can. J. Chem. Downloaded from www.nrcresearchpress.com by 210.87.254.42 on 09/05/12
For personal use only.

Phase Diagrams for the Sodium and Potassium Benzoate – Water Systems[1]

E. Colin W. Clarke and David N. Glew

Research and Development, Dow Chemical of Canada, Limited, Sarnia, Ontario N7T 7K7

Received March 11, 1974

E. Colin W. Clarke and David N. Glew. Can. J. Chem. **52**, 3281 (1974).

The low temperature phase diagrams have been determined for the potassium benzoate – water and the sodium benzoate – water systems. The ice eutectics with these anhydrous alkali benzoates were found at −11.8 °C with 34.89% potassium benzoate and at −14.5 °C with 39.7% sodium benzoate. Previously reported hydrates of potassium benzoate (3) were not observed. Concentrated sodium benzoate solutions below 0 °C were found to attain equilibrium with sodium benzoate only with the greatest difficulty.

E. Colin W. Clarke et David N. Glew. Can. J. Chem. **52**, 3281 (1974).

On a déterminé les diagrammes de phase à basse température des systèmes de benzoate de potassium – eau et benzoate de sodium – eau. On a trouvé que les eutectiques de glace pour ces benzoates alcalins anhydres sont à −11.8 °C avec 34.89% de benzoate de potassium et à −14.5 °C avec 39.7% de benzoate de sodium. On n'a pas observé les hydrates du benzoate de potassium (3) qui avaient été rapportés antérieurement. On a trouvé que les solutions concentrées de benzoate de sodium à des températures plus basses que 0 °C atteignent difficilement l'équilibre avec le benzoate de sodium. [Traduit par le journal]

Introduction

An interest in shipping aqueous potassium and sodium benzoate solutions in Canada prompted the need for us to know their low temperature phase diagrams. The potassium benzoate – water system had been previously much studied (2–4) but results were still incomplete. Results for the sodium benzoate – water system were fragmentary (2), despite the considerable use of sodium benzoate in the food and drug industries.

Experimental

Materials

Potassium benzoate was made by reaction of Fisher certified A.C.S. grade benzoic acid with Fisher certified A.C.S. grade potassium carbonate. The crude potassium benzoate was purified by recrystallization from ethanol containing about 10 vol% water. The potassium benzoate was shown to be anhydrous and dry by the zero weight loss of a sample after 24 h heating at 80 °C in a vacuum oven at 0.02 Torr. Equivalent weight determination (1) by perchloric acid titration in glacial acetic acid showed that the potassium benzoate was 99.8+% pure.

Fisher USP sodium benzoate was used both directly without purification and after recrystallization from water. A further sample was made by recrystallizing the product from the reaction of benzoic acid with sodium carbonate, both Fisher A.C.S. grade. Perchloric acid titration in glacial acetic acid (1) showed no detectable impurities in various preparations of sodium benzoate.

Saturated aqueous solutions of sodium benzoate invariably cooled to form voluminous gelatinous flocs from which it was difficult to filter the mother liquor; complete removal of water from the sodium benzoate gel was slow, requiring at least 24 h heating at 80 °C and 0.02 Torr.

Melting Point Determination

Equilibria between ice and aqueous benzoate solutions were determined by melting point measurements. The test solutions, containing 5 g water, were made up by weight in a stoppered test tube by first adding the solid benzoate and then the water. The test tube was cooled in a Dry Ice – acetone slush until the first solid separated from solution, after which the stopper was removed and a mercury-in-glass thermometer, marked every 0.2 °C from −38 to +42 °C, was inserted. The system was cooled slowly with continuous stirring by the thermometer until the temperature reached about −30 °C when the system was completely solid. The test tube was thermally insulated by inserting into a hole in a polyurethane foam block. The temperature was taken every 30 s and the system stirred when possible; this was continued until the temperature was at least 2 °C above that at which the last ice melted. The time–temperature plot indicated the eutectic melting point and the temperature at which the last crystal of ice melted.

Solubility Determination

Aqueous solubilities of the anhydrous benzoate salts were determined by an equilibrium method. The solubility vessel was a stoppered 50 ml volumetric flask which contained weighed quantities of salt and water, sufficient to yield 30 ml of saturated solution with about 10% of the solid undissolved at the experimental temperature. Stirring was effected by rotating the flask slowly in a water–glycol thermostat controlled within ±0.002 °C. The thermostat temperature was measured with a precision of 0.001 °C by a platinum resistance thermometer used with a Mueller bridge, amplifier, and galvanom-

[1]Contribution No. 197.

Can. J. Chem. Downloaded from www.nrcresearchpress.com by 210.87.254.40 on 09/05/12
For personal use only.

Can. J. Chem. Downloaded from www.nrcresearchpress.com by 210.87.254.40 on 09/05/12
For personal use only.

eter. After equilibration for at least 48 h a 2–3 ml sample of the solution was withdrawn through a glass wool filter via a hypodermic syringe, placed in a tared weighing bottle and weighed. The weight of salt in the sample was determined by evaporating the water slowly from the open weighing bottle initially on a hot plate at 90 °C and finally in a vacuum oven at 80 °C and 0.02 Torr.

Solid potassium benzoate settled rapidly leaving a clear saturated supernatant but the gel-like sodium benzoate did not settle over a period of hours and invariably plugged the glass wool filter so that it was difficult to withdraw a full 2 ml sample.

The saturated potassium benzoate solutions readily lost all water after 16 h on the hot plate so that further drying in the vacuum oven was unnecessary. However, the saturated sodium benzoate solutions were much more difficult to dry and did not give up all water even after 48 h on the hot plate. For these solutions water was evaporated by heating for 16 h on the hot plate and for at least 24 h in the vacuum oven.

Results and Discussion

Potassium Benzoate – Water System

The ice melting temperatures in aqueous potassium benzoate solutions are given in Table 1 and define curve AE in Fig. 1. Solubilities of anhydrous potassium benzoate are given in Table 2 and are plotted as curve CE. Values from the literature (2–4) are also plotted. Our measurements for the ice melting temperatures are in good agreement with those of Sidgwick and Ewbank (2), but differ systematically from Druzhinin and Sukhova (3). Our measurements for the solubility of anhydrous potassium benzoate are in good agreement with Pajetta (4) and in reasonable agreement with Sidgwick and Ewbank, but again differ systematically from Druzhinin and Sukhova. These latter authors claimed that their measurements between 9.2 and 38 °C represented the solubility of a stable potassium benzoate dihydrate phase; in contrast, Sidgwick and Ewbank, who were specifically searching for hydrates, were very definite that their equilibrium potassium benzoate solid phase was invariably anhydrous. We consider

TABLE 1. Ice melting temperatures and molal osmotic coefficients for potassium benzoate solutions

Potassium benzoate concentration (wt%)	Ice melting temperature (°C)	ϕ
11.49	−2.60	0.864
16.00	−3.95	0.895
20.01	−5.35	0.923
24.00	−6.95	0.951
27.03	−8.30	0.969
30.00	−9.40	0.949
31.50	−10.10	0.950
32.99	−10.65	0.936
34.89*	−11.80	0.953

*Eutectic.

TABLE 2. Aqueous solubility of potassium benzoate

Temperature (°C)	Potassium benzoate concentration (wt%)
25.00	42.28
24.99	42.21
24.99	42.23
24.99	42.28
24.99	42.17
20.01	41.30
15.00	40.47
9.99	39.53
5.01	38.57
0.02	37.50
0.01	37.52
−5.00	36.50
−8.00	35.76
−10.00	35.34
−11.50	34.96
−11.50	34.98

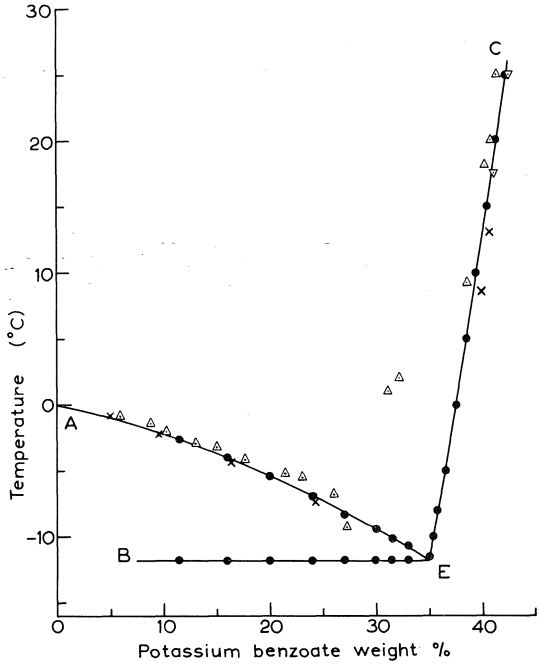

FIG. 1. Potassium benzoate – water phase diagram: ▽, Pajetta; ×, Sidgwick and Ewbank; △, Druzhinin and Sukhova; ●, this work.

Can. J. Chem. Downloaded from www.nrcresearchpress.com by 210.87.254.40 on 09/05/12
For personal use only.

that our curve CE represents the solubility of anhydrous potassium benzoate because no change in the physical appearance of the anhydrous potassium benzoate added initially took place during a 30 day equilibration period with continuous stirring.

We also tried to repeat the formation of potassium benzoate tetrahydrate under the conditions given by Druzhinin and Sukhova (3), but were unsuccessful. A saturated solution with excess anhydrous potassium benzoate was kept at 0 °C with continuous stirring for 42 days without the allegedly stable tetrahydrate (3) forming, despite the fact that each day the flask bottom was scratched firmly with a glass rod and the solution was shaken vigorously. Similarly, a saturated potassium benzoate solution with ice was maintained at −10 °C, with continuous stirring and with daily scratching and shaking, for 14 days without the tetrahydrate forming.

All melting point experiments showed well-defined eutectic arrests at −11.8 °C for periods of up to 50 min. This eutectic, characterizing the equilibrium coexistence of ice with anhydrous potassium benzoate, is represented in Fig. 1 by BE. The eutectic composition, 34.89 wt% potassium benzoate, was determined from extrapolation of our anhydrous potassium benzoate solubilities to −11.8 °C. Our melting point measurements above −11.8 °C did not show the thermal arrest which would have been expected for the ice–tetrahydrate eutectic (3).

The solution water activity, was calculated from the ice melting temperature using the freezing point equation given by Dorsey (5). The derived molal osmotic coefficients for water, ϕ, are included in Table 1 and plotted against potassium benzoate molality in Fig. 3. The composition dependence of ϕ is similar to that of sodium valerate solutions (6).

Sodium Benzoate – Water System

The ice melting temperatures for sodium benzoate solutions given in Table 3 define curve AE in Fig. 2. Three measurements by Sidgwick and Ewbank (2) are in general agreement with our results. When concentrated sodium benzoate solutions were being prepared the rate of solid dissolution was found to be much slower than for potassium benzoate. The sodium benzoate solutions at low temperatures were more viscous than corresponding potassium

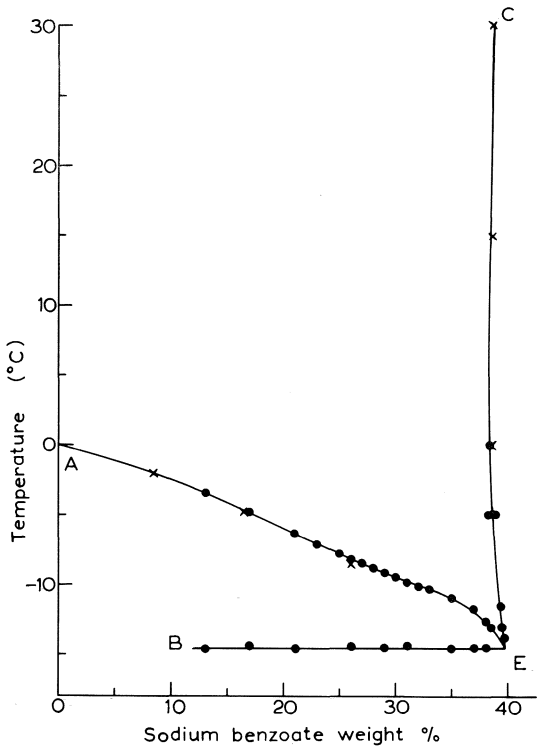

FIG. 2. Sodium benzoate – water phase diagram: ×, Sidgwick and Ewbank; ●, this work.

TABLE 3. Ice melting temperatures and molal osmotic coefficients for sodium benzoate solutions

Sodium benzoate concentration (wt%)	Ice melting temperature (°C)	ϕ
12.99	−3.45	0.897
17.01	−4.80	0.909
20.99	−6.30	0.921
23.00	−7.10	0.924
25.00	−7.80	0.910
26.01	−8.15	0.901
27.01	−8.40	0.883
27.99	−8.75	0.875
29.00	−9.10	0.867
30.02	−9.40	0.852
30.98	−9.85	0.854
31.97	−10.10	0.836
33.01	−10.30	0.813
35.01	−10.90	0.787
37.00	−11.70	0.776
38.01	−12.60	0.800
38.50	−13.10	0.815
39.7*	−14.50	0.858

*Eutectic.

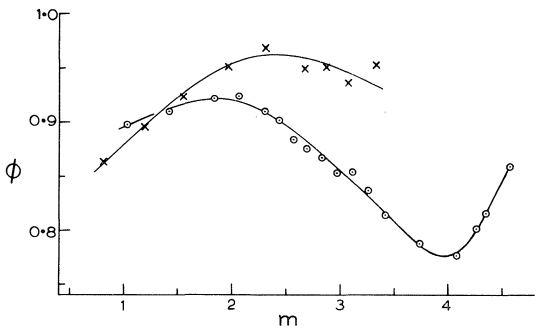

FIG. 3. Variation of molal osmotic coefficient with benzoate molality: ×, potassium benzoate; ○, sodium benzoate.

TABLE 4. Aqueous solubility of sodium benzoate

Temperature (°C)	Sodium benzoate concentration (wt%)
0.00	38.41±0.16
−5.00	38.60±0.23
−11.49	39.41
−11.49	39.38
−13.00	39.51
−13.81	39.91

benzoate solutions. The eutectic melting point for sodium benzoate was poorly defined in contrast with the well defined eutectic for potassium benzoate. The sodium benzoate system never exhibited an invariant eutectic temperature but only a decreased rate of temperature rise. Further, for experiments with similar sodium benzoate concentrations, sometimes the eutectic temperature discontinuity was readily apparent but at other times hardly perceptible. The eutectic temperature of −14.5 °C denoted by BE in Fig. 2 is the mean value for experiments where eutectic melting was clearly evident.

While prefreezing sodium benzoate solutions for the ice melting point experiments, we found that the viscosity became very high and yielded a sticky plastic mass which did not harden until below −20 °C. Further, the slope of the ice melting point curves at temperatures below the eutectic was always smaller than for the corresponding potassium benzoate system, indicating heat absorption and ice melting between −20 °C and the eutectic at −14.5 °C. This behavior of concentrated sodium benzoate solutions at low temperatures is caused by the slow attainment of equilibrium of the aqueous solution with solid sodium benzoate, resulting in supersaturation and glass phase formation.

Solubilities of anhydrous sodium benzoate are given in Table 4 and plotted as curve CE in Fig. 2. The values given in Table 4 for 0.00 and −5.00 °C are means and standard deviations for four and eleven determinations respectively. Solubility measurements by Sidgwick and Ewbank (2) are in general agreement with our results.

Further differences between the sodium benzoate – water and potassium benzoate – water systems were found during the solubility measurements. The addition of only a small quantity of sodium benzoate to a stirred mobile solution with a slight excess of solid resulted in transition to a thick gelatinous fluid from which no sample could be withdrawn. This contrasted with the potassium benzoate system where the stirred solution remained mobile and readily sampled when excess solid was added. A series of eleven measurements at −5.00 °C, extending over a total of 37 days and with four distinct initial compositions, demonstrated that equilibration with sodium benzoate was extremely slow, whereas with potassium benzoate solubility equilibrium was attained within 24 h.

Our measurements show that below 0 °C the temperature coefficient of solubility for sodium benzoate is small and negative in contrast to the more usual positive coefficient for potassium benzoate.

The water molal osmotic coefficients for sodium benzoate solutions are included in Table 3 and plotted against molality in Fig. 3. The shape of the ϕ curve bears a family resemblance to those for aqueous solutions of sodium valerate and sodium caproate (6).

1. The United States Pharmacopeia, 18th ed. Mack Publishing Company, Easton, Pa. 1970.
2. N. V. SIDGWICK and E. K. EWBANK. J. Chem. Soc. **121**, 1844 (1922).
3. I. G. DRUZHININ and S. I. SUKHOVA. Izv. Vyssh. Ucheb. Zaved., Khim. Khim. Tekhnol. **11**(2), 135 (1968).
4. R. PAJETTA. Gazz. chim. Ital. **36**, 67 (1906).
5. N. E. DORSEY. Properties of ordinary water substance. Reinhold Publishing Corporation, New York, N.Y. 1940. p. 562.
6. R. A. ROBINSON and R. H. STOKES. Electrolyte solutions. Butterworth Scientific Publications, London. 1955. p. 469.

Can. J. Chem. Downloaded from www.nrcresearchpress.com by 210.87.254.40 on 09/05/12
For personal use only.

Molecular Size Distribution in Random Polyfunctional Condensation with or without Ring Formation: Computer Simulation[1]

MICHAEL FALK AND RUTH E. THOMAS[2]

Atlantic Regional Laboratory, National Research Council of Canada, Halifax, Nova Scotia B3H 3Z1

Received January 14, 1974

MICHAEL FALK and RUTH E. THOMAS. Can. J. Chem. **52**, 3285 (1974).

We have re-examined the polymer size distribution in a model system initially composed of N_0 monomeric units RA_f, where each unit R carries f identical functional groups A. Self-condensation is postulated to proceed at random by the formation of A···A bonds until the fraction α of A groups have reacted. The controversy regarding the applicability of the Flory–Stockmayer (F.S.) and the Whiteway–Smith–Masson (W.S.M.) expressions to this model has been resolved. Two variants of this model are distinguished, depending on whether ring formation is allowed or forbidden. It is shown that in the limit of an infinite system the incidence of rings in the *rings allowed* model tends to zero below the critical value of α, $\alpha_c = 1/(f-1)$. Consequently, the limiting polymer size distributions for the *rings allowed* and *rings forbidden* models coincide over the range $0 \leqslant \alpha \leqslant \alpha_c$, and are both described by the F.S. expression. For the *rings forbidden* model, the F.S. equation fails above α_c, but for the *rings allowed* model it continues to apply over the entire accessible range $0 \leqslant \alpha \leqslant 1$. The W.S.M. equation represents the limiting distribution for the polymerization process in which one functional group per monomer is singled out (A*) and bonding is restricted to A···A* pairs. In that process, and in the limit of an infinite system, rings are not formed over the entire attainable range of α, from 0 to $2/f$.

MICHAEL FALK et RUTH E. THOMAS. Can. J. Chem. **52**, 3285 (1974).

On a réexaminé la dispersité d'un polymère au moyen d'un modèle composé initialement de N_0 unités monomères RA_f, dans lesquelles chaque unité R possède f groupes fonctionnels identiques A. On suppose qu'une autocondensation a lieu au hasard et mène à la formation de liaisons A···A jusqu'à ce qu'une fraction α des groupes A aient réagi. On a dissipé les doutes concernant la possibilité d'application des expressions de Flory–Stockmayer (F.S.) et de Whiteway–Smith–Masson (W.S.M.) pour ces modes. On distingue deux variantes de ce modèle, selon que la cyclisation soit permise ou interdite. On montre que, dans les limites d'un système infini, l'incidence des cycles dans le modèle de cyclisation permise tend vers zéro au-dessous de la valeur critique de α, $\alpha_c = 1/(f-1)$. Par conséquent la distribution numérique limite pour les modèles de cyclisation permise et de cyclisation interdite coincide dans le domaine $0 \leqslant \alpha \leqslant \alpha_c$, et peut être décrite par l'expression de F.S. Pour le modèle de cyclisation interdite l'équation F.S. n'est pas valable au dessus de α_c, tandis que pour le modèle de cyclisation permise elle continue de l'être dans tout le domaine accessible $0 \leqslant \alpha \leqslant 1$.

L'équation W.S.M. représente la distribution limite pour la réaction de polymérisation, dans laquelle un groupe fonctionnel (A*) par monomère peut être mis en évidence, la liaison se trouvant donc limitée aux paires A···A*. Au cours de cette réaction et dans les limites d'un système infini, les cycles ne se forment pas dans tout le domaine accessible de α, allant de 0 à $2/f$.

[Traduit par le journal]

This study deals with a controversy concerning the equilibrium distribution of polymer sizes in a simple model of random self-condensation of poly-functional monomers. The problem is an important one to settle because it is a standard reference case for equilibria in polymer science (1). Moreover, essentially the same mathematical problem arises in connection with other statistical processes (2–4). While we will employ the polymer chemist's vocabulary of "molecules", "residues", "reactive groups", "bonds", etc., the results are also applicable, with appropriate changes in terminology, to statistical branching processes outside of polymer chemistry.

Consider a model system initially composed of N_0 monomeric units RA_f, where R is a structural unit (residue), to which f equivalent functional groups A are attached. The A groups react with one another in pairs to form A···A bonds. The process is postulated to proceed *at*

[1]NRCC No. 14118.

[2]Summer student, May–August, 1973.

Can. J. Chem. Downloaded from www.nrcresearchpress.com by 210.87.254.105 on 09/05/12
For personal use only.

Can. J. Chem. Downloaded from www.nrcresearchpress.com by 210.87.254.105 on 09/05/12
For personal use only.

random until a fraction α of the A groups have reacted. What is the limiting distribution of monomers, dimers, trimers, etc., when N_0 tends to infinity?

Two variants of this model will be distinguished:

(i) Rings Allowed Model

In this variant, the reaction proceeds without restrictions. Since intramolecular reactions are allowed, rings of different sizes may be formed, including rings which involve two A groups on the same structural unit (Fig. 1*a*). The process may continue until $\alpha = 1$, when all A groups will have reacted and, if $f > 2$, a cross-linked network will have been formed. The random choice of reacting pairs, in the absence of restrictions, ensures that the principle of equal reactivity of all functional groups in the system is *always* fulfilled. This principle states that at every stage of the reaction the probability that a given unreacted functional group will react does not depend on the size or configuration of the molecule to which it is attached (*cf.* Appendix IV).

(ii) Rings Forbidden Model

In this variant, intramolecular bonds, *i.e.* pairings between A groups on the same polymer, are forbidden, so that rings cannot form (Fig. 1*b*). Bonding occurs at random between pairs of unreacted functional groups belonging to different molecules. Since all pairs of functional groups which belong to the same molecule are excluded from the reaction, the principle of equal reactivity of all functional groups is not in general valid, though it remains valid for special cases (*cf.* Appendix IV). The total number of molecules in the system, N, is a linear function of α, $N = N_0(1 - \alpha f/2)$, and the maximum value of α that may be reached is $\alpha_{max} = (2/f)(1 - 1/N_0)$, at which point $N = 1$, the system consisting of a single polymer of N_0 structural units joined by $N_0 - 1$ bonds. In the limit of N_0 becoming infinite, α_{max} becomes $2/f$.

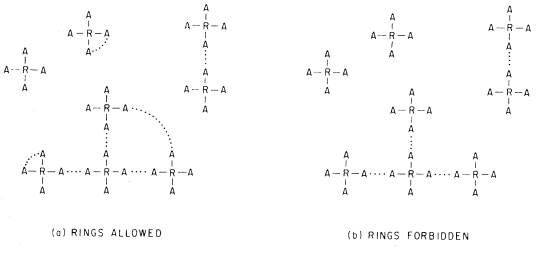

FIG. 1. Typical polymer mixtures formed by the self-condensation of the monomer RA_f for $f = 4$.

The polymer distributions corresponding to the *rings allowed* and *rings forbidden* models may be attained by other means than the two random growth processes outlined above. For example, asymptotic equilibrium-attainment processes may be envisaged in which the system initially consists of an arbitrary distribution of polymers, with a total number of bonds corresponding to the desired value of α. Bonds are then alternately broken and re-made at random, the total number of bonds remaining constant and rings being either allowed or forbidden. After a sufficient number of bonds have been broken and re-made, the distribution of polymer sizes in such systems should become statistically equivalent to that attained by the corresponding process of irreversible random growth.

The *rings allowed* and *rings forbidden* models are idealized representations of condensing or polymerizing molecules and represent limiting cases of more realistic but far more complex model systems. The *rings allowed* model corresponds to intermolecular and intramolecular bond formation proceeding with the same rate constant, which represents the limit of infinite concentration of reactive groups. The lack of dependence of the rate constant of ring closure on ring size corresponds to the absence of any geometrical restrictions imposed by the bonds, which may be approached by polymers having highly flexible backbones. The *rings forbidden* model, in complementary fashion, may be approached by polymers with a rigid backbone and a geometry which makes bonding between two unreacted groups on the same polymer unlikely. More elaborate models may be constructed (5–10) which set different probabilities for the closure of rings of different sizes or introduce additional variables. However, as the treatment of such models is far more difficult, in the present study we shall only be concerned with the simplest *rings allowed* and *rings forbidden* models defined above.

Flory declared that exact treatment of processes allowing ring formation is "hopeless at present" (ref. 11, p. 348). Approximate treatment has been presented by Harris (6) and Temple (10). The simplicity resulting from assigning equal reactivity to all pairs of unreacted groups in the system at all stages of reaction, which corresponds to the *rings allowed* model

Can. J. Chem. Downloaded from www.nrcresearchpress.com by 210.87.254.105 on 09/05/12
For personal use only.

defined above, does not appear to have been recognized before.

For what was stated to be the *rings forbidden* model, Flory[3] (11–13) and later Stockmayer (14) and others (as summarized in ref. 1) derived the following general expression for the number of x-mers (polymers of any configuration, containing x structural units)[4]:

$$[1]\quad N_x = N_0 \frac{f(fx - x)!}{(fx - 2x + 2)!x!} \times \alpha^{x-1}(1 - \alpha)^{fx-2x+2}$$

However, the Flory–Stockmayer (F.S.) expression has the disturbing mathematical property (11, 14) that the sums of the weight fractions and mole fractions of all x-mers, $\sum_{x=1}^{\infty} w_x$ and $\sum_{x=1}^{\infty} \mathrm{N}_x$ are unity only over the limited range of α from 0 to a critical value of α, $\alpha_c = 1/(f - 1)$. This is the value of α above which the probability of occurrence of infinite polymers becomes nonzero when $N_0 \to \infty$ for a process obeying equal reactivity of unreacted groups (ref. 11, p. 353). Beyond α_c, $\sum_{x=1}^{\infty} w_x$ is less than unity while $\sum_{x=1}^{\infty} \mathrm{N}_x$ is greater than unity. Flory's explanation (ref. 15, p. 192; ref. 11, p. 375) that the distribution equations include only species of finite size is unclear, because the derivation in ref. 11 did not specifically exclude infinite species. These difficulties have been at the root of recent debates (1, 16–18) regarding the applicability of the F.S. expression and of the alternative expression proposed by Whiteway, Smith, and Masson (W.S.M.) for what was declared to be the same system (19). Expressed in terms of the number of x-mers in the system, the W.S.M. expression is

$$[2]\quad N_x = N_0\left[1 - \frac{\alpha f}{2}\right] \frac{(fx - x)!}{(fx - 2x + 1)!x!} \times \left[\frac{\alpha f}{2(f - 1)}\right]^{x-1}\left[1 - \frac{\alpha f}{2(f - 1)}\right]^{fx-2x+1}$$

This expression yields weight and mole fractions for which

$$\sum_{x=1}^{\infty} w_x = 1 \quad \text{and} \quad \sum_{x=1}^{\infty} \mathrm{N}_x = 1$$

over the total range of α appropriate to the *rings forbidden* model, *i.e.* from $\alpha = 0$ to $\alpha = 2/f$. Equations 1 and 2 coincide when $f = 2$ but diverge for $f \geqslant 3$. Publication of the W.S.M. derivation (19, 20) led to a controversy (1, 16–18) which we now hope to settle by a re-examination of the problem, supported by computer simulation. A suggestion that the F.S.–W.S.M. controversy be settled by a computer simulation of the *rings forbidden* model has been made independently by Stepto (17).

Counting of Rings

In order to avoid any possible confusion in the counting of rings (21), we shall avoid the term "number of rings" and employ the term "number of ring closures", with the symbol C. We define the number of ring closures as the number of intramolecular bonds required to construct the system from ringless components. An alternative and equivalent definition is that it is the minimum number of bonds that must be broken to return the system to a ringless condition. Thus defined, the number of ring closures corresponds to the *cyclomatic number* in graph theory (22). The symbol $\bar{C}$ will be used for the number of ring closures per structural unit. As defined above, C and $\bar{C}$ obey the simple relations $C = N - N_0 + B$ and $\bar{C} = C/N_0$, where N is the number of molecules, N_0 the number of structural units, and B the total number of bonds in the polymer mixture.

Computer Simulation, Rings Allowed Model

The functional groups on the N_0 monomers initially present were represented by an array of $N_0 f$ numbers. The numbers from 1 to f were taken to correspond to the functional groups on monomer 1, the numbers $f + 1$ to $2f$ to the groups on monomer 2, and so on. Pairs of random numbers were used to select pairs of functional groups which were considered to form bonds. A record was kept of the groups which had reacted and of the structural units which had become bonded together, but details of connectivity were not recorded. Whenever a random number was selected which corresponded to a group which had already reacted, it was disregarded. If the two groups selected to

[3]See, however, footnote 7 in Appendix II.

[4]For the number of x-mers, N_x, one can derive the weight fraction of x-mers, $w_x = xN_x/N_0$, and the mole fraction of x-mers, $\mathrm{N}_x = N_x/N = N_x/N_0(1 - \alpha f/2)$, the last equality being valid only when rings are absent. The weight of material lost during a reaction step (*e.g.* H_2O molecules given off during etherification or esterification) is assumed to be negligible.

Can. J. Chem. Downloaded from www.nrcresearchpress.com by 210.87.254.105 on 09/05/12
For personal use only.

react happened to belong to the same polymer, a ring closure was recorded.

Each run consisted of a sequence of reaction steps carrying the system from $\alpha = 0$ to slightly below $\alpha = 1$. At specified values of α a record was made of the number of ring closures, the total number of molecules, and the number of monomers, dimers, etc., without rings. For every value of N_0 the results of a large number n of runs (100 to 400) were averaged and the means, standard deviations, σ, and estimated standard errors of the mean, $\sigma/\sqrt{n}$, were recorded. Standard deviations were lowest for the monomer, which was statistically the majority species, and gradually increased with x. The standard deviation was proportional to $1/N_0$, and thus the most accurate results were obtained at the highest values of N_0.

Figures 2, 3, and 4 show the partial results for a series of simulations with $f = 3$, $n = 100$, and $N_0 = 20$, 40, 80, 160, 320, 640, and 1280. The main parameters under study were the weight fractions[5] of monomers through tetramers without rings *i.e.* w_1, w_2, w_3, and w_4, as well as the total number of ring closures per residue, $\bar{C}$. The mean values of these five parameters were plotted against $1/N_0$. Such plots proved to be reasonably linear at high values of N_0 and the limiting values for $N_0 \rightarrow \infty$ were obtained by linear extrapolation as shown in Fig. 2. The standard errors on the limiting values, which appear as bars in the subsequent figures, were estimated graphically by combining the estimated uncertainty of the extrapolation with the standard error of the mean of the individual point at the highest value of N_0 (*cf.* Fig. 2).

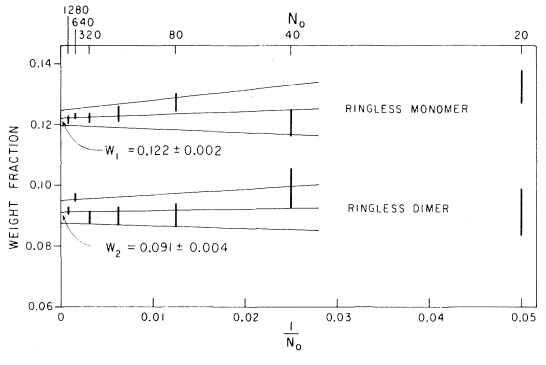

FIG. 2. An extrapolation of results from computer simulation. *Rings allowed*, $f = 3$, $N_0 = 20$ to 1280, $n = 100$, $\alpha = 0.5$.

[5]In the simulation with rings allowed, weight fractions are simpler to use than mole fractions, because the number of molecules at a given value of α varies from run to run.

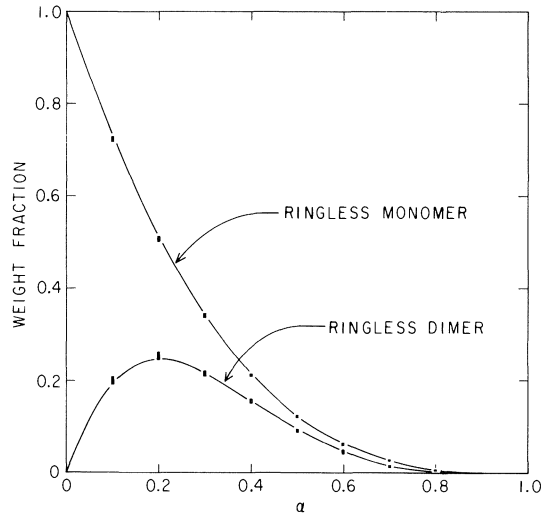

FIG. 3. Results of computer simulation. *Rings allowed*, $f = 3$. Limiting values of the weight fractions of ring-less monomers, w_1, and ring-less dimers, w_2, as a function of the extent of reaction, α. Solid lines: eq. 1.

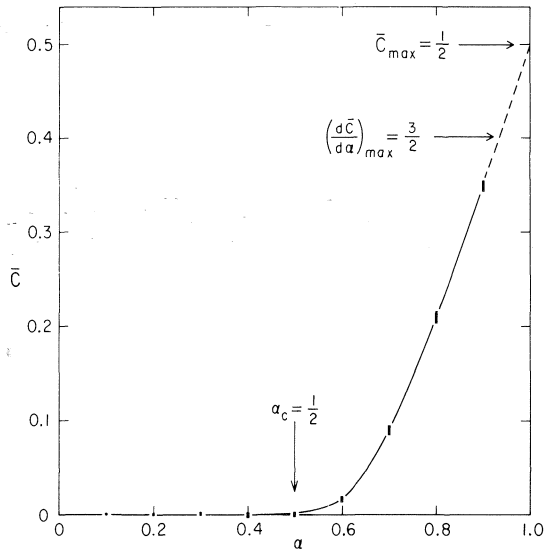

FIG. 4. Results of computer simulation. *Rings allowed*, $f = 3$. Limiting value of the number of ring closures per structural unit, $\bar{C}$, as a function of the extent of reaction, α.

Figure 3 shows the plot of the limiting values of w_1 and w_2, obtained from the above series of simulations. Figure 4 shows the limiting value of $\bar{C}$ as a function of α. The principal results are:

Can. J. Chem. Downloaded from www.nrcresearchpress.com by 210.87.254.105 on 09/05/12
For personal use only.

(*i*) The limiting values of w_1 and w_2 (as well as those of w_3 and w_4, not shown in Fig. 3) agree with the Flory expression over the entire range of α from 0 to 1. This confirms the deductions of Appendix II.

(*ii*) The limiting number of ring closures per structural unit, $\bar{C}$, is zero in the range of $0 \leqslant \alpha \leqslant \alpha_c$ (Fig. 4). This confirms the deductions of Appendix I.

(*iii*) Above α_c, $\bar{C}$ becomes finite and increases with α, approaching the final value $\bar{C}_{max} = 0.5$ at $\alpha = 1$. The slope, $d\bar{C}/d\alpha$, approaches the maximum value of 1.5. These values for $f = 3$ coincide with those deduced in Appendix III.

Computer Simulation, Rings Forbidden Model

This simulation was carried out similarly to the preceding one but with rings excluded. Whenever two numbers were selected which corresponded to unreacted groups on the same molecule, both numbers were disregarded and a new selection was made. Minor simplifications of record keeping were possible due to the absence of rings. The values of mole fractions, N_x, of monomers through tetramers (*i.e.* for $x = 1$, 2, 3, and 4) were recorded.

Table 1 and Figs. 5 to 8 report the results of simulations for $f = 2$, 3, and 4, $n = 400$, and values of N_0 ranging from 10 to 1000. The mean values of N_1, N_2, N_3, and N_4 were extrapolated to the limit of $1/N_0 = 0$, as before (Fig. 5). The limiting values of the mole fractions, with the estimated standard errors of extrapolation, are recorded in Table 1. In Figs. 6 to 8 the weight fractions as well as mole fractions of monomers, dimers, and trimers have been plotted against α. The principal results are:

(*i*) For $f = 2$, the F.S. and W.S.M. expressions coincide. Our limiting values of weight fractions and mole fractions of x-mers obtained by simulation fall on the joint F.S.–W.S.M. curve over the entire range of α (Fig. 6).

(*ii*) For $f = 3$ and $f = 4$, the F.S. and W.S.M. curves differ, the difference increasing with α. Our limiting weight and mole fractions (Figs. 7 and 8) fall on the F.S. curve in the range

$$0 \leqq \alpha \leqq \alpha_c$$

(*iii*) Above α_c our data deviate increasingly from the F.S. curve. The deviations are in the direction of the W.S.M. curve, but the data do not attain the W.S.M. values except in the limit

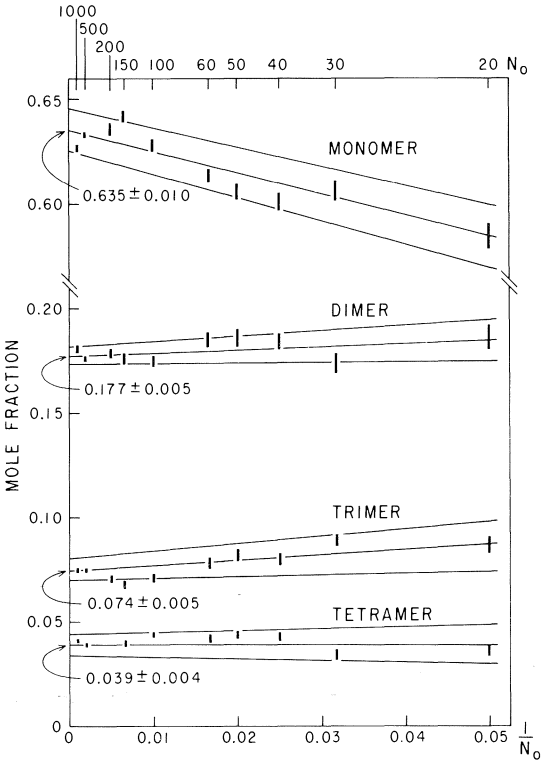

FIG. 5. An extrapolation of results from computer simulation. *Rings forbidden*, $f = 4$, $N_0 = 20$ to 1000, $n = 400$, $\alpha = 0.25$.

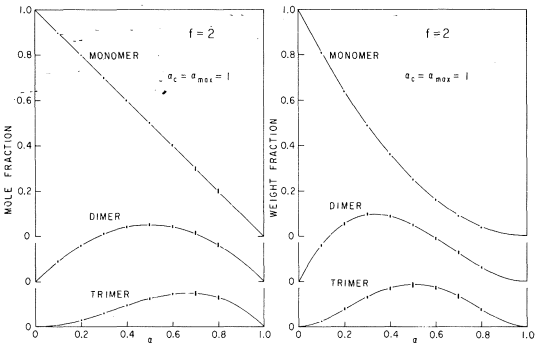

FIG. 6. Results of computer simulation. *Rings forbidden*, $f = 2$. Solid curve: eqs. 1 and 2. The ordinate scales of Figs. 6, 7, and 8 have been displaced for clarity.

of $\alpha \to \alpha_{max}$, and then only on the weight fraction scale.

(*iv*) In the limit of $\alpha \to \alpha_{max}$ the weight fractions of all x-mers tend toward zero, while their ratios, *e.g.* w_1/w_2, tend toward unity. At the same time for $f \geqslant 3$ the mole fraction of the monomer appears to increase toward unity,

Can. J. Chem. Downloaded from www.nrcresearchpress.com by 210.87.254.105 on 09/05/12
For personal use only.

TABLE 1. Limiting values for $N_0 \to \infty$ of mole fractions of monomers, dimers, trimers, and tetramers from computer simulation, *rings forbidden**

α	N_1	N_2	N_3	N_4
$f = 2$				
0.1	0.899 (2)	0.090 (2)	0.009 (1)	0.000 (0)
0.2	0.799 (3)	0.160 (4)	0.033 (2)	0.006 (2)
0.3	0.699 (5)	0.212 (4)	0.063 (3)	0.020 (5)
0.4	0.601 (5)	0.240 (4)	0.095 (4)	0.039 (4)
0.5	0.500 (6)	0.250 (5)	0.124 (7)	0.062 (5)
0.6	0.399 (6)	0.239 (7)	0.145 (7)	0.086 (8)
0.7	0.299(10)	0.216(10)	0.150(11)	0.100 (5)
0.8	0.197(10)	0.162 (9)	0.127(10)	0.102 (8)
$f = 3$				
0.2	0.731 (7)	0.179 (6)	0.057 (6)	0.020 (5)
0.3	0.621 (8)	0.199 (5)	0.079 (4)	0.043 (5)
0.4	0.540(12)	0.191 (8)	0.094 (4)	0.054 (5)
0.45	0.515 (8)	0.191(12)	0.094 (7)	0.056 (6)
0.5	0.506(15)	0.185(12)	0.094 (8)	0.055 (7)
0.55	0.512(15)	0.192(12)	0.093(10)	0.058 (8)
0.58	0.540(17)	0.190(20)	0.096 (8)	0.056(12)
0.6	0.565(25)	0.199(20)	0.090 (8)	0.050 (7)
0.62	0.609(15)	0.192(15)	0.083 (9)	0.049(10)
0.64	0.662(20)	0.187(20)	0.070(10)	0.041 (8)
0.65	0.700(25)	0.180(15)	0.062(10)	0.028 (8)
0.66	0.750(40)	0.173(25)	0.047(15)	0.014 (7)
$f = 4$				
0.1	0.821 (4)	0.131 (8)	0.033 (2)	0.010 (1)
0.2	0.685 (8)	0.174 (6)	0.064 (5)	0.030 (4)
0.25	0.635(10)	0.177 (5)	0.074 (5)	0.039 (4)
0.3	0.600(11)	0.177 (7)	0.076 (6)	0.041 (8)
0.33	0.591(10)	0.169 (6)	0.076 (5)	0.032 (5)
0.35	0.595(13)	0.176 (8)	0.077 (6)	0.042 (6)
0.38	0.605(12)	0.183 (7)	0.077 (4)	0.042 (4)
0.4	0.611(15)	0.181 (8)	0.076 (8)	0.039 (6)
0.42	0.634 (9)	0.182 (5)	0.076 (5)	0.035 (6)
0.44	0.667(10)	0.180 (5)	0.071 (5)	0.033 (4)
0.46	0.705(15)	0.174 (6)	0.064 (5)	0.030 (4)
0.48	0.765(10)	0.161(10)	0.045 (6)	0.017 (4)

*Numbers in parentheses are the estimated standard errors of extrapolation, expressed in units of the last decimal.

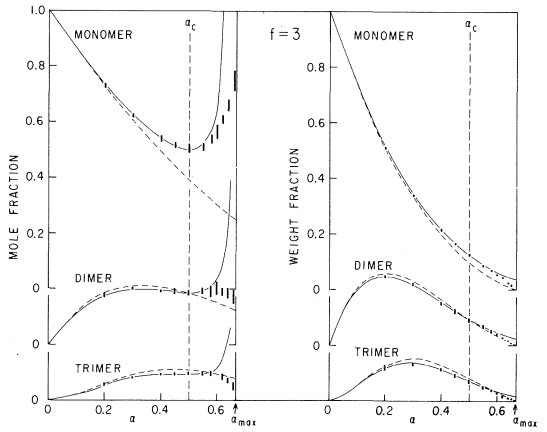

FIG. 7. Results of computer simulation. *Rings forbidden*, $f = 3$. Solid curve: eq. 1, broken curve: eq. 2.

while the mole fractions of the remaining species fall toward zero.

Verification of Computer Simulation for Low N_0

Expectation values of the mole fractions of various x-mers may be found by sequential enumeration of all possible states of the system, starting with $\alpha = 0$ and proceeding stepwise over all possible values of α. At each value of α the relative probability of every possible state is calculated from the number of possible ways to form that state.

As an illustration, let $N_0 = 5$, $f = 4$, and let rings be forbidden. Initially, all molecules are monomers, $\alpha = 0$, $N_1 = 5$, and $N_1 = 1$. The

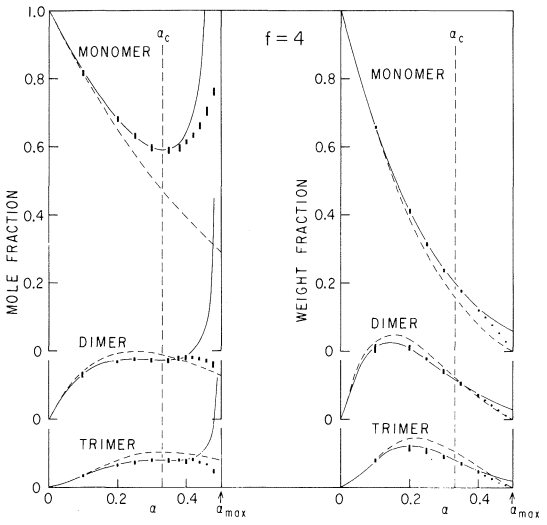

FIG. 8. Results of computer simulation. *Rings forbidden*, $f = 4$. Solid curve: eq. 1, broken curve: eq. 2.

first reaction step leads to the formation of one bond, leaving four molecules; the value of α is now $2/(5 \times 4) = 0.1$. The only possible state of the system is $N_1 = 3$, $N_2 = 1$. Hence, the expectation values of the mole fractions are $\mathrm{N}_1 = 3/4$ and $\mathrm{N}_2 = 1/4$, the remaining mole fractions being zero. After the next reaction step α equals 0.2. There are now two bonds and three molecules in the system and two states are possible: (*a*) $N_1 = 2$, $N_3 = 1$ and (*b*) $N_1 = 1$, $N_2 = 2$. From considerations of all possible pairings of unreacted groups at the previous stage of reaction, we obtain the relative probabilities 3/5 for (*a*) and 2/5 for (*b*). Hence the expectation values of the mole fractions are $\mathrm{N}_1 = (2 \times 3/5 + 1 \times 2/5)/3 = 8/15$; $\mathrm{N}_2 = (2 \times 2/5)/3 = 4/15$; $\mathrm{N}_3 = (1 \times 3/5)/3 = 3/15$. Similarly, after the next reaction step $\alpha = 0.3$. There are now three bonds and two molecules in the system and two states are possible: (*c*) $N_1 = 1$, $N_4 = 1$ and (*d*) $N_2 = 1$, $N_3 = 1$. The relative probabilities of these two states are calculated to be 11/17 for (*c*) and 6/17 for (*d*), so we obtain the following expectation values of mole fractions: $\mathrm{N}_1 = \mathrm{N}_4 = (1 \times 11/17)/2 = 11/34$; $\mathrm{N}_2 = \mathrm{N}_3 = (1 \times 6/17)/2 = 6/34$.

We have made such calculations for $f = 2$, 3, and 4 and for N_0 from 4 to 10, the latter value approaching the practical limit of hand calculations. The computer simulations of the corresponding systems yielded values of mean mole fractions which were statistically distributed about the calculated expectation values. This direct verification gives us additional confidence that our simulation is free from systematic errors.

Applicability of the Flory–Stockmayer Expression

It will be recalled that the F.S. equation appears to have been presented (11–14) as the limiting expression for the *rings forbidden* model. Our simulation results demonstrate the validity of the Flory equation for this model in the range $0 \leqslant \alpha \leqslant \alpha_c$; the reasons for the failure of this equation above α_c are discussed in Appendix IV. If may be noted that below α_c the F.S. expression describes the limiting distribution of polymer sizes in the *rings forbidden* model system *exactly*, and is not "somewhat inaccurate owing to the disregard of intramolecular reactions", as stated by Flory (ref. 15, p. 192; ref. 11, p. 348).

In addition, our simulation results show that the F.S. equation is the valid limiting equation for the *rings allowed* model, over the entire accessible range of α, $0 \leqslant \alpha \leqslant 1$. The applicability of the Flory equation in the *rings allowed* model is independently demonstrated in Appendix II. The limiting polymer size distributions in the two models coincide in the range $0 \leqslant \alpha \leqslant \alpha_c$, (Appendix I), and are both described by the F.S. expression.

For $f = 2$, the value of α_c is 1. In this special case the limiting distribution is independent of whether rings are allowed or forbidden, and is described by the F.S. expression over the entire attainable range of α, 0 to 1.

For $f \geqslant 3$, α_c lies below α_{max}, and for *rings forbidden* the Flory expression fails above α_c, as demonstrated in Figs. 7 and 8. There is at the present no analytical expression for the distribution of polymer sizes above α_c when rings are forbidden.

Applicability of the Whiteway–Smith–Mason Expression

The W.S.M. expression (eq. 2), like the Flory expression, has been proposed for the random polymerization of RA_f monomers with rings forbidden (19). However, our computer simulation of such polymerizations does not agree with the W.S.M. expression, except for the special case of $f = 2$ when that expression and the F.S. expression reduce to the same form.

Can. J. Chem. Downloaded from www.nrcresearchpress.com by 210.87.254.105 on 09/05/12
For personal use only.

Can. J. Chem. Downloaded from www.nrcresearchpress.com by 210.87.254.105 on 09/05/12
For personal use only.

It appears in fact that the W.S.M. equation represents the random polymerization of RA^*A_{f-1} monomers rather than that of RA_f monomers. RA^*A_{f-1} represents an *f*-functional monomer in which one of the *f* functional groups on each residue R, distinguished here by an asterisk, is singled out and only mixed pairs of groups, *i.e.* $A \cdots A^*$ but not $A \cdots A$ or $A^* \cdots A^*$, are allowed to form bonds. For this case, though with somewhat different notation, Flory (23) has derived an expression for the mole fraction of *x*-mers, which leads to the following expression for the number of *x*-mers:

$$[3] \quad N_x = N_0[1 - (f-1)\alpha_A] \times \frac{(fx - x)!}{(fx - 2x + 1)!x!}[\alpha_A]^{x-1}[1 - \alpha_A]^{fx-2x+1}$$

where α_A is defined as the fraction of unstarred A groups which have reacted. Equation 3 has validity over the entire attainable range of α_A from 0 to $1/(f-1)$. The maximum value of α_A coincides with the critical value of α_A at which infinitely large polymers appear. Therefore, in the limit of $N_0 \to \infty$, the incidence of rings becomes zero (*cf.* Appendix I) and the distinction between the *rings allowed* and *rings forbidden* variants vanishes.

The similarity of eq. 3 to the W.S.M. expression (eq. 2) may be immediately noted. To show the exact equivalence of the two expressions we introduce a new variable α defined, for the polymerization of RA^*A_{f-1}, as the fraction of all groups, A and A*, which have reacted. Since $\alpha_A = B/N_0(f-1)$ and $\alpha = 2B/N_0 f$, where *B* is the number of $A \cdots A^*$ bonds that have been formed, the relation between α_A and α is $\alpha_A = \alpha f/2(f-1)$. When this relation is substituted in eq. 3, we obtain eq. 2 exactly!

The exact correspondence of the W.S.M. expression with that for the polymerization of the RA^*A_{f-1} system shows that the W.S.M. counting procedure (19), which singles out one A group on every monomer, is equivalent to replacing random polymerization of RA_f monomers with rings forbidden by random polymerization of RA^*A_{f-1} monomers under the constraint that only $A \cdots A^*$ bonds may form. There is only one A* group per polymer of any size, hence, in the limiting case of an infinite system, the probability of an A group reacting with an A* group on the same molecule becomes zero. This ensures that rings do not form over the entire accessible range of α, 0 to $2/f$, in agreement with the original derivation of the W.S.M. expression in ref. 19.

Conclusions

(*i*) The Flory–Stockmayer expression describes the limiting (for $N_0 \to \infty$) distribution of ringless polymers in the random self-condensation of RA_f monomers with *rings allowed.*

(*ii*) In the above case, the limiting incidence of ring closures per residue is exactly zero below α_c but becomes non-zero above α_c; the occurrence of rings is limited to infinite polymers.

(*iii*) Below α_c but not above α_c the F.S. expression also represents the limiting distribution of polymer sizes in the random self-condensation of RA_f with *rings forbidden.*

(*iv*) There is presently no analytical expression valid for the *rings forbidden* model in the range $\alpha_c < \alpha \leqslant 2/f$. Some numerical parameters of the polymer distribution in this range were obtained by our computer simulation.

(*v*) The Whiteway–Smith–Masson expression represents the limiting distribution of polymer sizes in the random self-condensation of *f*-functional monomers RA^*A_{f-1} when bonding is restricted to $A \cdots A^*$ pairs. This mechanism ensures that rings do not form over the entire attainable range of α, 0 to $2/f$.

Computations

The computations were performed on the CDC 6600 computer of Dalhousie University, Halifax. Copies of the Fortran programs employed in this work are available on request.

We are indebted to Dr. C. R. Masson for bringing the problem to our attention, Mr. P. F. Seto for assistance in computations, Drs. C. R. Masson, S. G. Whiteway, A. G. McInnes, W. R. Smith, and W. Brostow for valuable discussions, and Professor Manfred Gordon for critical comments on the manuscript.

Appendix I

Probability of Ring Closures in the *Rings Allowed* Model

Consider a system of N_0 monomeric *f*-functional units ($N_0 \to \infty$), which has undergone random self-condensation without restrictions until the fraction α of all functional groups have reacted. The mixture may then contain mono-

Can. J. Chem. Downloaded from www.nrcresearchpress.com by 210.87.254.105 on 09/05/12
For personal use only.

mers, dimers, . . . , x-mers, . . . , some with rings and others without rings.

The probability that in a given reaction step a ring closure will occur on an x-mer, p_x^c, is equal to the probability that two unreacted groups chosen at random happen to belong to the same x-mer. Suppose that the current number of x-mers with or without rings is N_x'. The highest possible number of unreacted groups on one x-mer is $fx - 2x + 2$, corresponding to an x-mer without any rings. The total number of unreacted groups in the system is $N_0f(1 - \alpha)$. Therefore the probability that an unreacted group chosen at random will belong to some x-mer is not greater than $N_x'(fx - 2x + 2)/N_0f(1 - \alpha)$. The probability that the second group chosen at random will belong to *the same* x-mer is not greater than $(fx - 2x + 1)/N_0f(1 - \alpha) - 1$. We thus obtain

$$[A1] \quad p_x^c \leqslant N_x'(fx - 2x + 2) \times (fx - 2x + 1)/N_0f(1 - \alpha) \times [N_0f(1 - \alpha) - 1]$$

The above relation is true for any N_0. If N_0 approaches infinity, α may be treated as a continuous variable, which is incremented by $d\alpha = 2/N_0f$ in each reaction step. Unity may be neglected compared to $N_0f(1 - \alpha)$, and we may rewrite [A1] to obtain

$$[A2] \quad p_x^c \leqslant \left[\frac{N_x'(fx - 2x + 2)}{N_0f(1 - \alpha)}\right] \times \frac{(fx - 2x + 1)}{2} \frac{d\alpha}{(1 - \alpha)}$$

But the term in square brackets must be less than unity, as, for any value of α, $N_x'(fx - 2x + 2)$ is the maximum number of unreacted groups on the x-mers, while $N_0f(1 - \alpha)$ is the total number of unreacted groups in the system. Hence,

$$[A3] \quad p_x^c < \frac{fx - 2x + 1}{2} \frac{d\alpha}{1 - \alpha}$$

In order to obtain an upper bound for the number of ring closures on x-mers, C_x, we may integrate the upper bound for p_x^c from [A3] between $\alpha = 0$ and $\alpha = \alpha$. We obtain

$$[A4] \quad C_x < \tfrac{1}{2}(fx - 2x + 1) \ln\left(\frac{1}{1 - \alpha}\right)$$

which is *finite* for any finite x throughout the range $0 \leqslant \alpha < 1$. But in an infinite system, the total number of x-mers with or without rings, N_x', is infinite for any finite x throughout the range $0 < \alpha < 1$. Hence, the incidence of rings on x-mers, which we define as the ratio of x-mers which contain rings to the total number of x-mers, and which cannot be greater than C_x/N_x' (the incidence is smaller than C_x/N_x' if some x-mers contain several rings, and equal to C_x/N_x' if no x-mer contains more than one ring) must be zero for any finite x.

The total incidence of rings, which we define as the number of ring closures per residue, $\bar{C}$, is given by $\sum_{x=1}^{\infty} C_x/N_0$. Since each individual C_x is finite, the sum $\sum_{x=1}^{\infty} C_x$ remains finite so long as infinite polymers are absent from the system, *i.e.* in the range $0 < \alpha < \alpha_c$. Thus the incidence of rings, *i.e.* the expected number of ring closures per residue, for an infinite *rings allowed* system is zero below α_c. The polymer size distribution in such a system, below α_c, must therefore coincide with that of the *rings forbidden* system.

Some earlier workers have stated that the incidence of rings may be negligible in sufficiently concentrated systems undergoing polymerization (24, 25). However, the important facts that for the *rings allowed* model and in the limit of $N_0 \to \infty$ the expected incidence of rings on finite x-mers is exactly zero at any α, and that the total incidence of rings on all x-mers is exactly zero below α_c, do not appear to have been observed.

Appendix II

Derivation of the Flory Distribution as the Distribution of Ringless Polymers in the *Rings Allowed* Model

The following derivation follows closely the derivation by Flory in ref. 11, offerred for the *rings forbidden* model.[6] The present derivation is for the *rings allowed* model. Consider a system of f-functional units which has undergone random self-condensation *without restrictions*,

[6]Flory did not state unequivocally whether his model forbade ring formation or simply neglected it (*e.g.* ref. 11, p. 348). Stockmayer (ref. 14, p. 46) and most subsequent workers (1) have construed Flory's derivation to apply under the assumption that rings are forbidden.

Can. J. Chem. Downloaded from www.nrcresearchpress.com by 210.87.254.105 on 09/05/12
For personal use only.

as in Appendix I. The probability that an unreacted group selected at random belongs to an x-mer *without* rings, P_x, may be expressed in two ways.

Firstly, P_x is equal to the product of the probability p_x that the selected group belongs to a ringless x-mer of a given configuration, and the number ω_x of distinguishable configurations of ringless x-mers which start with the selected group

$$[A5] \qquad P_x = \omega_x p_x$$

The number of configurations, ω_x, has been shown (*cf.* ref. 11, p. 366) to be

$$[A6] \quad \omega_x = (fx - x)!/(fx - 2x + 1)!\,x!$$

Provided that the system is infinite and that the reaction has proceeded at random, without restrictions, the probability that a group encountered along the polymer is bonded or non-bonded is α or $(1 - \alpha)$, respectively, independent of the size of the polymer or the presence of ring-containing polymers in the system. The value of p_x is then

$$[A7] \qquad p_x = \alpha^{x-1}(1 - \alpha)^{fx-2x+1}$$

where $(x - 1)$ is the number of bonds on a ringless x-mer, while $(fx - 2x + 1)$ is the number of non-bonded groups, not counting the group originally selected. We therefore obtain

$$[A8] \quad P_x = [(fx - x)!/(fx - 2x + 1)!x!] \times \alpha^{x-1}(1 - \alpha)^{fx-2x+1}$$

Secondly, since the originally selected unreacted group was chosen at random, P_x must also equal the ratio of unreacted groups on ringless x-mers to the total number of unreacted groups in the system:

$$[A9] \quad P_x = N_x(fx - 2x + 2)/N_0 f(1 - \alpha)$$

where N_x is the number of ringless x-mers in the system. Eliminating P_x from eqs. A8 and A9, we obtain the Flory–Stockmayer expression (eq. 1). Our derivation formally recognizes the quantity N_x as *the number of ringless x-mers in a system which allows rings*. Our mode of derivation is general and implies that eq. 1 should be applicable over the entire accessible range of α, 0 to 1, whether or not the ringless polymers constitute the whole system or only a fraction of it. When the incidence of rings is non-zero, *i.e.* above α_c (*cf.* Appendix I), the total weight fraction of ringless polymers, given by the infinite sum

$$\sum_{x=1}^{\infty} w_x = \sum_{x=1}^{\infty} xN_x/N_0$$

must be less than unity. It has indeed been established (13, 14) that for the F.S. distribution this infinite sum equals unity for α between 0 and α_c, but deviates increasingly from unity above α_c, becoming zero at $\alpha = 1$.

Appendix III

Expected Number of Ring Closures at $\alpha = 1$

Consider a system composed of N_0 f-functional monomers ($N_0 \to \infty$), which has undergone complete self-condensation, without restrictions on ring formation, so that $\alpha = 1$. Let $\bar{C}$ represent the number of ring closures per residue. The *maximum* value of $\bar{C}$ is $f/2$ when f is even and $(f - 1)/2$ when f is odd (Table 2). The reason for this is that in order to maximize ring closures only the smallest possible rings must be constructed and these rings involve a pair of functional groups on the same residue. If f is odd, it can be seen that one functional group per residue, which cannot be used to form rings, always remains. The *minimum* value of $\bar{C}$ at $\alpha = 1$ is zero for $f = 1$ and $(f - 2)/2$ for $f \geqslant 2$, because the first two functional groups per residue may be used to form an infinite chain without any rings, but all remaining functional groups must then form rings.

When the self-condensation proceeds at random, the expectation value of $\bar{C}$ coincides with the minimum value. This is because in the limit of an infinite system the probability of ring closure is non-zero only for polymers of infinite size (Appendix I). In such polymers two functional groups per residue are involved in the formation of the backbone, so that only $f - 2$

TABLE 2. Minimum, maximum, and expected numbers of ring closures per residue, $\bar{C}$, for the complete self-condensation of a large number of f-functional monomers.

f	$\bar{C}_{min}$	$\bar{C}_{exp}$	$\bar{C}_{max}$
1	0	0	0
2	0	0	1
3	1/2	1/2	1
4	1	1	2
5	3/2	3/2	2
6	2	2	3
...	...	...	...
f	$(f - 2)/2$	$(f - 2)/2$	$f/2$ when f even $(f - 1)/2$ when f odd

Can. J. Chem. Downloaded from www.nrcresearchpress.com by 210.87.254.105 on 09/05/12
For personal use only.

functional groups per residue are available for ring formation, which leads to $(f - 2)/2$ ring closures per residue. The value of the derivative $d\bar{C}/d\alpha$ increases from 0 at $\alpha = \alpha_c$ to a maximum value when α approaches 1. The largest possible rate of ring formation is one ring closure per reaction step, *i.e.* $(\Delta\bar{C})_{\text{per step}} = 1/N_0$. Since $(\Delta\alpha)_{\text{per step}} = 2/N_0 f$, the maximum possible value of

$$d\bar{C}/d\alpha = \lim_{N_0 \to \infty} (\Delta\bar{C}/\Delta\alpha)$$

must be $(1/N_0)/(2/N_0 f) = f/2$. This value should be reached in the limit of $\alpha \to 1$, when all the residues will have polymerized into a single giant polymer and every remaining reaction step must result in ring closure.

Appendix IV

The Incompatibility of the Postulate of Equal Reactivity of Functional Groups with the Exclusion of Rings

The Flory–Stockmayer distribution has been derived in several ways. Apart from the derivation by Flory (ref. 11, p. 370), there are two reported derivations by Stockmayer (14), and one each by Good (26), Whittle (2), and by Gordon and Judd (1). These derivations postulate (*i*) that intramolecular reactions do not occur and (*ii*) that all unreacted functional groups are equally reactive regardless of the size of the polymer to which they are attached (1). The conditions under which these two postulates are mutually compatible do not appear to have been clearly noted.

In a random selection of pairs with rings allowed, the probability p_x that a particular unreacted group on an x-mer will be selected is $2/N_0 f(1 - \alpha)$, there being $N_0 f(1 - \alpha)$ unreacted groups in the system, each of them being equally likely to be selected. The value of p_x is independent of x, so that all groups are equally reactive as a result of the selection being random.

When ring formation is forbidden, those pairs of unreacted groups which belong to the same molecule are excluded from the reaction. An unreacted group on an x-mer is then forbidden to react with the other $(fx - 2x + 1)$ unreacted groups on the same x-mer and is allowed to react with only the remaining $N_0 f(1 - \alpha) - (fx - 2x + 1)$ unreacted groups in the system. Thus the reactivity of an unreacted group on an x-mer relative to one on a y-mer, defined as the relative probability of being selected to react, is

$$[A10] \quad \frac{p_x}{p_y} = \frac{N_0 f(1 - \alpha) - (fx - 2x + 1)}{N_0 f(1 - \alpha) - (fy - 2y + 1)}$$

When $f \geqslant 3$, this ratio approaches unity for finite x and y in the limit of $N_0 \to \infty$. (In the special case of $f = 2$, this ratio *is* unity for any value of N_0 and for any x and y, since then $fx - 2x + 1 = fy - 2y + 1 = 1$.) Thus, when $f \geqslant 3$, the compatibility of the postulate of equal reactivity of all unreacted groups with non-occurrence of rings requires (*i*) an infinite system, and (*ii*) absence of infinite polymers, which is fulfilled only below α_c. The derivations of the Flory expression in refs. 1, 2, 11, 14, and 26, which postulate simultaneously these two conditions, are therefore valid below α_c, and invalid above α_c.

1. M. Gordon and M. Judd. Nature, **234**, 96 (1971).
2. P. Whittle. Proc. Camb. Phil. Soc. **61**, 475 (1965).
3. M. E. Fisher and J. W. Essam. J. Math. Phys. **2**, 609 (1961).
4. T. E. Harris. The theory of branching processes. Springer-Verlag, Berlin. 1963.
5. H. Jacobson and W. H. Stockmayer. J. Chem. Phys. **18**, 1600 (1950).
6. F. E. Harris. J. Chem. Phys. **23**, 1518 (1955).
7. R. W. Kilb. J. Phys. Chem. **62**, 969 (1958).
8. V. S. Nanda and S. C. Jain. J. Chem. Phys. **49**, 1318 (1968).
9. M. Gordon and G. R. Scantlebury. J. Chem. Soc. B, 1 (1967).
10. W. B. Temple. Makromol. Chem. **160**, 277 (1972).
11. P. J. Flory. Principles of polymer chemistry. Cornell University Press, Ithaca, New York. 1953. Chapt. 9.
12. P. J. Flory. J. Am. Chem. Soc. **63**, 3082, 3091, 3096 (1941).
13. P. J. Flory. J. Am. Chem. Soc. **69**, 30 (1947).
14. W. H. Stockmayer. J. Chem. Phys. **11**, 45 (1943).
15. P. J. Flory. Chem. Rev. **38**, 137 (1946).
16. C. R. Masson, I. B. Smith, and S. G. Whiteway. Nature, **234**, 97 (1971).
17. R. F. T. Stepto. Can. J. Chem. **52**, 1188 (1974).
18. C. R. Masson and S. G. Whiteway. Can. J. Chem. **52**, 1190 (1974).
19. S. G. Whiteway, I. B. Smith, and C. R. Masson. Can. J. Chem. **48**, 33 (1970).
20. C. R. Masson, I. B. Smith, and S. G. Whiteway. Can. J. Chem. **48**, 201, 1456 (1970); **51**, 1422 (1973).
21. M. Bersohn. J. Chem. Soc. Perkin I, 1239 (1973).
22. J. W. Essam and M. E. Fisher. Rev. Modern Phys. **42**, 272 (1970).
23. P. J. Flory. J. Am. Chem. Soc. **74**, 2718 (1952).
24. W. H. Stockmayer. *In* Advancing fronts in chemistry. *Edited by* S. B. Twiss. Reingold Publ. Corp., New York. 1945. Chapt. 6.
25. R. H. Peters and R. F. T. Stepto. *In* The chemistry of polymerization processes. Monograph No. 20, Soc. Chem. Ind., London. 1965. p. 157.
26. I. J. Good. Proc. R. Soc. **A272**, 54 (1963).

Erratum: Primary Bond Formation in the Addition of Cyclopentenone to Chloroethylenes

R. O. Loutfy and P. de Mayo

Department of Chemistry, University of Western Ontario, London 72, Ontario

Received July 17, 1974

(Ref.: Can. J. Chem. **50**, 3465 (1972))

The name of N. A. Farid was inadvertently omitted from the list of authors of this article. The authors names should read R. O. Loutfy, P. de Mayo, and N. A. Farid.

Can. J. Chem. Downloaded from www.nrcresearchpress.com by 210.87.254.42 on 09/05/12
For personal use only.

Can. J. Chem. Downloaded from www.nrcresearchpress.com by 210.87.254.105 on 09/05/12
For personal use only.

Canadian Journal of Chemistry

Published by
THE NATIONAL RESEARCH COUNCIL OF CANADA

Journal canadien de chimie

Publié par
LE CONSEIL NATIONAL DE RECHERCHES DU CANADA

Volume 52 Number 19 October 1, 1974

Volume 52 numéro 19 1 octobre 1974

Conformations of Bridged Diphenyls. VI. Substituent Effects and Internal Rotation in Triply *Ortho*-substituted Diphenyl Ethers

HARM BENJAMINS, FAZAL HAQUE DAR, AND W. DAVID CHANDLER[1]

Department of Chemistry, University of Saskatchewan, Regina, Saskatchewan S4S 0A2

Received January 7, 1974

HARM BENJAMINS, FAZAL HAQUE DAR, and W. DAVID CHANDLER. Can. J. Chem. **52**, 3297 (1974).

Experimental evidence is presented to support the hypothesis that, in triply *ortho*-substituted diphenyl ethers, conformer interconversion involves both rings. The free energy barrier, measured by p.m.r., is sensitive to substituent effects arising in the ring having only one *ortho* substituent. The exceptionally high barrier found when an *ortho* iodine is present is consistent with the existence of a substituent-inside intermediate occurring during conformer conversion.

HARM BENJAMINS, FAZAL HAQUE DAR et W. DAVID CHANDLER. Can. J. Chem. **52**, 3297 (1974).

On rapporte une preuve expérimentale démontrant l'hypothèse selon laquelle les interconversions de conformères, dans les éthers diphénylés trisubstitués en position *ortho*, impliquent les deux noyaux. L'énergie de la barrière à la rotation, tel que mesuré par la r.m.n. du proton, est sensible aux effets de substituants découlant de la présence dans un noyaux de seulement un substituant en position *ortho*. La barrière exceptionnellement élevée qui est trouvée lorsqu'un iode est présent en position *ortho* est en accord avec l'existence d'un intermédiaire comportant un substituant à l'intérieur durant la conversion des conformères. [Traduit par le journal]

Introduction

Using rotational barriers, obtained from variable temperature p.m.r. spectra, a previous paper speculated on the mechanism by which stable conformers of doubly and triply *ortho*-substituted diphenyl ethers are interconverted (1). For the latter, it was proposed that ring rotation could take place through two butterfly conformations in which both rings make an angle of 90° with the central COC plane (Fig. 1). For the former, either a concerted rotation of the two rings (Fig. 2, X = H) or rotation through the butterfly intermediates could account for the experimentally observed free energy barriers. The importance of studies such as this lies in their potential for explaining the lack of success in resolving potentially chiral diphenyl ethers. The purpose of this paper is to present a more detailed mechanistic and topological analysis of isomerization for triply *ortho*-substituted diphenyl ethers along with experimental evidence for a mechanism involving both rings.

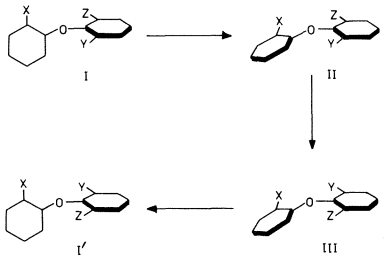

FIG. 1. Interconversion of stable, skew, H-inside conformers of triply *ortho*-substituted diphenyl ether through butterfly intermediates **II** and **III**.

[1]Author to whom all correspondence should be addressed.

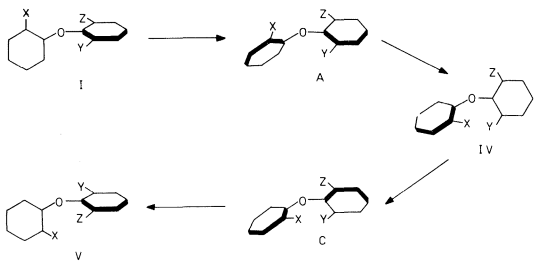

FIG. 2. Application of a concerted, cogwheel rotation to a skew, H-inside conformer of a triply *ortho*-substituted diphenyl ether.

For diphenyl ether itself, the stable conformation appears to be one in which the two rings are rotated from coplanarity in a conrotatory manner by angles estimated to be between 18 and 52° (2 and refs. therein). Since the energy barrier between possible conformers is small, there is a continuous and rapid interconversion of these at ordinary temperatures (2–5). A concerted or cogwheel mechanism, similar to that illustrated in Fig. 2, was suggested by Fong (3) as the prime method of internal motion in diphenyl ether. From a study of the potential energy surface calculated using an extended HMO method, Galasso *et al.* (2) concluded that the mechanism is more likely to involve a butterfly-like transition state. Nonetheless, the barriers for the cogwheel and the butterfly mechanisms were calculated to be only 0.3 kcal/mol apart.

In a very extensive analysis of isomerization due to restricted rotation of phenyl rings Gust and Mislow (6) labelled the concerted motion as a one-ring flip and the mechanism involving butterfly transition states as a two-ring flip. For the remainder of this paper the terms zero-ring flip, one-ring flip, and two-ring flip will be used as they have been defined by Gust and Mislow.

For *ortho*-substituted diphenyl ethers and many other bridged diphenyls there is ample evidence to suggest that the twist, H-inside conformations are the most stable (7–26). Figure 3, which was prepared in the manner of Gust and Mislow (6), displays all eight possible twist conformers for a triply *ortho*-substituted diphenyl ether. The four that have an *ortho* hydrogen inside or proximal (**A**, **B**, **A′**, and **B′**) occur in two pairs. The one pair, **A** and **B**, are interconvertible by a one-ring flip through the skew conformation, **I**. The other pair, **A′** and **B′**, are similarly interconvertible through **I′** where **A′**, **B′**, and **I′** are nonsuperimposable mirror images of the unprimed set.

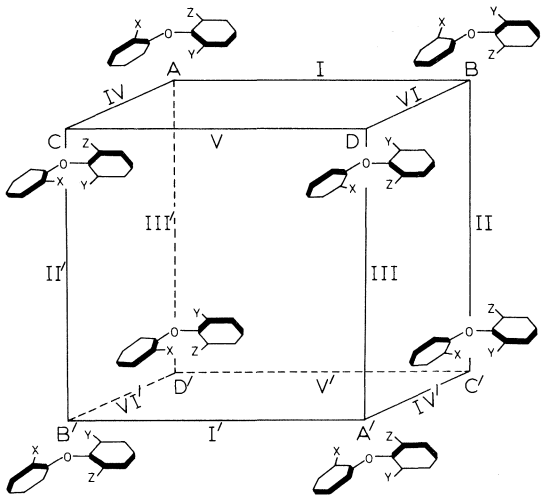

FIG. 3. Possible twist conformers for triply *ortho*-substituted diphenyl ether and ring-flip interconversions. The apices of the cube represent twist conformers. The roman numerals **I**, **IV**, **V**, **VI**, and their primed analogs represent skew conformers; **II**, **III**, and their primed analogs represent butterfly conformers. The horizontal edges are one-ring flips. The vertical edges are two-ring flips. Lines connecting diagonally opposite corners and passing through the center (not shown) are zero-ring flips.

Potential energy calculations (8) indicate that the barrier for the one-ring flip that interconverts **A** and **B** or **A′** and **B′** is very low. For this reason, several groups (2, 8, 23) have suggested that the conformation of these ethers in solution is best described as the average of each pair or the skew, H-inside conformation. Thus the interconversion of stable conformers is represented by **I** ↔ **I′** (See Fig. 1).

The topological analysis of conformer interconversion is clearly evident from Fig. 3. The eight horizontal edges represent one-ring flips through skew conformations **I**, **IV**, **V**, **VI**, and their mirror images (Figs. 1 and 2 as well); the vertical edges represent two-ring flips involving butterfly conformations **II**, **III**, and their mirror images; the four lines (not drawn) connecting diagonally opposite corners of this cube and passing through the center represent zero-ring flips through a planar conformation. To interconvert **I** and **I′** there are two types of mechanisms: (*i*) a zero-ring flip or (*ii*) a two-ring flip plus a one-ring flip. Rotation of the di-*ortho*-substituted ring alone is a zero-ring flip but this has been tentatively rejected because of the high energy needed to overcome *ortho* group repulsions in the planar transition state. The butterfly mech-

Can. J. Chem. Downloaded from www.nrcresearchpress.com by 210.87.254.105 on 09/05/12
For personal use only.

Can. J. Chem. Downloaded from www.nrcresearchpress.com by 210.87.254.105 on 09/05/12
For personal use only.

anism of Fig. 1 (**I** → **II** → **III** → **I′** or the equivalent **I** → **III′** → **II′** → **I′**) is analogous to a two-ring flip plus a one-ring flip. The concerted mechanism of Fig. 2 (**I** → **IV** → **V** or alternatively **I** → **VI** → **V**) can be ruled out as a possible method of conformer interconversion in this instance because **V** is a higher energy conformer that is not a mirror image of **I**. Rotation of the X-substituted ring alone, a one-ring flip, has the same effect so that the only processes that need be considered are rotation of the di-*ortho*-substituted ring alone or a double-ring mechanism such as that shown in Fig. 1.

Montaudo and his co-workers (7–10) have presented potential energy surfaces for some model doubly and triply *ortho*-substituted, bridged diphenyls, in all but one case using only nonbonded interactions to estimate the potential energy (10). Rowbotham (12) has obtained crude estimates of steric overlap between *ortho* substituents as well as the interaction of these substituents with the rings' π-clouds to arrive at similar diagrams of *allowed* and *forbidden* areas for diphenyl ether conformations. From these diagrams, the lowest energy route for interconversion of stable conformers can be assessed in a qualitative way.

For triply *ortho*-substituted diphenyl ethers Fig. 4 represents the results of these calculations including the areas of a number of conformations and several interconversion routes possible (8, 12). The shaded areas represent the stable conformational regions including H-inside twist and skew conformations. These are estimated to be

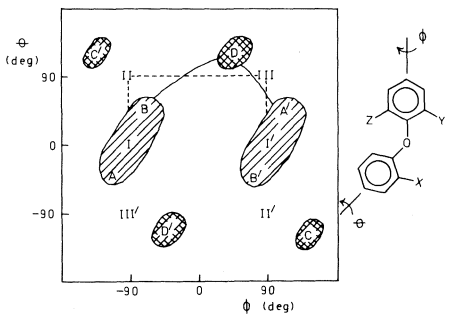

FIG. 4. Rotational map for a triply *ortho*-substituted diphenyl ether. θ = φ = 0° is the planar H-inside conformation. The shaded areas represent the stable time-average H-inside conformations; the cross-hatched areas represent the twist, X-inside conformations; - - - - - is rotation through butterfly intermediates as illustrated in Fig. 1; — is the lowest energy path for conformer interconversion as calculated by Montaudo *et al.* (8) and Rowbotham (12).

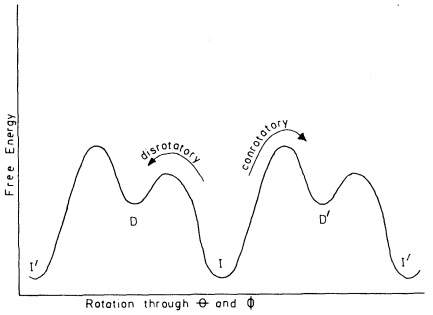

FIG. 5. Free energy diagram for interconversion of the conformers **I** and **I′** through a twist, X-inside intermediate **D** or **D′**.

several kcal/mol more stable than other twist conformations shown here as cross-hatched areas. Were Y and Z identical **I** and **I′** would be superimposable mirror images; otherwise they are enantiomeric and under certain conditions might be resolvable.

As expected the energy diagrams of Montaudo and Finocchiaro (8) and Rowbotham (12) indicate that the zero-ring flip or di-*ortho*-substituted ring rotation (**I** ↔ **I′** at constant θ) requires far too high an energy to be considered seriously. The suggested lowest energy, two-ring interconversion mechanism (solid line) probably involves a single intermediate rather than the two butterfly intermediates suggested earlier (dashed line). The intermediate would have a twist, X-inside conformation with φ and θ in the neighborhood of −45 and −120°, respectively. Because it has no plane of symmetry, the interconversion of **I** and **I′** should involve two *different* transition states (Fig. 5).[2] The higher energy one has large Z–X and Z–H interactions while the other has only a Z–X interaction. Interconversion of **I** and **I′** would then involve rotation of the two rings in a disrotatory fashion as the first step so that the measured barrier is that of this step.

Although a two-ring mechanism for conformer interconversion was postulated qualitatively in a previous paper (1) and energy contour diagrams suggest its existence as outlined above, experi-

[2]As long as Y and Z are substantially different there would be two different routes both with two transition states. These two routes would be **I** ↔ **D**, **D′** ↔ **I′** and **I** ↔ **C**, **C′** ↔ **I′**. **D** and **D′** being mirror images would have the same energy but **D** and **C** or D′ and **C′** would not. Figure 5 and the discussion above were prepared with the simplifying assumption that Z is the 'smaller' of the two substituents making **D** and **D′** more stable than **C** and **C′**. The interconversion route would then involve **D** or **D′** primarily.

mental verification has been lacking. In this paper we present evidence for such a mechanism using the two ether families **1** and **2**.

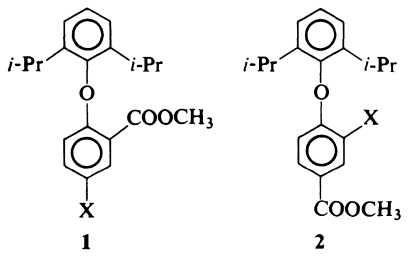

a X = NO_2
b X = NH_2
c X = I
d X = H

It has been shown that, for compounds such as **1** and **2**, the p.m.r. spectra of the isopropyl methyl groups are temperature dependent (1, 27). Below a temperature, T_c, there appear two doublets while at temperatures greater than T_c there is a single doublet. This phenomenon is explained in terms of rotation by 180° about the alkylated ring – O bond, a process which exchanges the identity of the two anisochronous methyls comprising each isopropyl. Thus the measured energy barrier for the methyl exchange is the barrier for whatever mechanism is involved in rotating the alkylated ring and, as a result, in converting, in this case, the two equivalent conformers **I** and **I′**. If the diisopropyl-substituted ring had no plane of symmetry **I** and **I′** would be enantiomers.

If the methyl exchange occurs by rotation of the alkylated ring alone, the barrier should be essentially independent of the variable substituent in both **1** and **2**. If, on the other hand, a two-ring mechanism is involved, the barrier would be expected to depend on the electronic character of X in **1** and on electronic and bulk effects in **2**. For example, in **1***a* where X = NO_2, a large mesomeric effect should be operating, increasing the double bond character of the Ar—O bond and lowering the energy of the stable, skew conformers **I** and **I′** relative to what would be expected in **1***d* where X = H. As the effect of the NO_2 on the transition state, being nearer the butterfly conformation, should be less, $\Delta G^{\ddagger}$ will be greater in **1***a*. When X = NH_2, as in **1***b*, the reverse mesomeric should operate and $\Delta G^{\ddagger}$ will be lower than for **1***d*. In fact one would expect $\Delta G^{\ddagger}$ to increase with changing *para*-substituent in the order $NH_2 < H < I < NO_2$.

The p.m.r. spectra of the eight compounds in families **1** and **2** were obtained over a wide range of temperatures and the coalescence data were extracted.

Results and Discussion

The coalescence data and $\Delta G^{\ddagger}$ values, calculated for an uncoupled AB system as outlined previously (1), are presented in Table 1. Clearly $\Delta G^{\ddagger}$ and T_c vary with substituent in both series beyond experimental error. For **1** the variation in $\Delta G^{\ddagger}$ is roughly as expected with a difference of 2.5 kcal/mol (measured at different temperatures) between X = NO_2 and X = NH_2. Thus, the electronic character of the groups substituted on one ring is important in influencing the barrier to rotation of the other ring, indicating the existence of a two-ring conformer conversion process. These results point out that in general the neglect of mesomeric effects in calculating potential energy contours could lead to erroneous results.

In series **2**, where steric effects may come into play, the results are also as expected for a two-ring process. $\Delta G^{\ddagger}$ is largest for the *ortho*-substituent with greatest size. Thus the barrier is greater when X = NO_2 than when X = NH_2 and is greater for **1***a* and **2***a*. When X = H the barrier is very low and another interconversion mechanism may be operative (1). In series **2** there is a much larger barrier for X = I than for X = NO_2 in spite of the fact that the nitro group, even if twisted out of the ring plane, is a stronger electron withdrawing substituent. The steric, *ortho*-substituent parameters, E_s, for iodine and nitro are −0.20 and −0.75, respectively (28), suggesting that NO_2 should have a larger steric effect in interacting with the isopropyl groups in the transition state of the two-ring mechanism. If that were so **2***a* should have a larger rotational barrier than **2***c* since virtually all the steric interaction would arise in the transition state.

However, several groups (29–31) have postulated the existence of an interaction between iodine and the π system of a phenyl ring in studies of the preferred conformations of some iodo-diphenyl ethers. Such an interaction would make the X-inside, twist conformation of Figs. 4 and 5 even lower in energy for **2***c*. If $\Delta G^{\ddagger}$ is to be abnormally large in this case, during the rotational process toward the intermediate the electron cloud about the iodine must become deformed in the direction of the phenyl ring. The interac-

Can. J. Chem. Downloaded from www.nrcresearchpress.com by 210.87.254.105 on 09/05/12
For personal use only.

TABLE 1. Coalescence data and $\Delta G^{\ddagger}$ values for series **1** and **2**

Compound	X	T_c (°C)	$\Delta\nu$ (Hz)[a]	k_c (s^{-1})	$\Delta G^{\ddagger}$ (kcal/mol)
1*a*	NO_2	100.5	6.4	14.2	20.0
1*b*	NH_2	53.3	6.6	14.7	17.5
1*c*	I	70.5	7.1	15.8	18.3
1*d*	H	76.5	7.0	15.5	18.6
2*a*	NO_2	66.5	6.5	14.4	18.1
2*b*	NH_2	52.6	7.3	16.1	17.3
2*c*	I	$\simeq 125$	6.5	14.4	$\simeq 21$
2*d*	H	< -70	7.0[b]	15.6[b]	< 10

[a]At 60 MHz.
[b]Estimate based on previous work (1). Temperatures considerably below T_c were unavailable using A-60A.

TABLE 2. Properties of diphenyl ethers in series **1** and **2**

Compound	Melting point (°C)	Analysis (%) Calculated C	H	N	I	Found C	H	N	I
1*a*	84–85	67.21	6.49	3.92	—	67.41	6.52	3.79	—
1*b*	131–133	73.37	7.70	4.28	—	73.22	7.78	4.14	—
1*c*	80–81	54.81	5.29	—	28.95	55.05	5.09	—	28.74
1*d*	79–80	76.89	7.74	—	—	76.70	7.63	—	—
2*a*	170–171/1 mm[a]	67.21	6.49	3.92	—	66.99	6.58	3.99	—
2*b*	155–156	73.37	7.70	4.28	—	73.52	7.84	4.09	—
2*c*	Viscous oil	54.81	5.29	—	28.95	55.01	5.43	—	29.18
2*d*	76–77	76.89	7.74	—	—	77.01	7.85	—	—

[a]Boiling point at 1 mm Hg.

tion between an isopropyl and the distorted electron cloud would then increase the energy of the transition state relative to that if NO_2 were the *ortho*-substituent. Such an argument requires that the iodine act as an *electron donor* in its interaction with the phenyl ring in the twist intermediate of **2***c*. Whatever the cause of the high barrier for **2***c* it is interesting to note that *ortho*-iodo-substituted biphenyls have long been known to have anomalously high rotational barriers (32, 33). It may be that chiral diphenyl ethers with an *ortho* iodine are best suited for resolution studies.

The results of Table 1 clearly support a two-ring mechanism for interconversion of the stable conformers of triply *ortho*-substituted diphenyl ethers and all the evidence is consistent with this mechanism involving a single, X-inside intermediate.

Experimental

The p.m.r. spectra were recorded on a Varian A-60A spectrometer. The data given are for samples dissolved in chloroform-*d* except **2***c* and **2***d* which required dimethylformamide-d_7 and acetone-d_6 as solvents, respectively. A discussion of the method used to calculate $\Delta G^{\ddagger}$ has been given previously (1).

The compounds were prepared by standard methods outlined earlier for other ethers (1, 14, 34). Table 2 gives the properties of these ethers.

The authors wish to acknowledge the generous support of the National Research Council of Canada for grants in aid of research and for a Scholarship to one of us (H.B.).

1. J. J. BERGMAN and W. D. CHANDLER. Can. J. Chem. **50**, 353 (1972).
2. V. GALASSO, G. DEALTI, and A. BIGOTTO. Tetrahedron, **27**, 6151 (1971).
3. F. K. FONG. J. Chem. Phys. **40**, 132 (1964).
4. J. E. KATON, W. R. FEAIRHELLER, JR., and W. R. LIPPINCOTT. J. Mol. Spectrosc. **13**, 72 (1964).
5. C. GARRIGOU-LAGRANGE, M. HORAK, R. K. KHANNA, and E. R. LIPPINCOTT. Coll. Czech. Chem. Commun. **35**, 3230 (1970).
6. D. GUST and K. MISLOW. J. Am. Chem. Soc. **95**, 1535 (1973).
7. G. MONTAUDO and P. FINOCCHIARO. J. Am. Chem. Soc. **94**, 6745 (1972).
8. G. MONTAUDO and P. FINOCCHIARO. J. Mol. Struct. **14**, 53 (1972).
9. G. MONTAUDO, P. FINOCCHIARO, and S. CACCAMESE. J. Org. Chem. **38**, 170 (1973).

Can. J. Chem. Downloaded from www.nrcresearchpress.com by 210.87.254.105 on 09/05/12
For personal use only.

10. G. W. BUCHANAN, G. MONTAUDO, and P. FINOCCHIARO. Can. J. Chem. **51**, 1053 (1973).
11. G. W. BUCHANAN, G. MONTAUDO, and P. FINOCCHIARO. Can. J. Chem. **52**, 767, (1974).
12. J. B. ROWBOTHAM. Ph.D. Thesis, Queen's University, Kingston, Ontario. 1970.
13. J. J. BERGMAN, W. D. CHANDLER, and R. Y. MOIR Can. J. Chem. **49**, 225 (1971).
14. J. J. BERGMAN, E. A. H. GRIFFITH, B. E. ROBERTSON, and W. D. CHANDLER. Can. J. Chem. **51**, 162 (1973).
15. H. BENJAMINS and W. D. CHANDLER. Can. J. Chem. **52**, 597 (1974).
16. G. MONTAUDO, P. FINOCCHIARO, E. TRIVELLONE, F. BOTTINO, and P. MARAVIGNA. Tetrahedron, **27**, 2125 (1971).
17. G. MONTAUDO, P. FINOCCHIARO, F. BOTTINO, S. CACCAMESE, P. MARAVIGNA, and E. TRIVELLONE. Proc. XXIII Int. Congr. Pure Appl. Chem. II, 1169 (1971).
18. G. MONTAUDO, S. CACCAMESE, P. FINOCCHIARO, and F. BOTTINO. Tetrahedron Lett. 877 (1970).
19. G. MONTAUDO, S. CACCAMESE, and P. FINOCCHIARO. J. Am. Chem. Soc. **93**, 4202 (1971).
20. G. MONTAUDO, P. FINOCCHIARO, and P. MARAVIGNA. J. Am. Chem. Soc. **93**, 4214 (1971).
21. G. MONTAUDO, P. FINOCCHIARO, and S. CACCAMESE. J. Org. Chem. **36**, 2860 (1971).
22. G. MONTAUDO, F. BOTTINO, and E. TRIVELLONE. J. Org. Chem. **37**, 504 (1972).
23. P. A. LEHMANN. Org. Magn. Res. **2**, 467 (1970).
24. P. A. LEHMANN and D. M. MCEACHERN. J. Mol. Struct. **7**, 253, 277 (1971).
25. D. M. MCEACHERN and P. A. LEHMANN. J. Mol. Struct. **7**, 267 (1971).
26. E. A. H. GRIFFITH, W. D. CHANDLER, and B. E. ROBERTSON. Can. J. Chem. **50**, 2963, 2972, 2979 (1972).
27. H. KESSLER, A. RIEKER, and W. RUNDEL. Chem. Commun. 475 (1968).
28. R. W. TAFT. *In* Steric effects in organic chemistry. *Edited by* M. Newman. John Wiley and Sons, New York. 1956. p. 556.
29. N. CAMERMAN and A. CAMERMAN. Science, **175**, 764 (1972).
30. N. CAMERMAN and A. CAMERMAN. Biochem. Biophys. Res. Commun. **48**, 1433 (1972).
31. P. A. LEHMANN. J. Med. Chem. **15**, 404 (1972).
32. L. N. FERGUSON. *In* The modern structural theory of organic chemistry. Prentice-Hall, Englewood Cliffs, N.J. 1963. p. 277.
33. M. S. LESLIE and E. E. TURNER. J. Chem. Soc. 1588 (1933).
34. W. D. CHANDLER, J. J. BERGMAN, and G. H. HAAS. Can. J. Chem. **49**, 583 (1971).

Can. J. Chem. Downloaded from www.nrcresearchpress.com by 210.87.254.105 on 09/05/12
For personal use only.

Protonation of Methyl Substituted Phenols in Super Acids[1,2]

R. F. CHILDS AND B. D. PARRINGTON

Department of Chemistry, McMaster University, Hamilton, Ontario L8S 4M1

Received April 1, 1974

R. F. CHILDS and B. D. PARRINGTON. Can. J. Chem. **52**, 3303 (1974).

The protonation of a series of methyl substituted phenols and anisoles in FSO_3H has been examined. When the *para* position of the phenol is unsubstituted, protonation was found to take place exclusively at this site. A methyl group on C-4 reduces the basicity of this carbon such that protonation on C-2, C-6 or oxygen can now compete with *para* protonation. Despite claims to the contrary, in FSO_3H no significant amount of *meta* protonation was observed for any of the phenols. In FSO_3H–SbF_5, 2,4,6-trimethylphenol is protonated on C-3 or C-5; however, it would appear that this *meta* protonation is accompanied by a modification of the hydroxy group by either further protonation or reaction with the Lewis acid SbF_5.

R. F. CHILDS et B. D. PARRINGTON. Can. J. Chem. **52**, 3303 (1974).

On a étudié la protonation, dans l'acide fluorosulphonique, d'une série de phénols substitués par des groupes méthyles ainsi que des anisoles. On a trouvé que la protonation se fait uniquement en position 4 lorsque le phénol ne porte aucun substituant en position *para*. L'introduction d'un groupe méthyle en position 4 réduit la basicité de ce carbone d'une façon telle que les carbones 2 et 6 ainsi que l'oxygène peuvent entrer en compétition avec la protonation en position *para*. Malgré les assertions du contraire, on n'observe, dans l'acide fluorosulphonique, aucune protonation en position *méta* des phénols. Dans un mélange FSO_3H–SbF_5, le triméthyl-2,4,6 phénol se protone en position 3 ou 5; toutefois il semble que cette protonation en *méta* est accompagnée par une modification du groupe hydroxyle soit par une protonation subséquent ou par réaction avec le SbF_5 qui agit comme acide de Lewis.

[Traduit par le journal]

Introduction

We have previously reported that protonated 2,4- and 2,5-cyclohexadienones undergo a series of rearrangements when irradiated in FSO_3H (2, 3). Protonated phenols, which are often observed as products of these reactions, undergo competing photoisomerizations. In order to understand these rearrangements, it is important to know in some detail the structures of the cations resulting from the protonation of these phenols in super acids.

There have been several reports of the protonation of phenols (4–9) and anisoles (10–14, 4, 5) in super acid media and some discussion as to the preferred site of proton attachment (15–17, 5, 8). When a phenol is unsubstituted at the *para* position, it is generally agreed that in FSO_3H protonation takes place at this site (18). The situation is more complex when the *para* position is substituted and in these cases oxygen, *ortho*, *meta*, and *para* protonation have all been claimed (7, 8).

We report here the results of a systematic study of the protonation of a series of methyl substituted phenols in FSO_3H and discuss the factors that determine the site(s) of protonation. These results differ in some respects to previous interpretations, particularly with regard to the question of *meta* protonation.

Experimental

General

Nuclear magnetic resonance spectra were obtained on Varian A-60 and HA-100 spectrometers fitted with variable temperature probes. The temperature of the probe was determined with a methanol sample and all spectra were run at temperatures between -55 and $-45°$. $(CH_3)_4N^+Cl^-$, taken as 3.1 δ, was used as an internal standard throughout. Ultraviolet spectra were obtained with a Cary 14 recording spectrophotometer using 1-cm quartz cells. The sample cell was maintained at low temperatures by mounting it in a Dewar with flat quartz windows that could be fitted in the Cary 14 spectrophotometer. The Dewar was cooled with a stream of N_2 gas obtained by boiling liquid N_2 and the temperature monitored with a thermocouple.

Materials

Fluorosulfuric acid (200 ml), to which NaF (2 g) was added, was distilled at atmospheric pressure through a 10 in. Vigreaux column. The middle fraction was collected and stored in sealed glass ampoules until required.

[1]We acknowledge helpful discussions with Dr. K. E. Richards whose results appear in an accompanying paper.

[2]A preliminary report of part of these findings has appeared (1).

Can. J. Chem. Downloaded from www.nrcresearchpress.com by 210.87.254.42 on 09/05/12
For personal use only.

TABLE 1. Site of protonation of methyl substituted phenols and anisoles*

Substituents	Compound	Acid	% protonation				
			Oxygen	C-2	C-3(C-5)	C-4	C-6
Phenols							
4-Methyl	**50**†	$HFSO_3$	55	40		5	‡
		$HFSO_3$–SbF_5	19	73.5		7.5	‡
2,3-Dimethyl	**1**	$HFSO_3$				100	
2,4-Dimethyl	**41**	$HFSO_3$	41			12	47
2,5-Dimethyl	**3**	$HFSO_3$				100	
2,6-Dimethyl	**5**	$HFSO_3$				100	
3,4-Dimethyl	**37**	$HFSO_3$		3		7	90
3,5-Dimethyl	**7**	$HFSO_3$				100	
2,3,4-Trimethyl	**21**	$HFSO_3$				17	83
2,3,5-Trimethyl	**9**	$HFSO_3$				100	
2,3,6-Trimethyl	**11**	$HFSO_3$				100	
2,4,5-Trimethyl	**22**	$HFSO_3$				85	15
2,4,6-Trimethyl	**32**	$HFSO_3$	42			58	
		$HFSO_3$–SbF_5			100		
3,4,5-Trimethyl	**23**	$HFSO_3$		57		43	‡
2,3,4,6-Tetramethyl	**18**	$HFSO_3$				100	
2,3,5,6-Tetramethyl	**13**	$HFSO_3$				100	
2,3,4,5,6-Pentamethyl	**17**	$HFSO_3$				100	
Anisoles							
2,4-Dimethyl	**45**	$HFSO_3$	23			5	72
2,4,6-Trimethyl	**35**	$HFSO_3$	100				

*Numbering scheme of phenol or anisole is maintained throughout.
†Some variation in the ratio of O to C protonation was observed with 50 depending on the batch of acid used. The ratio of the cations derived from protonation on C-2 and -4 remained constant with change of acid. The other phenols did not appear to exhibit a similar variation.
‡Positions 2 and 6 are equivalent.

Antimony pentafluoride was distilled twice and stored in Teflon bottles.

Most of the phenols are available commercially. Pentamethylphenol was prepared both by the method of Willstatter and Kubli (19) and by that of MacDonald and co-workers (20), m.p. 123–124° (lit. (21) m.p. 125°). 2,3,4-Trimethylphenol was obtained by the BF_3 catalyzed rearrangement of 2,3-dimethylanisole, m.p. 81–82° (lit. (22) m.p. 81°). 6,6-Dimethylcyclohexa-2,4-dienone was obtained from dimethylfulvene by the procedure of Alder *et al.* (23). Oxidation of 4,4-dimethylcyclohex-2-enone (24) was used to obtain 4,4-dimethylcyclohexa-2,5-dienone (25). 2,3,4,5,6,6-Hexamethylcyclohexa-2,4-dienone and 2,3,4,4,5,6-hexamethylcyclohexa-2,5-dienone were obtained by the procedures of Hart *et al.* (26, 27). 3,5,6-Trideuterio-2,4-dimethylphenol was prepared by refluxing the phenol in 5% D_2SO_4 in D_2O for 40 h. Integration of the n.m.r. spectrum of the product showed 94% of the ring protons had been replaced by deuterium.

Preparation of Cations

The phenol or dienone (30–50 mg) was placed in an n.m.r. tube and cooled to −78° before FSO_3H (0.6 ml) (or the appropriate mixture of FSO_3H–SbF_5), also cooled to −78°, was added. The suspension was stirred with a thin glass rod until solution occurred, A crystal of $(CH_3)_4N^+Cl^-$ was added to the solution as an internal standard.

Results

The cations produced upon protonation of the methyl substituted phenols in FSO_3H and FSO_3H–SbF_5 were identified by their low temperature n.m.r. spectra. In many cases protonation occurred at more than one site of the phenol and our findings are summarized in Table 1.

Protonation of Phenols Lacking a Para Substituent

The phenols shown in Scheme 1, which are all characterized by being unsubstituted in the 4 position, were all protonated on the *para* position when dissolved in FSO_3H. The n.m.r. spectra of these cations are completely consistent with the structures indicated and no other cations could be detected. The assignment of the various resonances, shown in Table 2, was made by considering their multiplicity and integration, together with the changes occurring in the spectra as the substitution pattern of the cation was altered. Similar results have been previously reported for the protonation of **7** (6, 7). The marked similarity in the n.m.r. spectra of these

Can. J. Chem. Downloaded from www.nrcresearchpress.com by 210.87.254.42 on 09/05/12
For personal use only.

Can. J. Chem. Downloaded from www.nrcresearchpress.com by 210.87.254.42 on 09/05/12
For personal use only.

TABLE 2. Proton chemical shifts of para protonated phenols and related materials in FSO_3H

Cation	Substituents	Chemical shift* C-2(C-6) Me	C-2(C-6) H	C-3(C-5) Me	C-3(C-5) H	C-4 Me	C-4 H	Coupling
53	4-Methyl	—	?	—	?	1.57d	?	J = 8 Hz
53†	4-Methyl	—	?	—	?	1.57d	?	J = 8 Hz
2	2,3-Dimethyl	2.22	7.18d	2.54	8.26d	—	4.15	J_{56} = 9 Hz
44	2,4-Dimethyl	—	?	—	?	1.55d	3.96q	J = 7 Hz
48	2,4-Dimethyl	—	?	—	?	1.55d	?	
4	2,5-Dimethyl	2.23	7.03	2.57	8.06	—	4.07	
6	2,6-Dimethyl	2.36	—	—	8.35	—	4.17	
39	3,4-Dimethyl	?	?	2.59	8.31	1.62d	3.82q	J = 8 Hz
8	3,5-Dimethyl	?	6.94	2.52	—	—	3.99	
24	2,3,4-Trimethyl	2.17	?	2.49	8.24d	1.54	3.82	J_{Me-H} = 8 Hz, $J_{5,6}$ = 8 Hz
10	2,3,5-Trimethyl	2.15	6.95	2.46	—	—	4.01	
12	2,3,6-Trimethyl	2.24, 2.26	—	2.53	8.04	—	4.11	
26	2,4,5-Trimethyl	2.21	7.03	2.53	8.03	1.55d	3.73q	J_{Me-H} = 8 Hz
33	2,4,6-Trimethyl	2.33	—	—	8.23	1.52d	3.88m	J_{Me-H} = 7 Hz
28	3,4,5-Trimethyl	—	6.93	2.53	—	1.60d	3.66q	J_{Me-H} = 8 Hz
20	2,3,4,6-Tetramethyl	2.23, 2.27	—	2.50	8.02	1.56d	3.73m	J_{Me-H} = 7 Hz
14	2,3,5,6-Tetramethyl	2.20	—	2.46	—	—	4.05	
19	2,3,4,5,6-Pentamethyl	2.16	—	2.42	—	1.52d	3.62q	J_{Me-H} = 8 Hz
15	4,4-Dimethyl	—	7.10d	—	8.38d	1.52	—	$J_{2,3}$ = 9 Hz
16	2,3,4,4,5,6-Hexamethyl	2.17	—	2.41	—	1.41	—	

*In p.p.m. from TMS using $(CH_3)_4N^+$ as internal standard. Numbering scheme of original phenol maintained in cations. d = doublet, q = quartet.
†FSO_3H–SbF_5 (4:1) solvent.

Can. J. Chem. Downloaded from www.nrcresearchpress.com by 210.87.254.42 on 09/05/12
For personal use only.

TABLE 3. Proton chemical shifts of ortho protonated phenols and related materials in FSO_3H

		Chemical shift (p.p.m.)*											
		C-2		C-3		C-4		C-5		C-6			
Cation	Substituents	Me	H	Me	H	Me	H	Me	H	Me	H	O—Me	Coupling
52	4-Methyl	—	7.13d	—	8.54d	2.26	—	—	7.35	—	4.36	—	J_{23} = 7 Hz
52†	4-Methyl	—	7.13d	—	8.54d	2.26	—	—	7.40	—	4.35	—	J_{23} = 7 Hz
42	2,4-Dimethyl	2.26	—	—	8.37	2.26	—	—	7.24	—	4.31	—	
46	2,4-Dimethyl	2.24	—	—	8.22	2.24	—	—	7.22	—	4.17	4.43	
38	3,4-Dimethyl	—	7.08	2.67	—	2.24	—	—	7.33	—	4.20	—	
40‡	4,5-Dimethyl	—	?	—	8.48	?	—	2.37	—	—	4.33	—	
25	2,3,4-Trimethyl	2.22§	—	2.62	—	2.25§	—	—	7.18	—	4.12	—	
27	2,4,5-Trimethyl	(2.21)	—	—	8.30	(2.21)	—	2.30	—	—	4.24	—	
29	3,4,5-Trimethyl	—	6.90	2.64	—	2.16	—	2.38	—	—	4.16	—	
30	6,6-Dimethyl	—	7.12m	—	8.58m	—	7.12m	—	7.62d,d	1.64	—	—	$J_{4,5}$ = 8.5 Hz
31	2,3,4,5,6,6-Hexamethyl	2.17	—	2.62	—	2.17	—	2.29	—	1.52	—	—	

*In p.p.m. from TMS using $(CH_3)_4N^+$ as internal standard. Numbering scheme of original phenol maintained in cations. d = doublet, d,d = doublet of doublets, m = multiplet.
†FSO_3H–SbF_5 (4:1) solvent.
‡Cation numbered so as to be consistent with the rest of the protonated phenols.
§Assignment may be reversed.

Can. J. Chem. Downloaded from www.nrcresearchpress.com by 210.87.254.42 on 09/05/12
For personal use only.

protonated phenols and those of the protonated cyclohexadienones **15** and **16** confirms their structural assignment (28–31).

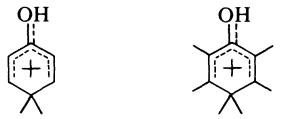

15 **16**

Protonation of Phenols with a 4-Methyl Substituent

Both pentamethylphenol, **17**, and the tetramethylphenol, **18**, were protonated only on the *para* position in FSO_3H at $-50°$ giving **19** and **20** respectively. The resonances of the methyl groups on C-2, -3, -5, and -6 of **19**, for example, display the requisite symmetry and occur in the regions expected on the basis of the spectra of

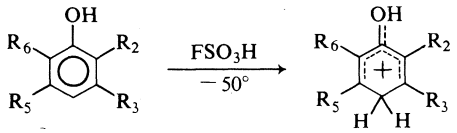

	R_2	R_3	R_5	R_6	
1	Me	Me	H	H	**2**
3	Me	H	Me	H	**4**
5	Me	H	H	Me	**6**
7	H	Me	Me	H	**8**
9	Me	Me	Me	H	**10**
11	Me	Me	H	Me	**12**
13	Me	Me	Me	Me	**14**

SCHEME 1

the previous cations. Coupling of the methyl protons and proton on C-4 results in the signal of the former being a doublet and the latter a quartet. The coupling constant, $J = 7$ Hz, for both **19** and **20**, is comparable to that observed for the hexamethylbenzenonium cation ($J = 6.87$ Hz) (13).

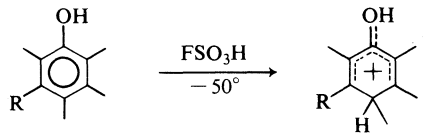

17 R=Me **19** R=Me
18 R=H **20** R=H

The n.m.r. spectra of solutions of the trimethylphenols **21**, **22**, and **23** in FSO_3H are more complex than can be accounted for on the basis of protonation at a single site. The presence of a cation resulting from *para* protonation was shown in each case by a high field doublet (*ca.* 1.5 δ) and a quartet (*ca.* 3.8 δ), characteristic of 4-methyl and 4-methine protons, respectively. As is shown in Table 2, the other resonances of these *para* protonated cations are quite in accord with their assigned structures.

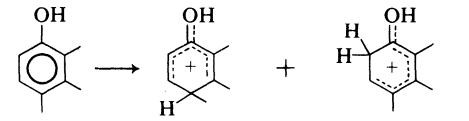

21 **24** 17% **25** 83%

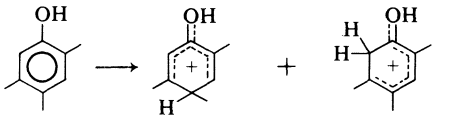

22 **26** 85% **27** 15%

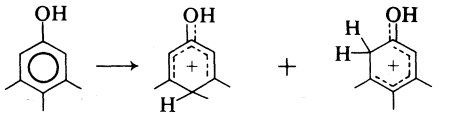

23 **28** 57% **29** 43%

Cations resulting from proton attachment at an *ortho* position are also present in FSO_3H solutions of these phenols. The protonated cyclohexadienones **30** and **31** are good models for the chemical shifts expected upon *ortho* protonation of a phenol and as can be seen from Table 3, there is a close correspondence between the chemical shifts of **25**, **27** and **29** with those of **30** and **31** (Table 3). If protonation had occurred at C-5 of any of these phenols, then the electron donating properties of the hydroxy group would be reduced and a considerable downfield shift of all the resonances would be expected as compared to the model cations (*vide infra*). The composition of the ions resulting from the protonation of these phenols was determined by integration of the n.m.r. spectra, see Table 1. Similar conclusions have been reached by Hartshorn *et al.* (7) for the protonation of **23**.

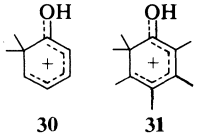

30 **31**

The n.m.r. spectrum of a solution of **32** in FSO_3H, shown in Fig. 1*A*, can be accounted for

TABLE 4. Proton chemical shifts of oxygen protonated phenols and related materials

Cation	Substituents	Chemical shift*		
		Me	Ring H	O–Me
51	4-Methyl	2.38	7.35	—
43	2,4-Dimethyl	2.36	7.24	—
47	2,4-Dimethyl	2.37	7.22	4.63
34	2,4,6-Trimethyl	2.31, 2.37	7.05	—
36	2,4,6-Trimethyl	2.26, 2.35	7.0	4.62

*In p.p.m. from TMS using $(CH_3)_4N^+$ as internal standard.

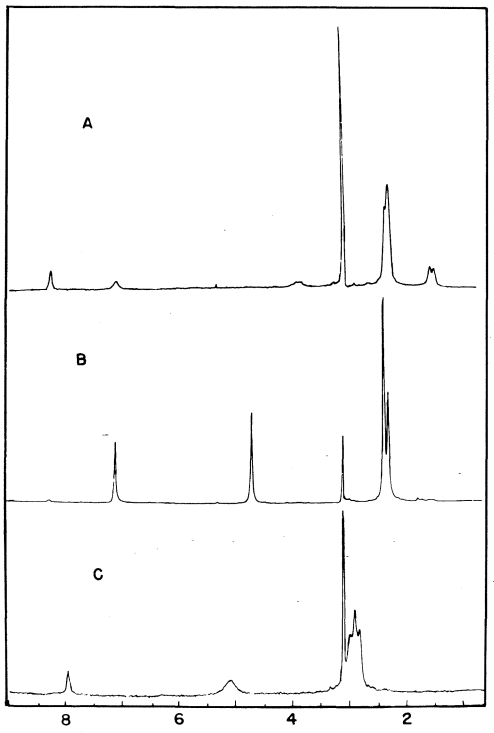

FIG. 1. Proton magnetic resonance spectra of 2,4,6-trimethylphenol in FSO_3H (*A*), in FSO_3H–SbF_5 (*C*), and 2,4,6-trimethylanisole in FSO_3H (*B*). (The singlet at 3.1 p.p.m. is due to tetramethylammonium chloride.)

on the basis of protonation both on oxygen and C-4. The high field doublet at 1.55, singlet at 2.33, broadened quartet at 3.88, and singlet at 8.23 δ can be attributed to **33**. The remaining signals at 2.31, 2.37, and 7.05 δ can be assigned to **34**.

The n.m.r. spectrum obtained from a FSO_3H solution of **35** which is shown in Fig. 1*b* indicates that only the oxygen protonated cation **36** is present. As is usually the case in FSO_3H, coupling between the methyl proton and proton

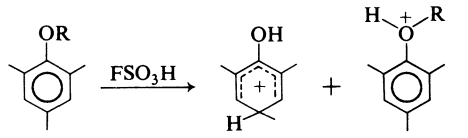

32 R = H
35 R = Me

33

34 R = H
36 R = Me

on the oxygen is not observed (9). There is very close agreement between the spectrum of **36** and the signals assigned to **34** in the more complex spectrum obtained from a FSO_3H solution of **32** (*cf.* Table 4).

The protonation of 3,4-dimethylphenol, **37**, has been previously reported to give **38** and **39** in a ratio of 90:10 (7). In this study both **38** and **39** were observed; however, in addition a small amount (~3%) of the isomer **40** was detected, as characterized by a low field doublet at 8.48 δ (J = 9 Hz), a singlet due to the methylene group at 4.33 δ, and methyl resonance at 2.37 δ. Other resonances attributable to **40** were not detected, probably due to their coincidence with those of **38** and **39**. The low temperature u.v. spectrum of a FSO_3H solution of **37** exhibited bands at 361 and 255 nm which is in accord with the major product being **38**. Protonated 2,4-cyclohexadienones have very similar u.v. spectra (2, 3, 30, 33).

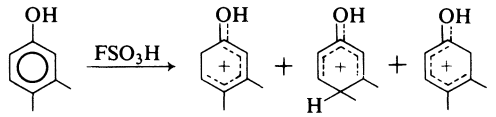

37

38 90%

39 7%

40 3%

Protonation of 2,4-dimethylphenol is particularly interesting in that it has been claimed that the corresponding anisole is partially protonated in the *meta* position in FSO_3H (9). The n.m.r. spectrum obtained from a solution of **41** in FSO_3H is indeed complex but in our opinion it

Can. J. Chem. Downloaded from www.nrcresearchpress.com by 210.87.254.42 on 09/05/12
For personal use only.

Can. J. Chem. Downloaded from www.nrcresearchpress.com by 210.87.254.42 on 09/05/12
For personal use only.

does not give any evidence for *meta* protonation. Rather, the spectrum is consistent with the formation of the three cations **42** (47%), **43** (41%), and **44** (12%). The cation **44** was readily characterized by a doublet and quartet attributable to the C-4 methyl and proton at 1.55 and 3.96 δ, respectively. While a methylene group resonance at 4.31 δ clearly indicated that protonation at C-6, -5, or -3 had occurred, its relative area showed that another cation must be present. This was identified as **43**, the oxygen protonated system, with resonances at 2.36 and 7.24 δ. Allowing for the resonances of **43** and **44**, this leaves a series of signals at 2.26, 4.31, 7.24, and 8.36 δ to be accounted for. Their multiplicity, area, and positions are completely consistent with the 6-protonated isomer **42** (Table 3). If proton addition to C-3 or -5 had occurred, then a much different charge distribution and hence chemical shifts of the proton resonances would be expected. Protonation of the trideuteriophenol **49** in FSO_3H and observation of the n.m.r. spectrum after 10 min at −50° showed that **42**, **43**, and **44** were formed. Complete replacement of all the deuteriums by hydrogen had taken place under these conditions.

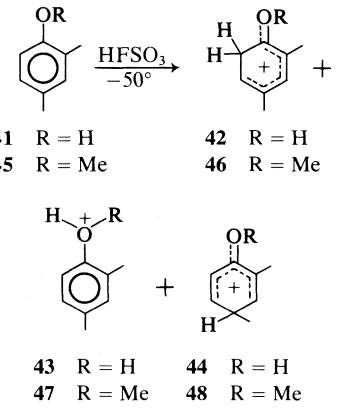

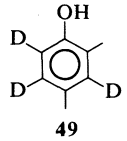

49

In view of the suggested *meta* protonation of the anisole **45**, we have repeated its protonation and find very similar results to those outlined above for the phenol. The products resulting from dissolution of **45** in FSO_3H were found to be **46** (72%), **47** (23%), and **48** (5%), the positions of the observed resonances in the n.m.r. spectrum being entirely consistent with the assigned structures. It is difficult to make a direct comparison between the chemical shifts published for **49** and those quoted here for **46** as different reference compounds and acid media are used. However, while the chemical shifts quoted for **49** and **46** differ in their absolute magnitude, there is a constant difference between the two sets of figures. This would suggest that these cations are indeed the same and result from *ortho* protonation of **45**.

Dissolution of *p*-cresol, **50**, in FSO_3H gave a solution of the three ions **51** (55%), **52** (40%), and **53** (5%). Both **51** and **52** have been detected before as protonation products of **50**, although it has been claimed that in FSO_3H only **51** is produced (9).

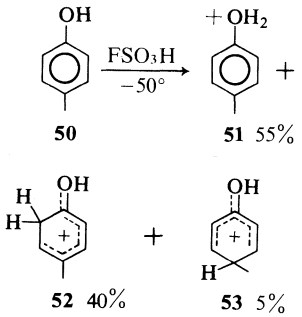

Protonations in SbF_5–FSO_3H

It has been shown in general that the addition of SbF_5 to a FSO_3H solution of a phenol results in an increase in the amount of carbon and reduction in the amount of oxygen protonation (9). Accordingly, to see if *C*-protonation could be enhanced in solutions of **32** and thus add further confirmation to the correctness of the spectral assignments, its protonation in a FSO_3H–SbF_5 mixture (4:1 v/v) was examined.

From the n.m.r. spectrum obtained from a solution of **32** in FSO_3H–SbF_5 (Fig. 1*c*), it is quite clear that protonation has not occurred as before on either oxygen or C-4 in this medium. The relative areas of the signals suggested that *meta* protonation had taken place to give **54**.

The resonances of **54** are all shifted downfield from those of the comparable protons of the protonated phenols shown in Tables 2 and 3. This is not unexpected as the hydroxy group (or modified hydroxy group) can no longer stabilize the positive charge on the benzenonium cation but rather would be an inductively elec-

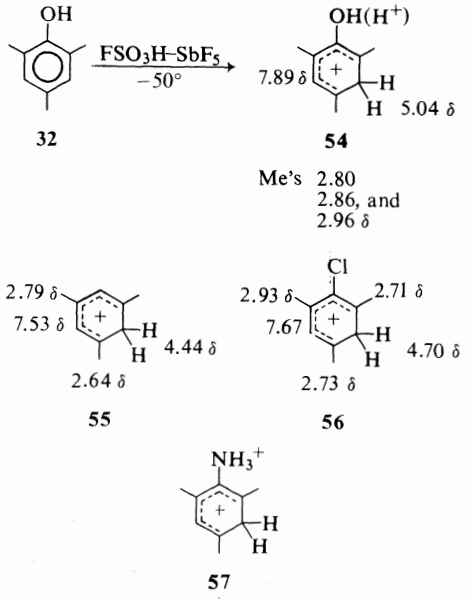

32 54 55 56 57

tron withdrawing group in this position. Evidence for this can be seen by comparing the chemical shifts of the proton resonances of **54** and protonated mesitylene, **55** (32). The resonances of **54** are occurring considerably further downfield than those of **55**. A better model for **54** is protonated chloromesitylene, **56** (33).[3] It is quite possible that the hydroxy group of **54** is further protonated to give a dication. No resonance attributable to the proton(s) on oxygen could be detected in the n.m.r. spectrum of **54**. A comparable diprotonation has been described with 2,4,6-trimethylaniline which in FSO_3H–SbF_5–SO_2 and HF–SbF_5 gives **57** (34, 18). It is difficult, however, to compare directly the chemical shifts of **54** and **57** as an external reference was used in reporting the latter resonances.

The *meta* protonated cation **54** was not detected by n.m.r. in FSO_3H solutions of **32** that did not contain SbF_5. However, the u.v. spectrum of a solution of **32** in FSO_3H exhibited bands at 270 and 308 nm, and a very weak absorption at 385 nm. The latter band, which cannot be attributed to either **33** or **34** (*cf.* 2, 3, 32), could conceivably originate from a small amount of **36**, too small to be detected by n.m.r. A FSO_3H solution of **56** showed a long wavelength absorption at 380 nm.

Discussion

A great deal of information is available on the basicities of aromatic hydrocarbons (35, 18). In particular, it is known that methyl substitution *ortho* or *para* to a given site on a benzene ring causes about a 1000-fold increase in its basicity, while methyl substitution in the *meta* position gives rise to only about a 5-fold increase. In contrast, substitution of a methyl upon the site of protonation reduces its basicity by a factor of about 20 (18). These effects are clearly operative within the series of phenols discussed in this paper.

Before discussing this, however, it is clearly important to know whether a kinetic or thermodynamic distribution of products is being obtained upon protonation of these phenols. The time invariance and reproducibility of the ratios of the cations produced from any individual phenol would suggest that a thermodynamic equilibrium is being reached. Direct evidence for this assertion comes from the results of the protonation of the trideuteriated phenol **49**, in which complete exchange of all the ring protons occurred prior to observation of the n.m.r. spectrum.

Phenol itself is protonated on carbon in FSO_3H, the proton being attached to C-4. Any methyl substituents upon C-2, -3, -5, or -6 of the phenol would be expected to enhance the basicity of the 4-position and have little effect upon the basicity of the oxygen. Indeed, all the phenols which lack a 4-methyl substituent are protonated in FSO_3H to give exclusively cations resulting from protonation *para* to the oxygen. No evidence for any other isomeric cations was found in any of these systems. Even in the case of 2,6-dimethylphenol, **5**, where the two methyls are situated so as to increase the basicity of C-3 and -5 by 10^6, no protonation in these positions could be detected. Clearly, the effect of the hydroxy group is overriding that of the methyl groups in phenols of this type.

The results in Table 1 show that when the 4-position of a phenol bears a methyl substituent, protonation of one of the two *ortho* positions or upon oxygen becomes possible. Protonation at C-2 or -6 of these systems is only observed when at least one of these sites is unsubstituted. Thus **17**, **18**, and **32** which all have methyls on C-2, -4,

[3]The chemical shifts of **56** quoted in ref. 34 are based upon internal tetramethylammonium chloride taken as 3.2 δ. The values quoted here have been modified to reflect the resonance position of tetramethylammonium chloride (3.1 δ) used in this paper.

Can. J. Chem. Downloaded from www.nrcresearchpress.com by 210.87.254.42 on 09/05/12
For personal use only.

Can. J. Chem. Downloaded from www.nrcresearchpress.com by 210.87.254.42 on 09/05/12
For personal use only.

and -6, show no indication of being protonated upon C-2 or -6. This is in accord with the known equilibrium position between **31** and **16** which lies heavily in favor of **16** (29–31).

31 **16**

The relative basicities of the ring carbons and oxygen of these 4-substituted phenols is very dependent upon the presence and position of other substituents on the ring. Thus *p*-cresol, **50**, is protonated to the extent of 55% on oxygen and 40% on C-2 and -6. With 2,4-dimethylphenol, **41**, a small increase in the amount of ring protonation is seen but clearly the additional methyl at C-2 has not influenced the relative basicities of the various sites to any great extent. This is in contrast to 3,4-dimethylphenol, **37**, where the additional methyl in the 3 position has so increased the basicity of C-2, -4, and -6, which are *ortho* or *para* to this 3-methyl group, that only ring protonation is detected.

It is interesting that for **37**, protonation at C-6, *para* to the 3-methyl group, is much favored over protonation at C-2, *ortho* to the 3-methyl group. A similar preference has been observed in the methyl substituted benzenonium cations (18).

The Question of Meta Protonation

The most favored case in which *meta* protonation might occur is 2,4,6-trimethylphenol, **32**; however, no *meta* protonated isomer could be detected in the n.m.r. spectrum of **32** when dissolved in FSO_3H. The three methyl groups on **32** would be expected to enhance the basicity of the *meta* position by some factor of 10^9 and yet would have little effect on the basicity of C-4 as compared to phenol. This suggests that there must be a factor of at least 10^9 difference in the relative basicities of the *meta* and *para* positions of phenol itself in FSO_3H. This being so, then without modification of the —OH group of any of these phenols, protonation on the C-3 or -5 position would not be expected to compete effectively with attack on the other positions.

As in FSO_3H–SbF_5 mixtures, **32** was protonated only in the *meta* position, the electron donating properties of the hydroxy group must be modified in this medium. One possibility is that diprotonation of this phenol is occurring in FSO_3H–SbF_5, a medium which is known to be much more acidic than FSO_3H itself (36). The most stable dication that could be formed is **59**, the now electron withdrawing oxygen substituent being sited on the position of highest electron density of the pentadienyl cation. The three methyl groups are ideally situated to stabilize this pentadienyl cation.

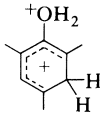

59

An alternative modification of the oxygen substituent which might be considered is its reaction with the Lewis acid, SbF_5. This could give either **60** or **61**, both of which would convert the oxygen function into an electron withdrawing substituent.

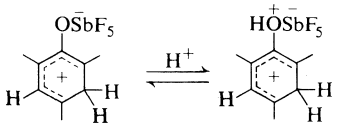

61 **62**

Some evidence for this type of reaction can be found in the reactions of the dienones **62** and **63** with a Lewis acid such as SO_3, when the zwitterion **64** is formed (31).

Whereas in FSO_3H, **62** and **63** were protonated to give **16** and **31**, respectively, in FSO_3H–SO_3 solution the *meta* isomer $\mathbf{64}H^+$ was observed. As it is known that the addition of SO_3 to FSO_3H has little effect on its acidity (36), it is unlikely that in FSO_3H–SO_3 the formation of the *meta* isomer can be attributed to diprotonation.

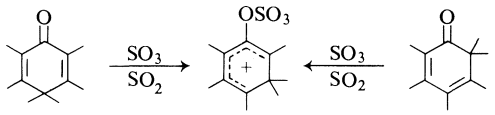

62 **64** **63**

The reaction of **63** with SbF_5 in SO_2 solution does not proceed cleanly as the ketone is oxidized in this medium. However, the initial spectra produced are indicative of the formation of the *meta* isomer corresponding to **64**, suggesting that the —O—$\overline{SbF_5}$ group is electron withdrawing. It is thus possible that in these acid media containing SbF_5, the Lewis acid is competing with

a proton for the Lewis base. Further studies are required to clarify this point; however, we feel caution should be employed in regarding the effect of the addition of SbF_5 to FSO_3H to be simply that of an increase in acidity.

We wish to thank the National Research Council of Canada for financial support.

1. R. F. CHILDS and B. D. PARRINGTON. Abstr. 55th Chemical Conference of the Chemical Institute of Canada, Quebec, June 1972. No. 67.
2. B. D. PARRINGTON and R. F. CHILDS. J. Chem. Soc. Chem. Commun. 1581 (1970).
3. N. FILIPESCU and J. W. PAVLIK. J. Am. Chem. Soc. **92**, 6062 (1970).
4. A. J. KRESGE, G. W. BARRY, K. R. CHARLES, and Y. CHIANG. J. Am. Chem. Soc. **84**, 4343 (1962).
5. T. BIRCHALL, A. N. BOURNS, R. J. GILLESPIE, and P. J. SMITH. Can. J. Chem. **42**, 1433 (1964).
6. R. W. ALDER and F. J. TAYLOR. J. Chem. Soc. B, 845 (1970).
7. M. P. HARTSHORN, K. E. RICHARDS, J. VAUGHAN, and G. J. WRIGHT. J. Chem. Soc. B, 1624 (1971).
8. K. E. HINE and R. F. CHILDS. J. Am. Chem. Soc. **93**, 2323 (1971).
9. G. A. OLAH and Y. K. MO. J. Org. Chem. **38**, 353 (1973).
10. D. M. BROUWER, E. L. MACKOR, and C. MACLEAN. Rec. Trav. Chim. Pays-Bas, **85**, 109, 114 (1966).
11. D. M. BROUWER, C. MACLEAN, and E. L. MACKOR. Disc. Faraday Soc. **39**, 121 (1965).
12. W. M. SCHUBERT and R. H. QUACCHIA. J. Am. Chem. Soc. **85**, 1278 (1963).
13. T. BIRCHALL and R. J. GILLESPIE. Can. J. Chem. **42**, 502 (1964).
14. G. A. OLAH, M. B. COMISAROW, E. NAMANWORTH, and B. RAMSEY. J. Am. Chem. Soc. **89**, 5259 (1967).
15. E. M. ARNETT and C. Y. WU. J. Am. Chem. Soc. **82**, 5660 (1960).
16. A. J. KRESGE and L. E. HAKKA. J. Am. Chem. Soc. **88**, 3868 (1966).
17. B. G. RAMSEY. J. Am. Chem. Soc. **88**, 5358 (1966).
18. D. M. BROUWER, E. L. MACKOR, and C. MACLEAN. *In* Carbonium ions. Vol. 2. *Edited by* G. A. Olah and P. von R. Schleyer. Wiley-Interscience, New York, N.Y. 1970. p. 837.
19. R. WILLSTATTER and H. KUBLI. Chem. Ber. **42**, 4151 (1909).
20. B. V. GREGOROVICH, K. S. Y. LIANG, D. M. CLUGSTON, and S. F. MACDONALD. Can. J. Chem. **46**, 3291 (1968).
21. A. W. HOFFMAN. Chem. Ber. **18**, 1821 (1885).
22. K. VON AUWERS and K. SAURWEIN. Chem. Ber. **55**, 2372 (1922).
23. K. ALDER, F. H. FLOCK, and H. LESSENICH. Chem. Ber. **90**, 1709 (1957).
24. W. G. DAUBEN, G. W. SHAFFER, and V. D. VIETMEYER. J. Org. Chem. **33**, 4060 (1968).
25. V. P. VITULLO. J. Org. Chem. **35**, 3976 (1970).
26. H. HART, P. M. COLLINS, and A. J. WARING. J. Am. Chem. Soc. **88**, 1005 (1966).
27. H. HART and D. W. SWATTON. J. Am. Chem. Soc. **89**, 1874 (1967).
28. K. L. COOK, M. J. HUGHES, and A. J. WARING. J. Chem. Soc. Perkin II, 1506 (1972).
29. V. G. SHUBIN, V. P. CHZHU, A. I. REZVUKHIN, A. A. TABATSKAYA, and V. A. KOPTYUG. Izvest. Akad. Nauk S.S.S.R. Ser. Khim. 2365 (1967).
30. V. G. SHUBIN, V. P. CHZHU, I. K. KOROBEINICHEVA, A. I. REZVUKHIN, and V. A. KOPTYUG. Izvest. Akad. Nauk S.S.S.R. Ser. Khim. 1742 (1970).
31. R. F. CHILDS. J. Chem. Soc. Chem. Commun. 946 (1969).
32. E. C. FRIEDRICH. J. Org. Chem. **33**, 413 (1968).
33. D. M. BROUWER. Rec. Trav. Chim. Pays-Bas, **87**, 335, 342 (1968).
34. G. A. OLAH, K. DUNNE, D. P. KELLY, and Y. K. MO. J. Am. Chem. Soc. **94**, 7438 (1972).
35. H. H. PERKAMPUS. Adv. Phys. Org. Chem. **4**, 195 (1966).
36. R. J. GILLESPIE and T. E. PEEL. Adv Phys. Org. Chem. **9**, 1 (1971).

Can. J. Chem. Downloaded from www.nrcresearchpress.com by 210.87.254.42 on 09/05/12
For personal use only.

Protonation of Polymethylphenols[1]

STEPHEN M. BLACKSTOCK, KENNETH E. RICHARDS, AND GRAEME J. WRIGHT
Department of Chemistry, University of Canterbury, Christchurch, New Zealand

Received April 1, 1974

STEPHEN M. BLACKSTOCK, KENNETH E. RICHARDS, and GRAEME J. WRIGHT. Can. J. Chem. **52**, 3313 (1974).

The protonation of a series of polymethylphenols in fluorosulfonic acid at $-50°$ has been studied. For those phenols with no substituent at C-4, protonaton occurs exclusively at that position. Isomeric ions were obtained for all phenols with a methyl substituent at C-4. 4-Methylphenol and 2,4-dimethylphenol each gave three ions, one from *O*-protonation and two from protonation at C-2 and C-4, whereas 2,4-dimethylphenol, 2,3,4-, 2,4,5-, and 3,4,5-trimethylphenol, and 2,3,4,5-tetramethylphenol gave only the *C*-protonated species. These studies establish that although electronic factors are important, steric factors play a predominant role in determining the relative proportions of the various species.

STEPHEN M. BLACKSTOCK, KENNETH E. RICHARDS et GRAEME J. WRIGHT. Can. J. Chem. **52**, 3313 (1974).

On a étudié, dans l'acide fluorosulphonique à $-50°$, la protonation d'une série de polyméthylphénols. Dans le cas des phénols ne portant aucun substituant en position 4, la protonation se fait exclusivement dans cette position. Des ions isomères sont obtenus pour tous les phénols portant un substituant méthyle en position 4. Les méthyl-4 et diméthyl-2,4 phénols donnent chacun trois ions: un provenant de la protonation sur l'oxygène et deux de la protonation en positions 2 et 4. Par ailleur les diméthyl-2,4 et triméthyl-2,3,4-, 2,4,5- et 3,4,5 phénols ainsi que le tétraméthyl-2,3,4,5 phénol ne donnent que des espèces protonés sur le carbone. Ces études ont permis d'établir que même si les facteurs électroniques sont importants, des facteurs stériques peuvent jouer un rôle prépondérant dans la détermination des proportions relatives de chacune des différentes espèces. [Traduit par le journal]

Introduction

The protonation of aromatic compounds in superacids has been studied extensively in recent years (1) and some of the factors which can affect the site of protonation can now be identified. One such factor is temperature; for example, for anisole in $HF–BF_3$, the strong temperature dependence (2) of the mode of protonation is shown by the change in the ratio of *C*-protonated to *O*-protonated species from 1.5 at —80° to over 50 at 0°. Another factor is the nature of the substituents in the aromatic system. Protonation of the 5-halo-*m*-xylenes (3) yields mixtures of two isomeric benzenonium ions **1***a*, *b*. The proportions of these two ions changes with the halogen from Cl (**1***a*:**1***b*, 2:1) to Br (0.56:1) to F (5:1). A similar substituent dependence is seen in the protonation of 1- and 2-substituted naphthalenes (4). A third factor is the nature of the superacid. For example anisole undergoes only *C*-protonation in fluorosulfonic acid (5) but in $HF–BF_3$ gives both *O*- and *C*-protonation (2).

We have previously (6) shown that *C*-protonation occurs in 3,4-dimethylphenol **2** and 3,4,5-trimethylphenol **3** not only *ortho* to the —OH to give ions **2***b*, **3***b* but also *para* to the —OH (and *ipso* to the C-4 methyl group) to give ions **2***a*, **3***a*. The proportions of these ions show a dramatic change in going from 3,4-dimethylphenol (ratio **2***b*:**2***a*, 11.5:1) to 3,4,5-trimethylphenol (ratio **3***a*:**3***b*, 1:1) and a similar effect is also observed with the corresponding methyl ethers.

In order to achieve a better understanding of the factors which influence the site of these protonations we have investigated the behavior of a series of methyl phenols in fluorosulfonic acid. We now report the results of this study. In order to reduce the number of variables we have in the first instance used fluorosulfonic acid only, at a temperature of $-50°$.

Results and Discussion

Proton magnetic resonance data for *para* protonated phenols is given in Table 1, for *ortho* protonated phenols in Table 2, and for oxonium ions in Table 3. The relative abundancies of ions obtained for each phenol are given in Table 4.

[1]We acknowledge helpful discussions with Dr. R. F. Childs whose results appear in an accompanying paper.

Can. J. Chem. Downloaded from www.nrcresearchpress.com by 210.87.254.40 on 09/05/12
For personal use only.

TABLE 1. Proton magnetic resonance data (p.p.m.)* for *para* protonated species in FSO_3H

	Positions 2 and 6		Positions 3 and 5		Position 4	
Cation	CH_3	H	CH_3	H	CH_3	H
4*a*	2.28	7.32	2.62	8.40	—	4.25 br s
5*a*	—	7.07	2.58	—	—	4.10 br s
6*a*	2.40	—	—	8.46	—	4.25 br s
7*a*	2.24	7.07	2.52	—	—	4.12 br s
8*a*	—	?	—	?	1.57 d $J_{Me,H}$ 7.0 Hz	?
2*a*	—	?	2.66	8.26	1.62 d $J_{Me,H}$ 7.5 Hz	3.88 q
9*a*	2.34	?	—	?	1.58 d $J_{Me,H}$ 7.0 Hz	4.10 q
11*a*	2.29	7.15	2.62	8.15	1.65 d $J_{Me,H}$ 7.5 Hz	3.84 q
3*a*	—	7.02	2.60	—	1.69 d $J_{Me,H}$ 7.5 Hz	3.76 q
12*a*	2.31	7.25	2.60	8.36	1.65 d $J_{Me,H}$ 7.5 Hz	3.92 q
13*a*	2.23	7.01	2.56	—	1.66 d $J_{Me,H}$ 7.5 Hz	3.76 q

*Internal $(CH_3)_4N^+$ marker.

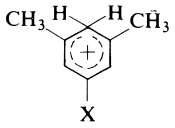

1*a* X = Cl, Br, F

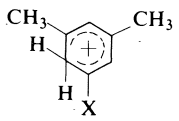

1*b* X = Cl, Br, F

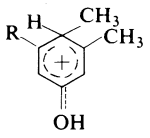

2*a* R = H
3*a* R = CH_3

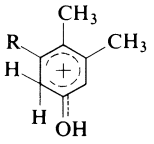

2*b* R = H
3*b* R = CH_3

The chemical shifts for hydrogen and methyl in the *para* protonated species fall into clearly discernible patterns (Table 1). For example, protons at positions 2 or 6 give rise to signals in the δ 7.0–7.25 region whereas those at the 3 position give signals at δ 8.15–8.50. Likewise with methyl substituents, those at positions 2 or 6 give signals in the δ 2.17–2.40 region while those at positions 3 or 5 appear at δ 2.50–2.60. Protons at C-4 show two ranges, δ 4.10–4.25 and δ 3.65–4.10, depending on whether the other 4-substituent is hydrogen or methyl.

A similar situation holds for the *ortho* protonated species (Table 2). The methylene group gives rise to signals in the δ 4.20–4.40 region, C-2 protons at δ 7.00–7.20 similar to the *para* protonated species. Methyls at positions 2 and 4 give signals in the region δ 2.20–2.40 with C-3 methyls at δ 2.70–2.80.

Protonation of 2,3-dimethylphenol, 3,5-dimethylphenol, 2,6-dimethylphenol, and 2,3,5-trimethylphenol occurs exclusively at C-4 to give the ions **4***a*, **5***a*, **6***a*, and **7***a*, respectively. This is in agreement with the observations (5) that both phenol and anisole *C*-protonate exclusively at C-4. For each of these compounds C-4 is clearly the most basic site, the *para* directing influence of the hydroxyl group being much stronger than the methyl directing influence. This is well illustrated in the case of 3,5-dimethylphenol where, although the C-2 and C-6 sites *ortho* to hydroxyl are activated by *para* and *ortho* methyl substituents, it is still the C-4 site which is protonated.

Olah and Mo have published details (7) of the protonation of 2,3-dimethylanisole and 3,5-di-

Can. J. Chem. Downloaded from www.nrcresearchpress.com by 210.87.254.40 on 09/05/12
For personal use only.

TABLE 2. Proton magnetic resonance data (p.p.m.)* for *ortho*-protonated species in FSO_3H

	Position 2		Position 3		Position 4	Position 5		Position 6
Cation	CH_3	H	CH_3	H	CH_3	CH_3	H	CH_2
8*b*	—	?	—	?	?	—	?	4.36 br s
2*b*	—	7.18	2.76	?	2.34	—	7.44	4.28 br s
9*b*	2.34	—	—	?	2.34	—	8.34	4.36 br s
11*b*	2.40	—	—	8.44	2.40	?	—	4.35 br s
3*b*	—	7.02	2.74	—	2.35	2.47	—	4.25 br s
12*b*	2.31	—	2.72	—	2.31	—	7.30	4.25 br s
13*b*	?	—	2.56	—	2.23	?	—	4.19 br s

*Internal $(CH_3)_4N^+$ marker.

TABLE 3. Proton magnetic resonance data (p.p.m.)* for oxonium ions in FSO_3H

	Positions 2 and 6		Positions 3 and 5		Position 4
Cation	CH_3	H	CH_3	H	CH_3
8*c*	—	7.35	—	7.35	2.38
9*c*	2.40	7.30	—	7.30	2.40

*Internal $(CH_3)_4N^+$ marker.

TABLE 4. Percentage of ions formed on protonation

	C-Protonated species (%)					
Phenol	*Para*-protonated		*Ortho*-protonated		*O*-Protonated species (%)	
4	**4***a*	(100)				
5	**5***a*	(100)				
6	**6***a*	(100)				
7	**7***a*	(100)				
8	**8***a*	(1)	**8***b*	(9)	**8***c*	(90)
2	**2***a*	(8)	**2***b*	(92)		
9	**9***a*	(6)	**9***b*	(31)	**9***c*	(63)
11	**11***a*	(80)	**11***b*	(20)		
3	**3***a*	(50)	**3***b*	(50)		
12	**12***a*	(20)	**12***b*	(80)		
13	**13***a*	(94)	**13***b*	(6)		

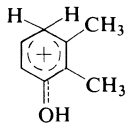

4*a*

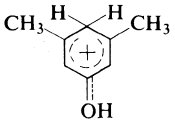

5*a*

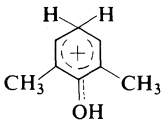

6*a*

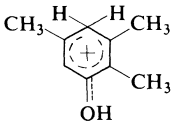

7*a*

methylanisole which are consistent with our own work on the phenols. However, protonation of 2,6-dimethylanisole gives only the *O*-protonated species in various acid systems (2, 7) and a di-protonated species in $HF–SbF_5(1:1)–SO_2ClF$ (7). This difference in behavior between the phenol and methyl ether arises because the flanking methyl groups, at C-2 and C-6, prevent coplanarity of the methoxy group with the benzene ring which is essential if *C*-monoprotonation is to occur.

Protonation of 4-methylphenol **8** gave us three

Can. J. Chem. Downloaded from www.nrcresearchpress.com by 210.87.254.40 on 09/05/12
For personal use only.

isomeric ions, the two *C*-protonated species **8***a* (1%) and **8***b* (9%), and the *O*-protonated species **8***c* (90%). The evidence for the ion **8***a* comes from a small methyl doublet at δ 1.57, $J = 7$ Hz. The effect of the methyl group is to reduce the basicity at C-4 relative to phenol and raise it slightly at C-2 so that the relative basicities at oxygen, C-2, and C-4 are 90:4.5:1. In the superacids used by Olah and Mo (7) no ion **8***a* was observed.

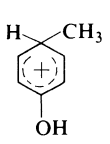

8*a*

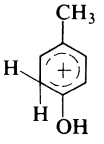

8*b*

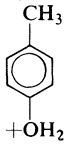

8*c*

For 3,4-dimethylphenol, as we have already shown (6), the introduction of the second methyl group at C-3 raises the basicity of the ring sufficiently to ensure that *C*-protonation only occurs. In this case the ions **2***a* (8%) and **2***b* (92%) are obtained. However, the position of the additional substituent makes a significant difference and 2,4-dimethylphenol gives the three isomeric ions **9***a* (6%), **9***b* (31%), and **9***c* (63%). The evidence for the structures of the *C*-protonated species is clear cut. For **9***a* a methyl doublet is obtained at δ 1.58, J = 7 Hz coupled to a one-proton quartet at δ 4.10. For **9***b* the chemical shifts are consistent with those for corresponding *ortho* species (see Table 2) some of whose structures have previously been confirmed by u.v. spectroscopy (6). Olah and Mo have reported (7) that 2,4-dimethylphenol gives a mixture of the *O*-protonated species **10***a* and the *C*-protonated species **10***b* in which protonation has occurred at C-5 *meta* to the methoxyl group. The chemical shifts given for **10***b* (external TMS) are similar to those obtained by us for ion **9***a* (internal $(CH_3)_4N^+$). We suggest that structure **10***b* can be only regarded as tentative until positive u.v. spectroscopic evidence is obtained.

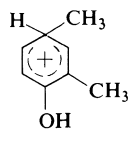

9*a*

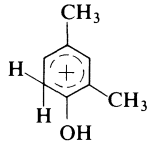

9*b*

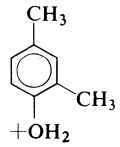

9*c*

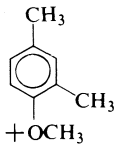

10*a*

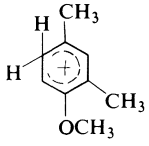

10*b*

That the position of the methyl substituents makes a significant difference to the nature and relative abundancies of the ions formed is well illustrated by the trimethylphenols. 2,4,5-Trimethylphenol gives the ions **11***a* (80%) and **11***b* (20%), 3,4,5-trimethylphenol gives **3***a* (50%) and **3***b* (50%), whereas 2,3,4-trimethylphenol gives **12***a* (20%) and **12***b* (80%). The chemical shifts for ions **11***a* and *b*, **12***a* and *b* are consistent with those for ions **3***a* and *b* whose structures are confirmed by u.v. spectroscopy (6). Protonation of 2,3,4,5-tetramethylphenol results in the predominance of the C-4 protonated species **13***a* (94%) over the *ortho* protonated species **13***b*.

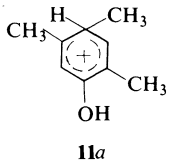

11*a*

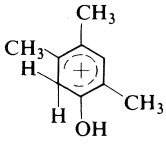

11*b*

An analysis of nitration and acetoxylation in the polymethylbenzenes (8) has shown that the complete set of product distributions can be satisfactorily accounted for in terms of four

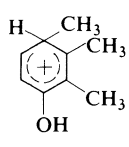

12*a*

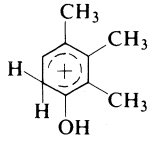

12*b*

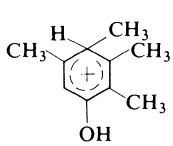

13*a*

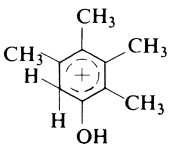

13*b*

Can. J. Chem. Downloaded from www.nrcresearchpress.com by 210.87.254.40 on 09/05/12
For personal use only.

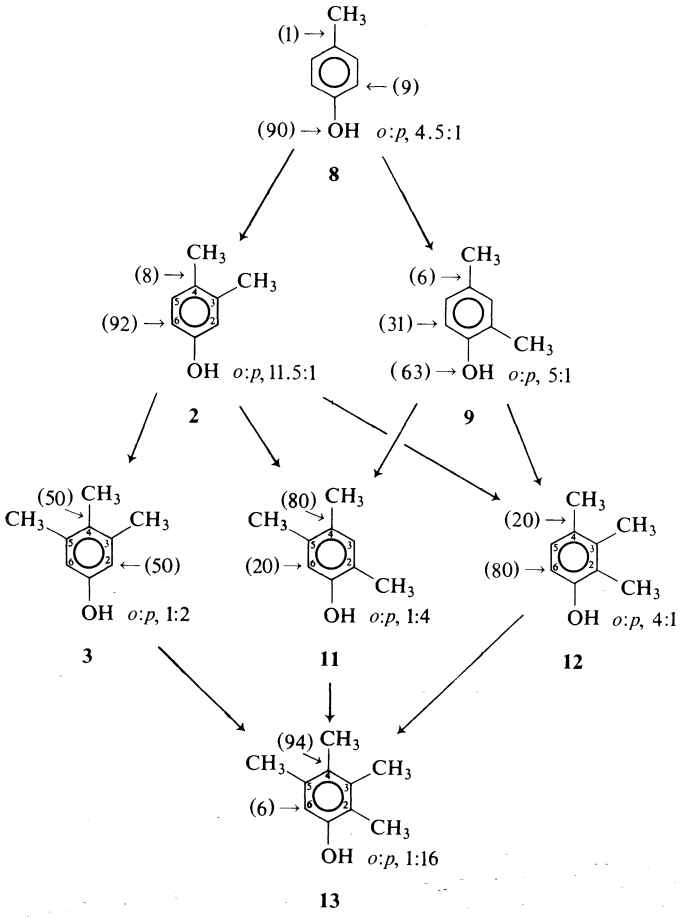

FIG. 1. Protonation of 4-methylphenols showing the effect of methyl substitution upon the reactivity of each site. (Figures in brackets give % protonation at a given site; *o*:*p*, statistical correction applied when two identical *ortho* sites are available.)

methyl partial rate factors, *ortho*, *meta*, *para*, and *ipso*. We now have sufficient data from this protonation study to allow calculation of a complete set of parameters (ρ, $\sigma_{o\text{-Me}}$, $\sigma_{o\text{-OH}}$, $\sigma_{i\text{-Me}}$) assuming additivity and using accepted values for $\sigma_{m\text{-Me}}$, $\sigma_{p\text{-Me}}$, and $\sigma_{p\text{-OH}}$ (9). However, no consistent set of these four parameters could be obtained from the data, although the values obtained are generally reasonable. For example, compounds **3** and **13** give a value of $\rho = -6.2$. It is possible to introduce an additional parameter to take some account of the effects of methyl buttressing (10) but again a consistent set of values cannot be obtained. At present, therefore, we are forced to discuss our results in qualitative terms.

The results are summarized in Fig. 1, which shows the relative extent of protonation at each site and the ratio of protonation *ortho* and *para* to the OH group in each compound (*o*/*p*; statistical correction applied where two identical *ortho* sites are available). Figure 1 allows the effect of methyl substitution in any given substrate to be readily assessed.

It is well established that for polymethylbenzenes the stability of ions formed by protonation at a methyl-bearing carbon is significantly less than that of ions formed by protonation at a hydrogen bearing site (1). This is reflected in the reduced basicity at methyl bearing sites and has been attributed to the loss of hyperconjugative interaction energy between the methyl group and the ring in the cation (1). Methyl substitution at the 3 position in indole and methylindoles reduces the basicity of that site by a factor of 10–20 (11). The presence of a similar effect for phenols

Can. J. Chem. Downloaded from www.nrcresearchpress.com by 210.87.254.40 on 09/05/12
For personal use only.

Can. J. Chem. Downloaded from www.nrcresearchpress.com by 210.87.254.40 on 09/05/12
For personal use only.

and their methyl ethers can be seen by comparing phenol and anisole with 4-methylphenol and 4-methylanisole (2), respectively. In the latter compounds, C-4 protonation is nonexistent or nearly so.

In the polymethylbenzene series the use of basicity constants (12, 13) has shown that replacing a hydrogen by a methyl group *ortho*, *para*, or *meta* to a given site increases the basicity of that site by a factor of a 1000 (*ortho* or *para*) or 5 (*meta*). Deuteration studies however indicate that a *para* methyl group has base-strengthening effect about twice that of an *ortho* methyl group (1), whereas n.m.r. spectroscopic work indicates an even greater difference between *ortho* and *para* (1). In addition to these electronic effects which might be expected to lead to predictable changes in protonation pattern with increasing methylation, other complicating effects can be expected. The first is the occurrence of *O*-protonation in **8** and **9**, which makes comparison between these substrates and the others difficult. Other complications undoubtedly arise from steric crowding between adjacent methyl groups (two such effects can be expected and one is well documented for the methyl group (10)). In a crowded environment, substitution at a methyl-bearing ring carbon should be favored because the methyl is moved out of the ring plane and strain is reduced. This steric compression has been demonstrated in desilylation reactions, where rates almost an order of magnitude above those predicted by additivity have been observed for protodesilylation and mercuridesilylation at $SiMe_3$ flanked by methyl groups (14, 15). The well documented buttressing effect is now known to reduce the ring activating effect of methyl groups in crowded environments. Reactivity is lower when the reaction site has *ortho* and *meta* methyl groups which are buttressed than when the methyl groups are unbuttressed (by about 17% in hydrogen–tritium exchange).

All these effects can be discerned in our results, though at present, as already stated, no quantitative description is possible. For compounds **2**, **3**, **11**, **12**, and **13** in which *O*-protonation is not observed, the effect of adding a methyl group can be studied from the pairs **2,3**; **2,11**; **2,12**; **3,13**; **11,13**; and **12,13**. Methylating **2** at the 6 position to give **11** (which changes the *o*:*p* ratio from 11.5:1 to 1:4) blocks the most basic ring position in **2** to all but *ipso* protonation, which has never been observed at a methyl *ortho* to the OH group. The additional methyl has clearly activated the free *meta* ring position (C-6[2]) since this position is now protonated; it has presumably also activated the C-4 *meta* position. The overall result is that because of the combination of electronic effects, the C-4 site becomes the most basic in **11**, position 6 not having a methyl *para* to it. Methylation of **2** at position 2 (to give **12**) also adds a methyl *ortho* to the hydroxyl group, but several effects will now operate. Carbons 4 and 6 should be electronically activated, C-4 should be activated by steric compression, and the activating effect of the methyl *para* to C-6 should be reduced by buttressing. The overall effect is a slight change in the relative basicities of carbons 4 and 6, compared with compound **2**, which is impossible to attribute to any one factor. Again, the change brought about by methylating **2** at C-5 (to give **3**) could be explained in terms of activation of C-4 by steric compression and *ortho* methylation, activation of C-2 by *para* methylation, deactivation of C-6 by buttressing of the C-3 methyl, or a combination of all of these.

As might be expected, steric effects are probably more discernible as methylation becomes more extensive. Methylation of **3** at C-2 (to give **13**) might be expected to increase the basicity of the two *meta* positions by roughly the same amount. This is clearly not the case; *ipso* protonation at C-4 is dramatically enhanced and this can be attributed to the gain in stability when the crowded 4-methyl group moves out of the ring plane. In moving from **10** to **13**, C-6 acquires a *para* methyl group but its effect will be diminished by buttressing and the C-4 reactivity enhanced by steric compression and *ortho* methyl activation. Again, methylating **11** at C-5 (to give **13**) should electronically activate C-4 and C-6 equally, but enhanced buttressing and steric compression combine to increase *ipso* protonation at the expense of C-6.

The difference in the electronic activating influence of a methyl *para*, *ortho*, and *meta* to a site with the minimum of steric effects is seen in the methylation of **8** to give **2** and **9** respectively. In going from **8** to **2** the addition of the C-3 methyl so activates the C-4 and C-6 sites that *O*-protonation is no longer competitive. The C-6 site is activated approximately twice as much as the

[2]Note, numbering alters in going from **2** to **11**.

C-4 site in line with earlier observations for the methylbenzene series (1). However in going from **8** to **9** the C-2 methyl activates both sites equally but this *meta* activation is not sufficient to remove *O*-protonation.

Experimental

All the phenols used were commercially available with the exception of 2,3,4-trimethylphenol and 2,3,4,5-tetramethylphenol which were prepared from the bromides by reaction of the Grignard Reagent with methylborate followed by 10% H_2O_2 (16). Fluorosulfonic acid was distilled under dry nitrogen before use. Proton magnetic resonance spectra were recorded on a Varian A60 spectrometer equipped with a variable temperature probe and spin decoupler. Chemical shifts were measured relative to $(CH_3)_4N^+BF_4^-$ as internal reference and converted to δ TMS by using δ TMS −3.20 for the reference ion.

We thank the Research Committee of the New Zealand Universities Grants Committee for financial support, and for the award of a Postgraduate Scholarship to Stephen M. Blackstock.

1. D. M. Brouwer, E. L. Mackor, and C. Maclean. *In* Carbonium ions. Vol. 2. *Edited by* G. A. Olah and P. von Schleyer. Wiley-Interscience, New York. 1970. p. 837.
2. D. M. Brouwer, E. L. Mackor, and C. Maclean. Rec. Trav. Chim. **85**, 109 (1966).
3. D. M. Brouwer. Rec. Trav. Chim. **87**, 335, 342 (1968).
4. G. A. Olah, G. D. Mateescu, and Y. K. Mo. J. Am. Chem. Soc. **95**, 1865 (1973).
5. T. Birchall, A. N. Bourns, R. J. Gillespie, and P. J. Smith. Can. J. Chem. **42**, 1443 (1964).
6. M. P. Hartshorn, K. E. Richards, J. Vaughan, and G. J. Wright. J. Chem. Soc. (B), 1624 (1971).
7. G. A. Olah and Y. K. Mo. J. Org. Chem. **38**, 353 (1973).
8. A. Fischer and G. J. Wright. Aust. J. Chem. In press.
9. C. D. Ritchie and W. F. Sagar. *In* Progress physical organic chemistry. Vol. 2. *Edited by* S. G. Cohen, A. Streitwiesser, and R. W. Taft. Interscience, New York. 1964. p. 323.
10. K. E. Richards, A. L. Wilkinson, and G. J. Wright. Aust. J. Chem. **25**, 2369 (1972).
11. R. L. Hinman and J. Lang. J. Am. Chem. Soc. **86**, 3796 (1964).
12. W. M. Laver and G. Stedman. J. Am. Chem. Soc. **80**, 6439 (1958).
13. E. L. Mackor, P. J. Smith, and J. H. van der Waals. Trans. Faraday Soc. **53**, 1309 (1957).
14. R. A. Benkeser, R. A. Hickner, D. I. Hoke, and O. H. Thomas. J. Am. Chem. Soc. **80**, 5289 (1958).
15. C. Eaborn and R. C. Moore. J. Chem. Soc. 3640 (1959).
16. M. F. Hawthorne. J. Org. Chem. **22**, 1001 (1957).

Can. J. Chem. Downloaded from www.nrcresearchpress.com by 210.87.254.40 on 09/05/12
For personal use only.

Degenerate Rearrangements in a Cyclohexenyl Cation. Independent Ring Carbon Interchange and Hydrogen Interchange Processes

RICHARD CONE, ROLLIN P. HASELTINE, PETER KAZMAIER, AND TED S. SORENSEN

Department of Chemistry, The University of Calgary, Calgary, Alberta T2N 1N4

Received April 1, 1974

RICHARD CONE, ROLLIN P. HASELTINE, PETER KAZMAIER, and TED S. SORENSEN. Can. J. Chem. **52**, 3320 (1974).

In a 1,2,4-trialkyl-substituted cyclohexenyl cation, two very facile degenerate rearrangements occur. One is simply a scrambling of a proton (C-3) on the allyl center with the C-4 proton. The more interesting process is one involving the specific interchange of the C-1 and -4 carbons and attached alkyl groups. Accurate rates have been measured for both these processes using specific deuterium labelling and the n.m.r. spin saturation technique, in order to probe the mechanism of the rearrangements.

RICHARD CONE, ROLLIN P. HASELTINE, PETER KAZMAIER et TED S. SORENSEN. Can. J. Chem. **52**, 3320 (1974).

Dans le cation cyclohexényle substitué par trois groupes alkyles en positions 1, 2 et 4, deux réarrangements dégénérés très faciles peuvent se produire. Un est simplement une compétition du proton en C-3 au centre allylique avec le proton en C-4. Le processus plus intéressant est celui qui implique les échanges spécifiques des carbones C-1 et C-4 avec les groupes alkyles qui leur sont attachés. Afin de mieux comprendre le mécanisme de ces réarrangements, des vitesses précises ont été mesurées pour chacun de ces processus utilisant le marquage au deutérium d'une façon spécifique et la technique de saturation des spins en r.m.n.

[Traduit par le journal]

Introduction

Previous work (1–3) in this laboratory has provided evidence for an unusual trialkyl-substituted cyclohexenyl cation rearrangement in which the carbon and attached alkyl groups at positions 1 and 4 specifically interchange (Scheme 1). In the earlier studies, the ion systems involved

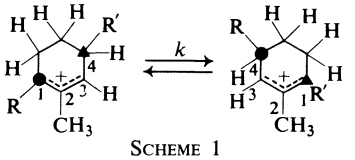

SCHEME 1

were somewhat complex (*e.g.* R and R′ different alkyl groups etc.) and it seemed desirable to settle conclusively the gross structural features of the process, and the mechanism, by using a simpler system. In the present study, both substituents are methyl groups and the rearrangement is therefore degenerate. The gross structural features of the rearrangement have been probed using specific deuterium labelling and this, together with a careful measurement of reaction kinetics, provides details concerning the mechanism.

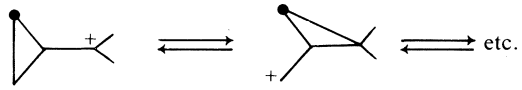

●≡"migrating center"

SCHEME 2

A second reason for this investigation was the hope that one might be able to *directly* observe the stereochemical consequences of the much studied cyclopropylcarbinyl–cyclopropylcarbinyl rearrangement (4) (Scheme 2). The mechanism which we have previously proposed for Scheme 1 involves intermediates which are postulated to undergo just this rearrangement. The key question concerns the stereochemical fate of the migrating cyclopropane center in the rearrangement (inversion or retention of configuration). By labelling the hydrogen at C-3 it should be possible in principle to distinguish these, *viz.* Scheme 3. Majerski and Schleyer (5) have used deuterium labelling in solvolytic studies of a simple cyclopropylcarbinyl system and found clean inversion of configuration during the rearrangement, so that the initial expectation in this work was for no exchange of the C-3 and -4 protons (see Scheme 3).

Can. J. Chem. Downloaded from www.nrcresearchpress.com by 210.87.254.5 on 09/05/12
For personal use only.

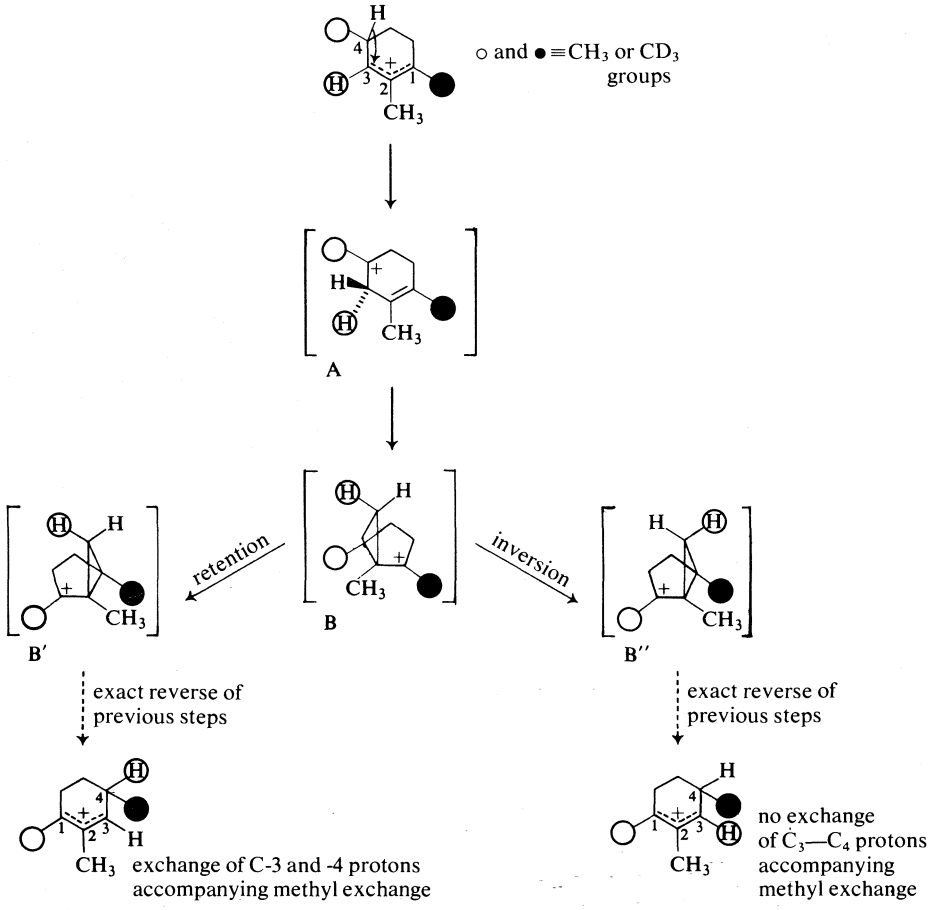

SCHEME 3. (*i*) All ions in brackets are assumed to be unobservable, high energy species. (*ii*) The homoallylic ion A may not be a distinct species, *i.e.* it may only lie on the energy surface. (*iii*) In B, both cyclopropane protons are unique. The actual experiment is not dependent on a particular assigned geometry: only that the overall reaction be symmetrical; *i.e.* if the migrating proton does become an "inner" proton in B, one assumes in a symmetrical process that this same "inner" proton in B′ or B″ will migrate back again. There is *a priori* no guarantee that B will retain a specific stereochemistry, however this point is tested by the proposed labelling scheme.

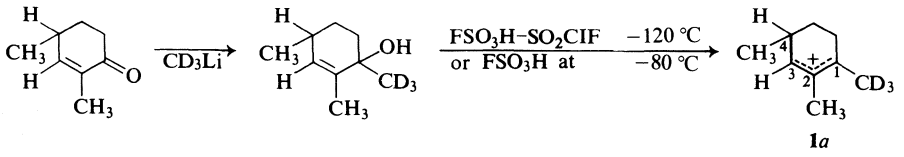

SCHEME 4

Results

Deuterium Labelling of the C-1 Methyl Group

In order to conclusively settle the gross structural features of the rearrangement (Scheme 1), the specifically deuterated ion **1***a* was prepared by the sequence shown in Scheme 4.

The unlabelled ion had been previously prepared and characterized (2) and the ^1H n.m.r. spectrum of **1***a* was identical except for the absence of the C-1 methyl peak at τ 6.99. As the temperature is raised to about −70 °C, one notes a gradual height decrease in the C-4 methyl peak

Can. J. Chem. Downloaded from www.nrcresearchpress.com by 210.87.254.5 on 09/05/12
For personal use only.

and the appearance of a C-1 methyl peak. The C-2 methyl peak remains unchanged! The actual rate of the reaction was measured by following the increase of the C-1 methyl signal, $k_1 = 4.4 \times 10^{-5}$ s^{-1} at -69.7 °C, and from the temperature dependence, $E_a = 15.3$ kcal/mol.

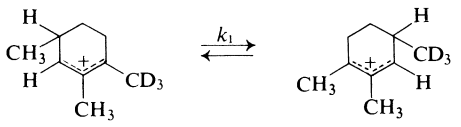

1*a* **1***b*

Although previous examples of this rearrangement were not studied quantitatively, they appear to occur at a similar rate.

At equilibrium, there appears to be equal deuterium (±5%) in the C-1 and -4 methyl groups, *i.e.* no measurable equilibrium isotope effect. It was also verified that no exchange of the cation deuterium with solvent protons occurs, a necessary condition, of course, for measuring accurate rearrangement rates.

Deuterium Labelling of the C-3 Hydrogen Position

Having established that the rearrangement occurred cleanly, we next turned our attention to the mechanistic details as outlined in the Introduction (Scheme 3). The 3-D ion **1***c* was prepared by the sequence outlined in Scheme 5.

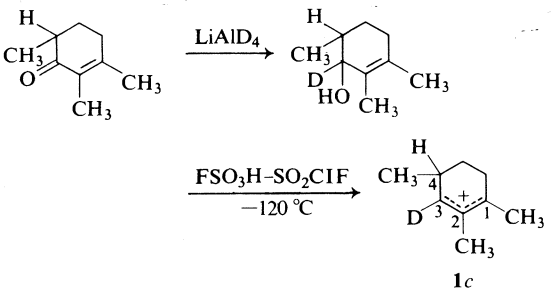

SCHEME 5

The ^{1}H n.m.r. spectrum of **1***c* was identical to the unlabelled ion except for the absence of the C-3 proton at τ 1.23. When the ion solution was warmed to about −80 °C, somewhat unexpectedly, a peak began to "grow" in the C-3 proton region. The C-4 proton is heavily coupled and obscured by the two C-6 protons and the C-1 methyl protons and the decrease in this peak is not easy to measure. The deuterium at C-3 is, however, specifically appearing at C-4 because

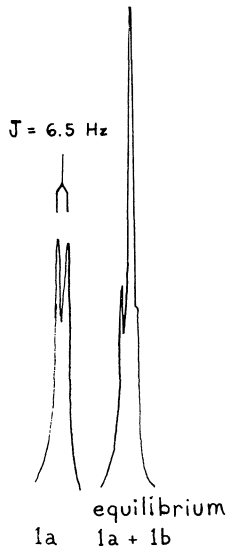

FIG. 1. The C-4 methyl group in ion **1***a* and after equilibration with **1***b* has been reached.

the original doublet for the C-4 methyl group changes progressively to a half-sized doublet and a singlet of about the same area (shown in Fig. 1). The rate for the process **1***c* ⇌ **1***d* was

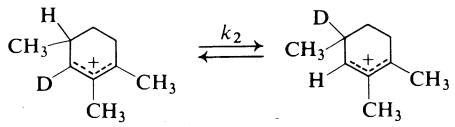

1*c* **1***d*

measured by following the area increase of the C-3 proton peak, $k = 1.4 \times 10^{-4}$ s^{-1} at −79.9 °C. Surprisingly, this rate is even faster than that measured for the methyl interchange and in order to obtain a same temperature comparison, the activation energy data for the k_1 process was used. Compared at −80 °C, the ratio of k_2/k_1 is 22.

In this reaction, like the k_1 measurement, there is no measurable (±10%) equilibrium isotope effect and the C-3–C-4 deuterium does not exchange with solvent protons at these temperatures.

The two isotope scrambling rates (k_1 and k_2) cannot be connected with the same rearrangement process unless one is observing improbably large and opposite kinetic isotope effects.

Detection of the Two Rearrangements by the Spin Saturation Technique

In elaborating the mechanistic details, it is obviously necessary to know for certain that one

Can. J. Chem. Downloaded from www.nrcresearchpress.com by 210.87.254.5 on 09/05/12
For personal use only.

Can. J. Chem. Downloaded from www.nrcresearchpress.com by 210.87.254.5 on 09/05/12
For personal use only.

is or is not dealing with two different rearrangements. Since the isotopic labelling results contain an element of uncertainty, the same two rearrangement processes were looked for in the unlabelled ion **1**. Of the techniques available, the n.m.r. line broadening method was clearly useless since an irreversible rearrangement of the ion **1** into **2** occurs rapidly above 0 °C (2), a temperature at which line broadening in the C-3 proton of **1** may just be observed.

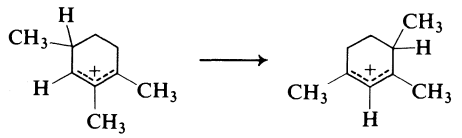

1 **2**

One technique previously used in this laboratory to measure reaction kinetics with rate constants in the range 0.1–10 s^{-1} is the saturation labelling technique of Forsén and Hoffman (6, 7). Straightforward extrapolation of the conventional kinetic rates observed for the deuterium-substituted cations suggests that the rates will be in the above range at approximately −20 to +10 °C. These temperatures are perilously close to the temperature where the irreversible **1** → **2** reaction becomes fairly fast but it was possible to confirm the presence of two different rates processes in the all proton ion **1**.

In Fig. 2 are shown the results obtained at various temperatures by observing the C-3 proton while irradiating the C-4 proton and separately, of observing the C-1 methyl protons while irradiating the C-4 methyl doublet. The qualitative difference in the two rates is readily apparent from Fig. 2. At −24 °C, the C-3 proton peak area is noticeably decreased but not the C-1 methyl area in the separate irradiation involving the methyls. However, at −4 °C, the C-1 methyl peak is now noticeably decreased while the C-3 proton area is approaching zero.

Under double irradiation, the area of an observed peak, M_z^{∞}, represents a steady-state condition where $M_z^0/M_z^{\infty} = 1 + T_1k$, k = rate constant for exchange of the irradiated nucleus with the nucleus being observed, T_1 = spin–lattice relaxation time of the observed nucleus and M_z^0 represents the original peak area (without double irradiation) of the nucleus being observed. In order to obtain accurate rate constants, it is necessary to study the time dependence of the magnetization decrease (from the original to the steady-state value) but in the present example, the rapid irreversible rearrangement of **1** to **2** makes this a doubtful exercise. The major concern in this work is a rate comparison rather than absolute rates and this comparison can be made provided only that one assumes the same T_1 value for both nuclei being observed in the two exchange processes. If the M_z^0/M_z^{∞} ratio is given the symbols R_1 and R_2 for the two systems, then $k_2/k_1 = (R_2 - 1)/(R_1 - 1)$. At −13 °C, R_2 for the C-3–C-4 protons system is *ca.* 6.3 while R_1 (the C-1 methyl – C-4 methyl) is *ca.* 1.25. This gives $k_2/k_1 = 25$, in reasonable agreement with the rate ratio observed in the labelled ions.

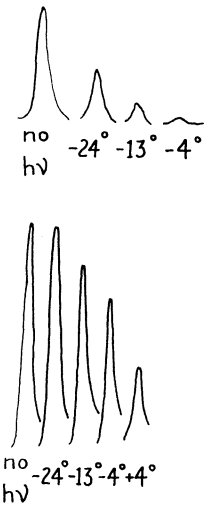

FIG. 2. Upper traces: the equilibrium peak sizes of the C-3 proton while irradiating (saturating) the C-4 proton. Lower traces: the equilibrium peak sizes of the C-1 methyl group while irradiating (saturating) the C-4 methyl region. In both traces, the areas have been corrected to take into account the decrease with time in the "no *hν*" peak through rearrangement (**1** → **2**).

The relaxation times T_1 of carbonium ion protons in FSO_3H solvent at these temperatures appear to be about 1–3 s (8). Substitution of a T_1 value of 2 s using the data (Fig. 2) for the C-1 methyl – C-4 methyl double irradiation at −4 °C yields a k_1 value of 0.3 s^{-1}. The extrapolated value at −4 °C from the Arrhenius plot of the labelled compound is 0.5 s^{-1}. Even if the agreement is somewhat fortuitous, it does support the overall method.

Both isotopic substitution and spin saturation methods yield the same conclusions: (*a*) there are two independent degenerate rearrangements

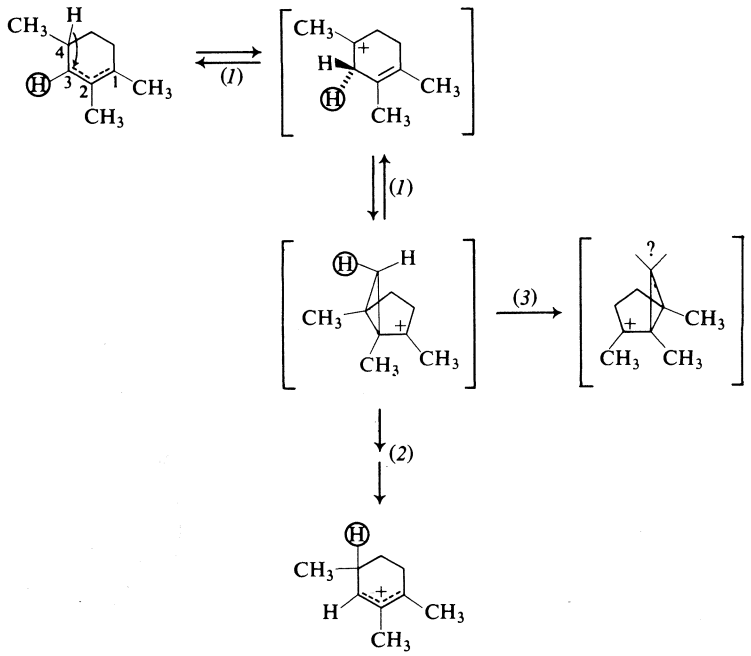

SCHEME 6

and (*b*) the C-3–C-4 proton exchange is *ca.* 20 times faster than the methyl exchange. The C-3–C-4 proton exchange does not imply a retention mechanism for the cyclopropylcarbinyl–cyclopropylcarbinyl cation step depicted in Scheme 3. It simply means that in this system all hope for testing the stereospecificity of this rearrangement is gone.

Discussion

Both degenerate rearrangements require the same initiating step, *i.e.* migration of a proton from C-4 to C-3. The resulting steady-state intermediate can proceed in three directions (Scheme 6): (*1*) return to the cyclohexenyl cation by the same transition state, in which case the reaction is completely "hidden"; (*2*) a bridge "flip" or any process which allows the other cyclopropyl proton (the original C-3 in **1**) to migrate to C-4 (the k_2 process observed in this work), or alternatively, the activation energy for process *1* may be higher than for process *2*, in which case k_2 is the rate of the hydride transfer (process *1*) step; (*3*) an experimentally slightly slower, cyclopropylcarbinyl–cyclopropylcarbinyl rearrangement. The interchanged C-1 methyl – C-4 methyl cyclohexenyl cation then subsequently results after the above H shift. In addition, the overall process (see Scheme 3) interchanges the C-1 and C-4 carbons and the C-5 and C-6 CH_2 groups. The rearrangement is not strictly degenerate since it actually interconverts optical isomers.

Nature of the Cyclopropylcarbinyl–Cyclopropylcarbinyl Step (3)

Wiberg and Szeimies (4) have considered in detail the various possible mechanisms for the sub-title rearrangement. One peculiarity of the present cyclohexenyl cation rearrangement is the apparent necessity for the C-2 alkyl group. In several cases involving 1,4-dialkyl-substituted cyclohexenyl cations, the interchange of these alkyl groups, if at all, must have been much slower.[1] This observation fits the "shuffle" mechanism for the cyclopropylcarbinyl–cyclopropylcarbinyl rearrangement, *i.e.* one step to the cyclobutyl cation and a second step to the "new" cyclopropylcarbinyl system (Scheme 7). The presence of a tertiary ion (C-2) at the cyclobutyl stage would provide a much lower energy transition state compared to the proton analog.

One other peculiarity of the rearrangement is

[1]In contrast to ions like **1**, the simple 1,4-dialkyl-substituted cyclohexenyl cations can also be interconverted by an acid–base equilibration mechanism and thus, when the interconversion (very much slower than in **1**) does occur, there is some doubt about the actual mechanism.

Can. J. Chem. Downloaded from www.nrcresearchpress.com by 210.87.254.5 on 09/05/12
For personal use only.

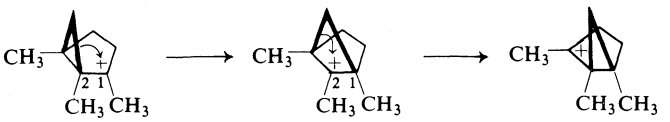

SCHEME 7

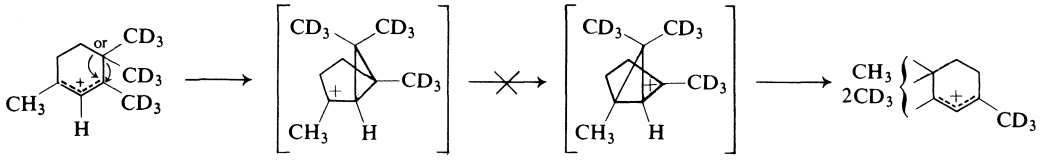

3*a* 3*b*

SCHEME 8

the dependence on the substitution at the cyclopropyl migrating center. This rearrangement (Scheme 7) has previously been looked for in the cyclohexenyl cation **3** (Scheme 8). Although there is excellent evidence (9) that the cyclopropylcarbinyl system is a very accessible intermediate, there is no sign of the rearranged cation **3***b* after 48 h at 25 °C.[2] A cyclopropylcarbinyl–cyclopropylcarbinyl rearrangement involving a tertiary migrating center has however been observed by Poulter and Winstein (10) and in this laboratory (11) and involves a simple allyl cation system.

Although the Scheme 1 rearrangement appears to require quite specific functionalization and is therefore not very general, it would appear that more complex organic molecules might offer interesting possibilities, for example, the decalenyl cations **4** and **5** should be interconvertible.

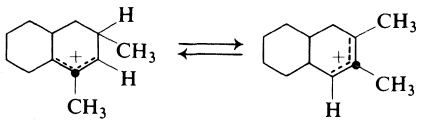

4 **5**

Experimental

1-Hydroxy-1,2,4-trimethylcyclohex-2-ene and the 1-CD_3 Analog

A solution of 2,4-dimethylcyclohex-2-enone (12) 1.007 g, 0.00805 mol, in 10 ml of ether was added under N_2 to an ice-cold solution of methyl lithium (prepared in the CD_3Li case from 1.12 g (0.16 mol), of Li metal, 2.038 g (0.0815 mol) of methyl iodide-d_3, and 20 ml of ether). After 3 h at 0 °C, the reaction mixture was allowed to warm to 25° and filtered through a glass wool plug, washing the plug with ether. The ether solution was cooled to 0° and 100 ml of cold saturated sodium bicarbonate added. The two layers were separated and the aqueous layer extracted with ether (4 × 30 ml). The combined ether layers were dried over anhydrous Na_2SO_4. The residue after removing the ether was distilled, b.p. 31–32 °C/0.075 mm, yield 0.91 g (79%).

Anal. Calcd. for $C_9H_{16}O$: C, 77.14; H, 11.4. Found: C, 77.37; H, 11.9.

Nuclear magnetic resonance, 60 MHz, CCl_4, indicates an approximate 40–60 mixture of the *cis* and *trans* alcohols (assignment uncertain) because two separate C-4 methyl peaks are observed at τ 9.08 (d, J = 6.5 Hz) and 9.04 (d, J = 6.5). The C-1 methyl is at 8.70, C-2 at 8.32 (b), and the C-3 proton at 4.83 (b). The remaining peaks are nondescript. Infrared spectra, CD_3 stretch at 2230 cm^{-1}.

1-Hydroxy-2,3,6-trimethylcyclohex-2-ene-1-d_1

A solution of 1.438 g (0.0104 mol) of 2,3,6-trimethylcyclohex-2-enone (12) in 10 ml of dry ether was added dropwise under N_2 to an ice-cold solution of 0.550 g (0.0131 mol) of $LiAlD_4$ in 10 ml of ether. After addition the mixture was refluxed for 2 h. The excess hydride was decomposed at 0 °C with methanol and water was then added to hydrolyze the mixture. The ether layer was separated and the aqueous layer extracted with ether (2 × 10 ml). The combined ether solutions were dried over anhydrous K_2CO_3. After removal of the ether, the residue was distilled at 38 °C/0.1 mm, yield 1.275 g (86%).

Anal. Calcd. for $C_9H_{15}DO$: C, 76.6. Found: C, 76.63.

Nuclear magnetic resonance, 60 MHz, CCl_4, 9.03 (d, J = 6.5 Hz), and 8.38 (b, 6H, two methyl groups). The remaining peaks are broad and nondescript. Infrared spectra C—D stretch at 2110 cm^{-1}.

Preparation of the Cations and Kinetic Procedures

The procedures used to prepare the ions were identical with previous descriptions (13). The kinetic measurements were carried out on n.m.r. samples (*ca.* 10% weight of alcohol per volume of solution) using a Varian Associates HA-100 to measure the ion spectra. Temperatures were monitored using a thermocouple placed directly in the sample (14) and temperature readings were made frequently and averaged. About 20 data points were collected for each run and the least-squares plot obtained.

[2]The cation **3** is in equilibrium with a cyclopentenyl cation (9) but this has no real bearing on Scheme 8.

Can. J. Chem. Downloaded from www.nrcresearchpress.com by 210.87.254.5 on 09/05/12
For personal use only.

For the **1***a*–**1***b* system, the height of the growing 1-CH_3 peak was measured and standardized in each case internally against the unchanging 2-CH_3 peak height to offset any machine variations. The same procedure was used for the growing 3H peak in the **1***c*–**1***d* case. Since K is experimentally 1 in both processes, the reaction can be treated by simple, as opposed to reversible, first-order kinetics. In each case, log $(X - X_e)$ *vs.* t was plotted, X_e, the equilibrium concentration of reactant, being obtained by letting the sample warm up to about $-50\,^{\circ}C$ for 30 min. The slope of this line is equal to $2k/2.303$.

Spin Saturation Transfer Experiments

Speed of operation was essential in these experiments since the ion **1** was rearranging fairly rapidly to **2** at the temperatures used. The experiment involves setting the power level of the external oscillator such that complete saturation of the irradiated proton is just obtained. The r.f. circuit was kept loaded at all times, the audio modulation being kept harmlessly several hundred cycles away from the desired frequency except when saturation of the peak was wanted and this could be accomplished by a simple switching process. The observing power was kept very low to avoid further saturation from this source. At a given temperature, a number of runs were quickly made by running over just the peak of interest while alternately irradiating on the exchanging proton position. The results shown in Fig. 2 are typical.

The authors wish to thank the National Research Council of Canada for generous financial support.

1. K. Rajeswari and T. S. Sorensen. Can. J. Chem. **50**, 2939 (1972).
2. T. S. Sorensen and K. Rajeswari. J. Am. Chem. Soc. **93**, 4222 (1971).
3. L. Huang, K. Ranganayakulu, and T. S. Sorensen. J. Am. Chem. Soc. **95**, 1936 (1973).
4. K. B. Wiberg and G. Szeimies. J. Am. Chem. Soc. **92**, 571 (1970).
5. Z. Majerski and P. von R. Schleyer. J. Am. Chem. Soc. **93**, 665 (1971).
6. S. Forsén and R. A. Hoffman. J. Chem. Phys. **39**, 2892 (1963).
7. F. A. L. Anet and A. J. R. Bourns. J. Am. Chem Soc. **89**, 760 (1967).
8. R. Haseltine. Unpublished results from this laboratory.
9. T. S. Sorensen and K. Ranganayakulu. J. Am. Chem. Soc. **92**, 6539 (1970).
10. C. D. Poulter and S. Winstein. J. Am. Chem. Soc. **94**, 2297 (1972).
11. T. S. Sorensen and K. Ranganayakulu. Tetrahedron Lett. 659 (1970).
12. G. Stork, A. Brizzolara, H. Landesman, J. Szmuszkovicz, and R. Terrell. J. Am. Chem. Soc. **85**, 207 (1963).
13. P. H. Campbell, N. W. K. Chiu, K. Deugau, I. J. Miller, and T. S. Sorensen. J. Am. Chem. Soc. **91**, 6404 (1969).
14. R. Bladek and T. S. Sorensen. Can. J. Chem. **50**, 2806 (1972).

Can. J. Chem. Downloaded from www.nrcresearchpress.com by 210.87.254.5 on 09/05/12
For personal use only.

Azatropolones. Part II.[1] The Schmidt Reaction of 2-Methoxy-5-methylbenzoquinone

COLIN G. HUGHES, ERROL G. LEWARS, AND ALUN H. REES
Department of Chemistry, Trent University, Peterborough, Ontario K9J 7B8

Received November 6, 1973[2]

COLIN G. HUGHES, ERROL G. LEWARS and ALUN H. REES. Can. J. Chem. **52**, 3327 (1974).

2-Methoxy-5-methylbenzoquinone undergoes reaction with sodium azide in sulfuric acid to give (*a*) 3-hydroxy-6-methyl-1*H*-azepin-2,5-dione, which undergoes ring contraction with base to give 5-methyl-4-pyridone-2-carboxylic acid; (*b*) 4-methoxy-7-methyl-1*H*-azepin-2,5-dione, which reacts with phosphorus oxychloride to give methyl 2-chloro-6-methylpyridine-4-carboxylate, not 2-chloro-4-methoxy-7-methyl-5*H*-azepin-5-one; (*c*) 7-methoxy-4-methyl-1*H*-azepin-2,5-dione. The reactions of these compounds are discussed and the evidence for their structures is presented.

COLIN G. HUGHES, ERROL G. LEWARS et ALUN H. REES. Can. J. Chem. **52**, 3327 (1974).

La méthoxy-2 méthyl-5 benzoquinone réagit avec l'azoture de sodium dans l'acide sulfurique pour donner (*a*) l'hydroxy-3 méthyl-6 1*H*-azépinedione-2,5 qui subit une contraction de cycle en présence de bases pour conduire à l'acide méthyl-5 pyridone-4 carboxylique-2; (*b*) la méthoxy-4 méthyl-7 1*H*-azépinedione-2,5 qui réagit avec l'oxychlorure de phosphore pour conduire à l'ester méthylique de l'acide chloro-2 méthyl-6 pyridinecarboxylique-4 et non pas à la chloro-2 méthoxy-4 méthyl-7 1*H*-azépinone-5; (*c*) la méthoxy-7 méthyl-4 1*H*-azépinedione-2,5. On discute des réactions de ces composés et l'on présente des preuves pour leur structure.
[Traduit par le journal]

The aromaticity of tropone (**1**, R = H) and tropolone (**1**, R = OH) (1) has recently been questioned (2). Having long been interested in aza analogs of tropolone (3), we now describe the synthesis of hydroxy derivatives of 5-azatropone (**2**) and discuss their nature.

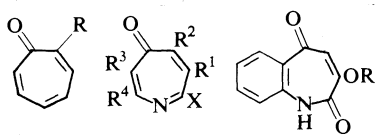

1 **2** **3**

The reaction of quinones with hydrogen azide has given azatropones (4*a*) and benzazatropones (4*b*). We have reported the ring expansion of alkoxynaphthoquinones to give benzazatropolones **3** (5). Hydroxyquinones undergo an alternative reaction leading to ring contraction (6).

When 2-methoxy-5-methylbenzoquinone (**4**) was treated with sodium azide in sulfuric acid, three of the four possible ring expansion products were isolated. These were compounds **5** (R = H), **6** (R = Me), and **7** (R = Me). Lactam **8** was not found. One of the products gave a red ferric chloride color, demethylation having occurred. By analogy with compound **3** which tends to demethylate (R = Me → H) on work-up, we suspected structure **5** (R = H) for our enolic product. When it was treated with diazomethane, it gave a methyl ether which differed from the two other ethers isolated.

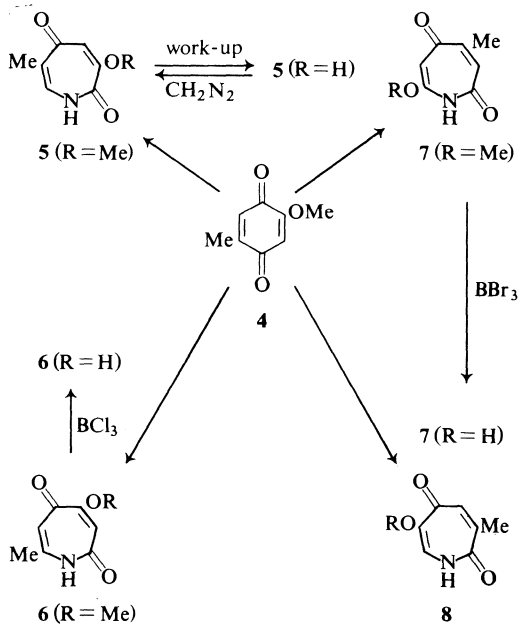

[1]For Part I see ref. 3.
[2]Revision received July 2, 1974.

Can. J. Chem. Downloaded from www.nrcresearchpress.com by 210.87.254.42 on 09/05/12
For personal use only.

Can. J. Chem. Downloaded from www.nrcresearchpress.com by 210.87.254.42 on 09/05/12
For personal use only.

Alkaline ring contraction of **5** (R = H) gave a methylpyridone carboxylic acid. Zinc dust pyrolysis of this acid gave a pyridine base identified by v.p.c.–m.s. as β-picoline.[3]

We synthesized 5-methyl-4-pyridone-2-carboxylic acid (7) and though the melting point differed from the literature value, the compound was identical in all respects with our ring contracted product, thus confirming the structure **9** and hence **5** (R = H) for the precursor.[4]

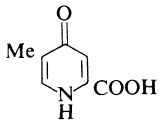

9

A less polar product isolated from the Schmidt reaction has been assigned structure **6** (R = Me). It was readily demethylated by boron trichloride to **6** (R = H), which gave a red color with ferric chloride.

The nonaromatic nature of **6** (R = H) became apparent on reaction with alkali when the molecule was completely hydrolyzed. Zinc dust pyrolysis of the alkaline reaction product did not yield any trace of picoline.

Reaction of **6** (R = H) with phosphorus oxychloride gave a polymer. When the ether **6** (R = Me) was treated with this reagent however, the product was methyl 2-chloro-6-methylisonicotinate (**10**), identical in all respects with a sample prepared from genuine 2-chloro-6-methylisonicotinic acid (8).[5] The least polar product from the Schmidt reaction was assigned structure **7** (R = Me). It could not be demethylated by boron trichloride (9). Boron tribromide gave **7** (R = H) which on structural grounds is not expected to give a ferric chloride color. None was in fact given. The n.m.r. (Table 1) and u.v. (Table 2) spectra are in accord with the proposed structure. Reaction of **7** (R = H) with alkali gave no characterizable product.

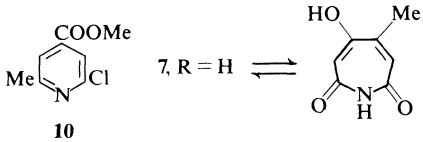

10

[3]We thank the Reilly Tar & Chemical Co. for generous samples of pure picolines.

[4]A significant point about this compound is that its n.m.r. spectrum (Table 1) shows strong coupling (8 Hz) between H-1 and H-7. This is within the range for *ortho* aromatic protons and suggests some bond delocalization as would be expected when mesomeric structures contribute. There are also tautomeric factors in the energy profile but their absence in the ether **5** (R = Me) does not alter $J_{1,7}$ which is still 8 Hz. This is at the lower end of the *ortho* coupling range of 7–10 Hz but still leaves the hetero atom with appreciable sp^2 character. A reasonable postulate is that the compound has some measure of aromaticity and may be termed an azatropolone.

[5]We thank Dr. H. Gutmann of Hoffmann-La Roche & Co. for a sample of this acid.

Experimental

Unless otherwise stated, i.r. spectra (Unicam S.P. 200) are in potassium bromide, quoting ν_{max} in cm^{-1}; u.v. spectra (S.P. 800) are in methanol, quoting λ_{max} in nm (log ε); n.m.r. spectra (Jeol Co. C60 HL) are in DMSO-d_6 quoting τ values relative to TMS (internal); mass spectra (A.E.I. M.S. 12) are at 70 eV on the probe quoting *m/e* (relative intensity); m.p.'s are taken in capillary tubes. Recrystallization solvents are given in parentheses after the melting point.

Vapor phase chromatography was done on a Pye 104 instrument using a 5 ft. × ¼ in. glass column of 10% SE-30 on Chromosorb W, carrier gas helium at 65°. Connection to the M.S. 12 was made via a Watson-Biemann separator.

The Schmidt Reaction of 2-Methoxy-5-methylbenzoquinone (4)

To 50 ml concentrated sulfuric acid, stirred at 0°, 5.84 g of **4** (10) was added over 20 min. Sodium azide, 2.6 g, was then added over 15 min and the red solution was stirred for 1 h (frothing). The flask was stoppered and stirred at 0° for 1 h and at 20° for 70 h. The solution was then poured into 500 ml water and extracted for 72 h in a chloroform extractor. The solvent flask then held 80 ml solution plus a solid which was collected.

The aqueous layer was re-extracted giving 80 ml clear solution. The filtrate from the first extraction was combined with this and concentrated to a small volume which was again filtered. The combined solid from both extracts was washed with chloroform and dried to give **5** (R = H) as a brown powder, m.p. 253–255°, 1.26 g, 22%; i.r. 3400, 3210, 1667, 1639, 1553, 1250, 1220; m.s. M^+ 153 (100).

Anal. Calcd. for $C_7H_7NO_3$: C, 54.9; H, 4.6; N, 9.15. Found: C, 54.9; H, 4.6; N, 9.0.

The filtrate from the collection of **5** (R = H) was diluted with 2 vol. of ether and the precipitated material was filtered off. From the concentrated filtrate, a second crop of solid was obtained, total yield of **6** (R = Me), 1.05 g, 16%. After sublimation (170°/0.1 mm), the compound had m.p. 226–226.5° (ethanol), almost colorless microcrystals; i.r. 3210, 1671, 1613br, 1225, 1155; m.s. M^+ 167 (35), 69 (100).

Anal. Calcd. for $C_8H_9NO_3$ (mol. wt. 167.0582): C, 57.5; H, 5.4; N, 8.4. Found (mol. wt. 167.0585): C,[6]; H, 5.5; N, 8.5.

The filtrate from the collection of **6** (R = Me) was

[6]The carbon analysis was variable. We thank Prof. A. G. Harrison of the University of Toronto for high resolution mass spectra.

TABLE 1. Nuclear magnetic resonance spectra of 2-methoxy-5-methylbenzoquinone and derived azepines

Compound	R	τ NH	CH = CMe	CH	OMe, s	OH
4		—	3.4d 8.05d	3.95d	6.25	—
5	H	−1.2d*	3.25d* 8.15d	3.65s	—	6.15
			J = 8 Hz			
			3.25s(br) after D_2O exchange			
6	Me	−1.0d*	3.25d* 8.15s(br)	3.75s	6.25	
	Me	−0.8	3.98br 7.85s	4.31br	6.25	
	H	−0.9	3.91d 7.8s	4.2br	—	−0.1
			J = 2 Hz			
7	Me	−0.4br	3.85br 7.9d	4.55s	6.3	—
			3.85q after D_2O exchange			
	H	−2.5	3.9q 7.9d	4.6s	—	0.6

*Each component of doublet broad.

TABLE 2. Ultraviolet spectra of 2-hydroxy-5-methylbenzoquinone, derived azepines and their methyl ethers

Compound	R	ν_{max} (log ε) Neutral	Alkaline*	Acidic*
4 (De-Me)		262	268	262
4		261 (4.28)	261	261
5	H	245 (4.41)	255 = 262 > 335	—
		~295br (3.41)		
	Me	245 (4.44)	245 > 339	245 > 300
		300br (3.54)		
6	Me	241 (4.43)	244 > 340	241 > 320
		320br (3.57)		
	H	240 (4.37)	259 > 315	240 > 322
		~322br (3.36)		
7	Me	277 (4.19)	277	277
		~315sh (3.95)	315sh	315sh
	H	277 (4.11)	277	277
		~315sh (3.84)		315sh

*One drop 2 N NaOH solution added to 1 cm cell for alkaline spectrum, then one drop concentrated HCl for acid spectrum.

chromatographed on Grade I neutral alumina, eluting with chloroform. Compound **7** (R = Me), 0.85 g, 13%, was obtained, m.p. 111–112° (dichloromethane–hexane), colorless prisms or feathery needles; i.r. 3400, 1710, 1674, 1613, 1200, 1180; m.s. M^+ 167 (75), 136 (100).

Anal. Calcd. for $C_8H_9NO_3$: C, 57.5; H, 5.45; N, 8.4. Found: C, 57.7; H, 5.5; N, 8.2.

*Conversion of 3-Hydroxy-5-methyl-1H-azepin-2,5-dione (**5**, R = H), to its Methyl Ether (**5**, R = Me)*

To a stirred suspension of the enol in excess methanol, diazomethane (*ca.* 10-fold excess) in ether was added. After 15 min the solvent was evaporated leaving **5** (R = Me), m.p. 285–287° (ethanol) in 100% yield; i.r. 3150, 1681, 1644, 1606, 1542, 1240, 1200; m.s. M^+ 167 (100), 139 (63), 65 (68).

Anal. Calcd. for $C_8H_9NO_3$: C, 57.5; H, 5.45; N, 8.4. Found: C, 57.6; H, 5.4; N, 8.15.

*Ring Contraction of **5** (R = H)*

Compound **5** (R = H), 200 mg in 2 ml 30% aqueous sodium hydroxide solution was refluxed 1 h, then cooled to 0°. Addition of concentrated hydrochloric acid precipitated a crystalline solid which was collected (centrifuge). After successive washing with water, ethanol, and ether, the compound was dried, 135 mg, 67%, m.p. 270–272° (ethanol); i.r. 3460, 3110, 1665, 1615, 1595br, 1220, 810.

We prepared with difficulty, see below, 5-methyl-4-pyridone-2-carboxylic acid **9** (7). In our hands, this had m.p. 270–271°, (lit. (7) m.p. 255–256°). Mixture m.p. with the ring contraction product above was 270–272°. The i.r. spectra of the two samples were identical.

*Synthesis of 5-Methyl-4-pyridone-2-carboxylic Acid **9***

2,5-Lutidine, 6 g, was converted (7) to 2-acetoxymethyl-5-methyl-4-nitropyridine, mobile orange liquid,

Can. J. Chem. Downloaded from www.nrcresearchpress.com by 210.87.254.42 on 09/05/12
For personal use only.

Can. J. Chem. Downloaded from www.nrcresearchpress.com by 210.87.254.42 on 09/05/12
For personal use only.

14% yield; i.r. (film) 1742 br, 1610, 1574, 1540, 1376, 1228, 1198, 1055. The alcohol had (hot-stage) m.p. 67–68° (dichloromethane–hexane), (lit. m.p. 66–67°); i.r. 3700, 1615, 1570, 1547; u.v. 226, 297; (H^+) 221, 291. This was oxidized to the aldehyde, m.p. 38° (ether–hexane) (lit. (7) m.p. 39–40°); i.r. (CH_2Cl_2) 1718, 1609, 1550; m.s. 166 (68), 149 (75), 138 (75), 120 (9), 92 (80), 65 (100).

The final stage succeeded only after adding nitric acid which is normally produced and consumed in the reaction.

The aldehyde, 157 mg, 8 ml 5% hydrogen peroxide, and 20 drops concentrated nitric acid were refluxed 1 h. After evaporation of the solution, water was added and evaporated off at 25°. This process was repeated then the residue was triturated with 3 ml water and filtered leaving 62 mg off-white solid which was dried over potassium hydroxide in vacuum. Compound **9**, colorless microprisms, had m.p. 270–271° (ethanol), (lit. m.p. 255–256° (acetic acid)); the m.p. of our sample remained 270–271° (acetic acid); u.v. 222, 255; (OH^-) 225, 269; (H^+) 218, 256; m.s. M^+ 153 (6), 109 (100). These spectra were identical with those of the ring contraction derived acid **9**, above.

Anal. Calcd. for $C_7H_7NO_3$: C, 54.9; H, 4.6; N, 9.15. Found: C, 55.0; H, 4.7; N, 9.2.

Zinc Dust Pyrolysis of the Ring Contracted Product ***9***

An intimate mixture of 27 mg **9** and an equal bulk of zinc dust was covered with 10 vol. of zinc dust and sealed in an evacuated glass tube. A break-seal divided this tube from the rest of an evacuated and sealed U-tube. The mixture was heated below red heat for 3 min. The break-seal was broken and the other arm of the U-tube was cooled in liquid nitrogen. The rest of the apparatus was warmed and the cooled tube was then cut off.

Methanol, 50 μl, was added to the frozen volatiles and the u.v. spectrum of a 2-μl portion was taken showing the presence of picoline, about 2.1 mg, 13% total. The remaining solution was injected into a g.c.–m.s. machine which showed that the pyrolysate consisted essentially of one component with the retention time and mass spectrum of β-picoline.

α-Picoline: m.s. M^+ 93 (100), 92 (20), 79 (14), 78 (15), 66 (30), 65 (13), 52 (15), 51 (15), 40 (14), 39 (20).

β-Picoline: m.s. M^+ 93 (100), 92 (20), 79 (9), 78 (17), 66 (30), 65 (15), 52 (9), 51 (12), 40 (18), 39 (20).

γ-Picoline: m.s. M^+ 93 (40), 92 (7), 79 (1), 78 (5), 66 (23), 65 (14), 52 (8), 51 (15), 40 (15), 39 (100).

The α- and β-isomers differ only slightly in mass spectrum but have quite different retention times. The γ-isomer which is not a theoretical product, has a retention time of the same order as the β-isomer but its mass spectrum is quite distinct.

*Reaction of 4-Methoxy-6-methyl-1H-azepin-2,5-dione (***6***, R = Me) with Phosphorus Oxychloride*

Compound **6**, (R = Me) 100 mg, was heated under nitrogen with 20 ml phosphorus oxychloride at 95° for 1 h. The dark solution was evaporated (80°/1 mm) and the residue was sublimed (150°/1 mm) twice, giving 41 mg, 37% white crystalline solid, m.p. 54–55° (hexane).

This product, unlike the starting material, was not demethylated by boron trichloride. Boron tribromide did effect demethylation but the product was an acid.

Authentic 2-chloro-6-methylpyridine-4-carboxylic acid was esterified (diazomethane). The ester had m.p. 56–57° (hexane), (8) mixture m.p. with the above sublimate, 56–57°. The spectra of the two samples were identical; i.r. 1730, 1600, 1560, 1310, 1220, 770; u.v. 219 (3.54), 290 (3.54); n.m.r. ($CDCl_3$) 7.4 (CMe), 6.1 (OMe), 2.45br (H5), 2.4br (H3); m.s. M^+ 185 (100), 154 (89).

Demethylation of ***6*** *(R = Me)*

A suspension of 104 mg **6** (R = Me), in 3 ml dichloromethane containing 500 mg boron trichloride was stirred at 25° for 20 h. The mixture was poured into water, extracted with 9 × 20 ml chloroform and the combined extracts were filtered. Evaporation of the filtrate gave 80 mg **6** (R = H) as an off-white solid, colorless microcrescents, m.p. 250–251° (dec.) (ethanol–cyclohexane); i.r. 3450, 1664, 1644, 1598, 1430, 1390, 1200, 770; m.s. 153 (43), 84 (100), 69 (27), 42 (60), 39 (13).

Anal. Calcd. for $C_7H_7NO_3$: C, 54.9; H, 4.6; N, 9.15. Found: C, 54.95; H, 4.6; N, 8.9.

Demethylation of ***7*** *(R = Me)*

Compound **7** (R = Me), 103 mg, was demethylated as above but by 536 mg boron tribromide (no reaction with the trichloride). The crude product, 94 mg of **7** (R = H), was an off-white solid. Pure, it has m.p. 197.5–199° (ethanol–hexane); i.r. 3410, 3300, 1706, 1691, 1649, 1430, 1390, 1180, 850; m.s. 153 (100), 136 (23), 109 (80), 68 (42), 39 (55).

Anal. Calcd. for $C_7H_7NO_3$: C, 54.9; H, 4.6; N, 9.15. Found: C, 54.9; H, 4.6; N, 9.0.

We thank the National Research Council of Canada for financial support.

1. T. Nozoe. Non-benzenoid aromatic compounds. *Edited by* D. Ginsberg. Interscience, London. 1959. Chapt. VII; A. Heusner. Angew. Chem. **70**, 643 (1958).
2. D. J. Bertelli and T. G. Andrews. J. Am. Chem. Soc. **91**, 5280 (1969); D. J. Bertelli, T. G. Andrews, and P. O. Crews. J. Am. Chem. Soc. **91**, 5286 (1969).
3. A. H. Rees. J. Chem. Soc. 3111 (1959).
4. (*a*) E. J. Moriconi and I. A. Maniscalco. J. Org. Chem. **37**, 208 (1972); (*b*) R. G. Cooke and I. M. Russell. Aust. J. Chem. **25**, 2421 (1972).
5. G. R. Birchall and A. H. Rees. Can. J. Chem. **52**, 610 (1974).
6. H. W. Moore and H. R. Sheldon. J. Org. Chem. **32**, 3603 (1967).
7. J. Koncewicz and Z. Skrowaczewska. Rocz. Chem. **42**, 1873 (1968); Chem. Abstr. **70**, 114972u (1969).
8. O. Isler, H. Gutmann, O. Straub, B. Fust, E. Bochni, and A. Studer. Helv. Chim. Acta, **38**, 1033 (1955).
9. F. M. Dean, J. Goodchild, L. E. Houghton, J. A. Martin, R. B. Morton, B. Parton, A. W. Price, and N. Somvichien. Tetrahedron Lett. 4153 (1966).
10. R. B. Woodward, F. Sondheimer, D. Taub, K. Heusler, and W. M. McLamore. J. Am. Chem. Soc. **74**, 4223, (1952).

Crystal and Molecular Structure of [2,3-Bis(dimethylarsino)-1,1,1,4,4,4,-hexafluorobut-2-ene-*As*, *As*]tricarbonyldiiodotungsten(II)

ANTHONY MERCER AND JAMES TROTTER

Department of Chemistry, University of British Columbia, Vancouver, British Columbia V6T 1W5

Received April 1, 1974

ANTHONY MERCER and JAMES TROTTER. Can. J. Chem. **52**, 3331 (1974).

Crystals of the title compound, $Me_2AsC(CF_3):C(CF_3)AsMe_2WI_2(CO)_3$, are monoclinic, $a = 15.37(2)$, $b = 9.529(1)$, $c = 15.967(3)$ Å, $\beta = 112.03(2)°$, $Z = 4$, space group $P2_1/c$. The structure was determined by Patterson and Fourier syntheses and refined by full-matrix least-squares procedures to a final R of 0.069 for 1823 observed (of a total of 2778) reflexions. The tungsten atom is seven-coordinate with a distorted capped octahedral environment, the capping group being a carbonyl (W—C, 1.94(3) Å). The capped face consists of the two remaining carbonyl groups (W—C, 1.97(4) and 2.00(4) Å) and one of the arsenic atoms from the bidentate ligand (W—As, 2.556(3) Å). The uncapped face contains the two iodine atoms (W—I, 2.848(2) and 2.856(2) Å) and the remaining arsenic atom (W—As, 2.618(3) Å), this bond length (*trans* to CO), being significantly longer (by 0.062 Å) than the other (*trans* to I) W—As distance.

ANTHONY MERCER et JAMES TROTTER. Can. J. Chem. **52**, 3331 (1974).

Les cristaux du composé $Me_2AsC(CF_3):C(CF_3)AsMe_2WI_2(CO)_3$, sont monocliniques. Les dimensions de la maille sont: $a = 15.37(2)$, $b = 9.529(1)$, $c = 15.967(3)$ Å, $\beta = 112.03(2)°$, $Z = 4$, groupe spatial $P2_1/c$. On a déterminé la structure par la méthode de Patterson et Fourier. La structure a été affinée par moindres carrés (matrice complète) jusqu'à une valeur finale du facteur d'accord (R) de 0.069 pour 1823 réflexions observées, sur un total de 2778. L'atome de tungstène est entouré de sept coordinats, et se trouve à l'intérieur d'un octaèdre coiffé déformé. Le groupe de recouvrement est un carbonyle (W—C = 1.94(3) Å). La face coiffée est constituée des deux autres groupes carbonyles (W—C = 1.97(4) et 2.00(4) Å) et d'un atome d'arsenic faisant partie du coordinat bidentate (W—As = 2.556(3) Å). La face non coiffée comprend les deux atomes d'iode (W—I = 2.848(2) et 2.856(2) Å) et l'atome d'arsenic restant (W—As = 2.618(3) Å). La longueur de cette liaison, en position *trans* par rapport au groupe carbonyle, est appréciablement plus grande (de 0.062 Å) que l'autre liaison W—As, en position *trans* par rapport à l'autre atome d'iode.

[Traduit par le journal]

Introduction

Preliminary n.m.r. data on [2,3-bis(dimethylarsino)-1,1,1,4,4,4,-hexafluorobut-2-ene-*As*,*As*]-tricarbonyldiiodotungsten(II) seemed consistent with stereochemical nonrigidity (1), the existence of which has also been observed for seven-coordinate tantalum (2). The X-ray crystal structure of $Me_2AsC(CF_3):C(CF_3)AsMe_2WI_2(CO)_3$ was undertaken to provide information, which could indicate the geometry of the most probable transition state, for the exchange processes occurring in solution.

Experimental

[2,3-Bis(dimethylarsino)-1,1,1,4,4,4,-hexafluorobut-2-ene-*As*,*As*]tricarbonyldiiodotungsten(II) was prepared by the dropwise addition of iodine to $Me_2AsC(CF_3):C(CF_3)AsMe_2W(CO)_4$, in CH_2Cl_2, with vigorous stirring under a N_2 atmosphere.

Anal. Calcd: C, 14.8; H, 1.4; I, 28.4. Found: C, 14.6; H, 1.2; I, 28.3.

Recrystallization from methylene chloride/hexane gave yellow plates. The crystal chosen for study was mounted with b parallel to the goniostat axis and was *ca.* 0.2 mm in length with a cross section of 0.2 × 0.04 mm. Unit-cell parameters were refined by a least-squares treatment of $\sin^2\theta$ values for 24 reflexions measured on a diffractometer with MoKα radiation. Crystal data are: $C_{11}H_{12}As_2F_6I_2O_3W$ f.w. = 893.40 Monoclinic, $a = 15.37(2)$, $b = 9.529(1)$, $c = 15.967(3)$ Å, $\beta = 112.03(2)°$, $U = 2167(2)$ Å^3, $\rho_o = 2.737(3)$, $Z = 4$, $\rho_c = 2.735(4)$, $F(000) = 1608$ (20 °C, MoKα, $\lambda = 0.71069$ Å, $\mu = 118$ cm^{-1}). Absent reflexions: $h0l$, $l \neq 2n$ and $0k0$, $k \neq 2n$ define uniquely the space group $P2_1/c$ (C_{2h}^5, No. 14).

Intensity data were measured for 2778 independent reflexions ($2\theta < 45°$) of which 942 had intensities less than $3\sigma(I)$ above the background, where $\sigma^2(I) = S + B + (0.05S)^2$ with S = scan count and B = background count. These reflexions were classified as unobserved.

Structure Analysis

The structure was determined by Patterson and Fourier syntheses and was refined by full-matrix least-squares methods, with minimization of $\sum w(F_o - F_c)^2$. The weighting scheme: $\sqrt{w} = 1$ if $|F_o| \leq 74.3$; $\sqrt{w} = 74.3/|F_o|$ if $|F_o| > 74.3$ and $\sqrt{w} = 0.0$ for unobserved reflexions gave constant average values of $w(F_o - F_c)^2$ over ranges of $|F_o|$ and was employed in the final stages of refinement. An absorption correction was applied (3)

Can. J. Chem. Downloaded from www.nrcresearchpress.com by 210.87.254.105 on 09/05/12
For personal use only.

Can. J. Chem. Downloaded from www.nrcresearchpress.com by 210.87.254.105 on 09/05/12
For personal use only.

TABLE 1. Final positional parameters (fractional × 10^4) with standard deviations in parentheses

Atom	*x*	*y*	*z*
W	6733(1)	3932(1)	3840(1)
I(1)	8344(1)	3338(2)	3427(1)
I(2)	5627(1)	2858(3)	2094(1)
As(1)	8053(2)	4102(3)	5396(2)
As(2)	6956(2)	1347(3)	4439(2)
F(1)	9743(20)	3296(32)	7073(19)
F(2)	10241(19)	2691(29)	6121(18)
F(3)	9903(23)	1333(36)	7008(23)
F(4)	7815(25)	−1202(36)	5435(22)
F(5)	9209(26)	−663(39)	5574(24)
F(6)	8701(23)	−530(37)	6578(24)
O(1)	6742(20)	6410(31)	2526(19)
O(2)	4737(21)	3648(31)	3926(19)
O(3)	6362(17)	6556(26)	4800(16)
C(1)	6688(24)	5473(39)	2978(23)
C(2)	5494(22)	3788(33)	3893(20)
C(3)	6485(25)	5613(40)	4431(24)
C(4)	8686(18)	2270(28)	5757(17)
C(5)	8218(19)	1142(30)	5422(18)
C(6)	9677(23)	2355(36)	6418(21)
C(7)	8525(40)	−394(58)	5735(36)
C(8)	8997(22)	5506(34)	5546(21)
C(9)	7715(23)	4521(37)	6430(21)
C(10)	6981(25)	−73(40)	3550(24)
C(11)	6092(24)	535(38)	4927(22)

and the final conventional *R* factor for 1823[1] observed reflexions using all the non hydrogen atoms was $R = 0.069$. The two CF_3 groups on the chelate ring had high isotropic temperature factors; however an F_o electron density map calculated using the phase from all the other found atoms did not reveal any evidence of disorder in the groups or individual atoms.

The final positional and thermal parameters are given in Tables 1 and 2 respectively. Measured and calculated structure factors have been placed in the Depository of Unpublished Data.[2]

Results and Discussion

The seven-coordinate geometry about the tungsten atom in **1**, [2,3,-bis(dimethylarsino)-1,1,1,4,4,4, - hexafluorobut - 2 - ene - *As*,*As*]tricarbonyldiiodotungsten(II) is similar to that found for **2** dibromotricarbonyl[1,2-bis(diphenylphosphino)ethane]molybdenum(II)-1-acetone (4), this type of geometry being described as a considerably distorted capped octahedron. In this

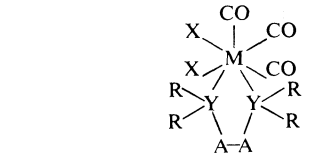

1
M = W
X = I
Y = As
R = CH_3

2
M = Mo
X = Br
Y = P
R = C_6H_5

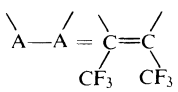

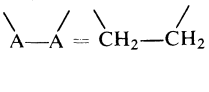

molecule the capping group is one of the carbonyls (C(3)—O(3)), the three atoms defining the capped face are C(1), C(2), and As(1), while the uncapped face consists of the two iodine atoms I(1) and I(2) and the remaining arsenic atom As(2). Figure 1 shows a projection down the W—C(3) bond. Although it would also be possible to describe the tungsten environment in terms of various distorted capped trigonal prisms (5), a detailed analysis of the differences between the basic polyhedra available for seven-coordinate molecules (6), indicates that in this type of molecule the ideal angle between the two larger coordinated atoms is 180° for a pentagonal bipyramid, *ca.* 90° for a capped octahedron, and 81.5° for a capped trigonal prism. From the

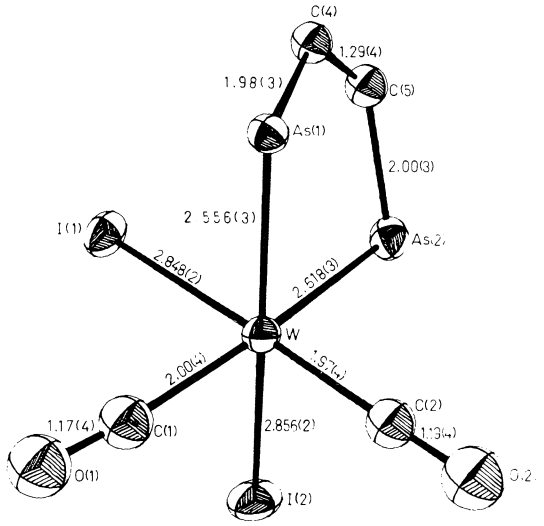

FIG. 1. Projection of the coordination sphere of the molecule viewed down the vector from the carbonyl group in the capping position (omitted from the diagram) to the tungsten atom.

[1]The thirteen highest intensity reflexions $10\bar{2}$, 106, $20\bar{4}$, $20\bar{2}$, 204, $30\bar{6}$, $50\bar{4}$, $50\bar{2}$, $60\bar{4}$, $1\bar{1}4$, $5\bar{1}4$, $0\bar{2}5$, and $2\bar{2}5$ were not included in the *R* factor calculation due to probable instrumental error.

[2]The structure factor table is available, at a nominal charge, from the Depository of Unpublished Data, National Science Library, National Research Council of Canada, Ottawa, Canada K1A 0S2.

TABLE 2. Final thermal parameters and their estimated standard deviations

(*a*) Anisotropic thermal parameters* (U_{ij} (Å^2) × 100)

Atom	U_{11}	U_{22}	U_{33}	U_{12}	U_{13}	U_{23}
W	4.18(6)	6.27(7)	4.15(6)	0.16(5)	1.49(4)	0.17(5)
I(1)	5.68(11)	9.35(15)	6.56(12)	−1.14(10)	3.27(9)	−1.43(10)
I(2)	6.39(12)	14.10(22)	5.15(11)	−0.22(13)	0.57(9)	−1.10(12)
As(I)	5.12(14)	4.59(15)	4.62(14)	−0.18(12)	1.50(11)	−0.11(11)
As(2)	6.37(17)	5.87(18)	5.61(16)	−1.83(14)	2.21(13)	−0.74(13)

*The anisotropic thermal parameters are U_{ij} in the expression $f = f_o \exp[-2\pi^2(U_{11}a^{*2}h^2 + U_{22}b^{*2}k^2 + U_{33}c^{*2}l^2 + 2U_{12}a^*b^*hk + 2U_{13}a^*c^*hl + 2U_{23}b^*c^*kl)]$.

(*b*) Isotropic thermal parameters

Atom	B (Å^2)	Atom	B (Å^2)
F(1)	11.7(7)	C(2)	5.8(6)
F(2)	11.0(7)	C(3)	7.0(8)
F(3)	13.6(9)	C(4)	4.5(5)
F(4)	13.5(9)	C(5)	4.9(6)
F(5)	15(1)	C(6)	5.9(7)
F(6)	13.6(9)	C(7)	11(1)
O(1)	9.3(7)	C(8)	6.1(7)
O(2)	9.5(7)	C(9)	6.5(7)
O(3)	7.4(5)	C(10)	7.4(8)
C(1)	6.9(8)	C(11)	6.9(7)

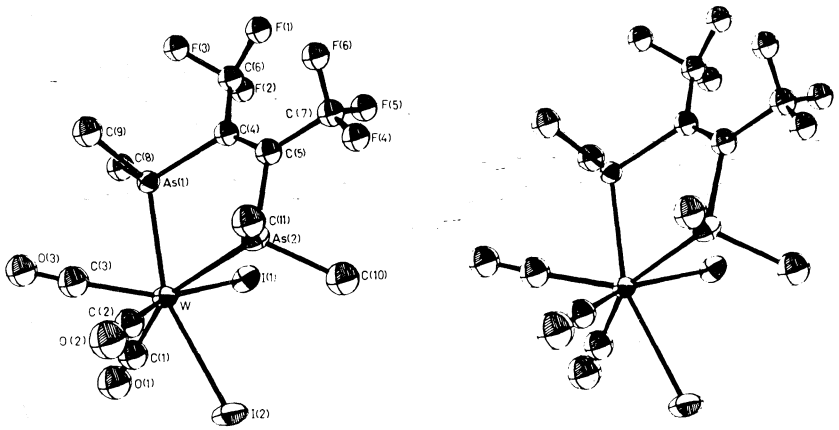

FIG. 2. A general stereoscopic view of the molecule showing the crystallographic numbering scheme.

I—W—I angle of 87.3° the choice of the capped octahedron would appear to describe the observed geometry more exactly. Figure 2 shows a general stereoscopic view of the molecule, with the atom labelling scheme. Individual bond lengths and angles with standard deviations are given in Tables 3 and 4 respectively.

The angles subtended at the tungsten atom by the unique carbon atom C(3) and the atoms in the capped face average to 74 and 128° respectively. These angles are very similar to those found in other capped octahedral structures, *i.e.* 73.6 and 125.5° in **2**, and 73 and 128° for [bis-(diphenylarsino)methane]dibromodicarbonylmolybdenum(II) (7). Similarly the angles subtended at the central metal atom by pairs of atoms in the capped, and pairs in the uncapped faces for both molecules **1** and **2** are comparable. In **1** they are an average of 112 and 86° respectively, while in **2** the mean values are 112.3 and 89.7°.

Another feature of a distorted capped octa-

Can. J. Chem. Downloaded from www.nrcresearchpress.com by 210.87.254.105 on 09/05/12
For personal use only.

TABLE 3. Bond lengths (Å) with standard deviations in parentheses

Bond	Length (Å)	Bond	Length (Å)
W—I(1)	2.848(2)	C(1)—O(1)	1.17(4)
W—I(2)	2.856(2)	C(2)—O(2)	1.19(4)
W—As(1)	2.556(3)	C(3)—O(3)	1.13(4)
W—As(2)	2.618(3)	C(4)—C(5)	1.29(4)
W—C(1)	2.00(4)	C(4)—C(6)	1.50(4)
W—C(2)	1.97(4)	C(5)—C(7)	1.56(6)
W—C(3)	1.94(3)	C(6)—F(1)	1.35(4)
As(1)—C(4)	1.98(3)	C(6)—F(2)	1.31(4)
As(1)—C(8)	1.92(3)	C(6)—F(3)	1.18(4)
As(1)—C(9)	1.95(3)	C(7)—F(4)	1.27(5)
As(2)—C(5)	2.00(3)	C(7)—F(5)	1.20(5)
As(2)—C(10)	1.97(4)	C(7)—F(6)	1.28(5)
As(2)—C(11)	1.93(3)		

hedron (5) demonstrated by this molecule, is the close non-bonded contacts made between the capping group and the three atoms in the capped face. Hence in **1**, C(3) is 2.46, 2.26, and 2.73 Å away from C(1), C(2), and As(1), compared to 2.29, 2.29, and 2.70 Å for the respective C(1) to C(2), C(3), and P(1) distances in molecule **2**.

The angle subtended at the central tungsten atom by the bidentate ligand is 75.9(1)°. This is similar to those subtended by the mutually *cis* atoms of the capped and uncapped faces (the mean value of six such angles being 78°). The ligand therefore seems ideally suited to occupy an edge of the capped octahedron. The three angles mutually *trans* are also very similar being 155, 159, and 161°, giving the geometry around the tungsten (see Fig. 1) a reasonable C_{3v} symmetry.

The tungsten–iodine distances of 2.848(2) and 2.856(2) Å would appear to be the first determinations of W—I bond lengths in a seven-coordinate environment. Tungsten–bromine distances in similar environments (8, 9) have already been found to have a mean value of 2.65 Å. Using a bromine covalent radius of 1.14 Å (10) we can estimate a W single bond radius of 1.51 Å for this compound. With use of 1.33 Å (10) for the iodine covalent radius, a predicted W—I bond length would be 2.84 Å, in reasonable agreement with the value found (mean value 2.852(2) Å). Assuming the radii of Mo(II) and W(II) are similar the value of 2.862 Å found for the Mo—I distance in $Mo(CNR)_6I^+$ (11) is also very close to these measured and predicted values. A similar argument predicts a W—As

TABLE 4. Bond angles (deg) with standard deviations in parentheses

Bonds	Angle (deg)	Bonds	Angle (deg)
I(1)—W—I(2)	87.3(1)	W—As(2)—C(5)	110(1)
I(1)—W—As(1)	78.2(1)	W—As(2)—C(10)	115(1)
I(1)—W—As(2)	83.8(1)	W—As(2)—C(11)	120(1)
I(1)—W—C(1)	78(1)	C(5)—As(2)—C(10)	103(1)
I(1)—W—C(2)	161(1)	C(5)—As(2)—C(11)	105(1)
I(1)—W—C(3)	128(1)	C(10)—As(2)—C(11)	103(1)
I(2)—W—As(1)	159.4(1)	As(1)—C(4)—C(5)	119(2)
I(2)—W—As(2)	88.2(1)	As(1)—C(4)—C(6)	115(2)
I(2)—W—C(1)	75(1)	C(5)—C(4)—C(6)	127(3)
I(2)—W—C(2)	77(1)	As(2)—C(5)—C(4)	118(2)
I(2)—W—C(3)	128(1)	As(2)—C(5)—C(7)	116(3)
As(1)—W—As(2)	75.9(1)	C(4)—C(5)—C(7)	126(3)
As(1)—W—C(1)	116(1)	W—C(1)—O(1)	174(3)
As(1)—W—C(2)	113(1)	W—C(2)—O(2)	178(3)
As(1)—W—C(3)	73(1)	W—C(3)—O(3)	177(3)
As(2)—W—C(1)	155(1)	C(4)—C(6)—F(1)	110(3)
As(2)—W—C(2)	85(1)	C(4)—C(6)—F(2)	116(3)
As(2)—W—C(3)	128(1)	C(4)—C(6)—F(3)	113(3)
C(1)—W—C(2)	108(1)	F(1)—C(6)—F(2)	106(3)
C(1)—W—C(3)	77(1)	F(1)—C(6)—F(3)	91(3)
C(2)—W—C(3)	71(1)	F(2)—C(6)—F(3)	117(3)
W—As(1)—C(4)	111(1)	C(5)—C(7)—F(4)	109(4)
W—As(1)—C(8)	117(1)	C(5)—C(7)—F(5)	108(5)
W—As(1)—C(9)	118(1)	C(5)—C(7)—F(6)	111(4)
C(4)—As(1)—C(8)	108(1)	F(4)—C(7)—F(5)	119(5)
C(4)—As(1)—C(9)	101(1)	F(4)—C(7)—F(6)	99(5)
C(8)—As(1)—C(9)	100(1)	F(5)—C(7)—F(6)	110(5)

Can. J. Chem. Downloaded from www.nrcresearchpress.com by 210.87.254.105 on 09/05/12
For personal use only.

Can. J. Chem. Downloaded from www.nrcresearchpress.com by 210.87.254.105 on 09/05/12
For personal use only.

bond length of 2.73 Å, compared to the 2.556(3) and 2.618(3) Å found experimentally. This significant shortening is thought to be due to some double bond character in the W—As bonds caused by (dπ–dπ) back donation from the central metal atom. The two W—As bonds are also significantly different from each other, which can be explained by consideration of the respective *trans* ligands. A *trans* ligand can affect the extent of back donation from the metal, hence the I(2) atom *trans* to As(1) is not as strong a dπ accepting group as the C(1)—O(1) group *trans* to As(2) which should result in a greater back donation to As(1). This will cause a shortening of the W—As(1) bond with respect to the W—As(2) bond, the difference found being 0.062 Å.

The W—C and C—O distances (mean values 1.97(4) and 1.16(4) Å) and the W—C—O angles (mean value 176(3)°) are similar to those found in other compounds with carbonyls joined to tungsten (12).

The five membered ring is in a "puckered" conformation. Table 5 gives the equation of a weighted least-squares mean plane, with deviations of the atoms from the plane, and values for the dihedral angles in the ring. This type of "puckered" conformation, with both carbon atoms on the same side of the weighted least-squares mean plane for the five membered ring, has been found in other compounds (13). The bend in the ring is probably to increase contacts between the methyl groups on the arsenic atoms and the adjacent carbonyl groups rather than the methyl–iodine contacts (14).

TABLE 5

(*a*) Equation of weighted least-squares mean plane* for the five membered ring

Atom	Δ (Å)	Δ/σ
W	0.0015	1.404
As(1)	−0.0105	3.822
As(2)	−0.0127	3.970
C(4)	0.7055	24.447
C(5)	0.6139	20.574

*Plane, $0.8945X - 0.1512Y - 0.4207Z - 4.2404 = 0$, X, Y, Z, are orthogonal coordinates in Å w.r.t. a, b, c^*, Δ is the deviation from the plane.

(*b*) Dihedral angles in the five membered ring

Atom 1	Atom 2	Atom 3	Atom 4	Angle (deg)	σ
As(2)	W	As(1)	C(4)	23	1
As(1)	W	As(2)	C(5)	−20	1
W	As(1)	C(4)	C(5)	−26	2
W	As(2)	C(5)	C(4)	12	2
As(1)	C(4)	C(5)	As(2)	8	2

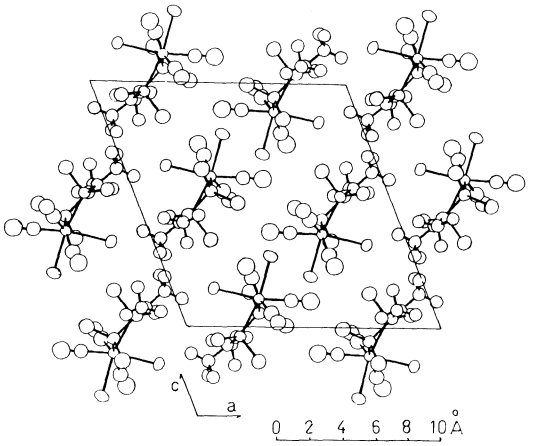

FIG. 3. A projection of the structure down the *b* axis.

Neither the carbon–carbon double bond length of 1.29(4) Å (expected 1.34 Å) (15), nor the W—As—C bond angle mean value of 110.5° (expected tetrahedral value of 109.5°) and the As—C—C bond angles, mean value of 118.5° (expected for sp^2 hybridized carbons of 120.0°) are significantly different from their stated expected values. Both the As(1)—C(4) and As(2)—C(5) bond distances of 1.98(3) and 2.00(3) Å are similar to the As—CH_3 bond lengths (mean, 1.98(3) Å) as is found in other similar ligands (16).

From the relative uncertainty of the positions of the two CF_3 groups, it seems unreasonable to attempt any meaningful discussion of their bond lengths and angles.

The intermolecular packing appears to be governed solely by van der Waals interactions. A projection of the structure down the *b* axis is shown in Fig. 3.

We thank Professor W. R. Cullen and Mr. L. Mihichuk for the crystals, the National Research Council of Canada for financial support, and the University of British Columbia Computing Centre for assistance.

1. L. MIHICHUK and W. R. CULLEN. Presented at C. I. C. Conference, Regina, June 1974.
2. P. MEAKIN, L. J. GUGGENBERGER, F. N. TEBBE, and J. P. JESSON. Inorg. Chem. **13**, 1025 (1974).
3. P. COPPENS, L. LEISEROWITZ, and D. RABINOVICH. Acta. Cryst. **18**, 1035 (1965).
4. M. G. B. DREW. J. Chem. Soc. Dalton, 1329 (1972).
5. (*a*) R. B. KING. J. Am. Chem. Soc. **92**, 6455 (1970);

(*b*) E. L. MUETTERTIES and C. N. WRIGHT. Q. Rev. **21**, 109 (1967).
6. M. G. B. DREW and J. D. WILKINS. J. Chem. Soc. Dalton, 1830 (1973).
7. M. G. B. DREW. J. Chem. Soc. Dalton, 626 (1972).
8. M. G. B. DREW, A. W. JOHANS, A. P. WOLTERS, and I. B. TOMKINS. Chem. Commun. 819 (1971).
9. M. G. B. DREW and A. P. WOLTERS. Chem. Commun. 457 (1972).
10. L. PAULING. Nature of the chemical bond. 3rd ed. Cornell University Press, Ithaca, New York. 1960, pp. 224–225.
11. D. F. LEWIS and S. J. LIPPARD. Inorg. Chem. **11**, 621 (1972).
12. (*a*) J. B. WILFORD and H. M. POWELL. J. Chem. Soc. A, 8 (1969); (*b*) M. ELDER and D. HALL. Inorg. Chem. **8**, 1273 (1969).
13. (*a*) M. R. CHURCHILL and T. A. O'BRIEN. J. Chem. Soc. A, 206 (1970); (*b*) J. H. CROSS and R. H. FENN. J. Chem. Soc. A, 3019 (1970).
14. M. G. B. DREW and J. D. WILKINS. J. Chem. Soc. Dalton, 2667 (1973).
15. Chem. Soc. Special Publ. No. 11, 1958 and No. 18, 1965.
16. I. W. NOWELL, S. RETTIG, and J. TROTTER. J. Chem. Soc. Dalton, 2381 (1972).

Can. J. Chem. Downloaded from www.nrcresearchpress.com by 210.87.254.105 on 09/05/12
For personal use only.

Koenigs–Knorr Syntheses of some α-1 → 2 and β-1 → 2 linked Nitro Disaccharides[1]

HANS H. BAER, JEAN M. J. FRÉCHET, AND URSULA WILLIAMS
Department of Chemistry, University of Ottawa, Ottawa, Canada K1N 6N5

Received May 31, 1974

HANS H. BAER, JEAN M. J. FRÉCHET, and URSULA WILLIAMS. Can. J. Chem. **52**, 3337 (1974).

2,3,4,6-Tetra-*O*-benzyl-α-D-glucopyranosyl bromide (**1**) and, in one instance, its α-D-*galacto* isomer (**2**) were condensed under conditions of the Helferich modification of the Koenigs–Knorr reaction with the four stereoisomeric methyl 4,6-*O*-benzylidene-3-deoxy-3-nitrohexopyranosides having the α-D-*galacto* (**3**), β-D-*galacto* (**4**), α-D-*gluco* (**5**), and β-D-*gluco* (**6**) configurations. Six new, 1 → 2 linked, fully blocked nitro disaccharides (**7**–**12**) were isolated. The configurations of the disaccharidic linkages were established by n.m.r. spectroscopy to be α in four of the products (**8**, **9**, **11**, and **12**) and β in two (**7** and **10**). The steric course of the disaccharide bond formation was found to depend on the anomeric as well as the over-all configuration of the alcoholic components **3**–**6**.

HANS H. BAER, JEAN M. J. FRÉCHET et URSULA WILLIAMS. Can. J. Chem. **52**, 3337 (1974).

Le bromure de 2,3,4,6-tétra-*O*-benzyl-α-D-glucopyranosyle (**1**) et, dans une expérience, son isomère α-D-*galacto* (**2**) ont été condensés avec les quatres méthyl-4,6-*O*-benzylidène-3-désoxy-3-nitrohexopyranosides stéréoisomériques ayant les configurations α-D-*galacto* (**3**), β-D-*galacto* (**4**), α-D-*gluco* (**5**) et β-D-*gluco* (**6**) dans les conditions de la modification d'Helferich à la réaction de Koenigs-Knorr. Six nouveaux nitro-disaccharides à liaison 1 → 2 et ayant leurs groupements fonctionnels protégés (**7**–**12**) ont été isolés. Les configurations des liaisons glycosidiques des disaccharides ont été établies par spectroscopie r.m.n. comme étant α pour quatre des produits (**8**, **9**, **11** et **12**), et β pour les deux autres (**7** et **10**). On a trouvé que l'anomérie et la configuration moléculaire des aglycones **3**–**6** avaient une influence sur le résultat stéréochimique de la réaction de formation du disaccharide.

The synthesis of nitro disaccharides has been the subject of previous articles from this laboratory (1–3). The methods used included an application of the nitromethane cyclization to a given disaccharide (1), the nucleophilic addition of partially blocked monosaccharides to nitro-olefinic sugar derivatives (2), and Koenigs–Knorr type condensations (3). The last-mentioned reactions were performed with per-*O*-acetylglycosyl bromides both under classical conditions (4–6) and by applying the Bredereck method (5–7) of trityl ether displacement, and moderate yields (14–25%) of β-1 → 6 linked nitro disaccharides were obtained.

The present work was undertaken with a view to exploring whether preparative advantages might be derived, in our special area of interest, from the Helferich modification (5,6,8,9) of the Koenigs–Knorr reaction, *i.e.*, the condensation promoted by mercuric cyanide. We were concurrently engaged in studies (10) on solvolyses of various glycosyl halides that bear the non-participating benzyl ether group at C-2, hoping to make advances in the complex problem (4–6) of steric control in glycosylation, particularly as regards the synthesis of such 1,2-*cis* glycosides as α-D-glucopyranosides and α-D-galactopyranosides. It was therefore decided to use 2,3,4,6-tetra-*O*-benzyl-α-D-glucopyranosyl bromide (**1**) and, in one instance, its α-D-*galacto* isomer (**2**) in a project of synthesizing new, 1 → 2 linked *O*-glycosyl derivatives of 3-deoxy-3-nitrohexoses. The hydroxylic components to be employed for condensation were the four stereoisomeric methyl 4,6-*O*-benzylidene-3-deoxy-3-nitrohexopyranosides having the α-D-*galacto* (**3**), β-D-*galacto* (**4**), α-D-*gluco* (**5**), and β-D-*gluco* (**6**) configurations. Recent reviews of the literature state that, in Koenigs–Knorr reactions with glycosyl halides which do not possess a participating group, the "steric outcome is extremely variable and may be either largely inversion or retention" (4) and that "practically, the steric result of the synthesis of an oligosaccharide under Helferich conditions seems now to be unpredictable" (5). Naturally this situation engendered our curiosity in the possible influ-

[1]Part XXXIV in a series on reactions of nitro sugars. For Part XXXIII, see ref. 13.

Can. J. Chem. Downloaded from www.nrcresearchpress.com by 210.87.254.42 on 09/05/12
For personal use only.

Can. J. Chem. Downloaded from www.nrcresearchpress.com by 210.87.254.42 on 09/05/12
For personal use only.

TABLE 1. Synthesis of disaccharides

Reactants	Product	Configuration of disaccharide linkage	Yield (%)*	Melting point (°C)	$[\alpha]_D^{25}$ in $CHCl_3$ (*c*, 1.8–2) (deg)	Analysis found† for $C_{48}H_{51}NO_{12}$		
						C	H	N
1 + 3	**7**	β	23.2 (66)	149–151	+84	68.88	6.05	1.73
1 + 4	**8**	α	34.3 (51)	159–160	+98.5	69.03	6.19	1.81
2 + 4	**9**	α	36.2 (72)	193	+88	68.95	6.06	1.84
1 + 5	**10**	β	77 (86.5)‡	171–173	+31.2	68.93	6.00	1.78
	11	α		99–102	+67	69.05	6.12	1.72
1 + 6	**12**	α	20‡	167–169	+32.8	69.11	6.15	1.79

*Isolated crystalline products, based on the amount of starting nitro glycoside introduced. In parentheses are given the yields calculated by taking into account any starting glycoside that was recovered unchanged.
†Calculated for $C_{48}H_{51}NO_{12}$ (833.9): C, 69.13; H, 6.16; N, 1.68.
‡See text.

Can. J. Chem. Downloaded from www.nrcresearchpress.com by 210.87.254.42 on 09/05/12
For personal use only.

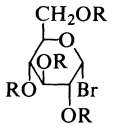

R = CH_2Ph

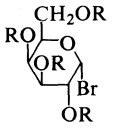

1 **2**

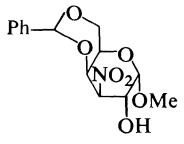

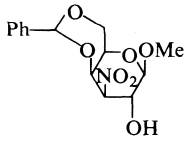

3 **4**

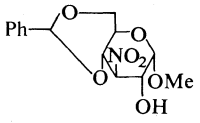

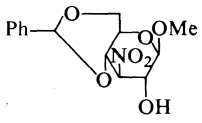

5 **6**

ence which the structure and stereochemistry of the alcoholic components **3**–**6** might exert on the configuration of the disaccharidic linkages produced.

The disaccharides obtained are listed in Table 1. The condensations were performed in the presence of mercuric cyanide in a benzene–nitromethane medium at 65°, with the exception of the synthesis of **9** which was conducted in a mixture of 1,2-dichloroethane and dichloromethane at room temperature. The products were isolated by column chromatography. The alcohols **3** and **4** afforded single disaccharides (**7**–**9**) in yields of 23–36%. Since a considerable proportion of the nitro monosaccharides could be recovered unchanged from most runs, the yields based on nitro monosaccharide actually expended ranged from 50 to 72%. Clearly, anomeric products that could conceivably have arisen and remained undetected in these particular reactions can only have played a minor role. By contrast, the alcohols **5** and **6** exhibited less stereoselectivity in their condensations. Thus, **5** gave **10** and **11** in a combined yield of 77% (crude mixture; 86.5% based on consumed **5**) but the mixture was difficult to separate by chromatography and fractional crystallization, and only 16.5% of pure **10** and 15% of **11** (which was not quite pure anomerically) were elaborated. There were indications suggesting that **10** constituted about two-thirds of the total disaccharide mixture formed. Similarly, the alcohol **6** gave a mixture of two disaccharides, according to t.l.c. Although only one of them (**12**) was isolated in 20% yield and could be characterized, the second isomer was revealed by an n.m.r. spectrum to be present, along with an about equal amount of **12**, in disaccharide fractions (yield, 24%) that were not separated.

In summary, an interesting trend in the steric course of these syntheses can be noted. The α-glycosidic alcohol components (**3** and **5**) furnished β-linked disaccharides, apparently as sole (**7**) or major (**10**) products. Conversely, the β-glycosidic alcohols (**4** and **6**) yielded α-linked disaccharides as the sole (**8** and **9**) or predominant (**12**) products. Furthermore, stereoselectivity seemed higher with the nitrogalactosides (**3** and **4**) than with the nitroglucosides (**5** and **6**). Although an explanation for these findings is not to be offered at this point, it is evident that both

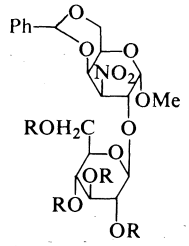

7

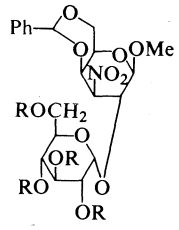

8

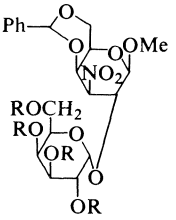

9

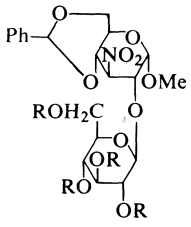

10

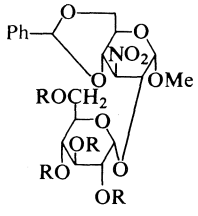

11

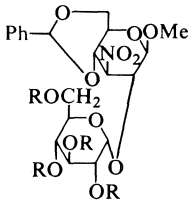

12

R = CH_2Ph

Can. J. Chem. Downloaded from www.nrcresearchpress.com by 210.87.254.42 on 09/05/12
For personal use only.

the configuration in the vicinity of the reaction site and the over-all configuration of the alcoholic component have a remarkable directive influence on the stereochemistry of the condensation.

The configurations of the disaccharide linkages of **7**–**12** were established by n.m.r. spectroscopy. The spectra (100 MHz in $CDCl_3$) of **8**, **9**, **11**, and **12** each showed a low-field doublet with small splitting (τ 4.3–4.5, J = 3–4 Hz), which was attributable to an equatorial, anomeric proton (H-1′) belonging to the terminal sugar moiety, and hence indicated the α-disaccharide configuration. Compounds **7** and **10** did not give anomeric proton signals in that region but exhibited doublets with larger splittings near τ 5.2, which were assignable to axial H-1′ protons indicative of the β-disaccharidic configuration. These signals were crowded together with others and for a better evaluation of the spectra it was useful to consider also the spectra of the methyl nitroglycosides **3**–**6**. Thus, the α-D-galactoside **3** gave a very simple spectrum, with a doublet (J = 2 Hz) at τ 5.04 for its equatorial H-1 and a broadened 3-proton singlet at τ 5.28 for H-2, -3, and -4 which fortuitously had nearly equal chemical shifts. In the disaccharide **7** derived from **3**, the effect of *O*-glycosyl substitution in position 2 was a downfield shift of H-1 by 0.3 p.p.m., and similar shifts of 0.2–0.3 p.p.m. were experienced by H-2 and H-3 which were now sufficiently separate to show vicinal coupling, and which were sufficiently shifted for the H-1′ doublet (J = 8 Hz) to be discernible at τ 5.20. Similarly, the signal of the equatorial H-1 at the methyl glycosidic center, which in the α-D-glucoside **5** occurred at τ 5.17, was shifted downfield by approximately 0.3 p.p.m. in the disaccharides **10** and **11** derived from **5** and did not interfere with the H-1′ signals at τ 5.20 and 4.50, respectively. In the β-D-galactoside **4**, the axial anomeric H-1 was expected to give a doublet with large splitting at relatively high field, and although the signal could not be located in a chloroform-*d* solution spectrum (it was at τ 5.70 in dimethylsulfoxide-d_6), it definitely was not present below τ 5.20. In the disaccharides **8** and **9** derived from **4**, the H-1 signals were likewise undistinguishable but must have been present in the 5–6 region and, in any event, would not have been mistaken for the H-1′ signals near τ 4.3. Finally, the β-D-glucoside **6** showed its H-1 signal at τ 5.66, and whereas in the disaccharide **12** the corresponding signal could not be discerned it must also have been in the τ 5–6 region, distinct from H-1′ with respect to both chemical shift and splitting.

We have recently recorded (11–13) the resonance positions of the glycosidic methoxyl protons in a large number of methyl nitroglycosides and found that, with few exceptions,[2] the signals fell in the range τ 6.40–6.56 in β-pyranosides and in the range 6.55–6.66 in α-pyranosides. One might therefore be tempted to take the chemical shift of a methoxyl resonance as a useful, if somewhat tenuous, indicator for anomeric configuration, provided it is not too close to the range boundary. The present series of compounds, however, exemplifies the need for circumspection in this regard. Thus, the α-anomeric methoxyl groups in **3** and **5** resonate (11) at τ 6.56 and 6.55, respectively, and they also resonate in the expected α-range in the disaccharides **7**, **10**, and **11** (τ 6.59, 6.59, and 6.63). On the other hand, the β-anomeric methoxyl signals occurring (11) at τ 6.40 and 6.46 in **4** and **6**, respectively, are shifted more markedly upfield in **8**, **9**, and **12** where they are found just outside the aforementioned β-range, at τ 6.58, 6.58, and 6.57, respectively. Obviously, α- and β-methyl glycosidic disaccharides of the structure here described cannot be differentiated on this basis.

Experimental

Reactions were routinely monitored by t.l.c. on silica gel G, normally with benzene–ether (4:1) as the irrigant. Melting points were determined in an electric aluminum block apparatus equipped with a calibrated thermometer. Optical rotations were measured with a Perkin-Elmer 141 automatic polarimeter, at room temperature. The n.m.r. data (100 MHz) refer to $CDCl_3$ solutions unless otherwise indicated.

2,3,4,6-Tetra-O-benzyl-α-D-glucopyranosyl Bromide (1)

2,3,4,6-Tetra-*O*-benzyl-α-D-glucose (14, 15) was *p*-nitrobenzoylated as described (15, 16) and the crystalline 1-*p*-nitrobenzoate was treated with anhydrous hydrogen bromide in dichloromethane (16). The procedure was the same as that detailed below for the preparation of **2**. Attempts to crystallize the bromide **1** had been unsuccessful earlier (16) and now again; freshly prepared, syrupy material was used.

2,3,4,6-Tetra-O-benzyl-1-O-p-nitrobenzoyl-β-D-galactopyranose

To an ice cold solution of 2,3,4,6-tetra-*O*-benzyl-D-galactose (17) (10.5 g) in pyridine (50 ml) was added

[2]These occurred in α-glycopyranosides presumed to have an axial nitro group at C-3 (12).

Can. J. Chem. Downloaded from www.nrcresearchpress.com by 210.87.254.42 on 09/05/12
For personal use only.

p-nitrobenzoyl chloride (8 g). The reaction mixture was stirred until it became homogeneous, stored overnight at room temperature, and then poured into ice water (600 ml). The semisolid material which separated was washed with cold 0.6 *N* hydrochloric acid and then with water. The product was dissolved in chloroform and the solution washed several times with 5% sodium bicarbonate solution and finally with water. Evaporation of the dried ($MgSO_4$) chloroform solution gave the *p*-nitrobenzoate (13 g, 97%) as an oil which according to t.l.c. and n.m.r. spectra was a mixture of α- and β-anomers in a ratio of about 1:2. Doublets given by the anomeric protons were at τ 3.37 ($J_{1,2}$ = 3.5 Hz) and τ 4.14 ($J_{1,2}$ = 7.8 Hz). Column chromatographic separation of the mixture on silica gel with benzene containing 0.5% of ether furnished the faster moving α-anomer as an oil (2.85 g) which failed to crystallize. Subsequent to an intermediate, mixed fraction (3 g), the pure β-anomer (7.2 g) was eluted. It crystallized from ether; m.p. 101–103°, $[\alpha]_D$ −39.7° (*c* 2, in $CHCl_3$).

Anal. Calcd. for $C_{41}H_{39}NO_9$ (689.8): C, 71.39; H, 5.70; N, 2.03. Found: C, 71.38; H, 5.68; N, 2.16.

2,3,4,6-Tetra-O-benzyl-α-D-galactopyranosyl Bromide (2)

The crystalline *p*-nitrobenzoate (β-anomer) just described (1 g) was dissolved in dichloromethane (50 ml, dried over CaH_2) and a stream of dry hydrogen bromide gas was passed through the solution at room temperature for 10 min. The precipitate of *p*-nitrobenzoic acid was removed by filtration through fritted glass in a dry atmosphere and the filtrate was evaporated *in vacuo* at room temperature. Several portions of added dichloromethane was evaporated from the syrupy residue. A residual, small amount of *p*-nitrobenzoic acid which crystallized in the syrup was removed by dissolution of the latter in a minimum amount of carbon tetrachloride followed by filtration and re-evaporation of the solution. A total of 240 mg (97%) of *p*-nitrobenzoic acid was isolated. The slightly yellow, syrupy **2** failed to crystallize. Dried *in vacuo*, it showed $[\alpha]_D$ +143° (*c* 1.9, in CH_2Cl_2). The n.m.r. spectrum showed a narrow 1-proton signal at τ 3.44 (H-1).

Synthesis of Disaccharides. General Remarks

Nitroglycosides 3–6

The preparation of the α-D-galactoside **3** (11), β-D-galactoside **4** (11, 18, 19) α-D-glucoside **5** (11, 18), and β-D-glucoside **6** (11, 19, 20) has been recorded. In addition to the published (11) chemical shift values of the benzylidene methine and methoxyl protons in these compounds, we here record further relevant n.m.r. data obtained by Dr. W. Rank in this laboratory. Compound **3**: τ 5.04 (d, $J_{1,2}$ = 2 Hz, H-1), 5.28 (broadened 3-H singlet, H-2, -3, -4), 5.80 (midpoint of 2 AB doublets, 2H, H-6, -6′), 6.27 (s, 1H, H-5). Compound **4** in $(CD_3)_2SO$: τ 4.99 (q, 1H, $J_{2,3}$ = 10 Hz, $J_{3,4}$ = 4 Hz, H-3), 5.31 (d, 1H, $J_{3,4}$ = 4 Hz, H-4), 5.70 (d, 1H, $J_{1,2}$ = 8 Hz, H-1), 5.8–6.1 (3H, 2-H singlet for H-6,6′ superposed on octet for H-2 which showed $J_{2,OH}$ = 4.5 Hz; the corresponding hydroxyl doublet was at τ 4.05), 6.26 (s, 1H, H-5). A good spectrum in $CDCl_3$ could not be obtained because of poor solubility, but it could be seen that there were no ring proton resonances below τ 5.2 in that solvent. Compound **5**: τ 5.17 (d, H-1, $J_{1,2}$ = 4 Hz), 5.19 (t, H-3, $J_{2,3}$ = $J_{3,4}$ = 10 Hz), 5.6–6.3 (5H, overlapping signals of H-2, -4, -5, -6, and -6′). Compound **6**: τ 5.28 (t, H-3, $J_{2,3}$ = $J_{3,4}$ = 10 Hz), 5.66 (d, H-1, $J_{1,2}$ = 7.5 Hz).

Procedure

The synthesis of **7** will hereafter be described in detail. Compounds **8–12** were obtained in the same fashion; minor variations in procedure are indicated where necessary. Yields, physical constants, and analytical data of the products are given in Table 1.

Methyl 4,6-O-Benzylidene-3-deoxy-3-nitro-2-O-(2,3,4,6-tetra-O-benzyl-β-D-glucopyranosyl)-α-D-galactopyranoside (7)

A magnetically stirred solution of **3** (0.65 g, 2.09 mmol) in nitromethane (25 ml) and benzene (25 ml) was azeotropically dried by boiling and allowing part of the solvent mixture (15 ml) to distil off, at atmospheric pressure. After cooling of the solution to 50° the bromide **1** (1.65 g, 2.73 mmol) and mercuric cyanide (0.69 g, 2.73 mmol) were added, and the mixture was then stirred for 40 h at 65°, with exclusion of moisture and light. Thin-layer chromatography showed that the fast-moving spot of **1** gradually disappeared and the slow-moving spot of **3** decreased in intensity (but did not disappear completely) while a new spot with intermediate mobility (**7**) arose. The reaction mixture was allowed to cool, diluted with chloroform, and washed successively with three portions of sodium bicarbonate solution and three portions of water. The organic solution was dried ($MgSO_4$) and evaporated to give an oil which was dissolved in a small amount of benzene for column chromatography. Approximately 40–60 parts of Silica Gel 7734 (Merck A. G.) per part of crude product was used for this and similar separations. Elution was started with pure benzene (*e.g.*, 600 ml), which removed fast-moving impurities, and it was continued with benzene–ether (98:2, v/v) until most of **7** had emerged. Evaporation of the appropriately pooled fractions gave **7** as an oil (405 mg) which was crystallized from ethyl acetate-petroleum ether (Table 1). The n.m.r. data: τ 4.5 (s, PhCH), 4.73 (d, H-1, $J_{1,2}$ = 3 Hz), 4.96 (q, H-2, $J_{1,2}$ = 3 and $J_{2,3}$ = 10 Hz), 5.10 (q, H-3, $J_{2,3}$ = 10 and $J_{3,4}$ = 2.5 Hz), 5.20 (d, *J* = 8 Hz, H-1′ ?), 6.59 (s, 3H, OCH_3).

Further elution of the column with benzene–ether (9:1) produced 420 mg of unchanged **3**, m.p. 167–168.5° dec., $[\alpha]_D$ +197° in chloroform (lit. (11) m.p. 166–167°, $[\alpha]_D$ +205°).

Methyl 4,6-O-Benzylidene-3-deoxy-3-nitro-2-O-(2,3,4,6-tetra-O-benzyl-α-D-glucopyranosyl)-β-D-galactopyranoside (8)

This disaccharide was obtained from **1** (2.8 g), **4** (1.0 g), and $Hg(CN)_2$ (1.1 g). The solvent was a mixture of benzene (35 ml) and nitromethane (35 ml), from which 20 ml had been removed by azeotropic distillation. Chromatography of the crude product gave **8** (920 mg) which crystallized from ethyl acetate – petroleum ether (Table 1), another disaccharide fraction (186 mg) with somewhat lower rotation ($[\alpha]_D$ +89°) and a wide melting range (135–150°), and 323 mg of unreacted **4** showing m.p. 231° dec. and $[\alpha]_D$ +29° (*c* 2, in dimethylformamide) (lit. (18) m.p. 230–231° dec., $[\alpha]_D$ +24.8°). The n.m.r. data of **8**: τ 4.28 (d, H-1′, $J_{1'2'}$ = 3.5 Hz), 4.51 (s, PhCH), 6.58 (s, 3H, OCH_3). There were no further ring proton signals downfield from τ 5.1.

*Methyl 4,6-O-Benzylidene-3-deoxy-3-nitro-2-O-(2,3,4,6-tetra-O-benzyl-α-D-galactopyranosyl)-β-D-galactopyranoside (**9**)*

To a solution of **4** (1.2 g) in dry 1,2-dichloroethane (10 ml) was added mercuric cyanide (0.7g) and a solution of **2** (1.58 g) in dichloromethane (10 ml). The mixture was stirred in the dark at room temperature for 70 h. Processing and chromatography furnished several minor fractions of unidentified products, a main fraction of **9** (1.162 g) and 595 mg of unchanged **4** showing m.p. 231–232° dec. and $[\alpha]_D$ +26° (*c* 1.5, in dimethylformamide). The n.m.r. data of **9**: τ 4.32 (d, H-1′, $J_{1',2'}$ = 3.5 Hz), 4.52 (s, PhCH), 6.58 (s, 3H, OCH_3). There were no further ring proton signals downfield from τ 5.05.

*Methyl 4,6-O-Benzylidene-3-deoxy-3-nitro-2-O-(2,3,4,6-tetra-O-benzyl-β-D-glucopyranosyl)-α-D-glucopyranoside (**10**) and Methyl 4,6-O-Benzylidene-3-deoxy-3-3-nitro-2-O-(2,3,4,6-tetra-O-benzyl-α-D-glucopyranosyl)-α-D-glucopyranoside (**11**)*

The materials used were **1** (2.28 g), **5** (1.0 g), mercuric cyanide (0.96 g), benzene (35 ml), and nitromethane (35 ml), and the procedure was the same as that employed for the syntheses of **7** and **8**. Chromatography yielded a first (impure) disaccharide fraction (0.74 g) which upon crystallization from ethyl acetate – petroleum ether gave **11** (361 mg) which was slightly contaminated by **10**. Recrystallization from isopropyl ether furnished **11** (212 mg) which still contained a small proportion of **10**, according to an n.m.r. spectrum. A subsequent impure fraction (1.32 g) from the column was similarly crystallized to give **10** (395 mg) which was slightly contaminated by **11**. Pure **10** (208 mg) was obtained by recrystallization from ethyl acetate – petroleum ether. Finally, a fraction (0.37 g) consisting largely of **5** was eluted. Upon recrystallization from ethanol–water, it weighed 114 mg and was identified spectroscopically by comparison with authentic **5**. The n.m.r. data of **10**: τ 4.49 (s, PhCH), 4.84 (d, H-1, with 3 Hz splitting, partly overlapped by a signal (H-3 ?) with large splittings, which adjoins upfield), 5.20 (d, H-1′, $J_{1,1'2'}$ = 7 Hz, superposed on other signals), 6.59 (s, 3H, OCH_3). Data of impure **11**: τ 4.50 (broadened singlet integrating to more than 1 proton, PhCH and H-1′), 4.84 (low-intensity doublet, H-1 of contaminating **10**), 4.90 (narrow doublet, H-1), 6.58 (weak singlet, OCH_3 of **10**), 6.63 (strong singlet, OCH_3).

*Methyl 4,6-O-Benzylidene-3-deoxy-3-nitro-2-O-(2,3,4,6-tetra-O-benzyl-α-D-glucopyranosyl)-β-D-glucopyranoside (**12**)*

The materials used for this condensation were **1** (1.43 g), **6** (0.75 g), mercuric cyanide (0.61 g), benzene (25 ml), and nitromethane (25 ml), and the procedure was as in the synthesis of **7**. Processing yielded a syrupy product (2.50 g) that contained several components. Treatment with ethyl acetate and petroleum ether resulted in the isolation of crystals (117 mg, m.p. 146–148°, $[\alpha]_D$ +14.2° in chloroform) which in t.l.c. exhibited two disaccharide spots of about equal intensity. The noncrystallizable, main part of the crude reaction product was subjected to column chromatography. The first fractions containing a single disaccharide were combined to give 398 mg of **12**; m.p. 163–168° raised to 167–169° after recrystallizations from ethyl acetate – petroleum ether and from carbon tetrachloride. Subsequent fractions yielded disaccharide mixtures similar to the one that had crystallized prior to chromatography (357 mg, $[\alpha]_D$ +12°). According to an n.m.r. spectrum, this material contained about equal amounts of **12** and another component, presumably the β-1 → 2 linked isomer. Hence it can probably be said that, whereas the yield of isolated **12** was 20%, the amount of disaccharide actually formed was at least about 32% of **12** and 12% of the isomer. The n.m.r. data of **12**: τ 4.49 and 4.51 (2H, sharp singlet of PhCH over the low-field line of doublet for H-1′, $J_{1',2'}$ = 3–4 Hz), 6.57 (s, 3H, OCH_3); there was no other ring proton signal below τ 5.05.

Further elution of the column produced mixtures of the two disaccharides and starting **6**. An impure end fraction was rich in levorotatary **6**, $[\alpha]_D$ −46° (*c* 0.9, in ethanol). (Lit. (20) $[\alpha]_D$ −72.5°).

Financial support of this work by the National Research Council of Canada is gratefully acknowledged.

1. H. H. Baer and A. Ahammad. Can. J. Chem. **44** 2893 (1966).
2. H. H. Baer and F. Kienzle. Can. J. Chem. **47**, 2819 (1969).
3. H. H. Baer, W. Rank, and F. Kienzle. Can. J. Chem. **48**, 1302 (1970).
4. C. Schuerch. Acc. Chem. Res. **6**, 184 (1973).
5. N. K. Kochetkov, O. S. Chizhov, and A. F. Bochkov. MTP Intern. Rev. Sci. Org. Chem. Ser. I, **7**, 147 (1973).
6. G. Wulff and G. Röhle. Angew. Chem. **86**, 173 (1974).
7. H. Bredereck, A. Wagner, G. Faber, H. Ott, and J. Rauther. Ber. **92**, 1135 (1959); H. Bredereck, A. Wagner, D. Geissel, P. Gross, U. Hutten, and H. Ott. Ber. **95**, 3056 (1962).
8. B. Helferich and K. F. Wedemeyer. Ann. **563**, 139 (1949).
9. H. M. Flowers. Methods Carbohyd. Chem. **6**, 474 (1972).
10. J. M. J. Fréchet and H. H. Baer. 166th ACS National Meeting, Chicago, Illinois. August 1973. Abstr. CARB 32. J. M. J. Fréchet, U. Williams, and H. H. Baer. 166th ACS National Meeting, Chicago, Illinois. August, 1973. Abstr. CARB 34.
11. H. H. Baer and W. Rank. Can. J. Chem. **50**, 1216 (1972).
12. H. H. Baer and W. Rank. Can. J. Chem. **51**, 2001 (1973).
13. H. H. Baer and W. Rank. Can. J. Chem. **52**, 2257 (1974).
14. O. T. Schmidt, T. Auer, and H. Schmadel. Ber. **93**, 556 (1960).
15. M. E. Tate and C. T. Bishop. Can. J. Chem. **41**, 1801 (1963).
16. T. Ishikawa and H. G. Fletcher, Jr. J. Org. Chem. **34**, 563 (1969).
17. P. W. Austin, F. E. Hardy, J. G. Buchanan, and J. Baddiley. J. Chem. Soc. 1419 (1965).
18. H. H. Baer, F. Kienzle, and T. Neilson. Can. J. Chem. **43**, 1829 (1965).
19. H. H. Baer. Methods Carbohyd. Chem. **6**, 302 (1972).
20. H. H. Baer and T. Neilson. Can. J. Chem. **43**, 840 (1965).

Can. J. Chem. Downloaded from www.nrcresearchpress.com by 210.87.254.42 on 09/05/12
For personal use only.

Phototropic Products from the Reactions of Aril Monoazines with Bases

PETER YATES,[1] E. M. LEVI, AND B. L. SHAPIRO

Departments of Chemistry, University of Toronto, Toronto, Ontario M5S 1A1 and Harvard University, Cambridge, Massachusetts

Received May 29, 1974

PETER YATES, E. M. LEVI, and B. L. SHAPIRO. Can. J. Chem. **52**, 3343 (1974).

Treatment of benzil monoazine with sodium methoxide gives 5-methoxy-1,2,5-triphenyl-3,4-diaza-2,4-pentadien-1-one (**2**), 5-benzoyl-4,5-dihydro-3,4,5-triphenylpyrazol-4-ol (**3**), and simple cleavage products. Compound **3** is hydrolyzed to 3,4,5-triphenylpyrazole and benzoic acid. It is phototropic, being reversibly converted on exposure to sunlight to a red product, which is readily autoxidized to benzil monoazine. Analogous phototropic products are formed on reaction of *p*-anisil monoazine and *p*-tolil monoazine with sodium methoxide. Reduction of the azines to the phototropic products may occur by cleavage to α-keto imine anions followed by their dimerization; such a pathway can also account for the formation of the cleavage products. Alternatively, reduction may proceed by hydride or electron transfer; that hydride transfer need not necessarily be involved is established by the observation that treatment of *p*-tolil monoazine with potassium *t*-butoxide also gives the corresponding phototropic product. It is proposed that the phototropic transformations involve intramolecular hydrogen abstraction to give enolic isomers of **3** and its analogs in which the heterocyclic ring has been cleaved.

PETER YATES, E. M. LEVI et B. L. SHAPIRO. Can. J. Chem. **52**, 3343 (1974).

Le traitement de la monoazine du benzile avec du méthylate de sodium conduit au méthoxy-5 triphényl-1,2,5 diaza-3,4 pentadien-2,4 one-1 (**2**) aux côtés du benzoyl-5 dihydro-4,5 triphényl-3,4,5 pyrazolol-4 (**3**) et d'autres composés de clivages simples. Le composé **3** peut être hydrolyzé pour fournir de l'acide benzoique et de la triphényl-3,4,5 pyrazole. C'est un composé phototropique qui se transforme d'une façon réversible sous l'action de la lumière du jour en un composé rouge qui est facilement autooxydé en un monoazine de benzile. D'autres composés phototropiques analogues sont formés par réaction des monoazines de *p*-anisile et de *p*-tolile avec le méthylate de sodium. La réduction des azines en produits phototropiques peut s'effectuer par clivage conduisant aux anions des α-céto imines qui peuvent alors se dimérisés; un tel processus peut aussi expliquer la formation des produits de clivage. La réduction peut aussi être effectuée par un hydrure ou un transfert d'électrons; le fait que le transfert d'hydrure n'est pas nécessairement impliqué est démontré par l'observation que le traitement de la monoazine du *p*-tolile avec du *t*-butylate de potassium donne aussi le produit phototropique correspondant. On propose donc que les transformations phototropiques impliquent un enlèvement d'hydrogène moléculaire conduisant aux isomères énoliques de **3** ainsi qu'à ses analogues dans lesquels l'hétérocycle a été coupé. [Traduit par le journal]

The reaction of benzil monoazine (**1**) with sodium methoxide was first investigated by Yates and Shapiro in connection with their studies of the reactions of α-diazo ketones with bases (1).

When a suspension of **1** and excess sodium methoxide in ether was boiled under reflux, the amount of suspended solid slowly decreased and the mixture acquired a deep purple color. The intensity of this color was not diminished after 15 days at reflux. Treatment of the mixture with water rapidly destroyed this color, giving an intensely yellow orange ethereal phase. Methyl benzoate, benzonitrile, and benzamide, together with unconsumed **1**, were isolated from the ethereal solution. In addition, two new crystalline compounds were obtained, each in *ca.* 10% yield; these are assigned structures **2** and **3** (Scheme 1).

Compound **2** is a very pale yellow substance, $C_{22}H_{18}N_2O_2$, that contains a methoxyl group and shows a strong band at 5.95 μ in its i.r. spectrum (*cf.* **1**, 5.95 μ) but no band in the 2.8–3.2 μ region. On hydrolysis in acid medium it gave **1**, benzil (**4**), benzoic acid, and hydrazine; basic hydrolysis gave deoxybenzoin (**5**), deoxybenzoin azine (**6**), and benzoic acid (Scheme 2). These hydrolysis products can be envisaged as arising via hydrolysis of the imino ether system of **2** to give **7** and hydrolysis of this

[1]To whom correspondence should be addressed at the Lash Miller Chemical Laboratories, University of Toronto, Toronto, Ontario M5S 1A1.

Can. J. Chem. Downloaded from www.nrcresearchpress.com by 210.87.254.5 on 09/05/12
For personal use only.

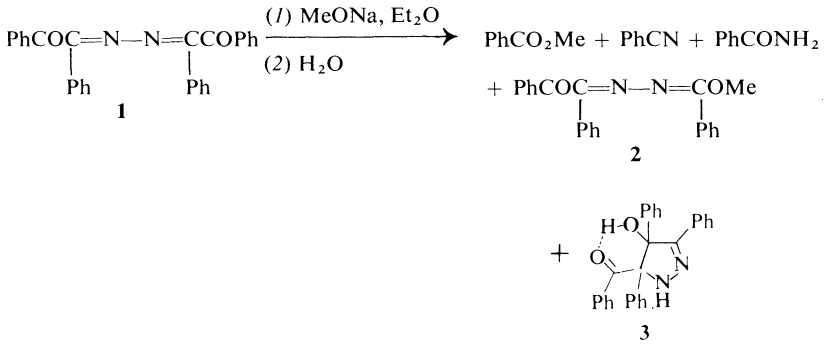

SCHEME 1

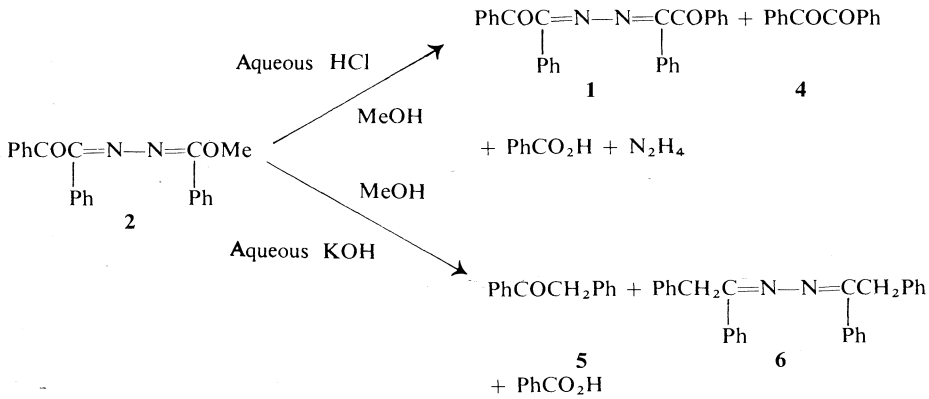

SCHEME 2

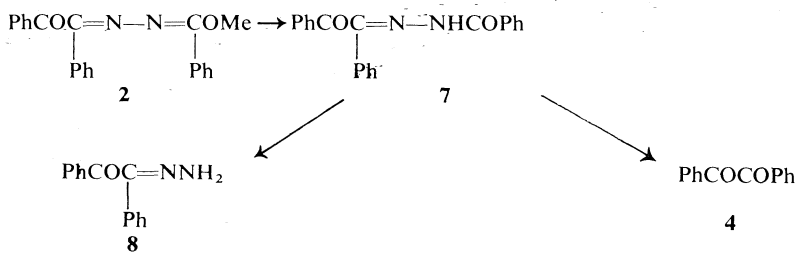

SCHEME 3

to benzil (**4**) or benzil monohydrazone (**8**) (Scheme 3). Facile Wolff-Kishner reduction of the monohydrazone of an α-diketone under mildly basic conditions has ample precedent (2).

The structural assignment **2** was confirmed by the independent synthesis of this compound in good yield from benzil monohydrazone (**8**) and trimethyl orthobenzoate (**9**) (Scheme 4).

Compound **3** is a yellow crystalline substance, $C_{28}H_{22}N_2O_2$, that undergoes decomposition on attempted recrystallization. Its most striking property is its phototropism; on exposure to light it is reversibly converted to a red substance that in turn is converted to **1** in the presence of air. For this reason it is necessary to carry out the reaction of **1** with sodium methoxide and the isolation of **3** in the dark or in subdued light. The i.r. spectrum of **3** shows a complex, medium intensity band at 3.01 μ and a single band in the carbonyl-stretching region at 6.03 μ. Its ^1H n.m.r. spectrum shows, in addition to signals corresponding to 20 aromatic protons, 2 one-proton singlets at δ 6.01 and 7.32 that are absent after treatment with D_2O. Compound **3** was

Can. J. Chem. Downloaded from www.nrcresearchpress.com by 210.87.254.5 on 09/05/12
For personal use only.

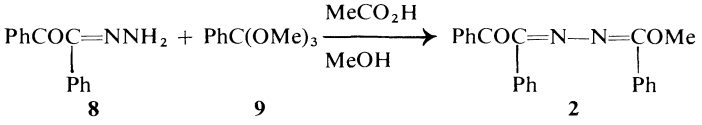

8 **9** **2**

SCHEME 4

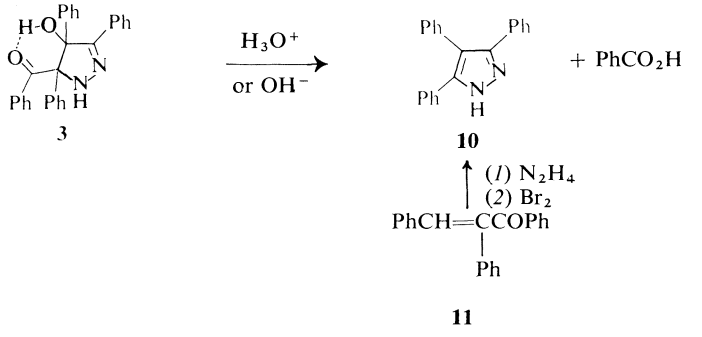

3 **10** **11**

SCHEME 5

hydrolyzed in either acidic or basic medium to give benzoic acid and 3,4,5-triphenylpyrazole (**10**), which was identified by comparison with an authentic sample prepared by treatment of α-phenylchalcone (**11**) with hydrazine followed by oxidation with bromine (Scheme 5).

The reconversion of the phototropic product to **1** in good yield under mild conditions suggests strongly that it retains the skeleton of **1** and this, together with its spectra and its hydrolysis to **10**, leads to the structural assignment **3**. This assignment requires that strong hydrogen bonding in the β-ketol system shifts the carbonyl-stretching band in the i.r. spectrum of **3** to an unusually long wavelength; such shifts have been observed previously for related β-ketols (3). Structure **3** is related by ring closure to the acyclic dihydroazine **12**; an alternative structure **13**, similarly related to **12**, cannot be absolutely excluded at this juncture,[2] although it seems very unlikely that hydrogen bonding in this structure would be sufficiently strong to account for the i.r. spectrum (*vide supra*).

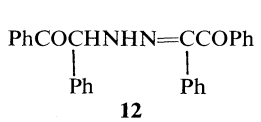

12

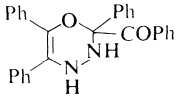

13

In order to obtain further spectroscopic data on which to base a definitive distinction between structures **3** and **13**, attempts were made to form an alkyl or acyl derivative of the phototropic compound. These were unsuccessful, and attention was turned to the reaction of sodium methoxide with other aril monoazines.

Reaction of *p*-anisil monoazine (**14**) gave methyl *p*-anisate, *p*-anisonitrile, *p*-anisamide, and a phototropic dihydro product that gave 3,4,5-tri-*p*-anisylpyrazole (**16**) on hydrolysis and is assigned structure **15** (Scheme 6); no product analogous to **2** was isolated, but no significance is attached to this circumstance since the weight balance of the products isolated was poor. Compound **15**, however, is more sensitive to oxidation than is **3** and was not investigated further.

Reaction of *p*-tolil monoazine (**17**) with sodium methoxide gave methyl *p*-toluate, *p*-tolunitrile, *p*-toluamide, and a phototropic dihydro product that gave 3,4,5-tri-*p*-tolylpyrazole (**19**) on hydrolysis and is assigned structure **18**; again no analog of **2** could be isolated. Compound **18** was isolated in 25% yield and formed a monoacetyl derivative on treatment with acetyl chloride. This derivative shows a single one-proton signal in its ^{1}H n.m.r. spectrum that is absent after D_2O treatment in contrast to its parent compound, which shows two such signals. Its i.r. spectrum shows a weak broad band at 2.8–3.1 μ and a strong band at 6.00 μ. The latter spectrum clearly indicates that, in terms of structure **18**, acylation has occurred on nitrogen to give **20**. In terms of structure **21**, the analog of

[2]The formation of **10** could be accommodated by the postulation of the intermediacy of **12** in the hydrolyses.

Can. J. Chem. Downloaded from www.nrcresearchpress.com by 210.87.254.5 on 09/05/12
For personal use only.

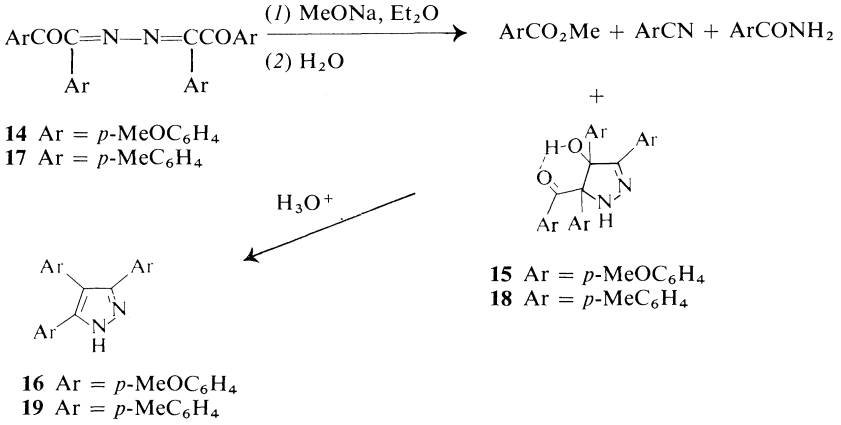

SCHEME 6

13, the acetylation product would have structure **22**.

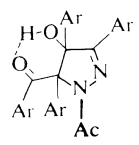

20 Ar = *p*-MeC_6H_4

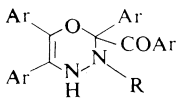

21 Ar = *p*-MeC_6H_4; R = H
22 Ar = *p*-MeC_6H_4; R = Ac

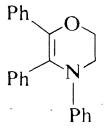

23

A definitive distinction could be made between these structures on the basis of ^{13}C n.m.r. spectroscopy. The ^{13}C spectrum of the acetylation product shows, in addition to signals attributable to methyl, aryl, and carbonyl carbons, signals at δ 83.9, 94.8, and 156.0. The first two of these can be assigned to the two sp^3 carbon atoms of the pyrazoline ring of **20** and the third to the pyrazoline C=N carbon atom (4). Structure **22** possesses only a single sp^3 carbon atom in addition to methyl carbon atoms and no carbon atom that would be expected to give rise to a signal at δ 156.0. The remote possibility that one of the ethylenic carbon atoms might give rise to a signal at δ < 100 was eliminated by examination of the ^{13}C spectrum of compound **23** (5); this showed only two methylene signals in the region δ < 120. Thus **22** can be excluded as the structure of the acetyl derivative.

One interpretation of the origin of compounds **2** and **3** from **1** is shown in Scheme 7. Here **3** arises from the dianion **25**, which is formed by dimerization of the anion **24**, itself formed together with methyl benzoate and benzonitrile by nucleophilic attack of methoxide ion on a carbonyl group of **1**. It may be noted that the anion **24** can be represented as the hybrid **24***a* with nitrenoid character. The origin of **2** is represented as involving initial attack by methoxide ion on an azomethine group of **1** to give an anion **26**, which is again attacked by methoxide ion to give methyl benzoate and the dianion **27**, which undergoes protonation and oxidation to **2** during the aqueous work-up. Alternatively, oxidation might occur before protonation by electron transfer from **27** to **1**, giving **2** and **25**. It is possible that the purple color of the reaction mixture arises from the dianions **25** and/or **27**; thus, treatment of **3** in ether with sodium hydride also generated this color.

A different interpretation of the origin of **3** is shown in Scheme 8. Here reduction of **1** is postulated to occur by hydride transfer from methoxide ion in a Meerwein-Ponndorf process, for which analogy exists (6), giving the monoanion **28**.

This view of the formation of **3** as involving a simple reduction process led us to investigate the possibility of preparing compounds of type **3** by the hydrogenation of aril monoazines. In the event, this has proved to be successful and to provide the best method for the preparation of such compounds (7).

The conception of Scheme 8 also led us to examine the reaction of an aril monoazine with

Can. J. Chem. Downloaded from www.nrcresearchpress.com by 210.87.254.5 on 09/05/12
For personal use only.

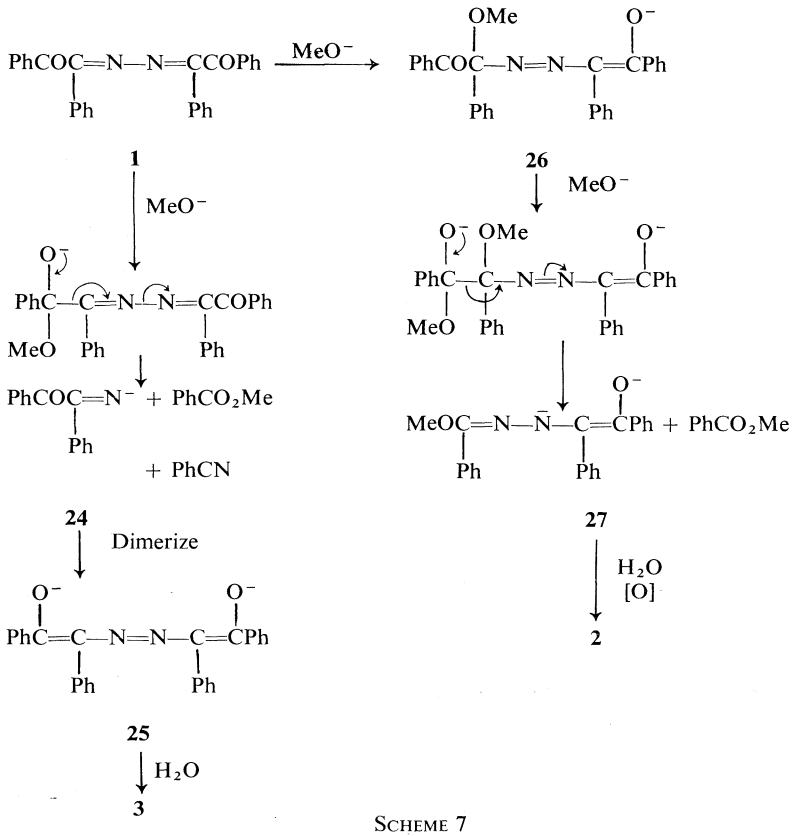

SCHEME 7

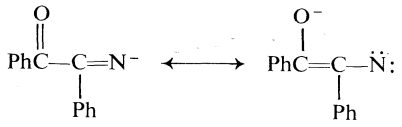

24*a*

potassium *t*-butoxide, an alkoxide without the potentiality for hydride ion transfer. Treatment of *p*-tolil monoazine (**17**) with potassium *t*-butoxide in boiling ether led to more rapid development of a deep-purple coloration than in the case of sodium methoxide. Aqueous work-up gave *t*-butyl *p*-toluate, *p*-tolunitrile, *p*-toluamide, the phototropic compound **18**, and *p*-tolil *p*-toluylhydrazone (**29**) (Scheme 9). The structure of **29** was established by its independent preparation from *p*-tolil monohydrazone and *p*-toluyl chloride; this product may well arise from compound **30**, the analog of **2**.

The formation of **18** by reaction of **17** with potassium *t*-butoxide demonstrates that reduction of **17** by an alkoxide can occur without the involvement of hydride ion transfer, although it does not, of course, exclude this as a possible pathway in the reaction of **17** with methoxide ion. Recent evidence that both methoxide and *t*-butoxide ion can react by electron transfer to systems with high electron affinity (8) leaves open the possibility that reduction of the aril monoazines occurs by such a pathway. However, we presently favor the process postulated in Scheme 7 since it provides an economical interpretation of the formation of both the phototropic compounds and the fragmentation products from the azines.

Finally we comment on the phototropism f **3** and its analogs. Exposure of **3** in the solid state or solution to light led to the formation of a red compound which reverted to **3** in the dark and gave **1** in the presence of air. This red compound could not be isolated, but it was shown to possess a strong i.r. band at 6.50 μ (see Experimental). Prolonged exposure of **3** to light and air led to its complete conversion to **1**. Similar observations were made in the case of compound **18**; however, its *N*-acetyl derivative, **20**, did not undergo these transformations. It is suggested

Can. J. Chem. Downloaded from www.nrcresearchpress.com by 210.87.254.5 on 09/05/12
For personal use only.

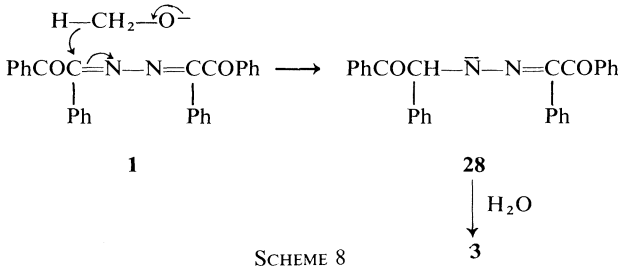

SCHEME 8

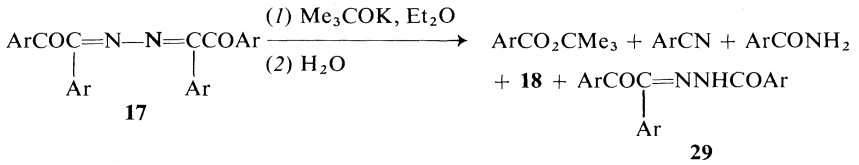

SCHEME 9
(Ar = *p*-MeC_6H_4)

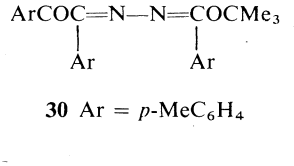

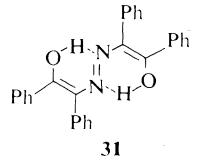

that the structure of the red intermediate is **31** and that it is formed via intramolecular hydrogen abstraction by the carbonyl oxygen atom in an excited state of **3**. It may be noted that **31** is the dienol corresponding to the dianion **25**.

Experimental

Hydrolysis of **2**

In Acid Medium

A solution of **2** (180 mg) (1) in a mixture of concentrated hydrochloric acid (10 ml), water (10 ml), and methanol (10 ml) was boiled under reflux for 5 h. The mixture was cooled, made basic with sodium hydroxide, and extracted with chloroform. The dried extract gave benzil monoazine (105 mg) and benzil (trace). Acidification of the aqueous phase and extraction gave benzoic acid (32 mg). The aqueous phase was again made basic with sodium hydroxide and the presence of hydrazine was established by the addition of a few drops of benzaldehyde; the pale yellow solid that separated after several hours was filtered, washed with water and a small amount of ice-cold 95% ethanol; m.p. 90–92°, undepressed on admixture with authentic benzalazine, m.p. 93–94° (lit.(9) m.p. 93°).

In Basic Medium

A solution of **2** (500 mg) and potassium hydroxide (20 g) in water (20 ml) and methanol (40 ml) was boiled under reflux for 26 h under nitrogen. The mixture was cooled, diluted with water, and extracted with dichloromethane. Evaporation of the extract and crystallization of the residue from 95% ethanol gave deoxybenzoin azine (**6**; 51 mg) as bright yellow crystals; three recrystallizations from ethanol–benzene gave material, m.p. 163–164°, undepressed on admixture with authentic deoxybenzoin azine, m.p. 163–164° (lit. (10) m.p. 164°). The mother liquor from the original crystallization of the azine was treated with 2,4-dinitrophenylhydrazine and hydrochloric acid to give deoxybenzoin 2,4-dinitrophenylhydrazone (120 mg) as pale orange crystals; three recrystallizations from chloroform–methanol gave shiny, orange prisms, m.p. 202–203°, undepressed on admixture with authentic deoxybenzoin 2,4-dinitrophenylhydrazone, m.p. 202–203° (lit. (11) m.p. 204°). Acidification of the original basic aqueous solution gave benzoic acid (265 mg).

Independent Synthesis of **2**

A solution of benzil monohydrazone (1.68 g), trimethyl orthobenzoate (3.08 g), and a few drops of acetic acid in anhydrous methanol (70 ml) was boiled under reflux for 72 h. The mixture was evaporated and the residue was taken up in benzene and chromatographed on neutral alumina. Evaporation of eluates obtained with benzene and 5% ether–benzene gave **2** (1.87 g; 73%) as a pale yellow crystalline solid; three recrystallizations from ether gave material, m.p. 124–125°, that was shown by mixture melting point and i.r. spectral comparison to be identical with the product, m.p. 124.5–125.5°, obtained from the reaction of **1** with sodium methoxide.

Hydrolysis of **3**: *Formation of* ***10***

In Acid Medium

A solution of **3** (450 mg) (1) in a mixture of methanol (50 ml), concentrated hydrochloric acid (15 ml), and benzene (15 ml) was boiled under reflux in the dark for 3.5 h. The solution was concentrated by evaporation to *ca.* 40 ml, cooled to room temperature, made basic with sodium hydroxide, and cooled at 0° overnight. The white needles that were deposited were collected, washed with a little cold aqueous sodium hydroxide and with water, and dried to give 3,4,5-triphenylpyrazole (**10**; 316 mg; 99%), m.p. 258–259.5°. Four recrystallizations from methanol gave material, m.p. 261–262°. The melting point of this product

Can. J. Chem. Downloaded from www.nrcresearchpress.com by 210.87.254.5 on 09/05/12
For personal use only.

Can. J. Chem. Downloaded from www.nrcresearchpress.com by 210.87.254.5 on 09/05/12
For personal use only.

was not depressed on admixture with authentic 3,4,5-triphenylpyrazole, m.p. 261–263° (*vide infra*).

Anal. Calcd. for $C_{21}H_{16}N_2$: C, 85.11; H, 5.44; N, 9.45. Found: C, 85.26; H, 5.22; N, 9.34.

Acidification of the original aqueous filtrate gave benzoic acid (118 mg; 90%).

In Basic Medium

Hydrolysis of **3** with boiling 20% aqueous methanolic potassium hydroxide for 14 h also gave 3,4,5-triphenylpyrazole (**10**) but in considerably lower yield (16%); the major product was benzil monoazine (55%).

*3,4,5-Triphenylpyrazole (**10**)*[3]

A solution of α-phenylchalcone (**11**; 5.68 g) (13), 95% hydrazine (750 mg), and two drops of acetic acid in ethanol (60 ml) was boiled under reflux for 12 h. The solution was cooled in an ice bath to give 3,4,5-triphenyl-2-pyrazoline as a white crystalline solid, which was filtered and washed with a little cold ethanol; concentration of the mother liquor gave a second crop of the same product (total yield, 95%). Four recrystallizations from ethanol (with minimal contact with the air) and drying *in vacuo* at room temperature gave an analytical sample, m.p. 166–168° (dec.); λ_{max} (CH_2Cl_2) 3.01 μ.

Anal. Calcd. for $C_{21}H_{18}N_2$: C, 84.53; H, 6.08; N, 9.39. Found: C, 84.41; H, 6.06; N, 9.27.

A solution of 3,4,5-triphenyl-2-pyrazoline (unrecrystallized: 4.50 g) in chloroform (50 ml) was treated with a solution of bromine in chloroform until the bromine color was no longer destroyed. A small additional portion of bromine solution was added and the mixture was boiled under reflux for 4 h. The mixture was evaporated with chloroform twice to dryness, the residue was taken up in hot 95% ethanol, and the solution was boiled under reflux for 30 min with aqueous 10% sodium hydroxide (50 ml). The resulting copious white precipitate was brought into solution by the addition of hot ethanol (400 ml) and the solution was filtered hot, allowed to cool slowly to room temperature, and then chilled in an ice bath to give 3,4,5-triphenylpyrazole (**10**), m.p. 259–261° (3.57 g; 80%). Three recrystallizations from methanol gave material, m.p. 261–263° (lit. (12) m.p. 265°).

*Irradiation of **3***

On exposure to visible light, compound **3** in the solid state or in solution rapidly acquired a very intense red color. A solution of **3** in dichloromethane in an i.r. cell was irradiated with strong sunlight for 5 min and the i.r. spectrum of the solution was immediately recorded three times in succession (20 min). The spectrum of the freshly irradiated solution showed a diminution of *ca.* 5% in the intensities of the bands of **3** and the appearance of a new band at 6.50 μ, together with weaker new bands in the 6.0–12.0 μ region. The second trace showed a marked decrease in intensity of the 6.50 μ band, and in the third trace this was almost entirely absent; the intensities of the bands of **3** increased in the second and third traces. During the recording of these three spectra the red color of the irradiated solution had faded almost completely, restoring the original color. Similar behavior was observed when the same solution was exposed to light for additional periods of 15 and 30 min. However, at the end of the third exposure, the 6.03 μ band of **3** had a distinct shoulder on the lower wavelength side that did not decrease in intensity with time. On prolonged exposure to sunlight (*ca.* 12 h) the red color faded gradually and the i.r. spectra showed the growth of the shoulder into the band of benzil monoazine at 5.95 μ and the eventual disappearances of the band of **3** at 6.03 μ. The solution was then bright yellow in color (perceptibly more intensely colored than the original pale yellow solution of **3**) and its i.r. and u.v. spectra showed the presence of benzil monoazine alone, which was recovered in essentially quantitative yield from the solution.

Addition of a small amount of hydroquinone to a solution of **3** before irradiation did not affect the rate of appearance of the red color. When a solution of **3** in dichloromethane was degassed by freezing in liquid nitrogen, pumping at 2×10^{-5}mm, thawing and refreezing five times, the rate of appearance of the red color was perceptibly faster than in the case of an undegassed solution.

*Reaction of p-Anisil Monoazine (**14**) with Sodium Methoxide: Formation of **15***

p-Anisil monoazine (**14**) was prepared from *p*-anisil and hydrazine dihydrochloride in aqueous ethanol; recrystallization from benzene – acetic acid gave yellow plates, m.p. 162–163.5° (lit. (14) m.p. 165°); λ_{max} ($CHCl_3$) 6.01 μ; λ_{max} (CH_2Cl_2) 293 nm (log ε 4.60), 347 nm (log ε 4.54); $^{H}\delta(CDCl_3)$ 3.71 (s, 6H), 3.81 (s, 6H), 6.73 (d, J = 8 Hz, 4H), 6.95 (d, J = 8 Hz, 4H), 7.48 (d, J = 8 Hz, 4H), 7.93 (d, J = 8 Hz, 4H); *m/e* (%) 536(4), 136(16), 135(100), 105(10), 77(16).

The azine **14** (6.43 g, 0.012 mol), sodium methoxide (2.22 g, 0.041 mol), and dry ether (300 ml) were placed in a dry, nitrogen-preswept, three-necked flask. The mixture was heated under reflux with stirring under a blanket of dry nitrogen. After *ca.* 2 h a faint red tinge was observed in the reaction mixture; after 16 h the reaction mixture was pink, after 1 day it was faint purple, and after 2 days it was dark purple. After 12 days the cooled reaction mixture was shaken with water (250 ml) at night under subdued light giving a dark orange ethereal solution and a pale yellow aqueous solution containing suspended yellow solid. This solid (1.99 g), m.p. 159–164°, was shown by i.r. spectroscopy to be *p*-anisil monoazine. The aqueous solution was extracted with ether, and the combined ethereal solutions were dried, filtered, and concentrated to 50 ml. Compound **15** separated as a yellow crystalline solid (690 mg, 11%),[4] m.p. 177–178°(dec.); λ_{max} ($CHCl_3$) 2.98 (complex), 6.05 μ; λ_{max} (CH_2Cl_2) 289 nm (log ε 4.39), 368 nm (log ε 3.47); *m/e* (%), 538(1), 536(9), 520(2), 510(13), 390(44), 386(10), 375(19), 358(11), 240(15), 227(100), 211(25), 137(11), 136(98), 135(100), 134(47), 133(17).

Anal. Calcd. for $C_{32}H_{30}N_2O_6$: C, 71.36; H, 5.61; N, 5.20. Found: C, 71.13; H, 5.67; N, 5.19.

The residual ethereal solution was evaporated to give an orange oil; this was taken up in petroleum ether –

[3]The preparation of **10** by this route has also been reported by Parham and Hasek (12); we include the details of our procedure here since it appears to have some advantage.

[4]In another run with **14** (6.43 g), sodium methoxide (3.33 g), and ether (500 ml) the yield of **15** was increased to 1.26 g (20%).

benzene, and the solution was chromatographed on alumina. Elution with petroleum ether – benzene (3:2) gave a colorless oil (771 mg) which had bands in its i.r. spectrum at 4.47 and 5.82 μ. Rechromatography of these fractions gave methyl *p*-anisate as a white solid (220 mg), m.p. 44–46° (lit. (11) m.p. 49°), λ_{max} (CCl_4) 5.82, 6.22 μ, eluted with petroleum ether, and a white solid, eluted with benzene – petroleum ether (1:3), which crystallized from petroleum ether to give *p*-anisonitrile (150 mg), m.p. 57–58.5°, λ_{max} (CCl_4) 4.47 μ, mixture m.p. 58–59° with an authentic sample (m.p. 59–60°). Elution of the original chromatographic column with petroleum ether – benzene (2:3) gave a yellow oil (630 mg) containing mainly *p*-anisil monoazine. Elution with methanol–chloroform (1:1) gave an oil (170 mg) which crystallized from water to give *p*-anisamide, m.p. 163–164° (lit. (11) m.p. 167°), identified by its i.r. spectrum.

The aqueous solution from work-up of the original reaction mixture was acidified to give *p*-anisic acid (240 mg), m.p. 184–185°, identified by mixture melting point and i.r. spectral comparison with an authentic sample (m.p. 182–185°).

*Hydrolysis of **15**: Formation of **16***

Compound **15** (263 mg) and a mixture of methanol, concentrated hydrochloric acid and benzene, (10:3:3; 64 ml) were heated under reflux. After *ca.* 30 min the original yellow color had faded. After 11 h the solution was concentrated under reduced pressure until crystals separated. Aqueous sodium hydroxide was added to neutralize the acid and the mixture was cooled at 0° overnight. Compound **16** separated as a white crystalline solid (186 mg; 99%), m.p. 211–220°. Four recrystallizations from methanol gave white needles, m.p. 225–225.5°; λ_{max} (KBr) 2.88, 6.21 μ; $^{H}\delta$ ($CDCl_3$) 3.42 (s, 2H; absent after D_2O treatment), 3.70 (s, 6H), 3.77 (s, 3H), 6.97 (m, 13H; 12H after D_2O treatment).[5]

Anal. Calcd. for $C_{24}H_{22}N_2O_3$: C, 74.59; H, 5.74; N, 7.25. Found: C, 74.17; H, 5.87; N, 7.23.

This product was shown to be **16** by mixture m.p. 224.5–225° with an authentic sample (m.p. 224–225.5°; *vide infra*). The i.r. and ^{1}H n.m.r. spectra of the two samples were indistinguishable.

The remaining aqueous solution was acidified and extracted with chloroform (100 ml); the chloroform extracts were dried and evaporated to give a white solid (85 mg) which crystallized from water to give *p*-anisic acid, m.p. 181–182°; mixture m.p. 182–185° with an authentic sample (m.p. 182–185°); the i.r. spectra of the two samples were indistinguishable.

*3,4,5-Tri-p-anisylpyrazole (**16**)*

Hydrogen chloride was passed through a cooled solution (ice bath) of deoxy-*p*-anisoin (14.0 g) and *p*-anisaldehyde (10 g) in ether (50 ml) for 30 min. The red solution was cooled at −20° overnight. The resulting cake was broken up under ethanol, filtered, washed with ice-cold ethanol, and dried, to give 3-chloro-1,2,3-tri-(*p*-anisyl)-1-propanone as a white solid (18.6 g), m.p. 134–139°; $^{H}\delta$($CDCl_3$) 3.67 and 3.70 (two s, 9H), 5.20 (d, J = 11 Hz, 1H), 5.72 (d, J = 11 Hz,1H), 6.7–7.0 (m, 8H), 7.48 (d, J = 9 Hz, 2H), 7.87 (d, J = 9 Hz, 2H). It was not further purified.

A suspension of 3-chloro-1,2,3-tri-(*p*-anisyl)-1-propanone (10 g), potassium acetate (8 g), and sodium carbonate (3 g) in methanol (100 ml) was boiled under reflux with stirring for 2 days. The methanol was evaporated, the residue was taken up in carbon tetrachloride, and the solution was filtered to remove suspended inorganic material and evaporated to give 1,2,3-tri-(*p*-anisyl)-2-propen-1-one as a yellow oil (7.5 g). The oil was taken up in benzene and chromatographed on silica gel. The purified material, eluted with ether–benzene (1:99), failed to crystallize; λ_{max} (CCl_4) 6.07 μ; $^{H}\delta$(CCl_4) 3.62 (s, 3H), 3.67 (s, 3H), 3.70 (s, 3H), 6.5–7.5 (m, 11H), 7.75 (d, J = 9 Hz, 2H).

A solution of 1,2,3-tri-(*p*-anisyl)-2-propen-1-one (as an oil; 6.92 g, 0.018 mol) and 95% hydrazine (620 mg, 0.018 mol) in absolute ethanol (60 ml) containing 2 drops of acetic acid was boiled under reflux for 2 days. The reaction mixture was cooled at −20° for 2 days and the supernatant decanted. The residual white solid was dissolved in chloroform (50 ml) and a solution of bromine in chloroform was added until the solution remained red colored. An additional 1 ml of the bromine solution was added and the resulting solution was boiled under reflux for 2 h. The chloroform was evaporated and the solid residue was taken up in hot 95% ethanol. Aqueous 10% sodium hydroxide (50 ml) was added, and the solution was cooled, to give 3,4,5-tri-(*p*-anisyl)pyrazole (**16**) as off-white needles (4.0 g). Four recrystallizations from 95% ethanol gave needles, m.p. 224–225.5°.

*Irradiation of **15***

Exposure of compound **15** to visible light in the solid state or in solution led rapidly to a red coloration. A solution of **15** in chloroform was exposed to light and air for three days. The i.r. spectrum of the irradiated solution showed that quantitative conversion of **15** to *p*-anisil monoazine (**14**) had occurred; this was confirmed by isolation of the product, m.p. 162–163°, which showed no depression on admixture with **14**.

*Reaction of p-Tolil Monoazine (**17**) with Sodium Methoxide: Formation of **18***

p-Tolil monoazine (**17**) was prepared from *p*-tolil and hydrazine dihydrochloride in aqueous ethanol. The crude product was dissolved in boiling benzene and the hot solution was filtered into boiling acetic acid; the benzene was removed by azeotropic distillation and the acetic acid solution was cooled to give **17**, m.p. 253–254° (lit. (15) m.p. 248°); λ_{max} ($CHCl_3$) 5.97 μ; λ_{max} (CH_2Cl_2) 266 nm (log ε 4.52), 327 nm (log ε 4.49); $^{H}\delta$ ($CDCl_3$) 2.37 (s, 6H), 2.25 (s, 6H), 7.03 (d, J = 8 Hz, 4H), 7.35 (m, 8H), 7.87 (d, J = 8 Hz, 4H).

p-Tolil monoazine (11.34 g, 0.024 mol), dry sodium methoxide (6.66 g, 0.12 mol), and dry ether (*ca.* 1 l) were placed in a dry, nitrogen-preswept flask. The mixture was boiled under reflux with stirring under a blanket of dry nitrogen. After *ca.* 2 h the reaction mixture had acquired a deep purple color. Reflux was continued for 15 days. The cooled reaction mixture was shaken with water (500 ml) at night under subdued light, to give a deep orange ethereal solution and a pale yellow aqueous solu-

[5]This material is considered to be the monohydrate of **16**; the analytical sample was subjected to intensive drying (at 100° and 6×10^{-4} mm for 45 h).

Can. J. Chem. Downloaded from www.nrcresearchpress.com by 210.87.254.5 on 09/05/12
For personal use only.

Can. J. Chem. Downloaded from www.nrcresearchpress.com by 210.87.254.5 on 09/05/12
For personal use only.

tion with discharge of the purple color. The aqueous solution was extracted with ether (3 × 100 ml) and the combined, dried ethereal solutions were concentrated under reduced pressure (at *ca.* 40°) to *ca.* 35 ml. Compound **18** separated as a pale yellow crystalline solid (2.50 g; 22%), m.p. 172–175°(dec.). This was treated with ether on a Hirsch funnel under slightly reduced pressure; insoluble azine contaminant remained on the filter paper and the filtrate was evaporated to give **18**, m.p. 173–175°(dec.) (very dependent on the rate of heating); λ_{max} ($CHCl_3$) 2.99 (complex), 6.05 μ; λ_{max} (CH_2Cl_2) 262 nm (log ε 4.22), 291 nm (log ε 4.23), 370 nm (log ε 3.29); $^{H}\delta$ ($CDCl_3$) 2.17 (s, 3H), 2.20 (s, 3H), 2.30 (s, 6H), 6.01 (s, broad, 1H; absent after D_2O treatment), 6.85–7.18 (m, 12H), 7.37 (s, sharp, 1H; absent after D_2O treatment), 7.50 (d, J = 8 Hz, 2H), 7.72 (d, J = 8 Hz, 2H); *m/e* (%), 474(3), 355(76), 238(15), 120(30), 119(95), 118(91), 117(100), 91(44).

Anal. Calcd. for $C_{32}H_{30}N_2O_2$: C, 80.98; H, 6.37; N, 5.90. Found: C, 80.89; H, 6.75; N, 6.01.

The ethereal mother liquor from the original crystallization of **18** was evaporated to an orange oil, which was taken up in benzene and chromatographed on alumina (500 g). Elution with benzene gave an oil (450 mg) whose i.r. spectrum, with bands at 4.50 and 5.80 μ, indicated the presence of a nitrile and an ester. *p*-Tolunitrile and methyl *p*-toluate were detected by comparison of v.p.c. retention times; they were separated by preparative v.p.c. and identified by i.r. spectral comparison with authentic samples; the estimated yields of nitrile and ester are 250 mg (8%) and 200 mg (6%), respectively. Further elution with benzene gave *p*-tolil monoazine (1.36 g). Elution with methanol–chloroform (1:1) gave an oil (1.36 g), which crystallized from benzene to give *p*-toluamide, m.p. 159–160°, identified by i.r. spectral comparison with an authentic sample, m.p. 158.5–160°.

The aqueous solution from the work-up of the original reaction mixture was acidified to give *p*-toluic acid (1.8 g), identified by i.r. spectral comparison with an authentic sample.

*Hydrolysis of **18**: Formation of **19***

Compound **18** (238 mg) and a mixture of methanol, concentrated hydrochloric acid, and benzene (10:3:3; 64 ml) were heated under reflux for 12 h; the yellow color of the solution faded within 30 min. The mixture was concentrated to 40 ml, neutralized with concentrated aqueous sodium hydroxide, and cooled to 0° to give **19** as a white crystalline solid (136 mg; 80%), m.p. 244–249°. Two recrystallizations from methanol gave white needles, m.p. 253–254°; λ_{max} ($CHCl_3$) 2.88 μ; λ_{max} (EtOH) 250 nm (log ε 4.38); *m/e* (%) 338(100), 337(25).

Anal. Calcd. for $C_{24}H_{22}N_2$: C, 85.17; H, 6.55; N, 8.28. Found: C, 85.10; H, 6.69; N, 8.32.

This compound was identified as **19** by mixture m.p. 253–254° with an authentic sample (m.p. 253–254°; *vide infra*).

The aqueous solution was acidified and extracted with ether to give *p*-toluic acid, identified by i.r. spectral comparison with an authentic sample.

*3,4,5-Tri-(p-tolyl)pyrazole (**19**)*

Hydrogen chloride was passed through a cooled solution of deoxy-*p*-toluoin (10.2 g) in *p*-tolualdehyde (8.0 g) until the solution set to a solid cake; this was then cooled at −20° overnight. The cake was broken up under ethanol, filtered, and washed with ice-cold ethanol and with ether, and dried to give 3-chloro-1,2,3-tri-(*p*-tolyl)-1-propanone as a white solid (12.0 g), m.p. 153–155°; $^{H}\delta$ ($CDCl_3$) 2.13 (s, 3H), 2.23 (s, 3H), 2.35 (s, 3H), 5.23 (d, J = 11 Hz, 1H), 5.73 (d, J = 11 Hz, 1H), 6.7–7.3 (m, 10H), 7.97 (d, J = 9 Hz, 2H).

A suspension of 3-chloro-1,2,3-tri-(*p*-tolyl)-1-propanone (10 g), potassium acetate (8 g), and sodium carbonate (3 g) in methanol (100 ml) was boiled under reflux for 1 day. The methanol was cooled and evaporated, and the residue was taken up in ether. The solution was filtered and cooled to give 1,2,3-tri-(*p*-tolyl)-2-propen-1-one (4.2 g). This was recrystallized from methanol to give greenish tinged needles, m.p. 116–117°; λ_{max} (CCl_4) 6.04 μ; $^{H}\delta$ (CCl_4) 2.23 (s, 3H), 2.43 and 2.45 (two s, 6H), 6.8–7.2 (m, 11H), 7.70 (d, J = 9 Hz, 2H).

Anal. Calcd. for $C_{24}H_{22}O$: C, 88.31; H, 6.79. Found: C, 88.28; H, 6.84.

A solution of 1,2,3-tri-(*p*-tolyl)-2-propen-1-one (2.30 g) and 95% hydrazine (200 mg) in ethanol (20 ml) containing 2 drops of acetic acid was boiled under reflux for 26 h. The solvent was evaporated to give an oil. This was taken up in chloroform, and a solution of bromine in chloroform was added until the bromine color persisted; a few additional drops of the bromine solution were then added. The resulting solution was boiled under reflux for 4 h. The chloroform was evaporated, and the solid residue was taken up in hot ethanol. Aqueous 10% sodium hydroxide was added and the solution was cooled to give 3,4,5-tri-(*p*-tolyl)pyrazole (**19**) as a white solid (2.0 g). This was recrystallized five times from methanol to give material, m.p. 253–254°.

*Acetylation of **18**: Formation of **20***

Compound **18** (1.20 g) was added to freshly distilled acetyl chloride (60 ml) in an aluminum foil-wrapped flask that had been preswept with nitrogen. The solution was boiled under reflux for 20 h under nitrogen. The red solution was stripped of acetyl chloride and the residue was taken up in chloroform (100 ml). The solution was washed with saturated aqueous sodium bicarbonate, dried, and evaporated. The residue was taken up in hot methanol, the solution was filtered from a yellow solid, and the filtrate was cooled to give **20** as a white crystalline solid (500 mg; 38%) that was recrystallized several times from methanol to give material, m.p. 196–198°; λ_{max} ($CHCl_3$) 2.8–3.1 (w), 6.00 μ; λ_{max} (MeOH) 260 nm (sh, log ε 4.23), 290 nm (log ε 4.30); $^{H}\delta$ ($CDCl_3$) 2.01 (s, 6H), 2.27 (s, 6H), 2.52 (s, 3H), 5.01 (br s, 1H; absent after D_2O treatment) 6.5–7.2 (m, 12H), 7.45 (d, J = 8 Hz, 2H), 7.63 (d, J = 8 Hz, 2H); *m/e* (%) 516(8), 397(20), 356(25), 355(83), 338(14), 280(23), 263(19), 238(50), 208(13), 146(14), 120(16), 119(100), 118(67), 91(54), 65(14).

Anal. Calcd. for $C_{34}H_{32}N_2O_3$; C, 79.04; H, 6.24; N, 5.42. Found: C, 79.14; H, 6.23; N, 5.51.

*Irradiation of **18***

Exposure of compound **18** in the solid state or solution to visible light led to a red coloration and eventual conversion to *p*-tolil monoazine. The development of the red color was more rapid than in the case of compounds **3** and **15**; however, in the solid state, the red intermediate appeared to be less sensitive to air oxidation since the

red color remained after exposure of a sample to light and air for 1 week.

Two solutions of compound **18** were prepared (*ca.* 60 mg/ml). One was preswept with oxygen and the other with nitrogen. The solutions were exposed to radiation from a Mineralite lamp (maximum emission at 254 nm). A red color appeared in the nitrogen-preswept solution in *ca.* 5 min while *ca.* 10 min were required for its appearance in the oxygen-preswept solution.

Two solutions of concentrations similar to that described above were exposed to a sunlamp. One solution was preswept with nitrogen, and the other was swept with oxygen throughout the irradiation, which was carried out for 30 min. Both solutions developed a red coloration within 1 min. After cessation of irradiation, the red color of the oxygen-swept solution disappeared within 2 min, while the color of the nitrogen-preswept solution faded more slowly, and could still be detected after 20 min. The i.r. spectrum of the oxygen-swept solution showed distinct bands due to *p*-tolil monoazine, whereas that of the nitrogen-preswept solution showed little conversion to azine.

*Reaction of p-Tolil Monoazine (**17**) with Potassium t-Butoxide*

p-Tolil monoazine (5.68 g, 0.012 mol), dry potassium *t*-butoxide (5.10 g, 0.045 mol), and dry ether (600 ml) were placed in a dry, nitrogen-preswept, 1-l two-necked flask. The suspension was boiled under reflux with stirring under a blanket of dry nitrogen. A deep purple color appeared within 2 min of mixing the reagents. After 7 days at reflux, the mixture was cooled and shaken with water (400 ml) at night under subdued light. The purple color was discharged, and an orange ethereal solution and a pale yellow aqueous solution were obtained. The aqueous solution was extracted with ether (250 ml) and the ethereal extract was dried, filtered, and evaporated to give compound **18** (1.21 g). Material recrystallized from ether and dried had an i.r. spectrum indistinguishable from that of material isolated from the reaction of *p*-tolil monoazine with sodium methoxide.

The ethereal mother liquor was evaporated and the residue was taken up in benzene. The solution was chromatographed on silica gel; elution with benzene gave (*i*) *t*-butyl *p*-toluate (100 mg), identified by spectral and v.p.c. comparison with an authentic sample prepared from *p*-toluyl chloride and *t*-butyl alcohol in pyridine; b.p. 126–128° (16 mm); λ_{max} (CCl_4) 5.86 μ; $^{H}\delta$ (neat) 1.58 (s, 9H), 2.27 (s, 3H), 7.07 (d, J = 8 Hz, 2H), 7.92 (d, J = 8 Hz, 2H); (*ii*) an oil (470 mg) containing *p*-tolunitrile (97%) and *t*-butyl *p*-toluate (3%) as shown by n.m.r. spectroscopy and v.p.c.; (*iii*) *p*-tolunitrile (170 mg), identified by i.r. and n.m.r. spectroscopy and v.p.c. Further elution with benzene and elution with ether–benzene mixtures (1:99, 1:49, and 3:97) gave *p*-tolil monoazine (970 mg). Further elution with ether–benzene mixtures (3:47 and 3:22) gave *p*-tolil *p*-toluylhydrazone, as a white solid (240 mg). Crystallization from ethanol gave material, m.p. 150–151°; λ_{max} ($CHCl_3$) 5.92, 6.05 μ; $^{H}\delta$ ($CDCl_3$) 2.40 (s, 3H), 2.47 (s, 6H), 7.1–7.4 (m, 8H, with a peak at 7.33), 7.62 (d, J = 8 Hz, 2H), 8.07 (d, J = hz, 2H), 9.33 (s, 1H; absent after D_2O treatment); *m/e* (%), 370(0.1), 369(0.1), 368(0.1), 367(0.1), 251(100), 208(12), 119(95), 118(11), 91(49).

Anal. Calcd. for $C_{24}H_{22}N_2O_2$: C, 77.81; H, 5.99; N, 7.56. Found: C, 78.15; H, 5.67; N, 7.63.

This compound was identified by i.r. spectral comparison and mixture m.p. 149–150° with an authentic sample of *p*-tolil *p*-toluylhydrazone, m.p. 149–150°, prepared from *p*-tolil monohydrazone and *p*-toluyl chloride in pyridine.

Elution with chloroform–ether mixtures gave *p*-toluic acid (290 mg). Elution with methanol–chloroform (3:22) gave a dark oil (260 mg) whose i.r. spectrum with bands at 2.89, 3.00, 6.02, and 7.35 μ indicated the presence of *p*-toluamide. In another run *p*-toluamide, m.p. 159–160°, was isolated and identified by i.r. spectral comparison with an authentic sample.

The aqueous solution from work-up of the original reaction mixture on acidification gave *p*-toluic acid (1.88 g), identified by i.r. spectral comparison with an authentic sample.

We thank Mr. G. Koves and Dr. A. M. Treasurywala for experimental contributions and the National Research Council of Canada for financial support.

1. P. Yates and B. L. Shapiro. J. Am. Chem. Soc. **81**, 212 (1959).
2. H. J. Bestmann, H. Buckschewski, and H. Leube. Chem. Ber. **92**, 1345 (1959).
3. E. Ghera and S. Shoua. J. Org. Chem. **37**, 1292 (1972). A. C. Huitric and W. D. Kumler. J. Am. Soc. **78**, 1147 (1956).
4. J. B. Stothers. Carbon-13 NMR spectroscopy. Academic Press, New York. 1972. G. C. Levy and G. L. Nelson. Carbon-13 nuclear magnetic resonance for organic chemists. Wiley-Interscience, New York. 1972.
5. G. Berti, G. Moretti, and D. Segnini. Farmaco (Pavia) Ed. Sci. **15**, 414 (1960); Chem. Abstr. **54**, 24515 (1960).
6. R. B. Woodward and P. Yates. J. Am. Chem. Soc. **85**, 553 (1963). W. von E. Doering and T. C. Aschner. J. Am. Chem. Soc. **75**, 393 (1953).
7. P. Yates and E. M. Levi. To be published.
8. S. M. Shein, L. V. Bryukhovetskaya, F. V. Pischugin, V. F. Starichenko, V. N. Panfilov, and V. V. Voevodskii. J. Struct. Chem. **11**, 228 (1970).
9. K. Miyatake. J. Pharm. Soc., Jap. **72**, 1162 (1952).
10. T. Curtius and A. Blumer. J. Prakt. Chem. [2], **52**, 117 (1895).
11. M. Frankel and S. Patai. Tables for identification of organic compounds. 2nd ed. The Chemical Rubber Co., Cleveland, Ohio. 1964.
12. W. E. Parham and W. R. Hasek. J. Am. Chem. Soc. **76**, 799 (1954).
13. E. P. Kohler and E. M. Nygaard. J. Am. Chem. Soc. **52**, 4128 (1930).
14. J. van Alphen. Rec. Trav. Chim. **48**, 1199 (1929).
15. T. Curtius and R. Kastner. J. Prakt. Chem. [2] **83**, 215 (1911).

Can. J. Chem. Downloaded from www.nrcresearchpress.com by 210.87.254.5 on 09/05/12
For personal use only.

Proton Magnetic Resonance Studies of 2′-Deoxythymidine, its 3′- and 5′-Monophosphates and 2′-Deoxythymidylyl-(3′,5′)-2′-deoxythymidine in Aqueous Solution[1]

DONALD J. WOOD, FRANK E. HRUSKA, AND KELVIN K. OGILVIE
Department of Chemistry, University of Manitoba, Winnipeg, Manitoba R3T 2N2

Received March 28, 1974

DONALD J. WOOD, FRANK E. HRUSKA, and KELVIN K. OGILVIE. Can. J. Chem. **52**, 3353, (1974).

Proton magnetic resonance studies of 2′-deoxythymidine, its 3′- and 5′-monophosphates and the dideoxynucleoside monophosphate, 2′-deoxythymidylyl-(3′,5′)-2′-deoxythymidine are described. Assignment of the spectral bands are carried out and the derived chemical shift and coupling constant data are discussed in terms of the conformational properties of these molecules. The main conclusion reached is that 3′- and 5′-phosphorylation as well as incorporation into the dinucleoside monophosphate at either the 3′- or 5′-terminus has only slight effects on the conformation of thymidine under the experimental conditions employed.

DONALD J. WOOD, FRANK E. HRUSKA et KELVIN K. OGILVIE. Can. J. Chem. **52**, 3353 (1974).

On rapporte des études de r.m.n. du proton de la déoxy-2′ thymidine ainsi que ses monophosphates-3′ et -5′ de même que le monophosphate du didéoxynucléoside, déoxy-2′ thymidylyl-(3′,5′) déoxy-2′ thymidine. L'attribution des bandes spectrales a été faites et les déplacements chimiques et les constantes de couplage qui ont été obtenus sont discutés en termes des propriétés conformationelles de ces molécules. La principale conclusion à laquelle on peut arriver est que la phosphorylation en 3′ ou 5′, de même que l'incorporation dans le dinucléoside de monophosphates soit en position 3′ ou 5′ n'a que des effets mineurs sur la conformation de la thymidine dans les conditions expérimentales utilisées. [Traduit par le journal]

Introduction

Considerable effort is being directed towards elucidation of the three-dimensional structures of polyribo- and polydeoxyribonucleotides. Valuable contributions towards our understanding of polymer structure are obtained from X-ray studies of the crystal and molecular structures of the component mononucleosides and mononucleotides (1–5). Recently, high-resolution X-ray analyses of several ribose dinucleoside monophosphates, adenylyl-(2′,5′)-uridine (6), uridylyl-(3′,5′)-adenosine (UpA) (7, 8), guanylyl-(3′,5′)-cytidine (GpC) (9), and adenylyl-(3′,5′)-uridine (ApU) (10) as well as of the deoxydinucleotide 5′-phosphoryl thymidylyl-(3′,5′)-thymidine (d(pTpT)) (11), have appeared in the literature. Since the pioneering efforts of Jardetzky (12) and Lemieux (13), it has been demonstrated that n.m.r. studies can provide detailed conformational information at the nucleoside (14–20), nucleotide (21–30), and dinucleoside monophosphate level (23, 31–36). To date only a limited number of n.m.r. studies of dideoxynucleoside monophosphates have appeared (32, 37). In the present study we report the p.m.r. analyses of 2′-deoxythymidine (dT), 2′-deoxythymidine-3′-monophosphate (3′dTMP), 2′-deoxythymidine-5′-monophosphate (5′dTMP), and thymidylyl-(3′,5′)-thymidine (d(TpT)) (Fig. 1). Assignments of the spectral bands of the dimer are carried out by comparison with monomer spectra and with spectral data for deoxy derivatives available in the literature (13, 15, 32). The chemical shifts and ^1H–^1H and ^1H–^{31}P coupling constants are discussed in terms of the respective molecular conformations. The main conclusion reached is that under the experimental conditions employed the conformational properties of the thymidine moiety are only slightly affected by 3′- and 5′-phosphorylation or by incorporation into the dideoxynucleoside monophosphate at either the 3′- or 5′-terminus.

Experimental

dT, 3′dTMP, and 5′dTMP (A grade) were obtained from Sigma and were used without further purification. d(TpT) was prepared according to the procedure of Letsinger *et al.* (38). Sodium-3-trimethylsilylpropionate-

[1]Presented in part at the 4th Harry Steenbock Symposium on the "Structure and Conformation of Nucleic Acids and Protein – Nucleic Acid Interactions", Madison June 16–19, 1974. Symposium Proceedings, in press, 1974.

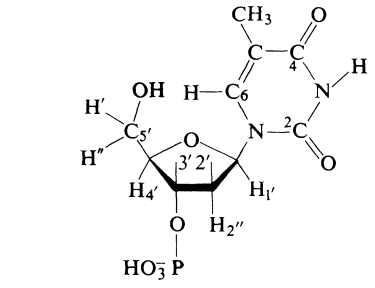

3′dTMP

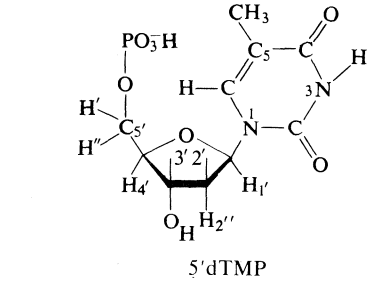

5′dTMP

d(*TpT*)

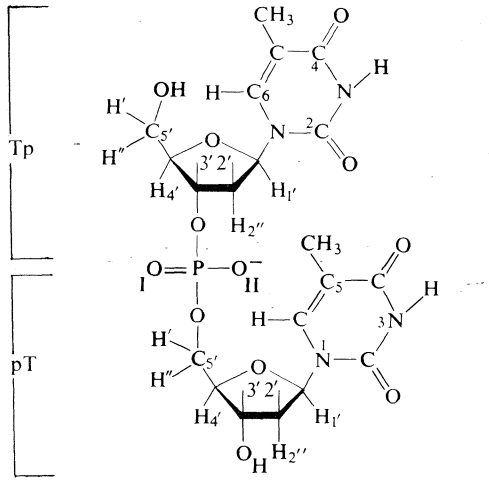

FIG. 1. Structural formulae of 2′-deoxythymidine-3′-monophosphate (3′dTMP), 2′-deoxythymidine-5′-monophosphate (5′dTMP), and 2′-deoxythymidylyl-(3′,5′)-2′-deoxythymidine (d(TpT)). Tp and pT refer to the free 5′- and 3′-nucleotide fragments of d(TpT), respectively.

2,2,3,3-d_4 (TSP) was used as an internal p.m.r. reference. Solutions of dT and d(TpT) (0.1 *M*, p*D* ~ 7.0) and of 3′dTMP and 5′dTMP (0.1 *M*, p*D* ~ 5.8)[2] were prepared and freeze-dried three times from 100% D_2O and finally dissolved in 100% D_2O. Spectra were obtained on Varian HA-100 and/or HR-220 MHz spectrometers. Calibration of spectra and spin-decoupling experiments were carried out by standard methods at both frequencies. Spectral analysis was carried out using LAME (39). Computer simulations of the spectra were used as a final test of the data (Figs. 2–4). In subsequent sections we describe spectral assignments which led to this simulation.

[2]The p*D* of the mononucleotide solution was kept at 5.8. At this p*D* the phosphate bears a single negative charge; this makes chemical shift comparison between monomer and dimer more relevant.

Results and Discussion

Spectral Assignment of dT, 3′dTMP, and 5′dTMP

The assignment of the 1′, 3′, and 4′ regions of a deoxyribose sugar and of the methyl and H_6 hydrogens of the thymine base is a straightforward matter in view of the characteristic patterns and location in the spectrum (13, 15, 32). Difficulties arise in the assignment of the pairs of methylene hydrogens at $C_{2'}$ and $C_{5'}$. No distinction can be made between the individual hydrogens *within* each pair in the case of 5′dTMP because of the strong coupling between $H_{2'}$ and $H_{2''}$ and between $H_{5'}$ and $H_{5''}$. It seems reasonable, on the basis of the arguments of Remin and Shugar (40), to assign the low- and high-field portions of the $H_{5'}$, $H_{5''}$ bands of dT and 3′dTMP bands to $H_{5'}$ and $H_{5''}$, respectively, although assignment is not crucial here because of the qualitative manner in which we treat our data in terms of molecular conformation.

In the following paragraphs we shall outline

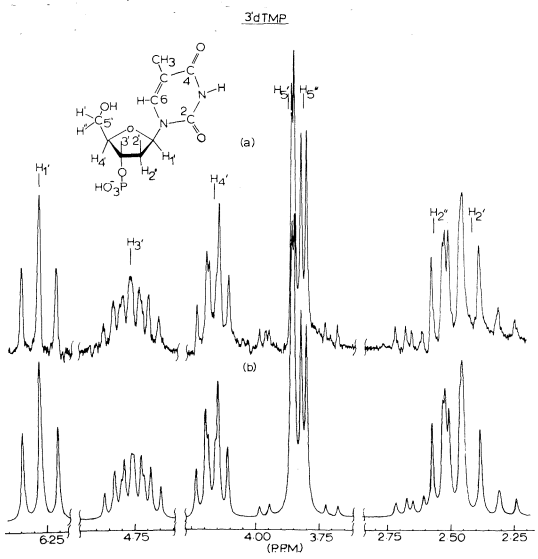

FIG. 2. (*a*) Single-scan, continuous-wave, 100 MHz spectrum of 3′dTMP (p*D* ≃ 5.8; 65 °C; 0.1 *M* in D_2O). Sweep width 250 Hz. (*b*) Computer simulated 100 MHz spectrum of 3′dTMP.

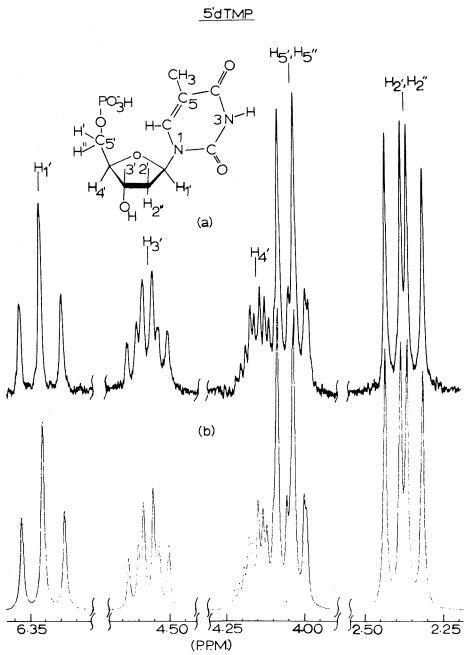

FIG. 3. (*a*) Single-scan, continuous-wave, 100 MHz spectrum of 5′dTMP (p$D \simeq 5.8$; 65 °C; 0.1 *M* in D_2O). Sweep width 250 Hz. (*b*) Computer simulated 100 MHz spectrum of 5′dTMP.

our reasoning based on the work of Fraser-Reid and Radatus (41) which leads to a plausible assignment of the 2′ and 2″ hydrogens of 3′dTMP. Our reasoning may appear circuitous since in our approach an assumption is made regarding the conformational behavior of the deoxyribose moieties in aqueous solution while in subsequent sections the conformational behavior is discussed in terms of the chemical shift and coupling constant data extracted from the assigned spectra. However, the assumption made is simply that the 2′-deoxyriboses in question may exist in either the 2′-*endo* or 3′-*endo* puckered modes.[3] Available n.m.r. data (13, 15, 17, 23, 32, 33, 43, 45) suggest that the 2′-deoxyriboses are best described in terms of a 2′-*endo* ↔ 3′-*endo* blend. However, we stress here that the major conclusions regarding the conformations of dT etc., do not rest on the assignment of $H_{2'}$ and $H_{2''}$. Nevertheless, the following exercise in assignment is useful since we demonstrate that a reasonable, internally consistent assignment in 3′dTMP is obtained. The absence of internal contradictions in the arguments used for spectral and for conformational assignment provide crosschecks on our reasoning and support our major conclusions.

Fraser-Reid and Radatus (41) have reported p.m.r. spectra (220 MHz) of 2′-deoxycytidines (dC) selectively deuterated at either the 2′(dC2′) or 2″(dC2″) positions (Fig. 5). The authors observed for dC2′ a symmetrical 1:2:1 triplet (4 Hz spacing) which was assigned to $H_{3'}$. Because of the first-order nature of the $H_{1'}$, $H_{2''}$, $H_{3'}$, and $H_{4'}$ bands they concluded (and we concur) that $J_{2''3'}$ and $J_{3'4'}$ are essentially equal ($\simeq$4.0 Hz) in dC. This near equality is entirely in accord with expectations for the following reasons. (*a*) The configurational relationship between the $H_{2''}$ and $H_{3'}$ pair and between the $H_{3'}$ and $H_{4'}$ pair is identical (one hydrogen is *endo* and one *exo* in each pair). (*b*) The gross conformational relationships are identical in that within each pair the hydrogens constitute a quasi equatorial–equatorial pair in the 2′-*endo* conformation and a quasi axial–axial pair in 3′-*endo*. Furthermore, $J_{3'4'}$ and $J_{2''3'}$ may safely be compared in conformational terms without electronegativity corrections since the $H_{2''}$—C—C—$H_{3'}$ and $H_{3'}$—C—C—$H_{4'}$ fragments bear a similar collection of substituents: a single oxygen ($O_{3'}$) and a collection of carbons and hydrogens whose electronegativity differences may be considered negligible. In addition we might add (since electronegativity effects upon $^3J_{HH}$ are known to be dependent on the *orientation* of the substituent (46)) that the $O_{3'}$ oxygen is identically placed on the two fragments: *gauche* to $H_{2''}$ and $H_{4'}$ in *both* the $C_{2'}$-*endo* and $C_{3'}$-*endo* conformations. Near equality of $J_{3'4'}$ and $J_{2''3'}$ is thus entirely expected in 2′-deoxyribosides except in those instances where severe distortion of the bond or conformational angles are likely. There appears no evidence which suggests this to be the case in any of the molecules studied here (1, 2, 11).

Fraser-Reid and Radatus (41) observed for the $H_{3'}$ hydrogen of dC2″ a quartet well separated from $H_{1'}$, $H_{2'}$, and $H_{4'}$ and thus,

[3]We are aware of the Altona and Sundaralingam (A.S.) (42, 43) discussion of furanose conformations with the N, S notations where N and S refer to two relatively narrow ranges of the pseudorotational cycle (41). We shall retain a more familiar notation (12), 2′-*endo* and 3′-*endo* which correspond to the S and N symbols, respectively. By 2′-*endo* we mean the broad envelope of conformations with negative τ_2 values and 3′-*endo*, the broad envelope of conformations with positive τ_2 values where τ_2 defines the rotation about $C_{2'}$—$C_{3'}$ (1).

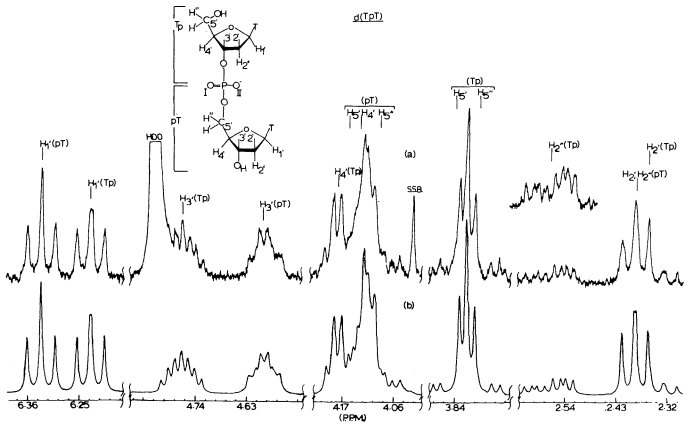

FIG. 4. (*a*) Single-scan, continuous-wave, 220 MHz spectrum of d(TpT) (p$D \simeq 7.0$; 18 °C; 0.1 M in D_2O). Sweep width 250 Hz. (*b*) Computer simulated 220 MHz spectrum of d(TpT).

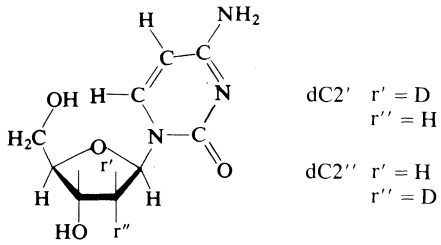

FIG. 5. Structural formulae of 2′-deoxycytidines deuterated at the 2′ or 2″-positions. From Fraser-Reid and Radatus (ref. 41).

bearing in mind that a hydrogen-to-deuterium substitution has negligible effect on vicinal H–H couplings, could extract a value of 6.7 Hz for $J_{2'3'}$ in dC. This information, coupled with our contentions that $J_{2''3'} \simeq J_{3'4'}$ and that the $J_{3'4'}$ values of dC (4.0 Hz), dT (3.7 Hz, 18 °C), and 3′dTMP (4.0 Hz, 18 °C) indicate similar conformations in this series of 2′-deoxyribosides, leads us to propose that the *low-field* components of the 2′,2″ region of 3′dTMP correspond to 2″ since only in this region do we find a spacing of about 4 Hz. In the high-field portion of the 2′,2″ region, which we assign to $H_{2'}$, couplings of 6.5, 7.2, and 14.3 Hz account for the pattern (see spectral simulation and Table 1).

To support the above rationale of the $J_{3'4'}$ and $J_{2''3'}$ values and the proposed spectral assignment, it would be useful to show that the magnitudes of other couplings in the ring are in line with our assignment, conformational assumptions and understanding of the influence of electronegative substituents on H–H vicinal couplings. To this end we shall make the following comparisons. (*a*) $J_{2'3'}$ and $J_{1'2'} + J_{3'4'}$ in 3′dTMP with corresponding values in *ribofuranosides* and (*b*) $J_{1'2''}$ in 3′dTMP with $J_{1'2''}$ in *arabinosides* (Fig. 6). These comparisons are made since they involve hydrogen pairs which are configurationally identical and since the couplings (and the sum) under comparison are expected to exhibit somewhat smaller variations with changes in the 2′-*endo* ↔ 3′-*endo* blend than, say, $J_{3'4'}$ which can range from about 0 to 10 Hz. This is so because of the *cis* (*gauche*) relationship of $H_{1'}$–$H_{2''}$ and $H_{2'}$–$H_{3'}$ pairs in all possible puckered modes of a deoxyribose ring and because of the inverse relationship between $J_{1'2'}$ and $J_{3'4'}$, a consequence of which is the fact that changes in the 2′-*endo* ↔ 3′-*endo* blend produce essentially equal but opposite effects on the individual couplings (14, 17, 43, 45). Thus differences in the compared values should exhibit reasonably well-defined trends in view of the structural differences between molecules compared (*i.e.* replacement of a hydroxyl by a hydrogen) and should reflect electronegativity and conformational effects of the 2′-hydroxyl.

In the large number of available p.m.r. data for furanosides, magnitudes of $J_{2'3'}$ lie in the range 5.2 ± 0.2 Hz while the sum $J_{1'2'} + J_{3'4'}$

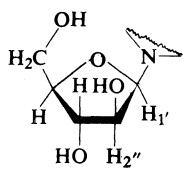

FIG. 6. Structure of an arabinose derivative.

TABLE 1. Proton magnetic resonance parameters[a] for D_2O solutions[b] of thymine derivatives

	dT	5′-dTMP		pT[c]		3′-dTMP		Tp[c]	
Parameter	18°	30°	65°	18°	65°	30°	65°	18°	65°
$\delta_{1'}$	6.28	6.34	6.31	6.34	6.32	6.31	6.28	6.23	6.24
$\delta_{2'}$	2.39[d]	2.37[d]	2.37[d]	2.38[d]	2.38[d]	2.41	2.41	2.36	2.36
$\delta_{2''}$	2.40[d]	2.38[d]	2.38[d]	2.39[d]	2.39[d]	2.55	2.56	2.58	2.57
$\delta_{3'}$	4.49	4.58	4.57	4.60	4.57	4.76	4.76	4.78	4.80
$\delta_{4'}$	4.04	4.17	4.16	4.13[e]	4.14[e]	4.18	4.17	4.19	4.19
$\delta_{5'}$	3.86	4.06[d]	4.05[d]	4.16[e]	4.16[e]	3.87	3.87	3.84	3.84
$\delta_{5''}$	3.79	4.05[d]	4.04[d]	4.09[e]	4.09[e]	3.81	3.81	3.79	3.79
$\delta_{5(CH_3)}$	1.89	1.93	1.93	1.91	1.92	1.91	1.91	1.90	1.90
δ_6	7.68	7.77	7.72	7.71	7.68	7.68	7.64	7.69	7.63
$J_{1'2'}$	6.9[f]	7.0	7.0	6.9	6.8	7.2	7.1	7.2	7.8
$J_{1'2''}$	6.9	7.0	7.0	6.9	6.8	6.5	6.6	6.1	6.3
$J_{2'2''}$	−14.2[g]	−13.8[g]	−14.4[g]	−14.1[g]	−14.2[g]	−14.3	−14.3	−14.0	−14.2
$J_{2'3'}$	5.6	4.8	4.9	5.8	5.4	6.8	6.9	6.0	6.6
$J_{2''3'}$	5.6	4.8	4.9	5.8	5.4	3.7	3.8	3.8	3.5
$J_{3'4'}$	3.7	2.9	3.3	4.0	3.7	4.0	3.7	3.2	3.6
$J_{4'5'}$	3.6	3.8	3.9	2.5[e]	2.5[e]	3.5	3.7	3.4	3.4
$J_{4'5''}$	4.9	3.8	3.9	4.0[e]	5.0[e]	4.8	5.0	4.2	5.5
$J_{5'5''}$	−12.6	−12.1[g]	−12.1[g]	−12.1[g]	−12.1[g]	−12.5	−12.5	−12.6	−12.3
J_{56}	1.1	1.1	1.2	1.3	1.2	1.2	1.2	1.0	1.2
$J_{P3'}$	—[h]	—	—	—	—	7.8	7.6	6.8	7.1
$J_{P4'}$	—	1.6	1.5	1.6[e]	1.6[e]	—	—	—	—
$J_{P5'}$	—	5.0	5.4	4.0[e]	4.0[e]	—	—	—	—
$J_{P5''}$	—	5.0	5.4	4.0[e]	5.0[e]	—	—	—	—
Σ^i	8.5	7.6	7.8	6.5[e]	7.5	8.3	8.7	7.6	8.9
Σ'^j	—	10.0	10.8	8.0[e]	9.0[e]	—	—	—	—

[a]Chemical shifts reported in p.p.m. from TSP. Coupling constants reported in Hz.
[b]Solutions 0.10 *M* in solute: mononucleotides at p*D* of 5.8; d(TpT) at p*D* of 7.0.
[c]See Fig. 1.
[d]The 0.01 p.p.m. chemical shift difference arbitrary in that $\delta_i \simeq \delta_j$.
[e]Due to the overlap of resonances these parameters are less certain than the other reported values.
[f]Due to the equivalence of the chemical shifts only the sum of the connected coupling constants is significant.
[g]Arbitrary. When $\delta_i = \delta_j$, the spectrum is independent of J_{ij}.
[h]Not observed or not applicable.
[i]$\Sigma = J_{4'5'} + J_{4'5''}$.
[j]$\Sigma' = J_{P5'} + J_{P5''}$.

is essentially constant at 10.1 ± 0.3 Hz.[4] In recent studies of arabinose derivatives (19, 47), values of about 5.0 Hz are noted for $J_{1'2''}$. The resultant changes in the above-mentioned couplings when a 2′-OH is removed from a ribose or an arabinose to produce a 2′-deoxy derivative are: $J_{2'3'}$ (3′dTMP − 5.2 Hz) = 1.6 Hz; $J_{1'2'} + J_{3'4'}$ (3′dTMP − 10.1 Hz) = 1.1 Hz; $J_{1'2''}$ (3′dTMP − 5.0 Hz) = 1.5 Hz. Thus larger values of the order of 1 Hz are evident for 3′dTMP.

Calculations according to Pachler (48) were carried out in order to estimate the effect of removal of the 2′-OH from ribose on $J_{2'3'}$ and $J_{1'2'} + J_{3'4'}$ and the effect of removal of the arabinose 2′-OH on $J_{1'2''}$. (For the calculations the A.S. geometry (42) was assumed and from the A.S. (42) method a 70% 2′-*endo* − 30% 3′-*endo* blend was derived (see below).) The calculations indicate that *each* of the compared values should be larger in the 2′-deoxyribose by about 0.5 to 1.0 Hz. Thus our observed differences are in qualitative (sign) agreement with the estimated OH effects. This agreement assures us that the proposed $H_{2'}$, $H_{2''}$ assignment is correct for 3′-dTMP (*i.e.* $H_{2''}$ to low field of $H_{2'}$). If the reverse assignment is assumed, then $J_{2''3'} = 6.8$ Hz and $J_{2'3'} = 4.0$ Hz for 3′-dTMP and arguments are now required to provide a simultaneous rationale of the large difference (2.8 Hz) between $J_{2''3'}$ and $J_{3'4'}$ and for the apparent reduction in $J_{2'3'}$ of about 1.2 Hz, brought about by the removal of the 2′-hydroxyl from a riboside.[5]

In summary then our exercise in 2′2″ assign-

[4]Exceptions to these trends occur for *syn* nucleosides (42).

[5]Contributions to the increase in compared values could also arise from flattening of the 2′-deoxyribose ring, relative to riboses. This flattening has been suggested by A.S. (42, 43).

TABLE 2. Proton magnetic resonance parameters of deoxyadenosine and deoxycytidine (at 18 °C)

	Value (p.p.m.)			Value (Hz)	
Chemical shift[a]	dA[b]	dC[c]	Coupling constant	dA[b]	dC[c]
$\delta_{1'}$	5.12	6.28	$J_{1'2'}$	7.5	6.8
$\delta_{2'}$	1.51	2.31	$J_{1'2''}$	6.1	6.3
$\delta_{2''}$	1.30	2.45	$J_{2'2''}$	−13.9	−14.0
$\delta_{3'}$	3.39	4.45	$J_{2'3'}$	6.2	6.6
$\delta_{4'}$	2.94	4.07	$J_{2''3'}$	3.1	3.9
$\delta_{5'}$	2.60	3.85	$J_{3'4'}$	3.0	4.0
$\delta_{5''}$	2.54	3.77	$J_{4'5'}$	3.0	3.7
δ_2 or δ_5	6.80	6.06	$J_{4'5''}$	4.2	5.0
δ_8 or δ_6	6.97	7.85	$J_{5'5''}$	−12.7	−12.5
			J_{56}	—	7.5

[a]Relative to *t*-BuOD for dA and to TSP for dC; 220 MHz.
[b]0.07 *M*, p*D* ≃ 7.3.
[c]0.10 *M*, p*D* ≃ 7.0.

ment requires the reasonable assumption that 2′-deoxyriboses populate 2′-*endo* and 3′-*endo* modes. An internally consistent picture of conformation, electronegativity effects, and trends in *J* values is obtained. The interlocking arguments provide mutual support for the various aspects of this problem.

Schleich *et al.* (15) have arrived at an identical assignment for $H_{2'}$,$H_{2''}$ of 2′-deoxyuridine (dU). However, the assignment was fortuitously arrived at since the authors misinterpreted the arguments of Lemieux and Lineback (49) regarding the influence of the *cis* oriented 3′-OH on $\delta_{2''}$. They attributed the position of $H_{2''}$ to low field of $H_{2'}$ to a *deshielding* effect of 3′-OH on $H_{2''}$, whereas Lemieux and Lineback have discussed the evidence that a *cis* oriented OH *shields* a vicinal hydrogen. Interestingly now Fang *et al.* (32), using the accepted interpretation of the influence of 3′-OH on $H_{2''}$, concluded that the $H_{2''}$ lies to high field of $H_{2'}$ in the *adenine* mononucleotides, 3′dAMP and 5′dAMP. We have considered the available coupling constant data of Fang *et al.* (3′-dAMP, $J_{1'2''}$ = 6.0 Hz; $J_{1'2'}$ = 6.9 Hz; $J_{2'-3'}$ = 5.8 Hz; $J_{2''3'}$ = 3.8 Hz) in the light of the work of Fraser-Reid and Radatus (41) and our arguments used in the assignment of 3′dTMP and must agree with this 2′,2″ assignment for the adenine derivatives as well as the fortuitously arrived at dU assignment. Thus an interesting situation arises in that there is a reversal of the relative positions of $H_{2'}$ and $H_{2''}$ hydrogens with a change in the base from a pyrimidine (thymine, uracil) to the purine, adenine. In Table 2 are found data for 2′-deoxycytidine (dC) and 2′-deoxyadenosine (dA) which demonstrate that the reversal of the 2′ and 2″ hydrogens occurs at the nucleoside level as well. This conclusion may be arrived at by noting the similarity in the magnitudes of $J_{2''3'}$ and $J_{3'4'}$ in dA as well as in dC. This allows us to assign the low-field portion of the 2′,2″ (dC) band and the high-field portion of the 2′,2″ (dA) band to the 2″ hydrogen. Clearly then some subtle shielding effects must be at play at the $C_{2'}$ position. Contributions to the relative 2′,2″ shift undoubtedly come from the ring currents associated with the base, as well as from the electric and anisotropic magnetic fields of the 3′-OH and the 2-keto group of a pyrimidine. Evaluation of the contributions from these factors is beyond the scope of this paper. However, it is interesting to note that when a purine derivative is puckered 2′-*endo* with a small (≃0°) χ value, $H_{2''}$ lies in the shielding region of the six-membered ring of the base whereas $H_{2'}$ lies near to the five-membered imidazole ring. Perhaps this arrangement, which points to a relatively large shielding contribution to $H_{2''}$, forms the basis for the location of $H_{2''}$ to high field of $H_{2'}$ in 3′- and 5′dAMP.

Spectral Assignment of d(TpT)

The first step taken in the spectral assignment of the d(TpT) dimer was the construction of a 220 MHz *composite* spectrum of 3′dTMP and 5′dTMP (using the mononucleotide parameters in Table 1) for a comparison of the widths and

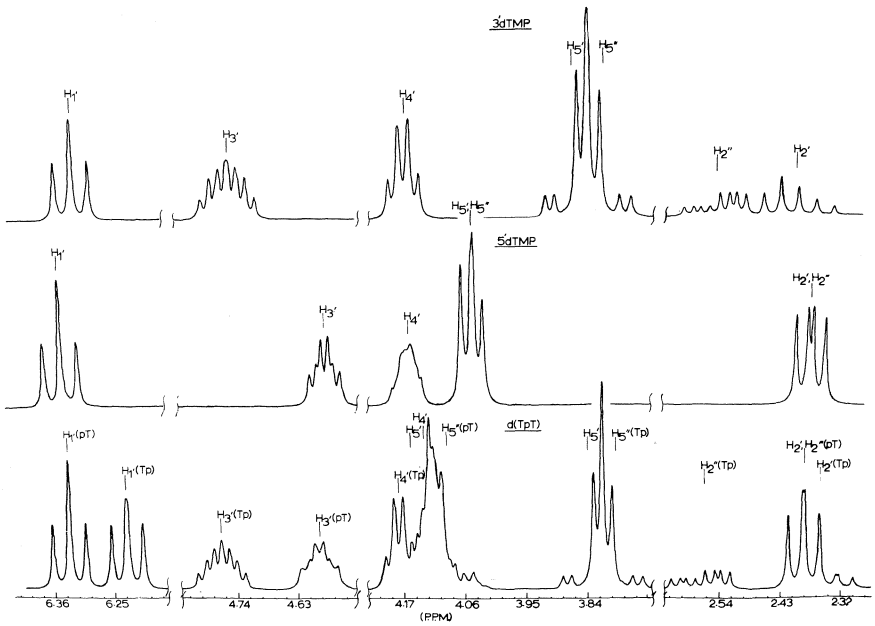

FIG. 7. Composite spectrum of 3′dTMP and 5′dTMP obtained by calculating 220 MHz spectra using experimental 100 MHz chemical shift and coupling constant data at 30° and computer simulated 220 MHz spectrum of d(TpT) using 18 °C data (Table 1).

splitting patterns of the observed dimer bands (Fig. 7). Using the arguments of Ts'o *et al.* (23) and the well-known phosphate effects (21, 22) the H_6, $H_{1'}$, and methyl hydrogens were assigned to the Tp and pT fragments as indicated in Fig. 7 and Table 1. The $H_{1'}$ assignment was later confirmed by double resonance experiments. In our composite 3′dTMP, 5′dTMP spectrum the $H_{3'}$ hydrogens appear as well-separated, characteristically shaped bands at 4.76 and 4.57 p.p.m., respectively. In d(TpT) the well-separated heptet (4.80 p.p.m.) and sextet (4.57 p.p.m.) were consequently assigned to $H_{3'}$(Tp) and $H_{3'}$(pT), respectively. This assignment is confirmed by our recent study (unpublished data) on d(TpTp) which corresponds to d(TpT) phosphorylated at the free 3′-hydroxyl of its pT fragment. Both $H_{3'}$ hydrogens in d(TpTp) appear in the vicinity of 4.8 p.p.m. with no $H_{3'}$ band in the 4.5–4.6 p.p.m. range.

Also recognizable is the d(TpT) heptet centered at 3.81 p.p.m. Its striking similarity in pattern and location to the $H_{5'}$,$H_{5''}$ band of 3′dTMP (centered at 3.84 p.p.m.) makes its assignment to $H_{5'}$, $H_{5''}$ (Tp) certain.

The multiplet around 2.40 p.p.m. is certainly due to the 2′,2″ hydrogens of pT and Tp. In addition to the similarity in the location of the 2′,2″ regions of the monomers and dimers, there are certain splitting and line intensity features in the d(TpT) spectrum which strongly resemble those in either 3′dTMP or 5′dTMP (see Fig. 7). Thus the appearance of the pair of quartets at lowest field in d(TpT) (centered at 2.66 and 2.52 p.p.m.) bears strong resemblance to the low field quartets of 3′dTMP (centered at 2.65 and 2.51 p.p.m.). The relatively intense four lines in the upper portion of d(TpT) (centered at 2.39 p.p.m.) resemble the 2′,2″ quartet of 5′dTMP (centered at 2.37 p.p.m.).

By the process of elimination the band centered around 4.15 p.p.m. must be assigned to the $H_{4'}$ (pT, Tp) and $H_{5'}$, $H_{5''}$ (pT) resonances.

With the assumption that the assignments of $H_{3'}$ (Tp) and $H_{3'}$ (pT) are correct, decoupling experiments were undertaken. The experiments were consistent with this assignment: the $H_{1'}$ triplet (6.34 p.p.m.), the strong quartet in the 2′,2″ region (2.39 p.p.m.) and the $H_{3'}$ band (4.60 p.p.m.) to the pT fragment *and* the $H_{1'}$ triplet (6.23 p.p.m.), the collection of weak (2′,2″) lines including the two quartets at lowest field, and the $H_{3'}$ band (4.78 p.p.m.)

to the Tp moiety. This is consistent with our tentative assignments based solely on chemical shift comparisons. We are further inclined to suggest that the pair of quartets at 2.66 and 2.52 p.p.m. are attributable to $H_{2''}$ (Tp) on the basis of their similarity in location (and appearance) to the low-field quartets of $H_{2''}$ (3′dTMP). Unfortunately the intense 2′,2″ (pT) quartet obscured most of the $H_{2'}$ (Tp) resonance. Final proof for the assignment was the excellent fit between experimental and calculated spectra (Fig. 4). At this point we draw attention to the near equality of $J_{3'4'}$ and $J_{2''3'}$ in both Tp and in 3′dTMP. Our reasoning above based on Fraser-Reid and Radatus (41) and these near equalities which follow from our assignment of the d(TpT) spectrum are mutually supporting.

Additional support for the 2′,2″ assignment of 3′dTMP and Tp is available through consideration of the effect of 3′- and 5′-phosphorylation on $H_{2'}$ and $H_{2''}$. A remarkable feature of the data in Table 1 is the constancy of $\delta_{2'}$ (2.38 ± 0.01 p.p.m.) over *all* entries. This contrasts sharply with the situation for $\delta_{2''}$: 2.39 ± 0.01 p.p.m. for dT, 5′dTMP, and pT and 2.57 ± 0.01 p.p.m. for Tp and 3′dTMP. These trends are entirely consistent with the spatial relationship between the 3′- and 5′-phosphates and $C_{2'}$ hydrogens, our 2′,2″ assignment for 3′dTMP and Tp and our understanding of the conformational features of these molecules. The *endo* hydrogen ($H_{2'}$) is not expected to be significantly influenced by phosphorylation at the 5′ position of dT since it is only when the molecules (pT, 5′dTMP) are simultaneously oriented *gauche–gauche* (gg) about $C_{4'}$—$C_{5'}$ and *trans′–gauche′* (t′g′) about $C_{5'}$—$O_{5'}$ (Fig. 8) that $H_{2'}$ is near to the negatively charged oxygens. However we have shown earlier (24–27) that in the case of 5′-mononucleotides, gg oriented systems favor g′g′ (Fig. 8) with virtual exclusion of t′g′ or g′t′ (*gauche′–trans′*) orientations. This exclusion of g′t′ and t′g′ conformations for gg 5′-monophosphates is apparent at the oligo- and polynucleotide level as well (1, 2, 7–11, and discussion below). For the cases of 3′-phosphorylation (3′dTMP, Tp), the presence of negative charge is expected to be sensed at $H_{2'}$ only when the molecule is simultaneously oriented 3′-*endo* and g(2′) (see Fig. 9 for definition of g(2′)). However, in subsequent sections we shall demonstrate that the 2′-*endo* pucker is favored and that a blend of the g(2′) and g(4′) conformers about $C_{3'}$—$O_{3'}$ is apparent. In conformations other than 3′-*endo*, g(2′) (and particularly in 2′-*endo*, g(4′)) the presence of charge on the 3′-phosphate of 3′dTMP and Tp is not expected to influence $\delta_{2'}$. Hence the constancy of $\delta_{2'}$ over all entries in Table 1 is understandable. The invariance of $\delta_{2''}$ for dT, 5′dTMP, and pT is also reasonable in view of the separation between the 5′ position and the *exo* hydrogen ($H_{2''}$). That 3′-phosphorylation should be reflected in $\delta_{2''}$ is, however, reasonable in view of the proximity between $H_{2''}$ and the phosphate oxygens, particularly in the favored 2′-*endo* (and g(2′)) conformations of 3′dTMP and Tp. Thus the single sharp range of $\delta_{2'}$ and dual sharp ranges of $\delta_{2''}$ values can be rationalized if our 2′,2″ assignment as well as our conformational conclusions are accepted.

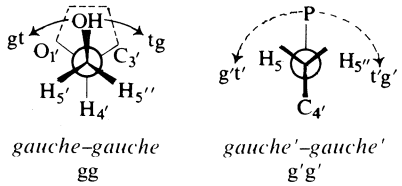

gauche–gauche gg *gauche′–gauche′* g′g′

FIG. 8. (*a*) Staggered conformations about $C_{4'}$—$C_{5'}$, gg (*gauche–gauche*), gt (*gauche–trans*), and tg (*trans–gauche*). (*b*) Staggered conformations about $C_{5'}$—$O_{5'}$, g′g′ (*gauche′–gauche′*), g′t′ (*gauche′–trans′*), and t′g′ (*trans′–gauche′*).

The Sugar–Base Torsion Angle

Considerable evidence now points to the preference for the *anti* (54) range of sugar–base torsion angles (χ) about the *N*-glycosyl linkage of pyrimidine nucleosides and nucleotides. Molecules displaying a preference for the *syn* range (with one exception, crystalline 4-thiouri-

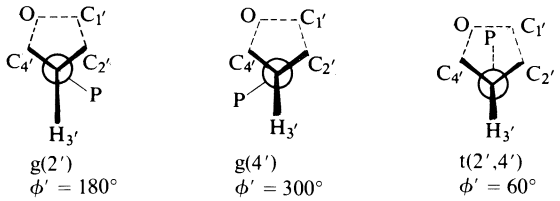

FIG. 9. Conformations about the $C_{3'}$—$O_{3'}$ bond of a 3′-nucleotide viewed from $C_{3'}$ to $O_{3'}$; (*a*) g(2′), phosphorus *gauche* to $H_{3'}$ and $C_{2'}$; (*b*) g(4′), phosphorus *gauche* to $H_{3'}$ and $C_{4'}$; (*c*) t(2′,4′), phosphorus *trans* to $H_{3'}$ and *gauche* to $C_{2'}$ and $C_{4'}$. ϕ' values according to the Sundaralingam convention (1).

dine (55)) possess a bulky group (methyl (56), carboxyl (57) etc.) at the 6 position of the base which forces the 2-keto oxygen to locate preferentially over the furanose ring. More specifically, X-ray, o.r.d., and n.m.r. evidence points to the preference for the *anti* range of dT, 3′dTMP, and 5′dTMP (1, 2, 21–23, 32, 58) as well as for the pTp and pT moieties of d(pTpT).

Prestegard and Chan (59) have argued that δ_6 should be sensitive to changes in χ since χ defines the spatial relationship of H_6 and the ethereal ring oxygen. On this basis the virtually invariant δ_6 for dT, 3′dTMP, and Tp is evidence that 3′-phosphorylation or incorporation into d(TpT) as the free 5′-terminus has no large effect on χ (thymidine). In fact $\delta_{1'}$ may be an even more sensitive monitor of χ changes since χ defines the disposition of $H_{1'}$ and the highly anisotropic and polar 2-keto oxygen. Thus some small variations in χ are indicated by the $\delta_{1'}$ (dT, 3′dTMP, Tp) data. Considering only the data for 3′dTMP and Tp at either temperature, an average deviation of only 0.03 p.p.m. is present for all hydrogens. This is entirely inconsistent with any drastic change of χ values concomitant with incorporation of the monomer into the dimer. A similar comparison of data for dT, 5′dTMP, and pT argues against any large influence upon χ (thymidine) due to 5′-phosphorylation or incorporation into d(TpT) at the free 3′-terminus under the present experimental conditions.

In the crystal state available χ values for thymidine residues (dT, 39.3°; 5′dTMP, 43.5°; pTp of d(pTpT), 27°; and pT of d(pTpT), 34°) reveal a remarkable degree of conformational similarity and the absence of drastic changes upon 3′- or 5′-phosphorylation or incorporation into a thymine dinucleoside(tide) (2, 11).

Puckering of the 2′-Deoxyfuranose Ring

Nuclear magnetic resonance evidence indicates that 2′-deoxyfuranose, as well as furanose, ring systems are best discussed in terms of a dynamic equilibrium between 2′-*endo* and 3′-*endo* puckered modes (14–17, 28, 30, 31, 50). Altona and Sundaralingam (42, 43) have suggested a method for estimating the conformational blend in the furanoses but as yet the authors have not presented a detailed extension for deoxy derivatives. However, it appears likely that the conformational blend in the molecules under examination here may be estimated from the expressions (43)

$$[1] \qquad \%\ 3'\text{-}endo \simeq 10J_{3'4'}$$

$$[2] \qquad \%\ 2'\text{-}endo = 100 - \%\ 3'\text{-}endo$$

In Table 2 are found calculated values for the molecules of interest here as well as for several ribose derivatives. Overall one can say that the deoxy derivatives display very similar puckering with a 60–70% bias for 2′-*endo*. However, within these limits some trends at the monomer level appear. (*a*) 3′-Phosphorylation has no noticeable effect on conformation whereas 5′-phosphorylation enhances the percentage of 2′-*endo* in both the ribose and 2′-deoxyribose series. Sundaralingam (2) has reviewed the evidence for the $C_{2'}$-*endo* bias of 5′-nucleotides in the ribo and deoxyribo series. (*b*) The removal of the 2′-hydroxyl leads to an enhancement of 2′-*endo*.[6] Discussions of this phenomenon which is apparent in both the crystal and solution state have appeared (1, 2, 17, 45). (*c*) Although the data do indicate some effect upon ring conformation following incorporation of dT or its monophosphates into the dimer, the changes are very small. In the crystal state (2) as well as in solution (17, 45) this prevailing tendency towards 2′-*endo* is apparent. In d(pTpT) both fragments assume this conformation (11).

Conformation About the Exocyclic $C_{4'}$—$C_{5'}$ and $C_{5'}$—$O_{5'}$ Bonds

In previous studies, simple relationships between Σ $(= J_{4'5'} + J_{4'5''})$ and P_{gg}, the fractional population of the *gauche–gauche* conformation (Fig. 8), and between Σ' $(= J_{P5'} + J_{P5''})$ and $P_{g'g'}$, the fractional population of the *gauche′–gauche′* conformation, were derived (26, 27).

$$[3] \qquad P_{gg} \simeq (13 - \Sigma)/10$$

$$[4] \qquad P_{g'g'} \simeq (24 - \Sigma')/18$$

These approximate relationships are particularly useful in those instances where, due to strong coupling between $H_{5'}$ and $H_{5''}$, only the values

[6]We have not considered any influence of this uracil-to-thymine base change in our comparison. However, other data indicate (2, 17) that this base change has little effect on the overall (2′-deoxy) furanose conformation.

of Σ and Σ' may be obtained from the spectrum (this is the case in 5′dTMP).[7]

In Table 4 we have calculated P_{gg} and $P_{g'g'}$ values for a series of molecules (crystal conformations are also included; those for d(pTpT) in ref. 11 are given under Tp and pT columns). We should point out here that some degree of uncertainty exists in the experimental Σ and Σ' values for the pT fragment. This is a consequence of the overlap of the $H_{4'}$, $H_{5'}$, and $H_{5''}$ (pT) bands and the absence of sufficient peaks required for iterative computer analysis. However, because of our approximate treatment of the data in terms of the conformational parameters we do not consider this greater uncertainty a serious matter. Furthermore, in a subsequent paragraph support for the qualitative conclusions based on Σ and Σ' values is provided through a consideration of the chemical shift data.

Several trends are apparent in Table 4. (*a*) At the monomer level, 3′-phosphorylation has little effect on P_{gg} in both the ribose and 2′-deoxyribose series. This situation holds in the crystal state for riboses (compare U (60) and 3′UMP (2) which are gg). No crystal data for 3′dTMP are available. However, 3′-phosphorylation results in a gt to gg change in 2′-deoxyuridine (2, 6). (*b*) 5′-Phosphorylation enhances P_{gg} at the monomer level. Sundaralingam and co-workers (2, 8) have argued that 5′-nucleotides are more "rigid" than the corresponding nucleoside or 3′-nucleotides, *i.e.* are expected (63), in solution, to have significantly enhanced P_{gg} values. The data in Table 4 indicate a substantial enhancement for U (56%) to 5′UMP (75%) in the ribose series but a considerably smaller change is noted for dT (45%) to 5′dTMP (54%) in the deoxyribose series. (*c*) Removal of the 2′-hydroxyl diminishes P_{gg} at the nucleoside, 3′-nucleotide, and 5′-nucleotide level. This influence of the 2′-OH has been discussed previously for the crystal and solution states (2, 17). (*d*) Incorporation of dT into d(TpT) increases the P_{gg} values slightly. (*e*) The $P_{g'g'}$ conformation of 5′dTMP is overwhelmingly favored (90%); our (less certain) Σ' (pT) suggests this to be the case in pT as well. This stronger bias for g′g′ conformations is entirely consistent with previous work carried out on a large number of 5′-nucleotides (26). In crystalline d(pTpT) both the pTp and pT fragments are oriented gg and g′g′.

The long-range four-bond $^4J_{P4'}$ couplings provide information about the $C_{4'}$—$C_{5'}$ and $C_{5'}$—$O_{5'}$ bond conformations (24–28), although they are expected to be less reliable than Σ and Σ' as conformational (P_{gg}, $P_{g'g'}$) probes due to their small size (0–3 Hz). In ref. 27 correlations are described between $^4J_{P4'}$ and Σ and Σ' values which were suggested to be of value in providing support for the conformational information derived from Σ and Σ'. (In this regard we should point out that recent measurements (27*b*) reveal a slight p*H* dependence upon $^4J_{P4'}$ *i.e.* protonation of the 5′-phosphate enhances it by about 0.5 Hz without a propor-

[7]A referee has suggested that the populations of the gt and tg conformers be separately evaluated rather than treated collectively as $1 - P_{gg}$. It is a simple matter to show that $P_{tg} - P_{gt} = \sigma/(J_t - J_g)$ where σ is defined as the *experimental* difference $J_{4'5'} - J_{4'5''}$. J_g and J_t are the *estimated gauche* and *trans* H–H couplings, respectively. In our derivation of eq. 3 (26) values of 1.5 Hz (J_t) were assumed. Thus $(P_{tg} - P_{gt}) = \sigma/10$. Given also P_{gg} (eq. 3) and $P_{tg} + P_{gt} = 1 - P_{gg}$, all P values can be estimated. Similarly for $C_{5'}$–$O_{5'}$ we can show that $(P_{t'g'} - P_{g't'}) = \sigma'/(J_t - J_g)$ where σ' is defined as the observed difference $J_{P5'} - J_{P5''}$. J_g and J_t are now the expected *gauche* and *trans* $^{31}P - {}^1H$ J values for the P—O—C—$H_{5'}$($H_{5''}$) fragments. In our derivation of eq. 4 (26), values of 3 Hz (J_g) and 21 Hz (J_t) were assumed. Thus with $P_{t'g'} - P_{g't'} = \sigma'/18$, $P_{g'g'}$ from eq. 4 and $P_{t'g'} + P_{g't'} = 1 - P_{g'g'}$ all $C_{5'}$—$O_{5'}$ P values can be estimated. We should stress that inherent in the use of equations are several assumptions, particularly that regarding the invariance of J_g and J_t for the three staggered conformers. They are however expected to vary since the molecules are not symmetrical about $C_{4'}$—$C_{5'}$ or $C_{5'}$—$O_{5'}$. Furthermore, it is well known that the *orientation* of electronegative substituents on H—C—C—H fragment is an important consideration (62). Thus in the gg conformer $J_{4'5''}$ will be *attenuated* relative to $J_{4'5'}$ since $O_{1'}$ lies *trans* to $H_{5''}$ and is expected to exert its maximal electronegativity effect on $J_{4'5''}$. However $O_{1'}$ lies *gauche* to $H_{5'}$ in gg; the $O_{1'}$ influence or $J_{4'5'}$ is thus expected to be much smaller. Similar considerations must be given to $J_{4'5'}$ in gt since $O_{1'}$ is now *trans* to $H_{5'}$. Corrections to the $J_{4'5'}$ and $J_{4'5''}$ values for the *trans* $O_{1'}$ influence are probably about 0.5 Hz. If they are not made, additional errors of about 5% in the calculated P's are introduced. Similar corrections (of unknown magnitude) to the P–H couplings seem warranted since rotation about the $C_{5'}$—$O_{5'}$ bond changes the disposition of the unshared pairs on $O_{5'}$ relative to $H_{5'}$, $H_{5''}$. Thus the accuracy in the calculated P's is at best $\pm 10\%$. However, though the absolute values of the P's must be considered with some reservation, we feel confident that trends in a particular P value over a series of molecules is meaningful. Our confidence is supported by the number of excellent correlations we have noted recently (17, 26, 45, 64). Finally assuming the Remin–Shugar (40) assignment of the 5′,5″ hydrogens, we estimate from the $J_{4'5'}$ and $J_{4'5''}$ values that P_{gt} and P_{tg} are 25 and 15%, respectively, for pT.

tionate (27) increase in Σ or Σ′.) The $^4J_{P4'}$ (5′-dTMP) values are consistent with $P_{gg} \sim 60\%$ and $P_{g'g'} \sim 80\%$. Due to the complexity of the $H_{4'}$, $H_{5'}$, $H_{5''}$ (pT) band, no $^4J_{P4'}$ (pT) can be extracted from the hydrogen spectra though it should be revealed in the ^{31}P spectra.

Our treatment of the $C_{4'}$—$C_{5'}$ and $C_{5'}$—$O_{5'}$ conformational problems in pT are hampered by the uncertainties in Σ and Σ′. Certainly we achieved some success (Fig. 4) in accounting for the $H_{4'}$, $H_{5'}H_{5''}$ (pT) band but the absence of sufficient fine structure precludes iterative computer analysis. Thus we resorted to a trial and error approach. A number of spectra were computed using large values of Σ and Σ′ (which would result if the molecule were *not* oriented gg or g′g′) but the fits with experimental spectra were poor. Thus we express some confidence in our suggestion that gg and g′g′ are slightly favored in their respective conformational blends. (However, we cannot claim to have exhausted all possible combinations of δ's and *J*'s.) Consideration of the chemical shift data support the contention that P_{gg} and $P_{g'g'}$ are similar for 5′dTMP and pT.

Examination of molecular models reveals a close approach of $O_{5'}$ to $H_{3'}$, and $H_{2'}$ in gg oriented 5′dTMP and pT. In the gt and tg conformations, $O_{5'}$ (and the negatively charged oxygens as well) approach $H_{4'}$. Nevertheless, $\delta_{2'}$, $\delta_{3'}$, and $\delta_{4'}$ values are remarkably constant for 5′dTMP and pT. This constancy seems consistent with the similarity in their estimated P_{gg}, $P_{g'g'}$ values in Table 4. It should also be noted that through our trial and error approach to the $H_{5'}H_{5''}$ (pT) analysis we have arrived at a somewhat enhanced magnetic nonequivalence between $H_{5'}$ and $H_{5''}$ (0.07 p.p.m. in pT compared with 0.01 p.p.m. in 5′dTMP). Similar enhancement of the magnetic nonequivalence has been observed for the pA fragment of adenylyl-(3′,5′)-adenosine by Kondo and Danyluk (35). In 5′AMP the authors note $\delta_{5'} - \delta_{5''} \simeq 0.02$ p.p.m. but in pA, the value was 0.19 p.p.m. (The enhancement in their purine and ribose derivative is larger than in our pyrimidine and deoxyribose derivative and the acidity conditions employed are not the same.) Nevertheless it is still encouraging to note that both in pA and in pT the enhanced magnetic nonequivalence is brought about by differential *deshielding* of $H_{5'}$ and $H_{5''}$ relative to the 5′ monophosphate. A discourse (64) on the 5′,5′′ magnetic nonequivalence and its relation to $C_{4'}$—$C_{5'}$ orientation has been provided.

Conformation About the $C_{3'}$—$O_{3'}$ Bond

Several possible conformations about the $C_{3'}$—$O_{3'}$ bond, which determine the disposition of the phosphate and the furanose ring, are available to 3′dTMP and Tp (Fig. 9). In the Sundaralingam notation these orientations are defined (1) by the angle φ′. In g(2′) the phosphorus in *gauche* to $H_{3'}$ and to $C_{2'}$ (φ′ = 180°); in g(4′) it is *gauche* to $H_{3'}$ and to $C_{4'}$ (φ′ = 300°); in t(2′,4′) it is *trans* to $H_{3'}$ and *gauche* to both $C_{2'}$ and $C_{4'}$ (φ′ = 60°). Space-filling models suggest that t(2′,4′) is an unlikely candidate for any 3′-mononucleotide fragment due to steric crowding. No X-ray data are as yet available for 2′-deoxy-3′-monophosphates but the (limited) data for the ribose series reveal a single broad range from 195 to 269° for φ′ with no entries for φ′, which places the P atom *gauche* to both $C_{2'}$ and $C_{4'}$ (t(2′,4′)). In *ribose* dinucleoside monophosphates a range from about 200 to 245° (2, 7–10) is observed; in the pTp fragment of d(pTpT) φ′ = 252° (11) (−108° in the notation (65) used by Camerman *et al.* in ref. 11). Nuclear magnetic resonance evidence based on ^1H–^{31}P and ^{13}C–^{31}P couplings have demonstrated a *preference* for g(2′) in the ribose derivatives uridine-3′-monophosphate (3′UMP) and polyuridylic acid for g(2′) (36, 66).

Bearing in mind the work of Hall and Malcolm (67), Davies and Danyluk (68), and Schleich *et al.* (15) it seems reasonable to suggest that the "small" values of $^3J_{P3'}$ (6.8–7.8 Hz) are consistent with virtual exclusion of t(2′,4′) in 3′dTMP and Tp since *trans* ^1H–^{31}P couplings in HCOP fragments are expected to be 21–24 Hz (67). The $^3J_{P4'}$ data do not, however, allow one to distinguish between g(2′) and in g(4′) since in each, $H_{3'}$ and P are oriented *gauche*.[8]

A consideration of the chemical shift data

[8] A 6.8–7.8 Hz $^3J_{P3'}$ value seems somewhat large for a classically oriented *gauche* (all angles 60°) H—C—O—P fragment (67). In the crystal state, however, a decided bias away from the classical g(2′) and g(4′) conformers towards a *cis* coplanar (φ′ = 240°) conformation is apparent (2). If this bias exists in solution as well, the somewhat enhanced $^3J_{P3'}$ values in 3′dTMP and Tp can be rationalized without invoking contributions from t(2′, 4′). Assuming a Karplus-like relationship and $^3J_{PH}$ (*trans*) = 21 Hz and $^3J_{PH}$ (*gauche*) = 3 Hz (67), a $^3J_{PH}$ value of about 7.0 Hz is calculated for a conformation biased 15° (φ′, 195 or 285°) towards the *cis* coplanar conformation.

provides additional conformational information. In view of the charge associated with the oxygen atoms (O(I) and O(II) in d(TpT), Fig. 1) and its proximity to $H_{4'}$ in g(4′) and to $H_{2''}$ in g(2′), we are inclined to suggest that the remarkable constancy in $\delta_{4'}$ (4.18 ± 0.01 p.p.m.) and $\delta_{2''}$ (2.57 ± 0.01 p.p.m.) for 3′dTMP and Tp argues for a blend of g(2′) and g(4′) which is similar in these compounds and essentially invariant over the temperature interval examined. This suggestion is substantiated by the constancy of other shift data: $\delta_{3'} = 4.78 \pm 0.02$ p.p.m.; $\delta_{2'} = 2.38 \pm 0.02$ p.p.m.

Although the $^3J_{P3'}$ values do not form a basis for quantitative discussions of the g(2′) ↔ g(4′) blend in 3′dTMP and Tp, our contention, based on the assessment of close contact interactions apparent in molecular models, is that, when 3′dTMP (Tp) assumes the *preferred* combination of ring pucker and $C_{4'}$—$C_{5'}$ orientation, *i.e.* 2′-*endo*, gg, there exists no significant bias towards either g(2′) or g(4′). In this conformational combination, g(2′) and g(4′) provide the 3′-phosphoryl group with an identical set of close contacts involving, in particular $H_{2''}$ and $H_{4'}$. In fact in the gg, 2′-*endo* (or 3′-*endo*) conformation the $H_{3'}$—$C_{3'}$—$O_{3'}$ plane defines a *local* mirror plane for the $C_{4'}$—$C_{3'}$—$C_{2'}$ fragment (and for the *important* contacts made by the 3′-phosphoryl in g(2′) and g(4′)). In the less probable combination (3′-*endo*, tg), a bias (probably towards g(2′)) is expected in view of the severe contacts made between the 5′-hydroxyl and 3′-phosphoryl groups when the molecule is g(4′). However our data (Tables 3 and 4) and X-ray data (1, 2) suggest that 3′-*endo*, tg cannot make important contributions to the overall conformational blend. In view of our statements regarding the similar steric environments experienced by the 3′-phosphoryl in g(2′) and g(4′) when 3′dTMP (Tp) assumes the preferred conformational combination 2′-*endo*, gg, it is interesting to point out the virtually identical effects of 3′-phosphorylation (or attachment of a pT fragment) upon $\delta_{2''}$ and $\delta_{4'}$ of a dT fragment. Relative to dT, $H_{2''}$ and $H_{4'}$ experience a 0.14 ± 0.01 and 0.17 ± 0.01 p.p.m. deshielding, respectively. We do not feel that these deshielding effects form a simple basis for a semiquantitative evaluation of the g(2′) ↔ g(4′) blend but, in view of the similar spatial disposition of $C_{2'}$—$H_{2''}$ and $C_{4'}$—$H_{4'}$ relative to $C_{3'}$—$O_{3'}$ in the 2′-*endo* and 3′-*endo* puckers, we should state that they are consistent with a near balance of g(2′) and g(4′) contributions. Mantsch and Smith (66) have provided n.m.r. evidence for a g(2′) preference in *ribose* 3′-mononucleotide (3′ UMP) in aqueous solution. In the crystalline state, 3′ UMP is g(4′) which suggests the importance of crystal packing forces on the $C_{3'}$—$O_{3'}$ orientation (2). We think it relevant to point out that in crystalline ribose 3′,5′-dinucleoside monophosphates the internal $C_{3'}$—$O_{3'}$ bond lies in the g(2′) range whereas in d(pTpT) it is in the g(4′) range.

TABLE 3. Calculated 2′-*endo* populations of the 2′-*endo* ↔ 3′-*endo* blend[a]

Compound	% 2′-*endo*
2′-Deoxyribosides	
dT	63[b]
3′dTMP	60(63)
5′dTMP	71(67)
Tp	68(64)
pT	67(60)
Ribosides	
U	46(49)[c]
3′UMP	45(45)[c]
5′UMP	61[d]

[a]Numbers in parentheses correspond to high temperature; other values are for ambient temperature, 18–30 °C.
[b]Probable error in calculated values ± 5%.
[c]Reference 15.
[d]Reference 24.

TABLE 4. Calculated rotamer populations (%) for the $C_{4'}$—$C_{5'}$ and $C_{5'}$—$O_{5'}$ bonds[a]

Compound	*P*gg	*P*g′g′
2′-Deoxyribosides		
dT	45[gt][b]	—
3′dTMP	47(43)	—
5′dTMP	54(52)[gg]	78(78)[g′g′]
Tp	54(47)[gg]	—
pT	65(55)[gg]	90(85)[g′g′]
Ribosides		
U	56[c][gg]	—
3′UMP	60[d][gg]	—
5′UMP	75[e][gg]	90[g′g′]

[a]Numbers in parentheses for high temperature (> 60 °C), other numbers for ambient temperature (18–30 °C); probable error ± 5%.
[b]Bracketed symbols give crystalline structure (refs. 1 and 2) except for Tp and pT where symbols are for d(pTpT) in ref. 11.
[c]References 15 and 16.
[d]Reference 15.
[e]Reference 24.

Conformation About the $O_{3'}$—P and $O_{5'}$—P Bonds

Unfortunately ^{1}H, ^{13}C, and ^{31}P coupling measurements cannot define the orientation about the $O_{3'}$—P and P—$O_{5'}$ bonds. The gene al similarity in the chemical shifts of corresponding hydrogens in the 3′dTMP–Tp and 5′dTMP–pT pairs[9] are suggestive of a similar conformational distribution about the relevant O—P bonds.

Base Stacking in d(TpT)

Detection of base stacking by n.m.r. between pyrimidines is difficult due to the absence of significant ring-current effects of the neighboring base. However, it is interesting to note that evaluation of the g(2′) contribution to the g(2′) ↔ g(4′) blend provides a measure of the upper limit of the population of base-stacked conformation since g(4′) precludes the formation of right-handed stacked forms. Furthermore, since destacking of a dimer probably results from O—P rotations (1, 2) and temperature increases should bring about destacking in the temperature interval examined (69), the absence of any substantial effects of temperature upon the shifts of hydrogens expected to be dependent on O—P rotations argues for small contributions from stacked forms. This is consistent with the presence of the extended form of d(pTpT) in the solid state (11). In aqueous solution ORD and CD measurements point to some ordering of 2′-deoxy dimers but the consensus of opinion is that pyrimidine bases have reduced stacking tendencies (69).

In conclusion, proton magnetic resonance studies of dT, 3′dTMP, 5′dTMP, and d(TpT) are discussed. Spectral assignment and analysis are carried out and the chemical shift and coupling constant data are discussed in terms of molecular conformation. The main conclusion reached is that little conformational change occurs in a 2′-deoxythymidine moiety upon 3′- or 5′-phosphorylation or upon incorporation into the dimer d(TpT). This conservation of the conformational parameters of a nucleoside fragment upon phosphorylation or incorporation into progressively more complex oligo- and polynucleotides has been discussed by Sundralingam (1, 2).

This research was supported in part by grants from the National Research Council of Canada, The Research Corporation of New York, The North Atlantic Treaty Organization, and The Faculty of Graduate Studies of the University of Manitoba. The authors acknowledge illuminating discussions with Professor T. Schaefer and the NMR group at the University of Manitoba. We thank Dr. A. A. Grey and Mrs. Valerie Robinson of the Canadian 220 MHz Centre, Sheridan Park Ontario, for obtaining 220 MHz spectra and Dr. J. B. Rowbotham for his assistance with the computer programs.

[9]Average difference over all deoxyribose hydrogens in each pair is 0.03 p.p.m.

1. M. Sundaralingam. Biopolymers, **7**, 821 (1969).
2. M. Sundaralingam. Proc. Intern. Symp. Conform. Biol. Mol. Polym. Symp. Quantum Biochem. *Edited by* B. Pullman and E. D. Bergmann. V5. 1973. p. 417.
3. W. Saenger. Angew. Chem. Int. Ed. **12**, 591 (1973).
4. A. Rahman and H. R. Wilson. Acta. Cryst. B**28** 2260 (1971).
5. S. Arnott and D. W. L. Hukins. Nature, **224**, 886 (1969).
6. E. Shefter, M. Barlow, R. Sparks, and K. Trueblood. J. Am. Chem. Soc. **86**, 1872 (1964).
7. N. C. Seeman, J. L. Sussman, H. M. Berman, and S. H. Kim. J. Mol. Biol. **66**, 403 (1972).
8. J. Rubin, T. Brennan, and M. Sundaralingam. Biochemistry, **11**, 3112 (1972).
9. R. O. Day, N. C. Seeman, J. M. Rosenberg, and A. Rich. Proc. Natl. Acad. Sci. U.S.A. **70**, 849 (1973).
10. J. M. Rosenberg, N. C. Seeman, J. P. Kim, F. L. Suddath, H. B. Nicholas, and A. Rich. Nature, **243**, 150 (1973).
11. N. C. Camerman, J. K. Fawcett, and A. Camerman. Science, **182**, 1142 (1973).
12. C. D. Jardetzky. J. Am. Chem. Soc. **84**, 62 (1962).
13. R. U. Lemieux. Can. J. Chem. **39**, 116 (1961).
14. F. E. Hruska, A. A. Grey, and I. C. P. Smith. J. Am. Chem. Soc. **92**, 4088 (1970).
15. T. Schleich, B. J. Blackburn, R. D. Lapper, and I. C. P. Smith. Biochemistry, **11**, 137 (1972).
16. B. J. Blackburn, A. A. Grey, I. C. P. Smith, and F. E. Hruska. Can. J. Chem. **48**, 2866 (1970).
17. F. E. Hruska. Proc. Intern. Symp. Conform. Biol. Mol. Polym. Symp. Quantum Biochem. *Edited by* B. Pullman and E. D. Bergmann. V5 1973. p. 345.
18. M. P. Schweizer, E. B. Banta, J. T. Witkowski, and R. K. Robins. J. Am. Chem. Soc. **95**, 3770 (1973).
19. M. Remin and D. Shugar. J. Am. Chem. Soc. **95**, 8146 (1973).
20. D. B. Davies and S. S. Danyluk. Can. J. Chem. **48**, 3112 (1970).
21. M. P. Schweizer, A. D. Broom, P. O. P. Ts'o, and D. P. Hollis. J. Am. Chem. Soc. **90**, 1042 (1968).
22. S. S. Danyluk and F. E. Hruska. Biochemistry, **7** 1038 (1968).
23. P. O. P. Ts'o, N. S. Kondo, M. P. Schweizer, and D. P. Hollis. Biochemistry, **8**, 997 (1969).
24. D. J. Wood, F. E. Hruska, R. J. Mynott, and R. H. Sarma. Can. J. Chem. **51**, 2571 (1973).
25. F. E. Hruska, D. J. Wood, R. J. Mynott, and R. H. Sarma. FEBS Lett. **51**, 153 (1973).
26. D. J. Wood, R. J. Mynott, F. E. Hruska, and R. H. Sarma. FEBS Lett. **31**, 323 (1973).
27. (*a*) R. H. Sarma, R. J. Mynott, D. J. Wood, and F. E. Hruska. J. Am. Chem. Soc. **95**, 6457 (1973); (*b*) D. J. Wood, F. E. Hruska, and R. H. Sarma. Unpublished results.

28. I. C. P. SMITH, H. H. MANTSCH, R. D. LAPPER, R. DESLAURIERS, and T. SCHLEICH. Proc. Intern. Symp. Conform. Biol. Mol. Polym. Symp. Quantum Biochem. *Edited by* B. Pullman and E. D. Bergmann. V5. 1973. p. 381.
29. P. A. HART and J. P. DAVIS. Proc. Intern. Symp. Conform. Biol. Mol. Polym. Symp. Quantum Biochem. *Edited by* B. Pullman and E. D. Bergmann. V5. 1973. p. 297.
30. T. DINH SON and C. CHACHATY. Biochem. Biophys. Acta, **335**, 1 (1973).
31. F. E. HRUSKA and S. S. DANYLUK. J. Am. Chem. Soc. **90**, 3266 (1968).
32. K. N. FANG, N. S. KONDO, P. S. MILLER, and P. O. P. Ts'o. J. Am. Chem. Soc. **93**, 6647 (1971).
33. S. I. CHAN and J. H. NELSON. J. Am. Chem. Soc. **91**, 168 (1969).
34. B. W. BANGERTER and S. I. CHAN. J. Am. Chem. Soc. **91**, 3910 (1969).
35. N. S. KONDO and S. S. DANYLUK. J. Am. Chem. Soc. **94**, 5121 (1972).
36. (*a*) G. GOVIL and I. C. P. SMITH. Biopolymers, **12**, 2589 (1973); (*b*) C. ALTONA, J. H. VAN BOOM, J. DE JAGER, H. J. KOENER, and G. VAN BENST. Nature, **247**, 560 (1974).
37. (*a*) A. D. CROSS and D. M. CROTHERS. Biochemistry, **10**, 4015 (1971); (*b*) C. C. MCDONALD, W. D. PHILIPS, and J. LAZAR. J. Am. Chem. Soc. **89**, 4166 (1967); (*c*) S. I. CHAN, B. W. BANGERTER, and H. H. PETER. Proc. Natl. Acad. Sci. (U.S.) **55**, 720 (1966).
38. R. L. LETSINGER, K. K. OGILVIE, and P. S. MILLER. J. Am. Chem. Soc. **91**, 3360 (1969).
39. C. W. HAIGH and J. M. WILLIAMS. J. Mol. Spectrosc. **32**, 398 (1969).
40. M. REMIN and D. SHUGAR. Biochem. Biophys. Res. Commun. **48**, 636 (1972).
41. B. FRASER-REID and B. RADATUS. J. Am. Chem. Soc. **93**, 6342 (1971).
42. C. ALTONA and M. SUNDARALINGAM. J. Am. Chem. Soc. **94**, 8205 (1972).
43. C. ALTONA and M. SUNDARALINGAM. J. Am. Chem. Soc. **95**, 2333 (1973).
44. L. D. HALL, P. R. STEINER, and C. PEDERSEN. Can. J. Chem. **48**, 1155 (1970).
45. F. E. HRUSKA, A. A. SMITH, and J. G. DALTON. J. Am. Chem. Soc. **93**, 4334 (1971).
46. (*a*) H. BOOTH. Tetrahedron Lett. 411 (1965); (*b*) D. H. WILLIAMS and N. S. BHACCA. J. Am. Chem. Soc. **86**, 2742 (1964).
47. F. E. HRUSKA, D. J. WOOD, J. G. DALTON, T. N. MCCAIG, and R. E. WASYLISHEN. In preparation.
48. K. G. R. PACHLER. J. Chem. Soc. 1936 (1972).
49. R. U. LEMIEUX and D. R. LINEBACK. Ann. Rev. Biochem. **32**, 155 (1963).
50. K. N. SLESSOR and A. S. TRACEY. Carbohydr. Res. **27**, 407 (1972).
51. D. J. WOOD and F. E. HRUSKA. In preparation.
52. C. GIESSNER-PRETTRE and B. PULLMAN. C.R. Acad. Sci. Paris, **261**, 13 (1965).
53. J. W. APSIMON and H. BEIERBECK. Can. J. Chem. **49**, 1328 (1971).
54. J. DONOHUE and K. N. TRUEBLOOD. J. Mol. Biol. **2**, 363 (1960).
55. W. SAENGER and K. H. SCHEIT. J. Mol. Biol. **50**, 153 (1970).
56. M. P. SCHWEIZER, J. T. WITKOWSKI, and R. K. ROBINS. J. Am. Chem. Soc. **93**, 277 (1971).
57. F. E. HRUSKA. J. Am. Chem. Soc. **93**, 1795 (1971).
58. T. R. EMERSON, R. J. SWAN, and T. L. V. ULBRICHT. Biochemistry, **6**, 843 (1967).
59. J. H. PRESTEGARD and S. I. CHAN. J. Am. Chem. Soc. **91**, 2843 (1969).
60. E. A. GREEN, R. SHIONO, R. D. ROSENSTEIN, and D. J. ABRAHAM. Chem. Commun. 53 (1971).
61. A. RAHMAN and H. R. WILSON. Acta Crystallogr. B**28**, 2260 (1972).
62. D. H. WILLIAMS and N. S. BHACCA. J. Am. Chem. Soc. **86**, 2742 (1964).
63. N. YATHINDRA and M. SUNDARALINGAM. Biopolymers, **12**, 297 (1973).
64. F. E. HRUSKA, D. J. WOOD, T. N. MCCAIG, A. A. SMITH, and A. HOLY. Can. J. Chem. **52**, 497 (1974).
65. S. H. KIM, H. M. BERMAN, N. C. SEEMAN, and M. D. NEWTON. Acta. Cryst. B**29**, 703 (1972).
66. H. H. MANTSCH and I. C. P. SMITH. Biochem. Biophys. Res. Commun. **46**, 808 (1972).
67. (*a*) L. D. HALL and R. B. MALCOLM. Can. J. Chem. **50**, 2092, 2102 (1972); (*b*) B. DONALDSON and L. D. HALL. Can. J. Chem. **50**, 2111 (1972).
68. D. DAVIES and S. S. DANYLUK. Abstr. Second Intern. Symp. NMR Spectrosc. Chemical Society, University of Surrey, July, 1972.
69. M. J. LOWE and J. A. SCHELLMAN. J. Mol. Biol. **65**, 91 (1972).

Anhydro Sugar Formation in Acid and Base Hydrolyses of 3,4-Di-*O*-methylsulfonyl-D-mannitol: a Rapid Route to 1,4:3,6-Dianhydro-D-iditol (D-Isoidide)[1]

DAVID ROY HICKS AND BERT FRASER-REID

Chemistry Department, University of Waterloo, Waterloo, Ontario N2L 3G1

Received May 2, 1974

DAVID ROY HICKS and BERT FRASER-REID. Can. J. Chem. **52**, 3367 (1974).

Brief acid hydrolysis of 1,2:5,6-di-*O*-isopropylidene-3,4-di-*O*-methylsulfonyl-D-mannitol (**1***a*), removes the isopropylidene groups giving the disulfonated hexitol, **2***a*. Upon continued acid hydrolysis of **2***a*, one sulfonate group is lost with formation of a sulfonated monoanhydro hexitol, **5***a*, then the second ester group is lost to give 1,4:3,6-dianhydro-D-iditol (D-isoidide, **3***a*). If the disulfonate, **2***a*, is treated with base, an isomeric dianhydro hexitol, the bisoxirane **4**, is formed. Under similar basic conditions, the monoanhydro hexitol, **5***a*, is stable. On acid hydrolysis, the bisoxirane, **4**, gives hexitols and only 20% of D-isoidide, which indicates that **4** cannot be an intermediate in the conversion of **2***a* to **3***a*. These results indicate that, in **2***a* at least, five-membered anhydro rings are formed preferentially in acid hydrolyses and three-membered rings in saponification.

The stage and course of hydrolysis of **2***a* are readily monitored by observing the τ 4–6 region in the n.m.r. spectra of D_2O samples of the hydrolysate.

DAVID ROY HICKS et BERT FRASER-REID. Can. J. Chem. **52**, 3367 (1974).

Une hydrolyse acide brève du di-*O*-isopropylidène-1,2:5,6 di-*O*-méthylsulfonyl-3,4 D-mannitol (**1***a*) enlève les groupes isopropylidènes et fournit l'hexitol disulfoné **2***a*. Si l'hydrolyse acide de **2***a* est continuée, un groupe sulfonate est perdu avec formation du monoanhydro hexitol sulfoné **5***a*; un deuxième groupe ester est ensuite perdu pour donner le dianhydro-1,4:3,6 D-iditol (D-isoidide, **3***a*). Si l'on traite le disulfonate **2***a* avec une base, un dianhydro hexitol isomère, le bisoxiranne **4**, se forme. Dans de telles conditions basiques, le monoanhydro hexitol **5***a* est stable. L'hydrolyse acide du bis oxiranne **4** donne des hexitols et seulement 20% de D-isoidide; ce résultat indique que **4** n'est pas un intermédiaire dans la transformation de **2***a* en **3***a*. Ces résultats indiquent que dans **2***a* au moins, les cycles anhydro à cinq membres se forment d'une façon préférentielle par hydrolyse acide et que les cycles à trois membres sont formés par saponification.

L'évolution de l'hydrolyse de **2***a* peut être facilement suivie grâce à la r.m.n.; les observations sont faites dans la région de 4 à 6 τ sur des échantillons de l'hydrolysat en solution dans de l'eau lourde. [Traduit par le journal]

Can. J. Chem. Downloaded from www.nrcresearchpress.com by 210.87.254.6 on 09/05/12
For personal use only.

An indication of the importance of anhydro sugars is provided by the fact that a recent review volume contained three articles dealing directly with their chemistry (2–4). As a sub-group of anhydro sugars, the alditol anhydrides are prominent, not only because of what their formation reveals about intramolecular interactions and rearrangements (5, 6) but also because of their increasing industrial biological importance (4, 7). The dianhydrohexitols, for example, have a range of clinical employment that includes coronary care,[2] regulation of glaucoma (8) and cerebro-spinal fluid pressures (9), and emulsifiers for injectable medications (10). In view of these broad interests, we wish to report herein studies that have led to ready syntheses of some anhydro iditols and which clarify some anomalies in the literature relating to the hydrolysis of certain sulfonated hexitols.

Some years ago we required the disulfonated hexitol **2***a* and attempted to obtain this from **1***a* by acid hydrolysis in keeping with a procedure described by Wiggins for the hydrolysis of **1***b* (11). His proof of structure for what he assumed was **2***b*, included treatment of his product with base whereupon a dianhydrohexitol **3***a* was obtained.

While our work was underway. Tipson and Cohen reported a detailed study (12) in which they followed the course of the hydrolysis by polarimetry which allowed them to isolate **2***a* and *b* in quantitative yields. They showed that

[1]For a preliminary account of this work, see ref. 1.

[2]For an impressive bibliography, see ref. 113 in our ref. 4.

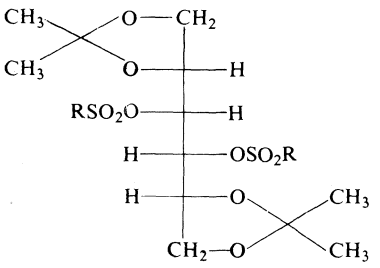

1

a R = CH_3
b R = $C_6H_4CH_3$

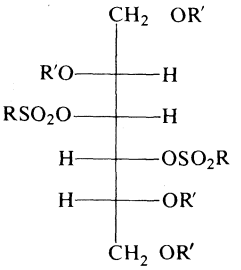

2

a R′ = H; R = CH_3
b R′ = H; R = $C_6H_4CH_3$
c R′ = Ac; R = CH_3
d R′ = Ac; R = $C_6H_4CH_3$

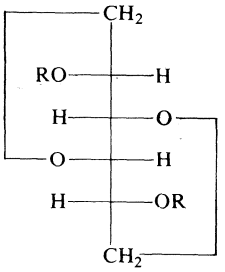

3

a R = H
b R = Ac
c R = $PhCO_2$
d R = Ms
e R = Ts

under Wiggins' conditions a considerable amount of sulfonic acid was liberated and, more seriously, that treatment of the disulfonate **2***a* or *b* with base produced not **3***a* but the isomeric dianhydride **4**.

We report herein our own observations which remove the apparent conflict in the results from both laboratories.

In an attempt to generate **2***a*, we treated the dimesylate **1***a* with ion exchange resin (H^+) and boiling water for 3 h and acetylated the product directly. However, the crystalline acetate contained no methanesulfonyl groups, judging from the absence of appropriate n.m.r. resonances $\tau \sim 6.8$. The possibility that the sulfonate groups had been lost during the acetylation step was excluded by showing (t.l.c.) that the hydrolysis product was regenerated upon saponification of the acetylated product. Direct comparison of derivatives of the hydrolysis product with those of the authentic L-enantiomer (see Experimental) established that 1,4:3,6 dianhydro-D-iditol (D-isoidide, **3***a*) had been produced.

Upon more cautious hydrolysis, it was found that if the suspension of **1***a* and resin in water was heated until dissolution just occurred, the desired dimesylate **2***a* could be obtained contaminated with ~10% of the monoanhydro product **5***a*. If the hydrolysis was permitted to go for 10 min beyond dissolution, compound **5***a* was the principal product. Continuation of the hydrolysis for 30 min gave D-isoidide, **3***a*, which underwent no further changes even after 4 h exposure to the reaction medium.

The structure of **2***a* was at first authenticated by treating the crude hydrolysis product with acetone and zinc chloride, whereupon the starting material (**1***a*) was regenerated in 79% yield. Subsequently, an authentic sample of the tetraacetate **2***c*[3] prepared by the method of Tipson and Cohen (12) was found to be identical to the corresponding material obtained from our preparation.

The gross structure of compound **5***a* was indicated by conversion to a crystalline triacetate **5***b* which gave correct elemental analysis. The 100 MHz spectrum of the latter (**5***b*) ($CDCl_3$; TMS) showed a multiplet for H-2 and H-5 at τ 4.4–4.8. The signal for H-3 was a prominent triplet at τ 4.98, $J_{23} = J_{34} = 6.0$ Hz. The triol **5***a* could be regenerated quantitatively from the triacetate (**5***b*) by hydrolysis with methanol–water–triethylamine. The location of the methylsulfonyl group at carbon-3 is based on the assumption that acid-catalyzed migration of the sulfonyl group is highly unlikely. The latter also suggests the D-talitol configuration for **5** and this conclusion is supported by the fact that acid hydrolysis of **5***a* affords 1,4:3,6-dianhydro-D-iditol (**3***a*), the displacement being assumed to occur with the usual inversion.

[3]We are grateful to Dr. Tipson for a specimen of **2***c* (12).

Can. J. Chem. Downloaded from www.nrcresearchpress.com by 210.87.254.6 on 09/05/12
For personal use only.

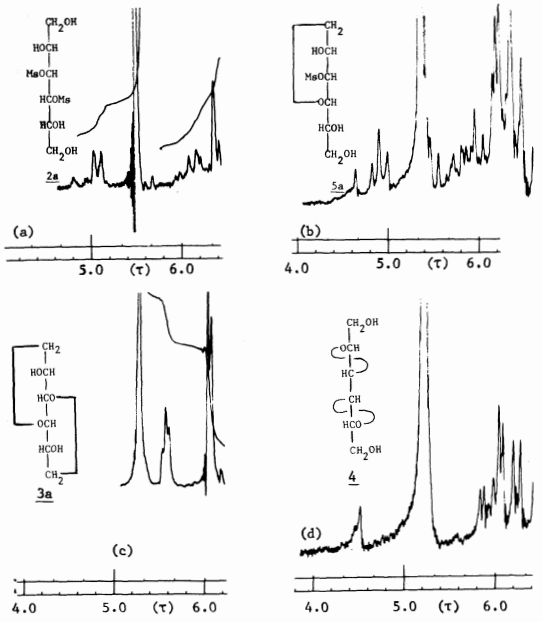

FIG. 1. Nuclear magnetic resonance spectra in D_2O (Me_2CO or TSP as internal standard): *a*, 3,4-di-*O*-methylsulfonyl-D-mannitol (**2***a*); *b*, 1,4-anhydro-3-*O*-methylsulfonyl-D-talitol (**5***a*); *c*, 1,4:3,6-dianhydro-D-iditol (D-isoidide) (**3***a*); *d*, 2,3:4,5-dianhydro-D-iditol (**4**).

The successive stages of hydrolysis of **1***a*, are conveniently determined by observing the low-field region of 60 MHz spectra of the hydrolysate in deuterium oxide (Fig. 1). Thus H-3 (≡H-4) of **2***a* appears as a doublet[4] with a spacing of 6.0 Hz at τ 5.03 (Fig. 1*a*). In compound **5***a* (Fig. 1*b*), H-3 is a triplet at τ 4.87, with a spacing of 6.0 Hz. In D-isoidide (**3***a*; Fig. 1*c*), there are no signals to low field of DOH and a triplet for H-2 (≡H-5) with a spacing of ~2 Hz is seen at τ 5.85. The singlet for H-3 (≡H4) is masked by the DOH peak.[4]

In addition to the data outlined in the preceding paragraph, the relative amounts of **2***a*, **3***a*, and **5***a* present at any stage can be readily determined by acetylating the crude mixture and studying its n.m.r. spectrum. This is particularly advantageous since the H-3 signals for **2***a* and **5***a* overlap (see Fig. 1*a* and *b*). In **2***c*, the methylsulfonyl groups are isochronous, occurring at τ 6.80, whereas in **5***b* the corresponding signal occurs at τ 6.83. With **3***b* the signal for H-3 (≡H-4) is a sharp spike at τ 5.54 (13*a*) in which region the other two compounds **2***b* and **5***b* give no signals.

We established that hydrolysis of the ditosylate **1***b* followed a course similar to that of the dimesylate **1***a* giving D-isoidide (**3***a*) when ion exchange resin was used as the acid catalyst. However, when the hydrolyses were done using aqueous acetic acid as described by Wiggins (11), the product, analyzed by t.l.c., showed only a small amount of D-isoidide (**3***a*) and no evidence of **2***b*. However it seemed clear that any D-isoidide he did obtain had been formed during the acid hydrolysis step and not during the saponification step as he had assumed.

The formation of the bisoxirane **4** from **2***a* as reported by Tipson and Cohen (12) was verified. Indeed the conversion of **2***a* to **4** could be accomplished more conveniently by allowing a solution of **2***a* in methanol–water–triethylamine to stand at room temperature for 30 min. The low-field portion of the n.m.r. spectrum of **4** in D_2O is shown in Fig. 1*d*. This portion of the spectra in Fig. 1, taken in conjunction with the absence of methylsulfonyl signals, allows **3***a* to be readily differentiated from **4**.

As a first step in clarifying the discrepancy in the results of Wiggins (11) and Tipson and Cohen (12), we established that the bisoxirane **4** was not an intermediate in the acid-catalyzed transformation of **2***a* to **3***a*. Thus treatment of **4** with the ion exchange resin (H^+) gave only ~20% of D-isoidide (**3***a*) as determined by n.m.r. spectroscopy. Furthermore, paper chromatography of the product revealed material with the same R_f as D-mannitol,[5] as well as other substances.

Scheme 1 summarizes some other observations on these materials. As was expected, D-isoidide, (**3***a*), was stable to lithium aluminum hydride but the bisoxirane **4** was cleaved giving several products. The monoanhydro compound **5***a*, which furnishes D-isoidide (**3***a*) on heating with acid, is stable to the methanol–water–triethylamine medium used for the conversion of **2***a* to **4** (*vide infra*).

The size of the anhydro rings formed during hydrolyses of sulfonate esters is influenced by a number of factors such as steric interactions, conformational changes, etc. However, in alkaline media three- and five-membered rings appear

[4]For detailed discussion of the p.m.r. spectra of dianhydro hexitols, see ref. 13*a*.

[5]Hydrolysis of **4** could conceivably give hexitols other than D-mannitol but this possibility was not examined.

Can. J. Chem. Downloaded from www.nrcresearchpress.com by 210.87.254.6 on 09/05/12
For personal use only.

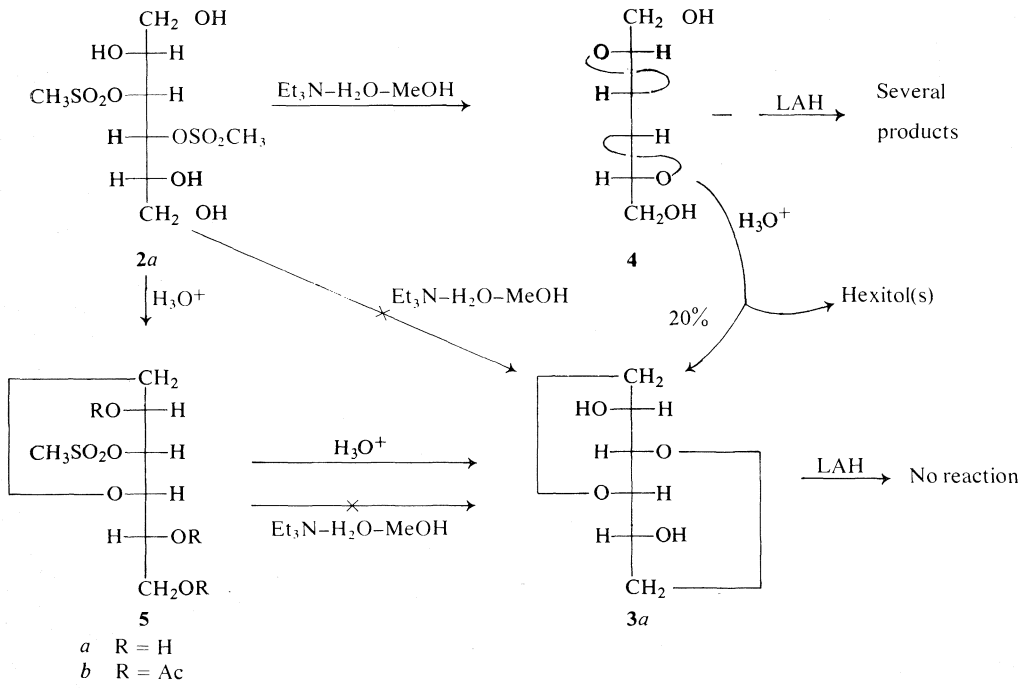

SCHEME 1

to be favored, the smaller ring being formed more readily (2–4, 6). This conclusion is upheld in the present study (Scheme 1) since base hydrolysis of **2***a* gave **4** but no **3***a*. Again, the stability of the monoanhydro compound **5***a* to base is revealing. Thus, while formation of a 2,3-oxirane from **5***a* is impossible since the 2-hydroxy and sulfonyloxy groups are in *cis* relationship, there are no steric barriers to the formation of **3***a*.

In contrast to the foregoing, anhydro rings formed in acidic media are invariably five-membered even when six- and/or three-membered rings are plausible alternatives (14). This situation is quite contrary to the preferences normally displayed in carbocyclic systems where three-membered rings are most readily formed (15). In this connection it is worthwhile to repeat that the possibility of **4** having been formed first in the acid hydrolysis of **2***a* and subsequently being converted to **3***a* has been excluded (*vide supra*).

Experimental

Melting points were determined on a Fischer-Johns heating stage and are uncorrected. Nuclear magnetic resonance spectra were determined using a Varian T-60 or Varian HA-100 spectrometer, solvents being D_2O (with acetone or sodium trimethylsilyl-2,2,3,3-tetradeuteriopropionate (TSP) as internal standards) or $CDCl_3$ (TMS).

*3,4-Di-O-methylsulfonyl-*D*-mannitol (2a) and its Tetraacetate (2c)*

(*a*) Compounds **2***a* and *c* were prepared in excellent yield, following the conditions of Tipson and Cohen (12).

(*b*) Distilled water (13 ml) was added to a mixture of 1,2:5,6-di-*O*-isopropylidene-3,4-di-*O*-methylsulfonyl-D-mannitol (**1***a*) (16) (1.0 g; 0.024 mol) and Dowex 50W-X2 (H^+ form) resin (2 g), contained in a 100-ml conical flask equipped with a reflux condenser and standing on an efficient magnetic stirrer hot plate. Vigorous stirring was begun and the heat was turned up to a maximum. When compound **1***a* had just dissolved, the flask was removed, cooled in an ice-water bath, and then filtered, the resin being washed with water. The filtrate was neutralized with barium carbonate and the mixture filtered once more. The filtrate was evaporated under reduced pressure and the residue, which invariably contained barium salts, was extracted with hot ethanol. The hot ethanol was filtered and evaporation of the filtrate gave syrupy material (0.78 g) whose 60 MHz n.m.r. spectrum in D_2O (acetone as internal standard) showed a doublet at τ 5.03 for H-3 ($\equiv$ H-4), J_{23} ($\equiv J_{45}$) = 6.0 Hz (see Fig. 1*a*), and a singlet at τ 6.83 for CH_3SO_3—.

The material was authenticated as being **2***a* by treating the syrupy product with anhydrous zinc chloride (0.7 g) and reagent grade acetone (5 ml), which had been dried over and distilled from anhydrous potassium carbonate, for 2 h at room temperature. The solution was poured into water (10 ml) containing dissolved potassium carbonate (1 g) and the organic substance recovered by extraction into methylene chloride. The extract was dried with sodium sulfate and evaporated to dryness dissolved in ethanol, whereupon a crystalline substance identical to the starting material (**1***a*) was obtained (0.79 g, 79% yield).

Can. J. Chem. Downloaded from www.nrcresearchpress.com by 210.87.254.6 on 09/05/12
For personal use only.

Can. J. Chem. Downloaded from www.nrcresearchpress.com by 210.87.254.6 on 09/05/12
For personal use only.

In another experiment, the syrupy preparation of **2***a* remaining after evaporation of the ethanol was acetylated for 7 h with acetic anhydride (5 ml) and pyridine (5 ml). Conventional work-up afforded a residue whose n.m.r. spectrum in $CDCl_3$ (TMS) showed two spikes for CH_3SO_3— at τ 6.80 and 6.83. By comparison with the pertinent signal in authentic **2***c* prepared by the method of Tipson and Cohen (12), the τ 6.80 signal was ascribed to **2***c*. The τ 6.83 signal arose from the monoanhydro compound **5***b*. The latter was present in 5–10% in all our preparations of compound **2** and undoubtedly inhibited crystallization of **2***a*. Chromatographic separation could not be achieved; however, fractional crystallization could be induced if the acetylated mixture containing **2***c* and **5***b* was seeded with crystalline **2***c* (12). In this way crystalline **2***c* (0.88 g; 70% from **1***a*), m.p. 80–83° (lit. (12) 81–83°) was obtained.

Nuclear magnetic resonance (100 MHz) of **2***c* ($CDCl_3$; TMS): τ 4.78 (s, 4, H-2,3,4,5); τ 5.40–584 (m, 4, H-1,1′, 6,6′), τ 6.80 (s, 6, CH_3SO_3); τ 7.88 (s, 6, CH_3CO_2), τ 7.94 (s, 6, CH_3CO_2).

*1,4-Anhydro-3-O-methylsulfonyl-*D*-talitol (5a) and its Triacetate (5b).*

The suspension of the diisopropylidene dimesylate (**1***a*) in water, was treated as described above for preparation of **2***a*. However, heating under reflux was continued for 10 min beyond dissolution before removing the flask and subjecting the contents to work-up as described for **2***a*. The n.m.r. spectrum of the product in D_2O (acetone as internal standard), Fig. 1*b*, showed a prominent triplet with a spacing of 5.0 Hz at τ 4.87, which was ascribed to H-3. In some preparations, small amounts (~5%) of D-isoidide (**3***a*), could be detected in the n.m.r. spectrum of the crude material by the presence of a characteristic triplet at τ 5.85.

The crude syrup was acetylated with acetic anhydride (5 ml) and pyridine (5 ml) for 7 h, and the acetylated material was recovered following customary work-up.

The residue crystallized from methanol, 0.72 g (82% from **1***a*), m.p. 103–104°; $[\alpha]_D^{23}$ +9.52° (*c*, 3.19 in $CHCl_3$).

Anal. Calcd. for $C_{13}H_{20}O_{10}S$: C, 42.38; H, 5.47; S, 8.70. Found: C, 42.58; H, 5.48; S, 8.74.

*1,4:3,6-Dianhydro-*D*-iditol (*D*-Isoidide, 3a)*

(*a*) The acid-catalyzed hydrolysis of compound **1***a* as described above, was allowed to continue for *at least* 30 min beyond dissolution, this being the minimum time for complete reaction. However, prolonged reflux for periods up to 4 h could be safely maintained, without affecting the yield or quality of product. The resin was removed by filtration and the organic material **3***a* was recovered as described above for **2***a*.

(*b*) The dimesylate, **1***a*, (5.0 g; 0.012 mol) or the ditosylate, **1***b*, (7.0 g; 0.012 mol) was dissolved in dioxan (40 ml), water (20 ml), and sulfuric acid (2.5 ml). The solution was refluxed for 3 h, cooled, neutralized with solid sodium bicarbonate, and evaporated. The organic material recovered, as in part *a*, was a syrup, (~2.3 g).

The syrups from either parts *a* or *b* failed to crystallize even though they were chromatographically pure (t.l.c. in ethyl acetate) with R_f 0.2 and gave almost quantitative yields of crystalline diacetate, dibenzoate, and dimesylate which were characterized as described below.

*2,5-Di-O-acetyl-1,4:3,6-dianhydro-*D*-iditol (3b)*

A sample of the syrupy 1,4:3,6-dianhydro-D-iditol (**3***a*) prepared as described in part *a* above from 6.0 g of dimesylate **1***a* was acetylated at room temperature with acetic anhydride (15 ml) and pyridine (15 ml) for 7 h. The mixture was cooled in ice and the excess acetic anhydride destroyed by adding 25 ml of methanol. Evaporation gave a syrup which was freed from pyridine by azeotropic distillation with toluene and was then set to crystallize from chloroform – petroleum ether (35–60°). The first (2.70 g; m.p. 49–52°) and second (0.32 g) crops of crystals amounted to 92% yield.

The material after two recrystallizations from methanol had the physical constants m.p. 55–56°; $[\alpha]_D^{23}$ −89.0° (*c*, 4.2 in $CHCl_3$). The corresponding values for an authentic sample of the enantiomer, 2,5-di-*O*-acetyl-1,4:3,6 dianhydro-L-iditol,[6] were 55–56°, mixture m.p. 59–66°, and +89.6°.

Anal. Calcd. for $C_{10}H_{14}O_6$: C, 52.17; H, 6.13. Found: C, 52.03; H, 6.15.

*2,6-Di-O-benzoyl-1,4:3,6-dianhydro-*D*-iditol (3c)*

The syrupy dianhydro derivative (**3***a*) prepared from the dimesylate, **1***a* (7.0 g; 0.017 mol) as described above in *a* was dissolved in pyridine (30 ml). To the ice-cold solution was added benzoyl chloride (9.0 ml; 0.076 mol) and the solution was allowed to warm up to, and stand at room temperature overnight. The mixture was poured into ice and water and the resulting oil was extracted with methylene chloride. After washing with 4 *N* sulfuric acid and saturated sodium bicarbonate the methylene chloride layer was dried and then evaporated. The syrup crystallized from ether – petroleum ether (5.2 g; 89%), m.p. 97–103°. The material after recrystallization from chloroform – petroleum ether, gave the following data: m.p. 110–111.5° $[\alpha]_D^{23}$ −132.0° (*c*, 2.17 in $CHCl_3$). The corresponding literature (13*c*) values for the L-enantiomer are 110–111° and +134.3°. Anal. Calcd. for $C_{20}H_{18}O_6$: C, 67.78; H, 5.12. Found: C, 67.09; H, 5.16.

*1,4:3,6-Dianhydro-2,5-di-O-methylsulfonyl and -di-O-p-tolylsulfonyl-*D*-iditol 3d and 3e, Respectively*

Samples of the syrupy dianhydro iditol, **3***a*, prepared as in *a* above, were mesylated and tosylated in a manner similar to that described for benzoylation above. The crystalline products had the following physical constants.

3*d*: m.p. 159–160°; $[\alpha]_D^{23}$ −31.60° (*c*, 1.77 in $(CH_3)_2CO$); corresponding values for authentic L-enantiomer,[6] m.p. 160–161° mixture m.p. 144–145°; $[\alpha]_D^{23}$ +31.65°.

3*e*: m.p. 105–106°; $[\alpha]_D^{23}$ −31.1° (*c*, 2.66 in $CHCl_3$); corresponding literature values for L-enantiomer 105.5–106°; +33.2° (13*b*).

*2,3:4,5-Dianhydro-*D*-iditol, 4*

(*a*) The diisopropylidene-dimesylate **1***a* (1.0 g), was deacetonated as described above to give syrupy **2***a* which was dissolved in 30 cc dry methanol. Barium methoxide (0.0048 mol) in 10 cc methanolic solution was added, and after 2 h the reaction mixture was processed as described by Tipson and Cohen (12) with the exception that the product was freed from inorganic salts by extraction into isopropyl alcohol and filtration. The

[6]We are grateful to Dr. G. H. S. Thomas for the authentic sample (13*a*).

filtrate was concentrated whereupon crystals of the desired material (**4**) formed spontaneously, 0.27 g (78%), m.p. 100–101°; $[\alpha]_D^{23}$ +78.1° (*c*, 1.04 in water) (lit. (12) m.p. 100–101°; $[\alpha]_D^{25}$ +82.1°).

(*b*) Syrupy **2***a* (0.5 g) was dissolved in 20 ml of methanol–water–triethylamine (5:4:1) mixture and allowed to stand for 30 min after which the solution was evaporated to dryness. It was redissolved in water (30 ml), and stirred with barium carbonate to remove the sulfonic acid. The solids were removed by filtration, the filtrate evaporated to dryness and extracted with isopropyl alcohol. Crystalline material (0.153 g) identical to that in part *a*, was obtained.

The low field n.m.r. spectrum of **4** is shown in Fig. 1*d* for comparison with the other materials in this series.

We are grateful to the National Research Council of Canada for financial support.

1. B. Fraser-Reid and D. R. Hicks. J. Chem. Soc. Chem. Commun. 19 (1972).
2. N. R. Williams. Adv. Carbohydr. Chem. Biochem. **25**, 109 (1970).
3. J. Defaye. Adv. Carbohydr. Chem. Biochem. **25**, 181 (1970).
4. S. Soltzberg. Adv. Carbohydr. Chem. Biochem. **25**, 229 (1970).
5. F. H. Newth. Quart. Rev. (London), **13**, 30 (1959); A. C. Cope and T. Y. Shen. J. Am. Chem. Soc. **78**, 5912 (1956); J. A. Mills. Adv. Carbohydr. Chem. **10**, 1 (1955).
6. D. H. Ball and F. W. Parrish. Adv. Carbohydr. Chem. **23**, 233 (1968); **24**, 139 (1969).
7. L. F. Wiggins. Adv. Carbohydr. Chem. **5**, 191 (1950).
8. B. Becker, A. E. Kolker, and T. Krupin. Arch. Opthalmol. **78**, 147 (1967).
9. B. L. Wise, J. L. Mathis, and J. H. Wright. J. Neurosurg. **25**, 183 (1966).
10. A. F. Woodhour and T. B. Stim. Chem. Abs. **61**, 13136 (1964).
11. L. F. Wiggins. J. Chem. Soc. 1403 (1947).
12. R. S. Tipson and A. Cohen. Carbohydr. Res. **7**, 232 (1968).
13. (*a*) F. J. Hopton and G. H. S. Thomas. Can. J. Chem. **47**, 2395 (1969). (*b*) A. C. Cope and T. Y. Shen. J. Am. Chem. Soc. **78**, 3177 (1956); H. G. Fletcher, Jr. and R. M. Geopp, Jr. J. Am. Chem. Soc. **68**, 939 (1946).
14. J. Defaye and J. Hildesheim. Tetrahedron Lett. 313 (1968).
15. H. O. House. Modern synthetic reactions. 2nd ed. W. A. Benjamin Inc., Menlo Park. 1972. p. 542.
16. P. Bladon and L. Owen. J. Chem. Soc. 598 (1950).

Can. J. Chem. Downloaded from www.nrcresearchpress.com by 210.87.254.6 on 09/05/12
For personal use only.

Photoelectron Spectrum and Electronic Structure of Tetrathiofulvalene (TTF)

A. John Berlinsky and James F. Carolan

Department of Physics, University of British Columbia, Vancouver, British Columbia V6T 1W5

AND

Larry Weiler

Department of Chemistry, University of British Columbia, Vancouver, British Columbia V6T 1W5

Received May 29, 1974

A. John Berlinsky, James F. Carolan, and Larry Weiler. Can. J. Chem. **52**, 3373 (1974).

The electronic structure of tetrathiofulvalene (TTF) has been determined from its photoelectron spectrum and the photoelectron data for the tetrahydro derivative of TTF and 1,3-dithiolane. Correlations of the ionization potentials (i.p.) and several molecular orbital calculations are used in the assignment of the photoelectron spectra of these three compounds. The first five i.p. of TTF and their assignment are as follows: 6.92 ($3b_{1u}$), 8.67 ($2b_{2g}$), 9.73 ($2b_{1u}$), 10.16 (a_u) and 10.49 eV (b_{3g}). The sixth i.p. at 11.00 eV is tentatively assigned to the $1b_{2g}$ level. The electronic structure of TTF is important in understanding the crystal packing and band structure of the highly conducting salt, TTF·TCNQ.

A. John Berlinsky, James F. Carolan et Larry Weiler. Can. J. Chem. **52**, 3373 (1974).

On a déterminé la structure électronique du tétrathiofulvalène (TTF); ces conclusions ont été obtenues à partir de son spectre photoélectronique et à l'aide de données photoélectroniques pour le tétrahydro-TTF et le dithiolane-1,3. Des corrélations d'ionisation potentiels (i.p.) et plusieurs calculs d'orbitales moléculaires sont utilisés pour déterminer les spectres photoélectrons de ces trois composés. Les cinq premiers i.p. de TTF et leur attribution sont les suivantes: 6.92 ($3b_{1u}$), 8.67 ($2b_{2g}$), 9.73 ($2b_{1u}$), 10.16 (a_u) et 10.49 eV (b_{3g}). Le sixième i.p. a une valeur de 11.00 eV et est attribué d'une façon non définitive au niveau $1b_{2g}$. La structure électronique du TTF est importante pour comprendre l'empilement cristallin et la structure des bandes du sel très conducteur TTF-TCNQ. [Traduit par le journal]

Recently there has been a surge of interest in the synthesis of crystalline charge transfer compounds and the study of their physical properties. One of these complexes, from tetrathiofulvalene (TTF, **1**) and tetracyanoquinodimethane (TCNQ, **2**)

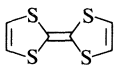

1

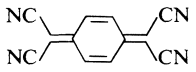

2

has been found to exhibit the highest electrical conductivity of any organic solid to date (1) and above 60 °K TTF·TCNQ possesses all the properties expected for a one dimensional metal (2). In addition a few crystals of TTF·TCNQ exhibit anomalously large peaks in their conductivity (1*b*). In all TTF·TCNQ crystals below 70 °K, there is a transition to a small gap semiconducting state (1). The high conductivity and this metal-semiconductor transition have recently been the subject of numerous experimental and theoretical papers. As part of our efforts to design new organic metals, we have undertaken a study of the electronic properties of TTF, TCNQ, and TTF·TCNQ from both a theoretical and experimental aspect. In a molecular orbital study of these compounds, we have calculated an approximate band structure for TTF·TCNQ which models the nearly one-dimensional behavior of the solid (3). In this paper we would like to present an electronic description of TTF based on photoelectron spectroscopy (p.e.s.), correlation of ionization potentials (i.p.) of related compounds, and molecular orbital calculations.

In Fig. 1 is shown the photoelectron spectrum of tetrahydrotetrathiofulvalene (THTTF, **3**) and

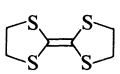

3

the first six vertical ionization potentials are listed in Table 1. The first σ i.p. of tetrahydrothiophene (**4**) and of 1,3-dithiolane (**5**) are at

Can. J. Chem. Downloaded from www.nrcresearchpress.com by 210.87.254.6 on 09/05/12
For personal use only.

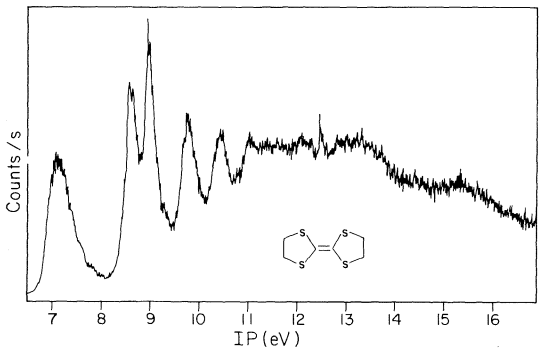

FIG. 1. Photoelectron spectrum of THTTF (**3**).

TABLE 1. Vertical ionization potentials of THTTF (**3**) in eV*

Measured	Assignment	Calculated EH†§	Calculated CNDO/2‡§
7.05	$\pi(3b_{1u})$	10.65 ($3b_{1u}$)	10.19 ($3b_{1u}$)
8.59	$\pi(2a_u)$	12.37 ($2a_u$)	11.45 ($2a_u$)
8.97	$\pi(2b_{3g})$	12.58 ($2b_{3g}$)	12.04 ($2b_{3g}$)
9.76	$\pi(2b_{2g})$	13.54 ($2b_{2g}$)	13.32 ($2b_{2g}$)
10.42	$\pi(2b_{1u})$	14.68 ($2b_{1u}$)	19.86 ($2b_{1u}$)
11.04	σ		

*Geometry was assumed to be planar with the same bond lengths and angles as TTF except that the CC single bond length was taken as 1.52 Å and the S—C_{sp^3} bond length as 1.80 Å.
†See ref. 7, using a hydrogen exponent of 1.3 and sulfur parameters as follows: 3s, exponent = 2.122 and $H_{ii} = -20.00$ eV; 3p, exponent = 1.827 and $H_{ii} = -13.30$ eV.
‡See ref. 6.
§There are several σ levels in the region of the π levels which have been omitted (see text).

10.92 (4) and 11.0 eV (5), respectively. Because of the additional sp^2 hybridized carbons in **3** compared to **5**, the σ i.p. of **3** must be greater than 10.5 eV. Hence the first five i.p. of **3** correspond to π ionizations. Both CNDO/2 (6) and

4

5

extended Hückel calculations (7) suggest the π level ordering given in Table 1 is correct, assuming the validity of Koopmans' theorem in these systems (8). A similar extended Hückel calculation on **3** using slightly different geometry, Slater exponents and Coulomb integrals for sulfur orbitals gave the same ordering of the π levels (9) as our calculation. Both of these calculations, especially the CNDO/2, place some σ levels in the same energy range as the π levels. We have chosen to ignore these σ levels in the calculations for the following reasons. The inductive argument above and comparison of the photoelectron data for **1**–**3** show that the first five i.p. in **3** must be due to ionization from π levels. Also, it is well known that because of the parameterizations in these calculations the first σ i.p. are underestimated relative to the π i.p. (6, 10). In the CNDO/2 calculations this may well be due to the overestimation of the interaction between levels of the same symmetry in these calculations (11). This may well explain the large gap between the $2b_{2g}$ and $2b_{1u}$ levels in the CNDO/2 calculations (Table 1). Finally we would suggest that the errors introduced in applying Koopmans' theorem to σ levels *may* be substantially greater than the errors applied to delocalized π levels because of the possibility of smaller correlation and reorganization effects in the π levels.

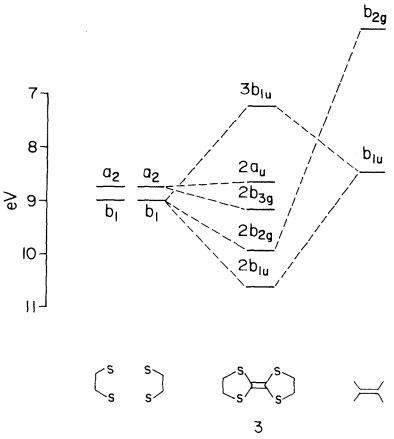

3

FIG. 2. Correlation diagram for the levels in **3**.

The correlation diagram, Fig. 2, can be constructed for THTTF (3). The π i.p. of the b_{1u} (π_{CC}) level in the octahydronaphthalene **6** is at

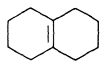

6

8.27 eV (12). Hence we have taken a value of 8.3 eV as an estimate of the "isolated" π_{CC} (b_{1u}) level in **3**. The position of the π* (b_{2g}) cannot readily be estimated. The π levels from the nonbonding sulfur levels (n_S) can be considered to arise from the interaction of two 1,2-dithioethane units (7). Molecular orbital calculations by us and others (13) indicate that for a planar geometry of **5** the a_2 (n_S) level will be at slightly higher energy than the b_1 (n_S) level. This is the ordering expected if the through space interaction is greater than the

Can. J. Chem. Downloaded from www.nrcresearchpress.com by 210.87.254.6 on 09/05/12
For personal use only.

7

through bond interaction (14). An estimate of the energies of these two levels is 8.64 eV and 8.90 eV from the photoelectron spectrum of 1,2-dimethylthioethane (13). These four sulfur levels (n_S) correlate with the b_{1u}, a_u, b_{3g}, and b_{2g} levels in **3**. There will be an additional interaction between the b_{1u} and b_{2g} (n_S) levels and the π_{CC} (b_{1u}) and π_{CC}^* (b_{2g}) in the central double bond of **3**.

The through space interaction of the two a_2 (n_S) levels would place the $2a_u$ level in **3** above the $2b_{3g}$ (n_S) as indicated in the calculations. The average of these two i.p. in THTTF (**3**) is 8.78 eV which is 0.14 eV greater than the i.p. of the isolated a_2 levels and represents the inductive effect of replacing a methyl group with a vinyl group adjacent to a sulfur atom. In addition, the through space interaction of the n_S (a_2) levels can be estimated from the splitting of the a_2 levels to be 0.38 eV. Interaction of the π_{CC} (b_{1u}) level and the n_S (b_{1u}) level give the two b_{1u} levels in **3**. The average of these i.p. in **3** is 8.74 eV and the average i.p. of the "isolated" b_{1u} levels is 8.6 eV which again reflects the small inductive effect on these levels and corroborates the proposed assignments in Table 1. The difference of 1.25 eV between the i.p. of the b_{1u} level in the "isolated" double bond and the i.p. of the $3b_{1u}$ level in **3** represents a measure of the direct conjugative interaction between the b_{1u} levels. This interaction stabilizes the $2b_{1u}$ level in **3** relative to the sulfur b_1 levels (Fig. 2) and can be estimated from these levels as follows. If we neglect the inductive effects (*vide supra*) the major effects stabilizing the $2b_{1u}$ level are the through space interaction of the two sulfur b_1 levels to generate the b_{2g} and a b_{1u} level, and the direct conjugative interaction of this b_{1u} level with the b_{1u} level associated with the central double bond. The through space interaction of the b_1 levels should be approximately the same as the through space interaction of the a_2 levels (0.38 eV). In this way, a second estimate of the direct b_{1u} interaction is 1.4 eV. Hence the average interaction of the b_{1u} levels $\langle n_S(b_{1u})|H|\pi_{CC}(b_{1u})\rangle$ is calculated to be 1.2 eV.

In Fig. 3 is shown the photoelectron spectrum of TTF (**1**), and the first seven vertical i.p. along

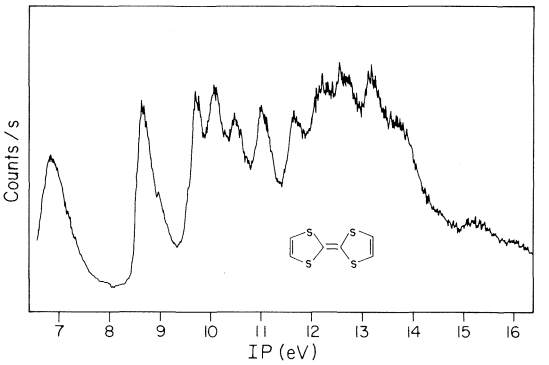

FIG. 3. Photoelectron spectrum of TTF (**1**).

with possible assignments and the results of two molecular orbital calculations are given in Table 2. Because the first σ i.p. in **1** is expected to be greater than 11 eV (*vide supra*), we can assign the first six bands to ionizations from π levels in **1**. The first band at 6.92 eV is assigned to ionization from the $3b_{1u}$ (π) level in agreement with our calculations and those of others (9, 13). The second band at 8.67 is assigned to ionization from the $2b_{2g}$ (π) level. Gleiter, *et al.* have also reported the photoelectron spectrum of TTF (**1**) recently (15). Their values for the i.p. and assignments of the first two i.p. are the same as those reported here. They experienced some difficulty in assigning the remaining i.p. From our assignment of the THTTF (**3**) photoelectron spectrum, the m.o. calculations, and the u.v. spectrum of the radical cation of TTF (16) we can assign the next four bands to ionization from the $2b_{1u}$, a_u, b_{3g}, and $1b_{2g}$ levels. This is the ordering of the π levels obtained from the extended

TABLE 2. Vertical ionization potentials of TTF (**1**) in eV*

		Calculated	
Measured	Assignment	EH†§	CNDO/2‡§
6.92	$\pi(3b_{1u})$	10.14 ($3b_{1u}$)	9.78 ($3b_{1u}$)
8.67	$\pi(2b_{2g})$	11.98 ($2b_{2g}$)	11.85 ($2b_{2g}$)
9.73	$\pi(2b_{1u})$	13.06 ($2b_{1u}$)	12.75 (a_u)
10.16	$\pi(a_u)$	13.34 (a_u)	13.06 (b_{3g})
10.49	$\pi(b_{3g})$	13.53 (b_{3g})	17.11 ($2b_{1u}$)
11.00	$\pi(1b_{2g})$	14.84 ($1b_{2g}$)	19.79 ($1b_{2g}$)
11.62	?	15.37 ($1b_{1u}$)	21.79 ($1b_{1u}$)

*Geometry of TTF from ref. 20.
†See ref. 7, using a hydrogen exponent of 1.3 and sulfur parameters as follows: 3s, exponent = 2.122 and H_{ii} = −20.00 eV; 3p, exponent = 1.827 and H_{ii} = −13.30 eV.
‡See ref. 6.
§There are several σ levels in the region of the π levels which have been omitted (see text).

Can. J. Chem. Downloaded from www.nrcresearchpress.com by 210.87.254.6 on 09/05/12
For personal use only.

Can. J. Chem. Downloaded from www.nrcresearchpress.com by 210.87.254.6 on 09/05/12
For personal use only.

Hückel calculations and also from a recent multiple scattering Xα calculation (17). The CNDO/2 calculations failed to give the correct ordering by misplacing the $2b_{1u}$ level. This may be due again to the fact that these calculations overemphasize the interaction between orbitals of the same symmetry (11). In this regard, note that the observed energy difference between the $1b_{2g}$ and the $3b_{1u}$ level is approximately 4 eV compared to a calculated value of 4.7 eV (extended Hückel) (EH) and 10 eV (CNDO/2). This clearly points out the difficulty in the CNDO/2 calculations.

A correlation diagram of the ionizations in TTF (**1**), THTTF (**3**), and two "isolated" cyclopentene π levels is shown in Fig. 4. The third i.p. at 9.83 eV is assigned to the $2b_{1u}$ ionization. The next two ionizations at 10.16 and 10.49 eV are assigned to the a_u and b_{3g} levels, respectively. The split between these levels in **1** is 0.33 eV and is essentially the same as that found in **3**, 0.36 eV. This would be expected if the $a_u(\pi,\pi^*)$ and $b_{3g}(\pi,\pi^*)$ interactions were the same in the correlation shown in Fig. 4. This is reasonable since the overlap and energy differences for these levels should be very similar. In both the extended Hückel and CNDO/2 calculations for **3** the coefficients of the $S(p_z)$ atomic orbitals are very nearly equal for the $a_u(\pi)$ and $b_{3g}(\pi)$ levels. These $a_u(\pi,\pi^*)$ and $b_{3g}(\pi,\pi^*)$ interactions stabilize the a_u and b_{3g} levels in **1** relative to **3**. The $b_{3g} \rightarrow 3b_{1u}$ transition in the radical cation of **1** would be calculated (18) to occur at 354 nm which is in good agreement with the observed transition at 338–340 nm (16). This further corroborates the assignments in Table 2. The band at 11.00 eV is tentatively assigned to the remaining $1b_{2g}$ ionization of **1**, mainly based on the inductive arguments outlined above and the last $1b_{1u}$ level remains unassigned. We feel that this is a reasonable ordering of the π level in TTF and the radical cation of TTF, and hence of the TTF in the charge transfer solid TCNQ·TTF. The absolute energies should be different for the m.o. in TTF and TTF^{+} but the relative ordering should remain unchanged as outlined above. The symmetry of the highest occupied orbital in TTF (and TTF^{+}) is very important in understanding the band structure in TTF·TCNQ (3).

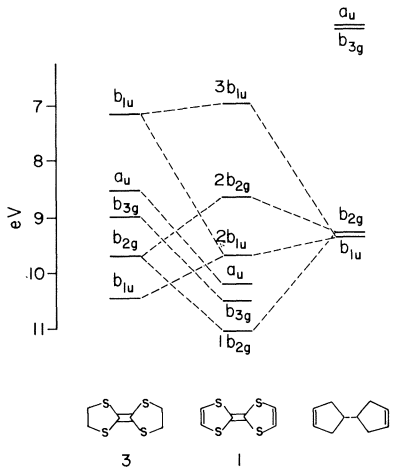

FIG. 4. Correlation diagram for the π levels in **1** and **3**.

Experimental

The photoelectron spectra of 1,3-dithiolane were recorded on a spectrometer described elsewhere (19). The photoelectron spectra of the tetrahydrotetrathiofulvalene (**3**) was recorded on a Perkin–Elmer, Model PS-16 Photoelectron Spectrometer with an inlet temperature of 89 °C and TTF (**1**) on the same intrument of 86 °C. All spectra were calibrated with the 9.55 and 10.12 eV i.p. of methyl iodide. Vertical i.p. are measured to ±0.03 eV.

We are grateful to Mr. Graham Sharp (University of Sussex) for the photoelectron spectra of TTF and THTTF, to Professor A. J. Heeger and Dr. Fred Wudl for samples of TTF and THTTF, to Dr. F. Herman and Dr. B. I. Bennett for the results of their multiple scattering Xα calculations, to Professor R. Hoffmann for a copy of his extended Hückel program, and to the National Research Council of Canada for financial support of this work.

1. (*a*) J. FERRARIS, D. O. COWAN, V. WALATKA, JR., and J. H. PERLSTEIN. J. Am. Chem. Soc. **95**, 948 (1973); (*b*) L. B. COLEMAN, M. J. COHEN, D. J. SANDMAN, F. G. YAMAGISHI, A. F. GARITO, and A. J. HEEGER. Solid State Commun. **12**, 1125 (1973).
2. A. F. GARITO and A. J. HEEGER. To be published.
3. A. J. BERLINSKY, J. F. CAROLAN, and L. WEILER. Solid State Commun. In press.
4. H. SCHMIDT and A. SCHWEIG. Tetrahedron Lett. 1437 (1973).
5. K. GOUGH and L. WEILER. Unpublished results.
6. J. A. POPLE and G. A. SEGAL. J. Chem. Phys. **44**, 3289 (1966).
7. R. HOFFMANN. J. Chem. Phys. **39**, 1397 (1963).
8. T. KOOPMANS. Physica, **1**, 104 (1934).
9. D. L. COFFEN, J. Q. CHAMBERS, D. R. WILLIAMS, P. E. GARRETT, and N. O. CANFIELD. J. Am. Chem. Soc. **93**, 2258 (1971).
10. R. L. ELLIS, H. H. JAFFÉ, and C. A. MASMANIDIS. J. Am. Chem. Soc. **96**, 2623 (1974).
11. (*a*) D. C. FROST, F. G. HERRING, A. KATRIB, R. A. N. MCLEAN, J. E. DRAKE, and N. P. C. WESTWOOD. Can. J. Chem. **49**, 4033 (1971); (*b*) G. AHLGREN. Tetrahedron Lett. 989 (1974).

12. P. BISCHOF, J. A. HASHMALL, E. HEILBRONNER, and V. HORNUNG. Tetrahedron Lett. 1033 (1970).
13. H. BOCK and G. WAGNER. Angew. Chem. Int. Ed. **11**, 150 (1972).
14. R. HOFFMANN. Acc. Chem. Res. **4**, 1 (1971).
15. R. GLEITER, E. SCHMIDT, D. O. COWAN, and J. P. FERRARIS. J. Electron Spectrosc. **2**, 207 (1973).
16. (*a*) F. WUDL, G. M. SMITH, and E. J. HUFNAGEL. Chem. Commun. 1453 (1970); (*b*) S. HUNIG, G. KIESSLICH, H. QUAST, and D. SCHEUTZOW. Liebigs. Ann. Chem. 310 (1973).
17. F. HERMAN and B. I. BENNETT. To be published.
18. F. G. HERRING and R. A. N. MCLEAN. Inorg. Chem. **11**, 1667 (1972).
19. J. C. BÜNZLI, D. C. FROST, and C. A. MCDOWELL. J. Electron Spectrosc. **1**, 481 (1972).
20. W. F. COOPER, N. C. KENNY, J. W. EDMONDS, A. NAGEL, F. WUDL, and P. COPPENS. Chem. Commun. 889 (1971).

Can. J. Chem. Downloaded from www.nrcresearchpress.com by 210.87.254.6 on 09/05/12
For personal use only.

A Study of Molecular Motion in *cis*- and *trans*-Dichlorodiamminepalladium(II)

S. E. ULRICH[1] AND B. A. DUNELL

Chemistry Department, University of British Columbia, Vancouver, British Columbia V6T 1W5

Received May 16, 1974

S. E. ULRICH and B. A. DUNELL. Can. J. Chem. **52**, 3378 (1974).

Spin–lattice relaxation 'null times' have been obtained for *cis*- and *trans*-$Pd(NH_3)_2Cl_2$. The presence of a low temperature minimum for the *trans* complex has been interpreted in terms of inequivalent ammine groups. The second moment values are consistent with both ammine groups in both complexes reorienting with sufficient rate above 77 K to narrow the n.m.r. line. Although whole molecule rotation does not occur in either complex, it is believed that libration does.

S. E. ULRICH et B. A. DUNELL. Can. J. Chem. **52**, 3378 (1974).

Les 'temps nuls' de relaxation spin–réseau ont été obtenus pour les $Pd(NH_3)_2Cl_2$ *cis* et *trans*. On interprète la présence d'un minimum à base température dans le complexe *trans* en termes de groupes ammines non-équivalents. Les valeurs du moment secondaire sont en accord avec l'interprétation selon laquelle les deux groupes ammines dans chacun des complexes se réorientent avec une vitesse telle au-dessus de 77 K que les lignes en r.m.n. sont amincies. Quoique la rotation de la molécule entière ne se produit pas ni dans l'un ni dans l'autre des complexes, on croit qu'il y a oscillation. [Traduit par le journal]

This study of molecular motion in solid *cis*- and *trans*-dichlorodiamminepalladium(II) by continuous wave and pulsed n.m.r. techniques is a continuation of a general study of transition metal complexes. Earlier work (1, 2) was devoted to octahedral cobalt complexes and we are extending our studies to complexes with square planar geometry in order to discover whether different configurations undergo different molecular motions.

Experimental

trans-$Pd(NH_3)_2Cl_2$ was prepared by adding HCl to $[Pd(NH_3)_4]Cl_2$ (3) until a yellow precipitate formed. The *trans*-$Pd(NH_3)_2Cl_2$ was filtered, washed with water and ethanol, and air dried. *cis*-$Pd(NH_3)_2Cl_2$ was prepared by adding $AgClO_4$ to $[Pd(NH_3)_4]Cl_2$ in a 0.2 *M* $HClO_4$ solution (4). The precipitated AgCl was filtered off and the solution left to stand overnight. A concentrated solution of NaCl was added (5) and the precipitated yellow solid was filtered, rapidly washed with water, followed by washings with ethanol and ether, and dried *in vacuo*. Both samples were evacuated for 48 h to insure removal of water and promote desorption of oxygen.

Proton continuous wave spectra were obtained from a 16 MHz spectrometer described elsewhere (6). T_1 values were obtained at 30 MHz as described previously (7). The calculated points shown in Fig. 1 were computed using a nonlinear least-squares program (BMD) (8).

Results and Discussion

The second moment values for both complexes undergo little change over the temperature range studied (77–300 K). The observed second moment for the *trans* complex is 10 ± 0.8 G^2 at 77 K and gradually decreases to about 7.5 G^2 at room temperature. The second moment for

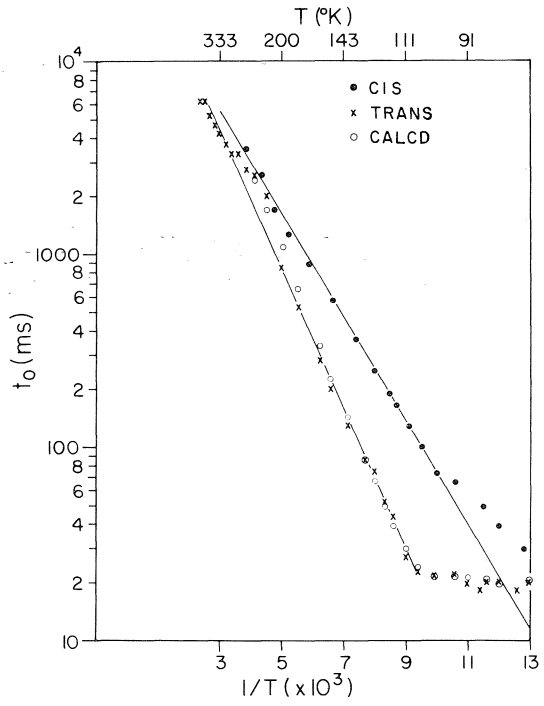

FIG. 1. t_0 *vs.* reciprocal temperature (°K).

[1]Present address: School of Chemical Sciences, University of Illinois, Urbana, Illinois 61801.

Can. J. Chem. Downloaded from www.nrcresearchpress.com by 210.87.254.40 on 09/05/12
For personal use only.

Can. J. Chem. Downloaded from www.nrcresearchpress.com by 210.87.254.40 on 09/05/12
For personal use only.

the *cis* complex is 6.5 ± 0.5 G^2 at 77 K and remains at this value to above 200 K, at which point saturation effects make spectral observation difficult for the size of sample available. The theoretical intra-ammine rigid lattice second moment is 33.6 G^2 (N—H assumed to be 1.02 Å and H—N—H angles assumed tetrahedral). The interammine, intramolecular contributions to the theoretical rigid lattice second moment are 0.09 G^2 for the *trans* isomer and 1.08 G^2 for the *cis* isomer (N—Pd assumed to be 2.1 Å and geometry assumed to be square planar). Intermolecular contributions can be estimated as 1 or 2 G^2 in each case. Reorientation of the NH_3 groups about their C_3 axes will reduce the intra-ammine theoretical second by a factor of 4 to 8.4 G^2 and reduce the small remaining second moment contributions by a factor of about 2. Thus the observed second moment of the *trans* isomer at 77 K is consistent with C_3 reorientation of both NH_3 groups about their N—Pd axes and the observed second moment of the *cis* isomer at 77 K indicates that there is some additional motion superimposed on C_3 reorientation of both ammine groups. A second moment value of 7.5 G^2 for the *trans* complex at 300 K is too large to be consistent with any whole molecule reorientation about an axis having an *n*-fold ($n \geq 3$) potential barrier. While the second moment might be consistent with a mechanism in which the whole molecule makes 180° jumps about a C_2 axis, such a mechanism is obviated by the discussion in the section on spin–lattice relaxation. Similar arguments apply to the *cis* complex. The observed changes in second moment for the *trans* complex appear to be consistent with libration of the whole molecule. A similar interpretation has been made of the results of second moment studies on *cis* and *trans* cobalt complexes (1). While there is no change in second moment with temperature for the *cis* complex, its value can also be explained by libration of the whole molecule superimposed on reorientation of both the ammine groups. That the second moment is unchanging with temperature suggests the angular amplitude of oscillation of the *cis* isomer is unchanging with temperature in the observed range. Given that these complexes are square planar, one assumes that libration about the axis through Pd and perpendicular to the plane of the complex will be most easily allowed by the lattice. For such an axis and for an interammine (including intermolecular) contribution of 1 to 2 G^2 in the given motional state, a librational amplitude of $30 \pm 10°$ will give a theoretical second moment agreeing with experiment for these isomers.

Figure 1 shows the results of spin–lattice relaxation time measurements for both complexes. Since the time dependence of the Z component of magnetization was clearly nonexponential throughout the temperature range studied, we have plotted the time t_0 at which $M_z = 0$, the so called 'null point' of the magnetization decay curve.

The t_0 curve for the *cis* complex is heading toward a presumed minimum. We believe this minimum would represent the C_3 reorientation of the ammine group(s). Since a minimum has not been reached we cannot state whether its depth corresponds to the reorientation of both ammine groups at approximately the Larmor frequency, for which the t_0 minimum would theoretically (1) be 10.5 ms, or to the reorientation of only one ammine group at this frequency, for which the theoretical minimum would be twice as large. A least squares fit of the linear portion of the log t_0 *vs.* T^{-1} curve gives an activation energy of 1.22 ± 0.01 kcal mol^{-1}.

The minimum in t_0 for the *trans* complex is broad and flat, and an attempt to fit the curve to an analytical form containing one BPP expression was very unsatisfactory. The best fit was obtained for a function which was the sum of two BPP terms (that is, $t_0^{-1} = t_{0A}^{-1} + t_{0B}^{-1}$). The experimental points were weighted by a factor t_0^2. This weighting corrected for the fact that the mean square error was computed on the difference between $1/t_{0(obs)}$ and $1/t_{0(calcd)}$. Since $\Delta(1/t_0)$ is small for large t_0, the fit was not satisfactory in the long t_0 region. Weighting by a factor t_0^2 in effect produced a fit in t_0 rather than $1/t_0$ and greatly improved the final agreement.

The parameters of best fit were: component A, $t_0(\text{min}) = 31$ ms, $\omega_0\tau_c^\circ = 6.2 \times 10^{-6}$, and activation energy = 1.8 kcal mol^{-1}; component B, $t_0(\text{min}) = 37$ ms, $\omega_0\tau_c^\circ = 5.2 \times 10^{-5}$, and $E =$ 1.9 kcal mol^{-1}. The uncertainties in the parameters for component A are large owing to a small number of data points in the range most affecting this component of the total t_0 curve.

The resolution into two minima (of about equal depth) necessitates the conclusion that two

ammine groups are inequivalent. The inequivalence of ammine groups has been observed in several cobalt ammine complexes (1, 9). We cannot, however, state with certainty that the two inequivalent ammine groups are attached to the same palladium atom. There is evidence (10) to suggest *trans*-$Pd(NH_3)_2Cl_2$ exists as a mixture of tetragonal and monoclinic forms at room temperature and this possibly accounts for the deviation from a straight line in Fig. 1 in the temperature range 200–250 K. This could, therefore, be an alternate explanation for the double minimum. Either interpretation is consistent with the suggestion from infrared work (11) that there is a more hindered ammine group.

If one assumes the bond lengths and angles noted earlier, together with the Pd—Cl = 2.3 Å, one obtains slightly closer contact between NH_3 and neighboring ligands on the same Pd in the *cis* configuration than in the *trans* configuration. The activation energy for ammine group reorientation in the *cis* complex is, however, lower than that in the *trans* complex. It seems, therefore, that the higher activation energy for ammine group reorientation in the *trans* isomer is a result of intermolecular interactions. Whether this is a consequence of denser packing (more Van der Waals interactions) or more hydrogen bonding we cannot state in the absence of X-ray work.

Because the internuclear H—H vector is not orthogonal to any C_2 axes except the N—Pd—N axis in the *trans* configuration or the N—Pd—Cl axis in the *cis* configuration, we suggested that a C_2 jump mechanism could account for the observed second moments. A shallow minimum in t_0 is predicted if such motion exists, and the absence of a minimum in t_0 above 100 K negates a C_2 jump motion in these systems.

We are grateful to the National Research Council of Canada for a grant-in-aid of this research.

1. S. E. Ulrich and B. A. Dunell. J. Chem. Soc. Faraday II, **69**, 1609 (1973).
2. S. E. Ulrich and B. A. Dunell. J. Magn. Res. **13**, 137 (1974).
3. Inorg. Syn. **8**, 234 (1966).
4. J. S. Coe, M. D. Hussain, and A. A. Malik. Inorg. Chim. Acta, **2**, 65 (1968).
5. J. S. Coe and J. R. Lyons. Inorg. Chem. **9**, 1775 (1970).
6. B. A. Dunell, C. A. Fyfe, C. A. McDowell, and J. Ripmeester. Trans. Faraday Soc. **65**, 1153 (1969).
7. S. E. Ulrich and B. A. Dunell. J. Chem. Soc. Faraday II, **68**, 680 (1972).
8. B. A. Dunell, M. D. Pachal, and S. E. Ulrich. Can. J. Chem. **51**, 1107 (1973).
9. G. R. Murray, Jr. and J. S. Waugh. J. Chem. Phys. **29**, 207 (1958).
10. R. Layton, D. W. Sink, and J. R. Durig. J. Inorg. Nucl. Chem. **28**, 1965 (1966).
11. K. Nakamoto, P. J. McCarthy, J. Fujita, R. A. Condrate, and G. T. Behnke. Inorg. Chem. **4**, 36 (1965).

Can. J. Chem. Downloaded from www.nrcresearchpress.com by 210.87.254.40 on 09/05/12
For personal use only.

New Synthesis of Nitroxyl Radicals of the Piperidine and Tetrahydropyridine Series[1]

LAWRENCE T. L. WONG, ROBERT SCHWENK,[2] AND J. CARLETON HSIA

Department of Pharmacology, Faculty of Medicine, University of Toronto, Toronto, Ontario M5S 1A8

Received November 16, 1973[3]

LAWRENCE T. L. WONG, ROBERT SCHWENK, and J. CARLETON HSIA. Can. J. Chem. **52**, 3381 (1974).

1-Oxyl-2,2,6,6-tetramethyl-4-piperidone cyanohydrin (**5**) was prepared by addition of HCN to 1-oxyl-2,2,6,6-tetramethyl-4-piperidone (**4**). The cyanohydrin was used to synthesize 1-oxyl-4-carboxy-2,2,6,6-tetramethylpiperidine (**2**) and 1-oxyl-4-carboxy-2,2,6,6-tetramethyl-1,2,5,6-tetrahydropyridine (**3**) which are useful nitroxyl radicals for spin labeling studies.

LAWRENCE T. L. WONG, ROBERT SCHWENK et J. CARLETON HSIA. Can. J. Chem. **52**, 3381 (1974).

La cyanohydrine de l'oxyl-1 tétraméthyl-2,2,6,6 pipéridone-4 (**5**) est préparée par addition de HCN sur la cétone correspondante **4**. La cyanohydrine peut être utilisée pour synthétiser l'oxyl-1 carboxy-4 tétraméthyl-2,2,6,6 pipéridine (**2**) ainsi que l'oxyl-1 carboxy-4 tétraméthyl-2,2,6,6 tétrahydro-1,2,5,6 pyridine (**3**) qui sont des radicaux nitroxyles utiles pour des études de marquage de spin. [Traduit par le journal]

Over the past several years, nitroxide free radicals have been extensively used as 'spin-label' probes to investigate the structures and conformations of biomacromolecules and biomembranes (1). Often, investigators will use two different types of nitroxide spin labels to reveal subtle conformational changes that may escape detection if only one type of spin label is used. McConnell and co-workers (2), for example, used both a pyrrolidine and piperidine spin label in their conformational study of spin labeled horse homoglobin. Recently, in our studies of the mode of action of drugs using the spin label technique, we required the carboxylic acid derivatives of the pyrrolidine and piperidine nitroxides (**1** and **2**, respectively). Although considerable effort has been spent in the synthesis of

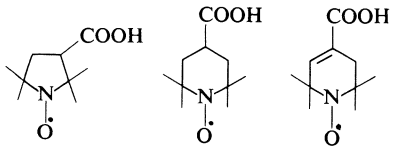

1 **2** **3**

pyrrolidine and piperidine nitroxyl radicals with various functional substituents (3), a review of the literature reveals that although the synthesis of the pyrrolidine derivative **1** has been reported, the synthesis of the piperidine derivative **2** and of the corresponding 1,2,5,6-tetrahydropyridine derivative **3**, have not. In this paper, therefore, we report the synthesis of these compounds in high yields starting from the parent ketone, 1-oxyl-2,2,6,6-tetramethyl-4-piperidone (**4**).

The syntheses of **2** and **3** are outlined in Scheme 1. The cyanohydrin **5** was prepared quite readily and in almost quantitative yield by addition of hydrogen cyanic acid (HCN) to the ketone (**4**). The cyanohydrin **5** was then dehydrated with phosphorus oxychloride and pyridine to give 1-oxyl-4-cyano-2,2,6,6-tetramethyl-1,2,5,6-tetrahydropyridine (**6**). The i.r. spectrum of compound **6** shows a strong absorption peak at 2220 cm^{-1}, indicating the presence of an α,β-unsaturated nitrile. Oxidation of **6** with hydrogen peroxide catalyzed by sodium tungstate – ethylenediaminetetraacetic acid sodium salt (4) gave 1-oxyl-4-carbamoyl-2,2,6,6-tetramethyl-1,2,5,6-tetrahydropyridine (**7**) which was then hydrolyzed in aqueous barium hydroxide solution to yield 1-oxyl-4-carboxyl-2,2,6,6-tetramethyl-1,2,5,6-tetrahydropyridine (**3**). The nitrile **6** can also be converted directly to the acid **3** using $Ba(OH)_2$.

For the synthesis of the saturated nitroxide carboxylic acid **2**, compound **3** was treated with diazomethane (5) to give the corresponding methyl ester derivative **8**, which was then hydrogenated at low pressure over Adam's platinum

[1]Supported by Grant MA-4129 and MRC-DA-6 from the Medical Research Council and Department of National Health and Welfare of Canada.

[2]MRC Postdoctoral Fellow, 1972–1973.

[3]Revision received June 21, 1974.

Can. J. Chem. Downloaded from www.nrcresearchpress.com by 210.87.254.5 on 09/05/12
For personal use only.

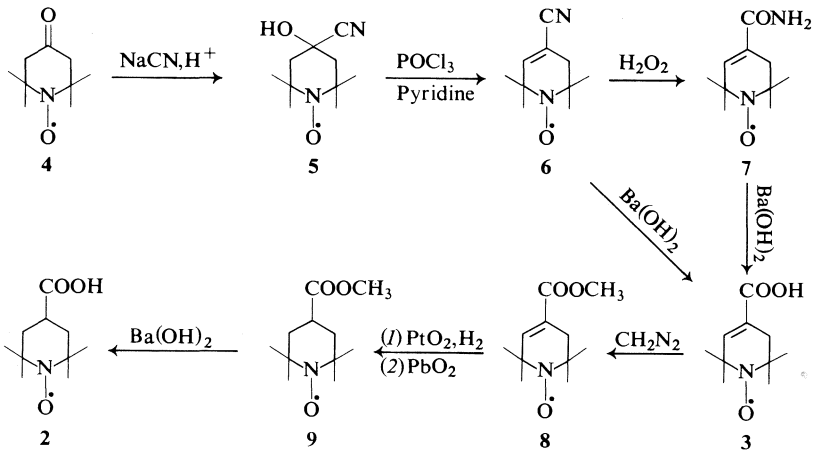

SCHEME 1

oxide catalyst to give 1-oxyl-4-methoxycarbonyl-2,2,6,6-tetramethylpiperidine (**9**). The hydrogenation was accompanied by the reduction of the nitroxide to the hydroxylamine (6) which, on exposure to air, was reoxidized slowly back to the nitroxide. Complete re-oxidation was ensured by treatment of the recovered product with lead dioxide (7). Compound **9** was hydrolyzed with $Ba(OH)_2$ to give 1-oxyl-4-carboxyl-2,2,6,6-tetramethylpiperidine (**2**) as pink needle crystals.

The successful preparation of 1-oxyl-2,2,6,6-tetramethyl-4-piperidone cyanohydrin (**5**) from ketone **4** demonstrates another selective reaction of the nitroxide free radical which does not involve reaction with the free valence. The carboxylic acid nitroxides **2** and **3** prepared can now be converted readily to useful spin labelling substrates for use to label and study biological systems in a manner similar to their five-membered ring counterparts (8, 9).

Experimental

Infrared spectra were recorded on a Perkin-Elmer model 710 A spectrometer. Mass spectra were recorded on a Bell and Howell 21-490 spectrometer. Column chromatography was performed using silica gel obtained from Davison Chemical (Grade 950, 60–200 mesh). All melting points were determined on a Fisher-Johns melting point apparatus and are uncorrected. Elemental analyses were performed by Microanalyses Laboratory, Toronto.

1-Oxyl-2,2,6,6-tetramethyl-4-piperidone Cyanohydrin (5)

To a solution of 30 g (0.176 mol) of 1-oxyl-2,2,6,6-tetramethyl-4-piperidone (**4**) in 100 ml of tetrahydrofuran was added a solution of 26 g (0.528 mol) of sodium cyanide in 100 ml of water and the resulting mixture was cooled to 5° in an ice bath. To this was added 52 g (0.528 mol) of 30% sulfuric acid at such a rate that the temperature of the reaction mixture never exceeded 15°. When the addition of sulfuric acid was complete, the solution was extracted with three 50-ml portions of ether. The ether extracts were combined, dried over magnesium sulfate, and evaporated under reduced pressure to give 35 g (100% yield) of 1-oxyl-2,2,6,6-tetramethyl-4-piperidone cyanohydrin (**5**) as a red syrup. Crystallization from hexane–ether gave orange crystals, m.p. 116–118°; i.r. ($CHCl_3$): 3570 cm^{-1} (free OH), 3300 cm^{-1} (H-bonded OH), 2240 cm^{-1} (C≡N, weak). Mass spectrum (*m/e*): M^+ 197; A_N ($CHCl_3$): 15.0 ± 0.1 G; *g* value = 2.0055 ± 0.0001.

Spins/mol calcd.: 6.0×10^{23}. Found: 6.1×10^{23}.

Anal. Calcd.: C, 60.91; H, 8.63; N, 14.21. Found: C, 60.88; H, 8.98; N, 14.00.

1-Oxyl-4-cyano-2,2,6,6-tetramethyl-1,2,5,6-tetrahydropyridine (6)

To a solution of 1 g (5 mmol) of the cyanohydrin **5** dissolved in 20 ml of dry pyridine was added 1 ml of freshly distilled phosphorus oxychloride and the resulting solution was stored at room temperature in the dark overnight. The excess phosphorus oxychloride was decomposed by slow addition of water (10 ml) and the solution was then exhaustively extracted with ether. The ether extracts were combined, washed with 1 *N* HCl, and dried over magnesium sulfate. Evaporation to dryness gave a brown solid which was purified by column chromatography using EtOAC–hexane (2:1 by volume) as the eluting solvent. From this there was obtained 0.7 g (78% yield) of 1-oxyl-4-cyano-2,2,6,6-tetramethyl-1,2,5,6-tetrahydropyridine (**6**) as a reddish-brown solid, m.p. 75–77°; i.r.: 2220 cm^{-1} (unsaturated C≡N, strong), 1650 (C=C); mass spectrum (*m/e*): M^+ 179, A_N ($CHCl_3$): 15.0 ± 0.1 G, *g* value: 2.0055 ± 0.0001.

Spins/mol calcd.: 6.0×10^{23}. Found: 6.0×10^{23}.

Anal. Calcd.: C, 67.04; H, 8.34; N, 15.64. Found: C, 66.83; H, 8.15; N, 15.37.

1-Oxyl-4-carbamoyl-2,2,6,6-tetramethyl-1,2,5,6-tetrahydropyridine (7)

To a solution of 0.3 g (1.68 mmol) of the nitrile **6** in 1 ml of methanol and 1 ml of water was added 0.5 ml of 30% hydrogen peroxide and catalytic amounts of sodium tungstate and Trilon-B (3, 7). The resulting solution was

Can. J. Chem. Downloaded from www.nrcresearchpress.com by 210.87.254.5 on 09/05/12
For personal use only.

Can. J. Chem. Downloaded from www.nrcresearchpress.com by 210.87.254.5 on 09/05/12
For personal use only.

stored at room temperature in the dark for 6 days. The solution was acidified to p*H* 2 with dilute hydrochloric acid and then extracted exhaustively with chloroform. The chloroform extracts were combined, dried over sodium sulfate, and evaporated under reduced pressure to give a brownish-orange solid. Recrystallization from chloroform–hexane gave 0.2 g (66% yield) of the amide as a light brown solid, m.p. 128–130°; i.r.: 3500, 3400 cm^{-1} (amide N—H), 1675 cm^{-1} (amide C=O), 1650 cm^{-1} (C=C); mass spectrum (*m/e*): M^+ 197; A_N ($CHCl_3$): 15.0 ± 0.1 G; *g* value: 2.0055 ± 0.0001.

Spins/mol calcd.: 6.0×10^{23}. Found: 5.9×10^{23}.

Anal. Calcd.: C, 60.91; H, 8.63; N, 14.21. Found: C, 61.07; H, 8.71; N, 14.26.

*1-Oxyl-4-carboxy-2,2,6,6-tetramethyl-1,2,5,6-tetrahydropyridine (**3**)*

*(a) From 1-Oxyl-4-carbamoyl-2,2,6,6-tetramethyl-1,2,5,6-tetrahydropyridine (**7**)*

A solution of 0.5 g (2.5 mmol) of the amide **7** and 0.8 g of $Ba(OH)_2 \cdot 8H_2O$ in 5 ml of water was heated at reflux until the evolution of ammonia had ceased. The solution was diluted with 10 ml of water and saturated with carbon dioxide. The resulting solution was acidified with diluted HCl to p*H* 2 and then extracted with chloroform. The chloroform solution was dried over sodium sulfate and evaporation to dryness gave 0.4 g (80% yield) of 1-oxyl-4-carboxy-2,2,6,6-tetramethyl-1,2,5,6,-tetrahydropyridine (**3**) which was recrystallized from chloroform–hexane to give a light orange solid, m.p. 190–192° (dec.); i.r.: 3500–2300 cm^{-1} (broad, acid OH), 1690 cm^{-1} (acid C=O), 1660 cm^{-1} (C=C); mass spectrum (*m/e*): M^+ 198; A_N ($CHCl_3$): 15.1 ± 0.1 G; *g* value: 2.0055 ± 0.0001.

Spins/mol calcd.: 6×10^{23}. Found: 6.0×10^{23}.

Anal. calcd.: C, 60.61; H, 8.08; N, 7.07. Found: C, 60.47; H, 8.02; N, 6.99.

*(b) From 1-Oxyl-4-cyano-2,2,6,6-tetramethyl-1,2,5,6-tetrahydropyridine (**6**)*

A solution of 0.2 g (1.12 mmol) of the nitrile **6** and 0.35 g of $Ba(OH)_2 \cdot 8H_2O$ in 3 ml of water was heated at reflux until the evolution of ammonia had ceased. The solution was worked up exactly as described in *a* to give 0.19 g of **3**, m.p. 190–192° (dec.).

*1-Oxyl-4-methoxycarbonyl-2,2,6,6-tetramethyl-1,2,5,6-tetrahydropyridine (**8**)*

A solution of 0.42 g (2 mmol) of **3** in 10 ml of anhydrous ether was treated with an excess of diazomethane in ether. The resulting solution was allowed to stand at room temperature for 15 min. The ether was evaporated under reduced pressure to give quantitative yield of **8** as a yellow solid, m.p. 57–60°; i.r.: 1710 cm^{-1} (ester C=O), 1665 cm^{-1} (C=C); mass spectrum (*m/e*): M^+ 212; A_N ($CHCl_3$): 15.1 ± 0.1 G; *g* value: 2.0055 ± 0.0001.

Spins/mol calcd.: 6.0×10^{23}. Found: 6.0×10^{23}.

Anal. calcd.: C, 62.26; H, 8.49; N, 6.60. Found: C, 62.12; H, 8.81; N, 6.47.

*1-Oxyl-4-methoxycarbonyl-2,2,6,6-tetramethylpiperidine (**9**)*

An excess of platinum oxide was added to a solution of 0.4 g (1.9 mmol) of the unsaturated ester (**8**) in 10 ml of 95% ethanol and the mixture was shaken under a slight pressure of hydrogen gas until the reaction was complete. The platinum oxide was removed by filtration and a small amount of lead dioxide was added to the filtrate. After stirring at room temperature for 1 h, the lead dioxide was removed and the resulting solution evaporated to dryness. Purification of the crude product by column chromatography (hexane–chloroform) afforded 0.29 g (74% yield) of **9** as an orange solid, m.p. 80–82°; i.r.: 1725 cm^{-1} (ester C=O); mass spectrum (*m/e*): M^+ 214; A_N ($CHCl_3$): 15.3 ± 0.1 G; *g* value: 2.0055 ± 0.0001.

Spins/mol calcd.: 6.0×10^{23}. Found: 5.9×10^{23}.

Anal. calcd.: C, 61.68; H, 9.34; N, 6.54. Found: C, 61.30; H, 9.14; N, 6.38.

*1-Oxyl-4-carboxy-2,2,6,6-tetramethylpiperidine (**2**)*

A solution of 0.15 g (0.7 mmol) of the saturated ester (**9**) and 0.35 g of $Ba(OH)_2 \cdot 8H_2O$ in 5 ml of water was refluxed for 16 h. The solution was then cooled and saturated with carbon dioxide. The resulting solution was acidified with dilute HCl to p*H* 2 and extracted exhaustively with chloroform. The chloroform extracts were combined, dried over magnesium sulfate, and evaporated under reduced pressure to give 0.13 g (86% yield) of **2**. Recrystallization from chloroform–hexane afforded pink needle crystals, m.p. 195–196°; i.r.: 3300–2400 cm^{-1} (broad, acid OH), 1705 cm^{-1} (acid C=O); mass spectrum (*m/e*): M^+ 200; A_N ($CHCl_3$): 15.5 ± 0.1 G; *g* value: 2.0054 ± 0.0001.

Spins/mol calcd.: 6.0×10^{23}. Found: 5.8×10^{23}.

Anal. calcd.: C, 60.00; H, 9.00; N, 7.00. Found: C, 59.90; H, 9.06; N, 7.04.

1. C. L. Hamilton and H. M. McConnell. Structural chemistry and molecular biology. *Edited by* A. Rich and N. Davidson. W. H. Freeman and Co., San Francisco, 1968. p. 115.
2. H. M. McConnell, W. Deal, and R. T. Ogata. Biochemistry, **8**, 2580 (1969).
3. E. G. Rozantsev. Free nitroxyl radical. *Edited by* H. Ulrich. Plenum Press, N.Y. 1970.
4. O. L. Lebedev and S. N. Kazarnovskii. Tr. Khim. Khim. Tekhnol. 649 (1959).
5. E. G. Rozantsev and L. A. Krinitskaya. Tetrahedron, **21**, 491 (1965).
6. E. G. Rozantsev and E. N. Gur-yanova. Iz. Akad. Nauk. SSR, Ser. Khim. 979 (1966).
7. D. J. Kosman and L. H. Piette. Chem. Commun. 926 (1969).
8. L. J. Berliner and H. M. McConnell. Proc. Nat. Acad. Sci. U.S.A. **55**, 708 (1966).
9. B. M. Hoffman, P. Schofield, and A. Rich. Biochemistry, **62**, 1195 (1969).

Chloride Quantum Yields from Photolysis of Chloropentammine and Chloropentakisalkylamino Chromium(III) Complexes

C. F. C. WONG AND A. D. KIRK[1]

Department of Chemistry, University of Victoria, Victoria, British Columbia V8W 2Y2

Received May 31, 1974

C. F. C. WONG and A. D. KIRK. Can. J. Chem. **52**, 3384 (1974).

Determination of chloride quantum yields in the photolysis of $[Cr(NH_3)_5Cl]^{2+}$ and chloropentakisalkylamino complexes has yielded values up to an order of magnitude lower than those reported in the literature. These determinations are described and the importance of the thermal production of chloride from the main photoproduct as a source of error is discussed. The similarity of the chloride quantum yields for the series of complexes confirm that our results for $[Cr(NH_3)_5Cl]^{2+}$, which are at least an order of magnitude lower than the lowest reported in the literature, are closer to the correct value than the earlier data.

C. F. C. WONG et A. D. KIRK. Can. J. Chem. **52**, 3384 (1974).

La détermination des rendements quantiques en chlorure lors de la photolyse des complexes $[Cr(NH_3)_5Cl]^{2+}$ et du chloropentakisalkylamino correspondant conduit à des valeurs qui sont plus basses que celles rapportées dans la littérature; les différences atteignent jusqu'à un ordre de grandeur. On décrit ces déterminations et on discute de l'importance de la production thermique de chlorure à partir du photoproduit principal comme source d'erreur. La similitude des rendements quantiques de chlorure pour une série de complexes confirme que nos résultats pour le $[Cr(NH_3)_5Cl]^{2+}$, qui sont au moins un ordre de grandeur plus bas que les plus bas rapportés dans la littérature sont plus proches de la réalité que les valeurs antérieures.

[Traduit par le journal]

Can. J. Chem. Downloaded from www.nrcresearchpress.com by 210.87.254.5 on 09/05/12
For personal use only.

Progress toward an understanding of chromium(III) photochemistry (see several papers in ref. 1) has placed fresh emphasis upon information on the ratios of reaction modes and their dependence on the nature of the ligands, the wavelength of irradiation, temperature, etc. As has been observed before (2) some of the data in the literature is inaccurate and not in unanimity. The quantum yield data for chloride release from chloropentammine chromium(III) ion (2–6), given in Table 1, is no exception. In the course of a study of solvent effects on the photolysis of chloropentammine and chloropentakisalkylamine chromium(III) complexes (7), we have had occasion to redetermine the photolysis quantum yield of chloride from the complexes. We have found yields at least an order of magnitude lower than previously reported.

Complexes of the type $[Cr(RNH_2)_5Cl]^{2+}$ show two photochemical reaction modes in acid solution

$$[1]\quad [Cr(RNH_2)_5Cl]^{2+} + H_3O^+ \xrightarrow{\phi_1} [Cr(RNH_2)_4H_2OCl]^{2+} + RNH_3^+$$

$$[2]\quad [Cr(RNH_2)_5Cl]^{2+} + H_2O \xrightarrow{\phi_2} [Cr(RNH_2)_5H_2O]^{3+} + Cl^-$$

where reaction 1 is favored. In addition the thermal reaction corresponding to [2] occurs slowly. Where one is working with relatively low intensity monochromatic light, the major problems in determining a quantum yield for chloride with any degree of precision are the thermal reaction 2 and the thermal lability of the major photoproduct, $[Cr(RNH_2)_4H_2OCl]^{2+}$, which releases chloride by the secondary thermal reaction

TABLE 1. Chloride quantum yield data for $[Cr(NH_3)_5Cl]^{2+}$

λ(nm)	ϕ_{Cl^-}	Reference
365	0.05	2
506	0.0072	3
430	0.004±0.002	6
564	<0.001*	5
503	0.01†	4
506	0.04	2
511	0.004±0.001	6
546	0.0045	3

*Measured in dimethylsulfoxide.
†Measured in 50% aqueous ethanol.

[1]To whom correspondence should be addressed.

Can. J. Chem. Downloaded from www.nrcresearchpress.com by 210.87.254.5 on 09/05/12
For personal use only.

[3] $[Cr(RNH_2)_4H_2OCl]^{2+} + H_2O \longrightarrow [Cr(RNH_2)_4(H_2O)_2]^{3+} + Cl^-$

Reaction 3 is often much faster than reaction 2. Amongst previous workers Moggi *et al.* (8), Langford and Tipping (5), and Wehry (6) apparently neglected this latter process, which may therefore have caused their chloride yields to be high; it should be noted, however, that Langford and Tipping quoted only an upper limit for the quantum yield of chloride in dimethyl sulfoxide. Wasgestian and Schläfer (3) applied an approximate correction which seems reasonable but their results are still much higher than ours. Because of the large wavelength variation of ϕ_{Cl^-} (3), this might have been due to the presence of short wavelength light.

The magnitude that the effect may assume was made clear during our initial study of $[Cr(CH_3NH_2)_5Cl]^{2+}$, for which, at 20 °C, the apparent ϕ_{Cl^-} rose from 3.0×10^{-3} to 1.0×10^{-2} for photolysis times of 1000 s (7% decomposition) and 2000 s (15% decomposition) respectively. Continuous monitoring of chloride ion yielded the curve shown in Fig. 1, which illustrates the more rapid rate of thermal decomposition of the photoproduct (at 20 °C, k_2 for $[Cr(CH_3NH_2)_5Cl]^{2+}$ is 8.8×10^{-8} s^{-1}, while k_3 for *cis*(?)-$[Cr(CH_3NH_2)_4H_2OCl]^{2+}$ is *ca.* 1.0×10^{-5} s^{-1}) and the overwhelming contribution that this makes to the overall chloride release. Consequently the method adopted for chloride determination in this work emphasized low conversions of complex and continuous chloride concentration measurements.

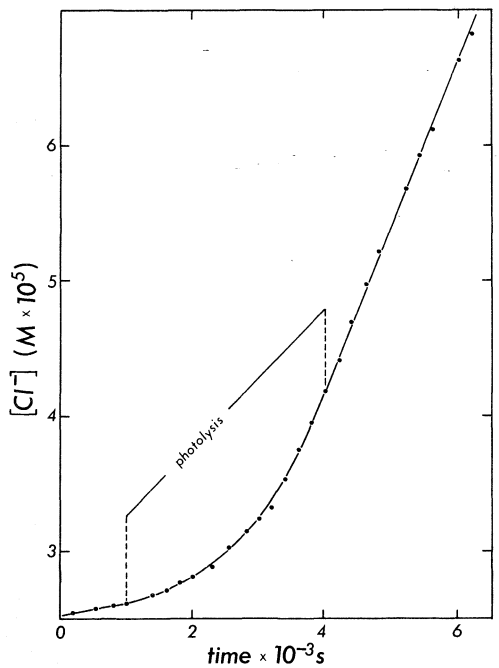

FIG. 1. Concentration *vs.* time for thermal and photochemical chloride release in the photolysis of $[Cr(CH_3NH_2)_5Cl]^{2+}$, temperature = 20 °C, complex = 1.0×10^{-2} *M* λ_{irrad} = 546 nm, p*H* = 3.0, ionic strength = 0.10.

The chloride concentration in the stirred solution was monitored continuously during irradiation using a chloride concentration cell (3), masked to avoid photovoltaic effects. Table 2 gives the conditions of the runs, and the measured chloride quantum yields calculated in two ways. In the first, reaction 3 was ignored and the total chloride assumed to be produced by reaction 2, photochemically and thermally. A correction for the thermal production of chloride by reaction 2 was then applied. Thus this should be an upper limit, in some cases generous, for ϕ_{Cl^-}. In the second, reaction 3 was corrected for by the method of Wasgestian and Schläfer, or by a modification thereof. As is seen, even the extreme upper limits for ϕ_{Cl^-} are an order of magnitude lower than the previously reported values.

The data in Table 2 show that for the whole series of complexes, both in water, and in the acetone/water solvent mixture necessary for solution of the higher alkylamine complexes, the chloride quantum yields for irradiation at 565 nm into the lowest energy quartet absorption band are consistently very small and lie in the range of $1 \rightarrow 4 \times 10^{-4}$. This we consider is good confirmatory evidence that the value of 3×10^{-4} or less found for $[Cr(NH_3)_5Cl]^{2+}$ is closer to the correct value than the earlier data quoted in Table 1.

These results illustrate that thermal reactions cannot always be corrected for by subtracting a dark thermal run from the irradiated sample. Of more significance, however, is the observation that the photochemical chloride yield drops off more rapidly with increasing wavelength than had previously been thought. Thus, for chloropentammine the results of Wasgestian and co-worker (3) show ϕ_{Cl^-} at 250 nm to be 0.2 falling off our value of $<3 \times 10^{-4}$ at 565 nm.

A fall off of this magnitude is probably more consistent than the earlier results with the

TABLE 2. Chloride quantum yield data for $Cr(RNH_2)_5Cl^{2+}$

RNH_2	λ(nm)	% conversion	ϕ_{Cl^-}*	ϕ_{Cl^-}†	Comments
NH_3	401	2.4		$(2\pm3)\times10^{-4}$	2×10^{-2} *M*
	565	3.5		$(0\pm3)\times10^{-4}$	in water
CH_3NH_2	401	3.2	2×10^{-3}	1×10^{-3}	2×10^{-2} *M*
	565	6.9	3×10^{-4}	2×10^{-4}	in water
$CH_3CH_2NH_2$	565	8.7	1×10^{-4}	8×10^{-5}	9×10^{-3} *M* in water
n-$PrNH_2$	565	4.5	2×10^{-4}	1×10^{-4}	1×10^{-2} *M* in 33% acetone

*This quantum yield represents an extreme upper limit calculated from photoproduced chloride plus any thermal Cl^- from the main photoproduct.
†Quantum yield, corrected as far as possible for thermal decomposition of the main photoproduct.

suggestion (3) that the chloride release in the first and second d–d transition regions arises from some charge transfer character in the corresponding excited states. In addition it shows that the ratio ϕ_{NH_3}/ϕ_{Cl^-} for irradiation into the first ligand field band is at least 1000, showing the photolysis mode for this complex is even more selective than previously thought.

The authors wish to acknowledge the financial support of the National Research Council of Canada and the University of Victoria Faculty Research Fund. C. F. C. Wong wishes to acknowledge the award of a University of Victoria Graduate Scholarship.

1. Symposium on inorganic and organometallic photochemistry. Mol. Photochem. 5(2) (1973).
2. V. BALZANI and V. CARASSITI. Photochemistry of coordination compounds. Academic Press, London and New York. 1970.
3. H. F. WASGESTIAN and H. L. SCHLÄFER. Zeit. Phys. Chem. N.F. **62**, 127 (1968).
4. E. ZINATO, P. TULLI, and P. RICCIERI. J. Phys. Chem. **75**, 3504 (1971).
5. C. H. LANGFORD and L. TIPPING. Can. J. Chem. **50**, 887 (1972).
6. E. L. WEHRY. J. Am. Chem. Soc. **95**, 2137 (1973).
7. C. F. C. WONG and A. D. KIRK. To be published.
8. L. MOGGI, F. BOLLETTA, and V. BALZANI. Ric. Sci. 1228 (1966).

Can. J. Chem. Downloaded from www.nrcresearchpress.com by 210.87.254.5 on 09/05/12
For personal use only.

Cationic Aryltetrazene Complexes of Iridium

ALAN B. GILCHRIST AND DEREK SUTTON[1]

Department of Chemistry, Simon Fraser University, Burnaby, British Columbia V5A 1S6

Received April 29, 1974

ALAN B. GILCHRIST and DEREK SUTTON. Can. J. Chem. **52**, 3387 (1974).

The details of the synthesis and properties of a number of cationic iridium aryltetrazene complexes of general formula $[Ir(CO)\{N_4(C_6H_4R)_2\}(PPh_3)_2]^+$ where R = H or *para*-F, Cl, Br, CF_3, or OCH_3 are presented. The complexes are compared with a number of other compounds possessing tetrazene or tetraazadiene ligands. A possible mechanism of formation is presented, consistent with presently available evidence.

ALAN B. GILCHRIST et DEREK SUTTON. Can. J. Chem. **52**, 3387 (1974).

On rapporte les détails de la synthèse et les propriétés d'un certain nombre de complexes cationiques iridium aryltétrazène de formule générale $[Ir(CO)\{N_4(C_6H_4R)_2\}(PPh_3)_2]^+$ dans lesquels R = H ou *para*-F, Cl, Br, CF_3 ou OCH_3. On compare ces complexes avec un certain nombre d'autres composés possédant des ligands tétrazène ou tétraazadiène. On présente un mécanisme possible pour la formation qui est en accord avec les données expérimentales disponibles actuellement. [Traduit par le journal]

Can. J. Chem. Downloaded from www.nrcresearchpress.com by 210.87.254.6 on 09/05/12
For personal use only.

Introduction

The tendency of nitrogen toward catenation is severely limited by the low enthalpy of the N—N single bond compared with that of N—N multiple bonds, so that examples are few. Two 1,4-substituted tetranuclear species have been described, 1,4-disubstituted tetraazadiene RN=N—N=NR′ and 1,4-tetrasubstituted tetrazene R(R′)N—N=N—NR″(R‴) (1). Examples of the tetrazene have been synthesized, but there appear to be no known examples of the tetraazadiene. In recent years, however, there have appeared a number of papers (2–9) describing compounds in which a ligand R_2N_4, formally of the tetraazadiene type, is bound to a transition metal. These include the preliminary details (8), and the X-ray structure determination (9) of one of the compounds described in this paper.

The structural and bonding features interrelating these two tetranitrogen species have their parallel in the possible representations for the binding of an R_2N_4 ligand to a metal ion, as illustrated in the following diagrams. Structure **1**

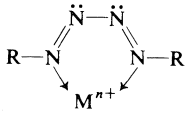

1

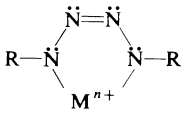

2

[1]To whom correspondence should be addressed.

involves conventional bidentate coordination of the tetraazadiene ligand, whereas in structure **2** we have an electron distribution closely analogous to that in the tetrazene itself, and which may be envisaged as arising from oxidative addition of the diene across M^{n+}

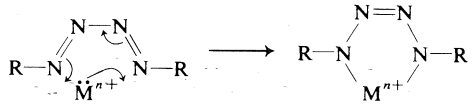

or viewed as coordination of the bidentate dianion to $M^{(n+2)+}$

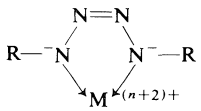

Whatever the description, the metal in structure **2** is formally $2e^-$-oxidized. By virtue of their delocalized π-systems, tetraazadienes clearly belong to the class of so-called "suspect" ligands like 1,2-diimines and 1,2-dithiolenes (10) with the result that observed dimensions within the metallocycle may approximate to either valence-bond extreme **1** or **2**, or may even be intermediate, depending on the nature of the metal and the other ligands present. Furthermore, there can occur involvement of unshared electrons on the coordinating nitrogen atoms in the π-electron system of the heterocycle through valence-bond structures such as **3***a* or **3***b*

Can. J. Chem. Downloaded from www.nrcresearchpress.com by 210.87.254.6 on 09/05/12
For personal use only.

TABLE 1. Elemental analyses and other data for the aryltetrazene complexes, $[Ir(CO)\{N_4(C_6H_4R)_2\}(PPh_3)_2]BF_4$ (**4***a–f*)

Compound (R)	Found (%)			Calculated (%)			ν(CO) cm^{-1}	Decomposition temperature[h] (°C)	Yield[a] (%)		Electronic spectrum[i] λ_{max}(nm)		
	C	H	N	C	H	N			*I*[b]	*S*[c]			
4*a*(H)	56.83	4.13	5.28	56.50	3.89	5.38	2037	180	15	21	390(5540)	440(5540)	500(3960)
4*b*(*p*-F)[d,e]	54.96	3.80	5.30	57.16	3.85	4.85	2057	150	45	50	400(6250)	440(6090)	500(3950)
4*c*(*p*-Cl)[f]	52.80	3.45	5.27	53.03	3.46	5.05	2057	150	23	50	406(8120)	440(7560)	500(5220)
4*d*(*p*-Br)[g]	49.84	3.59	4.44	49.66	3.54	4.45	2059	125	25	43	410(9420)	440(9120)	500(5820)
4*e*(*p*-CF_3)	51.99	3.67	4.56	52.00	3.30	4.75	2064		7	80	385(8660)	440(7240)	500(5180)
4*f*(*p*-OCH_3)	55.36	4.06	4.87	55.60	4.03	5.10	2035	140	< 10	15	360(4520)	420(4740) –90	500(4460)

[a]Based on a stoichiometry of 1 mol $IrCl(CO)(PPh_3)_2$ + 1 mol $ArN_2^+ \rightarrow$ 0.5 mol **4**.
[b]*I* = % yield of pure, isolated compound.
[c]*S* = % yield of product formed in solution during reaction, and calculated from the molar absorptivities, $\varepsilon_{500\ nm}$.
[d]Formulated with 1 mol C_6H_6 per 1 mol of complex; unable to obtain accurate carbon analysis, probably to varying benzene of crystallization.
[e]Anal. Calcd.: F, 9.87; P, 5.36. Found: F, 9.56; P, 5.10.
[f]Anal. Calcd.: F, 6.85. Found: F, 6.89.
[g]Formulated with 1 mol $(CH_3)_2CO$ per 1 mol of complex.
[h]Temperature at which evidence of decomposition first appears; **4***e* was not measured.
[i]In absolute ethanol at 25°, extinction coefficients in parentheses.

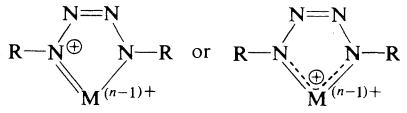

3*a* 3*b*

Compounds which, on various grounds, have been considered to approximate to extreme **1** have been generally referred to as tetraazadiene complexes (3, 7). The X-ray structural results on one of the iridium complexes reported here (9) indicate an electron distribution more closely approximating to **3**, and these compounds are therefore referred to as tetrazene complexes in this work.

Results and Discussion

The aryltetrazene complexes **4** were readily prepared by the addition of the requisite aryldiazonium tetrafluoroborate and ethanol or isopropanol to a benzene solution of Vaska's complex *trans*-$IrCl(CO)(PPh_3)_2$. The mole ratio of iridium compound to diazonium salt was held at 1:1. Although the apparent stoichiometry of the reaction suggests a 1:2 ratio this did not prove beneficial in practice as no significant improvement in yield resulted, and the product was then contaminated with a persistent small amount of diazonium salt. The alcohol:benzene

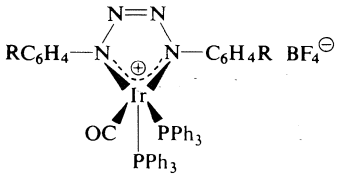

4

a R = H
b R = *p*-F
c R = *p*-Cl
d R = *p*-Br
e R = *p*-CF_3
f R = *p*-OCH_3

ratio used was 1:10 (v:v), since with this ratio the complex generally crystallized out easily on cooling or slow evaporation. Experiments employing a higher alcohol content usually resulted in no crystallization of tetrazene, and loss of tetrazene during the work up in the isolation of yellow aryldiazene (aryldiimide) co-products described elsewhere (11). Attempts to isolate derivatives other than those, **4***a–f*, listed in Table 1 were unsuccessful. Reactions with *p*-NEt_2 and *p*-OH phenyldiazonium ions showed no visible evidence (*e.g.*, color) for tetrazene formation and substantial amounts (*ca.* 70% for *p*-NEt_2) of the unreacted diazonium salt and iridium compound were recovered. Electron-donor substituents on the aromatic nucleus evidently hinder the formation of the complex, as indicated not only by these two unsuccessful reactions, but also by the low yield, and substantial amount of recovered diazonium salt (~10%) for the *p*-methoxy derivative. No isolation of complexes was accomplished for *ortho*- or *meta*-F, Cl, Br, NO_2, CH_3, and OCH_3 substituted phenyldiazonium salts, but the red solutions formed in these reactions exhibited electronic spectra containing the 500 nm band typically found for the characterized tetrazene complexes and the formation of analogous complexes in solution in these cases is inferred. Most notably, no evidence for the formation of tetrazene complexes is observed at all in the case of the *ortho* disubstituted diazonium salts examined (2,6-difluoro-, 2,6-dichloro, and 2,6-dimethylphenyldiazonium tetrafluoroborates). This is attributed to extreme steric interference at the carbon-bonded nitrogen atom, preventing its close approach to iridium.

The aryltetrazene complexes which were isolated are deep-red, diamagnetic crystalline solids. They are quite stable in air for prolonged periods and toward moderate heating as demonstrated by their decomposition temperatures (Table 1). They are soluble in ethanol, methanol, acetone, acetonitrile, nitromethane, chloroform, and dichloromethane and insoluble in diethyl ether, benzene, aliphatic hydrocarbons, and water. They appear to be unstable in chlorinated solvents, the product obtained on attempted recrystallization from CH_2Cl_2 giving high and irrational analysis for chlorine. The molar electrical conductance measured for **4***b* in nitromethane at 25° was $\Lambda_M = 105$ ohm^{-1} mol^{-1} cm^2 at 3.7×10^{-4} *M* and $\Lambda_M = 117$ at 1.5×10^{-4} *M*. These values are typical for 1:1 electrolytes (12) and comparable values were obtained for $[Ir(CO)Cl(NO)(PPh_3)_2]BF_4$ (13) ($\Lambda_M = 100$ (1.7×10^{-4} *M*) and 116 (6.6×10^{-4} *M*)) and $C_6H_5N_2BF_4$ ($\Lambda_M = 115$ at 4.5×10^{-4} *M*). Pyrolysis of **4***b* at 550° under high vacuum, and subsequent gas chromatographic analysis of the non-condensible gases yielded 1 mol CO and, significantly, 1 mol N_2 per mol complex rather than the 2 mol N_2 expected for a bisaryldiazo complex.

Can. J. Chem. Downloaded from www.nrcresearchpress.com by 210.87.254.6 on 09/05/12
For personal use only.

Can. J. Chem. Downloaded from www.nrcresearchpress.com by 210.87.254.6 on 09/05/12
For personal use only.

The infrared spectra of all the complexes exhibited a strong ν(CO) absorption in the region of 2050 cm^{-1}, (Table 1) representing a considerable upward wavenumber shift from ν(CO) in $IrCl(CO)(PPh_3)_2$ (1965 cm^{-1}) consistent with the assignment of a formal Ir(III) oxidation state. By comparison, $[IrCO(Cl)NO(PPh_3)_2]BF_4$ has ν(CO) at 2050 cm^{-1} (13). The value of ν(CO) increases with increasing positive value of the Hammett constant (σ_p) of the *p*-substituent R in the sequence OCH_3 ($\sigma_p = -0.27$) < H (0.0) < F (0.06) = Cl (0.23) < Br (0.23) < CF_3 (0.54). The relationship is not linear, and this may be a result of the ν(CO) values being determined from solid-state i.r. spectra. Nevertheless the general trend demonstrates that the electron withdrawing effect of an aryl substituent is relayed to the iridium decreasing the electron density at iridium available for back-bonding to the carbonyl group. No infrared bands assignable to NN-stretching of the tetrazene ligand were detected, and isotopic substitution with ^{15}N using $p\text{-}FC_6H_4{}^{14}N{\equiv}{}^{15}NBF_4$ in the synthesis failed to show a frequency shift for any of the observed i.r. bands of **4***b*. Raman spectra were unobtainable owing to decomposition under He–Ne laser irradiation.

The ^{19}F n.m.r. spectrum measured at 56.4 MHz for a $CDCl_3$ solution of **4***b* exhibited a weak signal at +6230 Hz and a strong signal at +8778 Hz (downfield relative to internal CCl_3F) assigned as due to the *p*-F and BF_4^- fluorines respectively. The shifts may be compared with values of +6135 Hz (*p*-F) and +8585 Hz (BF_4^-) reported for $[Pt(FC_6H_4NNH)(PEt_3)_2Cl]BF_4$ (14). The proton n.m.r. spectrum of **4***b* in $CDCl_3$ showed two broad multiplet peaks centered at τ 2.9 and τ 3.8 respectively, with integrated intensities corresponding to 40 protons and 4 protons respectively. A tentative assignment is that the τ 2.9 signal consists of a contribution from *m*-protons (relatively deshielded by the adjacent fluorine) of the tetrazene aryl substituents as well as the expected phenyl phosphine and benzene solvate contributions, whilst the less-deshielded *o*-protons give rise to the τ 3.8 signal.

The electronic spectra of the complexes (Table 1) consisted of three broad, intense overlapping bands in the region 350–600 nm. The detailed assignment of these bands is not known at the present time. The highest energy band (360–410 nm) varies in position with the nature of the *p*-substituent, but shows no simple trend. The remaining two bands, at *ca.* 440 and 500 nm do not show positional shifts. The extinction coefficients of all three bands are greater than 10^3 suggesting that they originate in relatively "allowed" electronic transitions, such as metal–ligand or intra-ligand (tetrazene) transitions. However, in view of the low symmetry of this pentacoordinate complex, and previously observed unusually intense d–d transitions in some pentacoordinate complexes (15), the possibility that the presently observed bands are due to d–d transitions cannot yet be excluded. An examination of the literature on other established (2, 3) or proposed (4–7) tetrazene/tetraazadiene complexes reveals that whilst these display a wide variety of colors, the actual spectral bands have seldom been reported. Thus it is not possible to say whether the presently observed spectrum contains features to be considered as typical of the tetrazene ligand.

The X-ray structure determination (9) carried out on **4***b* yielded dimensions within the metallocycle which were interpreted to indicate an electronic structure corresponding to a tetrazene, together with a degree of multiple bonding between the iridium atom and the adjacent nitrogen atoms, as depicted in the structure illustrated for **4**. A semi-empirical (CNDO) calculation (16*a*) performed on the simplified model ion $[Ir(N_4H_2)(CO)(PH_3)_2]^+$, whose geometry was assumed similar to that of **4***b*, agrees with this picture. For example, the bond order of the bond between the inner nitrogen atoms is calculated to be significantly greater than that of the outer N—N bonds, and the Ir atom contributes about $2e^-$ to the π-system of the metallocycle and is positively charged (*ca.* $0.33e^-$). These results contrast with the results of a similar calculation on the tetraazadiene complex $Fe\{N_4(CH_3)_2\}(CO)_3$ (16*b*).

We now turn to a discussion of the mechanism of the reaction. First, it should be noted that the sum of two aryldiazonium ions is two electrons short of being isoelectronic with a tetraazadiene ligand. Recognizing this, Carty (17) has proposed a mechanism involving a formal 2-electron transfer from the iridium atom in Vaska's complex in the process of coupling two diazonium ions. Unfortunately, this mechanism yields a hypothetical complex which is

TABLE 2. Comparison of yields

Reaction in C_6H_6/Pr^iOH*	Yield (mmol) Orthometallated diazene	Tetrazene	Acetone
p-$BrC_6H_4N_2^+ + V$	0.028	0.027	0.054
p-$FC_6H_4N_2^+ + AgBF_4 + V$	0.024	0.056	0.082
o-$F_2C_6H_3N_2^+ + V$	Nil	Nil	0.082

*V = Vaska's complex, $IrCl(CO)(PPh_3)_2$.

still two electrons short of being isoelectronic with **4**, since it must result in a tripositive *tetraazadiene* complex cation of iridium(III), whereas the observed compound is a monopositive *tetrazene* complex cation of iridium(III) (*i.e.*, isoelectronic with a monopositive tetraazadiene complex cation of Ir(I)). The proper overall reaction is represented in reaction 1

$$[1] \quad IrCl(CO)(PPh_3)_2 + 2ArN_2^+ \xrightarrow[-Cl^-]{+2e^-} \mathbf{4}$$

and the problem centers on the nature of the reduction process involved.

We have not yet been able to establish reaction conditions in which competing reactions giving rise to coproducts such as the aryldiazene complex (11) are more-or-less eliminated and so no detailed quantitative kinetic studies have yet been considered warranted. However, we have the following evidence that hydride abstraction from the alcohol occurs during the reaction, and we propose that this acts as the source of the electrons required for the reduction step (with the formation of H^+). Thus, tetrazene formation is not observed when ethanol is replaced by methanol, *t*-butanol, acetone, or acetic acid, but is observed for isopropanol, which like ethanol has an activated α-hydrogen atom. Repeating the synthesis with C_2H_5OD had no observable effect, whereas substituting C_2D_5OD caused a clearly observable drop in the rate of tetrazene formation (Fig. 1). Experimental difficulties did not allow the measurement of reliable approximate zero-time rates, so that no quantitative comparison of rate-constants can be made. However, the results point in favor of a primary isotope effect in C—H bond cleavage, presumably of an α-hydrogen atom, as in reaction 2.

$$[2] \quad R(R')C\overset{\curvearrowleft}{-}O\overset{\curvearrowleft}{-}H \rightarrow RR'C{=}O + H^+ + [H^-]$$

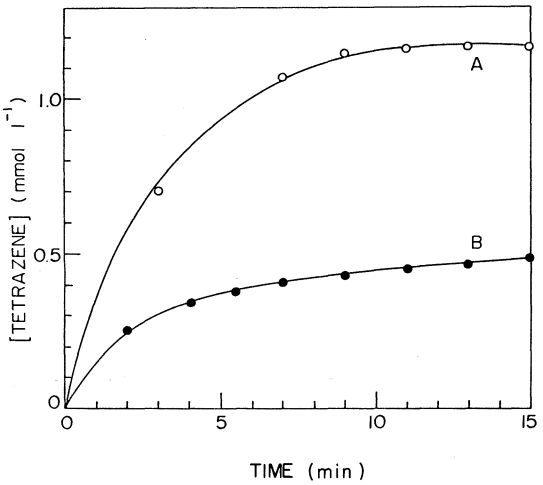

FIG. 1. Comparison of the formation of **4***d* in benzene–ethanol or benzene–C_2H_5OD (curve A), and benzene–ethanol-d^6 (curve B); p-$BrC_6H_4N_2BF_4$, 0.031 mmol; $IrCl(CO)(PPh_3)_2$, 0.031 mmol; benzene, 3.75 ml; and alcohol 1.25 ml; at 25°.

In agreement, acetone has been identified quantitatively in the isopropanol reactions, in amounts (Table 2) which suggest that the α-hydride abstraction may contribute to both tetrazene and aryldiazene (11) syntheses. As mentioned, the *ortho*-disubstituted diazonium ion o-$F_2C_6H_3N_2^+$ did not yield either the tetrazene or aryldiazene complex, nevertheless acetone was recovered in comparable quantity. A curious observation is that the normal reaction produces no tetrazene at all when conducted in pure isopropanol or ethanol (rather than mixtures of these with benzene), and no red color develops during the reaction (18). Possibly tetrazene formation requires a solvent less polar than the pure alcohol.

We propose the following tentative, but simple mechanism as a basis for further investigation. It envisages attack of diazonium

Can. J. Chem. Downloaded from www.nrcresearchpress.com by 210.87.254.6 on 09/05/12
For personal use only.

ion at the N^2 nitrogen atom[2] of an intermediate iridium aryldiazo or aryldiazene complex such as **5** or **6**. In the case of **5**, the ligand is formally

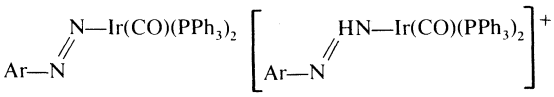

5 **6**

ArN_2^- (*i.e.*, the required $2e^-$ reduction of ArN_2^+ referred to above has been accomplished) and would have the doubly-bent geometry shown, as indicated by the X-ray structure determination of a comparable compound (19). Furthermore, this ligand is known to be capable of protonation at N^2 (20), so, by analogy, electrophilic attack by diazonium ion at N^2 in **5** (or in **6** with elimination of H^+) followed by electron rearrangement as in Scheme 1 yields the delocalized iridium(III) tetrazene complex cation **4** observed. There are two obvious routes by which these intermediates or their precursors can arise, which incidentally explain the role of the alcohol in the reaction.

(*i*) Since acetone was found in small quantities when diazonium ion alone was stirred in isopropanol there is the possibility of electrophilic attack of ArN_2^+ on the alcohol. In this case α-hydride abstraction would yield the unstable intermediate aryldiazene (21), ArN=NH which may react with $IrCl(CO)(PPh_3)_2$ by two routes; oxidative addition yields $Ir(N_2Ar)HCl(CO)(PPh_3)_2$ whereas Lewis base addition yields $Ir(HNNAr)Cl(CO)(PPh_3)_2$. Both are possible precursors of the intermediates **5** or **6**.

(*ii*) An alternative, to which we presently feel more inclined, is that α-hydride abstraction from the solvent is by an electrophilic iridium complex rather than diazonium ion. This type of reaction has been reported for both iridium(I) and iridium(III) complexes but not for Vaska's complex itself (22). In agreement, we ourselves have observed no reaction between Vaska's complex and either ethanol or isopropanol under a variety of conditions. In the presence of diazonium ion, Vaska's complex may be converted largely to the iridium(III) aryldiazo complex cation $[Ir(N_2Ar)Cl(CO)(PPh_3)_2]^+$ (23), which being coordinatively unsaturated is an excellent candidate for α-hydride abstraction to give the hydride complex $Ir(N_2Ar)HCl(CO)(PPh_3)_2$, or by subsequent "insertion" the aryldiazene complex $Ir(HNNAr)Cl(CO)(PPh_3)_2$, both referred to above.

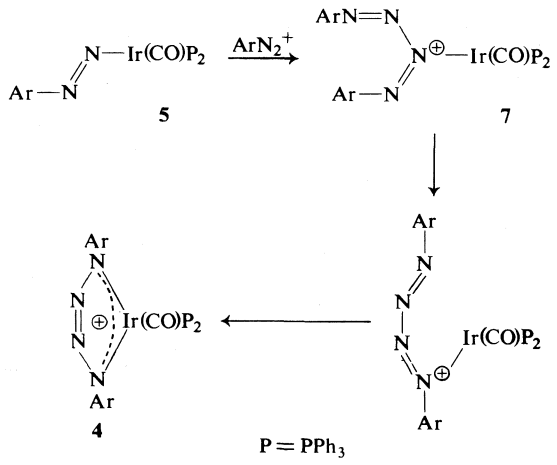

SCHEME 1

Farrell, in these laboratories, has recently shown that the iridium(I) hydride complex $IrH(CO)(PPh_3)_3$ will react in an "inert" solvent such as benzene–acetone with excess aryldiazonium ion (with loss of 1 mol PPh_3) to give the identical tetrazene, together with other products. We envisage that insertion of the diazonium ion into the Ir—H bond first occurs, to give the cationic aryldiazene complex **6**, $[Ir(HNNAr)(CO)(PPh_3)_2]^+$.

While we believe the above proposal to be a useful working hypothesis, we are aware of the possibility of alternative mechanisms, and experimental work to establish the mechanism of this reaction is continuing.

Experimental

Preparation of Complexes (4), [Ir(CO){$N_4(C_6H_4R)_2$}(PPh_3)$_2$]BF_4

The complexes **4***a–f* were all prepared in essentially similar fashion as follows. A solution of $IrCl(CO)(PPh_3)_2$ (0.125 mmol) in benzene (15 ml) was stirred magnetically under dry argon at room temperature. Solid aryldiazonium tetrafluoroborate (0.125 mmol) was added, followed immediately by absolute ethanol (1.5 ml). The diazonium salt quickly dissolved and the red solution was stirred for 1 h, at which time the yield of tetrazene was maximum judged from spectrophotometric measurements of the absorption intensity at 500 nm (see below). Red crystals of the product formed on cooling to 8° or after slow evaporation. Analyses and other data are included in Table 1. Infrared spectrum (**4***b*): 3060 w–m (νCH), 2057 (νCO), 1600 m, 1507 s, 1444 s (νCC skeletal), 1227 s (νCF), 1100–1030 vs,b (νBF_4^-), 845 m–s (δCH(C_6H_4F)), 750 s, 700 s (δCH(C_6H_5)), 560 m, 535 m–s, 515 s (δBF_4^- and aromatic).

[2]It is proposed that the nitrogen atoms in coordinated aryldiazo and related compounds be numbered Ar—N^1—N^2—M.

Can. J. Chem. Downloaded from www.nrcresearchpress.com by 210.87.254.6 on 09/05/12
For personal use only.

Reaction of Diazonium Salt or IrCl(CO)$(PPh_3)_2$ with Alcohols

The extent of reaction of diazonium ion or IrCl(CO)$(PPh_3)_2$ with alcohols was followed under various conditions by analyzing for acetaldehyde (from ethanol) or acetone (from isopropanol) by either gas chromatography of the collected volatiles or by carrying these under an argon stream through a solution of 2,4-dinitrophenylhydrazine. In the case of p-$BrC_6H_4N_2^+$ the formation of a meager amount of acetone was observed when stirred at room temperature with isopropanol. In the case of IrCl(CO)$(PPh_3)_2$ no evidence could be found of acetone or acetaldehyde formation at room temperature or under reflux, with or without added benzene. The i.r. spectrum of recovered solid was identical with that of the original, and no ν(Ir—H) absorptions were evident. In all cases, control experiments were conducted and the ability to detect acetone or acetaldehyde at the expected levels confirmed separately.

Physical Measurements

Infrared spectra were recorded using the Perkin–Elmer 457 and Beckman IR-12 instruments. Samples were pressed in KBr discs. Electronic spectra were recorded on Unicam SP 800 and Cary 14 spectrophotometers using optically matched cells. The electronic spectra were compared with the spectra of IrCl(CO)$(PPh_3)_2$ (λ_{max}(ε_{max}) values 339 (3160), 386 (3800), 436 (738)) and the aryldiazene co-product (11), showing absorption at 500 nm to be unique to the tetrazene. Syntheses were followed by measurement of the 500 nm absorbance of aliquots in order to determine the optimum reaction time and "spectrophotometric yield" listed in Table 1. ^{1}H n.m.r. spectra were recorded using Varian A60 and HA100 instruments, and τ values are relative to TMS as internal standard. ^{19}F n.m.r. spectra were obtained at 56.4 MHz employing a computer of average transients to enhance the very weak signals observed due to the relatively low solubility of **4***b* in $CDCl_3$.

Pyrolysis

Samples (*ca.* 3×10^{-8} mol) were heated at 550 °C for 3–4 h in an evacuated quartz tube attached to a vacuum system. After cooling to room temperature, the volatile contents were condensed in a liquid nitrogen trap and non-condensible gases transferred via a Toepler pump to a capillary, and sealed. These were then analyzed by gas chromatography (Porapak Q column at −78 °C; He carrier gas). The observed peak areas for N_2 and CO were compared with standard areas obtained for 1.122×10^{-5} mol each of N_2 and CO determined under the same gas chromatographic conditions.

We are grateful to Professor P. G. Perkins for communicating the results of the electronic structure calculations, to Drs. G. W. Rayner Canham and N. Farrell for stimulating discussions in connection with the mechanisms, to Professor T. N. Bell and Dr. A. Platt for assistance with gas chromatography and to A. P. Hitchcock and K. Jensen for experimental assistance. This work was supported by the National Research Council of Canada through operating grants.

1. P. A. S. Smith. The chemistry of open chain organic nitrogen compounds, Vol. II. W. A. Benjamin Inc., New York. 1966. Chapt. 12.
2. M. Dekker and G. R. Knox. Chem. Commun. 1243 (1967).
3. R. J. Doedens. Chem. Commun. 1271 (1968).
4. S. Otsuka and A. Nakamura. Inorg. Chem. **7**, 2542 (1968).
5. W. Beck, M. Bauder, G. La Monica, S. Cenini, and R. Ugo. J. Chem. Soc. A, 113 (1971).
6. G. La Monica, P. Sandrini, F. Zingales, and S. Cenini. J. Organomet. Chem. **50**, 287 (1973).
7. J. Ashley-Smith, M. Green, and F. G. A. Stone. J. Chem. Soc. Dalton, 1805 (1972).
8. F. W. B. Einstein, A. B. Gilchrist, G. W. Rayner Canham, and D. Sutton. J. Am. Chem. Soc. **93**, 1826 (1971).
9. F. W. B. Einstein and D. Sutton. Inorg. Chem. **11**, 2827 (1972).
10. F. A. Cotton and G. Wilkinson. Advanced inorganic chemistry, 3rd Ed. Wiley Interscience, New York. 1972. p. 724.
11. F. W. B. Einstein, A. B. Gilchrist, G. W. Rayner Canham, and D. Sutton. J. Am. Chem. Soc. **94**, 645 (1972).
12. W. J. Geary. Coord. Chem. Rev. **7**, 81 (1971).
13. D. J. Hodgson, N. C. Payne, J. A. McGinnety, R. G. Pearson, and J. A. Ibers. J. Am. Chem. Soc. **90**, 4486 (1968).
14. G. W. Parshall. J. Am. Chem. Soc. **87**, 2133 (1965).
15. M. J. Norgett, J. H. M. Thornley, and L. M. Venanzi. J. Chem. Soc. A, 540 (1967); G. Dyer and D. W. Meek. J. Am. Chem. Soc. **89**, 3982 (1967).
16. (*a*) P. G. Perkins. Personal communication; (*b*) D. R. Armstrong, P. G. Perkins, J. M. Scott, and J. J. P. Stewart. Theor. Chim. Acta, **26**, 237 (1972).
17. A. J. Carty. Organomet. Chem. Rev. A, **7**, 191 (1972).
18. N. Farrell and D. Sutton. Unpublished results.
19. A. P. Gaughan, B. L. Haymore, J. A. Ibers, W. H. Myers, T. E. Nappier, and D. W. Meek. J. Am. Chem. Soc. **95**, 6859 (1973).
20. K. R. Laing, S. D. Robinson, and M. F. Uttley. J. Chem. Soc. Dalton, 2713 (1973).
21. E. M. Kosower. Acc. Chem. Res. **4**, 193 (1971).
22. L. Vaska and J. W. Di Luzio. J. Am. Chem. Soc. **84**, 4989 (1962).
23. B. L. Haymore and J. A. Ibers. J. Am. Chem. Soc. **95**, 3052 (1973).

Can. J. Chem. Downloaded from www.nrcresearchpress.com by 210.87.254.6 on 09/05/12
For personal use only.

Application of Carbon-13 Nuclear Magnetic Resonance Spectroscopy to the Structural Determination of Chlorodeoxy Sugars

WALTER A. SZAREK[1] AND DOLATRAI M. VYAS
Department of Chemistry, Queen's University, Kingston, Ontario K7L 3N6
AND
STEPHAN D. GERO AND GABOR LUKACS
Institut de Chimie des Substances Naturelles, C.N.R.S., 91190 Gif-sur-Yvette, France
Received April 24, 1974

WALTER A. SZAREK, DOLATRAI M. VYAS, STEPHAN D. GERO, and GABOR LUKACS. Can. J. Chem. **52**, 3394 (1974).

The carbon-13 n.m.r. spectra of a series of chlorodeoxy sugars are reported. The results demonstrate the utility of this technique for the assignment of structure to this class of carbohydrate derivatives.

WALTER A. SZAREK, DOLATRAI M. VYAS, STEPHAN D. GERO et GABOR LUKACS. Can. J. Chem. **52**, 3394 (1974).

On rapporte les spectres r.m.n. du carbone 13 d'une série de sucres chlorodéoxylés. Les résultats démontrent l'utilité de cette technique pour attribuer des structures dans cette classe de dérivés de carbohydrates. [Traduit par le journal]

Can. J. Chem. Downloaded from www.nrcresearchpress.com by 210.87.254.105 on 09/05/12
For personal use only.

Introduction

An active area of investigation in several laboratories is the search for new methods of synthesis of halogenated carbohydrates. These derivatives are of interest, not only because of their potential intrinsic value in biochemistry and pharmacology, but also because of their utility in the synthesis of other rare sugars, such as deoxy and aminodeoxy sugars (1). In most cases, the structures of the chlorodeoxy sugars have been determined by chemical methods and occasionally with the aid of proton magnetic resonance (p.m.r.) spectroscopy. The chemical methods have sometimes been extremely laborious (*cf.* ref. 2). X-Ray crystallography has also been employed (3). In the present work, it has been demonstrated that the regiochemistry and stereochemistry of halogen substitution on a sugar molecule can be readily determined by carbon-13 magnetic resonance (c.m.r.) spectroscopy. Of relevance to this investigation is the work of Spiesecke and Schneider (4) who studied the effect of electronegativity and magnetic anisotropy of substituents on ^{13}C and proton chemical shifts in a series of alkyl halides; it was found that, unlike the chemical shifts of protons on the α carbon, the ^{13}C chemical shifts of the α carbon show larger deviations with a change in the inductive nature of substituents, especially as regards a change from chlorine to oxygen. On this basis, it seemed that c.m.r. spectroscopy would be a logical and more sensitive probe than p.m.r. spectroscopy for the structural elucidation of chlorodeoxy sugars. Some recent, pertinent applications of c.m.r. spectroscopy include structural and conformational studies on carbohydrates (5–11), nucleosides (12–14), and aminoglycoside antibiotics (15).

Results and Discussion

The ^{13}C chemical shifts of the chlorodeoxy sugars studied in this research and of some parent compounds are documented in Table 1. The signal assignments were made by a comparison of the spectra of the chlorodeoxy sugars with each other and with that of the corresponding parent glycoside or free sugar, and also on the basis of the general shielding properties associated with the various interactions observed by Perlin *et al.* (5) in the monosaccharide series. The effects on the chemical shifts resulting from the replacement of a hydroxyl group by a chloro

[1]To whom inquiries should be addressed.

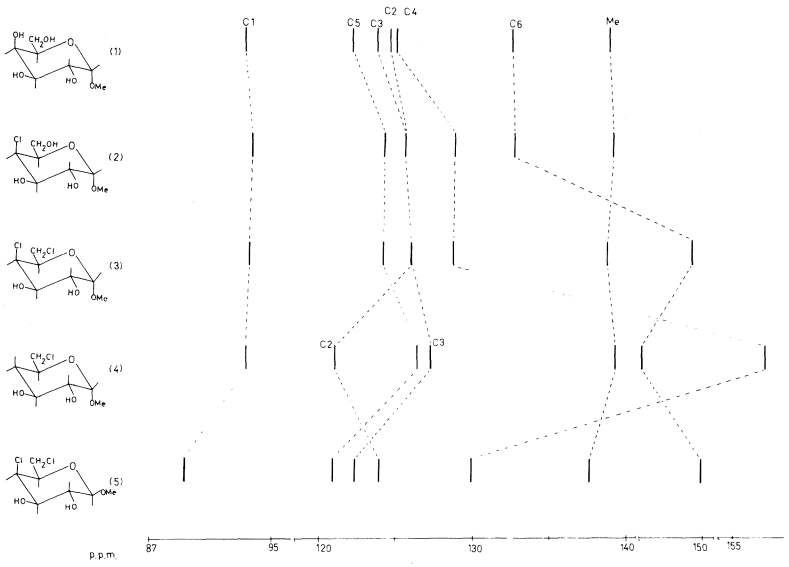

FIG. 1. ^{13}C chemical shift correlations for 4- and 6-monochloro- and 4,6-dichlorohexopyranosides.

group are discussed on the assumption that all of the molecules have the C1(D) conformation.[2]

Figure 1 shows the ^{13}C chemical shift correlation diagram for some 4- and 6-monochloro and 4,6-dichloro derivatives. The changes in ^{13}C shieldings resulting from the replacement of the axial hydroxyl group at C-4 in methyl α-D-galactopyranoside (**1**) by a chloro group are clearly evident. Thus, in the spectrum of methyl 4-chloro-4-deoxy-α-D-galactopyranoside (**2**) there is an ~3.7 p.p.m. upfield shift in the C-4 signal relative to the corresponding signal in the spectrum of compound **1**. This upfield shift may presumably be attributed to a difference in inductive effects between chlorine and oxygen. In compound **2**, C-2 is shielded relative to **1**, the upfield shift of the signal being 0.9 p.p.m. The shift of the C-2 signal can presumably be explained on the basis of the greater van der Waals' radius of chlorine than of an hydroxyl group (26). The chemical shifts of the signals for the anomeric carbon (C-1) and C-6 in the spectrum of compound **2** were essentially the same as those observed in the case of **1**; the C-6 assignment in the spectrum of **2** was confirmed by single frequency off-resonance decoupling (SFORD). The assignment of the signals for C-3 and C-5 in the spectrum of **2** was based on the expectation that the sequence of these signals would be the same as observed in the spectrum of the parent glycoside **1**. The upfield shift of the C-3 and C-5 signals relative to the corresponding signals in the spectrum of **1** may be attributed to a smaller β effect of chlorine than of an hydroxyl group.

The outstanding feature of the spectrum of methyl 4,6-dichloro-4,6-dideoxy-α-D-galactopyranoside (**3**) compared to that of methyl 4-chloro-4-deoxy-α-D-galactopyranoside (**2**) is the large upfield shift (16.6 p.p.m.) of the C-6 signal in the case of **3** (see Fig. 1) (*cf.* ref. 4). It was also observed that, in compound **3**, C-2, -3, -4, and -5 do not experience significantly different shieldings from those in **2**.

Significantly, the spectra of **2** and **3**, in addition to indicating the presence of a chloro group at C-4, were also consistent with this group being axially oriented and the sugar molecule having the C1(D) conformation. If the chloro group were

[2]In the present study, the assignments of the signals in the c.m.r. spectra of methyl α-D-galactopyranoside (**1**), methyl β-D-glucopyranoside (**7**), and β-D-allopyranose (**8**) in methyl sulfoxide-d_6 were made by a comparison with the assignments reported by Perlin *et al.* (5) for these compounds in deuterium oxide; solvent shifts of only 1–2 p.p.m. were observed. The assignments of the signals in the spectrum of methyl 4,6-*O*-benzylidene-α-D-allopyranoside (**9**) in methyl sulfoxide-d_6 were made by a comparison with the assignments reported by Conway *et al.* (8) for **9** in 1:4 methanol–chloroform-*d*; in this case, the chemical shifts were essentially identical.

Can. J. Chem. Downloaded from www.nrcresearchpress.com by 210.87.254.105 on 09/05/12
For personal use only.

TABLE 1. Carbon-13 chemical-shift data*

Compound	Synthesis reference	Carbon 1	2	3	4	5	6	Me
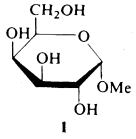 1	16	93.7	124.8	124.0	125.2	122.7	132.9	139.2
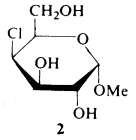 2	17	93.9	125.7	125.7	128.9	124.3	132.8	139.2
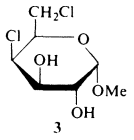 3	18	93.7	126.0	126.0	128.9	124.4	149.4	138.9
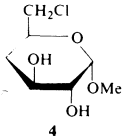 4	19	93.4	120.1	127.3	157.2	126.4	146.5	139.3
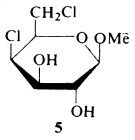 5	20	89.3	123.9	122.5	130.1	121.0	150.1	137.3
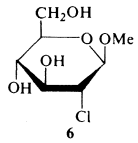 6	21	91.3	130.5	117.0	122.9	117.0	133.1	137.7
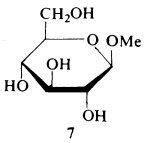 7		89.8	120.3	116.9	123.6	116.9	132.5	137.7
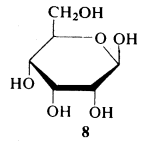 8	22	99.9	121.9	122.3	126.1	119.7	132.2	—
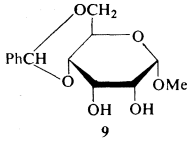 9	23	93.4	125.3	125.1	115.4	136.6	125.1	138.3

Can. J. Chem. Downloaded from www.nrcresearchpress.com by 210.87.254.105 on 09/05/12
For personal use only.

TABLE 1. (*Concluded*)

Compound	Synthesis reference	Carbon 1	2	3	4	5	6	Me
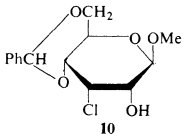 **10**	2, 24	93.4	125.8	130.3	117.7	130.3	124.9	137.3
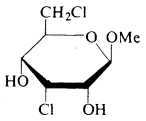 **11**	20*b*, 25	92.6	125.1	125.1	127.0	121.0	148.6	137.8
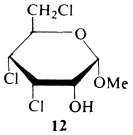 **12**	2	94.3	127.7	129.1	137.5	125.3	148.4	138.3

*In p.p.m. from CS_2 (external) in methyl sulfoxide-d_6.

equatorially oriented in this conformation, in other words, if the molecule possessed the D-*gluco* rather than the D-*galacto* configuration, then the C-2 and C-6 shieldings would have been expected to have been markedly different from those actually observed, since the relevant γ interactions in the D-*galacto* compound would be absent in the D-*gluco* compound; moreover, the chemical shifts of the C-3 and C-5 signals would also have been expected to have been different from those observed, since the β effect of an equatorially-oriented chloro group is presumably different from that of an axially-oriented group.

The importance of the effect of 1,3-diaxial nonbonded interactions on carbon shielding is illustrated clearly in the case of methyl 6-chloro-4,6-dideoxy-α-D-*xylo*-hexopyranoside (**4**) and methyl 4,6-dichloro-4,6-dideoxy-β-D-galactopyranoside (**5**). Thus, in the spectrum of compound **4**, the signal for C-2 is shifted downfield by 6.0 p.p.m., relative to the corresponding signal in the spectrum of **3**, and that for C-6 is shifted downfield by 3.9 p.p.m.; in each case the downfield shift can be ascribed to the diminished γ interaction resulting from replacement of an axial chlorine by hydrogen at C-4. The C-3 and C-5 signals in the spectrum of **4** are shifted upfield, surprisingly only by 1.3 and 2.0 p.p.m., respectively, relative to the corresponding signals in the spectrum of **3**; the upfield shift of the C-3 and C-5 signals can also be attributed to the absence of a chloro group at C-4 in compound **4**. An even more dramatic upfield shift (28.3 p.p.m.) was observed for the C-4 signal in the spectrum of **4**. The replacement of a chloro group by a hydrogen at C-4 not only removes the electron-withdrawing effect of a chlorine but also alters the magnitude of the vicinal gauche interactions and the γ steric interactions.

The signal assignments in the spectrum of methyl 4,6-dichloro-4,6-dideoxy-β-D-galactopyranoside (**5**) were made by a comparison of this spectrum with that of the α-anomer **3** in a manner analogous to that reported (5) for the spectra of methyl α- and β-D-galactopyranosides. In the case of **5** the absence of γ steric interactions is clearly reflected by the downfield shift of the C-3 and C-5 signals relative to the corresponding signals in the spectrum of **3**.

The effects of change in substitution in the carbohydrate derivatives **1**, **2**, **3**, and **4** on ^{13}C shieldings are summarized in Table 2. It is important to note that, because of the polyfunctionality of a carbohydrate molecule, a change of even one substituent can significantly alter the nature and magnitude of pertinent interactions, namely, vicinal gauche and 1,3-diaxial nonbonded interactions; both of these types of interaction can influence the ^{13}C shieldings of

Can. J. Chem. Downloaded from www.nrcresearchpress.com by 210.87.254.105 on 09/05/12
For personal use only.

TABLE 2. Effect of change of substituents on carbon-13 shieldings* in sugar derivatives

Conversions†	Δδ (p.p.m.)	Carbon 1	2	3	4	5	6
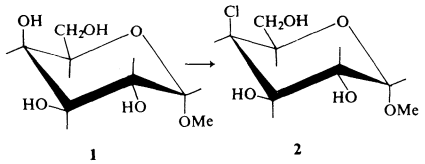 1 2	$\delta_2 - \delta_1$	0.2(+)	0.9(+)	1.7(+)	3.7(+)	1.6(+)	0.1(+)
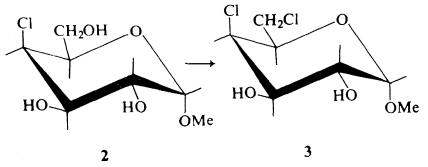 2 3	$\delta_3 - \delta_2$	0.2(+)	0.3(+)	0.3(+)	0	0.1(+)	16.6(+)
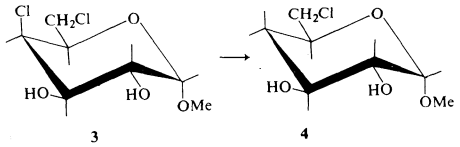 3 4	$\delta_4 - \delta_3$	0.3(−)	6.0(−)	1.3(+)	28.3(+)	2.0(+)	3.9(−)

*(+) denotes shielding and (−) denotes deshielding.
†The indicated conversions do not imply direct chemical transformation.

the carbon bearing the substituent as well as other carbons. The utility of c.m.r. spectroscopy for locating the site of change of substitution is further demonstrated with some other chlorodeoxy sugars.

The ^{13}C spectrum of methyl 2-chloro-2-deoxy-β-D-glucopyranoside (**6**), a compound which can be obtained by way of chloromethoxylation (27) of tri-*O*-acetyl-D-glucal, could be readily analyzed (see Table 1) by comparison with the spectrum of methyl β-D-glucopyranoside (**7**). Halogenations and halogenomethoxylations of glycals are known (28) to give mixtures of deoxyhalogeno sugars; in these studies p.m.r. spectroscopy was extensively used to determine the compositions of products and the configurations and conformations of the compounds obtained (see ref. 29). In the light of the present work, c.m.r. spectroscopy should be an effective tool for such studies.

An examination of the c.m.r. spectra of β-D-allopyranose (**8**), methyl 4,6-*O*-benzylidene-α-D-allopyranoside (**9**), methyl 4,6-*O*-benzylidene-3-chloro-3-deoxy-β-D-allopyranoside (**11**), and methyl 3,4,6-trichloro-3,4,6-trideoxy-α-D-allopyranoside (**12**) permitted assignments of the sites of halogenation in the latter three compounds (see Fig. 2). Thus, for example, in the spectrum of the 3-chloro derivative **10**, the most readily attributable signal is that of C-3; an upfield shift, relative to the corresponding signal in the spectrum of **9**, of 5.2 p.p.m. was observed. The assignments of the signals for C-2 and C-6 in the spectrum of **10** were made on the assumption that the chemical shifts of the C-6 signals in the spectra of **9** (see footnote 2) and **10** would be essentially the same. In the case of methyl 3,6-dichloro-3,6-dideoxy-β-D-allopyranoside (**11**), the presence of a chloro group at C-6 is clearly indicated by the large upfield shift (16.4 p.p.m.) of the C-6 signal relative to the corresponding signal in the spectrum of β-D-allopyranose (**8**) (see footnote 2); the assignments of the signals for C-2, -3, and -4 in the spectrum of **11** were made on the assumption that each of these carbons should be more shielded than the corresponding atoms in compound **8**. Finally, the signals in the spectrum of methyl 3,4,6-trichloro-3,4,6-trideoxy-α-D-allopyranoside (**12**) could be readily assigned by comparison with the spectra of compounds **10** and **11**. Thus, the C-2 signal in the spectrum of **12** would be expected to be at higher field than in the case of **10** or **11**, because of the presence in **12** of the

Can. J. Chem. Downloaded from www.nrcresearchpress.com by 210.87.254.105 on 09/05/12
For personal use only.

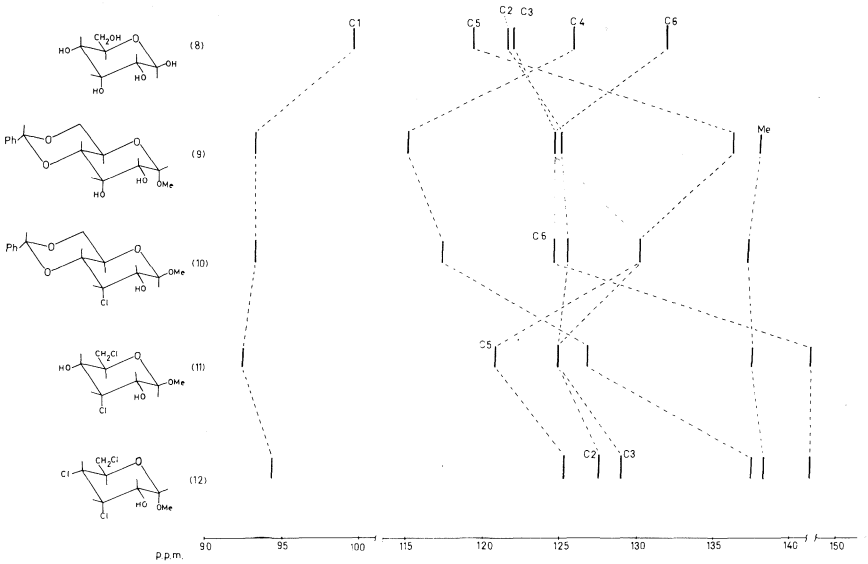

FIG. 2. ^{13}C chemical shift correlations for chlorinated D-allopyranosides.

shielding, vicinal gauche interaction between the axial methoxyl group at C-1 and the hydroxyl group at C-2; moreover, the upfield shift would be expected (*cf.* ref. 5) to be ~2 p.p.m. The assignment of the C-3 and C-5 signals was made on the basis of the expected, significant (~5 p.p.m.) upfield shift of the C-5 signal arising from the γ interaction between the axial methoxyl group at C-1 and the hydrogen at C-5 in **12**.

The data obtained in the present study suggest that the changes in ^{13}C shieldings resulting from the replacement of an hydroxyl group by a chloro group are configuration dependent. Thus, while replacement of an axial hydroxyl group by an axial chloro group results in a relatively small (2.5–4.0 p.p.m.) upfield shift of the signal of the substitution site (compare the C-4 signal of **1** and **2**, and also the C-3 signal of **8** and **11**), the shielding effect is markedly increased (~10 p.p.m.) if an equatorial hydroxyl group is replaced by an equatorial chloro group (compare the C-2 signal of **6** and **7**, and also the C-4 signal of **8** and **12**). The generality of this effect is under investigation.

Experimental

The compounds studied in this work were prepared by published procedures (see Table 1 for references). Carbon-13 magnetic resonance spectra were recorded in methyl sulfoxide-d_6 on a Bruker HX-90E Fourier transform spectrometer with tetramethylsilane (TMS) as internal standard; the chemical shift of the methyl sulfoxide-d_6 central line was 39.5 ± 0.2 p.p.m. with respect to TMS. The chemical shifts in this work are given in parts per million upfield from CS_2 (external), in order to conform with literature data (5, 12): $\delta^{CS_2} = 193.7 - \delta^{TMS}$ p.p.m.

The authors are grateful to the National Research Council of Canada for a grant (to W.A.S.), and to Professor J. K. N. Jones for his interest and encouragement.

1. (*a*) W. A. SZAREK. Advan. Carbohydr. Chem. Biochem. **28**, 225 (1973); (*b*) J. E. G. BARNETT. Advan. Carbohydr. Chem. **22**, 177 (1967); (*c*) S. HANESSIAN. Advan. Chem. Ser. **74**, 159 (1968).
2. H. J. JENNINGS and J. K. N. JONES. Can. J. Chem. **43**, 2372 (1965).
3. R. HOGE and J. TROTTER. J. Chem. Soc. A, 2165 (1969); G. H.-Y. LIN, M. SUNDARALINGAM, and J. JACKOBS. Carbohydr. Res. **29**, 439 (1973).
4. H. SPIESECKE and W. G. SCHNEIDER. J. Chem. Phys. **35**, 722 (1961).
5. A. S. PERLIN, B. CASU, and H. J. KOCH. Can. J. Chem. **48**, 2596 (1970).
6. D. E. DORMAN and J. D. ROBERTS. J. Am. Chem. Soc. **92**, 1355 (1970).
7. L. D. HALL and L. F. JOHNSON. Chem. Commun. 509 (1969).
8. E. CONWAY, R. D. GUTHRIE, S. D. GERO, G. LUKACS, A. M. SEPULCHRE, E. W. HAGAMAN, and E. WENKERT. Tetrahedron Lett. 4879 (1972).
9. S. HONDA, H. YUKI, and K. TAKIURA. Carbohydr. Res. **28**, 150 (1973).
10. P. A. J. GORIN and M. MAZUREK. Carbohydr. Res. **27**, 325 (1973).
11. D. R. BUNDLE, H. J. JENNINGS, and I. C. P. SMITH. Can. J. Chem. **51**, 3812 (1973).

Can. J. Chem. Downloaded from www.nrcresearchpress.com by 210.87.254.105 on 09/05/12
For personal use only.

12. A. J. JONES, D. M. GRANT, M. W. WINKLEY, and R. K. ROBINS. J. Am. Chem. Soc. **92**, 4079 (1970).
13. W. A. SZAREK, D. M. VYAS, A. M. SEPULCHRE, S. D. GERO, and G. LUKACS. Can. J. Chem. **52**, 2041 (1974).
14. W. VOELTER and E. BREITMAIER. Org. Magn. Res. **5**, 311 (1973).
15. P. W. K. WOO and R. D. WESTLAND. Carbohydr. Res. **31**, 27 (1973).
16. J. L. FRAHN and J. A. MILLS. Aust. J. Chem. **18**, 1303 (1965).
17. B. T. LAWTON. Ph.D. Thesis, Queen's University, Kingston, Ontario. 1969.
18. P. D. BRAGG, J. K. N. JONES, and J. C. TURNER. Can. J. Chem. **37**, 1412 (1959); H. J. JENNINGS and J. K. N. JONES. Can. J. Chem. **41**, 1151 (1963); B. T. LAWTON, W. A. SZAREK, and J. K. N. JONES. Carbohydr. Res. **14**, 255 (1970).
19. B. T. LAWTON, W. A. SZAREK, and J. K. N. JONES. Carbohydr. Res. **15**, 397 (1970).
20. (*a*) H. J. JENNINGS and J. K. N. JONES. Can. J. Chem. **40**, 1408 (1962); (*b*) D. M. DEAN, W. A. SZAREK, and J. K. N. JONES. Carbohydr. Res. **33**, 383 (1974).
21. E. FISCHER, M. BERGMANN, and H. SCHOTTE. Ber. **53**, 509 (1920).
22. J. D. STEVENS. Methods Carbohydr. Chem. **6**, 123 (1972).
23. B. R. BAKER and D. H. BUSS. J. Org. Chem. **30**, 2304 (1965).
24. E. H. WILLIAMS, W. A. SZAREK, and J. K. N. JONES. Can. J. Chem. **49**, 796 (1971).
25. R. G. EDWARDS, L. HOUGH, A. C. RICHARDSON, and E. TARELLI. Tetrahedron Lett. 2369 (1973).
26. J. R. CAVANAUGH and B. P. DAILEY. J. Chem. Phys. **34**, 1099 (1961).
27. R. U. LEMIEUX and B. FRASER-REID. Can. J. Chem. **42**, 532 (1964).
28. R. J. FERRIER. Advan. Carbohydr. Chem. **20**, 67 (1965); **24**, 199 (1969).
29. R. U. LEMIEUX and B. FRASER-REID. Can. J. Chem. **43**, 1460 (1965).

Can. J. Chem. Downloaded from www.nrcresearchpress.com by 210.87.254.105 on 09/05/12
For personal use only.

Electron Spin Resonance Studies of Aliphatic Ammonium Ion Radicals in Aqueous Sulfuric Acid Glasses[1]

HOWARD REGINALD FALLE[2] AND FREDERICK PETER SARGENT

Research Chemistry Branch, Atomic Energy of Canada Limited, Whiteshell Nuclear Research Establishment, Pinawa, Manitoba R0E 1L0

Received May 30, 1974

HOWARD REGINALD FALLE and FREDERICK PETER SARGENT. Can. J. Chem. **52**, 3401 (1974).

The reaction of hydrogen atoms with *n*-butylammonium ions in 6 *M* sulfuric acid glasses yields a characteristic eight-line e.s.r. spectrum, which is attributable to $CH_3\dot{C}HCH_2CH_2NH_3^+$. Evidence is drawn from computer simulated spectra and from the spectra of other alkylammonium radicals to account for this spectrum. Qualitative agreement between the simulated and experimental spectra is achieved by assuming that the $CH_3\dot{C}HCH_2$— moiety can adopt a range of conformations and can also undergo torsional motion about the sp^2 carbon – methylene carbon bond. The site of hydrogen abstraction from alkylammonium ions is evidently influenced by both NH_3^+ and CH_3 groups; abstraction tends to occur away from the former and adjacent to the latter.

HOWARD REGINALD FALLE et FREDERICK PETER SARGENT. Can. J. Chem. **52**, 3401 (1974).

La réaction des atomes d'hydrogène avec les ions *n*-butylammonium dans de l'acide sulfurique 6 *M* vitrifié conduit à un spectre r.p.e. caractéristique; ce spectre contient huit lignes et peut être attribué à $CH_3\dot{C}HCH_2CH_2NH_3^+$. On déduit ces conclusions de spectres simulés à l'aide d'ordinateurs et de spectres d'autres radicaux d'alkylammoniums. La correspondance qualitative entre les spectres simulés et expérimentaux est obtenue en faisant l'hypothèse que la portion $CH_3\dot{C}HCH_2$— peut adopter un grand nombre de conformations et peut aussi subir des mouvements de torsion autour du lien carbone sp^2 – carbone méthylénique. Le site de l'enlèvement de l'hydrogène des ions alkylammoniums est évidemment influencé à la fois par le NH_3^+ et le CH_3; l'enlèvement a tendance à se produire le plus loin possible du premier et le plus près possible du dernier. [Traduit par le journal]

Introduction

To determine whether or not certain free radicals trapped in aqueous glasses can adopt a range of conformations, we have investigated the reactions of hydrogen atoms with aliphatic ammonium ions in 6 *M* sulfuric acid. The possibility that $CH_3\dot{C}HCH_2CH_2NH_3^+$, for example, may adopt a range of conformations has important consequences, because of the angular dependence of β proton hyperfine couplings. The central issue in this study concerns the eight-line e.s.r. spectrum observed after the reaction of hydrogen atoms with *n*-butylammonium ions in 6 *M* H_2SO_4. To establish the structure of the predominant radical formed from $CH_3CH_2CH_2CH_2NH_3^+$, and to discuss conformational effects, we have drawn evidence from other alkylammonium radicals and from simulated e.s.r. spectra.

Pulse radiolysis and e.s.r. studies have shown that the species of radical formed by H atom abstraction depends on whether or not the amino group is protonated (1–7). In unprotonated amines, hydrogen abstraction by OH (or O^-) occurs primarily from the NH_2 group or from the methylene group adjacent to it. On the other hand, abstraction by OH (and H) from protonated amines occurs preferentially from positions further removed from the NH_3^+ group. The following example has been cited (4)

$$CH_3CH_2CH_2NH_2 \begin{cases} \rightarrow CH_3CH_2CH_2\dot{N}H \\ \rightarrow CH_3CH_2\dot{C}HNH_2 \end{cases}$$

$$CH_3CH_2CH_2NH_3^+ \begin{cases} \rightarrow CH_3\dot{C}HCH_2NH_3^+ \\ \rightarrow \dot{C}H_2CH_2CH_2NH_3^+ \end{cases}$$

This evidence suggests that $CH_3\dot{C}HCH_2CH_2NH_3^+$ would be the predominant radical formed by the reaction of H atoms with *n*-butylammonium ions in a 6 *M* H_2SO_4 glass. The character of the e.s.r. spectrum for $CH_3\dot{C}HCH_2R$ is markedly dependent on the orientation of the methylene protons with respect to the $2p_\pi$ orbital and the effect which a range of conformations can have on the spectrum pre-

[1]AECL No. 4860.

[2]NRCC Postdoctorate Fellow 1972–1974.

Can. J. Chem. Downloaded from www.nrcresearchpress.com by 210.87.254.105 on 09/05/12
For personal use only.

Can. J. Chem. Downloaded from www.nrcresearchpress.com by 210.87.254.105 on 09/05/12
For personal use only.

dicted for —ĊHCH$_2$— will be discussed in this context.

Experimental

The method used is one which has recently found application in a study of numerous biochemical and related substrates (8). Ultraviolet illumination of ferrous ions in 6 *M* H_2SO_4 at 77 K results in the formation of trapped hydrogen atoms, H_t

$$h\nu\,(254\text{ nm}) + \text{Fe (II)} + H^+ \rightarrow H_t + \text{Fe (III)}$$

When the sample is warmed to ~100 K, the 506 G e.s.r. doublet characteristic of H_t decreases in intensity (9). When the sample contains an organic solute, the decrease in the H_t signal is generally accompanied by a concomitant increase in a $g \sim 2$ free radical signal. Thus the radicals formed by the reaction of hydrogen atoms in 6 *M* H_2SO_4 with organic substrates can be characterized by interpreting the observed spectra. The e.s.r. spectrometer employed for the present studies was a Varian V4502-12 with Fieldial and low-temperature accessories.

The amines used were normally distilled under vacuum onto frozen H_2O (or D_2O) and subsequently thawed to make up aqueous solutions containing 1 mol/l amine. The *n*-hexylamine was dissolved in 1 *M* HCl. The sulfuric acid solutions were prepared by diluting H_2SO_4 to 6 mol/l (6 *M*) with triply distilled water. Sulfuric acid-d_2 in D_2O was prepared using SO_3 which had been distilled twice over P_2O_5 supported on glass wool (10). Iron powder was introduced into the sulfuric acid solutions as required, to produce ferrous ions. A Fe(II) concentration of 0.06 mol/l was used throughout and stock solutions of Fe(II) – 6 *M* sulfuric acid were kept no longer than 10 h. Micropipet portions of the 1 *M* amine solutions in H_2O (D_2O) were then mixed with aliquots of the Fe(II) – 6 *M* sulfuric acid solution to give ammonium ion concentrations of 0.02 to 0.10 mol/l. It should be noted that the amine–H_2O solutions were introduced into 6 *M* H_2SO_4 and the amine–D_2O solutions into 6 *M* D_2SO_4. When isopropylamine–D_2O was introduced into 6 *M* H_2SO_4, the radical found initially was $(CH_3)_2\dot{C}ND_3^+$ and not $(CH_3)_2\dot{C}NH_3^+$; the latter radical was observed only after the original solution had stood some 2 h at room temperature. The converse was observed for isopropylamine–H_2O in 6 *M* D_2SO_4, and similar behavior was observed in the case of ethylamine, establishing the presence of $CH_3\dot{C}HNH_3^+$.

The u.v. illumination of the glassy 6 *M* sulfuric acid samples was carried out at 77 K in a quartz e.s.r. cold finger Dewar. A Vycor filter and a Corning C37-54 (9863) visible filter were placed between the concentric spiral, low-pressure, Hg arc lamp and the Dewar, primarily to attenuate the unwanted 185 nm Hg emission. The samples were generally exposed to the 254 nm radiation at 77 K for 10 min.

The samples were subsequently transferred to the variable temperature insert in the spectrometer cavity, whereupon the decay in the H_t signal and the growth in the alkylammonium radical signal could be monitored at ~100 K. The samples were then annealled at ~120 K, which removed the residual D_t signal in the 6 *M* D_2SO_4 cases. After the samples were recooled and the spectra recorded at ~95 K, further warming was carried out up to ~150 K where the alkylammonium radical signal decayed. In the absence of an organic solute, relatively weak $g \sim 2$ signals were observed in both 6 *M* H_2SO_4 and 6 *M* D_2SO_4,[3] presumably due to H(D)SO_4 (1).

In certain cases, the observed spectrum must be attributed to more than one radical. Attempts to selectively thermal bleach the different species of radical were unsuccessful. Progressive annealling above ~140 K resulted in all cases in an irreversible decrease in the intensity of the alkylammonium radical signal and an increase in the presumed HSO_4 signal, but the essential features associated with the former remained much the same.

Spectra for —ĊHCH$_2$—

The magnitudes of the methylene proton splitting constants for —ĊHCH$_2$— depend on the azimuthal angle ξ defining the orientation of the protons with respect to the axis of the $2p_\pi$ orbital, *cf.* Fig. 1*a*.

$$[1] \qquad a_\alpha = \rho Q$$

$$[2] \qquad a_\beta = \rho[Q' + Q'' \cos^2 \xi] \cong \rho Q'' \cos^2 \xi$$

The expressions [1] and [2] relating α proton and β proton isotropic splitting constants, a_α and a_β, to the $2p_\pi$ orbital unpaired spin population, ρ, in hydrocarbon radicals are well established (11). For the majority of the computer simulated spectra discussed below, we have taken the values of the quantities ρQ and $\rho Q''$ for the α and β protons in —ĊHCH$_2$— to be 22 and 48 G, respectively; that is

$$[3] \qquad a_\alpha = 22 \text{ G}$$

$$[4] \qquad a_\beta = 48 \cos^2 \xi \text{ G}$$

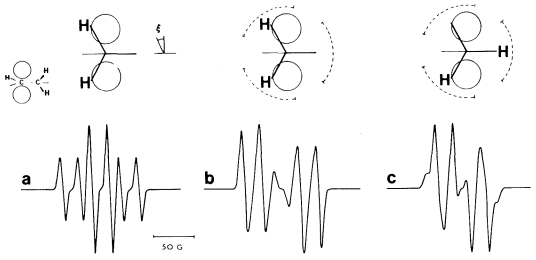

FIG. 1. Computer simulated e.s.r. spectra for the fragment —ĊHCH$_2$— calculated by means of [7–10] with $\Delta H_{pp} = 6$ G: (*a*) for the conformation in which $a_{\beta_1} = a_{\beta_2}$, ($\xi = 30°$); (*b*) by invoking the cosine probability distribution [10] of orientations from $\xi_{min} = -15°$ to $\xi_{max} = 75°$; and (*c*) using [10] for the range $\xi_{min} = 105°$ to $\xi_{max} = 195°$.

[3]The magnitude of this background signal was dependent on the source of the sulfuric acid and the iron; finally, Alfa iron powder (C, 99.5%) and B. D. H. Analar H_2SO_4 proved satisfactory.

Can. J. Chem. Downloaded from www.nrcresearchpress.com by 210.87.254.105 on 09/05/12
For personal use only.

Thus a_μ, the isotropic splitting constant for the protons of a freely rotating methyl group, is given by

$$[5] \qquad a_\mu = \rho Q'' \langle \cos^2 \xi \rangle = 24 \text{ G}$$

These splittings, a_α, a_β, and a_μ, were chosen in accord with the experimental splittings for $CH_3\dot{C}HCH_2CH_2NH_3^+$ (a_α = 22.0 G, a_β = 23.7 G, and a_μ = 25.6 G (2)) and may be compared with data for $CH_3\dot{C}HCH_2CH_3$ (12).

The overall width, Δ, predicted for the spectrum of $-\dot{C}HCH_2-$ also depends on the orientation of the methylene protons.

$$[6] \quad \Delta = \rho Q + \rho Q'' \{\cos^2 \xi + \cos^2 (\xi + 120°)\}$$

The value Δ_{max} = 94 G occurs when ξ = 30° and Δ_{min} = 58 G when ξ = 90°.[4] The spectrum for the configuration of $-\dot{C}HCH_2-$ in which the unpaired electron interacts equally with the two protons, ξ = 30°, is shown in Fig. 1*a*. Markedly different spectra are obtained when it is assumed that the methylene protons can adopt a range of orientations with respect to the adjacent $2p_\pi$ orbital.

To simplify the calculation of the "polycrystalline" e.s.r. spectra, we have omitted the anisotropic components of the proton hyperfine tensors and the **g**-tensor.

$$[7] \quad Y'(\xi) = Y_{max} \frac{2(\ln 2)}{\Gamma^2} [H - H_r(\xi)] \times \exp\left\{\frac{-(\ln 2)}{\Gamma^2} [H - H_r(\xi)]^2\right\}$$

The required spectra were simulated using [7], the equation for a Gaussian first-derivative lineshape $Y'(\xi)$, in which the maximum amplitude of the absorption is Y_{max} (11). The magnetic field at resonance is written $H_r(\xi)$ to emphasize the dependence on conformation in radicals of the form $-\dot{C}HCH_2-$. The half-width at half-height, Γ, of the normalized absorption and the peak-to-peak width, ΔH_{pp}, of the first-derivative line are related by

$$[8] \qquad \Delta H_{pp} = [2/\ln 2]^{1/2} \Gamma$$

The values used for ΔH_{pp} are included in the respective figure captions.

The total spectrum comprising the sum of each resonance line over all conformations was subsequently determined using

$$[9] \qquad Y_{tot}' = \sum_{\xi_{min}}^{\xi_{max}} Y'(\xi) \cdot P(\xi)$$

That is, individual spectra were calculated at 5° intervals of ξ over a designated range of conformations, ξ_{min} to ξ_{max}, each point $Y'(\xi)$ being multiplied by the probability factor $P(\xi)$. All conformations of $CH_3\dot{C}HCH_2R$ for example should not be equally probable and we have therefore employed the arbitrary but nevertheless reasonable cosine distribution

$$[10] \qquad P(\xi) = \cos\left(\frac{\pi}{2}\left[\frac{\xi - \hat{\xi}}{\delta\xi}\right]\right)$$

Here $\delta\xi$ defines the excursion of $\hat{\xi}$ for the particular conformation range and ξ is the azimuthal angle for the most probable conformation, so that $\xi_{min} = \hat{\xi} - \delta\xi$ and $\xi_{max} = \hat{\xi} + \delta\xi$. The spectrum in Fig. 1*b* was simulated for $-\dot{C}HCH_2-$ assuming the conformational distribution [10] over the range from ξ_{min} = 15° to ξ_{max} = 75°. The range ξ_{min} = 105° to ξ_{max} = 195° yielded a very different spectrum, Fig. 1*c*. It should be noted that the overall width of the spectrum in Fig. 1*b* is nearly the same as the value in Fig. 1*a*, which is Δ_{max}, the maximum value for $-\dot{C}HCH_2-$.

Results

$CH_3CH_2CH_2CH_2NH_3^+$

The spectrum in Fig. 2*a* was recorded at ~95 K following the decay of the trapped hydrogen atoms in 6 *M* H_2SO_4 samples containing $CH_3CH_2CH_2CH_2NH_3^+$. We will demonstrate that this spectrum arises predominantly from $CH_3\dot{C}HCH_2CH_2NH_3^+$ radicals which adopt a range of conformations. We have observed very similar spectra following hydrogen abstraction from *n*-pentylammonium and *n*-hexylammonium ions in 6 *M* H_2SO_4. To account for spectra derived from the *n*-alkylamino acids DL-norvaline and DL-norleucine, also very similar to Fig. 2*a*, it was proposed that $CH_3\dot{C}HCH_2R$ was the predominant species, and that the $CH_3\dot{C}HCH_2$-moieties were distributed over a range of conformations (8).

In γ-irradiated alkane single crystals (13–15), spectrum analysis is relatively straightforward because the species $CH_3\dot{C}HCH_2R$ and $R'CH_2\text{-}\dot{C}HCH_2R''$ are constrained, each to a particular

[4]Referring to Fig. 1*a*, Δ_{max} in fact occurs when the angle ξ equals 30° and 210°, and Δ_{min} occurs when ξ is 90, 120, 270, and 300°.

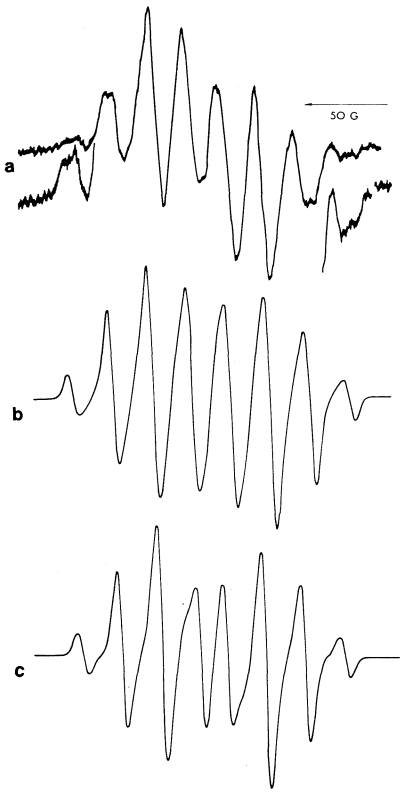

FIG. 2. The eight-line e.s.r. spectrum (*a*) was recorded at ~95 K following the reaction of hydrogen atoms with *n*-butylammonium ions in 6 *M* H_2SO_4, and is attributed to $CH_3\dot{C}HCH_2CH_2NH_3^+$ radicals. The spectra (*b*) and (*c*) were computed for $CH_3\dot{C}HCH_2$— assuming the probability distribution [10] with $\Delta H_{pp} = 6$ G; the range of conformations was from $\xi_{min} = -15°$ to $\xi_{max} = 75°$ for both, but the latter also includes torsional oscillation of amplitude $\chi = 30°$ using [14].

conformation. In a glass however, the nonuniform interactions between the substrate molecules and the matrix should allow more than one conformation. That is, molecules of the form $CH_3CH_2CH_2R$ could well be trapped in the sulfuric acid glasses with a certain distribution of conformations, and if so, the $CH_3\dot{C}HCH_2$— moieties of the resulting radicals should be similarly distributed about the most probable conformation.

In the lowest-energy conformation of *n*-butane, the carbon atoms lie in the *staggered* or *trans* configuration (16, 17). Abstraction of one of the methylene protons, forming $CH_3\dot{C}HCH_2CH_3$, would result in a rehybridization from sp^3 to sp^2 but this would not markedly alter the relative positions of the carbon atoms. Thus the lowest energy configuration of $CH_3\dot{C}HCH_2CH_3$, and analogously other $CH_3\dot{C}HCH_2R$ radicals, should also be *trans*, in the absence of an external potential field. In glass-forming media however, the nonuniform solute–solvent interactions constitute a potential field which could influence the equilibrium configurations of the substrate molecules and thus, in the case of $CH_3\dot{C}HCH_2R$, it is unlikely that all conformations would be equally probable.

The spectrum in Fig. 2*b* was computed for $CH_3\dot{C}HCH_2$— assuming the conformation distribution [10] for the range $\xi_{min} = -15°$ to $\xi_{max} = 75°$, that is with *trans* ($\hat{\xi} = 30°$) as the most probable conformation. The relative intensities and spacings of the eight lines correspond quite well with experiment. The overall width of the simulated spectrum is somewhat larger than the experimental width in Fig. 2*a* and this discrepancy is discussed below with reference to torsional motion in $\diagdown\dot{C}CH_2$—. The spectrum computed using [10] for 1° intervals instead of 5° was identical to Fig. 2*b*. The ranges $\xi_{min} = 5°$ to $\xi_{max} = 55°$ and $\xi_{min} = -15°$ to $\xi_{max} = 75°$ are, respectively, the minimum and maximum conformation ranges which lead to reasonable agreement with experiment. If the conformation range is extended or taken outside of the above ranges, the computed spectra no longer show good agreement with experiment. For example, a very different spectrum results from applying [10] over the range $\xi_{min} = 105°$ to $\xi_{max} = 195°$, where the most probable orientation ($\hat{\xi} = 150°$) corresponds to *gauche* $CH_3\dot{C}HCH_2$—.

Comparing Figs. 2*a* and 2*b*, we have thus found that the apparently anomalous eight-line spectrum observed as a result of hydrogen abstraction from *n*-butylammonium ions can be attributed to $CH_3\dot{C}HCH_2CH_2NH_3^+$ radicals when it is assumed that the $CH_3\dot{C}HCH_2$— moieties are distributed over a range of conformations in the 6 *M* H_2SO_4 glass. However, there are certain other possibilities which should be eliminated, thereby supporting the proposed occurrence of a range of conformations for the $CH_3\dot{C}HCH_2CH_2NH_3^+$ radicals. The crux of the argument is: can Fig. 2*a* be attributed to $CH_3\dot{C}HCH_2CH_2NH_3^+$ alone, or does it represent the sum of the spectra of several radicals?

There are four radicals which might be formed by hydrogen abstraction from *n*-butylammonium

Can. J. Chem. Downloaded from www.nrcresearchpress.com by 210.87.254.105 on 09/05/12
For personal use only.

Can. J. Chem. Downloaded from www.nrcresearchpress.com by 210.87.254.105 on 09/05/12
For personal use only.

ions: $\dot{C}H_2CH_2CH_2CH_2NH_3^+$, $CH_3\dot{C}HCH_2CH_2NH_3^+$, $CH_3CH_2\dot{C}HCH_2NH_3^+$, and $CH_3CH_2CH_2\dot{C}HNH_3^+$. Aliphatic amines would be incorporated into the sulfuric acid glasses in the protonated form: $RCH_2NH_3^+$ in 6 *M* H_2SO_4 and $RCH_2ND_3^+$ in 6 *M* D_2SO_4. Radicals of the form $R\dot{C}HNH_3^+$ should therefore be identifiable by a marked difference in spectrum compared with $R\dot{C}HND_3^+$, since the ammonium proton splitting constants in the former are 14–19 G (1, 8, 18–20). The introduction of *n*-butylamine–D_2O into 6 *M* D_2SO_4 resulted in a spectrum indistinguishable from Fig. 2*a* and so we conclude that the yield of $CH_3CH_2CH_2\dot{C}HNH_3^+$ cannot be significant.

The two radicals $\dot{C}H_2CH_2CH_2CH_2NH_3^+$ and $CH_3\dot{C}HCH_2CH_2NH_3^+$ with relative concentrations 1:2.8 have been identified as products of abstraction by OH from *n*-butylammonium ions in a Ti^{3+}–H_2O_2 flow system (2). It is unlikely that abstraction by H (or D) from *n*-butylammonium ions would be markedly less specific, or that these two radicals would have appreciably different isotropic splitting constants, in 6 *M* sulfuric acid glasses. To facilitate further discussion, it is necessary to interpret the spectra observed following hydrogen abstraction from other alkylammonium ions and then to draw comparisons with the foregoing results.

$CH_3CH_2NH_3^+$, $CH_3CH_2CH_2NH_3^+$, and $(CH_3)_2CHNH_3^+$

Comparison of the spectra derived from samples containing the above species gives a clear indication of the relative influences of the CH_3 and NH_3^+ groups on the site of hydrogen abstraction from ammonium ions in 6 *M* H_2SO_4 glasses. The spectra derived from ethylammonium ions in 6 *M* D_2SO_4 and in 6 *M* H_2SO_4 at ~95 K are shown in Figs. 3*a* and 3*b*, respectively, and the predominant five-line patterns can be attributed to $\dot{C}H_2CH_2ND(H)_3^+$. A similar spectrum has been reported at 155 K as a result of photo-induced decarboxylation of β-alanine in aqueous $K_3Fe(CN)_6$; the occurrence of a six-line spectrum at 95 K was taken to indicate that internal rotation in $\dot{C}H_2CH_2NH_3^+$ was more restricted than at 155 K (18). Unrestricted rotational motion about the C—C bond in $\dot{C}H_2CH_2NH_3^+$ would average the β proton hyperfine interaction, as in [5], so that the spectrum would consist of five lines, essentially 1:4:6:4:1 in relative intensity, with an overall width of $\Delta \sim 90$ G. We

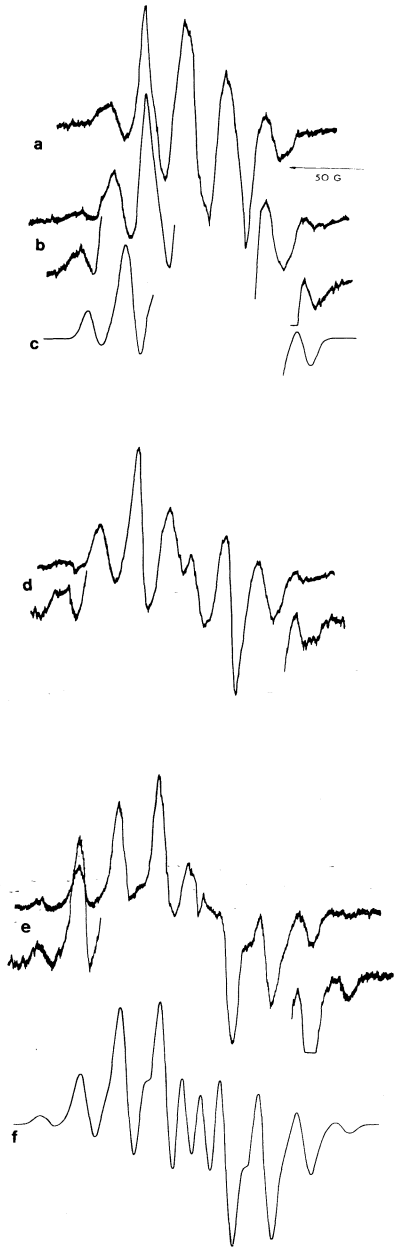

FIG. 3. The five-line spectrum (*a*) is ascribed to $\dot{C}H_2CH_2ND_3^+$, the predominant radical resulting from ethylammonium ions in 6 *M* D_2SO_4; the satellite lines observed in 6 *M* H_2SO_4 (*b*) are due to $CH_3\dot{C}HNH_3^+$; and (*c*) shows the outer lines of the spectrum computed for $CH_3\dot{C}HNH_3^+$. Spectrum (*d*) was observed following reaction of the hydrogen atoms with *n*-propylammonium ions in 6 *M* H_2SO_4. Spectrum (*e*) was observed as a result of hydrogen abstraction from isopropylammonium ions in 6 *M* H_2SO_4, and (*f*) was computed for $(CH_3)_2\dot{C}NH_3^+$ assuming fixed randomly oriented ammonium protons, with $\Delta H_{pp} = 10$ G.

Can. J. Chem. Downloaded from www.nrcresearchpress.com by 210.87.254.105 on 09/05/12
For personal use only.

note that the outermost lines in Fig. 3*a* are separated by ~105 G, whereas $\Delta_{max} = 116$ G for $\dot{C}H_2CH_2$—. The spectra of $\dot{C}H_2CH_2R$ radicals derived from other alkylammonium ions in 6 *M* H_2SO_4 glasses should have a similar appearance to Fig. 3*a*, assuming the same constraints on rotational averaging.

The satellite lines amplified in Fig. 3*b*, found in addition to the five major lines in 6 *M* H_2SO_4 but not in 6 *M* D_2SO_4, arise from $CH_3\dot{C}HNH_3^+$ (1). The outer lines of the spectrum simulated for $CH_3\dot{C}HNH_3^+$, using $a_\mu = 27$ G and $a_\alpha = 23$ G (18) and assuming a splitting of 12.5 G for the NH_3^+ proton, are shown in Fig. 3*c*. Simulation of the spectra of $\diagdown\!\!\dot{C}NH_3^+\!\!\diagup$ radicals in 6 *M* H_2SO_4 glasses is discussed further in conjunction with the results for $(CH_3)_2\dot{C}NH_3^+$.

Reaction of the H atom with *n*-propylammonium ions in 6 *M* H_2SO_4 yielded the spectrum in Fig. 3*d*. Since essentially the same spectrum was observed in 6 *M* D_2SO_4, the outermost lines cannot be due to $CH_3CH_2\dot{C}HNH_3^+$ but must arise from $CH_3\dot{C}HCH_2NH_3^+$. The overall width from Fig. 3*d* is $\Delta \sim 160$ G, while $\Delta_{max} = 116$ G for $\dot{C}H_2CH_2$—. The two most prominent lines are superimposable on the corresponding lines in the spectra derived from both ethylammonium and *n*-butylammonium ions. Thus it is uncertain whether the difference between the central portions of the spectra from $CH_3CH_2CH_2CH_2NH_3^+$ and $CH_3CH_2NH_3^+$ (Figs. 2*a* and 3*a*) means that the yield of $\dot{C}H_2CH_2$— radicals is appreciable or not. On statistical grounds alone, the ratio $\dot{C}H_2CH_2R:CH_3\dot{C}HR'$ from *n*-propylammonium would be between those ratios pertaining to the cases of ethylammonium and *n*-butylammonium ions.

Hydrogen abstraction from $(CH_3)_2CHND_3^+$ in 6 *M* D_2SO_4 yielded a seven-line spectrum with $\Delta = 145$ G attributable to $(CH_3)_2\dot{C}ND_3^+$, but in 6 *M* H_2SO_4 the markedly different spectrum in Fig. 3*e* with $\Delta = 180$ G was observed. The spectrum simulated for $(CH_3)_2\dot{C}NH_3^+$, using $a_\mu = 25$ G (18) and assuming a splitting of 12.5 G (*i.e.*, $\rho Q'' = 25$ G) for the NH_3^+ protons, is shown in Fig. 3*f*; the nitrogen splitting was omitted and instead the linewidth was increased to $\Delta H_{pp} = 10$ G. In accord with the results for $\dot{C}H(NH_3^+)CO_2H$ and $CH_3\dot{C}(NH_3^+)CO_2H$ in 6 *M* H_2SO_4 derived from glycine and alanine, respectively (8), we have assumed that the protons of the NH_3^+ groups adopt all possible fixed orientations, and on this basis the ammonium proton splitting was varied in order to achieve close agreement with Fig. 3*e*. Quite different spectra are predicted assuming a freely rotating NH_3^+ group. For the radical $\dot{C}H_2NH_3^+$, the ammonium proton and nitrogen splittings are 19 and 4 G, respectively (20); the deuteron splitting in $\dot{C}H_2ND_3^+$ would then be 3 G. Nitrogen and deuteron splittings of this magnitude are unlikely to be resolved in the 6 *M* sulfuric acid glasses. The smaller magnitude of the ammonium proton splittings for $\diagdown\!\!\dot{C}NH_3^+\!\!\diagup$ radicals in 6 *M* H_2SO_4 is presumably due to hydrogen bonding with the aqueous matrix.

$CH_3CH_2C(CH_3)_2NH_3^+$, $CH_3CH_2CH(CH_3)NH_3^+$, and $(CH_3)_3CNH_3^+$

The spectra derived from $CH_3CH_2C(CH_3)_2NH_3^+$ and $CH_3CH_2CH(CH_3)NH_3^+$ indicate the occurrence of hydrogen abstraction predominantly from the methylene group adjacent to the terminal methyl group. Reaction of the H atoms with *t*-pentylammonium ions resulted in the five-line spectrum in Fig. 4*a*. In comparison with the ethylammonium ion case, this spectrum shows that the $CH_3\dot{C}H$— species of radical is more abundant than $\dot{C}H_2CH_2$—.

The spectrum in Fig. 4*b* was obtained from a sample containing $CH_3CH_2CH(CH_3)NH_3^+$ and essentially the same spectrum was observed in 6 *M* D_2SO_4. The predominant form of radical is unlikely to be $\dot{C}H_2CH_2$—, and so this spectrum is ascribed to $CH_3\dot{C}HCH(CH_3)NH_3^+$. Although the conformation with $\xi = 45°$ predicts six equally spaced lines 1:5:10:10:5:1, as does rotational averaging of a_β, the observed spectrum can also be accounted for on the basis of a range of conformations. The spectrum in Fig. 4*c* was computed for $CH_3\dot{C}HCH\diagup\!\!\diagdown$ assuming the distribution [10] from $\xi_{min} = 25°$ to $\xi_{max} = 85°$. Very similar spectra have been obtained in the case of L-isoleucine (8).

For *t*-butylammonium ions, the expected 1:2:1 triplet from $\dot{C}H_2C(CH_3)_2NH_3^+$ was observed but compared with $CH_3CH_2C(CH_3)_2NH_3^+$, the H atoms were noticeably less reactive toward $(CH_3)_3CNH_3^+$.

Discussion

The foregoing results indicate that hydrogen abstraction from the CH_3CH_2R ammonium ion

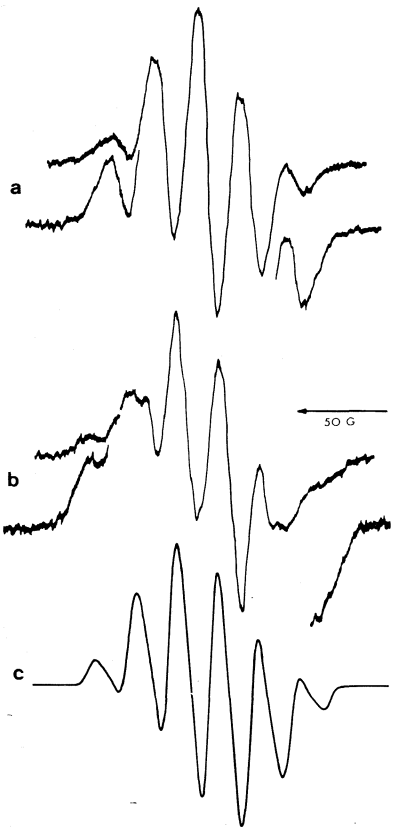

FIG. 4. Spectrum (*a*) is due to $CH_3\dot{C}HC(CH_3)_2NH_3^+$ formed by abstraction from *t*-pentylammonium ions in 6 *M* H_2SO_4. Spectrum (*b*) is attributed to $CH_3\dot{C}HCH(CH_3)NH_3^+$, and (*c*) was computed for $CH_3\dot{C}HCH\diagup\diagdown$ assuming [10] over the conformation range $\xi_{min} = 25°$ to $\xi_{max} = 85°$, $\Delta H_{pp} = 6$ G.

species in the 6 *M* sulfuric acid glasses occurs preferentially from the methylene group adjacent to a terminal methyl group, except in the case of $CH_3CH_2NH_3^+$. The influence of the NH_3^+ group on the site from which abstraction takes place can be seen from a comparison of $CH_3CH_2NH_3^+$ and $CH_3CH_2C(CH_3)_2NH_3^+$. That is, of the two types of radical, $\dot{C}H_2CH_2$— and $CH_3\dot{C}H$—, the former predominates in the case of ethylammonium and the latter in the case of *t*-pentylammonium ions. Evidently methyl groups also influence the sites of abstraction; comparing $CH_3CH_2NH_3^+$ with $(CH_3)_2CHNH_3^+$, the susceptibility of the carbon atom adjacent to the NH_3^+ toward abstraction is clearly increased by the second methyl group in $(CH_3)_2CHNH_3^+$. The $(CH_3)_3CNH_3^+$ case indicates that methyl groups adjacent to the NH_3^+ are not very susceptible to hydrogen abstraction.

Experiments involving OH reactions with alkylammonium ions in Ti^{3+}–H_2O_2 flow systems show a similar influence of the NH_3^+ group on the sites of abstraction. In the cases of *n*-propylammonium and *n*-butylammonium ions, only $\dot{C}H_2CH_2$— radicals were detected from the former, whereas the ratio of $CH_3\dot{C}HCH_2$— to $\dot{C}H_2CH_2$— radicals from the latter was 2.8:1 (2). On comparing these findings with the above results, it can be inferred that the relative yield of $CH_3\dot{C}HCH_2$— to $\dot{C}H_2CH_2$— from *n*-butylammonium ions in 6 *M* H_2SO_4 is at least 3 to 1. It is also noteworthy that $CH_3\dot{C}HCH_2$— was the predominant species found in γ-irradiated alkane crystals (13, 14); —$CH_2\dot{C}HCH_2$— radicals were detected in *n*-alkane crystals but even in the case of $CH_3(CH_2)_{34}CH_3$, a 3:1 ratio of $CH_3\dot{C}HCH_2$— to —$CH_2\dot{C}HCH_2$— was found (15).

As to the yields of $CH_3\dot{C}HCH_2$—, $\dot{C}H_2CH_2$—, and —$CH_2\dot{C}HCH_2$— radicals from *n*-butylammonium ions in 6 *M* H_2SO_4, it is probable that the trend toward a lower relative yield of $\dot{C}H_2CH_2$— continues as the number of methylene groups in $CH_3(CH_2)_nNH_3^+$ increases. It is probable too that the relative yield of —CH_2-$\dot{C}HCH_2$— radicals increases with increasing *n* ($n \geq 3$). Since the eight-line pattern attributed to $CH_3\dot{C}HCH_2$— also dominated the spectra derived from $CH_3(CH_2)_4NH_3^+$ and $CH_3(CH_2)_5$-NH_3^+, it is inferred that a low yield of —CH_2-$\dot{C}HCH_2$— radicals results from $CH_3CH_2CH_2$-$CH_2NH_3^+$. The latter inference is supported by the $CH_3CH_2CH_2CH(CO_2H)NH_3^+$ result (8); in fact, the spectra derived from both DL-norvaline and DL-norleucine are virtually indistinguishable from Fig. 2*a*.

With regard to the nature of the spectrum in Fig. 2*a* and its assignment $CH_3\dot{C}HCH_2CH_2$-NH_3^+, we note that the overall width is ~155 G and the relative intensities of the eight lines are in the approximate ratio 1:6:16:14:14:16:6:1. Now it is true that the spectrum predicted for the single conformation in which $\xi = 15°$ consists of eight equally spaced lines 1:5:11:15:15:11:5:1, with $\Delta = 163$ G. A superposition of this spectrum and that in Fig. 3*a* might resemble Fig. 2*a* but this possibility is discounted for two reasons: the *trans* form of $CH_3\dot{C}HCH_2$— ($\xi = 30°$) should have the lowest energy and we maintain that the nonhomogeneous solute–

Can. J. Chem. Downloaded from www.nrcresearchpress.com by 210.87.254.105 on 09/05/12
For personal use only.

Can. J. Chem. Downloaded from www.nrcresearchpress.com by 210.87.254.105 on 09/05/12
For personal use only.

solvent interactions in the aqueous glasses should preclude a single conformation. If the moiety $CH_3\dot{C}HCH_2$— could undergo relatively unrestricted rotational motion about the bond joining the trigonal carbon and the methylene carbon, a seven-line 1:6:15:20:15:6:1 spectrum with $\Delta = 142$ G would result and hence this alternative can be eliminated as well. We have already noted that the maximum width possible for $\dot{C}H_2CH_2CH_2CH_2NH_3^+$ should be ~120 G, as in the ethylammonium radical spectrum, Fig. 3*a*. If $\xi = 15°$ defined the orientation of both methylene groups in $CH_3CH_2\dot{C}HCH_2NH_3^+$, an eight-line 1:3:5:7:7:5:3:1 spectrum with $\Delta = 160$ G would result but again this is a single conformation and not the most stable. Thus the accumulated evidence gives every indication that $CH_3\dot{C}HCH_2CH_2NH_3^+$ is the radical responsible for the spectrum in Fig. 2*a* and does favor the proposal that $CH_3\dot{C}HCH_2R$ radicals adopt a range of conformations in 6 *M* sulfuric acid glasses.

The possible importance of torsional oscillations in the $CH_3\dot{C}H(CH_2)_nNH_3^+$ radicals remains to be discussed. In the classical approximation (21), torsional motion about the C—C bond in $\diagdown\dot{C}CH_2$— for example is considered to be sinusoidal. The time dependence of the angle defining the orientation of the methylene protons can be expressed as

$$[11] \qquad \bar{\xi}(t) = \xi + \chi \sin(2\pi t/\tau)$$

where χ is the amplitude and τ the period of the oscillation; the angle ξ now defines the equilibrium position for the β proton in question. The hyperfine splitting for the methylene protons can then be written

$$[12] \qquad a_\beta(t) = \rho Q'' \cos^2[\xi + \chi \sin(2\pi t/\tau)]$$

When τ is less than the value of $\tau_\beta \sim 3 \times 10^{-8}$ s typical of the β proton hyperfine interaction, [12] can be averaged over time.

$$[13] \quad \langle a_\beta(t)\rangle = \rho Q'' f(\xi, \chi) = \rho Q'' \left(\frac{1}{\pi}\right) \int_{-\pi/2}^{\pi/2} \cos^2(\xi + \chi \sin x)\, dx$$

Taking $\xi = 30°$ and $\chi = 30°$ for $\diagdown\dot{C}CH_2$— the value of the motional factor is $f(\xi, \chi) = 0.68$ (21), so that torsional oscillation of amplitude $\chi = 30°$ about the equilibrium configuration would yield $\langle a_{\beta_1}\rangle = \langle a_{\beta_2}\rangle = 33$ G. Thus the spectrum for $\diagdown\dot{C}CH_2$— undergoing rapid torsional motion of a given amplitude about $\xi = 30°$ would consist of a 1:2:1 triplet with an overall width in the range $72 < \Delta < 48$ G. On the other hand if $\tau > \tau_\beta$, the lines in the e.s.r. spectrum would show anomalous broadening since it would represent the sum of individual spectra for the various values of $\bar{\xi}(t)$ from [11].

However, it is conceivable that each member of an ensemble of $\diagdown\dot{C}CH_2$— fragments distributed over a range of conformations could undergo relatively rapid low-amplitude torsional motion. Thus [10] would express the distribution of the ξ_i, the equilibrium conformations of the radicals in question. With regard to $CH_3\dot{C}HCH_2$—, the magnitude of the hyperfine couplings for the α proton and for the protons of the freely rotating methyl groups would not be affected by oscillation about the bond joining the trigonal carbon and the methylene carbon; only the hyperfine lines due to the methylene protons would be affected by the torsional motion. Now the crucial point is that although the separations between the first three lines in both Fig. 2*a* and Fig. 2*b* are ~24 G, the two most intense lines are separated by ~61 G in the experimental spectrum and ~69 G in the computed spectrum. From previous results (21), it is clear than when $-45° < \xi < 45°$ the average $\langle a_{\beta_1}\rangle$ for $\diagdown\dot{C}CH_2$— as a result of torsional motion will be less than the magnitude of a_{β_1} given by [2] at the equilibrium angle ξ; conversely when $45° < \xi < 135°$ the value of $\langle a_{\beta_1}\rangle$ will be greater than a_{β_1} at ξ. The difference between these two quantities can be expressed as

$$[14] \quad \langle a_{\beta_1}\rangle - a_{\beta_1} = \rho Q'' f(0°, \chi) \sin[2(\xi - 45°)] = \delta a_{\beta_1}$$

Taking $f(0°, 30°) \sim 0.88$ (21) along with $\rho Q'' = 48$ G, this difference will be -6 G when $\xi = 0°$, zero when $\xi = 45°$, and $+6$ G when $\xi = 90°$; an analogous expression holds for δa_{β_2}. Thus if the various ξ_i for an ensemble of $\diagdown\dot{C}CH_2$— species are distributed as described by [10] from $-15°$ to 75°, the overall width of the resulting spectrum will decrease as χ increases, and we find $\Delta(\chi = 30°)/\Delta(\chi = 0°) = 0.90$. Similarly in the case of $CH_3\dot{C}HCH_2$—, the separation of the two most

intense lines is reduced to ~62 G, and so the lines of the computed spectrum in Fig. 2*c* become superimposable on the experimental lines in Fig. 2*a*.

The foregoing treatment is based on the validity of the approximation $Q' \sim 0$ in [2]. It is true that a negative value of Q' (22), rather than a small positive value (23), would reduce the overall width predicted for $>\dot{C}CH_2$—. In order to fit the spectrum for $CH_3\dot{C}HCH_2CH_2NH_3^+$ however, Q' or Q'' for the methyl protons would have to be quite different from the values for the methylene protons. We find it more reasonable to assume the same value of Q'' for both the methyl and methylene protons in $CH_3\dot{C}HCH_2$—, along with $Q' = 0$.

The overall width for $CH_3\dot{C}HCH_2NH_3^+$ is somewhat (<5 G) larger than Δ for $CH_3\dot{C}HCH_2CH_2NH_3^+$, possibly due to greater restrictions imposed by the matrix on the torsional motion. The widths of the spectra derived from $CH_3(CH_2)_4NH_3^+$ and $CH_3(CH_2)_5NH_3^+$ are approximately the same as the overall width from Fig. 2*a*. However, partial splitting of the outermost lines, presumably due to the anisotropic α proton and **g**-factor components, presents some difficulty in measuring certain overall widths.

Summary

The e.s.r. spectrum in Fig. 2*a* can be accounted for on the basis that $CH_3\dot{C}HCH_2CH_2NH_3^+$ radicals are responsible and that the $CH_3\dot{C}HCH_2$— moieties are distributed over a range of conformations. The qualitative agreement between the computed and experimental spectra can be improved by introducing torsional oscillation about the sp^2 carbon – methylene carbon bond. The spectrum in Fig. 4*b*, derived from $CH_3CH_2CH(CH_3)NH_3^+$ and ascribed to $CH_3\dot{C}HCH<$ radicals, can also be accounted for in terms of a range of conformations. Comparisons with the other alkylammonium radicals indicate that $\dot{C}H_2CH_2$— and —$CH_2\dot{C}HCH_2$— radicals contribute only slightly to the spectrum in Fig. 2*a*. We conclude that certain radicals trapped in low-temperature glasses are unlikely to be restricted to one particular conformation, and that the neglect of this possibility in characterizing the e.s.r. spectra could lead to confusion and to assignment errors.

H. R. Falle gratefully acknowledges the award of a National Research Council of Canada Postdoctorate Fellowship. We also thank D. R. Smith and M. Tomlinson for helpful criticism of the manuscript.

1. M. C. R. Symons. J. Chem. Soc. Perkin II, 797 (1973).
2. H. Taniguchi, K. Fukui, S.-I. Ohnishi, H. Hatano, H. Hasegawa, and T. Maruyama. J. Phys. Chem. **72**, 1926 (1968).
3. N. Getoff and F. Schwörer. Int. J. Radiat. Phys. Chem. **3**, 429 (1971).
4. N. Getoff and F. Schwörer. Int. J. Radiat. Phys. Chem. **5**, 101 (1973).
5. P. Neta and R. W. Fessenden. J. Phys. Chem. **75**, 738 (1971).
6. P. Wardman and D. R. Smith. Can. J. Chem. **49**, 1869 (1971).
7. P. Wardman and D. R. Smith. Can. J. Chem. **49**, 1880 (1971).
8. F. S. Dainton, H. R. Falle, and G. A. Salmon. Unpublished results.
9. C. J. Ultee and C. R. Kepford. Chem. Phys. Lett. **3**, 337 (1969).
10. G. Brauer. (Editor), Handbook of preparative inorganic chemistry. 2nd ed. Vol. I. Academic Press Inc., New York. 1963. p. 135. Inorg. Synth. **6**, 131 (1960); **7**, 155 (1961).
11. J. E. Wertz and J. R. Bolton. Electron spin resonance: elementary theory and practical applications. McGraw–Hill Inc., New York. 1972.
12. P. J. Krusic and J. K. Kochi. J. Am. Chem. Soc. **90**, 7156 (1968).
13. T. Gillbro, P.-O. Kinell, and A. Lund. J. Phys. Chem. **73**, 4167 (1969).
14. A. Lund. J. Phys. Chem. **76**, 1411 (1972).
15. A. Lund and L. Kevan. J. Phys. Chem. **77**, 2180 (1973).
16. M. Hanack. Conformation theory. Academic Press Inc., New York. 1965.
17. L. Radom and J. A. Pople. J. Am. Chem. Soc. **92**, 4786 (1970).
18. R. Poupko, I. Rosenthal, and D. Elad. Photochem. Photobiol. **17**, 395 (1973).
19. M. A. Collins and D. H. Whiffen. Mol. Phys. **10**, 317 (1966).
20. R. P. Kohin and P. G. Nadeau. J. Chem. Phys. **44**, 691 (1966).
21. E. W. Stone and A. H. Maki. J. Chem. Phys. **37**, 1326 (1962).
22. M. D. Sevilla. J. Phys. Chem. **74**, 669 (1970).
23. F. C. Adam and F. W. King. J. Chem. Phys. **58**, 2446 (1973).

Can. J. Chem. Downloaded from www.nrcresearchpress.com by 210.87.254.105 on 09/05/12
For personal use only.

An Electron Spin Resonance Study of Hydrogen Atom Reactions with Butenes Trapped in Aqueous Sulfuric Acid Glasses[1]

HOWARD REGINALD FALLE[2] AND FREDERICK PETER SARGENT

Research Chemistry Branch, Atomic Energy of Canada Limited, Whiteshell Nuclear Research Establishment, Pinawa, Manitoba R0E 1L0

Received May 30, 1974

HOWARD REGINALD FALLE and FREDERICK PETER SARGENT. Can. J. Chem. **52**, 3410 (1974).

Hydrogen atom reactions with butenes trapped in sulfuric acid glasses yield *sec*-butyl radicals by addition and methallyl radicals by abstraction. The character of the e.s.r. spectra due to the $CH_3\dot{C}HCH_2CH_3$ radicals depends on whether *cis*-2-butene or *trans*-2-butene was the precursor. Computer simulated spectra indicate that the most probable conformation for the $CH_3\dot{C}HCH_2CH_3$ radicals derived from *cis*-2-butene and *trans*-2-butene are '*oblique*' and '*trans*', respectively. Qualitative agreement between the simulated and experimental spectra is achieved by adding together the spectra computed for $CH_3\dot{C}HCH_2CH_3$ and $CH_3\bar{C}H\bar{C}H\bar{C}H_2$ in the percentage ratio 40:60. In computing the spectra for $CH_3\dot{C}HCH_2CH_3$, it is assumed that the radicals are distributed over a range of conformations and can undergo torsional motion.

HOWARD REGINALD FALLE et FREDERICK PETER SARGENT. Can. J. Chem. **52**, 3410 (1974).

Les réactions des atomes d'hydrogène avec des butènes piégés dans de l'acide sulfurique vitrifié produisent des radicaux butyles secondaires par addition et des radicaux méthallyles par enlèvement. Les caractéristiques des spectres r.p.e. dus aux radicaux $CH_3\dot{C}HCH_2CH_3$ dépendent de la stéréoisomérie *cis* ou *trans* du butène-2 qui leur donne naissance. Des spectres simulés à l'aide d'ordinateurs indiquent que la conformation la plus probable des radicaux $CH_3\dot{C}HCH_3$-CH_3 obtenus à partir des butènes-2 *cis* et *trans* sont respectivement *oblique* et *trans*. Une corrélation qualitative entre les spectres simulés et expérimentaux est obtenue en additionnant ensemble dans un rapport de 40:60, les spectres simulés du $CH_3\dot{C}HCH_2CH_3$ et $CH_3\bar{C}H\bar{C}H\bar{C}H_2$. Lorsque l'on simule le spectre du $CH_3\dot{C}HCH_2CH_3$, on fait l'hypothèse que les radicaux peuvent adopter un grand nombre de conformations et peuvent subir des mouvements de torsion.

[Traduit par le journal]

Introduction

In previous studies of ammonium ion radicals (1) and amino acid radicals (2), it was demonstrated that $CH_3\dot{C}HCH_2R$ radicals adopt a range of conformations in 6 *M* sulfuric acid glasses. Molecules of the form $CH_3CH_2CH_2R$ are trapped in these glasses with a certain distribution of conformations and in consequence the $CH_3\dot{C}HCH_2$— moieties of the radicals formed by hydrogen abstraction are similarly distributed about the most probable configuration. In the absence of an external potential field, the lowest-energy conformation of *n*-butane is the *staggered* or *trans* configuration (3) and by analogy the lowest-energy configuration of the $CH_3\dot{C}HCH_2R$ radicals should also be '*trans*'. However, the conformations of the individual substrate molecules will certainly be influenced by the nonhomogeneous solute–solvent interactions in glass-forming media and will become frozen as the viscosity increases. In the case of $CH_3\dot{C}HCH_2CH_2NH_3^+$, the equilibrium configurations must be largely determined by the solute–matrix interactions affecting the parent *n*-butylammonium ions as the glass sets (1).

On this basis, we inferred that the spectrum of $CH_3\dot{C}HCH_2CH_3$ radicals derived from each of the three isomeric butenes would provide further information about conformation effects in $CH_3\dot{C}HCH_2R$ radicals. If hydrogen atom addition to *trans*-2-butene yielded an eight-line spectrum similar to the $CH_3\dot{C}HCH_2CH_2NH_3^+$ case (1), this would clearly indicate nonuniform solute–matrix interactions. We assume that the planar geometry of the 2-butene molecules would remain unaltered on formation of 6 *M* sulfuric acid glasses but nonuniform fields would affect the conformations of the resulting $CH_3\dot{C}HCH_2$-CH_3 radicals. It follows that any differences in the spectra obtained after hydrogen atom addition to *cis*-2-butene and *trans*-2-butene must be ascribed to the different geometries of the pre-

[1]AECL No. 4862.

[2]NRCC Postdoctorate Fellow 1972–1974.

Can. J. Chem. Downloaded from www.nrcresearchpress.com by 210.87.254.105 on 09/05/12
For personal use only.

Can. J. Chem. Downloaded from www.nrcresearchpress.com by 210.87.254.105 on 09/05/12
For personal use only.

cursors. While hydrogen atom addition to 2-butene would give only $CH_3\dot{C}HCH_2CH_2$, $\dot{C}H_2CH_2CH_2CH_3$ could be formed as well from 1-butene. However, H atom addition to $RCH{=}CH_2$ in solid argon occurs predominantly (>95%) at the terminal sp^2 carbon (4). The H(D) atoms react quite readily with other 'gases' trapped in 6 *M* sulfuric acid glasses: C_2H_4, C_3H_8, CO, and N_2O for example, and further work on these systems is anticipated.

Experimental

A Varian V4502-12 e.s.r. spectrometer equipped with Fieldial, dual-cavity and low-temperature accessories was used. The *g*-factors were measured against DPPH ($g = 2.0036$).

Solutions containing 0.06 *M* Fe(II) were prepared by introducing iron powder into 6 *M* sulfuric acid and were saturated with nitrogen prior to use. The gases 1-butene, *cis*-2-butene, *trans*-2-butene, and 1,3-butadiene used in this study,[3] were bubbled into the Fe(II) – 6 *M* H_2SO_4 solutions at room temperature until saturation. Aliquots were then placed in e.s.r. sample tubes, cooled to 77 K, and subjected to 254 nm u.v. radiation for 10 min (1), yielding trapped hydrogen atoms, H_t. On subsequent examination of the glassy samples at ~100 K, the growth of a $g \sim 2$ hydrocarbon radical signal was observed concomitant with the decay in the H_t signal. Samples saturated with nitrogen showed only a weak background signal presumably due to HSO_4 (1). It should also be noted that the essential features of the spectra were not altered by annealling at ~140 K, implying that the matrix had remained rigid. On annealling the samples above 145 K, the e.s.r. signals decayed irreversibly.

Results and Discussion

The occurrence of hydrogen atom addition and abstraction reactions with *cis*-2-butene and *trans*-2-butene would result in the formation of *sec*-butyl (**1**) and methallyl (**2**) radicals. Our main thesis is that the spectra in Figs. 1*a* and 1*b*, observed after reaction of the H atoms in 6 *M* H_2SO_4 samples containing *trans*-2-butene and *cis*-2-butene, respectively, are not the same because the resulting $CH_3\dot{C}HCH_2CH_3$ radicals are confined to different conformation ranges. We base this on the assumption that the relative yields of **1** and **2** derived from *cis*-2-butene should be approximately the same as that from *trans*-2-butene. In radiolysis studies of olefins, the ratio of **1** to **2** (~1:2) from *cis*-2-butene was similar to the ratio from *trans*-2-butene, although not

[3]The butenes (CP grade, from Matheson of Canada Limited) were examined by gas chromatography and all three were found to contain <0.3% impurity; 1,3-butadiene was detected (0.07%) only in the *cis*-2-butene.

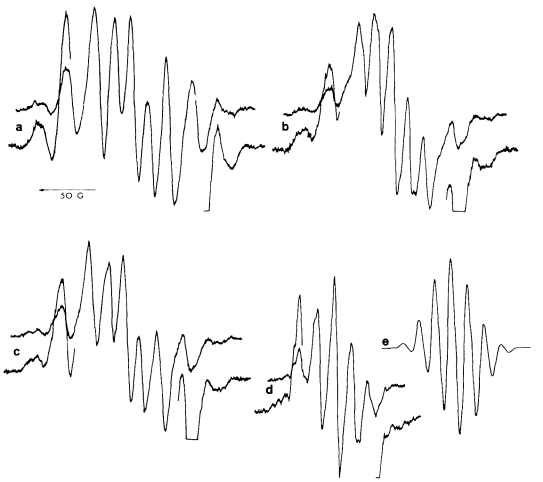

FIG. 1. The e.s.r. spectra recorded at 95 K after the reaction of hydrogen atoms with the three isomeric butenes trapped in 6 *M* H_2SO_4 glasses: (*a*) *trans*-2-butene, (*b*) *cis*-2-butene, and (*c*) 1-butene. The spectrum (*d*), recorded at 95 K after the reaction of H atoms with 1,3-butadiene, is attributable to $CH_3\dot{C}H\dot{C}H\dot{C}H_2$, and (*e*) is the computed spectrum for methallyl (**2**).

all of the radicals were formed by thermal hydrogen atoms (5).

The possibility that $CH_3\dot{C}HCH_2R$ radicals may adopt a range of conformations has important consequences because of the angular dependence of β proton hyperfine couplings. To a good approximation, the hyperfine splittings for the two methylene protons in $\diagdown\!\dot{C}CH_2\!-$ will be given by (6)

$$[1] \qquad a_{\beta_1} = \rho Q'' \cos^2 \xi$$
$$a_{\beta_2} = \rho Q'' \cos^2 (\xi + 120°)$$

where ξ is the azimuthal angle shown in the insets in Fig. 2 and Q'' is the proportionality constant relating the splitting constants, a_β, to the $2p_\pi$ orbital spin population, ρ (6). The total first-derivative spectrum for an ensemble of radicals of a given species was simulated using (1)

$$[2] \qquad Y_{tot}' = \sum_{\xi_{min}}^{\xi_{max}} Y'(\xi) \cdot P(\xi)$$

We have thus taken the sum of individual spectra, $Y'(\xi)$, calculated at 5° intervals of ξ over the designated range of conformations, ξ_{min} to ξ_{max}. The expression for a Gaussian line-shape contains the parameter Γ (1, 6), to which the peak-to-peak width of the first-derivative line is related by

Can. J. Chem. Downloaded from www.nrcresearchpress.com by 210.87.254.105 on 09/05/12
For personal use only.

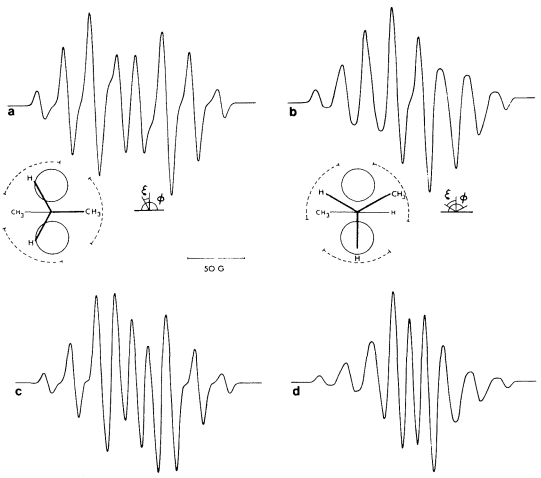

FIG. 2. The spectra (*a*) and (*b*) were computed for *sec*-butyl (**1**), on the basis of [1–4] with $\Delta H_{pp} = 6$ G, including torsional motion of amplitude $\chi = 30°$ about the sp^2 carbon – methylene carbon bond; (*a*) assumes the range $\xi_{min} = -10°$ to $\xi_{max} = 70°$, with '*trans*' as the most probable conformation and (*b*) assumes the range $\xi_{min} = 20°$ to $\xi_{max} = 100°$, with '*oblique*' as the most probable conformation. The spectra (*c*) and (*d*) are the renormalized sums: (1*e*) plus (2*a*) and (1*e*) plus (2*b*), respectively, both in the percentage ratios 60:40. In all cases $\Delta H_{pp} = 6$ G.

$$[3] \qquad \Delta H_{pp} = [2/(\ln 2)]^{1/2}\Gamma$$

The probability factor

$$[4] \qquad P(\xi) = \cos\left(\frac{\pi}{2}\left[\frac{\xi - \xi}{\delta\xi}\right]\right)$$

although arbitrary, is incorporated because all conformations should not be equally probable (1). Here $\hat{\xi}$ is the azimuthal angle for the most probable conformation and $\delta\xi$ defines the excursion of ξ over the conformation range from $\xi_{min} = \hat{\xi} - \delta\xi$ to $\xi_{max} = \hat{\xi} + \delta\xi$.

In simulating e.s.r. spectra for *sec*-butyl and methallyl, we have assumed the splitting constants (given in gauss, G) below.

$$\underset{24.5}{CH_3}\text{—}\underset{22}{\dot{C}H}\text{—}\underset{\begin{cases}49\cos^2\xi\\49\cos^2(\xi+(120°)\end{cases}}{CH_2}\text{—}CH_3$$

1

$$\underset{15.0}{CH_3}\text{—}\underset{14.0}{CH}\overset{\overset{4.0}{CH}}{\diagup\!\!\diagdown}\underset{14.0}{CH_2}$$

2

For **1** we have thus taken $\rho Q'' = 49$ G in [1], so that the methyl proton splitting is $a_\mu = \rho Q''\langle\cos^2\xi\rangle = 24.5$ G and $a_\alpha = \rho Q = 22$ G for the α-proton. These values may be compared with the following, also in G: $CH_3\dot{C}HCH_2CH_3$ (7), $a_\mu = 24.63$, $a_\alpha = 21.90$, $a_\beta = 27.20$; $CH_3\dot{C}HCH_2CH_2NH_3^+$ (8), $a_\mu = 25.6$, $a_\alpha = 22.0$, $a_\beta = 23.7$. The *cis* and *trans* isomers of **2** have been characterised in liquid solution (9), but would not be distinguishable in the sulfuric acid glasses since the difference in the splittings is less than the linewidth. For all of the simulated spectra herein, we have assumed a peak-to-peak linewidth of $\Delta H_{pp} = 6$ G.

It can be seen from Fig. 1 that the spectrum derived from butene-1, Fig. 1*c*, is similar to the one from *trans*-2-butene, Fig. 1*a*, whereas the spectrum derived from *cis*-2-butene is rather different, Fig. 1*b*. If we omit the central line, the eight-line pattern discernable in Fig. 1*a* is similar to the spectra attributed to $CH_3\dot{C}HCH_2CH_2NH_3^+$ (1) and $CH_3\dot{C}HCH_2CH(CO_2H)NH_3^+$ (2) in 6 *M* H_2SO_4 glasses, due to hydrogen abstraction from *n*-butylammonium and norvaline, respectively. It is noteworthy too that the spectrum from γ-irradiated *sec*-butylchloride at 77 K (10) appears not unike the $CH_3\dot{C}HCH_2CH_2NH_3^+$ spectrum in 6 *M* H_2SO_4.

Qualitative agreement between the spectrum simulated for $CH_3\dot{C}HCH_2CH_3$ and the eight-line pattern in Fig. 1*a* can be achieved by assuming a range of conformations and torsional oscillation, for the $>\dot{C}CH_2$— portion of the radical. The spectrum in Fig. 2*a* was computed for **1** assuming the conformation range $\xi_{min} = -10°$ to $\xi_{max} = 70°$, along with $\chi = 30°$ for the amplitude of the torsional motion about the sp^2 carbon – methylene carbon bond (1, 11). The maximum conformation range which yields a spectrum resembling Fig. 2*a* is $\xi_{min} = -15°$ to $\xi_{max} = 75°$, while the minimum range is $\xi_{min} = 5°$ to $\xi_{max} = 55°$. Spectra computed for conformation ranges outside the above limits are quite different from Fig. 2*a*. A decrease in the torsion amplitude increases the separation between the two most prominent lines but does not affect the separations of the outer lines. That is, the proton splittings arising from the $CH_3\dot{C}H$— portion of **1** remain unaffected by the torsional motion about the sp^2 carbon – methylene carbon bond.

Thus the above agreement is quite satisfactory except for the additional line in the centre of the eight-line pattern in Fig. 1*a*. Although the single configuration of $CH_3\dot{C}HCH_2$— in which $\xi = 30°$ would yield a spectrum (4 × 2 × 3 lines) having a central line, this possibility is contradicted by the evidence which depicts a range of con-

Can. J. Chem. Downloaded from www.nrcresearchpress.com by 210.87.254.105 on 09/05/12
For personal use only.

formations. An alternative interpretation is that the central line in each of the spectra in Fig. 1 arises from methallyl radicals (8, 12, 13). In Fig. 1*d*, we show the experimental spectrum of **2** in 6 *M* H_2SO_4, observed after reaction of the H atoms with 1,3-butadiene. The simulated spectrum for **2** consists of seven lines, as shown in Fig. 1*e* (ΔH_{pp} = 6 G). Gas chromatography of the butenes revealed 1,3-butadiene (0.07%) only in the *cis*-2-butene and so the source of the methallyl radicals seen in each of Figs. 1*a*, *b*, and *c* must be the butenes themselves. The *g*-factor measured at the midpoint of the central line was the same in Figs. 1*a–c*, within experimental error ($\pm$0.0002), as the value g = 2.0026 from the spectrum of **2** in Fig. 1*d*.

The spectrum in Fig. 2*c* represents the sum of the spectra in Figs. 2*a* and 1*e* in the percentage ratio 40:60, renormalized to the same maximum height, and matches the experimental spectrum in Fig. 1*a* from *trans*-2-butene quite well. Now the difference in overall appearance between Figs. 1*a* and *b*, derived from *trans*-2-butene and *cis*-2-butene, respectively, must reflect the difference in geometry of the $CH_3CH{=}CHCH_3$ precursors. Hydrogen atom addition to the CH_3-$CH{=}CHCH_3$ species leads to rehybridization of one of the carbon atoms from sp^2 to sp^3, accompanied by the loss of rigidity of the planar structure. The relative positions of the carbon atoms in the radicals are then more readily affected by intra- and intermolecular repulsions. In the case of *trans*-2-butene, the solute–matrix interactions force a range of conformations but the most probable configuration of the $CH_3\dot{C}H$-CH_2CH_3 radicals is still identifiable as '*trans*'.

However, the most probable configuration of the $CH_3\dot{C}HCH_2CH_3$ radicals derived from *cis*-2-butene would not remain '*cis*'; reorientation toward the '*trans*' form should occur since '*cis*' corresponds to the highest energy or *full-eclipsed* conformation of *n*-butane.[4] The computed spectrum in Fig. 2*b* was obtained assuming the conformation range ξ_{min} = 20° to ξ_{max} = 100°, again with a torsion amplitude of χ = 30°. In this case we have termed the most probable conformation '*oblique*'. A reasonable facsimile of the spectrum derived from *cis*-butene-2, Fig. 1*b*, is obtained when the methallyl spectrum is superimposed on Fig. 2*b*. The renormalized sum of Figs. 2*b* and 1*e* in the percentage ratio 40:60 is shown in Fig. 2*d*. Reorientation evidently does take place after H atom addition to *cis*-2-butene but the solute–matrix restrictions prevent '*trans*' from becoming the most probable configuration. Somewhat better agreement with experiment, particularly with regard to the intensities of the outer three lines in Fig. 2*d*, was obtained using ξ_{min} = 15° to ξ_{max} = 95° (ϕ = 155°), rather than the same range with ϕ = 150°. Although the range of conformations ξ_{min} = 140° to ξ_{max} = 220° with χ = 30° also leads to Fig. 2*b*, it is unlikely in view of the torsion amplitude and the conformation range that ϕ = 30° would be the most probable configuration, rather than '*gauche*' for example. The spectrum computed for the range ξ_{min} = 110° to ξ_{max} = 190° with '*gauche*' the most probable conformation is quite different from Figs. 2*a* and *b*.

Comparisons of the experimental and computed spectra suggest that abstraction from *cis*-2-butene and *trans*-2-butene occurs to the same extent, though the relative yields of **1** and **2** are open to question. However, the efficiency of hydrogen abstraction from the butenes in 6 *M* H_2SO_4 glasses is evidently comparable with that of H atom addition. In contrast we have found that reaction of the H atoms with propene yielded $CH_3\dot{C}HCH_3$ exclusively; the e.s.r. spectrum showed no trace of the allyl radical.

With regard to 1-butene, it is not clear whether *cis* (ϕ = 0°) or *skew* (ϕ = 120°) would be the more probable form trapped in the 6 *M* H_2SO_4 glass. An n.m.r. study (15) and an *ab initio* calculation (14) suggest that these rotational conformers might be about equally populated. In accord with the *cis*-2-butene results, we assume that the $CH_3\dot{C}HCH_2CH_3$ radicals formed from 1-butene, both *cis* and *skew*, would reorient towards '*trans*'. Unlike *cis*-2-butene however, it is probable that the geometries of the 1-butene conformers become altered in the 6 *M* H_2SO_4 glass, so that the precursors of **1** in the latter case would already be distributed over a range of conformations. These arguments may explain the minor differences between the spectra derived from butene-1 and *trans*-butene-2, Figs. 1*c* and *a*, respectively. The possibility that $\dot{C}H_2CH_2CH_2$-CH_3 also contributes to Fig. 1*c* may be unlikely in view of H atom addition to $RCH{=}CH_2$ in argon (4) but cannot be discounted.

[4]The conformers of *n*-butane are defined in terms of the CCCC dihedral angle ϕ (3, 14): for the *full-eclipsed* form ϕ = 0°, for *gauche* ϕ = 60°, while for the *trans* form ϕ = 180°. In the radical $CH_3\dot{C}HCH_2CH_3$, the '*oblique*' form corresponds to ϕ = 150°.

One limitation of the foregoing description is the symmetrical probability distribution [4]; the distribution of conformations of **1** may be unsymmetrical in the cases of 1-butene and *cis*-2-butene. Another limitation lies in the (classical) treatment of the torsional motion and the uncertainty in χ. It should be noted that the spectrum computed for the '*oblique*' form of **1** with $\chi = 0°$ and $\delta\xi = 40°$ is quite different from Fig. 2*b*. However, one essential difference between the butene isomers is geometry, the radicals **1** and **2** occupy the same holes in the 6 *M* H_2SO_4 glasses as the precursors, and hence we attribute the differences between Figs. 1*a*, *b*, and *c* to conformational differences in the species **1**.

Summary

Hydrogen atoms undergo reactions with *cis*-2-butene and *trans*-2-butene in 6 *M* H_2SO_4 which yield $CH_3\dot{C}HCH_2CH_3$ by addition and $CH_3CHCH\dot{C}H_2$ by abstraction. The e.s.r. spectra derived from samples containing *cis*-2-butene and *trans*-2-butene show differences which can be explained by assuming that the $CH_3\dot{C}HCH_2CH_3$ radicals in each case adopt different conformation ranges. Thus the eight-line pattern discernible in the spectrum in Fig. 1*a* can be simulated by assuming that '*trans*' $CH_3\dot{C}HCH_2CH_3$ is the most probable conformation. On the other hand, the spectrum obtained assuming '*oblique*' $CH_3\dot{C}HCH_2CH_3$ to be the most probable conformation is more compatible with Fig. 1*b*. The central line in each of the spectra in Fig. 1 is ascribed to $CH_3\bar{C}H\bar{C}H\bar{C}H_2$ radicals, and superposition of the computed spectra supports this assignment; *cf.* Figs. 2*c* and *d*.

In conclusion, the above results provide further evidence that radicals formed in glassy media can adopt a range of conformations. This occurrence might also be important in the study of free radicals in hydrocarbon glasses (16) and in argon matrix studies (4, 17).

H. R. Falle gratefully acknowledges the award of a National Research Council of Canada Postdoctorate Fellowship. We also thank D. R. Smith and M. Tomlinson for helpful criticism of the manuscript.

1. H. R. Falle and F. P. Sargent. Can. J. Chem. This issue.
2. F. S. Dainton, H. R. Falle, and G. A. Salmon. Unpublished results.
3. M. Hanack. Conformation theory. Academic Press Inc., New York. 1965.
4. J. E. Bennett and B. Mile. Faraday Trans. I, **69**, 1398 (1973).
5. R. A. Holroyd and G. W. Klein. J. Phys. Chem. **69**, 194 (1965).
6. J. E. Wertz and J. R. Bolton. Electron spin resonance: elementary theory and practical applications. McGraw-Hill Inc., New York. 1972.
7. P. J. Krusic and J. K. Kochi. J. Am. Chem. Soc. **90**, 7156 (1968).
8. H. Taniguchi, K. Fukui, S.-I. Ohnishi, H. Hatano, H. Hasegawa, and T. Maruyama. J. Phys. Chem. **72**, 1926 (1968).
9. J. K. Kochi and P. J. Krusic. J. Am. Chem. Soc. **90**, 7159 (1968).
10. P. B. Ayscough and C. Thomson. Trans. Faraday Soc. **58**, 1477 (1962).
11. E. W. Stone and A. H. Maki. J. Chem. Phys. **37**, 1326 (1962).
12. D. R. Smith, F. Okenka, and J. J. Pieroni. Can. J. Chem. **45**, 833 (1967).
13. T. Ohmori, T. Ichikawa, and M. Iwasaki. Bull. Chem. Soc. Japan, **46**, 1383 (1973).
14. L. Radom and J. A. Pople. J. Am. Chem. Soc. **92**, 4786 (1970).
15. A. A. Bothner-By, C. Naar-Colin, and H. Günther. J. Am. Chem. Soc. **84**, 2748 (1962).
16. D. J. Henderson and J. E. Willard. J. Am. Chem. Soc. **91**, 3014 (1969).
17. P. H. Kasai. Acc. Chem. Res. **4**, 329 (1971).

Can. J. Chem. Downloaded from www.nrcresearchpress.com by 210.87.254.105 on 09/05/12
For personal use only.

An Investigation of Substituent Effects on Coupling Constants to Vinyl Protons in Styrene Derivatives

WILLIAM F. REYNOLDS, IAN R. PEAT,[1] AND GORDON K. HAMER[2]
Department of Chemistry, University of Toronto, Toronto, Ontario, M5S 1A1

Received February 4, 1974

WILLIAM F. REYNOLDS, IAN R. PEAT, and GORDON K. HAMER. Can. J. Chem. **52**, 3415 (1974).

Experimental long-range phenyl proton – vinyl proton coupling constants in 4-substituted styrenes are substituent independent. This is also predicted by INDO – finite perturbation theory calculations of these coupling constants. Comparison with calculated and experimental long-range coupling constants for 4-substituted benzaldehydes suggests that the previously reported substituent dependence for the latter coupling constants arises from substituent-induced changes in molecular geometry.

Geminal vinyl coupling constants in 4-substituted styrenes, α-methylstyrenes, and α-*t*-butylstyrenes are substituent dependent with substituent effects increasing as phenyl and vinyl groups are twisted out of planarity. These trends are reproduced by INDO–FPT calculations. It is concluded that the substituent effects are primarily transmitted through space.

Both experimental and calculated vinyl ^{13}C–^{1}H coupling constants show strong stereospecific substituent effects. From the pattern of results (particularly the greater field dependence for $J_{C(\beta)H(9)}$ than $J_{C(\beta)H(8)}$) it is concluded that these coupling constants also reflect through-space substituent effects. This is supported by calculations on model compounds with no intervening phenyl group.

WILLIAM F. REYNOLDS, IAN R. PEAT et GORDON K. HAMER. Can. J. Chem. **52**, 3415 (1974).

Les constantes de couplage à longue distance mesurées entre les protons des phényles et les protons des groupements vinyles dans des styrènes substitués en position 4 sont indépendantes des substituants. Ce résultat est aussi prédit par les calculs INDO–FPT de ces constantes de couplage. La comparaison entre les valeurs calculées et les valeurs expérimentales des constantes de couplage à longue distance pour les benzaldéhydes subtitués en position 4 suggèrent que les résultats rapportés antérieurement sur la dépendance des substituants pour ces dernières constantes de couplage découlent de changements, induits par les substituants, dans la géométrie de la molécule.

Les constantes géminales des groupes vinyles dans les styrènes substitués en position 4 ainsi que dans des α-méthyles et α-*t*-butylstyrènes dépendent des substituants et ces effets augmentent lorsque les groupes phényles et vinyles sont déplacés hors du plan de la molécule. Ces tendances sont reproduites par des calculs INDO–FPT. On en conclut que les effets de substituants sont transmis principalement à travers l'espace.

Les constantes de couplage ^{13}C–^{1}H mesurées et calculées pour les groupes vinyles montrent de forts effets de substituants qui sont stéréospécifiques. Partant des variations dans les résultats (particulièrement la dépendance sur le champ qui est plus grand pour $J_{C(\beta)H(9)}$ que $J_{C(\beta)H(8)}$) on en conclut que ces constantes de couplage reflètent aussi des effets de substituants à travers l'espace. Cette conclusion est supportée par des calculs sur des composés modèles dans lesquels aucun groupe phényle n'intervient. [Traduit par le journal]

Introduction

While there have been numerous investigations of long-range coupling constants to side-chain protons in aromatic derivatives (1–3), there have been few systematic investigations of substituent effects on these coupling constants (4–6). Similarly, while molecular orbital calculations based on finite perturbation theory (7) in the CNDO/2 (8) and INDO (9) approximations have proved useful for investigations of ^{1}H–^{1}H coupling constants, these calculations have been used primarily to investigate mechanisms of transmission of coupling constants (3, 10–23) with lesser attention paid to substituent effects (11, 14, 20, 24).

Consequently, we decided to carry out an experimental and theoretical investigation of substituent effects on coupling constants in styrene derivatives. These compounds were

[1]Current address: Department of Chemistry, Florida State University, Tallahassee, Florida, 32306.
[2]Current address: School of Chemical Science, University of East Anglia, Norwich NOR 88C, England.

Can. J. Chem. Downloaded from www.nrcresearchpress.com by 210.87.254.42 on 09/05/12
For personal use only.

Can. J. Chem. Downloaded from www.nrcresearchpress.com by 210.87.254.42 on 09/05/12
For personal use only.

chosen not only because of the availability in our laboratory of numerous styrene derivatives (25) but also because of the geometric characteristics of styrene which make it a particularly useful model compound for investigating both substituent effects (25) and the mechanisms of transmission of coupling constants (12, 23).

Results of theoretical and experimental investigations of substituent effects on geminal, vicinal, and long-range ^1H–^1H coupling constants and directly bonded ^{13}C–^1H coupling constants are reported below.

Experimental

Compounds either were obtained commercially or else synthesized in this laboratory using methods described elsewhere (25, 26).

^1H spectra for 4-substituted styrenes were recorded on a Varian HA-100 spectrometer, operating in the frequency sweep mode at a probe temperature of 30 ± 1 °C. Internal tetramethylsilane (*ca.* 3 mol%) was used as a lock and reference signal. Spectra were measured at a sweep rate of 0.02 Hz/s and calibrated at less than 5 Hz intervals. Peak positions were obtained from the average of at least four scans (twice in each direction). Double resonance experiments were carried out using a Hewlett-Packard 4204A Oscillator.

Spectra for 4-nitrostyrene and 4-methoxystyrene were run in CS_2 whereas 4-dimethylaminostyrene and 4-ethynylstyrene were run in C_6D_6. C_6D_6 was used for the latter two compounds because it gave the largest chemical shift difference for the aromatic protons of the ethynyl derivative, facilitating analysis, and because the dimethylamino derivative reacted in CS_2 to give an intense yellow solution. All solutions contained 5 mol% of styrene derivative and 3 mol% of tetramethylsilane. Paramagnetic impurities were removed with a small magnet and then each solution was filtered into an n.m.r. tube which was degassed with at least four freeze–pump–thaw cycles and then sealed under vacuum.

It was necessary to decouple the methyl protons of the 4-methoxy and 4-dimethylamino derivatives and the ethynyl proton of 4-ethynylstyrene to remove long-range couplings of these groups to the vinyl protons.

Relative signs of long-range coupling constants in 4-nitrostyrene were determined by double-resonance 'tickling' experiments (27). Signs agreed completely with those determined previously for 3,4-dichloro- and 3-bromostyrene (12). The near constancy of long-range coupling constants in all of the 4-substituted styrenes justifies assigning the same signs for all these derivatives.

Experimental line frequencies and signs of coupling constants were used as input for iterative spectral analysis using the computer program LACX (28). Input parameters were estimated from observed splittings.

^{13}C–^1H coupling constants for α-methylstyrene and α-*t*-butylstyrene derivatives were determined from ^{13}C spectra obtained on a Varian XL-100-15 spectrometer operating in the pulsed Fourier transform mode at 25.160 MHz (probe temperature 32 ± 3 °C). ^1H coupled spectra were obtained in the 'gated gyrocode' mode in which the spectrometer is off during the acquisition time but on during a delay period to establish the nuclear Overhauser enhancement (29). ^{13}C spectra were obtained for 5–10 mol% solutions of styrene derivatives in CCl_4 with 8 mol% C_6D_{12} giving the lock signal.

^{13}C–^1H coupling constants could be estimated directly from the splittings in the ^{13}C spectra since the α-methyl- and α-*t*-butylstyrenes with $^{13}C(\beta)$, respectively, give AMR_3X and AMX spectra with splittings equal to coupling constants (precise calculations indicated a maximum deviation of 0.05 Hz from first-order splittings). In several of the α-*t*-butylstyrene derivatives, the central doublet of the X quartet was not resolved and only average ^{13}C–^1H coupling constants could be obtained (the peaks appeared to be broadened by unresolved coupling to the *t*-butyl hydrogens). In these cases, the coupling constants were measured from ^{13}C satellite peaks in ^1H spectra of 30 mol% solutions. The same approach was used to confirm the assignments of coupling constants in α-methylstyrene and its dimethylamino and nitro derivatives. In these compounds, ^1H and ^{13}C spectra gave coupling constants which agreed within 0.1 Hz, indicating no concentration dependence. It is estimated that the accuracy of individual coupling constants is ±0.2 Hz.

We also attempted to measure ^{13}C–^1H coupling constants for styrene derivatives. Unfortunately, these compounds give ABCX spectra with splittings in the $X(^{13}C)$ spectra not equal to the coupling constants. To obtain the latter, full spectral analysis is required, using the ^{13}C satellites in the ^1H spectrum. However, both the low intensity of the satelites plus the fact that both H(A) and H(B) satellites due to $^{13}C(\beta)$ are obscured by the main H(A) spectrum made it impossible to measure these peaks accurately.

Details of Calculations

CNDO and INDO finite perturbation calculations were performed using a modified version (19, 23) of a standard CNINDO program (30). Calculations were performed on an IBM-370 computer. Unless otherwise specified, standard bond lengths and angles (31) were used in the calculations.

Results and Discussion

Ring Proton – Vinyl Proton Coupling Constants

Experimental and calculated (INDO) values of long-range ^1H–^1H coupling constants for 4-substituted styrenes are summarized in Table 1. Both calculated and experimental coupling constants are an average of the values for the two planar conformations **1** and **2**. ^1H chemical shifts, intra-ring coupling constants, and pertinent computer fitting data from the spectral analysis of these derivatives are summarized in Table 2. Compounds were chosen to cover a wide range of substituent effects.

The most significant observation is that both experimental and calculated long-range couplings are substituent independent. This is

TABLE 1. Experimental and calculated[a] long-range coupling constants for 4-substituted styrene derivatives

Coupling[b] constant	Substituent: $N(CH_3)_2$ Exp.	$N(CH_3)_2$ Calcd.	OCH_3 Exp.	OCH_3 Calcd.	NO_2 Exp.	NO_2 Calcd.	C≡C—H Exp.	C≡C—H Calcd.
$\langle J_{27},J_{67}\rangle$	−0.51	−0.53	−0.53	−0.53	−0.52	−0.51	−0.52	−0.53
$\langle J_{28},J_{68}\rangle$	<0.07	+0.18	<0.07	+0.19	<0.07	+0.19	<0.07	+0.18
$\langle J_{29},J_{69}\rangle$	+0.11	+0.36	+0.15	+0.37	+0.16	+0.35	+0.15	+0.36
$\langle J_{37},J_{57}\rangle$	+0.36	+0.79	+0.36	+0.76	+0.39	+0.74	+0.39	+0.78
$\langle J_{38},J_{58}\rangle$	<0.07	−0.22	<0.07	−0.22	<0.07	−0.21	<0.07	−0.22
$\langle J_{39},J_{59}\rangle$	<0.07	−0.04	<0.07	−0.05	<0.07	−0.05	<0.07	−0.04

[a]INDO calculations.
[b]Numbering shown in **1** and **2**.

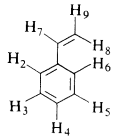

1

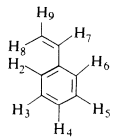

2

TABLE 2. Remaining N.M.R. parameters for 4-substituted styrenes

Parameter[a]	Compound: 4-$N(CH_3)_2$	4-OCH_3	4-NO_2	4-C≡C—H
$\delta_{(2,6)}$[b]	7.301	7.160	7.463	6.985
$\delta_{(3,5)}$	6.512	6.683	8.062	7.341
δ_7	6.702	6.524	6.746	6.398
δ_8	5.597	5.469	5.880	5.469
δ_9	5.040	5.006	5.439	5.020
J_{23},J_{56}[c]	8.60	8.53	8.56	8.03
J_{25},J_{36}	0.40	0.41	0.45	0.60
J_{26}	2.79	2.72	2.43	1.84
J_{35}	2.28	2.31	2.00	1.87
J_{78}	17.56	17.50	17.51	17.59
J_{79}	10.87	10.85	10.89	10.91
J_{89}	1.25	1.07	0.56	0.88
No. of peaks fitted	94	96	96	90
Worst fit (Hz)	0.059	0.063	0.062	0.042
Root mean square deviation	0.019	0.020	0.018	0.011
Probable errors of parameters	0.002–0.007	0.002–0.007	0.002–0.007	0.001–0.006
Solvent	C_6D_6	CS_2	CS_2	C_6D_6

[a]The lettering corresponds to **1** in Table 1.
[b]Chemical shifts in p.p.m. relative to internal tetramethylsilane.
[c]Coupling constant in Hz.

important since in our previous investigation of coupling constants in styrenes (12), ring substituents (Br or Cl) were used to simplify spectra and to force styrene into specific conformations. The results in Table 1 indicate that negligible errors were introduced by this procedure.

While methyl proton – ring proton couplings in toluenes are also insensitive to substituents (32), aldehyde proton – ring proton couplings in 4-substituted benzaldehydes show an experimentally significant substituent dependence (4). In an attempt to account for this difference, INDO calculations were started for a series of 4-substituted benzaldehydes. However, after calculations were performed for four derivatives (see Table 3), it became apparent that the electronic effect of a substituent introduced into an otherwise unperturbed molecule could not

Can. J. Chem. Downloaded from www.nrcresearchpress.com by 210.87.254.42 on 09/05/12
For personal use only.

TABLE 3. Experimental and calculated long-range coupling constants for some 4-substituted benzaldehyde derivatives

Coupling constant	Substituent: H		$N(CH_3)_2$		C≡N		NO_2	
	Exp.[a]	Calcd.[b]	Exp.[c]	Calcd.	Exp.[c]	Calcd.	Exp.[c]	Calcd.
$\langle J_{27},J_{67}\rangle$[d]	−0.10	−0.10	−0.23	−0.06	<0.06	−0.12	<0.06	−0.16
$\langle J_{37},J_{57}\rangle$	+0.38	+0.90	+0.47	+0.89	+0.38	+0.88	+0.41	+0.93

[a]From ref. 41.
[b]INDO calculations.
[c]From ref. 4.
[d]Numbering of benzaldehyde protons corresponds to that for styrenes (see **1** and **2**, Table 1) with H_7 the aldehyde proton.

TABLE 4. Calculated long-range coupling constants (in Hz) for benzaldehyde and styrene as a function of C(1)—C(α) bond length

(A) Benzaldehyde

Coupling constant	$J_{(CNDO)}$	$J_{(INDO(\sigma))}$	$J_{(INDO(\pi))}$[a]	$J_{(INDO)}$
$r_{C(1)-C(\alpha)} = 1.42$ Å				
$\langle J_{27},J_{67}\rangle$	+0.35	+0.14	−0.40	−0.26
$\langle J_{37},J_{57}\rangle$	+0.50	+0.63	+0.37	+1.00
$\langle J_{47}\rangle$	−0.01	−0.03	−0.33	−0.36
$r_{C(1)-C(\alpha)} = 1.46$ Å				
$\langle J_{27},J_{67}\rangle$	+0.40	+0.24	−0.34	−0.10
$\langle J_{37},J_{57}\rangle$	+0.46	+0.58	+0.32	+0.90
$\langle J_{47}\rangle$	0.00	−0.02	−0.27	−0.29
$r_{C(1)-C(\alpha)} = 1.50$ Å				
$\langle J_{27},J_{67}\rangle$	+0.47	+0.34	−0.28	+0.06
$\langle J_{37},J_{57}\rangle$	+0.43	+0.54	+0.27	+0.81
$\langle J_{47}\rangle$	0.00	−0.01	−0.22	−0.23

(B) Styrene

Coupling constant	$J_{(INDO)}$		
	$r = 1.42$ Å	$r = 1.46$ Å	$r = 1.50$ Å
$\langle J_{27},J_{67}\rangle$	−0.63	−0.53	−0.44
$\langle J_{37},J_{57}\rangle$	+0.90	+0.77	+0.65
$\langle J_{47}\rangle$	−0.30	−0.24	−0.20

[a]$J_{(INDO)} - J_{(INDO(\sigma))}$.

account for the experimental results. The calculated change in $\langle J_{27},J_{67}\rangle$ was not only too small but also of the wrong sign.

A plausible alternative explanation of the benzaldehyde results stems from the greater ability of a carbonyl group, compared to methyl or vinyl groups, to conjugate with the aromatic ring (33). Crystal structure data for 4-substituted benzoic acids show a variation of C(1)—C(α) bond length from 1.46 Å for the amino derivative to 1.50 Å for the nitro derivative (34). The corresponding benzaldehyde derivatives should show similar bond length changes.

To test the effect of this parameter, calculations were performed for benzaldehyde with the C(1)—C(α) bond length varying from 1.42 to 1.50 Å (Table 4). $\langle J_{27},J_{67}\rangle$ becomes less negative by 0.16 Hz for each 0.04 Å increase in bond length. This calculated change in $\langle J_{26},J_{67}\rangle$ is in the same direction as, and almost identical in magnitude to, that observed experimentally for 4-substituted benzaldehydes (−0.23 for the amino derivative, <0.06 Hz for the nitro derivative (4)). The calculations also correctly predict the smaller substituent dependence for the $\langle J_{37},J_{57}\rangle$ (total range 0.10 Hz (4)). Thus the

Can. J. Chem. Downloaded from www.nrcresearchpress.com by 210.87.254.42 on 09/05/12
For personal use only.

TABLE 5. Experimental and calculated vinyl ^1H–^1H coupling constants (in Hz) for some 4-substituted styrene derivatives

	Experimental[a]					Calculated[b]			
	Styrene			α-Methylstyrene	α-*t*-Butylstyrene	Styrene (ρ = 0°)			Styrene (ρ = 90°)
Substituent	J_{78}	J_{79}	J_{89}	J_{89}	J_{89}	J_{78}	J_{79}	J_{89}	J_{89}
H	17.56	10.90	1.09	1.62	1.79	26.15	9.08	5.00	4.93
$N(CH_3)_2$	17.51	10.87	1.26	1.74	2.07	26.28	9.13	5.02	5.04
CH_3	17.56	10.89	1.11	1.68	1.87	26.18	9.09	5.01	4.96
C≡C—H	17.57	10.92	0.93	—	—	26.14	9.07	4.97	—
F	17.56	10.93	0.93	1.53	1.68	26.13	9.05	4.91	4.86
CF_3	17.55	10.91	0.73	—	—	25.98	8.98	4.88	—
NO_2	17.57	10.93	0.58	1.07	1.19	25.92	8.94	4.83	4.69

[a]From ref. 25.
[b]INDO calculations.

substituent dependence of long-range couplings in 4-substituted benzaldehydes can be almost quantitatively accounted for by reasonable substituent-induced changes in the C(1)—C(α) bond length. However, this does not rule out the possibility that substituent-induced changes in either the C(α)—H bond length or the phenyl ring bonds may also affect the coupling constants.

The predicted change in $\langle J_{27},J_{67}\rangle$ for styrene is smaller (0.10 Hz for a 0.04 Å change in bond length) (Table 4). Furthermore, smaller changes in bond length would be expected since the vinyl group has only a slight tendency to accept or donate electrons (25).

Danyluk *et al.* (4) concluded that the substituent dependence of $\langle J_{27},J_{67}\rangle$ in benzaldehydes was primarily due to changes in σ contributions to these couplings. To test this conclusion, CNDO and INDO(σ) (10, 23) calculations were performed. Both calculations estimate only the fraction of the coupling constant transmitted entirely through the σ electron system. π contributions were estimated by taking J(INDO) − J(INDO(σ)) (10, 23). Results are in Table 4. The calculations suggest that substituent-induced changes in $\langle J_{27},J_{67}\rangle$ are due to changes in both σ and π contributions.

In addition to the planar 4-substituted styrenes, we attempted to measure long-range coupling constants in the nonplanar (25) 4-nitro-α-*t*-butylstyrene. However, the long-range coupling constants to the β vinyl protons were unmeasurably small, in agreement with INDO–FPT calculations which suggest that these coupling constants approach zero as the vinyl group is twisted out of conjugation with the phenyl group (12).

Geminal and Vicinal Vinyl Proton Coupling Constants

Geminal vinyl proton coupling constants in 4-substituted styrenes in cyclohexane vary from 0.58 Hz for the nitro derivative to 1.26 Hz for the dimethylamino derivative (25).

The substituent dependence of the geminal coupling constant $J_{H(8)H(9)}$, increases on going from styrene to α-*t*-butylstyrene; the total range of this coupling constant (from demethylamino to nitro derivatives) is 0.68 Hz for styrene, 0.67 Hz for α-methylstyrene, and 0.83 Hz for α-*t*-butylstyrene.

By contrast, *cis* and *trans* coupling constants for 4-substituted styrenes vary only slightly with substituent; the total range is 0.07 Hz in both cases (25). Electron-withdrawing groups may give rise to slightly larger coupling constants (Table 5), although the total range is comparable with the experimental uncertainty of ±0.03 Hz. Similarly, the *cisoid* and *transoid* allylic coupling constants to the methyl group in α-methylstyrene show no substituent effects. These results contrast with those of vinyl derivatives with directly bonded substituents where electronegative groups cause marked decreases in both geminal and vicinal coupling constants (35).

INDO calculations were performed for representative styrene derivatives with ρ = 0 and 90°, where ρ is the angle of twist between phenyl and vinyl groups (see Table 5). Calculations were not performed for the actual α-alkylstyrenes for reasons of computational economy. The calculations predict the increased substituent dependence of $J_{H(8)H(9)}$ as ρ increases (total range of 0.19 Hz for ρ = 0° and 0.35 Hz for ρ = 90°), although they underestimate the range of substituent effects in both planar and non-

Can. J. Chem. Downloaded from www.nrcresearchpress.com by 210.87.254.42 on 09/05/12
For personal use only.

TABLE 6. Experimental and calculated vinyl ^{13}C–^{1}H coupling constants (in Hz) for 4-substituted styrene derivatives

	Experimental coupling constants				Calculated coupling constants			
	α-Methylstyrene[c]		α-*t*-Butylstyrene		Styrene (ρ = 0°)		Styrene (ρ = 90°)	
Substituent	$J_{C(\beta)H(8)}$	$J_{C(\beta)H(9)}$	$J_{C(\beta)H(8)}$	$J_{C(\beta)H(9)}$	$J_{C(\beta)H(8)}$	$J_{C(\beta)H(9)}$	$J_{C(\beta)H(8)}$	$J_{C(\beta)H(9)}$
H	155.5	157.0[a]	156.6	155.7[b]	165.8	148.5	161.5	152.6
$N(CH_3)_2$	154.7	156.7[a]	156.7	154.4	166.0	148.5	161.5	150.9
$C(CH_3)_3$	155.4	156.9	156.7	155.1[b]	—	—	—	—
CH_3	155.4	156.7	156.8	155.1[b]	165.8	148.5	161.5	152.4
OCH_3	155.1	157.1	156.8	155.2	165.8	148.7	161.4	152.1
F	155.5	157.8[b]	156.9	155.6[b]	165.5	149.1	161.4	152.8
Cl	155.6	157.9	157.0	156.0[b]	—	—	—	—
Br	—	—	157.0	156.0[b]	—	—	—	—
NO_2	156.2	158.7[a]	157.1	157.3[b]	165.2	149.6	161.3	154.2
$Si(CH_3)_3$	155.7	157.1	—	—	—	—	—	—
$Sn(CH_3)_3$	155.6	157.1	—	—	—	—	—	—

[a]Assignments confirmed by ^{13}C satellites in ^{1}H spectra.
[b]Measured from ^{13}C satellites in ^{1}H spectra.
[c]All α-methylstyrenes had $J_{C(\beta)CH_3} = 6.0 \pm 0.1$ Hz.

planar derivatives. The calculations do not predict the increase in $J_{H(8)H(9)}$ with ρ for the unsubstituted styrenes (see Table 5). This is probably due to the omission of the α-alkyl group since a calculation for α-methylstyrene with ρ = 90° gave $J_{H(8)H(9)} = 6.53$ Hz. Unfortunately, the calculations also provide no explanation for the constancy of the vicinal coupling constants since they predict a marked decrease in J_{78} and J_{79} for electron-withdrawing groups.

While the calculations do not provide an explanation for the origin of substituent effects upon ^{1}H–^{1}H coupling constants, the pattern of experimental results suggests that it is due to through-space transmission of electronic effects. Through-bond effects (particularly conjugative effects) should decrease markedly with increase in ρ while through-space effects should be relatively insensitive to ρ (25). The small increase in the substituent dependence of $J_{H(8)H(9)}$ with ρ is thus more consistent with through-space than through-bond effects. Similarly, the experimental trends for styrenes parallel the solvent dependence of geminal and vicinal coupling constants in vinyl derivatives; the former are strongly solvent dependent while the latter show little solvent dependence (36). This suggests that the effect of a remote polar group in styrene is similar to that of a polar solvent molecule, *i.e.* essentially a through-space effect. Further evidence for through-space transmission of substituent effects is presented in the following section.

Directly Bonded Vinyl ^{13}C–^{1}H Coupling Constants

Vinyl ^{13}C–^{1}H coupling constants in α-methyl- and α-*t*-butylstyrene derivatives are summarized in Table 6. Calculated coupling constants for styrene at ρ = 0 and 90° are also included. α-Methylstyrene (ρ = 30°) and α-*t*-butylstyrene (ρ = 64°) lie between these extremes.

Both experimental results and calculations suggest that at large ρ, $J_{C(\beta)H(8)}$ is nearly constant while $J_{C(\beta)H(9)}$ shows a marked substituent dependence. On going from α-*t*-butyl- to α-methylstyrene the substituent dependence of $J_{C(\beta)H(8)}$ increases (total range of 1.5 compared to 0.5 Hz) whereas that of $J_{C(\beta)H(9)}$ decreases (2.0 compared to 2.9 Hz). The calculations predict the latter trend but not the former.

The greater sensitivity of $J_{C(\beta)H(9)}$ to substituent effects in both compounds again suggests a through-space transmission of substituent effects; the field due to a polar substituent acts almost directly along the C(β)H(9) bond but almost at right angles to C(β)H(8). However, these observations could also indicate a stereospecific transmission of electronic effects through the σ electron framework. This might be favored by the *trans* arrangement of C(1)—C(α) and C(β)—H(9) bonds (see ref. 23). To test this point, calculations were performed for CH_3X—

Can. J. Chem. Downloaded from www.nrcresearchpress.com by 210.87.254.42 on 09/05/12
For personal use only.

TABLE 7. Calculated geminal ^1H–^1H coupling constants and ^{13}C–^1H coupling constants for ethylene - methyl X pairs with C—X bond and ethylene molecule in the same relative orientation as the C(4)—X bond and vinyl group in 4-substituted styrenes (coupling constants in Hz)

CH_3X	$J_{H(8)H(9)}$	$J_{C(\beta)H(8)}$	$J_{C(\beta)H(9)}$	μ_{CH_3X}[a]	F[b]
CH_4	3.24	156.68	156.68	0.00	0.00
CH_3NH_2	3.24	156.65	156.70	0.46[c]	+0.04
CH_3OH	3.21	156.64	156.80	1.93[c]	+0.49
CH_3F	3.17	156.56	157.00	1.75	+0.71
CH_3NO_2	3.13	156.45	157.23	3.91	+1.11

[a]Dipole moment (Debye) from INDO calculation for CH_3X.
[b]Field substituent parameter (33) for X.
[c]Molecular dipole not parallel to C—X bond axis.

C_2H_4 pairs with the C—X bond and ethylene in the identical geometric arrangement to the C—X bond and the vinyl group in 4-substituted styrenes. Since there is no intervening phenyl group, these calculations should only reflect the field effect of the polar C—X bond. In fact, the calculated results of $J_{C(\beta)H(8)}$ and $J_{C(\beta)H(9)}$ (see Table 7) are entirely consistent with through-space field effects on these coupling constants. The increase in $J_{C(\beta)H(9)}$ and the smaller decrease in $J_{C(\beta)H(8)}$ parellel the magnitudes of the electric field vectors along these bonds (for styrene with the C(1)—C(α)—C(β) bond angle, α, = 120°, the resolved field component along C(β)H(8) is opposite in sign to that along C(β)H(9) (37)). Furthermore, the magnitudes of the changes in $J_{C(\beta)H(8)}$ and $J_{C(\beta)H(9)}$ closely parallel the polarizing ability of the C—X bond as measured either by the CH_3X dipole moment or the field substituent parameter for X (33). Furthermore, the calculations confirm that the substituent dependence of $J_{H(8)H(9)}$ is also at least partly due to through space effects.

In an attempt to obtain further information about the nature of the electronic substituent effects, calculated and experimental ^{13}C–^1H and geminal ^1H–^1H coupling constants were correlated with the field, F, and resonance, R, substituent parameters of Swain and Lupton (33) (see Table 8). In each case, the correlations reveal that $J_{C(\beta)H(9)}$ is more sensitive to field effects than $J_{C(\beta)H(8)}$. Furthermore, F contributions to $J_{H(8)H(9)}$, $J_{C(\beta)H(8)}$, and $J_{C(\beta)H(9)}$ are all almost independent of ρ. Both of these observations are entirely consistent with the presence of a through-space electric field effect which affects the coupling constants by C—H bond polarization. The magnitude of this polarization depends upon the component of the electric field vector acting along a given C—H bond (38). The only significant difference between calculated and experimental results is in the sign of the small field component to $J_{C(\beta)H(8)}$. Increase of the C(1)—C(α)—C(β) bond angle to a probably more realistic value of 130° (see ref. 25) would reverse the direction of the electric field component along C(β)—H(8), leading to a calculated positive field dependence for $J_{C(\beta)H(8)}$.

There have been previous suggestions that ^{13}C–^1H coupling constants are sensitive to electric field effects (39, 40). Raynes and Sutherley have estimated that the sensitivity of J_{C-H} to electric field effects is given by (39)

$$[1] \quad dJ_{C-H}/dE_z = +23 \times 10^{-6} \text{ Hz e.s.u.}^{-1}$$

where E_z is the field component along the C—H bond. This constant can also be estimated from our data. The difference in field contributions, Δf, to $J_{C(\beta)H(8)}$ and $J_{C(\beta)H(9)}$ is a measure of the electric field contribution to these coupling constants. For α-methyl- and α-*t*-butylstyrenes, $\Delta f \sim 0.83$ Hz. This can be used to estimate field contributions to $J_{C(\beta)H(9)} - J_{C(\beta)H(8)}$ (ΔJ) for individual derivatives. For example, for chloro derivatives, $F = 0.70$ (33). The field contribution to ΔJ is $F\Delta f$, *i.e.* ~ 0.58 Hz. The field effect of the polar C—Cl σ bond can be approximated by that of a point dipole of 1.86 D, acting halfway along the C—Cl bond (0.85 Å from Cl) (26). In this case, the difference in electric field components, ΔE_z ($\equiv E_z$ (C(β)H(9)) $- E_z$(C(β)H(8))) is $+1.50 \times 10^4$ for $\alpha = 120°$ or $+1.18 \times 10^4$ for $\alpha = 130°$ (electric field components are evaluated halfway along the C—H bond). Therefore dJ/dE_z is estimated to be between $(39 - 52) \times 10^{-6}$ Hz e.s.u.$^{-1}$, assuming α is between 120 and 130°. While this is larger than the value of Raynes (39), it is consistent with our observation

Can. J. Chem. Downloaded from www.nrcresearchpress.com by 210.87.254.42 on 09/05/12
For personal use only.

TABLE 8. Correlation of vinyl ^1H–^1H and ^{13}C–^1H coupling constants for 4-substituted styrenes with field, F, and resonance, R, substituent parameters

System	J	f^a	r^a	r^b
Styrene (exp.)[c]	$J_{H(8)H(9)}$	-0.38 ± 0.01	-0.37 ± 0.02	0.988
α-Methylstyrene (exp.)[c]	$J_{H(8)H(9)}$	-0.36 ± 0.04	-0.36 ± 0.07	0.966
α-*t*-Butylstyrene (exp.)[c]	$J_{H(8)H(9)}$	-0.40 ± 0.03	-0.57 ± 0.06	0.992
Styrene (calcd. $\rho = 0°$)	$J_{H(8)H(9)}$	-0.14 ± 0.02	-0.04 ± 0.02	0.981
Styrene (calcd. $\rho = 90°$)	$J_{H(8)H(9)}$	-0.18 ± 0.02	-0.20 ± 0.03	0.994
α-Methylstyrene (exp.)[c]	$J_{C(\beta)H(8)}$	$+0.37 \pm 0.05$	$+1.38 \pm 0.10$	0.985
	$J_{C(\beta)H(9)}$	$+1.17 \pm 0.13$	$+0.99 \pm 0.25$	0.960
α-*t*-Butylstyrene (exp.)[c]	$J_{C(\beta)H(8)}$	$+0.33 \pm 0.06$	$+0.02 \pm 0.12$	0.907
	$J_{C(\beta)H(9)}$	$+1.18 \pm 0.11$	$+1.99 \pm 0.21$	0.989
Styrene (calcd. $\rho = 0°$)	$J_{C(\beta)H(8)}$	-0.47 ± 0.05	-0.34 ± 0.09	0.987
	$J_{C(\beta)H(9)}$	$+0.85 \pm 0.11$	$+0.19 \pm 0.19$	0.976
Styrene (calcd. $\rho = 90°$)	$J_{C(\beta)H(8)}$	-0.17 ± 0.02	$+0.01 \pm 0.04$	0.975
	$J_{C(\beta)H(9)}$	$+1.22 \pm 0.23$	$+2.34 \pm 0.39$	0.983

[a]Coefficients for equation $J = J_0 + fF + rR$ where J_0 is the coupling constant for the unsubstituted styrene.
[b]Correlation coefficient.
[c]All compounds from ref. 25 included in correlation.

that field effects are enhanced for the styrene system, relative to aliphatic compounds (25). While it is undoubtedly an oversimplification to attribute the origins of the field dependence solely to C—H bond polarization (36), the pattern of results suggests that this is a major factor.

The correlations indicate resonance or conjugative contributions to both ^{13}C–^1H and geminal ^1H–^1H coupling constants which are more difficult to comprehend. The similar resonance contributions to $J_{C(\beta)H(8)}$ and $J_{C(\beta)H(9)}$ in α-methylstyrene appears reasonable, assuming resonance effects are transmitted through the Π electron system (25). The decreased resonance contribution to $J_{C(\beta)H(8)}$ for α-*t*-butylstyrene is also not unreasonable since conjugation should decrease as ρ increases. However, the increased resonance contributions to $J_{C(\beta)H(9)}$ and $J_{H(8)H(9)}$ with increased ρ are difficult to understand. For α-*t*-butylstyrene and for the styrene calculations at $\rho = 90°$, r values parallel f values. This suggests some through-space mechanism, possibly through-space transmission of the effect of Π electron density changes at C(1). However, unless one assumes that through-bond and through-space resonance contributions are of opposite sign, it is still difficult to rationalize the apparent increases in r with ρ. It is possible that the increased resonance dependence is not real but rather an artifact associated with some inadequacy in the correlations. However, the experimental results clearly suggest that there is an increased substituent dependence for $J_{H(8)H(9)}$ and $J_{C(\beta)H(9)}$ with increased ρ. Although the correlations underestimate the resonance dependence of these couplings, the calculations do indicate that the substituent dependence does increase with increasing ρ and the correlations again suggest that this is due to an increased resonance dependence.

To summarize, experimental measurements of long-range coupling constants in 4-substituted styrenes demonstrate that these coupling constants are not substituent dependent. Comparison of experimental and calculated long-range coupling constants for ring-substituted styrenes and benzaldehydes indicates that the previously reported (4) substituent dependence of these coupling constants in benzaldehydes is primarily due to changes in molecular geometry, particularly the C(1)—C(α) bond length.

The geminal vinyl proton coupling constants are strongly substituent dependent while the vicinal coupling constants are nearly constant. The pattern of results, the similarity of substituent effects and solvent effects and the results of INDO calculations on substituted styrenes and CH_3X–ethylene pairs suggest through-space transmission of electronic substituent effects.

Vinyl ^{13}C–^1H coupling constants in α-alkylstyrenes show strongly stereospecific substituent effects with $J_{C(\beta)H(9)}$ more sensitive than $J_{C(\beta)H(8)}$. Again both experimental results and INDO calculations indicate predominantly through-space electronic effects. Surprisingly, both $J_{C(\beta)H(9)}$ and $J_{H(8)H(9)}$ show increased substituent dependence with increasing ρ, apparently due to increased resonance effects.

Can. J. Chem. Downloaded from www.nrcresearchpress.com by 210.87.254.42 on 09/05/12
For personal use only.

Financial support from the National Research Council of Canada is gratefully acknowledged.

1. S. STERNHELL. Rev. Pure Appl. Chem. **14**, 15 (1964).
2. M. BARFIELD and B. CHAKRABARTI. Chem. Rev. **69**, 757 (1969).
3. J. ROWBOTHAM and T. SCHAEFER. Can. J. Chem. **51**, 953 (1973).
4. S. S. DANYLUK, C. L. BELL, and T. SCHAEFER. Can. J. Chem. **47**, 4005 (1969).
5. A. F. JANZEN and T. SCHAEFER. Can. J. Chem. **49**, 1818 (1971).
6. J. PEELING. Ph.D. Thesis, University of Manitoba, Winnipeg, Manitoba. 1973.
7. J. A. POPLE, J. W. MCIVER, JR., and N. S. OSTLUND. J. Chem. Phys. **49**, 2960 (1968); **49**, 2965 (1968).
8. J. A. POPLE and G. A. SEGAL. J. Chem. Phys. **43**, 5136 (1965).
9. J. A. POPLE, D. L. BEVERIDGE, and P. A. DOBOSH. J. Chem. Phys. **47**, 2026 (1967).
10. M. BACON and G. E. MACIEL. Mol. Phys. **21**, 257 (1971).
11. M. BARFIELD. J. Am. Chem. Soc. **93**, 1066 (1971).
12. M. BARFIELD, C. J. MACDONALD, I. R. PEAT, and W. F. REYNOLDS. J. Am. Chem. Soc. **93**, 4195 (1971).
13. R. WASYLISHEN and T. SCHAEFER. Can. J. Chem. **49**, 3216 (1971).
14. M. BARFIELD, R. J. SPEAR, and S. STERNHELL. J. Am. Chem. Soc. **93**, 5322 (1971).
15. M. BARFIELD and S. STERNHELL. J. Am. Chem. Soc. **94**, 1905 (1972).
16. R. WASYLISHEN and T. SCHAEFER. Can. J. Chem. **50**, 274 (1972).
17. R. WASYLISHEN and T. SCHAEFER. Can. J. Chem. **50**, 1852 (1972).
18. L. ERNST, W. M. HUTTON, and T. SCHAEFER. Can. J. Chem. **50**, 1863 (1972).
19. C. J. MACDONALD, G. K. HAMER, I. R. PEAT, and W. F. REYNOLDS. Can. J. Chem. **50**, 2035 (1972).
20. R. WASYLISHEN, J. B. ROWBOTHAM, L. ERNST, and T. SCHAEFER. Can. J. Chem. **50**, 2575 (1972).
21. I. R. PEAT and W. F. REYNOLDS. Can. J. Chem. **51**, 2968 (1973).
22. R. WASYLISHEN and T. SCHAEFER. Can. J. Chem. **51**, 3087 (1973).
23. I. R. PEAT and W. F. REYNOLDS. Can. J. Chem. **52**, 2403 (1974),
24. G. E. MACIEL, J. W. MCIVER, JR., N. S. OSTLUND, and J. A. Pople. J. Am. Chem. Soc. **92**, 4151 (1970); **92**, 4497 (1970); **92**, 4506 (1970).
25. G. K. HAMER, I. R. PEAT, and W. F. REYNOLDS. Can. J. Chem. **51**, 897 (1973); **51**, 915 (1973).
26. G. K. HAMER. Ph.D. Thesis, University of Toronto, Toronto, Ontario. 1973.
27. R. FREEMAN and W. A. ANDERSON. J. Chem. Phys. **37**, 2053 (1962).
28. C. W. HAIGH. Private communication.
29. (*a*) O. A. GANSOW and W. SCHITTENHELM. J. Am. Chem. Soc. **93**, 4294 (1971); (*b*) R. FREEMAN and H. D. W. HILL. J. Magn. Res. **5**, 278 (1971).
30. QUANTUM CHEMISTRY PROGRAM EXCHANGE PROGRAM 141.
31. D. L. BEVERIDGE and J. A. POPLE. Approximate molecular orbital theory. McGraw-Hill Book Company, New York, N.Y. 1970.
32. C. J. MACDONALD and W. F. REYNOLDS. Can. J. Chem. **48**, 1002 (1970).
33. C. G. SWAIN and E. D. LUPTON. J. Am. Chem. Soc. **90**, 4328 (1968).
34. R. W. G. WYCKOFF. Crystal structures. 2nd Ed. Vol. 6. Interscience Publishers, New York. 1969.
35. T. SCHAEFER and H. M. HUTTON. Can. J. Chem. **45**, 3153 (1967).
36. M. BARFIELD and M. D. JOHNSTON, JR. Chem. Rev. **73**, 52 (1973).
37. G. K. HAMER and W. F. REYNOLDS. Can. J. Chem. **46**, 3813 (1968).
38. A. D. BUCKINGHAM. Can. J. Chem. **38**, 300 (1960).
39. W. T. RAYNES and T. A. SUTHERLEY. Mol. Phys. **17**, 547 (1969).
40. J. C. HAMMEL and J. A. S. SMITH. J. Chem. Soc. (B), 1852 (1970).
41. R. J. KOSTELNIK, M. P. WILLIAMSON, D. E. WISNOSKY, and S. M. CASTELLANO. Can. J. Chem. **47**, 3313 (1969).

Can. J. Chem. Downloaded from www.nrcresearchpress.com by 210.87.254.42 on 09/05/12
For personal use only.

The Product of Homotropylium Cation Photolysis

P. A. CHRISTENSEN, Y. Y. HUANG, A. MEESTERS, AND T. S. SORENSEN

Department of Chemistry, The University of Calgary, Calgary, Alberta T2N 1N4

Received April 15, 1974

P. A. CHRISTENSEN, Y. Y. HUANG, A. MEESTERS, and T. S. SORENSEN. Can. J. Chem. **52**, 3424 (1974).

The product of homotropylium ion photolysis is the 1,2-dihydro-4H$^+$-pentalenyl cation. CNDO/2 and analogies to cyclopentenyl cation rearrangements allow one to rationalize the formation of this product.

P. A. CHRISTENSEN, Y. Y. HUANG, A. MEESTERS et T. S. SORENSEN. Can. J. Chem. **52**, 3424 (1974).

Le produit de photolyse de l'ion homotropylium est le cation dihydro-1,2 pentalényl-4H$^+$. Les calculs par CNDO/2 et des analogies avec les réarrangements du cation cyclopentényle nous permettent de rationaliser la formation de ce composé. [Traduit par le journal]

Introduction

Hogeveen and Gassbeck (1) have recently reported (from ^{1}H n.m.r.) that a single cation product results from the photolysis of protonated cyclooctatetraene **1** (homotropylium ion) but they were not able to assign a structure to this photoproduct. This product can now be identified as **2**, the 1,2-dihydro-4H$^+$-pentalenyl cation **2** and a logical mechanism for its formation can be arrived at.

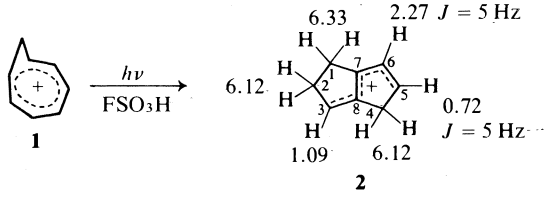

1 **2**

Results

Cation **2** was obtained by the careful protonation of the known 2,4-dihydropentalene **3** (2, 3) in 96% sulfuric acid at 0 °C. This ion remains unchanged after 2 h at 25 °C. Although three protonation sites (positions 1, 3, and 5) which lead to conjugated dienylic cations are present in **3**, only one leads to the linear dienylic cation **2**. Examples of the interesting cross-conjugated dienylic cations, which would result from protonation at the other two sites, are unknown. However, in agreement with the results of CNDO/2 calculations on both the simple dienylic cations **4** and **5** and on the actual systems **2**, **6**, and **7**, one predicts exclusive protonation at C-1 in **3** to give **2** (the relative total energies are noted with the structures and the partially optimized coordinates are listed in the Experimental section).

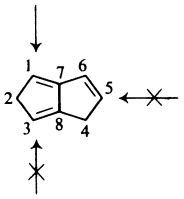

3

The structure assigned to **2** follows from the known structure of the neutral starting hydrocarbon and is also consistent with the chemical shifts observed for the ion (Fig. 1). Thus, the

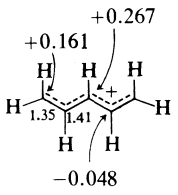

4
"W" conformation

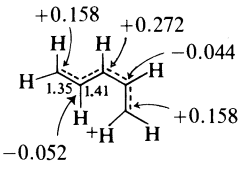

4
"sickle" conformation (the shape also in **2**)

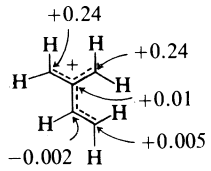

5

Relative E 0 +3.5 kcal/mol +42 kcal/mol

Can. J. Chem. Downloaded from www.nrcresearchpress.com by 210.87.254.42 on 09/05/12
For personal use only.

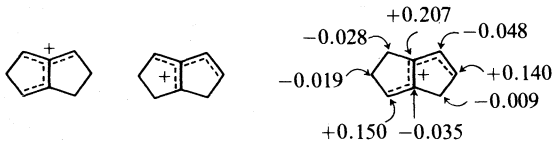

6 **7** **2**

Relative *E* +30 kcals/mol +15.5 kcal/mol 0

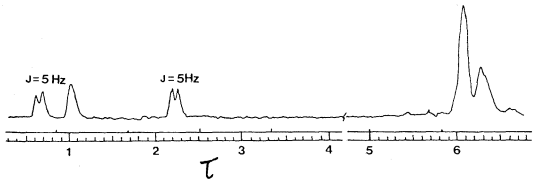

FIG. 1. The 60 MHz n.m.r. spectrum of **2** in 96% H_2SO_4 at *ca.* 35 °C.

smallish 5 Hz coupling observed for the vicinal protons in the partial structure **i** is typical of a five-membered enylic ring (*cf.* the cyclopentenyl cation **8**) (4).

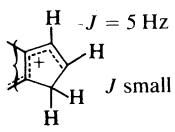

i

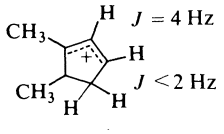

8

The small coupling in **2** between the protons at τ 0.72 and 1.09 and the respective methylene protons at 6.12 (accidentally equivalent) is also typical (*cf.* **8**). The large chemical shift separation of the vicinal protons on the dienylic cation center is a consequence of the alternating charge density on the carbons (substantiated by the CNDO/2 calculations). This same pattern has been observed in numerous other dienylic cations (4).

The chemical shift and coupling constant data reported by Hogeveen and Gassbeck (1) for their unknown product is identical to that observed for **2**, with the exception of small chemical shift differences, probably caused by small solvent effects and differences in referencing. None of the other possible bicyclo[3.3.0]octadienyl cations remotely fits the observed spectrum.

Discussion

The ring closure of the homotropylium ion appears to be closely analogous to that of the parent tropylium ion **9** (eq. 1) (1, 5, 6). This can

[1] 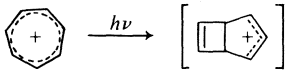

9

be regarded as an allowed disrotatory ring closure of the C-1 and C-5 π centers of a pentadienyl cation sub-unit. In the noncentrosymmetric homotropylium ion, there are three separate analogous ring closures. In rationalizing the experi-

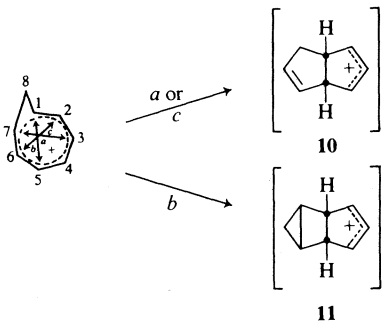

10 **11**

mental results, only the ion formed in closures *a* and *c* (**10**) easily leads to the observed product **2**. One predicts that the ion **10** will, however, be a very short-lived intermediate since a single hydride migration leads to a more stable (more highly alkyl substituted at the 1 or 3 position) allylic cation **12**. This process is almost exactly

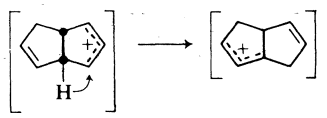

10 **12**

paralleled by the observed behavior of the presumed intermediate in the pentadienyl–cyclopentenyl cation closure shown in eq. 2 (4, 7). However, in the case of the cation **12**, this is also an unobserved intermediate since in this particular

[2] 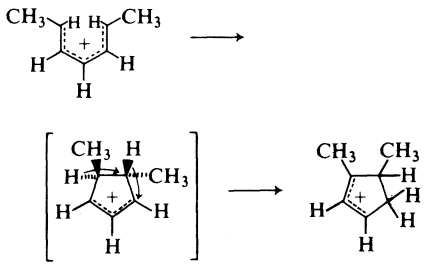

8 first observed product

Can. J. Chem. Downloaded from www.nrcresearchpress.com by 210.87.254.42 on 09/05/12
For personal use only.

Angle	2	6	7	14
123	110	108	111.4	104
234	104	109.5	110.3	108
345	103.9	102.6	104	112.5
451	112.1	109.8	104	107.9
512	110	110	110.3	107.6
128	107	110	108	101.7
287	113.9	110.6	110	103.4
876	106.9	105.9	110	101.5
761	104.5	104.5	102	111
612	108	109	110	111
328	143	142	140.6	147.2
516	142	141	139.7	141.4
Dihedral 8721				33.4

case there is predictably a considerable driving force leading to a fully conjugated dienylic cation. There is only one simple hydride-shift route leading to a dienylic cation (eq. 3). There are

[3] 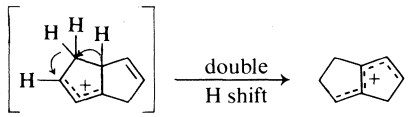

12 2

many analogies for such a double hydride shift in the rearrangements of numerous cyclopentenyl cations (7); that shown in eq. 2 being typical. An even closer analogy is shown in eq. 4.

[4] 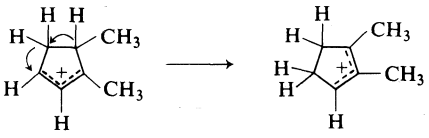

The only other mechanism for giving a conjugated dienylic cation is one involving deprotonation–protonation steps. In this case, three dienylic cations are possible from **12** (**2**, **13**, and **14** of eq. 5).

[5] 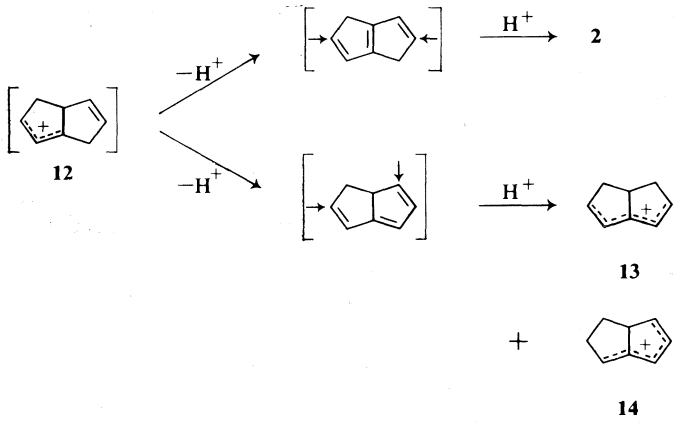

We have carried out CNDO/2 calculation on **14** and consistently (varying the nonplanar geometry) arrive at a higher energy (of the order of 30 kcal/mol) than that previously calculated for **2**. This is caused entirely by serious angle strain in **14** due to the tetrahedral bridgehead carbon. The angle strain – nonplanarity problems in **13** are even more serious and we did not attempt

Can. J. Chem. Downloaded from www.nrcresearchpress.com by 210.87.254.42 on 09/05/12
For personal use only.

a calculation on this ion. Thus this mechanism also predicts **2** as the sole stable product from the photolysis of **1**.

Experimental

The dihydropentalene **3** was prepared by the laborious route of Alder and Stein (2) and Katz and Rosenburger (3) starting from dicyclopentadiene. The preparation of **3** from the pyrolysis of cyclooctatetraene has been reported (8) but the crude product obtained by us contained starting material and benzene and it was difficult to obtain **3** in any reasonable amount from this route. The carbocation was prepared by adding dropwise a solution of dihydropentalene in carbon tetrachloride to a flask containing 96% sulfuric acid and an upper layer of carbon tetrachloride, cooled to 0° and stirred with a small magnetic bar. A Varian A-60 spectrometer was used for the n.m.r. measurements.

CNDO/2 Calculations (9)

For the five carbon pentadienyl cations, the optimum C—C bond lengths were obtained and these were used for the bicyclo[3.3.0]octadienyl cation calculations. The optimum C—C bond lengths were similar to those found in *ab initio* calculations (10), for example, bond lengths for the allyl system are 1.385 Å *vs.* 1.37 by the CNDO/2 method (10). The C—H bond lengths were taken from allyl *ab initio* calculations (10), 1.10 Å for terminal sp^2 C—H and 1.084 Å for internal sp^2 C—H bonds. For the five carbon cations, all assumed geometries were planar and angles of 120° were used. The optimum bond lengths were

and also for "sickle" conformer

For the cations **2**, **6**, **7**, an assumed planar geometry was used. All sp^2–sp^3 C—C bonds were made 1.50 Å and sp^3–sp^3 C—C bonds 1.54 Å. The sp^3 C—H bond was taken as 1.084 Å. All hydrogens were centered equally between nearest carbons and H—C—H angles were based on the corresponding C—C—C angles, *i.e.* if C—C—C was 103° (−6°), then H—C—H was taken as 115° (+6°). The C—C—C angles for **2**, **6**, **7**, and **14** are listed below. Although the external angles 328 and 516 are large, they can only be reduced significantly by severely decreasing two other angles. In **14**, C-8 is placed out of the plane of the remaining atoms in order to get better tetrahedral angles at C-2.

The authors wish to thank the National Research Council of Canada for generous operating support and the Killam Foundation for a scholarship to P.A.C. We also thank Dr. A. Rauk for helpful advice.

1. H. Hogeveen and C. J. Gassbeck. Rec. Trav. Chim. **89**, 1079 (1970); P. W. Cabell-Whiting and H. Hogeveen. Adv. Phys. Org. Chem. **10**, 132 (1973).
2. K. Alder and G. Stein. Ann. **485**, 223 (1931).
3. T. J. Katz and M. Rosenburger. J. Am. Chem. Soc. **84**, 865 (1962); T. J. Katz, M. Rosenburger, and R. K. O'Hara. J. Am. Chem. Soc. **86**, 249 (1964).
4. T. S. Sorensen. Can. J. Chem. **43**, 2746 (1965); **42**, 2768 (1964).
5. E. E. Van Tamelen, T. M. Cole, Jr., R. Greeley, and H. Schumacher. J. Am. Chem. Soc. **90**, 1372 (1968); E. E. Van Tamelen, R. H. Greeley, and H. Schumacher. J. Am. Chem. Soc. **93**, 6151 (1971).
6. R. F. Childs and V. Taguchi. Chem. Commun. 695 (1970).
7. R. Bladek and T. S. Sorensen. Can. J. Chem. **50**, 2806 (1972).
8. M. Jones, Jr. and L. O. Schwab. J. Am. Chem. Soc. **90**, 6549 (1968).
9. The Program CNINDO (P. A. Dobosh) Quantum Chemistry Program Exchange (QCPE), Bloomington, Indiana.
10. L. Radom, P. C. Hariharan, J. A. Pople, and P. V. R. Schleyer. J. Am. Chem. Soc. **95**, 6531 (1973).

Can. J. Chem. Downloaded from www.nrcresearchpress.com by 210.87.254.42 on 09/05/12
For personal use only.

Nonaromatic Primary Amine Tropolone Salts

BO LONG POH

School of Chemical Sciences, Universiti Sains Malaysia, Penang, Malaysia

Received May 29, 1974

BO LONG POH. Can. J. Chem. **52**, 3428 (1974).

Nonaromatic primary amines react rapidly with tropolone in nonpolar solvents such as carbon tetrachloride and benzene to give quantitative yields of the corresponding amine tropolone salts which when reacted with aqueous base give back tropolone and the original amines.

The reaction between nonaromatic primary amines and tropolone provides a convenient method of detecting and separating nonaromatic primary amines from other amines.

BO LONG POH. Can. J. Chem. **52**, 3428 (1974).

Les amines primaires non-aromatiques réagissent rapidement avec les tropolones dans des solvants nonpolaires tels que le tétrachlorure de carbone et le benzène pour donner avec des rendements quantitatifs le sel correspondant de l'amine avec la tropolone qui peut réagir avec des bases aqueuses pour redonner la tropolone et les amines originales.

La réaction entre les amines primaires non-aromatiques et la tropolone fournit donc une méthode simple de détecter et de séparer les amines primaires non-aromatiques des autres amines. [Traduit par le journal]

Introduction

This paper reports that tropolone reacts specifically and rapidly with nonaromatic primary amines in nonpolar solvents such as carbon tetrachloride and benzene to yield the corresponding yellow solid amine tropolone salts. All other amines give a clear solution. These salts react rapidly with aqueous base to give back the original amines and tropolone. This reaction provides a convenient method of detecting and separating nonaromatic primary amines from other amines.

Experimental

Preparation of Nonaromatic Primary Amine Tropolone Salts

Nonaromatic primary amine tropolone salts were prepared by the following general method: 5 mmol of the amine were added to 10 ml of carbon tetrachloride containing 5 mmol of tropolone. A yellow solid product precipitated immediately. It was suction filtered and washed with a small volume of carbon tetrachloride. The product was purified by vacuum sublimation. The yields were quantitative in all cases.

In cases where an amine has two primary amino groups, 2 equiv. of tropolone were used. Attempts to react tropolone with only one of the two primary amino groups in ethylenediamine, diethylenetriamine, and 1,2-diaminopropane by using an excess of the amines were not successful.

The identities of the amine tropolone salts were checked by elemental analyses and their n.m.r., i.r., and u.v. spectra. The n.m.r. spectra were taken with a Perkin-Elmer model R12B 60 MHz n.m.r. spectrometer, the i.r. spectra were recorded with a Beckman AccuLab 3 i.r. spectrophotometer, and the u.v. spectra were taken with a Perkin-Elmer 402 spectrophotometer. The extinction coefficients of each amine tropolone salt in water were determined at various concentrations of solute and found to obey Beer's law very closely. All the eight amine tropolone salts were found to absorb at the same wavelengths and have similar extinction coefficients. The average extinction coefficients were found to be 26 000 at 235 nm, 11 000 at 330 nm, and 7400 at 390 nm. Elemental analyses for C, H, and N were done by the Australian Microanalytical Service.

Tropolone and amines were purchased commercially.

Precipitation of a Nonaromatic Primary Amine in the Presence of Other Amines

Tropolone (5 mmol) was added to each of the following three solutions: solution A, 5 mmol each of cyclohexylamine and aniline in 15 ml of benzene; solution B 5 mmol each of cyclohexylamine and piperidine in 15 ml of benzene; and solution C, 5 mmol each of cyclohexylamine and triethylamine in 15 ml of benzene. In all the three cases, cyclohexylamine tropolone salt precipitated rapidly. The other three amines remained in the benzene.

Results and Discussion

All the nonaromatic primary amine tropolone salts prepared are stable, crystalline solids. They vary from pale yellow to lemon yellow in color. They are soluble in water and slightly soluble or insoluble in nonpolar solvents. Their solutions in water are basic. They were identified by elemental analyses and n.m.r., i.r., and u.v. spectra. These compounds can be represented by the general structure shown by **1**.

The results of the elemental analyses are given in Table 1. The calculated values agree with the values found.

Can. J. Chem. Downloaded from www.nrcresearchpress.com by 210.87.254.105 on 09/05/12
For personal use only.

TABLE 1. Melting points and analytical results of some non-aromatic primary amine tropolone salts

Compound	Color	Melting point*	% analysis C Found	C Calcd.	H Found	H Calcd.	N Found	N Calcd.
Benzylamine tropolone salt	Yellow	170–172	73.36	73.38	6.31	6.98	6.15	6.11
n-Butylamine tropolone salt	Yellow	143–145	68.01	67.71	8.74	8.71	6.92	7.18
t-Butylamine tropolone salt	Pale yellow	193–195	67.97	67.71	9.14	8.71	6.93	7.18
Cyclohexylamine tropolone salt	Pale yellow	184–185	70.69	70.61	8.63	8.59	6.52	6.33
1,6-Diaminohexane ditropolone salt	Lemon yellow	195	66.91	66.63	7.55	7.77	7.52	7.77
1,2-Diaminopropane ditropolone salt	Lemon yellow	155–156	64.18	64.16	6.88	6.91	9.01	8.80
Diethylenetriamine ditropolone salt	Yellow	178	62.36	62.27	7.03	7.20	12.34	12.10
Ethylenediamine ditropolone salt	Lemon yellow	155	63.21	63.11	6.50	6.57	8.88	9.20

*Uncorrected values. Melting points of all the samples were taken in sealed capillary tubes.

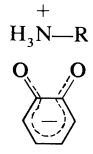

R = Alkyl, cycloalkyl

1

The n.m.r. spectra of these salts in D_2O and D_2O–NaOD are identical in the aromatic region. They show a multiplet in the τ = 2.7–3.2 p.p.m. region that is due to the ring proton resonances of tropolone and the proton resonances due to the amine molecule. Only cyclohexylamine tropolone salt is sufficiently soluble in $CDCl_3$ to enable the proton resonance of the protonated primary amino group to be observed. Integration of the tropolone ring protons and protons due to the amine molecule shows the composition of tropolone and amine in the salts (see Table 2).

The i.r. spectra of these salts show a broad band with discernable peaks in the 3000 cm^{-1} region which is characteristic of primary amine salts (1).

The u.v. spectra of these salts in water resemble that of tropolone in aqueous base. They show three bands at 235, 330, and 390 nm. The average extinction coefficients for these three bands for the eight amine tropolone salts are 26 000, 11 000, and 7400, respectively.

The original amine could be recovered from its tropolone salt by dissolving the salt in an aqueous base and extracting the freed amine with ether. The aqueous layer after acidification and extraction with dichloromethane gave back tropolone. The yields were quantitative. Since nonaromatic primary amine tropolone salts can be prepared with quantitative yields, tropolone is suitable for the separation of nonaromatic primary amines from other amines. For example, when tropolone was added to a mixture of cyclohexylamine and aniline in benzene, the former was precipitated as its tropolone salt whereas aniline remained in benzene. Similarly, cyclohexylamine was separated from piperidine and triethylamine. Table 3 gives the lower concentration limits for precipitation of some nonaromatic primary amines to occur.

The reaction between tropolone and nonaromatic primary amines is an acid–base reaction. Since secondary and tertiary aliphatic amines are as basic as primary aliphatic amines (pK_a about 10), they are also expected to react with tropolone. That such an acid–base reaction indeed occurs between them and tropolone is shown by the color change (from colorless to yellow) in these amine solutions in carbon tetrachloride or benzene when tropolone is added to them. The

Can. J. Chem. Downloaded from www.nrcresearchpress.com by 210.87.254.105 on 09/05/12
For personal use only.

TABLE 2. Nuclear magnetic resonance data of some nonaromatic primary amine tropolone salts*

Compound	Chemical shifts (τ) p.p.m.	Amine:tropolone†
Benzylamine tropolone salt	2.6 (s, 5 aryl H);‡; 2.7–3.2 (m, 5 tropolone ring H); 5.9 (s, 2 benzyl H)	1:1
n-Butylamine tropolone salt	2.7–3.2 (m, 5 tropolone ring H); 8.6–9.1 (m, 9 *n*-butyl H)	1:1
t-Butylamine tropolone salt	2.8–3.3 (m, 5 tropolone ring H); 8.85 (s, 9 *t*-butyl H)	1:1
Cyclohexylamine tropolone salt	2.5–3.2 (m, 5 tropolone ring H); 8.4–9.0 (b, 11 cyclohexyl H) 2.7 (m, 5 tropolone ring H); 5.7 (s, 3 amino H)§; 8.3–8.8 (b, 11 cyclohexyl H)	1:1 1:1
1,6-Diaminohexane ditropolone salt	2.7–3.2 (m, 2 × 5 tropolone ring H); 7.1 (b, 4 methylene H); 8.6 (b, 8 methylene H)	1:2
1,2-Diaminopropane ditropolone salt	2.6–3.2 (m, 2 × 5 tropolone ring H); 7.0 (d, 2 methylene H); 8.2 (1 methine H); 8.8 (d, 3 methyl H)	1:2
Diethylenetriamine ditropolone salt	2.5–3.2 (m, 2 × 5 tropolone ring H); 7.1 (sextet, 8 methylene H)	1:2
Ethylenediamine ditropolone salt	2.7–3.2 (m, 2 × 5 tropolone ring H); 5.35 (s, 4 methylene H)	1:2

*Taken in D_2O unless otherwise stated.
†This ratio is calculated from the integral of the tropolone ring protons and protons of the amine molecule.
‡b = broad; d = doublet; m = multiplet; s = singlet.
§Taken in $CDCl_3$.

TABLE 3. Lower concentration limits for the precipitation of some nonaromatic primary amines using tropolone

Amine	Lower concentration limits for precipitation (μg)*	
	CCl_4	C_6H_6
Benzylamine†	500	950
n-Butylamine†	730	730
t-Butylamine	140	140
Cyclohexylamine†	800	400
1,6-Diaminohexane	7	7
1,2-Diaminopropane	40	200
Diethylenetriamine	40	40
Ethylenediamine	36	36

*Each test was carried out by adding about 3 mg of tropolone to 0.5 ml of the solvent containing a known concentration of the amine.
†Precipitation occurred after about 4 min of shaking. However, precipitation occurred rapidly at higher concentrations of the amine.

appearance of the yellow color indicates that the acidic proton of tropolone ($pK_a = 6.71$) (2) is abstracted by the amines since tropolone anion gives a yellow solution whereas tropolone gives a colorless solution. However, no solid product was formed. When the solvent was evaporated, yellow solid nonaromatic secondary amine tropolone salts were obtained. They were purified by vacuum sublimation (see Table 4). A dark red viscous liquid was obtained for triethylamine. Thus, nonaromatic secondary amine tropolone salts are soluble in carbon tetrachloride and benzene whereas nonaromatic primary amine tropolone salts are insoluble. Tertiary aliphatic amines probably give the corresponding noncrystalline tropolone salts. When tropolone was added to aromatic amines in carbon tetrachloride or benzene there was no precipitation or formation of a yellow color. This can be explained by the fact that aromatic amines are weak bases (pK_a less than 5) and they do not abstract the acidic proton of tropolone to a sufficient extent.

The reaction between tropolone and amines can be used to differentiate amines as follows: a small drop of the unknown amine is dissolved in 0.3 ml of carbon tetrachloride or benzene. A few milligrams of tropolone[1] are then added to the amine solution. If a yellow precipitate is formed immediately, a nonaromatic primary amine is indicated. If there is no precipitate but the original colorless amine solution turns yellow, a nonaromatic secondary or tertiary amine is indicated. If there is no visible change, an aromatic amine is indicated. This method can be extended to microgram quantities of amines.

[1]It is recommended to add tropolone in the solid form rather than as a solution in the solvent used because nonaromatic primary amine tropolone salts precipitate rapidly in the former method. In the latter method *n*-butylamine tropolone salt precipitates very slowly.

Can. J. Chem. Downloaded from www.nrcresearchpress.com by 210.87.254.105 on 09/05/12
For personal use only.

TABLE 4. Melting points and n.m.r. data of some nonaromatic secondary amine tropolone salts

Compound	Melting point*	Chemical shifts† (τ) p.p.m.	Amine:tropolone‡
Diethylamine tropolone salt	159–161	0.3 (s, 2 amino H)§; 2.8–3.6 (m, 5 tropolone ring H); 7.1 (q, 2 × 2 methylene H); 8.8 (t, 2 × 3 methyl H)	1:1
Piperidine tropolone salt	146–147	1.56 (s, 2 amino H); 2.7–3.2 (m, 5 tropolone ring H); 6.9 (m, 4 methylene H); 8.3 (m, 6 methylene H)	1:1
Pyrrolidine tropolone salt	129–131	1.8 (s, 2 amino H); 2.9–3.4 (m, 5 tropolone ring H); 6.83 (m, 4 methylene H); 8.1 (m, 4 methylene H)	1:1

*Uncorrected values. Melting points of all the samples were taken in sealed capillary tubes.
†Taken in CCl_4.
‡This ratio is calculated from the integral of the tropolone ring protons and protons of the amine molecule.
§s = singlet; m = multiplet; q = quartet; t = triplet.

TABLE 5. Results of the reactions between amines and tropolone*

Compound	Observation	Compound	Observation
1,2-Diaminoethane	Yellow precipitate	Triethylamine	Yellow solution
1,6-Diaminohexane	Yellow precipitate	Triethanolamine†	Yellow solution
1,2-Diaminopropane	Yellow precipitate	Tribenzylamine‡	No visible change
Benzylamine	Yellow precipitate	8-Hydroxyquinoline	No visible change
n-Butylamine	Yellow precipitate	2,6-Dimethylpyridine	No visible change
t-Butylamine	Yellow precipitate	2-Picoline	No visible change
Cyclohexylamine	Yellow precipitate	Pyridine	No visible change
Diethylenetriamine	Yellow precipitate	Aniline	No visible change
Isopropylamine	Yellow precipitate	Diphenylamine	No visible change
Dicyclohexylamine	Yellow solution	4-Bromoaniline	No visible change
Diethylamine	Yellow solution	4-Chloroaniline	No visible change
Morpholine	Yellow solution	*N*-Ethylaniline	No visible change
Piperidine	Yellow solution	*N*-Benzylaniline	No visible change
Pyrrolidine	Yellow solution	*N*,*N*-Dimethylaniline	No visible change

*The reactions were carried out in carbon tetrachloride and benzene. Each test was carried out by adding about 3 mg of tropolone to a small drop of the amine (or a few crystals if it was a solid) dissolved in about 0.3 ml of the solvent.
†Very viscous liquid, does not mix well with the solvent.
‡Probably does not abstract the acidic proton of tropolone to a sufficient extent because tribenzylamine is a weak base. Its pK_a value was reported to be less than 8.4 in ref. 3 and estimated to be about 7.2 from the data given in ref. 4.

However, when the quantities of nonaromatic primary amines used are less than those given in Table 3 precipitation may not occur. Instead the amine solutions turn pale yellow when tropolone is added and in this case no distinction can be made between the nonaromatic amines. Some of the amines that were tested are given in Table 5.

The author wishes to thank Professor R. Stewart for a gift of tropolone. A short term research project grant from the Universiti Sains Malaysia is gratefully acknowledged.

1. K. NAKANISHI. *In* Infrared absorption spectroscopy—practical. Nankodo, Tokyo, 1962.
2. W. VON E. DOERING and L. H. KNOX. J. Am. Chem. Soc. **73**, 828 (1951).
3. H. GOLDSCHMIDT and R. M. SALCHER. Z. Physik. Chem. **29**, 89 (1899).
4. H. K. HALL, JR. J. Phys. Chem. **60**, 63 (1956).

Can. J. Chem. Downloaded from www.nrcresearchpress.com by 210.87.254.105 on 09/05/12
For personal use only.

The Synthesis and Properties of 4-Acetoxy-2,3-dihydro-3-oxo-4*H*-naphth[1,2-*b*] [1,4]oxazine, an Analog of Known Carcinogenic Hydroxamic Acids

R. T. COUTTS AND M. WOHLLEBE

Faculty of Pharmacy and Pharmaceutical Sciences, University of Alberta, Edmonton, Alberta T6G 2H7

Received May 23, 1974

R. T. COUTTS and M. WOHLLEBE. Can. J. Chem. **52**, 3432 (1974).

A synthesis of 4-acetoxy-2,3-dihydro-3-oxo-4*H*-naphth[1,2-*b*][1,4]oxazine (**4***a*) from 2-nitroso-1-naphthol is described. This compound (**4***a*) is substituted by various nucleophiles at position 5, with loss of the *N*-acetoxy group; in contrast, it did not react at physiological p*H* with the biological nucleophile methionine. On heating, **4***a* rearranges to the 2- and 5-acetoxy isomers.

R. T. COUTTS et M. WOHLLEBE. Can. J. Chem. **52**, 3432 (1974).

On décrit une synthèse de l'acétoxy-4 dihydro-2,3 oxo-3 [4*H*]-naphth [1,2-*b*] oxazine-1,4 (**4***a*) à partir du nitroso-2 naphthol-1. Le composé (**4***a*) subit des réactions de substitution par divers nucléophiles en position 5 avec perte du groupe *N*-acétoxy; toutefois il ne réagit pas au p*H* physiologique avec la méthionine agissant comme nucléophile biologique. Par chauffage, **4***a* se réarrange dans ses isomères acétoxy-2 ou -5. [Traduit par le journal]

Can. J. Chem. Downloaded from www.nrcresearchpress.com by 210.87.254.40 on 09/05/12
For personal use only.

N-Acetoxy-2-acetylaminofluorene (**1**) is a known carcinogenic compound which reacts *in vitro* with tissue nucleophiles such as methionine, at physiological p*H*. Attack by methionine occurs at positions 1 and 3 yielding 2-acetylamino-1-methylthiofluorene (**2**) and the corresponding 3-methylthio isomer (1, 2). *N*-Hydroxy-

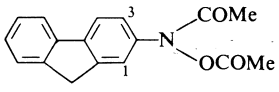

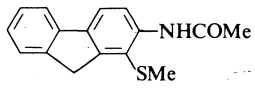

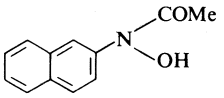

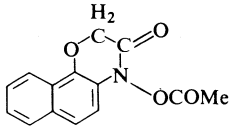

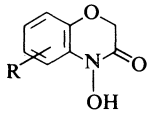

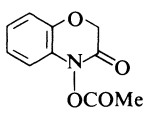

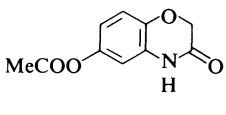

2-acetylaminonaphthalene (**3**) and compounds with related structures are also carcinogenic (3). So far, only acyclic hydroxamic acid derivatives such as **1** and **3** have been evaluated for their carcinogenic properties and their ability to react under mild conditions with tissue nucleophiles. We wished to determine whether cyclic hydroxamic acids possessed similar properties and selected 4-acetoxy-2,3-dihydro-3-oxo-4*H*-naphth[1,2-*b*][1,4]oxazine (**4***a*) as a suitable compound for investigation in view of its structural similarities to both compounds **1** and **3**, and its resemblence to 2*H*-1,4-benzoxazine hydroxamic acids (**5**) whose syntheses and properties have been previously investigated by us (4). Compound **4***a* possesses an *N*-acetoxy grouping and, since acetate is a good leaving group, **4***a* would be expected to be very reactive to nucleophilic reagents. As in compounds **1** and **3**, the position *para* to the N atom is blocked and, thus, nucleophilic attack might be expected at the *ortho* position.

The synthesis of **4***a* was achieved using 2-nitroso-1-naphthol (**6**) as starting material according to Scheme 1. Oxidation of **6** with hydrogen peroxide in acetic acid, according to a general procedure (5), gave 2-nitro-1-naphthol (**7**) which was converted to its potassium salt, then alkylated with ethyl bromoacetate to give ethyl (2-nitro-1-naphthoxy)acetate (**8**). The i.r. and p.m.r. spectra of this compound were consistent with its structure. Catalyzed sodium borohydride reduction (6) of **8** gave a product, $C_{12}H_9NO_3$, which was deduced to be the hydroxamic acid, 2,3-dihydro-4-hydroxy-3-oxo-

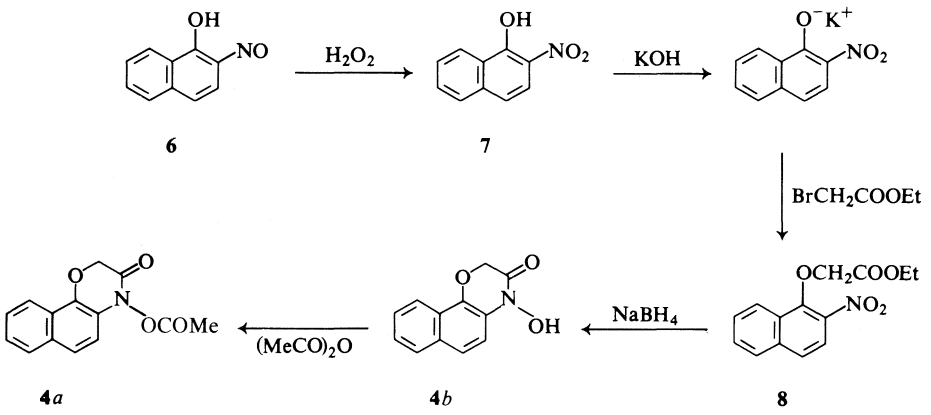

SCHEME 1

4*H*-naphth[1,2-*b*][1,4]oxazine (**4***b*) for the following reasons. It gave a purple color when treated with aqueous ferric chloride and was soluble in dilute sodium hydroxide solution, then reprecipitated on adding dilute hydrochloric acid. It also gave an i.r. spectrum (ν_{max} C=O 1645 and 1698 cm^{-1}) in support of structure **4***b* (7) as well as the expected p.m.r. spectrum which included a D-exchangeable OH signal at δ 10.90 (8, 9). Acetylation of **4***b* to **4***a* proved more difficult than envisaged but **4***a* was eventually obtained by acetylation of **4***b* with acetic anhydride in pyridine. This acetate was also characterized by its elemental analysis and its p.m.r. and i.r. spectra. One carbonyl stretching band was located at 1802 cm^{-1} which is characteristic of the *N*-acetoxy carbonyl group (7, 10).

Initial attempts to prepare **4***a* by reaction of **4***b* with acetyl chloride in benzene or with acetic anhydride in acetic acid were unsuccessful. The reaction product, obtained in 74% yield when **4***b* was treated with acetyl chloride was 5-chloro-2,3-dihydro-3-oxo-4*H*-naphth[1,2-*b*][1,4]oxazine (**4***c*). The same product was also obtained when a solution of **4***a* in benzene was saturated with anhydrous hydrogen chloride. When **4***b* was refluxed with acetic anhydride in acetic acid, 5-acetoxy-2,3-dihydro-3-oxo-4*H*-naphth[1,2-*b*][1,4]oxazine (**4***d*) was obtained in excellent yield. Refluxing a solution of **4***a* in acetic acid also gave **4***d*.

The formation of **4***c* when **4***b* was treated with acetyl chloride can be explained by the initial formation of **4***a* which then further reacted with the nucleophile, Cl^-, generated in the reaction medium. Similarly, when **4***b* was treated with acetic anhydride in acetic acid, the initially formed **4***a* reacted with acetate ions present in the reaction medium. Compound **4***a* was also found to react with dilute aqueous sulfuric acid to give 2,3-dihydro-5-hydroxy-3-oxo-4*H*-naphth-[1,2-*b*][1,4]oxazine (**4***e*), and with sulfuric acid in methanol to give 2,3-dihydro-5-methoxy-3-oxo-4*H*-naphth[1,2-*b*][1,4]oxazine (**4***f*).

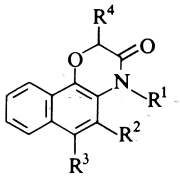

4

	R^1	R^2	R^3	R^4
a	OCOMe	H	H	H
b	OH	H	H	H
c	H	Cl	H	H
d	H	OCOMe	H	H
e	H	OH	H	H
f	H	OMe	H	H
g	H	H	OCOMe	H
h	H	H	H	OCOMe
k	H	SMe	H	H
m	H	H	H	H

The structural assignments for the products obtained by treating **4***a* with the nucleophiles just described were made mainly as a result of mechanistic considerations, and with supporting p.m.r. data. It is theoretically possible to obtain 5-, 8-, or 10-substituted lactams from **4***a* since three carbonium ion intermediates can be envisaged (Scheme 2) on the expulsion of the

Can. J. Chem. Downloaded from www.nrcresearchpress.com by 210.87.254.40 on 09/05/12
For personal use only.

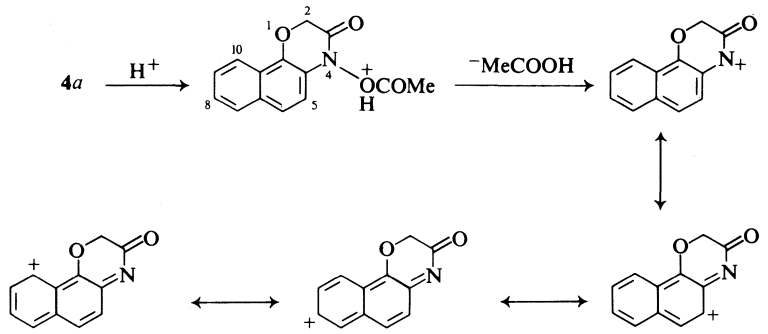

SCHEME 2

acetate group. The p.m.r. spectra of compounds **4***c–f* were quite distinctive. They all exhibited absorptions corresponding to —CH_2CO— and —N*H*—, as well as aromatic signals, each of which was comprised of an intense 1-proton singlet and a 4-proton complex multiplet. Since inter-ring coupling is negligible in naphthalene (11), an intense 1-proton singlet in the aromatic region signified that one of the naphthalene rings had a lone uncoupled proton and thus excluded the possibility that the nucleophiles had attacked the C-8 or C-10 positions.

In the case of the reaction of **4***a* with acetic acid, the possibility was considered that substitution could occur at the C-6 position (→ **4***g*) in light of our recent work (4) on the analogous benzoxazine, 4-acetoxy-3,4-dihydro-3-oxo-2*H*-1,4-benzoxazine (**9**), which, on refluxing in acetic acid gave the 6-acetoxy isomer (**10**). However, hydrolysis of the acetate **4***d* gave a phenolic lactam which was identical (i.r., p.m.r., m.p.) with the phenol **4***e* obtained from the reaction of **4***a* with dilute sulfuric acid.

When acetate **4***a* was refluxed in toluene, a mixture of isomeric acetates A and B was obtained. The isolated yields corresponded to a 3.4:1 ratio of A to B but the actual composition as determined by p.m.r. spectroscopy was 52:48. The structure **4***h* (Scheme 3) is assigned to A on the basis of its p.m.r. spectrum which showed unequivocally that the substituent nucleophile was located on the oxazine ring and not on the naphthalene portion of the molecule. Thus, **4***h* exhibited a 1-proton singlet at δ 6.84 corresponding to the H atom located at C-2, and a 6-proton multiplet at δ 7.28–8.12, indicative of there being six naphthalene protons in the molecule. In contrast, the p.m.r. spectrum of B exhibited a 2-proton singlet at δ 4.82 (O—CH_2—CO), a 1-proton singlet at δ 7.07 (C_6—*H*) and a 4-proton multiplet at δ 7.34–8.12 (remaining aromatic protons), which indicated identity with **4***d*. A mechanism explaining the formation of **4***d* from **4***a* is suggested (Scheme 4).

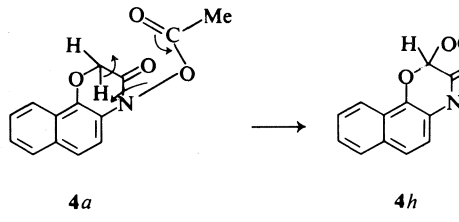

4*a* **4***h*

SCHEME 3

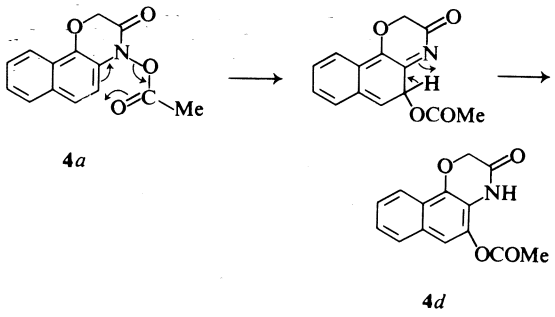

4*a* **4***d*

SCHEME 4

An examination of Dreiding models of **4***a* confirmed that the molecule can adopt conformations in which the ester carbonyl oxygen atom is in close proximity to C-2 or C-5. This thermal process, **4***a* → **4***d*, is analogous to the well-known Cope rearrangement. It is interesting that a cyclic carbinolamide analog of the antileukemic natural product, maytansine, shows nucleophilic addition reactions resembling those shown by **4***a* (12).

Can. J. Chem. Downloaded from www.nrcresearchpress.com by 210.87.254.40 on 09/05/12
For personal use only.

Can. J. Chem. Downloaded from www.nrcresearchpress.com by 210.87.254.40 on 09/05/12
For personal use only.

When a solution of **4***a* in ethanol–acetone was added to a solution of methionine in phosphate buffer (p*H* 7.8) at 40° under nitrogen, *i.e.*, conditions under which we have confirmed that **1** is converted to **2**, no methylthio compound (**4***k*) could be detected in the reaction mixture. Only a small amount of **4***m* was isolated and its structure confirmed by comparison with authentic material. Failure of **4***a* to react with methionine was thought to be due to the very low solubility of **4***a* in the solvent employed, so the reaction was repeated in 50% aqueous dimethylformamide. Again no **4***k* was obtained. In both instances, the reaction mixture turned dark purple, presumably indicative of undesired decomposition of **4***a*.

Experimental

Melting points (capillary tube) are uncorrected. Infrared spectra were recorded as Nujol mulls using a Beckman IR-10 spectrophotometer and p.m.r. spectra were obtained using a Varian A-60D spectrometer with DMSO-d_6 as solvent and TMS as the internal standard. Mass spectra were measured on an A.E.I. MS-12 mass spectrometer at an ionizing potential of 70 eV using the direct probe technique. Elemental analyses were performed by Mr. W. Dylke of our faculty.

2-Nitro-1-naphthol (7)

A stirred solution of 2-nitroso-1-naphthol (10 g), 30% hydrogen peroxide (150 ml), and concentrated nitric acid (10 ml, d 1.42) in glacial acetic acid (450 ml) was heated slowly (15 min) to 70° and for a further 15 min at this temperature. The mixture was poured onto ice (750 g) and the title compound (7.91 g), m.p. 126–128° separated (lit. (13) m.p. 128–129°). The product was used without purification in the synthesis of **8**.

Ethyl (2-Nitro-1-naphthoxy)acetate (8)

2-Nitro-1-naphthol (18.9 g) was added with vigorous stirring to a solution of potassium hydroxide (10 g) in absolute ethanol (100 ml). A thick red paste formed. Stirring was contined for a further 0.5 h, then the suspension was filtered and then washed with a mixture of ethanol and ether (1:1 v/v). The red potassium salt was suspended in acetone (75 ml) and dimethylformamide (75 ml) and ethyl bromoacetate (16.7 g) were added, and the resulting mixture was heated under reflux for 18 h. The mixture was filtered to remove potassium bromide and the filtrate flash-evaporated to a viscous brown oil. This was dissolved in chloroform (100 ml) and the chloroform solution was washed several times with water, then dried (K_2CO_3). Evaporation gave a yellow oil which solidified when triturated with cold ethanol. Recrystallization from ethanol gave the title compound (16.9 g) as yellow needles, m.p. 46–47°; i.r. ν_{max} 1750 cm^{-1} (C=O); p.m.r. δ 1.33 (t, 3H, J = 7 Hz, CH_3), 4.32 (q, 2H, J = 7 Hz, CH_2CH_3), 4.82 (s, 2H, —OCH_2CO), 7.58–8.67 (m, 6H, aromatic protons); mass spectrum *m/e* (% relative abundance) 275 (53) (M^+); 229 (44) (M − NO_2); 201 (100).

Anal. Calcd. for $C_{14}H_{13}NO_5$: C, 61.08; H, 4.76; N, 5.08. Found: C, 61. 31; H, 4.82, N, 5.24.

2,3-Dihydro-4-hydroxy-3-oxo-4H-naphth[1,2-b][1,4] oxazine (4b)

A solution of ethyl (2-nitro-1-naphthoxy)acetate (2.75 g) in dioxane (60 ml) was added dropwise over 15 min to a magnetically stirred suspension of 10% Pd–C (0.15 g) in water–dioxane (40:30, 50 ml) containing sodium borohydride (1.50 g). The mixture was stirred for a further 0.5 h and filtered through Celite. The solid remaining was washed with 10% Na_2CO_3 (20 ml) then water (50 ml) and these washings were added to the original filtrate. The combined solution was cooled in an ice bath and concentrated H_2SO_4 was added dropwise with stirring until the solution was acidic. The resulting white precipitate was collected, washed (H_2O) and dried *in vacuo* and yielded **4***b* (1.91 g), m.p. 199° after recrystallization (dioxane); i.r. ν_{max} 1645 and 1698 (C=O), 3100 (OH) cm^{-1}; p.m.r. δ 4.98 (s, 2H, CH_2), 7.40–8.12 (m, 6H, aromatic protons), 10.98 (s, 1H, D-exchangeable, N—OH); mass spectrum *m/e* (% relative abundance) 215 (33) (M^+); 199 (100).

Anal. Calcd. for $C_{12}H_9NO_3$: C, 66.97; H, 4.22; N, 6.50. Found: C, 67.08; H, 4.27; N, 6.29.

4-Acetoxy-2,3-dihydro-3-oxo-4H-naphth[1,2-b][1,4]-oxazine (4a)

A solution of the hydroxamic acid (**4***b*, 0.81 g) and acetic anhydride (2.5 ml) in pyridine (7.5 ml) was shaken at room temperature for 5 min then cooled in an ice bath. Cold water was added dropwise and the title compound (0.85 g) crystallized from solution. Recrystallization (pyridine–H_2O) gave cream-colored needles, m.p. 77–78°; i.r. ν_{max} 1700 (lactam C=O), 1802 (N—O—acetate C=O); p.m.r. δ 2.52 (s, 3H, CH_3); 5.18 (s, 2H, CH_2), 7.40–8.23 (m, 6H, aromatic protons); mass spectrum *m/e* (% relative abundance) 257 (39) (M^+); 215 (100) (M − CH_2=C=O)$^+$; 43 (79) [CH_3CO^+].

Anal. Calcd. for $C_{14}H_{11}NO_4$: C, 65.36; H, 4.31; N, 5.44. Found: C, 65.16; H, 4.42; N, 5.48.

5-Chloro-2,3-dihydro-3-oxo-4H-naphth[1,2-b][1,4]-oxazine (4c)

(*a*) A suspension of the hydroxamic acid (**4***b*, 0.47 g) in benzene (50 ml) containing acetyl chloride (5 ml) was refluxed under conditions which excluded the access of moisture. After 15 min a clear solution was obtained, then a colorless solid began to precipitate. After refluxing for an additional 45 min the mixture was cooled and filtered. The solid was washed with benzene and crystallized from chloroform–hexane to give the title compound (0.29 g), m.p. 270–272°; i.r. ν_{max} 1685 (C=O), 3165 (NH) cm^{-1}; p.m.r. δ 4.81 (s, 2H, CH_2), 7.32 (s, 1H, C_6-H), 7.49–8.16 (m, 4H, remaining aromatic protons), 10.90 (broad s, 1H, D-exchangeable, NH); mass spectrum *m/e* (% relative abundance) 233 (100), 235 (32) (M^+); 205 (19), 207 (9) (M − CO)$^+$; 192 (22), 194(7) [M − CH=C=O]$^+$.

Anal. Calcd. for $C_{12}H_{18}ClNO_2$: C, 61.68; H, 3.45; N, 6.00. Found: C, 61.86; H, 3.58; N, 5.98.

Can. J. Chem. Downloaded from www.nrcresearchpress.com by 210.87.254.40 on 09/05/12
For personal use only.

(*b*) A suspension of **4***a* (0.43 g) in benzene (25 ml) saturated with anhydrous HCl was stirred for 12 h. The resulting solid was crystallized from chloroform–hexane to give the title compound (0.36 g), m.p. 270–272°, whose i.r., p.m.r., and mass spectra were identical to those described immediately above.

*5-Acetoxy-2,3-dihydro-3-oxo-4H-naphth[1,2-b][1,4]-oxazine (**4***d*)

(*a*) A solution of the hydroxamic acid (**4***b*, 1.05 g) in glacial acetic acid (40 ml) and acetic anhydride (20 ml) was heated under reflux for 0.5 h, then poured into ice. The pale pink precipitate which formed was washed (H_2O), dried over KOH, and crystallized (ethyl acetate) to give the title compound as colorless needles (1.07 g), m.p. 235–236°; i.r. ν_{max} 1688 (lactam C=O), 1765 (ester C=O) and 3175 (NH) cm^{-1}; p.m.r. δ 2.44 (s, 3H, CH_3), 4.82 (s, 2H, CH_2), 7.07 (s, 1H, C_6-H), 7.34–8.12 (m, 4H, remaining aromatic protons), 10.90 (broad s, 1H, D-exchangeable, NH); mass spectrum *m/e* (% relative abundance) 257 (23) (M^+); 215 (100) ($M - CH_2{=}C{=}O)^+$; 43 (26) [CH_3CO^+].

Anal. Calcd. for $C_{14}H_{11}NO_4$: C, 65.36; H, 4.31; N, 5.44. Found: C, 65.26; H, 4.27; N, 5.44.

(*b*) When a solution of the acetate (**4***a*, 0.39 g) in glacial acetic acid (30 ml) was heated under reflux for 1 h, then poured into ice and treated further as described immediately above, the title compound (**4***d*, 0.34 g), m.p. 235–237° was obtained. Its i.r., p.m.r., and mass spectra were identical to those of the product obtained in reaction *a*.

*2,3-Dihydro-5-hydroxy-3-oxo-4H-naphth[1,2-b][1,4]-oxazine (**4***e*)

(*a*) The acetate (**4***a*, 0.80 g) was heated under reflux in 5% H_2SO_4 (150 ml) for 2 h. After standing overnight at room temperature, the reaction mixture was filtered and the solid which remained was washed (H_2O) and dried *in vacuo* to a pale brown solid (0.51 g), m.p. 272–282°. A solution of this product in 20% NaOH was declorized (charcoal) and the filtrate was acidified (HCl) to give the title compound (0.42 g), m.p. 293–294°; i.r. ν_{max} 1678 (C=O), 3160 (NH) cm^{-1}; p.m.r. δ 4.75 (s, 2H, CH_2), 6.83 (s, 1H, C_6—H), 7.30–8.32 (m, 4H, remaining aromatic protons), 10.14 (broad s, 1H, D-exchangeable, OH), 10.86 (broad s, 1H, D-exchangeable, NH); mass spectrum *m/e* (% relative abundance) 215 (100) (M^+); 187 (23) ($M - CO)^+$; 186 (11) ($M - HCO)^+$; 174 (14) ($M - CH{=}C{=}O)^+$.

Anal. Calcd. for $C_{12}H_9NO_3$: C, 66.97; H, 4.22; N, 6.50. Found: C, 67.04; H, 4.40; N, 6.64.

(*b*) Acetate **4***d* (0.48 g) was heated under reflux in 20% NaOH (10 ml) for 1 h. The reaction mixture was cooled and acidified (30% H_2SO_4) to give the title compound (**4***e*, 0.35 g), m.p. 292°, identical (i.r., p.m.r., mass spectrum) with the product obtained by procedure *a*.

(*c*) Acetate **4***d* (0.55 g) was heated under reflux in 5% H_2SO_4 (50 ml) for 2 h. The cooled solution was filtered to give **4***e* (0.44 g), m.p. 292°, identical (i.r. and p.m.r.) with the product obtained by procedure *a*.

*2,3-Dihydro-5-methoxy-3-oxo-4H-naphth[1,2-b][1,4]-oxazine (**4** f)*

A solution of the acetate (**4***a*, 0.82 g) in methanol (150 ml) and concentrated H_2SO_4 (1.0 ml) was heated under reflux for 4 h. The reaction mixture was concentrated until precipitation occurred. After cooling, the precipitate was collected, washed (H_2O), and dried *in vacuo* to give the title compound (0.63 g), m.p. 235–236° (from ethanol); i.r. ν_{max} 1692 (C=O), 3200 (NH) cm^{-1}; p.m.r. δ 3.98 (s, 3H, OCH_3), 4.76 (s, 2H, CH_2), 6.72 (s, 1H, C_6—H), 7.30–8.07 (m, 4H, remaining aromatic protons), 10.74 (broad s, 1H, D-exchangeable, NH); mass spectrum *m/e* (% relative abundance) 229 (100) (M^+); 214 (26) ($M - CH_3)^+$; 201 (7) ($M - CO)^+$.

Anal. Calcd. for $C_{13}H_{11}NO_3$: C, 68.11; H, 4.83; N, 6.11. Found: C, 67.93; H, 4.92; N, 5.80.

*2,3-Dihydro-3-oxo-4H-naphth[1,2-b][1,4]oxazine (**4***m*)

To a suspension of ethyl (2-nitro-1-naphthoxy)acetate (1.6 g) in concentrated HCl (15 ml) and ethanol (10 ml) was added $SnCl_2{\cdot}2H_2O$ (4.5 g) in ethanol (15 ml). The mixture was stirred for 10 h, during which time a clear yellow solution first formed, from which a colorless solid precipitated. The suspension was diluted with water (40 ml), filtered, and the precipitate was recrystallized (aqueous ethanol) to give the colorless title compound (0.76 g), m.p. 238–240°; i.r. ν_{max} 1722 (C=O), 3175 (NH) cm^{-1}; p.m.r. δ 4.86 (s, 2H, CH_2), 7.25–8.18 (m, 6H, aromatic protons), 11.02 (broad s, 1H, D-exchangeable, NH); mass spectrum *m/e* (% relative abundance) 199 (100) (M^+); 171 (28) ($M - CO)^+$; 170 (32) ($M - HCO)^+$, 158 (29) ($M - CH{=}C{=}O)^+$.

Anal. Calcd. for $C_{12}H_9NO_2$: C, 72.35; H, 4.55; N, 7.02. Found: C, 72.30; H, 4.49; N, 7.11.

*Thermal Rearrangements of 4-Acetoxy-2,3-dihydro-3-oxo-4H-naphth[1,2-b][1,4]oxazine (**4***a*)

A solution of **4***a* (0.76 g) in toluene (100 ml) was heated under reflux for 3 h, then filtered. The filtrate was flash-evaporated and gave a solid, m.p. 188–204°. Fractional crystallization from chloroform first gave 2-acetoxy-2,3-dihydro-3-oxo-4*H*-naphth[1,2-*b*][1,4]oxazine (**4***h*, 0.37 g), as a colorless solid, m.p. 222°; i.r. ν_{max} 1698 (lactam C=O), 1770 (ester C=O), 3175 (NH) cm^{-1}; p.m.r. δ 2.06 (s, 3H, $COCH_3$), 6.84 (s, 1H, OC*H*(OAc)CO), 7.28–8.12 (m, 6H, aromatic protons), 11.57 (broad s, 1H, D-exchangeable, NH); mass spectrum *m/e* (% relative abundance) 257 (42) (M^+); 215 (48) ($M - CH_2{=}C{=}O)^+$; 186 (100) (*m/e* 215 − HCO)$^+$.

Anal. Calcd. for $C_{14}H_{11}NO_4$: C, 65.36; H, 4.31; N, 5.44. Found: C, 65.54; H, 4.57; N, 5.48.

The chloroform filtrate was evaporated, and the residue was crystallized from ethyl acetate to yield 5-acetoxy-2,3-dihydro-3-oxo-4*H*-naphth[1,2-*b*][1,4]oxazine (**4***d*, 0.11 g), identical (i.r., p.m.r., m.p.) with the sample of **4***d* prepared as described earlier.

The authors wish to thank the Medical Research Council of Canada for financial assistance (Grant No. MT-2993), and Dr. A. M. Hogg and his associates, Chemistry Department, University of Alberta for the mass spectral data.

1. C. C. IRVING. *In* Metabolic conjugation and metabolic hydrolysis. Vol. 1. *Edited by* W. H. Fishman. Academic Press, New York. 1970. p. 53.
2. P. D. LOTLIKAR, J. D. SCRIBNER, J. A. MILLER, and E. C. MILLER. Life Sci. **5**, 1263 (1966).

3. E. Boyland and D. Manson. Biochem. J. **101**, 84 (1966).
4. R. T. Coutts and N. J. Pound. J. Chem. Soc. (C), 2696 (1971).
5. R. Kuhn and W. vanKlaveren. Chem. Ber. **71**, 779 (1938).
6. R. T. Coutts and E. M. Smith. Can. J. Chem. **45**, 975 (1967).
7. R. T. Coutts, K. W. Hindmarsh, S. J. Powell, J. L. Pound, and E. M. Smith. Can. J. Pharm. Sci. **3**, 49 (1968).
8. R. M. Acheson, C. J. Q. Brookes, D. P. Dearnaley, and B. Quest. J. Chem. Soc. (C), 504 (1968).
9. R. M. Acheson, R. G. Bolton, and I. Hunter. J. Chem. Soc. (C), 1067 (1970).
10. J. D. Loudon and I. Wellings. J. Chem. Soc. 3462 (1960).
11. J. D. Reinheimer and A. H. Kappelman. J. Org. Chem. **37**, 326 (1972).
12. A. I. Meyers and C. C. Shaw. Tetrahedron Lett. 717 (1974).
13. G. N. Burkhardt and H. Wood. J. Chem. Soc. 143 (1929).

Downloaded from www.interscience.com by 210.87.254.40 on 09/05/12
For personal use only.

The Mass Spectrometry of the Pyrolysis Products of Some Tetraalkylammonium and Bistetraalkylammonium Bromides

RONALD E. VERRALL[1] AND JOHN A. BURNS

Department of Chemistry and Chemical Engineering, University of Saskatchewan, Saskatoon, Saskatchewan S7N 0W0

Received May 15, 1974

RONALD E. VERRALL and JOHN A. BURNS. Can. J. Chem. **52**, 3438 (1974).

The mass spectra of three tetraalkylammonium bromide salts and two series of bistetraalkylammonium bromide salts, one saturated and the other unsaturated, have been studied. Substitution is the major process which occurs in the pyrolytic decomposition of these quaternary ammonium bromides when placed in the probe of the mass spectrometer. This leads to the production of a tertiary amine and an alkyl halide. The substitution reactions which occur are influenced by the proximity of the bromide anion(s) to the positively charged quaternary nitrogen centers in the crystal lattice. As well, a shorter distance between the positive nitrogen centers favors substitution reaction by means of an electron inductive effect.

RONALD E. VERRALL et JOHN A. BURNS. Can. J. Chem. **52**, 3438 (1974).

On a étudié les spectres de masse de trois bromures de tétraalkylammonium et deux séries de bromures de bistétraalkylammonium, une série est saturée l'autre insaturée. La substitution est la réaction principale qui se produit lors de la décomposition pyrolytique de ces bromures d'ammonium quaternaires lorsqu'ils sont placés dans la sonde d'un spectromètre de masse. Cette réaction conduit à la production d'une amine tertiaire et d'un halogénure d'alkyle. Les réactions de substitution qui se produisent sont influencées par la présence, dans le réseau cristallin, d'anions bromures à proximité des centres azotés quaternaires chargés positivement. Un facteur supplémentaire favorisant des réactions de substitution est la distance plus courte entre les centres azotés positifs qui résulte d'un effet électronique inductif. [Traduit par le journal]

Introduction

A search through the literature reveals that little attempt has been made at a detailed mass spectral study of the pyrolysis reactions of quaternary ammonium salts, either rigid or non-rigid systems, except for several recent publications (1–3). Quaternary ammonium salts yield complex spectra since, because of their general lack of volatility, they are subject to decomposition at high temperatures (4). However, these ionic salts normally do decompose according to set patterns (1, 2) depending on the steric and electronic effects of substituents located on the quaternary nitrogen center.

The usual thermal reaction (1) that occurs when tetraalkylammonium halides decompose is substitution which gives rise to an alkyl halide and a tertiary amine (eq. 1).

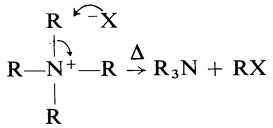

[1] $$R_4N^+X^- \xrightarrow{\Delta} R_3N + RX$$

Another typical pyrolytic process (1) of these salts is a type of Hofmann elimination as shown in eq. 2.

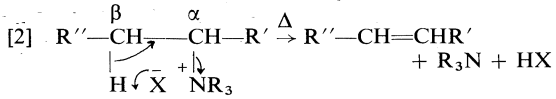

[2] $$R''\text{—}\overset{\beta}{C}H_2\text{—}\overset{\alpha}{C}H\text{—}R' \xrightarrow{\Delta} R''\text{—}CH{=}CHR' + R_3N + HX$$

In this work, the compounds investigated were comprised of 3 symmetrical tetraalkylammonium bromides, series 1, and 11 bistetraalkylammonium bromides, series 2 and 3, which are sometimes referred to as bolaform electrolytes. The compounds in series 1 are simple quaternary ammonium bromides from which the effect of alkyl group size on the rates of competing pyrolysis reactions can be deduced.

$$R_4NBr \begin{cases} \mathbf{1}\ R = CH_3 \\ \mathbf{2}\ R = CH_3CH_2 \\ \mathbf{3}\ R = CH_3CH_2CH_2CH_2 \end{cases}$$

Series 1

Series 2 provides a means of analyzing the effect of the proximity of an electron withdrawing substituent on the quaternary nitrogen during the pyrolysis reaction.

[1]To whom correspondence should be addressed.

Can. J. Chem. Downloaded from www.nrcresearchpress.com by 210.87.254.42 on 09/05/12
For personal use only.

TABLE 1. Major ions from the mass spectra of some tetraalkylammonium bromides at 70 eV. Intensity* of ions corresponding to the following designations

Compound	$R_3\overset{+\cdot}{N}$	$R'CH{=}\overset{+}{N}R_2$	$CH_2{=}\overset{+}{N}R_2$	$R\overset{+\cdot}{Br}$	$H\overset{+\cdot}{Br}(Br)$
1	8.4	20.9†	20.9†	16.2	1.6(2.0)
2	4.5	1.9	22.2	17.0	0.4(0.6)
3	1.6	0.3	21.9	1.4	0.2(0.2)

*Based on percentage of the sum of intensities of all the ions greater than $m/e = 25$, *i.e.*, $\% \Sigma_{25}$.
†Corresponds to same ion.

$[(C_2H_5)_3N(CH_2)_nN(C_2H_5)_3]Br_2$

4 $n = 2$
5 $n = 3$
6 $n = 4$
7 $n = 5$
8 $n = 6$
9 $n = 8$
10 $n = 10$

Series 2

In this series there are two types of α-carbons, those on the terminal head group, *i.e.*, in the ethyl group, and those in the bridging carbon chain. Cleavage of the α-carbon–β-carbon bond will be drastically different in the bridging carbon chain compared to the terminal ethyl groups when n is small. In series 3, the effect of unsaturated functional groups on the thermal degradation process of the bisquaternary ammonium bromides can be determined. The resultant pyrolysis products of quaternary ammonium halides ultimately are determined by the proximity of the halide ion to the positive nitrogen center.

$[(CH_2{=}CH{-}CH_2)_3N(CH_2)_nN(CH_2{-}CH{=}CH_2)_3]Br_2$ **11** $n = 2$, **12** $n = 3$

$[(CH_2{=}CH{-}CH_2)_2CH_3N(CH_2)_2NCH_3(CH_2{-}CH{=}CH_2)_2]Br_2$ **13**

$[(CH_2{=}CH{-}CH_2)_3NCH_2{-}CH{=}CH{-}CH_2N(CH_2{-}CH{=}CH_2)_3]Br_2$ **14**

Series 3

These three series should provide an insight into processes occurring during thermal degradation. In series 1, the steric effect of bulky substituents can be analyzed and in series 2 the effect of producing a more electron deficient nitrogen center can be assessed.

Results

Figure 1 shows the mass spectrum of compound **2** and is typical of the pyrolysis products at 70 eV obtained from the simple tetraalkylammonium bromides in series 1. A number of peaks were observed and these resulted from the predicted degradation processes. Since bromine gives two peaks of almost equal intensity, the intensity of the peak for an ion containing bromines is the sum of the two peaks observed.

It can be seen from Fig. 1 that the principal ions resulting from pyrolysis of tetraethylammonium bromide correspond to ethylene (m/e 28), to $C_2H_5\overset{+}{N}(H){=}CH_2$ (m/e 58), to $(C_2H_5)_2\overset{+}{N}{=}CH_2$ (m/e 86), to triethylamine (m/e 101), to the M − 1 fragment from triethylamine (m/e 100), and to ethylbromide (m/e 108, 110). Corresponding ions are observed for the other members of series 1. The major ions common to series 1 are listed in Table 1. From these data it is observed that there is a decrease in the relative percentage of the total ion current for the ions corresponding to $R_3\overset{+\cdot}{N}$ and $R\overset{+\cdot}{Br}$ as the size of the R group increases.

Figure 2 is the mass spectrum of compound **6** and is representative of the mass spectra of the pyrolysis products from the series 2 salts at 70 eV bombardment energy. Above m/e = 110 the ob-

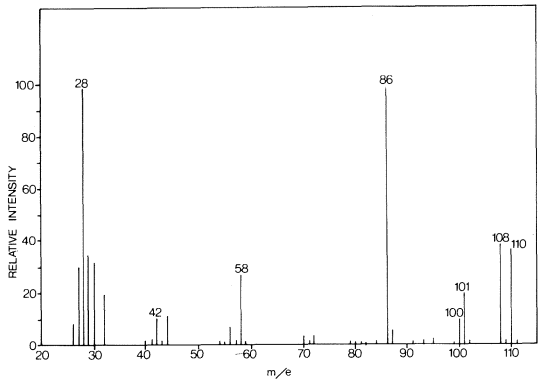

FIG. 1. Bar diagram of the mass spectrum of the pyrolysis products of compound **2**.

Can. J. Chem. Downloaded from www.nrcresearchpress.com by 210.87.254.42 on 09/05/12
For personal use only.

Can. J. Chem. Downloaded from www.nrcresearchpress.com by 210.87.254.42 on 09/05/12
For personal use only.

TABLE 2. Major ions from the mass spectra of some bistetraalkylammonium bromides at 70 eV. Intensity* of ions corresponding to the following designations

Compound	$Et_3\overset{+\cdot}{N}$	$CH_3CH{=}\overset{+}{N}Et_2$	$Et_2\overset{+}{N}{=}CH_2$	$\overset{+\cdot}{EtBr}$	$\overset{+\cdot}{HBr}(\overset{+}{Br})$	$Et_2\overset{+\cdot}{N}(CH_2)_nNEt_2$	$Et_2\overset{+\cdot}{N}(CH_2)_nBr$	$Et_2\overset{+}{N}(CH_2)_n$
4	2.6	4.3†	26.1	8.4	2.6(1.4)	—	0.8	4.3†
5	2.4	2.7	28.2	19.8	2.6(1.8)	—	0.8	1.4
6	2.4	1.1	16.2	13.4	1.0(1.4)	—	0.06	0.2
7	0.8	0.5	21.1	14.6	0.8(1.0)	0.2	—	0.6
8	1.3	0.5	21.0	25.2	0.8(1.0)	1.3	—	0.6
9	1.4	0.7	17.3	16.6	0.8(0.8)	1.9	—	0.2
10	1.2	0.7	16.4	13.8	0.6(1.0)	1.8	—	0.2

*Based on percentage of the sum of intensities of all ions greater than $m/e = 25$, *i.e.*, % Σ_{25}.
†Corresponds to same ion.

TABLE 3. Major ions from mass spectra of some unsaturated bistetraalkylammonium bromides at 70 eV. Intensity* of ions corresponding to the following designations

Compounds	$Allyl_3\overset{+\cdot}{N}$	$Allyl_2\overset{+}{N}=CH_2$	$CH_2=CH-CH=\overset{+}{N}Allyl_2$	$Allyl_2\overset{+}{N}(CH_2)_n$	$Allyl\overset{+\cdot}{Br}$	$H\overset{+\cdot}{Br}(\overset{+}{Br})$
11	—	13.0	0.3	0.7	13.0	0.8(1.6)
13	2.0†	11.0(4.7)†	(4.7)†	0.2(0.7)†	10.8(1.6)†	0.6(1.4)
12	1.2	13.4	0.8	0.7	7.6	0.6(0.6)
14	2.7	12.8	1.8	2.3	6.2	1.6(1.6)

*Based on percentage of the sum of intensities of ions greater than $m/e = 25$, *i.e.*, % Σ_{25}.
†Replace one allyl group by CH_3 for MDAAE.

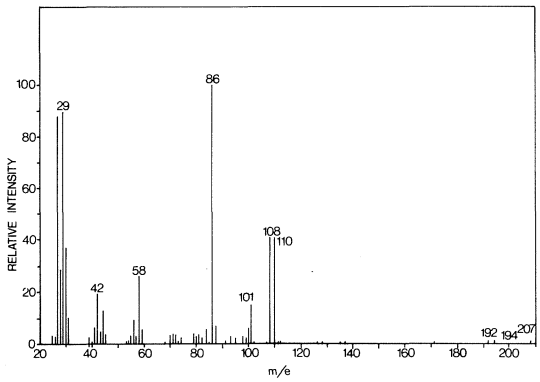

FIG. 2. Bar diagram of the mass spectrum of pyrolysis products of compound **6**.

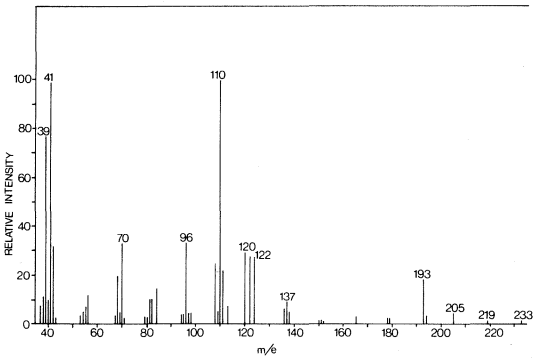

FIG. 3. Bar diagram of the mass spectrum of the pyrolysis products of compound **12**.

served ions have low intensities (some less than 1% of the total ion current); however, they are important when considering the degradation processes of these salts. In Fig. 2 weak ion intensities were observed for compound **6** corresponding to $(C_2H_5)_2\overset{+\cdot}{N}(CH_2)_4Br$ (*m/e* 207, 209), to

$$CH_2=\overset{+}{N}(C_2H_5)-(CH_2)_4Br$$

(*m/e* 192, 194), and to $(C_2H_5)_2\overset{+}{N}(CH_2)_4$ (*m/e* 128). Stronger intensity ions were observed corresponding to the ions discussed earlier for compound **2**. In other homologs of series 2 similar ions above *m/e* 110 were observed and for some, an ion corresponding to the bistertiary amine was present. Table 2 contains the ions of interest common to most of the mass spectra of the seven compounds in series 2.

A representative mass spectrum of the pyrolysis products of the bistetraalkylammonium bromides (compound **12**) which contain unsaturated alkyl groups, *i.e.*, series 3, is shown in Fig. 3. A comparison of Figs. 2 and 3 shows that there are more intense ions at higher mass values in the case of the unsaturated group, thus indicating less fragmentation for the series 3 compounds. Table 3 lists the important ions common to the partially unsaturated bisquaternary ammonium bromides at 70 eV electron bombardment energy. It is significant to note that none of the series 3 compounds shows the presence of the appropriate bistertiary amine as a parent product as was observed for series 2. This result indicates that there are notable differences in the pyrolysis processes of the saturated and unsaturated analogs of the bisquaternary ammonium bromides.

The tables list only the major ions which are useful for comparisons between the individual compounds and between the various series of compounds. A detailed set of data for the mass spectra of the 14 compounds studied can be obtained elsewhere (5). These compounds were also studied in the mass spectrometer at low electron bombardment energy (10–12 eV) and the most notable observation was the intensity of the ions corresponding to the bistertiary amine for series 2. The observed intensities were 2.8, 2.3, 2.3, 6.2, 20.9, 24.9, and 43.8 for compounds **4** to **10**, respectively.

Can. J. Chem. Downloaded from www.nrcresearchpress.com by 210.87.254.42 on 09/05/12
For personal use only.

Can. J. Chem. Downloaded from www.nrcresearchpress.com by 210.87.254.42 on 09/05/12
For personal use only.

In each individual case, there were other ions of significant intensity that were not singled out since they did not appear to contribute to the ensuing discussions. In most cases, the usual fragmentation patterns of tertiary amines (6) or halogenated hydrocarbons (7) explained the observed ions which have not been discussed.

Discussion

Generally, the patterns for the decomposition, ionization, and subsequent fragmentation are similar for the three series of pure crystalline compounds investigated except for some minor deviations. The relative yields of the competing pyrolysis reactions are to a large degree determined by the nature of the anion and the proximity of the anion with respect to the cationic nitrogen center. Compared to the smaller, more electronegative halide ions, bromide salts favor substitution as opposed to Hofmann degradation (8). The results of the work presented corroborate that the substitution process is preferred for bromide salts since only a low intensity of ions was found at 80 and 82 for HBr which would result from the Hofmann degradation process. In most of the compounds studied, the intensity of the HBr ions was less than 1% of the total ion current. One of the other products of Hofmann degradation as indicated in eq. 2, the olefin, cannot be used as a basis of comparison for preference of the process indicated in eq. 1 over that in eq. 2 since ethene is produced in subsequent rearrangements and fragmentation processes, for example, those shown in eqs. 3 and 4, respectively. In eq. 4, the $[R_2N(CH_2)_mCH_2CH_2]^+$ ion is a fragmentation product of one of the parent ions, the bistertiary amine for series 2 and 3. The process described in eq. 4 would not be found in series 1 since it is unlikely that the precursor ion would be favored for compounds **2** and **3** and could not be obtained for compound **1**.

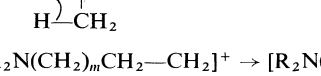

[3]

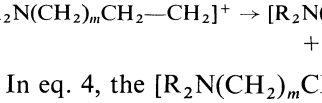

[4]

In contrast to the small amount of HBr observed for the quaternary ammonium compounds studied, the intensity of the ions corresponding to $R\dot{\overset{+}{N}}HBr$, where R is the alkyl group attached to the nitrogen in the parent salt, is much greater. The alkyl halide can only be derived by halide ion attack as shown by the degradation process in eq. 1. For series 2 and series 3 there are two possibilities for the attack of the halide ion during the thermal degradation process. There is the possibility of the halide ion attacking any one of the three similar alkyl groups attached to the nitrogen, *i.e.*,

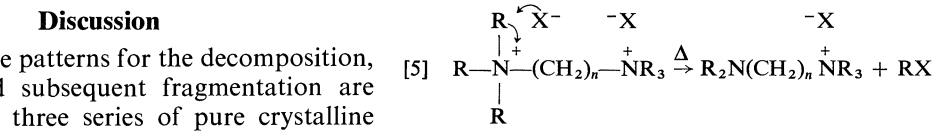

[5]

On the other hand, the halide ion could conceivably attack the bridging alkyl chain as shown in eq. 6.

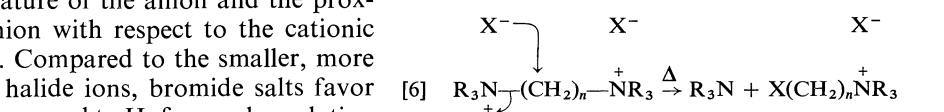

[6]

Furthermore, the substitution reaction is favored for the bistetraalkylammonium salts since the bromide anion preferably would be situated close to the nitrogen centers in order to aid in neutralizing the two positive charges on the same molecule. This will be more apparent when the nitrogen centers are close to one another.

The mass spectra of all the salts analyzed showed an ion equivalent to $CH_2{=}\overset{+}{N}R_2$, where R is the appropriate alkyl group for each salt. In most cases, this α-cleavage product was the base peak.

A comparison of the ions corresponding to $R_3\dot{\overset{+}{N}}$ and $R\dot{\overset{+}{B}}r$ for series 1 given in Table 1 shows that the substitution reaction occurs to a larger extent if the alkyl groups are small. This can be explained by the condition that it is possible for the bromide ion to be situated closer to the positive quaternary center when the alkyl groups are less bulky. The subsequent fragmentation of the $R_3\dot{\overset{+}{N}}$ and $R\dot{\overset{+}{B}}r$ ions for all three compounds must occur at a similar rate for this interpretation to be valid. However, it can be assumed that for compound **3** these ions will be fragmented more easily.

In theory, the bistetraalkylammonium salts should undergo thermal decomposition reactions similar to R_4NBr salts. However, in the series 2 and 3 compounds because of the requirement that the anions partially neutralize the two positive charges, the halide ions would necessarily be in close proximity to the nitrogen

Can. J. Chem. Downloaded from www.nrcresearchpress.com by 210.87.254.42 on 09/05/12
For personal use only.

centers. It is conceivable that the steric effects and location of the halide ion, for series 2, could systematically determine the ultimate degradation products. Since each bisquaternary bromide molecule must undergo two pyrolysis reactions, there is an added complication to its thermal degradation. Probably these reactions occur separately with the remaining quaternary center influencing the initial decomposition reaction, for example,

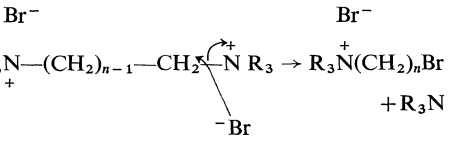

[7] $R_3\overset{+}{N}-(CH_2)_{n-1}-CH_2-\overset{+}{N}R_3 \rightarrow R_3\overset{+}{N}(CH_2)_nBr + R_3N$ (Br^- and ^-Br)

In eq. 7, the inductive effect of the quaternary nitrogen center on the left hand side of the molecule causes the methylene group adjacent to the righthand nitrogen to be somewhat electron deficient. When there are few bridging methylene groups, the conditions are suitable for bromide attack at these electropositive carbon centers. The salt on the right-hand side of eq. 7 then undergoes further decomposition.

For the series 2 salts the presence of fewer methylene groups between the nitrogen centers gives rise to a maximum inductive effect to yield the reaction outlined in eq. 7. As well, under these conditions, the bromide anions will be held closer to the nitrogen centers. Therefore, when n is small, *i.e.*, compounds **4** and **5**, there would be proportionately more bromide attack on bridging carbon (eq. 7) than for the larger homologs. The results in Table 2 confirm this as shown by the ions at $m/e = 179$ and 181 for compound **4**, 193 and 195 for compound **5**, and to a smaller extent 207 and 209 for compound **6**. Furthermore, at low electron bombardment energy, the parent ions obtained from the thermal decomposition show that the substitution reaction is favored.

The occurrence of bromide attack on the bridging carbon (eq. 7) was not observed for series 3 where it appears that the allyl substituents on the nitrogens are able to delocalize the positive charge. Hence, the essential conditions favoring bromide attack on the bridging carbon are removed.

From Table 2, it is possible to deduce some further general observations with regard to the thermal degradation of the compounds in series 2. First, the greater the number of methylenes between the nitrogen centers, the larger the amount of bistertiary amine observed. This can be explained by the process in eq. 7. For the larger members of series 2 loss of alkyl bromide is statistically preferred since the bridging carbon is not as electropositive as for the smaller members. Secondly, since there is relatively less triethylamine generated as one proceeds from compound **4** through to **10**, there is a definite indication that the bridging carbon–nitrogen bonds are weaker for the homologs with fewer bridging carbons.

It is concluded that the pyrolysis process of the tetraalkylammonium and bistetraalkylammonium bromides are primarily substitution reactions. In the pure crystalline state, the substitution reaction occurring during thermal degradation of quaternary ammonium halides is favored by (*a*) an electron withdrawing substituent on the nitrogen and (*b*) the location of the anion close to the attack site.

Experimental

The preparation and purification of the tetraalkylammonium and bistetraalkylammonium salts have been described elsewhere (4, 5). C, H, and N, analyses as well as gravimetric bromide indicated a purity of greater than 99.7%.

The mass spectra were determined at 10–12 eV and 70 eV using an MS-12 mass spectrometer. The samples were introduced using the direct probe technique and the ion source temperature was 210–230 °C. Contamination from substances previously analyzed in the spectrometer was reduced by baking the source and the probe vigorously before each analysis. The instrument was subsequently "flushed out" with a sample of the appropriate compound until several consecutive spectra obtained were identical.

The authors acknowledge financial support for this work from the National Research Council of Canada. J. A. B. gratefully acknowledges the award of an NRCC Scholarship. The authors thank Dr. P. J. Smith for his helpful discussions.

1. M. Hesse, W. Vetter, and H. Schmid. Helv. Chem. Acta, **48**, 674 (1965).
2. M. Hesse and H. Schmid. Liebigs Ann. Chem. **696**, 85 (1966).
3. P. J. Smith. Can. J. Chem. **52**, 365 (1974).
4. J. A. Burns and R. E. Verrall. Thermochim. Acta. **9**, 277 (1974).
5. J. A. Burns, Ph.D. Thesis, University of Saskatchewan, Saskatoon, Saskatchewan, 1973.
6. J. Collin. Bull. Soc. Roy. Sci. Liège, **21**, 446 (1952).
7. F. W. McLafferty. Anal. Chem. (*a*) **34**, 2 (1962); (*b*) **34**, 16 (1962).
8. H. Budzikiewicz, C. Djerassi, and D. H. Williams. Mass spectrometry of organic compounds. Holden-Day, San Francisco. 1967. Chapt. 3.

Canadian Journal of Chemistry

Published by
THE NATIONAL RESEARCH COUNCIL OF CANADA

Journal canadien de chimie

Publié par
LE CONSEIL NATIONAL DE RECHERCHES DU CANADA

Volume 52 Number 20 October 15, 1974 Volume 52 numéro 20 15 octobre 1974

Electronic Raman Spectroscopy and Magnetic Susceptibilities[1]

J. A. KONINGSTEIN AND C. J. KANE-MAGUIRE

Department of Chemistry, Carleton University, Ottawa, Canada K1S 5B6

Received April 30, 1974

J. A. KONINGSTEIN and C. J. KANE-MAGUIRE. Can. J. Chem. **52**, 3445 (1974).

Data from electronic Raman spectroscopy are employed to calculate temperature dependent magnetic susceptibilities for terbium aluminum garnet, terbium gallium garnet, europium gallium garnet, thulium aluminum garnet, and thulium gallium garnet. An electronic Raman spectrum of terbium gallium garnet is reported, as are newly observed electronic levels in thulium gallium garnet.

J. A. KONINGSTEIN et C. J. KANE-MAGUIRE. Can. J. Chem. **52**, 3445 (1974).

On utilise des données de spectroscopie Raman électronique pour calculer les susceptibilités magnétiques dépendantes de la température du grenat de terbium et d'aluminium, du grenat de terbium et de gallium, du grenat d'europium et de gallium, du grenat de thulium et d'aluminium et du grenat de thulium et de gallium. On rapporte aussi un spectre Raman électronique du grenat de terbium et de gallium ainsi que de nouveaux niveaux électroniques observés dans le grenat de thulium et de gallium. [Traduit par le journal]

Introduction

It is well known that the widths of electronic levels in the split *LSJ* manifolds of rare earth ions increase as the energies of the states increase. Thus although it is possible to determine from electronic Raman experiments the positions of low-lying crystal field states of the ground manifold and the states of lowest energy in other manifolds, it becomes difficult to observe Raman transitions which terminate on states with higher energy. The increasing width of the levels causes the transitions to be so broad that they escape detection. This proves troublesome if the data from electronic Raman spectroscopy (e.R.s.) are to be used in a crystal field analysis of certain of the *LSJ* manifold levels.

On the other hand, the electronic states situated up to several hundred reciprocal centimeters above the ground state contribute significantly to the value of the magnetic susceptibility of rare earth compounds, depending, of course, on the composition of the wave function and the number of ions in such states at a given temperature. Present experimental information suggests that the positions of these electronic states are more easily detected by e.R.s. than by far infrared or fluorescence spectroscopy. The technique of e.R.s. may fall short if employed in crystal field calculations, but at the same time one may be able to use it to calculate values of the magnetic susceptibility at various temperatures. Such calculations were recently reported for some crystals containing transition metal ions (1). In this communication we report on the results of e.R.s. and their relevance to the crystal

[1]Research supported by Grant A 2843 of the National Research Council of Canada.

Can. J. Chem. Downloaded from www.nrcresearchpress.com by 210.87.254.6 on 09/05/12
For personal use only.

field analysis and computations of magnetic susceptibilities of some rare earth garnets ($REAl_5O_{12}$ or $REGa_5O_{12}$).

Magnetic Susceptibilities of Terbium Aluminum Garnet, Terbium Gallium Garnet, and Europium Gallium Garnet

Trivalent rare earth ions experience a crystal field of orthorhombic symmetry in garnet crystals (2). Each crystal field component in the split LSJ manifolds of these ions belongs to one of the four representations of the group D_2. Electronic Raman transitions between such levels have been observed (3–13) in rare earth garnet crystals, and the intensity of each transition is related to the value of an element of a scattering matrix. From the form of this matrix the scattering tensor for transitions of the individual rare earth ions at their crystallographic sites can be determined. This, in turn, gives information about the symmetries of the electronic excited states, assuming that the symmetry of the ground state is known. Such symmetries depend on the magnitude and symmetry of the crystal field. Both properties are contained in the following expression for the crystal field potential V_{CF}.

$$[1] \qquad V_{CF} = \sum_n \sum_{m=n}^{-n} B_n^m r_i^n Y_n^m(\theta_i,\phi_i)$$

where the B_n^m are crystal field parameters, r_i^n is the expectation value of the radius of the ith f-electron, and the $Y_n^m(\theta_i,\phi_i)$ are spherical harmonics.

The crystal field potentials for terbium aluminum garnet (TbAlG) and europium galliam garnet (EuGaG) are well known (9, 13, 14), and were obtained from spectroscopic data which included the results of electronic Raman spectroscopy and in particular the polarization properties of the transitions. Not only was a good fit obtained between the computed and observed energy level diagrams for the split ^7F_J ($J = 6, 5, 4, \ldots, 0$) manifolds of Eu^{3+} and Tb^{3+}, but the wave functions for the crystal field levels became available.

The molar magnetic susceptibility χ_m for a rare earth ion with an even number of electrons depends on the electronic wave functions according to the following formula which was derived by Van Vleck:

$$[2] \quad \chi_m = \frac{N_0}{3}\left[\sum_J \exp(-E_j/kT)\right]^{-1} \times \sum_J \sum_\sigma \exp(-E_j/kT) \times \left[\frac{\langle J|\mu_\sigma|J\rangle^2}{kT} + \sum_{J\neq J'} \frac{2|\langle J|\mu_\sigma|J'\rangle|^2}{E_{J'} - E_J}\right].$$

The symbol J stands for the actual composition of the wave function (for the state at energy E_J) in terms of the $|J,J_z\rangle$ basis functions; N_0 is Avogadro's number. Equation 2 has been successfully applied (15) to relate χ_{TbAlG} with experimental results in the temperature interval 5 to 20 K.

In Fig. 1 a comparison of the results for the temperature range 0.5 to 20 K is shown. It is worthwhile to point out here that the first electronic excited state of Tb^{3+} in TbAlG has an energy of 2 cm^{-1} above the ground state and that both levels are crystal field components of the split $^7F_6$ manifold. Given such a small energy gap and provided that the wave functions of the states are of a specific composition, situations may arise (see Figs. 3 and 4) where the temperature dependent molar susceptibility is that as measured for terbium aluminum garnet (16). However in employing eq. 2 and

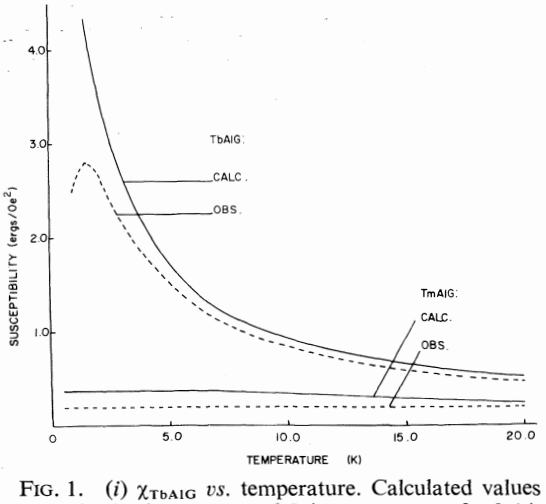

FIG. 1. (*i*) χ_{TbAlG} *vs.* temperature. Calculated values were derived using the crystal field parameters of ref. 14. (*ii*) χ_{TmAlG} *vs.* temperature. The following set of crystal field parameters (in cm^{-1}) were employed in the calculations: $A_2^0 = -200$, $A_4^0 = -300$, $A_6^0 = 40$, $A_2^2 = 275$, $A_4^2 = 223$, $A_6^2 = -150$, $A_4^4 = 1350$, $A_6^4 = 650$, and $A_6^6 = -120$. Observed values for χ_{TbAlG} and χ_{TmAlG} are those of ref. 15.

Can. J. Chem. Downloaded from www.nrcresearchpress.com by 210.87.254.6 on 09/05/12
For personal use only.

Can. J. Chem. Downloaded from www.nrcresearchpress.com by 210.87.254.6 on 09/05/12
For personal use only.

by substituting values of the energy of states as determined from e.R.s. and wave functions from a crystal field analysis which involved the complete ^7F manifold, values of χ_{TbAlG} are computed which do not show a maximum for $T \approx 1.5$ K. This particular compound becomes antiferromagnetic (17) below 1.35 K and the difference of calculated and experimental values of χ_{TbAlG} are attributed to magnetic ordering effects of the spins of the individual Tb^{3+} ions.

Recently Gavignet-Tillard *et al.* (18) used a crystal field calculation based on the positions of only some of the $^7F_6$ manifold levels, and computed values of χ_{TbAlG} which agreed quite well with experimental data. The crystal field they employed differed considerably from the one which was evaluated using the positions of many crystal field levels in all ^7F_J manifolds. Consequently, the present calculations of χ_{TbAlG} based on the latter should be considered to be more accurate.

Contrary to the case of TbAlG are the data available for TbGaG. The experimentally determined values of χ_{TbGaG} have been published (16) but the positions of the crystal field levels were not known. In Fig. 2 is shown part of a Raman spectrum of a TbGaG single crystal, and the electronic Raman transitions of the trivalent terbium are indicated. This assignment is based on a similarity of the Raman spectra of TbAlG and TbGaG. Strong electronic Raman effects occur to crystal field states of the split $^7F_6$ manifold with an energy $< 100\ cm^{-1}$ above the ground state. Such a similarity exists also between the spectra with shifts of 2100–2500 cm^{-1} due to $^7F_6$–$^7F_5$ transitions. The crystal field potential of the compounds EuGaG and DyGaG has been calculated from spectroscopic data which included the results of e.R.s. (11, 15). Using the crystal field parameters for these compounds, the calculations were made for the terbium compound and the results are shown in Table 1. It is seen that the observed energies of the states of TbGaG are intermediate between the value of levels calculated using the Eu-garnet parameters and those found from Dy-garnet parameters. Such a result is not unexpected because the radius of Tb^{3+} is intermediate between that of Eu^{3+} and Dy^{3+}. As a result of the closeness of the first excited state to the ground state it is difficult to determine the symmetries of the electronic levels from the symmetries of the observed transitions. The crystal field analyses using the DyGaG and EuGaG parameters indicate that the ground state belongs to the representation A or B_3, respectively, and the first excited state to the species B_3 or A, respectively, of the point group D_2, which describes the symmetry at the site of the rare earth ion. In Fig. 3 a comparison is made of the calculated and experimental values (16) of χ_{TbGaG} as a function of T. In the calculations the computed position and wave functions of all $^7F_6$ levels were employed.

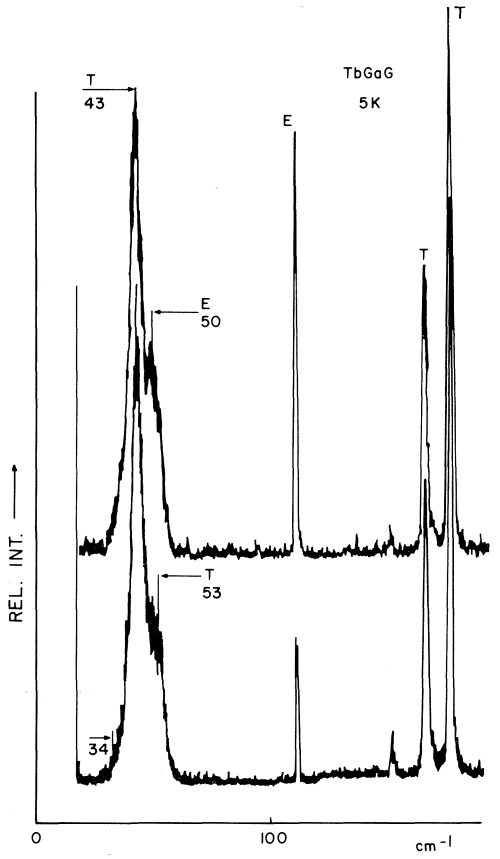

FIG. 2. Low energy region of the Raman spectrum of TbGaG excited with the 4880 Å radiation of an argon laser. All electronic Raman transitions occur with shifts $< 100\ cm^{-1}$ and those $> 100\ cm^{-1}$ are phonons of TbGaG. The symbols E and T stand for the symmetries E_g and T_{2g}, respectively, of the space group O_h^{10}. The intensities of transitions of the polarization spectra were so chosen that those of symmetry T remained the same but all E transitions are reduced by a factor of three.

TABLE 1. The positions of the low-lying $^7F_6$ electronic levels of Tb^{3+} in TbGaG

Observed value (cm^{-1})	Calculated value (cm^{-1})*	
	(*a*)	(*b*)
0	0	0
—	0.7	3.5
34	41.0	34.4
43	41.7	36.2
50	85.7	42.0
53	85.7	51.6

*The calculated values are for crystal field parameters equal to those of EuGaG (*a*) and DyGaG (*b*). A similar comparison is obtained between calculated and observed positions of the crystal field levels of the split $^7F_5$ manifold.

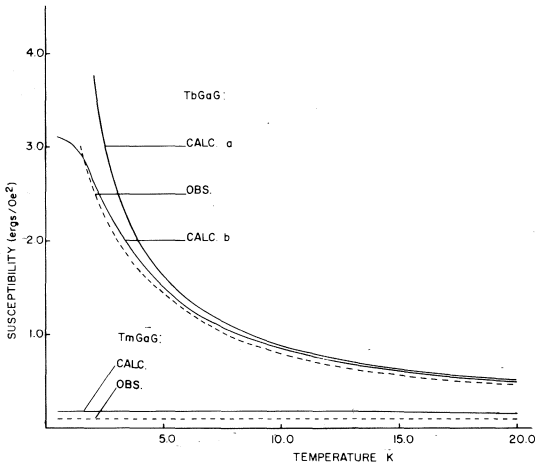

FIG. 3. (*i*) χ_{TbGaG} *vs.* temperature. Calculation (*a*) employed the EuGaG parameters of ref. 14, whereas calculation (*b*) used the DyGaG parameters of ref. 10. (*ii*) χ_{TmGaG} *vs.* temperature. Calculated values were derived using the parameters given in Table 2. Observed values for χ_{TbGaG} and χ_{TmGaG} are those of ref. 15.

Calculation of χ_{TbGaG} with values of crystal field parameters between those for EuGaG and DyGaG shows that $\chi_{exp} > \chi_{theo}$ for $T > 2.5$ K. Covalency effects have been neglected in the crystal field calculations. They tend to quench the orbital momentum of the electrons of the centrally located rare earth ions, and as a result, lower the *g*-value and thus the magnetic susceptibility. Presently it is not clear if covalency effects are responsible for the lower values of χ_{exp}. It is seen in the case of TbAlG (Fig. 1) that alignment of the spins of the individual Tb^{3+} ions also lowers the value of χ_{exp} compared to χ_{theo}.

The ground state of trivalent europium in EuGaG is $^7F_0$ and the excited states which can contribute to χ_{EuGaG} are those of the $^7F_1$ and $^7F_2$ manifolds. The manifolds are split for EuGaG and the crystal field components are (14, 15) at 308, 329, 411 cm^{-1} ($^7F_1$) and 819, 834, 855, 1324, 1341 cm^{-1} ($^7F_2$). Those for $^7F_3$ are at an energy >1832 cm^{-1}. In Fig. 4 the calculated values of χ_{EuGaG} for different values of T are shown, but experimental data are not available to test the accuracy of the calculations.

Low-lying Electronic Levels and Magnetic Susceptibilities of Thulium Aluminum Garnet and Thulium Gallium Garnet

There have been several reports (5, 19, 20) in literature dealing with the positions of crystal field states in the split $^3H_6$ ground manifold of Tm^{3+} in thulium aluminum garnet (TmAlG) and thulium gallium garnet (TmGaG). Schieber *et al.* (19) interpreted the temperature dependent values of χ_{TmGaG} on the basis of a crystal field of pure cubic symmetry, and concluded that the first electronic state was situated at an energy >104 cm^{-1} above the ground state. On the other hand Pearson *et al.* (20) concluded from optical measurements that the lowest levels lie at 85, 113, 123, and 184 cm^{-1}. These states were thought to be electronic in origin, although the effect of vibronic coupling was considered.

Electronic Raman spectroscopy has several advantages in this respect over absorption and emission techniques. Vibronic coupling can complicate the assignment of Raman spectra, but only totally symmetric vibrations can couple.

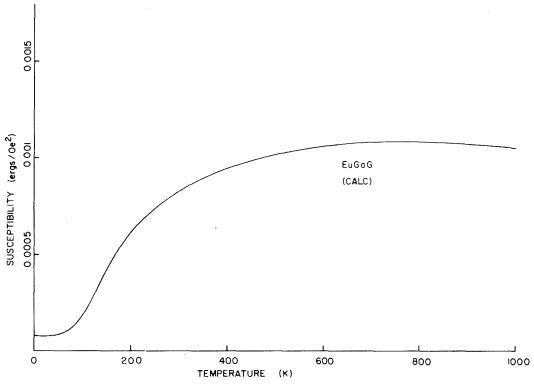

FIG. 4. χ_{EuGaG} *vs.* temperature. The parameters of ref. 14 were employed in the calculations.

Can. J. Chem. Downloaded from www.nrcresearchpress.com by 210.87.254.6 on 09/05/12
For personal use only.

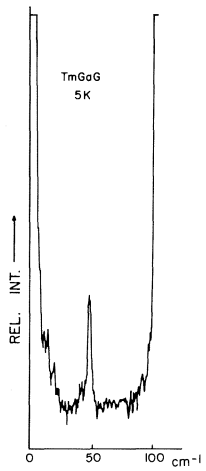

FIG. 5. Low-energy region of the Raman spectrum of TmGaG, showing the electronic transition at 45 cm^{-1}. $T \cong 5$ K.

In addition, the vibro-electronic Raman effect is only allowed if the symmetries of the electronic states are the same (21). Another advantage of electronic Raman spectroscopy is that for cubic crystals symmetries can be assigned to the electronic states from a knowledge of the symmetry of the scattering matrix. The electronic Raman scattering form TmGaG was recently observed at low temperature; the spectrum of the oriented crystal for small shifts is shown in Fig. 5. The positions and symmetries of the observed electronic levels for Tm^{3+} in TmGaG are shown in Table 2.

TABLE 2. Low-lying $^3H_6$ electronic levels of Tm^{3+} in TmGaG

Experimental		Calculated*	
$E(cm^{-1})$	Γ	$E(cm^{-1})$	Γ
192	B_1	191	B_1
189	B_2	189	B_2
185	B_3	170	B_3
245	A	34	A
0	B_1	0	B_1

*Calculated values refer to the following set of crystal field parameters (in cm^{-1}): $A_2^0 = -120$, $A_4^0 = -223$, $A_6^0 = 30$, $A_2^2 = 50$, $A_4^2 = 246$, $A_6^2 = -60$, $A_4^4 = 970$, $A_6^4 = 590$, and $A_6^6 = -50$.

Using the dysprosium garnet parameters for the initial fit, the splitting patterns for $^3H_6$ of Tm^{3+} in TmGaG and TmAlG were calculated. The computed energy levels for TmGaG were found to be close to the observed levels given in Table 2. The ground state for TmGaG is of symmetry B_1 and the first excited state at $\sim 45\ cm^{-1}$ is of symmetry A. According to group theory a transition between levels of

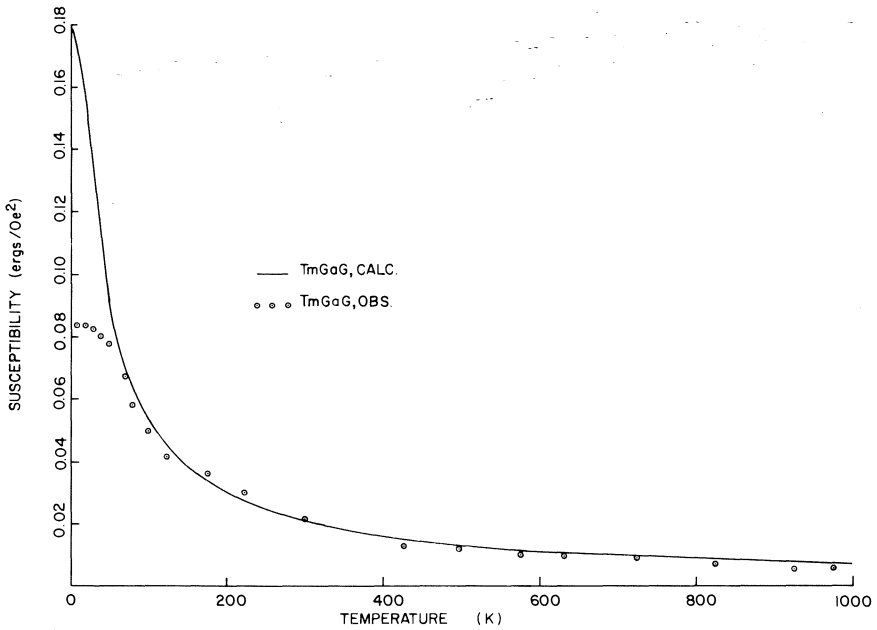

FIG. 6. χ_{TmGaG} *vs.* temperature. Parameters employed in the calculation are given in Table 2. Observed values for χ_{TmGaG} are those of ref. 18.

Can. J. Chem. Downloaded from www.nrcresearchpress.com by 210.87.254.6 on 09/05/12
For personal use only.

symmetry A and B_1 for Tm^{3+} at the D_2 site results in a Raman band of symmetry T_{2g} (in O_h) for the entire cubic crystal. The observed spectrum (Fig. 5) is in agreement with this prediction, and in the final computations the crystal field parameters $A_n^m = \langle r^n \rangle B_n^m$ were allowed to deviate from the Dy garnet parameters so that the calculated symmetries and positions of the excited states agreed with the experimental data of Table 2. The calculated results are tabulated there for comparison. The same procedure was followed for TmAlG, but the crystal field calculations were less satisfying.

From the energy level schemes, the temperature dependent magnetic susceptibilities for TmGaG and TmAlG were calculated. The comparison of experimental (19) *vs.* calculated results for χ_{TmGaG} in the temperature range 0.5–1000 K is presented in Figs. 3 and 6. The difference of the curves for $T < 60$ K may (as in the case for TbAlG) be due to magnetic ordering effects. There exists also a large difference of calculated and observed values of χ_{TmAlG} (see Fig. 1).

Conclusive Remarks

Recently the crystal field was determined for some cubic rare earth garnet crystals. Good agreement exists between calculated and observed splitting patterns and also the symmetry of the states agrees with the calculations. In this work we present the results of a computation of the molar magnetic susceptibility of these crystals and the role of electronic Raman spectroscopy is emphasized. Because of the good agreement of computed and observed values of the magnetic susceptibility for large temperature ranges it is felt that e.R.s. is an important technique in the study of magnetic properties of the crystals.

1. D. H. Boal, J. T. Hoff, P. Grünberg, J. Preudhomme, and J. A. Koningstein. J. Raman Spectrosc. **1**, 489 (1973).
2. S. Geller. Z. Kristallogr. **125**, 1 (1967).
3. J. A. Koningstein. J. Chem. Phys. **46**, 2811 (1967).
4. J. A. Koningstein. Chem. Phys. Lett. **2**, 213 (1968).
5. J. A. Koningstein and Toa-Ning Ng. Can. J. Chem. **47**, 1395 (1969).
6. J. A. Koningstein. Solid State Commun. **7**, 351 (1969).
7. J. A. Koningstein and G. Mace. Chem. Phys. Lett. **3**, 343 (1969).
8. J. A. Koningstein and G. Schaack. J. Opt. Soc. Am. **60**, 755 (1970).
9. J. A. Koningstein and G. Schaack. Phys. Rev. B**2**, 1242 (1970).
10. B. E. Argyle, R. L. Wadsack, and R. K. Chang. J. Appl. Phys. **42**, 1478 (1971).
11. R. L. Wadsack, Joan L. Lewis, B. E. Argyle, and R. K. Chang. Phys. Rev. B**3**, 4342 (1971).
12. J. A. Koningstein and P. Grünberg. Can. J. Chem. **49**, 2336 (1971).
13. I. Dabrowski, B. Grünberg, and J. A. Koningstein. J. Chem. Phys. **56**, 1264 (1972).
14. J. P. VanderZiel and L. G. Van Uitert. Phys. Rev. **186**, 332 (1969).
15. D. Boal, P. Grünberg, and J. A. Koningstein. Phys. Rev. B**7**, 4757 (1973).
16. W. P. Wolf, M. Ball, M. T. Hutchings, M. J. M. Leask, and A. F. G. Wyatt. J. Phys. Soc. Jap. **17**, B**1**, 443 (1962).
17. A. M. Cooke, T. L. Thorp, and M. R. Wells. Proc. Phys. Soc. **92**, 400 (1967).
18. A. Gavignet-Tillard, J. Hammann, and L. DeSeze. J. Phys. Chem. Solids, **34**, 241 (1973).
19. M. M. Schieber, C. C. Lin, and J. H. VanVleck. J. Phys. Chem. Solids, **27**, 1041 (1966).
20. J. J. Pearson, G. F. Herrmann, and R. A. Buchanan. J. Appl. Phys. **39**, 980 (1968).
21. C. J. Kane-Maguire and J. A. Koningstein. J. Chem. Phys. **59**, 1899 (1973).

Can. J. Chem. Downloaded from www.nrcresearchpress.com by 210.87.254.6 on 09/05/12
For personal use only.

Photolysis of SO_2 in the Presence of Foreign Gases. VI. Acetylene and Allene[1]

MENACHEM LURIA[2] AND JULIAN HEICKLEN

Department of Chemistry and Center for Air Environment Studies, The Pennsylvania State University, University Park, Pa. 16802

Received October 30, 1973[3]

MENACHEM LURIA and JULIAN HEICKLEN. Can. J. Chem. **52**, 3451 (1974).

The photolysis of SO_2 at 3130 Å and 25 °C in the presence of C_2H_2 leads to CO, and, in the presence of allene to CO and C_2H_4 as gas phase products. In the C_2H_2 system, the CO comes from the two non-emitting triplet states of SO_2, 57% from SO_2** and 43% from $SO_2{}^+$. In the allene system, the two excited singlet states of SO_2, and possibly the emitting triplet state, also participate. The relative importance of the contributions from each state can be estimated to be >35% from $^1SO_2$, <16% from $^3SO_2$, 8% from SO_2*, 12% from SO_2**, and 29% from $SO_2{}^+$.

MENACHEM LURIA et JULIAN HEICKLEN. Can. J. Chem. **52**, 3451 (1974).

La photolyse du SO_2 à 3130 Å et 25 °C, en présence de C_2H_2, conduit à la formation de CO; en présence d'allène il y a formation de CO et de C_2H_4. Lors de la réaction en présence de C_2H_2, le CO provient de deux états triplets du SO_2, soit 57% à partir de SO_2** et 43% à partir de $SO_2{}^+$. Lors de la réaction en présence d'allène, les deux états excités singulets du SO_2 et possiblement l'état triplet émettant participent à la réaction. L'importance relative des contributions de chaque état peut être estimé de la façon suivante: >35% pour $^1SO_2$, <16% pour $^3SO_2$, 8% de SO_2*, 12% pour SO_2** et 29% de $SO_2{}^+$.

[Traduit par le journal]

Introduction

In the photolysis of SO_2 at 3130 Å in the presence of CO, it has been shown that at least four excited electronic states are involved (1, 2). The emitting singlet and triplet states are readily quenched by all foreign gases, the triplet being particularly easily quenched by the known triplet quenchers NO and biacetyl. At high pressures, these states are not chemically important and CO_2 is produced from two other states: a singlet, SO_2*, not quenched by any gas tested, and a triplet, SO_2**, quenched by the triplet quenchers NO and biacetyl, but not by other inactive gases such as N_2 or CO_2.

In a more recent study involving the SO_2 sensitized emission of biacetyl (3), it was found that H_2O readily quenches SO_2**. In addition another triplet state, $SO_2{}^+$, was found which is not quenched by N_2, CO_2, or H_2O, but is readily quenched by biacetyl, thiophene, and presumably NO.

It has also been found in our laboratory that photoexcited SO_2 reacts readily with C_2H_2 to produce CO and a solid (4), and with allene to produce CO, C_2H_4, and an oil (5). It is of interest to know which electronic states are involved in the photochemical reactions. To examine this problem we have now measured the gas phase products in the presence of various quenchers, and the results are presented here.

Experimental

The reaction was carried out in a cylindrical cell 50 cm long and 5 cm in diameter, containing quartz windows at both ends. To insure complete mixing the gases were introduced into the reaction vessel through a Pyrex tube with 10 pinholes equally spaced along its length, which was placed in the vessel close to its surface and ran along its length. The radiation was from a Hanovia 200 W U-shape type SH mercury arc and passed through an Ealing 3130 Å interference filter before entering the reaction vessel. The gases used were from the Matheson Co. These included SO_2, C_2H_2, C_3H_4, CO_2, N_2, NO, and C_2H_4. The purification and handling of these gases is described in previous publications (2, 4, 5). Distilled H_2O was used after degassing at −95 °C.

The reaction cell was connected through a stopcock to a gas chromatographic sample tube of volume 350 cc. The chromatograph utilized a Gow Mac power supply and thermistor detector at 0 °C. Two columns were used. One was 8 ft long containing 5Å molecular sieves and was used for N_2 and CO analysis. The other was 30 ft long and contained dimethylsulfolane; it was used to measure C_2H_4. All gaseous products could be detected at pressure of ≥0.1 mTorr. He with a flow rate of 100 cc/min was the carrier gas in both columns.

Actinometry was done with $(CH_3)_2N_2$, which gives a

[1]CAES Report No. 330–73.

[2]Present address: Stanford Research Institute, Menlo Park, California 94025.

[3]Revision received July 3, 1974.

Can. J. Chem. Downloaded from www.nrcresearchpress.com by 210.87.254.42 on 09/05/12
For personal use only.

Can. J. Chem. Downloaded from www.nrcresearchpress.com by 210.87.254.42 on 09/05/12
For personal use only.

TABLE 1. Photolysis of SO_2 in the presence of C_2H_2*

M	[M] (Torr)	$\Phi(CO)(\times 10^3)$
$[C_2H_2] = 0.22$ Torr		
—	0	18
—	0	20
H_2O	2	8.5
H_2O	5	7.3
H_2O	10	8.5
$[C_2H_2] = 2.2$ Torr		
—	0	33
—	0	34
—	0	35
CO_2	750	35
NO	10	0†
NO	10	0†
H_2O	2	26
H_2O	5	20
H_2O	10	15
$[C_2H_2] = 22.0$ Torr		
—	0	39

*$[SO_2] = 2.2$ Torr, $I_a = 2.7$ mTorr/min, irradiation time = 30 min.
†$\Phi(CO) < 1.2 \times 10^{-3}$.

quantum yield of N_2 of 1.0 (6). All actinometry runs were done at the same $(CH_3)_2N_2$ absorbance as used in the SO_2 runs, using the measured extinction coefficients (to base 10) at 3130 Å of 3.8×10^{-3} and 1.5×10^{-4} $Torr^{-1}$ cm^{-1}, respectively, for SO_2 and $(CH_3)_2N_2$.

Results and Discussion

The CO quantum yields, $\Phi(CO)$, in the photolysis of SO_2–C_2H_2 mixtures are given in Table 1. The addition of excess CO_2 has no effect so that $^1SO_2$ and $^3SO_2$ (the emitting singlet and triplet states, respectively) play no role. Also 10 Torr of NO completely suppresses the reaction; thus SO_2* is not involved. The addition of excess H_2O reduces $\Phi(CO)$ to a limiting value 43% of that in the absence of H_2O. Since H_2O quenches SO_2** but not $SO_2{}^{\ddagger}$ it can be concluded that CO is produced 43% of the time from $SO_2{}^{\ddagger}$ and 57% of the time from SO_2**.

The results of similar experiments in the SO_2–allene system are shown in Table 2. Here the addition of CO_2 drops $\Phi(CO)$ to 49% of its value in the absence of CO_2. Thus the emitting $^1SO_2$ and $^3SO_2$ are presumably responsible for 51% of the reaction. If NO is also added, the reaction is not quenched to zero as with C_2H_2, but 8% of the CO remains. This can be attributed to SO_2*, since the other four states are quenched. When both CO_2 and H_2O are present, 37% of the CO remains. Since this 37% is from SO_2* and $SO_2{}^{\ddagger}$, the contribution from $SO_2{}^{\ddagger}$ is 29%. By subtraction, the SO_2** contribution becomes 12%. When NO is added, the three triplet states and some fraction of $^1SO_2$ are quenched. The CO is reduced to 43%. Since the contribution from SO_2* is 8%, then that from $^1SO_2$ is >35%. By difference $^3SO_2$ accounts for <16%, and probably a lot less. The results for both C_2H_2 and C_3H_4 are summarized in Table 3. The estimated uncertainty is about ±10%.

The $\Phi(C_2H_4)/\Phi(CO)$ ratio in the allene system

TABLE 2. Photolysis of SO_2 in the presence of allene*

M	[M] (Torr)	$\Phi(CO)(\times 10^3)$	$\Phi(C_2H_4)/\Phi(CO)$
$[C_3H_4] = 0.22$ Torr			
—	0	9.8	0.22
H_2O	10	4.5	0.16
$CO_2 + H_2O$	750 + 10	3.6	—
$CO_2 + H_2O + NO$	750 + 10 + 10	1.4	—
$[C_3H_4] = 2.2$ Torr			
—	0	17.8†	0.28†
—	0	17.2	0.31
CO_2	750	8.3	—
CO_2	750	8.9	—
NO	10	8.3	—
NO	10	6.8	0.29
CO_2 + NO	750 + 10	1.4	—
H_2O	10	7.7	0.15
$[C_3H_4] = 22.0$ Torr			
—	0	23.0†	0.24†

*$[SO_2] = 2.2$ Torr, $I_a = 2.8$ mTorr/min, irradiation time = 60 min.
†Irradiation time = 30 min.

TABLE 3. Percentage of CO from each excited state of SO_2

State	Quencher	% CO from C_2H_2	% CO from C_3H_4
$^1SO_2$	CO_2, NO, H_2O	0	>35
$^3SO_2$	CO_2, NO, H_2O	0	<16
SO_2*	None	0	8
SO_2**	NO, H_2O	57	12
SO_2+	NO	43	29

is somewhat scattered, but is about 0.27 ± 0.05 in the absence or presence of NO. With excess CO_2 present, experimental difficulties interfered with the C_2H_4 analysis since C_2H_4 and CO_2 have similar gas chromatographic retention times. However, with H_2O present, $\Phi(C_2H_4)/\Phi(CO)$ dropped noticeably to 0.16. We have no explanation for this observation.

Experiments were done with excess hydrocarbon to obtain the upper limiting values for $\Phi(CO)$. These are 0.039 for C_2H_2 and 0.023 for allene. They can be compared to the value of ~ 0.05 obtained for $\Phi(CF_2O)$ in the SO_2–C_2F_4 system, where the emitting states, $^1SO_2$ and $^3SO_2$, are not important (7). It is interesting that the upper limiting value for $\Phi(CO)$ is smaller for allene even though more excited electronic states are involved than for C_2F_4 or C_2H_2. Presumably removal of excited SO_2 by allene does not lead to CO production all the time.

This work was supported by the Environmental Protection Agency under Grant No. 800874, for which we are grateful.

1. L. STOCKBURGER, III, S. BRASLAVSKY, and J. HEICKLEN. J. Photochem. **2**, 15 (1973).
2. E. CEHELNIK, J. HEICKLEN, S. BRASLAVSKY, L. STOCKBURGER, III, and E. MATHIAS. J. Photochem. **2**, 31 (1973).
3. A. M. FATTA, E. MATHIAS, J. HEICKLEN, L. STOCKBURGER, III, and S. BRASLAVSKY. J. Photochem. **2**, 119 (1973).
4. M. LURIA, R. G. DE PENA, K. J. OLSZYNA, and J. HEICKLEN. J. Phys. Chem. **78**, 325 (1974).
5. M. LURIA, K. J. OLSZYNA, R. G. DE PENA, and J. HEICKLEN. J. Aerosol Sci. In press.
6. J. CALVERT and J. N. PITTS. Photochemistry. John Wiley, New York. 1966. p. 463.
7. E. CEHELNIK, C. W. SPICER, and J. HEICKLEN. J. Am. Chem. Soc. **93**, 5371 (1971).

Can. J. Chem. Downloaded from www.nrcresearchpress.com by 210.87.254.42 on 09/05/12
For personal use only.

Palladium(II) Complexes with Dithiomalonamide and *N,N'*-Diphenyldithiomalonamide

GIAN CARLO PELLACANI

Istituto di Chimica Generale e Inorganica, University of Modena, 41100 Modena, Italy

Received December 20, 1973

GIAN CARLO PELLACANI. Can. J. Chem. **52**, 3454 (1974).

Dithiomalonamide (Hdtma) and *N,N'*-diphenyldithiomalonamide (Hdpma) form diamagnetic square-planar complexes PdL_2 and $PdL_2 \cdot 2DMF$. For these complexes a $[PdS_4]$ coordination was suggested by their electronic and i.r. spectra. The splitting orbital parameters, Δ_1, indicates that these anionic ligands assume an intermediate position in the spectrochemical series of sulfur donors. These ligands also form $Pd(HL)_2X_2$ (X = Cl, Br, I, ClO_4) and $PdHLX_2$ (X = Cl, Br, I) complexes in which spectroscopic evidence suggests an S,N bidentate ligand coordination, forming six-membered rings. ν(PdN) and ν(PdS) are tentatively assigned. For $Pd(Hdpma)_2X_2$ complexes from the far i.r. and electronic spectra we propose a *cis*-PdN_2S_2 configuration. The Δ_1 parameters in the six-membered ring $Pd(HL)_2X_2$ complexes indicate a ligand strength greater than in the analogous S,N coordinated five-membered ring complexes of dithiooxamides and show an inversion of the order found in $Ni(HL)_2X_2$ (HL=Hdtma, Hdpma) complexes. In $PdHLX_2$ complexes the presence of two bands assignable to $\nu_{asym}(PdX)$ and $\nu_{sym}(PdX)$ supports a *cis*-halogen configuration.

GIAN CARLO PELLACANI. Can. J. Chem. **52**, 3454 (1974).

Le dithiomalonamide (Hdtma) et le *N,N'*-diphényldithiomalonamide (Hdpma) forment des complexes diamagnétiques plan-carré PdL_2 et $PdL_2 \cdot 2DMF$. On suggère pour ces complexes une coordination $[PdS_4]$ à cause de leurs spectres électroniques et infrarouges. Les paramètres Δ_1 de dédoublement des orbitales indiquent que ces liaisons coordinées anioniques admettent une position intermédiaire dans les séries spectrochimiques où le soufre agit comme donneur. Ces coordinats forment aussi les complexes $Pd(HL)_2X_2$ (X = Cl, Br, I, ClO_4) et $PdHLX_2$ (X = Cl, Br, I) pour lesquels on suggère grâce à des données spectroscopiques, que les coordinats agissent par le S et le N comme groupe à deux liaisons coordinées et forment des noyaux hexagonaux. On peut trouver les valeurs de ν(PdN) et ν(PdS). En se basant sur les spectres électroniques et de l'infrarouge lointain des complexes $Pd(Hdpma)_2X_2$, on propose une configuration *cis* pour PdN_2S_2. Les paramètres Δ_1 dans les complexes à noyau hexagonal $Pd(HL)_2X_2$ montrent que la force de coordination est plus élevée que celle observée dans les complexes analogues du dithiooxamide à cinq chainons et liés par le S et le N; ces paramètres montrent aussi une inversion de l'ordre trouvé dans les complexes $Ni(HL)_2X_2$ (HL = Hdtma, Hdpma). Dans les complexes $PdHLX_2$, la présence de deux bandes attribuées à $\nu_{asym}(PdX)$ et $\nu_{sym}(PdX)$ appuie l'hypothèse d'une configuration dans laquelle les halogènes sont en position *cis*. [Traduit par le journal]

Introduction

Research into dithiomalonamide (Hdtma) and *N,N'*-diphenyldithiomalonamide (Hdpma) as ligands for transition metal ions is limited (1, 2), despite their similarity with β-dithioketones and the advantage they have over the latter of being isolable ligands, which can be comparatively studied with their complexes.

Previously we studied the nickel(II) dithiomalonamides (3) and found that they act both as chelating agents, in which the replacement of a proton by a metal cation produces six-membered chelate rings with the two donor sulfur atoms, and as coordinating agents through nitrogen and sulfur, forming six-membered rings.

As these ligands permit considerable expansion of the chemistry of $[MS_4]$ and $[MS_2N_2]$ complexes (4), containing six-membered rings, we have now studied the dithiomalonamide palladium(II) complexes. All the palladium(II) dithiomalonamides prepared are new, and were investigated in order to compare them with the analogous nickel(II) complexes (3) and with the palladium(II) dithiooxamides, containing S,N-coordinated ligands and forming five-membered rings, which were studied previously (5, 6).

Experimental

Dithiomalonamide and *N,N'*-diphenyldithiomalonamide were prepared as previously described (3). The acids were used at the following concentrations: HAc, glacial;

Can. J. Chem. Downloaded from www.nrcresearchpress.com by 210.87.254.42 on 09/05/12
For personal use only.

TABLE 1. Analytical data and molar conductivities (Ω^{-1} cm^2 mol^{-1})

Compound	Color	Pd(%) Calcd.	Pd(%) Found	S(%) Calcd.	S(%) Found	N(%) Calcd.	N(%) Found	λ_M†
$Pd(dtma)_2$	Red-orange	28.54	28.62	34.41	34.19	15.03	14.91	
$Pd(dtma)_2 \cdot 2DMF$	Orange	20.52	20.46	24.71	24.63			
$Pd(Hdtma)_2Cl_2$	Yellow	23.87	23.76	28.78	29.30			54
$Pd(Hdtma)_2I_2$	Yellow	16.93	16.76	20.40	19.93			145
$Pd(Hdtma)_2(ClO_4)_2$	Yellow	18.55	18.67	22.36	22.58			145

Compound	Color	Pd(%) Calcd.	Pd(%) Found	C(%) Calcd.	C(%) Found	H(%) Calcd.	H(%) Found	λ_M†
$Pd(Hdtma)_2Br_2$	Yellow	19.90	19.39	13.47	13.87	2.26	2.65	125
$Pd(Hdtma)Cl_2$	Maroon	34.15	34.62	11.56	11.60	1.94	2.02	39
$Pd(Hdtma)Br_2$	Orange	26.56	26.86	8.99	9.24	1.51	1.69	61
$Pd(dpma)_2$	Red	15.72	15.29	53.18	53.28	3.87	3.98	
$Pd(dpma)_2 \cdot 2DMF$	Orange	12.93	12.46	52.49	52.31	4.90	5.18	
$Pd(Hdpma)_2Cl_2$	Yellow	14.19	13.67	48.01	47.83	3.76	4.08	58
$Pd(Hdpma)_2Br_2$	Yellow	12.68	12.65	42.94	42.61	3.36	3.41	130
$Pd(Hdpma)_2I_2$	Yellow	11.40	12.18	38.61	38.17	3.03	3.24	151
$Pd(Hdpma)_2(ClO_4)_2$*	Yellow	12.11	12.85					160
$Pd(Hdpma)Cl_2$	Brown-yellow	22.93	22.70	38.85	38.38	3.04	3.13	42
$Pd(Hdpma)Br_2$	Red-orange	19.25	19.33	32.59	31.70	2.55	2.70	56
$Pd(Hdpma)I_2$	Red	16.45	15.92	27.86	27.58	2.18	2.30	54

*S(%): calcd. 14.60; found 15.03.
†10^{-3} *M* solution in DMF.

$HClO_4$, 60%; HCl, 37%; HBr, 48%; HI, 57%. All reagents were of pure chemical grade.

$Pd(OH)_2$, used as a starting material for some complex preparations, was prepared by adding an aqueous solution of $KHCO_3$ (10%) to an aqueous solution of $Pd(NO_3)_2 \cdot 2H_2O$ until p*H* 8 was reached. A complete precipitation of $Pd(OH)_2$ ensued, which was then centrifuged and washed with H_2O.

The following methods gave the best crystalline products:

$Pd(dtma)_2$ and $Pd(dpma)_2$: from HAc solutions of ligands and $Pd(OH)_2$ with molar ratio M:L = 1:2.

$PdL_2 \cdot 2DMF$: by adding diethylether to a dimethylformamide (DMF) solution of the PdL_2 complexes.

$Pd(Hdtma)_2Cl_2$: 2 m*M* $PdCl_2$ in 30 ml HCl to 4.5 m*M* L in 360 ml HAc + 30 ml HCl.

$Pd(Hdtma)_2X_2$ (X = Br, I): 0.18 m*M* $Pd(OH)_2$ in 3 ml HX to 8 m*M* L in 12 ml EtOH + 8 ml H_2O.

$Pd(Hdtma)_2(ClO_4)_2$: 2 m*M* $Pd(OH)_2$ in 2.5 ml $HClO_4$ to 9 m*M* L in 35 ml HAc.

$Pd(Hdtma)X_2$ (X = Cl, Br): 0.5 m*M* L in 25 ml EtOH to 1.7 m*M* PdX_2 in 3 ml HX.

$Pd(Hdpma)_2Cl_2$; 0.3 m*M* $PdCl_2$ in 2 ml HCl + 2 ml H_2O to 1.2 m*M* L in 20 ml EtOH.

$Pd(Hdpma)_2X_2$ (X = Br, I, ClO_4) : 0.6 m*M* $Pd(OH)_2$ in 4 ml HX + 4 ml H_2O to 1.2 m*M* L in 20 ml EtOH.

$Pd(Hdpma)X_2$ (X = Cl, Br, I): 0.38 m*M* (for Cl), 0.4 m*M* (for Br), and 0.28 m*M* (for I) L in 4 ml EtOH to 1.14, 1.22, and 0.84 m*M*, respectively, PdX_2 in 2 ml HX.

The compounds cannot be recrystallized and were analyzed by conventional methods. Palladium(II) was analyzed by EDTA titration (7). Physical measurements were made as previously described (3).

Analyses and molar conductivities are reported in Table 1.

Results and Discussion

The complexes of palladium(II) with dithiomalonamide and *N,N'*-diphenyldithiomalonamide have different stoichiometries depending on the media in which they were prepared. Inner complexes, PdL_2, were isolated from glacial acetic acid, while from strong acid media, in which the undissociated ligand form prevails, $Pd(HL)_2X_2$ (X = Cl, Br, I, ClO_4) cationic and $PdHLX_2$ (X = Cl, Br, I) neutral complexes were isolated.

All of the complexes are diamagnetic. They are insoluble in nonpolar solvents, while in polar solvents, such as dimethylformamide (DMF), methylcellusolve (MCS), and ethanol, the inner complexes give a solution of $\sim 10^{-3}$ *M* concentration, this level of concentration being given by the cationic and neutral complexes only in DMF.

The i.r. assignments given for Hdtma by Jensen and Nielsen (8) and the previous results of nickel(II) dithiomalonamides (3) were used for the interpretation of the spectra of the complexes.

Can. J. Chem. Downloaded from www.nrcresearchpress.com by 210.87.254.42 on 09/05/12
For personal use only.

TABLE 2. Characteristic i.r. bands of the inner complexes*

	Frequency (cm^{-1})			
	$Pd(dtma)_2$	$Pd(dtma)_2 \cdot 2DMF$	$Pd(dpma)_2$	$Pd(dpma)_2 \cdot 2DMF$
ν(C···N)	1524vs	1494vs	1488vsb	1480vsb
ν(C···C) + δ(C—H)	1428s	1428s	1445w	1446w
δ(C—H) + ν(C···C)	1319vsb	1321vsb	1310s	1313m
ν(C···C)	1248ms	1250ms	1243vs	1265s
π(C—H)	803m	807s	787s	810ms
ν(C···S)	652s	642s	644s	657s
ν(M—S)	401m	406m	393sb	368vs
	329sb	358s	327m	329s
Ring def.	153w	152w	200vw	193vw

*v = very, s = strong, m = medium, w = weak, b = broad.

Inner Complexes

The great similarity of the i.r. spectra of the PdL_2 and $PdL_2 \cdot 2DMF$ (L = dtma, dpma) (Table 2) with those of $Pd(dtaa)_2$ (dtaa = dithioacetylacetonate) (9, 10) and NiL_2 (L = dtma, dpma) (3), the increase of ν(CN) and the decrease of ν(CS) frequencies, with respect to the ligand, and the existence of two ν(PdS) bands suggest a $[PdS_4]$ square-planar coordination (3, 9, 11–13). By removal of a proton from the CH_2 group the six-membered ring acquires some aromatic character as in acetylacetonates monothio- and dithio-acetylacetonates.

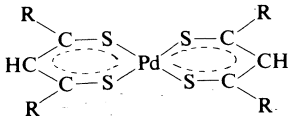

R = NH_2, NHφ (this work), CH_3 (9)

The position of ν(CS) at 657–642 cm^{-1} in these complexes indicates a C—S bond order and a metal–sulfur bond strength in dithiomalonamides intermediate between dithiocarbamates and dithioacetylacetonates (9). The assignments of the PdS bands were made on this basis and in accordance with the values of the NiS stretching vibrations found in the analogous NiL_2 complexes (3), as the NiS and PdS stretching frequencies do not differ appreciably if the ligand is the same (14). The i.r. spectra of the $PdL_2 \cdot 2DMF$ complexes are equivalent to the sum of PdL_2 and free DMF.

The electronic spectra of the inner complexes are essentially the same in the solid state as in MCS, DMF, or strongly-coordinating pyridine and confirm an S_4-coordination on account of their analogies with the spectra of the $Pd(dtaa)_2$ (15) (Table 3) and NiL_2 (L = dtma, dpma) (3) complexes. In particular, no variation in energy of the band at 20.3–20.4 kK indicates a very stable $[PdS_4]$ square-planar environment with negligible axial σ interactions and permits the assignment of this band to the $^1A_{1g} \rightarrow {}^1B_{1g}$ ($x^2 - y^2 \rightarrow xy$) in-plane transition. The orbital parameters Δ_1 (16), calculated from the d–d transition by assuming a correction factor (17) ($F_2 = 10F_4 = 600$) of 2100 cm^{-1}, places these ligand anions in the spectrochemical series of sulfur donors for palladium(II) planar complexes (15, 17, 18) as follows: maleonitriledithiolate (17800) < dithioacetylacetonate (20200) < diphenyldithiomalonamide anion (22380) < dithiomalonamide anion (22510) < diethyldithiophosphate (23900) < diethyldithiocarbamate (24300) < dithiooxalate (28100).

The order Δ_1 [Pd(II)] > Δ_1 [Ni(II)] (3) for dithiomalonamides is as expected (18). The assignments of charge-transfer bands are supported by comparison with NiL_2 (L = dtma, dpma) complexes (3), as the energy relationship $PdL_2 > NiL_2$ is also characteristic of this type of transition (16, 19).

Cationic and Neutral Complexes

In all the cationic and neutral dithiomalonamide complexes the major change in the positions of the fundamental bands mainly due to ν(NH), ν(CN), and ν(CS) (Table 4) are similar to those of the cationic nickel dithiomalonamides, already reported and discussed (3). This suggests that the ligands are bidentate, coordinating with the palladium through sulfur and nitrogen, to form six-membered rings. The new bands, appearing in the far i.r. spectra of the complexes, assigned to the prevailing contribution of ν(PdN) and ν(PdS) agree with the values of ν(NiN) and ν(NiS) in the analogous nickel dithiomalonamides (3) and lie within the range of

Can. J. Chem. Downloaded from www.nrcresearchpress.com by 210.87.254.42 on 09/05/12
For personal use only.

TABLE 3. Electronic spectra (in kK, log ε in parentheses) of $Pd(dtma)_2$ and $Pd(dpma)_2$ in methylcellusolve and $Pd(dtaa)_2$ (15)

	Observed (maximum)		
	$Pd(dtma)_2$	$Pd(dpma)_2$	$Pd(dtaa)_2$
d–d			
$^1A_g \rightarrow {}^1B_{1g}(x^2 - y^2 \rightarrow xy)$	20.4(2.39)	20.3(2.90)	18.1(2.65)
$^1A_g \rightarrow {}^1B_{3g}(xz \rightarrow xy)$			19.8(3.25)
M → L change transfer			
$^1A_g \rightarrow {}^1B_{2u}(xz \rightarrow L(\pi^*))$	25.3sh(3.71)	23.9sh(4.15)	19.8(3.25)
$^1A_g \rightarrow {}^1B_{3u}(yz \rightarrow L(\pi^*))$	26.9(3.99)		20.5(3.20)
L → M charge transfer			
$^1A_g \rightarrow {}^1B_{2u}, {}^1B_{3u}(L(\pi) \rightarrow xy)$		32.3sh(4.54)	33.4(4.11)
$^1A_g \rightarrow {}^1B_{2u}, {}^1B_{3u}(L(\sigma) \rightarrow xy)$	44.1(4.45)	42.6sh(4.51)	46.3(4.08)
L → L*			
$^1A_g \rightarrow {}^1B_{2u}$	33.3(4.62)	29.0(4.65)	29.3(3.82)
$^1A_g \rightarrow {}^1B_{1u}$	39.3(4.74)	39.4(4.61)	39.5(4.53)

TABLE 4. More relevant i.r. bands (cm^{-1}) of $Pd(HL)_2X_2$ (X=Cl, Br, I, ClO_4) and $Pd(HL)X_2$ (X=Cl, Br, I) complexes

Complex	ν(CN)			ν(CS)		
Hdtma		1440vs			800ms	
$Pd(Hdtma)_2X_2$	1455–75vs	1405–08w	1300–10s	931–33w	720–800m	689–710s
$Pd(Hdtma)X_2$*	1459vs	1389–98m	1307–08s	913–925m		693–97s
Hdpma		1513vs			680vs	
$Pd(Hdpma)_2X_2$	1548–57vs		1433–40vs	687–90vs		639–48m
$Pd(Hdpma)X_2$†	1528–43vs		1420–30vs	687–97vs		615–17w

*ν(PdCl) for $Pd(Hdtma)Cl_2$: 301vsb, 294sh; ν(PdBr) for $Pd(Hdtma)Br_2$: 231sb.
†ν(PdCl) for $Pd(Hdpma)Cl_2$: 305vsb, 291m; ν(PdBr) for $Pd(Hdpma)Br_2$: 242s, 222s; ν(PdI) for $Pd(Hdpma)I_2$: 150mb.

the values found for Pd(II)-complexes of other thioamidic ligands (5, 14, 20). In particular no new additional bands are observed in the complexes in this spectral region.

In the $Pd(Hdtma)_2X_2$ (X = Cl, Br, I, ClO_4) complexes the presence of one Pd—S at 358–364 cm^{-1} and one Pd—N at 466–489 cm^{-1} stretching mode suggest that the PdS_2N_2 skeletons are *trans*-planar (14, 21), while in the $Pd(Hdpma)_2X_2$ complexes, the two new bands appearing at 486–490 and 475–479 cm^{-1} assignable to ν(PdN) and two at 334–336 and 324–325 cm^{-1} assignable to ν(PdS), indicate that the PdS_2N_2 skeletons of these complexes are *cis* (14, 21).

The i.r. bands of ClO_4 groups are characteristic of ClO_4 ions (22).

In $Pd(HL)X_2$ (X = Cl, Br, I), two Pd—L bands (one ν(PdN) at 481–492 cm^{-1} and one ν(PdS) at 326–363 cm^{-1}) and two PdX bands $\nu_{asym}(PdX)$ and $\nu_{sym}(PdX)$ (Table 4) lead to the conclusion that the complexes are monomer with one S,N-bidentate six-membered ring ligand and two *cis*-halogen atoms (5, 13, 21, 23–25).

The electronic spectra of the solid $Pd(HL)_2X_2$ (X = Cl, Br, I, ClO_4) complexes (Table 5) are very similar and do not seem to be affected by the change of the anion. The shoulder at 22.7–23.8 kK may be assigned to a d–d band ($^1A_g \rightarrow {}^1B_{1g}$), the other d–d bands lying under the strong charge-transfer band at 26.3–29.4 kK. The corrected orbital parameter Δ_1 calculated for the perchlorato complexes, places Hdtma, Hdpma, and dithiooxamides (5) in the following S,N donor spectrochemical series for palladium planar complexes: dithiooxamide (19340) < *N,N'*-dimethyldithiooxamide (21150) < Hdpma (25100) < Hdtma (25900).

Δ_1 (25900 and 25100 cm^{-1} for cationic complexes) > Δ_1 (22510–22380 cm^{-1} for inner complexes) confirms an S_2N_2 coordination for the cationic complexes. $\Delta_1[PdS_2N_2] > \Delta_1[NiS_2N_2]$ (3) agrees with the spectrochemical order of these metal ions. The position of Hdpma which, in the nickel(II) series (3), is after Hdtma offers additional evidence for a *cis*-S_2N_2 skeleton for the $Pd(Hdpma)_2X_2$ complexes, because the great steric hindrance due to the *cis*-configuration, and which weakens the Pd—N bonds, prevails over the ligand field strength.

Can. J. Chem. Downloaded from www.nrcresearchpress.com by 210.87.254.42 on 09/05/12
For personal use only.

TABLE 5. Electronic spectra (in kK) of solid complexes and their DMF solutions (log ε in parentheses)

Compound	State		d–d band
$Pd(Hdtma)_2X_2$	Solid	23.0–23.8sh	28.6–29.4
	DMF + L(0.01 *M*)	21.4(2.40)	27.6(4.04)
$Pd(Hdpma)_2X_2$	Solid	22.7–23.0sh	26.3–27.0
	DMF + L(0.01 *M*)	20.4sh(~3.00)	23.6sh 25.2sh
$Pd(Hdtma)Cl_2$	Solid	19.2sh	26.0sh
	DMF	19.4(2.50)	23.8sh 25.5sh 29.0(3.97) 31.6(4.06) 37.7(4.41)
$Pd(Hdtma)Br_2$	Solid	18.7sh	22.9sh
	DMF	19.0(2.37)	23.8sh 25.3sh 28.5(3.92) 31.6sh 35.3(4.29)
$Pd(Hdpma)Cl_2$	Solid	19.6sh	24.4
	DMF	20sh(~2.71)	24.0(3.86) 27.8(4.40) 36.4sh
$Pd(Hdpma)Br_2$	Solid	19.0sh	23.5sh
	DMF	19.1sh(~2.57)	23.5sh 28.0(4.42) 34.2(4.46)
$Pd(Hdpma)I_2$	Solid	18.5sh	20.8sh 26.7
	DMF	17.2sh(~2.57)	23.6sh 30.1(4.51)

The assignment of the d–d band in the spectra of the $PdHLX_2$ (X = Cl, Br, I) complexes (Table 5) is confirmed, as the decreasing energy in the sequence Cl > Br > I corresponds to the position of the halides in the spectrochemical series.

The DMF solution electronic spectra (Table 5) of $Pd(HL)_2X_2$ complexes are identical with one another, different from the solid electronic spectra and do not seem to be affected by the presence of excess ligand, indicating the same solvent effect in the primary coordination sphere of the metal ion. Therefore, while the λ_M values (Table 1) of $Pd(HL)_2X_2$ (X = Br, I, ClO_4) complexes are typical of 1:2 electrolytes in DMF (26), the low values for $Pd(HL)_2Cl_2$ complexes are indicative of strong interactions between $Pd(HL)_2^{2+}$ cation and chloro anions. The DMF solution electronic spectra of the $PdHLX_2$ complexes, except $Pd(Hdpma)X_2$ (X = Cl, Br), may suggest a strong solvent effect in the primary coordination sphere of the metal ions. The λ_M values for $PdHLX_2$ complexes indicate a partial dissociation of complexes in DMF solution.

The author is grateful to Professor Giorgio Peyronel for stimulating discussion and for his kind support. This work was supported by the financial aid of the Consiglio Nazionale delle Ricerche of Italy.

1. V. N. ODNORALOVA and G. I. KUDRYAVTSEV. Vysokomolekul. Soedin. **4**, 1314 (1962).
2. G. BARNIKOW and H. KUNZEK. Z.Chem. **6**, 343 (1966).
3. G. PEYRONEL, G. C. PELLACANI, G. BENETTI, and G. POLLACCI. J. Chem. Soc. Dalton, 879 (1973).
4. R. H. HOLM and M. J. O'CONNOR. Progr. Inorg. Chem. **14**, 241 (1971).
5. G. PEYRONEL, A. C. FABRETTI, and G. C. PELLACANI. J. Inorg. Nucl. Chem. **35**, 973 (1973).
6. A. C. FABRETTI, G. C. PELLACANI, and G. PEYRONEL. Gazz. Chim. Ital. **103**, 397 (1973).
7. W. M. MACNEVIN and O. H. KRIEGE. Anal. Chem. **27**, 535 (1955).
8. K. JENSEN and P. H. NIELSEN. Acta Chem. Scand. **20**, 597 (1966).
9. O. SIIMANN and J. FRESCO. Inorg. Chem. **8**, 1846 (1969) and references cited therein.
10. O. SIIMANN and J. FRESCO. J. Chem. Phys. **54**, 734 (1971).
11. J. OJIMA, T. ONISHI, T. IWAMOTO, N. INAMOTO, and K. TAMARU. Inorg. Nucl. Chem. Lett. **6**, 65 (1970).
12. D. M. ADAMS and J. B. CORNELL. J. Chem. Soc. 1299 (1968).
13. D. M. ADAMS. Metal–ligand and related vibrations. E. Arnold Publ., London. 1967. pp. 225, 302, 325, 326.
14. C. W. SCHLAPFER and K. NAKAMOTO. Inorg. Chim. Acta, **6**, 177 (1972).
15. O. SIIMANN and J. FRESCO. J. Am. Chem. Soc. **92**, 2652 (1970).
16. H. B. GRAY and C. J. BALLHAUSEN. J. Am. Chem. Soc. **85**, 260 (1963).
17. A. R. LATHAM, V. S. HASCALL, and H. B. GRAY. Inorg. Chem. **4**, 789 (1965).
18. H. B. GRAY. Trans. Metal. Chem. **1**, 239 (1965).
19. B. G. WERDEN, E. BILLIG, and H. B. GRAY. Inorg. Chem. **5**, 78 (1966).
20. U. AGARWALA and LAKSHMI AGARWALA. J. Inorg. Nucl. Chem. **34**, 251 (1972).
21. J. R. FERRARO. Low-frequency vibrations of inorganic and coordination compounds. Plenum Press, New York. 1971. pp. 162, 166, 205.
22. B. J. HATHAWAY and A. E. UNDERHILL. J. Chem. Soc. 3091 (1961).
23. W. KITCHING, G. J. MOORE, and D. DODDRELL. Inorg. Chem. **9**, 521 (1970).
24. J. PLUSCEC and A. D. WESTLAND. J. Chem. Soc. 5371 (1965).
25. E. A. ALLEN, N. P. JOHNSON, D. T. ROSEVEAR, and W. WILKINSON. J. Chem. Soc. 2137 (1970).
26. W. J. GEARY. Coord. Chem. Rev. **7**, 81 (1971).

Can. J. Chem. Downloaded from www.nrcresearchpress.com by 210.87.254.42 on 09/05/12
For personal use only.

Solubility of Indium Trichloride and Some Double Salts

ELINOR M. KARTZMARK
University of Manitoba, Winnipeg, Manitoba R3T 2N2

Received May 1, 1974

ELINOR M. KARTZMARK. Can. J. Chem. **52**, 3459 (1974).

The solubility of indium trichloride in water has been determined in the range 25 to 110 °C. The ternary systems: indium chloride – sodium chloride – water; indium chloride – calcium chloride – water, and indium chloride – dioxane – water, have been investigated at 25 °C. Three double salts have been found to occur, having the formulas: $6(InCl_3 \cdot 3H_2O) \cdot 5(CaCl_2 \cdot 4H_2O)$; $InCl_3 \cdot 3C_4H_8O_2 \cdot 2H_2O$, and $InCl_3 \cdot 2C_4H_8O_2 \cdot 2H_2O$.

ELINOR M. KARTZMARK. Can. J. Chem. **52**, 3459 (1974).

On a déterminé la solubilité du trichlorure d'indium dans l'eau dans l'intervalle de température de 25 à 110 °C. On a examiné à 25 °C les systèmes ternaires: chlorure d'indium, chlorure de sodium, eau; chlorure d'indium, chlorure de calcium, eau et chlorure d'indium et dioxanne, eau. On a trouvé que trois sels doubles peuvent exister et qu'ils répondent aux structures suivantes: $6(InCl_3 \cdot 3H_2O) \cdot 5(CaCl_2 \cdot 4H_2O)$; $InCl_3 \cdot 3C_4H_8O_2 \cdot 2H_2O$ et $InCl_3 \cdot 2C_4H_8O_2 \cdot 2H_2O$.
[Traduit par le journal]

Can. J. Chem. Downloaded from www.nrcresearchpress.com by 210.87.254.40 on 09/05/12
For personal use only.

For some time, in this laboratory we have been studying the thermodynamic properties and electrical conduction of solutions of indium trichloride in water and in water–dioxane mixtures (1, 2). To round out this work, it seemed desirable to study the solubility of this salt in water and water–dioxane mixtures and in ternary systems with other salts.

This paper reports on the systems: indium chloride – sodium chloride – water, indium chloride – calcium chloride – water, and indium chloride – dioxane – water, all at 25 °C, as well as the solubility of indium chloride in water, in the temperature range 25–110 °C.

The only relevant data in the literature appear in a series of papers by Ensslin *et al.* (3), which are quoted in the compilation of solubilities by Linke and Seidell (4), where little comment is given as to their reliability. Ensslin *et al.* report a high solubility of indium chloride in many non-aqueous solvents and the formation of a remarkable number of hydrated ternary compounds between indium chloride and other salts. Their experimental method of determining the formulas of the compounds is quite unacceptable. They prepared saturated solutions of the salts in question in a desiccator over phosphorus pentoxide, at room temperature. They removed the solid phase by filtration, pressed it dry with filter paper, and analyzed. Obviously, such solids are not pure phases. The well-known "wet rest" method of Schreinemakers (5) is the only satisfactory method of determining the composition of double salts. For example, in the system: indium chloride – calcium chloride – water, Ensslin *et al.* report compounds of "formulas" $CaCl_2 \cdot 2InCl_3 \cdot 12H_2O$, $3CaCl_2 \cdot 4InCl_3 \cdot 30H_2O$, $CaCl_2 \cdot InCl_3 \cdot 8H_2O$.

On the face of it, the existence of so many double salts appeared doubtful. No work has been reported in the literature on indium chloride in water–dioxane mixtures.

Experimental

Materials

The indium chloride was obtained in the form of pure, concentrated solution from Cominco (1). Fisher certified dioxane was purified by the method of Hess and Frahm (6). The sodium chloride and calcium chloride were reagent grade and were used without further purification.

Temperature Control

Solutions were equilibrated for 24 to 48 h, in a thermostat at 25 ± 0.01 °C. The high temperature bath consisted of a high boiling oil controlled to ±0.05 °C.

(A) Solubility of Indium Chloride in Water

Saturated solutions of indium chloride at low temperatures are exceedingly viscous and therefore difficult to filter. An apparatus which permitted filtration within the oil bath was designed, so that the lengthy filtration process was done at bath temperature, using air pressure. Saturation was approached from both higher and lower temperatures to ensure equilibrium.

The indium chloride was determined by precipitation of Cl^- as silver chloride (7), with a reproducibility of 0.02%. The actual error in solubility determination is greater than this, due to problems encountered in filtration. The solubilities in weight % are plotted against

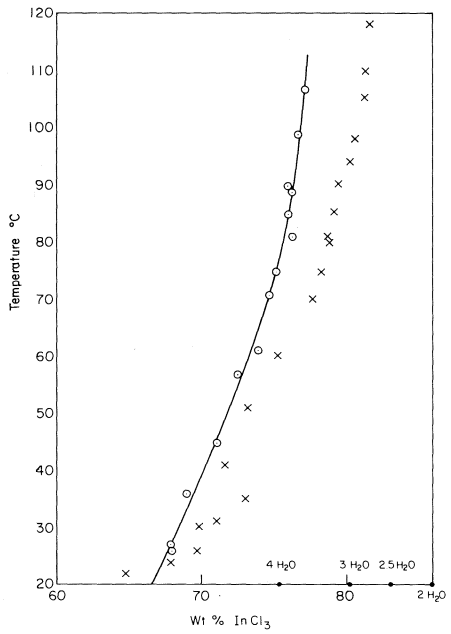

FIG. 1. Solubility of indium chloride in water. ⊙, this work; ×, Ensslin *et al.* (3).

temperature in Fig. 1; the data are to be found in the Depository of Unpublished Data.[1]

(B) System: Indium Chloride – Sodium Chloride – Water, at 25 °C

Analysis for Cl^- was done as in (*A*). Indium was determined by precipitation with ammonia. The indium hydroxide was converted to In_2O_3 by heating in an electric furnace at 600 °C. The reproducibility of this method is not better than 0.1%. The sodium chloride was obtained by difference. The data are to be found in the Depository of Unpublished Data[1] and are plotted in Fig. 2.

(C) System: Indium Chloride – Calcium Chloride – Water at 25 °C

This system was analyzed as in (*B*), calcium chloride being determined by difference. The data are to be found in the Depository of Unpublished Data[1] and are expressed graphically in Fig. 3.

(D) System: Indium Chloride – Dioxane – Water, at 25 °C

This system became of interest when an attempt was made to precipitate indium chloride from the highly concentrated stock solution (57 wt%) by addition of *p*-dioxane. A heavy white precipitate appeared immediately. Since the precipitate was not deliquescent, as are $InCl_3$ and $InCl_3 \cdot 3H_2O$, it was obvious that a new

[1]These data may be obtained, at a nominal charge, from the Depository of Unpublished Data, National Science Library, National Research Council of Canada, Ottawa, Canada K1A 0S2.

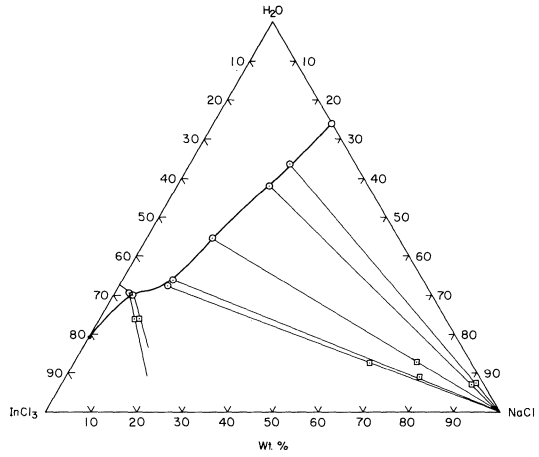

FIG. 2. System $InCl_3$–NaCl–H_2O at 25 °C. ⊙, composition of liquid; ⊡, composition of "wet rest."

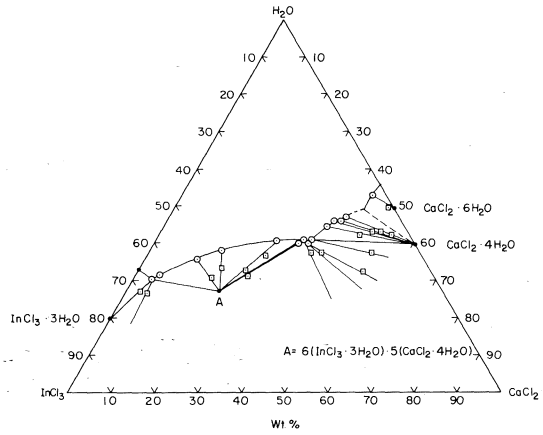

FIG. 3. System $InCl_3$–$CaCl_2$–H_2O at 25 °C. ⊙, composition of liquid; ⊡, composition of "wet rest."

compound had formed. The solubilities were determined as follows: indium chloride was determined by chloride analysis. A second property is necessary for the analysis of a ternary system and for this purpose refractive index was chosen.

The refractive indices of solutions made by adding different weights of water to indium chloride, to dioxane, and to four pseudobinary systems:

(*1*) 85.71% indium chloride – 14.29% dioxane; (*2*) 69.23% indium chloride – 30.77% dioxane; (*3*) 45.00% indium chloride – 55.00% dioxane; (*4*) 33.33% indium chloride – 66.67% dioxane; were measured and plotted *vs.* water content, for the six systems (refractive indices were measured using a Pulfrich refractometer, thermostatically controlled at 25°). Lines of equal refractive index were constructed on a very large triangular diagram (about 32 in. side). The analysis of an unknown consisted in determining its refractive index and indium chloride content, the composition of the solution lying at the point of intersection of the two lines. Analysis of "known"

Can. J. Chem. Downloaded from www.nrcresearchpress.com by 210.87.254.40 on 09/05/12
For personal use only.

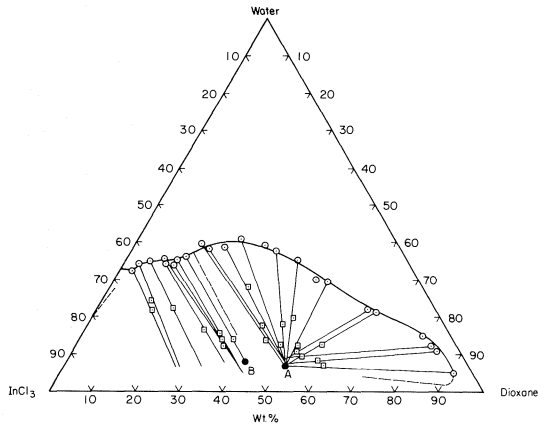

FIG. 4. System $InCl_3$–dioxane–H_2O at 25 °C. A = $InCl_3 \cdot 3$dioxane$\cdot 2H_2O$. B = $InCl_3 \cdot 2$dioxane$\cdot 2H_2O$. ⊙, composition of liquid; ⊡, composition of "wet rest".

solutions by this method gave indium chloride (as $AgCl_2$) to ±0.05% and dioxane to ±0.5%. Because of the rather large error in the dioxane determination it was necessary to prepare an unusually large number of saturated solutions in order to obtain the compositions of the compounds without ambiguity. The data are plotted in Fig. 4.

Discussion

The solubilities quoted by Ensslin *et al.* (3) are considerably higher than those of the present work where great care was taken to ensure equilibrium had been established. Apparently on the basis of three "breaks" in the solubility curve, they claimed the existence of four hydrates, *viz.* $InCl_3 \cdot 4H_2O$; $InCl_3 \cdot 3H_2O$; $InCl_3 \cdot 2.5\ H_2O$; and $InCl_3 \cdot 2H_2O$; the tetrahydrate being stable at 25 °C. The solubilities in wt% obtained in this work plot on a smooth curve, within the experimental error (Fig. 1); the existence of several hydrates would have to be demonstrated by thermal analysis or a systematic study of suitable ternary systems at different temperatures. The ternary systems at 25 °C show that the stable hydrate is the trihydrate at this temperature. The solubility data are to be found in the Depository of Unpublished Data[1] in terms of wt% and molality, *vs.* temperature. When subjected to a least squares program fitted to the equation

$$y = y_{24^\circ} + a(t - 24)^{1/2} + b(t - 24) + c(t - 24)^{3/2} + d(t - 24)^2$$

the constants have the following values: for y (wt%), $y_{24^\circ} = 67.70$, $a = -0.2593$, $b = 0.1795$, $c = 0.01806$, $d = -0.002453$ (standard error of the estimate 0.2715); for y (molality), $y_{24^\circ} = 9.420$, $a = 0.02803$, $b = -0.02204$, $c = 0.03109$, $d = -0.002347$ (standard error of the estimate 0.1869).

The system: indium chloride – sodium chloride – water (Fig. 2) shows no features of interest except that the invariant solution contains little sodium chloride (3.8%). There are no compounds or solid solutions.

In Fig. 3, the existence of a congruently saturating double salt of the formula, $6(InCl_3 \cdot 3H_2O) \cdot 5(CaCl_2 \cdot 4H_2O)$, is proved. The system calcium chloride – water is well known to show a transition

$$CaCl_2 \cdot 6H_2O \rightarrow CaCl_2 \cdot 4H_2O + 2H_2O$$

at 30 °C. The temperature of this transition is decreased below 25 °C, due to the presence of indium chloride and results in both hydrates having a range of stability in the ternary system at 25 °C. A summary of the solubility data at the invariant points is given below.

Wt%		
$InCl_3$	$CaCl_2$	Nature of solid phase
—	44.5	$CaCl_2 \cdot 6H_2O$
7.0	43.0 (estimated)	$CaCl_2 \cdot 6H_2O$ + $CaCl_2 \cdot 4H_2O$
24.6	35.0	$CaCl_2 \cdot 4H_2O$ + double salt
43.0	18.5	Double salt, $6(InCl_3 \cdot 3H_2O) \cdot 5(CaCl_2 \cdot 4H_2O)$
64.2	4.90	Double salt + $InCl_3 \cdot 3H_2O$
67.6	—	$InCl_3 \cdot 3H_2O$

There is no evidence for the existence of the compounds reported by Ensslin *et al.* (3).

Attempts to obtain the solubility of indium chloride in dioxane in the apparatus which was open to the atmosphere failed, due to the presence of a small amount of water. The heat of solution in dioxane (measured approximately as greater than −9 kcal/mol) suggests the formation of a compound between indium chloride and dioxane. Two ternary compounds were found to exist: A, having formula $InCl_3 \cdot 3$dioxane$\cdot 2H_2O$, which is congruently saturating in water and occupies a large area of the ternary diagram (Fig. 4), and B, $InCl_3 \cdot 2$dioxane$\cdot 2H_2O$ which resulted when dioxane was added to the stock solution containing 57% $InCl_3$. The analyses of wet solid residues showed limited solid solubility of $InCl_3 \cdot 3H_2O$ in $InCl_3 \cdot 2$dioxane$\cdot 2H_2O$. It is inter-

Can. J. Chem. Downloaded from www.nrcresearchpress.com by 210.87.254.40 on 09/05/12
For personal use only.

esting that, despite their size, three molecules of dioxane have replaced one of water from the trihydrate to form compound A, while two molecules of dioxane have replaced one of water in compound B. This matter will be investigated further by a single crystal analysis.

1. A. N. CAMPBELL. Can. J. Chem. **51**, 3006 (1973).
2. A. N. CAMPBELL, E. M. KARTZMARK, and O. N. BHATNAGAR. Can. J. Chem. **52**, 1954 (1974).
3. F. ENSSLIN, B. ZIEMECK, and L. DE SCHAEPDRYVER. Z. Anorg. Chem. **254**, 293 (1947); **254**, 297 (1947).
4. W. F. LINKE and A. SEIDELL. Solubilities of inorganic and metal organic compounds. Vol. 1. 4th ed. ACS, Washington. 1958.
5. F. A. H. SCHREINEMAKERS. Z. Phys. Chem. **11**, 76 (1893).
6. K. HESS and H. FRAHM. Ber. **71**, 2627 (1938).
7. I. M. KOLTHOFF and E. B. SANDELL. Textbook of quantitative inorganic analysis. 3rd ed. MacMillan, New York. 1952. p. 307.

Can. J. Chem. Downloaded from www.nrcresearchpress.com by 210.87.254.40 on 09/05/12
For personal use only.

The Dipole Polarizability of the Hydrogen Molecular Ion: A Variational Two-Center Calculation

R. P. McEachran and Sharon Smith
Physics Department, York University, Toronto, Ontario M3J 1P3

AND

M. Cohen
School of Chemistry, The Hebrew University, Jerusalem, Israel

Received November 15, 1973[1]

R. P. McEachran, Sharon Smith, and M. Cohen. Can. J. Chem. **52**, 3463 (1974).

The electric dipole polarizability tensor of the hydrogen molecule-ion has been calculated variationally over a wide range of internuclear separations, using the accurate two center James (ref. 3) orbital as the unperturbed wavefunction. Our most accurate values, obtained with first order functions containing between three and five variational parameters, are in good agreement with some recent moment function values calculated by Bates (ref. 7).

R. P. McEachran, Sharon Smith et M. Cohen. Can. J. Chem. **52**, 3463 (1974).

On calcule d'une façon variationnelle, le tenseur de polarisabilité du dipôle électrique de la molécule-ion d'hydrogène sur un grand intervalle de séparations internucléaires, en utilisant l'orbitale exacte James à deux centres (ref. 3) comme une fonction d'onde non-perturbée. Les valeurs les plus précises, obtenues par des fonctions de premier ordre contenant entre trois et cinq paramètres variables, sont en bon accord avec quelques valeurs de fonctions récemment calculées par Bates (ref. 7). [Traduit par le journal]

Introduction

The calculation of molecular dipole polarizabilities provides a classic example of the use of Rayleigh–Schrödinger (R.S.) perturbation theory. The hydrogen molecule-ion, H_2^+, is actually the simplest physical system for which the relevant differential equation cannot be solved in closed form. It was shown by Rahman (1) that, whereas the field-free Schrödinger equation of H_2^+ is separable in confocal elliptic coordinates, the first order R.S. equation corresponding to a uniform electric field in any chosen direction is *not* separable. Thus, approximate methods are required in its solution.

Fortunately, the energy of polarization is a second order quantity whose calculation may be cast in a variational form. The standard variational procedure is based on a *minimum* principle for the second order energy and would yield a rigorous *lower* bound to the dipole polarizability if the *exact* unperturbed orbital $\psi^{(0)}$ were used as zero-order approximation. But when an *approximate* unperturbed orbital $\phi^{(0)}$ is used, the resulting value of the polarizability may no longer provide a bound. A good example is provided by some recent calculations of Adamov *et al.* (2) on H_2^+. At $R = 2$ a.u. (the equilibrium separation) they obtain the following lower bounds for the parallel polarizability (in a.u.): $\alpha^{(1)} \geqslant 3.442$ ($\phi^{(0)}$ a single parameter approximation), $\alpha^{(2)} \geqslant 5.173$ ($\phi^{(0)}$ a two parameter approximation). Since the two parameter unperturbed orbital due to James (3) is known to be highly accurate not only from the point of view of its energy but also from its very high overlap with the exact $\psi^{(0)}$ (4) it seems reasonable to assume that $\alpha^{(2)}$ is highly accurate. In fact, this value is very close to that obtained by Rahman (1) ($\alpha_{\|} = 5.059$) from a very refined approximate calculation based on the exact $\psi^{(0)}$ of Johnson (5), yet it is clear that the Adamov *et al.* value is *not* a rigorous lower bound. The formal difficulty is resolved by recognizing that any approximate $\psi^{(0)}$ introduces an effective (or model) Hamiltonian in place of the exact physical Hamiltonian, so that the calculations are really appropriate to a model system similar to, but not identical with, the physical one.

In the present paper, we give a brief review of the theory, as well as a description of our calculations together with an assessment of our results in the light of earlier work.

[1]Revision received June 27, 1974.

Can. J. Chem. Downloaded from www.nrcresearchpress.com by 210.87.254.6 on 09/05/12
For personal use only.

Can. J. Chem. Downloaded from www.nrcresearchpress.com by 210.87.254.6 on 09/05/12
For personal use only.

Theory

Consider a system of charged particles whose field-free motion is described by a Hamiltonian $H^{(0)}$. When the system is placed in a uniform electric field $\boldsymbol{F}$, the electrostatic interaction between its dipole moment $\boldsymbol{d}$ and the field $\boldsymbol{F}$ modifies the Hamiltonian to

$$[1] \qquad H = H^{(0)} - \boldsymbol{d}\cdot\boldsymbol{F}$$

and it is usual to expand the energy eigenfunctions $\psi(\boldsymbol{F})$ and the corresponding eigenvalues $E(\boldsymbol{F})$ of the complete Hamiltonian H in powers of the *field strength* $\boldsymbol{F}$

$$[2] \quad \psi(F) = \psi^{(0)} + F\psi^{(1)} + F^2\psi^{(2)} + ...$$

$$[3] \quad E(\boldsymbol{F}) = E^{(0)} - \boldsymbol{\mu}\cdot\boldsymbol{F} - \tfrac{1}{2}!\,(\boldsymbol{\alpha} : \boldsymbol{FF}) - .....$$

For atoms and homonuclear molecules, the permanent dipole moment $\boldsymbol{\mu}$ vanishes, so that the leading energy correction is *second* order in the field and its magnitude is related to the elements of the polarizability tensor $\boldsymbol{\alpha}$. Comparison of eq. 3 with the conventional R.S. energy expansion

$$[4] \quad E(\boldsymbol{F}) = E^{(0)} + FE^{(1)} + F^2E^{(2)} + ...$$

indicates that we must calculate second order energies $E^{(2)}$, which require the first order functions $\psi^{(1)}$ appropriate to fields $\boldsymbol{F}$ in various directions.

For a linear molecule with cylindrical symmetry about the internuclear axis (conventionally labelled the z-axis) the polarizability tensor has only three non-vanishing diagonal elements. These are called the parallel component $\alpha_{\|}$ where

$$[5] \qquad \alpha_{\|} = -2\langle\psi_z^{(1)}|d_z|\psi^{(0)}\rangle$$

and the perpendicular components, $\alpha_{\perp}$, where

$$[6a] \qquad \alpha_{\perp} = -2\langle\psi_x^{(1)}|d_x|\psi^{(0)}\rangle$$

$$[6b] \qquad = -2\langle\psi_y^{(1)}|d_y|\psi^{(0)}\rangle$$

from symmetry.

For simplicity of presentation, we discuss here the calculation of $\alpha_{\|}$ only; the case of $\alpha_{\perp}$ is completely analogous.

In eq. 5, $\psi_z^{(1)}$ is the well behaved solution of the first-order R.S. equation

$$[7] \qquad (H^{(0)} - E^{(0)})\,\psi_z^{(1)} = d_z\psi^{(0)}$$

The formal solution of this equation may be written

$$[8] \qquad \psi_z^{(1)} = \sum_{k\neq 0} \frac{\langle\psi^{(0)}|d_z|\psi_k\rangle}{E_k - E^{(0)}}\,\psi_k$$

where the ψ_k are exact excited state solutions of the field-free Schrödinger equation with corresponding exact energies E_k, and the "sum" includes contributions from the continuum as well as from an infinite number of discrete excited states. The polarizability may then be written

$$[9a] \qquad \alpha_{\|} = 2\sum_{k\neq 0} \frac{|\langle\psi^{(0)}|d_z|\psi_k\rangle|^2}{E_k - E^{(0)}}$$

$$[9b] \qquad = 3\sum_{k\neq 0} f_k^{\|}/(E_k - E^{(0)})^2$$

where we have introduced the parallel oscillator strength $f_k^{\|}$. Equation 9*b* has been used to calculate the polarizability of H_2^+ (6, 7) from accurate oscillator strengths, and the resulting values are strictly lower bounds since only a *finite* number of discrete transitions and transitions to various continua are included in the summation. Direct solution of eq. 7 should avoid the uncertainties inherent in the infinite sums. Now, provided that the field free eigenfunction $\psi^{(0)}$ and energy $E^{(0)}$ are known exactly, the accurate calculation of $\alpha_{\|}$ is limited only by the accuracy of the solution $\psi_z^{(1)}$. Since eq. 7 is not separable and must therefore be solved approximately, it is usual to employ a variational procedure due to Hylleraas (8) in which the functional

$$[10] \quad J_{\|} = \langle\phi_z^{(1)}|H^{(0)} - E^{(0)}|\phi_z^{(1)}\rangle - 2\langle\phi_z^{(1)}|d_z|\psi^{(0)}\rangle$$

is minimized. The minimum value of $J_{\|}$ then provides a *lower bound* to the polarizability

$$[11] \qquad \alpha_{\|} \geqslant -2J_{\|}$$

However, for most electronic systems other than the hydrogen atom, $\psi^{(0)}$ and $E^{(0)}$ are known only *approximately*. In the case of H_2^+, virtually exact eigenfunctions are available (for a review see Bates and Reid (9)) but their form is quite complicated.

It is therefore more convenient to use an approximate form $\phi^{(0)}$ for $\psi^{(0)}$. We are then faced with a choice of alternative procedures. If we write an effective Hamiltonian $\mathfrak{H}^{(0)}$ corresponding to $\phi^{(0)}$ with eigenvalue $\varepsilon^{(0)}$ we may seek a variational solution of an approximate

Can. J. Chem. Downloaded from www.nrcresearchpress.com by 210.87.254.6 on 09/05/12
For personal use only.

equation similar to eq. 7 by minimizing the functional

$$[12a]\quad J_{\|} = \langle \phi_z^{(1)} | \mathfrak{H}^{(0)} - \varepsilon^{(0)} | \phi_z^{(1)} \rangle - 2\langle \phi_z^{(1)} | d_z | \phi^{(0)} \rangle$$

However, on the assumption that $\phi^{(0)}$ is an accurate representation of $\psi^{(0)}$, it may be thought preferable to use the exact $H^{(0)}$ instead of the effective $\mathfrak{H}^{(0)}$. Then, in order for the functional to remain invariant under addition of arbitrary multiples of $\phi^{(0)}$ to the first-order $\phi_z^{(1)}$, we must for consistency use $\bar{E} = \langle \phi^{(0)} | H^{(0)} | \phi^{(0)} \rangle$ as the energy parameter in the functional

$$[12b]\quad J_{\|} = \langle \phi_z^{(1)} | H^{(0)} - \bar{E} | \phi_z^{(1)} \rangle - 2\langle \phi_z^{(1)} | d_z | \phi^{(0)} \rangle$$

This is the procedure implicitly followed by Kaneko and Inokuti (10) in their calculations on the hydrogen atom.

Since $\phi^{(0)}$ is not exact, the variational calculation based on [12*a*] now guarantees a lower bound to the polarizability of a *model* system with Hamiltonian $\mathfrak{H}^{(0)}$. On the other hand, the variational calculation based on [12*b*] cannot yield a bound, but it is to be expected that the two sets of values will be very similar provided that $\phi^{(0)}$ is a sufficiently good representation of $\psi^{(0)}$.

Calculations

For $\phi^{(0)}$, we have used a two parameter orbital due to James (3)

$$[13]\quad \phi^{(0)} = N e^{-a\lambda}(1 + b\mu^2)$$

Here, λ and μ are the usual confocal elliptical coordinates, and N is a normalization constant. The variational parameters a and b have been calculated by Jackson *et al.* (11) over a wide range of internuclear separations ($0.2 \leqslant R \leqslant 6.0$ a.u.). The energy calculated with this $\phi^{(0)}$ is within 2% of the most accurate values available (12) over the entire range of internuclear separations studied. The overlap of this $\phi^{(0)}$ with the virtually exact $\psi^{(0)}$ of Bates *et al.* (13) ranges from 0.9999 at $R = 1$ a.u. to 0.9995 at $R = 4$ a.u. (14). Thus, it is clear that this $\phi^{(0)}$ represents a very good approximation to the unperturbed orbital $\psi^{(0)}$.

An effective Hamiltonian $\mathfrak{H}^{(0)}$ corresponding to $\phi^{(0)}$ may be written in confocal elliptic coordinates

$$[14]\quad \mathfrak{H}^{(0)} = -\frac{2}{R^2(\lambda^2 - \mu^2)}\left\{\frac{\partial}{\partial\lambda}\left[(\lambda^2 - 1)\frac{\partial}{\partial\lambda}\right] + \frac{\partial}{\partial\mu}\left[(1 - \mu^2)\frac{\partial}{\partial\mu}\right] + \frac{(\lambda^2 - \mu^2)}{(\lambda^2 - 1)(1 - \mu^2)}\frac{\partial^2}{\partial\phi^2} + 2a\lambda + a^2(1 - \mu^2) + \frac{2b(3\mu^2 - 1)}{1 + b\mu^2}\right\}$$

where R is the internuclear separation in atomic units.

In the case of $\alpha_{\|}$, the perturbation operator d_z is given explicitly as

$$[15]\quad d_z = R\lambda\mu$$

and the symmetry of d_z and $\phi^{(0)}$ suggests the following trial form for $\phi_z^{(1)}$:

$$[16]\quad \phi_z^{(1)} = \phi^{(0)} \sum_{m=0}^{\infty} f_{2m+1}(\lambda)\, P_{2m+1}(\mu)$$

with

$$[17]\quad f_{2m+1}(\lambda) = \sum_{n=0}^{\infty} a_n^{(2m+1)}\, P_n(\lambda)$$

where $P_n(\lambda)$ is the usual Legendre polynomial of order n.

In the case of $\alpha_{\perp}$, for which the perturbation operator d_x is given by

$$[18]\quad d_x = R(\lambda^2 - 1)^{1/2}(1 - \mu^2)^{1/2}\cos\phi$$

the appropriate form of $\phi_x^{(1)}$ is

$$[19]\quad \phi_x^{(1)} = \phi^{(0)}(\lambda^2 - 1)^{1/2}(1 - \mu^2)^{1/2} \times \cos\phi \sum_{m=0}^{\infty} f_{2m}(\lambda) P_{2m}(\mu)$$

with

$$[20]\quad f_{2m}(\lambda) = \sum_{n=0}^{\infty} a_n^{(2m)} P_n(\lambda)$$

Thus, the practical calculations involve the determination of the expansion coefficients $a_n^{(2m+1)}$ and $a_n^{(2m)}$ through minimization of the functionals $J_{\|}$ and $J_{\perp}$. The functional forms of $\phi_z^{(1)}$ and $\phi_x^{(1)}$ are the same, whether we use the effective $\mathfrak{H}^{(0)}$ of [12*a*] or the exact $H^{(0)}$ of [12*b*].

Results and Discussion

In Table 1, we present values of $\alpha_{\|}$ and $\alpha_{\perp}$ (in a.u.) calculated using [12*a*]. These are con-

TABLE 1. Dipole polarizability of H_2^+ (a.u.)

R	$\alpha_\parallel$	$\alpha_\perp$
0.2	0.3296 (3,0)*	0.3231 (2,0)
0.4	0.4411 (3,1)	0.4098 (2,0)
0.6	0.6091 (3,1)	0.5235 (2,1)
0.8	0.8442 (3,1)	0.6589 (2,1)
1.0	1.165 (3,1)	0.8143 (2,1)
1.2	1.596 (3,1)	0.9878 (2,1)
1.4	2.168 (3,2)	1.178 (2,1)
1.6	2.925 (3,2)	1.384 (2,1)
1.8	3.911 (3,2)	1.601 (2,1)
2.0	5.199 (3,2,1)	1.829 (2,1)
2.5	10.32 (3,2,1)	2.428 (2,1)
3.0	19.94 (3,2,1)	3.040 (2,1,1)
4.0	70.23 (3,2,1,1)	4.132 (2,1,1,1)
5.0	236.7 (3,2,1,1)	4.937 (2,1,1,1)
6.0	783.5 (3,2,1,1)	5.551 (2,1,1,1)

*$(n_1, n_3, \ldots)$ means that in eq. 17 the first n_1 terms corresponding to a_n^1, the first n_3 terms corresponding to a_n^3, etc. were used in the calculation.

verged values, correct to 4 significant figures. Beside each value we give the smallest numbers of expansion coefficients required to reproduce these values, the expansions being ordered with increasing m. At each internuclear separation, we made far more elaborate variational calculations with a maximum of (5,4,3,2) terms for $\alpha_\parallel$ and (5,4,3,2,1) terms for $\alpha_\perp$. In no case do the values obtained with these larger expansions differ by more than one unit in the last figure from the values given in Table 1.

Previous calculations performed for H_2^+ over a wide range of internuclear separations are by Dalgarno and Lewis (6), Calvert and Davison (15), and Bates (7). Calvert and Davison (15) solved the first-order perturbation equation numerically, but took as $\phi^{(0)}$ a series of single-center numerical functions of increasing degrees of refinement. Both Dalgarno and Lewis (6) and Bates (7) used the oscillator strength sum rule, eq. 9*b*, directly.

It seems likely that the results of Bates (7) are, for the most part, reliable. Both our present values and those of Calvert and Davison (15) are in good agreement with those of Bates except at very small internuclear separations, and it seems probable that the continuum contribution may have been underestimated slightly by Bates.

Rahman (1) and more recently Adamov *et al.* (2) have performed accurate first order variational calculations near the equilibrium separation at $R = 2.0$ a.u. Their results, together with our own and those of Calvert and Davison (15) and Bates (7) are collected together in Table 2 for ease for reference. Also presented are our values of $\alpha' = \partial\alpha/\partial R$ and $\alpha'' = \partial^2\alpha/\partial R^2$ at equilibrium; these were determined by a parabolic fit of the data from an additional series of calculations in the neighborhood of $R = 2.00$ a.u. Rahman (1) has demonstrated the importance of these "anharmonic" α' terms in the calculation of transition moments even for low lying vibrational states. In Table 3, we give a sample of our results for $\alpha_\parallel$, calculated using two different zero order functions $\phi^{(0)}$, a one parameter "united atom" orbital (16), as well as the two parameter James orbital. For each $\phi^{(0)}$, we used both functionals [12*a*] and [12*b*]. It is clear from this comparison, that the single parameter $\phi^{(0)}$ is inadequate as a representation of $\psi^{(0)}$ except at very small separations, and this is reflected in the divergence of the values obtained from the two functionals. The more accurate two parameter $\phi^{(0)}$ yields almost identical values of $\alpha_\parallel$ over the entire range of R-values.

These results confirm the reliability of the two parameter James orbital as a representation of the exact $\psi^{(0)}$, and suggest that the variational procedure has produced polarizabilities of

TABLE 2. Dipole polarizability of H_2^+ at equilibrium (a.u.)

	Value				
Parameter	Reference 2	Reference 15	Reference 7	Reference 1	This work
$\alpha_\parallel$	5.173	5.084	5.06	5.061	5.199
$\alpha_\perp$	1.847	1.767	1.76	1.758	1.829
$\alpha_\parallel'$				7.209	7.307
$\alpha_\parallel''$				10.098	9.607
$\alpha_\perp'$				1.132	1.150
$\alpha_\perp''$				0.198	0.227

Can. J. Chem. Downloaded from www.nrcresearchpress.com by 210.87.254.6 on 09/05/12
For personal use only.

TABLE 3. Dipole polarizability $\alpha_{\parallel}$ of H_2^+ using different $\phi^{(0)}$ and different variational functionals

	$\phi^{(0)}$ single parameter		$\phi^{(0)}$ two parameter	
R	[12a]	[12b]	[12a]	[12b]
0.4	0.431	0.429	0.441	0.435
1.0	1.033	1.081	1.165	1.145
2.0	3.475	4.471	5.199	5.143
3.0	8.937	17.58	19.94	19.84

acceptable accuracy over the entire range of internuclear separations studied.

One of us (M.C.) wishes to acknowledge the hospitality of the Physics Department, York University, where part of this research was carried out.

We are grateful to a referee whose critical comments on an earlier version of this work led to a substantially improved version.

This work was supported in part by the National Research Council of Canada.

1. A. RAHMAN. Physica, **19**, 145 (1953).
2. M. N. ADAMOV, T. K. REBANE, and R. A. EVAESTOV. Opt. Spectrosc. **22**, 389 (1967).
3. H. M. JAMES. J. Chem. Phys. **3**, 9 (1935).
4. J. GOODISMAN. J. Chem. Phys. **41**, 820 (1964).
5. V. A. JOHNSON. Phys. Rev. **60**, 373 (1941).
6. A. DALGARNO and J. T. LEWIS. Proc R. Soc. A, **240**, 284 (1957).
7. D. R. BATES. Chem. Phys. Lett. **17**, 184 (1972).
8. E. A. HYLLERAAS. Z. Phys. **65**, 209 (1930).
9. D. R. BATES and R. H. G. REID. Adv. Atom. Mol. Phys. **4**, 13 (1968).
10. S. KANEKO and M. INOKUTI. Chem. Phys. Lett. **23**, 275 (1973).
11. M. JACKSON, R. P. McEACHRAN, and M. COHEN. Chem. Phys. Lett. **10**, 143 (1971).
12. H. WIND. J. Chem. Phys. **42**, 2371 (1965).
13. D. R. BATES, K. LEDSHAM, and A. L. STEWART. Philosoph. Trans. *A*, **246**, 215 (1953).
14. J. KATRIEL. Private communication.
15. J. McI. CALVERT and W. D. DAVISON. Chem. Phys. Lett. **4**, 327 (1969).
16. M. COHEN and R. P. McEACHRAN. Can. J. Phys. **44**, 2809 (1966).

Can. J. Chem. Downloaded from www.nrcresearchpress.com by 210.87.254.6 on 09/05/12
For personal use only.

Erratum: A Kinetic Model of the Accommodation Pumping Phenomenon

GRAHAM RICHARD BRANTON AND STEPHEN ALAN RYCE
Department of Chemistry, University of Victoria, Victoria, British Columbia V8W 2Y2

Received July 26, 1974
(Ref.: Can. J. Chem. **52**, 2073 (1974))

The positions of the labels for Boundary B and Boundary C in Fig. 1 of this article were interchanged inadvertently during printing.

Can. J. Chem. Downloaded from www.nrcresearchpress.com by 210.87.254.5 on 09/05/12
For personal use only.

Some Rhodium(III) Complexes of Linear Tetraamines

ROBERT W. HALLIDAY AND RICHARD H. COURT
Adelphi University, Garden City, New York 11530

Received February 13, 1974

ROBERT W. HALLIDAY and RICHARD H. COURT. Can. J. Chem. **52**, 3469 (1974).

We report the preparation of rhodium(III) complexes of 2,3,2 tet; 3,2,3 tet, 3,3,3 tet, and 3,4,3 tet. In the case of the [Rh(2,3,2 tet)Cl_2]Cl complex, both the *cis*-α and *trans* forms were isolated. In the remaining cases, only the *trans* form was isolated.

ROBERT W. HALLIDAY et RICHARD H. COURT. Can. J. Chem. **52**, 3469 (1974).

On rapporte la préparation de complexes du rhodium(III) avec les 2,3,2 tet, 3,2,3 tet, 3,3,3 tet et 3,4,3 tet. Dans le cas du complexe [Rh(2,3,2 tet)Cl_2]Cl, on a isolé les deux formes *cis*-α et *trans*. Dans les autres cas, seule la forme *trans* a été isolée. [Traduit par le journal]

Can. J. Chem. Downloaded from www.nrcresearchpress.com by 210.87.254.105 on 09/05/12
For personal use only.

During the past several years, a large number of complexes with linear tetraamines as ligands have been prepared. The linear tetraamines have the general formula, $NH_2(CH_2)_nNH(CH_2)_mNH(CH_2)_nNH_2$, where *n* may or may not equal *m*.[1] Three geometric isomers are possible in these complexes, one *trans* and two *cis*. In the *cis*-α isomer the terminal nitrogens of the tetraamine are *trans* to one another, while in the *cis*-β isomer the terminal nitrogens are *cis* to one another.

The isomers of the cobalt(III) complexes of these tetradentate ligands which have previously been prepared are summarized in Table 1. The *cis*-α $[Co(2,3,2\text{ tet})Cl_2]^+$ could only be prepared by the decomposition of the corresponding carbonate complex (3). The *cis*-β isomer in the 2,3,2 tet case occurred only when a bidentate ligand occupied the remaining two positions (4, 6). Similarly, only *cis*-α $[Co(3,2,3\text{ tet})ox]^+$ has been prepared (4). Barefield (13) had difficulty in preparing $[Co(3,3,3\text{ tet})Cl_2]^+$ and did not fully characterize the complex, but suggested that the *trans* topology was formed exclusively.

Rhodium(III) complexes with 2,2,2 tet and 2,3,2 tet have been prepared and characterized (7, 8). While the 2,2,2 tetraamine forms the *cis*-α configuration exclusively, the only reported preparation of $[Rh(2,3,2\text{ tet})Cl_2]^+$ shows the *trans* isomer (7).

In this study, the preparation of four new rhodium complexes with 2,3,2 tet, 3,2,3 tet, 3,3,3 tet, and 3,4,3, tet are reported.

[1]Systematic abbreviations have been developed for these linear tetraamines in which the number of methylene groups are given as a prefix to the ligand abbreviation tet. Thus, the ligand with the formula $NH_2(CH_2)_3NH(CH_2)_2NH(CH_2)_3NH_2$ would be abbreviated as 3,2,3 tet. This system will be used exclusively in this paper.

TABLE 1. Cobalt(III) complexes of the linear tetraamines

Ligand	Isomers	References
2,2,2 tet	*cis*-α, *cis*-β, *trans*	1, 2
2,3,2 tet	*cis*-α, *cis*-β, *trans*	3, 4
3,2,3 tet	*cis*-β, *trans*	4–6
3,3,3 tet	*trans*	13

Experimental

Materials

The rhodium trichloride trihydrate (99.9%) used in the synthesis was obtained from ROC-RIC Corporation and used as received. The diamines and dibromides used in the preparation of 2,3,2 tet, 3,2,3 tet, and 3,3,3 tet were obtained from Aldrich Chemical Co. and used as received. The 3,4,3 tet was commercially available from J. T. Baker (Baker Grade) and was converted to the tetrahydrochloride salt before use.

Preparation of the Linear Tetraamines

We used a procedure similar to that of Brubaker and Schaefer (4). In this method, 2 mol of diamine ($NH_2(CH_2)_nNH_2$) are reacted with 1 mol of dibromide ($Br(CH_2)_mBr$). We note that care should be taken when combining these reagents. They should be mixed slowly and carefully while maintaining the temperature between 25 and 35 °C. This will avoid an overly vigorous reaction. The resultant linear tetraamine was separated from unreacted starting materials and by-products by vacuum distillation.

The crude products of this preparation were converted to the tetrahydrochlorides by the slow addition of a slight excess of concentrated HCl to an alcoholic solution of the tetraamine free base. The precipitate which formed was filtered and recrystallized repeatedly from ethanol–water until the CHN analysis was correct for the tetrahydrochlorides. The purified tetraamine tetrahydrochlorides were used in the preparation of the rhodium complexes.

Analyses

Anal. Calcd. for $C_7H_{20}N_4 \cdot 4HCl$ (2,3,2 tet·4HCl): C, 27.47; H, 7.90; N, 18.30. Found: C, 27.65; H, 8.05; N, 17.99.

Can. J. Chem. Downloaded from www.nrcresearchpress.com by 210.87.254.105 on 09/05/12
For personal use only.

Anal. Calcd. for $C_8H_{22}N_4 \cdot 4HCl$ (3,2,3 tet·4HCl): C, 30.02; H, 8.19; N, 17.50. Found: C, 29.95; H, 7.95; N, 17.10.

Anal. Calcd. for $C_9H_{24}N_4 \cdot 4HCl$ (3,3,3 tet·4HCl): C, 32.35; H, 8.45; N, 16.77. Found: C, 32.16; H, 8.44; N, 16.08.

Anal. Calcd. for $C_{10}H_{26}N_4 \cdot 4HCl$ (3,4,3 tet·4HCl): C, 34.50; H, 8.68; N, 16.09. Found: C, 34.42; H, 8.67; N, 16.56.

Preparation of cis-α-Dichloro-N,N-bis(2-aminoethyl)-1,3-propanediaminerhodium(III) Chloride Monohydrate

A procedure similar to that of Johnson and Basolo (8) was employed. In a typical preparation, 0.99 g of $RhCl_3 \cdot 3H_2O$ (3.76×10^{-3} mol) was dissolved in 50 ml of distilled water in a 500 ml round bottom flask fitted with a condenser. A 1.16 g portion of 2,3,2 tet·4HCl (3.79×10^{-3} mol) was added with stirring. The solution slowly changed from its original dark red color to orange. A 50 ml portion of a 100 ml solution containing 0.90 g of KOH (16.0×10^{-3} mol) was added and the solution refluxed for approximately 10 min until it cleared. To the now light orange solution the remaining 50 ml of KOH solution in 5 ml portions at 2 min intervals was added. After the addition of the remaining KOH the golden yellow solution was evaporated to dryness on a steam bath. The solid which was obtained was recrystallized several times from ethanol–water which removed large quantities of KCl. The pale yellow needles so obtained were washed with ethanol and dried in the oven at 100 °C.

Anal. Calcd. for $RhC_7H_{20}N_4Cl_3 \cdot H_2O$: C, 21.69; H, 5.72; N, 14.46. Found: C, 21.65; H, 5.68; N, 14.4.

Preparation of trans-Dichloro-N,N-bis(2-aminoethyl)-1,3-propanediaminerhodium(III) Chloride Hemihydrate

When the solutions from the recrystallization of the *cis*-α-[Rh(2,3,2 tet)Cl_2]Cl were taken to dryness, a dark yellow powder was obtained. When recrystallized from ethanol/H_2O, the product gave the correct analysis for $RhC_7H_{20}N_4Cl_3 \cdot \frac{1}{2}H_2O$.

Anal. Calcd. for $RhC_7H_{20}N_4Cl_3 \cdot \frac{1}{2}H_2O$: C, 22.21; H, 5.59; N, 14.80. Found: C, 22.44; H, 5.53; N, 14.44.

Preparation of trans-Dichloro-N,N-bis(3-aminopropyl)-1,2-ethane-diaminerhodium(III) Nitrate

This method was similar to that used above with the exception that the ligand was 3,2,3 tet·4HCl, and that concentrated nitric acid was added after partial evaporation due to the difficulty in isolating the chloride in pure form. Dark yellow prisms were obtained.

Anal. Calcd. for $RhC_8H_{22}N_5Cl_2O_3$: C, 23.42; H, 5.40; N, 17.07. Found: C, 23.50; H, 5.50; N, 17.22.

Preparation of trans-Dichloro-N,N-bis(3-aminopropyl)-1,3-propanediaminerhodium(III) Nitrate Hemihydrate

The method was similar to that previously employed with the exception that the ligand was 3,3,3 tet·4HCl. Dark yellow prisms were obtained.

Anal. Calcd. for $RhC_9H_{24}N_3Cl_2O_3 \cdot \frac{1}{2}H_2O$: C, 24.96; H, 5.82; N, 16.17. Found: C, 24.74; H, 6.03; N, 16.22.

Preparation of trans-Dichloro-N,N-bis(3-aminopropyl)-1,4-butanediaminerhodium(III) Chloride

The method was similar to that previously employed with the exceptions that the ligand was 3,4,3 tet·4HCl and that no concentrated nitric acid was added. An orange powder was obtained.

Anal. Calcd. for $RhC_{10}H_{26}N_4Cl_3$: C, 29.18; H, 6.37; N, 13.61. Found: C, 29.28; H, 6.05; N, 13.82.

Elemental Analyses

Carbon, hydrogen, and nitrogen analyses were performed by Schwarzkopf Microanalytical Laboratory, Inc., Woodside, N.Y. or the Analytical Research Department, Ciba-Geigy Corp., Ardsley, N.Y.

Absorption Spectra

Ultraviolet and visible absorption spectra were determined using a Cary 14 or Beckman Acta III recording spectrophotometer. Standard 1 cm quartz cells were used. Ultraviolet spectral measurements were made on aqueous solutions of known concentrations immediately after preparation. The solutions were in the concentration range of 1.0×10^{-2} *M*.

Infrared Spectroscopy

Infrared spectra were obtained using a Perkin–Elmer 257 double beam, grating spectrophotometer. The samples were prepared as potassium bromide pellets.

Results

In this work, we have prepared complexes of rhodium(III) with 2,3,2 tet, 3,2,3 tet, 3,3,3 tet, and 3,4,3 tet. In all cases the procedure employed used trichlorotriaquorhodium(III) as starting material (8).

Anderson and Basolo (9) have shown that for the chloride salts of $[Rh(2,2,2\text{ tet})Cl_2]^+$ the *cis* isomer is less soluble than the *trans* isomer, while for the nitrate salts of the same complex the *trans* isomer is less soluble than the *cis*. In all of our preparations we initially isolated the chloride salts of the complexes and thus favored the isolation of any *cis* isomer formed. In the case of the 2,3,2 tet ligand, unlike previous workers (7), we have isolated both the *cis*-α and *trans* complexes with the rhodium(III) ion. With all other ligands, only a *trans* isomer could be found. In some cases, it was necessary to reprecipitate the original chlorides as nitrates in order to achieve analytical purity.

The topology that these complexes assume was determined principally by their ultraviolet–visible absorption spectra. The peak positions and molar extinction coefficients of the complexes prepared in this study are given in Table 2, along with those of similar rhodium(III) compounds prepared by other workers.

The absorption spectra of the chlorides prepared in this study clearly indicated the *trans* geometry for all but the one to which we assign

TABLE 2. Summary of absorption spectra of rhodium(III) complexes

Complex	λ_{max} (μ)	ε_{max}
cis-$[Rh(en)_2Cl_2]^+$*	352, 295	155, 180
cis-$[Rh(2,2,2\text{ tet})Cl_2]^+$*	352, 293	250, 200
cis-$[Rh(2,3,2\text{ tet})Cl_2]^+$	349, 295	212, 234
trans-$[Rh(en)_2Cl_2]^+$*	406, 286	75, 130
trans-$[Rh(m\text{-bn})_2Cl_2]^+$*†	409, 290 (sh)	75, 120
trans-$[Rh(2,3,2\text{ tet})Cl_2]^+$	408, 286 (sh)	78, 120
trans-$[Rh(3,2,3\text{ tet})Cl_2]^+$	412, 288 (sh)	82, 208
trans-$[Rh(3,3,3\text{ tet})Cl_2]^+$	424, 301	84, 175
trans-$[Rh(3,4,3\text{ tet})Cl_2]^+$	427, 298	131, 196

*Reference 8.
†*m*-bn is *meso*-2,3-butanediamine.

the *cis*-α geometry. We have made these geometric assignments based on work previously done by Basolo and co-worker (8). For a series of *cis* and *trans* $[Rh(en)_2X_2]^+$ complexes (where X = NO_2^-, I^-, Br^-, Cl^-), Basolo and co-worker were able to unequivocally assign the *cis* geometry by the resolution of a *cis* complex into its optical enantiomers. They have also shown that in the series of $[RhN_4X_2]^+$ complexes, the *cis* isomers absorb at a significantly lower wavelength than the *trans* isomers. In addition, both theoretical (10) and experimental (8) considerations indicate that the *cis* isomer exhibits the more intense absorption.

Our results for the $[Rh(2,3,2\text{ tet})Cl_2]^+$ ion are in agreement with the above, *i.e.* the *cis* isomer exhibits a more intense, lower wavelength absorption than does the *trans* isomer. In Table 2 a comparison can also be made between the spectra of the *cis*-α isomer prepared in this study and *cis*-$[Co(en)_2Cl_2]^+$ whose structure was unequivocally determined by resolution into its optical enantiomers. Furthermore, the electronic spectra of the *trans* $[Rh(2,3,2\text{ tet})Cl_2]^+$ prepared in this study is in essential agreement with that of previous workers (λ_{max}, 410 and 290 μ) (7). Since the three remaining complexes in this series have absorptions at wavelengths similar to those of the *trans*-$[Rh(2,3,2\text{ tet})Cl_2]^+$, we have also assigned the *trans* configuration to these complexes.

While the electronic absorption spectra are sufficient for the assignment of *cis* and *trans* topologies they are somewhat ambiguous in determining if the *cis* complex is the α or β geometry. The infrared spectra of these complexes, however, clearly distinguishes between the two possibilities.

A summary of the infrared absorption spectra in the NH stretching (3000–3300 cm^{-1}) and the NH_2 antisymmetric deformation (1560–1600 cm^{-1}) regions is given in Table 3. A rather unexpected result is the observation of two strong absorptions in the NH_2 deformation region of the *trans*-$[Rh(2,3,2\text{ tet})Cl_2]^+$ ion. Casual observation of the spectrum in this region alone would lead to the incorrect assignment of the *cis*-β geometry to this complex. That this structure assignment is in direct opposition to the previous electronic spectral data, which unequivocally established the *trans* geometry for this complex, suggests that one must consider the entire infrared spectra in making structural assignments. A similar problem was encountered by Worrell and Busch (11). The *cis*-α-$[Co(eee)Cl_2]Cl$ complex[2] they prepared exhibited two strong absorptions in the 1560–1600 cm^{-1} region from which the *cis*-β topology would be implied in opposition to the n.m.r. and electronic spectral data. The remaining complexes prepared in this study all exhibit only a single strong absorption in the deformation region which would be consistent with either the *trans* or *cis*-α configuration.

However, in the other regions that are characteristic of configuration, the infrared spectra is in agreement with the assignment of *cis*-α and *trans* geometry to complexes prepared in this study. The absorptions are summarized in Table 4.

As Buckingham and Jones (12) conclude, the 990–1100 cm^{-1} region distinguishes topologies clearly. This region, which they tentatively assign to modes involving NH_2 twisting, exhibits four strong bands for complexes of *cis*-β geometry, three strong bands for *trans* geometry, and only two strong bands for complexes of *cis*-α geometries. As can be seen, the *cis* complex prepared in this study has two sharp bands, while the *trans* complexes have three sharp bands.

An additional region of note is that of the CH_2 bending (1430–1490 cm^{-1}) mode. Here, the spectra becomes less complicated and more intense in the order *cis*-α, *cis*-β, *trans* as would be expected from a decrease in the number of nonbonded interactions (12). The *cis*-α$[Rh(2,3,2\text{ tet})Cl_2]^+$ exhibits four strong to medium bands while the *trans*-$[Rh(2,3,2\text{ tet})Cl_2]^+$ exhibits only three more intense bonds.

Based on the previous discussion we assign the

[2]eee = $H_2N(CH_2)_2S(CH_2)_2S(CH_2)_2NH_2$.

Can. J. Chem. Downloaded from www.nrcresearchpress.com by 210.87.254.105 on 09/05/12
For personal use only.

TABLE 3. NH stretching and antisymmetric deformation frequencies (cm^{-1}) for the *cis* and *trans*-dichlorotetraaminerhodium(III) compounds

Compound	N—H stretch	N—H deformation
cis-α-[Rh(2,3,2 tet)Cl_2]$^+$	3240, 3190, 3130, 3080	1590
cis-α-[Rh(2,2,2 tet)Cl_2]$^+$*	3251, 3205, 3105, 3045	1582
trans-[Rh(2,3,2 tet)Cl_2]$^+$	3240, 3180, 3090	1600, 1592
trans-[Rh(3,2,3 tet)Cl_2]$^+$	3220, 3190, 3130, 3060	1565
trans-[Rh(3,3,3 tet)Cl_2]$^+$	3190, 3130, 3050	1585
trans-[Rh(3,4,3 tet)Cl_2]$^+$	3230, 3170, 3050	1570

*Reference 12.

TABLE 4. Characteristic infrared frequencies (cm^{-1})*

	Frequencies				
	1430–1490	1350–1400	1250–1290	990–1090	860-920
cis-β-[Co(2,2,2 tet)Cl_2]$^+$†	1481 (m)	1390 (w)	1281 (m)	1070 (s)	918 (m)
	1451 (s)	1374 (w)	1265 (w)	1049 (s)	898 (m)
		1364 (w)	1249 (m)	1027 (s)	862 (m)
		1354 (m)		1013 (w)	
				994 (s)	
cis-α-[Co(2,2,2 tet)Cl_2]$^+$†	1491 (w)	1390 (w)	1270 (m)	1058 (m)	905 (m)
	1480 (m)	1374 (m)	1245 (w)	1038 (s)	871 (m)
	1440 (s)	1362 (m)		1005 (w)	
	1431 (s)				
cis-α-[Rh(2,3,2 tet)Cl_2]$^+$	1470 (m)	1400 (m)	1272 (m)	1090 (m)	
	1460 (s)	1380 (s)	1248 (m)	1023 (s)	890 (m)
	1450 (s)	1360 (m)		1052 (s)	862 (m)
	1430 (m)				
trans-[Co(2,2,2 tet)Cl_2]$^+$†	1482 (m)	1381 (w)	1262 (m)	1030 (s)	926 (m)
	1452 (s)	1376 (w)	1250 (w)	1018 (s)	912 (m)
	1433 (w)	1362 (w)	1241 (m)	999 (s)	847 (m)
trans-[Rh(2,3,2 tet)Cl_2]$^+$	1475 (m)	1390 (w)	1292 (m)	1090 (s)	
	1460 (s)	1370 (m)	1265 (w)	1051 (s)	895 (m)
	1448 (m)	1360 (w)	1250 (w)	1032 (s)	872 (m)

*Intensities are estimated as: s, strong; m, medium; w, weak.
†Reference 12.

cis-α topology to the *cis* compound isolated in this study. This result is in agreement with that of the analogous cobalt(III) complexes of 2,3,2 tet prepared by Hamilton and Alexander (3). In that study, they isolated the *trans* isomer and were able to prepare only the *cis*-α salt from the *trans* complex.

Conclusion

In the series of rhodium(III) complexes with linear tetraamines, the size of the ligand appears to determine the configuration of the complex when monodentate ligands occupy the remaining octahedral sites. With the smallest ligand of the series, 2,2,2 tet, only *cis*-α [Rh(2,2,2 tet)Cl_2]Cl was isolated (8). With the next larger ligand, 2,3,2 tet, the complex has been isolated as both the *cis*-α and *trans* isomers. The larger ligands studied here (3,2,3 tet, 3,3,3 tet, and 3,4,3 tet) all assumed the *trans* configuration. Since they were obtained in low yield in most cases, and the major products were not isolated and identified, it is possible that there is considerable strain even in the *trans* configuration of the complex. Molecular models support this theory and indicate the major source of steric strain is possibly in the middle ring formed by the secondary nitrogens and the rhodium ion.

Can. J. Chem. Downloaded from www.nrcresearchpress.com by 210.87.254.105 on 09/05/12
For personal use only.

1. D. A. BUCKINGHAM, P. A. MARZILLI, and A. M. SARGESON. Inorg. Chem. **6**, 1032 (1967).
2. A. M. SARGESON and G. H. SEARLE. Inorg. Chem. **6**, 787 (1967).
3. H. G. HAMILTON, JR. and M. D. ALEXANDER. Inorg. Chem. **5**, 2060 (1966).
4. G. R. BRUBAKER and D. P. SCHAEFER. Inorg. Chem. **10**, 968 (1971).
5. M. D. ALEXANDER and H. G. HAMILTON, JR. Inorg. Chem. **8**, 2131 (1969).
6. G. R. BRUBAKER and D. P. SCHAEFER. Inorg. Chem. **9**, 2373 (1970).
7. B. BOSNICH, R. D. GILLARD, E. D. MCKENZIE, and G. A. WEBB. J. Chem. Soc. A, 1331 (1966).
8. S. A. JOHNSON and F. BASOLO. Inorg. Chem. **1**, 925 (1962).
9. R. ANDERSON and F. BASOLO. J. Am. Chem. Soc. **82**, 4423 (1960).
10. C. J. BALLHAUSEN. Progress in inorganic chemistry, Vol. 2. Interscience Publ. Inc., N.Y. 1960. p. 251.
11. J. H. WORRELL and D. H. BUSCH. Inorg. Chem. **8**, 1563 (1969).
12. D. A. BUCKINGHAM and D. JONES. Inorg. Chem. **4**, 1387 (1965).
13. E. KENT BAREFIELD. Private communication.

Can. J. Chem. Downloaded from www.nrcresearchpress.com by 210.87.254.105 on 09/05/12
For personal use only.

Cycloaddition Reactions of Silyldiazoalkanes Involving Rearrangements from Carbon to Nitrogen

A. R. BASSINDALE AND A. G. BROOK

Department of Chemistry, Lash Miller Chemical Laboratories, University of Toronto, Toronto, Ontario M5S 1A1

Received April 18, 1974

A. R. BASSINDALE and A. G. BROOK. Can. J. Chem. **52**, 3474 (1974).

The products obtained from the 1,3 cycloadditions of a variety of silyldiazoalkanes, R_3SiCN_2R', to several alkenes were studied: the data are consistent with the initial formation of the expected Δ^1-pyrazoline. However, when R′ = Ph, COOEt, but not Me, a thermal 1,3 rearrangement of the silyl group from carbon to nitrogen subsequently occurs. Base-catalyzed isomerizations of the Δ^1 to Δ^2-pyrazolines were noted, as was the desilylation of the Δ^1-pyrazolines in refluxing methanol. Mechanisms are proposed for the various reactions.

A. R. BASSINDALE et A. G. BROOK. Can. J. Chem. **52**, 3474 (1974).

On a étudié les produits obtenus par la cycloaddition 1,3 de plusieurs silyldiazoalcanes, R_3SiCN_2R', à plusieurs alcènes; les résultats obtenus sont en accord avec la formation initiale de la Δ^1 pyrazoline attendue. Toutefois lorsque R′ = Ph ou COOEt (mais pas dans le cas où R′ est égal à Me), un réarrangement thermique 1,3 du groupe silyle se produit subséquemment du carbone vers l'azote. On a noté des isomérisations catalysées par les bases des Δ^1 pyrazolines vers les Δ^2 de même que la désilylation des Δ^1 pyrazolines dans le méthanol à reflux. Des mécanismes sont proposés pour ces diverses réactions.

[Traduit par le journal]

Introduction

Although the cycloaddition reactions of α-silyldiazoalkanes have been the subject of several studies (1–7), the role of organosilicon substituents in determining the reaction products is by no means established. Three types of simple addition compounds have been found to be products, namely the Δ^1-(4), Δ^2-(H-1) (2–6), and Δ^2-(Si-1) (7) pyrazolines (Scheme 1). It is

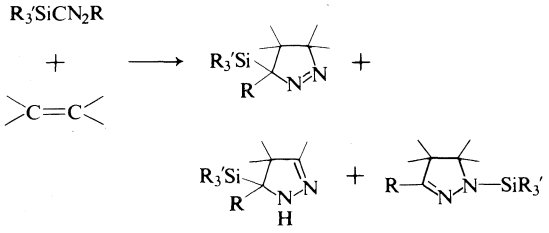

SCHEME 1

well known (9) that most Δ^1-pyrazolines are unstable and readily isomerize to the tautomeric Δ^2-pyrazolines. It is not known how this rearrangement is affected by an organosilicon substituent on the pyrazoline ring. We were particularly interested by the report that the product of cycloaddition of ethyl 1-trimethylsilyl diazoacetate to diethyl fumarate was a Δ^2-pyrazoline with the trimethylsilyl group on N-1. This is one of the very few examples of a Si—C → Si—N rearrangement. The authors (7) proposed the following reaction.

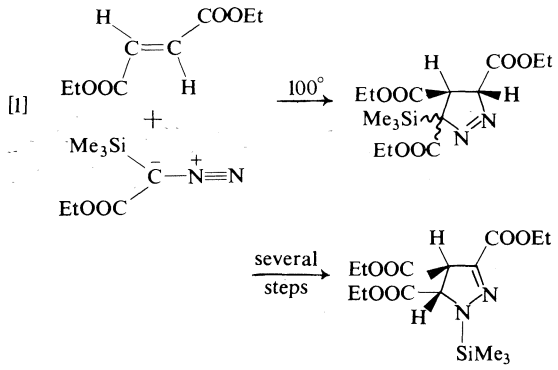

Although the above 'several step' rearrangement is possible, we considered that a 1,3 suprafacial migration of the trimethylsilyl group would be more likely. This rearrangement would give the same product as the several step rearrangement and would be analogous to the known β-ketosilane rearrangement (8). Therefore, we set out to investigate the rearrangement further, and to study in more detail the effects of the organosilicon group ($R_3'Si$) and the organic group (R) on the cycloaddition reactions of diazoalkanes ($R_3'SiCN_2R$) with alkenes.

In this study, the following diazoalkanes were used: 1-trimethylsilyl-1-diazoethane (**1**),1-phe-

Can. J. Chem. Downloaded from www.nrcresearchpress.com by 210.87.254.5 on 09/05/12
For personal use only.

Can. J. Chem. Downloaded from www.nrcresearchpress.com by 210.87.254.5 on 09/05/12
For personal use only.

nyl - 1 - trimethylsilyldiazomethane (**2**),1 - triphenylsilyl-1-diazoethane (**3**), 1-phenyl-1-triphenylsilyldiazomethane (**4**), and ethyl 1-trimethylsilyldiazoacetate (**5**). The addition reactions of **1**–**5** to one or more of the following alkenes were studied; diethyl fumarate, diethyl maleate, methyl acrylate, acrylonitrile, and maleic anhydride.

Results and Discussion

The relative rates of addition of diazoalkanes **1**–**5** to diethyl fumarate were measured. The data given below are for a carbon tetrachloride solution, *ca.* 0.5 M in both diazoalkane and alkene, at room temperature.[1] It was found that the rates decreased in the following order, with the relative rates for complete reaction as shown.

	Me_3SiCN_2Me	>	Me_3SiCN_2Ph	>
Relative rate	1		2×10^{-2}	
	1		**2**	

Ph_3SiCN_2Me	>	Ph_3SiCN_2Ph	>	Me_3SiCN_2COOEt
25×10^{-4}		$\sim 2.5 \times 10^{-6}$		$\sim 2.5 \times 10^{-7}$
3		**4**		**5**

The time for complete reaction of **1** and diethyl fumarate under the stated conditions was 5 min. There is, therefore, a very large substituent effect as illustrated by the differences in rate of greater than 10^6 between **1** and **5**. In order to understand this difference, it is necessary to examine factors affecting both the ground state stabilities of diazoalkanes and the transition state during cycloaddition.

Organosilyldiazoalkanes exhibit enhanced thermal stability compared to simple diazoalkanes (2, 10). There is a hypsochromic shift of *ca.* 50 nm in the u.v. spectrum of silyldiazoalkanes relative to the analogous diazoalkane. The stabilization and spectra have been explained (4, 10) in terms of increased resonance stabilization of the silyldiazoalkane using the silicon 'd' orbitals.

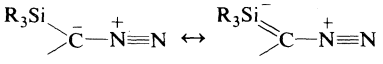

A recent crystallographic study questions the extent of (p → d) π interactions because the bond lengths and angles are quite 'normal' (11). We have carried out CNDO/2 (12) calculations on diazoethane and 2-siladiazoethane both with and without the *d* function in the basis set. Our calculations show that both the highest occupied molecular orbital (HOMO) and lowest unoccupied molecular orbital (LUMO) are lower in energy in 2-siladiazoethane than in diazoethane due to overlap with the silicon 3d orbitals. The lowering of energy is greater for the HOMO than the LUMO, explaining the hypsochromic shift in the u.v. spectra of siladiazoalkanes. It can be shown by a simple perturbation approach (13, 14) that the cycloaddition of a diazoalkane with an electron-deficient alkene is controlled by the perturbation between the HOMO of the diazoalkane and LUMO of the alkene. A lowering of the HOMO of the diazoalkane thus decreases the perturbation and hence the reactivity. We conclude that (p–d) π interactions affecting frontier orbitals are responsible for the anomalous spectra and thermal stability of silyldiazoalkanes and suggest that in determining the effects of 'd' orbitals on the reactivity of organosilicon compounds, it is more fruitful to examine the frontier orbitals than the bond lengths and angles.

Two other effects must be considered in interpreting the reactivity of silyldiazoalkanes. Firstly, diazoalkanes with a carbonyl group adjacent to the diazo group are stabilized by resonance effects which probably affect the frontier orbitals. Secondly, the transition state for cycloaddition to diethyl fumarate is highly crowded and the reaction is thus susceptible to steric inhibition when bulky groups are involved.

By using a combination of the above three factors, the relative reactivity of compounds **1**–**5** can be readily understood. The quite small difference between **1** and **2** is explained by a combination of the greater size of a phenyl group relative to a methyl group and a small extra resonance stabilization of the HOMO of **2** by interaction with the phenyl π molecular orbitals. The large differences between **1** and **3**, and **2** and **4** result from increased transition state energies in the additions of **3** and **4** caused by the greater bulk of Ph_3Si relative to Me_3Si. The combined stabilizing effects of a carboethoxyl group and a trimethylsilyl group on the HOMO cause **5** to exhibit extraordinary ground state stability, and therefore low reactivity.

The present study has been chiefly concerned with the influence of the silicon-containing group on the course of the cycloaddition reac-

[1]The rates of these reactions were found to be relatively solvent independent, as is usual for cycloadditions (9).

tions. The definitive experiment was the addition of trimethylsilylphenyldiazomethane, **2**, to diethyl fumarate. An equimolar mixture of **2** and diethyl fumarate in pure dry carbon tetrachloride was allowed to react at ambient temperature. The progress of the reaction was followed by n.m.r. spectroscopy. After 2 h, the reaction was *ca.* 50% complete. The n.m.r. spectrum showed resonances due to starting materials and one product which had a spectrum consistent with it being 4,5-dicarboethoxy-3-phenyl-3-trimethylsilyl-1-pyrazoline **6**. The

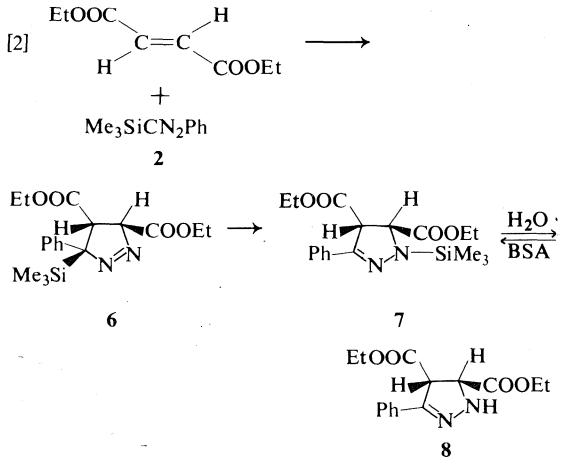

n.m.r. spectrum of **6** showed the H-4 and H-5 methine proton resonances as doublets at δ 3.5 and 5.7 p.p.m., respectively, with $J = 7$ Hz. These resonances are characteristic of protons attached to sp^3 hybridized carbon atoms bearing the groups shown in the above structure. The *trans* geometry about C_4—C_5 is based on the knowledge that cycloadditions with *trans* olefins usually result in retention of geometry (14) and is supported by a comparison of the coupling constant with those of the products of addition to *cis* olefins. The n.m.r. spectra were invaluable in assigning structures to the cycloadducts. Isomeric compounds could be characterized readily and the salient features of some of these spectra are given in Tables 1–3. The stereochemistry about C_3—C_4 is based on the observations that there was only one isomer produced and that the resonances due to one carboethoxyl group were shielded by 0.6 p.p.m. relative to the normal positions. Examination of a model of **6** showed that the carboethoxyl group on C-4 was in the shielding cone of a *cis* phenyl group but not a *trans* phenyl group. The isomer expected on steric grounds is **6**. It was not possible to obtain pure **6** since as the reaction neared completion a second product appeared, the amount of which increased at the expense of **6**. After 5 h at ambient temperature the reaction was 90% complete. After a further hour at reflux, 4,5-dicarboethoxy-3-phenyl-1-trimethylsilyl-2-pyrazoline, **7**, was isolated as the sole product.

TABLE 1. Methine proton resonances in some Δ^1-pyrazolines

Compound	H-4 (δ)	H-5 (δ)	$J_{4,5}$ (Hz)
6	3.50	5.70	7
9	3.70	5.72	9.5
10	3.58	5.90	10
15	3.02	5.55	8

TABLE 2. Methine proton resonances in some Δ^2(Si-1)-pyrazolines

Compound	H-4 (δ)	H-5 (δ)	$J_{4,5}$ (Hz)
7	4.45	4.8	5
11	4.70	5.0	12
12	4.44	4.72	9

TABLE 3. Methine proton resonances in some Δ^2(N-1)-pyrazolines

Compound	H-4 (δ)
23	4.2
16	3.8

The structure of **7** was confirmed spectroscopically. In the n.m.r. spectrum H-4 and H-5 appeared as AB doublets at δ 4.45 and 4.80 p.p.m., respectively, with $J = 5$ Hz. Thus comparing the spectrum of **7** relative to **6**, H-4 was deshielded by 1.3 p.p.m. due to a rehybridization of C-3 from sp^3 to sp^2, and H-5 was shielded by 0.9 p.p.m. due to rehybridization of N-1 from sp^2 to sp^3. The two carboethoxyl groups in **7** had similar resonances since the C-4 carboxyl group was no longer in the phenyl shielding cone. There was only one i.r. carbonyl absorption which appeared at 5.77 μ indicating that both ester carbonyl groups were nonconjugated. After 30 s shaking with methanol **7** was quantitatively desilylated to 4,5-dicarboethoxy-3-phenyl-2-pyrazoline, **8**.

The extreme sensitivity of **7** to hydrolysis and solvolysis by protic solvents is characteristic of

Can. J. Chem. Downloaded from www.nrcresearchpress.com by 210.87.254.5 on 09/05/12
For personal use only.

Can. J. Chem. Downloaded from www.nrcresearchpress.com by 210.87.254.5 on 09/05/12
For personal use only.

compounds containing N—Si bonds (18). The H-4 and H-5 resonances in the n.m.r. spectra of **7** and **8** were almost identical, showing that no major rearrangements had taken place. There was an absorption at 2.9 μ in the i.r. spectrum of **8**, characteristic of compounds containing N—H bonds. There were no absorptions due to Me_3Si in either the i.r. or n.m.r. spectra of **8**. Treatment of a CH_2Cl_2 solution of **8** with bistrimethylsilylacetamide (BSA) resulted in quantitative conversion back to **7**, further proof for its structure.

The rearrangement **6** → **7** which followed first-order kinetics was the first unambiguous observation of a 1,3 migration of a silyl group from carbon to nitrogen, a process directly analogous to the β-ketosilane to siloxyalkene rearrangement (8).

Another example of a rearrangement of silicon from carbon to nitrogen was observed during the addition of 1-phenyl-1-trimethylsilyldiazomethane, **2**, to maleic anhydride. After 4 h the reaction mixture was completely decolorized and the n.m.r. spectrum indicated that three products were present. These were the two epimers of 3-phenyl-3-trimethylsilyl-1-pyrazoline-4,5 dicarboxylic acid anhydride, **9** and **10**, and 3-phenyl-1-trimethylsilyl-2-pyrazoline-4,5 dicarboxylic acid anhydride, **11**.

[3]

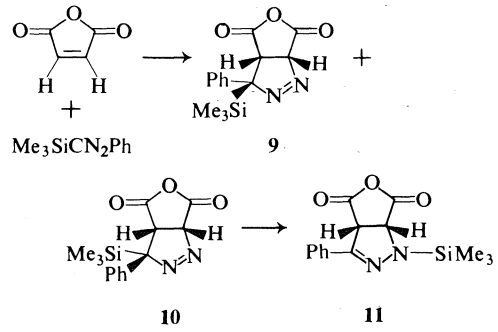

The n.m.r. spectrum was taken frequently after the mixture had decolorized. The H-3 and H-4 doublets due to **10** rapidly disappeared leaving only those ascribed to **9** and **11**. The doublets due to **9** disappeared at a rate corresponding to the growth of the doublets of **11**. A plot of log [**9**] *vs.* *t* was an excellent straight line. The rearrangement **9** → **11** was therefore first order and had a rate constant of 54×10^{-3} min^{-1} at 25°. After 2 days pure **11** was deposited from the solution in the form of white needle-shaped crystals. The crystals obtained were highly moisture sensitive and their i.r. spectrum showed carbonyl absorbances at 5.35 and 5.58 μ as expected for an unconjugated anhydride.

The rearrangement of a $\Delta^1 \rightarrow \Delta^2$ pyrazoline via 1,3-silyl migration could not always be observed directly. In the addition of **2** to diethyl maleate the reaction was so slow at ambient temperature that after several days only a small amount of product had formed. After completion of the reaction by 24 h reflux the reaction mixture contained two isomeric products in approximately equal amounts, believed to be the two epimers of 4,5-dicarboethoxy-3-phenyl-1-trimethylsilyl-2-pyrazoline, **7** and **12**. The intermediate Δ^1-pyrazoline could not be observed because rearrangement was much more rapid than addition, both at ambient temperature and reflux. The evidence for the structures assigned is based on the previous identification of **7**, which accounted for half of the observed resonances in the n.m.r. spectrum and an analysis of the remaining signals. In addition to the similarities in the n.m.r. spectra of **7** and **12** further evidence for the epimeric nature of these compounds was gained from the observation that on heating, the mixture completely epimerized to the more stable **7**, presumably by intermolecular prototropy.

[4]

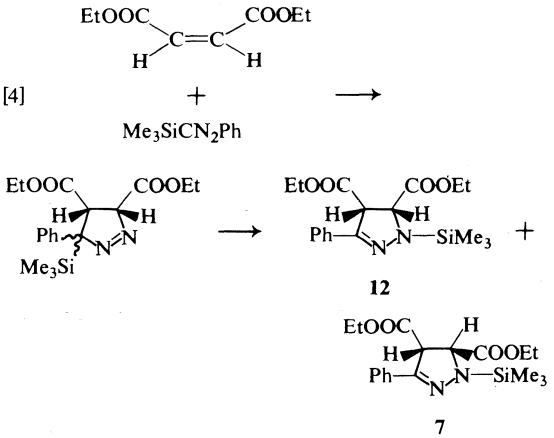

In the addition of ethyl trimethylsilyldiazoacetate, **5**, to diethyl fumarate at 100–140°, previously reported by Schöllkopf (7), the rearranged product, 3,4,5-tricarboethoxy-1-trimethylsilyl-2-pyrazoline, **13**, was the only observed product. We repeated this reaction at ambient temperature, following the progress by n.m.r. spectroscopy. The reaction, in the absence of solvents, was complete in 4 weeks. During this time the only signals observed in the

n.m.r. were those due to **13**. The structure of **13** was confirmed by shaking with methanol for 30 s to completely desilylate to the known 3,4,5-tricarboethoxy-2-pyrazoline, which was then quantitatively resilylated by BSA to **13**. We conclude that in this case the rearrangement of the Δ^1 to Δ^2 pyrazoline by 1,3 silyl migration is too fast to measure at ambient temperature.

[5] 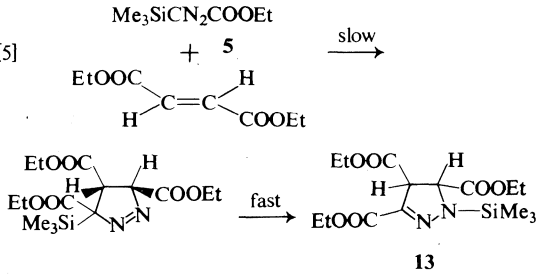

13

In contrast to the behavior where the silyldiazoalkane bears an electron-releasing methyl group, the addition of the diazoalkane **1** to diethyl fumarate in dry carbon tetrachloride at ambient temperature gave 4,5-dicarboethoxy-3-methyl-3-trimethylsilyl-1-pyrazoline, **15**, as the sole product. On heating **15** isomerized to **16**

[6] 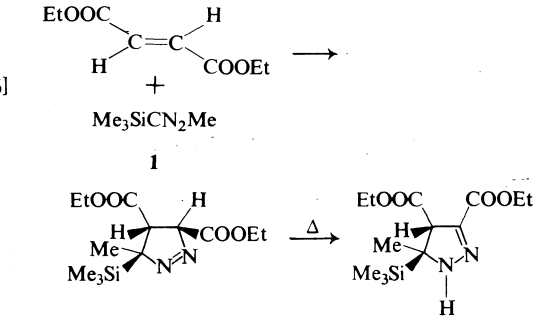

1

15 **16**

quantitatively, rearrangement resulting from 1,3-hydrogen migration, rather than 1,3 silyl migration. The product, 3,4-dicarboethoxy-5-methyl-5-trimethylsilyl-2-pyrazoline, **16**, was identified by the presence of an NH absorbance at 2.9 μ and both conjugated and nonconjugated carbonyl i.r. absorptions. The n.m.r. spectrum integrated correctly for the proposed structure and contained singlets at δ 1.10 and 3.80 p.p.m. corresponding to the methyl group on C-5 and the single uncoupled proton H-4.

The addition of **1** to methyl acrylate (R = COOMe) at ambient temperature gave a mixture of the two epimers of 5-carbomethoxy-3-methyl-3-trimethylsilyl-1-pyrazoline, **17** and **18**, (R = COOMe) in a ratio of about 1:4.

[7] 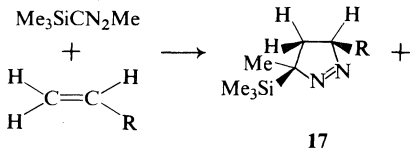

R = COOMe, CN

17

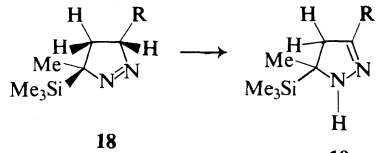

18 **19**

These compounds could not be isolated since they isomerized readily to the single Δ^2-pyrazoline 3-carbomethoxy-5-methyl-5-trimethylsilyl-2-pyrazoline, **19**. The minor product, **17**, isomerized more rapidly than **18**.

The addition of **1** to acrylonitrile (R = CN) was similar to the addition to methylacrylate and a mixture of two Δ^1-pyrazolines **17**, **18** (R = CN) was formed initially. The mixture could not be separated; after 2 h at ambient temperature isomerization to 3-cyano-5-methyl-5-trimethylsilyl-2-pyrazoline, **19** (R = CN) was complete. Again, the more hindered epimer was the faster to rearrange. The more rapid isomerization of the cyano compounds relative to the carboethoxyl compounds was probably due to the more strongly electron-withdrawing cyano group in the former case which made H-3 particularly susceptible to tautomerism.

The addition of 1-triphenylsilyldiazoethane, **3**, to acrylonitrile resulted in a mixture of the two Δ^1-pyrazolines **20** and **21** which on heating at 60° isomerized rapidly to the Δ^2-pyrazoline, **22**, 3-cyano-5-methyl-5-triphenylsilyl-2-pyrazoline.

[8] 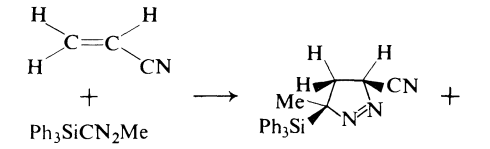

20

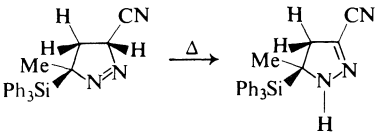

21 **22**

Can. J. Chem. Downloaded from www.nrcresearchpress.com by 210.87.254.5 on 09/05/12
For personal use only.

Can. J. Chem. Downloaded from www.nrcresearchpress.com by 210.87.254.5 on 09/05/12
For personal use only.

From these results it appears that triphenylsilyl and trimethylsilyl pyrazolines behave similarly, in marked contrast to the difference in behavior between *C*-phenyl- and *C*-methyl-substituted silylpyrazoline (as in **7** or **11**).

From the above results it is obvious that the rates of rearrangement of Δ^1- to Δ^2-pyrazolines by 1,3-silyl migration are very susceptible to differences in the substituents on the carbon atom bearing the trimethylsilyl group. The transition state for the 1,3-silyl migration can be represented as follows.

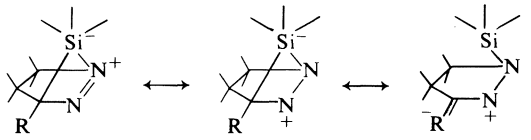

a b c

Where R is electron-withdrawing, charge is delocalized through canonical form **c**, which is product like, and the reaction is facilitated. Methyl and other electron-releasing groups are unable to stabilize the transition state in this manner accounting for the difference in rates in the cases where R = CO_2Et and R = Me. The differences in rates of silyl migration were substantial, since for R = CO_2Et the rearrangement was too fast to observe at ambient temperature, whereas for R = Me the reaction was evidently very slow even at 80° since only products arising from tautomerism were observed in all cases.

The tautomerism of $\Delta^1 \rightarrow \Delta^2$-pyrazolines is known (9) to be catalyzed by bases and acids, and in this case was strongly catalyzed by traces of water or amines, particularly diethylamine. In the addition of **1** to diethyl fumarate or diethyl maleate in the presence of traces of water, the product obtained was the conjugated Δ^2-pyrazoline, **16**, there being no trace of the initially formed Δ^1-pyrazoline.

In the addition of 1-phenyl-1-trimethylsilyldiazomethane, **2**, to diethyl fumarate or diethyl maleate at ambient temperature in the presence of traces of moisture, the Δ^2-pyrazoline 3,4-dicarboethoxy-5-phenyl-5-trimethylsilyl-2-pyrazoline, **23**, was the exclusive product.

Therefore at ambient temperature the presence of a trace of moisture was sufficient to accelerate the hydrogen migration to such an extent that 1,3 silyl migration was no longer the favored reaction. Probably the silyl migration is not catalyzed by moisture (or base since the same situation obtains in the presence of traces of diethylamine); a small increase in rate of the silyl migration should have been sufficient to have ensured the observation of at least traces of the N—Si product. However, the only product obtained on addition of diazoalkane **2** to diethyl maleate or diethyl fumarate at reflux was the one, **7**, resulting from **6** undergoing a 1,3 silyl migration. The mechanism we propose in this case is shown in eq. 9. This scheme was confirmed by refluxing a solution of the Δ^2-pyrazoline **23** in dry carbon tetrachloride, where no reaction was observed over 1/2 h. Addition of a trace of water to the refluxing solution of **23** resulted in the quantitative conversion to **7** during 1/2 h. The rate determining step for the reaction **23** → **7** was probably the step **23** → **6** since it was observed that the reaction **6** → **7** was quite facile at ambient temperature (*vide supra*).

The addition of **5** to diethyl fumarate, in the presence of traces of amines or water, at both

[9]

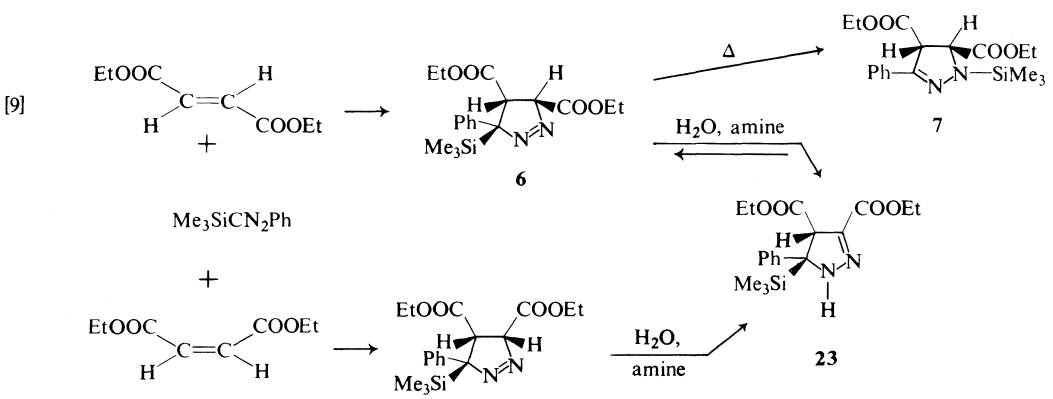

ambient temperature and 100°, followed the same course as was followed in the absence of catalysis, namely rearrangement to the Δ^2-pyrazoline **13**, via 1,3 silyl migration. Evidently the silyl migration is so facile when a carboethoxy group is on the adjacent carbon that even the strongly catalyzed tautomerism cannot compete. This information permits establishment of the relative activating effect of a group on silyl migration as

$$R = EtOOC > Ph \gg Me$$

This order parallels the trends in σ and σ^- values for the above groups (15) confirming the suggestion that increasing electron-withdrawing ability should stabilize the transition state for rearrangement.

During the course of these studies a further interesting reaction was discovered. Treatment of the Δ^1-pyrazoline **15** with refluxing methanol for 1/2 h resulted in the formation of a small amount of **16** but the major product was 4,5-dicarboethoxy-3-methyl-2-pyrazoline, **24** which was also characterized by air oxidation to the pyrazole **25**.

[10]

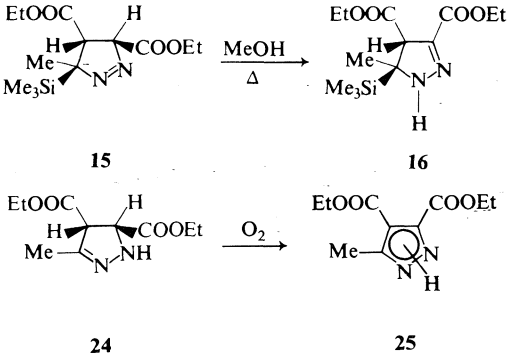

Two mechanisms which could account for the formation of **24** are outlined in eqs. 11 and 12.

[11]

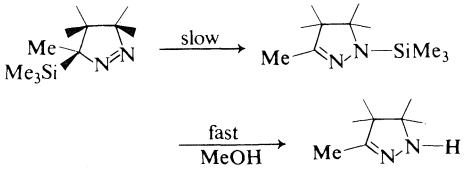

[12]

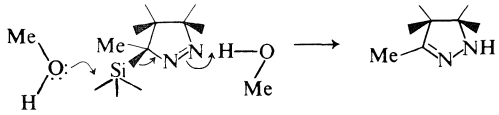

The route involving 1,3 silyl migration, followed by the facile cleavage of the N—Si bond seems improbable on the grounds that heating **15** in a variety of aprotic solvents failed to catalyze the 1,3 silyl migration. The second route (eq. 12) appears more probable, this mechanism being analogous to that proposed for the facile cleavage of several systems, including trimethylsilylacetonitrile, where a trimethylsilylmethyl group is adjacent to an unsaturated center (16). A high degree of solvent participation in the transition state must be involved if the product is to be, as found, the thermodynamically unstable pyrazoline **24**. The cleavage of **15** → **24** was base-catalyzed, which is further evidence supporting the second mechanism. The sensitivity to acid catalysis could not be estimated; traces of acid in the reaction mixture resulted in unidentified side reactions taking place.

In contrast a methanolic solution of the epimeric Δ^1-pyrazolines **17** and **18** (R = CN), obtained by addition of **1** to acrylonitrile, was completely isomerized to **19**, by refluxing for an hour, there being no traces of loss of the trimethylsilyl group. Presumably H-3 is activated by the adjacent cyano group to such an extent that rearrangement is much faster than cleavage.

In conclusion, the major results reported herein can be summarized as follows. (*i*) Δ^1-pyrazolines may rearrange by either 1,3 silyl migration or hydrogen migration (tautomerism), silyl migration being favored, all other factors being equal. Both rearrangements are facilitated by electron-withdrawing groups bonded to the α-carbon. The tautomerism is strongly catalyzed by both water and bases and in some cases can become the favored route by (*a*) increasing the electron supply to the silyl α-carbon or (*b*) adding traces of catalysts or by a combination of both of these; (*ii*) Δ^1-pyrazolines, silyl substituted at C-3 can undergo facile allylic cleavage of the trimethylsilyl group by methanol.

Experimental

All diazoalkanes were prepared by the method of Brook and Jones (4), except for 1-trimethylsilylethyldiazoacetate which was prepared by the method of Schöllkopf *et al.* (7).

The n.m.r. spectra were recorded on Varian A56/60 and T60 spectrometers using TMS as internal standard. The i.r. spectra were recorded on a Perkin Elmer 237B instrument with polystyrene calibration. An AEI-MS 902

Can. J. Chem. Downloaded from www.nrcresearchpress.com by 210.87.254.5 on 09/05/12
For personal use only.

Can. J. Chem. Downloaded from www.nrcresearchpress.com by 210.87.254.5 on 09/05/12
For personal use only.

mass spectrometer was used for recording mass spectra. Melting points are uncorrected and were measured on a Fisher-Johns hot-stage instrument. Microanalyses were performed by A. B. Gygli, Toronto.

*The Addition of 1-Phenyl-1-trimethylsilyldiazomethane, **2**, to Diethyl Fumarate*

(*a*) Diethyl fumarate (0.19 g, 1.1 mmol) was added over 2 min to **2** (0.19 g, 1 mmol) in 2 ml of carefully dried CCl_4, at ambient temperature. The progress of the reaction was followed by n.m.r. spectroscopy. After 2 h the reaction was 50% complete. The n.m.r. spectrum showed resonances due to starting materials and one other compound, the Δ^1 pyrazoline **6**; n.m.r. (CCl_4) δ 7.3 (s, phenyl), 5.70 (d, H-5, $J_{4,5}$ = 7 Hz), 4.3 (q, C-5, $CO_2CH_2CH_3$, J = 7 Hz), 3.7 (q, C-4, $CO_2CH_2CH_3$, J = 7 Hz), 3.5 (d, H-4, $J_{4,5}$ = 7 Hz), 1.45 (t, C-5, $CO_2CH_2CH_3$, J = 7 Hz), 1.0 (t, C-4, $CO_2CH_2CH_3$, J = 7 Hz), 0.14 (s, $SiMe_3$).

Compound **6** could not be isolated from the reaction mixture but the resonance positions, coupling constants, and *relative* integrations are in accord with the assigned structure. After a further 5 h at ambient temperature the reaction was nearing completion and the n.m.r. contained resonances due to starting materials, **6**, and a new compound **7**. The reaction mixture was heated at reflux for 1 h, the volatile materials were removed on a vacuum line, and the residual oil was analyzed immediately. (Any attempts at further purification resulted in loss of the trimethylsilyl group from the molecule.) This procedure afforded 0.36 g (95%) of 4,5-dicarboethoxy-3-phenyl-1-trimethylsilyl-2-pyrazoline, **7**; i.r. (film) 5.77 (C=O), 6.93 (C—Ph), 8.0 (Si—Me) μ; n.m.r. (CCl_4) δ 7.2–7.9 (m, 5H, phenyl), 4.80 (d, 1H, H-5, $J_{4,5}$ = 5 Hz), 4.45 (d, 1H, H-4, $J_{4,5}$ = 5 Hz), 4.2 (2 overlapping q separated by 3 Hz, 4H, C-4, C-5, $CO_2CH_2CH_3$, J = 7 Hz), 1.3 (q, 6H, C-4, C-5, $CO_2CH_2CH_3$, J = 7 Hz), 0.42 (s, 9H, $SiMe_3$) p.p.m.; mass spectrum, *m/e* calcd. for $C_{18}H_{26}N_2O_4Si$: 362, found: 362.

Anal. Calcd. for $C_{18}H_{26}N_2O_4Si$: C, 59.63; H, 7.21; N, 7.73. Found: C, 59.67; H, 7.28; N, 7.66.

Shaking a methanolic solution of **7** for 30 s followed by removal of the volatile materials under reduced pressure was sufficient to remove the trimethylsilyl group from the ring. The n.m.r. and i.r. spectra were consistent with the new compound being 4,5-dicarboethoxy-3-phenyl-2-pyrazoline, **8**. The n.m.r. spectrum of **8** differs from that of **7** only in that the trimethylsilyl protons' resonance at δ 0.42 has been replaced by an NH absorbance at δ 7.0. Similarly in the i.r. spectrum, a new band characteristic for NH appeared at 2.9 μ replacing the Me_3Si group absorptions at 8.0, 12.0, and 13.3 μ. Treatment of a solution of **8** in CH_2Cl_2 with BSA resulted in quantitative conversion to **7**.

(*b*) *Cycloaddition in CCl_4, Containing a Trace of Water, at Ambient Temperature*

Diethyl fumarate (0.19 g, 1.1 mmol) was added over 2 min to diazoalkane **2** (0.19 g, 1 mmol) in 2 ml of CCl_4 containing a trace of water. After 24 h at ambient temperature the reaction was completely colorless and n.m.r. spectroscopy showed no resonances due to starting materials. The oil obtained on removal of volatile components was crystallized from benzene–hexane to yield 0.31 g (85%) of 3,4-dicarboethoxy-5-phenyl-5-trimethylsilyl-2-pyrazoline, **23**; i.r. (CCl_4) 3.0 (broad) (NH), 5.8 (C=O), 5.9 (C=O), 6.94 (C—Ph), 8.0 ($SiMe_3$); n.m.r. (CCl_4), δ 7.6 (s, 1H, NH), 7.2 (s, 5H, phenyl), 4.15 (q, 2H, C-3, $CO_2CH_2CH_3$, J = 7 Hz), 4.20 (s, 1H, H-4), 3.6 (q, 2H, C-4, $CO_2CH_2CH_3$, J = 7 Hz), 1.32 (t, 3H, C-3, $CO_2CH_2CH_3$, J = 7 Hz), 0.73 (t, 3H, C-4, $CO_2CH_2CH_3$, J = 7 Hz), 0.10 (s, 9H, $SiMe_3$), p.p.m.; mass spectrum, *m/e* calcd. for $C_{18}H_{20}N_2O_4Si$: 362, found: 362.

Anal. Calcd. for $C_{18}H_{20}N_2O_4Si$: C, 59.63; H, 7.23; N, 7.73. Found: C, 59.86; H, 7.41; N, 7.79.

(*c*) *Cycloaddition in CCl_4 Containing Traces of Moisture, at Reflux Temperature*

A reaction mixture identical in composition to *b* was refluxed for 2 h and after work-up 0.30 g (81%) of **7**, characterized by n.m.r., was obtained.

*The Addition of Phenyltrimethylsilyldiazomethane (**2**) to Maleic Anhydride*

To maleic anhydride (0.61 g, 0.62 mmol) in 5 ml of CCl_4 at 0° was added **2** (0.118 g, 0.62 mmol). The solution was colorless after 4 h. The n.m.r. indicated that there are three products, **9**, **10**, and **11**. This mixture could not be isolated nor the components separated; however, the following n.m.r. data are consistent with the proposed structures: **9**, n.m.r. (CCl_4) δ 7.5–8.5 (m, 5H, phenyl (this includes the phenyl resonances due to **10** and **11**)), 5.72 (d, 0.9H, H-5, $J_{4,5}$ = 9.5 Hz), 3.70 (d, 0.9H, H-4, $J_{4,5}$ = 9.5 Hz), 0.04 (s, Me_3Si, 9.55H (this includes the Me_3Si resonance of **10**)); **10**, n.m.r. (CCl_4) δ 7.5–8.5 (m, phenyl), 5.90 (d, 0.05H, H-5, $J_{4,5}$ = 10 Hz), 3.58 (d, 0.05H, H-4, $J_{4,5}$ = 10 Hz), 0.04 (s, Me_3Si); **11**, n.m.r. (CCl_4) δ 7.5–8.5 (m, phenyl), 5.00 (d, 0.05H, H-5, $J_{4,5}$ = 12 Hz), 4.70 (d, 0.05H, H-4, $J_{4,5}$ = 12 Hz), 0.38 (s, 0.45H, Me_3Si).

The reaction mixture was warmed to 25 °C and the n.m.r. spectrum was taken periodically and after a few minutes the concentration of **10** was negligible. The rate of the rearrangement **9** → **11** was then measured. The relative concentration of **9** in the mixture of **9** and **11** was calculated from the integration of the H-4 plus H-5 resonances of **9** and **11**, respectively. A plot of the logarithm of the concentrations thus obtained *vs.* time was an excellent straight line giving rise to a first-order rate constant of 54×10^{-3} min^{-1} at 25 °C. After standing for 2 days 0.17 g (94%) of white needle-shaped crystals of pure **11** were deposited. These moisture sensitive crystals were dried and analyzed immediately, m.p. 94–95°; n.m.r. *vide supra*.

Anal. Calcd. for $C_{14}H_{16}N_2O_3Si$: C, 58.30; H, 5.50; N, 9.71. Found: C, 58.60; H, 5.50; N, 9.79.

*The Addition of **2** to Diethyl Maleate*

To a solution of diethyl maleate (0.64 g, 4.4 mmol) in 3 ml of carefully dried CCl_4 was added **2** (0.835 g, 4.4 mmol). The mixture was heated at reflux under a dry nitrogen atomosphere. After 24 h the reaction was complete, the color of the diazoalkane being completely discharged, and g.l.c. analysis showed two products to be present in approximately equal amounts. Analysis of the n.m.r. showed one component to be **7**, whereas the other component had spectral properties consistent with it being **12**, the epimer of **7**. The two components could not be separated; however, the mixture of **7** and **12** had the

Can. J. Chem. Downloaded from www.nrcresearchpress.com by 210.87.254.5 on 09/05/12
For personal use only.

following characteristics: i.r. almost identical to that of **7**; n.m.r. (CCl_4) signals due to **7** plus those ascribed to **12**, δ 7.2–7.9 (m, phenyl), 4.72 (d, 1H, H-5, $J_{4,5}$ = 9 Hz), 4.44 (d, 1H, H-4, $J_{4,5}$ = 9 Hz), 4.20 (m, C-4, C-5, $CO_2CH_2CH_3$), 1.4 (m, C-4, C-5, $CO_2CH_2CH_3$), 0.40 (s, $SiMe_3$, 9H).

Anal. Calcd. for $C_{18}H_{26}N_2O_4Si$: C, 59.63; H, 7.33; N, 7.73. Found: C, 59.90; H, 7.29; N, 7.88.

Shaking the above mixture with methanol at ambient temperature removed all the trimethylsilyl groups as methoxytrimethylsilane. The n.m.r. spectrum of the mixture produced was similar to that of the original mixture, with the exception that there was no trimethylsilyl proton resonances, and an NH absorption had appeared (*ca.* δ 6.5 p.p.m.). This desilylated mixture was readily silylated by BSA to a mixture of **7** and **12**.

Heating a mixture of **7** and **12** at 80° for several days resulted in complete conversion of **12** to **7**.

*Addition of Ethyl Trimethylsilyldiazoacetate (**5**) to Diethyl Fumarate*

The procedure of Schöllkopf (7) was followed and a 90% yield of **13** was obtained. This product was quantitatively desilylated, on brief shaking with methanol, to the known 3,4,5-tricarboethoxy-2-pyrazoline, m.p. 98–99° (lit. (17) m.p. 98–99°) which was quantitatively resilylated to **13** by BSA.

The same product, **13**, was obtained when the reaction was carried out at ambient temperature, 4 weeks being required for completion in the absence of solvent. No evidence for the formation of compounds other than **13** was obtained at any stage of the reaction from the i.r. or n.m.r. spectra.

*The Addition of Methyltrimyethlsilyldiazomethane (**1**) to Diethyl Fumarate*

In a typical experiment, **1** (0.64 g, 5 mmol) was added over 5 min to a stirred solution of diethyl fumarate (0.86 g, 5 mmol) in 5 ml of carefully dried (4A molecular sieves) carbon tetrachloride. About 3 min after addition the mixture had decolorized. A crude oil was obtained from evaporation of volatile materials (1.6 g, 95%). This oil was purified by rapid passage down a 10 × 1 cm alumina (Woelm, neutral, grade 1) column with benzene as eluent, affording 1.2 g (68%) of **15**: u.v. λ_{max} (ε) (C_6H_{12}), 218 (1300), 285 (750) nm; n.m.r. (CCl_4) δ 5.55 (d, 1H, H-3, $J_{3,4}$ = 8 Hz), 4.10 (m, 4H, C-3, C-4, $CO_2CH_2CH_3$, J = 7 Hz), 3.02 (d, 1H, H-4, $J_{3,4}$ = 8 Hz), 1.25 (t, 6H, C-3, C-4, $CO_2CH_2CH_3$, J = 7 Hz), 1.20 (s, 3H, C-5, CH_3), 0.08 (s, 9H, Me_3Si).

Anal. Calcd. for $C_{13}H_{24}O_4N_2Si$: C, 51.97; H, 8.05; N, 9.30. Found: C, 52.31; H, 8.10; N, 9.04.

Quantitative isomerization of **15** to 3,4-dicarboethoxy-5-methyl-5-trimethylsilyl-2-pyrazoline, **16**, was accomplished by 1/2 h reflux of a solution of **15** in carbon tetrachloride, benzene, cyclohexane or ether. This transformation was catalyzed at ambient temperature by traces of water or amines. In a typical experiment a solution of **15** (1 g) in 5 ml of carbon tetrachloride was refluxed for 1/2 h. After this time the volatile components were removed on a rotary evaporator and the remaining oil (1 g, 100%) was identified as **16**; u.v. λ_{max} (ε) (C_6H_{12}), 205 (1900), 225 (1700), 285 (3900) nm; i.r. 2.95 (NH), 5.82 (C=O), 5.92 (C=O conjugated), 8.0 (Si—CH_3) μ; n.m.r. (CCl_4) δ 6.6 (broad s, 1H, NH), 4.0 (m, 4H, C-3, C-4, $CO_2CH_2CH_3$), 3.8 (s, 1H, H-4), 1.30 (m, 6H, C-3, C-4, $CO_2CH_2CH_3$), 1.10 (s, 3H, CH_3), 0.10 (s, 9H, Me_3Si) p.p.m.

Anal. Calcd. for $C_{13}H_{24}O_4N_2Si$: C, 51.97; H, 8.05; N, 9.30. Found: C, 52.10, H, 8.08; N, 9.13.

*Solvolysis of 4,5-Dicarboethoxy-3-phenyl-3-trimethylsilyl-1-pyrazoline, **15**, by Methanol*

A solution of **15** (0.3 g) in 5 ml of dry methanol was refluxed for 1/2 h under N_2. Gas–liquid chromatography analysis after this time showed the presence of methanol, methoxytrimethylsilane, the Δ^2-pyrazoline **16** (*ca.* 5%), and a new compound, **27**. Repeated attempts to purify the new compound were unsuccessful. It is believed that **27** is 4,5-dicarboethoxy-3-methyl-2-pyrazoline. The crude oil obtained by removal of methanol and methoxytrimethylsilane had the following characteristics; n.m.r. (CCl_4) δ 6.0 (broad s, 1H, NH), 4.44 (d, 1H, H-5, $J_{4,5}$ = 8 Hz), 4.05 (m, 4H, C-4, C-5, $CO_2CH_2CH_3$), 3.90 (d, 1H, H-4, $J_{4,5}$ = 8 Hz), 1.92 (s, 3H, CH_3—C=N—), 1.10 (m, 6H, C-4, C-5, $CO_2CH_2CH_3$). There were also resonances attributed to **16**, (*ca.* 5%).

Anal. Calcd. for $C_{10}H_{16}N_2O_4$: C, 52.62; H, 7.06; N, 12.27. Found: C, 51.41; H, 7.00; N, 11.42.

As the analysis for **24** was not satisfactory, it was characterized by oxidation to 2-methyl-3,4-dicarboethoxypyrazole, **25**. A methanolic solution of **16** and **24** was refluxed in the presence of air for 24 h and after this time pure **25** was obtained by distillation, (60–80%), b.p. 140°/0.2 mm (Kugelröhr); i.r. 5.94 μ (C=O); n.m.r. (CCl_4) δ 7.4 (s, 1H, NH), 4.22, 4.18 (2q, 4H, C-4, C-5, $CO_2CH_2CH_3$, J = 7 Hz), 2.40 (s, 3H, C-5, CH_3), 1.25 (t, 6H, C-4, C-5, $CO_2CH_2CH_3$, J = 7 Hz).

Anal. Calcd. for $C_{10}H_{14}N_2O_4$: C, 53.08; H, 6.23; N, 12.38. Found: C, 53.00; H, 6.33; N, 12.30.

The solvolysis of **15** was dependent on the methanol used. In some cases after reflux, *only* **16** was obtained (by tautomerism) rather than allylic cleavage of the $SiMe_3$ group. This was probably due to variations in the amount of base present in the sample of methanol, although this was not verified.

*The Reaction of **1** with Methyl Acrylate*

To methyl acrylate (0.86 g, 10 mmol) in 5 ml of dry carbon tetrachloride was added **1** (1.28 g, 10 mmol) dropwise. The reaction was complete after 5 min at ambient temperature. The volatile materials were removed by evaporation and the remaining oil (2.0 g, 93%). was examined. Gas-liquid chromatography analysis indicated the presence of two compounds; the n.m.r. spectrum strongly suggested that these were the two epimeric Δ^1-pyrazolines **17** and **18** in a ratio of 1 to 4, respectively: **17**, n.m.r. (CCl_4) δ 5.21 (X component of ABX, 0.2H, H-5), 3.8 (s, 3H, OCH_3 of **17** and **18**), 1.1–1.5 (AB component of ABX, 2H, H_A, H_B of **17** and **18**), 1.30 (s, 0.6H, C-3, CH_3), 0.14 (s, 9H, $SiMe_3$ of **17** and **18**); **18**, 4.82 (X of ABX, 0.8H, H-5), 1.52 (s, 2.4H, CH_3), 0.14 (s, $SiMe_3$); i.r. (CCl_4): 5.75 (C=O), 8.0 (CH_3—Si) μ.

The solution of isomers further rearranged slowly to 3-carbomethoxy-5-methyl-5-trimethylsilyl-2-pyrazoline, **19**. After 2 days at ambient temperature **17** had completely rearranged to **19**, whereas after 20 days, **18** had *ca.* 50% rearranged to **19**. For characterization the mixture of **17** and **18** was isomerized to **19** by dissolving for 1/2 h in a 10% diethylamine–ether solution, after which

time **19** was obtained by Kugelröhr distillation, b.p. 65°/0.1 mm, 1.6 g (74%); i.r. (CCl_4) 2.95 (NH), 5.88 (C═O), 8.0 (Si—CH_3); n.m.r. (CCl_4) δ 6.8 (s, 1H, NH), 3.70 (s, 3H, OCH_3), 2.73 (AB q, 2H, H_A, H_B, J = 16 Hz), 1.07 (s, 3H, C—CH_3), 0.14 (s, 9H, Si$(CH_3)_3$); mass spectrum, *m/e* calcd. for $C_9H_{18}N_2O_2Si$: 214, found: 214.

*The Addition of **1** to Acrylonitrile*

To a solution of acrylonitrile (0.064 g, 1.2 mmol) in 2 ml of carbon tetrachloride at 0° was added **1** (0.15 g, 1.2 mmol). The reaction was complete after 5 min. At this point the n.m.r. was complex but corresponded to a mixture of the two epimeric Δ^1-pyrazolines **17** and **18**; i.r. 4.42 μ (unconjugated nitrile); n.m.r. **17**, (CCl_4) δ 5.35 (X component of ABX, 0.4H, H-5) *ca.* 2.15 (AB component of ABX, 0.8H, H_A, H_B), 1.30 (s, 1.2H, CH_3), 0.09 (s, 3.6H, $SiMe_3$): **18**, 4.80 (X component of ABX, 0.6H, H-5), *ca.* 1.6 (AB of ABX, 1.2H, H_A, H_B), 1.48 (s, 1.8H, CH_3), 0.05 (s, 5.4H, $SiMe_3$) p.p.m.

After standing for 2 h the mixture of **17** and **18** had completely isomerized to 5-cyano-3-methyl-3-trimethylsilyl-2-pyrazoline, **19**, which was obtained as an oil (0.15 g, 71%) on evaporation of the volatile materials; i.r. (film) 2.95 (NH), 4.50 (C≡N), 8.0 (Si—CH_3) μ; n.m.r. (CCl_4) δ 6.8 (s, 1H, NH), 2.6 (AB q, 2H, H_A, H_B, J_{AB} = 16 Hz), 1.02 (s, 3H, CH_3), 0.05 (s, 9H, $SiMe_3$).

Anal. Calcd. for $C_8H_{15}N_3Si$: C, 52.99; H, 8.33; N, 23.17. Found: C, 52.50; H, 8.46; N, 23.01.

When a mixture of **17** and **18**, obtained from low temperature addition of **1** to acrylonitrile, was refluxed for 1/4 h with methanol the exclusive product is **19**.

*The Addition of Diazoalkane **3** to Acrylonitrile*

A solution of 1-triphenylsilyl-1-diazoethane (0.43 g, 1.37 mmol) in 3 ml of acrylonitrile was completely decolorized after 1/4 h. The solvent was removed under reduced pressure, the residue was taken up in carbon tetrachloride, and the n.m.r. spectrum was consistent with a mixture of **20**, **21**, and **22**. Heating the solution for 1/4 h at 60° resulted in completion conversion to **22**, which could be crystallized to afford 0.36 g (72%) of white needles from benzene–hexane, m.p. 184–186°; n.m.r. (CCl_4) δ 7.2–7.6 (m, 15H, Ph_3Si), 3.0 (AB q, 2H, J = 17 Hz, H_A, H_B), 1.30 (s, 3H, CH_3) p.p.m.; i.r. (CCl_4) 2.95 (NH), 4.50 (C≡N), 7.0 (SiPh) μ.

Anal. Calcd. for $C_{23}H_{21}N_3Si$: C, 75.13; H, 5.76; N, 11.43. Found: C, 75.03; H, 5.53; N, 11.06.

1. K-D. KAUFMANN and K. RÜHLMANN. Z. Chem. **7**, 263 (1968).
2. D. SEYFERTH, A. W. DOW, H. MENZEL, and T. C. FLOOD. J. Am. Chem. Soc. **90**, 1080 (1968).
3. D. SEYFERTH, A. W. DOW, H. MENZEL, and T. C. FLOOD. J. Organomet. Chem. **44**, 279 (1972).
4. A. G. BROOK and P. F. JONES. Can. J. Chem. **49**, 1841 (1971).
5. M. F. LAPPERT and J. S. POLAND. Chem. Commun. 156 (1969).
6. M. F. LAPPERT and J. S. POLAND. J. Chem. Soc. (C), 3910 (1971).
7. U. SCHÖLLKOPF, D. HOPPE, N. RIEBER, and V. JACOBI. Ann. Chem. **730**, 1 (1969).
8. A. G. BROOK, D. M. MACRAE, and W. W. LIMBURG. J. Am. Chem. Soc. **89**, 5493 (1967).
9. R. HUISGEN. Angew. Chem. Int. Ed. **2**, 633 (1963).
10. D. SEYFERTH and T. C. FLOOD. J. Organomet. Chem. **29**, C25 (1971).
11. C. GLIDEWELL and G. M. SHELDRICK. J. Chem. Soc. Dalton, 2409 (1972).
12. A. BASSINDALE. Unpublished calculations using CNDO/2. P. A. Dobush, Program Number 141. Quantum chemistry program exchange. University of Indiana, Bloomington, Indiana.
13. K. N. HOUK, J. SIMS, C. R. WATTS, and L. J. LUSKUS. J. Am. Chem. Soc. **95**, 7301 (1973).
14. R. SUSTMANN. Tetrahedron Lett. 2717, 2721 (1971).
15. J. HINE. Physical organic chemistry. 2nd Ed. McGraw-Hill, New York, N.Y. 1962. p. 87 ff.
16. M. PROBER. J. Am. Chem. Soc. **77**, 3224 (1955).
17. E. BUCHNER and C. v. D. HEIDL. Ber. **34**, 345 (1901).
18. C. EABORN. Organosilicon compounds. Butterworth. London. 1960. p. 345.

Can. J. Chem. Downloaded from www.nrcresearchpress.com by 210.87.254.5 on 09/05/12
For personal use only.

Chlorine Nuclear Quadrupole Resonance Spectra of 1-Substituted 2-Chloropolyfluorocycloalkenes

LIAN SAI CHIA,[1] WILLIAM R. CULLEN, MICHAEL C. L. GERRY, AND POH SIEW YIAW[1]

Department of Chemistry, University of British Columbia, Vancouver, British Columbia V6T 1W5

Received April 30, 1974

LIAN SAI CHIA, WILLIAM R. CULLEN, MICHAEL C. L. GERRY, and POH SIEW YIAW. Can. J. Chem. **52**, 3484 (1974).

Chlorine nuclear quadrupole resonance frequencies are reported for the compounds $YC{=}CCl(CF_2)_n$ (n = 2,3,4; Y = H, CH_3, C_2H_5, $Si(CH_3)_3$, F, OCH_3, N_3, NR_2, Cl, SCH_3, $P(C_6H_5)_2$, $As(CH_3)_2$, $Mn(CO)_5$, π-$C_5H_5Fe(CO)_2$, but not all combinations). The values range from 38.999 MHz (n = 3; Y = F) to 34.668 MHz (n = 2; Y = π-$C_5H_5Fe(CO)_2$) and are roughly related to the electronegativity of Y and to the ring size. The mean temperature coefficients of the frequencies lie in the range -0.9×10^{-4} to -1.8×10^{-4}/°K.

LIAN SAI CHIA, WILLIAM R. CULLEN, MICHAEL C. L. GERRY et POH SIEW YIAW. Can. J. Chem. **52**, 3484 (1974).

On rapporte les fréquences de résonance quadrupolaire du chlore dans les composés $YC{=}CCl(CF_2)_n$ (n = 2,3,4; Y = H, CH_3, C_2H_5, $Si(CH_3)_3$, F, OCH_3, N_3, NR_2, Cl, SCH_3, $P(C_6H_5)_2$, $As(CH_3)_2$, $Mn(CO)_5$, π-$C_5H_5Fe(CO)_2$, mais toutes les combinaisons n'ont pas été inclus). Les valeurs s'étalent entre 38.999 MHz (n = 3; Y = F) à 34.668 MHz (n = 2; Y = π-$C_5H_5Fe(CO)_2$) et sont généralement reliées à l'électronégativité d'Y et à la grandeur du cycle. Les coefficients de température moyenne des fréquences varient entre -0.9×10^{-4} à -1.8×10^{-4}/°K. [Traduit par le journal]

Introduction

Although extensive chlorine nuclear quadrupole resonance (n.q.r.) spectral studies of chlorinated hydrocarbons have been made (1–3), there are few corresponding studies on chlorinated polyfluoroaliphatic compounds. To our knowledge, data for only five polyfluoroalkenes have been reported in the literature (4–6) prior to the present work in spite of the fact that the chemistry of fluorocarbon compounds is quite different from that of their hydrocarbon analogs (*e.g.* the double bond of a fluoroalkene is electron deficient, whereas that of a hydroalkene is usually electron rich (7)). Thus, it seemed desirable to study the chlorine n.q.r. spectra of a range of chloropolyfluoroalkenes. In particular in recent years, a number of substituted chloropolyfluorocycloalkenes $YC{=}CCl(CF_2)_n$ has been synthesized. These compounds, which have a vinylic substituent Y and a vinylic chlorine atom on the adjacent carbon atoms, are somewhat related to *ortho* substituted aromatic compounds, and data for them are presented in this paper.

In earlier studies ^{19}F n.m.r. data for some substituted perfluorocyclobutenes, $YC{=}CF(CF_2)_2$ have been described (8, 9). One interesting feature is the large variation in chemical shift of the vinylic fluorine atom. Notably when Y is a NR_2 group, the resonance of the vinylic fluorine is well upfield. Cullen and Dhaliwal have rationalized this in terms of a shielding of the vinylic fluorine atom due to contributions from canonical forms such as $R_2\overset{\oplus}{N}{=}C{-}\overset{\ominus}{C}F(CF_2)_2$. Since n.q.r. is a powerful tool for elucidating electronic effects, chlorine n.q.r. studies on the related systems $YC{=}CCl(CF_2)_n$ with Cl replacing F might be expected to show parallel behavior.

Experimental

The 1,2-dichloropolyfluorocycloalkenes $ClC{=}CCl(CF_2)_n$ (n = 2,3,4) and 2,3-dichlorohexafluorobutene were obtained from Peninsular Chemresearch Inc., Gainesville, Florida. The derivatives of these compounds were prepared by literature procedures as indicated in Table 1.

[1]This work includes part of the material submitted by Lian Sai Chia and Poh Siew Yiaw in partial fulfilment of the requirements for the Ph.D. and B.Sc. degrees, respectively, University of British Columbia.

Can. J. Chem. Downloaded from www.nrcresearchpress.com by 210.87.254.5 on 09/05/12
For personal use only.

TABLE 1. ^{35}Cl n.q.r. frequencies for chloropolyfluoroalkenes at $-196°$ (in MHz)[a]

Y		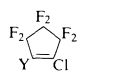	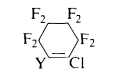	Reference No.
F	38.311(30) 38.425(30)	38.999(100)	[b]	18
Cl	37.001(600)[c] 37.113(600)	38.039(350)[d]	38.666(32)	
OMe	37.101(400)	37.909(60)	[b]	19
N_3	36.866(50)	37.844(25)		20
H	36.495(40)	37.487(60)	[b]	21
NEt_2		37.768(20), 37.331(21) 37.222(18)		9
NMe_2	36.276(8)	37.232(50) 37.415(80)	37.965(15)	9
Me	[b]	[b]		22
Et	36.030(45) 36.252(33)	[b]		22
$SiMe_3$	35.825(65)	[b]		23
SMe	[b]	36.713(30)		19
$AsMe_2$	35.648(62) 35.675(45)	36.711(60)		8
PPh_2	[b]	36.638(30)		24
$Mn(CO)_5$	34.801(30)			25
$(\pi\text{-}C_5H_5)Fe(CO)_2$	34.668(100)			25

[a]Experimental uncertainty is ±0.050 MHz. Figures in parentheses are signal-to-noise ratios.
[b]No n.q.r. signal was obtained.
[c]From ref. 5.
[d]From ref. 6.

The desired products were purified by distillation or recrystallization, and identified by means of their b.p. or m.p. and known i.r., ^1H n.m.r. and ^{19}F n.m.r. spectral data.

Initial n.q.r. measurements were made with the spectrometer described previously (10). These were repeated and extended with a Decca instrument using Zeeman modulation. The resonance frequencies were measured with the aid of the frequency marker on the instrument and checked with a Hewlett Packard 5246L electronic counter.

Variable temperature studies were done by allowing the sample to warm from liquid nitrogen temperature. By this means a slow temperature variation from $-196\,°C$ to room temperature was obtained in about 4 h. Temperatures were measured with a calibrated copper–constantan thermocouple.

Results and Discussion

The ^{35}Cl n.q.r. frequencies observed for the compounds investigated are listed in Table 1. Some of the compounds, not unexpectedly, have more signals than the number of chlorine atoms in the molecule. The corresponding ^{37}Cl resonance frequencies were also measured although they are not listed. In all cases these were of lower intensity and their frequency was approximately 1.27 times that of the ^{35}Cl signal, consistent with the expected value.

For chlorine ($I = 3/2$), the n.q.r. frequency is related to the coupling constant by the equation:

$$\nu = \frac{e^2Qq}{2h}\left(1 + \frac{\eta^2}{3}\right)^{1/2}$$

However, since the Cl atoms in the compounds studied are involved in only one bond, η will probably be less than 0.2, so the error caused by neglecting η is less than 0.7% (2). Thus, to a good approximation, the coupling constant can be obtained simply by doubling the observed frequency.

Substituent Effects

From Table 1 it can be seen that the chlorine n.q.r. frequencies of the cyclobutene compounds decrease in the order listed: F > Cl > OMe > N_3 > H > NR_2 > Et > $SiMe_3$ ~ SMe ~

Can. J. Chem. Downloaded from www.nrcresearchpress.com by 210.87.254.5 on 09/05/12
For personal use only.

$AsMe_2 \sim PPh_2 > Mn(CO)_5 > (\pi\text{-}C_5H_5)Fe(CO)_2$. The order is essentially that of decreasing electronegativities of the substituents. The implication then is that the variations in n.q.r. frequencies with substituent are due chiefly to inductive effects, though other factors, particularly conjugative effects, may also be significant. Following Semin and co-workers (11) we have attempted to put this on a more quantitative basis by fitting the data to equations of the following form:

$$[1] \qquad \nu = \nu_0 + a\sigma_I + b\sigma_C$$

Here ν is the n.q.r. frequency. The parameters σ_I and σ_C provide a measure of the inductive and conjugative transmission effects of the various substituents; ν_0, a, b are coefficients to be determined in the fit. The values of the σ parameters used in the present work are taken from Exner (12).

Least-squares fits were made to eq. 1 for both $YC{=}CCl(CF_2)_2$ and $YC{=}CCl(CF_2)_3$ using σ_I and σ_C but in most cases the coefficients of σ_C had standard errors larger than the value of b itself. Thus the dependence on σ_C was indeterminate, and the dependence on σ_I alone was evaluated as follows.

For $YC{=}CCl(CF_2)_2$:

$$[2] \quad \nu = (36.211 \pm 0.181) + (2.723 \pm 0.569)\sigma_I \qquad (R = 0.89)$$

For $YC{=}CCl(CF_2)_3$:

$$[3] \quad \nu = (36.793 \pm 0.335) + (3.018 \pm 1.024)\sigma_I \qquad (R = 0.77)$$

There is a fairly reasonable dependence on σ_I, although for the cyclopentenes the coefficient of σ_I has again a rather large standard error. Two noteworthy points emerge: (*i*) The values of 'a' in eqs. 2 and 3 are the same within their standard errors, suggesting that the dependence on σ_I is purely a function of the substituent and independent of the rest of the ring. (*ii*) The correlation of ν with σ_I is only fair in both cases.

The most likely cause of the scatter is differences in extra-molecular potentials caused by variations in the crystal lattice sites of the chlorine atoms. These typically result in frequency variations of up to ± 0.5 MHz (13) in organic molecules. Since the molecules considered here are rather complex, with complex substituents, large variations in crystal structure, and consequent scatter of the n.q.r. frequencies can be expected. Steric effects of the substituents might also give small frequency variations, and there might also be differences in the C=C(Cl) angle and C—Cl bond length having similar effects. All these contributors could well mask any dependence of frequency on σ_C.

The n.q.r. data can basically be rationalized in terms of two simple canonical forms, namely **1** and **2**, in which Cl is covalently (by a single bond) and ionically bonded, respectively, to carbon. By analogy with other ethylenic com-

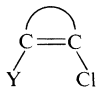

1

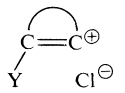

2

pounds (14, 15), these forms probably contribute roughly 70 and 20%, respectively, to the resonance hybrid, with the result that e^2Qq for ^{35}Cl is approximately 70 MHz, as found in this work. As the electronegativity of the substituent Y increases, the s-character of carbon in the C—Cl bond increases; this in turn increases the electronegativity of the carbon atom and decreases the ionic character of the C—Cl bond (*i.e.* decreases the contribution of structure **2**) (15). Since e^2Qq of Cl in **2** is zero, the net result should be an increase in n.q.r. frequency with electronegativity (and σ_I) of Y, as found.

As mentioned in the introduction, electronegativity alone cannot be used to rationalize the ^{19}F chemical shifts of the vinylic fluorine atom in the compounds $YC{=}CF(CF_2)_2$ and contributions from canonical forms of the type **3** (X = F) needed to be considered (8, 9). Although there is a good correlation ($R = 1.00$) between ν (^{35}Cl) and δ (^{19}F) for the compounds $YC{=}CXCF_2CF_2$ (X = Cl or F) for Y = F, OCH_3, $N(CH_3)_2$ ($\nu = (45.933 \pm 0.303) - (0.062 \pm 0.002)\delta$) which suggests they are affected by the same factors, the relationship fails when compounds with other groups Y are included. Overall there appears to be no obvious relationship between the n.q.r. frequency and the corresponding ^{19}F chemical shift. Perhaps it is expecting too much for there to be one since, as indicated above, canonical

Can. J. Chem. Downloaded from www.nrcresearchpress.com by 210.87.254.5 on 09/05/12
For personal use only.

Can. J. Chem. Downloaded from www.nrcresearchpress.com by 210.87.254.5 on 09/05/12
For personal use only.

forms such as **1** and **2** are needed to rationalize the n.q.r. data but canonical forms such as **3** and **4** appear to make a significant contribution to the resonance hybrid when X = F.

3 4

Indeed the known (7) great susceptibility of vinylic fluorine atoms to nucleophilic attack when Y is an electronegative group is indicated by **4**. Its diminished activity (but still great) when Y is $N(CH_3)_2$, OCH_3 etc. is indicated by **3**. Canonical form **3** may give a hint as to why when Y = F, OCH_3, $N(C_3H_3)_2$ there is the correlation between $\nu(^{35}Cl)$ and $\delta(^{19}F)$ for this restricted group. Interestingly this same small group together with $Y = N_3$ can be fitted to an equation of the type [1] with a good correlation ($R = 1.00$) with both σ_I and σ_C ($\nu = (35.103 \pm 0.016) + (5.220 \pm 0.026)\sigma_I - (0.736 \pm 0.016)\sigma_C$) which could be an indication that canonical forms such as **3** do make a small contribution when X = Cl.

Effect of Ring Size

From Table 1 it can be seen that the resonance frequency of the ring compounds increases as the ring size increases. Two reasons can be suggested for this change. Firstly, the increase in the number of electron withdrawing CF_2 groups will decrease the contribution from **2** and hence increase the frequency. Secondly, the increase in the exocyclic

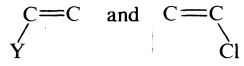

bond angles will decrease the s-character of C in the C—Cl bond, and hence increase the effective electronegativity difference between C and Cl. However, 2,3-dichlorohexafluorobutene, which should have essentially the same exocyclic bond angles as 1,2-dichlorooctafluorocyclohexene, has a higher frequency (6) (39.491 MHz) than the latter (38.666 MHz), which could indicate that the former is the main reason, provided these small differences are significant.

The n.q.r. frequencies of 1,2-dichlorodifluorocyclopropene at −196° are 38.14, 38.37, 38.58, and 38.75 MHz (4). Here the vinylic chlorine atoms have higher resonance frequencies instead of lower than those of 1,2-dichlorotetrafluorocyclobutene. This may be due in part to a contribution from the ionic form

5

to the ground state of the former compound. The canonical form **5**, which is in this particular case favored because of its aromaticity, results in reduced withdrawal of charge from the ring to chlorine.

Temperature Dependence of n.q.r. Frequencies

The temperature dependence of the resonance frequency of hydrocarbons has been well documented (2, 13) but little is known about fluoroalkenes. Figure 1 shows the temperature dependence curves of some of the fluorocycloalkenes investigated here. The frequency decreases with increasing temperature which is the same behavior expected from Bayer's theory (16), although the curvature of curve *h*

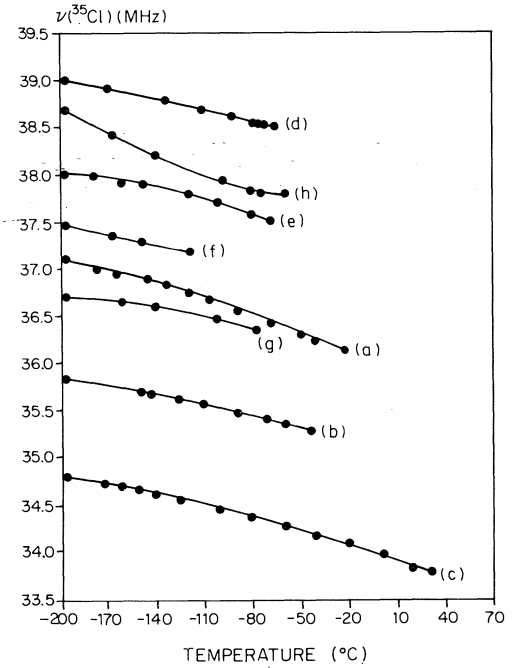

FIG. 1. Temperature dependence of the resonance frequency of $YC{=}CCl(CF_2)_n$ ($n = 2$; (*a*) Y = OMe, (*b*) Y = $SiMe_3$, (*c*) Y = $Mn(CO)_5$, $n = 3$; (*d*) Y = F; (*e*) Y = Cl, (*f*) Y = H; (*g*) Y = $AsMe_2$; $n = 4$; (*h*) Y = Cl).

seems abnormal. The shape of each curve is smooth, indicating that there are probably no phase transitions in the region investigated. The mean temperature coefficients $a \simeq -0.9 \times 10^{-4}$ to -1.8×10^{-4} °K are not unusual (2, 3, 17).

The authors wish to thank the National Research Council of Canada for their financial support of this work in the form of operating grants to W.R.C. and M.C.L.G. and also for the funds to purchase the spectrometer. The International Nickel Company of Canada, Limited, is thanked for the award of a scholarship to L.S.C.

1. T. P. Das and E. L. Hahn. Nuclear quadrupole resonance spectroscopy. Academic Press, New York, N.Y. 1958.
2. E. A. C. Lucken. Nuclear quadrupole coupling constants. Academic Press, New York, N.Y. 1969.
3. I. P. Biryukov, M. G. Voronkov, and I. A. Safin. Tables of nuclear quadrupole resonance frequencies. Israel Program for Scientific Translations, Jerusalem. 1969.
4. R. M. Smith and R. West. Tetrahedron Lett. **26**, 2141 (1969).
5. C. Brevard and J. M. Lehn. J. Chim. Phys. **65**, 727 (1968).
6. E. A. C. Lucken. J. Chem. Soc. 2954 (1959).
7. W. A. Sheppard and C. M. Sharts. Organic fluorine chemistry. W. A. Benjamin, Inc., New York, N.Y. 1969.
8. W. R. Cullen, P. S. Dhaliwal, and G. E. Styan. J. Organometal. Chem. **6**, 364 (1966).
9. W. R. Cullen and P. S. Dhaliwal. Can. J. Chem. **45**, 719 (1967).
10. J. K. B. Bishop, W. R. Cullen, and M. C. L. Gerry. Can. J. Chem. **49**, 3910 (1971).
11. G. K. Semin, A. A. Neimysheva, and T. A. Babushkina. Izv. Akad. Nauk. SSSR, Ser. Khim. **2**, 486 (1970).
12. O. Exner. The Hammett equation—the present position. *In* Advances in linear free energy relationships. *Edited by* N. B. Chapman and J. Shorter. Plenum Press, New York, N.Y. 1972.
13. A. Weiss. Top. Curr. Chem. **30**, 1 (1972).
14. M. C. L. Gerry. Can. J. Chem. **49**, 255 (1971).
15. R. G. Stone and W. H. Flygare. J. Mol. Spectrosc. **32**, 233 (1969).
16. H. Bayer. Z. Physik. **130**, 227 (1951).
17. W. Pies, H. Rager, and A. Weiss. Org. Magn. Res. **3**, 147 (1971).
18. R. L. Johnson. Ph.D. Thesis. University of Iowa. 1966.
19. W. R. Cullen, D. S. Dawson, and P. S. Dhaliwal. Can. J. Chem. **45**, 683 (1967).
20. C. O. Parker. J. Am. Chem. Soc. **81**, 2183 (1961).
21. D. J. Burton and R. L. Johnson. J. Am. Chem. Soc. **86**, 5361 (1964).
22. J. D. Park and R. Fontanelli. J. Org. Chem. **28**, 258 (1963).
23. W. R. Cullen and G. E. Styan. J. Organomet. Chem. **6**, 633 (1966).
24. R. F. Stockel. Can. J. Chem. **46**, 2625 (1968).
25. R. B. King and A. Efraty. J. Fluorine Chem. **1**, 283 (1971).

Can. J. Chem. Downloaded from www.nrcresearchpress.com by 210.87.254.5 on 09/05/12
For personal use only.

The Proton Magnetic Resonance Spectrum of *p*-Methylbenzylbromide. Conformational Preference of the Bromomethyl Rotor

KALVIN CHUM,[1] J. BRIAN ROWBOTHAM,[2] AND TED SCHAEFER

Department of Chemistry, University of Manitoba, Winnipeg, Manitoba R3T 2N2

Received March 11, 1974

KALVIN CHUM, J. BRIAN ROWBOTHAM, and TED SCHAEFER. Can. J. Chem. **52**, 3489 (1974).

A complete analysis is given of the nine-spinproton magnetic resonance spectrum of *p*-methylbenzyl bromide as a 20 mol% solution in acetone-d_6. The long-range coupling constants between methyl and ring protons are the same as those in toluene. The coupling constants between the methylene protons and the other protons in the molecule are consistent with a two-fold barrier of 500 ± 200 cal/mol for the bromomethyl group, the preferred conformation having the C—Br bond in a plane perpendicular to the aromatic plane. An alternative model, in which a C—H bond of the bromomethyl rotor prefers the aromatic plane to the extent of 3 kcal/mol, is considered unlikely.

KALVIN CHUM, J. BRIAN ROWBOTHAM et TED SCHAEFER. Can. J. Chem. **52**, 3489 (1974).

On donne une analyse complète du spectre de résonance magnétique nucléaire du proton pour les neuf spins du bromure de *p*-méthylbenzyle en solution à 20 mol% dans l'acétone-d_6. Les constantes de couplage à longue distance entre le méthyle et les protons du cycle sont les mêmes que celles observées dans le toluène. Les constantes de couplage entre les protons méthyléniques et les autres protons de la molécule sont en accord avec l'hypothèse que la rotation du groupe bromométhyle implique une barrière binaire possédant une énergie de 500 ± 200 cal/mol et que le groupe bromométhyle existe dans une conformation privilégiée impliquant un lien C—Br dans un plan perpendiculaire au plan du noyau aromatique. On considère comme improbable le modèle dans lequel un lien C—H du rotor bromométhyle serait dans le plan aromatique jusqu'à concurrence de 3 kcal/mol.

[Traduit par le journal]

Introduction

The long-range spin–spin coupling constants between protons or fluorine nuclei in methyl or fluoromethyl groups and the ring protons in toluene and its derivatives are stereospecific (1–6). The coupling over six bonds, $^6J_p^{H,CH}$ or $^6J_p^{H,CF}$, has a $\sin^2\theta$ dependence, θ being the angle defined in **1**, and is transmitted by a σ–π electron mechanism (4, 7). Its magnitude also

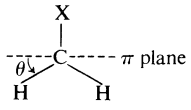

1

depends on the electronegativity, E_X, of the substituent, X (3). The couplings over five bonds, $^5J_m^{H,CH}$, and four bonds, $^4J_o^{H,CH}$, have a more complex dependence on θ (4, 7, 8).

In principle, the preferred conformation about the Csp^2—Csp^3 bond can be deduced from these couplings. When the barrier to rotation is large, say 2 kcal/mol or more, the ground state conformation is well defined and can be easily deduced from the magnitudes of the coupling constants (2, 3, 6). When the barrier is low, conformational preferences can still be identified under favorable circumstances. For example, a recent analysis (5) of the spin–spin coupling data on benzal fluoride and a number of its dichloro derivatives, suggests a barrier of rather less than 0.5 kcal/mol (almost free rotation) and a ground state conformation in which the C—H bond of the CHF_2 group lies in the plane of the ring. An *ab initio* molecular orbital calculation gave the same ground state and a barrier of 0.180 kcal/mol (9).

Such a calculation predicts a similar barrier in benzyl fluoride, the C—F bond favoring an in-plane conformation. The proton magnetic resonance spectrum of this compound has not yet yielded to analysis.

As the size of the substituent, X, in the CH_2X group increases, an in-plane conformation of the C—X bond becomes less favorable for steric reasons and it is interesting to see whether the coupling constants will reflect the situation. Con-

[1]Research Assistant.
[2]Research Associate 1973–1974.

Can. J. Chem. Downloaded from www.nrcresearchpress.com by 210.87.254.6 on 09/05/12
For personal use only.

TABLE 1. Proton chemical shifts* and coupling constants† of *p*-methylbenzylbromide in acetone

Parameter		LACX	LAME		NUMAR
decoupling		CH_2 and CH_3	CH_3	CH_2	—
ν_A		707.682 (0.010)‡	707.945 (0.003)‡	707.959 (0.002)‡	707.96
ν_B		723.950 (0.010)	724.272 (0.003)	724.267 (0.002)	724.27
ν_{CH_2Br}		—	447.938 (0.003)	—	447.86
ν_{CH_3}		—	—	225.456 (0.002)	225.49
$^3J_o^{H,H}$		7.862 (0.015)	7.830 (0.004)	7.856 (0.003)	7.843
$^4J_m^{H,H}$	H_B	2.019 (0.017)	2.021 (0.005)	2.011 (0.003)	2.015
		2.018 (0.017)	2.020 (0.005)	2.010 (0.003)	2.015
$^5J_p^{H,H}$		0.562 (0.013)	0.559 (0.004)	0.535 (0.002)	0.547
$^4J_o^{H,CH_3}$		—	—	−0.712 (0.001)	−0.730
$^5J_m^{H,CH_3}$		—	—	0.349 (0.001)	0.375
$^4J_o^{H,CH_2Br}$		—	−0.393 (0.003)	—	−0.420
$^5J_m^{H,CH_2Br}$		—	0.253 (0.003)	—	0.280
$^7J_p^{CH_2,CH_3}$		—	—	—	0.34±0.03
Root mean square error		0.028	0.019	0.013	—
Largest error		0.055	0.041	0.040	—
Lines assigned		24	128	208	—
Lines calculated		24	128	215	—

*In Hz to low field of internal tetramethylsilane for a 20 mol% acetone-d_6 solution at 100 MHz.
†In Hz, see **2** in text for labelling of ring protons.
‡Probable errors.

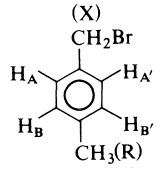

2

sequently, the p.m.r. spectrum of *p*-methylbenzylbromide, **2**, was analyzed as a nine-spin, $[AB]_2X_2R_3$ system. The methyl group actually simplifies the analytical procedure and its coupling data serve as a reference point in the discussion of the coupling between the methylene protons and the ring or methyl protons. Comparison with data for related molecules and with molecular orbital calculations may then yield conformational information about the CH_2Br group.

Experimental

A 20 mol% solution of recrystallized *p*-methylbenzylbromide (Koch-Light) in acetone-d_6, containing a small amount of tetramethylsilane (TMS), was degassed by the freeze–pump–thaw technique. Proton magnetic resonance spectra were calibrated on an HA100D spectrometer at sweep rates of 0.01 and 0.02 Hz/s in a manner described previously (10). The acetone solution had a spectral range sufficient for accurate analyses. Decoupling experiments yielded the four-spin ring proton spectrum, $[AB]_2$, the six-spin spectrum, $[AB]_2X_2$, and the seven-spin spectrum, $[AB]_2R_3$.

Results and Discussion

Spectral Analysis

The four-spin system was analyzed with the computer program LACX (11), yielding the ring proton spectral parameters in column 2 of Table 1. The six- and seven-spin spectra were analyzed with the program LAME (12) and gave the results in columns 3 and 4 of Table 1. As shown in the table, most calculated transitions were assigned, 208 of the 215 calculated transitions being assigned in the seven-spin system.

The noniterative program NUMAR (13) gave fits to the nine-spin spectrum. Initial calculations took mean values of the spectral parameters from the LAME results, and $^7J_p^{CH_2,CH_3}$ was varied between 0.25 and 0.40 Hz in steps of 0.05 Hz. For each value of this coupling the line widths at half-height were varied between 0.15 and 0.20 Hz and asymmetry factors (14) of 0.7 and 0.6 were tried. Later calculations included variations in the couplings between ring and side-chain protons. The final parameters are given in column 5 of Table 1. The final fit gave $^7J_p^{CH_2,CH_3}$ as 0.34

Can. J. Chem. Downloaded from www.nrcresearchpress.com by 210.87.254.6 on 09/05/12
For personal use only.

Can. J. Chem. Downloaded from www.nrcresearchpress.com by 210.87.254.6 on 09/05/12
For personal use only.

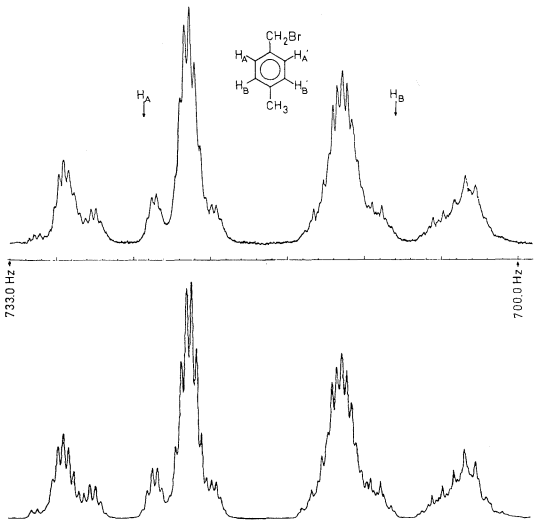

FIG. 1. The observed (top) and calculated ring p.m.r. spectrum of *p*-methylbenzyl bromide as a 20 mol % solution in acetone-d_6. The frequency scale is in Hz at 100 MHz to low field of internal tetramethylsilane. The calculated spectrum assumes a line width at half-height of 0.2 Hz and an asymmetry factor of 0.5. Note that the line width of the H_A protons is observed to be larger than that of the H_B protons.

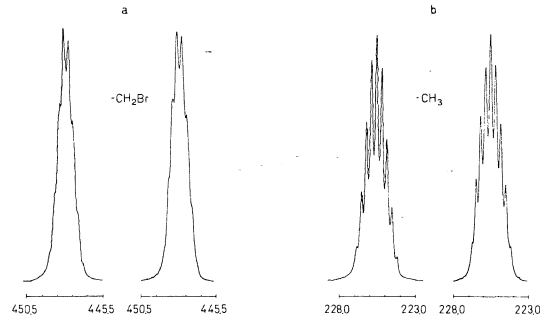

FIG. 2. The observed and calculated spectra of the methylene and methyl protons of *p*-methylbenzyl bromide under conditions described in the caption to Fig. 1. The calculated spectra assume a line width of 0.2 Hz and an asymmetry factor of 0.6. In both *a* and *b* the calculated spectrum occurs at the left.

Hz, values of 0.30 or 0.38 Hz leading to marked deviations of the calculated from the observed spectra.

In Figs. 1 and 2 the observed and calculated spectra indicate good agreement and suggest the reliability of the parameters. The line widths of the ring protons *ortho* to the CH_2Br groups were larger than those of the other ring protons (see figure caption). T_1 measurements are needed for an elucidation of this fact.

Long-range Couplings and Conformational Preferences

(a) Methyl Proton – Ring Proton Couplings

$^4J_o^{H,CH_3}$ is -0.72 ± 0.01 Hz and $^5J_m^{H,CH_3}$ is 0.36 ± 0.02 Hz in *p*-methylbenzyl bromide, well within experimental error of the corresponding values in toluene (1). These results bear out previous statements (3) that such long-range couplings are insensitive to solvent and ring substituent effects. In toluene, the barrier to rotation is 0.014 kcal/mol (15), so that the observed couplings are those for free rotation of the methyl group.

(b) Coupling Over Seven Bonds, $^7J_p^{CH_2,CH_3}$

In compounds of the type **3** it has been shown that $^6J_p^{H,CH_2X}$ decreases in magnitude as the

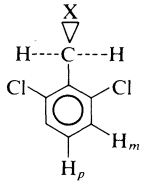

3

electronegativity *E*X increases (3). In particular, $^6J_p^{H,CH_3}$ is -0.63 Hz in **3** (X = H) and is -0.61 Hz in toluene. One may write (3, 16)

$$[1] \qquad {}^6J_p^{H,CH_3} = B \sin^2 \theta$$

where θ is defined above, and for free rotation $\langle \sin^2 \theta \rangle = 0.5$. Therefore $B = -1.2_4$ Hz. When X = Br in **3**, $^6J_p^{H,CH_2}$ is -0.21 Hz (3) so that *B* becomes -0.84 Hz, because $\theta = 30°$.

In *p*-xylene (8) and various derivatives (7, 8) $^7J_p^{CH_3,CH_3}$ has the same magnitude as, but opposite sign to, $^6J_p^{H,CH_3}$ in toluene, as expected for a mechanism in which σ–π interaction occurs between the C—H bonds of the side chain and the π electron system of the aromatic ring. Hence

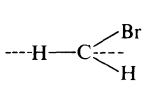

4

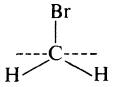

5

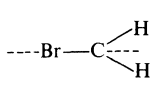

6

one may use the value of 0.34 Hz for $^7J_p^{CH_2,CH_3}$ in *p*-methylbenzyl bromide in an attempt to discriminate among **4**, **5**, **6**, and/or a free rotation

Can. J. Chem. Downloaded from www.nrcresearchpress.com by 210.87.254.6 on 09/05/12
For personal use only.

model for the CH_2Br group. For example, for **4** one has $^7J_p^{CH_2,CH_3} = 0.84(\sin^2 0° + \sin^2 60°)/2 = 0.32$ Hz as the predicted value and almost exactly equal to the observed constant. For **5** the predicted number is 0.21 Hz and is 0.63 Hz for **6**. For free rotation the coupling constant should be 0.42 Hz, also *well* outside the value which gives agreement with experiment.

This result is based on a classical approach and is only valid if **4** is more stable than **5** or **6** by about 3 kcal/mol or more (the barrier in **3** (X = Br) is greater than 10 kcal/mol (17)). Such a high barrier is unlikely for *p*-methylbenzylbromide and a quantum mechanical approach is therefore necessary. The problem in which a coupling constant with a $\sin^2\theta$ dependence is partially averaged by rotation about a two-fold barrier has been solved (18). It is then a simple matter to fit our ratio of 0.34/0.84 to a curve giving this ratio as a function of barrier to obtain 500 ± 200 cal/mol. The rather generous error limits reflect possible errors in coupling constants and in the approximate solutions to the Mathieu equation.

Le Fèvre and co-workers (19) arrived at **4** as the preferred conformation of *p*-methylbenzylbromide in CCl_4 solution *if* molecular rigidity is to be expected, in agreement with our result. We prefer the lower barrier which predicts **5** as the lowest energy conformation, **6** as the highest. Then **4** does not lie at a local minimum on a two-fold potential energy curve. The conformation **5** relieves nonbonded repulsive interactions between the C—Br and the ring C—H bonds.

A barrier of 500 cal/mol means that substantial classical oscillations occur about the minimum and maximum conformations. With that reservation it may be noted that the fractional populations are $p_5 = 0.7$ and $p_6 = 0.3$ at 32 °C. Consequently, a 100° change in temperature will change ^7J by at most 0.03 Hz.

The barrier estimate depends only on the assumption of a $\sin^2\theta$ dependence of ^7J and on our experimental estimate of B in eq. 1. The $\sin^2\theta$ dependence is strongly supported by the fact that $^7J^{CH_3,CH_3} = -^6J^{CH_3,H}$ in *p*-xylene and toluene, respectively. Furthermore, these parameters are insensitive to the presence of ring substituents, as discussed above.

Of course, a confirmation of the present barrier estimate by microwave or far i.r. techniques is advisable, in our opinion.

(c) Coupling Over Four Bonds: $^4J_o^{H,CH_2}$

The angular dependence of $^4J_o^{H,CH_2}$ and of $^5J_m^{H,CH_2}$ is likely to be considerably more complex than that of $^6J^{H,CH_2}$ of $^7J^{CH_2,CH_3}$. The experimental evidence pertains only to a few angles. Calculations of the angular dependence of ^4J, ^5J, and ^6J can be made at the level of approximate molecular orbital theory. The $\sin^2\theta$ dependence of ^6J and ^7J is well reproduced by these calculations (4) although the magnitudes do not always agree with experiment.

The following discussion of ^4J and ^5J should be viewed as a heuristic one, in that it is an attempt at using approximate theoretical J values in conjunction with a few experimental measurements to obtain agreement with the more firmly based conformational data deduced above.

In toluene the observed value of $^4J_o^{H,CH_3}$ is -0.75 Hz (1) while the mean INDO MO FPT value is -0.92 Hz (4). CNDO/2 calculations, using geometries and convergence procedures as described previously (4), yield less than 0.03 Hz for all conformations. The INDO MO FPT program has not been parameterized for atomic numbers higher than nine. Therefore, fluorine was chosen to simulate an electronegative substituent on the methyl group (bromine). The conformational angle, θ, is defined in **7** and the results of the computations following the parameterization in ref. 20 are given in Table 2. CNDO/2 values, untabulated, for $^4J_o^{H,CH_2F}$ lie between 0.03 and 0.13 Hz.

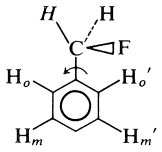

$\theta = 0°$, F above plane; an increase in θ brings F farther out of plane

7

From Table 2, the predicted values of $^4J_o^{H,CH_2}$ for conformations **4**, **5**, and **6** are -0.61, -0.45, and -1.11 Hz, respectively. A plot of ^4J_o in Table 2 *vs.* θ is not a $\sin^2\theta$ curve, peaking as it does at 105°, but a very rough estimate of the reduction in these three predicted values caused by motional averaging is obtained by multiplying by a factor of 0.8 obtained from the observed and free rotation value for $^7J_p^{CH_2,CH_3}$ (0.34 and 0.42 Hz). One finds -0.49, -0.36, and -0.89 Hz for **4**, **5**, and **6**, respectively. The best agreement is therefore found for **5** as the low-

TABLE 2. Computed long-range proton–proton coupling constants of the methyl or methylene protons in toluene and benzyl fluoride by INDO MO FPT†

θ* (deg)	$^4J_o^{H,CH_2F}$	$^4J_o^{H',CH_2F}$	$^5J_m^{H,CH_2F}$	$^5J_m^{H',CH_2F}$
0	−0.194	−0.486	0.141	0.887
15	−0.190	−0.477	0.138	0.883
30	−0.315	−0.576	0.201	0.895
45	−0.543	−0.755	0.320	0.916
60	−0.819	−0.963	0.474	0.931
75	−1.075	−1.139	0.633	0.921
90	−1.243	−1.225	0.771	0.871
105	−1.285	−1.189	0.872	0.773
120	−1.200	−1.032	0.931	0.637
135	−1.017	−0.795	0.948	0.480
150	−0.796	−0.537	0.934	0.329
165	−0.602	−0.321	0.907	0.209
180	−0.486	−0.194	0.887	0.141

*The angle θ is defined by **7** of the text.
†See **7** in the text for the definition of the H′ in $^4J_o^{H',CH_2F}$. As θ increases, the C—F bond moves farther out of the aromatic plane.

energy confirmation, the observed value of $^4J_o^{H,CH_2}$ being −0.41 Hz. In view of the approximations underlying this estimate, the rough agreement is hardly a confirmation of the conclusions based on ^7J. However, it is encouraging to note that **6** is contraindicated as the low energy form, in agreement with the ^7J data and with chemical intuition based on steric interactions.

(c) Coupling Over Five Bonds, $^5J_m^{H,CH_2}$

The INDO values for benzylfluoride are given in Table 2, their mean value being 0.66 Hz. For toluene the mean of the ^5J values, also calculated at 15° intervals in the angle θ, is 0.69 Hz (4), indicating an inappreciable change in ^5J induced by an electronegative atom. The theoretical J values in Table 2 yield 0.65, 0.55, and 0.78 Hz for **4**, **5**, and **6**, respectively.

It is known that INDO overestimates $^5J_m^{H,CH_3}$, in that $^5J_m^{H,CH_3}$ in toluene is 0.36 Hz (1), whereas the calculated value is 0.69 Hz for free rotation. Reduction of the predicted values by 0.36/0.69 gives 0.34, 0.29, and 0.40 Hz for **4**, **5**, and **6**, respectively. The observed value in *p*-methylbenzylbromide is 0.27 Hz.

We do not suggest that ^4J and ^5J can be used to determine the barrier to rotation nor the preferred conformation of the bromomethyl group (although **6** does appear to be an unlikely candidate for the stable form). It does appear, however, that the above discussion indicates the absence of glaring contradictions between the conclusions based on ^7J and the magnitudes of ^4J and ^5J in *p*-methylbenzylbromide.

(e) Solvent Effects on Conformational Stability

The classical solvation theory of Abraham *et al.* (21, 22) implies that the more polar solute conformer is favored by an increase in the dielectric constant of the solution. Although acetone has a relatively high dielectric constant, the dipole moments of **4**, **5**, and **6** differ at most by 0.1 D in 1.6 D, **6** having the lowest moment. This statement is based on CNDO/2 and INDO calculations on benzyl fluoride. It is apparent that solvation energy differences are very small and that the Kerr constant data in CCl_4 solution (19) may be compared with spin coupling data in acetone solution. The difference in dipole moments between **4** and **5** is about 0.02 D.

Conclusions

To conclude, the long-range proton–proton spin–spin coupling constant in *p*-methylbenzylbromide are interpreted in terms of a two-fold barrier to internal rotation of about 500 cal/mol for the bromomethyl rotor. The stable conformation has the C—Br bond in a plane perpendicular to the aromatic plane. An alternative but unlikely model implies a barrier of at least 3 kcal/mol with a low-energy conformation in which a C—H bond of the CH_2Br group prefers the plane of the aromatic ring. The barrier of 500 cal/mol compares with an *ab initio* molecular

Can. J. Chem. Downloaded from www.nrcresearchpress.com by 210.87.254.6 on 09/05/12
For personal use only.

orbital calculation (9) on benzyl fluoride in which the C—F bond prefers the aromatic plane by 250 cal/mol.

We are grateful to Dr. J. S. Martin for a copy of the program NUMAR and to the National Research Council of Canada for financial assistance. We thank a referee for very helpful suggestions.

1. M. P. Williamson, R. J. Kostelnik, and S. M. Castellano. J. Chem. Phys. **49**, 2218 (1968).
2. T. Schaefer, R. Schwenk, C. J. Macdonald, and W. F. Reynolds. Can. J. Chem. **46**, 2187 (1968).
3. A. F. Janzen and T. Schaefer. Can. J. Chem. **49**, 1818 (1971).
4. R. Wasylishen and T. Schaefer. Can. J. Chem. **50**, 1852 (1972).
5. J. B. Rowbotham, A. F. Janzen, J. Peeling, and T. Schaefer. Can. J. Chem. **52**, 481 (1974).
6. H. M. Hutton, J. B. Rowbotham, B. H. Barber, and T. Schaefer. Can. J. Chem. **49**, 2033 (1971).
7. C. J. Macdonald and W. F. Reynolds. Can. J. Chem. **48**, 1002 (1970).
8. J. B. Rowbotham and T. Schaefer. Can. J. Chem. **52**, 489 (1974).
9. W. J. Hehre, L. Radom, and J. A. Pople. J. Am. Chem. Soc. **94**, 1496 (1972).
10. R. Wasylishen and T. Schaefer. Can. J. Chem. **49**, 94 (1971).
11. C. W. Haigh. Private communication.
12. C. W. Haigh and J. M. Williams. J. Mol. Spectrosc. **32**, 398 (1969).
13. A. R. Quirt and J. S. Martin. Private communication.
14. J. B. Rowbotham and T. Schaefer. Can. J. Chem. **50**, 2344 (1972).
15. H. Rudolph, H. Dreizler, A. Jaeschke, and P. Wendling. Z. Naturforsch. **22***a*, 940 (1967).
16. C. Heller and H. M. McConnell. J. Chem. Phip. **32**, 1535 (1960).
17. J. Peeling, L. Ernst, J. B. Rowbotham, and T. Schaefer. Can. J. Chem. **52**, 2414 (1974).
18. E. W. Stone and A. H. Maki. J. Chem. Phys. **37**, 1326 (1962).
19. K. E. Calderbank, R. J. W. Le Fèvre, and R. K. Pierens. J. Chem. Soc. B, 1463 (1970).
20. J. A. Pople, J. W. McIver, Jr., and N. S. Ostlund. J. Chem. Phys. **49**, 2960, 2965 (1968).
21. R. J. Abraham and Z. L. Rossetti. J. Chem. Soc. Perkin II, 582 (1973).
22. R. J. Abraham. J. Phys. Chem. **73**, 1192 (1969).

Can. J. Chem. Downloaded from www.nrcresearchpress.com by 210.87.254.6 on 09/05/12
For personal use only.

Epithermal Electron Ranges and Thermal Electron Mobilities in Liquid Aromatic Hydrocarbons[1]

KYOJI SHINSAKA[2] AND GORDON R. FREEMAN

Chemistry Department, University of Alberta, Edmonton, Alberta T6G 2G2

Received May 22, 1974

Can. J. Chem. Downloaded from www.nrcresearchpress.com by 210.87.254.105 on 09/05/12
For personal use only.

KYOJI SHINSAKA and GORDON R. FREEMAN. Can. J. Chem. **52**, 3495 (1974).

Radiolysis free ion yields were measured as functions of electric field strength and temperature in benzene, toluene, 1,2-, 1,3-, and 1,4-dimethylbenzene, 1,2,3-, 1,2,4-, and 1,3,5-trimethylbenzene, 1,2,3,4- and 1,2,4,5-tetramethylbenzene, pentamethylbenzene, hexamethylbenzene, naphthalene, and anthracene. Secondary electron ranges b_{GP} were estimated from the yields. The density-normalized ranges $b_{GP}d$ were almost constant, 34–38 $\times 10^{-8}$ g/cm^2, from benzene up to the tetramethylbenzenes, then increased to 47 $\times 10^{-8}$ in pentamethyl- and 52 $\times 10^{-8}$ in hexamethylbenzene. In naphthalene and anthracene the normalized ranges were 32 and $\sim$20 $\times 10^{-8}$ g/cm^2, respectively. Electron mobilities in the liquids at 293 K, and their activation energies, expressed in (cm^2/V s, kcal/mol) were: benzene (0.114, 7.4); toluene (0.063, 3.4); 1,2-dimethylbenzene (0.018, 4.4); 1,3-dimethylbenzene (0.057, 4.5); 1,4-dimethylbenzene (0.062, —); 1,2,3-trimethylbenzene (0.022, 4.8); 1,2,4-trimethylbenzene (0.035, 4.3); 1,3,5-trimethylbenzene (0.17, 3.2); 1,2,3,4-tetramethylbenzene ($\sim$0.02, 5). The mobilities reflect migration retarding influences of the aromatic ring and molecular asymmetry, and a slight ring-shielding effect of methyl groups that tends to enhance the mobility.

KYOJI SHINSAKA et GORDON R. FREEMAN. Can. J. Chem. **52**, 3495 (1974).

Les rendements radiolytiques en ions libres ont été mesurés en fonction du champ électrique et de la température, en phase liquide, dans le benzène, le toluène, le di-, tri-, tétra-, penta-, et hexaméthylebenzène, le naphthalène et l'anthracène. Les parcours b_{GP} des électrons secondaires ont été deduits à partir de ces rendements, et normalisés en les multipliant par les densites d des liquides: $b_{GP}d$ = 34–38 $\times 10^{-8}$ g/cm^2 dans le benzène, le toluène, et les di-, tri- et tétraméthylebenzenes; $b_{GP}d$ augmente à 47 $\times 10^{-8}$ g/cm^2 pour le pentaméthyl et atteint 52 $\times 10^{-8}$ g/cm^2 avec l'hexaméthylebenzène. Pour le naphthalène et l'anthracène, les parcours normalisés sont respectivement de 32 et $\sim$20 $\times 10^{-8}$ g/cm^2. Les mobilités des électrons à 293 K et les energies d'activation correspondantes, en unités de (cm^2/V s, kcal/mol), sont (0.114, 7.4) pour le benzène, (0.063, 3.4) pour le toluène, (0.018, 4.4) pour le diméthyl-1,2 benzène, (0.057, 4.5) pour le diméthyl-1,3 benzène, (0.062, —) pour le diméthyl-1,4 benzène, (0.022, 4.8) pour le triméthyl-1,2,3 benzène, (0.035, 4.3) pour le triméthyl-1,2,4 benzène, (0.17, 3.2) pour le triméthyl-1,3,5 benzène, et (0.02, 5) pour tétraméthyl-1,2,3,4 benzène. L'asymétrie moléculaire et une certaine affinité du noyau aromatique entravent la migration de l'électron, à l'inverse de l'éffect écran dû aux groupements méthyles. Les mobilités refletent ces diverses influences.

Introduction

Liquid aromatic hydrocarbons are poorer insulators than are liquid alkanes (1–6). The conductance of the former is several orders of magnitude larger than that of the latter. It has been suggested that the conductance of liquid benzene and methyl-substituted benzenes is due to electron transfer from molecule to molecule by a hopping mechanism (4, 5). The activation energy of conductance (9.7 $\pm$ 0.2 kcal/mol, 40 $\pm$ 1 kJ/mol) is four-fold greater than that of viscous flow (2.3 kcal/mol, 10 kJ/mol), which seems to indicate that the contribution of ionic diffusion is negligible (4). The activation energy of anionic mobility E_- in liquid hydrocarbons is equal and opposite to that of viscosity E_η, while that of cationic mobility E_+ is $E_+ \approx -(1.0 - 1.5)E_\eta$ (7).

The conductivity κ of a liquid is proportional to the sum of the products of the charge carrier concentrations n_i and their mobilities u_i.

$$[1] \qquad \kappa = \sum_i n_i z_i e u_i$$

where $z_i e$ is the charge on carrier i and z_i may be assumed to be unity in liquid hydrocarbons. The Arrhenius temperature coefficient of con-

[1]Assisted financially by the National Research Council of Canada.

[2]I. W. Killam Memorial Postdoctoral Fellow, 1971–1973.

TABLE 1. Specific conductances of purified liquids

Liquid	Melting point (K)	T (K)	Specific conductance[a] (10^{-17} Ω^{-1} cm^{-1})	E_{sc}[b] (kcal/mol)
Benzene	279	292	2[c], 7[d]	[c], 8[d]
Methylbenzene	178	292	1[c]	[c]
1,2-Dimethylbenzene	248	292	5	10
1,3-Dimethylbenzene	225	292	7	8
1,4-Dimethylbenzene	286	292	60	8
1,2,3-Trimethylbenzene	248	292	9	9
1,2,4-Trimethylbenzene	229	292	3	6
1,3,5-Trimethylbenzene	228	293	2	7
1,2,3,4-Tetramethylbenzene	267	292	70	6
1,2,4,5-Tetramethylbenzene	352	358	540	11
Pentamethylbenzene	327	333	660	6
Hexamethylbenzene	438	448	24 000	—
Naphthalene	354	357	6 000	10
Anthracene	489	500	1×10^6	—
Cyclohexane	280	293	0.02	
Neopentane	257	293	0.02	

[a]Measured at temperature T and d.c. field 19 kV/cm about 0.5 h after the field was applied.
[b]Arrhenius activation energy of specific conductance.
[c]Erratic change with temperature.
[d]Benzene given a preliminary treatment with acid.

ductance is equal to the weighted sum of those of n_i and u_i. The above mentioned activation energy of conductance of benzene and the methyl benzenes might therefore indicate an appreciable temperature dependence of the charge injection mechanism rather than an unusually large temperature coefficient of electron transport.

Values of electron mobilities in benzene and toluene have been reported (8), but not their temperature dependences. The present article records electron mobilities and activation energies in benzene and a series of methyl-substituted benzenes. The data provide a test of the proposed conductance mechanism in the liquid benzenes (5) and extend knowledge about electron transport processes in liquids.

Penetration ranges of low energy (secondary) electrons into liquid aromatic hydrocarbons, including naphthalene, are also given.

Experimental

Materials

The benzene was Phillips Research Grade, with stated purity 99.9%. The methyl-substituted benzenes were obtained from Chemical Samples Co. The stated purities were 99.9%, except those of 1,2,3-trimethyl- (99%), 1,2,4-trimethyl- (99.6%), 1,2,3,4-tetramethyl- (99%), 1,2,4,5-tetramethyl- (99.8%), pentamethyl- (99%), and hexamethyl- (99%) benzene.

Zone refined naphthalene and anthracene, each 99.9% pure, were obtained from Aldrich Chemical Co. The anthracene came in sealed glass ampoules containing an inert atmosphere.

The standard purification for compounds that were liquid at room temperature was to pour ~50 cm^3 of liquid into a reservoir on a grease-free vacuum line, bubble for 30 min with ultrahigh purity argon, degas by evacuation for a minute or two without freezing the sample, distil onto ~2 g of degassed KOH pellets and stir for ~3 h, distil onto ~2 g of degassed $LiAlH_4$ powder and stir for ~3 h, distil onto ~5 g of Na/K alloy and stir for ~15 h, distil into an electrolysis cell (stainless steel electrodes) and electrolyse at 1.5 kV/cm for ~5 h, distil into conductance cell, freeze at 77 K, and evacuate to 10^{-6} Torr (10^{-4} Nm^{-2}). The cell was then sealed with a flame.

One batch of benzene was given the following preliminary treatment: shake with concentrated sulfuric acid for 5 h, separate from acid and shake with several changes of doubly distilled water, separate from water and shake 1 h with CaO, then distill the benzene from the CaO. The benzene was then treated in the usual way with argon, KOH, etc. The resulting liquid had a higher specific conductance than the benzene that had not been treated with acid (Table 1), but the free ion yields in the two samples were the same, within experimental error.

Compounds that were solid at room temperature were treated in a sublimation apparatus. The crystals were first evacuated at room temperature for ~30 min to remove gas, then melted and the liquid passed through a sintered glass plug (150 μ mesh) into a reservoir containing Na/K alloy. The reservoir was then cooled in liquid nitrogen and sealed with a flame. The reservoir was then warmed to a few degrees above the melting point of the hydrocarbon and the material stirred for ~5 h. The hydrocarbon was then sublimed through a break-seal and sintered glass plug into the reservoir of the conduc-

Can. J. Chem. Downloaded from www.nrcresearchpress.com by 210.87.254.105 on 09/05/12
For personal use only.

Can. J. Chem. Downloaded from www.nrcresearchpress.com by 210.87.254.105 on 09/05/12
For personal use only.

tance cell. After final pumping at 77 K to 10^{-6} Torr, the cell was sealed with a flame.

The Na/K alloy treatment was omitted for hexamethylbenzene, due to the high temperatures involved, and for naphthalene and anthracene, due to their reactivity with the alloy.

The specific conductances of the purified aromatic hydrocarbon liquids were in the vicinity of 10^{-16} Ω^{-1} cm^{-1} at 292 K and increased with temperature (Table 1). The values for benzene and toluene were two orders of magnitude smaller than those reported earlier for the liquids containing air (5), and an order of magnitude smaller than that reported for freshly distilled and degassed benzene (4). The conductance of our di- and trimethylbenzenes were mostly an order of magnitude smaller than those reported for the liquids containing air (5). The activation energies of conductance were similar, within a large experimental scatter (Table 1), and may be taken to be 8 ± 2 kcal/mol, independent of the presence (5) or absence of air. The observed activation energy does not indicate an electron hopping mechanism (5), since the electron scavenger oxygen has no effect on it. The magnitude of the conductance seems to be governed by impurities and the high activation energy is not understood.

By comparison, the specific conductances of cyclohexane and neopentane purified in a similar manner were each 2×10^{-19} Ω^{-1} cm^{-1} at 293 K, two orders of magnitude smaller than those of the aromatic liquids.

Conductance Cell

The cell was a slight modification of that shown in Fig. 1 of ref. 9. Copper braid was put on the outside of the glass tube containing the high tension lead, in addition to that containing the collector lead, and the two inner-ends of the braids were connected by a wire around the cell or by soldering part of the braids together. The glass tube that covered the lead to the guard ring was cut off and the guard ring was grounded to the braid on the outside of the collector lead. This modification decreased the noise level. The collector electrode area was 7.8 cm^2 and the gap between the stainless steel electrodes was 3.3 mm.

Irradiation Procedures and Dosimetry

The methods are described in refs. 9 and 10. Briefly, a 1 μs pulse of 1.7 MeV X-rays delivered ~5×10^{10} eV/g to the sample. Free ion yields $G_{fi}{}^{E}$ were measured at electric field strengths between 2 and 40 kV/cm, using the charge clearing technique, and extrapolated to zero field strength by means of a theoretical model. Thermal electron mobilities u were determined at field strengths between 5 and 20 kV/cm, using the magnitude of the electron conductance transient as a measure of $G_{fi}{}^{E}u$ and taking the ratio $(G_{fi}{}^{E}u/G_{fi}{}^{E}) = u$. The positive ion mobilities were small compared to those of the electrons. Ion conductance transients (11) in the presence of an electron scavenger gave mobilities typically 10^{-4}–10^{-3} cm^2/V s.

The high temperature samples were thermostated in a clear Dewar flask, rather than in an asbestos box, so that the melting of the solid samples could be observed and temperature uniformity checked. The Dewar was fitted with an asbestos lid. Two copper–constantan thermocouples were attached to the surface of the conductance cell, using silicone rubber adhesive. One thermocouple was used for temperature control, the other for measurement.

Physical Properties of the Liquids

The densities (12–14) and dielectric constants (13–17) of some of the liquids were available in the literature. The rest were measured. The methods of measurement will be reported elsewhere, with tables of values for many compounds. Values needed in the present work are listed in Table 2.

The total ionization yields in the liquid are not known. It has been assumed that $G_{tot} = 4.3$ in all liquids, equal to the gas phase value for benzene (18).

Results

Free Ion Yields

The free ion yield $G_{fi}{}^{E}$ in a given liquid increases with increasing applied electric field strength E and with increasing temperature. Typical results for benzene are shown in Fig. 1.

The yields were extrapolated to $E = 0$ by using eq. 2.

$$[2] \qquad G_{fi}{}^{E} = G_{tot} \int_0^\infty F(y)\phi(y,E)\,dy$$

where G_{tot} is the total number of ion–electron pairs generated per 100 eV absorbed by the liquid, $F(y)dy$ is the fraction of thermalized electron–ion pairs that have initial intrapair separation distances between y and $y + dy$, and $\phi(y, E)$ is the probability that a pair with a given separation distance y will escape geminate neutralization (become free ions) in the presence of an applied field E (9, 19).

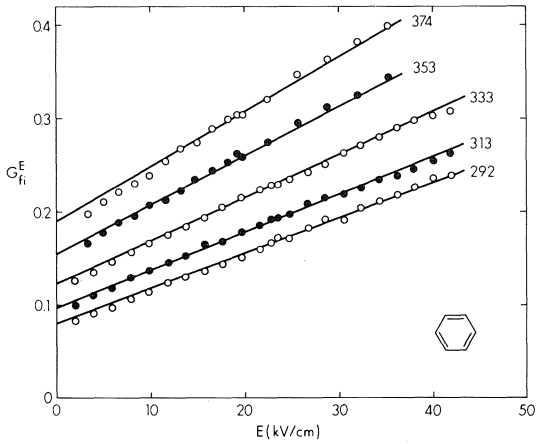

FIG. 1. Free ion yields $G_{fi}{}^{E}$ at field strength E in benzene. The numbers at the ends of the curves are °K. The lines were calculated from eqs. 2–4 using the values of b_{GP} and G_{tot} listed in Table 2.

TABLE 2. G_{fi}^{0} and most probable range b_{GP} in liquids

Liquid	T (K)	d (g/cm^3)	ε	G_{fi}^{0}	b_{GP} (Å)[a]	$b_{GP}d$ (10^{-8} g/cm^2)	$b_{GP}d_{av}$ (10^{-8} g/cm^2)
			Aromatic hydrocarbons				
Benzene[b]	374	0.793	2.13	0.19	50	39	38
	353	0.815	2.17	0.15	48	39	
	345	0.823	2.18	0.13	46	38	
	333	0.837	2.21	0.12	45	38	
	324	0.846	2.22	0.105	44	37	
	313	0.858	2.24	0.098	43	37	
	304	0.867	2.26	0.087	42	37	
	292	0.880	2.29	0.081	42	37	
	281	0.891	2.31	0.072	42	37	
Toluene	354	0.811	2.25	0.15	45	37	38
	322	0.840	2.32	0.12	44	37	
	292	0.868	2.39	0.093	43	37	
	253	0.904	2.49	0.066	42	38	
	212	0.941	2.57	0.044	41	39	
1,2-DMB	413	0.778	2.25	0.20	43	34	35
	373	0.812	2.36	0.15	41	34	
	333	0.846	2.46	0.12	40	34	
	292	0.881	2.57	0.094	40	35	
	253	0.914	2.67	0.069	39	36	
1,3-DMB	383	0.787	2.20	0.16	44	35	35
	353	0.813	2.26	0.13	42	35	
	323	0.838	2.32	0.10	41	35	
	292	0.865	2.38	0.082	41	35	
	263	0.890	2.45	0.066	40	36	
	233	0.916	2.54	0.049	39	36	
1,4-DMB	400	0.768	2.10	0.16	44	34	34
	362	0.801	2.16	0.12	42	33	
	333	0.826	2.20	0.099	41	34	
	313	0.844	2.23	0.084	41	34	
	292	0.863	2.27	0.073	41	35	
1,2,3-TrMB	445	0.773	2.23	0.27	47	36	37
	414	0.798	2.31	0.23	47	38	
	387	0.819	2.38	0.20	44	36	
	354	0.846	2.47	0.17	42	36	
	324	0.870	2.55	0.14	41	36	
	292	0.895	2.64	0.12	42	37	
	265	0.917	2.71	0.093	41	38	
1,2,4-TrMB	414	0.779	2.15	0.22	47	36	36
	383	0.804	2.21	0.17	44	35	
	353	0.836	2.26	0.13	42	35	
	323	0.852	2.32	0.10	40	34	
	292	0.877	2.38	0.083	41	36	
	263	0.900	2.44	0.065	40	36	
	232	0.925	2.49	0.048	40	37	
1,3,5-TrMB	383	0.791	2.01	0.21	54	42	38
	352	0.817	2.10	0.15	49	40	
	323	0.841	2.19	0.12	46	38	
	293	0.865	2.28	0.087	43	38	
	262	0.891	2.37	0.063	41	37	
	232	0.915	2.46	0.046	39	36	

Can. J. Chem. Downloaded from www.nrcresearchpress.com by 210.87.254.105 on 09/05/12
For personal use only.

TABLE 2. (*Concluded*)

Liquid	T (K)	d (g/cm^3)	ε	$G_{fi}{}^0$	b_{GP} (Å)[a]	$b_{GP}d$ (10^{-8} g/cm^2)	$b_{GP}d_{av}$ (10^{-8} g/cm^2)
1,2,3,4-TeMB	413	0.816	2.29	0.25	47	38	38
	383	0.839	2.35	0.21	45	38	
	353	0.861	2.41	0.17	44	38	
	323	0.883	2.48	0.14	43	38	
	292	0.906	2.55	0.11	42	38	
	271	0.922	2.60	0.086	41	37	
1,2,4,5-TeMB	402	0.800	2.15	0.20	46	37	38
	383	0.815	2.18	0.18	46	38	
	358	0.835	2.22	0.15	45	38	
PMB	414	0.822	2.23	0.38	59	48	47
	394	0.837	2.26	0.33	57	48	
	373	0.852	2.29	0.29	56	47	
	353	0.867	2.33	0.25	54	47	
	333	0.890	2.36	0.22	53	47	
HMB	448	0.823	2.17	0.6	74	61	61
Naphthalene	376	0.956	2.51	0.11	33	32	32
	357	0.972	2.54	0.094	33	32	
Anthracene	500	0.964	2.65	~0.1	~20	~20	~20
			Cycloalkane				
Cyclohexane[c]	294	0.778	2.02	0.19	66	51	51
			Cycloalkene				
Cyclohexene[c]	293	0.813	2.23	0.20	62	50	51[c]

[a]Based on $G_{tot} = 4.3$, the gas phase value for benzene (ref. 18).
[b]Average values of $G_{fi}{}^0$ from three samples.
[c]Reference 9.

$$[3]\quad \phi(y,E) = e^{-r/y}\left(1 + e^{-\beta y}\sum_{n=1}^{\infty}\frac{(\beta y)^n}{(n+1)!} \times \sum_{j=0}^{n-1}(n-j)\frac{(r/y)^{j+1}}{(j+1)!}\right)$$

where $r = \xi^2/\varepsilon kT$, $\xi = 4.803 \times 10^{-10}$ e.s.u., ε is the dielectric constant of the liquid, k is Boltzmann's constant, T is the absolute temperature, and $\beta = (\xi E/300kT)$.

The distribution function $F(y)$ was taken to have the form [4], which has been designated Y_{GP} (9).

$$[4]\quad \begin{cases} F(y) = 0.96(4y^2/\pi^{1/2}b_{GP}{}^3)\exp(-y^2/b_{GP}{}^2) & y < 2.4b_{GP} \\ F(y) = 0.96[(4y^2/\pi^{1/2}b_{GP}{}^3)\exp(-y^2/b_{GP}{}^2 + 0.5b_{GP}{}^2/y^3] & y > 2.4b_{GP} \end{cases}$$

where 0.96 is a normalization factor that was

Can. J. Chem. Downloaded from www.nrcresearchpress.com by 210.87.254.105 on 09/05/12
For personal use only.

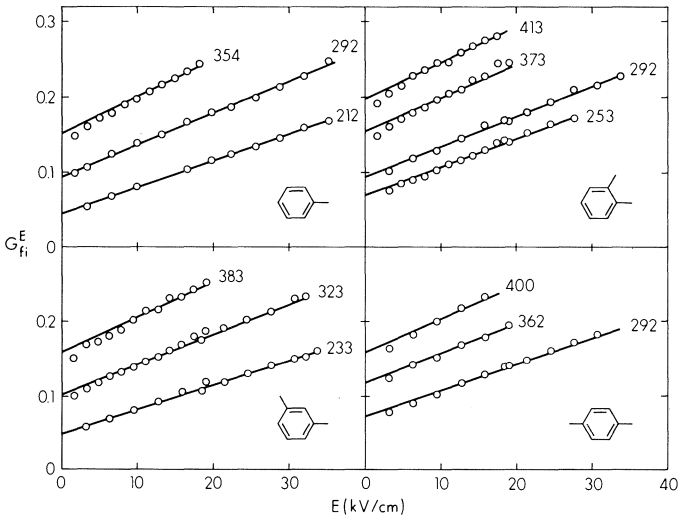

FIG. 2. Free ion yields G_{fi}^{E} at field strength E in toluene, 1,2-dimethylbenzene, 1,3- and 1,4-dimethylbenzene. The temperature in °K is marked at the end of each curve. The lines were calculated using eqs. 2–4, with b_{GP} and G_{tot} from Table 2.

omitted earlier by typographical error (9), and b_{GP} is the adjustable dispersion parameter.[3] The latter is also the most probable value of y and is a direct function of G_{fi}^{0}/G_{tot}, where G_{fi}^{0} is the free ion yield at zero field strength. Distribution function [4] is a gaussian to which has been added a power function at large y values. Within the framework of the single ion pair spur model, [4] gives satisfactory results for many dielectric liquids (9).

To calculate a value of G_{fi}^{E} from eqs. 2–4 one requires values for G_{tot} and b_{GP}. For lack of better information, the gas phase ionization yield in benzene, $G_{tot} = 4.3$ (17), was used for all the liquids. A preliminary value of b_{GP} was then assumed and G_{fi}^{E} was calculated for each experimental value of E. Calculated and experimental yields were compared by calculating the average % error:

$$[5] \quad \text{Average \% error} = 100\sum|G_{fi,calc}^{E} - G_{fi,exp}^{E}|/\sum G_{fi,exp}^{E}$$

The calculations were repeated with a series of b_{GP} values to find the one that gave the minimum average % error. This value of b_{GP} was then used to calculate G_{fi}^{0}.

$$[6] \quad G_{fi}^{0} = G_{tot}\int_{0}^{\infty} F(y)\, e^{-r/y}\, dy$$

The best-fit curves calculated for benzene at

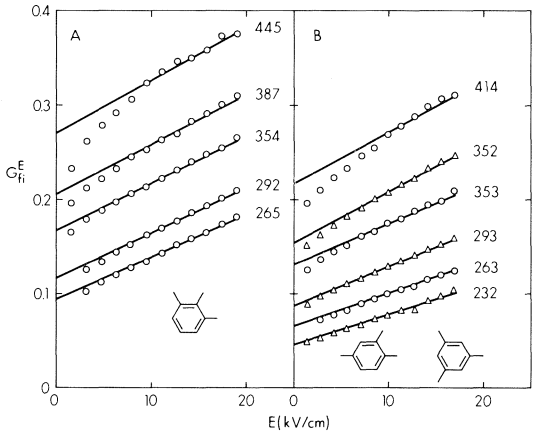

FIG. 3. Free ion yields G_{fi}^{E} at field strength E in trimethylbenzenes A: 1,2,3-TrMB. B: 1,2,4-TrMB, ○; 1,3,5-TrMB, △. The temperatures are marked in °K. The lines were calculated using eqs. 2–4, with b_{GP} and G_{tot} from Table 2.

[3]An essentially equivalent function for Y_{GP}, of a slightly simpler form suggested by Yaffe and Jarnagin (28), is

$$[4'] \quad \begin{cases} F(y) = (4y^2/\pi^{\frac{1}{2}}b_{GP}^{3})\exp(-y^2/b_{GP}^{2}) & y < 2.1b_{GP} \\ F(y) = 0.44b_{GP}^{2}/y^{3} & y > 2.1b_{GP} \end{cases}$$

[4] and [4′] contain discontinuities at $2.4b_{GP}$ and $2.1b_{GP}$, respectively, but the calculations are not noticeably affected by them. The two portions of the function could be adjusted to eliminate the discontinuity and renormalized, but the extra manipulation would not improve the calculated yields.

Can. J. Chem. Downloaded from www.nrcresearchpress.com by 210.87.254.105 on 09/05/12
For personal use only.

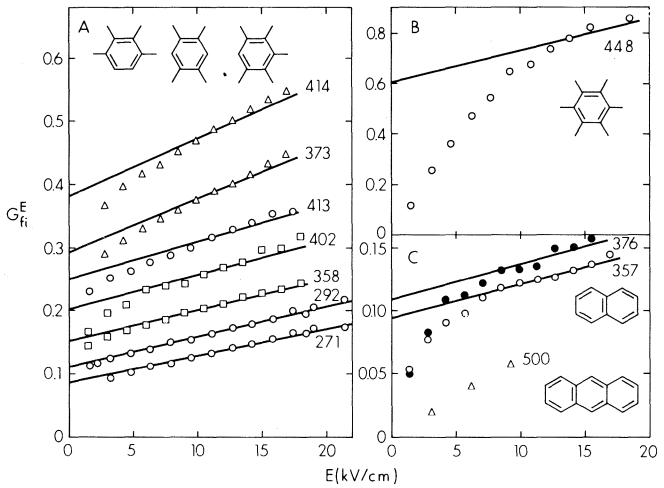

FIG. 4. Free ion yields $G_{fi}{}^{E}$ at field strength E in aromatic C_{10}—C_{14} hydrocarbon liquids. *A*: 1,2,3,4-tetramethylbenzene (1,2,3,4-TeMB), ○; 1,2,4,5-TeMB, □; pentamethylbenzene, △. *B*: hexamethylbenzene. *C*: naphthalene, ○, ●; anthracene, △. The temperatures are marked in °K. The lines were calculated using eqs. 2–4, with b_{GP} and G_{tot} from Table 2. No calculated line is shown for anthracene.

a series of temperatures are shown in Fig. 1. The parameter values are listed in Table 2. The curves pass through the experimental points at the lower temperatures, but the theoretical slope is somewhat smaller than the experimental slope at the highest temperature.

The free ion yields in toluene and the dimethylbenzenes (Fig. 2), trimethylbenzenes (Fig. 3), and tetramethylbenzenes (Fig. 4*A*) are similar to those in benzene. The yields in pentamethylbenzene and hexamethylbenzene are somewhat larger, while those in naphthalene and anthracene are smaller than those in the other liquids at similar temperatures (Fig. 4).

The difference between the calculated curve and the experimental yields is greatest in the liquids that have the highest intrinsic conductances (Fig. 4 and Table 1). The difference appears to indicate incomplete collection of the radiolytic free ions at the lower fields. The radiolytic free ions can be neutralized by intrinsic charge carriers as well as by each other. The mean lifetime of the free ions decreases with increasing concentration of intrinsic charge carriers. The field strength required to collect essentially all of the free ions at the electrodes increases with decreasing lifetime. Therefore, the field strength required to sweep the free ions to the electrodes before being neutralized tends to increase with increasing intrinsic conductance. The relationship is not simple because the required field strength depends mainly on the charge carrier concentration n, while the intrinsic conductance depends on nu, where u is the mobility.

In anthracene the background conductance became so noisy at fields greater than 9 kV/cm that charge clearing measurements of the radiolytic free ions became impossible.[4] Complete collection of the free ions was not attained at 9 kV/cm in anthracene. By comparing the points for anthracene with those for naphthalene and hexamethylbenzene (Fig. 4), and the relative intrinsic conductances of the liquids (Table 1), one may estimate that complete collection of free ions in anthracene would require $E \gtrsim 20$ kV/cm. It therefore appears that $G_{fi}{}^{0} \approx 0.1$ in liquid anthracene at 500 K.

Electron Mobilities

Mobilities were measured as functions of temperature in benzene, toluene, the dimethyl- and trimethylbenzenes, and 1,2,3,4-tetramethylbenzene. The mobilities were independent of field strength over the range measured, 5–20 kV/cm, and are listed in Table 3. Arrhenius activation energies were obtained from the plots in Fig. 5 and are given in Table 3.

[4]NOTE ADDED IN PROOF: See Electric field induced light emission and conductance-loss transients in liquid anthracene (29).

Can. J. Chem. Downloaded from www.nrcresearchpress.com by 210.87.254.105 on 09/05/12
For personal use only.

TABLE 3. Thermal electron mobilities and their activation energies in aromatic hydrocarbons

Liquid	T (K)	u ($cm^2/V\,s$)	E_u (kcal/mol)
Benzene[a]	342	0.69	7.4
	333	0.52	
	324	0.40	
	314	0.28	
	306	0.19	
	293	0.114	
	282	0.074	
Toluene	304	0.077	3.4
	292	0.063	
1,2-DMB	356	0.069	4.4
	333	0.049	
	310	0.032	
	292	0.018	
1,3-DMB	351	0.21	4.5
	330	0.14	
	313	0.11	
	292	0.057	
1,4-DMB	293	0.062	—
1,2,3-TrMB	354	0.092	4.8
	344	0.081	
	333	0.064	
	324	0.054	
	315	0.044	
	303	0.030	
	293	0.022	
1,2,4-TrMB	377	0.21	4.3
	353	0.14	
	333	0.11	
	312	0.061	
	292	0.035	
1,3,5-TrMB	324	0.26	3.2
	315	0.22	
	306	0.20	
	293	0.16	
1,2,3,4-TeMB	353	0.091	5
	343	0.081	
	333	0.065	
	323	0.040	

[a]Average of two samples.

Electron conductance signals were not obtained from the liquified compounds that were solid at room temperature, such as 1,2,4,5-tetramethylbenzene (Table 1). This might have been due to the difficulty of purifying and transferring, keeping pure, the high-melting substances. Similar problems had been encountered earlier with high-melting globular alkanes such as 2,2,3,3-tetramethylbutane (20), in which the short lifetimes of the electron signals were attributed to scavenging by impurities.

Discussion

Free Ion Yields and Electron Ranges

The free ion yield obtained in benzene at 292 K, $G_{fi}^{0} = 0.081$, was 50% greater than the value 0.053 reported earlier (26).

Electron ranges in a given liquid are inversely proportional to the liquid density d, so for comparison purposes the ranges were normalized by multiplying by the density (Table 2). Molecular and liquid structure effects were sought by comparing the normalized ranges $b_{GP}d$.

Can. J. Chem. Downloaded from www.nrcresearchpress.com by 210.87.254.105 on 09/05/12
For personal use only.

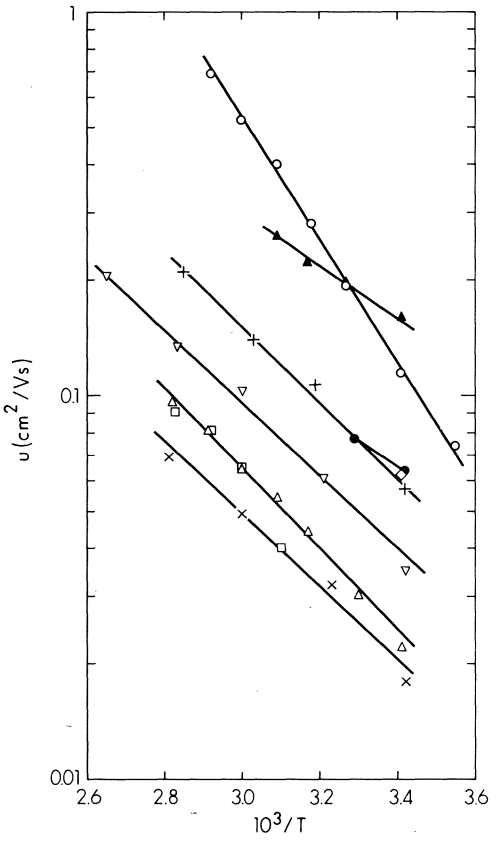

FIG. 5. Arrhenius plots of thermal electron mobilities in aromatic hydrocarbon liquids. Benzene, ○; toluene ●; 1,2-dimethylbenzene, ×; 1,3-dimethylbenzene, +; 1,4-dimethylbenzene, ◇; 1,2,3-trimethylbenzene, △; 1,2,4-trimethylbenzene, ▽; 1,3,5-trimethylbenzene, ▲; 1,2,3,4-tetramethylbenzene, □.

The normalized ranges are the same whether there are 0, 1, 3, or 4 methyl groups on the benzene ring (Table 2). The small decrease of range in the dimethylbenzenes is slightly beyond the experimental scatter. The range is significantly greater in pentamethylbenzene and is still larger in the hexamethyl compound (Table 2).

The gas phase ionization potentials (21), and presumably the electron affinities (22), of the benzenes decrease monotonously with increasing number of substituted methyl groups (21). There is, therefore, no apparent correlation between the electron ranges in the liquids and the gas phase ionization potentials or electron affinities of the molecules. Nor is there a correlation between the electron ranges and the relative liquid phase ionization potentials, as reflected by the relative optical excitation energies of charge transfer complexes of the benzenes (23) (see Table 4).

The gas phase dipole moments of some of the substituted benzenes are zero, while those of others are up to 0.6 D (24, 25) with no observable effect on the electron range (Table 4). The permanent dipoles of these molecules are evidently so diffuse that polarization and short range interactions between the electrons and liquid phase molecules dominate the electron energy loss processes.

The range in benzene is much smaller than that in cyclohexane or cyclohexene (Table 4). Attachment of up to four methyl groups to the benzene ring causes little or no change in the electron range, but attachment of five results in a larger range, and six methyl groups restore the range to the cyclohexane value. The abrupt effect of methyl substitution in the last two positions of the benzene ring is difficult to understand in view of the unimportance of symmetry in the less-substituted benzenes.

The range in benzene is smaller than that in *n*-butane, but greater than that in butene-1 (Table 4).

The ranges in naphthalene and anthracene are lower than that in benzene (Table 4), indicating that the electron energy loss interactions are stronger with the fused ring molecules than with benzene. The normalized range in the conjugated diolefin butadiene-1,3 lies between those in naphthalene and anthracene (Table 4).

Several factors, including the degree of sphericity and "chemical reactivity" of the molecules appear to affect the electron energy loss probabilities in liquid hydrocarbons. The detailed pattern of the factors is not yet clear.

Thermal Electron Mobilities

The mobilities in benzene and toluene, interpolated to 300 K in Fig. 5, are respectively 4-fold and 7-fold smaller than those reported earlier (8). Technical difficulties with the background currents decreased the accuracy of the earlier measurements and prevented the determination of the temperature coefficients of the mobilities (8).

The mobility in benzene at 293 K is only 12% of that in cyclohexene, but is double that in butene-1 (Table 4). The correlation between epithermal electron ranges and thermal electron

Can. J. Chem. Downloaded from www.nrcresearchpress.com by 210.87.254.105 on 09/05/12
For personal use only.

TABLE 4. Electron ranges and mobilities (at 293 K) in liquid hydrocarbons, and molecular properties

Liquid	$b_{GP}d_{av}$[a] (10^{-8} g/cm^2)	Ionization potential[b] (eV)	$h\nu_{max}$[c] (eV)	μ (D)	u_{293} (cm^2/V s)
	38	9.25	3.23	0.0[d,e]	0.114
	38	8.82	3.05	0.36[e]	0.063
	35	8.56	2.88	0.6[e]	0.018
	35	8.56	2.82	0.4[f]	0.057
	34	8.45	2.70	0.0[d]	0.062
	37	8.48	—	0.6[f]	0.022
	36	8.27	—	0.3[f]	0.035
	38	8.39	2.69	0.0[d]	0.17
	38	—	—	0.6[g]	~0.02
	38	8.03	—	0.0[d]	—
	47	7.92	—	0.4[h]	—
	52	7.85	2.27	0.0[d]	—
	32	8.12	—	0.0[d]	—
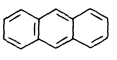	~20	7.23	—	0.0[d]	—
	51[i]	9.88	—	0.0[d]	0.4[j,k]

Can. J. Chem. Downloaded from www.nrcresearchpress.com by 210.87.254.105 on 09/05/12
For personal use only.

TABLE 4. (*Concluded*)

Liquid	$b_{GP}d_{av}$[a] (10^{-8} g/cm^2)	Ionization potential[b] (eV)	$h\nu_{max}$[c] (eV)	μ (D)	u_{293} (cm^2/V s)
	51[i]	8.95	—	0.55[e]	1.0[j]
	50[i]	10.63	—	≤0.05[e]	0.4[k]
	33[i]	9.58	—	0.31[e]	0.064[j]
	27[i]	9.07	—	0.0[d,e]	0.00[j,l]

[a]Secondary electron range, normalized for the different liquid densities.
[b]Gas phase ionization potential (ref. 21).
[c]Optical excitation energy at the band maximum, of charge transfer complexes of the benzenes with tetracyanoethylene in dichloromethane solvent (ref. 23).
[d]On the basis of molecular symmetry.
[e]Reference 24.
[f]Reference 25.
[g]By comparison with the values for 1,2-dimethyl- and 1,2,3-trimethylbenzene.
[h]Assumed equal to the value for toluene.
[i]Reference 9, Fig. 10.
[j]Reference 10.
[k]Reference 26, 296 K.
[l]Electrons react with the conjugated diolefin to form negative ions.

mobilities noted in other systems (10, 20) extends to these three liquids. However, in the series of methyl-substituted benzenes variation in the mobilities is somewhat different from that in the ranges (Table 4). The two quantities appear to have gross dependences on similar properties of the media, but the fine structure dependences are different. The relative variations in the mobilities are much greater than those in the ranges (10, 20, and Table 4).

Substitution of methyl groups for hydrogen atoms on the benzene ring tends to decrease the electron mobility through the resultant molecular asymmetry and dipole moment. This is shown by the decrease in u as one proceeds from benzene to toluene to 1,2-dimethylbenzene (Table 4). There is also a reverse effect, perhaps through shielding of the aromatic ring, indicated by the increase of u on going from benzene to 1,3,5-trimethylbenzene. Benzene has a higher degree of symmetry than does 1,3,5-trimethylbenzene; one expects that in a sufficiently pure sample of hexamethylbenzene the mobility would be the highest in the series. Hexamethylbenzene has approximately the same degree of symmetry as benzene.

The mobility in 1,2,3,4-tetramethylbenzene is similar to that in its symmetry-analog 1,2-dimethylbenzene, but the accuracy of the former value needs improvement. When better purification and measurement techniques have been developed it will be informative to compare the mobilities in the symmetrically analogous pairs 1,2,4,5-tetramethylbenzene and 1,4-dimethylbenzene, pentamethylbenzene and toluene, and in hexamethylbenzene and benzene. Quantitative information about the opposing effects of methyl substitution should be obtainable from the comparison.

The activation energies E_u of the mobilities are 4 ± 1 kcal/mol, with the exception of that in benzene, 7.4 kcal/mol (Table 3). Measurement of E_u in two different preparations of benzene gave 7.4 ± 0.4 and 7.6 ± 0.8 kcal/mol, while the averaged mobilities shown in Fig. 5 give 7.4 ± 0.4 kcal/mol. The large activation energy might be due to the participation of equilibrium 7.

[7] $$e^- + C_6H_6 \rightleftharpoons C_6H_6^-$$

The anion is more stable at low temperatures, at least when formed by reaction between the hydrocarbon and solvated electrons in dimethoxyethane (27). Negative ions have lower mobilities than do electrons, so the apparent mobility of electrons would be smaller the greater is the fraction of their lifetime that they

Can. J. Chem. Downloaded from www.nrcresearchpress.com by 210.87.254.105 on 09/05/12
For personal use only.

spend as $C_6H_6^-$. The observed temperature coefficient of electron migration would therefore be the actual electron mobility activation energy plus a contribution from the temperature dependence of [7].

Electrons attach less readily to the dimethylbenzenes (27), presumably because methyl groups donate electron density to the aromatic ring and decrease its electron affinity. Equilibria analogous to [7] would therefore contribute less to the temperature coefficient of electron migration in the methyl-substituted benzenes. The lower mobilities in the methylbenzenes would be attributed to electron solvation processes rather than to negative ion formation.

The mobilities of electrons and positive holes in anthracene crystals are each ~ 1 cm^2/V s at ~ 300 K, and the photocurrent has an activation energy of 4 kcal/mol (3). Melting the crystals increased the photocurrent at the melting point by three orders of magnitude, and the increase was attributed to increased electronic mobility (3). Although the electron mobility could not be measured in liquid anthracene in the present work, the short range of epithermal electrons in the liquid (Table 4) makes the existence of a low lying conduction band in liquid anthracene highly improbable. The increase in photocurrent observed on melting (3) was probably due to more efficient charge carrier generation in the liquid phase.

We wish to thank the personnel of the Radiation Research Center for aid with the electronics.

1. N. V. RIEHL. *In* Symposium on electrical conductivity in organic solids. *Edited by* H. Kallman and M. Silver. Interscience, New York. 1961. p. 61.
2. G. DREHFAHL and H. J. HENKEL. Z. Phys. Chem. Leipzig, **206**, 93 (1956).
3. (*a*) J. KOMMANDEUR, G. J. KOSINEK, and W. G. SCHNEIDER. Can. J. Chem. **36**, 513 (1958); (*b*) J. KOMMANDEUR. *In* Physics and chemistry of the organic solid state, Vol. 2. *Edited by* J. Fox, M. M. Labes, and A. Weissberger. Interscience, New York. 1965. p. 1.
4. E. O. FORSTER. J. Chem. Phys. **37**,1021 (1962).
5. E. O. FORSTER. J. Chem. Phys. **40**, 86 (1964).
6. E. O. FORSTER. J. Chem. Phys. **40**, 91 (1964).
7. I. ADAMCZEWSKI and B. JACHYM. Acta Phys. Pol. **30**, 767 (1966).
8. R. M. MINDAY, L. D. SCHMIDT, and H. T. DAVIS. J. Phys. Chem. **76**, 442 (1972).
9. J.-P. DODELET, K. SHINSAKA, U. KORTSCH, and G. R. FREEMAN. J. Chem. Phys. **59**, 2376 (1973).
10. J.-P. DODELET, K. SHINSAKA, and G. R. FREEMAN. J. Chem. Phys. **59**, 1293 (1973).
11. M. G. ROBINSON and G. R. FREEMAN. Can. J. Chem. **52**, 440 (1974).
12. R. R. DREISBACH. Adv. Chem. Ser. **15**, (1959); **22** (1959).
13. E. W. WASHBURN. International critical tables, Vols. 1 (1926) and 6 (1929). McGraw–Hill, New York.
14. Beilstein's Handbuch der Organischen Chemie, 4 auflage, 3 ergänzungswerk, 5 Bd., Springer–Verlag, Berlin.
15. J. TIMMERMANS. Physico-chemical constants of pure organic compounds, Vol. 2. Elsevier Publishing Co., New York. 1965.
16. A. A. MARYOTT and E. R. SMITH. Circ. U.S. Natl. Bur. Stand. 514 (1951).
17. H. LANDOLT and H. JAHN. Z. Phys. Chem. **10**, 289 (1892).
18. R. M. LEBLANC and J. A. HERMAN. J. Chim. Phys. **63**, 1055 (1966).
19. G. R. FREEMAN. J. Chem. Phys. **39**, 1580 (1963).
20. J.-P. DODELET and G. R. FREEMAN. Can. J. Chem. **50**, 2667 (1972).
21. R. W. KISER. Introduction to mass spectrometry and its applications. Prentice–Hall, Englewood Cliffs, N.J. 1965. Appendix IV.
22. A. STREITWIESER, JR. Molecular orbital theory for organic chemists. Wiley, New York. 1961. Chapt. 7.
23. E. M. KOSOWER. An introduction to physical organic chemistry. Wiley, New York. 1968. p. 182.
24. R. D. NELSON, JR., D. R. LIDE, JR., and A. A. MARYOTT. Selected values of electric dipole moments for molecules in the gas phase. NSRDS-NBS 10, U.S. Govt. Printing Office, Washington, D.C. 1967.
25. A. L. MCCLELLAN. Tables of experimental dipole moments. Freeman, San Francisco. 1963.
26. W. F. SCHMIDT and A. O. ALLEN. J. Chem. Phys. **52**, 2345 (1970); **52**, 4788 (1970).
27. T. R. TUTTLE, JR. and S. I. WEISSMAN. J. Am. Chem. Soc. **80**, 5342 (1958).
28. M. YAFFE and R. C. JARNAGIN. Private communication.
29. K. SHINSAKA and G. R. FREEMAN. Can. J. Chem. This issue.

Can. J. Chem. Downloaded from www.nrcresearchpress.com by 210.87.254.105 on 09/05/12
For personal use only.

The Adsorption, Desorption, and Exchange Reactions of Oxygen, Hydrogen, and Water on Platinum Surfaces. I. Oxygen Interaction

Y. K. PENG AND P. T. DAWSON[1]

Chemistry Department and Institute for Materials Research, McMaster University, Hamilton, Ontario L8S 4M1

Received May 23, 1974

Can. J. Chem. Downloaded from www.nrcresearchpress.com by 210.87.254.5 on 09/05/12
For personal use only.

Y. K. PENG and P. T. DAWSON. Can. J. Chem. **52**, 3507 (1974).

The kinetics of adsorption and desorption of oxygen on a platinum filament have been studied by temperature-programmed desorption mass spectrometry. Oxygen adsorption becomes significant only after any carbon contamination is removed from the surface. At 300 °K oxygen adsorbs dissociatively into an atomic β-state which contains four overlapping sub-states. The initial sticking probability is 0.16 but this falls off rapidly with increasing coverage. A kinetic analysis for desorption from the β_2- and β_4-states gave $E_{des}^{\ddagger}(\beta_2) = 39$ kcal mol^{-1} and $E_{des}^{\ddagger}(\beta_4) = 54$ kcal mol^{-1}. The desorption was first order suggesting a lack of mobility of the adatoms at the desorption temperature (~700 °K). No oxygen atom desorption could be detected in a line-of-sight experiment. Adsorption of a mixture of $^{32}O_2$ and $^{36}O_2$ resulted in complete isotopic mixing on desorption. At 115 °K, the β-state still populates first with the same initial sticking probability indicating adsorption is nonactivated. Moreover, the sticking probability remains at its high initial value for a much more extensive coverage range, suggesting a precursor state to adsorption. After the β_3- and β_4-states are fully occupied, further adsorption into the β-state is competitive with occupation of an α-state which desorbs at low temperatures (~150 °K) with first order kinetics and $E_{des}^{\ddagger}(\alpha) \sim 6$ kcal mol^{-1}. No isotope mixing occurred in the α-state which is undoubtedly molecular. Prior population of the β_1- and β_2-states at 300 °K reduced the α-state adsorption at 115 °K suggesting that α and β occupy the same sites. Each site can adsorb either an atom or molecule since each molecule added to the β-state excludes two molecules from the α-state.

Y. K. PENG et P. T. DAWSON. Can. J. Chem. **52**, 3507 (1974).

La cinétique de l'adsorption et de la désorption de l'oxygène sur filament de platine a été étudiée par désorption à température programmée en spectrométrie de masse. L'adsorption de l'oxygène devient importante seulement lorsque toute contamination due au carbone est éliminée de la surface. A 300 °K, l'oxygène s'adsorbe en se dissociant à l'état atomique β qui contient quatre sous-états superposés. La probabilité initiale d'adhésion est 0.16 mais décroît rapidement à mesure que le recouvrement augmente. Une analyse cinétique de la désorption des états β_2 et β_4 donne $E_{des}^{\ddagger}(\beta_2) = 39$ kcal/mol et $E_{des}^{\ddagger}(\beta_4) = 54$ kcal/mol. La désorption est un phénomène du premier ordre ce qui permet de suggérer une absence de mobilité des atomes adsorbés à la température de désorption (~ 700 °K). Aucune désorption des atomes d'oxygène n'a été détectée au cours d'une expérience en ligne directe. L'adsorption d'un mélange de $^{32}O_2$ et de $^{34}O_2$ a conduit à un mélange isotopique complet lors de la désorption. A 115 °K, l'état β est encore occupé en premier avec la même probabilité initiale d'adhésion indiquant ainsi que l'adsorption n'est pas activée. De plus, la probabilité d'adhésion demeure à son niveau initial élevé sur une gamme beaucoup plus étendue de recouvrement, ce qui laisse croire à l'existence d'un état précédant l'adsorption. Lorsque les états β_3 et β_4 sont complètement occupés, l'adsorption additionnelle sous l'état β entre en compétition avec l'occupation d'un état α qui se désorbe à basse température (~150 °K) suivant une cinétique du premier ordre et $E_{des}^{\ddagger}(\alpha) \sim 6$ kcal/mol. Il n'y a pas de mélange isotopique à l'état α qui est sans doute moléculaire. La population préalable des états β_1 et β_2 à 300 °K diminue l'adsorption de l'état α à 115 °K ce qui suggère que α et β occupent les mêmes sites. Chaque site peut adsorber soit un atome, soit une molécule puisque chaque molécule ajoutée à l'état β exclut deux molécules de l'état α.

[Traduit par le journal]

Introduction

Early studies (1, 2) and more recent ultra-high vacuum investigations (3–6) of the adsorption of oxygen on polycrystalline platinum surfaces indicate that oxygen does adsorb on platinum at room temperature. On platinum films the calorimetric heat of adsorption varied from 69 kcal mol^{-1} at low coverage to 36 kcal mol^{-1} at high coverage (1). On polycrystalline wires and ribbons, initial sticking probabilities in the range

[1]To whom correspondence should be addressed.

Can. J. Chem. Downloaded from www.nrcresearchpress.com by 210.87.254.5 on 09/05/12
For personal use only.

0.14 to 0.2 have been reported (4–6), whereas the values reported for the saturation coverage at room temperature vary from 1×10^{14} (4), through $2–3 \times 10^{14}$ (6) to 4×10^{14} molecules cm^{-2} (5).

In contrast, more recent studies on the interaction of oxygen with platinum single crystal planes indicate that oxygen does not chemisorb on platinum (7) or that it does so with an exceedingly small sticking coefficient of $\sim 7 \times 10^{-7}$ (8, 9). However, in earlier low energy electron diffraction (LEED) studies, changes in LEED patterns were attributed to oxygen adsorption (10). In attempting to resolve these conflicting results, Weinberg *et al.* (8, 9) have speculated that oxygen does not chemisorb on clean platinum surfaces but that carbon contamination stimulates the adsorption of oxygen. This is a surprising and certainly not a widely accepted conclusion making the question as to whether clean platinum chemisorbs oxygen to an appreciable extent or not a very contentious issue; see, for example, the discussion following ref. 8.

This paper is the first of a series describing thermal desorption and field electron emission studies of the reactions important to an understanding of hydrogen–deuterium exchange between hydrogen and water on platinum surfaces. Clearly, it is important to establish whether clean platinum can chemisorb oxygen. The ability of a contaminated surface to chemisorb oxygen was determined and then extra care was taken to ensure that a non-carbon contaminated surface was generated and its adsorption properties were investigated.

Experimental Methods

Apparatus

The ultra-high vacuum system used in this work has been described previously (11). The sample filament, a 12 cm length of 0.01 in. diameter platinum wire (Johnson Matthey and Mallory, Grade I) equipped with 0.003 in. diameter sensing leads for temperature measurement and control, was spot welded to the heavy tungsten leads of a four lead press seal. In low temperature experiments a filament temperature of ~115 °K was obtained by immersing the press seal in liquid nitrogen. The entire system was baked at 400 °C for prolonged periods and the ultimate pressure in the system was 5×10^{-10} Torr.

Oxygen pressures were monitored with a quadrupole mass spectrometer which was calibrated against an ion gauge attached directly to the reaction vessel (ion gauge G_1, ref. 11). Generation of CO and CO_2 by the hot ion gauge filament seriously complicates this calibration at low oxygen pressures; thus, when oxygen was allowed to flow through the system at a pressure less than 10^{-7} Torr a steady increase in pressure was observed with the ion gauge whereas the mass spectrometer indicated a constant oxygen pressure. At higher pressures this effect was negligible in the time required for the calibration. Therefore, the calibration was carried out in the pressure range $1–5 \times 10^{-7}$ Torr and mass spectrometer ion currents corresponding to lower oxygen pressures were obtained by extrapolation. To avoid contamination of the sample filament, the ion gauge used for the calibration (G_1) was removed from the system before the sample filament was installed.

Slow thermal desorption spectra with a linear heating rate were obtained using a motorized potentiometer as the comparison resistor in a Kelvin double-bridge temperature control circuit. In order to avoid high oxygen pressures, which caused a reduction in mass spectrometer emission current during desorption, and to obtain good resolution, a very slow heating rate of 5.6 deg s^{-1} was used.

Generation of carbon monoxide within the system could also cause contamination during adsorption so ion gauge G_2 (11) was never operated during adsorption, even though this gauge did not have a line-of-sight with the sample filament. For coverage measurements using the flash (*i.e.* fast heating rate) desorption experiments this gauge was used to monitor the pressure burst, but only for a short period of time between the adsorption sequences, and only after the oxygen had been pumped from the system. During the entire course of this work constant checks for CO contamination proved to be negative.

Oxygen $^{32}O_2$ was purified by diffusion through silver, the oxygen $^{36}O_2$, with a specified isotopic purity of 99%, was supplied by Stohler Isotope Chemicals in a Pyrex flask with a break seal and was used without further purification. Hydrogen was purified by diffusion through palladium and carbon monoxide of 99.9% purity was obtained from Matheson in a Pyrex flask with a break seal.

Cleaning the Sample Filament

The platinum filament used in this work was cleaned by high temperature treatment with oxygen. During the cleaning process, changes in its ability to absorb hydrogen and oxygen have been followed. On a freshly installed filament which had been heated at 1300 °K for several minutes in vacuum, neither hydrogen adsorption at 115 °K nor oxygen adsorption at 300 °K could be detected. Heating the filament at this temperature for 3 h enabled adsorption of both hydrogen and oxygen, but the extent was still very small. It has been reported that, based on Auger electron spectroscopy experiments, all contaminants except carbon can be removed from platinum by *in situ* heating (12, 13). Thus the surface on which adsorption of hydrogen and oxygen were negligible must have been contaminated with carbon. This was further confirmed by a sharp increase in CO partial pressure when the filament was heated at temperatures higher than 1100 °K with oxygen flowing through the system. The hypothesis that carbon contamination on platinum surfaces is essential to stimulate the adsorption of oxygen (9), contradicts this observation.

Heating the filament at 1300 °K in 5×10^{-6} Torr oxygen for 2 h seemed to remove the carbon contaminant completely and increased the amounts of hydrogen and

Can. J. Chem. Downloaded from www.nrcresearchpress.com by 210.87.254.5 on 09/05/12
For personal use only.

oxygen adsorbed to a constant value which could not be affected by further oxygen treatment. The results reported in this paper were obtained with filaments which have been cleaned in this manner.

Measurement of Sticking Probability and Coverage

Both sticking probability and coverage were determined using the pressure–time method (14). Usually in this method the filament is maintained at a high enough temperature to prevent adsorption during introduction of gas into the system. In these experiments the platinum filament could not be maintained at a temperature higher than 1100 °K, since the hot filament atomizes oxygen above this temperature. Thus some oxygen could be adsorbed on the cool ends of the filament before the adsorption was started. On account of such complications caused by the temperature distribution of the filament, an additional procedure was used in which the sample was flashed clean and cooled in vacuum before oxygen was introduced into the system. Whereas the first method might be expected to give low values for the initial sticking probability and coverage, adsorption on parts of the system other than the sample filament could lead to values which are too high in the second method. A comparison of the results obtained by both methods may reveal such effects and give a more reliable result.

The sticking probability, s, and coverage, n, were determined from these curves using the relationships (14)

$$[1] \qquad s = \frac{QV}{zAP}\left[\frac{P_0 - P}{\tau} - \frac{dP}{dT}\right]$$

$$[2] \qquad n = \frac{QV}{A\tau}\left[\int_0^t (P_0 - P)dt - \tau(P_0 - P)\right]$$

where A is the area of the filament, τ the characteristic pumping time, P_0 the steady state pressure when the surface is saturated, V the volume of the system, z the collision frequency per unit area per unit pressure, and Q the number of molecules in the gas phase per unit volume per unit pressure. The characteristic pumping time, τ, was measured before and after each adsorption sequence.

Whereas the sticking probability determined in this way is independent of mass spectrometer calibration errors, the accuracy of the coverage depends directly on this calibration, which, as already discussed, could not be carried out in the actual pressure range where the pressure–time curves were obtained. To check the coverage determined from eq. 2, the amount of oxygen adsorbed was also measured by flashing the filament to 1100 °K in a closed system after the oxygen leak was closed and the system pumped out. The pressure burst during the flash was measured with the ion gauge and the coverage was calculated after a small correction was made for pumping by the hot ion gauge filament. It was found that, for identical doses, the coverage determined by this method was smaller than that calculated from eq. 2 by a factor of ~1.8.

A smaller amount of oxygen desorbing than that which had apparently adsorbed could be caused by a portion of the adsorbed oxygen desorbing as either platinum oxides or oxygen atoms. This has been suggested by Vanselow and Schmidt (3) and Weber *et al.* (5) who observed similar, but coverage dependent, differences between the amounts adsorbing and desorbing. Olivei (15) has recently reported results indicating that oxygen atoms and, to a lesser extent, oxides are the dominant species desorbing from oxygen covered platinum surfaces and that molecular oxygen desorption is insignificant!

We have carried out experiments using a line-of-sight geometry between the sample filament and the mass spectrometer to check on the extent of atomic oxygen desorption. The experimental details are similar to those described in ref. 16. The mass 32 and mass 16 desorption spectra are recorded in Fig. 1*a*; the mass 16 spectrum is imperceptibly different from that observed for cracking of molecular oxygen in the ionization chamber of the mass spectrometer. To show that this experiment would successfully demonstrate atomic oxygen desorption were it to occur, the experiment was repeated using a tungsten filament, Fig. 1*b*. In this case, the dominant mass 16 spectrum satisfactorily shows the desorption of oxygen in the atomic state. Thus there is no evidence to suggest that oxygen desorbs from platinum as atoms. The reasons for the differences between these results and those of Olivei are not obvious.

Procop and Völter obtained reasonable agreement between the amounts of oxygen adsorbing and desorbing (6). Thus, considering the difficulties encountered in measuring accurate oxygen pressures, we tentatively attribute the differences observed in this experiment to mass spectrometer calibration errors. In experiments using hydrogen as adsorbate, for which pressures were known with greater accuracy, both methods of coverage measurement gave good agreement. The coverages reported in this paper are thus the values which have been normalized to fit the coverages determined by the flash desorption method.

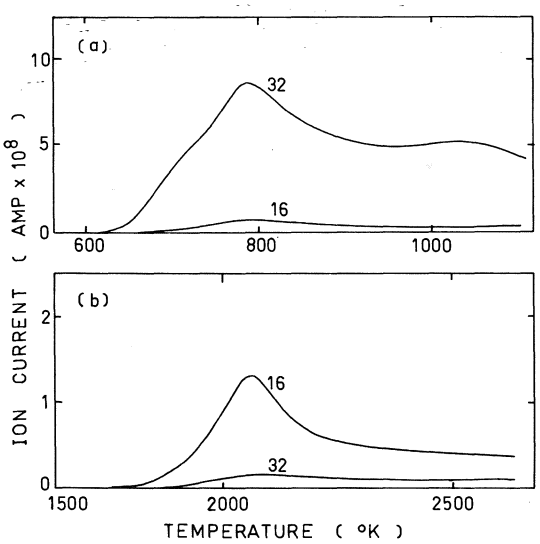

FIG. 1. Mass 16 and 32 desorption spectra obtained with line-of-sight geometry after oxygen adsorption on (*a*) platinum and (*b*) tungsten surfaces. The reaction vessel wall was at 77 °K in both (*a*) and (*b*) and the oxygen exposures were ~10^{-5} and 10^{-6} Torr s respectively.

Can. J. Chem. Downloaded from www.nrcresearchpress.com by 210.87.254.5 on 09/05/12
For personal use only.

Results

Room Temperature Adsorption

Thermal Desorption Spectra

The thermal desorption spectra obtained from a platinum filament after exposure to various doses of oxygen are shown in Fig. 2. Adsorption at 300 °K produces, at least superficially, a single desorption peak in agreement with previous observations (5, 6). This peak has been designated by Fusy *et al.* as arising from a β-state (17). In this paper we will follow this traditional way of labelling desorption features but must point out that it is widely recognized that a direct correspondence between desorption features and binding states does not necessarily obtain; thus, for example, a single adsorbed state can give rise to two desorption peaks because of two different desorption mechanisms. The fine structure in the spectra indicate that the oxygen desorbing from this tightly bound β-state is composed of several sub-states which populate successively as the coverage increases. They are labelled the β_1-, β_2-, β_3-, and β_4-states.

The most tightly bound β_4-state populates first and desorbs at ~820 °K, whereas the most weakly bound β_1-state only populates at high coverage and desorbs at a considerably lower temperature, ~650 °K. The shoulder at ~1100 °K must arise from the pumping effect of the hot sample filament which becomes significant above 1100 °K. A very small peak has always been observed at much higher temperatures, ~1300 °K, but its origin is not yet clear.

The pretreatment of the sample filament affects the fine structure of the desorption spectra. After prolonged annealing very low resolution was observed between the β_3- and β_4- peaks and often a single peak was observed. It is probable that this single peak arose from overlap of the β_3- and β_4- peaks, a point which will be further discussed in the analysis of the desorption kinetics.

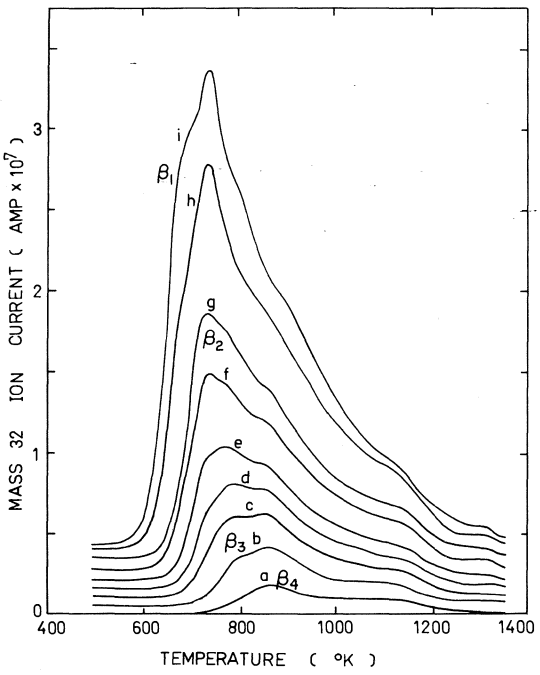

FIG. 2. Thermal desorption spectra obtained after oxygen adsorption on platinum at 300 °K for (*a*) 2×10^{-7}; (*b*) 4×10^{-7}; (*c*) 8×10^{-7}; (*d*) 1.6×10^{-6}; (*e*) 3.2×10^{-6}; (*f*) 1.2×10^{-5}; (*g*) 2×10^{-5}; (*h*) 2×10^{-4}; and (*i*) 2×10^{-3} Torr s. The curves are offset.

Sticking Probability

The pressure–time curves obtained by the two methods described in the experimental section are shown in Fig. 3. Curve A was obtained by allowing the filament to cool from 1100 to 300 °K with oxygen flowing through the cell whereas curve B was obtained by introducing the oxygen into the system after the filament had been flash-cleaned and cooled in vacuum. The variation of filament temperature with time for curve A is also indicated. A comparison between curves A and B reveals that, except in the initial stages of

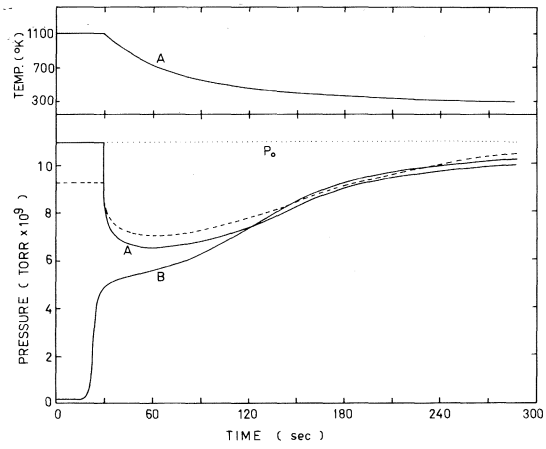

FIG. 3. Pressure–time curves for oxygen adsorption on platinum. For curve *A*, the filament was cooled from 1100 to 300 °K with oxygen flowing through the system. The filament temperature during this experiment is also shown. The effect of cooling from 1200 °K is shown by the dashed curve. For curve *B*, oxygen was introduced after the filament had been flash-cleaned and cooled in vacuum.

Can. J. Chem. Downloaded from www.nrcresearchpress.com by 210.87.254.5 on 09/05/12
For personal use only.

adsorption, the agreement is quite good. During the initial adsorption period in method A the filament temperature was still high which could account for the small difference between curves A and B. However, Procop and Völter report an initial sticking probability which is relatively independent of temperature between 323 and 773 °K (6). Alternative explanations could be adsorption of oxygen on parts of the system in addition to the filament for method B, or lack of adsorption on the precovered cool ends of the filament in method A.

The dashed curve shown in this figure was obtained when the filament was maintained at 1200 °K, rather than 1100 °K, before it was allowed to cool and adsorb oxygen. The pumping effect of the filament makes such experiments inadequate.

The variation of sticking probability with surface coverage is shown in Fig. 4. The curves A and B were obtained from pressure–time curves A and B of Fig. 2; the data points shown indicate the coverage intervals used in graphical integration of these curves. It is evident from curve B that the sticking probability is quite high, ~0.16, at low coverage and drops rapidly with increasing coverage. At a coverage of 5×10^{13} molecules cm^{-2}, it has a value less than 10^{-2}. The observed high initial sticking probability is in good agreement with that of 0.14 determined by Weber *et al.* on a filament (5), and by Procop and Völter on a foil (6).

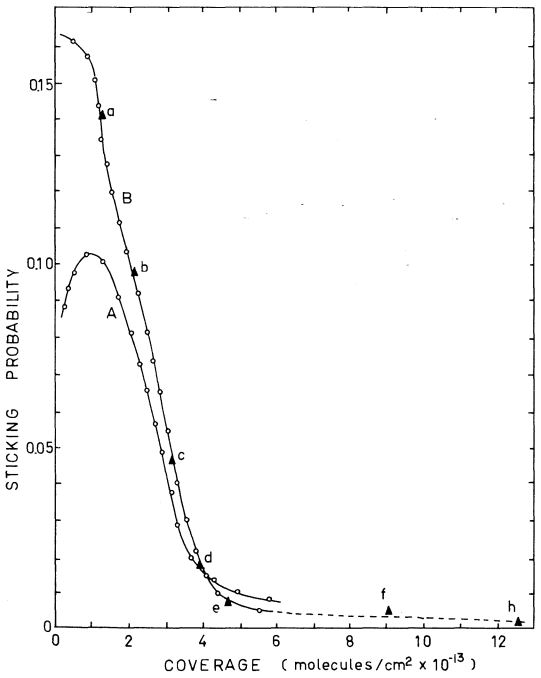

FIG. 4. Variation of sticking probability with surface coverage. Curves *A* and *B* were obtained from pressure–time curves *A* and *B* of Fig. 3. The triangles represent sticking probabilities determined independently from desorption spectra *a–h* of Fig. 2. The coverages in curves *A* and *B* were reduced by a factor of 1.8.

The triangles shown in Fig. 4 represent independently determined sticking probabilities for the coverages corresponding to the desorption spectra (*a*)–(*h*) of Fig. 2. These coverages were determined by comparing the areas under each spectrum and normalizing them to fit the coverages determined by the flash desorption method using a closed system. The sticking probabilities were determined directly from the surface coverage and the exposure. For coverages higher than 5×10^{13} molecules cm^{-2} this was the only method used, since the pressure–time method was not sufficiently accurate for measuring low sticking probabilities.

Comparison of Fig. 2 with Fig. 4 shows that the high initial sticking probability corresponds to filling of the β_3- and β_4-states and that filling of the β_1- and β_2-states has a sticking probability less than 10^{-2}.

The highest coverage determined in this work, $\sim 1.7 \times 10^{14}$ molecules cm^{-2}, was obtained after an exposure of 2×10^{-3} Torr s at an oxygen dosing pressure of 2×10^{-6} Torr. This coverage was mainly contributed by the β_1- and β_2-states.

Desorption Kinetics

For a thermal desorption process with constant activation energy, $E^{\ddagger}$, for which a high pumping speed and a linear heating rate, b deg s^{-1}, are used it can be shown that the desorption rate is a maximum at the temperature of the maximum in the desorption peak, T_m, and that (18)

$$[3] \qquad \frac{E^{\ddagger}}{RT_m^2} = \frac{\nu_1}{b} \exp\left[-\frac{E^{\ddagger}}{RT_m}\right]$$

for a first order process or

$$[4] \qquad \frac{E^{\ddagger}}{RT_m^2} = \frac{n_0 \nu_2}{b} \exp\left[-\frac{E^{\ddagger}}{RT_m}\right]$$

for a second order process, where ν_1 and ν_2 are frequency factors and n_0 is the initial coverage. Thus for both first and second order processes, the kinetic parameters $E^{\ddagger}$ and ν can be deter-

Can. J. Chem. Downloaded from www.nrcresearchpress.com by 210.87.254.5 on 09/05/12
For personal use only.

mined from the variation of T_m with b at constant n_0. Alternatively, according to [4], for second order processes, $E^{\ddagger}$ and ν can be calculated from the variation of T_m with n_0 at constant b.

β_2-*State*: From Fig. 2 we can see that T_m for the β_2-state is independent of coverage and thus this state obeys first order desorption kinetics. The variation of T_m with b was determined and a plot of log (T_m^2/b) *vs.* $1/T_m$ is shown in Fig. 5. The plot is satisfactorily linear and from its slope we determine $E^{\ddagger}(\beta_2) = 39$ kcal mol^{-1} and therefore, from [3], $\nu_1 = 1.4 \times 10^{11}$ s^{-1}.

The desorption spectra shown in Fig. 2 seem to indicate that the other substates also follow first order desorption kinetics, although this conclusion cannot be drawn unambiguously when there is such extensive overlap between the desorption peaks. Weber *et al.* (5) and Procop and Völter (6) have reported that the desorption is second order, however in one case (5) the method of analysis used is suspect when desorption is not from a single state, and in the other (6) no evidence was presented.

β_4-*State*: The activation energy for desorption of the most tightly bound β_4-state was determined from the variation of peak maximum temperature with heating rate at constant initial coverage. The plot (Fig. 5) indicates $E^{\ddagger}(\beta_4) =$ 54 kcal mol^{-1} at $n_0 = 10^{13}$ molecules cm^{-2}. The first or second order frequency factors were then calculated from eqs. 3 and 4 as $\nu_1 = 4.7 \times 10^{12}$ s^{-1} and $\nu_2 = 9.7 \times 10^{-2}$ cm^2 mol^{-1} s^{-1} respectively. These frequency factors are of the expected order of magnitude for a desorption process with inappreciable entropy of activation.

As already noted, after prolonged annealing the filament often gave desorption spectra with only a single peak in the temperature range where the β_3- and β_4-states desorb. The peak maximum temperature of this single peak shifted to lower temperatures with increasing coverage, a characteristic of second order desorption processes. Analysis of the peak as a second order process by plotting log $(T_m^2 n_0)$ *vs.* $1/T_m$ led to a confusing result; this plot indicated a surprisingly low activation energy of 28 kcal mol^{-1}, whereas a plot of log (T_m^2/b) *vs.* $1/T_m$ at constant coverage gave a value of 51 kcal mol^{-1} which is in good agreement with that already determined for the β_4-state. The explanation for this conflicting result is presumably that this single peak arose from overlap of the β_3 and β_4 peaks. If this is the case, then a failure of the kinetic analysis using the shift of T_m with coverage is to be expected.

Isotope Mixing

The observation of high activation energies for desorption of the β_2- and β_4-states suggests that oxygen is dissociatively adsorbed on platinum at room temperature. This conclusion was checked more directly by exposing the sample filament to a mixture of $^{32}O_2$ and $^{36}O_2$ in approximately equal amounts and determining the isotopic composition of the gas which subsequently is desorbed. The mass 32, 34, and 36 desorption spectra are shown in Fig. 6*a* and can be seen to have identical shapes; the fraction of $^{34}O_2$ in the desorbing gas was determined from the areas of

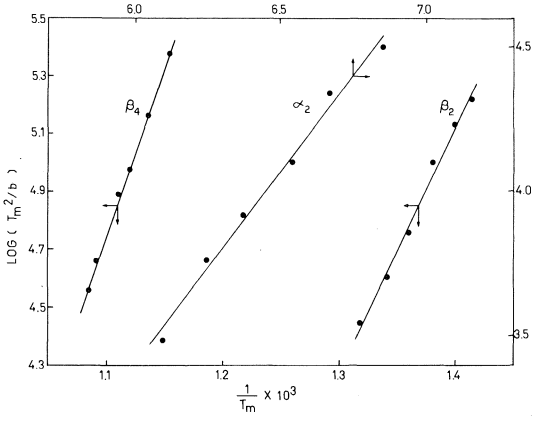

FIG. 5. Plots of log (T_m^2/b) *vs.* $(1/T_m)$ for the α_2-, β_2-, and β_4- desorption peaks, where T_m is the peak maximum temperature and b is the heating rate.

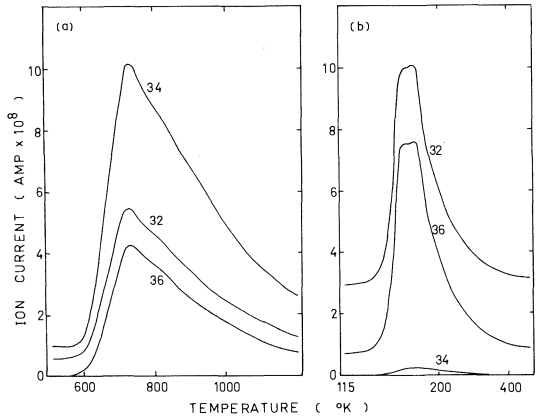

FIG. 6. Mass 32, 34, and 36 desorption spectra obtained after the platinum filament had been exposed to an approximately equimolar mixture of $^{32}O_2$ and $^{36}O_2$ at (*a*) 300 °K, and (*b*) 115 °K. The curves are offset.

Can. J. Chem. Downloaded from www.nrcresearchpress.com by 210.87.254.5 on 09/05/12
For personal use only.

the desorption peaks and corresponds to the value required for statistical mixing. These observations substantially confirm that oxygen adsorbs dissociatively in the β-state.

Low Temperature Adsorption

Thermal Desorption Spectra

In addition to the tightly bound β-state, oxygen can also adsorb in a weakly bound state at 115 °K as indicated in Fig. 7. This weakly bound state has been designated as the α-state (17); however, the fine structure in the desorption spectra indicates that this is not a single peak but is composed of three overlapping peaks which are designated as the α_1-, α_2-, and α_3-states. Whereas the α_2- and α_3-states populate almost simultaneously, filling of the α_1-state begins only after these states are extensively populated.

Annealing of the sample filament has an effect on the ratio of the amounts adsorbed in the α- and β-states, n_α/n_β, and those in the α_2- and α_3-states, $n_{\alpha_2}/n_{\alpha_3}$. Both of these ratios increase significantly after the filament has been annealed at 1100 °K for 24 h in vacuum. Further annealing at this temperature for prolonged periods had little effect on these ratios.

Relative Populations of the α- and β-States

The amounts of oxygen desorbing in the α- and β-states after adsorption at 115 °K are plotted as a function of exposure in Fig. 8. For comparison, the total amount adsorbed at 300 °K (in the β-state) is also shown. If it is assumed that

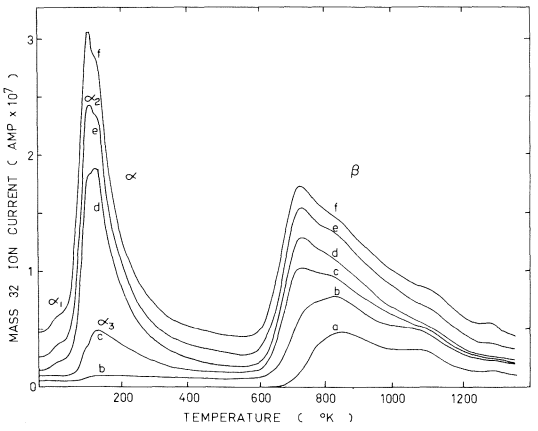

FIG. 7. Thermal desorption spectra obtained after oxygen adsorption at 115 °K for (*a*) 2 × 10^{-7}; (*b*) 3 × 10^{-7}; (*c*) 4 × 10^{-7}; (*d*) 8 × 10^{-7}; (*e*) 1.6 × 10^{-6}; and (*f*) 3.2 × 10^{-6} Torr s. The curves are offset.

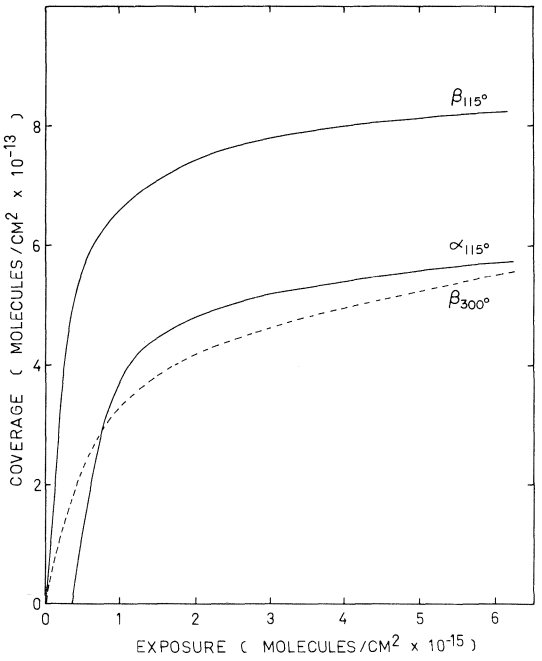

FIG. 8. Variation of the amount adsorbed in the α- and β-states with exposure at 115 °K. The amount adsorbed at 300 °K is given by the dashed curve.

the desorption spectra reflect the distribution of oxygen in different binding states at the adsorption temperature, a point which will be discussed more fully later, then filling of the α-state starts only after the β-state has been extensively populated, to ~5 × 10^{13} molecules cm^{-2}; this corresponds to the coverage in the β_3- and β_4-states. The initial sticking probability in the β-state at 115 °K is approximately the same as at 300 °K but it remains constant at this high value, ~0.15, for a much larger coverage range, *i.e.* to almost 5 × 10^{13} molecules cm^{-2}. However, the sticking probability drops rapidly at higher coverage such that for a large exposure of 1.8 × 10^{17} molecules cm^{-2}, the amount adsorbed in the β-state at 115 °K is 1 × 10^{14} molecules cm^{-2} compared with 1.3 × 10^{14} molecules cm^{-2} at 300 °K. For this same exposure the coverage in the α-state at 115 °K is 0.9 × 10^{14} molecules cm^{-2}. The α-state populates only after the β-state has reached half its maximum coverage at 115 °K.

Effect of Prior Population of the β-State on Adsorption into the α-State

A relationship between the formation of the α-state and that of the β-state is suggested by the

Can. J. Chem. Downloaded from www.nrcresearchpress.com by 210.87.254.5 on 09/05/12
For personal use only.

data shown in Figs. 7 and 8. To further investigate this relationship the β-state was prepopulated to varying extents, by adsorbing oxygen at 300 °K, and then the surface was saturated at 115 °K; the total dose was 2.4×10^{-4} Torr s in each case. The desorption spectra obtained for three different preadsorbed β-coverages are shown in Fig. 9. When the β-state is prepopulated to 5×10^{13} molecules cm^{-2}, *i.e.* the β_3- and β_4-states, there is little effect on the subsequent adsorption into the α-state; compare curves *a* and *b*. This is consistent with the observation that at 115 °K the α-state populates only after the β-state has attained a coverage of 5×10^{13} molecules cm^{-2}. As the amount of preadsorbed oxygen is further increased, so that the β_1- and β_2-states have been populated at 300 °K, an exclusion effect is observed. Note also that there is a sequential reduction in population of the α-substates, with the α_2-state preceding the α_3-state as the β_2- and then the β_1-states are prepopulated. This suggests that filling of the α_2- and α_3-states is closely related to that of the β_2- and β_1-states, respectively.

Desorption Kinetics

Since the peak maximum temperatures, T_m, for both the α_2- and α_3-states are independent of coverage, both of these states desorb with first order kinetics. The plot of log (T_m^2/b) *vs.* $1/T_m$ for the α_2-state is shown in Fig. 5 and from this plot we can calculate $E^{\ddagger}(\alpha_2) = 6$ kcal mol^{-1} and $\nu_1 = 1.2 \times 10^8$ s^{-1}. However, since in the temperature range where this state desorbs the temperature was not exactly linear in time these kinetic parameters are less reliable than the others determined in this work.

Isotope Mixing

A state desorbing by first order kinetics with such a low activation energy might be expected to be adsorbed molecularly, *i.e.* non-dissociatively. This is confirmed by an isotope mixing experiment, Fig. 6*b*. In contrast to the β-state, adsorption of a mixture of $^{32}O_2$ and $^{36}O_2$ resulted in no isotopic mixing in the α-desorption peak. Oxygen adsorbed in the α-state undoubtedly remains molecular.

Interaction of Preadsorbed Oxygen with Hydrogen and Carbon Monoxide at 300 °K

The sample filament was saturated with oxygen at a pressure of 2×10^{-6} Torr, and then exposed to hydrogen or carbon monoxide gas for various time intervals. The desorption spectra obtained after interaction with hydrogen at 4×10^{-8} Torr are shown in Fig. 10. Preadsorbed oxygen was removed from the surface completely after 400 s and desorption of hydrogen was observed only after all the oxygen had been removed.

Similar results were obtained with carbon monoxide. The preadsorbed oxygen was completely removed from the surface after an exposure of 8×10^{-6} Torr s at a carbon monoxide pressure of 2×10^{-8} Torr. After the preadsorbed oxygen had been partially removed from the surface, desorption spectra for CO_2, CO,

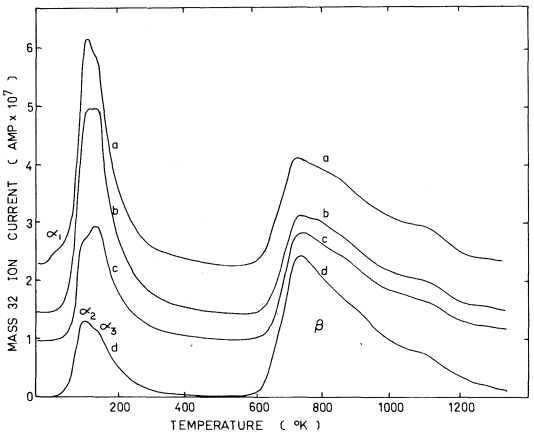

FIG. 9. Thermal desorption spectra obtained after oxygen adsorption at 115 °K and after prepopulation of the β-state at 300 °K; (*a*) without preadsorption and with (*b*) 5×10^{13}, (*c*) 9×10^{13}, and (*d*) 1.3×10^{14} molecules cm^{-2} preadsorbed. The curves are offset.

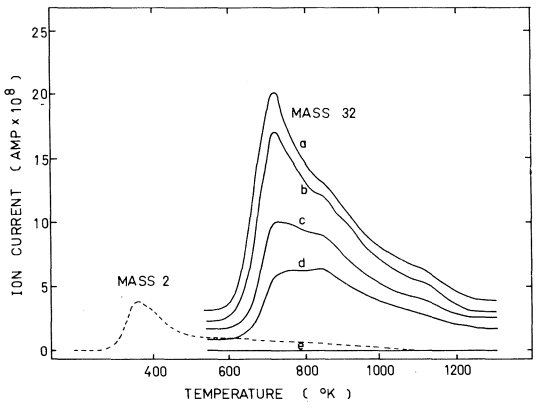

FIG. 10. Thermal desorption spectra obtained after the interaction of adsorbed oxygen with gaseous hydrogen at 4×10^{-8} Torr for (*a*) 0; (*b*) 100; (*c*) 150; (*d*) 200; and (*e*) 400 s. After 400 s oxygen had been completely removed and a hydrogen desorption spectrum was observed (dashed curve). The curves are offset.

Can. J. Chem. Downloaded from www.nrcresearchpress.com by 210.87.254.5 on 09/05/12
For personal use only.

and O_2 were observed. Since CO_2 does not adsorb on platinum at room temperature (19), this observation suggests that CO and O_2 can be co-adsorbed on the surface at room temperature. The oxidation of carbon monoxide on a Pt(110) crystal surface has been extensively investigated by Bonzel and Ku (20, 21).

Thus, in agreement with earlier investigations (22), hydrogen and carbon monoxide can remove adsorbed oxygen from platinum surfaces to produce H_2O and CO_2 respectively. In ultra-high vacuum systems hydrogen and carbon monoxide are the main components in the residual gas. Thus it seems most probable that studies in which oxygen adsorption is not observed on platinum surfaces (7) or is observed with a low sticking probability (8, 9) have been performed in systems with too large a residual gas pressure (23).

Discussion

Conversion Between States during Desorption

The sticking probability for the β_3- and β_4-states was observed to remain at its high initial value for a much greater range of coverage at 115 °K than at 300 °K; moreover, no α-desorption was observed until the β_3- and β_4-states were filled (Fig. 8). The straightforward interpretation of these observations is that the desorption spectra accurately reflect the population of the binding states at the adsorption temperature and thus there is no activation energy for dissociative adsorption into the β_3- and β_4-states. However, one must consider the alternative interpretation that at the adsorption temperature the oxygen is adsorbed molecularly in the α-state but that during thermal desorption the activation energy for conversion to the β-state is acquired before desorption as the α-state at temperatures ~130 °K.

Such a conversion between the α- and β-states was checked by using a fast heating rate for the desorption spectrum in which desorption of the α-state was complete within 500 ms compared with ~20 s for the slow desorption spectra of Fig. 7. The results were substantially the same as for spectra *a* and *b* of Fig. 7, showing only a β-desorption peak. If the activation energy for conversion between the α- and β-states is sufficiently small that it occurs completely in the temperature interval 115 to 130 °K even at highest heating rate, then presumably this conversion would also take place during the adsorption period at 115 °K. This argument has been presented in detail by Ehrlich in discussing interconversion between the γ- and β-states for nitrogen adsorbed on tungsten (24).

Direct adsorption of oxygen into the dissociatively adsorbed β-state at low temperatures is further supported by the high initial heat of adsorption of greater than 40 kcal mol^{-1} observed for oxygen adsorption on platinum black at 77 °K (22). Thus the conversion to the tightly bound state occurs on a calorimetric time scale even at 77 °K.

A further possibility is that the conversion takes place via the gas phase, *i.e.* oxygen desorbs in the α-state but readsorbs into the β-state at higher filament temperatures. For the low coverages of spectra 7*a* and *b* this readsorption would need to be quantitative which is impossible. At higher coverage, where α-desorption is appreciable, the sticking coefficient for the β-state is so low that less than one-hundredth of a monolayer could readsorb during the period of the desorption spectrum.

Thus we consider the desorption spectra satisfactorily represent the distribution of adsorbed oxygen between the α- and β-states at the adsorption temperature. However, in contrast, it is quite possible that the β- (and α-) substates do not represent different binding states but could represent different desorption mechanisms for adatoms which prior to desorption are indistinguishable (11) or variations in desorption energy resulting from adatom interactions. These possibilities are additional to the more obvious interpretation involving an intrinsically heterogeneous surface.

Sticking Probability and Characteristics of the Binding States

To facilitate discussion and comparison, the salient observations will be summarized.

Oxygen adsorbs on platinum in two states:

(*a*) A dissociatively adsorbed atomic state, the β-state, which is tightly-bound ($E_{des}^{\ddagger} \sim$ 39–54 kcal mol^{-1}) and desorbs at high temperatures (~700–800 °K). Isotope mixing occurs freely in desorption from this state.

(*b*) An associatively adsorbed molecular state, the α-state, which is weakly-bound ($E_{des}^{\ddagger} \sim 6$ kcal mol^{-1}) and desorbs by first order kinetics at low temperatures (~150 °K). Isotope mixing does not occur in this state.

The sticking probability has the following characteristics:

Can. J. Chem. Downloaded from www.nrcresearchpress.com by 210.87.254.5 on 09/05/12
For personal use only.

(*c*) The initial sticking probability is approximately the same, ~0.16, for filament temperatures of 300 and 115 °K suggesting that the adsorption is non-activated, at least in its early stages. This is further confirmed by the observations of Procop and Völter between 323 and 673 °K (6). Since the β-state populates first, even at 115 °K, dissociative adsorption requires no activation energy.

(*d*) While at 300 °K the sticking probability falls off rapidly to values less than 10^{-2}, the sticking probability remains at its high initial value for a much more extensive coverage range at 115 °K.

(*e*) At 115 °K, the α-state populates only after the β-coverage has reached 5×10^{13} molecules cm^{-2}, *i.e.* half its maximum value at 115 °K.

(*f*) The maximum β-coverage at 115 °K (1×10^{14} molecules cm^{-2}) is less than for the same exposure at 300 °K (1.3×10^{14} molecules cm^{-2}). The maximum β-coverage observed at 300 °K was $\sim 1.7 \times 10^{14}$ molecules cm^{-2} ($\theta \sim 1/3$).

(*g*) Prior adsorption at 300 °K into the β-state to coverages greater than 5×10^{13} molecules cm^{-2} reduces the amount which can be subsequently adsorbed into the α-state at 115°K.

Qualitatively these observations show remarkable similarity to those for the nitrogen–tungsten system (24). A possible exception is the temperature dependence observed for the initial sticking probability of nitrogen on tungsten observed by Ehrlich (24), although Kisliuk observed a constant sticking probability between 196 and 473 °K (25).

The observation, (*d*), of higher sticking probabilities at lower temperatures is most readily interpreted by an adsorption model involving a weakly adsorbed precursor state to chemisorption; the α-state is probably the precursor state. In this model the sticking probability does not decrease with increasing coverage in the manner expected for the decrease in probability of collisions from the gas phase with vacant sites because a weakly-bound precursor provides a pool of adsorbate molecules on the surface. The concentration of precursor molecules decreases with increasing temperature accounting for the decrease in sticking probability. Several developments of this model have been presented (26–28).

Results for oxygen adsorption on a Pt(111) single crystal surface (23) were found to obey an Elovich-type of equation in that the sticking probability varied logarithmically with the coverage at 543 and 603 °K. A similar plot for the sticking probability data at 300 °K presented in this paper was not linear. The lack of agreement is not unexpected since a simple result obtained for a single crystal may not be reproduced on a polycrystalline filament surface where different surfaces could be contributing in different coverage ranges. However, the temperature dependent sticking probability proposed to explain the logarithmic plot seems unlikely in view of the data presented in this same paper (23) together with that presented here and ref. 6.

Some insight into the nature of the α- and β-binding sites can be deduced from the manner in which the adlayer grows. Thus the initial adsorption into the β-state is non-activated and occurs rapidly even at 115 °K. However, once the β_3- and β_4-states are occupied the sticking coefficient drops rapidly and subsequent adsorption into the β_1-, β_2-, and α-states occurs simultaneously and competitively. Thus prepopulation of the β_1- and β_2-states reduces the amount of oxygen which can be subsequently adsorbed into the α-state. The simplest explanation for these observations is that α- and β-states occupy the same sites and that dissociative adsorption into the β_1- and β_2-states is activated. Thus at 115 °K a fraction of the molecules could remain undissociated on these sites producing the α-state. When adsorption occurs at 300 °K these molecules dissociate to form more of the β_1- and β_2-states, thus reducing the amounts which can be subsequently adsorbed in the α-state at 115 °K. A comparison of the spectra *a* and *d* of Fig. 9 supports this conclusion; the decrease in the α-coverage when the β-state is prepopulated at 300 °K is close to twice the increase in the β-coverage. Thus an individual site is capable of taking up either one molecule in the α-state or an atom in the β-state.

Heterogeneity of the surface complicates the adsorption model. Thus the sequential reduction in the α-substates with increasing amounts of preadsorbed oxygen suggests that the α_2- and β_2-states are adsorbed on the same plane and the α_3- and β_1-states occupy a different plane. The effect of annealing on the n_α/n_β and $n_{\alpha_2}/n_{\alpha_3}$ ratios also suggests complicating effects from a variable distribution of crystal facets. Clearly any further progress in our understanding of this adsorption system must await detailed studies on different single crystal planes.

Desorption Kinetics

The first order kinetics observed for the molecularly adsorbed α-states requires no discussion. However, first order kinetics were also deduced for the atomically adsorbed β_2-state and this is worth comment. Recombination of adsorbed atoms would be bimolecular and thus second order if the adatoms were completely mobile at the desorption temperature, *i.e.* $E_{diff}^{\ddagger} \ll E_{des}^{\ddagger}$. Thus the observation of a first order desorption process for the β_2-state implies that the adatoms are not completely mobile at ~700 °K. This is in agreement with the field emission microscope observations of Lewis and Gomer (29). Boundary diffusion of a chemisorbed layer at high coverage occurred with $E_{diff}^{\ddagger} = 27$ kcal mol^{-1} at 450–500 °K whereas at low coverage, boundary-free diffusion occurs only at temperatures higher than 500 °K with $E_{diff}^{\ddagger} = 34$ kcal mol^{-1}. Since $E_{des}^{\ddagger}(\beta_2) = 39$ kcal mol^{-1}, we can see that the activation energies for diffusion and desorption are comparable. This condition, $E_{diff}^{\ddagger} \sim E_{des}^{\ddagger}$, is just what would be required for a first order recombination of adjacent adatoms which have restricted mobility (11). An alternative, but not entirely independent, interpretation has been suggested for oxygen desorption from tungsten in which bond breaking in a surface oxide is rate limiting in the desorption process (30).

The authors wish to thank Atomic Energy of Canada Limited, Chalk River Nuclear Laboratories for their support of this research.

1. D. Brennan, D. O. Hayward, and B. M. W. Trapnell. Proc. R. Soc. Lond. A**256**, 81 (1960).
2. M. A. H. Lanyon and B. M. W. Trapnell. Proc. R. Soc. Lond. A**227**, 387 (1955).
3. R. Vanselow and E. A. Schmidt. Z. Naturforsch. **22**a, 717 (1967).
4. B. J. Wood, N. Endow, and H. Wise. J. Catal. **18**, 70 (1970).
5. B. Weber, J. Fusy, and A. Cassuto. J. Chim. Phys. **66**, 708 (1969).
6. M. Procop and J. Völter. Z. Phys. Chem. Leipzig, **250**, 387 (1972).
7. A. E. Morgan and G. A. Somorjai. Surf. Sci. **12**, 405 (1968).
8. W. H. Weinberg, R. M. Lambert, C. M. Comrie, and J. W. Linnett. Proc. Vth Int. Conf. Catal. Miami Beach, Florida. 1972. p. 513.
9. W. H. Weinberg, R. M. Lambert, C. M. Comrie, and J. W. Linnett. Surf. Sci. **30**, 299 (1970).
10. C. W. Tucker. J. Appl. Phys. **35**, 1897 (1964).
11. P. T. Dawson and Y. K. Peng. Surf. Sci. **33**, 565 (1972).
12. T. W. Haas, J. T. Grant, and G. J. Dooley. J. Vac. Sci. Technol. **7**, 43 (1970).
13. T. W. Haas, J. T. Grant, and G. J. Dooley. Phys. Rev. B**1**, 1449 (1970).
14. P. A. Redhead. Trans. Faraday Soc. **57**, 641 (1961).
15. A. Olivei. J. Less-Common Met. **29**, 11 (1972).
16. Y. K. Peng and P. T. Dawson. Can. J. Chem. **52**, 1147 (1974).
17. J. Fusy, J. J. Ehrhardt, and A. Cassuto. Colloque CNRS sur la structure et les proprietes des surfaces des solides, Paris. 1969. p. 163.
18. P. A. Redhead. Vacuum, **12**, 203 (1962).
19. W. L. Winterbottom. Surf. Sci. **36**, 195 (1973).
20. H. P. Bonzel and R. Ku. J. Vac. Sci. Technol. **9**, 663 (1972).
21. H. P. Bonzel and R. Ku. Surf. Sci. **33**, 91 (1972).
22. J. G. Aston. J. Phys. Chem. **67**, 2042 (1963).
23. H. P. Bonzel and R. Ku. Surf. Sci. **40**, 85 (1973).
24. G. Ehrlich. J. Chem. Phys. **34**, 29 (1961).
25. P. Kisliuk. J. Chem. Phys. **30**, 174 (1959).
26. G. Ehrlich. J. Phys. Chem. **59**, 473 (1955).
27. G. Ehrlich. J. Phys. Chem. Solids, **1**, 3 (1956).
28. P. Kisliuk. J. Phys. Chem. Solids, **3**, 95 (1957); **5**, 78 (1958).
29. R. Lewis and R. Gomer. Surf. Sci. **12**, 157 (1968).
30. C. Kohrt and R. Gomer. J. Chem. Phys. **52**, 3283 (1970).

Can. J. Chem. Downloaded from www.nrcresearchpress.com by 210.87.254.5 on 09/05/12
For personal use only.

Photolysis of Thietane–Cyclopentadiene Mixtures. Reactions of Monomeric Thioformaldehyde[1]

DAVID R. DICE AND RONALD P. STEER[2]

Department of Chemistry and Chemical Engineering, University of Saskatchewan, Saskatoon, Saskatchewan S7N 0W0

Received May 22, 1974

DAVID R. DICE and RONALD P. STEER. Can. J. Chem. **52**, 3518 (1974).

The 313 nm photolysis of thietane–cyclopentadiene mixtures in the vapor phase at temperatures between 25 and 235 °C has been studied. 2-Thiabicyclo[2.2.1]hept-5-ene (TBH) results from the concerted, thermal, 1,4-Diels–Alder cycloaddition of thioformaldehyde to cyclopentadiene. Other products arise via nonconcerted processes involving biradical intermediates. Thioformaldehyde is scavenged quantitatively with high added pressures of cyclopentadiene and thus the yield of TBH may be used as a measure of the amount of monomeric CH_2S produced in the system.

DAVID R. DICE et RONALD P. STEER. Can. J. Chem. **52**, 3518 (1974).

On a étudié la photolyse, à 313 nm en phase vapeur et à des températures allant de 25 à 235 °C, de mélanges de thiétane avec du cyclopentadiène. Le thia-2 bicyclo[2.2.1]heptène-5 (TBH) qui se forme résulte d'une réaction Diels–Alder-1,4 (cycloaddition concertée et thermique) du thioformaldéhyde sur le cyclopentadiène. D'autres produits proviennent de processus nonconcertés impliquant des intermédiaires biradicalaires. Le thioformaldéhyde est piégé quantitativement lorsque du cyclopentadiène sous haute pression est utilisé; les rendements en TBH obtenu peuvent donc être utilisés comme une mesure de la quantité de CH_2S, sous forme monomérique, produite dans le système. [Traduit par le journal]

Introduction

Increasing interest has been shown recently in the photochemical and thermal reactions of thiocarbonyl compounds. The generally high ground state reactivity of these substances has hampered their investigation however and, to the present, substantial work has been done only on the most stable thiones. Thus, studies have been made of the thermal (1, 2) and photochemical (3–6) cycloaddition reactions of thiocarbonyls, particularly thiobenzophenone, the internal photocyclization of aromatic thiobenzoyl compounds (7), and the photothioenolization of some bicyclic thiones (8). Measurement of the electronic absorption (9, 10) and emission (3, 11) spectra of only a limited number of thiones and thials in condensed media has been possible.

The simplest thiocarbonyl compound is thioformaldehyde, which has been postulated to be an unstable product in a number of photolytic and thermolytic systems. Based largely on stoichiometric arguments, it has been inferred that CH_2S is a product of the self-disproportionation of CH_3S radicals in the gas phase (12) and some spectroscopic data is available to substantiate this hypothesis (9, 13). It has also been suggested that CH_2S is a product of the photodecomposition of several cyclic sulfides (14, 15) and we have recently advanced arguments that CH_2S and C_2H_4 should be formed in equal yields in the direct photolysis of thietane vapor (16). Despite the fact that a substantial amount of spectral data for CH_2S has been gathered in these experiments, no satisfactory method of quantitative analysis of this species has been developed.

The chemical reactions of CH_2S also remain largely unstudied. In part this is due to the inherent instability of the thials which polymerize readily (17, 18). In addition, until now there has been no satisfactory means of producing the monomer cleanly.

In this paper we present conclusive evidence that monomeric thioformaldehyde is produced in high yield by direct photolysis of thietane vapor. We have also studied a method whereby the monomer may be trapped and analyzed quantitatively via its reaction with cyclopentadiene.

[1]From the Ph.D. thesis of D. R. Dice, University of Saskatchewan, 1974.

[2]To whom correspondence should be addressed.

Can. J. Chem. Downloaded from www.nrcresearchpress.com by 210.87.254.6 on 09/05/12
For personal use only.

Can. J. Chem. Downloaded from www.nrcresearchpress.com by 210.87.254.6 on 09/05/12
For personal use only.

Experimental

The photolysis system used in this study has been described previously (16). A PEK, Model 15, 500 W high pressure mercury arc lamp was used in conjunction with a liquid filter ($NiSO_4$, K_2CrO_4) to isolate the 313 nm region of the lamp's emission spectrum. Photolyses were carried out to no more than 1% decomposition of the substrate.

Thietane (Eastman) was purified by preparative gas chromatography. Cyclopentadiene, prepared by thermally cracking dicylopentadiene (Aldrich), was purified by preparative gas chromatography immediately prior to each run. Cyclopentadiene prepared in this way contained small variable amounts of the dimer. An authentic sample of 2-thiabicyclo[2.2.1]hept-5-ene (TBH) was prepared according to the method of Johnson *et al.* (19).

Products noncondensable at −130 °C (*n*-pentane slush) were ethylene and propylene which were analyzed by gas chromatography using a 10 ft × ¼ in. Porapak Q column. The −130 °C condensable products, principally TBH, 1,2-dithiocane, a product with a molecular weight of 140 and reactants, were separated and analyzed by f.i.g.c. using a 15 ft × ⅛ in. tricresyl phosphate column (5% w/w) with temperature programming from 50 to 120 °C.

Products were identified by comparing their gas chromatography retention times with those of authentic samples and by mass spectrometry.[3] In some cases analyses were performed using a gas chromatograph coupled directly to the mass spectrometer. Absolute errors in the analysis of C_2H_4 and C_3H_6 were estimated to be ±3%, while those for TBH and 1,2-dithiocane were estimated to be ±5%.

Results and Discussion

We have previously shown (16) that ethylene, propylene, and, by inference, thioformaldehyde are products of the direct photolysis of thietane vapor at 313 nm. Further study has now shown that 1,2-dithiocane (DTO) is also produced in small yield (maximum of 7% of that of C_2H_4). We have also previously advanced evidence (16) that propylene is a secondary product arising from the reaction of thioformaldehyde with the substrate.

When cyclopentadiene–thietane mixtures were photolyzed at 313 nm, two additional products appeared. The one formed in high yield was identified as 2-thiabicyclo[2.2.1]hept-5-ene (TBH). The second product, generally formed in small yields, had a molecular mass of 140. The mass spectrum of this product is consistent with any of the following three structures, each of which could be formed by the addition of a C_3H_6S moiety to cyclopentadiene.

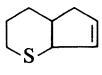

2-thiabicyclo[4.3.0]non-8-ene
(8-TBN)

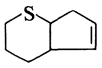

2-thiabicyclo[4.3.0]non-7-ene
(7-TBN)

2-thiabicyclo[4.2.1]oct-7-ene
(TBO)

Unfortunately, insufficient quantities of this product were formed to permit elucidation of its structure by an independent method. Knowledge of the precise identity of this product is not necessary to sustain a discussion of the chemical processes which are responsible for its formation, however.

The effects on the product yields of changing the pressure of cyclopentadiene when cyclopentadiene–thietane mixture were photolyzed at various temperatures are given in Table 1. Several trends are evident from this data.

At all temperatures there is a rapid rise in the yield of TBH as the pressure of cyclopentadiene (CP) is increased. The rate of this rise increases as the temperature increases and at all temperatures the yield of TBH levels off at high CP pressures. The yield of the mass 140 product also increases rapidly as the pressure of CP is increased but, unlike TBH, reaches a maximum and then falls off at still higher pressures. The maximum yield of the mass 140 product decreases and is reached at lower CP pressures as the temperature is decreased. The yields of ethylene and DTO decrease slightly and the yield of propylene falls rapidly to zero as the pressure of CP increases.

These observations may be explained satisfactorily on the basis of the following reaction scheme.

The above scheme predicts that the yield of C_2H_4 should equal the yield of TBH at CP

[3]Mass spectra of the sulfides produced in this study may be obtained, at a nominal charge, from the Depository of Unpublished Data, National Science Library, National Research Council of Canada, Ottawa, Canada K1A 0S2.

TABLE 1. Effect of added cyclopentadiene on the photolysis of thietane vapor at various temperatures*

		Rates (μmol min^{-1})				
T (°C)	P(CP) (Torr)	C_2H_4 ($\times 10^2$)	C_3H_6 ($\times 10^3$)	TBH ($\times 10^2$)	DTO† ($\times 10^3$)	(m.w. = 140)‡ ($\times 10^3$)
235	0	4.6	21	0	3.8	0
	23	4.6	1.5	4.0	2.9	2.7
200	0	4.6	2.6	0	3.3	0
	0.05	4.6	2.4	0.8	3.3	0.07
	0.25	4.3	1.9	2.1	3.3	0.13
	0.66	4.6	1.7	1.9	3.0	0.43
	1.05	4.5	1.3	2.9	3.1	2.4
	1.74	4.3	0.82	2.9	3.3	3.7
	4.0	4.3	1.0	2.9	3.3	4.7
	8.0	4.0	0.81	3.0	3.0	6.7
	9.3	4.0	0.44	3.0	3.0	8.7
	15.0	4.3	0.91	3.5	2.9	8.3
	23	4.2	0.80	3.6	2.6	9.0
	46	4.0	0.72	3.9	2.0	7.0
	73	3.9	0.32	3.6	2.2	7.0
	98	3.1	—	3.0	1.0	4.3
	201	3.3	—	—	—	1.8
100	0	3.7	1.8	0	2.0	0
	0.12	3.9	0.86	0.60	2.0	0.67
	1.2	3.8	0.63	2.2	1.7	2.0
	3.5	3.7	0.47	2.5	1.9	3.3
	5.8	3.9	—	2.8	1.5	4.3
	10	3.8	—	3.0	1.8	5.3
	23	3.7	—	2.8	1.3	3.0
	46	3.3	—	3.1	1.2	2.2
	112	3.4	—	3.3	1.2	1.2
	181	3.0	—	3.0	1.0	1.3
25	0	3.3	—	0	1.2	0
	0.5	3.4	—	0.56	1.0	0.13
	1.0	3.5	—	0.80	0.70	0.25
	5.0	3.4	—	1.5	0.17	0.21
	8.0	3.3	—	2.0	0.17	0.03
	10	3.5	—	2.5	0.13	0.03
	20	3.4	—	2.4	0.13	0.02
	46	3.5	—	2.6	0.10	0.02
	70	3.2	—	2.5	—	0.02
	150	3.2	—	2.6	—	—

*λ = 313 nm, P(THT) = 23 Torr, time = 30 min, $I_a = 5.17 \times 10^{-8}$ E min^{-1}.
†Assuming flame response equivalent to that of *n*-propyl disulfide.
‡Product of molecular weight = 140 (*cf.* text). Flame response equivalent to that of TBH is assumed.

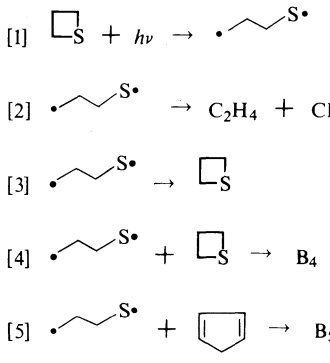

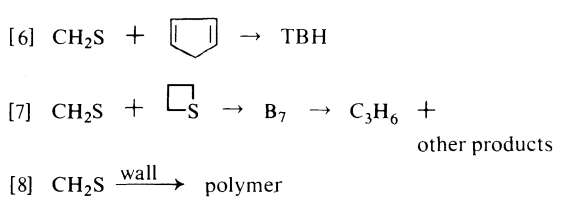

pressures large enough to scavenge CH_2S quantitatively. Within experimental error, the data are in accord with this prediction although agreement is better at higher than at lower temperatures. It may be that at 25 °C scavenging

Can. J. Chem. Downloaded from www.nrcresearchpress.com by 210.87.254.6 on 09/05/12
For personal use only.

Can. J. Chem. Downloaded from www.nrcresearchpress.com by 210.87.254.6 on 09/05/12
For personal use only.

is incomplete at the highest CP pressures used, but because of the thermal instability and low volatility of TBH, it is more likely that the imbalance is due to the loss of small portions of TBH in the analysis.

The above scheme does not account for the observed decrease in the yields of the mass 140 product at high CP pressures. The explanation for this latter phenomenon must lie in the fact that reaction 5 is nonconcerted and proceeds via an intermediate biradical, B_5, which can add to further CP molecules at a rate which is competitive with its rate of ring closure. Higher molecular weight products formed in such reactions would not have been detected.

The yield of DTO is expected to decrease with increasing CP pressure at constant thietane pressure since the rate of reaction 5 will increase relative to that of reaction 4. Moreover, if reaction 4 is nonconcerted and proceeds via a biradical intermediate, B_4, then this biradical could also react with CP and decrease the DTO yield.

It has been shown previously (16) that both CH_2S and a scavengeable biradical intermediate (identified as B_7) are involved in the sequence of reactions leading to propylene. The fact that the C_3H_6 yield decreases rapidly with increasing CP pressure confirms this earlier work since the scavenging of CH_2S in reaction 6 and the possible scavenging of B_7 by CP will greatly reduce the overall rate of reaction 7.

The question of the nature of reaction 6 is an important one. On the basis of thermochemical (20, 21) and spectroscopic (9, 10, 13) data and theoretical calculations (22), it is possible that the CH_2S formed in reaction 2 could be in its (n,π*) excited state. It is also possible that excited CH_2S could be formed as a result of the direct adsorption of light at 313 nm by ground state thioformaldehyde in a secondary photolytic process (16). It is therefore possible that TBH could arise via a (presumably nonconcerted) 1,4-cycloaddition of electronically excited CH_2S to CP. The weight of evidence is against this being an important reaction pathway, however.

First, by analogy with the aliphatic aldehydes (23) and several thiones (3, 4), reaction of CH_2S in its (n,π*) excited state with CP is expected to proceed, at least in part, via a concerted 1,2-cycloaddition pathway leading to thietane derivatives. Only one product of mass 112 was found, however, and its structure is that of TBH. Second, if reaction 6 were nonconcerted a biradical intermediate having a structure which resembles that of B_5 would be involved. However, the yields of C_2H_4 and TBH are equal at high CP pressure and the yield of TBH does not diminish as the pressure of CP is increased whereas DTO, the mass 140 product and C_3H_6, all of which have biradical precursors, are formed with yields which do diminish with increasing CP pressure. This suggests that no scavengeable biradical intermediate is formed in reaction 6 and that reaction 6 is concerted. Although a 1,4-cycloaddition of excited CH_2S to CP cannot be eliminated altogether, the bulk of the evidence does suggest that reaction 6 is an example of a gas phase, concerted, thermal, 1,4-Diels–Alder cycloaddition.

Diels–Alder addition of thiophosgene, $CSCl_2$, to CP in condensed phase has previously been reported (19) and constitutes the first step in a multi-step synthesis of TBH and other similar compounds. Thioacetophenone has also been reported (24) to form a 1:1 adduct with CP. It is therefore possible that the photolysis of mixtures of CP and thietane (or its derivatives) could be used as a simple preparative route to TBH and other similar compounds. We also believe that reaction with CP may very well be used to detect and analyze for monomeric CH_2S (and perhaps other thials) in other photochemical systems in which such analysis has been impossible previously.

Based upon the proposed reaction scheme and assuming that steady states in $\cdot CH_2CH_2CH_2S\cdot$ and CH_2S are both achieved in times which are short compared with the length of photolysis (30 min), then one obtains

$$[9] \qquad \frac{R(C_2H_4)}{R(TBH)} = 1 + \frac{k_8 + k_7[THT]}{k_6[CP]}$$

$R(C_2H_4)$ and R(TBH) are the rates of C_2H_4 and TBH formation respectively, [THT] is the concentration of thietane, and k_7 is the rate constant for the removal of CH_2S in reaction 7. Because the thietane concentration was held constant, $k_8 + k_7[THT] = k'$, a constant. Therefore, a plot of $R(C_2H_4)/R(TBH)$ *vs.* $[CP]^{-1}$ should be a straight line with a slope of k'/k_6 and an intercept of 1.0. Such a graph is shown in Fig. 1. Data taken at CP pressures less than 0.5 Torr have not been used because at these low pressures a substantial fraction of the CP will be consumed during the photolysis.

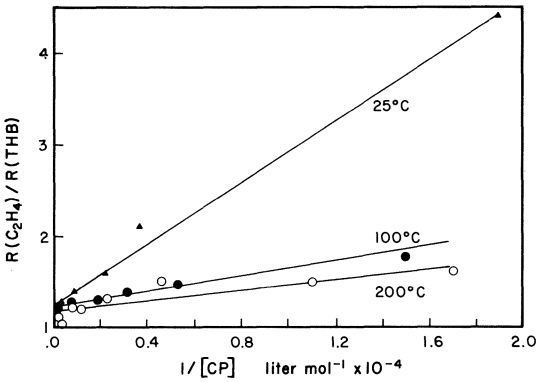

FIG. 1. Data of Table 1 fit to eq. 9.

With experimental error, straight line plots of unit intercept are obtained for temperatures of 25, 100, and 200 °C, in accord with the proposed mechanism. The half life of CH_2S in 30 Torr of pure thietane at 200 °C in this reaction system has been estimated previously (16) to be about 3 min, in agreement with other workers (25). Thus k' will have a value of about 5×10^{-3} s^{-1} and k_6 is about 2×10^2 l mol^{-1} s^{-1} at 200 °C.

This research was supported by grants from the National Research Council of Canada and from the Research Corporation for which the authors express their gratitude. One of us (D.R.D.) was the recipient of an N.R.C.C. studentship.

1. H. J. MIDDLETON, W. F. SHARKEY, and E. C. HOWARD. J. Am. Chem. Soc. **83**, 2589 (1961).
2. N. SUGIAMA, M. YOSHIOKA, H. AOYAMA, and T. NISHIO. J. Chem. Soc. Chem. Commun. 1063 (1971).
3. D. R. KEMP, A. H. LAWRENCE, C. C. LIAO, R. O. LOUTFY, P. DE MAYO, A. A. NICHOLSON, and S. PASZYC. XXIII International Conference of Pure and Applied Chemistry, Vol. 1. Boston. 1971. p. 367.
4. P. DE MAYO and A. A. NICHOLSON. Israel J. Chem. **10**, 341 (1972).
5. A. OHNO, Y. OHNISHI, and G. TSUCHIHASHI. J. Am. Chem. Soc. **91**, 5038 (1969).
6. P. DE MAYO and H. SHIZUKA. J. Am. Chem. Soc. **95**, 3942 (1973).
7. R. LAPOUYADE and P. DE MAYO. Can. J. Chem. **50**, 4068 (1972).
8. D. L. L. BLACKWELL and P. DE MAYO. J. Chem. Soc. Chem. Commun. 130 (1973).
9. KJ. ROSENGREN. Acta Chem. Scand. **16**, 2284 (1962).
10. J. FABIAN and R. MAYER. Spectrochim. Acta, **20**, 229 (1964).
11. A. H. LAWRENCE and P. DE MAYO. J. Am. Chem. Soc. **95**, 4084 (1973).
12. D. R. TYCHOLIZ and A. R. KNIGHT. J. Am. Chem. Soc. **95**, 1726 (1973).
13. A. JONES and F. P. LOSSING. J. Phys. Chem. **71**, 4111 (1967).
14. H. A. WEIBE and J. HEICKLEN. J. Am. Chem. Soc. **92**, 7031 (1970).
15. S. BRASLAVSKY and J. HEICKLEN. Can. J. Chem. **49**, 1316 (1971).
16. D. R. DICE and R. P. STEER. J. Phys. Chem. **77**, 434 (1973).
17. R. D. LIPSCOMB and W. H. SHARKEY. J. Polym. Sci. **8**, 2187 (1970).
18. E. E. REID. Organic chemistry of bivalent sulfur, Vol. 3. Chemical Publishing Co., New York. 1960. Chapt. 2.
19. C. R. JOHNSON, J. E. KEISER, and J. C. SHARP. J. Org. Chem. **34**, 861 (1969).
20. H. MACKLE. Tetrahedron. **19**, 1159 (1963).
21. J. D. COX. Tetrahedron, **19**, 1175 (1963)
22. N. C. BAIRD and J. R. SWENSON. J. Phys. Chem. **77**, 277 (1973).
23. D. R. ARNOLD. Adv. Photochem. **6**, 301 (1968).
24. T. NISHIO, M. YOSHIOKA, H. AOYAMA, and N. SUGIAMA. Bull. Chem. Soc. Jap. **46**, 2253 (1973).
25. D. R. JOHNSON, F. X. POWELL, and W. H. KIRCHHOFF. J. Mol. Spectrosc. **39**, 136 (1971).

Can. J. Chem. Downloaded from www.nrcresearchpress.com by 210.87.254.6 on 09/05/12
For personal use only.

Diffusion in Partially Ion Exchanged Molecular Sieves

D. M. RUTHVEN

Department of Chemical Engineering, University of New Brunswick, Fredericton, New Brunswick

Received May 9, 1974

D. M. RUTHVEN. Can. J. Chem. **52**, 3523 (1974).

Results of a simple idealized numerical simulation are presented showing the variation of sorbate diffusivity with degree of ion exchange in a system such as the Na–Ca A zeolites. Theoretical curves showing the expected variation of diffusivity, diffusional activation energy, and pre-exponential factor are given. The pattern of behavior predicted depends on the ratio of the diffusivities for the extreme ionic forms. When this ratio is small there is a gradual variation in diffusivity, activation energy, and pre-exponential factor over the entire range of ionic compositions but for large ratios there is an abrupt change at a particular ionic composition. Limited experimental data for the diffusion of *n*-butane in partially Ca^{2+} exchanged 4A sieve are presented and interpreted in terms of the theoretical model.

D. M. RUTHVEN. Can. J. Chem. **52**, 3523 (1974).

On présente les résultats d'une simulation numérique idéalisée simple montrant la variation de la diffusibilité des espèces adsorbées avec le degré d'échange ionique dans un système tel que les zéolithes-A Na–Ca. On donne les courbes théoriques montrant les variations attendues en se basant sur la diffusibilité l'énergie d'activation de la diffusion et les facteurs pré-exponentiels. Les schémas de comportements qui sont prédits dépendent des taux de diffusibilité pour les formes ioniques extrêmes. Quand ce rapport est petit il y a une variation continue dans la diffusibilité, l'énergie d'activation et le facteur pré-exponentiel sur tout l'intervalle des compositions ioniques mais aux rapports plus élevés il y a un changement subit à une composition ionique particulière. Des données expérimentales limitées pour la diffusion du *n*-butane sur des tamis moléculaires 4A partiellement échangés avec Ca^{2+} sont présentées et interprétées en termes du modèle théorique. [Traduit par le journal]

Can. J. Chem. Downloaded from www.nrcresearchpress.com by 210.87.254.105 on 09/05/12
For personal use only.

It is well established that the sorptive properties of many zeolites may be profoundly modified by ion exchange. For example, by exchanging the sodium cations of the 4A zeolite for calcium, the effective sieve diameter may be increased from about 4 to 5 Å, thus admitting the straight chain hydrocarbons which are effectively excluded from the 4A sieve. This change in sorptive properties was noted by Breck *et al.* (1) in their original paper and further examples have been given by Rees and Berry (2), Wolf and Pilchowski (3), and, more recently, by Takaishi *et al.* (4). Experimental data for such systems have usually been presented, in quasi-equilibrium terms, as graphs showing the variation of apparent saturation capacity with the degree of ion exchange. It is however clear that, in general, the sorption cut-off arises from a kinetic effect rather than from any real difference in equilibrium capacity. Given sufficient time linear hydrocarbons can penetrate the lattice of the 4A sieve but, at ordinary temperatures, the time required is inordinately long.

A theoretical treatment of the adsorption cut-off phenomenon has been given by Hammersley (5) in his discussion of the percolation problem. Assuming a random distribution of blocked and unblocked pores in a cubic lattice Hammersley calculated how the fraction of crystal accessible to the sorbate would vary with the fraction of blocked pores. This approach, however, gives no information concerning the kinetics of sorption in a partially ion exchanged sieve which is the subject of the present paper.

Theoretical Considerations

We consider a cubic pore structure such as exists in the type A zeolites and assume that there are two types of window, randomly distributed through the lattice. In the case of the type A zeolite the two types of window would correspond to *open* windows characteristic of the 5A sieve and *closed* windows, containing, for example, a sodium ion as in the 4A sieve. The fraction of open windows is denoted by x and the diffusivities of the sorbate in crystals containing all *open* and all *closed* windows are denoted respectively by D_A and D_B with the ratio $r \equiv D_A/D_B$. Considering the diffusion

process as a random walk with a step size equal to the lattice parameter one may calculate by numerical simulation, for any specified values of r and x, the relative value of the diffusivity, expressed as the ratio D/D_A (or D/D_B).

The numerical simulation, which was carried out using the I.B.M. 370 computer at the University of New Brunswick, was based on a standard random number generating subroutine. The zeolite lattice was first constructed and each window was then designated as either open or closed according to an assigned probability (x). A trial molecule was placed in the (0,0,0) cavity and a random number between 1 and 6 was called in order to decide the direction of the first attempted jump. If the window encountered by the molecule moving in this direction was *open* the jump was considered successful and the coordinates of the molecule were adjusted to move the molecule into the neighboring cavity. If the molecule encountered a *closed* window another random number was called in order to decide whether or not the jump was successful, the probability of successfully completing the jump through a *closed* window being $1/r$. This procedure was repeated N times and the mean square displacement of the molecule λ^2 was calculated. With unit probability of success assigned to a jump through an open window and the displacement measured in lattice units, it follows, from the theory of random walks, that

$$[1] \qquad D/D_A = \lambda^2/N$$

The calculation was repeated for a sufficiently large number of steps so that the value of λ^2/N became independent of N. In general this required $N > 2000r$.

The results of these calculations are shown in Figs. 1 and 2. Figure 1, in which the ratio D/D_A is plotted against x with r as a parameter, shows the way in which diffusion through an *open* sieve is restricted by the introduction of some *closed* windows. For sufficiently large values of r the curves become asymptotic to the line

$$[2] \qquad D/D_A = 1.5x - 0.5 \; (x > 1/3)$$

which defines the limiting behavior for the case in which the *closed* windows are completely closed ($D_B = 0$, $r = \infty$). The way in which a *closed* sieve is opened up by the introduction of some *open* windows is illustrated in Fig. 2. For large values of r the curves again approach a

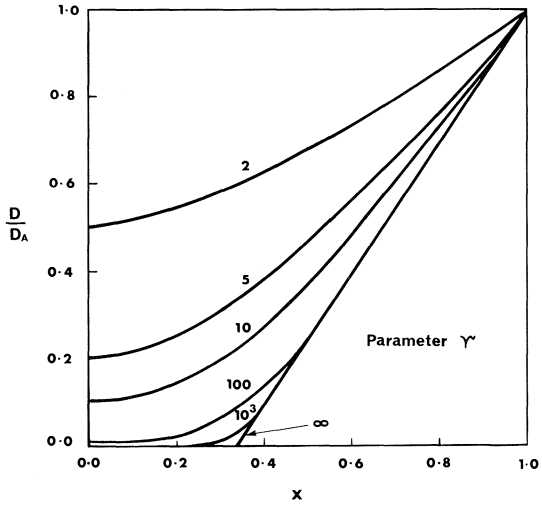

FIG. 1. Variation of diffusivity with fraction of *open* windows.

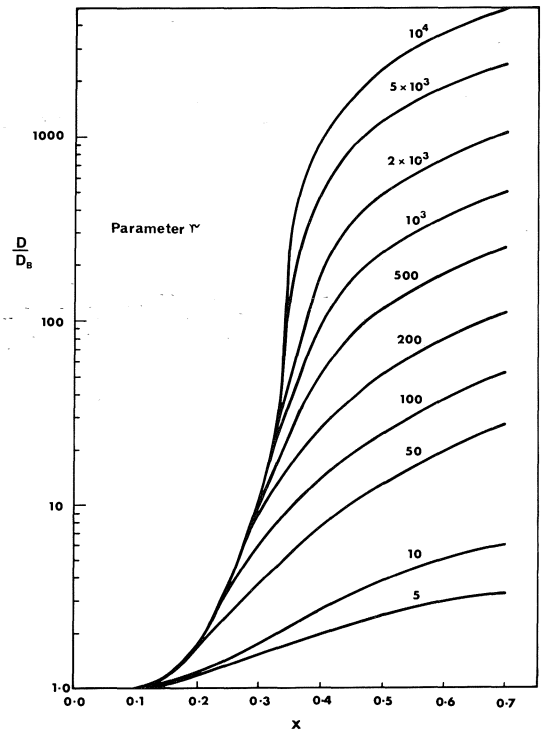

FIG. 2. Variation of diffusivity with fraction of *open* windows.

single curve but the form of this curve cannot easily be deduced by straightforward consideration of the limiting case ($D_B = 0$). The opening of the sieve corresponds physically to an increase in the mean diffusion path as a result of the

Can. J. Chem. Downloaded from www.nrcresearchpress.com by 210.87.254.105 on 09/05/12
For personal use only.

Can. J. Chem. Downloaded from www.nrcresearchpress.com by 210.87.254.105 on 09/05/12
For personal use only.

removal of some of the barriers to diffusion. The effect becomes significant when about 15% of the windows are open. For high values of r the transition to the behavior defined by eq. 2 is very sharp and occurs at $x = 1/3$. For lower values of r the transition commences at lower values of x and is more gradual.

If it is assumed that the temperature dependence of the diffusivities can be represented by the Eyring equations:

$$[3] \qquad D_A = D_{*A}e^{-E_A/RT} \qquad D_B = D_{*B}e^{-E_B/RT} \qquad D = D_*e^{-E/RT}$$

the variation of the apparent diffusional activation energy E with r and x may be calculated, since

$$[4] \qquad \frac{\partial \log (D/D_B)}{\partial \log r} = \frac{E_B - E}{E_B - E_A} \qquad (E_B > E > E_A)$$

The results of this calculation are shown in Fig. 3 in which $(E_B - E)/(E_B - E_A)$ is plotted against x with r as a parameter. The corresponding variation in the pre-exponential factor, calculated for the case in which $D_{*A} = D_{*B}$, is shown in Fig. 4. For relatively small values of r the activation energy changes gradually from E_A to E_B over a wide range of x while the pre-exponential factor shows only a relatively small variation. By contrast, for large values of r, there is a step change in both activation energy and pre-exponential factor at $x = \frac{1}{3}$. For $x < \frac{1}{3}$ the activation energy is essentially the same as for a closed sieve (E_B) and the increase in diffusivity with increasing x arises from the increased distance travelled between successive high energy barriers, leading to a rapidly increasing pre-exponential factor. For $x > \frac{1}{3}$ transport occurs almost entirely through the open windows so that the activation energy is essentially the same as for an *open* sieve (E_A) while the pre-exponential factor decreases linearly with the fraction of blocked windows.

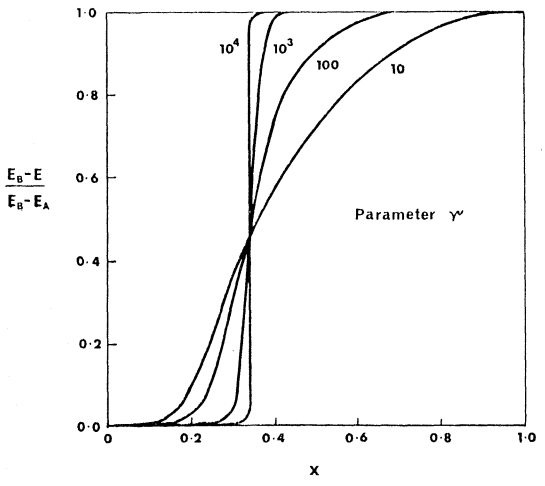

FIG. 3. Variation of diffusional activation energy with fraction of *open* windows.

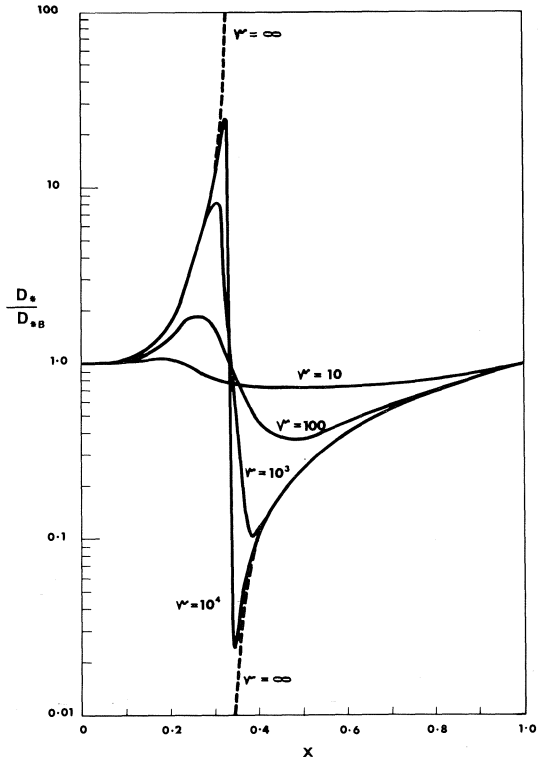

FIG. 4. Variation of pre-exponential factor with fraction of *open* windows.

Experimental

A limited experimental study of the diffusion of *n*-butane in partially ion exchanged 4A zeolite was undertaken using the gravimetric apparatus of Clarke (6) and a similar apparatus at the University of New Brunswick. The theory presented above is strictly applicable only to differential diffusivity data since the effect of a concentration dependent diffusivity is not considered. Zeolitic diffusivities are in general strongly concentration dependent but at low sorbate concentrations a limiting value is approached asymptotically. For systems in which the diffusivity increases with sorbate concentration, as is the case for the diffusion of *n*-butane in type A zeolites, the rate of desorption is much less sensitive than the rate of adsorption to the range of concentration over which the

Can. J. Chem. Downloaded from www.nrcresearchpress.com by 210.87.254.105 on 09/05/12
For personal use only.

sorption curve is measured (9, 10). For such a system the integral diffusivity, calculated from a transient desorption curve measured at a low concentration, provides a good approximation to the limiting differential diffusivity and the validity of this approximation is assumed in the present study.

The zeolite sample was first equilibrated, at the desired temperature, with *n*-butane at a pressure of 10 Torr, this being the saturation vapor pressure at −78 °C. The equilibrated sample was then desorbed to a liquid nitrogen trap and the course of the desorption was followed gravimetrically. The rate of the process was sufficiently slow so that the diffusivity could be calculated from the initial slope of the desorption curve, plotted against the square root of time (7):

$$[5] \qquad \frac{m_t}{m_\infty} = \frac{2A}{V}\sqrt{\frac{Dt}{\pi}}$$

(valid for $m_t/m_\infty < \sim 0.3$)

Here m_t/m_∞ is the ratio of the quantity of sorbate desorbed during time t to the total quantity desorbed as $t \to \infty$ and A/V is the ratio of surface area to volume for the zeolite sample. Diffusivities were also calculated from the long time solution of the diffusion equation, duly corrected for crystal shape and size distribution (8). The values so obtained agreed well with the value from the initial rates. One of the desorption measurements was carried out in two stages with the sample being isolated and allowed to equilibrate after approximately half the sorbate had desorbed. The diffusivities calculated from both steps were essentially the same thus confirming the validity of the approximation to the limiting differential diffusivity.

In some cases the adsorption curves were also followed. In general the integral diffusivities for adsorption, calculated from eq. 5, were higher than the corresponding values obtained from the desorption curves, as is to be expected for a system in which the diffusivity increases with concentration (9). At the highest temperature (175 °C) the equilibrium isotherm is practically linear over the range 0–10 Torr so that, within this range, the diffusivity is essentially constant. At this temperature the difference between the adsorption and desorption rates was found to be very small.

Results and Discussion

Diffusivities were measured at several temperatures within the range 0–175 °C for four samples of type A sieve containing 30.5–35.5% prepared by Clarke (6) and one sample containing 52.1% equivalents Ca^{2+} (expressed as % of original Na^+ ions which have been replaced by Ca^{2+}). The values of A/V which were determined by photomicrography are noted in Table 1. The diffusivities are plotted against reciprocal temperature in Fig. 5 and the diffusional activation energies and pre-exponential factors (eq. 3) are summarized in Table 1, which includes also the values of D_* and E for diffusion of *n*-butane

TABLE 1. Activation energies and pre-exponential factors in the expression $D = D_* e^{-E/RT}$

%Ca^{2+}	E (kcal/mol)	$D_* \times 10^7$ (cm^2/s)
4A[a]	9.45	0.073
4A[b]	8.5	0.042
30.55	9.7	0.481
32.54	9.6	1.30
34.10	9.2	2.57
35.48	9.4	12.1
52.1	3.64	0.015
5A[c]	4.0	0.073

[a]Value estimated from experimental data for 30.5–35.4% Ca^{2+} sieves ($A/V = 2.7 \times 10^4$ cm^{-1}).
[b]Values from high temperature data of Walker *et al.* (15) ($A/V = 1.5 \times 10^4$ cm^{-1}).
[c]Values from Ruthven *et al.* (11) ($A/V = 1.7 \times 10^4$ cm^{-1}).

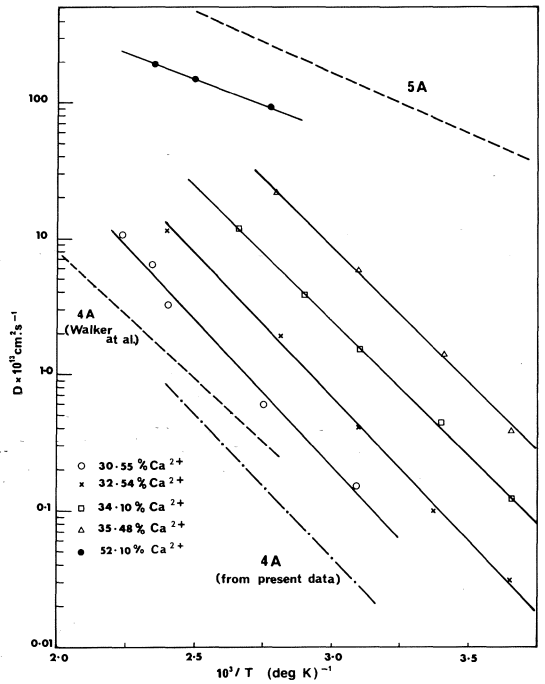

FIG. 5. Temperature dependence of diffusivity for butane in various ion exchanged type A zeolites.

in the *open* 5A sieve (11) and the *closed* 4A sieve (15). Figure 6 shows the diffusivity at 91 °C plotted against % Ca^{2+}.

In each cavity of the type A zeolite there are 8 type I sites, located near the centers of the 6-membered oxygen rings, and six type II sites within the 8-membered oxygen windows, each shared between two cavities (13, 14). The type I and type II sites can accommodate 11 cations per cavity. The twelfth cation which is present in the pure sodium form of the zeolite (4A) is

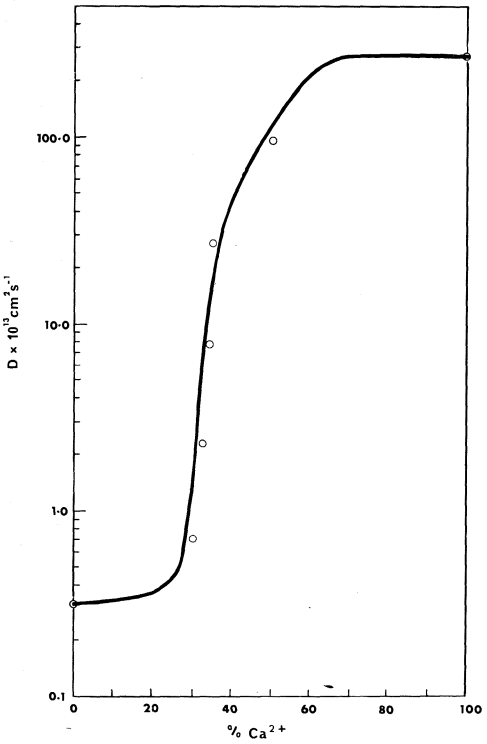

FIG. 6. Variation of diffusivity at 91 °C with $\%Ca^{2+}$ exchange (theoretical line, experimental points).

located near one of the four membered oxygen rings (14) but this site is less favorable energetically than the sites of types I and II and is probably not occupied to any significant extent in sieves containing less than 11 cations per cavity. The type I sites are energetically more favorable than the type II sites and are preferentially occupied, leading to opening of the windows with increasing Ca^{2+} exchange. The precise distribution of the cations between these sites will be governed by a complex equilibrium but, for any given composition (Na^+/Ca^{2+}), the maximum possible value of x may be estimated by assuming that all type I sites are occupied before any of the type II sites. The theoretical curve shown in Fig. 6 was calculated on the basis of this assumption with $r = 860$, this being the ratio of diffusivities for *open* and *closed* sieves at 91 °C as estimated from the available diffusivity data for 5A and 4A sieves (11, 15). This curve gives a good representation of the observed variation of diffusivity with Ca^{2+} exchange.

The experimental activation energies are broadly consistent with the theory which predicts an abrupt change from the value for a 4A sieve to the value for a 5A sieve at a Ca^{2+} composition ($\geq 33.3\%$) such that slightly less than two-thirds of the type II sites are occupied by cations. The activation energies for the 30.5–35.5% Ca^{2+} sieves are essentially constant although somewhat larger than the value given by Walker *et al.* for the 4A sieve (15). The data of Walker *et al.* were however obtained at much higher temperatures (350–450 °C) and over a wide temperature range some variation in activation energy may be expected. The activation energy for the 52.1% Ca^{2+} sieve is similar to that for the 5A sieve (11).

For the diffusion of methane (12) it has been shown that the difference in diffusivity between the 4A and 5A sieves arises mainly from the difference in activation energy and that the pre-exponential factors for the 4A and 5A sieves are essentially the same. If it is assumed that this is true also for the diffusion of *n*-butane one may use the value of D_* for the 5A sieve in conjunction with the mean experimental activation energy for the 30.5–35.5% Ca^{2+} sieves to estimate the diffusivity of butane in the 4A sieve within the present temperature range. The values estimated in this way lie somewhat below the extrapolation of the data of Walker *et al.* as may be seen from Fig. 5.

Using a value of r based on the experimental diffusivity for the 5A sieve and the derived diffusivity for the 4A sieve, values of x' for the partially exchanged sieves may be obtained by matching experimental and theoretical diffusivities. These values are compared in Table 2 with the values (x'') calculated from the Na^+/Ca^{2+} analysis on the assumption that all type I sites are occupied before any of the type II sites. The values of x' are all similar to but slightly

TABLE 2. Fraction of open windows in partially Ca^{2+} exchanged type A sieve[a]

$\%Ca^{2+}$	n	x'	x''	f
30.55	10.17	0.27	0.28	0.996
32.54	10.11	0.31	0.32	0.996
34.10	9.95	0.32	0.35	0.985
35.48	9.87	0.33	0.37	0.983
52.1	8.87	0.57	0.71	0.895

[a] n = total number of cations per cavity, calculated from Ca^{2+} content; x' = fraction of open windows calculated from diffusivity data; x'' = fraction of open windows calculated from n assuming all type I sites occupied; f = fraction of type I sites occupied, as calculated from x' and n.

Can. J. Chem. Downloaded from www.nrcresearchpress.com by 210.87.254.105 on 09/05/12
For personal use only.

smaller than the corresponding values of x''. This is consistent with an equilibrium between the two types of sites such that a small fraction of the type I sites may remain vacant while some of the type II sites are occupied. From general considerations such an equilibrium seems qualitatively reasonable but, in view of the uncertainties inherent in the Ca^{2+}/Na^{+} determination (6), further analysis is probably not justified.

It is of interest to note that the sharp decline in diffusivity which is predicted when the Ca^{2+} content of the sieve falls below about 30% (Fig. 6) corresponds closely with the cut off observed by Breck *et al.* (1) for the sorption of nitrogen, propane, and *n*-heptane in Na–Ca A zeolite. The limiting case in which a sorbate molecule has zero probability of passing through a blocked window is covered by Hammersley's analysis (2, 5) which, applied to the Na–Ca A zeolite, predicts that the capacity for such a sorbate should fall to a negligibly low value at $x = 0.23$ (approximately 28% Ca^{2+}). The present analysis shows that, even when the rate of diffusion in the *closed* sieve is finite, the decline in diffusivity in this region of ionic composition may be so sharp as to lead to an effective sorption cut-off. For such a system (*e.g.* propane or butane in Na–Ca A) the precise form of the quasi equilibrium capacity curve would depend on the duration of the experiment.

Conclusion

The theory presented above provides a method by which the kinetics of sorption in a partially ion exchanged sieve may be predicted if the diffusivities for the two extreme ionic forms of the sieve are known. The assumptions involved in the theory are simple and physically realistic and the generalized curves presented in Figs. 1–4 should therefore provide a useful basis for the analysis of experimental diffusivity data for such systems. The theory appears to provide a satisfactory interpretation of the limited experimental data available for the diffusion of *n*-butane in partially calcium exchanged A-type zeolites but a full verification of the theory would require a more extensive experimental study with a variety of sorbates and covering a wider range of zeolite compositions.

The apparatus of Clarke was made available to the author through the kind cooperation of Professor R. M. Barrer, Imperial College, London. The author is also grateful to Professor Barrer for a number of helpful comments made during the preparation of the manuscript. The assistance of Dr. D. R. Garg with the numerical simulation and of Dr. R. I. Derrah. who made the experimental measurements for the 52.1% Ca^{2+} sieve, is also gratefully acknowledged.

1. D. W. Breck, W. G. Eversole, R. M. Milton, and T. B. Reed. J. Am. Chem. Soc. **78**, 5963 (1956).
2. L. V. C. Rees and T. Berry. Molecular sieves. Society of Chemical Industry, London. 1968. p. 149.
3. F. Wolf and K. Pilchowski. Chem. Techn. **23**, 672 (1971).
4. T. Takaishi, A. Yusa, and Y. Yatsurugi, 3rd Int. Conf. Mol. Sieves, Zurich, Sept. 3–7, 1973. report no. 134.
5. J. M. Hammersley. Methods in computational physics. Vol. 1. Academic Press, New York, 1963. p. 281.
6. D. J. Clarke. Ph.D. Thesis. Imperial College, London, England. 1972.
7. R. M. Barrer and D. W. Brook. Trans. Faraday Soc. **49**, 1049 (1954).
8. D. M. Ruthven and K. F. Loughlin. Chem. Eng. Sci. **26**, 577 (1971).
9. J. Crank. Mathematics of diffusion. Oxford University Press, 1956. p. 280.
10. D. R. Garg and D. M. Ruthven. Chem. Eng. Sci. **27**, 417 (1972).
11. D. M. Ruthven, K. F. Loughlin, and R. I. Derrah. Adv. Chem. **121**, 330 (1973).
12. D. M. Ruthven and R. I. Derrah. Faraday Trans I, **68**, 2332 (1972).
13. L. Broussand and D. P. Shoemaker. J. Am. Chem. Soc. **82**, 1041 (1960).
14. R. Y. Yanagida, A. A. Amaro, and K. Seff. J. Phys. Chem. **77**, 805 (1973).
15. P. L. Walker, L. G. Austin, and S. P. Nandi. Chem. Phys. Carbon, **2**, 257 (1966).

Can. J. Chem. Downloaded from www.nrcresearchpress.com by 210.87.254.105 on 09/05/12
For personal use only.

The Effects of α-Halogen Substitution on the Configuration of Alkyl Radicals in Solution by Electron Spin Resonance

KUANG S. CHEN AND JAY K. KOCHI[1]

Departments of Chemistry, University of Western Ontario, London, Ontario, and Indiana University, Bloomington, Indiana 47401

Received February 26, 1974

KUANG S. CHEN and JAY K. KOCHI. Can. J. Chem. **52**, 3529 (1974).

The e.s.r. spectra of a variety of alkyl radicals with α-halogen substituents have been examined in solution. The configurations of α-halogen substituted ethyl and β,β,β-trifluoroethyl radicals are correlated with the hyperfine splittings of α-methyl protons and α-trifluoromethyl fluorines, respectively. For an α-fluorine substituent, electronegativity plays an important role in determining the pyramidal configuration of the radical center, whereas size appears to be a more important factor with chlorine and bromine in promoting a less pyramidal configuration at the radical center. Two α-halogen substituents have a disproportionately greater effect than one halogen in influencing the configuration at the radical site. The *g*-factors of fluoroalkyl radicals are qualitatively analyzed in order to discuss possible mechanisms of β-fluorine hyperfine interactions and the effect of trifluoromethyl substitution on the configuration of the radical site.

KUANG S. CHEN et JAY K. KOCHI. Can. J. Chem. **52**, 3529 (1974).

On a examiné les spectres r.p.e. d'un certain nombre de radicaux alkyles possédant des substituants halogènes en position α. Les configurations des radicaux éthyles substitués en α par des hydrogènes et les radicaux β,β,β-trifluoroéthyles sont reliées respectivement avec les couplages hyperfins des groupes α-méthyles et α-trifluorométhyles. Dans le cas d'un substituant fluor en α, l'électronégativité joue un rôle important sur la configuration pyramidale du centre radicalaire; toutefois dans le cas du chlore et du brome, il apparait que la grosseur est un facteur plus important pour promouvoir un centre radicalaire ayant une configuration moins pyramidale. Deux substituants halogènes en position α ont un effet proportionnellement beaucoup plus grand qu'un halogène en vue d'influencer la configuration du site radicalaire. Les facteurs *g* des radicaux fluoroalkyles sont analysés qualitativement en vue de pouvoir discuter des mécanismes possibles d'interactions hyperfines des hydrogènes en β et l'effet de la substitution d'un groupe trifluorométhyle sur la configuration du site radicalaire.

[Traduit par le journal]

Introduction

The conformations of free radicals can be directly affected by steric interactions imposed by α-substituents (1). A notable example is provided by the change in the stable conformation **1** of the *n*-propyl radical to **2** in the *t*-amyl analog by replacement of the two α-protons with methyl groups (1*d*).

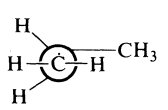

1

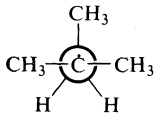

2

For the *n*-propyl radical, e.s.r. studies in the solid state at 4 °K are in accord with deductions of its conformation in solution at higher temperatures (1). Conformations of alkyl radicals in solution are based on the magnitude and the temperature dependence of the β-proton hyperfine splittings together with the selective variations in the spectral linewidths (1*b–f*).

Substitution in the α-position of alkyl radicals may also exert a conformational change in free radicals by altering the configuration at the radical site. For example, the decrease in the extent of bridging in α,α-difluoro-β-chloroethyl radical **3** compared to the conformationally frozen β-chloroethyl radical **4** has been ascribed

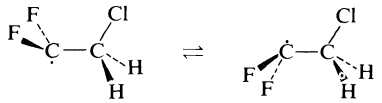

3

to an increasingly pyramidal configuration at the radical center (1*i*, 2).

The measurement of ^{13}C splittings represents

[1]To whom all correspondence should be addressed.

Can. J. Chem. Downloaded from www.nrcresearchpress.com by 210.87.254.42 on 09/05/12
For personal use only.

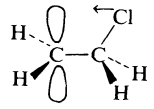

4

the best approach for determining the configuration at the α-carbon in simple alkyl radicals by e.s.r. Thus, Fessenden and Schuler have quantitatively estimated the degree of bending in the series of fluorinated methyl radicals CH_nF_{3-n} from ^{13}C hyperfine splittings (3). Due to problems associated with routine determination of ^{13}C splittings, however, it is desirable to utilize additional probes such as the more readily measurable α-proton, fluorine, chlorine, methyl proton, and trifluoromethyl fluorine h.f.s. to determine the configuration of radical sites in alkyl radicals (4, 5). In this paper we wish to discuss several methods for deducing the configurations of halogenated alkyl radicals from the isotropic e.s.r. parameters.

Results and Discussion

Proton Hyperfine Splittings of α-Methyl Groups

On the basis of the α-hydrogen and α-methyl proton hyperfine coupling constants, a_H^{α} and a_{CH_3}, of a series of alkyl radicals: methyl, ethyl, *i*-propyl, and *t*-butyl, Fessenden and Schuler concluded that a_{CH_3} can be correlated by the expression (1*a*)

$$[1] \qquad a_{CH_3} = Q_H^{CH_3}\rho_\alpha$$

$Q_H^{CH_3}$ is a constant with a value of 29.30 G and ρ_α, the spin density at the α-carbon is given by eq. 2,

$$[2] \qquad \rho_\alpha = (1 - 0.081)^n$$

where n is the number of α-methyl groups. Equation 2 implies that each α-methyl group withdraws about 8% of the spin density from the carbon center. A relationship given in eq. 3 which is applicable more generally to alkyl radicals with nonpolar or monopolar substituents has been developed by Fischer employing this concept (6).

$$[3] \qquad \rho_\alpha = \prod_{i=1}^{3} [1 - \Delta(X_i)]$$

$\Delta(X_i)$ is a parameter which measures the spin-withdrawing influence of an α-substituent denoted as X_i. A series of $\Delta(X_i)$ values has been derived for various substituents by an iterative procedure from experimentally measured values of a_{CH_3}, although no values have been recorded heretofore for any halogen substituent.

The hyperfine splitting constants and *g*-factors for a series of α-haloalkyl radicals are listed in Table 1. The values of a_{CH_3} are independent of temperature between −40 and −130 °C, and they have been used to determine $\Delta(X_i)$ for fluorine, chlorine, and bromine substituents.

The unusually small value of the proton h.f.s. in $CH_3CF_2^{\cdot}$ (a_H = 13.99 G) is striking for an α-methyl group in comparison with those in other alkyl radicals (23–26 G). Two factors may be considered for this unusual observation: (*a*) the bond polarization by an α-fluorine substituent, and (*b*) the configuration of the methyl group relative to the half-filled orbital at C_α. It is unlikely that bond polarization plays an important role since a single α-fluorine is insufficient to cause a proportional reduction on a_{CH_3}, and the value of the methyl splitting in CH_3CHF (24.48 G), is similar to that in the ethyl radical (26.99 G). We suggest that the pyramidal geometry at the α-carbon is the most important factor in causing the unusually small h.f.s. of the α-methyl proton in $CH_3CF_2^{\cdot}$. The INDO–MO method[2] was used to determine the stable configuration at C_α and the conformation of both CH_3CHF and CH_3CF_2 by optimizing the calculated proton and fluorine h.f.s. to the experimental values. Interestingly, the geometry resulting from the optimization listed in Table 2 is close to the minimized total energy. Furthermore, the geometries of best fit at C_α for CH_3CHF and CH_3CF_2 are almost the same as those obtained experimentally and theoretically for H_2CF and HCF_2, respectively (3, 7). This result implies that the configuration of the radical center is affected very little on replacement of a hydrogen by a methyl group.

INDO results of CH_3CF_2 in Table 2 also indicate that bond polarization does not contribute significantly to the small α-methyl proton h.f.s. since the methyl splitting increases substantially from 14.35 to 25.64 G simply by constraining the radical site in CH_3CF_2 to a planar configuration. Furthermore, nonplanarity is also

[2]An INDO program obtained from QCPE, Indiana University, has been converted for the CDC 6600. In spite of the approximations involved, the semiempirical INDO method has been shown to predict the geometry of fluorinated methyl radicals fairly reliably in comparison with those involving *ab initio* calculations (7).

Can. J. Chem. Downloaded from www.nrcresearchpress.com by 210.67.234.42 on 09/09/12
For personal use only.

TABLE 1. Electron spin resonance parameters of α-halogen substituted ethyl radicals

Radical	T (°C)	$\langle g \rangle$	Hyperfine splitting (G) a_X^α	a_H^α	a_H^β	ρ_α*	ϕ† (deg)	Mode of generation‡
CH_3CH_2	−113	2.00260	—	22.37	26.99	0.919	0	P, S
CH_3CHF	−106	2.00366	59.21	17.31	24.48	0.836	10	P
CH_3CF_2	−78	2.00361	94.01	—	13.99	0.478	25	H, S
CH_3CCl_2	−108	2.00727	4.34	—	19.70	0.672	12	S
CH_3CHBr	−77	2.00751	<0.2	20.47	24.71	0.843	0	P
$(CH_3)_2CH$	−113	2.00267	—	22.12	24.75	0.845	0	P, S
$(CH_3)_2CF$	−48	2.00360	60.85	—	21.11	0.721	14	H
$(CH_3)_2CCl$§	—	—	2.3	—	22.3	0.761	0	
$(CH_3)_2CCH_3$	−113	2.00270	—	—	22.93	0.776	0	P, S

*From eq. 1.
†From eq. 7 and $\Delta(H) = 0.0$, $\Delta(CH_3) = 0.081$, $\Delta(F) = 0.024$, $\Delta(Cl) = 0.099$.
‡P = *t*-butyl perester, S = halogen abstraction by R_3S_i, H = hydrogen abstraction by *t*-BuO or CF_3O.
§Reference 4*b*.

TABLE 2. Conformational dependence of electron spin resonance parameters in α-fluorinated ethyl radicals by INDO–MO

Structural and e.s.r. parameters*	CH_3CH_2	CH_3CHF		CH_3CF_2	
	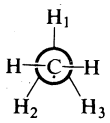	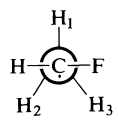	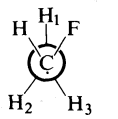	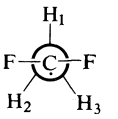	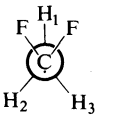
$\angle C_\beta C_\alpha H_\alpha$	120	120	121	—	—
$\angle C_\beta C_\alpha F_\alpha$	—	120	119	120	115
$\angle H_\alpha C_\alpha H_\alpha$	120	—	—	—	—
$\angle H_\alpha C_\alpha F_\alpha$	—	120	119	—	—
$\angle F_\alpha C_\alpha F_\alpha$	—	—	—	120	106
$r(C_\alpha—C_\beta)$	1.40	1.52	1.52	1.50	1.51
a_{H_1}	53.41	51.02	52.28	49.90	37.21
a_{H_2}	14.69	13.70	11.10	13.51	2.92
a_{H_3}	14.69	14.11	13.64	13.51	2.92
$\frac{1}{3}(a_{H_1} + a_{H_2} + a_{H_3})$	27.60	26.28	25.67	25.64	14.35
$\frac{1}{2}(a_{H_2} + a_{H_3})/a_{H_1}$	0.27	0.27	0.24	0.27	0.078
a_H^α	−20.36	−20.76	−18.58	—	—
a_F^α	—	58.55	61.95	49.89	93.69
$a_{^{13}C}^\alpha$	39.9	38.12	44.56	36.86	142.50
$a_{^{13}C}^\beta$	−12.4	−11.88	−11.22	−11.80	0.89
Total energy (a.u.)	—	−43.0290	−43.0303	−68.7258	−68.7374

*$r(C_\alpha—H_\alpha) = 1.08$ Å, $r(C_\beta—H_\beta) = 1.08$ Å, $r(C_\alpha—F_\alpha) = 1.35$ Å, C_β = tetrahedral; angles in degrees, bond lengths in Å, and h.f.s. in G.

reflected in the rather high barrier to rotation about the $C_\alpha—C_\beta$ bond in CH_3CF_2 (2.2 kcal mol^{-1}), in contrast to the essentially free rotation of the methyl groups in the alkyl analogs, such as ethyl, isopropyl, and *t*-butyl radicals (1*a–e*, 5).

Since eqs. 1 and 3 have not been tested for any α-halogen substituted ethyl radicals, we have calculated values of $\Delta(F)$ for α-fluoroethyl radicals from the observed values of a_{CH_3}, and found them to vary from 0.091 to 0.279 for $CH_3\dot{C}HF$ and $CH_3\dot{C}F_2$, respectively. The variation is not unexpected because the value of a_{CH_3}, which results largely from a hyperconjugative interaction in radicals of the π-type (8), will be proportional to the spin density at the α-carbon, ρ_α, only if the half-filled orbital has the same amount of p-character. Two factors may be considered for this variation: (*a*) the effect of bond polarization by an α-fluorine substituent on the value of $Q_H^{CH_3}$ and (*b*) the change in p-character induced by an increase in the pyramidal configuration at the radical site by successive replacement of hydrogen by fluorine.

A unique value of $\Delta(F) = 0.024$, on the other hand, was obtained from INDO calculated

Can. J. Chem. Downloaded from www.nrcresearchpress.com by 210.87.254.42 on 09/05/12
For personal use only.

values of a_{CH_3} for both $CH_3\dot{C}HF$ and $CH_3\dot{C}F_2$ in hypothetical planar configurations by using eqs. 1 and 3, and a value of $Q_H^{CH_3} = 29.30$ G. The same values of $Q_H^{CH_3} = 29.30$ G obtained for $CH_3\dot{C}H_2$, $CH_3\dot{C}HF$, and $CH_3\dot{C}F_2$, when they are all constrained to the same planar configurations, suggests that the hyperfine splitting produced by a (full) electron in a pure p-orbital on freely rotating methyl protons is the same for an α-fluorinated ethyl as well as for an ethyl radical. The latter may not be unexpected, since the extent of mixing between the p-orbital and a CH_3 group orbital of the correct symmetry will depend upon the energy difference between the two. Indeed, the energy of a p-orbital at a planar carbon center to which one fluorine is attached (*i.e.*, the half-filled molecular orbital energy = −0.3890 a.u. from an INDO calculation) is about the same as that (−0.3811 a.u.) for a p-orbital on carbon to which two fluorines are bonded. Thus, the assumption that there is a constant energy separation between the half-filled p-orbital and the methyl group orbital may be a reasonable one for planar α-fluoroalkyl radicals, as it has been suggested by Fessenden and Schuler (1*a*) for alkyl radicals. Furthermore, the unusually small value of $\Delta(F)$ is consistent with the high electronegativity of the fluorine atom, which presumably makes a smaller contribution in the canonical structure **6** to the total wave function for the radical with X = F compared to CH_3.

5 6

The excellent agreement between the experimental results and the INDO calculations suggests that the reduction in the value of the methyl splitting in CH_3CF_2 is mainly due to the change in the configuration of the methyl group relative to the half-filled orbital at the pyramidal radical center. It also suggests that a quantitative correlation between the observed value of a_{CH_3} and the configuration at the radical site may be more generally applicable to other radicals.

If θ describes the dihedral angle between the β-CH bond and the p-orbital at the carbon radical center, the hyperfine splitting constant for the β-proton is given by eq. 4 (9), where A and B are constants.

$$[4] \qquad a_H^{\beta} = A + B\cos^2\theta$$

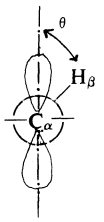

For planar radicals, the β-proton h.f.s. arises largely from a hyperconjugative interaction (*i.e.*, A is negligible in comparison with B in eq. 4),

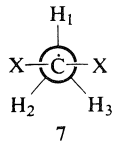

7

where X = H, CH_3, Cl, F, Br and the ratio R of the hyperfine splitting constants for $H_{2,3}$ and H_1 in **7** will be a constant and independent of the α-substituents. According to eq. 5, a constant value of $R = 0.25$ is expected if $A \ll B$. Indeed, the

$$[5] \qquad R = \frac{\frac{1}{2}(a_{H_2} + a_{H_3})}{a_{H_1}} = \frac{A + B\cos^2 120^\circ}{A + B\cos^2 0^\circ} = \frac{A + \frac{1}{4}B}{A + B}$$

calculated ratio of 0.27 for $\frac{1}{2}(a_{H_2} + a_{H_3})/a_{H_1}$ in Table 2 is the same for the ethyl radical as well as for α-fluoro and α,α-difluoroethyl radicals in a hypothetical planar configuration. On the other hand, the ratio of the calculated hyperfine splitting constants for $H_{2,3}$ and H_1 as well as the methyl proton h.f.s., a_{CH_3}, are strongly dependent on the degree of bending at the radical center as shown in Table 3 and Fig. 1. By analogy, we assume that related radicals have values for R which are also mainly determined by the degree of bending at the radical site.

For bent radicals, Fessenden and Schuler quantitatively estimated the degree of bending at radical site for fluoromethyl radicals from the observed α ^{13}C splitting using eq. 6,

$$[6] \qquad a_C(\phi) = a_C(0) + 1190(2\tan^2\phi)$$

where φ is the angle between a C—F bond and a plane normal to the three-fold symmetry axis, and $a_C(0)$ is the ^{13}C splitting of a planar methyl radical and equal to 30 G (3). The term $2\tan^2\phi$

Can. J. Chem. Downloaded from www.nrcresearchpress.com by 210.87.254.42 on 09/05/12
For personal use only.

TABLE 3. Conformational dependence of the β-proton hyperfine splitting for α,α-difluoroethyl radical by INDO–MO*

∠FCαF (deg)	∠CβCαF (deg)	Hyperfine splitting (G) a_{CH_3}	a_{H_1}	$a_{H_{2,3}}$	R
106	115	14.35	37.21	2.92	0.078
109	116	15.81	39.70	3.87	0.097
112	117	17.34	42.21	4.91	0.116
116	118	19.76	45.87	6.71	0.146
120	120	25.64	49.90	13.51	0.271

*r(Cβ—Hβ) = 1.08 Å, r(Cα—Fα) = 1.35 Å, r(Cα—Cβ) = 1.51 Å, Cβ is tetrahedral.

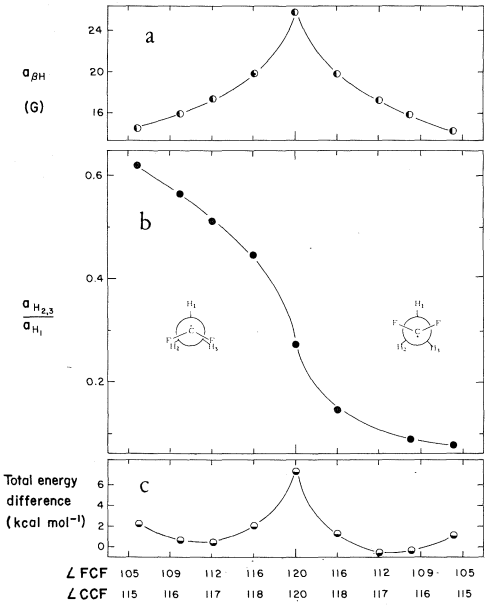

FIG. 1. Electron spin resonance parameters of CH_3CF_2 as a function of the configuration at the radical as determined by INDO-MO: (*a*) β-proton h.f.s., (*b*) ratio of β-proton splittings, (*c*) difference in the total energy relative to the optimized structure with ∠FCF = 106° and ∠CCF = 115°.

corresponds to the s-character of the orbital containing the unpaired electron, suggesting that the spin density at the α-carbon atom is reduced from ρ_α to $\rho_\alpha(1 - 2\tan^2\phi)$ where the term $(1 - 2\tan^2\phi)$ corresponds to the p-character of the orbital containing the unpaired electron. A set of modified equations which correlate a_{CH_3} with the spin density at the α-carbon atom for bent radicals can be obtained from the corresponding eqs. 1 and 3.

$$[1] \qquad a_{CH_3} = Q_H^{CH_3}\rho_\alpha$$

where $Q_H^{CH_3} = 29.30$ G

$$[7] \qquad \rho_\alpha = (1 - 2\tan^2\phi)\prod_{i=1}^{3}[1 - \Delta(X_i)]$$

where $\Delta(X_i)$ is a parameter which measures the spin-withdrawing influence of an α substituent X_i on a planar radical configuration, namely via bond polarization. For bent radicals, the spin density at α-carbon depends on bond polarization as well as the angle of bending exerted by α-substituents.

In Table 1, ρ_α was calculated from eq. 1 and the observed value of a_{CH_3}. ϕ was obtained from ρ_α by the use of eq. 7.

Fluorine Hyperfine Splittings for the α-Trifluoromethyl Group (a_{CF_3})

Fessenden and Schuler obtained eq. 1 with $Q_H^{CH_3} = 29.30$ G and $\Delta(CH_3) = 0.081$ by using an iterative procedure from the experimentally observed value of a_{CH_3} for ethyl, isopropyl, and *t*-butyl radicals (1*a*). In Table 4, we have summarized the e.s.r. parameters of a series of radicals which result from the successive replacement of a hydrogen atom in the methyl radical with a trifluoromethyl group, namely CF_3CH_2, $(CF_3)_2CH$, and $(CF_3)_3C$. The value of a_{CF_3} are temperature independent in the range of −40 to −130 °C for CF_3CH_2 and $(CF_3)_2CH$.[3]

There is some current disagreement as to the effect which successive replacement of a hydrogen by a methyl group has on the configuration of alkyl radicals. In the series: ethyl, *i*-propyl, and *t*-butyl radicals, and especially for $\cdot C(CH_3)_3$, an argument based on the magnitude and the sign of the temperature dependence of ^{13}C splitting has suggested that the *t*-butyl radical is non-planar (10). However, Symons, Ingold, and

[3]The temperature dependence of the β-fluorine h.f.s. of $(CF_3)_3C\cdot$ has not been studied (4*c*), but it is not unreasonable to assume that this β-fluorine h.f.s. is temperature independent.

Can. J. Chem. Downloaded from www.nrcresearchpress.com by 210.87.254.42 on 09/05/12
For personal use only.

TABLE 4. Electron spin resonance parameters of α-trifluoromethyl substituted methyl radicals

Radical	T (°C)	$\langle g \rangle$	a_H^α (G)	a_F^β Exptl.	a_F^β Calcd.†	Δa_F^β (G)‡	ρ_α*
CH_3	−113	2.00262	22.88				1
CF_3CH_2	−113	2.00234	23.77	29.61	29.43	0.18	0.778
$(CF_3)_2CH$	−113	2.00221	24.61	22.64	22.90	−0.26	0.605
$(CF_3)_3C$§	−60	2.0015		17.9	17.81	0.09	0.471

*See text.
†a_F^β (calcd) = 37.83 G × ρ_α.
‡$\Delta a_F^\beta = a_F^\beta$ (exptl) − a_F^β (calcd).
§Taken from ref. 4c.

Fischer have pointed out that the evidence used to deduce the nonplanarity at the radical site is not rigorous (1*g*, 11). The nearly constant values of the *g*-factors and the α-proton splittings, as well as the small change of the α ^{13}C splittings from 38.34 G in methyl radical to 45.2 G in *t*-butyl radical suggest that the effect of α-methyl substitution on the bending of the radical site is quite small.

The essentially free rotation in the β,β,β-trifluoroethyl radical can be attributed to a low barrier associated with the 6-fold rotation symmetry along the C_α—C_β bond as a result of planarity at the trigonal α-carbon center (12). There is a small but significant increase in the α-proton h.f.s. in going from CF_3CH_2 to $(CF_3)_2CH$, but the change is also accompanied by an increase in steric repulsion due to the presence of an additional bulky CF_3 group. It appears unlikely that the configuration of $(CF_3)_2CH$ and $(CF_3)_3C$ could be anything but planar. Since CF_3 is more electronegative than hydrogen, Pauling's argument (13) that substitution of more electronegative groups should increase the bending does not seem to hold for the series of radicals with the structure, $CH_n(CF_3)_{3-n}$.[4] The effect of electronegativity may be offset by the steric effects of the CF_3 groups in these radicals. A correlation of the fluorine h.f.s. in α-trifluoromethyl groups similar to eq. 1 for α-methyl proton h.f.s. can be obtained by an iterative procedure

$$a_{CF_3} = Q_F^{CF_3}\rho_\alpha \quad [8]$$

with $Q_F^{CF_3} = 37.83$ G and $\Delta(CF_3) = 0.222$.

The unique values of $Q_F^{CF_3}$ and $\Delta(CF_3)$ indicate that the variations in the p-character of the half-filled orbital are relatively small amongst the radicals considered here. The latter also implies that α-trifluoromethyl substituents do not dramatically affect the configuration of alkyl radicals. The rather large spin-withdrawing influence of a CF_3 group in which $\Delta(CF_3) = 0.222$, suggest that structures such as **6** for X = CF_3 are relatively unimportant to the total wave-function for the radical.

Due to the intrinsic features of the INDO program (14), the lack of agreement between the calculated and experimental β-fluorine h.f.s. is noteworthy. Nonetheless, a relationship similar to eq. 4 for β-proton splittings (with a negligible A_F in comparison with B_F) has been proposed for the β-fluorine h.f.s. of planar radicals such as **8** (15) and $R' = [\frac{1}{2}(a_{F_2} + a_{F_3})/a_{F_1}] = 0.25$

$$a_F^\beta = B_F \cos^2\theta \quad [9]$$

was obtained. Similarly, a dependence of R' on bending will be expected. Indeed, a value for R'

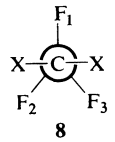

8

of −3.14/40.4 or −0.078 can be extracted from the results of Meakin and Krusic for the perfluoroethyl radical from their low temperature e.s.r. study (16). The bending at the radical site of perfluoroethyl radical has been supported by INDO calculations (4*c*), and it is also reflected in the rather high barrier to rotation about the C_α—C_β bond (16) (2.85 kcal mol^{-1}). Accordingly, eqs. 7 and 8 can be used to correlate a_{CF_3} with the spin density at the α-carbon atom for bent β,β,β-trifluoroethyl radicals. The e.s.r. parameters for α-halogen substituted β,β,β-trifluoroethyl radicals are given in Table 5, together with values for ρ_α and ϕ calculated

[4]For recent theoretical arguments to the FCF and CF_3CCF_3 bond angles, see ref. 28.

Can. J. Chem. Downloaded from www.nrcresearchpress.com by 210.87.254.42 on 09/05/12
For personal use only.

TABLE 5. Electron spin resonance parameters of α-halogen substituted β,β,β-trifluoroethyl radicals

Radical	T (°C)	$\langle g \rangle$	a_X^α (G)	a_H^α (G)	a_F^β (G)	ρ_α*	ϕ* (deg)	Mode of generation§
CF_3CH_2	−113	2.00234	—	23.77	29.61	0.778	0	S
CF_3CHF	−106	2.00363	66.18	21.47	25.25	0.668	14	P
CF_3CF_2	−84	2.00386	87.26	—	11.36	0.300	29	P
CF_3CHCl†	−60	—	3.7	22.2	23.4	0.619	13	
CF_3CCl_2	−81	2.00797	4.14	—	18.56	0.491	18	S
$(CF_3)_2CH$	−113	2.00221	—	24.61	22.64	0.605	0	P
$(CF_3)_2CF$‡	−60	2.0033	67.4	—	19.2	0.508	15	

*See text.
†Taken from ref. 15*b*.
‡Taken from ref. 4*c*.
§S = halogen abstraction by R_3S_i, P = photolysis of *t*-butyl peresters.

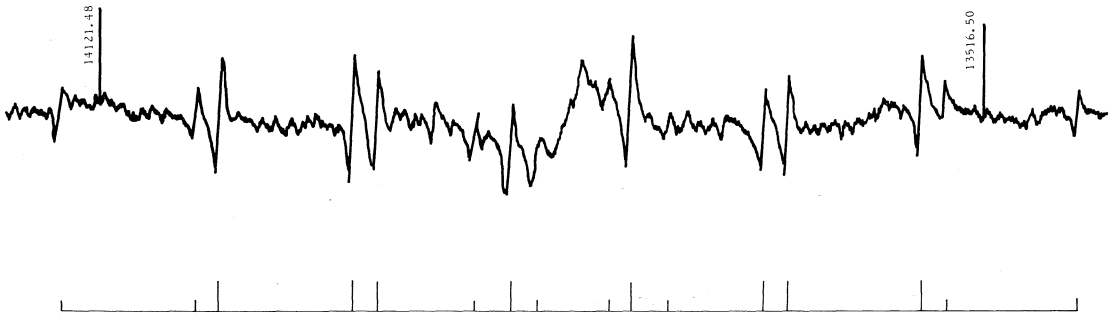

FIG. 2. Electron spin resonance spectrum of α,β,β,β-tetrafluoroethyl radical in cyclopropane solution at −100 °C. The stick spectrum shows theoretical binomial intensity ratios.

from eqs. 7 and 8. The e.s.r. spectrum of α,β,β,β-tetrafluoroethyl radical is given in Fig. 2.

The Effect of α-Halogen Substitution on the Configuration of Alkyl Radicals

Based on the observed α-chlorine and methyl proton h.f.s., Cooper *et al.* concluded that 2-chloroisopropyl radical is essentially planar (4*b*). We obtain a value of Δ(Cl) = 0.099 from the observed a_{CH_3} and the use of eqs. 1 and 3. Using this value of Δ(Cl) and eqs. 1, 7, and 8, we obtained values of ρ_α and ϕ for α-chlorinated ethyl and β,β,β-trifluoroethyl radicals which are given in Tables 1 and 5.

For the α-bromoethyl radical, Fig. 3, a value of a_{CH_3} equal to 24.71 G is very close to 24.48 G obtained for a_{CH_3} of the α-fluoroethyl radical. However, the smaller electronegativity and the bulkier nature of the bromine atom suggest that the radical is planar or nearly planar. A value of Δ(Br) = 0.082 was calculated on this basis using eqs. 2 and 3.

g-Factors and the Mechanism of β-Fluorine Hyperfine Splittings

There are two principal mechanisms which have been proposed to account for the interaction between a β-fluorine substituent and an unpaired electron at the radical center. The first involves an interaction between the lowest unoccupied antibonding orbital of the trifluoromethyl group and the half-filled orbital of radical (17). The second mechanism involves a 1–3 homoconjugation between the half-filled p-orbital and the lone-pair p-orbital of the fluorine (18).

The second mechanism can only make a positive contribution to the *g*-factor since the half-filled orbital at the carbon center is of higher energy than the lone-pair p-orbital of fluorine (19). However, a positive or negative contribution to the *g*-factor may arise from the first mechanism. The sign of the contribution depends on the difference between $(\varepsilon^0 - \varepsilon^b)$ and $(\varepsilon^0 - \varepsilon^a)$ where ε^0, ε^b, and ε^a are the half-filled orbital, the highest occupied bonding orbital, and the lowest unoccupied antibonding orbital energies, respectively.

The monotonic decrease in the isotropic *g*-factor with an increasing number of α-trifluoromethyl substituents shown in Table 4 is in

Can. J. Chem. Downloaded from www.nrcresearchpress.com by 210.87.254.42 on 09/05/12
For personal use only.

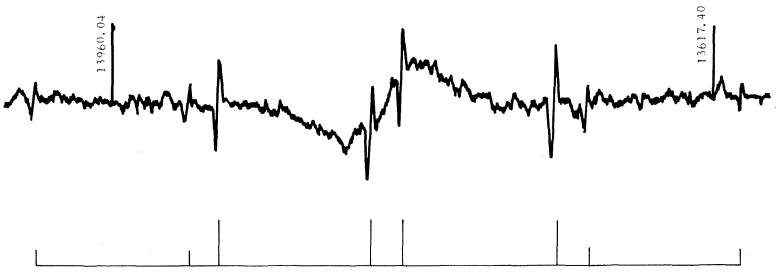

FIG. 3. Electron spin resonance spectrum of α-bromoethyl radical in cyclopropane solution at −77 °C. The stick spectrum shows the binomial intensity ratios. The proton n.m.r. field markers are in kHz.

striking contrast to the essentially constant *g*-factors for the hydrocarbon analogs. The trend in *g*-factors noted above for α-CF_3 substituted alkyl radicals suggests that the second mechanism does not contribute in a major way to the spin-transfer process. The first mechanism has been used to interpret the difference between the large fluorine h.f.s. in hexafluoroacetone ketyl and the small one in the isoelectronic nitroxide (20*c*). Thus, the diagram shown in Fig. 4 illustrates that the energy difference between the lowest unoccupied antibonding orbital of the CF_3 group and the half-filled orbital of the carbonyl group is indeed smaller than that in the nitroxide function.

According to the first mechanism, a_F^β is approximately inversely proportional to the energy difference between the lowest unoccupied antibonding orbital of the trifluoromethyl group and the half-filled orbital at the radical center. From the observed value of $a_{CF_3} = 22.64$ G for $(CF_3)_2CH$ in comparison with 34.7 G for $(CF_3)_2C\dot{O}^-$ and 8.26 G for $(CF_3)_2N\dot{O}$, we conclude that the half-filled orbital of the CH group has an energy close to 0 a.u. (20, 21). Thus, the difference $(\varepsilon^0 - \varepsilon^a) \approx 0.3$ a.u. is expected to be smaller than $(\varepsilon^0 - \varepsilon^b) \approx 0.7$ a.u., and an α-CF_3 group would make a negative contribution to the *g*-factor if the first mechanism were responsible for the observed β-fluorine h.f.s. Such a conclusion is consistent with the observed monotonic decrease of the *g*-factors of the radicals resulting from successive replacement of a hydrogen with a CF_3 group. Therefore, we interpret the decrease of the *g*-factor as a support for a mechanism of spin transfer into the antibonding orbital of the CF_3 group similar to that formulated for hexafluoroacetone ketyl. Such an effect would not be expected in methyl compounds since the highest unoccupied orbital of the methyl group is of higher energy than the level in the trifluoromethyl group due to the smaller electronegativity of the proton. The latter is in accord with the nearly invariant *g*-factor of the series of alkyl radicals: methyl, ethyl, isopropyl, and *t*-butyl.

On the other hand, the *g*-factors of ethyl or β,β,β-trifluoroethyl radicals with one α-halogen substituent are always greater than those of the parent radicals as listed in Tables 1 and 5. The larger *g*-factor in these radicals is consistent with the findings of McConnell and Robertson (22), that in planar π-radicals, the successive substitution of hydrogen by an atom with a lone pair of electrons at a position where the spin density is appreciable, causes a progressive increase in the *g*-factor. This effect can be attributed to the delocalization of the spin onto the lone pair orbital of the α-halogen atom, which affords a positive contribution to the *g*-factor

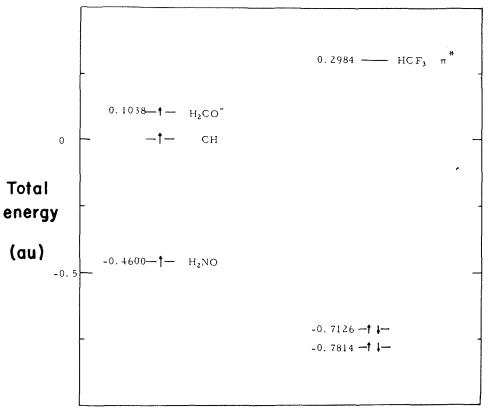

FIG. 4. Highest occupied and lowest unoccupied orbital energies for HCF_3, $H_2C\dot{O}^-$, and $H_2N\dot{O}$ as calculated from INDO-MO. The energy levels are drawn to scale. Data are taken from reference 17*c*. For the energy level of $\rangle\dot{C}H$ see text.

Can. J. Chem. Downloaded from www.nrcresearchpress.com by 210.87.254.42 on 09/05/12
For personal use only.

Can. J. Chem. Downloaded from www.nrcresearchpress.com by 210.87.254.42 on 09/05/12
For personal use only.

due to the lower energy level of lone pair orbital in comparison with the half-filled orbital at the radical center. When a second halogen atom is introduced, however, there is only a small increase or even a decrease in the *g*-factor. Evidently as the degree of bending increases due to the introduction of the second α-halogen, the effect of delocalization on to halogen which is associated with a positive contribution to *g*-factor is increasingly offset by a factor associated with a negative contribution. A similar change in *g*-factors has been previously noted in the series of $\dot{C}H_nF_{3-n}$ and $\dot{S}iH_nF_{3-n}$ (3, 23).

Conclusion

An equation has been derived to estimate the angle of bending at the radical site due to α-halogen substitution in alkyl radicals which is based on the experimentally observed α-methyl proton or α-trifluoromethyl fluorine hyperfine splitting constants. Two α-fluorine substituents have a disproportionately greater influence on bending than one fluorine, in accord with results calculated by INDO. The effect of an α-chlorine or bromine substituent is akin to that of a methyl group, and suggests that size has an important influence. The effect of an α-trifluoromethyl group on the *g*-factor has been qualitatively correlated with the energy levels of the CF_3 group. The observed monotonic decrease of the *g*-factors on successive replacement of an hydrogen atom in the methyl radical by a CF_3 group is consistent with the hyperconjugative mechanism proposed for the β-fluorine splitting. The positive contribution to the *g*-factor by α-halogen substituents is offset to an increasing extent by the increasing degree of bending at the radical site.

Experimental Section

The modified Varian X-band spectrometer, microwave frequency measurements, light source, and sample tubes are as described previously (1*d*).

To minimize the error in the *g*-value determinations, all measurements were made on spectra recorded on the same day for increasing magnetic field. Perylene cation radical $g = 2.00258$ (24) was used as standard in the configuration employed. The accuracy of the measurements is estimated as ± 0.00003. Hyperfine splittings were corrected for second-order shifts and confirmed by computer simulation.

For photolytic reduction of alkyl halides, equal volumes of di-*t*-butyl peroxide and triethylsilane were diluted with sufficient cyclopropane (and ethane) to give a final ratio of approximately 1:1:1:4 (v/v). For the photolysis of acyl peresters, a small amount of the perester (*ca.* 100 mg) was dissolved in a relatively large volume (15:1) of cyclopropane or cyclopropane–ethane mixtures. For the photolytic abstraction of hydrogen atom from the fluorohydrocarbons, a solution with a half-volume of di-*t*-butyl peroxide or bis-trifluoromethyl peroxide was diluted with cyclopropane or Freon-12 (CF_2Cl_2) to give a final ratio of approximately 1:0.5:4. For the generation of 1,1-difluoroethyl radical from 1,1-difluoroethane, bis-trifluoromethyl peroxide was used, since di-*t*-butyl peroxide under the same conditions did not afford sufficiently high concentrations of radicals for e.s.r. measurements. For the generation of 2-fluoropropyl radical from the photolytic abstraction of hydrogen from 2-fluoropropane, spectra of radicals with good signal-to-noise could only be observed at temperatures higher than −80 °C.

Materials

Di-*t*-butyl peroxide was obtained from Shell Chemical Co., washed with water, dried, passed through an alumina column, and redistilled at reduced pressure prior to use. Triethylsilane was obtained from Columbia Chemicals Co., refluxed over molecular sieve and redistilled prior to use. Bis-trifluoromethyl peroxide was obtained from PCR, Inc. 1,1,1,-trichloroethane (Matheson), 1,1,1-trifluoro-2-bromoethane (Pierce Chemical Co.), and 1,1,1-trichlorotrifluoroethane, (PCR, Inc.) were washed with water, dried, and redistilled prior to use. Perfluoropropyl bromide was obtained from PCR, Inc. and used as such. 1,1-Difluoroethane (Genetron 152A) and 1,1-difluoro-1-chloroethane (Genetron 142B) were obtained from Matheson Co. Perfluoropropionyl chloride was obtained from Pierce Chemical Co.

t-Butyl Hexafluoroisobutyryl Perester was prepared via the acid chloride (25) (n.m.r.: δ 1.31 (s), 4.03 (septet)).

t-Butyl β,β,β-trifluoro-α-fluoropropionyl Perester was prepared via the anhydride. (n.m.r.: δ 1.31(s), 5.17 (d × q)).

t-Butyl α-fluoropropionyl Perester

Ethyl methanesulfonyl-lactate was prepared by the method of Crossland and Servis (26). Yield 95%. (n.m.r.: δ 1.32 (t), 1.58 (d), 3.07 (s), 4.25 (q), 5.04 (q)). The lactate (20 g) and 12 g anhydrous potassium fluoride in 65 ml of hexamethylphosphoric triamide were heated and stirred at 100 °C over a period of 24 h. The reaction mixture was cooled, diluted with cold water, and extracted with anhydrous ether. The extracts were washed with water, dried over anhydrous magnesium sulfate, and distilled (b.p. = 51 °C at 93 mm). Yield of ethyl α-fluoropropionate, 50% (n.m.r.: δ 1.30 (t), 1.50 (d × d), 4.20 (q), 4.87 (d × q)). Ethyl α-fluoropropionate (15 g) and 100 ml of 10% potassium hydroxide aqueous solution were stirred at room temperature over a period of 3 h. The reaction mixture was extracted with ether, dried, and distilled (b.p. = 84–85 °C at 54 mm). Yield α-fluoropropionic acid 70% (n.m.r.: (δ 1.62 (d × d), 5.06 (d × q)). *t*-Butyl-α-fluoropropionyl perester was prepared via the acid chloride (n.m.r.: (δ 1.31 (s), 1.63 (d × d), 5.14 (d × q)). 2-Fluoropropane was prepared by the method of Edgell and Parts (27) via the mesylate (n.m.r.: δ 1.32 (d × d), 4.86 (d × septet)). *t*-Butyl-α-bromopropionyl perester was prepared from α-bromopropionic acid via the acid bromide (n.m.r.: δ 1.33(s), 1.84(d), 4.36(q)).

We wish to thank the National Science Foundation for financial support and Dr. D. R. Eaton for helpful criticisms.

1. (*a*) R. W. Fessenden and R. H. Schuler. J. Chem. Phys. **39**, 2147 (1963); (*b*) R. W. Fessenden. J. Chim. Phys. **61**, 1570 (1964); (*c*) J. K. Kochi and P. J. Krusic. Chem. Soc. Spec. Publ. **24**, 147 (1970); (*d*) P. J. Krusic and J. K. Kochi. J. Am. Chem. Soc. **93**, 846 (1971); (*e*) P. J. Krusic, P. Meakin, and J. P. Jesson. J. Phys. Chem. **75**, 3438 (1971); (*f*) K. S. Chen, D. J. Edge, and J. K. Kochi. J. Am. Chem. Soc. **95**, 7036 (1973); (*g*) D. Griller and K. U. Ingold. J. Am. Chem. Soc. **95**, 6459 (1973); (*h*) F. J. Adrian, E. L. Cochran, and V. A. Bowers. J. Chem. Phys. **59** 3946 (1973); (*i*) K. S. Chen, P. J. Krusic, and J. K. Kochi. J. Phys. Chem. In press.
2. K. S. Chen, D. Y. H. Tang, L. K. Montgomery, and J. K. Kochi. J. Am. Chem. Soc. **96**, 2201 (1974).
3. R. W. Fessenden and R. H. Schuler. J. Chem. Phys. **43**, 2704 (1965).
4. (*a*) A. J. Dobbs, B. C. Gilbert, and R. O. C. Norman. J. Chem. Soc. A, 124 (1971); (*b*) J. Cooper, A. Hudson, and R. A. Jackson. Mol. Phys. **23**, 209 (1972); (*c*) R. V. Lloyd and M. T. Rogers. J. Am. Chem. Soc. **95**, 1512 (1973).
5. K. S. Chen and J. K. Kochi. Chem. Phys. Lett. **23**, 233 (1973); J. Am. Chem. Soc. **96**, 794 (1974).
6. H. Fischer. Z. Naturforsch. **19***a*, 866 (1964); **20***a*, 428 (1965).
7. (*a*) K. Morokuma, L. Pederson, and M. Karplus. J. Chem. Phys. **48**, 4801 (1968); (*b*) D. L. Beveridge, P. A. Dobosh, and J. A. Pople. J. Chem. Phys. **48**, 4802 (1968).
8. A. D. McLachlan. Mol. Phys. **1**, 233 (1958).
9. C. Heller and H. M. McConnell. J. Chem. Phys. **32**, 1535 (1960).
10. D. E. Wood, L. F. Williams, R. F. Sprecher, and W. A. Lathan. J. Am. Chem. Soc. **94**, 6241 (1972).
11. (*a*) M. C. R. Symons. Tetrahedron Lett. 207 (1973); (*b*) H. Paul and H. Fischer. Helv. Chim. Acta, **15**, 1575 (1973).
12. (*a*) A. J. Bowles, A. Hudson, and R. A. Jackson. Chem. Phys. Lett. **5**, 552 (1970); (*b*) D. J. Edge and J. K. Kochi. J. Am. Chem. Soc. **94**, 6485 (1972).
13. L. Pauling. J. Chem. Phys. **51**, 2767 (1969).
14. G. R. Underwood. Private communication.
15. (*a*) M. Iwasaki. Fluorine Chem. Rev. **5**, 1 (1971); (*b*) A. Hudson and K. D. J. Root. Adv. Magn. Reson. **5**, 1 (1971).
16. P. Meakin and P. J. Krusic. J. Am. Chem. Soc. **95**, 8185 (1973).
17. (*a*) M. J. S. Dewar. Hyperconjugation. Ronald Press, New York, N.Y. 1962. p. 159; (*b*) W. R. Knolle and J. R. Bolton. J. Am. Chem. Soc. **91**, 5411 (1969); (*c*) K. Morokuma. J. Am. Chem. Soc. **91**, 5412 (1969).
18. W. A. Sheppard. J. Am. Chem. Soc. **87**, 2410 (1965).
19. A. J. Stone. Proc. R. Soc. Ser. A, **271**, 424 (1963); Mol. Phys. **6**, 509 (1963); **7**, 311 (1964).
20. E. G. Janzen and J. L. Gerlock. J. Phys. Chem. **71**, 4577 (1967).
21. W. D. Blackley and R. R. Reinhard. J. Am. Chem. Soc. **87**, 802 (1965).
22. H. M. McConnell and R. E. Robertson. J. Phys. Chem. **61**, 1018 (1957).
23. M. V. Merritt and R. W. Fessenden. J. Chem. Phys. **56**, 2353 (1972).
24. B. G. Segal, M. Kaplan, and G. K. Fraenkel. J. Chem. Phys. **43**, 4191 (1965).
25. P. D. Bartlett and R. R. Hiatt. J. Am. Chem. Soc. **80**, 1398 (1958).
26. R. K. Crossland and K. L. Servis. J. Org. Chem. **35**, 3195 (1970).
27. W. F. Edgell and L. Parts. J. Am. Chem. Soc. **77**, 4899 (1955).
28. R. C. Bingham and M. J. S. Dewar. J. Am. Chem. Soc. **95**, 7182 (1973). P. Kollman. J. Am. Chem. Soc. **96**, 4363 (1974).

Can. J. Chem. Downloaded from www.nrcresearchpress.com by 210.87.254.42 on 09/05/12
For personal use only.

Structure Cristalline de $TlVO_3$

MARCEL GANNE, YVES PIFFARD ET MICHEL TOURNOUX

Laboratoire de Chimie Minérale B, U.E.R. de Chimie, Faculté des Sciences de Nantes, B.P. 1044, 44037, Nantes, cedex, France

Reçu le 26 fevrier 1974

M. GANNE, Y. PIFFARD et M. TOURNOUX. Can. J. Chem. **52**, 3539 (1974).

Le métavanadate de thallium $TlVO_3$ cristallise dans une maille orthorhombique (groupe spatial *Pbcm*) de paramètres $a = 5.16$, $b = 11.22$, $c = 5.73$ Å avec $Z = 4$. La structure a été déterminée à partir de 255 réflexions indépendantes mesurées à l'aide d'un diffractomètre automatique.

Dans cette structure le vanadium adopte une coordinence tétraédrique. Les tétraèdres s'associent par mise en commun de deux atomes d'oxygène pour former des chaînes $(VO_3)_n^{n-}$ parallèles à l'axe *c*.

$TlVO_3$ s'avère être isotype des métavanadates MVO_3 (M = K, NH_4, Rb, Cs). Le thallium adopte une coordinence dix analogue à celle des alcalins. L'étude structurale montre que le doublet $6s^2$ du thallium est stéréochimiquement inactif dans $TlVO_3$.

M. GANNE, Y. PIFFARD, and M. TOURNOUX. Can. J. Chem. **52**, 3539 (1974).

Thallium metavanadate ($TlVO_3$) crystallizes in an orthorhombic lattice (space group *Pbcm*) with parameters $a = 5.16$, $b = 11.22$, $c = 5.73$ Å with $Z = 4$. The structure was determined using 255 independent reflections measured with an automatic diffractometer.

Vanadium has a tetrahedral coordination in this structure. The tetrahedra are joined by having two oxygens in common to form chains $(VO_3)_n^{n-}$ parallel to the *c* axis.

$TlVO_3$ is established to be isomorphous to the metavanadates MVO_3 (M = K, NH_4, Rb, Cs). Thallium has a coordination number of ten analogous to that of the alkali metals. The study demonstrates that the $6s^2$ doublet of thallium is sterochemically inactive in $TlVO_3$.

[Journal translation]

Introduction

L'étude structurale d'un grand nombre de composés oxygénés ternaires du thallium révèle une évolution progressive du rôle stéréochimique joué par le doublet solitaire du thallium I avec la teneur en thallium de ces composés. Dans les composés pauvres en thallium I celui-ci présente une coordinence élevée et son comportement est analogue à celui des alcalins, K et Rb; il y a souvent une relation d'isotypie entre les composés de même formulation. Au contraire dans les phases riches en thallium I, la coordinence de cet élément est faible; tous les anions sont situés d'un même côté par rapport au thallium, les distances thallium–oxygène sont très courtes ($\simeq 2.50$ Å) ce qui est l'indice de l'établissement de liaisons de covalence; le doublet solitaire du thallium I joue alors un rôle stéréochimique. La structure des composés Tl_4O_3 (1), Tl_3PO_4 (2), Tl_3BO_3 (3), Tl_2TiO_3 (4), et Tl_2SnO_3 (5) illustre ce comportement.

Les métavanadates anhydres d'éléments monovalents présentent tous des caractéristiques communes: coordinence tétraédrique du vanadium, présence de chaînes infinies $(VO_3)_n^{n-}$. Trois types structuraux ont été caractérisés: $LiVO_3$ (6) de groupe spatial *Cc* dont la structure présente de grandes analogies avec celle du diopside $CaMg(SiO_3)_2$ et du spodumène, $NaVO_3$ (7) qui est isotype du diopside et MVO_3 avec (M = K, NH_4, Rb, Cs); dans ce dernier groupe les structures de KVO_3 et de NH_4VO_3 ont été déterminées (8–11).

L'examen des paramètres de la maille élémentaire de $TlVO_3$ que nous avons déjà donnée dans une publication récente (12) suggère l'isotypie de ce composé et des métavanadates de potassium et d'ammonium (tableau 1).

Nous avons toutefois entrepris l'étude structurale de $TlVO_3$ dans le but de pouvoir comparer les environnements du thallium et du potassium dans le cadre d'une étude générale sur le système Tl_2O–V_2O_5 et sur l'activité stéréochimique du doublet solitaire du thallium I.

Partie expérimentale

Le composé $TlVO_3$ est préparé par voie humide par action d'une solution de nitrate thalleux sur une solution diluée de métavanadate d'ammonium. L'évaporation

Can. J. Chem. Downloaded from www.nrcresearchpress.com by 210.87.254.105 on 09/05/12
For personal use only.

Can. J. Chem. Downloaded from www.nrcresearchpress.com by 210.87.254.105 on 09/05/12
For personal use only.

TABLEAU 1. Données cristallographiques des métavanadates isotypes

Composé	Groupe spatial	a (Å)	b (Å)	c (Å)	Z
KVO_3	*Pbcm*	5.22	10.82	5.90	4
NH_4VO_3	*Pbcm*	4.90	11.79	5.82	4
$TlVO_3$	*Pbcm*	5.16	11.22	5.73	4
$RbVO_3$	*Pbcm*	4.99	11.98	5.65	4
$CsVO_3$	*Pbcm*	5.38	12.20	5.78	4

lente, à température ambiante, de la solution obtenue conduit à la formation de cristaux transparents, aciculaires à base carrée.

Données cristallographiques

$TlVO_3$ p.m. = 303.4 orthorhombique, *Pbcm*, $a = 5.16(1)$, $b = 11.22(2)$, $c = 5.73(1)$ Å, $V = 331.8$ Å^3, $\rho_o = 6.02(3)$ g/cm^3, $\rho = 6.05$ g/cm^3, $Z = 4$, (20 °C, CuKα, $\lambda = 1.54050$ Å), $\mu = 514$ cm^{-1} (20 °C, MoKα, $\lambda = 0.70926$).

Ces données cristallographiques ont été obtenues lors de l'étude préliminaire effectuée sur monocristal à l'aide des méthodes photographiques classiques. Les conditions d'existence observées $0kl$, $k = 2n$; $h0l$, $l = 2n$ sont compatibles avec les groupes spatiaux *Pbcm* et $Pbc2_1$. Les tests physiques: piezoélectricité et doublage de fréquence laser effectués au C.N.E.T. de Lannion se sont avérés négatifs. Un test statistique portant sur la distribution des facteurs de structure normalisés ne s'est pas avéré suffisamment significatif pour permettre le choix entre les deux groupes spatiaux possibles (13). L'affinement a été conduit dans un premier temps dans le groupe centrosymétrique *Pbcm*. Un calcul effectué avec le groupe $Pbc2_1$ ne conduit pas à une amélioration du facteur de reliabilité. La densité a été mesurée sur poudre, après dégazage sous vide primaire (10^{-2} Torr), par la méthode de la poussée hydrostatique. Le tétrachlorure de carbone, étalonné par rapport à l'eau bidistillée, a été utilisé comme liquide pycnométrique.

Un cristal de dimensions $0.15 \times 0.02 \times 0.02$ mm, assimilable à un cylindre a été retenu pour l'enregistrement des intensités diffractées au moyen d'un diffractomètre automatique "Nonius" CAD-3, utilisant le rayonnement MoK$_\alpha$. Dans le demi-espace réciproque compris entre $\theta = 3.5°$ et $\theta = 35°$, les intensités de 1784 réflexions ont été mesurées avec un balayage θ–2θ. Elles correspondent à 737 réflexions indépendantes. Seules les corrections de Lorentz et celles de polarisation ont été effectuées sur les intensités des 255 réflexions indépendantes satisfaisant au test $\sigma(I)/I = 0.25$. Dans le domaine de θ exploré l'erreur maximale, liée à l'absorption d'un cylindre dont $R = 0.60$, n'excède pas 2% pour les facteurs de structure observés; la correction d'absorption n'a pas été effectuée. Les écarts-types sont évalués par application de la statistique de Poisson régissant les mesures par comptage. Le rapport $\sigma(I)/I$ est donné par la relation

$$\frac{[T + \tau^2(F_1' + F_2')]^{1/2}}{T - \tau(F_1' + F_2')}$$

où T est l'intensité brute de la réflexion, F_1' et F_2' les intensités des fonds continus à gauche et à droite et $\tau = t/2t'$ le rapport des temps de comptage de la réflexion et des fonds continus. Les mesures d'intensité ont été effectuées en choisissant la valeur $\tau = \frac{1}{2}$.

Détermination de la structure

L'interprétation de la fonction de Patterson tridimensionnelle à l'aide de la matrice de Patterson a permis de retenir la position 4d pour l'atome de thallium. L'atome de vanadium a pu être localisé sur une position 4d grâce à une synthèse de Fourier tridimensionnelle. Après quatre cycles d'affinement des coordonnées atomiques du thallium et du vanadium, le facteur de reliabilité classique

$$R = \sum(|F_o| - Z|F_c|)/\sum|F_o|$$

est de 0.123.

L'affinement des paramètres atomiques et des coefficients d'agitation thermique a été réalisé par la méthode des moindres carrés (matrice complète) en minimisant la quantité $S = \sum W(|F_o| - Z|F_c|)^2$ où W est le facteur de pondération et Z le facteur d'échelle.

Une série de Fourier différence permet de placer les trois atomes d'oxygène. Deux correspondent à une position 4d et l'autre à la position 4c du groupe *Pbcm*. Après quatre cycles d'affinement en isotropie thermique avec des facteurs de pondération unitaires, le facteur R atteint la valeur 0.085. Lors d'un dernier affinement comprenant trois cycles, le tenseur d'agitation thermique du thallium ainsi qu'un schéma de pondération ont été introduits. Le facteur de pondération s'exprime en fonction de l'écart type par la relation $W = 1/[\sigma^2(F)]$.

Nous avons utilisé le schéma de pondération de Hughes (14) avec les bornes $F_1 = 1.5$, $F_2 = 75$, $F_3 = 140$ et $F_4 = 240$. En fin d'affinement 7 réflexions telles que $|F_o - F_c|/\sigma \geq 20$ ont été rejetées.

Dans ces conditions, le facteur résiduel atteint la valeur R = 0.055 et le facteur

$$R_W = [\sum W(|F_o| - Z|F_c|)^2/\sum W(|F_o|)^2]^{1/2}$$

la valeur 0.066.

Ces calculs d'affinement ont été effectués à l'aide du programme SFLS 5 (15) sur ordinateur CDC 6400. Les facteurs de diffusion atomique sont extraits des tables de Moore (16). La liste

TABLEAU 2. Coordonnées atomiques ($\times 10^4$) et coefficients d'agitation thermique ($\times 10^3$)[a,b]

Atome	X	Y	Z	U_{11} (ou U)*	U_{22}	U_{33}	U_{12}	U_{13}	U_{23}
Tl	774 (3)	4018 (1)	1/4	33 (1)	20 (1)	31 (1)	3 (1)	0	0
V	5384 (10)	1678 (4)	1/4	17 (1)*					
O(2)	8501 (54)	1612 (27)	1/4	36 (1)*					
O(3)	4144 (73)	351 (26)	1/4	34 (1)*					
O(1)	4307 (52)	1/4	0	17 (1)*					

[a]Le facteur de température de chaque atome s'exprime sous la forme exp $[-2\pi^2(a^{*2}h^2U_{11} + b^{*2}k^2U_{22} + c^{*2}l^2U_{33} + 2a^*b^*hkU_{12} + 2a^*c^*hlU_{13} + 2b^*c^*klU_{23})]$ ou exp $[-2\pi^2(U.1/d^2)]$.
[b]Les écarts-types sont indiqués entre parenthèses.

des facteurs de structure observés et calculés a été versée au dépôt des données non publiées.[1]

Les valeurs des divers paramètres atomiques sont données dans le tableau 2.

Description de la structure

La fig. 1 représente une vue de la structure, projetée sur le plan (001). $TlVO_3$ est isotype de KVO_3 et de NH_4VO_3. Le tableau 3 permet de comparer les principaux angles et distances interatomiques dans $TlVO_3$ avec les résultats obtenus par Evans (11) pour KVO_3 et NH_4VO_3.

Tous les atomes à l'exception des atomes d'oxygène notés O(1) sont situés dans les plans miroirs; ils occupent les positions 4d du groupe *Pbcm*. L'atome O(1) occupe la position 4c correspondant à l'axe binaire.

Les atomes de vanadium sont au centre de tétraèdres formés par les atomes d'oxygène. Chaque groupement VO_4 partage deux de ces atomes d'oxygène avec deux autres tétraèdres. Cette association par des sommets conduit à des chaînes $(VO_3)_n^{n-}$ infinies parallèles à l'axe c. Les atomes de thallium assurent la cohésion entre les chaînes en adoptant une coordinence 10 irrégulière. Chaque thallium relie quatre chaînes de tétraèdres.

Les angles O—V—O sont très voisins de ceux observés pour KVO_3 et NH_4VO_3 et ne s'écartent que de très peu de la valeur idéale: 109.5°. L'écart le plus important est observé pour l'angle O(1)—V—O(1): 106.2° qui concerne les deux sommets non partagés des tétraèdres. On constate comme dans le cas de KVO_3 et de NH_4VO_3 deux types de longueur de liaisons V—O selon que l'oxygène est ou non commun à deux tétraèdres. Cette différence significative est, comme l'a indiqué Evans (11), l'indice d'un caractère π de la liaison vanadium–oxygène non partagé.

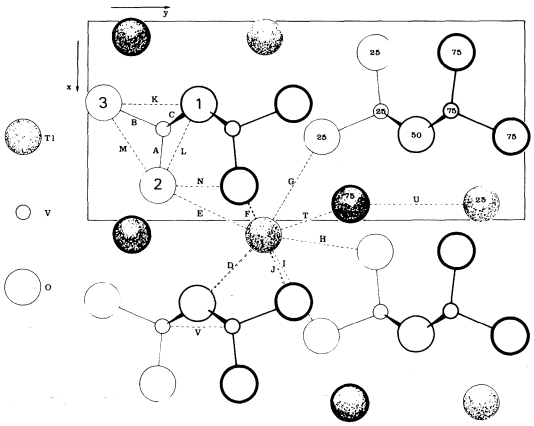

FIG. 1. Projection de la structure cristalline de $TlVO_3$ sur le plan (001).

La fig. 2 représente l'environnement du thallium I dont la coordinence est 10. Le polyèdre de coordination est très comparable à celui du potassium dans KVO_3. Les distances M^I—O

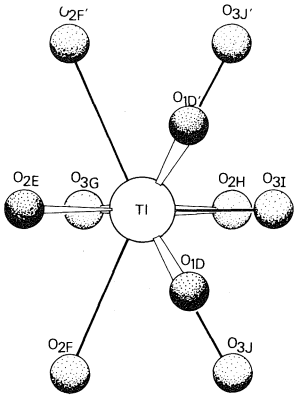

FIG. 2. Environnement oxygéné du thallium I dans la structure cristalline de $TlVO_3$.

[1]On peut obtenir la série complète de données des tableaux à un prix nominal, en s'adressant au Dépôt des données non publiées, Bibliothèque scientifique nationale, Conseil national de recherches du Canada, Ottawa, Canada K1A 0S2.

Can. J. Chem. Downloaded from www.nrcresearchpress.com by 210.87.254.105 on 09/05/12
For personal use only.

Can. J. Chem. Downloaded from www.nrcresearchpress.com by 210.87.254.105 on 09/05/12
For personal use only.

TABLEAU 3. Principales distances interatomiques et principaux angles de valence[a] dans KVO_3, NH_4VO_3 et $TlVO_3$

Liaisons	Segments	KVO_3	$TlVO_3$[c]	NH_4VO_3
V—O(2)	A	1.66±0.010	1.61 (3)	1.67±0.03
V—O(3)	B	1.65±0.010	1.62 (3)	1.65±0.03
V—O(1)	C	1.81±0.010	1.79 (1)	1.80±0.03
O(1)—O(3)	K	2.84±0.015	2.80 (2)	2.85±0.05
O(1)—O(2)	L	2.86±0.015	2.78 (3)	2.82±0.05
O(2)—O(3)	M	2.70±0.015	2.66 (4)	2.67±0.05
O(3)—O(3)	N	3.60±0.015	3.49 (2)	3.50±0.05
M—O(1)[b]	D	2.80±0.012	2.88 (2)	2.96±0.05
M—O(2)	E	2.91±0.012	2.94 (3)	3.00±0.05
M—O(2)[b]	F	3.12±0.012	3.17 (1)	3.19±0.05
M—O(3)	G	2.76±0.012	2.94 (3)	2.85±0.05
M—O(2)	H	2.79±0.012	2.93 (3)	3.06±0.05
M—O(3)	I	3.16±0.012	3.02 (3)	3.40±0.05
M—O(3)[b]	J	3.45±0.012	3.42 (2)	2.85±0.05
M—M	T	3.71±0.008	3.70 (1)	4.77±0.05
M—M	U	4.24±0.008	4.45 (1)	3.66±0.05
V—V	V	3.43±0.007	3.41 (1)	3.42±0.005
Angles de valence				
O(2)—V—O(3)		109±0.8°	107±2°	110.6 (10)
O(1)—V—O(2)		111±0.8°	108±2°	109.5 (7)
O(1)—V—O(3)		110±0.8°	111±2°	110.5 (8)
O(1)—V—O(1)		104±0.8°	108±2°	106.2 (4)
V—O(1)—V		143±0.8°	145±2°	143.9 (6)

[a]Les distances sont exprimées en Angström, les angles en degrés.
[b]Ces valeurs interviennent deux fois dans l'environnement du thallium.
[c]Les écarts-types sur les données concernant $TlVO_3$ sont indiqués entre parenthèses. Pour KVO_3 et NH_4VO_3 nous avons reproduit l'estimation qui nous semble contestable de l'erreur donnée par Evans (11).

(tableau 3) sont comprises entre 2.76 et 3.45 Å pour KVO_3; leur dispersion est un peu moins importante pour $TlVO_3$: 2.88 et 3.42 Å. Les principaux angles O—M^I—O sont rassemblés dans le tableau 4.

La comparaison des deux polyèdres indique que le doublet $6s^2$ du thallium est stéréochimiquement inactif dans cette structure. Cette activité lorsqu'elle se manifeste, se traduit en effet par de très courtes distances thallium–oxygène (1–5) indiquant un caractère covalent de la liaison et par une disposition des anions conforme à la théorie de Gillespie et Nyholm (17).

Conclusion

Cette étude structurale confirme la relation d'isotypie que laissait pressentir le comparaison des paramètres des mailles élémentaires de $TlVO_3$ et des métavanadates des alcalins de grand rayon ionique. Elle n'a pas permis de mettre en évidence un début d'activité stéréochimique du doublet $6s^2$ du thallium I. Orgel (18) calculant l'effet du champ cristallin sur les cations d'éléments lourds et polarisables des groupes B a discuté de la manifestation de cette activité et des propriétés physiques susceptibles d'en résulter.

TABLEAU 4. Principaux angles O—M^I—O dans $TlVO_3$ et KVO_3[a]

Angles	$TlVO_3$	KVO_3 (11)
O2E—Tl—O2F′	69.43 (0.51)	73.40 (0.20)
O2E—Tl—O1D′	73.11 (0.42)	75.37 (0.17)
O2E—Tl—O3G	97.02 (0.57)	96.63 (0.24)
O2E—Tl—O3J′	113.05 (0.54)	115.87 (0.22)
O2E—Tl—O3I	143.18 (0.56)	139.61 (0.23)
O3G—Tl—O2F′	78.15 (0.55)	75.62 (0.22)
O3G—Tl—O2H	66.80 (0.57)	70.29 (0.24)
O3G—Tl—O3J′	109.42 (0.57)	107.66 (0.24)
O3G—Tl—O3I	119.78 (0.60)	123.74 (0.26)
O3G—Tl—O1D′	147.84 (0.47)	147.81 (0.22)
O2H—Tl—O3I	52.98 (0.57)	53.44 (0.22)
O2H—Tl—O3J′	74.37 (0.54)	69.83 (0.22)
O2H—Tl—O2E	163.83 (0.53)	166.93 (0.23)
O2H—Tl—O1D′	120.42 (0.42)	115.58 (0.18)
O3I—Tl—O3J′	57.09 (0.56)	55.71 (0.22)
O3I—Tl—O1D′	75.09 (0.47)	70.08 (0.20)
O3I—Tl—O2F′	115.53 (0.54)	113.64 (0.22)
O1D′—Tl—O3J′	51.97 (0.46)	52.86 (0.19)
O1D′—Tl—O2F′	69.70 (0.41)	72.21 (0.17)
O1D′—Tl—O1D	59.71 (0.25)	61.24 (0.11)
O3J′—Tl—O3J	113.53 (0.52)	111.41 (0.22)
O3J′—Tl—O2F′	58.58 (0.51)	57.94 (0.20)
O2F′—Tl—O2F	128.90 (0.49)	132.55 (0.20)

[a]La nomenclature utilisée pour les atomes d'oxygène correspond aux notations de la fig. 2. Le ′ permet de distinguer deux atomes qui se correspondent par l'opération réflexion. Les angles sont exprimés en degrés avec l'écart-type entre parenthèses.

Il est probable qu'elle se manifestera dans le système Tl_2O–V_2O_5 pour des composés plus riches en thallium tels que Tl_3VO_4 dont l'étude est en cours.

1. R. MARCHAND et M. TOURNOUX. C.R. Acad. Sc. Paris, **277**, série C, 863 (1973).
2. M. GANNE et M. TOURNOUX. C.R. Acad. Sc. Paris, **276**, série C, 1755 (1973).
3. R. MARCHAND, Y. PIFFARD et M. TOURNOUX. C.R. Acad. Sc. Paris, **276**, série C, 177 (1973).
4. A. VERBAERE, M. DION et M. TOURNOUX. J. Solid State Chem. A paraître.
5. A. VERBAERE, M. DION et M. TOURNOUX. J. Solid. State. Chem. A paraître.
6. P. MAHE et M. R. LEE. C.R. Acad. Sc. Paris, **277**, série C, 307 (1973).
7. H. SORUM. Kong norske Vidensk. Selsk., Forh. **15**, 39 (1942).
8. V. SYNECEK et F. HANIC. Czech. J. Phys. **4**, 120 (1954).
9. H. T. EVANS, JR. et S. BLOCK. Am. Mineral. **39**, 326 (1954).
10. M. PETRASOVA, J. MADAR et F. HANIC. Chem. Svesti, **12**, 410 (1958).
11. H. T. EVANS, JR. Z. Krist. **114**, 257 (1960).
12. M. GANNE et M. TOURNOUX. C.R. Acad. Sc. Paris, **272**, série C, 1858 (1971).
13. I. L. KARLE et J. KARLE. Acta Cryst. **21**, 849 (1966).
14. E. W. HUGHES. J. Am. Chem. Soc. **63**, 1737 (1941).
15. C. T. PREWITT. Fortran IV full matrix cristallographic least squares, Program SFLS-5, 1966.
16. F. H. MOORE. Acta Cryst. **16**, 1169 (1963).
17. R. J. GILLESPIE et R. NYHOLM. Q. Rev. Chem. Soc. **11**, 339 (1957).
18. L. E. ORGEL. J. Chem. Soc. 3815 (1959).

Can. J. Chem. Downloaded from www.nrcresearchpress.com by 210.87.254.105 on 09/05/12
For personal use only.

Arrhenius Parameter for Some Gas-phase Cycloaddition Reactions of Singlet Molecular Oxygen

R. D. ASHFORD AND E. A. OGRYZLO

Department of Chemistry, University of British Columbia, Vancouver, British Columbia V6T 1W5

Received June 10, 1974

R. D. ASHFORD and E. A. OGRYZLO. Can. J. Chem. **52**, 3544 (1974).

Rate constants have been determined for several reactions of $O_2(^1\Delta_g)$ in the gas phase, at temperatures between 300 and 550 °K. The following values were obtained when the data was fitted to the Arrhenius equation:

$$k(\text{cyclopentadiene}) = 2 \times 10^8 \exp(-3900/RT)\ \text{l mol}^{-1}\ \text{s}^{-1}$$

$$k(\text{1,3-cyclohexadiene}) = 1.5 \times 10^8 \exp(-5500/RT)\ \text{l mol}^{-1}\ \text{s}^{-1}$$

$$k(\text{furan}) = 1.5 \times 10^8 \exp(-5300/RT)\ \text{l mol}^{-1}\ \text{s}^{-1}$$

$$k(\text{2-methylfuran}) = 2 \times 10^8 \exp(-3900/RT)\ \text{l mol}^{-1}\ \text{s}^{-1}$$

A charge-transfer interaction in the transition-state is invoked to account for the data available for such reactions.

R. D. ASHFORD et E. A. OGRYZLO. Can. J. Chem. **52**, 3544 (1974).

On a déterminé, à des températures allant de 300 à 550 °K, les constantes de vitesse de plusieurs réactions de $O_2(^1\Delta_g)$ en phase gazeuse. Lorsque les données ont été traitées à l'aide de l'équation d'Arrhénius, on a obtenu les valeurs suivantes:

$$k(\text{cyclopentadiène}) = 2 \times 10^8 \exp(-3900/RT)\ \text{l mol}^{-1}\ \text{s}^{-1}$$

$$k(\text{cyclohexadiène-1,3}) = 1.5 \times 10^8 \exp(-5500/RT)\ \text{l mol}^{-1}\ \text{s}^{-1}$$

$$k(\text{furanne}) = 1.5 \times 10^8 \exp(-5300/RT)\ \text{l mol}^{-1}\ \text{s}^{-1}$$

$$k(\text{méthyl-2 furanne}) = 2 \times 10^8 \exp(-3900/RT)\ \text{l mol}^{-1}\ \text{s}^{-1}$$

On fait appel à une interaction de transfert de charge dans l'état de transition pour expliquer les données disponibles pour ces réactions. [Traduit par le journal]

Can. J. Chem. Downloaded from www.nrcresearchpress.com by 210.87.254.40 on 09/05/12
For personal use only.

The addition of $O_2(^1\Delta_g)$ to conjugated dienes provides a novel illustration of the well known Diels–Alder cycloaddition reaction (1). Reaction is believed to occur by means of a concerted attack at the 1 and 4 positions of the diene to form a cyclic endoperoxide as illustrated in the following equation for cyclopentadiene (2).

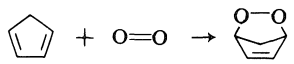

diene singlet oxygen Raniform endoperoxide

These reactions have been studied in some detail in solution (3). However, in the gas phase, no activation energies have been reported, and only a few preliminary rate constants can be found in the literature (4). These suggest a much slower rate for the same reaction in the gas phase. The present study was undertaken to measure the rate constants and activation energies for the gas-phase reactions in order to determine whether such data can shed any light on the detailed mechanism of these reactions.

Experimental Section

Singlet oxygen was produced in a conventional discharge-flow system (5) using a 100 W microwave generator in Matheson extra-dry oxygen. The major portion of the oxygen atoms were removed with a mercuric oxide ring formed immediately after the discharge by distilling a very small amount of mercury through the discharge. The remaining trace of atomic oxygen was scavenged by the addition of sufficient NO_2, after the discharge, to completely eliminate the faint O + NO afterglow.

The reaction tube was 70 cm long and had an internal diameter of 4.9 cm. It was surrounded with an electrically heated jacket which allowed the temperature to be varied between room temperature and 200 °C. The pumping rate was adjusted to produce a relatively slow linear flow rate of about 85 cm/s, when the pressure was 2.5 Torr. Under these conditions the partial pressure of $O_2(^1\Delta_g)$ was about 0.1 Torr and about 10% is deactivated along the length of the reaction tube (chiefly in collisions with ground state oxygen molecules).

The $O_2(^1\Delta_g)$ concentration was monitored with an RCA-7265 photomultiplier which measured the "dimol"

TABLE 1. Rate constants and Arrhenius parameters for the gas phase reactions of $O_2(^1\Delta_g)$[a]

Substrate	log A	E^* (kcal/mol)	k (25 °C) (M^{-1} s^{-1})
Cyclopentadiene	8.3±0.2	3.9±0.25	3.5×10^5
1,3-Cyclohexadiene	8.2±0.15	5.5±0.2	1.6×10^4
Furan	8.2±0.15	5.3±0.2	2.1×10^4
2-Methylfuran	8.3±0.2	3.9±0.25	3.5×10^5

[a]The errors quoted represent 95% confidence limits.

Can. J. Chem. Downloaded from www.nrcresearchpress.com by 210.87.254.40 on 09/05/12
For personal use only.

emission at 6340 Å (6) through an interference filter and a "honeycomb" collimator. The photomultiplier was calibrated with an isothermal-calorimetric measurement of the $O_2(^1\Delta_g)$ concentration (7). The calorimeter could not be used throughout the experiment because the cobalt catalyst was found to lose its effectiveness for deactivating $O_2(^1\Delta_g)$ on exposure to hydrocarbons at the elevated temperatures used in these experiments.

An E.A.I. Quad 1100 mass spectrometer was used to follow the concentration of the diene at a fixed position at the end of the reaction tube. The position of the hydrocarbon inlet was continuously variable along the reaction tube. A sufficiently small amount of the diene was admitted so that (*a*) the $O_2(^1\Delta_g)$ was not significantly consumed by reaction, and (*b*) the peak-height registered by the mass spectrometer was strictly proportional to the partial pressure of the hydrocarbon in the system. To monitor the diene concentration a large mass-peak was chosen which displayed the largest drop when $O_2(^1\Delta_g)$ was introduced, *i.e.* one which showed the smallest contribution from fragmentation of the products. This was not difficult because the fragmentation pattern of the endoperoxide was quite different from that of the parent diene.

Results

Since the $O_2(^1\Delta_g)$ in the reaction tube was not measurably consumed in the observation tube when the dienes were added, the reaction could be treated as pseudo first order, and the rate constant calculated with the equation

$$[1] \qquad \ln([\text{Diene}]^0/[\text{Diene}]) = k[^1\Delta_g]t$$

$[^1\Delta_g]$ is the average singlet oxygen concentration along the reaction tube while $[\text{Diene}]^0$ and [Diene] are the concentrations of diene initially and at time t respectively. Using eq. 1, rate constants were determined at a series of temperatures between 298 and 477 °K for four dienes. The results are presented in the form of an Arrhenius plot in Fig. 1 and the Arrhenius parameters obtained by a least squares analysis are listed in Table 1 together with the rate constants at 25 °C.

Discussion

Activation energies for these reactions of singlet oxygen in the gas phase have not been reported previously. Huie and Herron (4) obtained a value of $k = 6.8 \times 10^4$ l mol^{-1} s^{-1} for the reaction with 1,3-cyclohexadiene and 1.0×10^6 l mol^{-1} s^{-1} for the reaction with 2-methylfuran at room temperature.[1] The differences between these values and those reported in Table 1 are surprising because both determinations used essentially the same technique. However, it may be significant that at least the value for 1,3-cyclohexadiene was apparently obtained by Huie and Herron without added NO_2. It is therefore possible that their higher value could be the result of interference from oxygen atoms.

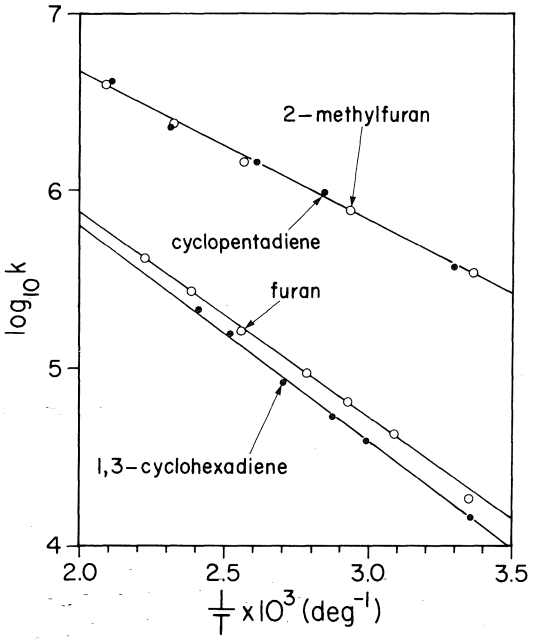

FIG. 1. Arrhenius plot of the rate constants for the reaction of $O_2(^1\Delta_g)$ with the four molecules identified on the figure.

[1]A value of 10^5 for the rate constant in the $O_2(^1\Delta_g)$ – 2-methylfuran reaction is a typographical error (19).

TABLE 2. Arrhenius parameters for some Diels–Alder reactions (8)

System	log A	E^* (kcal/mol)	k (25 °C) (M^{-1} s^{-1})
In the gas phase			
Acrolein + isoprene	6.0	18.7	2.8×10^{-8}
Acrolein + butadiene	6.2	19.7	1.2×10^{-9}
Acrolein + cyclopentadiene	6.2	15.2	1.5×10^{-5}
In dioxane			
Maleic anhydride + cyclohexadiene	5.2	12.6	8×10^{-4}
Maleic anhydride + cyclopentadiene	5.4	8.9	9×10^{-2}

The most noteworthy point which arises from our temperature dependent studies is that for this set of dienes the pre-exponential factor remains essentially constant, and the differences in reactivity can be attributed to differences in the activation energies. This also appears to be true for other Diels–Alder reactions when a given dienophile is added to a series of dienes. Some typical systems are listed in Table 2. Our results can be considered to confirm the suggestion that with a given dienophile the geometry of the transition state in the Diels–Alder reaction is fixed and hence the entropy of activation (and pre-exponential factor) shows little variation. Varying reactivities can then be identified chiefly with changes in the potential-energy barrier for the reaction.

The fact that the activation energies for these singlet oxygen reactions are much lower than those for other dienophiles can be attributed to the greater electrophilicity of singlet oxygen. It has been shown (9) that for almost all Diels–Alder reactions the rate is increased by electron-donating substituents on the diene and electron-withdrawing substituents on the dienophile. Alternatively, such substituents can be considered to lower the ionization energy of the diene and raise the electron affinity of the donor (10). The large electron affinity of singlet oxygen ($\sim$1.8 eV) could therefore also be considered the source of its higher reactivity. However, rationalization of the results is also possible in quantum mechanical terms and we will consider such a description in more detail.

The basic theoretical work of Kearns and Khan (2) established orbital and state correlation diagrams essential for the prediction of reaction products, and the elimination of orbitally forbidden paths. However the effect of substituents on reactivity was not considered. Chalvet *et al.* (11) have attempted to predict the effect of substituents in the reaction of singlet oxygen with aromatic hydrocarbons. Their calculations showed that the electron densities in the hydrocarbon were not useful criteria for predicting reactivities. However they were able to predict the point of attack on the ring system from the extent of delocalization in the assumed transition state. Such delocalization depends on the magnitude of the interaction between certain frontier orbitals (12) recently used by Sustman (13) to describe substituent effects in Diels–Alder reactions. This model assumes that only the highest occupied molecular orbital (h.o.m.o.) and the lowest unoccupied molecular orbital (l.u.m.o.) need to be considered for most chemical reactions. The change in orbital energies during the course of the reaction can be calculated, and it is a fundamental assumption of this approach that the activation energy for a reaction is determined principally by the magnitude of this interaction in the transition state. This interaction energy is most easily estimated with perturbation-theory (14), and the most significant qualitative result is that the interaction is greatest when the orbitals of the correct symmetry have similar energies. In the case of the normal Diels–Alder reactions which display the substituent effects discussed above, the arrangement of the relevant orbitals is shown in Fig. 2. Orbital occupancy is indicated with arrows. The relative positions of the orbital energy-levels on the reactant have been estimated from their ionization energies. It can be seen that with this orbital arrangement the initially dominant interaction is most probably between the π^* orbital on the dienophile and ψ_2 on the diene since π and ψ_3 have a much greater energy separation. The merit of this approach lies in its ability to account for the rate-accelerating effect of electron with-

Can. J. Chem. Downloaded from www.nrcresearchpress.com by 210.87.254.40 on 09/05/12
For personal use only.

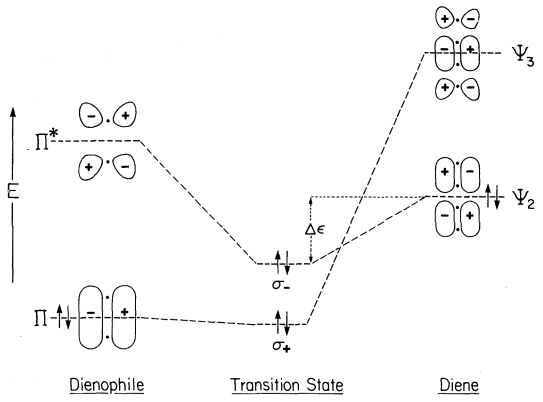

FIG. 2. An illustration of the h.o.m.o.–l.u.m.o. interactions in the normal Diels–Alder reaction.

drawing substituents on the dienophile and electron donating groups on the diene. Both changes would bring the two levels closer together causing a greater interaction in the transition state and thus a lower activation energy for the reaction.

There is, however, a difficulty when an attempt is made to fit the reactivity of $O_2(^1\Delta_g)$ into this orbital model. Since the effect of substituents on the diene parallels that observed for the normal Diels–Alder reaction, it is tempting to simply disregard the fully occupied antibonding π^* orbital (π_y^*) and bonding π orbital (π_y) on the oxygen (since they have the wrong symmetry for interaction with the diene) and then identify the π_x^* and π_x orbitals with the l.u.m.o. and h.o.m.o. orbitals of the normal dienophile discussed above. This would yield an energy-level diagram for the singlet oxygen reaction which is qualitatively similar to that shown in Fig. 2. In this way the effect of substituents on the diene is accounted for as it was with other dienophiles, and the greater reactivity of $O_2(^1\Delta_g)$ could be attributed to a better energetic-coincidence between π_x^* and ψ_2. However, when an attempt is made to justify the positioning of these energy levels using the ionization energy of $O_2(^1\Delta_g)$, difficulties arise. The ionization energies of the dienes lie between 8 and 9 eV, which fixes the position of ψ_2. However, the 11 eV ionization energy of $O_2(^1\Delta_g)$ is now a measure of the π^*-orbital energy (rather than the π-orbital as it was for ethylene derivatives). The position of the π-orbital has been established at 15.3 eV with photoelectron spectroscopy (15). This places the π^* orbital about 4.3 eV above the π orbital in agreement with the observed $\pi \rightarrow \pi^*$ transition energy in O_2 (16). This reasoning leads to the positions of the orbitals on an energy level diagram as illustrated in Fig. 3. Substituents on the diene which raise the level of ψ_2 now cause a decrease in the interaction between π_x and ψ_2. However, it can be seen from an examination of Fig. 3 that it is not the magnitude of this interaction which is important now, it is the position of the new orbital (σ^-) in the transition state relative to ψ_2 on the diene, *i.e.* the magnitude of ΔE, and this is determined mainly by the energy gap between ψ_2 and π_x^*. The addition of electron-donating substituents on the diene would still have the effect of raising the level of ψ_2, but this would lead to a larger value of ΔE, causing a greater stabilization in the transition state and a lower activation energy for the reaction.

If the above description of the system is correct, the reaction is driven chiefly by a true charge-transfer interaction rather than an orbital-interaction such as may occur in the "normal" Diels–Alder reaction.[2] Consequently

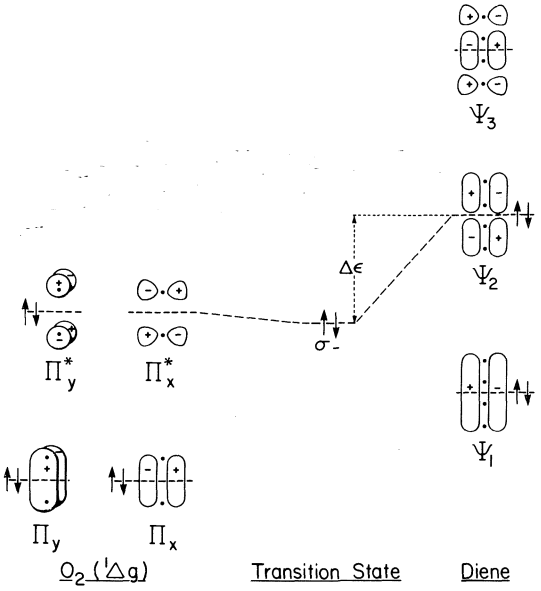

FIG. 3. Orbital interactions between dienes and singlet oxygen if the l.u.m.o. on oxygen lies below the h.o.m.o. on the diene.

[2]Fukui (12) has described the normal Diels–Alder reaction in terms of "electron-flow". However, this is qualitatively different from the present system in which the energy levels of the isolated reactants have not been significantly altered at the point where charge transfer occurs.

Can. J. Chem. Downloaded from www.nrcresearchpress.com by 210.87.254.40 on 09/05/12
For personal use only.

TABLE 3. Rate constants and Arrhenius parameter for reactions of $O_2(^1\Delta_g)$ in methanol (3)

Substrate	log A	E^* (kcal/mol)	k (25 °C) (M^{-1} s^{-1})
Cyclopentadiene	7.7	0.25	3.5×10^7
1,3-Cyclohexadiene	7.2	1.3	5×10^6
Furan	7.6	0.2	3.2×10^7
2-Methylfuran	7.8	0.4	3.8×10^7

one would predict a polar transition state and hence a significant solvent effect on the reaction. These reactions have been studied in solution and the results reported by Koch (3) are given in Table 3. It is difficult to assess the complex procedure through which Koch obtained these activation energies, and it is unfortunate that the lifetimes of singlet oxygen which are consistent with his data are somewhat different from those obtained later by more direct techniques (16). The values of k (25 °C) and log A in Table 3 have been calculated from his data using the more recent value for the singlet oxygen lifetime in methanol (17). It will be noted that the rate constants are between 10^2 and 10^3 times greater in solution and this is due to the very much lower activation energy for the reactions in solution. Such a large difference between the gas and condensed phase parameters is not observed for the normal Diels–Alder reaction (18), but is consistent with the "charge transfer" mechanism discussed above for the singlet oxygen reaction since the solvent would be expected to produce a more stable charge transfer transition state. With an activation energy approaching zero in methanol a great variation in the rate constant would not be expected when the solvent is changed. This is indeed the experimental observation reported by Young *et al.* (17) for the very fast reaction with 2,5-diphenylfuran.

Summary

A consideration of the orbital energy levels in $O_2(^1\Delta_g)$ relative to those in most cyclic dienes which form endoperoxides suggests that the reaction rate may be governed by the magnitude of the charge-transfer interaction in the transition state. This view is supported by the large increase in rate constant which occurs when these reactions are carried out in solution. The data available indicates that this increased reactivity can be identified with a decrease in activation energy to almost zero in the condensed phase. Consequently no appreciable variation in the rate constant would be anticipated when the solvent is changed. Indeed, changes in the pre-exponential factor could more than compensate for the effect of any further change in E^* by the solvent. Unfortunately, activation energies for these reactions, in different solvents, have not yet been reported.

Financial assistance from the National Research Council of Canada is gratefully acknowledged.

1. K. GOLLNICK and G. O. SCHENK. *In* Organic chemistry. vol. 8. 1,4-Cycloaddition reactions. *Edited by* J. Hamer. Academic Press, New York, N.Y. 1967. pp. 255–344.
2. D. R. KEARNS and A. U. KHAN. Photochem. Photobiol. **10**, 193 (1969).
3. E. KOCH. Tetrahedron, **24**, 6295 (1968).
4. R. E. HUIE and J. H. HERRON. Int. J. Chem. Kinet. **5**, 197 (1973).
5. K. FURUKAWA, E. W. GRAY, and E. A. OGRYZLO. Ann. N.Y. Acad. Sci. **171**, 175 (1970).
6. J. S. ARNOLD, R. J. BROWNE, and E. A. OGRYZLO. Photochem. Photobiol. **4**, 963 (1965).
7. L. W. BADER and E. A. OGRYZLO. Discuss. Faraday Soc. **37**, 46 (1964).
8. A. WASSERMAN. Diels–Alder reactions. Elsevier Publishing Co., Amsterdam. 1965. p. 50.
9. J. SAUER. Angew. Chem. Int. Ed. **6**, 16 (1967).
10. A. I. KONOVALOV, V. D. KISELEV, and O. A. VIGDOROVICH. Zhur. Org. Khim. **3**, 2085 (1967).
11. O. CHALVET, R. DANDEL, G. H. SCHMID, and J. RIGARIDY, Tetrahedron, **26**, 365 (1970).
12. K. FUKUI. Acc. Chem. Res. **4**, 57 (1971).
13. R. SUSTMAN. Tetrahedron Lett. 2721 (1971).
14. W. C. HENDRON. Chem. Rev. **72**, 157 (1972).
15. M. I. ALJOBOURY, D. P. MAY, and D. W. TURNER. J. Chem. Soc. 616 (1965).
16. G. HERZBERG. Spectra of diatomic molecules. Van Nostrand Co. Inc., Princeton, N.J. 1950.
17. R. H. YOUNG, K. WEHRLY, and R. L. MARTIN. J. Am. Chem. Soc. **93**, 5774 (1971).
18. S. W. BENSON. Foundations of chemical kinetics. McGraw–Hill Book Co., N.Y. 1960. p. 509.
19. J. H. HERRON and R. E. HUIE. Private communication.

Can. J. Chem. Downloaded from www.nrcresearchpress.com by 210.87.254.40 on 09/05/12
For personal use only.

An Electron Spin Resonance Study of the Spin Adducts of OH and HO_2 Radicals with Nitrones in the Ultraviolet Photolysis of Aqueous Hydrogen Peroxide Solutions[1]

JOHN R. HARBOUR, VIVIAN CHOW, AND JAMES R. BOLTON[2]

Photochemistry Unit, Department of Chemistry, University of Western Ontario, London, Ontario N6A 3K7

Received May 16, 1974

JOHN R. HARBOUR, VIVIAN CHEW, and JAMES R. BOLTON. Can. J. Chem. **52**, 3549 (1974).

The photolysis of H_2O_2 in aqueous solution has been used to study and characterize electron spin resonance (e.s.r.) spectra of the ·OH and HO_2· radical spin adducts with the spin traps 5,5-dimethyl-1-pyrroline-1-oxide (DMPO) and phenyl-*t*-butyl nitrone (PBN). At high concentrations of spin trap and low concentrations of H_2O_2 an e.s.r. spectrum is obtained which we assign to the ·OH radical adduct (for DMPO, $a^N = 15.3$ G, $a_\beta^H = 15.3$ G, $a_{\gamma_1}^H = 0.61$ G, $a_{\gamma_2}^H = 0.25$ G, and $g = 2.0060$; for PBN, $a^N = 15.3$ G, $a_\beta^H = 2.75$ G, and $g = 2.0057$). At low concentrations of spin trap and high concentrations of H_2O_2 a second spin adduct spectrum is obtained which we assign to the spin adduct of the HO_2· radical (for DMPO, $a^N = 14.3$ G, $a_\beta^H = 11.7$ G, $a_\gamma^H = 1.25$ G, $g = 2.0061$; for PBN, $a^N = 14.8$ G, $a_\beta^H = 2.75$ G, and $g = 2.0057$).

JOHN R. HARBOUR, VIVIAN CHEW et JAMES R. BOLTON. Can. J. Chem. **52**, 3549 (1974).

On utilise la photolyse du peroxyde d'hydrogène en solution aqueuse pour étudier et caractériser les spectres rpe des adduits de ·OH et de HO_2· avec les pièges à spin diméthyl-5,5 pyrroline-1 oxyde-1 (DMPO) et phényl *t*-butyl nitrone (PBN). A des hautes concentrations de piège à spin et à de basses concentrations de H_2O_2, un spectre rpe est obtenu qui peut être assigné à l'adduit du radical ·OH (pour DMPO, $a^N = 15.3$ G, $a_\beta^H = 15.3$ G, $a_{\gamma_1}^H = 0.61$ G, $a_{\gamma_2}^H = 0.25$ G et $g = 2.0060$; pour PBN, $a^N = 15.3$ G, $a_\beta^H = 2.75$ G et $g = 2.0057$). A des basses concentrations de piège à spin et à de hautes concentrations de H_2O_2, un deuxième spectre rpe est obtenu qui peut être assigné à l'adduit du radical HO_2· (pour DMPO, $a^N = 14.3$ G, $a_\beta^H = 11.7$ G, $a_\gamma^H = 1.25$ G, $g = 2.0061$; pour PBN, $a^N = 14.8$ G, $a_\beta^H = 2.75$ G et $g = 2.0057$). [Traduit par le journal]

Introduction

The technique of spin trapping of short-lived radical intermediates (R·) by nitrones and other spin traps has become a valuable addition to the methods of studying reaction mechanisms. This technique has been reviewed recently by Janzen (1). The basic reaction can be described as

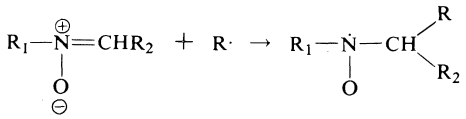

The resultant spin adduct is usually a relatively stable nitroxide radical which can be characterized by electron spin resonance (e.s.r.) spectroscopy. In favorable cases it is possible to identify the radical R· from the parameters of the nitroxide e.s.r. spectra (principally *g* factors and hyperfine splittings). Eventually through the compilation of the e.s.r. parameters for a wide variety of spin adducts, one should be able to identify an unknown radical intermediate by a comparison of the e.s.r. parameters.

The two nitrone spin traps which have found wide use are 5,5-dimethyl-1-pyrroline-1-oxide (DMPO)

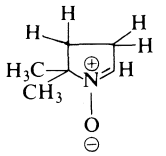

and phenyl-*t*-butylnitrone (PBN)

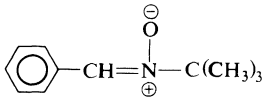

DMPO has the advantage that the β-hydrogen hyperfine splitting of the spin adduct is quite sensitive to the nature of R· (ref. 2 gives an

[1]Contribution No. 111 of the Photochemistry Unit, University of Western Ontario, London, Ontario.

[2]To whom correspondence should be addressed.

Can. J. Chem. Downloaded from www.nrcresearchpress.com by 210.87.254.42 on 09/05/12
For personal use only.

Can. J. Chem. Downloaded from www.nrcresearchpress.com by 210.87.254.42 on 09/05/12
For personal use only.

extensive list of spin adducts with DMPO); whereas PBN has the advantage of forming very stable spin adducts.

We have recently begun a study of photochemically induced electron transfer processes in aqueous solution. In the course of this work we detected spin adducts from what appeared to be the hydroxyl radical. However, a search of the literature revealed that no validated case of such spin adducts in aqueous solution has been presented. In this paper we hope to provide the evidence necessary to characterize the spin adducts of not only the ·OH radical but also the HO_2· radical, radicals which are of considerable importance as intermediates in chemical, photochemical, and radiolysis processes in aqueous solution.

Previous work (3–8) has indicated that ·OH and HO_2· radicals are the major intermediates generated in the u.v. photolysis of aqueous hydrogen peroxide. We have utilized both DMPO and PBN as spin traps in this system, and we will demonstrate that indeed ·OH and HO_2· radicals can be trapped and the spin adduct e.s.r. spectra characterized for these radicals.

Materials and Methods

Electron spin resonance spectra were obtained on a Varian E12 electron spin resonance spectrometer. Second derivative spectra were obtained by combining the 100 and 1 kHz modulation and detection systems. The u.v. irradiation source was a Hanovia Model 977B-1 KW Hg–Xe lamp in a Schoeffel Model LH 151N lamp housing. For some experiments a flash photolysis apparatus manufactured by Photochemical Research Associates was used in conjunction with the e.s.r. The flash lamp used was a Novatron 185 manufactured by Xenon Corporation. This apparatus and technique have been described elsewhere (9).

H_2O_2 (30%) was obtained from Anachemia Chemicals Ltd. Dilution was carried out with twice distilled, deionized water. PBN was a gift from Dr. E. G. Janzen and DMPO was a gift from Dr. K. S. Chen.

D_2O_2 (1%) was prepared by diluting 70% H_2O_2 (a gift from E. I. DuPont of Nemours and Company) with 99.7 atom% D_2O (Merck, Sharp and Dohme of Canada Ltd.).

Results and Discussion

Ultraviolet photolysis of a 1% aqueous H_2O_2 solution in the presence of DMPO generates the e.s.r. signal ($g = 2.0060 \pm 0.0002$) seen in Fig. 1*a*. The 1:2:2:1 quartet pattern[3] ($a =$ 15.3 G)[4] can be explained by the accidental equality of a^N and a^H. A pH study over the range $1 \leq$ p$H \leq 9.5$ showed no variation in either g factor or in the observed splitting. Variation of the DMPO concentration over the range 10^{-4} to 10^{-1} M affects only the intensity of the e.s.r. signal.

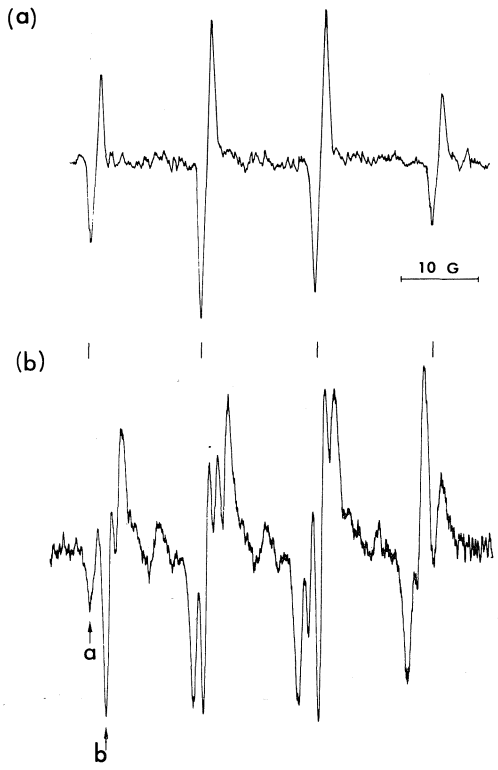

FIG. 1. Electron spin resonance spectra (microwave power 10 mW; modulation amplitude 0.5 G; time constant 0.3 s; scan time 4 min) obtained upon u.v. photolysis of H_2O_2 solutions in the presence of DMPO. (*a*) 1% H_2O_2 and 1×10^{-2} M DMPO; (*b*) 30% H_2O_2 and 8×10^{-2} M DMPO.

On increasing the H_2O_2 concentration to 30% in the presence of 8×10^{-2} M DMPO a second e.s.r. signal appears (see Fig. 1*b*) under u.v. photolysis. This signal is characterized by $g = 2.0061 \pm 0.0002$[5] $a^N = 14.3$ G, $a_\beta^H = 11.7$ G, and $a_\gamma^H = 1.25$ G. Both of these spectra decay upon termination of illumination

[3]Additional small hyperfine splittings are seen under high resolution (see below).

[4]Hyperfine splittings are quoted with a confidence limit of $\pm 1\%$ or ± 0.03 G whichever is the larger.

[5]Although the absolute error in g is ± 0.0002, there is no doubt that this spectrum is centered at a lower field from the spectrum in Fig. 1*a* and hence has a slightly higher g factor.

Can. J. Chem. Downloaded from www.nrcresearchpress.com by 210.87.254.42 on 09/05/12
For personal use only.

but with different rates, the spectrum in Fig. 1*a* decaying more rapidly. Hence, under continuous illumination, the observed ratio of the two signals is continuously changing. In order to bypass this problem we employed the technique of flash photolysis–e.s.r. (9). A single flash under our experimental conditions was sufficient to generate an observable signal. By monitoring at fields *a* and *b* (see Fig. 1*b*), the intensity increase following a single flash I_a and I_b and the resultant ratio I_a/I_b could be measured.[6]

Using the flash technique, I_a/I_b was found to vary extensively as a function of reactant concentrations. At high concentrations of DMPO in a 30% H_2O_2 solution, I_a/I_b is large, that is the 1:2:2:1 quartet dominates; while at low concentrations of DMPO I_a/I_b is small indicating that the second radical signal is the major spin adduct observed.

These results can be interpreted in terms of the following mechanism. Ultraviolet light initially causes the homolytic cleavage of H_2O_2

[1] $$H_2O_2 \xrightarrow{h\nu} 2\cdot OH$$

In the presence of DMPO, the ·OH radical can be trapped

[2] 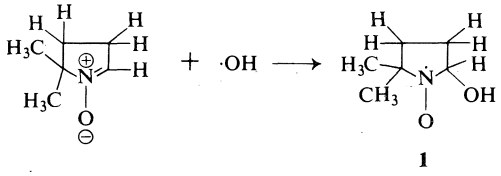

1

Radical **1** is assumed to be responsible for the 1:2:2:1 quartet spectrum.

However, some of the ·OH radicals may react with H_2O_2.

[3] $$\cdot OH + H_2O_2 \rightarrow H_2O + HO_2\cdot$$

The HO_2· radical may also be trapped by DMPO

[4] 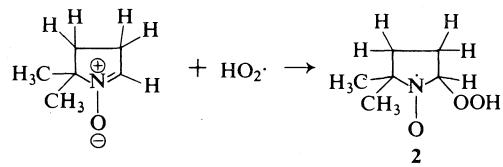

2

[6]The rate of decay of the signals is slow compared to the time necessary to record the signal amplitude following a flash.

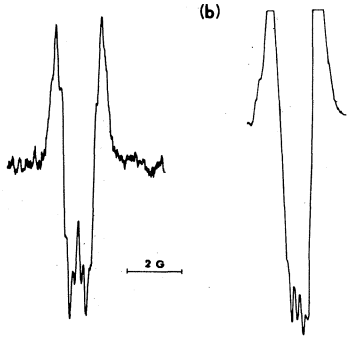

FIG. 2. Second derivative e.s.r. spectra (microwave power 4 mW; modulation amplitude 0.1 G; time constant 1.0 s; scan time 8 min) of the low field line of the hydroxy adduct obtained upon u.v. photolysis of: (*a*) 1% D_2O_2 in D_2O with 1×10^{-2} *M* DMPO; (*b*) 1% H_2O_2 in H_2O with 1×10^{-2} *M* DMPO.

Radical **2** is assumed to be responsible for the second radical spectrum in Fig. 1*b*.

Experiments carried out using 1% D_2O_2 in D_2O provided additional confirmation of the assignment of the spin adducts. In radical **1** one would expect a slightly narrower linewidth due to the replacement of the OH proton by a deuteron ($\gamma_H/\gamma_D = 6.5$) providing the OH proton hyperfine splitting contributes to the overall linewidth. Indeed a 10–15% narrowing of the radical **1** linewidths was observed. In addition, some additional hyperfine structure became apparent in the D_2O_2 system. In order to confirm this, a second-derivative recording was made to enhance the resolution. This spectrum along with the corresponding OH adduct signal are shown in Fig. 2. The improved resolution in the OD adduct spectrum is clearly evident. The two γ proton hyperfine splittings are $a_{\gamma_1}^{H} = 0.61$ G and $a_{\gamma_2}^{H} = 0.25$ G. The observation of a γ hyperfine splitting is important since all previous oxy adducts reported exhibit at least one γ hyperfine splitting (2).

At low concentrations of spin trap (or in the absence of spin trap) evolution of oxygen is evident upon illumination as indicated through the formation of bubbles in the e.s.r. sample cell. O_2 evolution in this system is thought to originate according to one or more of the following three mechanisms (3, 10)

[5] $$HO_2\cdot + HO_2\cdot \rightarrow H_2O_2 + O_2$$

[6] $$\cdot O_2^- + \cdot O_2^- + 2H_2O \rightarrow H_2O_2 + O_2 + 2OH^-$$

or

Can. J. Chem. Downloaded from www.nrcresearchpress.com by 210.87.254.42 on 09/05/12
For personal use only.

[7] $$\begin{cases} HO_2\cdot + \cdot OH \rightarrow H_2O_3 \\ H_2O_3 \rightarrow H_2O + O_2 \end{cases}$$

($HO_2\cdot$ and $\cdot O_2^-$ are in equilibrum. See below.) Thus the formation of $HO_2\cdot$ or $\cdot O_2^-$ is a necessary prerequisite for O_2 evolution. Hence, the observation of the $HO_2\cdot$ spin adduct at low concentrations of DMPO is consistent with the above mechanisms.

At high concentrations of DMPO where the trapping of the ·OH radical predominates, no oxygen evolution can be detected. This is consistent with the fact that $HO_2\cdot$ cannot be formed when most of the ·OH radicals are trapped.

We have obtained similar results with the PBN spin trap as illustrated in Fig. 3*a* and *b*. At 1% H_2O_2 concentration the ·OH radical adduct is observed with $a^N = 15.3$ G and $a_\beta^H = 2.75$ G. At 30% H_2O_2 concentration the $HO_2\cdot$ radical adduct is detected with $a^N = 14.8$ G and $a_\beta^H = 2.75$ G. Both radicals have a g factor of 2.0057. Hence either nitrone can act as an effective trap for ·OH and $HO_2\cdot$ radicals, although DMPO provides a more distinct differentiation between the two radical adducts.

The ·OH radical adduct of PBN has been reported by Janzen *et al.* (11) in a benzene solution. They obtained $a^N = 14.63$ G and $a_\beta^H = 2.88$ G. Our results for aqueous solutions are close to their values when consideration is made of the solvent dependence of nitroxide hyperfine splittings.

It is of importance to mention the acid–base equilibrium of the $HO_2\cdot$ radical

[8] $$HO_2\cdot \rightleftharpoons H^+ + \cdot O_2^-$$

The pK_a for this equilibrium is 4.4 ± 0.4 (3, 10). This raises the question of whether or not these spin traps are capable of initially trapping $\cdot O_2^-$ followed by protonation to yield the HO_2 adduct. Previous studies (1) suggest that only neutral radicals are trapped by nitrones. In order to test this we carried out a study of the pH dependence of the spin trapping reaction in 30% H_2O_2 over a pH range of 2.5 to 5.5. There was relatively little change in the ratio I_a/I_b. There are two interpretations of this result. Either $HO_2\cdot$ and $\cdot O_2^-$ are trapped by the nitrones at about the same rate, or $HO_2\cdot$ is trapped before the acid–base equilibrium can be established. Czapski and Bielski (3) report that the $HO_2\cdot$ radical relaxes to equilibrium in about 1 μs. Thus a considerable amount of spin trapping could occur before equilibration if spin trapping occurs at a diffusion controlled rate.

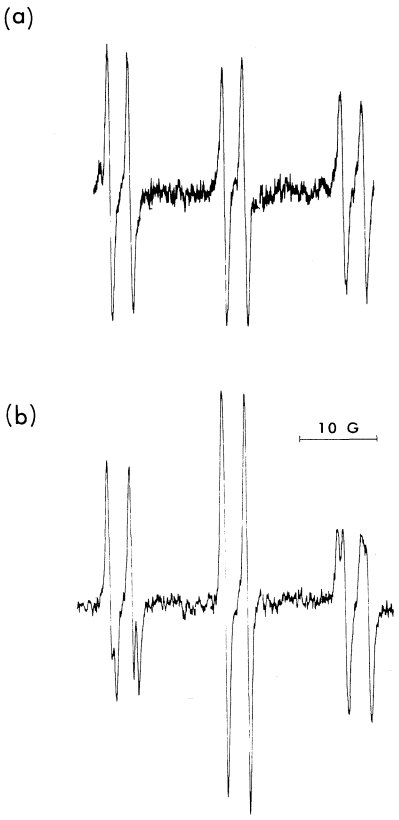

FIG. 3. Electron spin resonance spectra (microwave power 10 mW; modulation amplitude 0.5 G; time constant 0.3 s; scan time 4 min) obtained upon u.v. photolysis of H_2O_2 solutions in the presence of a saturated solution of PBN. (*a*) 1% H_2O_2; (*b*) 30% H_2O_2.

At a pH near 7.0, the $HO_2\cdot$ adduct did increase relative to the ·OH radical adduct. However, at this pH, the base catalyzed decomposition of H_2O_2 becomes important since O_2 evolution in the dark is apparent. $HO_2\cdot$ is known to be an intermediate in that reaction.

Conclusion

We believe we have provided conclusive evidence for the identification of the ·OH and $HO_2\cdot$ radical adducts with the spin traps DMPO and PBN in aqueous solution. The e.s.r. parameters for these spin adducts can now be used with confidence in the study of re-

actions involving ·OH or HO_2· radical intermediates in aqueous solution.

1. E. G. JANZEN. Acc. Chem. Res. **4**, 31 (1971).
2. E. G. JANZEN and J. I-PING LIU. J. Magn. Reson. **9**, 510 (1973).
3. G. CZAPSKI and B. H. BIELSKI. J. Phys. Chem. **67**, 2180 (1963).
4. I. SAFARIK. Magy. Kem. Foly. **73**, 382 (1967).
5. K. TAKAKURA and B. RANBY. J. Phys. Chem. **72**, 164 (1968).
6. S. J. WYARD, R. C. SMITH, and F. J. ADRIAN. J. Chem. Phys. **49**, 2780 (1968).
7. C. H. BAMFORD and R. P. WAYNE. Photochemistry and reaction kinetics. *Edited by* P. G. Ashmore, F. S. Dainton, and T. M. Sugden. Cambridge University Press, Cambridge, U.K. 1967. Chapt. 3.
8. K. KUWATA, Y. KOTAKE, K. INADA, and M. ONO. J. Phys. Chem. **76**, 2061 (1972).
9. J. R. BOLTON and J. T. WARDEN. *In* Creation and detection of the excited state, Vol. 2. *Edited by* W. R. Ware. Marcel Dekker, New York. In press.
10. K. SEHESTED, O. L. RASMUSSEN, and H. FRICKE. J. Phys. Chem. **72**, 626 (1968).
11. E. G. JANZEN, T. KASAI, and K. KUWATA. Bull. Chem. Soc. Jap. **46**, 2061 (1973).

Can. J. Chem. Downloaded from www.nrcresearchpress.com by 210.87.254.42 on 09/05/12
For personal use only.

Can. J. Chem. Downloaded from www.nrcresearchpress.com by 210.87.254.6 on 09/05/12
For personal use only.

Di-(1-adamantyl)iminoxy. Preparation and Dipole Moment[1]

D. LINDSAY, E. C. HORSWILL, D. W. DAVIDSON, AND K. U. INGOLD

Division of Chemistry, National Research Council of Canada, Ottawa, Canada K1A 0R9

Received May 24, 1974

D. LINDSAY, E. C. HORSWILL, D. W. DAVIDSON, and K. U. INGOLD. Can. J. Chem. **52**, 3554 (1974).

The di-(1-adamantyl)iminoxy radical, $(1\text{-Ad})_2C{=}NO\cdot$, has been prepared from the corresponding imine. It is a blue, crystalline material that is stable indefinitely in air at room temperature in the solid state. Dipole moments have been measured in benzene at 30° for the radical (2.90 D), for $(1\text{-Ad})_2C{=}NH$ (2.49 D), and for $(1\text{-Ad})_2C{=}NOMe$ (0.79 D). In the radical the unpaired spin density on nitrogen is estimated to be *ca.* 25%.

D. LINDSAY, E. C. HORSWILL, D. W. DAVIDSON et K. U. INGOLD. Can. J. Chem. **52**, 3554 (1974).

On a préparé, à partir de l'imine correspondante, le radical di(adamantyl-l) iminoxyle, $(Ad\text{-}1)_2C{=}NO\cdot$. Ce composé est bleu et cristallisé; à la température de la pièce et à l'air, il est stable indéfiniment dans cet état. On a mesuré les moments dipolaires du radical (2.90 D), du $(Ad\text{-}1)_2C{=}NH$ (2.49 D) et de $(Ad\text{-}1)_2C{=}NOMe$ (0.79 D) dans le benzène à 30°. On estime que dans le radical, la densité de spin d'électron non pairé sur l'azote est d'environ 25%.

[Traduit par le journal]

Di-*t*-butyliminoxy, $(t\text{-Bu})_2C{=}NO\cdot$, was prepared in these laboratories a few years ago (1). It was the first σ radical (2) to be isolated (a sky-blue liquid, f.p. −21°). In an attempt to obtain a longer-lived and, particularly, a crystalline[2] iminoxy we have prepared di-(l-adamantyl)iminoxy, $(1\text{-Ad})_2C{=}NO\cdot$, from the parent imine[3] (3) by the procedure used for $(t\text{-Bu})_2C{=}NO\cdot$ (1).

$$(1\text{-Ad})_2C{=}NH \xrightarrow{H_2NOH} (1\text{-Ad})_2C{=}NOH \xrightarrow{Ag_2O} (1\text{-Ad})_2C{=}NO\cdot$$

Compound	Melting point (°C)	Nuclear magnetic resonance data* (p.p.m.)	Infrared† (cm^{-1}) C=N	Infrared† (cm^{-1}) N—O
$(1\text{-Ad})_2C{=}NH$	140–143 (lit.(3) 113–116)	1.70 (12 H), 1.95 (18 H)	1582 (strong, sharp)	
$(1Ad)_2C{=}NOH$	268–271	Insoluble	1610 (weak, broad)	930 (strong, sharp)
$(1\text{-Ad})_2C{=}NO$	121—122.5		1595 (strong, sharp)	

*The n.m.r. spectra in $CDCl_3$ are quoted in p.p.m. downfield from TMS.
†The i.r. spectra were measured in KBr.

The radical was purified by passage through Woelm 'dry column' silica in hexane. The pale-blue crystalline radical is stable indefinitely in air at room temperature. In degassed benzene solutions the e.s.r. spectral parameters are: $a^{14N} = 31.14$, $a^{15N} = 43.3$, $a^{13C} = 8.0$ and 13.6 G, $g = 2.00481$, and the extinction coefficient is 5.7 (800 nm). These solutions were of sufficient

[1]NRCC No. 14226.

[2]We had hoped to determine the structure by X-ray crystallography but unfortunately it was not possible to obtain sufficient data from the crystals of $(1\text{-Ad})_2C{=}NO\cdot$.

[3]All compounds had appropriate mass spectra and analyzed acceptably for C, H, and N.

stability for us to measure the radical's dipole moment. This was done in order to obtain a measure of the extent of delocalization of the unpaired electron towards nitrogen from its formal site on oxygen.

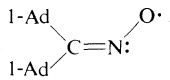

1

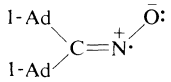

2

Dielectric constant measurements were made in benzene solution at 30° and 10 kHz with a three-terminal cell and a GR 1615-A Capacitance bridge. Dipole moments were evaluated by the method of Guggenheim as described elsewhere (4). Measurements were made on $(1\text{-Ad})_2C{=}NH$, $(1\text{-Ad})_2C{=}NO\cdot$, and (since the oxime was too insoluble) on $(1\text{-Ad})_2C{=}NOMe$ which was prepared by methylation with MeI of $(1\text{-Ad})_2C{=}NONa$ in dimethyl formamide (m.p. 117–118°; n.m.r. 1.67 (12 H), 1.96 (12 H), 2.28 and 2.32 (6 H), 3.73 (3 H); i.r. no C=N band (1480–1700), but strong, sharp bands at 893, 998, and 1045). The following dipole moments were obtained: $(1\text{-Ad})_2C{=}NH$, 2.49 ± 0.04 D; $(1\text{-Ad})_2C{=}NO\cdot$, 2.90 ± 0.07 D; and $(1\text{-Ad})_2C{=}NOMe$, 0.79 ± 0.08 D.

While various assumptions *could* be made about the detailed structures of these compounds and the individual bond moments, we feel that, so far as the question of electron delocalization goes, the following approach is justified by its simplicity. For $(1\text{-Ad})_2C{=}NOMe$, we take the C=N—O angle to be *ca.* 110° (as in $Me_2C{=}NOH$ (5)) and the N—O—Me angle to be similar. The Me→O group moment is presumably the same as that in ethers, *viz.* (6), 1.2 D (*i.e.*, 0.8 D for C→O plus 0.4 D for H_3→C), and the N→O bond moment is 0.5 D (6). If the $(1\text{-Ad})_2C{\Rightarrow}N$ moment is represented by x, and if there is a *trans* configuration about the N—O bond, we have:

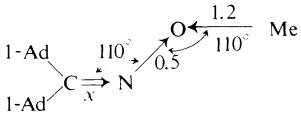

i.e.,

$$0.79 = [(x + 0.5\cos(70°) - 1.20)^2 + (0.5\sin 70°)^2]^{\frac{1}{2}}$$

which yields $x = 1.68$ D. This value is in satisfactory agreement[4] with an estimated $(alkyl)_2C{\Rightarrow}N$ moment of 1.8 D (*i.e.*, 1.4 D for C⇒N (7) and *ca.* 0.4 D for $(alkyl)_2$→C).

Theoretical calculations by the INDO method have suggested that in the $H_2C{=}NO\cdot$ radical the C=N—O angle is 135° (8). The N→O bond moment in $(1\text{-Ad})_2C{=}NO\cdot$, y, is therefore given by,

$$2.90 = [(x + y\cos(45°))^2 + (y\sin 45°)^2]^{\frac{1}{2}}$$

which yields $y = 1.76$ D. The extent to which this dipole moment represents delocalization of the electron is somewhat uncertain, since delocalization must reduce the "normal" N→O bond moment of 0.5 D. We compromise between 1.76 and 1.26 D and assign 1.51 ± 0.25 D to delocalization. If the N—O bond length is taken to be 1.25 Å,[5] the extent of delocalization, q, is given by,

$$q = \frac{1.51 \pm 0.25 \text{ D}}{4.8 \times 10^{-10} \text{ e.s.u.} \times 1.25 \text{ Å}} = 0.25 \pm 0.04$$

We conclude that the unpaired spin density on nitrogen, $\rho_N(=q)$, is *approximately* 25%, or canonical structures **1** and **2** contribute *ca.* 75% and 25%, respectively, to the radical.

From the anisotropic e.s.r. spectra of a number of iminoxys, Fox and Symons (10) have estimated $\rho_N = 41 \pm 5\%$. Our own value for ρ_N is in reasonable agreement with this, considering the uncertainties in the interpretation of the two types of data. It is also worth noting, that dipole moment measurements on a dialkyl nitroxide radical have given a lower value for ρ_N (27% (11)) than that estimated from e.s.r. spectra (50% (12)). However, the O—H bond strengths, D[O—H], in hydroxylamines and in oximes make it certain that the unpaired electron is delocalized to a greater extent in nitroxides than in iminoxys. It is perhaps even justifiable to estimate ρ_N from D[O—H] as follows. For

[4]This agreement tends to confirm the *trans* geometry of the N—O bond since a conformation having the Me group out of the C=N—O plane will reduce x. For example, if the Me—O bond made an angle of 30° with the plane, $x = 1.08$ D. Rotation about the N—O bond is completely prevented by the *syn*-adamantyl group.

[5]The N—O bond length in $Me_2C{=}NOH$ is 1,36 Å (5) and in a bicyclic nitroxide radical it is 1.29 Å (9). The bond length is expected to be shorter in an iminoxy than in a nitroxide. Theoretical calculations (8) on $H_2C{=}NO\cdot$ indicate a value of 1.225 Å. Using this same geometry (8) our own INDO calculations yield a dipole moment of 1.8 D for $H_2C{=}NO\cdot$ and $\rho_N = 12\%$.

Can. J. Chem. Downloaded from www.nrcresearchpress.com by 210.87.254.6 on 09/05/12
For personal use only.

alkoxy radicals, D[O—H] is 104 kcal/mol (13) and the spin density on oxygen, ρ_O, ~1.0. For unhindered[6] dialkyl nitroxides, D[O—H] is 72–75 kcal (14) and $\rho_O \sim \rho_N \sim 0.5$ (12). For unhindered dialkyliminoxys, D[O—H] is 84–86 kcal (14), which yields, by a linear interpolation, $\rho_O \sim 71\%$ corresponding to $\rho_N \sim 29\%$.

The $(1\text{-Ad})_2C{=}NH$ dipole moment of 2.49 D indicates that there is a large N←H bond moment in imines. This is consistent with the fact that the proton must be fairly acidic since the imine can form a sodium salt. No dipole moment has been previously reported on any $R_2C{=}NH$ compound, presumably because of their general instability.

1. J. L. BROKENSHIRE, G. D. MENDENHALL, and K. U. INGOLD. J. Am. Chem. Soc. **93**, 5278 (1971); G. D. MENDENHALL and K. U. INGOLD. J. Am. Chem. Soc. **95**, 2963 (1973).
2. M. C. R. SYMONS. J. Chem. Soc. 2276 (1965).
3. J. H. WIERINGA, H. WYNBERG, and J. STRATING. Tetrahedron Lett. 2071 (1972).
4. R. WALKER and D. W. DAVIDSON. Can. J. Chem. **37**, 492 (1959).
5. T. K. BIERLIN and E. C. LINGAFELTER. Acta Cryst. **4**, 450 (1951).
6. J. W. SMITH. Electric dipole moments. Butterworths, London. 1955. Chapt. 4.
7. K. B. EVERARD and L. E. SUTTON. J. Chem. Soc. 2318 (1949).
8. M. F. CHIU, B. C. GILBERT, and B. T. SUTCLIFFE. J. Phys. Chem. **76**, 553 (1972).
9. A. CAPIOMONT, B. CHION, and J. LAJEROWICZ. Acta Cryst. Sect. B, **27**, 322 (1971).
10. W. M. FOX and M. C. R. SYMONS. J. Chem. Soc. A, 1503 (1966).
11. E. G. ROZANTSEV and E. N. GUR'YANOVA. Izv. Akad. Nauk SSSR, Ser. Khim. 979 (1966).
12. H. HAYAT and B. L. SILVER. J. Phys. Chem. **77**, 72 (1973).
13. S. W. BENSON and R. SHAW. Adv. Chem. Series, **75**, 288 (1968).
14. L. R. MAHONEY, G. D. MENDENHALL, and K. U. INGOLD. J. Am. Chem. Soc. **95**, 8610 (1973).

[6]Since steric factors influence the hydroxylamine or oxime to a much greater extent than the radicals (14), it is the values of D[O—H] for unhindered compounds which are appropriate in estimating ρ_O.

Can. J. Chem. Downloaded from www.nrcresearchpress.com by 210.87.254.6 on 09/05/12
For personal use only.

Electron Mobilities and Ranges in Solid Neopentane: Effect of Liquid–Solid Phase Change[1]

KYOJI SHINSAKA AND GORDON R. FREEMAN

Chemistry Department, University of Alberta, Edmonton, Alberta T6G 2G2

Received June 27, 1974

KYOJI SHINSAKA and GORDON R. FREEMAN. Can. J. Chem. **52**, 3556 (1974).

The mobility of thermal electrons, the radiolysis free ion yield, and the penetration range of epithermal electrons in neopentane increase on going from the liquid to the solid phase at the triple point (257 K). The mobility is $u = 71$ cm²/V s in the liquid at 258 K and 154 cm²/V s in the solid at 257 K; the density normalized penetration range of the secondary electrons in X-radiolysis is $b_{GP}d = 1.25 \times 10^{-6}$ g/cm² in the liquid (296–258 K) and 1.72×10^{-6} g/cm² in the solid (253–202 K). The increases at the triple point are presumably due to the greater degree of order in the solid. Electron mobility in the solid increases with decreasing temperature, $u(\text{solid}) \approx 6.8 \times 10^5 T^{-3/2}$ cm²/V s. The scattering length of neopentane is ~8 Å in the solid and ~9 Å in the liquid near the triple point.

KYOJI SHINSAKA et GORDON R. FREEMAN. Can. J. Chem. **52**, 3556 (1974).

La mobilité des électrons thermiques, le rendement en ion libre lors de la radiolyse et les taux de pénétration des électrons épithermaux dans le néopentane augmente lorsqu'on passe de la phase liquide à la phase solide au point triple (257 K). La mobilité est de $u = 71$ cm²/V s à l'état liquide à 258 K et de 154 cm²/V s à l'état solide à 257 K; le taux de pénétration normalisé pour la densité des électrons secondaires à la radiolyse-X est de

[1]Assisted by the National Research Council of Canada.

alkoxy radicals, D[O—H] is 104 kcal/mol (13) and the spin density on oxygen, ρ_O, ~1.0. For unhindered[6] dialkyl nitroxides, D[O—H] is 72–75 kcal (14) and $\rho_O \sim \rho_N \sim 0.5$ (12). For unhindered dialkyliminoxys, D[O—H] is 84–86 kcal (14), which yields, by a linear interpolation, $\rho_O \sim 71\%$ corresponding to $\rho_N \sim 29\%$.

The $(1\text{-Ad})_2C{=}NH$ dipole moment of 2.49 D indicates that there is a large N←H bond moment in imines. This is consistent with the fact that the proton must be fairly acidic since the imine can form a sodium salt. No dipole moment has been previously reported on any $R_2C{=}NH$ compound, presumably because of their general instability.

1. J. L. BROKENSHIRE, G. D. MENDENHALL, and K. U. INGOLD. J. Am. Chem. Soc. **93**, 5278 (1971); G. D. MENDENHALL and K. U. INGOLD. J. Am. Chem. Soc. **95**, 2963 (1973).
2. M. C. R. SYMONS. J. Chem. Soc. 2276 (1965).
3. J. H. WIERINGA, H. WYNBERG, and J. STRATING. Tetrahedron Lett. 2071 (1972).
4. R. WALKER and D. W. DAVIDSON. Can. J. Chem. **37**, 492 (1959).
5. T. K. BIERLIN and E. C. LINGAFELTER. Acta Cryst. **4**, 450 (1951).
6. J. W. SMITH. Electric dipole moments. Butterworths, London. 1955. Chapt. 4.
7. K. B. EVERARD and L. E. SUTTON. J. Chem. Soc. 2318 (1949).
8. M. F. CHIU, B. C. GILBERT, and B. T. SUTCLIFFE. J. Phys. Chem. **76**, 553 (1972).
9. A. CAPIOMONT, B. CHION, and J. LAJEROWICZ. Acta Cryst. Sect. B, **27**, 322 (1971).
10. W. M. FOX and M. C. R. SYMONS. J. Chem. Soc. A, 1503 (1966).
11. E. G. ROZANTSEV and E. N. GUR'YANOVA. Izv. Akad. Nauk SSSR, Ser. Khim. 979 (1966).
12. H. HAYAT and B. L. SILVER. J. Phys. Chem. **77**, 72 (1973).
13. S. W. BENSON and R. SHAW. Adv. Chem. Series, **75**, 288 (1968).
14. L. R. MAHONEY, G. D. MENDENHALL, and K. U. INGOLD. J. Am. Chem. Soc. **95**, 8610 (1973).

[6]Since steric factors influence the hydroxylamine or oxime to a much greater extent than the radicals (14), it is the values of D[O—H] for unhindered compounds which are appropriate in estimating ρ_O.

Can. J. Chem. Downloaded from www.nrcresearchpress.com by 210.87.254.5 on 09/05/12
For personal use only.

Electron Mobilities and Ranges in Solid Neopentane: Effect of Liquid–Solid Phase Change[1]

KYOJI SHINSAKA AND GORDON R. FREEMAN

Chemistry Department, University of Alberta, Edmonton, Alberta T6G 2G2

Received June 27, 1974

KYOJI SHINSAKA and GORDON R. FREEMAN. Can. J. Chem. **52**, 3556 (1974).

The mobility of thermal electrons, the radiolysis free ion yield, and the penetration range of epithermal electrons in neopentane increase on going from the liquid to the solid phase at the triple point (257 K). The mobility is $u = 71$ cm²/V s in the liquid at 258 K and 154 cm²/V s in the solid at 257 K; the density normalized penetration range of the secondary electrons in X-radiolysis is $b_{GP}d = 1.25 \times 10^{-6}$ g/cm² in the liquid (296–258 K) and 1.72×10^{-6} g/cm² in the solid (253–202 K). The increases at the triple point are presumably due to the greater degree of order in the solid. Electron mobility in the solid increases with decreasing temperature, $u(\text{solid}) \approx 6.8 \times 10^5 T^{-3/2}$ cm²/V s. The scattering length of neopentane is ~8 Å in the solid and ~9 Å in the liquid near the triple point.

KYOJI SHINSAKA et GORDON R. FREEMAN. Can. J. Chem. **52**, 3556 (1974).

La mobilité des électrons thermiques, le rendement en ion libre lors de la radiolyse et les taux de pénétration des électrons épithermaux dans le néopentane augmente lorsqu'on passe de la phase liquide à la phase solide au point triple (257 K). La mobilité est de $u = 71$ cm²/V s à l'état liquide à 258 K et de 154 cm²/V s à l'état solide à 257 K; le taux de pénétration normalisé pour la densité des électrons secondaires à la radiolyse-X est de

[1]Assisted by the National Research Council of Canada.

$b_{GP}d = 1.25 \times 10^{-6}$ g/cm² à l'état liquide (296 à 258 K) et de 1.72×10^{-6} g/cm² à l'état solide (253 à 202 K). On fait l'hypothèse que l'augmentation au point triple est probablement due à un plus grand degré d'ordre dans le solide. La mobilité des électrons à l'état solide augmente lorsque la température diminue, u(solide) est pratiquement $\approx 6.8 \times 10^5 T^{-3/2}$ cm²/V s. La longueur de diffusion du néopentane est ~8 Å à l'état solide et de ~9 Å à l'état liquide près du point triple. [Traduit par le journal]

Can. J. Chem. Downloaded from www.nrcresearchpress.com by 210.87.254.5 on 09/05/12
For personal use only.

The effect of molecular and liquid structure on the mobilities of thermal electrons in liquids is currently of great interest (1–8). Although the behavior is partially understood (1, 3, 9), many aspects remain unexplained (5, 10).

The effect of the liquid–solid phase change on the mobility of electrons in a hydrocarbon is of interest. An early report (6) indicated that the mobility in solid *n*-hexane at ~30° below the melting point was at least five times greater than that expected for electrons in the liquid at the melting point. Neopentane would be a better candidate for study because electron mobility in the liquid is relatively high (9) and the material forms a plastic crystal (11) rather than a rigid solid upon freezing. Both of these properties increase the probability of obtaining a measurable electron conductance signal in the solid. Molecules in the plastic crystal retain a significant degree of freedom of rotational motion, which would tend to inhibit the formation of fixed traps for electrons (9) in the solid.

It was also possible to measure the effect of the liquid–solid phase change on the penetration ranges of the secondary electrons in the X-irradiated hydrocarbon.

Electron mobilities and free ion yields were measured by pulse radiolysis techniques. The mobility u was calculated from eq. 1.

$$[1] \qquad u = d^2/Vt$$

where d is the distance between the plane, parallel electrodes, V is the applied voltage, and t is the electron transit time (measured at the base of the electron conductance transient signal). The positive ion mobility in the solid was $< 10^{-5}$ cm²/V s, sufficiently small that the positive ion current could not be accurately integrated. The free ion yield was therefore determined by integrating the electron current and multiplying it by two. Other procedures were the same as those used earlier (10, 12). To minimize the build-up of space charge in the solid samples, the pulse dose (1×10^{10} eV/cm³), frequency (<1/min), and total number (14/temperature) were kept small.

The electron mobility was independent of field strength over the range used, which was 2–10 kV/cm in the solid and 2–15 kV/cm in the liquid. The mobility in the liquid was virtually independent of temperature, in agreement with earlier reports (9, 13). However, upon freezing the neopentane the electron mobility increased abruptly by a factor of two; $u = 71$ cm²/V s in the liquid at 258 K and 154 cm²/V s in the solid at 257 K. The mobility continued to increase as the solid was cooled (Fig. 1). The curve through the points for solid neopentane was arbitrarily drawn with the $T^{-3/2}$ variation characteristic of electron drift that is limited by acoustic-mode scattering (14). The curve provides a reasonable interpretation of the data.

Similar behavior had been observed earlier for electrons in argon (14). The value of the ratio of mobilities (u_{solid}/u_{liquid}) near the triple point is ~2.2 in argon (14) and 2.3 in neopentane. According to the theory of Cohen and Lekner (15) the thermal electron mobility is given by eq. 2.

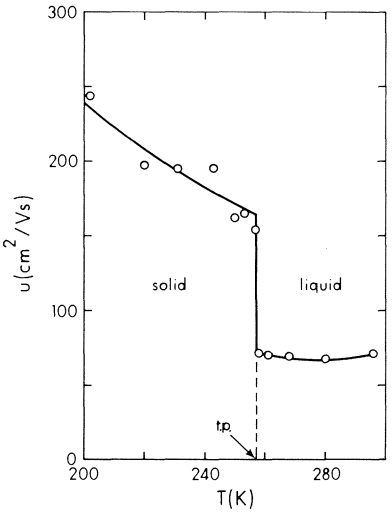

FIG. 1. Electron mobility in solid and liquid neopentane as a function of temperature. The triple point is t.p. = 257 K. The curve for the solid was arbitrarily drawn with the equation $u = 240\ (T/200)^{-3/2}$ cm²/V s.

TABLE 1. Electron ranges b_{GP} and mobilities u in liquid and solid neopentane

T(K)	ε*	d (g/cm³)†	b_{GP} (Å)‡	$b_{GP}d$ (10^{-8} g/cm²)	u (cm²/V s)
			Liquid		
296	1.78	0.588	212	125	71
280	1.81	0.606	204	124	67
261	1.84	0.624	205	128	70
258	1.85	0.627	193	121	71
			Solid		
253	1.97	0.690	254	175	165
243	1.98	0.695	248	172	195
231	1.99	0.701	243	170	195
220	2.00	0.706	247	174	197
202	2.01	0.715	235	168	244

*The dielectric constants were measured in the present work for the liquid, and for the solid just below the triple point; extrapolated for the lower temperature solids, using the Clausius–Mosotti equation (P = 25.4 cm³/mol).
†The densities were measured in the present work.
‡Based upon the single pair spur model (12), using range distribution YGP and G_{tot} = 4.5.

$$[2]\quad u = \frac{e}{1800a^2n^2\chi_T}\left(\frac{2\pi}{m}\right)^{1/2}\left(\frac{1}{kT}\right)^{3/2}\ \text{cm}^2/\text{V s}$$

where e and m are the electron charge and mass, respectively, a is the electron scattering length of the molecules, n is the number of molecules/cm³, χ_T is the isothermal compressibility of the medium, k is Boltzmann's constant, and T is the temperature. For solid argon just below the triple point $u \approx 1000$ cm²/V s (13), $n = 2.45 \times 10^{22}$ atom/cm³ (16), and $\chi_T = 9.5 \times 10^{-11}$ cm²/dyn (17); the scattering length is therefore $a = 1.8$ Å. A similar calculation yields $a = 2.0$ Å for liquid argon near the triple point. The compressibilities of solid and liquid neopentane are not known, but from the densities and the electron mobilities one obtains $a^2\chi_T = 6.2 \times 10^{-25}$ and 1.7×10^{-24} cm⁴/dyn for the solid at 253 K and liquid at 258 K, respectively. By comparison with the compressibilities of other hydrocarbons (18), the values for neopentane near the triple point may be $\sim 1 \times 10^{-10}$ cm²/dyn for the solid and $\sim 2 \times 10^{-10}$ cm²/dyn for the liquid, about the same as those for argon (17). The scattering length of neopentane would then be ~8 Å in the solid and ~9 Å in the liquid.

The values of the quantity $(n^2a^2\chi_T)$ for solid argon and neopentane near their triple points are similar to each other, being 1.8×10^{19} and 2.0×10^{19} cm^{-2} dyn^{-1}, respectively. This indicates that the electron scattering properties of the bulk materials are similar for the two substances.

The free ion yield in neopentane also increased upon freezing (Fig. 2). The larger yield in the solid implies that the secondary electron ranges are greater in the solid than in the liquid. Theoretical yields were calculated using the electric field effect model (12). The calculated curves are shown in Fig. 2 and the corresponding values of the electron range parameter b_{GP} are listed in Table 1. The density normalized range $b_{GP}d$ increases from 1.25×10^{-6} g/cm² in the liquid to 1.73×10^{-6} g/cm² in the solid.

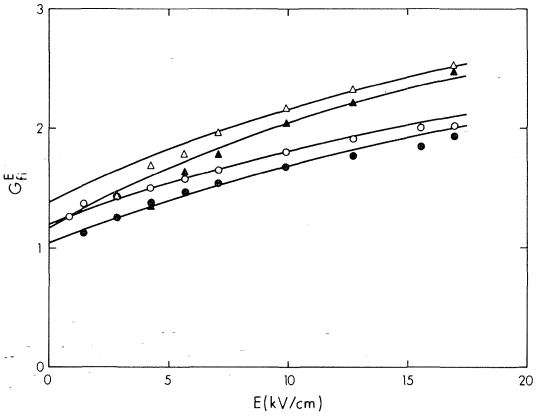

FIG. 2. Free ion yields G_{fi}^E in X-irradiated neopentane as functions of applied electric field strength E and temperature. Solid phase: ▲, 220 K; △, 253 K. Liquid phase: ●, 261 K; ○, 296 K. The curves were calculated using equations from ref. 12 and the parameter values in Table 1. The experimental yields for the solid at low applied field strengths are probably low due to space charge effects.

The correlation between thermal electron mobility and secondary electron range that exists when changing from one liquid to another

Can. J. Chem. Downloaded from www.nrcresearchpress.com by 210.87.254.5 on 09/05/12
For personal use only.

(10) extends also to the liquid-solid phase change in neopentane.

We would like to thank the staff of the Radiation Research Center for aid with the electronics.

1. N. R. KESTNER and J. JORTNER. J. Chem. Phys. **59**, 26 (1973).
2. M. G. ROBINSON and G. R. FREEMAN. Can. J. Chem. **52**, 440 (1974).
3. J. LEKNER and A. R. BISHOP. Phil. Mag. **27**, 297 (1973).
4. L. G. CHRISTOPHOROU, R. P. BLAUNSTEIN, and D. PITTMAN. Chem. Phys. Lett. **18**, 509 (1973).
5. J. A. JAHNKE, N. A. W. HOLZWARTH, and S. A. RICE. Phys. Rev. **5A**, 463 (1972).
6. R. M. MINDAY, L. D. SCHMIDT, and H. T. DAVIS. J. Chem. Phys. **54**, 3112 (1971).
7. W. F. SCHMIDT and G. BAKALE. Chem. Phys. Lett., **17**, 617 (1972).
8. A. V. RUDNEV, A. V. VANNIKOV, and N. A. BAKH. High Energy Chem. **6**, 416 (1972).
9. J.-P. DODELET and G. R. FREEMAN. Can. J. Chem. **50**, 2667 (1972).
10. J.-P. DODELET, K. SHINSAKA, and G. R. FREEMAN. J. Chem. Phys. **59**, 1293 (1973).
11. R. RUDMAN and B. POST. Mol. Cryst. **5**, 95 (1968).
12. J.-P. DODELET, K. SHINSAKA, U. KORTSCH, and G. R. FREEMAN. J. Chem. Phys. **59**, 2376 (1973).
13. R. M. MINDAY, L. D. SCHMIDT, and H. T. DAVIS. J. Phys. Chem. **76**, 442 (1972).
14. L. S. MILLER, S. HOWE, and W. E. SPEAR. Phys. Rev. **166**, 871 (1968).
15. M. H. COHEN and J. LEKNER. Phys. Rev. **158**, 305 (1967).
16. V. G. FASTOVSKII, A. E. ROVINSKII, and YU. V. PETROVSKII. Inert gases. Engl. trans. Israel Program for Scientific Translations, Jerusalem. 1967.
17. P. A. EGELSTAFF. An introduction to the liquid state. Academic Press, London. 1967. p. 4.
18. LANDOLT-BÖRNSTEIN. Zahlenwerte und Funktionen. 6th ed. Vol. 2. Springer–Verlag, Berlin. 1971. Part 1.

Can. J. Chem. Downloaded from www.nrcresearchpress.com by 210.87.254.5 on 09/05/12
For personal use only.

Electric Field Induced Light Emission and Conductance-Loss Transients in Liquid Anthracene[1]

KYOJI SHINSAKA[2] AND GORDON R. FREEMAN

Chemistry Department, University of Alberta, Edmonton, Alberta T6G 2G2

Received July 2, 1974

KYOJI SHINSAKA and GORDON R. FREEMAN. Can. J. Chem. **52**, 3559 (1974).

Liquid anthracene has an unusually high electrical conductivity for a hydrocarbon, being 2×10^{-11} mho cm^{-1} at 507 K. At electric field strengths above 3 kV/cm the conductance suffers transient *decreases* that last < 3 μs and are irregularly spaced in time. The average frequency of occurrence and magnitude of the transients increase rapidly with increasing field above the threshold. The conductance loss transients are accompanied by emission of light. These phenomena may be related to that of semiconductor laser emission.

KYOJI SHINSAKA et GORDON R. FREEMAN. Can. J. Chem. **52**, 3559 (1974).

L'anthracène en phase liquide possède une conductance électrique de 2×10^{-11} mho cm^{-1} à 507 K, qui est une valeur très élevée pour un hydrocarbure. Aux champs électriques supérieurs à 3 kV/cm la conductance subit des *décroissances* éphémères. Celles-ci durent moins de 3 μs et se présentent à des intervals irréguliers. La fréquence et la grandeur moyenne des décroissances éphémères augmentent en fonction du champ électrique au dessus du seuil de 3 kV/cm. Les pertes de conductance coincident avec l'émission de lumière. Ces phénomènes sont peut-être reliées a l'émission des lasers à semiconducteurs.

During a recent attempt to measure the X radiolysis free ion yield in liquid anthracene (1), difficulty was encountered due to inconstancy of the intrinsic conductance of the liquid at high electric fields. At field strengths above 3 kV/cm the intrinsic conductance signal was marked by irregularly spaced transient *decreases* in conductance (Fig. 1). The observed duration of a given transient was equal to and probably limited by the response time of the amplifier (PAR model 113, response time ~ 3 μs, gain $10^3 \times 10^4$ Ω).

[1]Assisted financially by the National Research Council of Canada.

[2]I. W. Killam Memorial Postdoctoral Fellow.

(10) extends also to the liquid-solid phase change in neopentane.

We would like to thank the staff of the Radiation Research Center for aid with the electronics.

1. N. R. KESTNER and J. JORTNER. J. Chem. Phys. **59**, 26 (1973).
2. M. G. ROBINSON and G. R. FREEMAN. Can. J. Chem. **52**, 440 (1974).
3. J. LEKNER and A. R. BISHOP. Phil. Mag. **27**, 297 (1973).
4. L. G. CHRISTOPHOROU, R. P. BLAUNSTEIN, and D. PITTMAN. Chem. Phys. Lett. **18**, 509 (1973).
5. J. A. JAHNKE, N. A. W. HOLZWARTH, and S. A. RICE. Phys. Rev. **5A**, 463 (1972).
6. R. M. MINDAY, L. D. SCHMIDT, and H. T. DAVIS. J. Chem. Phys. **54**, 3112 (1971).
7. W. F. SCHMIDT and G. BAKALE. Chem. Phys. Lett., **17**, 617 (1972).
8. A. V. RUDNEV, A. V. VANNIKOV, and N. A. BAKH. High Energy Chem. **6**, 416 (1972).
9. J.-P. DODELET and G. R. FREEMAN. Can. J. Chem. **50**, 2667 (1972).
10. J.-P. DODELET, K. SHINSAKA, and G. R. FREEMAN. J. Chem. Phys. **59**, 1293 (1973).
11. R. RUDMAN and B. POST. Mol. Cryst. **5**, 95 (1968).
12. J.-P. DODELET, K. SHINSAKA, U. KORTSCH, and G. R. FREEMAN. J. Chem. Phys. **59**, 2376 (1973).
13. R. M. MINDAY, L. D. SCHMIDT, and H. T. DAVIS. J. Phys. Chem. **76**, 442 (1972).
14. L. S. MILLER, S. HOWE, and W. E. SPEAR. Phys. Rev. **166**, 871 (1968).
15. M. H. COHEN and J. LEKNER. Phys. Rev. **158**, 305 (1967).
16. V. G. FASTOVSKII, A. E. ROVINSKII, and YU. V. PETROVSKII. Inert gases. Engl. trans. Israel Program for Scientific Translations, Jerusalem. 1967.
17. P. A. EGELSTAFF. An introduction to the liquid state. Academic Press, London. 1967. p. 4.
18. LANDOLT-BÖRNSTEIN. Zahlenwerte und Funktionen. 6th ed. Vol. 2. Springer–Verlag, Berlin. 1971. Part 1.

Can. J. Chem. Downloaded from www.nrcresearchpress.com by 210.87.254.5 on 09/05/12
For personal use only.

Electric Field Induced Light Emission and Conductance-Loss Transients in Liquid Anthracene[1]

KYOJI SHINSAKA[2] AND GORDON R. FREEMAN

Chemistry Department, University of Alberta, Edmonton, Alberta T6G 2G2

Received July 2, 1974

KYOJI SHINSAKA and GORDON R. FREEMAN. Can. J. Chem. **52**, 3559 (1974).

Liquid anthracene has an unusually high electrical conductivity for a hydrocarbon, being 2×10^{-11} mho cm^{-1} at 507 K. At electric field strengths above 3 kV/cm the conductance suffers transient *decreases* that last < 3 μs and are irregularly spaced in time. The average frequency of occurrence and magnitude of the transients increase rapidly with increasing field above the threshold. The conductance loss transients are accompanied by emission of light. These phenomena may be related to that of semiconductor laser emission.

KYOJI SHINSAKA et GORDON R. FREEMAN. Can. J. Chem. **52**, 3559 (1974).

L'anthracène en phase liquide possède une conductance électrique de 2×10^{-11} mho cm^{-1} à 507 K, qui est une valeur très élevée pour un hydrocarbure. Aux champs électriques supérieurs à 3 kV/cm la conductance subit des *décroissances* éphémères. Celles-ci durent moins de 3 μs et se présentent à des intervals irréguliers. La fréquence et la grandeur moyenne des décroissances éphémères augmentent en fonction du champ électrique au dessus du seuil de 3 kV/cm. Les pertes de conductance coincident avec l'émission de lumière. Ces phénomènes sont peut-être reliées a l'émission des lasers à semiconducteurs.

During a recent attempt to measure the X radiolysis free ion yield in liquid anthracene (1), difficulty was encountered due to inconstancy of the intrinsic conductance of the liquid at high electric fields. At field strengths above 3 kV/cm the intrinsic conductance signal was marked by irregularly spaced transient *decreases* in conductance (Fig. 1). The observed duration of a given transient was equal to and probably limited by the response time of the amplifier (PAR model 113, response time ~ 3 μs, gain $10^3 \times 10^4$ Ω).

[1]Assisted financially by the National Research Council of Canada.

[2]I. W. Killam Memorial Postdoctoral Fellow.

TABLE 1. Field dependence of transient decreases in the intrinsic conductance of liquid anthracene at 507 K

E (kV/cm)	i* (μA)	No. of transients/s	Ave. Δi† (nA)	$-10^3\Delta i/i$
0	0.0	0	0.0	—
3	0.5	0	0.0	0.0
6	1.0	600	−0.1	0.1
9	1.5	2 600	−0.6	0.4
12	2.0	3 000	−2.4	1.2
15	2.5	8 000	−10.0	4.0
18	2.7	25 000	−30.0	11.0

*Intrinsic current, steady state. Specific conductivity = 2×10^{-11} mho cm^{-1}.
†Time averaged decrease of the intrinsic current due to the transients: (coulombs/transient) × (transients/s).

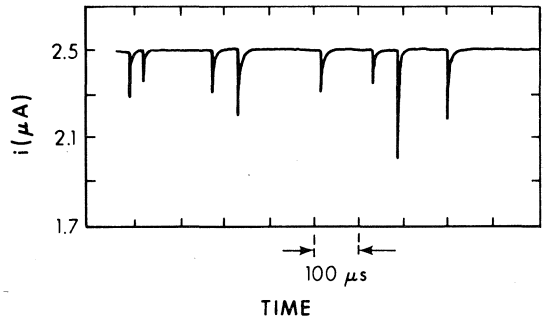

FIG. 1. Transient decreases in the intrinsic conductance of liquid anthracene at 507 K and 15 kV/cm. The cell had stainless steel electrodes and a guard ring (ref. 1).

The average frequency of occurrence of the transients increased with field strength (Table 1). The magnitude of the transients also increased with increasing field (Fig. 2). It is curious that the graphs in Fig. 2 display structure. Transients of certain magnitudes are favored: 30, 60, 100, etc. nA. A transient corresponds to the sudden *loss* of a large group of charge carriers. Integration of a transient with respect to time indicates that a 30 nA peak corresponds to the loss of $\sim 10^6$ charge carriers, which seems to be a unit quantity in the present effect.

The time averaged decrease of the intrinsic current due to the transients may be represented by Δi, and the normal intrinsic current by i. The fractional loss $\Delta i/i$ increased rapidly with increasing field strength (Table 1).

The conductance loss transients were accompanied by the emission of light. The light emission consisted of transient specs of bluish-greenish-white light at both electrode surfaces, detected visually in a darkened room. Time coincidence studies of conductance loss and light emission were not made, but the electric field threshold and the field dependence of the relative frequency of the two processes were similar. Light emission began at 4 kV/cm and the number of spec flashes per second on the electrode surfaces increased rapidly with increasing field strength above the threshold (*cf.* Table 1).

The concomitance of light emission and conductance loss, each in transient bursts, implies that the luminescence was coupled to annihilation of charge carriers or of their precursors. This electroluminescence may be related to semiconductor laser emission (2). Anthracene is apparently a semiconductor in both the solid and liquid phases (3). The fact that light is emitted in tiny specs might indicate that charges are injected into the anthracene from minute irregularities on the electrode surfaces.

Electroluminescence has also been observed in solid anthracene (4). It would be worthwhile to

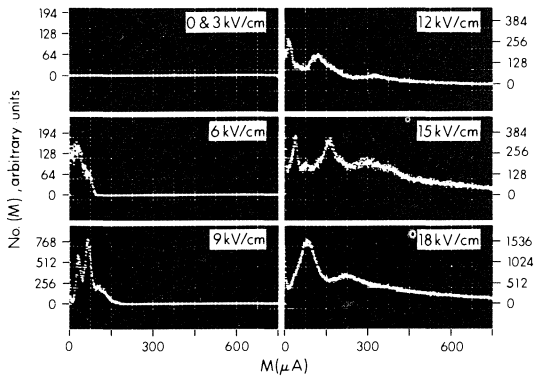

FIG. 2. Transient decreases in the intrinsic conductance of liquid anthracene at 507 K. Relative numbers of transients of magnitude M plotted as a function of the transient magnitude M. The field strengths are indicated in the Figure. The transients were counted for 20 s at each field strength.

Can. J. Chem. Downloaded from www.nrcresearchpress.com by 210.87.254.5 on 09/05/12
For personal use only.

look for transient losses in the steady state conductance of that material and to test for time coincidence between conductance loss and light emission. Solid anthracene would be much easier to work with than the liquid material. The latter requires inconveniently high temperatures, although it has the advantages of clear transparency and uniform contact with the electrodes.

1. K. SHINSAKA and G. R. FREEMAN. Can. J. Chem. This issue.
2. H. RIECK. Semiconductor lasers. Macdonald, London. 1970.
3. J. KOMMANDEUR, G. J. KOSINEK, and W. G. SCHNEIDER. Can. J. Chem. **36**, 513 (1958).
4. W. HWANG and K. C. KAO. J. Chem. Phys. **60**, 3845 (1974).

Can. J. Chem. Downloaded from www.nrcresearchpress.com by 210.87.254.5 on 09/05/12
For personal use only.

S_N2 Displacement at Tertiary Carbon[1]

OLIVER E. EDWARDS AND CIRO GRIECO[2]
Division of Biological Sciences, National Research Council of Canada, Ottawa, Canada K1A 0R6

Received June 20, 1974

OLIVER E. EDWARDS and CIRO GRIECO. Can. J. Chem. **52**, 3561 (1974).

Evidence is presented for classical[3] S_N2 displacement of bromine by azide ion from a tertiary α-bromo lactone, a tertiary α-bromo ester, and two tertiary α-bromo ketones.

OLIVER E. EDWARDS et CIRO GRIECO. Can. J. Chem. **52**, 3561 (1974).

On présente la preuve du déplacement classique[3] S_N2 du brome par un ion azidure d'une α-bromo lactone tertiaire, d'un α-bromo ester tertiaire et deux α-bromo cétones tertiaires.

[Traduit par le journal]

Recent investigation of possible S_N2 reactions at tertiary carbon have led to evidence in various structural types for a spectrum of S_N2-like mechanisms ranging from displacement on an ion-pair intermediate (1), through cases in which considerable positive charge develops in the transition state (2) to a classical[3] S_N2-type displacement (3).

In connection with a need for tertiary α-azido-γ-lactones we considered the possibility of S_N2 displacement on the corresponding α-halo lactones since: (*a*) The adjacent carbonyl should suppress S_N1 and accelerate S_N2 reaction. (*b*) The ring constraint and the trigonal carbon adjacent to the reaction site would minimize repulsive interactions in an S_N2 transition state. (*c*) The linear azide ion, which is a good nucleophile, in dipolar aprotic solvents would provide minimal steric compression in the transition state. In accord with this, bromo lactone **1** in dimethyl formamide containing 3 equiv. of lithium azide was converted into the azido lactone **2** in 5 min at room temperature. In dimethyl formamide at 0° the reaction gave good second-order kinetics with $k_2 = 1.3 \times 10^{-3}$ l mol^{-1} s^{-1}. This promp-

[1]Issued as NRCC No. 14238.

[2]Guest worker from Department of Pharmaceutical Chemistry and Toxicology, Universita Delgli Studi di Napoli.

[3]Defined as biomolecular displacement of a group attached to carbon in which no positive charge develops on the carbon in the transition state.

look for transient losses in the steady state conductance of that material and to test for time coincidence between conductance loss and light emission. Solid anthracene would be much easier to work with than the liquid material. The latter requires inconveniently high temperatures, although it has the advantages of clear transparency and uniform contact with the electrodes.

1. K. SHINSAKA and G. R. FREEMAN. Can. J. Chem. This issue.
2. H. RIECK. Semiconductor lasers. Macdonald, London. 1970.
3. J. KOMMANDEUR, G. J. KOSINEK, and W. G. SCHNEIDER. Can. J. Chem. **36**, 513 (1958).
4. W. HWANG and K. C. KAO. J. Chem. Phys. **60**, 3845 (1974).

Can. J. Chem. Downloaded from www.nrcresearchpress.com by 210.87.254.6 on 09/05/12
For personal use only.

S_N2 Displacement at Tertiary Carbon[1]

OLIVER E. EDWARDS AND CIRO GRIECO[2]
Division of Biological Sciences, National Research Council of Canada, Ottawa, Canada K1A 0R6

Received June 20, 1974

OLIVER E. EDWARDS and CIRO GRIECO. Can. J. Chem. **52**, 3561 (1974).

Evidence is presented for classical[3] S_N2 displacement of bromine by azide ion from a tertiary α-bromo lactone, a tertiary α-bromo ester, and two tertiary α-bromo ketones.

OLIVER E. EDWARDS et CIRO GRIECO. Can. J. Chem. **52**, 3561 (1974).

On présente la preuve du déplacement classique[3] S_N2 du brome par un ion azidure d'une α-bromo lactone tertiaire, d'un α-bromo ester tertiaire et deux α-bromo cétones tertiaires.

[Traduit par le journal]

Recent investigation of possible S_N2 reactions at tertiary carbon have led to evidence in various structural types for a spectrum of S_N2-like mechanisms ranging from displacement on an ion-pair intermediate (1), through cases in which considerable positive charge develops in the transition state (2) to a classical[3] S_N2-type displacement (3).

In connection with a need for tertiary α-azido-γ-lactones we considered the possibility of S_N2 displacement on the corresponding α-halo lactones since: (*a*) The adjacent carbonyl should suppress S_N1 and accelerate S_N2 reaction. (*b*) The ring constraint and the trigonal carbon adjacent to the reaction site would minimize repulsive interactions in an S_N2 transition state. (*c*) The linear azide ion, which is a good nucleophile, in dipolar aprotic solvents would provide minimal steric compression in the transition state. In accord with this, bromo lactone **1** in dimethyl formamide containing 3 equiv. of lithium azide was converted into the azido lactone **2** in 5 min at room temperature. In dimethyl formamide at 0° the reaction gave good second-order kinetics with $k_2 = 1.3 \times 10^{-3}$ l mol^{-1} s^{-1}. This promp-

[1]Issued as NRCC No. 14238.

[2]Guest worker from Department of Pharmaceutical Chemistry and Toxicology, Universita Delgli Studi di Napoli.

[3]Defined as biomolecular displacement of a group attached to carbon in which no positive charge develops on the carbon in the transition state.

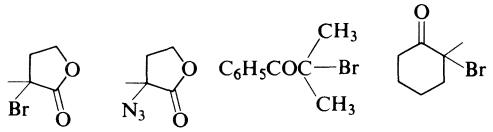

1 2 3 4

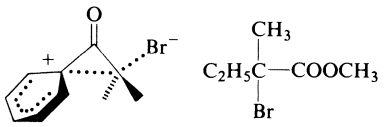

5 6

ted us to study the reaction in dry methanol. Again bimolecular kinetics[4] with $k_2 = 2.9 \times 10^{-4}$ l mol^{-1} s^{-1} was found at 60 °C for ratios of lithium azide to bromo lactone from 3:1 to 1:2. Similar second-order kinetics was observed for ketones **3** ($k_2 = 4.5 \times 10^{-3}$ at $-20°$ in DMF) and **4** ($k_2 = 1.2 \times 10^{-2}$ at 0° in DMF) and ester **6** ($k_2 = 9 \times 10^{-4}$ at 25° in DMF).

The work of Bordwell and Mecca (1) shows that these criteria are insufficient to eliminate from consideration displacement on a tight ion pair. However, the following observations strongly support a classical S_N2 mechanism[3] for the α-bromo carbonyl compounds: (*i*) Reaction of **3** with SCN^- in methanol at 60 °C gave thiocyanate as the only product. (*ii*) No solvolysis products were detected from **1** or **3** at 60° in aqueous methanol containing lithium azide. (*iii*) No rearranged products arising from **3** via phenonium ion **5** were observed from reaction with LiN_3 in methanol.[5] (*iv*) A negative salt effect was found for reaction of **1** with azide ion in 60% methanol – 40% water. (*v*) The rate of reaction of bromo ketone **4** was nine times that of bromo lactone **1** in DMF at 0 °C. This is the opposite of what one would expect if there were significant positive charge development on carbon in the transition state.[6]

Partial resolution of 2-bromo-2-methylbutyric acid was achieved. Reaction of the acid and methyl ester **6** with azide in DMF is summarized in the table below.

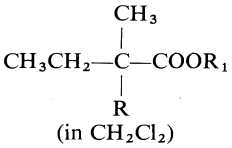

R (in CH_2Cl_2)	$[\alpha]_D$ (+)-Acid	(−)-Acid	(+)-Ester	(−)-Ester
Br	+0.37	−0.72	+0.35	−0.59
N_3	+4.4	−5.2	−5.7	+6.8

Because of low yields in the resolution and difficulty in purifying the small amounts of active products these results lack precision. However, they point to retention of configuration for the acid and inversion for the ester. Alternative tests for the extent of inversion are being explored.

1. F. G. Bordwell and T. G. Mecca. J. Am. Chem. Soc. **94**, 2119 (1972).
2. C. A. Grob, K. Seckinger, S. W. Tam, and R. Traber. Tetrahedron Lett. 3051 (1973).
3. U. Miotti and A. Fava. J. Am. Chem. Soc. **88**, 4274 (1966).
4. A. C. Cope and E. S. Graham. J. Am. Chem. Soc. **73**, 4702 (1951).

[4]A small amount (*ca.* 3%) of elimination took place. Linear plots were obtained using biomolecular rate equations, to greater than 80% reaction. Activity coefficients are unknown and were ignored in the calculations.

[5]An analogue of this type of reaction would be the silver ion assisted Favorskii rearrangement (4).

[6]The ^{13}C n.m.r. shift of the carbonyl carbon of an ester (*ca.* 175 p.p.m. is less than that of a ketone (*ca.* 215 p.p.m.) suggesting considerably greater electron deficiency on that of the ketone. If so, positive charge development adjacent to the ketone carbonyl would be opposed more than if adjacent to the ester carbonyl. The larger chemical shift (*ca.* 44 p.p.m.) of the α-carbon of saturated ketones relative to that of esters (34 p.p.m.) seems in harmony with this conclusion.

Can. J. Chem. Downloaded from www.nrcresearchpress.com by 210.87.254.6 on 09/05/12
For personal use only.

Reaction of Cuprate Reagents with Pyridine in the Presence of Chloroformate. A Novel Synthesis of 1,4-Dihydropyridine Derivatives[1]

EDWARD PIERS AND MARCEL SOUCY[2]

Department of Chemistry, University of British Columbia, 2075 Wesbrook Place, Vancouver, British Columbia V6T 1W5

Received June 21, 1974

EDWARD PIERS and MARCEL SOUCY. Can. J. Chem. **52**, 3563 (1974).

Reaction, under appropriate conditions, of lithium dialkyl- or diarylcuprates with pyridine in the presence of methyl chloroformate afforded, in good yields, 1-carbomethoxy-4-alkyl (or aryl)-1,4-dihydropyridines. Also formed, in limited but varying amounts (~2–11%), were the corresponding 1,2-dihydropyridine derivatives.

EDWARD PIERS et MARCEL SOUCY. Can. J. Chem. **52**, 3563 (1974).

Dans des conditions appropriées, la réaction des cuprates de dialkyl ou de diaryl lithium avec la pyridine en présence du chloroformate de méthyle conduit, avec de bons rendements, aux carbométhoxy-1 alkyl (ou aryl)-4 dihydro-1,4 pyridines. Il se forme aussi, en quantités plus petites mais variables (≃2–11%) les dérivés correspondants du dihydro-1,2 pyridine.

[Traduit par le journal]

Dihydropyridines play a role as intermediates in certain reactions (*e.g.* nucleophilic substitution) of pyridines and also serve as important synthetic precursors for the latter (1). Furthermore, various substituted dihydropyridines (particularly 1,4-dihydropyridines) have been shown to possess a variety of useful physiological properties (1).

It is known that the reaction of pyridine and derivatives with alkyl- or aryllithium reagents (1–3), with Grignard reagents in the presence of an appropriate electrophile (1, 4, 5), or with sodium borohydride in the presence of methyl chloroformate (6) results primarily in 1,2-addition, with the predominant formation of the corresponding 1,2-dihydropyridine derivative. Thus, until now, it has been extremely difficult to prepare simply substituted 1,4-dihydropyridines. We report here a novel, convenient method for the synthesis of 4-substituted 1,4-dihydropyridine derivatives. The method involves the reaction of lithium dialkyl- or diarylcuprates with pyridine in the presence of an electrophilic reagent, *e.g.* methyl chloroformate.

Our initial studies were carried out with lithium dimethylcuprate (7). Addition of methyl chloroformate to a solution of pyridine and the cuprate reagent in ether, followed by appropriate work-up, afforded in 81% yield 1-carbomethoxy-4-methyl-1,4-dihydropyridine (**1**), accompanied by a small amount (2%) of the corresponding 1,2-dihydropyridine derivative. These materials were identified by spectral data and by hydrogenation to the corresponding piperidine derivatives, which were then compared with authentic samples. It should be noted that electrophilic reagents other than chloroformate could also be used. For example, reaction of lithium dimethylcuprate with pyridine in the presence of diethyl phosphorochloridate yielded the novel 1,4-dihydropyridine derivative **2**.[3]

The investigation of the above type of reaction was extended to include other dialkyl- and diarylcuprates and the results are summarized in Table 1. In general, good yields of 1-carbomethoxy-4-alkyl(or aryl)-1,4-dihydropyridines **5** were obtained.[4] Varying amounts of the corresponding 1,2-dihydropyridine derivatives **6** were also formed, although it was found that the quantities of **6** produced could be minimized to some extent by use of low reaction temperatures. The formation of small amounts of the 1,2-dihydropyridine derivatives does not detract from the usefulness of the above syntheses, since

[1]Financial support for this work by the National Research Council of Canada is gratefully acknowledged.

[2]NRCC Postdoctorate Fellow.

[3]Separate control experiments showed that the cuprate reagent did not react with pyridine directly. For example, when a solution of pyridine and lithium dimethylcuprate in ether was stirred at 0° for 1 h and was then worked up without addition of methyl chloroformate, pyridine could be recovered in greater than 80% yield. These results indicated that the products were probably formed by reaction of the cuprate reagent with the initially formed pyridinium salts **3** and **4** (see ref. 4).

[4]It should be noted that the compounds **5** are potentially convenient synthetic precursors for 4-alkyl(or aryl)pyridines. Investigations into this possibility are proceeding.

Can. J. Chem. Downloaded from www.nrcresearchpress.com by 210.87.254.5 on 09/05/12
For personal use only.

TABLE 1. Reaction of lithium dialkyl- and diarylcuprates with pyridine in the presence of methyl chloroformate

Cuprate (R)[a]	Product yield (%)[b]	Ratio (**5**:**6**)[c]
CH_3—[d]	81	98:2
CH_3CH_2—	67	96:4
$CH_3(CH_2)_3$—	86	98:2
$(CH_3)_2CH$—	65	89:11
$CH_3CH_2\underset{\vert}{C}HCH_3$	56	89:11
C_6H_5—	70	90:10
p-$CH_3C_6H_4$—	65	92:8

[a]Prepared by addition of 2 equiv. commercial alkyl- or aryllithium reagent (Ventron Corporation) to a slurry of purified cuprous iodide in ether.
[b]Yield of distilled product.
[c]As determined by g.l.c. analysis of distilled product.
[d]This experiment was carried out at 0° and worked-up by filtration through silica gel. All other experiments were done as described in the text.

1 R = $COOCH_3$ **3** R = $COOCH_3$
2 R = $PO(OC_2H_5)_2$ **4** R = $PO(OC_2H_5)_2$

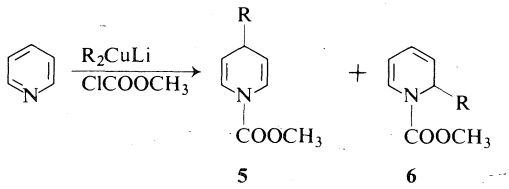

5 **6**

it has been shown (6) that these materials can readily be separated from 1,4-dihydropyridines by treatment of the mixture with maleic anhydride.

The following experimental procedure is representative. To a solution of lithium di-*n*-butylcuprate (**8**) (6 mmol) in dry ether (25 ml) at −78° under an atmosphere of argon was added 5 mmol of pyridine. A solution of methyl chloroformate (20 mmol) in dry ether (25 ml) was added dropwise over a period of 10 min. The resulting mixture was stirred at −78° for 30 min, warmed to 0° (ice water bath) and then stirred for an additional 30 min. Florisil (3g) was added to the reaction mixture, the latter was stirred for a few seconds, and then filtered through a short column (4.5 cm diameter) of florisil (35 g). The column was eluted with an additional 350 ml of ether. Evaporation of the ether, followed by distillation (air bath temperature 90–92°; 0.1 mm) of the residual oil afforded 835 mg (86%) of a mixture of **5** (R = *n*-Bu) and **6** (R = *n*-Bu), in a ratio of approximately 98:2. A sample of pure **5** (R = *n*-Bu) exhibited i.r. (film) ν_{max} 1730, 1693, 1633, 1440, 1412, 1372, 1342, 1310, 1196, 1115, 950, 740, 722 cm^{-1}; p.m.r. τ 3.20 (broad d, 2H, $—C_2H$ and $—C_6H$, J = 8 Hz), 5.13 (d of d, 2H, $—C_3H$ and $—C_5H$, J = 8 Hz, 3.5 Hz), 6.20 (s, 3H, $—COOCH_3$), 7.05 (unresolved m, 1H, $—C_4H$), 8.40–8.88 (m, 6H, $—CH_2CH_2CH_2—$), 9.12 (m, 3H, $—CH_3$).

1. U. EISNER and J. KUTHAN. Chem. Rev. **72**, 1 (1972).
2. C. S. GIAM and E. E. KNAUS. Tetrahedron Lett. 4961 (1971).
3. R. F. FRANCIS, W. DAVIS, and J. T. WISENER. J. Org. Chem. **39**, 59 (1974).
4. G. FRAENKEL, J. W. COOPER, and C. M. FINK. Angew. Chem. Intern. Ed. **9**, 523 (1970).
5. L. M. THIESSEN, J. A. LEPOIVRE, and F. C. ALDERWEIRELDT. Tetrahedron Lett. 59 (1974).
6. F. W. FOWLER. J. Org. Chem. **37**, 1321 (1972).
7. H. O. HOUSE, W. L. RESPESS, and G. M. WHITESIDES. J. Org. Chem. **31**, 3128 (1966).
8. C. R. JOHNSON and G. A. DUTRA. J. Am. Chem. Soc. **95**, 7777 (1973).

Can. J. Chem. Downloaded from www.nrcresearchpress.com by 210.87.254.5 on 09/05/12
For personal use only.

Can. J. Chem. Downloaded from www.nrcresearchpress.com by 210.87.254.42 on 09/05/12
For personal use only.

Canadian Journal of Chemistry

Published by
THE NATIONAL RESEARCH COUNCIL OF CANADA

Journal canadien de chimie

Publié par
LE CONSEIL NATIONAL DE RECHERCHES DU CANADA

Volume 52 Number 21 November 1, 1974 Volume 52 numéro 21 1 novembre 1974

A Proton Magnetic Resonance Study of 1,4-Dibromobenzene-^{13}C Partially Oriented in Nematic Phases

E. E. BURNELL AND M. A. J. SWEENEY

Chemistry Department, University of British Columbia, Vancouver V6T 1W5

Received May 27, 1974

E. E. BURNELL and M. A. J. SWEENEY. Can. J. Chem. **52**, 3565 (1974).

Proton magnetic resonance spectra of 1,4-dibromobenzene (^{13}C and ^{12}C) partially oriented in nematic phases have been measured and analyzed, and the geometry of the molecule has been determined. The angle $\angle HC_2C_3$ is found to be 120.02 ± 0.01° and the angle $\angle C_1C_2C_3$ 120 ± 2°; with the assumption that all CC bond distances are of equal length the angle $\angle C_1C_2C_3$ = 119.88 ± 0.05°. The J_{CH} are determined using three spectra of samples with differing degrees of orientation.

E. E. BURNELL et M. A. J. SWEENEY. Can. J. Chem. **52**, 3565 (1974).

On a mesuré et analysé les spectres de résonance magnétique nucléaire de proton du dibromo-1,4 benzène (^{13}C et ^{12}C) partiellement orienté dans des phases nématiques; on a aussi déterminé la géométrie de la molécule. L'angle $\angle HC_2C_3$ est de 120.02 ± 0.01° et l'angle $\angle C_1C_2C_3$ est de 120 ± 2°; en faisant l'hypothèse que toutes les distances CC sont de longueurs égales, l'angle $\angle C_1C_2C_3$ = 119.88 ± 0.05°. On a déterminé les constantes de couplage J_{CH} en utilisant trois spectres d'échantillons avec des degrés différents d'orientation.

[Traduit par le journal]

Introduction

The n.m.r. spectra of molecules partially oriented in nematic phases have been used extensively for the determination of relative internuclear distances (1, 2). In the majority of cases studied, only information about the proton geometries has been reported. Using time-averaging techniques, the proton spectra of molecules containing ^{13}C in natural abundance are obtainable (3, 4), and hence more complete geometrical information is available. A serious problem is that the spectral line positions in the spectra of partially oriented molecules are sensitive only to the sum $2D_{CH} + J_{CH}$. The scalar indirect spin–spin coupling constants, J_{CH}, are not always known or cannot be completely determined from isotropic spectra. D_{CH} is the direct dipole–dipole coupling between nuclei C and H, and in general

$$[1] \qquad D_{ij} = -\frac{h\gamma_i\gamma_j}{4\pi^2}\frac{S_{ij}}{r_{ij}^3}$$

where i and j specify the nuclear pair, S_{ij} is the orientation parameter for the ij direction, and γ_i is the magnetogyric ratio for the ith nucleus (1). The problem of separating D_{CH} and J_{CH} has been circumvented in the case of 1,4-dichlorobenzene by studying two spectra with differing degrees of orientation (5). Equation 1 shows that the D_{CH} change with orientation, whereas the scalar J_{CH} are independent of orientation.

Here we report the results of a p.m.r. study of partially oriented 1,4-dibromobenzene (^{12}C and ^{13}C) (Fig. 1). Spectra with three different degrees of orientation were used in the analysis. The proton geometry of the molecule has been reported previously (6), but the ^{13}C satellites

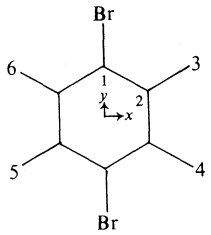

FIG. 1. 1,4-Dibromobenzene.

were not observed. The two sums ($D_{CH} + \frac{1}{2}J_{CH}$) for ^{13}C in position 1, the four sums ($D_{CH} + \frac{1}{2}J_{CH}$) for ^{13}C in position 2, and the three D_{HH} have been determined for each spectrum and used to obtain the molecular geometry and some information about the J_{CH}. Corrections for molecular vibrations (7) have not been applied because mean-square vibrational amplitudes are not available.

Experimental

Three time-averaged proton spectra were used for the analysis. The spectra were similar to those of partially oriented 1,4-dichlorobenzene reported earlier (5). Spectra I and II were run on a Varian HA-100 spectrometer operated in the HA mode using one of the lines of the 1,4-dibromobenzene-^{12}C spectrum to provide a lock signal. Spectrum III was run on a Varian XL-100 spectrometer using FT techniques and an external proton lock. Sample I was ~20 mol% 1,4-dibromobenzene dissolved in the nematic phase of *N*-(*p*-ethoxybenzylidene)-*p'*-*n*-butylaniline (EBBA) and 150 scans were accumulated at ~30 °C with a line width of ~4 Hz. Sample II was ~30 mol% in EBBA and 119 scans were accumulated at ~30 °C with a line width of ~5 Hz. Sample III was ~15 mol% in EBBA and 2000 transients were accumulated at ~42 °C with a resultant line width of ~3 Hz. For each sample only one of the upfield or downfield multiplet of peaks was time averaged and drawn out using a scale of 1000 Hz = 50 cm for samples I and II, and 1100 Hz = 50 cm for sample III. The splitting between low- and high-field multiplets ($=3D_{34}$) was measured using one scan of the entire spectrum in each case and did not change significantly during the time taken to accumulate the ^{13}C side-band spectrum. A modified version (5) of LEQUOR (8) was used to analyze simultaneously the three spectra: (*i*) ^{13}C at position 1, (*ii*) ^{13}C at position 2, and (*iii*) no ^{13}C. The parameters obtained, fitting to about 30 lines for each sample, are listed in Table 1.

Results and Discussion

With the assumption of D_{2h} symmetry, four geometrical coordinates are needed to specify the relative carbon and proton geometry of 1,4-dibromobenzene. In addition, two orientation parameters are needed to specify the time-averaged orientation of the molecule in the magnetic field. To yield absolute values for orientation parameters and geometrical coordinates some scale must be chosen; in the present case the calculations are scaled to a C_2C_3 bond length of 1.3974 Å, the value for benzene (9). Knowledge of the J_{CH} is also required because only the sum $2D_{CH} + J_{CH}$ is obtainable from the spectrum. For the calculations we assume $J_{23} = 167.93$ Hz, $J_{25} = J_{24} - 1.9$ Hz, and $J_{26} = J_{24} + 5.5$ Hz from ref. 10. This leaves J_{24}, J_{13}, and J_{14} to be determined.

The iterative weighted least-squares program SHAPE (11) was modified to fit the 27 equations resulting from the three sets of D_{ij} reported in Table 1 to determine the four relative geometrical parameters, the six orientational parameters, and the three indirect spin–spin coupling constants. Results are in Table 2, case A, where the weighted r.m.s. error of the fit from SHAPE was 0.4 Hz. The coordinates of the protons and of C_2 are well determined. J_{24}, J_{25}, and J_{26} are determined to better accuracy than in the case of 1,4-dichlorobenzene (5). However, as in the case of 1,4-dichlorobenzene, the position of C_1 has a large uncertainty, as do the values of J_{13} and J_{14}. This inaccuracy may partly be due to the large covariance between D_{13} and D_{14} (5), and partly to the small range of orientation parameters used to separate D_{CH} and J_{CH}.

In an attempt to increase the accuracy of the information about C_1, a second calculation was performed using SHAPE and imposing the restriction that all CC bond lengths are equal (case B, Table 2). This makes the value of the y coordinate of nucleus 1 ($y(1)$) dependent on the coordinates of C_2. The proton coordinates are unchanged, as are the coordinates of C_2. J_{13}, J_{14}, and $y(1)$ have lower errors than in case A but their values depend on the ratio of the values chosen for the bond distances C_1C_2 and C_2C_3.

The coordinates in Table 2 can be used to calculate various bond distances and bond angles. The results of such calculations for both cases A and B are in Table 3. We note that case A gives a C_1C_2 bond distance of 1.41 ± 0.03 Å; the error spans the value assumed for case B. The angle $\angle C_1C_2H_3$ is close to the values of 119° 37′ and 119° 43′ reported by Bulthuis *et al.* (6), where they assumed $r_{CH} = 1.084$ Å, $r_{CC} = 1.395$ Å, and that the carbons formed a regular hexagon. The angle $\angle H_3C_2C_3 = 120.02 \pm 0.01°$ is accurately determined, as is the value of the CH bond length of 1.106 ± 0.001 Å. The effects

Can. J. Chem. Downloaded from www.nrcresearchpress.com by 210.87.254.42 on 09/05/12
For personal use only.

TABLE 1. Spectral parameters (in Hz) from the p.m.r. spectra of 1,4-dibromobenzene-^{13}C partially oriented in EBBA

Parameter	Value		
	Sample I	Sample II	Sample III
$D_{13}+\frac{1}{2}J_{13}$	334.6±0.9	259.5±3.0	382.4±0.9
$D_{14}+\frac{1}{2}J_{14}$	−78.6±1.0	−67.4±3.1	−93.8±0.9
$D_{23}+\frac{1}{2}J_{23}$	539.2±0.5	413.1±1.8	575.4±0.5
$D_{24}+\frac{1}{2}J_{24}$	−569.2±0.5	−436.5±1.8	−656.1±0.5
$D_{25}+\frac{1}{2}J_{25}$	6.1±1.8	10.0±9.1	10.8±2.2
$D_{26}+\frac{1}{2}J_{26}$	86.0±1.9	60.2±9.3	92.9±2.3
D_{34}	−2057.8±0.1	−1568.8±0.5	−2361.7±0.2
D_{35}	19.6±0.1	14.2±0.2	21.2±0.1
D_{36}	171.5±0.1	129.6±0.2	195.4±0.1
J_{34}*	8.41		
J_{35}*	0.46		
J_{36}*	2.38		
Root-mean-square error	0.3	0.9	0.4

*Assumed from ref. 10.

TABLE 2. Geometrical, orientational, and indirect spin–spin coupling parameters of 1,4-dibromobenzene*

Parameter	Value	
	Case A	Case B
$x(1)$ (Å)	(0)	(0)
$x(2)$ (Å)	1.212±0.001	1.212±0.001
$x(3)$ (Å)	2.170±0.001	2.170±0.001
$y(1)$ (Å)	1.41±0.06	1.395±0.001†
$y(2)$‡ (Å)	(0.6987)	(0.6987)
$y(3)$ (Å)	1.252±0.001	1.252±0.001
S_{xx}		
Sample I	−0.1170±0.0002	−0.1170±0.0002
Sample II	−0.0882±0.0002	−0.0882±0.0002
Sample III	−0.1326±0.0002	−0.1326±0.0002
S_{zz}		
Sample I	−0.1522±0.0002	−0.1522±0.0002
Sample II	−0.1170±0.0002	−0.1170±0.0002
Sample III	−0.1763±0.0002	−0.1763±0.0002
J_{13} (Hz)	−2±15	−4.9±1.3
J_{14} (Hz)	11.5±1.6	11.7±1.3
J_{23}§ (Hz)	(167.93)	(167.93)
J_{24} (Hz)	1.6±0.5	1.6±0.6
J_{25}‖ (Hz)	(−0.3)	(−0.3)
J_{26}‖ (Hz)	(7.1)	(7.1)

*Weighted r.m.s. error from SHAPE = 0.4 Hz for case A and 0.4 Hz for case B. Values in brackets are assumed. The origin is taken as the center of symmetry of the molecule. In case A, the C_2C_3 distance is given the value 1.3974 Å (from benzene (9)). In case B, the distance C_1C_2 is also set to 1.3974 Å.

†For case B, the value of $y(1)$ is dependent on the coordinates of C_2 and is restricted by C_1—C_2 = 1.3974 Å.

‡Assumed from benzene (9).

§From Read *et al.* (10).

‖Set from ref. 10 so that $J_{25} = J_{24} - 1.9$ Hz and $J_{26} = J_{24} + 5.5$ Hz.

Can. J. Chem. Downloaded from www.nrcresearchpress.com by 210.87.254.42 on 09/05/12
For personal use only.

TABLE 3. Bond lengths and bond angles determined for 1,4-dibromobenzene from the geometrical coordinates in Table 2*

Parameter	Value	
	Case A	Case B
$r_{C_1C_2}$ (Å)	1.41 ± 0.03	(1.3974)†
$r_{C_2C_3}$ (Å)	(1.3974)†	(1.3974)†
r_{CH} (Å)	$1.106_4 \pm 0.001_3$	$1.106_4 \pm 0.001_3$
$\angle C_1C_2C_3$ (°)	120 ± 2	119.88 ± 0.05
$\angle H_3C_2C_3$ (°)	120.02 ± 0.01	120.02 ± 0.01
$\angle C_1C_2H_3$ (°)	120 ± 2	120.10 ± 0.05

*Values in brackets are assumed.
†Assumed from benzene (9).

of molecular vibrations might be expected to reduce this value. In the case of benzene, the reduction was 0.041 Å (7).

The ratio $r_{36}:r_{34}$ of 1.733 ± 0.001 is a little larger than the values of 1.721 ± 0.007 and 1.723 ± 0.010 previously reported (6). However, the difference is not significant.

In conclusion, a comparison with the data for 1,4-dichlorobenzene (5) shows only slight differences. The angle $\angle H_3C_2C_3$ equals $120.3 \pm 0.1°$ for the dichlorobenzene, about 0.3° larger than in the present case. Comparing the coordinates, only the value of $x(3)$ differs outside the experimental errors ($=2.162 \pm 0.005$ Å for dichlorobenzene). These differences are less than two standard deviations and hence are not significant. In both dichlorobenzene and dibromobenzene the J_{CH} values involving C_2 agree with those determined for benzene (12). However, J_{13} and J_{14} for dibromobenzene are larger than those reported for benzene (12). Because of the large errors associated with J_{13} and J_{14}, and their covariance with $y(1)$ (or in case B their dependence on the assumed value of the C_1C_2 bond length) no confidence can be placed in the differences from the values for benzene.

These experiments demonstrate the power of the use of the n.m.r. of partially oriented molecules for the determination of geometrical structure in the liquid phase, and also for the determination of those indirect spin–spin coupling constants which may be difficult, or impossible, to obtain from high-resolution n.m.r. spectra of isotropic liquids. The technique of using ^{13}C in natural abundance is limited to systems with simple proton spectra, where the lines from the ^{13}C satellites are not obscured by the more intense proton lines.

The authors wish to thank Professor P. Diehl and Dr. W. Niederberger for helpful discussions. The authors are grateful to the National Research Council of Canada for financial support.

1. P. DIEHL and C. L. KHETRAPAL. NMR—basic principles and progress. Vol. 1. Springer-Verlag, New York. 1969.
2. P. DIEHL and P. M. HENRICHS. Specialist periodical reports—nuclear magnetic resonance. Vol. 1. Chemical Society, London. 1972. p. 321.
3. M. COCIVERA. J. Chem. Phys. **47**, 3061 (1967).
4. L. C. SNYDER and S. MEIBOOM. J. Chem. Phys. **47**, 1480 (1967).
5. E. E. BURNELL, P. DIEHL, and W. NIEDERBERGER. Can. J. Chem. **52**, 151 (1974).
6. J. BULTHUIS, J. GERRITSEN, C. W. HILBERS, and C. MACLEAN. Rec. Trav. Chim. **87**, 417 (1968).
7. P. DIEHL and W. NIEDERBERGER. J. Magn. Res. **9**, 495 (1973).
8. P. DIEHL, H. P. KELLERHALS, and W. NIEDERBERGER. J. Magn. Res. **4**, 352 (1971).
9. A. LANGSETH and B. P. STOICHEFF. Can. J. Phys. **34**, 350 (1956).
10. J. M. READ, JR., R. W. GRECELY, and J. H. GOLDSTEIN. J. Mol. Spectrosc. **25**, 107 (1968).
11. P. DIEHL, P. M. HENRICHS, and W. NIEDERBERGER. Mol. Phys. **20**, 139 (1971).
12. G. ENGLERT, P. DIEHL, and W. NIEDERBERGER. Z. Naturf. **26**a, 1829 (1971).

Can. J. Chem. Downloaded from www.nrcresearchpress.com by 210.87.254.42 on 09/05/12
For personal use only.

The Reaction of Propiolic Acid Esters with Tertiary Amines. Formation of Betaines[1,2]

A. W. McCULLOCH AND A. G. McINNES

Atlantic Regional Laboratory, National Research Council of Canada, Halifax, Nova Scotia B3H 3Z1

Received May 9, 1974

A. W. McCULLOCH and A. G. McINNES. Can. J. Chem. **52**, 3569 (1974).

Reaction of propiolate esters, H—C≡C—CO_2R, with tertiary alkylamines R'_3N in highly aqueous media yields betaines of the type *trans* $R'_3N^+ \cdot CH{=}CH \cdot CO_2^-$. The spectral and chemical properties of these derivatives are discussed as well as the mechanism of their formation. The major by-product of reaction is the corresponding *trans*-3-alkoxyacrylate RO—CH=CH—CO_2R.

A. W. McCULLOCH et A. G. McINNES. Can. J. Chem. **52**, 3569 (1974).

La réaction des esters du type H—C≡C—CO_2R avec des amines tertiaires du type R'_3N dans des milieux aqueux conduit aux bétaïnes $R'_3N^+ \cdot CH{=}CH \cdot CO_2^-$ *trans*. On discute des propriétés chimiques et spectrales de ces dérivés de même que de leurs mécanismes de leur formation. Le produit secondaire, formé d'une façon prépondérante dans cette réaction, est l'alkoxy-3 acrylate RO—CH=CH—CO_2R *trans* correspondant. [Traduit par le journal]

Introduction

Tertiary alkylamines are widely used as catalysts for nucleophilic additions to acetylenic esters (1–4) and are also useful as polymerization catalysts (5, 6). Catalyzed dimerization of a propiolate ester H—C≡C—CO_2R can be effected readily. When carried out in an inert solvent with exclusion of H_2O the major product is the vinyl acetylene **1** (4, 7, 8). In the presence of a small amount of H_2O a good yield of the symmetrical ether **2** is obtained (4, 7).

We have observed that interaction of tertiary alkylamines with esters of propiolic acid in the presence of a large amount of H_2O gives (in good yield) betaines of type **3**. This communication describes the formation and properties of some of these derivatives.

Results and Discussion

Observations

Equimolar amounts of ethyl propiolate (EP) and Et_3N were reacted at room temperature using a solvent mixture of H_2O–CH_2Cl_2 (1:1 v/v). The organic phase of the reaction contained the 3-ethoxyacrylate **4***a* (12%) and a small amount of **2***a* (0.7%); compound **1***a* could not be detected. Evaporation of the aqueous phase and trituration of the residue with acetone gave the betaine **3***a* as a dihydrate in about 60% yield. Under the same conditions reaction of Et_3N with methyl propiolate (MP) gave **3***a* (56%) and methyl 3-methoxyacrylate **4***b* (28%). As expected, increasing the relative concentration of H_2O in these experiments increased the yield of **3***a* (up to 80%).

Analogous reactions were carried out between Me_3N and EP (or MP). Under highly aqueous

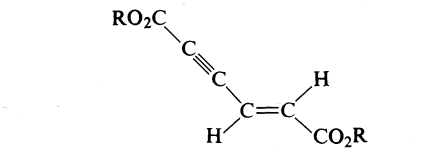

1

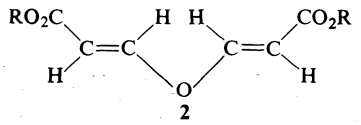

2

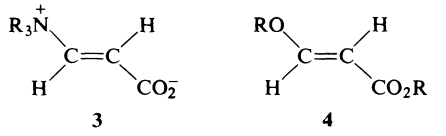

3 **4**

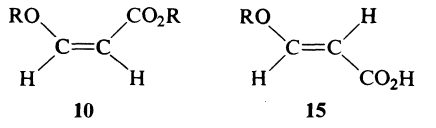

10 **15**

a R=Et; *b* R=Me; *c* R=*n*-Bu

[1]Issued as NRCC No. 14202.

[2]Reported in part at the 56th Canadian Chemical Conference of the Chemical Institute of Canada, Montreal, Quebec, June, 1973.

Can. J. Chem. Downloaded from www.nrcresearchpress.com by 210.87.254.42 on 09/05/12
For personal use only.

conditions the major products were **3***b* and **4***a* (or *b*): in the presence of limited concentrations of H_2O significant amounts of **1***a* (or *b*) and **2***a* (or *b*) were formed, with decreased yields of **3***b* and **4***a* (or *b*).

Betaines **3***c* and **5** were similarly obtained from reactions of EP with tri-*n*-butylamine and *N*-methylpiperidine.

Under identical conditions the reaction between propiolic acid and Et_3N afforded only the 1:1 salt **6**.

Mechanisms

In the absence of H_2O the tertiary amine may abstract the acidic hydrogen of the alkyl propiolate. Nucleophilic attack by the resultant anion on a second molecule of the acetylenic ester may then proceed as shown in Scheme 1*a*. Protonation of the allene intermediate affords the vinyl acetylene **1**. The stereospecificity of the reaction, which gives only the *trans* olefin, requires that the proton source (R_3N^+H) be oriented *cis* to the attacking nucleophile. Such an orientation may be attributed to residual coordination between the triethylammonium ion (BH) and the acetylenic moiety (A). A similar effect has been proposed by Brady to explain the stereospecificity of the reaction of $Me_3N \cdot HCl$ with EP in CH_2Cl_2, which yields only **7** (9).

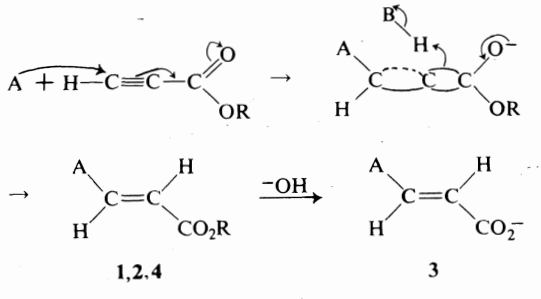

1,2,4 **3**

	A	B—H	Product
a	$RO_2C-C\equiv C^-$	$R_3\overset{+}{N}H$	**1**
b	HO^-	$R_3\overset{+}{N}H$	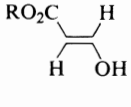
	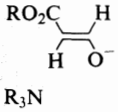	$R_3\overset{+}{N}H$	**2**
c	R_3N	HOH	**3**
d	RO^-	$R_3\overset{+}{N}H$ or HOH	**4**

SCHEME 1

In the presence of a limited amount of H_2O, attack by hydroxide on the propiolate (Scheme 1*b*) may lead to the *trans* β-hydroxyacrylate: the vinyloxide anion can react subsequently in the same way with a second molecule of propiolate to afford the divinyl ether **2**.

Formation of the betaines **3** may be rationalized as shown in Scheme 1*c*. The initial allene intermediate **8** is again protonated stereospecifically on the *cis* side,[3] the proton source presumably being H_2O associated with the solvated quaternary ammonium center. The resultant quaternary hydroxide, being a strong base, undergoes self-catalyzed ester hydrolysis, leading to stabilization of the negative charge on the carboxylate grouping. Formation of **3** clearly does not involve initial hydrolysis to propiolic acid and subsequent reaction with the tertiary amine, since the latter reaction yields only the 1:1 salt.[4]

The primary by-product under highly aqueous conditions is **4**. Attack by alkoxide (derived from the alcohol released by hydrolysis of the ester group during formation of **3**) leads once more to an allene intermediate (Scheme 1*d*). There are two possible proton sources: R_3N^+H and H_2O. *Cis* protonation is presumably assured in this case by hydrogen bonding between the alkoxyl oxygen and water.

It is interesting to note that reaction of MP with MeOH (solvent) in the presence of an equimolar amount of Et_3N gave the ether **4***b*, along with its *cis* isomer **10***b*. The product ratio (**4***b*:**10***b* ≈ 7:3) is consistent with that observed by Winterfeldt for the same reaction catalyzed by *N*-methyl morpholine (3). Under these conditions protonation (by MeOH) is likely from either side, leading to a mixture of isomeric products.

Structures

Compounds **1***b* (4, 7), **2***a* (11), **2***b* (4, 7), **4***a*

[3]Intermediates of type **8** have been postulated in the reactions of pyridines with dimethyl acetylenedicarboxylate (1, 2, 10) and MP (11): such an intermediate has in fact been trapped in the reaction of pyridine with dimethyl acetylenedicarboxylate (12).

[4]The detection in the product from EP and Et_3N of small amounts of **9** (formed by reaction of **6** with EP (13)) suggests that hydrolysis to propiolic acid constitutes a minor reaction pathway.

Can. J. Chem. Downloaded from www.nrcresearchpress.com by 210.87.254.42 on 09/05/12
For personal use only.

TABLE 1. 60 MHz p.m.r. parameters for **1**, **2**, **4**, **15**, and **16** ($CDCl_3$)

	Olefinic hydrogens: AX (or AB)				Other hydrogens* (δ)
	Integral	Centroid (δ)	J_{AX}(Hz)	$\Delta\nu_{AX}$(Hz)	—OR, —CO_2R, —NR
1*a*	2H	6.63	16.0	19.1	1.32 (3H, t), 1.34 (3H, t), 4.25 (2H, q), 4.28 (2H, q)
1*b*	2H	6.65	16.1	18.7	3.80 (3H, s), 3.83 (3H, s)
2*a*	4H	6.66	12.3	120.1	1.28 (6H, t), 4.21 (4H, q)
2*b*	4H	6.64	12.2	116.1	3.75 (6H, s)
4*a*	2H	6.40	12.8	144.2	1.27 (3H, t), 1.34 (3H, t), 3.93 (2H, q), 4.16 (2H, q)
4*b*	2H	6.38	12.7	144.9	3.68 (6H, s)
15*a*	2H	6.47	12.7	149.7	1.34 (3H, t), 3.98 (2H, q), 10.50 (1H, s)
15*b*	2H	6.47	12.6	150.3	3.74 (3H, s), 11.57 (1H, s)
16	2H	6.02	13.1	171.7	1.16 (6H, t), 1.26 (3H, t), 3.20 (4H, q), 4.14 (2H, q)

*s = singlet, t = triplet, q = quartet.

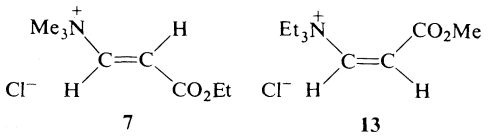

7

13

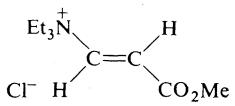

14

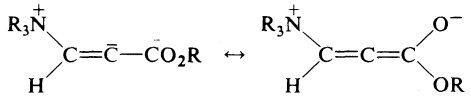

8

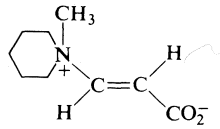

5

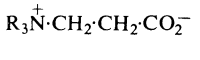

11

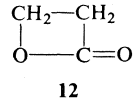

12

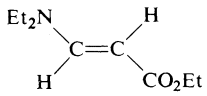

16

(14), and **4***b* (3) have all been reported previously. The physical constants and properties of our products were in all cases consistent with those reported.[5] Product **1***a* was readily identified by comparison of its mode of formation and spectral properties with those of **1***b*. Proton magnetic resonance data for all by-products are given in Table 1.

Betaine **3***a* is a colorless hygroscopic solid, insoluble in common organic solvents but readily soluble in H_2O. Crystallization from EtOH gave an alcoholate from which the anhydrous compound could be obtained by drying under vacuum. All the betaines isolated in this study exhibited wide melting ranges, with decomposition, which were dependent on the rate of heating. These properties are paralleled closely by those reported for betaines of type **11**, prepared by reaction of tertiary amines with β-propiolactone **12** (15) or with α,β-unsaturated carboxylic acids (16).

The p.m.r. spectra of **3***a–c* and **5** are very simple, showing only an AB quartet for two olefinic hydrogens and signals for the hydrogens of the amine substituents (Table 2). As expected, the signal for the $N^+\cdot CH_2$ hydrogens of **3***a* is significantly shifted downfield (by 1 p.p.m.) relative to that (2.53 δ) of the N—CH_2 hydrogens of Et_3N. The i.r. spectrum of **3***a* is characterized by strong carboxylate absorption at 1595 cm^{-1} and C=C absorption at 1660 cm^{-1}.

The *trans* stereochemistry of the double bond in **3***a–c* and **5** has been assigned on the basis of p.m.r. evidence. Irradiation of the methylene hydrogens of **3***a* caused a 15% enhancement (nuclear Overhauser effect) of the signals of *both* olefinic hydrogens. Such a dual effect is only possible where the internuclear distance between each olefinic hydrogen and the methylene protons is similar and would clearly be impossible if the two hydrogens were *cis*. The *trans* assignment is further supported by the

[5]A discrepancy exists in the reported m.p. of **2***b* (133° (4), 158–159° (7)). The correct value is that given by Wenkert *et al.* (7).

Can. J. Chem. Downloaded from www.nrcresearchpress.com by 210.87.254.42 on 09/05/12
For personal use only.

TABLE 2. 60 MHz p.m.r. parameters for **3***a–c*, **5**, **9**, **13**, **14**, and **18** (D_2O)

CPD	Olefinic hydrogens: Centroid of AB (δ)	$\Delta\nu_{AB}$(Hz)	J_{AB}(Hz)	Other signals* (δ)
3*a*†	6.48	11.7	14.2	1.28 (9H, t); 3.55 (6H, q)
3*b*	6.70	29.4	14.2	3.38 (9H, s)
3*c*	6.51	16.7	14.6	0.8–2.0 (21H, m); 3.3–3.7 (6H, m)
5	6.65	21.1	14.3	1.80 (6H, m); 3.27 (3H, s); 3.65 (4H, m)
9	6.88	31.7	14.5	1.36 (12H, t); 3.67 (6H, q); 4.36 (2H, q); 3.16 (1H, s)
13	6.35	16.3	11.0	1.32 (9H, t); 3.72 (6H, q); 3.86 (3H, s)
14	6.86	31.8	14.6	1.32 (9H, t); 3.63 (6H, q); 3.87 (3H, s)
18	6.60	25.9	14.5	1.32 (9H, t); 3.60 (6H, q); 3.23 (1H, s)

*s = singlet, t = triplet, q = quartet, m = multiplet.
†Nuclear Overhauser experiments were performed at 100 MHz on a 5% degassed solution of **3***a* in dimethyl sulfoxide-d_6. Irradiation of the methylene hydrogens (δ 3.46) caused a 15% enhancement in the signals for both olefinic hydrogens.

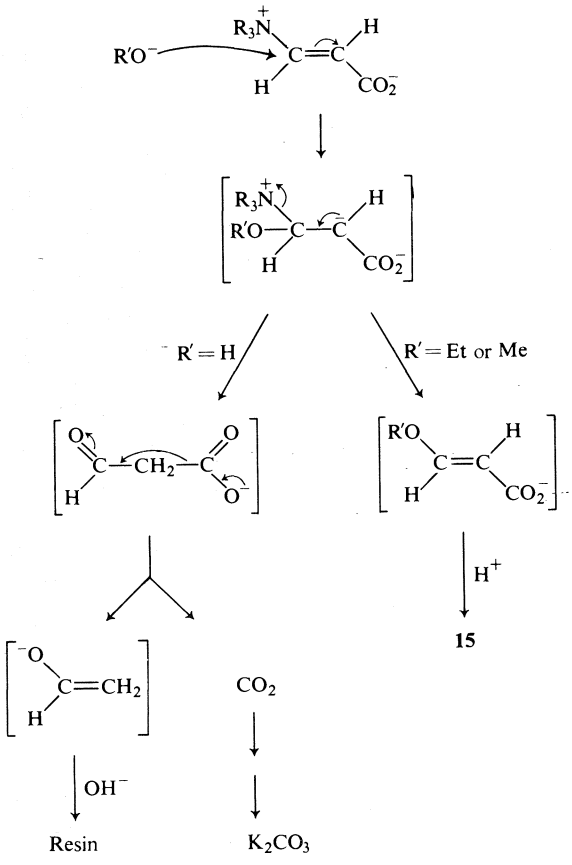

SCHEME 2

coupling constant (*ca.* 14.3 Hz) between the two olefinic hydrogens (Table 2). The *cis* and *trans* salts **13** and **14**, obtained from the reaction of MP with $Et_3N \cdot HCl$, were used as models. Data are also included in Table 2 for **9** and **18**.

Properties

The characteristic behavior of these betaines is illustrated by the following reactions of **3***a*.

(*a*) When **3***a* was refluxed with *ethanolic KOH* for 5 h a crystalline solid precipitated from the hot solution. This was identified as potassium carbonate (yield 32%). After reacidification of the solution a 20% yield of *trans* β-ethoxyacrylic acid **15***a* was isolated. The major product from the corresponding reaction of **3***a* with *methanolic KOH* was the β-methoxy acid **15***b* (35% in 4.5 h): in this case no K_2CO_3 precipitated. A similar yield of **15***b* was obtained using *methanolic KOMe*.

The formation of both K_2CO_3 and **15** can be accounted for by nucleophilic attack by hydroxide and alkoxide, respectively, giving an intermediate complex which can then eliminate the tertiary amine (Scheme 2). Mechanisms of this type have been proposed for nucleophilic substitutions at olefinic (17) and aromatic (18) carbons.

In the case of attack by hydroxide the product formed may readily decarboxylate ($\rightarrow K_2CO_3$) and the aldehydic fragment would be expected to polymerize spontaneously. Supporting evidence for this pathway is obtained by the isolation of material similar to that formed by resinification of acetaldehyde under basic conditions. The alternative decarboxylative elimination mechanism, occurring during pyrolysis (see below) and shown in Scheme 3, does not operate under these conditions. No gaseous products were evolved: all CO_2 formed was trapped and precipitated *in situ* as K_2CO_3.

The reaction ($KOH–CH_3OH$) was repeated using **3***a* in which both olefinic hydrogens had

Can. J. Chem. Downloaded from www.nrcresearchpress.com by 210.87.254.42 on 09/05/12
For personal use only.

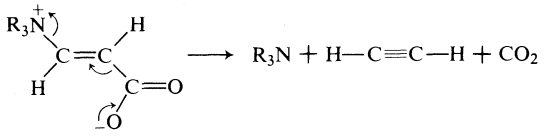

SCHEME 3

been replaced by deuterium (use of D_2O in its preparation). In the initial stages of reaction (<15 min) the small amount of **15***b* isolated showed negligible exchange of either olefinic deuterium. This is consistent with Scheme 2, and invalidates any mechanism involving a triple-bonded intermediate. The improved conversion to **15** in methanolic solution (relative to that in EtOH) may be attributed to the greater acidity of CH_3OH, leading to a higher concentration of RO^- in this solvent.

(*b*) Catalytic reduction of **3***a* occurred smoothly, 2 mol hydrogen being absorbed. High conversion to propionic acid and Et_3N was observed. This reduction presumably occurs by stepwise hydrogenation of the olefinic bond, elimination of Et_3N and reduction of the regenerated double bond.

(*c*) Under controlled conditions *pyrolysis* of **3***a* (no solvent) afforded a mixture of products. The major among these were CO_2 (isolated as $BaCO_3$), C_2H_2 (obtained as cuprous acetylide), Et_3N (isolated as its hydrochloride), and the enamino ester **16**. Formation of the first three products presumably involves the decarboxylative elimination shown in Scheme 3. Formation of **16** is difficult to rationalize unless we assume intermolecular transfer of the ethyl group. Isomerization of the double bond, placing the N^+Et_3 and CO_2^- groups in a *cis* juxtaposition suitable for facile transfer of the ethyl group from N to O seems unlikely since the product stereochemistry is also *trans*, indicating that reisomerization would have had to occur.

(*d*) Reaction of **3***a* with *anhydrous HCl* in *MeOH* afforded the corresponding ester salt **14** in good yield. The latter, together with its *cis* stereoisomer **13**, was also prepared by reaction of MP with $Et_3N \cdot HCl$ in MeOH (*cf.* 9, 19). Structurally similar *trans* (β-acylvinyl) trimethylammonium chlorides have been prepared by reaction of the corresponding *trans* β-chlorovinyl ketones with $Me_3N \cdot HCl$ (20).

Reaction of **3***a* with *propiolic acid* gave the *trans* β-triethylammonium acrylic acid salt **18**.

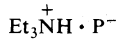

6

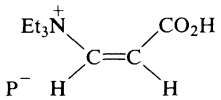

17

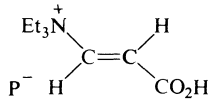

18

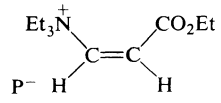

19

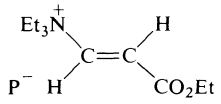

9

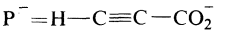

We have also observed that salt **6** slowly rearranges on standing to give **18** together with its *cis* isomer **17**. In addition the corresponding ester salts **19** and **9** could be obtained by reaction of **6** with EP (13).

To conclude, the tendency of molecules such as **3** to undergo stereospecific nucleophilic attack at the carbon atom carrying the positively charged N atom offers considerable synthetic potential. We are investigating the use of these readily obtainable betaines in synthesis of this type and also their possible application to insertion of an unsubstituted double bond (by use of **3**, **13**, or **14** as a dienophile and subsequent elimination of the carboxyl and amino functions).

Experimental

Proton magnetic resonance spectra were obtained on a Varian A-60A spectrometer. Tetramethylsilane was used as internal standard in $CDCl_3$: in D_2O sodium 3-trimethylsilylpropionate-2,2,3,3-d_4 was employed. The i.r. spectra were recorded on Perkin-Elmer 521 or 237 spectrometers and mass spectra using a Dupont 21-491 spectrometer. Chromatographic separations were carried out on Mallinckrodt silicic acid (100–150 mesh), with $CHCl_3$ as eluant.

Ethyl Propiolate with Triethylamine

Et_3N (5.05 g, 0.05 mol) was added dropwise over a period of 10 min to a well-stirred mixture of EP (4.90 g, 0.05 mol), CH_2Cl_2 (25 ml), and H_2O (25 ml), the rate of addition being controlled to maintain the temperature < 32°. Stirring was continued for 1 h at room temperature. The CH_2Cl_2 phase was separated and the aqueous phase extracted with CH_2Cl_2. The combined CH_2Cl_2 solutions were then dried (Na_2SO_4) and evaporated to afford a reddish oil (1.09 g). Compound **4***a* could be obtained from this by column chromatography, as a sweet-smelling yellow oil (859 mg, 12%), n_D^{20} = 1.4438 (lit. (14) n_D^{20} = 1.4471). Very weak parent ion at *m/e* 144; ($C_7H_{12}O_3$

Can. J. Chem. Downloaded from www.nrcresearchpress.com by 210.87.254.42 on 09/05/12
For personal use only.

Can. J. Chem. Downloaded from www.nrcresearchpress.com by 210.87.254.42 on 09/05/12
For personal use only.

requires 144); prominent ions at *m/e* 99 and 71. Compound **4***a* could also be purified by distillation. Later fractions contained **2***a* (73 mg, 0.7%).

The aqueous phase of the reaction mixture was azeotroped to dryness under reduced pressure using dioxane. The residue was triturated with acetone[6] to afford the dihydrate of betaine **3***a* as a colorless solid (6.54 g). This was dried under vacuum overnight at room temperature to give **3***a* as a beige powder (5.34 g, 63%), m.p. (dec.) 205–210°; ν_{max} (KBr): 1660, 1595, 1380 cm^{-1}. The material is very hygroscopic, insoluble in Et_2O and $CHCl_3$, but readily soluble in cold H_2O or MeOH. Crystallization from a small amount of absolute EtOH gave the ethanolate as colorless prisms.

The yield of **3***a* was dependent on the solvent ratio H_2O–CH_2Cl_2 and varied from 40% at 1:9 to 80% at 9:1.

Methyl Propiolate with Triethylamine

Et_3N (7.58 g, 0.075 mol) and MP (6.30 g, 0.075 mol) in CH_2Cl_2 (35 ml) and H_2O (35 ml) were reacted as above. The organic layer afforded a red oil: distillation gave **4***b* as a pale yellow oil (2.43 g, 28%), b.p. 162–164° (lit. (3,21) 155–156°/755 mm). The aqueous layer gave **3***a* as its dihydrate (8.75 g, 56%).

Reaction of MP (8.40 g, 0.1 mol), Et_3N (10.10 g, 0.1 mol), CH_2Cl_2 (20 ml), and H_2O (80 ml) gave **3***a* (13.02 g, 76%).

Ethyl Propiolate with Trimethylamine

25% aqueous Me_3N (35 ml) was reacted with EP (7.35 g), CH_2Cl_2 (35 ml), and H_2O (35 ml) in the same way. The CH_2Cl_2 layer afforded a pale yellow oily solid: p.m.r. indicated a mixture of **2***a*, **4***a*, and **1***a* (see below) in a molar ratio of 5:4:1. Trituration with petroleum ether (b.p. 30–60°) left **2***a* as colorless needles (2.86 g, 30%), m.p. 115–116°. Highest molecular ion at *m/e* 214 ($C_{10}H_{14}O_5$ requires 214); prominent ions at *m/e* 169, 141, 99, and 73. ν_{max} (KBr): 1720, 1695, 1680, 1615 cm^{-1}.

The aqueous phase gave the hydrated betaine **3***b* as a colorless solid. Drying under vacuum at room temperature gave **3***b* as an amorphous cream-colored solid (2.57 g, 27%), m.p. (dec.) 240–245°.

An improved yield (54%) of **3***b* was obtained using a solvent ratio of H_2O–CH_2Cl_2, 3:1.

Methyl Propiolate with Trimethylamine

(*a*) 25% aqueous Me_3N (25 ml) was similarly reacted with MP (4.20 g) in CH_2Cl_2 (25 ml). The mixture turned dark brown immediately, while the CH_2Cl_2–H_2O ratio was high. The CH_2Cl_2 layer yielded a dark gummy residue (3.34 g). Extraction of the latter with hot petroleum ether (b.p. 30–60°) left a brown amorphous solid (750 mg), which was then thoroughly extracted with Et_2O. Evaporation and crystallization of the residue from Et_2O gave **2***b* as colorless needles (431 mg, 5%), m.p. 157.5–159° (lit. (7) 158–159°). Highest molecular ion at *m/e* 186 ($C_8H_{10}O_5$ requires 186); prominent ions at *m/e* 155, 127, 85, and 59. The petrol extract gave a sticky yellow solid (1.81 g). Crystallization from petroleum ether (b.p. 30–60°) afforded **1***b* as pale yellow needles (1.38 g, 16%), m.p. 54–55° (lit. (4) 55°).

[6]Proton magnetic resonance examination of the acetone-soluble residue (0.88 g) indicated **3***a* and **9** in a molar ratio of approximately 3:2.

The aqueous layer yielded a very dark brown viscous oil (1.70 g), which was not investigated.

(*b*) The reaction was repeated, in this case the 25% aqueous Me_3N (35 ml) being added to MP (6.30 g), CH_2Cl_2 (35 ml), *and* H_2O (35 ml). The mixture turned yellow, but became no darker during the reaction. The CH_2Cl_2 layer gave a sticky colorless solid (2.56 g) the p.m.r. of which indicated a mixture of **4***b*, **2***b*, and **1***b* in a molar ratio of 9:1:1. Trituration with acetone gave **2***b* as colorless needles (465 mg, 3%).

The aqueous layer afforded **3***b* (4.37 g, 45%).

Betaine 3c

Tributylamine (9.25 g, 0.05 mol) was added in the usual way to a mixture of EP (4.90 g, 0.05 mol), CH_2Cl_2 (25 ml), and H_2O (25 ml). After 1 h at room temperature the organic phase was separated (p.m.r. showed unreacted Bu_3N, **4***a*, and a small amount of **2***a*). The aqueous phase gave **3***c* directly as a colorless crystalline solid (8.79 g, 69%), m.p. (dec.) 195–200°. This compound is insoluble in EtOAc, acetone, or Et_2O but is quite soluble in $CHCl_3$ and readily soluble in cold H_2O.

Betaine 5

N-Methylpiperidine (4.95 g, 0.05 mol) was added to a mixture of EP (4.90 g, 0.05 mol), CH_2Cl_2 (25 ml), and H_2O (25 ml). After 1 h at room temperature the organic layer was separated and discarded. The aqueous layer afforded betaine **5** (2.80 g, 33%), m.p. (dec.) 180–185°.

Propiolic Acid with Triethylamine

Et_3N (6.55 g, 0.065 mol) and propiolic acid (4.55 g, 0.065 mol) were reacted in CH_2Cl_2 (25 ml) and H_2O (75 ml) for 1 h at room temperature. The aqueous layer afforded a quantitative yield of the 1:1 salt **6**.

The same product was obtained by addition of Et_3N (5.06 g, 0.05 mol) to propiolic acid (3.50 g, 0.05 mol) in CH_2Cl_2 (50 ml) at 0°. Evaporation of solvent gave **6** as a very hygroscopic colorless crystalline solid (8.51 g, ~100%). δ ($CDCl_3$): 1.34 (9H, t), 2.67 (1H, s), 3.15 (6H, q).

Vinylacetylene 1a

EP (10.0 g, 0.1 mol) and *N*-methylpiperidine (10.0 g, 0.1 mol) were reacted in dry benzene (100 ml) for 1 h according to the procedure of Wenkert *et al.* for the preparation of **1***b* (7). Column chromatography of the product afforded **1***a* (6.0 g, 60%) as a yellow oil, n_D^{25} = 1.4882. Highest molecular ion at *m/e* 196 ($C_{10}H_{12}O_4$ requires 196); prominent ions at *m/e* 151, 123, 89, 87, and 50. ν_{max} (liquid film): 2234, 1725, 1625 cm^{-1}.

Reaction of Methyl Propiolate with Triethylamine in Methanol

Et_3N (3.03 g, 0.03 mol) in MeOH (12 ml) was added to a well-stirred solution of MP (2.52 g, 0.03 mol) in MeOH (25 ml). The mixture was stirred at room temperature for 2 h Evaporation afforded an oily solid (2.76 g); p.m.r. indicated a mixture of **4***b* and **10***b* in a ratio of 7:3 (*cf.* ref. 3).

Properties of 3a

(*a*) *Reaction with KOH–EtOH*

A solution of **3***a* (3.42 g, 0.02 mol) in 100% EtOH (25 ml) was added to a hot solution of KOH (1.12 g, 0.02 mol) in EtOH (25 ml) and the mixture refluxed for 5 h, during

Can. J. Chem. Downloaded from www.nrcresearchpress.com by 210.87.254.42 on 09/05/12
For personal use only.

which a crystalline solid was deposited. This solid (880 mg, 32%) was filtered and identified as K_2CO_3 by its characteristic reactions with dilute HCl, $MgSO_4$, $HgCl_2$, $AgNO_3$, and $CaCl_2$. The red filtrate was concentrated and the residue taken up in H_2O. The aqueous solution was extracted with Et_2O. This afforded a strong-smelling red-brown gum (120 mg). (This material was very similar (appearance, smell, p.m.r.) to that obtained by dropwise addition of acetaldehyde into refluxing ethanolic KOH, evaporation of the solvent, and extraction of an aqueous solution of the residue with Et_2O).

The aqueous solution was then acidified with HCl and the acid solution extracted with Et_2O: the dried extract gave a yellow solid. Crystallization from benzene – petroleum ether gave **15***a* as pale yellow needles (480 mg, 20%), m.p. 109.5–110° (lit. (22) 109°). No gaseous products could be detected from the above reaction.

(*b*) *Reaction with KOH–MeOH*

(*i*) A solution of **3***a* (3.42 g, 0.02 mol) in MeOH (20 ml) was added to a hot solution of KOH (1.12 g, 0.02 mol) in MeOH (30 ml) and the mixture refluxed for 24 h. The bulk of the solvent was then evaporated and the residue dissolved in H_2O. The aqueous solution was extracted with Et_2O (only 71 mg dark red gum) and then acidified with HCl. The acid solution was extracted with Et_2O: the dried extract gave **15***b* as a cream-colored crystalline solid (925 mg, 45%), m.p. 102–103° (lit. (22) 102°). A separate experiment showed 35% conversion to **15***b* in 4.5 h.

(*ii*) Dideuterated **3***a* (1.9 g, 0.011 mol) in MeOH (15 ml) was added to a hot solution of KOH (650 mg, 0.012 mol) in MeOH (20 ml). The mixture was refluxed for 1 h and was then worked up as in *i* to give **15***b* (133 mg, 11.5%). Analysis by p.m.r. indicated 10 and 25% exchange of the low and high-field olefinic deuteriums. Negligible exchanges were observed in the **15***b* (2.5%) obtained in a similar experiment after only 15 min.

(*c*) *Reaction with KOMe–MeOH*

To **3***a* (1.71 g) in MeOH (15 ml) was added a 0.465 *N* solution (22 ml) of KOMe in MeOH, to give a mixture equimolar in **3***a* and KOMe. This was refluxed for 22 h. The bulk of the solvent was evaporated and the residue dissolved in cold H_2O (30 ml) and acidified with HCl. The acid solution was then extracted with Et_2O to give **15***b* (476 mg, 47%).

(*d*) *Catalytic Reduction*

(*i*) A solution of **3***a* (2.0 g) in MeOH (150 ml) was hydrogenated at room temperature and pressure using Adams' catalyst (150 mg) until uptake of H_2 was complete (30 min). The solution was filtered and treated with gaseous HCl for 5 min at 0°. Evaporation of solvent gave $Et_3N \cdot HCl$ as a colorless solid (1.32 g, 82%), m.p. (dec.) 255–260°, identical to an authentic sample.

(*ii*) The reaction mixture from an experiment identical to *i* was evaporated to give an orange oil (1.18 g). This was dissolved in Et_2O (75 ml) and the solution treated with gaseous HCl at 0° to give $Et_3N \cdot HCl$ (410 mg, 26%), m.p. (dec.) 255–260°. Evaporation of the filtrate afforded propionic acid as a pungent oil (292 mg, 34%), identical to an authentic sample.

(*e*) *Pyrolysis*

(*i*) The betaine **3***a* was recovered as its alcoholate after refluxing for 60 h in 100% EtOH.

(*ii*) Solid **3***a* (2.0 g) was heated in an oil bath to 150°, a side arm connected to the flask being led into a saturated $Ba(OH)_2$ solution. Heating was maintained at 140–160° for 1 h, during which gas was liberated. The precipitated $BaCO_3$ (552 mg, 24%) was filtered and dried.

(*iii*) Experiment *ii* was repeated with the side arm being led in this case to an ammoniacal cuprous chloride solution. A heavy precipitate of red cuprous acetylide was deposited.

(*iv*) Solid **3***a* (13.5 g) was heated in an oil bath, the temperature being maintained at 130–140° for 1 h: although decomposition started, no distillate was collected. When the bath temperature was increased to 150–175° a fraction of boiling range 65–85° was collected. A $CHCl_3$ solution of this fraction was saturated with gaseous HCl. Evaporation of solvent and trituration of the residue with Et_2O gave a brownish solid. Crystallization from EtOH gave $Et_3N \cdot HCl$ as colorless needles (2.18 g, 20%), m.p. (dec.) 258–260°.

The residue in the pyrolysis flask was a dark red oil (7.06 g). This was distilled under reduced pressure (60 mm). Pure **16** (2.31 g, 17%) was collected as a pale yellow oil, b.p.160–162° (lit. (23) b.p.129–130°/180 mm), identical to the product obtained from reaction of Et_2NH with EP.

(*f*) *Reaction with HCl–MeOH*

A stirred solution of **3***a* (2.90 g) in MeOH (75 ml) was treated for 5 min at 0° with gaseous HCl. After stirring for a further 90 min the solvent was evaporated. The oily residue solidified and was triturated with acetone to give the *trans* ester chloride **14** (2.81 g, 75%), m.p. (dec.) 165–170°, identical to a sample prepared from $Et_3N \cdot HCl$ and MP (see below).

(*g*) *Reaction with Propiolic Acid*

A solution of propiolic acid (1.40 g, 0.02 mol) in MeOH (10 ml) was added to a stirred solution of **3***a* (3.42 g, 0.02 mol) in MeOH (40 ml). Evaporation of the solvent gave a paste. Trituration of the latter with acetone gave **18** as a colorless crystalline solid (3.92 g, 81%), m.p. (dec.) 119–122°.

The above compound, together with its *cis* isomer **17**, was also obtained when salt **6** was allowed to stand at room temperature (13).

*Preparation of Salts **13** and **14** (cf. 9, 19)*

(*i*) A solution of $Et_3N \cdot HCl$ (2.41 g, 0.018 mol) and MP (2.96 g, 0.035 mol) in MeOH (200 ml) was refluxed for 2 h. Evaporation of the solvent gave a solid residue. Trituration with acetone afforded **14** (3.55 g, 91%), m.p. (dec.) 167–170°.

(*ii*) A solution of $Et_3N \cdot HCl$ (2.91 g, 0.02 mol) and MP (1.86 g, 0.02 mol) in MeOH (200 ml) was refluxed for 2 h. Work-up as in *i* gave **14** (1.81 g, 37%) and in addition, from the acetone-soluble fraction, compound **13** as a very viscous and unstable colorless oil (2.09 g, 43%).

We wish to acknowledge the contributions made to this work by A. P. Korn (NRCC summer student, 1971), B. V. Brackett (research assistant, 1971–1972), and D. Ettinger (research assistant, 1972–1973).

1. E. WINTERFELDT. Angew. Chem. Int. Ed. **5**, 423 (1967).
2. E. WINTERFELDT. *In* Chemistry of acetylenes. *Edited*

by H. G. Viehe. Marcel Dekker, New York. 1969. Chapt. 4. p. 267.
3. E. WINTERFELDT and H. PREUSS. Chem. Ber. **99**, 450 (1966).
4. E. WINTERFELDT. Chem. Ber. **97**, 1952 (1964).
5. C. I. SIMIONESCU and T-H. KIM. Rev. Roum. Chim. **14**, 1519 (1969); Chem. Abstr. **73**, 4236m (1970).
6. B. J. MACNULTY. Polymer, **1**, 275 (1966).
7. E. WENKERT, K. A. H. ADAMS, and C. L. LEICHT. Can. J. Chem. **41**, 1844 (1963).
8. K. A. POLLART. U.S. Patent 3,383,403. Chem. Abstr. **69**, 35475k (1968).
9. D. G. BRADY. Ph.D. Thesis. Purdue University. Lafayette, Indiana. Univ. Microfilms, 66–13, 175. 1966.
10. L. M. JACKMAN, A. W. JOHNSON, and J. C. TEBBY. J. Chem. Soc. 1579 (1960).
11. R. M. ACHESON and J. M. WOOLLARD. J. Chem. Soc. C, 3296 (1971).
12. R. M. ACHESON and A. O. PLUNKETT. J. Chem. Soc. 2676 (1964).
13. A. W. MCCULLOCH and A. G. MCINNES. Unpublished work.
14. W. J. CROXALL and H. J. SCHNEIDER. J. Am. Chem. Soc. **71**, 1257 (1949).
15. T. L. GRESHAM, J. E. JANSEN, F. W. SHAVER, R. A. BANKERT, and F. T. FIEDOREK. J. Am. Chem. Soc. **73**, 3168 (1951).
16. A. LEBERRE and A. DELACROIX. Bull. Soc. Chim. Fr. 2404 (1973).
17. D. E. JONES, R. O. MORRIS, C. A. VERNON, and R. F. M. WHITE. J. Chem. Soc. 2349 (1960).
18. J. F. BUNNETT. Q. Rev. 1 (1960).
19. W. E. TRUCE and D. G. BRADY. J. Org. Chem. **31**, 3543 (1966).
20. W. R. BENSON and A. E. POHLAND. J. Org. Chem. **29**, 385 (1964).
21. K. BOWDEN. Can. J. Chem. **44**, 661 (1966).
22. L. N. OWEN and H. M. B. SOADE. J. Chem. Soc. 1030 (1947).
23. F. STRAUSS and W. VOSS. Chem. Ber. **59***b*, 1681 (1926).

Can. J. Chem. Downloaded from www.nrcresearchpress.com by 210.87.254.42 on 09/05/12
For personal use only.

The Synthesis of Specifically Deuterated Phenanthrenes

J. L. CHARLTON, B. KOSTYK, AND H. K. LAI

Department of Chemistry, University of Manitoba, Winnipeg, Manitoba R3T 2N2

Received May 7, 1974

J. L. CHARLTON, B. KOSTYK, and H. K. LAI. Can. J. Chem. **52**, 3577 (1974).

Synthetic methods for the preparation of phenanthrene-1,3-d_2, -2,4-d_2, -1,2,3,4-d_4, -1,3,6,8-d_4, and -2,4,5,7-d_4 are described.

J. L. CHARLTON, B. KOSTYK et H. K. LAI. Can. J. Chem. **52**, 3577 (1974).

On décrit des méthodes de synthèse pour la préparation des phénanthrène-1,3-d_2, -2,4-d_2, -1,2,3,4-d_4, -1,3,6,8-d_4 et -2,4,5,7-d_4. [Traduit par le journal]

Can. J. Chem. Downloaded from www.nrcresearchpress.com by 210.87.254.105 on 09/05/12
For personal use only.

Due to an interest in the effect of deuteration on the spectroscopic properties of aromatic molecules, we have recently synthesized a series of specifically deuterated anthracenes (1). As we wished to continue our spectroscopic studies on phenanthrene derivatives it became necessary to devise a synthetic scheme for the preparation of specifically deuterated phenanthrenes. As we required symmetrically deuterated material we discarded all approaches such as a Haworth-like synthesis in which the rings are added sequentially in a Friedel Crafts addition of succinic anhydride. We have also found that replacement of halogen by deuterium in the completed molecule can be difficult (2) although this approach has been used successfully by others (3). In any event, there is no obvious route to the symmetrically halogenated precursors.

Only two methods for preparation of the carbon skeleton from suitably deuterated precursors occurred to us. The first is the Diels–Alder addition of butadiene to orthobenzoquinone. A similar method had been used successfully for the synthesis of deuterated anthracenes (1). The second method is the cylization–oxidation of the appropriately deuterated stilbenes (4). Since a review of the literature revealed that orthobenzoquinones were difficult to work with, we turned our attention to the preparation of specifically deuterated stilbenes and their cyclization to phenanthrenes.

Results and Discussion

The deuterated phenanthrenes prepared during the course of this work are listed in Table 1 and they have all been synthesized by cyclization of a corresponding stilbene. The cyclization–oxidation procedure has been reported previously (4).

Four of the stilbenes listed in Table 1 are prepared from benzaldehyde-2,4,6-d_3 and -2,5-d_2. The trideuterio aldehyde was prepared from aniline in the following way. Aniline hydrochloride was heated in D_2O at 100 °C to exchange the *ortho* and *para* protons. The free amine was then diazotized and reacted with cuprous cyanide to give benzonitrile-2,4,6-d_3. This was subsequently reduced with stannous chloride to give the benzaldehyde. Benzaldehyde-3,5-d_2 was prepared from *p*-toluidine which was exchanged as its hydrochloride in D_2O. The free amine was diazotized and treated with cuprous bromide to give *p*-bromotoluene-3,5-d_2. After removing the bromine via a Grignard reaction the methyl group was oxidized with chromium trioxide in acetic anhydride to give the toluene diacetate. Hydrolysis and steam distillation gave pure aldehyde. Scheme 1 contains the general scheme for the preparation of the deuterated benzaldehydes.

The conversion of benzaldehyde to stilbene has been described by Fieser (5) and stilbene-2,2′,4,4′,6,6′-d_6 and -3,3′,5,5′-d_4 were prepared by this method. Stilbene-2,4,6-d_3 and -3,5-d_2 were prepared by treating the deuterated benzaldehydes with benzyl magnesium bromide followed by dehydration. Stilbene-2,3,4,5,6-d_5 was synthesized from phenylacetaldehyde and perdeuteriophenylmagnesium bromide with subsequent dehydration. Perdeuteriobromobenzene was prepared by the method of Vogel (6). The three stilbene preparations are illustrated in Scheme 2.

The isotopic purities of the phenanthrenes synthesized were determined by mass spectometry (8 eV) and are recorded in Table 1. The yields for many of these reactions are often low but do not represent any attempt at maximization.

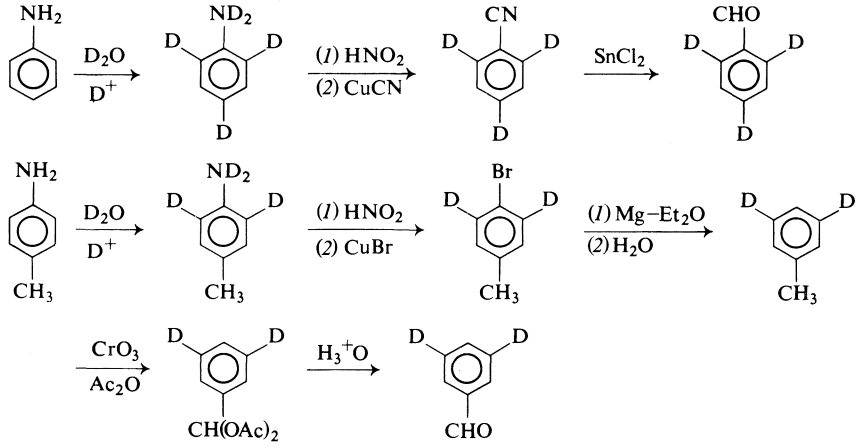

SCHEME 1

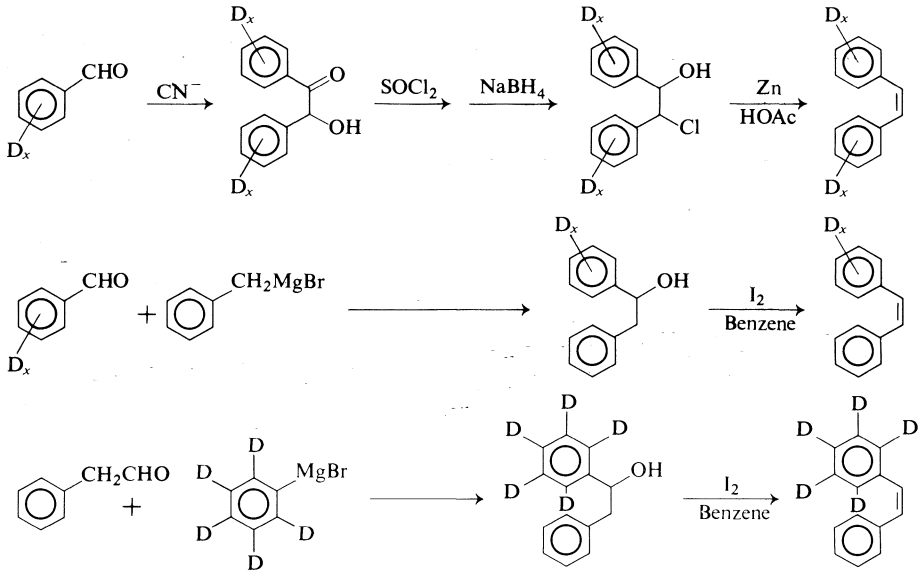

SCHEME 2

TABLE 1. Deuterated phenanthrenes and their isotopic purities

Phenanthrene	From stilbene	Phenanthrene purity (%)*
1,3,6,8-d_4	2,2′,4,4′,6,6′-d_6	98 d_4
2,4,5,7-d_4	3,3′,5,5′-d_4	13 d_3, 85 d_4
1,3-d_2	2,4,6-d_3	98 d_4
2,4-d_2	3,5-d_2	3 d_1, 97 d_2
1,2,3,4-d_4	2,3,4,5,6-d_5	98 d_4

*Mol% isotopic composition. Values are precise to only ±2%.

Experimental

Mass spectra were recorded on a Finnigan 1015 mass spectrometer at an ionization energy of 8 eV. Mass ratios were calculated from peak heights and are precise only to ±2%. Ultraviolet (u.v.) spectra of the deuterated phenanthrenes were recorded in ethanol (95%) on a Unicam recording spectrometer. The nondeuterated phenanthrene exhibited λ_{max} 251 (64 000) nm.

Aniline-2,4,6-d_3

This compound was prepared essentially by the method of Best and Wilson (7). The exchange was continued until

Can. J. Chem. Downloaded from www.nrcresearchpress.com by 210.87.254.105 on 09/05/12
For personal use only.

Can. J. Chem. Downloaded from www.nrcresearchpress.com by 210.87.254.105 on 09/05/12
For personal use only.

the mass peak at *m/e* 95 was less than 2% of the peak *m/e* 96 in the free amine which had been reexchanged in H_2O.

Benzonitrile-2,4,6-d_3

The method of Vogel (8) was used. The cuprous cyanide solution was prepared from $CuSO_4 \cdot 5H_2O$ (45.5 g), $NaHSO_3$ (12.6 g), and KCN (12.6 g). Aniline-2,4,6-d_3 (14 g) was diazotized at 0–5 °C with $NaNO_2$ (10.9 g) in 6 *N* HCl (75 ml). Care was taken to ensure that the temperature of the solution was not allowed to rise above 5 °C during addition of the amine to prevent exchange. After work-up in the prescribed manner a yield of 11.6 g (74.3%) of the nitrile was obtained. A mass spectrum (8 eV) exhibited mass peaks only at *m/e* 106 and 107 (^{13}C).

Benzaldehyde-2,4,6-d_3

The method of Williams (9) was used with little modification. Anhydrous stannous chloride (41.2 g) was used to reduce benzonitrile-d_3 (11.2 g) using the described method. The yield of benzaldehyde-d_3 was 7.39 g (63%). A mass spectrum exhibited mass peaks only at *m/e* 109 and 110 (^{13}C).

Benzoin-2,2′,4,4′,6,6′-d_6

The method of Fieser was used without modification (5). The benzoin was prepared from benzaldehyde-2,4,6-d_3 (5.0 ml) using KCN (0.5 g) in 80% ethanol–water (25 ml). The yield of crude benzoin was 3.67 g (71%). A mass spectrum confirmed its molecular weight at 218 with the peak at 217 less than 2% relative intensity.

Stilbene-2,2′,4,4′,6,6′-d_6

The method of Fieser was used without modification (5). The benzoin-d_6 (3.0 g) was reacted sequentially with $SOCl_2$ (3.0 ml), $NaBH_4$ (270 mg), and Zn (1.5 g) in the prescribed manner. Work-up yielded 0.856 g (33.4% overall). A mass spectrum confirmed the molecular weight at 186 with again less than 2% relative intensity at *m/e* 185.

Phenanthrene-1,3,6,8-d_4

The stilbenes were cyclized and oxidized using a method similar to that of Mallory *et al.* (4). The stilbene-d_6 (0.540 g) was added to a solution of iodine in cyclohexane (0.038 g in 300 ml). The solution was irradiated for 2 h using a Hanovia 450 W mercury lamp (Serial No. 679 A36) in a water cooled quartz jacket, immersed in the solution. Oxygen was bubbled through the solution during the irradiation. The pink solution was evaporated *in vacuo* and the residue chromatographed on alumina (Woelm neutral, Grade 1) with cyclohexane as eluant. The first few fractions yielded white crystals which were recrystallized from 95% ethanol to give 0.206 g (39%). A mass spectrum showed only the mass peak at 182 and its carbon-13 isotope at 183; u.v. λ_{max} 251 (62 000) nm.

Stilbene-2,4,6-d_3

Magnesium (1 g), benzyl bromide (1.2 ml), and ether (anhydrous, 20 ml) were refluxed together for 1 h under a dry tube. Benzaldehyde-2,4,6-d_3 (1 g) in ether (20 ml) was added dropwise over 10 min with stirring. After refluxing ½ h the solution was poured onto ice and dilute sulfuric acid added. The solution was then extracted with ether, the extracts dried ($MgSO_4$), and evaporated *in vacuo*. The oily residue, which crystallizes on standing, was dissolved in benzene (100 ml), a large crystal of iodine added, and the mixture refluxed 2 days. Evaporation of the solvent and repeated evaporation of small aliquots of CCl_4 removed most of the iodine. Chromatography on alumina (Woelm neutral, Grade 1, eluant benzene) and recrystallization from 95% ethanol yielded 0.510 g of stilbene-2,4,6-d_3 (29%). A mass spectrum confirmed its molecular weight at 183 with less than 2% relative intensity at *m/e* 182.

Phenanthrene-1,3-d_2

The stilbene-2,4,6-d_3 (510 mg) from above was treated in a manner similar to that used in the preparation of phenanthrene-1,3,6,8-d_4 to yield 0.131 g of phenanthrene-1,3-d_2 (27%). The mass spectrum showed only a peak at 180 and the carbon-13 isotopic peak at 181 u.v. λ_{max} 251 (63 000) nm.

p-Toluidine-2,6-d_2

Toluidine (20 g) was dissolved in 95% ethanol (50 ml) and 6 *N* HCl (100 ml) added. The ethanol was evaporated *in vacuo* and the solution cooled. The crystals were collected, washed with a little acetone, and air dried to give 20 g of the hydrochloride.

The hydrochloride was exchanged in D_2O and the deuterated toluidine isolated in a manner analogous to that described for aniline-2,4,6-d_3. The yield was 16 g and the material was used without purification. For mass spectrum analysis the amino protons were re-exchanged in H_2O. Mass spectrum *m/e* (relative intensity) 94 (7), 95 (100), 96 (8).

p-Bromotoluene-3,5-d_2

The toluidine-2,6-d_2 was diazotized and treated with cuprous bromide as described by Vogel (6). The cuprous bromide was prepared from $CuSO_4 \cdot 5H_2O$ (9.45 g), copper turnings (3 g), sodium bromide (16.3 g), and 2.4 ml H_2SO_4 in 150 ml of water. The toluidine (16 g) was powdered and added slowly to a cold (0–5 °C) sulfuric acid solution (16 ml in 120 ml H_2O) and then diazotized by adding $NaNO_2$ (10.5 g). The *p*-bromotoluene-3,5-d_2 was isolated by steam distillation and extraction with ether to give 8.0 g (32%).

Toluene-3,5-d_2

p-Bromotoluene-3,5-d_2 (12.0 g) was treated with magnesium (2.0 g) in anhydrous ether (50 ml). After refluxing 2 h water was added dropwise followed by dilute sulfuric acid. This was extracted with ether, the extracts dried ($MgSO_4$), and the ether distilled off through an 8 in. column packed with raschig rings. The yield of toluene-3,5-d_2 was 6.5 g or 100%. A mass spectrum confirmed its molecular weight at *m/e* 94.

Benzaldehyde-3,5-d_2

Toluene-3,5-d_2 (6.5 g), acetic acid (98 ml), and acetic anhydride (98 ml) were placed in a 500 ml flask. H_2SO_4 (15 ml, concentrated) was added slowly with stirring, keeping the temperature below 10 °C. After cooling to 0 °C, CrO_3 (14 g, powdered) was added over 2 h keeping the temperature below 10 °C. After stirring 1 h the solution was poured onto ice (300 ml by volume) and a little benzene–pentane (80:20) added. The ice was filtered off and the solution extracted well with benzene–pentane. These extracts were washed with 20% K_2CO_3 and then

dried ($MgSO_4$) and evaporated *in vacuo*. The residue was covered with 200 ml of 0.05 *N* H_2SO_4 and steam distilled. The distillate was extracted with ether, the extracts dried and evaporated *in vacuo* to leave 3.31 g of benzaldehyde-3,5-d_2 (39%). The molecular weight was confirmed by mass spectrometry.

Benzoin-3,3′,5,5′-d_4

Benzoin-3,3′,5,5′-d_4 was prepared from benzaldehyde-3,5-d_2 (2.3 g) by refluxing $\frac{1}{2}$ h in ethanol–water (4.6 and 2.3 ml) with KCN (0.250 g). This was diluted with water, extracted with ether, the extracts dried ($MgSO_4$) then evaporated *in vacuo*, and the residue recrystallized from 95% ethanol to give 800 mg (40%).

Stilbene-3,3′,5,5′-d_4

The method of Fieser was again used without modification (5). The benzoin (800 mg) was reacted sequentially with $SOCl_2$ (5 ml), $NaBH_4$ (75 mg), and Zn (0.70 g) in the prescribed manner. Work-up and recrystallization from 95% ethanol yielded 200 mg of stilbene-3,3′,5,5′-d_4 (67%). Mass spectrum: *m/e* (relative intensity) 182(2), 183(16), 184(100), 185(16).

Phenanthrene-2,4,5,7-d_4

The stilbene-3,3′,5,5′-d_4 from above (200 mg) was irradiated in cyclohexane (200 ml) in the presence of iodine (38 mg) and oxygen (saturated) for $1\frac{3}{4}$ h as previously described. Work-up yielded 50 mg of phenanthrene-2,4,5,7-d_4 after recrystallization from 95% ethanol (25%). Mass spectrum: *m/e* (relative intensity) 180(3), 181(15), 182(100), 183(17); u.v. λ_{max} 251 (63 000) nm.

Stilbene-3,5-d_2

Stilbene-3,5-d_2 was prepared from benzaldehyde-3,5-d_2 (1 g) in a manner identical to that described above for stilbene-2,4,6-d_3. The yield of recrystallized product was 629 mg (83%). Mass spectrum: *m/e* (relative intensity) 179(7), 180(100), 181(13).

Phenanthrene-2,4-d_2

This was prepared from stilbene-3,5-d_2 (540 mg) as described previously for phenanthrene-1,3-d_2. The yield of recrystallized product was 183 mg (33%). Mass spectrum: *m/e* (relative intensity) 179(10), 180(100), 181(17); u.v. λ_{max} 251 (64 000) nm.

Bromobenzene-d_5

Bromobenzene-d_5 was prepared from deuteriobenzene (Matheson, Coleman and Bell, 99.5 atom %D) using the method of Vogel (6). Benzene-d_6 (5 g), pyridine (1 drop), and bromine (4 ml) were stirred overnight on a steam bath.

The solution was diluted with ether and extracted with water, 5% NaOH, then again with water. The ether extract was dried ($MgSO_4$) and distilled, collecting the fraction that boils at 154–157 °C. Yield was 7.5 g (75%).

Stilbene-2,3,4,5,6-d_5

Magnesium (0.6 g), bromobenzene-d_5 (3.0 g), and ether (20 ml, anhydrous) were refluxed together for 1 h. Phenyl acetaldehyde (2.22 g) in ether (20 cc) was added dropwise over 10 min with stirring. The mixture was refluxed $\frac{1}{2}$ h, poured onto ice, diluted with dilute H_2SO_4, then extracted with ether.

The extracts were dried ($MgSO_4$) and evaporated *in vacuo*. Petroleum ether was added (60–80 °C) and the crystalline precipitate collected to yield 2 g (53%) of α-hydroxydiphenylethane-2,3,4,5,6-d_5. The alcohol (1.2 g) was refluxed in benzene (100 ml) containing a large crystal of iodine for 3 days. This, after evaporation *in vacuo* and treatment with charcoal yielded 540 mg of recrystallized (95% ethanol) stilbene-2,3,4,5,6-d_5 (53%).

Phenanthrene-1,2,3,4-d_4

The stilbene-2,3,4,5,6-d_5 (540 mg) was converted to the corresponding phenanthrene as previously described. The yield of phenanthrene-1,2,3,4-d_4 was 185 mg (48%) of recrystallized (95% ethanol) material. Mass spectrum shows only peaks corresponding to the tetradeuterated material and its carbon-13 analog; u.v. λ_{max} 251 (66 000) nm.

The financial assistance of the National Research Council of Canada is gratefully acknowledged. The technical assistance of M. Arneson was also appreciated.

1. J. L. CHARLTON and R. AGAGNIER. Can. J. Chem. **51**, 1852 (1973).
2. H. BOUAS-LAURENT, R. CALAS, and M. JOSIEN. C.R. **252**, 285 (1961).
3. B. CHENON, L. C. LEITHCH, R. N. RENAUD, and L. PICHAT. Bull. Soc. Chim. Fr. 38 (1964).
4. F. B. MALLORY, C. S. WOOD, and J. T. GORDON. J. Am. Chem. Soc. **86**, 3094 (1964).
5. L. F. FIESER. *In* Experiments in organic chemistry. 3rd ed. rev. D. C. Heath and Company, Boston. 1957.
6. A. I. VOGEL. *In* Elementary practical organic chemistry. Part 1. Longmans, Green and Co. Ltd., New York. 1957.
7. A. P. BEST and C. L. WILSON. J. Chem. Soc. 239 (1946).
8. A. I. VOGEL. *In* A textbook of practical organic chemistry. 3rd ed. Longmans, Green and Co. Ltd., New York. 1956. p. 608.
9. J. W. WILLIAMS. J. Am. Chem. Soc. **61**, 2248 (1939).

Can. J. Chem. Downloaded from www.nrcresearchpress.com by 210.87.254.105 on 05/05/12
For personal use only.

Stereochemical Implications from the Conformational Analysis of the Seven-membered Ring in 5-Oxabenzocycloheptene

LOUIS CANUEL AND MAURICE ST-JACQUES[1]

Département de Chimie, Université de Montréal, Montréal, Québec H3C 3V1

Received May 8, 1974

LOUIS CANUEL and MAURICE ST-JACQUES. Can. J. Chem. **52**, 3581 (1974).

The computer analysis (LAOCN-3 program) of the p.m.r. spectrum of 5-oxabenzocycloheptene (**3**) at $-105°$ has provided values for all coupling constants about the C_3—C_4 bond, while the complete line-shape simulation (DNMR program) has provided the following activation parameters: $\Delta G^{\ddagger} = 9.5$ kcal/mol (at $-57°$), $\Delta H^{\ddagger} = 9.9$ kcal/mol, and $\Delta S^{\ddagger} = 1.5$ e.u. A novel long distance (transannular) deuterium isotope effect has been discovered during the analysis of the spectrum of a partially deuterated derivative of **3**. A comparison of the p.m.r. parameters for 5-oxabenzocycloheptene and benzocycloheptene provides the basic data from which stereochemical and conformational inferences can be made for more complex derivatives in this series.

LOUIS CANUEL et MAURICE ST-JACQUES. Can. J. Chem. **52**, 3581 (1974).

La simulation à l'ordinateur (programme LAOCN-3) du spectre r.m.p. de l'oxa-5 benzocycloheptène (**3**) à -105 °C a permis d'obtenir toutes les valeurs des constantes de couplage pour la liaison C_3—C_4; de plus la simulation des formes raies (programme DNMR) a permis d'obtenir les paramètres d'activation suivants: $\Delta G^{\ddagger} = 9.5$ kcal/mol (à -57 °C), $\Delta H^{\ddagger} = 9.9$ kcal/mol et $\Delta S^{\ddagger} = 1.5$ e.u. Un nouvel effet isotopique (transannulaire) a été mis en évidence durant l'analyse du spectre d'un dérivé partiellement deutérié de **3**. Une comparaison des paramètres r.m.p. entre l'oxa-5 benzocycloheptène et le benzocycloheptène établit les données de base permettant de faire des déductions stéréochimiques et conformationnelles pour des dérivés plus complexes dans cette série. [Traduit par le journal]

Nuclear magnetic resonance spectroscopy is a particularly well-suited technique to investigate the conformational and stereochemical properties of cyclic organic molecules. Whereas five- and six-membered rings have been investigated extensively in the last 10 years (1–3), relatively little information is available on basic seven-membered cyclic compounds (2–6). In fact, it was only recently that the conformation of benzocycloheptene (**1**) was identified and fully characterized through a p.m.r. study (7) at $-120°$; that work provided accurate vicinal coupling constants for this basic molecule from which reliable dihedral angles were determined for all vicinal protons about the C_3—C_4 (and C_6—C_7) bond.

Our continuing systematic investigation of the cycloheptene–benzocycloheptene system (7–9) has led us to study the effect of oxygen on both the static and dynamic conformational properties of this system and possible inferences on the future stereochemical applications of the Karplus theory (10, 11) to derivatives containing heteroatoms. Although much has been written about the effect of heteroatoms on vicinal coupling constants (11, 12) and significant improvements have been made to account for deviations caused by oxygen (13–15), it now appears that generalizations are limited to well-defined sets of compounds and cannot be transplanted confidently from one set to another.

Our first objective therefore was to obtain accurate vicinal coupling constants for the basic 5-oxabenzocycloheptene system while our second aim was to determine accurately the effect of oxygen on the activation parameters and especially on $\Delta S^{\ddagger}$ from which inferences about ring inversion pathways might be drawn. Our approach first involved the analysis of the low temperature p.m.r. spectra of the deuterated derivatives **3***a* and **3***b* prepared directly from **2** through catalytic deuteration in the presence of palladium-on-charcoal (16). The trial p.m.r. parameters thus obtained then enabled the complete line-shape analysis of the spectral change of 5-oxabenzocycloheptene (**3**) itself at various temperatures.

Results

The 5-oxabenzocycloheptene-*cis*-3,4-*cis*-6,7-d_4 consists of a mixture of the *syn* and *anti* isomers, **3***a* and **3***b*, prepared in essentially equivalent

[1]Author to whom correspondence should be addressed.

Can. J. Chem. Downloaded from www.nrcresearchpress.com by 210.87.254.5 on 09/05/12
For personal use only.

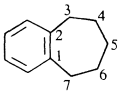

1

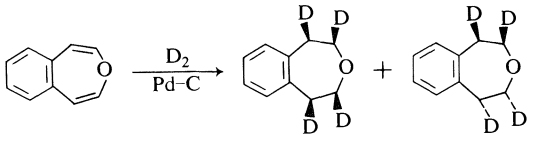

2 3*a* 3*b*

amounts by the method described above. In the following discussion, this mixture of isomers will be referred to collectively as **3***ab*.

The p.m.r. spectra (100 MHz, deuterium decoupled) of **3***ab* at +25° and −105° are shown in Fig. 1. The spectrum at −105° is relatively straightforward to analyze; it consists of two distinct AX patterns, one with components at δ 3.37 and 2.72 showing no visible splitting and the other with components at δ 4.11 and 3.23 showing a 2.0 Hz splitting. First-order spectral analysis therefore reveals that the two possible *cis* arrangements of protons about the C_3—C_4 bond are characterized by a coupling constant of 2.0 Hz and another that is small enough not to be resolved under the present experimental conditions. As shown below, the spectrum at +25° allows an accurate estimate of this small coupling constant.

The spectrum of **3***ab* at +25° shown in Fig. 1

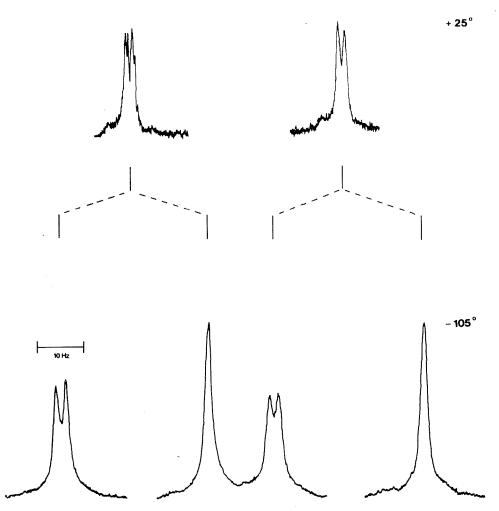

FIG. 1. The nonaromatic portion of the 100 MHz deuterium decoupled p.m.r. spectrum of **3***ab* at +25 and −105°.

reveals clearly that the lines of the upfield doublet are separated by 1.3 Hz. Since this value represents the average of the two coupling constants at −105°, it follows that 0.6 Hz is the value of the small coupling constant not resolved at low temperature. The observation that the low-field multiplet of the spectrum at +25° is not a doublet but actually a pair of doublets (with 1.3 Hz splitting) separated by 0.5 Hz supports the above analysis and further suggests that a particular isotope effect is responsible for the additional fine structure. It will be demonstrated later, in the next section, that a small transannular isotope effect is present and accounts for small differences in chemical shifts of the protons in **3***a* and **3***b*. Furthermore, it will be shown that this new isotope effect is able to manifest itself explicitely only in the low-field component of the spectrum of **3***ab* at +25°.

The 100 MHz spectrum of 5-oxabenzocycloheptene (**3**) at ambient temperature, being essentially of the AA′XX′ type (17), is characterized by two multiplets. As the temperature is decreased, the spectrum changes markedly and, as shown in Fig. 2, contains three complex multiplets at −105°. This spectrum can be analyzed as an ABCD assuming that cross-ring coupling only broadens the experimental lines. Trial parameters obtained from the low temperature spectrum of **3***ab* enable the exact simulation of this spectrum by means of the LAOCN-3 program (18) as shown in Fig. 2. The parameters obtained from the computer iterative analysis are reported collectively in Table 1 where the labels 3e, 4a, etc. refer to the different proton environments in accord with identifications made in the next section.

The p.m.r. parameters obtained by iterative

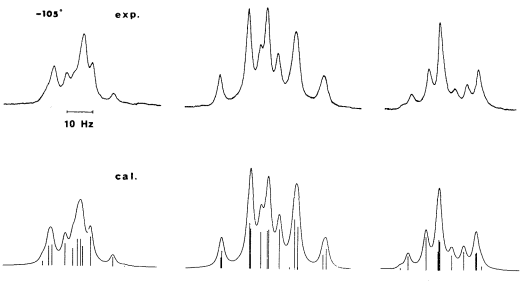

FIG. 2. Experimental and iterative computer simulated spectra (LAOCN-3 program) for the three multiplets of the methylene protons of **3** at −105°.

Can. J. Chem. Downloaded from www.nrcresearchpress.com by 210.87.254.5 on 09/05/12
For personal use only.

TABLE 1. Proton magnetic resonance parameters obtained from the computer simulation of the spectrum of **3** at $-105°$

(*A*) Chemical shifts[a]

δ_{4e}[b]	δ_{4a}	δ_{3a}	δ_{3e}
4.122	3.359	3.230	2.726

(*B*) Coupling constants[c]

J_{3gem}	J_{4gem}	$J_{3a,4a}$	$J_{3a,4e}$	$J_{3e,4a}$	$J_{3e,4e}$
−15.3	−11.8	11.2	2.0	0.6	5.0

[a]In p.p.m. for solutions in chlorodifluoromethane at 100 MHz relative to internal TMS.
[b]The numbers refer to the carbon position on the ring and the letters identify the protons as axial or equatorial in accord with the conclusion of the discussion section. They may be considered only as a label at this point.
[c]In Hz; estimated error ±0.2 Hz.

computer analysis of the spectrum of **3** at $-105°$ together with T_2 values and the appropriate axial–equatorial pattern of chemical shift exchange during ring inversion provided the necessary input data which enabled the simulation of spectra as a function of a variable rate constant (k in s^{-1}) with the DMMR-2 program (19). Figure 3 shows the excellent matching obtained for several experimental and calculated spectra. It is evident from this observation that the complexity of the spectral change enabled spectral simulation and comparison with the experimental spectra over a significantly broad temperature interval (about 50°) and consequently permitted very accurate determinations of rate constants for various temperatures within this range.

The rate constants thus obtained within $-41.6°$ to $-91.4°$ were then used to calculate the characteristic activation parameters for conformational interconversion through a least-square regression analysis using the computer program (20) ACTENG modified slightly to supply the Arrhenius plot shown in Fig. 4. The parameters calculated using a transmission coefficient of one-half are: $\Delta G^{\ddagger} = 9.5 \pm 0.2$ kcal/mol (at $-57°$), $\Delta H^{\ddagger} = 9.9 \pm 0.2$ kcal/mol, $\Delta S^{\ddagger} = 1.5 \pm 1.0$ e.u., and $E_a = 10.3 \pm 0.2$ kcal/mol.

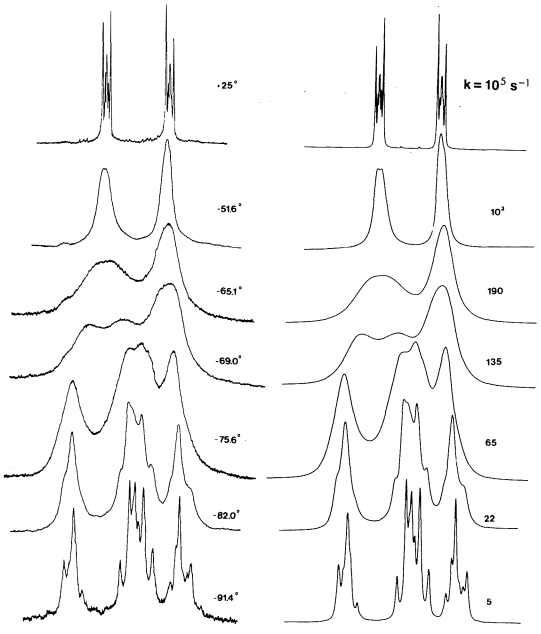

FIG. 3. Experimental (left) p.m.r. spectra of the methylene protons of **3** at various temperatures and matching calculated spectra (DNMR program).

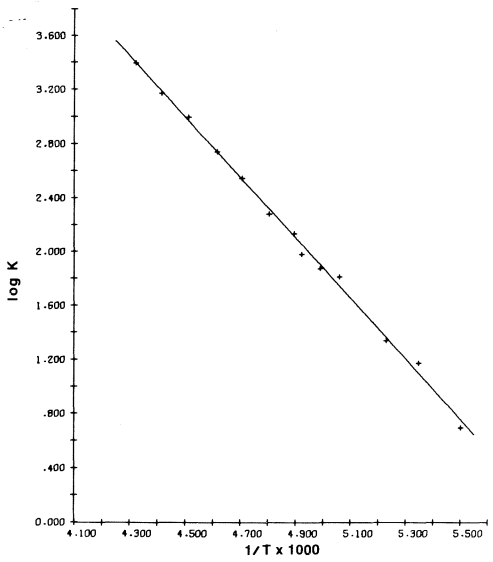

FIG. 4. Arrhenius plot for compound **3**.

Can. J. Chem. Downloaded from www.nrcresearchpress.com by 210.87.254.5 on 09/05/12
For personal use only.

Can. J. Chem. Downloaded from www.nrcresearchpress.com by 210.87.254.5 on 09/05/12
For personal use only.

Discussion

Conformational Interconversion

It has been clearly established that the ring conformation of benzocycloheptene is a chair (7) and consequently the stable conformation of 5-oxabenzocycloheptene is undoubtedly also a chair. Experimental (9) and theoretical (21) studies on the inversion mechanism of the cycloheptene chair have shown that the inversion pathway involves boat intermediates (**6**) and that the rate determining step involves a wagging of carbons 1 and 2, the highest energy conformation being **5** which effectively contains six coplanar carbon atoms.

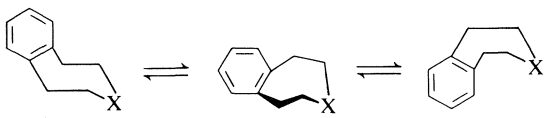

4 **5** **6**

The p.m.r. spectral changes of **3***ab* and **3** are consistent with such an interconversion pathway. In this case, the inversion is characterized by a free energy of activation of 9.5 kcal/mol which is only slightly lower than the value of 10.7 kcal/mol characteristic of benzocycloheptene. Since the complex spectral change of 5-oxabenzocycloheptene takes place over a temperature interval of about 50°, computer simulation is able to provide accurate rate constants over this range and data treatment can therefore provide significant $\Delta S^{\ddagger}$ and $\Delta H^{\ddagger}$ activation parameters (2, 22). The value of $\Delta S^{\ddagger}$ calculated for a transmission coefficient of one-half (which takes into consideration the fact that once a molecule reaches the boat family, it can either come back to the initial chair or go to an inverted chair (7)) is 1.5 ± 1 e.u., a value of magnitude comparable to the value of -0.2 ± 2 e.u. determined for the inversion of 5,5-difluorocycloheptene (23). Since contributions to the entropy of activation from differences in vibrational and rotational partition functions are expected to be small and positive for ring inversion of similar compounds in inert solvents (2, 24), the value of $\Delta S^{\ddagger}$ obtained in this work can be considered to be reliably characteristic of the cycloheptene system. It is therefore justifiable to assume that $\Delta\Delta G^{\ddagger} = \Delta\Delta H^{\ddagger}$ in this family.

The lower barrier observed for **3** appears to reflect partly on the lower barrier to rotation about the C_4—C_5 and C_5—C_6 bonds as suggested from a comparison with simple models such as methyl ether and propane for which barriers to methyl rotation are 2.5 and 3.3 kcal/mol, respectively (25, 26). The barrier reduction of 1.2 kcal/mol is thus best explained by a decrease in torsional energy about the C_4—C_5 and C_5—C_6 bonds for **3** in the conversion of **4** into **5**.

Isotope Effect

In addition to the well-known deuterium isotope upfield shift resulting from α and β deuteration, the spectrum of **3***ab* further reveals a novel type of long distance isotope effect on chemical shifts. This suggestion builds on the recent report of a stereochemical dependence (27, 28) of the upfield shift resulting from β deuteration (*i.e.* through three bonds). The more complex isotope effect discovered is transmitted through four bonds and as shown below is capable of explaining the multiplicity of the low-field component of the room temperature spectrum of **3***ab* (Fig. 1).

Further definition of this new transannular isotope effect requires a careful examination of interconverting chair conformations for **3***a* and **3***b* shown below as **7** ⇌ **8** and **9** ⇌ **10**, respectively (structures **8** and **10** have been rotated for direct comparison with **7** and **9**). Conformations **7** and **8** are characterized by pairs of *cis* protons in a *syn* relationship whereas **9** and **10** possess *anti* pairs of *cis* protons.

The above interconversions reveal that ring inversion exchanges C-3 with C-7 and C-4 with C-6 of the chair skeleton and concomitantly axial and equatorial proton (or deuteron) on each pair of exchanging carbon atoms. Now, if it is assumed that both sides of the molecules **3***a* and **3***b* are independent of each other, then

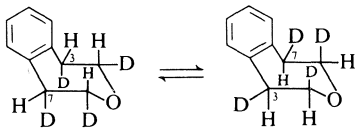

7 **8**

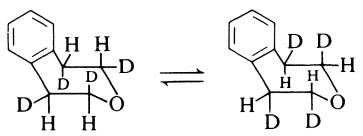

9 **10**

TABLE 2. Comparison of the p.m.r. parameters for 5-oxabenzocycloheptene and benzocycloheptene

Compound	Chemical shifts (p.p.m.)		Coupling constants (Hz)					
	$\delta_{3a,3e}$	$\delta_{4a,4e}$	$J_{3a,4a}$	$J_{3a,4e}$	$J_{3c,4a}$	$J_{3c,4e}$	J_{3gcm}	J_{4gem}
5-Oxabenzocycloheptene (**3**)	−0.504	0.763	11.2	2.0	0.6	5.0	−15.3	−11.8
Benzocycloheptene (**1**)[a]	−0.106	0.737	12.6	1.1	1.1	6.6	−14.1	−13.8

[a]The data for **1** are taken from ref. 7.

the rapidly inverting molecules should give rise to superposed averaged AX patterns. Clearly this is not observed. On the other hand, if both sides of the molecules were not independent of each other in at least one of the conformations **7** to **10** because there existed a long range isotope effect, the averaged AX doublet characteristic of each molecule would no longer necessarily be superposed. The resulting hypothetical spectrum at 25° would then consist of two pairs of doublets.

One such pair of doublets, separated by 0.5 Hz, is clearly observed at low field in the spectrum of **3***ab* at 25°. The signal at high field, on the other hand, does not show this expected pattern but instead consists of a broad doublet. The existence of coupling between benzylic and aromatic protons (29) is believed to give rise to appreciable broadening and prevent the resolution of finer structure if it existed.

Analysis of the spectrum **3***ab* at −105° (Fig. 1) together with the computer simulations for **3** reveal that the chemical shift order from low to high field for the various protons is: H_{4e}, H_{4a}, H_{3a}, and H_{3e}. Furthermore, the spectrum which is characteristic of protons in conformations **7** to **10** shows no visible isotopic splitting in any of the signals and consequently the pair of protons $H_{4e}H_{3a}$ constitutes an AX pattern (J = 2.0 Hz) while the protons $H_{4a}H_{3e}$ constitute another AX pattern (J = 0.6 Hz, nonresolved).

At present, the origin of the isotopic effect on chemical shifts is not well understood (27) and any proposed explanation must first consider the stereochemical requirements for transmission of the isotopic information. In the present context this question involves an examination of the various transmission pathways possible between deuterons and protons on C-4 and C-6: (*a*) a di-axial pathway (*e.g.* between H_{4a} and D_{6a} in **9**), (*b*) a di-equatorial pathway (*e.g.* between D_{4e} and H_{6e} in **9**), (*c*) axial–equatorial pathway (*e.g.* H_{4a} and D_{6e} in **7**).

Further analysis of the properties of structures **7** to **10** shows that pathways *a* and *b* are possible only in the *anti* isomer **3***b* (*i.e.* in conformations **9** and **10**) whereas pathway *c* is possible only in the *syn* isomer **3***a* (*i.e.* in conformations **7** and **8**). It therefore follows that since protons in **7** and **8** account for about 50% of the total intensity of the signals of both H_{4a} and H_{4e} (also H_{6a} and H_{6e}), only protons in **9** and **10** (accounting for the other 50% of total intensity) would be split up by an isotopic effect occurring through either pathway *a* or *b*.

Unfavorable conformation populations together with probable long distance coupling between protons on C-4 and C-6 in **9** and **10** therefore make it hazardous to select a particular pathway in the absence of observable fine splitting at −105°. It is therefore clear that a proper explanation of the long range isotope effect discovered must await additional experimental and theoretical work.

Properties of the Chair Conformation

The p.m.r. parameters characteristic of **1** and **3** are listed in Table 2. Although both sets are in accord with generalized chair geometries, significant differences do exist especially for the values of $\delta_{3a,3e}$ and the various vicinal coupling constants.

The common observation that the signal of the equatorial proton on C-3 (H_{3e}) is at higher field than the axial proton (H_{3a}) and opposite the order for the protons on C-4 can be explained in part by the presence of the aromatic ring whose anisotropic effect on chemical shift is expected to be stronger for nearby protons. Furthermore, the oxygen atom in **3** is expected to shift H_{3e} upfield significantly (30) in accord with the larger absolute value of $\delta_{3a,3e}$.

Can. J. Chem. Downloaded from www.nrcresearchpress.com by 210.87.254.5 on 09/05/12
For personal use only.

Can. J. Chem. Downloaded from www.nrcresearchpress.com by 210.87.254.5 on 09/05/12
For personal use only.

Differences in coupling constants, on the other hand, could be due to the following two factors: distortion of the chair geometry and the electronegativity of the heteroatom in **3**. Because an understanding of the origin of these differences is important prior to the utilization of the p.m.r. method for rapid stereochemical and conformational deductions in more complex seven-membered derivatives, it is necessary to evaluate the various contributions as accurately as possible.

The use of modified Karplus equations to obtain dihedral angles from values of vicinal coupling constants has met with limited success when applied to systems containing electronegative substituents. A systematic study (31) of the effect of heteroatoms on ethane derivatives, for which rapid rotation between staggered conformations was assumed, has provided equations capable of accounting for the various trends observed. Extrapolation of these results to ring systems where rotational angles are no longer staggered has however presented problems. Horton and co-workers (13) have devised a modified Karplus equation which has been found useful in the carbohydrate field although several notable exceptions were reported. Recently, Slessor and Tracey (32) have invented a new method of assigning dihedral angles to hydrogens adjacent to a methylene group. Although promising, the DAERM method is particularly limited when electronegative substituents are bonded directly to the molecular segment under consideration and the error introduced is expected to be maximal when the electronegative substituent is antiperiplanar to one of the hydrogen nuclei under consideration. It is therefore clear that these quantitative treatments are not able to define the precise geometry of **3** for comparison to that of **1** which has been determined accurately (7).

Recently, the *R* method (33, 34) has been useful to characterize the overall shape of six-membered rings. The new parameter, the *R* value, is defined as a ratio of averaged vicinal coupling constants J_{trans}/J_{cis} where $J_{trans} = \frac{1}{2}(J_{aa} + J_{ee})$ and $J_{cis} = \frac{1}{2}(J_{ae} + J_{ea})$ for a $-CH_2CH_2-$ fragment in a ring system. Thus, it has been shown that compared to cyclohexane ($R = 2.16$) tetrahydropyran ($R = 1.91$) is slightly flattened. By analogy, *R* values calculated for **1** and **3** from the data given in Table 2 suggest that 5-oxabenzocycloheptene ($R = 6.2$) is slightly more flattened than benzocycloheptene ($R = 8.7$), although both cycloheptene derivative chairs are much more puckered than the six-membered chairs.

Quantitative application of the *R* method was proposed by Buys (33) whose treatment assumes that a given $X-CH_2CH_2-Y$ fragment possesses pseudotrigonal projection symmetry. Expressions for dihedral angles have been developed and their successful application to benzocycloheptene (7) suggests interesting possibilities for **3**. Using $R = 6.2$, the following angles characterizing structure **12** are obtained: $\phi_1 = \phi_3 = 70.5°$, $\phi_2 = 49.5°$, $\phi_4 = 190.5°$, and $\psi = 70.5°$. A comparison of these angles with those obtained for benzocycloheptene (7) ($\phi_1 = \phi_3 = 73°$, $\phi_2 = 44°$, $\phi_4 = 189°$, and $\psi = 74°$) suggests that to a first approximation, chair distortion could account partly for some of the differences in vicinal coupling constants reported in Table 2.

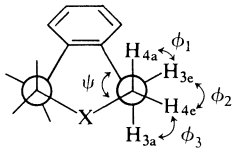

11 X = CD_2
12 X = O

The stereochemical effect of oxygen on the magnitude of vicinal coupling constants has been studied from two different approaches using six-membered rings as substrates. In one investigation Booth (35) determined the effect of axial and equatorial substituents on vicinal coupling. In addition to decreasing the value of the coupling constants, the effect was found to be stereochemically dependent whereby the decrease is maximum when the O—C—C—H relationship is *trans* coplanar as illustrated in structure **13**.

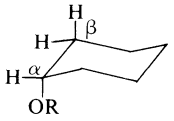

13

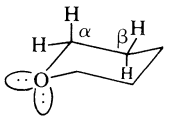

14

Later, work by Anteunis (14) and Crabb and co-workers (15) revealed that the stereochemical dependence of the influence of oxygen is even more subtle when the heteroatom is part of the ring as in heterocycle of structure **14**.

Can. J. Chem. Downloaded from www.nrcresearchpress.com by 210.87.254.5 on 09/05/12
For personal use only.

It has been suggested (14) that, in addition to the above effect, eclipsing of a lone-pair on oxygen with an adjacent C—H (on C(α) in structure **14**) significantly raises vicinal couplings involving this proton. But since eclipsing is expected to be small in both six- and seven-membered cyclic compounds existing in a chair conformation, the predominant effect of oxygen will be through the β-proton *trans* to it, namely H_{3e} in the case of **3** as seen in projection **12**.

It therefore appears that an estimate of the contribution of ring flattening to the various vicinal couplings can be obtained from the calculation of the values of $^3J_{HH}$ corresponding to the dihedral angles characteristic of the chair conformation (**12**) of 5-oxabenzocycloheptene by means of the equation (7): $^3J_{HH} = 12.95 \cos^2 \phi$. This approach reveals that the value of $J_{3e,4e}$ corresponding to $\phi_2 = 49.5°$ is 5.4 Hz and consequently that flattening accounts for most of the change in this parameter between **1** and **3**. On the other hand, flattening is unable to explain the changes in magnitudes observed for the other three vicinal couplings listed in Table 2 and consequently electronegativity effects must be predominantly responsible for the observed differences.

The decrease of J_{4gem} between **1** and **3** (−13.8 to −11.8 Hz) is analogous to the reduction observed between cyclohexane (36) and tetrahydropyran (37) (−13.05 to −11.2 Hz); flattening appears responsible for the change in both series.

Since oxygen is more electronegative than nitrogen and sulfur, benzocycloheptene derivatives containing either of these heteroatoms at position 5 are expected to yield vicinal coupling constants within the range given in Table 2. The results reported therefore constitute the basic data from which stereochemical and conformational inferences can be made rapidly for more complex molecules in this series. Furthermore, it is believed that stereochemical studies of analogous seven-membered derivatives bearing electronegative substituents can now be undertaken with reasonable confidence. Such analyses would require the adaptation of the basic data through incorporation of corrective terms now available from studies of electronegativity effects of various substituents on model six-membered cyclic compounds.

Experimental

The v.p.c. analyses and separations were carried out on a Varian-aerograph A90-P3 instrument using ¼ in. SE-30 columns and helium as carrier gas. Mass spectral analyses were performed on an Associated Electrical Industries model MS-902 mass spectrometer operating at 70 and 12 eV on an Hitachi-Perkin-Elmer model RMU-6-D instrument.

Routine analytical p.m.r. spectra were recorded on a JEOL C-60H spectrometer operating at 60 MHz in the external lock mode. The low temperature p.m.r. spectra were obtained at 100 MHz using a JEOL JNM-4H-100 spectrometer. Solutions in chlorodifluoromethane containing a small quantity of TMS were degassed and sealed. Deuterium decoupling, when required, was effected by means of the JEOL Hetero Spin Decoupler model JNM-SD-HC.

Temperatures were monitored by means of a JEOL temperature control unit model JES-VT-3 and determined accurately with a calibrated thermocouple placed inside a solvent-containing dummy n.m.r. tube. Temperature measurements were taken before and after recording several p.m.r. spectra at each reported temperature. A variation of less than 0.5° was ordinarily observed between the two sets of temperature readings.

Rate constants were obtained from a visual comparison of experimental and computer calculated spectra. For this purpose, five to eight spectra were recorded at a sweep rate of 0.15 Hz/s without saturation at each temperature. The spectra were calculated by means of programs described in the text on a CDC CYBER 74 computer and traced on a CALCOMP plotter.

5-Oxabenzocycloheptene(3)

This known compound was prepared by catalytic reduction of 3-benzoxepin (16) using palladium-on-charcoal (5%) in methanol at a pressure of 2 atm. The product was purified through preparative v.p.c. and characterized by its p.m.r. spectrum in chlorodifluoromethane: multiplets at δ 2.95 (two CH_2), 3.72 (two CH_2), and 7.72 (four aromatic protons).

5-Oxabenzocycloheptene-d_4 (3ab)

To 0.15 g of 3-benzoxepin dissolved in 45 ml of methanol was added 0.70 g of catalyst (Pd–C, 5%). The flask was then attached to a compact hydrogenation apparatus (38). The mixture was then stirred vigorously and allowed to react with deuterium gas slightly above atmospheric pressure for 18 h. Having removed the catalyst by filtration, the compound was then isolated by preparative v.p.c. and characterized by its p.m.r. spectrum (described in the text) and its high resolution mass spectrum.

Mol. Wt. Calcd. for $C_{10}H_8D_4O$: 152.1139. Found (mass spectrum at 70 eV): 152.1138.

The isotopic composition obtained from a mass spectrum at 10 eV is: $d_6 = 2\%$, $d_5 = 3\%$, $d_4 = 77\%$, $d_3 = 15\%$, $d_2 = 3\%$.

We wish to acknowledge the assistance of Dr. Michel Bernard with the computer programs and of Mr. Robert Mayer with the recording of the p.m.r. spectra at low temperatures. We are very grateful to the National Research Council of Canada for financial assistance.

1. H. BOOTH. *In* Progress in NMR spectroscopy. *Edited by* J. W. Emsley, J. Feeney, and C. H. Sutcliffe. Vol. 5. Pergamon Press, Toronto. 1969. p. 149.
2. G. BINSCH. *In* Topics in stereochemistry. *Edited by* E. L. Eliel and N. L. Allinger. Vol. 3. Interscience, New York. 1968. p. 97.
3. I. O. SUTHERLAND. *In* Annual reports on NMR spectroscopy. Vol. 4. *Edited by* E. F. Mooney. Academic Press, New York. 1971. p. 71.
4. (*a*) S. KABUSS, H. G. SCHMID, H. FRIEBOLIN, and W. FAISST. Org. Magn. Res. **1**, 451 (1969); (*b*) K. V. BREDOW, A. JAESCHKE, H. G. SCHMID, F. FRIEBOLIN, and S. KABUSS. Org. Magn. Res. **2**, 543 (1970).
5. J. B. HENDRICKSON, R. K. BOECKMAN, J. D. GLICKSON, and E. GRUNDWALD. J. Am. Chem. Soc. **95**, 495 (1973).
6. M. CHRISTL and J. D. ROBERTS. J. Org. Chem. **37**, 3443 (1972).
7. M. ST-JACQUES and C. VAZIRI. Org. Magn. Res. **4**, 77 (1972).
8. M. ST-JACQUES and C. VAZIRI. Can. J. Chem. **51**, 1192 (1973).
9. M. ST-JACQUES and C. VAZIRI. Can. J. Chem. **49**, 1256 (1971).
10. M. KARPLUS. J. Am. Chem. Soc. **85**, 2870 (1963).
11. R. GRINTER. *In* Nuclear magnetic resonance. Vol. 2. *Edited by* R. K. Harris. The Chemical Society, London. 1973. p. 83.
12. H. BOOTH. *In* Progress in NMR spectroscopy. Vol. 5. *Edited by* J. W. Emsley, J. Feeney, and C. H. Sutcliffe. Pergamon Press, Toronto. 1969. p. 161.
13. P. L. DURETTE and D. HORTON. Org. Magn. Res. **3**, 417 (1971).
14. M. ANTEUNIS. Bull. Soc. Chim. Belges, **75**, 413 (1966).
15. Y. ALLINGHAM. T. A. CRABB, and R. F. NEWTON. Org. Magn. Res. **3**, 37 (1971).
16. K. DIMROTH, G. POHL, and H. FOLLMANN. Chem. Ber. **99**, 634 (1966).
17. J. W. EMSLEY, J. FEENEY, and L. H. SUTCLIFFE. High resolution nuclear magnetic resonance spectroscopy. Vol. 1. Pergamon Press, Toronto. 1965.
18. S. CASTELLANO and A. A. BOTHNER-BY. *In* Computer programs for chemistry. Vol. 1. *Edited by* D. F. Detar. W. A. Benjamin, New York. 1968.
19. G. BINSCH. J. Am. Chem. Soc. **91**, 1304 (1969). A copy of the DNMR program was obtained from QCPE, Bloomington, Indiana.
20. D. F. DETAR. Computer programs for chemistry. Vol. 3. W. A. Benjamin, New York. 1969.
21. N. L. ALLINGER and J. T. SPRAGUE. J. Am. Chem. Soc. **94**, 5734 (1972).
22. A. ALLERHAND, H. A. GUTOWSKY, J. JONAS, and R. A. MEINGER. J. Am. Chem. Soc. **88**, 3185 (1966).
23. R. KNORR, G. GANTER, and J. D. ROBERTS. Angew. Chem. Int. Ed. Eng. **6**, 556 (1967).
24. R. K. HARRIS and N. SHEPPARD. J. Mol. Spectrosc. **23**, 231 (1967).
25. J. R. DURIG and Y. S. LI. J. Mol. Struct. **13**, 459 (1972).
26. J. P. LOWE. Prog. Phys. Org. Chem. **6**, 1 (1968).
27. J. B. LAMBERT and L. G. GREIFENSTEIN. J. Am. Chem. Soc. **95**, 6150 (1973).
28. F. A. L. ANET and F. LEYENDECKER. J. Am. Chem. Soc. **95**, 156 (1973).
29. L. M. JACKMAN and S. STERNHELL. Applications of nuclear magnetic resonance spectroscopy in organic chemistry. 2nd Ed. Pergamon Press, Toronto. 1969. p. 330.
30. M. ANTEUNIS, D. TAVERNIER, and F. BORREMANS. Bull. Soc. Chim. Belges, **75**, 396 (1966).
31. L. PHILLIPS and V. WRAY. J. Chem. Soc. Perkin II, 536 (1972).
32. K. N. SLESSOR and A. S. TRACEY. Can. J. Chem. **49**, 2874 (1971).
33. H. R. BUYS. Rec. Trav. Chim. Pays-Bas, **88**, 1003 (1970).
34. J. B. LAMBERT. Acc. Chem. Res. **4**, 87 (1971).
35. H. BOOTH. Tetrahedron Lett. **7**, 411 (1965).
36. E. W. GARBISH and M. G. GRIFFITH. J. Am. Chem. Soc. **90**, 6543 (1968).
37. J. B. LAMBERT, C. E. MIXAN, and D. H. JOHNSON. J. Am. Chem. Soc. **95**, 4634 (1973).
38. H. O. HOUSE. Modern synthetic reactions. 2nd Ed. W. A. Benjamin, Menlo Park, Calif. 1972. p. 2.

Can. J. Chem. Downloaded from www.nrcresearchpress.com by 210.87.254.5 on 09/05/12
For personal use only.

Photolysis of Aqueous Solutions of Hydrogen Peroxide Containing β-Ammonio Alcohols

TERRY FOSTER AND PAUL RONALD WEST

Department of Chemistry, University of Victoria, Victoria, British Columbia V8W 2Y2

Received October 9, 1973[1]

TERRY FOSTER and PAUL RONALD WEST. Can. J. Chem. **52**, 3589 (1974).

During the photolysis of aqueous H_2O_2 added β-ammonio alcohols suffer oxidative attack initiated through hydrogen abstraction by the ·OH radical. At p*H* 7.0 the initially formed radical, $(R)_3\overset{+}{N}CH_2\dot{C}OHR'$, undergoes fragmentation to yield $R_3\overset{+}{N}H$ and CH_3COR' exclusively. At p*H* 1.0 fragmentation is less important and direct oxidation to $(R)_3\overset{+}{N}CH_2COR'$ dominates. A radical deprotonation step is proposed to account for the p*H* dependence.

TERRY FOSTER et PAUL RONALD WEST. Can. J. Chem. **52**, 3589 (1974).

Lors de la photolyse du peroxyde d'hydrogène dans des solutions aqueuses contenant des β-ammino alcools, ces derniers sont oxydés et l'étape préliminaire de cette réaction est l'enlèvement d'un hydrogène par le radical ·OH. A p*H* 7.0, le radical formé initialement, $(R)_3\overset{+}{N}CH_2\dot{C}OHR'$, se fragmente pour conduire exclusivement à $R_3\overset{+}{N}H$ et CH_3COR'. A p*H* 1.0, la fragmentation est moins importante et l'oxydation directe en $(R)_3\overset{+}{N}CH_2COR'$ domine. Afin d'expliquer la dépendance sur le p*H*, on propose une étape impliquant une déprotonation radicalaire. [Traduit par le journal]

Introduction

Interest in the chemical reactivity of the β-ammonio alcohols, **1**, arises from the biological importance of several members of the general

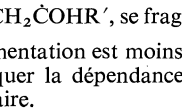

1

class. Choline (**1**, R = CH_3, R′ = H, R″ = H) and its acetyl ester play firmly established roles in the transmission of nerve impulses. Ethanolamine and its *N*-methyl derivatives ($CH_3NHCH_2CH_2OH$ and $(CH_3)_2NCH_2CH_2OH$) are vital intermediates in the biosynthesis of choline.[2] Moreover, ethanolamine, choline, and serine (**1**, R = H, R′ = H, R″ = CO_2^-) all occur widely as structural units in complex lipids.

In radiation damage to biological systems the attack of the electrophilic oxidizing species ·OH on β-ammonio alcohols will occur at the carbinol carbon to generate secondary organic radicals, (reaction 1). Using the Ti(III)·H_2O_2 reaction in a rapid aqueous flow system monitored by an e.p.r. spectrometer, the radical

[1] $(R)_3\overset{+}{N}CH_2CHOHR' \xrightarrow{\cdot OH} (R)_3\overset{+}{N}CH_2\dot{C}OHR'$

R, R′ = H, CH_3 **2**

intermediates, **2**, have been identified at p*H* 2.5 (1, 2). At p*H* 6.5–7.5 the observed signal corresponds to an α-carbonyl radical **3** generated by fragmentation (reaction 2) (2).

[2] $(R)_3\overset{+}{N}CH_2\dot{C}OHR' \longrightarrow (R)_3\overset{+}{N}H + \cdot CH_2COR$

3

Similar eliminations of radicals have been documented for electronegative β-substituents such as OH (3), Cl (3), and $OCOCH_3$ (1). The acid catalyzed reaction has been studied by e.p.r. spectroscopy at p*H* 1.5, reaction 3.

[3] $HOCH_2\dot{C}HOH \xrightarrow{H^+} \cdot CH_2CHO + H_2O$

However, pulse radiolysis (4) and steady-state radiolysis (5) have demonstrated that fragmentation to yield $\cdot CH_2CHO$ must be a process that occurs under neutral and basic conditions for 1,2-ethanediol.

In the case of β-ammonio substituents, by far the best documented example of the fragmentation reaction is the γ-radiolysis of the α-form of choline chloride. It is the most radiosensitive crystalline organic solid known *G*(fragmenta-

[1]Revision received July 15, 1974.

[2]Protonated at *in vivo* p*H*, and included in the general class of β-*ammonio* alcohols.

Can. J. Chem. Downloaded from www.nrcresearchpress.com by 210.87.254.105 on 09/05/12
For personal use only.

Can. J. Chem. Downloaded from www.nrcresearchpress.com by 210.87.254.105 on 09/05/12
For personal use only.

tion) = 55 000 (6). In consequence its radiolysis has attracted careful studies on the products (only CH_3CHO and $(CH_3)_3\overset{+}{N}HCl^-$) (7), on the e.p.r. of occluded radicals at 77 °K (6) and at room temperature (8), and on the role of trapped electrons in the chain elimination (9).

In the present study, the products of photolysis of aqueous hydrogen peroxide solutions that contained added β-ammonio alcohols have been carefully examined under both neutral and acidic conditions. The experiments serve to complement and quantitatively affirm the conclusions of the e.p.r. spectroscopic studies (2). The clear-cut pattern that emerges permits extrapolation of the results to the γ-radiolysis of the crystalline choline salts.

Experimental

General

Commercially available 2-hydroxyethyltrimethylammonium chloride (henceforth *choline chloride*), 2-(*N,N*-dimethylaminoethanol and 1-(*N,N*-dimethylamino)-2-propanol were of Fisher Certified Reagent or Aldrich reagent grade. 2-Hydroxypropyltrimethylammonium chloride (henceforth β-*methyl choline*) was prepared as previously described (2). The quaternary salts were purified by repeated recrystallization from ethanol–ether and vacuum desiccation until no trace of solvent remained (n.m.r. spectroscopy). The tertiary amines were distilled until judged pure (n.m.r. spectroscopy), then converted to the hydrochloride salts by passing HCl gas through an aqueous ethanolic solution. The salts were then recrystallized from ethanol–ether and stored under vacuum desiccation. All n.m.r. spectra were recorded on a Perkin–Elmer R12A spectrometer employing water as solvent and tetramethylsilane as external reference. Hydrogen peroxide was Fisher Certified reagent 30% and was used without further treatment. The neutral photolysis solutions were maintained by a p*H* 7.0 phosphate buffer prepared from 1.0 *M* potassium hydrogen phosphate (250 ml) and 1.0 *M* sodium hydroxide (144 ml).

Photolysis Experiments

Procedure

An Hanovia 450 W medium pressure mercury lamp suspended in an Hanovia quartz photochemical reactor well with water cooling jacket was the light source employed. A thin cylindrical reaction vessel was fitted as a sleeve around the commercial well allowing 20 ml of solution to spread as an annulus in the path of the light beam. The Pyrex vessel (H_2O_2 photolyzed by 313 nm line) was equipped with an efficient oxygen-free (Fieser's solution) nitrogen purge to remove volatile products as they formed. The outlet was fitted with a water condenser to minimize solvent loss, and then analytical traps as required, usually Dry Ice – methylene chloride cooled.

In a typical experiment, the substrate was dissolved in 25 ml of phosphate buffer, 0.1 *N* hydrochloric acid or water (unbuffered system) and hydrogen peroxide (3.3 ml) was added. The total charge was made up to 30 ml. Finally 20 ml were placed in the photolysis apparatus and thoroughly purged with N_2 prior to photolyzing for a period from 6 to 10 h. In a long series of experiments a given lamp efficiency falls necessitating longer reaction time. By the same token, no attempt was made to exactly reproduce percentage decomposition from one experiment to another.

Analysis

After irradiation, the reaction mixture was made up to 50 ml (volumetric flask). At that time the 10 ml aliquot set aside in the dark was also made up to 50 ml. Hydrogen peroxide consumption was then determined iodometrically using samples from the photolyzed and unreacted solutions.

Quantitative estimation of the products and the overall stoichiometry was accomplished by adding a known weight of sodium acetate to both the unreacted and product solutions. The integrated intensity of the n.m.r. signal from the acetate methyl was then compared with the other resonances.

Qualitative experiments were carried out establishing (*i*) the stability of the reaction mixture (n.m.r.) and (*ii*) the nature and relative amounts of the products. Hence, experiments providing estimation of yields (Tables 3 and 4) are supported by additional qualitative runs where the sodium acetate standard was not introduced.

Identification of the products was made by preparing standard samples of the reaction mixture containing the assigned products adjusted to near the concentrations observed in the photolyzed solutions. For clarity the n.m.r. data are presented in Table 1. Note that 1-(*N,N*-dimethylamino)-2-propanone was available from the companion e.p.r. studies (2). The synthesis of 1-(*N,N,N*-trimethylamino)-2-propanone was carried out by treatment of 1-(*N,N*-dimethylamino)-2-propanone with chloromethane in aqueous solution using the procedure adopted for the synthesis of β-methylcholine chloride (2). In view of the sensitivity of the quaternary ketone, it was prepared by reacting the dimethylamino ketone to completion as judged by n.m.r. The resultant solution showed the required integration and contained no residual dimethylamino ketone resonances. The aqueous solution so obtained was then used in preparing the standard sample.

Quantitative estimation of acetaldehyde in the cold trap was made by oxidation to acetic acid with alkaline H_2O_2 and back titration with standard acid (10). Acetone was determined spectrophotometrically by comparison of its alkaline salicylaldehyde color reaction with that of standard samples (11).

Control Procedures

The photostability of a buffered p*H* 7.0 solution of choline chloride was demonstrated by n.m.r. analysis after a 10 h photolysis. Trimethylamine hydrochloride (38 mmol in 30 ml of buffer) similarly was photostable. Photolysis of aqueous H_2O_2 (buffer) containing excess acetone (34 mmol in 20 ml) showed 10% of acetic acid based on remaining acetone after 6 h. No 2-propanol derivatives showed any acetic acid formation from such secondary reaction. Under dark conditions the choline–H_2O_2 buffer system showed a 2% fall in peroxide titer in 10 h, but no products of molecular oxidation were detected by n.m.r. Similarly after reflux of a choline reaction mixture containing H_2O_2 in 0.1 *N* HCl for 6 h,

TABLE 1. Proton magnetic resonance spectral data for β-ammonio alcohols and photolysis products

Compound (p*H* = 6.8)	Chemical shift (τ)				
	$CH_3\overset{+}{N}$—	—CH_2—$\overset{+}{N}$—	—CHO—	CH_3—C—	CH_3C=O
$(CH_3)_3\overset{+}{N}CH_2CH_2OH$	6.68	6.42	5.92	—	—
$(CH_3)_3\overset{+}{N}CH_2CO_2H$	6.79	5.98	—	—	—
$(CH_3)_3\overset{+}{N}CH_2CHOHCH_3$	6.71	6.51, 6.61*	5.2†	8.64‡	—
$(CH_3)_3\overset{+}{N}CH_2COCH_3$	6.83	6.10	—	—	7.88
$(CH_3)_2\overset{+}{N}HCH_2CHOHCH_3$	6.98	6.72, 6.84*	5.3†	8.64‡	—
$(CH_3)_2\overset{+}{N}HCH_2COCH_3$	6.92	6.10†	—	—	7.57
$(CH_3)_2\overset{+}{N}HCH_2CH_2OH$	6.95	6.70	5.90	—	—
$(CH_3)_3\overset{+}{N}H$	7.06	—	—	—	—
$(CH_3)_2\overset{+}{N}H_2$	7.15	—	—	—	—
CH_3COCH_3	—	—	—	—	8.10
$CH_3CH(OH)_2$	—	—	—	—	8.52§
CH_3CO_2H	—	—	—	—	8.05

*J = 0.5 Hz.
†Not resolved in the p*H* 6.8 buffer.
‡J = 7.0 Hz.
§J = 6.0 Hz.

complete decomposition of the peroxide was observed without any additional resonances in the n.m.r. spectrum.

Results

Oxidative Attack on Choline, β-Methylcholine, and Related Tertiary Amines

Neutral Aqueous Solution (Buffered)

(a) Products

At p*H* 6.8 (phosphate buffer), photolysis of 1.0 *M* aqueous H_2O_2 containing 1 *M* choline chloride, $(CH_3)_3\overset{+}{N}CH_2CH_2OH\ Cl^-$, gave acetaldehyde and trimethyl ammonium chloride as the major products after 35% decomposition of the peroxide. A trace of acetic acid attributed to further oxidation of acetaldehyde is also detected by n.m.r.

Confirmation of each product was obtained by standard methods. Acetaldehyde was swept from the solution during photolysis, and identified directly by n.m.r. and mass spectra and as its 2,4-dinitrophenyl hydrazone derivative. It was the sole material in the cold trap. Trimethylamine was established by n.m.r. spectroscopy, both in the photolyzed solution (as the cation) and after sweeping it from the basified reaction mixture into aqueous HCl. After the latter procedure, no n.m.r. resonances remained other than those due to choline and a trace of acetate (high gain). Moreover extraction of the reaction mixture with ether provided no residue on evaporation of the extracts.

Similar thorough examination of reaction mixtures from other substrates showed only the products expected from fragmentation of the radical obtained by hydrogen abstraction from the carbinol carbon (reactions 1 and 2).

[1] $R_3\overset{+}{N}CH_2CHOHR' \xrightarrow{\cdot OH} R_3\overset{+}{N}CH_2\dot{C}OHR'$

R, R′ = CH_3 or H

[2] $R_3\overset{+}{N}CH_2\dot{C}OHR \longrightarrow R_3\overset{+}{N}H + \dot{C}H_2\overset{O}{\overset{\|}{C}}R \xrightarrow[\text{donor}]{\text{hydrogen}} CH_3\overset{O}{\overset{\|}{C}}R$

In Table 2 the results of these experiments are summarized. Nuclear magnetic resonance signals appropriate to the analysis are given in the Experimental section. For both quaternary and

Can. J. Chem. Downloaded from www.nrcresearchpress.com by 210.87.254.105 on 09/05/12
For personal use only.

TABLE 2. Products of photolysis reactions in aqueous solutions of H_2O_2

Substrate*	p*H*	Products: Fragmentation process†	Products: Oxidation (intact)
$(CH_3)_3\overset{+}{N}CH_2CH_2OH$‡	6.8	$(CH_3)_3\overset{+}{N}H$, CH_3CHO	Nil
	1.0	$(CH_3)_3\overset{+}{N}H$, CH_3CHO	$(CH_3)_3\overset{+}{N}CH_2CO_2H$
$(CH_3)_2\overset{+}{N}HCH_2CH_2OH$‡§	6.8	$(CH_3)_2\overset{+}{N}H_2$, CH_3CHO	Nil
$(CH_3)_3\overset{+}{N}CH_2CHOHCH_3$	6.8	$(CH_3)_3\overset{+}{N}H$, $CH_3\overset{O}{\overset{\|\|}{C}}CH_3$	Nil
	1.0	$(CH_3)_3\overset{+}{N}H$, $CH_3\overset{O}{\overset{\|\|}{C}}CH_3$	$(CH_3)_3\overset{+}{N}CH_2\overset{O}{\overset{\|\|}{C}}CH_3$
$(CH_3)_2\overset{+}{N}HCH_2CHOHCH_3$	6.8	$(CH_3)_2\overset{+}{N}H$, $CH_3\overset{O}{\overset{\|\|}{C}}CH_3$	Nil
	1.0	$(CH_3)_2\overset{+}{N}H$, $CH_3\overset{O}{\overset{\|\|}{C}}CH_3$	$(CH_3)_2\overset{+}{N}HCH_2\overset{O}{\overset{\|\|}{C}}CH_3$

*Concentration 0.8–1.0 *M*, $[H_2O_2]_{initial} = 1.0$ *M*.
†Note that no *net* oxidation of the substrate is involved in the fragmentation. However, the amine and carbonyl components of the reaction mixture do result from *oxidative* attack on the substrate.
‡Under all conditions trace quantities of CH_3CO_2H are detected.
§Not studied at p*H* 1.0.

tertiary amines, the photo-induced reaction apparently proceeds via this one pathway at p*H* 6.8.

(b) Estimation of Yields at pH 6.8

(i) Amine: In the n.m.r. spectrum, the separation of the *N*-methyl signals of the substrate cations and the product amine cations allowed quantitative estimation of both species. Comparison with the initial concentration of quaternary ammonium salt allowed a percentage recovery to be estimated with considerable reliability. As a further check on amine concentration, a basic solution was swept into acetic acid/acetic anhydride and titrated with 0.1 *N* perchloric acid in acetic acid (12). The methods agreed within $\pm 2\%$. In Table 3, the results of such estimations for all substrates show recovery at a lower limit of 96% but more often quantitative. These results strongly suggest a clear-cut reaction pathway.

(ii) Carbonyl Products: Quantitative evaluation of the carbonyl product yields presented great difficulties. The oxygen produced constitutes an interference, and must be continually swept from solution. As well, acetaldehyde hydrate $CH_3CH(OH)_2$ has a highly reactive methine hydrogen, and competes effectively with the less reactive cationic substrate for hydroxyl radical. Deliberate initial addition of the usual theoretical yield of acetaldehyde to a choline photolysis dropped amine production by 80%. Hydrogen peroxide consumption doubled (6 h) but acetic acid became a major product. Hence purging the reaction continuously with nitrogen is necessary to remove both oxygen and acetaldehyde. Under such conditions adequate trapping of the volatile carbonyl components was not readily achieved. In a control, sweeping an unphotolyzed choline solution (10-fold excess of acetaldehyde, normal reactant concentrations) gave only 35% recovery (Dry Ice – methylene chloride). In actual runs we isolated 20% of theoretical acetaldehyde, and 60% of theoretical acetone from $(CH_3)_3\overset{+}{N}CH_2CHOHCH_3$ as substrate. Similar efficiencies were obtained either by using two aqueous sodium bisulfite traps (13) or by gravimetric 2,4-dinitrophenylhydrazone recovery (two traps). However, considering the mechanical losses in the control experiments and the absence of other products, we are satisfied the designated carbonyl products are the stoichiometric partners of the amines. Success in the n.m.r. analyses of the latter components led us to abandon any further attempts at acetaldehyde and acetone isolation.

(c) Hydrogen Peroxide Consumption

Iodometric analysis provided a measure of

Can. J. Chem. Downloaded from www.nrcresearchpress.com by 210.87.254.105 on 09/05/12
For personal use only.

TABLE 3. Product yields in neutral (buffered) aqueous solution*

Substrate	Amount† Initial	Amount† Final	Amine produced†	Recovery (%)	H_2O_2 consumption (I)‡	Amine yield (%)§
$(CH_3)_3\overset{+}{N}CH_2CH_2OH$	29.9	27.3	1.6	96.7	7.0	23
$(CH_3)_3\overset{+}{N}CH_2CH_2OH$	25.3	23.1	2.2	100.0	8.2	27
$(CH_3)_3\overset{+}{N}CH_2CHOHCH_3$	22.5	20.9	1.5	99.6	7.2	21
$(CH_3)_3\overset{+}{N}CH_2CHOHCH_3$	23.3	19.8	2.9	97.4	10.6	28
$(CH_3)_3\overset{+}{N}CH_2CHOHCH_3$	25.8	24.2	1.6	100.0	5.6	29
$(CH_3)_3\overset{+}{N}CH_2CHOHCH_3$	26.0	24.8	1.0	99.2	6.0	17
$(CH_3)_2\overset{+}{N}HCH_2CH_2OH$	20.6	15.0	5.6	100.0	21.8	26
$(CH_3)_2\overset{+}{N}HCH_2CHOHCH_3$	20.6	19.2	1.7	101.5	5.4	32

*Quantities to ±0.1 mmol based on three integration measurements.
†Quantity in 20 ml photolysis aliquot.
‡Total charge of hydrogen peroxide = 20-25 mmol in 20 ml.
§% Amine = amine/H_2O_2 consumption × 100%.

peroxide consumption (Table 3). The accepted primary event in the photolysis of hydrogen peroxide provides two hydroxyl radicals for each molecule of H_2O_2 (reaction 4) (14, 15). Ideally

[4] $$H_2O_2 \xrightarrow{h\nu} HO\cdot + \cdot OH$$

then two abstraction radicals would be formed from the ammonio alcohol (reaction 1).[3] However competition from attack on hydrogen peroxide leading to a chain decomposition (reactions 5–7) will serve to reduce this optimum formation of abstraction radicals.

[5] $$HO\cdot + H_2O_2 \longrightarrow H_2O + HO_2\cdot$$

[6] $$HO_2\cdot + H_2O_2 \longrightarrow H_2O + O_2 + \cdot OH$$

[7] $$HO_2\cdot + HO_2\cdot \longrightarrow H_2O_2 + O_2$$

Furthermore, if the α-carbonyl radical formed from reaction 2 attacks another molecule of ammonio alcohol a second chain reaction forming amine will ensue. If chain lengths were short, we might expect to see dimeric termination products by n.m.r. spectroscopy. Additional n.m.r. methylene or methyl resonances due to 1,4-butanedial ($\cdot CH_2CHO$ dimerization) and 2,4-hexanedione ($\dot{C}H_2\overset{O}{\overset{\|}{C}}CH_3$ dimerization) are absent at highest gain settings. Alternatively, termination may occur by formation of $\cdot O_2H$ radicals, *e.g.* reaction 8 followed by their

[8] $$\cdot CH_2\overset{O}{\overset{\|}{C}}R + H_2O_2 \longrightarrow CH_3\overset{O}{\overset{\|}{C}}R + HO_2\cdot$$

dimerization via reaction 7. We detect oxygen mass spectrometrically during photolysis of both acidic and neutral solutions, consistent with the occurrence of reaction 7.

Clearly yields quoted as percentages in Table 3 serve to reflect similar overall behavior of all the cationic substrates, and do not establish the competitive position of the two possible chain reactions (See Discussion section).

Acidic Aqueous Solution

Products

At p*H* 1.0 (0.1 *N* HCl) photolysis of the quaternary and tertiary ammonium salts in 1.0 *M* H_2O_2 solution gave less net reaction, and a substantially different product distribution. In each case the "fragmentation products" observed in the experiments at p*H* 6.8 were present.

[3]Electron spin resonance studies using the Ti(III)·H_2O_2·RH system show that the substrates, though less reactive than neutral alcohols (*e.g.* $CH_3CHOHCH_3$ and CH_3CH_2OH), do provide spectra that indicate moderately favorable attack relative to hydrogen peroxide (2). As an illustration, for acetone, a substrate comparable to H_2O_2 in reactivity toward ·OH, we require a four-fold higher concentration than in the case of ammonio alcohol to obtain similar e.s.r. signal intensity.

Can. J. Chem. Downloaded from www.nrcresearchpress.com by 210.87.254.105 on 09/05/12
For personal use only.

TABLE 4. Product yields in acidic aqueous solution*

Substrate	Yield: Oxidation (*i*)	Yield: Fragmentation (*ii*)	H_2O_2 consumption (*iii*)	Products (% of *iii*)†: (*i*)	(*ii*)	Combined
$(CH_3)_3\overset{+}{N}CH_2CH_2OH$	0.6	0.4	7.2	8.4	5.6	14
$(CH_3)_3\overset{+}{N}CH_2CHOHCH_3$	0.8	0.2	7.8	10.3	2.6	13
$(CH_3)_2\overset{+}{N}HCH_2CHOHCH_3$	3.3	0.4	9.8	33.7	4.1	38

*Consumption and yields refer to mmol in 20 ml of reaction mixture. Initial H_2O_2 = *ca.* 20 mmol; initial substrate = 20 mmol.
†Expressed as mmol product/H_2O_2 × 100%; for comparison with neutral conditions.

However now the dominant product from choline, β-methylcholine, and 1-(*N*,*N*-dimethylamino)-2-propanol resulted from oxidation of the primary or secondary alcohol function without elimination. In Table 1 these involatile cationic products are summarized. In each case identification was made by n.m.r. through comparison with synthetic mixtures containing the authentic compounds and the reactants. No other products were detected. A thorough search was made for new (unsplit) C-methyl signals in the reaction mixture from 2-propanol derivatives where the species $(R)_3\overset{+}{N}CH_2C(CH_3)(OH)C(CH_3)(OH)\underline{C}H_2\overset{+}{N}R_3$ might have been formed.

Reaction Yields at pH 1.0

Quantitative analysis by the n.m.r. integration technique was hampered by the sharply reduced yield of products and by the juxtaposition of *N*-methyl resonances from the amines and the "intact" cationic oxidation products. In Table 4 relative yields of the processes were determined by comparison of product resonances and the signal due to added acetate. No attempt to quantify *N*-methyl recovery (*cf.* p*H* 6.8) was made in view of the overwhelming excess of substrate. Clearly the fragmentation process is highly p*H* dependent, for oxidation of the alcohol function now dominates the product distribution. Moreover, the reduced molar yield of amine indicates that a facile fragmentation pathway available at p*H* 6.8 has been lost.

Unbuffered Aqueous Solution

During the photolysis of neutral unbuffered choline or β-methyl choline solutions, the gradual accumulation of acidic products (*e.g.* $(CH_3)_3\overset{+}{N}H$, CH_3CO_2H, $(CH_3)_3\overset{+}{N}CH_2CO_2H$) provides a final solution of p*H* 1.0–2.5. Such unbuffered experiments showed both fragmentation and oxidation products. To correlate with *in vivo* conditions a p*H* 6.8 buffer (1 *M* phosphate) was adopted. No significant change in p*H* was observed before and after reaction. At 1 *M* buffer a slight drop to p*H* 5.7 was observed with the two tertiary amines; however only fragmentation products were observed. At these buffer concentrations we cannot readily account for the decrease. We note that the recorded p*H* is uncorrected for activity in a solution of high ionic strength provided by a changing ionic composition.

Other control experiments including direct photolysis of the substrate and of the amine cations, molecular oxidation of the substrate, and reaction of the substrate with the buffer were negative. (See Experimental section.)

Discussion

Neutral Conditions

Reaction of the β-ammonio alcohols during the photolysis of aqueous hydrogen peroxide shows a p*H* dependence that agrees entirely with the observations by e.p.r. spectroscopy using the rapid flow system (Ti(III)–H_2O_2 reaction) (2). At p*H* 6.8 only fragmentation products are formed during photolysis. In the e.p.r. studies at neutrality an α-carbonyl radical intermediate is detected while the precursor abstraction radical signal observed in acidic medium is absent.

It is proposed that the results of both experiments are compatible with hydrogen abstraction from the carbinol (alcohol) carbon followed by rapid deprotonation and fragmentation of the conjugate base of the radical. For example, consider 1-(*N*,*N*-dimethylamino)-2-propanol, Scheme 1. In the photolysis, only acetone and trimethylamine are formed. In the e.p.r. spectrum the acetonyl radical $\cdot CH_2COCH_3$ and

Can. J. Chem. Downloaded from www.nrcresearchpress.com by 210.87.254.105 on 09/05/12
For personal use only.

Can. J. Chem. Downloaded from www.nrcresearchpress.com by 210.87.254.105 on 09/05/12
For personal use only.

Hydrogen Peroxide
Initiation

[4] $H_2O_2 \longrightarrow 2\phi_a HO\cdot$

Propagation

[5] $H_2O_2 + \cdot OH \xrightarrow{k_5} H_2O + HO_2\cdot$

[6] $HO_2\cdot + H_2O_2 \xrightarrow{k_6} H_2O + O_2 + \cdot OH$

Termination

[7] $2HO_2\cdot \xrightarrow{k_7} H_2O_2 + O_2$

Ammonio Alcohol
Initiation

[9] $\cdot OH + (CH_3)_2\overset{+}{N}HCH_2CHOHCH_3 \xrightarrow{k_9}$

$(CH_3)_2\overset{+}{N}HCH_2\dot{C}OHCH_3$

$(CH_3)_2\overset{+}{N}HCH_2CHOHCH_2\cdot$

Propagation

[10] $(CH_3)_2\overset{+}{N}HCH_2\dot{C}CH_3 \xrightarrow[OH^-]{H_2O} (CH_3)_2\overset{+}{N}HCH_2C\cdot CH_3$ (OH; O^-)

[11] $(CH_3)_2\overset{+}{N}HCH_2\dot{C}CH_3 \xrightarrow{k_{11}}$ (O^-)

$(CH_3)_2NH + \dot{C}H_2COCH_3$

[12] $\dot{C}H_2\overset{O}{\overset{\|}{C}}CH_3 + (CH_3)_2\overset{+}{N}HCH_2CHCH_3 \xrightarrow{k_{12}}$ (OH)

$CH_3\overset{O}{\overset{\|}{C}}CH_3 + (CH_3)_2\overset{+}{N}HCH_2\dot{C}CH_3$ (OH)

Termination

[13] $H_2O_2 + R\cdot \xrightarrow{k_{13}} RH + HO_2\cdot$

$R = (CH_3)_2\overset{+}{N}HCH_2CHOH\dot{C}H_2$

$\dot{C}H_2COCH_3$

[7] $2HO_2\cdot \xrightarrow{k_7} H_2O_2 + O_2$

SCHEME 1

a signal due to adjacent methyl attack, *e.g.* $(CH_3)_3\overset{+}{N}CH_2CHOH\dot{C}H_2$ appear at p*H* 6.0. In the present study, photolysis of H_2O_2 to give two hydroxyl radicals is the initiating process, Scheme 1. Reduction of peroxide by Ti(III) is the analogous event in the flow experiments (reaction 14) (2).

[14] $Ti(III)(EDTA) + H_2O_2 \xrightarrow{H^+}$

$Ti(IV)(EDTA) + \cdot OH + H_2O$

The mechanism assumes that the pK_a of the abstraction radical is markedly lowered relative to the substrate alcohol. Electron spin resonance studies have shown that the pK_a of an α-alcohol radical is lower by from 4–8 units. For instance, 2-propanol has pK_a = 17.1 while $(CH_3)_2\dot{C}OH$ has pK_a = 12.03 (16). Noting that the effect of the charged ammonio substituent should lower the pK_a of both alcohol and abstraction radical (*e.g.* compare $(CH_3)_3\overset{+}{N}CH_2CO_2H$, p$K_a$ = 1.83; CH_3CO_2H, pK_a = 4.75) we propose that deprotonation will occur under neutral conditions.[4] Indeed using pulse radiolysis, Henglein and coworkers have observed the conversion of 1,2-dihydroxy ethyl radical, **4**, to acetaldehyde radical at p*H* 8.5 (reaction 15) (4). The ammonio

[15] $HOCH_2\dot{C}HOH \underset{}{\overset{OH^-}{\rightleftharpoons}} HOCH_2\dot{C}HO^- \longrightarrow$

4 **5**

$\dot{C}H_2CHO + OH^-$

radicals will be more acidic than **4**, and in consequence will undergo the process of fragmentation at lower p*H*. Radical species **5** (reaction 15) loses OH^- faster than the protonation equilibrium can be established. By analogy elimination of the deprotonated radical $(CH_3)_2\overset{+}{N}HCH_2\dot{C}O\bar{C}H_3$ should also be rapid, a prediction confirmed by observation of $\dot{C}H_2COCH_3$ under steady state conditions of transient radical concentration in the e.s.r. flow experiment.

Three distinct modes of further reaction of the acetonyl radical are possible in the system: (*i*) attack on ammonio alcohol to form a second abstraction radical tending to perpetuate a chain reaction (reaction 12); and either (*ii*) simple dimerization or (*iii*) abstraction of hydrogen from H_2O_2 (reaction 13). Both of the latter processes serve to terminate the chain reaction.

Assessment of the length of the chain is not possible on the basis of present data as the following analysis indicates. First, $\cdot CH_2\overset{O}{\overset{\|}{C}}CH_3$ (in general any α-carbonyl radical) should be electrophilic, and exhibit reactivity not drastically at variance with the hydroxyl radical itself (consider **6** and **7**).

[4]Note that if elimination from the deprotonated form is kinetically favored the reaction can be observed at a p*H* lower than the radical pK_a.

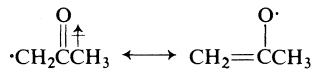

6 7

Therefore we might expect that if ·OH attacks both alcohol and hydrogen peroxide, *e.g.* rate constants k_9 and k_5 being comparable; then the acetonyl radical will have the analogous rates k_{12} and k_{13} competitive.

Now consider reactions 5 to 7 for the H_2O_2 chain decomposition in conjunction with reactions 9 to 12 for chain production of amine allowing only the sequence [13], [7] for termination (see Scheme 1). By steady state approximation for all radical species, and for zero order peroxide photodecomposition, equations 16 and 17 are derived

$$[16]\quad \phi(-H_2O_2) = 2\phi_a + 2k_6\left(\frac{\phi_a}{k_7 I_a}\right)^{1/2}[H_2O_2]$$

$$[17]\quad \phi(\text{amine}) = \left[2\phi_a + k_6\left(\frac{\phi_a}{k_7 I_a}\right)^{1/2}[H_2O_2]\right] \times \left[1 + \frac{k_{12}[\text{alcohol}]}{k_{13}[H_2O_2]}\right] \times \left[1 + \frac{k_5[H_2O_2]}{k_9[\text{alcohol}]}\right]^{-1}$$

The chain decomposition of the hydrogen peroxide (eq. 16) is unaffected by the alcohol, having the same form as originally proposed by Weiss (17). From eq. 17, it is apparent that under the equimolar alcohol and peroxide concentrations used that if $\dot{C}H_2CCH_3$ (O) and ·OH had exactly the same reactivity *e.g.* $k_{12}/k_{13} = k_5/k_9$ then the second (chain) term in $\phi(-H_2O_2)$ would be just twice that for amine production.

In the absence of direct measurement of I_a it is not possible to assess the chain lengths involved. Experiments are being undertaken to measure the quantum yields $\phi(-H_2O_2)$ and ϕ(amine) to shed light on this question.

Although $(CH_3)_2\overset{+}{N}HCH_2CHOH\dot{C}H_2$ is evident as an intermediate (e.s.r.) no products attributed to it are detected in the photolysis studies. Attack on H_2O_2 to reform substrate (reaction 13) or disproportionation forming substrate and undetected amounts of $(CH_3)_2\overset{+}{N}HCH_2CCH_3$ (O) could account for these intermediate radicals. It is also possible that this radical would react with the ammonio alcohol as has been demonstrated for simple alcohols (18).

Acid Conditions

At p*H* 1.0 oxidation of the abstraction radical becomes the most important process for all substrates. Specifically in the case of $(CH_3)_2\overset{+}{N}HCH_2\dot{C}OHCH_3$ a moderately efficient oxidation (33%) is observed. Such α-hydroxy tertiary radicals are normally reactive as reducing agents, (19) (reaction 18).

[18] 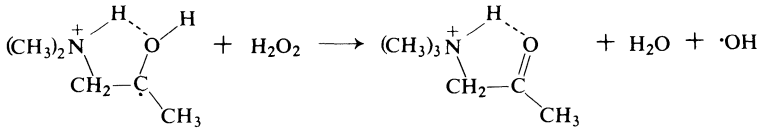

Intramolecular hydrogen-bonding in this particular radical has been demonstrated by e.s.r., and apparently facilitates the electron transfer in spite of the destabilizing influence of the positive charge. Indeed the corresponding quaternary cation shows less inclination toward oxidation, (reaction 19).

[19] 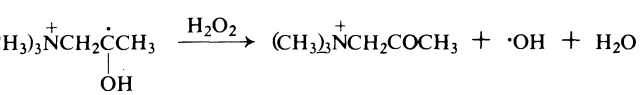

Again we speculate that the less ready oxidation of the two quaternary cations at p*H* 1.0 may be

Can. J. Chem. Downloaded from www.nrcresearchpress.com by 210.87.254.105 on 09/05/12
For personal use only.

assigned to competition from repair by hydrogen transfer from H_2O_2.[5] In addition disproportionation would produce the ketone but at reduced efficiency, reaction 20.

[20] $$2(CH_3)_3\overset{+}{N}CH_2\overset{OH}{\overset{|}{\dot{C}}}-CH_3 \longrightarrow (CH_3)_3\overset{+}{N}CH_2\overset{O}{\overset{\|}{C}}CH_3 + (CH_3)_3\overset{+}{N}CH_2\overset{OH}{\overset{|}{C}}HCH_3$$

Fragmentation also persists at p*H* 1.0 in the photolysis experiments. Our results do not bear on the question of the alternative homolytic process occurring in the absence of base catalysis, (reaction 21).

[21] $$(CH_3)_3\overset{+}{N}CH_2\dot{C}HOH \longrightarrow (CH_3)_3N^{+\cdot} + CH_2{=}CHOH$$

Observation of the e.p.r. signal of $(CH_3)_3N^{+\cdot}$ at p*H* 1.0 has been reported (1).[6] However it has been noted that the reducing potentials of $\cdot CH_2\overset{+}{C}H{=}OH$ and $(CH_3)_3N{:}$ are clearly similar (E = *ca.* −0.8 V) and that $(CH_3)_3N^{+\cdot}$ may arise via electron transfer (reaction 22) (2).

[22] $$(CH_3)_3\overset{+}{N}-CH_2\dot{C}HOH \longrightarrow (CH_3)_3\ddot{N}\ \dot{C}H_2\overset{\overset{+}{O}H}{\overset{\diagup\!\!\diagup}{C}}\overset{H}{\diagdown} \longrightarrow (CH_3)_3N^{+\cdot}\ CH_2{=}\overset{OH}{\overset{|}{C}}H$$

Relevance to γ-Irradiation of Choline Chloride

In spite of numerous studies (6–9), the intrinsic reason for the instability of the α-crystalline form of choline chloride is not definitely established. Symons has advanced a mechanism in which $(CH_3)_3N^{+\cdot}$ is the chain propagating species for decomposition to aldehyde and amine (8). However, it is also the species that is observed in the e.p.r. spectrum of γ-irradiated choline chloride at room temperature. As the chain carrier it is not likely to accumulate as the major paramagnetic species, particularly with G(fragmentation) = 55 000. Alternatively Lemmon and co-workers have proposed the central role of a biradical species **8**, (9, 20). It is presumed to react with a detrapped electron after or accompanying the diffusing apart of the radicals forming $\bar{C}H_2CH_2OH^*_9$, the excited ethanol anion, as the chain carrier.

$$(CH_3)N^{+\cdot}\cdots\dot{C}H_2CH_2OH\cdots Cl^-$$

8

On the basis of the observed p*H* dependent decomposition of β-ammonio alcohol radicals we suggest that electron detrapping occurs to quench the "biradical", but forming trimethylamine. In Scheme 2 choline I represents this species accepting the electron in the first stage. In stage 2 the reactive primary radical abstracts a hydrogen from choline II, and as in solution the amine moiety (base) removes the OH proton. Now rapid decomposition of the deprotonated radical ensues (stage 3). The last propagation step (stage 4) is the generation of a new abstraction radical from choline III creating CH_3CHO and the ion $(CH_3)_3\overset{+}{N}H$. Accumulation of cation radical $(CH_3)N^{+\cdot}$ may indicate termination by the homolytic or electron transfer pathways (reactions 21 and 22) when base catalysis does not occur in the propagation step (stage 4).

The orientation of the molecules in Scheme 2 is based on the disposition along the *b* axis of the crystal as proposed by Senko and co-worker (21).

[5]No substantial thermodynamic stabilization of α-hydroxy radicals is predicted. Their formation arises as a consequence of kinetic control that can be rationalized in terms of a stable polar transition state for electrophilic ·OH attack.

[6]Note $(CH_3CH_2)_3\overset{+}{N}CH_2CH_2OH$ oxidation at p*H* 2.5 does give $\cdot CH_2CHO$ radical spectra (2).

Can. J. Chem. Downloaded from www.nrcresearchpress.com by 210.87.254.105 on 09/05/12
For personal use only.

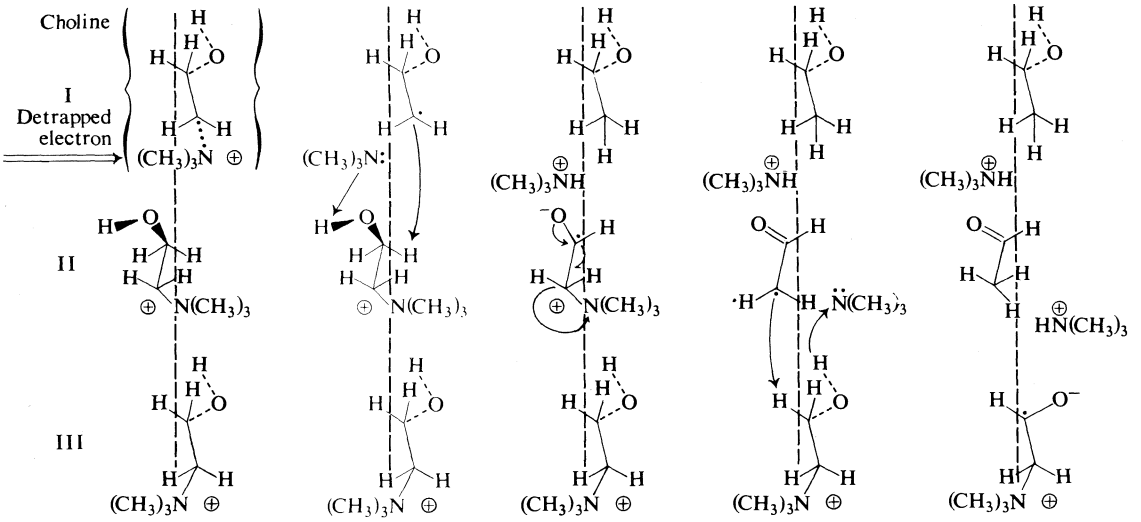

SCHEME 2

We would like to thank the National Research Council of Canada and the University of Victoria for generous support of the project through operating grants. A referee's helpful suggestion concerning the competitive chain reactions is acknowledged.

1. B. C. GILBERT, J. P. LARKIN, and R. O. C. NORMAN. J. Chem. Soc. Perkin II, 794 (1972).
2. T. FOSTER and P. R. WEST. Can. J. Chem. **51**, 4009 (1973).
3. R. J. PRITCHETT and R. O. C. NORMAN. J. Chem. Soc. B, 849 (1966).
4. K. M. BANSAL, M. GRÄTZEL, A. HENGLEIN, and E. JANATA. J. Phys. Chem. **77**, 16 (1973).
5. C. E. BURCHILL and K. M. PERRON. Can. J. Chem. **49**, 2382 (1971).
6. R. O. LINDBLOM, R. M. LEMMON, and M. CALVIN. J. Am. Chem. Soc. **83**, 2484 (1961).
7. M. A. SMITH and R. M. LEMMON. J. Phys. Chem. **69**, 3370 (1965).
8. M. C. R. SYMONS. J. Chem. Soc. Faraday Trans. II, **68**, 216 (1972).
9. A. NATH, R. AGARWAL, L. MARTON, V. SUBRAMANYAN, and R. M. LEMMON. J. Am. Chem. Soc. **93**, 2103 (1971).
10. C. N. SATTERFIELD, R. E. WILSON, R. M. LECLAIR, and R. C. RIED. Anal. Chem. **26**, 1792 (1954).
11. S. BERNTSSON. Anal. Chem. **28**, 1337 (1956).
12. S. SIGGIA and W. MAXCY. Anal. Chem. **19**, 1023 (1947).
13. R. M. CUNDIFF and J. A. RIDDICK. Anal. Chem. **24**, 910 (1952).
14. D. H. VOLMAN and J. C. CHEN. J. Am. Chem. Soc. **81**, 4141 (1959).
15. F. S. DAINTON and J. ROWBOTTOM. Trans. Faraday Soc. **49**, 1160 (1953).
16. G. P. LAROFF and R. W. FESSENDEN. J. Phys. Chem. **77**, 1283 (1973).
17. J. WEISS. Faraday Soc. Discuss. **12**, 161 (1952).
18. C. E. BURCHILL and I. S. GINNS. Can. J. Chem. **48**, 1232 (1970).
19. R. O. C. NORMAN and P. R. WEST. J. Chem. Soc. B, 389 (1969).
20. T. TOMKIEWICZ, R. AGARWAL, and R. M. LEMMON. J. Am. Chem. Soc. **95**, 3144 (1973).
21. M. E. SENKO and D. H. TEMPLETON. Acta Cryst. **13**, 281 (1960).

Can. J. Chem. Downloaded from www.nrcresearchpress.com by 210.87.254.105 on 09/05/12
For personal use only.

The Addition of Arylselenium Trichlorides *vs.* Areneselenenyl Chlorides to *cis*- and *trans*-1-Phenylpropene[1]

DENNIS G. GARRATT AND GEORGE H. SCHMID

Lash Miller Chemical Laboratories, Department of Chemistry, University of Toronto, Toronto, Ontario M5S 1A1

Received February 4, 1974

DENNIS G. GARRATT and GEORGE H. SCHMID. Can. J. Chem. **52**, 3599 (1974).

2,4-Dinitrophenylselenium trichloride has been found to add to *cis*- and *trans*-1-phenylpropene in an *anti* stereospecific manner to yield *threo-dl*- and *erythro-dl*-β-chloroalkyl 2,4-dinitrophenyl selenide dichlorides, respectively. Comparison is made with the adducts from the addition of 2,4-dinitrobenzeneselenenyl chlorides. β-Chloroalkyl 2,4-dinitrophenyl selenides react with chlorine or sulfuryl chloride to yield β-chloroalkyl 2,4-dinitrophenyl selenide dichlorides. β-Chloroalkyl selenide dichlorides were observed to decompose into 1,2-dichloro adducts and areneselenenyl chloride. 2,4-Dinitrobenzeneselenenyl acetate was shown to add to alkenes in an *anti* stereospecific manner.

DENNIS G. GARRATT et GEORGE H. SCHMID. Can. J. Chem. **52**, 3599 (1974).

On a trouvé que le trichlorure de dinitro-2,4 phénylsélénium s'additionne sur les phényl-1 propène *cis* et *trans* d'une façon stéréospécifique *anti* conduisant respectivement aux dichlorures de *thréo-dl* et *érythro-dl*-β-chloroalkyle dinitro-2,4 phénylsélénure. On a fait une comparaison avec les produits provenant de l'addition des chlorures de dinitro-2,4 benzènesélénenyle. Les β-chloroalkyle dinitro-2,4 phénylsélénures réagissent avec le chlore ou le chlorure de sulfuryle pour conduire aux dichlorures de β-chloroalkyl dinitro-2,4 phénylsélénure. On a observé que les dichlorures de β-chloroalkyle sélénures se décomposent en adduits dichloré-1,2 et en chlorure d'arènesélénenyle. On a montré que l'acétate de dinitro-2,4 benzènesélénenyle s'additionne aux alcènes d'une façon stéréospécifique *anti*. [Traduit par le journal]

2,4-Dinitrophenylselenium trichloride has been reported to react with cyclohexene (eq. 1) to give *trans*-2-chlorocyclohexyl-1 2′,4′-dinitrophenyl selenide (1). This has been interpreted as support for an equilibrium between arylselenium trichloride, areneselenenyl chloride, and chlorine (eq. 2). To account for the results it was assumed that the selenenyl chloride was the most reactive electrophile.

[1] 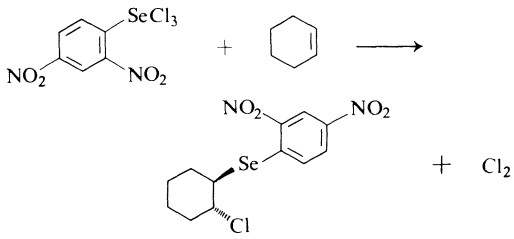

[2] 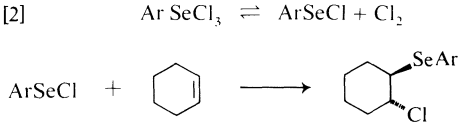

Ar = 2,4-Dinitrophenyl

In contrast to this, de Moura Campus and Petragnani (2) in a study of the analogous tellurium system reported that aryltellurium trichlorides add to cyclohexene to give aryl *trans*-2-chlorocyclohexyl telluride dichlorides. The reaction, however, was not general since some olefins did not react with tellurium derivatives and others produced elemental tellurium by reduction and halogenated products. *Anti* addition to the double bond was assumed but no structural proof was given. Selenium tetrachloride (3) and tellurium tetrachloride (2, 4) have been found to add to olefins to form β-chloroalkylselenium trichlorides and β-chloroalkyltellurium trichlorides, respectively, which are then capable of reacting with a further mole of olefin to yield bis(β-chloroalkyl) selenide dichloride and telluride dichloride, respectively. The additions are reported to occur in a predominately Markownikoff sense, with assumed *anti* addition to the double bond.

We wish to report evidence which indicates that arylselenium trichlorides react with alkenes to form β-chloroalkyl aryl selenide dichloride adducts in a stereospecific *anti* manner. These adducts are thermally unstable, decomposing into 1,2-dichloro adducts and areneselenenyl

[1]Organoselenium Chemistry. Part IV. For Part III see ref. 16.

Can. J. Chem. Downloaded from www.nrcresearchpress.com by 210.87.254.42 on 09/05/12
For personal use only.

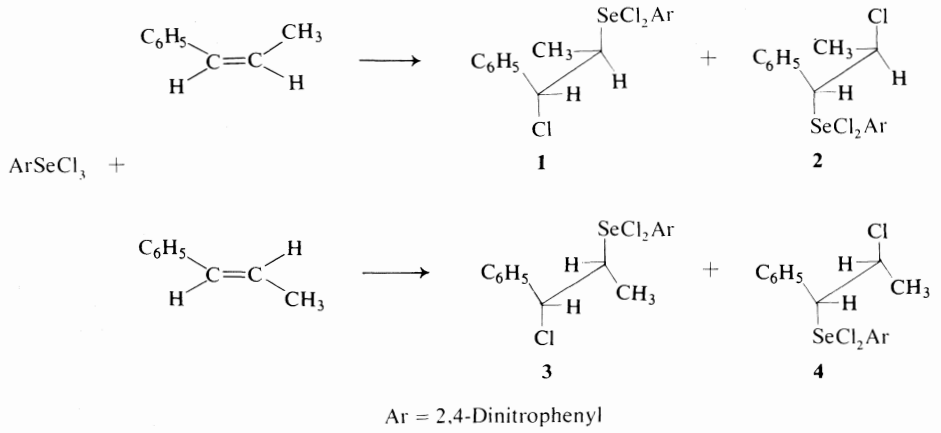

chloride (eq. 3). In the presence of excess olefin the areneselenenyl chloride reacts to form a β-chloroalkyl aryl selenide in an *anti* stereospecific manner.

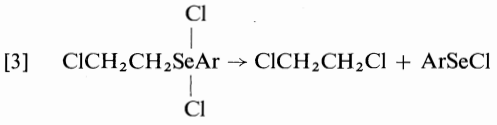

[3] $ClCH_2CH_2SeAr \rightarrow ClCH_2CH_2Cl + ArSeCl$

$ArSeCl + H_2C{=}CH_2 \rightarrow ArSeCH_2CH_2Cl$

Results and Discussion

2,4-Dinitrophenylselenium trichloride reacts readily with *cis*- and *trans*-1-phenylpropene in methylene chloride solution at 25° to yield a mixture of Markownikoff[2] and *anti*-Markownikoff β-chloroalkyl 2,4-dinitrophenyl selenide dichlorides, **1**–**4**. Addition to the *cis* alkene gives compounds **1** and **2**, whereas addition to the *trans* alkene yields compounds **3** and **4**, respectively. No higher aggregates were observed in the presence of an excess of either starting material. Compounds **1** and **2** decompose on standing to yield *threo-dl*-1,2-dichloro-1-phenylpropane (5), whereas **3** and **4** yield the *erythro-dl*-isomer (6). Compounds **5** and **6** are equivalent in all respects to samples made independently via the addition of chlorine to *cis*- and *trans*-1-phenylpropene (5).

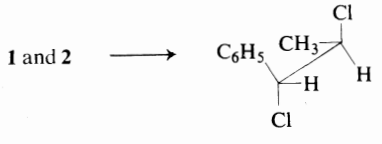

[2]The Markownikoff isomer is designated as the one in which the chlorine is bonded to the benzylic carbon.

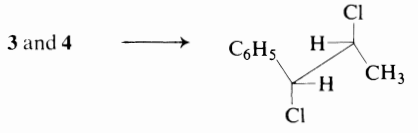

The regiospecificity of the addition is determined from the c.m.r. and p.m.r. data of compounds **1**–**4** which are summarized in Table 1. The following points are to be noted: (*i*) The aliphatic protons are identified on the basis of their chemical shifts. It has been observed that protons α to a selenide dichloride group are generally deshielded relative to those α to a chlorine atom. Further protons α to a chlorine are deshielded relative to those α to a bivalent organic sulfur or selenium group (Table 3). The above observation holds as long as equivalent environments with respect to the remaining two groups are maintained. (*ii*) Confirmation of the assignment of the proton chemical shifts can be obtained from double resonance experiments. Irradiation of the methyl doublet of **1** and **3** decoupled the adjacent proton yielding a simple doublet in each case. At high spectral amplitude, we were able to clearly distinguish the ^{77}Se–^{1}H spin–spin coupling interactions, thus establishing the regiochemistry. Vicinal ^{77}Se–C–C–^{1}H coupling interactions were much weaker or not observable. (*iii*) The assignments of the ^{13}C chemical shifts of the aliphatic carbons is made on the basis of the coupled ^{13}C spectrum. The β-methyl carbon atom appears as a quartet while both the benzylic and the β-carbon atom appear as doublets. The distinction between the two is based upon the observation that the ^{13}C chemical shifts are affected by

Can. J. Chem. Downloaded from www.nrcresearchpress.com by 210.87.254.42 on 09/05/12
For personal use only.

TABLE 1. Proton and carbon magnetic resonance parameters for the products of the addition of 2,4-dinitrophenylselenium trichloride to *cis*- and *trans*-1-phenylpropene

β-Chloroalkyl selenide dichloride	Configuration	*Nucleus* ^1H Chemical shifts* αH	βH	βCH_3
1	*threo*-M	4.75 (d)	4.21 (m)	1.55 (d)
2	*threo*-aM	4.81 (d)	4.18 (m)	1.26 (d)
3	*erythro*-M	4.78 (d)	4.17 (m)	1.58 (d)
4	*erythro*-aM	4.82 (d)	4.17 (m)	1.34 (d)

β-Chloroalkyl selenide dichloride	Configuration†	*Nucleus* ^{13}C Chemical shifts αC	βC	βCH_3	$J^{77}Se$–^{13}C
1	*threo*-M	62.7	75.9	19.1	48
2	*threo*-aM	82.0	63.4	15.4	47
3	*erythro*-M	63.7	72.8	18.4	51
4	*erythro*-aM	79.3	63.9	14.7	55

*Chemical shifts δ, p.p.m. downfield from internal TMS; *J* in Hz.
†M, Markownikoff; aM, anti-Markownikoff.

neighboring sulfur, selenium, and chlorine in the same way as are proton chemical shifts. The benzylic and β-carbon were further distinguished on the basis of their respective geminal ^{13}C proton couplings. Thus the benzylic carbon appears as a doublet, $J_{CH} = 125$ Hz, with doublet fine structure, $J_{CCH} \simeq 5$ Hz, whereas β-carbon appears as a doublet, $J_{CH} = 125$ Hz, but has doublet of quartet fine structure, $J_{CCH} = 5$ Hz. (*iv*) The ^{77}Se–^{13}C coupling in the decoupled ^{13}C spectra can be observed for all four isomers. For **2** and **4**, coupling between the benzylic carbon and selenium is observed while no coupling is observed between the β-carbon and selenium. For **1** and **3**, the reverse is found. The magnitude of this coupling was in the range 47–55 Hz in contrast to that observed for bivalent selenides, $J_{sec} = 62$–67 Hz (see Tables 1 and 2). (*v*) The stereochemistry of the addition has been determined from the chemical shift of the β-methyl protons in isomers **1**–**4**. It is known that in the p.m.r. spectra of a series of racemic *erythro* and *threo* isomers of 1,2-disubstituted 1-arylpropanes (6) the β-methyl protons of the *erythro* isomer always appear at lower field than those of the *threo* isomer.

From these data, it is concluded that the addition of 2,4-dinitrophenylselenium trichloride to *cis*- and *trans*-1-phenylpropene is *anti* stereospecific. Thus, compounds **1** and **3**, resulting from Markownikoff addition to *cis*- and *trans*-1-phenylpropene, are the *threo-dl* and *erythro-dl* isomers, respectively, whereas compounds **2** and **4** are the *threo-dl* and *erythro-dl* isomers, respectively, of *anti*-Markownikoff addition.

Addition of 2,4-dinitrobenzeneselenenyl chloride, in methylene chloride solution at 25° to *cis*- and *trans*-1-phenylpropene yields *threo-dl*- and *erythro-dl*-1-chloro-1-phenylpropyl-2 2′,4′-dinitrophenyl selenide, **7** and **8**, respectively.

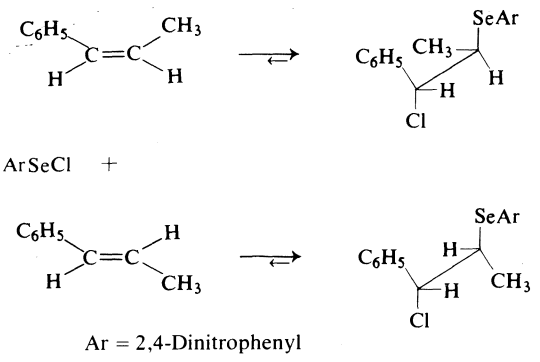

Ar = 2,4-Dinitrophenyl

These reactions were observed to yield only 75 and 80% of **7** and **8**, respectively. The remainder of the reaction mixture was unreacted starting material. Warming the solutions was generally observed to cause a reversible formation of the starting material. This suggests that an equilibrium had been obtained at 75 and 80% conversion to products at 25° for **7** and **8**, respectively.

Can. J. Chem. Downloaded from www.nrcresearchpress.com by 210.87.254.42 on 09/05/12
For personal use only.

TABLE 2. ^{13}C magnetic resonance parameters for adducts of 2,4-dinitrobenzeneselenenyl and sulfenyl chlorides with *cis*- and *trans*-1-phenylpropene and selected model compounds

Compound	Chemical shifts* and coupling constants						
	X = Se				X = S		
	αC	βC	βCH$_3$	$J^{77}Se^{13}C$	αC	βC	βCH$_3$
PhCHCHCH$_3$ (Cl, XAr)							
threo							
Ar = 4-ClC$_6$H$_4$	Unknown				65.82	51.24	17.52
Ar = 4-CH$_3$C$_6$H$_4$	65.9	54.7	17.2	62	65.90	51.39	17.31
Ar = 2,4-(NO$_2$)$_2$C$_6$H$_3$(7)	65.3	52.2	17.5	63	65.60	49.65	18.09
erythro							
Ar = 4-ClC$_6$H$_4$	Unknown				67.28	51.35	17.70
Ar = 4-CH$_3$C$_6$H$_4$	67.1	53.4	17.8	67	67.29	51.30	17.31
Ar = 2,4-(NO$_2$)$_2$C$_6$H$_3$(8)	66.8	51.4	18.1	66	66.76	49.80	17.85
PhCHCHCH$_3$ (XAr, Cl)							
threo							
Ar = 4-ClC$_6$H$_4$	Unknown				59.81	61.18	22.13
Ar = 4-CH$_3$C$_6$H$_4$	59.0	59.9	20.5	65	59.94	61.33	21.68
Ar = 2,4(NO$_2$)$_2$C$_6$H$_3$	Unknown				59.41	59.73	23.24
erythro							
Ar = 4-ClC$_6$H$_4$	Unknown				59.93	61.41	23.41
Ar = 4-CH$_3$C$_6$H$_4$	60.1	62.0	23.8	67	60.23	61.78	23.68
Ar = 2,4-(NO$_2$)$_2$C$_6$H$_3$	Unknown				Unknown		

*Reported δ = p.p.m. from internal TMS in chloroform-*d*; *J* in Hz.

The Markownikoff orientation of the adducts was established by c.m.r. spectroscopy. The ^{13}C spectral data of **7** and **8** along with the Markownikoff and *anti*-Markownikoff adducts of some sulfur analogs are given in Table 2. The ^{13}C chemical shift values of **7** and **8** more closely resemble the Markownikoff than the *anti*-Markownikoff adducts. In addition, the β-carbons of both **7** and **8** show ^{77}Se–^{13}C spin–spin coupling interactions. As in the case of the arylselenium trichloride adducts, the ^{13}C chemical shifts were assigned on the basis of the proton coupled spectra.

The stereochemistry of the adducts was again established from the chemical shifts of the β-methyl protons in the p.m.r. spectra of **7** and **8**. The data are given in Table 3. On the basis of the observation that β-methyl protons of the *erythro* isomer always appear at lower field than those of the *threo* isomer (6), **7** is assigned the *threo* configuration while **8** is assigned the *erythro*. Thus, 2,4-dinitrobenzeneselenenyl chloride adds to *cis*- and *trans*-1-phenylpropene in an *anti* stereospecific manner. This result provides evidence supporting the widely assumed stereochemistry of areneselenenyl chloride addition to alkenes (7, 8).

The structural assignment of **7** and **8** is further substantiated by their reaction with equimolar amounts of chlorine or sulfuryl chloride in methylene chloride or carbon tetrachloride at 25° to form **1** and **3** respectively.

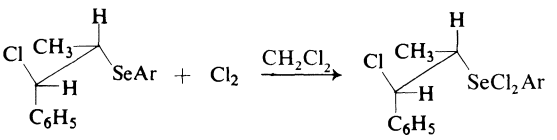

7 **1**

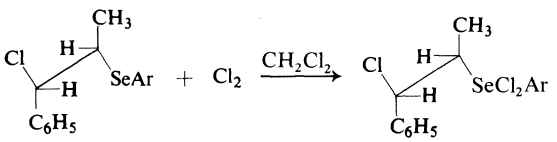

8 **3**

Can. J. Chem. Downloaded from www.nrcresearchpress.com by 210.87.254.42 on 09/05/12
For personal use only.

TABLE 3. Proton magnetic resonance parameters* for adducts of 2,4-dinitrobenzeneselenenyl chloride and 2,4-dinitrobenzenesulfenyl chloride with *cis*- and *trans*-1-phenylpropene in acetic acid at 25°

Compound*	No.	H_a	J_{ab}	H_b	J_{bc}	H_c	Melting point (°)
Ph—CH^a(Cl)—CH^b(SeAr)—CH_3^c *erythro*-M	**8**	5.06 (a)†	7.0	3.86 (o)	6.5	1.70 (d)	89–92
Ph—CH^a(Cl)—CH^b(SAr)—CH_3^c *erythro*-M	**8′**	5.06 (d)	7.0	3.99 (q)	7.0	1.66 (d)	92–93
Ph—CH^a(Cl)—CH^b(SeAr)—CH_3^c *threo*-M	**7**	5.12 (d)	5.0	3.96 (m)	7.0	1.56 (d)	97
Ph—CH^a(Cl)—CH^b(SAr)—CH_3^c *threo*-M	**7′**	5.12 (d)	6.0	4.07 (q)	7.0	1.45 (d)	75–76
Ph—CH^a(OAc)—CH^b(SeAr)—CH_3^c *erythro*-M	**10**	4.80 (d)	6.5	3.96 (m)	6.5	1.63 (d)	138
Ph—CH^a(OAc)—CH^b(SeAr)—CH_3^c *threo*-M	**9**	4.67 (d)	7.2	3.82 (m)	7.6	1.48 (d)	166

*Ar = 2,4-Dinitrophenyl.
†d, doublet; q, quintet; o, octet; m, multiplet.
‡δ (p.p.m.) from internal TMS; *J* in Hz.

In the presence of excess chlorine **7** and **8** rapidly decompose to a complex mixture of 1,2-dichloro-1-phenylpropane, 2,4-dinitrophenylselenium trichloride, bis(2,4-dinitrophenyl) diselenide, bis(2,4-dinitrophenyl)selenide, bis(2,4-dinitrophenyl)selenide dichloride, and elemental selenium. Similar reactions have been found with tellurium derivatives (4) and are consistent with known reactions of organoselenium compounds (2, 4).

It is of interest that whereas the thermolysis of the selenide dichlorides to 1,2-dichloro adducts was stereospecific with retention of configuration at carbon, the chlorination of the selenide dichloride species was stereoselective. The reactions of **1** with chlorine proceeded with 30% retention of configuration.

Secondary rearrangement between Markownikoff and *anti*-Markownikoff adducts of the nature observed on the addition products of olefins with sulfenyl halides (9) seems to be of little consequence in β-chloroalkyl selenides (10). Compounds **7** and **8** show no tendency to isomerize to their corresponding *anti*-Markownikoff isomers over a period of three months in methylene chloride, chloroform, or acetic acid. Similar results have been observed with the analogous sulfur compounds (9).

When **7** and **8**, the products of the addition of 2,4-dinitrobenzeneselenenyl chloride to *cis*- and *trans*-1-phenylpropene, are allowed to stand in acetic acid in the dark, they are slowly converted to the Markownikoff acetate products **9** and **10**, respectively. Authentic samples of **9** and **10** were prepared via the addition of 2,4-dinitrobenzeneselenenyl acetate to *cis*- and *trans*-1-phenylpropene, respectively. The addition of selenenyl acetate was found to be regiospecific in the Markownikoff sense and *anti* stereospecific as hypothesized by Jenny (11) based upon the p.m.r. data given in Table 3.

On the basis of our results, we can reexamine the addition of 2,4-dinitrophenylselenium trichloride first reported by Kharasch and propose

Can. J. Chem. Downloaded from www.nrcresearchpress.com by 210.87.254.42 on 09/05/12
For personal use only.

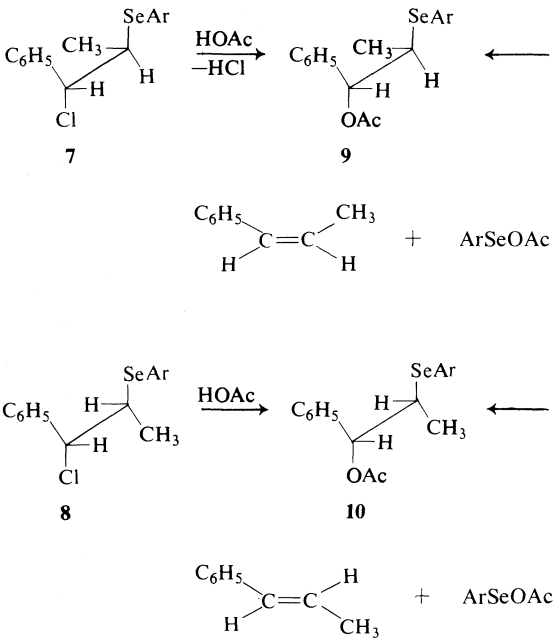

an alternate mechanism. Lawson and Kharasch (1) explained their results on the arylselenium trichloride – areneselenenyl chloride equilibrium. Experimental confirmation of the trichloride to selenenyl chloride equilibrium was first demonstrated by Foster (12) for phenylselenium trichloride. The actual products in this case were hydrogen chloride and 4-chlorobenzeneselenenyl chloride (eq. 5). It was further

[5] $C_6H_5SeCl_3 \rightleftarrows C_6H_5SeCl + Cl_2$
$\rightarrow 4\text{-}ClC_6H_4SeCl + HCl$

shown by Foster that chlorine reacts with benzeneselenenyl chloride to form 4-chlorobenzeneselenenyl chloride and hydrogen chloride. Further, 4-chlorobenzeneselenenyl chloride and chlorine react to form 4-chlorophenylselenium trichloride (eq. 6), and 4-chlorobenzeneselenenyl chloride is in equilibrium with the trichloride and the diselenide species (eq. 7).

[6] $4\text{-}ClC_6H_4SeCl + Cl_2 \rightleftarrows 4\text{-}ClC_6H_4SeCl_3$

[7] $3(4\text{-}ClC_6H_4SeCl) \rightleftarrows 4\text{-}ClC_6H_4SeCl_3 + (4\text{-}ClC_6H_4)_2Se_2$

2,4-Dinitrophenylselenium trichloride was found via competition experiments to react much faster than 2,4-dinitrobenzeneselenenyl chloride with 1-phenylpropenes, in nonpolar solvents such as carbon tetrachloride. In more polar solvents such as methylene chloride or 1,2-dichlorethane, addition of areneselenenyl chlorides became more competitive.

Thus Kharasch's hypothesis (1) that the selenenyl chloride was more reactive than the selenium trichloride in neat cyclohexene appears to be in error. Under Kharasch's reaction conditions the 2,4-dinitrophenylselenium trichloride most likely reacted forming the β-chloro selenide dichloride (eq. 8) which was thermally unstable and decomposed to 1,2-dichlorocyclohexane and 2,4-dinitrobenzeneselenenyl chloride (eq. 9). The dissociation of acyclic aliphatic aryl selenide dichlorides to give areneselenyl chlorides and alkyl chloride is well documented (12, 13) and is often utilized in the synthesis of areneselenenyl chlorides without contamination of trichloride, a common problem in most synthesis. The 2,4-dinitrobenzeneselenenyl chloride thus generated can react with the excess cyclohexene to yield the observed β-chloro selenide (eq. 10).

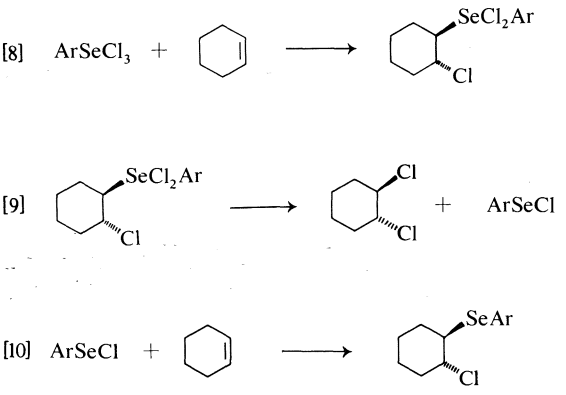

Ar = 2,4-Dinitrophenyl

Experimental

General

All experiments were carried out in a nitrogen-filled glove box or on a standard vacuum line using Schlenk type apparatus. In view of the malodorous and toxic nature of some of the compounds scrupulous avoidance of contact was maintained throughout this work.

Proton and carbon-13 magnetic resonance samples were run in amberized sample tubes as chloroform-*d* solutions using Varian T-60 and XL-100-15 ^{13}CFT ^{13}C spectrometers, respectively. All nitrogen was predried and deoxygenated prior to use by bubbling through traps containing: (*a*) pyridine, triphenylmethane, and $LiAlH_4$, (*b*) concentrated H_2SO_4, and (*c*) activated alumina. Melting points were determined on a Fisher-Johns block and were uncorrected.

Chemicals

cis- and *trans*-1-Phenylpropene were purchased from

Can. J. Chem. Downloaded from www.nrcresearchpress.com by 210.87.254.42 on 09/05/12
For personal use only.

Can. J. Chem. Downloaded from www.nrcresearchpress.com by 210.87.254.42 on 09/05/12
For personal use only.

Chemical Samples Co. and used without further purification. Acetic acid (C.I.L. Glacial) was purified by refluxing for 48 h with a calculated 3% excess of acetic anhydride, followed by fractional distillation. Methylene chloride was shaken with portions of concentrated H_2SO_4 until the acid layer remained colorless, then washed with water, aqueous 5% Na_2CO_3, then water again, predried with $CaCl_2$, and distilled over $CaSO_4$. Carbon tetrachloride was purified in a similar manner with prior refluxing for 2 h over mercury to remove sulfides. Freshly distilled solvent was used in each case.

2,4-Dinitrophenylselenium Trichloride, m.p. 75–83° dec. (lit. (1) m.p. 80–85° dec.) and *2,4-dinitrobenzeneselenenyl chloride*, m.p. 89–90° (lit. (1) m.p. 88–89°) were prepared by the method of Lawson and Kharasch (1).

2,4-Dinitrobenzeneselenenyl acetate was prepared by the method of Jenny (11, 14) and Behaghel (15) in 97% yield and recrystallized from pentane, m.p. 133°.

Anal. Calc. for $C_8H_6N_2O_4Se$: C, 31.49; H, 1.98; N, 9.18. Found: C, 31.25; H, 2.03; N, 8.89.

*erythro-dl-2-Chloro-1-phenylpropyl-1 2′,4′-Dinitrophenyl Selenide Dichloride (**4**)*

To a solution of 0.416 g (0.001 mol) 2,4-dinitrophenylselenium trichloride in 50 ml of anhydrous deoxygenated methylene chloride under nitrogen was added slowly 0.188 g (0.002 mol) *trans*-1-phenylpropene. The solution turned dark orange within 2 h. At this point the solution was warmed to ≃40° and the solvent evaporated to yield a yellow brown oil in 79% yield. Proton magnetic resonance analysis showed a 55:45 mixture of **4** and **3**. Attempts to isolate pure **4** by fractional crystallization, t.l.c., and g.l.c. failed either because of isomerization of **4** to **3** or decomposition to **6**.

*threo-dl-2-Chloro-1-phenylpropyl-1 2′,4′-Dinitrophenyl Selenide Dichloride (**2**)*

This compound was prepared in an analogous method to that of **4** above. A 60:40 mixture of **2** and **1** was obtained under kinetic control. There was evidence of isomerization of **2** to **1**; however, a thermodynamically controlled distribution was not obtained because of competitive decomposition.

*erythro-dl-1-Chloro-1-phenylpropyl-2 2′,4′-Dinitrophenyl Selenide (**8**)*

To a solution of 0.522 g (0.00186 mol) 2,4-dinitrobenzeneselenenyl chloride in 20 ml of methylene chloride was added slowly 0.221 g (0.00187 mol) of *trans*-1-phenylpropene. The entire reaction was carried out under nitrogen. The flask was stoppered and kept at room temperature in the dark for 1 week, at which point an apparent equilibrium was obtained at approximately 80% completion as determined by p.m.r. Attempts to increase the yield by warming the solution gave only starting material and decreased yields of product. Removal of the solvent under nitrogen gave a crude orange-red oil in 72% based on starting olefin, crystallized from CCl_4, m.p. 92°

Anal. Calcd. for $C_{15}H_{13}N_2O_4SeCl$: C, 45.08; H, 3.18; N, 7.01. Found: C, 45.45; H, 3.33; N, 7.11.

Mass spectrum M^+ *m/e* 400, mol. wt. calcd. 399.692.

*threo-dl-1-Chloro-1-phenylpropyl-2 2′,4′-Dinitrophenyl Selenide (**7**)*

This was prepared as for the *erythro* isomer above. An apparent equilibrium was established at ≃75% conversion to product as determined by p.m.r. Crystallized from CCl_4, yield 52%, m.p. 76°.

Anal. Calcd. for $C_{15}H_{18}N_2O_4SeCl$: C, 45.08; H, 3.28; N, 7.01. Found: C, 45.09; H, 3.34; N, 7.23.

*erythro-dl-1-Chloro-1-phenylpropyl-2 2′,4′-Dinitrophenyl Selenide Dichloride (**3**)*

To a solution of 0.799 g (0.002 mol) **8** in 25 ml CCl_4 was added 0.540 g (0.004 mol) of freshly distilled sulfuryl chloride. The reactants were kept for 3 h at room temperature under nitrogen, then the solvent and unreacted SO_2Cl_2 were pumped off, and the resultant crude yellow brown oil was crystallized from 1,2-dichloroethane, m.p. 110° dec.

Anal. Calcd. for $C_{15}H_{13}N_2O_4SeCl_3$: C, 38.24; H, 2.86; Cl, 22.15; N, 6.01. Found: C, 38.10; H, 2.86; Cl, 22.15; N, 6.01.

Note: this compound is thermally unstable and very readily hydrolyzed in the presence of moisture.

*threo-dl-1-Chloro-1-phenylpropyl-2 2′,4′-Dinitrophenyl Selenide Dichloride (**1**)*

This was prepared as above but using **7** instead of **8**. Crystallized from 1,2-dichloroethane, m.p. 137° dec. Decomposed before analysis could be performed, in three attempts.

*erythro-dl-1-Acetoxy-1-phenylpropyl-2 2′,4′-Dinitrophenyl Selenide (**10**)*

To a solution of 0.400 g (0.001 mol) **8** in 10 ml of anhydrous acetic acid was added 0.167 g (0.001 mol) silver acetate. The mixture was stirred for 1 h at room temperature, filtered under nitrogen to remove AgCl, and the solvent evaporated. Yield 98%; crystallized from 1,2-dichloroethane, m.p. 138°.

Alternatively 2,4-dinitrobenzeneselenenyl acetate 0.610 g (0.002 mol) was added to 0.222 g *trans*-1-phenylpropene in 25 ml methylene chloride under nitrogen at 25°. The solvent was removed by bubbling nitrogen through the solution after having let the solution stand for 2 days in the dark. A deep reddish orange oil was recovered, which recrystallized as above, m.p. 138°, yellow-orange crystals.

Anal. Calcd. for $C_{17}H_{16}N_2O_6Se$: C, 49.94; H, 3.95, N, 6.85. Found: C, 49.93; H, 3.75; N, 7.25.

*threo-dl-1-Acetoxy-1-phenylpropyl-2 2′,4′-Dinitrophenyl Selenide (**9**)*

This was prepared as for **10**. Yellow crystalline solid, m.p. 166°.

Found: C, 49.75; H, 4.00; N, 7.11.

*Decomposition of **1**, **2**, **3**, and **4***

Solutions of **1**, **2**, **3**, and **4** in CCl_4, CH_2Cl_2, or HOAc were found to be unstable, yielding 1,2-dichloro-1-phenylpropanes **5** and **6** (**6**, *erythro-dl* isomer p.m.r. δ(p.p.m.) CCl_4: 1.68, d(3H), 4.27, m(1H), 4.80, d(1H), 7.28, s(5H)); **5**, *threo-dl* isomer p.m.r.: 1.41, d(3H), 4.30, m(1H), 4.92, d(1H), 7.29, s(5H)) and 2,4-dinitrobenzeneselenenyl chloride, m.p. 88–89°. Repetitive runs showed no trace of either **6** upon decomposition of *threo-dl*-β-chloroalkyl selenide dichloride **1** and **2** or **5** upon decomposition of **3** or **4** as determined by p.m.r. and g.l.c. (1/4 in. × 13 ft 5% Carobwax on Chromosorb G).

TABLE 4. Percentage product distributions* from competition experiments as a function of solvent and olefin stucture

					% product distribution*	
$ArSeCl_3$	ArSeCl	*cis*-Olefin	*trans*-Olefin	Solvent	Se^{IV}	Se^{II}
1	1	0.4	—	CCl_4	100	0
1	1	—	0.4	CCl_4	100	0
1	10	0.4	—	CCl_4	100	0
1	10	—	0.4	CCl_4	100	0
1	1	0.4	—	CH_2Cl_2	95	5
1	1	—	0.4	CH_2Cl_2	90	10
1	10	0.4	—	CH_2Cl_2	46	54
1	10	—	0.4	CH_2Cl_2	33	66

*These distributions represent % composition as determined upon total consumption of olefin and as such may not represent absolute measurements of relative reactivity due to the reversible nature of the reactions involved.

*Reaction of **1** with Excess Chlorine*

To a solution of 0.941 g (0.002 mol) **1** in 30 ml of CCl_4 was bubbled predried chlorine gas for 30 min. A black insoluble material precipitated and was removed by filtration. The filtrate contained 1,2-dichloro-1-phenylpropenes and some soluble organoselenium compounds. Proton magnetic resonance and g.l.c. analysis of the dichlorophenylpropanes established a distribution of 65% *threo*- to 35% *erythro-dl*-1,2-dichloro-1-phenylpropane. Mass spectral analysis of the organoselenium compounds and comparison with spectra of authentic samples gave the mixture reported in the test. No attempt was made to determine the relative amounts of each component or to determine the composition of the insoluble material, believed to be mainly elemental selenium.

Competition experiments were carried out in a variety of solvents using different ratios of 2,4-dinitrophenylselenium trichloride, 2,4-dinitrobenzeneselenenyl chloride, and *cis*- and *trans*-1-phenylpropene. Product ratios of selenide dichloride to selenide are given in Table 4 for representative runs in carbon tetrachloride and methylene chloride solvents at 25°.

Continued financial support of the National Research Council of Canada is gratefully acknowledged. A University of Toronto Special Open Fellowship awarded to one of us (D.G.G.) is also very much appreciated.

1. D. LAWSON and N. KHARASCH. J. Org. Chem. **24**, 857 (1959).
2. M. DE MOURA CAMPUS and N. PETRAGNANI. (*a*) Tetrahedron, **18**, 521 (1962); (*b*) Tetrahedron Lett. **6**, 11 (1959).
3. R. F. RILEY, J. FLATO, and D. BENGELS. J. Org. Chem. **27**, 2652 (1962); H. BRINTZINGER, K. PFANNSTIEL, and H. VOGEL. Z. Anorg. Allgem. Chem. **256**, 75 (1948).
4. M. OGAWA and R. ISHIOKA. Nippon Kagalcukai Bull. **43**(2), 496 (1970).
5. R. C. FAHEY and C. SCHUBERT. J. Am. Chem. Soc. **87**, 5172 (1965).
6. G. H. SCHMID. Can. J. Chem. **46**, 3415 (1968).
7. H. J. REICH. J. Org. Chem. **39**, 428 (1974).
8. K. B. SHARPLESS and R. F. LAUER. J. Org. Chem. **39**, 429 (1974).
9. G. H. SCHMID, V. M. CSIZMADIA, V. J. NOWLAN, and D. G. GARRATT. Can. J. Chem. **50**, 2457 (1972).
10. G. F. LAUTENSCHLAGER. J. Org. Chem. **34**, 4002 (1969).
11. W. JENNY. Helv. Chim. Acta, **36**, 1278 (1953); W. JENNY. Helv. Chim. Acta, **41**, 593 (1958).
12. D. G. FOSTER. Rec. Trav. Chim. **53**, 405 (1934).
13. O. BEHAGHEL and K. HOFMANN. Ber. **72B**, 697 (1939).
14. W. JENNY. Helv. Chim. Acta, **35**, 1591 (1952).
15. O. BEHAGHEL and W. MÜLLER. Ber. **68**, 1540 (1935).
16. D. G. GARRATT, P.-T. CHENG, S. C. NYBURG, and G. H. SCHMID. Cryst. Struct. Commun. **3**, 361 (1974).

Can. J. Chem. Downloaded from www.nrcresearchpress.com by 210.87.254.42 on 09/05/12
For personal use only.

Preparation, Infrared Spectra, Electronic Spectra, and Magnetic Moments of Copper(II) Complexes of *N*-Acetylglycine and Their Amine Adducts

G. MARCOTRIGIANO
Cattedra di Chimica, Facoltà di Medicina-Veterinaria, Università di Bari, Italy
AND
G. C. PELLACANI
Istituto di Chimica Generale e Inorganica, Università di Modena, Italy

Received March 29, 1974

G. MARCOTRIGIANO and G. C. PELLACANI. Can. J. Chem. **52**, 3607 (1974).

Compounds of the type $[CuA_2 \cdot H_2O]_2$ and $[CuA_2 \cdot 4H_2O]_2$ have been prepared, where A is *N*-acetylglycine (aceturic acid). Amine adducts of the type CuA_2B (B = piperazine, 2,2′-bipyridine, and 1,10-phenantroline) and CuA_2B_2 (B = *N*-methylpiperazine, piperidine, morpholine, pyridine, and ethylenediamine) were obtained by reaction of the amines with $CuA_2 \cdot 4H_2O$. Each complex was characterized by elemental analysis, infrared spectrum, electronic spectrum, and magnetic moment. For the piperazine and ethylenediamine adducts a square-planar pattern of coordination about copper(II) ion is probable, while for the other amine adducts a square-pyramidal structure is proposed. For all the complexes the coordination of the *N*-acetylglycine occurs only through the terminal carboxyl oxygen in a monodentate arrangement.

G. MARCOTRIGIANO et G. C. PELLACANI. Can. J. Chem. **52**, 3607 (1974).

On a préparé les composés du type $[CuA_2 \cdot H_2O]_2$ et $[CuA_2 \cdot 4H_2O]_2$ dans lesquels A est égal à *N*-acétylglycine. Les produits d'addition avec les amines, du type CuA_2B (B = piperazine, bypyridine-2,2′ et phénantroline-1,10) et CuA_2B_2 (B = *N*-méthylpipérazine, pipéridine, morpholine, pyridine et éthylènediamine), sont obtenus par la réaction des amines avec $CuA_2 \cdot 4H_2O$. Chaque complexe est caractérisé par son analyse élémentaire, son spectre infrarouge, son spectre électronique et son moment magnétique. Pour les produits d'addition avec la pipérazine et l'éthylènediamine on croit que la coordination autour du cuivre(II) se fait suivant un plan carré alors que pour les autres composés d'addition avec les amines on propose une structure pyramidale à base carré. Pour les complexes de la *N*-acétylglycine, la coordination se fait uniquement par l'intermédiaire de l'oxygène du carboxyle terminal.
[Traduit par le journal]

Introduction

An amino acid like *N*-acetylglycine (aceturic acid) is of special interest in that in a simple environment it contains a peptide bond, which is the link that unites individual amino acids into proteins. While its crystal structure is well known (1, 2), its complexing ability toward the transition metal ions has not been extensively investigated, at least not as regards the preparation and study of the complexes in the solid state. Previous works treat the potentiometric study of complex compounds of zinc(II) in aqueous solution (3), the stability constant study for some 1:1 metal complexes in aqueous solution (4), and the catalase and peroxidase properties of copper(II) and cobalt(II) complexes in solution (5, 6).

In this work we have prepared and investigated by spectral and magnetic measurements the copper(II) complexes with *N*-acetylglycine (abbreviation A) and their adducts with nitrogen donor ligands such as aliphatic heterocyclic amines (piperazine (pz), *N*-methylpiperazine (CH_3-pz), piperidine (pd), and morpholine (mf)), aromatic heterocyclic amines (pyridine (py), 2,2′-bipyridine (bipy), and 1,10-phenantroline (phen)), and ethylenediamine (en). This work is an extension of our previous investigations into the adducts of the bis(β-keto-enolates) and bis(carboxylates)metal(II) (metal = Co, Ni, Cu) of aliphatic heterocyclic amines (7–10). The effect of these amines on the carboxylate (acetate and propionate) coordination leads to an asymmetrical bidentate coordination of carboxylates (10).

Can. J. Chem. Downloaded from www.nrcresearchpress.com by 210.87.254.40 on 09/05/12
For personal use only.

Can. J. Chem. Downloaded from www.nrcresearchpress.com by 210.87.254.40 on 09/05/12
For personal use only.

Experimental

Preparation of the Complexes

The reagents were of pure commercial grade.

$CuA_2 \cdot 4H_2O$: 2×10^{-2} *M* of solid $Cu(ClO_4)_2 \cdot 6H_2O$ were dissolved in a 4×10^{-2} *M* solution in methanol (120–150 ml) of *N*-acetylglycine neutralized with a 4×10^{-2} *M* solution of NaOH in H_2O (10 ml) + MeOH (30 ml). After concentration of the solution (until 40 ml) the blue solid compound was separated by cooling at 0 °C.

$CuA_2 \cdot H_2O$ (green) was obtained by recrystallization from absolute ethanol of $CuA_2 \cdot 4H_2O$.

$CuA_2 \cdot pz$ (violet) was obtained by mixing a methanolic solution (12 ml) of $CuA_2 \cdot 4H_2O$ (1 m*M*) with an excess of piperazine (4 m*M*) in ethanol (12 ml) and by cooling at 0 °C.

CuA_2B_2 (*B* = *CH_3-pz, pd*) (blue) were prepared by dissolving $CuA_2 \cdot 4H_2O$ (2 m*M*) in an excess of the amine (8–10 ml), adding ethanol until a limpid solution was obtained, and cooling at 0 °C.

$CuA_2(mf)_2$ (blue) was obtained by adding an excess of morpholine (5 m*M*) to an ethanolic solution (20 ml) of $CuA_2 \cdot 4H_2O$ (1 m*M*) and cooling at 0 °C.

$CuA_2(py)_2$ (blue) was obtained by adding an excess of pyridine (5 ml) to an ethanolic solution (10 ml) of $CuA_2 \cdot 4H_2O$ (1 m*M*), treating with ethyl ether, and cooling at 0 °C.

CuA_2B_2 (*B* = *phen, bipy*) (blue) were obtained by mixing a methanolic solution (10 ml) of $CuA_2 \cdot 4H_2O$ (1 m*M*) with a methanolic solution (5 ml) of the amine (1 m*M*), adding ethyl ether, and cooling at 0 °C.

$CuA_2(en)_2$ (violet) was obtained by mixing an ethanolic solution of $CuA_2 \cdot 4H_2O$ to an ethanolic solution containing an excess of en, adding ethyl ether, and cooling at 0 °C. The same compound was obtained with a 1:1 metal salt/amine molar ratio.

Analyses

Copper was determined by complexometric titration with EDTA (ethylenediaminetetraacetic acid), nitrogen by the Kjeldahl method, hydrogen and carbon by the standard combustion method.

Physical Measurements

Physical measurements were made as previously described (7). μ_{eff}, at room temperature, were calculated from the relationship $\mu_{eff} = 2.83 (\chi_M^C T)^{1/2}$, where χ_M^C is the molar susceptibility corrected by diamagnetic contribution using Pascal's constants (11).

Results and Discussion

The compounds prepared and their analyses are listed in Table 1. By reaction of $CuA_2 \cdot 4H_2O$ with bases the water molecules can be replaced to give compounds of the type CuA_2B (B = pz, phen, bipy) and CuA_2B_2 (B = CH_3–pz, pd, mf, py, en). Attempts to determine molecular weights of these adducts were frustrated by their low solubility in solvents such as benzene or nitrobenzene.

The room temperature magnetic moments are reported in Table 2. The rather low magnetic moment observed for $CuA_2 \cdot H_2O$ is evidence that its structure is unique among the complexes studied and this is the only stereochemical information available from these measurements. Comparisons with other works (12–15) suggest that $CuA_2 \cdot H_2O$ probably has a dimeric structure.

The more relevant i.r. bands are reported in Table 3. The formation of coordinate bonds in bis(*N*-acetylglycine)copper(II) adducts of the aliphatic heterocyclic amines is immediately apparent from the considerable shifts to lower frequencies (50–160 cm^{-1}) of $\nu(NH)^{(b)}$ that occur in the case of coordinated but not of uncoordinated amines. These shifts show that pz, CH_3-pz, pd, and mf are coordinated to the metal by means of the nitrogen atom of their NH group (8–10). In the mf adduct the shift of the C—O—C stretching vibration at 1115 cm^{-1} with respect to free mf (1095 cm^{-1}) excludes a possible oxygen-to-metal coordination (8–10, 16).

The assignment of all of the bands has not been made, but those of NH stretching, CO ketonic stretching, and antisymmetric and symmetric carboxy stretching frequencies in *N*-acetylglycine (17) and *N*-acetylglycinate are straightforward. Of primary concern for the coordination are the positions of the symmetric and antisymmetric carboxy stretching frequencies and their separation. These are listed in Table 3 for all complexes together with some data for sodium and potassium salts, assumed to typify ionic *N*-acetylglycinate spectra. As for the acetate (18, 19), it is noted that both the OCO stretching bands of *N*-acetylglycine are shifted in the same direction upon coordination. The separation (199–216 cm^{-1}) of the observed carboxy group frequencies of the complexes, which is very close to those of ionic *N*-acetylglycinate salts (195 cm^{-1} for KA and 200 cm^{-1} for NaA), could suggest that the coordination occurs through the terminal carboxyl oxygen in a monodentate or monodentate-bridging arrangement. It agrees with that observed in other carboxylate complexes (13, 19). The observed $\nu(NH)^{(a)}$ and $\nu(CO)^{(a)}$ bands of *N*-acetylglycine after coordination exclude the coordination of these groups with the copper ion. The variation of the $\nu(NH)^{(a)}$ values in the complexes in the range of 3250–3350 cm^{-1} may suggest that this group is involved in the hydrogen bonds.

In view of the relative insolubility, low magnetism, i.r. spectrum, with the $\nu_{as}(OCO)$ at 1625

TABLE 1. Analytical results

	Analysis (%)							
	Cu		C		H		N	
Compound*	Calcd.	Found	Calcd.	Found	Calcd.	Found	Calcd.	Found
$CuA_2 \cdot H_2O$	20.26	19.95	30.61	31.18	4.50	4.83	8.93	9.17
$CuA_2 \cdot 4H_2O$	17.28	17.20	26.11	26.53	5.48	6.18	7.62	7.65
$CuA_2 \cdot pz$	16.64	16.25	37.72	37.62	5.81	6.61	14.68	14.74
$CuA_2(CH_3\text{-}pz)_2$	12.81	12.69	43.56	43.59	7.32	7.35	16.95	16.76
$CuA_2(pd)_2$	13.64	13.48	46.37	46.21	7.36	7.62	12.03	11.91
$CuA_2(mf)_2$	13.52	14.16	40.87	41.40	6.44	6.75	11.93	11.74
$CuA_2(py)_2$	14.00	13.98	47.60	47.88	4.89	5.16		
$CuA_2(en)_2$	15.20	15.39	34.63	35.29	6.79	6.85	20.21	20.48
$CuA_2 \cdot bipy$	14.93	14.80	45.10	45.96	4.26	4.82		
$CuA_2 \cdot phen$	13.36	13.00	50.45	50.99	4.24	4.72		

*A, *N*-acetylglycine; pz, piperazine; CH_3-pz, *N*-methylpiperazine; pd, piperidine; mf, morpholine; py, pyridine; en, ethylenediamine; bipy, 2,2′-bipyridine; phen, 1,10-phenantroline.

TABLE 2. Electronic spectra (nm) and magnetic moments (B.M.)

Compound	State	μ_{eff}*	λ (nm)†	
$CuA_2 \cdot H_2O$	Solid	1.42	720	370sh
$CuA_2 \cdot 4H_2O$	Solid	1.95	780sh 620	
$CuA_2 \cdot pz$	Solid	1.95	655sh 515	
$CuA_2(CH_3\text{-}pz)_2$	Solid	1.81	665	
	In chloroform		685(63)	
$CuA_2(pd)_2$	Solid	1.96	730sh 625	
	In chloroform		670(75)	415sh
$CuA_2(mf)_2$	Solid	1.94	750sh 635	
	In chloroform		670(34)	
$CuA_2(py)_2$	Solid	1.90	730sh 625	
	In methanol + py		650(70)	
$CuA_2(en)_2$	Solid	1.85	540	
	In methanol		570(71)	
$CuA_2 \cdot bipy$	Solid	1.85	750sh 635	390sh
	In chloroform		670(63)	
$CuA_2 \cdot phen$	Solid	1.99	680	
	In chloroform		670(56)	

*At room temperature.
†ε values in parenthesis; sh = shoulder.

cm^{-1} (higher than compounds with other types of *N*-acetylglycinate ions), indicating bidentate bridging carboxyl groups, as found in similar situations, despite the Δν value of 210 cm^{-1} (18, 19), and electronic spectrum (Table 2) of the $CuA_2 \cdot H_2O$ complex, it seems likely that this complex has a dimeric structure like $[Cu(acetate)_2 \cdot H_2O]_2$ (12) and other similar compounds (12, 13).

The solid $CuA_2 \cdot 4H_2O$ complex exhibits normal paramagnetic behavior and has an electronic spectrum similar to that observed for copper(II) hippurate dimer (20), which is consistent with a distorted square-pyramidal field and a coordination sphere of five bonded oxygen atoms (20). A monodentate coordination of *N*-acetylglycine in this compound agrees with this proposed structure, like that found for $[Cu(hippurate)_2 \cdot 4H_2O]_2$ (20, 21).

In the pz complex a linear polymeric chain with piperazine "bridging" two copper ions may be suggested by its insolubility, by the presence of one $(NH)^{(b)}$ stretching vibration and by the similarity of its i.r. spectrum with that of $CdCl_2 \cdot pz$, containing long-chain piperazine molecules in the chair configuration "bridging" metal-ions (22).

The electronic spectra of the amine adducts in the solid state (Table 2) are consistent with either a square-planar, or severely tetragonally dis-

Can. J. Chem. Downloaded from www.nrcresearchpress.com by 210.87.254.40 on 09/05/12
For personal use only.

TABLE 3. More important infrared bands (cm^{-1})*

Compound	ν(NH)[a]	ν(NH)[b]	ν(CO)[a]	$\nu(OCO)_{as}$	$\nu(OCO)_s$	Δν
HA	3352vs		1590vsb	1720vs	1350s	
NaA	3320m		1630sb	1600vsb	1400vs	200
	3260sh					
KA	3308vs		1640s	1600vs	1405s	195
$CuA_2 \cdot H_2O$	3350vs		1640sh	1625vsb	1415vs	210
$CuA_2 \cdot 4H_2O$	3310vs		1613vsb	1614vsb	1397ms	216
$CuA_2 \cdot pz$	3355s	3170s	1658vs	1611vs	1402vs	209
$CuA_2(CH_3\text{-}pz)_2$	3290mb	3290mb	1671vs	1609vs	1394vs	205
$CuA_2(pd)_2$	3347s	3247s	1650vs	1608vs	1383vs	215
		3163s				
$CuA_2(mf)_2$	3347s	3245s	1650vs	1608vs	1385vs	213
		3152s				
$CuA_2(py)_2$	3250vs		1625vsb	1605sh	1406vs	199
$CuA_2(en)_2$	3295s	3162m	1650s	(1560vsb)	1388vs	
	3265s	3120m				
$CuA_2 \cdot bipy$	3300sb		1635vsb	1608s	1396vs	212
$CuA_2 \cdot phen$	3275sb		1630vsb	1590sh	1388s	202

*Vibrations of acetyl group (a) and of aliphatic heterocyclic amines (b); v = very, s = strong, b = broad, m = medium, sh = shoulder.

torted octahedral structure, or with a distorted square-pyramidal structure, like $[CuA_2 \cdot 4H_2O]_2$. A square-planar or square-pyramidal structure agree with a monodentate or monodentate-bridging coordination of the carboxyl group of the *N*-acetylglycine and with the invariably bidentate nature of phen and bipy. In fact, a six-coordinate structure containing one phen or one bipy molecule and two carboxylate molecules around a metal ion, has necessarily a *cis*-structure. Such a *cis*-structure with *cis*-(CuO_4N_2) chromophores has an electronic spectrum characterized by two distinct bands at 1100–1000 and 755–700 nm (23). While in the case of pz and en adducts, the electronic spectra may suggest an essentially square-planar structure, for the other amine adducts the electronic spectra, very similar to those of $[CuA_2 \cdot 4H_2O]_2$, may indicate a square-pyramidal structure.

The "red-shift" of the principal band of the electronic spectra in chloroform solution, which are identical with one another, indicates a diminished tetragonal distortion about the copper ion (10, 24), arising from coordination of solvent molecules on axial positions of a square-planar complex, in fact, the energy of d_{z^2} is most sensitive to the degree of tetragonality of the ligand field (24), or could also arise from other courses such as dissociation of amine ligands.

Conclusions

Although the *N*-acetylglycinate anion possesses four potential coordination sites, the coordination seems to occur only through the terminal carboxyl oxygen in a monodentate arrangement. This was not foreseen since bidentate coordination through the carboxyl oxygens may be suggested (25) by the pK_A value of *N*-acetylglycine (pK_A = 3.60 (26), 3.632 (27), or 3.9 (in 20% dioxane) (28)) and bidentate coordination through the nitrogen and terminal carboxyl oxygen would have led to a five-membered chelate ring as has been found in similar situations (29, 30). The experimental results could suggest that the carboxylates, in the adducts of the aliphatic heterocyclic amines, do not give an asymmetrically bidentate coordination, as previously found for the copper(II) acetate and propionate adducts (10), therefore the mono or bidentate carboxylate coordination depends only on the nature of the carboxylic acids.

Only in the $(CuA_2 \cdot H_2O)_2$ complex does the *N*-acetylglycine act as bidentate ligand bridging two metal ions.

1. G. B. KARPENTER and J. DONOHUE. J. Am. Chem. Soc. **72**, 2315 (1950).
2. J. DONOHUE and R. E. MARSH. Acta Cryst. **15**, 941 (1962).
3. F. KARCZYNSKI. Zesz. Nauk. Mat. Fiz. Chem. Wyzsza Szk. Pedagog. Gdansku, Wydz. Mat. Fiz. Chem. **7**, 149 (1967).
4. J. W. BUNTING and K. M. THONG. Can. J. Chem. **48**, 1654 (1970).
5. A. YA. SICHEV and BUI NGOK THO. Zh. Fiz. Khim. **43**, 503, 1173 (1969); Zh. Fiz. Khim. **44**, 93 (1970); Izv. Vyssh. Ucheb. Zaved. Khim. Tekhnol. **13**, 1054 (1970).

Can. J. Chem. Downloaded from www.nrcresearchpress.com by 210.87.254.40 on 09/05/12
For personal use only.

6. A. YA. SICHEV, BUI NGOK THO, and S. F. NEDOPEKINA. Kinet. Katal. **13**, 308 (1972).
7. G. MARCOTRIGIANO, R. BATTISTUZZI, and G. C. PELLACANI. Can. J. Chem. **50**, 2557 (1972).
8. G. C. PELLACANI, R. BATTISTUZZI, and G. MARCOTRIGIANO. J. Inorg. Nucl. Chem. **35**, 2243 (1973).
9. G. MARCOTRIGIANO and G. C. PELLACANI. Inorg. Nucl. Chem. Lett. **9**, 957 (1973).
10. G. MARCOTRIGIANO, G. C. PELLACANI, and C. PRETI. Z. Anorg. Allgem. Chem. In press.
11. B. N. FIGGIS and J. LEWIS. Technique of inorganic chemistry: magnetochemistry. Vol. IV. John Wiley, New York. 1965. p. 142.
12. M. KATO, H. B. JONASSEN, and J. C. FANNING. Chem. Rev. **64**, 99 (1964).
13. J. R. WASSON, CHIN-I-SHYR, and C. TRAPP. Inorg. Chem. **7**, 469 (1968) and references cited therein.
14. S. F. A. KETTLE and A. J. P. PIOLI. J. Chem. Soc. 1243 (1968).
15. R. W. JOTHAM and S. F. A. KETTLE. J. Chem. Soc. 2821 (1969).
16. I. S. AHUJA and A. GARG. Inorg. Nucl. Chem. Lett. **7**, 937 (1971).
17. F. MICHEEL and B. SCHLEPPINGHOFF. Chem. Ber. **88**, 763 (1955).
18. K. NAKAMOTO, Y. MORIMOTO, and A. E. MARTELL. J. Am. Chem. Soc. **83**, 4528 (1961).
19. N. F. CURTIS. J. Chem. Soc. 1579 (1968).
20. J. N. BROWN, H. R. EICHELBERGER, E. SCHAEFFER, M. L. GOOD, and L. M. TREFONAS. J. Am. Chem. Soc. **93**, 6290 (1971) and references cited therein.
21. J. N. BROWN and L. M. TREFONAS. Inorg. Chem. **12**, 1730 (1973).
22. P. J. HENDRA and D. B. POWELL. J. Chem. Soc. 350, 5105 (1960); Spectrochim. Acta. **18**, 229 (1962).
23. D. ATTANASIO, I. COLLAMATI, C. ERCOLANI, and G. ROTILIO. J. Chem. Soc. 2242 (1973).
24. L. L. FUNCK and T. R. ORTOLANO. Inorg. Chem. **7**, 567 (1968).
25. B. HAMMOND, F. H. JARDINE, and A. G. VOHRA. J. Inorg. Nucl. Chem. **33**, 1017 (1971).
26. M. ZIEF and J. T. EDSALL. J. Am. Chem. Soc. **59**, 2245 (1937).
27. A. NEUBERGER. Proc. R. Soc. Lond. A**158**, 68 (1937).
28. YU. I. KHURGIN and I. V. VIKHA. Izv. Akad. Nauk. SSSR, Ser. Khim. **6**, 1245 (1968).
29. C. M. WEEKS, A. COOPER, and D. A. NORTON. Acta Cryst. B, **25**, 443 (1969).
30. T. UEKI, T. ASHIDA, Y. SASADA, and M. KAKUDO. Acta Cryst. B, **24**, 1361 (1968).

Can. J. Chem. Downloaded from www.nrcresearchpress.com by 210.87.254.40 on 09/05/12
For personal use only.

On the Hydrogen Bond Breaking Ability of Fluorocarbons Containing Higher Halogens

THÉRÈSE DI PAOLO AND C. SANDORFY

Département de Chimie, Université de Montréal, Montréal, Québec

Received May 24, 1974

THÉRÈSE DI PAOLO and C. SANDORFY. Can. J. Chem. **52**, 3612 (1974).

Infrared measurements show that fluorocarbons containing higher halogens are able to open O—H---O, N—H---N, S—H---S, N—H---O=C type hydrogen bonds. This is probably due to a competitive mechanism of association consisting in the formation of donor–acceptor complexes. It is suggested that the breaking or perturbation of hydrogen bonds by this mechanism is of importance for the explanation of the anesthetic activity of these compounds.

THERÉSÈ DI PAOLO et C. SANDORFY. Can. J. Chem. **52**, 3612 (1974).

Une importante propriété des fluorocarbures contenant des halogènes supérieurs peut être mise en évidence par des mesures de spectres infrarouges: ils peuvent rompre des liaisons hydrogène de type O—H---O, N—H---N, S—H---S, N—H---O=C, en solution. Cela est probablement lié à la formation de complexes donneur–accepteur qui entre en compétition avec celle des liaisons hydrogène. Nos observations portent à croire que la rupture ou la perturbation de liaisons hydrogène peut constituer une étape importante dans le mécanisme de l'anesthésie causée par ces molécules.

Can. J. Chem. Downloaded from www.nrcresearchpress.com by 210.87.254.105 on 09/05/12
For personal use only.

Introduction

It has been reported, in a previous note from this laboratory (1), that 1,2-dibromotetrafluoroethane (CF_2Br–CF_2Br, also known as fluorocarbon or Freon 114-B-2) when used as a solvent component for secondary aliphatic amines acts as a hydrogen bond breaking agent. In our first experiments the solvent was a 1:1 mixture of CCl_3F and CF_2Br–CF_2Br (henceforth abbreviated as FR) and the hydrogen bonds were of the N—H---N type formed by the self-association of the amine molecules (2). The solvent FR can be used down to liquid nitrogen temperature where it forms a glass. It has been observed that as temperature was lowered (and contrary to expectation), the intensity of the free (unassociated) i.r. N—H stretching band increased while the intensity of the N—H stretching band of the hydrogen bonded N—H group decreased and disappeared completely at -190 °C (*cf.* Fig. 1 in ref. 1). This striking phenomenon is due to CF_2Br–CF_2Br: when instead of FR a 1:1 mixture of CCl_3F and methylcyclohexane (FM) was used we observed the normal increase of the associated band and decrease of the free band when temperature was lowered.

It has been also observed that in the case of aromatic amines (3, 4) and alcohols (1, 5) the presence of CF_2Br–CF_2Br lowered the degree of self-association.

The breaking of the hydrogen bonds of the N—H---N or O—H---O types was interpreted in terms of a competition between hydrogen bond and donor–acceptor complex formation. (Hydrogen bonding is not considered as a case of donor–acceptor complex formation in this paper.)

In view of the very important role played by hydrogen bonds in living organisms it was decided to start a detailed investigation of this phenomenon. The hypothesis underlying this investigation is that association by hydrogen bonding and association by donor–acceptor complex formation constitute two competitive mechanisms which the living organism might use for opening and closing hydrogen bonds.

Some of the fluorocarbons are widely used as anesthetics and have a variety of biological activity. This makes it natural to ask if there could be a relation between their anesthetic potency and their hydrogen bond breaking ability.

In the work presented here we first studied the hydrogen bond breaking properties of the following bromofluorocarbons: perfluoro-*n*-propylbromide (n-C_3F_7Br); 1,2-dibromotetrafluoroethane (CF_2Br–CF_2Br); dibromodifluoromethane (CF_2Br_2); 1-bromo-2-chloro-1,2-trifluoroethane (CF_2Br–$CFClH$)(H′); 1,1,1-trifluoro-2-chloro-2-bromoethane (CF_3–$CClBrH$)(H). H is a widely used anesthetic under the name of halothane or fluothane.

We then added to this series the following

Can. J. Chem. Downloaded from www.nrcresearchpress.com by 210.87.254.105 on 09/05/12
For personal use only.

fluorocarbons having chlorine or iodine as the highest halogen: 1,1-dichloro-2,2,2-trifluoroethane (CCl_2H–CF_3); trichlorofluoromethane (CCl_3F); perfluoro-*n*-propyliodide (n-C_3F_7I); perfluoroisopropyliodide (i-C_3F_7I); 1-iodo-2-bromotetrafluoroethane (ClF_2–$CBrF_2$); 1-iodo-2,2,2-trifluoroethane (ClH_2–CF_3); 1-iodo-2-chloro-1,2,2-trifluoroethane ($ClFH$–$CClF_2$).

The effect of these fluorocarbons was studied on the following hydrogen bonded systems: self-associated diethylamine, pyrrole, indole, 2,2,4-trimethyl-3-pentanol, *tert*-butanol, 2,6-diisopropylphenol, *n*-propylthiol, *N*-methylpivalamide (N22 trimethylpropionamide), *N*-ethylacetamide, *N*-methylbenzamide, acetanilide, δ-valerolactam. These systems contain weak or moderately strong hydrogen bonds ($\Delta H \sim 2$–6 kcal/mol).

The amines, alcohols, phenols, amides, and thiols were dissolved in mixtures of one of the above mentioned fluorocarbons and of CCl_3F or methylcyclohexane at concentrations depending on experimental conditions and the i.r. spectra were measured at temperatures ranging from 22 to −190 °C. The evolution of the pattern of associations was followed as a function of temperature. The role of low temperatures in these experiments has been to magnify the changes observed in the spectra by facilitating complex formation so that we can study them better. To a lesser degree these changes exist also at room temperature as is shown below in a few examples.

Experimental

The spectra were measured on a Perkin–Elmer model 621 spectrometer. The low temperature cells we used were described in previous publications from this laboratory (2, 6).

Our samples of diethylamine and δ-valerolactam were 'Baker-analyzed' products, indole 'Fisher-certified'; our samples of pyrrole, 2,2,4-trimethyl-3-pentanol, 2,6-diisopropylphenol, and *n*-propylthiol were highly purified products of the Aldrich Chemical Company and the amides were Eastman Reagent Chemicals. They were further purified by distillation or recrystallization and were dried and stored over calcium sulfate or molecular sieves and kept in a dry box under nitrogen atmosphere. The i.r. spectra were checked against previously published ones and were found to be identical.

The fluorocarbons were high purity samples supplied by the E.I. Du Pont de Nemours Company with the exception of (^1H) and the iodides which came from the PCR, Inc., Gainesville, Florida. Methylcyclohexane and methylcyclopentane came from the Phillips Petroleum Company. They were distilled and stored over P_2O_5 in a dry box. The preparation of the solutions and the filling of the cells was also carried out in a dry box. The cell lengths varied from 0.24 to 0.46 mm. The concentrations refer to the total volume of each solution and the i.r. spectra are given in molar extinction coefficients ($\varepsilon = 1/cl \log I_0/I$) against wave numbers. They were corrected for changes in density with temperature. The concentrations used for the calculation of the ε's are the overall concentrations and not those of given associated species. Also, because of environmental changes due to changes in temperature the ε's have temperature dependence even in cases of no specific association. For these reasons our molar extinction coefficients (absorptivities) should be considered as apparent and approximate; they are convenient for comparing spectra taken at different initial concentrations but are not to be used to obtain quantitative relationships.

Results

N—H---N Type Hydrogen Bonds in Aliphatic Secondary Amines

Figure 1 shows the results of a concentration study on a 0.6 *M* solution of diethylamine carried out at −190 °C. In a 1:1 mixture of CCl_3F and methylcyclohexane (FM), that is with no bromine in the solvents, we find a weak free NH band at 3308 cm^{-1} and a much stronger associated band at 3214 cm^{-1} (curve *G*). If we add 0.08 *M* of n-C_3F_7Br to the solution the associated band becomes broader and undergoes a shift to lower frequencies. The band is obviously a com-

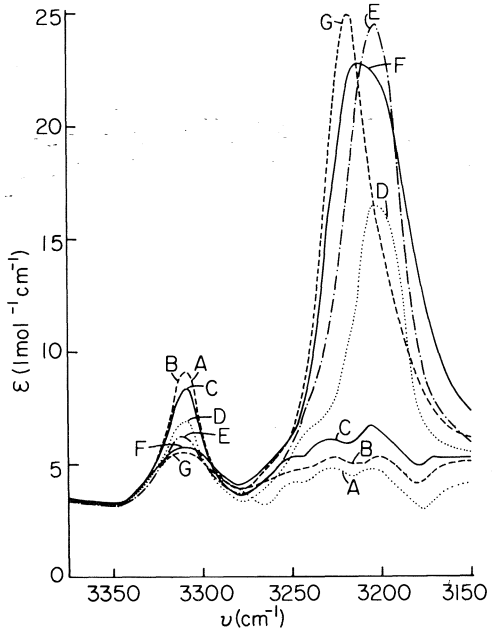

FIG. 1. The i.r. spectra of a 0.6 *M* solution of diethylamine in a 1:1 mixture of CCl_3F and methylcyclohexane (FM) at −190 °C in the presence of variable amounts of n-C_3F_7Br: *A*, 1.04 *M*; *B*, 0.87 *M*; *C*, 0.62 *M*; *D*, 0.42 *M*; *E*, 0.32 *M*; *F*, 0.08 *M*; *G*, 0.

plex band. When we increase the proportion of n-C_3F_7Br to about 0.32 M the peak appears at 3202 cm^{-1} (curve E). It is clear from the comparison of these three curves that the first result of the perturbation by n-C_3F_7Br is the formation of a weak aggregate to which the peak of curve E is related and that curve F contains comparable amounts of both the bromine-unperturbed species and this aggregate. The latter is likely to be the dimer containing the N—H---N type hydrogen bond with an additional solvent perturbation by the bromine containing molecule —Br:N—H---:N—H. The formation of N—H---Br type hydrogen bonds is considered unlikely since the corresponding N—H band would be expected to have a higher frequency (perhaps 3250–3270 cm^{-1}) but this possibility is not entirely ruled out. At higher n-C_3F_7Br concentrations (curves D, C, B, and A) the intensity of this band decreases rapidly and when n-C_3F_7Br and diethylamine are at about the same concentration only weak associated bands remain and at the same time the free NH band increased in intensity and became the only prominent NH band in the spectrum. It is seen that the aggregate which was the first result of the perturbation was destroyed at higher n-C_3F_7Br concentrations and that the new complex is not a hydrogen bonded adduct and that it is essentially a 1:1 complex. A charge transfer from the N lone pair to n-C_3F_7Br is naturally suspected (*cf.* ref. 1).

Similar low temperature concentration studies have been carried out with CF_2Br–CF_2Br and CF_2Br_2. The observations are essentially the same: we again see evidence for the formation of a weak initial aggregate followed by the breaking of hydrogen bonds. These molecules are somewhat more potent hydrogen bond breaking agents as it appears from the concentrations needed to bring about the same relative decrease in the intensity of the associated N—H band. Its virtual disappearance is again obtained when the concentrations of the amine and of the fluorocarbon are the same so that the final complex must be again 1:1 despite the presence of two bromine atoms in the fluorocarbon.

While so far we have described the results of fluorocarbon concentration studies at a given temperature (−190 °C) and a given amine concentration (about 0.6 M), Fig. 2 shows the temperature dependence of the spectra at a given amine (0.6 M) and a similar CF_2Br–CF_2Br concentration. This cannot be done at room temperature as the bands are too weak and too diffuse, therefore, the curves we show are those taken between −80 and −190 °C. The gradual disappearance of the associated N—H---N band as temperature decreases (and conditions for complex formation become more favorable) is easily followed. The shoulders at about 3250 cm^{-1} are likely to be due to the remaining hydrogen bonded species. The main observation is that more and more hydrogen bonds are broken as temperature decreases, as shown by the increasing strength of the free NH band near 3310 cm^{-1}. n-C_3F_7Br and CF_2Br_2 gave similar results.

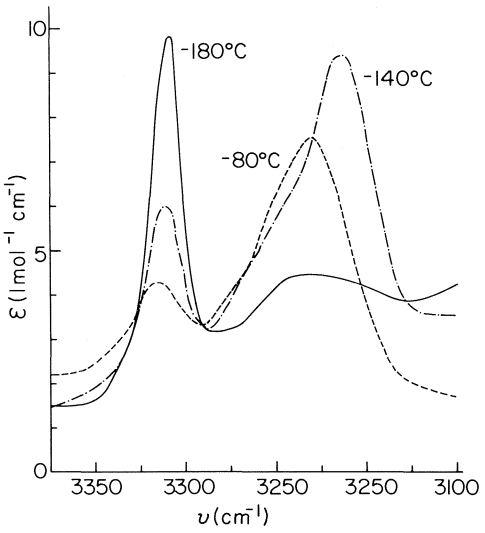

FIG. 2. The i.r. spectra of a 0.60 M solution of diethylamine in a 1:1 mixture of CCl_3F and methylcyclohexane in the presence of 0.66 M CF_2Br–CF_2Br at different temperatures.

We compared the spectra of aliphatic secondary amines taken in purely hydrocarbon solvents and in CCl_3F. Although we have encountered solubility problems we could observe that the degree of N—H---N association was slightly lower in CCl_3F. Fluorocarbons containing hydrogen like CCl_2H–CF_3 or CBrClH–CF_3 reacted with the solute giving a precipitate.

Self-associated Pyrrole

The above results demonstrate the generality of the hydrogen bond breaking ability of bromine containing fluorocarbons. As a next step we shall inquire if this phenomenon still exists with stronger N—H---N type hydrogen bonds. We examined the case of indole and pyrrole.

Can. J. Chem. Downloaded from www.nrcresearchpress.com by 210.87.254.105 on 09/05/12
For personal use only.

Can. J. Chem. Downloaded from www.nrcresearchpress.com by 210.87.254.105 on 09/05/12
For personal use only.

Bernard-Houplain and Sandorfy (4) found that when temperature decreased the intensity of the associated band increased gradually but much more slowly in the presence of CF_2Br–CF_2Br than in the absence of it. This means that in the case of these stronger hydrogen bonds the effect of the bromine containing fluorocarbon consists in retarding association but a higher proportion of the hydrogen bonds remains unbroken than for diethylamine under similar conditions.

We have now studied these conditions more systematically. Pyrrole in FM, *i.e.* in the absence of bromine atoms, behaves regularly: with decreasing temperature the free band gradually disappears and the much stronger associated band increases in intensity. At 0.124 *M* the free band has practically disappeared at −100 °C (4). In FR, even at higher dilution (0.03 *M*) the free band is still fairly strong at −140 °C. If instead of FR we use a 1:1 mixture of methylcyclohexane and C_3F_7Br or CF_2Br_2 the results are similar. Figure 3 shows the spectrum of pyrrole in a 1:1 mixture of CCl_3F and halothane. It is a more effective hydrogen bond breaker than CF_2Br–CF_2Br or the other fluorocarbons mentioned above. The intensity of the free band decreases and the intensity of the associated band increases with decreasing temperature but the free band is quite intense even at −180 °C. The same experiments were carried out with compound H′ with essentially the same results as for halothane (H).

The frequencies of both the 'free' and associated bands vary somewhat with temperature. This is probably due to additional solvent effects on both the hydrogen bonded and donor–acceptor complexes, the latter having an NH frequency close to that of the free NH band.

As stated above the purpose of taking the spectra at low temperature is magnification: making conditions more favorable to association. However, the effects develop gradually and, to a lower degree, they are also present at room temperatures. Pyrrole constitutes a typical example of this. Figure 4 shows its spectrum in pure CCl_3F and in pure halothane at room temperature. The associated band is much weaker in halothane.

Figure 5 gives the spectra of 0.08 *M* pyrrole in FM solution with 1 *M* CCl_2H–CF_3 added. The effect is comparable to that of halothane at similar concentrations.

n-C_3F_7I is an even stronger inhibitor to hydrogen bond formation. We studied its effect at a series of temperatures. Figure 6 shows the spectra taken at −140 °C (0.12 *M* pyrrole in FM with (*a*) 0.13 *M*, (*b*) 0.24 *M*, (*c*) 0.41 *M* *n*-C_3F_7I). These iodide concentrations are lower than were the bromide concentrations in the figures shown above. Even so, the associated band at 3375 cm^{-1} undergoes a greater decrease in intensity. The situation is more complicated, however. The 'free' band is present near its usual frequency (3485 cm^{-1}) but a new band appears near 3450 cm^{-1}. We cannot identify the species to which this band is due. It could be a dimer while the 3375 cm^{-1} band is a higher oligomer. It is possible, too, that the latter corresponds to the dimer while the 3450 cm^{-1} band is due to an

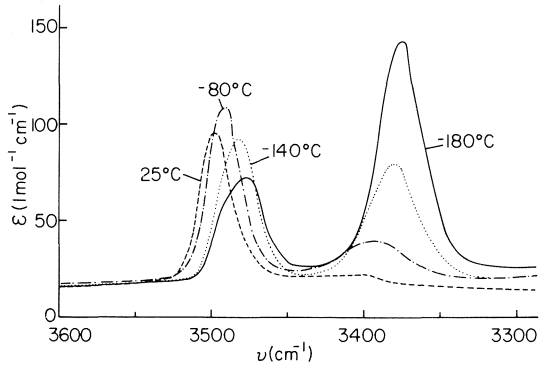

FIG. 3. The i.r. spectra of a 0.18 *M* solution of pyrrole in a 1:1 mixture of CCl_3F and halothane at different temperatures.

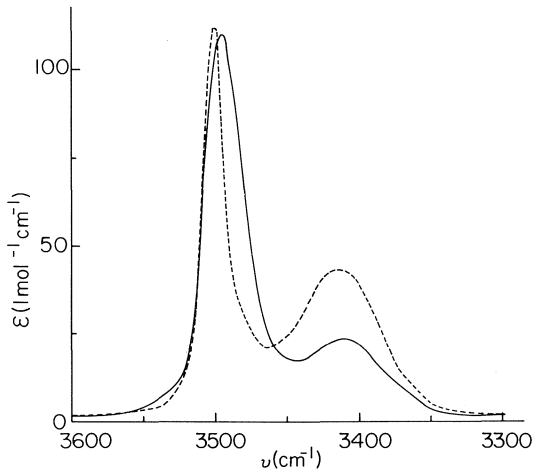

FIG. 4. Comparison of the room temperature spectra of a 0.54 *M* solution of pyrrole in CCl_3F (---) and a 0.57 *M* solution of pyrrole in halothane (—).

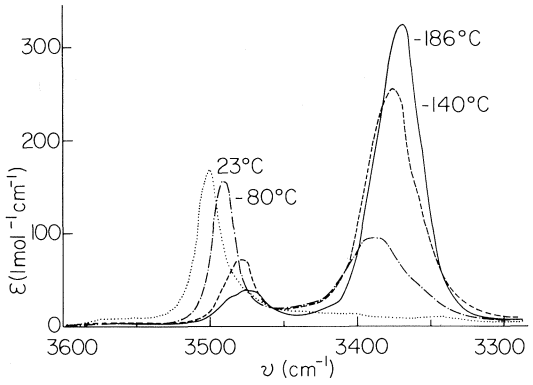

FIG. 5. The i.r. spectra of a 0.08 *M* solution of pyrrole in a 1:1 mixture of CCl_3F and methylcyclohexane in the presence of 1.0 *M* CCl_2H–CF_3 at different temperatures.

N—H---I type hydrogen bond or to a strong pyrrole–iodide complex. Obviously, the iodides exert a stronger perturbation than the bromides. For our present purposes it is sufficient to note their strong hydrogen bond breaking power as observed on the 'associated band' at 3375 cm^{-1}.

Indole behaves in a way similar to pyrrole.

O—H---O Type Hydrogen Bonds

The low temperature spectra of sterically hindered alcohols were studied by Bourdéron *et al.* (5). We measured the spectra of some of these in FM, in FR, and in halothane under similar conditions. 2,2,4-Trimethyl-3-pentanol at an initial concentration of about 0.1 *M* has its free band disappear at −100 °C in FM (Fig. 7). In CF_2Br–CF_2Br containing FR it disappears more slowly (at about −120 °C). The same is true for CF_2Br_2. In the presence of H it is still well pronounced at −140 °C and seen as a weak band at −190 °C (Fig. 8). At the same time the intensity of the associated band increases but much more slowly than in FM. At −80 °C in H the associated band near 3400 cm^{-1} is still very weak (probably oligomers only) and it is only at lower temperatures that the typical 'polymer' band near 3350 cm^{-1} develops. The results remain essentially the same if instead of H we use H′. Thus, the behavior of this sterically hindered alcohol is similar to that of pyrrole, the main effect being a hindering of association. The effect is somewhat less pronounced than in pyrrole and this is in keeping with the greater energy of the

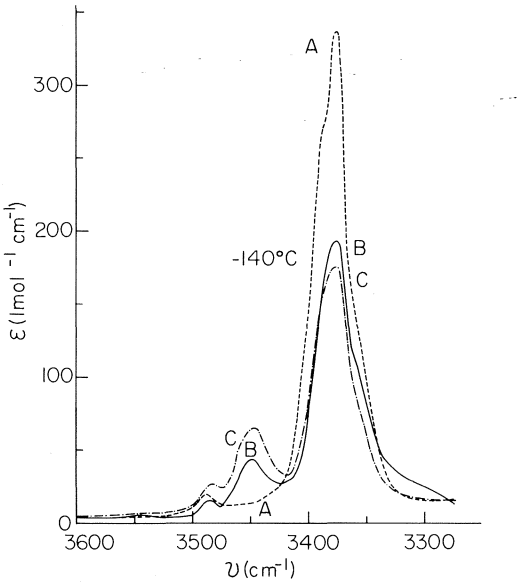

FIG. 6. The i.r. spectra of a 0.12 *M* solution of pyrrole in a 1:1 mixture of CCl_3F and methylcyclohexane at −140 °C in the presence of variable amounts of *n*-C_3F_7I: A, 0.13 *M*; B, 0.24 *M*; C, 0.41 *M*.

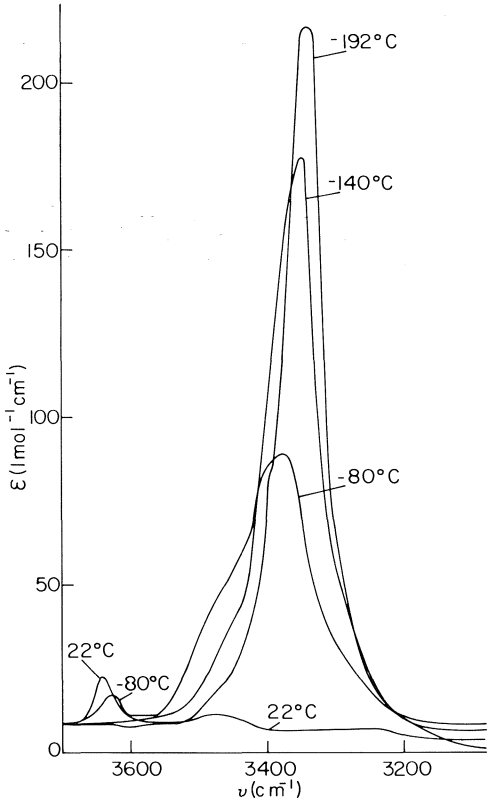

FIG. 7. The i.r. spectra of a 0.094 *M* solution of 2,2,4-trimethyl-3-pentanol in a 1:1 mixture of CCl_3F and methylcyclohexane at different temperatures.

Can. J. Chem. Downloaded from www.nrcresearchpress.com by 210.87.254.105 on 09/05/12
For personal use only.

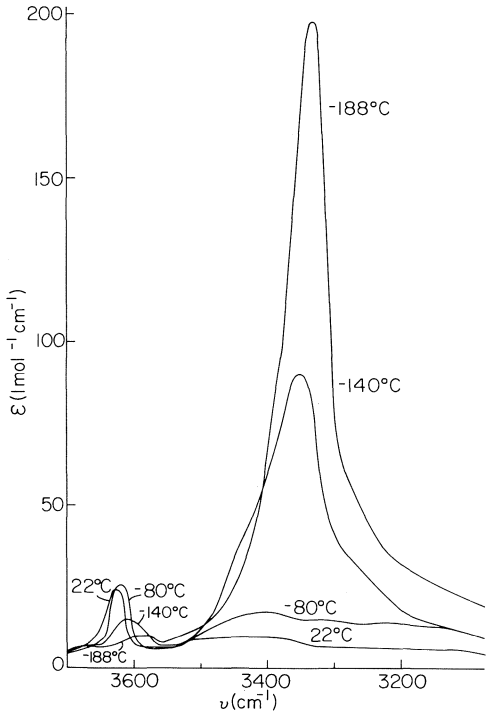

FIG. 8. The i.r. spectra of a 0.087 *M* solution of 2,2,4-trimethyl-3-pentanol in a 1:1 mixture of CCl_3F and halothane at different temperatures.

hydrogen bond in the case of the alcohol. The slight changes in frequency of both the free and associated bands with temperature show that just as in the case of amines we have, in addition to the hydrogen bond – charge transfer competition, some weaker solvent effects influencing the frequencies. The shoulder at 3450–3400 cm^{-1} seen in the low temperature spectra is probably due to O—H---O oligomers; O—H---Br is unlikely since this shoulder appears in FM also.

CCl_2H-CF_3 has an effect similar to the bromides. This also applies to *n*-C_3F_7I but the same effects are obtained with lower concentrations.

In the case of *tert*-butanol (*cf.* ref. 6) we can make essentially the same observations but the effect is less pronounced.

2,6-Diisopropylphenol (DIPP) was subjected to more detailed investigation. It has been shown previously (1, 5) that whereas in FM this molecule gives only strong associated bands at −190 °C, in FR at the same temperature an oligomer band is the most intense and is located near 3500 cm^{-1}. At −120 °C the free band is still present and it is more intense than in FM (1). The same is observed with *n*-C_3F_7Br.

We made a concentration study at −184 and at −140 °C (Fig. 9) but using CF_2Br_2 instead of CF_2Br–CF_2Br. The results are similar. However, the three curves shown in Fig. 9 represent solutions in FM, in FM containing 1.1 *M* of CF_2Br_2, and a 1:1 mixture of CF_2Br_2 and methylcyclohexane, respectively, so that the last solvent does not contain CCl_3F. The 3500 cm^{-1} oligomer band is seen even in FM but it becomes much more intense when CF_2Br_2 is added to the solution showing that many hydrogen bonded polymers were transformed into oligomers.

Figure 10 compares the spectrum of DIPP taken in FM and in the presence of H. The strong hydrogen bond breaking ability of halothane is demonstrated strikingly by these curves. At −140 °C in FM we see a huge polymer band and a weaker oligomer band. In H the polymer absorption decreases dramatically, the oligomer band is better seen and a quite strong free band appears above 3600 cm^{-1}. When temperature further decreases to −186 °C the oligomer band becomes the strongest but the free band is still well pronounced. The results are very similar with H′ except that H is slightly more effective in disassociating DIPP.

Figure 11 shows the spectrum of DIPP at

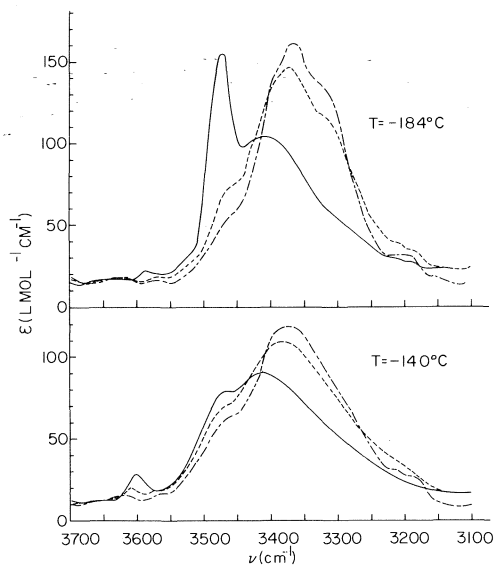

FIG. 9. The i.r. spectra of 0.1 *M* 2,6-diisopropylphenol at −184 and −140 °C in solutions of a 1:1 mixture of CF_2Br_2 and methylcyclohexane (—); a 1:1 mixture of CCl_3F and methylcyclohexane containing 1.1 *M* CF_2Br_2 (---); and a 1:1 mixture of CCl_3F and methylcyclohexane (-·-·-).

Can. J. Chem. Downloaded from www.nrcresearchpress.com by 210.87.254.105 on 09/05/12
For personal use only.

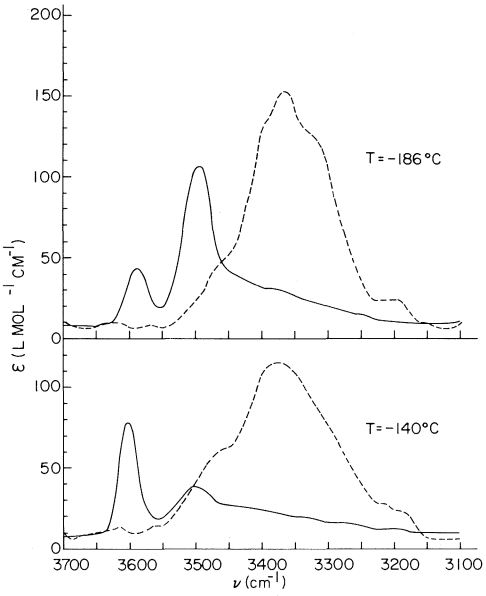

FIG. 10. The i.r. spectra of 0.13 *M* 2,6-diisopropylphenol in a 1:1 mixture of CCl_3F and halothane (—) and in a 1:1 mixture of CCl_3F and methylcyclohexane (---) at −186 and −140 °C.

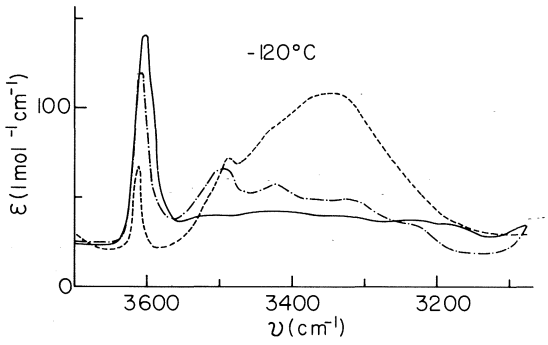

FIG. 11. The i.r. spectra of 0.05 *M* 2,6-diisopropylphenol at −120 °C in a 1:1 mixture of CCl_3F and methylcyclohexane (---), in a 1:1 mixture of CCl_3F and methylcyclohexane containing 1.1 *M* CCl_2H–CF_3 (-·-·-) and in a 1:1 mixture of CCl_3F and CCl_2H–CF_3 (—).

−120 °C in FM, in FM with 1.0 *M* CCl_2H–CF_3 and in a 1:1 mixture of CCl_3F and CCl_2H–CF_3. In FM the intense and broad 'polymer' band dominates the spectrum. Upon addition of CCl_2H–CF_3 this band is considerably weaker and in the 1:1 mixture it disappeared completely. An oligomer band appears at about 3480 cm^{-1} and increases in intensity with the CCl_2H–CF_3 concentration. At lower temperatures (Fig. 12) this appears even more clearly. At these

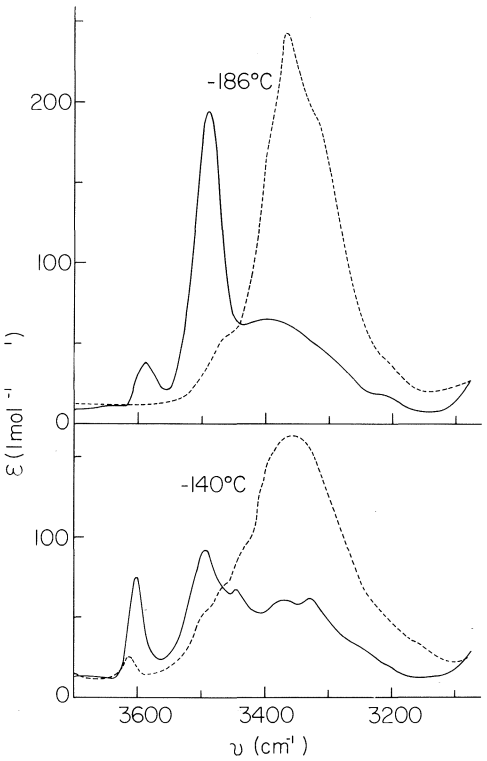

FIG. 12. The i.r. spectra of 0.054 *M* 2,6-diisopropylphenol at −140 and −186 °C in solutions of a 1:1 mixture of CCl_3F and methylcyclohexane containing 1.1 *M* CCl_2H–CF_3 (—) and a 1:1 mixture of CCl_3F and methylcyclohexane (---).

temperatures the change is essentially from polymer to oligomer and it is spectacular. The free band is also present, however.

With normal and iso-C_3F_7I we observe the same effect but at lower (0.5 *M*) iodide concentration. The destruction of hydrogen bonds seems to halt at the oligomer level and in spite of the stronger hydrogen bond breaking ability of the iodides the free band has disappeared at −190 °C while it is present for the bromides. It is possible that the oligomer band receives an important part of its intensity from a strong DIPP–iodide complex.

S—H---S Type Hydrogen Bonds

We studied only one system of this kind, self-associated *n*-propylthiol. Figure 13 shows the spectra of a 1.0 *M* solution in FM and in FR. The hydrogen bond breaking ability of the bromine containing solvent is clearly demonstrated. The free band (near 2580 cm^{-1}) appears at low temperatures in FR and the associated

Can. J. Chem. Downloaded from www.nrcresearchpress.com by 210.87.254.105 on 09/05/12
For personal use only.

band (near 2525 cm^{-1}) is considerably weakened with respect to its strength in FM.

These systems were studied (in FR) in a detailed manner in this laboratory by Bicca de Alencastro and Sandorfy (7). For obtaining the spectra given in Fig. 13 fully deuterated methylcyclohexane had to be used instead of methylcyclohexane, because of its strong absorption in the 2500–2600 cm^{-1} region.

We did not study this system with other fluorocarbons.

N—H---O=C Type Hydrogen Bonds

These are hydrogen bonds of utmost importance for the living organism. Some amides were studied previously (8) in solutions containing CF_2Br–CF_2Br. Figure 14 compares the spectra of a 0.048 *M* solution of *N*-methylpivalamide (N22 trimethylpropionamide) in a 1:1 mixture of CCl_3F and CF_3–CHClBr (halothane) and in a 1:1 mixture of CCl_3F and methylcyclohexane. The effect is already evident at room temperature: in the halothane containing solvent the associated band near 3400 cm^{-1} which is due to the N—H---O=C hydrogen bond is much weaker and the free band at 3490 cm^{-1} is much stronger than in the other solvent. At −80 °C the effect takes spectacular proportions: in FM the free band has almost disappeared and the associated band is very intense whereas in (CCl_3F + halothane) the free band is prominent and the associated band is weak. The effect of halothane is stronger than that of CF_2Br–CF_2Br (8).

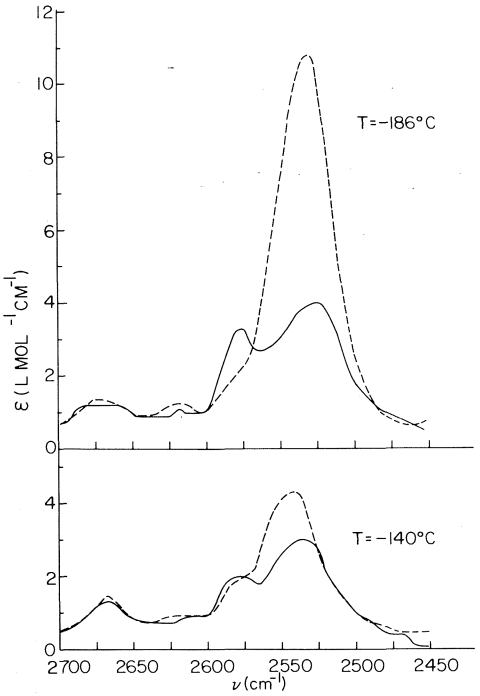

FIG. 13. The i.r. spectra of 1.1 *M* of propylthiol in a 1:1 mixture of CCl_3F and CF_2Br–CF_2Br (—) and in a 1:1 mixture of CCl_3F and methylcyclohexane-d_{14} (---) at −186 and −140 °C.

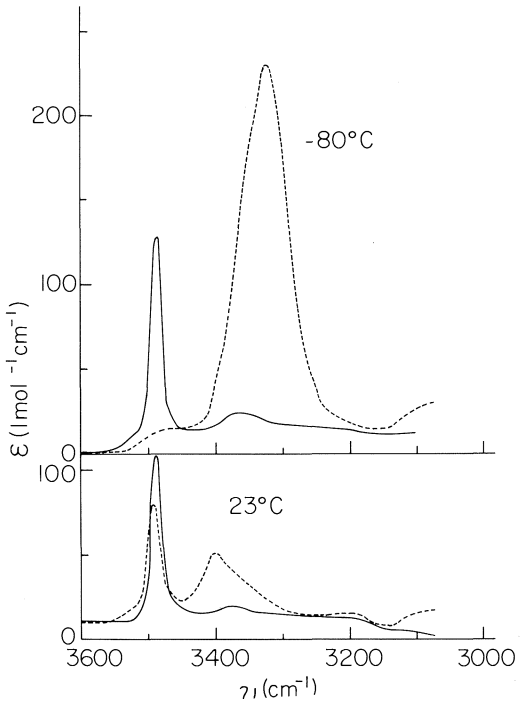

FIG. 14. The i.r. spectra of a 0.048 *M* solution of *N*-methylpivalamide at 23 and −80 °C in a 1:1 mixture of CCl_3F and CF_3–CClBrH (—) and in a 1:1 mixture of CCl_3F and methylcyclohexane (---).

Figure 15 gives the spectrum of *N*-methylpivalamide (0.045 *M* in FM) at room temperature and at −80 °C in the presence of 1.0 *M* CCl_2HCF_3. At room temperature the free species is already clearly favored and at low temperature the associated band is much weaker and the free band is much stronger. With *n*-C_3F_7I we obtain a quite similar picture with 0.2 *M* of iodide.

Thus it is seen that the N—H---O=C bond of the amides is affected by fluorocarbons in much the same way as amines and alcohols. *N*-methylacetamide (8), *N*-ethylacetamide (8), *N*-methylbenzamide, and acetanilide gave essentially similar results. For the aromatic amides low

Can. J. Chem. Downloaded from www.nrcresearchpress.com by 210.87.254.105 on 09/05/12
For personal use only.

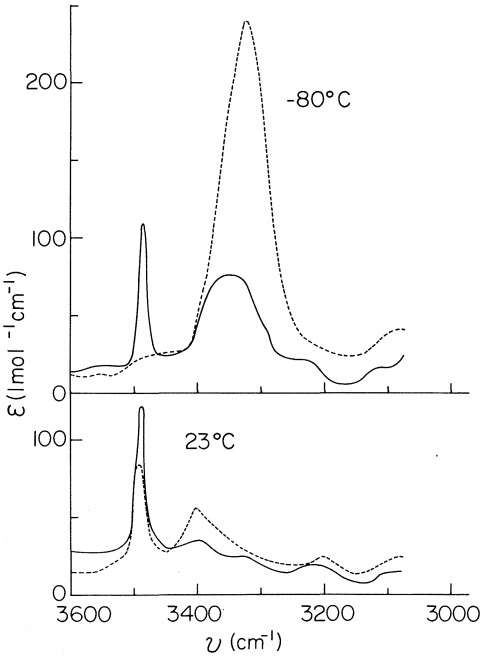

FIG. 15. The i.r. spectra of a 0.045 *M* solution of *N*-methylpivalamide at 23 and −80 °C in a 1:1 mixture of CCl_3F and methylcyclohexane (---) and in the same solvent with 1.0 *M* CF_3–$CHCl_2$ added (—).

solubility prevented us from doing a complete study.

δ-Valerolactam's spectrum at room temperature is given in Fig. 16. In FM the solubility was not sufficient but the comparison of the spectra taken in (CCl_3F + halothane) and in FR (dashed curve) shows that again the relative intensity of the free band is greater with halothane as has been observed in all other cases.

Discussion

Real and apparent spectral intensities depend on a number of factors and this is even more true when we are dealing with cases of molecular association. It seems to us, therefore, that any attempt to establish a quantitative relationship between observed spectral intensities and hydrogen bond breaking potency would be unwarranted at this stage. It is quite possible, however, by prospection of the spectra and allowing for the concentrations of both the hydrogen bonding molecule and the fluorocarbon, to make qualitative comparisons for one given system at a given temperature in order to obtain a loose relationship. The following general trends are clearly discerned: (*i*) Perfluorinated molecules have no

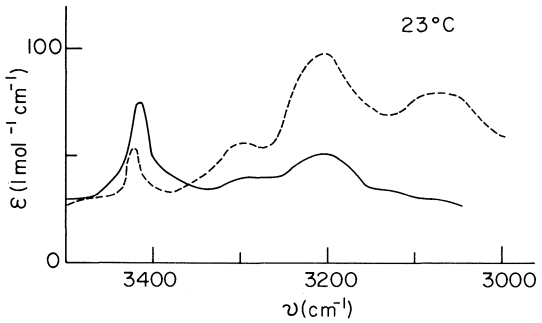

FIG. 16. The i.r. spectra of a 0.05 *M* solution of δ-valerolactam at 23 °C in a 1:1 mixture of CCl_3F and CF_3–$CClBrH$ (—) and in a 1:1 mixture of CCl_3F and CF_2Br–CF_2Br.

hydrogen bond breaking potency; (*ii*) fluorocarbons containing only chlorine in addition to carbon and fluorine have only a weak effect; (*iii*) Br and I containing fluorocarbons are strong hydrogen bond breakers and the order of potency is Cl < Br < I; (*iv*) chlorine containing fluorocarbons become strong hydrogen bond breakers if they contain a hydrogen atom. For example, whereas CF_3–CCl_3 has only a slight potency, CF_3–$CHCl_2$ is a strong hydrogen bond breaker. Bromine containing fluorocarbons also become stronger hydrogen bond breakers if they contain a hydrogen atom.

Now, it is very significant that an obvious parallelism exists between the hydrogen bond breaking ability and the anesthetic potency of fluorocarbons. To substantiate this contention we can cite the works of Krantz and Rudo (9), Larsen (10), and Clayton (11) on the relative anesthetic potency of fluorocarbons. Summarizing their extensive studies involving a very great number of fluorocarbons Krantz and Rudo stated that "Halogenation of hydrocarbons and ethers increases potency in the following order: F < Cl < Br < I"; "One or more hydrogen atoms in the molecule are necessary for effective central nervous system depression"; "Complete hydrogen substitution by fluorine usually produces a physiologically inert compound." Similar conclusions can be drawn from the data of Larsen and Clayton.

All this is in excellent qualitative agreement with our results on the hydrogen bond breaking potency of fluorocarbons. We found no hydrogen bond breaking action with perfluoro compounds and only a weak one with compounds containing only fluorine and chlorine. As stated

Can. J. Chem. Downloaded from www.nrcresearchpress.com by 210.87.254.105 on 09/05/12
For personal use only.

Can. J. Chem. Downloaded from www.nrcresearchpress.com by 210.87.254.105 on 09/05/12
For personal use only.

above, the presence of a hydrogen atom increases the hydrogen bond breaking potency of fluoro- and chlorocarbons greatly. CF_3–$CHCl_2$, for example, is almost as good a hydrogen bond breaker as halothane. The order F < Cl < Br < I was clearly established. There is thus a *striking parallelism* between the anesthetic potency and hydrogen bond breaking ability of fluorocarbon inhalation anesthetics.

We should like to add some speculation on the possible nature of the complex which provides the competitive mechanism of association leading to the breaking of hydrogen bonds. Since the enthalpies of formation of the hydrogen bonds which are involved are of the order of 2–6 kcal/mol, donor–acceptor complexes seem to be eligible. The lowest ionization potentials of amines (12, 13), alcohols (14, 15), amides (16), and thiols (13) are in the 8–10 eV range whereas those of the fluorocarbons are in the 11–13 eV range (17, 18). Thus we should expect the amines, alcohols, etc. to be the electron donors and the fluorocarbons the electron acceptors. Exceptions might occur for some iodides which have ionization potentials between 10 and 11 eV but we did not examine this case in detail. The complexes then might be of the charge transfer type with the nonbonding N, O, S, lone pairs as electron donors and the lowest excited orbitals of the fluorocarbons as acceptors. The latter are thought to be antibonding in the C—Cl or C—Br bonds (17, 19). The related u.v. transitions are of the $(C—Cl)^* \leftarrow \overline{Cl}$ or $(C—Br)^* \leftarrow \overline{Br}$ type departing from an essentially halogen lone pair orbital and have high excitation energies, about 6 eV for the bromides. They usually follow the trend in the lowest ionization potentials. Some numerical values for these i.p.'s are collected in Table 1.

It is interesting to remark in this respect that the lowest i.p.'s of these fluorocarbons, which are always related to an essentially halogen lone pair orbital, follow the same trend as the hydrogen bond breaking potency *and* anesthetic potency. Only molecules with the same number of (nonfluorine) identical halogens should be compared since in the presence of more than one the interaction of their lone pair atomic orbitals creates several molecular orbitals built of lone pair atomic orbitals.

Fluorocarbon anesthetics are known to act without undergoing chemical reactions in the organism. Therefore a mechanism involving complex and hydrogen bond formation or breaking seems to be well adapted to the explanation of their action. The hydrogen bonds which are involved might be protein to water, water to water, the N—H---O=C or N—H---N=C type bonds keeping the helices of the proteins or nucleic acids together, etc. All the hydrogen bonds discussed in this paper are of types frequently occurring in the organism. It is significant in this respect that certain fluorocarbons are known to interfere with cell division (20). Complex formation and the breaking of hydrogen bonds might alter the conformation of basic biological molecules necessary to the proper function of the organism. These considerations are in line with recent ideas of Eyring *et al.* (21) and Ueda and Kamaya (22) which are based on thermodynamic principles. The often emphasized lipid solubility of fluorocarbons (23, 24) appears to be a necessary condition for their action and it is in no way contradictory to the suggestions contained in this paper. It is, of course, not meant that *all* inhalation anesthetics exert their action through the same mechanism. Not all of them are fluorocarbons. We are planning to develop these biological implications in a forthcoming publication.

In conclusion, fluorocarbons containing higher halogens can break hydrogen bonds of the N—H---N, O—H---O, S—H---S, N—H---O=C and probably other types. The order of increasing hydrogen bond breaking potency is F < Cl <

TABLE 1. The lowest vertical ionization potential (in eV) of some fluorocarbons determined by photoelectron spectroscopy using a Perkin–Elmer PS-16 instrument

Compound	Lowest Cl, Br, or I lone pair i.p. (eV)	Reference No.
CF_3Cl	13.0	17
C_2F_5Cl	13.0	18
CF_3Br	12.0	17
C_2F_5Br	12.0	25
n-C_3F_7Br	12.0	25
CF_3I	10.8	27
C_2F_5I	10.7	27
n-C_3F_7I	10.6	27
CF_2HCl	12.6	
CF_2BrCl	11.8	26
CF_2Br–$CFClH$	11.7	25
CF_3–CClBrH (halothane)	11.2	16
CF_2Cl_2	12.3	17
CF_2Br_2	11.2	26
$CFHCl_2$	12.0	17
CF_2Br–CF_2Br	11.4	25

Br < I for fluorocarbons containing no hydrogen. The presence of hydrogens in the chloro- or bromofluorocarbons increases this potency a great deal. This phenomenon is probably due to competitive donor–acceptor complex formation. There is a striking parallelism between the hydrogen bond breaking and anesthetic potencies of fluorocarbons. Therefore we are putting forward the idea that donor–acceptor complex formation together with a breaking or perturbing of hydrogen bonds is an important step in the mechanism of the anesthetic action of fluorocarbons.

We thank the National Research Council of Canada for financial support and for a postgraduate scholarship to one of us (T.D.P.). This work has been supported by the E.I. Du Pont de Nemours Company of Wilmington, Delaware to whom we express our sincere thanks. Our special thanks are due to Dr. R. L. McCarthy and Dr. C. S. Hoffman who helped us in every possible manner.

1. M.-C. Bernard-Houplain, C. Bourdéron, J.-J. Péron, and C. Sandorfy. Chem. Phys. Lett. **11**, 149 (1971).
2. M.-C. Bernard-Houplain and C. Sandorfy. J. Chem. Phys. **56**, 3412 (1972).
3. M.-C. Bernard-Houplain, G. Bélanger, and C. Sandorfy. J. Chem. Phys. **57**, 530 (1972).
4. M.-C. Bernard-Houplain and C. Sandorfy. Can. J. Chem. **51**, 1075 (1973).
5. C. Bourdéron, J.-J. Péron, and C. Sandorfy. J. Phys. Chem. **76**, 864 (1972).
6. M. Asselin and C. Sandorfy. J. Mol. Struct. **8**, 145 (1971).
7. R. Bicca de Alencastro and C. Sandorfy. Can. J. Chem. **50**, 3594 (1972).
8. M.-C. Bernard-Houplain and C. Sandorfy. Can. J. Chem. **51**, 3640 (1973).
9. J. C. Krantz and F. G. Rudo. *In* Handbook of experimental pharmacology. Vol. XX/I. Springer, Berlin. 1966. pp. 520–522.
10. E. R. Larsen. Fluorine Chem. Rev. **3**, 1 (1969).
11. J. W. Clayton. Fluorine Chem. Rev. **1**, 197 (1967).
12. K. Watanabe, T. Nakayama, and J. Mottl. J. Quant. Spectrosc. Radiat. Transfer, **2**, 369 (1962).
13. A. D. Baker and D. Betteridge. Photoelectron spectroscopy. Pergamon Press, Oxford. 1972.
14. M. B. Robin and N. A. Kuebler. J. Electron spectrosc. **1**, 13 (1972/73).
15. A. D. Baker, D. P. May, and D. W. Turner. J. Chem. Soc. B, **22**, (1968).
16. D. W. Turner, C. Baker, A. D. Baker, and C. R. Brundle. Molecular photoelectron spectroscopy. Wiley-Interscience, London. 1970.
17. J. Doucet, P. Sauvageau, and C. Sandorfy. J. Chem. Phys. **58**, 3708 (1973).
18. J. Doucet, P. Sauvageau, and C. Sandorfy. J. Chem Phys. In press.
19. C. R. Zobel and A. B. F. Duncan. J. Am. Chem. Soc. **77**, 2611 (1955).
20. J. F. Nunn, J. D. Lovis, and K. L. Kimball. Brit. J. Anaesth. **43**, 524 (1971).
21. H. Eyring, J. W. Woodbury, and J. S. D'Arrigo. Anesthesiology, **38**, 415 (1973).
22. I. Ueda and H. Kamaya. Anesthesiology, **38**, 425 (1973).
23. P. Seeman. Pharmacol. Rev. **24**, 589 (1972).
24. H. Meyer and H. Hemmi. Biochem. Z. **277**, 39 (1935).
25. R. Routhier, P. Sauvageau, and C. Sandorfy. J. Chem. Phys. In press.
26. J. Doucet, R. Gilbert, P. Sauvageau, and C. Sandorfy. To be published.
27. R. A. Boschi and D. R. Salahub. Mol. Phys. In press.

Can. J. Chem. Downloaded from www.nrcresearchpress.com by 210.87.254.105 on 09/05/12
For personal use only.

A New Chlorinated Cyclopentenone Produced by a *Cryptosporiopsis* Species

GEORGE M. STRUNZ, PAVLE I. KAZINOTI, AND MERLYN A. STILLWELL

Canadian Forestry Service, P.O. Box 4000, Fredericton, New Brunswick E3B 5G4

Received March 13, 1974

GEORGE M. STRUNZ, PAVLE I. KAZINOTI, and MERLYN A. STILLWELL. Can. J. Chem. **52**, 3623 (1974).

A new metabolite, isolated from cultures of a *Cryptosporiopsis* sp., is shown to be (1*R*,5*S*)-2-cyclopentene-1-carboxylic acid, 2-*trans*-allyl-3-chloro-1,5-dihydroxy-4-oxo methyl ester.

GEORGE M. STRUNZ, PAVLE I. KAZINOTI et MERLYN A. STILLWELL. Can. J. Chem. **52**, 3623 (1974).

Un nouveau métabolite, isolé des cultures d'une espèce inconnue de *Cryptosporiopsis*, s'avéra l'acide (1*R*,5*S*)-2-cyclopentène-1-carboxylique, ester méthylique 2-*trans*-allyle-3-chloro-1, 5-dihydroxy-4-oxo.

Can. J. Chem. Downloaded from www.nrcresearchpress.com by 210.87.254.5 on 09/05/12
For personal use only.

Chlorine-containing cyclopentenones **1**–**3**, apparently of polyketide origin, have been isolated from fermentations of *Sporormia affinis* Sacc., Bomm and Rouss (1). In independent studies the compound **1**, designated cryptosporiopsin (2), was reported as a metabolic product of *Cryptosporiopsis* sp. (2) and *Periconia macrospinosa* (3). The diol **4** was also isolated from the latter source (3). In addition, *S. affinis* and *P. macrospinosa* give rise to a series of biogenetically related dihydroisocoumarins containing chlorine (3, 4).

We report here on a new metabolite, **5**, isolated together with crytosporiopsin from recent fermentations of a *Cryptosporiopsis* sp.

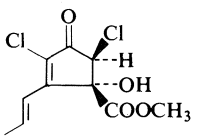

1

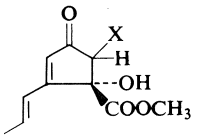

2 X = β-Cl
3 X = α-Cl

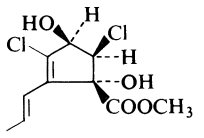

4

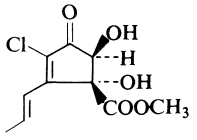

5

The new compound, $C_{10}H_{11}O_5Cl$, displayed spectroscopic characteristics (see Experimental) which demonstrated clearly its structural relationship with cryptosporiopsin (1, 2). The u.v. and n.m.r. spectra were particularly revealing in this respect. The latter shows, besides the characteristic signals indicative of methyl ester and *trans*-allyl protons, a broadened singlet at δ 4.63 attributable to the C-5 hydrogen (δ 4.57 in cryptosporiopsin), and broad absorption at *ca.* δ 4.2–5.0, corresponding to two hydroxyl protons. The presence of two hydroxyl groups, one secondary and the other tertiary, was confirmed by the n.m.r. spectrum of the diacetate (see Experimental).

The structure **5** (C-5 stereochemistry not included) was corroborated by the isolation of cryptosporiopsin (**1**) (1*S*,5*S*) among the products resulting from treatment of the metabolite with methane sulfonyl chloride (mesyl chloride) in pyridine. The similarity of the c.d. and o.r.d. curves of the new metabolite with those of cryptosporiopsin (Table 1), *cf.* ref. 1, suggests that the configuration of the former at C-5 is *S* as in **5**.

The "unexpected" configuration at C-5 in the mesyl chloride reaction product, cryptosporiopsin (**1**), may be rationalized in several ways and is not incompatible with the stereochemistry assigned to **5**. The possibility that a displacement product with *R* configuration at C-5 could undergo epimerization at this centre under the reaction conditions employed, was demonstrated by the observation that the C-5 hydrogen in cryptosporiopsin underwent deuterium exchange on treatment with methanol-d_1 in pyridine-d_5. Furthermore, since epimerization at C-5 was not observed on pyridine treatment of cryptosporiopsin, it can be concluded that the C-5 chlorine atom is in the more stable configuration in this compound or that protonation

TABLE 1. Circular dichroism and optical rotatory dispersion data for metabolite **5** and cryptosporiopsin

Circular dichroism λ (nm) (θ × 10^{-3})		Optical rotatory dispersion λ (nm) (φ × 10^{-3})	
Metabolite **5***	Cryptosporiopsin†	Metabolite **5***	Cryptosporiopsin†
410 (0)	395 (0)		
337 (+8.10)	332 (+10.2)	366 (+5.55)	360 (+3.77)
304 (+2.77)	303 (+0.38)	313 (−3.41)	310 (−9.05)
278 (+12.4)	277 (+8.30)	295 (0)	286 (−3.77)
253 (0)	254 (0)	247 (−17.5)	245 (−15.5)
226 (−20.5)	228 (−19.8)	216 (+3.41)	216 (+4.52)

*Metabolite 5 : 1.172 × 10^{-2} *M* in MeOH; 0.1 mm cell.
†Cryptosporiopsin : 1.326 × 10^{-2} *M* in MeOH; 0.1 mm cell.

of the enolate or enol from the α side is strongly favored. The metabolite **5** was also recovered unchanged after pyridine treatment.

In contrast with cryptosporiopsin (5), metabolite **5** was devoid of antifungal activity against selected test organisms (disc assay, 100 μg/disc). In the same bioassays 5-dechlorocryptosporiopsin was also inactive.

Experimental

Melting points were determined on a hot-stage apparatus and are uncorrected. Infrared spectra were recorded on a Beckman IR-10 spectrophotometer. Ultraviolet spectra were obtained using either a Beckman DK-2A or Perkin-Elmer 402 spectrophotometer. Nuclear magnetic resonance spectra were recorded with a Varian T-60 instrument employing tetramethylsilane as internal standard. Mass spectra were obtained with an Hitachi Perkin-Elmer RMU-6D mass spectrometer. The instrument used for o.r.d. and c.d. measurements was a Durrum Jasco model ORD/UV-5 optical rotatory dispersion recorder with SS-20-2 modification (Sproul Scientific). Microanalysis was performed by Spang Microanalytical Laboratory, Ann Arbor, Michigan.

Production and Isolation of **5**

Material extracted with chloroform from filtered culture medium[1] that had supported growth of *Cryptosporiopsis* sp. (liquid shake culture, temperature *ca.* 22°) for 12–14 days, was chromatographed on a column of Kieselgel (100–200 mesh, Gebr. Herrmann, Köln). Cryptosporiopsin was eluted with benzene–chloroform (3:2) and metabolite **5** was obtained from the chloroform eluates. The latter was further purified by crystallizations from benzene–cyclohexane to give crystals, m.p. 126–134°; for c.d. and o.r.d. data see Table 1; i.r. (KBr) *inter alia* 3360 (br), 1737, 1710, 1632, 1562, 978, 785, and 762 cm^{-1}; i.r. (CCl_4) 3500 (br), 1737, and 1649 cm^{-1}; u.v. λ_{max} (EtOH) 288 nm (ε 17 700); n.m.r. ($CDCl_3$; 60 MHz) δ 1.98 (3H, d, $J \sim 6$ Hz), 3.82 (3H, s), 4.63 (1H, s), 4.2–5.0 (2H, m) (exchangeable with D_2O), 6.33–7.22 (2H, AB part of ABX_3, J_{AB} 16–17 Hz); mass spectrum, *m/e* 246 (M^+), ($M^+ + 2$) 35%, 228 $(M - H_2O)^{\ddagger}$, and 187 (base peak) $(M - COOCH_3)^+$.

Anal. Calcd. for $C_{10}H_{11}O_5Cl$: C, 48.69; H, 4.50; Cl, 14.38. Found: C, 48.64; H, 4.60; Cl, 14.26.

Diacetate of **5**

A solution of **5** (40 mg) in acetic anhydride (2.5 ml) was stirred with zinc chloride (10 mg) in a nitrogen atmosphere at 0° for 3.5 h. The yellow oily product obtained on work-up was purified by preparative-layer chromatography on silica gel plates yielding the diacetate as an almost colorless oil which resisted crystallization attempts; i.r. (CCl_4) 1762, 1748, and 1638 cm^{-1}; n.m.r. ($CDCl_3$; 60 MHz) δ 1.98 (3H, d, $J \sim 6$ Hz), 2.18 (6H, s), 3.80 (3H, s), 6.13 (1H, s), 6.31–7.13 (2H, AB part of ABX_3, J_{AB} 16–17 Hz); mass spectrum (with isotope peaks for ^{37}Cl), 330 (M^+), 288 $(M - C_2H_2O)^{\ddagger}$, 246 $(M - C_4H_4O_2)^{\ddagger}$ 228 (base peak) $(M - C_4H_6O_3)^{\ddagger}$, 196 $(M - C_5H_{10}O_4)^{\ddagger}$, and 187 $(M - C_6H_7O_4)^+$.

Mol. Wt. Calcd. for $C_{14}H_{15}O_7Cl$: 330. Found: 330.

Mesyl Chloride Treatment of **5**

A solution of **5** (123 mg, 0.499 mmol) in dry pyridine (1.5 ml) was treated with mesyl chloride (0.05 ml, 74 mg, 0.646 mmol) under anhydrous conditions at 0° for 2 h. The resulting dark brown solution was poured into ice water and the mixture was made acidic by dropwise addition of concentrated hydrochloric acid. Material obtained from the chloroform extracts was subjected to preparative-layer chromatography on silica gel plates, using the solvent system benzene–acetone (9:1).

The separation yielded 19 mg of gum which gave colorless crystals from methylene chloride – cyclohexane, m.p. 128–134°. This product was identified as cryptosporiopsin by comparison of c.d., i.r., u.v., n.m.r., mass spectra, t.l.c. behavior, and mixture melting point with an authentic sample.

A second (more polar) product (13 mg) isolated as a gum in the chromatographic separation had spectroscopic characteristics appropriate for a monomesylate: i.r. ($CHCl_3$) 3490, 1743, 1635, and 1378 cm^{-1}; n.m.r. ($CDCl_3$; 60 MHz) δ 1.98 (3H, d, $J \sim 6$ Hz), 3.28 (3H, s), 3.85 (3H, s), 4.42 (1H, br s) (exchangeable with D_2O), 5.30 (1H, s), 6.31–7.12 (2H, AB part of ABX_3, J_{AB} 16–17 Hz); mass spectrum (with isotope peaks for ^{37}Cl) *m/e* 324 (M^+) and 265 $(M - COOCH_3)^+$.

Mol. Wt. Calcd. for $C_{11}H_{13}O_7SCl$: 324. Found: 324.

[1]The culture medium was the basal synthetic medium of Jennison *et al.* (6) with added KCl (0.1 g/l) and p*H* adjusted to 3.5 with HCl.

Can. J. Chem. Downloaded from www.nrcresearchpress.com by 210.87.254.5 on 09/05/12
For personal use only.

We thank Mr. M. Kakushima for experimental assistance, Mr. J. Hoyle, University of Alberta for the o.r.d. and c.d. measurements, and Mrs. M. Austria, University of New Brunswick for mass spectra determinations.

1. W. J. McGahren, J. H. van den Hende, and L. A. Mitscher. J. Am. Chem. Soc. **91**, 157 (1969).
2. G. M. Strunz, A. S. Court, J. Komlossy, and M. A. Stillwell. Can. J. Chem. **47**, 2087 (1969); **47**, 3700 (1969).
3. D. Giles and W. B. Turner. J. Chem. Soc. C, 2187 (1969).
4. W. J. McGahren and L. A. Mitscher. J. Org. Chem. **33**, 1577 (1968).
5. M. A. Stillwell, F. A. Wood, and G. M. Strunz. Can. J. Microbiol. **15**, 501 (1969).
6. M. W. Jennison, M. D. Newcomb, and R. Henderson. Mycologia, **47**, 275 (1955).

Can. J. Chem. Downloaded from www.nrcresearchpress.com by 210.87.254.5 on 09/05/12
For personal use only.

Reaction of Acetaldehyde and Malononitrile. 2,2,4,4-Tetracyano-3,5-dimethylcyclohexylmalononitrile

JOHN J. KRAJEWSKI AND JAMES W. MOYER

DeSoto, Incorporated, 1700 South Mount Prospect Road, Des Plaines, Illinois 60018

Received December 11, 1972[1]

JOHN J. KRAJEWSKI and JAMES W. MOYER. Can. J. Chem. **52**, 3626 (1974)

The condensation of acetaldehyde and malononitrile is reported to yield 1,1,3,3-tetracyano-2,4-dimethylcyclobutane. The n.m.r. spectrum of this material and several of its derivatives, however, was found to best fit the title compound. A reaction scheme for the formation of the title compound is suggested.

JOHN J. KRAJEWSKI et JAMES W. MOYER. Can. J. Chem. **52**, 3626 (1974)

Il a été rapporté que la condensation de l'acétaldéhyde avec le malononitrile conduit au tétracyano-1,1,3,3 diméthyl-2,4 cyclobutane. On trouve toutefois que le spectre r.m.n. de ce composé et plusieurs de ces dérivés correspond mieux à la structure tétracyano-2,2,4,4 diméthyl-3,5 cyclohexylemalononitrile. [Traduit par le journal]

The study of the condensation of simple aldehydes with malononitrile is historically old (1). The reaction of formaldehyde with malononitrile, which has been studied by a number of investigators (2–5), is unique and may, under the appropriate conditions, give several products.

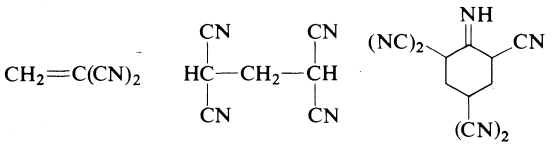

1 **2** **3**

The simplest condensation product, vinylidene cyanide (**1**), was isolated, characterized, and found to be extremely reactive (2). Condensation of **1** with malononitrile in vapor or liquid phase occurs readily without base catalysis to form 1,1,3,3-tetracyanopropane (**2**) (2–4). Further condensation of **1** with **2** via Michael and Thorpe reactions yields 2,2,4,4,6-pentacyanocyclohexanonimine (**3**) (5).

The reaction of acetaldehyde with malononitrile follows a somewhat similar course. The simplest isolable product was found to be 1,1,3,3-tetracyano-2-methylpropane (**4**) (6). Although ethylidene malononitrile (**5**) has not been isolated and characterized, its existence in equilibrium with malononitrile and **4** has been demonstrated by n.m.r. spectroscopy (7).

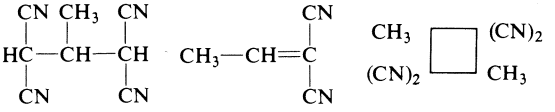

4 **5** **6**

Primarily on the basis of elemental analysis and a cryoscopic molecular weight determination in acetic acid, a second equimolar condensation product of malononitrile and acetaldehyde was reported to be 1,1,3,3-tetracyano-2,4-dimethylcyclobutane (**6**), m.p. 184.5° (6).

In view of the similarity of the reaction of formaldehyde and acetaldehyde with malononitrile to produce unstable alkylidene malononitriles and subsequently 1,1,3,3-tetracyano-2-alkylpropanes, it was felt that the structure assigned to the acetaldehyde malononitrile condensation product, **6**, melting at 184° was incorrect. If the parallelism between the two aldehydes were to follow, one might anticipate instead the formation of 2,2,4,4,6-pentacyano-3,5-dimethylcyclohexanonimine (**7**). For this reason, the condensation of acetaldehyde and malononitrile was reexamined.

The condensation of 2 mol malononitrile with 1 mol acetaldehyde in ethanol, by a preparation slightly modified from that reported by Diels *et al.* (3), gave a product melting at 81–83°. Although melting points of 113–114° and 99–100° were reported (3, 7), the compound analyzed correctly for $C_8H_6N_4$ (7). The n.m.r. spectrum confirmed the findings of Hart and Freeman (7), that is, 1,1,3,3-tetracyano-3-methylpropane (**4**)

[1]Revision received July 31, 1974.

Can. J. Chem. Downloaded from www.nrcresearchpress.com by 210.87.254.6 on 09/05/12
For personal use only.

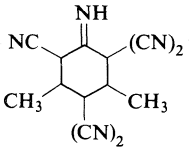

7

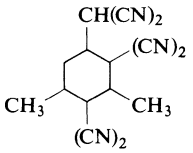

8

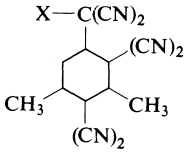

9 X = Br
10 X = Cl

exists in equilibrium with malononitrile and ethylidene malononitrile (**5**). It is therefore clear that sharpness of melting point and accuracy of elemental analysis are insufficient criteria for the purity of 1,1,3,3-tetracyano-2-alkylpropanes. These results are brought about by shifts in the Michael-type equilibrium.

Condensation of equimolar quantities of acetaldehyde and malononitrile gave a compound having elemental analysis and melting point in agreement with those reported for **6** (6). Examination of the i.r. spectrum indicated the presence of nitrile groups but an absence of any N—H, C=C, or C=N bonds. Thus, the correct structure for this product cannot be 2,2,4,4,6-pentacyano-3,5-dimethylcyclohexanonimine (**7**) but instead some structure (**8**) which at this point was uncharacterized.

Several attempts to repeat the reported (6) cryoscopic molecular weight determination in glacial acetic acid failed because of severe supercooling. A determination of the ebulioscopic molecular weight in acetic acid gave a value of 287 (mol. wt. calcd. for $C_{15}H_{12}N_6$: 276).

The mass spectrum of **8** shows a molecular ion peak (M^+) at *m/e* 276 and an $(M + 1)^+$ ion peak at *m/e* 277. The presence of the $(M + 1)^+$ ion peak is consistent with a nitrile containing structure since peaks at mass (M + 1) are characteristic of nitriles (8). The relatively large intensity of the $(M + 1)^+$ peak in comparison with the intensity of the molecular ion is attributed to a large number of nitrile groups in the structure. Significant fragment ion peaks support the proposed structure as follows: *m/e* 211, loss of $CH(CN)_2$; *m/e* 185 (base peak), loss of $CH(CN)_2$ and CN; *m/e* 66 and 65, $(CH_2(CN)_2)^+$ and $(CH_2(CN)_2)^+$; *m/e* 41, $(CH_3CN)^+$; *m/e* 27 and 26, $(HCN)^+$ and $(CN)^+$. At lower electron ionization voltages, the relative intensities of the peaks at *m/e* 276 and 277 increase with respect to fragmentation ion peaks, thus supporting their assignment as M^+ and $(M + 1)^+$ ion peaks, respectively. The mass spectral data in general are consistent with the proposed structure for **8**. Consequently, the correct structure corresponds to a compound analyzing for $C_{15}H_{12}N_6$.

The n.m.r. spectrum of **8** was determined in deuterated nitromethane and deuterated pyridine. If one assigns a value of 1 proton for the integral of the smallest peak, the integration curves are then consistent with a total of 12 protons. This is in agreement with a $C_{15}H_{12}N_6$ (**8**) structure. Two doublets of three protons each correspond to two nonequivalent methyl groups attached to methine carbons. The methine proton coupled exclusively to one of the methyl groups appears as a quartet at δ 3.06 in deuterated nitromethane and at δ 3.66 in deuterated pyridine. The coupling of this methine proton to the methyl group at δ 1.90 in deuterated nitromethane was confirmed by double resonance experiments. One proton appearing as a doublet at δ 4.70 in deuterated nitromethane and as a singlet at δ 8.59 in deuterated pyridine is assigned to $CH(CN)_2$ and $C(CN)_2^- \cdot C_5D_5N^+H$, respectively. Further complex multiplets between δ 1.9–3.0 account for the methylene group and the remaining ring methine proton. These protons form the ABC part of an $ABCMX_3$ spin system whose chemical shifts and coupling constants cannot be readily determined. These spectral features are consistent with 2,2,4,4,-tetracyano-3,5-dimethylcyclohexylmalononitrile (**8**). Consequently, the structure **6** which was assigned to the compound melting at 184° is incorrect.

An examination of the proposed structure for **8** will show that it is stereochemically complex. 2,2,4,4-Tetracyano-3,5-dimethylcyclohexylmalononitrile (**8**) has three asymmetric carbons which give rise to four possible pairs of enantiomorphs. These enantiomorphic pairs are diasteriomeric with respect to each other. Attempts to separate these diasterioisomers by thin-layer or column chromatography on several supports with several solvents and their mixtures were unsuccessful.

The Michael and Knoevenagel condensation reactions leading to the formation of **8** are known

Can. J. Chem. Downloaded from www.nrcresearchpress.com by 210.87.254.6 on 09/05/12
For personal use only.

Can. J. Chem. Downloaded from www.nrcresearchpress.com by 210.87.254.6 on 09/05/12
For personal use only.

to be reversible and may, therefore, lead to the epimerization of **8**, particularly about the 1 position. Consequently, further attempts at a total structure proof including stereochemical and conformational analysis were abandoned in favor of a gross structure proof.

Bromination and chlorination of **8** resulted in the mono halogenation products, bromo-2,2,4,4-tetracyano-3,5-dimethylcyclohexylmalononitrile (**9**) and chloro-2,2,4,4-tetracyano-3,5-dimethylcyclohexylmalononitrile (**10**), respectively, as evidenced by elemental analysis and n.m.r. spectroscopy.

The n.m.r. spectra of **9** and **10** are much simplified in that the $CH(CN)_2$ proton is replaced by a halogen atom. The resonance of the proton at C-1 for **10** is thus reduced to a doublet of doublets with couplings of 11.8 and 3.0 Hz. These couplings very likely arise from an axial–axial interaction and an axial–equatorial interaction, respectively, with the two protons at C-6. This establishes axial conformation for the proton at C-1 (and equatorial conformation for the dicyanochloromethyl group).

The condensation of acetone with malononitrile or mesityl oxide with malononitrile is reported to yield 2,2,6-tricyano-3,3,5-trimethylcyclohex-5-eneonimine (**12**) via the same intermediate (9, 10).

The possibility that the noncyclic malononitrile adduct of crotonaldehyde (**14**) might similarly be an intermediate to **8** was investigated. The only solid material resulting from the condensation of crotonaldehyde and malononitrile was concluded to have an empirical formula $C_{10}H_8N_4$. The mass spectrum showed a molecular ion at *m/e* 184 and base peak at *m/e* 41 (CH_3CN^+) which is consistent with structures having nitrile groups in close steric proximity with a methyl group. The i.r. spectrum indicated the presence of nitrile (2260 cm^{-1}), N—H (*ca.* 3270 cm^{-1}), and C=C or C=N (1660 and 1620 cm^{-1}). These data are consistent with 2,2,6-tricyano-3-methylcyclohex-5-enonimine (**13***a*) and its tautomer 2,2,6-tricyano-3-methylcyclohexa-4,6-dienamine (**13***b*). These results preclude the possibility that a noncyclic crotonaldehyde–malononitrile adduct (**14**) is a common precursor to **8** and **13**. It is likely, however, on the basis of analogy to the reported mechanism for α,β-unsaturated ketone–malononitrile condensations (9, 10), that the noncyclic crotonaldehyde–malononitrile adduct (**14**) is the precursor to **13**.

Equimolar quantities of acetaldehyde and **4** upon refluxing in ethanol with a trace of piperidine was found to afford a 40.8% yield of **8**.

Upon mixing equimolar quantities of acetaldehyde and malononitrile in ethanol, with or without catalytic quantities of piperidine, a spontaneous exotherm occurs with the formation of a high yield of **4**. This reaction mixture contains 50 mol% **4** and 50 mol% acetaldehyde. Upon refluxing this reaction mixture, it may be assumed that the unreacted acetaldehyde undergoes aldol condensation to yield crotonaldehyde. After the reaction mixture has been refluxed for about 2 h, **8** appears as a precipitate in 84% yield. By refluxing a solution of $\frac{2}{3}$ mol **4** with $\frac{1}{3}$ mol crotonaldehyde in the presence of piperidine for about 2 h, a 37% yield of **8** (identified by i.r. and n.m.r. spectroscopy) resulted. When a solution of equimolar quantities of **4**, crotonaldehyde and malononitrile in ethanol containing one drop of piperidine is refluxed for 15–20 min, **8** (identified by i.r. and n.m.r. spectroscopy) precipitates from the reaction mixture in 52% yield. The above observations coupled with knowledge that the formation of **4** and **5** is reversible, leads the authors to suggest a reaction route for the formation of **8** outlined in Scheme 1.

Experimental

Melting points were determined in capillaries with a Fisher-Johns apparatus and are uncorrected. The n.m.r. spectra were obtained on JEOL C-60H and Varian A-60 spectrometers with tetramethylsilane as an internal standard; chemical shifts are expressed on the δ scale. The following abbreviations are used to designate multiplicity of the n.m.r. signals: s, singlet; d, doublet; t, triplet; q, quartet; and m, multiplet. Infrared spectra were determined on Beckman IR-5A and IR-12 grating spectrophotometers.

The mass spectra were determined on a DuPont 21-491 double focusing mass spectrometer with a source temperature of 200 °C, a probe temperature of 300 °C with electron ionization voltage varying from 5 to 72 eV.

1,1,3,3-Tetracyano-3-methylpropane (4)

The title compound was prepared by a method slightly modified from that reported by Diels *et al.* (3). A solution of malononitrile (54 g) and acetaldehyde (18 g) in ethanol (200 ml) was stirred overnight at room temperature. The resulting mixture was chilled, filtered, and the solids dried to yield crude **4** (53.4 g, 83%), m.p. 74–80°. Recrystallization twice from Skelly Solve C afforded an analytical sample, m.p. 81.2–83° (lit. (6) m.p. 113–114°). The n.m.r. spectrum of this material was in agreement with that published by Hart and Freeman (7), that is n.m.r. (CD_3SOCD_3): **4**, δ 1.60 (d, J = 7.0 Hz, 3H, $CHCH_3$ at C-2) δ 3.24 (m, 1H at C-2) δ 5.28 (d, J = 5.2 Hz, 2H at C-1 and C-3); malononitrile δ 4.47 (s, 2H); **5**, δ 2.25 (d, J = 7.2 Hz, 3H, $CHCH_3$) δ 7.98 (q, J = 7.2 Hz, 1H).

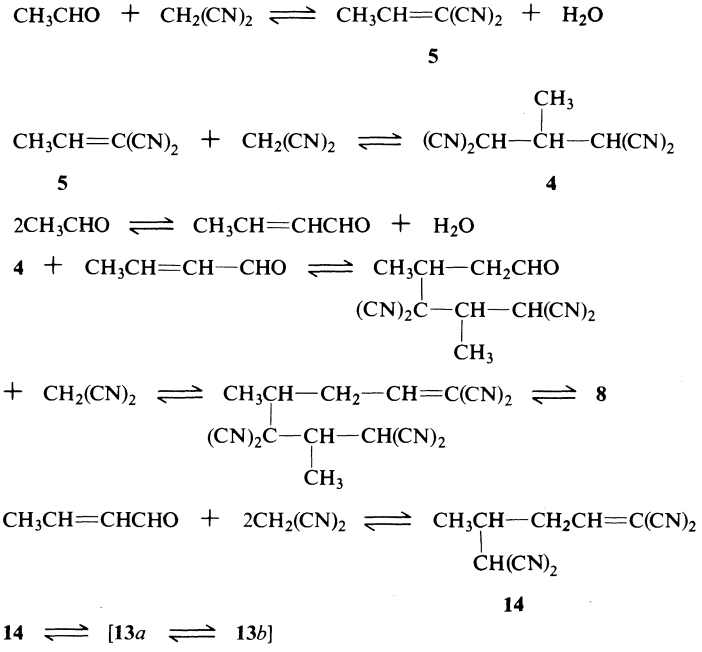

SCHEME 1

Anal. Calcd. for $C_8H_6N_4$: C, 60.8; H, 3.8; N, 35.4. Found: C, 60.7; H, 3.8; N, 35.2.

*2,2,4,4-Tetracyano-3,5-dimethylcyclohexylmalononitrile (**8**)*

A solution of malononitrile (66 g), acetaldehyde (45 g), and piperidine (2 drops) in ethanol (200 ml) was refluxed for 2 h. The resulting solid was filtered with suction, washed with water, and dried to yield crude **8** (77 g, 84%), m.p. 181–183°. An analytical sample was prepared by recrystallization from dimethyl sulfoxide–ethanol (1:10), m.p. 186–188° (lit. (6) m.p. 184–185°), mass spectrum (72 eV) *m/e* (relative intensity) 277(3.7), 276(0.7), 211(26), 185(100), 148(24), 147(24), 119(35), 93(33), 92(57), 66(30), 65(20), 52(34), 41(87), 27(38), 26(9). ν_{max} (KBr) 2230 cm^{-1} (saturated CN), no absorptions for C=C or C=NH; n.m.r. (CD_3NO_2): δ 1.51 (d, J = 6.0 Hz, 3H, $CHCH_3$ at C-5), δ 1.90 (d, J = 7.0 Hz, 3H, $CHCH_3$ at C-3), δ 1.9–3.0 (m, 1H, $CHCH_3$ at C-5) and m, 2H at C-6), δ 3.06 (q, J = 7.0 Hz, 1H, $CHCH_3$ at C-3), δ 3.1 (m, 1H at C-1), and δ 4.70 (d, J = 4.4 Hz, 1H, $CH(CN)_2$); n.m.r. (C_5D_5N): δ 1.23 (d, J = 6.0 Hz, 3H, $CHCH_3$ at C-5), δ 1.81 (d, J = 7.0 Hz, 3H, $CHCH_3$ at C-3), δ 3.66 (q, J = 7.0 Hz, 1H, $CHCH_3$ at C-3), δ 3.51 (d of d, J = 10.3 Hz, J = 3.0 Hz, 1H, at C-1), and δ 8.59 (s, 1H, $C(CN)_2^- \cdot C_5D_5NH^+$).

Mol. Wt. Calcd. for $C_{15}H_{12}N_6$: 276. Found (ebullioscopic molecular weight in acetic acid): 287. (Blank, acetanilide, Calcd.: 135. Found: 133.4.)

Anal. Calcd. for $C_{15}H_{12}N_6$: C, 65.2; H, 4.3.; N, 30.4. Found: C, 65.3; H, 4.3; N, 30.4.

*Bromo-2,2,4,4-tetracyano-3,5-dimethylcyclohexylmalononitrile (**9**)*

To a stirred solution of **8** (12 g) in glacial acetic acid (300 ml) was added bromine (11 g). The resulting solution was treated with an equal volume of water, the solids filtered, washed with water and air dried to yield pure **9** (14.5 g, 94%), m.p. 168–169° (dec.), n.m.r. (CD_3SOCD_3): δ 1.40 (d, J = 6.0 Hz, 3H, $CHCH_3$ at C-5), δ 1.75 (d, J = 7.0 Hz, 3H, $CHCH_3$ at C-3), δ 1.9–2.9 (m, 1H, $CHCH_3$ at C-5 and m, 2H at C-6), δ 3.58 (q, J = 7.0 Hz, 1H, $CHCH_3$ at C-3), δ 3.92 (d of d, J = 11.8 Hz, J = 3.0 Hz, 1H at C-1).

Anal. Calcd. for $C_{15}H_{11}BrN_6$: C, 50.7; H, 3.1; N, 23.7; Br, 22.5. Found: C, 50.6; H, 3.2; N, 23.8; Br, 22.4.

*Chloro-2,2,4,4-tetracyano-3,4-dimethylcyclohexylmalononitrile (**10**)*

Into a stirred solution of **8** (10 g) in glacial acetic acid (300 ml) and water (50 ml) was bubbled chlorine until no further change was noted. The reaction mixture was treated with an equal volume of water, the solids filtered, washed with water, and dried to yield crude **10** (9.8 g, 87%), m.p. 162–164° (dec.). An analytical sample was prepared by recrystallization three times from ethanol and water, m.p. 171° (dec.); n.m.r. (CD_3NO_2): δ 1.54 (d, J = 6.0 Hz, 3H, $CHCH_3$ at C-5), δ 1.97 (d, J = 7.0 Hz, 3H, $CHCH_3$ at C-3), δ 1.9–2.8 (m, 1H, $CHCH_3$ at C-5 and m, 2H at C-6), δ 3.14 (q, J = 7.0 Hz, 1H, $CHCH_3$ at C-3), and δ 3.52 (d of d, J = 11.8 Hz, J = 3.0 Hz, 1H, at C-1).

Anal. Calcd. for $C_{15}H_{11}ClN_6$: C, 58.0; H, 3.5; N, 27.1; Cl, 11.4. Found: C, 57.8; H, 3.6; N, 27.1; Cl, 11.2.

8 from Acetaldehyde and 4

A solution of 1,1,3,3-tetracyano-2-methylpropane (**4**) (15.8 g), acetaldehyde (4.5 g), piperidine (one drop) in ethanol (200 ml) was refluxed for 1 h. The resulting solid (7.5 g, 54%) was shown by its melting point (m.p. 182–183°) and i.r. spectrum to be **8**.

Can. J. Chem. Downloaded from www.nrcresearchpress.com by 210.87.254.6 on 09/05/12
For personal use only.

8 from Crotonaldehyde and 4

A solution of **4** (10.4 g), 2.33 g crotonaldehyde, one drop piperidine in 80 ml ethanol was refluxed for 2 h to yield a solid precipitate. This crude product was identified by i.r. and n.m.r. spectroscopy as **8**. The yield was 4.5 g (49.5%).

8 from 4, Crotonaldehyde, and Malononitrile

A solution of 15.8 g **4** in 60 ml ethanol was treated with 7 g crotonaldehyde and 1 drop of piperidine. The reaction mixture was stirred at room temperature for 15 min, treated with 6.6 g malononitrile and refluxed for 15–20 min to yield 14.5 g (52%) **8**. (Identified by i.r. and n.m.r. spectroscopy.)

2,2,6-Tricyano-3-methylcyclohex-5-enonimine (13)

A solution of malononitrile (33 g) and crotonaldehyde (17.5 g) in ethanol (200 ml) was treated with piperidine (one drop) and refluxed for 2 h. The resulting solution was chilled, filtered, and the solids dried to yield **13** (17 g, 37%) melting above 305°; ν_{max} (KBr) 3270 (NH), 2260 (CN), 1660 and 1620 cm^{-1} (C=C or C=N); mass spectrum (78 eV) *m/e* (relative intensity) M^+ 184 (3), major fragment 41(100).

Anal. Calcd. for $C_{10}H_8N_4$: C, 65.2; H, 4.3; N, 30.4. Found: C, 65.3; H, 4.4; N, 29.3.

The authors wish to thank Dr. R. E. Wolf for his encouragement, and Dr. E. P. Lira for many interesting discussions.

1. F. Freeman. Chem. Revs. **69**, 591 (1969).
2. A. E. Ardis *et al.* J. Am. Chem. Soc. **72**, 1305 (1950).
3. O. Diels, H. Gartner, and R. Kaack. Chem. Ber. **55**, 3439 (1922).
4. O. Diels and B. Conn. Chem. Ber. **56**, 2076 (1923).
5. J. C. Westfahl and T. L. Gresham. J. Org. Chem. **21**, 319 (1956).
6. O. Diels, H. Gartner, and R. Kaack. Chem. Ber. **55**, 3445 (1922).
7. H. Hart and F. Freeman. Chem. Ind. (London), 333 (1963).
8. J. H. Beynon, R. A. Saunders, and A. E. Williams. The mass spectra of organic molecules. Elsevier Publ. Co., New York, N.Y. 1968. p. 308.
9. J. W. ApSimon, J. W. Hooper, and B. A. Laishes. Can. J. Chem. **48**, 3064 (1970).
10. J. K. Williams, J. Org. Chem. **28**, 1054 (1963).

Can. J. Chem. Downloaded from www.nrcresearchpress.com by 210.87.254.6 on 09/05/12
For personal use only.

Radiolysis of Ethane + Sulfur Hexafluoride and Ethylene + Sulfur Hexafluoride Gaseous Systems. Formation of SF_5 · Radical and its Reactivity

JANUSZ GAWŁOWSKI[1] AND JAN A. HERMAN

Département de chimie et Centre de recherche sur les atomes et les molécules, Université Laval, Québec, Québec G1K 7P4

Received May 24, 1974

JANUSZ GAWŁOWSKI and JAN A. HERMAN. Can. J. Chem. **52**, 3631 (1974).

Neutralization processes of ions in radiolysis of ethane or ethylene + sulfur hexafluoride systems lead to the formation of the SF_5· radical. Compounds of the general formula RSF_5 are formed as a result of recombination reactions with hydrocarbon radicals. In the mixture ethane + 0.3% sulfur hexafluoride the radiochemical yield of SF_5· is $G_{SF_5} = 2.8 \pm 1$. The presence of ammonia decreases G_{SF_5} to *ca.* 0.2, suggesting that the neutralization process of $NH_4^+(NH_3)_n$ with SF_6^- ions follows some unknown path. In the present work some reactions of the SF_5· radical are studied. Preliminary results indicate that the presence of SF_6 influences very little, if at all, the yield of atomic hydrogen.

JANUSZ GAWŁOWSKI et JAN A. HERMAN. Can. J. Chem. **52**, 3631 (1974).

Les processus de neutralisation des ions pendant la radiolyse des systèmes: éthane ou éthylène + hexafluorure de soufre conduisent à l'apparition du radical SF_5·. Celui-ci forme des composés du type RSF_5 dans des réactions de recombinaison avec des radicaux hydrocarbonés. Dans le mélange éthane + 0.3% hexafluorure de soufre, le rendement en radicaux SF_5· est $G_{SF_5} = 2.8 \pm 1$. L'addition de l'ammoniac diminue ce rendement à $G \approx 0.2$, ce qui suggère que la neutralisation des ions $NH_4^+(NH_3)_n$ avec SF_6^- suit une voie encore inconnue. Quelques réactions du radical SF_5· sont étudiées dans le présent travail. Les résultats préliminaires indiquent que la présence de SF_6 influence peu ou pas du tout le rendement en hydrogène atomique.

Introduction

Sulfur hexafluoride is very often used as an electron scavenger in radiolytical studies. Recently, new effects caused by the presence of SF_6 were brought to light: (*a*) chain *cis–trans* isomerization of olefins (1–6), (*b*) elimination of some highly unsaturated hydrocarbons produced in radiolysis (6–8), (*c*) energy transfer to SF_6 from excited species formed in liquid systems during radiolysis (9). The assumption was advanced that the former two effects should be attributed to SF_5· radicals formed in ion neutralization processes

[1] $$RH^+ + SF_6^- \rightarrow SF_5\cdot + \text{products}$$

In this work we present arguments in favor of the formation of the SF_5· species and its participation in radical reactions.

Experimental

Ethane and ethylene (Matheson Co., C.P. grade) were purified from higher hydrocarbons by adsorption at −76 °C on active charcoal. Ethane was further passed through $Hg(ClO_4)_2$ adsorbed on Chromosorb P in order to eliminate remaining olefins. Ethylene was additionally purified from acetylene by passing through a solution of $AgNO_3$ in ethylene glycol adsorbed on a suitable support. After a bulb-to-bulb distillation at liquid nitrogen temperature the C_2H_6 and C_2H_4 were stored over pulverized metallic sodium which eliminated remaining traces of water and oxygen (10). Gas chromatography (g.c.) showed that the ethane was practically pure, while in the ethylene only C_2H_6 was present ($\leq 0.1\%$).

1,3-Butadiene, ammonia, and sulfur hexafluoride (Matheson Co.) were purified by bulb-to-bulb distillation and dried over Molecular Sieve 3A. Immediately before its use oxygen (medical grade) was passed through cold traps maintained at liquid nitrogen temperature.

The irradiation glass cells (200–250 ml) were fired at 500 °C for at least 30 min before the introduction of the gaseous sample. Then they were sealed and irradiated in a AECL 220 Gammacell ^{60}Co γ-ray source at a dose rate of 0.08 Mrad/h.

All analyses were performed in a Victoreen 4000 g.c. equipped with flame ionization (f.i.d.) and electron capture (e.c.d.) detectors. The following columns were used: (*1*) squalane columns (9 m × 6.4 mm o.d. and 9 m × 3.2 mm o.d.) at 25 and 60 °C for identification of radiolysis products; (*2*) 20% oxydipropionitrile on Chromosorb P (30–60 mesh) (5 m × 6.4 mm o.d.) at 25 °C for quantitative analysis of RSF_5 compounds; (*3*) Porapak Q (4 m × 3.2 mm o.d.) at 70 and 100 °C for analysis of hydrocarbons and C_2H_5F; (*4*) Silicone oil SF30 (6%) (1.5 m × 3.2 mm o.d.) programmed between 100 and 250 °C at 5 °C/min for analysis of high boiling products.

Sometimes in order to make the analysis easier an additional short column (10 cm) containing $Hg(ClO_4)_2$ on Chromosorb P was inserted between the analytical

[1]Permanent address: Laboratory of Radiochemistry and Radiation Chemistry, Warsaw University, Warsaw, Poland.

Can. J. Chem. Downloaded from www.nrcresearchpress.com by 210.87.254.40 on 09/05/12
For personal use only.

TABLE 1. Radiolytical product yields from ethane: total pressure 200 Torr

Composition	Dose (Mrad)	Radiolytical yields				
		CH_3SF_5	$C_2H_5SF_5$	C_2H_5F	C_3H_8	n-C_4H_{10}
C_2H_6 + 0.3% SF_6	0.32	0.8	1.8	n.d.*	n.d.	n.d.
C_2H_6 + 0.29% SF_6	0.64	0.83	1.55	n.d.	n.d.	n.d.
C_2H_6 + 0.32% SF_6	1.28	0.75	1.68	0.27	0.64	1.36
C_2H_6	1.28	—	—	—	1.0	2.1
C_2H_6 + 0.4% SF_6	1.92	0.88	1.55	0.35	0.65	1.40

*n.d. = not determined.

column and the detector; this removed all unsaturated compounds.

The radiolysis products containing the build-up fragments of SF_6 were first distinguished on chromatograms by electron capture, and then identified by mass spectrometry on a Varian MAT CH7 instrument.

High molecular weight compounds deposited on the wall during radiolysis were dissolved in 0.5 ml of benzene and introduced into the g.c. in samples of *ca.* 20 μl.

Results

Radiolysis of C_2H_6 + SF_6 System

Among the radiolytical products two were found characterized by very strong signals on e.c.d. Their retention indexes on squalane column are $I_R(I) = 323$ and $I_R(II) = 439$ respectively. The following mass spectrum for 70 V electrons of compound (I) was measured (the relative intensities are shown in parentheses): *m/e* 127, SF_5^+ (100); 123, $SF_4CH_3^+$ (16); 108, SF_4^+ (3); 89, SF_3^+ (68); 70, SF_2^+ (10); 15, CH_3^+ (10). From this mass spectrum it was concluded that compound (I) corresponds to CH_3SF_5. The mass spectrum of compound (II), *m/e* 137, $SF_4C_2H_5^+$ (3); 127, SF_5^+ (20); 108, SF_4^+ (2); 89, SF_3^+ (34); 70, SF_2^+ (8); 51, SF^+ (4); 29, $C_2H_5^+$ (100); 27, $C_2H_3^+$ (60), points to a $C_2H_5SF_5$ molecular formula. The mass spectra of these compounds are not described in the literature, and standard samples are unavailable owing to very difficult syntheses (11). Besides these two intense peaks on e.c.d. other much smaller signals were observed. We did not attempt to identify these smaller products, however, since their yields were low as estimated from g.c. analysis with flame ionization detection.

The RSF_5 compounds being unavailable the direct determination of f.i.d. sensitivity coefficients was impossible. Therefore, we proceeded in an indirect way assuming that: (*a*) the SF_5 group, by analogy with other functional groups, brings into the f.i.d. sensitivity coefficient a constant contribution independent of the size of the hydrocarbon radical (12), and (*b*) the sensitivity of the electron capture is identical for the CH_3SF_5 and $C_2H_5SF_5$; then the comparison of the areas of peaks for the f.i.d. and e.c.d. gives a contribution of -0.75 for the $-SF_5$ group, if a value of 4.0 corresponds to n-C_4H_{10}. The calculated radiolytical yields by this procedure are certainly not precise, especially in the case of CH_3SF_5; however, they can be used in relative measurements.

In addition to the two aforementioned radiolytical products ethyl fluoride ($I_R = 268$ on squalane) was positively identified, and probably methyl fluoride too. The yield of the latter compound was not measured owing to the adjacent very strong peak of ethane, which makes the measurement doubtful. In Table 1 are presented the *G*-values (yields per 100 eV of absorbed energy) for CH_3SF_5, $C_2H_5SF_5$, C_2H_5F, C_3H_6, and n-C_4H_{10} for different absorbed doses of radiation. Figure 1 shows the yield of $C_2H_5SF_5$ as a function of ammonia concentration.

Radiolysis of C_2H_4 + SF_6 System

The analysis with e.c.d. of gaseous products formed during radiolysis of C_2H_4 + 0.3% SF_6 shows two main compounds characterized by retention indexes on squalane $I_R(II) = 439$ and $I_R(III) = 632$ respectively, and several smaller components among which $I_R(I) = 323$ is present. The compounds having retention indexes 439 and 323 were previously identified as $C_2H_5SF_5$ and CH_3SF_5. The mass spectrum of compound (III) is as follows: *m/e* 127, SF_5^+ (4); 89, SF_3^+ (8); 70, SF_2^+ (7); 57, $C_4H_9^+$ (50); 56, $C_4H_8^+$ (26); 55, $C_4H_7^+$ (13); 41, $C_3H_5^+$ (97); 29, $C_2H_5^+$ (100). On the basis of the highest mass fragments compound (III) was tentatively identified as $C_4H_9SF_5$.

The radiolytical yields of these products for

Can. J. Chem. Downloaded from www.nrcresearchpress.com by 210.87.254.40 on 09/05/12
For personal use only.

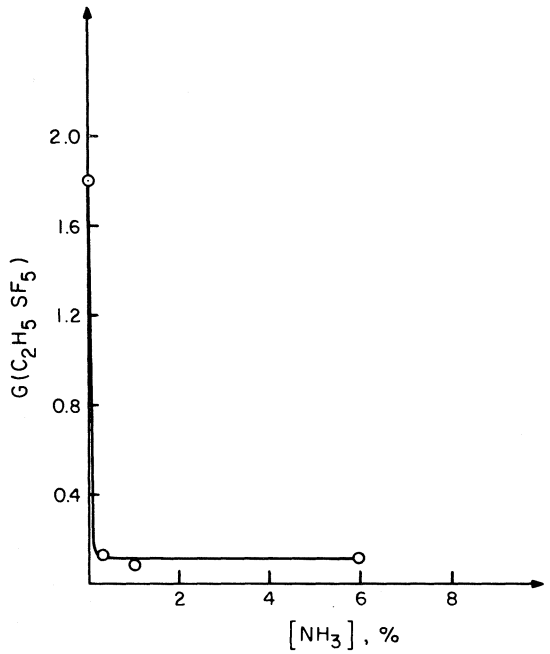

FIG. 1. $G(C_2H_5SF_5)$ as a function of ammonia concentration in the C_2H_6 + 0.3% SF_6 system. Total pressure 200 Torr.

irradiation of the C_2H_4 + 0.4% SF_6 system (p = 400 Torr, dose = 1.9 Mrad) were found to be $G(CH_3SF_5) = 0.02$, $G(C_2H_5SF_5) = 0.23$, and $G(C_4H_9SF_5) = 0.27$. Other products giving signals on e.c.d. were not identified, their yields being small, $G \leqslant 0.01$. Some were saturated products ($Hg(ClO_4)_2$ did not react with them) but probably not pure hydrocarbons, since they give an ill-defined signal on e.c.d. Among these products only one was positively recognized as being C_2H_5F, the others are probably alkyl fluoro derivatives also.

The addition of 1% or more of ammonia to the C_2H_4 + 0.3% SF_6 system (p = 400 Torr) diminishes dramatically the yields of RSF_5 compounds to such an extent that their determination by f.i.d. was practically impossible, but their presence could be seen with the e.c.d. On this basis it was established that yields of these products are about 20 times less in the presence of NH_3 than in the absence of this scavenger. Once these low yields of RSF_5 products are reached in the presence of small quantities of NH_3, further addition does not influence the $G(RSF_5)$ values. Oxygen (0.7%) or butadiene (0.3%) added to the C_2H_4 + 0.35% SF_6 (p = 400 Torr) system scavenged totally CH_3SF_5, $C_2H_5SF_5$, and $C_4H_9SF_5$.

In Fig. 2 are shown chromatograms of high molecular weight electron-attaching compounds formed during radiolysis of the C_2H_4 + 0.3% SF_6 system in the absence and presence of NH_3 or 1,3-C_4H_6. The chromatograms are qualitative only, the electron-capture detector working far from linearity near the saturation limits in the case of strong signals. In the presence of oxygen (0.7%) the high molecular weight electron-attaching compounds are not formed.

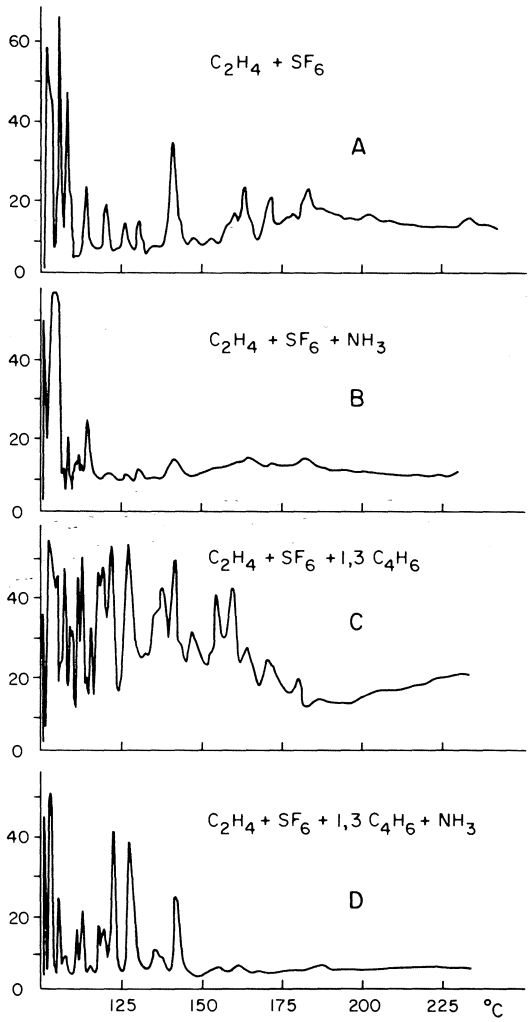

FIG. 2. Chromatograms of electron-attaching high molecular weight products formed in the presence of scavengers during radiolysis of the C_2H_4 + 0.3% SF_6 system. Total pressure 400 Torr, dose 0.64 Mrad, column 1.5 m × 0.32 mm o.d. 6% SE 30 silicone oil, temperature program 5 °C/min from 100 to 250 °C.

Can. J. Chem. Downloaded from www.nrcresearchpress.com by 210.87.254.40 on 09/05/12
For personal use only.

Can. J. Chem. Downloaded from www.nrcresearchpress.com by 210.87.254.40 on 09/05/12
For personal use only.

Discussion

C_2H_6 + SF_6 System

In previous published work (6) the assumption was made that neutralization processes of hydrocarbon ions with SF_6^- lead to the formation of $SF_5^{\cdot}$ radicals:

[1] $$RH^+ + SF_6^- \rightarrow SF_5^{\cdot} + \text{products}$$

In order to test this assumption ethane was chosen, because the radical processes in C_2H_6 radiolysis are relatively simple, $CH_3^{\cdot}$ and $C_2H_5^{\cdot}$ being virtually the only hydrocarbon radicals produced. Our results presented in Table 1 for pure ethane are similar to those obtained by other authors for higher pressures of C_2H_6 (13, 14).

In the presence of SF_6 new products, CH_3SF_5, $C_2H_5SF_5$, and C_2H_5F, are formed in relatively important yields, which seem to be independent of the absorbed dose. On the other hand the yields of propane and butane decrease. Assuming that CH_3SF_5, $C_2H_5SF_5$, and C_2H_5F result from recombination–disproportionation processes [2], [3], and [4] of $SF_5^{\cdot}$ with $CH_3^{\cdot}$ and $C_2H_5^{\cdot}$ radicals

[2] $$CH_3^{\cdot} + SF_5^{\cdot} \rightarrow CH_3SF_5$$

[3] $$C_2H_5^{\cdot} + SF_5^{\cdot} \rightarrow C_2H_5SF_5$$

[4] $$C_2H_5^{\cdot} + SF_5^{\cdot} \rightarrow C_2H_5F + SF_4$$

one can estimate the radiolytical yield of the $SF_5^{\cdot}$ radical. It is found that $G_{SF_5} = 2.8 \pm 1$.

The high error limit is due to the following: (*a*) the sensitivity coefficients of the flame ionization detection are measured indirectly; particularly the error in $G(CH_3SF_5)$ may be important; (*b*) the disproportionation reaction

[5] $$CH_3^{\cdot} + SF_5^{\cdot} \rightarrow CH_3F + SF_4$$

is not taken into account; (*c*) a possible disproportionation reaction

[6] $$C_2H_5^{\cdot} + SF_5^{\cdot} \rightarrow SF_5H + C_2H_4$$

was not evident from our results; (*d*) the recombination of two $SF_5^{\cdot}$ radicals into S_2F_{10} (not determined) is not considered.

Such a high yield of $SF_5^{\cdot}$ radicals indicates that during radiolysis of the ethane – sulfur hexafluoride system the process [1] is the main neutralization path for ions, but probably not the only one. Indeed, some unidentified radiolytical products giving signals on e.c.d. were observed; however, their yields were very small compared to $G(CH_3SF_5)$ and $G(C_2H_5SF_5)$.

The comparison of yields of $CH_3^{\cdot}$ and $C_2H_5^{\cdot}$ radicals in the absence and presence of SF_6 gives some unexpected results. Considering that yields of propane and butane formed at 200 Torr in nonradical processes are 0.1 and 0.2 (15), and that for the reactions $CH_3^{\cdot} + C_2H_5^{\cdot}$ and $C_2H_5^{\cdot} + C_2H_5^{\cdot}$ the ratios k_d/k_c are 0.04 and 0.14 (16), one finds in the presence and absence of SF_6 the following *G*-values for methyl and ethyl radical formation: $G_{CH_3} = 1.5$ and 1.1, $G_{C_2H_5} = 5.1$ and 5.2 respectively. Consequently, within the experimental error, the yield of the ethyl radical, $G_{C_2H_5}$, does not depend on the presence of $SF_6^{\cdot}$. Since an important fraction of $C_2H_5^{\cdot}$ radicals is formed by the reaction of atomic hydrogen with ethane (17), it then follows that under our experimental conditions the atomic hydrogen is not generated by the neutralization of ions with electrons or, if it is, only in very low yield. This is only a preliminary conclusion. In our opinion, the problem of atomic hydrogen formation in neutralization processes needs further detailed investigation. However, on the basis of present results, it is obvious that any calculation of radiolytical yields of radicals, in hydrocarbon + SF_6 systems, can lead to important error if the reactions of the $SF_5^{\cdot}$ radical are not taken into account.

C_2H_6 + SF_6 + NH_3 System

It is generally admitted that the presence of ammonia in irradiated systems leads to proton transfer from positive RH^+ ions to NH_3

[7] $$RH^+ + NH_3 \rightarrow R + NH_4^+$$

Therefore, it is expected that the neutralization processes will involve solvated NH_4^+ ions. When ammonia is added to the $C_2H_6 + SF_6$ system the $G(C_2H_5SF_5)$ decreases sharply to a constant value, which is then independent of further addition of NH_3 (Fig. 1). The yield of CH_3SF_5 decreases in a similar way to a new low value, $G(CH_3SF_5) \leqslant 0.05$. The total yield of $SF_5^{\cdot}$ radical production in the presence of NH_3 calculated from the *G*-values of CH_3SF_5 and $C_2H_5SF_5$ can be estimated to be $G_{SF_5} \leqslant 0.2$. This is about 15 times less than the value found in the absence of ammonia. The decrease of G_{SF_5} cannot be ascribed to the reaction of the SF_5 radical with NH_3, because in this case a progressive decrease of $G(C_2H_5SF_5)$ as a function of the ammonia concentration should be observed, which clearly is not the case (Fig. 1). A similar influence of ammonia is noted in the

radiolysis of the C_2H_4–SF_6 system (see Results). This effect appears to be characteristic for ammonia and not of the nature of the radiolyzed hydrocarbon. This suggests that the neutralization process

[8] $NH_4^+(NH_3)_n + SF_6^- \rightarrow SF_5^{\cdot} + \text{products}$

occurs with a low yield. It was shown in previous work (6) that the disappearance yield of SF_6 in the radiolysis of hydrocarbon + SF_6 system is nearly equal to the ionic yield, $G(-SF_6) \simeq G_{ion}$, and is independent of the presence of ammonia. Therefore, products other than SF_5 radical must be formed in the neutralization processes of ammonia ions. In the system C_2H_6 + SF_6 + NH_3 other organic compounds characterized by strong electronegative groups were not found in yields exceeding 0.05. On this basis we can assume that the neutralization of NH_4^+ with SF_6^- gives inorganic decomposition products (*i.e.* SF_4) which are relatively unreactive towards hydrocarbons and radicals. We did not search for such compounds in the present work.

The above discussion calls into question a previous hypothesis (6) that the $SF_5^{\cdot}$ radical is responsible for the *cis–trans* chain isomerization of gaseous 2-butene. In those experiments ammonia had practically no influence on isomerization yields, and we have to admit that another product formed in the presence of SF_6 (with a yield independent of NH_3) causes the isomerization.

C_2H_4 + SF_6 System

The identification of CH_3SF_5, $C_2H_5SF_5$, and $C_4H_9SF_5$ among radiolytical products reinforces the previous assumption that reaction 1 is taking place during γ-radiolysis of gaseous ethylene–SF_6 mixtures. These compounds can only be formed by the recombination of $SF_5^{\cdot}$ with alkyl radicals generated in the radiolysis of ethylene (reactions 2, 3, and 9).

[9] $C_4H_9^{\cdot} + SF_5^{\cdot} \rightarrow C_4H_9SF_5$

These processes are corroborated by the radical scavenging action of oxygen, and also by the fact that yields of $C_2H_5SF_5$ and $C_4H_9SF_5$ are much higher than that of CH_3SF_5, and are approximately in the ratio of yields of the respective radicals formed in radiolysis of pure C_2H_4 (18).

Our results do not allow us to determine the yield of the $SF_5^{\cdot}$ radical in this system for the following reasons. (*a*) Low dose-rate irradiation of ethylene gives a very complex overall picture of the radical processes (18). One of the consequences of the addition of radicals to the double bond of C_2H_4 is that high molecular radicals are formed, $C_6H_{13}^{\cdot}$, $C_8H_{17}^{\cdot}$ etc., and these might also react with $SF_5^{\cdot}$. Furthermore, the lack of data concerning the ratios of disproportionation/recombination rate constants for alkyl radicals with $SF_5^{\cdot}$

[10*a*] $C_nH_{2n+1} + SF_5^{\cdot} \rightarrow C_nH_{2n+1}SF_5$

[10*b*] $\rightarrow C_nH_{2n+1}F + SF_4$

[10*c*] $\rightarrow C_nH_{2n} + SF_5H$

makes any quantitative interpretation difficult. (*b*) High molecular electron-attaching products are formed in the radiolysis of the C_2H_4 + SF_6 system for which the probable precursor is the SF_5 radical (see later in the text).

The addition of 0.3% of 1,3-C_4H_6 to the C_2H_4 + 0.3% SF_6 system totally scavenges CH_3SF_5, $C_2H_5SF_5$, and $C_4H_9SF_5$ and simultaneously new strong peaks appear for the high molecular weight products (Fig. 2*C*). These results can be explained by assuming a fast reaction 11 (6, 8).

[11] $SF_5^{\cdot} + 1,3\text{-}C_4H_6 \rightarrow SF_5C_4H_6^{\cdot}$

In consequence the steady state concentration of $SF_5^{\cdot}$ radicals is so low that even the very sensitive e.c.d. cannot detect traces of $C_2H_5SF_5$ and $C_4H_9SF_5$. The new radical $SF_5C_4H_6^{\cdot}$ can further condense with ethylene or butadiene and finally recombine with other radicals giving high molecular weight products.

An alternate assumption that the high molecular weight molecules are formed directly in ionic or neutralization processes is very improbable. Indeed, the analysis of chromatograms (Fig. 2) indicates that NH_3 strongly decreases the yields of high molecular weight products, but has a small influence on their qualitative composition. If these products are produced directly by ion neutralization, then the presence of NH_3, capturing the positive ions before the occurrence of neutralization, should make their formation impossible. The decrease in the yield of high molecular weight products can be explained by the decrease in the yield of the $SF_5^{\cdot}$ radical in the presence of NH_3 (a similar behavior is noted in C_2H_6 + SF_6 mixture). The scavenging action of oxygen on high molecular weight products also points out the radical nature of the formation of these compounds.

Can. J. Chem. Downloaded from www.nrcresearchpress.com by 210.87.254.40 on 09/05/12
For personal use only.

All these results confirm the already advanced assumption that the $SF_5^{\cdot}$ radicals are responsible for removing the highly unsaturated products formed during radiolysis of ethylene (or other hydrocarbons) in the presence of SF_6 (6, 8).

Summary

The $SF_5^{\cdot}$ radical is formed in neutralization processes of ions during radiolysis of gaseous ethane and ethylene added with SF_6. In a mixture of 0.3–0.4% SF_6 in C_2H_6 the yield of this radical is $G_{SF_5} = 2.8 \pm 1$. The $SF_5^{\cdot}$ radical reacts further with other hydrocarbon radicals giving compounds of general formula SRF_5.

There is a decrease of about 15 times in the $SF_5^{\cdot}$ yield in the presence of ammonia. This suggests that the neutralization process of SF_6^- with $NH_4^+(NH_3)_n$ follows a new path not yet understood. The present results only partially confirm a previous assumption concerning the behavior of the $SF_5^{\cdot}$ radical in radiolyses of hydrocarbons mixed with sulfur hexafluoride (6). This radical is certainly responsible for removing highly unsaturated hydrocarbon products formed during radiolysis of ethylene and butylenes. On the other hand the *cis-trans* chain isomerization of olefins by $SF_5^{\cdot}$ is questionable. Preliminary results indicate that in the radiolysis of C_2H_6 the presence of SF_6 influences very little, if at all, the yield of atomic hydrogen.

This work was made possible through the financial assistance of the National Research Council of Canada. We are grateful to Mr. F. Bouchard for technical assistance.

1. R. W. HUMMEL. Nature, **218**, 1050 (1970).
2. R. B. CUNDALL and W. TIPPETT. Adv. Chem. Ser. **82**, 387 (1968).
3. J. W. F. VAN INGEN and W. A. CRAMER. J. Phys. Chem. **74**, 1134 (1970).
4. J. GAWŁOWSKI, J. NIEDZIELSKI, J. SOBKOWSKI, and A. ZECHOWSKA. Radiat. Eff. **11**, 85 (1971).
5. L. W. SIECK, S. G. LIAS, L. HELLNER, and P. AUSLOOS. J. Res. Natl. Bur. Stand. **76A**, 115 (1972).
6. J. NIEDZIELSKI and J. GAWŁOWSKI. J. Chem. Phys. **77**, 2853 (1973).
7. P. T. HOLLAND and J. A. STONE. Can. J. Chem. **48**, 3277 (1970).
8. J. NIEDZIELSKI and J. GAWŁOWSKI. Int. J. Radiat. Phys. Chem. **5**, 239 (1973).
9. U. I. PITCHOOZHKIN, H. YAMAZAKI, and S. SHIDA. Bull. Chem. Soc. Jap. **46**, 67 (1973).
10. J. GAWŁOWSKI and J. NIEDZIELSKI. Rocz. Chem. **44**, 685 (1970).
11. R. D. DRESDNER and J. A. YOUNG. J. Am. Chem. Soc. **81**, 574 (1959).
12. J. C. STERNBERG, W. S. GALLAWAY, and D. T. L. JONES. *In* Gas chromatography, third international symposium. Academic Press, New York, N.Y. 1962. p. 231.
13. K. YANG and P. L. GANT. J. Phys. Chem. **65**, 1861 (1961).
14. C. M. WODETZKI, P. A. MCCUSTER, and D. B. PETERSON. J. Phys. Chem. **69**, 1045 (1965).
15. H. H. CARMICHAEL, R. GORDEN JR., and P. AUSLOOS. J. Chem. Phys. **42**, 343 (1965).
16. J. A. KERR and E. RATAJCZAK. Second supplement tables of bimolecular gas reactions. University of Birmingham, England. 1972.
17. C. M. WODETZKI, P. A. MCCUSKER, and D. B. PETERSON. J. Phys. Chem. **69**, 1056 (1965).
18. J. GAWŁOWSKI and J. NIEDZIELSKI. Int. J. Radiat. Phys. Chem. **5**, 419 (1973).

Can. J. Chem. Downloaded from www.nrcresearchpress.com by 210.87.254.40 on 09/05/12
For personal use only.

Les phases cyanures de nickel(II) hydratés

Y. MATHEY ET C. MAZIERES

Laboratoire de Physicochimie Minérale, Bâtiment 420, Université Paris-Sud 91405 Orsay

Reçu le 14 mai 1974

Y. MATHEY et C. MAZIERES. Can. J. Chem. **52**, 3637 (1974).

L'étude de la préparation et des propriétés des composés $Ni(CN)_2 \cdot xH_2O$ montre l'existence de trois phases "cyanure complexe de Ni(II) hydraté". Elles résultent toutes d'empilements de couches complexes polymères $[Ni(H_2O)_2Ni(CN)_4]_\infty$ analogues aux couches $[Ni(NH_3)_2Ni(CN)_4]_\infty$ rencontrées dans les amminocyanures de nickel, et contiennent des H_2O interlamellaires non coordinées. Leur caractérisation, par diffraction X et spectroscopie électronique u.v.–visible, est précisée. Toutes trois possèdent la symétrie orthorhombique et répondent à la formule $Ni(H_2O)_2Ni(CN)_4 \cdot yH_2O$.

Y. MATHEY and C. MAZIERES. Can. J. Chem. **52**, 3637 (1974).

A critical study of the preparation and properties of the hydrated forms of Ni cyanide shows the existence of three different phases in the compounds $Ni(CN)_2 \cdot xH_2O$. By X-ray diffraction and u.v.–visible spectroscopy, it is found that all three phases are formed by different stacking of polymeric $[Ni(H_2O)_2Ni(CN)_4]_\infty$ layers similar to the $[Ni(NH_3)_2Ni(CN)_4]_\infty$ layers existing in Ni amminocyanides, with interlamellar noncoordinated H_2O molecules. All three phases are indexed in the orthorhombic system and can be given as $Ni(H_2O)_2Ni(CN)_4 \cdot yH_2O$.

Introduction

Utilisés dès 1897 comme intermédiaires dans la préparation du réseau d'accueil du Clathrate d'Hofmann $Ni(CN)_2NH_3, C_6H_6$ (1) les "cyanures de nickel" sont connus pour leur aptitude à former avec l'ammoniac ou avec de nombreuses molécules organiques polaires, *n* alkylamines en particulier, des complexes du type $Ni(NH_2R)_2Ni(CN)_4$ (1 à 13) dont la structure semble mieux comprise que celle des nombreux cyanures $Ni(CN)_2 \cdot xH_2O$ décrits à ce jour. En effet, bien que l'existence d'entités plan carré $[Ni(CN)_4]$ d'une part, et le rôle de ligand joué par certaines molécules H_2O d'autre part, soient admis dans chacun de ces complexes hydratés, l'état des connaissances dans ce domaine, tel qu'il est donné dans le tableau 1 est encore insuffisant et imprécis; le but de cet article est de l'unifier et de le compléter. Une étude, par spectroscopie électronique u.v. – visible – proche i.r., des entités complexes participant à chaque type d'édifices, nous permet de proposer des modèles structuraux en accord avec les spectres de diffraction X.

Quant aux composés quasi anhydres de formule voisine de $Ni(CN)_2$ (6, 14, 17, 19, 22, 23), nous avons trouvé que l'absence de molécules polaires pouvant jouer le rôle de ligand modifie considérablement la nature et le mode d'association des entités complexes centrées sur les atomes de nickel. L'étude de ces composés, généralement beaucoup moins bien organisés (11, 18, 24) est reportée à un prochain article.

Partie expérimentale

Nous avons repris toutes les méthodes décrites (7, 11, 13, 15, 17, 20, 21) et trouvé qu'elles peuvent être ramenées aux schémas suivants:

(*A*) addition, avec agitation, d'une solution aqueuse diluée de KCN à une solution aqueuse diluée de $Ni\,SO_4$ ou $Ni\,Cl_2$. Lavages répétés (eau puis alcool) du précipité bleu vert obtenu.

(*B*) addition lente, avec agitation, d'une solution diluée de KCN à une solution diluée de $NiSO_4$ à 100 °C. Lavages.

(*C*) addition lente simultanée, avec agitation, d'une solution diluée de $NiSO_4$ et d'une solution diluée de KCN à de l'eau légèrement acidifiée et portée à ébullition. Lavages.

(*D*) addition lente avec agitation, d'une solution N de H_2SO_4 à une solution aqueuse diluée de $K_2Ni(CN)_4$ portée à ébullition. Lavages du précipité violet obtenu.

Le mode de séchage s'est avéré un facteur très important de la préparation.

Analyse élémentaire

Le nickel est dosé par complexométrie (EDTA): détermination globale après destruction à chaud par H_2SO_4 concentré; détermination successive des nickel N coordinés (en solution fortement ammoniacale) puis des nickel C coordinés (après leur déplacement des cations complexes $[Ni(CN)_4]^{2-}$ par action de Ag^+). Le contenu en CN est estimé par dosage en retour des ions Ag^+ inutilisés dans la destruction des plans $[Ni(CN)_4]^{2-}$ selon

$$2\,Ag^+ + [Ni(CN)_4]^{2-} \rightarrow 2[Ag(CN)_2]^- + Ni^{2+}$$

Le contenu en H_2O est déterminé soit par thermogravimétrie, soit par différence à partir des quantités en nickel et groupements cyano.

Can. J. Chem. Downloaded from www.nrcresearchpress.com by 210.87.254.105 on 09/05/12
For personal use only.

Can. J. Chem. Downloaded from www.nrcresearchpress.com by 210.87.254.105 on 09/05/12
For personal use only.

TABLEAU 1. "Cyanures de nickel" hydratés: données expérimentales précédentes

N°	Formule proposée, x = degré d'hydratation après sèchage	Mode préparatoire: Type (voir texte)	Mode préparatoire: Séchage	d_{hkl} en Å des raies les plus intenses et intensités relatives	Moment effectif (T amb) en μ_B	Références
I	$Ni(CN)_2 \cdot 7H_2O$	*A*	?	?	?	15, 14
II	$Ni(CN)_2 \cdot 4H_2O$*	?	?	4.39 3.67 3.53 (100) (10) (10)	?	16
III	$Ni(CN)_2 \cdot 3H_2O$	*A*	Air T amb	"amorphe"	2.20	17
IV	$Ni(CN)_2 \cdot 3H_2O$	*B*	?	"cristallisé"	?	7
V	$Ni(CN)_2 \cdot xH_2O$ ($x > 2.3$)	*A*	Air T amb	4.60 6.14 5.61 3.57 (100) (30) (20) (20)	? ?	11
VI	$Ni(CN)_2 \cdot 2.3H_2O$ produit Hopkin et Williams	?	?	4.37 4.44 3.54 3.67 (100) (30) (16) (12)		11
VII	$Ni(CN)_2 \cdot 2H_2O$*	?	?	?	2.28	18
VIII	$Ni(CN)_2 \cdot 2H_2O$	?	?	?	2.46	19
IX	$Ni(CN)_2 \cdot 2H_2O$	*D*	Air 60 °C	cubique a = 10.10 Å 5.05 3.57 3.36 4.12 (100) (100) (20) (10)	2.3	20, 21
X	$Ni(CN)_2 \cdot 1.5H_2O$	*A*	?		?	13
XI	$Ni(CN)_2 \cdot 1.5H_2O$	*C*	Air 60 °C	Orthorhombique a = 7.27 Å, b = 14.08 Å, c = 8.83 Å 4.42 4.40 3.53 3.64 (100) (100) (100) (70)	2.2	20, 21

*Deux composés signalés l'un comme cyanure tétrahydraté (Hoffmann et Höchtlen (2), l'autre comme dihydraté (Ray et Sahu (17), sont en réalité des ammoniacates analogues au produit préparé et étudié par Rayner et Power (4). Ils ne figurent pas dans le tableau 1.

TABLEAU 2. Les différentes phases cyanure de Ni

Mode préparatoire (*cf*: partie expérimentale)	Phase $Ni(CN)_2 \cdot xH_2O$	Domaine de variation de x
D	K (spectre *a*, fig. 1)	1.5–2.5
A, *B*, ou *C* séchage à l'air *T* ambiante	L_0 (spectre *b*, fig. 1)	>2.5
A, *B*, ou *C* séchage à l'air 60 °C	L_1 (spectre *c*, fig. 1)	1–2

Analyse radiocristallographique

Par transmission (chambre de Guinier, diamètre 114 mm $\lambda K\alpha_1$ Cu) et par reflexion (chambre Debye Scherrer, diamètre 114 mm $\lambda K\alpha$Cu, ou diffractomètre $\lambda K\alpha_1$ Cu). Dans ce dernier cas, l'échantillon est déposé sur la plaque support (quartz) par sédimentation de la poudre préalablement mise en suspension, puis séchage.

Absorption ultraviolette – visible – proche infrarouge

Par transmission, sur spectromètre SHIMADZU MPS 502. Echantillons solides, soit dispersés dans une pastille de KBr (concentration variable de 0.5 à 5% selon le ε des bandes étudiées), soit déposés sur la plaque transparente utilisée en diffractométrie X.

Absorption infrarouge

Spectres réalisés sur échantillons en suspension dans le nujol ou en dilution dans KBr (concentration ~1%) avec un spectromètre à réseaux HITACHI EPI G2.

Mesures magnétiques

A l'ambiante; montage type Gouy avec étalon $Mn_2P_2O_7$ ou montage type Faraday avec étalon $HgCo(NCS)_4$.

Résultats et discussion

(I) Préparation et identification

La préparation *D* conduit toujours à un cyanure cristallisé $Ni(CN)_2 \cdot xH_2O$ de couleur violette; son spectre de diffraction (fig. 1*a*) est identique à celui du produit IX (Tableau 1); x varie entre 1.5 et 2.5 selon que le séchage est fait à l'air ou en température jusqu'à 60 °C. Le moment effectif μ_{eff} par atome de nickel est compris entre 2.15 et 2.20.

Les preparations *A*, *B*, et *C* conduisent, après séchage à l'air, à une autre catégorie de produits: bleu vert, avec $x > 2.5$, $\mu_{eff} \sim 2.3$; leurs spectres de diffraction X (fig. 1*b*) comportent en particulier 12 raies signalées par Walker (produit V). Les produits I et III appartiennent vraisemblablement aussi à cette seconde catégorie.

Une troisième catégorie de cyanure de nickel est obtenue à partir des préparations *A*, *B*, et *C* suivie d'un séchage à 60 °C ou d'un très long abandon à l'atmosphère ambiante. Pour ces produits, x est toujours supérieur à 1, parfois à 2, μ_{eff} mesuré est encore voisin de 2.3 μ_B mais leurs spectres de diffraction X sont complètement différents des précédents (Fig. 1*c*). Les produits II, VI, X ainsi que le produit XI indexé par Ludi et Hügi appartiennent certainement à cette catégorie.

La dispersion des valeurs de x à l'intérieur d'une même catégorie de produits sans incidence sur les spectres X de poudre, révèle l'existence (confirmée par spectrométrie d'absorption infrarouge) de molécules H_2O relativement peu liées. Elle s'explique probablement par des différences de conditionnement ou de conservation des produits, et il parait artificiel de classer les cyanures $Ni(CN)_2 \cdot xH_2O$ selon la seule valeur de x. Nous proposons (tableau 2) un classement basé sur l'identification par diffraction X, retenant qu'il existe trois modes préparatoires conduisant chacun à une phase type $Ni(CN)_2 \cdot xH_2O$, de degré d'hydratation x variable entre certaines limites et bien cristallisée. Ces phases types seront notées K, L_0, et L_1 dans la suite de ce travail.[1] Leur analyse conduit toujours à un rapport CN/Ni égal à 2 avec deux types d'atomes de nickel en quantités égales, l'un déplaçable par l'EDTA, l'autre non.

(II) Etude par spectroscopie électronique ultraviolette – visible – proche infrarouge.

Les spectres électroniques des trois phases K, L_0, L_1 ont été comparés à ceux de complexes connus du Ni(II) ($3d^8$) (tableau 3). Leur spectre semble toujours résulter, en première approximation, de la juxtaposition d'un spectre de bandes de transfert de charge (entités plan carré $[Ni(CN)_4]^{2-}$) dans le domaine u.v. et d'un spectre de bandes de transition d–d (entités octaédriques $[NiL_6]$) dans le domaine proche u.v.–visible–proche i.r. Ce résultat, joint à celui des analyses chimiques et magnétiques, permet de généraliser à chacune des phases K, L_0, L_1

[1] K, "quasi cubique"; L_0, Lamellaire à zéro intercalaire; L_1, Lamellaire à 1 intercalaire.

Can. J. Chem. Downloaded from www.nrcresearchpress.com by 210.87.254.105 on 09/05/12
For personal use only.

Can. J. Chem. Downloaded from www.nrcresearchpress.com by 210.87.254.105 on 09/05/12
For personal use only.

TABLEAU 3. Maximum d'absorption en kK

Espèces	μ_B	$^3A_{2g} \rightarrow {}^3T_{2g}$ (F)	$^3A_{2g} \rightarrow {}^1E_g$ (D)	$^3A_{2g} \rightarrow {}^3T_{1g}$ (F)	$^3A_{2g} \rightarrow {}^3T_{1g}$ (P)	$^1A_{1g} \rightarrow {}^1B_{1g}$	$^1A_{1g} \rightarrow {}^1A_{2g}$	$^1A_{1g} \rightarrow {}^1E_g$
K	2.15–2.20	11.3	(13.8)	18.4	*	33.0	35.4	38.3
L_0	2.27	11.0	—	16.9	*	33.0	35.6	38.6
L_1	2.40	9.5 et 11.75	(14.0)	17.2	*	32.9	35.4	38.3
$Ni(NH_3)_2Ni(CN)_4.\frac{1}{4}H_2O$ (présent travail)	2.18	10.35	13.6	17.2	*	32.9	35.3	38.2
$[Ni(NH_3)_6]^{2+}$ (25, 27)		10.75	13.15	17.5	28.2	—	—	—
$[Ni(H_2O)_6]^{2+}$ (25, 27)		8.5	(15.4)	(13.5)	25.3	—	—	—
$K_2Ni(CN)_4$ (26)	—	—	—	—	—	32.3	35.2	37.6

*La bande $^3A_{2g} \rightarrow {}^3T_{1g}$ (P) de $[Ni(H_2O)_2N_4]$, dissimulée sous le transfert de charge $^1A_{1g} \rightarrow {}^1B_{1g}$ de $[Ni(CN)_4]$ beaucoup plus intense, ne peut être repérée. Aucune mesure de l'interaction $^3T_{1g}$ (F) $\rightarrow {}^3T_{1g}$ (P) ne peut donc être effectuée dans ce cas.

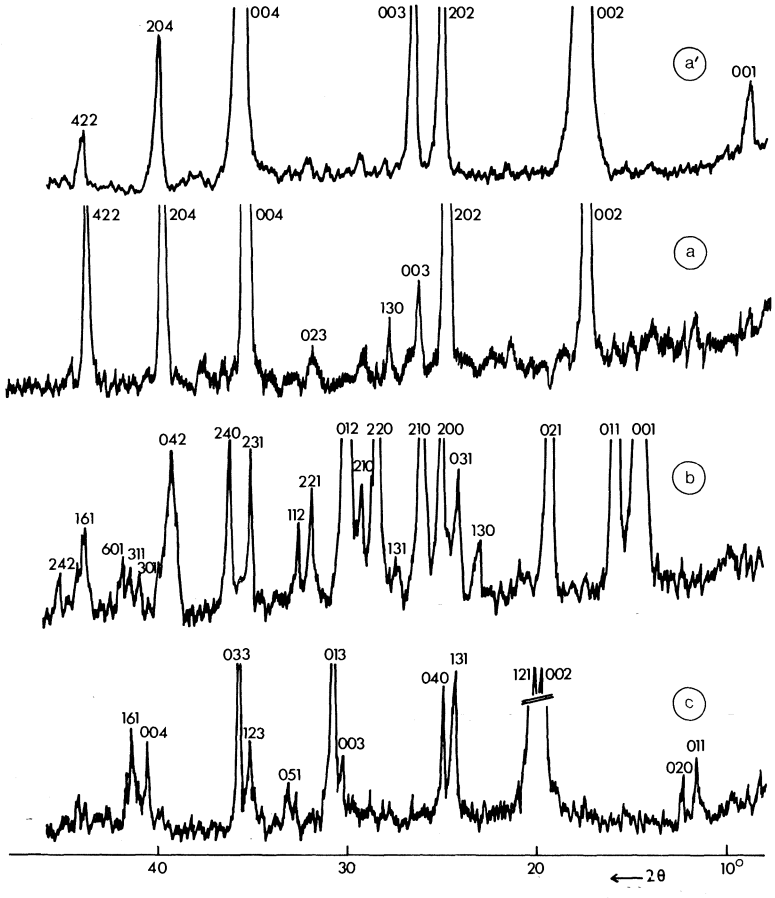

FIG. 1. Diffractogrammes ($\lambda K\alpha_1 Cu$): (*a'*) Phase K (orientation privilégiée due au dépot par sédimentation); (*a*), (*b*), (*c*), respectivement phases K, L_0, et L_1.

la conclusion de Ludi et Hügi (21) concernant le composé XI (phase L_1): la moitié des atomes de Ni occupent le centre d'entités complexes diamagnétiques $[NiC_4]$ de géométrie plan carré; les autres, liés aux atomes N des groupements cyano, occupent le centre d'entités complexes octaédriques seules responsables du paramagnétisme. L'observation par i.r. d'un glissement important de la bande d'élongation ν_{CN} vers les plus grands nombres d'onde (2170 cm^{-1} environ au lieu de 2130 cm^{-1} dans $K_2Ni(CN)_4$) confirme que les ligands CN ne sont plus terminaux et qu'ils assurent le pontage entre les deux types d'atomes métalliques. De la répétition de ce pontage Ni—CN—Ni dans les deux dimensions du plan des complexes $[Ni(CN)_4]^{2-}$ résulte un réseau plan où alternent des entités $[NiC_4]$ et $[NiN_4]$. De part et d'autre de ce réseau bidimensionnel, véritable polymère, les sites de coordination encore disponibles sur les Ni N-coordinés acceptent des molécules H_2O par paires en *trans* des plans $[NiN_4]$. Ainsi, les phases K, L_0, L_1 correspondent aux formules $Ni(H_2O)_2Ni(CN)_4 \cdot yH_2O$, comme le clathrate d'Hofmann et les complexes aminés correspondent à $Ni(NH_3)_2Ni(CN)_4 \cdot 2C_6H_6$ et $Ni(NH_2R)_2Ni(CN)_4$ respectivement.

Bien que, dans les trois phases K, L_0, et L_1, les couches polymères soient constituées de façon analogue, leur mode d'empilement spécifique affecte la position et la forme des bandes d–d: en particulier, la manifestation attendue de la descente en symétrie $O_h \rightarrow D_{4h}$

O_h	$^3A_{2g}$	$^3T_{2g}$ (F)	$^3T_{1g}$ (F)
↓	↓	↙ ↘	↙ ↘
D_{4h}	$^3B_{1g}$	$^3B_{2g}$ ^3E_g	$^3A_{2g}$ ^3E_g

sur les bandes d–d des entités $[Ni(H_2O)_2N_4]$, n'est observée que dans le cas de L_1 pour lequel le niveau $^3T_{2g}$ (F) est notablement dédoublé.

Can. J. Chem. Downloaded from www.nrcresearchpress.com by 210.87.254.105 on 09/05/12
For personal use only.

TABLEAU 4. Caractéristiques des mailles K, L_0 et L_1

	K orthorhombique	L_0 orthorhombique	L_1 orthorhombique
Paramètres	$a = 10.09$ Å $b = 10.15$ Å $c = 10.12$ Å	$a = 7.09$ Å $b = 13.84$ Å $c = 6.10$ Å	$a = 7.26$ Å $b = 14.20$ Å $c = 8.88$ Å
Intervalle caractéristique entre deux couches successives (Basal spacing)	$c/2 = 5.06$ Å	$c = 6.10$ Å	$c/2 = 4.44$ Å
Formule développée	$Ni(H_2O)_2Ni(CN)_4 \cdot yH_2O$ $1 < y < 3$	$Ni(H_2O)_2Ni(CN)_4 \cdot yH_2O$ $y > 3$	$Ni(H_2O)_2Ni(CN)_4 \cdot yH_2O$ $0 < y < 2$
Z: nombre de formule par maille	4	2	4
Masse volumique g/cm^3	Calculée pour $y = 1:1.76$ Calculée pour $y = 2:1.89$ Expérimentale: 1.82	Calculée pour $y = 7:2.13$ Calculée pour $y = 8:2.23$ Expérimentale: 2.18	Calculée pour $y = 0.5:1.93$ Calculée pour $y = 1:2.00$ Expérimentale: 2.00

Du fait de la faible intensité des bandes de transition d–d d'une part, de leur élargissement par effet de taille de grain et l'absorption interne d'autre part, la détermination des fréquences d'absorption n'est pas excellente; cependant nous avons toujours obtenu avec les cyanures complexe étudiés des valeurs supérieures à celles de Ludi et Hügi.

Pour K et L_0, l'écart à la symétrie octaédrique est sans doute trop faible pour se traduire autrement que par l'élargissement asymétrique observé sur les bandes. Dans le cas de la phase K, la symétrie ponctuelle des entités $[Ni(H_2O)_2N_4]$ semble même être restée suffisamment proche de celle d'un complexe NiL_6 pour que l'on puisse appliquer la règle de l'environnement moyen: le calcul de Dq(N), paramètre de champ cristallin pour les atomes N des groupements cyano, effectué à partir de notre valeur expérimentale $(Dq)_{exp} = 1.13$ kK et de la valeur classique (25, 27) $(Dq)_{[Ni(H_2O)_6]^{2+}} = 0.85$ kK, conduit à une valeur de 1.27 kK pour —NC qui situerait ce ligand parmi les plus forts des ligands N coordinés, comparable à l'*O*-phénantroline (25). Ce résultat ne concorde pas avec les conclusions de Shriver et coll. concernant la force du champ de ligand dans le cyanure cubique $K_2NiFe(CN)_6$ (28), où pourtant les distances M—CN—Ni—NC—M et les fréquences ν_{CN} sont voisines de celles observées pour la phase K. Pour expliquer le désaccord concernant Dq(N), on peut penser que du fait de l'empilement des couches $[Ni(H_2O)_2Ni(CN)_4]_\infty$ l'influence des molécules H_2O ligands sur le Ni auquel elles se coordonnent est beaucoup plus importante que dans le complexe hexaquo nickel(II) et qu'il y a eu sous-estimation dans le calcul de Dq(N) de la valeur du paramètre $Dq(H_2O)$.

(III) Indexation et modèles structuraux

L'indexation des diffractogrammes de K, L_0, et L_1 (fig. 1*a–c*) conduit à trois mailles orthorhombiques (tableau 4 et fig. 2). La maille L_1 (fig. 2*c*) est manifestement celle proposée par Ludi et Hügi pour XI ($a = 7.27$ Å; $b = 14.08$ Å; $c = 8.83$ Å). La maille L_0 (fig. 2*b*) est nouvelle et la maille orthorhombique K (fig. 2*a*) diffère fondamentalement de la maille cubique ($a = 10.10$ Å) proposée pour IX (20), malgré la similitude des spectres.

Les masses volumiques calculées à partir de ces résultats sont en bon accord avec les valeurs obtenues par picnométrie en adoptant, dans la formule $Ni(H_2O)_2Ni(CN)_4 \cdot yH_2O$, les valeurs de y fournies par l'analyse. Le mode d'empilement des couches polymères (fig. 2*a–c*) permet de comprendre les différences entre les intensités diffractées observées respectivement dans les spectres de poudre des échantillons non orientés et ceux des échantillons obtenus par sédimentation (fig. 1*a* et *a'*).

En effet, lors de la sédimentation, les différents grains, dont la croissance s'est déjà effectuée en respectant un principe d'empilement, se disposent en couches grossièrement parallèles à la plaque support. L'intensité diffractée par les plans réticulaires auxquelles ces couches s'identifient est alors fortement modifiée et des diffractions d'ordre élevé ($n = 8$) peuvent être observées. Ceci parait incompatible avec une symétrie cubique. La disposition des atomes Ni de la phase K aux nœuds d'un réseau quasi

Can. J. Chem. Downloaded from www.nrcresearchpress.com by 210.87.254.105 on 09/05/12
For personal use only.

Can. J. Chem. Downloaded from www.nrcresearchpress.com by 210.87.254.105 on 09/05/12
For personal use only.

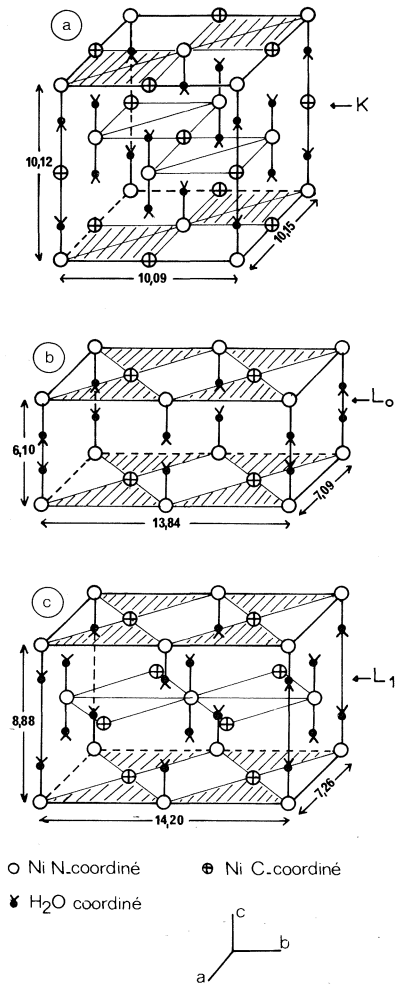

FIG. 2. Mailles élémentaires et modes d'empilement: (*a*), phase K; (*b*), phase L_0; (*c*), phase L_1.

cubique pourrait bien être le résultat fortuit d'une similitude entre la distance Ni—CN—Ni dans la couche et le double de l'intervalle séparant deux couches successives. Par ailleurs si, après empilement des couches, on avait un réseau tétragonal, l'existence de la raie 001 imposerait que la maille soit primitive: la déformation des couches par les yH_2O non coordinées pourrait alors être responsable d'un nouvel abaissement de symétrie: tétragonal → orthorhombique et la maille pourrait être soit primitive, soit à base centrée. C'est à cette dernière éventualité que conduit l'indexation proposée ici (fig. 1) pour K. Tous les indices respectent les règles d'extinction particulières suivantes: $hkl \rightarrow h + k = 2n$; $hk0 \rightarrow h + k = 2n$; $0kl \rightarrow k = 2n$; $h00 \rightarrow h = 2n$; $h0l \rightarrow h = 2n$; $0k0 \rightarrow k = 2n$, et il est possible de suggérer comme groupe d'espace pour la phase K, *C*222, *Cmm*2, *Cmma*, ou *Cmmm*, ce dernier correspondant au shéma de maille proposé fig. 2*a*. Aucune restriction ne semble imposée aux paramètres des deux autres types: leurs mailles sont très probablement primitives.

(IV) Stabilité

S'il est possible d'identifier les trois phases types par leur seul spectre de RX, il est impossible de préciser leur stabilité relative sans tenir compte du rôle essentiel joué par les molécules yH_2O en position interlamellaire. Seule, en effet, l'occupation de l'espace interlamellaire par une quantité importante de molécules H_2O, non coordinées mais en interaction avec leur environnement, rend possible un édifice aussi "aéré" que la phase L_0. La stabilité de cette phase dépend donc de ce remplissage entre les couches successives et l'on comprend l'importance déterminante du mode de séchage sur l'identité du produit après les préparations de type *A*, *B*, ou *C* (tableau 1). La diminution de y au-dessous d'un seuil voisin de 2, lente à $T_{amb.}$, rapide à 60 °C, se traduit par un écroulement (local d'abord, généralisé ensuite) de l'édifice, transformant la phase L_0 (dont l'intervalle fondamental entre couches successives est égal à 6.10 Å) en une phase plus compacte, très comparable, la phase L_1 (d'intervalle fondamental 4.44 Å). Cette transformation $L_0 \rightarrow L_1$ présente d'ailleurs une grande analogie avec la transformation de la phase clathrate en phase ammino-cyanure lors du départ des molécules encagées de $Ni(NH_3)Ni(CN)_4 \cdot 2C_6H_6$ (29).

Enfin nous avons trouvé que la deshydratation ménagée ($60 \leq t \leq 150$ °C) des cyanures hydratés de structure K entraine aussi des modifications structurales vers la phase L_1. Le mécanisme de cette transformation ne peut s'expliquer aussi simplement que celui de la transformation $L_0 \rightarrow L_1$ mais il semble qu'il ne soit plus possible de conserver la structure K pour un complexe $Ni(H_2O)_2Ni(CN)_4 \cdot yH_2O$ en dessous de $y = 1$. En définitive, seule la phase L_1 (issue de L_0 ou de K) pourrait être conservée avec des valeurs de y inférieures à l'unité.

Conclusion

L'étude des spectres de poudre des composés $Ni(CN)_2 \cdot xH_2O$ issus de nombreuses prépara-

tions mentionnées dans la littérature a permis de montrer qu'il n'existe que trois phases distinctes notées K, L_0, et L_1. L'individualité de chacune de ces structures découle surtout du mode d'empilement des couches complexes polymères $[Ni(H_2O)_2Ni(CN)_4]_\infty$ qui les constituent.

La stabilité de ces cyanures hydratés $Ni(H_2O)_2Ni(CN)_4 \cdot yH_2O$, est liée à la présence de y molécules d'eau non coordinées, bloquées en position interlamellaires; interagissant entre elles et avec les molécules d'eau coordinées, elles augmentent considérablement la cohésion entre couches successives. Cependant, comme le montrent les modifications des spectres de transition d–d des pseudo-octaèdres $[Ni(H_2O)_2N_4]$ et la disparition de la symétrie tétragonale dans les réseaux considérés, ces interactions se traduisent par la déformation des couches complexes.

1. K. A. Hofmann et Küspert. Z. Anorg. Chem. **15**, 204 (1897).
2. K. A. Hofmann et Höchtlen. Chem. Ber. **36**. 1149 (1903).
3. J. H. Rayner et H. M. Powell. J. Chem. Soc. 319 (1952).
4. J. H. Rayner et H. M. Powell. J. Chem. Soc. 3412 (1958).
5. E. E. Aynsley et W. A. Campbell. J. Chem. Soc. 4137 (1957).
6. E. E. Aynsley et W. A. Campbell. J. Chem. Soc. 1723 (1958).
7. A. Weiss et R. Frank. Kolloid-Z. **177**, 47 (1961).
8. G. Gawalek, H. Trautmann et H. G. Könnecke. Chem. Techn. Berlin, **7**, 409 (1964).
9. A. I. M. Rae et E. N. Maslen. Z. Krist. **123**, 391 (1966).
10. J. Cano Ruiz, J. M. Esteban Bermudez et E. Gutierrez Rios. Anales Real Soc. Espan. Fis. Quim. **61B**, 1055 (1965).
11. G. F. Walker et D. G. Hawthorne. Trans. Faraday. Soc. **63**, 166 (1966).
12. G. F. Walker et D. G. Hawthorne. Polym. Lett. **6**, 593 (1968).
13. G. F. Walker et D. G. Hawthorne. J. Catal. **15**, 83 (1969).
14. D. M. Bose. Nature, **125**, 708 (1930).
15. H. E. Williams. Cyanogen Compounds. Arnold, London. 1948.
16. J. D. Hanawalt, H. W. Rinn et L. K. Frevel. Ind. Eng. Chem. **10**, 457 (1938).
17. P. Ray et H. Sahu. J. Indian Chem. Soc. **23**, 161 (1946).
18. L. Cambi, A. Cagnasso et E. Tremolada. Gazz. Chim. Ital. **64**, 758 (1934).
19. R. A. Fereday. Proc. Phys. Soc. Lond. **46**, 214 (1934).
20. A. Ludi et R. Hügi. Helv. Chim. Acta, **50**, 1283 (1967).
21. A. Ludi et R. Hügi. Helv. Chim. Acta, **51**, 349 (1968).
22. A. Serres. Ann. Phys. **20**, 441 (1933).
23. W. Biltz, W. Eschweiler et A. Bodenseik. Z. Anorg. Allg. Chem. **170**, 161 (1928).
24. V. M. Bhatnagar et J. A. R. Cloutier. Can. J. Chem. **40**, 1708 (1962).
25. C. K. Jørgensen. Absorption spectra and chemical bonding. Pergamon Press, Oxford. 1962.
26. H. B. Gray et C. J. Ballhausen. J. Am. Chem. Soc. **85**, 260 (1963).
27. O. Bostrup et C. K. Jørgensen. Acta Chem. Scand. **11**. 1223 (1957).
28. D. F. Shriver. S. A. Shriver et S. E. Anderson. Inorg. Chem. **4**. 725 (1965).
29. Y. Mathey et C. Mazieres. Bull. Soc. Chim. **11**, 2918 (1973).

Can. J. Chem. Downloaded from www.nrcresearchpress.com by 210.87.254.105 on 09/05/12
For personal use only.

The Detection of Alkoxy and Other Radicals in the Gamma Radiolysis of Alcohols by an Electron Spin Resonance and Spin Trapping Method[1]

FREDERICK PETER SARGENT AND EDWARD MICHAEL GARDY

Research Chemistry Branch, Atomic Energy of Canada Limited, Whiteshell Nuclear Research Establishment, Pinawa, Manitoba R0E 1L0

Received June 17, 1974

FREDERICK PETER SARGENT and EDWARD MICHAEL GARDY. Can. J. Chem. **52**, 3645 (1974).

The radicals produced during γ radiolysis of methanol, ethanol, 1-propanol, 2-propanol, and *t*-butanol have been trapped by reaction with 2-nitroso-2-methylpropane (*t*-nitrosobutane) to give nitroxides which are detected by e.s.r.

$$R\cdot + t\text{-BuNO} \rightarrow t\text{-BuN}(O\cdot)\text{—R}$$

All the alcohols gave alkoxy radicals and, with the exception of *t*-butanol, radicals derived by the loss of an H atom from the carbon atom adjacent to the OH group. Methyl radicals were detected in *t*-butanol.

FREDERICK PETER SARGENT et EDWARD MICHAEL GARDY. Can. J. Chem. **52**, 3645 (1974).

On a piégé les radicaux produits lors de la radiolyse gamma du méthanol, de l'éthanol, du propanol-1, du propanol-2, et du *tert*-butanol avec du nitroso-2 méthyle-2 propane (*tert*-nitrosobutane) qui conduisent à des radicaux nitroxydes qui peuvent être détectés par r.p.e.

$$R\cdot + t\text{-BuNO} \rightarrow t\text{-BuN}(O\cdot)\text{—R}$$

Tous les alcools donnent des radicaux alcoxy et, sauf l'exception du *tert*-butanol, les radicaux se forment par perte d'un atome d'hydrogène provenant de l'atome de carbone adjacent au groupe OH. Dans le *tert*-butanol, on a détecté des radicaux méthyles.

[Traduit par le journal]

Introduction

The radiation chemistry of alcohols, and in particular that of methanol, has been explained in terms of e_s, H, and $\dot{C}H_2OH$ (1). However, mass spectrometric studies show that the primary ion, CH_3OH^+, can undergo ion molecule reactions 1 and 2 with almost equal probability (2–4).

[1] $CH_3OH^+ + CH_3OH \rightarrow \dot{C}H_2OH + CH_3OH_2^+$

[2] $\rightarrow CH_3O\cdot + CH_3OH_2^+$

It seems reasonable that these reactions should also take place in the liquid phase. There is indirect evidence of methoxy radicals, $CH_3O\cdot$, in irradiated methanol. For example, anisole is formed in mixtures of methanol and benzene (5) and the higher yields of formaldehyde and correspondingly lower yields of glycol in methanolic solutions of KI were attributed to the oxidation of iodide ions by methoxy radicals (6). Although the presence of an oxidizing radical has been demonstrated for pulse irradiated methanol (7, 8), there has been no direct evidence of the formation of methoxy radicals. Electron spin resonance (e.s.r.) studies should provide proof of their existence but none were detected by *in situ* radiolysis (9, 10) of alcohols with 3 MeV electrons (11). This failure to detect alkoxy radicals, RO·, can be attributed to two causes: (*1*) their lifetime is so short that it would be outside the millisecond time resolution of the e.s.r. spectrometer and (*2*) alkoxy radicals would be expected to be similar to OH radicals and to have an orbitally degenerate ground state. This latter characteristic leads to large spin–orbit coupling, fast spin–lattice relaxation, and hence, very broad and undetectable e.s.r. lines.

Although alkoxy radicals, RO·, are not visible by direct e.s.r. examination, they can be made visible by means of a spin trapping technique. This involves the addition of a radical, R·, to a nitroso compound to give a nitroxide (12) which

[1]AECL No. 4799.

Can. J. Chem. Downloaded from www.nrcresearchpress.com by 210.87.254.105 on 09/05/12
For personal use only.

Can. J. Chem. Downloaded from www.nrcresearchpress.com by 210.87.254.105 on 09/05/12
For personal use only.

is long-lived and may be detected by e.s.r. The method has been used to observe alkoxy radicals formed in chemical and photochemical oxidations (13, 14) and we have used it to trap and identify the radicals produced in γ radiolysis of alcohols. We chose to use the trapping compound 2-nitroso-2-methylpropane, *t*-BuNO, because of the greater sensitivity of the e.s.r. spectra of the nitroxide formed in reaction 3 to changes in the nature of the trapped radical, R·.

[3] $$R\cdot + t\text{-BuNO} \rightarrow t\text{-BuN}(O\cdot)\text{—R}$$

The trapping of alkyl radicals in this way results in a nitroxide with a nitrogen coupling constant of 14–16 G, whereas trapping of alkoxy radicals gives values of 27–30 G (12).

During the course of this work, we discovered a paper by Wargon and Williams (15) reporting a similar study which, however, was restricted to methanol. They concentrated on the relative yields of methoxy and hydroxymethyl radicals in the γ radiolysis of methanol at -78 °C. However, we have shown that the results obtained by the *t*-BuNO trapping method should only be used to identify the radicals formed (16). It cannot be used to measure the relative yields of radicals unless the stability of the nitroxides formed on trapping is established. In the case of the alcohols, some of the nitroxides formed by trapping with *t*-BuNO are unstable (16, 17) and decay to an equilibrium value. Therefore, this paper deals only with the identity of the radicals trapped. No conclusions are drawn about their relative yields but it will be shown that alkoxy, alkyl, and hydroxy-alkyl radicals are formed in the γ radiolysis of alcohols.

Experimental

2-Nitroso-2-methylpropane was prepared by the method of Stowell (18). Although this compound exists as a dimer in the solid state, it dissociates to its monomeric form in solution. Stowell gives the equilibrium constants at various temperatures in carbon tetrachloride and suggests that the equilibrium is established in a few minutes. We wished to determine these properties in the alcohols and chose methanol as our typical solvent. This was done by means of n.m.r. of concentrated solutions of *t*-BuNO at various temperatures. The dissociation constants at 54, 37, and 23 °C were 5.9, 2.0, and 1.4 mol l^{-1} respectively. Therefore 0.1 and 0.01 *M* solutions[2] are 89 and 99% dissociated at 23 °C. The kinetic analysis of the establishment of the equilibrium showed it to be a simple dissociation of dimer into monomer. It was found that at 23 °C, a 0.1 *M* solution of *t*-BuNO in methanol was 80% dissociated after 30 min. Therefore all solutions were prepared and stored for at least 1 h before use. Since exposure to light gives unwanted e.s.r. signals from di-*t*-butyl nitroxide (19, 20), they were always stored and used in the dark. The solutions of *t*-BuNO were outgassed on a vacuum line, γ irradiated in an AECL-220 Gamma Cell, and examined with a Varian V4500 e.s.r. spectrometer.[3] Those samples irradiated at -80 °C in a Dry-ice/methanol bath were cooled just prior to radiolysis. Using n.m.r., it was shown that rapidly cooling the solutions to -80 °C does not change the percentage dissociation of the *t*-BuNO over a period of 30 min. Therefore all solutions, after being equilibrated at room temperature, are assumed to be at least 90% dissociated even when cooled to lower temperatures.

The alcohols were of the best quality available commercially. Fractional distillation following refluxing with acidified 2,4-dinitrophenylhydrazine had no effect on the experimental results.

Results

Methanol

Gamma radiolysis of a 0.1 *M* *t*-BuNO solution in methanol at -80 °C gave the spectrum shown in Fig. 1A. This consists of three groups of four lines which are clearly due to interaction with a nitrogen nucleus and three equivalent protons of 29.5 and 1.54 G respectively. This spectrum is from the nitroxide, **1**, formed by the scavenging of methoxy radicals as in reaction 4.

[4] $$CH_3O\cdot + t\text{-BuNO} \rightarrow t\text{-BuN}(O\cdot)\text{—}OCH_3$$

1

The coupling constants agree quite well with the values of 29.4 and 1.4 G found in photochemical studies (12–14). Almost identical spectra were obtained for 0.01 *M* solutions. These results show that γ radiolysis of methanol produces methoxy radicals.

For 0.001 *M* solutions of *t*-BuNO, the spectra showed scavenging of not only methoxy radicals but also hydroxy methyl, CH_2OH. The nitroxide **2** formed by the trapping of the latter, as in reaction 5

[5] $$\dot{C}H_2OH + t\text{-BuNO} \rightarrow t\text{-BuN}(O\cdot)\text{—}CH_2OH$$

2

[2]Concentrations of *t*-BuNO throughout this paper are expressed in mol of monomer.

[3]The synthetic fused quartz sample tubes gave a small e.s.r. peak following γ radiolysis. This has been marked Q in the spectra.

Can. J. Chem. Downloaded from www.nrcresearchpress.com by 210.87.254.105 on 09/05/12
For personal use only.

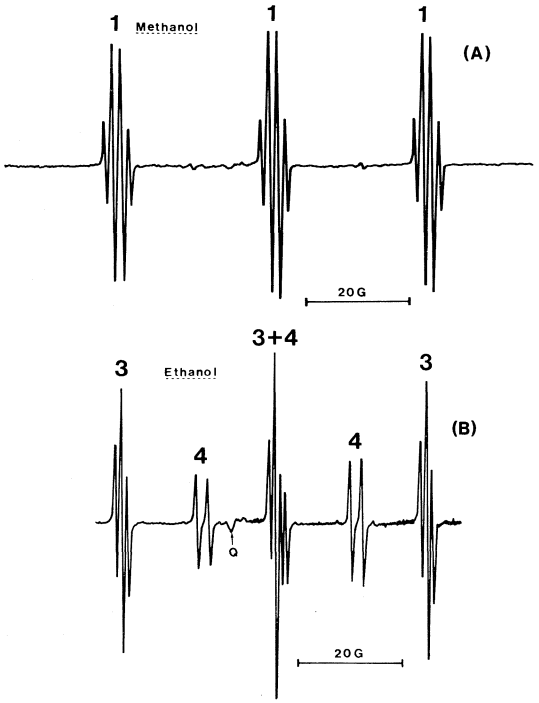

FIG. 1. The e.s.r. spectra observed after γ radiolysis of 0.1 *M* *t*-BuNO solutions at −80 °C.[3] (*a*) Methanol; (B) ethanol.

has a nitrogen coupling constant of 14.4 and the —CH_2— protons coupling is 4.0 G. These spectra demonstrate that γ radiolysis of methanol produces both $CH_3O\cdot$ and $\dot{C}H_2OH$ radicals. The absence of any trapping of $\cdot\dot{C}H_2OH$ in the more concentrated solutions of *t*-BuNO might suggest that $CH_3O\cdot$ is the precursor of all the $\cdot CH_2OH$ radicals (15), by reaction 6,

[6] $CH_3O\cdot + CH_3OH \rightarrow \dot{C}H_2OH + CH_3OH$

but we have shown previously that this is not the case (16). The absence of trapped $\dot{C}H_2OH$ in the 0.1 *M* *t*-BuNO solutions is caused by the instability of nitroxide **2**. This seems to be related to the concentration of the *t*-BuNO and is currently being investigated.

Ethanol

Gamma radiolysis of 0.1 *M* *t*-BuNO solutions in ethanol at −80 °C gave the spectrum shown in Fig. 1B. This is derived from the two nitroxides **3** and **4** formed by the trapping of $CH_3CH_2O\cdot$ and $CH_3\dot{C}HOH$ respectively as in reactions 7 and 8,

[7] $CH_3CH_2O\cdot + t\text{-BuNO} \rightarrow t\text{-BuN}(O\cdot)\text{—}OCH_2CH_3$

3

[8] $CH_3\dot{C}HOH + t\text{-BuNO} \rightarrow t\text{-BuN}(O\cdot)\text{—}C(CH_3)(H)\text{—}OH$

4

The coupling constants are 29.1 and 1.1 G for the nitrogen and the $\cdot OCH_2$— protons respectively in nitroxide **3**, which is in good agreement with the values of 28.9 and 1.1 G reported for the tetraacetate oxidation of ethanol (14). The nitroxide **4** had nitrogen and —$\dot{C}$H— proton couplings of 14.5 and 2.0 G respectively.

1-Propanol

Gamma radiolysis of a 0.1 *M* *t*-BuNO solution in 1-propanol gave the spectrum shown in Fig. 2A which is due to nitroxides **5** and **6** formed by trapping $CH_3CH_2CH_2O\cdot$ and $CH_3CH_2\dot{C}HOH$ respectively, as in reactions 9

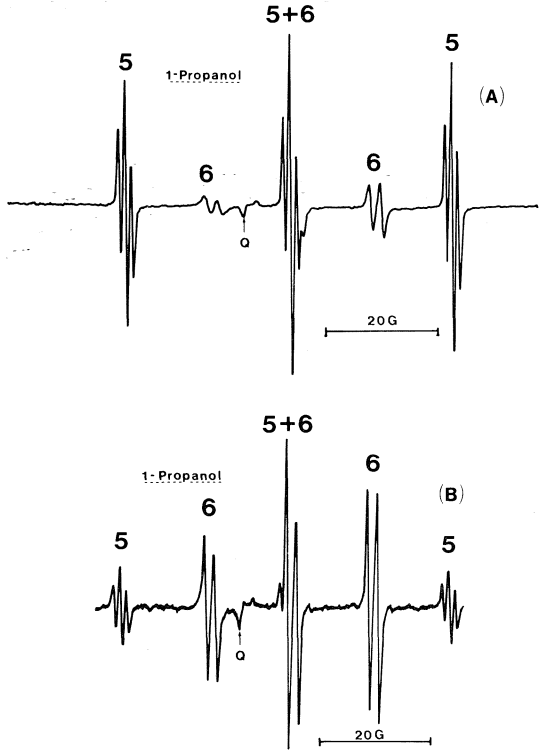

FIG. 2. The e.s.r. spectra observed after γ radiolysis of 0.1 *M* *t*-BuNO solutions in 1-propanol at −80 °C.[3] (A) Recorded at −80 °C; (B) recorded at −20 °C.

Can. J. Chem. Downloaded from www.nrcresearchpress.com by 210.87.254.105 on 09/05/12
For personal use only.

and 10. Since trapping of either $CH_3CH_2\dot{C}HOH$ or $CH_3\dot{C}HCH_2OH$ would give similar spectra, the assignment of **6** is ambiguous; however, by analogy with the other alcohols $CH_3CH_2\dot{C}HOH$ is the most probable.

[9]
$$CH_3CH_2CH_2O\cdot + t\text{-BuNO} \rightarrow t\text{-BuN}(O\cdot)\text{—}OCH_2CH_2CH_3$$
5

[10]
$$CH_3CH_2\dot{C}HOH + t\text{-BuNO} \rightarrow t\text{-BuN}(O)\text{—}CH(OH)\text{—}CH_2CH_3$$
6

The coupling constants for **5** were 29.4 and 1.2 G for the nitrogen and $—OCH_2—$ protons respectively. The values for **6** were 14.5 and 1.8 G for the nitrogen and the —CH— proton respectively. The spectrum of nitroxide **6** appears to be weak in Fig. 2A because the high viscosity of 1-propanol at −80 °C makes the lines broad. These became much more intense on warming to −20 °C, Fig. 2B. However, double integration of the peaks showed that the area remained the same and that the effect was due to changes in the line widths only.

2-Propanol

Gamma radiolysis of a solution of 0.1 *M* *t*-BuNO in 2-propanol at −80 °C gave the spectrum in Fig. 3A. This is due to the nitroxides **7** and **8** which are formed by trapping of $(CH_3)_2CHO\cdot$ and $(CH_3)_2\dot{C}OH$ respectively as in reactions 11 and 12,

[11]
$$(CH_3)_2CHO\cdot + t\text{-BuNO} \rightarrow t\text{-BuN}(O)\text{—}OCH(CH_3)_2$$
7

[12]
$$(CH_3)_2\dot{C}OH + t\text{-BuNO} \rightarrow t\text{-BuN}(O\cdot)\text{—}C(OH)(CH_3)_2$$
8

The nitroxide **7** has a nitrogen coupling constant of 28.4 G but gives no resolvable proton splitting. This is in agreement with the reported spectra (13). Nitroxide **8** also showed only a nitrogen coupling of 15.9 G. This nitroxide, formed by trapping $(CH_3)_2\dot{C}OH$, is less intense than expected. This is linewidth effect caused by the high viscosity of the 2-propanol at −80° C. At higher temperatures the lines narrow and become correspondingly more intense. At −40 °C this nitroxide decays and at 0 °C its half life is 3.0 s. This explains the failure by Perkins *et al.* to detect $(CH_3)_2\dot{C}OH$ in their photochemical studies at room temperature (20).

t-Butanol

Since the melting point of *t*-butanol is 25 °C solutions of 0.1 *M* *t*-BuNO were prepared, γ-irradiated, and examined at about 30 °C. The spectrum shown in Fig. 3B was recorded 5 min after radiolysis. The peaks labelled **9** are due to the trapping of *t*-butoxy radicals by reaction 13

[13]
$$t\text{-BuO}\cdot + t\text{-BuNO} \rightarrow t\text{-BuN}(O\cdot)\text{—}Ot\text{—Bu}$$
9

The nitrogen coupling constant for **9** was 27.0 G. The peaks marked **10** are not identified but they have a nitrogen coupling of 16.0 G. The weaker peaks were examined at higher gains and some of them were shown to be due to the nitroxide formed by trapping methyl radicals. Some other less intense peaks in the spectra are tentatively assigned to trapping of $\cdot CH_2C(CH_3)_2OH$.

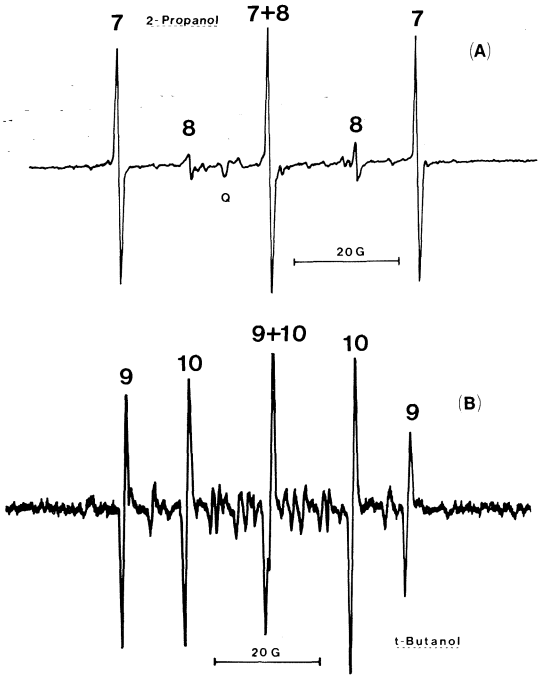

FIG. 3. The e.s.r. spectra observed after γ radiolysis of 0.1 *M* *t*-BuNO solutions in (A) 2-propanol at −80 °C and (B) *t*-butanol at +30 °C.[3]

Can. J. Chem. Downloaded from www.nrcresearchpress.com by 210.87.254.105 on 09/05/12
For personal use only.

Discussion

The results show that γ radiolysis of all the alcohols studied produced alkoxy radicals which are trapped by the *t*-BuNO. Apart from *t*-butanol, all the alcohols also produced hydroxy alkyl radicals by the loss of a hydrogen atom from the carbon adjacent to the hydroxyl group. This suggests that in all cases the primary cation formed in the γ radiolysis can react to give alkoxy radicals in reaction 14

[14] $ROH^+ + ROH \rightarrow RO\cdot + ROH_2^+$

With the exception of *t*-butanol, the primary cation can also react to give α-hydroxy alkyl radicals by reaction 15

[15] $RR'CHOH^+ + RR'CHOH \rightarrow RR'\dot{C}OH + RR'CHOH_2^+$

Although it has been shown previously (16) that the relative yields of the nitroxides detected does not necessarily reflect the relative yields of the radicals formed in the radiolysis, the results in the present study show that alkoxy radicals are not the sole products of the radiolysis.

In *t*-butanol, methyl radicals were trapped. These are undoubtedly the precursors of the molecular yields of methane and ethane from this alcohol (21). The failure to detect methyl trapping in the other alcohols does not preclude their formation. The resulting nitroxides are unstable and the net trapping efficiency will be less because the viscosity is less and the rate of H abstraction by methyl radicals is higher.

The unidentified nitroxide **10** observed in *t*-butanol has a nitrogen coupling of 16 G which must come from trapping an alkyl-like radical. Although **10** might be in part derived from the trapping of radicals produced in the γ radiolysis, it more likely originates from the decomposition of **9**. This has been shown (22) to proceed by reaction 16 and the *t*-butyl radicals formed would then be trapped by *t*-BuNO to give di-*t*-butyl nitroxide 17.

[16] $t\text{-BuN}(\text{O})\text{O}t\text{-Bu} \rightarrow t\text{-Bu}\cdot + \text{N}(\text{O})\text{O}t\text{-Bu}$

[17] $t\text{-Bu}\cdot + t\text{-BuNO} \rightarrow t\text{-BuN}(\text{O})t\text{-Bu}$

Therefore nitroxide **10** is identified as di-*t*-butyl nitroxide.

The failure to detect H atoms or electrons seems to be in conflict with the recent observations of Mao and Kevan (23, 24) who report the trapping of H atoms in methanol by a nitrone. However, we have shown that the H and (or) electron adduct of *t*-BuNO are unstable and rapidly decay even at −80 °C (16). This might also explain the failure to detect the H-atom transfer from $(CH_3)_2\dot{C}OH$ to *t*-BuNO reported by Perkins *et al.* (20). These authors used a continuous production method and therefore were able to detect the steady state concentration of *t*-BuNHO·. It should also be pointed out that since they did not detect the trapping of $(CH_3)_2\dot{C}OH$ it is possible that the system is more complicated than it first appears. We observe that $(CH_3)_2\dot{C}OH$ is trapped but that it decays at ambient temperatures. It is possible that the product of this decay produces *t*-BuNHO· in the Perkins system or that only a very small fraction of the $(CH_3)_2\dot{C}OH$ radicals undergo the H-atom transfer reaction.

Spin trapping studies such as the ones described in this report are providing information about the role of free radicals in radiation chemistry of liquids. By using a direct method of radiolysis and detection (16), we hope to be able to extend this approach to the measurement of yields and rate constants.

We thank Professor M. J. Perkins for drawing our attention to the Stowell synthesis of *t*-BuNO and Dr. H. R. Falle for his assistance in preparing this compound. We wish also to thank Richard Dickinson and the Department of Chemistry of the University of Manitoba for some of the n.m.r. spectra.

1. J. W. T. Spinks and R. J. Woods. An introduction to radiation chemistry. Wiley, New York. 1964.
2. L. P. Theard and W. H. Hamill. J. Am. Chem. Soc. **84**, 1134 (1962).
3. J. C. J. Thynne, F. K. Amenu-Kpodo, and A. G. Harrison. Can. J. Chem. **44**, 1655 (1966).
4. D. J. Hyatt, E. A. Dodman, and M. J. Henchman. Ion–molecule reactions in the gas phase. Adv. Chem. Ser. No. 58, Am. Chem. Soc. Washington. 1966. p. 131.
5. A. Ekstrom and J. L. Garnett. J. Phys. Chem. **70**, 324 (1966).
6. L. M. Theard and M. Burton. J. Phys. Chem. **67**, 59 (1963).
7. R. V. Bensasson and J. K. Thomas. Int. J. Radiat. Phys. Chem. **1**, 185 (1969).
8. (*a*) F. S. Dainton, I. Janovski, and G. A. Salmon. Proc. R. Soc. A, **327**, 305 (1972); (*b*) D. H. Ellison, G. A. Salmon, and F. Wilkinson. Proc. R. Soc. A, **328**, 23 (1972).

9. R. W. FESSENDEN and R. H. SCHULER. J. Chem. Phys. **39**, 2147 (1963).
10. K. EIBEN and R. W. FESSENDEN. J. Phys. Chem. **75**, 1186 (1971).
11. F. P. SARGENT and E. M. GARDY. J. Phys. Chem. **78**, 1977 (1974).
12. E. G. JANZEN. Acc. Chem. Res. **4**, 31 (1971).
13. (*a*) A. MACKOR, TH. A. J. W. WAJER, and TH. J. DEBOER. Tetrahedron Lett. 385 (1967); (*b*) S. FORSHULT, C. LAGERCRANTZ, and K. TORSELL. Acta Chem. Scand. **23**, 522 (1969).
14. A. LEDWITH, P. J. RUSSELL, and L. H. SUTCLIFFE. Proc. R. Soc. Lond. A, **332**, 151 (1973).
15. J. A. WARGON and F. WILLIAMS. J. Am. Chem. Soc. **94**, 7917 (1972).
16. F. P. SARGENT, E. M. GARDY, and H. R. FALLE. Chem. Phys. Lett. **24**, 120 (1974).
17. (*a*) D. F. BOWMAN, J. L. BROKENSHIRE, T. GILLAN, and K. U. INGOLD. J. Am. Chem. Soc. **93**, 6551 (1971); (*b*) D. F. BOWMAN, T. GILLAN, and K. U. INGOLD. J. Am. Chem. Soc. **93**, 6555 (1971).
18. J. C. STOCKWELL. J. Org. Chem. **36**, 3055 (1971).
19. A. MACKOR, TH. A. J. W. WAJER, and TH. J. DEBOER. Tetrahedron Lett. 2115 (1966).
20. M. J. PERKINS, P. WARD, and A. HORSFIELD. J. Chem. Soc. B, 395 (1970).
21. R. H. JOHNSEN and D. A. BECKER. J. Phys. Chem. **67**, 831 (1963).
22. M. J. PERKINS and B. P. ROBERTS. J. Chem. Soc. Perkin II, 297 (1974).
23. S. W. MAO and L. KEVAN. Chem. Phys. Lett. **24**, 505 (1974).
24. S. W. MAO and L. KEVAN. J. Phys. Chem. **78**, 91 (1974).

Can. J. Chem. Downloaded from www.nrcresearchpress.com by 210.87.254.105 on 09/05/12
For personal use only.

The Oxidation of Acetals by Ozone[1]

PIERRE DESLONGCHAMPS,[2] PAUL ATLANI,[3] DANIEL FRÉHEL, ALAIN MALAVAL, AND CLAUDE MOREAU[4]

Laboratoire de synthèse organique, Département de chimie, Université de Sherbrooke, Sherbrooke, Québec J1K 2R1

Received April 29, 1974

PIERRE DESLONGCHAMPS, PAUL ATLANI, DANIEL FRÉHEL, ALAIN MALAVAL, and CLAUDE MOREAU. Can. J. Chem. **52**, 3651 (1974).

Ozone reacts very smoothly with acetals to give the corresponding esters. There are six *gauche* conformations that are theoretically possible for an acetal function. It is shown that only three of them are reactive toward ozone. It is proposed that a reactive acetal function must take a conformation in which each oxygen must have an electron pair orbital oriented antiperiplanar to the C—H bond. The mechanism of this reaction is also discussed.

PIERRE DESLONGCHAMPS, PAUL ATLANI, DANIEL FRÉHEL, ALAIN MALAVAL et CLAUDE MOREAU. Can. J. Chem. **52**, 3651 (1974).

Les acétals se transforment facilement en esters correspondants sous l'action de l'ozone. Il y a six conformations *gauches* pour une fonction acétal dont trois seulement sont réactives avec l'ozone. Il est de plus proposé que chaque atome d'oxygene de la fonction acétal doit posséder une orbitale d'électrons libres orientée de manière antipériplanaire par rapport au lien C—H pour qu'elle soit réactive avec l'ozone. Le mécanisme de réaction est aussi discuté.

Can. J. Chem. Downloaded from www.nrcresearchpress.com by 210.87.254.105 on 09/05/12
For personal use only.

We reported in 1971 (1) in preliminary form that ozone reacts in essentially quantitative yield and in a completely specific fashion with the acetal function of an aldehyde to give the corresponding ester.

$$\underset{\displaystyle H}{\underset{|}{R—C}}(OR')_2 + O_3 \rightarrow R—COOR' + R'—OH + O_2$$

In 1972, we also published in a preliminary communication (2) the relationship between the precise conformation of the acetal function and its reactivity toward ozone. We have now completed this work and wish to report in detail the result of our entire investigation.

Table 1 describes the results of the oxidation of different types of simple acetals. It clearly indicates that this new oxidation reaction is a general one; the nature of the alkyl groups (R and R′) of the acetal function does not influence the final result. Each example shows that this reaction proceeds in essentially quantitative yield.

However, there exists a tremendous difference in the rate of reaction as particularly shown by examples 1–5 (Table 1): the cyclic acetals react much faster than the acyclic ones. For instance, 10 mmol of dimethoxy acetal was completely oxidized after 15 h, while the same molar quantity of the five-membered ring dioxolane acetal required only 10 min. In fact, this last reaction is practically instantaneous since the ozone was generated at a rate of 1 mmol per minute and the ozone generator was stopped after 10 min, just when the blue color of ozone appeared in the reaction mixture. This result suggests that a completely new method for the titration of ozone at −78° can in principle be developed by utilizing this remarkably fast and specific reaction between ozone and dioxolane acetals. We took advantage of this instantaneous reaction to establish the stoichiometry of the reaction. A saturated solution of ozone in ethyl acetate was prepared at −78°. A solution (0.01 *M*) of a dioxolane acetal in ethyl acetate was slowly added at −78°. The blue color of ozone disappeared rapidly. During the addition, there was a constant formation of a gas which was measured. The molar quantity of oxygen produced was found identical to the amount of acetal used. This indicated that 1 mol of ozone

[1]Support for this work by the National Research Council of Canada, the Alfred P. Sloan Foundation, and by the "Ministère de l'Education" Québec, is gratefully acknowledged.

[2]A. P. Sloan Fellow, 1970–1972. To whom all correspondence should be addressed.

[3]Holder of a "bourse postdoctorale France–Québec", 1971–1972. Deceased January 1974.

[4]Holder of a "bourse postdoctorale France–Québec", 1973–1974.

TABLE 1. Oxidation of various types of acetals[a]

Reaction No.	Acetal	Product	Reaction time	Yield (%)[d]
1	n-C_6H_{13}—$CH(OCH_3)_2$	n-C_6H_{13}—$COOCH_3$[b]	15 h	91
2	n-C_6H_{13}—$CH(OC_2H_5)_2$	n-C_6H_{13}—$COOC_2H_5$[b]	8 h	94
3	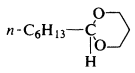	n-C_6H_{13}—COO—CH_2—CH_2—OH[c]	2 h	97
4	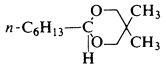	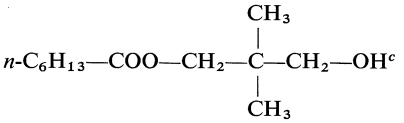	1 h	98
5	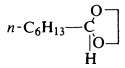	n-C_6H_{13}—COO—CH_2—CH_2—OH[c]	10 min	98
6	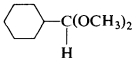	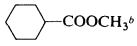	13 h	98
7	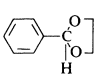	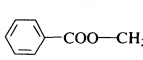	10 min	100

[a]Reaction was carried out at −78° in ethyl acetate using 10 mmol of acetal; rate of ozone: 1 mmol/min.
[b]Spectroscopic (i.r., n.m.r.) data was obtained for this compound which was also compared with an authentic sample.
[c]This product was isolated as the corresponding acetate derivative (Ac_2O–pyridine). Spectroscopic (i.r., n.m.r.) and satisfactory analytical data have been obtained for this derivative.
[d]Yield of isolated material.

reacts at −78° with 1 mol of acetal yielding 1 mol of ester and 1 mol of oxygen.

Table 2 shows that the oxidation of open-chain acetals (dialkoxy acetal) can be achieved more conveniently if the reaction is simply carried out at room temperature. This large difference in rates between cyclic and acyclic acetals is easily explained when the preferred conformation of each acetal is taken into consideration (*vide infra*).

This new reaction constitutes a novel method for converting an aldehyde into an ester.[5] It is likely that it proceeds via the insertion of ozone into the C—H bond of the acetal (**1**) forming an intermediate[6] such as **2** or **3** which then breaks down to give the reaction products, the ester **4** and the alcohol **5**. Such an insertion reaction has been shown to be operative in the reaction of ozone with simple ethers, silanes, hydrocarbons (anthrone), and aldehydes (6). Based on our study of the oxidation of various complex acetals by ozone (2), the results obtained on the hydrolysis of complex orthoesters (4), and the work of King and Allbutt (7) on the stereoselective hydrolysis of dioxolenium ions and of orthoesters, we conclude that the ozonolysis of acetals doubtless proceeds via the formation of an intermediate analogous to a hemiorthoester.

TABLE 2. Effect of temperature on the rate of oxidation of n-C_6H_5—$CH(OCH_3)_2$ in ethyl acetate

Acetyl (mmol)	Reaction temperature (°C)	Reaction time (h)
13.6	−78	15
13.5	0	1.5
23.2	25	1.5

All the acetals studied so far were symmetrical, since the OR groups were identical. It was of interest to examine the oxidation of unsymmetrical acetals. If a tetrahedral intermediate is formed during the oxidation of an acetal function, a substrate such as **6** should lead to an

[5]For a practical example of the conversion of a dimethoxy acetal into a methyl ester, see ref. 3.

[6]We have recognized very early during our work that the intermediate which is formed during the oxidation of acetals is either identical or equivalent to a hemiorthoester which is the tetrahedral intermediate formed during the transesterification of esters. This finding has led us to the development of a new stereoelectronic theory for the hydrolysis of esters (4), and later, of amides (5).

Can. J. Chem. Downloaded from www.nrcresearchpress.com by 210.87.254.105 on 09/05/12
For personal use only.

TABLE 3. Oxidation of tetrahydropyranyl ether[a]

Acetal	Amount (mmol)	Product[b]	Reaction time (h)	Yield[c] (%)
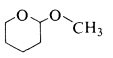	40	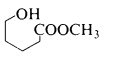	2	99
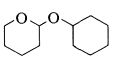	10	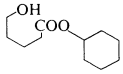	1	91
	30	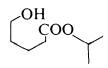	2	95
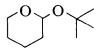	12.6	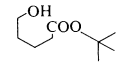	3	91

[a]Reaction carried out at −78° in ethyl acetate; rate of ozone: 1 mmol/min.
[b]This product was isolated as the corresponding acetate derivative (Ac_2O–pyridine). Spectroscopic (i.r., n.m.r.) and satisfactory analytical data have been obtained for this derivative.
[c]Yield of isolated material.

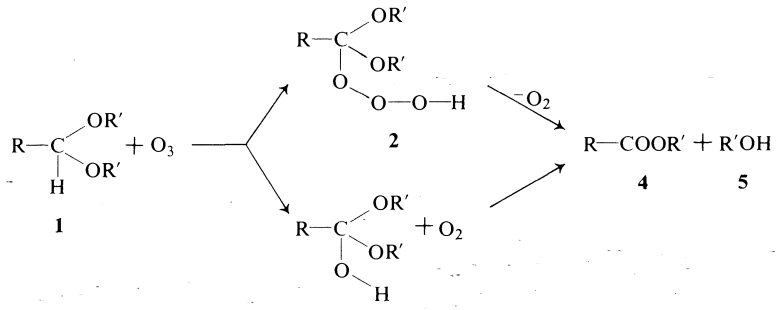

intermediate such as **7** which can in principle decompose in two different ways to give the hydroxy ester **8**, or the lactone **9** plus the alcohol **10**. We found experimentally, that ozone reacts

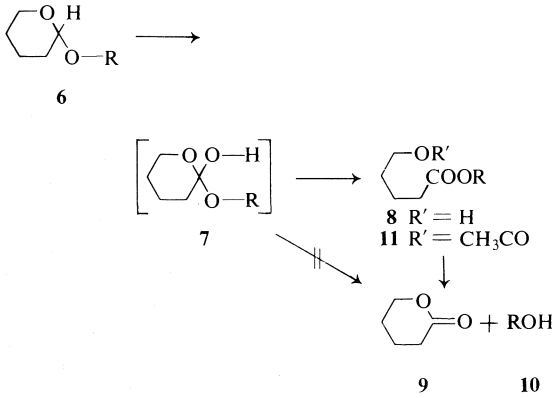

very smoothly with tetrahydropyranyl ethers (an unsymmetrical acetal) in a completely specific manner, yielding the hydroxy ester **8** exclusively. No trace of lactone **9** could be detected. These results are summarized in Table 3. This reaction also constitutes a new highly efficient method for the cleavage of the tetrahydropyranyl ether protecting group under neutral conditions. Simple heating of the resulting hydroxy ester **8**, in a neutral solvent, produces δ-valerolactone (**9**) and liberates the alcohol **10**.[7]

[7]The hydroxy ester **8** can be esterified (Ac_2O–pyridine) to give the acetoxy ester **11**. Therefore, whenever an alcohol function needs to be protected by an acid sensitive blocking group and then by an ester type protecting group which is not as sensitive to acid, a tetrahydropyranol ether can be used, transformed by ozone into the hydroxy ester **8** which can then be acetylated to give the acetoxy ester **11**.

Can. J. Chem. Downloaded from www.nrcresearchpress.com by 210.87.254.105 on 09/05/12
For personal use only.

We have also demonstrated that tetrahydrofuranyl ethers (**12**) (8) were smoothly oxidized by ozone to the hydroxy ester **14** exclusively (Table 4), thus the specific opening of a tetra-

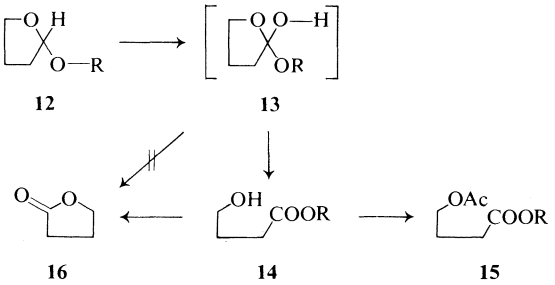

12 **13** **16** **14** **15**

hedral intermediate (**13** → **14**) was again observed. In these experiments, acetic anhydride and sodium acetate was used as solvent in order to trap the hydroxy ester **14** which was subsequently isolated as the corresponding acetoxy ester **15**. The use of this solvent system was found to be a very convenient means of preventing lactonization of the hydroxy ester (**14** → **16**). We have also found that it served another purpose when the ozonolysis reaction had to be carried out for long periods of time at room temperature with excess of ozone; it protected against further oxidation of the primary and secondary alcohols which are formed during the reaction. In cases where there is no need to trap an alcohol function, it was our experience that reagent grade ethyl acetate was the best solvent. However, other solvents which do not react with ozone can be used with success such as carbon tetrachloride, dichloromethane, and glacial acetic acid. When the reaction is carried out at room temperature and takes a few hours, large excesses of ozone–oxygen gas go through the solution, therefore a high boiling solvent is preferred to reduce the amount of solvent lost by evaporation.

TABLE 4. Oxidation of tetrahydrofuranyl ether[a]

Acetal	Product[b]	Yield[c] (%)
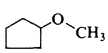	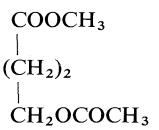	85
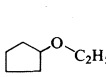	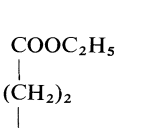	87

[a]Reaction carried out with 10 mmol of acetal at room temperature for 6 h in acetic anhydride – sodium acetate; rate of ozone: 1 mmol/min.
[b]Spectroscopic (i.r., n.m.r.) and satisfactory analytical data (±0.3) have been obtained for this product.
[c]Yield of isolated material.

After completing our work on the simple tetrahydropyranyl ethers, the next logical step was to study this new reaction on tetrahydropyranyl ethers which possess a rigid chair conformation. Consequently, the oxidation of a series of conformationally rigid α- and β-methyl glycopyranosides was undertaken. We found that β-methyl glycopyranosides were converted smoothly into their corresponding 5-acetoxy aldonic acid methyl esters whereas the α-methyl glycopyranosides were recovered unchanged in quantitative yield. β-Anomers of methyl 2,3,4,6-tetra-*O*-acetyl-D-glucopyranoside (**17**), -D-mannopyranoside (**18**)[8], and -D-galactopyranoside (**19**)[8] were converted into their corresponding penta-*O*-acetyl-D-aldonic acid methyl esters **20**, **21**, and **22**. However, their respective α-anomers **23**, **24**, and **25**[8] were found to be completely inert toward ozone. Poly-*O*-acetyl methyl β-glycosides were used because the oxidation of the anomeric center is a fairly slow reaction and the hydroxyl groups need protection against ozone. Acetic anhydride – sodium acetate was used as solvent to trap *in situ* the newly formed hydroxyl group at position 5 so that a good yield of poly-*O*-acetyl aldonic acid methyl ester could be isolated. When there is no substituent at position 2, as in methyl 2-deoxy-3,4,6-tri-*O*-acetyl-β-D-glucopyranoside (**26**), the oxidation of the anomeric center is sufficiently rapid that there is no need to protect the 5-hydroxyl group which is being formed. When glacial acetic acid is used as solvent, methyl 2-deoxy-3,4,6-tri-*O*-acetyl-5-hydroxy-D-gluconate (**27**) can be isolated in good yield. Acetylation of **27** gave methyl tetra-*O*-acetyl-2-deoxy-D-gluconate (**28**), which can also be obtained directly by carrying out the oxidation of **26** in acetic anhydride and sodium acetate. The nonreactivity of the α-glucosides suggests a new method for the separation and the purification of α-glycoside from a mixture of α and β. We have used this method successfully to purify methyl 2-deoxy-3,4,6-tri-*O*-acetyl-α-D-glucopyranoside (**29**). Triacetyl glucal was trans-

[8]We are grateful to Professor A. S. Perlin (McGill University) for his generous gift of this compound.

Can. J. Chem. Downloaded from www.nrcresearchpress.com by 210.87.254.105 on 09/05/12
For personal use only.

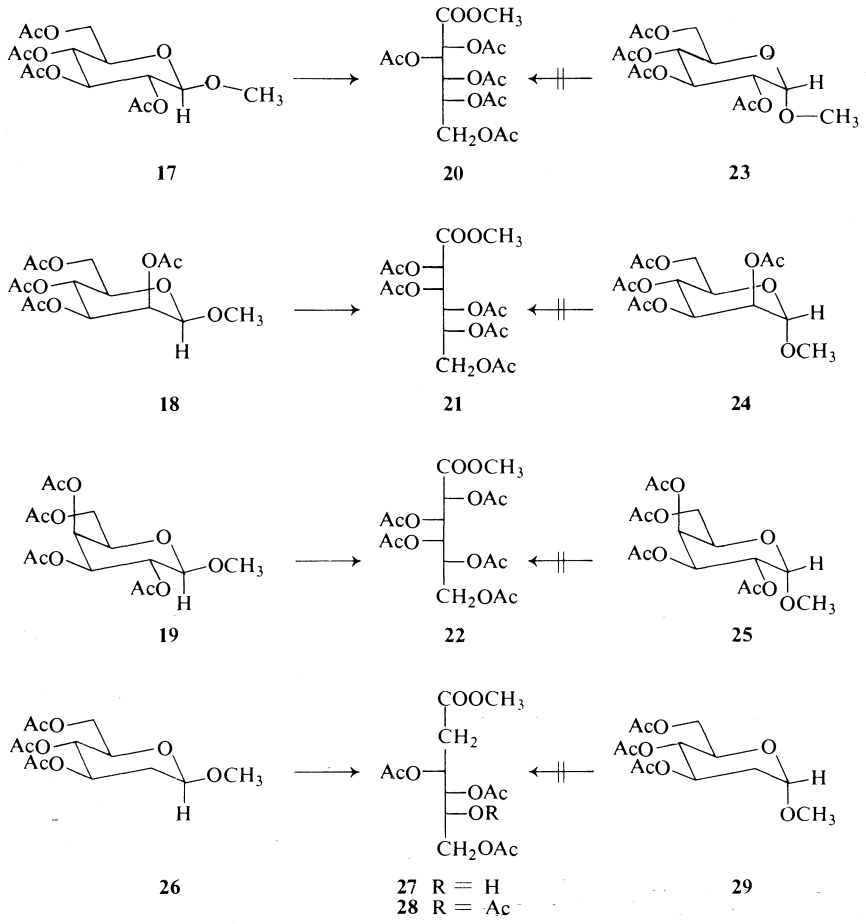

formed into a mixture of the two anomers of methyl 2-deoxy-3,4,6-tri-*O*-acetyl-D-glucopyranoside (9). The pure β-anomer (**26**) was obtained by crystallization. The remaining mixture of α- and β-anomers in the mother liquor was then treated with ozone in ethyl acetate. This process converted the β-anomer into methyl 5-hydroxy-2-deoxy-3,4,6-tri-*O*-acetyl gluconate (**27**) which has a much lower R_f value on thin-layer chromatography than the unreacted α-anomer. The α-anomer **29** was easily obtained pure by a simple column chromatography.

So far we have shown that cyclic acetals react with ozone, dialkoxy acetals react but the rate is low, β-glycosides are reactive, and α-glycosides are inert. It was clear from these results that there was a relationship between the conformation of the acetal function and its reactivity toward ozone. This led us to propose that any reactive conformer must have on each oxygen atom a lone pair orbital oriented antiperiplanar to the C—H bond of the acetal function (1).

This requirement was met with dioxolane acetal (**30**) and the most stable rotamer of β-glycoside (**31**) (10). In an α-glycoside, which can be represented as its favored rotamer by structure **32**, the ring oxygen orbitals are not oriented antiperiplanar to the C—H bond; it is the ring carbon – oxygen bond which is antiperiplanar. The lone pair orbitals of the ring oxygen in an α-glycoside (regardless of the rotamer) are never available, indicating that the oxidation does not proceed if only one oxygen has the proper orbital orientation. Furthermore, dialkoxy acetals are known (11) to exist in one preferred conformation (**33**) which is identical to the favored rotamer of an α-glycoside (**32**). This is quite normal because this conformer is the only one which avoids the anomeric effect (10). This conformer is inert toward ozone. In order to react with ozone, the

Can. J. Chem. Downloaded from www.nrcresearchpress.com by 210.87.254.105 on 09/05/12
For personal use only.

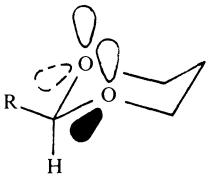

30

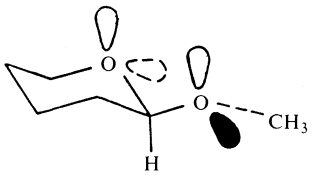

31

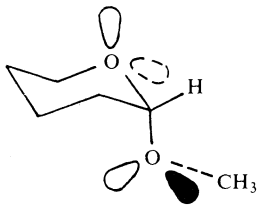

32

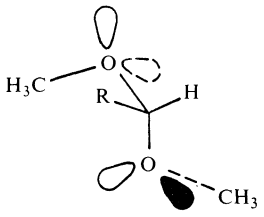

33

dialkoxy acetal must adopt another conformation which has proper orbital orientation. This is possible with the dialkoxy acetal but impossible with chair-rigid α-glycosides. However, any reactive conformer of the dialkoxy acetal will be present only in a very small amount at equilibrium because such a conformer has to overcome the anomeric effect which exists when two lone pair orbitals are in a 1,3-synperiplanar arrangement.[9] Consequently, the reaction rate which is dependent upon the concentration of the reactive conformer is going to be fairly low.

It was clear at this stage of our investigation that the postulate of the orientation of the lone pairs had to be verified in a more rigorous manner. Consequently, we had to consider all the possible *gauche* conformers that an acetal function can assume, make rigid chemical models of each of them if possible, and verify their respective reactivity with ozone.

Scheme 1 shows the nine *gauche* conformers that are theoretically possible for an acetal function. Conformers A, B, and D have no plane of symmetry and in fact conformers A′, B′, and D′ are their respective mirror images, therefore chemically equivalent. The remaining conformers C, E, and F possess a plane of symmetry. Consequently, there are only six conformers (A, B, C, D, E, and F) which are chemically different for an acetal function. Of those, only conformers A, C, and F possess a lone pair orbital on each oxygen oriented antiperiplanar to the C—H bond. Conformers B and D have only one oxygen with a lone pair properly oriented, and conformer E has none. Consequently if our postulate is valid, conformers B, D, and E should be inert and conformers A, C, and F should be reactive toward ozone.

Scheme 2 describes the conformers of Scheme 1 in which a six-membered ring has been incorporated. One can observe that the first three conformers A, B, and C represent the three rotamers of a conformationally rigid β-glycoside. Conformers D, E, and B′ correspond to the three conformers of a rigid α-glycoside (10). We have found that α-glycosides are inert toward ozone; conformers D, E, and B′ are therefore not reactive. Conformer B′ is chemically equivalent to conformer B, they are mirror image in Scheme 1, B is therefore not reactive. These conformers were further eliminated by observing that *cis*-1,8-dioxaoctahydronaphthalene (**34**) does

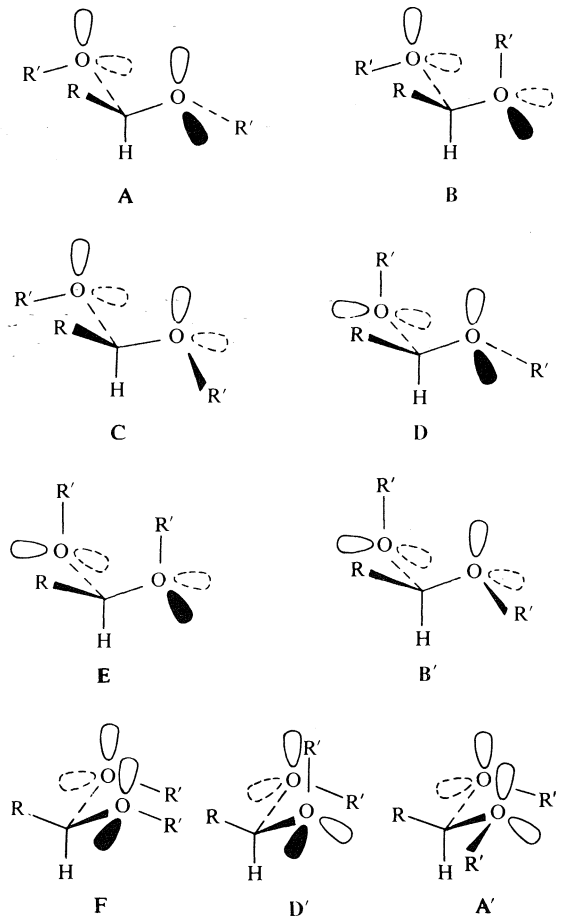

SCHEME 1

[9]A 1,3-synperiplanar arrangement is equivalent to a 1,3-diaxial arrangement in a six-membered ring.

Can. J. Chem. Downloaded from www.nrcresearchpress.com by 210.87.254.105 on 09/05/12
For personal use only.

Can. J. Chem. Downloaded from www.nrcresearchpress.com by 210.87.254.105 on 09/05/12
For personal use only.

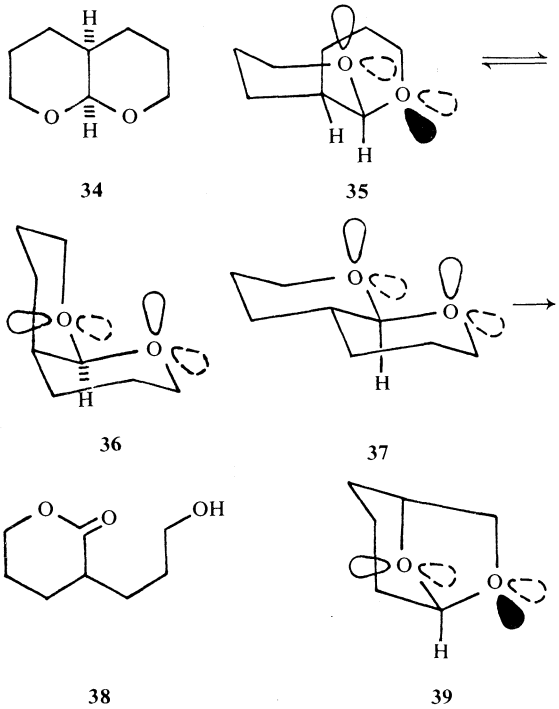

34 35 36 37 38 39

not react with ozone. Being a *cis* decalin, this compound (**34**) is conformationally mobile and exists in the two conformations, **35** and **36**, which are in perfect equilibrium since they are mirror images; they also correspond to conformers B and B′, respectively, and constitute ideal chemical models for these two conformers. *trans*-1,8-Dioxaoctahydronaphthalene (**37**) is an excellent rigid model for conformer C and it was readily oxidized by ozone to hydroxy lactone **38** in quantitative yield within 1.5 h at −78°. 6,8-Dioxabicyclo[3.2.1]octane (**39**)[10] is a rigid model for conformer E and it was found to be unreactive toward ozone. This result has to be taken with some reserve because this compound is not the most appropriate rigid model for E since the hydrogen of the acetal function is incorporated in a bridgehead. Conformer D is the most stable rotamer of an α-glycoside; since α-glycosides are inert to ozone, D is eliminated as a reactive conformer and there is no need to look for a more rigid chemical model for this one. Conformer A or its mirror image A′ represents the most stable rotamer for a β-glycoside and it is very likely that A is a reactive conformer. The best chemical model that we have studied for conformer A is the β-glycoside. It is very difficult to construct a rigid bicyclic model starting with the preferred rotamer (10) of a β-glycoside; the direction that the O—R′ bond is taking makes it difficult to reattach this side chain to the ring in a rigid manner. Finally, 1,3-dioxane acetals represent an ideal model for conformer F and such acetals have been shown to be reactive with ozone.

The relationship between the conformation of the acetal function and its reactivity toward ozone was further confirmed by a study of the

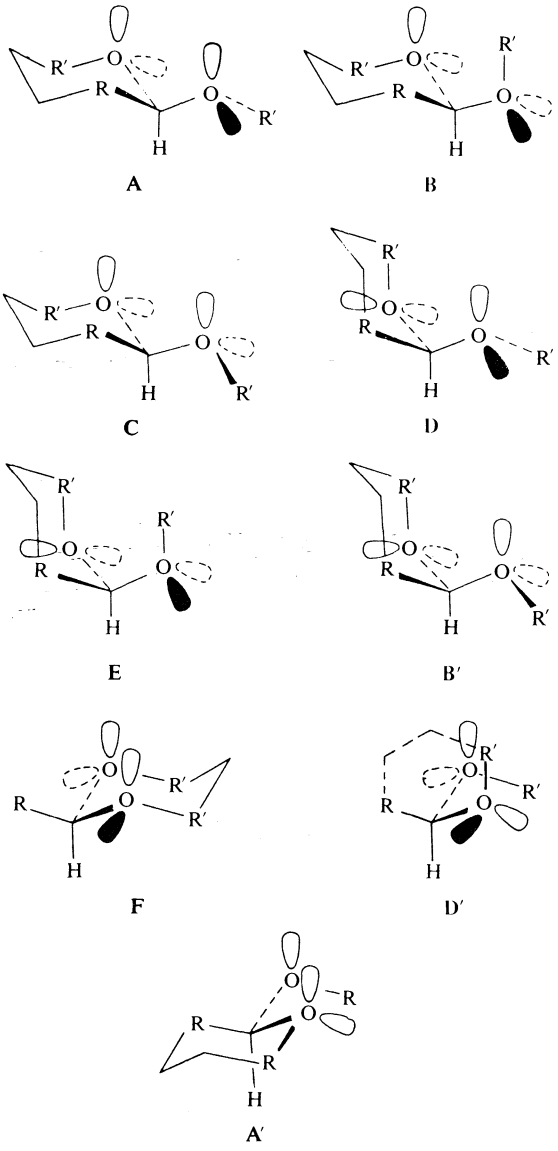

A B C D E B′ F D′ A′

SCHEME 2

[10]We are grateful to Professor R. K. Brown (University of Alberta) for his generous gift of this compound.

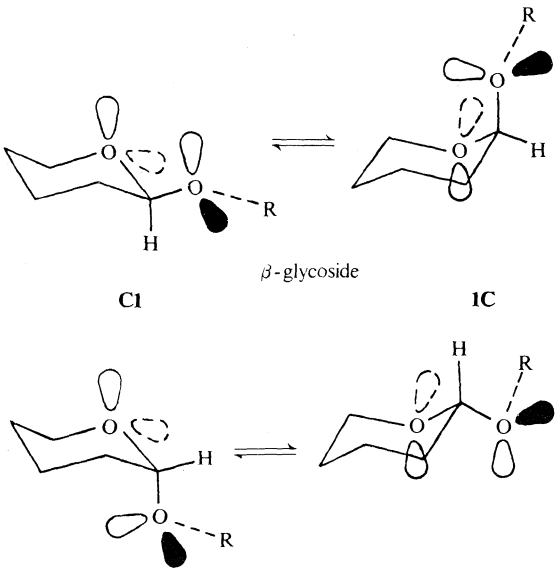

SCHEME 3

ozonolysis of some labile glycopyranosides as well as some glycofuranosides. Chair-rigid methyl α- and β-glycopyranosides are known to exist in their respective Cl conformations (Scheme 3). There are some α- and β-methyl glycopyranosides which are known to be conformationally labile; they exist as an equilibrium mixture of their Cl and 1C conformations (12). If our postulate is valid, both anomers should be reactive: the β-anomer through its Cl conformation and the α-anomer through its 1C conformation. Furthermore, their respective rates of reaction should depend mainly on the concentration of the Cl conformer for the β-anomer and the concentration of the 1C conformer for the α-anomer.

Methyl 2,3,4-tri-*O*-acetyl-β-D-xylopyranoside (**40**) exists mainly in conformation Cl (81%) (12); it is converted smoothly within 8 h into methyl 2,3,4,5-tetra-*O*-acetyl-D-xylonate (**41**). Methyl 2,3,4-tri-*O*-acetyl-α-D-xylopyranoside (**42**) exists in a small proportion (<2%) in conformation lC (12). Consequently, it should react with ozone but the rate of the reaction should be fairly low. This was found to be the case since the oxidation of this α-anomer was not complete (92% of conversion) after 71 h of reaction. It is the first example of a reactive α-anomer toward ozone. The methyl α- and β-arabinopyranosides represent an interesting pair of anomers. It is known (12) that the tri-*O*-acetyl β anomer **43** exists to a large extent in the abnormal lC conformation (≃97%). The tri-*O*-acetyl α-anomer **45** also exists preferentially in the lC conformation (83%). The α-anomer **45** in the arabinose series should therefore be oxidized at a much faster rate than the β-anomer **43** and this conclusion agrees with the experimental results. Methyl 2,3,4-tri-*O*-acetyl-α-D-arabinopyranoside (**45**)[11] was completely oxidized into methyl 2,3,4,5-tetra-*O*-acetyl-D-arabinonate (**44**) within 7 h. The β-anomer **43** was only partially oxidized (71% of conversion) after 80 h. This pair, **43** and **45**, represent the first examples of an α-anomer being more reactive than the corresponding β-anomer. No conformational rigidity can normally be expected from a five-membered ring. Consequently, in methyl glycofuranoside, each anomer should be able to take a conformation which would have proper orbital orientation. Thus, both anomers should react with ozone. Methyl 2,3,5-tri-*O*-acetyl-β-D-ribofuranoside (**46**) as well as its α-anomer (**48**) are both converted into methyl 2,3,4,5-tetra-*O*-acetyl-D-ribonate (**47**) at approximately the same rate (≃16 h) at room temperature.

The preceding experimental results establish fairly rigorously that of the six possible *gauche* conformers for an acetal function, three (A, C, and F) are reactive and three (B, D, and E) are inert toward ozone. Consequently, the postulate that each reactive *gauche* conformer of an acetal function needs to have a lone pair orbital on each oxygen oriented antiperiplanar to the C—H bond has been verified. To obtain the real chemical significance of this postulate, a good knowledge of the mechanism of the ozonolysis reaction has to be gained so that we can understand the role of the orientation of the lone pair orbitals in the reaction.

A detailed study of the mechanism of the oxidation of acetals by ozone has not yet been achieved. However, we think that enough evidence has been obtained to propose a mechanism. As we have already mentioned, this reaction very likely proceeds through the formation of an intermediate which is either identical or equivalent to a hemiorthoester. No direct evidence has yet been obtained but indirect evidence strongly supports this proposal. There appears to be very little doubt that the hydrolysis of orthoesters

[11]We are grateful to Professor J. K. N. Jones (Queen's University) for his generous gift of this compound.

Can. J. Chem. Downloaded from www.nrcresearchpress.com by 210.87.254.105 on 09/05/12
For personal use only.

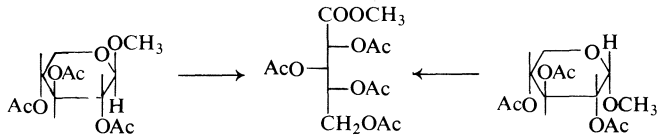

40 41 42

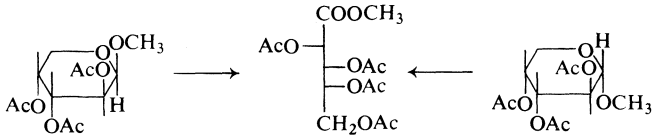

43 44 45

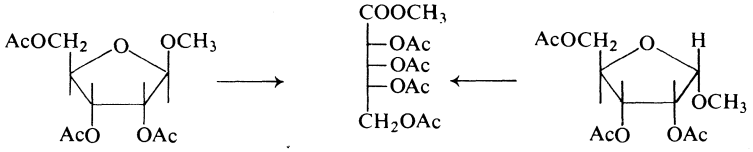

46 47 48

proceeds through the formation of a hemiorthoester (4, 7). We have shown that the ozonolysis of acetals gives the same products obtained from the acid hydrolysis of orthoesters. This observation strongly suggests that the same kind of intermediate is formed in the ozonolysis reaction (2).

Experiments have been carried out to get information on the mechanism by which the C—H bond of the acetal is oxidized, in order to get the proposed tetrahedral intermediate. Diacetoxy acetal (**49**) as well as α- and β-D-glucose pentaacetate (**50** and **51**) do not react with ozone. These results suggest that a positive charge must be developed at the carbon of the acetal function in the transition state of the reaction. Proper alignment of the lone pair orbitals of the ether oxygens can easily stabilize such a positive charge, but the acetoxy group cannot. Ethyl diethoxyacetate (**52**) was found to be completely inert, confirming this suggestion. At the same time this eliminated the possibility of a free radical mechanism, which would lead to the formation of an intermediate such as **53**. A carbethoxy group should facilitate the formation of such a radical intermediate. Finally, competitive oxidation experiments between *para*-substituted benzaldehyde acetals have been carried out. These experiments show that **54** (R = OCH_3) is twice as reactive as **54** (R = H) which in turn is also twice as reactive as **54** (R = NO_2). Thus, an electron-donating group enhances the rate of the reaction, while an electron-attracting group retards the rate. The effect of the methoxy or the nitro group on the rate of the reaction is not very pronounced. We suggest that this is because of the two oxygens of the acetal function which are directly linked to the reacting carbon. These oxygens are in a much better position to stabilize the positive charge than a remote electronic group. Thus, groups in the *para*-position cannot have an important effect on the rate.[12] On the other hand, in compound **52** the carbethoxy group is directly attached to the

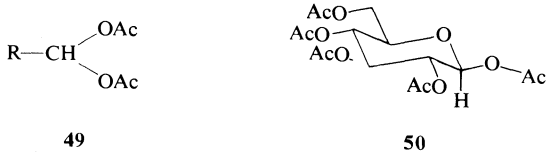

49 50

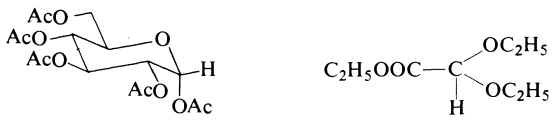

51 52

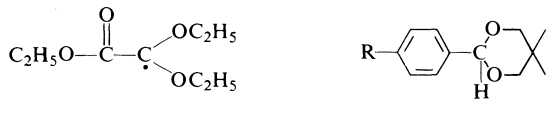

53 54

[12]Professor S. Fliszár (Université de Montréal, personal communication, results to be published) has made a kinetic investigation of this reaction. He has found that the rate correlates well with σ with a ρ value of −1.10, in agreement with the above discussion.

Can. J. Chem. Downloaded from www.nrcresearchpress.com by 210.87.254.105 on 09/05/12
For personal use only.

Can. J. Chem. Downloaded from www.nrcresearchpress.com by 210.87.254.105 on 09/05/12
For personal use only.

carbon which is going to become positively charged and its electron-withdrawing property will therefore play a major role. Its role must be predominant since **52** is inert toward ozone.

At present, we think that the most appealing mechanism which comes to mind is the following. Ozone would insert in a 1,3-fashion into the C—H bond of the acetal function (6) to form either a hemiorthoester and molecular oxygen or a hydrotrioxide hemiorthoester (Scheme 4). The latter would then break down to give the ester and alcohol products. We should emphasize that ozone would insert only when the acetal function has a conformation in which each oxygen has a lone pair orbital antiperiplanar to the C—H bond. The breakdown of the tetrahedral intermediate is also governed by the same type of stereoelectronic rule, specific cleavage of a carbon–oxygen bond taking place when the other oxygens of the tetrahedral intermediate each have a lone pair orbital oriented antiperiplanar to the departing *O*-alkyl group (4).

For example, a tetrahydropyranyl ether would react through its most stable rotamer giving specifically a tetrahedral intermediate. This intermediate has proper orbital orientation to break the ring oxygen–carbon bond, thus forming the hydroxy ester (Scheme 5). Loss of the OR group to generate the δ-lactone is not possible through an orbital-assisted mechanism simply because the lone pair orbitals of the ring oxygen cannot be used; they are not properly oriented. It is the C_6—O bond of the ring oxygen which is antiperiplanar to the OR group.

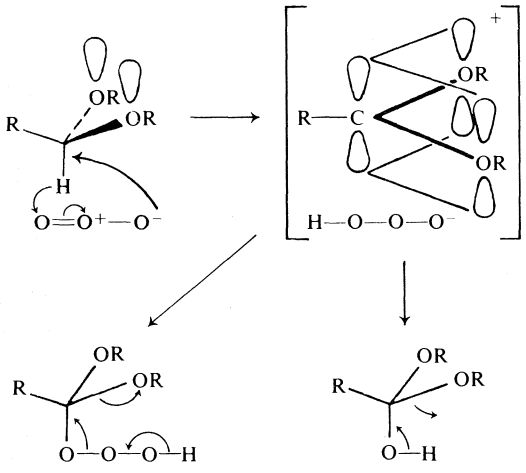

SCHEME 4

Various oxidations of aldehyde acetals into esters have been reported and we believe that these reactions proceed also through a hydride transfer (or its equivalent) from the acetal to the oxidizing agent. Different types of acetals (13) have been oxidized by *N*-bromosuccinimide and no evidence has yet been obtained against a hydride transfer from the acetal to a bromonium ion as one of the key steps. Oxidation of acetal by hydride transfer with triethyloxonium tetrafluoroborate (14, 15) and with triphenylmethane tetrafluoroborate (15) has also been described. Angyal and his co-workers have reported the oxidation of acetals by chromium trioxide in acetic acid (16). This last reaction is quite interesting since the same stereospecificity and outcome of the reaction has been observed with α- and β-glycoside.

We believe that the oxidation of acetals and the hydrolysis of hemiorthoesters (4) and of hemiorthoamides (5) are isolated examples of a general chemical process. The reactions described in Scheme 6 also belong to the same class: (*a*) the haloform reaction, (*b*) the basic fragmentation of α-diketone monothioketals (17), (*c*) the Grob fragmentation with two heteroatoms (18) and related reactions (19), (*d*) the retro-Claisen condensation, and (*e*) the benzilic rearrangement. The Cannizaro reaction, the facile opening of cyclopropanone (Favorski rearrangement), and the cleavage of nonenolizable ketone by sodium amide (Haller–Bauer reaction (20)) and by hydroxide ion (21) can also be added to the preceding list of reactions. The combination of two heteroatoms with proper orbital orientation is a very powerful driving force for expelling a leaving group. The reaction should be easier if one of the two heteroatoms is negatively charged; if both heteroatoms can bear a negative charge, it should proceed with even greater ease and work with an even poorer leaving group.

Thus, this general chemical process can take place whenever two heteroatoms (oxygen and/or nitrogen) and a leaving group are linked to the same carbon. The only requirement is a stereoelectronic one where each heteroatom should have a lone pair orbital oriented antiperiplanar to the leaving group.

Experimental

The i.r. spectra were taken on a Perkin-Elmer 257 Spectrophotometer; n.m.r. spectra (τ values) were recorded on a Varian A-60 spectrometer in the solvents

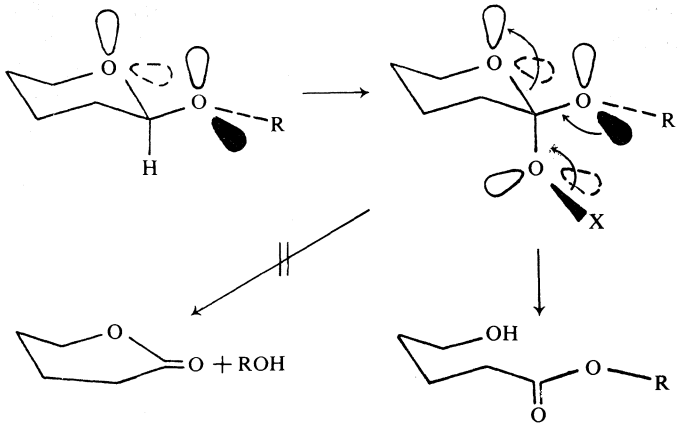

SCHEME 5

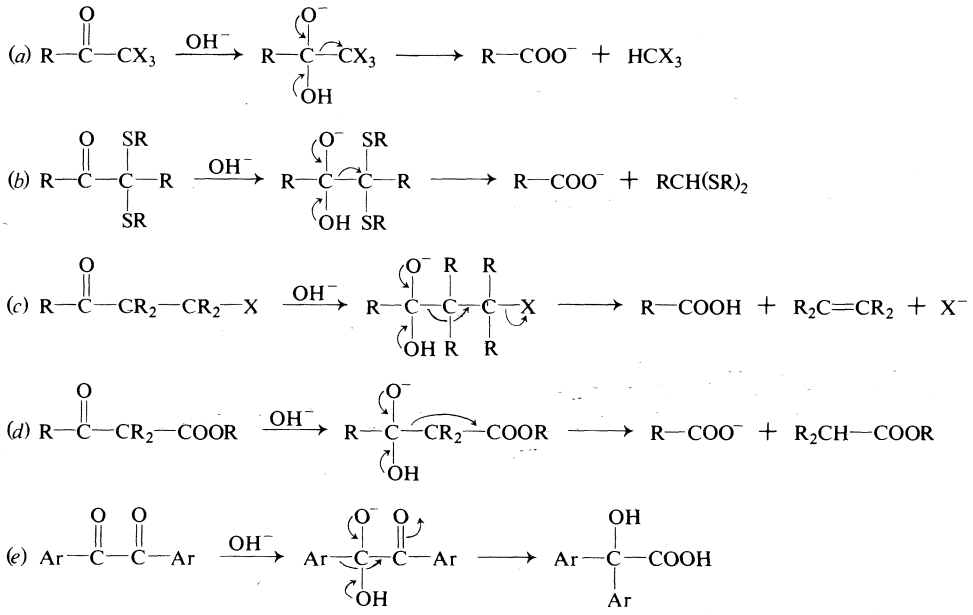

SCHEME 6

Can. J. Chem. Downloaded from www.nrcresearchpress.com by 210.87.254.105 on 09/05/12
For personal use only.

indicated and with TMS as standard. The v.p.c. analyses were done on a Varian Aerograph, model 90-P. The ozonolysis reactions were carried out with a Welsbach Ozonator, model T-816. Organic solution were dried over anhydrous magnesium sulfate and Silica gel was used in all the chromatography (columns and plates). Microanalysis were performed by Dr. C. Daesslé, Organic Microanalyses and by Mr. J. Tamas, Laboratoire de Microanalyse, Université de Sherbrooke.

Stoichiometry of the Reaction

A stream of ozone–oxygen gas was passed through cold (−78°) ethyl acetate (50 ml) for 1 h. A cold solution (−78°) of 2-phenyl-1,3-dioxolan (1.5 g, 10 mmol) in ethyl acetate (10 ml) was then added. The blue color of ozone disappeared after 20 s and the volume of gas formed was ≃60 ml (≃2.7 mmol). The solvent was then evaporated to dryness. The two compounds which were present in the reaction mixture were identified (n.m.r.) as 2-phenyl-1,3-dioxolan (≃7.2 mmol) and ethyl 2-hydroxybenzoate (≃2.8 mmol). This experiment was repeated twice.

The same experiment was also carried out with 2-*n*-hexyl-1,3-dioxolan and an analogous result was obtained. In this case, it took approximately 3 min for the blue color of ozone to disappear.

Typical Procedures for the Ozonolysis of Acetals

(a) 1,1-Dimethoxyheptane

1,1-Dimethoxyheptane (3.716 g, 23.22 mmol) in ethyl acetate (100 ml) was ozonized at room temperature (rate of ozone: 1 mmol/min). The reaction was followed by proton n.m.r. analysis of aliquots and was found to be complete after 1.5 h. Excess ozone was removed by

Can. J. Chem. Downloaded from www.nrcresearchpress.com by 210.87.254.105 on 09/05/12
For personal use only.

flushing the system with nitrogen. The solvent was removed by evaporation and the residue was dissolved in ether. This solution was washed with aqueous sodium carbonate and water. The dried ethereal solution was concentrated *in vacuo*; the resulting product was distilled to give pure methyl heptanoate (3.017 g, 91%), identified by comparison with an authentic sample. The same experiment was carried out at −78° but the reaction required a longer time to go to completion (Table 2).

(b) 2-n-Hexyl-1,3-dioxolan

2-*n*-Hexyl-1,3-dioxolan (1.589 g, 10.05 mmol) was ozonized in ethyl acetate (100 ml) at −78° (rate of ozone: 1 mmol/min). After 10 min, the blue color of ozone appeared in the solution and the ozone generator was stopped. Excess ozone was removed by flushing the system with nitrogen. The solvent was removed by evaporation and the residue was dissolved in ether (200 ml); this solution was washed once with brine then dried. Removal of solvent *in vacuo* gave ethyl 2-hydroxyheptanoate (1.772 g, 100%); i.r.: ν_{max} (film) 3500 and 1740 cm^{-1}; n.m.r.: δ ($CDCl_3$) 4.30 (2H, multiplet, CH_2OCO) and 3.90 (2H, multiplet, CH_2O).

This crude material was then treated with a mixture of pyridine (5 ml) and acetic anhydride (5 ml). After 15 h, this solution was taken to dryness *in vacuo*. The residue thus obtained was dissolved in ether and then washed with aqueous sodium carbonate and water. The dried ethereal solution was evaporated *in vacuo* to give ethyl 2-acetoxyheptanoate (2.120 g, 98%). An analytical sample was prepared by microdistillation; i.r.: ν_{max} ($CHCl_3$) 1740 cm^{-1}; n.m.r.: δ ($CDCl_3$) 4.32 (4H, singlet, OCH_2CH_2O) and 2.10 (3H, singlet, CH_3COO).

Anal. Calcd. for $C_{11}H_{22}O_4$: C, 61.09; H, 9.32. Found: C, 61.18; H, 9.58.

(c) 2-Methoxytetrahydropyran

2-Methoxytetrahydropyran (5.588 g, 48.17 mmol) was ozonized in ethyl acetate (100 ml) at −78° (rate of ozone: 1 mmol/min). The reaction was followed by proton n.m.r. analysis of aliquots and was found to be complete after 2 h. Residual ozone was removed by flushing the system with nitrogen, then the solvent was removed *in vacuo*. The crude material was treated with a mixture of pyridine (10 ml) and acetic anhydride (10 ml). After 15 h, this solution was evaporated to dryness; the residue obtained was dissolved in ether. This solution was washed with aqueous sodium carbonate and brine. The dried ethereal solution was evaporated *in vacuo* to give methyl 5-acetoxypentanoate (6.380 g, 94%). An analytical sample was prepared by microdistillation; i.r.: ν_{max} (film) 1740 cm^{-1}; n.m.r.: (δ) 4.05 (2H, diffuse triplet, CH_2OAc), 3.63 (3H, singlet, $COOCH_3$), 2.34 (2H, multiplet), 2.00 (3H, singlet, $OCOCH_3$), and 1.70 (2H, multiplet).

Anal. Calcd. for $C_8H_{14}O_4$: C, 55.16; H, 8.10. Found: C, 55.06; H, 8.05.

(d) 2-Methoxytetrahydrofuran (8)

Sodium acetate (4 g) was added to a solution of 2-methoxytetrahydrofuran (1.02 g, 10 mmol) in acetic anhydride (100 ml). This mixture was ozonized (rate of ozone: 1 mmol/min) at room temperature. The reaction was followed by proton n.m.r. analysis of aliquots and was complete after 6 h. Residual ozone was removed by flushing the system with nitrogen. The mixture was heated (oil bath temperature 100°) for 2 h, then taken to dryness *in vacuo*. Water was added and the aqueous phase was extracted with chloroform. The extract was treated with activated charcoal, then filtered through celite. The filtrate was evaporated and the resulting residue was dissolved in ether. This was washed with aqueous sodium carbonate and brine. The ethereal solution was dried and evaporated *in vacuo*. The material thus obtained was distilled to give methyl 4-acetoxybutyrate (1.36 g, 85%); i.r.: ν_{max} (film) 1740 cm^{-1}; n.m.r.: δ ($CDCl_3$) 4.06 (2H, diffuse triplet, CH_2O), 3.63 (3H, singlet, OCH_3), and 2.0 (3H, singlet, CH_3COO).

Anal. Calcd. for $C_7H_{12}O_4$: C, 52.49; H, 7.55. Found: C, 52.76; H, 7.65.

Ozonolysis of Glycosides

*(a) Methyl 2,3,4,6-Tetra-O-acetyl-β-D-glucopyranoside (**17**) (22)*

Sodium acetate (4 g) was added to a solution of methyl 2,3,4,6-tetra-*O*-acetyl-β-D-glucopyranoside (602 mg, 1.66 mmol) in acetic anhydride (100 ml). This mixture was ozonized (rate of ozone: 0.3 mmol/min) at room temperature; the reaction was complete after 16 h. Excess ozone was removed by flushing the system with nitrogen. The mixture was evaporated *in vacuo* and water was added. The aqueous phase was extracted with ether. The extract was washed with aqueous sodium carbonate and brine, then dried. Evaporation to dryness gave a residue which was purified by column chromatography (chloroform–ether, 4:1). This gave methyl penta-*O*-acetyl-D-gluconate (**20**, 667 mg, 92%) which was crystallized from ethanol – petroleum ether, m.p. 120–121°, $[\alpha]_{578}$ ($CHCl_3$) 9.4° (lit. (23) m.p. 124°, $[\alpha]_D$ ($CHCl_3$) 9.2°); n.m.r.: δ ($CDCl_3$) 3.78 (3H, singlet, OCH_3), 2.22 (3H, singlet, CH_3COO), and 2.1–2.13 (12 H, two signals corresponding to four acetate groups). This compound was found identical to an authentic sample (23).

The corresponding α-anomer **23** (22) was recovered unchanged after being subjected to the reaction conditions described above.

The following methyl glycosides were submitted to the same experimental conditions. The reactions were followed by proton n.m.r. analysis.

*(b) Methyl 2,3,4,6-Tetra-O-acetyl-β-D-mannopyranoside (**18**) (24)*

Compound **18** (155 mg, 0.43 mmol) gave (reaction time, 10 h) methyl penta-*O*-acetyl-D-mannonate (**21**, 132 mg, 74%) after preparative t.l.c. This product was crystallized from ether – petroleum ether, m.p. 80–81°, $[\alpha]_{578}$ ($CHCl_3$) +22°; n.m.r.: δ ($CDCl_3$) 3.68 (3H, singlet, OCH_3), 2.11 (3H, singlet, CH_3COO), 2.08 (3H, singlet, CH_3COO), 2.04 (3H, singlet, CH_3COO), and 2.02 (6H, singlet, two CH_3COO).

Anal. Calcd. for $C_{17}H_{24}O_{12}$: C, 48.57; H, 5.75. Found: C, 48.56; H, 5.80.

The corresponding α-anomer **24** (24) was recovered unchanged after the same treatment.

*(c) Methyl 2,3,4,6-Tetra-O-acetyl-β-D-galatopyranoside (**19**) (25)*

Compound **19** (225 mg, 0.62 mmol) gave (reaction time, 6 h) methyl penta-*O*-acetyl-D-galactonate (**22**, 241 mg, 92%) after preparative t.l.c. This product was crystallized with ether – petroleum ether, m.p. 125–126°, (lit. (23) m.p. 126–127°); n.m.r.: δ ($CDCl_3$) 3.68 (3H, singlet, OCH_3), 2.14, 2.09, 2.06, 2.01, and 1.99 (15 H, five singlets corresponding to five acetate groups).

Can. J. Chem. Downloaded from www.nrcresearchpress.com by 210.87.254.105 on 09/05/12
For personal use only.

The corresponding α-anomer **25** (25) was recovered unchanged after the same treatment.

*(d) Methyl 3,4,6-Tri-O-acetyl-2-deoxy-β-D-glucopyranoside (**26**) (9)*

Method 1. Compound **26** (912 mg, 3 mmol) was treated with ozone under the conditions described above to give (reaction time, 1 h) methyl tetra-*O*-acetyl-2-deoxy-D-gluconate (**28**, 1.03 g, 81%) which was crystallized from ether – petroleum ether, m.p. 55–57°, $[\alpha]_{578}$ ($CHCl_3$) + 33°; n.m.r.: δ ($CDCl_3$) 3.67 (3H, singlet, OCH_3), 2.14 (3H, singlet, CH_3COO), and 2.04–2.07 (9H, two signals corresponding to three acetate groups).

Anal. Calcd. for $C_{15}H_{22}O_{10}$: C, 49.72; H, 6.12. Found: C, 49.79; H, 6.09.

Method 2. Compound **26** (580 mg, 1.9 mmol) was ozonized in glacial acetic acid (100 ml) during 1.5 h at room temperature. The solvent was removed *in vacuo* and purification of the residue by preparative t.l.c. gave pure methyl 3,4,6-tri-*O*-acetyl-2-deoxygluconate (**27**, 486 mg, 80%) which was crystallized from chloroform – petroleum ether, m.p. 106–107°, $[\alpha]_{578}$ ($CHCl_3$) +64°; n.m.r.: δ ($CDCl_3$) 3.68 (3H, singlet, OCH_3), and 2.05–2.10 (9H, two signals corresponding to three acetate groups).

Compound **27** (208 mg) was then treated with a mixture of pyridine (5 ml) and acetic anhydride (5 ml) for 17 h at room temperature. After evaporation of the solvent, the residue was dissolved in chloroform and the organic solution was washed with aqueous sodium bicarbonate and brine. The dried chloroform solution was evaporated to dryness and the residue was purified by preparative t.l.c. to give pure methyl 3,4,5,6-tetra-*O*-acetyl-2-deoxy-D-gluconate (**28**, 178 mg).

The α-anomer **29** (9) was treated by ozone in acetic anhydride – sodium acetate and it was recovered unchanged.

*(e) Methyl 2,3,4-Tri-O-acetyl-β-D-xylopyranoside (**40**) (26)*

Compound **40** (645 mg, 2.20 mmol) gave (reaction time, 8 h) methyl tetra-*O*-acetyl-D-xylonate (**41**, 602 mg, 78%) after purification by preparative t.l.c. An analytical sample was prepared by microdistillation; $[\alpha]_{578}$ ($CHCl_3$) −6°; n.m.r.: δ ($CDCl_3$) 3.75 (3H, singlet, OCH_3), 2.19, 2.09, 2.06, and 2.04 (12 H, four singlets corresponding to four acetate groups).

Anal. Calcd. for $C_{14}H_{20}O_{10}$: C, 48.28; H, 5.79. Found: C, 48.10; H, 5.66.

The corresponding α-anomer **42** (689 mg, 240 mmol (26)) was ozonized for 71 h and gave unreacted **42** (8%) and methyl tetra-*O*-acetyl-D-xylonate (**41**, 92%) which were separated by preparative t.l.c.

*(f) Methyl 2,3,4-Tri-O-acetyl-α-D-arabinopyranoside (**45**) (12)*

Compound **45** (2.0 g, 6.8 mmol) gave (reaction time, 7 h) methyl tetra-*O*-acetyl-D-arabonate (**44**, 2.28 g, 95%) after purification by preparative t.l.c. This material was crystallized from ethanol; m.p. 128–129° (lit. (27) m.p. 116°); n.m.r.: δ ($CDCl_3$) 3.74 (3H, singlet, OCH_3), 2.17 (3H, singlet, CH_3COO), and 2.06 (9H, two signals corresponding to three acetate groups).

Anal. Calcd. for $C_{14}H_{20}O_{10}$: C, 48.28; H, 5.75. Found: C, 48.11; H, 5.82.

The corresponding β-anomer **43** (242 mg, 0.8 mmol (12)) was ozonized for 80 h and gave unreacted **43** (39%) and methyl tetra-*O*-acetyl-D-arabonate (**44**, 71%) which were separated by preparative t.l.c.

*(g) Methyl 3,4,5-Tri-O-acetyl-β-D-ribofuranoside (**46**) (28)*

Compound **46** (0.3 g, 1.18 mmol) gave (reaction time, 16 h) methyl tetra-*O*-acetyl-D-ribonate (**47**, 0.32 g, 90%); m.p. 89–90°, $[\alpha]_D$ ($CHCl_3$) −12.7° (lit. (29) m.p. 90°, $[\alpha]_D$ ($CHCl_3$) −13°); n.m.r.: δ ($CDCl_3$) 3.77 (3H, singlet, OCH_3), and 2.03–2.13 (12 H, signals corresponding to four acetate groups).

The corresponding α-anomer **48** (28) also gave compound **47** (reaction time, 18 h).

Ozonolysis of Model Compounds

*(a) trans-1,8-Dioxaoctahydronaphtalene (**37**) (30)*

Compound **37** (926 mg, 6.52 mmol) was ozonized in ethyl acetate (75 ml) at −78° (rate of ozone: 1 mmol/min). The reaction was found to be complete after 1.5 h. Residual ozone was removed by flushing the system with nitrogen, then, the solvent was removed *in vacuo* to yield crude hydroxy lactone **38** (1.140 g, ≃100%), i.r.: ν_{max} (film) 3450 and 1740 cm^{-1}; n.m.r.: δ ($CDCl_3$) 4.35 (3H, multiplet, CH_2OCO), and 3.75 (2H, multiplet, CH_2OH).

Crude hydroxy lactone **38** was then treated with a mixture of pyridine (5 ml) and acetic anhydride (5 ml). After 15 h, the solution was taken to dryness *in vacuo* to give compound **38** (H = CH_3CO) which was purified by column chromatography (1.025 g, 80%). An analytical sample was prepared by microdistillation; i.r.: ν_{max} (film) 1740 cm^{-1}; n.m.r.: δ ($CDCl_3$) 4.38 (2H, diffuse triplet, J = 6 Hz, CH_2—OCO), 4.15 (2H, diffuse triplet, J = 6 Hz, CH_2OAc), and 2.06 (3H, singlet, CH_3COO).

Anal. Calcd. for $C_7H_{12}O_4$: C, 59.98; H, 8.05. Found: C, 59.79; H, 7.96.

*(b) cis-1,8-Dioxaoctahydronaphtalene (**34**) (30)*

Compound **34** (865 mg, 6.52 mmol) was recovered unchanged after being subjected to the reaction conditions described above.

(*c*) The following compounds were found to be inert toward ozone (room temperature, ethyl acetate): ethyl diethoxy acetate (**52**, 3 h), β-D-glucosepentaacetate (**50**, 6 h), α-D-glucosepentaacetate (**51**, 6 h), 6,8-dioxabicyclo-[3.2.1]octane (**39**, (31), 6 h), and 1,1-diacetoxyheptane (**49**, (32), 2 h in glacial acetic acid).

*Ozonolysis of Para-substituted Benzaldehyde Acetal (**54**)*

(*a*) A mixture of phenyl 2,2-dimethyl-1,3-dioxan (0.01 *M*) and *p*-methoxyphenyl 2,2-dimethyl-1,3-dioxan (0.01 *M*) in ethyl acetate was ozonized at −78° during 10 min. The resulting mixture was analyzed by vapor phase chromatography (SE-30, temperature 135°). This experiment was repeated three times. Phenyl 2,2-dimethyl-1,3-dioxan was converted into 3-hydroxy-2,2-dimethylpropyl benzoate to the extent of 28%; *p*-methoxyphenyl 2,2-dimethyl-1,3-dioxan was transformed into 3-hydroxy-2,2-dimethylpropyl *p*-methoxybenzoate to the extent of 60%.

(*b*) Using the technique described above, an equimolar mixture (0.01 *M*) of *p*-methoxyphenyl 2,2-dimethyl-1,3-dioxan and *p*-nitrophenyl 2,2-dimethyl-1,3-dioxan was ozonized. The first compound was converted into 3-hydroxy-2,2-dimethylpropyl *p*-methoxybenzoate to the extent of 70% while the second compound was transformed into 3-hydroxy-2,2-dimethylpropyl *p*-nitrobenzoate to the extent of 20%.

Similarly, an equimolar mixture (0.01 *M*) of phenyl 2,2-dimethyl-1,3-dioxan and *p*-nitrophenyl 2,2-dimethyl-1,3-dioxan gave 3-hydroxy-2,2-dimethylpropyl benzoate (86%) and 3-hydroxy-2,2-dimethylpropyl *p*-nitrobenzoate (40%).

1. P. DESLONGCHAMPS and C. MOREAU. Can. J. Chem. **49**, 2465 (1971).
2. P. DESLONGCHAMPS, C. MOREAU, D. FRÉHEL, and P. ATLANI. Can. J. Chem. **50**, 3402 (1972).
3. P. SOUCY, T.-L. HO, and P. DESLONGCHAMPS. Can. J. Chem. **50**, 2047 (1973).
4. P. DESLONGCHAMPS, P. ATLANI, D. FRÉHEL, and A. MALAVAL. Can. J. Chem. **50**, 3405 (1972).
5. P. DESLONGCHAMPS, C. LEBREUX, and R. J. TAILLEFER. Can. J. Chem. **51**, 1665 (1973).
6. C. C. PRICE and A. L. TUMOLO. J. Am. Chem. Soc. **86**, 4691 (1964); R. E. ERICKSON, R. T. HANSEN, and J. HARKINS. J. Am. Chem. Soc. **90**, 6777 (1968); L. SPIALTER, L. PAZDERNIK, S. BERSTEIN, W. A. SWANSIGER, G. L. BUELL, and M. E. FREEBURGER. Ozone reactions with organic compounds. Adv. Chem. Ser. No. 112. American Chem. Soc. Wash., D.C. p. 65, 1972; J. E. BATTERBEE and P. S. BAILEY. J. Org. Chem. **32**, 3899 (1967); P. S. BAILEY and H. M. WHITE. J. Org. Chem. **30**, 3037 (1965).
7. J. F. KING and A. D. ALLBUTT. Can. J. Chem. **48**, 1754 (1970); Tetrahedron Lett. **49** (1967).
8. D. FRÉHEL and P. DESLONGCHAMPS. Can. J. Chem. **50**, 1783 (1972).
9. G. R. INGLIS, J. C. P. SCHWARZ, and L. MACLAREN. J. Chem. Soc. 1014 (1962).
10. R. U. LEMIEUX. Molecular rearrangements. Pt. 2. *Edited by* Paul de Mayo. Interscience, New York. 1964; R. U. LEMIEUX. Abstract of Papers, Am. Chem. Soc. **135**, 5E (1959); R. U. LEMIEUX. Pure Appl. Chem. **25**, 527 (1971).
11. O. EXNER, V. JEHLIČA, and B. UCHYTIL. Coll. Czech. Chem. Commun. **33**, 2862 (1968).
12. P. L. DURETTE and D. HORTON. Carbohydr. Res. **18**, 403 (1971).
13. E. N. MARVEL and M. J. JONCICH. J. Am. Chem. Soc. **73**, 973 (1951); A. RIECHE, E. SCHMITZE, W. SCHADE, and E. BEYER. Chem. Ber. **94**, 2926 (1961); J. D. PRUGH and W. C. MCCARTHY. Tetrahedron Lett. 1351 (1966); S. HANESSIAN. Carbohydr. Res. **2**, 96 (1966); S. HANESSIAN and N. R. PLESSAS. J. Org. Chem. **34**, 1035, 1045, 1053 (1969); D. L. FAILLA, T. L. HULLAR, and S. B. SISKIN. Chem. Commun. 716 (1966).
14. H. MEERWEIN, V. HEDERICK, H. MORSHEL, and K. WUNDERLICH. Annalen, **635**, 1 (1960); ST. SLOMKOWSKI and ST. PENCZEK. Chem. Commun. 1347 (1970).
15. D. H. R. BARTON, P. D. MAGNUS, G. SMITH, G. STRECKERT, and D. ZURR. J. Chem. Soc. Perkin I, 542 (1972).
16. S. J. ANGYAL and K. JAMES. Aust. J. Chem. **23**, 1209 (1970); **24**, 1219 (1971); S. S. ANGYAL and M. E. EVANS. Aust. J. Chem. **25**, 1495, 1513 (1972); M. BERTOLINI and C. P. J. GLAUDEMANS. Carbohydr. Res. **17**, 449 (1971).
17. J. A. MARSHALL and H. ROEBKE. Tetrahedron Lett. 1555 (1970); J. A. MARSHALL, C. T. BUSE, and D. E. SEITZ. Synt. Commun. **3**, 85 (1973).
18. C. A. GROB. Angew. Chem. Int. Ed. **6**, 1 (1967); **8**, 535 (1969); S. JULIA and G. LINSTRUMENTELLE. Bull. Soc. Chim. Fr. 3490 (1966); W. KRAUS and W. ROTHENWOHRER. Tetrahedron Lett. 1007 (1968); P. G. GASSMAN and J. M. HORNBACK. J. Am. Chem. Soc. **91**, 5817 (1969).
19. W. EISELE, C. A. GROB, E. RENK, and H. VON TSCHAMMER. Helv. Chim. Acta, **51**, 816 (1968).
20. K. E. HAMLIN and A. H. WESTON. Organic reactions. Vol. IX. John Wiley and Sons, Inc., New York. 1957. p. 1.
21. P. G. GASSMAN and F. V. ZALAR. Tetrahedron Lett. 3031, 3251 (1964); P. G. GASSMAN, J. T. LUMB, and F. V. ZALAR. J. Am. Chem. Soc. **89**, 946 (1967).
22. C. S. HUDSON and J. K. DALE. J. Am. Chem. Soc. **37**, 1264 (1915).
23. R. T. MAJOR and E. W. COOK. J. Am. Chem. Soc. **58**, 5474 (1936); G. B. ROBBINS and F. W. UPSON. J. Am. Chem. Soc. **62**, 1074 (1940).
24. J. K. DALE. J. Am. Chem Soc. **46**, 1046 (1924).
25. P. A. LEVENE and H. SOBOTKA. J. BIOL. Chem. **67**, 759 (1926); J. K. DALE and C. S. HUDSON. J. Am. Chem. Soc. **52**, 2534 (1930).
26. C. S. HUDSON and J. K. DALE. J. Am. Chem. Soc. **40**, 997 (1918).
27. W. J. HUMPHLETT. Carbohydr. Res. **4**, 157 (1967).
28. C. T. BISHOP and F. P. COOPER. Can. J. Chem. **41**, 2743 (1963).
29. M. L. WOLFROM, A. THOMPSON, and EVAN F. EVANS. J. Am. Chem. Soc. **67**, 1793 (1945).
30. Y. BAHUREL, M. LISSAC-CAHU, G. DESCOTES, M. GELIN, J. DESMAU, and J. DUPLAN. Bull. Soc. Chim. Fr. 4006 (1970).
31. T. P. MURRAY, C. S. WILLIAMS, and R. K. BROWN. J. Org. Chem. **36**, 1311 (1971).
32. E. SPÄTH. Monatsh. **36**, 29 (1915).

Can. J. Chem. Downloaded from www.nrcresearchpress.com by 210.87.254.105 on 09/05/12
For personal use only.

The Reaction of Methyl Radicals with Molecular Hydrogen

PETER C. KOBRINSKY AND PHILIP D. PACEY
Department of Chemistry, Dalhousie University, Halifax, Nova Scotia B3H 3J5

Received June 17, 1974

PETER C. KOBRINSKY and PHILIP D. PACEY. Can. J. Chem. **52**, 3665 (1974).

Mixtures of neopentane and hydrogen were pyrolyzed in a flow system at 826–968 K and 27–400 mm Hg. Measurements of the yields of CH_4 and C_2H_6 at various conditions enabled calculation of the rate constant for

$$CH_3 + H_2 \rightarrow CH_4 + H$$

at 926 and 829 K. The Arrhenius plot of these and earlier measurements from 372 to 1370 K is a curve, which can be represented by

$$k = 10^{2.9}T^2 \exp(-40 \text{ kJ mol}^{-1}/RT) \times 1 \text{ mol}^{-1} \text{ s}^{-1}$$

PETER C. KOBRINSKY et PHILIP D. PACEY. Can. J. Chem. **52**, 3665 (1974).

On a pyrolysé des mélanges de néopentane et d'hydrogène dans un système continue à 826–968 K et 27–400 mm Hg. La mesure des rendements en CH_4 et en C_2H_6 sous diverses conditions permettent de calculer la constante de vitesse pour la réaction

$$CH_3 + H_2 \rightarrow CH_4 + H$$

à 926 et 829 K. Une courbe d'Arrhénius, réunissant ces mesures et d'autres antérieures à 372–1370 K, peut être représentée par l'équation

$$k = 10^{2.9}T^2 \exp(-40 \text{ kJ mol}^{-1}/RT) \times 1 \text{ mol}^{-1} \text{ s}^{-1}$$

[Traduit par le journal]

Introduction

The reaction between methyl radicals and molecular hydrogen has recently been investigated by Clark and Dove (1) using reflected shock waves through hydrogen–azomethane–neon mixtures at 1272–1370 K. The rate coefficient measured was five times faster than predicted on the basis of earlier experiments at lower temperatures (372–591 K). The kinetic isotope effect for this reaction has also been studied recently, for thermal methyl radicals at 399–645 K by Shapiro and Weston (2) and for photolytically "hot" methyl radicals by Ting and Weston (3).

The reaction is of experimental interest because it occurs in the industrial pyrolysis of hydrocarbons and because several theoretical calculations of the potential energy surface for the reaction have been performed, most recently by Raff (4).

In the present study, neopentane–hydrogen mixtures have been pyrolyzed in a flow system; the decomposition of neopentane provided the source of methyl radicals.

The main reactions expected to occur in this system are:

[1] $C_5H_{12} \rightarrow CH_3 + t\text{-}C_4H_9$

[2] $t\text{-}C_4H_9 \rightarrow i\text{-}C_4H_8 + H$

[3] $H + C_5H_{12} \rightarrow H_2 + C_5H_{11}$

[4] $C_5H_{11} \rightarrow i\text{-}C_4H_8 + CH_3$

[5] $CH_3 + C_5H_{12} \rightarrow CH_4 + C_5H_{11}$

[6] $CH_3 + H_2 \rightarrow CH_4 + H$

[7] $2CH_3 \rightarrow C_2H_6$

This mechanism is identical with that proposed for the pyrolysis of pure neopentane (5), with the exception of the reaction under investigation (reaction 6), which is an additional source of CH_4.

The hydrogen atoms formed in [6] should regenerate H_2 by reaction 3, consuming more neopentane in the process. Thus, provided the mechanism is correct and provided reaction 6 occurs at a measureable rate, hydrogen should act as a homogeneous catalyst for neopentane decomposition.

Can. J. Chem. Downloaded from www.nrcresearchpress.com by 210.87.254.105 on 09/05/12
For personal use only.

Can. J. Chem. Downloaded from www.nrcresearchpress.com by 210.87.254.105 on 09/05/12
For personal use only.

Analysis of the mechanism leads to the following relation between the initial rates of formation of CH_4 and C_2H_6, $R^0_{CH_4}$ and $R^0_{C_2H_6}$,

$$[8] \quad k_5 + k_6 \frac{[H_2]}{[C_5H_{12}]} = \frac{R^0_{CH_4}(k_7)^{1/2}}{[C_5H_{12}](R^0_{C_2H_6})^{1/2}}$$

A plot of the right hand side of this expression *vs.* $[H_2]/[C_5H_{12}]$ should be linear with a slope of k_6 and intercept k_5.

As was true in the case of pure neopentane pyrolysis, the rate coefficient, k_1, for the initiation reaction, may be calculated from the expression,

$$[9] \quad k_1 = R^0_{C_2H_6}/[C_5H_{12}]$$

Experimental

The basic apparatus and experimental technique were the same as for the flow pyrolysis of pure neopentane (5).

Hydrogen (Linde zero gas, 99.95%) was passed through a deoxo unit and a molecular sieve column at −196 °C to remove any oxygen or trace hydrocarbons. Neopentane (Phillips Research Grade, 99.88%) was purified by trap-to-trap distillation and by degassing at −196 °C or at −95 °C. Typical concentrations of CH_4 and C_2H_6 as impurities in the reactant mixtures prepared were 1–20 p.p.m. and 0.1–1 p.p.m., respectively.

Two 75 cm long quartz reactors described in ref. 5 were reused: reactor *i*, 1.7 cm inside diameter, surface to volume ratio (S/V) = 3.1 cm^{-1}, and reactor *iii* 0.2 cm inside diameter, S/V = 23 cm^{-1}. Temperature measurements at intervals along the reactors, interpreted with the computer program described previously (6), indicated that 93% of the reaction occurred within ±8 °C of the average temperature for a typical experiment.

Flow rates of neopentane were limited to 0.1 mol/h or less to prevent the cooler entering gases from distorting the temperature profile (5). Because of its larger thermal conductivity and smaller heat capacity, hydrogen should not distort the profile significantly.

The reaction products were analyzed by gas chromatography as in ref. 5.

Results

More than 300 experiments[1] have been performed at reactor temperatures close to 829, 926, and 968 K, pressures from 27 to 400 mm Hg, $[H_2]/[C_5H_{12}]$ from 0 to 3.1, and reactor residence times from 0.01 to 5.5 s, corresponding to conversions of neopentane from 0.1 to 6%.

Dependence of Rates on Reaction Time

The dependence of the rates of formation of CH_4 and C_2H_6 on reactor residence times for fixed reagent pressures and compositions at 826 and 968 K are shown in Figs. 1*a* and *b*. In all four cases the rates of product formation decrease as the reaction time increases. A similar effect was observed with pure neopentane (5) and was attributed to self inhibition of the reaction by the isobutene formed.

The solid lines in the figures were obtained by the method of least squares. The extrapolated initial rates reported in the following sections agreed with the nearest observed rates within 10%.

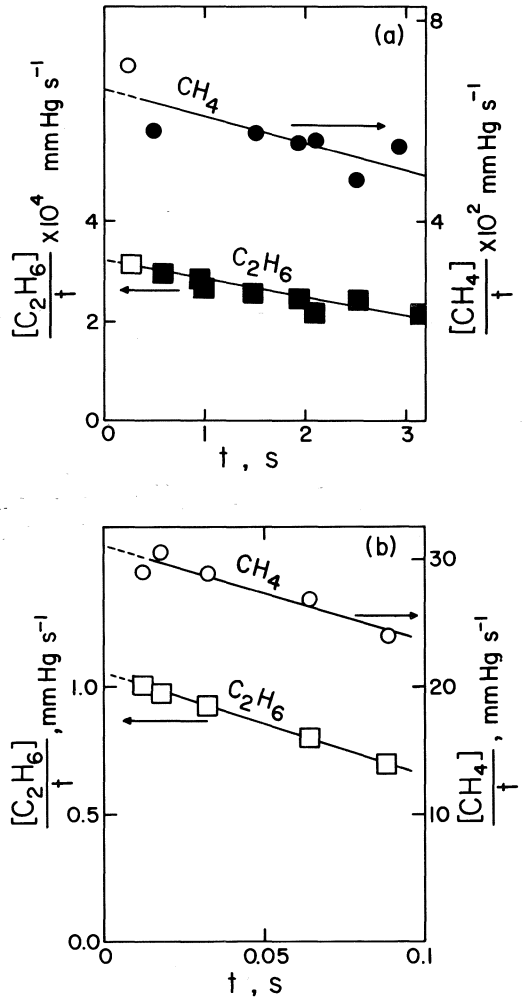

FIG. 1. Rates of formation of CH_4 and C_2H_6 as a function of reactor residence time for pyrolysis of (*a*) 22 mm Hg of C_5H_{12} and 38 mm Hg of H_2 at 826 K and (*b*) 36 mm Hg of C_5H_{12} and 72 mm Hg of H_2 at 968 K. Filled points, reactor *i*, S/V = 3.1 cm^{-1}; open points, reactor *iii*, S/V = 23 cm^{-1}.

[1]Tables of data are available, at a nominal charge, from the Depository of Unpublished Data, National Science Library, National Research Council of Canada, Ottawa, Canada K1A 0R6.

Can. J. Chem. Downloaded from www.nrcresearchpress.com by 210.87.254.105 on 09/05/12
For personal use only.

Addition of hydrogen did accelerate the decomposition of neopentane; at 923 K, on pyrolysis of 86 mm Hg of pure C_5H_{12}, $R^0_{CH_4}$ (which is 94% of the rate of decomposition of C_5H_{12} at these conditions) was 11 mm Hg s^{-1}, but on pyrolysis of 82 mm Hg of C_5H_{12} with 164 mm Hg of H_2, $R^0_{CH_4}$ was 24 mm Hg s^{-1}.

Dependence of Rates on Pressure

Dependence of the initial rates of formation of CH_4 and C_2H_6 on total pressure in the reactor is shown in Figs. 2 and 3 for pyrolysis at 829 K of a mixture with $[H_2]/[C_5H_{12}] = 1.69$ and at 926 K with $[H_2]/[C_5H_{12}] = 2.0$, respectively.

Both sets of data for C_2H_6 correlate well with the dashed lines of slope equal to 1.0. This behavior is predicted by the mechanism, provided the chain initiation reaction is first order and provided reaction 7 is the only termination reaction.

The order of CH_4 production in Fig. 2 agrees with the dashed line of slope 1.5 predicted by the mechanism. In Fig. 3, CH_4 production deviates from an order of 1.5 at low pressure; a similar effect was attributed to the pressure dependence of the recombination rate coefficient, k_7, in ref. 5.

To avoid uncertainty regarding the value of k_7, used in eq. 8, it is necessary either to work at conditions where k_7 is pressure independent or to extrapolate to high pressures. Two Lindemann–Hinshelwood plots, for 926 K and $[H_2]/[C_5H_{12}] = 2.0$ and 829 K and $[H_2]/C_5H_{12}] = 1.69$, are shown in Fig. 4. The straight lines were determined by the method of least squares. According to eq. 8, k_7 is inversely proportional to distance along the vertical axis. At 829 K, k_7 appears to be independent of pressure. At 926 K, the intercept, or infinite pressure extrapolated value, is within 10% of the nearest observed value. At 968 K (not shown in Fig. 4) the extrapolations were too long to be reliable and will not be quoted further.

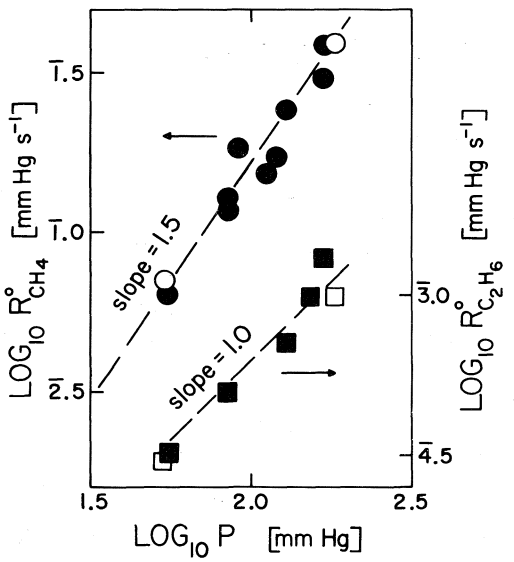

FIG. 2. Order plots for CH_4 and C_2H_6 formation for $[H_2]/[C_5H_{12}] = 1.69$ at 829 K. Filled points, reactor *i*; open points, reactor *iii*. The dashed lines have slopes of exactly 1.5 and 1.0, predicted by the mechanism.

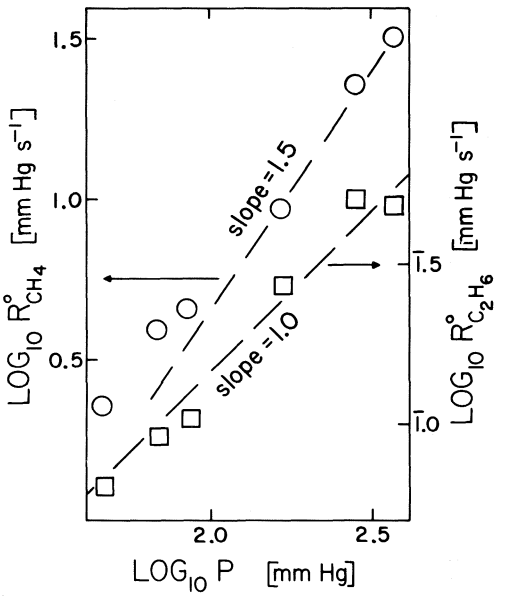

FIG. 3. Order plots for CH_4 and C_2H_6 formation for $[H_2]/[C_5H_{12}] = 2.0$ in reactor *iii* at 926 K. The dashed lines have slopes of 1.5 and 1.0, as would be predicted by the mechanism if k_7 were independent of pressure.

Variation of $[H_2]/[C_5H_{12}]$ Ratio

Values of k_1 calculated using eq. 9 showed no trends with changing ratio of $[H_2]$ to $[C_5H_{12}]$. The average results (with standard deviation) from this study of $4.2(\pm 0.7) \times 10^{-3}$ s^{-1} at 926 K and $1.4(\pm 0.2) \times 10^{-5}$ s^{-1} at 829 K agreed with the values of 4×10^{-3} s^{-1} and 1.6×10^{-5} s^{-1}, respectively, calculated from the Arrhenius expression of ref. 5.

The effect of added hydrogen on values of $k_5 + k_6[H_2][C_5H_{12}]^{-1}$ calculated from expression 8 are shown in Fig. 5. The high pressure limiting value of k_7 was taken as 2.43×10^{10} l mol^{-1} s^{-1} (7). There has been some criticism of this number (8) but any error would affect

TABLE 1. Arrhenius parameters for reaction 6

Experimental system	Measure of $[CH_3]$	T(K)	$\log_{10} A$ (l mol^{-1} s^{-1})	E_A (kJ mol^{-1})
H_2CCO photolysis ref. 9	Reaction 7	372–480	8.5	43
$(CH_3)_2CO$ photolysis refs. 10, 11	Reaction 7	403–563	8.5	42
$(CH_3)_2CO$ photolysis ref. 12	Reaction 10	409–591	8.4	41
$(CH_3)_2CO$ photolysis ref. 2	Reaction 10	399–645	8.7	45
C_5H_{12} pyrolysis this work	Reaction 7	829–926	10.1 ± 0.4	59 ± 7
Combination of experiment and theory, ref. 1		1340, 1500	10.2 ± 0.3	65

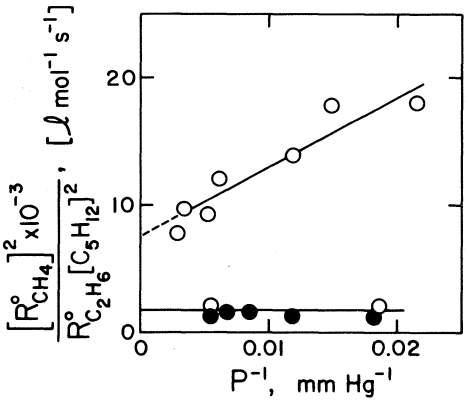

FIG. 4. Lindemann–Hinshelwood style plots for the experimental function, $R^0CH_4{}^2[C_5H_{12}]^{-2}R^0C_2H_6{}^{-1}$, for $[H_2]/[C_5H_{12}] = 2.0$, $T = 926$ K (upper line) and $[H_2]/[C_5H_{12}] = 1.69$, $T = 829$ K (lower line). ●, Reactor *i*; ○, reactor *iii*.

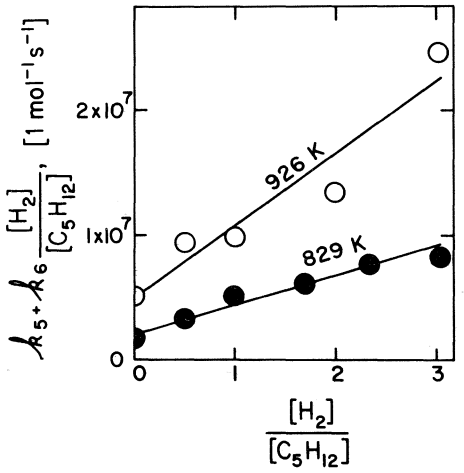

FIG. 5. Values of $k_5 + k_6[H_2][C_5H_{12}]^{-1}$, calculated from eq. 8, as a function of $[H_2]/[C_5H_{12}]$ at 926 K, ○, and 829 K, ●.

earlier low temperature measurements of k_6 in the same way. At 926 K, values of $R^0{}_{CH_4}[C_5H_{12}]^{-1}(R^0{}_{C_2H_6})^{-1/2}$, required in eq. 8, were obtained as the square roots of intercepts of Lindemann–Hinshelwood plots like Fig. 4. At 829 K, average values of $R^0{}_{CH_4}[C_5H_{12}]^{-1}(R^0{}_{C_2H_6})^{1/2}$ for a particular mixture were calculated.

The lines on Fig. 5 were calculated using the method of least squares. The intercepts give values of k_5 of $5.0(\pm 1.0) \times 10^6$ l mol^{-1} s^{-1} at 926 K and $2.0(\pm 0.2) \times 10^6$ l mol^{-1} s^{-1} at 829 K. The averages agree within 1 and 12%, respectively, with values calculated from the Arrhenius expression in ref. 5.

The slopes in Fig. 5 give values of k_6 of $5.8(\pm 0.6) \times 10^6$ l mol^{-1} s^{-1} at 926 K and $2.4(\pm 0.1) \times 10^6$ l mol^{-1} s^{-1} at 829 K. The Arrhenius expression calculated from these values is $\log k_6 = 10.1 - 59$ kJ mol^{-1}/2.3 RT.

Discussion

Comparison with Other Work

Values of k_6 from this work and from previous studies are shown in the form of an Arrhenius plot in Fig. 6. The corresponding Arrhenius parameters appear in Table 1. The low temperature data of Gesser and Steacie (9) and Majury and Steacie (10) are based on photolytic experiments with methods of calculation like those of the present work. The other low temperature data were calculated from the results of the kinetic isotope effect experiments of Davison and Burton (12) and Shapiro and Weston (2) and from the Arrhenius parameters for

[10] $$CH_3 + D_2 \rightarrow CH_3D + D$$

measured by Chanmugam and Burton (13). There is some uncertainty regarding the rate of the latter reaction (14) but both the Arrhenius parameters and the absolute rates measured by

Can. J. Chem. Downloaded from www.nrcresearchpress.com by 210.87.254.105 on 09/05/12
For personal use only.

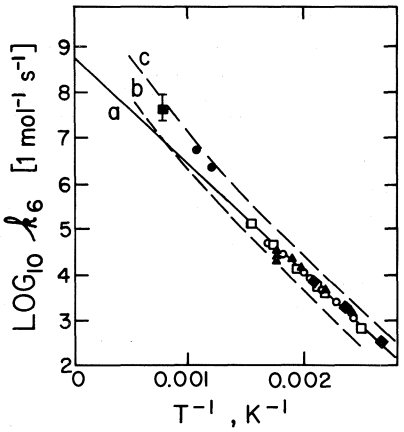

FIG. 6. Arrhenius plot for k_6; ◆, measured by Gesser and Steacie (9); ▲, Majury and Steacie (10); ○, Davison and Burton (12, 13); □, Shapiro and Weston (2, 13); ●, this work; ■, Clark and Dove (1). The straight, solid line (*a*) is a least-squares fit to the data of ref. 2. The dashed curves (*b*) and (*c*) were calculated using activated complex theory by Johnston and Parr (16) and by Clark and Dove (1), respectively.

Chanmugam and Burton represent reasonable average values. The highest temperature point in Fig. 6 is taken from the recent experiments of Clark and Dove (1) on the shock tube pyrolysis of azomethane with added hydrogen. Clark and Dove made use of several other rate constants, previously determined by measuring the concentration of methyl radicals with a mass spectrometer during the shock tube pyrolysis of azomethane with no hydrogen added. An additional calculation of k_6 by Benson and Jain (15) has been omitted, since it was based on the assumption that the Arrhenius plot for the reaction

[11] $CH_3 + H_3COCH_3 \rightarrow CH_4 + H_2COCH_3$

is a straight line, whereas the Arrhenius plots for several similar reactions are now believed to be curved (1, 5, 6). Values of k_6 calculated by Clark and Dove from thermochemistry and the rate of the reverse reaction have been omitted because of uncertainty in the thermochemistry required (1).

The four sets of low temperature data shown are in agreement with each other. The solid, straight line in Fig. 6 is drawn through the data of Shapiro and Weston (2), which came closest to predicting the high temperature rate constants. Even so, the values of k_6 from the present work at 829 K are 3.0 times faster than would be predicted from this straight-line extrapolation and 3.2, 3.6, and 4.1 times faster than predicted from refs. 10, 9, and 12, respectively. This supports the conclusion of Clark and Dove that the Arrhenius plot is best described by a curve.

The Arrhenius parameters in Table 1 from the present work are also significantly greater than those determined at lower temperatures.

To obtain an expression to fit all the data, values of k_6 were calculated for the end of each experimental range from the Arrhenius parameters in Table 1. The values were fitted by least squares to expressions of the form, $\log k_6 - n \log T = B - CT^{-1}$, where n is an integer or half-integer and B and C are constants. The best fit (taken as the maximum correlation coefficient) was obtained for $n = 2$ and $k_6 = 10^{2.9\pm0.1}T^2 \exp(-40 \pm 1 \text{ kJ mol}^{-1}/RT)$ l mol^{-1} s^{-1}. This expression has not been illustrated in Fig. 6, as other techniques of data fitting could have led to different expressions.

Possible Competing Reactions

The formation of extra CH_4 by the reaction,

[12] $CH_3 + H \rightarrow CH_4$

can be ruled out since this is a termination reaction, and cannot exceed the rate of the initiation reaction 1. The rate of initiation, measured as $R^0_{C_2H_6}$, was only 0.5 to 3% of the rate of formation of CH_4. Furthermore the value of k_1, calculated assuming reaction 12 did not occur, was constant at a particular temperature, as expected. Surface reactions can be ruled out because of the insensitivity to surface-to-volume ratio, demonstrated in Figs. 1*a*, 2, and 4. Other potential sources of CH_4 and the possibility of curvature of the Arrhenius plot for k_7 can be eliminated by arguments similar to those in ref. 5.

Comparison with Theory

The dashed lines in Fig. 6 show the theoretical calculations of Johnston and Parr (16) and of Clark and Dove. Both sets of calculations are based on potential energy surfaces calculated by the bond-energy-bond-order (BEBO) technique and both employ activated complex theory, with tunnelling corrections for an unsymmetrical Eckart barrier.

In contrast to the straight line *a*, both curves duplicate the observed curvature well, although they disagree regarding the absolute magnitude of the rate coefficient. Johnston and Parr do not

Can. J. Chem. Downloaded from www.nrcresearchpress.com by 210.87.254.105 on 09/05/12
For personal use only.

give full details of their calculation but they chose a bond dissociation energy, $D_e(H_3C—H)$, of 439 kJ mol^{-1}, whereas Clark and Dove chose 465 kJ mol^{-1}. The resulting differences in potential energy between activated complex and reactants, ΔV_{act}, were 63 kJ mol^{-1} (16) and 52 kJ mol^{-1} (1). Other theoretical treatments have yielded values of ΔV_{act} from 30 to 100 kJ mol^{-1} (4).

In conclusion, it has been demonstrated that neopentane pyrolysis is a clean source of methyl radicals for reaction with other molecules, and that reaction 7 can be used as a measure of $[CH_3]$ under these conditions. Reaction 6 is sufficiently rapid that addition of hydrogen should accelerate most thermal decompositions in which methyl radicals play a major role. Activated complex theory, though unable yet to predict uniquely the absolute rate, does provide a satisfactory explanation for the observed curvature of the Arrhenius plot for the reaction of methyl radicals with molecular hydrogen.

The authors wish to thank the National Research Council of Canada for a grant in support of this research.

1. T. C. Clark and J. E. Dove. Can. J. Chem. **51**, 2155 (1973).
2. J. S. Shapiro and R. E. Weston, Jr. J. Phys. Chem. **76**, 1669 (1972).
3. C. T. Ting and R. E. Weston, Jr. J. Phys. Chem. **77**, 2257 (1973).
4. L. M. Raff. J. Chem. Phys. **60**, 2220 (1974).
5. P. D. Pacey. Can. J. Chem. **51**, 2415 (1973).
6. P. D. Pacey and J. H. Purnell. J. Chem. Soc. Faraday Trans. I, **68**, 1462 (1972).
7. H. E. Van Den Berg, A. B. Callear, and R. J. Norstrom. Chem. Phys. Lett. **4**, 101 (1969).
8. A. M. Bass and A. H. Laufer. Ber. Bunsenges. physik. Chem. **78**, 198 (1974).
9. H. Gesser and E. W. R. Steacie. Can. J. Chem. **34**, 113 (1956).
10. T. G. Majury and E. W. R. Steacie. Can. J. Chem. **30**, 800 (1952).
11. E. Whittle and E. W. R. Steacie. J. Chem. Phys. **21**, 993 (1953).
12. S. Davison and M. Burton. J. Am. Chem. Soc. **74**, 2307 (1952).
13. J. Chanmugam and M. Burton. J. Am. Chem. Soc. **78**, 509 (1956).
14. P. Gray, A. A. Herod, and A. Jones. Chem. Rev. **71**, 247 (1971).
15. S. W. Benson and D. V. S. Jain. J. Chem. Phys. **31**, 1008 (1959).
16. H. S. Johnston and C. Parr. J. Am. Chem. Soc. **85**, 2544 (1963).

Can. J. Chem. Downloaded from www.nrcresearchpress.com by 210.87.254.105 on 09/05/12
For personal use only.

New Route to Cyclic Azomethine Imines

P. C. Ip, K. Ramakrishnan, and J. Warkentin
Department of Chemistry, McMaster University, Hamilton, Ontario, L8S 4M1

Received May 23, 1974

P. C. Ip, K. Ramakrishnan, and J. Warkentin. Can. J. Chem. **52**, 3671 (1974).

Cyclic azomethine imines, in which the ring is four-membered, have been synthesized by thermal decomposition of the readily available 2-hydrazono-Δ^3-1,3,4-oxadiazolines. Possible mechanisms, involving the intermediacy of an iminooxirane, are discussed.

P. C. Ip, K. Ramakrishnan et J. Warkentin. Can. J. Chem. **52**, 3671 (1974).

On a synthétisé des azométhines imines cycliques contenant un cycle à quatre par la décomposition thermique des hydrazono-2 Δ^3-oxadiazolines-1,3,4 facilement accessibles. On discute de différents mécanismes possibles impliquant la formation d'un iminooxyranne comme intermédiaire. [Traduit par le journal]

Can. J. Chem. Downloaded from www.nrcresearchpress.com by 210.87.254.6 on 09/05/12
For personal use only.

Azomethine imine ylids are readily available through a variety of routes including hydrogen abstraction from *N*-amino pyridinium salts (1, 2), photochemical ring contraction of a phthalazine to an isoindole ylid (3), reaction of azocyanides (4) or azocarbonyl compounds (5) with diazoalkanes, and reaction of 3-pyrazolidones with ketones (6–8). Cyclic azomethine imines, containing a four- or five-membered ring, were reported in 1968 by Greenwald and Taylor (9, 10), who prepared them according to eqs. 1 and 2. Such compounds are useful in synthesis of other heterocyclic

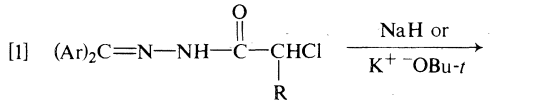

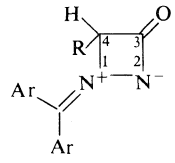

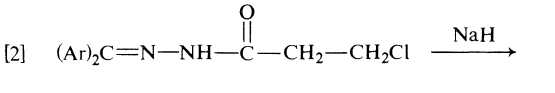

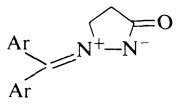

molecules (10, 11). Moreover, the four-membered ylid (eq. 1) has interesting structural features; the X-ray crystal structure showing an ortho hydrogen of the *Z*-oriented aromatic ring within hydrogen bonding distance from N-2 (12).

We report a new synthesis of 4,4-disubstituted, cyclic, azomethine imines (**3**), which complements the previous route (eq. 1) (10, 11) and which extends to new members of the family, particularly 4,4-disubstituted systems, not available by the previous route (11).

Results and Discussion

Scheme 1 illustrates the sequence of reactions by which carbonyl compounds and carbohydrazide are converted to 2-hydrazono-Δ^3-1,3,4-oxadiazolines (**2**) and to 3-oxo-1,2-diazetidinium hydroxide inner salts (**3**).

Table 1 lists some compounds (**2**) which were synthesized in connection with the present work. Oxidative cyclization of carbohydrazones (Scheme 1) gave only one of the configurations possible at the exocyclic double bond (13). Such selectivity has been observed also in oxidative cyclization of 4-substituted semicarbazones of ketones (14), which leads to 2-imino-Δ^3-1,3,4-oxadiazolines with the *Z*-configuration at the exocyclic double bond (15). Compounds **2** are tentatively assigned the *Z*-configuration by analogy.

Table 2 lists the new dipolar compounds (**3**) which have been synthesized by thermolysis of **2**. The scope of Scheme 1 for the synthesis of **3** is currently limited to the following substituent types: R_1, R_2 = aryl; R_2 = H, R_1 = aryl; and R_3, R_4 = alkyl. The spirocyclic compound **2***i* (Table 1) decomposed to a complex mixture containing the appropriate product **3** (n.m.r. evidence) but a pure sample could not be isolated. In the case of **2***h* (Table 1), the pyrolysis mixture was again complex and there was no evidence that it contained the expected

Can. J. Chem. Downloaded from www.nrcresearchpress.com by 210.87.254.6 on 09/05/12
For personal use only.

TABLE 1. 2-Hydrazono-Δ^3-1,3,4-oxadiazolines (**2**)[a]

Compound	R_1	R_2	R_3	R_4	Melting point (°C)	%C Calcd.	%C Found	%H Calcd.	%H Found	%N Calcd.	%N Found
2*a*	C_6H_5	C_6H_5	CH_3	CH_3	110–112		[b]		[b]		[b]
2*b*	*p*-C_6H_4Cl	*p*-C_6H_4Cl	CH_3	CH_3	143–145 (dec)	56.53	56.48	3.91	4.11	15.50	15.39[d]
2*c*	*p*-C_6H_4Br	*p*-C_6H_4Br	CH_3	CH_3	173–174 (dec)	45.36	45.29	3.14	3.30	12.45	12.41[e]
2*d*	C_6H_5	CH_3	CH_3	CH_3	115–116	62.59	62.66	6.13	6.50	24.33	24.30
2*e*	C_6H_5	H	CH_3	CH_3	95	61.10	60.95	5.59	5.78	25.91	25.90
2*f*	*p*-$C_6H_4CH_3$	H	CH_3	CH_3	108–110	62.59	62.67	6.13	6.23	24.33	24.19
2*g*	C_6H_5	H	CH_3	CH_2CH_3	44[c]						
2*h*	C_6H_5	H	$(CH_2)_5$		Oil[c]						
2*i*	C_6H_5	H	$(CH_2)_4$		104	64.45	64.25	5.82	5.80	23.12	23.35

[a]Yields were in the range 57–78%, based on amounts isolated. Some of the oxidations have been carried out only once and in no case was optimization of the yield attempted.
[b]Previously reported (13).
[c]This low-melting material was not obtained analytically pure. Its n.m.r. and i.r. spectra (13) were consistent with the assigned structure and it gave the expected molecular weight (mass spectrometric).
[d]%Cl: calcd., 19.62; found, 19.51.
[e]%Br: calcd., 35.50; found, 35.39.

TABLE 2. Azomethine imine ylids (**3**)[a]

Compound	R_1	R_2	R_3	R_4	Melting point (°C)	%C Calcd.	%C Found	%H Calcd.	%H Found	%N Calcd.	%N Found
3*a*	C_6H_5	C_6H_5	CH_3	CH_3	171–173	77.27	77.22	6.06	6.15	10.61	10.65
3*b*	*p*-C_6H_4Cl	*p*-C_6H_4Cl	CH_3	CH_3	200–201	61.27	61.27	4.23	4.26	8.41[b]	8.46[b]
3*c*	*p*-C_6H_4Br	*p*-C_6H_4Br	CH_3	CH_3	210–211		[c]				
3*d*	C_6H_5	H	CH_3	CH_3	191	70.21	69.76	6.38	6.53	14.89	14.76
3*f*	*p*-$C_6H_4CH_3$	H	CH_3	CH_3	211	71.29	70.81	6.93	7.20	13.86	13.47
3*g*	C_6H_5	H	CH_3	CH_2CH_3	154	71.29	71.33	6.93	7.07	13.86	13.80

[a]Yields of pure material were in the range 32–36% in all cases listed.
[b]%Cl: calcd., 21.27; found, 20.98.
[c]This material was not analyzed. Its identity was established by means of an X-ray crystal structure (16).

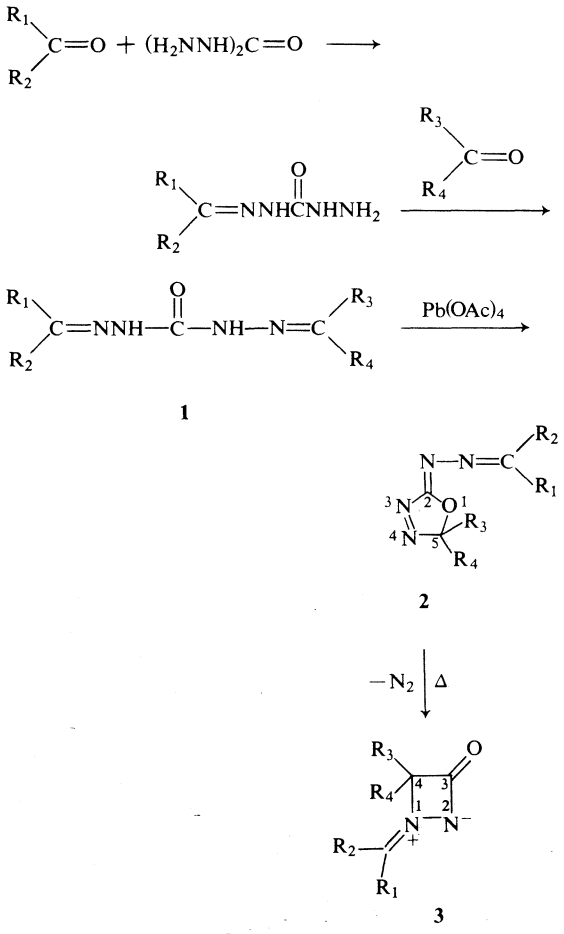

SCHEME 1

azomethine imine. The small C-3, C-4, N-1 bond angle (81°) of the azomethine imines (12, 16) would tend to enlarge the angle between exocyclic bonds to C-4, a geometry that could be mildly resisted in spiranes of the type under consideration. Whether strain at C-4 is a cause of the very low yields of such spiranes is not clear at this time.

Attempts to prepare **3** with R_1 and/or R_2 = alkyl have been unsuccessful to date, possibly because such products undergo subsequent reactions involving proton transfer from the allylic positions of the imminium function. Compounds **3** with R_3 = H and/or R_4 = H are also not available via Scheme 1 because the required precursors (**2**, R_3 = H and/or R_4 = H) undergo rapid azo–hydrazone tautomerism, precluding their isolation. Fortunately, the site selectivity in oxidation of unsymmetric carbohydrazones (**1**, $R_3 = R_4$ = alkyl; $R_1 = R_2$ = aryl or R_1 = aryl, R_2 = H) is just that depicted in Scheme 1 (13), placing alkyl substituents at C-5 of the ring and aryl substituents (or aryl and H) at the exocyclic hydrazono function of **2**. Thus the new synthetic route nicely complements Taylor's method (eq. 1), which cannot be adapted to the synthesis of 4,4-disubstituted members of the family **3** because tertiary chloroacyl hydrazones give only products of elimination on treatment with NaH or *t*-BuO^-K^+, and which also does not lead to systems **3** in which R_2 = H (11).

Two configurations of **3** are possible if $R_1 \neq R_2$. In the cases studied to date, we have obtained only the *Z*-isomers (R_2 = H, R_1 = aryl). Assignment of the configuration is based on the finding that diaryl compounds ($R_1 = R_2$ = aryl) have proton magnetic resonance (p.m.r.) spectra in which the chemical shift of two aryl protons is 8.0 δ while eight aryl protons (for the diphenyl system) absorb near 7.4 δ. The lower-field signal has been assigned to the two *ortho* protons of the *Z*-oriented phenyl group (11), since these are in close proximity to the negative amido nitrogen. All compounds **3** of Table 2, which have only one aryl group at the imminium carbon, have a two-proton signal near 8.0 δ. They must therefore be the *Z*-isomers.

The crystal structures of two members of the family **3** ($R_3 = R_4 = CH_3$, $R_1 = R_2$ = *p*-C_6H_4X, X = Cl, Br) have been determined (16). These not only confirm the assigned structure but also the close proximity between one ortho hydrogen of the *Z*-oriented aryl group and negative ring nitrogen, which has been described as a hydrogen bond (12, 16). In solution that interaction, if the term hydrogen bond is appropriate, is quite small. At −90°, in CH_2Cl_2, the n.m.r. spectrum of **3***a* showed two *ortho* hydrogens in equivalent environments, at 8.0 δ.

Several mechanisms can be envisioned for the formation of **3** from **2** (Scheme 2). There is precedent for decomposition of 2-imino oxadiazolines both to ketone and isonitrile (path *a*, Scheme 2) and to isocyanate and diazoalkane (path *c*) (17). Reactions of isocyanides with ketones are known (Passerini reaction) and an iminooxirane intermediate has been proposed (18). Evidence against operation of path *a* in the present system was obtained by decom-

Can. J. Chem. Downloaded from www.nrcresearchpress.com by 210.87.254.6 on 09/05/12
For personal use only.

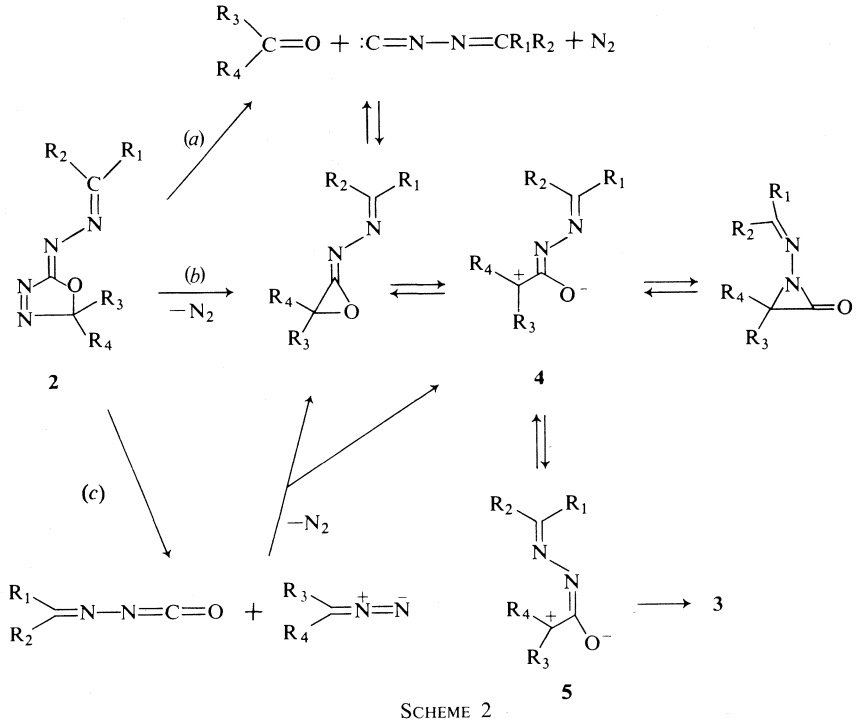

SCHEME 2

position of **2** ($R_3 = R_4 = CH_3$, $R_1 = R_2 = C_6H_5$) in 2-butanone, which was not incorporated. Path *c*, involving isocyanate and diazoalkane as primary intermediates from a retro 1,3-dipolar cycloaddition has not been ruled out. Those products could recombine with loss of nitrogen to form an iminooxirane or the latter could arise more directly from **2** (path *b*). Iminooxiranes have never been isolated but there is evidence that they can undergo thermolysis to isocyanides and carbonyl compounds (19) and that they are interconvertible with α-lactams (20), probably through a dipolar intermediate analogous to that involved in polymerization of α-lactones (21).

The dipolar intermediate in the present system has available a third ring closure option, to form **3**. Such closure is not possible, however, until the amido nitrogen has inverted configuration. Inversion of that configuration could occur via the α-lactam, in which resonance (22) would give the amido nitrogen's lone pair more p-character, or it could occur in the zwitterion, which must have C—N bond orders below two because of conjugation. Once the amido nitrogen is inverted the azine system has the unstable *s-cis* configuration. It could either return to **4** or else the second nitrogen could invert to achieve another *s-trans* configuration (**5**), which is geometrically suited for closure to **3**. Inversion of the second nitrogen, however, converts from the *E*-configuration ($R_1 = C_6H_5$, $R_2 = H$) of aldazine **2** (23), or of iminooxirane, to the *Z*-configuration. Thus the mechanism can account for the apparent selectivity of ring closure to the *Z*-isomers of **3***d*–**3***g*. The stereoselectivity, it should be emphasized, is not firmly established at this time for the stability of corresponding (unknown) *E*-isomers to the reaction conditions has not been demonstrated.

The mechanism of formation of **3** is under investigation.

Experimental

Carbohydrazones were synthesized according to Scheme 1; the aldehyde or aryl ketone moiety being introduced first and the aliphatic ketone last. Yields in these straightforward condensations were in the range 65–90% for each step. A typical synthesis is described below. The procedures for oxidative cyclization of carbohydrazones and for thermolysis of oxadiazolines are also described below. Properties and analyses of compounds are gathered in Tables 1–2. Melting points are uncorrected.

Can. J. Chem. Downloaded from www.nrcresearchpress.com by 210.87.254.6 on 09/05/12
For personal use only.

*Benzaldehyde-4-aminosemicarbazone (**6**)*

Carbohydrazide (5.0 g, 0.056 mol) and benzaldehyde (4.5 g, 0.042 mol) in 50 ml of absolute ethanol were heated at the reflux temperature for 1 h. The product which separated on cooling was filtered, washed with hot water, and recrystallized from ethanol: m.p. 165° (lit. (24) m.p. 173°); 86% yield.

*Crossed Carbohydrazone of Acetone and Benzaldehyde (**7**)*

A solution of **6** (20 g) in excess acetone (80 ml) was refluxed for 3 h. The solution was concentrated to 20 ml and the crystals which separated on cooling were filtered: yield 82%; m.p. 188–191°.

*5,5-Dimethyl-2-(benzylidenehydrazono)-Δ^3-1,3,4-oxadiazoline (**2e**)*

A solution of lead tetraacetate (LTA, 6.0 g, 0.0135 mol) in 25 ml of methylene chloride was cooled with ice. Gradual addition of **7** (2.0 g, 0.0092 mol) with stirring, was completed in 10 min; the temperature in the reaction vessel remaining below 5°. Stirring was continued for 15 min before ice water (50 ml) was added. After stirring for 10 min more, the dark brown slurry was filtered through Celite and the pale yellow organic layer was separated, washed with cold water (3 × 50 ml), with saturated sodium bicarbonate (50 ml), with cold water (3 × 50 ml), and dried with $MgSO_4$. Filtration and evaporation left a yellow solid (65%) which was recrystallized from petroleum ether: m.p. 95°; p.m.r. ($CDCl_3$) δ 1.8 (s, 6), 7.5 (m, 5), 8.5 (s, 1). All aldehyde derivatives **2** (R_1 = H) showed a one-proton singlet near 8.5 δ. All compounds **2** gave infrared spectra characteristic of 2-alkylidenehydrazono-Δ^3-1,3,4-oxadiazolines (13). Melting points and analyses are in Table 1.

*1-((Z)-phenylmethylene)-4,4-dimethyl-3-oxo-1,2-diazetidinium Hydroxide, Inner Salt (**3d**)*

A solution of **2e** (0.20 g, 1.05 × 10^{-3} mol) in chlorobenzene (10 ml) was refluxed for 24 h. About 7 ml of the solvent was distilled out. Cooling of the residual solution and addition of petroleum ether caused separation of a white solid which was filtered, washed with petroleum ether, and recrystallized from petroleum ether – chloroform to yield **3d** (37%): m.p. 191°; p.m.r. ($CDCl_3$) δ 1.74 (s, 6), 7.1 (s, 1), 7.45 (m, 3), 8.05 (m, 2); m.s. 188 (molecular ion). Melting points and analyses of members of the family **3** synthesized by analogous procedures, are in Table 2.

2-Methoxy-2-methyl-N-(diphenylmethylenimino)-propionamide

2-Methoxy-2-methylpropanoic acid (25) was esterified with methanol and sulfuric acid (25). The ester (2.95 g, 0.022 mol) was heated on the steam bath for 5 h with hydrazine hydrate (99%, 1.55 g, 0.031 mol). Evaporation of liquid in a rotary evaporator at 80° left 1.63 g (55%) of crude 2-methoxy-2-methylpropanoic acid hydrazide as a colorless oil. The hydrazide (1.63 g, 0.0123 mol) was heated with benzophenone (4.5 g, 0.025 mol) in 20 ml of ethanol for 17 h before the alcohol was removed at the water pump (65°). Washing of the solid residue with petroleum ether and recrystallization from ethyl ether in petroleum ether gave 0.34 g (10%) of the title compound: m.p. 125–126°; p.m.r. (CCl_4) δ 1.30 (s, 6, CH_3), 2.97 (s, 3, OCH_3), 7.13–7.73 (m, 10, phenyl); i.r. 3345 cm^{-1} (N—H), 1710 cm^{-1} (CO). This product was identical to that obtained from heating **3a** with methanol in a sealed tube at 150° for 30 h.

This work was supported by the National Research Council of Canada.

1. R. Gosl and A. Neuwsen. Chem. Ber. **92**, 2521 (1959).
2. W. Schneider and W. Riedel. Ber. Dtsch. Chem. Ges. **74**, 1252 (1941).
3. B. Singh. J. Am. Chem. Soc. **91**, 3670 (1969).
4. R. Huisgen, R. Fleischmann, and A. Eckell. Tetrahedron Lett. 1 (1960).
5. G. F. Bettinetti and L. Capretti. Gazz. Chem. Ital. **95**, 33 (1965).
6. W. O. Godtfredsen and S. Vangedal. Acta Chem. Scand. **9**, 1498 (1955).
7. J. C. Howard, G. Gever, and P. Wei. J. Org. Chem. **28**, 868 (1963).
8. H. Dorn and A. Otto. Angew. Chem. Intern. Ed. Engl. **7**, 214 (1968).
9. R. B. Greenwald and E. C. Taylor. J. Am. Chem. Soc. **90**, 5272 (1968).
10. R. B. Greenwald and E. C. Taylor. J. Am. Chem. Soc. **90**, 5273 (1968).
11. N. F. Haley. Ph.D. Thesis, Princeton University, 1971; Diss. Abstr. **32**, 3851-B (1972).
12. C. J. Fritchie, Jr. and J. L. Wells. Chem. Commun. 917 (1968).
13. P. R. West and J. Warkentin. J. Org. Chem. **33**, 2089 (1968).
14. A. M. Cameron, P. R. West, and J. Warkentin. J. Org. Chem. **34**, 3230 (1969).
15. A. Prakash, C. Calvo, A. M. Cameron, and J. Warkentin. J. Cryst. Mol. Struct. **3**, 71 (1973).
16. C. Calvo, P. C. Ip, N. Krishnamachari, and J. Warkentin. Can. J. Chem. **52**, 2613 (1974).
17. P. R. West and J. Warkentin. J. Org. Chem. **34**, 3233 (1969).
18. T. Saegusa, N. Taka-ishi, and H. Fujii. Tetrahedron **24**, 3795 (1968).
19. K. Bott. Tetrahedron Lett. 3323 (1968).
20. (*a*) J. C. Sheehan and I. Lengyel. J. Am. Chem. Soc. **86**, 746 (1964); (*b*) J. C. Sheehan and I. Lengyel. Angew. Chem. Intern. Ed. **7**, 25 (1968).
21. (*a*) P. D. Bartlett and L. B. Gortler. J. Am. Chem. Soc. **85**, 1864 (1963); (*b*) R. Wheland and P. D. Bartlett. J. Am. Chem. Soc. **92**, 6057 (1970); (*c*) W. Adam and R. Rucktäschel. J. Am. Chem. Soc. **93**, 557 (1971). (*d*) O. L. Chapman, P. W. Wojtkowksi, W. Adam, O. Rodriquez, and R. Rucktäschel. J. Am. Chem. Soc. **94**, 1365 (1972).
22. E. R. Talaty, A. E. Dupuy, Jun., and T. H. Golson. Chem. Commun. 49 (1969).
23. J. Elguero, R. Jacquier, and C. Marzin. Bull. Soc. Chim. Fr. 1374 (1969).
24. A. C. Brown, E. C. Pickering, and F. J. Wilson. J. Chem. Soc. 107 (1927).
25. C. H. Weizmann, M. Sulzbacher, and E. Bergmann. J. Am. Chem. Soc. **70**, 1153 (1948).

Can. J. Chem. Downloaded from www.nrcresearchpress.com by 210.87.254.6 on 09/05/12
For personal use only.

Etude des fluorures et oxyfluorures de chlore ClF_5 et $ClOF_3$ liquides par résonance magnétique nucléaire

MICHEL ALEXANDRE ET PAUL RIGNY

Centre d'Etudes Nucléaires de Saclay, Service de Chimie-Physique, BP N° 2, 91190, Gif-sur-Yvette, France

Reçu le 28 mars 1974

MICHEL ALEXANDRE et PAUL RIGNY. Can. J. Chem. **52**, 3676 (1974).

Les mesures de temps de relaxation des aimantations nucléaires ainsi que l'interprétation des formes de raies d'absorption du fluor dans ClF_5 et $ClOF_3$ permettent de compléter les données relatives à ces composés. Ainsi le déplacement chimique entre fluors inéquivalents de $ClOF_3$ a été trouvé égal à 50 ± 2 p.p.m. La constante de couplage chlore ^{35}Cl – fluor dans ClF_5 est égale à 192 Hz pour le fluor axial, et inférieure à 20 Hz pour les fluors équatoriaux. Enfin, des informations supplémentaires telles que la vitesse de l'échange chimique entre fluors de $ClOF_3$, ainsi les couplages chlore–fluor moyens dans ClF_3 et $ClOF_3$ ont été obtenues.

MICHEL ALEXANDRE and PAUL RIGNY. Can. J. Chem. **52**, 3676 (1974).

Nuclear relaxation time measurements and interpretations of absorption line shape in ClF_5 and $ClOF_3$ allow one to complete data for these compounds. Thus, the chemical shift between non-equivalent fluorine atoms in $ClOF_3$ has been found equal to 50 ± 2 p.p.m. The coupling constant, chlorine ^{35}Cl – fluorine is 192 Hz for the axial fluorine, and less than 20 Hz for the equatorial fluorines. In addition to other information, such as exchange times between fluorine atoms in $ClOF_3$, and the mean coupling constant chlorine–fluorine in $ClOF_3$ and ClF_3, is reported.

Introduction

On connait les fluorures et oxyfluorures de chlore suivants: ClF, ClF_3, ClF_5; ClOF, $ClOF_3$, ClO_2F, ClO_2F_3, ClO_3F, ClO_4F. L'existence de certains d'entre eux n'est pas encore établie avec certitude (ClOF), d'autres sont connus et caractérisés depuis peu: ClF_5 (1), $ClOF_3$ (2, 3). Ce caractère récent, lié à une très grande réactivité qui en rend le maniement délicat, explique le peu d'études structurales dont ces corps ont fait l'objet.

A l'exception de ClO_nF, ils mettent en défaut la règle de l'octet, et la description des liaisons chimiques dans ces molécules a fait l'objet de nombreux travaux (4). Pour les composés dont la structure est connue, l'une des liaisons Cl—F (liaison courte) présente un catactère covalent comparable au composé ClF, tandis que les autres liaisons Cl—F, plus longues, s'expliquent par un caractère semi-ionique ou une hybridation d'orbitales à 3 centres – 4 électrons. Sauf pour le trifluorure et le pentafluorure, le spectre r.m.n. haute résolution du fluor apporte peu d'information sur la structure moléculaire, soit parce que la molécule ne contient qu'un seul type de fluor, soit parce que l'échange chimique est rapide, et une seule raie est observée.

Nous présentons ici une étude des composés ClF_5 et $ClOF_3$ par la relaxation nucléaire. La mesure des temps de relaxation peut se faire par l'étude des formes de raies, ou, plus facilement, à l'aide de la spectroscopie r.m.n. par impulsions. De telles mesures apportent ici plus de renseignements que la spectroscopie à haute résolution (tableau 1). Ainsi, il nous a été possible de déterminer les constantes de couplages chlore-fluor pour les deux types de fluor de ClF_5, et de confirmer la structure de la molécule $ClOF_3$, déterminée par spectroscopie Raman (5). L'existence de deux types de fluors inéquivalents en échange rapide a été vérifiée; leur déplacement chimique a pu être obtenu par l'interprétation des temps de relaxation dans le référentiel tournant ainsi que par la forme de la raie d'absorption à 250 MHz.

La relaxation magnétique; théorie

Dans un champ magnétique statique H_0, un système de spins possède une aimantation $M_0 = \chi H_0$, où χ est la susceptibilité. Si cette aimantation est perturbée de sa valeur initiale, la composante parallèle à H_0 revient à sa position d'équilibre en un temps T_1, tandis que la composante perpendiculaire décroit en un temps T_2. Cette relaxation est provoquée par les couplages spin–réseau, fonctions aléatoires du temps. Sans entrer dans les détails, rappelons que les fluctuations rapides (c'est-à-dire de temps caractéristique τ_c tel que $\gamma H_0 \tau_c \ll 1$) contribuent de façon égale aux relaxations longitudinales et trans-

Can. J. Chem. Downloaded from www.nrcresearchpress.com by 210.87.254.105 on 09/05/12
For personal use only.

TABLEAU 1. Données magnétiques relatives à quelques fluorures et oxyfluorures de chlore

	ClF_3 [a]		ClF_5 [a]		$ClOF_3$ [a]		
	F_1	F_2	F_1	F_2	F_1	F_2	ClO_3F
Déplacements chimiques (p.p.m.) [b]	13	−113 [d]	−425 [e]	−260 [e]	−308	−254	−287 [f]
Constante de couplage $J_{F_1F_2}$ (Hz)		403 [d]		133 [e]			
Constante de couplage $J_{^{35}Cl-F}$		260 [c]	192	≤20		195 [c]	278 [g]

[a] ClF_1: liaison courte, ClF_2 liaison longue.
[b] Déplacements chimiques exprimés à partir de CCl_3F.
[c] Il s'agit de la constante de couplage chlore–fluor moyenne.
[d] Voir réf. 6.
[e] Voir réf. 7.
[f] Voir réf. 8.
[g] Voir réf. 9.

versales, tandis que les fluctuations lentes ne sont pratiquement efficaces que pour la relaxation transversale (11).

Dans les cas qui nous occupent ici, la relaxation longitudinale des noyaux de fluor est provoquée par les fluctuations de l'interaction spin–rotation et des couplages dipolaires (10) tandis que celle des noyaux de chlore (^{35}Cl ou ^{37}Cl) est due aux fluctuations du couplage quadrupole–gradient de champ électrique. L'étude de ces mécanismes apporte peu d'information sur les propriétés chimiques des composés mais renseigne sur les mouvements moléculaires (15). Il n'en est pas de même de la relaxation transversale. Les mouvements lents qui déterminent cette dernière pourront être la relaxation longitudinale du chlore (T_{1Cl}), qui module les couplages chlore–fluor J_{Cl-F}, ou l'échange chimique entre fluors inéquivalents. L'aspect des phénomènes étudiés dépend de la vitesse du mécanisme par rapport à la grandeur modulée. Dans ces composés, on sera toujours dans la situation $J_{ClF}T_{1Cl} \ll 1$: les couplages chlore–fluor ne donnent pas de structure fine, mais contribuent à la relaxation transversale des fluors.

Pour l'échange chimique entre fluors, qui peut être ou bien rapide, ou bien lent devant la différence de déplacement chimique $(\sigma_1 - \sigma_2)\nu_0$ (ν_0, fréquence de Larmor), plusieurs cas sont à distinguer:

(*a*) échange chimique très lent (ou inexistant):

Si le spectre observé est du premier ordre (cas de ClF_5 à 56.4 MHz), les raies observées correspondent aux transitions d'un spin, et ont une largeur $1/T_{2i}$ (transition du fluor i) (11)

$$[1] \qquad 1/T_{2i} = 1/T_{1i} + 5\pi^2 J_{Cl-Fi}{}^2 T_{1Cl}$$

(*b*) si l'échange chimique est rapide, $2\pi\nu_0(\sigma_1 - \sigma_2)\tau_e \ll 1$ (τ_e temps d'échange), on n'observe plus qu'une seule raie, de largeur (*cf.* Appendice):

$$[2] \qquad \frac{1}{T_2} = \frac{1}{T_1} + \frac{8}{9}\pi^2\nu_0{}^2(\sigma_1 - \sigma_2)^2\tau_e + \frac{1}{T_{2s}}$$

Le dernier terme $1/T_{2s}$ est la vitesse de relaxation due à la modulation des couplage chlore–fluor par la relaxation du chlore et (ou) par l'échange interfluor. Son calcul détaillé (10) nécessite la connaissance τ_e, T_{1Cl}, des constantes de couplages J_{Cl-F_1}, J_{Cl-F_2} et du mécanisme d'échange (intramoléculaire ou intermoléculaire). Il peut s'écrire:

$$[3] \qquad 1/T_{2s} = 5\pi^2\langle J^2\rangle\tau_s$$

avec

$$\langle J^2\rangle = \tfrac{1}{3}J_{Cl-F_1}{}^2 + \tfrac{2}{3}J_{Cl-F_2}{}^2$$

et

$$\tau_s{}^{-1} = T_{1Cl}{}^{-1} + \tau_e{}^{-1}$$

Une analyse détaillée montre que l'expression 3 est en général approximative, mais n'entraine qu'une erreur faible.

(*c*) A fréquence de Larmor élevée (250 MHz), les déplacements chimiques sont beaucoup plus grands que les couplages scalaires fluor–fluor, et les effets de ceux-ci peuvent être négligés. La raie d'absorption a approximativement l'équation suivante, (cas d'un échange entre deux sites de population $\frac{1}{3}$ et $\frac{2}{3}$):

$$[4] \qquad S(\nu - \nu_0) = \text{Reel}\left\{\frac{\frac{1}{2\pi\tau_e} + i\left(\frac{\sigma\nu_0}{3} + \nu\right)}{2\pi\left(\frac{\sigma^2\nu_0{}^2}{9} - \nu_0{}^2 - \frac{\sigma\nu}{3}\nu_0\right) + i\frac{\nu}{\tau_e}}\right\}$$

avec ν_0, fréquence de Larmor, $\sigma = \sigma_1 - \sigma_2$.

Can. J. Chem. Downloaded from www.nrcresearchpress.com by 210.87.254.105 on 09/05/12
For personal use only.

Can. J. Chem. Downloaded from www.nrcresearchpress.com by 210.87.254.105 on 09/05/12
For personal use only.

Il est intéressant d'observer aussi la relaxation en présence d'irradiation: on crée une situation où l'aimantation nucléaire est transversale et l'on irradie la substance de telle sorte que, dans le référentiel tournant, l'aimantation soit colinéaire au champ magnétique de radiofréquence H_1 (spin locking). Dans ces conditions, l'aimantation transversale décroît avec une constante de temps $T_{1\rho}$. En échange rapide, on peut écrire (12):

$$[5] \quad \frac{1}{T_{1\rho}} = \frac{8}{9}\frac{\pi^2\nu_0^2(\sigma_1 - \sigma_2)^2\tau_e}{1 + \gamma_F^2 H_1^2 \tau_e^2} + \frac{1}{T_{1\rho s}}$$

Le deuxième terme peut être négligé à fréquence de Larmor ν_0 suffisamment élevée. Les mesures des temps T_2, complétées par celles des temps $T_{1\rho}$ conduisent dans ce cas au déplacement chimique $(\sigma_1 - \sigma_2)$ et au temps d'échange τ_e.

Dans l'utilisation des expressions 1 et 3 aux composés chlorés on doit tenir compte de l'hétérogénéité isotopique du chlore (75% de ^{35}Cl et 25% de ^{37}Cl), qui se manifeste aussi bien sur les constantes de couplage J_{Cl-F} que sur les temps de relaxation $T_1(^{35}Cl)$ ou $T_1(^{37}Cl)$. Par suite des valeurs relatives des rapports gyromagnétiques et des constantes quadrupolaires des deux isotopes du chlore, il y a à peu près compensation des deux effets:

$$[6] \quad \frac{J_{^{35}Cl-F}^2}{J_{^{37}Cl-F}^2}\frac{T_1(^{35}Cl)}{T_1(^{37}Cl)} = \left(\frac{\gamma(^{35}Cl)}{\gamma(^{37}Cl)}\right)^2\left(\frac{Q(^{35}Cl)}{Q(^{37}Cl)}\right)^2 \simeq 0.9$$

Par contre, l'expression 3 doit se récrire (nous négligerons l'effet isotopique sur τ_s):

$$[7] \quad \langle J^2\rangle = \tfrac{3}{4}\langle J_{35}^2\rangle + \tfrac{1}{4}\langle J_{37}^2\rangle$$

avec

$$\langle J_{35}^2\rangle = \tfrac{1}{3}J_{^{35}Cl-F_1}^2 + \tfrac{2}{3}J_{^{35}Cl-F_2}^2$$

idem pour ^{37}Cl.

Préparation des échantillons et méthodes expérimentales

Les composés ClF_3 et ClF_5 proviennent de sources commerciales, et sont ensuite soigneusement distillés. La dernière distillation de ClF_3 est effectuée en présence de fluorure de potassium, afin de retenir les traces d'acide fluorhydrique présentes. Malgré ces précautions, les différents échantillons de ClF_3 préparés présentaient de grandes différences quant à la vitesse d'échange des atomes de fluor.

Le trifluorure de chlore monoxyde a été synthétisé au laboratoire, par la méthode de Pilipovich *et al.* (2), par réaction entre le fluor et le nitrate de chlore. $ClOF_3$ est ensuite stocké à l'état de complexe avec le fluorure de potassium et transféré dans des tubes de Kel-F juste avant l'emploi. Cette procédure évite la présence de produits de décomposition.

Les temps de relaxation du fluor ont été mesurés par les méthodes habituelles de la spectrométrie pulsée (13): séquence d'impulsions π–$\pi/2$ pour le temps T_1 et $\pi/2$–π pour le temps T_2. Les spectromètres à impulsions ont été construits au laboratoire et permettent de travailler soit à fréquence de Larmor variable (2–60 MHz), soit à fréquence fixe (30 MHz) pour les mesures dans le référentiel tournant. Les spectres d'absorption du fluor ont été obtenus sur un spectromètre Varian NV-14 à 56.4 MHz et un spectromètre CAMECA à 250 MHz.

Résultats

(1) Relaxation transversale en haut champ et échange rapide (Fig. 1)

Si l'échange chimique entre fluors inéquivalents (F_1 et F_2) est suffisamment rapide, il est possible de choisir une fréquence de Larmor ν_0 tel que $\nu_0(\sigma_1 - \sigma_2)\tau_e \ll 1$ et $\nu_0^2(\sigma_1 - \sigma_2)^2\tau_e \gg 1/T_{2s}$

Dans ces conditions, la mesure du temps $T_2(F)$ (ou du temps $T_{1\rho}$ si H_1 tend vers 0) conduit à la quantité $(\sigma_1 - \sigma_2)^2\tau_e$, tandis que la pente de la droite $T_{1\rho} = f(H_1^2)$, (H_1 varie de 0.5 à 3 G) donne le terme $\tau_e/(\sigma_1 - \sigma_2)^2$. Les temps τ_e et les déplacements chimiques de $ClOF_3$ déduits de ces mesures sont rassemblés dans le tableau 2. A la

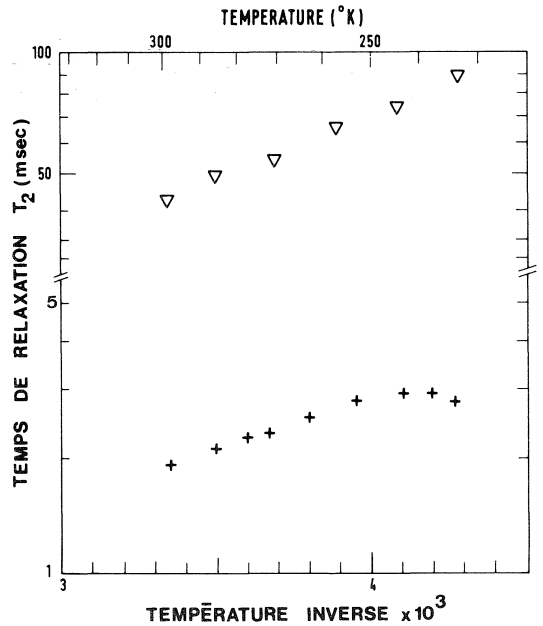

FIG. 1. Temps de relaxation T_2 du fluor ^{19}F de $ClOF_3$, en fonction de la température aux fréquences de Larmor $\nu_0 = 30$ MHz (+) et $\nu_0 = 1.7$ MHz (▽).

Can. J. Chem. Downloaded from www.nrcresearchpress.com by 210.87.254.105 on 09/05/12
For personal use only.

TABLEAU 2. Déplacements chimiques et temps d'échange entre fluors de $ClOF_3$ à diverses températures, déduits des mesures de relaxation dans le référentiel tournant

Température (°C)	Différence de déplacement chimique (p.p.m.)	Temps d'échange ($\times 10^5$) (s)
−34	50.5	1.60
−10	49.6	1.80
+22.5	51.2	2.5

précision des mesures près (10%), le déplacement chimique est trouvé indépendant de la température, égal à 50 ± 2.5 p.p.m. et reproductible d'un échantillon à l'autre. Le temps d'échange, au contraire, a un comportement anormal: il tend à augmenter lorsque la température s'élève. Ce serait paradoxal s'il s'agissait d'un processus simple (réaction du premier ordre), mais peut se comprendre dans le cas d'une cinétique d'échange complexe. Quand les échantillons vieillissent, le temps τ_e évolue, mais le déplacement chimique trouvé $\sigma_1 - \sigma_2$ reste constant. Ceci est compatible avec un échange catalysé par des impuretés, qui, à faible concentration ne peuvent avoir d'influence sur le déplacement chimique observé. Une meilleure compréhension de cet aspect nécessiterait une identification des espèces présentes dans l'échantillon; celle-ci n'est nullement possible ni en r.m.n. ni en spectroscopie Raman.

(2) Relaxation transversale en bas champ (Fig. 1)

En choisissant ν_0 assez petit pour que $\nu_0^2(\sigma_1 - \sigma_2)^2\tau_e \ll 1/T_{2s}$, on aura $1/T_2 \sim 1/T_{2s}$. En tenant compte du fait que

$$[8] \qquad \frac{J_{^{35}Cl-F}{}^2}{J_{^{37}Cl-F}{}^2} = \frac{\gamma(^{35}Cl)^2}{\gamma(^{37}Cl)^2}$$

et connaissant le temps τ_s (τ_e est déduit des mesures à haut champ et $T_1(Cl) = T_2(Cl)$ a été mesuré d'après la largeur de la raie d'absorption du chlore ^{35}Cl) l'expression 3 permet d'évaluer la constante de couplage moyenne fluor–chlore ^{35}Cl. On aboutit aux résultats suivants:

$$ClF_3, \quad (\langle J_{^{35}Cl-F}{}^2\rangle)^{1/2} = 260 \text{ Hz}$$

$$ClOF_3, (\langle J_{^{35}Cl-F}{}^2\rangle)^{1/2} = 195 \text{ Hz}$$

Ces constantes sont du même ordre de grandeur que celles des liaisons Cl—F dans ClO_3F, $J_{^{35}Cl-F} = 278$ Hz (9) ou ClF_6^+: $J_{^{35}Cl-F} = 337$ Hz (14).

(3) Etude des spectres d'absorption du fluor

(a) Spectre de $ClOF_3$ à 250 MHz

A 250 MHz, d'après les valeurs du tableau 2, on voit que $2\pi\nu_0(\sigma_1 - \sigma_2)\tau_e \simeq 1$. La forme de la raie d'absorption est complexe et donnée par l'expression 4. En ajustant la courbe théorique au spectre expérimental (Fig. 2), on est conduit aux valeurs suivantes pour la différence de déplacement chimique et le temps d'échange (à +20 °C):

$$\sigma_1 - \sigma_2 = 53.8 \pm 2.5 \text{ p.p.m.}$$

et

$$\tau_e = 1.7 \times 10^{-5} \text{ s}$$

L'accord entre le déplacement chimique obtenu par analyse de la forme de raie à 250 MHz et celui déduit des temps de relaxation est excellent. Les mesures à haut champs conduisent, de plus, aux valeurs relatives des déplacements chimiques (par rapport à $CFCl_3$):

$$\sigma_1 \text{ (liaison courte)} = -308 \pm 2 \text{ p.p.m.}$$

$$\sigma_2 \text{ (liaisons longues)} = -254 \pm 2 \text{ p.p.m.}$$

(b) Spectre de ClF_5 à 56.4 MHz

Le spectre haute résolution du fluor de ClF_5 (7) correspond à celui attendu pour une molécule de symétrie C_{4v}, avec un atome de fluor axial (F_A) et quatre atomes équatoriaux (F_E). A 56.4 MHz ce spectre est du premier ordre et composé d'un doublet et d'un quintuplet avec $\nu_0(\sigma_{F_A} - \sigma_{F_E}) = 9300$ Hz et $J_{F_A-F_E} = 133$ Hz. Un examen approfondi du spectre réalisé sur un appareil de bonne résolution révèle que, d'une part, les raies du quintuplet sont beaucoup plus larges que les

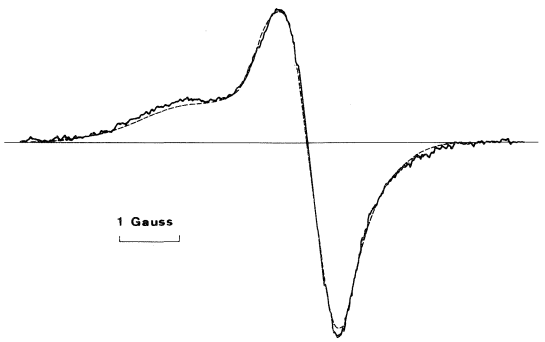

FIG. 2. Dérivée de la raie d'absorption du fluor ^{19}F de $ClOF_3$ à $\nu_0 = 250$ MHz. La courbe pointillée est calculée d'après la dérivée de l'expression 4.

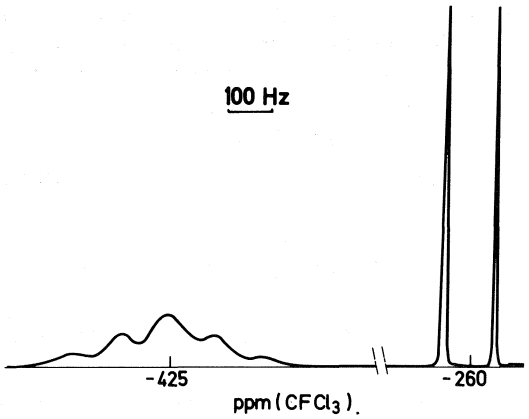

FIG. 3. Spectre haute-résolution de ClF_5 à $-20\,°C$ ($\nu_0 = 56.4$ MHz).

raies du doublet (Fig. 3), et que d'autre part, chaque raie du doublet se décompose en deux raies d'intensités 3:1 et décalées de 0.09 p.p.m. (Fig. 4). Nous attribuons ce dédoublement à un effet des isotopes du chlore sur la liaison Cl—F; sa valeur est voisine de celle qui a été observée pour $^{35}ClF_6^+$–$^{37}ClF_6^+$ (14) 0.15 ± 0.02 p.p.m.).

L'échange entre fluors dans ClF_5, s'il existe, est trop lent pour affecter les propriétés de r.m.n. Les autres mécanismes susceptibles de contribuer aux largeurs des raies sont:

(a) les fluctuations rapides (couplages dipole–dipole et spin–rotation) qui contribuent également à la relaxation longitudinale (typiquement de l'ordre de 1 Hz).

(b) le fait que l'approximation AX_4 (couplage fluor–fluor traité au premier ordre en perturbation) n'est pas suffisante. Au second ordre, cette perturbation provoque l'apparition d'une structure fine d'écartement $J_{F_AF_E}{}^2/\nu_0(\sigma_A - \sigma_E) \simeq 2$ Hz. Ici cette structure fine n'est pas résolue, mais participe à l'élargissement des raies du doublet.

(c) le couplage chlore–fluor, modulé par la relaxation du chlore (expression 1).

Pour les raies du quintuplet (largeur à mi-hauteur 37 Hz à $-73\,°C$), les deux premières causes d'élargissement sont négligeables et l'expression 1 (le temps $T_1(Cl) = T_2(Cl)$ est déduit de la largeur de la raie d'absorption du chlore ^{35}Cl (10)) conduit à

$$|J_{^{35}Cl-F_A}| = 192 \text{ Hz}$$

Les raies du doublet sont beaucoup plus étroites (4 Hz). La différence entre la largeur observée et les deux premières causes d'élargissement est de l'ordre de grandeur de l'erreur expérimentale (0.5 Hz). On n'a alors qu'une limitation supérieure de la contribution scalaire à la relaxation transversale

$$|J_{^{35}Cl-F_E}| \leqslant 20 \text{ Hz}$$

Les mesures de couplage chlore–fluor soulignent la différence entre les deux types de liaison chlore–fluor. La constante de couplage chlore–fluor axial, correspondant à la liaison courte (de caractère covalent) est beaucoup plus grande que celle de la liaison chlore–fluor équatorial, qui présente un caractère plus ionique.

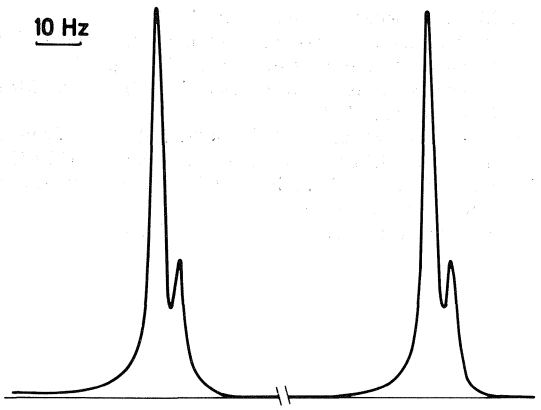

FIG. 4. Doublet du spectre haute-résolution de ClF_5 à $-62\,°C$ ($\nu_0 = 56.4$ MHz).

Conclusion

L'étude de la relaxation nucléaire, par mesure directe des temps T_2 et T_1 ainsi que par l'interprétation des largeurs de raies dans la série des fluorures et oxyfluorures de chlore permet de compléter les informations obtenues par r.m.n. haute résolution du fluor. On a pu étudier les couplages scalaires chlore–fluor dans ClF_5, ClF_3, $ClOF_3$. On a pu aussi mesurer le déplacement chimique entre fluors inéquivalents de $ClOF_3$, malgré un échange chimique rapide, et mesurer cette vitesse d'échange.

Nous sommes heureux de pouvoir remercier ici Madame D. Martin, Messieurs R. Bougon et Tue Buy Huy tant pour la préparation des échantillons que pour leurs conseils et les discussions fructueuses qu'ils nous ont permis d'avoir.

Can. J. Chem. Downloaded from www.nrcresearchpress.com by 210.87.254.105 on 09/05/12
For personal use only.

Can. J. Chem. Downloaded from www.nrcresearchpress.com by 210.87.254.105 on 09/05/12
For personal use only.

Appendice

Expression de la vitesse de relaxation transversale du fluor dans les fluorures de chlore en présence d'échange chimique rapide

Pour des molécules telles que ClF_3 ou $ClOF_3$, l'échange chimique induit trois mécanismes susceptibles de participer à la relaxation transversale du fluor: (*1*) les différences de déplacements chimiques entre fluors; (*2*) les couplages fluor–fluor; (*3*) les couplages chlore–fluor.

Si la vitesse d'échange est rapide devant la différence de déplacement chimique, seuls les mécanismes (*1*) et (*3*) contribuent à la relaxation:

$$1/T_2 = 1/T_1 + \tfrac{2}{9}4\pi^2\nu_0{}^2(\sigma_1 - \sigma_2)^2\tau_e + 1/T_{2s}$$

$1/T_1$ = relaxation due aux autres mécanismes que ceux envisagés ci-dessus; $\sigma_1 - \sigma_2$ = différence de déplacement chimique entre fluors, ν_0 = fréquence de Larmor, τ_e = temps d'échange, $1/T_{2s}$ = relaxation due aux couplages scalaires chlore–fluor.

L'expression ci-dessus s'établit comme suit: L'hamitonien fluctuant total, modulé par l'échange, s'écrit

$$\mathscr{H}_f(t) = 2\pi\nu_0 \sum_i \sigma_i(t) I_z{}^i + 2\pi \sum_{i<j} J_{ij}(t)\boldsymbol{I}^i \cdot \boldsymbol{I}^j + 2\pi \sum J_{i,\alpha}(t)\boldsymbol{I}^i \cdot \boldsymbol{S}^\alpha$$

$\boldsymbol{I}^i$, spin de l'atome i de fluor; $\boldsymbol{S}^\alpha$, spin de l'atome α de chlore. $\sigma_i(t)$, déplacement chimique du spin i à l'instant t ($\sigma_i = \sigma_1$ ou σ_2); $J_{i,\alpha}(t)$, couplage entre les spins i et α à l'instant t ($J_{i,\alpha} = J_1$ ou J_2 si i et α sont sur la même molécule; $J_{i,\alpha} = 0$ si i et α sont sur des molécules différentes).

$J_{ij}(t)$ couplage entre les spins i et j à l'instant t.

La vitesse de relaxation est déterminée par l'équation (11).

$$\frac{d}{dt}\langle\rho I_x\rangle = -\int_0^\infty d\tau \mathscr{T}r\langle[\mathscr{H}_f{}^*(0),[\mathscr{H}_f(\tau), I_x]]\rho\rangle$$

où ρ est la matrice densité et $I_x = \sum_i I_x{}^i$.

Dans les hypothèses suivantes: $2\pi\nu_0(\sigma_1 - \sigma_2)\tau_e \ll 1$; $2\pi(\nu_0 - \nu_{Cl})T_{1Cl} \gg 1$ et en observant que: (*1*) il ne peut y avoir de terme linéaire en ν_0; (*2*) les couplages fluor–fluor ne participent pas à la relaxation:

$$[J_{ij}(t)\boldsymbol{I}^i\boldsymbol{I}^j, I_x] = 0$$

la relaxation des fluors est exponentielle et caractérisée par un temps T_2:

$$\frac{1}{T_2} = 4\pi^2\nu_0{}^2 \int_0^\infty \langle\sigma_i(0)\cdot\sigma_i(\tau)\rangle\, d\tau + 5\pi^2 \int_0^\infty \langle J_{i,\alpha}(0)\cdot J_{i,\alpha}(\tau)\rangle\, e^{-\tau/T_{1Cl}}\, d\tau$$

Le premier terme ne dépend pas du mécanisme d'échange envisagé et est égal à $4\pi^2\nu_0{}^2\frac{2}{9}(\sigma_1 - \sigma_2)^2\tau_e$. Par contre le second terme dépend du mécanisme d'échange (intermoléculaire ou intramoléculaire).

1. D. F. Smith. Sciences, **141**, 1039 (1963).
2. D. Pilipovich, C. G. Lindhal, C. J. Schack, R. D. Wilson et K. O. Christe. Inorg. Chem. **11**, 2189 (1972).
3. R. Bougon, J. Isabey et P. Plurien. C. R. Acad. Sci. Ser. C, **271**, 1366 (1970).
4. R. D. Brown et J. B. Peel. Aust. J. Chem. **11**, 2605 (1968).
5. K. O. Christe et E. C. Curtis. Inorg. Chem. **11**, 2196 (1972).
6. E. L. Muetterties et W. D. Phillips. J. Am. Chem. Soc. **79**, 322 (1957).
7. D. Pilipovich, W. Maya, E. A. Lawton, H. F. Bauer, D. F. Sheehan. N. N. Ogimachi, R. D. Wilson, F. C. Gunderloy et V. E. Bedwell. Inorg. Chem. **6**, 10, 1918 (1967).
8. H. Agahigian, A. P. Gray et G. D. Vickers. Can. J. Chem. **40**, 157 (1962).
9. J. Bacon, R. J. Gillespie et J. W. Quail. Can. J. Chem. **41**, 3063 (1963).
10. M. Alexandre. Thèse. Orsay, 1974.
11. A. Abragam. Les principes du magnétisme nucléaire, Presses Universitaires de France, 1968. p. 311.
12. C. Deverell, R. E. Morgan et J. H. Strange. Mol. Phys. **18**, 553 (1970).
13. T. C. Farrar et E. D. Becker. Pulse and Fourier transform N.M.R. Academic Press, New York. 1971.
14. K. O. Christe, J. F. Hon et D. Pilipovich. Inorg. Chem. **12**, 84 (1973).
15. M. Alexandre et P. Rigny. A publier.

Arrhenius Parameters for Reaction of the *tert*-Butylperoxy and 2-Ethyl-2-propylperoxy Radicals with some Nonhindered Phenols, Aromatic Amines, and Thiophenols[1]

J. H. Bernard Chenier, Edward Furimsky, and James Anthony Howard

Division of Chemistry, National Research Council of Canada, Ottawa, Canada K1A 0R9

Received March 19, 1974

J. H. Bernard Chenier, Edward Furimsky, and James Anthony Howard. Can. J. Chem. **52**, 3682 (1974).

Preexponential factors and activation energies are reported for the transfer of a hydrogen atom from phenol, β-naphthol, aniline, β-naphthylamine, thiophenol, and β-naphthalenethiol to a tertiary alkylperoxy radical ($(CH_3)_3COO^\cdot$ and $C_2H_5C(CH_3)_2OO^\cdot$). The *A*-factors fall in the range 2×10^4 to 2×10^7 M^{-1} s^{-1} and increase in the order $C_6H_5SH \sim$ β-$C_{10}H_7SH \sim$ β-$C_{10}H_7NH_2 <$ $C_6H_5NH_2 \sim$ β-$C_{10}H_7OH <$ C_6H_5OH while the activation energies fall in the range 1 to 5 kcal mol^{-1} and increase in the order $C_6H_5SH \sim$ β-$C_{10}H_7SH <$ β-$C_{10}H_7NH_2 \sim$ β-$C_{10}H_7OH <$ $C_6H_5OH \sim C_6H_5NH_2$. Differences in activation energies and preexponential factors are not consistent with a reaction mechanism which attributes low activation parameters solely to an equilibrium between the reactants and a hydrogen bonded free radical – reactant complex, followed by H-atom transfer within the complex.

J. H. Bernard Chenier, Edward Furimsky et James Anthony Howard. Can. J. Chem. **52**, 3682 (1974).

On rapporte les facteurs préexponentiels et les énergies d'activation pour le transfert de l'atome d'hydrogène du phénol, β-naphthol, de l'aniline, de la β-naphthylamine, du thiophénol et du β-naphthalènethiol à un radical alkylperoxy tertiaire ($(CH_3)_3COO^\cdot$ et $C_2H_5C(CH_3)_2OO^\cdot$). Les facteurs *A* varient entre 2×10^4 et 2×10^7 M^{-1} s^{-1} et augmentent dans l'ordre $C_6H_5SH \sim$ β-$C_{10}H_7SH \sim$ β-$C_{10}H_7NH_2 <$ $C_6H_5NH_2 \sim$ β-$C_{10}H_7OH <$ C_6H_5OH alors que les énergies d'activation varient entre 1 et 5 kcal mol^{-1} et augmentent dans l'ordre de $C_6H_5SH \sim$ β-$C_{10}H_7SH <$ β-$C_{10}H_7NH_2 \sim$ β-$C_{10}H_7OH <$ $C_6H_5OH \sim C_6H_5NH_2$. Les différences dans les énergies d'activation et dans le facteur préexponential ne sont pas en accord avec un mécanisme réactionnel qui n'attribue des paramètres d'activation bas qu'à un équilibre entre les réactifs et un complexe réactif – radical libre liés par un pont hydrogène suivi par un transfert d'atome d'hydrogène à l'intérieur du complexe. [Traduit par le journal]

Introduction

We have recently reported the results of a kinetic electron spin resonance (e.s.r.) study of reaction of the *tert*-butylperoxy radical with some hindered phenols and aromatic amines (1), compounds that are widely used as antioxidants. This work showed directly that the preexponential factors (10^4–10^5 M^{-1} s^{-1}) and activation energies (0.5–1.0 kcal mol^{-1}) for these hydrogen atom transfers are significantly smaller than Arrhenius parameters that are usually associated with bimolecular reactions (2, 3).

In this paper we report the results of a similar kinetic e.s.r. study of reaction of the *tert*-butylperoxy radical (and also the 2-ethyl-2-propylperoxy radical) with some nonhindered phenols (phenol and β-naphthol), aromatic amines (aniline and β-naphthylamine), and thiophenols (benzenethiol and β-naphthalenethiol), AH,

$$\text{ROO}^\cdot + \text{AH} \xrightarrow{k_1} \text{ROOH} + \text{A}^\cdot \qquad [1]$$

where R is *tert*-butyl and 2-ethyl-2-propyl, k_1 is the reaction rate constant, and $A^\cdot$ is either a phenoxy, anilino or thiophenoxy radical.

It was hoped that a knowledge of the Arrhenius parameters for hydrogen atom donors with the reaction site not protected by bulky *ortho* substituents might offer some insight into the mechanism for the transfer of a hydrogen atom from a heteroatom (O, N, and S) to an oxyl radical.

Experimental

tert-Butylperoxy radicals were generated by photolysis of 2,2′-azoisobutane (0.01–0.02 *M*) in oxygen saturated isopentane–toluene (90:1 by vol) in the presence of a large excess of the reactant. 2-Ethyl-2-propylperoxy radicals were formed by photolysis of 5–10% di-*tert*-butyl peroxide in oxygen saturated isopentane (also in the pres-

[1]NRCC No. 14225.

Can. J. Chem. Downloaded from www.nrcresearchpress.com by 210.87.254.40 on 09/05/12
For personal use only.

ence of the reactant). The peroxy radical concentration was followed as a function of time after the initiating light was interrupted by e.s.r. spectroscopy (4). The order with respect to each component was determined by working at different initial peroxy radical and reactant concentrations. Stoichiometric factors were determined either by the e.s.r. induction period method described previously (1) or, for the compounds which did not give sharp induction periods, by an alternative 'dark' e.s.r. method. This method involved photochemical generation of a known concentration of $(CH_3)_3COO^\bullet$ (usually about 10^{-4} *M*) in the cavity of the spectrometer in the absence of the reactant at -100 °C. A fraction of these radicals was then destroyed by addition of a known concentration of reactant (*ca.* $1/4[(CH_3)_3COO^\bullet]_0$) in the dark. Because of the uncertainties involved in the determination of accurate absolute radical concentrations stoichiometric factors were determined relative to 2,6-di-*tert*-butyl-4-methylphenol, which is known to react with 2 equiv. of peroxy radicals (1).

The phenols, aromatic amines, thiophenols, azoisobutane, toluene, isopentane, fluorotrichloromethane, *tert*-butyl hydroperoxide, and *tert*-butyl alcohol were commercial samples which were purified by the usual techniques. Deuteration of β-naphthol was accomplished by the method described previously (1).

Results and Discussion

Stoichiometric Factors

The overall reaction of a peroxy radical ($ROO^\bullet$) with a hydrogen atom donating reactant (XH) is given by

[2] $$n\,ROO^\bullet + XH \rightarrow \text{Nonradical products}$$

where n is the stoichiometric factor.

Boozer *et al.* (5) found and it has since been confirmed (6), using the hydrocarbon autoxidation induction period method, that $n = 2$ for phenol and β-naphthol. The analogous e.s.r. induction period method could not be used for these compounds, aniline, and β-naphthylamine because they were destroyed by continuous photolysis much faster than 2,6-di-*tert*-butyl-4-methylphenol. Stoichiometric factors of 2.0 were, however, obtained when a known concentration of $(CH_3)_3COO^\bullet$ was destroyed by a smaller concentration of the phenols and aromatic amines in the dark.

The e.s.r. induction period method could be used for thiophenol and β-naphthalenethiol and gave n-factors of 2.0 for these compounds.

Product studies and stoichiometric factors equal to 2.0 have conclusively demonstrated that reaction 2 for hindered phenols (A′H) consists of the elementary reactions

[1′] $$ROO^\bullet + A'H \rightarrow ROOH + A'^\bullet$$

[3] $$ROO^\bullet + A'^\bullet \rightarrow A'OOR$$

Exhaustive product studies have not been reported for reaction of peroxy radicals with C_6H_5OH, β-$C_{10}H_7OH$, $C_6H_5NH_2$, β-$C_{10}H_7NH_2$, C_6H_5SH, and β-$C_{10}H_7SH$. However, the fact that each molecule of these compounds reacts with 2 *tert*-butylperoxy radicals strongly suggests that in our system reaction 1 is followed by a reaction analogous to [3], *i.e.*,

[3′] $$ROO^\bullet + A^\bullet \xrightarrow{k_3'} ROOA$$

The only circumstance in which the stoichiometric factor would not be equal to 2.0 would be if the dimerization of $A^\bullet$ radicals were occurring, *i.e.*,

[4] $$2A^\bullet \xrightarrow{2k_4} AA$$

The occurrence of reaction 4 in our system is most unlikely because, at the concentrations of AH used, $k_3'[ROO^\bullet][A^\bullet] \gg 2k_4[A^\bullet]^2$ since $[ROO^\bullet] \gg [A^\bullet]$ and $k_3' \geq 2k_4$, at least for phenoxy radicals (7, 8).

Kinetics

Rate laws for hydrocarbon autoxidation inhibited by nonhindered phenols and aromatic amines can be complex (9). This is because the nonhindered phenoxy and anilino radicals ($A^\bullet$) produced in reactions analogous to [1] (where $ROO^\bullet$ would be the peroxy radical derived from the hydrocarbon) can undergo chain propagating reactions with the substrate (RH) and accumulated hydroperoxide (ROOH)

[5] $$A^\bullet + RH \rightarrow AH + R^\bullet$$

[6] $$A^\bullet + ROOH \rightarrow AH + ROO^\bullet$$

Despite this problem absolute values of k_1 have been estimated for several alkylperoxy radicals and a number of nonhindered phenols and aromatic amines (10). It is, however, difficult (and probably impossible) to determine reliable Arrhenius parameters for k_1 from kinetic investigations of inhibited autoxidations.

Our method of investigating reactions of the *tert*-butylperoxy radical with reactive substrates (1, 4) is more suitable for kinetic studies of reaction 1 because it cannot be complicated by reaction 5 (because of the absence of RH) and is unlikely to be complicated by reaction 6 because $[(CH_3)_3COO^\bullet] \geq (CH_3)_3COOH$ and $k_6 < k_3'$.

Rates of disappearance of $(CH_3)_3COO^\bullet$ in the presence of a large excess of phenol, β-naphthol,

Can. J. Chem. Downloaded from www.nrcresearchpress.com by 210.87.254.40 on 09/05/12
For personal use only.

Can. J. Chem. Downloaded from www.nrcresearchpress.com by 210.87.254.40 on 09/05/12
For personal use only.

aniline, β-naphthylamine, thiophenol, and β-naphthalenethiol were exactly first order in the radical concentration, *i.e.*, $-d[ROO^{\bullet}]/dt = k_{\psi}[ROO^{\bullet}]$ where k_{ψ} is the pseudo first-order rate constant ($nk_1[AH]$). Bimolecular rate constants (k_1) did not vary by more than a factor of 2 when [AH] was changed by at least a factor of 10. Reaction 1 can, therefore, be accurately described by the rate law

$$-d[ROO^{\bullet}]/dt = 2k_1[ROO^{\bullet}][AH]$$

Rates of disappearance of $(CH_3)_3COO^{\bullet}$ in the presence of β-$C_{10}H_7OH$, β-$C_{10}H_7NH_2$, C_6H_5-SH, and β-$C_{10}H_7SH$ were not influenced by the addition of 0.1 *M* *tert*-butyl hydroperoxide. On the other hand, values of k_1 for phenol and aniline were about one half as large in the presence of this concentration of hydroperoxide as they were in its absence. Rate reductions of a similar magnitude were obtained when *tert*-butyl alcohol was used instead of *tert*-butyl hydroperoxide. It would, therefore, appear that intermolecular hydrogen bonding lowers the reactivity of phenol and aniline at such high hydroperoxide concentrations.

At low temperatures and high reactant concentrations self-association could possibly influence the reactivity of some of the hydrogen donors studied in this work. Of the six compounds that we have studied phenol would be expected to give the most stable hydrogen bonded dimer. The thermodynamic parameters for the self-association of this compound in CCl_4 are $\Delta H^0 = -2.3$ kcal mol^{-1} and $\Delta S^0 = -1.3$ e.u. (11). Consequently at $-100°$ a 10^{-3} *M* solution in isopentane (the lowest temperature and highest phenol concentration used) should be at least 75% dissociated. Clearly, self-association should have little or no influence on reactant reactivity in our systems.

Intermolecular H-bonding between the reactant and solvent is, however, more important for nonhindered phenols than for hindered phenols. For instance the value of k_1 for β-$C_{10}H_7OH$ at 20° in the presence of acetonitrile (1 *M*) is approximately 25% (8×10^3 M^{-1} s^{-1}) of the value in the absence of acetonitrile (3.2×10^4 M^{-1} s^{-1}) whereas for hindered phenols acetonitrile (4 *M*) only reduces the rate constant by a factor of 2 (1).

Absolute values of the bimolecular rate constant, k_1, for β-$C_{10}H_7OH$ in isopentane from −93 to +20 °C are listed in Table 1. Below about −20° radicals produced from azoisobutane and from di-*tert*-butyl peroxide and isopentane gave rate constants which were the same within experimental error. At +20°, however, the former method gave rate constants consistently about a factor of 2 smaller than the latter method. Bennett and co-workers (12) have recently suggested that the decay of $(CH_3)_3COO^{\bullet}$ (produced from azoisobutane) can be influenced by radical regeneration from thermolysis of *cis*-azoisobutane (produced during irradiation) during the dark reaction. Consequently, at temperatures above −20° values of k_1 for β-$C_{10}H_7OH$ (and the other compounds studied in this work) were determined for radicals formed by photolysis of di-*tert*-butyl peroxide in oxygen saturated isopentane; below −20° rate constants were determined for radicals produced by both methods.

TABLE 1. Absolute rate constants for reaction of $C_2H_5C(CH_3)_2OO^{\bullet}$ [a] and $(CH_3)_3COO^{\bullet}$ [b] with β-naphthol in isopentane

Temperature (°C)	$10^{-3}k_1(M^{-1}$ s$^{-1})$
20	32.0[a]
−3	18.5[a]
−25	14.5[a]
−30	9.0[a]
−32	10.0[b]
−40	7.5[a]
−42	7.0[a]
−56	4.75[a]
−56	8.0[b]
−60	6.5[a]
−60	7.5[b]
−70	2.0[a]
−70	4.0[b]
−80	2.1[a]
−80	3.3[b]
−90	2.2[b]
−93	1.8[a]

A plot of $\log(k_1/M^{-1}$ s$^{-1})$ against the reciprocal of the absolute temperature for β-$C_{10}H_7OH$ is shown in Fig. 1. This plot afforded the Arrhenius equation $\log(k_1/M^{-1}$ s$^{-1}) = 6.4 - 2.6/\theta$, where $\theta = 2.303RT$ kcal mol^{-1}.

These Arrhenius parameters are significantly smaller than the values of $\log(A/M^{-1}$ s$^{-1}) = 8.9$ and $E = 7.3$ kcal mol^{-1} reported by Tsepalov and Shlyapintokh for reaction of the 1-phenylethylperoxy radical with β-naphthol (13).

Extrapolation of the Arrhenius equation found

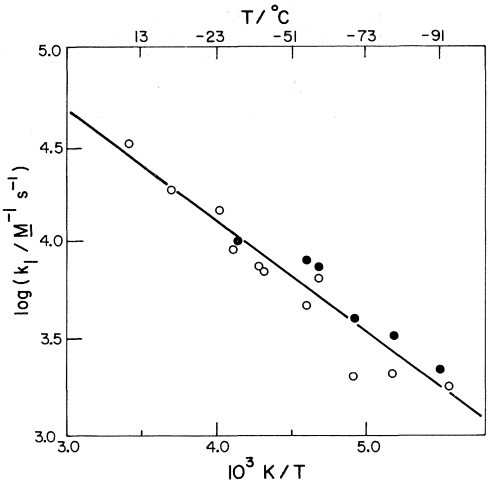

FIG. 1. A plot of log $(k_1/M^{-1}\,s^{-1})$ for the reaction of $(CH_3)_3COO^{\cdot}$ (●) and $C_2H_5C(CH_3)_2OO^{\cdot}$ (○) with β-naphthol against the reciprocal of the absolute temperature.

in the present work to 60° yields a value of $k_1 = 5.0 \times 10^4\ M^{-1}\,s^{-1}$, in excellent agreement with a rate constant of $3.3 \times 10^4\ M^{-1}\,s^{-1}$ that can be calculated for reaction of the 9-peroxy-9,10-dihydroanthracene radical with β-naphthol at this temperature[2] (14).

β-Naphthol is approximately 10 times less reactive than α-naphthol to ROO· at −95° whereas at 60° it is only about 4 times less reactive. The difference in reactivity between the two naphthols is due to a difference in activation energies $(E_1^{\beta} - E_1^{\alpha} \sim 1$ kcal mol$^{-1})$ since $A_1^{\alpha}/A_1^{\beta} \sim 1.0$.

A significant reduction in reactivity occurred when the phenolic hydrogen in β-naphthol was replaced by deuterium. Absolute values of k_1 for the deuterated compound fit the equation $\log(k_1/M^{-1}s^{-1}) = 6.5 - 3.9/\theta$. The difference in activation energies between β-$C_{10}H_7OD$ and β-$C_{10}H_7OH$ $(E_1^{D} - E_1^{H} = 1.3$ kcal mol$^{-1})$ is very close to the value of 1.4 kcal mol^{-1} calculated on the basis of a simple zero point energy effect. Within our experimental accuracy there was no difference between A_1^{H} and A_1^{D}.

The linearity of the Arrhenius plot for β-naphthol over a 120° temperature range and the similarity between A_1^{D} and A_1^{H} confirm our previous conclusion (1) that quantum mechanical tunneling has very little influence on the transfer of a hydrogen atom from a phenol to a peroxy radical.

Kinetic parameters[3] for reaction of the tertiary alkylperoxy radicals with C_6H_5OH, $C_6H_5NH_2$, β-$C_{10}H_7NH_2$, C_6H_5SH, and β-$C_{10}H_7SH$ are listed in Table 2. Since absolute values of k_1 are accurate to within a factor of 2 at any one temperature the activation energies and pre-exponential factors listed in this table are accurate to ±0.5 kcal mol^{-1} and ±0.5 log unit, respectively.

The A-factors increase in the order $C_6H_5OH >$ β-$C_{10}H_7OH \sim C_6H_5NH_2 >$ β-$C_{10}H_7NH_2 \sim C_6H_5SH \sim$ β-$C_{10}H_7SH$ and the activation energies in the order $C_6H_5OH \sim C_6H_5NH_2 >$ β-$C_{10}H_7OH \sim$ β-$C_{10}H_7NH_2 >$ β-$C_{10}H_7SH \sim C_6H_5SH$. The A-factor for C_6H_5OH is close to the "normal" value while those for $C_6H_5NH_2$, β-$C_{10}H_7NH_2$, C_6H_5SH, and β-$C_{10}H_7SH$ are low.

The phenols are more reactive than their nitrogen analogs because of larger A-factors while β-naphthol and β-naphthylamine are more reactive than their phenyl analogs because of lower activation energies. The thiophenols are somewhat anomalous in that both Arrhenius parameters for the phenyl and naphthyl derivatives are of similar magnitude. These parameters are, however, significantly smaller than the Arrhenius parameters for the analogous phenols.

Arrhenius parameters have not been previously reported for reaction of any of these compounds with peroxy radicals. There are, therefore, no published values with which we can compare our results.

[2]The value of the rate constant for reaction of the 9-peroxy-9,10-dihydroanthracene radical with β-naphthol was calculated from Mahoney's (14) rate constant ratio of $k_5/k_3 = 39.0$ at 60°, where k_5 and k_3 are the rate constants for reaction of the 9-peroxy-9,10-dihydroanthracene radical with β-naphthol and 9,10-dihydroanthracene, respectively. The value of k_3 was estimated to be $850\ M^{-1}\,s^{-1}$ from a rotating sector study of the autoxidation of 9,10-dihydroanthracene and assuming that the A_3-factor for 9,10-dihydroanthracene is equal to the A_3-factor of $5.6 \times 10^6\ M^{-1}\,s^{-1}$ for tetralin (10). The agreement between directly and indirectly determined values of k_1 really is remarkable in view of the circuitous way in which the indirect value of k_1 was obtained. This agreement must increase considerably our faith in relative rate constants obtained from hydrocarbon autoxidation and absolute rate constants determined by the rotating sector technique.

[3]A complete compilation of the values of k_1 is available, at nominal charge, from the Depository of Unpublished Data, National Science Library, National Research Council of Canada, Ottawa, Canada K1A 0S2.

Can. J. Chem. Downloaded from www.nrcresearchpress.com by 210.87.254.40 on 09/05/12
For personal use only.

TABLE 2. Arrhenius parameters and rate constants at 30° for reaction of $(CH_3)_3COO^\cdot$ and $C_2H_5C(CH_3)_2OO^\cdot$ with some phenols, aromatic amines, and thiophenols in isopentane

Substrate	$\log (A_1/M^{-1}\,s^{-1})^a$	$E_1{}^b$/kcal mol^{-1}	$10^{-3}k_1(M^{-1}\,s^{-1})$ at 30° ^{c}
C_6H_5OH	7.2	5.2	2.8
β-$C_{10}H_7OH$	6.4	2.6	33
$C_6H_5NH_2$	6.3[d]	5.0	0.5[d]
β-$C_{10}H_7NH_2$	4.7[d]	2.3	1.1[d]
C_6H_5SH	4.5	1.1	5.1
β-$C_{10}H_7SH$	4.8	1.5	5.2

[a] ± 0.5 log units.
[b] ± 0.5 kcal mol^{-1}.
[c] Calculated from the appropriate Arrhenius equation.
[d] Per active hydrogen.

Absolute values of the rate constants for reaction of phenol with the poly(peroxystyryl)peroxy radical (k_1' at 65° = 5 × 10^3 M^{-1} s^{-1}) (10) and with the 9-peroxy-9,10-dihydroanthracene radical (k_1' at 60° = 8.2 × 10^3 M^{-1} s^{-1}) (14) have been reported. These values are very similar to the extrapolated values of k_1 for phenol at these temperatures (k_1 at 60° = 6.0 × 10^3 M^{-1} s^{-1} and k_1 at 65° = 7.0 × 10^3 M^{-1} s^{-1}).

A rate constant of approximately 316 M^{-1} s^{-1} has been estimated for reaction of aniline with the poly(peroxystyryl)peroxy radical at 65° (15) which is somewhat smaller than our estimated reactivity of this compound (k_1 = 1200 M^{-1} s^{-1}) with $(CH_3)_3COO^\cdot$ at this temperature.

We have previously concluded (16) that 2,6-di-*tert*-butylphenol (BP) is less reactive than phenol (P) at 65° to peroxy radicals because the steric protection afforded by the two bulky *ortho tert*-butyl groups overshadows the accelerating effect due to electron release by these substituents. It is now clear that the differences in reactivity of these phenols ($k_1{}^{BP}/k_1{}^{P}$ = 185 at −95° and $k_1{}^{BP}/k_1{}^{P}$ = 1.0 at 40°) are the result of differences in *both* A_1 ($\log A_1{}^{P}/A_1{}^{BP}$ = 2.9) and E_1 ($E_1{}^{P} - E_1{}^{BP}$ = 4.2 kcal mol^{-1}). This means that adding two *ortho tert*-butyl substituents to phenol *decreases* the entropy of activation for the transfer of a H-atom to a peroxy radical by about 13 e.u. and *decreases* the enthalpy of activation for this process by about 4 kcal mol^{-1}.

The low Arrhenius parameters for reaction of the *tert*-butylperoxy radical with hindered phenols and aromatic amines (A'H) have been attributed (1) to the formation of a hydrogen bonded free radical–reactant complex, followed by transfer of a hydrogen atom within the complex (17).

$$\mathrm{ROO^\cdot + A'H} \underset{k_b}{\overset{k_a}{\rightleftharpoons}} \mathrm{ROO\cdots HA'}$$

$$\mathrm{ROO\cdots HA'} \xrightarrow{k_c} \mathrm{ROOH + A'}$$

According to this mechanism the overall activation energy will be low by an amount equivalent to the heat of formation of the hydrogen bonded complex (ΔH^0) and the preexponential factor will be low by an amount equivalent to the loss in entropy on formation of the complex (ΔS^0). The differences in $\Delta S^{\neq}$ and $\Delta H^{\neq}$ for phenol and 2,6-di-*tert*-butylphenol are consistent with this mechanism since values of $-\Delta H^0$ and $-\Delta S^0$ for the formation of a hydrogen bonded complex between tetrahydrofuran and 2,6-di-*tert*-butylphenol are 4 kcal mol^{-1} and 20 e.u. larger than the corresponding thermodynamic parameters for phenol and tetrahydrofuran (18).

The similarity between $\Delta\Delta H^{\neq}$ and $\Delta\Delta H^0$ for phenol and 2,6-di-*tert*-butyphenol implies that *all* of the difference in E_1 could be due to $\Delta\Delta H^0$. There must, however, be some contribution to ΔE_1 from the difference in the strengths of the O—H bonds that are broken because the abstraction of a H-atom from 2,6-di-*tert*-butylphenol by ROO$^\cdot$ is approximately 9 kcal mol^{-1} more exothermic than from phenol.[4] If the reaction of these phenols with ROO$^\cdot$ follows a Polanyi relation with a value of α = 0.63 (22)

[4] The strength of the OH bond in 2,6-di-*tert*-butylphenol can be estimated to be ~81.0 kcal mol^{-1} (19) while the value of $D_{(O-H)}$ in phenol is ~90 kcal mol^{-1} (20). The lower value for BP is not surprising when one considers that ~8 kcal mol^{-1} of strain energy will be partially relieved with the loss of a hydrogen atom (19). Furthermore the barrier to rotation of the hydroxyl group in 2,4,6 tri-*tert*-butylphenol is at least 1.6 kcal mol^{-1} lower than in phenol (21).

Can. J. Chem. Downloaded from www.nrcresearchpress.com by 210.87.254.40 on 09/05/12
For personal use only.

Can. J. Chem. Downloaded from www.nrcresearchpress.com by 210.87.254.40 on 09/05/12
For personal use only.

ΔE_1 would be ~ 6 kcal mol^{-1}. Clearly all of ΔE_1 between phenol and 2,6-di-*tert*-butylphenol can be accounted for either by the difference in the heats of formation of an H-bonded radical–reactant complex or by the difference in the exothermicities of the reaction. It is, however, much more reasonable to conclude that both factors may influence ΔE_1.

Aromatic amines and thiophenols do not form detectable concentrations of a H-bonded complex with tetrahydrofuran at ambient temperatures, almost certainly because values of $-\Delta H^0$ are very small. Consequently, the low values of log A_1 and E_1 for these compounds cannot be attributed to a transition state which is stabilized by a H-bonded free radical – reactant complex.

The differences in E_1 for the compounds listed in Table 2 must, therefore, be almost entirely due to differences in the strengths of the X—H bond that is broken. Unfortunately although estimates of D(N—H) for $C_6H_5NH_2$ (~ 88 kcal mol^{-1}) and β-$C_{10}H_7NH_2$ (~ 82 kcal mol^{-1}) have been made (23) there are no reliable estimates of D(S—H) for C_6H_5SH and β-$C_{10}H_7SH$.

The differences in log A_1, particularly the very low values for the thiophenols, are more difficult to rationalize. There does, however, appear to be a semi-qualitative relationship between $\Delta H^{\neq}$ and $\Delta S^{\neq}$ which implies that the transition states with less bond breaking and more bond making (*i.e.*, the more exothermic reactions) are 'tighter' or more rigid.

Phenol is considerably more reactive than toluene ($k_1^{C_6H_5OH}/k_1^{C_6H_5CH_3} \sim 3 \times 10^5$ at 30°) to $(CH_3)_3COO^{\cdot}$ even though the heats of these H-atom transfers are comparable (20). This difference is principally due to a difference in activation energy ($E^{C_6H_5CH_3} - E^{C_6H_5OH} \sim 6.0$ kcal mol^{-1}) since log ($A^{C_6H_5OH}/A^{C_6H_5CH_3} \sim 1.0$).[5] The lower activation energy for phenol is consistent with the involvement of a H-bonded radical–reactant complex in the transition state, the similarity between the A-factors for these two compounds is, however, not consistent with this mechanism.

Both Mahoney (20) (using Johnston and Parrs' bond-energy-bond-order calculation (25)) and Zavitsas (26) (using his modification of the BEBO method (27)) have suggested that abstraction of a H-atom from oxygen by an oxy radical is energetically more favorable than abstraction from carbon because the anti-bonding or triplet repulsion energy for the transition state ROO$\cdot\cdot\cdot$H$\cdot\cdot\cdot$OC$_6$H$_5$ is smaller than for ROO$\cdot\cdot\cdot$H$\cdot\cdot\cdot$CH$_2$C$_6$H$_5$. Very qualitative BEBO calculations of these systems tentatively imply that the difference in activation energies could be as large as 5 kcal mol^{-1}. Unfortunately these calculations are even more qualitative when they are extended to aromatic amines and thiophenols.

To conclude, low activation parameters for reaction of hindered and nonhindered phenols with *t*-ROO$^{\cdot}$ can be partially attributed to a reaction mechanism that involves an equilibrium between the reactants and a H-bonded free radical – reactant complex, followed by the transfer of a H-atom within the complex. This mechanism, however, cannot be invoked to explain the low activation parameters for reaction of thiophenols with *tert*-ROO$^{\cdot}$. Some of the differences in activation energies for reaction of C_6H_5XH (where X = CH_2, O, NH and S) with *tert*-ROO$^{\cdot}$ may be due to differences in the strengths of the X—H bond. The differences in the *A*-factors may then be the result of a correlation between $\Delta S^{\neq}$ and $\Delta H^{\neq}$.

One of us (E. F.) thanks the Chevron Research Company for financial support in the form of a Fellowship.

1. J. A. Howard and E. Furimsky. Can. J. Chem. **51**, 3738 (1973).
2. S. W. Benson. Thermochemical kinetics. John Wiley and Sons, Inc., New York. 1968.
3. D. M. Golden. Fourteenth symposium (international) on combustion. The Combustion Institute, Pittsburgh. 1973 p. 121.
4. E. Furimsky and J. A. Howard. J. Am. Chem. Soc. **95**, 369 (1973).
5. C. E. Boozer, G. S. Hammond, C. E. Hamilton, and J. N. Sen. J. Am. Chem. Soc. **77**, 3233 (1955).
6. E. C. Horswill, J. A. Howard, and K. U. Ingold. Can. J. Chem. **44**, 985 (1966).
7. L. R. Mahoney. J. Am. Chem. Soc. **89**, 1895 (1967).
8. L. R. Mahoney and S. A. Weiner. J. Am. Chem. Soc. **94**, 585 (1972).
9. L. R. Mahoney. Angew. Chem. Intern. Ed. Engl. **8**, 547 (1969).
10. J. A. Howard. Adv. Free Radical Chem. **4**, 49 (1972).
11. S. N. Vinogradov and R. H. Linnell. Hydrogen bonding. Van Nostrand Reinhold Co., New York. 1971. p. 125.
12. J. E. Bennett, J. A. Eyre, C. P. Rimmer, and R. Summers. Chem. Phys. Lett. **26**, 69 (1974).

[5]The *A*-factor and activation energy for reaction of $(CH_3)_3COO^{\cdot}$ with toluene have not been measured. They must, however, be very similar to the values reported for *p*-xylene (24).

13. V. F. TSEPALOV and V. YA. SHLYAPINTOKH. Dokl. Akad. Nauk SSSR, **124**, 883 (1959).
14. L. R. MAHONEY. J. Am. Chem. Soc. **89**, 1895 (1967).
15. K. U. INGOLD. Free radicals, **2**, 37 (1973).
16. J. A. HOWARD and K. U. INGOLD. Can. J. Chem. **41**, 2800 (1963).
17. L. R. MAHONEY and M. A. DAROOGE. J. Am. Chem. Soc. **94**, 7002 (1972).
18. S. SINGH and C. N. R. RAO. J. Am. Chem. Soc. **88**, 2142 (1966).
19. L. A. MAHONEY, F. C. FERRIS, and M. A. DAROOGE. J. Am. Chem. Soc. **91**, 3883 (1969).
20. L. R. MAHONEY. Private communication.
21. K. U. INGOLD and D. R. TAYLOR. Can. J. Chem. **39**, 471 (1961).
22. I. B. AFANASEV. Usp. Khim. **40**, 216 (1971).
23. E. T. DENISOV. Usp. Khim. **42**, 361 (1973).
24. S. KORCEK, J. H. B. CHENIER, J. A. HOWARD, and K. U. INGOLD. Can. J. Chem. **50**, 2285 (1972).
25. H. S. JOHNSTON and C. PARR. J. Am. Chem. Soc. **85**, 2544 (1963).
26. A. A. ZAVITSAS. Private communication.
27. A. A. ZAVITSAS. J. Am. Chem. Soc. **94**, 2779 (1972).

Can. J. Chem. Downloaded from www.nrcresearchpress.com by 210.87.254.40 on 09/05/12
For personal use only.

Can. J. Chem. Downloaded from www.nrcresearchpress.com by 210.87.254.40 on 09/05/12
For personal use only.

Synthesis of Lactose-Operator Gene Fragments by the Improved Triester Method[1]

K. ITAKURA, N. KATAGIRI, AND S. A. NARANG

Division of Biological Sciences, National Research Council of Canada, Ottawa, Canada K1A 0R6

Received August 19, 1974

K. ITAKURA, N. KATAGIRI, and S. A. NARANG. Can. J. Chem. **52**, 3689 (1974).

The synthesis of lactose-operator gene fragments have been achieved by the improved triester methodology and new phosphorylating and condensing reagents.

K. ITAKURA, N. KATAGIRI, et S. A. NARANG. Can. J. Chem. **52**, 3689 (1974).

La synthèse des fragments du gêne opérant de la lactose a été réalisée par la méthode améliorée du triester en utilisant de nouveaux agents de phosphorylation et de condensation.

[Traduit par le journal]

The lactose-operator gene constitutes a unique sequence of 21–24 bases in *E. coli* which has the remarkable property of regulating the biological function of the lactose-operon (1). Recently Gilbert and his co-worker (2) have presented a unique sequence of 24 base pairs (see Scheme 1) by determining the sequence of RNA transcription copies of this fragment. In this communication, we wish to report the application of our improved triester approach for the chemical syntheses of pentadeca- (**1**), dodeca- (**2**), nona- (**3**), and hexanucleotides (**4**) representing the twofold symmetrical region of the lac-operator gene sequence.

The basic feature of the triester approach as reported by most other laboratories (3–6), involved a "two-step", reaction, *i.e.* phosphorylation followed by subsequent coupling at each synthetic step. However, we observed that the initial phosphorylation did not give a pure 3′-phosphodiester component in quantitative yield thus leading to very complicated reaction mixtures on addition of the second component. We overcame this problem by using 5′-protected nucleosides containing fully protected 3′-phosphate groups **5** as starting material (7). Thus 5′-dimethoxytrityl nucleoside **6** was phosphorylated with bistriazolide of *p*-chlorophenyl phosphate **7**,[2] a new and highly efficient phosphorylating reagent (8). This reaction went to completion in 6 h at room temperature and on subsequent treatment with β-cyanoethyl alcohol, a fully protected mononucleotide **5** was obtained in quantitative yield after isolation by silica gel chromatography. Treatment of **5** with 80% acetic acid afforded 5′-hydroxy 3′-fully protected nucleotide **8**, whereas a very mild alkaline treatment (0.05 *N* sodium hydroxide, dioxane–water) selectively removed the β-cyanoethyl group to give a 5′-protected nucleoside 3′-phosphodiester product **9**. Using triisopropylbenzenesulfonyl chloride (TPS) as condensing reagent and the synthetic path outlined in the scheme, we observed that the yields of oligonucleotides containing purine bases (especially guanine) were consistently low (*ca.* 20%) (9, 10). By introducing two new condensing reagents, mesitylenesulfonyl triazolide (MST) (10) and *p*-nitrobenzenesulfonyl triazolide[3] (m.p. 147–149°) (8) (*p*-NBST),

[1]NRCC No. 14252.

[2]It was prepared by condensing *p*-chlorophenyl phosphodichloridate (1 equiv.) with 1*H*-1,2,4-triazole (2 equiv.) in the presence of triethylamine (2 equiv.) in dioxane. Due to extremely labile nature of bistriazolide of *p*-chlorophenyl phosphate, the reaction mixture was used immediately after the removal of triethylammonium hydrochloride.

[3]It was prepared in the quantitative yield according to the published procedure (10). It was characterized satisfactorily by elemental and spectral analyses.

Can. J. Chem. Downloaded from www.nrcresearchpress.com by 210.87.254.40 on 09/05/12
For personal use only.

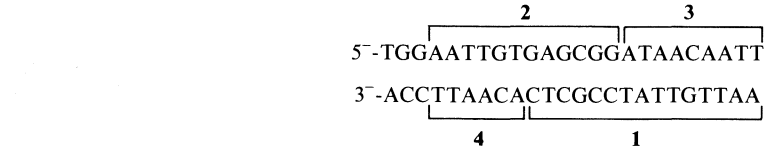

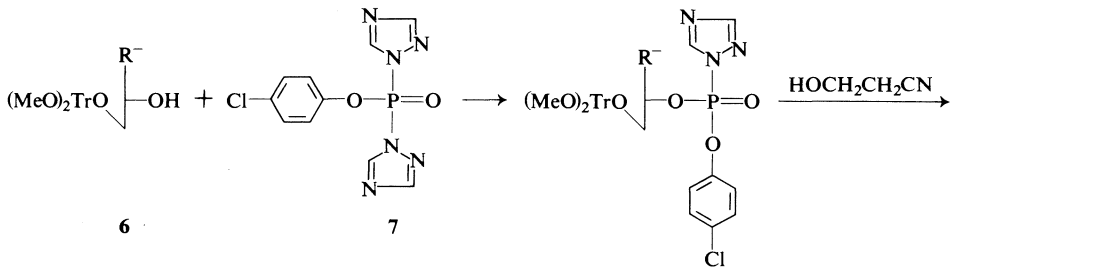

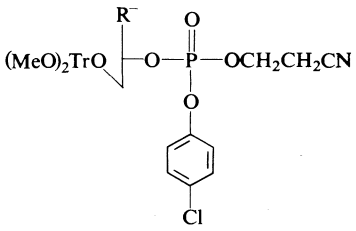

5

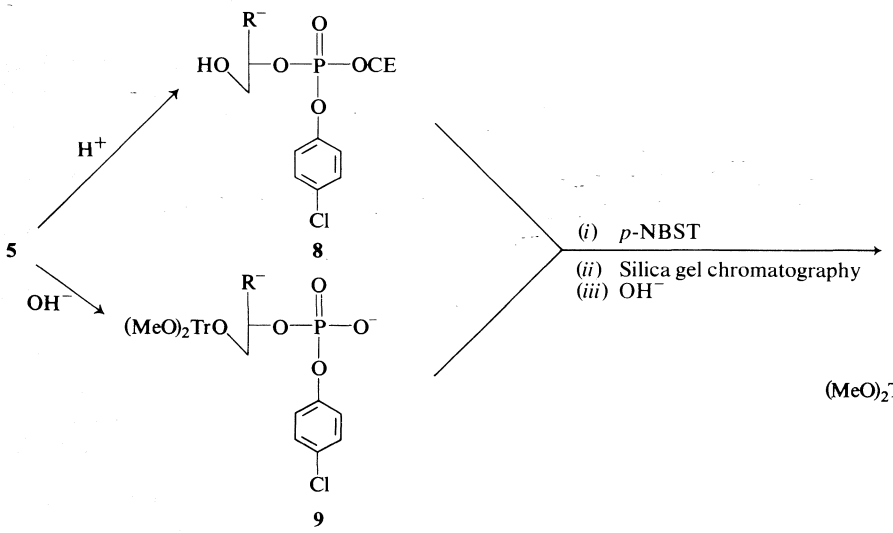

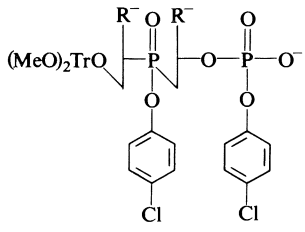

10

10 + 8 → (i) p-NBST; (ii) Silica gel chromatography; (iii) OH^-

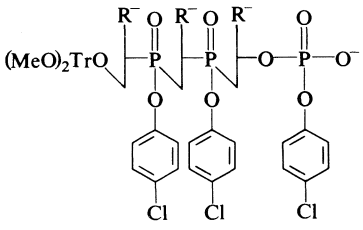

11

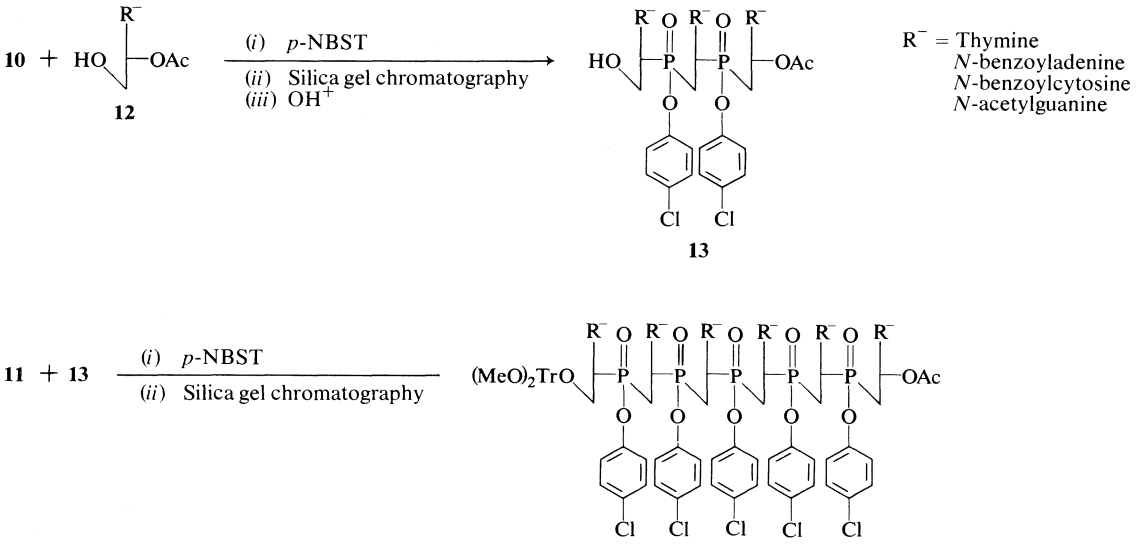

SCHEME 1. Lactose-operator gene sequence

substantially higher yields were realized at each step. For example, the protected dodecanucleotide [$(MeO)_2$Tr]dbzA-bzA-T-T-acG-T-acG-bzA-acG-bzC-acG-acG(Ac) was synthesized by condensing [$(MeO)_2$Tr]dbzA-bzA-T-T-acG-Tp(Cl-Ph) (0.5 mmol) with dacG-bzA-acG-bzC-acG-acG(Ac) (0.4 mmol) in the presence of *p*-nitrobenzenesulfonyl triazolide[4] (*p*-NBST) (2.5 mmol) for 2 days. The reaction was then taken up in chloroform (25 ml) which was washed with 0.1 *M* triethylammoniumbicarbonate buffer (5 ml × 3) and finally with water (10 ml). The organic layer was dried over anhydrous sodium sulphate and evaporated. The resulting residue was co-evaporated with toluene three times to remove pyridine and applied to silica gel column[5] (10 × 5 cm) in chloroform (10 ml). The column was eluted with a mixture of chloroform–methanol (10%, 1 l). Fractions of 2 ml/5 min were collected at room temperature.[6] The fully protected dodecanucleotide (0.98 g) was isolated from fraction 36–44 in 41%. By using the similar experimental conditions, we obtained the following isolated yields of hexa- (60–65%), nona- (55–60%), and pentadecamer (30–40%) (see Table 1).

The complete deprotection of fully protected dodecanucleotide (0.1 g) was carried out with 0.1 *N* sodium hydroxide – dioxane (100 ml) at room temperature for 48 h. After neutralization with Dowex-50 (pyridinium form), the concentrated residue was treated with concentrated ammonia (50 ml) for 2 days at room temperature and finally with 80% acetic acid (50 ml) for 20 min at room temperature. The deprotected compound was isolated by gel filtration on Sephadex G-25 (SF).

The homogeneity of each unprotected compound was checked rigorously by (*i*) t.l.c. on silica gel using aqueous solvent systems (11); (*ii*) homochromatography of 5′-^{32}P-labeled compound according to Sanger (12) and Wu (13) techniques; (*iii*) complete digestion with snake venom or spleen phosphodiesterase enzymes to their expected ratios of nucleoside to nucleotides. Finally the sequence of each fragment was confirmed by two-dimensional chromatography (electrophoresis on cellulose acetate strip at p*H* 3.5, pyridine–acetate buffer followed by homochromatography on DEAE cellulose thin-layer plates in 2% partially hydrolyzed RNA containing 7 *M* urea) of 5′-labeled oligomers partially digested with snake venom phosphodiesterase enzyme. Each oligomer gave the expected finger-printing pattern (14).

In conclusion, with this improved triester approach and the new phosphorylating and condensing reagents, we have been able to achieve large scale syntheses of longer oligonucleotides of defined sequence in high yields using approximately equimolar ratios of each component.

[4]It did not cause any sulfonation of 5′-hydroxyl group of oligonucleotide. Moreover the condensation reaction using (*p*-NBST) afforded the very clean reaction as compared with TPS.

[5]Thin-layer chromatographic silica gel was used for column chromatography.

[6]Every second fraction was checked on silica gel t.l.c. plates in chloroform–methanol (9:1) solvent.

Can. J. Chem. Downloaded from www.nrcresearchpress.com by 210.87.254.40 on 09/05/12
For personal use only.

Can. J. Chem. Downloaded from www.nrcresearchpress.com by 210.87.254.40 on 09/05/12
For personal use only.

TABLE 1. Reaction conditions of various condensation steps and the yields

3′-Phosphodiester component		5′-Hydroxyl component			Product			
							Completely deblocked compound	
Identity	Amount (mmol (g))	Identity	Amount (mmol (g))	*p*-NBST[a] (mmol)	Identity	Yield (% (g))	Identity	Yield (%)
$[(MeO)_2Tr]$[b]dbzA-bzC[c]-bzAp(ClPh)	1.1 (2.1)	dbzA-T-T(Ac)	1 (1.3)	3	$[(MeO)_2Tr]$dbzA-bzC-bzA-bzA-T-T(Ac)	62 (2)	A-C-A-A-T-T **4**	71
$[(MeO)_2Tr]$dbzA-T-bzAp(ClPh)	0.5 (0.95)	dbzA-bzC-bzA-bzA-T-T(Ac)	0.48 (1.40)	2	$[(MeO)_2Tr]$dbzA-T-bzA-bzA-bzC-bzA-bzA-T-T(Ac)	57 (1.30)	A-T-A-A-C-A-A-T-T **3**	64
$[(MeO)_2Tr]$bzA-bzA-T-T-acG-Tp(ClPh)	0.5 (1.62)	dacG-bzA-acG-bzC-acG-acG(Ac)	0.4 (1.10)	2.5	$[(MeO)_2Tr]$dbzA-bzA-T-T-acG-T-acG-bzA-acG-bzC-acG-acG(Ac)	41 (0.98)	A-A-T-T-G-T-G-A-G-C-G-G **2**	52
$[(MeO)_2Tr]$dbzA-bzA-T-T-acG-Tp(ClPh)	0.15 (0.49)	dT-bzA-T-bzC-bzC-acG-bzC-T-bzC(Ac)	0.1 (0.43)	0.65	$[(MeO)_2Tr]$dbzA-bzA-T-T-acG-T-T-bzA-T-bzC-bzC-acG-bzC-T-bzC(Ac)	35 (0.26)	A-A-T-T-G-T-T-A-T-C-C-G-C-T-C **1**	45

[a]*p*-NBST signifies *p*-nitrobenzenesulfonyl triazolide, a new condensing reagent used in the present studies.
[b]Abbreviation are as suggested by the IUPAC–IUB Commission (15).
[c]Benzoyl protecting group was found to be stable under the reaction condition using *p*-nitrobenzenesulfonyl triazolide as condensing reagent.

1. F. JACOB and J. MONOD. J. Mol. Biol. **3**, 318 (1961).
2. W. GILBERT and A. MAXAM. Proc. Natl. Acad. Sci. **70**, 3581 (1973).
3. R. L. LETSINGER and K. K. OGILVIE. J. Am. Chem. Soc. **89**, 4801 (1967); R. L. LETSINGER and K. K. OGILVIE. J. Am. Chem. Soc. **91**, 3350 (1969).
4. C. B. REESE and R. SAFFHILL. Chem. Commun. 767 (1968); C. B. REESE and R. SAFFHILL. Chem. Commun. 869 (1971); N. J. CUSACK, C. B. REESE, and J. H. VAN BOOM. Tetrahedron Lett. 2209 (1973).
5. F. ECKSTEIN and I. RIZK. Chem. Ber. **102**, 2326 (1969).
6. T. NEILSON and E. S. WERSTIUK. Can. J. Chem. **49**, 3004 (1971); T. NEILSON and E. S. WERSTIUK. J. Am. Chem. Soc. **96**, 2295 (1974).
7. K. ITAKURA, C. P. BAHL, N. KATAGIRI, J. J. MICHNIEWICZ, R. H. WIGHTMAN, and S. A. NARANG. Can. J. Chem. **51**, 3649 (1973).
8. N. KATAGIRI, K. ITAKURA, and S. A. NARANG. Unpublished work.
9. T. C. CATLIN and F. CRAMER. J. Org. Chem. **38**, 245 (1973).
10. N. KATAGIRI, K. ITAKURA, and S. A. NARANG. Chem. Commun. 325 (1974).
11. J. J. MICHNIEWICZ, C. P. BAHL, K. ITAKURA, N. KATAGIRI, and S. A. NARANG. J. Chromatogr. **85**, 159 (1973).
12. G. G. BROWNLEE and F. SANGER. Europ. J. Biochem. **11**, 395 (1969).
13. E. JAY, R. BAMBARA, P. PADMANABHAN, and R. WU. Nucleic Acids Res. **1**, 331 (1974).
14. C. P. BAHL, K. J. MARIANS, R. WU, S. A. NARANG, K. ITAKURA, and N. KATAGIRI. In preparation.
15. IUPAC–IUB. Biochemistry, **9**, 4022 (1970).

Can. J. Chem. Downloaded from www.nrcresearchpress.com by 210.87.254.40 on 09/05/12
For personal use only.

Can. J. Chem. Downloaded from www.nrcresearchpress.com by 210.87.254.6 on 09/05/12
For personal use only.

Canadian Journal of Chemistry

Published by
THE NATIONAL RESEARCH COUNCIL OF CANADA

Journal canadien de chimie

Publié par
LE CONSEIL NATIONAL DE RECHERCHES DU CANADA

Volume 52 Number 22 November 15, 1974

Volume 52 numéro 22 15 novembre 1974

Cobalt-59 Nuclear Quadrupole Resonance Studies on Five-coordinate Cobalt Complexes

LIAN SAI CHIA, WILLIAM R. CULLEN, AND MICHAEL C. L. GERRY

Chemistry Department, University of British Columbia, Vancouver, British Columbia V6T 1W5

Received June 17, 1974

LIAN SAI CHIA, WILLIAM R. CULLEN, and MICHAEL C. L. GERRY. Can. J. Chem. **52**, 3695 (1974).

The n.q.r. spectra of a number of complexes of the type $[Y_3PCo(CO)_3]_2$ have been recorded. The results are compared with those from related studies.

LIAN SAI CHIA, WILLIAM R. CULLEN et MICHAEL C. L. GERRY. Can. J. Chem. **52**, 3695 (1974).

On a enregistré les spectres n.q.r. d'un certain nombre de complexes du type $[Y_3PCo(CO)_3]_2$. Les résultats sont comparés avec ceux rapportés dans des études apparentés.

[Traduit par le journal]

Recently there has been an interest in the cobalt-59 nuclear quadrupole resonance (n.q.r.) of axially symmetric five-coordinate cobalt compounds (1–5). These studies have mainly been concerned with complexes of the type $Y_3MCo(CO)_4$ (Y = Cl, CH_3, C_6H_5, etc., M = Ge, Sn) and their carbonyl substituted derivatives. The n.q.r. spectra of other axially symmetric cobalt complexes have received little attention. For example, for the large class of dimeric complexes of the form $[Y_3PCo(CO)_3]_2$, which contain a Co—Co σ bond and the Y_3P groups in the axial positions (6–9), only one spectrum has been reported (3) (for Y = C_6H_5). Similarly for the ionic complexes $[(Y_3P)_2Co(CO)_3]^+X^-$ only one spectrum (3) (for Y = C_6H_5, X = $Co(CO)_4$) has previously been described.

To determine the effects of the substituents Y and the anions X^- on the n.q.r. spectra of these complexes, both dimeric and ionic, we have obtained the spectra of several examples.

The following compounds were prepared by literature methods as follows: $[Y_3ECo(CO)_3]_2$: (E = P; Y = C_6H_5O (10, 11), C_2H_5O (10), CH_3O (10), *n*-C_4H_9 (10), C_6H_5 (10); Y_3 = $(C_6H_5)_2(CH_3O)$ (10); Y_3E = $(C_6H_5)_3As$ (10), $(C_6H_5)_3Sb$ (10)); $(Y_3P)_2Co(CO)_3{}^+X^-$: (Y = C_6H_5 or *n*-C_4H_9, X = $Co(CO)_4$ or $B(C_6H_5)_4$ (12)); $[(CH_3O)_3P]_3Co(CO)_2{}^+B(C_6H_5)_4{}^-$ (13).

Nuclear quadrupole resonance spectra were recorded using a Decca instrument as described previously (14). The recorded frequencies are listed in Table 1. Note that some compounds did not give a detectable signal in the region 7–60 MHz. No signal attributable to the ion $Co(CO)_4{}^-$ was found.

Results and Discussion

For ^{59}Co, which has $I = 7/2$, both the quadrupole coupling constant e^2Qq and the asymmetry parameter η can be obtained from the experimental frequencies using a series of approximations for the transition frequencies (15). The resulting values can be confirmed with a frequency ratio plot (16). To carry out this procedure a computer program was written to cal-

TABLE 1. ^{59}Co n.q.r. spectra of $[(Y_3P)_2Co(CO)_3]^+X^-$ and $[Y_3PCo(CO)_3]_2$ complexes

Compound	Temperature (°C)	Frequency[a] (MHz)	η	e^2Qq (MHz)
$[(C_6H_5)_3P]_2Co(CO)_3{}^+Co(CO)_4{}^-$	25[b]	34.20 22.77	0.05	159.7
	33	34.124(9) 22.564(10) 12.125(4)	0.136	159.534
$[(C_6H_5)_3P]_2Co(CO)_3{}^+BPh_4{}^-$	30	33.641(8) 22.006(7)	0.219	157.754
$[(C_6H_5O)_3PCo(CO)_3]_2$	0	33.440(30) 22.281(36) 11.219(16)	0.0392	156.104
	30	33.474(23) 22.295(30) 11.224(14)	0.0414	156.230
$[(CH_3O)_3PCo(CO)_3]_2$	0	30.868(100) 20.573(115) 10.372(83)	0.0460	144.080
	28	30.849(90) 20.550(100) 10.345(70)	0.0405	143.982
$[(C_2H_5O)_3PCo(CO)_3]_2$	0	30.249(80) 20.232(95) 10.169(65)	0.0265	141.674
	24	30.345(40) 20.228(46) 10.181(28)	0.0320	141.655
$[(n\text{-}C_4H_9)_3PCo(CO)_3]_2$	0	30.272(12) 20.170(10) 10.163(7)	0.0386	141.291
	30	30.125(10) 20.080(9) 10.107(6)	0.0333	140.627
$[(C_6H_5)_3PCo(CO)_3]_2$[b]	25	31.46 20.96	0	146.8

[a]The numbers in parentheses are signal to noise ratios. The first line gives ν_3, the second line ν_2, and the third line ν_1. Experimental errors: ± ~0.050 MHz.
[b]Reference 3.

culate the energy levels and transition frequencies for any values of the nuclear spin, e^2Qq, and η (17).

Since $I = 7/2$ for ^{59}Co each nucleus should give three strong transitions, having frequencies ν_1, ν_2, ν_3, which are directly proportional to e^2Qq, so that the ratios ν_2/ν_1, ν_3/ν_2, and ν_3/ν_1 are independent of e^2Qq, though dependent on η. Accordingly the program was used to calculate the values for these ratios for a series of values of η differing by 0.0001. The observed ratios were then compared with the calculated ones to obtain η. In a similar fashion, because the transition frequencies are directly proportional to e^2Qq, the calculated frequencies were obtained with $e^2Qq = 1$. With η obtained, the calculated frequencies were divided into the observed values to evaluate e^2Qq for the complex. The averaged values of both e^2Qq and η are given in Table 1.

Table 1 also contains the results of Ogino and Brown (3). It is noteworthy that our data for $[(C_6H_5)_3P)_2Co(CO)_3]^+Co(CO)_4{}^-$ are in excellent agreement with theirs, with our frequencies slightly lower at the higher temperature. We were unable to repeat their measurements for $[(C_6H_5)_3PCo(CO)_3]_2$; this was probably a function of the nature of our sample.

The crystal structures of a number of derivatives of the type $[Y_3PCo(CO)_3]_2$ have been determined, and have the general structure **1** (6–9) where each cobalt atom is five-coordinate with the group V base in the axial positions. The low values of η recorded for the compounds in

Can. J. Chem. Downloaded from www.nrcresearchpress.com by 210.87.254.6 on 09/05/12
For personal use only.

TABLE 2. Comparison of the ^{59}Co n.q.r. constants[a] and asymmetry parameters[a] of substituted cobalt carbonyl dimers and related compounds

Compound	L = CO	L = $P(OCH_3)_3$	L = $P(OC_6H_5)_3$	L = $P(C_6H_5)_3$	L = $P(n\text{-}C_4H_9)_3$
$[Co(CO)_3L]_2$		143.98(0.04)[b]	156.23(0.04)[b]	146.8(0)[c]	140.63(0.03)[b]
$(C_6H_5)_3SnCo(CO)_3L$	104.11(0.05)[e]	104.19(0.04)[d]	110.44(0.27)[d]	114.53(0.10)[i]	103.18(0.04)[d]
$(CH_3)_3SnCo(CO)_3L$	97.70(0)[i]		103.88(0.03)[d]		
	95.63(0)[i]				
$Cl_3SnCo(CO)_3L$	163.4(0)[e]		159.46(0.03)[d]	~160[c]	173.6(0)[c]
$Cl_3Ge(CO)_3L$	161.6(0)[e,g]			156.9(0.08)[c]	166.0(0)[c]
	159.3(0)[e,g]				
$Cl_3SCo(CO)_3L$	130.7(0.13)[e]				113.9(0)[c]
$Co(CO)_3L_2^+$				159.5(0.14)[b,h]	
				157.7(0.22)[b,h]	
$Fe(CO)_4L$	2.60[f]			2.54[f]	

[a]Coupling constants are in MHz, except for $Fe(CO)_4L$, which are in mm s^{-1}. Asymmetry parameters (in parentheses) are unitless.
[b]Present work.
[c]From ref. 3.
[d]From ref. 4.
[e]From ref. 2.
[f]From ref. 21.
[g]Two different resonances from the same complex.
[h]Resonances from two different complexes.
[i]From ref. 5; $T = 77$ °K.

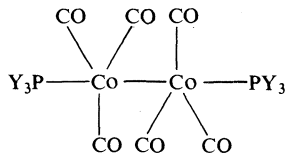

1

Table 1 are certainly in keeping with this structure. It is interesting that the triphenylphosphite derivative is normal in this respect since Boyd and Brown (4) found that η for $(C_6H_5)_3SnCo(CO)_3P(OC_6H_5)_3$ was significantly greater than for other similar phosphine and phosphite derivatives. This increase was ascribed to conformational effects of the triphenylphosphite. However, these same authors report that η for $Cl_3SnCo(CO)_3P(OC_6H_5)_3$ is normal.

The infrared spectra (12, 13) of the $((C_6H_5)_3P)_2Co(CO)_3^+X^-$ compounds (X = $Co(CO)_4$, BPh_4) show only one CO band attributable to the cation; this indicates a D_{3h} structure **2**. The small η values (0.1–0.2) of these compounds are also consistent with the proposed structure. The variation in the values of η observed indicates once again the great sensitivity of that

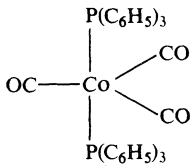

2

parameter to intermolecular interactions in the solid state (18).

Table 2 contains a summary of the coupling constants obtained in the present work together with data for related complexes. The coupling constants can be discussed in terms of the following simple equation (1):

$$[1]\quad e^2Qq_{mol} = e^2Qq_{320}[N_{d_{z^2}} + \tfrac{1}{2}(N_{d_{xz}} + N_{d_{yz}}) - (N_{d_{xy}} + N_{d_{x^2-y^2}})]$$

where N_d is the population of the appropriate Co 3d orbital; e^2Qq_{320} is the coupling constant of a single $3d_{z^2}$ electron. It has been shown (1) that e^2Qq_{320} is negative, whereas e^2Qq_{mol} is most likely positive, so that the last, negative term in the parentheses is greater than the sum of the first two.

Boyd and Brown (4) have suggested that the variations in ^{59}Co resonance frequencies for $XCo(CO)_3L$ complexes depend not only on the nature of X and L individually, but also on the interactions between them. Thus, for example, the trends observed on variation of L are expected to be different when X is a strong π-acceptor from when X is a weak π-acceptor. In the case of the complexes studied in this work L is PY_3 and X is $Y_3PCo(CO)_3$. Since the Co—Co bond is symmetrical a net σ- or π-electron drift from one cobalt atom to the other is not expected. The complexes thus form the basis for a description when X is a very weak σ-donor and π-acceptor. Indeed, one can go further and

Can. J. Chem. Downloaded from www.nrcresearchpress.com by 210.87.254.6 on 09/05/12
For personal use only.

say that in the Co—Co bonded complexes, unlike all the other compounds in Table 2, the variations in e^2Qq are functions of PY_3 alone. It is clear from our data that these variations are slight (about 6%). According to eq. 1 $N_{d_{z^2}}$ gives a measure of σ-donor ability, and $(N_{d_{xz}} + N_{d_{yz}})$ a measure of the π-acceptor ability of PY_3. The small variation of coupling constants suggests that these orbital populations, and consequently the bonding properties of PY_3, are virtually independent of Y. The same conclusions can be reached for $(C_6H_5)_3Sn$, $(CH_3)_3Sn$, Cl_3Sn, indeed for every other X.

Comparison of the coupling constants of the Co—Co bonded complexes with those of $(C_6H_5)_3Sn$— and $(CH_3)_3Sn$— derivatives illustrates two noteworthy points: (*i*) The trends on varying Y in PY_3 are essentially the same and (*ii*) the coupling constants of the Sn derivatives are consistently 40–50 MHz below those of the dimers. Now $(C_6H_5)_3Sn$— and $(CH_3)_3Sn$— are relatively weak π-acceptors (1, 4), and since Sn has a slightly higher electronegativity than Co they are probably slight σ-acceptors as well. Thus there is little surprise in the trends with Y in PY_3. The 40–50 MHz general decrease of e^2Qq in the Sn compounds cannot be accounted for in terms of the σ- or π-acceptor abilities of Sn, since both these should *increase* e^2Qq. The decrease must thus result from a lowering of $(N_{d_{xy}} + N_{d_{x^2-y^2}})$, presumably as a secondary effect from the reduction of $N_{d_{z^2}}$, $N_{d_{xz}}$, and $N_{d_{yz}}$.

When the ligands X are strong π-acceptors (*e.g.* Cl_3Sn—, Cl_3Ge—) the ^{59}Co coupling constants increase again, presumably because of a decrease of $(N_{d_{xz}} + N_{d_{yz}})$. This applies also to the ion $Co(CO)_3[P(C_6H_5)_3]_2^+$. The effect of decreased σ-donor ability when Cl replaces C_6H_5 and CH_3 also helps increase e^2Qq by decreasing $N_{d_{z^2}}$.

At the time of submitting this paper, we became aware that others (19, 20) have studied some of the compounds described here. Their data are in good agreement with ours.

The authors are grateful to the National Research Council of Canada for financial support of this work in the form of operating grants (to W.R.C. and M.C.L.G.) and funds to purchase the spectrometer. One of us (L.S.C.) wishes to thank the International Nickel Company of Canada, Limited, for the award of a scholarship. They would also like to thank Dr. T. L. Brown for comments and information concerning related work.

1. T. L. Brown, P. A. Edwards, C. B. Harris, and J. L. Kirsch. Inorg. Chem. **8**, 763 (1969).
2. D. D. Spencer, J. L. Kirsch, and T. L. Brown. Inorg. Chem. **9**, 235 (1970).
3. K. Ogino and T. L. Brown. Inorg. Chem. **10**, 517 (1971).
4. T. E. Boyd and T. L. Brown. Inorg. Chem. **13**, 422 (1974).
5. A. N. Nesmeyanov, G. K. Semin, E. V. Bryukhova, K. N. Anisimov, N. E. Kolobova, and V. N. Khandozhko. Izv. Akad. Nauk SSSR Ser. Khim. 1936 (1969).
6. J. A. M. Case. Ph.D. Thesis. University of Wisconsin, 1967.
7. A. S. Foust, Jr. Ph.D. Thesis. University of Wisconsin, 1970.
8. J. A. Ibers. J. Organomet. Chem. **14**, 423 (1968).
9. R. F. Bryan and A. R. Manning. Chem. Commun. 1316 (1968).
10. A. Sacco. Ann. Chim. Rome, **43**, 495 (1953).
11. G. H. Whitfield and H. W. B. Reed. J. Chem. Soc. 1931, 1940 (1954).
12. (*a*) W. Hieber and W. Freyer. Chem. Ber. **91**, 1230 (1958); **93**, 462 (1960). (*b*) A. Sacco and M. Freni. J. Inorg. Nucl. Chem. **8**, 566 (1954).
13. S. Attali and R. Poilblanc. Inorg. Chim. Acta, **6**, 475 (1972).
14. L. S. Chia, W. R. Cullen, M. C. L. Gerry, and S. Y. Poh. Can. J. Chem. In press.
15. G. K. Semin and E. I. Fedin. Zh. Strukt. Khim. **1**, 252 (1960).
16. H. G. Robinson. Phys. Rev. **100**, 1731 (1955).
17. L. S. Chia. Ph.D. Thesis. University of British Columbia, Vancouver, British Columbia. 1974.
18. M. G. Clark. Chem. Phys. Lett. **13**, 316 (1972).
19. T. L. Brown. Acc. Chem. Res. In press.
20. T. E. Boyd. Ph.D. Thesis. University of Illinois, Urbana, Illinois. 1973.
21. R. L. Collins and R. Pettit. J. Am. Chem. Soc. **85**, 2332 (1963); J. Chem. Phys. **39**, 3433 (1963).

Can. J. Chem. Downloaded from www.nrcresearchpress.com by 210.87.254.6 on 09/05/12
For personal use only.

Sorption of Water, Ammonia, Ethyl Chloride, and Methane on Na—X Zeolite and Associated Framework Distortion

D. L. RIMMER AND R. MCINTOSH

Department of Chemistry, Queen's University, Kingston, Ontario K7L 3N6

Received April 17, 1974

D. L. RIMMER and R. MCINTOSH. Can. J. Chem. **52**, 3699 (1974).

Length change and sorption isotherms have been determined for water, ammonia, ethyl chloride, and methane on compacted samples of zeolite NaX. Methane sorption at 0 °C and ethyl chloride sorption at −10 °C were accompanied by little or no framework distortion as monitored by length change measurements; sorption of ammonia in the temperature range −50 to −70 °C produced more appreciable distortion; and water sorption at room temperature caused large changes. In each case the framework distortion was correlated with different stages in the sorption process. The sorption isotherms for the ammonia/NaX system indicated the possibility at high uptakes of two-dimensional condensation or multilayer formation. The critical temperature for two-dimensional condensation would be −70 °C.

D. L. RIMMER et R. MCINTOSH. Can. J. Chem. **52**, 3699 (1974).

On détermine le changement de longueur et les isothermes de sorption de l'eau, de l'ammoniac, du chlorure d'éthyle et du méthane sur des échantillons agglomérés de zéolithe NaX. En se basant sur des mesures de changement de longueur, on en conclut que la sorption du méthane à 0 °C et celle du chlorure d'éthyle à −10 °C sont accompagnées de peu ou pas de déformation du squelette; la sorption de l'ammoniac dans l'intervalle de températures de −50 à −70 °C produit une déformation plus appréciable et la sorption de l'eau à température de la pièce cause de grands changements. Dans chaque cas, la déformation du squelette est reliée aux différents stades du procédé de sorption. Les isothermes de sorption du système ammoniac/NaX indiquent la possibilité, aux adsorptions élevées, d'une condensation bidimensionnelle ou d'une formation à couches multiples. La température critique de la condensation bidimentionnelle est de −70 °C.

[Traduit par le journal]

Introduction

Valuable additional information about the sorption process may sometimes be obtained when measurement of the sorbent's length changes is made in conjunction with conventional measurements of sorption isotherms. Certain processes taking place during sorption cannot be detected, or inferred, from the sorption isotherm alone. In earlier studies of this kind (see, for example refs. 1–4) porous silica glass has been employed as the sorbent. However this had the disadvantage of having a random and poorly defined pore structure, which made the interpretation of the results more difficult. A zeolite was chosen as the sorbent in the present work to lessen this difficulty. Zeolite pore structures and, to a degree, the location of the cations within the structures are defined crystallographically, so that the shape and size of the pores and their interconnecting channels are all known (5, 6). Zeolites have two disadvantages however: (*i*) the mobility of some of the cations and (*ii*) the necessity of compacting zeolite powder in order to produce rod-like samples. The mobility of the cations results in uncertainty in their location, and the use of a compact introduces the possibility of length changes due to rearrangement of the zeolite crystallites. Two earlier studies of sorption and associated length changes for the water NaA zeolite system (7, 8) had demonstrated the feasibility of such studies. In this work a different, but related, zeolite (NaX) was employed along with a variety of sorbates in the hope of coming to more general conclusions than the earlier studies permitted.

Experimental

Materials

The sorbent was a compacted powder sample of Linde Molecular Sieve type 13X (NaX). Pellets, 7 mm diameter and 10–25 mm length, were produced in a die with pressure being applied by means of a hydraulic press via a plunger. A moisture content of ~5% and pressures in the range 18 500–55 000 p.s.i. were found to be the optimum conditions for obtaining satisfactory pellets, in agreement with the findings of earlier workers (9, 10). By varying the applied pressure six samples were obtained with densities in the range 55–83% of the single crystal density. Only the least dense and most dense of these

Can. J. Chem. Downloaded from www.nrcresearchpress.com by 210.87.254.105 on 09/05/12
For personal use only.

Can. J. Chem. Downloaded from www.nrcresearchpress.com by 210.87.254.105 on 09/05/12
For personal use only.

varied significantly in their sorption and length change behavior when water was sorbed. Good agreement was obtained for the remaining four samples, which covered the range 62 to 76% of the single crystal value.

The samples were outgassed under vacuum in the sorption cell by raising the temperature gradually from 90 to 400 °C in steps of approximately 60 °C. The temperature was only raised when the pressure had fallen to $< 10^{-4}$ mm Hg and the temperature was maintained at 400 °C until a pressure $< 5 \times 10^{-6}$ mm Hg was reached. This outgassing procedure was found to produce an irreversible shrinkage in the pellets, causing them to become loose in their clamps. Repeated heating caused no further macroscopic shrinkage; thus it became a standard procedure to "preshrink" the samples in a muffle furnace at 400 °C overnight, before loading into the cell. The shrinkage could not be attributed to a sintering of the particles, because X-ray powder diffraction patterns showed no loss of crystallinity and scanning electron micrographs showed no increase in agglomeration of the particles in three samples which were: (*1*) uncompacted, (*2*) compacted, and (*3*) compacted and heat treated. It is thought that the shinkage was caused by particle redistribution which removed density inhomogeneities, such as found by Duwez and Zwell (11) in their studies of metal powder compacts. Such rearrangement would result in a more uniformly dense, but smaller sample.

The sorbates used were methane (Matheson Ultra High Purity grade, 99.97% minimum purity), ethyl chloride (Matheson USP grade, 99.7% minimum purity), and ammonia (Matheson Anhydrous grade, 99.99% minimum purity). The methane was simply passed through a molecular sieve trap before use to remove moisture. The ethyl chloride and ammonia were similarly passed through the molecular sieve trap and then condensed in liquid nitrogen cooled traps. They were outgassed by successive cycles of pumping, warming to melting point, cooling and pumping, and then they were fractionally distilled under vacuum.

Apparatus

The apparatus was based on that of Kipkie *et al.* (4, 12) and comprised four main parts: (*i*) the vacuum system, used in sorbate and sorbent preparation and in the operation of the volumetric system for adding gases, (*ii*) the sorption cell which housed the sorbent and the length change measuring transducer, (*iii*) the electrical circuitry associated with the transducer operation, and (*iv*) the thermostat system, which provided an adjustable constant temperature environment for the cell. The vacuum system was capable of producing a vacuum of 10^{-6} mm Hg, the transducer could detect length changes as small as 0.05 μm, and the temperature control in the range 0 to −130 °C was ±0.05 °C for periods up to a week. It was necessary to modify the sorption cell design which had been used by Kipkie *et al.* (4), because of the different sorbent being studied. Firstly, the section below the flange was shortened because the compacts employed were much shorter than Kipkie's porous glass rods. Secondly, the base of the cell was redesigned so as to be removable and was screwed into position. A vacuum-tight seal was obtained by use of a gold gasket. This modification was necessary because the maximum outgassing temperature of 400 °C was sufficiently high to volatilize certain metals from the silver solder connection which was incorporated in the former design. It was also necessary to replace the brass clamps, which held the compacted samples in place, by stainless steel ones for the same reason. In order to protect the transducer, located at the top of the cell, from overheating during the high temperature outgassing procedure, a very small furnace was constructed which heated only the lower part of the cell, corresponding to the sample position; and above this, but below the flange, a removable brass water jacket was installed to maintain the upper part of the cell at temperatures below 100 °C.

Water Sorption Measurements

This very simple set of experiments was designed initially to test the effect of sample density on sorption and length change behavior. However the results proved to be of more general interest and will be discussed fully later. The six samples of varying density were dehydrated at 400 °C in a muffle furnace for 2 days. After weighing and measuring to obtain their dry weights and lengths, they were placed in a desiccator held at a fixed relative humidity by a sulfuric acid – water solution. Fluctuations in the relative humidity caused by temperature changes were limited by keeping the desiccator in a constant temperature room. The samples were removed from the desiccator after periods of from 1 to 3 days and weighed on an analytical balance to the nearest 0.1 mg, and their lengths measured with a micrometer gauge to the nearest 0.0001 in. Weighing and measuring were continued until equilibrium in both weight uptake and length change was obtained. By successive dilution of the sulfuric acid, the relative humidity was increased in steps and the samples allowed to equilibrate at each value. In this way approximate sorption and length change isotherms were obtained.

Results and Discussion

Methane Sorption at 0 °C

The sorption data agreed quite well with those of Barrer and Sutherland (13). Slightly higher uptakes were found in this study which might well be due to the higher outgassing temperature. The sorption was accompanied by no significant expansion or contraction. Barrer and Sutherland had calculated that the isosteric heat of sorption for this system in the 0–25 °C temperature range was 4.1–4.5 kcal/mol. It seems that such weak interaction is insufficient to cause any major distortion of the zeolite framework.

Ethyl Chloride Sorption at −10 °C

Ethyl chloride was chosen as the next sorbate for study. Because of its polar nature it was expected to interact strongly with the zeolite and the shape of the sorption isotherm (Fig. 1*a*) tends to confirm this hypothesis. However only very small length changes were measured (Fig. 1*b*), and this can best be explained by a consideration of the size of the sorbate molecule in relation to the zeolite structure. Ethyl chloride is too large a molecule to penetrate the sodalite unit

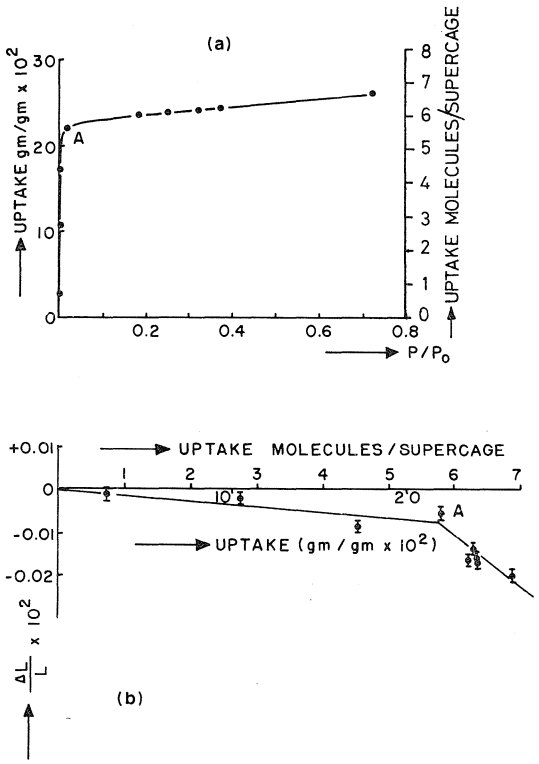

FIG. 1. (*a*) Sorption isotherm for ethyl chloride on sodium zeolite at −10 °C. (*b*) Length change isotherm for ethyl chloride at −10 °C.

because its limiting cross-section is of the order of 4 Å, compared with the 2.2 Å diameter sodalite entrance window. Consequently sorption is limited to the supercages. Point A in Fig. 1 corresponds to an uptake of ~46 molecules of ethyl chloride/unit cell of the zeolite, or ~6 molecules/supercage. Each unit cell contains ~88 Na^+ ions; 16 of these are located in SI, SI′, and SII′ sites and are thus inaccessible to the ethyl chloride molecules. A further 24–32 Na^+ ions are thought to be in SII sites in the windows connecting the supercages to the sodalite units (14, 15). This leaves 40–48 Na^+ ions/unit cell, or 5–6 Na^+ ions/supercage, in the most accessible sites within the supercages. Thus it appears that the sorption of one ethyl chloride molecule/supercage Na^+ ion represents the first phase of the sorption phenomenon. The supercage Na^+ ions will be the highest energy sites for a polar molecule and the first ethyl chloride molecules sorbed will probably be localized on these sites. This process will disturb the crystal field within the zeolite, the result of which is a slight distortion of the zeolite lattice which is manifested as an overall contraction. After point A the ethyl chloride molecules are most likely to locate on the next most energetically favorable sites which are the SII Na^+ ions. The fact that the contraction is more marked after this point leads to the conclusion that the crystal field is more strongly disturbed by interaction of the sorbate with SII Na^+ ions.

The estimated saturation value of the amount adsorbed corresponds with about 7 molecules/supercage. At −10 °C the molar volume of ethyl chloride is closely 69 cm^3 or about 115 $Å^3$ per molecule (16). The free diameter of the large cage is about 12 Å and its free volume about 820 $Å^3$ (17). Thus 7 molecules of ethyl chloride almost exactly fill this volume and the condition at saturation seems clear.

Ammonia Sorption at −50 °C

This sorbate was chosen because it is polar yet much smaller than ethyl chloride and there is the possibility of its entering the sodalite unit. The results for run 8 are shown in Fig. 2*a* and *b*, but the experiment was repeated twice (runs 9 and 10) to check reproducibility. The sorption isotherms were very reproducible and the length change isotherms only varied in the magnitude of the initial contraction. The extent of the contraction in each, expressed as $\Delta L/L \times 10^2$, was as follows: run 8, −0.027; run 9, −0.053; and run 10, −0.075.

Only partially complete desorption branches were obtained because it was difficult to reach low pressures with the apparatus used. However sufficient information was obtained to show the existence of marked hysteresis over a wide range of relative pressure. At high relative pressures capillary condensation between the crystals which make up the compact undoubtedly causes some of the hysteresis. However an alternative explanation is needed to explain its persistence to lower values of P/P_0. Barrer and Gibbons (18) found no hysteresis in the isotherms that they measured in the temperature range 100–180 °C. In the same paper they presented evidence that ammonia could diffuse into the sodalite units of basic sodalite but only extremely slowly at room temperature and more rapidly at temperatures over 100 °C. Consequently at −50 °C the diffusion of ammonia molecules into the sodalite units of the zeolite is also likely to be extremely slow. Once within the sodalite unit the molecules

Can. J. Chem. Downloaded from www.nrcresearchpress.com by 210.87.254.105 on 09/05/12
For personal use only.

Can. J. Chem. Downloaded from www.nrcresearchpress.com by 210.87.254.105 on 09/05/12
For personal use only.

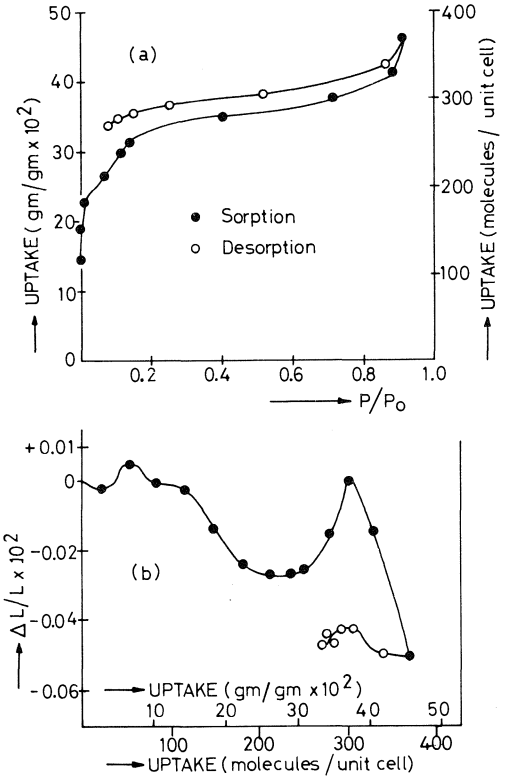

FIG. 2. (*a*) Sorption isotherm for ammonia on sodium zeolite at −50 °C. (*b*) Length change isotherm for ammonia at −50 °C.

are unlikely to be desorbed except at elevated temperatures. Irreversibility of this kind could explain the hysteresis observed at −50 °C.

A second interesting feature of the sorption isotherms is their unusual shape in the relative pressure range 0.05 to 0.15. Associated with this region of the isotherm is a minimum in the curve of fractional length change. There is thus additional evidence of a change in the mechanism of sorption within the relative pressure range. As the initial sorption appears to be associated with Na^+ ions in the supercages, and these are sites of high energy of interaction, subsequent sorption presumably occurs on a more energetically homogeneous surface. The shape of the isotherm suggests the formation of interacting sorbate molecules, which, with diminishing temperature, could exhibit a phenomenon analogous to two-dimensional condensation. Isotherms at lower temperatures were obtained and the rate of increase of amount sorbed with increasing pressure was exaggerated until the isotherm at −70 °C suggests a step in the isotherm resembling what would be expected for a first order phase change. These data are illustrated in Fig. 3. If this explanation is feasible, an experimental estimate of the critical temperature for condensation is approximately −70 °C. Cassel (19) and Hill (20) have shown theoretically that the ratio of two to three-dimensional critical temperatures (T_{2c}/T_{3c}) should be 0.50. Since T_{3c} is 133 °C, T_{2c} would be −70 °C, so that some additional support is given the hypothesis in spite of the rather narrow range of temperatures over which the isotherms have been determined. A necessary condition for two-dimensional condensation is an energetically homogeneous surface. The zeolite surface is certainly not homogeneous, but the inflection in the isotherm does not appear until considerable sorption has occurred on the high energy sites. A calorimetric study of the sorption of ammonia on NaX by Avgul *et al.* (21) showed a levelling off of the heat of sorption at high uptakes, which indicates a more homogeneous surface. In a second study Barrer and Gibbons (18) found evidence of a slight rise in the calculated isosteric heats of adsorption at higher coverages similar to that for water sorption on NaX in the fractional coverage range $\theta = 0.3$ to 0.9 reported by Barrer and Bratt (22). They attributed the rise to exothermic water–water interactions. As suggested earlier the ammonia isotherm suggests interactions of the ammonia in the sorbed state.

Other explanations of the shape of the isotherm may be sought. One which appears feasible is the onset of multilayer formation in the usual sense and another is capillary condensation in pores which may have been created in compacting the particles. Of these two the former

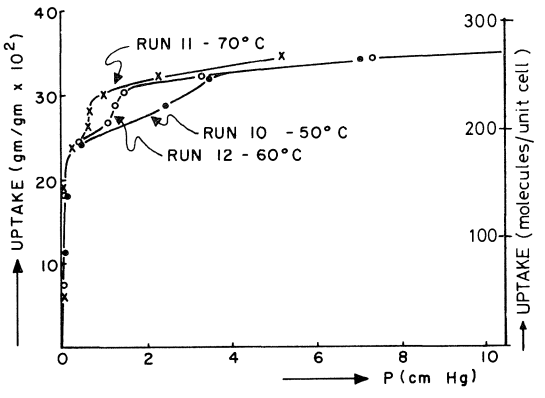

FIG. 3. Sorption isotherms for ammonia on sodium zeolite at −50, −60, and −70 °C.

Can. J. Chem. Downloaded from www.nrcresearchpress.com by 210.87.254.105 on 09/05/12
For personal use only.

seems the more likely since the relative pressure for spontaneous filling would exceed a relative pressure of 0.3 and there was no evidence from X-ray or electron microscope examination that the crystallites suffered damage in preparing the compacts. Moreover, the mechanism of capillary condensation should increase the contraction (1), but multilayer formation would increase the spreading pressure and could lead to the minimum in the curve.

The main features of the length change isotherms are as follows: during the sorption of the first 100 molecules/unit cell there is no marked expansion or contraction; between 100 and 200 molecules/unit cell there is a marked contraction; between 200 and 250 molecules/unit cell there is a minimum; from 250 to 300 molecules/unit cell there is a marked expansion; and above 300 molecules/unit cell another contraction takes place. The desorption points for run 8 indicate that the final contraction is almost totally irreversible. This was confirmed in run 9 when the adsorption was terminated before the final contraction and the desorption points were found to coincide with the adsorption points.

The sorption of the first 100 molecules/unit cell takes place in the highest energy sites, *i.e.* the Na^+ ions in the supercages. As with ethyl chloride this initial sorption caused little distortion of the framework. Stamires (23) has suggested in interpreting conductivity measurements for this system that 100 sorbed molecules/unit cell represents the point at which the mobile supercage cations are fully solvated.

Subsequent sorption between 100 and 200 molecules/unit cell which is accompanied by a contraction takes place on or near cations in sites SII and to a lesser extent, because of slow diffusion into the sodalite unit, sites SII′, SI′, and SI. The variation in the magnitude of the contraction can be explained if it is assumed that the location of the cations is not identical at the start of each experiment. The distortion of the aluminosilicate framework, which is manifested as expansions and contractions of the compact, will depend greatly on the position of the cations, which are the initial sorption sites. The cations are present to balance the negative charge of the framework; movement of the cations will cause a perturbation of the crystal field of the zeolite and a distortion of the framework. In order to have reproducible length changes during initial sorption, it would be necessary to have identical starting conditions. If this is not the case then it could explain the differences in the magnitude of the initial contraction. In this respect the SII cations will be of primary importance because: (*1*) they are the next most energetically favorable sorption sites when the supercage ions are fully solvated, and being more intimately bound up with the alumino-silicate framework than the latter the sorption process is more likely to cause framework distortion, the magnitude of which will depend on the exact location of the cation; and (*2*) they are located at access windows to the sodalite unit and will affect the rate of diffusion of ammonia molecules into the sodalite unit. It is postulated in connection with water sorption that sorption within the sodalite unit is responsible for large contractions in the length change measurements. Consequently if the same is true for ammonia sorption then the extent of penetration of the sodalite unit will also determine the magnitude of the contraction. Such a postulate can also help to explain why the contractions for water are an order of magnitude greater than for ammonia sorption. Additionally infrared spectroscopic studies (24–26) have shown that initially sorbed water molecules are oriented with respect to the cations in such a way that one of the hydrogen atoms of the molecule is hydrogen-bonded to a framework oxygen, while the other hydrogen atom is directed away from the surface. This is likely to cause more framework distortion than ammonia sorption which calorimetric and i.r. spectroscopic measurements (21, 27) have shown to take place with the ammonia molecules probably oriented with their nitrogen atoms towards the surface and all their hydrogen atoms away from it.

The position of the minimum in the length change measurements covers the range 200–250 molecules/unit cell, or 25–31 g/g $\times 10^{-2}$ uptake. This corresponds to the stage in the sorption process at which two-dimensional condensation is postulated to be taking place. The minimum and the condensation both indicate that the sorption is no longer taking place on high energy cation sites, because these are now fully occupied and the zeolite with its solvated cations is energetically more homogeneous. The position of the minimum, the magnitude of the subsequent expansion, and the position of that maximum appear to be reproducible. This evidence indicates that the state of the system at the minimum is a stable, reproducible one.

Sorption of a further 50 molecules/unit cell is accompanied by an expansion of ~ 0.027 $\Delta L/L \times 10^{-2}$ in all cases. This corresponds to the less pronounced uptake of ammonia in the relative pressure range 0.15 to 0.75. The decrease in sorption as a function of pressure and the expansion which accompanies the sorption in this region indicate that the zeolite cavities are approaching saturation.

Sorption beyond 300 molecules/unit cell causes the irreversible contraction mentioned above. It is thought that the process responsible for this contraction is capillary condensation between the zeolite crystals. The section of the sorption isotherm corresponding to the contraction is the final section which is convex to the pressure axis. This "turn up" in the isotherm is indicative of capillary condensation. Such a process is likely to cause the crystals to rearrange and the rearrangement would be in such a way as to give a more densely packed and stable compact. Prior to the experiment the compact had been outgassed at 400 °C. This process is likely to have caused the compact to expand and become less densely packed. If the subsequent cooling process was insufficient to allow the compact to return to its most stable state, then any later rearrangement would tend to cause an irreversible contraction as found here.

Length change isotherms were also measured at -60 and -70 °C but were very similar to those at -50 °C. The magnitude of the initial contraction varied, but did not correlate with decrease in temperature or increasing sharpness of the adsorption step. The extent of contraction in each case fell within the range found in the three runs at -50 °C.

Water Sorption at Room Temperature (~ 20 °C)

The data presented in this section are only approximate (see Experimental section for details). Six samples of varying bulk density were employed and gave similar results. Those for the sample with density 67.1% of the single crystal value are shown in Fig. 4. Sorption was followed by desorption; a second sorption cycle was carried out after the sorbent had been heated to 400 °C for 2 days. The values obtained at very low relative pressures were non-equilibrium values and are so indicated by the dotted line of Fig. 4*b*. In Fig. 4*a* the isotherm of Barrer and Bratt (22), obtained at 30 °C, is shown for comparison. The difference appears to be due to the better removal of zeolitic water in their case because of evacuation at 350 °C for 12 h. Correction of our data by 5 g/g $\times 10^{-2}$ is made in discussing our data so that, for example, the minimum in the data for length change may be considered to occur at 21 g/g $\times 10^{-2}$ instead of 16 g/g $\times 10^{-2}$.

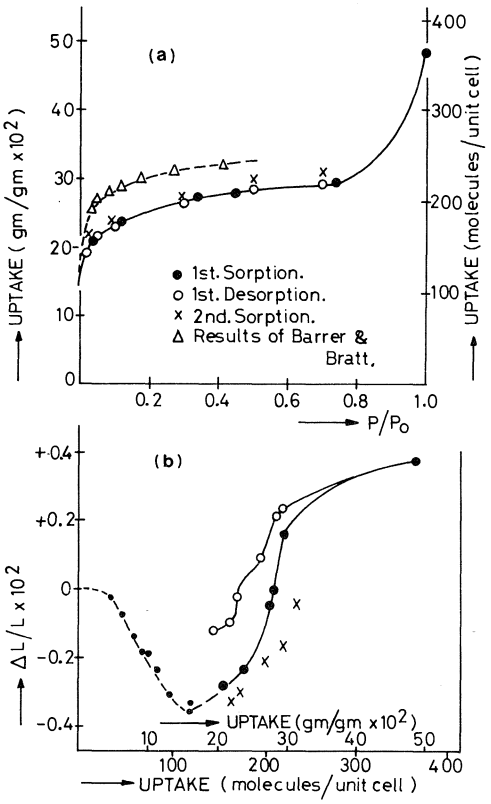

FIG. 4. (*a*) Sorption isotherm for water on sodium zeolite at approximately 20 °C. Sample density 67.1% of single crystal value. (*b*) Length change isotherm for water on sodium zeolite at approximately 20 °C. Sample density 67.1% of single crystal value.

Barrer (28) has reported that removal of water causes the unit cell edge dimension to diminish and then to expand, which he attributes to the behavior of capillary condensed sorbate with menisci creating negative hydrostatic pressure which diminishes as sorbate is removed. The hydrated crystal contained 26 g/g $\times 10^{-2}$ of water and had a smaller unit cell than the dehydrated one. At an equivalent degree of hydration the work reported here shows that the compact has contracted by about 0.2% in agreement with the X-ray work. Olson (15, 29) has also em-

Can. J. Chem. Downloaded from www.nrcresearchpress.com by 210.87.254.105 on 09/05/12
For personal use only.

Can. J. Chem. Downloaded from www.nrcresearchpress.com by 210.87.254.105 on 09/05/12
For personal use only.

ployed X-ray data to show that the lattice parameter a_0 decreases from 25.099 to 25.028 Å during hydration to 29.4 g/g $\times 10^{-2}$. This corresponds to a contraction of 0.283%. In the second sorption cycle of the present study at the corrected uptake of 29.4 g/g $\times 10^{-2}$ the contractions of all samples fell within the range 0.23 to 0.33%. Thus it is probable that the initial contraction is due to framework distortion and that rearrangement of particles makes little contribution.

As in the case of ammonia the contraction begins after initial sorption on the Na^+ ions of the supercage, and apparently 100 molecules/unit cell are sorbed in that way in the case of water. The contraction which follows extends to a corrected uptake of $\sim$22.5 g/g $\times 10^{-2}$, or $\sim$165 molecules/unit cell, and its magnitude is about 0.35%. This is an order of magnitude greater than for ammonia or ethyl chloride and the difference is thought to be due to the ease with which water molecules may enter the sodalite units and interact with the $SINa^+$ ions. There is no published study of ion positions in a dehydrated sample of NaX, but in a hydrated sample only 9 of 16 possible SI sites were occupied by Na^+ ions (15). Evidence for other fanjasite type zeolites points to migration of SI cations into the sodalite unit in many cases during hydration (6). Any movement of these ions will cause a large distortion.

Expansion from the minimum to 32.5 g/g $\times 10^{-2}$ is in the order of 0.43%. Part of this expansion is irreversible as the desorption points show. Because of absence of hysteresis in the sorption isotherms the irreversibility must be attributed to particle rearrangement in the compact. Expansions from corrected uptakes of 32.5 g/g $\times 10^{-2}$ to saturation vary from sample to sample and are greater for the denser samples.

The length changes for the second sorption are less than for the first probably because of a reduction in the irreversible part of the expansion.

Finally, interesting comparisons can be made between this work and the earlier work of Sereda and Feldman (7) and Kononyuk *et al.* (8) who also studied sorption and length changes for water sorbing on a zeolite. Direct comparisons are impossible, however, because they both used NaA zeolite. In all three studies: the extent of the expansions and contractions are in order of magnitude agreement; a minimum occurred in the length changes, at which point the sample was smaller than its original length; and the minimum was followed by a large expansion which took the sample to a point where it was larger than its original length. In the region of initial sorption: Kononyuk *et al.* found an expansion followed by a steep contraction leading to the minimum; Sereda and Feldman found a gradual contraction leading to the minimum; and the present work indicated a region of no movement followed by a steep contraction leading to the minimum. This lack of agreement only emphasizes an earlier point made in this paper concerning the lack of reproducibility of the magnitude of the contraction for ammonia sorption at -50 °C, namely that the length changes during initial sorption will depend greatly on the original positions of the cations. Because of their mobility these are bound to vary and consequently so will the initial length changes. In the interpretation of the results the authors agree with Kononyuk *et al.* in thinking that the minimum in the length changes corresponds to the completion of the hydration of the cations and that subsequent sorption represents filling of the zeolite cavities and sorption on the external surfaces of the zeolite particles.

Summary

In the light of the data presented above certain tentative generalizations can be made about the factors affecting distortion of the NaX zeolite framework during sorption. These are:

(*1*) the polarity of the sorbate: non-polar sorbates do not cause significant framework distortion, whereas polar sorbates do.

(*2*) the size of the sorbate: large molecules that are excluded from the sodalite unit cause less distortion; water which can readily enter the sodalite unit causes more distortion; and ammonia which can only slowly diffuse into the sodalite unit causes intermediate distortion.

(*3*) the stage of the sorption process: initial sorption on mobile supercage Na^+ ions causes little distortion; subsequent sorption on the SII (and in certain cases SII′, SI′, and SI) cations causes appreciable distortion which is manifested as a contraction; completion of the solvation of the cations is marked by a minimum in the length change measurements; and further sorption during which the zeolite cavities fill with sorbate causes distortion which appears as an expansion.

(*4*) the orientation of those molecules sorbed

on cations: if the sorbed molecule is oriented in such a way as to interact with both the cation and the framework the distortion of the latter will be greater.

We would like to acknowledge financial assistance for this work from the National Research Council of Canada and also the Province of Ontario, which provided a Graduate Fellowship for one of us (D.L.R.). Some of the ideas in this paper were first discussed during the Ph.D. examination of one of the authors (D.L.R.) and we would particularly like to mention the contribution of Dr. Ralph Feldman, the external examiner, in this respect.

1. C. AMBERG and R. MCINTOSH. Can. J. Chem. **30**, 1012 (1952).
2. D. J. C. YATES. J. Phys. Chem. **60**, 513 (1956).
3. A. A. ANTONIOU. J. Phys. Chem. **68**, 2754 (1964).
4. W. B. KIPKIE, R. MCINTOSH, and B. KELLY. J. Coll. Interface Sci. **38**, 3 (1972).
5. W. M. MEIER and D. H. OLSON. *In* Molecular sieve zeolites. Adv. Chem. Ser. 101, Am. Chem. Soc., Washington, D.C. 1971.
6. J. V. SMITH. *In* Molecular sieve zeolites. Adv. Chem. Ser. 101, Am. Chem. Soc., Washington, D.C. 1971.
7. P. J. SEREDA and R. F. FELDMAN. J. Appl. Chem. **13**, 150 (1963).
8. V. F. KONONYUK, A. I. SARAKHOV, and M. M. DUBININ. Dokl. Phys. Chem. **198**, 456 (1971).
9. D. C. FREEMAN, JR. and D. N. STAMIRES. J. Chem. Phys. **35**, 799 (1961).
10. V. BOSACEK, M. M. DUBININ, O. KADLEC, K. O. MURMAN, and V. NARRATIL. Dokl. Phys. Chem. **174**, 305 (1967). V. BOSACEK and Z. TRARUZKORA. Coll. Czech. Chem. Commun. **36**, 551 (1971).
11. P. DUWEZ and L. ZWELL. Trans. Am. Inst. min. (metall.) Eng. **185**, 137 (1949).
12. W. B. KIPKIE. Ph.D. Thesis, Queen's University, Kingston, Ontario. 1970.
13. R. M. BARRER and J. W. SUTHERLAND. Proc. R. Soc. Lond. A**237**, 439 (1956).
14. L. BROUSSARD and D. P. SHOEMAKER. J. Am. Chem. Soc. **82**, 1041 (1960).
15. D. H. OLSON. J. Phys. Chem. **74**, 2758 (1970).
16. T. MCMULLEN, E. D. CROZIER, and R. MCINTOSH. Can. J. Chem. **46**, 2945 (1968).
17. D. W. BRECK. Zeolite molecular sieves: structure, chemistry and use. Wiley–Interscience, New York. 1973. p. 430.
18. R. M. BARRER and R. M. GIBBONS. Trans. Farraday Soc. **59**, 2569, 2875 (1963).
19. H. M. CASSEL. J. Phys. Chem. **48**, 195 (1944).
20. T. L. HILL. J. Chem. Phys. **14**, 441 (1946).
21. N. N. AVGUL, A. V. KISELEV, L. YA. KURDYUKOVA, and M. V. SERDOBO. Russ. J. Phys. Chem. **42**, 96 (1968).
22. R. M. BARRER and G. C. BRATT. J. Phys. Chem. Solids, **12**, 130, 146, 154 (1959).
23. D. N. STAMIRES. J. CHEM. Phys. **36**, 3174 (1962).
24. L. BERTSCH and H. W. HABGOOD. J. Phys. Chem. **67**, 1621 (1963).
25. J. L. CARTER, P. J. LUCCHESI, and D. J. C. YATES. J. Phys. Chem. **68**, 1385 (1964).
26. C. L. ANGELL and P. C. SCHAFFER. J. Phys. Chem. **69**, 3463 (1965).
27. V. N. ABRAMOV, A. V. KISELEV, and V. I. LYGIN. Russ. J. Phys. Chem. **38**, 1020 (1964).
28. R. M. BARRER. Experentia, Suppl. VII, page 113 (1957).
29. D. H. OLSON. Private communication.

Can. J. Chem. Downloaded from www.nrcresearchpress.com by 210.87.254.105 on 09/05/12
For personal use only.

Fluorescence différée et émissions photostimulées du carbazole et de la diphénylamine dans une matrice rigide d'éther à 77 °K

D. MULLER,[1] M. EWALD[2] ET G. DUROCHER

Département de chimie, Université de Montréal, C.P. 6210, Montréal, Québec H3C 3V1

Reçu le 30 mai 1974

D. MULLER, M. EWALD et G. DUROCHER. Can. J. Chem. **52**, 3707 (1974).

La fluorescence différée ainsi que la fluorescence et la phosphorescence photostimulée par la lumière visible à 6000 Å dans les systèmes diphénylamine (DPA) – éther vitreux et carbazote (C) – éther vitreux à 77 °K ont été enregistrées. L'analyse de la recombinaison électron–cation après stimulation dans le visible a été élaborée en utilisant un modèle cinétique préalablement décrit (10). Les rendements en triplet de la DPA et du C sont calculés et comparés aux valeurs expérimentales existantes. Le rapport (β) du peuplement de l'état triplet T_1 en fonction de l'état singulet S_1, après recombinaison est égal à 2 environ aussi bien pour la DPA que pour le C. Une valeur de 4.4 avait été obtenue pour l'indole et le tryptophane dans l'éther. Cette différence ne peut s'expliquer qu'en termes des énergies des états S_1 des molécules de soluté considérées ainsi qu'en fonction de la longueur d'onde utilisée lors de la stimulation.

D. MULLER, M. EWALD, and G. DUROCHER. Can. J. Chem. **52**, 3707 (1974).

The isothermal delayed fluorescence along with the visible (6000 Å) photostimulated fluorescence and phosphorescence emissions have been recorded and analyzed in the following systems: diphenylamine (DPA) – ether rigid glass and carbazole (C) – ether rigid glass at 77 °K. The electron–cation recombination after visible light stimulation has been analyzed in terms of a kinetic model already described (10). The triplet quantum yields of the DPA and C molecules are calculated and compared to the existing experimental values. The rate constant ratio (β) of populating the first triplet (T_1) relative to populating the first excited singlet (S_1) after the recombination event has taken place, is equal to about 2 in both systems investigated here. A value of 4.4 was obtained for indole and tryptophan in the same matrix. This difference can only be explained in terms of various singlet state energies for these molecules and also in terms of the stimulating energies used in these experiments.

Introduction

Il est connu depuis longtemps que la diphénylamine (DPA) ainsi que le carbazole (C) peuvent être photoionisés à 77 °K dans une matrice d'EPA (éther, isopentane et alcool 5:5:2) (1, 2). Dans le cas des amines aromatiques, la photoionisation s'effectue par l'intermédiaire de l'état triplet de la molécule de soluté qui absorbe un second photon de façon à ce que le système soluté–matrice atteigne le premier continuum d'ionisation (3–5). L'électron ainsi dégagé de la molécule de soluté peut être piégé dans la matrice ou encore se recombiner avec la molécule mère pour produire une luminescence isotherme appelée également émission différée. La fluorescence différée de la DPA n'avait pu être mise en évidence lors des premières études sur cette molécule (2) et ce n'est que tout récemment que l'observation et l'étude cinétique de cette émission dans diverses matrices a pu être réalisée (4, 5).

Un deuxième type de recombinaison concerne surtout les électrons fortement piégés dans la matrice. Ces électrons peuvent être piégés "physiquement" dans des "défauts" de la matrice ou encore "chimiquement" s'ils forment avec les molécules de soluté ou de solvant des ions négatifs ou des radicaux. L'excitation de ces électrons par une lumière infrarouge, visible ou ultraviolette provoque une luminescence de recombinaison appelée émission photostimulée. Albrecht *et coll.* (6, 7) furent les premiers à étudier de façon exhaustive ce type de recombinaison: d'autres chercheurs poursuivirent ces études (8, 9). Les émissions photostimulées de l'indole et du tryptophane ont fait l'objet d'une publication récente dans laquelle il a été démontré l'importance de la grandeur des interactions entre l'électron piégé et la matrice en ce qui concerne le processus de recombinaison électron–cation (10).

Dans le présent article nous mettons en évi-

[1]Adresse actuelle: Centre Universitaire, Place du 8 mai 1945, St.-Denis, France.

[2]Adresse actuelle: Département de chimie physique, Université de Bordeaux I, 33-Talence, France.

dence la fluorescence différée du carbazole de même que les émissions photostimulées de la DPA et du carbazole dans une matrice vitreuse d'éther à 77 °K. L'étude du rapport d'intensité de la phosphorescence et de la fluorescence stimulées est analysée en terme des énergies disponibles de la paire électron–cation au moment de la recombinaison.

Techniques expérimentales

(1) Produits et solutions

La DPA (Eastman Kodak) après cristallisation dans l'éthanol a été purifiée par fusion de zone sous atmosphère d'hélium. Après 20 passages, les cristaux de DPA ont été retirés de la partie supérieure de la colonne. Le carbazole est un produit monocristallin provenant de la maison James Hinton et purifié également par fusion de zone. La pureté est de 99.999%. L'éther diéthylique était un produit Mallinckrodt "éther anhydre", il a été sèché, sur sodium, puis distillé avant chacune des expériences. Il a été démontré expérimentalement qu'aux sensibilités utilisées lors des expériences d'émission différée ou stimulée, aucune trace d'impureté du solvant n'est présente. Les solutions ont toutes été préparées à l'obscurité. Une concentration de 10^{-3} *M* en DPA et en C dans l'éther à température ambiante a été utilisée au cours de ce travail.

(2) Observation des luminescences

Les spectres d'émissions différées et stimulées de même que les courbes de déclin ont tous été obtenus avec un spectrofluorimètre-phosphorimètre Aminco–Bowman muni d'un dispositif à miroir ellipsoidal de condensation de la lumière sur la fente d'entrée du monochromateur d'excitation. L'appareil de même que son mode opérationnel ont été décrits antérieurement (4, 10).

Pour l'observation des émissions photostimulées nous avons suivi la méthode cyclique suivante à tous les 10 nm: (*a*) 0–120 s: excitation à 290 nm avec un faisceau contenant 4×10^{-9} einstein $cm^{-2} s^{-1}$, (*b*) 120–240 s: période d'obscurité permettant ainsi le déclin complet de la fluorescence et de la phosphorescence naturelle, (*c*) 240–360 s: stimulation à 600 nm à l'aide du monochromateur d'excitation muni de filtres Wratten appropriés (2B et 16) pour ne laisser passer que la lumière entre 500 et 700 nm. Cette méthode cyclique nous procure à chacune des longueurs d'onde d'émission une impulsion du type de celles tracées sur les figs. 3 et 7. Ces signaux sont par la suite intégrés et corrigés en unités relatives de quanta $cm^{-2} s^{-1}$. C'est ainsi que les spectres de fluorescence et de phosphorescence stimulées sont obtenus sur les figs. 4 et 8. Des renseignements supplémentaires sur la partie expérimentale peuvent être obtenus dans un article récent (10).

Résultats

(A) Diphénylamine

Les spectres reproduits sur la fig. 1 sont très similaires à ceux déjà obtenus pour la DPA dans d'autres milieux vitreux comme l'EPA et le 3-MP (4, 5). En trait plein sur la figure, la fluo-

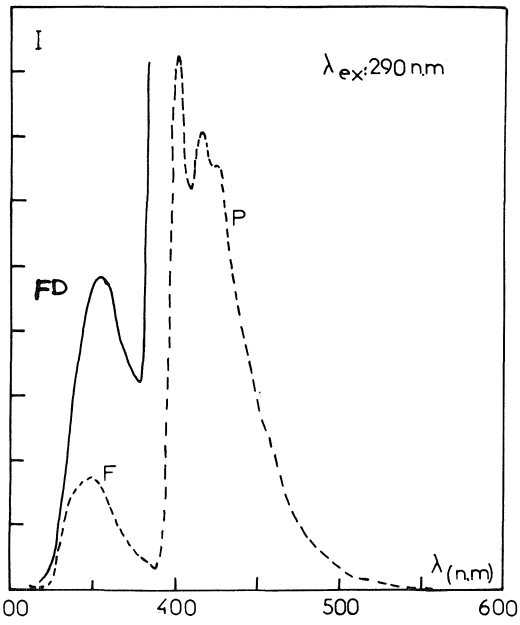

FIG. 1. DPA 10^{-3} *M* dans l'éther à 77 °K: (---) fluorescence et phosphorescence naturelle non-corrigée pour le système de détection et sans phosphoroscope; (—) fluorescence à longue durée de vie (isotherme ou différée) non corrigée et observée à l'aide d'un phosphoroscope. Ces émissions ont été excitées à 290 nm. L'ordonnée est en unités relatives.

rescence isotherme (différée) (FIIIB) est au même endroit que la fluorescence naturelle. Le déclin de cette fluorescence différée est très long et non-exponentiel comme le montre la fig. 2. Cependant il a été démontré récemment que la forme de cette courbe de déclin dépend fortement de la longueur d'onde d'excitation (5). La durée de vie de la phosphorescence est de 1.9 ± 0.2 s dans l'éther. La fluorescence différée est ici caractérisée par la composante lente de la courbe de déclin. Nous ne pouvons encore affirmer avec certitude que la partie rapide appartient à la fluorescence différée (5). Il se pourrait qu'une annihilation triplet–triplet (FIV) soit également à l'origine de cette partie rapide (4). Nous avons observé les rapports d'intensité suivants: $I_p \propto I_0$ et $I_{FLD} \propto I_0^{2.0}$ montrant bien la dépendance biphotonique de la fluorescence à longue durée (FLD), I_0 étant l'intensité de la lumière excitatrice.

La fig. 3 nous montre la forme des impulsions de fluorescence et de phosphorescence stimulées de la DPA à deux longueurs d'onde 350 et 400 nm. La montée de la fluorescence est instantanée (constante de temps de l'appareil enregistreur)

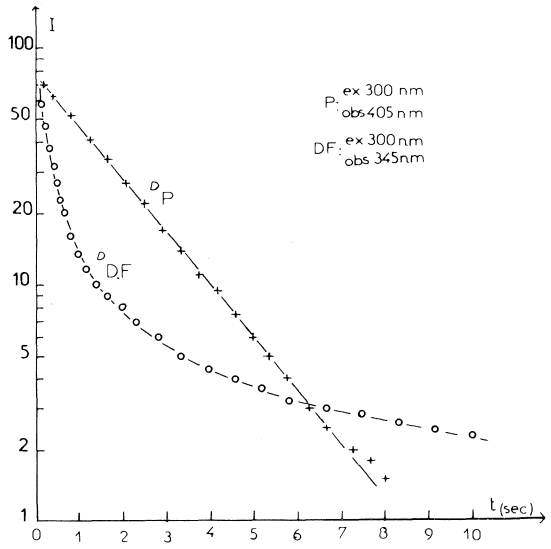

FIG. 2. DPA 10^{-3} M dans l'éther à 77 °K: courbes de déclin de la fluorescence différée (DF) et de la phosphorescence observées à l'aide d'un phosphoroscope. Le filtre Corning 7–60 a été utilisé devant le PM lors de l'observation de la fluorescence différée de façon à réduire le recouvrement des spectres de fluorescence et de phosphorescence.

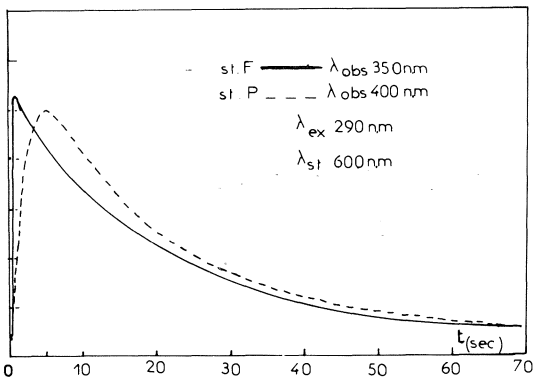

FIG. 3. DPA 10^{-3} M dans l'éther à 77 °K: variation avec le temps de stimulation de la fluorescence et de la phosphorescence stimulées observées à 350 et 400 nm respectivement. La lumière de stimulation (600 nm) est appliquée au temps $t = 0$. L'échantillon avait été irradié pendant 2 min à 290 nm au préalable. Par la suite un temps de noirceur de 2 min a été alloué avant que ne débute la stimulation.

alors que celle de la phosphorescence stimulée possède une constante de temps de 1.9 s correspondant à la durée de vie de la phosphorescence de la DPA dans l'éther. La décroissance de la stimulation suit une loi du premier ordre pour la première minute de la décroissance ce qui semble démontrer que ce sont les électrons piégés dans les défauts physiques de la matrice qui sont impliqués dans le processus de recombinaison (11). Les émissions naturelles de même que les émissions stimulées corrigées sont comparées à la fig. 4. Le rapport $(I_P/I_F)_N$ des émissions naturelles est égal à 5.9 ± 0.3. I_P et I_F sont les surfaces sous les courbes de fluorescence et phosphorescence en quanta $cm^{-3}\ s^{-1}$. Dans un régime où l'état stationnaire s'applique $I_P/I_F = \phi_P/\phi_F$. Le rapport des rendements quantiques n'est pas connu pour la DPA dans l'éther. Ermolaev obtint un rapport ϕ_P/ϕ_F de 7.3 ± 0.4 pour la DPA dans un verre d'alcool et d'éther (12) alors que des rapports de 6.6 et 6.1 ont été obtenus plus récemment dans l'EPA (15, 16).

Le rapport des émissions stimulées $(I_P/I_F)_{st}$ est égal à 22.1 ± 0.6 montrant une nette augmentation relative de la phosphorescence stimulée sur la phosphorescence naturelle. Un résultat similaire avait été obtenu pour l'indole et le tryptophane dans l'éther (10). Il est à noter que les

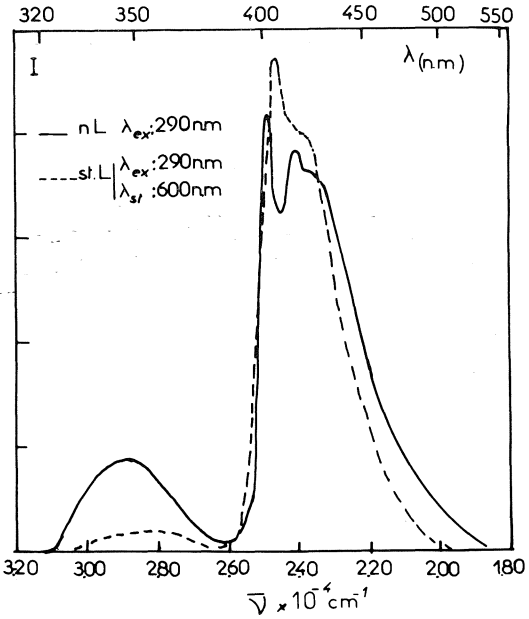

FIG. 4. DPA 10^{-3} M dans l'éther à 77 °K: (—) Spectres de fluorescence et de phosphorescence naturelles, excitées à 290 nm, et enregistrés sans phosphoroscope, corrigés pour le système de détection et transformés en unités relatives de quanta $cm^{-2}\ s^{-1}$. (---) Luminescence stimulée obtenue en traçant point par point à tous les 10 nm l'intégration graphique des courbes comme celles représentées à la fig. 3. Les corrections et transformations en unités relatives de quanta $cm^{-2}\ s^{-1}$ ont également été apportées.

erreurs mentionnées plus haut indiquent la reproductibilité des résultats sur un ensemble de trois mesures différentes effectuées sur trois échantillons différents de concentration égale.

(B) Carbazole

La fig. 5 nous montre les spectres de fluorescence et de phosphorescence naturelle pris sans phosphoroscope ainsi que la phosphorescence et la fluorescence de longue durée (FLD) pris avec phosphoroscope. Comme lors de l'étude de la DPA, la courbe de déclin de la FLD peut se décomposer en au moins deux composantes (fig. 6). L'une de ces composantes possède un temps de vie supérieur à la durée de vie de la phosphorescence qui est de 7.6 ± 0.1 s et peut être assignée à la fluorescence isotherme (différée) du carbazole. On remarque l'effet important que possède la longueur d'onde excitatrice sur l'intensité de cette composante isotherme qui devient très faible lorsque l'excitation s'effectue dans le premier système d'absorption du carbazole à 330 nm. Cet effet fait actuellement l'objet d'une étude plus approfondie qui sera publiée plus tard. Encore ici $I_p \propto I_0^{1.0}$ et $I_{FLD} \propto I_0^{2.0}$ montrent bien la dépendance biphotonique de l'émission longue.

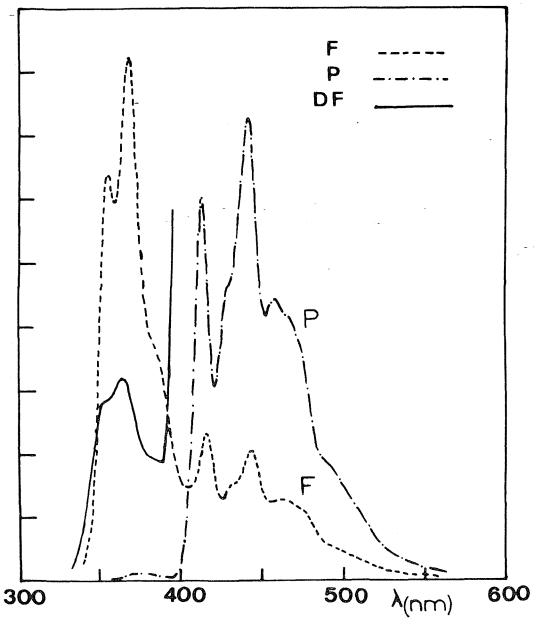

FIG. 5. Carbazole 10^{-3} *M* dans l'éther à 77 °K: (---) Fluorescence et phosphorescence naturelle non corrigée pour le système de détection; (—) fluorescence différée (DF) non-corrigée et observée à l'aide d'un phosphoroscope; (------) même spectre mais enregistré à une sensibilité moindre permettant ainsi l'observation de la phosphorescence du carbazole. Ces émissions ont été excitées à 290 nm. L'ordonnée est ici en unités relatives.

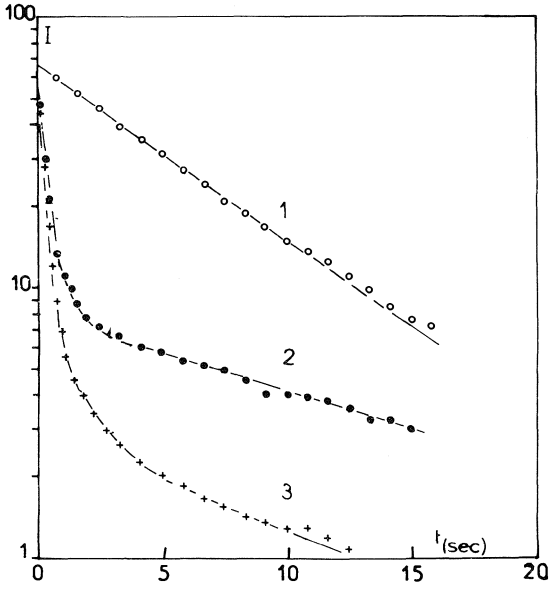

FIG. 6. Carbazole 10^{-3} *M* dans l'éther à 77 °K: (*1*) déclin de la phosphorescence du carbazole, excitée à 290 nm et observée à 415 nm; (*2*) déclin de la fluorescence différée excitée à 290 nm et observée à 370 nm; (*3*) déclin de la fluorescence différée excitée à 330 nm et observée à 370 nm. Le filtre Corning 7-60 du côté du PM a été utilisé pour l'observation du déclin des fluorescences différées.

La montée de l'impulsion de phosphorescence stimulée (fig. 7) possède encore ici une constante de temps égale à la durée de vie de phosphorescence du carbazole dans l'éther soit 7.6 s. Comme pour la DPA, la décroissance des émissions stimulées obéit à une loi du premier ordre. Le rapport des intensités des émissions naturelles $(I_P/I_F)_N$ est égal à 0.44 ± 0.04 alors que le rapport ϕ_P/ϕ_F donné par Ermolaev dans un mélange alcool–éther est de 0.55 ± 0.05 (12). En émission stimulée, le rapport est fortement augmenté à $(I_P/I_F)_{st} = 4.3 \pm 0.4$.

(C) Spectre d'action des émissions photostimulées

Le spectre d'action corrigé de la fluorescence stimulée de la DPA dans l'éther est représenté à la fig. 9 entre 500 et 700 nm qui sont les limites de notre instrumentation actuelle. Pour que ce spectre soit équivalent au spectre d'absorption des entités responsables de la recombinaison il faudrait que le rendement quantique de fluo-

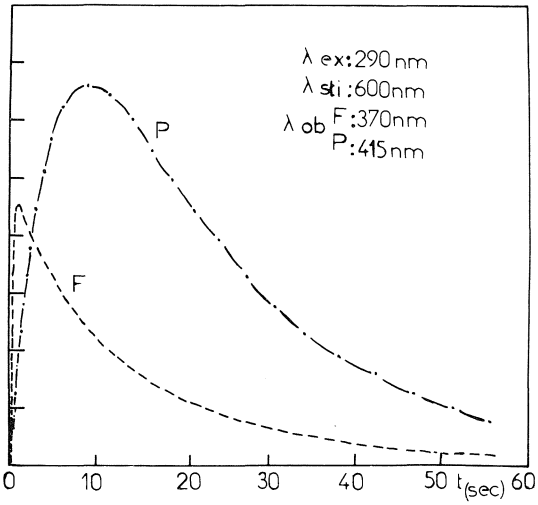

FIG. 7. Carbazole 10^{-3} *M* dans l'éther à 77 °K: Variation avec le temps de stimulation de la F et de la P stimulées observées à 370 et 415 nm respectivement. La lumière de stimulation (600 nm) est appliquée au temps $t = 0$. L'échantillon avait été irradié pendant 2 min à 290 nm au préalable. Par la suite un temps de noirceur de 2 min a été alloué avant le début de la stimulation.

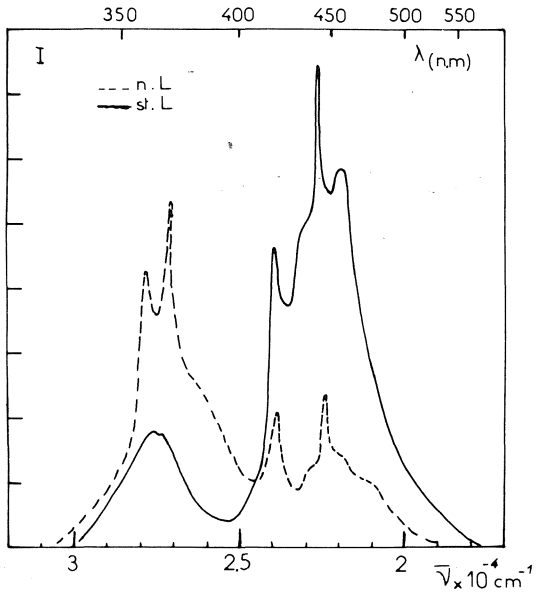

FIG. 8. Carbazole 10^{-3} *M* dans l'éther à 77 °K: (---) Spectres de F et P naturelles, excitées à 290 nm, enregistrés sans phosphoroscope, corrigés pour le système de détection; (—) luminescence stimulée obtenue en traçant point par point à tous les 10 nm l'intégration graphique des courbes comme celles représentées à la fig. 7. Ces deux spectres sont donnés en unités relatives de quanta $cm^{-2}\,s^{-1}$.

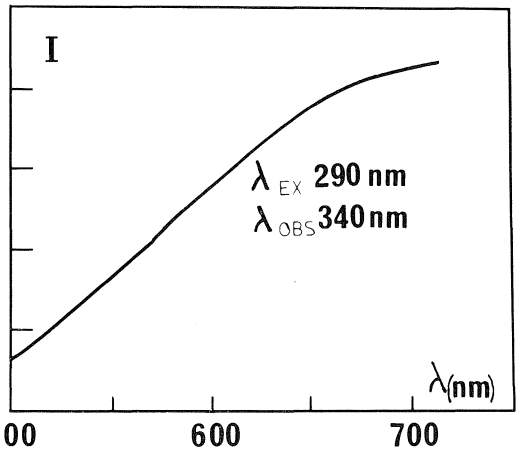

FIG. 9. Spectre d'action corrigé des fluorescences stimulées de la DPA et du carbazole d'abord irradiés à 290 nm dans l'éther à 77 °K. L'observation de la fluorescence stimulée s'est faite à 340 nm pour les deux molécules.

rescence stimulée soit indépendant de la longueur d'onde de stimulation. Cependant, nous avons actuellement certains indices du contraire et cela fera l'objet d'une publication future. On pourrait croire que ce spectre d'action correspond à une partie du spectre d'absorption des électrons dans l'éther dont le maximum se situe à 8066 cm^{-1} dans le proche infrarouge (13).

Discussion

(a) Cinétique de la luminescence photostimulée

Le modèle cinétique de McClain et Albrecht (6) a été utilisé lors de l'étude des émissions photostimulées de l'indole et du tryptophane et une description détaillée des constantes utilisées a été donnée (10). Le résultat important se retrouve à l'éq. 14 de la réf. 10 où

$$\frac{(I_p/I_F)_{st}}{(I_p/I_F)_N} = 1 + \frac{\beta(\lambda)}{\phi_T}$$

Les symboles à gauche de l'équation sont familiers et ces intensités ont toutes été mesurées pour la DPA et le C. ϕ_T est le rendement en triplet de la molécule de soluté dans la matrice vitreuse considérée. $\beta(\lambda) = k_{AT}/k_{AS}$ se définit comme étant le rapport du peuplement de l'état triplet T_1 relativement à celui de l'état singulet S_1 lors des processus de recombinaison ou encore $\beta(\lambda)$ correspond, à un temps donné après la stimulation, au nombre de molécules de soluté au niveau triplet T_1 comparativement au nombre

TABLEAU 1. Paramètres utilisés pour le calcul du rendement en triplet de la diphénylamine et du carbazole

Soluté	$\eta = N_H/N_H + N_C$	E_T (cm^{-1})	k_{ip}* (s^{-1})	$\tau_P = (k_P + k_{ip})^{-1}$ (s)	q_P† $= k_P/k_P + k_{ip}$	ϕ_P/ϕ_F	ϕ_F‡	$\phi_T = \phi_P/q_P$
Diphénylamine	0.458	25150	0.102	1.9	0.83	5.9	0.12	0.85
Carbazole	0.409	24540	0.039	7.6	0.70	0.44	0.44	0.21

*k_{ip} caractérise la constante de désactivation non-radiative $T_1 \rightsquigarrow S_0$ et est calculée par la théorie de Siebrand (20).
†q_P est souvent désigné l'efficacité quantique de la phosphorescence qui est différente du rendement ϕ_P.
‡Les rendements de fluorescence sont tirés des réfs. 15 et 16.

de molécules au niveau singulet S_1. Il est à noter que la cinétique pour être valable ne doit impliquer aucun processus d'intercombinaison entre les singulets et les triplets supérieurs à S_1 et T_1 après l'étape déterminante de la recombinaison (21). k_{AT} et k_{AS} sont les constantes de vitesse du premier ordre qui caractérisent le peuplement des triplets et des singulets au moment des recombinaisons.

Il a été démontré dans un article antérieur (10) que ce paramètre $\beta(\lambda)$ dépendait fortement de l'énergie mise en jeu lors du processus de recombinaison. En effet la matrice éthylène – glycol (EG) – eau (W) est reconnue pour piéger les électrons plus fortement que la matrice d'éther (13) et donc lors de la stimulation à 650 nm du système indole–matrice préalablement photoionisé, $\beta(650) = 4.4$ dans l'éther alors que $\beta(650) = 20$ dans le mélange EG–W. Ceci démontre clairement que la profondeur des pièges influence directement l'énergie disponible au moment de la recombinaison: très peu de processus de recombinaison semble être suffisamment énergétique pour produire l'état S_1 dans l'EG–W. Le paramètre $\beta(\lambda)$ devrait également varier avec l'énergie de la lumière stimulatrice pour la même raison énergétique discutée plus haut. Enfin ce paramètre devrait être sensible à l'énergie des niveaux premier singulet des molécules de soluté considérées.

Dans le présent article, deux molécules de soluté sont étudiées dans la même matrice (éther) et à la même longueur d'onde de stimulation soit 600 nm. Seule la différence d'énergie entre le premier singulet de la DPA et celui du carbazole pourrait modifier le paramètre $\beta(\lambda)$ entre les deux systèmes. Le premier état singulet (bande 0–0) de la DPA dans l'éther se situe à environ 31 000 cm^{-1}, le maximum d'absorption se situe à 35 000 cm^{-1} mais aucune structure fine vibrationnelle n'est observée en absorption et en fluorescence. Par contre la bande 0–0 du carbazole se situe à 29 600 cm^{-1} dans un spectre bien structuré (14).

(b) Rendement en triplet de la DPA et du carbazole

Plusieurs auteurs ont publié les valeurs des constantes non-radiatives de l'état premier singulet de ces molécules piégées en matrices vitreuses (12, 15, 16). Ces constantes non-radiatives sont cependant assimilées aux constantes k_i (10) régissant l'intercombinaison S_1–T_1 ce qui revient à utiliser l'hypothèse qu'en matrice vitreuse la somme du rendement de fluorescence et du rendement en triplet est égale à l'unité. Bagdasaryan *et coll.* (17) ont mesuré le rendement triplet de ces molécules dans un verre d'éthanol à 77 °K par la méthode de Keller et Hadley (18), et on en conclu que la somme de $\phi_F + \phi_T$ n'est pas égale à l'unité. En effet pour le carbazole $\phi_T = 0.23 \pm 0.03$ alors que $\phi_F = 0.44$ (15, 16) et pour la DPA, $\phi_T = 0.47 \pm 0.09$ alors que $\phi_F = 0.12$ (15, 16). D'autre part, Sveshnikova et Snegov obtiennent pour le rendement en triplet de la DPA dans un verre d'alcool et d'éther à 90 °K mesuré par la méthode du transfert d'énergie triplet–triplet, une valeur de 0.87 ± 0.08 (19). Ce résultat confirmerait l'hypothèse des auteurs précédents (12, 15, 16).

Face à ces résultats expérimentaux il est intéressant de comparer ces valeurs de ϕ_T avec celles que l'on a obtenues théoriquement par la méthode de Siebrand (20) en assimilant l'atome d'azote à un atome de carbone. Un calcul identique a été décrit antérieurement (10). Le tableau 1 indique les valeurs des paramètres utilisées ainsi que le résultat final.

Il est remarquable de constater qu'un tel calcul approximatif nous fournisse une valeur de ϕ_T pour le carbazole identique à toute fin pratique à la valeur expérimentale mesurée de 0.23 (17). Le calcul devrait cependant être moins valable lorsqu'appliqué à la DPA qui est une molécule non planaire. Mais encore là le résultat de 0.85 est en accord avec celui obtenu par Sveshnikova *et coll.* (19) mais en désaccord avec celui de Bagdasaryan *et coll.* (17).

(c) Calcul du rapport des constantes de vitesse relatives au peuplement des états S_1 et T_1 (paramètre β).

Utilisant les valeurs publiées ou calculées des rendements quantiques en triplet des deux molécules considérées, la paramètre $\beta(600)$ est rapporté au tableau 2 et obtenu à l'aide de l'équation cinétique donnée à la partie (*a*) de ce chapitre. La première constatation est que le paramètre β est nettement inférieur à 3 et se rapproche de 2 pour les deux molécules considérées dans le cadre de l'utilisation des valeurs de ϕ_T calculées. Ce résultat est important en ce sens qu'il était généralement acquis que lors du piégeage dans une matrice solide à 77 °K la relaxation de spin avait le temps de se produire au moment de la recombinaison de façon à produire un rapport

TABLEAU 2. Valeurs du paramètre β pour une stimulation à 600 nm dans une matrice d'éther à 77 °K

	$(I_P/I_F)_{st}$	$(I_P/I_F)_N$	ϕ_T	β (600)
DPA	22.1 (±0.6)	5.9 (±0.3)	0.85	2.3 (±0.3)
	22.1 (±0.6)	5.9 (±0.3)	0.47*	1.3 (±0.1)
Carbazole	4.3 (±0.4)	0.44 (±0.04)	0.21	1.9 (±0.3)

*Valeur tirée de Bagdasaryan *et coll.* (17).

statistique états triplets/états singulets de 3:1 (22). Cette hypothèse avait été utilisée dans un article précédent dans lequel la valeur minimum de β (λ) avait été fixée à 3. Les valeurs supérieures à 3 étaient alors interprètées par des facteurs énergétiques impliquant la paire électron–cation au moment de la recombinaison (10). Une valeur minimum inférieure à 3 pour β(λ) pourrait être interprètée par une recombinaison très rapide, le spin de l'électron n'ayant pas le temps de se réorienter (23): si cela est possible en émission différée nous ne croyons pas en cette possibilité en émission stimulée. D'autre part depuis quelques années, il a été démontré que les vitesses de peuplement des trois sous-niveaux du triplet T_1 à partir du premier état singulet excité étaient variables (24). Toutefois cette différence de population est d'abord causée par la sélectivité du couplage spin–orbital entre les états S_1 et T_1. Il est donc difficile au stade actuel de nos connaissances d'expliquer théoriquement ce résultat expérimental.

La seconde constatation qui doit être faite à l'examen du tableau 2 est qu'il ne semble pas être plus difficile de peupler l'état singulet de la DPA que celui du carbazole au moment de la recombinaison électron–cation car β(DPA) $\lesssim$ β(carbazole) peu importe la valeur de ϕ_T utilisée. On doit donc en conclure que la faible différence d'énergie existant entre les états S_1 de la DPA et du carbazole soit environ 1400 cm^{-1} n'est pas un facteur d'empêchement de la recombinaison au niveau S_1 de la DPA lorsque la stimulation est effectuée à 600 nm dans un verre d'éther. La stimulation à 600 nm semble donc apporter aucune contrainte énergétique pour la recombinaison aux singulets de la DPA et du carbazole. Il est à noter que les deux constatations mentionnées ci-haut à partir des résultats du tableau 2 ne seraient aucunement modifiées, pour toutes valeurs de ϕ_T de la DPA comprises entre 0.4 et 0.9. Ces conclusions sont en fait indépendantes de l'incertitude qui existe sur la valeur absolue de ϕ_T.

Ces résultats peuvent difficilement être comparés à ceux obtenus sur l'indole et le tryptophane dans une matrice d'éther où β(650) = 4.4 (10). D'une part la longueur d'onde de stimulation n'est pas la même et d'autre part le premier état singulet de l'indole et du tryptophane dans l'éther se situe à 34 600 cm^{-1} soit 3600 et 5000 cm^{-1} plus élevé que les niveaux S_1 de la DPA et du carbazole. Il est cependant évident que ces deux derniers facteurs devraient contribuer à l'augmentation du paramètre β telle qu'observée. L'importance de chacun de ces deux facteurs énergétiques est actuellement à l'étude dans notre laboratoire.

Nous désirons remercier le Conseil national de recherches du Canada pour avoir subventionné ce travail. Nous remercions également M. Aurèle Blanchette pour l'assistance technique prodiguée au cours d'une partie de ce travail.

1. G. N. LEWIS et D. LIPKIN. J. Am. Chem. Soc. **64**, 2801 (1942).
2. H. LINSCHITZ, M. G. BERRY et D. SCHWEITZER. J. Am. Chem. Soc. **76**, 7833 (1954).
3. K. D. CADOGAN et A. C. ALBRECHT. J. Chem. Phys. **43**, 2550 (1965); J. Phys. Chem. **72**, 929 (1968).
4. M. EWALD, D. MULLER et G. DUROCHER. Spectrochim. Acta, **29**A, 1051 (1973).
5. A. MOUSNIER. Thèse de Doctorat (3è cycle). Université de Bordeaux, Bordeaux, France. 1973.
6. W. M. MCCLAIN et A. C. ALBRECHT. J. Chem. Phys. **43**, 465 (1965).
7. E. DOLAN et A. C. ALBRECHT. J. Chem. Phys. **37**, 1149 (1962).
8. YU. A. VLADIMIROV, D. I. ROSHCHUPKIN et E. E. FESENKO. Photochem. Photobiol. **11**, 227 (1970).
9. R. SANTUS, M. AUBAILLY et C. HELENE. C.R. Ac. Sci, **272**, 2008 (1971).
10. D. MULLER, M. EWALD et G. DUROCHER. Can. J. Chem. **52**, 407 (1974).
11. J. BLAIS et M. GAUTHIER. Chem. Phys. Lett. **16**, 68 (1972).
12. V. L. ERMOLAEV. Opt. Spectrom. **11**, 266 (1961).
13. T. SHIDA, S. IWATA et T. WATANABE. J. Phys. Chem. **76**, 3683 (1972).
14. A. BLANCHETTE et G. DUROCHER. Résultats non publiés.
15. J. E. ADAMS, W. W. MANTULIN et J. R. HUBER. J. Am. Chem. Soc. **95**, 5477 (1973).

16. E. C. LIM et M. KEDZIERSKI. Chem. Phys. Lett. **20**, 242 (1973).
17. KH. S. BAGDASARYAN, YU. I. KIRJUKHIN et Z. A. SINITSINA. J. Photochem. **1**, 225 (1972/73).
18. R. A. KELLER et S. G. HADLEY. J. Chem. Phys. **42**, 2382 (1965).
19. E. B. SVESHNIKOVA et M. I. SNEGOV. Opt. Spectrom. **29**, 265 (1970).
20. W. SIEBRAND. J. Chem. Phys. **47**, 2411 (1967); The triplet state. Cambridge University Press, 1967.
21. E. H. GILMORE, G. E. GIBSON et D. S. MCCLURE. J. Chem. Phys. **20**, 829 (1952); **23**, 399 (1955).
22. B. BROCKLEHURST. Nature, **221**, 921 (1969); B. BROCKLEHURST, G. PORTER et J. M. YATES. J. Phys. Chem. **68**, 203 (1964).
23. J. O. MAGEE. Comparative effects of radiation. *Edité par* M. Burton, J. S. Kirby Smith et J. L. Magee. J. Wiley and Son, 1960. p. 130.
24. M. SCHWOERER et H. SIXL. Chem. Phys. Lett. **2**, 14 (1968); M. S. ELSAYED, D. S. TINTI et D. V. OWENS. Chem. Phys. Lett. **3**, 339 (1969); M. S. DEGROOT, I. A. HESSELMANN, J. SCHMIDT et J. H. VANDERWAALS. Mol. Phys. **15**, 17 (1968).

The Crystal and Molecular Structure of a Nickel Complex of the Schiff Base, Bis(trifluoroacetylacetone)triethylenetetraamine[1]

MARY FRANCES RICHARDSON

Department of Chemistry, Brock University, St. Catharines, Ontario L2S 3A1

Received June 17, 1974

MARY FRANCES RICHARDSON. Can. J. Chem. **52**, 3716 (1974).

The Schiff base, bis(trifluoroacetylacetone)triethylenetetraamine (H_2L), forms a nickel complex with the composition $NiC_{16}F_6H_{22}N_4O_2$ (NiL). Crystals of NiL belong to the monoclinic space group $P2_1/c$ with $a = 10.040(2)$, $b = 15.077(7)$, $c = 13.943(7)$ Å, $\beta = 111.88(5)°$, $D_c = 1.610$ g/cc, $D_o = 1.61(2)$ g/cc, $Z = 4$. A total of 1686 independent reflections with $F^2 \geq 2\sigma(F^2)$, $2\theta \leq 42°$ were measured on a Picker 4-circle diffractometer by the θ–2θ scan technique with MoKα radiation. A full matrix least squares refinement of the structure yielded an unweighted R factor of 0.057. The structure confirms that condensation of triethylenetetraamine with trifluoroacetylacetone occurs through the acetyl group, not through the trifluoroacetyl group. The nickel atom is octahedrally coordinated by the four nitrogen and two oxygen atoms of the L^{2-} ligand. The triethylenetetraamine moiety has the α-configuration, so that the oxygen atoms occupy *cis* positions on the octahedron. Distortions in the octahedral geometry are due to the three contiguous five-membered rings in the complex; the average N—Ni—N angle is 81.1°. The trifluoroacetylacetone fragments are essentially planar, with an average O—Ni—N angle of 90.6°. These rings are folded about the O—N lines, the folding angles being 17.1 and 8.0° for the two rings. The average Ni—O, Ni—N (trigonal), and Ni—N-(tetrahedral) distances are 2.037, 2.044, and 2.128 Å, respectively.

MARY FRANCES RICHARDSON. Can. J. Chem. **52**, 3716 (1974).

La base de Schiff, bis(trifluoroacétylacétone)triéthylènetétramine (H_2L), forme un complexe avec le nickel de composition $NiC_{16}F_6H_{22}N_4O_2$ (NiL). Les cristaux NiL appartiennent au groupe d'espace monoclinique $P2_1/c$ avec $a = 10.040(2)$, $b = 15.077(7)$, $c = 13.943(7)$ Å, $\beta = 111.88(5)°$, $D_c = 1.610$ g/cc, $D_o = 1.61(2)$ g/cc, $Z = 4$. On a déterminé un total de 1686 réflexions indépendantes avec $F^2 \geq 2\sigma(F^2)$, $2\theta \leq 42°$ à l'aide d'un diffractomètre à quatre cercles Picker par la technique de balayage θ–2θ avec la radiation MoKα. La structure est affinée par la méthode des moindres carrés (matrice complète) et conduit à un facteur non-pondéré R de 0.057. La structure confirme que la condensation de la triéthylènetétramine avec la trifluoroacétylacétone se produit par l'intermédiaire du groupe acétyle et non par le groupe trifluoroacétyle. L'atome de nickel est coordonné d'une façon octaédrique par les quatre atomes d'azote et les deux atomes d'oxygène du ligand L^{2-}. La portion triéthylènetétramine a la configuration α ce qui amène les atomes d'oxygène à occuper les positions *cis* sur l'octaèdre. Les distorsions dans la géométrie octaédrique sont dus à la présence de trois cycles à cinq contigus dans le complexe; la valeur moyenne de l'angle N—Ni—N est de 81.1°. Les fragments trifluoroacétyleacétone sont à toute fin pratique planaires avec une valeur moyenne de l'angle O—Ni—N de 90.6°. Ces cycles sont pliés autour des liens O—N; les angles de plissement sont de 17.1° et de 8.0° pour les deux cycles. Les distances moyennes de Ni—O, Ni—N (trigonal) et Ni—N (tétraédrique) sont respectivement de 2.037, 2.044 et 2.128 Å.

[Traduit par le journal]

Introduction

Condensation of triethylenetetraamine (trien) with β-diketones yields a variety of linear and macrocyclic Schiff base ligands which readily coordinate to transition metal ions (1–3). The linear, potentially hexadentate ligand, bis(trifluoroacetylacetone)triethylenetetraamine (H_2L) forms three complexes with nickel: NiL, Ni(HL)Cl.$3H_2O$, and Ni(H_2L)Cl_2.$4H_2O$ (2). NiL is a brown paramagnetic complex, presumably octahedral, while the other two are orange and diamagnetic, and therefore probably square planar. Thus, the extent of ionization of the ligand affects the coordination about the nickel. Structure determinations of NiL and Ni(H_2L)Cl_2.$4H_2O$ were undertaken to determine the structural details of the complexes, and thus to evaluate the relative importance of steric *vs.* electronic factors in the coordination. The results for NiL are reported herein.

[1]Presented at the Summer Meeting of the American Crystallographic Association, Pennsylvania State University, August, 1974.

Can. J. Chem. Downloaded from www.nrcresearchpress.com by 210.87.254.6 on 09/05/12
For personal use only.

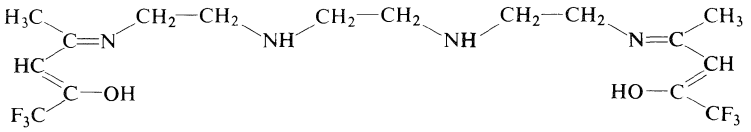

H_2L

Experimental

Data Collection

Crystals of NiL were prepared (2) and given to us by Dr. S. C. Cummings, Department of Chemistry, Wright State University, Dayton, Ohio. Cell dimensions were determined at 23 ± 3° from scans of the *h*00, 0*k*0, 00*l*, and *h*0*l* reflections, as well as by direct measurement of the angle between the a^* and c^* axes, on two crystals, one of which was aligned about b^* and the other about c^*. The scans were performed on a manual Picker 4-circle diffractometer out to $2\theta = 60°$ with MoKα_1 radiation ($\lambda = 0.70926$ Å) at a take-off angle of 1.5°. Standard deviations on the cell parameters were estimated in two ways: from the variance on each set of measurements for a given crystal and from the variance between the two crystals. The larger of these estimated standard deviations is given below for each cell dimension.

$NiC_{16}F_6H_{22}N_4O_2$ m.w. = 475.0

Monoclinic, $a = 10.040(2)$, $b = 15.077(7)$, $c = 13.943(7)$ Å, $\beta = 111.88(5)°$, $V = 1958.6$ Å^3, $D_m = 1.61(2)$ g/cc, $D_c = 1.61$ g/cc, $Z = 4$, space group $P2_1/c$, $\mu = 10.72$ cm^{-1} (MoKα radiation, $\lambda = 0.7107$ Å).

The data crystal was a slightly irregular column, 0.2 × 0.2 × 0.6 mm, parallel to the *a*, *b*, and *c* axes, respectively. It was mounted on a glass fiber with epoxy cement, and aligned about the c^* axis on the diffractometer. Data were collected with MoKα radiation at a take-off angle of 4.0°. The θ–2θ scan technique was used. The scan was made at a rate of 1°/min over a 2° range, from 1° below the calculated peak position to 1° above. Background was counted for 20 s at each end of the scan. Filters were inserted whenever the peak counting rate exceeded 40 000 c.p.s. A standard reflection was monitored every 2 h; it showed minor fluctuations, largely dependent on the temperature and humidity.

The intensities were corrected for background, for variation in the standard reflection, and for the extra filters inserted; Lorentz-polarization corrections were then applied to convert the net intensities, *I*, to structure factors. No absorption corrections were made. Standard deviations on the structure factors, $\sigma(F)$, were calculated by the procedure detailed in Stout and Jensen (4):

$$\sigma(F) = 0.5(\mathrm{Lp})^{-1/2}\left|\frac{N_T + N_B + (0.05N_P)^2}{N_T - N_B}\right|^{1/2}$$

where N_T, N_B, and N_P are the total counts, the background, and the net peak counts, respectively. A total of 2086 reflections were obtained with $2\theta \leq 42°$, of which 1686 had $I \geq 2\sigma(I)$ and were classified as observed. The unobserved reflections were assigned zero weights during the refinement, and were not included in the *R*-factor calculations.

Structure Determination and Refinement

The atomic scattering factors for neutral Ni, F, O, N, C, and H atoms were taken from the International tables for X-ray crystallography (5), as were the real and imaginary parts of the anomalous scattering of nickel. Major computer programs employed included local adaptations of Zalkin's FORDAP, Busing and Levy's ORFLS, and Busing, Martin, and Levy's ORFFE. In the least squares refinements, the function minimized was $\Sigma w\Delta^2$, where $w = 1/\sigma^2(F)$ and $\Delta = ||F_o| - |F_c||$. Unweighted and weighted residuals, R_1 and R_2, respectively, were calculated after each refinement:

$$R_1 = \Sigma\Delta/\Sigma|F_o|$$

$$R_2 = \Sigma w\Delta^2/\Sigma wF_o^2$$

A three dimensional unsharpened Patterson synthesis revealed the nickel atom positions. The structure solution then proceeded routinely. After the 29 atoms heavier than hydrogen had been located and refined isotropically ($R_1 = 0.109$, $R_2 = 0.146$), anisotropic thermal parameters were introduced for the nickel and fluorine atoms ($R_1 = 0.075$, $R_2 = 0.105$). The positions of all hydrogen atoms (except those on the methyl groups) were calculated by assuming $d_{N-H} = d_{C-H} = 1$ Å and the appropriate angles for trigonal and tetrahedral carbon and nitrogen atoms. These were introduced as fixed parameters, along with isotropic thermal parameters 1 Å^2 greater than the carbon or nitrogen atom to which the hydrogen was bonded ($R_1 = 0.060$, $R_2 = 0.082$). One more cycle of refining all 152 variables by full-matrix least squares yielded final values of R_1 and R_2 equal to 0.057 and 0.079, respectively. The average (parameter shift)/(sigma) was 0.4 on this cycle, and the refinement was regarded as complete. The goodness of fit, $(\Sigma w\Delta^2/(N_o - N_v))^{1/2}$, was 1.8, where N_o and N_v are the number of observations and the number of variables, respectively.

A weighting analysis was performed and showed no serious systematic dependence of $w\Delta^2$ on $\sin\theta$ or on *F*. A difference Fourier synthesis revealed no peaks higher than about 0.5 e/Å^3. A few of these peaks were located in the vicinities of the methyl carbon atoms C(1) and C(16), but were too ill-defined to warrant including them as hydrogen atoms.

The structure factor table is in the Depository of Unpublished Data.[2]

Results and Discussion

Tables 1 and 2 present the positional and

[2]Copies may be obtained at a nominal charge, upon request, from the Depository of Unpublished Data, National Science Library, National Research Council of Canada, Ottawa, Canada K1A 0S2.

Can. J. Chem. Downloaded from www.nrcresearchpress.com by 210.87.254.6 on 09/05/12
For personal use only.

Can. J. Chem. Downloaded from www.nrcresearchpress.com by 210.87.254.6 on 09/05/12
For personal use only.

TABLE 1. Atomic positional parameters and isotropic thermal parameters, with estimated standard deviations in parentheses

Atom	x	y	z	B (Å^2)
Ni	0.22208(10)	0.32461(6)	0.43532(6)	*
O(1)	0.0255(5)	0.2816(3)	0.4268(4)	3.84(10)
F(1)	−0.2181(6)	0.2031(5)	0.4518(5)	*
F(2)	−0.2354(6)	0.2307(6)	0.2994(5)	*
F(3)	−0.2062(6)	0.1009(4)	0.3537(6)	*
C(1)	−0.1645(10)	0.1834(6)	0.3813(7)	5.13(20)
C(2)	−0.0049(8)	0.1993(5)	0.4186(5)	3.22(14)
C(3)	0.0827(8)	0.1274(5)	0.4382(6)	3.79(16)
C(4)	0.2384(8)	0.1293(5)	0.4766(5)	3.39(15)
C(5)	0.3122(10)	0.0387(6)	0.5045(7)	5.15(20)
N(1)	0.3074(6)	0.2022(4)	0.4864(4)	3.18(12)
C(6)	0.4665(10)	0.1994(6)	0.5257(7)	5.07(19)
C(7)	0.5265(10)	0.2913(7)	0.5263(7)	5.50(20)
N(2)	0.4341(7)	0.3410(5)	0.4360(5)	4.83(15)
C(8)	0.4338(11)	0.3051(7)	0.3356(7)	5.76(22)
C(9)	0.2983(12)	0.3300(7)	0.2517(8)	6.25(23)
N(3)	0.1729(7)	0.3006(4)	0.2761(5)	4.36(14)
C(10)	0.0418(10)	0.3513(7)	0.2229(7)	5.38(21)
C(11)	0.0528(10)	0.4455(6)	0.2653(6)	4.90(19)
N(4)	0.1316(6)	0.4443(4)	0.3794(4)	3.50(12)
C(12)	0.0675(9)	0.6043(6)	0.3797(6)	4.56(18)
C(13)	0.1383(8)	0.5170(5)	0.4302(5)	3.38(15)
C(14)	0.2143(8)	0.5206(5)	0.5416(6)	3.84(16)
C(15)	0.2749(8)	0.4513(5)	0.6024(5)	3.18(14)
C(16)	0.3529(10)	0.4693(6)	0.7173(7)	4.82(18)
O(2)	0.2830(5)	0.3695(3)	0.5832(4)	3.64(10)
F(4)	0.3072(7)	0.4148(4)	0.7750(3)	*
F(5)	0.3364(7)	0.5497(4)	0.7496(4)	*
F(6)	0.4896(6)	0.4547(6)	0.7488(5)	*

*Atom refined with anisotropic thermal parameters.

TABLE 2. Anisotropic thermal parameters (×10^4) and estimated standard deviations*

Atom	β_{11}	β_{22}	β_{33}	β_{12}	β_{13}	β_{23}
Ni	94.9(1.4)	34.4(0.6)	40.9(0.7)	−0.4(0.6)	23.6(0.7)	−0.9(0.4)
F(1)	154(9)	152(6)	141(6)	−13(6)	101(6)	−51(5)
F(2)	116(8)	153(7)	146(6)	−19(6)	−2(6)	43(5)
F(3)	164(9)	79(4)	222(7)	−53(5)	97(7)	−54(5)
F(4)	359(13)	71(4)	52(3)	−14(6)	50(5)	−2(3)
F(5)	339(13)	55(3)	70(4)	−8(5)	30(5)	−26(3)
F(6)	142(9)	185(7)	103(5)	27(6)	−28(5)	−60(5)

*The expression for the anisotropic temperature factor is $T_i = \exp(-\beta_{11}h^2 - \beta_{22}k^2 - \beta_{33}l^2 - \beta_{12}hk - \beta_{13}hl - \beta_{23}kl)$.

thermal parameters, and the standard deviations estimated in the course of the least squares refinement, of all atoms heavier than hydrogen. Table 3 lists the calculated hydrogen atom positions. A view of the NiL molecule is shown in Fig. 1. The bond distances and angles in Tables 4 and 5 are arranged in pairs which are related by an approximate C_2 axis which passes through the nickel atom and the midpoint of the C(8)—C(9) bond. The sizes and orientations of the anisotropic thermal ellipsoids are listed in Table 6. The standard deviations quoted in Tables 4–7 are estimates obtained from the variances of the individual parameters.

The Coordination of Nickel

There are four possible geometrical isomers[3] for the octahedral coordination of a linear hexa-

[3]These four refer only to the relative placement of the ligand atoms. The actual number of isomers is larger because the N(2)—N(3) ring can exist in two principal conformations: a *gauche* form in which the H(N2) and H(N3) atoms are on opposite sides of the N(2)—Ni—N(3) plane, and an envelope form in which the two hydrogen atoms are on the same side of this plane.

Can. J. Chem. Downloaded from www.nrcresearchpress.com by 210.87.254.6 on 09/05/12
For personal use only.

TABLE 3. Calculated positions of the hydrogen atoms

Atom	x	y	z
H(C6A)	0.507	0.175	0.596
H(C6B)	0.497	0.062	0.477
H(C7A)	0.527	0.323	0.589
H(C7B)	0.623	0.289	0.487
H(N2)	0.470	0.405	0.443
H(C8A)	0.438	0.236	0.340
H(C8B)	0.521	0.324	0.314
H(C9A)	0.301	0.398	0.248
H(C9B)	0.299	0.306	0.185
H(N3)	0.152	0.236	0.252
H(C10A)	−0.046	0.322	0.230
H(C10B)	0.021	0.357	0.146
H(C11A)	−0.051	0.470	0.250
H(C11B)	0.098	0.486	0.230
H(C3)	0.038	0.067	0.423
H(C14)	0.219	0.580	0.576

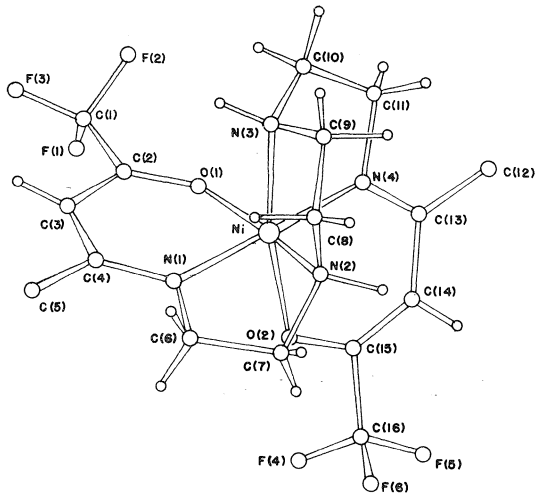

FIG. 1. View of the NiL molecule. The hydrogen atoms are shown but labels have been omitted for clarity.

dentate ligand such as L^{2-}. These are depicted in Fig. 2; the nomenclature is based on the configuration of the trien moiety (6). While the β-configuration of trien is strongly favored in octahedral complexes (7), this configuration is unable to accommodate the trigonal nitrogen atoms N(1) and N(4), and the associated planar trifluoroacetylacetonate residues in the hexadentate L^{2-} ligand. Molecular models suggest that the *cis*-α_1 isomer with a *gauche* N(2)—N(3) ring is the most nearly strain-free isomer, and it is the one actually found in the structure of NiL (Fig. 1). The *cis*-α_1 isomer has also been found in bis-salicylidenetriethylenetetraamine nickel (8).

The nickel atom is coordinated to the four

TABLE 4. Bond distances in NiL (e.s.d.'s in parentheses)

Bond	d (Å)	Bond	d (Å)
Ni—O(1)	2.038(6)	Ni—O(2)	2.036(5)
Ni—N(1)	2.048(6)	Ni—N(4)	2.040(6)
Ni—N(2)	2.139(8)	Ni—N(3)	2.118(7)
F(1)—C(1)	1.319(14)	F(4)—C(16)	1.345(12)
F(2)—C(1)	1.309(11)	F(5)—C(16)	1.325(11)
F(3)—C(1)	1.323(11)	F(6)—C(16)	1.295(11)
C(1)—C(2)	1.508(12)	C(15)—C(16)	1.523(11)
C(2)—O(1)	1.273(9)	C(15)—O(2)	1.271(9)
C(2)—C(3)	1.358(11)	C(14)—C(15)	1.340(10)
C(3)—C(4)	1.452(11)	C(13)—C(14)	1.454(9)
C(4)—C(5)	1.533(12)	C(12)—C(13)	1.536(11)
C(4)—N(1)	1.279(10)	C(13)—N(4)	1.293(10)
N(1)—C(6)	1.484(11)	N(4)—C(11)	1.490(10)
C(6)—C(7)	1.510(14)	C(10)—C(11)	1.526(14)
C(7)—N(2)	1.462(10)	C(10)—N(3)	1.463(11)
N(2)—C(8)	1.500(13)	C(9)—N(3)	1.489(15)
C(8)—C(9)	1.474(13)		

nitrogen and two oxygen atoms of the L^{2-} ligand. The average Ni—O, Ni—N(trigonal), and N—N(tetrahedral) distances are 2.037, 2.044, and 2.128 Å, respectively. These values compare favorably with distances found in other octahedral nickel complexes; *e.g.* Ni—O = 2.018 Å in nickel acetylacetonate dihydrate (9), and Ni—N = 2.124 Å in $Ni(en)_3SO_4$ (10). The difference in the Ni—N(trigonal) and Ni—N (tetrahedral) distances is at least partly due to the smaller radius of sp^2-hybridized nitrogen as compared to sp^3.

The coordination polyhedron is a slightly distorted octahedron whose dimensions are given in Table 7. The deviations from idealized octahedral geometry are due to the presence of three five-membered rings in the complex. The average N—Ni—N angle in these rings is 81.1°, close to the value of 82.1° found in $Ni(en)_3SO_4$ (10). In the six-membered rings, the average angle at the nickel atom is 90.6°, much closer to the idealized value of 90°. Of the three octahedral axes, only one, the N(1)—Ni—N(4) axis, is close to 180° (177.8°). The O(1)—Ni—N(2) and O(2)—Ni—N(3) angles of 167.7 and 169.5° reflect the constraints imposed by the five-membered rings.

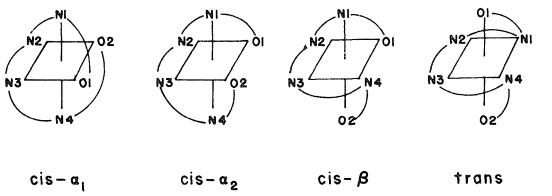

FIG. 2. Possible isomers for octahedral coordination of a linear hexadentate ligand.

Can. J. Chem. Downloaded from www.nrcresearchpress.com by 210.87.254.6 on 09/05/12
For personal use only.

TABLE 5. Bond angles in NiL (e.s.d.'s in parentheses)

Bonds	Angle	Bonds	Angle
F(1)—C(1)—F(2)	106.7(8)	F(4)—C(16)—F(5)	104.0(8)
F(1)—C(1)—F(3)	104.8(9)	F(4)—C(16)—F(6)	104.4(7)
F(2)—C(1)—F(3)	104.4(7)	F(5)—C(16)—F(6)	106.9(8)
F(1)—C(1)—C(2)	112.6(7)	F(4)—C(16)—C(15)	111.4(7)
F(2)—C(1)—C(2)	112.1(9)	F(5)—C(16)—C(15)	116.1(7)
F(3)—C(1)—C(2)	115.5(8)	F(6)—C(16)—C(15)	113.0(9)
C(1)—C(2)—O(1)	112.0(7)	C(16)—C(15)—O(2)	110.3(6)
C(1)—C(2)—C(3)	117.9(7)	C(14)—C(15)—C(16)	117.4(7)
C(3)—C(2)—O(1)	130.1(7)	C(14)—C(15)—O(2)	132.3(6)
C(2)—C(3)—C(4)	125.9(7)	C(13)—C(14)—C(15)	125.5(7)
C(3)—C(4)—C(5)	115.3(7)	C(12)—C(13)—C(14)	115.2(7)
C(5)—C(4)—N(1)	123.1(7)	C(12)—C(13)—N(4)	123.7(6)
C(3)—C(4)—N(1)	121.5(7)	C(14)—C(13)—N(4)	121.1(7)
C(4)—N(1)—C(6)	118.7(6)	C(13)—N(4)—C(11)	118.2(6)
Ni—N(1)—C(4)	126.7(5)	Ni—N(4)—C(13)	128.0(4)
Ni—N(1)—C(6)	114.0(5)	Ni—N(4)—C(11)	113.7(5)
N(1)—C(6)—C(7)	110.4(7)	N(4)—C(11)—C(10)	109.6(7)
C(6)—C(7)—N(2)	110.0(7)	C(11)—C(10)—N(3)	111.6(7)
C(7)—N(2)—C(8)	113.5(7)	C(9)—N(3)—C(10)	114.0(7)
Ni—N(2)—C(7)	104.8(6)	Ni—N(3)—C(10)	104.9(6)
Ni—N(2)—C(8)	107.4(5)	Ni—N(3)—C(9)	107.6(5)
N(2)—C(8)—C(9)	109.2(9)	N(3)—C(9)—C(8)	110.6(9)
Ni—O(1)—C(2)	120.7(5)	Ni—O(2)—C(15)	121.1(4)

TABLE 6. Sizes and orientations of the thermal ellipsoids*

Atom	R	$\overline{U}_R$	θ_x	θ_y	θ_z
Ni	1	0.185(2)	103(4)	81(5)	13(5)
	2	0.199(2)	96(12)	170(5)	80(4)
	3	0.205(2)	14(7)	94(13)	98(5)
F(1)	1	0.190(18)	22(4)	101(3)	130(3)
	2	0.313(7)	112(4)	118(2)	127(3)
	3	0.453(7)	90(2)	30(2)	118(2)
F(2)	1	0.215(7)	33(2)	88(2)	79(3)
	2	0.336(11)	67(3)	50(3)	139(3)
	3	0.450(8)	111(2)	40(3)	51(3)
F(3)	1	0.208(11)	42(5)	53(4)	91(3)
	2	0.297(12)	48(5)	133(4)	121(2)
	3	0.460(7)	91(2)	114(2)	31(2)
F(4)	1	0.205(8)	97(2)	90(4)	14(2)
	2	0.284(8)	97(3)	173(3)	87(4)
	3	0.409(8)	10(2)	97(3)	105(2)
F(5)	1	0.189(10)	90(2)	47(3)	47(3)
	2	0.295(6)	86(3)	137(3)	53(3)
	3	0.409(9)	4(3)	87(3)	115(2)
F(6)	1	0.197(8)	54(3)	83(2)	59(2)
	2	0.319(12)	44(3)	122(2)	133(3)
	3	0.511(8)	68(2)	33(2)	121(2)

*Principal axes R of the anisotropic temperature factors. The root-mean-square displacements ($\overline{U}_R$) along the principal axes are given in Å. θ_x, θ_y, and θ_z are the direction axes (in degrees) with respect to the crystallographic a, b, and c axes.

It should be noted that, while the bond parameters related by the approximate C_2 axis are usually equal within a standard deviation, this is not the case for the N(1)—N(2) and N(3)—N(4) bites and the N(1)—Ni—N(2) and N(3)—Ni—N(4) angles, where the differences are on the order of six standard deviations. The only structural feature which might be related to this is the extent of folding of the six-membered rings (*vide infra*); the O(1)—N(1) ring has a more

TABLE 7. Dimensions of the coordination polyhedron of nickel

Bond	Distance (Å)	Bonds	Angle (deg)
O(1)—N(1)	2.895(8)	O(1)—Ni—N(1)	90.2(2)
N(1)—N(2)	2.675(10)	N(1)—Ni—N(2)	79.4(3)
N(2)—N(3)	2.804(8)	N(2)—Ni—N(3)	82.4(3)
N(3)—N(4)	2.718(10)	N(3)—Ni—N(4)	81.6(2)
N(4)—O(2)	2.905(7)	N(4)—Ni—O(2)	90.9(2)
O(1)—O(2)	2.999(6)	O(1)—Ni—O(2)	94.8(2)
O(1)—N(4)	2.848(9)	O(1)—Ni—N(4)	88.6(2)
O(1)—N(3)	3.001(10)	O(1)—Ni—N(3)	92.4(2)
N(1)—N(3)	3.110(8)	N(1)—Ni—N(3)	96.6(2)
N(1)—O(2)	2.914(8)	N(1)—Ni—O(2)	91.1(2)
N(2)—N(4)	3.238(10)	N(2)—Ni—N(4)	101.5(3)
N(2)—O(2)	3.003(10)	N(2)—Ni—O(2)	92.0(2)
		O(1)—Ni—N(2)	167.7(2)
		O(2)—Ni—N(3)	169.5(3)
		N(1)—Ni—N(4)	177.8(2)

TABLE 8. Coefficients of the best planes ($\times 10^4$) through selected sets of atoms*

Plane	Atoms in plane	*A*	*B*	*C*	*D*	Deviation of Ni (Å)	Average deviation (Å)
I	Ni, O(1), N(1), N(2), N(4)	981	−3217	−9417	−68187	0.06	0.05
II	Ni, O(1), N(2), N(3), O(2)	−2024	9402	−2741	30470	0.02	0.14
III	Ni, N(1), N(3), N(4), O(2)	−9460	−3224	−329	−17757	0.04	0.07
IV	O(1), C(1)–C(5), N(1)	3197	−444	−9465	−59689	0.41	0.04
V	O(2), C(12)–C(16), N(4)	9690	2119	−1268	1062	0.18	0.04

The equation of the plane has the form $AX + BY + CZ = D$, where X, Y, and Z are orthogonal coordinates (in Å) of the atoms in a system where the x, y, and z axes are parallel to the a, b, and c axes of the unit cell, respectively.

pronounced fold about the O—N line than the O(2)—N(4) ring.

The ligand bites are normal, with an average of 2.73 Å for the N—N distances in the five-membered rings and 2.90 Å for the N—O distances in the six-membered rings. The polyhedron edges which are not contained in a chelate ring are generally somewhat longer than those which are.

Unweighted least squares planes (Table 8) were calculated for the three ligand belts: Ni—O(1)—N(1)—N(2)—N(4), Ni—O(1)—N(3)—N(2)—O(2), and Ni—O(2)—N(1)—N(3)—N(4). There is a small, but significant, ruffling of the planes, with the ligand atoms alternating above and below the planes.

The L^{2-} Ligand

Condensation of triethylenetetraamine with trifluoroacetylacetone is expected to occur through the acetyl group rather than through the trifluoroacetyl group. The present structure confirms that this is indeed the case.

In general, the bond distances and angles in the L^{2-} ligand are similar to those quoted for bis(acetylacetone)ethylenediamine Schiff base complexes (11). The CF_3 groups introduce only small perturbations in the bond distances in the rest of the ligand. The average C—F distance is 1.32 Å, and the CF_3 groups have fairly well-defined geometries. The thermal parameters of these groups suggest that they are librating about the C(1)—C(2) and C(15)—C(16) bonds (Table 6).

The N(2) and N(3) atoms in the ligand are tetrahedral. The N(1) and N(4) atoms are trigonally hybridized, with the nickel atom nearly lying in the planes defined by the C(4)—N(1)—C(6) and C(11)—N(4)—C(13) fragments. (The distances of the nickel atom from these planes are 0.25(3) and 0.06(3) Å, respectively.) The acetylacetoniminate rings (not including the nickel atom) are almost planar (planes IV and V, Table 8). These rings are folded about their O—N bites, the O(1)—N(1) ring making an angle of 17.1° with the Ni—O(1)—N(1) plane and the O(2)—N(4) ring making an angle of 8.0° with the Ni—O(2)—N(4) plane. Such folding is common, and apparently occurs in order to optimize the molecular packing or to relieve steric strain within the molecule. The direction of folding is

Can. J. Chem. Downloaded from www.nrcresearchpress.com by 210.87.254.6 on 09/05/12
For personal use only.

toward the N(3) atom for the O(1)—N(1) ring, and towards the N(2) atom for the O(2)—N(4) ring.

The conformations of the ethylenediamine-like rings are most readily described in terms of the distances of the carbon atoms from the N—Ni—N planes. The central N(2)—N(3) ring has a symmetrical *gauche* form, which is the most stable form for an isolated ethylenediamine chelate ring (12). The C(8) atom is 0.34 Å above the N(2)—Ni—N(3) plane while C(9) is 0.34 Å below it. The other two rings are so distorted from the *gauche* conformation that they are best described as having the envelope form. The C(6) and C(7) atoms both lie below the N(1)—Ni—N(2) plane (0.41 and 0.84 Å, respectively), while C(10) and C(11) both lie above the N(3)—Ni—N(4) plane (0.76 and 0.31 Å, respectively). The ring conformations can also be described by the intersection angles of the N—C—C planes in each ring (13): these angles are 37.1(11), 54.5(10), and 37.9(11)° in the N(1)—N(2), N(2)—N(3), and N(3)—N(4) rings, respectively. Thus, the overall configuration of the trien fragment is similar to that found in α- and *trans*-coordinated trien ligands (3, 6, 8, 14), but differs from that observed for β-trien complexes (15).

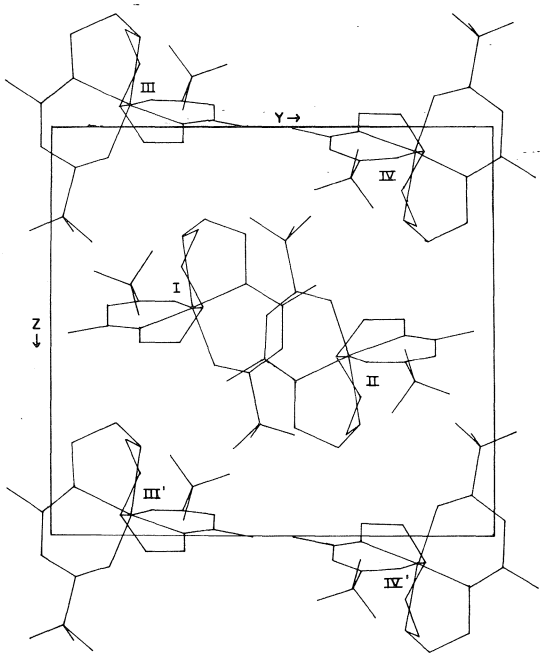

FIG. 3. Molecular packing in the NiL crystal. The three molecules on the right are part of a layer at $x \approx 0.78$; the three on the left are part of a layer at $x \approx 0.22$.

Molecular Packing

The packing of the NiL molecules within the unit cell is shown in Fig. 3. Molecule I is the molecule shown (slightly rotated) in Fig. 1. Molecules II, III, and IV are related to Molecule I by the inversion center at (1/2, 1/2, 1/2), the *c*-glide plane intersecting the *y* axis at 1/4, and the screw axis parallel to *y*, respectively. The primes denote translation by one unit along the *z* axis. The shortest intermolecular contacts are not much less than the sum of the van der Waals radii of the corresponding atoms. The hydrogen atoms on N(2) and N(3) do not seem to be involved in hydrogen bonding to any other atoms in the structure; the N(2) and N(3) atoms make no intermolecular contacts shorter than 3.5 Å.

The author is grateful to the National Research Council of Canada and to the J. P. Bickell Foundation for the financial support of this research. She also acknowledges the competent assistance of Mr. Kenneth Franklin during the data collection.

1. S. C. CUMMINGS and R. E. SIEVERS. Inorg. Chem. **11**, 1483 (1972).
2. J. G. MARTIN, R. M. C. WEI, and S. C. CUMMINGS. Inorg. Chem. **11**, 475 (1972).
3. M. F. RICHARDSON and R. E. SIEVERS. J. Am. Chem. Soc. **94**, 4134 (1972).
4. G. H. STOUT and L. H. JENSEN. X-ray structure determination. A practical guide. Macmillan Company, New York. 1968. pp. 454–458.
5. International tables for X-ray crystallography. Vol. III. The Kynoch Press, Birmingham. 1968. p. 201, Table 3.3.1 A, and p. 215, Table 3.3.2 C.
6. M. DWYER and I. E. MAXWELL. Inorg. Chem. **9**, 1459 (1970).
7. B. BOSNICH, R. D. GILLARD, E. D. MCKENZIE, and G. A. WEBB. J. Chem. Soc. A, 1331 (1966).
8. P. D. CRADWICK, M. E. CRADWICK, G. G. DODSON, D. HALL, and T. N. WATERS. Acta Crystallogr. B**28**, 45 (1972).
9. H. MONTGOMERY and E. C. LINGAFELTER. Acta Crystallogr. **17**, 1481 (1964).
10. MAZHAR-UL-HAQUE, C. N. CAUGHLAN, and K. EMERSON. Inorg. Chem. **9**, 2421 (1970).
11. M. CALLIGARIS, G. NARDIN, and L. RANDACCIO. Coord. Chem. Rev. **7**, 385 (1972).
12. E. J. COREY and J. C. BAILAR, JR. J. Am. Chem. Soc. **81**, 2620 (1959).
13. K. N. RAYMOND, P. W. R. CORFIELD, and J. A. IBERS. Inorg. Chem. **7**, 843 (1968).
14. G. MARONGIU, E. C. LINGAFELTER, and P. PAOLETTI. Inorg. Chem. **8**, 2763 (1969).
15. D. A. BUCKINGHAM, I. E. MAXWELL, A. M. SARGESON, and H. C. FREEMAN. Inorg. Chem. **9**, 1921 (1970).

Can. J. Chem. Downloaded from www.nrcresearchpress.com by 210.87.254.6 on 09/05/12
For personal use only.

Laser Spectrofluorimetry of Chlorophylls

ROGER M. LEBLANC, GENEVIÈVE GALINIER, ALAIN TESSIER, AND LISE LEMIEUX

Groupe de Recherche en Biophysique, Département de Chimie-Biologie, Université du Québec, Trois-Rivières, Québec G9A 5H7

Received June 11, 1974

ROGER M. LEBLANC, GENEVIÈVE GALINIER, ALAIN TESSIER, and LISE LEMIEUX. Can. J. Chem. **52**, 3723 (1974).

A device has been set up to determine quantitatively the weak fluorescence intensities of pigment molecules. It consists of a laser spectrofluorimeter. The excitation beam can be produced with either a He/Cd laser (441.6 nm) or a He/Ne laser (632.8 nm). This system allows us to detect the fluorescence of dilute chlorophyll *a* or *b* solutions of the order of 10^{-12} mol/l. This sensitivity also permits the study of the emission spectra from chlorophyll in monomolecular or solid states, and since a polarization rotator has been incorporated into our apparatus, one may presume some possible orientation of the molecules.

ROGER M. LEBLANC, GENEVIÈVE GALINIER, ALAIN TESSIER et LISE LEMIEUX. Can. J. Chem. **52**, 3723 (1974).

On a mis au point un appareil pour déterminer quantitativement les faibles intensités de fluorescence des molécules de pigments. Il s'agit d'un spectrofluorimètre à laser. Le faisceau excitant peut être produit soit par un laser He/Cd (441.6 nm) soit par un laser He/Ne (632.8 nm). Ce système nous permet de déceler la fluorescence de solutions diluées de chlorophylle *a* ou *b* de l'ordre de 10^{-12} mol/l. Cette sensibilité permet aussi d'étudier les spectres d'émission de la chlorophylle à l'état monomoléculaire ou à l'état solide: on peut prévoir certaines orientations possibles des molécules à l'aide du rotateur de polarisation incorporé à notre appareil.

[Traduit par le journal]

Introduction

All biological membranes, animal and vegetal, are built on the same model. However, the second possesses the extraordinary power of transforming electromagnetic energy into chemical energy. This transformation in green plants is due to the presence of various pigments such as chlorophylls and carotenoïds. The steps of this mechanism are still obscure on certain points. Several models such as micells (1), B.L.M. (2, 3), and monolayers (4, 5) are proposed to simulate the membrane layer structure.

In our laboratory, we study the fluorescence of pigments in the monomolecular state to get an insight about the primary processes in photosynthesis. In this state, pure chlorophyll *a* monolayer shows very weak fluorescence due to the self-quenching effect. To study this fluorescence, we must deal with very low fluorescence intensities. In solution, this phenomenon exists for chlorophyll *a* concentrations higher than 10^{-6} mol/l.

Since available apparatus on the market is insufficiently sensitive, our group constructed a laser spectrofluorimeter capable of detecting very weak fluorescence signals.

To increase spectrophotometer sensitivity, many research workers have used expensive devices of detection: lock-in amplifier, photon counting, computer, etc., while still using conventional excitation sources such as tungsten, xenon, and mercury lamps.

These systems have several advantages, but we already know (6) that it is possible to increase the fluorescence intensity by an order of two using an appropriate continuous gas laser as the excitation source while retaining conventional detection devices. Since it is not difficult to get commercial lasers with variable frequencies, the objections to their high specificity are no longer true.

Recently, Aoshima *et al.* (7) have described a system for measuring the fluorescence of chlorophyll monolayers using the photon counting technique. Measurements of fluorescence intensities of chlorophyll in pure and mixed monolayers, solid films, and solution, have been taken with a laser spectrofluorimeter built in our laboratory.

By using Currie's criteria (8) to determine detection limits and the method of Shcherbov *et al.* (9) for estimating our sensitivity, we obtained a sensitivity as high as Aoshima, even by setting a monochromator at the emission.

Can. J. Chem. Downloaded from www.nrcresearchpress.com by 210.87.254.5 on 09/05/12
For personal use only.

Can. J. Chem. Downloaded from www.nrcresearchpress.com by 210.87.254.5 on 09/05/12
For personal use only.

Furthermore, we kept the advantages of using a laser as an excitation source and the possibility of changing the incident beam angle in regard to the molecules in the monomolecular state.

Experimental Methods

Chemical Products

Chlorophyll *a*, free of chlorophyll *b*; and chlorophyll *b*, free of chlorophyll *a* were obtained from the Sigma Chemical Company, St. Louis, Mo. These products were stored at 0 °C in the dark. Arachidic acid, 99 + % pure, was purchased from Eastman Organic Chemical Company, New York. Cadmium chloride, a Baker Analysed reagent, was supplied by Baker Chemical Company, New Jersey. The diethyl ether, ANALAR, was obtained from the British Drug House, Montreal.

Equipment

He/Cd laser, Spectra Physics, $\lambda = 441.6$ nm, 75 mW; He/Ne laser, Spectra Physics, $\lambda = 632.8$ nm, 5 mW; aluminum coated surface mirrors, Ealing Company; monochromator, Jarrell–Ash 82–410, focal length 0.25 m, *f*/3.5, resolution 0.3 nm, slit 1.0 mm; cut off filter, Corning Type RG 645; photomultiplier, EMI 9558 QB; power supply, Velonex Nimpac 105, stability 200 mV ± 0.003%, range 0 to 3000 V; nanoammeter, Gencom, model 911; recorder, Yew No. 3043; polarization rotator, Spectra Physics No. 310–21, λ from 400 to 700 nm, accuracy of rotation 0.2°.

Langmuir Method

To simulate the pigment monomolecular state in the chloroplast, we have worked out a technique from Langmuir *et al.* (10) allowing us to get a pure or mixed chlorophyll *a* monolayer. Our adapted apparatus is a temperature controllable trough (35.0 cm × 14.9 cm × 5.0 cm) cemented together with a water or solvent nonsoluble cement; an horizontal mica float (13.0 cm × 0.7 cm × 0.0012 cm); gold foil (0.00024 cm) which attaches the float to the lateral walls of the trough. A stainless steel wire, 10 cm above the surface goes through a very light aluminum piece, this being attached to the mica float by means of two nylon threads. A graduated circular scale is attached to the torsion wire to determine the degree of rotation of the wire.

By exerting a certain pressure on the molecules spread at the air/water interface, this force is transmitted to the mica float and then to the torsion wire by the means of the aluminum balance. A glass barrier, covered with Teflon tape, moves on the lateral walls of the trough along a graduated scale compressing the molecules.

Before deposition of the pigments on quartz slides, the balance is calibrated and the pressure area curves have been studied. The results are compared to the literature and found to be identical to those results obtained by Gaines *et al.* (11, 12). A meticulous cleaning of the aqueous subphase surface and instruments is necessary before each run if one wants to obtain reproducible data.

Under a given surface pressure, specific for each type of compound, we immerse the quartz slide. During deposition, the surface pressure is kept constant by manually controlling barrier displacement. An electric motor with a speed of one revolution per three minutes guarantees the uniform movement of the slide. Very often, pigment molecules are deposited on slides already covered by a lipidic base, usually consisting of cadmium arachidate multilayers. It has two roles: to be the salt of a cell fatty acid and to get a uniform slide surface at a molecular level. This technique of depositing the fatty acid is one developed by Blodgett–Langmuir (13).

Laser Spectrofluorimeter Device

A block diagram of the apparatus and components is shown in Fig. 1.

An excitation source of coherent light from a He/Cd laser or from a He/Ne laser emits a polarized beam (99.9%) directly on the sample. The pigment solution is placed on a quartz slide or in a quartz cell which is situated in a closed dark box on a circular disk. This disk allows the orientation angle of the sample to change in respect to the incident beam. Furthermore, the slide support may be moved laterally to prevent the intense light emitted by the laser from radiating through the same point of monolayer. Behind the slide, the laser beam hits a front surface mirror and is reflected through the sample again to hit a second front surface mirror almost parallel to the first.

In this manner, the light is reflected a dozen times through the slide. However, the number of passages can be changed easily. The sample's fluorescence is focused by a converging lens, focal length 3.5 cm, which gathers the beam from a diaphragm (0.9 cm × 0.6 cm). The diaphragm cuts out most of the stray light. The light converges onto a monochromator slit fixed to the dark box, a sharp cut off filter eliminates the light at wavelength shorter than 645 nm. A photomultiplier, joined to the monochromator, is cooled with dry ice. A stable power supply provides the photomultiplier voltage. A nanoammeter and a recorder complete the system.

A broad band polarization rotator may be mounted directly to one laser or to the other.

Results and Discussion

A comparative study of the sensitivity of our device was done.

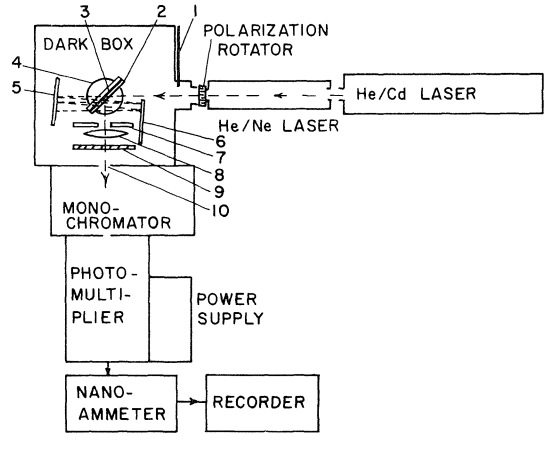

FIG. 1. Block diagram of the laser spectrofluorimeter: 1, obturator; 2, slide support; 3, quartz slide; 4, rotative disk; 5, 6, front surface mirrors; 7, diaphragm; 8, convergent lens; 9, filter; 10, slit.

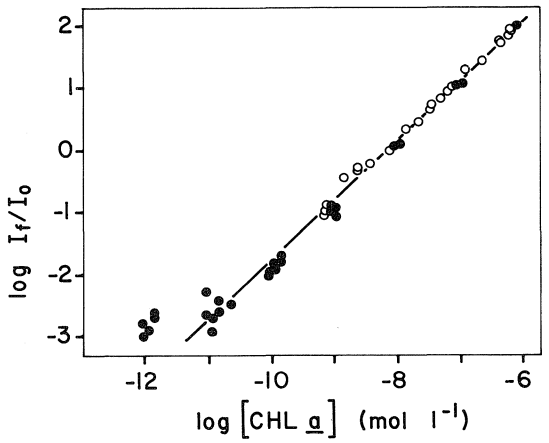

Fig. 2. Relative fluorescence intensity of pigment solutions as a function of chlorophyll *a* concentration; spectrofluorimeters: ○, Perkin–Elmer MPF-2A; ●, He/Cd laser; $\lambda_{exct.} = 441.6$ nm.

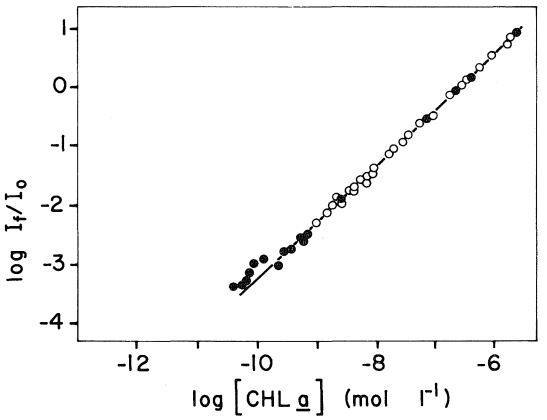

FIG. 3. Relative fluorescence intensity of pigment solutions as a function of chlorophyll *a* concentration; spectrofluorimeters: ○, Perkin–Elmer MPF-2A; ●, He/Ne laser; $\lambda_{exct.} = 632.8$ nm.

Figure 2 shows the results we obtained for the relative fluorescence intensity of a chlorophyll *a* solution (I_f) when the concentration varies from 10^{-13} to 10^{-6} mol/l. The reference (I_0) was a solution of chlorophyll *b*, 1.6×10^{-8} mol/l. We can see that there is a linear relationship between the relative intensity of emitted light and the pigment concentration. At concentration less than 10^{-8} mol/l, the laser spectrofluorimeter is the only equipment capable of reliable data. For very weak concentrations, lower than 10^{-12} mol/l, qualitative determinations are still possible. The difficulty in obtaining quantitative results at these concentrations arises from stray light.

Figure 3 represents the same phenomenon when the He/Ne laser is used as the excitation beam. In this case, too, our spectrofluorimeter remains the most sensitive for weak pigment concentrations.

Results about monomolecular chlorophyll *a* fluorescence spectrum appear in Fig. 4 for both systems. We noted that at wavelength higher than 680 nm, the response of a Perkin–Elmer spectrofluorimeter is less accurate than ours. This means that the laser spectrofluorimeter has a better detecting device, enabling us to work with a certain confidence in the red end of the spectrum.

Chlorophyll *a* monolayers were deposited and we used lamella with a deposition ratio of 0.95 to 1.05. This ratio is defined as A_l/A_s where A_l is the decrease of area occupied by the monolayer at the air/water interface and A_s is the area coated by the monolayer at the air/solid interface.

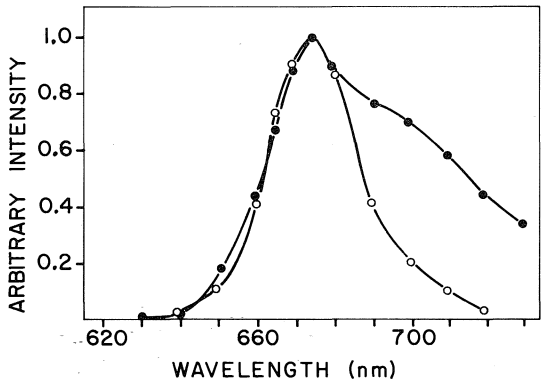

FIG. 4. Fluorescence spectra of chlorophyll *a* monolayers with the Perkin–Elmer MPF-2A, ○; and He/Cd laser spectrofluorimeters, ● ($\lambda_{exct.} = 441.6$ nm).

In Fig. 5, we have the fluorescence spectra of chlorophyll *a* monolayers when pure and when diluted with phytol. The effect of self-quenching in the first case is quite evident.

When the polarization rotator is adjusted to the laser, fluorescence spectra of chlorophyll *a* monolayers can be taken for various polarization angles of the excitation light. Figure 6 is an example of what we obtained with the He/Ne laser under such conditions. Relative fluorescence intensity of the chlorophyll *a* monolayer is plotted as a function of different polarization angles of the incident beam. The results show that there is a certain orientation of chlorophyll *a* molecules on the surface of the quartz slides. As

Can. J. Chem. Downloaded from www.nrcresearchpress.com by 210.87.254.5 on 09/05/12
For personal use only.

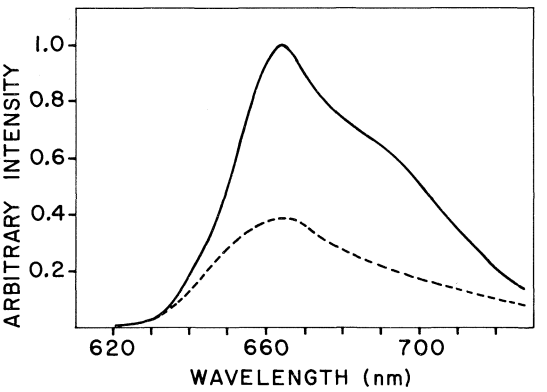

FIG. 5. Fluorescence spectra of pure and diluted chlorophyll *a* monolayer (He/Cd laser spectrofluorimeter): —, chlorophyll *a* + phytol (1:1); ---, pure chlorophyll *a*.

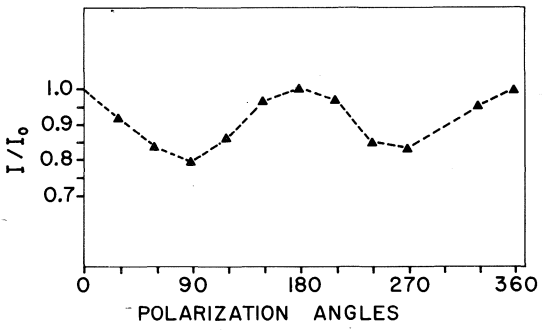

FIG. 6. Fluorescence polarization of chlorophyll *a* monolayers (He/Ne laser spectrofluorimeter). *I* is the fluorescence intensity of the monolayer when the excitation beam is polarized at the given angles, I_0 is the fluorescence intensity of the same monolayer when the excitation beam is polarized at 0°.

a matter of fact, it seems probable that this situation prevails at the air–water interface and in biological membranes too.

Using clean quartz slides or five layers of cadmium arachidate on each side of a quartz slide, we do not detect any variation of light intensity when changing the polarization angles of the incident beam.

Aoshima *et al.* (7) experienced some difficulties in trying to detect very weak fluorescence. Furthermore, some curious facts have to be pointed out. In the deposition of chlorophyll monolayers, the pressure areas of 360 Å^2/molecule for chlorophyll *a* and 490 Å^2/molecule for chlorophyll *b* are much too high to ensure that their monolayers were pure and not mixed with impurities. Usually chlorophyll *a* monolayer is deposited at a surface pressure of 24 dyn/cm which corresponds to 100 Å^2/molecule while chlorophyll *b* is usually deposited at 28 dyn/cm or 60 Å^2/molecule.

In comparing our apparatus with that of Aoshima, they were constructed to measure very weak fluorescence originating from monolayers. If we consider only the sensitivity of the two spectrofluorimeters both have achieved their goal; both are able to record fluorescence of the pigment monolayer.

The first advantage of our apparatus is the use of a monochromator; this increases the resolution (3.5 nm at 632.8 nm) and saves time since we do not have to manipulate filters. This lowers the risk of error. Using the photon counting technique (7), a certain time interval is necessary for the weak signal to be registered; this interval is inconvenient since we are dealing with a molecule which *undergoes degradation upon exposure to light*. The problem of stray light is diminished with the use of a laser as the source. The reason for this is that the beam is very parallel. Furthermore, the light from the laser is polarized, and with this, we can easily change the angle of polarization without affecting the intensity of the laser light.

On the concept of our spectrofluorimeter, we thought it advantageous to have the possibility of changing the angle of incidence onto the slide. We believe that the molecules are indeed oriented on the slide and that the angle at which the light strikes the slide has a definite effect on the coefficient of absorption.

We are the first to admit that our apparatus can be improved. For example, we could significantly increase our signal-to-noise ratio by modulating the laser beam and by using part of the beam as a reference; and then, by using a lock-in to capture the two signals, we could subtract the reference beam signal from the sample beam signal. We could also incorporate a system which would give us a corrected spectrum directly. However, our spectrofluorimeter does satisfy our needs.

The utilization and adaptation of our system would provide a good source of information. In the field of energy transfer between molecules, one may benefit by this device since it is capable of detecting very weak fluorescence.

This work was supported by grants from the National Research Council of Canada and the Université du Québec à Trois-Rivières.

Can. J. Chem. Downloaded from www.nrcresearchpress.com by 210.87.254.5 on 09/05/12
For personal use only.

1. J. S. C. WESSELS and M. VAN KOTEN HERTOGS. Philips Tech. Rev. **27**, 241 (1966).
2. P. MUELLER, H. T. TIEN, and W. C. WESCOTT. Circulation, **26**, 1167 (1962).
3. N. T. VAN and H. T. TIEN. J. Phys. Chem. **74**, 3559 (1970).
4. G. L. GAINES. Insoluble monolayers at liquid–gas interface. John Wiley and Sons. New York. 1966.
5. S. M. DE B. COSTA, J. R. FROINES, J. M. HARRIS, R. M. LEBLANC, B. H. ORGER, and G. PORTER. Proc. R. Soc. Lond. A **326**, 503 (1972).
6. E. F. WYNER, J. A. SOUSA, J. F. ROACH, and M. Nakashima. Am. Dyest. Rep. **62**, 21 (1973).
7. R. AOSHIMA, K. IRIYAMA, and H. ASAI. Appl. Opt. **12**, 2748 (1973).
8. L. A. CURRIE. Anal. Chem. **40**, 586 (1968).
9. D. P. SHCHERBOV, I. N. ASTOF'EVA, and R. N. PLOTNIKOVA. Issled. Obl. Khim. Fiz. Metod. Anal. Miner. Syr'ya. 76 (1971).
10. I. LANGMUIR, V. J. SCHAEFFER, and H. SABOTKA. J. Am. Chem. Soc. **59**, 1751 (1937).
11. G. L. GAINES, W. D. BELLAMY, and A. G. TWEET. J. Chem. Phys. **41**, 538 (1964).
12. G. L. GAINES, A. G. TWEET, and W. D. BELLAMY. J. Chem. Phys. **42**, 2193 (1965).
13. K. B. BLODGETT and I. LANGMUIR. Phys. Rev. **51**, 964 (1937).

Can. J. Chem. Downloaded from www.nrcresearchpress.com by 210.87.254.5 on 09/05/12
For personal use only.

The Quenching of Singlet Oxygen ($^1\Delta_g$) by Transition Metal Chelates[1]

D. J. CARLSSON, T. SUPRUNCHUK, AND D. M. WILES
Division of Chemistry, National Research Council of Canada, Ottawa, Canada K1A 0R9

Received May 17, 1974

D. J. CARLSSON, T. SUPRUNCHUK, and D. M. WILES. Can. J. Chem. **52**, 3728 (1974).

Various transition metal chelates were found to quench $^1O_2$ in the liquid phase. $^1O_2$ was generated either photochemically, from an ozonide, or with a microwave source and reacted with rubrene or 3-methyl-2-pentene. Rate constants for $^1O_2$ quenching by the chelates were measured in various solvents using the three $^1O_2$ sources, and compared with the constants of previously known $^1O_2$ quenchers. The most efficient chelates quenched $^1O_2$ at close to the diffusion controlled rate, as did β-carotene. Some quenchers of $^1O_2$ in the liquid phase were qualitatively shown to quench in the solid state. The possible $^1O_2$ quenching mechanisms of the chelates are discussed.

D. J. CARLSSON, T. SUPRUNCHUK et D. M. WILES. Can. J. Chem. **52**, 3728 (1974).

Des chélates de divers métaux de transition permettent l'extinction de $^1O_2$ en phase liquide. On produit $^1O_2$ soit par une réaction photochimique à partir d'un ozonide, soit par une source microonde, et il réagit avec le rubrène ou le méthyl-3 pentène-2. On mesure les constantes de vitesse de l'extinction de $^1O_2$ par les chélates dans des solvants variés en utilisant les trois sources de $^1O_2$ et on les compare avec les constantes d'extincteurs connus. L'extinction de $^1O_2$ par les chélates les plus efficaces se fait près de la vitesse contrôlée de diffusion, comme le fait le β-carotène. On a montré qualitativement que quelques extincteurs de $^1O_2$ en phase liquide provoquent aussi l'extinction en phase solide. On discute des mécanismes possibles de l'extinction de $^1O_2$ par les chélates. [Traduit par le journal]

Can. J. Chem. Downloaded from www.nrcresearchpress.com by 210.87.254.105 on 09/05/12
For personal use only.

Since the initial discovery of singlet oxygen ($^1\Delta_g$, $^1O_2$) reactions with organic substrates in 1939 (1) and their rediscovery in 1963 (2), the study of $^1O_2$ reactions has grown at an explosive rate (3–5). Commercial interest in singlet oxygen chemistry has now reached a high level because of known involvement, or postulated intervention of $^1O_2$ in processes such as air pollution, cancer formation, rancidification of edible oils, and deterioration of many polymeric materials (rubbers, plastics, fibers, biopolymers, etc. (6)). Although $^1O_2$ has been suggested to be an important component of photochemical smogs (*7a*), its atmospheric concentration is probably always low in comparison with other airborne oxidants such as ozone (*7b*). Nevertheless, significant quantities of $^1O_2$ may be generated in solids or liquids either under the influence of ozone (8), or by the near u.v. (sunlight) excitation of impurities, which are then quenched by $^3O_2$ to give $^1O_2$ (6).

The commercial importance of $^1O_2$ should lead to a growing interest in the prevention of $^1O_2$ reactions, especially by quenching to ground state ($^3O_2$) oxygen by reaction 1.

[1] $$^1O_2 + \text{Quencher} \xrightarrow{k_q} \text{Quencher} + {}^3O_2$$

[1]NRCC No. 14264.

Various compounds have been reported to quench $^1O_2$ in the liquid or gas phases. These compounds include the carotenoids, aliphatic and aromatic amines, sulfides, phenols, etc. (9). However, all of these compounds are either inefficient quenchers ($k_q < 10^8\ M^{-1}\ s^{-1}$ in the liquid phase) or are themselves unstable and subject to photo or thermal oxidative degradation (especially the carotenoids and the aromatic amines). In recent preliminary communications we have reported that certain transition metal chelates are very efficient $^1O_2$ quenchers both in liquid and solid states (10, 11). Since many of these chelates also possess extremely high u.v. stability and good thermal stability, they should find wide commercial application, and also be useful in the diagnosis of $^1O_2$ reactions. In this paper we discuss in detail the quenching ability of these chelates in the presence of various $^1O_2$ acceptors, using $^1O_2$ derived from widely different sources.

Experimental

Singlet Oxygen Generation

Photochemical

$^1O_2$ was generated in the liquid phase either by the irradiation of rubrene (9,10,11,12-tetraphenylnaphthacene) at 520 ± 20 nm or tetraphenylporphine at 390 ± 20 nm. Air saturated solutions (~$1 \times 10^{-3}\ M$

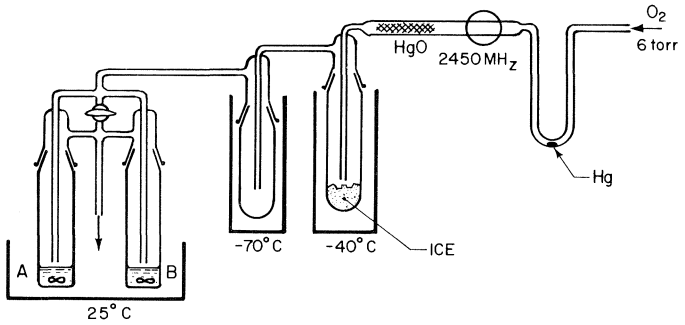

FIG. 1. Microwave system and twinned reaction cells.

in O_2) were irradiated in 1 cm path fluorescence cells, in a Farrand Spectrofluorometer (MK1 xenon arc source, IP28 Photomultiplier). Sensitizer fluorescence emissions in the presence of $^1O_2$ quenchers were periodically monitored at 545 nm (rubrene) and 650 nm (tetraphenylporphine).

Thermal

Ozone was added to solutions of triphenylphosphite in methanol at −70 °C to give a solution of the ozonide adduct, $(\phi O)_3P\ldots O_3$. A rubrene or rubrene/quencher solution containing traces of methanol and pyridine (final concentration 5% in each case) was cooled to −70 °C and then added to the ozonide solution. A rapid evolution of $^1O_2$ resulted (reaction 2).

[2] $$(\phi O)_3P\ldots O_3 \rightarrow (\phi O)_3PO + {}^1O_2$$

Microwave

Oxygen at 6 Torr was led over a mercury droplet and through a microwave discharge (2450 MHz, 70 W) in a quartz tube. Atomic oxygen, ozone, $^1\Delta_g$ and $^1\Sigma_g^+$ singlet oxygen species were generated (reaction 3).

[3] $$^3O_2 \xrightarrow{\text{microwave}} {}^1O_2(^1\Delta_g, {}^1\Sigma_g^+), O\cdot, O_3$$

The trace of mercury vapor formed mercuric oxide rings inside the quartz tube, and prevented O_3 and O· concentrating in the emergent gas stream (12*a*). Any $^1\Sigma_g^+$ (emerging from the discharge zone) was deactivated to $^1\Delta_g$ by a low pressure of water vapor (from a trap containing ice at −40 °C) and water vapor was removed by a trap at −78 °C. However, a low stationary concentration of $^1\Sigma_g^+$ is rapidly established in the flow system by an energy pooling process between $^1\Delta_g$ molecules (12*b*). We are grateful to a referee for pointing out that the H_2O trap system probably does not influence this low $^1\Sigma_g^+$ concentration in the reaction cells at our pumping rate (~500 cm s^{-1} flow). The $^1O_2$ stream was split into two identical gas streams, each of which passed over a stirred rubrene solution (2.0 ml), one solution with a quencher, and one quencher free (Fig. 1). This procedure allowed comparative experiments to be performed, so as to compensate for fluctuations in the $^1O_2$ concentration coming from the discharge. Owing to the low pressure in the microwave system, only involatile solvents can be used.

Reagents

Rubrene was recrystallized from benzene. Hexadecane was rendered hydroperoxide- and olefin-free by repeated tumbling with concentrated H_2SO_4, and fractionation under reduced pressure. All hydrocarbons were passed through activated alumina immediately before use. 3-Methyl-2-pentene was Phillips Research Grade. Squalene (2,6,10,15,19,23-hexamethyltetracosane-2,6,10,14,18,22-hexaene) was distilled under reduced pressure. All solvents were spectroscopic grade. Chelates were purified by recrystallization or column chromatography.

Product Analysis

Rubrene consumption was measured spectrophotometrically at 520 nm, since singlet oxygen reaction produces a colorless endoperoxide. In the case of the tetraphenylporphine/3-methyl-2-pentene system, hydroperoxide concentrations were estimated spectrophotometrically after the liberation of I_3^- from NaI solution in isopropanol, as described previously (13).

Treatment of Results

Rubrene and many olefins react rapidly with $^1O_2$ to yield respectively an endoperoxide (14) and a hydroperoxide (4).

Photochemical $^1O_2$ Generation

Rubrene can act as both sensitizer and substrate in photooxidations (14) whereas an olefin requires a sensitizer such as tetraphenylporphine. For the oxidation of the rubrene or olefin substrates, concentration [A], in the presence of a quencher, concentration [Q], reactions 1 and 4 to 6 are now well established (9, 14)

[4] $$^3O_2 + [\text{Sensitizer}]^* \rightarrow {}^1O_2 + \text{Sensitizer} \qquad (\text{Rate} = R_i)$$

[5] $$^1O_2 + A \xrightarrow{k_{ox}} AO_2$$

[6] $$^1O_2 \xrightarrow{k_d} {}^3O_2$$

and lead to the rate expression

[7] $$-d[A]/dt = k_{ox}[A]R_i/(k_d + k_{ox}[A] + k_q[Q])$$

A stationary concentration of $^1O_2$ is assumed and R_i is the rate of $^1O_2$ generation in solution.

Can. J. Chem. Downloaded from www.nrcresearchpress.com by 210.87.254.105 on 09/05/12
For personal use only.

Then in the absence of quencher

$$[8] \qquad -\frac{1}{d[A]/dt} = \frac{1}{R_i} + \frac{k_d}{k_{ox}[A]R_i}$$

It follows from [7]

$$[9] \qquad \left[\frac{(d[A]/dt)_0^0}{(d[A]/dt)_0^Q} - 1\right]^{-1} = \frac{k_{ox}[A]_0 + k_d}{k_q[Q]}$$

where subscript 0 refers to initial values, and superscripts Q and 0 refer to rates in the presence and absence of quencher respectively.

Thermal $^1O_2$ Generation

The kinetics of the generation of $^1O_2$ by the decomposition of $(\phi O)_3P\ldots O_3$ in the presence of pyridine have been discussed by Mendenhall (15), who has shown that $^1O_2$ is generated quantitatively from the ozonide. If no $^1O_2$ is lost from the solution, then from reactions 1, 2, 5, and 6,

$$[10] \quad d[(\phi O)_3P\ldots O_3]/d[A] = 1 + (k_d + k_q[Q])/k_{ox}[A]$$

Integration of eq. 10 yields the following expression after complete ozonide decomposition (at time ∞).

$$[11] \quad \frac{k_q}{k_{ox}} = \frac{1}{[Q]} \times \left(\frac{[(\phi O)_3PO_3]_0 - [A]_0 + [A]_\infty}{\ln [A]_0/[A]_\infty} - \frac{k_d}{k_{ox}}\right)$$

In the absence of quencher, k_d/k_{ox} can be derived from expression 11.

Microwave $^1O_2$ Generation

Reactions 1, 3, 5, and 6 lead to the rate expression 7. Integrating this expression up to a time t, both in the presence and absence of quencher leads to the relationship

$$[12] \quad \frac{k_q}{k_{ox}} = \frac{[A]_t^Q - [A]_t^0 + (k_d/k_q)\ln [A]_t^Q/[A]_t^0}{[Q]\ln [A]_0/[A]_t^Q}$$

Results

Photochemical $^1O_2$ Generation

The loss of rubrene during irradiation at 520 nm in air-saturated solutions was followed spectrophotometrically. Some rubrene consumption curves are shown in Fig. 2. In the rubrene photo-oxidation, the rate of rubrene consumption is a complex function of the rubrene concentration, since rubrene is involved as both sensitizer (reaction 4) and substrate for $^1O_2$ (reaction 5). Consequently the ratios of initial rates, $(d[A]/dt)_0^0/(d[A]/dt)_0^Q$ were always used in the calculation of rate constant ratios. Two distinct kinetic effects were observed depending on the solvent employed. In iso-octane, the rate ratios measured at fixed quencher concentrations were virtually independent of the rubrene concentrations, as shown by the examples in Table 1. In methylene chloride the rate ratio was dependent on rubrene concentration; the methylene chloride data are plotted in Fig. 3. From expression 9, the slopes and intercepts shown in Fig. 3 lead to k_d/k_{ox} and k_q/k_{ox} values of $(1.76 \pm 0.4) \times 10^{-4}\ M$ and 117 ± 30 (β-carotene), $(0.90 \pm 0.07) \times 10^{-4}\ M$ and 0.19 ± 0.02 [Ni(II)bis(O-butyl 3,5-di-*t*-butyl-4-hydroxybenzyl phosphonate)], and $(1.25 \pm 0.08) \times 10^{-4}\ M$ and 2.0 ± 0.4 (Ni(II)bis-acetylacetonate) respectively Kinetic data for rubrene photo-oxidation at various quencher concentrations are shown in Table 2.

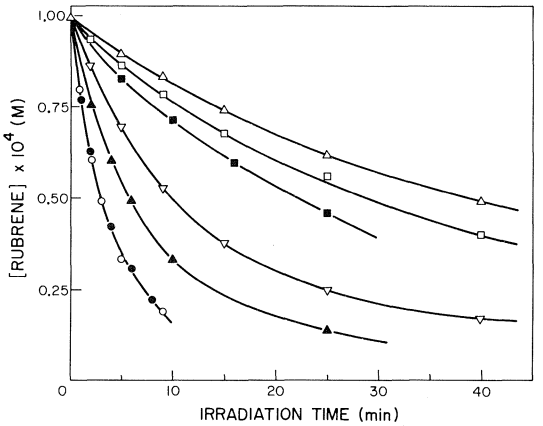

FIG. 2. Rubrene photooxidation in the presence of $^1O_2$ quenchers. Irradiation at 520 ± 20 nm. Rubrene in iso-octane; quencher: ○, none; ▽, DABCO ($4 \times 10^{-3}\ M$); □, Ni(II) bis[2,2′-thiobis-4-(1,1,3,3-tetramethylbutyl)phenolate] ($4 \times 10^{-3}\ M$); △, Ni(II) [2,2′-thiobis-4-(1,1,3,3-tetramethylbutyl)phenolate]-*n*-butylamine ($4 \times 10^{-3}\ M$). Rubrene in methylene chloride; quencher: ●, none; ■, β-carotene ($1 \times 10^{-5}\ M$); ▲, Ni(II) bis-acetylacetonate ($1 \times 10^{-4}\ M$).

Hydroperoxide is produced on the irradiation at 390 ± 20 nm of a tetraphenylporphine solution containing the olefin 3-methyl-2-pentene (Fig. 4). In the absence of a quencher, the reciprocal rate is linearly dependent on the

Can. J. Chem. Downloaded from www.nrcresearchpress.com by 210.87.254.105 on 09/05/12
For personal use only.

TABLE 1. Rubrene photooxidation in the presence of quenchers in *i*-octane

Rubrene [A] × 10^4 (M)	Rate rubrene loss (× 10^7) ($M\,s^{-1}$)		$(d[A]/dt)_0^0$ / $(d[A]/dt)_0^Q$	k_q/k_d (× 10^{-3}) (M^{-1})
	$-(d[A]/dt)_0^0$*	$-(d[A]/dt)_0^Q$†		
1,4-Diazabicyclo[2.2.2]octane (4×10^{-3} M)				
1.0	3.8	1.15	3.30	0.57
0.75	2.25	0.75	3.00	0.50
0.59	1.74	0.55	3.16	0.54
0.43	0.96	0.34	2.82	0.45
0.22	0.30	0.093	3.23	0.56
Nickel(II) bis[2,2′-thiobis-4-(1,1,3,3-tetramethylbutyl)phenolate] (4×10^{-3} M)				
1.0	3.80	0.38	10.0	2.2
0.89	3.49	0.32	11.2	2.5
0.78	2.25	0.25	9.0	2.0
0.61	1.74	0.18	9.7	2.2
0.43	0.96	0.11	8.7	1.9
Nickel(II) [2,2′-thiobis-4-(1,1,3,3-tetramethylbutyl)phenolate]-*n*-butylamine (4×10^{-3} M)				
1.0	3.80	0.31	12.2	2.8
0.89	3.49	0.27	12.9	3.0
0.78	2.25	0.19	11.8	2.7
0.61	1.74	0.14	12.4	2.8
0.43	0.96	0.079	12.2	2.8
N-Isopropyl-*N*′-phenyl-*p*-phenylene diamine (4×10^{-4} M)				
1.0	2.29	0.80	2.86	4.6
0.78	1.74	0.60	2.90	4.7
0.65	1.19	0.42	2.83	4.6
0.43	0.64	0.23	2.78	4.4
0.33	0.43	0.155	2.77	4.4

*Without quencher.
†With quencher, at same light intensity as *.

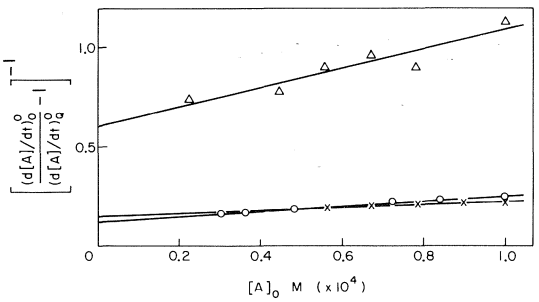

FIG. 3. Rubrene photooxidation in methylene chloride. ×, β-carotene (1.5×10^{-5} M); ○, Ni(II) bis[O-butyl 3,5-di-*t*-butyl-4-hydroxybenzyl phosphonate] (4×10^{-3} M); △, Ni(II) bis-acetylacetonate (1.0×10^{-4} M).

reciprocal olefin concentration (Fig. 5). From eq. 8 the intercept of this plot gives the rate of $^1O_2$ generation in solution (4.3×10^{-7} $M\,s^{-1}$) and the slope allows the calculation of $k_d/k_{ox} = 1.64 \times 10^{-2}$ M in chlorobenzene solutions. Sensitized photo-oxidation of 3-methyl-2-pentene ($1.0–5.2 \times 10^{-2}$ M) in the presence of nickel(II) [2,2′-thiobis-4-(1,1,3,3-tetramethylbutyl)phenolate]-*n*-butylamine ($7.4–32 \times 10^{-4}$ M) led to an average k_q/k_{ox} of 80 ± 5.

Irradiation of either a sensitizer-free solution of 3-methyl-2-pentene in chlorobenzene or an olefin-free solution of tetraphenylporphine in chlorobenzene yielded no detectable hydroperoxide ($< 5 \times 10^{-6}$ M). Many metal chelates are rapid decomposers of hydroperoxides (6, 16). However, separate dark experiments with oxidized 3-methyl-2-pentene solutions showed that the hydroperoxide concentrations did not decrease either in the presence of nickel(II) [2,2′-thiobis-4-(1,1,3,3-tetramethylbutyl)phenolate]-*n*-butylamine or of the sensitizer.

Thermal $^1O_2$ Generation

Rubrene is bleached by the $^1O_2$ evolved rapidly from $(\phi O)_3PO_3$ on the addition of a trace of pyridine. The validity of expression 11 for the $(\phi O)_3PO_3$ production of $^1O_2$ in a rubrene solution has been confirmed by Mendenhall (15). Rubrene concentrations before and after ozonide decomposition are shown in

Can. J. Chem. Downloaded from www.nrcresearchpress.com by 210.87.254.105 on 09/05/12
For personal use only.

TABLE 2. Effect of quencher concentration on rubrene photooxidation*

Quencher	[Quencher] $\times 10^4$ (M)	$(d[A]/dt)_0^0$ $\times 10^7$ ($M\,s^{-1}$)	$(d[A]/dt)_0^Q$ $\times 10^7$ ($M\,s^{-1}$)	$k_q/k_d \times 10^{-3}$ (M^{-1})
Ni(II) bis(di-*n*-butyldithiocarbamate)†	40	5.3_4	0.0089	150
	2.1	2.5_4	0.044_3	270
	0.21	2.5_4	0.23_0	470
Ni(II) bis(2-hydroxy-5-methoxyphenyl-*N*-*n*-butyl aldimine)†	10	1.6_8	0.087_5	18
	2.4	1.6_8	0.21_5	28
	0.60	1.9_5	0.42_5	60
	0.060	1.2_1	0.90_1	57
Ni(II) [2,2′-thiobis-4-(1,1,3,3-tetramethylbutyl)-phenolate]-*n*-butylamine†	50	5.35	0.337	3.0
	10	2.2_2	0.35_5	5.3
	1.7	1.5_6	0.90_5	4.3
Fe(III) tri(di-isopropyldithiocarbamate)‡	10	5.2_3	0.0236	0.053§
	1.0	4.2_1	0.203	0.052§

*Unquenched initial rate fluctuations due to variations in Xe arc intensity.
†Rubrene concentration 1.0×10^{-4} M in *i*-octane.
‡Rubrene concentration 1.0×10^{-4} M in CH_2Cl_2.
§k_q/k_{ox}.

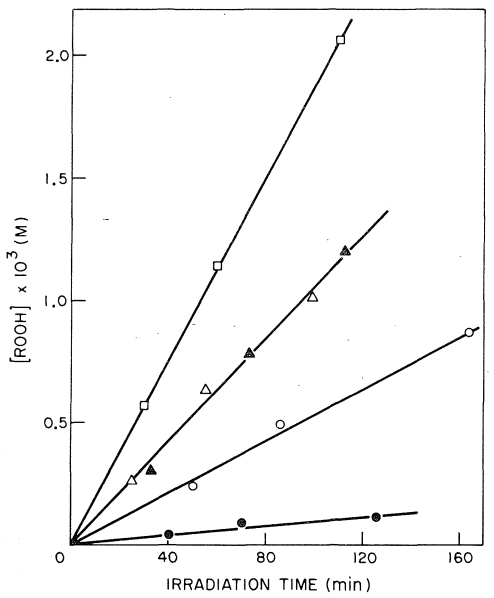

FIG. 4. Sensitized photooxidation of 3-methyl-2-pentene. Sensitizer tetraphenylporphine (7.5×10^{-6} M) in chlorobenzene, irradiated at 390 ± 20 nm. Quencher: Ni(II) [2,2′-thiobis-4-(1,1,3,3-tetramethylbutyl)phenolate]-*n*-butylamine. Concentrations, olefin: ○, 0.52×10^{-2} M; △, 1.02×10^{-2} M; □, 5.2×10^{-2} M; olefin, quencher: ●, 1.02×10^{-2}, 3.25×10^{-3} M; ▲, 5.2×10^{-2}, 7.49×10^{-3} M.

Table 3 for various quenchers. The rate ratios k_d/k_{ox} for $^1O_2$ deactivation in methylene chloride and iso-octane are calculated from [11] in the absence of a quencher. In the presence of a quencher, k_q/k_{ox} ratios were also calculated from expression 11, using the appropriate experimental k_d/k_q value.

Microwave $^1O_2$ Generation

Rubrene is rapidly bleached by oxygen which has passed through a microwave discharge. Although a microwave discharge is a convenient source of $^1O_2$ it is difficult to control consistently the concentration of $^1O_2$ dissolved in a liquid exposed to the $^1O_2$-containing stream. This problem was largely overcome by the simultaneous exposure of solutions in the twinned reaction cells (Fig. 1), one cell containing only rubrene solution, the other rubrene and a dissolved quencher. The discharge was usually continued until 60–70% of the rubrene in the quencher free solution had been oxidized to the colorless endoperoxide. Rubrene bleaching

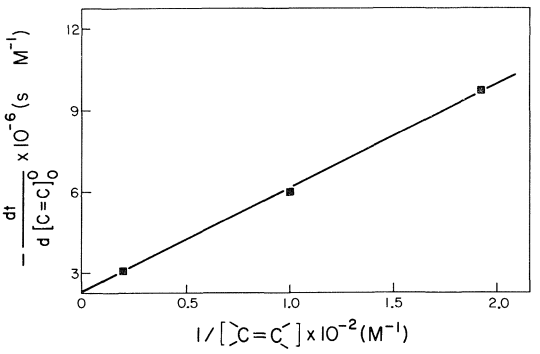

FIG. 5. Sensitized photooxidation of 3-methyl-2-pentene. Tetraphenylporphine (7.5×10^{-6} M) sensitizer in chlorobenzene. No quencher.

Can. J. Chem. Downloaded from www.nrcresearchpress.com by 210.87.254.105 on 09/05/12
For personal use only.

TABLE 3. $^1O_2$ from $(\phi O)_3P\ldots O_3$ in the presence of quenchers

Quencher*	Initial $[(\phi O)_3P\ldots O_3] \times 10^3$ (M)	Rubrene $\times 10^4$ (M) Initial $[A]_0$	Rubrene $\times 10^4$ (M) Final $[A]_\infty$	$k_d/k_q \times 10^4$ (M)	k_q/k_{ox}
—	2.36	4.0	0.19	6.7†	—
—	1.42	4.0	0.65	6.2†	—
—	0.94	4.0	0.10	1.0‡	—
DABCO	0.94	6.0	3.4	—	0.45‡
DABCO	1.42	4.0	2.1	—	0.53†
Ni(II) bis(O-butyl 3,5-di-*t*-butyl-4-hydroxybenzyl phosphonate)	0.94	6.0	1.77	—	0.14‡
Ni(II) [2,2′-thiobis-4-(1,1,3,3-tetramethylbutyl)-phenolate]-*n*-butylamine	1.42	4.0	3.50	—	4.1†
	2.36	4.0	3.07	—	3.3†
Ni(II) bis[2,2′-thiobis-4-(1,1,3,3-tetramethylbutyl)-phenolate]	1.42	4.0	3.33	—	2.7†
	2.36	4.0	2.88	—	2.6†
Ni(II) bis(2-hydroxy-5-methoxyphenyl-*N*-*n*-butyl aldimine)	2.36	4.0	3.89	—	48†

*2.4 $\times 10^{-3}$ M.
†In iso-octane/MeOH/pyridine 90:5:5.
‡In CH_2Cl_2/MeOH/pyridine 90:5:5.

TABLE 4. $^1O_2$ From the microwave discharge in the presence of quenchers

Quencher	[Quencher] $\times 10^3$ (M)	[Rubrene] $\times 10^4$ (M) Initial $[A]_0$	Final $[A]_t^0$	Final $[A]_t^Q$	k_q/k_{ox}
Ni(II) [2,2′-thiobis-4-(1,1,3,3-tetramethylbutyl)-phenolate]-*n*-butylamine	3.02	1.5	0.12	0.82	1.4*
	3.77	1.89	0.21	1.06	3.8†
N-Isopropyl-*N*′-phenyl-*p*-phenylene diamine	0.79	2.01	0.12	0.93	4.9*
Ni(II) bis(di-*n*-butyldithiocarbamate)	3.13	2.01	0.28	1.88	14*
	2.12	2.01	0.30	1.85	13*
	1.06	2.01	0.19	1.70	13*
Ni(II) bis(2-hydroxy-5-methoxyphenyl-*N*-*n*-butyl aldimine)	4.88	1.05	0.19	0.96	5.7*
	1.22	1.45	0.19	1.00	4.8*
Ni(II) bis-acetylacetonate	4.25	1.89	0.55	0.83	1.2†
	4.25	1.89	0.62	0.83	0.84†
$NiCl_26H_2O$	4.62	1.89	0.27	1.32	4.9†
$CoCl_26H_2O$	3.50	1.89	0.30	0.50	0.66†
$MnCl_24H_2O$	4.83	1.89	0.27	0.27	<0.01†

*In hexadecane, using $k_d/k_{ox} = 9.0 \times 10^4$ s^{-1}, calculated from DABCO quenching data.
†In 2-butoxyethanol, using $k_d/k_{ox} = 38 \times 10^4$ s^{-1}, calculated from DABCO quenching data.

data are shown in Table 4 for the microwave system.

Experimental difficulties and the complexity of the integrated rate expression 12 prevent the direct estimation of k_d/k_{ox} ratios for the solvents employed in the microwave work. Indirect k_d/k_{ox} ratios were calculated from competitive experiments involving rubrene and rubrene/DABCO (1,4-diaza-bicyclo[2.2.2]octane) solutions. k_q/k_{ox}(DABCO) was assumed to be 0.49 and solvent independent as found from the ozonide decomposition data (Table 3), and this value was used together with eq. 12 to calculate the respective k_d/k_{ox} values. The k_d/k_{ox} values derived from the various $^1O_2$ generation techniques are collected in Table 5.

Can. J. Chem. Downloaded from www.nrcresearchpress.com by 210.87.254.105 on 09/05/12
For personal use only.

TABLE 5. Experimental k_d values in various solvents

This work*				Literature values	
$^1O_2$ Source/substrate	Solvent	$k_d/k_{ox} \times 10^3$	$k_d \times 10^{-4}$ (s^{-1})	Solvent	$k_d \times 10^{-4}$ (s^{-1})
Photo/rubrene	CH_2Cl_2	0.13	0.95	$CHCl_3$	1.7‡
$(\phi O)_3PO_3$/rubrene	CH_2Cl_2	0.10	0.73		
$(\phi O)_3PO_3$/rubrene	*i*-Octane	0.64	4.7	cyC_6H_{12}	5.9‡
Microwave/rubrene	Hexadecane	1.2	9.0		
Microwave/rubrene	2-Butoxyethanol	5.2†	38	CH_3OH	14‡
Photo $\phi_4$porphine/3-Me-2-pentene	ϕCl	0.16†	1.1	C_6H_6	4.0‡§

*Assuming $k_{ox} = 7.3 \times 10^7\ M^{-1}\ s^{-1}$ (rubrene) and $1.0 \times 10^6\ M^{-1}\ s^{-1}$ (3-Me-2-pentene).
†Calculated from DABCO quenched solutions, assuming $k_q(DABCO) = 3.5 \times 10^7\ M^{-1}\ s^{-1}$.
‡Reference 25.
§Reference 18.

k_q/k_{ox} values were calculated from the microwave data using expression 12 and are shown in Table 4.

Since alkanes have been suggested to react with $^1O_2$ (17), hexadecane (3.4 *M*) was exposed for 5 h to microwave-generated $^1O_2$. Hydroperoxide was not detectable after this treatment ($< 5 \times 10^{-6}\ M$). However, when undiluted squalene was similarly exposed ~2.0 *M* hydroperoxide was formed, but no $\diagdown C{=}O \diagup$ products could be detected by i.r. spectroscopy ($< 1 \times 10^{-4}\ M$ from ~1715 cm^{-1} $\diagdown C{=}O \diagup$ absorption).

Exposure of chelate solutions in hexadecane to 1 h of $^1O_2$ from the microwave source resulted in no detectable changes in the u.v. absorption of the solutions, for all of the chelates listed in Table 6. A similar resistance to $^1O_2$ attack has been reported for nickel(II) Schiff-base complexes (18).

Discussion

All convenient methods for the generation of $^1O_2$ are plagued by experimental problems. Of the three methods used in this work, problems can arise from the following sources.

In the photochemical routes, deactivation of the excited singlet or triplet states of sensitizers by the $^1O_2$ quencher under investigation can lead to high apparent k_q/k_{ox} values for $^1O_2$ quenching, since $(R_i)_0^Q$ is no longer equal to $(R_i)_0^0$, but instead smaller. Singlet quenching can be detected by observing the fluorescence of the sensitizer (at 545 nm for rubrene and 650 nm for tetraphenylporphine). All of the quenchers examined had negligible effect on the fluorescence of these sensitizers (<10% decrease in emission). Unfortunately the phosphorescence emissions from the sensitizer triplets were experimentally inaccessible. However, from the data of Adamczyk and Wilkinson (19), who showed that polynuclear aromatic triplets are quenched by Ni(II) Schiff base complexes with rate constants of $\sim 3 \times 10^9\ M^{-1}\ s^{-1}$ and of Porter and co-workers (20), who showed that $^3O_2$ quenching of polynuclear aromatic triplets occurred with a rate constant of $\sim 2 \times 10^9\ M^{-1}\ s^{-1}$, chelate quenching of rubrene triplets can be expected to be important in comparison with $^3O_2$ quenching (reaction 4) only when the chelate concentration exceeds $\sim 1 \times 10^{-3}\ M$ (dissolved $^3O_2$ concentration $\sim 1 \times 10^{-3}\ M$ in air saturated solutions (20)). In fact, the three upper chelates listed in Table 2 show k_q/k_{ox} values which increase as the chelate concentration decreases (the converse of the effect expected to result from rubrene triplet quenching), but became approximately constant at below $1 \times 10^{-4}\ M$. This unexpected effect might stem from chelate association (trimer, tetramer formation) at higher concentrations as has been reported for some Ni(II) chelates in solution (21).

Problems occur in the decomposition of $(\phi O)_3P\ldots O_3$ to $^1O_2$ because of the possibility of direct reaction between the ozonide and either the substrate or the quencher. Although the catalytic decomposition of the ozonide at −70 °C will minimize direct attack, nickel(II) bis(di-*n*-butyldithiocarbamate), a well known antiozonant, did react directly with the ozonide to give a brown precipitate. Ozonide reaction

Can. J. Chem. Downloaded from www.nrcresearchpress.com by 210.87.254.105 on 09/05/12
For personal use only.

TABLE 6. Quenching of singlet oxygen ($^1\Delta_g$) in rubrene solutions*

Quencher†	$k_q \times 10^{-8}$ (M^{-1} s^{-1})*					
	Rubrene $\xrightarrow{h\nu}$		$(\phi O)_3PO_3$		Microwave discharge	
	i-Octane	CH_2Cl_2	*i*-Octane	CH_2Cl_2	Hexadecane	2-BuEtOH
DABCO	0.30		0.39	0.33		
N-Isopropyl-*N'*-phenyl-*p*-phenylene diamine	2.1				4.0	
β-Carotene		130‡				
Ni(II) bis(di-*n*-butyldithiocarbamate)	170‡	90		>10§	10	
Ni(II) bis(2-hydroxy-5-methoxyphenyl-*N*-*n*-butyl aldimine)	26‡	20	35		4.0	
Fe(III) tri(di-isopropyldithiocarbamate)		43			12	
Co(II) bis(di-isopropyldithiocarbamate)	19				9.0	
$NiCl_26H_2O$						3.1
Ni(II) [2,2'-thiobis-4-(1,1,3,3-tetramethylbutyl)-phenolate]-*n*-butylamine‖	2.0‡		2.7		1.0	2.8
Ni(II) bis[2,2'-thiobis-4-(1,1,3,3-tetramethylbutyl)phenolate]	0.96		2.0		1.3	
Ni(II) bisacetylacetonate		1.5				0.75
$CoCl_26H_2O$						0.48
Ni(II) bis(O-butyl 3,5-di-*t*-butyl-4-hydroxybenzyl phosphonate)		0.14		0.10		0.34
$MnCl_24H_2O$	<0.01					
Zn(II) bis(di-*n*-butyldithiocarbamate)	<0.01					

*Averaged values at 25 °C in the indicated solvent, calculated from k_d values taken from our data in Table 4 and k_{ox}(rubrene) = 7.3×10^7 M^{-1} s^{-1}.
†Quencher concentration 4×10^{-3} to 1×10^{-4} M unless specified.
‡Quencher concentration $< 2 \times 10^{-4}$ M.
§Interference by some chelate-ozonide reaction.
‖$k_q = 0.8 \times 10^8$ M^{-1} s^{-1} from tetraphenylporphine/3-methyl-2-pentene system.

with rubrene has been shown to be negligible (22).

The effluent from an oxygen microwave discharge contains O_3, O·, $^1\Sigma_g^+$($^1O_2$) etc. as well as $^1\Delta_g$($^1O_2$). The use of a slow mercury distillation into the discharge to give mercuric oxide rings and the presence of a low vapor pressure of water can minimize the concentrations of O_3, O·, and $^1\Sigma_g^+$ in the effluent stream (12). The absence of O_3 and O· in the $^1\Delta_g$($^1O_2$) stream from our apparatus was confirmed by the absence of carbonyl products ($< 1 \times 10^{-4}$ M) on exposure of squalene so as to generate a high hydroperoxide level (2.0 M). Both O_3 and O· would have produced large amounts of carbonyl products.

Absolute k_d and k_q values may be calculated from the k_d/k_{ox} and k_q/k_{ox} ratios if literature values for k_{ox} are assumed. For rubrene, $k_{ox} = 6.0 \times 10^7$ M^{-1} s^{-1} can be calculated from the k_d/k_{ox} value of 1.4×10^{-3} M (23) in methanol, where $k_d = 9 \times 10^4$ s^{-1} (23). A very similar value of k_{ox} (rubrene) = 7.8×10^7 M^{-1} s^{-1} can be derived from β-carotene quenching data (k_{ox}(rubrene) = $3k_{ox}$(tetramethylethylene) (24) = $150k_{ox}$(2-methyl-2-pentene) (3), k_q(β-carotene)/k_{ox}(2-methyl-2-pentene) = 2×10^4 (9) and k_q(β-carotene) = 1.3×10^{10} M^{-1} s^{-1} (18)). The k_{ox} value for 3-methyl-2-pentene was assumed to be identical to that of 2-methyl-2-pentene (1.0×10^6 M^{-1} s^{-1}) as derived above.

Experimental k_d/k_{ox} and calculated k_d values for the various solvents employed are collected in Table 5. The calculated k_d values (Table 5) are in fair agreement with values published for comparable solvent systems (18, 25). The indirectly estimated hexadecane and 2-butoxyethanol k_d values seem somewhat high, and may indicate the presence of some $^1O_2$ quenching impurities, or some solvent dependence of k_q/k_{ox} for DABCO.

In iso-octane, the rate ratio $(dA/dt)^0/(dA/dt)^Q$ was found to be independent of the rubrene concentration, under fixed photolysis conditions (Table 1). This result is to be expected from the relative values of k_d in iso-octane (4.7×10^4 s^{-1}) and $k_{ox}[A]$ (always $< 7 \times 10^3$ s^{-1}), when (from eq. 9)

$$[13] \quad (dA/dt)_0{}^0/(dA/dt)_0{}^Q \simeq 1 + \frac{k_q[Q]}{k_d}$$

(The limited solubility of rubrene in iso-octane

Can. J. Chem. Downloaded from www.nrcresearchpress.com by 210.87.254.105 on 09/05/12
For personal use only.

precludes working at higher concentrations.) The k_q/k_d values calculated from expression 13 for the iso-octane solutions of various chelates are shown in Tables 1 and 2. k_q values were calculated from these k_q/k_d ratios, using $k_d = 4.7 \times 10^4\ s^{-1}$ (Table 5), and are listed in Table 6. In methylene chloride, $k_d = 8 \times 10^3\ s^{-1}$, and is comparable to $k_{ox}[A]$ so that [9] is valid, as is confirmed by the linearity of the plots shown in Fig. 3. The slopes and intercepts of these lines in Fig. 3 allow the direct estimation of k_d/k_{ox} and k_q/k_{ox}. In addition, the linearity of these rate plots is indicative of the absence of any significant quenching of $^1O_2$ by rubrene itself.

Despite the inherent problems with each method of $^1O_2$ generation the fair agreement between the k_q values collected in Table 6 for a given quencher is an indication of both the absence of significant side reactions and the general validity of the assumptions made in the calculation of k_q/k_{ox} for each technique. The collected k_q values for the metal chelates are in fair agreement with the few published values available. The semiquantitative data of Guillory and Cook (21) and Felder and Schumacher (27) are in good agreement with Table 6, and agreement with the k_q data of Flood *et al.* (28) who used methylene blue sensitization of 1,3-diphenylbenzofuran oxidation is excellent. Very recently Farmilo and Wilkinson (18) have also shown that certain nickel(II) Schiff-base complexes can quench $^1O_2$ at close to the diffusion controlled rate in benzene solution.

The k_q values for DABCO, β-carotene, and *N*-isopropyl-*N'*-phenyl-*p*-phenylenediamine in Table 6 are included largely for comparison with literature values of 1.6×10^7 (in 1:1:1 benzene, methanol, diglyme) (9), 1.3×10^{10} in benzene (18), and $1.5 \times 10^9\ M^{-1}\ s^{-1}$ in ethanol respectively. The latter value is calculated from the data of Dalle *et al.* (26), using a literature value (25) of $k_d = 8.3 \times 10^4\ s^{-1}$ in ethanol. Aliphatic and aromatic amines have been shown (23) to quench $^1O_2$ by the formation of a charge transfer complex (reaction 15).

[15] $R_3N + {}^1O_2 \rightleftharpoons [{}^1O_2{}^{\delta-} \ldots NR_3{}^{\delta+}] \rightarrow {}^3O_2 + R_3N$

Our amine k_q values are lower than the published values perhaps because of a solvent polarity effect as suggested by Young *et al.* (23). Our low polarity solvents would not stabilize a $^1O_2$–amine charge transfer complex as effectively as the high polarity solvents employed previously (9, 26). β-Carotene has been proven (18) to quench by an energy transfer process to a low lying β-carotene triplet (reaction 16), and quenching is accompanied by *cis–trans* isomerization.

[16] ^{1}(β-carotene) + $^1O_2 \rightarrow {}^3$(β-carotene) + $^3O_2$

It is interesting to speculate on the mechanism by which the chelates quench $^1O_2$. Chelate quenching seems to be a specific property of the chelate as a whole, since the free ligands (where stable) either do not quench $^1O_2$, or quench at a much lower efficiency (10, 28). The quenching effect is apparently not related to coordination or magnetism, since octahedral (paramagnetic) (*e.g.* $NiCl_2 6H_2O$) and square planar (diamagnetic) (*e.g.* nickel(II) bis(di-*n*-butyldithiocarbamate)) complexes quench $^1O_2$, as does an octahedral trimeric complex (*e.g.* nickel(II) bis-acetylacetonate). For the hydrated chlorides (Table 6) $^1O_2$ quenching efficiency increases in the sequence Mn(II) ≪ Co(II) < Ni(II). Both cobaltous and nickelous chlorides have vacant electronic energy levels at 8000–9000 cm^{-1}, whereas the d^5 manganous complex has none (29). This infers that energy transfer might be important for these chlorides, since the oxygen $^1\Delta_g \rightarrow {}^3\Sigma_g{}^+$ transition occurs at ~8000 cm^{-1}. A similar conclusion was reached by Farmilo and Wilkinson from a consideration of Ni(II) and Pd(III) chelates, and ferrocene quenching of $^1O_2$ (18). However, both the charge transfer process [15] and the energy transfer reaction 16 might well operate for different transition metal chelates. Another attractive source of $^1O_2$ quenching by some of the metal chelates involves the formation of a loose complex, possibly analogous to those formed between $^3O_2$ and many Co, Ni, and Fe complexes (30, 31). Although the high stability of many cobalt–oxygen complexes would preclude efficient $^1O_2$ quenching, a transient association could lead to efficient quenching.

Since $^1O_2$ attack is now being considered as an important source of degradation of rubbers and plastics (6), it is important to know whether any of the compounds listed in Table 6 can quench $^1O_2$ in the solid state. This was investigated by either co-depositing a solid layer of a quencher with rubrene by evaporation of a solution in the cells of the microwave apparatus or by coating one of the $^1O_2$ delivery tubes

Can. J. Chem. Downloaded from www.nrcresearchpress.com by 210.87.254.105 on 09/05/12
For personal use only.

(Fig. 1) with a thin solid coating of the quencher, just above a stirred rubrene solution. With both methods, on exposure to $^1O_2$, appreciable reduction in rubrene bleaching was found with the quenchers *N*-isopropyl-*N'*-phenyl-*p*-phenylenediamine, β-carotene, nickel(II) bis(di-*n*-butyldithiocarbamate), nickel(II) bis(2-hydroxy-5-methoxyphenyl-*N*-*n*-butyl aldimine), and nickel(II)[2,2'-thiobis-4-(1,1,3,3-tetramethylbutyl)-phenolate]-*n*-butylamine. Meaningful quantitative solid state quenching data would require the deposition of uniform mono-molecular layers, rather than the polycrystalline layers produced by the above techniques.

The authors wish to express their appreciation for the help and guidance given by Dr. G. D. Mendenhall during the early stage of this work.

1. H. KAUTSKY. Trans. Faraday Soc. **35**, 216 (1939).
2. C. S. FOOTE and S. WEXLER. J. Am. Chem. Soc. **86**, 3879 (1964).
3. C. S. FOOTE. Acc. Chem. Res. **1**, 104 (1968).
4. D. R. KEARNS. Chem. Rev. **71**, 395 (1971).
5. M. L. KAPLAN. Chem. Tech. 621 (1971).
6. D. J. CARLSSON and D. M. WILES. Rubber Chem. Technl. In press.
7. (*a*) W. S. GLEASON, A. D. BROADBENT, E. WHITTLE, and J. N. PITTS. J. Am. Chem. Soc. **92**, 2068 (1970); (*b*) R. M. KUMMLER and M. H. BORTNER. Am. Chem. Soc. Preprints Divn. Petroleum Chem. **16**, (4) A44 (1971).
8. R. W. MURRAY and M. L. KAPLAN. J. Am. Chem. Soc. **90**, 537 (1968).
9. C. S. FOOTE, R. W. DENNY, L. WEAVER, Y. CHANG, and J. PETERS. Ann. N.Y. Acad. Sci. **171**, 139 (1970).
10. D. J. CARLSSON, G. D. MENDENHALL, T. SUPRUNCHUK, and D. M. WILES. J. Am. Chem. Soc. **94**, 8960 (1972).
11. D. J. CARLSSON, T. SUPRUNCHUK, and D. M. WILES. J. Polym. Sci. Polym. Lett. **11**, 61 (1973).
12. (*a*) M. L. KAPLAN and P. G. KELLEHER. Science, **169**, 1207 (1970); (*b*) S. J. ARNOLD and E. A. OGRYZLO. Can. J. Phys. **45**, 2053 (1967).
13. D. J. CARLSSON and D. M. WILES. Macromolecules, **2**, 597 (1969).
14. T. WILSON. J. Am. Chem. Soc. **88**, 2898 (1966).
15. G. D. MENDENHALL. Ph.D. Thesis, Harvard University, Boston, Mass. 1970.
16. J. A. HOWARD, Y. OHKATSU, J. H. B. CHENIER, and K. U. INGOLD. Can. J. Chem. **51**, 1543 (1973).
17. M. L. KAPLAN and P. G. KELLEHER. J. Polym. Sci. Polym. Lett. **9**, 565 (1971).
18. A. FARMILO and F. WILKINSON. Photochem. Photobiol. **18**, 447 (1973).
19. A. ADAMCZYK and F. WILKINSON. J. Chem. Soc. Faraday Trans. II **68**, 2031 (1972).
20. O. L. J. GIJZEMAN, F. KAUFMAN, and G. PORTER. J. Chem. Soc. Faraday Trans. II, **69**, 708 (1973).
21. J. P. GUILLORY and C. F. COOK. J. Polym. Sci. **11**, 1927 (1973).
22. P. D. BARTLETT, G. D. MENDENHALL, and A. P. SCHAAP. Ann. N.Y. Acad. Sci. **171**, 79 (1970).
23. R. H. YOUNG, R. L. MARTIN, D. FERIOZI, D. BREWER, and R. KAYSER. Photochem. Photobiol. **17**, 233 (1973).
24. B. E. ALGAR and B. STEVENS. J. Phys. Chem. **74**, 3029 (1970).
25. P. B. MERKEL and D. R. KEARNS. J. Am. Chem. Soc. **94**, 7244 (1972).
26. J. P. DALLE, R. MAGOUS, and M. MOUSSERON-CANET. Photochem. Photobiol. **15**, 411 (1972).
27. B. FELDER and R. SCHUMACHER. Angew. Makromol. Chem. **31**, 35 (1973).
28. J. FLOOD, K. E. RUSSELL, and J. K. S. WAN. Macromolecules, **6**, 669 (1973).
29. F. A. COTTON and G. WILKINSON. Advanced inorganic chemistry. 2nd ed. Interscience, New York, N.Y. 1966. Chapt. 28.
30. S. OTSUKA, A. NAKAMURA, Y. TATSUNO, and M. MIKI. J. Am. Chem. Soc. **94**, 3761 (1972).
31. L. H. VOGT, F. M. FAIGENBAUM, and S. E. WIBERLEY. Chem. Rev. **63**, 269 (1963).

Can. J. Chem. Downloaded from www.nrcresearchpress.com by 210.87.254.105 on 09/05/12
For personal use only.

Apparent Molal Volumes and Heat Capacities of Alkaline Earth Chlorides in Water at 25 °C

GÉRALD PERRON AND JACQUES E. DESNOYERS[1]

Department of Chemistry, Université de Sherbrooke, Sherbrooke, Québec

AND

FRANK J. MILLERO

Rosenstiel School of Marine and Atmospheric Science, University of Miami, Miami, Florida 33149

Received May 3, 1974

GÉRALD PERRON, JACQUES E. DESNOYERS, and FRANK J. MILLERO. Can. J. Chem. **52**, 3738 (1974).

The densities and volumetric specific heats of the alkaline earth chlorides have been measured in water at 25 °C in the concentration range 0.01 to 0.4 *M* with a flow densimeter and a flow microcalorimeter. Apparent molal volumes and heat capacities have been derived.

GÉRALD PERRON, JACQUES E. DESNOYERS et FRANK J. MILLERO. Can. J. Chem. **52**, 3738 (1974).

Les masses volumiques et les capacités calorifiques des chlorures des alcalino-terreux ont été mesurées dans l'eau à 25 °C dans le domaine de concentration 0.01 à 0.4 *M* au moyen d'un densimètre et d'un microcalorimètre dynamiques. Les capacités calorifiques et volumes apparents molaires correspondants ont été calculés.

Can. J. Chem. Downloaded from www.nrcresearchpress.com by 210.87.254.6 on 09/05/12
For personal use only.

There seems to be very few precise measurements of the heat capacity of multivalent salts in water. These data would be very useful to predict the temperature dependence of activity data and to gain information on solute–solvent interactions. Such measurements are now readily obtainable with flow microcalorimeters (1). With this technique, the relative difference in volumetric specific heat σ (J K^{-1} cm^{-3}) with respect to that of a reference σ_0, usually taken as the pure solvent, is obtained. From the change $(\sigma - \sigma_0)/\sigma_0$, the apparent molal heat capacities are derived from the relation

$$[1] \qquad \phi_C = \phi_V\sigma_0 + 1000\,(\sigma - \sigma_0)/c$$

or

$$[2] \qquad \phi_C = Mc_p + 1000\,(c_p - c_p{}^0)/m$$

where c and m are respectively the molarity and the molality, M is the solute molecular weight, c_p is the weight specific heat ($c_p = \sigma/d$ where d is the density), and ϕ_V is the apparent molal volume. The purpose of the present paper is to report ϕ_C data for alkaline earth chlorides at 25 °C.

As it can be seen from eqs. 1 and 2, ϕ_C can be calculated from σ only if ϕ_V or density data of comparable accuracy are known. Precise densities of some of the alkaline earth chlorides have been determined by Dunn (2) and by Wirth and Bangert (8). However, we felt it would be useful to repeat all the densities using a flow densimeter (4) since an agreement with the literature values would at least serve as a check of the purity of our salts.

The apparent molal volumes were calculated in the usual way from the densities of the solutions d and of the solvent d_0 with

$$[3] \qquad \phi_V = M/d_0 - 1000(d - d_0)/cd_0$$

The techniques used for specific heat measurements with a flow microcalorimeter (1) and for density measurements with a flow densimeter (4) have been described previously. The relative change in specific heat $\Delta\sigma/\sigma_0$ can be obtained to $\pm 0.3\%$ (3) up to the limit of the sensitivity on $\Delta\sigma$ which is $\pm 7 \times 10^{-5}$ J K^{-1} cm^{-3}. Differences in densities $d - d_0$ can be measured to $\pm 3 \times 10^{-6}$ g cm^{-3}.

Stock solutions were made of all the salts with reagent grade Fisher Chemicals (without further purification). The concentrations of the stock solutions were determined by making weight titrations with $AgNO_3$. The stock solutions were used to prepare the other solutions by weight dilution. Deionized water (Millipore Super Q)

[1]To whom correspondence should be addressed.

TABLE 1. Apparent molal volumes and heat capacities of alkaline earth chlorides in water at 25 °C

m	c	$(d - d_0) \times 10^3$ (g cm^{-3})	ϕ_V (cm^3 mol^{-1})	$\left[\frac{\sigma - \sigma_0}{\sigma_0}\right] \times 10^3$	ϕ_C (J K^{-1} mol^{-1})	c_p (J K^{-1} g^{-1})
Magnesium chloride						
0.00386	0.00385	0.311	14.44			
0.01332	0.01328	1.065	15.04	−0.98	−246.6	4.1707
0.02320	0.02312	1.849	15.29	−1.70	−241.8	4.1645
0.03312	0.03301	2.630	15.57	−2.31	−226.6	4.1587
0.06610	0.06583	5.214	16.06	−4.64	−227.0	4.1383
0.13161	0.13093	10.287	16.70	−9.11	−220.4	4.0989
0.19730	0.19606	15.316	17.14	−13.55	−216.5	4.0603
0.26330	0.26132	20.313	17.53	−17.69	−209.1	4.0234
0.34096	0.33790	26.142	17.90	−22.53	−203.3	3.9808
Calcium chloride						
0.01256	0.01252	1.156	18.70	−1.01	−257.5	4.1703
0.02235	0.02227	2.051	18.95	−1.75	−247.6	4.1634
0.03287	0.03275	3.003	19.34	−2.58	−248.8	4.1560
0.06635	0.06607	6.047	19.52	−5.12	−241.2	4.1328
0.13065	0.12992	11.808	20.16	−9.76	−229.0	4.0901
0.19623	0.19486	17.621	20.62	−14.38	−221.7	4.0477
0.26325	0.26103	23.504	21.01	−19.04	−216.4	4.0053
0.32800	0.32476	29.135	21.34	−23.43	−211.6	3.9655
Strontium chloride						
0.00374	0.00373	0.519	19.26			
0.01261	0.01257	1.750	19.36	−1.05	−268.3	4.1676
0.02186	0.02179	3.031	19.44	−1.78	−258.7	4.1592
0.03250	0.03238	4.491	19.89	−2.63	−255.9	4.1496
0.06524	0.06496	8.992	20.16	−5.22	−250.6	4.1203
0.12923	0.12851	17.715	20.73	−9.99	−237.5	4.0653
0.19752	0.19612	26.937	21.24	−14.84	−226.9	4.0090
0.25129	0.24920	34.142	21.58	−18.64	−221.8	3.9656
0.32856	0.32524	44.417	22.03	−24.07	−216.6	3.9048
Barium chloride						
0.00388	0.00387	0.715	23.44			
0.01562	0.01557	2.871	23.93			
0.02736	0.02726	5.009	24.57	−2.43	−268.6	4.1483
0.03879	0.03864	7.088	24.87	−3.40	−262.8	4.1357
0.07881	0.07842	14.341	25.45	−6.75	−252.7	4.0922
0.15690	0.15580	28.389	26.11	−13.05	−239.3	4.0107
0.23647	0.23428	42.502	26.92	−19.18	−228.9	3.9316
0.31614	0.31251	56.554	27.36	−25.06	−220.2	3.8558
0.38688	0.38165	68.920	27.75	−30.04	−212.3	3.7917

and water redistilled from an alkaline permanganate solution were both used. Both types of water gave similar results inside the experimental error. The molalities were converted to molarities whenever necessary using the measured solution densities. In all calculations, d_0 and σ_0 were taken as 0.997047 g cm^{-3} (5) and 4.1793 J K^{-1} cm^{-3} (6) at 25 °C.

The experimental data and derived ϕ_V, ϕ_C, and c_p are given in Table 1. The apparent molal quantities can be expressed either in terms of c or m using a Redlich type equation (7)

$$[4] \quad \phi_V = \phi_V^0 + A_V c^{1/2} + B_V' c + \ldots$$

$$[5] \quad \phi_V = \phi_V^0 + A_V (d_0 m)^{1/2} + B_V m + \ldots$$

$$[6] \quad \phi_C = \phi_C^0 + A_C c^{1/2} + B_C' c + \ldots$$

$$[7] \quad \phi_C = \phi_C^0 + A_C (d_0 m)^{1/2} + B_C m + \ldots$$

The A_V and A_C coefficients can be calculated from the Debye-Hückel limiting law and have the values 9.706 and 150.6 for 2:1 electrolytes in water at 25 °C for ϕ_V and ϕ_C expressed in cm^3 mol^{-1} and J K^{-1} mol^{-1}.

Can. J. Chem. Downloaded from www.nrcresearchpress.com by 210.87.254.6 on 09/05/12
For personal use only.

Can. J. Chem. Downloaded from www.nrcresearchpress.com by 210.87.254.6 on 09/05/12
For personal use only.

Plots of $\phi_V - A_V c^{1/2}$ *vs.* c are shown in Fig. 1. The ϕ_V data of Dunn (2) and of Wirth and Bangert (8) are also included for comparison; the agreement between the difference sets of data is usually inside 0.1 cm^3 mol^{-1}. The only disagreement is with the high dilution values of $MgCl_2$ where the present ϕ_V data are somewhat lower. It is not obvious which set of values are the most reliable, but, at these high dilutions, the error implied on ϕ_V causes an uncertainty on ϕ_C which is smaller than that arising from $\sigma - \sigma_0$.

The concentration dependence of the heat capacity is shown in Fig. 2. It is difficult to appraise the accuracy of the present ϕ_C data because of the sparcity of literature data on 2:1 electrolytes. The only system which has been studied extensively is $BaCl_2$. The data of White (9) and Richards and Dole (10) show a larger scatter and are in general 5 to 10 J K^{-1} mol^{-1} more negative than the present. Similarly, the infinite dilution value ϕ_C^0 of Criss and Cobble (11) obtained from heats of solution data is -304 compared with the present -293 J K^{-1} mol^{-1}. The mean values of the data of Kapustinsky and Dezideryeva (12) for $SrCl_2$ agree with the present ones despite their larger scatter. Lewis and Randall (13) report rounded ϕ_C values for $CaCl_2$ based on the data of Richards and Dole (10) and of Rutskov (14). The average values of Lewis and Randall (not shown) and those of Richard and Dole agree well with the present ones. The only data on $MgCl_2$ (15) are outside the range of the present measurements. The excellent agreement of our ϕ_V data and the general agreement of our

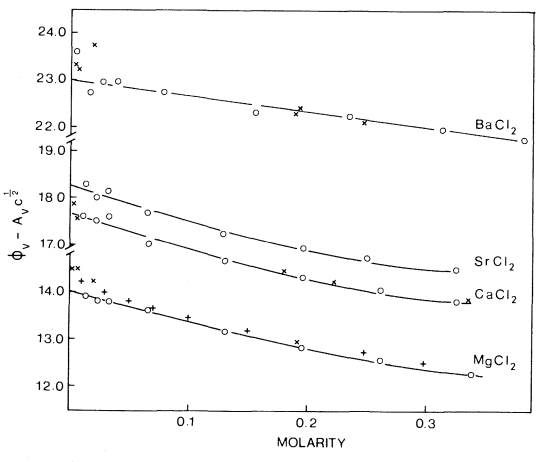

FIG. 1. Apparent molal volume of alkaline earth chlorides in water at 25 °C: ○, present work; ×, Dunn (2); +, Wirth and Bangert (8).

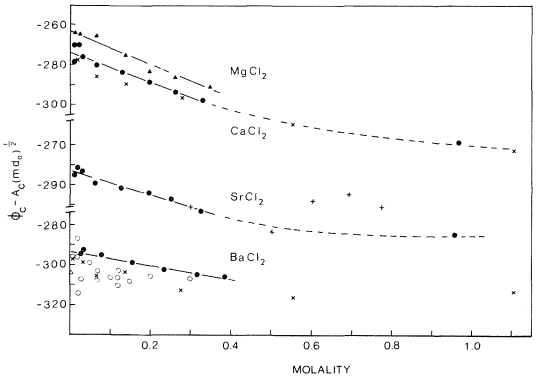

FIG. 2. Apparent molal heat capacity of alkaline earth chlorides in water at 25 °C: ▲, ●, present work; ×, Richards and Dole (10); ○, White (9); +, Kapustinsky and Dezideryeva (12); △, Criss and Cobble (11).

ϕ_C data with those of the literature lead us to believe that the present measurements are reliable to better than 5 J K^{-1} mol^{-1}.

The parameters of eqs. 4 and 5, derived from a weighted least-squares fitting of the present data, are summarized in Table 2. It can be shown (3) that the same ϕ_V^0 and ϕ_C^0 are obtained inside the experimental uncertainty whether the data are expressed in c or m; ϕ_C^0 and ϕ_V^0 were therefore fixed at the values given from eqs. 4 and 6 and the parameters B_C, B_V, C_C, and C_V determined from eqs. 5 and 7. With ϕ_C of all the salts and ϕ_V of $BaCl_2$, a term in c or m is sufficient to represent the data up to 0.4 M. With ϕ_V of the other salts a term in $c^{3/2}$ or $m^{3/2}$ is also required. An examination of the parameters ϕ_V^0, B_V, ϕ_C^0, and B_C show that they vary in a systematic way with the size of the cations with the exception of B_V of $BaCl_2$ which seems too positive with respect to the others. However, an examination of Fig. 1 gives us no reason to expect that our data or that of Dunn could be in error. The concentration dependence of ϕ_V and ϕ_C of the alkaline earth chlorides does not show any evidence of strong ion-pair formation, as in the case of $MgSO_4$ (16), but does not preclude the possibility of a small degree of association.

Conventional ionic standard partial molal heat capacities, based on $\bar{C}_p^0(H^+) = 0$ at 25 °C, can be obtained by subtracting from ϕ_C^0 twice the conventional value for Cl^-, -123.1 J K^{-1} mol^{-1} (3). These values are: Mg^{2+}, -16; Ca^{2+}, -28; Sr^{2+}, -36; Ba^{2+}, -46 J K^{-1} mol^{-1}. Nothing can be said on the sign of the $\bar{C}_p^0$ (conv) since these are not absolute values. However, these

TABLE 2. Parameters of eqs. 4 to 7 of alkaline earth chlorides in water for ϕ_C and ϕ_V given respectively in J K^{-1} mol^{-1} and cm^3 mol^{-1}

Salt	ϕ_V^0	B_V	C_V	B_V'	C_V'	ϕ_C^0	B_C	B_C'
$MgCl_2$	14.02	−8.32	5.36	−8.38	5.48	−262.2	−87.7	−87.7
$CaCl_2$	17.65	−10.45	8.38	−10.55	8.58	−274.5	−71.3	−71.0
$SrCl_2$	18.26	−11.25	10.16	−11.37	10.42	−282.0	−62.6	−62.2
$BaCl_2$	22.98	−3.28		−3.24		−292.2	−38.3	−37.5

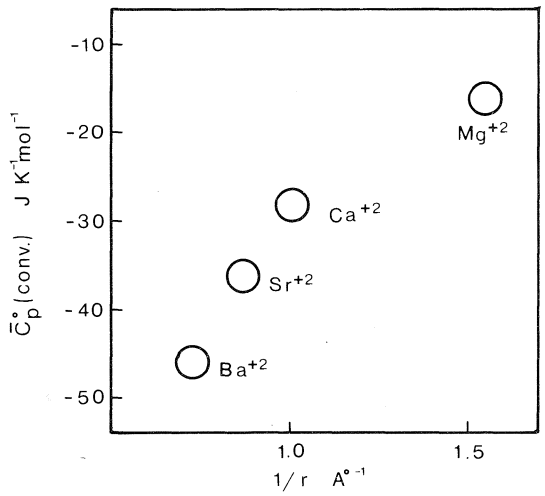

FIG. 3. Conventional standard partial molal heat capacities of alkaline earth ions in water at 25 °C.

$\bar{C}_p^0$ (conv) increase with decreasing ionic size (Fig. 3) while the Born equation (17) predicts a decrease. Therefore, as in the case of alkali halides (3), the Born equation fails to account for the size dependence of partial molal heat capacities and other types of interactions such as structural ones have to be considered.

J.E.D. wishes to acknowledge the support of the Defence Research Board of Canada (Grant 5401-05) and F.J.M. of the Office of Naval Research (contract N00014-67-A-0201-0013) and Oceanographic Branch of the National Science Foundation (GA-17386).

1. P. PICKER, P. A. LEDUC, P. R. PHILIP, and J. E. DESNOYERS. J. Chem. Thermodyn. **3**, 631 (1971).
2. L. A. DUNN. Trans. Faraday Soc. **62**, 2348 (1966).
3. J. L. FORTIER, P. A. LEDUC, and J. E. DESNOYERS. J. Solution Chem. **3**, 323 (1974).
4. P. PICKER, E. TREMBLAY, and C. JOLICOEUR. J. Solution Chem. **3**, 377 (1974).
5. G. S. KELL. J. Chem. Eng. D. **12**, 66 (1967).
6. H. F. STIMSON. Am. J. Phys. **23**, 614 (1955).
7. O. REDLICH. Naturwissenschaften, **19**, 251 (1930); O. REDLICH and D. M. MEYER. Chem. Rev. **64**, 221 (1964).
8. H. E. WIRTH and F. K. BANGERT. J. Phys. Chem. **76**, 3488 (1972).
9. C. M. WHITE. J. Am. Chem. Soc. **58**, 1615 (1936).
10. T. W. RICHARDS and M. DOLE. J. Am. Chem. Soc. **51**, 794 (1929).
11. C. M. CRISS and J. W. COBBLE. J. Am. Chem. Soc. **83**, 3223 (1961).
12. A. F. KAPUSTINSKY and I. P. DEZIDERYEVA. Trans. Faraday Soc. **42**, 69 (1946).
13. G. N. LEWIS and M. RANDALL. Thermodynamics. *Revised by* K. S. Pitzer and L. Brewer. McGraw–Hill, New York. 1961. p. 653.
14. A. P. RUTSKOV. Zhur. Prik. Khim. **21**, 8 (1948).
15. M. EIGEN and E. WICKE. Z. Electrochem. **55**, 354 (1951).
16. G. PERRON, J. E. DESNOYERS, and F. J. MILLERO. To be published.
17. R. M. NOYES. J. Am. Chem. Soc. **86**, 971 (1964).

Can. J. Chem. Downloaded from www.nrcresearchpress.com by 210.87.254.6 on 09/05/12
For personal use only.

Comments on the Crystal Structure of Polypivalolactone and Deviation of Ester Groups from *trans* Planarity

J. CORNIBERT,[1] N. V. HIEN, F. BRISSE, AND R. H. MARCHESSAULT[2]

Department of Chemistry, Université de Montréal, C.P. 6210, Montréal, Québec H3C 3V1

Received May 13, 1974

J. CORNIBERT, N. V. HIEN, F. BRISSE, and R. H. MARCHESSAULT. Can. J. Chem. **52**, 3742 (1974).

The crystalline conformation of polypivalolactone was determined by analysis of the chain conformational energies and it was found that the minimum energy corresponds to a planar *trans* conformation for the ester group. The result was compared to published X-ray data based on fiber diffraction which show a significant deviation from *trans* planarity. This difference is discussed in terms of the relative energies involved and by comparison with literature crystallographic results of low molecular weight carboxylic esters. It is stressed that because of the paucity of information in fiber diffraction, internal energy considerations are important for assigning internal rotation angles. Crystallographic results for low molecular weight compounds show that deviations greater than 10° from *trans* planarity are rare for ester groups.

J. CORNIBERT, N. V. HIEN, F. BRISSE et R. H. MARCHESSAULT. Can. J. Chem. **52**, 3742 (1974).

On a déterminé la conformation cristalline de la polypivalolactone par analyse des énergies conformationnelles de chaînes; on a trouvé que l'énergie minimum correspond à une conformation *trans* coplanaire pour le groupe ester. Ce résultat est comparé avec les données de rayons-X publiées, basées sur la diffraction de fibre, qui montrent une déviation notable de la planarité *trans*. On discute de cette différence en termes d'énergies relatives impliquées et par comparaison avec les résultats cristallographiques rapportés dans la littérature pour des esters carboxyliques de faible poids moléculaire. On fait remarquer que, dû au peu d'information de la diffraction des fibres, la considération d'énergie internee est importante pour attribuer les angles de rotation interne. Les résultats cristallographiques pour des composés de bas poids moléculaires montrent que des déviations plus grandes que 10° par rapport à la planarité *trans* sont rares dans les groupes esters. [Traduit par le journal]

Introduction

The detailed crystal structure of polypivalolactone (PPL) was first reported by Carazzolo (1) based on analysis of an X-ray fiber diagram of this polymer; from the measured fiber repeat of 6.02 Å and evidence for a 2_1 helix, the author proposed a chain model of type T_2G_2 (2) which would place all the ester groups in a planar *trans* conformation. This structure was referred to by Knobloch and Statton (3) who also discovered a second crystalline conformation involving a planar *zig-zag* chain with a fiber repeat of 4.74 Å.

In a more recent paper by Perego *et al.* (4), the crystal structure of PPL was studied by an analysis of the observed intensities in the fiber diagram of the 2_1 helical form. The internal rotation angles corresponding to the proposed crystalline conformation are such that the chain atoms of the ester group 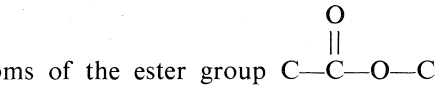 are not in a planar *trans* conformation such as is usually the case in the crystalline conformations of low molecular weight acetates, benzoates, and other carboxylic esters (5–39). In Fig. 1 is shown the distribution of the important internal rotation angle (ω, see Fig. 2) of the ester groups of low molecular weight compounds; the most frequent value of ω is found to be less than 1°, the mean value is calculated to be 4°, and of the 64 ester groups surveyed no value higher than 14° is reported.

We have been studying the crystallography and conformation of polyesters based on the propiolactone backbone, that is polyester chains of the type $+CHR—CR'R''—COO+_n$, and have consistently found that minimum energy is attained only when the ester group has a near planar *trans* conformation. In order to compare our results for PPL with those of Perego *et al.* (4), who have used a slightly

[1]Present address: Institut de Recherche Clinique de Montréal, Boulevard des Pins, Montréal, Québec.

[2]To whom correspondence should be addressed.

Can. J. Chem. Downloaded from www.nrcresearchpress.com by 210.87.254.105 on 09/05/12
For personal use only.

TABLE 1. List of bond lengths and angles used in this study (44) and by Perego *et al.* (4) for PPL (*cf.* Fig. 2*a*)

	Length (Å)			Angle (deg)	
Bond	Ref. 4	Ref. 44	Angle	Ref. 4	Ref. 44
a	1.54	1.53	***ab***	108.5	109.5
b	1.52	1.53	***bc***	109.0	115.0
c	1.31	1.36	***cd***	112.0	114.0
d	1.44	1.45	***da***	111.5	110.0
e	1.25	1.23	***be***	127.0	120.0
f	1.54	1.54	***af***	109.5	109.5

different set of bond lengths and bond angles than those used in our study (*cf.* Table 1), we have repeated the conformational energy calculation using their molecular parameters (*cf.* Table 2). Our calculations are based strictly on energy considerations and show that a deviation of 16°, as proposed by Perego *et al.* (4) for poly-pivalolactone from the *trans* conformation of the ester group would be energetically costly for the crystalline conformation which they propose.

Those results are contained in Table 3 where the internal rotation angles used by Perego *et al.* (4) following the notation of Natta *et al.* (46) have been converted to the ω, θ, ψ, φ notation[3] which we defined in a previous paper (45) as is shown in Fig. 2.

Summary of Conformational Calculations

The choice of bond lengths and angles which we have made is based on the standard values for organic molecules (47) and on the results of electron diffraction and microwave spectroscopy of methyl formate and acetate (48, 49). These values are close to those used by Brant *et al.* (50) and Ooi *et al.* (51) in their work on poly-L-lactic acid and poly-β-methyl-L-aspartate. For angle *da* (*cf.* Fig. 2*a*), the value of 110° has been used, it agrees with the results from the interpretation of microwave spectra of ethyl formate (52) and it is the average value of angle C—C—OH for alcohols (47).

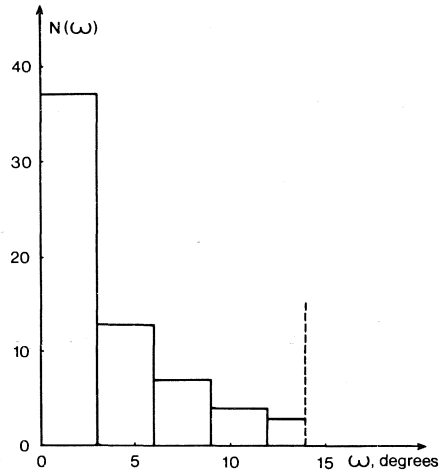

FIG. 1. Distribution of ester rotation angle ω (*cf.* Fig. 2) from crystallographic data of 64 carboxylic esters of low molecular weight compounds (refs. 5–39).

For PPL, there are four internal rotation angles to vary. Therefore in constructing Ramachandran maps (54) it is necessary to work in four dimensions *i.e.* one map for each ω and θ. Then lines of constant energy, of constant fiber repeat, and of constant number of monomers per turn of helix are plotted as functions of ψ and φ (*e.g.* in Fig. 3). Different maps are obtained as ω and θ take on different values. By inspection, when a region of correct helical parameters and of low energy is recognized, another program is used to do the refined search for the minimum energy (44).

The conformational energy calculated takes into account the following intramolecular contributions to the total energy U of the chain:

[3]The internal rotation angles used by Perego *et al.* follow Natta's notation wherein σ of a bond is zero when this bond together with two immediate neighbors in the chain are arranged in a *cis* conformation, while in our notation the angle is zero when a *trans* conformation is obtained. If we consider any three successive chain bonds, L_1, L_2, and L_3, looking along L_2 from L_1 the positive internal rotation angle σ is the angle which L_3 has been rotated clockwise away from the conformation where σ = 0 (*cis* in the notation of Perego *et al.* and *trans* in our notation). Figure 1 serves to identify the different bonds and internal rotation angles in PPL.

To convert from the notation of Perego *et al.* to ours use the formula $\psi = 180 + \sigma_a$.

Can. J. Chem. Downloaded from www.nrcresearchpress.com by 210.87.254.105 on 09/05/12
For personal use only.

TABLE 2. Conformational energies for conformations satisfying crystalline parameters n and h

Conformation*					
ω (deg)	θ (deg)	ψ (deg)	φ (deg)	Reference	Energy†
0.00	28.1	239.5	214.4	This study (min. energy)	−2.475
16.0	−2.0	221.0	241.0	Perego *et al.*	−0.342‡
2.0	14.5	235.4	224.6	This study (min. energy)	−1.74
16.0	−2.0	221.0	241.0	Perego *et al.*	−0.12

*All these conformations correspond to right-handed "crystalline" helices.
†Unit for energy is kcal/mol of monomer.
‡This conformation is possible only for a slightly greater fiber repeat of 6.18 Å.

(*a*) Electrostatic energy (U_E): it is caused by dipole–dipole interaction of the ester groups and is calculated by Coulomb's law with the concept of partial charges; data on partial charges come from Smyth (55) and we used the same dielectric constant 3.0 as Brant *et al.* (50).

(*b*) Energy of interaction between non-bonded atoms (U_{NB}): this energy is calculated by the classical "6–12" relation of Lennard–Jones (53, 54); the parameters used come from Yan *et al.* (56). Following a suggestion by Gibson and Scheraga (57), the hydrogen atoms of the methyl groups were incorporated in an enlarged carbon atom.

(*c*) Torsional energy around the single bonds (U_T) (58): this energy complements U_{NB} in explaining the height of the energy barrier involved in free rotation (53, 54). By the method of Scott and Scheraga (58), the torsional barrier used in a periodic function is obtained from lower weight molecules. The torsional barrier of the angle ω is very high, 8.75 kcal/mol of monomer.

TABLE 3. Atomic coordinates* of PPL monomer corresponding to minimum energy as shown in Fig. 4

Atom	x (Å)	y (Å)	z (Å)
C^{α}	1.890	0.0	0.0
C (carbonyl)	0.933	−0.804	0.883
O (ester)	−0.193	−0.142	1.260
C^{β}	−1.085	−0.923	2.095
O (carbonyl)	1.211	−1.960	1.198
$H^{\beta,1}$	−1.768	−1.489	1.479
$H^{\beta,2}$	−0.514	−1.608	2.705
$C^{\delta,1}$	2.818	0.837	0.883
$C^{\delta,2}$	2.725	−0.958	−0.852

*The coordinates are referred to an orthogonal system of axes with z as helix axis.

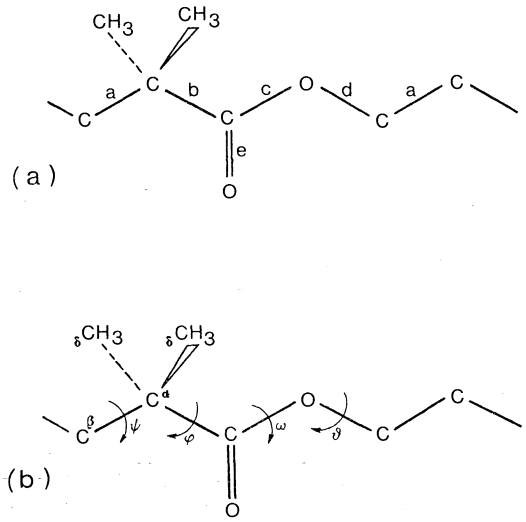

FIG. 2. Identification of bonds: (*a*) Perego *et al.* (4); (*b*) internal rotation angles used in this study.

Discussion

In Table 2, different conformations of PPL and their calculated energies are listed. It is noted that, for either choice of molecular parameters, the minimum energy conformation always includes angle $\omega \simeq 0°$ such as to keep the chain atoms of the ester group in the same plane. The calculated energies are found to be especially sensitive to changes in angle ω, and much less so to changes in the other three angles, at least in the region where $\omega \simeq 0°$. The conformation proposed by Perego *et al.* has relatively high energy (−0.12 kcal/mol of monomer) as compared to the helix of minimum energy (−1.74 kcal/mol of monomer) which also satisfies the fiber repeat and symmetry considerations dictated by the X-ray data.

Can. J. Chem. Downloaded from www.nrcresearchpress.com by 210.87.254.105 on 09/05/12
For personal use only.

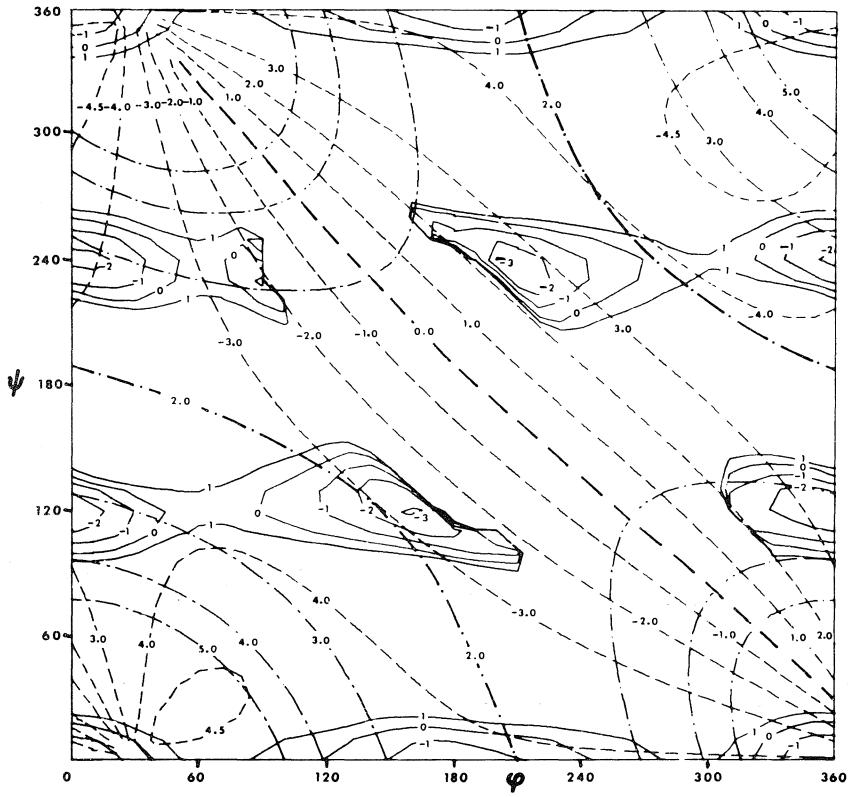

FIG. 3. Conformational map of polypivalolactone for $\omega = 0°$ and $\theta = 331.9°$: energy contour — in kcal/mol and curves giving n (number of monomers per turn) ----- and h (advance per monomer) --- in Å, sign + or − for respectively right-handed or left-handed helicoidal conformations.

Using our choice of bond distances and angles, the conformation of Perego *et al.* is still found to have energy far from the minimum, whereas the conformation proposed here (*cf.* Fig. 4) has the lowest energy of all.

Figure 3 shows the φ,ψ map corresponding to the minimum energy for the 2_1 chain with fiber repeat of 6.02 Å. The map has $\omega = 0°$ and $\theta = 331.9°$ as parameters, the minimum energy can be seen to occur at $\varphi = 145.6°$ and $\psi = 120.5°$ where the curves $n = 2$ and $h = -3$ intersect each other (these angles correspond to a left-handed helix, a right-handed helix of equal energy in this case would have $\omega = 0°$, $\theta = 28.1°$, $\varphi = 214.4°$, and $\psi = 239.5°$, see Table 2). Figure 4 shows projections of the helix corresponding to this energy minimum and whose atomic coordinates are listed in Table 3.

We have also studied the crystalline conformations of two other polyesters, poly-β-hydroxybutyrate (PHB) (43) and poly-β-propiolactone (PL) (42), which possess the same main chain backbone atoms as PPL but different lateral groups. In the crystalline state, these three polyesters adopt the same type of helix, 2_1, but with slightly different advances per monomer, 2.98, 3.51, and 3.01 Å for PHB, PL, and PPL respectively. For the minimum energy of all these polymers, we have found no deformation of the planarity of the ester group, *i.e.* $\omega \simeq 0°$ even in the case of PHB which has an asymmetric carbon due to the lateral methyl group in the β position.

In their studies of polyethylene adipate, $[(CH_2)_2—OCO—(CH_2)_4—COO]_n$, and polyethylene suberate, $[(CH_2)_2—OCO—(CH_2)_6—COO]_n$, Turner-Jones and Bunn (42) proposed a planar zig-zag conformation for the aliphatic acid chain section. All of the internal rotations of bonds, accounting for an observed shortening of 0.5 Å in the fiber repeat as compared to the ideal planar conformation of the chain were

Can. J. Chem. Downloaded from www.nrcresearchpress.com by 210.87.254.105 on 09/05/12
For personal use only.

Can. J. Chem. Downloaded from www.nrcresearchpress.com by 210.87.254.105 on 09/05/12
For personal use only.

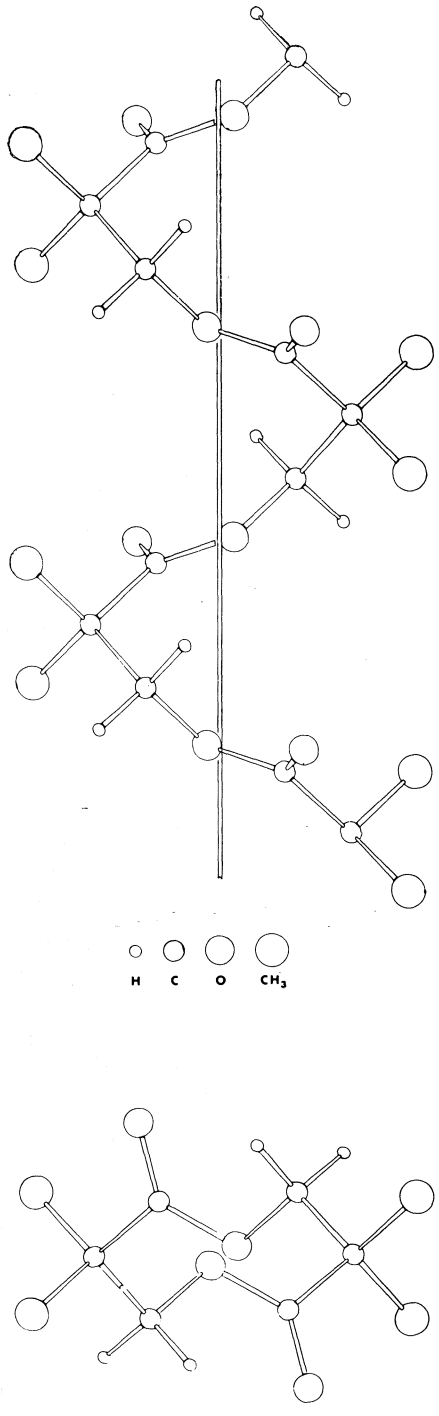

FIG. 4. Conformation of polypivalolactone corresponding to minimum energy conformation in Fig. 3 (left-handed helix, $\omega = 0°$, $\theta = 331.9°$, $\varphi = 145.6°$, $\psi = 120.5°$).

in the ester portion of the polymer backbone. Based only on fiber diffraction analysis (42), this proposal is correct as stated. The ester group internal rotation angles derived by these authors were: $\theta = 66°$, $\omega = 18°$, $\varphi = 10°$. In our calculations it is noted that the torsional barrier energies for θ, ω, and φ are 0.0, 8.75, and 0.2 kcal/mol, respectively, this suggests that ω should be more restricted than φ and by combining potential energy calculations with X-ray analysis these authors would probably have arrived at values of internal rotation angles somewhat different than proposed. The relatively large value for ω is particularly suspect (*cf.* Fig. 1).

Kim (43) determined the crystal structure of polytetramethylene adipate, $[(CH_2)_4—OCO—(CH_2)_4—COO]_n$, and found an ideal planar zig-zag conformation. In this case there is no shortening of the fiber repeat as in the cases studied by Turner-Jones and Bunn (42). It should be interesting to look at the crystal structures of ethylene glycol diesters which could serve as model compounds for understanding why polyesters based on ethylene glycol have a distinctly non-planar ester conformation.

Bittiger and Marchessault (40) studied the crystal structure of poly-ε-caprolactone by interpretation of X-ray diffraction patterns of the fiber and found the ester group to have planar *trans* conformation. Independently, Chatani *et al.* (41) studied the crystallography of the same polymer and proposed a conformation with $\omega = 7°$ well within the limits shown in Fig. 1.

In conclusion, refinements of polymer crystal structures by comparison of observed and calculated X-ray intensities allow rather poor precision when there is a choice of conformational angles. Polymer crystallographers have a variety of approaches to systematically minimize the chain conformational energy and compare observed and calculated intensities. An approach along these lines was made for PPL by Perego *et al.* but, as this note is intended to show, it is noteworthy that their conformation does not coincide with the minimum energy "crystalline" conformation. It is always possible for lattice energy to compensate for an unfavorable chain conformational energy, but the small molecule examples cited in Fig. 1 lead

one to expect that the minimum energy of the independent chain and the actual conformation in the crystal in the case of linear homopolyesters will involve ω values close to zero.

1. G. CARAZZOLO. Chem. Ind. **46**, 525 (1964).
2. A. E. ALEXANDER. X-Ray diffraction methods in polymer science. Wiley-Interscience, New York. 1969. p. 365.
3. F. W. KNOBLOCH and W. O. STATTON. U.S. Patent, 3, 299, 171 (1967).
4. G. PEREGO, A. MELIS, and M. CERASI. Die Makromol. Chem. **157**, 269 (1972).
5. A. CAMERMAN and J. TROTTER. Acta Cryst. **18**, 197 (1965).
6. A. M. O'CONNELL and I. PASCHER. Acta Cryst. B**25**, 2553 (1969).
7. P. W. R. CORFIELD, J. D. MOKREN, P. L. DURETTE, and D. HORTON. Carbohydr. Res. **23**, 158 (1972).
8. F. LEUNG and R. H. MARCHESSAULT. Can. J. Chem. **51**, 1215 (1973).
9. B. L. BARNETT and R. E. DAVIS. Acta Cryst. B**26**, 326 (1970).
10. W. R. KRIGBAUM and P. G. BARBER. Acta Cryst. B**27**, 1884 (1971).
11. H. AKIMOTO and Y. IITAKA. Acta Cryst. B**25**, 1491 (1969).
12. R. C. PETTERSEN. J. Am. Chem. Soc. **93**, 5629 (1971).
13. A. E. SMITH, R. KALISH, and E. J. SMUTNY. Acta Cryst. B**28**, 3494 (1972).
14. B. JENSEN. Acta Chem. Scand. **25**, 3388 (1971).
15. S. ALEBY and E. VONSYDOW. Acta Cryst. **13**, 487 (1960).
16. K. LARSSON. Ark. Kemi. **23**, 1 (1965).
17. D. C. HODGKIN and E. N. MASLEN. Biochem. J. **79**, 393 (1961).
18. S. ABRAHAMSSON. Acta Cryst. **16**, 409 (1963).
19. T. A. HAMOR, W. S. CAUGHEY, and J. L. HOARD. J. Am. Chem. Soc. **87**, 2305 (1965).
20. A. F. CAMERON, K. K. CHEUNG, G. FERGUSON, and J. M. ROBERTSON. J. Chem. Soc. B, 559 (1969).
21. P. COGGON, A. T. MCPHAIL, and G. A. SIM. J. Chem. Soc. B, 534 (1969).
22. E. J. GABE and W. H. BARNES. Acta Cryst. **16**, 796 (1963).
23. C. S. GIBBONS and J. TROTTER. J. Chem. Soc. B, 840 (1969).
24. I. C. PAUL, G. A. SIM, T. A. HAMOR, and J. M. ROBERTSON. J. Chem. Soc. Lond. 4133 (1962).
25. J. A. HAMILTON, A. T. MCPHAIL, and G. A. SIM. J. Chem. Soc. Lond. 708 (1962).
26. J. K. FAWCETT and J. TROTTER. J. Chem. Soc. B, 174 (1966).
27. A. T. MCPHAIL and G. A. SIM. J. Chem. Soc. B, 962 (1968).
28. M. DOBLER, J. D. DUNITZ, and B. T. KILBOURN. Helv. Chim. Acta, **52**, 2573 (1969).
29. J. W. MONCRIEF and W. N. LIPSCOMB. Acta Cryst. **21**, 322 (1966).
30. N. SAKABE and Y. HIRATA. Tetrahedron Lett. 965 (1966).
31. C. S. GIBBONS and J. TROTTER. J. Chem. Soc. B, 840 (1969).
32. M. NATSUME and Y. IITAKA. Acta Cryst. **20**, 197 (1966).
33. I. L. KARLE and J. KARLE. Acta Cryst. B**24**, 81 (1968).
34. C. TAMURA, O. AMAKUSA, Y. SASADA, and K. TSUDA. Acta Cryst. **21**, 226 (1966).
35. E. M. GOPALAKRISNA, A. COOPER, and D. A. NORTON. Acta Cryst. B**25**, 143 (1969).
36. E. M. GOPALAKRISNA, A. COOPER, and D. A. NORTON. Acta Cryst. B**25**, 1601 (1969).
37. H. SAKURAI, N. SAKABE, and Y. HIRATA. Tetrahedron Lett. 6309 (1966).
38. J. SYGUSCH, F. BRISSE, and S. HANESSIAN, Acta Cryst. B**30**, 40 (1974).
39. F. LEUNG and R. H. MARCHESSAULT. Private communication.
40. H. BITTIGER and R. H. MARCHESSAULT. Acta Cryst. B**26**, 1923 (1970).
41. Y. CHATANI, Y. OKITA, H. TADOKORO, and Y. YAMASHITA. Polym. J. **1**, 555 (1970).
42. A. TURNER-JONES and C. W. BUNN. Acta Cryst. **15**, 105 (1962).
43. C. W. KIM. Ph.D. Thesis. University of Delaware, 1971.
44. J. CORNIBERT. Ph.D. Thesis. Département de Chimie, Université de Montréal, Montréal, Québec. 1972.
45. J. CORNIBERT and R. H. MARCHESSAULT. J. Mol. Biol. **71**, 735 (1972).
46. G. NATTA, P. CORRADINI, and I. W. BASSI. J. Polym. Sci. **51**, 505 (1961).
47. H. J. M. BOWEN and L. E. SUTTON. Tables of interatomic distances and configurations in molecules and ions. The Chemical Society, London (1956), supplement (1965).
48. J. M. O'GORMAN, W. SHAND JR., and V. SHOEMAKER. J. Am. Chem. Soc. **72**, 4222 (1969).
49. R. F. CURL. J. Chem. Phys. **30**, 1529 (1959).
50. D. A. BRANT, A. E. TONNELI, and P. J. FLORY. Macromolecules, **2**, 228 (1969).
51. T. OOI, R. A. SCOTT, G. VANDERKOOI, and H. A. SCHERAGA. J. Chem. Phys. **46**, 4410 (1967).
52. J. M. RIVEROS and E. B. WILSON. J. Chem. Phys. **46**, 4605 (1967).
53. H. A. SCHERAGA. Advances in physical organic chemistry. Vol. 6. *Edited by* V. Gold. Academic Press, London. 1968. p. 103.
54. G. N. RAMACHANDRAN and V. SASISEKHARAN. Advances in protein chemistry. Vol. 23. *Edited by* C. B. Anfinsen *et al.* Academic Press, New York. 1968. p. 283.
55. C. P. SMYTH. Dielectric behavior and structure. McGraw–Hill, New York. 1955.
56. J. F. YAN, G. VANDERKOOI, and H. A. SCHERAGA. J. Chem. Phys. **49**, 2713 (1968).
57. K. D. GIBSON and H. A. SCHERAGA. Proc. Natl. Acad. Sci., U.S., **58**, 420 (1967).
58. R. A. SCOTT and H. A. SCHERAGA. J. Chem. Phys. **42**, 2209 (1965).

Can. J. Chem. Downloaded from www.nrcresearchpress.com by 210.87.254.105 on 09/05/12
For personal use only.

Chemical Behavior of Charge-transfer Complexes. VI.[1] Catalysis of Acetolysis of 2,4,7-Trinitro-9-fluorenyl *p*-Toluenesulfonate by Aromatic Hydrocarbon Donors

ALLAN K. COLTER, ARTHUR L. MCKENNA, III,[2] AND M. A. KASEM

Departments of Chemistry, Carnegie-Mellon University, Pittsburgh, Pennsylvania 15213 and University of Guelph, Guelph, Ontario N1G 2W1

Received July 30, 1973[3]

ALLAN K. COLTER, ARTHUR L. MCKENNA, III, and M. A. KASEM. Can. J. Chem. **52**, 3748 (1974).

The catalytic effectiveness of eleven aromatic hydrocarbon donors in the acetolysis of 2,4,7-trinitro-9-fluorenyl *p*-toluenesulfonate (TNF-OTs) has been examined. For nine of these donors, the kinetic data were analyzed to obtain the rate constant, k_c, for acetolysis of the 1:1 donor–substrate complex, and the 1:1 donor–substrate association constant, K. Two measures of catalytic effectiveness, log k_c and log k_cK correlate well with the highest occupied molecular orbital energy of the donor, E(HOMO), calculated by the Hückel molecular orbital (HMO) method. The success of these correlations is considered to mean that the transition state for acetolysis resembles a π-complex. A model based on Mulliken's charge-transfer theory in its simplest form leads to an estimate of 0.11 of an electron transferred from the donor to the acceptor substrate in the complexed transition state.

ALLAN K. COLTER, ARTHUR L. MCKENNA, III et M. A. KASEM. Can. J. Chem. **52**, 3748 (1974).

On a examiné l'utilité catalytique de 11 donneurs hydrocarbonés aromatiques pour l'acétolyse du *p*-toluènesulfonate de trinitro-2,4,7 fluorènyl-9 (TNF-OTs). Pour 9 de ces donneurs, on a analysé les données cinétiques pour obtenir une constante de vitesse, k_c, pour l'acétolyse du complexe donneur substrat 1:1 et la constante d'association, K, pour le donneur substrat 1:1. Deux mesures d'efficacité catalytique, log K_c et log k_cK assurent une bonne corrélation avec l'énergie HOMO calculée par la méthode HMO des orbitales moléculaires d'Hückel. On considère que le succès de ces corrélations signifie que l'état de transition pour l'acétolyse ressemble à un complexe π. Un modèle, basé sur la théorie de transfert de charge de Mulliken dans sa forme la plus simple, permet d'estimer à 0.11 la quantité d'électron transférée du donneur au substrat accepteur dans l'état de transition complexé.

[Traduit par le journal]

Introduction

Earlier work has shown that acetolysis of 2,4,7-trinitro-9-fluorenyl *p*-toluenesulfonate (TNF-OTs) is strongly catalyzed by aromatic

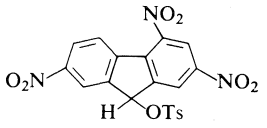

TNF-OTs

donors (1–3) and that the magnitude of the rate enhancements is sensitive to donor structure. For example, at 99.3°, 0.02 *M* phenanthrene, acenaphthene, and anthracene increase the observed rate constants by factors of 1.9, 5.1, and 10, respectively (1). These rate enhancements parallel the frequencies of the charge-transfer absorption maxima of complexes of these donors with the acceptors trinitrobenzene, chloranil, and tetracyanoethylene (1).

Our interpretation of these catalytic effects has been based on the mechanistic scheme [1] in which D is donor, D·TNF-OTs is a 1:1

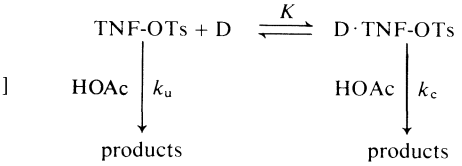

[1]

donor–substrate π-complex or complexes, k_u and k_c are rate constants for acetolysis of uncomplexed and complexed substrate, respectively, and K is the 1:1 donor–substrate association constant. The enhanced reactivity of the π-complex is presumed to be a result of charge transfer from donor to substrate in the electronically-deficient transition state. According to

[1]Part V of this series, ref. 3.

[2]Taken in part from the Ph.D. thesis of A. L. McKenna, III (25).

[3]Revision received August 9, 1974.

Can. J. Chem. Downloaded from www.nrcresearchpress.com by 210.87.254.105 on 09/05/12
For personal use only.

Can. J. Chem. Downloaded from www.nrcresearchpress.com by 210.87.254.105 on 09/05/12
For personal use only.

this interpretation, the observed rate constant in the presence of a fixed concentration of donor is a function of both k_c and K.

The previous paper in this series (3) reports an attempt to obtain a more quantitative understanding of donor catalytic effectiveness in acetolysis of TNF-OTs. For a series of methoxy- and dimethoxynaphthalene donors at 85.3°, there was a reasonably good linear correlation between log k_cK and the coefficient m_i of the highest occupied molecular orbital (HOMO) of the donor (where the energy, E, is expressed in the form $\alpha + m_i\beta$) calculated by the Hückel molecular orbital (HMO) method. These data, however, did not permit a test of a correlation between log k_c and E(HOMO) due to large relative experimental uncertainties in the k_c values. The large uncertainties are a result of the low values of K (0.4–2.9 l mol^{-1}) and the limited range of donor concentrations possible (ref. 4 and references cited therein). It is a characteristic of the estimation of k_c and K from values of the observed rate constant at different donor concentrations, that errors in k_c and K are inversely related (*i.e.*, overestimation of one results in underestimation of the other) while the product k_cK can be determined with much greater accuracy.

On theoretical grounds (see Discussion) it was felt that log k_c should be more directly related to E(HOMO) of the donor than log k_cK. A primary objective of the present work was to investigate this prediction for a series of donors having sufficiently large association constants to permit a precise determination of k_c. A series of aromatic hydrocarbon donors was chosen for this study, using methyl substitution to increase solubility and to provide a greater spread in π donor strength. The results show that log k_c correlates *at least* as well as log k_cK with E(HOMO). The mechanistic implications of these correlations are considered in more detail in this paper. In addition, a model based on the Mulliken charge-transfer theory (5, 6) has been developed which leads to an estimate of the extent of charge transfer from donor to substrate in the transition state for acetolysis of the 1:1 donor–substrate complex.

Results

The donors studied in this work were 2-methyltriphenylene (2-Me-T), acenaphthylene (Acen), fluoranthene (F), 2,6-dimethylnaphthalene (2,6-Me_2-N), 2,3,6-trimethylnaphthalene (2,3,6-Me_3-N), 1,5-dimethylnaphthalene (1,5-Me_2-N), 1,2-benzanthracene (Bza), pyrene (Py), 1-methylpyrene(1-Me-Py),9-methylanthracene(9-Me-An) and 9,10-dimethylanthracene (9,10-Me_2-An).

Table 1 lists observed first order rate constants for acetolysis of TNF-OTs at 70.0° in the presence of the above donors. First order behavior was observed with all donors except Acen, Bza, and 9,10-Me_2-An. In these cases calculated first order rate constants varied in an approximately linear manner with per cent reaction and the rate constants reported in Table 1 were obtained by extrapolation to 0% reaction. With Bza and 9,10-Me_2-An, calculated first order rate constants showed small but regular decreases with extent of reaction, the decreases being consistent with consumption of TNF-OTs and donor in a 1:1 molar ratio. Infrared and proton n.m.r. spectra of the product formed in the presence of Bza were consistent with a trinitro-9-fluorenylbenzanthracene but a complete characterization was not carried out. Similar reactions have been observed by Okamoto *et al.* (7) in acetolysis of the closely related 2,4,7-trinitro-9-fluorenyl (+)camphor-10-sulfonate in the presence of aromatic donors. Alkylation reactions almost certainly occur to varying extents with some, but not all (see Discussion), of the other donors studied in this work as well, however with donor concentrations around 0.05 M or higher the decrease in the calculated first order rate constant is smaller than the experimental error. The low solubilities of Bza and 9,10-Me_2-An in acetic acid limited the rate measurements to lower donor concentrations. Acetolyses in the presence of Acen were complicated by concurrent reactions consuming both donor and *p*-toluenesulfonic acid. First order rate constants calculated from the theoretical infinity titer increased with extent of reaction in an approximately linear manner. Apparently Acen is converted to a donor of greater catalytic effectiveness, probably the dimer or polymers (8). The nature of the acid-consuming reaction was not investigated.

The assumed mechanism, [1], together with the equilibrium condition for 1:1 complexation between TNF-OTs and D, leads to [2](2), where

$$[2]\quad 1/(k_{obs} - k_u) = 1/(k_c - k_u) + 1/\{K(k_c - k_u)c_D\}$$

k_{obs} is the observed first order rate constant in

TABLE 1. Rates of acetolysis of 2,4,7-trinitro-9-fluorenyl *p*-toluenesulfonate[a] in the presence of aromatic hydrocarbon donors at 70.0°

Donor[b]	10^2 [Donor] (M)[c]	10^6 k_{obs} (s^{-1})[d]
None	—	0.842±0.007[e]
	—	0.839±0.005[e]
2-Me-T	0.96	1.80 ±0.02
	1.44	2.20 ±0.02
	1.91	2.57 ±0.03
	2.39	2.94 ±0.02
	2.88	3.28 ±0.02
Acen	4.79	4.46 ±0.04[f]
	5.75	5.17 ±0.02[f]
	7.18	5.94 ±0.12[f]
	9.57	6.96 ±0.10[f]
F	4.79	2.70 ±0.01
	5.75	2.99 ±0.02
	7.18	3.34 ±0.02
	8.61	3.67 ±0.03
	9.57	3.90 ±0.01
2,6-Me_2-N	4.79	4.77 ±0.05
	5.75	5.36 ±0.09
	7.18	6.16 ±0.02
	8.61	6.87 ±0.07
	9.57	7.40 ±0.08
2,3,6-Me_3-N	4.79	11.7 ±0.1
	5.75	13.6 ±0.1
	7.18	15.9 ±0.1
	8.61	18.2 ±0.1
	9.57	19.7 ±0.1
1,5-Me_2-N	4.79	24.1 ±0.2
Bza	0.48	6.00 ±0.01[f]
	0.96	10.8 ±0.1[f]
	1.44	15.2 ±0.1[f]
Py	0.38	3.19 ±0.07
1-Me-Py	4.71	52.1 ±0.8
	5.75	61.1 ±0.5
	7.18	68.4 ±0.5
	8.45	73.9 ±1.1
	9.57	79.9 ±0.7
9-Me-An	4.79	91.2 ±0.3
	5.75	105 ±1
	7.18	124 ±1
	8.61	136 ±1
	9.57	148 ±1
9,10-Me_2-An	0.96	42.0 ±0.1[f]
	0.97	37.8 ±0.2[f]
	1.44	57.4 ±0.1[f]
	1.91	75.5 ±0.1[f]
	2.39	90.0 ±0.3[f]

[a]Concentration of ester, 0.002 M.
[b]See text for abbreviations.
[c]At 70.0°.
[d]Averages of 9–13 values, listed with average deviations, except as noted.
[e]A value of 0.840 × 10^{-6} s^{-1} was used for k_u in subsequent calculations.
[f]Obtained by least squares extrapolation of calculated k_{obs} to 0% reaction, listed with standard deviation.

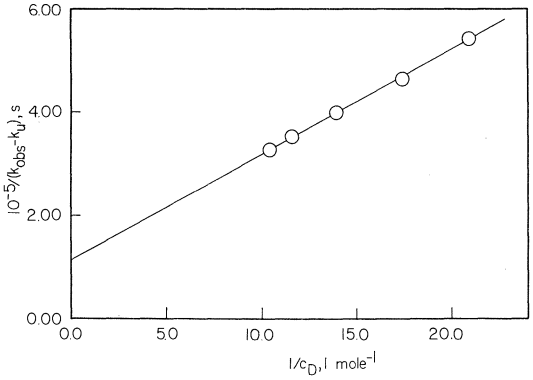

FIG. 1. Plot of data for fluoranthene according to eq. 2.

the presence of stoichiometric concentration of donor, c_D. The equation predicts a linear relation between $1/(k_{obs} - k_u)$ and $1/c_D$ from which both k_c and K can be obtained. In all nine systems for which such an analysis was carried out, the plots were in fact strictly linear with practically no noticeable scatter from the best fit straight line (Fig. 1). Values of k_c and K obtained from analysis of the kinetic data according to eq. 2 (see Experimental) are listed in Table 2. Also listed for these nine donors are values of k_c/k_u, the factor by which complexation increases the rate of acetolysis of TNF-OTs.

No analysis of this kind was possible for Py because of its low solubility, and insufficient data were obtained with 1,5-Me_2-N. For these donors only estimates of the product k_cK are listed. Rearrangement of [2] leads to the following expression for the observed rate constant in the presence of donor:

$$[3] \quad k_{obs} = k_u + K(k_c - k_u)c_D/(1 + Kc_D)$$

From [3] it is evident that the initial slope of a plot of k_{obs} *vs.* c_D is equal to $(k_c - k_u)K$, or, where $k_c \gg k_u$, approximately k_cK. With all of the donors studied at more than one concentration, plots of k_{obs} *vs.* c_D showed decreasing slope with increasing c_D as predicted by eq. 3.

Following our earlier work (3) we wished to examine the relationship between donor catalytic effectiveness and donor strength. Since no complete set of ionization potentials (or other experimental quantities related to ionization potentials) were available for the group of donors studied, we chose instead to use the HOMO energies as calculated by the HMO method as a measure of donor strength. Such energies correlate well with experimental ionization poten-

Can. J. Chem. Downloaded from www.nrcresearchpress.com by 210.87.254.105 on 09/05/12
For personal use only.

TABLE 2. Results of analysis of kinetic data[a]

Donor	K (1 mol^{-1})	$10^5 k_c$ (s^{-1})	$10^4 k_c K$ (1 mol^{-1} s^{-1})	k_c/k_u
2-Me-T	9.41±0.37	1.23 ± 0.05	1.16	14.6
Acen	5.04±0.94	2.00 ± 0.34	1.01	23.8
F	5.87±0.17	0.932± 0.023	0.547	11.1
Ph[b]	2.2 ±0.7	2.1 ± 0.5	0.462	25
2,6-Me_2-N	5.18±0.19	2.05 ± 0.07	1.06	24.4
2,3,6-Me_3-N	3.91±0.15	6.91 ± 0.25	2.70	82.3
1,5-Me_2-N	—	—	4.85[c]	—
Bza	8.73±0.47	12.9 ± 0.7	11.3	154
Py	—	—	6.17[c]	—
1-Me-Py	11.4 ±0.8	15.2 ± 0.9	17.2	181
9-Me-An	6.39±0.35	38.7 ± 1.9	24.7	461
9,10-Me_2-An	6.91±2.83	63.7 ±25.8	44.0	758

[a]Values of K and k_c obtained from weighted least squares treatment of data according to eq. 2, listed with standard deviations.
[b]From ref. 2.
[c]From initial slope of plot of k_{obs} *vs.* c_D.

tials, polarographic oxidation potentials, and charge-transfer absorption energies for a series of complexes with a common acceptor (9, 10). For our purposes it was necessary also to have a reliable estimate of the influence of a methyl group on the E(HOMO) of the donor. Although methyl groups are known to enhance donor strength, no systematic investigation of the best model for inclusion of a methyl group into the simple HMO method has been reported. In the present work, 3 models were chosen for examination, mostly on the basis of precedent. These were:

(*a*) An inductive (I) model, approximated by first order perturbation theory (11). The energy of the ith molecular orbital, E_i, of the substituted hydrocarbon was calculated from E_i for the parent hydrocarbon using the expression

$$[4]\quad E_i(\text{Ar-CH}_3) = E_i(\text{Ar-H}) + h\sum_r c_{ir}{}^2\beta$$

where r identifies the carbon atoms to which methyl groups are attached, c_{ir} is the coefficient of the rth atomic orbital in the ith molecular orbital, and h is a constant, taken to be −0.21 (11).

(*b*) A heteroatom (H) model (12, 13). This model treats the methyl group as a heteroatom which contributes a pair of electrons to the π system (**1**). Values of the coulomb (α) and bond

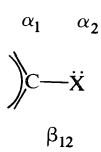

1

(β) integrals used were (13): $\alpha_1 = \alpha$, $\alpha_2 = \alpha + 2.0\beta$, and $\beta_{12} = 0.7\beta$, where α and β are the standard parameters used for the aromatic rings.

(*c*) A conjugation (C) model (13, 14). This model treats the methyl group as a modified vinyl group (**2**).

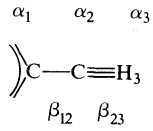

2

The parameters used were (15): $\alpha_1 = \alpha$, $\alpha_2 = \alpha - 0.1\beta$, $\alpha_3 = \alpha - 0.3\beta$, $\beta_{12} = 0.8\beta$, $\beta_{23} = 2.8\beta$.

The E(HOMO) values obtained in the calculations are listed, for the donors included in the kinetic study, in Table 3. Although there are minor qualitative differences between the three

TABLE 3. Donor highest occupied molecular orbital energies[a]

	E(HOMO)[c,d]		
Donor[b]	C	I	H
2-Me-T	0.674	0.661	0.639
2,6-Me_2-N	0.606	0.589	0.559
2,3,6-Me_3-N	0.602	0.574	0.549
1,5-Me_2-N	0.590	0.541	0.505
1-Me-Py	0.436	0.416	0.403
9-Me-An	0.403	0.373	0.359
9,10-Me_2-An	0.391	0.333	0.298

[a]Listed as the coefficient, m, where $E_i = \alpha + m_i\beta$.
[b]Abbreviations as in Table 1.
[c]Abbreviations: C, conjugation model; I, inductive model; H, heteroatom model.
[d]E(HOMO) values for unsubstituted donors: Acen, 0.638; F, 0.618; Ph, 0.605; Bza, 0.452; Py, 0.445.

Can. J. Chem. Downloaded from www.nrcresearchpress.com by 210.87.254.105 on 09/05/12
For personal use only.

TABLE 4. Charge-transfer spectral data

Donor[a]	λ_{max} (nm)	$10^{-3}\Delta\bar{\nu}_{max}$ (cm^{-1})	$10^{-3}\Delta\bar{\nu}_{max}/\Delta m_i$(HOMO) C	I	H
N	560 ± 5^b				
1,5-Me_2-N	623 ± 5^b	1.8 ± 0.3^b	64 ± 11	23 ± 4	16 ± 3
2,6-Me_2-N	617 ± 5^b	1.6 ± 0.3^b	133 ± 25	55 ± 5	27 ± 5
2,3,6-Me_3-N	621 ± 5^b	1.8 ± 0.3^b	113 ± 19	41 ± 7	26 ± 4
Py	732 ± 5^b				
	620 ± 5^c				
1-Me-Py	770 ± 5^b	0.67 ± 0.18^b	78 ± 21^b	23 ± 6^b	16 ± 4^b
	661 ± 5^c	1.0 ± 0.24^c	116 ± 28^c	34 ± 8^c	24 ± 6^c
An	632 ± 10^c				
	542 ± 10^d				
9-Me-An	684 ± 5^c	1.2 ± 0.4^c	109 ± 36^c	29 ± 10^c	22 ± 7^c
	556 ± 10^d	0.47 ± 0.66^d	43 ± 60^d	11 ± 16^d	9 ± 12^d
9,10-Me_2-An	737 ± 5^c	2.3 ± 0.3^c	100 ± 13^c	28 ± 4^c	20 ± 3^c
	601 ± 5^d	1.4 ± 0.5^d	61 ± 22^d	17 ± 6^d	12 ± 4^d

[a]Abbreviations as in Table 1.
[b]Tetracyanoethylene.
[c]Chloranil.
[d]2,4,7-Trinitrofluorenone.

models, the major distinction is the magnitude of the effect of methyl substitution, which increases in the order C < I < H. That is, the extent to which the E(HOMO) is raised by methyl substitution appears to be more a function of the particular parameters used rather than any inherent differences between the models, at least for these donors.

In order to have an independent experimental criterion for choosing between the three models, we measured the wavelengths of charge-transfer absorption maxima for complexes of selected methyl-substituted donors and the corresponding unsubstituted donors with the acceptors tetracyanoethylene (TCNE), chloranil (CA), and 2,4,7-trinitrofluorenone (TNF) (Table 4). Good linear correlations between the frequency of the charge-transfer absorption and m_i(HOMO) calculated by the HMO method have been demonstrated for complexes of aromatic hydrocarbon donors with these 3 acceptors (eq. 5), where values of a have been determined

$$[5] \qquad \bar{\nu}_{max} = am_i(\text{HOMO}) + b$$

as 24.2×10^3 cm^{-1} β^{-1} (16) and 26.3×10^3 cm^{-1} β^{-1}(17) for TCNE, 25.8×10^3 cm^{-1} β^{-1} for CA (17), and 24.8×10^3 cm^{-1} β^{-1} (17) for TNF. Therefore, the shift in charge transfer absorption, $\Delta\bar{\nu}_{max}$, resulting from methyl substitution should be approximately 25×10^3 times the calculated Δm_i(HOMO). The data in Table 4 reveal that the C model consistently underestimates the effect of methyl substitution while the I and H models (with the parameters used in these calculations) are generally satisfactory, probably giving reasonable estimates of the minimum and maximum effects of methyl substitution, respectively.

Plots of log K, log k_cK, and log k_c *vs.* m_i(HOMO) (using the H model values) are shown in Figs. 2, 3, and 4. Although there is a rough trend toward higher K values with decreasing m_i(HOMO), the first correlation is very poor. Table 5 summarizes the results of least squares analyses of plots of log k_cK and log k_c *vs.* m_i(HOMO) for the three models investigated. The kinetic data correlate approximately equally well with the I and H values, with the C values giving a somewhat poorer correlation.

Discussion

These results again show the striking dependence of donor catalytic effectiveness on donor structure. The factor by which the substrate reactivity is increased by complexation, k_c/k_u, varies from 11 (F) to 758 (9,10-Me_2-An) for the donors included in this study.

Both K and k_c are expected to increase monotonically with increasing E(HOMO) (decreasing m_i(HOMO)) of the donor (5, 6, 9, 18). We will first consider the qualitative significance of Figs. 2, 3, and 4; the quantitative significance of Figs. 3 and 4 is discussed below. The absence of a close correlation between the equilibrium constant K and the calculated E(HOMO) (or various experimental quantities which are

Can. J. Chem. Downloaded from www.nrcresearchpress.com by 210.87.254.105 on 09/05/12
For personal use only.

TABLE 5. Correlation of log k_cK and log k_c with E(HOMO)

Model	Slope ± std. dev.	Intercept ± std. dev.	Correlation coefficient
	log k_cK[a]		
C	−5.90±0.80	4.74±0.44	0.906
	(−6.39±0.74)	(4.99±0.41)	(0.939)
I	−5.71±0.56	4.53±0.30	0.947
	(−5.87±0.56)	(4.61±0.30)	(0.957)
H	−5.63±0.48	4.41±0.25	0.959
	(−5.68±0.51)	(4.43±0.27)	(0.961)
	log k_c		
C	−5.62±0.64	4.80±0.35	0.942
I	−5.19±0.45	4.47±0.24	0.964
H	−5.01±0.41	4.32±0.22	0.968

[a]Values in parentheses are with 1,5-Me_2-N and Py omitted.

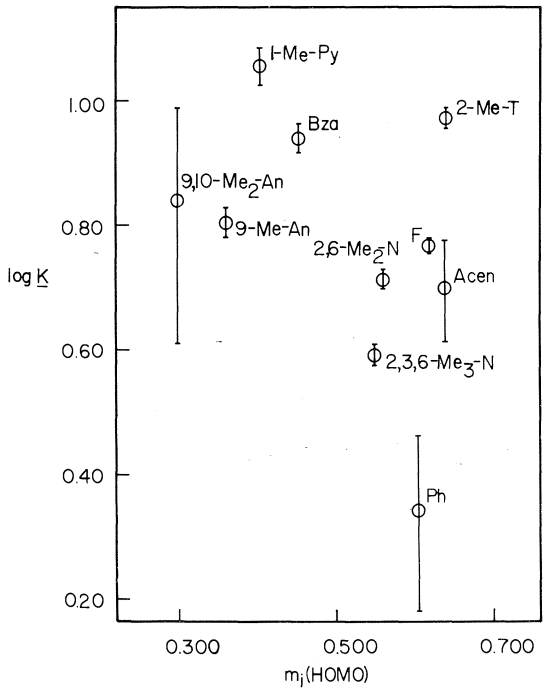

FIG. 2. Plot of log K *vs.* m_i(HOMO) (heteroatom model).

linearly related to E(HOMO)) is in line with most previous work (3, 9, 10, 19; see, however, ref. 20) and may mean that charge-transfer forces make a relatively unimportant contribution to the binding of these complexes in the reaction ground state (18, 19). Connors and co-workers (21, 22) have observed a correlation between complex stability and the estimated area of contact for complexes of theophylline and other xanthines in aqueous solution. A similar relationship is evident from the present results in that the complexation constants appear to increase as the size of the donor increases, independent of the calculated E(HOMO).

The significance of the two measures of catalytic effectiveness, log k_cK and log k_c, have been

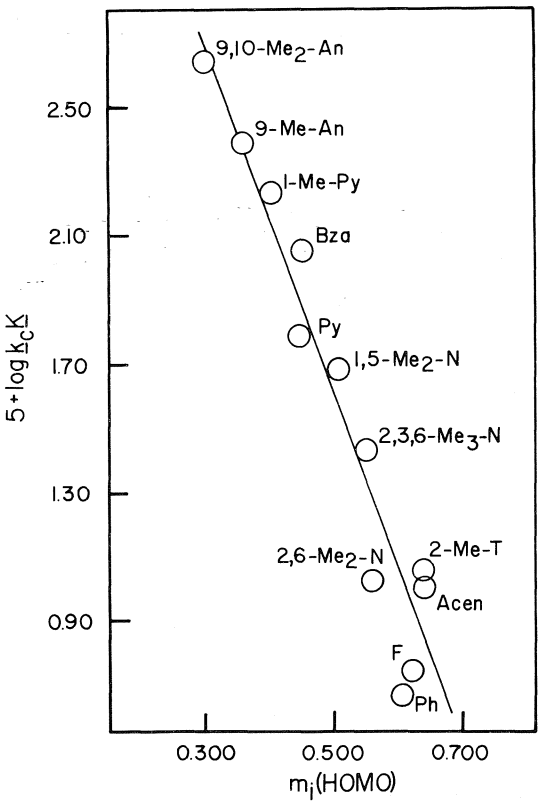

FIG. 3. Plot of log k_cK *vs.* m_i(HOMO) (heteroatom model).

Can. J. Chem. Downloaded from www.nrcresearchpress.com by 210.87.254.105 on 09/05/12
For personal use only.

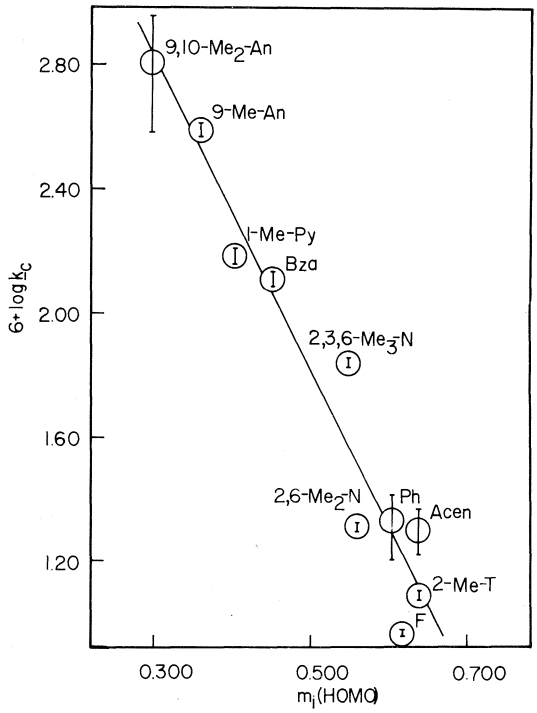

FIG. 4. Plot of log k_c *vs.* m_i(HOMO) (heteroatom model).

discussed previously (3) where the following relationships were derived:

$$[6] \quad -RT \ln k_c K = \Delta G_{\ddagger}^{0} + \text{constant}$$

$$[7] \quad -RT \ln k_c = \Delta G_{\ddagger}^{0} - \Delta G^{0} + \text{constant}'$$

The quantity $\Delta G_{\ddagger}^{0}$ is the standard free energy difference between the complexed transition state and the uncomplexed transition state plus donor (23), while ΔG^{0} is the standard free energy of formation of the reaction ground state complex from reactant and donor. Figure 3, therefore, shows the dependence of the stability of the transition state complex (relative to uncomplexed transition state plus donor) on the calculated m_i(HOMO). The success of this correlation indicates that in complexes of donors with the more electronically-deficient transition state, charge-transfer interaction and other interactions which are expected to increase with increasing E(HOMO) (18, 19) are now of dominant importance.

If the geometries of complexes of a particular donor with the reactant and its acetolysis transition state are similar, we might expect steric and other interactions not depending on donor E(HOMO) to cancel to some extent in the difference $\Delta G_{\ddagger}^{0} - \Delta G^{0}$. Although the experimental errors associated with the separation of k_c and K (above) make this test difficult, it is clear from Table 5 that the correlation of $\Delta G_{\ddagger}^{0} - \Delta G^{0}$ (*i.e.*, log k_c) with m_i(HOMO) is *at least as good* as that between $\Delta G_{\ddagger}^{0}$ (*i.e.*, log $k_c K$) and m_i(HOMO). This conclusion is not changed by exclusion of the points for 1,5-Me_2-N and Py from the log $k_c K$ correlation, so that the two correlations are based on the same 10 donors. Furthermore, some further improvement in the log k_c correlation could still result from more accurate separation of k_c and K, while no significant portion of the scatter in the log $k_c K$ correlation can be due to experimental error.

The striking success of the correlations of log $k_c K$ and log k_c with m_i(HOMO) has important mechanistic implications. Acetolysis of TNF-OTs in the presence of certain donors leads to varying amounts of alkylation products. The alkylation reaction predominates for some donors, *e.g.*, Bza and 9,10-Me_2-An while for others, *e.g.*, Ph and Py, there is no evidence for any consumption of donor. The reaction of the 1:1 complex is pictured as proceeding via slow formation of a π-complexed carbonium ion or ion pair intermediate which may react with acetic acid to give acetate ester (1) or with the donor to give alkylation product (reaction 8). However,

$$[8] \quad \text{D·TNF-OTs} \xrightarrow{\text{slow}} \text{D·TNF}^{+}\text{OTs}^{-} \xrightarrow{\text{HOAc}} \text{D·TNF-OAc} + \text{HOTs}$$

$$\text{D·TNF}^{+}\text{OTs}^{-} \longrightarrow \text{alkylation product(s)} + \text{HOTs}$$

the kinetics are equally consistent with rate-determining formation of a σ-complex intermediate which partitions itself in the same way (reaction 9). To the extent that alkylation products are formed, the two alternatives represent extremes in a spectrum of mechanisms for Friedel–Crafts reactions and possibly other electrophilic aromatic substitutions (24). If the transition state resembles a σ-complex, log k_c should be linearly related to the cation localization energy, L_r^{+}, for the most reactive position in the donor (ref. 13, chapt. 11). Since m_i(HOMO) and L_r^{+} (most reactive position) tend to parallel each other with polynuclear aromatic hydrocarbons, the series of donors studied in this work does not provide the

Can. J. Chem. Downloaded from www.nrcresearchpress.com by 210.87.254.105 on 09/05/12
For personal use only.

[9] D·TNF-OTs $\xrightarrow{\text{slow}}$ *e.g.*,

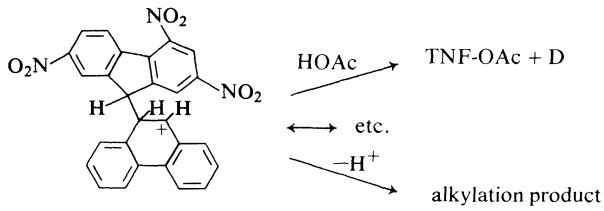

most sensitive test for distinguishing between mechanisms 8 and 9. Nevertheless, both log k_c and log k_cK were found to correlate significantly less well (*e.g.*, for log k_c, $r = 0.82$, relative standard deviation in slope = 22%) with L_r^+ than with m_i(HOMO) where both quantities were calculated by the H model. Of more significance than the poorer correlation, however, is the observation that the order of catalytic effectiveness of the two pairs of naphthalene and anthracene donors is opposite to that predicted by L_r^+ values (*i.e.*, L_r^+ for the 1-position in 2,6-Me_2-N is less than that for 2,3,6-Me_3-N and L_r^+ for the 9-position in 9-Me-An is less than that for 9,10-Me_2-An). Similarly, the order of catalytic effectiveness of 1-methoxy- and 2-methoxynaphthalene (3) is opposite to that predicted by their L_r^+ values. Further, the *order* of reactivity predicted by m_i(HOMO) or L_r^+ within each of these groups, cannot be changed by varying the parameters used in any reasonable model for methyl substitution. On the other hand, the donors with the lower L_r^+ values are those for which alkylation is most extensive, in agreement with either mechanism.

In units of electron volts, the correlations shown in Figs. 3 and 4 are given by eqs. 10 and 11.

$$[10]\quad \Delta G_{+}^{0} = (0.383 \pm 0.033)m_i - (0.300 \pm 0.017)$$

$$[11]\quad \Delta G_{+}^{0} - \Delta G^{0} = (0.341 \pm 0.028)m_i - (0.294 \pm 0.015)$$

The slopes are roughly 10–15% of those observed in similar correlations of ionization potential with m_i(HOMO) (ref. 13, p. 191, 25). It is clear that these slopes must reflect the extent of electron transfer from the donor to the acceptor in the complexed transition state. A more quantitative understanding of this relationship can be obtained from the charge-transfer theory of Mulliken and co-workers (5, 6). According to the theory in its simplest form, the wave function, Ψ_N, of a donor–acceptor complex in its electronic ground state can be expressed as [12]

$$[12]\quad \Psi_N = a\Psi_0(\mathrm{D,A}) + b\Psi_1(\mathrm{D^+A^-})$$

where Ψ_0(D,A) is a hypothetical no-bond wave function and $\Psi_1(D^+A^-)$ a dative wave function corresponding to transfer of an electron from the donor HOMO to the lowest vacant molecular orbital of the acceptor. For weak complexes, the enthalpy of formation (from separated D and A), ΔH^0, is given by (5, 6)

$$[13]\quad \Delta H^0 = W_0 - \frac{\beta_0^2}{W_1 - W_0}$$

where W_0 is the energy of the pure no-bond form (*i.e.*, $\langle\Psi_0\mathscr{H}\Psi_0\rangle$), W_1 is the energy of the pure dative form ($\langle\Psi_1\mathscr{H}\Psi_1\rangle$), and β_0 is defined by $\beta_0 = H_{01} - W_0S_{01}$, where $H_{01} = \langle\Psi_0\mathscr{H}\Psi_1\rangle$ and $S_{01} = \langle\Psi_0\Psi_1\rangle$. The energies W_0 and W_1 are taken relative to the total energy of the separated donor and acceptor molecules in eq. 13. The ratio of the coefficients b/a in the wave function Ψ_N is given approximately by

$$[14]\quad b/a = \frac{\beta_0}{W_1 - W_0}$$

so that

$$[15]\quad \Delta H^0 = W_0 - \frac{b^2}{a^2}(W_1 - W_0).$$

The energy W_1 (relative to separated donor and acceptor) is given by

$$[16]\quad W_1 = I - A + C$$

where I is the vertical ionization potential of the donor, A the vertical electron affinity of the acceptor, and C the electrostatic attraction between D^+ and A^- in D^+A^-. Assuming that the coulomb term C is approximately constant for the donors studied in this work, and that W_0 is small and very nearly constant, we can write

$$[17]\quad \frac{\partial\Delta H^0}{\partial W_1} \approx \frac{\partial\Delta H^0}{\partial I} = \frac{b^2}{a^2}$$

Can. J. Chem. Downloaded from www.nrcresearchpress.com by 210.87.254.105 on 09/05/12
For personal use only.

Can. J. Chem. Downloaded from www.nrcresearchpress.com by 210.87.254.105 on 09/05/12
For personal use only.

Since b/a increases with decreasing ionization potential of the donor, ΔH^0 is not a linear function of I, though the relation may be expected to be approximately linear over a limited range of I. The assumption that $\partial W_0/\partial I \approx 0$ is equivalent to assuming that all of the variation in ΔH^0 is a result of variation in charge-transfer interaction. The fact that a smooth relationship between ΔH^0 and I is ordinarily not observed (above) may be due in part to the fact that this assumption is false (19). Since $\partial I/\partial m_i(\text{HOMO}) = \beta$, the relationship between ΔH^0 and m_i-(HOMO) is given by [18].

$$[18] \qquad \frac{\partial \Delta H^0}{\partial m_i(\text{HOMO})} = \beta \frac{b^2}{a^2}$$

For complexes of a series of structurally-related donors with the same acceptor a rough proportionality between ΔH^0 and ΔS^0 of complexation is often observed (9, 10). If the relationship between ΔH^0 and ΔS^0 is written as $\Delta H^0 = B\Delta S^0 +$ constant, an equation analogous to [18] can be written for ΔG^0:

$$[19] \qquad \frac{\Delta G^0}{\partial m_i(\text{HOMO})} = \beta\left(\frac{B - T}{B}\right)\frac{b^2}{a^2}$$

However, for the polynucleararomatic donors used in this study, the available data indicate that ΔS^0 is very nearly constant (*i.e.*, B is very large) for trinitrobenzene (26) and chloranil (27) complexes. In any case, we believe that it is more correct to correlate ΔG^0 with m_i(HOMO) than ΔH^0 (ref. 13, chapt. 11) (*i.e.*, that ΔG^0 should replace ΔH^0 in [18]). This is particularly true because eqs. 13–18 take no account of solvent effects. We therefore assume that $(B - T)/B \approx 1$.

Normalization of eq. 12 leads to

$$[20] \qquad a^2 + b^2 + 2abS_{01} = 1$$

For weak complexes S_{01} is small and $a^2 + b^2 \approx 1$. Taking a value of 3.0 eV for β (ref. 13, p. 191, 25) eq. 10 leads to an estimate of 0.11 for b^2, or 11% charge-transfer in the complexed acetolysis transition state. From eq. 11 the same analysis indicates that the extent of charge-transfer increases by about 10% in going from complexed ground state to complexed transition state. If the integral S_{01} is taken as approximately 0.1 (6), the extent of charge-transfer is now approximately $a^2 + b^2 + abS_{01}$ (6) and the estimate of the extent of charge-transfer in the complexed transition state now becomes about 14%.

In addition to the assumptions leading to eq. 19 we have assumed that the structure of the trinitrofluorenyl portion of the complexed transition state is independent of the donor. This assumption can only be valid over a limited range of donor ionization potentials. With sufficiently low ionization potentials we expect complete electron transfer to accompany or even precede (ref. 28 and subsequent papers in this series) ionization.

Experimental

Reagents

2,4,7-Trinitro-9-fluorenyl *p*-toluenesulfonate was prepared as previously described (29). 1-Methylpyrene, m.p. 70–71°, was prepared from pyrene following the procedure of Vollman *et al.* (30). 2-Methyltriphenylene, m.p. 103–104°, was prepared from phenanthrene according to the method of Fieser and Joshel (31). Commercially available donors were chromatographed on alumina, recrystallized twice from 95% ethanol or methanol, and dried under vacuum before use. Compounds purified in this manner had the following m.p.: acenaphthylene, 92–93°; fluoranthene, 108–110°; 2,6-dimethylnaphthalene, 108–110°; 2,3,6-trimethylnaphthalene, 100–102°; 1,5-dimethylnaphthalene, 81–83°; benzanthracene, 159–160°; pyrene, 148–150°; 9-methylanthracene, 78–79°; 9,10-dimethylanthracene, 176–178°. Naphthalene, m.p. 78–80°, was further purified by vacuum sublimation. Tetracyanoethylene (Aldrich) was crystallized twice from chlorobenzene and vacuum sublimed twice to give white crystals, m.p. 198–200°. Chloranil (Eastman Practical Grade) was crystallized from benzene, chromatographed on calcium carbonate, and vacuum sublimed to give yellow flakes, m.p. 292–294° (sealed tube). Trinitrofluorenone, prepared as described by Woolfolk and Orchin (33) was crystallized twice from benzene, m.p. 175°.

Kinetic Measurements

The kinetic measurements were carried out as described previously (2), as was analysis of the data to obtain k_c and K.

Charge-transfer Spectra

All spectral measurements were made at room temperature (20 °C) in a 1 cm cell in the range of 360–800 nm on a Cary Model 14 Spectrophotometer. Solutions were prepared by mixing equal volumes of 0.02 M donor and acceptor solutions in spectral grade methylene chloride. Charge transfer maxima estimated from the spectrophotometer traces are estimated to be accurate within the limits stated in Table 4. Where two bands seriously overlapped, the observed maxima were corrected using the procedure of Voigt and Reid (32). Such corrections varied from 0–3 nm with the TCNE spectra and 0–8 nm with the CA and TNF spectra but are all smaller than the stated experimental uncertainty.

This research was supported by the National Science Foundation (Grant GP-6380) and by the National Research Council of Canada. The authors are also grateful to Dr. Colin Fyfe for helpful discussions.

1. A. K. COLTER and S. S. WANG. J. Am. Chem. Soc. **85**, 114 (1963).
2. A. K. COLTER, S. S. WANG, G. H. MEGERLE, and P. S. OSSIP. J. Am. Chem. Soc. **86**, 3106 (1964).
3. A. K. COLTER and S. HUI. J. Org. Chem. **33**, 1935 (1968).
4. D. A. DERANLEAU. J. Am. Chem. Soc. **91**, 4044 (1969).
5. R. S. MULLIKEN. J. Am. Chem. Soc. **64**, 811 (1950).
6. R. S. MULLIKEN and W. B. PERSON. Molecular complexes: a lecture and reprint volume. Wiley–Interscience, 1969.
7. K. OKAMOTO, I. NITTA, and H. SHINGU. Bull. Chem. Soc. Jap. **41**, 1433 (1968).
8. J. DOLINKSKY and K. DZIEWONSKI. Chem. Ber. **48**, 1917 (1915).
9. G. BRIEGLEB. Elektronen-donator-acceptor-komplexe. Springer–Verlag, Berlin. 1961.
10. R. FOSTER. Organic charge-transfer complexes. Academic Press, New York. 1969.
11. A. R. LEPLEY. J. Am. Chem. Soc. **86**, 2545 (1964).
12. F. A. MATSEN. J. Am. Chem. Soc. **72**, 5243 (1950).
13. A. STREITWIESER, JR. Molecular orbital theory for organic chemists. John Wiley and Sons, Inc., New York. 1961. pp. 131–135.
14. R. S. MULLIKEN, C. A. RIEKE, and W. G. BROWN. J. Am. Chem. Soc. **63**, 41 (1949).
15. A. STREITWIESER, JR. and P. M. NAIR. Tetrahedron, **5**, 149 (1959).
16. M. J. S. DEWAR and A. R. LEPLEY. J. Am. Chem. Soc. **83**, 4560 (1961).
17. M. NEPRĂS and R. ZAHRADNIK. Collect. Czech. Chem. Commun. **29**, 1545 (1964).
18. M. W. HANNA and J. L. LIPPERT. *In* Molecular complexes. Vol. 1. Elek Science, London. 1973. Chapt. 1.
19. M. J. S. DEWAR and C. C. THOMPSON, JR. Tetrahedron Suppl. **7**, 97 (1966).
20. R. E. MERRIFIELD and W. D. PHILLIPS. J. Am. Chem. Soc. **80**, 2778 (1950).
21. K. A. CONNORS, M. H. INFELD, and B. J. KLINE. J. Am. Chem. Soc. **91**, 3597 (1969).
22. J. L. COHEN and K. A. CONNORS. J. Pharm. Sci. **59**, 1271 (1970).
23. J. L. KURZ. J. Am. Chem. Soc. **85**, 987 (1963).
24. G. A. OLAH, M. TASHIRO, and S. KOBAYASHI. J. Am. Chem. Soc. **92**, 6369 (1970).
25. A. L. MCKENNA, III. Ph.D. Thesis, Carnegie-Mellon University, Pittsburgh, Pennsylvania. 1970.
26. A. BIER. Rec. Trav. Chim. Pays-Bas. **75**, 866 (1956).
27. G. BRIEGLEB, J. CZEKALLA, and G. REUSS. Z. Phys. Chem. (Frankfurt am Main). **30**, 333 (1961).
28. R. C. KERBER, G. C. URRY, and N. KORNBLUM. J. Am. Chem. Soc. **87**, 4250 (1965).
29. A. K. COLTER and S. S. WANG. J. Org. Chem. **27**, 1517 (1962).
30. H. VOLLMAN, H. BECKER, M. CORELL, and H. STREICK. Ann. Chem. **521**, 107, 112 (1937).
31. L. F. FIESER and L. M. JOSHEL. J. Am. Chem. Soc. **61**, 2958 (1939).
32. E. M. VOIGT and C. REID. J. Am. Chem. Soc. **86**, 3931 (1964).
33. E. O. WOOLFOLK and M. ORCHIN. Org. Synth. Coll. Vol. III, 837 (1955).

Can. J. Chem. Downloaded from www.nrcresearchpress.com by 210.87.254.105 on 09/05/12
For personal use only.

Further Studies on the Homogeneous Hydrogenation of Olefins Catalyzed by a Cyclic Phosphine Complex of Rhodium(I) Hydride

DAVID G. HOLAH, IAN M. HOODLESS, ALAN N. HUGHES, BENJAMIN C. HUI, AND DOUGLAS MARTIN

Department of Chemistry, Lakehead University, Thunder Bay, Ontario P7B 5E1

Received March 26, 1974

DAVID G. HOLAH, IAN M. HOODLESS, ALAN N. HUGHES, BENJAMIN C. HUI, and DOUGLAS MARTIN. Can. J. Chem. **52**, 3758 (1974).

The use of $RhH(DBP)_3$[1] as a very active homogeneous hydrogenation catalyst is described and the equilibrium constant for its dissociation to the catalytically active $RhH(DBP)_2$ evaluated.

DAVID G. HOLAH, IAN M. HOODLESS, ALAN N. HUGHES, BENJAMIN C. HUI et DOUGLAS MARTIN. Can. J. Chem. **52**, 3758 (1974).

On décrit l'utilisation du $RhH(DBP)_3$ comme catalyseur d'hydrogénation homogène très actif; on évalue la constante d'équilibre pour sa dissociation en $RhH(DBP)_2$ qui est catalytiquement actif. [Traduit par le journal]

We have recently reported (1) kinetic studies on the homogeneous hydrogenation of olefins catalyzed by $RhH(DBP)_4$[1] and the interpretation of our data is based on the complete dissociation of $RhH(DBP)_4$ in the initial step [1]

$$[1] \qquad RhH(DBP)_4 \rightleftharpoons RhH(DBP)_3 + DBP$$

with the catalytically active species being the bis(phosphine) complex arising from reaction 2

$$[2] \qquad RhH(DBP)_3 \overset{K}{\rightleftharpoons} RhH(DBP)_2 + DBP$$

The equilibrium constant K was estimated to be between $(1.6\text{–}8.9) \times 10^{-5}$ M.

Reaction 1 lies essentially to the right and this is demonstrated by the fact that addition of ethanol to a benzene solution of $RhH(DBP)_4$ precipitates only $RhH(DBP)_3$. Addition of an excess of DBP to a benzene solution of the latter, followed by removal of the solvent under vacuum did not produce $RhH(DBP)_4$ and it seems therefore that reaction 1 is not reversible under these conditions.

That the above precipitate is indeed $RhH(DBP)_3$ is suggested by analytical data, by the infrared spectrum which shows a weak peak at $\nu = 1975\ cm^{-1}$ assignable to the Rh—H stretch, by the n.m.r. spectrum (100 MHz) which shows for both $RhH(DBP)_4$ and $RhH(DBP)_3$ a broad weak hydride peak at $\tau 20.47$ in chlorobenzene at room temperature, and by the reduction of carbon tetrachloride to chloroform by the compound presumed to be $RhH(DBP)_3$.

Benzene solutions of $RhH(DBP)_3$, like $RhH(DBP)_4$, catalyze the homogeneous hydrogenation of olefins at room temperature and less than 1 atm of hydrogen pressure. The selectivity is the same as in the case of $RhH(DBP)_4$ suggesting that a similar intermediate is probably involved. The rate of hydrogenation is $\sim 10\%$ faster than in the $RhH(DBP)_4$ system under similar conditions, and can be attributed to the absence of the inhibiting effect arising from the presence of the DBP ligand dissociated from the tetrakis compound. The dependence of the rate of hydrogenation on substrates and on catalyst concentration (Fig. 1) are similar to the $RhH(DBP)_4$ system. The catalyst dependence approximates to half order at higher concentrations (Fig. 2), where reasonably good straight lines can be drawn when the rate is plotted against $[RhH(DBP)_3]^{1/2}$.

The mechanism proposed for the tetrakis(phosphine) system, which includes reactions 1 to 4

$$[3] \qquad RhH(DBP)_2 + \text{olefin} \overset{k_1}{\underset{k_{-1}}{\rightleftharpoons}} Rh(\text{alkyl})(DBP)_2$$

$$[4] \qquad Rh(\text{alkyl})(DBP)_2 + H_2 \overset{k_2}{\rightarrow} RhH(DBP)_2 + \text{alkane}$$

can be simplified when applied to the present catalyst. Thus, omitting reaction 1 and assuming K to be small, we arrive at the rate law

[1]DBP is 5-phenyl-5*H*-dibenzophosphole 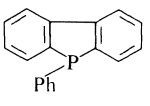

Can. J. Chem. Downloaded from www.nrcresearchpress.com by 210.87.254.6 on 09/05/12
For personal use only.

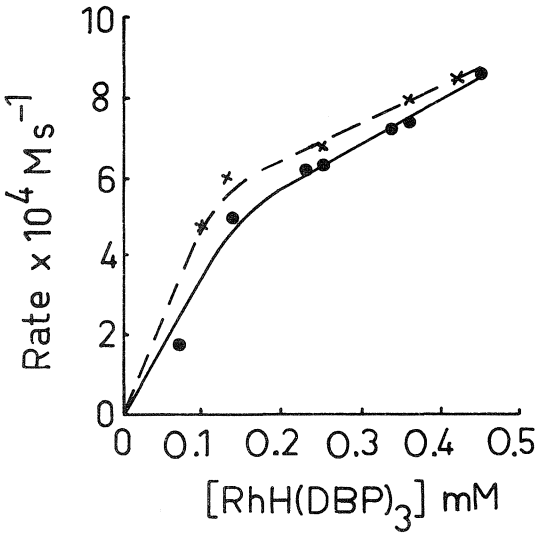

FIG. 1. Dependence of the rate of hydrogenation of 1-hexene and 1-decene in benzene at 20° on the concentration of $RhH(DBP)_3$. ●, 1-hexene; ×, 1-decene.

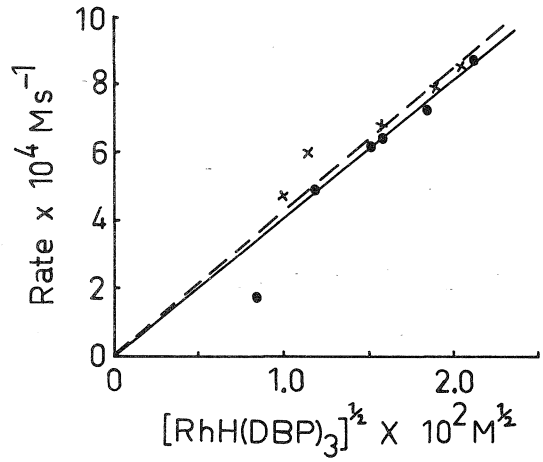

FIG. 2. Plot of rate *vs.* $[RhH(DBP)_3]^{1/2}$. ×, 1-decene; ●, 1-hexene.

$$[5] \quad \text{Rate} = \frac{K^{1/2}k_1[\text{Rh}]^{1/2}[\text{Olefin}][\text{H}_2]}{k_{-1}/k_2 + [\text{H}_2]}$$

Using the data obtained in the $RhH(DBP)_4$ system (for 1-hexene $k_1 = 70.5\ M^{-1}\ s^{-1}$ and $k_2/k_{-1} = 285\ M^{-1}$) and with $[H_2] = 3.9 \times 10^{-3}$ M, [1-hexene] = 0.25 M, K is estimated from the slope of the plot in Fig. 2 to be 1.6×10^{-5} M, entirely consistent with our results using $RhH(DBP)_4$.

Recently (2) the use of $RhH(PPh_3)_4$ in homogeneous hydrogenation reactions has been briefly reported. It shows, as might be expected, a rate dependence on the catalyst concentration similar to the one observed by us for the analogous DBP complex.

Spectrophotometric studies have produced (3) a value of K for the loss of a PPh_3 molecule from $RhCl(PPh_3)_3$ at 1.4×10^{-4} M, and recent hydrogenations studies using this catalyst (4) resulted in $K < 1.0 \times 10^{-5}$ M. Our data, as for the $RhCl(PPh_3)_3$ compound, emphasises again the great reactivity of the bis(ligand) species as the active catalyst in spite of its very low concentration.

Experimental

Experimental procedures, the syntheses of DBP and $RhH(DBP)_3$ and catalytic experiments were as previously described (1).

We thank the National Research Council of Canada for generous financial support of this work and Dr. D. Webster for kindly running some n.m.r. spectra.

1. D. BUDD, D. G. HOLAH, A. N. HUGHES, and B. C. HUI. Can. J. Chem. **52**, 775 (1974).
2. J. HJORTKJAER. 166th ACS Meeting, Chicago, Illinois. 1973. Abstract INDE 10.
3. H. ARAI and J. HALPERN. J. Chem. Soc. Chem. Commun. 1571 (1971).
4. J. HALPERN and C. S. WONG. J. Chem. Soc. Chem. Commun. 629 (1973).

Can. J. Chem. Downloaded from www.nrcresearchpress.com by 210.87.254.6 on 09/05/12
For personal use only.

Catalytic Hydrogenation of Unsaturated Carboxylic Acids Using *N,N*-Dimethylacetamide Solutions of Ruthenium(I) Chlorides[1]

BENJAMIN C. HUI[2] AND BRIAN R. JAMES

Department of Chemistry, University of British Columbia, Vancouver, British Columbia V6T 1W5

Received July 15, 1974

BENJAMIN C. HUI and BRIAN R. JAMES. Can. J. Chem. **52**, 3760 (1974).

N,N-Dimethylacetamide solutions of dimeric ruthenium(I) chlorides catalyze homogeneously the hydrogenation of ethylene and unsaturated carboxylic acids under mild conditions. Kinetic and mechanistic studies show that the catalysis involves a monomeric Ru(I) complex which forms reversibly a steady state concentration of a $Ru(III)H_2$ species; this reacts with olefinic substrate to yield saturated product by two successive single hydrogen atom transfers with regeneration of the Ru(I) catalyst. The overall hydrogen addition to fumaric acid is *cis*. Hydrogenation of maleic acid is accompanied by an efficient isomerization to fumaric acid.

BENJAMIN C. HUI et BRIAN R. JAMES. Can. J. Chem. **52**, 3760 (1974).

Les solutions du dimère du chlorure de ruthénium(I) dans la *N,N*-diméthylacétamide, catalysent d'une manière homogène, l'hydrogénation de l'éthylène et des acides carboxyliques insaturés dans des conditions de réaction très douces. Les études cinétiques et des mécanismes de réaction démontrent que la catalyse met en jeu un complexe monomère de Ru(I) qui produit réversiblement une concentration constante d'un composé $Ru(III)H_2$; ce dernier réagit avec le substrat oléfinique pour conduire au composé saturé par deux transferts successifs d'un seul atome d'hydrogène avec regénération du catalyseur Ru(I). Globalement l'addition d'hydrogène sur l'acide fumarique se fait *cis*. L'hydrogénation de l'acide maléique est accompagnée d'une isomérisation en acide fumarique. [Traduit par le journal]

Introduction

We recently reported on the production of ruthenium(I) chlorides in *N,N*-dimethylacetamide (DMA) solution by the hydrogen reduction of ruthenium(III) chloride (1). This discovery came about through attempts to use ruthenium(II) chlorides in nonacidic media for catalytic hydrogenation of olefins (2); such solutions did catalyze ethylene hydrogenation but the systems were complicated by accompanying reduction of the ruthenium(II) to ruthenium(I). This led to investigation of the ruthenium(I) chloride solutions themselves as hydrogenation catalysts, and this paper describes these studies, especially on the kinetics and mechanism of the hydrogenation of maleic and fumaric acids. Some of the work presented here has been reported briefly elsewhere (3, 4). Rylander *et al.* (5) reported some years ago that solutions of $RuCl_3$ in dimethylformamide homogeneously hydrogenated dicyclopentadiene but no kinetic data or mechanism were presented.

[1]Taken from the Ph.D. thesis of B.C. Hui, University of British Columbia, 1969.

[2]Present address: Department of Chemistry, Lakehead University, Thunder Bay, Ontario P7B 5E1.

Experimental

Ruthenium(III) trichloride trihydrate was obtained as $RuCl_3 \cdot 3H_2O$ (40.59% Ru) from Johnson Matthey Limited. Other materials used and the procedure used for following H_2-uptake of constant pressure have been described previously (2, 6). The brown DMA solutions of ruthenium(I) chlorides were prepared (1) by subjecting DMA solutions of $RuCl_3 \cdot 3H_2O$ to 1 atm H_2 at 80° until gas uptake ceased (~2 h). Solid substrates such as maleic acid (MA) and fumaric acid (FA) were then added from glass buckets held over the ruthenium solutions via the use of side-arms on the reaction vessel.

Results

The Ru(I) chloride complexes in DMA were found to be efficient catalysts for the homogeneous hydrogenation of maleic and fumaric acids at mild conditions (60–80°, $\leqslant$1 atm H_2). Figure 1 shows typical H_2-uptake plots at 80° for various ruthenium concentrations and H_2 pressures at one particular maleic acid concentration (0.051 *M*). The total gas uptake corresponded to stoichiometric reduction to succinic acid which was readily isolated and identified by infrared and melting point. There was no H_2 uptake, of course, in the absence of substrate.

The visible absorption spectrum of the brown

Can. J. Chem. Downloaded from www.nrcresearchpress.com by 210.87.254.5 on 09/05/12
For personal use only.

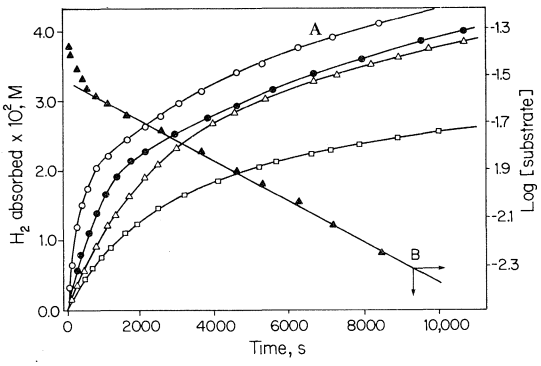

FIG. 1. Uptake and log plots for the Ru(I)-catalyzed hydrogenation of maleic acid in DMA at 80°, 0.051 *M* maleic acid. ○, 0.021 *M* Ru, 725 mm H_2; ●, 0.0053 *M* Ru, 725 mm H_2; △, 0.0026 *M* Ru, 725 mm H_2; □, 0.0053 *M* Ru, 200 mm H_2; ▲ (*B*) is a plot of log [substrate] *vs.* time for curve *A*.

Ru(I) chloride solution shows a continuum from 400–700 nm with intensity decreasing with increasing wavelength. The spectra at a series of concentrations do not follow Beer's Law; for example, at 500 nm, $\varepsilon = 435$ for a 0.02 *M* solution while $\varepsilon = 700$ for a 10^{-4} *M* solution. These data together with data on an isolated solid complex $(Ru(I)_2Cl_3(HDMA)$, where HDMA indicates protonated DMA (7)) indicate that a dimer $\rightleftharpoons$ monomer equilibrium is involved, the dimer having chloride bridges and possibly a Ru—Ru bond. There was no evidence for the formation of a Ru(I) – maleic acid complex as the absorption spectrum remained unchanged on adding this excess substrate to a Ru(I) solution; the Ru(I) solution was also visibly unreactive toward H_2.

The visible spectra of the brown solutions also remained essentially constant throughout the catalytic hydrogenation experiments, and we were unable to detect by n.m.r. or i.r. any ruthenium hydride species. Such observations do not rule out equilibria 1–3

$$[1] \qquad Ru(I) + H_2 \rightleftharpoons Ru(III)H_2$$

$$[2] \qquad Ru(I) + H_2 \rightleftharpoons Ru(I)H^- + H^+$$

$$[3] \qquad 2Ru(I) + H_2 \rightleftharpoons 2Ru(II)H$$

which illustrate the established modes of hydrogen activation (dihydride formation, heterolytic splitting, and homolytic splitting, respectively (ref. 4, p. 6)), and which could lie essentially completely to the left.

The catalytic hydrogenation rates illustrated in Fig. 1 show a continual fall-off with time. The uptake plots do not analyze overall for a first-order dependence on MA (Fig. 1, curve *B*), although after about 1500 s the curves do give good pseudo first-order log plots (constant H_2 pressure) for the substrate concentration (initial [MA] = 0.022–0.11 *M*). When FA was used as substrate at concentrations up to ~0.05 *M*, the uptake plots show a good first-order dependence on FA for the complete hydrogenation (Fig. 2). The more complex character for the MA systems is due to an accompanying isomerization of the substrate to fumaric acid (see below). Generally there was a short induction period of about 100–200 s for all the catalytic hydrogenations.

Table 1 summarizes kinetic data for the hydrogenation of the maleic acid systems at 80°. The initial rates could be measured with reasonable accuracy and these refer to the hydrogenation of maleic acid. The pseudo first-order rate constants k' were evaluated from the linear log plots obtained for the later regions of the uptake plots. Table 2 summarizes data for the fumaric acid systems; the k' values were evaluated from the good first-order log plots obtained at the lower fumaric acid concentrations; at higher concentrations (≥ 0.073 *M*) good log plots were not obtained and consequently the initial rates were taken. It is clear that the k' values measured in the maleic acid systems refer in fact to hydrogenation of fumaric acid, the *trans* isomerization product of maleic acid (this is seen by a comparison of the starred values of k' in Tables 1 and 2, which are essentially the same). Fumaric acid

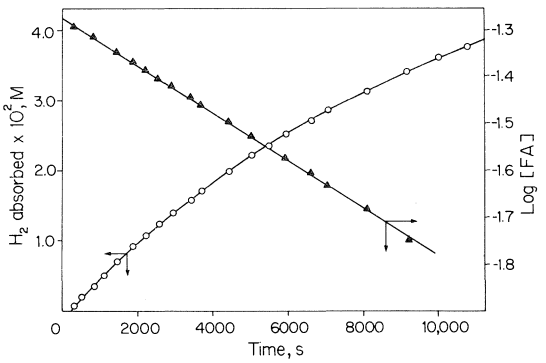

FIG. 2. Uptake and log plots for the Ru(I)-catalyzed hydrogenation of fumaric acid in DMA at 80°. 0.0053 *M* Ru, 0.052 *M* fumaric acid, 725 mm H_2.

Can. J. Chem. Downloaded from www.nrcresearchpress.com by 210.87.254.5 on 09/05/12
For personal use only.

Can. J. Chem. Downloaded from www.nrcresearchpress.com by 210.87.254.5 on 09/05/12
For personal use only.

TABLE 1. Ru(I)-catalyzed hydrogenation of maleic acid systems at 80°

[Ru(I)] ($\times 10^2$) (M)	H_2 (mm)	[H_2] ($\times 10^3$) (M)	[MA] ($\times 10^2$) (M)	Initial rate ($\times 10^5$) ($M\,s^{-1}$)	k'† ($\times 10^4$) (s^{-1})
2.10	725	2.32	5.10	4.75	2.05
1.05	725	2.32	5.05	3.13	1.52
0.53	725	2.32	5.05	2.49	1.02
0.26	725	2.32	5.05	1.75	0.92
0.11	725	2.32	5.05	0.99	0.59
0.53	651	2.08	5.00	2.18	1.12
0.53	400	1.28	5.05	1.52	0.73
0.53	200	0.64	5.10	0.87	0.39
0.53	725	2.32	2.13	1.16	1.21*
0.53	725	2.32	3.25	1.73	1.26*
0.53	725	2.32	6.50	2.70	1.30*
0.53	725	2.32	10.90	3.68	1.28*
0.53	725	2.32	5.30	1.72[a]	1.23[a]
0.53	725	2.32	5.05	1.73[b]	0.63[b]
0.53	725	2.32	5.00	1.42[c]	0.41[c]
0.53	725	2.32	5.00	1.20[d]	0.30[d]
0.53	725	2.32	5.00	0.82[e]	0.18[e]
0.53	725	2.32	4.90	2.28[f]	1.15[f]
0.53	725	2.32	5.10	2.37[g]	1.31[g]

*To be compared with starred values in Table 2.
†The k' values refer in fact to hydrogenation of fumaric acid (see text): [a]D_2 in place of H_2; [b]0.013 M LiCl; [c]0.026 M LiCl; [d]0.05 M LiCl; [e]0.10 M LiCl; [f]0.05 M p-toluenesulfonic acid; [g]0.10 M p-toluenesulfonic acid.

was detected during the later stages of hydrogenation of maleic acid solutions.

The Ru(I) solutions did not react with 1 atm C_2H_4 at 80°, but hydrogenation of ethylene to ethane was observed on subjecting the solutions to C_2H_4/H_2 mixtures. The uptake plots were linear (rate = 0.54×10^{-6} $M\,s^{-1}$ with 0.02 M Ru(I), 430 mm C_2H_4, and 295 mm H_2). Again no change in visible absorption spectrum of the solution was observed during the reaction, and the pseudo zero-order uptake plot is consistent with a constant [Ru(I)] while maintaining the H_2 and C_2H_4 pressures and concentrations constant in the uptake apparatus.

TABLE 2. Ru(I)-catalyzed hydrogenation of fumaric acid; [Ru(I)] = 0.53×10^{-2} M, 725 mm H_2, 80°

[FA] ($\times 10^2$) (M)	k' ($\times 10^4$) (s^{-1})	Initial rate ($\times 10^6$) ($M\,s^{-1}$)
15.60	—	11.10
10.70	—	9.70
10.70	—	6.45†
7.25	—	7.97
5.17	1.20*	6.20
3.00	1.36*	4.10
1.80	1.23*	2.20

*To be compared with starred values in Table 1.
†D_2 in place of H_2.

The Maleic Acid System

The hydrogenation rates of MA (initial rates, column 5 of Table 1) were measured as a function of H_2 pressure, and concentrations of Ru(I), MA, added chloride, and added acid. The rate is not linearly dependent on catalyst concentration but shows a good half-order dependence on Ru(I) (Fig. 3). The rate shows a good first-order dependence on H_2 up to 725 mm (Fig. 4). A kinetic isotope effect ($rate_{H_2}/rate_{D_2}$) of 1.35 was observed. The dependence on [MA] is shown in Fig. 5, which also gives corresponding data at 70 and 60°; the rates are first-order at low concentration, but become less than one and approach zero-order at higher concentrations.

A marked inverse dependence on added chloride was noted over the range 0.0–0.1 M, and a reasonably linear relationship was obtained on plotting $(\text{initial rate})^{-1}$ *vs.* [added Cl^-] (Fig. 6). Unfortunately the total salt strength could not be kept constant in these experiments since perchlorate ion (commonly added to give constant ionic strength) was found to oxidize the Ru(I) solutions. Addition of a strong acid (p-toluenesulfonic acid) had essentially no effect on the hydrogenation rate.

The Fumaric Acid System

A plot of k' for the hydrogenation of FA

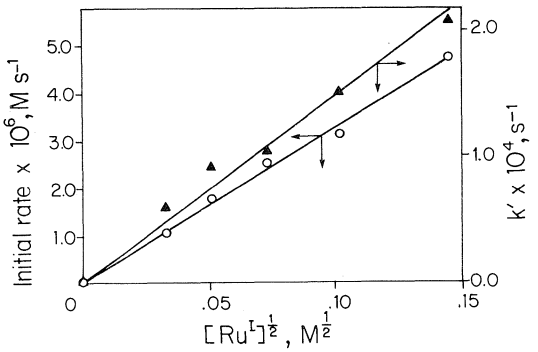

FIG. 3. Dependence of hydrogenation rates on $[Ru(I)]^{1/2}$ in DMA at 80°, 725 mm H_2. ○, 0.051 *M* maleic acid; ▲, ~0.025 *M* fumaric acid.

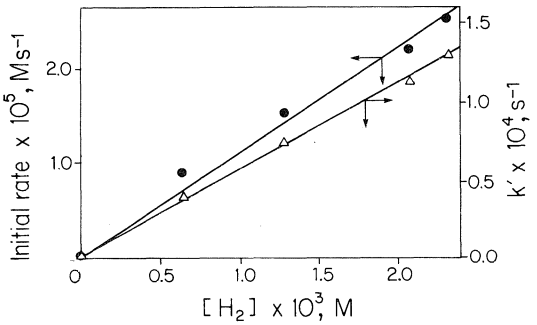

FIG. 4. Dependence of hydrogenation rates on $[H_2]$ in DMA at 80°, 0.0053 *M* Ru(I). ●, 0.051 *M* maleic acid; △, ~0.025 *M* fumaric acid.

against $[Ru(I)]^{1/2}$ (Fig. 3) is linear, and again shows a half-order dependence on catalyst concentration. A first-order dependence on H_2 is also evident (Fig. 4). The dependence of the initial rate (either measured or calculated from k' values) on the fumaric acid concentration is shown in Fig. 7; it is similar to that for the maleic acid system being first-order at lower olefin concentrations and approaching zero-order at higher concentrations. This dependence shows clearly why good first-order log plots are not obtained at the higher substrate concentrations. The ratio of rate of reduction using H_2 to that using D_2 was about unity at lower [FA] (Table 1) but was ~1.5 at higher concentrations (Table 2). As in the maleic acid systems, an inverse dependence on chloride concentration was observed (Fig. 6), and there was no significant dependence on adding acid.

The deuterated succinic acid products formed from deuteration of fumaric acid were characterized by i.r. (see below).

Discussion

Kinetics of Hydrogenation

The ruthenium(I) chloride solutions almost certainly contain some dimeric species, and the half-order kinetic dependence on Ru supports this. The kinetic data alone are consistent with a dimer ⇌ monomer pre-equilibrium followed by reaction of the monomer Ru(I) species with H_2 or olefin according to Scheme 1 (ligands omitted). Activation of H_2 must occur by processes such

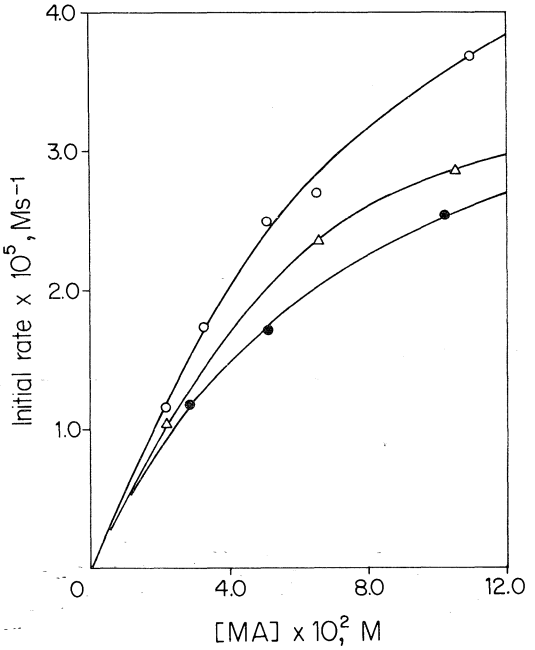

FIG. 5. Dependence of maleic acid hydrogenation rate on maleic acid concentration in DMA, 0.0053 *M* Ru. ○, 80°, 2.32 × 10^{-3} *M* H_2; △, 70°, 2.22 × 10^{-3} *M* H_2; ●, 60°, 2.18 × 10^{-3} *M* H_2.

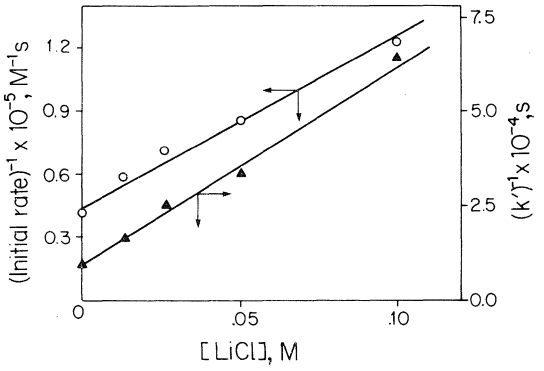

FIG. 6. Inverse dependence of hydrogenation rates on [LiCl] in DMA at 80°, 0.0053 *M* Ru(I), 725 mm H_2. ○, 0.05 *M* maleic acid; ▲, ~0.025 *M* fumaric acid.

Can. J. Chem. Downloaded from www.nrcresearchpress.com by 210.87.254.5 on 09/05/12
For personal use only.

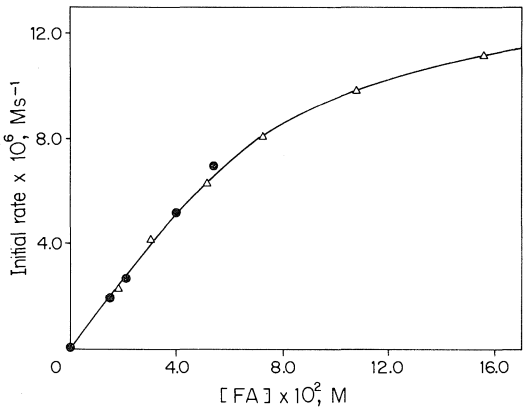

FIG. 7. Dependence of fumaric acid hydrogenation rate on fumaric acid concentration in DMA at 80°, 0.0053 *M* Ru, 725 mm H_2. △, from fumaric acid systems (Table 2); ●, from maleic acid systems (calculated from *k'* starred values in Table 1).

as [1]–[3]. Reaction 3 can be ruled out because of the observed Ru dependence. Reaction 2 is possible in the polar DMA solvent and has been invoked previously (1). However, the observed dependence on olefin together with the independence on acid are consistent only with reaction 1 for hydrogen activation (see below).

Scheme 1 incorporates the two general paths that have been recognized for transfer of the H_2

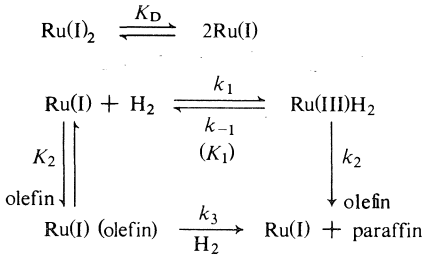

SCHEME 1

molecule to an olefin via a catalyst complex (ref. 4, p. 400): (*1*) attack of uncomplexed olefin on a dihydro complex at a vacant site to give a transition state in which both hydrogen and olefin are bound to the metal atom (k_2 path); (*2*) attack of H_2 on an olefin complex to give the same transition state (k_3 path). The k_2 and k_3 paths are indistinguishable kinetically if the equilibria K_1 and K_2 are set up rapidly since the rate of H_2 uptake is given by

$$[4]\quad \frac{-d[H_2]}{dt} = \frac{(k_2K_1 + k_3K_2)[H_2][MA][Ru(I)]_T}{1 + K_2[MA] + K_1[H_2] + [Ru(I)]_T/K_D}$$

where subscript T refers to total concentration. This is the expression for reaction by both paths; the k_2K_1 and k_3K_2 terms refer respectively to the k_2 and k_3 paths; k_3K_2 becomes zero if the k_2 path predominates and *vice versa*. The terms in the denominator, taken from left to right, represent the amounts present as monomer, olefin complex, hydride complex, and dimer, respectively. The observed first-order dependence on H_2 implies that the $K_1[H_2]$ term is small, which means that Ru(III)H_2 will not be detectable; however, the observed first- to zero-order dependence on olefin would imply that the K_2[MA] is significant and that there is an appreciable concentration of the olefin complex in solution at higher olefin concentrations. However, the Ru solutions do not react with maleic acid, and the spectrum of the reacting solution remained unchanged throughout a kinetic run. All the observations can be accounted for if the reaction occurs solely by the k_2 path with the hydride formation not being a rapid equilibrium, *i.e.*

$$[5]\quad Ru(I)_2 \overset{K_D}{\rightleftarrows} 2Ru(I)$$

$$[6]\quad Ru(I) + H_2 \underset{k_{-1}}{\overset{k_1}{\rightleftarrows}} Ru(III)H_2 + (Cl^-)$$

$$[7]\quad Ru(III)H_2 + \text{olefin} \xrightarrow{k_2} Ru(I) + \text{product}$$

Such a mechanism assuming a steady state concentration of Ru(III)H_2 yields the rate-law

$$[8]\quad \text{Rate} = \frac{-d[H_2]}{dt} = \frac{-d[\text{olefin}]}{dt} = \frac{k_1k_2K_D'[Ru(I)]_T^{1/2}[\text{olefin}][H_2]}{k_{-1}[Cl^-] + k_2[\text{olefin}]}$$

where $K_D' = (K_D/2)^{1/2}$ and $[Ru(I)]_T$ is the total ruthenium(I) chloride concentration expressed as monomer. The derivation of this rate-law giving the half-order in ruthenium involves the assumption that K_D is small, that is, practically all the ruthenium is present as dimer at the concentrations used in the kinetic runs. Since no H_2-uptake

Can. J. Chem. Downloaded from www.nrcresearchpress.com by 210.87.254.5 on 09/05/12
For personal use only.

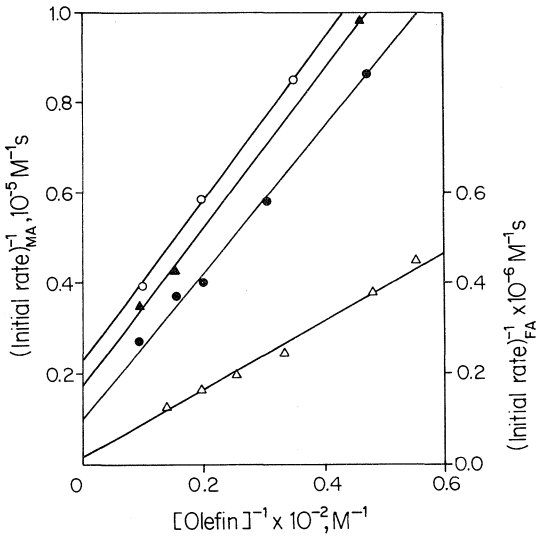

FIG. 8. Dependence of initial hydrogenation rates plotted in accord with eq. 9. Maleic acid data of Fig. 5 (○, 60°; ▲, 70°; ●, 80°). △, fumaric acid data of Table 2.

is observed in the absence of olefin, k_{-1} must be greater than k_1. Reaction 6 is written involving a molecular dihydride since a heterolytic splitting of H_2 would give proton production and such a mechanism would give an inverse dependence of the rate on added acid at lower olefin concentrations, which was not observed. Evidence for the production of a ruthenium(III) hydride species in the presence of triphenylphosphine by a reaction such as [6] will be given later. Reaction 6 will involve displacement of Cl^- or solvent ligand; rate-law 8 has been written assuming the former. If a solvent molecule is involved, $k_{-1}[Cl^-]$ will be replaced by k_{-1}[solvent], or k_{-1}' (a pseudo first-order constant).

Equation 8 can be rewritten in the form

$$[9] \quad (\text{Rate})^{-1} = \frac{k_{-1}[Cl^-][\text{olefin}]^{-1}}{k_1 k_2 K_D'[H_2][\text{Ru(I)}]_T^{1/2}} + \frac{1}{k_1 K_D'[H_2][\text{Ru(I)}]_T^{1/2}}$$

Figure 8 shows a plot of (rate)$^{-1}$ *vs.* [olefin]$^{-1}$ for the maleic and fumaric acid systems; the linear relationships are in accord with eq. 9, and yield the values of k_1K_D' and $k_{-1}[Cl^-]/k_2$ given in Table 3. The k_1K_D' values determined at 80° from the lines drawn are essentially independent of the two substrates used and this gives strong

TABLE 3. Ru(I)-catalyzed hydrogenation of unsaturated carboxylic acids. Temperature dependence of some kinetic data; [Ru(I)] = 0.53 × 10^{-2} *M*, 725 mm H_2

Temperature (°C)	Substrate	$k_{-1}[Cl^-]/k_2$ (*M*)	k_1K_D' ($M^{-1/2}$ s^{-1})
80	Maleic acid	0.16	0.59
70	Maleic acid	0.10	0.34
60	Maleic acid	0.06	0.22
80	Fumaric acid	0.55	0.45

support for the suggested mechanism, although the determined values are very sensitive to the intercept values. The k_2 value for the MA system is about four times that for the FA one.

The k_1K_D' values for the MA system give a good Arrhenius plot and an apparent $\Delta H^{\ddagger}$ value of 10.9 ± 1.0 kcal mol^{-1}. Reaction 5 is expected to be somewhat endothermic, so that the activation energy for k_1 is likely to be somewhat greater than 10.9 kcal. From the half-order dependence on Ru, even at the lowest [Ru(I)] used (~10^{-3} *M*), the upper limit of K_D must be ~10^{-5} *M*,[3] and hence the lowest value of k_1 is ~100 M^{-1} s^{-1} at 80°. Assuming such a value for k_1, and a $\Delta H_1^{\ddagger}$ value of 11 kcal, gives $\Delta S_1^{\ddagger}$ ~ −20 e.u. These admittedly very crude activation parameters are similar to those observed for oxidative addition of H_2 to square planar d^8 systems (8), and are in the normal range for a bimolecular reaction in solution between an ion and a neutral molecule (9).

The inverse dependence on chloride could result from the reverse of reaction 6 according to rate-law 8, and in accord with eq. 9 a plot of (initial rate)$^{-1}$ *vs.* [Cl^-] at constant concentrations of olefin, H_2, and Ru(I) yields straight lines for the MA and FA systems. The abscissa represents the added chloride and does not include any contribution from the starting compound, $RuCl_3 \cdot 3H_2O$; including this unknown amount would displace each abscissa value by a constant increment. The slopes would be unaffected by this correction and they yield values of 7.0 $M^{1/2}$ s (MA) and 85.0 $M^{1/2}$ s (FA) for $k_{-1}/k_1k_2K_D'$ at

[3]It is of interest that the noted divergence from Beer's Law in the visible absorption spectrum at 20° becomes evident at concentrations below ~10^{-3} *M*, which again indicates that K_D (as defined by eq. 5) would be of the order 10^{-5} *M*.

Can. J. Chem. Downloaded from www.nrcresearchpress.com by 210.87.254.5 on 09/05/12
For personal use only.

80°. These values are not too consistent with the data in Table 3 since the k_2 value for FA should be about four times less than the value for the MA system. The composite factors determined from the chloride dependence indicate a factor of twelve between the k_2 values. Further, assuming that the chloride contribution from the trichloride for these studies at 0.53×10^{-2} M Ru(I) is about 0.01 M, the estimated intercepts on the ordinate axis yield k_1K_D' values at 80° of about 0.3 $M^{1/2}$ s^{-1} and 0.04 $M^{1/2}$ s^{-1} for the MA and FA systems, respectively. These should be independent of the substrate used, and should also agree with the values determined from the olefin dependence studies (*cf.* Table 3). The discrepancies could arise from either failure to maintain a constant ionic strength in the chloride variation experiments, or added chloride affecting the distribution of ruthenium(I) chloride complexes present. The linear plots obtained for the chloride variation could be fortuitous.

At higher olefin concentration eq. 8 takes the limiting form, rate $= k_1K_D'[Ru(I)]_T^{1/2}[H_2]$, and the deuterium isotope effect of 1.5 measured at higher [FA] then refers to the k_1 value for dihydride formation (eq. 6). The small value suggests a synchronous breaking of the H—H bond and making of Ru—H bonds. Similar small isotope effects have been observed for oxidative addition of H_2 to a number of iridium(I) and rhodium(I) species (6, 10, 11). At lower [FA], the rate law takes the limiting form

$$\text{Rate} = k_1k_2K_D'[Ru(I)]_T^{1/2}[\text{olefin}][H_2]/k_{-1}[Cl^-]$$

and the measured isotope effect of about unity is a composite one relating to the k_1k_2/k_{-1} term.

Isomerization and Deuteration

The isomerization of maleic acid is catalyzed at a Ru center, since no such process is observed in DMA solution at 80° in the absence of metal complexes (6). No evidence was found for complexing between MA and Ru(I), and isomerization was evident only under hydrogenation conditions. A well-established mechanism for double-bond migration in olefins involves the reversible formation of metal alkyls through metal olefin hydride complexes via an insertion reaction (12). A similar mechanism may be invoked to explain *cis–trans* isomerization:

[10] 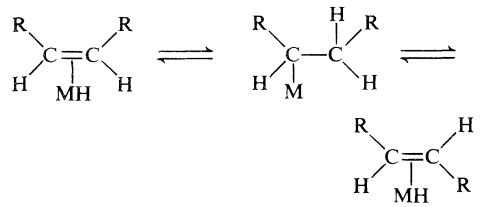

In the present system such a mechanism can exist if the H_2 molecule transfer occurs in two consecutive single hydrogen transfer steps:

$$\text{[11]}\quad Ru(III)H_2 + \text{olefin} \overset{(1)}{\rightleftharpoons} Ru(III)H_2(\text{olefin}) \overset{(2)}{\rightleftharpoons} Ru(III)H(\text{alkyl}) \overset{(3)}{\rightarrow} Ru(I) + \text{saturated product}$$

Such stepwise transfer of hydrogen is well documented for hydrogenation catalyzed by $RhCl(PPh_3)_3$ (ref. 4, p. 213). The observed isomerization in the present ruthenium system implies that the reverse of steps 1 and 2 successfully compete with step 3, the reductive elimination of product.

Deuterium reduction has been used to determine the stereochemistry of the H_2-addition to maleic and fumaric acids (2), since the corresponding dideuterosuccinic acids have been characterized by i.r. (13). From fumaric acid, the isolated succinic acid product had bands at 7.5–7.7 μ (broad), 8.09 μ (strong), 8.47 μ (sharp shoulder), 8.65 μ (shoulder), 9.45 μ (weak), and 11.65 μ (medium), which is consistent with a mixture of DL-sym-1,2-dideuterosuccinic acid and unsymmetrical dideuterosuccinic acid ($HO_2CCH_2CD_2CO_2H$). Such data can be rationalized in terms of Scheme 2 for the detailed path of the reactions shown in eq. 11. The DL-acid results from the transfer of the second coordinated deuterium in **1**; the unsymmetrical acid results from successive transfer of deuterium and hydrogen in a species **2** formed from **1**. The catalyst is regenerated as the monomeric Ru(I) species. The overall *cis* addition of H_2 (fumaric acid → the DL-acid) requires that decomposition of the alkyl hydride **1** (reductive elimination of the DL-acid) involves retention of configuration at the carbon atom attached to the metal. Such retention has been demonstrated recently for a corresponding decomposition of a hydridoalkylmolybdenum complex (14).

For the k_2 step (eq. 11), it seems more likely

Can. J. Chem. Downloaded from www.nrcresearchpress.com by 210.87.254.5 on 09/05/12
For personal use only.

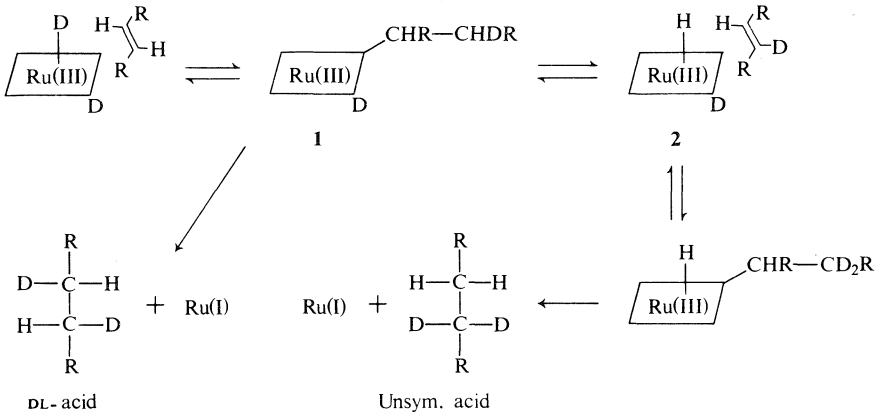

SCHEME 2

that olefin complexation to the dihydridoruthenium species is rate-determining (at lower [olefin]) rather than the subsequent hydrogen transfer steps. The lower hydrogenation rate (k_2) for FA compared to MA is then attributable to a steric effect, the *trans* isomer being more hindered in forming the π-hydrido complex.

The Hydrogen Activation Step

The monomeric Ru(I) complex is a d^7 system, and the hydrogen activation step is written as involving oxidative addition to a d^5 Ru(III)H_2 product; such a process has not been reported previously. Oxidative addition of H_2 to a d^7 system is well-documented only in the case of the pentacyanocobaltate(II) ion, but this involves a termolecular reaction to give a d^6 Co(III)H; that is, the oxidation number increases by one (15):

[12] $2Co(II)(CN)_5^{3-} + H_2 \rightarrow 2Co(III)(CN)_5H^{3-}$

Oxidative addition of alkyl halides to the same Co(II) system again gives Co(III) products but via a bimolecular free-radical mechanism (15):

[13] $Co(CN)_5^{3-} + RX \xrightarrow{k} Co(CN)_5X^{3-} + R\cdot$

[14] $Co(CN)_5^{3-} + R\cdot \rightarrow Co(CN)_5R^{3-}$

which give

[15] $2Co(CN)_5^{3-} + RX \rightarrow Co(CN)_5X^{3-} + Co(CN)_5R^{3-}$

Clearly it is possible to suggest formation of a Ru(II)H via reactions corresponding to reactions 13–15, which would also be consistent with formation of a hydride via a bimolecular rate-determining step and not leading to an inverse acid dependence (*cf.* reaction 6):

[16] $Ru(I) + H_2 \underset{k_{-1}}{\overset{k_1}{\rightleftharpoons}} Ru(II)H + H\cdot$

[17] $Ru(I) + H\cdot \rightarrow Ru(II)H$

which give

[18] $2Ru(I) + H_2 \rightarrow 2Ru(II)H$

However, such a free-radical H atom mechanism seems highly unlikely, and it also becomes difficult to account for the observed kinetics of the catalytic hydrogenations.

Some direct support for a reaction such as [6] was evidenced by reaction of the Ru(I) solutions with H_2 in the presence of triphenylphosphine. Addition of PPh_3 to the brown DMA solutions of Ru(I) (PPh_3:Ru = 3) resulted in a darkening of the coloration; this solution, in contrast to the initial one, slowly absorbed H_2 at 80° up to a 1:1 ratio of H_2:Ru. A reaction such as [19]

[19] $(PPh_3)_nRu(I) + H_2 \rightarrow (PPh_3)_nRu(III)H_2$

would be consistent with the data, although further studies are necessary to confirm such dihydride formation. The product is certainly not the phosphine-stabilized Ru(II) monohydride complex $HRuCl(PPh_3)_3$ (*cf.* reaction 18) which has been formed by subjecting DMA solutions of Ru(II) to hydrogen in the presence of PPh_3 (1).

Can. J. Chem. Downloaded from www.nrcresearchpress.com by 210.87.254.5 on 09/05/12
For personal use only.

We thank the National Research Council of Canada for financial support and Johnson Matthey Limited for loan of ruthenium.

1. B. C. HUI and B. R. JAMES. Can. J. Chem. **52**, 348 (1974).
2. J. HALPERN, J. F. HARROD, and B. R. JAMES. J. Am. Chem. Soc. **88**, 5150 (1966).
3. B. C. HUI and B. R. JAMES. Chem. Commun. 198 (1969).
4. B. R. JAMES. Homogeneous hydrogenation. Wiley–Interscience, New York. 1973. p. 95.
5. P. N. RYLANDER, N. HIMELSTEIN, D. R. STEELE, and J. KREIDL. Englehard Ind. Tech. Bull. **3**, 61 (1962).
6. B. R. JAMES and G. L. REMPLE. Discuss. Faraday Soc. **46**, 48 (1968).
7. B. R. JAMES, R. S. MCMILLAN, and E. OCHIAI. Inorg. Nucl. Chem. Lett. **8**, 239 (1972).
8. L. VASKA and M. F. WERNEKE. Trans. N.Y. Acad. Sci. **31**, 70 (1971).
9. A. A. FROST and R. G. PEARSON. Kinetics and mechanism. 2nd ed. Wiley, New York. 1961. p. 147.
10. P. B. CHOCK and J. HALPERN. J. Am. Chem. Soc. **88**, 3511 (1966).
11. C. O'CONNOR and G. WILKINSON. J. Chem. Soc. A, 2665 (1968).
12. M. ORCHIN. Adv. Catal. **16**, 1 (1966).
13. C. R. CHILDS and K. BLOCH. J. Org. Chem. **26**, 1630 (1961).
14. A. NAKAMURA and S. OTSUKA. J. Am. Chem. Soc. **95**, 7262 (1973).
15. J. HALPERN. Acc. Chem. Res. **3**, 386 (1970).

Can. J. Chem. Downloaded from www.nrcresearchpress.com by 210.87.254.5 on 09/05/12
For personal use only.

Some Electrical and Thermodynamic Properties of the System: Indium Trichloride – Dioxane – Water

ALAN N. CAMPBELL

Department of Chemistry, University of Manitoba, Winnipeg, Manitoba R3T 2N2

Received June 27, 1974

ALAN N. CAMPBELL. Can. J. Chem. **52**, 3769 (1974).

The following properties have been investigated: conductance in water and in water–dioxane, the solubility products of indium hydroxide and of indium iodate, e.m.f.'s of the cell: In(s)/$InCl_3$(m)/sat. KCl/Hg_2Cl_2 in sat. KCl/Hg and resulting activity coefficients, heats of solution of indium trichloride in water, water–dioxane, and pure dioxane, freezing point diagram of dioxane–water, heats of mixing of dioxane–water, heats of mixing of indium chloride – water with dioxane–water, change in volume on mixing of water–dioxane, and of water – indium chloride with water–dioxane.

ALAN N. CAMPBELL. Can. J. Chem. **52**, 3769 (1974).

On étudie les propriétés suivantes: la conductance dans l'eau et dans le système eau–dioxanne, les produits de solubilité de l'hydroxyde d'indium et de l'iodate d'indium, la f.e.m. de la pile: In(s)/$InCl_3$(m)/KCl sat./Hg_2Cl_2 dans KCl sat./Hg et les coefficients d'activité qui en résultent, les chaleurs de dissolution du trichlorure d'indium dans l'eau, dans le mélange eau–dioxanne et dans le dioxanne pur, le diagramme de solidification du système dioxane–eau, les chaleurs de mélange du dioxanne–eau, les chaleurs de mélange du chlorure d'indium – eau avec du dioxanne–eau, le changement de volume au cours du mélange eau–dioxanne et eau – chlorure d'indium dans le système eau–dioxanne. [Traduit par le journal]

Introduction

Many of the properties of indium chloride and its derived salts have recently been determined in this laboratory (1).[1] Thus, the limiting conductance of $\frac{1}{3}In^{3+}$ has been determined by a method which can only be justified on the ground of expediency (1). For the lack of anything better, the figure of 56.3 mho at 25° may stand for the time being. The difficulty lies in the hydrolysis of indium trichloride, as was first observed by Thiel (2). It occurred to the author that by using a mixed solvent of water and dioxane the hydrolysis might be obviated but it soon became clear that the conductance of a very weak solution in a dioxane–water solvent is almost as great as in pure water. In the absence of hydrolysis, and assuming validity of the Walden rule, $\Lambda^0\eta$ = constant, it would have been possible to obtain Λ in pure water.

Having entered on the subject of mixed dioxane–water solvent for indium trichloride, it was decided to pursue the subject and more or less to repeat the previous work on indium trichloride in water (1). All the experimental methods have been described previously (3–5).

[1]I am indebted to the generosity of Cominco (of Trail, B.C.) for a supply of aqueous solution of pure indium trichloride (57.88% weight of $InCl_3$).

Results

Electrical Properties

Equivalent Conductance

The results of equivalent conductance measurements of indium chloride in water and in 51.55 wt. % dioxane–water solutions are shown in Fig. 1. The numerical data are to be found in the Depository of Unpublished Data.[2]

Solubility Products of Indium Hydroxide, $In(OH)_3$, and of Indium Iodate, $In(IO_3)_3$

Indium hydroxide was prepared by precipitation of indium trichloride with ammonia and indium iodate by precipitation with potassium iodate. Both precipitates were washed thoroughly with hot water but this procedure is insufficient to remove all traces of soluble electrolyte. The method of procedure was to place excess of the powdered product in a Shedlovsky conductance cell, filled with conductance water. At intervals of 24 h, measurements of conductance were taken until a maximum occurred. The liquid was then poured off, fresh conductance water added, and the procedure repeated. Finally, a state of affairs was

[2]These data may be obtained, at a nominal charge, from the Depository of Unpublished Data, National Science Library, National Research Council of Canada, Ottawa, Canada K1A 0S2.

Can. J. Chem. Downloaded from www.nrcresearchpress.com by 210.87.254.6 on 09/05/12
For personal use only.

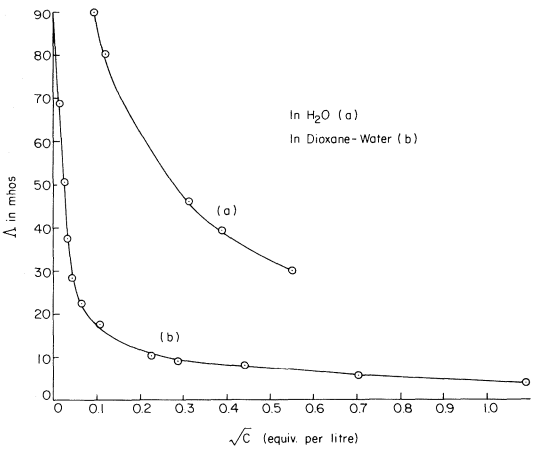

FIG. 1. Equivalent conductance of $InCl_3$ in water and in water–dioxane.

reached when the conductance did not increase on standing and this was accepted as the true conductance of a saturated solution. The following values were obtained at 25°: $In(OH)_3$, $K_s = 5.115 \times 10^{-20}$; $In(IO_3)_3$, $K_s = 3.007 \times 10^{-4}$ (corresponds to a solubility of 0.6568 g/l.) The value for $In(IO_3)_3$ is a maximum value because of the hydrolysis of the salt.

Unsaturated solutions of indium iodate were also prepared and the equivalent conductance determined as follows: $c = 0.002676$ equiv/l, $\Lambda = 187.1$ mho; $c = 0.001067$ equiv/l, $\Lambda = 195.1$ mho. Obviously the same hydrolysis occurs as with $InCl_3$.

Electromotive Force Measurements

The e.m.f. of the cell

$$In(s)/InCl_3(m)/sat.\ KCl/Hg_2Cl_2 \text{ in sat. } KCl/Hg$$

was investigated at various concentrations. From the observed E and m values, the activity coefficients were calculated by the method of Harned *et al.* (6). The results are given in Table 1. In Fig. 2, the results of these measurements are plotted along with previous results obtained from freezing point depression (4); all the figures lie on the same curve. Extrapolation to zero concentration gives E^0 ($In^{3+} + 3e \rightarrow In$) = −0.327 V, as against the values of −0.340 V of Hattox and de Vriess (7).

Calorimetric Results

Powdered indium metal dissolves in concentrated hydrochloride acid sufficiently rapidly for calorimetric work.

TABLE 1. Electromotive force of the cell $In(s)/InCl_3(m)/sat.\ KCl/Hg_2Cl_2$ in sat. KCl/Hg

m (in mol/1000 g H_2O)	E (cell voltage)	γ
6.1386	0.5943	0.1549
1.3905	0.6793	0.0572
0.8264	0.6988	0.0544
0.3707	0.7174	0.0705
0.1679	0.7310	0.1046
0.0661	0.7477	0.1633
0.0261	0.7640	0.2567
0.00558	0.7840	0.6706

$$In + 3HCl.aq = InCl_3.aq + 1.5H_2(g)$$
$$\Delta H = -22.51 \pm 0.97 \text{ kcal}$$

The concentration of indium chloride produced was small enough to be considered infinite dilution. From the enthalpy of the above reaction that of $InCl_3$.aq is calculated to be − 130.01 kcal, in good agreement with the value of Klemm and Bräutigam (8) if their result refers to $InCl_3$.aq. On the basis of my own figure (*cf.* infra) for the heat of solution of anhydrous $InCl_3$ in water, we have

$$InCl_3(s) + aq = InCl_3.aq$$
$$\Delta H = -16.77 \text{ kcal}$$

and from this $InCl_3(s)$ results as −113.24 kcal.

Heat of Solution of Anhydrous $InCl_3$ in Water

$\Delta H = -16.77 \pm 0.72$ kcal ($m = 0.511$).

Heat of Solution in Pure Dioxane

$\Delta H = -8.92$ kcal ($m = 0.1532$). Reaction may not be complete so that the above figure is a minimum.

Heat of Solution in a Solvent of Composition $3D.2H_2O$: D = dioxane (cf. Kartzmark (9))

$\Delta H = -17.75 \pm 0.76$ kcal. The heat of solution is approximately the same as that in water.

Heat of Dilution of a Saturated Solution of $InCl_3$ in a Solvent of Composition 49.35 wt. % dioxane

Concentration of saturated solution = 1.0109 m: (*i*) initial molality = 1.0109, final molality = 0.5242, ΔH/mole of mixture = −1159 cal; (*ii*) initial molality = 0.5242, final molality = 0.2062, ΔH/mole of mixture = −703.8 cal. These results are practically identical with the corresponding results for water as solvent.

Can. J. Chem. Downloaded from www.nrcresearchpress.com by 210.87.254.6 on 09/05/12
For personal use only.

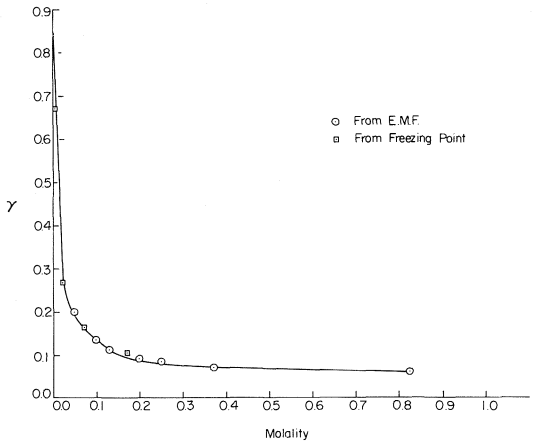

FIG. 2. Activity coefficients from e.m.f. and from freezing point measurements.

Freezing Point Diagram and Heats of Mixing of Dioxane–Water Mixture

As a preliminary to using water–dioxane as a solvent, the work of Goates and Sullivan (10) on water–dioxane mixture was repeated. The results for the freezing point diagram are in essential agreement, as Fig. 3 shows. It had been intended to study the effect of indium chloride on the eutectic mixture, but the indefiniteness of eutectic composition and temperature made accurate work impossible.

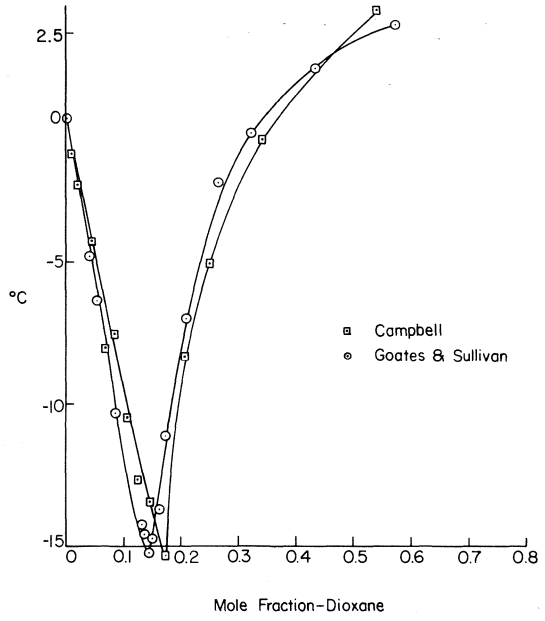

FIG. 3. Freezing points of dioxane–water.

The values for the heats of mixing are given in the Depository of Unpublished Data[2] and graphically in Fig. 4. The agreement is excellent. The limiting value of ΔH per mole of dioxane results as -2400 cal per mol (*cf.* data in the Depository of Unpublished Data).

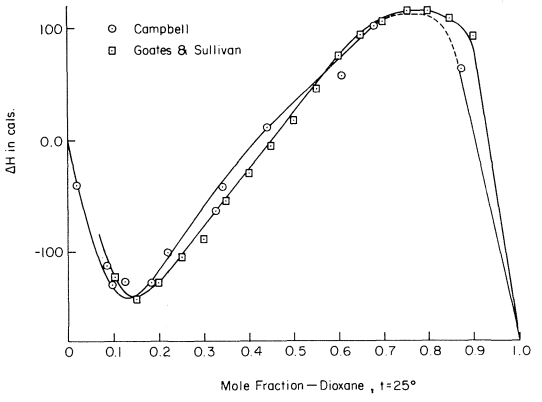

FIG. 4. Heats of mixing of dioxane–water. $t = 25°$.

Discussion

It is apparent from Fig. 1, that the addition of dioxane to water has reduced the mobility or the number, or both, of conducting ions of indium chloride but has had little or no effect on the hydrolysis in very dilute solution.

The solubility of indium hydroxide is lower than that of aluminum hydroxide but higher than that of ferric hydroxide; that of indium chlorate agrees with the known solubility. The two numerical results for the conductance of indium iodate in dilute solution show that it, like the chloride, undergoes hydrolysis.

When the activity figures for indium chloride from e.m.f. measurements are plotted on the same graph with those previously obtained from freezing point measurements (4) they are seen to lie on the same curve. The value of E^c ($In^{3+} + 3e \rightarrow In$) from the e.m.f. measurements (-0.327 V) is in reasonable agreement with that of Hatto and de Vries (7) (-0.34). The work of Ferri (11) shows that the ionization (hydrolysis) equilibrium of $InCl_3$ is not simple, but this should not have any bearing on my evaluation of γ.

This work on the freezing point diagram and heats of mixing of dioxane and water was done in ignorance of the work of Goates and Sullivan so the good agreement must be considered very satisfactory.

Nothing need be said about the heat of solu-

Can. J. Chem. Downloaded from www.nrcresearchpress.com by 210.87.254.6 on 09/05/12
For personal use only.

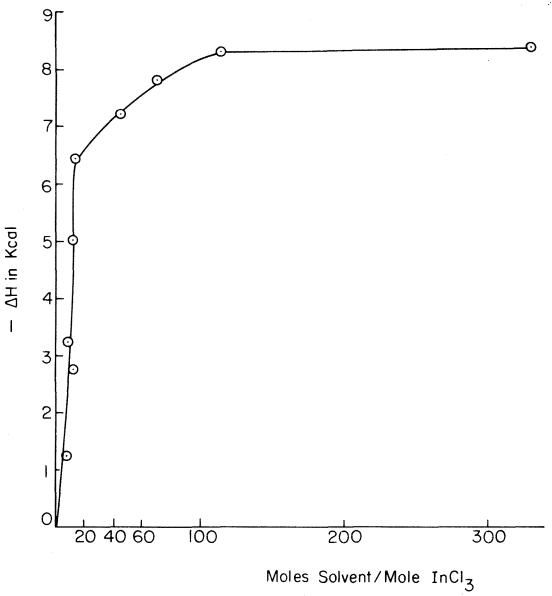

FIG. 5. Heat of mixing of 57% indium chloride – water with 57% dioxane–water.

tion of metallic indium in concentrated hydrochloric acid or that of indium chloride in various solvents, but the heats of mixing of 57% indium chloride – water with 57% dioxane–water are of interest. In contrast with the beautiful curve for dioxane–water, with its marked maximum and minimum, the results for the solvents containing indium chloride appear anomalous, but this is because two independent variables are involved, *viz.* the concentrations of indium chloride and of dioxane. If, however, the heat of mixing is plotted against moles solvent (total) per mole

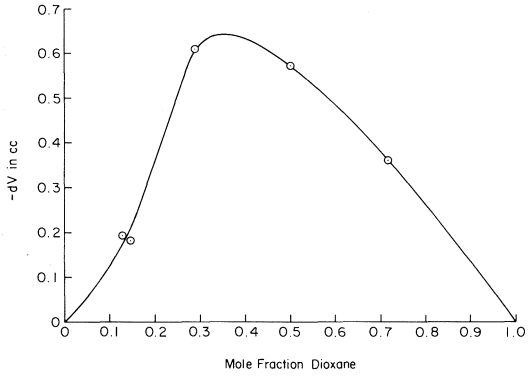

FIG. 6. Contraction in volume on mixing dioxane and water.

$InCl_3$, a constant value of -8 kcal is obtained above 100 mol of solvent (Fig. 5).

The plot of excess volumes of mixing of water with dioxane shows a maximum between 0.3 and 0.4 mole fraction dioxane, of -0.65 cc (Fig. 6).

The figure obtained for the enthalpy of $InCl_3(s)$ permits the calculation of the lattice energy of $InCl_3(s)$. The Born–Haber cycle is

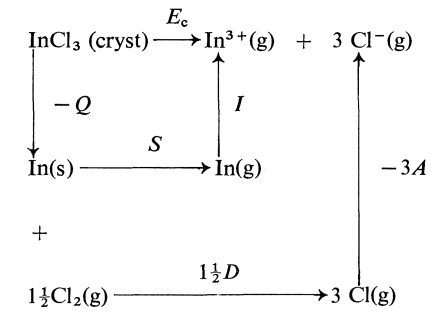

Where Q = heat of formation of $InCl_3$(cryst) (-113.24 kcal) and S = heat of sublimation of In, which can be calculated from the known heat of fusion (0.780 kcal/mol) and Trouton's rule to be 38.7 kcal. The figure agrees exactly with that of Robert (12). I = ionisation potential of In(g) (= 643.5 kcal); A = electron affinity of Cl (g) (= 88 kcal); D = heat of dissociation of Cl_2(g) (= 54 kcal). Hence $E_c = -Q + S + 1\frac{1}{2}D + I - 3A = 612.4$ kcal. This figure seems not unreasonable for the complete ionization of indium chloride triply charged ion compared with that of sodium chloride (190 kcal, singly charged ion).

1. A. N. CAMPBELL. Can. J. Chem. **51**, 3006 (1973).
2. A. THIEL. Zeit. Anorg. Chem. **40**, 332 (1904).
3. A. N. CAMPBELL, E. M. KARTZMARK, and S. C. Anand. Can. J. Chem. **48**, 1579 (1970).
4. A. N. CAMPBELL, E. M. KARTZMARK, and OM N. BHATNAGAR. Can. J. Chem. **52**, 1954 (1974).
5. I. BROWN and F. SMITH. Aust. J. Chem. **15**, 1 (1962).
6. H. S. HARNED *et al.* J. Am. Chem. Soc., **54**, 1350 (1932); **55**, 2179 (1933); **58**, 989 (1936).
7. E. M. HATTOX and T. DE VRIESS. J. Am. Chem. Soc. **58**, 2128 (1936).
8. W. KLEMM and M. BRÄUTIGAM. Z. Anorg. Chem. **163**, 232 (1927).
9. E. M. KARTZMARK. Can. J. Chem. **52**, 3459 (1974).
10. J. R. GOATES and R. J. SULLIVAN. J. Phys. Chem. **62**, 188 (1957).
11. D. FERRI. Acta Chem. Scand. **26**, 733 (1972).
12. C. ROBERT. Helv. Phys. Acta, **9**, 426 (1936).

Can. J. Chem. Downloaded from www.nrcresearchpress.com by 210.87.254.6 on 09/05/12
For personal use only.

The Kinetics of the Insertion Reaction of Tin(II) Chloride with Hexacarbonylbis(triphenylphosphite)dicobalt

PETER FOWLER BARRETT

Department of Chemistry, Trent University, Peterborough, Ontario K9J 7B8

Received November 26, 1973[1]

PETER FOWLER BARRETT. Can. J. Chem. **52**, 3773 (1974).

The kinetics of the thermal insertion reaction of $SnCl_2$ with the metal–metal bonded complex $[P(OC_6H_5)_3Co(CO)_3]_2$ have been studied by following the change in the visible spectrum in THF over the temperature range 35.0 to 55.0 °C. The activation enthalpy and entropy for the reaction are 24.7 ± 0.4 kcal/mol and 2.4 ± 1.3 cal mol^{-1} deg^{-1} respectively. The data are consistent with a two-stage mechanism identical to that proposed for the corresponding reaction with $[P(n\text{-}C_4H_9)_3Co(CO)_3]_2$ and from a comparison of the two reactions it is concluded that the cobalt–cobalt bond is slightly weakened when tributylphosphine is replaced by the better π-electron acceptor triphenylphosphite. The insertion products $[LCo(CO)_3]_2SnCl_2$ are shown to undergo further reaction with $[LCo(CO)_3]_2$ to form $[LCo(CO)_3]_3SnCl$ (L = CO, $P(n\text{-}C_4H_9)_3$, $P(OC_6H_5)_3$).

PETER FOWLER BARRETT. Can. J. Chem. **52**, 3773 (1974).

Les cinétiques de la réaction d'insertion thermique de $SnCl_2$ avec le complexe à lien métal–métal $[P(OC_6H_5)_3Co(CO)_3]_2$ ont été étudiées en suivant la variation du spectre visible dans le THF dans l'intervalle de température de 35.0 à 55.0 °C. L'enthalpie d'activation et l'entropie de la réaction sont respectivement de 24.7 ± 0.4 kcal/mol et de 2.4 ± 1.3 cal mol^{-1} deg^{-1}. Les résultats sont conformes à un mécanisme en deux étapes, identique à celui proposé pour la réaction correspondante avec $[P(n\text{-}C_4H_9)_3Co(CO)_3]_2$, et de la comparaison des deux réactions on déduit que la liaison cobalt–cobalt est légèrement affaiblie lorsque la tributylphosphine est remplacée par la triphénylphosphite qui est un meilleur accepteur d'électrons. Les produits d'insertion $[LCo(CO)_3]_2SnCl_2$ peuvent subir des changements en réagissant à nouveau avec $[LCo(CO)_3]_2$ pour former $[LCo(CO)_3]_3SnCl$ (L = CO, $P(n\text{-}C_4H_9)_3$, $P(OC_6H_5)_3$).

[Traduit par le journal]

Introduction

The kinetics of the insertion of tin(II) halides into the metal–metal bond of a number of transition metal carbonyl complexes have been reported recently (1–4). On the basis of the proposed mechanisms for these reactions, it has been possible in a number of cases to interpret the data in a way which provides a measure of the metal–metal bond strengths.

In an attempt to determine the effect of substituents on metal–metal bond strengths, a kinetic investigation of the thermal insertion of $SnCl_2$ into the metal–metal bond of $[P(OC_6H_5)_3Co(CO)_3]_2$ is reported here and the results compared with those of the similar reaction with $[P(n\text{-}C_4H_9)_3Co(CO)_3]_2$ (4). Under the kinetic conditions, only the insertion reaction was observed to occur, although at much lower concentrations of $SnCl_2$ a different product was obtained and is concluded to be the tris substituted complex $[P(OC_6H_5)_3Co(CO)_3]_3SnCl$. The preparation by similar routes of the analogous complexes $[LCo(CO)_3]_3SnCl$ (L = CO, $P(n\text{-}C_4H_9)_3$) as well as the tetrakis complex $[Co(CO)_4]_4Sn$ are reported, and the ease of formation of these products is used to corroborate the kinetic evidence regarding the relative cobalt–cobalt bond strengths in $[LCo(CO)_3]_2$ (L = $P(n\text{-}C_4H_9)_3$, $P(OC_6H_5)_3$).

Experimental and Results

Materials

Hexacarbonylbis(triphenylphosphite)dicobalt was prepared by the method of Sacco (5) and dichlorobis(tetracarbonylcobalt) tin(IV) by the method of Graham and co-worker (6). Tin(II) chloride and bromide were dehydrated using acetic anhydride (7), the entire operation being carried out in an atmosphere of nitrogen in a glove bag. Tetrahydrofuran was purified by refluxing over sodium wire, and was freshly distilled and deoxygenated by bubbling nitrogen through it for about 20 min before being used in the kinetic runs.

Kinetics

The thermal insertion of tin(II) chloride into the metal–metal bond of $[P(OC_6H_5)_3Co(CO)_3]_2$ was studied by following the disappearance of the starting material at

[1]Revision received August 15, 1974.

Can. J. Chem. Downloaded from www.nrcresearchpress.com by 210.87.254.42 on 09/05/12
For personal use only.

570 nm using a Unicam SP1800 spectrophotometer. Infrared spectra of the reaction products were recorded on a Perkin–Elmer 621 spectrophotometer and showed that at concentrations of $SnCl_2$ greater than 0.1 *M*, only the insertion product was formed, but that at lower concentrations increasing quantities of another product were being formed. This byproduct proved to be the tris complex $[P(OC_6H_5)_3Co(CO)_3]_3SnCl$, and in order to keep its formation to a minimum in the kinetic runs, it was necessary to avoid using solutions of low $SnCl_2$ concentration. Reaction solutions approximately 5×10^{-3} *M* in $[P(OC_6H_5)_3Co(CO)_3]_2$ were prepared as reported earlier (1).

Pseudo first order kinetics were observed in all cases with the tin(II) chloride in excess. Plots of $\log (A_t - A_\infty)$ against time, where A_t and A_∞ refer to the absorbances at 570 nm at times t and ∞, respectively, were linear for between 50 to 75% of the reaction. A_∞ was measured experimentally for the faster reactions and estimated in other cases.

The pseudo first order rate constants, k_{obs}, are plotted in Fig. 1 as a function of tin(II) chloride concentration. The lines drawn through the experimental points are theoretical ones calculated on the basis of rate parameters derived by a least-squares treatment (8).

Reactions of SnX_2 and $[LCo(CO)_3]_2SnX_2$ with $[LCo(CO)_3]_2$

Dichlorobis(tricarbonyltriphenylphosphitecobalt)-tin(IV), $[P(OC_6H_5)_3Co(CO)_3]_2SnCl_2$

To a refluxing solution of $SnCl_2$ (1.3 g, 6.9 mmol) in 20 ml THF under N_2 was added gradually $[P(OC_6H_5)_3Co(CO)_3]_2$ (0.40 g, 0.43 mmol). After 45 min the THF was removed under reduced pressure, the residue extracted with CH_2Cl_2, filtered, and the residue obtained on evaporation recrystallized from ethanol yielding the desired product (9).

Chlorotris(tricarbonyltriphenylphosphitecobalt)tin(IV), $[P(OC_6H_5)_3Co(CO)_3]_3SnCl$

Method A: A solution of $[P(OC_6H_5)_3Co(CO)_3]_2$ (0.40 g, 0.43 mmol) and $SnCl_2$ (0.05 g, 0.26 mmol) in 25 ml THF was refluxed under N_2 for 45 min. The THF was then removed under reduced pressure and the residue extracted with ethanol, filtered, and recrystallized from ethanol yielding 0.15 g of orange platelet crystals, m.p. 119–122 °C.

Anal. Calcd. for $[P(OC_6H_5)_3Co(CO)_3]_3SnCl$: C, 49.98; H, 3.00; Cl, 2.34. Found: C, 49.26; H, 3.55; Cl, 2.62.

Method B: A solution of $[P(OC_6H_5)_3Co(CO)_3]_2$ (0.064 g, 0.068 mmol) and $[P(OC_6H_5)_3Co(CO_3]_2SnCl_2$ (0.064 g, 0.058 mmol) in 20 ml THF was refluxed under N_2 for 30 min. The THF was removed under reduced pressure and 0.03 g product isolated as in Method A.

Bromotris(tricarbonyltriphenylphosphitecobalt)tin(IV), $[P(OC_6H_5)_3Co(CO)_3]_3SnBr$

This compound was prepared in an identical manner to that employed in Method A for the chloro analog using 0.40 g (0.43 mmol) $[P(OC_6H_5)_3Co(CO)_3]_2$ and 0.06 g (0.22 mmol) $SnBr_2$ in 25 ml THF yielding 0.14 g of orange needle crystals, m.p. 128–131 °C.

Anal. Calcd. for $[P(OC_6H_5)_3Co(CO)_3]_3SnBr$: C, 48.56; H, 2.91; Br, 5.13. Found: C, 47.98; H, 3.21; Br, 4.63.

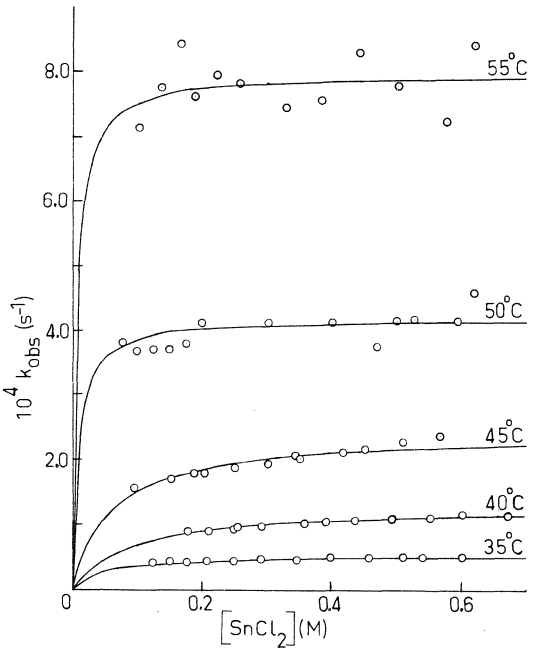

FIG. 1. Plot of the observed pseudo first order rate constant *vs.* tin(II) chloride concentration for the thermal reaction $[P(OC_6H_5)_3Co(CO)_3]_2 + SnCl_2 \rightarrow [P(OC_6H_5)_3Co(CO)_3]_2SnCl_2$ in THF. The curves drawn through the experimental points are theoretical lines calculated from the rate constants in Table 2.

Dichlorobis(tricarbonyltri-n-butylphosphinecobalt)-tin(IV), $[P(n\text{-}C_4H_9)_3Co(CO)_3]_2SnCl_2$

A solution of $[P(n\text{-}C_4H_9)_3Co(CO)_3]_2$ (0.40 g, 0.58 mmol) and $SnCl_2$ (0.40 g, 2.1 mmol) in 20 ml THF was refluxed under N_2 for 1 h. The THF was removed under reduced pressure and the residue extracted with CH_2Cl_2. The remainder of the isolation procedure was identical to that reported by Bonati *et al.* (9) yielding 0.25 g of product.

Chlorotris(tricarbonyltri-n-butylphosphinecobalt)-tin(IV), $[P(n\text{-}C_4H_9)_3Co(CO)_3]_3SnCl$

A solution of $[P(n\text{-}C_4H_9)_3Co(CO)_3]_2SnCl_2$ (0.20 g, 0.23 mmol) and $[P(n\text{-}C_4H_9)_3Co(CO)_3]_2$ (0.16 g, 0.23 mmol) in 20 ml THF was refluxed under N_2 for 5 h. The THF was removed under reduced pressure and the residue extracted with boiling methanol, filtered, and recrystallized from methanol–water yielding 0.11 g orange crystals, m.p. 151–155 °C.

Anal. Calcd. for $[P(n\text{-}C_4H_9)_3Co(CO_3]_3SnCl$: C, 45.42; H, 6.86; Cl, 2.98. Found: C, 46.62; H, 7.34; Cl, 2.28.

Chlorotris(tetracarbonylcobalt)tin(IV), $[Co(CO)_4]_3SnCl$ and Tetrakis(tetracarbonylcobalt)tin(IV), $[Co(CO)_4]_4Sn$

A solution of $[Co(CO)_4]_2$ (0.20 g, 0.59 mmol) and $[Co(CO)_4]_2SnCl_2$ (0.20 g, 0.38 mmol) in 20 ml THF was stirred under N_2 for 10 min at room temperature. The THF was removed under reduced pressure and the residue extracted with *n*-pentane, filtered, and crystallized

Can. J. Chem. Downloaded from www.nrcresearchpress.com by 210.87.254.42 on 09/05/12
For personal use only.

TABLE 1. Infrared spectra

Compound	ν(CO) in CH_2Cl_2 (cm^{-1})
$[P(OC_6H_5)_3Co(CO)_3]_3SnCl$	2058w, 2031m, 1989vs, ~1960m, sh
$[P(OC_6H_5)_3Co(CO)_3]_3SnBr$	2057w, 2030m, 1986vs, 1960m, sh
$[P(n\text{-}C_4H_9)_3Co(CO)_3]_3SnCl$	2029w, 2001m, 1954vs, 1927m, sh

Compound	ν(Sn—X) in CsI disc (cm^{-1})
$[Co(CO)_4]_2SnCl_2$	332s, 322s (Nujol mull)*
$[Co(CO)_4]_2SnBr_2$	234m, s, 222s (Nujol mull)*
$[P(OC_6H_5)_3Co(CO)_3]_2SnCl_2$	311s
$[P(OC_6H_5)_3Co(CO)_3]_3SnCl$	293m
$[P(OC_6H_5)_3Co(CO)_3]_3SnBr$	<200
$[P(n\text{-}C_4H_9)_3Co(CO)_3]_2SnCl_2$	301s
$[P(n\text{-}C_4H_9)_3Co(CO)_3]_3SnCl$	276m

*From ref. 16.

from *n*-pentane yielding a red product which the infrared indicated was a mixture of unreacted $[Co(CO)_4]_2$ and $[Co(CO)_4]_3SnCl$ (10). An infrared spectrum of the red material not soluble in the *n*-pentane extractions indicated it to be the tetrakis product $[Co(CO)_4]_4Sn$ (11).

Table 1 gives the infrared spectra in the carbonyl region for those complexes first reported here and also the tin–halogen frequencies for these and a number of other related complexes.

Discussion

Figure 1 shows the variation of the pseudo first order rate constants k_{obs} with the concentration of tin(II) chloride for the thermal insertion reaction of $[P(OC_6H_5)_3Co(CO)_3]_2$ with excess $SnCl_2$ in THF at the temperatures indicated. Although at a given temperature the observed rate constants do not vary considerably, there does appear to be a tendency for them to increase with increasing $SnCl_2$ concentration. This behavior could be explained by postulating that both a unimolecular and bimolecular mechanism were operating simultaneously. Under these circumstances a straight line could be drawn through the experimental points, and from the intercept and slope the rate constants for these two mechanisms determined. Inspection of the experimental points indicates that because of the low values of the slopes that would be obtained, the bulk of the reaction would have to proceed via the unimolecular mechanism.

Alternatively, the following two-step mechanism that has been postulated in a number of similar reactions (1, 3, 4) could account for the observed behavior:

$$A_2 \underset{k_{-1}}{\overset{k_1}{\rightleftharpoons}} A_2^* \xrightarrow[B]{k_2} ABA$$

where A_2 represents the metal–metal bonded complex $[P(OC_6H_5)_3Co(CO)_3]_2$, A_2^* is a reactive intermediate, B is the tin(II) chloride, and ABA the insertion product. On the basis of this mechanism, the observed rate constants should level off at a constant value of k_1 at high concentrations of $SnCl_2$. All the experimental values can be interpreted as having nearly approached the limiting value of k_1 even at concentrations of $SnCl_2$ as low as 0.1 *M*. Unfortunately, due to the production of the byproduct $[P(OC_6H_5)_3Co(CO)_3]_3SnCl$ at lower concentrations of $SnCl_2$, it was not possible to determine whether the rate constants dropped dramatically under these conditions. In a limited kinetic study using $SnBr_2$ there was little change in the observed rate constants with changing $SnBr_2$ concentration and the magnitude of these rate constants was very near the limiting value of the rate constants determined at high $SnCl_2$ concentrations at the same temperature. In other reactions in which a bimolecular mechanism has been proposed for the attack of stannous halides on metal–metal bonds (2, 4), $SnBr_2$ has reacted much more readily than $SnCl_2$. Since no such difference has been found here, it is reasonable to conclude that no bimolecular mechanism is operating in this reaction, and the two-step mechanism is therefore proposed to account for our results.

As discussed previously (1), the rate law for this mechanism can be expressed

$$[1] \quad -\frac{d[A_2]}{dt} = \frac{k_1 k_2 [B]/k_{-1}}{1 + k_2[B]/k_{-1}}[A_2] = k_{obs}[A_2]$$

Can. J. Chem. Downloaded from www.nrcresearchpress.com by 210.87.254.42 on 09/05/12
For personal use only.

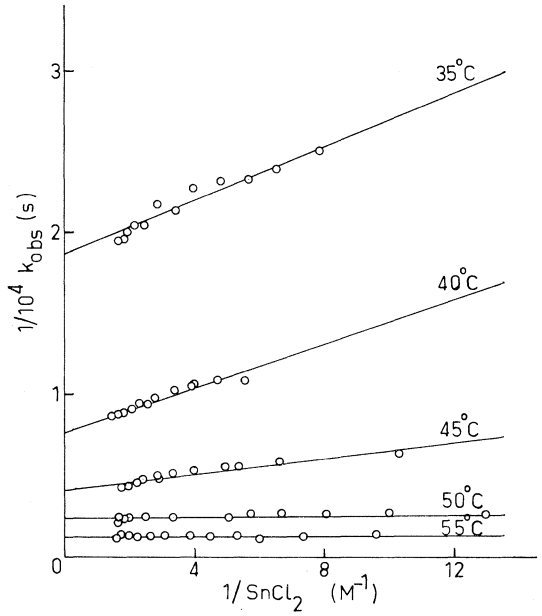

FIG. 2. Plot showing linear relationship between values of $1/k_{obs}$ and $1/[SnCl_2]$ taken from Fig. 1. The straight lines are least-squares plots and lead to the rate constants given in Table 2.

and by rearrangement of eq. 1 the following expression can be obtained

$$[2] \qquad 1/k_{obs} = 1/k_1 + k_{-1}/k_1k_2[B]$$

A plot of $1/k_{obs}$ against $1/[B]$ should yield a straight line with slope k_{-1}/k_1k_2 and intercept $1/k_1$. Figure 2 shows plots of this type for the reaction of $[P(OC_6H_5)_3Co(CO)_3]_2$ with $SnCl_2$. Table 2 gives the kinetic parameters obtained from a least squares treatment assuming equal uncertainties for all values of k_{obs}. The activation enthalpy and entropy were obtained from a weighted least-squares treatment of the kinetic parameters (8).

The corresponding activation enthalpy and entropy for the analogous reaction of $SnCl_2$ with $[P(n\text{-}C_4H_9)_3Co(CO)_3]_2$ have been reported to be 26.4 ± 0.7 kcal/mol and 5 ± 2 cal mol^{-1} deg^{-1} (4). The $\Delta H^{\ddagger}$ for the reaction of the triphenylphosphite complex is marginally smaller (1.7 kcal/mol) than for the tributylphosphine complex while the $\Delta S^{\ddagger}$ is essentially the same within experimental error for the two complexes. Since the two reactions are so similar in all respects, it would therefore seem reasonable to assume that they also react by the same mechanism.

A possible reactive intermediate, A_2*, proposed in the reaction of the tributylphosphine complex was a radical pair trapped in a solvent cage, in which the Co—Co bond had been homolytically broken and the $\Delta H^{\ddagger}$ could be regarded as a measure of the energy required to break this bond. Alternatively, a singly carbonyl bridge species

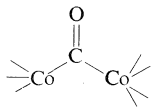

was postulated in which the metal–metal bond had also been broken, and in this case the $\Delta H^{\ddagger}$ could be regarded as the lower limit of the energy required to break the Co—Co bond because the degree of bond making involved in forming the carbonyl bridge could offset the energy to break the Co—Co bond. Carbonyl bridged intermediates have been proposed for a number of reactions (12, 13) and might well be anticipated in the reactions of the cobalt complexes because all complexes of the type $[LCo(CO)_3]_2$ (L = CO, or Group Va ligand) have been postulated to exist as bridged as well as non-bridged isomers in solution (14, 15).

Regardless of what the actual mechanism is, as long as it can be assumed that the tributylphosphine and triphenylphosphite complexes react via the same mechanism, it has been shown that replacement of tributylphosphine by triphenylphosphite in the cobalt carbonyl complex results in a slight reduction (1.7 kcal/mol) in the $\Delta H^{\ddagger}$. Since the greatest contribution to this activation energy results from the breaking of the Co—Co bond according to any of the proposed mechanisms, we can conclude that this bond is weaker in the triphenylphospite complex than in the tributylphosphine complex.

It has been shown that the complexes $[LCo(CO)_3]_2$ react not only with $SnCl_2$ to form $[LCo(CO)_3]_2SnCl_2$, but also with $[LCo(CO)_3]_2$-

TABLE 2. Kinetic parameters for the $SnCl_2$ thermal reaction*

Temperature (°C)	10^4k_1 (s^{-1})	$10^2k_{-1}/k_2$ (mol l^{-1})
35.0	0.53±0.02	4.4±1.0
40.0	1.30±0.03	9.0±0.8
45.0	2.42±0.07	6.0±0.3
50.0	4.19±0.09	0.8±0.3
55.0	7.95±0.25	0.6±0.7

*The uncertainties are standard deviations; $\Delta H_1^{\ddagger} = 24.7 \pm 0.4$ kcal mol^{-1}; $\Delta S_1^{\ddagger} = 2.4 \pm 1.3$ cal mol^{-1} deg^{-1}.

Can. J. Chem. Downloaded from www.nrcresearchpress.com by 210.87.254.42 on 09/05/12
For personal use only.

$SnCl_2$ to form $[LCo(CO)_3]_3SnCl$, (L = CO, $P(OC_6H_5)_3$, or $P(n\text{-}C_4H_9)_3$). Patmore and Graham (11) have reported the similar reaction of SnX_2 (X = F, acetate) with $[Co(CO)_4]_2$ to form $[Co(CO)_4]_3SnX$. The ease of these reactions depends very much on L, and the rates decrease with changing L in the order CO > $P(OC_6H_5)_3$ > $P(n\text{-}C_4H_9)_3$ which parallels the order of decreasing π-accepting ability of L and hence increasing electron density on the cobalt atoms. Adams *et al.* (16) have suggested that this should result in a weakening of the Sn—Cl bond and this is borne out in the dramatic decrease in the Sn—Cl stretching frequencies along both the $[LCo(CO)_3]_2SnCl_2$ and $[LCo(CO)_3]_3SnCl$ series.

In the following proposed reaction to produce the tris-substituted complexes,

$$[LCo(CO)_3]_2 + [LCo(CO)_3]_2SnCl_2 \rightarrow [LCo(CO)_3]_3SnCl + \underset{\text{decomposes}}{LCo(CO)_3Cl(?)}$$

both Co—Co bonds and Sn—Cl bonds must be broken. Since the ease of the reaction decreases with L in the order CO > $P(OC_6H_5)_3$ > $P(n\text{-}C_4H_9)_3$, and since this is the order of *decreasing* Sn—Cl bond strengths, it would seem logical that it must be the order of *increasing* Co—Co bond strengths. Although such an argument does not carry much weight alone in the absence of any information regarding the mechanism of the reaction, it does help to substantiate the conclusions drawn from the kinetic study of the insertion reaction.

As has been discussed in a previous paper (1), the substitution of tributylphosphine by the stronger π-electron acceptor ligand triphenylphosphite might be expected to affect the metal–metal bond in two ways, one of which could strengthen the bond, the other weaken it. Decreased electron density on the metals could strengthen the bond by reducing the repulsion between electrons in filled nonbonding orbitals on the metals, while at the same time shrinking of the σ-bonding orbitals would occur which would tend to weaken the bond. While the former effect has been proposed to predominate in reactions of some compounds containing Fe—Fe and Mo—Mo bonds (1), the latter is evidently more important in reactions of the Co—Co complexes. Hence while it may be possible to predict the effect of substituents on metal–metal bond strengths for a given metal system, it would clearly be a dangerous assumption to make generalizations to other systems.

The author is indebted to the National Research Council of Canada for financial support, and to Mr. L. L. Annett for performing the kinetic experiments.

1. P. F. Barrett and W. J. Jacobs. Can. J. Chem. **50**, 972 (1972).
2. P. F. Barrett and R. R. Clancy. Can. J. Chem. **49**, 2627 (1971).
3. P. F. Barrett and Kenneth K. W. Sun. Can. J. Chem. **48**, 3300 (1970).
4. P. F. Barrett and A. J. Poë. J. Chem. Soc. A, 429 (1968).
5. A. Sacco. Ann. Chim. Italy, **43**, 495 (1953).
6. D. J. Patmore and W. A. G. Graham. Inorg. Chem. **5**, 1405 (1966).
7. G. Brauer (*Editor*). Handbook of preparative inorganic chemistry, Vol. 1. Academic Press, New York. 1963. p. 728.
8. J. Mandel. The statistical analysis of experimental data. Interscience, New York. 1964. pp. 141–144 and pp. 272–278.
9. F. Bonati, S. Cenini, D. Morelli, and R. Ugo. J. Chem. Soc. A, 1052 (1966).
10. D. J. Patmore and W. A. G. Graham. Inorg. Chem. **5**, 2222 (1966).
11. D. J. Patmore and W. A. G. Graham. Inorg. Chem. **7**, 771 (1968).
12. L. I. B. Haines, D. Hopgood, and A. J. Poë. J. Chem. Soc. A, 421 (1968).
13. L. I. B. Haines and A. J. Poë. J. Chem. Soc. A, 2826 (1968).
14. A. R. Manning. J. Chem. Soc. A, 1135 (1968).
15. G. Capron-Cotigny and R. Poilblanc. Bull. Soc. Chim. Fr. 1440 (1967).
16. D. M. Adams, J. N. Crosby, and R. D. W. Kemmitt. J. Chem. Soc. A, 3056 (1968).

Can. J. Chem. Downloaded from www.nrcresearchpress.com by 210.87.254.42 on 09/05/12
For personal use only.

^{13}C Chemical Shifts of Methylquinolizidines and Correlations with the Chemical Shifts of Methyl Substituted *trans*-Decalins

ROBERT T. LALONDE AND THOMAS N. DONVITO

Department of Chemistry, State University of New York, College of Environmental Science and Forestry, Syracuse, New York 13210

Received May 29, 1974

ROBERT T. LALONDE and THOMAS N. DONVITO. Can. J. Chem. **52**, 3778 (1974).

^{13}C chemical shifts are reported for quinolizidine and eight methylquinolizidines. Assignments of methylquinolizidine resonances are made with the assistance of the previously made assignments of quinolizidine, the methyl substituted *trans*-decalins and the methyl parameters of Grant. A more careful comparison of the quinolizidines with the *trans*-decalins is made through correlations with experimental data for four decalins and calculated data for six decalins.

ROBERT T. LALONDE et THOMAS N. DONVITO. Can. J. Chem. **52**, 3778 (1974).

On rapporte les déplacements chimiques du ^{13}C pour la quinolizidine et huit méthylquinolizidines. Les attributions des résonances des méthylquinolizidines sont faites à l'aide des attributions précédemment faites de la quinolizidine et des méthyl-*trans*-décalines. Les paramètres des groupes méthyle établie par Grant sont également utilisés pour aider á faire ces attributions. Une comparaison plus soignée des quinolizidines avec les *trans*-décalines est faite par l'intermédiaire de deux corrélations. Une corrélation utilise les données expérimentales pour quatre décalines tandis que l'autre utilise les données calculées pour six décalines.

Introduction

The ^{13}C spectra of methylquinolizidines have been examined to facilitate assignments in Nuphar and other quinolizidine alkaloids. Thus the objective of our study was to collect the data for quinolizidine, **1**, and methylquinolizidines **2–9** and assign their chemical shifts aided by the experimental and calculated data for the corresponding *trans*-decalins **10–15**. The comparison of the quinolizidine and *trans*-decalin data was appropriate since the more stable form of quinolizidine and methylquinolizidines is the *trans*-fused form (1).

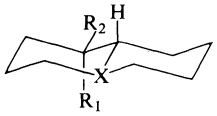

1 $R_1 = R_2 = H$; X = N

10 $R_1 = R_2 = H$; X = CH*

2 $R_1 = H$; $R_2 = CH_3$; X = N

11 $R_1 = H$; $R_2 = CH_3$; X = CH*

3 $R_1 = CH_3$; $R_2 = H$; X = N

12 $R_1 = CH_3$; $R_2 = H$; X = CH*

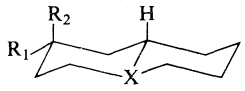

4 $R_1 = H$; $R_2 = CH_3$; X = N

13 $R_1 = H$; $R_2 = CH_3$; X = CH*

5 $R_1 = CH_3$; $R_2 = H$; X = N

14 $R_1 = CH_3$; $R_2 = H$; X = CH*

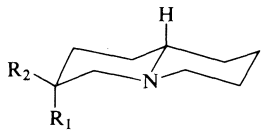

6 $R_1 = H$; $R_2 = CH_3$

7 $R_1 = CH_3$; $R_2 = H$

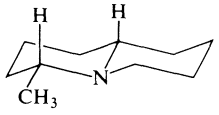

8

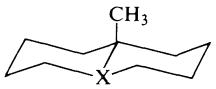

9 X = N

15 X = CH†

NOTE: *Bridgehead hydrogens are *anti*; †bridgehead hydrogen and methyl group are *anti*.

Can. J. Chem. Downloaded from www.nrcresearchpress.com by 210.87.254.42 on 09/05/12
For personal use only.

Can. J. Chem. Downloaded from www.nrcresearchpress.com by 210.87.254.42 on 09/05/12
For personal use only.

Eggert and Djerassi (2) showed a single linear relation between the observed chemical shift of ^{13}C in aliphatic acyclic amines and the calculated shift (3) in hydrocarbons wherein CH replaces the nitrogen of the amine. Similarly Hart and Ford (4) correlated the calculated hydrocarbon shifts (3) with tetraalkylammonium ions, tetraalkylboride ions and trialkylboranes. We obtained similar correlations, one using the experimental decalin data of Dalling *et al.* (5) and the second by employing the calculated decalin shifts of the same authors.

Experimental

Materials

Quinolizidine was prepared by a modified method of Boeckelheide *et al.* (6). The 3-methylquinolizidines **6** and **7** and 10-methylquinolizidine, **9**, were prepared by a modified procedure of Leonard *et al.* (7). All the other quinolizidines were prepared by the method of Katritzky and co-workers (1*a*).

Measurements

The spectra of all the compounds were determined at ambient temperature in 0.3–0.5 *M* $CDCl_3$ solutions containing approximately 1% TMS in 12 mm tubes. Chemical shift values were determined relative to TMS = δ 0.00 p.p.m. The spectrometer was a Varian XL-100-15 operating at 25.16 MHz, equipped for pulsed Fourier transformation and controlled by a Varian VFT-100 computer. The Fourier transformations were based on 8192 data points and employed the absorption spectrum. Field/frequency lock was established on the deuterium resonance of the $CDCl_3$ solvent. Between 1 and 10 K transients were used for most fully decoupled spectra and about four times that number for off-resonance decoupled spectra. Because of the small quantity of *t*-2-methylquinolizidine, **4**, available, it was necessary to use 193 K transients for the fully decoupled spectrum and no off-resonance decoupled spectrum was obtained.

Results and Discussion

Observed chemical shifts and assignments for the nine quinolizidines are presented in Table 1. The assignments were made with the aid of off-resonance decoupled spectra, peak intensities, known chemical shift differences and comparisons with the corresponding decalins (*vide infra*). The assignments for the parent quinolizidine, **1**, have already been made (8). Therefore by comparing the spectra of *trans*-decalin (5) and quinolizidine an approximate value for the shift associated with replacement of a bridgehead CH by N was determined for quinolizidine. With this information and the observed (5) chemical shifts of the methyldecalins, **11**, **14**, and **15**, the resonance signals of *t*-1[1] (**2**), *c*-2 (**5**), *t*-3 (**6**), *c*-4 (**8**), and 10-methylquinolizidine (**9**) were assigned. The case of *t*-3-methylquinolizidine, **6**, will be used as an example. The resonances of C-3 and C-10 were the only doublets and the lower field one (62.64 p.p.m.) was assigned to C-10 since the latter is α to nitrogen. Of the two remaining low-field signals (64.66 and 56.72 p.p.m.), both triplets, the one at lower field was assigned to C-4 since the latter is both α to nitrogen and β to the C-3 equatorial methyl. The higher field triplet was assigned to C-6 by default. The remaining resonances, all triplets, were assigned by matching observed chemical shifts with the nearest shifts calculated by assuming that the CH by N replacement differentials for *trans*-decalin and quinolizidine would be the same for *trans-syn*-2-methyldecalin (**14**) and *t*-3-methylquinolizidine (**6**). These calculated shifts, presented in Table 2, agree with those given in Table 1.

In the second method of resonance assignment, Dalling and Grant's methyl parameters (9) were applied to quinolizidine. Chemical shifts calculated for *t*-3-methylquinolizidine (**6**) by this method also appear in Table 2. This second method was used of necessity in those cases where data for the appropriate methyldecalin was lacking. Thus by using the two methods the methylquinolizidine chemical shifts were assigned unequivocally for all carbons except those which possessed both the same off-resonance splitting and a chemical shift difference of 1 p.p.m. or less.

Essentially, the first of the above-described assignment methods was the basis for a more sophisticated comparison of methyl decalins and methylquinolizidines. The experimentally determined methylquinolizidine shifts were plotted against the experimentally determined methyl substituted *trans*-decalin shifts[2] obtained by Dalling *et al.* (5). This procedure was followed separately for α-, α-bridgehead, β-, and γ-carbons where α, β, and γ refer to the carbon one, two, and three bonds removed from the nitrogen of the quinolizidine or the corresponding bridgehead CH of the *trans*-decalin.

[1]The symbols for designating configuration and position of methyl groups are those of Katritzky and co-workers (1*a*).

[2]δ^{TMS}. Original data converted using $\delta^{TMS} = 128.82 - \delta^{C_6H_6}$.

TABLE 1. ^{13}C Chemical shifts of quinolizidines and decalins

Compound	Carbon[b]	Splitting	δ ^{13}C in p.p.m.[a] Quinolizidine Obsd.	Quinolizidine Calcd. Method 1[c]	Quinolizidine Calcd. Method 2[d]	Decalin Calcd.[e]
1	1	t	33.62	33.46	33.97	35.27
	2	t	24.76	24.91	25.30	26.78
	3	t	26.04	26.08	26.09	26.78
	4	t	56.85	56.36	56.52	35.27
	10	d	63.20	63.23	63.29	43.79
2	1	d	36.60	37.05	37.25	38.80
	2	t	34.20	34.63	33.94	35.27
	3	t	25.87	26.35	26.09	26.78
	4	t	57.06	57.02	56.52	35.27
	6	t	57.06	56.92	56.52	35.27
	7	t	25.53	26.07	26.09	26.78
	8	t	24.87	24.57	25.30	26.78
	9	t	29.92	29.84	29.74	30.71
	10	d	69.46	69.81	68.81	48.78
	CH_3	q	18.73			19.28
3	1	d	32.96		30.75	31.80
	2	t	32.38		30.38	31.77
	3	t	20.89		21.86	22.22
	4	t	57.55		56.52	35.27
	6	t	57.34		56.52	35.27
	7	t	25.83		26.09	26.78
	8	t	25.13		25.30	26.78
	9	t	30.33		29.74	30.71
	10	d	65.88		64.94	45.28
	CH_3	q	13.75			11.38
4	1		39.29		38.60	40.26
	2		29.84		25.33	26.81
	3		31.35		30.72	31.77
	4		50.68		51.65	30.71
	6		56.54		56.52	35.27
	7		25.92		26.09	26.78
	8		24.81		25.30	26.78
	9		33.33		33.97	35.27
	10		56.96		58.26	39.23
	CH_3		17.81			15.33
5	1	t	42.26	41.82	41.84	43.75
	2	d	31.18	30.66	32.46	33.81
	3	t	34.41	34.36	33.97	35.27
	4	t	56.58	55.91	56.52	35.27
	6	t	56.58	55.91	56.52	35.27
	7	t	26.00	25.94	26.09	26.78
	8	t	24.63	24.76	25.30	26.78
	9	t	33.47	32.89	33.97	35.27
	10	d	62.63	62.48	63.29	43.79
	CH_3	q	22.17			23.84

The resulting correlations were linear, being represented by the general eq. 1,

$$[1] \qquad \delta_Q = A\delta_D + B$$

where δ_Q and δ_D are respectively the quinolizidine and decalin ^{13}C chemical shifts for a single type of carbon, *i.e.* α-, α-bridgehead, etc. The constant A is the slope of the best straight line as determined by computer using a least squares program and B is the y-intercept of this line. The values of these constants and some of the pertinent statistical data are given in Table 3.

Can. J. Chem. Downloaded from www.nrcresearchpress.com by 210.87.254.42 on 09/05/12
For personal use only.

TABLE 1 (*Concluded*)

Compound	Carbon[b]	Splitting	δ ^{13}C in p.p.m.[a] Quinolizidine Obsd.	Quinolizidine Calcd. Method 1[c]	Quinolizidine Calcd. Method 2[d]	Decalin Calcd.[e]
6	1	t	33.34	33.03	33.97	35.27
	2	t	33.51	33.20	33.94	35.27
	3	d	31.33	31.83	32.62	33.81
	4	t	64.66	65.03	65.57	43.75
	6	t	56.72	55.76	56.52	35.27
	7	t	25.97	25.94	26.06	26.78
	8	t	24.81	24.76	25.30	26.78
	9	t	33.61	33.03	33.97	35.27
	10	d	62.64	62.37	63.29	43.79
	CH_3	q	19.77			23.84
7	1	t	28.50		29.74	30.71
	2	t	30.14		30.38	31.77
	3	d	28.63		26.12	26.81
	4	t	62.05		61.85	40.26
	6	t	56.98		56.52	35.27
	7	t	25.70		26.09	26.78
	8	t	24.84		25.30	26.78
	9	t	32.96		33.97	35.27
	10	d	63.42		63.29	43.79
	CH_3	q	18.26			15.33
8	1	t	34.16	34.10	33.97	35.27
	2	t	24.75	25.18	25.30	26.78
	3	t	35.45	35.78	33.97	35.27
	4	d	59.21	60.08	60.29	38.80
	6	t	51.90	52.60	51.65	30.71
	7	t	26.39	25.74	26.09	26.78
	8	t	24.62	24.90	25.30	26.78
	9	t	33.97	34.00	33.97	35.27
	10	d	63.23	63.05	63.29	43.79
	CH_3	q	20.78			19.28
9	1	t	40.45	40.97	40.75	42.57
	2	t	20.33	20.09	20.66	22.22
	3	t	26.22	26.33	26.09	26.78
	4	t	49.97	50.92	51.65	30.71
	10		53.18	53.49	52.03	33.60
	CH_3	q	10.07			15.31

[a]Relative to TMS.
[b]The number given refers to the carbon of the quinolizidine and corresponds to the same carbon position in the decalin. However the actual numbering may be different in the decalin.
[c]From eq. 1 and *A* and *B* constants obtained by the use of the experimental chemical shift values of decalin. See Table 3.
[d]From eq. 1 and *A* and *B* constants obtained by the use of the calculated chemical shift values of decalin. See Table 4.
[e]For the corresponding *trans*-decalins from the hydrocarbon parameters of ref. 6, or taken from ref. 6 for decalins **11**, **14**, and **15**.

Particularly noteworthy is that the values of *A* are near unity and that the replacement of CH by N has the same large effect only on the α- and α-bridgehead carbons as indicated by the values of *B*. Table 3 also shows that the standard deviations are less than 1 p.p.m. Moreover, the maximum deviations are less than 1 p.p.m. and occur in no systematic manner. Thus the observed linear relations mean that decalin and quinolizidine chemical shift data are nearly interchangeable for β- and γ-carbons and also interchangeable for α-carbons when an adjustment (*B* value) is made for the chemical shift differences due to CH by N replacement.

A single expression for both types of α-carbons was generated in the following manner. First an

Can. J. Chem. Downloaded from www.nrcresearchpress.com by 210.87.254.42 on 09/05/12
For personal use only.

TABLE 2. Calculated chemical shift values for *t*-3-methylquinolizidine

Carbon	On the basis of CH by N replacement differentials[a]	By application of methyl parameters to quinolizidine[b]
1	33.28	33.67
2	33.25	33.79
3	31.93	32.00
4	65.42	65.88
6	56.26	56.63
7	25.89	26.04
8	24.61	24.76
9	33.18	33.62
10	62.37	62.98

[a]See Table 1 for the differentials and the text for differential definition.
[b]Reference 10.

expression for obtaining an adjusted chemical shift value for the appropriate decalin α-bridgehead carbons was obtained by subtracting the α-bridgehead carbon relation from the α-carbon relation and letting $\delta_Q^{\alpha} - \delta_Q^{\alpha_B} = 0$, where $\delta_Q^{\alpha_B}$ and δ_Q^{α} are respectively the chemical shifts of the bridgehead α- and nonbridgehead α-carbons of the quinolizidines. The resulting expression is given by eq. 2,

$$[2] \qquad \delta_D^{\alpha_A} = 1.0207\delta_D^{\alpha_B} - 3.6032$$

where $\delta_D^{\alpha_A}$ is the adjusted chemical shift for the appropriate decalin α-bridgehead carbons. The $\delta_D^{\alpha_A}$ values and the chemical shifts for the nonbridgehead α-carbons (δ_D^{α}) then were plotted together against the quinolizidine α-carbon chemical shifts to obtain a new linear relation. Thus values for *A* and *B* constants for both adjusted and nonbridgehead α-carbons are included together in Table 3 under the designation α_A. The corresponding *A* and *B* constants can be used along with $\delta_D^{\alpha_A}$ or δ_D^{α} in eq. 1 for calculating the quinolizidine α-carbon chemical shifts regardless of bridgehead or nonbridgehead character of the α-carbon.

The observed quinolizidine chemical shifts were plotted also against the decalin shifts calculated (Table 1) from the hydrocarbon parameters of Dalling *et al.* (5). The chief purpose of making this second correlation was to confirm the assignments in quinolizidines **3**, **4** and **7**, compounds for which the corresponding experimental decalin shift data was lacking. The correlation was represented once again by the general eq. 1. Values of constants *A* and *B* and pertinent statistical data are given in Table 4.[3] As expected, bridgehead α-carbons again had to be adjusted to conform to the same linear relation as nonbridgehead α-carbons. The adjusted value ($\delta_D^{\alpha'_A}$) of the calculated chemical shift ($\delta_D^{\alpha'_B}$) is given by eq. 3 obtained in a manner similar to eq. 2.

[3]The second correlation is less precise than the first because of the error introduced in calculating the decalin chemical shifts. When chemical shifts of the three methyl substituted *trans*-decalins, **11**, **14**, **15**, were calculated using Grant's hydrocarbon parameters, an average error of 0.57 p.p.m. and a maximum error of 1.85 p.p.m. were obtained when compared to the reported experimental values.

TABLE 3. Values of constants and statistical data for the correlation: $\delta_Q = A\delta_D + B$; obtained by plotting experimental quinolizidine and *trans*-decalin ^{13}C chemical shifts

Carbon position	No. of points	Values for constants *A*	Values for constants *B*	Standard deviations (p.p.m.)[a]	Maximum deviations (positive and negative) Carbon No.	Compound	Value
α	10	1.013	21.16	0.69	6	**6**	0.95
					4	**9**	−0.94
α_B	6	1.034	17.51	0.26	10	**6**	0.28
					10	**2**	−0.35
β	20	0.975	−0.41	0.38	7	**8**	0.65
					7	**2**	−0.54
γ	10	0.977	−1.64	0.33	2	**5**	0.52
					2	**8**	−0.43
α_A	16	1.011	21.22	0.56	6	**6**	0.96
					4	**9**	−0.95

[a]Standard deviation in p.p.m. for the prediction of quinolizidine chemical shift.

Can. J. Chem. Downloaded from www.nrcresearchpress.com by 210.87.254.42 on 09/05/12
For personal use only.

TABLE 4. Values of constants and statistical data for the correlation: $\delta_Q = A\delta_D + B$; obtained by plotting experimental quinolizidine chemical shifts against calculated *trans*-decalin ^{13}C chemical shifts

Carbon position	No. of points	Values for constants		Standard deviations (p.p.m.)[a]	Maximum deviations (positive and negative)		
		A	*B*		Carbon No.	Compound	Value
α′	16	1.070	18.76	0.76	4	**3**	1.04
					4	**9**	−1.66
α'_B	9	1.107	14.81	0.88	10	**9**	1.07
					10	**4**	−1.33
β′	32	0.928	1.23	0.86	3	**7**	2.51
					3	**6**	−1.29
γ′	16	1.018	−1.95	1.39	2	**4**	4.51
					2	**5**	−1.28
α'_A	25	1.068	18.86	0.76	10	**9**	1.15
					4	**9**	−1.68

[a]Standard deviation in p.p.m. for the prediction of quinolizidine chemical shift.

[3] $$\delta_D{}^{\alpha'A} = 1.0346\delta_D{}^{\alpha'B} - 3.692$$

The quinolizidine chemical shifts obtained from both methods of correlation are listed in Table 1, inspection of which reveals that the first method gives results which are more accurate than the second. However the second method has wider application since it does not depend on the availability of experimental decalin data.

In concluding, two interrelated features of the results will be noted. The effect of equatorial or axial methyl substitution on the chemical shift of the substituted carbon or any other carbon can be obtained by comparing the chemical shifts of **2**–**8** with those of **1**. Secondly, as expected on the basis of other studies (8, 9) the chemical shift of an axial methyl is always upfield from that of the epimeric equatorial methyl.

The authors are grateful to the National Science Foundation for an equipment grant to the Department of Chemistry, State University of New York, College of Environmental Science and Forestry toward the purchase of the XL-100-15 spectrometer and the VFT 100 computer used in this study. Support of this work by the National Institutes of Health, U.S. Public Health Service (Grant No. AI-10188) is gratefully acknowledged. We also acknowledge the assistance of L. McCandless in determining the spectra, H. Howell for preparing a mixture of 3-methylquinolizidine, and the Computer Center for processing the spectral data used in the correlations.

1. (*a*) T. M. MOYNEHAN, K. SCHOFIELD, R. A. Y. JONES, and A. R. KATRITZKY. J. Chem. Soc. 2637 (1962); (*b*) C. D. JOHNSON, R. A. Y. JONES, A. R. KATRITZKY, C. R. PALMER, K. SCHOFIELD, and R. J. WELLS. J. Chem. Soc. 6797 (1965).
2. H. EGGERT and C. DJERASSI. J. Am. Chem. Soc. **95**, 3710 (1973).
3. L. P. LINDEMAN and J. Q. ADAMS. Anal. Chem. **43**, 1245 (1971).
4. D. J. HART and W. T. FORD. J. Org. Chem. **39**, 363 (1974).
5. D. K. DALLING, D. M. GRANT, and E. G. PAUL. J. Am. Chem. Soc. **95**, 3718 (1973).
6. (*a*) V. BOEKELHEIDE and V. ROTHCHILD. J. Am. Chem. Sol. **71**, 879 (1949); (*b*) V. BOEKELHEIDE and D. LODGE. J. Am. Chem. Soc. **73**, 3681 (1951); **76**, 1832 (1954); **77**, 569i (1955).
7. (*a*) N. J. LEONARD, A. S. HAY, R. W. FULMER, and V. W. GASH. J. Am. Chem. Soc. **77**, 439 (1955); (*b*) N. J. LEONARD, R. FULMER, and A. S. HAY. J. Am. Chem. Soc. **78**, 3457, 3463 (1956).
8. D. W. COCHRAN. Ph.D. Dissertation, Indiana University, Bloomington, Indiana. 1971.
9. D. K. DALLING and D. M. GRANT. J. Am. Chem. Soc. **94**, 5318 (1972).

Can. J. Chem. Downloaded from www.nrcresearchpress.com by 210.87.254.42 on 09/05/12
For personal use only.

Cleavage of the Methylenedioxy Ring in the Grignard Reaction of 3,4-Methylenedioxybenzonitrile[1]

JANET E. FORREST AND RONALD A. HEACOCK
Atlantic Regional Laboratory, National Research Council of Canada, Halifax, Nova Scotia B3H 3Z1
AND
THOMAS P. FORREST
Chemistry Department, Dalhousie University, Halifax, Nova Scotia B3H 3J5

Received April 16, 1974

JANET E. FORREST, RONALD A. HEACOCK and THOMAS P. FORREST. Can. J. Chem. **52**, 3784 (1974).

The reaction of 3,4-methylenedioxybenzonitrile (**2**) with ethyl magnesium bromide gives products resulting from opening of the methylenedioxy ring, namely 4-hydroxy-3-*n*-propoxypropiophenone (**3**) and 3-hydroxy-4-*n*-propoxypropiophenone (**4**) in addition to the expected product 3,4-methylenedioxypropiophenone (**1**). The isomeric hydroxy-*n*-propoxy ketones were differentiated on the basis of their spectroscopic properties.

JANET E. FORREST, RONALD A. HEACOCK et THOMAS P. FORREST. Can. J. Chem. **52**, 3784 (1974).

La réaction du méthylène-3 dioxy-4 benzonitrile (**2**) avec le bromure d'éthylmagnésium conduit à des produits résultant de l'ouverture du cycle méthylènedioxy, à savoir l'hydroxy-4*n*-propoxy-3 propiophénone (**3**) et l'hydroxy-3 *n*-propoxy-4 propiophénone (**4**) en plus du produit attendu la méthylène-3 dioxy-4 propiophénone (**1**). Les hydroxy *n*-propoxy cétones isomères ont été identifiées en se basant sur leurs propriétés spectroscopiques.

[Traduit par le journal]

During the course of a recently completed investigation, involving the synthesis of certain new aromatic compounds, found in the spices nutmeg and mace (1–4), it was necessary to prepare some suitably substituted propiophenone derivatives. In the synthesis of one such derivative, 3,4-methylenedioxypropiophenone (**1**), from 3,4-methylenedioxybenzonitrile (**2**) by a Grignard reaction, products from the opening of the methylenedioxy ring were obtained as well as the required product. Although this reaction has been described previously (5) no ring-opened products were found, presumably because the reaction was carried out at a lower temperature (in refluxing benzene as opposed to refluxing toluene in this case). A few reports of the opening of the methylenedioxy ring by Grignard reagents have appeared in the early literature (6–9).

Thin-layer chromatography (t.l.c.) of the products from the reaction of **2** with ethyl magnesium bromide indicated that in addition to **1**, several other products were formed. The two major by-products appeared, by virtue of the colors they gave with chromogenic reagents, to be both ketonic and phenolic in character.

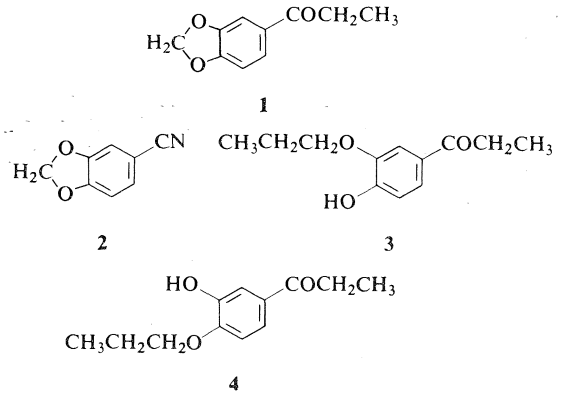

The main phenolic reaction products were separated from the crude reaction mixture and purified by preparative t.l.c. Both compounds had the same molecular formula, $C_{12}H_{16}O_3$ (elemental analysis and mass spectral data) suggesting that in fact some opening of the methylenedioxy ring had occurred during the Grignard reaction and that the two products were the isomeric hydroxy-*n*-propoxypropiophenones **3** and **4**.

[1]Issued as NRCC No. 14237.

Can. J. Chem. Downloaded from www.nrcresearchpress.com by 210.87.254.6 on 09/05/12
For personal use only.

TABLE 1. Ultraviolet–visible absorption spectral characteristics of some alkoxyhydroxypropiophenones, their derivatives, and some related compounds

Compound	Solvent	λ_{max}, nm (ε)		
4-Hydroxy-3-*n*-propoxypropiophenone (**3**)	MeOH	306 (11 000)	275 (13 700)	229 (21 000)
	MeOH–NaOH	342 (28 000)	295 (sh)	249 (13 000)
3-Hydroxy-4-*n*-propoxypropiophenone (**4**)	MeOH	306 (12 000)	273 (17 000)	229 (26 000)
	MeOH–NaOH	345 (9 000)	283 (12 000)	248 (35 000)
4-Hydroxypropiophenone	MeOH	273 (10 400)		218 (7800)
	MeOH–NaOH	323 (16 000)		235 (4200)
3-Hydroxyacetophenone	MeOH	308 (3100)	249 (9000)	217 (21 500)
	MeOH–NaOH	340 (2720)	265 (sh)	235 (26 000)
4-Hydroxy-3-*n*-propoxypropiophenone 2,4-dinitrophenylhydrazone (**5**)	MeOH	390 (21 400)		
	MeOH–NaOH	438 (17 500)		
3-Hydroxy-4-*n*-propoxypropiophenone 2,4-dinitrophenylhydrazone (**6**)	MeOH	388 (33 500)		
	MeOH–NaOH	400 (27 000)		
4-Hydroxypropiophenone 2,4-dinitrophenylhydrazone	MeOH	388 (29 400)		
	MeOH–NaOH	424 (26 700)		
3-Hydroxyacetophenone 2,4-dinitrophenylhydrazone	MeOH	375 (48 000)		
	MeOH–NaOH	384 (43 500)		

As expected, the i.r. spectra of **3** and **4** exhibited broad peaks in the —OH stretching region at *ca.* 3400 cm^{-1} and sharp peaks at *ca.* 1670 cm^{-1} in the carbonyl region. The n.m.r. spectra of **3** and **4** were practically identical and in complete agreement with the proposed structures.

The assignment of the structures **3** and **4** to the individual isomers were made on the basis of a comparison of the u.v. spectra, under basic and neutral conditions, of the products with the spectra of the model compounds 3-hydroxyacetophenone and 4-hydroxyacetophenone (see Table 1) and other similar compounds (see refs. 10–12). This assignment was verified by the u.v.–visible spectra of the 2,4-dinitrophenylhydrazones (see Table 1).

Experimental

The melting points were determined on a Fisher-Johns Apparatus and are uncorrected. The i.r., u.v.–visible, n.m.r., and mass spectra were obtained on a Perkin–Elmer model 237 recording spectrophotometer, a Unicam SP 8000 recording spectrophotometer, a Varian A-60A instrument and a Dupont/C.E.C. 21-491 mass spectrometer, respectively.

The Reaction Between 3,4-Methylenedioxybenzonitrile (2) and Ethyl Magnesium Bromide

A solution of 3,4-methylenedioxybenzonitrile (14.7 g) in toluene (200 ml) was added dropwise, with stirring, during 30 min to a solution of ethyl magnesium bromide (prepared from ethyl bromide (18.66 ml) and magnesium (6.07 g) in dry ether (200 ml)). The resulting suspension was heated with stirring and the ether removed by distillation, the total volume of the reaction mixture being maintained at *ca.* 500 ml by the slow addition of toluene. After removal of the ether was complete, the reaction mixture was boiled under reflux for 3 h and then poured, with stirring, into ice water (1 l) containing concentrated hydrochloric acid (30 ml). The toluene layer was removed and the aqueous layer extracted with ether (4 × 100 ml). The aqueous phase, which contained the ketimine hydrochloride was heated for a short time to remove residual organic solvents and was then boiled under reflux for $2\frac{1}{2}$ h to completely hydrolyze the ketimine. The resulting dark colored oily suspension was extracted with ether (4 × 100 ml). Phenolic (and other acidic) products were removed from these latter ether extracts by extraction with 4% aqueous sodium hydroxide (5 × 200 ml). The remaining ether phase containing neutral products gave, after drying (Na_2SO_4) and concentrating to dryness *in vacuo*, a reddish brown oil. Chromatography of this oil on a short silica gel column (4 in. × $1\frac{1}{2}$ in.) (Koch-Light, 100–200 mesh size) using benzene as eluting solvent yielded 3,4-methylenedioxypropiophenone (9.0 g) as a colorless crystalline solid, m.p. 39–40° (lit. (5, 13) m.p. 38–39°). A quantity of unreacted nitrile (2.2 g) was recovered from the earlier fractions and combined toluene layer and prehydrolysis extracts (see above).

The combined alkaline extracts were cautiously acidified with concentrated HCl and re-extracted with ether (4 × 200 ml). This ether extract was dried (Na_2SO_4) and concentrated to dryness, after being washed with aqueous sodium bicarbonate and water, to give a brown oil. Preliminary t.l.c. examination of this material indicated that it contained two major products and five minor products. The two major products were obtained as pale yellow crystalline solids after purification by preparative t.l.c. on Merck silica gel (F_{254}) plates (20 × 40 cm; thickness 2 mm); the best separations were obtained with triple development using chloroform as solvent.

The slower running major band contained 3-hydroxy-

Can. J. Chem. Downloaded from www.nrcresearchpress.com by 210.87.254.6 on 09/05/12
For personal use only.

4-*n*-propoxypropiophenone (**4**) (0.8 g) which was finally obtained as very pale yellow elongated flat plates, m.p. 81.5–82.5°, after repeated recrystallization from light petroleum (b.p. 80–100°); λ_{max} (MeOH) nm (ε): (see Table 1); ν_{max} (Nujol): 3410, 1670 cm^{-1}; n.m.r. δ ($CDCl_3$): 1.05 (3H, t, $J = 7.5$, $—CH_3$ of $CH_3CH_2CH_2O—$), 1.20 (3H, t, $J = 7.2$, $—CH_3$ of $CH_3CH_2CO—$), 1.87 (2H, sextuplet, $—CH_2—$ adjacent to CH_3 of $CH_3CH_2CH_2O—$), 2.92 (2H, q, $J = 7.2$, $—CH_2—$ of $CH_3CH_2CO—$), 4.08 (2H, t, $J \simeq 6.5$, $—CH_2—$ adjacent to $—O—$ of $CH_3CH_2CH_2O—$), 5.75 (1H, s, exchangeable with D_2O, OH), 6.87 (1H, d, $J = 9$, aromatic proton at C-5), 7.45–7.63 (2H, m, aromatic protons at C-2 and C-6); mass spectrum: M^+ 208; Calcd. for $C_{12}H_{16}O_3$: 208, *m/e* (relative intensity): 208 (19), 179 (31), 137 (100), 109 (10), 43 (16).

Anal. Calcd. for $C_{12}H_{16}O_3$: C, 69.21; H, 7.74. Found: C, 69.21; H, 7.69%.

3-Hydroxy-4-*n*-propoxypropiophenone 2,4-dinitrophenylhydrazone, (**6**), bright orange needles from xylene, m.p. 180–181°. Mass spectrum M^+ 388; Calcd. for $C_{18}H_{20}N_4O_6$: 388.

Anal. Calcd. for $C_{18}N_{20}N_4O_6$: C, 55.66; H, 5.19; N, 14.43. Found: C, 55.65; H, 5.00; N, 14.43%.

The faster running band contained 4-hydroxy-3-*n*-propoxypropiophenone (**3**) (0.66 g) which was finally obtained in colorless needles m.p. 76.5–77° after several recrystallizations from light petroleum (b.p. 80–100°); λ_{max} (MeOH) nm (ε): (see Table 1); ν_{max} (Nujol): 3390, 1670 cm^{-1}; n.m.r. δ ($CDCl_3$): 1.05 (3H, t, $J = 7.5$, CH_3 of $CH_3CH_2CH_2O—$), 1.21 (3H, t, $J = 7.2$, $—CH_3$ of $CH_3CH_2CO—$), 1.85 (2H, sextuplet, $—CH_2—$ adjacent to CH_3 of $CH_3CH_2CH_2O—$), 2.95 (2H, q, $J = 7.2$, $—CH_2—$ of $CH_3CH_2CO—$), 4.10 (2H, t, $J \simeq 6.5$, $—CH_2—$ adjacent to $—O—$ of $CH_3CH_2CH_2O—$), 6.18 (1H, s, exchangeable D_2O, OH), 6.94 (1H, d, $J = 9$, aromatic proton at C-5), 7.46–7.64 (2H, m, aromatic protons at C-2 and C-6); mass spectrum: M^+ 208; Calcd. for $C_{12}H_6O_3$: 208, *m/e* (relative intensity): 208 (28); 179 (58); 137 (100); 109 (11); 43 (12).

Anal. Calcd. for $C_{12}H_{16}O_3$: C, 69.21; H, 7.74. Found: C, 69.20; H, 7.79%.

4-Hydroxy-3-*n*-propoxypropiophenone 2,4-dinitrophenylhydrazone (**5**), deep red needles from absolute alcohol, m.p. 167–168°. Mass spectrum M^+ 388; Calcd. for $C_{18}H_{20}N_4O_6$: 388.

Anal. Calcd. for $C_{18}H_{20}N_4O_6$: C, 55.66; H, 5.19; N, 14.43. Found: C, 55.72; H, 5.18; N, 14.34%.

The authors wish to thank Mr. G. McCully of the Atlantic Regional Laboratory for recording some of the spectra.

1. J. E. Forrest and R. A. Heacock. Lloydia, **35**, 440 (1972).
2. J. E. Forrest, R. A. Heacock, and T. P. Forrest. Experientia. **29**, 139 (1973).
3. T. P. Forrest, J. E. Forrest, and R. A. Heacock. Naturwissenschaften, **60**, 257 (1973).
4. J. E. Forrest, R. A. Heacock, and T. P. Forrest. J. Chem. Soc. (Perkin I), 205 (1974).
5. R. C. Fuson, R. Gaertner, and D. H. Chadwick. J. Org. Chem. **13**, 489 (1948).
6. E. Späth. Monatsh. Chem. **35**, 319 (1914).
7. K. Kafuku, N. Ishikawa, and R. Kato. J. Pharm. Soc. Jap. No. 533, 587 (1926); Chem. Abstr. **21**, 2256 (1927).
8. E. Späth and H. Quietensky. Ber. **60B**, 1882 (1927).
9. K. Kafuku, N. Ishikawa and R. Kato. Bull. Ind. Res. Gov. Formosa, **24**, 1 (1928); Chem. Abstr. **23**, 1889 (1929).
10. H. W. Lemon. J. Am. Chem. Soc. **69**, 2998 (1947).
11. L. Doub and J. M. Vandenbelt. J. Am. Chem. Soc. **69**, 2714 (1947).
12. L. Doub and J. M. Vandenbelt. J. Am. Chem. Soc. **71**, 2414 (1949).
13. P. Hoering. Ber. **38**, 3464 (1905).

Can. J. Chem. Downloaded from www.nrcresearchpress.com by 210.87.254.6 on 09/05/12
For personal use only.

On the Origin of the Bohlmann Bands

SAUL WOLFE, H. BERNHARD SCHLEGEL,[1] AND MYUNG-HWAN WHANGBO[2]
Department of Chemistry, Queen's University, Kingston, Ontario K7L 3N6
AND
FERNANDO BERNARDI
Laboratorio C.N.R. dei Composti del Carbanio contenenti eteroatomi, Ozzano E., Bologna, Italy
Received June 5, 1974

SAUL WOLFE, H. BERNHARD SCHLEGEL, MYUNG-HWAN WHANGBO, and FERNANDO BERNARDI. Can. J. Chem. **52**, 3787 (1974).

A perturbational molecular orbital analysis has been performed of the strengths of the CH bonds of methylamine and methanol in their staggered conformations. This analysis leads to the prediction that a CH bond *anti*-coplanar to a directed lone pair is stronger than a *gauche* CH bond, and is in disagreement with experimental observation. The origin of the disagreement is to be found in the underestimation of the role of the nuclear–nuclear contribution to the bond strengths. *Ab initio* computation of the *gauche* and *anti* stretching force constants of methylamine provides quantitative theoretical support for the view that these differ because of a nuclear-dominated effect. It is suggested that effects, analogous to those observed in the Bohlmann bands, may be seen even in the absence of nonbonded electron pairs.

SAUL WOLFE, H. BERNHARD SCHLEGEL, MYUNG-HWAN WHANGBO et FERNANDO BERNARDI. Can. J. Chem. **52**, 3787 (1974).

On effectue une analyse orbitale moléculaire, par la méthode des perturbations, des forces des liaisons CH de la méthylamine et du méthanol dans leurs conformations décalées. Cette analyse conduit à la prévision que le lien CH, *anti*-coplanaire par rapport à un doublet libre dirigé, est plus fort qu'une liaison CH *gauche*; cette prévision est en désaccord avec l'observation expérimentale. La sous-estimation du rôle de la contribution noyau–noyau dans les forces des liaisons est à l'origine de ce désaccord. Un calcul ab initio des constantes des forces de valence *gauche* et *anti* de la méthylamine fournit un appui théorique quantitatif à l'idée qu'elles diffèrent à cause de l'effet nucléaire dominant. On suggère que des effets analogues à ceux observés dans les bandes Bohlmann, peuvent être observés même en l'absence de doublets électroniques non-liés. [Traduit par le journal]

Introduction

The Bohlmann bands are found in the 2800–2650 cm^{-1} region of the i.r. spectra of amines (1). They have been correlated (2) with the stretching of carbon–hydrogen bonds that are *anti*-coplanar to the nitrogen lone pair and this correlation has been used extensively for the assignment of configuration to the quinolizidine alkaloids (1) and other piperidine derivatives (2, 3). Simple aliphatic alcohols and thiols also exhibit the phenomenon (4).

Because of the nature of the empirical correlation, it has seemed natural to rationalize the existence of the Bohlmann bands in terms of some kind of interaction between an axial (directed) lone pair and an *anti*-coplanar σ_{CH} bond. Thus, Hamlow (5) and Krueger (2, 4) and their co-workers have suggested that participation of the lone pair in a $\sigma_{CH_{ax}}$* orbital would lead to an electronic weakening of the CH_{ax} bond, and cause its stretching frequency to be shifted away from the normal CH stretching envelope.

Mechanical coupling between the vibrations of two CH bonds *anti* to a nitrogen lone pair, via a pulsating vibration of the nitrogen, has been offered as an alternative mechanism (6). However, such coupling appears to be small (7, 8) and unable to account for the observed shifts. Moreover, primary amines, which can have only one CH bond *anti* to the nitrogen lone pair, and thus cannot display such mechanical coupling, have Bohlmann bands (2).

Recent Raman studies of partially deuterated quinolizidines and piperidines (8) have shown

[1]Holder of a National Research Council of Canada 1967 Science Scholarship, 1972 – present.
[2]Holder of a National Research Council of Canada Studentship, 1972 – present.

Can. J. Chem. Downloaded from www.nrcresearchpress.com by 210.87.254.42 on 09/05/12
For personal use only.

Can. J. Chem. Downloaded from www.nrcresearchpress.com by 210.87.254.42 on 09/05/12
For personal use only.

that Fermi resonance between the low-lying CH stretching mode and the first overtone of a CH deformation can, in some cases, contribute to the Bohlmann bands. However, from a partial valence force field analysis of their data, Ernstbrunner and Hudec (8) found the CH bond *anti* to the nitrogen lone pair still to be significantly weaker than the corresponding *gauche* CH bond. Consequently it appears that Fermi resonance may serve to amplify the effect of an already weakened CH bond in producing low frequency CH stretching bands but is not the primary cause of these bands.

We have become interested in the origin of the Bohlmann bands because of the implications of two kinds of observations made in the course of theoretical studies related to the *gauche* effect (9). First, lone electron pairs seem to be less important to the understanding of stereochemical observations than bonding electron pairs, because of their quasi-spherical behavior (10). Clearly, if the lone pairs of amines, alcohols, and thiols were to behave as nondirected ligands, it would not be possible to specify the geometric relationship between these lone pairs and vicinal CH bonds as required by the electronic argument of Hamlow *et al.* (5). Secondly, certain stereochemical observations seem to be the result of nuclear–nuclear repulsion effects which override electronic interactions (11). Extension of these two findings to the present problem could be possible if it could be demonstrated that the weakening of the *anti* CH bonds occurs, not in response to the presence of a directed lone pair but rather *to the absence of a nucleus*.

The purpose of this paper is to show, qualitatively, by a more complete treatment than that employed previously (2, 4, 5) that orbital interaction predicts that the effect of a directed lone pair upon an *anti* CH bond serves to *strengthen* this bond, *i.e.*, that the Bohlmann bands cannot be attributed to interactions of the type depicted in Fig. 1. We then provide, by nonempirical SCF–MO computations, quantitative support for this conclusion and for the view that the Bohlmann bands are the result of a nuclear-dominated effect. Some experimental consequences of this result are also considered.

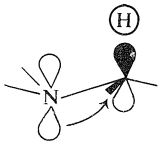

FIG. 1. The model of Hamlow *et al.* (5), showing charge transfer from N_{lp} to $\sigma^*_{CH_{ax}}$.

Results and Discussion

The treatment of Hamlow *et al.* (5) supposes charge transfer from the nitrogen lone pair (N_{lp}) to the antibonding axial CH molecular orbital ($\sigma^*_{CH_{ax}}$) and is depicted schematically in Fig. 1. It predicts partial double bond character in the CN bond, an increase in the charge at the axial hydrogen atom, and a weakening of the axial CH bond. Charge transfer from N_{lp} to the antibonding CH equatorial molecular orbital ($\sigma^*_{CH_{eq}}$) is not considered, because N_{lp} and $\sigma^*_{CH_{eq}}$ do not overlap. This analysis represents a simplified perturbational treatment of the problem. However, it is a well-established consequence of perturbation theory (12) that the interaction between two orbitals depends not only upon their symmetries but also upon the differences in their orbital energies.

We have selected methylamine and methanol as our model systems. Following the usual procedure (13), we treat these molecules in terms of the interactions between the CH_3 and NH_2 (CH_3 and OH) groups. The coordinate system for methylamine and the approximate molecular orbitals of CH_3 and NH_2 groups are shown in Fig. 2. The most important interactions are those between HOMO and LUMO. According to perturbation theory, the stabilization of an occupied orbital by an unoccupied orbital means that the occupied orbital has a small contribution from the unoccupied orbital and this may be interpreted in terms of charge transfer from the former to the latter (14).

From the interaction diagram in Fig. 2 it is evident that *1* and *2* are the most important interactions. Interaction *1* corresponds to charge transfer from N_{lp} to π_x^*. This is a π-type interaction and its effect is to weaken all of the CH bonds. But since the CH bond which is *anti* to N_{lp} has more antibonding character in the π_x^* orbital than the *gauche* CH bonds, it may reasonably be argued that the weakening of the *anti* CH bond will be greater and that the *anti* hydrogen will have a higher atomic charge than the *gauche* hydrogens. This analysis resembles closely the one given by Hamlow *et al.* Interaction *2* corresponds to charge

Can. J. Chem. Downloaded from www.nrcresearchpress.com by 210.87.254.42 on 09/05/12
For personal use only.

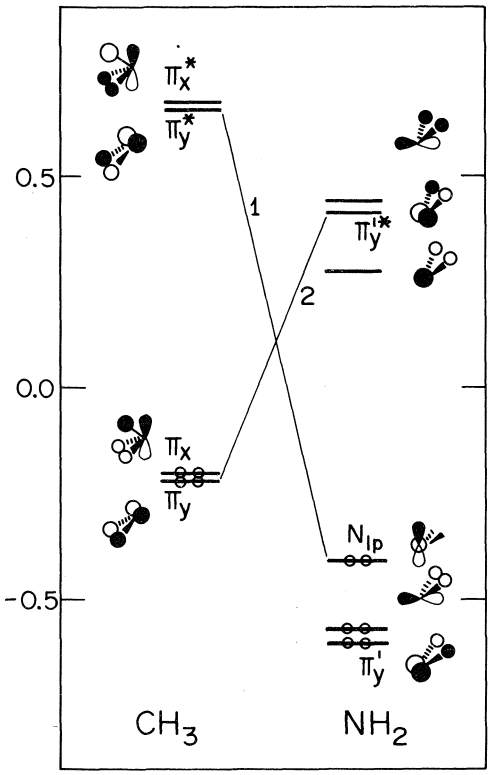

FIG. 2. Orbital interaction model employed to determine the strengths of the *gauche* and *anti* CH bonds of CH_3NH_2. The symmetries and energy levels shown in Figs. 2 and 3 have been taken from *ab initio* wavefunctions computed for CH_3^-, NH_3, and H_2O. Although the absolute positions of the various orbital levels depend upon the particular choice of wavefunction, the relative orderings remain the same for wavefunctions of the same quality. For the extended Hückel level orderings and symmetries of some simple molecules, see ref. 25.

transfer from π_y to $\pi_{y'}^*$, and its effect is to decrease the bonding character of the *gauche* CH bonds and, thus, weaken these relative to the *anti* CH bond. Again the *anti* hydrogen is predicted to have a higher atomic charge.

It must now be noted that interaction *2* is more important than interaction *1*, because the energy difference between HOMO and LUMO is smaller in the case of *2*. Consequently, the effect of this more complete description of the problem is to reverse Hamlow's conclusion. An interesting consequence of the analysis is the finding that the classical conjugative interaction depicted in Fig. 1, which predicts greater charge at the axial hydrogen, is supported; but this is not associated with a weakening of the CH_{ax} bond.

Extension of this model to the treatment of methanol is shown in Fig. 3. Here the dominant interaction is *1*, and leads to greater weakening of the CH bond which is anti to the OH *bond*, *i.e.*, that CH bond which is *not anti*-coplanar to an oxygen lone pair.

It is clear that, in both cases, the prediction of the perturbation model is in disagreement with the experimental facts. However, such orbital interaction models can underestimate the effects of nuclear–nuclear repulsion upon the total energy of the system. This can be seen more clearly from the expression of the total energy in a one-determinantal treatment:

$$[1] \qquad E_T = 2\sum_i^{occ} \varepsilon_i - V_{ee} + V_{nn}$$

where ε_i, V_{ee}, and V_{nn} are, respectively, the orbital energy of the ith orbital, the electron–electron, and the nuclear–nuclear repulsion energies. The success of the model depends explicitly upon the assumption that there is cancellation of the last two terms of eq. 1 (15).

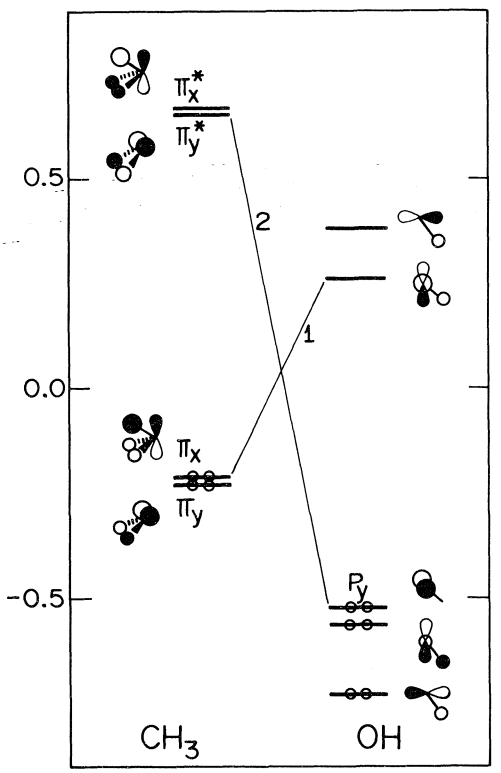

FIG. 3. Orbital interaction model employed to determine the strengths of the *gauche* and *anti* CH bonds of CH_3OH.

TABLE 1. The total energy of methylamine and its nuclear and electronic components at several *anti* and *gauche* CH bond lengths

CH bond length (Å)		Energy (Hartree)		
Anti	*Gauche*	Electronic	Nuclear	Total
1.09	1.09	−136.977299	41.912882	−95.064416
1.04	1.09	−137.166092	42.103195	−95.062897
1.14	1.09	−136.798767	41.735948	−95.062819
1.09	1.04	−137.166996	42.103590	−95.063406
1.09	1.14	−136.797889	41.735658	−95.062231
1.089*	1.081			−95.064525

*Optimized geometry and energy as determined from the parabolic fit to the above data.

TABLE 2. The computed and experimental CH stretching force constants of methylamine

	Force constant (mdyn/Å)			
C—H Bond	Total	Electronic	Nuclear	Experimental*
Anti	5.435	−17.895	23.329	4.652 (4.732)†
Gauche	5.572	−17.941	23.512	4.760 (4.939)
Gauche–anti	0.137	−0.046	0.183	0.108 (0.207)

*See ref. 18.
†Values in parentheses are for the deuterated species.

That such cancellation does not always occur has been noted recently (16). Should this situation exist in the case of the Bohlmann bands it would follow that the weakening of the CH bond *anti* to an adjacent lone pair would be the result of the nuclear contribution to the force constant. It was necessary, therefore, to test the validity of this argument by an *ab initio* computation of the nuclear and electronic components of CH stretching force constants of bonds *gauche* and *anti*-coplanar to a lone pair.[3]

The computations were performed on methylamine in its stable (staggered) conformation, using the CDC version[4] of Gaussian 70 (17), the extended (4–31 G) basis set and, initially, the following geometry: C—N, 1.48 Å; N—H, 1.02 Å; ∠HNH = ∠CNH = 106.0°. The force constants of the CH_{anti} and the two CH_{gauche} bonds were obtained from eq. 2, where

$$[2] \qquad f_{JK} = \partial^2 E/\partial R_J \partial R_K$$

the second derivative of the total energy E is taken with respect to the nuclear coordinates at equilibrium.

The total energy was calculated at several CH_{anti} and CH_{gauche} bond lengths close to the equilibrium values (see Table 1) and two parabolic fits to these values were obtained. The second derivatives of these parabolas were then calculated and these numbers, shown in Table 2, are taken as estimates of the two stretching force constants. Both computed harmonic force constants are within 15% of the experimental values (18), the CH_{anti} force constant being lower. In addition, the difference between the *gauche* and *anti* force constants is in the range given for the experimental values.

Ab initio computations of force constants are well established in the theoretical chemical literature (19) and it is usually found that, at the Hartree–Fock level, stretching force constants are overestimated by 10–15%, as in the present work. The origin of the error is to be found in the neglect of electron pair correlation. A similar situation exists in the *ab initio* computation of conformational energies. Though correlation effects contribute significantly to absolute energies, the contribution to energy differences is small because of the conforma-

[3]It is convenient to employ the traditional notion of a directed lone pair to facilitate the description of the geometry of the system.

[4]We thank Professor W. J. Hehre for this version of the programme.

Can. J. Chem. Downloaded from www.nrcresearchpress.com by 210.87.254.42 on 09/05/12
For personal use only.

Can. J. Chem. Downloaded from www.nrcresearchpress.com by 210.87.254.42 on 09/05/12
For personal use only.

tional invariance of the correlation energy term (20). It is generally agreed, therefore, that calculations within the Hartree–Fock framework contain all of the information required for the understanding of conformational problems (20). Since the present computations are performed at geometries close to the energy minimum of the molecule, and differing energetically from the energy minimum by less than the energy difference between the eclipsed and staggered conformations, it seems valid to assume that a similar invariance exists in the computation of force constants, and that the *difference* in the calculated *gauche* and *anti* force constants is significant.

We have, therefore, proceeded with the partitioning of each force constant into its nuclear and electronic components. This partitioning has the form (21)

$$[3] \qquad f_{JK} = f_{\text{nucl}} + f_{\text{elec}}$$

where

$$[4] \qquad f_{\text{nucl}} = \partial^2\Omega/\partial R_J \partial R_K$$

and Ω is the potential energy associated with nuclear repulsion, given by

$$[5] \qquad \Omega = \sum_{J>K=1}^{N} Z_J Z_K R_{JK}^{-1}$$

The contribution of f_{nucl} could thus be computed readily and f_{elec} obtained by difference. The results are included in Table 2.

It is evident that the nuclear contribution to the *gauche–anti* difference in force constants is dominant; and it is larger than the total because the electronic component *strengthens* rather than weakens the CH_{anti} bond. A rationalization of this result can be found in the orbital interaction model presented above. Alternatively, the result can be considered to be a natural consequence of the variational principle, which allows electron density to flow into those regions of space in which maximum stabilization (*i.e.*, greatest nuclear–electron attraction) is achieved. Table 3 displays the computed net atomic charges in methylamine and shows higher electron density in the *anti* CH bond, as predicted by the interaction model. This increases the attraction between this bond and the two *gauche* amino hydrogens, and results in an electronic strengthening of the *anti* CH bond.

We conclude that the change from a bond to a lone pair has a less important effect upon the potential hypersurface than the removal of a nucleus. Since the presence of the lone pair is thus not essential to the observed weakening of an *anti* CH bond, it may be speculated that such weakening could also be observable in a hydrocarbon containing a suitably nonsymmetric nuclear–nuclear term. For example, the infrared spectrum of 2,3-dimethylbutane, which exists in both *gauche* and *anti* conformations (22), exhibits a strong band at 2877 cm^{-1} (23), which may be assigned to the stretching of the tertiary hydrogens of the *gauche* conformation. As seen in **1**, these hydrogens are *anti*-coplanar to methyl groups. In addition, the infrared spectrum has a weak band at 2810 cm^{-1}, which might be caused by the antisymmetric stretch of the tertiary hydrogens of the *anti* conformation. As seen in **2**, these hydrogens are *anti*-coplanar to each other. If such an interpretation were correct, it would follow that the difference in the effects of H and CH_3 upon the stretching of an *anti*-coplanar CH bond is of the same order of magnitude as observed for the Bohlmann bands. A more detailed examination of the infrared spectra of 2,3-dimethylbutane and its deuterated analogs would, therefore, seem to be desirable.[5]

TABLE 3. The computed net atomic charges in methylamine

Atom	Net atomic charge
Carbon	−0.279
Nitrogen	−0.778
Hydrogen	
Amino	0.296
Gauche	0.168
Anti	0.129

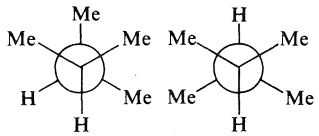

1 **2**

Finally, we wish to emphasize that the present results, although highly suggestive, should be regarded as a preliminary analysis of the problem, because only two of the diagonal

[5]The 2800 cm^{-1} region of the spectrum is free from overtone bands.

harmonic force constants of methylamine have been computed *ab initio*. What is now needed is a computation of the anharmonic force field of the whole molecule. A prerequisite to this study is the development of an *ab initio* program for the calculation of harmonic and anharmonic force fields. This programming phase of the work has been completed recently (24) and its application to the Bohlmann bands is presently under investigation.

We thank the Petroleum Research Fund, administered by the American Chemical Society, N.A.T.O., the Italian C.N.R., and the National Research Council of Canada for financial support of this work.

1. F. BOHLMANN. Angew. Chem. **69**, 641 (1957); Chem. Ber. **91**, 2157 (1958).
2. J. SKOLIK, P. J. KRUEGER, and M. WIEWOROWSKI. Tetrahedron, **24**, 5439 (1968), and references cited therein.
3. (*a*) J. B. LAMBERT, R. G. KESKE, R. E. CARHART, and A. P. JOVANOVICH. J. Am. Chem. Soc. **89**, 3761 (1967); (*b*) T. A. CRABB and E. R. JONES. Tetrahedron, **26**, 1217 (1970).
4. P. J. KRUEGER, J. JAN, and H. WIESER. J. Mol. Struct. **5**, 375 (1970).
5. H. P. HAMLOW, S. OKUDA, and N. NAGAKAWA. Tetrahedron Lett. 2553 (1964).
6. J. KONARSKI. Chem. Phys. Lett. **12**, 249 (1971); J. Mol. Struct. **5**, 389 (1970); J. Mol. Struct. **7**, 337 (1971).
7. D. C. MCKEAN. Chem. Commun. 1373 (1971).
8. E. E. ERNSTBRUNNER and J. HUDEC. J. Mol. Struct. **17**, 249 (1973).
9. S. WOLFE. Acc. Chem. Res. **5**, 102 (1972).
10. (*a*) S. WOLFE, A. RAUK, L. M. TEL, and I. G. CSIZMADIA. J. Chem. Soc. B, 136 (1971); (*b*) S. WOLFE, L. M. TEL, J. H. LIANG, and I. G. CSIZMADIA. J. Am. Chem. Soc. **94**, 1361 (1972); (*c*) S. WOLFE, L. M. TEL, W. J. HAINES, M. A. ROBB, and I. G. CSIZMADIA. J. Am. Chem. Soc. **95**, 4863 (1973).
11. (*a*) S. WOLFE, L. M. TEL, and I. G. CSIZMADIA. Can. J. Chem. **51**, 2423 (1973); (*b*) A. LIBERLES, A. GREENBERG, and J. E. EILERS. J. Chem. Educ. **50**, 676 (1973).
12. L. SALEM. J. Am. Chem. Soc. **90**, 543 (1968).
13. R. HOFFMANN, L. RADOM, J. A. POPLE, P. V. R. SCHLEYER, W. J. HEHRE, and L. SALEM. J. Am. Chem. Soc. **94**, 6221 (1972).
14. N. D. EPIOTIS. J. Am. Chem. Soc. **94**, 1924 (1972).
15. R. HOFFMANN. J. Chem. Phys. **39**, 1397 (1963).
16. N. D. EPIOTIS. J. Am. Chem. Soc. **95**, 3087 (1973).
17. (*a*) W. J. HEHRE, R. F. STEWART, and J. A. POPLE. J. Chem. Phys. **51**, 2657 (1969); (*b*) R. DITCHFIELD, W. J. HEHRE, and J. A. POPLE. J. Chem. Phys. **54**, 724 (1971).
18. A. Y. HIRAKAWA, M. TSUBOI, and T. SHIMANOUCHI. J. Chem. Phys. **57**, 1236 (1972).
19. (*a*) K. F. FREED. J. Chem. Phys. **52**, 253 (1970); (*b*) P. PULAY. Mol. Phys. **17**, 197 (1969); (*c*) P. PULAY. Mol. Phys. **18**, 473 (1970); (*d*) P. PULAY and W. MEYER. J. Chem. Phys. **57**, 3337 (1972).
20. L. C. ALLEN. Ann. Rev. Phys. Chem. **20**, 315 (1969).
21. J. GERRAT and I. M. MILLS. J. Chem. Phys. **49**, 1719, 1730 (1968).
22. (*a*) G. J. SZASZ and N. SHEPPARD. J. Chem. Phys. **17**, 93 (1949); (*b*) D. W. E. AXFORD and D. H. RANK. J. Chem. Phys. **18**, 51 (1950); (*c*) E. J. JACOB, H. B. THOMPSON, and L. S. BARTELL. J. Chem. Phys. **47**, 3736 (1967); (*d*) A. L. VERMA, W. F. MURPHY, and H. J. BERNSTEIN. J. Chem. Phys. **60**, 1540 (1974).
23. Selected infrared spectral data. American Petroleum Institute Research Project 44. Serial No. 811.
24. H. B. SCHLEGEL and S. WOLFE. Unpublished results.
25. B. M. GIMARC. J. Am. Chem. Soc. **93**, 593 (1971).

Can. J. Chem. Downloaded from www.nrcresearchpress.com by 210.87.254.42 on 09/05/12
For personal use only.

The Crystal and Molecular Structure of Dichloro(acetylacetonato)-2,2′-bipyridylindium(III)

J. G. CONTRERAS[1] AND F. W. B. EINSTEIN[2]

Department of Chemistry, Simon Fraser University, Burnaby, B.C. V5A 1S6

AND

D. G. TUCK

Department of Chemistry, University of Windsor, Windsor, Ontario N9B 3P4

Received June 19, 1974

J. G. CONTRERAS, F. W. B. EINSTEIN, and D. G. TUCK. Can. J. Chem. **52**, 3793 (1974).

The molecular structure of dicholoro(acetylacetonato)-2,2′-bipyridylindium(III) has been determined from three dimensional X-ray data collected by counter methods. The structure has been refined by least-squares techniques to a conventional R factor of 4.3% for the 3524 observed reflections. Crystals of $Cl_2In(acac)(bipy)$ are monoclinic, $a = 11.340(3)$, $b = 12.198(3)$, $c = 14.330(3)$ Å, $\beta = 120.25(2)°$, $z = 4$, space group $P2_1/c$. The chloride ligands are *cis*, with In—Cl at distances of 2.443(1) and 2.394(1) Å; the In—O bond lengths are 2.124(3) and 2.164(3) Å, and the In—N bond distances are 2.276(4) and 2.299(4) Å.

J. G. CONTRERAS, F. W. B. EINSTEIN et D. G. TUCK. Can. J. Chem. **52**, 3793 (1974).

On a déterminé la structure moléculaire du dichloro(acétylacétonato) bispyridyl-2,2′ indium(III) à partir des données de diffraction des rayons-X en trois dimensions mesurées par les méthodes des compteurs. La structure a été affinée par la méthode des moindres carrés à un facteur R de 4.3% pour les 3524 réflexions observées. Les cristaux de $Cl_2In(acac)(bipy)$ sont monocliniques $a = 11.340(3)$, $b = 12.198(3)$, $c = 14.330(3)$ Å, $\beta = 120.25(2)°$, $z = 4$ groupe d'espace $P2_1/c$. Les chlores agissant comme ligands sont *cis* avec des distances InCl de 2.443(1) et 2.394(1) Å; les longueurs des liaisons In—O sont de 2.124(3) et 2.164(3) Å et les distances In—N sont de 2.276(4) et 2.299(4) Å. [Traduit par le journal]

Introduction

In a previous paper (1), we described a new and interesting route to indium(III) complexes involving the oxidation of indium(I) halides by refluxing acetylacetonate (acac). The reaction product is a mixture of $In(acac)_3$ and $X_2In(acac)$ (X = Cl, Br, or I) and although the latter compounds could not be isolated, it was possible to prepare two types of crystalline derivatives $[X_2IN(acac)L^{II}]EtOH$ (L^{II} 2,2′-bipyridyl or 1,10-phenanthroline) and $[X_2In(acac)L_2]EtOH$ (L = pyridine or pyridine-d_5). The presence of an $InO_2N_2X_2$ kernel in these compounds was confirmed by the usual spectroscopic methods.

A number of the structural problems of such compounds could not be solved by vibrational spectroscopy. In particular, it was not possible to distinguish between *cis* and *trans* stereochemistry, since the overall symmetry is too low in either case to permit unambiguous assignment of the appropriate bands in the vibrational spectra. An additional complication is that the acetylacetonate ligand may be in either the expected bidentate chelate form, bonding through its two oxygen atoms, or bonded to the metal via the γ-carbon atom (2, 3). In order to confirm the actual situation in the $X_2In(acac)L^{II}$ case, we have now carried out a single crystal X-ray structure determination of the title compound.

One interesting question was not answered in this X-ray study. The earlier preparative and spectroscopic work showed clearly that the compounds always contained 1 molecule of ethanol per indium and that this ethanol was sufficiently firmly held in the lattice that some type of chemical interaction seemed probable (1). Unfortunately the crystals obtained from ethanol solution were not suitable for X-ray analysis and the material which crystallized from acetylacetone–acetonitrile mixtures contained no ethanol. The nature of the strong interaction of ethanol with $X_2In(acac)$ adducts therefore still remains to be identified.

[1]Present address: Instituto de Quimica, Universidad de Concepción, Casilla 3-C, Concepción, Chile.

[2]Author to whom correspondence should be addressed.

Can. J. Chem. Downloaded from www.nrcresearchpress.com by 210.87.254.6 on 09/05/12
For personal use only.

Can. J. Chem. Downloaded from www.nrcresearchpress.com by 210.87.254.6 on 09/05/12
For personal use only.

Experimental

Dichloro(acetylacetonato)-2,2′-bipyridylindium(III) was prepared by the method reported previously (1). Crystals suitable for Weissenberg and precession photographs and data collection were obtained from a 1:1 mixture of acetonitrile–acetylacetone. A small colorless crystal, parallelepiped in shape, with dimensions of 0.55 × 0.26 × 0.30 mm, was used for photographs and data collection.

Precession photographs of the *h*0*l*, *h*1*l*, *h*2*l*, 1*k*2*h*, 2*k*2*h*, and *hk*2*h* layers about the *b* axis and Weissenberg photographs indicated the Laue symmetry 2/*m* and the systematic absences *h*0*l*, $l = 2n + 1$, and 0*k*0 when $k = 2n + 1$, leading to unequivocal identification of the space group as $P2_1/c$.

Accurate cell dimensions were determined from a least-squares fit of 20 strong reflections selected from the photographs. The 2θ values were accurately measured on a Picker FACS-1 computer controlled four-circles diffractometer, using MoK_{α_1} radiation ($\lambda = 0.70926$ Å) with a take-off angle of 1.0°. The crystal was in a general orientation. Crystal data are as follows:

$Cl_2InC_{15}O_2N_2H_{15}$ Mol. wt. = 440.82

Monoclinic, $P2_1/c$, $a = 11.340(3)$, $b = 12.198(3)$, $c = 14.330(3)$ Å, $\beta = 120.25(2)°$, $v = 1712$ Å^3, $\rho_0 = 1.69(5)$ g cm^{-3} (flotation), $\rho_c = 1.70$ g cm^{-3}, $z = 4$, $\mu = 16.8$ cm^{-1}, $MoK_{\alpha_1} = 0.7107$ Å, $T = 20$ °C.

Intensity data for one quarter of the limiting sphere or reflection with $2\theta \leq 60°$ were collected by the θ–2θ scan method using niobium-filtered MoK_α radiation and a scintillation counter equipped with a pulse height discriminator. The take-off angle for data collection was 1.5° and each reflection was symmetrically scanned for 2° in 2θ, plus allowance for α_1–α_2 dispersion. The background was counted for 10 s at each end of the scan range. Two standard reflections were measured every 70 reflections and there was ±5% variation over the entire set of data. The net intensities were corrected for Lorentz and polarization effects. Any reflection for which $I < 3\sigma(I)$ was considered 'unobserved' and not used in the structure solution and refinement. 4988 reflections were measured; 3524 of these were considered as 'observed.'

Structure Determination

The positions of the indium and chlorine atoms were found from a three-dimensional Patterson map. A full matrix least-squares refinement of the scale and the atomic coordinates gave $R = 27.5\%$, where $R = \Sigma(|F_o| - |F_c|)/\Sigma|F_o|$. An electron density Fourier difference synthesis revealed all the nonhydrogen atoms. Two cycles of least-squares refinement with indium and chlorines assigned anisotropic thermal parameters reduced R to 5.7%. An electron density difference Fourier synthesis allowed the location of all hydrogen atoms except those bonded to the C(12) and C(15), *i.e.* the methyl hydrogens. At this point the weights assigned to individual reflections were changed from unit values to those based on counter statistics $(1/\sigma F)^2$. Two further cycles of refinement with all nonhydrogen atoms except C(12) and C(15) anisotropic gave a residual index $R = 4.7\%$. A new difference Fourier function revealed the coordinate positions of two methyl hydrogens; the remaining four positions were calculated from the coordinate positions of the parent carbon atoms and of the identified methyl hydrogens. An examination of bond lengths and angles indicated that the calculated hydrogen positions were reasonable.

Two cycles of least-square refinement[3] with all nonhydrogen atoms anisotropic gave a final residual index $R = 4.3\%$ for all the observed data. At no time were the positions or temperature factors of the hydrogen atoms refined directly, although their positions were recalculated after each refinement. In the structure factor calculations, the atomic scattering factors for In, Cl, O, N, and C were taken from ref. 4; the factor for In was corrected for anomalous dispersion. The final atomic coordinates and temperature factors are listed in Table 1 and the interatomic distances and angles in Table 2, along with the estimated standard deviation. Mean planes through appropriate groups of atoms are presented in Table 3. The crystallographic computer programs used in this work have been cited elsewhere (5).

Discussion

The molecular structure of dichloro(acetylacetonato)-2,2′-bipyridylindium(III) consists of a six coordinate indium atom surrounded by two *cis* chlorine atoms, a bidentate bipyridyl group, and a bidentate acetylacetonate anion (Fig. 1). The $InO_2N_2Cl_2$ group possesses the distorted octahedral configuration to be expected for a complex having three different ligands. In general, this information confirms the structure deduced on the basis of the earlier preparative and spectroscopic work (1).

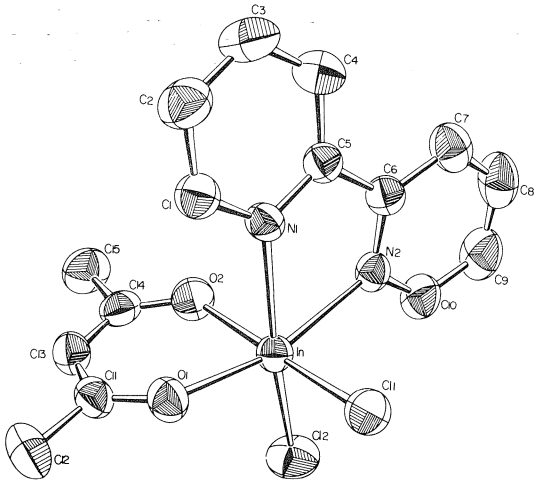

FIG. 1. Measured and calculated structure factors. (Those values with F measured $< 3\sigma$ are given a negative value and were treated as 'unobserved.')

[3]A complete set of tabular data is available, at nominal charge, from the Depository of Unpublished Data, National Science Library, National Research Council of Canada, Ottawa, Canada K1A 0S2.

TABLE 1. Final fractional coordinates and thermal parameters[a,b,c]

Atom	x	y	z	U_{11}	U_{22}	U_{33}	U_{12}	U_{13}	U_{23}
In	19230(3)	28606(2)	30890(2)	422(2)	374(2)	398(2)	−14(1)	235(1)	−7(1)
Cl(1)	4060(1)	1977(1)	4398(1)	439(6)	495(7)	666(8)	23(5)	183(6)	67(6)
Cl(2)	1328(2)	1594(1)	1643(1)	980(11)	643(8)	549(8)	−101(8)	405(8)	−203(7)
N(1)	2398(4)	4389(3)	4130(3)	48(2)	38(2)	45(2)	−6(2)	28(2)	−2(2)
N(2)	3035(4)	4091(3)	2583(3)	45(2)	47(2)	46(2)	3(2)	28(2)	5(2)
O(1)	0918(3)	2130(3)	3845(3)	54(2)	54(2)	58(2)	0(2)	33(3)	8(2)
O(2)	0025(3)	3731(3)	2116(3)	53(2)	53(2)	60(2)	7(2)	27(2)	11(2)
C(1)	1925(5)	4530(4)	4806(4)	69(3)	48(3)	58(3)	−5(2)	43(3)	−5(2)
C(2)	2121(6)	5489(4)	5370(4)	80(4)	59(3)	64(3)	2(3)	45(3)	−7(3)
C(3)	2850(6)	6306(4)	5256(4)	94(4)	45(3)	67(3)	4(3)	44(3)	−9(3)
C(4)	3347(6)	6162(4)	4554(4)	69(3)	42(2)	65(3)	−6(2)	32(3)	−1(2)
C(5)	3099(4)	5194(3)	3996(3)	41(2)	38(2)	43(2)	2(2)	19(2)	5(2)
C(6)	3548(4)	4994(4)	3210(3)	43(2)	40(2)	43(2)	3(2)	21(2)	7(2)
C(7)	4426(5)	5683(4)	3096(4)	54(3)	59(3)	61(3)	−5(2)	28(3)	11(3)
C(8)	4747(5)	5466(5)	2300(5)	66(4)	84(4)	79(4)	−2(3)	51(3)	20(4)
C(9)	4202(6)	4570(5)	1659(5)	79(4)	81(4)	75(4)	6(3)	58(3)	13(3)
C(10)	3359(5)	3900(4)	1829(4)	67(3)	61(3)	62(3)	3(2)	45(3)	6(2)
C(11)	0339(5)	2166(4)	3548(4)	53(3)	50(3)	52(3)	−13(2)	32(2)	−12(2)
C(12)	0761(6)	1402(5)	4136(5)	63(3)	78(3)	73(3)	−23(3)	40(3)	−3(3)
C(13)	1301(5)	2839(4)	2738(4)	45(3)	57(3)	63(3)	−6(2)	31(2)	−9(3)
C(14)	1090(5)	3578(4)	2087(4)	44(3)	42(2)	56(3)	2(2)	19(2)	−12(2)
C(15)	2260(6)	4240(5)	1267(5)	56(4)	65(4)	76(4)	13(3)	23(3)	4(3)

Atom	x	y	z	U_{iso}
H(1)	144	395	491	53
H(2)	174	557	582	61
H(3)	299	697	564	63
H(4)	387	673	447	58
H(7)	480	630	355	57
H(8)	534	593	220	71
H(9)	441	440	111	67
H(10)	299	327	140	55
H(12a)	−018	157	489	68
H(12b)	−169	151	393	68
H(12c)	−064	065	401	68
H(13)	−221	279	261	53
H(15a)	−188	488	115	70
H(15b)	−279	386	060	70
H(15c)	−288	445	151	70

[a]The estimated standards in the last significant figures are given in parentheses in this and subsequent tables.
[b]U_{iso} in 10^3 A^2.
[c]Coordinate parameters for In × 10^5, for H × 10^3, for all other atoms × 10^4. U_{ij} for In, Cl(1), and Cl(2) are in 10^4 A^2, and in 10^3 A^2 for all other atoms. The anisotropic temperature factor has the form exp $\{-2\pi^2(a^{*2}h^2U_{11} + \ldots + 2a^*b^*hkU_{12} + \ldots +)\}$.

Indium–Acetylacetonate

The acetylacetonate ligand is bonded to indium through the two oxygen atoms. This same mode has been reported for $In(acac)_3$, which has been shown by X-ray powder methods to be isostructural with $Fe(acac)_3$ (6), although no bond lengths are available for $In(acac)_3$. An evaluation of the In—O lengths (2.124 and 2.164 Å) in terms of a detailed bonding scheme is difficult, firstly because of the two different values and secondly because of the small number of other indium–oxygen donor systems which have been studied. The bond lengths are in fact close to those reported for the *cis*$[InI_2(dmso)_4]^+$ cation (dmso = dimethylsulfoxide), in which In—O ranges between 2.15 and 2.20 Å (7). Since the In—O interaction in this cation is most probably σ donation via a single bond, it seems that there can be little, if any, multiple bonding in the In—O bond in the present compound. The

Can. J. Chem. Downloaded from www.nrcresearchpress.com by 210.87.254.6 on 09/05/12
For personal use only.

TABLE 2. Interatomic distances (Å) and angles (deg)

(a) Interatomic bonded contacts

Atom pair	Distance	Atom pair	Distance
In—Cl(1)	2.443(1)	In—Cl(2)	2.394(1)
In—O(1)	2.124(3)	In—O(2)	2.164(3)
In—N(1)	2.276(4)	In—N(2)	2.299(4)
N(1)—C(1)	1.335(6)	N(2)—C(10)	1.327(6)
N(1)—C(5)	1.337(5)	N(2)—C(6)	1.354(6)
C(1)—C(2)	1.375(7)	C(10—C(9)	1.369(7)
C(2)—C(3)	1.357(8)	C(9)—C(8)	1.361(8)
C(3)—C(4)	1.390(8)	C(8)—C(7)	1.387(8)
C(4)—C(5)	1.373(6)	C(7)—C(6)	1.374(6)
C(5)—C(6)	1.472(6)		
O(1)—C(11)	1.266(5)	O(2)—C(14)	1.258(5)
C(11)—C(12)	1.488(7)	C(14)—C(15)	1.490(7)
C(11)—C(13)	1.392(7)	C(14)—C(13)	1.402(7)

(b) Interatomic angles (deg)

Bond	Angle	Bond	Angle
Cl(1)—In—Cl(2)	96.8(1)	N(1)—In—O(2)	81.4(1)
O(1)—In—O(2)	85.4(1)	N(2)—In—Cl(1)	92.3(1)
N(1)—In—N(2)	71.7(1)	Cl(2)—In—O(1)	100.4(1)
Cl(1)—In—O(1)	90.2(1)	N(2)—In—O(2)	90.1(1)
N(1)—In—O(1)	91.2(1)	N(2)—In—Cl(2)	96.2(1)
Cl(1)—In—N(1)	92.4(1)	O(2)—In—Cl(2)	90.2(1)
In—N(1)—C(1)	122.2(3)	In—N(2)—C(10)	124.3(3)
In—N(1)—C(5)	118.0(3)	In—N(2)—C(6)	116.3(3)
C(1)—N(1)—C(5)	119.7(4)	C(6)—N(2)—C(10)	118.7(4)
N(1)—C(1)—C(2)	122.1(5)	N(2)—C(10)—C(9)	123.1(5)
C(1)—C(2)—C(3)	118.8(5)	C(10)—C(9)—C(8)	118.7(5)
C(2)—C(3)—C(4)	119.2(5)	C(9)—C(8)—C(7)	119.4(5)
C(3)—C(4)—C(5)	119.4(5)	C(8)—C(7)—C(6)	119.1(5)
C(4)—C(5)—C(6)	122.7(4)	C(7)—C(6)—C(5)	122.7(4)
In—O(1)—C(11)	128.1(3)	In—O(2)—C(14)	127.3(3)
O(1)—C(11)—C(12)	114.7(4)	O(2)—C(14)—C(15)	115.3(5)
O(1)—C(11)—C(13)	125.3(4)	—C(13)	125.4(4)
C(12)—C(11)—C(13)	120.1(4)	C(15)—C(14)—C(13)	119.4(4)

(c) Selected intramolecular nonbonded contacts

Atom pair	Distance	Atom pair	Distance
In—C(13)	3.430(5)		
In—C(5)	3.134(4)		
In—C(6)	3.143(4)		
Cl(1)—Cl(2)	3.616(2)	N(1)—O(2)	2.897(5)
Cl(1)—N(1)	3.409(4)	Cl(2)—O(2)	3.233(4)
Cl(1)—N(2)	3.422(4)	O(1)—O(2)	2.907(4)
Cl(1)—O(1)	3.242(4)	N(2)—O(2)	3.161(5)
Cl(2)—N(2)	3.494(4)	N(1)—O(1)	3.144(5)
Cl(2)—O(1)	3.476(4)	—N(2)	2.739(6)

(d) Intermolecular contacts shorter than 4.0 Å

Atom pair	Distance	Atom pair	Distance
Cl(1)—C(8)	3.80(4)(4)[a]	Cl(2)—C(1)	3.35(5)(3)
Cl(1)—C(9)	3.68(2)(3)	Cl(2)—C(2)	3.49(8)(3)
Cl(1)—C(15)	3.77(6)(2)	Cl(2)—C(12)	3.99(1)(3)
		Cl(2)—C(14)	3.94(2)(1)
		Cl(2)—C(15)	3.89(1)(3)

[a]Figures in this column refer to the following symmetry transformations with respect to atoms in column one; (1) x, y, z; (2) $x, \frac{1}{2} + y, \frac{1}{2} - z$; (3) $x, \frac{1}{2} - y, z - \frac{1}{2}$; (4) $1 - x, y - \frac{1}{2}, \frac{1}{2} - z$.

Can. J. Chem. Downloaded from www.nrcresearchpress.com by 210.87.254.6 on 09/05/12
For personal use only.

Can. J. Chem. Downloaded from www.nrcresearchpress.com by 210.87.254.6 on 09/05/12
For personal use only.

TABLE 3. Mean planes as $Ax + By + Cz + D = 0$

Plane	Atoms defining the plane and their deviations (Å)			A	B	C	D	χ^2
1	In (0.008)	Cl(1) (−0.032)	O(1) (−0.292)	0.1851	−0.7181	−0.7609	5.0880	23 093.2
	O(2) (−0.215)	N(2) (−0.349)						
2	In (−0.003)	Cl(1) (−0.011)	Cl(2) (0.064)	0.7676	0.5400	0.3454	−0.5292	11 500.6
	N(1) (0.395)	O(2) (−0.127)						
3	In (−0.003)	Cl(2) (0.045)	N(1) (0.275)	−0.6810	0.4632	−0.5671	0.5157	5589.7
	N(2) (−0.060)							
4	O(1) (−0.008)	O(2) (0.008)	C(11) (0.019)	0.1520	−0.7346	−0.6613	5.3111	48.2
	C(13) (0.002)	C(14) (−0.002)						
5	N(1) (−0.0001)	C(1) (−0.006)	C(2) (0.011)	−0.5455	0.3749	−0.7496	1.6806	7.1
	C(3) (−0.006)	C(4) (−0.004)	C(5) (0.005)					
6	N(2) (−0.006)	C(6) (0.012)	C(7) (−0.010)	−0.5276	0.5399	−0.6559	0.2296	15.06
	C(8) (−0.002)	C(9) (0.010)	C(10) (−0.001)					

distances are less than in acetato(dimethyl)-indium(III), or its diethyl analog (8, 9), but in these compounds the 'bite' of the acetate ligand is clearly restricted and this may affect the In—O bond length.

The InO_2C_3 ring system shows some structural deviations from coplanarity (see Table 3). We do not believe these deviations to be chemically significant. The two C—C bonds in the ring are equal within experimental error, at an average value (1.396 Å) which lies between a typical single (1.54 Å) and double (1.33 Å) carbon–carbon bond. The carbon–oxygen bonds are also equal (average 1.262 Å) and intermediate in value between single and double bonds, so that the overall picture is of delocalized bonding over the O—C—C—O portion of the metal–ligand ring system. This is entirely analogous to the situation in other acetylacetonate complexes, except that the indium–oxygen bonds are not involved in this delocalization (see above).

Indium–2,2′-Bipyridyl

The indium–nitrogen bonds differ significantly in length but are in the range of expected value for an In—N single bond.

Analysis for the planarity of the bipyridyl ligand showed that whereas one of the heterocyclic rings is planar, the other (that containing the N(2) atom) presents a statistically significant deviation from planarity. The deviation of this ring from planarity (and that observed for the acetylacetonato ligand) is small and from a chemical point of view apparently unimportant. The dihedral angle between the heterocyclic rings is 10.9°.

Indium–Chlorine

The chlorine atoms are *cis* located, one *trans* to O(2) and the other *trans* to N(1). The observed In—Cl bond lengths are 2.443(1) and 2.394(1) Å for In—Cl(1) and In—Cl(2), respectively. The difference in the In—Cl bond lengths is in agreement with the difference in electronegativity of the *trans* ligand. One might expect that the σ bond competition would lead to In—Cl(1) being longer as a result of being *trans* to O(2). The In—Cl bond distances are in good agreement with those reported earlier for indium(III) complexes (10–12); the bonds are longer than in tetrahedral $InCl_4^-$ (2.33 Å) but shorter than in $InCl_6^{3-}$ (2.52 Å).

There remains the question of the *cis* stereochemistry of the complex which is in keeping with the apparently preferred configuration in *cis*$[InI_2(dmso)_4]^+$ (7). The problem of assessing the relative stabilities of InX_4L_2 species has been discussed in detail elsewhere (13) on the basis of the model of ligand steric angles developed by Zahrobsky (14). The general conclusion is that the *cis* isomer will be the more stable of the two, since the total repulsive nonbonded contacts are minimized in this form. The present results clearly show that $Cl_2In(acac)(bipy)$ provides a further example of a *cis* isomer being the predominant form.

This work was supported by operating grants from the National Research Council of Canada. One of us (J.G.C.) acknowledges a leave of absence from the Universidad de Concepción.

1. J. G. Contreras and D. G. Tuck. J. Chem. Soc. (Dalton), 1249 (1974).
2. K. Nakamoto. Infrared spectra of inorganic and coordination compounds. John Wiley and Sons Inc. 2nd ed. New York. 1971.
3. B. N. Figgis, J. Lewis, R. F. Long, R. Mason, R. S. Nyholm, P. J. Pauling, and G. B. Robertson. Nature, **195**, 1278 (1962).
4. D. T. Cromer and J. T. Waber. Acta Cryst. **18**, 104, (1965).
5. F. W. B. Einstein and R. D. G. Jones. Inorg. Chem. **11**, 395 (1972).
6. V. I. Ivanov and O. M. Petrukhim. Kristallografika, **15**, 576 (1970).
7. F. W. B. Einstein and D. G. Tuck. Chem. Commun. 1182 (1970).
8. F. W. B. Einstein, M. M. Gilbert, and D. G. Tuck. J. Chem. Soc. (Dalton), 248 (1973).
9. H. D. Hansen. J. Organomet. Chem. **39**, C37 (1972).
10. J. Trotter, F. W. B. Einstein, and D. G. Tuck. Acta Cryst. B**25**, 603 (1969).
11. D. W. Brown, F. W. B. Einstein, and D. G. Tuck. Inorg. Chem. **8**, 14, (1969).
12. J. G. Contreras, F. W. B. Einstein, M. M. Gilbert, and D. G. Tuck. Submitted for publication.
13. A. J. Carty and D. G. Tuck. Prog. Inorg. Chem. In press.
14. R. F. Zahrobsky. J. Am. Chem. Soc. **93**, 3313 (1971).

Can. J. Chem. Downloaded from www.nrcresearchpress.com by 210.87.254.6 on 09/05/12
For personal use only.

Charge Distributions and Chemical Effects. VIII. Ionization Potentials of Normal and Branched Alkanes

HERVÉ HENRY AND SÁNDOR FLISZÁR

Département de Chimie, Université de Montréal, Montréal, Québec H3C 3V1

Received June 17, 1974

HERVÉ HENRY and SÁNDOR FLISZÁR. Can. J. Chem. **52**, 3799 (1974).

The comparison of adiabatic ionization potentials of normal and branched alkanes with carbon net charges indicates a lowering of the i.p.'s with increasing electron population of the electron-richest pair of bonded C—C atoms in the molecules. In terms of "inductive charges", it is found that $n = -4.4083$, *i.e.*, precisely the same ordering of charges previously determined from ^{13}C n.m.r. shifts. The relative C charges can thus be calculated from ^{13}C chemical shifts and used in the equation i.p. $= 13.15\bar{q} - 1.50$ eV, where $\bar{q}$ = one half the sum of charge on the pair of electron-richest bonded C atoms, to give i.p.'s with a standard error of 0.044 eV. The relevance of these charges with respect to carbon 1s binding energies is discussed.

HERVÉ HENRY et SÁNDOR FLISZÁR. Can. J. Chem. **52**, 3799 (1974).

La comparaison des potentiels d'ionisation adiabatique des alcanes normaux et ramifiés avec les charges nettes du carbone montre une chute des p.i. avec l'augmentation de la population électronique de la paire d'atomes liés C—C la plus riche en électrons dans les molécules. En termes de "charges inductives", on trouve que $n = -4.4083$, *i.e.* exactement le même ordre des charges antérieurement déterminé par les déplacements r.m.n, du ^{13}C. On peut alors calculer les charges relatives à partir des déplacements chimiques du ^{13}C et les utiliser dans l'équation p.i. $= 13.15\bar{q} - 1.50$ eV, où $\bar{q}$ = la moitié de la somme des charges sur la paire d'atomes C liés la plus riche en électrons; on obtient les p.i. avec un écart-type de 0.044 eV. On discute de l'importance de ces charges par rapport aux énergies de liaison 1s du carbone.

[Traduit par le journal]

The object of this paper is to present a correlation between ionization potentials (i.p.) of normal and branched alkanes and charge distributions. Crude justifications for such a study can be found in the work of Widing and Levitt (1) who described numerous correlations between adiabatic i.p.'s and Taft's inductive substituent constants (an indirect way of correlating i.p.'s with charges) and in a note by Streitwieser (2) who justified to some extent a dependence of i.p.'s on local charge densities.

Here, attention is focussed on the charges to be used for studying such a correlation. This question has been discussed recently (3, 4) in terms applying to any molecular property involving charges. The equations for the carbon net (*i.e.*, nuclear minus gross) charges which were derived from the "inductive theory" (3) are given in Table 1.

These charges are expressed in relative units, with respect to q_C(ethane) = 1. Multiplication of these relative charges by a unity factor, β = C net charge of ethane, yields net populations in charge units. The set of "inductive" charge distributions $f(n, \beta)$ has been shown to represent a summary of sets of theoretical results, each of which can be generated by inserting the appropriate n and β values in the "inductive" equations. For example, the optimized STO-3G charges (5) are obtained using $n = 1.3325$ and $\beta = -20.96$ (10^{-3} electron units = m*e*), whereas Hoyland's BO *ab initio* results (6) are reproduced by letting $n = 25$ and $\beta = -504$ m*e*. In short, it appeared that the "inductive equations" are quite general whereas the choice of any particular theoretical method in fact reduces to choosing a particular n value, that corresponding to the method selected.

The question about the "true" n value has also been discussed (4): the use of the correct n value is critical in any study of a property–charge relationship since the relative ordering of the C charges depends on n. It has been found (4) that carbon-13 n.m.r. shifts, δ_C, are related to the C net charges q (in relative units) by eq. 1, provided

$$[1] \quad \delta_C = -237.1q + 242.64 \qquad (\pm 0.3 \text{ p.p.m., from TMS})$$

that $n = -4.4122$. It is important to note that *any n value other than* ~ -4.4 *would destroy the*

Can. J. Chem. Downloaded from www.nrcresearchpress.com by 210.87.254.6 on 09/05/12
For personal use only.

TABLE 1. "Inductive" charges, adiabatic ionization potentials, and ^{13}C chemical shifts of alkanes

Molecule	No.[a]	Ionization potential (eV)	q		δ (p.p.m. from TMS)	
			C-1	C-2	C-1	C-2
CH_4		12.98	$4(n+1)/3n$		−2.1	
$\overset{*}{C}H_3\overset{*}{C}H_3$	1	11.65	1.000	1.000	5.9	5.9
$\overset{*}{C}H_3\overset{*}{C}H_2CH_3$	2	11.07	$(3n+0.55)/3n$	$(2n-3.8)/3n$	15.6	16.1
$CH_3\overset{*}{C}H_2\overset{*}{C}H_2CH_3$	3	10.63	$(2n-3.35)/3n$	$(2n-3.35)/3n$	25.0	25.0
$\overset{*}{C}H_3\overset{*}{C}H(CH_3)_2$	4	10.57	$(3n+1.03)/3n$	$(n-7.7)/3n$	24.3	25.2
$CH_3\overset{*}{C}H_2\overset{*}{C}H_2CH_2CH_3$	5	10.35	$(2n-3.46)/3n^b$	$(2n-2.8)/3n$	22.6	34.5
$\overset{*}{C}H_3\overset{*}{C}(CH_3)_3$	6	10.35	$(n+0.49)/n$	$-4/n$	31.5	27.9
$CH_3\overset{*}{C}H_2\overset{*}{C}H(CH_3)_2$	7	10.32	$(2n-2.95)/3n^b$	$(n-7.46)/3n^b$	31.8	29.9
$CH_3CH_2\overset{*}{C}H_2\overset{*}{C}H_2CH_2CH_3$	8	10.18	$(2n-2.94)/3n^b$	$(2n-2.94)/3n^b$	32.0	32.0
$(CH_3)_2\overset{*}{C}H\overset{*}{C}H_2CH_2CH_3$	9	10.12	$(n-7.58)/3n^b$	$(2n-2.39)/3n^b$	27.8	41.8
$CH_3\overset{*}{C}H_2\overset{*}{C}H(CH_3)CH_2CH_3$	10	10.08	$(2n-3.09)/3n^b$	$(n-7.08)/3n^b$	29.3	36.7
$(CH_3)_3\overset{**}{C}CH_2CH_3$	11	10.06	$-11.85/3n^b$	$(2n-2.67)/3n^b$	30.4	36.7
$(CH_3)_2\overset{*}{C}H\overset{*}{C}H(CH_3)_2$	12	10.02	$(n-7.23)/3n^b$	$(n-7.23)/3n^b$	34.1	34.1

[a]Refers to points in Fig. 1.
[b]"Inductive" charges from ^{13}C n.m.r. shifts as explained in the text; others from ref. 3.

monotonic dependence of ^{13}C n.m.r. shifts on C charges. It is noteworthy that this "experimental" n value is remarkably close to that predicted (−4.4) by assuming that in the alkanes all the C atoms are as similar as possible among themselves, as far as their charges are concerned (4).

Whenever the "inductive" charges were known from the "inductive theory" and/or from optimized *ab initio* calculations, eq. 1 appeared to be in excellent agreement with experimental δ_C results. Indeed, the standard deviation (0.3 p.p.m.) is small in comparison with the error (~ 2.4 p.p.m.) in δ_C which would correspond to a 1% error in the estimate of q. On these grounds, eq. 1 is now used to derive the expressions for C charges when these are not known from previous work. This is simply done by calculating q ($n = -4.4122$) from eq. 1 and, therefrom, the appropriate x values from the general equations: $(3n + x)/3n$ (primary C), $(2n + x)/3n$ (secondary C), $(n + x)/3n$ (tertiary C), and $-x/n$ (quaternary C atom) (Table 1). The chemical shifts which were used in these calculations are those determined by Grant and Paul (7).

We have now available the expressions for the C atomic charges required for the comparison with adiabatic ionization potentials (8). Two questions need now be answered: (*i*) which atom(s) of each molecule shall be considered for the correlation with the i.p.'s and (*ii*) what is the "proper" n value to be associated with the equations of Table 1? The form of the correlation (linear or other) is not of any particular interest at this stage: all that is required is that the dependence be monotonic.

Several attempts were made, including attempts to correlate the i.p.'s with the net charge of the electron-richest C atom of each molecule or with a combination of the electron-richest carbon–hydrogen pair of each molecule, all of which failed in giving any monotonic dependence of i.p.'s on these quantities, whatever numerical choice was made for n. The only monotonic correlation was obtained when comparing the ionization potentials with the electron-richest pair of bonded C atoms in each molecule. This correlation turned out to be linear (Fig. 1), although such a linearity had not been postulated *a priori*.

The least-square analysis of the data, using

Can. J. Chem. Downloaded from www.nrcresearchpress.com by 210.87.254.6 on 09/05/12
For personal use only.

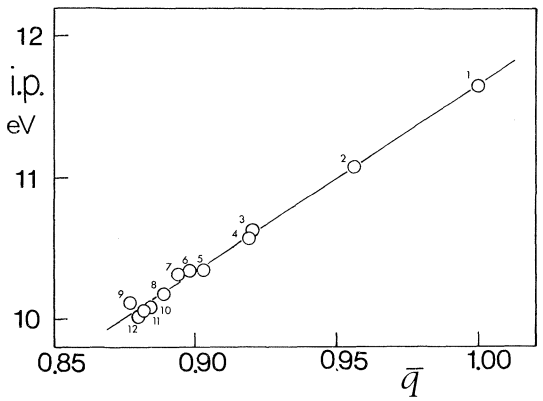

FIG. 1. Verification of eq. 2.

the equations of Table 1, indicated that $n = -4.4083$ and that

$$[2] \qquad \text{i.p.} = 13.15\bar{q} - 1.50 \text{ eV}$$

with a standard deviation of 0.044 eV. In eq. 2, $\bar{q}$ is one half the sum of the relative net charges of the electron-richest pair of bonded C atoms in each alkane molecule.

At this point it must be stressed that although some of the charges used in this paper were obtained from ^{13}C chemical shifts (for which $n = -4.4122$), in this least-square analysis of the i.p.'s n was allowed to assume freely any value which would give the best correlation. In this respect, $n = -4.4083$ can be regarded as a really independent "experimental" n value.

Discussion

The above results point at the role of the electron-richest bonded C—C pair in the molecules, a result which is similar to that obtained by Widing and Levitt (1) for the normal alkanes and to that observed for alkyl-substituted ethylenes (9). In the latter case, linear correlations were obtained between i.p.'s and the sum of charges on the unsaturated C atoms, whereby any increase of their electron density due to substituent effects leads to a lowering of the molecular ionization potential. Similarly, the results presented in Fig. 1 indicate that the i.p.'s of the alkanes decrease as the joint electron population of the pair of electron-richest C atoms increases.

Such results are in general accord with common views: the electron attracting power of otherwise similar atoms is diminished as their electron populations are increased. On these grounds, the relative ordering of the C charges obtained with $n \simeq -4.4$ appears to be intuitively acceptable. The importance of this argument regarding charges can be inferred from the fact that the reverse ordering of charges would be obtained with any $n > 0$, a result given by most theoretical calculations (3).

The obvious advantage of the present analysis derives from the use of the "inductive" charges, which are equivalent to those given by numerous theoretical methods, except for the n value which differs from method to method (3). In that, we have used the most general approach for studying a property–charge relationship, in letting n be a quantity to be calibrated by experiment.[1] It is then remarkable that the n value deduced from i.p.'s is virtually identical to that calculated from chemical shifts and to that predicted (4) for a situation where the various C atoms carry as similar charges as possible. It is important to stress that both in ^{13}C shifts and i.p.'s the $n \simeq -4.4$ value is the only one which permits a monotonic property–charge relationship. Here, we take advantage of this fact which enables us to use chemical shifts for calculating charges (eq. 1) and then to use these charges for calculating the ionization potentials (eq. 2).

There is an additional important point associated with $n \simeq -4.4$. At this level, the C atoms become increasingly electron-richer (*i.e.*, less positive, since the polarities are C^+—H^-) as the number of their α-CH_3 substituents is increased (3, 4). These charges are therefore in accord with the results of Thomas (10) who observed that in alkanes the carbon 1s binding energy decreases when a hydrogen is replaced by an alkyl group and concluded therefrom that the replacement of a hydrogen attached to a C atom with a carbon apparently results in an increased electron density at the carbon. The difficulties pointed out by Thomas, to the effect that experimental 1s binding energies are seemingly *not* consistent with MO calculations, can thus be ascribed simply to the fact that charge densities corresponding to $n > 0$ were used in his comparisons[2], *i.e.*, charges whose relative

[1]It has been shown (4) that n can be associated with the mode of partitioning C—H overlap populations. In this sense, the evaluation of the "proper" n can be regarded as an experimental calibration of the mode of distributing overlap populations between bonded C—H atoms.

[2]The charges which were used by Thomas (10) are those calculated by Palke and Lipscomb (11) and correspond to $n \simeq 13.8$, with $\beta = -372$ m*e*.

Can. J. Chem. Downloaded from www.nrcresearchpress.com by 210.87.254.6 on 09/05/12
For personal use only.

ordering is reversed with respect to that corresponding to $n \simeq -4.4$.

The financial aid given by the National Research Council of Canada is gratefully acknowledged.

1. H. F. WIDING and L. S. LEVITT. Tetrahedron, **30**, 611 (1974).
2. A. STREITWIESER. J. Phys. Chem. **66**, 368 (1962).
3. S. FLISZÁR, G. KEAN, and R. MACAULAY. J. Am. Chem. Soc. **96**, 4353 (1974).
4. S. FLISZÁR, A. GOURSOT, and H. DUGAS. J. Am. Chem. Soc. **96**, 4358 (1974).
5. G. KEAN and S. FLISZÁR. Can. J. Chem. **52**, 2772 (1974).
6. J. R. HOYLAND. J. Chem. Phys. **50**, 473 (1969).
7. D. M. GRANT and E. G. PAUL. J. Am. Chem. Soc. **86**, 2984 (1964).
8. K. WATANABE, T. NAKAYAMA, and J. MOTTL. J. Quant. Spectrosc. Radiat. Transfer, **2**, 369 (1962).
9. J. GRIGNON and S. FLISZÁR. Can. J. Chem. **52**, 2766 (1974).
10. T. D. THOMAS. J. Chem. Phys. **52**, 1373 (1970).
11. W. E. PALKE and W. N. LIPSCOMB. J. Am. Chem. Soc. **88**, 2384 (1966).

Can. J. Chem. Downloaded from www.nrcresearchpress.com by 210.87.254.6 on 09/05/12
For personal use only.

Nucleic Acid Related Compounds. 14. 3′-*O*-Aminoacyl-2′-*O*-methyladenosines and 2′-*O*-Aminoacyl-3′-*O*-methyladenosines Related to Charged tRNA Termini[1,2]

MORRIS J. ROBINS, MALCOLM MACCOSS,[3] AND G. RAMANI[4]

Department of Chemistry, The University of Alberta, Edmonton, Alberta T6G 2G2

Received June 3, 1974

MORRIS J. ROBINS, MALCOLM MACCOSS, and G. RAMANI. Can. J. Chem. **52**, 3803 (1974).

Aminoacyl nucleosides derived from 2′-*O*-methyladenosine and 3′-*O*-methyladenosine have been isolated as pure solids and completely characterized for the first time. Coupling of 5′-*O*-(mono-*p*-methoxytrityl)-2′-*O*-methyl- (and 3′-*O*-methyl-) adenosines (**1** and **6**, respectively) with *N*-*tert*-butyloxycarbonyl(*N*-*t*BOC)-amino acid anhydrides (**2***a–c*) (generated *in situ* from the corresponding *N*-*t*BOC-amino acids and *N*,*N*′-dicyclohexylcarbodiimide) in the presence of 4-*N*,*N*-dimethylaminopyridine gave the 3′-*O*-(*N*-*t*BOC-aminoacyl)-5′-*O*-(mono-*p*-methoxytrityl-2′-*O*-methyladenosines (**3***a–c*) and 2′-*O*-(*N*-*t*BOC-aminoacyl)-5′-*O*-(mono-*p*-methoxytrityl-3′-*O*-methyladenosines (**7***a–c*), respectively, in good yields. The L-leucine (*a*), L-phenylalanine (*b*), and L-methionine (*c*) compounds were prepared in each series. Complete deblocking was effected using 98% formic acid since usual procedures had disadvantages with these molecules. The 3′-*O*-(L-aminoacyl)-2′-*O*-methyladenosines (**4***a–c*) and 2′-*O*-(L-aminoacyl)-3′-*O*-methyladenosines (**8***a–c*) were obtained in high yields with no detectable hydrolysis of the aminoacyl or glycosidic bonds under these conditions.

N-Formylmethionyl and *N*-acetylphenylalanyl derivatives were prepared in each series by acylation of the deblocked products with acetic formic anhydride and *p*-nitrophenyl acetate, respectively. Biochemical rationale for the use of these compounds in the study of protein biosynthesis and initiation processes are discussed. The puromycin-like activity of 3′-*O*-phenylalanyl-2′-*O*-methyl-adenosine (**4***b*) was confirmed.

MORRIS J. ROBINS, MALCOLM MACCOSS et G. RAMANI. Can. J. Chem. **52**, 3803 (1974).

Les nucléosides d'aminoacylés dérivés de la 2′-*O*-méthyladénosine et du 3′-*O*-méthyladénosine ont été isolés pour la première fois sous forme de solides et entièrement caractérisés. Le couplage des 5′-*O*-(mono-*p*-méthoxytrityl)-2′-*O*-méthyl(et -3′-*O*-méthyl) adénosines (respectivement **1** et **6**) avec les anhydrides d'acides aminés *N*-*tert*-butylonycarbonylé (*N*-*t*BOC) (**2***a–c*) (par réaction des acides aminés *N*-*t*BOC avec la *N*,*N*′-dicyclohexylcarbodiimide) en présence de 4-*N*,*N*-diméthylaminopyridine, donnent avec de bons rendements les 3′-*O*-(*N*-*t*BOC-aminoacyl)-5′-*O*-(mono-*p*-méthoxytrityl)-2′-*O*-méthyladénosines (**3***a–c*) et 2′-*O*-(*N*-*t*BOC-aminoacyl)-5′-*O*-(mono-*p*-méthoxytrityl)-3′-*O*-méthyladénosines (**7***a–c*). Les composés L-leucine (*a*), L-phénylalanine (*b*) et L-méthionine (*c*) ont été préparés dans chaque série. La déprotection complète a été effectuée en utilisant l'acide formique à 98% car les procédés habituels présentaient des inconvénients avec ces molécules. Les 3′-*O*-(L-aminoacyl)-2′-*O*-méthyladénosines (**4***a–c*) et les 2′-*O*-(L-aminoacyl)-3′-*O*-méthyladénosines (**8***a–c*) ont été obtenus avec des rendements élevés sans hydrolyse détectable des liaisons aminoacyle ou glycosidique dans ces conditions.

Les dérivés *N*-formylméthionylé et *N*-acétylphénylalanilé ont été préparés dans chaque série en acylant les produits déprotégés au moyen de l'anhydride mixte acétique et formique et de l'acétate de *p*-nitrophényle respectivement. On discute la raison biochimique fondamentale de l'utilisation de ces composés dans l'étude de la biosynthèse des protéines ainsi que les processus d'initiation. On a confirmé l'activité de type puromycine de la 3′-*O*-phénylalanyl-2′-*O*-méthyl-adénosine (**4***b*). [Traduit par le journal]

The nucleoside antibiotic puromycin (**i***a*) has been found to function as an aminoacyl tRNA simulator in accepting the growing peptide chain at a site on the ribosome (see for example, ref. 1, a recent concise review, ref. 2, and references therein). Numerous 3′(2′)-*O*-aminoacyl nucleoside (**ii**), nucleotide, and oligonucleotide derivatives, analogs of the 3′-termini of charged tRNA, have been prepared and investigated biochemically (see ref. 3 and references therein). However, prior to the initiation of our studies (3), no

[1]Generous support from the National Research Council of Canada (A5890), the National Cancer Institute of Canada, the Defence Research Board of Canada, and the University of Alberta is gratefully acknowledged.

[2]For the previous paper in this series see ref. 33.

[3]Postdoctoral Fellow 1972–Present.

[4]Postdoctoral Fellow 1971–1973.

Can. J. Chem. Downloaded from www.nrcresearchpress.com by 210.87.254.6 on 09/05/12
For personal use only.

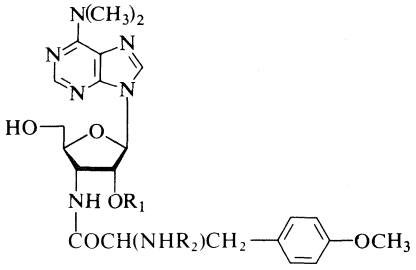

i

a $R_1 = R_2 = H$
b $R_1 = COCH_3$; $R_2 = H$
c $R_1 = H$; $R_2 = COCH_3$

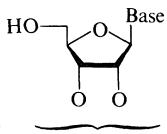

H; $COCH(NH_2)R$

ii

aminoacyl nucleosides of rigorously defined purity or specific 2′ isomeric structure had been reported. Most biochemical studies had been effected using "stock solutions" or freeze–dried solids obtained from reaction sequences involving amino acid coupling with nucleoside derivatives. These incompletely characterized preparations invariably contained free nucleosides and amino acid (from cleavage of the aminoacyl linkage during deblocking) plus both isomers indicated in **ii** in the case of ribosides. Rich and co-workers (4) had proposed that protein biosynthesis might proceed by initial transfer of the growing peptide chain from peptidyl-tRNA to the 2′(3′)-hydroxyl group of a 3′(2′)-*O*-aminoacyl-tRNA at the receptor site. Intramolecular transfer of the $O^{2'(3')}$-peptidyl function to the free α-NH_2 of the $O^{3'(2')}$-aminoacyl moiety would constitute the peptide bond-forming step of protein biosynthesis. Their finding that such an intramolecular reaction occurred in 2′,3′-bis-*O*-(L-phenylalanyl)adenosine and that 2′-*O*-acetylpuromycin (**i***b*) rearranged to the *N*-acetyl derivative (**i***c*) made the synthesis of aminoacyl nucleosides with the *cis*-vicinal hydroxyl group missing or specifically blocked of significant interest. Žemlička *et al.* (5) described a preparation of 3′-*O*-(L-phenylalanyl)-2′- deoxyadenosine which was found to have essentially no peptide acceptor activity (6). The 2′-hydroxyl function was assumed to be necessary for accepting activity in substrate or binding function(s) (6).

A most interesting study was reported very recently by Sprinzl and Cramer (7) which demonstrated 2′-hydroxyl charging of a tRNA terminating with 3′-deoxyadenosine (cordycepin) by phenylalanyl-tRNA synthetase. This charged tRNA, however, was unable to function in the peptide elongation step. In contrast, the corresponding tRNA terminating with 2′-deoxyadenosine could not be charged at the 3′-hydroxyl by the synthetase. These authors (7), therefore, suggested a scheme involving initial 2′ charging followed by aminoacyl migration to 3′ before peptide chain elongation.

Chládek *et al.* (8) have studied phenylalanyl esters of 2(*R*)-(adenin-9-yl)-4(*R*)-hydroxymethyl-3-oxapentan-1,5-diol (obtained by periodate oxidation of a 5′-*O*-blocked adenosine and subsequent borohydride reduction of the resulting dialdehyde). In agreement with the work of Sprinzl and Cramer (7), the 5-ester (**iii***a*) (corresponding to a 3′-*O*-aminoacyl nucleoside) had

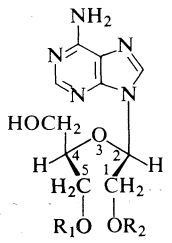

Phe = $COCH(NH_2)CH_2C_6H_5$

iii

a R_1 = Phe, $R_2 = H$
b $R_1 = R_2$ = Phe
c $R_1 = H$, R_2 = Phe

peptide acceptor activity whereas the 1-ester (**iii***c*) (corresponding to a 2′-*O*-aminoacyl nucleoside) was virtually inactive. The 1,5-bis-ester (**iii***b*) (corresponding to a 2′,3′-bis-*O*-aminoacyl nucleoside (9)) was a slightly better acceptor than **iii***a* (8). These combined results suggest that the 3′-*O*-aminoacyl function is obligatory for accepting activity.[5] However, once charging (2′-hydroxyl required (7)) has occurred, the status of the 2′-hydroxyl function may be relatively unimportant.[5] The positive accepting results re-

[5]NOTE ADDED IN PROOF: Cramer and co-workers (35) have now found accepting activity (although at a low rate) for a tRNA terminating with a 2′-*O*-aminoacylnucleoside or analog (**iii***c*) but noted that no further participation in peptide elongation occurred.

Can. J. Chem. Downloaded from www.nrcresearchpress.com by 210.87.254.6 on 09/05/12
For personal use only.

Can. J. Chem. Downloaded from www.nrcresearchpress.com by 210.87.254.6 on 09/05/12
For personal use only.

ported (8) with **iii***b* would appear to obviate the Rich proposal for intramolecular transfer (at least in this system) since an 11-membered cyclic transition state would be required for acylation of the α-amino function of the 5-*O*-phenylanyl moiety by the 1-*O*-phenylalanyl carboxyl group. Since **iii***b* is actually more active than **iii***a* in this system, such an energetically (entropy) unfavorable possibility seems unreasonable and the C-2′ analogous substituent may be involved in binding and/or favorable conformational effects.

These findings raise possibilities for the design of molecules which could specifically interfere with the amino acid charging step independently of the peptide chain lengthening process (*i.e.* the puromycin reaction). In this regard it is interesting that the tRNA terminating with 2′-deoxyadenosine was reported (7) to act as a competitive inhibitor of synthetase charging of the naturally occurring tRNA terminating with adenosine.

Effective coupling and deblocking procedures for the synthesis of chemically pure, "crystalline" 3′-*O*-aminoacyl-2′-deoxyadenosines and 2′-*O*-aminoacyl-3′-deoxyadenosines have been developed in this laboratory (3). It has been found that 2′-*O*-methyladenosine and certain of its nucleotide and polynucleotide compounds behave analogously to the corresponding adenosine products but dramatically different from the 2′-deoxyadenosine analogs with respect to conformational effects, binding and association, recognition, enzyme reactions, etc. (see for example refs. 10–15 and references therein). As well, 2′-*O*-methyl nucleosides are well studied and ubiquitous components of tRNA (16) and are thus attractive natural products for 2′-hydroxyl blocked 3′-*O*-aminoacyl nucleosides. A facile synthetic route to 2′-*O*- and 3′-*O*-methyl nucleosides has been developed (17, 18) making both products readily available. During the course of this work, a preliminary communication appeared (19) reporting the preparation and puromycin-like activity of 3′-*O*-phenylalanyl-2′-*O*-methyladenosine. We now wish to report a convenient route to the first "crystalline" completely characterized 3′-*O*-aminoacyl-2′-*O*-methyladenosines and 2′-*O*-aminoacyl-3′-*O*-methyladenosines.

Treatment of 2′-*O*- or 3′-*O*-methyladenosine (17, 18) with mono-*p*-methoxytrityl chloride in pyridine gave 5′-*O*-(mono-*p*-methoxytrityl)-2′-*O*-methyladenosine (**1**) or 5′-*O*-(mono-*p*-methoxytrityl)-3′-*O*-methyladenosine (**6**), respectively, in reasonable yields (see Scheme 1). Symmetrical *N-tert*-butyloxycarbonyl(*N-t*BOC)-amino acid anhydrides (**2***a–c*) of L-leucine (*a*), L-phenylalanine (*b*), and L-methionine (*c*) were prepared *in situ* from the *N-t*BOC-amino acid and dicyclohexylcarbodiimide (DCC) according to the general procedure of Khorana (20). Acylation at *O*-3′ or *O*-2′ of **1** or **6**, respectively, with the anhydrides **2***a–c* in ethyl acetate proceeded readily in the presence of 4-*N*,*N*-dimethylaminopyridine. This catalyst dramatically facilitates acylations with hindered substrates (21) and was found to be mandatory when using *N*-trityl-amino acids (3). The fully blocked products (**3***a–c* and **7***a–c*), obtained in 60–80% chromatographically pure yields, were "recrystallized"[6] and fully characterized (see Tables 1 and 2).

Our initial studies on hydrogenolytic removal of the commonly used *N*-carbobenzyloxy (*N*-CBZ) blocking group indicated partial loss of the amino acid from the nucleoside, as observed by others (22). As expected, trifluoroacetic acid effected complete deblocking of both the mono-*p*-methoxytrityl and *t*BOC protected functions of **3***a–c* or **7***a–c*. However, evaporation of the reaction solution followed by repeated coevaporation with various solvents, precipitation of the product using several solvent combinations, and extended drying of the samples *in vacuo* at elevated temperatures over various drying agent combinations including potassium hydroxide pellets, all failed to completely remove trifluoroacetate as evidenced by a residual peak in the ^{19}F n.m.r. spectra. Attempted chemical absorption of the remaining trifluoroacetic acid from solutions of product using solid barium carbonate, weakly basic resins, etc., led to some cleavage of amino acid from the nucleoside. Therefore, this approach (used in the preparation of an uncharacterized (19) preparation of **4***b*) was abandoned since biochemical evaluation of samples with even trace quantities of the highly toxic trifluoroacetate could be subject to question. Experiments using boron trifluoride etherate or mineral acids in various solvents gave products containing residual BF_3 or failed to achieve complete deblocking without causing

[6]These products were subjected to the usual process of recrystallization (*i.e.* dissolved by warming in solvent and found to separate from solution upon cooling). However, most of the samples did not exhibit diffracting properties under a polarizing microscope and are probably amorphous or microcrystalline solids.

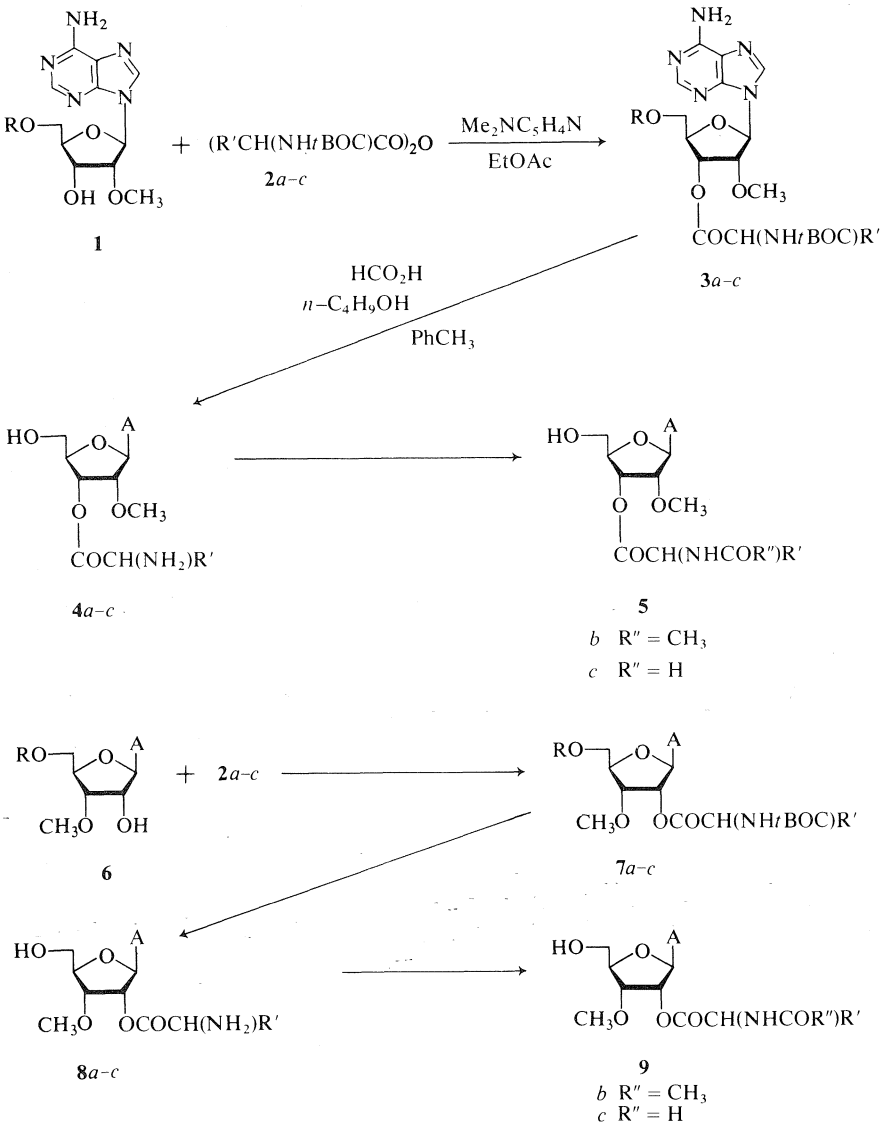

a R' = $CH_2CH(CH_3)_2$; *b* R' = $CH_2C_6H_5$; *c* R' = $CH_2CH_2SCH_3$

A = Adenine-9; R = $C(C_6H_5)_2(p\text{—}C_6H_4OCH_3)$; *t*BOC = $COOC(CH_3)_3$

SCHEME 1

observable amino acid cleavage from the nucleoside.

Treatment of **3***a–c* or **7***a–c* with 98% formic acid at room temperature effected rapid removal of the mono-*p*-methoxytrityl function followed by slower deblocking of the *N*-tBOC-amino moiety. After 3–4 h (see Experimental) **4***a–c* or **8***a–c* were the only products observable by thin-layer chromatography (t.l.c.). Toluene and 1-butanol were added to prevent *N*-formylation during evaporation of the reaction solution and to effect smooth azeotropic removal of formic acid and water. Generally high yields of the free aminoacyl nucleosides (**4***a–c* or **8***a–c*) were ob-

Can. J. Chem. Downloaded from www.nrcresearchpress.com by 210.87.254.6 on 09/05/12
For personal use only.

Can. J. Chem. Downloaded from www.nrcresearchpress.com by 210.87.254.6 on 09/05/12
For personal use only.

TABLE 1. Fully blocked aminoacyl derivatives[a]

Compound	Yield (%)	Formula	Elemental analysis (%) Calculated C	H	N	S	Found C	H	N	S	Ultraviolet spectra[b] (nm (ε)) Maximum	Minimum
3*a*	63	$C_{42}H_{50}N_6O_8$	65.78	6.57	10.96	—	65.72	6.75	10.76	—	233(17 700) 258(15 600)	225(15 800) 243(13 400)
3*b*	68	$C_{45}H_{48}N_6O_8$	67.48	6.04	10.49	—	67.27	6.14	10.27	—	233(20 200) 260(16 800)	227(19 500) 246(14 800)
3*c*	79	$C_{41}H_{48}N_6O_8S$	62.73	6.16	10.71	4.08	62.55	6.20	10.73	4.14	234(18 000) 259(16 300)	225(15 800) 244(13 900)
7*a*	71	$C_{42}H_{50}N_6O_8$	65.78	6.57	10.96	—	65.88	6.76	10.88	—	235(16 600) 260(13 700)	223(14 100) 244(12 600)
7*b*	69	$C_{45}H_{48}N_6O_8$	67.48	6.04	10.49	—	67.23	6.29	10.25	—	234(17 300) 260(14 500)	223(15 600) 244(12 600)
7*c*	71	$C_{41}H_{48}N_6O_8S$	62.73	6.16	10.71	4.08	62.53	6.35	10.42	4.22	233(17 800) 259(15 300)	223(15 500) 244(13 300)

[a]Samples were recrystallized[5] from ethyl acetate – pentane (for **7***a–c*) or diisopropyl ether (for **3***a–c*) and were dried for 20 h at 56°/0.1 mm over Drierite (anhydrous calcium sulfate) and paraffin wax. No clearly defined melting behavior was observed and all samples softened and melted at about 90–105°.
[b]Determined in methanol.

TABLE 2. Nuclear magnetic resonance data on fully blocked aminoacyl derivatives[a]

Compound	6-NH_2[b]	$H_{1'}$	$H_{2'}$	$H_{3'}$	$TrOCH_3$[b]	2′(3′)-OCH_3[b]	Amino acid	*t*-BOC[b]
3*a*	6.25	6.08[c]	4.82[d]	5.56[e]	3.76	3.37	0.93[f]	1.43
3*b*	6.30	5.98[c]	4.84[d]	5.49[e]	3.74	3.32	3.07[g]	1.41
3*c*	5.92	6.03[c]	4.83[d]	5.56[e]	3.74	3.34	2.05[h]	1.43
7*a*	6.45	6.18[i]	6.04[j]	4.50[k]	3.72	3.34	0.92[f]	1.42
7*b*	6.13	6.12[i]	5.95[j]	4.46[k]	3.75	3.34	3.12[g]	1.40
7*c*	6.19	6.15[i]	5.98[j]	4.50[k]	3.76	3.36	2.07[h]	1.44

[a]Chemical shifts in δ from TMS internal in $CDCl_3$; D_2O exchange employed when 6-NH_2 and $H_{1'}$ overlap occurred.
[b]Singlet.
[c]Doublet $J_{1'-2'} \sim 6$ Hz.
[d]"Triplet" $J_{2'-1'} \sim J_{2'-3'} \sim 6$ Hz.
[e]"Quartet" $J_{3'-2'} \sim 6$ Hz, $J_{3'-4'} \sim 3.5$ Hz.
[f]Doublet $J \sim 6$ Hz, $-CH(CH_3)_2$.
[g]Doublet $J \sim 6.5$ Hz, $-\underset{|}{CH}-CH_2Ph$.
[h]Singlet, $-SCH_3$.
[i]Doublet $J_{1'-2'} \sim 4$ Hz.
[j]"Triplet" $J_{2'-1'} \sim J_{2'-3'} \sim 4$ Hz.
[k]Multiplet, overlapped with amino acid proton.

tained. These products were purified by "recrystallization"[6] and were completely characterized by elemental analysis and physical data[7] (see Tables 3 and 4).

Protein synthesis in *Escherichia coli* (23) and probably in prokaryotic systems in general (see ref. 24 for a review) is initiated by a specific species of *N*-formylmethionyl-tRNA (fMet-$tRNA_f^{Met}$). This initiation process was shown to be simulated by *N*-acetylphenylalanyl-tRNA (25). Therefore, *N*-formylmethionyl and *N*-acetylphenylalanyl derivatives of the 2′-*O*- and 3′-*O*-methylaminoacyl nucleosides were prepared in order to investigate possible effects on the initiation processes and any biological species selectivity which may exist.

The "active ester" approach of Bodánszky (26) employing *p*-nitrophenyl acetate was used to prepare the *N*-acetyl-L-phenylalanyl products **5***b* and **9***b* from **4***b* and **8***b*, respectively. Acetic formic anhydride in cold methanol gave selective formylation of the amino acid moiety of **4***c* and **8***c* to yield the *N*-formylmethionyl products **5***c* and **9***c*, respectively.

Monoaminoacyl derivatives of a *cis*-vicinal glycol system as found in charged tRNA's exhibit very rapid $O_{2'} \rightleftarrows O_{3'}$ isomerization in aqueous solution (27). They are also rather unstable with respect to hydrolysis with typical half-lives of 5–30 min at about 30° and near neutrality (20, 28, 29). The present 3′ (and 2′)-*O*-aminoacyl-2′(and 3′)-*O*-methyladenosines, of course, have uniquely defined structure with no $O_{2'} \rightleftarrows O_{3'}$ isomerism possible. In addition, removal of the *cis*-vicinal hydroxyl would be expected to confer hydrolytic stability since the hydrogen-bonded hydrolytic transition state postulated (30) for aminoacyl ribonucleosides is now precluded. Indeed, the present series of compounds (except for the methionine products) exhibit little or no observable cleavage in distilled water at ~30° for 18 h. However, they break down over an extended period of time to give some of the *O*-methyladenosine plus amino acid even when stored as solids at 4° in a desiccator. The more amorphous products and methionine products appear to be less stable. The optical rotations also vary with time for certain of the compounds and must be viewed with some caution. No racemization of the amino acids was anticipated under the mild reaction conditions employed. This was confirmed by mild basic hydrolysis of the free aminoacyl nucleosides followed by substrate specificity evaluation using L-amino acid oxidase (31).

The acceptor activity (puromycin reaction (1)) of 3′-*O*-phenylalanyl-2′-*O*-methyladenosine (**4***b*) was found to be less than 40% that of puromycin in the system studied (1).[8] This confirms the general results previously noted (19), although markedly different experimental conditions, systems, and activity levels were observed. Therefore, the intramolecular transfer mechanism of peptide bond formation suggested by

[7]After submission of this manuscript, Chládek, *et al.* (34) reported the preparation (using *N*-carbobenzyloxyphenylalanine) and qualitative characterization of the two phenylalanyl esters defined in the present study.

[8]C. Coutsogeorgopoulos. Private communication.

Can. J. Chem. Downloaded from www.nrcresearchpress.com by 210.87.254.6 on 09/05/12
For personal use only.

TABLE 3. 3′(2′)-*O*-Aminoacyl-2′(3′)-*O*-methyladenosines[a]

Compound	Yield (%)	Formula	Elemental analysis (%) Calculated C	H	N	S	Found C	H	N	S	Ultraviolet spectra[b] (nm (ε)) Maximum	Minimum	$[\alpha]_D^{23}$[c]
4*a*	58	$C_{17}H_{26}N_6O_5$	51.76	6.64	21.31	—	52.07	6.69	21.25	—	259(14 000)	226(1800)	−58.4°
4*b*[d]	89	$C_{20}H_{24}N_6O_5 \cdot 0.5\ HCO_2H \cdot 0.6\ CH_3CO_2C_2H_5$	54.70	5.92	16.68	—	54.78	5.81	16.83	—	258(14 100)	227(2000)	−39.3°
4*c*	95	$C_{16}H_{24}N_6O_5S$	46.59	5.86	20.38	7.77	46.74	5.97	20.08	7.69	259(15 000)	227(2250)	−57.1°
8*a*	84	$C_{17}H_{26}N_6O_5$	51.76	6.64	21.31	—	51.56	6.69	21.02	—	260(12 800)	225(1800)	−59.3°
8*b*	81	$C_{20}H_{24}N_6O_5$	56.07	5.65	19.61	—	55.99	5.78	19.38	—	260(12 300)	226(2700)	−48.6°
8*c*	95	$C_{16}H_{24}N_6O_5S$	46.59	5.86	20.36	7.77	46.22	6.04	20.07	7.50	260(14 100)	223(3500)	−72.1°

[a]All analytical samples were recrystallized[5] from dry ethyl acetate (sometimes with addition of pentane) and dried at 56°/0.1 mm for 1–4 days over potassium hydroxide pellets and paraffin wax.
[b]Determined in methanol.
[c]Determined in dimethyl formamide (freshly distilled from phosphorus pentoxide at reduced pressure) at concentrations between 0.9–1.1.
[d]Solvation of crystalline product (m.p. 113–114°) determined by integration of appropriate peaks in the n.m.r. spectrum and verified by the elemental analysis. This sample, when precipitated from acetone – pentane yielded an amorphous white powder. Calcd. for $C_{20}H_{24}N_6O_5 \cdot 0.5H_2O$ (verified by n.m.r.) C, 54.91; H, 5.76; N, 19.21. Found: C, 54.63; H, 5.84; N, 18.83.

Can. J. Chem. Downloaded from www.nrcresearchpress.com by 210.87.254.6 on 09/05/12
For personal use only.

TABLE 4. Nuclear magnetic resonance data on 3′(2′)-*O*-aminoacyl-2′(3′)-*O*-methyladenosines[a]

Compound	6-NH_2[b]	$H_{1'}$	$H_{2'}$	$H_{3'}$	OCH_3[b]	Amino acid
4*a*	7.34	6.00[c]	4.70[d]	5.46[e]	3.24	0.87 and 0.94[f]
4*b*	7.38	5.96[c]	4.68[d]	5.40[e]	3.20	2.90[g] and 7.27[h]
4*c*	7.37	6.02[c]	4.70[d]	5.49[e]	3.22	2.06[i]
8*a*	7.32	6.16[j]	5.78[k]	4.22[l]	3.34	0.80 and 0.86[f]
8*b*	7.35	6.18[j]	5.76[k]	4.16[l]	3.32	2.85[g] and 7.16[h]
8*c*	7.32	6.15[j]	5.78[k]	4.24[l]	3.34	2.02[i]

[a]Chemical shifts in δ from TMS internal in DMSO-d_6.
[b]Singlet.
[c]Doublet, $J_{1'-2'} \sim 7.2$ Hz.
[d]Doublet of doublets, $J_{2'-1'} \sim 7.5$ Hz, $J_{2'-3'} \sim 5.5$ Hz.
[e]Doublet of doublets, $J_{3'-2'} \sim 5.5$ Hz, $J_{3'-4'} \sim 2$ Hz.
[f]Two doublets, $J \sim 2$ Hz, $—CH(CH_3)_2$.
[g]Doublet, $J \sim 7$ Hz, $—CHCH_2Ph$.
[h]Phenyl.
[i]$—SCH_3$.
[j]Doublet, $J_{1'-2'} \sim 5$ Hz.
[k]"Triplet", $J_{2'-1'} \sim J_{2'-3'} \sim 5$ Hz.
[l]"Triplet", $J_{3'-2'} \sim J_{3'-4'} \sim 5$ Hz.

Rich and co-workers (4) appears to be precluded in this model system. Details of biochemical and microbiological evaluation of these series of aminoacyl nucleosides will be published (in collaboration with C. Coutsogeorgopoulos and A. Bloch).

It would be highly desirable to study these compounds in other precisely defined charging, initiation, and elongation systems and the procedures presently described make them readily available.

Experimental

Melting points were determined on Gallenkamp or Reichert microstage apparatus and are uncorrected. Ultraviolet (u.v.) spectra were determined in methanol using Cary 14 or 15 spectrophotometers. Nuclear magnetic resonance spectra were recorded on a Varian HA-100 instrument and chemical shift data is reported in p.p.m. from TMS internal standard on the δ scale. Optical rotations were measured using a Perkin-Elmer Model 141 polarimeter with a 10-cm 1-ml micro cell. Elemental analyses were obtained by the microanalytical laboratory of this department and Schwarzkopf Microanalytical Laboratory. Thin-layer chromatography (t.l.c.) was effected using Eastman Kodak sheets (silica gel No. 13181) in solvent systems indicated; developed chromatograms were detected by 2537 Å light (chromophore), 20% perchloric acid spray (mono-*p*-methoxytrityl functions show orange), and ninhydrin spray (slow development of yellow color upon warming for the free aminoacyl nucleosides). Column chromatography was performed on alumina (J. T. Baker No. 0537 aluminum oxide) or silica gel (Gebr. Hermann, Kieselgel) unless specified. Evaporations were effected using a Büchler rotating evaporator with Dry-Ice cooled Dewar condenser under aspirator or mechanical oil pump vacuum at 30° or lower.

*N-t*BOC-L-leucine, *N-t*BOC-L-phenylalanine, *N-t*BOC-L-methionine, and L-amino acid oxidase were purchased from Sigma Chemical Company. The preparation and separation of 2′-*O*-methyladenosine and 3′-*O*-methyladenosine have been described in detail (17, 18). Ethyl acetate was dried by distillation from P_2O_5 and stored over Linde molecular sieves (4A, dried at 200°). Pyridine was dried by refluxing over and distillation from CaH_2.

Possible racemization was evaluated by hydrolyzing a 1 mg sample of the deblocked aminoacyl nucleoside in 0.1 ml of 0.05 *M* tris(hydroxymethyl)aminomethane (p*H* 8.5 at 37°) for 20 h at 37°. The hydrolyzate was treated with 0.0196 units (in 0.1 ml) of L-amino acid oxidase and compared by paper chromatography (Whatman No. 1, *n*-BuOH–HOAc–H_2O, 12:3:5, descending) with synthetic mixtures of D and L enantiomers of the same amino acid treated under identical conditions. In all cases investigated, less than 5% ninhydrin positive material was observed in the hydrolyzates.

*5′-O-(Mono-p-methoxytrityl)-2′-O-methyladenosine (**1**)*

A 1.95 g (0.007 mol) portion of 2′-*O*-methyladenosine was treated with 3.2 g (0.011 mol) of mono-*p*-methoxytrityl chloride in 50 ml of dry pyridine and the reaction mixture was stirred at 15° for 50 h in the dark. MeOH (100 ml) was added and the solution was stirred for 1.5 h at room temperature. This solution was then poured into 400 ml of ice water and the resulting emulsion was extracted with 300 ml of $CHCl_3$. The aqueous phase was extracted with 2 × 100 ml of $CHCl_3$ and the combined organic layers were washed with 2 × 100 ml of cold saturated aqueous $NaHCO_3$ solution and then 2 × 100 ml of H_2O. The organic solution was evaporated to dryness and the residue coevaporated *in vacuo* using acetone. The cream-colored solid foam (5.7 g) was dissolved in 15 ml of $CHCl_3$ and applied to a column (3.8 × 38 cm, 350 g) of Merck neutral alumina (packed in $CHCl_3$). The column was washed with 2100 ml of $CHCl_3$ to elute rapidly migrating (t.l.c., MeOH–$CHCl_3$, 3:97) impurities. Elution was begun with MeOH–$CHCl_3$ (6:94) and the first 350 ml also contained fast (t.l.c.) impurities. After 1000 ml, the elution solvent was changed to MeOH–$CHCl_3$ (20:80) and the t.l.c. homogeneous fractions were pooled and evaporated to dryness. The resulting solid foam was dissolved in a small volume of $CHCl_3$ and precipitated into stirred pentane to give 2.37 g (62%) of pure **1**. A 0.1 g sample was recrystallized from diisopropyl ether (10 ml) and dried at 60°/0.1 mm for 65 h over Drierite and paraffin wax to give **1**; m.p. 99–101°; u.v. max 233, 258 nm (ε 16 200, 14 500); u.v. min 225, 243 nm (ε 14 600, 12 200); n.m.r. ($CDCl_3$, TMS internal) δ 2.92

Can. J. Chem. Downloaded from www.nrcresearchpress.com by 210.87.254.6 on 09/05/12
For personal use only.

Can. J. Chem. Downloaded from www.nrcresearchpress.com by 210.87.254.6 on 09/05/12
For personal use only.

(br, 1, 3′-OH), 3.4–3.6 (m, 2, $H_{5',5''}$), 3.54 (s, 3, 2′-OCH_3), 3.76 (s, 3, $C_6H_4OCH_3$), 4.19 (m, 1, $H_{4'}$), 4.43 (m, 2, $H_{2'}$ and $H_{3'}$), 5.79 (s, 2, 6-NH_2), 6.11 (d, $J_{1'-2'}$ = 4.0 Hz, 1, $H_{1'}$), 6.7–7.5 (m, 14, aromatic), 8.0 (s, 1, H_2), 8.27 (s, 1, H_8).

Anal. Calcd. for $C_{31}H_{31}N_5O_5$: C, 67.25; H, 5.64; N, 12.65. Found: C, 67.14; H, 5.93; N, 12.78.

5′-O-(Mono-p-methoxytrityl)-3′-O-methyladenosine (6)

A 5.71 g (0.02 mol) portion of 3′-*O*-methyladenosine was treated with 9.29 g (0.03 mol) of mono-*p*-methoxytrityl chloride in 125 ml of dry pyridine and subjected to an analogous procedure to that described above for **1**. The appropriate eluate from the alumina column was evaporated and the residue recrystallized from acetone to give 5.90 g (53%) of colorless needles of **6**; m.p. 118–120°; u.v. max 233, 260 n.m. (ε 16 700, 13 200); u.v. min 225, 246 n.m. (ε 15 200, 11 600); n.m.r. (Me_2CO-d_6, TMS internal) δ 2.84 (br, 1, 2′-OH), 3.34–3.58 (m, 1, $H_{3'}$), 3.48 (s, 3, 3′-OCH_3), 3.78 (s, 3, $C_6H_4OCH_3$), 4.24 (m, 2, $H_{5',5''}$), 5.04 (t, $J_{2'-1'}$ = 4.5 Hz, 1, $H_{2'}$), 6.00 (d, $J_{1'-2'}$ = 4.5 Hz, 1, $H_{1'}$), 6.62 (br, s, 2, 6-NH_2), 6.74–7.6 (m, 14, aromatic), 8.15 (s, 2, H_2 and H_8).

Anal. Calcd. for $C_{31}H_{31}N_5O_5$: C, 67.25; H, 5.64; N, 12.65. Found: C, 67.29; H, 5.92; N, 12.40.

Preparation of 3′-O-(N-tBOC-aminoacyl)-5′-O-(mono-p-methoxytrityl)-2′-O-methyladenosines (3a–c) and 2′-O-(N-tBOC-aminoacyl)-5′-O-(mono-p-methoxytrityl)-3′-O-methyladenosines (7a–c)

These blocked derivatives were prepared from the corresponding *N-t*BOC-amino acid anhydrides (**2***a–c*) (generated *in situ* from the *N-t*BOC-amino acids by the general procedure of Rammler and Khorana (20)) and **1** (for **3***a–c*) or **6** (for **7***a–c*) (see Tables 1 and 2 for data) by the following general procedure illustrated for **3***c*.

3′-O-(N-tBOC-L-Methionyl)-5′-O-(mono-p-methoxytrityl-2′-O-methyladenosine (3c)

To a solution of 1.6 g (0.0065 mol) of *N-t*BOC-L-methionine (previously dried at room temperature/0.1 mm over KOH pellets) in 25 ml of dry EtOAc was added 1.34 g (0.0065 mol) of *N,N′*-dicyclohexylcarbodiimide (DCC). Precipitation of *N,N′*-dicyclohexylurea (DCU) began almost immediately and the mixture was stirred at room temperature for 1.5 h. The mixture was filtered directly into a solution of 1.5 g (0.0027 mol) of dried **1** and 0.2 g of 4-*N,N*-dimethylaminopyridine in dry EtOAc and the DCU filter cake (0.7 g) was washed with 15 ml of dry EtOAc. The combined reaction mixture was stirred at 14° for 48 h and then filtered. The resulting DCU filter cake (0.5 g) was washed with 50 ml of EtOAc. The combined filtrate was washed with 2 × 100 ml of ice-cold saturated aqueous $NaHCO_3$ solution, 2 × 100 ml of ice water, and evaporated. Coevaporation of the residue with acetone gave a pale yellow solid foam which was dissolved in 10 ml of $CHCl_3$ and precipitated slowly into 350 ml of vigorously stirred pentane. The resulting white solid was filtered to give 2.31 g of crude product which was dissolved in 12 ml of $CHCl_3$ and applied to a column (2.5 × 30 cm, 150 g, packed in $CHCl_3$) of alumina. The column was washed with $CHCl_3$ and the first 225 ml contained only fast migrating materials (t.l.c., Me_2CO–$CHCl_3$, 2:8). Homogeneous product was eluted in the following 1000 ml and these combined fractions were evaporated to give 1.76 g (83%) of **3***c* as a dried solid foam. Precipitation of this material from $CHCl_3$ (8 ml) into pentane (400 ml) gave 1.67 g (79%) of **3***c* as a white powder. A sample for analysis was recrystallized[6] from diisopropyl ether and dried at 65°/0.1 mm over Drierite and Paraffin wax for 65 h. (See Tables 1 and 2 for data.)

Deblocking to give the 3′-O-Aminoacyl-2′-O-methyladenosines (4a–c) and 2′-O-Aminoacyl-3′-O-methyladenosines (8a–c)

These compounds were prepared by one-step deblocking of **3***a–c* and **7***a–c*, respectively, by the same general procedure illustrated below for **4***c*.

3′-O-(L-Methionyl)-2′-O-methyladenosine (4c)

A solution of 1.67 g (0.0021 mol) of **3***c* in 35 ml of 98% formic acid was allowed to stand at room temperature for 3.5 h. Toluene (200 ml) and 1-butanol (200 ml) were added to the orange solution and the resulting colorless solution was evaporated to approximately 10 ml (vacuum pump, < 20°). This procedure was repeated with two additional 400 ml portions of toluene–1-butanol (1:1) and finally with 200 ml of toluene to give a white solid upon evaporation to dryness. This material was stirred (triturated) with 4 × 200 ml of pentane. The supernatant washes were decanted and the fourth filtered to give 0.85 g (95%) of a chromatographically homogeneous (t.l.c., MeOAc–MeOH, 94:6) white powder of **4***c* hemiformate. A sample for analysis was recrystallized[6] from dry EtOAc (filtered quickly and washed with pentane to prevent oiling)[9] and dried at 40°/0.1 mm for 3 days over KOH pellets and paraffin wax. (See Tables 3 and 4 for data.)

3′-O-(N-Acetyl-L-phenylalanyl)-2′-O-methyladenosine (5b)

A solution prepared by warming 0.1 g (0.0002 mol) of **4***b* and 0.36 g (0.002 mol) of *p*-nitrophenyl acetate in 5 ml of absolute EtOH was stirred at room temperature for 22 h. An additional 0.1 g of *p*-nitrophenyl acetate was added and stirring was continued for 5 h. Thin-layer chromatography (MeOH–MeOAc, 6:94) indicated complete conversion of **4***b* to **5***b* and 25 ml of H_2O was added. The mixture was extracted with 4 × 25 ml of $CHCl_3$ and the combined organic layers were evaporated to dryness. The residue was dissolved in 5 ml of $CHCl_3$ and applied to a column (1.5 × 28 cm, 15 g) of silica gel (packed in $CHCl_3$). The column was washed with $CHCl_3$–Me_2CO (8:2) until all rapidly migrating (t.l.c.) impurities were eluted. Solvent was changed to absolute EtOH and the chromatographically homogeneous fractions were pooled and evaporated. Coevaporation of the white solid residue with Et_2O and drying *in vacuo* gave **5***b* in quantitative yield. This material was recrystallized[6] from $CHCl_3$ – diisopropyl ether to give 0.068 g (72%) of **5***b*; m.p. softens 110° completely melted at 155°; $[\alpha]_D^{24}$ −68.4° (*c* 0.99, DMF) u.v. max 259 nm (ε 17 000); u.v. min 227 n.m. (ε 2800); n.m.r. (DMSO-d_6, TMS internal) δ 1.82 (s, 3, $COCH_3$) 3.02 (m, 2, —CH_2Ph), 3.19 (s, 3, 2′-OCH_3), 3.29 (s, 2, H_2O; verified by D_2O exchange and reintegration), 3.59 (m, 2, $H_{5',5''}$), 3.91 (m, 1, $H_{4'}$), 4.39–4.77 (m, 2, $H_{2'}$ and —*CH*(NHAc)CH_2Ph), 5.40 (d of d, 1, $H_{3'}$), 5.60 (br, 1, 5′-OH), 5.95 (d, $J_{1'-2'}$ = 7 Hz, 1, $H_{1'}$), 7.28 (s, 5, Ph), 7.37 (s, 2, 6-NH_2), 8.17 (s, 1, H_2), 8.41 (s, 1, H_8), 8.35–8.53 (d overlapped with H_8, 1, N*H*Ac).

[9]In certain cases filtration in a dry box under nitrogen was required to prevent oiling.

Anal. Calcd. for $C_{22}H_{26}N_6O_6 \cdot H_2O$: C, 54.09; H, 5.78; N, 17.21. Found: C, 54.15; H, 5.50; N, 17.19.

3′-O-(N-Formyl-L-methionyl-2′-O-methyladenosine (5c)

A solution of 0.30 g (0.00069 mol) of **4c**.hemiformate in 30 ml of MeOH at −10° was treated with 0.06 ml of cold acetic formic anhydride (32) and the solution was allowed to stir at −10°. Complete conversion of **4c** to **5c** was indicated by t.l.c. (MeOH–MeOAc, 6:94) in 5 min and 40 ml of toluene – 1-butanol (1:1) was added. After stirring for 20 min at room temperature, the solution was evaporated to dryness and the residue was coevaporated with absolute EtOH. This product was precipitated from EtOAc into pentane to give 0.28 g (92%) of **5c** which was dried at 40°/0.1 mm for 2 days and then at 56°/0.1 mm for 4 days over KOH pellets and paraffin wax. This sample had $[\alpha]_D^{24}$ −75° (*c* 1.04, DMF) u.v. max 259 nm (ε 13 800); u.v. min 226 n.m. (ε 2600); n.m.r. (DMSO-d_6, TMS internal) δ 1.8–2.18 (m, 2, $CH_2CH_2SCH_3$), 2.07 (s, 3, SCH_3), 2.36–2.7 (m, 2, CH_2SCH_3), 3.22 (s, 3, 2′-OCH_3), 3.66 (m, 2, $H_{5',5''}$). 4.16 (m, 1, $H_{4'}$), 4.28–4.80 (m, 2, $H_{2'}$ and —*CH*(NHCO*H*)), 5.4–5.7 (m, 2, $H_{3'}$ and 5′-OH), 6.02 (d, $J_{1'-2'}$ = 7 Hz, $H_{1'}$), 7.37 (s, 2, 6–NH_2), 8.14 (s, 1, NHCOH), 8.18 (s, 1, H_2), 8.44 (s, 1, H_8), 8.65 (*d*, *J* = 7.8 Hz, 1, —N*H*COH).

Anal. Calcd. for $C_{17}H_{24}N_6O_6S$: C, 46.35; H, 5.49; N, 19.08; S, 7.28. Found: C, 46.15; H, 5.69; N, 18.80.; S, 7.17.

2′-O-(N-Acetyl-L-phenylalanyl)-3′-O-methyladenosine (9b)

This compound was prepared from 0.1 g (0.0002 mol) of **8b** and 0.48 g (0.0027 mol) of *p*-nitrophenyl acetate as described above for the conversion of **4b** → **5b**. The solid resulting from evaporation of the silica gel column eluate was precipitated from EtOAc into pentane to give 0.094 g (81%) of **9b** which was dried at 56°/0.1 mm for 20 h over KOH pellets and paraffin wax; $[\alpha]_D^{23}$ −60.6° (*c* 1.0, DMF); u.v. max 260 nm (ε 15 700); u.v. min 218 nm (ε 3800); n.m.r. (DMSO-d_6, TMS internal) δ 1.77 (s, 3, $COCH_3$), 2.80–3.10 (br t, 2, CH_2Ph), 3.33 (s, 3, 3′-OCH_3), 3.56–3.78 (m, 4, $H_{5',5''}$ and H_2O), 4.2 (m, 3, $H_{4'}$, *CH*(NHAc), 5′-OH), 4.33–4.65 (m, 1, $H_{3'}$), 5.79 (t, $J_{2'-1'} \sim J_{2'-3'} \sim 5.3$ Hz, 1, $H_{2'}$), 6.18 (d, $J_{1'-2'}$ = 5.6 Hz, 1, $H_{1'}$), 7.20 (s, 5, Ph), 7.36 (s, 2, 6-NH_2), 8.18 (s, 1, H_2), 8.38 (m, 2, N*H*Ac, H_8).

Anal. Calcd. for $C_{22}H_{26}N_6O_6 \cdot H_2O$: C, 54.09; H, 5.78; N, 17.21. Found: C, 54.20; H, 5.56; N, 17.08.

2′-O-(N-Formylmethionyl)-3′-O-methyladenosine (9c)

This compound was prepared from 0.3 g (0.0007 mol) of **8c** and 1.5 ml of acetic formic anhydride in methanol at −10° as described above for the conversion of **4c** → **5c**. The product was precipitated from EtOAc into pentane to give 0.25 g (77%) of **9c** which was dried at 56°/0.1 mm for 20 h over KOH pellets and paraffin wax. This sample had $[\alpha]_D^{23}$ −75.1° (*c* 1.0, DMF); u.v. max 260 nm (ε 14 100); u.v. min 225 nm (ε 3100); n.m.r. DMSO-d_6, TMS internal) δ 1.69–2.23 (m, 2, $CH_2CH_2SCH_3$), 2.03 (s, 3, SCH_3), 2.34–2.70 (m, 2, CH_2SCH_3), 3.34 (s, 3, 3′-OCH_3), 3.64 (m, 2, $H_{5',5''}$), 4.0–4.6 (m, 3, $H_{4'}$, $H_{3'}$, and *CH*(NHCOH)), 5.44 (br, 1, 5′-OH), 5.80 (m, 1, $H_{2'}$), 6.13 (d, $J_{1'-2'}$ = 5.0 Hz, 1, $H_{1'}$), 7.3 (s, 2, 6-NH_2), 8.02 (s, 1, NHCO*H*), 8.13 (s, 1, H_2), 8.35 (s, 1, H_8), 8.58 (d, 1, CH(N*H*COH).

Anal. Calcd. for $C_{17}H_{24}N_6O_6S$: C, 46.35; H, 5.49; N, 19.08; S, 7.28. Found: C, 46.14; H, 5.77; N, 18.86; S, 7.37.

We thank Dr. Frank A. Norris for useful preliminary experiments and Mr. Alan S. K. Lee for the preparation of some starting materials. We thank Drs. C. Coutsogeorgopoulos and A. Bloch for communication of preliminary biochemical results.

1. C. Coutsogeorgopoulos. Biochemistry, **6**, 1704 (1967).
2. R. J. Suhadolnik. Nucleoside antibiotics. Wiley-Interscience, New York, N.Y. 1970. Chapt. 1.1.
3. M. J. Robins, R. A. Jones, and M. MacCoss. Biochemistry, **13**, 553 (1974).
4. H. Neumann, V. E. Shashoua, J. C. Sheehan, and A. Rich. Proc. Natl. Acad. Sci. U.S. **61**, 1207 (1968).
5. J. Žemlička, S. Chládek, Z. Haladová, and I. Rychlík. Collect. Czech. Chem. Commun. **34**, 3755 (1969).
6. I. Rychlík, J. Černá, S. Chládek, J. Žemlička, and Z. Haladová. J. Mol. Biol. **43**, 13 (1969).
7. M. Sprinzl and F. Cramer. Nature, New Biol. **245**, 3 (1973).
8. S. Chládek, D. Ringer, and J. Žemlička. Biochemistry, **12**, 5135 (1973).
9. J. Černá, S. Chládek, I. Rychlík, and J. Žemlička. Biochim. Biophys. Acta, **199**, 291 (1970).
10. F. Rottman and K. Heinlein. Biochemistry, **7**, 2634 (1968).
11. F. Rottman and K. L. Johnson. Biochemistry, **8**, 4354 (1969).
12. A. M. Bobst, F. Rottman, and P. A. Cerutti. J. Mol. Biol. **46**, 221 (1969).
13. A. R. Price and F. Rottman, Biochemistry, **9**, 4524 (1970).
14. B. Żmudzka, M. Tichy, and D. Shugar. Acta Biochim. Pol. **19**, 149 (1972).
15. I. Tazawa, S. Tazawa, J. L. Alderfer, and P. O. P. Ts'o. Biochemistry, **11**, 4931 (1972).
16. R. H. Hall. The modified nucleosides in nucleic acids. Columbia University Press, New York, N.Y. 1971.
17. M. J. Robins and S. R. Naik. Biochim. Biophys. Acta, **246**, 341 (1971).
18. M. J. Robins, S. R. Naik, and A. S. K. Lee. J. Org. Chem. **39**, 1891 (1974).
19. V. A. Pozdnyakov, Yu. V. Mitin, M. K. Kukhanova, L. V. Nikolaeva, A. A. Krayevsky, and B. P. Gottikh. Fed. Eur. Biochem. Soc. Lett. **24**, 177 (1972).
20. D. H. Rammler and H. G. Khorana. J. Am. Chem. Soc. **85**, 1997 (1963).
21. W. Steglich and G. Höfle. Angew. Chem. Int. Ed. Engl. **8**, 981 (1969).
22. S. Chládek, P. Pulkrábek, J. Sonnenbichler, J. Žemlička, and I. Rychlík. Coll. Czech. Chem. Commun. **35**, 2296 (1970).
23. B. F. C. Clark and K. A. Marcker. J. Mol. Biol. **17**, 394 (1966).

Can. J. Chem. Downloaded from www.nrcresearchpress.com by 210.87.254.6 on 09/05/12
For personal use only.

24. J. LUCAS-LENARD and F. LIPMANN. Ann. Rev. Biochem. **40**, 409 (1971).
25. J. LUCAS-LENARD and F. LIPMANN. Proc. Natl. Acad. Sci. U.S. **57**, 1050 (1967).
26. M. BODÁNSZKY. Nature, **175**, 685 (1955).
27. C. S. MCLAUGHLIN and V. M. INGRAM. Biochemistry, **4**, 1442; 1448 (1965).
28. J.-P. WALLER, T. ERDÖS, F. LEMOINE, S. GUTTMANN, and E. SANDRIN. Biochim. Biophys. Acta, **119**, 566 (1966).
29. H. G. ZACHAU and H. FELDMANN. Prog. Nucleic Acid Res. Mol. Biol. **4**, 217 (1965).
30. T. C. BRUICE and T. H. FIFE. J. Am. Chem. Soc. **84**, 1973 (1962).
31. B. RINIKER and R. SCHWYZER. Helv. Chim. Acta, **44**, 658 (1961).
32. L. I. KRIMEN. Org. Synth. **50**, 1 (1970).
33. M. J. ROBINS and E. M. TRIP. Tetrahedron Lett. In press.
34. S. CHLÁDEK, D. RINGER, and K. QUIGGLE. Biochemistry, **13**, 2727 (1974).
35. G. CHINALI, M. SPRINZL, A. PARMEGGIANI, and F. CRAMER. Biochemistry, **13**, 3001 (1974).

Can. J. Chem. Downloaded from www.nrcresearchpress.com by 210.87.254.6 on 09/05/12
For personal use only.

A Study of the Donor Properties of the Phenoxachalcogenines. I. Tetracyanoethylene and Chloranil as Acceptors

CHARLES A. HELLER, RALPH A. ZINGARO, AND EDWARD A. MEYERS
Department of Chemistry, Texas A&M University, College Station, Texas 77843

Received April 17, 1974

CHARLES A. HELLER, RALPH A. ZINGARO, and EDWARD A. MEYERS. Can. J. Chem. **52**, 3814 (1974).

The phenoxachalcogenines have been studied as donors toward tetracyanoethylene (TCNE) as the acceptor. It was found that the thermodynamic values for the interactions show no significant trends when the chalcogenine atom is varied from Te to Se to S to O. For the four 1:1 complexes studied, the following average values for the thermodynamic properties were obtained at 20 °C (the total range for each quantity is given in parentheses): K = 1.4 (1.0) l mol^{-1}, ΔG = 0.2 (0.4) kcal mol^{-1}, ΔH = −2.0 (0.2) kcal mol^{-1}, ΔS = −7.0 (0.5) cal deg^{-1} mol^{-1}. The lack of any significant changes in the thermodynamic values is explained on the basis that all of the complexes involve similar interactions, probably of the π–π molecular complex type. The results were essentially the same for the interaction between phenoxatellurine (PTe) and chloranil (TCQ).

CHARLES A. HELLER, RALPH A. ZINGARO et EDWARD A. MEYERS. Can. J. Chem. **52**, 3814 (1974).

On a étudié les propriétés des phénoxachalcogénines comme donneur vis à vis le tétracyanoéthylène (TCNE) comme accepteur. On a trouvé que les valeurs thermodynamiques pour les interactions ne montrent aucune tendance particulière quand l'atome de la chalcogénine passe du Te au Se au S et à O. Pour les quatres complexe un à un qui ont été examinés, les valeurs moyennes suivantes ont été obtenues pour les propriétés thermodynamiques à 20° (les variations totales pour chaque quantité sont données entre parenthèse): K = 1.4 (1.0) l mol^{-1}, ΔG = 0.2 (0.4) kcal mol^{-1}, ΔH = 2.0 (0.2) kcal mol^{-1}, ΔS = −7.0 (0.5) cal deg^{-1} mol^{-1}.Le manque de changement significatif dans les valeurs thermodynamiques est expliqué sur la base que tous les complexes impliquent des interactions similaires probablement du type de complexe moléculaire π–π. Les résultats sont essentiellement les mêmes que ceux obtenus pour les interactions entre le phénoxatellurine (PTe) et le chloranil (TCQ). [Traduit par le journal]

Introduction

When phenoxatellurine (**1**) is oxidized with concentrated nitric acid, white phenoxatellurine 10,10-dinitrate (**2**) is formed according to the following reaction:

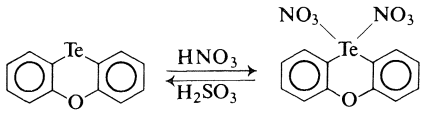

1 **2**

Phenoxatellurine 10,10-dinitrate (**2**), when heated with sulfurous acid, is reduced to phenoxatellurine. During the oxidation and reduction reactions, a violet intermediate is formed (2). The formation of a violet-colored solid is also observed when crystals of **1** and **2** are mixed in the solid state (1,2). In our investigations of this interesting interaction (1) we have encountered a number of difficulties in studying this reaction on a quantitative basis in solution. For example, in acetone, an irreversible reaction takes place which results in the formation of 10-acetonylphenoxatellurine nitrate (3). In methylene chloride, at room temperature, (**1**) and (**2**) react irreversibly to precipitate bis(phenoxatelluronium)dinitrate (4). Because of these difficulties, in order to acquire some basic information on the nature of the charge–transfer interactions of molecules of this type, the study which is the subject of the present report was carried out.

The phenoxachalcogenines (**3**) and related compounds such as thianthrene (**4**) have been used as donors in studies involving several

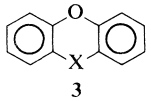

3

X = O	Diphenylene dioxide	DPDO
X = S	Phenoxathiin	PS
X = Se	Phenoxaselenine	PSe
X = Te	Phenoxatellurine	PTe

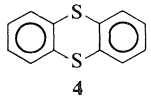

4

Thianthrene PSS

Can. J. Chem. Downloaded from www.nrcresearchpress.com by 210.87.254.105 on 09/05/12
For personal use only.

Can. J. Chem. Downloaded from www.nrcresearchpress.com by 210.87.254.105 on 09/05/12
For personal use only.

charge–transfer systems. Kuboyama (5) investigated PSS, PS, and DPDO as donors toward iodine and chloranil (tetrachloroquinone, TCQ). He found that 1:1 complexes were formed in all cases and obtained the values given in Table 1 for the equilibrium constants of the iodine system using the method of Ketelaar *et al.* (6). Hillebrand and her co-workers (7) have studied PS and some of its derivatives as donors toward tetrachlorophthalic anhydride (TPA) and the somewhat stronger acceptors, tetracyanoethylene (TCNE) and 2,3-dichloro-5,5-dicyanobenzoquinone (DDQ) (8). However, they did not report equilibrium constants, extinction coefficients, or thermodynamic values.

Hetnarski and Hofman (9) studied PTe as a donor toward 1,3,5-trinitrobenzene (TNB), picric acid, and picryl chloride. In all cases 1:1 complexes were reported to form in solution. The equilibrium constants and extinction coefficients were calculated using the method of Benesi–Hildebrand (10). Table 1 lists the important results of the study. The solid compound formed between PTe and TNB was also found to have a 1:1 stoichiometry.

Hetnarski and Grabowska (11) studied the phenoxachalcogenines, DPDO, PS, PSe, and PTe as donors toward TNB in 1,2-dichloroethane. They report that in all cases 1:1 charge–transfer complexes are formed. DPDO gave a solid 2:1 complex in which two TNB molecules were coordinated to one of DPDO. The pertinent results of the study using the method of Benesi–Hildebrand (10) for calculating the equilibrium constants and extinction coefficients are also given in Table 1.

Results and Discussion

Typical spectra for the phenoxachalcogenine–TCNE and PTe–TCQ systems are shown in Fig. 1. Job's plots were prepared for each system (1). Maxima appeared at mol fractions of 0.5 and these correspond to the formation of 1:1 complexes. In all cases, the maxima are fairly broad, which is characteristic of weak complexing systems. In addition, the Job's plots were symmetrical on either side of the maxima. This suggests an absence of termolecular complexes (12). While this does not rule out the possibility of the formation of higher complexes in these systems, it does mean, that over the range of experimental concentrations used in the present study, the 1:1 complex clearly predominates.

Values for the equilibrium constant, K, and extinction coefficient, ε_c, were calculated using the method of Rose and Drago (13). Examination of the results presented in Table 2 for the equilibrium constants and extinction coefficients for the phenoxachalcogenine charge-transfer complexes, shows that all of the equilibrium constants are less than 10, and that all the extinction coefficients are relatively small, of the order of a few hundred to about a thousand. The small values for the equilibrium constants indicate that the complexes formed are relatively weak, probably being of the π–π charge–transfer type (14). There may well be a much stronger charge-transfer band located at shorter wavelengths but the uncomplexed components absorb very strongly in this region, so that observation of such a band is precluded.

When attempts are made to calculate values for equilibrium constants and the extinction coefficients for weak complexes, a number of difficulties are encountered (15–20). Person (15) discusses some of these problems and points out that there are three regions to consider when one plots the absorbance of the system *vs.* the concentration of one of the components while maintaining a constant concentration of the other component. When the donor concentration is small compared to that of the acceptor, the increase in absorbance with increasing donor concentration is linear. While the product of the extinction coefficient and the equilibrium constant may be obtained, the individual values cannot be determined with certainty. When the concentration of the donor is large with respect to that of the acceptor, the absorbance remains essentially unchanged as the concentration of the donor is increased, indicating that complete

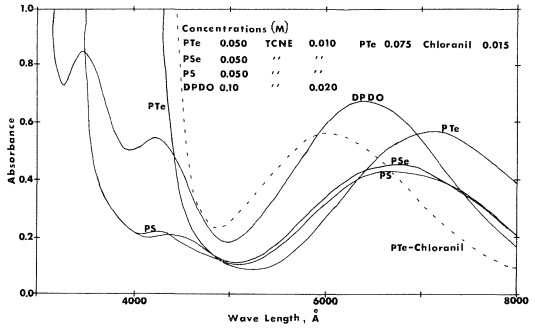

FIG. 1. Absorption spectra for mixtures of the various phenoxachalcogenines with TCNE and chloranil in dichloromethane at 20°.

Can. J. Chem. Downloaded from www.nrcresearchpress.com by 210.87.254.105 on 09/05/12
For personal use only.

TABLE 1. Literature values of equilibrium constants, extinction coefficients, and thermodynamic constants for phenoxachalcogenine complexes

Donor	Acceptor	Solvent	λ_{max} (Å)	Extinction coefficient (average) value)	$K_c(20°)$	$-\Delta H$ (kcal mol^{-1})	$-\Delta S$ (e.u.)	Reference No.
Thianthrene	Iodine	CCl_4	3710	13 350	1.34	3.82	12.4	3
	Chloranil	CCl_4	5150–5200 4180–4200					
	Iodine	CH_2Cl_2	3750	12 300	1.09	3.71	12.5	3
	Chloranil	CH_2Cl_2	5250					
Phenoxathiin	Iodine	CCl_4	3960	14 200	0.95	4.12	14.3	3
	Chloranil	CCl_4	5800,4000					
	Iodine	CH_2Cl_2	4000	14 800	0.74	4.12	14.6	3
	Chloranil	CH_2Cl_2	5870					
Diphenylene dioxide	Iodine	CCl_4	3995	(3280?)	0.27			
	Chloranil	CCl_4	5580					
	Iodine	CH_2Cl_2	3940					
	Chloranil	CH_2Cl_2	5600					
Phenoxatellurine	1,3,5-Trinitro-benzene	CH_2ClCH_2Cl	4400	1020	13.2±2.0*	1.0±0.8 $\Delta G = -1.52\pm0.09$		7, 9
	Picric acid	CH_2ClCH_2Cl	4200	900	8.4±1.8*			7
	Picryl chloride	CH_2ClCH_2Cl	4200	820	8.0±2.1*			7
Phenoxaselenine	1,3,5-Trinitro-benzene	CH_2ClCH_2Cl	4150–4200	725	11.2±1.7*			9
Phenoxathiin	Benzene	CH_2ClCH_2Cl	4200	650	12.8±1.5*	3.2±1.3		9
Diphenylene dioxide	Benzene	CH_2ClCH_2Cl	4100–4150	125	12.2±0.3*	3.2±0.4		9

*(mol fraction)$^{-1}$ at 23°.

Can. J. Chem. Downloaded from www.nrcresearchpress.com by 210.87.254.105 on 09/05/12
For personal use only.

complexation has occurred. The extinction coefficient may be obtained under these conditions using the method of Yoe and Jones (21). To obtain meaningful results for both K and ε_c from spectrophotometric methods, the concentrations of the donor must be such that the absorbance is no longer linear with respect to concentration of the donor.

Plots of the donor concentrations *vs.* absorbance are observed to deviate slightly from a linear relationship. A sample plot for the PTe–TCNE system is presented in Fig. 2. It is in this region of deviation from linearity that the methods of Rose and Drago (13), Benesi and Hildebrand (10), Scott (22), and Ketelaar *et al.* (23) are used, and selection of K and ε is difficult, because the deviation from linearity is small.

Other investigators, such as Asmus (24), Momoki *et al.* (25), and Likussar and Boltz (26) have reinvestigated the equations based upon the application of spectral data to various equilibrium problems. They have recast the equations into linear forms suitable for graphical portrayal and for detailed analysis. These methods are most useful when the deviations from linearity are pronounced and/or when the equilibrium constants are large. Since neither condition is met in our experiment, other methods of data treatment were tested.

Consider the equilibrium expression

$$[1] \qquad K = \frac{C}{(C_0 - C)(C_v - C)}$$

where C_0 is the initial acceptor concentration which is kept constant throughout the experiment and C_v is the initial donor concentration which is changed from run to run. C is the concentration of the complex. If the expression is expanded and solved for C, [2] is obtained.

$$[2] \quad C = \{(C_0 + C_v + 1/K) - [(C_v + C_0 + 1/K)^2 - 4C_0C_v]^{1/2}\}/2$$

When a series of plots of C_v *vs.* C for different values of C_0, C_v, and K are constructed, plots such as Fig. 3 are obtained. The limiting slope of the curve for $C = 0$, $C_v = 0$ is given by

$$[3] \qquad \left(\frac{dC}{dC_v}\right)_0 = \frac{KC_0}{KC_0 + 1}$$

The limiting slope for various values of K is shown in Fig. 3.

If lines are drawn tangent to the plots of absorbance of the complex *vs.* concentration of PTe at the origin such as in Fig. 2, an estimate of the value $K\varepsilon_c$ for the various complexes can be obtained from the slope, $(dA/dC_v)_0$. The slope is related to K and ε_c by expression [4], which is obtained directly from [3].

$$[4] \qquad M = \left(\frac{dA}{dC_v}\right)_0 = \frac{\varepsilon_c(KC_0)}{KC_0 + 1}$$

There are two important limiting values for [4]. When $KC_0 \gg 1$, $M \cong \varepsilon_c$. This situation is encountered in all of the systems utilized in the study of Momoki *et al.* (25). Under this condition it is possible to estimate the maximum absorption to be expected from the complex, provided that its formula is known. Otherwise, a trial and error analysis of the data, with various

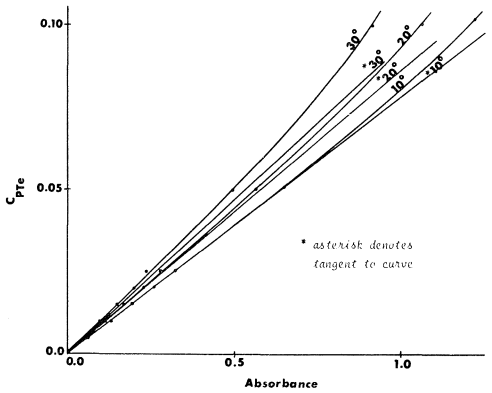

FIG. 2. Plot of the concentration of phenoxatellurine *vs.* the absorbance of the complex for 0.01 M TCNE.

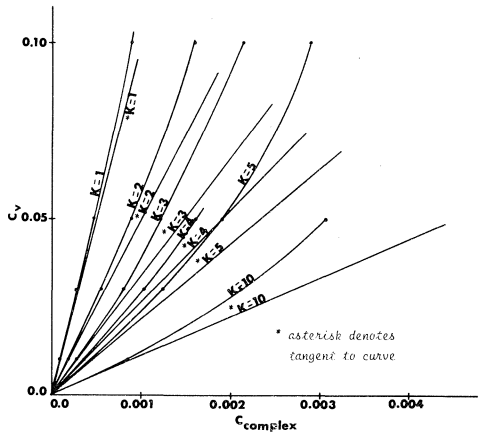

FIG. 3. Plot of the calculated concentration of the complex for various values of K *vs.* the variable concentration of the donor at 0.01 M acceptor concentration.

TABLE 2. Calculated values for the equilibrium constant and extinction coefficient by the method of Rose and Drago

Donor	Acceptor	λ_{max} (Å)	Temperature (°C)	ε_c	Average ε_c	K^{-1}	K (l mol^{-1})	$K\varepsilon_c$
PTe	Chloranil	5900–6100	10.0	200		0.24	4.2	820
			20.0	170	180	0.25	4.0	700
			30.0	160		0.27	3.7	600
PTe	TCNE	7100–7200	10.0	1400		0.81	1.24	1700
			20.0	1000	1000	0.90	1.10	1140
			30.0	750		1.03	0.97	730
PSe	TCNE	6600–6800	10.0	*				
			20.0	300	330	0.44	2.27	680
			30.0	350		0.52	1.9	670
PS	TCNE	6700–6800	10.0	380		0.29	3.5	1330
			20.0	340	320	0.32	3.1	1060
			30.0	250		0.37	2.7	680
DPDO	TCNE	6400–6500	10.0	80		0.19	5.3	420
			20.0	100	90	0.22	4.5	450
			30.0	90		0.24	4.2	380

*Not enough crossovers for determination of a value.

assumed values of the maximum absorption must be made in order to apply their methods. In the second case, $KC_0 \ll 1$ and $M \cong \varepsilon_c KC_0$. These conditions are the ones that are encountered for the complexes which are the subject of this study.

Table 3 lists the slopes obtained from Fig. 2 and the other plots of the concentrations of phenoxachalcogenine *vs.* the absorbance of the various complexes and the corresponding values of K, ε_c, and $K\varepsilon_c$ calculated from the slopes. Table 4 lists the various values of K, ε_c, and $K\varepsilon_c$ obtained by fitting point by point the calculated curves in Fig. 4 to the experimental values plotted in Fig. 2 and related plots. When the derivative of ln M is taken with respect to $(1/T)$, eq. 5 results after the combining of terms and simplification.

$$[5] \qquad \frac{\mathrm{d} \ln M}{\mathrm{d}(1/T)} = \frac{1}{(KC_0 + 1)} \frac{\mathrm{d} \ln K}{\mathrm{d}(1/T)}$$

The enthalpy for a reaction, ΔH, can be obtained from K by

$$[6] \qquad \frac{\mathrm{d} \ln K}{\mathrm{d}(1/T)} = \frac{-\Delta H}{R}$$

Combining [5] and [6] yields

$$[7] \qquad \frac{-\Delta H}{R} = \frac{\mathrm{d} \ln M}{\mathrm{d}(1/T)} (KC_0 + 1)$$

M is defined as the slope $(\mathrm{d}A/\mathrm{d}C_v)_0$ so that ΔH can be calculated from the slopes of the various plots such as those in Fig. 2. Figure 4 shows the plots of log $(\mathrm{d}A/\mathrm{d}C_v)_0$ *vs.* $1/T$ for the complexes. Table 5 lists the values of ΔH calculated using this method. It is the opinion of the authors, that this approach for the calculation of values for ΔH is better than that which utilizes the changes in the calculated values of K. This is perhaps because the values are obtained more directly from experimentally observed values of the optical absorption.

The major source of uncertainty in this treat-

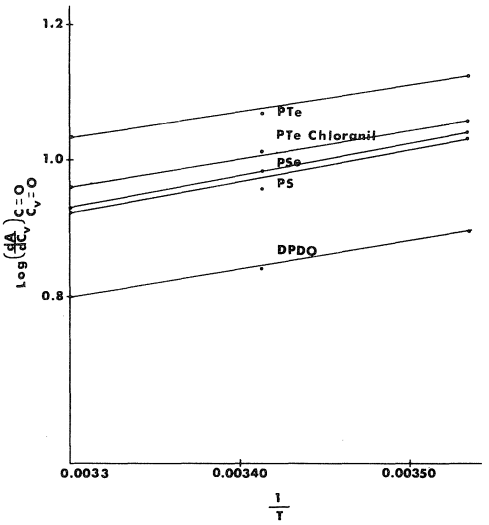

FIG. 4. Plots of log $(\mathrm{d}A/\mathrm{d}C_v)_0$ *vs.* $1/T$ for complexes studied in this work.

Can. J. Chem. Downloaded from www.nrcresearchpress.com by 210.87.254.105 on 09/05/12
For personal use only.

TABLE 3. Calculated values of slopes, K, ε_c, and $K\varepsilon_c$ for the phenoxachalcogenine complexes obtained from Fig. 5 and similar plots

Donor	Acceptor	Temperature (°C)	Slope	K	ε_c	$K\varepsilon_c$
PTe	Chloranil	10	11.39	1	1125	1125
				2	581	1162
				3	391	1173
PTe	Chloranil	20	10.31	1	1041	1041
				2	526	1052
				3	354	1062
PTe	Chloranil	30	9.09	1	918	918
				2	364	928
				3	312	936
PTe	TCNE	10	13.2	1	1330	1330
				2	674	1348
				3	453	1360
PTe	TCNE	20	11.63	1	1175	1175
				2	593	1186
				3	400	1200
PTe	TCNE	30	10.72	1	1082	1082
				2	548	1095
				3	368	1104
PSe	TCNE	10	10.87	1	1098	1098
				2	554	1108
				3	373	1120
PSe	TCNE	20	9.62	1	972	972
				2	491	981
				3	330	991
PSe	TCNE	30	8.43	1	851	851
				2	430	860
				3	289	867
PS	TCNE	10	10.75	1	1086	1086
				2	548	1097
				3	369	1107
PS	TCNE	20	9.12	1	921	921
				2	465	930
				3	313	939
PS	TCNE	30	8.40	1	848	848
				2	428	857
				3	288	865
DPDO	TCNE	10	7.81	1	789	789
				2	398	796
				3	279	805
DPDO	TCNE	20	6.89	1	696	696
				2	352	704
				3	237	710
DPDO	TCNE	30	6.28	1	635	635
				2	310	641
				3	216	647

ment is the measurement of the slopes of $(dA/dC_v)_0$ from the plots of A *vs.* C_v in Fig. 2 and related plots. Another possible source of error is in the value of K used in eq. 7 but since the values of K involved are all quite small (1–3) and the value of C_0 is on the order of 1 to 2×10^{-2} M, the maximum uncertainty from this source is of the order of a few percent. The

Can. J. Chem. Downloaded from www.nrcresearchpress.com by 210.87.254.105 on 09/05/12
For personal use only.

TABLE 4. Comparison of experimental curves in Fig. 5 with the calculated curves in Fig. 4 to obtain values of K, ε_c, and $K\varepsilon_c$ at 20°

Donor	Acceptor	C_0	K	C_v	$C \times 10^4$	A	ε_c*	$C\varepsilon_c$	$K\varepsilon_c$
PTe	Chloranil	0.015	1	0.015	2.184	0.148		0.129	592
				0.03	4.306	0.255	592.2		
				0.075	10.31	0.563		0.611	
				0.15	19.28	1.024		1.14	
PTe	Chloranil	0.015	2	0.015	4.24	0.148		0.129	608
				0.03	8.39	0.255	304		
				0.075	19.01	0.563		0.578	
				0.150	33.58	1.024		1.02	
PTe	Chloranil	0.015	3	0.015	6.36	0.148		0.137	
				0.03	11.87	0.255	214.8		644†
				0.075	26.44	0.563		0.551	
				0.15	45.02	1.024		0.899	
PTe	Chloranil	0.015	4	0.015	8.01	0.148		0.135	
				0.03	15.18	0.255			
				0.075	32.81	0.563		0.551	
				0.15	53.54	1.024		0.899	
PTe	TCNE	0.01	1	0.01	0.979	0.115		0.1157	1182†
				0.03	2.877	0.340	1181.8		
				0.05	4.696	0.565		0.555	
				0.1	8.90	1.062		1.052	
PTe	TCNE	0.01	2	0.01	1.923	0.115		0.118	1223
				0.03	5.55	0.340	612.6		
				0.05	8.915	0.565		0.546	
				0.1	15.90	1.062		0.974	
PTe	TCNE	0.01	3	0.01	2.831	0.115		0.120	1271
				0.03	8.023	0.340	423.8		
				0.05	12.037	0.565		0.546	
				0.1	21.40	1.062		0.974	
PSe	TCNE	0.01	1	0.01	0.979	0.09		0.092	939†
				0.03	2.877	0.27	938.5		
				0.05	4.696	0.45		0.441	
PSe	TCNE	0.01	2	0.01	1.923	0.09		0.094	973
				0.03	5.550	0.27	486.5		
				0.05	8.915	0.45		0.434	
PSe	TCNE	0.01	3	0.01	2.831	0.09		0.095	1010
				0.03	8.023	0.27	336.5		
				0.05	12.037	0.45		0.405	
PS	TCNE	0.01	1	0.01	0.979	0.093		0.092	939†
				0.03	2.877	0.270	938.5		
				0.05	4.696	0.455		0.441	
				0.1	8.90	0.890		0.835	
PS	TCNE	0.01	2	0.01	1.923	0.093		0.094	973
				0.03	5.55	0.270	486.5		
				0.05	8.915	0.455		0.434	
				0.1	15.9	0.89		0.744	
PS	TCNE	0.01	3	0.01	2.831	0.093		0.095	1010
				0.03	8.023	0.270	336.5		
				0.05	12.037	0.455		0.405	
				0.1	21.40	0.89		0.720	
DPDO	TCNE	0.02	1	0.02	3.845	0.133		0.1336	347†
				0.04	7.542	0.262	347.4		
				0.1	17.83	0.673		0.6194	
				0.2	32.70	1.31		1.136	

Can. J. Chem. Downloaded from www.nrcresearchpress.com by 210.87.254.105 on 09/05/12
For personal use only.

TABLE 4. (*Concluded*)

Donor	Acceptor	C_0	K	C_v	$C \times 10^4$	A	ε_c*	$C\varepsilon_c$	$K\varepsilon_c$
DPDO	TCNE	0.02	2	0.02	7.398	0.133		0.136	368
				0.04	14.25	0.262	183.9		
				0.1	32.09	0.673		0.590	
				0.2	55.12	1.31		1.014	
DPDO	TCNE	0.02	3	0.02	10.69	0.133		0.138	388
				0.04	20.25	0.262	129.4		
				0.1	43.71	0.673		0.566	
				0.2	71.39	1.31		0.924	

*$\varepsilon_c = A/C$, for the value of C indicated.
†Best value.

assumptions inherent in this procedure are that the extinction coefficient of the complex is temperature independent and that the absorption is proportional to the concentration of the complex.

Another approach for evaluating ΔH for the reactions being studied can be made from the change in absorbance with temperature. Consider the case which corresponds to the maximum absorption in the Job's plots for the various complexes. At the maximum, for 1:1 complexes, the concentrations of the donor and acceptor are equal and eq. 1 becomes

$$[8] \qquad K = \frac{C}{(C_0 - C)^2}$$

Expressing [8] in logarithmic form and differentiating with respect to $(1/T)$, [9] is obtained after simplification and rearrangement.

$$[9] \qquad \frac{\mathrm{d} \ln K}{\mathrm{d}(1/T)} = \frac{\mathrm{d}C}{\mathrm{d}(1/T)}[(1/C + 2/(C_0 - C)]$$

If the assumption is now made that C is always much smaller than C_0 (and this is the case because of the small values of K obtained) then the term $1/C$ in [9] is considerably larger than the second term and the approximation in [10] can be made.

TABLE 5. Values of enthalpy of reaction obtained from the slopes of $(\mathrm{d}A/\mathrm{d}C_v)$; $C = 0$, $C_v = 0$

Donor	Acceptor	ΔH(kcal mol^{-1})
PTe	Chloranil	-2.0 ± 0.3
PTe	TCNE	-1.8 ± 0.3
PSe	TCNE	-2.2 ± 0.3
PS	TCNE	-2.1 ± 0.3
DPDO	TCNE	-1.9 ± 0.2

$$[10] \qquad \frac{\mathrm{d} \ln K}{\mathrm{d}(1/T)} = \frac{\mathrm{d}C}{\mathrm{d}(1/T)}(1/C)$$

When Beer's law (pathlength taken as unity) is expressed in logarithmic form and differentiated with respect to $1/T$, [11] is obtained.

$$[11] \qquad \frac{\mathrm{d} \ln A}{\mathrm{d}(1/T)} = \frac{\mathrm{d} \ln \varepsilon_c}{\mathrm{d}(1/T)} + \frac{\mathrm{d} \ln C}{\mathrm{d}(1/T)}$$

The extinction coefficient is assumed to be temperature independent so [11] reduces to

$$[12] \qquad \frac{\mathrm{d} \ln A}{\mathrm{d}(1/T)} = \frac{\mathrm{d} \ln C}{\mathrm{d}(1/T)}$$

By combining eqs. 10, 12, and 6, eq. 13 is obtained.

$$[13] \qquad \frac{\mathrm{d} \ln A}{\mathrm{d}(1/T)} = \frac{-\Delta H}{R}$$

If the log of A *vs.* $1/T$ is plotted, ΔH can be obtained from the slope and eq. 13. The only approximations made were that ε_c is temperature independent and that the second term in [9] can be neglected.

Considering the values of K, ε_c, $K\varepsilon_c$, and ΔH calculated by the various methods, Table 6 represents the best values obtained. Included in Table 6 are also the values of the peak-width at half of maximum intensity, $\Delta\nu_{1/2}$, the frequency of the band maximum, ν_{max}, the oscillator strength, f, obtained from ref. 27

$$[14] \qquad f = 1.35 \times 10^{-8}\, \varepsilon_{max}\, (\nu_{max} - \Delta\nu_{1/2})$$

and the transition dipole moment, D, obtained from ref. 28

$$[15] \qquad D = 0.0958\, (\varepsilon_{max}\, \Delta\nu_{1/2}/\nu_{max})$$

where ν_{max} corresponds to the value calculated for ε_c.

Can. J. Chem. Downloaded from www.nrcresearchpress.com by 210.87.254.105 on 09/05/12
For personal use only.

TABLE 6. Calculated values for the phenoxachalcogenine complexes formed with tetracyanoethylene at 20°

Donor	Acceptor	K (l mol^{-1})	ε_c	$K\varepsilon_c$	ΔH (kcal mol^{-1})	λ_{max} (Å)	$\nu_{max} \times 10^{-3}$ cm^{-1}
PTe	Chloranil	3.0±1.0	200± 50	650±100	−1.2 ±1.0	5900–6100	16.65
PTe	TCNE	1.0±0.3	1100±100	1100±100	−2.0 ±0.4	7000–7200	14.08
PSe	TCNE	1.5±0.5	485±100	970±100	−2.1 ±0.2	6600–6800	14.93
PS	TCNE	2.0±0.5	400±100	900±100	−2.1 ±0.3	6700–6800	14.81
DPDO	TCNE	1.0±0.5	200±100	300±100	−1.95±0.2	6400–6500	15.50

Donor	Acceptor	$\Delta\nu_{1/2} \times 10^{-3}$cm^{-1}	f	D (Debye)	ΔG_{293} (kcal mol^{-1})	ΔS (e.u.)	I_d (eV)
PTe	Chloranil	4.66	0.032	5.36	−0.06±0.02	−4.0±3.0	
PTe	TCNE	3.84	0.152	28.74	0.0 ±0.02	−6.8±1.3	7.59
PSe	TCNE	4.89	0.066	15.22	−0.02±0.02	−7.2±0.7	7.71
PS	TCNE	5.12	0.053	13.25	−0.04±0.02	−7.2±1.0	7.69
DPDO	TCNE	4.60	0.029	5.69	0.0 ±0.02	−6.7±0.7	7.79

The ionization potentials of the phenoxachalcogenines were calculated using the empirical equation from ref. 29

[16] $$h\nu = 0.87\, I_d - 4.86$$

An examination of the data presented in Table 6 for the values of K, ε_c, ΔH, and related quantities, leads to the conclusion that the interactions between the phenoxachalcogenines and TCNE are essentially of the same type. In spite of the variations in the electronegativities of the chalcogen atoms in the series O > S > Se > Te, there is very little variation in the extinction coefficients, the wavelengths of maximum absorption, or the thermodynamic values, from compound to compound. This suggests that the interaction for the series is basically of the same type, and almost certainly involves a delocalized π orbital on the donor molecule rather than a localized n orbital of the chalcogen.

This conclusion is different than that reached by Hetnarski and Grabowska (11). They used TNB as an acceptor with the phenoxachalcogenines in 1,2-dichloroethane as a solvent. They suggest that the interaction between this acceptor and the phenoxachalcogenines is of a localized n to π type in the case of PTe, PSe, and PS, and of the π to π type in the case of DPDO. In view of the obvious lack of any meaningful differences in the thermodynamic values and equilibrium constants obtained by Hetnarski and Grabowska (11), listed in Table 1, and the similar results obtained in the present study for K and ΔH, their conclusion is questionable.

These investigators observed that diethyl sulfide and diphenyl ether form charge–transfer complexes with TNB and that these complexes have absorption maxima very close to those formed with PS and DPDO, respectively. Mixtures of diethyl, di-*n*-propyl, or di-*n*-butyl ether with TNB were found not to absorb in the visible region.

They proposed that, since diethyl sulfide and PS absorb at essentially the same wavelength, both must act as n-type donors. Similarly, since DPDO and diphenyl ether also absorb at nearly the same wavelength, they must have essentially the same type of interaction with TNB. Since it is difficult to propose that oxygen acts as a n-type donor toward a relatively weak acceptor such as TNB, they assumed that a π-type interaction involving the aromatic ring was operative in the case of DPDO. In rebuttal, it may be noted that PS and DPDO absorb at nearly the same frequencies, so that this criterion does not appear to serve as a basis for differentiating between the n- and π-type alternatives for PS and DPDO.

These investigators also reported the existence of a linear relationship between the location of the respective absorption maxima and the electronegativities of the S, Se, and Te atoms. The electronegativity values used in making their correlations were those of Allred and Rochow (30). If one examines critically the relationship of the λ_{max} to electronegativity, it is difficult to see any greater correlation other than the trend in λ_{max} of Te > Se = S = O while the electronegativity changes O > S = Se > Te. The change of λ_{max} with electronegativity is a little more apparent in the case of our study, being of the order Te > Se = S > O, but again, considering the number of factors that can affect ΔH, ε_c,

Can. J. Chem. Downloaded from www.nrcresearchpress.com by 210.87.254.105 on 09/05/12
For personal use only.

Can. J. Chem. Downloaded from www.nrcresearchpress.com by 210.87.254.105 on 09/05/12
For personal use only.

and K, the interactions for the entire series do not seem to change sufficiently to require the hypothesis of basically different types of charge–transfer interactions.

An example of the magnitude in this change that has been observed in other work on n-type complexes may help to clarify the discussion. Zingaro and co-workers in a series of studies (31–33) have examined the interaction of molecules of the type R_3PX (X = O, S, Se) with iodine in chloroform. They have shown that the donor properties of R_3PX are of a localized n-type.

Thus, for R = cyclohexyl and X = O, S, and Se, the respective values are for λ_{max}: 370, 421 and 319 nm, for K: 39, 1820, and 46 600; for R = 1-naphthyl and X = S and Se, the respective values are for λ_{max}: 430 and 325 nm, for K: 96 and 9090, for ΔH: −4.66 and −10.45 kcal mol^{-1}, for ΔG: −2.70 and −5.40 kcal mol^{-1} and for ΔS: −6.58 and −16.94 e.u.; for R = phenyl, or mixed aryl groups, the trends in these values follow a very similar pattern. This is in marked contrast with the results obtained with the phenoxachalcogenine complexes with TNB.

The differences that have been observed in the $R_3PX{\cdot}I_2$ system have been explained as being due to several factors (34), including ionization potentials and π interactions.

Hillebrand *et al.* (8) in their study of the interaction of PS with TCNE have suggested that the absorption band at 6700–6800 Å is due to the transition from the last occupied molecular orbital on the donor to the lowest empty molecular orbital on the acceptor. The absorption peak which occurs at about 4300–4500 Å was assigned to a somewhat higher energy transition from the second highest filled molecular orbital on the donor to the lowest unfilled orbital on the acceptor.

The phenoxachalcogenines all exhibit similar maxima, with an absorption band (6400–7200 Å) shown in Fig. 1, which is formed on interaction with TCNE. A second somewhat less intense band is also seen close to 4500 Å in all of the systems except the PTe–TCNE system. PTe itself possesses characteristic absorption at wavelengths shorter than about 4500 Å. This presumably precludes the observation in the complex of a second band near 4500 Å. Since all of the complexes absorb at approximately the same region of the visible spectrum, it is reasonable to assume that the absorption band at these longer wavelengths is due to a related transition, *viz.*, from the highest occupied molecular orbital on the donor to the lowest empty molecular orbital on the acceptor. It further appears that the absorption band which appears at 4500 Å is due to a transition from the second highest molecular orbital on the donor to the lowest orbital on the acceptor (8). This appears to be true for all of the phenoxachalcogenine–TCNE complexes, although there may be another common type of transition occurring.

On the basis of the evidence presented in this work, together with a re-evaluation of those data resulting from previous studies, the donor actions discussed above for this group of molecules appear to be of π to π type.

Experimental

Reagents

Details on the preparation of the donors are described elsewhere (1). Phenoxatellurine, purified by several resublimations at 80° (0.05–0.1 Torr), melted at 76–77°; phenoxaselenine, purified by resublimation and recrystallization from ethanol, melted at 85–86°. Phenoxathiin was purchased from Eastman Organic Chemicals and was recrystallized from petroleum ether to a constant melting point of 56–57°. Diphenylene dioxide was purchased from K&K Laboratories and recrystallized to a constant melting point of 120–121°. Tetracyanoethylene was purchased from the Aldrich Chemical Company and sublimed through activated wood charcoal to a melting point of 200–201° (sealed tube). Chloranil was purchased from Eastman Organic Chemicals and recrystallized from toluene to a constant melting point of 291–292° (sealed tube).

The dichloromethane was Reagent A. C. S. grade, purchased from Matheson, Coleman and Bell. It was refluxed over P_2O_5 and distilled over this reagent under a dry nitrogen atmosphere.

Spectra of the thermostatted samples (±0.1°) were recorded on a Cary Model 14 spectrometer.

This work has been assisted by a grant from the Robert A. Welch Foundation, Houston, Texas, and the National Science Foundation (Grant No. GP-27588). The Selenium-Tellurium Development Assn., Inc., has kindly furnished assistance in defraying the costs of publication.

1. C. A. HELLER. Ph.D. Dissertation, Texas A&M University. 1972.
2. H. D. K. DREW. J. Chem. Soc. 3054 (1926).
3. M. M. MANGION, M. R. SMITH, and E. A. MEYERS. J. Heterocycl. Chem. **10**, 537 (1973).
4. M. M. MANGION, M. R. SMITH, and E. A. MEYERS. J. Heterocycl. Chem. **10**, 543 (1973).
5. A. KUBOYAMA. J. Am. Chem. Soc. **86**, 164 (1964).
6. J. A. A. KETELAAR, C. VAN DE STOLPE, A. GOUDSMIT, and W. DZCUBAS. Rec. Trav. Chim. Pays-Bas, **71**, 1104 (1952).

7. M. HILLEBRAND, O. MAIOR, V. EM SAHINI, and E. VOLANSCHI. J. Chem. Soc. B, 775 (1969).
8. M. HILLEBRAND, O. MAIOR, and V. EM SAHINI. Rev. Roum. Chim. **15**, 149 (1970).
9. B. HETNARSKI and W. HOFMAN. Bull. Acad. Pol. Sci. Ser. Sci. Chim. **17**, 1 (1969).
10. H. A. BENESI and J. H. HILDEBRAND. J. Am. Chem. Soc. **71**, 2703 (1949).
11. (*a*) B. HETNARSKI and A. GRABOWSKA. Bull. Acad. Pol. Sci. Ser. Sci. Chim. **17**, 333 (1969). (*b*) B. HETNARSKI and A. GRABOWSKA. Rocz. Chem. **44**, 1713 (1970).
12. B. DODSON, R. FOSTER, A. A. S. BRIGHT, M. I. FOREMAN, and J. GORTON. J. Chem. Soc. B, 1283 (1971).
13. N. J. ROSE and R. S. DRAGO. J. Am. Chem. Soc. **81**, 6138 (1959).
14. R. S. MULLIKEN and W. B. PERSON. Molecular complexes. Wiley-Interscience, New York. 1969, p. 304.
15. W. B. PERSON. J. Am. Chem. Soc. **87**, 167 (1965).
16. D. A. DERANLEAU. J. Am. Chem. Soc. **91**, 4044 (1969).
17. P. H. EMSLIE, R. FOSTER, C. A. FYFE, and I. HORMAN. Tetrahedron, **21**, 2843 (1965).
18. P. H. EMSLIE and R. FOSTER. Tetrahedron, **21**, 2851 (1965).
19. S. CARTER, J. N. MURRELL, and E. J. ROSCH. J. Chem. Soc. 2048 (1965).
20. M. J. S. DEWAR and C. C. THOMPSON, JR. Tetrahedron Suppl. 7, 97 (1966).
21. J. H. YOE and A. L. JONES. Ind. Eng. Chem. Anal. Ed. **16**, 111 (1944).
22. R. L. SCOTT. Rec. Trav. Chim. Pays-Bas, **78**, 787 (1956).
23. J. A. A. KETELAAR, C. VAN DE STOLPE, and H. R. GERSMANN. Rec. Trav. Chim. Pays-Bas, **70**, 499 (1951).
24. E. ASMUS. Z. Anal. Chem. **178**, 104 (1960).
25. K. MOMOKI, J. SEKINO, H. SATO, and N. YAMAGUCHI. Anal. Chem. **41**, 1286 (1969).
26. W. LIKUSSAR and D. F. BOLTZ. Anal. Chem. **43**, 1265 (1971).
27. R. FOSTER. Organic charge–transfer complexes. Academic Press, London. 1969, p. 73.
28. H. TSUBOMURA and R. LANG. J. Am. Chem. Soc. **83**, 2085 (1961).
29. H. KURODA, M. KOBAYASHI, M. KINOSHITA, and S. TAKEMOTO. J. Chem. Phys. **36**, 457 (1962).
30. A. L. ALLRED and E. G. ROCHOW. J. Inorg. Nuclear Chem. **5**, 264 (1958).
31. R. A. ZINGARO, R. E. MCGLOTHLIN, and E. A. MEYERS. J. Phys. Chem. **66**, 2579 (1962).
32. W. TEFTELLER, JR. and R. A. ZINGARO. Inorg. Chem. **5**, 2151 (1966).
33. B. R. CONDRAY, R. A. ZINGARO, and M. V. KUDCHADKER. Inorg. Chim. Acta, **2**, 309 (1968).
34. W. TEFTELLER, JR. Ph.D. Dissertation. Texas A&M University. 1966.

Can. J. Chem. Downloaded from www.nrcresearchpress.com by 210.87.254.105 on 09/05/12
For personal use only.

Can. J. Chem. Downloaded from www.nrcresearchpress.com by 210.87.254.40 on 09/05/12
For personal use only.

Oxidative Transfer Dehydrogenation of α,β-Unsaturated Carbinols to α,β-Unsaturated Ketones Catalyzed by Ruthenium Complexes

YOEL SASSON AND GARRY L. REMPEL

Inorganic Chemistry Laboratory, Department of Chemical Engineering, University of Waterloo, Waterloo, Ontario, N2L 3G1

Received July 11, 1974

YOEL SASSON and GARRY L. REMPEL. Can. J. Chem. **52**, 3825 (1974).

The homogeneous competitive intermolecular and intramolecular hydrogen transfer from unsaturated carbinols to vinyl ketones in the presence of a number of ruthenium complexes is reported. The oxotriruthenium complex, $Ru_3O(OOCCH_3)_7$ was used in applying this process for the oxidative transfer dehydrogenation of unsaturated carbinols to unsaturated ketones.

YOEL SASSON et GARRY L. REMPEL. Can. J. Chem. **52**, 3825 (1974).

On rapporte le transfert homogène d'hydrogène de carbinols non-saturés à des vinyl cétones en présence d'un certain nombre de complexes de ruthénium; la réaction implique une compétition inter- et intramoléculaire. On a utilisé le complexe oxotriruthénium, $Ru_3O(OOCCH_3)_7$ afin d'appliquer ce processus à la déhydrogénation impliquant un transfert oxydant d'hydrogène des carbinols insaturés en cétones non-saturées. [Traduit par le journal]

Recently we have investigated (1) the homogeneous rearrangement of unsaturated secondary alcohols to the corresponding saturated ketones via an intramolecular hydrogen transfer (reaction 1).

[1] $RCH{=}CHCH(OH)R' \rightarrow RCH_2CH_2COR'$

Reaction 1 was carried out in the presence of a number of ruthenium complexes; the oxotriruthenium acetate complex, $Ru_3O(OOCCH_3)_7$, being the most active and selective complex for the intramolecular hydrogen transfer process.

While studying the effects of various co-catalysts or potential inhibitors for reaction 1 we have found that in the presence of vinyl ketones reaction 1 is significantly inhibited and a competitive intermolecular hydrogen transfer process (reaction 2) is found to occur.

[2] $RCH{=}CHCH(OH)R' + CH_2{=}CHCOR'' \rightarrow RCH{=}CHCOR' + CH_3CH_2COR''$

For example, when a mixture of 1-hexene-3-ol (0.5 g, 50 mmol) methyl vinyl ketone (0.35 g, 50 mmol), and $RuCl_2(P(C_6H_5)_3)_3$ (19 mg, 2×10^{-2} mmol) was maintained under nitrogen[1] in a sealed tube at 100 °C a clear reddish-orange solution resulted. Analysis of the solution by g.l.c. after 4.5 h indicated that the mixture contained 0.285 g (28.5 mmol) hexene-3-one, 0.215 g (21.5 mmol) 3-hexanone, 0.200 g (28.5 mmol) 2-butanone, and 0.150 g (21.5 mmol) of the remaining methyl vinyl ketone. Thus, in this case, 43% of the 1-hexene-3-ol reacted via the intramolecular route to yield 3-hexanone and 57% yielded the intermolecular product 1-hexene-3-one.[2]

Results of similar experiments with a number of catalysts under various conditions are summarized in Table 1.

As was found for the intramolecular process (1), $Ru_3O(OOCCH_3)_7$ was also the most active and selective complex for the intermolecular reaction. The results in Table 1 indicate that the efficiency and selectivity of the catalyst depend on its concentration, donor: acceptor molar ratio, and reaction temperature. Highest yields of intermolecular transfer were obtained using 0.02 m*M* $Ru_3O(OOCCH_3)_7$ at 100 °C with a donor:

[1]The nitrogen atmosphere is not essential and reactions of this type also take place in the presence of air.

[2]It should be noted that after some 1-hexene-3-one is formed it can itself be reduced to 3-hexanone via the intermolecular route. However, relative rate studies have indicated that this path is of minor importance.

TABLE 1. Hydrogen transfer of 1-hexene-ol in the presence of methyl vinyl ketone*

Catalyst	Concentration (m*M*)	Molar ratio donor/acceptor	% Intermolecular transfer	% Intramolecular transfer	Time† (h)
$RuCl_3 3H_2O$	0.02‡	1/1	56	38	4.0
$RuCl_2(P(C_6H_5)_3)_3$	0.02	1/1	57	43	4.7
	0.08	1/1	58	42	4.3
	0.02	1/5	64	36	14.0
$RuHCl(P(C_6H_5)_3)_3$	0.02	1/1	49	51	5.3
$RuH(OOCCH_3)(P(C_6H_5)_3)_3$	0.02	1/1	37	63	4.7
$RhCl(P(C_6H_5)_3)_3$	0.02	1/1	24	76	1.5
$Ru_3O(OOCCH_3)_7$	0.0075§	1/1	59	41	0.75
	0.02	1/1	70	30	0.58
	0.02	1/5	89	11	0.42
	0.02	1/8	88	12	0.42
	0.005	1/5	87	13	1.17
	0.0025	1/5	78	22	2.50
	0.02‖	1/5	80	20	7.5
	0.02¶	1/5	83	17	0.25

*Reaction conditions: 50 mmol 1-hexene-3-ol plus appropriate amount of methyl vinyl ketone and the catalyst in a sealed tube under N_2 at 100 °C. Separation of products on a 1.8 m 10% Carbowax 20M on chromosorb W column at 70 °C.
†Time required for complete disappearance of 1-hexene-3-ol.
‡6% of dehydration and hydrogenolysis products identified (2).
§In all experiments where $Ru_3O(OOCCH_3)_7$ was used, 0.5 ml ethylene glycol was added as co-solvent. The co-solvent played no part in the transfer reaction itself.
‖85 °C.
¶115 °C.

TABLE 2. Oxidative transfer dehydrogenation of unsaturated alcohols to unsaturated ketones with methyl vinyl ketone catalyzed by $Ru_3O(OCCH_3)_7$*

Alcohol	Product	Temperature (°C)	Time (h)	Yield (%)
$CH_3CH_2CH(OH)CH{=}CH_2$	$CH_3CH_2COCH{=}CH_2$	100	0.5	90
$CH_3CH_2CH_2CH(OH)CH{=}CH_2$	$CH_3CH_2CH_2COCH{=}CH_2$	100	0.4	89
$CH_3(CH_2)_3CH(OH)CH{=}CH_2$	$CH_3(CH_2)_3COCH{=}CH_2$	100	0.5	89
$CH_3(CH_2)_4CH(OH)CH{=}CH_2$	$CH_3(CH_2)_4COCH{=}CH_2$	100	0.5	91
$CH_3CH{=}CHCH(OH)CH_3$	$CH_3CH{=}CHCOCH_3$	140	5.0	82
$CH_2CH_2CH{=}CHCH(OH)CH_2$	$CH_2CH_2CH{=}CHCOCH_2$	140	5.0	87

*Reaction conditions: 50 mmol of alcohol, 250 mmol methyl vinyl ketone, 40 mg of $Ru_3O(OCCH_3)_7$ in 0.5 ml ethylene glycol. Products were separated on a 1.8 m 10% Carbowax 20M on Chromosorb W Column at 70 °C.

acceptor molar ratio of 1/5. It is of interest to note that $RuCl_2(P(C_6H_5)_3)_3$ is quite different in its behavior when excess of acceptor is present; the selectivity for intermolecular transfer is slightly improved but the reaction rate is very much lower.

Other common alcoholic donors (3) (*i.e.* benzyl alcohols) were not reactive for reduction of vinyl ketones. Also other potential acceptors (3, 4) (*i.e.* chalcone, benzalacetone, acetophenone) also did not react with unsaturated alcohols under the conditions noted in Table 1. The combination of unsaturated alcohols as hydrogen donors and vinyl ketones as acceptors in the presence of $Ru_3O(OOCCH_3)_7$ or $RuCl_2(P(C_6H_5)_3)_3$ is apparently the most reactive homogeneous intermolecular hydrogen transfer system so far reported (3–6).

Although the intermolecular hydrogen transfer reaction may have some practical value for selective reduction of vinyl ketones to ethyl ketones, the major utility of the process is for the oxidative transfer dehydrogenation of unsaturated carbinols.[3] In this manner we have oxidized some 1-alkene-3-ols to the corresponding 1-alkene-3-ones; other unsaturated alcohols requiring somewhat stronger conditions for oxidation. In Table 2, results of some of these oxidations are provided.

[3]Similar oxidation of diols have previously been reported (7).

Can. J. Chem. Downloaded from www.nrcresearchpress.com by 210.87.254.40 on 09/05/12
For personal use only.

At present, no detailed mechanism can be deduced for the intermolecular hydrogen transfer, however, the following general remarks are applicable. The inhibition effect of the added vinyl ketone on the intramolecular route (reaction 1) suggests that coordination and activation of the acceptor (*i.e.* the vinyl ketone) occurs prior to the coordination of the donor. This fact is particularly evident in the case of the catalyst $RuCl_2(P(C_6H_5)_3)_3$ where in the presence of an excess of acceptor, the reaction rate is extremely slow; apparently due to blocking of the coordination sites on the catalyst by the unsaturated ketone. Since the competitive intermolecular and intramolecular reactions proceed essentially at the same rate, they probably involve a similar rate determining step. Based on previous related studies (4, 6, 8) it would appear that this step involves the breaking of the C—H bond α to the hydroxyl in the donor. The hydride is then transferred directly, or via a metal hydride intermediate, to the bound unsaturated ketone or intramolecularly to the 3-position of the unsaturated alcohol.

We thank the National Research Council of Canada and the University of Waterloo for financial support, and Engelhard Industries for the loan of ruthenium.

1. Y. Sasson and G. L. Rempel. To be published.
2. M. Dedieu and Y. L. Pascal. C. R. Acad. Sc. Paris C, **277**, 1257 (1973).
3. Y. Sasson and J. Blum. Tetrahedron Lett. 2167 (1971).
4. Y. Sasson, P. Albin, and J. Blum. Tetrahedron Lett. 833 (1974).
5. J. Trocha-Grimshaw and H. B. Henbest. Chem. Commun. 544 (1967); M. Gulloti and R. Ugo. J. Chem. Soc(C), 139 (1971); T. Nishiguchi and F. Fukuzumi. Bull. Chem. Soc. Jap. **45**, 1656 (1972); T. Nishiguchi and K. Fukuzumi. J. Am. Chem. Soc. **96**, 1893 (1974).
6. H. Imai, T. Nishiguchi, and K. Fukuzumi. J. Org. Chem. **39**, 1622 (1974).
7. S. L. Regen and G. M. Whitesides. J. Org. Chem. **37**, 1832 (1972).
8. F. G. Cowherd and J. L. von Rosenberg. J. Am. Chem. Soc. **91**, 2157 (1969); G. Eadon and M. Y. Shiekh. J. Am. Chem. Soc. **96**, 2289 (1974); Y. Sasson and J. Blum. Chem. Commun. 309 (1974).

Can. J. Chem. Downloaded from www.nrcresearchpress.com by 210.87.254.40 on 09/05/12
For personal use only.

Can. J. Chem. Downloaded from www.nrcresearchpress.com by 210.87.254.42 on 09/05/12
For personal use only.

Canadian Journal of Chemistry

Published by
THE NATIONAL RESEARCH COUNCIL OF CANADA

Journal canadien de chimie

Publié par
LE CONSEIL NATIONAL DE RECHERCHES DU CANADA

Volume 52 Number 23 December 1, 1974

Volume 52 numéro 23 1 décembre 1974

Substrate Activation in the Carboxypeptidase A Catalysis of Ester Hydrolysis

JOE MURPHY AND JOHN W. BUNTING

Department of Chemistry, University of Toronto, Toronto, Ontario M5S 1A1

Received June 17, 1974

JOE MURPHY and JOHN W. BUNTING. Can. J. Chem. **52**, 3829 (1974).

The hydrolyses of the *O*-hippuryl derivatives of glycolic acid (**1***a*), 2-methyllactic acid (**1***b*), and *p*-chloromandelic acid (**1***c*) by bovine carboxypeptidase A display substrate activation. The hydrolyses of the latter two esters also display substrate inhibition at high substrate concentrations (> 0.03 and > 0.05 *M* respectively). Partial kinetic analyses are presented, and these phenomena are discussed in terms of reaction schemes which involve substrate binding at both activating and inhibiting regulatory sites.

The hydrolysis of **1***b* by this enzyme is the first indication that the presence of a hydrogen atom on the α-carbon atom of the alcohol moiety is not obligatory for ester substrates of carboxypeptidase A. The binding of **1***c* at the catalytic site is approximately 1000 times weaker than for *O*-hippurylmandelic acid and indicates a dramatic influence for the *p*-chloro substituent on the binding of the phenyl ring of the mandelic acid unit.

JOE MURPHY et JOHN W. BUNTING. Can. J. Chem. **52**, 3829 (1974).

L'hydrolyse des dérivés *O*-hippuryle des acides glycolique (**1***a*), 2-méthyllactique (**1***b*) et *p*-chloromandélique (**1***c*) par la carboxypeptidase A de bovin démontre une activation du substrat. L'hydrolyse de ces deux derniers esters démontre aussi une inhibition du substrat à haute concentration en substrat (respectivement > 0.03 et > 0.05 *M*). Des analyses cinétiques partielles sont présentées et ces phénomènes sont discutés en termes de schémas réactionnels impliquant un lien du substrat à chaque site activateur et inhibiteur.

L'hydrolyse de **1***b* par cet enzyme est la première indication, que la présence d'un atome d'hydrogène sur l'atome de carbone en alpha sur une partie de l'alcool, n'est pas obligatoirement requise pour les substrats esters de la carboxypeptidase A. Le lien de **1***c* au site catalytique est approximativement 1000 fois plus faible que pour l'acide *O*-hippurylmandélique et indique une influence critique pour le substituant *p*-chloro sur le lien du cycle phényle du groupe acide mandélique. [Traduit par le journal]

Substrate activation and inhibition effects are often observed in the hydrolysis of dipeptide substrates and their ester analogs by bovine carboxypeptidase A. Although many cases of substrate inhibition of ester hydrolysis are known (1–3), only one example of substrate activation of ester hydrolysis has been reported (4). Thus, *O*-hippurylglycolic acid (**1***a*) displays a sigmoid dependence of initial velocity of enzymic hydrolysis upon substrate concentration. In this communication, we wish to report two further examples of substrate activation in the hydrolysis of esters of hippuric acid by carboxypeptidase A. Each of these examples is important in further illuminating the substrate specificity of this enzyme.

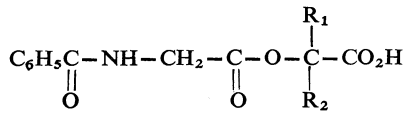

a $R_1 = R_2 = H$
b $R_1 = R_2 = CH_3$
c $R_1 = H$; $R_2 = p\text{-}ClC_6H_4$

Can. J. Chem. Downloaded from www.nrcresearchpress.com by 210.87.254.42 on 09/05/12
For personal use only.

Experimental

Synthesis of Substrates

O-Hippurylglycolic acid (**1***a*): A mixture of hippuric acid (0.055 mol), benzyl chloroacetate (0.050 mol), and triethylamine (0.050 mol) in acetonitrile (100 ml) was heated under reflux for 16 h. After cooling, the triethylammonium chloride was filtered off and the acetonitrile removed on the rotary evaporator. The residue was dissolved in dichloromethane (30 ml) and extracted with 3 *M* HCl (100 ml) and then with saturated aqueous sodium bicarbonate (200 ml). After drying over magnesium sulfate the dichloromethane was removed under vacuum to give an oil which crystallized on standing. This crude benzyl 2-hippuroxyacetate was recrystallized from a benzene–hexane mixture; yield 89%; m.p. 100–102°. This benzyl ester (0.040 mol) in ethyl acetate (400 ml) was hydrogenated at 1 atm. and room temperature in the presence of 5% Pd–C (0.5 g) until uptake of hydrogen ceased. Acetone (400 ml) was added, and the solution was heated to boiling and filtered. Removal of the solvents under vacuum gave the crude *O*-hippurylglycolic acid in essentially quantitative yield. After recrystallization from 8:1 1,2-dichloroethane–acetonitrile: m.p. 166–167° (lit. (4) 165–166°); p.m.r. (CF_3CO_2D)δ: 4.58 (2H, s), 4.97 (2H, s), 7.70 (5H, m).

O-Hippuryl-2-methyllactic acid (**1***b*): A stirred mixture of hippuryl chloride (0.184 mol), 2-methyllactic acid (0.216 mol), and tetrahydrofuran (500 ml) was treated dropwise with pyridine (40 ml, 0.48 mol). After further stirring for 15 h at room temperature, the pyridine hydrochloride was filtered off and the tetrahydrofuran was removed under vacuum. The residue was dissolved in dichloromethane (500 ml). Upon extraction of this solution with 3 *M* HCl (500 ml), large quantities of colorless crystals separated. The contents of the extraction funnel were filtered and the solid washed with dichloromethane. The crude ester was recrystallized from 3:2 1,2-dichloroethane–acetonitrile; yield 85%; m.p. 167–168°; p.m.r. (CF_3CO_2H)δ: 1.77 (6H, s), 4.50 (2H, broad s), 7.67 (5H, m), 8.13 (1H, broad s).

Anal. Calcd. for $C_{13}H_{15}NO_5$: C, 58.9; H, 5.70; N, 5.28. Found: C, 59.0; H, 5.95; N, 5.26.

DL-*O-Hippuryl-p-chloromandelic acid* (**1***c*): By the pyridine-catalyzed esterification of hippuryl chloride with DL-*p*-chloromandelic acid as described above; yield 69%; m.p. 199–200° (1:1 1,2-dichloroethane–acetonitrile); p.m.r. (CF_3CO_2H)δ: 4.67 (2H, d, J_{CH-NH} = 4 Hz), 6.25 (1H, s), 7.52–7.70 (10H, m).

Anal. Calcd. for $C_{17}H_{14}ClNO_5$: C, 58.7; H, 4.06; Cl, 10.2; N, 4.03. Found: C, 58.9; H, 4.37; Cl, 10.7; N, 4.05.

Kinetics

Carboxypeptidase A was obtained as a toluene-preserved suspension from Worthington Biochemical Corporation (Code COA). Stock solutions of this enzyme and of the substrates were prepared as described previously (5).

All hydrolyses (enzymic and nonenzymic) were followed on a Radiometer p*H*-Stat in aqueous solution at 25°, ionic strength 0.5 (substrate + NaCl). The general experimental technique and estimation of the velocities for the enzymic hydrolyses (performed at p*H* 7.5) have been described elsewhere (5). Calculations for the racemic ester **1***c* are based on the assumption that only the L-ester is hydrolyzed and that the D-ester is neither a substrate nor a competitive inhibitor.[1] This has been established for several carboxypeptidase A substrates (1, 6–8) and was supported by the observation that only 50 ± 2% of the ester **1***c* had been hydrolyzed by carboxypeptidase A at equilibrium. The esters **1***a* and **1***b* were completely hydrolyzed by enzyme, and all three substrates were completely hydrolyzed in aqueous base (p*H* 10–11). Pseudo first-order rate constants for the nonenzymic reactions were obtained from the slopes of linear first-order plots, and in each case, except **1***b*, the values of k_{OH} were obtained by averaging four runs in the region p*H* 10–11. The hydrolysis of **1***b* was so slow that k_{OH} was estimated from the initial rate at p*H* 11.

Results

The dependence of the initial velocity on substrate concentration for the hydrolysis of each of the esters **1***a*, *b*, *c* by carboxypeptidase A at p*H* 7.5, ionic strength 0.5 and 25° is indicated in Figs. 1–3. In each case, at low substrate concentrations, the velocity shows a greater than linear dependence on substrate concentration, which is typical of substrate activation. The data for *O*-hippurylglycolic acid agree closely at all but the highest substrate concentrations with the data previously reported for this ester by Kaiser and co-workers (4) under the same experimental conditions. At high substrate concentrations, the esters **1***b* and *c* each display substrate inhibition with the velocities passing through maxima at substrate concentrations of approximately 0.03 and 0.05 *M* for **1***b* and *c*, respectively.

Lineweaver–Burk plots (E/v *vs.* $1/S$) of the data in Figs. 1–3 confirm the presence of substrate activation for the esters **1***a*, *b*, *c*. These plots are linear only at very low substrate concentrations ($< 1.0 \times 10^{-3}$ *M* for **1***a*; $< 1.6 \times 10^{-3}$ *M* for **1***b*; $< 4 \times 10^{-4}$ *M* for **1***c*) and show negative deviations typical of substrate activation at higher concentrations. Extrapolations from these linear regions pass through the origin (*e.g.* Fig. 4 for **1***b*) and the slopes of these lines may be used to evaluate k_{cat}/K_m in the absence of substrate activation (*i.e.* for formation and reaction of an E·S complex). Values of k_{cat}/K_m for each ester are collected in Table 1, and the broken lines in Figs. 1–3 indicate this predicted behavior in the absence of substrate activation.

[1]A recent analysis (J. Murphy and J. W. Bunting (15)) of the influence of the D-ester on the hydrolysis of *O*-hippuryl-L-mandelic acid by carboxypeptidase A is consistent with this assumption; see also ref. 14.

Can. J. Chem. Downloaded from www.nrcresearchpress.com by 210.87.254.42 on 09/05/12
For personal use only.

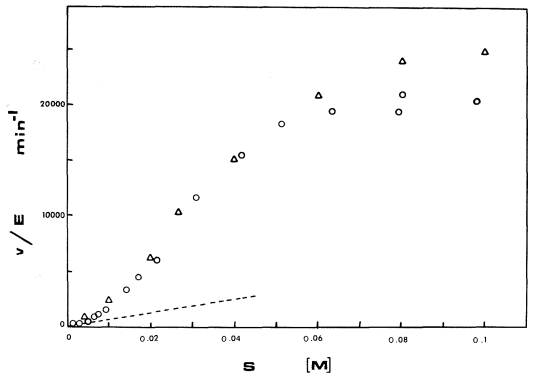

FIG. 1. Dependence of initial velocity on substrate concentration for the hydrolysis of *O*-hippurylglycolic acid (**1***a*) by carboxypeptidase A (25°, p*H* 7.5, ionic strength 0.5). ○ present work; △ data of ref. 4. The broken line indicates k_{cat}/K_m for nonactivated hydrolysis.

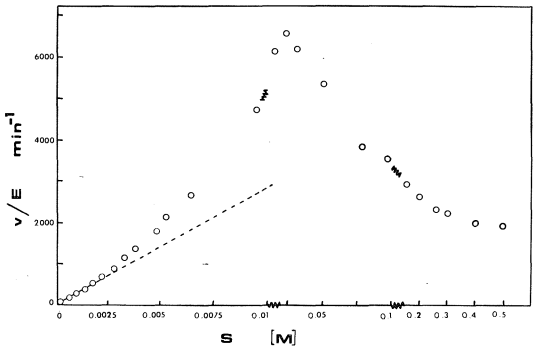

FIG. 2. Dependence of initial velocity on substrate concentration for the hydrolysis of *O*-hippuryl-2-methyllactic acid (**1***b*) by carboxypeptidase A (25°, p*H* 7.5, ionic strength 0.5). The broken line indicates k_{cat}/K_m for nonactivated hydrolysis.

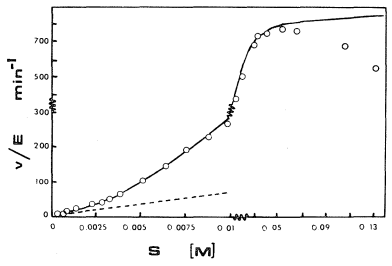

FIG. 3. Dependence of initial velocity on substrate concentration for the hydrolysis of *O*-hippuryl-DL-*p*-chloromandelic acid (**1***c*) by carboxypeptidase A (25°, p*H* 7.5, ionic strength 0.5). The broken line indicates k_{cat}/K_m for nonactivated hydrolysis. The full line is an iterative fit (see text) using $K_1^{app} = 0.14\ M$, $K_3^{app} = 2.0 \times 10^{-3}\ M$, $k_2^{app} = 1.0 \times 10^3\ min^{-1}$, $k_3 = 860\ min^{-1}$ (average error = 5.2%).

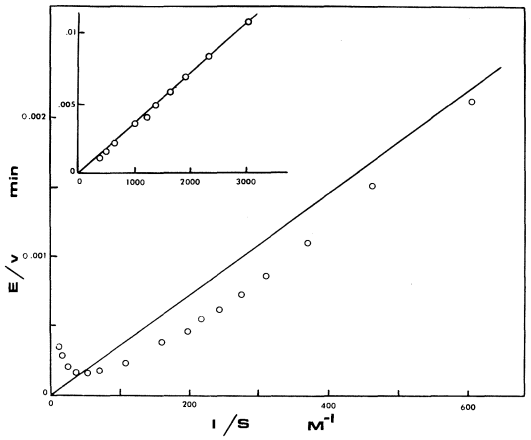

FIG. 4. Lineweaver–Burk plot for the hydrolysis of **1***b*. The line of the major figure is defined in the inset at lower substrate concentrations.

The simplest general reaction scheme that is capable of fitting the observed substrate activation phenomena seems to be Scheme 1.

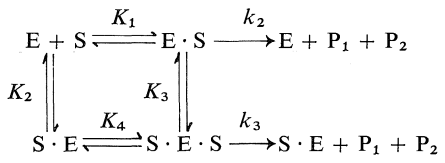

SCHEME 1

Assuming that the equilibria are established rapidly relative to k_2 and k_3, this scheme gives the rate eq. 1.

$$[1]\quad \frac{v}{E} = \frac{\dfrac{k_2 S}{(1 + K_1/K_2)} + \dfrac{k_3 S^2}{K_3(1 + K_1/K_2)}}{\dfrac{K_1}{(1 + K_1/K_2)} + S + \dfrac{S^2}{K_3(1 + K_1/K_2)}}$$

Thus, at low substrate concentrations, the observed k_{cat}/K_m is equivalent to k_2/K_1 and is the real specificity constant for nonactivated substrate hydrolysis by the enzyme. At high substrate concentrations, and in the absence of substrate inhibition, this scheme predicts $v/E \approx k_3$. Plots of E/v against $1/S^2$ for **1***a*, *b*, *c* at substrate concentrations less than that at which the maximum velocity occurs in Figs. 2 and 3 may be conveniently extrapolated to $1/S^2 = 0$ (Fig. 5), and values for k_3 derived in this way (reciprocal of the ordinate intercept) are included in Table 1.

Equation 1 is a second-degree equation of the form that we have previously fitted to experi-

TABLE 1. Kinetic parameters for the hydrolysis of $C_6H_5CONHCH_2CO_2CR_1R_2CO_2^-$ by carboxypeptidase A[a]

R_1	R_2	k_2/K_1 (M^{-1} min^{-1})[b]	k_3 (min^{-1})[c]	$K_1^{app}(M)$[d]	k_2^{app} (min^{-1})[d]	$K_3^{app}(M)$[e]	$K_1K_3(M^2)$[f]
H	H	6×10^4	2.5×10^4	$>1\times10^{-1}$	$>6\times10^3$	$<1\times10^{-2}$	1×10^{-3}
CH_3	CH_3	3×10^5	8×10^3	$>3\times10^{-3}$	$>1\times10^3$	$<2\times10^{-2}$	6×10^{-5}
H	p-ClC_6H_4	1×10^4	9×10^2	$>5\times10^{-2}$	$>2\times10^2$	$<4\times10^{-3}$	2×10^{-4}
H	C_6H_5[g]	9×10^6	4.5×10^2	1.5×10^{-3}	1.3×10^4	1.6×10^{-3}	—
H	C_2H_5[g]	2×10^7	2.2×10^2	3.7×10^{-4}	7.2×10^3	9.4×10^{-4}	—

[a]At 25°, pH 7.5, ionic strength 0.5.
[b]From reciprocal of slope of linear portion of E/v *vs.* $1/S$ (at low S); *i.e.* k_{cat}/K_m.
[c]From reciprocal of ordinate intercept of E/v *vs.* $1/S^2$ at substrate concentrations less than that at which the maximum velocity occurs.
[d]Minimum estimates obtained from the iteration procedure.
[e]Maximum estimates obtained from the iteration procedure.
[f]From slope of E/v *vs.* $1/S^2$ (see text).
[g]All data for this ester from ref. 3.

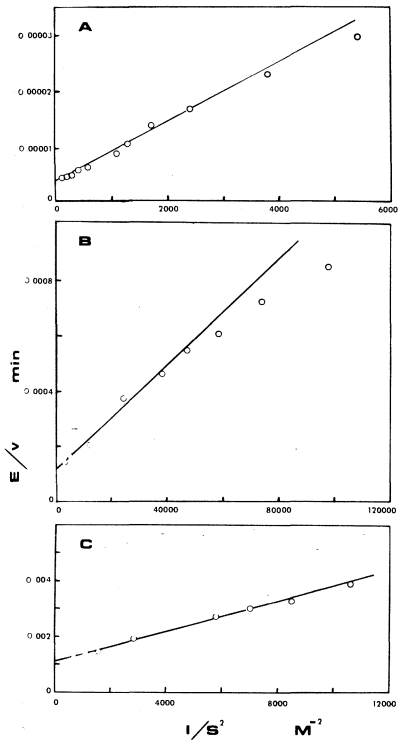

FIG. 5. Dependence of E/v on $1/S^2$ at substrate concentrations lower than that at which the maximum velocity occurs for **1***a* (A), **1***b* (B), and **1***c* (C).

mental data by an iteration procedure (9). However, attempts to fit the present activation data to eq. 1 by this iteration technique lead to an infinite number of mathematically acceptable solutions for the parameters $k_2^{app} = k_2/(1 + K_1/K_2)$, $K_1^{app} = K_1/(1 + K_1/K_2)$, and $K_3^{app} = K_3(1 + K_1/K_2)$, which arise because of the non-convergence of the iteration technique for the present experimental data. These solutions are characterized by approximately constant values for k_3, $K_1^{app}K_3^{app} = K_1K_3$ and $k_2^{app}/K_1^{app} = k_2/K_1$, but widely varying individual values for k_2^{app}, K_1^{app}, and K_3^{app}. For example a solution with $K_1^{app} = x$, $k_2^{app} = y$, $K_3^{app} = z$, and $k_3 = k_3$ gives the same close fit to the experimental data as a solution with $K_1^{app} = 10x$, $k_2^{app} = 10y$, $K_3^{app} = 0.1z$, and $k_3 = k_3$. Unfortunately, a distinction of the physically meaningful solution does not seem possible for any of these esters. (See Fig. 3 for one set of parameters for **1***c* and the curve generated according to eq. 1.)

Despite these shortcomings in the kinetic analysis, partial solutions with physical meaning can still be obtained. For example, the ratio of k_2 to K_1 can be derived for each substrate, as discussed previously. As discussed above, values for k_3 can also be estimated by extrapolating to $1/S^2 = 0$ plots of E/v *vs.* $1/S^2$ at substrate concentrations less than that at which the maximum velocity occurs. This extrapolation also suggests that over the linear region of this plot eq. 1 may be approximated by:

$$\frac{v}{E} = \frac{k_3S^2/K_3^{app}}{K_1^{app} + S^2/K_3^{app}}$$

i.e.

$$\frac{E}{v} = \frac{1}{k_3} + \frac{K_1^{app}K_3^{app}}{k_3S^2}$$

Thus the product $K_1^{app}K_3^{app}$ may also be obtained from the slope of this plot (Fig. 5), and these values for **1***a*, *b*, *c* obtained in this way are included in Table 1 and are in reasonable agreement with the same product evaluated by the attempted iteration technique. Lastly, minimum estimates for k_2^{app} and K_1^{app} can be obtained directly from the multiple solutions of the

Can. J. Chem. Downloaded from www.nrcresearchpress.com by 210.87.254.42 on 09/05/12
For personal use only.

TABLE 2. Base-catalyzed hydrolysis of hippurate and acetate esters

$C_6H_5CONHCH_2CO_2CR_1R_2CO_2^-$				$CH_3CO_2CH_n(CH_3)_{3-n}$	
R_1	R_2	k_{OH} (M^{-1} min^{-1})[a]	Relative k_{OH}	n	Relative k_{OH}[b]
H	H	129	1	2	1
H	C_2H_5	25.1	0.19	1	0.24
CH_3	CH_3	1.4	0.011	0	0.014
H	C_6H_5	71.4	0.55		
H	p-ClC_6H_4	102	0.78		

[a]At 25°, ionic strength 0.5.
[b]From ref. 10.

iteration procedure, since acceptable fits[2] to the experimental data seem to occur only if k_2^{app} and K_1^{app} exceed certain values. This method also affords maximum values for K_3^{app}, since the process of minimizing K_1^{app} simultaneously maximizes K_3^{app} (because $K_1^{app}K_3^{app}$ appears to be constant in all of the mathematically acceptable solutions, as discussed previously). Values for k_3, minimum estimates for k_2^{app} and K_1^{app}, and maximum estimates for K_3^{app} are listed in Table 1.

The reasons for the multiple solutions that are obtained in the attempted parameter evaluations by the iteration technique are clear from the relative values for K_1^{app} and K_3^{app} in Table 1 in the cases of **1***a* and *c*. For each of these esters, K_1^{app} is at least a factor of 10 larger than K_3^{app}, which indicates that the affinity of E·S complexes for S to form E·S_2 is much greater than the affinity of E for S to form E·S. Thus at substrate concentrations at which activation is exhibited, the predominant enzyme–substrate complex present in solution is E·S_2, with very little E·S being present. The $k_2^{app}S$ term therefore contributes very little to the total observed velocity, and so the calculated velocities in eq. 1 are relatively insensitive to the variation of k_2^{app} over a relatively wide range of possible values.

Also included in Table 1 for comparison, are similar parameters for the esters **1**: R_1 = H; R_2 = C_2H_5 and **1**: R_1 = H; R_2 = C_6H_5 which display substrate inhibition that we have previously fitted (3) by an equation of the same form as eq. 1.

The nonenzymic base-catalyzed hydrolysis of each of the esters in Table 1 has also been measured. The second-order rate constants, k_{OH}, for these reactions are collected in Table 2. The observed dependences of k_{OH} on structural variations in the alcohol moiety of these esters are typical of those usually observed in base-catalyzed hydrolyses of carboxylate esters (10).

Only for ester **1***b* were substrate inhibition data obtainable over a relatively wide range of substrate concentrations under the present experimental conditions. A plot of v/E *vs.* $1/S$ for **1***b* at high substrate concentrations (Fig. 6) is approximately linear, and extrapolation to $1/S$ = 0 (*i.e.* infinite substrate concentration) indicates that the velocity apparently does not approach zero but rather 1.3×10^3 min^{-1} (ordinate intercept) at high substrate concentrations.

Discussion

The hydrolysis of the esters **1***a*, *b*, and *c* by carboxypeptidase A is characterized by substrate activation, at least over part of the substrate concentration range examined. Like the substrate inhibition previously observed for other hippuric acid esters (3) the activation curves can be fitted by Scheme 1, indicating that

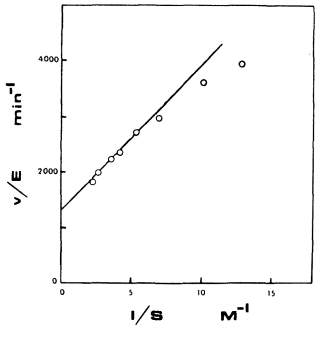

FIG. 6. Dependence of v/E on $1/S$ for **1***b* at high substrate concentrations.

[2]An acceptable fit is defined here as having a set of parameters for which the average percentage difference between the calculated and experimental velocities is not greater than the experimental error in the velocity data (~5–8%).

Can. J. Chem. Downloaded from www.nrcresearchpress.com by 210.87.254.42 on 09/05/12
For personal use only.

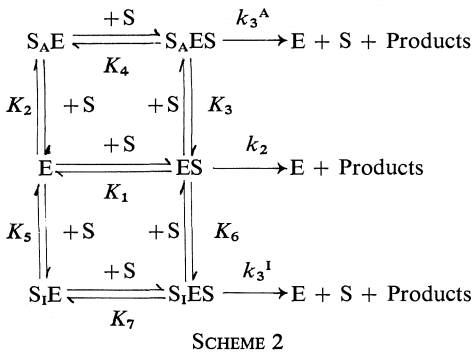

SCHEME 2

the substrate activation is caused by binding of two molecules of substrate to the enzyme.

The existence of substrate activation in the hydrolysis of the present esters can be rationalized in two different ways. It is possible that the enzyme possesses not one, but *two* regulatory sites, one of which is associated with substrate inhibition and the other with substrate activation. A kinetic scheme consistent with this hypothesis is shown in Scheme 2. Here, substrate may bind to the active site (S), an inhibiting regulatory site (S_I), or an activating regulatory site (S_A), and hydrolysis within these complexes is such that $k_3^I < k_2 < k_3^A$. Substrate activation or inhibition is then caused by preferential binding of substrate to the activating or inhibiting regulatory sites, respectively. The main problem with this interpretation is that the activating regulatory site would have to possess an unusual specificity towards binding of hippuric acid esters in order to accommodate the three examples of substrate activation that are observed in the present work. For example, the activating site would appear to bind esters with large R side chains (**1**: $R_1 = H$; $R_2 = p$-ClC_6H_4) and small R side chains (**1**: R_1, $R_2 = H$ or CH_3) and yet is apparently unable to accommodate side chains of intermediate size like phenyl, benzyl, or aliphatic groups like ethyl, propyl, etc. This seems highly improbable.

An alternative explanation for substrate activation and inhibition can be devised which involves only one regulatory site. According to this interpretation, substrate activation and inhibition are simply different aspects of the same basic phenomenon, whose manifestation as substrate activation rather than inhibition (or vice-versa) is dependent only on the relative values of the kinetic parameters k_2^{app}, K_1^{app}, k_3, and K_3^{app}. The simplest kinetic scheme which describes the enzymic hydrolysis of the hippuric acid esters is Scheme 1, which generates the rate eq. 1. The condition that substrate activation should occur is thus given by inequality (2), which simplifies to the inequality (3). Similarly substrate inhibition is predicted by the inequality (4). Clearly, substrate activation will always occur if $k_3 > k_2^{app}$, independent of the substrate concentration. Activation can also arise even when k_2^{app} is greater than k_3, however, provided K_1^{app} is sufficiently large and the substrate concentration is such that (3) is valid. The inequalities (3) and (4) seem to suggest that the existence of substrate

$$[2]\quad \frac{k_2^{app}S + k_3S^2/K_3^{app}}{K_1^{app} + S + S^2/K_3^{app}} > \frac{k_2^{app}S}{K_1^{app} + S}$$

$$[3]\quad K_1^{app} > \left[\frac{k_2^{app}}{k_3} - 1\right]S$$

$$[4]\quad K_1^{app} < \left[\frac{k_2^{app}}{k_3} - 1\right]S$$

activation or inhibition is independent of the value of K_3^{app}. The difference ΔV, in the rates of activated and nonactivated hydrolysis (eq. 5) is strongly influenced by K_3^{app}, however, so that experimental observation of substrate activation is dependent on the value of this parameter, even if the theoretical existence of substrate activation is not. A similar argument pertains to the experimental detection of substrate inhibition.

$$[5]\quad \Delta V = \frac{k_2^{app}S + k_3S^2/K_3^{app}}{K_1^{app} + S + S^2/K_3^{app}} - \frac{k_2^{app}S}{K_1^{app}S}$$

As discussed earlier, a detailed kinetic analysis of the substrate activation curves for the esters **1***a*, *b*, *c* is prohibited by the inability to discern physically meaningful sets of kinetic parameters from the infinite number of solutions. The only parameter in Scheme 1 that can be confidently evaluated is k_3, and comparison of this parameter for **1***a*, *b*, *c* with k_3 for those hippurate esters which show only substrate inhibition according to Scheme 1 is of interest (Table 1). Although k_3 for **1***c*: $R_1 = H$; $R_2 = p$-ClC_6H_4 (9×10^2 min^{-1}) and **1**: $R_1 = H$; $R_2 = C_6H_5$ (4.5×10^2 min^{-1}) are similar, k_3 for **1***b*: $R_1 = R_2 = CH_3$ (8×10^3 min^{-1}) is 40 times larger than for **1**: $R_1 = H$; $R_2 = C_2H_5$ (2.2×10^2 min^{-1}). The relative k_3 values for these latter two esters are inverted relative to what one might expect

Can. J. Chem. Downloaded from www.nrcresearchpress.com by 210.87.254.42 on 09/05/12
For personal use only.

Can. J. Chem. Downloaded from www.nrcresearchpress.com by 210.87.254.42 on 09/05/12
For personal use only.

based upon the usual effects of R_1 and R_2 substituents on the α-carbon atom of the alcohol moiety upon the nonenzymic hydrolysis rates of esters (*cf.* k_{OH} in Table 2). This then suggests that the k_3 values for these latter two esters do not represent hydrolysis in equivalent $E \cdot S_2$ complexes, and so Scheme 2 which involves different S_IES and S_AES species seems to be indicated. Further, the relative k_3 values for **1***a* and **1**: $R_1 = H$; $R_2 = C_2H_5$ show a greater than 100-fold enhancement for **1***a*, which is much greater than the fivefold difference in k_{OH}, and further support different S_IES and S_AES complexes. On the other hand, while the relative k_3 values for **1***a* and *b* are *qualitatively* consistent with the expected decrease in reactivity of **1***b* as a result of the increased substitution at the α-carbon atom of the alcohol moiety, it must be admitted that the *quantitative* agreement for the relative k_3 and k_{OH} values for **1***a* and *b* is poor (Table 2). In this regard, it may be significant that **1***b* is the only ester substrate studied to date which does not bear a hydrogen atom on the α-carbon atom of the alcohol group. It is therefore possible that the enhanced k_3 values for **1***b* relative to **1***a* may result from a displaced binding mode for **1***b* in which the catalytically active enzyme functional groups are somewhat more effectively oriented towards the ester carboxyl group.

The close correspondence between the relative k_3 and k_{OH} values for **1***c* and **1**: $R_1 = H$; $R_2 = C_6H_5$, suggests that k_3 represents the hydrolysis of equivalent $E \cdot S_2$ complexes for these two esters; *i.e.* the substrate activation and inhibition that is observed for these two esters both arise from Scheme 1, but with the inequalities (3) and (4) holding, respectively. The considerably larger K_1^{app} value observed for **1***c* (Table 1) than for the unsubstituted mandelic acid derivative is also consistent with this interpretation.

The above arguments suggest, then, that substrate activation for **1***a* and *b* is best reconciled with Scheme 2; *i.e.* different regulatory sites for substrate activation and inhibition. On the other hand, the activation phenomenon for **1***c* is probably more readily reconciled with the use of the same regulatory site as is involved in the more usual substrate inhibition phenomena for hippuric acid esters with this enzyme. This attribution of substrate activation to two different causes also does away with the necessity for endowing the regulatory activation site with the curious substrate specificity that was remarked upon earlier in this discussion.

It is also noteworthy that the specificity constants k_2/K_1 for the hydrolysis of the esters **1***a*, *b*, *c* which show substrate activation are several orders of magnitude smaller than for analogous hippuric acid esters which display substrate inhibition (see Table 1). Since carboxypeptidase A is known to show a preference for hydrophobic substituents on the α-carbon atom of the alcohol moiety, these small values of k_2/K_1 for **1***a* and *b* may simply be due to increases in K_1 resulting from weaker binding of **1***a* and *b* to form the $E \cdot S$ complex relative to those hippurate esters having more hydrophobic alcohol moieties. This is also suggested by the minimum values derived for K_1^{app} (Table 1). However, the decrease in k_2/K_1 by close to a factor of 10^3 by the introduction of a *p*-chloro substituent into the mandelic acid unit is quite unexpected. As was pointed out earlier, the relative k_3 values for **1***c*: $R_1 = H$; $R_2 = p\text{-}ClC_6H_4$ and **1**: $R_1 = H$; $R_2 = C_6H_5$ are quite consistent with the expected influence of the *p*-chloro substituent on the rate of ester hydrolysis. If it is assumed that the observed substituent effect on k_3 would also be reflected in k_2, then it is clear that the large difference in the specificity constants for the chloro- and unsubstituted mandelic acid derivatives arise from differences in K_1 rather than in k_2; *i.e.* the *p*-chloro substituent substantially hinders (by a factor of approximately 10^3) binding of the phenyl ring of the mandelic acid moiety of these esters. This is also consistent with the observed K_1^{app} values for these esters in Table 1, since K_1^{app} must represent a minimum value for K_1. Thus, the relatively trivial structural modification of introducing a chlorine substituent into the mandelic acid phenyl ring not only relieves the substrate inhibition effects that are present for the unsubstituted ester, but also induces substrate activation. A similar effect of a chlorine substituent upon the binding of inhibitor ions to this enzyme has also recently been observed in our laboratory.[3] Thus, benzoic acid is a competitive inhibitor of esterase activity ($K_i = 6.0$ mM (7)), whereas *p*-chlorobenzoic acid is a noncompetitive inhibitor ($K_i = 15$ mM) and consequently must bind at a different site to that of the unsubstituted benzoate anion.

[3]J. W. Bunting and C. D. Myers, unpublished observations.

Can. J. Chem. Downloaded from www.nrcresearchpress.com by 210.87.254.42 on 09/05/12
For personal use only.

The relative k_3 values for **1***a* and *b* are qualitatively consistent with the expected decrease in reactivity due to the increased substitution at the α-carbon atom of the alcohol moiety. On the other hand, k_2/K_1 for the more highly substituted methyllactic acid ester is fivefold greater than for the glycolic acid ester; this suggests that K_1 for **1***b* is significantly smaller than for **1***a* if it can again be assumed that the observed substituent effects on k_3 will also be reflected in k_2. Thus, the methyllactic acid ester appears to bind to the enzyme more strongly than does the glycolic acid ester. While this is in agreement with the observed enzymic preference for hydrophobic substituents on the α-carbon of the alcohol moiety, it is unexpected since all previously known substrates for carboxypeptidase A show a strict requirement for the α-amino acid or α-hydroxy acid to bear a hydrogen atom on the α-carbon atom (13). The ester **1***b* therefore represents the first indication that this enzyme can accept substrates having a methyl group on the α-carbon atom in place of the previously obligatory hydrogen atom.

Two possible explanations for the observed decrease in velocity at very high substrate concentrations (Figs. 2 and 3) are apparent. Bethune (11) has shown that a wide variety of carboxylic acids containing an aromatic ring (including hippuric acid at concentrations similar to those at the higher end of our substrate concentration scale) are able to promote association between carboxypeptidase A molecules to produce oligomers of various degrees of polymerization, which may have reduced catalytic activity. Alternatively, it is possible that substrate inhibition becomes important through the formation of catalytically less active higher-order enzyme–substrate complexes ($E \cdot S_3$, etc.). This latter proposal is clearly inherent in Scheme 2 provided that substrate molecules which bind at the activation and inhibition regulatory sites are not mutually exclusive. Extension of Scheme 2 to include an ESS_IS_A complex which is catalytically active with rate constant k_4 will result in the extension of eq. 1 to eq. 6, where K_4^{app} is the

$$[6] \quad \frac{v}{E} = \frac{k_2^{app}S + k_3S^2/K_3^{app} + k_4S^3/K_3^{app}K_4^{app}}{K_1^{app} + S + S^2/K_3^{app} + S^3/K_3^{app}K_4^{app}}$$

apparent dissociation constant of ESS_IS_A to $E \cdot S_2$ type species (*cf.* K_3^{app} for dissociation of S_AES to S_AE and $E \cdot S$). For large S in eq. 6, v/E approaches k_4, and thus Fig. 6 suggests that for **1***b*, $k_4 = 1.3 \times 10^3$ min^{-1}.

Finally, it should be noted that the hydrolysis of some peptide substrates by this enzyme also seems to be complicated by substrate activation effects which give way to substrate inhibition at higher substrate concentrations (12). The present work represents the first examples, to the best of our knowledge, of the occurrence of *both* substrate activation and inhibition in the kinetics of carboxypeptidase A catalyzed hydrolysis of ester substrates.

We appreciate the continued support of this work by the National Research Council of Canada.

1. W. O. McClure, H. Neurath, and K. A. Walsh. Biochemistry, **3**, 1897 (1964).
2. S. Awazu, F. W. Carson, P. L. Hall, and E. T. Kaiser. J. Am. Chem. Soc. **89**, 3627 (1967).
3. J. W. Bunting and J. Murphy. Biochem. Biophys. Res. Commun. **48**, 1316 (1972).
4. E. T. Kaiser, S. Awazu, and F. W. Carson. Biochem. Biophys. Res. Commun. **21**, 444 (1965).
5. J. W. Bunting and J. Murphy. Can. J. Chem. **52**, 2640 (1974).
6. J. R. Whitaker, F. Menger, and M. L. Bender. Biochemistry, **5**, 386 (1966).
7. J. W. Snoke and H. Neurath. J. Biol. Chem. **181**, 789 (1949).
8. E. T. Kaiser and F. W. Carson. J. Am. Chem. Soc. **86**, 2922 (1964).
9. J. W. Bunting and J. Murphy. Can. J. Biochem. **50**, 1369 (1972).
10. C. K. Ingold. Structure and mechanism in organic chemistry. 2nd ed. Cornell University Press, Ithaca, N.Y. 1969. p. 1135.
11. J. L. Bethune. Biochemistry, **4**, 2698 (1965).
12. R. C. Davies, J. F. Riordan, D. S. Auld, and B. L. Vallee. Biochemistry, **7**, 1090 (1968).
13. F. A. Quiocho and W. M. Lipscomb. Adv. Protein Chem. **25**, 1 (1971).
14. L. G. Lange III, D. S. Auld, and J. F. Riordan. Biochemistry, **13**, 1983 (1974).
15. J. Murphy and J. W. Bunting. Can. J. Chem. In press.

Decomposition Mechanism of 1,2-Dioxetane

GENE BARNETT[1]

Facultad de Ciencias, Universidad de Chile, Santiago de Chile

Received March 29, 1974

GENE BARNETT. Can. J. Chem. **52**, 3837 (1974).

An orbital correlation diagram was constructed for the thermal decomposition of 1,2-dioxetane into products that allow chemiluminescence. A decomposition mechanism is proposed that gives a temperature dependent rupture of the OO bond, thus allowing ring twisting which is followed by the rupture of the CC bond. This mechanism is consistent with results of the thermochemical analysis for this type of reaction. The equilibrium structure of 1,2-dioxetane was determined from the molecular orbital calculations and gave a planar configuration for the COOC ring.

GENE BARNETT. Can. J. Chem. **52**, 3837 (1974).

On a construit un diagramme de corrélation orbitalaire pour la décomposition thermique du peroxyde d'éthylène en produits permettant une chimioluminescence. On propose un mécanisme de décomposition qui donne une rupture du lien OO dépendant de la température, ceci permet une torsion du cycle suivie par une rupture de la liaison CC.Ce mécanisme est cohérent avec les résultats obtenus lors de l'analyse thermochimique pour ce type de réaction. Un calcul d'orbitale moléculaire nous a permis de déterminer la structure à l'équilibre du peroxyde d'éthylène. Ce calcul indique une configuration planaire pour le cycle COOC.

[Traduit par le journal]

Introduction

Reactivity of 1,2-dioxetane molecules is a topic of great interest as the reaction of molecular species originally in their ground electronic states results in a product molecule which is in an electronically excited state. This chemiluminescence process is being actively studied to elucidate the kinetics (1), solvent dependence (2), reaction efficiency (3), and mechanism (4) for the energy producing reaction. We have constructed the reaction coordinate which describes the addition of diatomic oxygen to ethylene to form the reaction intermediate 1,2-dioxetane which then undergoes thermal decomposition into known products that allow chemiluminescence. Our primary concern is the nature of the thermal decomposition. The result of our study is to propose a decomposition mechanism that can be tested directly by experimentation. For the O_2 addition to the carbon double bond it has been established that the diatom is in an excited singlet state which can be generated in several ways (5, 6). The rate of singlet addition to olefins is observed to decrease with increasing ionization potential of the olefin (7). The olefins can be classified according to reactivity, using the rate of peroxide product formation relative to decay of excited O_2 to the ground state to set up a reactivity scale (8). The 1,2-dioxetanes have been in evidence as reaction intermediates for a number of years and recently a number of them have been isolated.[2] Kopecky and Mumford (9) first prepared and studied the thermal decomposition of 3,3,4-trimethyl-1,2-dioxetane while Turro and Lechtken (10) later studied the decomposition and chemiluminescence of tetramethyl-1,2-dioxetane. The kinetic data of Kopecky and Mumford (9) was used in a thermochemical analysis of decomposition kinetics of methylated 1,2-dioxetanes by O'Neal and Richardson (11). The more recent data of Turro and Lechtken (10) was in good agreement with their predictions. Chemiluminescence of the decomposition products has been observed in many cases (9, 12) but only recently has the yield of electronic excited singlet and triplet states been quantitatively determined (10, 13). In view of these experimental observations we develop the reaction coordinate by the use of the tools of quantum chemistry in an effort to gain a better understanding of the processes involved in the overall reaction. We consider the unsubstituted 1,2-dioxetane, H_2COOCH_2, as our system as it is more economical in computer studies and

[1]Present address: School of Pharmacy, University of California, San Francisco, California 94122.

[2]See footnote 1 of ref. 3 for a comprehensive bibliography.

Can. J. Chem. Downloaded from www.nrcresearchpress.com by 210.87.254.40 on 09/05/12
For personal use only.

Can. J. Chem. Downloaded from www.nrcresearchpress.com by 210.87.254.40 on 09/05/12
For personal use only.

because the O'Neal and Richardson (11) analysis supports the view that this is a typical system. All reactants, products, and the intermediate are described by molecular orbitals (MO's) calculated in the CNDO/2 approximation. Details of this method can be obtained from the book, and references therein, of Pople and Beveridge (14). The computer program is available through the Quantum Chemistry Program Exchange (15). The CNDO/2 method has been applied to a large number of molecules and comparison with experimental data established that the method does an acceptable job of predicting bond lengths and bond angles in noncyclic molecules (14). While the method has not been extensively applied to cyclic systems yet, our results for the equilibrium structure of 1,2-dioxetane are quite reasonable based on the structural information available from chemical studies. In all calculations we find the optimum geometry (minimize the total energy) as this removes uncertainty in that we finally have all MO's for the "best CNDO geometry." Our calculations for O_2, C_2H_4, and H_2CO are repetitions of work reported (14). The final geometry for 1,2-dioxetane is presented in Table 1.

Structure of 1,2-Dioxetane

From Table 1, and comparing with data in Pople and Beveridge (14), it is seen that in the equilibrium structure of 1,2-dioxetane the OO bond length is a good CNDO estimate of a peroxide bond while the CO length corresponds well to an alcohol bond and the CC length is a single-bond value. The H_2CC angle shows the hydrogens are tilted by 20° away from the planar configuration they had in the ethylene reactant whereas the two CH_2 groups are in an eclipsed configuration. The four-member ring COOC is planar and has the highly strained angles of 85° for the CCO angles and COO angles of 95°. This is the geometry that gives the lowest total energy for 1,2-dioxetane which implies by the variation principle that we have the best wave function description for the molecule within the approximations of the CNDO method of calculation. The final structure has C_{2v} symmetry which allows us to consider the reaction coordinate under this symmetry and with "best CNDO geometries" throughout.

TABLE 1. Geometry of 1,2-dioxetane[a]

Bond	Length (Å)	Bond angle	Degrees
OO	1.23	COO	95
OC	1.37	CCO	85
CC	1.46	HCO	112
CH	1.16	HCC	119
		HCH	108
		H_2CC	20

[a]The dipole moment has a value of 2.84 D and the net charges on the atomic centers are −0.11, +0.13, −0.01 for O, C, and H, respectively.

The planar ring was not in keeping with our early expectations, considering the nonplanarity of cyclobutane which is isoelectronic with 1,2-dioxetane. But if it is assumed that the nonplanarity of cyclobutane is the result of hydrogen–hydrogen interactions between methylene groups being sufficiently strong to overcome resistance to decreasing the ring angles (16), we have considerable difference in the interactions within 1,2-dioxetane. It has only two pairs of hydrogen–hydrogen interactions, compared to eight for cyclobutane, with the remaining interactions involving lone-pair electrons on the oxygens. The comparison of cyclobutane with trimethylene oxide (17) shows the latter is planar with no barrier to ring puckering by 17° in the ground state (18). This planar structure of trimethylene oxide indicates a weaker interaction for lone-pairs, which one might expect as lone-pairs are rather diffuse for long-range interactions. Thus we think the molecular structure of 1,2-dioxetane as reported in Table 1 is a reasonable description of the molecule in its ground electronic state within the Born–Oppenheimer approximation.

Orbital Correlation Diagram

In Fig. 1 are listed the MO energy levels for the reaction coordinate under C_{2v} point group symmetry for $O_2 + C_2H_4$, H_2COOCH_2, and $H_2CO + OCH_2$. The relative orientations of the molecules are shown in the figure and the orbital notation is defined below the figure. The 1,2-dioxetane energy levels are labeled by their C_{2v} irreducible representation symmetry with the COOC ring in the xz-plane. The dioxetane symmetry orbitals and their energies are given in Table 2 in terms of important atomic orbitals of O and C (the atomic orbitals not included have coefficients at least an order of magnitude smaller than the listed ones). The MO's of O_2 and C_2H_4 as reactants at infinite separation are taken in $\pm$

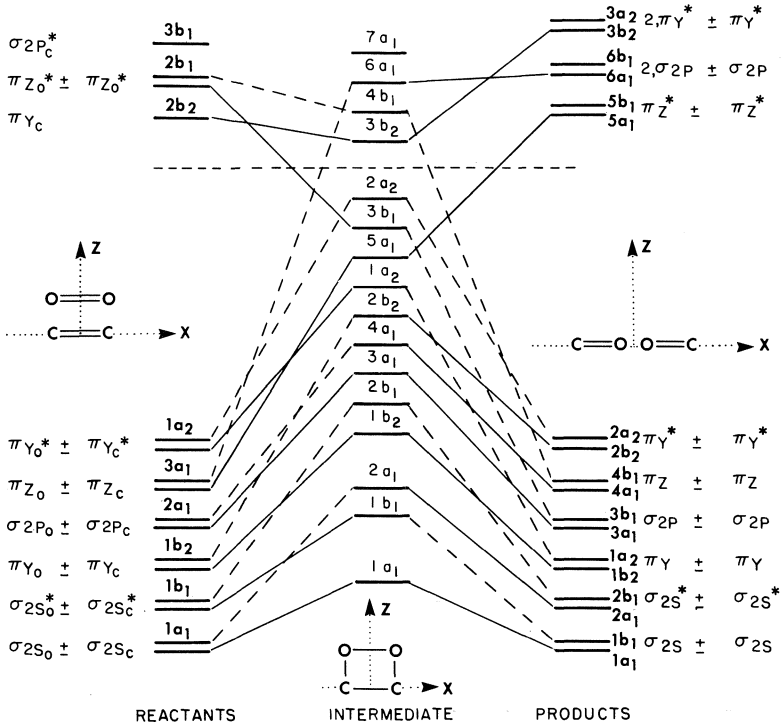

FIG. 1. Orbital correlation diagram. Reactants: The notation is $\sigma_{2sO} \pm \sigma_{2sC} = (2sO_L + 2sO_R) \pm (2sC_L + 2sC_R)$ and $\pi_{yO}^* \pm \pi_{yC}^* = (2pyO_L - 2pyO_R) \pm (2pyC_L - 2pyC_R)$ where $2pyC_L$ is a $2py$ orbital centered on the left (L) carbon atom in the above diagram. Except for $2b_2 = \pi_{yC}$ and $3b_1 = \sigma_{2pC}^*$ the reactant orbitals occur in degenerate pairs of the same symmetry; thus $\pi_{zO} + \pi_{zC}$ and $\pi_{zO} - \pi_{zC}$ are both of $3a_1$ symmetry. Intermediate: The molecular orbitals are defined in Table 2 with reference to the above diagram. The point group symmetries and calculated molecular orbital energies are also given in Table 2. Products: The notation is $\sigma_{2s}^* \pm \sigma_{2s}^* = (2sC_L - 2sO_L) \pm (2sO_R - 2sC_R)$. The product orbitals always occur in degenerate pairs where the symmetry of the upper level is for the minus combination; thus $\pi_y + \pi_y$ has $1b_2$ symmetry and $\pi_y - \pi_y$ has $1a_2$ symmetry.

TABLE 2. Molecular orbitals for 1,2-dioxetane[a]

Energy (a.u.)	Symmetry (C_{2v})	Major atomic orbital components for O and C[a]
−2.07	$1a_1$	$0.5(2s_O) + 0.3(2s_C)$
−1.32	$1b_1$	$-0.5(2\bar{s}_O) + 0.3(2\bar{s}_C) - 0.2(2px_O) - 0.2(2px_C)$
−1.31	$2a_1$	$-0.3(2s_O) + 0.4(2s_C) - 0.2(2pz_O) - 0.2(2pz_C)$
−1.06	$1b_2$	$0.5(2py_O) + 0.5(2py_C)$
−0.95	$2b_1$	$-0.4(2\bar{s}_O) - 0.3(2\bar{s}_C) - 0.1(2px_O) + 0.2(2px_C) - 0.1(2pz_O) + 0.2(2pz_C)$
−0.93	$3a_1$	$-0.2(2s_O) - 0.2(2\bar{p}x_O) + 0.3(2\bar{p}x_C) - 0.4(2pz_O) + 0.3(2pz_C)$
−0.89	$4a_1$	$-0.5(2\bar{p}x_O) + 0.3(2\bar{p}x_C) + 0.3(2pz_O) - 0.3(2pz_C)$
−0.69	$2b_2$	$-0.5(2py_O) + 0.3(2py_C)$
−0.68	$1a_2$	$0.4(2\bar{p}y_O) - 0.4(2\bar{p}y_C)$
−0.57	$5a_1$	$-0.4(2\bar{p}x_O) - 0.5(2\bar{p}x_C)$
−0.55	$3b_1$	$-0.6(2\bar{p}z_O) - 0.4(2\bar{p}z_C)$
−0.47	$2a_2$	$-0.6(2\bar{p}y_O) - 0.2(2\bar{p}y_C)$
+0.24	$3b_2$	$0.5(2py_C)$
+0.25	$4b_1$	$0.5(2\bar{s}_C) - 0.2(2\bar{p}z_C)$
+0.27	$6a_1$	$-0.4(2s_C) + 0.3(2\bar{p}x_C) - 0.1(2pz_O)$
+0.33	$7a_1$	$0.4(2pz_O) + 0.5(2pz_C)$

[a]The following notation is used: $(2s_O) = 2s_{O1} + 2s_{O2}$ and $(2\bar{P}x_C) = 2px_{C1} - 2px_{C2}$.

Can. J. Chem. Downloaded from www.nrcresearchpress.com by 210.87.254.40 on 09/05/12
For personal use only.

Can. J. Chem. Downloaded from www.nrcresearchpress.com by 210.87.254.40 on 09/05/12
For personal use only.

combinations that transform under the C_{2v} group operations for the respective MO's that have the closest energy matching. Thus the π_y MO of O_2 (π_{yO}) is combined with the π_y of ethylene (π_{yC}) to give two MO's for the reactant complex. Under the group symmetry operations $\hat{E}$, $\hat{C}_2(z)$, $\hat{\sigma}(xz)$, $\hat{\sigma}(yz)$, one can readily show that $\pi_{yO} + \pi_{yC}$ and $\pi_{yO} - \pi_{yC}$ both transform as the b_2 irreducible representation. In an ordering of lowest energy first, they are the first MO's of b_2 symmetry to appear and are labeled $1b_2$. The product orbital levels are formed from $\pm$ combinations of the MO's for two formaldehyde molecules at infinite separation with the orientation shown in Fig. 1. By application of the group symmetry operations $\sigma_{2p} + \sigma_{2p}$ has $3b_1$ symmetry while $\sigma_{2p} - \sigma_{2p}$ had $3a_1$ symmetry. The lines between levels in the diagram are correlated on the basis of symmetry; only orbital levels of the same symmetry are connected and lines between levels of the same symmetry do not cross. The levels for the K shells of C and O are not shown as the K electrons stay within these levels and are energetically much lower than the ones displayed here. For the order of energy levels of ethylene and formaldehyde the agreement of our results with other more sophisticated calculations is excellent for occupied levels (those of negative energy) while matching for virtual or unoccupied levels is less good, as one might expect since our orbital basis is extremely limited (19).

Discussion

With the orbital correlation diagram of Fig. 1 we will consider the decomposition of 1,2-dioxetane into a product that allows one formaldehyde molecule in the ground state and the other in an electronic excited state. The electron configuration for the ground state of H_2CO is

$$...(\sigma_{2s})^2(\sigma_{2s}{}^*)^2(\pi_y)^2(\sigma_{2p})^2(\pi_z)^2(\pi_y{}^*)^2$$

while the 1-electron excitations that allow a molecule in one of the low lying experimentally observed electronic excited states are

$$\pi_y{}^* \rightarrow 2\pi_y{}^*,\ \pi_y{}^* \rightarrow \pi_z{}^*,\ \pi_y{}^* \rightarrow 2\sigma_{2p}$$

The $\pi_y{}^* \rightarrow 2\sigma_{2p}$ excited state would allow a chemiluminescence band around 1700 Å from the $^1B_2$ state; the $\pi_y{}^* \rightarrow 2\pi_y{}^*$ $^1A_1$ state emits at approximately 1550 Å; the most likely excited state is $\pi_y{}^* \rightarrow \pi_z{}^*$ with a band at 3530–2300 Å which is assigned to the transition from $^1A_2$ to the ground state (20). The electronic configuration for the excited molecule will be assumed as

$$...(\sigma_{2s})^2(\sigma_{2s}{}^*)^2(\pi_y)^2(\sigma_{2p})^2(\pi_z)^2(\pi_y{}^*)^1(\pi_z{}^*)^1$$

A closer inspection of the MO's shows that this $\pi_y{}^* \rightarrow \pi_z{}^*$ assignment is the one often referred to as the carbonyl $n \rightarrow \pi^*$ transition (21). We must emphasize that *this choice of excited state is arbitrary*. One could consider many possibilities but this choice has the following virtues: (*i*) this choice is consistent with the expected experimental observation of chemiluminescence; (*ii*) the corresponding triplet state $^3A_2$ lies close in energy; (*iii*) this is only a one-electron excited state as opposed to a many-electron one; (*iv*) this result correlates with the more reasonable assignment for the 1,2-dioxetane intermediate as other choices would force more electron excitations or excitations to much higher states.

The ground electron configuration for the 1,2-dioxetane intermediate as seen from Table 2 is

$$...(3a_1)^2(4a_1)^2(2b_2)^2(1a_2)^2(5a_1)^2(3b_1)^2(2a_2)^2$$

With our choice of product state described above a two-electron excited state for 1,2-dioxetane is required in order to obey the symmetry restrictions of the orbital correlation diagram. The excitations are $2b_2 \rightarrow 4b_1$ and $5a_1 \rightarrow 4b_1$, thus the electron configuration of the excited state that correlates to the desired products is

$$...(4a_1)^2(2b_2)^1(1a_2)^2(5a_1)^1(3b_1)^2(2a_2)^2(4b_1)^2$$

The $2b_2$, $5a_1$, and $4b_1$ symmetry MO's for 1,2-dioxetane are shown in simplified form in Fig. 2. It is seen that $2b_2$ describes π bonding in the OO and CC bonds and some antibonding in the CO bonds. The $5a_1$ orbital is primarily σ bonding in the OO and CC bonds whereas $4b_1$ is π^* antibonding for the CC bond. The result of this double promotion is to greatly weaken, or break, the OO bond and also greatly increase the antibonding character of the CC bond thus causing it to weaken or break as well. O'Neal and Richardson (11) demonstrated that the kinetic data for thermal decomposition is consistent with a two-step mechanism. Since the 1,2-dioxetanes have an estimated half-life stability at 60 °C that ranges from 10 s (for the unmethylated compound) to over 2 h, it is reasonable to assume that 1,2-dioxetane is excited from its ground state during the decomposition pro-

Can. J. Chem. Downloaded from www.nrcresearchpress.com by 210.87.254.40 on 09/05/12
For personal use only.

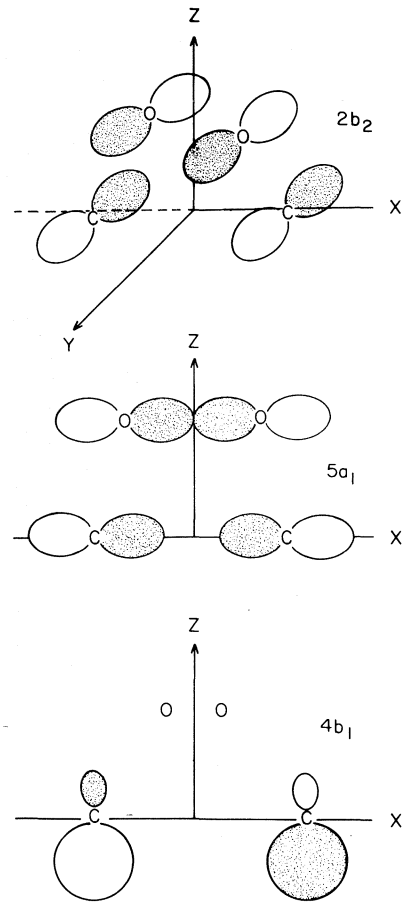

FIG. 2. Approximate representation of the $2b_2$, $5a_1$, and $4b_1$ molecular symmetry orbitals of 1,2-dioxetane.

cess. One can speculate that the $2b_2 \rightarrow 4b_1$ excitation would occur first as the $2b_2$ orbital, having π_y character, is more spatially available for a collision excitation in the solvent–solute reaction vessel. Then the second step, $5a_1 \rightarrow 4b_1$, can occur as the molecule undergoes twisting to remove ring strain (estimated at 26 kcal/mol (11). Thus we can represent the proposed decomposition mechanism as

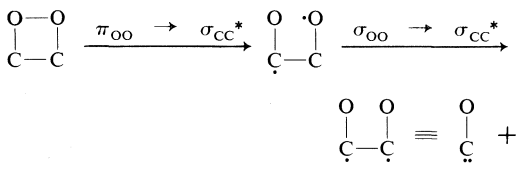

which is consistent with the O'Neal and Richardson (11) model based solely on thermochemical arguments. They found the first step to be rate limiting and report estimated activation energies of about 22 kcal/mol. The energy to break the OO bond is about 10 kcal/mol greater than this so we must account for the smaller activation energy which has been verified experimentally for the two methylated compounds. Both sets of kinetic data (9, 10) were obtained at elevated temperatures in a benzene solvent. Thus one expects considerable excitation of the ring-bending mode of vibration while solvent–solute interactions, which can be rather strong since 1,2-dioxetane has a sizable dipole moment as noted in Table 1, can enhance the anharmonicity of this mode and thus allow curve crossing at lowered energies. This proposed mechanism makes it plausible that the first step for the mechanism is slow and temperature dependent while the second step, which would depend on the possibility for ring twisting about the CC bond, would be relatively fast. The increase in decomposition rate with increasing temperature has been observed for 3,3-dimethyl-1,2-dioxetane and 3-methyl-3-phenyl-1,2-dioxetane (1). A pertinent experiment then is to study decomposition kinetics for a substituted 1,2-dioxetane where ring twisting cannot occur easily. While this proposed mechanism requires a double excitation of the intermediate molecule it still has the statistical probability of a single excitation process. The first excitation must happen phenomenologically but the second step is a spontaneous movement to release the highly strained condition of the ring system.

An alternative mechanism has been proposed by Turro and Lechtken (4). They suggest that the decomposition proceeds via a concerted process where vibronic interaction enhances a spin–orbit effect great enough to cause rotation about the CO bond thus breaking the OO bond. They report solvent effects on the decomposition of tetramethyl-1,2-dioxetane in support of this mechanism (4). However it has now been reported that, while there is a solvent dependence for the decomposition reaction, the luminescence pathway is independent of solvent (2). As further rebuttal of their mechanism we note that the quantum mechanical expression for the vibronic–spin–orbit interaction appears only in the second-order of perturbation theory (22). While it has been pointed out that for systems similar to the COOC planar ring these interactions may have a greater effect than usual, it would seem unlikely that a second-order pertur-

Can. J. Chem. Downloaded from www.nrcresearchpress.com by 210.87.254.40 on 09/05/12
For personal use only.

bation would effect the breaking of a chemical bond. The spin–orbit coupling in a light atom such as oxygen is usually considered negligible compared to the heavy atoms and heavy atom coupling is generally much less significant when the atom is part of a planar aromatic molecular system (23).

One would like to predict whether the decomposition leading to chemiluminescence will give fluorescence or phosphorescence emission. Unfortunately with orbital correlation diagrams one cannot determine if the preferred pathway is via the singlet or triplet excited product molecule. This is a very interesting question that seems to depend on the substituent nature of the 1,2-dioxetane molecule. A theoretical approach would best be to use configuration interaction calculations in order to construct a state correlation diagram although Pople (24) has considered a method using complex MO's, as opposed to real MO's used here, that might throw light on this problem.

The remaining process on the reaction coordinate then is the interaction of singlet molecular oxygen with the ethylene olefin to form the intermediate, a topic that has received extensive general coverage (6, 25). The concerted addition of oxygen to an olefin has been considered in terms of mechanisms that involve various types of intermediates in addition to dioxetanes, including peroxiranes, ionic and radical intermediates. Our study can contribute nothing new to this general problem as we do not know in which electronic configuration the 1,2-dioxetane is initially formed. If we assume it is formed in the ground electronic state then one possible process is for oxygen to add to C_2H_4 which must have a double excitation $(\pi_y)^2 \rightarrow (\pi_z^*)^2$. This excited state of ethylene has been considered in the theoretical study of Kaldor and Shavitt (19). They found it to lie slightly above the ionization threshold for the molecule which is in keeping with our introductory considerations of the experimental data.

We need to consider one last point briefly. On thermochemical grounds O'Neal and Richardson (11) suggested that the unmethylated 1,2-dioxetane will only give chemiluminescence if the decomposition product is an eximer. To consider this question directly requires state energy levels. However, in addition to the mechanism presented above, the 1,2-dioxetane could decompose via a $(5a_1)(2a_2) \rightarrow (4b_1)^2$ process giving the ion pair $H_2CO^+ + {}^-OCH_2$, a process that seems less probable than the one discussed above.

Conclusions

By application of approximate molecular orbital calculations we have found a planar structure for 1,2-dioxetane as reported in Table 1. On the basis of the microwave study of trimethylene oxide we can expect the ring to have very little, if any, barrier to puckering in the zero vibrational level. The bond lengths seem quite reasonable.

Using an orbital correlation diagram we are able to propose a mechanism for the thermal decomposition of 1,2-dioxetane that is consistent with the available experimental data on the process. Further our mechanism is consistent with that proposed solely on thermochemical considerations and it is the simplest mechanism that will give such agreement. This mechanism is amenable to direct experimental verification.

In conclusion then, we believe this study has given useful information on both the question of the structure of 1,2-dioxetane and the thermal decomposition mechanism for this molecule. The stability of the methylated compounds is such that we can expect some experimental studies on the structures to be reported in the near future. We would expect molecular orbital studies to give a nonplanar ring structure for methylated compounds but the proposed mechanism for the thermal decomposition would remain essentially unchanged. Experimental studies on the decomposition mechanism, a temperature dependent step followed by a step dependent on the possibility for ring twisting, need to be carried out.

We acknowledge stimulating discussions with W. D. Jones and W. H. Richardson of San Diego, and R. Van Fossen of Santiago. Valuable comments of the referee were greatly appreciated.

1. W. H. Richardson, M. B. Yelvington, and H. E. O'Neal. J. Am. Chem. Soc. **94**, 1619 (1972).
2. T. Wilson, M. E. Landis, A. L. Baumstark and P. D. Bartlett. J. Am. Chem. Soc. **95**, 4765 (1973).
3. W. H. Richardson, F. C. Montgomery, M. B. Yelvington, and G. Ranney. J. Am. Chem. Soc. **96**, 4045 (1974).
4. N. J. Turro and P. Lechtken. J. Am. Chem. Soc. **95**, 264 (1973); Pure Appl. Chem. **33**, 363 (1973).

5. W. H. RICHARDSON and V. HODGE. J. Org. Chem. **35**, 1216 (1970).
6. D. R. KEARNS. Chem. Rev. **71**, 395 (1971).
7. D. R. KEARNS. J. Am. Chem. Soc. **95**, 6554 (1969).
8. C. S. FOOTE. Acc. Chem. Res. **1**, 104 (1968).
9. K. R. KOPECKY and C. MUMFORD. Can. J. Chem. **47**, 709 (1969).
10. N. J. TURRO and P. LECHTKEN. J. Am. Chem. Soc. **94**, 2886 (1972).
11. H. E. O'NEAL and W. H. RICHARDSON. J. Am. Chem. Soc. **92**, 6553 (1970).
12. F. MCCAPRA and R. A. HANN. Chem. Commun. 422 (1969).
13. E. H. WHITE, P. D. WILDES, J. WIECKO, H. DOSHAN, and C. C. WEI. J. Am. Chem. Soc. **95**, 7050 (1973); W. H. RICHARDSON, F. C. MONTGOMERY, and M. B. YELVINGTON. J. Am. Chem. Soc. **94**, 9277 (1972).
14. J. A. POPLE and D. L. BEVERIDGE. Approximate molecular orbital theory. McGraw-Hill Co., New York. 1970.
15. Quantum Chemistry Program Exchange. No. 91, Chemistry Department, Indiana University, Bloomington, Indiana.
16. J. D. ROBERTS and M. C. CASERIO. Basic principles of organic chemistry. Benjamin Inc., New York. 1965.
17. E. L. ELIEL, N. L. ALLINGER, S. J. ANGYAL, and G. A. MORRISON. Conformational analysis. John Wiley & Sons, Inc., New York. 1965.
18. S. I. CHANN, J. ZINN, and W. D. GWINN. J. Chem. Phys. **34**, 1319 (1961).
19. (*a*) U. KALDOR and I. SHAVITT. J. Chem. Phys. **48**, 191 (1968); (*b*) J. L. WHITTEN and M. HACKMEYER. J. Chem. Phys. **51**, 5584 (1969).
20. G. HERZBERG. Molecular spectra and molecular structure. Vol. III. Van Nostrand Co., Inc., New York. 1966.
21. M. ORCHIN and H. H. JAFFÉ. Symmetry, orbitals and spectra. John Wiley & Sons, Inc., New York. 1971.
22. A. C. ALBRECHT. J. Chem. Phys. **38**, 354 (1963).
23. S. P. MCGLYNN, T. AZUMI, and M. KONOSHITA. The triplet state. Prentice-Hall, Englewood Cliffs, N.J. 1969. pp. 261, 409.
24. J. A. POPLE. Int. J. Quantum Chem. **5**, 175 (1971).
25. S. INAGAKI, S. YAMABE, H. FUJIMOTO, and K. FUKUI. Bull. Chem. Soc. Japan. **45**, 3510 (1972).

Can. J. Chem. Downloaded from www.nrcresearchpress.com by 210.87.254.40 on 09/05/12
For personal use only.

Synthesis of 4-*O*-β-D-Galactopyranosyl-L-rhamnopyranose

GWENDOLYN M. BEBAULT, GUY G. S. DUTTON, AND NORMAN A. FUNNELL
Department of Chemistry, The University of British Columbia, Vancouver, British Columbia V6T 1W5

Received May 14, 1973[1]

GWENDOLYN M. BEBAULT, GUY G. S. DUTTON, and NORMAN A. FUNNELL. Can. J. Chem. **52,** 3844 (1974).

4-*O*-β-D-Galactopyranosyl-L-rhamnopyranose has been synthesized in 60% yield by condensation of 2,3,4,6-tetra-*O*-acetyl-α-D-galactopyranosyl bromide with methyl 2,3-*O*-isopropylidene-α-L-rhamnopyranoside using mercuric cyanide in acetonitrile (Helferich reaction). The disaccharide is a syrup but the derived alditol and alditol peracetate are crystalline compounds.

GWENDOLYN M. BEBAULT, GUY G. S. DUTTON et NORMAN A. FUNNELL. Can. J. Chem. **52,** 3844 (1974).

4-*O*-(β-D-Galactopyrannosyle)-L-rhamnopyrannose a été synthétisé avec un rendement de 60% par une réaction de condensation du α-D-tétraacétylbromogalactose avec le méthyl-2,3-*O*-isopropylidène-α-L-rhamnopyrannoside en utilisant le cyanure mercurique dans l'acétonitrile (réaction de Helferich). Le disaccharide est une huile visqueuse tandis que l'alditol correspondant et le peracétate de l'alditol sont des composés cristallins.

Can. J. Chem. Downloaded from www.nrcresearchpress.com by 210.87.254.42 on 09/05/12
For personal use only.

Although L-rhamnose is widely distributed in nature only one glycosylrhamnose (1) had been synthesized prior to 1972. Hence, the synthesis of a series of disaccharides with L-rhamnose linked through position 4 as the aglycon, was undertaken (2–6). We now report the synthesis of another member of this series, namely, 4-*O*-β-D-galactopyranosyl-L-rhamnose (**6**). Such disaccharides are important reference compounds in structural studies and for immunological investigations. The disaccharide described here (**6**) has been found as part of the structure of the capsule of *Klebsiella* K-type 47 (7). The rationale for such syntheses and detailed experimental procedures for many of the steps have already been given (2). Since this work has been completed and reported (8) an additional synthesis of **6** has been published (9).

Crystalline 2,3,4,6-tetra-*O*-acetyl-α-D-galactopyranosyl bromide (**1**), prepared by the method of Fletcher (10), was condensed with methyl 2,3-*O*-isopropylidene-α-L-rhamnopyranoside (**2**) in acetonitrile using mercuric cyanide. Methyl 2,3-*O*-isopropylidene-4-*O*-(2,3,4,6-tetra-*O*-acetyl-β-D-galactopyranosyl-α-L-rhamnopyranoside (**3**) was obtained crystalline in 85% yield. The isopropylidene group is very labile and such yields can be obtained only if all traces of water, acid, and alcohol are removed from the reagents. For this reason the use of crystalline **1** is to be preferred rather than a syrup. Treatment of **3** with trifluoroacetic acid in chloroform (11) removed the isopropylidene group to give **4**, acetolysis of which gave the fully acetylated disaccharide (**5**) as a syrup. Deacetylation provided the syrupy disaccharide (**6**) that was characterized as the crystalline disaccharide alditol (**7**), m.p. 179–180°, and crystalline alditol peracetate (**8**), m.p. 114–115°. The disaccharide (**6**) was obtained in an overall yield of 60% based on **2**.

The structure of the disaccharide follows from the method of synthesis and from methylation analysis, and the products from periodate oxidation of the methyl glycoside of the disaccharide.

Experimental

General methods and experimental procedures are essentially as described previously (2). Melting points were taken between glass slides on a Fisher–Johns apparatus and are uncorrected. Optical rotations were measured with a Perkin–Elmer model 141 polarimeter at 23 ± 1°. Nuclear magnetic resonance spectra were recorded on a Varian XL-100 instrument using tetramethylsilane as internal standard except as noted. Gas–liquid partition chromatography was carried out on an F and M 720 instrument at a gas flow rate of 60 ml/min using columns: (*a*) 2 ft × 1/4 in. 20% SE 30 (F and M Division, Hewlett Packard Avondale, Pennsylvania), (*b*) 4 ft × 1/4 in. 5% butanediol succinate on 80–100 mesh Diatoport S and (*c*) 6 ft × 1/4 in. 15% OS 138 on 100–120 mesh Gas Chrom Q. Thin-layer chromatography was carried out using solvent systems A and B (see below) on silica gel G (EM Reagents). The dried plates were visualized by spraying with 35% ethanolic sulfuric acid and heating to about 150° for 3–5 min. Paper chromatographic separa-

[1]Revision received August 21, 1974.

Can. J. Chem. Downloaded from www.nrcresearchpress.com by 210.87.254.42 on 09/05/12
For personal use only.

tions were carried out on Whatman No. 1 paper using the upper layer of solvent systems C and D (see below) and were visualized using silver nitrate in acetone for non-reducing compounds (12) and *p*-anisidine spray (13) in trichloroacetic acid for reducing sugars. Solvent A, ethyl ether – toluene (2:1); B, butanone–water azeotrope; C, ethyl acetate – pyridine – water (4:1:1); D, 1-butanol–ethanol–water (4:1:5). Solutions were concentrated below 50° *in vacuo*.

*2,3,4,6-Tetra-O-acetyl-α-D-galactosyl Bromide (**1**)*

This was prepared in 80% yield from β-D-galactose pentaacetate (14) by the method of Fletcher (10). The product (**1**) was recrystallized from ethyl ether at 0° and had m.p. 80–82°; $[\alpha]_D$ +217° (*c* 1.0, chloroform) (lit. (15) m.p. 83–84°); $[\alpha]_D$ +215° (*c* 1, chloroform). Preparation of **1** by other methods (16, 17) was less satisfactory.

*Methyl 2,3-O-Isopropylidene-α-L-rhamnopyranoside (**2**)*

This was prepared by the method of Levene and Muskat (18) with the addition of 2,2-dimethoxypropane (5% of the volume of acetone) or as previously reported (2). If the latter method is employed the ion-exchange resin should be soaked overnight in methanol rather than acetone to avoid the formation of condensation products.

*Methyl 2,3-O-Isopropylidene-4-O-(2,3,4,6-tetra-O-acetyl-β-D-galactopyranosyl)-α-L-rhamnopyranoside (**3**)*

To a solution of **2** (883 mg, 4.0 mmol, dried at 60°/1 mm for 2 h) and dry mercuric cyanide (0.90 g) in dry acetonitrile (8.8 ml) was added in one portion with stirring the freshly prepared crystalline bromide **1** and stirring was continued for 1 h at which time t.l.c. in solvent A showed the reaction to be complete. Conventional work-up (2) gave **3** (1.87 g, 3.4 mmol, 85%) which, after recrystallization from ethanol (25 ml/g), had m.p. 192–193°; $[\alpha]_D$ −24.4° (*c* 2.05, chloroform); R_f (t.l.c. solvent A) 0.61; n.m.r. ($CDCl_3$): τ 6.64 (3H singlet, C-1 OCH_3), 7.84–8.02 (12H, OAc's), 8.72 (3H doublet, $J_{5,6}$ = 6 Hz, CH_3), 8.47, 8.66 (3H singlets isopropylidene CH_3's).

Anal. Calcd. for $C_{24}H_{36}O_{14}$: C, 52.55; H, 6.62. Found: C, 52.44; H, 6.64.

*Methyl 4-O-(2,3,4,6-Tetra-O-acetyl-β-D-galactopyranosyl)-α-L-rhamnopyranoside (**4**)*

A solution of **3** (1.0 g) in chloroform (45 ml) was reacted at room temperature for 1 h with trifluoroacetic acid containing 1% water (5 ml). The product (**4**) was obtained as a syrup which showed only one spot on t.l.c. R_f 0.06 (solvent A) and 0.70 (solvent B); yield 0.92 g; n.m.r. ($CDCl_3$): 6.64 (3H singlet, C-1 OCH_3), 7.84–8.02 (12H, OAc's), 8.68 (3H doublet, $J_{5,6}$ = 6 Hz, CH_3).

*1,2,3-Tri-O-acetyl-4-O-(2,3,4,6-tetra-O-acetyl-β-D-galactopyranosyl)-α-L-rhamnopyranose (**5**)*

Compound **4** (0.90 g) in acetic anhydride (5 ml) was shaken with 10 ml of a solution of concentrated sulfuric acid in acetic anhydride (2%, v/v) at room temperature for 3 h. The product (**5**, 0.83 g) showed a major component on t.l.c. with R_f 0.43 (solvent A) and $[\alpha]_D$ −55° (*c* 2.0, chloroform) but neither preparative t.l.c. nor silica gel column chromatography yielded crystalline material; n.m.r. ($CDCl_3$) τ 4.03 (1H doublet, $J_{1,2}$ = 1.5 Hz, H-1), 7.82–8.05 (21H OAc's), 8.66 (3H doublet, $J_{5,6}$ = 6 Hz, CH_3).

*4-O-β-D-Galactopyranosyl-L-rhamnose (**6**)*

Deacetylation of **5** (0.80 g) gave **6** (0.40 g) as a syrup which showed only one spot on paper chromatography (solvent C, 48 h) with $R_{glucose}$ 0.80; $[\alpha]_D$ −8° (*c* 2.2, water); n.m.r. (D_2O, external TMS): τ 4.83 (1H doublet, $J_{1,2}$ = 1.5 Hz, H-1 of α-L-rhamnose), 5.07 (1H singlet, H-1 of β-L-rhamnose), 5.29 (1H doublet, $J_{1',2'}$ = 6.8 Hz, H-1'), 8.60 (3H doublet, $J_{5,6}$ = 6 Hz, CH_3).

Gas–liquid chromatography of the per(trimethylsilyl) disaccharide (column *a* at 230°) gave two peaks at 14.4 (82%) and 17.1 min (18%); per(trimethylsilyl)sucrose 22.7 min.

*4-O-β-D-Galactopyranosyl-L-rhamnitol (**7**)*

Reduction of the disaccharide (**6**, 0.15 g) gave **7** which crystallized from methanol (1 g/10 ml). Recrystallization from methanol gave pure **7**, m.p. 179–180°; $[\alpha]_D$ +2.8° (*c* 2.2, water); $R_{glucose}$ 0.53 (solvent C, 48 h); n.m.r. (D_2O, external TMS): τ 5.48 (1H doublet, $J_{1',2'}$ = 7.7 Hz, H-1'), 8.71 (3H doublet, $J_{5,6}$ = 6 Hz, CH_3).

Anal. Calcd. for $C_{12}H_{24}O_{10}$: C, 43.90; H, 7.37. Found: C, 43.78; H, 7.37.

Gas–liquid chromatography of the per(trimethylsilyl)-alditol (column *a* at 240°) gave one peak at 12.0 min; per(trimethylsilyl)sucrose 16.3 min.

Acetylation of **7** gave 4-*O*-β-D-galactopyranosyl-L-rhamnitol octaacetate (**8**) which, after recrystallization from ethanol (80 ml/g) had m.p. 114–115°; $[\alpha]_D$ −62.8° (*c* 2.1, chloroform); R_f 0.35 (t.l.c., solvent A); n.m.r. ($CDCl_3$); τ 7.84–8.04 (24H, OAc's), 8.67 (3H doublet, $J_{5,6}$ = 6Hz, CH_3).

Anal. Calcd. for $C_{28}H_{40}O_{18}$: C, 50.60; H, 6.07. Found: C, 50.64; H, 6.20.

*Methyl 4-O-β-D-Galactopyranosyl-α-L-rhamnopyranoside (**9**)*

Deacetylation of **4** (0.70 g) gave syrupy **9** (0.40 g) which showed one spot on paper chromatography (solvent C) with $R_{glucose}$ 2.93; $[\alpha]_D$ −49° (*c* 1.6, methanol); n.m.r. (D_2O, external TMS): τ 5.40 (1H doublet, $J_{1',2'}$ = 7.7 Hz, H-1'), 6.70 (3H singlet, C-1 OCH_3), 8.73 (3H doublet, $J_{5,6}$ = 5.5 Hz, CH_3).

Methylation

Compound **9** (0.52 g) in dry methyl sulfoxide (1 ml) was reacted with methyl sulfinyl anion (1.5 *M*, 1 ml) for 4 h and then shaken with methyl iodide (0.5 ml) overnight. The product was recovered as a syrup having R_f 0.13 (t.l.c., solvent A); $[\alpha]_D$ −39° (*c* 1.1, chloroform); n.m.r. ($CDCl_3$): τ 5.35 (1H doublet, $J_{1,2}$ = 1.5 Hz, H-1), 5.48 (1H doublet, $J_{1',2'}$ = 7.5 Hz, H-1'), 6.51–6.71 (21H, OCH_3's), 8.76 (3H doublet, $J_{5,6}$ = 6 Hz, CH_3). Hydrolysis, reduction, and acetylation followed by g.l.c. on column *c* at 225° gave two components the retention times and mass spectra of which were consistent with 1,4,5-tri-*O*-acetyl-2,3-di-*O*-methyl-L-rhamnitol (19.7 min) and 1,5-di-*O*-acetyl-2,3,4,6-tetra-*O*-methyl-D-galactitol (27.2 min).

Periodate Oxidation

Reaction of compound **9** with sodium metaperiodate (0.05 *M*, 100 ml) at 4° in the dark showed a rapid uptake of 2 mol of periodate with the consumption becoming constant (2.95 mol) in 24 h. Reduction and methanolysis gave a syrup, paper chromatography (solvent D) of

which indicated the presence of 1-deoxy-D-erythritol and glycerol. Gas–liquid chromatography of the acetylated syrup (column *b* at 125°) gave components with retention times and mass spectra identical to the peracetylated derivatives of 1-deoxy-D-erythritol (10 min) and glycerol (16 min).

The authors thank the National Research Council of Canada for the award of Scholarships (to N.A.F. and G.M.B.) and for a grant that made this work possible.

1. R. J. BEVERIDGE, W. A. SZAREK, and J. K. N. JONES. Carbohydr. Res. **19**, 107 (1971).
2. G. M. BEBAULT and G. G. S. DUTTON. Can. J. Chem. **50**, 3373 (1972).
3. G. M. BEBAULT and G. G. S. DUTTON. Can. J. Chem. **52**, 678 (1974).
4. J. M. BERRY and G. G. S. DUTTON. Can. J. Chem. **52**, 681 (1974).
5. G. M. BEBAULT, G. G. S. DUTTON, and C. K. WARFIELD. Carbohydr. Res. **34**, 174 (1974).
6. G. M. BEBAULT and G. G. S. DUTTON. Carbohydr. Res. In press.
7. H. BJÖRNDAL, B. LINDBERG, J. LÖNNGREN, K. G. ROSELL, and W. NIMMICH. Carbohydr. Res. **27**, 373 (1973).
8. G. M. BEBAULT, J. M. BERRY, G. G. S. DUTTON, N. FUNNELL, and C. K. WARFIELD. 165th National Meeting, Dallas, Texas, April, 1973. Abstr. CARB 35.
9. R. R. KING and C. T. BISHOP. Carbohydr. Res. **32**, 239 (1974).
10. H. G. FLETCHER, JR. Methods Carbohydr. Chem. **2**, 228 (1963).
11. A. J. ACHER, Y. RABINSOHN, E. S. RACHAMAN, and D. SHAPIRO. J. Org. Chem. **35**, 2436 (1970).
12. W. E. TREVELYAN, D. P. PROCTER, and J. S. HARRISON. Nature, **166**, 444 (1950).
13. L. HOUGH, J. K. N. JONES, and W. H. WADMAN. J. Chem. Soc. 1702 (1950).
14. F. J. BATES (*Editor*). Polarimetry, saccharimetry and the sugars. U.S. Govt. Print. Off. Washington, 1942, p. 488.
15. J. CONCHIE and G. A. LEVVY. Methods Carbohydr. Chem. **2**, 335 (1963).
16. J. K. DALE. J. Am. Chem. Soc. **38**, 2187 (1916).
17. T. ISHIKAWA and H. G. FLETCHER, JR. J. Org. Chem. **34**, 563 (1969).
18. P. A. LEVENE and I. E. MUSKAT. J. Biol. Chem. **105**, 431 (1934).

Can. J. Chem. Downloaded from www.nrcresearchpress.com by 210.87.254.42 on 09/05/12
For personal use only.

The Kinetics of the Isotopic Exchange of Oxygen-18 with the Oxygen of Copper(II) Molybdate

D. G. KLISSURSKI, R. A. ROSS, AND T. J. GRIFFITH

Faculty of Science, Lakehead University, Thunder Bay, Ontario P7B 5E1

Received April 16, 1974

D. G. KLISSURSKI, R. A. ROSS, and T. J. GRIFFITH. Can. J. Chem. **52**, 3847 (1974).

The kinetics of the exchange of gas-phase oxygen-18 with the oxygen of copper(II) molybdate has been studied in an all-glass "static-circulation" apparatus using a quartz differential reactor. The activation energy of the exchange between 522 and 601 °C was 40 kcal mol^{-1} and the reaction order was 0.7 in the oxygen partial pressure range 5 to 30 Torr. The structure and physical properties of the molybdate were determined by X-ray, i.r., thermal and chemical analysis.

It is shown that the exchange reactivity of the surface and bulk oxygen in copper(II) molybdate is closer to the reactivity of oxygen in MoO_3 than it is to the oxygen in CuO. From current theories on the relationships between exchange rates and catalytic properties, it is deduced that copper(II) molybdate would be expected to exhibit properties similar to those of V_2O_5 in catalytic oxidation reactions.

D. G. KLISSURSKI, R. A. ROSS et T. J. GRIFFITH. Can. J. Chem. **52**, 3847 (1974).

On étudie la cinétique de l'échange en phase gazeuse de l'oxygène-18 avec l'oxygène du molybdate de cuivre(II) dans un appareil de "circulation statique" tout en verre en utilisant un réacteur différentiel en quartz. L'énergie d'activation de cet échange entre 522 et 601 °C est de 40 kcal mol^{-1}; l'ordre de la réaction est de 0.7 pour une pression partielle d'oxygène variant entre 5 et 30 Torr. On détermine la structure et les propriétés physiques du molybdate par les rayons-X, l'infrarouge et des analyses thermiques et chimiques.

La réactivité d'échange de l'oxygène dans le molybdate de cuivre(II), en surface et en gros, est plus proche de la réactivité de l'oxygène dans MoO_3 que de l'oxygène dans CuO. En se basant sur les théories actuelles sur les relations entre les taux d'échange et les propriétés catalytiques, on déduit que le molybdate de cuivre(II) doit présenter des propriétés similaires à celles de V_2O_5 dans les réactions d'oxydation catalytique. [Traduit par le journal]

Can. J. Chem. Downloaded from www.nrcresearchpress.com by 210.87.254.42 on 09/05/12
For personal use only.

Introduction

Transition metal molybdates are often basic components of numerous catalysts that are used in selective oxidation reactions. For this reason it is of interest to investigate the reactivity of oxygen in the surface layer of the compounds by the oxygen isotopic exchange technique. From such investigations information can be obtained concerning the bonding energy of oxygen on the catalyst surface, the degree of surface heterogeneity and the rate of diffusion of oxygen from the surface layer into the bulk lattice of the compounds.

While single oxides have been studied systematically (1–7) and correlations proposed for exchange rates and activation energies with the activities and selectivities of the oxides in a large group of redox reactions (6–8), very few studies have been reported for complex oxide catalysts. It was felt that such studies might lead to the introduction and development of new selective heterogeneous catalysts for partial or complete oxidation processes and hence the present communication reports results obtained from an investigation on the exchange of molecular oxygen with the oxygen of copper(II) molybdate.

Experimental

Materials

Copper(II) molybdate was prepared by a combined method of precipitation and solid state reaction. Solutions of ammonium paramolybdate, $(NH_4)_6Mo_7O_{24}\cdot 4H_2O$ (0.1 *M*), and copper nitrate, $Cu(NO_3)_2\cdot 6H_2O$ (0.2 *M*), were mixed vigorously at 25 °C and the suspension evaporated to dryness. After prolonged grinding, the dry precipitate was calcined for 30 h at 620 °C in an oxygen atmosphere with intermediate grinding at 5 h intervals. The copper(II) molybdate obtained was deep green in color and of high purity as confirmed by X-ray and chemical analysis and by i.r. spectroscopy. The i.r. spectrum obtained by KBr disc technique and shown in Fig. 1 is in general agreement with that obtained by Clark and Doyle (9). However, a characteristic absorption band was observed at 965 cm^{-1} while the bands reported at 845 and 990 cm^{-1} were not registered. It was assumed that these bands could be attributed to the presence of free molybdena (characteristic bands at 830 and 985 cm^{-1}) in the previous preparation (9).

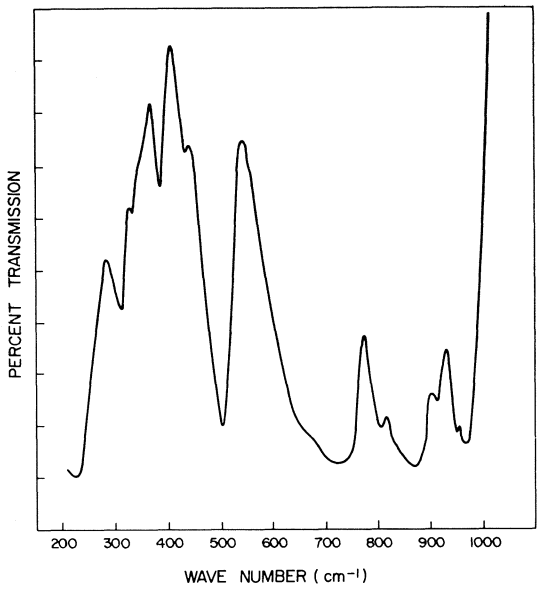

FIG. 1. Infrared spectrum of copper(II) molybdate.

The *d* values and the respective percent intensities as determined by X-ray analysis were in the order: 9.20–10%, 5.54–33%, 3.96–26%, 3.72–100%, 3.36–91%, 3.30–50%, 3.21–40%, 3.11–25%, 2.97–73%, 2.71–45%, 2.58–26%, and 2.50–26%. These data are in agreement with those of Nassau and Abrahams (10) and consistent with the established values for the lattice parameters of this compound (11).

DTA and TGA runs in air showed that decomposition commenced at about 750 °C and was intensive at 820 and 825 °C as indicated by a large endothermic peak on the DTA curve. A peritectic decomposition at 825 °C was previously noted also by Nassau and Abrahams (10).

A fraction of the powder with grain size 0.5–1 mm was used for the kinetic studies. The specific area of the fraction was 0.48 $m^2\ g^{-1}$ (BET, krypton, $\delta = 19.4$ Å^2).

The oxygen isotope mixture contained ~20% $^{18}O_2$ and was prepared by dilution of oxygen-18 enriched gas (99%) oxygen-18, Isomet Corp.) with previously-dried high-purity oxygen (Matheson Ltd.).

Apparatus and Procedure

The kinetic measurements were carried out with the all-glass static circulation apparatus described previously (12) utilizing a quartz differential reactor. The total volume of the circulation loop of the apparatus was 470 ml and analysis of the isotopic composition of the gaseous oxygen was carried out with a Hitachi–Perkin–Elmer model RMU-7 double-focussing mass spectrometer.

Samples were heat treated at 600 °C for 2 h in dry circulating oxygen, 20 Torr, in order to remove adsorbed gases and to stabilize the oxygen content in the surface layer. The trap before the reactor was cooled in liquid nitrogen. After pretreatment, the reactor was thermostated at the desired temperature and circulation of the oxygen isotope mixture was started. The oxygen pressure was measured at the beginning and at the end of each experiment by mercury and dibutylphthalate U-tube manometers. The difference between the values did not exceed 3–5% and was associated with the collection of samples in previously-evacuated ampoules. Experiments were mostly carried out at 10 Torr, while the pressure was varied between 5 and 30 Torr for the determination of the reaction order.

Results

Treatment of the Experimental Data

The specific rate of exchange was calculated from the equation

$$[1] \qquad R = \frac{N_s \ln (1 - F)}{S(1 + \lambda)\tau \cdot 2}$$

where F, the extent to which equilibrium has been approached, is defined as $F = (C_0 - C)/(C_0 - C_\infty)$. C_0 is the initial concentration of ^{18}O (at .%); C is the concentration of ^{18}O at the time of exchange, τ; and C_∞ is the equilibrium concentration of ^{18}O calculated on the basis of a material balance. $\lambda = N_s/N_g$, where N_s is the number of the exchangeable oxygen atoms in the sample, N_g is the number of the oxygen atoms in the gas phase, S is the total surface area of the sample, cm^2, and R is the exchange rate per unit area, molecules $O_2\ cm^{-2}\ s^{-1}$.

The applicability of eq. 1 for the calculation of the exchange rates is shown in Fig. 2 in which the dependence of log $(1 - F)$ on the duration of the exchange is plotted for a series of experiments.

A slight deviation from linear dependence was observed in the case of a few samples which had been preheated above 750 °C. It was felt that this was probably due to the partial decomposition of the compound. The main kinetic results are summarized in Table 1.

The temperature dependence of the exchange rate is presented as an Arrhenius-type plot in

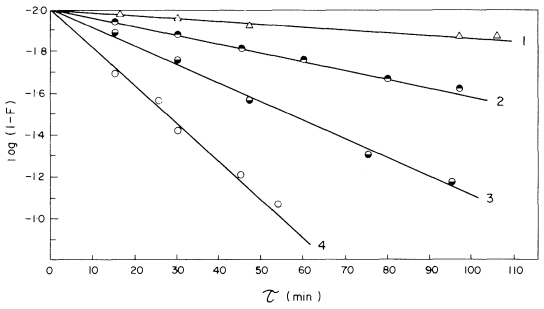

FIG. 2. The dependence of log $(1 - F)$ on time of exchange: *1*, 522 °C; *2*, 540 °C; *3*, 501 °C, and *4*, 601 °C. (The values of log $(1 - F)$ at 501 °C are multiplied 10 times.)

Can. J. Chem. Downloaded from www.nrcresearchpress.com by 210.87.254.42 on 09/05/12
For personal use only.

Can. J. Chem. Downloaded from www.nrcresearchpress.com by 210.87.254.42 on 09/05/12
For personal use only.

TABLE 1. The influence of temperature and oxygen pressure on the specific rate of exchange of oxygen-18 with the oxygen of copper(II) molybdate

No.	Temperature (°C)	P_{O_2} (Torr)	Rate (molecules cm^{-2} s^{-1}) ($\times 10^{11}$)
1	501	10	0.38
2	503	10	0.51
3	522	10	0.71
4	523	10	0.83
5	540	10	1.6
6	543	10	1.8
7	567	10	4.6
8	601	10	8.3
9	606	10	10.5
10	606	10	11.5
11	540	5	1.1
12	540	6.5	1.3
13	540	10	1.8
14	540	15	2.5
15	540	20	2.8
16	540	30	4.1

Fig. 3. A value of 40 kcal mol^{-1} was calculated for the activation energy of exchange from these results.

Figure 4 shows the dependence of the specific rate of exchange on the presence of the oxygen isotope mixture between 5 and 30 Torr. The value determined for the reaction order was 0.7.

For a comparison the kinetic characteristics of the exchange for several other compounds are given in Table 2.

Discussion

Previous studies (1–8) have shown that metal oxides may be subdivided into three groups. The first group includes some transition metal oxides, Co_3O_4, NiO etc., whose surface oxygen exhibits energetically non-uniform behavior (12, 19), and the rate of exchange decreases with an increase of the degree of exchange. The oxides in the second group, such as Fe_2O_3 and MgO, exchange their surface oxygen at a constant rate, but the exchangeable oxygen is only a few monolayers deep. Finally, the third group includes oxides which exchange not only surface but also lattice oxygen with a constant rate. This feature can be explained mainly through the occurrence of the fast self-diffusion of oxygen in these compounds; for example V_2O_5 (5), CeO_2 (14), and Nb_2O_5 (13). MoO_3 and CuO, which can be regarded as precursors of copper(II) molybdate, possess quite different oxygen reactivities with

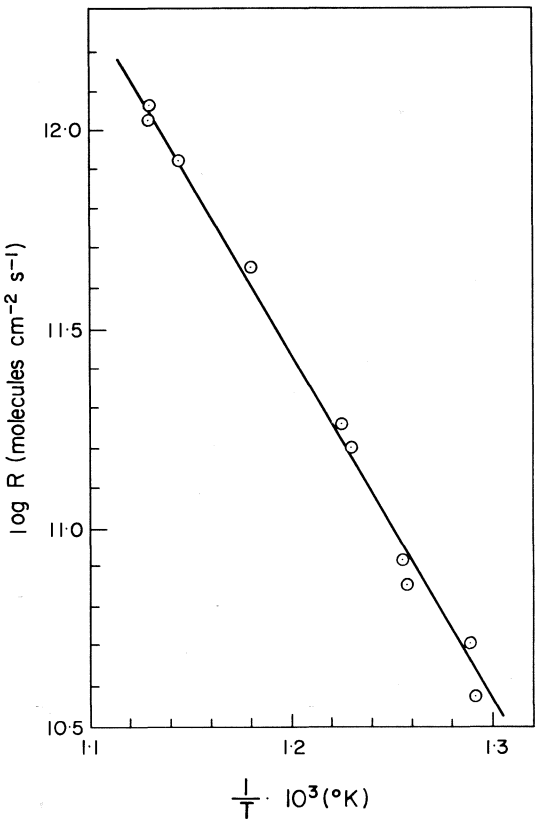

FIG. 3. The temperature dependence of the rate of exchange.

respect to the isotopic exchange and belong to the third and first groups, respectively.

As can be seen from the comparative date in Table 2, the exchange reactivity of the surface and bulk oxygen in copper(II) molybdate is closer to the reactivity of oxygen in MoO_3 than it is to that for CuO (Table 2). Further, copper(II) molybdate shows a close similarity in reactivity to cobalt(II) and iron(III) molybdates (16), and to the other molybdates of the fourth period metals (15). In general the reactivity of oxygen in these molybdates is closer to the reactivity of oxygen in MoO_3 than it is to that of oxygen in the other oxide component. While the rate of exchange of molecular oxygen with the oxygen of the oxides of the fourth period metals varies over several orders of magnitude (2, 15), the rate of exchange for the pure molybdates changes within the limits of one order of magnitude (15). Such an "equalization" may be related to the nature of the oxygen bonds in these compounds and to their lattice structures.

TABLE 2. Kinetic characteristics of oxygen isotopic exchange for copper(II) molybdate, molybdena, cupric oxide, and vanadium pentoxide

Compound	Temperature interval of measurements (°C)	Experimental conditions: Temperature (°C)	Oxygen pressure (Torr)	Rate of exchange (molecules/cm² s)	Activation energy (kcal/mol)	Reference
$CuMoO_4$	500–610	601	10	8.3×10^{11}	40	—
MoO_3	520–630	600	10	2.5×10^{11}	58	15
CuO	250–350	300	40	7×10^{11}	26	2
V_2O_5	450–500	500	11	5×10^{9}	46	20
		600	11	1.6×10^{11}*	—	

*Extrapolated.

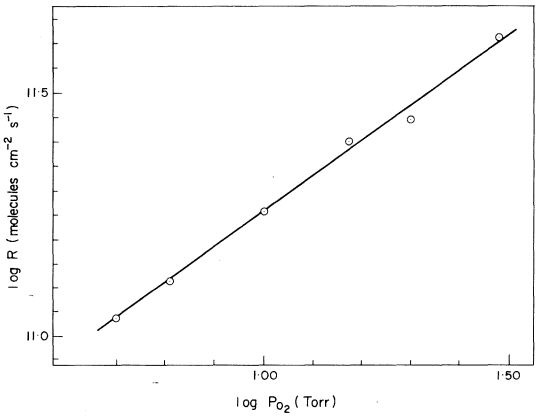

FIG. 4. The dependence of the specific rate of exchange on oxygen pressure at 540 °C.

According to some recent proposals (17–19) the oxygen species in solid catalysts which is active in catalytic processes is bound to one metal atom and theoretical calculations (18) show that when bonds are formed with several metal atoms a significant increase of the bond strength results. Since the activity of the molybdates in the exchange reaction, reflects mainly the activity of the MoO_3 component (the bivalent or trivalent cations in these compounds have only a small influence) it can be assumed that the oxygen form which is most active in the exchange with molecular oxygen is bound only to one molybdenum atom.

It is interesting to note that the rate of exchange of molecular oxygen with the oxygen of copper(II) molybdate, other conditions being equal, is significantly higher than the rate of exchange with the molybdates of other bivalent metals from the fourth period of the Periodic Table (15). This phenomenon could be explained by the lower bonding energy of oxygen in this particular compound since according to Nassau and Abrahams (10), the optical transmission curve indicates that there is a looser binding of oxygen in copper(II) molybdate than in compounds with the scheelite structure. This is consistent with the lower coordination numbers and the lower melting point of copper(II) molybdate.

Current concepts suggest that a correlation may exist between the rate of exchange of molecular oxygen with the oxygen of oxides and their activity and selectivity in a large number of redox-type catalytic reactions. In the case of loosely-bound and highly-reactive surface oxygen, oxidation processes lead to complete oxidation. Surface oxygen possessing lower reactivity favors partial oxidation processes and the subsequent reactions that would lead to complete oxidation are almost totally suppressed.

For a series of oxidation reactions, the valid use of a Brønsted–Polanyi expression

$$E = E_0 \pm q \qquad [2]$$

has been demonstrated (6), where E is the activation energy of the catalyzed reaction and q is the bonding energy of oxygen in the surface layer of the catalyst. The established relationship between q and the activation energy of the oxygen isotopic exchange, E_e

$$E_e = \beta q \qquad [3]$$

where β is a coefficient of proportionality, permits the activation energy and the rate of exchange to be used for a prognosis of the properties of oxidation catalysts. For copper(II) molybdate, the activation energy and the rate of oxygen exchange are not very far removed from those values for vanadium(V) oxide and on this basis

Can. J. Chem. Downloaded from www.nrcresearchpress.com by 210.87.254.42 on 09/05/12
For personal use only.

it can be supposed that copper(II) molybdate, if stable at the reaction conditions, will reflect properties similar to those of vanadium(V) oxide as an oxidation catalyst.

1. E. R. S. WINTER. Advances in catalysis. Vol. 10. Academic Press, New York. 1959. p. 196.
2. G. K. BORESKOV. Advances in catalysis. Vol. 15. 1964. p. 285.
3. G. K. BORESKOV. Disc. Faraday Soc. **41**, 263 (1966).
4. E. R. S. WINTER. J. Chem. Soc. (A), 2889 (1968).
5. J. NOVAKOVA. Catal. Rev. **4**, 77 (1971).
6. G. K. BORESKOV. Kinet. Catal. **14**, 7 (1973).
7. E. F. MCCAFFREY, D. G. KLISSURSKI, and R. A. ROSS. Proc. Vth Int. Congress on Catalysis, Palm Beach, 1972. North Holland, Amsterdam, 1973.
8. D. G. KLISSURSKI. Proc. IVth Int. Congress on Catalysis. Moscow, 1968. Ed. Academy Kiado, Budapest, 1970.
9. G. M. CLARK and W. P. DOYLE. Spectrochim. Acta, **22**, 1441 (1966).
10. N. NASSAU and S. C. ABRAHAMS. J. Cryst. Growth, **2**, 136 (1968).
11. S. C. ABRAHAMS, J. L. BERNSTEIN, and P. B. JAMIESON. J. Chem. Phys. **48**, 2619 (1968).
12. V. V. POPOVSKII and G. K. BORESKOV. Kinet. Catal. **1**, 566 (1960).
13. R. A. ROSS, D. G. KLISSURSKI, and T. J. GRIFFITH. Z. Phys. Chem. (N.F.), **86**, 50 (1973).
14. G. V. ANTOSHIN, KH. M. MINACHEV, and R. V. DMITRIEV. Kinet. Catal. **9**, 816 (1968).
15. R. A. ROSS, D. G. KLISSURSKI, and T. J. GRIFFITH. To be published.
16. G. K. BORESKOV, V. S. MUZYKANTOV, G. I. PANOV, and V. V. POPOVSKII. Kinet. Catal. **10**, 1043 (1969).
17. T. V. ADAMIYA, YU. A. MISCHENKO, and A. I. GEL'BSTEIN. Kinet. Catal. **11**, 734 (1970).
18. N. N. BULGAKOV, YU. A. BORISSOV, and V. V. POPOVSKII. Kinet. Catal. **14**, 468 (1973).
19. F. TRIFIRO, I. PASQUON, and P. CENTOLA. J. Catal. **10**, 86 (1968).
20. V. S. MUZYKANTOV, V. V. POPOVSKII, and N. I. MIKICHUR. Kinetika i kataliz (Russ.), **5**, 745 (1964).

Can. J. Chem. Downloaded from www.nrcresearchpress.com by 210.87.254.42 on 09/05/12
For personal use only.

The Chlorine Atom Sensitized Oxidation and the Ozonolysis of C_2Cl_4[1]

ECKART MATHIAS,[2] EUGENIO SANHUEZA,[3] I. C. HISATSUNE, AND JULIAN HEICKLEN

Department of Chemistry and Center for Air Environment Studies, The Pennsylvania State University, University Park, Pa., 16802

Received April 16, 1973[4]

Can. J. Chem. Downloaded from www.nrcresearchpress.com by 210.87.254.42 on 09/05/12
For personal use only.

ECKART MATHIAS, EUGENIO SANHUEZA, I. C. HISATSUNE, and JULIAN HEICKLEN. Can. J. Chem. **52**, 3852 (1974).

The chlorine atom initiated oxidation of C_2Cl_4 was studied both in the absence and presence of O_3 at 24 and 32 °C. In the absence of O_3, the products are $CCl_3CCl(O)$ and CCl_2O, and they are produced in a long-chain process in a ratio of 2.5 at 24 °C and 3.0 at 32 °C. The product producing step involves the decay of C_2Cl_5O radicals

[6*a*] $$C_2Cl_5O \rightarrow CCl_3CCl(O) + Cl$$

[6*b*] $$\rightarrow CCl_3 + CCl_2O$$

The ratio k_{6a}/k_{6b} is 5.0 at 24 °C and 6.0 at 32 °C since CCl_3 reacts with O_2 to produce another CCl_2O molecule. In the presence of O_3 the ratio $\Phi\{CCl_3CCl(O)\}/\Phi\{CCl_2O\}$ drops, $\overline{CCl_2CCl_2O}$ is produced, and the chain length is reduced. The change in $\Phi\{CCl_3CCl(O)\}/\Phi\{CCl_2O\}$ is a function of $[O_3]/[O_2]$ and is attributed to the additional reactions

[12*a*] $$C_2Cl_5 + O_3 \rightarrow CCl_3CCl(O) + Cl + O_2$$

[12*b*] $$\rightarrow CCl_2O + CCl_3 + O_2$$

The epoxide yield is a function of $[C_2Cl_4]/[O_3]$ and is attributed to the reaction of ClO with C_2Cl_4. The ClO is produced by the reaction of $Cl\cdot$ with O_3

[10] $$Cl + O_3 \rightarrow ClO + O_2$$

which competes with

[2] $$Cl + C_2Cl_4 \rightarrow C_2Cl_5$$

The ratio $k_2/k_{10} = 6.7$. The reduction in yield as O_3 is added results from the terminating reaction

[15*b*] $$ClO + O_3 \rightarrow ClO_2 + O_2$$

The ClO_2 reacts further with O_3 to produce Cl_2O_7.

The reaction of O_3 with C_2Cl_4 at 24 °C also produces mainly $CCl_3CCl(O)$ and CCl_2O with $\overline{CCl_2CCl_2O}$ as a minor product. Other minor products detected after extended conversions included Cl_2, CO, and CO_2. However *c*-C_3Cl_6 was not found. The ratio $[CCl_3CCl(O)]/[CCl_2O]$ is < 1. Moreover, the addition of O_2 retarded the reaction, indicating a long chain mechanism in which both free radicals (species with an odd number of electrons) and CCl_2 were absent. A diradical chain mechanism is presented which explains the main features. The chain step is the addition of CCl_2O_2 to C_2Cl_4

[25] $$CCl_2O_2 + C_2Cl_4 \rightarrow CCl_2O_2C_2Cl_4$$

The adduct then reacts with O_3 in a chain regenerating step or with O_2 in a chain terminating step.

ECKART MATHIAS, EUGENIO SANHUEZA, I. C. HISATSUNE et JULIAN HEICKLEN. Can. J. Chem. **52**, 3852 (1974).

On a étudié, à 24 et à 32 °C, en présence et en absence de O_3, l'oxydation initiée par des atomes de chlore de C_2Cl_4. En l'absence de O_3, les produits sont $CCl_3CCl(O)$ et CCl_2O; ils sont produits par un processus en chaîne dans un rapport de 2.5 à 24 °C et de 3.0 à 32 °C. Les étapes amenant la formation de ces produits impliquent la décomposition des radicaux C_2Cl_5O

---

[1]CAES Report No. 304–73.

[2]Present address: General Electric Company, Plastics Division, 1 Plastics Avenue, Pittsfield, Mass., 01201.

[3]Fulbright Fellow: 1972–1974.

[4]Revision received June 5, 1974.

[6a] $C_2Cl_5O \rightarrow CCl_3CCl(O) + Cl$

[6b] $\rightarrow CCl_3 + CCl_2O$

Le rapport k_{6a}/k_{6b} est égal à 5.0 à 24 °C et à 6.0 à 32 °C puisque CCl_3 réagit avec O_2 pour amener la formation d'une autre molécule de CCl_2O. En présence de O_3, le rapport $\Phi[CCl_3CCl(O)]/\Phi[CCl_2O]$ diminue alors que $\overline{CCl_2CCl_2O}$ est produit et que la longueur de la chaîne est réduite. Le changement dans le rapport $\Phi[CCl_3CCl(O)]/\Phi[CCl_2O]$ est une fonction de $[O_3]/[O_2]$ et est attribué aux réactions supplémentaires:

[12a] $C_2Cl_5 + O_3 \rightarrow CCl_3CCl(O) + Cl + O_2$

[12b] $\rightarrow CCl_2O + CCl_3 + O_2$

Le rendement en époxyde est une fonction de $[C_2Cl_4]/[O_3]$ et on l'attribue à la réaction du ClO sur le C_2Cl_4. Le ClO est produit par la réaction de $Cl\cdot$ avec O_3

[10] $Cl + O_3 \rightarrow ClO + O_2$

qui est en compétition avec

[2] $Cl + C_2Cl_4 \rightarrow C_2Cl_5$

Le rapport k_2/k_{10} est égal à 6.7. La réduction de rendement, observé lorsque du O_3 est additionné, résulte de la réaction de terminaison

[15b] $ClO + O_3 \rightarrow ClO_2 + O_2$

Le ClO réagit avec O_3 pour conduire à Cl_2O_7.

La réaction de O_3 avec C_2Cl_4 à 24 °C conduit aussi à la formation de $CCl_3CCl(O)$ et de CCl_2O comme produits principaux aux côtés de $\overline{CCl_2CCl_2O}$ sous forme de produit mineur. D'autres produits mineurs ont été détectés après plusieurs conversions et ceci inclus Cl_2, CO et CO_2. On n'a toutefois jamais trouvé de c-C_3Cl_6. Le rapport de $[CCl_3CCl(O)/[CCl_2O]$ est moins que un. Toutefois l'addition de O_2 retarde la réaction; on peut en déduire que le mécanisme de la réaction est un mécanisme à longue chaîne duquel CCl_2 et les radicaux libres (les entités avec un nombre impairs d'électrons) sont absents. Un mécanisme en chaîne impliquant un bi-radical est présenté qui explique les caractéristiques principales de la réaction. L'initiation de la chaîne est l'addition CCl_2O_2 sur C_2Cl_4

[25] $CCl_2O_2 + C_2Cl_4 \rightarrow CCl_2O_2C_2Cl_4$

L'adduit réagir alors avec O_3 dans une étape regénérant la chaîne ou avec O_2 dans une étape terminant la chaine. [Traduit par le journal]

Introduction

The chlorine atom initiated oxidation of C_2Cl_4 has been studied in several laboratories (1–4), and the results reviewed (5). In all the studies, the major products were $CCl_3CCl(O)$ and CCl_2O. The reaction was a long chain reaction with chain lengths of about 300 independent of light intensity, I_a, or any of the reactant pressures if the O_2 pressure was sufficiently high. The ratio of product quantum yields $\Phi\{CCl_3CCl(O)\}/\Phi\{CCl_2O\}$ was 5.7 at 80–100 °C (4) and 4.0 at 40–80 °C (3). The ratio has not been measured at lower temperatures.

The main features of the mechanism of the reaction were worked out in a brilliant paper by Huybrechts *et al.* (4), who found different intensity dependences for the rate of the O_2-inhibited chlorination ($I_a^{1/2}$) and the chlorine atom initiated oxidation (I_a). They argued that since these two reactions are coupled, they have common chain-breaking steps which must be bimolecular in radicals to explain the $I_a^{1/2}$ dependence of the rate of chlorination. Therefore, the oxidation must be propagated by a radical–radical reaction. This led them to propose the following mechanism

[1] $Cl_2 + h\nu \rightarrow 2Cl$

[2] $Cl + C_2Cl_4 \rightarrow C_2Cl_5$

[3] $C_2Cl_5 + O_2 \rightarrow C_2Cl_5O_2$

[4a] $2C_2Cl_5O_2 \rightarrow 2C_2Cl_5O + O_2$

[4b] $\rightarrow (C_2Cl_5O)_2 + O_2$

[5] $C_2Cl_5O_2 + C_2Cl_5 \rightarrow (C_2Cl_5O)_2$

[6a] $C_2Cl_5O \rightarrow CCl_3CCl(O) + Cl$

[6b] $\rightarrow CCl_2O + CCl_3$

They proposed that the CCl_3 radical somehow reacted with O_2 to regenerate Cl atoms

[7] $CCl_3 + O_2 \rightarrow CCl_2O + Cl + \frac{1}{2}O_2$

Reaction 7 is of course not an elementary reac-

Can. J. Chem. Downloaded from www.nrcresearchpress.com by 210.87.254.42 on 09/05/12
For personal use only.

Can. J. Chem. Downloaded from www.nrcresearchpress.com by 210.87.254.42 on 09/05/12
For personal use only.

tion, but would presumably occur via the sequence

$$CCl_3 + O_2 \rightarrow CCl_3O_2$$

$$2CCl_3O_2 \rightarrow 2CCl_3O + O_2$$

$$CCl_3O \rightarrow CCl_2O + Cl$$

Their mechanism does not include the ClO radical as an intermediate.

There is an alternative to reaction 7 in which the ClO radical is an intermediate, but CCl_3O is not

[8] $$CCl_3 + O_2 \rightarrow CCl_2O + ClO$$

[9] $$ClO + C_2Cl_4 \rightarrow C_2Cl_5O$$

In order to test the two possibilities, we have examined the chlorine atom sensitized oxidation of C_2Cl_4 in the presence of O_3. The O_3 will react with chlorine atoms in the well-established reaction (6, 7)

[10] $$Cl + O_3 \rightarrow ClO + O_2$$

It should also react with CCl_3 and C_2Cl_5 as follows

[11] $$CCl_3 + O_3 \rightarrow CCl_3O + O_2$$

[12] $$C_2Cl_5 + O_3 \rightarrow C_2Cl_5O + O_2$$

With either mechanism, the $[CCl_3CCl(O)]/[CCl_2O]$ ratio will be unchanged unless the ratio k_{6a}/k_{6b} is different for the C_2Cl_5O radicals produced in reactions 4*a*, 9, and 12. In that case, the addition of O_3 will shift the product ratio, regardless of the mechanism. However, if the pathway suggested by Huybrechts *et al.* (4) is correct, the addition of O_3 will produce ClO radicals only by a competition of O_3 and C_2Cl_4 for Cl atoms, while the alternative pathway will also lead to a suppression of ClO by increasing the $[O_3]/[O_2]$ ratio. Furthermore if new products are formed, they must come from the new radical (either ClO or CCl_3O, as the case may be) as a precursor.

Before the studies in the presence of O_3 were done it was necessary to reexamine the chlorine atom initiated oxidation of C_2Cl_4 at lower temperatures to obtain the ratio $[CCl_3CCl(O)]/[CCl_2O]$. Also, we needed to study the dark reaction between O_3 and C_2Cl_4 both in the absence and presence of O_2. The results of these studies are reported here.

Experimental

For the experiments at 24 °C the reactant gases were mixed in an infrared cell and the reaction monitored by infrared spectroscopy. The kinetic apparatus has been described previously (8). For most of the reactions, the gases were mixed directly in the cell, but for some reactions, the reactants were frozen into a cold finger on the infrared cell and then permitted to vaporize. The kinetic apparatus was connected to a glass vacuum line (one stage glass oil diffusion pump) provided with stopcocks greased with high vacuum silicone grease (Dow Corning).

The infrared cell consisted of a 10.3 cm long Pyrex cylinder (4.8 cm o.d.) provided with NaCl or KCl windows sealed onto the cell with high vacuum silicone grease (Dow Corning).

The irradiation experiments were carried out in the infrared cell by exposing the length side of the cell to radiation emitted from a GE-H100-A4/T medium pressure mercury lamp with a Pyrex envelope. The radiation was filtered through a 3.08 cm thick Corning 7–54 filter to remove visible radiation.

Two infrared spectrophotometers were used. Relatively fast reactions were followed with a Perkin–Elmer 112, single beam, infrared spectrophotometer with a CaF_2 prism. Slow reactions were followed with a Perkin–Elmer 521 grating infrared spectrophotometer.

The rates of slow reactions were followed by scanning repeatedly over the absorption bands corresponding to the carbonyl absorptions of both the phosgene and the trichloroacetyl chloride. Reactions which were too fast for this procedure were followed by monitoring continuously the appearance of the carbonyl absorption bands of the products.

The infrared bands used for analysis and their respective peak extinction coefficients (to base 10) are: C_2Cl_4, 920 cm^{-1}, 0.0165 $Torr^{-1}$ cm^{-1}; O_3, 1055 cm^{-1}, 0.003 $Torr^{-1}$ cm^{-1}; $CCl_3CCl(O)$, 1810 cm^{-1}, 0.0145 $Torr^{-1}$ cm^{-1}; CCl_2O, 1830 cm^{-1}, 0.0180 $Torr^{-1}$ cm^{-1}. The extinction coefficient for the 1810 cm^{-1} band of CCl_2O was also measured to be 0.0140 $Torr^{-1}$ cm^{-1}. This value was needed for computation of the $CCl_3CCl(O)$ pressure, since both compounds absorb at 1810 cm^{-1}.

Tetrachloroethylene was supplied by J. T. Baker (Analyzed, chlorine free) and degassed, at first several times at −196 °C and subsequently several times at −23 °C. Finally, it was distilled *in vacuo* from a −23 °C bath to a cold finger (at −196 °C) of the permanent storage bulb.

Nitrogen and oxygen were supplied by Philip Wolf and Sons. Nitrogen was used without further purification. Oxygen was purified by the method described by Nightingale *et al.* (9).

Chlorine (Matheson, 99.5% purity) was degassed thoroughly, and then repeatedly exposed to KOH pellets to remove the HCl. The absence of HCl was confirmed by infrared analysis. The chlorine was then slowly distilled into the storage vessel by keeping the KOH–H_2O–KCl mixture at as low a temperature as practical.

Ozone was produced as needed from a static electric discharge (Tesla coil) of oxygen and collected at −196 °C. The O_3 was then degassed at −196 °C two or three times to remove any excess oxygen.

The gas pressures of tetrachlorethylene, O_3, Cl_2, and low pressures of oxygen were measured using a cathetometer and a Kel-F oil (grade KF-3) manometer. Nitrogen and high pressures of oxygen were measured with a mercury manometer.

TABLE 1. Chlorine atom sensitized oxidation of C_2Cl_4 in the absence of O_3

$[O_2]$ (Torr)	$[C_2Cl_4]$ (Torr)	$\Phi\{CCl_3CCl(O)\}$	$\Phi\{CCl_2O\}$	$\frac{\Phi\{CCl_3CCl(O)\}}{\Phi\{CCl_2O\}}$	$-\Phi\{C_2Cl_4\}$	$\frac{-\Phi\{C_2Cl_4\}^*}{\Phi\{ox\}}$
		$T = 24\,°C$, $[Cl_2] = 2.76 \pm 0.20$ Torr, $I_a = 1.29 \pm 0.09$ mTorr/s				
5.8	3.00	21	8.6	2.4	—	—
49	3.95	79	33	2.4	—	—
535	2.32	252†	96†	2.6	—	—
		$T = 32\,°C$, $[Cl_2] = 1.93 \pm 0.13$ Torr, $I_a = 0.30 \pm 0.04$ mTorr/s				
3.23	1.26	60	20	3.0	—	—
8.9	1.68	90	30	3.0	—	—
23.3	1.73	82.5	28	2.95	92	0.95
32.2	3.26	171	56	3.1	193	0.93
88.1	1.88	211	76	2.85	248	0.99
91.0	3.21	226	73	3.1	277	1.06
436	1.77	260†	80†	3.2	278	0.93
450	1.80	257	84	3.1	—	—

*$\Phi\{ox\} = \Phi\{CCl_3CCl(O)\} + \frac{1}{2}\Phi\{CCl_2O\}$.
†Actinometer for all runs (with and without O_3) at 24 and 32 °C, respectively. Assumed $\Phi\{ox\} = 300$.

The experiments at 32 °C were done slightly differently than those at 24 °C. The light source was a Hanovia medium-pressure mercury lamp, and the radiation passed through a Pyrex filter and a Corning 7-54 filter to isolate the 3660 Å line before entering a T-shaped reaction cell which was situated in the sample beam of a Beckman IR-10 spectrophotometer.

The O_3 was distilled at −186 °C before use, and its pressure was measured with a H_2SO_4 manometer. The C_2Cl_4, Cl_2, and low O_2 pressures were measured with a silicone oil manometer. High pressures of O_2 were measured with a Wallace and Tiernan absolute pressure indicator.

The epoxide $\overline{CCl_2CCl_2O}$ was analyzed by following its infrared absorption band at 1340 cm^{-1}. Its peak extinction coefficient was estimated to be 3.1×10^{-3} $Torr^{-1}$ cm^{-1}. This estimate was based on the consumption of C_2Cl_4 in experiments at high $[O_3]/[C_2Cl_4]$ where the epoxide is the main product.

The infrared bands used for analysis in the 32 °C runs were the same as at 24 °C. Because a different instrument was used the peak extinction coefficients were slightly different: C_2Cl_4, 920 cm^{-1}, 0.0178 $Torr^{-1}$ cm^{-1}; CCl_2O, 1830 cm^{-1}, 0.0152 $Torr^{-1}$ cm^{-1}; $CCl_3CCl(O)$, 1810 cm^{-1}, 0.009 $Torr^{-1}$ cm^{-1}.

Results

Cl Atom Oxidation

When mixtures of Cl_2, O_2, and C_2Cl_4 are photolyzed with radiation principally at 3660 Å, the products of the reaction are $CCl_3CCl(O)$ and CCl_2O exclusively; there is no indication of tetrachloroethylene oxide, $\overline{CCl_2CCl_2O}$, production. The results are summarized in Table 1. The quantum yields for both products increase with O_2 pressure approaching an upper limiting value. For actinometric purposes we assume the upper limiting value to be 300 for $\Phi\{CCl_3CCl(O)\} + \frac{1}{2}\Phi\{CCl_2O\}$ in accordance with earlier workers (1–5). The ratio of products, $\Phi\{CCl_3CCl(O)\}/\Phi\{CCl_2O\}$ is 2.5 ± 0.1 at 24 °C and 3.0 ± 0.2 at 32 °C. This trend is in keeping with that found by others, *i.e.* 4.0 at 40–80 °C (3) and 5.7 at 80–100 °C (4). Thus $k_{6a}/k_{6b} = 5.0$ at 24 °C and 6.0 at 32 °C, since each CCl_3 gives an additional CCl_2O.

With O_3 also present $\overline{CCl_2CCl_2O}$ is also produced, and at high $[O_3]/[C_2Cl_4]$ becomes almost the exclusive product. In addition, small amounts of a compound with an infrared absorption band at 1300 cm^{-1} were produced. When high O_3 pressures were used a weaker peak at 1025 cm^{-1} was also seen. These bands belong to Cl_2O_7 (10), a known product of the photochemical reaction between Cl_2 and O_3 (5). The reaction products are produced rapidly during irradiation and also slowly in the dark when O_3 and C_2Cl_4 are present at fairly high pressures. The dark rate is never more than 10% of the photochemical rate. The Cl_2O_7 apparently attacks the NaCl windows of the reaction cell as a band at 1100 cm^{-1}, characteristic of a Cl—O stretch mode, is observed. This band remains after the reaction mixture is removed from the cell, and can only be partially removed by prolonged pumping, suggesting that the residual band intensity belongs to a chlorate or perchlorate.

The results of the photochemical reaction in the presence of O_3 are summarized in Table 2. For these runs the C_2Cl_4, O_3, and O_2 pressures were varied by factors of 10, 23, and 526,

Can. J. Chem. Downloaded from www.nrcresearchpress.com by 210.87.254.42 on 09/05/12
For personal use only.

Can. J. Chem. Downloaded from www.nrcresearchpress.com by 210.87.254.42 on 09/05/12
For personal use only.

TABLE 2. Chlorine atom sensitized oxidation of C_2Cl_4 in the presence of O_3

$\frac{[C_2Cl_4]}{[O_3]}$*	$\frac{[O_3]}{[O_2]}$†	$[C_2Cl_4]$‡ (Torr)	$[O_3]$‡ (Torr)	$[O_2]$ (Torr)	$[Cl_2]$ (Torr)	I_a§ (mTorr/s)	Irradiation time (s)	$-\Phi\{O_3\}$	$\Phi\{CCl_3CCl(O)\}$	$\Phi\{CCl_2O\}$	$\Phi\{\overline{CCl_2CCl_2O}\}$	$\frac{\Phi\{CCl_3CCl(O)\}}{\Phi\{CCl_2O\}}$
							$T = 32\,°C$					
0.030	0.28	1.00 (0.69)	24.3 (23.1)	86.0	2.00	0.30	200	35.5	2.21	0.84	7.5	2.63
0.037	3.3	1.18 (0.60)	17.1 (15.9)	5.2	1.90	0.28	200	—	3.00	2.00	15.7	1.50
0.062	7.7	1.45 (0.93)	16.3 (15.0)	2.1	2.15	0.32	—	20.5	3.4	2.22	9.9	1.53
0.070	0.57	1.18 (0.77)	12.0 (11.1)	21.0	4.94	0.74	60	37	4.7	—	13.4	—
0.076	0.62	1.17 (0.77)	11.5 (10.2)	18.6	0.59	0.088	500	57	5.4	3.7	10.7	1.46
0.13	0.125	1.84 (1.16)	11.5 (9.0)	92.0	1.92	0.29	150	117	14.1	3.7	15.6	3.8
0.156	0.36	3.4 (2.95)	20.0 (18.9)	54.0	1.5	0.23	100	95	19.2	8.6	15.3	2.23
0.17	0.50	2.33 (1.68)	10.6 (10.0)	21.2	5.13	0.77	42	39	10.7	4.5	18.4	2.38
0.18	0.44	1.02 (0.90)	5.1 (4.9)	11.5	1.7	0.26	40	39	15.0	5.8	15.0	2.59
0.17	0.52	1.94 (1.62)	10.5 (9.8)	20.0	0.51	0.076	150	144	20.9	15.0	24	1.39
0.18	0.41	2.36 (1.82)	10.6 (10.0)	26.0	5.13	0.077	40	40	12.1	4.3	20.8	2.8
0.19	0.52	2.39 (1.89)	11.5 (10.0)	22.0	1.94	0.29	100	106	11.5	8.2	18.7	1.40
0.23	0.51	2.69 (2.25)	10.5 (9.8)	20.7	0.59	0.088	150	98	36.0	18.2	22.1	1.98
0.23	0.29	1.90 (1.44)	7.0 (6.3)	24.1	1.5	0.23	50	120	36.4	13.5	36.4	2.70
0.24	0.32	4.80 (4.13)	18.6 (17.5)	58.4	1.7	0.26	80	104	27.9	12.4	30.0	2.25
0.255	0.33	7.00 (6.45)	26.2 (25.3)	79.0	1.5	0.23	40	150	42	23.0	52.0	1.83
0.284	0.20	1.87 (1.20)	5.3 (4.22)	25.5	1.8	0.27	100	80	28.4	9.2	16.2	3.09
0.32	27	10.0 (8.67)	27.0 (25.2)	1.0	2.1	0.31	200	57	13.3	20.7	17	0.64
0.36	0.077	2.87 (2.03)	7.02 (5.62)	91.0	1.90	0.28	100	96	39.3	12.2	13.9	3.22
0.40	0.058	2.21 (1.50)	5.35 (3.76)	91.0	2.0	0.3	100	106	34.5	10.2	14.7	3.4
0.45	0.30	3.21 (2.65)	6.62 (5.88)	22.2	1.93	0.28	50	105	54	18.5	17.0	2.9
0.56	0.28	2.90 (2.12)	5.1 (3.80)	18.0	1.94	0.29	100	92	33	17	17.0	1.9
0.57	0.067	3.65 (2.41)	6.2 (4.20)	92.0	2.1	0.31	110	113	50	18.3	13	2.7
0.70	14.0	10.0 (8.75)	14.0 (12.5)	1.0	2.0	0.30	100	101	39	40	13	0.97
0.95	1.4	2.0	2.1	1.45	1.8	0.27	100	89	41‖	31‖	—	1.3
1.0	0.117	3.8 (2.35)	3.4 (2.3)	29.0	2.13	0.31	100	45	71	32	7.5	2.2
1.3	0.116	3.54 (2.4)	3.2 (1.9)	27.5	1.93	0.28	50	170	96	67	—	1.4
1.84	0.0022	4.1 (2.5)	2.14 (1.36)	97	1.90	0.28	110	50	84	36	<4	2.3
2.64	0.073	5.1 (3.57)	1.9 (1.35)	26	1.84	0.28	110	40	93	40	<4	2.3
							$T = 24\,°C$‖					
1.17	0.049	2.77	2.37	48	2.76	1.29	—	—	32	7.3	<3	2.3
1.28	0.0061	3.03	2.37	385	2.76	1.29	—	—	23	5.8	<3	2.5
1.82	0.0022	2.13	1.17	526	2.76	1.29	—	—	41	15.8	<3	2.6
1.92	0.28	4.55	2.37	8.4	2.76	1.29	—	—	16.4	10.3	<3	1.6
3.42	0.22	4.00	1.17	5.3	2.76	1.29	—	—	19	10.5	<3	1.8
4.65	0.024	5.45	1.17	48	2.76	1.29	—	—	41	17.5	<3	2.4

*Ratios of the average pressures.
†Ratios of the initial pressures.
‡The values in parenthesis are the average pressure during the run.
§Actinometry based on results in Table 1.
‖Quantum yields obtained by extrapolation to zero time.

Can. J. Chem. Downloaded from www.nrcresearchpress.com by 210.87.254.42 on 09/05/12
For personal use only.

respectively, the absorbed intensity, I_a, by a factor of 17, and the ratios $[C_2Cl_4]/[O_3]$ and $[O_3]/[O_2]$ by factors of 155 and 10^4 respectively. The parameter which influences the results most is $[C_2Cl_4]/[O_3]$. As this ratio rises $\Phi\{CCl_3CCl(O)\}$ and $\Phi\{CCl_2O\}$ rise. $\Phi\{\overline{CCl_2CCl_2O}\}$ at first rises reaching a maximum value of about 30 for a ratio of about 0.25, and then falls with further increases in the ratio. The ratio $\Phi\{CCl_3CCl(O)\}/\Phi\{CCl_2O\}$ shows a mild dependence on $[O_3]/[O_2]$. This is seen more easily in Fig. 1. There is considerable scatter in the data, but the ratio drops from about 3.0 in the absence of O_3 to about 1.0 at $[O_3]/[O_2] > 10$. The data points at 24 °C lie below those at 32 °C, as they do in the absence of O_3.

Another manifestation of the same effect is seen for extended photolysis during a reaction. Results for such a run are shown in Fig. 2. At the earliest measured time, the ratio of $[CCl_3CCl(O)]$ to $[CCl_2O]$ is about 1.3, but as the run progresses the $[O_3]/[O_2]$ drops, and the ratio rises to 1.75.

In a number of runs in Table 2, the quantum yield of O_3 consumption, $-\Phi\{O_3\}$, exceeded the sum of those for product formation, indicating that O_3 is consumed at a faster rate than C_2Cl_4 in those runs.

Ozonolysis

The dark reaction of O_3 with C_2Cl_4 was studied at 24 °C. The products were O_2, CCl_2O, and $CCl_3CCl(O)$, with minor amounts of $\overline{CCl_2CCl_2O}$ also observed. A small amount of HCOOH was also found, but this undoubtedly comes from the hydrolysis of $CCl_3CCl(O)$. The more thoroughly the reactants were dried, the smaller the amount of HCOOH produced. In some cases, for very extended conversions, trace amounts of Cl_2, CO, and CO_2 were also found. There was no evidence at all of c-C_3Cl_6 formation.

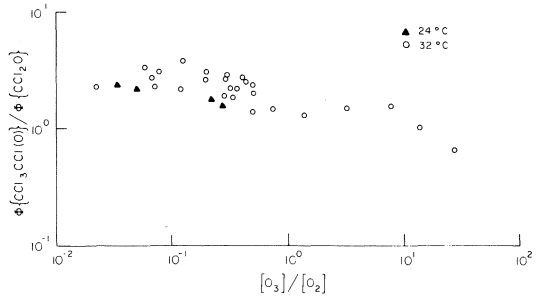

FIG. 1. Log–log plot of the ratio of the quantum yields of $CCl_3CCl(O)$ and CCl_2O *vs.* $[O_3]/[O_2]$ in the chlorine atom sensitized oxidation of C_2Cl_4 by O_2 and O_3.

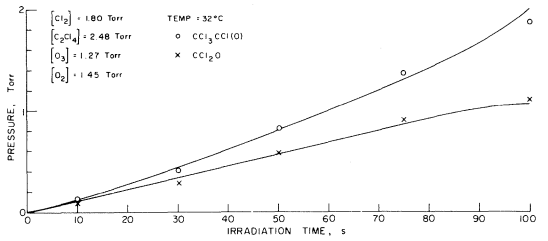

FIG. 2. Plot of the $CCl_3CCl(O)$ and CCl_2O pressures *vs.* irradiation time in the chlorine atom sensitized oxidation of C_2Cl_4 by O_2 and O_3 at 32 °C.

It was difficult to measure quantitatively the $\overline{CCl_2CCl_2O}$ formation because it was a minor product, and its optimum band for infrared analysis at 900 cm^{-1} was obscured by the C_2Cl_4 band at 920 cm^{-1}. The weaker band at 1340 cm^{-1} was observed early in the run at high O_3 pressures ($\sim$12 Torr), and all the bands could be observed if the C_2Cl_4 was reacted to completion. The other carbon-containing products and the reactants could be monitored continually. For a typical run, the results are shown in Fig. 3. Initially, the reaction proceeds smoothly, but after some time, the rate slows markedly, and finally almost stops, even though the reactants are not exhausted. The inhibition is due to the

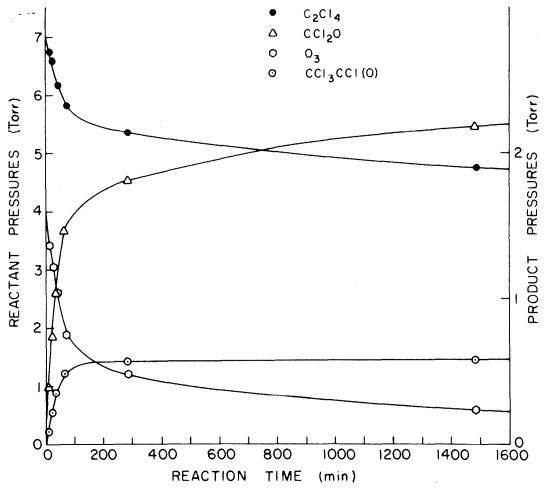

FIG. 3. Plot of reactant and product pressures (note different scales) *vs.* reaction time in the ozonolysis of C_2Cl_4 at 24 °C. The initial reactant concentrations were $[C_2Cl_4]_0 = 6.9$ Torr and $[O_3]_0 = 4.1$ Torr.

TABLE 3. Reaction of O_3 with C_2Cl_4 at 24 °C

$[C_2Cl_4]_0$ (Torr)	$[O_3]_0$ (Torr)	$[N_2]$ (Torr)	$R_i\{CCl_2O\}$ (Torr/min)	$R_i\{CCl_3CCl(O)\}$ (Torr/min)	$\frac{R_i\{CCl_2O\}}{R_i\{CCl_3CCl(O)\}}$
3.85	6.15	121	0.015	—	—
4.50	3.8	0	0.013	0.012	1.1
6.9	4.1	0	0.025	0.019	1.3
9.0	6.05	120	0.039	0.023	1.7
18.0	3.01	113	0.18	0.15	1.2
18.0	5.38	112	0.12	0.098	1.2

accumulation of O_2, since if O_2 is initially present, the initial reaction rate is very much reduced, at least by a factor of 10.

The initial rates of formation of CCl_2O and $CCl_3CCl(O)$, $R_i\{CCl_2O\}$ and $R_i\{CCl_3CCl(O)\}$ respectively, are listed in Table 3 for several runs at different initial reactant pressures, $[C_2Cl_4]_0$ and $[O_3]_0$. The initial rates are difficult to obtain because the inhibition starts soon in the run. Nevertheless, within the large uncertainty, some conclusions can be reached. The initial rates increase rapidly with C_2Cl_4 pressure. They are not much affected by the presence of N_2 or the initial O_3 pressure. In the case of O_3, the initial pressure variation was only a factor of two, so that this conclusion is tentative. It was difficult to obtain accurate initial rates for higher or lower O_3 pressures to confirm this observation, since at low O_3 pressures, the reaction did not proceed sufficiently before inhibition occurred to make accurate measurements, and at high O_3 pressures the initial rates were too rapid for accurate measurement. Whereas in the chlorine atom initiated oxidation, $CCl_3CCl(O)$ was always produced in excess of CCl_2O, the reverse happens in the O_3–C_2Cl_4 dark reaction.

Discussion

The chlorine atom initiated oxidation of C_2Cl_4 is a long-chain process. Corroboration comes from this work, since the addition of O_3 can inhibit the reaction, and inhibition by additives only occurs for chain processes. Likewise, the ozonolysis of C_2Cl_4 is a long-chain process, since the addition of O_2 inhibits the reaction. This is a highly interesting and unusual situation, since the two chain oxidations are inhibited by each other's oxidizing agent. This implies that the chain carriers in the two systems are different; otherwise addition of the second oxidant in the first system, or *vice versa*, should enhance the chain length or have no effect.

Cl Atom Oxidation

The mechanism for the chlorine atom oxidation is a free radical mechanism as outlined in the Introduction. Our results confirm those of earlier workers (1–4). In the absence of O_3, the mechanism predicts that if termination is exclusively by reaction 5, then

$$[13]\quad \Phi\{CCl_3CCl(O)\} + \tfrac{1}{2}\Phi\{CCl_2O\} = \left(\frac{2k_3{}^2k_{4a}}{k_5{}^2}\right)^{1/3}\left(\frac{[O_2]^2}{I_a}\right)^{1/3}$$

However, if termination is exclusively by reaction 4*b*, then

$$[14]\quad \Phi\{CCl_3CCl(O)\} + \tfrac{1}{2}\Phi\{CCl_2O\} = 2k_{4a}/k_{4b}$$

Equation 13 applies at low values of $[O_2]^2/I_a$, whereas eq. 14 applies at high values of $[O_2]^2/I_a$. Figure 4 is a log–log plot of $\Phi\{CCl_3CCl(O)\} + \frac{1}{2}\Phi\{CCl_2\Phi\}$ *vs.* $[O_2]^2/I_a$. The plot behaves as predicted. At high $[O_2]^2/I_a$, the quantum yields are constant giving $k_4/k_{4b} = 150$. At low $[O_2]^2/I_a$, the log–log plot is fitted by a slope of $\frac{1}{3}$, though there is considerable scatter in the

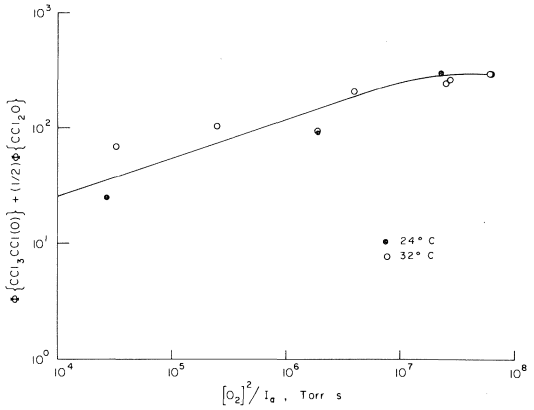

FIG. 4. Log–log plot of $\Phi\{CCl_3CCl(O)\} + \frac{1}{2}\Phi\{CCl_2O\}$ *vs.* $[O_2]^2/I_a$ in the chlorine atom sensitized oxidation of C_2Cl_4 in the absence of O_3.

Can. J. Chem. Downloaded from www.nrcresearchpress.com by 210.87.254.42 on 09/05/12
For personal use only.

Can. J. Chem. Downloaded from www.nrcresearchpress.com by 210.87.254.42 on 09/05/12
For personal use only.

data. The intercept gives $(2k_3^2k_4/k_5^2)^{1/3} \sim 1.2$ $(\text{Torr s})^{-1/3}$.

In the presence of O_3 there are three main effects. These are: (*1*) the ratio $\Phi\{CCl_3CCl(O)\}/\Phi\{CCl_2O\}$ drops as the $[O_3]/[O_2]$ ratio is increased, but is unaffected as the $[O_3]/[C_2Cl_4]$ ratio is changed; (*2*) $\overline{CCl_2CCl_2O}$ is produced, its quantum yield depending mainly on the $[C_2Cl_4]/[O_3]$ ratio; and (*3*) the overall rate of the reaction is reduced as $[O_3]/[C_2Cl_4]$ is raised.

Based on the mechanism outlined in the Introduction, the products of the photochemical oxidation result from the decomposition of the C_2Cl_5O radical. Consequently, the change in ratio of the products implies that the C_2Cl_5O radicals produced by an additional route in the presence of O_3, *i.e.* either by reactions 9 or 12, must be energetically different from those produced by reaction 4*a*, and thus have a different decay ratio k_{6a}/k_{6b}. That ClO is actually produced in the presence of O_3 can be established by comparing the rate constants for reactions 2 and 10. These are respectively, $k_2 = 1.3 \times 10^{10}\ M^{-1}\ s^{-1}$ (11), and $k_{10} > 4 \times 10^8\ M^{-1}\ s^{-1}$ (7). In one of the runs in Table 2, $[C_2Cl_4]/[O_3] = 0.030$, so that some of the chlorine atoms have been converted to ClO before addition to C_2Cl_4.

The change in $\Phi\{CCl_3CCl(O)\}/\Phi\{CCl_2O\}$ depends on the $[O_3]/[O_2]$ ratio, a result to be expected if the C_2Cl_5O radicals produced in reaction 12 are different than those produced from reaction 3 followed by 4*a*. Presumably the C_2Cl_5O radicals produced in reaction 4*a* are nearly thermal neutral, since the excess energy of reaction tends to appear mainly in newly formed bonds, in this case the O_2 molecule. Support for this hypothesis comes from the fact that small temperature changes noticeably influence the ratio $\Phi\{CCl_3CCl(O)\}/\Phi\{CCl_2O\}$. Such an effect would not be expected to show up if the radicals contained a considerable amount of excess energy. On the other hand any C_2Cl_5O radicals produced from the reaction of C_2Cl_5 and O_3 would be expected to contain a considerable portion of the ~50 kcal/mol energy of reaction. Thus their decomposition should lead to $\Phi\{CCl_3CCl(O)\}/\Phi\{CCl_2O\}$ even larger than 3.0. Actually the ratio was diminished rather than enhanced. This suggests that reaction 12 does not proceed through C_2Cl_5O (unless the excess energy is highly organized in specific reaction modes), and that reaction 12 should be written

[12*a*] $C_2Cl_5 + O_3 \rightarrow CCl_3CCl(O) + Cl + O_2$

[12*b*] $\rightarrow CCl_2O + CCl_3O_2$ (or $CCl_3 + O_2$)

There is also the possibility that the epoxide could be produced in this reaction. However the ratio of the epoxide to the other products depends primarily on $[C_2Cl_4]/[O_3]$ and not $[O_3]/[O_2]$. Thus another route must be mainly responsible for the epoxide, and for simplicity we ignore the channel of reaction 12 that could lead to epoxide production.

The epoxide must come from a radical precursor which is absent in the absence of O_3, *i.e.* either ClO or CCl_3O, as the case may be. In the former case, $(\Phi\{CCl_3CCl(O)\} + \frac{1}{2}\Phi\{CCl_2O\})/\Phi\{\overline{CCl_2CCl_2O}\}$ would depend on $[C_2Cl_4]/[O_3]$, whereas in the latter case, on $[O_3]/[O_2]$. Since the dependence is on $[C_2Cl_4]/[O_3]$, we conclude that epoxide comes from ClO, that ClO is absent in the absence of O_3, and that the mechanism of Huybrechts *et al.* (4) is correct. The route to epoxide formation is reaction 9, the possible reaction channels being

[9*a*] $ClO + C_2Cl_4 \rightarrow \overline{CCl_2CCl_2O} + Cl$

[9*b*] $\rightarrow CCl_3CCl(O) + Cl$

[9*c*] $\rightarrow CCl_2O + CCl_3$

The termination step introduced by O_3, as well as the routes to Cl_2O_7 production, come from the interaction of ClO with O_3

[15*a*] $ClO + O_3 \rightarrow Cl + 2O_2$

[15*b*] $\rightarrow ClO_2 + O_2$

The ClO_2 reacts further with O_3 to give the higher chlorine oxides.

Since the chain length is long under all conditions, the mechanism predicts that

$$[16]\quad \frac{(\Phi\{CCl_3CCl(O)\} + \frac{1}{2}\Phi\{CCl_2O\})}{\Phi\{\overline{CCl_2CCl_2O}\}} = \frac{k_{9b} + k_{9c}}{k_{9a}} + \frac{k_2k_{15}}{k_{9a}k_{10}} + \frac{k_2k_9[C_2Cl_4]}{k_{10}k_{9a}[O_3]}$$

The left-hand side of the equation is plotted *vs.* $[C_2Cl_4]/[O_3]$ in Fig. 5. The data can be fitted by a straight line, and this line passes through the origin. There is no significant trend with $[O_3]/[O_2]$, thus justifying our neglecting epoxide formation through reaction 12. The slope gives $k_2k_9/k_{10}k_{9a} = 6.7$ and the lack of intercept

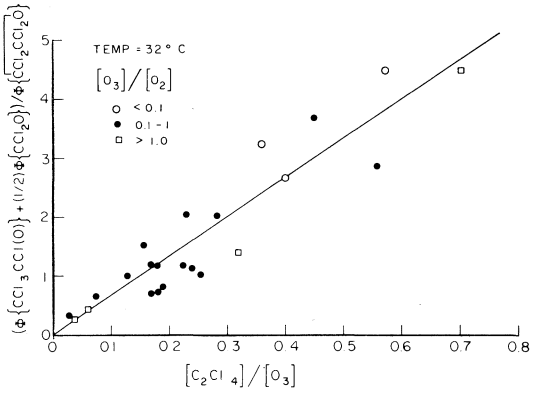

FIG. 5. Plot of $(\Phi\{CCl_3CCl(O)\} + \frac{1}{2}\Phi\{CCl_2O\})/\Phi\{\overline{CCl_2CCl_2O}\}$ *vs.* $[C_2Cl_4]/[O_3]$ in the chlorine atom sensitized oxidation of C_2Cl_4 by O_2 and O_3 at 32 °C.

gives $(k_{9b} + k_{9c})/k_{9a} + k_2k_{15}/k_{9a}k_{10} \sim 0$. Thus $k_2/k_{10} = 6.7$. Since $k_2 = 1.3 \times 10^{10}\ M^{-1}\ s^{-1}$, $k_{10} = 1.9 \times 10^9\ M^{-1}s^{-1}$.

The result that k_{15}/k_{10} is too small to play any role requires that some other reaction must be incorporated to explain the fact that the O_3 consumption can exceed C_2Cl_4 consumption (see Table 2). The possible reactions are

$$C_2Cl_5O_2 + O_3 \rightarrow C_2Cl_5O + 2O_2$$

$$CCl_3O_2 + O_3 \rightarrow CCl_3O + 2O_2$$

$$ClO_2 + O_3 \rightarrow ClO + 2O_2$$

The first two reactions lead to no changes in the mechanistic rate laws developed. The third reaction, if it occurs, would tend to make k_{10} appear smaller than it really is, but otherwise would not change the rate law.

The rate law for individual product quantum yields depends on the termination step. Since there are three termination steps there are three limiting sets of rate laws. These are:

Case I: Termination by Reaction 15b

$$[17]\quad \Phi\{\overline{CCl_2CCl_2O}\} = 2k_{9a}[C_2Cl_4]/k_{15b}[O_3]$$

$$[18]\quad \Phi\{CCl_3CCl(O)\} + \tfrac{1}{2}\Phi\{CCl_2O\} = \frac{2k_2k_9}{k_{10}k_{15b}}\left(\frac{[C_2Cl_4]}{[O_3]}\right)^2$$

Case II: Termination by Reaction 4b

$$[19]\quad \Phi\{\overline{CCl_2CCl_2O}\} = \frac{2k_{10}k_4}{k_2k_{4b}}\left(1 + \frac{k_{12}[O_3]}{k_3[O_2]}\right)\frac{[O_3]}{[C_2Cl_4]}$$

$$[20]\quad \Phi\{CCl_3CCl(O)\} + \tfrac{1}{2}\Phi\{CCl_2O\} = \left(1 + \frac{k_{12}[O_3]}{k_3[O_2]}\right)2k_4/k_{4b}$$

Case III: Termination by Reaction 5

$$[21]\quad \Phi\{\overline{CCl_2CCl_2O}\} = \frac{k_{10}}{k_2}\left(1 + \frac{k_{12}[O_3]}{k_3[O_2]}\right) \times \left(\frac{2k_3^2k_4}{k_5^2}\right)^{1/3}\left(\frac{[O_2]^2}{I_a}\right)^{1/3}\frac{[O_3]}{[C_2Cl_4]}$$

$$[22]\quad \Phi\{CCl_3CCl(O)\} + \tfrac{1}{2}\Phi\{CCl_2O\} = \left(\frac{2k_3^2k_4}{k_5^2}\right)^{1/3}\left(1 + \frac{k_{12}[O_3]}{k_3[O_2]}\right)\left(\frac{[O_2]^2}{I_a}\right)^{1/3}$$

Since all three termination steps can occur, the overall rate law should be complex indeed, and a detailed analysis of the data for additional rate coefficient ratios is not possible.

The rate coefficient ratios obtained in this study are summarized in Table 4.

Ozonolysis

The fact that O_2 inhibits the ozonolysis of C_2Cl_4 implies that free radicals (*i.e.* species with an odd number of electrons) are absent. Certainly, the free-radical chain carriers in the chlorine atom sensitized oxidation are absent, or else the addition of O_2 would enhance the reaction. Additional support for this conclusion comes from the fact that the product ratio $[CCl_3CCl(O)]/[CCl_2O]$ exceeds unity in the chlorine atom sensitized oxidation, but is less than unity in the ozonolysis.

To explain the ozonolysis, a diradical mechanism must be invoked. Even for this mechanism, the simplest diradical, CCl_2, must be absent also, because it leads to mono free radicals (*i.e.* Cl and ClO) when it reacts with O_2 (12). We propose a mechanism very similar to that proposed for the ozonlysis of $C_2H_2Cl_2$ (8).

$$[23]\quad O_3 + C_2Cl_4 \rightarrow CCl_2O + CCl_2O_2$$

$$[24]\quad CCl_2O_2 + O_3 \rightarrow CCl_2O + 2O_2$$

$$[25]\quad CCl_2O_2 + C_2Cl_4 \rightarrow CCl_2O_2C_2Cl_4$$

$$[26a]\quad CCl_2O_2C_2Cl_4 + O_3 \rightarrow CCl_2O_2C_2Cl_4O_3$$

$$[26b]\quad \rightarrow CCl_2O_2 + C_2Cl_4O + O_2$$

$$[27]\quad CCl_2O_2C_2Cl_4O_3 + C_2Cl_4 \rightarrow CCl_2O_2 + 2CCl_2O + C_2Cl_4O$$

Can. J. Chem. Downloaded from www.nrcresearchpress.com by 210.87.254.42 on 09/05/12
For personal use only.

TABLE 4. Summary of rate coefficient ratios

Ratio	Value	Units	Source
k_{6a}/k_{6b}	5.0 ± 0.2(24 °C)	None	$\Phi\{CCl_3CCl(O)\}/\Phi\{CCl_2O\}$
k_{6a}/k_{6b}	6.0 ± 0.4(32 °C)	None	$\Phi\{CCl_3CCl(O)\}/\Phi\{CCl_2O\}$
k_4/k_{4b}	150	None	Eq. 14, Fig. 4
$k_3^2k_4/k_5^2$	~0.9*	$Torr^{-1}\ s^{-1}$	Eq. 13, Fig. 4
k_2/k_{10}	6.7 ± 1.0	None	Eq. 16, Fig. 5
$(k_{9b} + k_{9c})/k_{9a}$	~0 (<0.1)	None	Eq. 16, Fig. 5
k_{15}/k_{10}	~0 (<0.06)	None	Eq. 16, Fig. 5

*At least a factor of 2 uncertainty.

where C_2Cl_4O includes both $CCl_3CCl(O)$ and $\overbrace{CCl_2CCl_2O}$. Other reactions are also possible, but for simplicity, they have been omitted.

The above mechanism leads to the simple rate laws

$$[28]\quad R_i\{CCl_2O\} = 2k_{23}[O_3][C_2Cl_4] + 2k_{23}k_{25}k_{26a}[C_2Cl_4]^2/k_{24}k_{26}$$

$$[29]\quad R_i\{C_2Cl_4O\} = k_{23}k_{25}[C_2Cl_4]^2/k_{24}$$

For long chains, eq. 28 further simplifies to

$$[30]\quad R_i\{CCl_2O\} \sim 2k_{23}k_{25}k_{26a}[C_2Cl_4]^2/k_{24}k_{26}$$

in which case

$$[31]\quad R_i\{CCl_2O\}/R_i\{C_2Cl_4O\} = 2k_{26a}/k_{26}$$

The mechanism predicts no dependence on $[O_3]$, in conformance with the experimental findings.

Figure 6 is a log–log plot of $R_i\{CCl_2O\}$ *vs.* $[C_2Cl_4]$. The line which best fits the data has a slope of 1.8 which compares favorably with the value of 2.0 predicted by eq. 30. Thus, within the large experimental uncertainty, the mechanism conforms to the results.

For the runs in Table 3, $R_i\{CCl_2O\}/R_i\{CCl_3CCl(O)\} = 1.3 \pm 0.2$. Then from eq. 31, $k_{26a}/k_{26} = 0.65$.

In the presence of O_2 the chain is presumably terminated via the reaction sequence

$$[32]\quad CCl_2O_2C_2Cl_4 + O_2 \rightarrow CCl_2O_2C_2Cl_4O_2$$

$$[33]\quad CCl_2O_2C_2Cl_4O_2 + C_2Cl_4 \rightarrow 3CCl_2O + C_2Cl_4O$$

Then the limiting rate law at high O_2 pressure would become

$$[34]\quad R_i\{CCl_2O\} = 4k_{23}[O_3][C_2Cl_4]$$

In our experiments with excess O_2, $R_i\{CCl_2O\} \sim 4 \times 10^{-3}$ Torr/min for $[C_2Cl_4] = 7.5$ Torr and $[O_3] = 3.5$ Torr. Since part of this reaction might be attributed to the slow heterogeneous decay of O_3, $k_{23} \leq 0.012\ M^{-1}\ s^{-1}$.

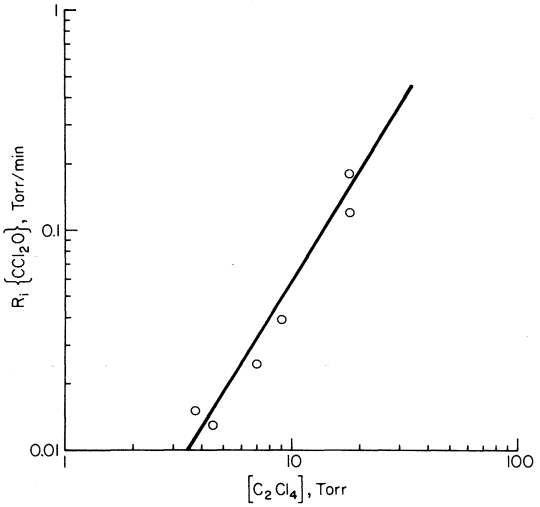

FIG. 6. Log–log plot of initial rate of CCl_2O formation *vs.* the C_2Cl_4 pressure in the ozonolysis of C_2Cl_4 at 24 °C.

The only previously reported work on the O_3–C_2Cl_4 reaction was by Williamson and Cvetanović (13) in CCl_4 solution. They found the reaction to be first order in both O_3 and olefin concentrations with a rate constant $1.0\ M^{-1}\ s^{-1}$, about 100 times that found here. It is interesting to note that their rate coefficient for the O_3–CH_2CCl_2 reaction in CCl_4 solution was about 10 times larger than that found in the gas phase (8).

This work was supported by the Environmental Protection Agency under Grant No. R800949 for which we are grateful.

1. R. G. DICKINSON and J. A. LEERMAKERS. J. Am. Chem. Soc. **54**, 3852 (1932).
2. R. G. DICKINSON and J. L. CARRICO. J. Am. Chem. Soc. **56**, 1473 (1934).

Can. J. Chem. Downloaded from www.nrcresearchpress.com by 210.87.254.42 on 09/05/12
For personal use only.

3. C. SCHOTT and H. J. SCHUMACHER. Z. Phys. Chem. B**49**, 107 (1941).
4. G. HUYBRECHTS, J. OLBRECHTS, and K. THOMAS. Trans. Faraday Soc. **63**, 1647 (1967).
5. J. HEICKLEN. Adv. Photochem. **7**, 57 (1969).
6. W. D. MCGRATH and R. G. W. NORRISH. Z. Phys. Chem. Frankfurt, **15**, 245 (1958).
7. M. A. A. CLYNE and J. A. COXON. Proc. R. Soc. A**303**, 207 (1968).
8. L. A. HULL, I. C. HISATSUNE, and J. HEICKLEN. Can. J. Chem. **51**, 1504 (1973).
9. R. E. NIGHTINGALE, A. R. DOWNIE, D. L. ROTENBERG, B. L. CRAWFORD, JR., and R. A. OGG, JR. J. Phys. Chem. **58**, 1047 (1954).
10. R. SAVOIE and P. A. GIGUÉRE. Can. J. Chem. **40**, 991 (1962).
11. J. A. FRANKLIN, G. HUYBRECHTS, and C. CILLIEN. Trans. Faraday Soc. **65**, 2094 (1969).
12. E. SANHUEZA and J. HEICKLEN. Can. J. Chem. This issue.
13. D. G. WILLIAMSON and R. J. CVETANOVIĆ. J. Am. Chem. Soc. **90**, 4248 (1968).

Can. J. Chem. Downloaded from www.nrcresearchpress.com by 210.87.254.42 on 09/05/12
For personal use only.

The Hg 6(^{3}P)-Photosensitized Oxidation of C_2Cl_4[1]

EUGENIO SANHUEZA[2] AND JULIAN HEICKLEN

Department of Chemistry and Center for Air Environment Studies, Pennsylvania State University, University Park, Pennsylvania 16802

Received April 16, 1973[3]

EUGENIO SANHUEZA and JULIAN HEICKLEN. Can. J. Chem. **52**, 3863 (1974).

The Hg 6(^{3}P) sensitized photolysis of C_2Cl_4 was studied at 25 °C both in the absence and presence of N_2O and O_2. For C_2Cl_4 alone, the only products are polymer and Hg_2Cl_2. The quantum yield of C_2Cl_4 disappearance, $-\Phi\{C_2Cl_4\} \sim 1$. Thus, the photolysis produces C_2Cl_3 radicals and Hg_2Cl_2, the C_2Cl_3 radicals dimerize, and the resultant 1,3-C_4Cl_6 polymerizes. The relative quenching of Hg 6(^{6}P) by C_2Cl_4 compared to N_2O is 3.0.

In the presence of O_2 the products are $CCl_3CCl(O)$ and CCl_2O which are formed in a radical chain process in a ratio of 2.6 independent of reaction conditions. CO is also produced with a quantum yield of unity. The quantum yields of the chlorine-containing products are independent of the O_2 pressure and the absorbed intensity, but are proportional to the C_2Cl_4 pressure, the proportionality constants being 1.4 and 3.7 Torr^{-1}, respectively, for CCl_2O and $CCl_3CCl(O)$. A detailed mechanism, based on the chlorine atom chain oxidation, is presented, and appropriate rate constant ratios are evaluated.

EUGENIO SANHUEZA et JULIAN HEICKLEN. Can. J. Chem. **52**, 3863 (1974).

On a étudié à 25 °C, en présence et en absence de N_2O et O_2, la photolyse du C_2Cl_4 sensibilisé par le Hg 6(^{3}P). Lorsque le C_2Cl_4 est seul on n'isole comme produits qu'un polymère et du Hg_2Cl_2. Le rendement quantique pour la disparition du C_2Cl_4, $-\Phi\{C_2Cl_4\}$, est pratiquement égal à 1. Donc la photolyse produit des radicaux C_2Cl_3 et du Hg_2Cl_2; les radicaux C_2Cl_3 se dimérisent et le C_4Cl_6-1,3 qui en résulte se polymérise. La facilité relative, pour C_2Cl_4 comparé à N_2O, de piéger Hg 6(^{6}P) est égale à 3.0.

En présence d'oxygène les produits sont le $CCl_3CCl(O)$ et le CCl_2O qui se forment par un processus radicalaire en chaîne dans un rapport de 2.6 qui est indépendant des conditions réactionnelles. Du CO est aussi produit avec un rendement quantique égal à l'unité. Les rendements quantiques de produits contenant du chlore sont indépendants de la pression d'oxygène et de l'intensité absorbée, mais ils sont proportionnels à la pression de C_2Cl_4; les constantes de proportionnalités sont respectivement de 1.4 et 3.7 Torr^{-1} pour CCl_2O et $CCl_3CCl(O)$. On présente un mécanisme détaillé basé sur l'oxydation en chaîne par les atomes de chlore; de plus on évalue les rapports des constantes de vitesse appropriées.

[Traduit par le journal]

Introduction

The chlorine atom initiated oxidation of C_2Cl_4 has been studied in several laboratories (1–4), and the results reviewed (5). More recently a study was made in our laboratory (6). In all the studies, the major products were $CCl_3CCl(O)$ and CCl_2O, the reaction was a long chain reaction with chain lengths of about 300 independent of light intensity, I_a, or any of the reactant pressures if the O_2 pressure was sufficiently high. The ratio of product quantum yields $\Phi\{CCl_3CCl(O)\}/\Phi\{CCl_2O\}$ was 5.7 at 80–100 °C (4), 4.0 at 40–80 °C (3), 3.0 at 32 °C (6), and 2.5 at 24 °C (6).

The main features of the mechanism of the reaction were worked out in a remarkable paper by Huybrechts *et al.* (4) who found different intensity dependences for the rates of the O_2 inhibited chlorination ($I_a^{1/2}$) and the chlorine atom initiated oxidation (I_a). They argued that since these two reactions are coupled, they have common chain-breaking steps, which must be bimolecular in radicals to explain the $I_a^{1/2}$ dependence of the rate of chlorination. Therefore, the oxidation must be propagated by a bimolecular radical reaction. Their mechanism is

[1] $Cl_2 + h\nu \rightarrow 2Cl$

[2] $Cl + C_2Cl_4 \rightarrow C_2Cl_5$

[3] $C_2Cl_5 + O_2 \rightarrow C_2Cl_5O_2$

[4a] $2C_2Cl_5O_2 \rightarrow 2C_2Cl_5O + O_2$

[4b] $\rightarrow (C_2Cl_5O)_2 + O_2$

[5] $C_2Cl_5O_2 + C_2Cl_5 \rightarrow (C_2Cl_5O)_2$

[1]CAES Report No. 306-73.
[2]Fulbright Fellow: 1972-1974.
[3]Revision received June 5, 1974.

Can. J. Chem. Downloaded from www.nrcresearchpress.com by 210.87.254.105 on 09/05/12
For personal use only.

Can. J. Chem. Downloaded from www.nrcresearchpress.com by 210.87.254.105 on 09/05/12
For personal use only.

[6a] $C_2Cl_5O \rightarrow CCl_3CCl(O) + Cl$

[6b] $\rightarrow CCl_2O + CCl_3$

[7] $CCl_3 + O_2 \rightarrow CCl_3O_2$

[8] $CCl_3O_2 \rightarrow CCl_2O + Cl + \frac{1}{2}O_2$

In our laboratory, we are engaged in an extensive program to study halocarbon oxidation. In this paper we report the results of the Hg-photosensitized oxidation of C_2Cl_4. These results are compared to those obtained by chlorine atom initiation to see whether a radical-chain mechanism is involved.

Experimental

The experiments utilized conventional static photochemical techniques. The working part of the vacuum system was greaseless, employing Teflon stopcocks and greaseless joints with Viton O-rings. For pressures < 5 Torr, a Consolidated Vacuum Corp. McLeod gauge was used whenever possible. Pressures between 5 and 50 Torr were measured in a Wallace and Tiernan absolute pressure indicator. Pressures larger than 50 Torr were measured in a mercury manometer.

All gases were Matheson C.P. grade. When it was possible, they were purified by bulb-to-bulb distillation in the vacuum line and degassed at -196 °C before each run. The C_2Cl_4 was Baker Analyzed, chlorine free. The fraction volatile at -21 °C but condensable at -90 °C was used. It was degassed before each run from a trap at -90 °C. The $CCl_3CCl(O)$ was from Eastman Kodak and was fractionated in the same manner as C_2Cl_4 before use. The gases were saturated with mercury vapor at room temperature and mixed directly in the cell.

Three reaction cells were used. Cell No. 1 was a cylindrical quartz vessel 5 cm in diameter and 10 cm long. Cells No. 2 and 3 were Pyrex T-shaped cells. For each cell the stem of the T had a 5 cm diameter quartz window to permit entrance of the radiation. The top of the T had two NaCl windows, each 5 cm in diameter, for infrared analysis. The windows were attached to the cells with Carter's epoxy cement. The length of the tops of the T cells were 6.7 and 12.7 cm, respectively, and were situated in the sample beam of a Beckman IR-10 infrared spectrometer for continual analysis of C_2Cl_4, CCl_2O, and $CCl_3CCl(O)$. Each cell contained a drop of Hg.

Irradiation was from a Hanovia flat-spiral low-pressure mercury resonance lamp. Before entering the reaction cell, the radiation passed through a Corning 9-54 filter to remove radiation below 2200 Å. When reduced intensities were desired, Corning 9-30 filters were inserted between the lamp and reaction vessel. Actinometry was obtained from the Hg-photosensitized decomposition of N_2O in the presence of 1–2% C_2F_4 to scavenge the $O(^3P)$ atoms produced. For this system, $\Phi\{N_2\} = 1.0$ (7).

When cell No. 1 was used, the fraction of the contents condensable at -196 °C was transferred to an infrared cell for analysis of C_2Cl_4, CCl_2O, and $CCl_3CCl(O)$ after irradiation. For a number of experiments, the condensables at -196 °C were separated at -90 °C. The volatile fraction contained N_2O and CCl_2O, the condensable fraction, C_2Cl_4 and $CCl_3CCl(O)$. Both fractions were analyzed separately by infrared analysis, the results being the same as when fractionation was not done.

When cells No. 2 and 3 were used, infrared analysis was done continually during irradiation. The C_2Cl_4, CCl_2O, and $CCl_3CCl(O)$ were analyzed from their respective absorption bands at 910, 1835, and 1015 cm^{-1}. Calibration of these bands gave peak extinction coefficients of 1.86×10^{-2}, 1.58×10^{-2}, and 5.6×10^{-3} $Torr^{-1}$ cm^{-1}, respectively. The band of $CCl_3CCl(O)$ at 1810 cm^{-1} interfered with the CCl_2O analysis, so it was calibrated also, and corrections made. Its peak extinction coefficient was found to be 1.37×10^{-2} $Torr^{-1}$ cm^{-1}.

For a few runs analysis was made for CO and CO_2 by gas chromatography. For CO, the column used contained 5A molecular sieves and was 10 ft long. It operated at 0 °C with a He flow rate of 60 cc/min. In one run, gas chromatographic analysis for CO_2 was made utilizing a 24 ft long column packed with Porapak Q operating at 25 °C with a H_2-carrier gas flow rate of 60 cc/min.

For the actinometer runs as well as those with N_2O and C_2Cl_4 present, N_2 was measured by expansion of the gas noncondensable at -196 °C.

The absence of Cl_2 was checked by ultraviolet analysis on a Cary 14 spectrometer. During photolysis the mercury drop became coated with Hg_2Cl_2, as verified by dissolving the drop in nitric acid solution followed by the addition of $AgNO_3$. The characteristic AgCl precipitate was obtained.

In order to remove the polymer which was formed in the absence of O_2 from the reaction cell No. 1, air was admitted, and the cell was heated with an oxygen gas torch to about 500 °C before each experiment. When cell No. 2 was used, it was cleaned by rinsing with acetone and isopropanol.

Results

The Hg $6(^3P)$-sensitized photolysis of C_2Cl_4 at 25 °C yields polymer and Hg_2Cl_2 as the exclusive products. The polymer was not identified, but the Hg_2Cl_2 coated the Hg drop and the presence of chloride was verified by dissolving the drop in nitric acid followed by the addition of $AgNO_3$ to precipitate AgCl. No other products were found. In particular, both Cl_2 and c-C_3Cl_6 were absent, an upper limit to the quantum yield of the latter compound being 0.05.

The loss of C_2Cl_4 was monitored and the results are in Table 1. It is somewhat difficult to obtain accurate quantum yields since the products coat the windows and reduce the light intensity as the run progresses. The quantum yield of C_2Cl_4 loss, $-\Phi\{C_2Cl_4\}$, is listed in Table 1. Within the large experimental uncertainty, $-\Phi\{C_2Cl_4\} \sim 1.0$. Thus a long chain polymerization of C_2Cl_4 is not involved.

In order to measure the rate constant for the quenching of Hg $6(^3P)$ by C_2Cl_4, experiments were done with both N_2O and C_2Cl_4 present and the quantum yield of N_2 formation, $\Phi\{N_2\}$, was measured. Short exposures were used so that

Can. J. Chem. Downloaded from www.nrcresearchpress.com by 210.87.254.105 on 09/05/12
For personal use only.

TABLE 1. Hg-sensitized photolysis of C_2Cl_4 at 25 °C

$[C_2Cl_4]$ (Torr)	I_a (mTorr/s)	Irradiation time (s)	$-\Phi\{C_2Cl_4\}$
2.20	0.40*	1800	0.76
3.20	0.40*	900	0.83
4.80	0.40*	3300	0.72
4.80	3.2*	500	0.90
5.20	1.7*	500	1.20
1.00	1.0†	—	1.4‡
1.66	1.3†	—	0.9‡
4.10	1.7†	—	1.2‡
6.50	2.0†	—	0.9‡

*I_a, average value from actinometries at the beginning and at the end of the run.
†I_a at the beginning of the run.
‡Based on initial rates (0 time).

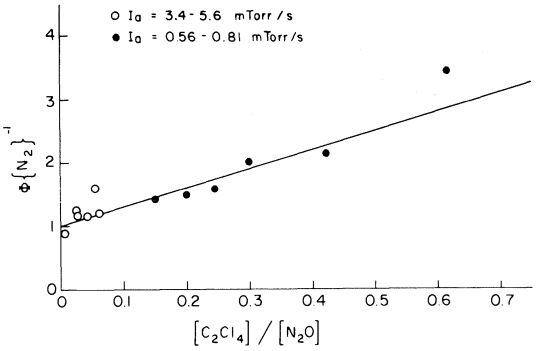

FIG. 1. Plot of the reciprocal nitrogen quantum yield *vs.* $[C_2Cl_4]/[N_2O]$ in the Hg-photosensitized decomposition of C_2Cl_4–N_2O mixtures at 25 °C.

actinometer experiments before and after each run gave similar results. The values for $\Phi\{N_2\}$ for the various experiments are listed in Table 2. $\Phi\{N_2\}$ drops as $[C_2Cl_4]/N_2O]$ is raised, as expected from the competition

[9] $Hg\ 6(^3P) + N_2O \rightarrow Hg\ 6(^1S) + N_2 + O(^3P)$

[10] $Hg\ 6(^3P) + C_2Cl_4 \rightarrow$ removal of $Hg\ 6(^3P)$

Reactions 9 and 10 lead to the simple rate law

[11] $$\Phi\{N_2\}^{-1} = 1 + k_{10}[C_2Cl_4]/k_9[N_2O]$$

Figure 1 shows a plot of $\Phi\{N_2\}^{-1}$ *vs.* $[C_2Cl_4]/[N_2O]$. The plot is linear and passes through an intercept of one. The slope gives $k_{10}/k_9 = 3.0 \pm 0.5$. Since the value (5) for $k_9 = 2.2 \times 10^{11}\ M^{-1}\ s^{-1}$, then $k_{10} = 6.6 \times 10^{11}\ M^{-1}\ s^{-1}$.

For the $Hg\ 6(^3P)$-sensitized photolysis of C_2Cl_4–O_2 mixtures, the major products of the reaction were CCl_2O and $CCl_3CCl(O)$. The quantum yields of these compounds were large, exceeding unity, thus indicating a chain process. The polymer, which was still produced, was relatively much less important. Also produced was Hg_2Cl_2 and CO. In one run with a C_2Cl_4 pressure of 4.8 Torr and an O_2 pressure of 35 Torr, an analysis was made for CO_2. It was a very minor product, its quantum yield being about 0.1. Since this run was done at a high O_2 pressure and should favor CO_2 formation, it can be concluded that CO_2 is unimportant. As in the absence of O_2, no c-C_3Cl_6 was produced. Cl_2 was not detected, but of course if it were produced, it would have reacted with the Hg.

Several runs were made and the C_2Cl_4 disappearance monitored. The results for five runs are plotted as a first order rate plot in Fig. 2. The five runs were followed to 70–75% depletion of the C_2Cl_4. The absorbed intensities, I_a, and the initial C_2Cl_4 pressure both vary over a factor of 6. All the runs fit the same rate law, which is

[12] $$\ln([C_2Cl_4]_0/[C_2Cl_4]) = kI_at$$

where $[C_2Cl_4]_0$ is the initial C_2Cl_4 pressure. From Fig. 2, k is found to be $4.4 \pm 0.4\ Torr^{-1}$.

For a number of runs, quantum yield measurements were made based on either initial rates or average rates for a given exposure. These results are listed in Table 3. For several runs including the three listed in Table 3, $\Phi\{CO\}$ was measured and found to be 1.0 ± 0.1. These runs were for O_2 pressures about 6 Torr, but covered C_2Cl_4 pressures from 2.5–9.9 Torr and I_a from 0.25 to 1.60 mTorr/s. The runs listed in Table 3 cover a C_2Cl_4 pressure range of a factor 13.7, an O_2

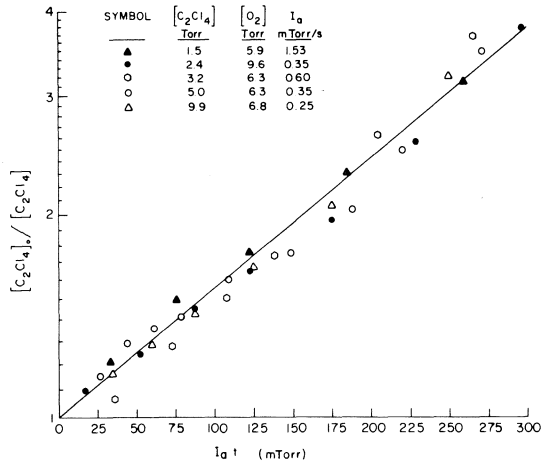

FIG. 2. Semilog plot of $[C_2Cl_4]_0/[C_2Cl_4]$ *vs.* I_at in the Hg-photosensitized oxidation of C_2Cl_4 for five experiments at 25 °C.

TABLE 2. Hg-sensitized photolysis of mixtures of C_2Cl_4 and N_2O at 25 °C

$\frac{[C_2Cl_4]}{[N_2O]}$	$[C_2Cl_4]$ (Torr)	$[N_2O]$ (Torr)	I_a (mTorr/s)	Irradiation time (s)	$\Phi\{N_2\}$
0.0064	1.00	155	3.4	30	1.1
0.0226	3.10	137	5.3	30	0.81
0.0268	3.05	114	4.6	50	0.85
0.043	1.10	25.6	5.3	30	0.83
0.054	1.10	20.5	5.6	30	0.63
0.061	1.12	18.4	0.81	150	0.83
0.148	1.32	8.9	0.81	100	0.70
0.201	1.55	7.7	0.65	200	0.67
0.246	1.60	6.5	0.68	100	0.63
0.297	2.20	7.4	0.59	200	0.50
0.42	1.60	3.8	0.81	100	0.47
0.61	3.30	5.4	0.56	200	0.29

TABLE 3. Hg-sensitized photooxidation of C_2Cl_4 at 25 °C

$[C_2Cl_4]$* (Torr)	$[O_2]$ (Torr)	I_a (mTorr/s)	$\Phi\{CCl_2O\}$	$\Phi\{CCl_3CCl(O)\}$	$-\Phi\{C_2Cl_4\}$‖
0.72(1.15)	7.3	0.36	0.96	2.5	4.6
1.03	5.2	0.60	1.13	3.16	4.4
1.50	5.9	1.53	3.04	8.25	9.15(6.6)
1.75(2.10)	6.0	0.35	1.57	4.8	6.7
2.2	5.8	0.14	2.85	7.0	7.6
2.2	6.0	0.17	3.38	8.25	10.6
2.2	5.5	0.29	3.44	10.0	12.6
2.3	5.1	0.74	5.0	13.5	15.5
2.4	9.6	0.35	2.9	7.8	10.3(10.5)
2.5	45.5	0.60	5.0	12.5	13.7
2.9(5.1)	28.9	0.35	4.9	12.0	14.0
3.0(3.6)	6.8	0.35	3.4	6.7	10.0
3.2	6.3	0.60	4.6	12.8	14.7(14.0)
3.6(4.9)	67.0	0.35	5.3	13.2	23.0
4.2(5.0)	6.2	0.35	3.6	10.0	15.0
4.2(4.8)	6.3	1.73	7.0	19.5	21.2
5.0	6.3	0.35	5.8	16.0	31(22)
5.0†	6.3	0.60	7.5	21.0	25
5.4	5.5	1.10	8.0	23.0	—
5.6(7.7)	7.0	0.35	9.4	20.0	32
7.1‡	6.6	0.25	8.0	24	36
7.9(9.9)	6.5	0.35	13.0	—	—
8.8(11.7)	4.2	0.35	15.0	36	56
9.9§	6.8	0.25	14.4	35	37(43)

*For those runs with quantum yields based on extensive photolysis, the average C_2Cl_4 pressure is listed. The value in parenthesis is the initial C_2Cl_4 pressure. The other runs are all based on initial rates.
†$\Phi\{CO\} = 1.00$.
‡$\Phi\{CO\} = 0.93$.
§$\Phi\{CO\} = 1.13$.
‖Values in parentheses obtained from using the slope in Fig. 2.

pressure range of a factor of 15.9, and an I_a range of 12.3. Within the scatter of the data, the quantum yields of the chlorine containing species are independent of $[O_2]$, essentially independent of I_a (there appears to be a slight increase in yields with I_a), and increase with the C_2Cl_4 pressure. Thus, these results are consistent with those in Fig. 2.

A few runs were done with C_2Cl_4, O_2, and either SO_2, CO, or NO present. The affect of these gases on the quantum yields of the chlorine containing compounds is shown in Table 4. The

Can. J. Chem. Downloaded from www.nrcresearchpress.com by 210.87.254.105 on 09/05/12
For personal use only.

TABLE 4. Hg-sensitized photooxidation of C_2Cl_4 in the presence of SO_2, CO, and NO at 25 °C, I_a = 0.35 mTorr/s, and $[O_2]$ = 5.6 ± 0.3 Torr

[M] (Torr)	$[C_2Cl_4]$‡ (Torr)	$\Phi\{CCl_2O\}$	$\Phi\{CCl_3CCl(O)\}$	$-\Phi\{C_2Cl_4\}$	$\frac{\Phi\{CCl_3CCl(O)\}}{\Phi\{CCl_2O\}}$
		M = SO_2			
0.0*	3.8	5.3	14.1	17.1	2.6
0.40	3.6(2.8)	3.7	11.4	15.2	3.1
1.10	4.8(4.0)	4.2	9.5	16.5	2.3
3.40	4.6(3.8)	3.3	9.4	16.2	2.9
		M = CO			
0.0*	4.2	5.9	15.6	13.8	2.6
0.42	5.1(4.4)	3.9	10.4	14.9	2.6
0.80	4.8(4.1)	4.9	—	14.7	—
		M = NO			
0.0*	5.0	7.0	18.6	22.0	2.6
0.044	5.4(5.2)	1.31	3.14	4.3	2.4
0.088	5.6(5.4)	0.91	1.35	1.0	1.5
0.088†	5.8(5.6)	0.63	0.95	—	1.5
0.093	2.9(2.8)	0.91	0.84	—	0.9
0.195	4.8(4.6)	0.79	1.25	—	1.6

*For [M] = 0, quantum yields obtained from Fig. 3.
†$[O_2]$ = 56.7 Torr.
‡All irradiations were for 300 s. The $[C_2Cl_4]$ listed is the initial pressure. The value in parenthesis is the average value for the 300 s irradiation.

addition of SO_2 or CO does not have much, if any, effect. However, only small amounts of NO greatly reduce the quantum yields, suggesting that NO is scavenging the free radical chain carriers.

Finally, one run was done in which 7.1 Torr of Cl_2 was photolyzed by a medium-pressure Hg lamp in the presence of 5.2 Torr of C_2Cl_4 and 20.0 Torr of O_2 in a Pyrex cell. In this experiment, in which the oxidation of C_2Cl_4 is initiated by chlorine atoms, the ratio $\Phi\{CCl_3CCl(O)\}/\Phi\{CCl_2O\}$ was found to be 2.7, in good agreement with the work of Mathias *et al.* (6).

Discussion

In the absence of O_2, the only products are Hg_2Cl_2 and polymer, but $-\Phi\{C_2Cl_4\} \sim 1$. Consequently the quenching of Hg 6(^{3}P) by C_2Cl_4 must cleave a C—Cl bond. This might occur directly

[10*a*] $\quad Hg\ 6(^3P) + C_2Cl_4 \rightarrow C_2Cl_3 + HgCl$

or by energy transfer first

[10*b*] $\quad Hg\ 6(^3P) + C_2Cl_4 \rightarrow Hg\ 6(^1S) + C_2Cl_4^*$

followed by

[13] $\quad Hg\ 6(^1S) + C_2Cl_4^* \rightarrow C_2Cl_3 + HgCl$

where $C_2Cl_4^*$ is an electronically excited C_2Cl_4 molecule. In either case, the C_2Cl_3 radical would dimerize, and the resulting 1,3-C_4Cl_6 molecule would polymerize.

In the presence of O_2, the quantum yields are unaffected by changes in the O_2 pressure. This result must be reconciled with the fact that O_2 is as efficient as N_2O in quenching Hg 6(^{3}P) via the process (5)

[14] $\quad Hg\ 6(^3P) + O_2 \rightarrow Hg\ 6(^1S) + O_2^*$

where O_2^* is electronically excited O_2. Presumably, the explanation is that O_2^* can transfer its energy to C_2Cl_4 in the same manner as it does with the perfluoroolefins (5)

[15] $\quad O_2^* + C_2Cl_4 \rightarrow O_2 + C_2Cl_4^*$

and this reaction is followed by reaction 13.

The results of the Hg-photosensitized oxidation of C_2Cl_4 are very similar to those in the Cl-initiated oxidation, *i.e.* the major products are $CCl_3CCl(O)$ and CCl_2O produced in a ratio of 2.6 independent of conditions. Furthermore, the quantum yields are independent of I_a and O_2 pressure. Consequently, the mechanism consisting of reactions 2–8 must be operative in both systems.

The only difference between the two systems is that for Hg sensitization, the quantum yields are

Can. J. Chem. Downloaded from www.nrcresearchpress.com by 210.87.254.105 on 09/05/12
For personal use only.

TABLE 5. Summary of rate constant ratios

Ratio	Value	Units	Source	
			Equation	Figure
k_{10}/k_9	3.0±0.5	None	11	1
$k_{18}k_4/k_{17}k_{4b}$	4.4±0.4	$Torr^{-1}$	12	2
$k_{18}k_4/k_{17}k_{4b}$	4.4±1.0	$Torr^{-1}$	22	3
$\frac{2k_{6b}k_4k_{18}}{k_6k_{4b}k_{17}}$	1.4±0.3	$Torr^{-1}$	20	3
$\frac{k_{6a}k_4k_{18}}{k_6k_{4b}k_{17}}$	3.7±1.0	$Torr^{-1}$	21	3
$k_{6a}/2k_{6b}$	2.6±0.2	None	20, 21	3

proportional to the C_2Cl_4 pressure, whereas for chlorine atom initiation, there is no dependence on C_2Cl_4 pressure. The explanation for the difference must be in the mechanism that initiates chlorine atom production in the Hg-sensitized system. The simplest mechanism consistent with the observation is

[16] $C_2Cl_3 + O_2 \rightarrow C_2Cl_3O_2$

[17] $C_2Cl_3O_2 \rightarrow$ CO by termination

[18] $C_2Cl_3O_2 + C_2Cl_4 \rightarrow C_2Cl_5 + (CClO)_2$

Reaction 17 is needed to satisfy the observations that $\Phi\{CO\} = 1.0$ and that there is no dependence on I_a, *i.e.* termination is first order in radicals. How reaction 17 proceeds is not clear. Possibly it is a wall reaction. Reaction 18 is the chain initiating reaction and produces $(CClO)_2$. However we presume reaction 18 to be much less important than reaction 17, so that insufficient $(CClO)_2$ would be produced to detect.

The mechanism consisting of reactions 2–8, 10, and 13–18 leads to the following rate laws if the rate of reaction 18 is small compared to that for reaction 17, and the rates of reactions 4*b* and 5 are small compared to that for reaction 4*a*.

[19] $$\Phi\{CO\} = 1$$

[20] $$\Phi\{CCl_2O\} = \frac{2k_4k_{6b}k_{18}}{k_{4b}k_6k_{17}}[C_2Cl_4]$$

[21] $$\Phi\{CCl_3CCl(O)\} = \frac{k_4k_{6a}k_{18}}{k_{4b}k_6k_{17}}[C_2Cl_4]$$

[22] $$-\Phi\{C_2Cl_4\} - 1 = \frac{k_4k_{18}}{k_{4b}k_{17}}[C_2Cl_4]$$

In agreement with eq. 19, $\Phi\{CO\}$ was found to be one. Figure 3 shows log–log plots of $\Phi\{CCl_2O\}$, $\Phi\{CCl_3CCl(O)\}$, and $-\Phi\{C_2Cl_4\} - 1$ *vs.* the C_2Cl_4 pressure. As predicted by eqs. 20–22, all the plots can be well fitted by lines of slope one. From the three graphs the rate constant ratios in eqs. 20–22 are found to be 1.4 ± 0.3, 3.7 ± 1.0, and 4.4 ± 1.0 $Torr^{-1}$ respectively. The ratio $\Phi\{CCl_3CCl(O)\}/\Phi\{CCl_2O\} = k_{6a}/2k_{6b} = 2.6 \pm$

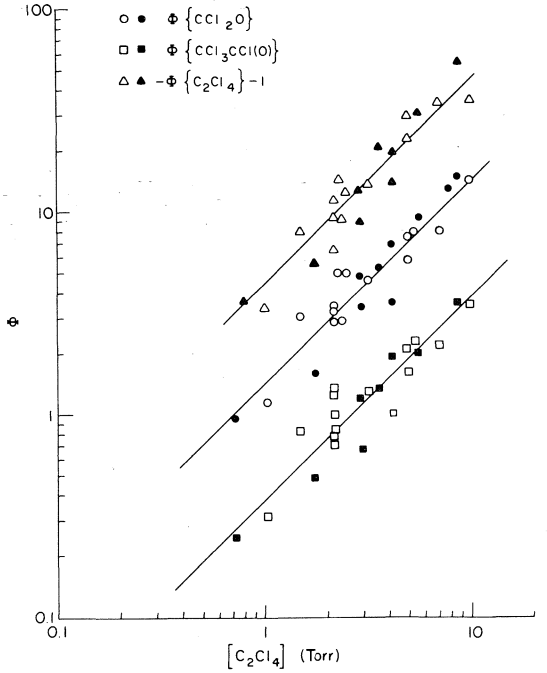

FIG. 3. Log–log plots of the quantum yields *vs.* C_2Cl_4 pressure in the Hg-photosensitized oxidation of C_2Cl_4 at 25 °C. The open points represent results from initial slopes; the filled points represent average values for runs at extended conversions. For clarity, the plot for $\Phi\{CCl_3CCl(O)\}$ has been displaced downward by a factor of 10.

Can. J. Chem. Downloaded from www.nrcresearchpress.com by 210.87.254.105 on 09/05/12
For personal use only.

0.2 is in excellent agreement with that found in the Cl initiated reaction (6). Also, mass balance requires that $-\Phi\{C_2Cl_4\} - 1 \simeq \Phi\{CCl_3CCl(O)\} + \frac{1}{2}\Phi\{CCl_2O\}$; the value for $-\Phi\{C_2Cl_4\} - 1$ of $4.4[C_2Cl_4]$ agrees exactly with the value for $\Phi\{CCl_3CCl(O)\} + \frac{1}{2}\Phi\{CCl_2O\}$ of $4.4[C_2Cl_4]$. Finally, the value of $(k_4/k_{4b})(k_{18}/k_{17})$ of 4.4 found from Fig. 3 agrees exactly with the same value found from Fig. 2.

A summary of the rate constant ratios found in this work is given in Table 5.

We wish to thank R. Shortridge, M. Luria, and T. Osif for help with the experiments and I. C. Hisatsune and E. Mathias for useful discussions. This work was supported by the Environmental Protection Agency under Grant No. R 800949 for which we are grateful.

1. R. G. Dickinson and J. A. Leermakers. J. Am. Chem. Soc. **54**, 3852 (1932).
2. R. G. Dickinson and J. L. Carrico. J. Am. Chem. Soc. **56**, 1473 (1934).
3. C. Schott and H. J. Schumacher. Z. Phys. Chem. B**49**, 107 (1941).
4. G. Huybrechts, J. Olbrechts, and K. Thomas. Trans. Faraday Soc. **63**, 1647 (1967).
5. J. Heicklen. Adv. Photochem. **7**, 57 (1969).
6. E. Mathias, E. Sanhueza, I. C. Hisatsune, and J. Heicklen. Can. J. Chem. This issue.
7. R. J. Cvetanović. Adv. Photochem. **1**, 115 (1963).

Can. J. Chem. Downloaded from www.nrcresearchpress.com by 210.87.254.105 on 09/05/12
For personal use only.

The Reaction of $O(^3P)$ with C_2Cl_4 [1]

EUGENIO SANHUEZA[2] AND JULIAN HEICKLEN

Department of Chemistry and Center for Air Environment Studies, Pennsylvania State University, University Park, Pa. 16802

Received April 16, 1973[3]

EUGENIO SANHUEZA and JULIAN HEICKLEN. Can. J. Chem. **52**, 3870 (1974).

The reaction of $O(^3P)$, prepared from Hg photosensitization of N_2O with C_2Cl_4 was studied at 25 °C. The exclusive products of the reaction in the absence of O_2 were CCl_2O and polymer (as well as N_2 from the N_2O). The quantum yield of CCl_2O production, $\Phi\{CCl_2O\}$, was 0.19 independent of the C_2Cl_4 pressure or the absorbed intensity, I_a. There was no evidence for CO, Cl_2, c-C_3Cl_6, $CCl_3CCl(O)$, or $\overline{CCl_2CCl_2O}$ production. The reaction mechanism is

$$O(^3P) + C_2Cl_4 \rightarrow CCl_2O + CCl_2 \quad [12a]$$

$$\rightarrow C_2Cl_4O^* \quad [12b]$$

with $k_{12a}/k_{12} = 0.19$. The CCl_2 radical dimerizes and the energetic $C_2Cl_4O^*$ intermediate polymerizes. By competitive kinetics, the ratio k_{12}/k_{13} was found to be 0.10, where $k_{12} \equiv k_{12a} + k_{12b}$ and k_{13} is the rate coefficient of the $O(^3P) + C_2F_4$ reaction.

In the presence of O_2, a chain process is involved in which $CCl_3CCl(O)$ and CCl_2O are the major products. They are formed in a ratio of 2.0 independent of reaction conditions, but the chain length is proportional to $[C_2Cl_4]/I_a^{1/2}$. Also produced is CO with a quantum yield of ~0.18. The ratio $\Phi\{CCl_3CCl(O)\}/\Phi\{CCl_2O\} = 2.0$ is similar to that of 2.5 found in the Cl atom initiated oxidation. This result is interpreted to mean that chlorine atoms are involved in the chain. The reaction which initiates monoradicals in the system is

$$CCl_2 + O_2 \rightarrow ClCO + ClO \quad [21]$$

EUGENIO SANHUEZA et JULIAN HEICKLEN. Can. J. Chem. **52**, 3870 (1974).

On a étudié, à 25 °C, la réaction de C_2Cl_4 avec $O(^3P)$ préparé par photosensibilisation au mercure du N_2O. Les seuls produits formés au cours de la réaction, en absence d'oxygène, sont le CCl_2O et un polymère (il se forme aussi du N_2 à partir du N_2O). Le rendement quantique pour la production de CCl_2O, $\Phi\{CCl_2O\}$, est de 0.19 et est indépendant de la pression de C_2Cl_4 ou de l'intensité absorbée, I_a. On n'a trouvé aucune indication concernant la production de CO, Cl_2, c-C_3Cl_6, $CCl_3CCl(O)$ ou $\overline{CCl_2CCl_2O}$. Le mécanisme réactionnel est

$$O(^3P) + C_2Cl_4 \rightarrow CCl_2O + CCl_2 \quad [12a]$$

$$\rightarrow C_2Cl_4O^* \quad [12b]$$

pour lesquels $k_{12a}/k_{12} = 0.19$. Le radical CCl_2 se dimérise et l'intermédiaire $C_2Cl_4O^*$ qui contient beaucoup d'énergie se polymérise. A l'aide de cinétiques compétitives, on a trouvé que le rapport k_{12}/k_{13} est de 0.10; dans cette équation $k_{12} = k_{12a} + k_{12b}$ et k_{13} est le coefficient de vitesse pour la réaction $O(^3P) + C_2F_4$.

En présence d'oxygène, un processus en chaîne est impliqué dans lequel $CCl_3CCl(O)$ et $CCl_2(O)$ sont les produits prédominants. Ils se forment dans un rapport de 2.0 qui est indépendant des conditions de la réaction mais la longueur de la chaîne est proportionnelle à la quantité $[C_2Cl_4]/I_a^{1/2}$. Du CO est aussi produit avec un rendement quantique d'environ 0.18. Le rapport $\Phi\{CCl_3CCl(O)\}/\Phi\{CCl_2O\} = 2.0$ est semblable à la valeur de 2.5 trouvé pour les réactions d'oxydation initiées par des atomes de chlore. On interprète ce résultat comme signifiant que les atomes de chlore sont impliqués dans la chaîne. La réaction qui provoque la formation initiale de monoradicaux dans ce système est

$$CCl_2 + O_2 \rightarrow ClCO + ClO \quad [21]$$

[Traduit par le journal]

Introduction

The chlorine atom initiated oxidation of C_2Cl_4 has been studied in several laboratories (1–4), and the results reviewed (5). More recently, a study was made in our laboratory (6). In all the studies, the major products were $CCl_3CCl(O)$ and CCl_2O. The reaction was a long chain reaction with chain lengths of about 300 independent of light intensity, I_a, or any of the reactant pressures if the O_2 pressure was suffi-

[1]CAES Report No. 305–73.
[2]Fulbright Fellow 1972–1974.
[3]Revision received August 9, 1974.

ciently high. The ratio of product quantum yields $\Phi\{CCl_3CCl(O)\}/\Phi\{CCl_2O\}$ was 5.7 at 80–100 °C (4), 4.0 at 40–80 °C (3), 3.0 at 32 °C (6), and 2.5 at 24 °C (6).

The main features of the mechanism of the reaction were worked out by Huybrechts *et al.* (4).

[1] $Cl_2 + h\nu \rightarrow 2Cl$

[2] $Cl + C_2Cl_4 \rightarrow C_2Cl_5$

[3] $C_2Cl_5 + O_2 \rightarrow C_2Cl_5O_2$

[4*a*] $2C_2Cl_5O_2 \rightarrow 2C_2Cl_5O + O_2$

[4*b*] $\rightarrow (C_2Cl_5O)_2 + O_2$

[5] $C_2Cl_5O_2 + C_2Cl_5 \rightarrow (C_2Cl_5O)_2$

[6*a*] $C_2Cl_5O \rightarrow CCl_3CCl(O) + Cl$

[6*b*] $\rightarrow CCl_2O + CCl_3$

[7] $CCl_3 + \frac{1}{2}O_2 \rightarrow CCl_2O + Cl$

Reaction 7 is, of course, not a fundamental reaction, but proceeds through the sequence.

$$CCl_3 + O_2 \rightarrow CCl_3O_2$$
$$2CCl_3O_2 \rightarrow 2CCl_3O + O_2$$
$$CCl_3O \rightarrow CCl_2O + Cl$$

In addition, for systems in which ClO radicals are present, they also can carry the chain via

[8*a*] $ClO + C_2Cl_4 \rightarrow CCl_3CCl(O) + Cl$

[8*b*] $\rightarrow CCl_2O + CCl_3$

[8*c*] $\rightarrow \overline{CCl_2CCl_2O} + Cl$

The above mechanism involves only monoradicals. The ozonolysis is also a chain process, but the product ratio $[CCl_3CCl(O)]/[CCl_2O]$ is less than one (6). In that system, only diradicals are involved, and the mechanism presumably involves such reactions as (6)

[9] $CCl_2O_2 + C_2Cl_4 \rightarrow CCl_2O_2C_2Cl_4$

[10] $CCl_2O_2C_2Cl_4 + O_2 \rightarrow CCl_2O_2C_2Cl_4O_2$

[11] $CCl_2O_2C_2Cl_4O_2 + C_2Cl_4 \rightarrow 3CCl_2O + C_2Cl_4O$

In our laboratory, we are engaged in an extensive program to study halocarbon oxidation. In this paper, we report the results of the oxidation of C_2Cl_4 initiated by oxygen atoms. These results are compared to those obtained by chlorine atom initiation and ozonolysis to see whether a monoradical or diradical mechanism is involved.

Experimental

Gas mixtures were photolyzed in a 10 cm long by 5 cm diameter quartz cell containing a drop of mercury. Irradiation was from a Hanovia flat-spiral low-pressure mercury resonance lamp. The radiation passed through a 9-54 Corning filter to remove radiation below 2200 Å. One or two Corning 9-30 filters were used to reduce the light intensity when desired.

The reaction mixture exited continuously, prior to and during each photolysis, through a pinhole into 8 mm Pyrex tubing which led through a second pinhole into a modified E.A.I. 160 quadrupole mass spectrometer. Complete details of the apparatus and procedure have been described previously (7). The leak-rate of the first pinhole was sufficiently small so that the pressure drop in the reaction vessel was negligible during the time of the experiment ($\leq$600 s).

All gases were Matheson C.P. grade. When it was possible, they were purified by bulb-to-bulb distillation in the vacuum line and degassed, before each run, at −196 °C. The tetrachloroethylene was Baker Analyzed, chlorine free. The fraction volatile at −21 °C but condensable at −90 °C was used. It was degassed before each run from a slush at −90 °C. The trichloroacetyl chloride was from Eastman Kodak and was fractionated in the same manner as the C_2Cl_4 before use.

The working part of the vacuum system was greaseless, employing Teflon stopcocks and greaseless joints with Viton O-rings. For pressures less than 5 Torr, a Consolidated Vacuum Corporation McLeod gauge was used whenever possible. Pressures between 5 and 50 Torr were measured in a calibrated Wallace and Tiernan absolute pressure indicator. Pressures higher than 50 Torr were measured in a mercury manometer.

In order to measure quantum yields, the *m/e* peak ratios (63/44), (94/44), and (117/44) were plotted *vs.* time. The slopes of these plots yielded the rates of production of CCl_2O (63/44) and $CCl_3CCl(O)$ (117/44) and disappearance of C_2Cl_4 (94/44), when corrected for the relative sensitivity calibration factor and multiplied by the pressure of N_2O present. These products rates were converted to quantum yields by dividing by the N_2 production rate.

For a number of the experiments, the reaction mixture was collected at −196 °C, the noncondensable gases were removed, and the condensables were warmed at −90 °C. The N_2O and CCl_2O were removed and the C_2Cl_4–$CCl_3CCl(O)$ fraction was retained. Both fractions were analyzed separately by infrared spectrometry in a Beckman IR-10 spectrometer.

Additional experiments were made in a T-shaped cell situated in the sample beam of the I.R.-10 spectrometer. Thus the halogenated products could be monitored continuously by infrared analysis. Some runs were done with C_2F_4 added to study the competition between C_2Cl_4 and C_2F_4 for O(³P). The product CF_2O was monitored at 1960 cm^{-1} using its peak extinction coefficient (to base 10) of 0.016 $Torr^{-1}$ cm^{-1}.

In some runs the gases noncondensable at −196 °C were analyzed by gas chromatography using an 8 ft long 5A molecular sieve column at 0 °C with a He flow rate of 100 cc/min. Gas chromatographic analysis for CO_2 was made utilizing a 24 ft long column packed with Porapak Q operating at 25 °C and a H_2 carrier gas flow rate of 60 cc/min.

TABLE 1. Reaction of $O(^3P)$ with C_2Cl_4 at 25 °C by mass spectral analysis

$[C_2Cl_4]$ (Torr)	$R\{N_2\}$ (mTorr/s)	Irradiation time (s)	$\Phi\{CCl_2O\}$*	$-\Phi\{C_2Cl_4\}$†
	$I_a \sim 10$ mTorr/s,‡ $[N_2O] = 138 \pm 10$ Torr			
0.95	6.0	185	0.22	0.9
1.20§	6.0	205	0.21	—
1.90	3.68	210	0.19	—
3.70	4.35	230	0.16	—
5.70	1.35	240	0.21	1.9
	$I_a \sim 6.8$ mTorr/s,‡ $[N_2O] = 204 \pm 10$ Torr			
1.55	4.6	205	0.15	—
1.90‖	3.91	200	0.16	—
2.37	5.1	205	0.17	1.0
3.10	5.3	255	0.14	1.1
	$I_a \sim 2.1$ mTorr/s,‡ $[N_2O] = 197 \pm 3$ Torr			
1.40	1.6	600	0.17	1.25
2.90	1.4	600	0.18	1.0
			Ave = 0.18 ± 0.04	

*$\Phi\{CCl_2O\}$ computed as the ratio of CCl_2O to N_2 produced.
†$-\Phi\{C_2Cl_4\}$ computed as the ratio of C_2Cl_4 consumed to N_2 produced.
‡I_a at the beginning of the run as determined from the N_2 produced from the irradiation of N_2O in the presence of 1–2% of C_2F_4.
§$[N_2O] = 197$ Torr.
‖Analysis of this run by infrared spectroscopy rather than mass spectroscopy.

TABLE 2. Reaction of $O(^3P)$ with C_2Cl_4 at 25 °C by infrared spectral analysis*

$[C_2Cl_4]$ (Torr)	$[N_2O]$ (Torr)	I_a (mTorr/s)	Irradiation time (s)	$R\{N_2\}$ (mTorr/s)	$\Phi\{CCl_2O\}$†	$-\Phi\{C_2Cl_4\}$‡
0.90	58	1.4	1000	0.57	0.22	1.5
0.94	500	0.8	2250	0.135	0.17	1.85
1.70	165	1.0	600	0.38	0.23	1.67
1.76	388	1.2	630	0.53	0.15	1.69
3.5	208	1.2	900	0.52	0.20	2.20
					Ave = 0.19 ± 0.04	

*Continuous infrared analysis in a T-shaped cell. The CCl_2O was analyzed with a scale expander and auxiliary recorder.
†$\Phi\{CCl_2O\}$ computed as the ratio of CCl_2O to N_2 produced.
‡$-\Phi\{C_2Cl_4\}$ computed as the ratio of C_2Cl_4 consumed to N_2 produced.

In order to remove the polymer from the reaction cell, air was admitted, and the cell was heated with an oxygen gas torch to about 500 °C before each experiment.

Results

The mercury-sensitized photolysis of N_2O in the presence of C_2Cl_4 at 25 °C yields N_2, CCl_2O, and polymer as exclusive products. A careful search was made for CO, Cl_2, c-C_3Cl_6, $CCl_3CCl(O)$, and $\overline{CCl_2CCl_2O}$, but they were absent. For the latter two compounds, an upper limit of 0.05 could be placed on their quantum yields. There was also no evidence for copious amounts of Hg_2Cl_2 production, since the Hg drop did not become coated. However, since polymer was produced the cell had to be cleaned periodically by flaming. Thus, some Hg_2Cl_2 might have been produced and removed in the cleaning process.

The results of the photolyses are shown in Tables 1 and 2. The absorbed intensity, I_a, at the beginning of a run was measured from the mercury-sensitized photolysis of N_2O in the presence of 1–2% C_2F_4 (to scavenge the $O(^3P)$ atoms produced). In this system $\Phi\{N_2\} = 1.0$ (5, 8). During the irradiation of N_2O–C_2Cl_4 mixtures, the polymer coats the window and I_a is continuously reduced. This was verified by actinometry experiments (*i.e.* the N_2O–C_2F_4 system) after the irradiation. However, the amount

TABLE 3. Reaction of O(³P) with C_2Cl_4 in the presence of C_2F_4 at 25 °C and $I_a \sim 10$ mTorr/s at the beginning of the run. Analysis by mass spectroscopy

$\frac{[C_2Cl_4]}{[C_2F_4]}$	$[C_2Cl_4]$ (Torr)	$[C_2F_4]$ (Torr)	$[N_2O]$ (Torr)	$R\{N_2\}$ (mTorr/s)	Irradiation time (s)	$\Phi\{CCl_2O\}$*
1.86	1.95	1.05	130	4.4	210	0.025
2.48	1.71	0.69	162	5.6	200	0.035
3.55	2.38	0.67	164	2.8	250	0.040
4.00	2.96	0.74	164	2.8	215	0.045
5.00	5.90	1.18	129	2.6	205	0.065
5.89	5.17	0.88	154	2.4	220	0.075
9.75	6.44	0.66	161	1.8	210	0.085

*$\Phi\{CCl_2O\}$ computed as the ratio of CCl_2O to N_2 produced. CCl_2O normalized to fit infrared data.

TABLE 4. Reaction of O(³P) with C_2Cl_4 in the presence of C_2F_4 at 25 °C and $I_a \sim 1.3$ mTorr/s at the beginning of the run. Analysis by infrared spectroscopy

$\frac{[C_2Cl_4]}{[C_2F_4]}$	$[C_2Cl_4]$ (Torr)	$[C_2F_4]$ (Torr)	$[N_2O]$ (Torr)	$R\{N_2\}$ (mTorr/s)	$\Phi\{CCl_2O\}$*	$\Phi\{CF_2O\}$*
1.04	1.32	1.27	382	1.43	—	0.85
2.17	1.33	0.62	248	0.60	—	0.78
4.03	2.5	0.62	375	0.71	<0.07	0.74
5.8	2.9	0.51	200	0.37	0.075	0.64
10.4	5.2	0.51	204	0.42	0.09	0.50

*Quantum yields computed by comparison with N_2 production.

of N_2 produced during the photolysis of the N_2O–C_2Cl_4 mixtures can be used as an internal actinometer to measure the amount of O(³P) atoms produced. Thus in Tables 1 and 2, the quantum yields are computed on the basis of the N_2 produced.

In the experiments in Tables 1 and 2, the initial I_a is varied by a factor of 12, and the C_2Cl_4 pressure by a factor of 6.3. The quantum yield of CCl_2O production, $\Phi\{CCl_2O\}$, is 0.19 ± 0.04 insensitive to variations in any of the parameters.

The quantum yield of C_2Cl_4 loss, $-\Phi\{C_2Cl_4\}$, is somewhat difficult to measure, and the results are scattered. However the values range between 0.9 and 2.2.

In order to measure the rate constant for the reaction of O(³P) with C_2Cl_4, the mercury-sensitized decomposition of N_2O was studied in the presence of mixtures of C_2Cl_4 and C_2F_4. The data are listed in Tables 3 and 4. (In Table 3, the absolute values of $\Phi\{CCl_2O\}$ were obtained by comparison to infrared data, rather than by direct mass spectral calibration.) It can be seen that $\Phi\{CCl_2O\}$ rises and $\Phi\{CF_2O\}$ falls as the $[C_2Cl_4]/[C_2F_4]$ ratio rises as expected from the competition

[12*a*] $O(^3P) + C_2Cl_4 \rightarrow CCl_2O + CCl_2$

[12*b*] $\rightarrow$ not CCl_2O

[13] $O(^3P) + C_2F_4 \rightarrow CF_2O +$

From the results of Tables 1 and 2, the fraction $k_{12a}/k_{12} = 0.19$ independent of reaction conditions. Then reactions 12 and 13 lead to the simple rate laws

$$[14a] \quad \Phi\{CCl_2O\}/(\Phi_0\{CCl_2O\} - \Phi\{CCl_2O\}) = k_{12}[C_2Cl_4]/k_{13}[C_2F_4]$$

$$[14b] \quad (1.0 - \Phi\{CF_2O\})/\Phi\{CF_2O\} = k_{12}[C_2Cl_4]/k_{13}[C_2F_4]$$

where $\Phi_0\{CCl_2O\}$ is $\Phi\{CCl_2O\}$ in the absence of C_2F_4, *i.e.* $\Phi_0\{CCl_2O\} = 0.19$.

Figure 1 shows a plot of the left-hand side of eqs. 14*a* and *b* *vs.* $[C_2Cl_4]/[C_2F_4]$. The plot is linear and passes through the origin. Its slope gives $k_{12}/k_{13} = 0.10$. Since O(³P) reacts equally efficiently with C_2F_4 and C_2H_4 at 25 °C, our result is in agreement with the qualitative result of Huie *et al.* (9) that O(³P) reacts less readily with C_2Cl_4 than with C_2H_4.

In the presence of O_2, three additional products were found: CO, CO_2, and $CCl_3CCl(O)$. There was still no evidence for *c*-C_3Cl_6, Cl_2, Hg_2Cl_2, or CCl_2CCl_2O. In particular, the upper

TABLE 5. Reaction of $O(^3P)$ with C_2Cl_4 in the presence of O_2 at 25 °C

$[C_2Cl_4]/I_a^{1/2}$ ((Torr s)$^{1/2}$)	$[C_2Cl_4]$ (Torr)	I_a§ (mTorr/s)	$[O_2]$ (Torr)	$[N_2O]$ (Torr)	$\Phi\{CCl_2O\}$	$\Phi\{CCl_3CCl(O)\}$	$-\Phi\{C_2Cl_4\}$	$\Phi\{CO\}$‖
9.9	0.85	7.3	2.35	199	0.67	—	0.70	—
11.6	1.00	7.5	2.40	199	0.90	—	1.80	—
15.9	1.56	9.7	0.79	188	1.0	—	1.80	—
17.3	1.40	6.5	1.80	200	0.40	—	0.90	—
24.1	1.92	6.4	0.58	205	0.75	—	1.70	—
26.3	2.15	6.6	6.20	194	1.3	—	—	—
27.4	2.20	6.5	0.80	195	1.9	—	—	—
28.6	2.37	6.9	2.40	190	1.7	—	2.5	—
29.1	2.38	6.7	8.90	190	1.1	—	2.5	—
30.0	2.45	6.7	2.30	200	1.4	—	2.3	—
36.4	2.35	4.2	4.05	167	—	3.0	—	—
40.6*	2.50	3.8	4.40	226	1.5	3.8	7.0	—
43.0‡	1.50	1.20(0.80)	4.60	332	1.8	5.0	6.6	0.14
48.0	2.95	3.8	3.35	219	—	2.6	—	—
50.0‡	2.00	1.7(1.30)	5.50	518	2.0	5.0	7.0	0.19
63.0†	2.0	1.01	4.2	230	—	—	—	0.15
63.3‡	2.0	1.0(0.80)	4.7	453	2.2	5.5	5.6	0.25
75.4	6.40	7.2	2.30	198	2.3	—	5.6	—
79.6*	5.35	4.5	5.60	214	2.5	7.5	11.8	—
84	6.30	4.5	5.60	201	—	4.5	—	—
85	5.10	3.6	6.30	185	—	5.4	—	—
89	6.55	7.4	9.35	189	2.0	—	3.5	—
89	7.50	7.1	3.85	212	2.8	—	4.7	—
90	1.80	0.40	2.60	200	5.1	—	—	—
94‡	4.20	2.00(1.0)	2.20	486	5.4	13.0	13.0	0.16
99	8.30	7.1	8.90	202	3.5	—	7.0	—
101	1.97	0.38	3.40	191	5.2	—	8.7	—
103	2.05	0.40	2.80	199	5.0	—	—	—
107†	4.3	1.58	6.7	222	—	—	—	0.23
119	2.10	0.31	2.50	193	—	6.7	7.5	—
120	2.20	0.34	2.78	207	—	11.5	8.2	—
127*	8.50	4.5	5.60	194	4.3	10.3	17.0	—
148†	4.7	1.01	6.3	244	—	—	—	0.15
152	5.0	1.09	6.0	200	—	12.0	—	—
153	4.65	1.09	5.85	200	7.8	—	—	—
159*	5.4	1.15	5.3	150	6.0	12.5	22.0	—
163	5.3	1.05	6.0	209	6.7	—	9.0	—
175*	11.2	4.1	6.2	228	5.4	9.5	18.0	—

*Analysis by infrared spectroscopy rather than mass spectrometry.
†Analysis by gas chromatography.
‡Analysis of chlorinated compounds by continuous monitoring with infrared analysis in a T-shaped reaction cell. CO and CO_2 analysis by gas chromatography. For these runs $\Phi\{CO_2\} < 0.1$ (based on N_2 production). These runs done for extended reaction times to increase accuracy of CO and CO_2 analysis.
§Values in parentheses are from N_2 measured.
‖$\Phi\{CO\}$ based on N_2 production.

limit for the quantum yield of the last compound was 0.1.

For four of the runs in Table 5, analysis for CO_2 showed it to be minor, its quantum yield being <0.1 in all cases. In order to promote CO_2 formation, one run was done with 40 Torr of O_2 ($[C_2Cl_4] = 4.6$ Torr, $[N_2O] = 214$ Torr). This run contained four times as much O_2 as in any of the runs listed in Table 5. Yet for this run $\Phi\{CO_2\}$ was <0.15. Thus, we conclude that CO_2 is not an important product under our conditions.

The chlorine-containing products were produced with a slight induction of a few seconds, after which they were produced linearly with irradiation time. Quantum yield measurements are based on the slopes of the straight-line portions of the curves of growth for CCl_2O, $CCl_3CCl(O)$, and C_2Cl_4.

Results of the photolyses in the presence of O_2 are given in Table 5. The quantum yields of CCl_2O and $CCl_3CCl(O)$ production are large; thus extensive irradiation was not necessary for analysis, and polymer build-up was less exten-

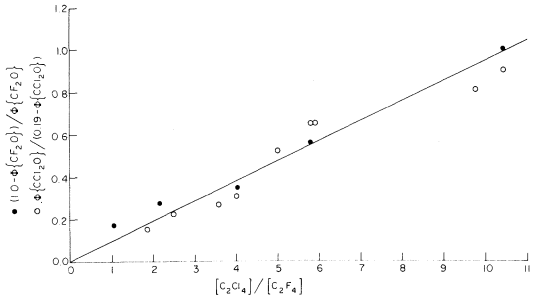

FIG. 1. Plots of $\Phi\{CCl_2O\}/(0.19 - \Phi\{CCl_2O\})$ and $(1 - \Phi\{CF_2O\})/\Phi\{CF_2O\}$ *vs.* $[C_2Cl_4]/[C_2F_4]$ for the reaction of $O(^3P)$ with mixtures of C_2Cl_4 and C_2F_4 at 25 °C.

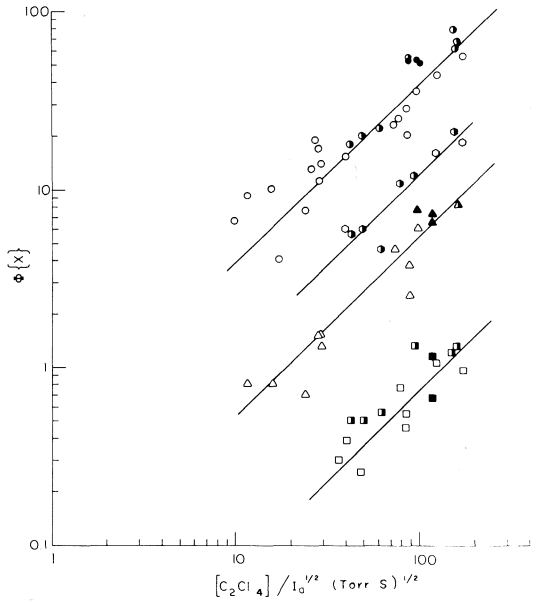

FIG. 2. Log–log plots of $-\Phi\{C_2Cl_4\} - 1$, $\Phi\{CCl_3CCl(O)\}$, and $\Phi\{CCl_2O\}$ *vs.* $[C_2Cl_4]/I_a^{1/2}$ for the reaction of $O(^3P)$ with C_2Cl_4 in the presence of O_2 at 25 °C. The circles represent $\Phi\{CCl_2O\}$; the squares, $\Phi\{CCl_3CCl(O)\}$; the triangles, $-\Phi\{C_2Cl_4\}$ as measured by mass spectroscopy; and the hexagons, $-\Phi\{C_2Cl_4\}$ as measured by infrared spectroscopy. The open points are for I_a = 3.5–10 mTorr/s; the half-filled points are for I_a = 1.0–2.0 mTorr/s; and the filled points are for I_a = 0.3–0.4 mTorr/s. For clarity, the curve for $\Phi\{CCl_2O\}$ is displaced upwards by a factor of 10, that for $\Phi\{CCl_3CCl(O)\}$ is displaced downward by a factor of 10.

sive than in the absence of O_2. External actinometry using the N_2O–C_2F_4 system could be used to obtain reliable quantum yields. An actinometry run was made before and after each experiment with O_2, and the average actinometric value used.

Experiments were done in which the O_2 pressure was varied from 0.58 to 9.35 Torr, the C_2Cl_4 pressure from 0.85 to 11.2 Torr, and I_a from 0.31 to 9.7 mTorr/s. $\Phi\{CCl_2O\}$, $\Phi\{CCl_3CCl(O)\}$, and $-\Phi\{C_2Cl_4\}$ all increase with the C_2Cl_4 pressure, but decrease as I_a is raised. Though there is considerable scatter at low O_2 pressure, there is no trend in the quantum yields as the O_2 pressure is varied. The best description of the data is that the quantum yields increase proportionately with $[C_2Cl_4]/I_a^{1/2}$. The plots illustrating this dependence are shown in Fig. 2. The log–log plots are fitted by straight lines of slope one. The proportionality constants that relate the quantum yields with $[C_2Cl_4]/I_a^{1/2}$ are 0.036 (Torr s)$^{1/2}$ for $\Phi\{CCl_2O\}$ and 0.072 (Torr s)$^{1/2}$ for $\Phi\{CCl_3CCl(O)\}$. For $-\Phi\{C_2Cl_4\}$ the data by mass spectral analysis lie below those for infrared analysis, showing some experimental discrepancy. The proportionality constants obtained by the two methods are 0.068 and 0.135 (Torr s)$^{1/2}$, respectively, for mass spectral and infrared analysis.

We believe that the discrepancy in the two analyses for C_2Cl_4 loss is due to the fact that C_2Cl_4 adheres very strongly to the wall of the reaction vessel. Thus, in the mass spectrometric experiments, C_2Cl_4 continues to enter the gas phase as it is depleted, and the measured loss rate is too low. However, for infrared analysis, the gas is transferred from the reaction vessel to the infrared cell, some of the C_2Cl_4 remains behind, and the measured loss is too large.

For a few runs CO was measured at the end of the run by gas chromatography. $\Phi\{CO\} = 0.18 \pm 0.04$ for these runs.

A few runs were made with either NO or SO_2 present. These results are summarized in Table 6. In the absence of O_2, the presence of 0.076 Torr of NO may reduce $\Phi\{CCl_2O\}$ somewhat, but 0.308 Torr of SO_2 has no effect. In neither case is polymer production inhibited. With O_2 present, both gases noticeably reduce product formation. In the case of NO, 0.085 Torr reduces product formation by at least a factor of 4. For 0.46 Torr of SO_2, the drop is at least a factor of 2.

Discussion

In the absence of O_2, the mechanism of the reaction is straightforward

[15] $\quad Hg + h\nu \rightarrow Hg^*$

TABLE 6. Reaction of $O(^3P)$ with C_2Cl_4 in the presence of NO and SO_2 at 25 °C

$[C_2Cl_4]/I_a^{1/2}$ ((Torr s)$^{1/2}$)	$[C_2Cl_4]$ (Torr)	I_a (mTorr/s)	[X] (Torr)	$[N_2O]$ (Torr)	$\Phi\{CCl_2O\}$	$\Phi\{CCl_3CCl(O)\}$
			X = NO, O_2 absent			
—*	3.0	8.5	0.076	173	0.12	—
			X = SO_2, O_2 absent			
—	2.7	8.5	0.308	200	0.19	—
			X = NO, $[O_2]$ = 6.2–7.6 Torr			
165†	—	—	0.0	—	6.0	11.9
154	5.1	1.09	0.087	203	1.7	—
169	5.5	1.06	0.080	201	—	1.7
171*	5.7	1.12	0.085	160	1.2	1.8
			X = SO_2, $[O_2]$ = 5.4–6.0 Torr			
155†	—	—	0.0	—	5.6	11.1
145	4.9	1.15	0.460	125	3.1	3.9
152	5.0	1.09	0.462	186	3.6	—
160	5.2	1.06	0.380	178	3.7	—
164	5.4	1.09	0.370	205	2.4	4.3

*Analysis by infrared rather than mass spectrometry.
†From Fig. 2.

[16] $Hg^* + N_2O \rightarrow Hg + N_2 + O(^3P)$

[12*a*] $O(^3P) + C_2Cl_4 \rightarrow CCl_2O + CCl_2$

[12*b*] $\rightarrow C_2Cl_4O^*$

[17] $C_2Cl_4O^* \rightarrow$ polymer

[18] $2CCl_2 \rightarrow C_2Cl_4$

where $C_2Cl_4O^*$ is an energetically excited adduct of $O(^3P)$ and C_2Cl_4. The absence of $\overline{CCl_2CCl_2O}$ and *c*-C_3Cl_6 as products indicates, respectively, that all the $C_2Cl_4O^*$ polymerizes and that none of the CCl_2 adds to C_2Cl_4 under our experimental conditions. The mechanism predicts that

[19] $$\Phi\{CCl_2O\} = k_{12a}/k_{12}$$

[20] $$-\Phi\{C_2Cl_4\} = 1 - k_{12a}/2k_{12}$$

$\Phi\{CCl_2O\} = 0.19$ independent of reaction conditions, so this is the value of k_{12a}/k_{12}. With this value, $-\Phi\{C_2Cl_4\}$ should be 0.9. From Tables 1 and 2, it can be seen that $-\Phi\{C_2Cl_4\}$ varies between 0.9 and 2.2. For those runs in which $-\Phi\{C_2Cl_4\} > 0.9$, some additional C_2Cl_4 must be incorporated into the polymer.

With O_2 present, $CCl_3CCl(O)$ is produced. Since the reaction of $O(^3P)$ with C_2Cl_4 does not produce this molecule, it apparently does not result from intramolecular chlorine atom migration. Therefore, monoradicals must be involved in the oxidation. Furthermore, a long chain oxidation is indicated which gives $\Phi\{CCl_3CCl(O)\}$ and $\Phi\{CCl_2O\}$ in a ratio similar to that for the chlorine atom initiated chain oxidation (6). A mechanism similar to the one in that system must be involved. However, in the $O(^3P)$–C_2Cl_4–O_2 system, the quantum yields (except for CO) increase proportionately with $[C_2Cl_4]/I_a^{1/2}$, whereas in the chlorine atom sensitized oxidation, the quantum yields are independent of $[C_2Cl_4]$ and I_a.

In the $O(^3P)$–C_2Cl_4–O_2 system, the oxidation must be initiated by reaction of either $C_2Cl_4O^*$ or CCl_2 with O_2. It is difficult to see why the interaction of $C_2Cl_4O^*$ with O_2 should lead to monoradical production. Also the CO produced is equal to the number of CCl_2 radicals produced, *i.e.* $\Phi\{CO\}$ in the presence of O_2 is equal to $\Phi\{CCl_2O\}$ in the absence of O_2.

Clearly the indicated initiating reaction is

[21] $CCl_2 + O_2 \rightarrow ClCO + ClO$

This reaction differs from that for CF_2 where the exclusive product with O_2 is the adduct (5). Possibly some adduct is also produced with CCl_2, but it cannot be important in initiating the chain process. The reason for the difference in the CCl_2 and CF_2 systems is energetics. Reaction 21 is at least 24 kcal/mol exothermic, whereas the corresponding reaction for CF_2 is markedly endothermic (5).

Since the rate law for the chain process depends on $[C_2Cl_4]/I_a^{1/2}$, the chain terminating steps are radical–radical reactions, in which one of the radicals must be the chain-carrier that reacts with C_2Cl_4. The other radical must be one that is absent in the chlorine atom sensitized oxidation, *i.e.* ClCO. Thus the possible reactions of ClCO are

[22] $$ClCO \rightarrow Cl + CO$$

[23] $$Cl + ClCO \rightarrow Cl_2 + CO$$

[24*a*] $$ClO + ClCO \rightarrow Cl_2O + CO$$

[24*b*] $$\rightarrow Cl_2 + CO_2$$

In our studies, both CO and CO_2 were found. However, the CO_2 was found at high O_2 pressures where it might have been produced by

[25] $$ClCO + O_2 \rightarrow ClO + CO_2$$

The chain terminating steps require the production of Cl_2 and/or Cl_2O. If these molecules were formed they would react readily with Hg to produce Hg_2Cl_2. There was no positive evidence for Hg_2Cl_2 formation, but, under our conditions, the small amounts produced would have escaped detection as checked in separate experiments in which small amounts of Cl_2 were reacted with Hg.

The observed proportionality of the quantum yields on $[C_2Cl_4]/I_a^{1/2}$ can be explained if reactions 22 and 23 are neglected and if reaction 8 is assumed to be less important than reaction 24. Then, the concentrations of ClO and ClCO are each approximately equal to $[(k_{12a}/k_{12})I_a/k_{24}]^{1/2}$.

The chain propagating steps are those outlined in the Introduction, *i.e.* reactions 2, 3, 4*a*, 6*a*, 6*b*, 7, 8*a*, 8*b*, and 8*c*. For long chain lengths, the mechanism leads to the following rate laws

[26] $$\Phi\{CO\} + \Phi\{CO_2\} = k_{12a}/k_{12}$$

[27] $$\Phi\{CCl_2O\} = \frac{k_{12a}}{k_{12}} + 2\alpha\left(\frac{k_{6b}}{k_6}\frac{k_{4a}}{k_{4b}} + \frac{k_{8b}}{k_8}\right)\frac{[C_2Cl_4]}{I_a^{1/2}}$$

[28] $$\Phi\{CCl_3CClO\} = \alpha\left(\frac{k_{6a}}{k_6}\frac{k_{4a}}{k_{4b}} + \frac{k_{8a}}{k_8}\right)\frac{[C_2Cl_4]}{I_a^{1/2}}$$

[29] $$-\Phi\{C_2Cl_4\} = 1 + \alpha\left(1 + \frac{k_4}{k_{4b}}\right)\frac{[C_2Cl_4]}{I_a^{1/2}}$$

where

$$\alpha \equiv k_8(k_{12a}/k_{12}k_{24})^{1/2}$$

Since $k_{12a}/k_{12} = 0.19$, eq. 27 predicts that $\Phi\{CO\} + \Phi\{CO_2\} = 0.19$ in conformance with our findings. The value of k_{12a}/k_{12} is small compared with $\Phi\{CCl_2O\}$, so that the last term in eq. 27 is dominant. Also, since $k_{4a}/k_{4b} \gg 1$, the terms k_{8a}/k_8 and k_{8b}/k_8 are negligible. Then eqs. 27 and 28 simplify to

[30] $$\Phi\{CCl_2O\} \simeq \frac{2k_{4a}}{k_{4b}}\frac{k_{6b}}{k_6}\frac{[C_2Cl_4]}{I_a^{1/2}}$$

[31] $$\Phi\{CCl_3CCl(O)\} \simeq \frac{k_{4a}}{k_{4b}}\frac{k_{6a}}{k_6}\frac{[C_2Cl_4]}{I_a^{1/2}}$$

Figure 2 shows that both $\Phi\{CCl_2O\}$ and $\Phi\{CCl_3CCl(O)\}$ are proportional to $[C_2Cl_4]/I_a^{1/2}$. From this figure the proportionality gives

$$2(k_{4a}k_{6b}/k_{4b}k_6)\alpha = 0.038 \text{ (Torr s)}^{-1/2}$$

and

$$(k_{4a}k_{6a}/k_{4b}k_6)\alpha = 0.072 \text{ (Torr s)}^{-1/2}$$

The ratio of these values gives $2k_{6b}/k_{6a} = 0.52$, slightly larger than the value of 0.40 found by Mathias *et al.* (6). The value found here is high, both because k_{12a}/k_{12}, k_{8a}/k_8, and k_{8b}/k_8 are not negligible in eqs. 30 and 31, and because the chains are not of infinite length.

The scatter in the data for $-\Phi\{C_2Cl_4\}$ is large, and the two methods of analysis give different results. However, within the scatter, eq. 29 is approximately obeyed. From Fig. 2, the quantity $\alpha(1 + k_4/k_{4b})$ lies between 0.05 and 0.12 (Torr s)$^{-1/2}$. When divided by $(k_{4a}k_{6a}/k_{4b}k_6)\alpha$, a value between 0.7 and 1.7 is found for k_6/k_{6a} which brackets the value of 1.25 found from the CCl_2O and $CCl_3CCl(O)$ quantum yields.

The few results in Table 6 show the effect of added NO or SO_2. Small quantities of these gases were used so that they would not compete effectively with C_2Cl_4 for the O(³P) atom. Thus with O_2 absent, the results are not much affected. However, in the presence of O_2, the chain length of oxidation is reduced, thus indicating that both species can react with one or more of the radical intermediates.

We wish to thank R. Shortridge, M. Luria, and T. Osif for help with the experiments and I. C. Hisatsune and E. Mathias for useful discussions. This work was sup-

ported by the Environmental Protection Agency under Grant No. R800949 for which we are grateful.

1. R. G. DICKINSON and J. A. LEERMAKERS. J. Am. Chem. Soc. **54**, 3852 (1932).
2. R. G. DICKINSON and J. L. CARRICO. J. Am. Chem. Soc. **56**, 1473 (1934).
3. C. SCHOTT and H. J. SCHUMACHER. Z. Phys. Chem. B**49**, 107 (1941).
4. G. HUYBRECHTS, J. OLBRECHTS, and K. THOMAS. Trans. Faraday Soc. **63**, 1647 (1967).
5. J. HEICKLEN. Adv. Photochem. **7**, 57 (1969).
6. E. MATHIAS, E. SANHUEZA, I. C. HISATSUNE, and J. HEICKLEN. Can. J. Chem. This issue.
7. H. A. WIEBE, A. VILLA, T. M. HELLMAN, and J. HEICKLEN. J. Am. Chem. Soc. **95**, 7 (1973).
8. R. J. CVETANOVIĆ. Adv. Photochem. **1**, 115 (1963).
9. R. E. HUIE, J. T. HERRON, and D. D. DAVIS. Int. J. Chem. Kinet. **4**, 521 (1972).

Acid and Base Catalysis in the Oxidation of 6,7,8-Trimethyllumazine. I. Products of the Reaction[1]

KIYOTAKA OYAMA AND ROSS STEWART

Department of Chemistry, University of British Columbia, Vancouver, British Columbia V6T 1W5

Received May 27, 1974

KIYOTAKA OYAMA and ROSS STEWART. Can. J. Chem. **52**, 3879 (1974).

The permanganate oxidation of 6,7,8-trimethyllumazine (**1**), a pteridine derivative, is subject to catalysis by acids and bases. Above p*H* 3.5, the reaction products are 6,8-dimethyl-7-oxolumazine and formaldehyde. Below p*H* 3.5, the reaction products are hydroxybiacetyl and the methylamide of alloxanic acid.

Oxidation of **1** by potassium *trans*-1,2-diaminocyclohexanetetraacetatomanganate(III) at p*H* 6.0 under an oxygen atmosphere gave the oxolumazine and formaldehyde. Under a nitrogen atmosphere coupled products were obtained, indicating that radical intermediates are formed with this oxidant.

KIYOTAKA OYAMA et ROSS STEWART. Can. J. Chem. **52**, 3879 (1974).

L'oxydation par le permanganate du triméthyl-6,7,8 lumazine (**1**), un dérivé de la pteridine, est soumis à une catalyse par les acides et par les bases. Au-dessus d'un p*H* de 3.5, les produits de la réaction sont le diméthyl-6,8 oxo-7-lumazine et la formaldéhyde. En dessous d'un p*H* de 3.5, les produits de la réaction sont l'hydroxybiacétyle et la méthylamide de l'acide alloxanique.

L'oxydation de **1** par le *trans*-diamino-1,2 cyclohexane tétraacétatomenganate de potassium à un p*H* de 6.0 sous un atmosphère d'oxygène conduit à l'oxolumazine et à la formaldéhyde. Sous un atmosphère d'azote des produits de couplage sont obtenus indiquant que des intermédiaires radicalaires se forment avec cet oxydant.

[Traduit par le journal]

Introduction

Riboflavin **2**, (R = ribityl) and other flavin nucleotides occupy a central position in the reaction chain that is responsible for oxidation in living systems. Because of the close similarity in structure between riboflavin and 6,7,8-trimethyllumazine (**1**) (2,4-dihydroxy-6,7,8-trimethylpteridine), the latter can be used as a model compound for these oxidative nucleotides.

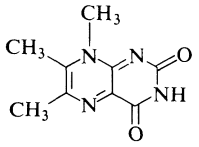

1

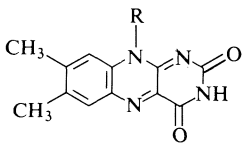

2

In 1969, Paterson and Wood (1) reported that the methyl protons at the 7-position of 6,7-dimethyl-8-ribityllumazine, a precursor in nature of **2**, undergo deuterium exchange and almost at the same time two other groups (2, 3) reported independently the occurrence of this reaction in the same or closely related compounds. Stewart and McAndless (2, 4) carried out kinetic studies of the exchange of **1** and showed the reaction to be subject to both general-acid and general-base catalysis. Satisfactory mechanisms were elucidated for both routes (1–5).

The dihydro derivative of **1**, **3**, is readily oxidized by potassium ferricyanide in alkaline solution, first to **1** and then to 6,8-dimethyl-7-oxolumazine, **5** (6). Such a facile oxidative demethylation is highly unusual and makes the reaction intriguing from the point of view of mechanism.

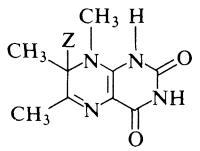

3 (Z = H)
4 (Z = OH)

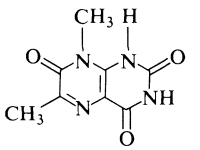

5

The reaction is also important for two other reasons. Firstly, permanganate oxidation has been used to locate sites of hydration in heterocyclic compounds, the carbon atom which is oxidized to a carbonyl group being assumed to be that on which the hydroxyl group was located (7, 8).

[1]Taken in part from the Ph.D. Thesis of K. Oyama, University of British Columbia, 1973.

Can. J. Chem. Downloaded from www.nrcresearchpress.com by 210.87.254.105 on 09/05/12
For personal use only.

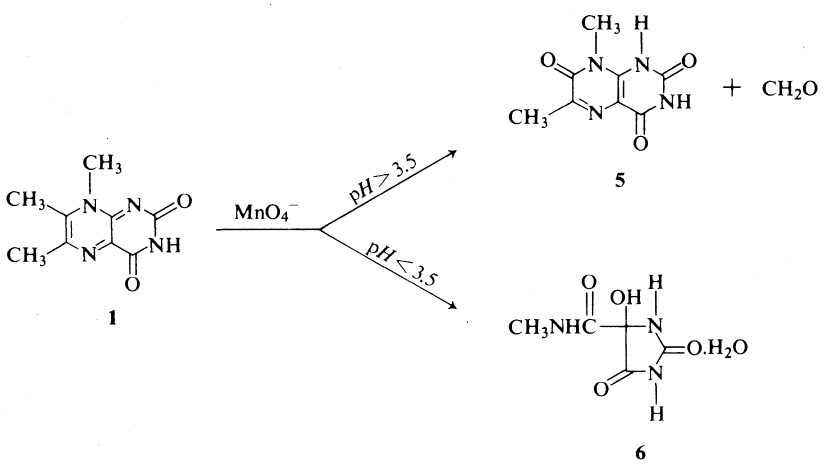

This method has been used even when a methyl group is present at the suspected site of hydration, making the derived alcohol tertiary in nature (9) as in **4**. The basis of this approach needs further examination.

Secondly 6,7-dimethyl-8-ribityllumazine (a derivative of **1**) is known to be a precursor of 6-methyl-7-oxo-8-ribityllumazine (a derivative of **5**) in biological systems (10). Although the mechanism of this transformation has received considerable attention, it remains unclarified (10, 11).

It was hoped that an investigation of the permanganate oxidation of 6,7,8-trimethyllumazine would shed light on the matters referred to above. To aid these studies the oxidation of **1** by potassium *trans*-1,2-diaminocyclohexanetetraacetatomanganate(III), $KMn^{III}CyDTA$, was also investigated.

The products of the oxidation vary with the identity of the oxidant and with the reaction conditions and these matters are described in the present paper. Reaction kinetics and mechanism are discussed in the accompanying paper.

Results and Discussion

Reaction Products

The rate of the oxidation of **1** with permanganate in aqueous solution varies markedly with p*H*, showing a minimum at p*H* 3.5. The course of the reaction is also strongly p*H* dependent since, at p*H* values greater than 3.5, the principal products of the reaction are the 7-oxo compound **5** and formaldehyde, whereas below p*H* 3.5 the principal product is the hydantoin derivative **6**.

Compound **6** was identified by comparison with an authentic sample produced by the reaction of alloxan and methylamine (12). Its structure, about which some doubt has existed (13), was determined with the help of i.r., p.m.r., and ^{13}C magnetic resonance spectroscopy.

The n.m.r. spectrum of this compound in dry DMSO-d_6 consists of a singlet at $\delta = 2.52$ p.p.m. and a broad peak centered at $\delta = 7.90$ p.p.m. (from tetramethylsilane as an external reference.) The ratio of the integral value of the former and the latter is 1:2. This ratio corresponds to three and six protons respectively; the presence of nine hydrogens is indicated by the empirical formula. When a few drops of D_2O were added to the DMSO-d_6 solution, the n.m.r. peak at lower field disappeared completely, with the one at higher field remaining unchanged, indicating that six protons are attached to nitrogen or oxygen atoms and three protons to a carbon atom. The i.r. spectrum shows a very wide absorption between 2500 and 3500 cm^{-1}, suggesting the presence of strong hydrogen bonds, and there are two absorptions in the carbonyl region.

The carbon-13 spectrum of the reaction product shows the presence of five nonequivalent nuclei, as required for **6**, absorbing at 25.8, 86.3, 159.8, 171.5, and 176.5 p.p.m. from TMS. The original structure **6** for the product of the alloxan-methylamine reaction, put forward by Blitz and Lachmann (12), was questioned by Clarke-Lewis and Edgar (13), who favored the salt structure, **10**. The chemical shift of the methyl carbon atom in amides falls in general near 25 p.p.m. whereas those in quaternary salts fall near 55 p.p.m. (14–16). Furthermore, absorption of the carbonyl carbon atom of amides

Can. J. Chem. Downloaded from www.nrcresearchpress.com by 210.87.254.105 on 09/05/12
For personal use only.

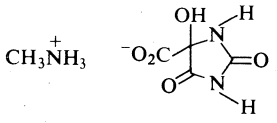

10

generally appears near 170 p.p.m. in amides (15) and at lower field than 180 p.p.m. in carboxylate salts (17). The ^{13}C spectrum of the reaction product is thus in considerably better agreement with **6** than with **10**. (We assign the carbon atom resonances as follows: methyl, 25.8; quaternary carbon atom, 86.3; ring carbonyl flanked by two nitrogens, 159.8; sidechain amide, 171.5; ring carbonyl flanked by one nitrogen, 176.5. (ref. 14, spectrum No. 178).)

The broad absorption between 2500 and 3500 cm^{-1} in the i.r. might seem to support the ionic structure **10**. However, it can equally well be accommodated by **6** if extensive hydrogen bonding exists, as shown in **6′**. The additional molecule of water, shown as water of crystallization in **6**, would also contribute to broadened i.r. absorption in this region.

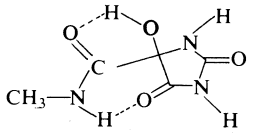

6′

The hydantoin **6** probably arises as a result of oxidative cleavage of the pyrazine ring of **1** followed by contraction of the pyrimidine ring. We have shown that 5-amino-6-methylamino-2,4-dioxopyrimidine, **7**, which is a model compound for **8**, a likely intermediate in the oxidation scheme, is oxidized by permanganate at p*H* 1.0 to give **6**. The conversion of **7** and **8** to **6** probably proceeds via the alloxan–methylamine adduct **9**, since **6** can be prepared by treating alloxan with aqueous methylamine (12). The path from **1** to **6** would seem, therefore, to involve the following intermediates.

The pyrazine ring in **1** is cleaved to produce hydroxybiacetyl, which has been identified as a reaction product. The oxidation by permanganate is not affected by conducting the reaction in the absence of oxygen.

Potassium *trans*-1,2-diaminocyclohexanetetraacetatomanganate(III) ($KMn^{III}CyDTA$) is an exclusively 1-equiv. oxidant and is known to react with organic anions by means of electron transfer

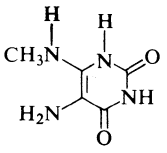

7

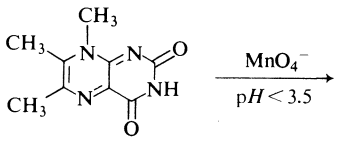

1

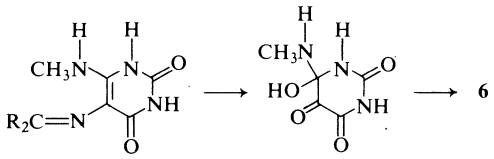

8 9

(18, 19). When the oxidation of **1** by KMn^{III}-CyDTA was conducted in phosphate buffer at p*H* 6.0 under an oxygen atmosphere 6,8-dimethyl-7-oxolumazine (**5**) and formaldehyde were produced, the yield of the former being greater than 81%. The reaction rate is affected by p*H* and by the presence of buffers, indicating that, here too, acid–base catalysis occurs.

When the reaction was carried out under nitrogen at p*H* 6.0 a large quantity of yellow precipitate appeared (approximately 90% of the weight of starting material). It was found that the reaction produced two kinds of product depending upon the amount of $KMn^{III}CyDTA$ used. The product was assigned structure **11** when equimolar quantities of oxidant and TML were used and structure **12** when two equiva-

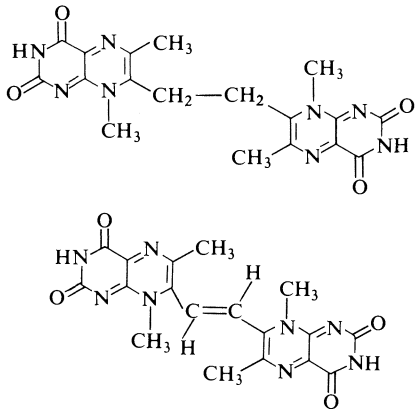

12

Can. J. Chem. Downloaded from www.nrcresearchpress.com by 210.87.254.105 on 09/05/12
For personal use only.

Can. J. Chem. Downloaded from www.nrcresearchpress.com by 210.87.254.105 on 09/05/12
For personal use only.

lents of oxidant (molar ratio 2 $KMn^{III}CyDTA$: 1 TML) were used, on the basis of the products' mass spectra (see Experimental).

There is little doubt that **11** is produced by the coupling of two 7-methyl radicals produced from **1**, either by hydrogen-atom abstraction or, more likely, by proton loss followed by electron abstraction from the resulting anion. The alkene, **12**, is then produced by further reaction of the activated methylene groups in **11**.

Experimental

Materials

Compounds **1** and **5** were prepared by the methods of Birch and Moye (21) and McAndless (6). One of the intermediates in these syntheses, 4-methylamino-5-amino-2,6-dihydroxypyrimidine, tends to decompose while being recrystallized. In the present work we have found that its bisulfite salt may be successfully recrystallized from water containing a small amount of sodium dithionite.

Buffer solutions, made in the usual way, were freshly prepared each week.

Product Identification

Permanganate Oxidation of **1** *at pH 6.0*

It was found that 1 mol of **1** was completely consumed when 4/3 mol of permanganate were used at p*H* 6.0 (Na_2HPO_4 = 0.1 *M*).

The u.v. spectrum of the solution after completion of the reaction was identical with that of an authentic sample of 6,8-dimethyl-7-oxolumazine, **5**. The calculation based on the initial concentration of **1** and the known extinction coefficient at 346 nm of **5** revealed that **1** was converted to **5** in nearly quantitative yield (95%). Other organic products were determined by dissolving **1** (20 mg, 0.1 mmol) in 10 ml of phosphate buffer (p*H* = 6.0, Na_2HPO_4 = 0.1 *M*). To this was added the permanganate solution (20 mg, 0.13 mmol in 5 ml of the same buffer). The reaction mixture was allowed to stand at room temperature for 10 min with stirring and then any deposited manganese dioxide was filtered off. The filtrate was added to a freshly prepared solution of 1,2-dianilinoethane (30 mg) in 10 ml of 40% aqueous acetic acid. A copious white precipitate immediately separated out. This was collected, dried in a vacuum desiccator, and then weighed (16 mg). Recrystallization of the crude product from hot methanol gave white needles whose melting point is 125–126°. The melting point indicates this compound to be the condensation product of formaldehyde with 1,2-dianilinoethane (lit. (22) m.p. 126°). This is confirmed by the result of the elemental analysis.

Anal. Calcd. for $C_{15}H_{16}N_2$: C, 80.31; H, 7.20; N, 12.49. Found: C, 80.59; H, 7.16; N, 12.30.

The yield of formaldehyde based on the crude condensation product was 73%.

Oxidation of **1** *at pH 1.0 with Stoichiometric Amount of Permanganate*

A solution of an accurately weighed amount of **1** (500 mg, 2.43 mmol) in 30 ml of phosphate buffer (p*H* = 1.0, Na_2HPO_4 = 0.1 *M*) was titrated by 0.05 *M* permanganate solution containing the same buffer. Each drop was added with vigorous stirring and only after the pink color of the preceding drop had completely disappeared. The titration was stopped when the pink color of permanganate was retained longer than 15 s. Calculation of the uptake of permanganate showed that approximately $\frac{4}{5}$ of a mol of permanganate were consumed for 1 mol of **1**. The color of the reaction mixture at the end point was pale yellow and no deposit of manganese dioxide was observed. When the solution was made alkaline, a white precipitate, presumably manganese hydroxide, separated out. This indicates all of the permanganate was reduced to the 2+ stage under the present conditions.

The reaction mixture was divided into two aliquots and one of them was added to a freshly prepared solution of 600 mg (3 mmol) of 2,4-dinitrophenylhydrazine in 3 ml of 50% sulfuric acid. The solution was then heated on the steam bath for 10 min. After cooling the solution, an orange colored precipitate was collected, dried in a vacuum desiccator, and then weighed (240 mg). The crude 2,4-dinitrophenylhydrazone was recrystallized from nitrobenzene to give reddish-orange colored needles whose m.p. is 255–265° (dec.).

Anal. Calcd. for $C_{16}H_{14}O_9N_8$: C, 41.56; H, 3.05; N, 24.24. Found: C, 41.44; H, 3.05; N, 24.14.

Melting point and elemental analysis showed the compound to be the di-2,4-dinitrophenylhydrazone of hydroxybiacetyl (23). The yield of hydroxybiacetyl based on the crude phenylhydrazone was 44%.

The other aliquot of the reaction mixture was made basic by the addition of sodium bicarbonate powder. After standing for 1 h the precipitate of white manganese hydroxide was filtered off and the filtrate was made slightly acidic (p*H* 5~6) by addition of dilute sulfuric acid. The solution was then evaporated to dryness by means of a rotary evaporator. To the residue was added methanol (30 ml) and the mixture was then boiled on a steam bath and filtered. This was repeated two more times. The methanol extracts were combined and evaporated to dryness on a rotary evaporator. The residue was dried in a vacuum desiccator and weighed (220 mg). Two recrystallizations of the crude product from methanol–ether solution, with a charcoal treatment included in the first recrystallization, gave 30 mg of a white granular solid, m.p. 149–151° (dec.).

Anal. Calcd. for $C_5H_9N_3O_5$: C, 31.42; H, 4.74; N, 21.99. Found: C, 31.38; H, 4.83; N, 21.95.

This compound was shown to be alloxanic acid methylamide monohydrate, the product obtained by treating alloxan with methylamine (12), by means of u.v. and i.r. spectral comparisons and by means of mixture m.p.; it has been assigned structure **6**.

Oxidation of **1** *at pH 1.0 with Excess of Permanganate*

A solution of 206 mg of **1** (1 mmol) in 50 ml of 0.1 *M* phosphate buffer at p*H* 1.0 was mixed with a solution of 15.8 g (0.1 mol) of potassium permanganate dissolved in 180 ml of the buffer. After 1 min (about 5 half-lives) (23) excess permanganate was quenched by sodium bisulfite. The subsequent work-up, conducted as before, gave **6**, the yield of which was 160 mg (84%), based on the crude compound. Attempts to isolate other likely products, hydroxybiacetyl and biacetyl, by 2,4-dinitrophenylhydrazine treatment failed. By using gas–liquid chromatography, acetic acid and some unidentified compounds were detected. Ammonia was also detected using Nessler's reagent.

Can. J. Chem. Downloaded from www.nrcresearchpress.com by 210.87.254.105 on 09/05/12
For personal use only.

Oxidation of **1** *by* $KMn^{III}CyDTA$

A solution of 20 mg of **1** in 10 ml of 0.1 *M* phosphate buffer at p*H* 6.0 was placed in a two-neck flask, both necks being fitted with rubber caps through which syringe needles were inserted. High-purity nitrogen was passed through one needle, which was dipped below the surface of the solution. A nitrogen-flushed solution of $KMn^{III}CyDTA$ (45 mg, 0.1 mmol or 90 mg, 0.2 mmol) in 5 ml of the same buffer was then added in one of two ways; (*i*) dropwise, when equimolar quantities of $KMn^{III}CyDTA$ and **1** were used; (*ii*) all at once, when 2 equiv. of $KMn^{III}CyDTA$ were used. After 3 h, a yellow precipitate was collected by filtration, washed thoroughly with distilled water, dried in a vacuum desiccator, and weighed. In all cases the amount of the product was 17 mg or more. It was found from the mass spectra of the products that the reaction produced two kinds of product, depending upon the ratio of the oxidant and the substrate. Both compounds melt with decomposition at high temperatures and are extremely insoluble in all common solvents, making purification extremely difficult and preventing good analytical data being obtained. However, the locations of the parent peaks in the mass spectra were such as to allow assignment of structure **11** to the compound obtained with equimolar quantities of reactants and **12** to that obtained with a onefold excess of oxidant. The compound assigned structure **11** melts with decomposition at 304–306° and has a parent peak at 205, exactly half the formula weight of **11**. The absence of a 410 peak is easily accounted for since scission between the methylene groups is to be expected. The compound assigned structure **12**, shown as the *trans* isomer, melts with decomposition at 313–315° and has a parent peak at 408 (the exact formula weight of **12**), with a large peak at 217, the mass of the expected fragment **13**.

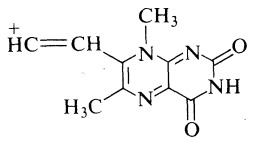

13

The carbon-13 n.m.r. spectrum of **6** in D_2O was recorded on Varian XL-100-15 with Fourier transform computer system by using *p*-dioxane as an internal reference. The chemical shifts from TMS were then obtained by adding 67.4 p.p.m. (ref. 17, p. 23) to the observed values. Mass spectra were obtained by using A.E.I. MS 902 mass spectrometer.

Grateful acknowledgement is made to the National Research Council of Canada for financial support and to Professor James F. King for helpful discussions.

1. T. Paterson and H. C. S. Wood. Chem. Commun. 290 (1969).
2. J. M. McAndless and R. Stewart. Can. J. Chem. **48**, 263 (1970).
3. R. L. Beach and G. W. E. Plaut. Biochemistry, **9**, 760 (1970).
4. R. Stewart and J. M. McAndless. J. Chem. Soc. Perkin II, 376 (1972).
5. F. J. Bullock and O. Jardetzky. J. Org. Chem. **30**, 2056 (1965).
6. J. M. McAndless. Ph.D. Thesis, University of British Columbia, Vancouver, B.C. 1969.
7. A. Albert. Angew. Chem. Int. Ed. Engl. **6**, 919 (1967).
8. A. Albert and W. L. F. Armarego. *In* Advances in heterocyclic chemistry. Vol. 4. *Edited by* A. R. Katritzky. Academic Press, New York. 1965. pp. 1–42.
9. N. W. Jacobsen. J. Chem. Soc. C, 1065 (1966).
10. (*a*) S. Kuwada, T. Masuda, T. Kishi, and M. Asai. J. Vitaminol. (Japan), **4**, 217 (1958). (*b*) M. Asai, K. Mizuno, and S. Kuwada. Chem. Pharm. Bull. (Japan), **9**, 85, 503 (1961).
11. (*a*) T. Masuda, T. Kishi, M. Asai, and S. Kuwada. Chem. Pharm. Bull. (Japan), **6**, 523 (1958). (*b*) G. M. Brown. Physiol. Rev. **40**, 331 (1960). (*c*) F. Korte, H. U. Aldag, G. Ludwig, W. Paulus, and K. Storiko. Ann. **619**, 70 (1958). (*d*) H. Mitsuda, F. Kawai, and J. Suzuki. Vitamins (Japan), **23**, 415 (1961). (*e*) T. Rowan, H. C. S. Wood, and P. Hemmerich. Proc. Chem. Soc. 261 (1961). (*f*) M. Asai, K. Mizuno, and S. Kuwada. Chem. Pharm. Bull. (Japan), **10**, 243 (1962); **11**, 23 (1963).
12. H. Blitz and F. Lachmann. J. Prakt. Chem. **113**, 310, 317, 318 (1926).
13. J. W. Clark-Lewis and J. A. Edgar. J. Chem. Soc. 3887 (1962).
14. L. F. Johnson and W. C. Jankowski. Carbon-13 n.m.r. spectra. John Wiley and Sons, New York. 1972.
15. G. C. Levy and G. C. Nelson. Carbon-13 nuclear magnetic resonance for organic chemists. Wiley-Interscience, New York. 1972. p. 123.
16. G. C. Levy and G. C. Nelson. J. Am. Chem. Soc. **94**, 4897 (1972).
17. J. B. Stothers. Carbon-13 n.m.r. spectroscopy. Academic Press, New York. 1972. p. 295.
18. R. E. Hamm and M. A. Suwyn. Inorg. Chem. **6**, 142 (1967).
19. B. L. Poh and R. Stewart. Can. J. Chem. **50**, 3432, 3437 (1972).
20. A. J. Birch and C. J. Moye. J. Chem. Soc. 2622 (1958).
21. H. W. Wanzlick and W. Loechel. Ber. **86**, 1463 (1953).
22. G. Hesse and H. Stahl. Ber. **89**, 2424 (1956).
23. K. Oyama and R. Stewart. This issue.

Acid and Base Catalysis in the Oxidation of 6,7,8-Trimethyllumazine. II. Kinetics and Mechanism[1]

ROSS STEWART AND KIYOTAKA OYAMA

Department of Chemistry, University of British Columbia, Vancouver, British Columbia V6T 1W5

Received May 27, 1974

ROSS STEWART and KIYOTAKA OYAMA. Can. J. Chem. **52**, 3884 (1974).

The kinetics of the oxidation of 6,7,8-trimethyllumazine, **1**, by permanganate in aqueous solution is examined. The p*H*–rate plot shows a minimum at p*H* 3.5 and there is catalysis by buffers. Above p*H* 3.5 the 7-keto compound, **5**, is produced by a general base catalyzed route the rate of which is identical to that of the reaction that causes exchange at the 7-methyl group. The kinetic isotope effect for oxidation of the 7-CD_3 compound is 6.89 at 31.4°.

Below p*H* 3.5 scission of the pyrazine ring occurs, there is a small isotope effect, and the rate is somewhat faster than that observed for exchange of the 7-methyl group. There appear to be three routes leading to product; one, a permanganate-independent reaction catalyzed by general acids, a second which is also permanganate independent and involves hydration of the substrate, and a third which is permanganate dependent and involves attack by permanganate on the conjugate acid of the substrate.

The utility of oxidation as a means of locating hydration sites in heterocyclic compounds is discussed and some comments are made on the mechanism of the enzymic oxidation of the ribityl analog of **1**.

ROSS STEWART et KIYOTAKA OYAMA. Can. J. Chem. **52**, 3884 (1974).

On a examiné la cinétique de l'oxydation du triméthyl-6,7,8 lumazine, **1**, par le permanganate en solution aqueuse. La relation entre la vitesse et le p*H* montre un minimum à un p*H* 3.5 et il y a catalyse par les tampons. Au-dessus du p*H* 3.5, il y a formation du composé cétonique en position 7, **5**, par un processus impliquant une catalyse basique générale dont la vitesse de laquelle est identique à celle de la réaction qui produit l'échange du groupe méthyle en position 7. L'effet isotopique cinétique pour l'oxydation du composé contenant un CD_3 en position 7 est de 6.89 à 31.4°.

En-dessous du p*H* de 3.5, il y a coupure du cycle pyrazine; ceci s'effectue avec un petit effet isotopique et la vitesse est passablement plus rapide que celle observée pour l'échange du groupe méthyle en position 7. Il semble que trois routes peuvent conduire à ce produit: la première, une réaction indépendante du permanganate catalysée d'une manière générale par les acides; une seconde qui est aussi indépendante du permanganate et qui implique une hydratation du substrat; une troisième est dépendante du permanganate et implique une attaque du permanganate sur l'acide conjugué du substrat.

On discute de l'utilité de l'oxydation comme méthode de déterminer les sites d'hydratation dans les hétérocycles et on fait quelques commentaires sur le mécanisme de l'oxydation enzymatique de l'analogue ribitylé de **1**. [Traduit par le journal]

Kinetics

The reaction of 6,7,8-trimethyllumazine, **1**, with permanganate in unbuffered aqueous solution is extremely slow, except under strongly acidic or strongly basic conditions. The rate of the oxidation is dependent on p*H* and, at a given p*H*, is more rapid in buffered than in unbuffered solutions. Outside the region p*H* 1–6 the reaction in phosphate buffer ($[Na_2HPO_4] = 0.1\ M$) is too rapid to be followed by the usual spectrophotometric methods. Within the p*H* range 1–6, excellent first-order plots were obtained when a large excess of permanganate was used (Fig. 1), showing the reaction to be first order with respect to **1**.

The kinetic order with respect to permanganate is somewhat more complicated. The effect of permanganate concentration on the rate was examined between p*H* 1 and 6 with the buffer concentration and the ionic strength kept at constant values. The variation of the pseudo first-order rate constant k_1', with permanganate concentration at p*H* 1.0, 1.4, 2.0, and 5.0 is exhibited graphically in Fig. 2. These results suggest that there are two paths, one with a rate depending on permanganate concentration and the other with a rate independent of permanganate con-

[1]Taken in part from the Ph.D. Thesis of K. Oyama, University of British Columbia, 1973.

Can. J. Chem. Downloaded from www.nrcresearchpress.com by 210.87.254.6 on 09/05/12
For personal use only.

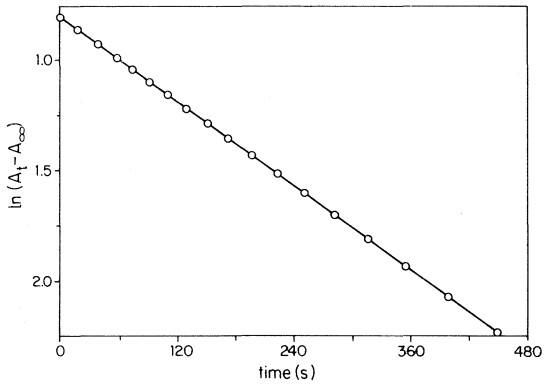

FIG. 1. A typical pseudo first-order rate plot for the permanganate oxidation of 6,7,8-trimethyllumazine (**1**); pH = 2.4, $[Na_2HPO_4]$ = 0.10 M, μ = 0.42, T = 31.4°, [**1**] = 5.10×10^{-5} M, $[KMnO_4] = 2.18 \times 10^{-3}$ M.

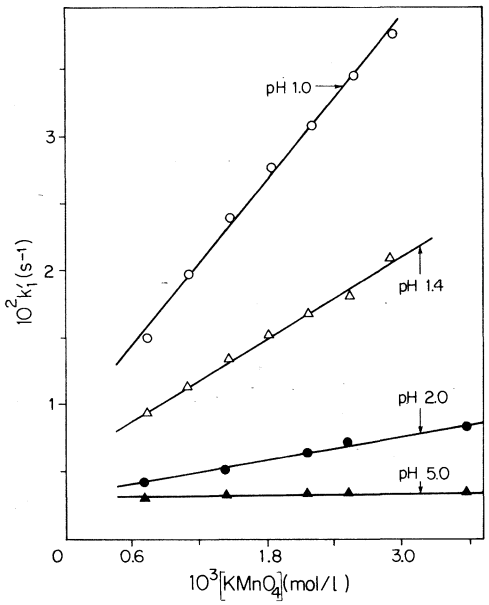

FIG. 2. Relation between rate constant and permanganate concentration in the oxidation of **1** at various pH values; $[Na_2HPO_4]$ = 0.10 M, [**1**] = 5.10×10^{-5} M, μ = 0.42, T = 31.4°.

centration. The rate law is given in eq. 1.

$$[1] \qquad \frac{-d[\mathbf{1}]}{dt} = k_1^0[\mathbf{1}] + k_2[\mathbf{1}][MnO_4^-]$$

Effect of Buffer Concentration on the Rate

The oxidation is very much more rapid in buffered solution than in unbuffered solution. The effect of the buffer concentration on the rate at pH 6 is shown in Fig. 3. A straight line extrapolated to zero buffer concentration passes close to the origin of the graph, indicating the uncatalyzed oxidation to be extremely slow (Fig. 3).

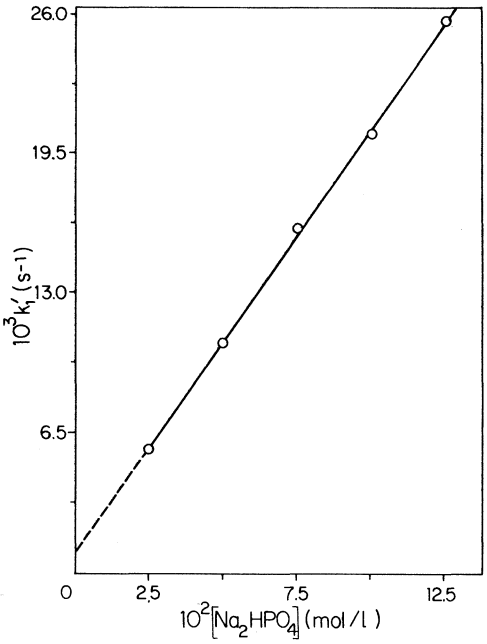

FIG. 3. Effect of buffer concentration on the rate of oxidation of **1** at pH 6.0; $[KMnO_4] = 3.0 \times 10^{-3}$ M, [**1**] = 5.10×10^{-5} M, μ = 0.42, T = 31.4°.

At pH 2.0 pseudo first-order rate constants k_1' were recorded for different permanganate and buffer concentrations. When k_1' was plotted against permanganate concentration at fixed buffer concentration, parallel straight lines were obtained (Fig. 4). One can conclude that the permanganate-dependent rate (k_2, obtained from the slope) is not subject to general acid catalysis, since it is unaffected by changes in the buffer concentration. On the other hand the permanganate-independent rate (k_1^0, obtained from the intercept) is clearly affected by changes in the buffer concentration and is therefore subject to general acid catalysis. A plot of k_1^0 against buffer concentration, gave a good straight line (Fig. 5); extrapolation of the line to zero buffer concentration intercepted the ordinate somewhat above the origin, which is distinctly different from the case at pH 6.0.

The slopes (k_2) and the intercepts (k_1^0) of the plots of k_1' against permanganate concentration at various values of pH are shown in Fig. 6 and 7 as a function of pH. When the logarithm of k_2 was plotted against pH a straight line with nearly

Can. J. Chem. Downloaded from www.nrcresearchpress.com by 210.87.254.6 on 09/05/12
For personal use only.

Can. J. Chem. Downloaded from www.nrcresearchpress.com by 210.87.254.6 on 09/05/12
For personal use only.

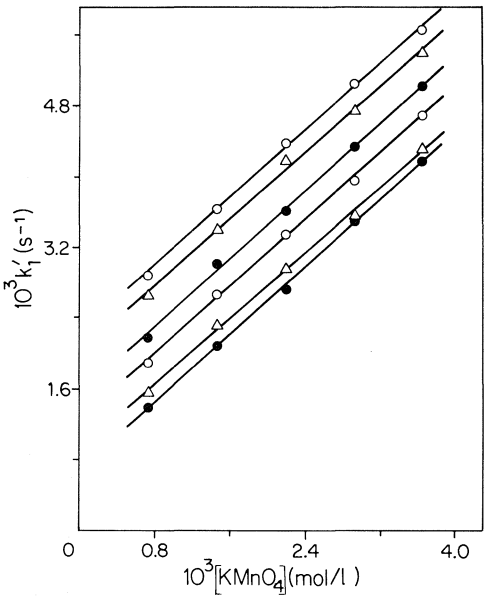

FIG. 4. Effect of permanganate concentration on the rate of oxidation of **1** at different buffer concentrations; pH = 2.0, [**1**] = 5.10 × 10^{-5} M, μ = 0.42, T = 31.4°; Reading from top to bottom the buffer concentrations, slopes (k_2, l mol^{-1} s^{-1}), and intercepts ($k_1°$, s^{-1}) are: 0.125, 1.48, and 0.00349; 0.100, 1.46, and 0.00314; 0.075, 1.49, and 0.00238; 0.050, 1.46, and 0.00195; 0.025, 1.44, and 0.00154; 0.100, 1.40, and 0.00127 (compound **2**).

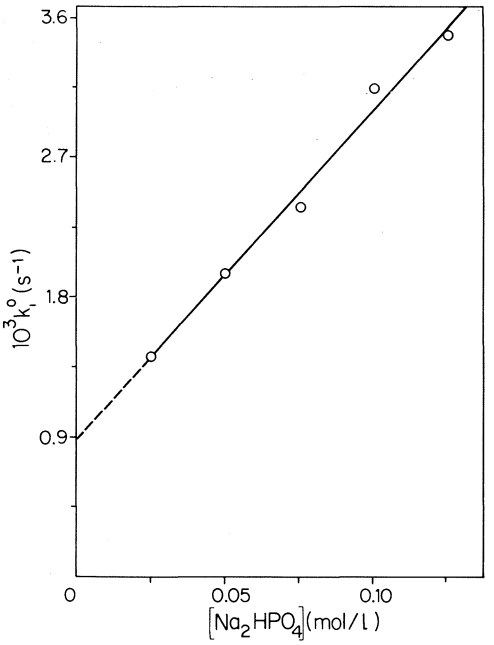

FIG. 5. Effect of buffer concentration on the rate for the permanganate-independent path; pH = 2.0, μ = 0.42, T = 31.4°.

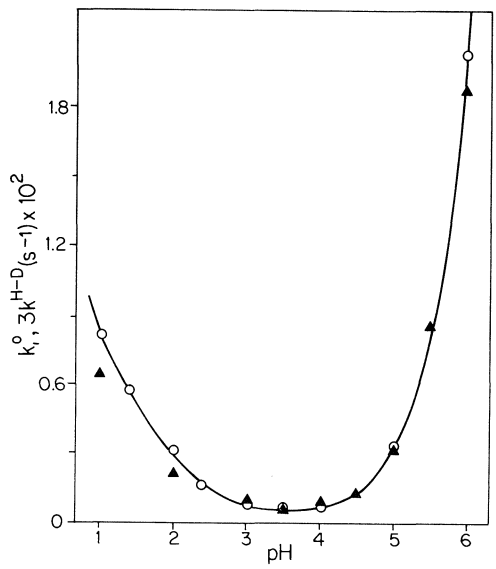

FIG. 6. pH–rate profiles for oxidation of **1** by permanganate-independent path, $k_1°$, (circles) and for deuterium exchange of **1**, $3k^{H-D}$ (triangles) [$NaHPO_4$] = 0.10 M, μ = 0.42, T = 31.4°.

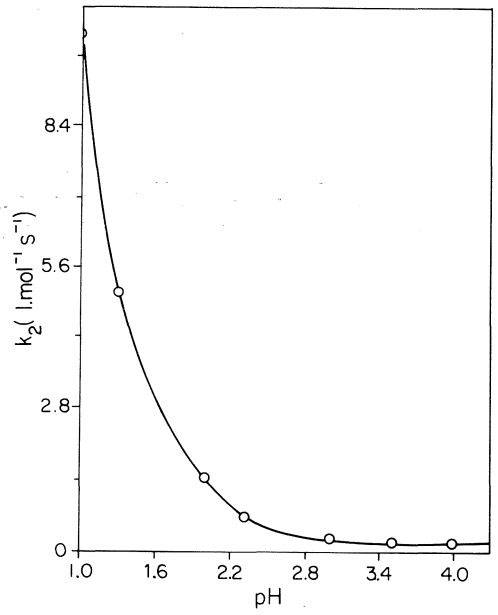

FIG. 7. pH–rate profile for the permanganate-dependent path in the oxidation of **1**; [Na_2HPO_4] = 0.10 M, μ = 0.42, T = 31.4°.

unit slope (0.88) was observed between pH 1 and 2.4. This result, coupled with the fact that k_2 is not affected by the concentration of the buffer (Fig. 4), clearly indicates that the reaction whose rate is dependent on permanganate concentra-

tion (*i.e.*, the permanganate-dependent path) is catalyzed by only hydronium ion, or in other words, is subject to specific acid catalysis.

Kinetic Isotope Effect

Permanganate oxidation of **1** deuterated at the 7-methyl group, **2**, was studied at p*H* 6.0 and 2.0 in aqueous buffered H_2O.

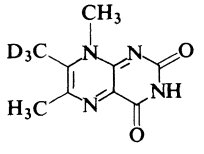

2

In the experiment at p*H* 6.0 the concentration of permanganate was made high enough so that the rate was independent of the permanganate concentration. The rates thus obtained were compared with those for the protium compound under the same conditions. At p*H* 2.0 pseudo first-order rate constants (k_1') for the deuterated compound were determined at different permanganate concentrations. The results at p*H* 6 and 2 are collected in Table 1. At each p*H* plots of logarithm of the absorbance at 416 nm *vs* time gave excellent straight lines up to 2 half-lives, with correlation coefficients always greater than 0.999, and there were no signs of acceleration of the reaction, which would have resulted from any appreciable replacement of deuterium by hydrogen.

The rate plot at p*H* 2.0 was a good straight line parallel to, but lower than, that for the protium compound. The kinetic isotope effect on k_2, the permanganate-dependent path was obtained from the slope and found to be 1.04; from the intercept the effect on k_1^0, the permanganate-independent path, was found to be 2.47. At p*H* 6.0 the average deuterium isotope effect is 6.89, also at 31.4°.

TABLE 1. Rate constants for the permanganate oxidation of 6,8-dimethyl-7-trideuteriomethyllumazine, **2**

(a) pH 6.0

$[Na_2HPO_4]$ (mol/l)	k_1' (s^{-1})*	k_H/k_D
0.100	2.83×10^{-3}	7.21
0.075	2.44×10^{-3}	6.56
		Mean 6.89

*$\mu = 0.42$, $T = 31.4°$, $[2] = 5.10 \times 10^{-5}$ *M*, $[MnO_4^-] = 3.00 \times 10^{-3}$ *M*.

(b) pH 2.0

$[MnO_4^-]$ (mol/l)	k_1' (s^{-1})†‡	k_H/k_D
7.32×10^{-4}	2.30×10^{-3}	
1.46×10^{-3}	3.20×10^{-3}	1.04 (k_2)
2.19×10^{-3}	4.29×10^{-3}	2.47 (k_1^0)
2.93×10^{-3}	5.51×10^{-3}	
3.66×10^{-3}	6.31×10^{-3}	

†$\mu = 0.42$, $T = 31.4°$, $[Na_2HPO_4] = 0.100$ *M*, $[2] = 5.10 \times 10^{-5}$ *M*.
‡Slope (k_2, l mol^{-1} s^{-1}) = 1.40, intercept (k_1^0 s^{-1}) = 1.27×10^{-3} correlation coefficient = 0.997.

Mechanism

Permanganate-independent Path

The permanganate-independent path is subject to both general-acid and general-base catalysis with the reaction being slowest near p*H* 3.5. These kinetic features are remarkably similar to those of the hydrogen–deuterium exchange reaction of the 7-methyl group, which is also subject to both general-acid and general-base catalysis and has its minimum rate near p*H* 3.5 (2). Such similarities suggest that the oxidation via the permanganate-independent path and the exchange reaction might go via the same intermediates. The intermediates in the exchange reaction are the enolate anion **3** in the general-base catalyzed route and the enol **3***a* in the general-acid catalyzed route, their formation being rate-determining (see Scheme 1). If the oxidation in fact proceeds via these intermediates, then the rates of the oxidation and the exchange should be identical. However, for the comparison of two rates one has to consider the statistical effects at the 7-methyl group, because the exchange involves removal of all three hydrogens whereas the oxidation may require removal of only one hydrogen atom. It can be shown (3, 4) that the observed oxidation rate will be three times as great as the observed exchange rate, provided both reactions proceed via rate-determining formation of the enol or the enolate anion. Hence, the exchange rates for **1** obtained by McAndless and Stewart (2) under the same conditions as the oxidation were multiplied by a factor of three, and these values ($3k_{obs}^{H-D}$), as well as the oxidation rates, are plotted against p*H* in Fig. 6. Although the oxidation is somewhat faster than the exchange at lower p*H*, the general agreement between the two rates is very close, suggesting that the reactive intermediates in the oxidation are the enolate anion for $pH > 3.5$ (general base catalysis

Can. J. Chem. Downloaded from www.nrcresearchpress.com by 210.87.254.6 on 09/05/12
For personal use only.

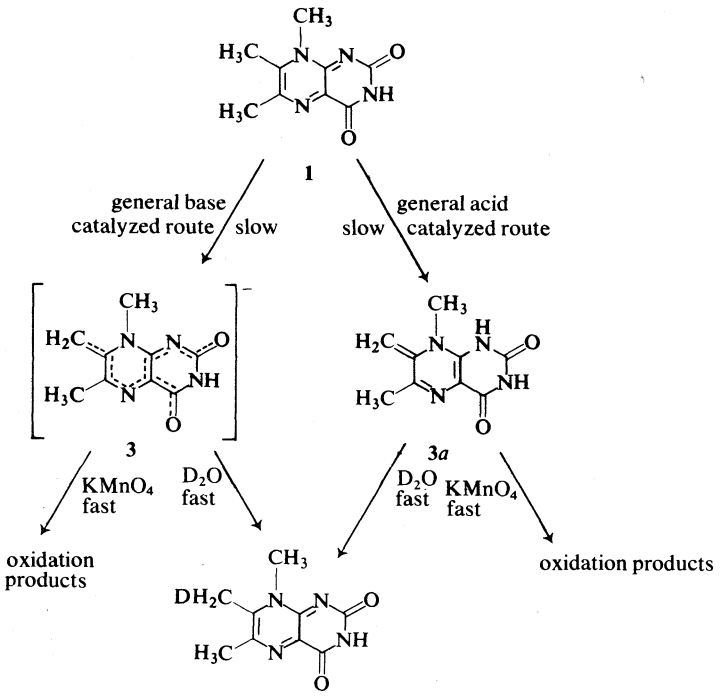

SCHEME 1. Oxidation and exchange reactions of **1** via the same intermediates.

region) and the enol for pH < 3.5 (general acid catalysis region).

Above pH 3.5

The principal results for the oxidation of **1** by the permanganate-independent path above pH 3.5 are: (*i*) The reaction produces formaldehyde and the 7-keto lumazine. (*ii*) The reaction is first order in **1** and is subject to general base catalysis. (*iii*) The rate is almost identical with that of the exchange reaction multiplied by a factor of three. (*iv*) There is a primary isotope effect, k_1/k_2 = 6.89, at 31.4°. (*v*) Presence of oxygen affects neither the rate nor the products.

These observations and other pieces of evidence can be accommodated by the mechanism shown in Scheme 2. The fact that coupled products result from the oxidation of **1** by Mn^{III} (1) shows that the radical **4** can indeed be formed. The failure to detect such coupling products in the permanganate case is probably due to further rapid reaction of the radical intermediate with permanganate, by further one-electron transfer to the permanganate or, more likely, by formation of a manganate(VI) ester, as in Scheme 2.

Although manganate(VI) and manganate(V) ions disproportionate rapidly in neutral and acidic solution Wiberg *et al.* (5) have recently shown that esters of these manganate species are formed as intermediates in the course of the permanganate oxidation of olefins and that they are relatively stable even under neutral conditions. Lee and Brownridge (6) have also provided spectrophotometric evidence for a cyclic manganate(V) ester intermediate in the permanganate oxidation of cinnamic acid. An alternative mechanism to Scheme 2 is a 2-equiv. reaction of permanganate at the double bond of the enolate anion. We prefer Scheme 2 because the reaction at the double bond under acidic conditions gives different products (next section) than those found here.

Below pH 3.5

The results obtained for the oxidation of **1** by the permanganate-independent path in this pH region can be summarized as follows: (*i*) The reaction is first order in **1** and zero order in permanganate. (*ii*) The reaction is subject to general acid catalysis. (*iii*) The oxidation is somewhat faster than the exchange rate multiplied by a factor of three. (*iv*) A kinetic isotope effect of 2.46 at 31.4° was obtained for the oxidation of **2**. (*v*) The isolated products are hydroxybiacetyl,

Can. J. Chem. Downloaded from www.nrcresearchpress.com by 210.87.254.6 on 09/05/12
For personal use only.

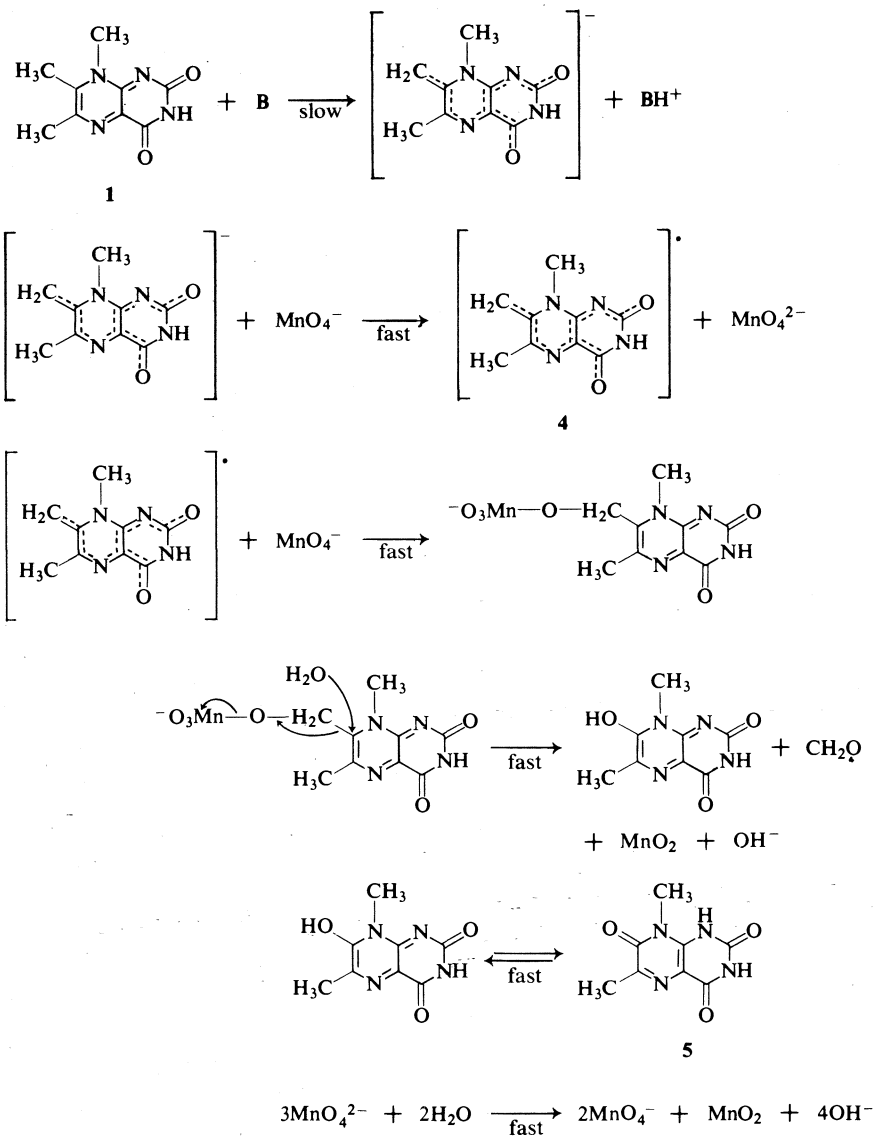

SCHEME 2. Mechanism of oxidation of **1** via general base catalyzed route. The general bases are denoted by B.

ammonia, and compound **6**, the methyl amide of alloxanic acid (1).

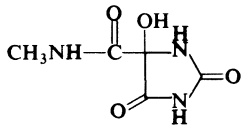

6

These results suggest the mechanism outlined in Scheme 3.

It seems certain that the oxidation of **1** is preceded by enolization. Thus, as in the deuterium exchange reaction, the initial step involves a reversible formation of the protonated species, which is then deprotonated at the 7-methyl group by attack of conjugate bases of the buffer acids to give the enol form of **1**. All the facts, except for the small isotope effect, summarized at the beginning of this section are consistent with the second step being rate determining. The value of 2.46 is rather small for a primary deuterium isotope effect. This, and the fact that the oxidation is somewhat faster than the exchange, are to be discussed later.

Can. J. Chem. Downloaded from www.nrcresearchpress.com by 210.87.254.6 on 09/05/12
For personal use only.

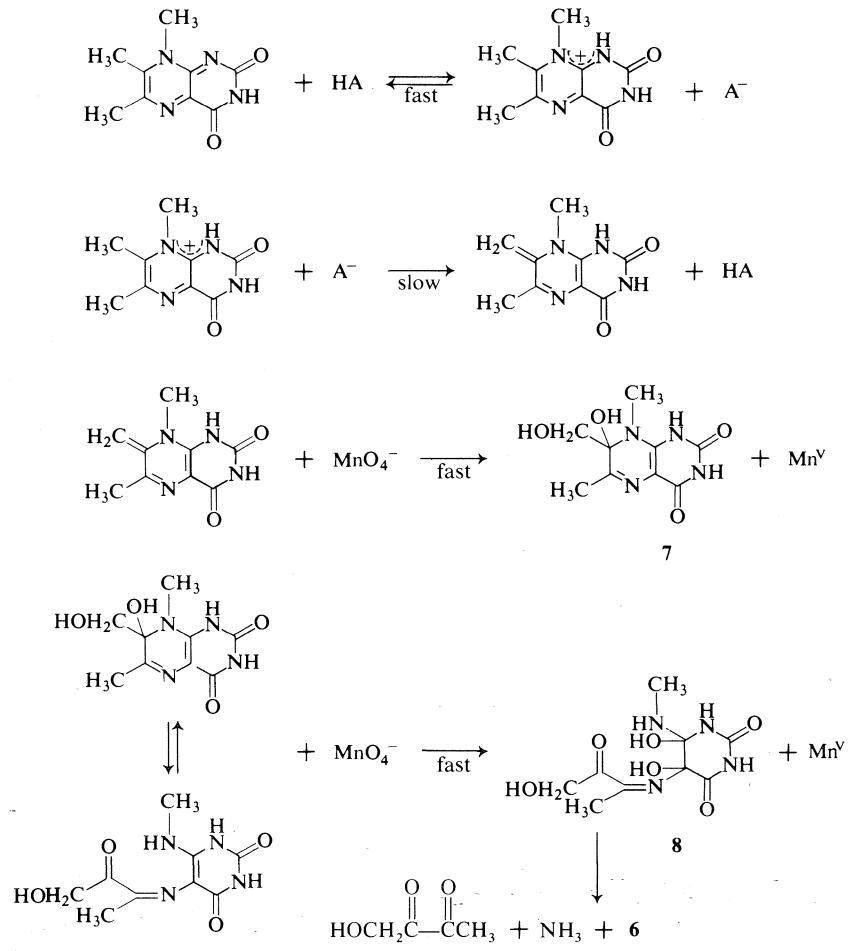

SCHEME 3. Mechanism of oxidation of **1** via enolization route (where HA denotes the buffer acids).

2,4-Dioxo-5-amino-6-methylaminopyrimidine, which may be regarded as the model for the suggested reaction intermediates **7** and **8**, is in fact oxidized to **6** at p*H* 1.0 (1, 4).

As mentioned before, difficulties were met in interpreting the small kinetic isotope effect and the faster rate of the oxidation than the exchange in the more acidic solutions. These facts can be explained by assuming the presence of another permanganate-independent path, in addition to the enolization route. It is known that 8-substituted lumazine derivatives, including **1**, undergo acid- and base-catalyzed hydration (8). It would be expected that the double bond of the pyrimidine moiety of the hydrated species, which is essentially the same as the intermediate in the enolization route (**7** in Scheme 3), is oxidized readily by permanganate. Therefore, if there were acid-catalyzed hydration, as well as enolization, an oxidation mechanism via hydration might occur, as shown in Scheme 4.

The final products for the hydration route would be expected to be ammonia, **6**, and biacetyl. Ammonia and **6** are produced by both the enolization and hydration routes and, of course, were found as reaction products. Attempts to isolate biacetyl were unsuccessful, however, probably because of further oxidation, which takes place with excess permanganate, the conditions of the product-analysis experiments (1).

Support for the occurrence of the hydration route was obtained in a study of the permanganate oxidation of 6,7-diphenyl-8-methyllumazine, a compound which cannot form the enol or the enol anion. It was indeed found that the rate of the permanganate-independent path for this compound is identical to the reported

Can. J. Chem. Downloaded from www.nrcresearchpress.com by 210.87.254.6 on 09/05/12
For personal use only.

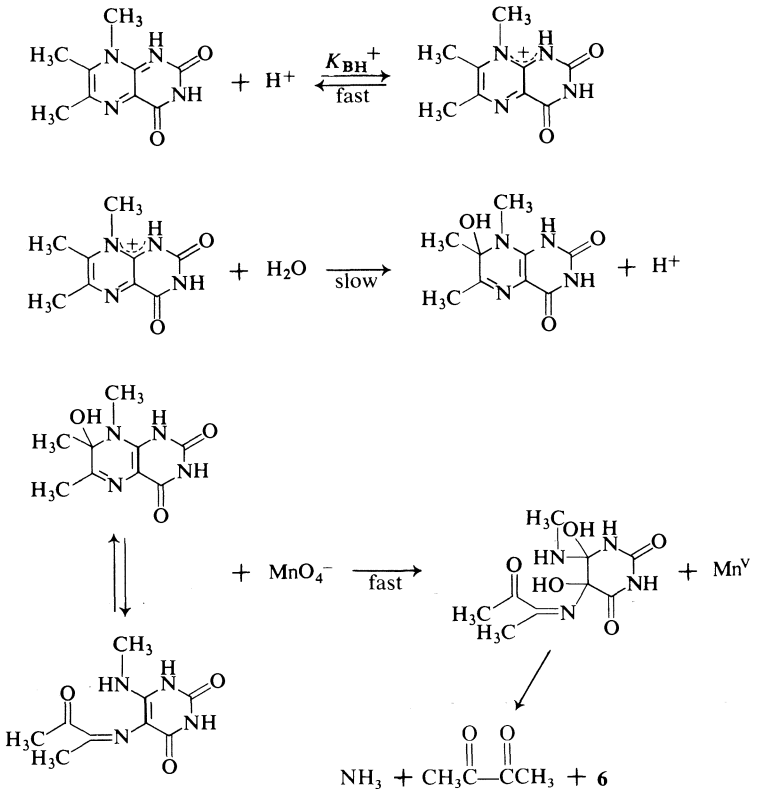

SCHEME 4. Mechanism of the oxidation of **1** via the hydration route.

hydration rate (8). Furthermore, benzil, the analog of biacetyl, was found as a reaction product (4, 7).

It seems reasonable to assume that the hydration route contributes to the permanganate-independent path and that there is no kinetic isotope effect associated with it. This would account for the low isotope effect found with **2**.

Permanganate-dependent Path

The results for this reaction, which is observed in acid solution, may be summarized as follows: (*i*) The rate of the reaction is first order in **1**, permanganate, and hydronium ion. (*ii*) The rate is independent of the buffer concentration. (*iii*) Substitution of the hydrogens of the 7-methyl group by deuterium does not affect the rate of the reaction.

These results are in agreement with the rate-controlling step being attack by permanganate ion on the conjugate acid of **1** (Scheme 5). It would be expected that a plot of log (rate) *vs.* p*H* would tend to curve near the pK_{BH^+} of **1**, 0.85 (8) and finally level off when the acidity of the solution is high enough to protonate most of the compound. Unfortunately, it was not possible to study the p*H* region below 1.0, the reaction being too fast to follow. (The permanganate oxidation of 6,7-diphenyl-8-methylumazine is slower than that of **1** and it was thus possible to study this compound in the highly acidic region. It was indeed found that the rate of the permanganate-dependent path levels off when protonation is complete (7).)

Cleavage of the C—H bond in the 7-methyl group is not involved in the reaction between protonated **1** and permanganate and this accounts for there being no kinetic isotope effect observed for the oxidation of **2** in this region. The reaction likely occurs via addition of the permanganate to the carbon–carbon double bond at the 6,7-position of protonated **1**, which may be somewhat more reactive than the unprotonated species because of the interruption in conjugation. Permanganate addition to the double bond will lead to a dihydroxy compound which will then split into biacetyl, ammonia, and **6**. The mechanism for the oxidation via the per-

Can. J. Chem. Downloaded from www.nrcresearchpress.com by 210.87.254.6 on 09/05/12
For personal use only.

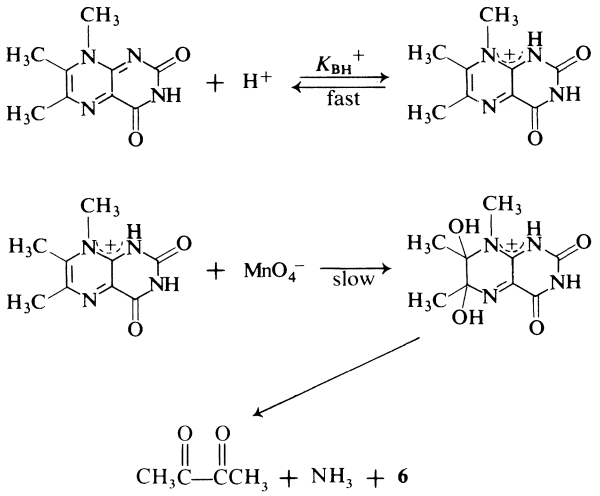

SCHEME 5. Mechanism of oxidation of **1** via the permanganate-dependent path.

manganate-dependent path may be depicted in Scheme 5.

A referee has quite reasonably pointed out that oxidation processes are much more commonly activated by protonation of the oxidant than by protonation of the substrate, as shown in Scheme 5. Nonetheless, we hesitate to invoke permanganic acid and neutral lumazine as the reactants (a kinetically equivalent mechanism) because of the enormous rate constant required to accommodate the kinetics (4).

Conclusions Regarding the Oxidation Mechanism

Above p*H* 3.5 the permanganate oxidation of **1** takes place via initial formation of the enolate anion by removal of a proton from the 7-methyl group. The oxidation is very facile and produces the demethylated 7-oxo compound and formaldehyde, an unusual product for an oxidative demethylation. This characteristic feature of the oxidation can be attributed to the unique properties of **1**; firstly the strongly acidic character of the 7-methyl protons and secondly its tendency to undergo hydration at the 7-position. The first property is responsible for the facile reaction and the second for the unusual products.

In the acidic region (pH < 3.5), there seem to be three routes involved in the reaction. Each of the routes involves initial protonation of **1**, followed by three competitive and rate-determining steps: enolization, hydration, and oxidation.

Comments on the Use of Oxidation as a Means of Locating the Site of Hydration in Heterocyclic Systems

A frequently used method to locate the site of hydration in heterocyclic systems is that developed by Albert and Armarego (9) and others (10). It is based on the idea that heterocyclic compounds that have water covalently bound across a —C=N— bond are by nature secon-

dary alcohols and can thus be oxidized to the corresponding oxo compounds. In 1966, Jacobsen (11) showed that 6,7,8-trimethyl derivatives of some amino- and hydroxypteridines underwent rapid oxidative demethylation with permanganate in basic solution to produce the corresponding 7-oxo compounds in very good yield. He assumed that the reaction takes place by initial hydration at the 7-position to give a tertiary alcohol, followed by oxidative demethylation (considered as oxidation followed by decarboxylation), and on this basis he considered such oxidative demethylations could be used as an additional means to locate the position of hydration.

Oxidation and subsequent decarboxylation of tertiary alcohols usually requires vigorous conditions or prolonged reaction times and it has become apparent from the present study that such facile oxidative demethylations occur via initial ionization of the 7-methyl group rather

Can. J. Chem. Downloaded from www.nrcresearchpress.com by 210.87.254.6 on 09/05/12
For personal use only.

Can. J. Chem. Downloaded from www.nrcresearchpress.com by 210.87.254.6 on 09/05/12
For personal use only.

than via initial hydration at the 7-position. In spite of such uncertainty in the oxidation mechanism, this method has been applied to locate the site of hydration of several pteridine derivatives which have a methyl group at the suspected site of the hydration (11, 12).

Recently, Paterson and Wood (13) applied the oxidation method to 8-substituted pyrido[2,3-*d*]pyrimidines. They noticed that these compounds showed a large hypsochromic shift in their u.v. spectra in acidic solution. On the assumption that this is due to covalent hydration occurring at the 7-position, they attempted to convert these compounds to the corresponding 7-oxo compounds by using permanganate in acidic solution. The attempts failed, however, and they were forced to leave their hypothesis that the hydration is taking place in these systems unconfirmed, even though the u.v. spectra provided strong support for this.

The present study of the permanganate oxidations of **1** and 6,7-diphenyl-8-methyllumazine shows that the hydrated forms of these molecules are oxidized rapidly at the double bond in the pyrimidine moiety. From this and the general tendency of permanganate to react faster with double bonds than with alcohols, it seems very likely that the hydrated species studied by Paterson and Wood (13) are oxidized at the double bond of the pyrimidine moiety, rather than at the hydrate site.

These considerations lead to the conclusion that the oxidation method with permanganate is unsatisfactory in the case when the hydrate contains a reactive double bond. This latter criterion should be added to the limitations already noted by Albert and Armarego (9*a*) with regard to the oxidation method.

Comments on the Mechanism of the Enzymic Conversion of 6,7-Dimethyl-8-ribityllumazine to 6-Methyl-7-oxo-8-ribityllumazine

In 1956 Masuda (14) reported isolation of three compounds, riboflavin, 6,7-dimethyl-8-ribityllumazine (**9**), and 6-methyl-7-oxo-8-ribityllumazine (**10**) from the fermentation product of Eremothecium ashbyii. Compounds **9** and **10** are the ribityl analogs of compounds **1** and **5** studied herein. It soon became clear that **9** is the precursor of both riboflavin (15–18) and **10** (19, 20) in biological systems. Kuwada and his co-workers (21) found that treatment of **9** with the enzyme solution prepared from *Eremothecium ashbyii* produced **10**, formaldehyde, and formic acid. They found that the conversion occurred only above p*H* 4, the yields of the products improving with a rise of p*H*. They considered the enol to be the intermediate but a detailed mechanism of the reaction has not yet been proposed.

Their results resemble those found in the present study. The fact that the yields of the products are higher at higher p*H* suggests that ionization of the 7-methyl group is also involved in the enzymic conversion. The ionization may have been achieved by the action either of the enzyme or of general bases present in the living systems and it may well be that electron transfer takes place from the enolate anion to the enzyme, as in the oxidation of **1** by permanganate or by $KMn^{III}CyDTA$ in the presence of oxygen (1).

Experimental

The wavelength maximum of neutral **1** is at 404 nm. By contrast, permanganate ion has a minimum at 416 nm and even when a 50-fold excess of the stoichiometric concentration of permanganate is present the absorbance at this wavelength due to permanganate is relatively small. Kinetic data were therefore obtained by observing the disappearance of the lumazine absorption at 416 nm. In all of the kinetic experiments the pseudo first-order technique was used, the initial oxidant concentration being in at least 12-fold excess.

Stock solutions of **1** and potassium permanganate were prepared by weighing accurately the appropriate amount of material into a 10 ml volumetric flask and making up to the mark with distilled water. The amount of **1** in the stock solution was chosen to give a concentration close to 5×10^{-5} *M* (giving an initial absorbance of approximately 0.6) when 25 μl. of the stock solution was diluted into 2.5 ml of a buffer solution. On the other hand, the amount of permanganate was chosen to give a 12- or 60-fold excess of the stoichiometric concentration when 10 or 50 μl of the stock solutions were added to 2.5 ml of buffer.

The stock solutions of permanganate and the lumazines were stable over several days but, in general, fresh solutions were prepared daily.

The typical kinetic run was carried out as follows: the buffer solution (2.5 ml) and a stock solution of **1** (25 μl) were added to an optical cell by means of syringes equipped with Chaney adapters. To the lumazine solution thus obtained, an appropriate volume (usually 10–50 μl) of permanganate stock solution was added by means of a microsyringe. The cell was stoppered with a Teflon stopper, thoroughly mixed by shaking, placed in the cell compartment of the spectrophotometer, and the absorbance at 416 nm was followed with respect to time. The cell and all reaction components were thermostated at the desired temperature prior to use.

It was found that the kinetics of the reaction of **1** with permanganate were unaffected by conducting the reaction under a nitrogen or oxygen atmosphere instead of under air.

The methyl group at the 7-position of **1** undergoes facile deuterium exchange. Thus, **1** deuterated at the 7-methyl group, **2**, was produced in the following way. An accurately weighed amount of **1** was dissolved in a known volume of deuterium oxide (99.5% pure) buffered by an appropriate amount of sodium phosphate. The solution was allowed to stand for 7 to 10 half-lives of the exchange reaction, as estimated from the exchange rate (2). The deuterated compound thus formed was used without being isolated. Prior to the kinetic study, the n.m.r. spectrum was run on an aliquot of the solution to make sure that the protium compound was completely converted to the deuterium compound.

The oxidation reaction was started by adding a small volume of this solution (25 μl) to a much larger volume of the permanganate in buffered H_2O (2.5 ml). The change of absorbance at 416 nm was then recorded with respect to time.

The exchange rates shown in Fig. 6 are those obtained by McAndless and Stewart (2). In their experiments the measured pH was not corrected to give the corresponding pD values. The conversion of pH obtained by a glass–calomel pH assembly to the corresponding pD can be done by the addition of the scale-factor of 0.4 to the measured pH (22). The change in the solvent from H_2O to D_2O results in changes in the concentrations of each phosphate species as well as **1**. Since the reactions are subject to general catalysis by the phosphate buffer species and by hydronium ion, such changes in the concentrations of the buffer species makes unequivocal comparison of H_2O and D_2O systems impossible. However, the change in pK values of **1** and phosphoric acid in going to D_2O may be largely compensated by the scale-factor of 0.4, since these changes occur in the same direction with about the same magnitude (22, 23). Such a view is substantiated by the fact that both reactions have minimum rates at the same pH.

All the kinetic data were analyzed by the method of least squares by arranging the data in a linear form of $y = ax + b$. The least-squares analysis and the subsequent plotting were performed by a Hewlett-Packard calculator and plotter, model 9125A.

The financial support of the National Research Council of Canada is gratefully acknowledged.

1. K. Oyama and R. Stewart. Can. J. Chem. This issue.
2. J. M. McAndless and R. Stewart. Can. J. Chem. **48**, 263 (1970).
3. C. Rappe. Acta Chem. Scand. **20**, 2236 (1966).
4. K. Oyama. Ph.D. Thesis. University of British Columbia, Vancouver, B.C. 1973.
5. K. B. Wiberg, C. J. Deutsch, and J. Rocek. J. Am. Chem. Soc. **95**, 3034 (1973).
6. D. G. Lee and J. R. Brownridge. J. Am. Chem. Soc. **95**, 3033 (1973).
7. K. Oyama and R. Stewart. To be published.
8. W. Pfleiderer, J. Bunting, D. D. Perrin, and G. Nubel. Ber. **99**, 3503 (1966).
9. (*a*) A. Albert and W. L. F. Armarego. *In* Advances in heterocyclic chemistry. Vol. 4. *Edited by* A. R. Katritzky. Academic Press, New York. 1965. pp. 1–42. (*b*) A. Albert, W. L. F. Armarego, and E. Spinner. J. Chem. Soc. 2689 (1961). (*c*) W. L. F. Armarego. J. Chem. Soc. 4094, 5030 (1962).
10. (*a*) D. D. Perrin. J. Chem. Soc. 645 (1962). (*b*) D. J. Brown and S. F. Mason. J. Chem. Soc. 3443 (1956).
11. N. W. Jacobsen. J. Chem. Soc. (C), 1065 (1966).
12. T. Rowan and H. C. S. Wood. J. Chem. Soc. (C), 452 (1968).
13. T. Paterson and H. C. S. Wood. J. Chem. Soc. Perkin I, 1041 (1972).
14. (*a*) T. Masuda. Pharm. Bull. (Japan), **4**, 71, 72, 375 (1956); **5**, 28 (1957). (*b*) T. Masuda, T. Kishi, and M. Asai. Pharm. Bull. (Japan), **5**, 598 (1957); Chem. Pharm. Bull. (Japan), **6**, 291 (1958).
15. G. F. Maley and G. W. E. Plaut. J. Biol. Chem. **234**, 641 (1959).
16. G. F. Maley and G. W. E. Plaut. Fed. Proc. **17**, 268 (1958).
17. T. Kishi, M. Asai, T. Masuda, and S. Kuwada. Chem. Pharm. Bull. (Japan), **7**, 515 (1959).
18. F. Korte and H. U. Aldag. Ann. **628**, 144 (1959).
19. S. Kuwada, T. Masuda, T. Kishi, and M. Asai. Chem. Pharm. Bull. (Japan), **6**, 618 (1958).
20. M. Asai, K. Mizuno, and S. Kuwada. Chem. Pharm. Bull. (Japan), **9**, 85, 503 (1961).
21. M. Asai, K. Mizuno, and S. Kuwada. Chem. Pharm. Bull. (Japan), **10**, 243 (1962); **11**, 23 (1963).
22. P. K. Glasoe and F. A. Long. J. Phys. Chem. **64**, 188 (1960).
23. R. Gary, R. G. Bates, and R. A. Robinson. J. Phys. Chem. **68**. 3806 (1964).

Can. J. Chem. Downloaded from www.nrcresearchpress.com by 210.87.254.6 on 09/05/12
For personal use only.

A Carbon-13 Nuclear Magnetic Resonance Investigation of Some Substituted Methyl Phenyl Sulfides, Sulfoxides, and Sulfones

GERALD W. BUCHANAN, CESAR REYES-ZAMORA, AND DOUGLAS E. CLARKE
Department of Chemistry, Carleton University, Ottawa, Canada K1S 5B6

Received July 2, 1974

GERALD W. BUCHANAN, CESAR REYES-ZAMORA, and DOUGLAS E. CLARKE. Can. J. Chem. **52**, 3895 (1974).

Carbon-13 chemical shifts for 33 methyl phenyl sulfides, sulfoxides, and sulfones are reported. Observed trends are discussed in terms of the steric and electronic influences of the substituent groups. Additivity correlations for *para*-disubstituted materials are noted. In general, the shieldings of methyl carbons bonded to sulfur are rather insensitive to the nature of the aromatic substituents. By contrast to the proton shieldings, the CH_3SO and CH_3SO_2 carbons exhibit nearly identical chemical shifts.

GERALD W. BUCHANAN, CESAR REYES-ZAMORA et DOUGLAS E. CLARKE. Can. J. Chem, **52**, 3895 (1974).

On rapporte les déplacements chimiques du carbone-13 pour 33 méthyl phényl thioéthers, sulfoxydes et sulfones. Les tendances observées sont discutées en termes des influences stériques et électroniques des substituants.

On note des corrélations additives pour les composés *para*-disubstitués. En général, les blindages des méthyles carbonés liés au soufre sont plutôt insensibles à la nature des substituants aromatiques. Par opposition aux blindages du proton, les carbones des groupes CH_3SO et CH_3SO_2 présentent sensiblement les mêmes déplacements chimiques.

[Traduit par le journal]

Can. J. Chem. Downloaded from www.nrcresearchpress.com by 210.87.254.42 on 09/05/12
For personal use only.

Introduction

Since early investigations in ^{13}C n.m.r., a great deal of attention has been focussed on the resonances for substituted benzenes (1–13). A paucity of data, however, exists for sulfur containing substituents and a recent survey (14) indicates that no studies for groups of this nature have been carried out. In view of the current interest (15, 16) in the nature of the bonding between sulfur and π electron systems the n.m.r. properties of such molecules should be of interest. Accordingly we wish to report a systematic investigation of the ^{13}C spectra of a series of 33 substituted methyl phenyl sulfides, sulfoxides, and sulfones. Substituents have been selected with a view to providing information regarding both steric and electronic influences on the carbon shieldings.

Results and Discussion

Methyl Phenyl Sulfides

^{13}C chemical shifts for methyl phenyl sulfide **1** and 10 derivatives are presented in Tables 1 and 2. Values in parentheses indicate ambiguities in the assignments. For **1**, differentiation between resonances for C-2,6 *vs.* C-3,5 was not possible experimentally. In the proton n.m.r. spectrum there is no significant chemical shift between the aromatic protons and thus selective ^1H decoupling cannot be employed. Spin–lattice relaxation times are expected to be similar for C-2,6 and C-3,5; and the spectra were not affected substantially by lanthanide shift reagents. It is known, however, that *para*-subsituent effects on aromatic ^{13}C resonances are usually additive within ± 1 p.p.m. (4–14), and thus the possibility of using the *para*-substituted materials **4** and **7–11** to check the tentative assignments for **1** seemed attractive. Additivity parameters for the CH_3, OCH_3, Br, Cl, F, and NO_2 functions employed here have been well documented (14).

Table 3 contains the predicted (relative to benzene 128.7 p.p.m.) shifts for the aromatic carbons of **4** and **7–11**, with the observed values in parenthesis. Much more satisfactory agreement is obtained using the C-2,6 and -3,5 resonances of **1** as indicated rather than the reversed values. With the exception of C-2,6 for **7** and **11**, the agreement between calculated and experimental findings is near ± 1 p.p.m.

For **1**, shielding effects relative to benzene are observed at the C-2,6 and C-4 carbons. In the electronically excited state of **1** it has been suggested (17, 18) that sulfur acts as an electron donor, and if this were the case in the ground state, contributions from the resonance forms

Can. J. Chem. Downloaded from www.nrcresearchpress.com by 210.87.254.42 on 09/05/12
For personal use only.

TABLE 1. ^{13}C chemical shifts for some alkylated methyl phenyl sulfides (δ_C from TMS ± 0.1)*

Compound	Substituent	S-CH_3	C-1	C-2	C-3	C-4	C-5	C-6	2-CH_3	3-CH_3	4-CH_3	2- $CH(CH_3)_2$	4- $CH(CH_3)_2$	2- $CH(CH_3)_2$	4- $CH(CH_3)_2$
1	—	15.9	138.6	126.8	128.8	125.0	128.8	126.8							
2	2-CH_3	16.0	137.8	136.0	129.9	(124.8)	(125.4)	126.6	19.9						
3	3-CH_3	16.1	(138.6)	127.9	(138.5)	126.1	128.8	124.3		21.2					
4	4-CH_3	16.5	(135.1)	127.8	129.6	(134.9)	129.6	127.8			20.8				
5	2,4,6-CH_3	18.3	137.9	142.5	128.9	132.1	128.9	142.5	21.5		20.9			31.5	34.4
6	2,4,6-Isopropyl	21.1	130.5	152.8	121.8	149.4	121.8	152.5				24.5	23.9		

*0.2 *M* solution in $CDCl_3$.

TABLE 2. ^{13}C chemical shifts for *para*-substituted methyl phenyl sulfides (δ_C from TMS ± 0.1)*

Compound	Substituent	C-1	C-2	C-3	C-4	C-5	C-6	S-CH_3	O-CH_3
7	4-OCH_3	129.2	130.3	114.8	158.5	114.8	130.3	17.9	55.3
8	4-Br	137.9	128.6	131.8	118.9	131.8	128.6	16.1	
9	4-Cl	137.3	128.2	128.9	131.1	128.9	128.2	16.1	
10	4-F	133.8	129.8	116.0	161.5	116.0	129.8	17.1	
11	4-NO_2	145.3	125.5	123.9	148.9	123.9	125.5	15.0	

*0.2 *M* solutions in $CDCl_3$.

TABLE 3. Predicted and observed* aryl carbon shieldings relative to benzene for *para*-substituted methyl phenyl sulfides

Compound	Substituents	C-1	C-2,6	C-3,5	C-4
1	—	(+9.9)	(−1.9)	(+0.1)	(−3.1)
4	4-CH_3	+6.8(+ 6.4)	−2.1(−0.9)	+0.7(+ 0.9)	+5.4(+ 6.2)
7	4-OCH_3	+1.3(+ 0.5)	−1.7(+1.6)	−14.8(−13.9)	+26.8(+29.8)
8	4-Br	+8.9(+ 9.2)	+0.3(−0.1)	+3.4(+ 3.1)	−9.1(− 9.8)
9	4-Cl	+7.9(+ 8.6)	−0.9(−0.5)	+0.3(+ 0.2)	+2.7(+ 2.4)
10	4-F	+5.5(+ 6.1)	−0.2(+0.1)	−14.0(−12.7)	+31.4(+32.8)
11	4-NO_2	+15.9(+16.6)	−1.1(−3.2)	−5.2(− 4.8)	+15.9(+20.2)

*In parentheses.

below (**1***a–c*) would lead to increased shielding at the *ortho* and *para*-ring positions.[1]

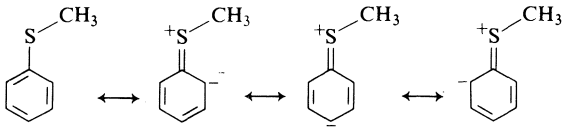

1 **1***a* **1***b* **1***c*

An alternate rationale for the shielding at the *ortho* carbons comes from the conclusion, based on Kerr constant measurements (19) that the favoured conformation of **1** is planar. In this event there would be a 'γ' steric interaction between the CH_3 group and the *ortho* carbon which would be expected to shield the *ortho* position (20).

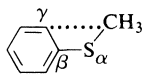

For the monomethyl derivatives **2–4**, no unusual trends are evident. The *ortho*-methyl group in **2** is shielded relative to its *meta* and *para* counterparts in **3** and **4** respectively, an observation consistent with a variety of related methyl substituted benzene derivatives (1, 4, 14, 20). No substantial change in the S—CH_3 chemical shift is evident in the series **1–4**.

By contrast, the S—CH_3 resonance in **5** is *ca.* 2 p.p.m. deshielded relative to **1–4**. For related anisoles (9, 21) a similar effect is noted in the O—CH_3 resonance in di-*ortho*-methylated molecules. Clearly this deshielding cannot arise from steric inhibition of resonance by the *ortho*-CH_3 groups, since this would be expected to cause attenuation of electron release by sulfur and thus *shield* the S—CH_3 resonance. Also, the possibility of *d*-orbital participation in sulfur compounds should make them less susceptible to steric inhibition of resonance than their oxygenated analogs, since rotation about the aryl–S bond causes one orbital of the proper symmetry to replace another in a bonding position as the S—CH_3 group is rotated (15). A number of examples of large (up to 10 p.p.m.) deshielding effects have been reported for sterically compressed 'δ' functional groups (22) and accordingly, a possible origin for the deshielding of the S—CH_3 in **5** is the δ steric interaction between the S—CH_3 and the *ortho*-CH_3 function in the planar conformation. Notably the *ortho*-CH_3 groups of **5** are also deshielded by *ca.* 2 p.p.m. relative to the mono-*ortho*-alkylated compound **2**. No doubt the planar form of **5** will be populated only to a minor extent and thus the magnitude of the effect (*ca.* 2 p.p.m.) is considerably smaller than in systems such as 1,8 dimethylnaphthalene where the deshielding δ effect on the CH_3's is *ca.* 7 p.p.m.

[1]Throughout this paper, it is assumed that the shielding at carbon should increase with increasing electron density.

Can. J. Chem. Downloaded from www.nrcresearchpress.com by 210.87.254.42 on 09/05/12
For personal use only.

Can. J. Chem. Downloaded from www.nrcresearchpress.com by 210.87.254.42 on 09/05/12
For personal use only.

TABLE 4. ^{13}C chemical shifts for some alkylated methyl phenyl sulfoxides (δ_C from TMS ± 0.1)*

Compound	Substituent	$SOCH_3$	C-1	C-2	C-3	C-4	C-5	C-6	$2\text{-}CH_3$	$3\text{-}CH_3$	$4\text{-}CH_3$	2- $CH(CH_3)_2$	4- $CH(CH_3)_2$	2- $CH(CH_3)_2$	4- $CH(CH_3)_2$
12	—	44.0	146.3	123.6	129.4	131.0	129.4	123.6							
13	$2\text{-}CH_3$	42.2	144.2	134.0	(130.7)	(130.6)	127.5	123.1	18.4						
14	$3\text{-}CH_3$	43.9	145.9	123.7	139.4	131.6	129.2	120.6		21.3					
15	$4\text{-}CH_3$	44.1	143.4	123.7	130.1	141.5	130.1	123.7			21.3				
16	$2,4,6\text{-}CH_3$	44.4	143.2	139.6	132.3	134.9	132.3	139.6			20.9				
17	2,4,6-Isopropyl	41.1	136.0	149.8	123.2	152.3	123.2	149.8				24.7, 24.2	23.8	28.1	34.3

*0.2 *M* solutions in $CDCl_3$.

TABLE 5. ^{13}C chemical shifts for *para*-substituted methyl phenyl sulfoxides (δ_C from TMS ± 0.1)

Compound	Substituent	C-1	C-2	C-3	C-4	C-5	C-6	$SOCH_3$	OCH_3
18	4-OCH_3	137.4	125.5	115.0	162.2	115.0	125.5	44.0	55.6
19	4-Br	145.2	125.2	132.6	125.3	132.6	125.2	44.0	
20	4-Cl	144.9	125.0	129.5	137.0	129.5	125.0	44.0	
21	4-F	142.4	126.3	116.9	164.7	116.9	126.3	44.3	
22	4-NO_2	154.0	124.9	124.6	150.1	124.6	124.9	44.2	

*0.2 *M* solution in $CDCl_3$, except **22** which was 0.02 *M* in $CDCl_3$.

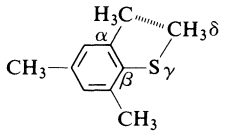

In the triisopropyl compound **6**, the interacting CH_3 groups are 'ε' to each other and a further deshielding of the S—CH_3 resonance of *ca.* 3 p.p.m. is evident. Similar effects were noted in 2,6-diisopropyl anisole (21).

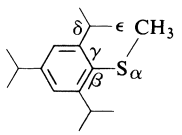

It is interesting that the 2,6-CH_3 resonances of the isopropyl group are 0.6 p.p.m. below those for the 4-isopropyl function, indicative of a mutual deshielding interaction here. Recently (23) results for [2,2]-metacyclophanes indicate deshielding effects for sterically compressed ε carbons up to 7.3 p.p.m.

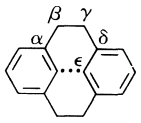

The primary cause of the effect is suggested to be a decrease in the π-electron density at the ε carbons due to transannular van der Waals repulsion.

In an attempt to examine the influence of polar groups the *para*-substituted compounds **4** and **7**–**11** were studied. Ring carbon shieldings are reasonably close to those predicted from additivity (Table 3). Regarding the S—CH_3 chemical shifts, however, some unusual features are evident. For **7** it has been suggested (15) that the vacant d-orbitals on sulfur will accept electrons from the *para*-methoxy function and on this basis a shielding of the S—CH_3 resonance is expected in **7** relative to **1**. Surprisingly, the S—CH_3 resonance of **7** is deshielded by *ca.* 2 p.p.m. compared to **1**. Conversely for **11**, the electron withdrawing inductive effect of the *para*-nitro moiety is expected to deshield the S—CH_3 group but a shielding of 1 p.p.m. relative to **1** is found. These trends are contrary to results for *para*-substituted anisoles (9) where a plot of the OCH_3 shifts *vs.* Hammett σ values gives a fair correlation. The 4-CH_3, -Cl, and -Br functions have little influence on the S—CH_3 resonances relative to methyl phenyl sulfide itself, a trend consistent with the corresponding anisoles.

In this regard the S—CH_3 proton shifts for **1**, **4**, and **7**–**11** are of interest. With the exception of **11** ($\delta = 2.55$) the resonances are nearly identical, appearing at $\delta = 2.45 \pm 0.01$ p.p.m. The deshielding in **11** can be explained on the basis of the inductive influence of the *para*-nitro group. Certainly more investigation is needed to clarify the ^{13}C trends here but it is evident that the S—CH_3 shieldings must be affected substantially by factors other than substituent polarity.

Methyl Phenyl Sulfoxides

^{13}C chemical shifts for methyl phenyl sulfoxide **12** and 10 derivatives are shown in Tables 4 and 5. As was the case for the sulfides the assignments for C-3,5 *vs.* C-2,6 of **12** are supported by the very satisfactory additivity correlations noted in Table 6. *A priori*, the methylsulfinyl group might be expected to show resonance properties which are some blend of lone pair donation and d-orbital acceptance. On the basis of dipole moments (24), ^{19}F n.m.r. (25) and pK_a values (16–28) however, the d-orbital acceptance properties are considered to be predominant. Accordingly the observed deshielding at the *para*-carbon of **12** relative to benzene is reasonable. The recent proposal of Katritsky and co-workers (16) that the CH_3SO group is a net resonance donor, based on infrared intensities is inconsistent with present findings.

For **13**, the data suggest that the preferred

Can. J. Chem. Downloaded from www.nrcresearchpress.com by 210.87.254.42 on 09/05/12
For personal use only.

TABLE 6. Predicted and observed* aryl carbon shieldings relative to benzene for *para*-substituted methyl phenyl sulfoxides

Compound	Substituent	C-1	C-2,6	C-3,5	C-4
12	—	(+17.6)	(−5.1)	(+0.7)	(+2.3)
15	4-CH_3	+14.5(+14.7)	−5.3(−5.0)	+1.3(+ 1.4)	+11.4(+12.8)
18	4-OCH_3	+8.7(+ 8.7)	−5.1(−3.2)	−14.8(−13.7)	+32.5(+33.5)
19	4-Br	+16.6(+16.5)	−2.9(−3.5)	+4.0(+ 3.9)	−3.1(− 3.4)
20	4-Cl	+15.6(+16.2)	−4.1(−3.7)	+0.9(+ 0.8)	+8.7(+ 8.3)
21	4-F	+13.2(+13.7)	−3.5(−2.4)	−13.4(−11.8)	+37.4(+36.0)
22	4-NO_2	+23.6(+25.3)	−4.3(−3.8)	−4.6(− 4.1)	+21.9(+21.4)

*In parentheses.

conformation is as depicted below. The γ steric interaction between the $SOCH_3$ and C-6 would

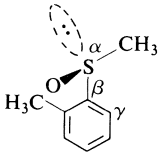

be expected to shield both these resonances relative to **12**, as is observed. In this form, the dihedral angle between the S=O or the S lone pair and the C_2—CH_3 bond is near 60°, thus attenuating any deshielding anisotropic influence (29) of the S=O group or a deshielding δ effect. This argument will be extended in the discussion for **16**.

No remarkable trends are apparent for **14** or **15**. For **16**, however, the $SOCH_3$ chemical shift is nearly identical to those of **12**, **14**, and **15**. Recently it has been found in this laboratory (30) that the barrier to aryl–S rotation in **16** is 9.2 kcal/mol whereas that for **12** is below 6 kcal/mol, indicating considerable steric influence of the ortho CH_3 groups. Therefore it is somewhat surprising that no detectable effect on the CH_3SO resonance is apparent.

Consideration of the preferred conformation for **16** is helpful here and the two possible extremes for the ground state geometry are shown below. Since severe van der Waals repulsion is expected between the *ortho*-CH_3's and the

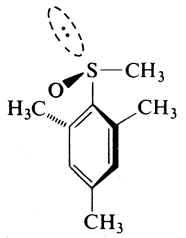

16*a*

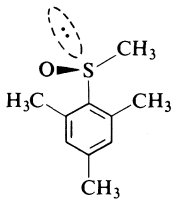

16*b*

$SOCH_3$ of **16***b*, **16***a* is likely to predominate. In this conformation the $SOCH_3$ methyl is perpendicular to the plane of the ring and thus the δ steric interaction with the *ortho*-CH_3's will be minimized. However the *ortho*-CH_3's are deshielded by *ca.* 4 p.p.m. relative to **13**, a finding that may originate either from the anisotropic influence of the S=O group (29) or a van der Waals δ deshielding due to the close spatial proximity of the oxygen atom, since the dihedral angle between the bonds bearing the δ groups is near 20° in **16***a*.

In the triisopropyl sulfoxide **17** the CH_3SO resonance is shielded by *ca.* 3 p.p.m. relative to **12**, **14**–**16**. The sterically interacting methyl groups are ε to each other as was pointed out for **6**, but the shielding trend is in the *opposite* direction. Very recently (31) a shielding ε effect was found in the methyl phenanthrenes, which is *ca.* 4.6 p.p.m. in the 4,5-dimethyl derivative.

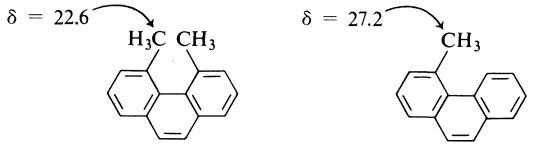

It thus appears that ε steric interactions can be either shielding or deshielding and further studies are required to elucidate the origin of these results.

Since the sulfur atom in sulfoxides is a chiral center the isopropyl methyl groups are diastereotopic (32). Accordingly the 0.5 p.p.m. chemical shift difference between these ortho groups in **17** is not unexpected. The *para*-isopropyl methyls are also diastereotopic but they are farther from the site of asymmetry and no shift difference between them is apparent.

From the results in Table 5 it is clear that the effects of polar substituents on the CH_3SO carbon chemical shifts are negligible. This apparent lack of sensitivity to substitution was also noted

Can. J. Chem. Downloaded from www.nrcresearchpress.com by 210.87.254.42 on 09/05/12
For personal use only.

Can. J. Chem. Downloaded from www.nrcresearchpress.com by 210.87.254.42 on 09/05/12
For personal use only.

by Mislow and co-workers (33, 34) who found that the rates of thermal racemization of various methyl phenyl sulfoxides are relatively unaffected by the electronic nature of *para* groups. The proton chemical shifts for the CH_3SO groups of **12**, **15**, **18**–**21** are $\delta = 2.71 \pm 0.01$ p.p.m., using 0.2 *M* solutions in $CDCl_3$. For **22** a small downfield shift to $\delta = 2.79$ is noted which suggests some inductive electron withdrawal by the $—NO_2$ function.

Methyl Phenyl Sulfones

Tables 7 and 8 contain the ^{13}C chemical shifts for methyl phenyl sulfone **23** and 10 derivatives. Assignments for **23** are unambiguous from selective ^1H decoupling, since it is known (35) that aromatic protons *ortho* to the SO_2 groups are considerably deshielded relative to the *meta* hydrogens. Results in Table 9 show that the agreement between calculated and observed shifts is, in most cases, within 1 p.p.m. In general the most remarkable observation in the sulfones is the close similarity between the ^{13}C shieldings for the SO_2CH_3 groups and the $SOCH_3$ results for the sulfoxides. Introduction of the second electronegative oxygen in the sulfones might have been expected to deshield the methane sulfonyl carbon but no effect is noted. The proton chemical shifts seem more in accord with expectation, the shifts for the SO_2CH_3 group being *ca.* 0.35 p.p.m. downfield from those of the sulfoxides. The *para*-nitro substituted compound *33* has the largest deshielding, appearing at $\delta = 3.12$.

X-Ray (36) and dipole moment studies (37) have shown that methyl phenyl sulfones adopt the conformation below preferentially.

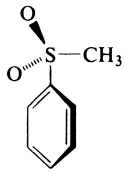

Since the $S—CH_3$ group is perpendicular to the plane of the phenyl ring it is relatively unaffected by *ortho*-CH_3 substitution as indicated by the very similar $S—CH_3$ shieldings for **23**–**27**. The deshielding of the C-2,6-CH_3 resonances of **27** relative to **24** is puzzling however. In **28**, the ε effect on the SO_2CH_3 carbon is deshielding as in **6** but this is not a general observation as indicated earlier. The pronounced deshieldings at C-2,4 and 6 of **28** are a consequence of increased β substitution as previously noted for diphenyl ethers and anisoles (21).

As in the case of the sulfoxides, the ^{13}C shieldings for the SO_2CH_3 group are insensitive to the electronic nature of the *para* substituent. Table 8 shows shifts near 44.5 ± 0.3 for compounds **29**–**33**.

A number of groups (1, 3, 14) have pointed out the apparent correlation between *para*-carbon chemical shifts and the electronic properties of substituents for monosubstituted benzenes. In general, electron withdrawing groups tend to deshield the *para* carbon while electron releasing functions shield it. Results for **1**, **12** and **23** are in accord with this trend, since the σ_p values for the $—SCH_3$, $—SOCH_3$, and $—SO_2CH_3$ groups are -0.047, $+0.567$, and $+0.728$, respectively (50). As a summary of results for 24 monosubstituted aromatics is available (14), a detailed treatment of the correlations here seems unwarranted.

From the present work it is clear that although both steric and electronic factors are operative, the trends are by no means general. The monosubstituted compounds **1**, **12** and **23** exhibit shifts consistent with the electronic properties of the substituents. By contrast, the lack of sensitivity of the $S—CH_3$ shieldings in the three series to the nature of the *para* groups suggests a minor amount of conjugation between the phenyl ring and the sulfur atom. Additional evidence has been put forward for carbon steric shifts when the interacting groups are in a δ or an ε orientation. For ε interactions the effects can be shielding *or* deshielding.

Experimental

Spectra

^{13}C spectra were obtained using the pulsed Fourier transform method at 25.16 MHz on a Varian XL-100-12 n.m.r. spectrometer. The free induction decays were stored in a Nicolet BNC-12 computer (20 K memory) and were transformed after a sufficient number had been accumulated. Normally 4096 data points were used in the interferogram accumulation and spectral widths of 5000 and 1000 Hz were employed.

All samples were examined as 0.2 *M* solutions in $CDCl_3$ containing 4% TMS as an internal standard. Tube size was 5 mm outer diameter. Normally spectra were recorded with complete proton noise decoupling. For the selective decoupling experiments irradiation was performed at low decoupler power in the absence of noise modulation.

Materials

With the exception of **17** and **28**, all compounds examined have been reported previously, with references for each shown as follows: **1**, **6**, **8** (38); **3**, **4**, **7**, **9**–**11** (15); **12**,

Can. J. Chem. Downloaded from www.nrcresearchpress.com by 210.87.254.42 on 09/05/12
For personal use only.

TABLE 7. ^{13}C chemical shifts for some alkylated methyl phenyl sulfones (δ_C from TMS ± 0.1)*

Compound	Substituent	SO_2CH_3	C-1	C-2	C-3	C-4	C-5	C-6	2-CH_3	3-CH_3	4-CH_3	2- $CH(CH_3)_2$	4- $CH(CH_3)_2$	2- $CH(CH_3)_2$	4- $CH(CH_3)_2$
23	—	44.3	141.0	127.2	129.3	133.5	129.3	127.2							
24	2-CH_3	43.7	139.6	137.8	132.4	133.6	126.9	129.3	20.0						
25	3-CH_3	44.5	141.1	127.7	139.7	134.4	129.3	124.5		21.2					
26	4-CH_3	44.6	138.5	127.5	130.0	144.6	130.0	127.5			21.5				
27	2,4,6-CH_3	44.4	142.4	138.8	131.5	134.5	131.5	138.8	22.4		20.8				
28	2,4,6-Isopropyl	46.6	134.2	150.9	124.1	153.7	124.1	150.9				25.0	23.6	29.6	34.3

*0.2 *M* solution in $CDCl_3$.

TABLE 8. ^{13}C chemical shifts for *para*-substituted methyl phenyl sulfones (δ_C from TMS ± 0.1)*

Compound	Substituent	C-1	C-2	C-3	C-4	C-5	C-6	SO_2CH_3	OCH_3
29	4-OCH_3	132.5	129.5	114.6	163.8	114.6	129.5	44.8	55.7
30	4-Br	140.2	128.9	132.7	128.7	132.7	128.9	44.4	
31	4-Cl	139.6	128.9	129.6	140.1	129.6	128.9	44.3	
32	4-F	137.5	130.3	116.7	165.8	116.7	130.3	44.5	
33	4-NO_2	146.9	128.9	124.6	151.3	124.6	128.9	44.3	

*0.2 *M* solutions in $CDCl_3$.

TABLE 9. Predicted and observed* aryl carbon shieldings relative to benzene for *para*-substituted methyl phenyl sulfones

Compound	Substituent	C-1	C-2,6	C-3,5	C-4
23	—	(+12.3)	(−1.5)	(+0.6)	(+4.8)
26	4-CH_3	+9.2(+ 9.8)	−1.7(−1.2)	+1.2(+ 1.3)	+13.9(+15.9)
29	4-OCH_3	+3.4(+ 3.8)	−1.5(+0.8)	−14.9(−14.1)	+35.0(+35.1)
30	4-Br	+11.3(+11.5)	+0.7(+0.2)	+3.9(+ 4.0)	−0.6(− 0.0)
31	4-Cl	+10.3(+10.9)	−0.5(+0.2)	+0.8(+ 0.9)	+11.2(+11.4)
32	4-F	+7.9(+ 8.8)	+0.1(+1.6)	−13.5(−12.0)	+39.9(+37.1)
33	4-NO_2	+18.3(+18.2)	−0.7(+0.2)	−4.7(− 4.1)	+24.4(+22.6)

*In parentheses.

14, **15**, **18–23**, **25**, **26**, **29–33** (16); **16** (34); **27** (39); **5** (40); **2** (41); **13** (42); **24** (43); **19** (44) and **30** (45).

2,4,6-Triisopropyl methyl phenyl sulfoxide **17** was prepared starting with 1,3,5-triisopropylbenzene, which had been obtained commercially from K and K laboratories, Plainview, New York. Chlorosulfonation with chlorosulfonic acid according to the procedure of Huntress and Carten (46) yielded 2,4,6-triisopropylbenzenesulfonyl chloride in 80% yield. Reduction to the thiol was accomplished in 74% yield via the procedure of Adams and Marvel (47). Methylation with methyl sulfate in base (48) converted the material to the methyl sulfide in 94% yield. Sodium metaperiodate oxidation (49) gave the sulfoxide **17** in 87% yield; m.p. 106.5–108°, which was characterized by its infrared and ^1H n.m.r. spectra.

Anal. Calcd. for $C_{16}H_{26}SO$: C, 72.12; H, 9.84; S, 12.03. Found: C, 72.11; H, 9.76; S, 12.17.

Oxidation of the sulfide with a fourfold excess of H_2O_2 in refluxing HOAc, according to the published procedure (28) yielded the sulfone **28** in 72% yield; m.p. 132–133°, which was characterized by infrared and proton n.m.r. spectra.

Anal. Calcd. for $C_{16}H_{26}SO_2$: C, 68.04; H, 9.28; S, 11.35. Found: C, 67.99; H, 9.41; S, 11.39.

Elemental analyses were carried out by Spang Microanalytical Laboratory, Ann Arbor, Michigan.

Financial support from the National Research Council of Canada is gratefully recognized.

1. P. C. LAUTERBUR. J. Am. Chem. Soc. **83**, 1846 (1961).
2. P. C. LAUTERBUR. Tetrahedron Lett. 274 (1961).
3. H. SPIESECKE and W. G. SCHNEIDER. J. Chem. Phys. **35**, 731 (1961).
4. P. C. LAUTERBUR. J. Chem. Phys. **38**, 1406, 1415, 1432 (1963).
5. G. B. SAVITSKY. J. Phys. Chem. **67**, 2723 (1963).
6. G. E. MACIEL and J. J. NATTERSTAD. J. Chem. Phys. **42**, 2427 (1965).
7. C. P. NASH and G. E. MACIEL. J. Phys. Chem. **68**, 832 (1964).
8. K. S. DHAMI and J. B. STOTHERS. Can. J. Chem. **43**, 479, 510 (1965).
9. K. S. DHAMI and J. B. STOTHERS. Can. J. Chem. **44**, 2855 (1966).
10. K. S. DHAMI and J. B. STOTHERS. Can. J. Chem. **45**, 233 (1967).
11. T. F. PAGE, JR. Mol. Phys. **13**, 523 (1967).
12. F. W. WEHRLI, J. W. DE HAAN, A. I. M. KEULEMANS, O. EXNER, and W. SIMON. Helv. Chim. Acta, **52**, 103 (1969).
13. G. L. NELSON, G. C. LEVY, and J. D. CARGIOLI. J. Am. Chem. Soc. **94**, 3089 (1972).
14. J. B. STOTHERS. Carbon-13 n.m.r. spectroscopy, Academic Press, New Nork, N.Y. 1972.
15. N. C. CUTRESS, T. B. GRINDLEY, A. R. KATRITSKY, and R. D. TOPSOM. J. Chem. Soc. Perkin II, 263 (1974).
16. N. C. CUTRESS, T. B. GRINDLEY, A. R. KATRITSKY, M. SHOME, and R. D. TOPSOM. J. Chem. Soc. Perkin II, 268 (1974).
17. T. S. GOVINDARAJAN. Ph.D. Thesis, Annamolai University. 1957.
18. A. MANGINI and R. PASSERINI. J. Chem. Soc. 1168 (1952).
19. M. J. ARONEY, R. J. W. LE FÈVRE, R. K. PIERENS, and M. G. N. THE. J. Chem. Soc. B, 1132 (1971).
20. W. R. WOOLFENDEN and D. M. GRANT. J. Am. Chem. Soc. **88**, 1496 (1966).
21. G. W. BUCHANAN, G. MONTAUDO, and P. FINOCCHIARO. Can. J. Chem. **52**, 767 (1974).
22. S. H. GROVER, J. P. GUTHRIE, J. B. STOTHERS, and C. T. TAN. J. Magn. Res. **10**, 227 (1973).
23. T. SATO, T. TAKEMURA, and M. KAINOSHO. Chem. Commun. 97 (1974).

Can. J. Chem. Downloaded from www.nrcresearchpress.com by 210.87.254.42 on 09/05/12
For personal use only.

24. H. GOETZ, B. KLABUHU, F. MARSCHNER, H. HOHBERG, and W. SKUBALLA. Tetrahedron, **27**, 999 (1971).
25. W. A. SHEPPARD and R. W. TAFT. J. Am. Chem. Soc. **94**, 1919 (1972).
26. F. G. BORDWELL and G. D. COOPER. J. Am. Chem. Soc. **74**, 1058 (1952).
27. F. G. BORDWELL and H. M. ANDERSEN. J. Am. Chem. Soc. **75**, 6019 (1953).
28. F. G. BORDWELL and P. J. BOUTAN. J. Am. Chem. Soc. **79**, 717 (1957).
29. R. D. G. COOPER, P. V. DE MARCO, J. C. CHENG, and N. D. JONES, J. Am. Chem. Soc. **91**, 1408 (1969).
30. G. W. BUCHANAN, C. REYES-ZAMORA, and D. E. CLARKE. J. Org. Chem. In press.
31. J. B. STOTHERS. Private communication.
32. K. MISLOW and M. RABAN. Top. stereochem. **1**, 1 (1967); **2**, 199 (1967).
33. D. R. RAYNER, E. G. MILLER, P. BICKART, A. J. GORDON, and K. MISLOW. J. Am. Chem. Soc. **88**, 3138 (1966).
34. D. R. RAYNER, A. J. GORDON, and K. MISLOW. J. Am. Chem. Soc. **90**, 4854 (1968).
35. G. MONTAUDO and P. FINOCCHIARO. J. Mol. Struct. **16**, 299 (1973).
36. C. RERAT and G. TSOUCARIS. Bull. Soc. Fr. Miner. Cristallogr. **87**, 100 (1964).
37. H. LUMBROSO and R. PASSERINI. Bull. Soc. Chim. Fr. 1179 (1955).
38. V. BALIAH and M. URNA. Tetrahedron, **19**, 455 (1963).
39. S. N. BHATTACHARYA, C. EABORN, and D. R. M. WALTON. J. Chem. Soc. C, 1367 (1969).
40. D. CAGNIANT and P. CAGNIANT. Bull. Soc. Chim. Fr. 228 (1966).
41. J. H. BOWIE, S. O. LAWRESON, J. O. MADSEN, G. SCHROLL, and D. H. WILLIAMS. J. Chem. Soc. B, 951 (1966).
42. D. CARNIMEO and R. CURCI. Boll. Sci. Fac. Chim. Ind. Bologna, **23**, 293 (1965).
43. G. KRESZE and W. AMANN. Spectrochim. Acta, A **25**, 393 (1969).
44. R. CURCI and G. MODENA. Tetrahedron Lett. 863 (1965).
45. G. KRESZE, U. UHLICH, E. RUPTE, and B. SCHRADER. Z. Anal. Chem. **197**, 283 (1963).
46. E. H. HUNTRESS and F. H. CARTEN. J. Am. Chem. Soc. **62**, 511 (1940).
47. R. ADAMS and C. S. MARVEL. Org. Syn. Coll. **1**, 504 (1941).
48. E. I. VOGEL. A textbook of practical organic chemistry. 3rd ed. 1956. p. 670.
49. C. R. JOHNSON and J. E. KEISER. Org. Syn. **46**, 78 (1966).
50. H. H. JAFFE. Chem. Rev. **53**, 191 (1953).

Can. J. Chem. Downloaded from www.nrcresearchpress.com by 210.87.254.42 on 09/05/12
For personal use only.

ω-Aldehydo Sugars Prepared by Ninhydrin Oxidation

ALAN R. GIBSON,[1] LAURENCE D. MELTON,[2] AND KEITH N. SLESSOR
Department of Chemistry, Simon Fraser University, Burnaby, British Columbia V5A 1S6

Received June 12, 1974

ALAN R. GIBSON, LAURENCE D. MELTON, and KEITH N. SLESSOR. Can. J. Chem. **52**, 3905 (1974).

The reaction of ninhydrin with 6-amino-6-deoxy-hexopyranosyl sugars has been investigated. 6-Aldehydocyclohexaamylose and 1,2:3,4-di-*O*-isopropylidene-α-D-*galacto*-hexodialdo-1,5-pyranose have been prepared by oxidative deamination of 6-amino-deoxycyclohexaamylose and 6-amino-6-deoxy-1,2:3,4-di-*O*-isopropylidene-α-D-galactopyranose, respectively, using ninhydrin. The preparation of the two aldehydes by the ninhydrin reaction is compared with the method of photolysis of the corresponding azido sugars. The mass spectra of the perdimethylsilyl derivatives of cyclohexaamylose and *O*-methyl oxime of 6-aldehydocyclohexaamylose have been recorded.

ALAN R. GIBSON, LAURENCE D. MELTON et KEITH N SLESSOR. Can. J. Chem. **52**, 3905 (1974).

On a étudié la réaction de la ninhydrine avec les sucres amino-6 déoxy-6 hexopyrannosyles. Les composés aldéhydo-6 cyclohexaamylose et 1,2:3,4-di-*O*-isopropylidène-α-D-*galacto*-hexodialdo-1,5-pyrannose ont été préparés respectivement par une déamination oxydante du 6-amino-6-déoxycyclohexaamylose et du 6-amino-6-déoxy-1,2:3,4-di-*O*-isopropylidène-α-D-galactopyrannose en utilisant la ninhydrine. La préparation des deux aldéhydes par la réaction de la ninhydrine est comparée à la méthode de photolyse des sucres azido correspondants. On a pris les spectres de masse des dérivés perdiméthylsilylés de la cyclohexaamylose et du *O*-méthyl oxime de la 6-aldéhydocyclohexaamylose. [Traduit par le journal]

Introduction

The preparation of ω-aldehydo sugars is of considerable importance because of the utility of these compounds as synthetic intermediates in monosaccharide and polysaccharide chemistry. Among the older methods for preparing ω-aldehydo derivatives are the Rosenmund catalytic reduction of glycuronic acid chloride and glycol cleavage reactions using lead tetraacetate or periodate oxidation (for a review see ref. 1). However, all these methods require suitably protected sugars, as does the oxidation of the primary hydroxyl group using dimethyl sulphoxide – *N*,*N*′-dicyclohexylcarbodiimide (Pfitzner–Moffatt reagent) or other dimethyl sulphoxide oxidizing mixtures; preparations of aldehydes with dimethyl sulphoxide reagents other than the Pfitzner–Moffatt reagent have not been so successful because of side reactions (2–4). Recently, chromium trioxide – dipyridine complex has been found to oxidize the primary hydroxyl groups of various monosaccharides to aldehydes but this approach also requires protected sugars (5).

[1]Department of Chemistry, Queen's University, Kingston, Ontario K7L 3N6.

[2]Unilever Research, Colworth House, Sharnbrook, Bedford, England MK44 1LQ.

The methods of preparation of ω-aldehydo derivatives from unprotected sugars are limited. D-*gluco*-Hexodialdose has been prepared from D-glucurono-γ-lactone in a very low yield by reduction with sodium borohydride and from a 6-deoxy-6-nitro derivative in a moderate yield by the Nef degradation (6). Oxidation of methyl hexopyranosides with potassium ferrate (7) gave the corresponding 6-aldehyde in moderate yields. Photolysis of 6-azido derivatives of glycosides and polysaccharides has been shown by Horton and co-workers (8) to produce the corresponding ω-aldehydo sugars in good yields. Another approach to the synthesis of ω-aldehydo sugars is by oxidative deamination of the corresponding unprotected amino sugar. Ninhydrin (2,2-dihydroxy-1,3-indandione) (9) has long been known to bring about the oxidative deamination of simple organic compounds containing a primary amine to yield aldehydes (9, 10). In this report, the applicability of the ninhydrin reaction to carbohydrates containing an amino group attached to a primary carbon is discussed.

Results and Discussion

6-Amino-6-deoxycyclohexaamylose (**2**) (11), in which the hydroxyl groups are unsubstituted, and 6-amino-6-deoxy-1,2:3,4-di-*O*-isopropyli-

Can. J. Chem. Downloaded from www.nrcresearchpress.com by 210.87.254.5 on 09/05/12
For personal use only.

Can. J. Chem. Downloaded from www.nrcresearchpress.com by 210.87.254.5 on 09/05/12
For personal use only.

dene-α-D-galactose (**5**) were treated with ninhydrin. The monoaminocyclohexaamylose was converted quantitatively to 6-aldehydocylohexaamylose (**3**) by the ninhydrin oxidation, according to t.l.c. (thin-layer chromatography). The yield of 60% for the pure isolated aldehyde is reasonable considering the nature of the compound. In another preparation of the monoaldehydocyclohexaamylose from monoaminocyclohexaamylose which contained ~5% cyclohexaamylose as impurity, a somewhat higher yield was obtained allowing for the contaminating cyclohexaamylose. As it proved difficult to remove the cyclohexaamylose impurity from the product, it was simpler to purify the monoaminocyclohexaamylose before carrying out the oxidation. β-Elimination of ω-aldehydo sugars is known to occur under basic conditions (4, 12) and this would involve the breaking of the adjacent glycosidic linkage in a maltodextrin (13). However, no opening of the cyclohexaamylose torus was detected under the mild conditions used for the ninhydrin oxidation. The pure aldehyde reduced Fehling's solution and the optical rotatory dispersion indicated that the aldehyde existed in the hydrated form in aqueous solution. The freeze-dried aldehyde analyzed as a trihydrate and it was further characterized by the mass spectrometry of its perdimethylsilyl methyl oxime derivative.

Production of aldehydocyclohexaamylose by photolysis (8) of the azido compound (**4**) (11)

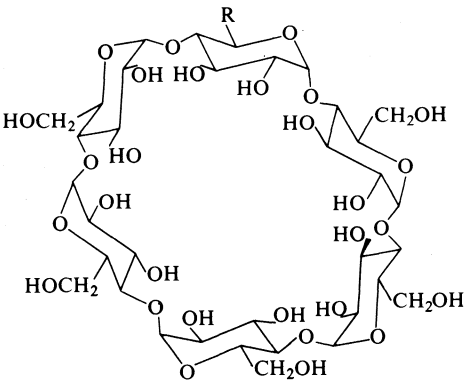

1 R = CH_2OH

2 R = CH_2NH_2

3 R = CHO

4 R = CH_2N_3

FIG. 1. Cyclohexaamylose and some of its derivatives.

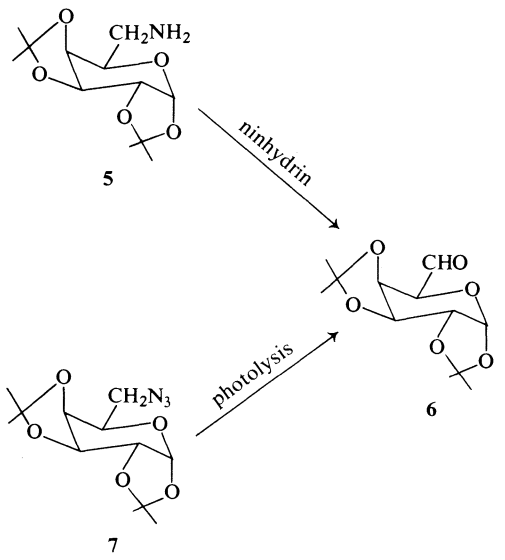

FIG. 2. Synthetic routes to 1,2:3,4-di-*O*-isopropylidene-α-D-*galacto*-hexodialdo-1,5-pyranose (**6**).

resulted in a product whose properties were consistent with those expected for **3**. The formation of a side product, suggested to be an amine, during the photolysis of 6-azido-6-deoxyamylose has been reported recently (13). The pure aldehydocyclohexaamylose produced by the ninhydrin reaction had the same characteristics on t.l.c. and p.c. (paper chromatography) as the aldehyde produced by photolysis. Both aldehydes could be reduced by sodium borohydride to compounds which had the same chromatographic characteristics as cyclohexaamylose (**1**). Since azido sugars can be reduced virtually quantitatively to amines, oxidative deamination by ninhydrin appears to be an equivalent method of preparing ω-aldehydes of unprotected sugars to photolysis of azido sugars.

The general applicability of the ninhydrin reaction was confirmed by using it to prepare the known aldehyde, 6-aldehydo-1,2:3,4-di-*O*-isopropylidene-α-D-galactose (**6**) (14, 15) from 6-amino-6-deoxy-1,2:3,4-di-*O*-isopropylidene-α-D-galactose (**5**). No side products were detected during this preparation. The aldehyde was also synthesized by photolysis (8) of 6-azido-6-deoxy-1,2:3,4-di-*O*-isopropylidene-α-D-galactose (**7**). The aldehydes produced by the two different methods had the same physical properties and the same characteristics on t.l.c. The two aldehydes were characterized and proven identical by comparison of their crystalline *p*-nitrophenylhy-

Can. J. Chem. Downloaded from www.nrcresearchpress.com by 210.87.254.5 on 09/05/12
For personal use only.

drazones. The two methods gave comparable yields of aldehyde (38% by ninhydrin reaction and 43% by photolysis). Hence, it appears that for fully protected sugars neither method of aldehyde preparation has a distinct advantage over the other.

Only a few examples of oxidative deamination by ninhydrin are known in preparative carbohydrate chemistry. Ninhydrin has been used to convert 3-*O*-β-D-glucopyranosyl-2-amino-2-deoxy-D-gluconic acid to 2-*O*-β-D-glucopyranosyl-D-arabinose (16) and 3-*O*-(methyl β-D-glucopyranosyluronate)-2-amino-2-deoxy-D-galactose to 2-*O*-β-D-glucopyranosyluronic acid-D-lyxose (17). More recently Veyrières and Jeanloz (18) treated muramic acid with ninhydrin to give 2-*O*-D-lactyl-D-arabinose in 62% yield. In all these examples the amino group is at the C-2 carbon and in each case the sugars undergo oxidative deamination with concomitant cleavage of the C-1 — C-2 bond to produce an aldehyde containing one less carbon atom.

In some trial experiments to evaluate the possibility of producing ketoses from 2-amino-2-deoxyhexitols, we have observed only C-1 — C-2 bond cleavage. 2-Amino-2-deoxy-D-glucitol yielded on ninhydrin oxidation, arabinose as the only observable chromatographic product. No fructose was detected.

There appears to be no previous investigation of the action of ninhydrin on amino groups attached to primary carbons of sugars. In the present work it has been shown that ninhydrin reacts with an amine attached to a primary carbon of a sugar to give an aldehyde but, unlike amino sugars in which the amine is at C-2, there was no carbon–carbon bond cleavage. This is in agreement with the earlier work of Moubasher and Othman (10) who found that ethylamine, *n*-butylamine, and benzylamine were oxidized by ninhydrin to yield acetaldehyde, butyraldehyde, and benzaldehyde, respectively. Furthermore, this result is in agreement with the current theory (9) of the ninhydrin reaction.

In order to confirm the structure of 6-aldehydocyclohexaamylose, the perdimethylsilyl methyl oxime was examined by mass spectrometry. The perdimethylsilyl methyl oxime was prepared from the aldehyde in a one-pot reaction (compare the preparation of pertrimethylsilyl methyl oximes of sugars (19)). As the substances currently available for calibrating mass spectrometers, perfluorokerosene, and perfluoroheptyltriazine (20), only allow a mass of 1185 to be reached and the molecular ion of the perdimethylsilyl methyl oxime of 6-aldehydocyclohexaamylose is 1985 a.m.u., it was decided to use perdimethylsilyl cyclohexaamylose ($M^+ = 2016$) as a reference compound as well as a model compound. Beadle (21) has reported the difficulty of preparing a pure pertrimethylsilyl derivative of cyclohexaamylose for gas chromatography and has shown the advantages of the perdimethylsilyl derivative. The present mass spectral work confirms the incompleteness of trimethylsilylation and the utility of the perdimethylsilyl derivative. The molecular ions of the cyclohexaamylose and aldehydocyclohexaamylose derivatives (Table 1) were observed and no peaks were detected at higher *m/e* values. Table 1 also lists the most intense *m/e* peaks that were detected. One distinguishing feature of the mass spectra is the particularly high relative abundances of the molecular ions compared to those found for straight chain pertrimethylsilylated oligosaccharides. This is comparable to what is observed for cyclic peptides compared to linear peptides; see for instance ref. 22.

The major fragmentation pathways can be grouped in series for perdimethylsilylcyclohexaamylose (Table 2). The corresponding series for the *O*-methyl oxime are given in Table 3. The mass difference of 336 between adjacent members of a series is due to the following cleavage.

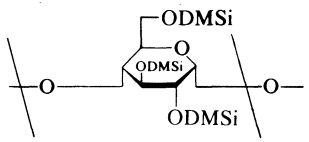

The members of series I are caused by cleavage of a glycosidic linkage plus the loss of a hydrogen and subsequent loss of glucosidic residues. The structure of series I members for cyclohexaamylose may be postulated as

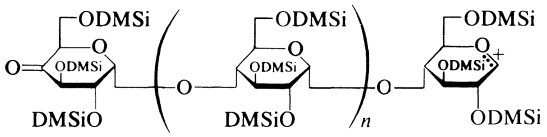

where $n = 0, 1, 2, 3$, or 4, and the 335 fragment would then be

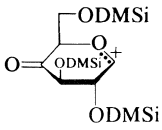

TABLE 1. Selected peaks from the mass spectra of perdimethylsilyl derivatives of cyclohexaamylose and *O*-methyl oxime of 6-aldehydocyclohexaamylose

Cyclohexaamylose		Aldehydocyclohexaamylose		
m/e	%	*m/e*	%	Species
2016	0.14	1985	0.18	M^+
2001	0.11			$(M - CH_3)^+$
		1955	0.09	$(M - 2CH_3)^+$
1940	0.22	1909	0.05	$(M - DMSiOH)^+$
207	49.0	207	63.5	—
189	23.5	189	16.5	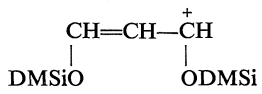
176	100	176	100	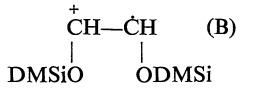 (B)
163	14.1	163	14.4	$(CH_3)_2HSiOCH{=}\overset{+}{O}SiH(CH_3)_2$
149	48.0	149	49.3	—
133	35.2	133	30.0	$(CH_3)_2HSi\overset{+}{O}Si(CH_3)_2$
117	38.8	117	41.3	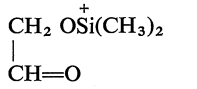
59	72.5	59	73.3	$(CH_3)_2\overset{+}{H}Si$

Series II could be formed by cleavage of a glycosidic linkage, loss of one or more glucosyl residues and transfer of a hydrogen to the charge retaining species. Possible structures for this series are

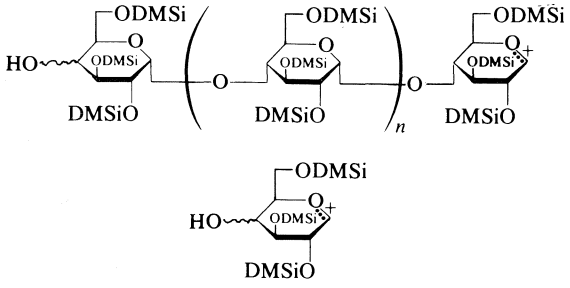

m/e 337

where $n = 0$, 1, 2 or 3.

Series III, which occurs 30 mass units higher than series I, might be postulated as

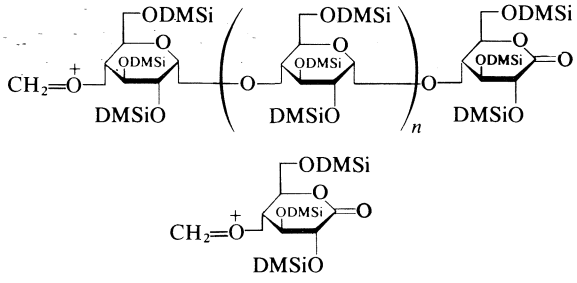

m/e 365

where $n = 0$, 1, 2 or 3.

Series IV, by analogy with trimethylsilyl derivatives of oligosaccharides (23), could be postulated as

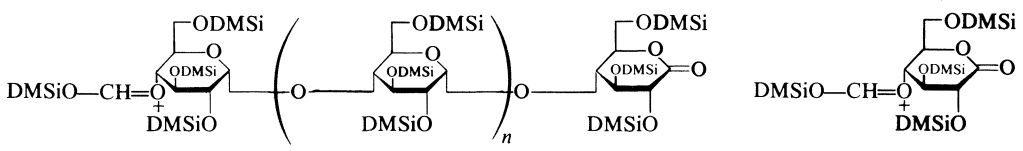

m/e 439

where $n = 0$, 1, 2 or 3.

Can. J. Chem. Downloaded from www.nrcresearchpress.com by 210.87.254.5 on 09/05/12
For personal use only.

TABLE 2. The major fragmentation series in the mass spectrum of perdimethylsilyl cyclohexaamylose

No. of intact pyranose rings	Series I		Series II		Series III		Series IV		Series V	
	m/e	%	*m/e*	%	*m/e*	%	*m/e*	%	*m/e*	%
6	2015	0.09								
5	1679	—	1681	—	1709	0.08	1783	0.23	1882	0.09
	1603*	0.16	1605†	0.04						
4	1343	—	1345	—	1373	0.08	1447	0.05	1546	0.10
	1267‡	0.20								
3	1007	0.33	1009	0.32	1037	0.25	1111	0.14	1210	0.11
2	671	0.59	673	0.51	701	0.30	775	0.36	874	0.10
1	335	4.77	337	1.57	365	0.69	439	0.59	538	—

*1603 = 1679 − DMSiOH (76)
†1605 = 1681 − DMSiOH
‡1267 = 1343 − DMSiOH

TABLE 3. Fragmentation series in the mass spectrum of perdimethylsilyl 6-aldehydocyclohexaamylose *O*-methyl oxime

No. of intact pyranose rings	Series I		Series II		Series III		Series IV		Series V	
	m/e	%	*m/e*	%	*m/e*	%	*m/e*	%	*m/e*	%
6	1984	0.16								
5	1648	0.06	1650	0.05	1678	0.08	1752	0.13	1851	0.05
4	1312	0.42	1314	0.64	1342	0.41	1416	0.34	1515	0.04
3	976	0.39	978	0.26	1006	0.27	1080	0.21	1179	—
									1103*	0.33
2	640	0.33	642	0.34	670	0.40	744	0.54	843	0.22
1	304	1.18	306	1.38	334	0.58	408	0.74	507	0.60

*1103 = 1179 − DMSiOH (76)

Series V, also by analogy with trimethylsilyl derivatives, may be postulated as

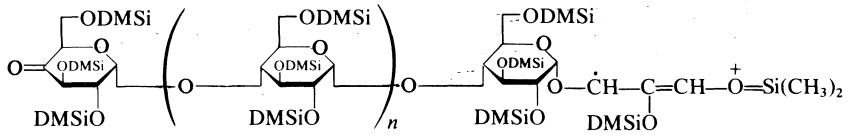

where n = 0, 1, 2 or 3.

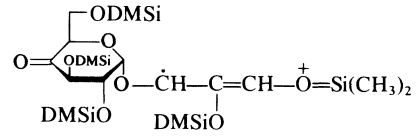

m/e 538

Series I–V of the aldehydocyclohexaamylose derivative are analogous to the corresponding series for cyclohexaamylose except for the mass difference of 31 a.m.u. due to the replacement of one —CH_2ODMSi group by —CH = $NOCH_3$.

The initial assumption in interpreting the mass spectra of the perdimethylsilyl derivatives was that the fragmentation pathways were analogous to those established (24) for pertrimethylsilyl derivatives of sugars (see for example the intense low mass peaks given in Table 1). However, series I–III are not found as major series in the fragmentation of pertrimethylsilyl ethers of sugars and their appearance may be due to the cyclic nature of cyclohexaamylose or to differences in properties of dimethylsilyl and trimethylsilyl ethers. In the mass spectra of both compounds there are additional series of 2 a.m.u. higher than series III–V as is series II to series I. It is not surprising that the mass spectrum of the aldehyde derivative contains the smaller mass members of the series from cyclohexaamylose as they would be readily formed by loss of the residue containing the *O*-methyl oxime group. Those seen are *m/e* 671 (0.70%) and *m/e* 335 (0.79%) of series I; *m/e* 673 (0.24%) and *m/e* 337 (0.62%) of series II; *m/e* 701 (0.29%) and *m/e* 365 (0.66%) of series III; *m/e* 1111 (0.11%), *m/e* 775

Can. J. Chem. Downloaded from www.nrcresearchpress.com by 210.87.254.5 on 09/05/12
For personal use only.

(0.46%), and *m/e* 439 (0.46%) of series IV; and *m/e* 874 (0.26%) of series V.

Experimental

General

Melting points were determined on a Fisher-Johns apparatus and are uncorrected. Evaporations were conducted on a Buchi rotary evaporator at bath temperatures not exceeding 45°. Optical rotations were measured on a Perkin-Elmer Model P22 spectropolarimeter. Pyridine was dried by distilling from barium oxide and then kept over Linde molecular sieve Tpye 4A. Ninhydrin was purchased from Fisher Scientific Co. and used without further purification. Activated charcoal, Darco, G-60, 20–40 mesh, was purchased from Matheson, Coleman, and Bell. The reagents for preparing derivatives for mass spectrometry were bought from Pierce Chemical Co., Illinois. Thin-layer chromatography was performed on Silica gel G with solvents: A, butanone – methanol – 1.0 *N* acetic acid 12:3:5; B, butanone–methanol–water 14:3:3; C, butanone – water 9:1 and D, diethyl ether – toluene 2:1. Paper chromatography using Whatman 3MM paper was run by the descending technique with the solvent ethyl acetate – pyridine – water 5:4:3. All sugars were detected after t.l.c. with 10% aqueous sulphuric acid spray followed by heating. Aldehydo derivatives were observed on t.l.c. plates by spraying with 2,4-dinitrophenylhydrazine (0.3%) in 2 *N* hydrochloric acid. Ninhydrin (0.2%) in ethanol was sprayed to detect amines after t.l.c. and p.c. Iodine vapour was used to detect cyclohexaamylose and its derivatives on thin-layer and paper chromatograms. The R_f values of cyclohexaamylose derivatives were measured relative to cyclohexaamylose (R_c).

6-Amino-6-deoxycyclohexaamylose (2)

This compound was prepared from cyclohexaamylose (**1**) as previously described (11) and was further purified by application of 1.12 g of material to a column (37 × 2.3 cm) of activated charcoal in an aqueous solution (40 ml). The column was washed with 12.5% ethanol (1400 ml). The ethanolic eluate, which contained monoaminocyclohexaamylose, was collected in 100 ml fractions. The purity was checked by t.l.c. (solvent A) and the appropriate fractions were combined, concentrated to approximately 50 ml on a rotary evaporator, filtered through a Celite pad, and freeze–dried to yield the monoamine (**2**) (0.45 g).

6-Aldehydocyclohexaamylose (3)

6-Amino-6-deoxycyclohexaamylose (**2**) (0.40 g) was dissolved in aqueous solution (40 ml) containing sodium bicarbonate (0.50 g) and ninhydrin (0.40 g) added. The solution, which became purple on addition of ninhydrin, was heated on a boiling water bath. Thin-layer chromatography, solvent A, showed the reaction was complete in 10 min to give only one carbohydrate product (R_c 0.95, brown with iodine vapour and yellow with 2,4-dinitrophenylhydrazine spray). During the reaction an intermediate was seen by t.l.c. (R_c 1.1, yellow with iodine vapour). On standing overnight at room temperature a brown precipitate formed, which was removed by filtration. The filtrate was applied to a charcoal column (20 × 2.5 cm). The column was eluted with 12.5% ethanol (1.0 l) and 25% ethanol (1.2 l). The 25% ethanol eluate was collected in 100 ml fractions. Concentrated ammonia was added dropwise to neutralize each fraction and then the fractions were evaporated to dryness. Thin-layer chromatography (solvent A) indicated 12.5% ethanol eluate contained no unreacted amine and 25% ethanol eluted pure monoaldehydocyclohexaamylose. The monoaldehydocyclohexaamylose in the appropriate fractions was dissolved in water and the combined fractions were filtered through a Celite pad. On evaporation to dryness a colorless material was obtained, which weighed 0.24 g after freeze–drying. A portion of this material was crystallized from a concentrated aqueous solution, m.p. 205° (dec.), $[\alpha]_D^{20}$ +123° (*c* 1.00, water).

Anal. Calcd. for $C_{36}H_{58}O_{30}\cdot 3H_2O$: C, 42.19; H,6.30. Found: C, 42.37; H, 6.52.

The product gave a positive test with Fehling's solution. A sample of the monoaldehydocyclohexaamylose (10 mg) was dissolved in water (1 ml) and reduced with sodium borohydride (5 mg) overnight at room temperature. The excess borohydride was destroyed by adding 1 *N* acetic acid to p*H* 4.5. The solution was passed through Dowex 50(H^+) resin and then evaporated five times with methanol (2 ml), with 2 drops of 1 *N* hydrochloric acid added to the first three evaporations. Paper chromatography showed the aldehyde (R_c = 0.7, brown with iodine) had been completely reduced to a substance with the same R_f and iodine reaction (purple) as cyclohexaamylose (**1**).

Photolysis of 6-Azido-6-deoxycyclohexaamylose (4)

Freeze–dried 6-azido-6-deoxycyclohexaamylose (11) (200 mg) was dissolved in water (95 ml) and under nitrogen was irradiated for 6 h. The source of radiation, a medium pressure mercury lamp (unfiltered), was placed in a water-cooled quartz immersion well. Thin-layer chromatography (solvent A) showed the reaction was over in 3 h giving one major product (*ca.* 90%). The major component of the mixture exhibits the same characteristics on t.l.c. and p.c. as the monoaldehydocyclohexaamylose prepared by ninhydrin oxidation (t.l.c.: solvent A, R_c = 0.95; solvent B, R_c = 1.0; brown with iodine, yellow with 2,4-dinitrophenylhydrazine and p.c.: R_c = 0.7, brown with iodine). An attempt to purify the aldehyde by complexing with 1,1,2,2-tetrachloroethane (11) did not effect the purification desired. After reduction of the mixture (10 mg) with sodium borohydride (see above) the major component had the same characteristics on p.c. as cyclohexaamylose (**1**).

Mass Spectrometry

The mass spectra were recorded on a Varian MAT 711 spectrometer. The ionizing potential was 70 eV, the accelerating voltage 4 kV, the ion source temperature 250°, and the sample inlet temperature 190°. Spectra were calibrated with a mixture of perfluorokerosene and 2,4,6-tris(perfluoroheptyl)-1,3,5-triazine and by direct counting. Before preparing derivatives for mass spectrometry, the material was freeze–dried and then dried over phosphorus pentoxide at 50°, 10^{-4} Torr, overnight.

Perdimethylsilyl Cyclohexaamylose

Cyclohexaamylose (1 mg) was dissolved in pyridine (0.5 ml) and tetramethyldisilazane (0.1 ml) and dimethylchlorosilane (0.05 ml) added. The mixture was shaken vigorously and heated at 40° for 1 h. The solution was evaporated to dryness and the solid extracted with

Can. J. Chem. Downloaded from www.nrcresearchpress.com by 210.87.254.5 on 09/05/12
For personal use only.

Can. J. Chem. Downloaded from www.nrcresearchpress.com by 210.87.254.5 on 09/05/12
For personal use only.

n-hexane. The *n*-hexane extract was evaporated in a sample cup.

Perdimethylsilyl 6-Aldehydocyclohexaamylose O-methyl Oxime

6-Aldehydocyclohexaamylose (0.15 mg) was dissolved in pyridine (0.2 ml), methoxylamine hydrochloride (4 mg) was added, and the solution was kept at 80° for 2 h. After cooling to room temperature, tetramethyldisilazane (0.05 ml) and dimethylchlorosilane (0.025 ml) were added and the mixture was heated at 40° for 1 h. The remainder of the procedure is as given for perdimethylsilylcyclohexaamylose.

6-Azido-6-deoxy-1,2:3,4-di-O-isopropylidene-α-D-galactopyranose (7)

1,2:3,4-Di-*O*-isopropylidene-6-*O*-*p*-tolylsulphonyl-α-D-galactopyranose (25) (49 g) was converted to 6-azido-6-deoxy-1,2:3,4-di-*O*-isopropylidene-α-D-galactopyranose by the method of Szarek and Jones (26). The resulting pale yellow oil was further purified by distillation to yield a colorless syrup, b.p. 99° at 0.06 mm, $[\alpha]_D^{22}$ −99° (*c* 1.59, $CHCl_3$) (lit. (26) $[\alpha]_D^{21}$ −92.1° (*c* 1.48 in chloroform containing 0.75% ethanol). The n.m.r. spectrum of the product was consistent with that expected for the title compound (**7**). Thin-layer chromatography (solvent D) indicated the product contained a small amount (*ca.* 5%) of side product.

6-Amino-6-deoxy-1,2:3,4-di-O-isopropylidene-α-D-galactopyranose (5)

6-Azido-6-deoxy-1,2:3,4-di-*O*-isopropylidene-α-D-galactopyranose (**7**) (19.5 g) was dissolved in methanol (200 ml) and hydrogenated for 48 h at 30 p.s.i. with palladium black as a catalyst. The mixture was filtered and evaporated to yield a yellow syrup. After distillation (b.p. 92°, 0.03 Torr) t.l.c. (solvent C) showed a small amount of starting material was present. The syrup was dissolved in diethyl ether – petroleum ether (30–60°) 1:1 (40 ml) and extracted with water (40 ml) eight times. The combined water extracts were evaporated to a syrup which was redissolved in the ether – petroleum ether mixture (40 ml) and the extraction procedure was repeated. The resulting syrup (9.6 g) was pure according to t.l.c. (solvent C). The n.m.r. spectra of the product and of the product which had undergone deuterium exchange were consistent with that expected for the title compound (**5**). The product had $[\alpha]_D^{22}$ −56.4° (*c* 1.00, chloroform) (lit. (26) $[\alpha]_D^{28}$ −44.0° (*c* 1.31, methanol); lit. (27) $[\alpha]_D^{21}$ −40.1° (*c* 2.04, methanol).

Preparation of 1,2:3,4-Di-O-isopropylidene-α-D-galacto-hexodialdo-1,5-pyranose (6) by the Ninhydrin Reaction

6-Amino-6-deoxy-1,2:3,4-di-*O*-isopropylidene-α-D-galactose (**5**) (5.0 g) was dissolved in an aqueous solution (500 ml) containing sodium bicarbonate (5.0 g) and ninhydrin (15.0 g). Thin-layer chromatography (solvent C) showed the reaction was complete in less than 5 min and no side products were detected. The brown precipitate which formed when the reaction mixture was allowed to stand overnight was removed by filtering through Celite. The aqueous filtrate (400 ml) was extracted eight times with ethyl acetate (150 ml). The combined ethyl acetate extracts were dried with magnesium sulfate, filtered, and evaporated to a dark purple syrup. The syrup was distilled twice (b.p. 90–98°, 0.1 Torr (lit. (14) 104–105°, 0.5 Torr; lit. (15) 96–100°, 0.1 Torr)) to yield a pale yellow syrup (1.9 g) which was pure on t.l.c. The n.m.r. spectrum of the product had the same features as those previously found (14) for 1,2:3,4-di-*O*-isopropylidene-α-D-*galacto*-hexodialdo-1,5-pyranose. The aldehyde had $[\alpha]_D^{22}$ −87° (*c* 1.1, chloroform) (lit. (14) $[\alpha]_D^{20}$ −131° (*c* 0.9, chloroform); lit. (15) $[\alpha]_D$ −113° (*c* 3.4).

The procedure of Horton and co-workers (14) was used to prepare 1,2:3,4-di-*O*-isopropylidene-α-D-*galacto*-hexodialdo-1,5-pyranose 6-(*p*-nitrophenyl)hydrazone from the aldehyde (400 mg). Crystallization from benzene gave yellow needles of the hydrazone (110 mg), m.p. 214–215°, $[\alpha]_D^{22}$ −93° (*c* 1.0, chloroform) (lit. (14) m.p. 214–215°, $[\alpha]_D^{22}$ −83.5° (*c* 1.0, chloroform); lit. (3) m.p. 208–209°, $[\alpha]_D^{23}$ −90° (*c* 1.5, chloroform).

Preparation of 1,2:3,4-Di-O-isopropylidene-α-D-galacto-hexodialdo-1,5-pyranose (6) by Photolysis

6-Azido-6-deoxy-1,2:3,4-di-*O*-isopropylidene-α-D-galactopyranose (**7**) (4.4 g) was dissolved in benzene (100 ml) and photolyzed for 13.5 h under the conditions given above for the photolysis of 6-azido-deoxycyclohexaamylose. After evaporation of benzene, the syrup was dissolved in diethyl ether – petroleum ether and purified as described for **5**. Distillation (b.p. 105°, 0.05 Torr) gave a syrup (1.7 g) with $[\alpha]_D^{22}$ −83° (*c* 0.94, chloroform) (for literature values see ninhydrin reaction). Thin-layer chromatography (solvents C and D) showed the aldehyde prepared by photolysis had the same R_f values as the aldehyde prepared by ninhydrin oxidation. The n.m.r. spectra of the aldehydes produced by photolysis and ninhydrin oxidation are identical and in agreement with the reported spectrum (14).

The aldehyde (410 mg) was converted to 1,2:3,4-di-*O*-isopropylidene-α-D-*galacto*-hexodialdo-1,5-pyranose 6-(*p*-nitrophenyl)hydrazone (80 mg) by the method of Horton and co-workers (14). The hydrazone was crystallized from benzene, m.p. 212–214°, $[\alpha]_D^{22}$ −96° (*c* 1.0, chloroform). The mixture melting point of the *p*-nitrophenylhydrazones produced by ninhydrin oxidation and photolysis was 214–215° (see ninhydrin reaction for literature values).

We wish to thank the National Research Council of Canada for financial support in the form of an operating grant and a post-graduate fellowship (LDM). We are indebted to Professor J. Lorberth for running the mass spectra.

1. L. HOUGH and A. C. RICHARDSON. *In* Rodd's chemistry of carbon compounds. Vol. I, Part F, 2nd Ed. *Edited by* S. Coffey. Elsevier, Amsterdam. 1967. p. 294.
2. G. H. JONES and J. G. MOFFATT. Methods Carbohydr. Chem. **6**, 315 (1972).
3. D. J. WARD, W. A. SZAREK, and J. K. N. JONES. Carbohydr. Res. **21**, 305 (1972).
4. D. M. MACKIE and A. S. PERLIN. Carbohydr. Res. **24**, 67 (1972).
5. R. E. ARRICK, D. C. BAKER, and D. HORTON. Carbohydr. Res. **26**, 441 (1973).
6. D. L. MACDONALD and H. O. L. FISCHER. J. Am. Chem. Soc. **78**, 5025 (1956).

7. J. N. BeMiller, V. G. Kumari, and S. D. Darling. Tetrahedron Lett. 4143 (1972).
8. D. Horton, A. E. Luetzow, and O. Theander. Carbohydr. Res. **26**, 1 (1973).
9. D. J. McCaldin. Chem. Rev. **60**, 39 (1960).
10. R. Moubasher and A. M. Othman. J. Am. Chem. Soc. **72**, 2666 (1950).
11. L. D. Melton and K. N. Slessor. Carbohydr. Res. **18**, 29 (1971).
12. E. F. L. J. Anet. Carbohydr. Res. **7**, 453 (1968).
13. D. Horton, A. E. Luetzow, and O. Theander. Carbohydr. Res. **27**, 268 (1973).
14. D. Horton, M. Nakadate, and J. M. J. Tronchet. Carbohydr. Res. **7**, 56 (1968).
15. G. B. Howarth, D. G. Lance, W. A. Szarek, and J. K. N. Jones. Can. J. Chem. **47**, 75 (1969).
16. B. Weissman and K. Meyer. J. Am. Chem. Soc. **76**, 1753 (1954).
17. E. A. Davidson and K. Meyer. J. Am. Chem. Soc. **77**, 4796 (1955).
18. A. Veyrières and R. W. Jeanloz. Biochemistry, **9**, 4153, (1970).
19. E. C. Horning and M. G. Horning. Methods Med. Res. **12**, 396 (1970).
20. T. Aczel. Anal. Chem. **40**, 1917 (1968).
21. J. B. Beadle. J. Chromatogr. **42**, 201 (1969).
22. B. J. Millard. Tetrahedron Lett. 3041 (1965).
23. J. P. Kamerling, J. F. G. Vliegenthart, J. Vink, and J. J. de Ridder. Tetrahedron, **27**, 4275 (1971).
24. D. C. DeJongh, T. Radford, J. D. Hribar, S. Hanessian, M. Bieber, G. Dawson, and C. C. Sweeley. J. Am. Chem. Soc. **91**, 1728 (1969).
25. R. S. Tipson. Methods Carbohydr. Chem. **2**, 246 (1963).
26. W. A. Szarek and J. K. N. Jones. Can. J. Chem. **43**, 2345 (1965).
27. V. I. Veksler, L. N. Kovalenko, and A. V. Markovich. J. Gen. Chem. U.S.S.R. **34**, 708 (1964).

Can. J. Chem. Downloaded from www.nrcresearchpress.com by 210.87.254.5 on 09/05/12
For personal use only.

Synthesis of 2-*O*-, 3-*O*-, and 4-*O*-β-D-Glucopyranosyl-L-rhamnose, and of 2-*O*-β-D-Galactopyranosyl-L-rhamnose[1]

RUSSELL R. KING[2] AND CLAUDE T. BISHOP

Division of Biological Sciences, National Research Council of Canada, Ottawa, Canada K1A 0R6

Received August 16, 1974

RUSSELL R. KING and CLAUDE T. BISHOP. Can. J. Chem. **52**, 3913 (1974).

Reaction of 2,3,4,6-tetra-*O*-acetyl-α-D-glucopyranosyl bromide with benzyl-α-L-rhamnopyranoside in the presence of silver carbonate yielded benzyl 2-*O*-, 3-*O*-, and 4-*O*-(2,3,4,6-tetra-*O*-acetyl-β-D-glucopyranosyl)-α-L-rhamnopyranosides in a molar ratio of 1.0:3.6:1.6. The products were separated by preparative t.l.c. Deacetylation followed by hydrogenolysis afforded the unsubstituted disaccharides. Proton magnetic resonance spectra of each derivative and methylation analysis of the disaccharide benzyl glycosides provided confirmation of the structures. The preparation, by a similar method, of benzyl 2-*O*-β-D-galactopyranosyl-α-L-rhamnopyranoside, characterized as its crystalline acetate, is also described.

RUSSELL R. KING et CLAUDE T. BISHOP. Can. J. Chem. **52**, 3913 (1974).

La réaction du bromure de 2,3,4,6-tetra-*O*-acetyl-α-D-glucopyranosyle avec benzyl-α-L-rhamnopyranoside, en présence du carbonate d'argent, conduit aux benzyl 2-*O*-, 3-*O*-, et 4-*O*-(2,3,4,6-tetra-*O*-acetyl-β-D-glucopyranosyl)-α-L-rhamnopyranosides dans la proportion molaire de 1.0:3.6:1.6. On a separé les trois produits par la chromatographie sur couche mince. La déacétylation suivit par l'hydrogenolyse conduit aux disaccharides non substitués. La spectroscopie r.m.n. de chaque dérivatif et l'analyse par méthylation des glycosides benzyliques des disaccharides ont confirmé les structurs. On décrit aussi la synthèse, par un procédé semblable, de benzyl 2-*O*-β-D-galactopyranosyl-α-L-rhamnopyranoside, caracterisé comme son cristallin dérivatif acetylé.

The successful syntheses of 3-*O*- and 4-*O*-β-D-galactopyranosyl-L-rhamnose and of 3-*O*-(2-acetamido-2-deoxy-β-D-glucopyranosyl)-L-rhamnose (1) indicated a potential route to a number of other useful rhamnose-containing disaccharides. That work showed that the variation in reactivity of hydroxyl groups in benzyl-α-L-rhamnopyranoside resulted in preferential formation of the 3-*O*-linked disaccharide and that secondary products could be recovered by chromatography.

The present paper reports an extension of those studies to clarify the generality of the method and to provide β-D-glucopyranosyl-rhamnoses for structural and serological studies on a number of bacterial polysaccharides that are reported (2) to contain these two sugars.

Reaction of 2,3,4,6-tetra-*O*-acetyl-α-D-glucopyranosyl bromide (**1**) with benzyl-α-L-rhamnopyranoside (**2**) in the presence of silver carbonate furnished, by t.l.c., two seemingly homogeneous disaccharide fractions. One of these was oxidizable by periodate indicating a 1 → 2 or 1 → 4 linkage. The periodate resistant fraction crystallized readily and t.l.c. of a fully acetylated sample confirmed that the compound was homogeneous. It was tentatively assigned the structure, benzyl 3-*O*-(2,3,4,6-tetra-*O*-acetyl-β-D-glucopyranosyl)-α-L-rhamnopyranoside (**3**).

The fraction that was oxidizable by periodate also gave an isopropylidene derivative when reacted with acetone and concentrated sulfuric acid. This result suggested that the material was predominantly the 1 → 4 linked derivative (**4**). However, because the compound could not be crystallized its homogeneity was checked by t.l.c. of a fully acetylated sample. Another minor component was thereby revealed and the mixture was separated to yield two crystalline hexaacetates tentatively identified as benzyl 2,3-di-*O*-acetyl-4-*O*-(2,3,4,6-tetra-*O*-acetyl-β-D-glucopyranosyl)-α-L-rhamnopyranoside (**6**, major component) and benzyl 3,4-di-*O*-acetyl-2-*O*-(2,3,4,6-tetra-*O*-acetyl-β-D-glucopyranosyl)-α-L-rhamnopyranoside (**7**, minor component).

Deacetylation of the tetraacetate **3** and the hexaacetates **6** and **7** yielded benzyl 3-*O*-β-D-glucopyranosyl-α-L-rhamnopyranoside (**8**), benzyl 4-*O*-β-D-glucopyranosyl-α-L-rhamnopyranoside (**9**), and benzyl 2-*O*-β-D-glucopyranosyl-α-L-rhamnopyranoside (**10**). Hydro-

[1]Issued as NRCC No. 14271.

[2]NRCC Postdoctorate Fellow, 1972–1974.

Can. J. Chem. Downloaded from www.nrcresearchpress.com by 210.87.254.6 on 09/05/12
For personal use only.

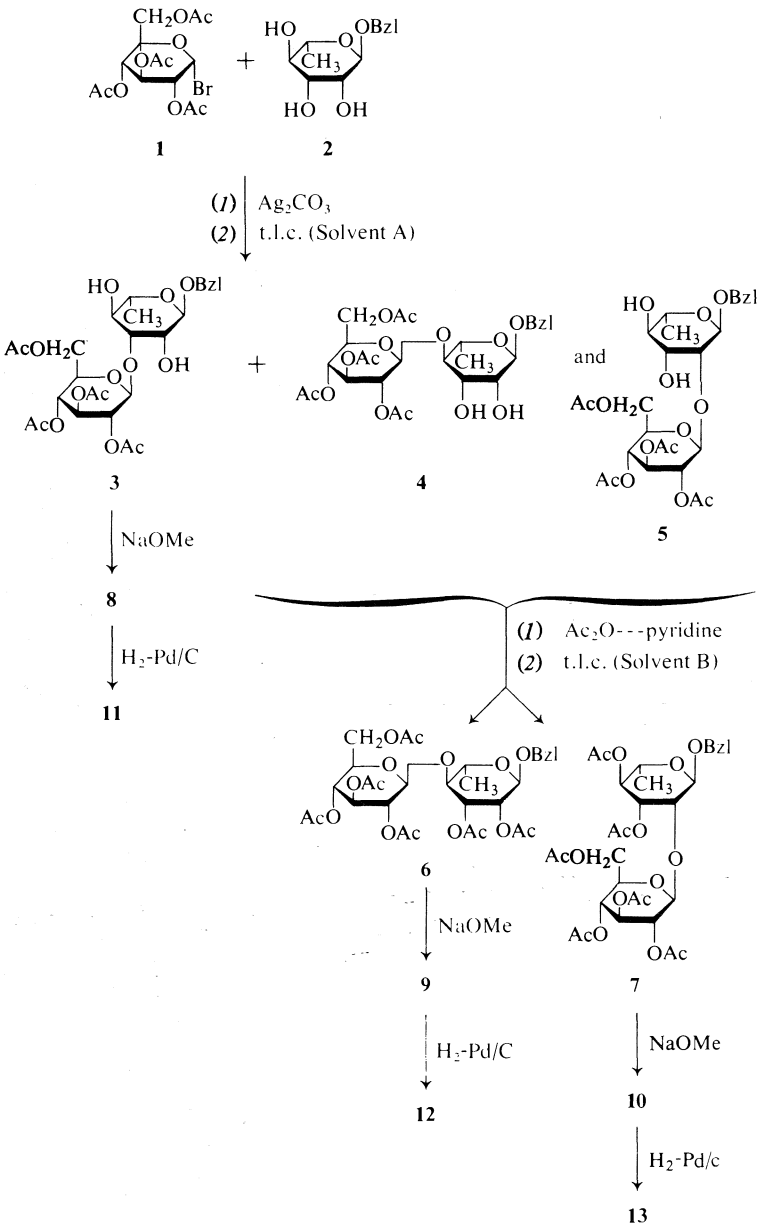

genolysis of these benzyl glycosides furnished the disaccharides 3-*O*-β-D-glucopyranosyl-L-rhamnose (**11**), 4-*O*-β-D-glucopyranosyl-L-rhamnose (**12**), and 2-*O*-β-D-glucopyranosyl-L-rhamnose (**13**). The p.m.r. spectra of the disaccharides **11**, **12**, and **13** indicated $J_{1',2'} =$ 7.5, 8.5, and 7.5 Hz, respectively, consistent with a β-D-glucopyranosyl linkage (3). The structures were confirmed by methylation analysis of the benzyl glycosides **8**, **9**, and **10**, the hydrolysis products after methylation being characterized by mass spectrometry of their alditol acetates (4).

Both the optical rotation and the p.m.r. spectrum of compound **12** were similar to those given by the disaccharide derived from condensation of 2,3,4,6-tetra-*O*-acetyl-α-D-glucopyranosyl bromide with methyl 2,3-*O*-isopropylidene-α-L-rhamnopyranoside in the presence of mercuric cyanide in acetonitrile (5). A disaccharide identified as 3-*O*-β-D-glucopyranosyl-L-rhamnose by methylation analysis and

Can. J. Chem. Downloaded from www.nrcresearchpress.com by 210.87.254.6 on 09/05/12
For personal use only.

Can. J. Chem. Downloaded from www.nrcresearchpress.com by 210.87.254.6 on 09/05/12
For personal use only.

p.m.r. spectroscopy has been isolated recently by partial hydrolysis of *Klebsiella* K72 capsular polysaccharide (6). The p.m.r. spectrum reported for that compound is in agreement with that found for the synthetic product, **11**.

Discovery of the $1 \rightarrow 2$ linked disaccharide in the glucosyl-L-rhamnose series prompted a reexamination of the products from reaction of 2,3,4,6-tetra-*O*-acetyl-α-D-galactopyranosyl bromide with benzyl α-L-rhamnopyranoside (1). Following the same separation scheme, t.l.c. of the acetylated, periodate-sensitive fraction from this latter condensation led to isolation of benzyl 3,4-di-*O*-acetyl-2-*O*-(2,3,4,6-tetra-*O*-acetyl-β-D-galactopyranosyl)-α-L-rhamnopyranoside (**14**). The structure was confirmed by methylation analysis of the benzyl glycoside and p.m.r. spectroscopy of the free disaccharide as outlined above.

It may be noted that yields of disaccharides from benzyl α-L-rhamnopyranoside were in the same order, *i.e.* $1 \rightarrow 3 > 1 \rightarrow 4 > 1 \rightarrow 2$, with either the D-glucosyl or D-galactosyl halide tetraacetate. There is little doubt that this order of reactivity is determined almost exclusively by the relative reactivities of the free hydroxyls in the aglycone and that similar results would be obtained with other glycosyl halide tetraacetates. The method therefore provides a facile route to other disaccharides in which L-rhamnose is the aglycone. Furthermore, this condensation of unprotected glycosides with glycosyl halides and subsequent separation of products offers an attractive route to disaccharides where a specifically blocked aglycone is either inaccessible or difficult to prepare. Clearly, the greater reactivity of primary hydroxyl groups would lead to a predominance of $1 \rightarrow 6$ linked disaccharides from hexopyranosides. However, specific blocking at that position is easily achieved, *e.g.* *O*-trityl group, thus opening the route for reaction at the other hydroxyls.

Experimental

Melting points are uncorrected and were determined on a Kofler hot stage microscope. Optical rotations were measured with a Perkin-Elmer 141 polarimeter and are equilibrium values unless stated otherwise. Proton magnetic resonance spectra were recorded on a Varian Anaspect EM360 NMR spectrometer with tetramethylsilane as an internal standard except as noted. A Hewlett-Packard Model 402 gas chromatograph with a flame ionization detector was used for g.l.c.; the column was a glass U-tube (150 × 0.3 cm) filled with 3% SE30 on Chromosorb W. Thin-layer chromatograms were run on glass plates coated with Silica Gel F-254 unless noted otherwise. Solvent mixtures used were (v/v): (A) ethyl acetate – petroleum ether (40–60), 3:2, (B) ethyl acetate – petroleum ether 4:5, (C) ethyl acetate – petroleum ether, 3:7, (D) *n*-butanol–pyridine–water, 6:4:3. Separated components were detected by u.v. irradiation (for all benzyl glycosides) or by charring after a spray of 5% sulfuric acid in ethanol. Reducing sugars were detected by *p*-anisidine. Mass spectra were recorded on a Hitachi RMU-6D mass spectrometer.

Reaction of 2,3,4,6-Tetra-O-acetyl-α-D-glucopyranosyl Bromide with Benzyl α-L-Rhamnopyranoside

Benzyl α-L-rhamnopyranoside, **2** (1) (2.8 g) was dissolved in chloroform (70 ml) and the solution was stirred with silver carbonate (6 g) and Drierite (10 g) for 18 h. 2,3,4,6-Tetra-*O*-acetyl-α-D-glucopyranosyl bromide, **1** (7) (6.5 g) was added to the stirred mixture over a period of 1 h and stirring was continued for 18 h. The inorganic salts were removed by filtration, washed with chloroform (2 × 50 ml), and the combined filtrate and washings were evaporated to dryness under diminished pressure. The sirupy residue was fractionated by t.l.c. (solvent A) to yield two fractions.

The fraction (734 mg) of higher mobility crystallized from ether. The compound did not react with an excess of aqueous sodium metaperiodate at 24° and it was therefore designated as benzyl 3-*O*-(2,3,4,6-tetra-*O*-acetyl-β-D-glucopyranosyl)-α-L-rhamnopyranoside, **3**; m.p. 138–139°; $[\alpha]_D^{24}$ −37.5° (*c*, 1.0 in chloroform); p.m.r. ($CDCl_3$) τ 2.62 (5H singlet, aromatic protons), 7.96 (12H singlet, 4 × 0Ac), 8.65 (3H doublet, $J = 6.0$ Hz, CH_3).

Anal. Calcd. for $C_{27}H_{36}O_{14}$: C, 55.47; H, 6.17. Found: C, 55.41; H, 5.91.

As a further test of homogeneity this fraction was fully acetylated (acetic anhydride and pyridine) and the hexaacetate was examined by t.l.c. (solvent B); only a single component was found.

The fraction (520 mg) of lower mobility was sensitive to oxidation by aqueous sodium metaperiodate (reaction monitored t.l.c.). Reaction of a small sample of this fraction with acetone containing a trace of concentrated sulfuric acid gave rise to a new, faster running compound on thin-layer chromatograms (solvent B) indicating that an *O*-isopropylidene derivative had been formed. Acetylation of this fraction (500 mg) with acetic anhydride (10 ml) and pyridine (15 ml) yielded a mixture of hexaacetates that was separable into two compounds by t.l.c. in solvent B.

The hexaacetate of higher mobility in solvent B crystallized from ether and was shown subsequently to be benzyl 3,4-di-*O*-acetyl-2-*O*-(2,3,4,6-tetra-*O*-acetyl-β-D-glucopyranosyl)-α-L-rhamnopyranoside, **7** (149 mg): m.p. 147–148°; $[\alpha]_D^{24}$ −46.6° (*c*, 1.0 in chloroform).

Anal. Calcd. for $C_{31}H_{40}O_{16}$: C, 55.69; H, 5.99. Found: C, 55.83; H, 6.02.

The hexaacetate of lower mobility in solvent B crystallized from absolute ethanol and was shown subsequently to be benzyl 2,3-di-*O*-acetyl-4-*O*-(2,3,4,6-tetra-*O*-acetyl-β-D-glucopyranosyl)-α-L-rhamnopyranoside, **6** (232 mg): m.p. 104–105°; $[\alpha]_D^{24}$ −76.8° (*c*, 1.0 in chloroform).

Can. J. Chem. Downloaded from www.nrcresearchpress.com by 210.87.254.6 on 09/05/12
For personal use only.

Anal. Calcd. for $C_{31}H_{40}O_{16}$: C, 55.69; H, 5.99. Found: C, 55.75; H, 6.08.

*Benzyl 2-O-, 3-O-, and 4-O-β-D-Glucopyranosyl-α-L-rhamnopyranoside (**10**, **8**, and **9**)*

The tetraacetate **3** and the hexaacetates **6** and **7** (690, 210, and 140 mg, respectively) were each deacetylated in methanol (10 ml) by sodium methoxide (0.1 *N*, 25, 10, and 10 ml, respectively). The solutions were deionized with Amberlite IR-120 and evaporated to dryness to yield the following benzyl glycosides.

(*a*) Benzyl 3-*O*-β-D-glucopyranosyl-α-L-rhamnopyranoside, **8** (506 mg) was obtained as a sirup; $[\alpha]_D^{24}$ −68.4° (*c*, 1.0 in ethanol); p.m.r. (D_2O, external TMS) τ, 2.67 (5H singlet, aromatic protons), 5.15 (1H doublet, $J_{1,2}$ = 1.6 Hz, H-1), 5.41 (1H doublet, $J_{1',2'}$ = 7.4 Hz, H′-1), 5.44 (2H doublet, J = 3.0 Hz, benzylic protons), 8.70 (3H doublet, J = 6.0 Hz, CH_3).

Anal. Calcd. for $C_{19}H_{28}O_{10}$: C, 54.80; H, 6.78. Found: C, 54.58; H, 6.54.

(*b*) Benzyl 4-*O*-β-D-glucopyranosyl-α-L-rhamnopyranoside, **9** (129 mg) crystallized from acetone, m.p. 96–98°; $[\alpha]_D^{24}$ −75.6° (*c*, 1.0 in ethanol); p.m.r. (D_2O, external TMS) τ, 2.68 (5H singlet, aromatic protons), 5.25 (1H doublet, $J_{1,2}$ = 1.5 Hz, H-1), 5.30 (1H doublet, $J_{1',2'}$ = 7.5 Hz, H′-1), 5.51 (2H doublet, J = 2.5 Hz, benzylic protons), 8.70 (3H doublet, J = 6.0 Hz, CH_3).

Anal. Calcd. for $C_{19}H_{28}O_{10}$: C, 54.80; H, 6.78. Found: C, 54.68; H, 6.62.

(*c*) Benzyl 2-*O*-β-D-glucopyranosyl-α-L-rhamnopyranoside, **10** (81 mg) was obtained as a sirup; $[\alpha]_D^{24}$ −48.8° (*c*, 1.0 in ethanol); p.m.r. (D_2O, external TMS) τ, 2.64 (5H singlet, aromatic protons), 4.88 (1H doublet, $J_{1,2}$ = 0.8 Hz, H-1), 5.41 (2H doublet, J = 2.5 Hz, benzylic protons), 5.57 (1H doublet, $J_{1',2'}$ = 7.2 Hz, H′-1), 8.74 (3H doublet, J = 6.0 Hz, CH_3).

Anal. Calcd. for $C_{19}H_{28}O_{10}$: C, 54.80; H, 6.78. Found: C, 54.52; H, 6.55.

Methylation Analysis

A portion (10 mg) of each benzyl glycoside (**8**, **9**, and **10**) was methylated (8) with methyl iodide (0.1 ml) and sodium hydride (20 mg) in *N*,*N*-dimethylformamide (5 ml). Each product was purified by t.l.c. (solvent A), hydrolyzed (0.54 *M* sulfuric acid, 1.0 ml, 100°, 6 h), reduced by sodium borohydride, and acetylated (acetic anhydride – pyridine) to furnish a 1:1 mixture (determined by g.l.c.) of two partially methylated alditol acetates. Each mixture was separated by t.l.c. (solvent C) and the products were identified by mass spectrometry (4) as follows: 1,5-di-*O*-acetyl-2,3,4,6-tetra-*O*-methyl-D-glucitol (*m/e* 117, 161, 205) from each benzyl glycoside **8**, **9**, and **10**; 1,3,5-tri-*O*-acetyl-2,4-di-*O*-methyl-L-rhamnitol (*m/e* 117, 131, 233) from compound **8**; 1,4,5-tri-*O*-acetyl-2,3-di-*O*-methyl-L-rhamnitol (*m/e* 117, 203) from compound **9**; 1,2,5-tri-*O*-acetyl-3,4-di-*O*-methyl-L-rhamnitol (*m/e* 131, 189) from compound **10**. The identification of these partially methylated L-rhamnitol acetates proved that the benzyl glycosides **8**, **9**, and **10** were respectively the 1 → 3, 1 → 4, and 1 → 2 linked disaccharide derivatives.

*2-O-, 3-O-, and 4-O-β-D-Glucopyranosyl-L-rhamnose (**13**, **11**, and **12**)*

Each benzyl glycoside **8**, **9**, and **10** (400, 112, and 70 mg, respectively) in 95% ethanol (25 ml) was shaken overnight with palladium black (50 mg) under hydrogen at atmospheric pressure. The catalyst was removed by filtration and evaporation of the filtrates yielded the following disaccharides as sirups.

(*a*) 2-*O*-β-D-Glucopyranosyl-L-rhamnose (**13**, 44 mg) showed only one spot on t.l.c. (cellulose, solvent D) with $R_{glucose}$ = 1.38; its trimethylsilyl derivative gave a single peak on g.l.c. with $T_{sucrose}$ = 0.87; $[\alpha]_D^{24}$ +9.5° (*c*, 2.0 in water); p.m.r. (D_2O, external TMS) τ, 4.64 (⅔H doublet, $J_{1,2}$ = 1.5 Hz, H-1 of α-L-form), 5.19 (⅓H doublet, $J_{1,2}$ = 1.0 Hz, H-1 of β-L-form), 5.43 (1H doublet, $J_{1',2'}$ = 8.5 Hz, H′-1), 8.75 (3H doublet, J = 6.0 Hz, CH_3).

(*b*) 3-*O*-β-D-Glucopyranosyl-L-rhamnose (**11**, 272 mg) also showed one spot on t.l.c. (cellulose, solvent D), $R_{glucose}$ = 1.42 and one peak on g.l.c. of its trimethylsilyl derivative, $T_{sucrose}$ = 0.94; $[\alpha]_D^{24}$ −11.4° (*c*, 2.0 in water); p.m.r. (D_2O, external TMS) τ, 4.96 (⅔H doublet, $J_{1,2}$ = 1.8 Hz, H-1 of α-L-form), 5.19 (⅓H doublet, $J_{1,2}$ = 1.0 Hz, H-1 of β-L-form), 5.40 (1H doublet, $J_{1',2'}$ = 7.5 Hz, H′-1), 8.77 (3H doublet, J = 6.0 Hz, CH_3).

(*c*) 4-*O*-β-D-Glucopyranosyl-L-rhamnose (**12**, 68 mg) showed one spot on t.l.c. (cellulose, solvent D), $R_{glucose}$ = 1.24, and one peak on g.l.c. of its trimethylsilyl derivative, $T_{sucrose}$ = 0.92; $[\alpha]_D^{24}$ −24.5° (*c*, 1.0 in H_2O) (lit. (5) $[\alpha]_D$ −24.2° (in water)); p.m.r. (D_2O, external TMS) τ, 4.87 (⅔H doublet, $J_{1,2}$ = 1.5 Hz, H-1 of α-L-form), 5.12 (⅓H doublet, $J_{1,2}$ = 1.0 Hz, H-1 of β-L-form), 5.27 (1H doublet, $J_{1',2'}$ = 7.5 Hz, H′-1), 8.77 (3H doublet, J = 6.0 Hz, CH_3).

Isolation of 2-O-β-D-Galactopyranosyl-L-rhamnose

The mixture obtained from reaction of benzyl α-L-rhamnopyranoside with 2,3,4,6-tetra-*O*-acetyl-α-D-galactopyranosyl bromide (1) was separated into periodate-resistant and periodate-sensitive fractions by t.l.c. in solvent A. The periodate-sensitive fraction (490 mg) was acetylated with acetic anhydride (14 ml) and pyridine (16 ml). The mixture of hexaacetates was then resolved by t.l.c. in solvent B and the faster running component proved to be benzyl 3,4-di-*O*-acetyl-2-*O*-(2,3,4,6-tetra-*O*-acetyl-β-D-galactopyranosyl)-α-L-rhamnopyranoside (**14**, 149 mg). The compound crystallized from ether and had m.p. 154–155°; $[\alpha]_D^{24}$ −54.2° (*c*, 1.0 in chloroform).

Anal. Calcd. for $C_{31}H_{40}O_{16}$: C, 55.69; H, 5.99. Found: C, 55.66; H, 5.81.

The compound was deacetylated, methylated, hydrolyzed, reduced, and acetylated as described above to yield 1,5-di-*O*-acetyl-2,3,4,6-tetra-*O*-methyl-D-galactitol (*m/e* 45, 117, 161, 205) and 1,2,5-tri-*O*-acetyl-3,4-di-*O*-methyl-L-rhamnitol (*m/e* 131, 189) analyzed by t.l.c. and mass spectrometry as before. These results prove the 1 → 2 disaccharide linkage.

Deacetylation and hydrogenolysis of compound **14** (135 mg) as described above yielded 2-*O*-β-D-galactopyranosyl-L-rhamnose (**15**, 58 mg) as a sirup. It showed only one spot on t.l.c. (cellulose, solvent D); $[\alpha]_D^{24}$ −7.5° (*c*, 2.0 in water); p.m.r. (D_2O, external TMS) τ, 4.91 (⅔H doublet, $J_{1,2}$ = 1.5 Hz, H-1 of α-L-form), 5.16 (⅓H doublet, $J_{1,2}$ = 1.0 Hz, H-1 of β-L-form), 5.34 (1H doublet, $J_{1',2'}$ = 8.0 Hz, H′-1), 8.70 (3H doublet, J = 6.0 Hz, CH_3).

We thank F. P. Cooper for the p.m.r. spectra and H. Seguin for the microanalyses and mass spectra.

1. R. R. KING and C. T. BISHOP. Carbohydr. Res. **32**, 239 (1974).
2. M. HEIDELBERGER. *In* Research in immunochemistry and immunobiology. Vol. 3. *Edited by* J. B. G. Kwapinski and E. D. Day. University Park Press, Baltimore. 1973. pp. 1–40.
3. J. N. C. WHYTE. Anal. Biochem. **42**, 476 (1971).
4. H. BJÖRNDAL, C. G. HELLERQVIST, B. LINDBERG, and S. SVENSSON. Angew. Chem. Int. Ed. Engl. **9**, 610 (1970).
5. G. M. BEBAULT and G. G. S. DUTTON. Can. J. Chem. **50**, 3373 (1972).
6. Y-M. CHOY and G. G. S. DUTTON. Can. J. Chem. **52**, 684 (1974).
7. J. K. DALE. J. Am. Chem. Soc. **38**, 2187 (1916).
8. J. S. BRIMACOMBE, B. D. JONES, M. STACEY, and J. J. WILLARD. Carbohydr. Res. **2**, 167 (1966).

Can. J. Chem. Downloaded from www.nrcresearchpress.com by 210.87.254.6 on 09/05/12
For personal use only.

The Dimerization Constant of Nitrobenzene in Benzene: A Critique of Partition as a Thermodynamic Method

SAUL GOLDMAN AND WAYNE C. DUER

Department of Chemistry, University of Guelph, Guelph, Ontario

Received June 10, 1974

SAUL GOLDMAN and WAYNE C. DUER. Can. J. Chem. **52**, 3918 (1974).

The dimerization constant (K) of nitrobenzene in benzene was determined at 5.5 and 25 °C by means of partition (solvent extraction). A hydration study was performed at these temperatures to determine the extent of hydration of nitrobenzene in the benzene phase. Published freezing point depression data for the anhydrous benzene–nitrobenzene system were used to obtain a value of K at 5.5 °C. The heats of solution of nitrobenzene in benzene (anhydrous) were determined at 25 °C. The heat of solution and freezing point depression data were combined to obtain a value of K for the anhydrous system at 25 °C. At each of 5.5 and 25 °C the value of K determined by partition was significantly smaller than the corresponding value of K for the anhydrous system, and the discrepancy was larger at 25 than at 5.5 °C. It was found that by fitting a simple electrostatic model to the difference in the values of K found at 5.5 °C, the difference at 25 °C could be predicted.

SAUL GOLDMAN et WAYNE C. DUER. Can. J. Chem. **52**, 3918 (1974).

On détermine par partage (extraction par solvant) la constante de dimérisation (K) du nitrobenzène dans le benzène à 5.5 et à 25 °C. On effectue une étude de l'hydratation à ces températures pour déterminer le degré d'hydratation du nitrobenzène dans la phase benzénique. On utilise les données publiées sur l'abaissement du point de congélation du système benzène–nitrobenzène anhydre pour obtenir une valeur de K à 5.5 °C. On détermine les chaleurs de dissolution du nitrobenzène dans le benzène (anhydre) à 25 °C. On obtient une valeur de K à 25 °C pour le système anhydre par combinaison des données sur les chaleurs de dissolution et l'abaissement du point de congélation. Les valeurs de K déterminées par partage à 5.5 et 25 °C sont significativement plus petites que les valeurs correspondantes de K pour le système anhydre, et la différence est plus grande à 25 °C qu'à 5.5 °C. On peut prédire la différence à 25 °C en ajustant un simple modèle électrostatique à la différence observée pour les valeurs de K à 5.5 °C. [Traduit par le journal]

Introduction

Partition, at first sight, is an attractive technique for the determination of the stoichiometric activity coefficient (or the degree of aggregation) of a solute in an organic solvent. The method consists of determining the equilibrium distribution ratio of a solute between water and a second immiscible solvent. If the stoichiometric activity coefficient of the solute in water is known, or if the solute in the aqueous phase is sufficiently dilute to be considered ideal, then the stoichiometric activity coefficient in the organic phase can be deduced. By repeating the experiment at different total solute concentrations, the concentration-dependence of the stoichiometric activity coefficient in the organic phase can be obtained. The method is attractive because it is potentially applicable to a wide variety of systems. The solute can be either an electrolyte (1, 2) or a nonelectrolyte (3). The experimental temperature can readily be varied (2, 4) and the choice of nonaqueous solvents is limited only in that the solvent must be immiscible with water.

There is, unfortunately, a problem inherent in the use of partition, and this problem derives from the fact that all solvents have some mutual solubility. Thus the solvent in the aqueous phase is not pure water, but water saturated with the organic solvent, and similarly the solvent in the organic phase is the water-saturated organic solvent. Therefore in principle at least, thermodynamic data obtained by partition may differ from data obtained by other methods.

It is generally assumed that the effect of the dissolved organic solvent on the extent of solute–solute interaction in the aqueous phase is negligible. This is because the systems chosen for study are generally such that the extent of solute–solute interaction in the aqueous phase is small, so that the effect of a perturbation on this interaction will also be small.

In several previous studies (5–7), this same view was taken of the role of dissolved water in

Can. J. Chem. Downloaded from www.nrcresearchpress.com by 210.87.254.42 on 09/05/12
For personal use only.

Can. J. Chem. Downloaded from www.nrcresearchpress.com by 210.87.254.42 on 09/05/12
For personal use only.

the organic phase. Specifically, Davies and Griffiths (5, 6) and Huq and Lodhi (7) assumed that the presence of dissolved water in the organic phase had no effect on the dimerization equilibria of carboxylic acids in that phase. However the extent of solute–solute interaction is generally much greater in the organic phase than in the aqueous phase, so that the magnitude of a perturbation due to dissolved foreign solvent is likely to be much greater in the organic phase. Thus Christian *et al.* found that the values of the dimerization constants of carboxylic acids obtained by partition are consistently lower than the values obtained by other methods wherein the system is studied under anhydrous conditions (4). These authors attributed the lower values obtained by partition to specific preferential hydration of the monomer relative to the dimer in the organic phase. The extent of hydration of the solute in the organic phase was determined, and therefrom a method of correcting the partition results to the anhydrous state was derived (4, 8). However, when the extent of hydration of the solute is fairly large, as it is with carboxylic acids in the benzene phase, the accuracy with which this hydration correction can be made is not very good. Furthermore it is implicitly assumed in this method of correction that the dissolved water in the organic phase that is not directly bound to the solute has no effect on the stoichiometric activity coefficient of the solute. However the mere existence of unbound water in the organic phase means that we are dealing with a mixed (rather than pure) solvent in that phase. Therefore corrections to the partition results based on bound water alone cannot, at least in principle, be complete.

Thus the extent to which partition results can be corrected to give thermodynamic data relevant to anhydrous systems remains unresolved. However the resolution of this question is of considerable importance, because if partition results can be corrected reliably to the anhydrous state, then the results of partition could be used interchangeably with those of other more conventional thermodynamic or spectroscopic methods. It is thus the object of the present work to test partition against other thermodynamic methods and in the process, to inquire further into the factors that affect partition results.

Our approach is to select a system wherein the known complicating factors of the partition method are minimal. Subsequently, the partition results for this system will be compared with those for the corresponding anhydrous system. These latter results will be obtained by other thermodynamic methods. We therefore seek a system with the following properties: (*1*) the aqueous phase concentration of the solute in the partition experiments should be low. This is to ensure that complications due to possible nonideality of the solute in the aqueous phase are minimal; (*2*) the extent of hydration of the solute in the organic phase should be very small, so that the above mentioned uncertainties in the correction for hydration are small; (*3*) the binary system consisting of the solute in the anhydrous organic solvent should be amenable to study by classical thermodynamic methods, so that thermodynamic data are available for comparison with the data obtained by partition.

After a preliminary search, it was decided that the system nitrobenzene in benzene most nearly met the above conditions. In this work, the aqueous phase nitrobenzene concentration never exceeded 2.5×10^{-3} *m*; the extent of hydration of nitrobenzene in the benzene phase was found to be very small; for the anhydrous system accurate freezing point depression data were available and it was also possible, with the anhydrous system, to carry out accurate heat of solution measurements. Vapor pressure data for the anhydrous system at high temperatures (50–70 °C) are also available (9), but we found in preliminary calculations, that these data lacked the accuracy required for the present purpose.

Experimental

Materials

The benzene used was taken from laboratory stock. This was reagent grade benzene, further purified as described previously (10). The benzene used in the calorimetric experiments was dried by allowing it to be in contact with drierite for several weeks. The water content of the dried benzene was found to be of the order of 1 part in 10^5.

Certified grade nitrobenzene was further purified as described below. The reagent was first dried over calcium chloride. The dried product was fractionally crystallized four successive times; about $\frac{1}{3}$ of the material was discarded on each crystallization. This was followed by two successive vacuum distillations from P_2O_5 wherein the central $\frac{2}{3}$ fraction was retained each time. Chromatographic analysis on the final product revealed no significant impurities; the water content was of the order of

Can. J. Chem. Downloaded from www.nrcresearchpress.com by 210.87.254.42 on 09/05/12
For personal use only.

4 parts in 10^5; the freezing point was 5.75 ± 0.01 °C (lit. (11) 5.76 ± 0.01 °C); the density at 25 °C was 1.19834 ± 0.00001 (lit. (12) 1.1983 ± 0.0002). The final product was stored in the dark.

Distilled water was used for all the equilibrations.

Apparatus and Procedures

Partition

Stock solutions of nitrobenzene, both in water and in benzene, were prepared by weighing the nitrobenzene followed by accurate dilution with the appropriate solvent.

The two phases of the partition system were equilibrated in 175 ml milk-dilution bottles fitted with bakelite screw caps having Teflon inserts. The bottles were clamped lengthwise on a Plexiglass rotor immersed in a water thermostat the temperature of which was maintained to within 0.02 °C of the required value. The bottles were given end-over-end rotation at 20 r.p.m.

In all the partition experiments the initial volumes of the benzene and aqueous phases were 25 and 125 ml respectively. After equilibration the bottle was removed from the rotor, and was suspended vertically in the water bath with only the cap and neck of the bottle above the water surface; the upper level of the lighter benzene phase was well under the surface of the bath water. In sampling the aqueous phase both pipets and syringes were used. A positive air pressure was maintained in the sampling device during its descent through the upper benzene phase. The results were unaffected by the choice of the sampling device; *i.e.* pipets and syringes gave indistinguishable results.

Equilibrium was established both by using different equilibration times and by approaching equilibrium from both under-saturation and super-saturation with respect to the aqueous phase (achieved by having all the nitrobenzene initially in the organic phase, and all the nitrobenzene initially in the aqueous phase, respectively). In general 2 h were allowed for equilibration.

The equilibrium nitrobenzene concentrations in the aqueous phases were determined spectrophotometrically with a Pye Unicam SP500 Series 2 spectrophotometer. Matched pairs of Spectrosil cells having path lengths of 0.1, 1, and 10 cm were used. The measurements were made at a wavelength of 284 nm. At this wavelength the extinction coefficient of nitrobenzene was large, while that of benzene was very small. Nevertheless a small blank correction for the benzene dissolved in the aqueous phase was required and was made. For purposes of calibration, standard solutions of nitrobenzene were made up in water that had been presaturated with benzene. Thus, nitrobenzene was found to obey Beer's law over the concentration range 2×10^{-6} to 2×10^{-3} M; its extinction coefficient in this solvent at 22.5 ± 0.5 °C and 284 nm was $(5.58 \pm 0.05) \times 10^3$ cm^{-1} mol^{-1} l. This value of the extinction coefficient was used to calculate the equilibrium aqueous phase nitrobenzene concentrations. From these concentrations, and from the known initial amounts of benzene, nitrobenzene, and water, it was possible to calculate the corresponding equilibrium nitrobenzene concentrations in the benzene phase (see below). It was also found that nitrobenzene obeyed Beer's law in pure water (over the range 2×10^{-6} to 2×10^{-3} M) and that its extinction coefficient in pure water was experimentally indistinguishable from the above value. This supports the view that the extent of interaction between nitrobenzene and benzene in the aqueous phase is small.

In order to calculate the equilibrium nitrobenzene concentration in each phase, it was necessary to take several factors into account. First, a small correction was made at each temperature for the loss of benzene (due to solubility) to the aqueous phase. It was of the order of 1%. Second, the effect of temperature on the volume of each phase was taken into account in calculating the equilibrium phase volumes. Corrections both for loss of water to the benzene phase (due to solubility), and for loss of material (benzene, nitrobenzene, or water) to the vapor space were found under the present conditions to be negligible, and were omitted.

Hydration

Stock solutions of nitrobenzene in benzene were prepared by weighing the nitrobenzene, followed by accurate dilution with benzene. In these experiments 10 ml of water were equilibrated with 150 ml of the benzene phase. Under these conditions the equilibrium nitrobenzene concentration in the benzene phase is not significantly different (within 0.1%) from its initial concentration in that phase. The temperature was maintained to within 0.02 °C of the desired value.

It was found in preliminary work that dried nitrobenzene had no effect on the Karl Fischer end point. All the analyses were for the total water concentration in the benzene phase. These analyses were performed with an Aquatest II automatic Karl Fischer Titrator (model 702, Photovolt). The techniques used for equilibration, sampling, and analysis of the benzene phase for water, have all been previously described (10).

Calorimetry

The heats of solution of nitrobenzene in benzene over the concentration range 0.04–1 m nitrobenzene were determined with an LKB 8700 Precision Calorimetry System. Sample introduction was accomplished both by means of ampoules and by an automatic dosimeter (Metrohm Herisau Dosimat). A 100 ml capacity vessel was used in each case. The calorimeter vessel and the relevant glassware were dried prior to use. The solution compositions were computed from the weights of benzene and nitrobenzene.

Results

The results of the partition experiments are given in Table 1. The average sample standard deviation for the measured aqueous phase nitrobenzene concentration was about 0.5%. The number of replicates (given in Table 1) represents the number of separate equilibrations and analyses that were performed.

The hydration results are given in Table 2. The equilibrium nitrobenzene concentration in the benzene phase was taken to be equal to its initial concentration in that phase (see previous section). In practice the total water concentrations were obtained in units of molarity. The results were converted to molalities using the solution density at each composition. Each

TABLE 1. Partition data for nitrobenzene between water and benzene. Equilibrium stoichiometric molality of nitrobenzene ($\times 10^6$)

5.5 °C			25 °C		
Aqueous phase	Benzene phase	Number of replicates	Aqueous phase	Benzene phase	Number of replicates
2.88	1 180	2	2.86	1 137	3
5.64	2 362	3	5.77	2 275	3
11.21	4 725	2	11.53	4 550	3
16.88	7 088	3	17.17	6 828	3
22.43	9 453	3	22.81	9 107	3
26.69	11 010	6	28.38	11 390	3
27.05	11 320	3	28.85	11 620	2
28.08	11 820	1	29.07	11 520	3
53.70	22 670	3	57.93	23 070	3
128.2	55 030	3	115.0	46 250	3
206.1	90 540	3	171.0	69 530	2
251.0	112 200	3	227.2	92 900	3
251.5	111 500	3	271.7	112 400	3
251.9	111 200	3	272.1	112 600	3
260.5	114 300	1	274.8	115 000	2
267.3	119 400	2	524.5	227 100	3
484.1	225 400	3	1004	464 100	3
912.5	460 500	3	1460	711 500	2
1 308	706 000	3	1845	970 200	3
1 660	962 300	3	2263	1 232 000	3
2 005	1 226 000	3			

TABLE 2. Equilibrium hydration data for nitrobenzene in benzene. Equilibrium stoichiometric concentrations in benzene

5.5 °C		25 °C	
Nitrobenzene (molal)	Water* (molal $\times 10^2$)	Nitrobenzene (molal)	Water* (molal $\times 10^2$)
Nil	2.00	Nil	4.03
0.05745	2.05	0.05745	4.10
0.1155	2.14	0.1155	4.17
0.2932	2.19	0.2932	4.31
0.6020	2.32	0.6020	4.52
1.271	2.65	1.271	5.06

*Mean of duplicate determination.

entry in columns 2 and 4 of Table 2 represents the mean of a duplicate determination. The average sample standard deviation for the water analyses was about 1%. The solubility of water in pure benzene was in accord with previously determined values (10, 13).

The results of the calorimetric experiments are given in Table 3. The estimated uncertainty in each heat of solution (each value of q) is about 1%.

The freezing point depression data were taken from published values. The freezing point depression of benzene by nitrobenzene has been studied by a number of workers (14–18). However Bury and Jenkins (17) point out that all of the studies prior to their own were based on Beckmann's supercooling method which, Bury and Jenkins argue, is subject to a number of errors. Consequently Bury and Jenkins used an equilibrium method in their work. They studied the benzene–nitrobenzene system over the concentration range 0.1–1.3 m nitrobenzene. Subsequently Davison (18), in a very careful investigation, used a Kraus-type twin cell in conjunction with the equilibrium method to extend the concentration range for this system down to 0.0055 m nitrobenzene. Davison also proved that the benzene–nitrobenzene system

Can. J. Chem. Downloaded from www.nrcresearchpress.com by 210.87.254.42 on 09/05/12
For personal use only.

TABLE 3. The heat of solution of nitrobenzene in benzene at 25.0±0.2 °C

n* (mol × 10^3)	m_i† (molal)	m_f† (molal)	q‡ (cal)
3.877	0.0	0.04471	1.675
3.930	0.0	0.04499	1.732
7.658	0.08876	0.1764	3.018
7.788	0.2659	0.3550	2.787
7.790	0.0	0.08906	3.295
7.800	0.4573	0.5594	2.463
7.818	0.3550	0.4573	2.597
7.825	0.1764	0.2659	2.921
7.827	0.5594	0.6618	2.349
8.033	0.0	0.09211	3.370
9.152	0.0	0.1046	3.882
24.33§	0.1114	0.4211	8.711
48.67§	0.4211	1.0402	14.251

*n = number of moles of nitrobenzene added to the calorimeter.
†m_i, m_f = initial and final stoichiometric nitrobenzene molality respectively.
‡q = heat that accompanies each nitrobenzene addition.
§These two additions were made with an automatic dosimeter; the other additions were made by means of ampoules.

TABLE 4. Freezing point depression of benzene by nitrobenzene

[Nitrobenzene] (molal)	θ* (°C)
Reference 18	
0.00550	0.02763
0.01371	0.07126
0.01908	0.09859
0.02618	0.1312
0.02950	0.1508
0.03608	0.1874
0.04355	0.2158
0.04888	0.2446
0.05111	0.2572
0.07063	0.3511
Reference 17	
0.1016	0.4900
0.1045	0.5070
0.1652	0.7960
0.2027	0.9600
0.2602	1.226
0.3725	1.722
0.4157	1.921
0.4854	2.220
0.5960	2.675
0.7142	3.178
0.7342	3.265
0.8684	3.806
0.9008	3.940
1.089	4.653
1.174	4.980
1.271	5.313
1.293	5.387

*θ = freezing point depression of solution relative to pure benzene.

did not form solid solutions. Both Davison and Bury and Jenkins made a deliberate effort to exclude moisture from their experimental systems.

It is here considered that of the available freezing point depression data, those due to Davison, and Bury and Jenkins, are the most reliable. We found that these authors' data were consistent with each other, but were not consistent with much of the earlier data obtained by the supercooling method. We have therefore combined Davison's and Bury and Jenkins' data into one set, and these data are given in Table 4.

Treatment of the Data

Partition

The nitrobenzene in the aqueous phase is assumed to be ideal (the stoichiometric molal activity coefficient is taken as unity) for all the experimental concentrations ($\sim 3 \times 10^{-6}$ to 2×10^{-3} m). This assumption is considered reasonable in view of the very low concentrations of nitrobenzene in the aqueous phase. Furthermore, it is consistent with the observed constancy of the extinction coefficient of nitrobenzene in the aqueous phase.

The nitrobenzene in the benzene phase is assumed to exist in the form of monomers and dimers, and these species are themselves taken to be ideal. This formulation attributes all the nonideality of the nitrobenzene in the benzene phase to the existence of dimers in that phase. We will later derive an exact thermodynamic relationship between the dimerization constant, thus defined, and the stoichiometric activity coefficient of the nitrobenzene.

The dimerization constant K, and the partition coefficient P, refer to the equilibria

$$2M_b \overset{K}{\rightleftarrows} D_b$$

$$M_{aq} \overset{P}{\rightleftarrows} M_b$$

where the subscripts b and aq denote the benzene and aqueous phases respectively, and M and D mean monomers and dimer, respectively. From their definitions, and the foregoing considerations

$$[1] \qquad K \equiv \frac{{}^{D}a_b}{{}^{M}a_b{}^2} = \frac{[{}^{D}m_b]}{[{}^{M}m_b]^2}$$

Can. J. Chem. Downloaded from www.nrcresearchpress.com by 210.87.254.42 on 09/05/12
For personal use only.

Can. J. Chem. Downloaded from www.nrcresearchpress.com by 210.87.254.42 on 09/05/12
For personal use only.

[2] $$P \equiv \frac{{}^{M}a_b}{{}^{M}a_{aq}} = \frac{[{}^{M}m_b]}{[m_{aq}]}$$

where a and $[m]$ denote activity and molality, respectively. From the condition of mass balance in the benzene phase

[3] $$[{}^{s}m_b] = [{}^{M}m_b] + 2[{}^{D}m_b]$$

where ${}^{s}m_b$ is the stoichiometric molality of nitrobenzene in the benzene phase. On combining eqs. 1 to 3:

[4] $$\frac{[{}^{s}m_b]}{[m_{aq}]} = P + 2KP^2[m_{aq}]$$

In order to obtain the values of P and K, eq. 4 was fitted by weighted least-squares to the partition data in Table 1. Each point was weighted in proportion to the number of replecate determinations corresponding to the point. From the least-squares estimates of the slope and intercept of eq. 4, the quantities $2KP^2$ and P were respectively obtained, and subsequently K was calculated from

[5] $$K = \tfrac{1}{2}(\text{slope}/\text{intercept}^2)$$

The values of P and K thus obtained, are given in Table 5 together with the estimated values of the standard deviations of these quantities. These latter estimates were obtained by the application of simple methods of error analysis (19) to eq. 4.

It was found that eq. 4 adequately represented the partition data over our entire experimental concentration range, and this is demonstrated in Fig. 1. Thus the postulated monomer–dimer equilibrium in the benzene phase adequately accounts for the partition data.

Hydration

The increase in the total (stoichiometric) water concentration in the benzene phase, as a function of the stoichiometric nitrobenzene concentration in that phase, is illustrated in Fig. 2. It is seen that, at each temperature, the data can be represented by an equation of the form

[6] $$[{}^{s}m_w]_b = [{}^{0}m_w]_b + \bar{n}[{}^{s}m_b]$$

where $[{}^{s}m_w]_b$ is the stoichiometric molality of water in the benzene phase, and $[{}^{0}m_w]_b$ and $\bar{n}$ are constants. The intercept of eq. 6, $[{}^{0}m_w]_b$, represents the free or unbound water concentration in the benzene phase, which is identified with the solubility of water in pure benzene. Thus even at finite nitrobenzene concentrations the free water concentration in the benzene phase is assumed constant. The slope of eq. 6, $\bar{n}$, is taken to be the average number of bound moles of water per mole of nitrobenzene. Therefore we interpret the increase in the water content of the benzene phase as being due to water bonding to (sticking to) the nitrobenzene. The justification for this view is that different solutes (*e.g.* benzoic acid *vs.* nitrobenzene, see Fig. 2) "salt in" water to very different degrees, so that it seems likely that this is due to water specifically bonding to the polar functional groups in the molecule.

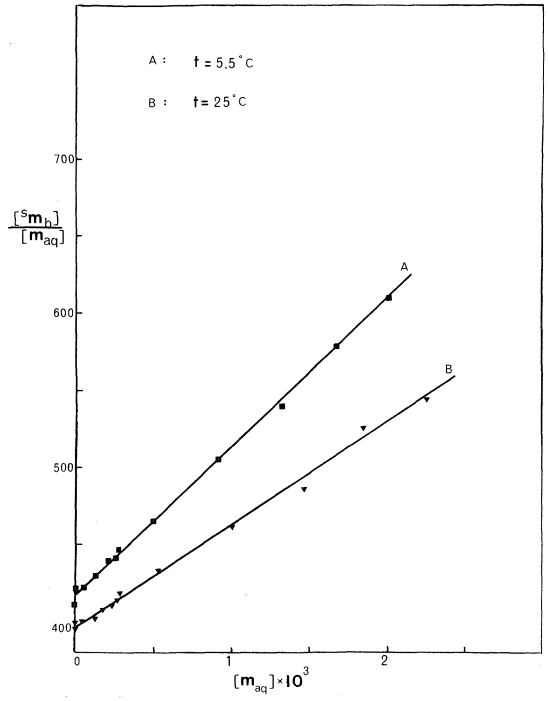

FIG. 1. The partition of nitrobenzene between water and benzene. The lines are the least-squares fits of eq. 4 to the data in Table 1. The points are from the data in Table 1.

TABLE 5. Values of the partition coefficient and dimerization constant of nitrobenzene obtained by partition

Temperature (°C)	P*	K† (molal^{-1})
5.5	416.8±0.5	0.280±0.007
25.0	396.2±0.5	0.212±0.011

*P ≡ partition coefficient of nitrobenzene (see eq. 2).
†K ≡ dimerization constant of nitrobenzene in benzene (see eq. 1).

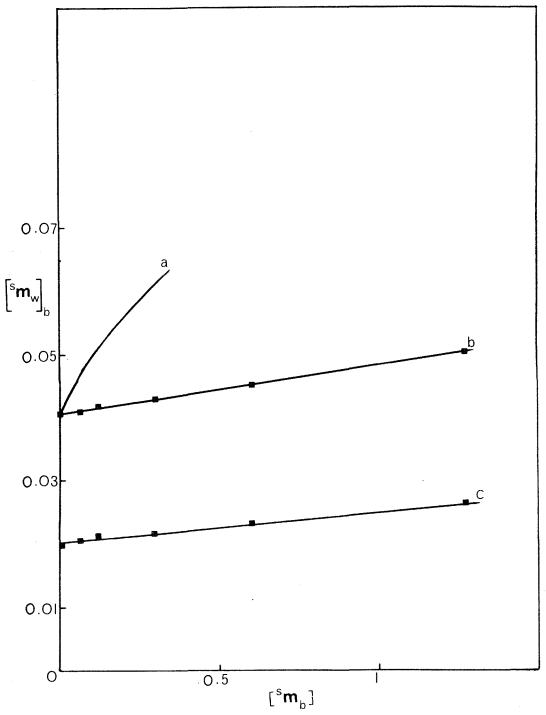

FIG. 2. The dependence of the total water concentration in the benzene phase on the total solute concentration in the benzene phase. (*a*) Solute is benzoic acid, $t = 25\,^\circ C$, curve obtained from ref. 8. (*b*) Solute is nitrobenzene, $t = 25\,^\circ C$, this work. (*c*) Solute is nitrobenzene, $t = 5.5\,^\circ C$, this work.

Equation 6 was fitted to the hydration data by least-squares, and the least-squares estimates of $[^0m_w]_b$ and $\bar{n}$ are given in Table 6 together with the estimated standard deviations of these quantities. These latter estimates were obtained by an application of the law of accumulation of errors (19) to eq. 6.

For comparison, we include in Fig. 2 a plot of the corresponding functions for benzoic acid in wet benzene at 25 °C. These data were taken from published values (8). There are two noteworthy differences between the hydration data for the two systems. First it is clear that nitrobenzene is much less extensively hydrated (per mole of solute) than is benzoic acid. Second, whereas $\bar{n}$ (the slope) is not concentration-dependent in the nitrobenzene system, in the benzoic acid system it decreases with benzoic acid concentration.

TABLE 6. Least-squares parameters for hydration of nitrobenzene in benzene

Temperature (°C)	$[^0m_w]_b$* (molal)	$\bar{n}$†
5.5	0.0204±0.0002	0.0048±0.0003
25.0	0.0405±0.0001	0.0079±0.0002

*$[^0m_w]_b$ = solubility of water in benzene (intercept of eq. 6).
†$\bar{n}$ = hydration number of nitrobenzene in wet benzene (slope of eq. 6).

By extending previously published work (20), it may be shown that the constancy of $\bar{n}$ demonstrated in Fig. 2 leads to the result that hydration of the nitrobenzene in the benzene phase is such that the monomers and the dimers are equally stabilized. That is, because of the constancy of $\bar{n}$, the inclusion of hydrates of nitrobenzene in the treatment of the partition data would lead to no change whatever in the calculated value of the dimerization constant.

Freezing Point Depression

Our approach is to first treat the freezing point depression data so as to obtain the stoichiometric activity coefficients of nitrobenzene in benzene. A thermodynamic relationship between the stoichiometric activity coefficient and the dimerization constant is derived, and therefrom a value for the dimerization constant of nitrobenzene in benzene is obtained.

The freezing point data are treated in the conventional way (21). It was found that the data in Table 4 could be represented by a Lewis and Randall *j*-function of the form

$$[7] \qquad j = a[m] + b[m]^2 + c[m]^3$$

where a, b, and c are constants

$$j \equiv 1 - \frac{\theta}{[m]\lambda}$$

where $[m] \equiv$ the stoichiometric molality of the solution (the notation $[^s m_b]$ for this quantity is used only with the two-phase system), $\theta \equiv$ the freezing point depression corresponding to molality $[m]$.

$$\lambda \equiv \frac{RT_0^2}{\bar{L}_0} \cdot \frac{W}{1000}$$

where $T_0 \equiv$ the freezing point of pure benzene, $\bar{L}_0 \equiv$ the latent molal heat of fusion of benzene at T_0, $W \equiv$ the molecular weight of benzene, and $R \equiv 1.9872$ cal/mol deg. From a published study on the properties of benzene (22) we obtain the values: $T_0 = 278.69\,^\circ C$; $\bar{L}_0 = 2358$ cal/mol, and hence $\lambda = 5.113$ deg/molal. It is also possible to estimate λ directly from the

Can. J. Chem. Downloaded from www.nrcresearchpress.com by 210.87.254.42 on 09/05/12
For personal use only.

Can. J. Chem. Downloaded from www.nrcresearchpress.com by 210.87.254.42 on 09/05/12
For personal use only.

freezing point depression data. Thus Bury and Jenkins (17) found the value 5.122 deg/molal, and Davison (18) found λ to be 5.088 deg/molal. It is seen that the calculated value 5.113, selected for use here, lies between these two estimates.

The values of a, b, and c were found by fitting eq. 7 to the data in Table 4 by least-squares. Thus the values of a, b, and c were found to be: 0.40205, −0.43900, and 0.18635 respectively.

The connection between the j-function and the stoichiometric molal activity coefficient of nitrobenzene is

$$[8] \quad -\ln \gamma = j + \int_0^{[m]} j\,\mathrm{d} \ln [m] - \xi_1 \lambda I_1 - \xi_2 \lambda I_2$$

where $\gamma \equiv$ stoichiometric molal activity coefficient of nitrobenzene in benzene

$$I_1 \equiv \int_0^{\theta} (1 - j)\mathrm{d}\theta$$

$$I_2 \equiv \int_0^{\theta} \theta(1 - j)\mathrm{d}\theta$$

$$\xi_1 \equiv \left(\frac{2000}{WRT_0^2}\right)\left(\frac{\bar{L}_0}{T_0} - \frac{\bar{J}}{2}\right)$$

$$\xi_2 \equiv \left(\frac{3000}{WRT_0^3}\right)\left(\frac{\bar{L}_0}{T_0} - \frac{2\bar{J}}{3}\right)$$

$\bar{J} \equiv$ The difference between the molal heat capacities of liquid and solid benzene. It will be assumed to be invariant with temperature.

Equation 8 is obtained by expanding the logarithm of the solvent activity in terms of the freezing point depression of the solution, and this is followed by a Gibbs–Duhem integration. This equation (except for the fourth term on the right-hand side) is derived in a standard reference book (21). The fourth term on the right-hand side of eq. 8 results from retaining a cubic term in the expansion of the logarithm of the solvent activity. This term was retained as a precaution; in practice we found that its contribution to $\ln \gamma$ was completely negligible. The contribution of the third term to $\ln \gamma$ was small, but not quite negligible ($\sim$5%). The values of ξ_1 and ξ_2 required with eq. 8 were obtained from the properties of benzene. From $\bar{J} = 0.76$ cal/mol deg (22), and the previously given values of $\bar{L}_0$ and T_0 we find: $\xi_1 = 13.4 \times 10^{-4}$ molal/°K^2; $\xi_2 = 7.103 \times 10^{-6}$ molal/°K^3.

It was possible to derive analytic expressions for each of the terms on the right-hand side of eq. 8. These expressions are given in Appendix A. Using these expressions, the least-squares values of a, b, and c, and eq. 8 we can calculate (over the range 0–1.3 $[m]$) the value of γ at any $[m]$. However in order to compare the freezing point depression results with those obtained by partition, it was necessary to re-express the freezing point data in terms of a dimerization constant. The thermodynamic relationship between the stoichiometric molal activity coefficient and the dimerization constant (where the dimerization constant is defined so as to include all the nonideality manifested by the solute) is

$$[9] \quad (1 - \gamma)/\gamma^2 = 2[m]K$$

Equation 9 is derived in Appendix B. Thus the value of K from the freezing point data was obtained as the slope of the least-squares fit of $(1 - \gamma)/\gamma^2$ *vs.* $2[m]$. The fit is demonstrated in Fig. 3, wherein the values of γ were calculated as described above. By means of an error analysis, it was possible to estimate the standard deviation of K. This analysis is given in Appendix C. Thus it was found that the value of K obtained from the freezing point depression data

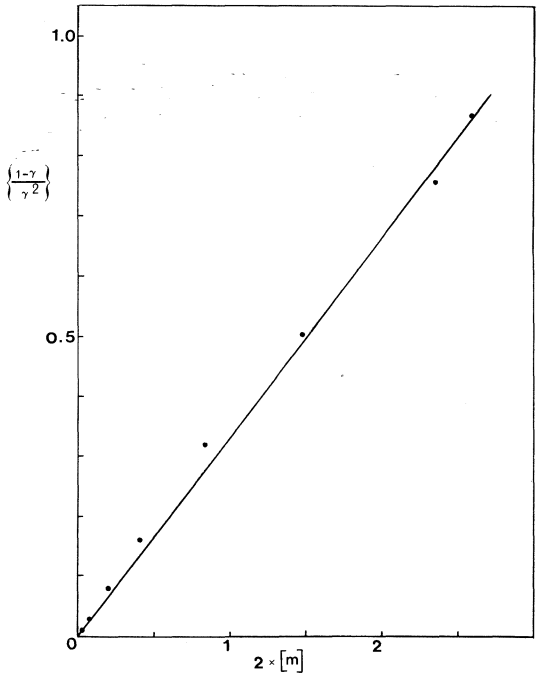

FIG. 3. The determination of K from freezing point depression data by eq. 9.

(written with one standard deviation) was $K = 0.335 \pm 0.011$ molal^{-1}.

Since the temperature of the freezing point experiments is a variable, in principle this value of K represents an average value over the temperature range 5.50–0.13 °C (see values of θ in Table 4). For the anhydrous benzene–nitrobenzene system however, it will be shown in the subsequent calorimetry section that K varies only very slightly with temperature (~0.001 units in K per degree). Therefore we take the above value of K to refer to the temperature 5.5 °C.

Calorimetry

The heat of solution data are treated so as to obtain values for the molal enthalpy of solution of nitrobenzene in benzene at infinite dilution, $\Delta H_\infty{}^0$, and the standard state molal enthalpy of dimerization of nitrobenzene in benzene $\Delta H_D{}^0$. This latter quantity is subsequently used, together with the value of K obtained from the freezing point data, to calculate a value of K for the anhydrous system at 25 °C.

As with our approach taken with the other techniques, we assume that the monomers and dimers of nitrobenzene are themselves ideal at all concentrations, and that the nonideality of the solute results solely from the existence of the monomer–dimer equilibrium. Consequently it may be shown that

$$[10] \qquad \left(\frac{q}{n}\right) = \Delta H_\infty{}^0 + \Delta H_D{}^0\left(\frac{(n_D)_f - (n_D)_i}{n}\right)$$

where $q \equiv$ the measured quantity of heat that accompanies the addition of n moles of nitrobenzene to the calorimeter and $(n_D)_f$, $(n_D)_i \equiv$ the number of moles of nitrobenzene dimer that are respectively present, after and before the addition of the nitrobenzene. The values of n were obtained from the weight of nitrobenzene corresponding to each addition. The quantity $(n_D)_f$ was obtained from

$$[11] \qquad (n_D)_f = [m_D]_f w_f$$

where $w_f \equiv$ weight (in kg) of benzene in the calorimeter vessel and $[m_D]_f \equiv$ molality of nitrobenzene dimers in the calorimeter after addition of a sample. $[m_D]_f$ was calculated by the equation

$$[12] \qquad [m_D]_f = \frac{(-1 + \sqrt{1 + 8K[m]_f})^2}{16K}$$

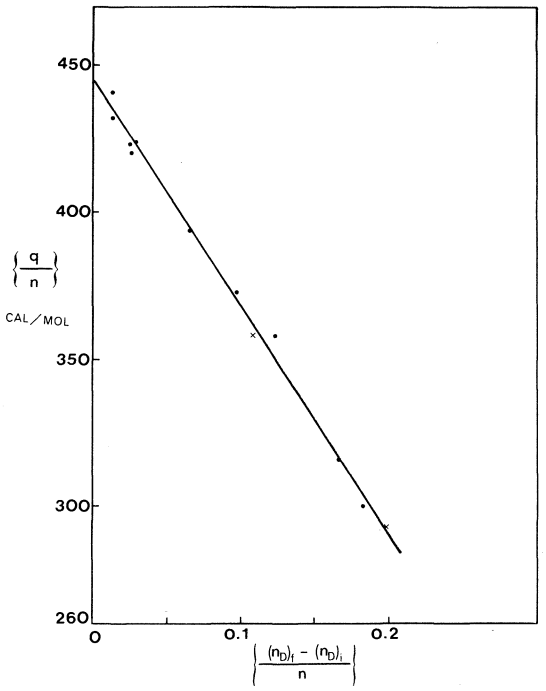

FIG. 4. The fit of eq. 10 to the calorimetric data. ×, obtained by dosimeter; ●, obtained by ampoules.

where $[m]_f \equiv$ stoichiometric molality of nitrobenzene in the calorimeter after sample addition. Equation 12 is obtained by combining the equations

$$K = \frac{[m_D]_f}{[m_M]_f{}^2}$$

and

$$[m]_f = [m_M]_f + 2[m_D]_f$$

The equations used to calculate $(n_D)_i$ are obtained by substituting the subscript i for f in eqs. 11 and 12.

In order to obtain the values of $\Delta H_\infty{}^0$ and $\Delta H_D{}^0$ from eq. 10 we require a value for K at 25 °C for use in eq. 12. This, in turn, could be obtained from the value of K at 5.5 °C if a value of $\Delta H_D{}^0$ were available. The problem was resolved by means of the iterative scheme described below.

The assumption that is used in this scheme is that $\Delta H_D{}^0$ is invariant with temperature over the range 5.5 to 25 °C. An initial value for K at 25 °C was guessed, and this value was used with eqs. 11 and 12 to calculate, at each n, a value of the ratio $((n_D)_f - (n_D)_i)/n$ for use in eq. 10. Equation 10 represents a straight line

Can. J. Chem. Downloaded from www.nrcresearchpress.com by 210.87.254.42 on 09/05/12
For personal use only.

with intercept $\Delta H_\infty{}^0$ and slope $\Delta H_D{}^0$. Therefore eq. 10 was fitted by least-squares to the data in Table 3 to obtain a first estimate for both $\Delta H_\infty{}^0$ and $\Delta H_D{}^0$. This estimate for $\Delta H_D{}^0$ is then used to obtain a second value of K at 25 °C by the equation

$$[13]\quad \ln \frac{K_{25}}{K_{5.5}} = \frac{\Delta H_D{}^0}{R}\left(\frac{1}{278.65} - \frac{1}{298.15}\right)$$

For $K_{5.5}$ in eq. 13 we use the value 0.335, obtained from the freezing point depression data. The second value of K_{25} is then used to obtain a second estimate of both $\Delta H_\infty{}^0$ and $\Delta H_D{}^0$. The entire procedure, which generates new values of K_{25}, $\Delta H_\infty{}^0$, and $\Delta H_D{}^0$ upon each iteration was repeated for a total of 10 times. Convergence was achieved after 5 iterations. The final values of K_{25}, $\Delta H_\infty{}^0$, and $\Delta H_D{}^0$ were independent of the initially chosen value of K_{25}. Thus we obtained the values: $K_{25} = 0.306 \pm 0.011\ m^{-1}$, $\Delta H_\infty{}^0 = 445 \pm 2$ cal/mol, $\Delta H_D{}^0 = -769 \pm 17$ cal/mol. The standard deviations given with $\Delta H_\infty{}^0$ and $\Delta H_D{}^0$ were obtained by application of the law of accumulation of errors to eq. 10 (19). The standard deviation given with K_{25} is simply the value that was obtained for the standard deviation of $K_{5.5}$. The justification for this estimate lies in the fact that by applying eq. C2 to eq. 13, it is found that the additional uncertainty in K_{25} (beyond that in $K_{5.5}$), induced by the uncertainty in $\Delta H_D{}^0$ is essentially negligible.

Discussion

We will not, in this article, attempt a molecular interpretation, of the actual values of K. This interesting but fairly complex question will form the subject of a separate study. Rather, in this discussion we will attempt to account for the differences in the values obtained for K in the wet and dry solvents. Clearly, the factors that cause these differences are germane to an understanding of partition.

The values of the dimerization constant of nitrobenzene in wet and dry benzene are summarized in Table 7. It is clear from Table 7 that, at each temperature, the value of K in wet benzene is significantly smaller than the corresponding value in the anhydrous system. This was confirmed by a t-test at the 1% level of significance. It is also seen from Table 7 that the difference in the values of K (dry *vs.* wet) increases with temperature.

TABLE 7. Dimerization constant of nitrobenzene in water-saturated and anhydrous benzene

Temperature (°C)	K^* (molal^{-1})	
	Water-saturated	Anhydrous
5.5	0.280±0.007	0.335±0.011
25.0	0.212±0.011	0.306±0.011

*The values of K are given with 1 standard deviation.

We have therefore shown, for the present system, that the results of partition are significantly different from those obtained with the corresponding anhydrous system. Indeed, the value of K at 25 °C in dry benzene is almost 50% greater than it is in wet benzene despite the fact that this particular system was chosen so as to minimize the difficulties inherent in the partition method. In view of this it seems unlikely that partition, applied to less propitious systems, would give results that are in accord with those for the corresponding anhydrous state.

It is noteworthy that the values of the dimerization constant of carboxylic acids in wet benzene are also lower than their corresponding values in dry benzene (4). In this respect, our results for nitrobenzene are consistent with those for the carboxylic acids. However, carboxylic acids in wet benzene are much more extensively hydrated than is nitrobenzene in this medium (see Fig. 2), so that it is particularly significant that this phenomenon (getting a lower value of K in the wet solvent) persists with nitrobenzene. A possible explanation for this is put forward below.

It was concluded from the hydration data that the existence of hydrates of nitrobenzene in the benzene phase (inferred from the fact that $\bar{n} > 0$) would not (because of the constancy of $\bar{n}$) lead to a different value of K. However apart from this water of hydration, the benzene phase also contains free (nonbonded) water. We now postulate that this water also interacts with the solute.

Whereas the values of K differ significantly for the wet and dry systems, the difference represents only a very small difference in the standard state Gibbs free energy of dimerization. At 5.5 °C the difference in this quantity (given by $RT \ln (K(\text{dry})/K(\text{wet}))$ is only ~0.1 kcal/mol. Since both nitrobenzene and water are polar

Can. J. Chem. Downloaded from www.nrcresearchpress.com by 210.87.254.42 on 09/05/12
For personal use only.

Can. J. Chem. Downloaded from www.nrcresearchpress.com by 210.87.254.42 on 09/05/12
For personal use only.

molecules, we postulate that this difference is due to a weak, dipole–dipole interaction between the free (nonbonded) water and the nitrobenzene in the benzene phase. Furthermore we postulate that this interaction energy stabilizes the nitrobenzene monomer relative to the dimer, and that this differential effect results in a lower value of K in the wet solvent.

In order to test this idea numerically, we use a simple electrostatic model to represent the monomer–water interaction. The model, which contains one adjustable parameter, is fitted to the difference in the values of K (wet *vs.* dry) at 5.5 °C, and therefrom the value of the adjustable parameter is obtained. This value of the parameter is subsequently used with the model and the experimental value of K(dry) at 25 °C to predict a value for K(wet) at this temperature and this prediction is compared with the corresponding experimental result.

We assume that the free water in the benzene phase stabilizes the nitrobenzene monomer through a weak dipole–dipole interaction, but that it does not interact with the nitrobenzene dimer. The potential energy of interaction between the water and the monomer is assumed to be given by Keesom's equation (23). This equation, for the angle-averaged dipole–dipole interaction energy, modified for the dielectric constant of the medium, is

$$[14] \qquad u_{23}(r) = -\frac{2}{3}\frac{U_2^2 U_3^2}{\varepsilon k T r^6}$$

where $u_{23}(r)$ is the potential energy of interaction between the monomer and the water, ε is the dielectric constant of benzene, and U_2 and U_3 are the dipole moments in benzene of nitrobenzene and water, respectively, and r is the center-to-center distance between the monomer and the water.

Because of the reaction field of the solvent, the dipole moment of a polar solute in solution is greater than what it is in the gas phase. We estimate the dipole moments of water and nitrobenzene in benzene by the equation (24)

$$[15] \qquad U = u_g\left[\frac{2\varepsilon + 1}{2\varepsilon + n_D^2}\cdot\frac{n_D^2 + 2}{3}\right]$$

where U is the dipole moment of the solute in solution, u_g is the gas phase dipole moment of the solute, n_D is the refractive index of the solute for sodium light, and ε (as in eq. 14) is the dielectric constant of benzene.

From the foregoing considerations it may be shown that

$$[16] \qquad \ln\frac{K_d}{K_w} = \frac{16\pi\tilde{N}U_2^2U_3^2[^0m_w]_b d_0}{9000\sigma_{23}^3\varepsilon(kT)^2}$$

where K_d and K_w mean K(dry) and K(wet) respectively. The only unknown in eq. 16 is σ_{23}, the effective hard-sphere diameter between water and the nitrobenzene monomer. Therefore a value of σ_{23} can be obtained by applying eq. 16 to our data at either 5.5 or 25 °C. However, because of the approximations upon which eq. 16 is based, the value of σ_{23} thus obtained is unlikely to be very meaningful. On the other hand, if the model is basically correct, then eq. 16 should be of the correct functional form. Consequently we should be able to predict the value of K_w at one temperature, from the value of K_d at that temperature and the value of σ_{23} obtained by applying eq. 16 to our data at the other temperature. Thus, we apply eq. 16 to our experimental value of $\ln(K_d/K_w)$ at 5.5 °C to obtain a value of σ_{23}. This value is then used with eq. 16 and our experimental value of K_d at 25° to predict a value for K_w at 25°.

At 5.5 °C, by eqs. 15 and 16 and the values: $\ln(K_d/K_w) = 0.179$ (see Table 7); $(n_D)_2 = 1.55$ (ref. 25, p. 836); $(n_D)_3 = 1.33$ (ref. 25, p. 2936); $\varepsilon = 2.313$ (ref. 25, p. 2513); $(u_g)_2 = 1.85$ D (ref. 25, p. 2532); $(u_g)_3 = 4.27$ D (ref. 25, p. 2539); $d_0 = 0.89420$ (12); $T = 278.65$; $[^0m_w]_b = 0.0204\,m$; we find $\sigma_{23} = 2.19 \times 10^{-8}$ cm.

With this value of σ_{23}, eqs. 15 and 16, and the values at 25 °C: $K_d = 0.306$ molal^{-1} (see Table 7); $(n_D)_2$, $(n_D)_3$, $(u_g)_2$, $(u_g)_3$ the same as above; $\varepsilon = 2.274$ (ref. 25, p. 2513); $d_0 = 0.87365$ (10); $[^0m_w]_b = 0.0405$ (see Table 6); we find $(K_w)_{25} = 0.225$ molal^{-1}. The experimental value for this quantity is $(K_w)_{25} = 0.212 \pm 0.011$ molal^{-1}. Thus the proposed model predicts the value of $(K_w)_{25}$ to well within two standard deviations of the experimental value. By means of a t-test applied at the 1% level of significance, it was confirmed that the predicted value of $(K_w)_{25}$ was not significantly different from the experimental value.

The success of this prediction lends support to our explanation for the lower values of K found for nitrobenzene in the wet solvent. Furthermore, since carboxylic acids are polar, it is likely that our postulated effect is at least partly responsible for the lower values of the

dimerization constant obtained when partition is applied to carboxylic acids.

We are grateful to the National Research Council of Canada and the Chemistry Department of the University of Guelph for financial assistance. We also acknowledge the kind cooperation of Professors W. A. E. McBryde and Don Irish in making their calorimeter available to us.

1. S. Goldman and G. C. B. Cave. Can. J. Chem. **49**, 1726 (1971).
2. S. Goldman and G. C. B. Cave. Can. J. Chem. **49**, 4096 (1971).
3. E. M. Woolley, J. G. Travers, B. P. Erno, and L. G. Hepler. J. Phys. Chem. **75**, 3591 (1971).
4. S. D. Christian, H. E. Affsprung, and S. A. Taylor. J. Phys. Chem. **67**, 187 (1963).
5. M. Davies and D. M. L. Griffiths. Z. Phys. Chem. N. F. **2**, 353 (1954).
6. M. Davies and D. M. L. Griffiths. Z. Phys. Chem. N. F. **6**, 143 (1956).
7. A. K. M. Shamsul Huq and S. A. K. Lodhi. J. Phys. Chem. **70**, 1354 (1966).
8. R. Van Duyne, S. A. Taylor, S. D. Christian, and H. E. Affsprung. J. Phys. Chem. **71**, 3427 (1967).
9. J. Hurwic and J. Radzikowski. *In* Nitro compounds. Proc. Int. Symp., Warsaw. 1963. p. 419.
10. S. Goldman. Can. J. Chem. **52**, 1668 (1974).
11. A. Weissburger and E. S. Proskauer. Organic solvents. 2nd ed. Vol. VII. Interscience Publishers, Inc., New York. 1955. p. 223.
12. R. F. Brumel and K. V. Bibber. *In* International critical tables. Vol. III. McGraw–Hill Book Company, Inc., New York. 1929. p. 29.
13. J. R. Johnson, S. D. Christian, and H. E. Affsprung. J. Chem. Soc. A. 77 (1966).
14. E. Beckmann. Z. Phys. Chem. **2**, 729, 734 (1888).
15. Dahms. Ann. Phys. **54**, 496 (1895).
16. L. G. Davy and N. V. Sidgwick. J. Chem. Soc. 281 (1933).
17. C. R. Bury and H. O. Jenkins. J. Chem. Soc. 688 (1934).
18. J. A. Davison. J. Am. Chem. Soc. **67**, 228 (1945).
19. V. V. Nalimov. The application of mathematical statistics to chemical analysis. Pergamon Press, London. 1963. pp. 34, 167.
20. S. Goldman and G. C. B. Cave. Can. J. Chem. **49**, 1716 (1971).
21. R. A. Robinson and R. H. Stokes. Electrolyte solutions. 2nd rev. ed. Butterworths, London. 1959. p. 183.
22. G. D. Oliver, M. Eaton, and H. M. Huffman. J. Am. Chem. Soc. **70**, 1502 (1948).
23. W. H. Keesom. Phys. Z. **22**, 129 (1921).
24. C. J. F. Böttcher. Theory of electric polarisation. Elsevier Publishing Company, Houston, Texas. 1952. p. 70.
25. Handbook of chemistry and physics. 41st ed. The Chemical Rubber Company, Cleveland, Ohio. 1959–1960.
26. J. E. Freund. Mathematical statistics. Prentice–Hall Inc., Englewood Cliffs, N.J. 1962. p. 174.
27. K. A. Brownlee. Statistical theory and methodology in science and engineering. 2nd ed. John Wiley and Sons, Inc., New York. 1965. pp. 431–447.

Can. J. Chem. Downloaded from www.nrcresearchpress.com by 210.87.254.42 on 09/05/12
For personal use only.

Appendix A

Analytic Expressions used in the Calculation of ln γ by Equation 8

There are four terms on the right-hand side of eq. 8; the expressions used for each of these terms are given below.

The first term, j, is obtained directly from eq. 7.

The second term is

$$\int_0^{[m]} j\,\mathrm{d}\ln[m] = \int_0^{[m]} \frac{j\mathrm{d}[m]}{[m]} = a[m] + \tfrac{1}{2}b[m]^2 + \tfrac{1}{3}c[m]^3$$

The third term is $-\xi_1\lambda I_1$ where

$$I_1 \equiv \int_0^{\theta} (1 - j)\mathrm{d}\theta.$$

From the definition of the j-function

$$\theta = [m]\lambda(1 - j) \qquad [A1]$$

Combining eq. 7 with eq. A1

$$\theta = \lambda([m] - a[m]^2 - b[m]^3 - c[m]^4)$$

Hence

$$(1 - j)\mathrm{d}\theta = f_1([m])\mathrm{d}[m]$$

where

$$f_1([m]) = \lambda(1 - 3a[m] + (2a^2 - 4b)[m]^2 + (5ab - 5c)[m]^3 + (6ac + 3b^2)[m]^4 + 7bc[m]^5 + 4c^2[m]^6)$$

$$\therefore \qquad I_1 = \int_0^{\theta} (1 - j)\mathrm{d}\theta = \int_0^{[m]} f_1([m])\mathrm{d}[m]$$

Thus

$$-\xi_1\lambda I_1 = -\xi_1\lambda^2\left\{[m] - \tfrac{3}{2}a[m]^2 + \frac{(2a^2 - 4b)}{3}[m]^3 + \frac{(5ab - 5c)}{4}[m]^4 + \frac{(6ac + 3b^2)}{5}[m]^5 + \frac{7bc}{6}[m]^6 + \frac{4c^2}{7}[m]^7\right\}$$

The fourth term is obtained by the same procedure as that used for the third term. It is

$$-\xi_2\lambda I_2 = -\xi_2\lambda^3\left\{\tfrac{1}{2}[m]^2 - \frac{4a}{3}[m]^3 + \frac{(5a^2 - 5b)}{4}[m]^4 + \frac{(12ab - 6c - 2a^3)}{5}[m]^5 + \frac{(14ac + 7b^2 - 7a^2b)}{6}[m]^6 + \frac{(16bc - 8ab^2 - 8a^2c)}{7}[m]^7 + \frac{(9c^2 - 18abc - 3b^3)}{8}[m]^8 - \frac{(10ac^2 + 10b^2c)}{9}[m]^9 - \frac{11bc^2}{10}[m]^{10} - \frac{4c^3}{11}[m]^{11}\right\}$$

Appendix B

The Relation Between the Stoichiometric Activity Coefficient of a Solute and the Dimerization Constant

For a situation in which a solute is believed to be partially dimerized, we may calculate the total Gibbs free energy of the system by two methods: (*a*) by considering the solute at stoichiometric molality $[m]$ to have a stoichiometric molal activity coefficient γ, (*b*) by considering the solute to be nonideal solely because of the existence of a monomer–dimer equilibrium wherein the monomers and dimers are themselves ideal. We designate method (*b*) by a prime, and consider the solute, in both methods to be dissolved in 1 kg of benzene. We have, according to the two points of view

[B1] $$G = [m]\bar{G}_2 + \frac{1000}{78.11}\bar{G}_1$$

and

[B2] $$G' = [m_M']\bar{G}_M' + [m_D']\bar{G}_D' + \frac{1000}{78.11}\bar{G}_1$$

Since the value of Gibbs free energy of the system is unaffected by the way we choose to express it, *i.e.* since

[B3] $$G = G'$$

Therefore:

[B4] $$[m]\bar{G}_2 = [m_M']\bar{G}_M' + [m_D']\bar{G}_D'$$

But in situation (*b*), the monomers and dimers are in equilibrium, *i.e.*

[B5] $$\bar{G}_D' = 2\bar{G}_M'$$

Therefore from eq. B4

[B6] $$[m]\bar{G}_2 = \bar{G}_M'\{[m_M'] + 2[m_D']\}$$

or

[B7] $$\bar{G}_2 = \bar{G}_M'$$

Therefore

[B8] $$\bar{G}_2^{\,0} + RT\ln\gamma[m] = \bar{G}_M^{\,0\prime} + RT\ln[m_M']$$

Choosing the same standard state with both points of view

[B9] $$\gamma = \frac{[m_M']}{[m]} = \frac{[m_M']}{[m_M'] + 2K[m_M']^2}$$

Hence, from eq. B9

[B10] $$\gamma = \frac{1}{1 + 2K[m_M']} = \frac{1}{1 + 2K\gamma[m]}$$

Rearranging terms

[B11] $$\frac{1 - \gamma}{\gamma^2} = 2[m]K$$

Can. J. Chem. Downloaded from www.nrcresearchpress.com by 210.87.254.42 on 09/05/12
For personal use only.

Can. J. Chem. Downloaded from www.nrcresearchpress.com by 210.87.254.42 on 09/05/12
For personal use only.

Appendix C

Estimation of the Standard Deviation of the Dimerization Constant Obtained from Freezing Point Depression

The values of γ used to obtain K (by eq. 9) were calculated from the complete expression for $\ln\gamma$ *i.e.* by eq. 8. As mentioned in the body of this article (see Treatment of Data, Freezing Point Depression), the third and fourth terms in eq. 8 contribute relatively little to the value of $\ln\gamma$. Moreover the inclusion of these terms in an error analysis would be very cumbersome. Therefore for purposes of this error analysis they are omitted.

Our approach is to first use a truncated form of eq. 8 to obtain an expression for the variance of γ. Subsequently, this expression is used to obtain an estimate of the standard deviation of K.

The truncated form of eq. 8 is

$$[C1] \quad -\ln\gamma = j + \int_0^{[m]} j\,d\ln[m] = 2a[m] + \tfrac{3}{2}b[m]^2 + \tfrac{4}{3}c[m]^3$$

We use the symbols var (x) and cov (x) to represent the variance and covariance of x respectively. Introducing the approximation (valid for $\gamma \sim 1$), $\gamma \simeq 1 + \ln\gamma$, and applying the theorem (26)

$$[C2] \quad \operatorname{var}\left\{\sum_{j=1}^{m} c_j x_j\right\} = \sum_{j=1}^{m} c_j^2 \operatorname{var}(x_j) + 2\sum\sum_{j<l} c_j c_l \operatorname{cov}(x_j, x_l)$$

to eq. C1, we obtain

$$[C3] \quad \operatorname{var}(\gamma_i) \simeq \operatorname{var}(\ln\gamma_i) = 4[m_i]^2 \operatorname{var}(a) + 9/4[m_i]^4 \operatorname{var}(b) + 16/9[m_i]^6 \operatorname{var}(c) + 6[m_i]^3 \operatorname{cov}(a,b) + 16/3[m_i]^4 \operatorname{cov}(a,c) + 4[m_i]^5 \operatorname{cov}(b,c)$$

The variances and covariances required with eq. C3 were obtained by the application of regression theory to eq. 7. Specifically, the variances and covariances were obtained from the diagonal and off-diagonal elements respectively of the c-matrix (27).

The value of K was obtained by the application of least-squares to eq. 9; *i.e.* from

$$[C4] \quad K = \frac{\sum_{i=1}^{n} (2[m_i])\left(\frac{1-\gamma_i}{\gamma_i^2}\right)}{\sum_{i=1}^{n} (2[m_i])^2}$$

From the law accumulation of errors (19):

$$[C5] \quad \text{st. dev. } (K) = \sqrt{\sum_{i=1}^{n} \left(\frac{\partial K}{\partial \gamma_i}\right)^2 \operatorname{var}(\gamma_i)}$$

From eq. C4

$$[C6] \quad \left(\frac{\partial K}{\partial \gamma_i}\right)^2 = \left(\frac{2[m_i]\left(\frac{\gamma_i - 2}{\gamma_i^3}\right)}{\sum_{i=1}^{n} (2[m_i])^2}\right)^2$$

Thus, eq. C5 together with eqs. C6 and C3 were used to calculate the standard deviation of K.

Gas–Solid Exchange Reaction: Zinc Vapor and Polycrystalline Zinc Orthosilicate

ETALO A. SECCO,[1] HARI PADA DHAR, AND CHIEN-HUO SU

Chemistry Department, St. Francis Xavier University, Antigonish, Nova Scotia

Received July 2, 1974

ETALO A. SECCO, HARI PADA DHAR, and CHIEN-HUO SU. Can. J. Chem. **52**, 3932 (1974).

The exchange kinetics of zinc vapor with polycrystalline zinc orthosilicate have been studied in a static system in the temperature range 760–1000 °C.

The kinetic data reveal two rate laws. The initial rate is assigned to a transport step, *i.e.* mobility of zinc with $D = 10^{-8} \exp(-34 \pm 5 \text{ kcal}/RT) \text{ cm}^2 \text{ s}^{-1}$. The rate at high annealing times is a composite of the initial rate and a particle growth process, *e.g.* sintering.

ETALO A. SECCO, HARI PADA DHAR et CHIEN-HUO SU. Can. J. Chem. **52**, 3932 (1974).

On étudie la cinétique de l'échange de vapeur de zinc avec l'orthosilicate de zinc polycristallin dans un système statique entre 760 et 1000 °C.

Les données cinétiques révèlent deux lois de vitesses. On attribue la vitesse initiale à une étape de transport, c.-à-d. mobilité du zinc avec $D = 10^{-8} \exp(-34 \pm 5 \text{ kcal}/RT) \text{ cm}^2 \text{ s}^{-1}$. La vitesse aux temps élevés de recuit est une combinaison de la vitesse initiale et d'un procédé de croissance des grains tel que le frittage. [Traduit par le journal]

Introduction

This study is a continuation of a program of research on heterogeneous isotopic exchange reactions involving a metallic vapor and its metal bearing solid compound. The results of previous studies on binary compounds of the Zn–ZnX type systems, where X = O, S, Se, and Te (1, 2), have shown the exchange rate to be controlled by two processes, an initial first-order rate followed by a diffusion rate. These two rate-determining processes were interpreted in terms of two limiting conditions: (*i*) the first-order rate prevails when the ambient gas has ready access to the solid exchange sites and (*ii*) the diffusion rate predominates when the ambient vapor has access to the solid exchange sites only via a rate-controlling transport step.

To extend our understanding of gas–solid exchange reactions we deemed it desirable to study a solid which incorporated a well-defined structural and compositional variable with respect to one of the binary compounds already investigated. Zn_2SiO_4 appeared to us to fill this requirement since its composition may be expressed as $SiO_2.2ZnO$ and its lattice arrangement shows each oxygen atom to be common to one SiO_4 tetrahedron and two ZnO_4 tetrahedra which contrasts with the wurtzite lattice of ZnO where each oxygen is common to four ZnO_4 tetrahedra. That is, the SiO_4 interlocking unit could be visualized as a defect in the ZnO_4 network. This rupture of ZnO_4 continuity might reveal additional information regarding the energetics and rate-controlling steps in the gas–solid exchange reaction. Furthermore, solid Zn_2SiO_4 fulfills the exchange requisite conditions, *i.e.* nonvolatile, stable, etc.

Experimental

The zinc orthosilicate powder used in this work was from two sources: A. D. MacKay, Inc., New York, chemically pure quality (hereafter referred to as silicate MK) and Semi-Elements Inc., Saxonburg, Pennsylvania with stated impurity $< 0.001\%$ (hereafter referred to as silicate SE). The X-ray diffractograms of the two powders showed only peaks characteristic of Zn_2SiO_4 (3) and thermal analyses, DTA and TG, exhibited no thermal effect on heating the powders to 1000 °C. The surface area of silicate SE was measured to be 0.9 m^2/g from N_2 adsorption measurements, using a AMINCO SorBET instrument, which yields a mean spherical radius of 8.5×10^{-5} cm. The silicate samples were stored in an oven at 140 °C before use.

The exchange runs were carried out in a static system using quartz reaction vessels and the reaction fraction α was determined by the uptake of radioactive zinc in the solid, as previously described (1).

Results and Discussion

The semi-log plots of $(1 - \alpha)$ *vs.* time for Zn exchange in silicate MK, untreated and preannealed in zinc vapor for 10 h at 900 °C are presented in Figs. 1*a* and 1*b*, respectively; the exchange reaction was carried out at constant

[1]To whom correspondence should be addressed.

Can. J. Chem. Downloaded from www.nrcresearchpress.com by 210.87.254.6 on 09/05/12
For personal use only.

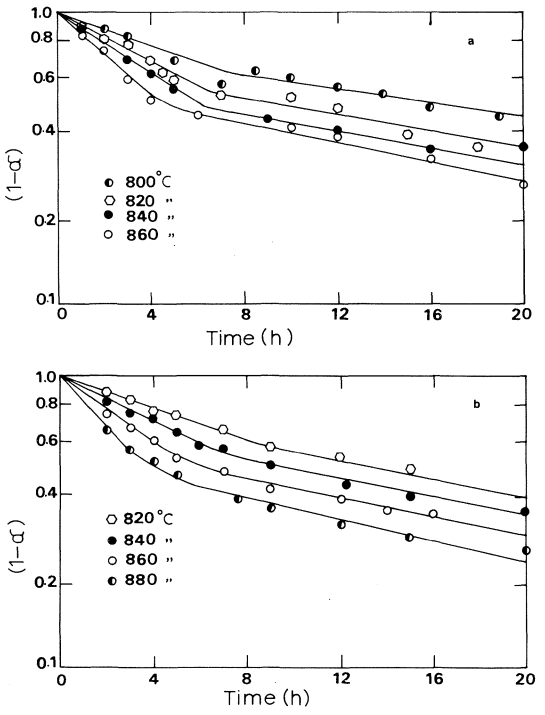

FIG. 1. (*a*) Plot of log $(1 - \alpha)$ *vs.* time for untreated silicate MK. (*b*) Plot of log $(1 - \alpha)$ *vs.* time for preannealed silicate MK.

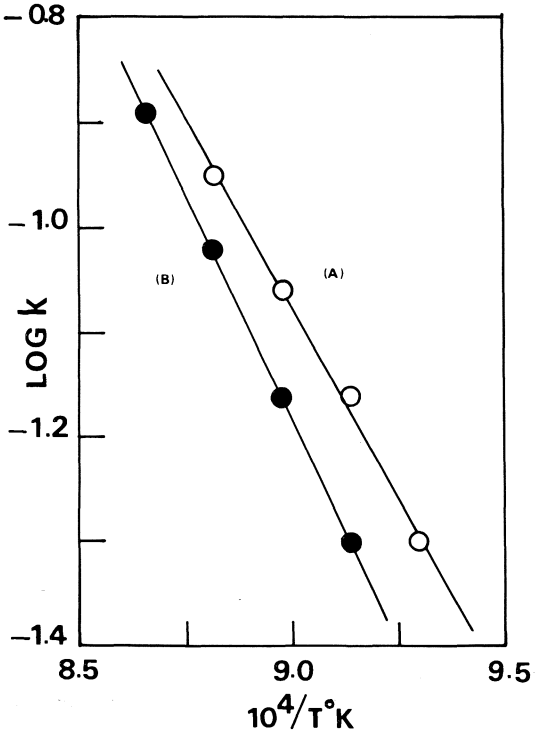

FIG. 2. Plot of log k *vs.* $10^4/T$ °K for untreated silicate MK, line *a*, and for preannealed silicate MK, line *b*.

$P_{Zn} = 0.10$ atm and constant $s = 0.5$ mole fraction of zinc in the system. The plots reveal two apparent processes with less scatter for the preannealed sample. The logarithm of the rate constants, k_{1MK} and k_{1MK}' for untreated and pretreated silicate MK, respectively obtained from the slopes of the straight lines for the initial process are plotted against the reciprocal of absolute temperature in Fig. 2. The Arrhenius equations are found to be

$$k_{1MK} = A_1 \exp(-33 \pm 6 \text{ kcal}/RT)\ \text{s}^{-1}$$

and

$$k_{1MK}' = A_1' \exp(-39 \pm 2 \text{ kcal}/RT)\ \text{s}^{-1}$$

The step in the exchange reaction at high reaction times exhibits a reduced temperature dependence with an activation energy E_a estimated to be ~5 kcal/mol.

The plot of the exchange fraction α *vs.* time at various temperatures and the semi-log plot of $(1 - \alpha)$ *vs.* time at 760, 800, 900, and 1000 °C for untreated silicate SE are displayed in Figs. 3*a* and 3*b*, respectively. The irregularity of the 1000 °C isotherm in the region $\alpha \sim 0.7$ compared to the rest of the isotherms is evident. The Arrhenius equation for each step in the temperature range 760–900 °C was calculated to be

$$k_{1SE} = A_1 \exp(-35 \pm 5 \text{ kcal}/RT)\ \text{s}^{-1}$$

and

$$k_{2SE} = A_2 \exp(-8 \pm 6 \text{ kcal}/RT)\ \text{s}^{-1}$$

The fitting of the exchange data to a diffusion rate expression is shown in Fig. 4. The diffusion equation involves a plot of Dt/r^2, taken from a theoretical plot (4), *vs.* time (D is the diffusion coefficient and r the radius of the spherical particle bathed in an atmosphere of a diffusant). A straight line with zero intercept, as required for a diffusion-controlled rate, obtains only at 760 °C.

In order to identify the origin of the deviation from a linear diffusion relation in silicate SE above 760 °C, the solid was preannealed in inactive zinc vapor at 0.10 atm and 1000 °C for 20 h. Prolonged time exposure and high temperature treatment can enhance the sintering reaction; sintering effects an increase in particle size r with a resultant inverse effect on the diffusion plot slope, *i.e.* slope $= D/r^2$. The

Can. J. Chem. Downloaded from www.nrcresearchpress.com by 210.87.254.6 on 09/05/12
For personal use only.

Can. J. Chem. Downloaded from www.nrcresearchpress.com by 210.87.254.6 on 09/05/12
For personal use only.

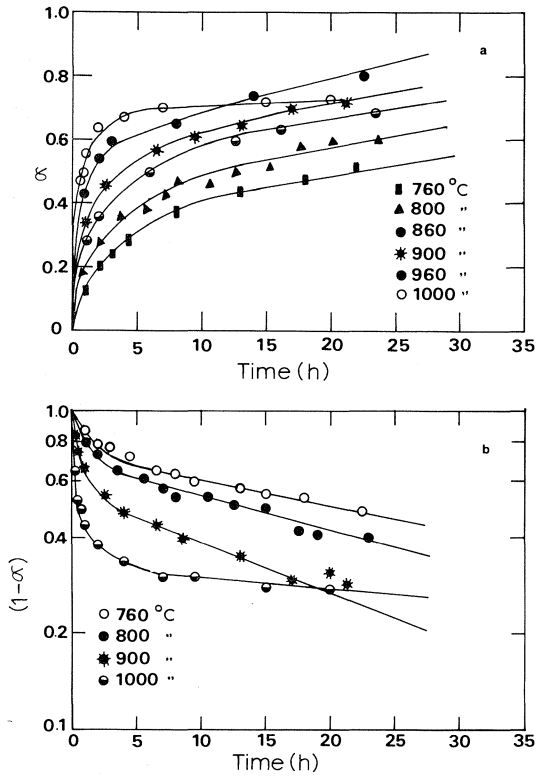

FIG. 3. (*a*) Plot of α *vs.* time for untreated silicate SE. (*b*) Plot of log (1 − α) *vs.* time for untreated silicate SE.

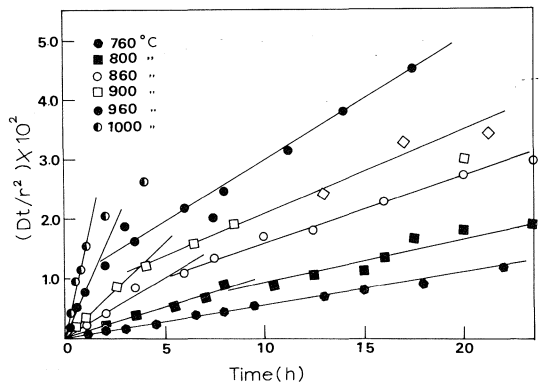

FIG. 4. Diffusion equation plot of Dt/r^2 *vs.* time for untreated silicate SE.

acceptable fit of the exchange data to the diffusion equation as a result of pretreatment is evident in Fig. 5 and the activation energy from these slopes is calculated to be 34 ± 5 kcal/mol. This E_a value is in agreement with the value for the initial step in both silicate MK and silicate SE; the constant E_a value, within experimental limits, suggests a common rate process which is insensitive to the purity of Zn_2SiO_4 within the limits of the two silicate sources.

The exchange rate dependence on the pressure of zinc vapor was also studied and the results are presented in Fig. 6. These results suggest a condition associated with low adsorption coverage where $RT \gg KP_{Zn}$ in the overall exchange rate equation (1), *viz.*

$$k = \frac{ak_eKP_{Zn}}{(RT) + KP_{Zn}}$$

where a = total number of available adsorption sites, k_e = exchange rate constant, K = equilibrium constant for adsorption, P_{Zn} = zinc vapor pressure, R = gas constant, and T in °K, which yields $k = cP_{Zn}$, where $c = (ak_eK/RT)$ for a specific solid at a fixed T.

Experiments carried out at constant time, T,

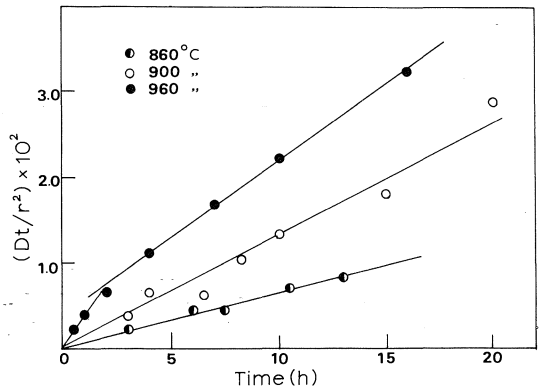

FIG. 5. Diffusion equation plot of Dt/r^2 *vs.* time for preannealed silicate SE.

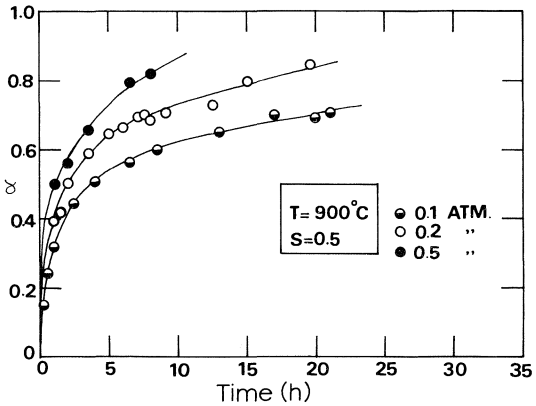

FIG. 6. Plot of α *vs.* time at various pressures of zinc vapor.

P_{Zn}, and s using radiozinc of varying specific activity, *viz.* 6–20 counts, yielded the same activity uptake in the solid. This result rules out any momentary or initial excess uptake of radiozinc vapor by the solid silicate.

The E_a value from Fig. 5 yields the diffusion coefficient $D = 10^{-8} \exp(-34 \pm 5 \text{ kcal}/RT)$ $\text{cm}^2\ \text{s}^{-1}$ for the untreated silicate SE. This D value is in good agreement with the interstitial mobility D_i (1) suggesting that the interstitial mobility of zinc is the rate-controlling process precluding any secondary effect, such as sintering. This agreement lends convincing support to the reaction model postulated for the Zn–ZnO exchange and Zn oxidation studies.

Assuming sintering to be responsible for the decreasing slopes in Figs. 1*a*, 1*b*, and 3*b*, we can evaluate the energy associated with sintering. The apparent temperature dependence of 5–10 kcal represents a net value for the two processes, interstitial mobility and sintering, suggesting then an energy of 30–35 kcal for the sintering step under the experimental conditions.

The authors are indebted to the National Research Council of Canada for financial support.

1. E. A. SECCO. *In* Sixth international symposium on reactivity of solids. *Edited by* J. W. Mitchell, R. C. DeVries, R. W. Roberts, and P. Cannon. Wiley–Interscience, Division of John Wiley and Sons, Toronto, Ontario. 1968. p. 523.
2. E. A. SECCO and RICHARD S.-C. YEO. Can. J. Chem. **49**, 1953 (1971).
3. A.S.T.M. Index to powder diffraction file. 1963. No. 8-492.
4. J. CRANK. The mathematics of diffusion. Clarendon Press, Oxford. 1956. p. 53.

Can. J. Chem. Downloaded from www.nrcresearchpress.com by 210.87.254.6 on 09/05/12
For personal use only.

The Molecular Structure of Trimethylindium by Vapor Phase Electron Diffraction

GERALD BARBE, J. LAWRENCE HENCHER, QUANG SHEN, AND DENNIS G. TUCK

Department of Chemistry, University of Windsor, Windsor, Ontario

Received June 7, 1974

GERALD BARBE, J. LAWRENCE HENCHER, QUANG SHEN, and DENNIS G. TUCK. Can. J. Chem. **52**, 3936 (1974).

The molecular structure of trimethylindium has been redetermined by vapor phase electron diffraction. The independent structural parameters assuming three-fold axial symmetry based on the r_g distances and their estimated uncertainties (2σ) are r(InC) = 209.3 ± 0.6 pm, r(CH) = 114 ± 3 pm, and $<$HCIn = 112.7 ± 0.8°. A slight nonplanarity (3.0 ± 2.5°) was attributed to a shrinkage effect in r(C···C) of 0.4 pm. The analysis was insensitive to the rotational position of the methyl groups relative to the InC_3 frame. The root mean square amplitudes were not accurate due to a problem with the indium phase factor.

GERALD BARBE, J. LAWRENCE HENCHER, QUANG SHEN et DENNIS G. TUCK. Can. J. Chem. **52**, 3936 (1974).

On détermine de nouveau la structure moléculaire du triméthylindium par diffraction électronique en phase vapeur. Les paramètres structuraux indépendants, en admettant une symétrie axiale d'ordre trois basée sur les distances r_g et leurs erreurs estimées (2σ), sont r(InC) = 209.3 ± 0.6 pm, r(CH) = 114 ± 3 pm et $<$HCIn = 112.7 ± 0.8°. La légère déformation du plan (3.0 ± 2.5°) est attribuée aux distances r(C···C) plus courtes de 0.4 pm. L'analyse ne dépend pas de la position rotationnelle des groupes méthyles par rapport au squelette InC_3. Les valeurs quadratiques moyennes ne sont pas précises à cause d'un problème dû au facteur de phase de l'indium. [Traduit par le journal]

Introduction

Trimethylindium, one of the simplest of the organometallic compounds of indium, presents a number of interesting structural features. In the vapor phase, the compound has been shown by vapor pressure measurements (1) to be monomeric above 90 °C, and an early electron diffraction study (2) established the trigonal planar structure, with an indium–carbon bond length of 216 pm (≡ 2.16 Å). The monomeric nature of the vapor, and the D_{3h} structure, have subsequently been confirmed by mass spectrometry (3) and vibrational spectroscopy (4, 5).

In the solid state, X-ray crystal structure work (6*a*) shows a rather different situation. The basic unit is a tetramer, in which three different short In—C bond lengths are found, at 216, 224, and 225 pm, and longer bonds of 310 and 360 pm. These longest bonds serve as bridges to neighboring tetrameric units. The structure is electron deficient, and in that way resembles the trimethyl compounds of other group III elements (Messmer and Amma as referenced in ref. 6*a*. Values quoted are the results of the reanalysis of the data of Amma and Rundle (6*b*)).

In view of the fact that the vapor phase study cited above was carried out more than thirty years ago, we have redetermined the structure using a new electron diffraction camera and microdensitometer constructed in this department. A further rationale for this study is that trimethylindium is the parent of a number of other interesting organoindium species, on which further studies are planned.

Experimental

Instrumentation

The geometry of the electron diffraction camera was similar to that described by Bartell (7). The electron microsource, single condenser lens, and power supplies were taken from an RCA Type EMU3B electron microscope. The high voltage was 58 kV and the collected beam current was about 5×10^{-7} A with a 0.750 mm aperture in the pole piece.

Two nozzle positions approximately 95 and 295 mm from the photographic plate could be measured with the instrument under vacuum. The nozzle was sighted through a window with a precision cathetometer (±0.01 mm) and its position was measured with respect to a previously calibrated mark located on the front of the vacuum chamber. The aluminum nozzle had a 0.5 mm hole slightly tapered on the inside to a knife edge. The distance from the nozzle tip to the beam center was about 0.5 mm as measured from its shadow on the diffraction pattern of an MgO sample located above the nozzle. The r^3 sector and its mounting were constructed of aluminum. The inner part of the sector and the edges of the mounting were machined to 45° on the under side to reduce extraneous scattering.

Can. J. Chem. Downloaded from www.nrcresearchpress.com by 210.87.254.40 on 09/05/12
For personal use only.

Can. J. Chem. Downloaded from www.nrcresearchpress.com by 210.87.254.40 on 09/05/12
For personal use only.

The high voltage was regulated to 0.01%, so that a wavelength stability of $\Delta\lambda/\lambda = 5 \times 10^{-5}$ was expected. The overall precision of the nozzle-to-plate distance was better than ± 0.05 mm. Diffraction patterns were recorded on 4 × 5 in. Kodak Electron Image Plates. The typical vacuum was $1\text{–}2 \times 10^{-5}$ Torr.

Optical densities were obtained with a single beam microdensitometer which was specially constructed to scan electron diffraction patterns. The photographic plate was spun at 300 r.p.m. on a stationary stage, while a carriage bearing the light source (tungsten filament), optics, and detector (silicon phototransistor FPT 100) moved continuously across the plate diameter at 1 mm per minute. The center of the diffraction pattern was located by a spot produced by a brief exposure of the undeflected beam. The coincidence of the spot with the pattern center was checked by rotating the sector and viewing the beam on a fluorescent screen with a telescope. Measurements of MgO ring *diameters* revealed no ring ellipticity within ± 0.02 mm (experimental precision) for the sharpest rings. Readings of detector voltage were made with an integrater/digital voltmeter combination at 3 s intervals for a period of 600 ms. Under these conditions an annulus of 0.050 mm was covered during each reading. The distance travelled between readings was found to be 0.1095 mm.

General

The sample of trimethylindium was prepared by Freeland of this department by exchange of pure indium with dimethylmercury (8). The sample purity was checked by n.m.r. and found to be better than 99%.

Exposures of the diffraction patterns of $In(CH_3)_3$ were made with the nozzle at 21 °C. The vapor pressure of the solid at this temperature is 3 Torr. With this vapor pressure longer exposures (70 s) than usual (25 s) were needed to record the molecular scattering which was weak compared to the background. In the same experiment separate carbon disulfide patterns were recorded for the electron wavelength calibration.

The photographic plates were developed for 3 min in undiluted Kodak D19 containing 1 g l^{-1} of benzotriazole as an antifogging agent. Developing solutions were maintained at 20 °C.

Analysis

The experimental molecular scattering component was obtained as

$$[1] \qquad sI_m(s) = s^5 I_a(s)[I(s)/B(s) - 1]$$

where $I(s)$ was the experimental sectored total intensity, $B(s)$ was the background, and $I_a(s)$ was the calculated atomic scattering, and $s = (4\pi/\lambda) \sin(\theta/2)$, ($\lambda$ = electron wavelength, θ = angle of diffraction). The theoretical molecular intensity (7) was given by

$$[2] \quad sI_m(s) = 2 \sum_{i<j} C_{ij}(s) \exp(-l_{ij}^2 s^2/2) r_{ij}^{-1} \times \sin[s(r_{ij} - \phi(s))]$$

where the sum is over all pairs of atoms taken once, l_{ij} is the mean square amplitude, r_{ij} is the interatomic distance, and $\phi(s)$ was an asymmetry factor to correct for anharmonicity (9).

$$[3] \qquad r_{ij} = r_g(0) - l_{ij}^2/r_{ij}$$

where $r_g(0)$ was the thermal average interatomic distance (9). The factor $C_{ij}(s)$ was defined as

$$[4] \qquad C_{ij}(s) = |f_i(s)||f_j(s)| \cos[\eta_i(s) - \eta_j(s)]$$

where the atomic scattering factors, $f_i(s)$, and phase factors, $\eta_i(s)$, were those calculated by Schäfer *et al.* (10). The inelastic scattering factors used in the calculation of $I_a(s)$ (7) were those of Tavard *et al.* (11).

The $r_g(0)$ distances were calculated in terms of an independent set of structural parameters which were refined by least squares (12). The weight matrix (13) was taken as a unit matrix, since inclusion of the factor $s^5 I_a(s)$ (which is an increasing function of s) in eq. 1 was thought to account adequately for uncertainty in drawing the background at small values of s.

The s scale was established from the CS_2 scattering patterns by the following procedure. A trial wavelength, λ_0, was assumed and $I(s_0)$ was obtained from the 400 microdensitometer readings by a four point Lagrange interpolation using the measured nozzle to plate distance. A trial background was hand drawn and refined by back Fourier transformation of the radial distribution curve for $r < 80$ pm. The molecular scattering was obtained by eq. 1 and analyzed by least squares to give a calculated C—S bond length, r_0. A refined wavelength was then calculated as $\lambda = (r_c/r_0)\lambda_0$, where r_c, the standard bond length was taken from the CS_2 structure quoted by Kuchitsu (14). By reiteration of this process, r_0 was brought into agreement with r_c. The analysis of the CS_2 plates was limited to the range $23 < q < 54$ Å^{-1} (Å = 100 pm)[1] because of the difficulty of drawing the background for $q < 20$ Å^{-1}. The results of the wavelength calibration are given in Table 1.

The experimental molecular intensity of $In(CH_3)_3$ was weak compared to the total intensity and was observed to diminish very rapidly with increasing scattering angle. Similar behavior was observed in the case of InC_5H_5 by

[1]Since the experimental intensities were taken at intervals of $(\pi/10)$ in s, it was convenient to use the variable $q = (10/\pi)s$ in the remaining discussion.

Can. J. Chem. Downloaded from www.nrcresearchpress.com by 210.87.254.40 on 09/05/12
For personal use only.

TABLE 1. Wavelength calibration from CS_2 scattering

Parameter	Observed	Standard*
r(CS)	155.7 ± 0.1 pm	155.7 ± 0.1 pm
l(CS)	3.9 ± 0.2 pm	3.9 ± 0.1 pm
κ(CS)†	0.64 pm^3	0.64 pm^3
l(SS)	4.6 ± 0.3 pm	4.1 ± 0.1 pm
κ(SS)†	0.49 pm^3	0.49 pm^3
R‡	0.0539	—
λ	5.060 pm	—
L	296.32 ± 0.05 mm	—

*The standard structure is based on r_a distances which are related to $r_g(0)$ by $r_a = r_g(0) - l^2/r$.
†The anharmonicity parameter in $\phi(s) = \kappa s^2$ was constrained in the analysis.
‡$R = \{\Sigma_s[sI_m(s)_{exp} - sI_m(s)_{th}]^2 W(s)/\Sigma_s[sI_m(s)_{exp}]^2 W(s)\}^{1/2}$ is a measure of goodness of fit. See ref. 12.

TABLE 2. Structural parameters for $In(CH_3)_3$[a]

	r_{ij} (pm)	l_{ij} (pm)	K_{ij} (pm)	δ_{ij} (pm)[c]
In—C	209.3 ± 0.6[b]	8.6 ± ?[b]		
		(5.6)[c]	(0.7)[c]	
C—H	114 ± 3	9 ± 3		
<InC$_3$[d]	3 ± 2.5°	—	—	
<HCIn	112.7 ± 0.8°	—	—	
C···C	362.0[e]	20 ± 10		0.4
		(16)	(0.3)	
In···A	274.4[e]	15 ± 3		
R[f]	0.081			
R[g]	1.078			

[a]Based on the $r_g(0)$ distances as defined in eq. 3.
[b]The quoted uncertainties are $3\sigma^*$ (σ^* = estimated random error from the least squares analysis), which is approximately 2σ (where $\sigma = (\sigma^{*2} + \sigma^2 \text{ systematic})^{1/2}$) or the 95% confidence limit. The value of l_{InC} is not accurate due to the inaccurate In scattering factor as discussed in the text.
[c]Mean square amplitudes, l_{ij}, and perpendicular corrections to the interatomic distances, K_{ij}, calculated from observed vibrational frequencies are in parentheses in the table. δ_{ij} is the observed shrinkage.
[d]The angle of deviation from planarity, see text.
[e]Dependent parameters not refined in the least squares.
[f]See Table 1, footnote ‡.
[g]Index of resolution $\mathbf{R}(\Sigma|sI_m(s)_{theor}|/\Sigma|sI_m(s)_{exp}|)$.

Shibata *et al.* (15) who showed that it was due to the indium–carbon phase factor difference.

Useful intensity data could only be obtained for the range $10 < q < 50$ Å^{-1}. The molecular component beyond $q = 50$ Å^{-1} was too weak to be isolated from the noise in either long camera or short camera plates. A weak extraneous background at $q > 50$ Å^{-1} also obscured the molecular scattering on the long camera plates. Intensity calculations later showed that the molecular envelope fell from 1/200 of the total intensity at $q = 50$ Å^{-1} to 1/1000 at $q = 56$ Å^{-1} (Å = 100 pm). Intensities from three good long camera plates were corrected for plates flatness (7) by dividing by $\cos^3\theta$ (θ = diffraction angle) and combined to produce the experimental sectored intensity $I(q)$ which is available from the Depository of Unpublished Data.[2] The optical density of the $In(CH_3)_3$ plates was 0.31–0.72. The emulsion linearity correction (7) was taken as zero.

The experimental background had a broad smooth fluctuation which was due to deviation of the sector from the r^3 shape.[3] Various smooth backgrounds, with and without the fluctuations, were tested. The $sI_m(s)$ curve obtained in each case was analyzed by least squares. The results revealed no significant variation in the major geometrical parameter values but the In—C mean square amplitude varied from 8.6 to 11.0 pm. The final structural parameter values based on the C_{3v} model are presented in Table 2. The molecular intensity, $sI_m(s)$ and the radial distribution are given in Figs. 1 and 2, respectively. The correlation matrix is given in Table 3.

A normal coordinate analysis based on the frequency assignments of Hall *et al.* (5) was

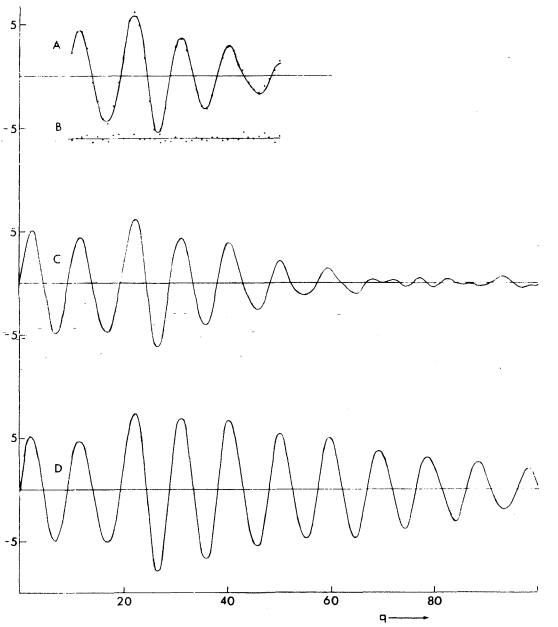

FIG. 1. The molecular intensity of trimethylindium. (*A*) Experimental (dots) and theoretical (solid curve) $sI_m(s)$ calculated from refined structural parameters of Table 2. (*B*) (Experimental–theoretical) $sI_m(s)$. (*C*) $sI_m(s)$ calculated from refined structural parameters but with $l_{InC} = 5.6$ pm. (*D*) $sI_m(s)$ calculated as in *C* but without the phase factors.

[2]Tables of relative intensities are available at a nominal charge from the Depository of Unpublished Data, National Science Library, National Research Council of Canada, Ottawa, Canada K1A 0S2.
[3]The sector shape was determined by direct measurement with a travelling microscope.

TABLE 3. Correlation matrix

	r(In—C)	$<(InC_3)$	r(C—H)	$<(HCl_n)$	l_{In-C}	$l_{C...C}$	$l_{In...H}$	l_{C-H}
σ*	0.2	3.8	1.6	1.0	0.3	6.3	1.0	1.5
	1.000							
	−0.015	1.000						
	−0.056	−0.035	1.000					
	−0.146	0.108	−0.721	1.000				
	0.072	−0.034	0.338	−0.274	1.000			
	0.021	−0.503	0.096	−0.220	0.065	1.000		
	−0.112	0.073	−0.061	0.109	−0.151	−0.152	1.000	
	0.019	−0.012	0.065	−0.066	−0.045	0.014	0.011	1.000

*σ in pm for distances, degrees for angles.

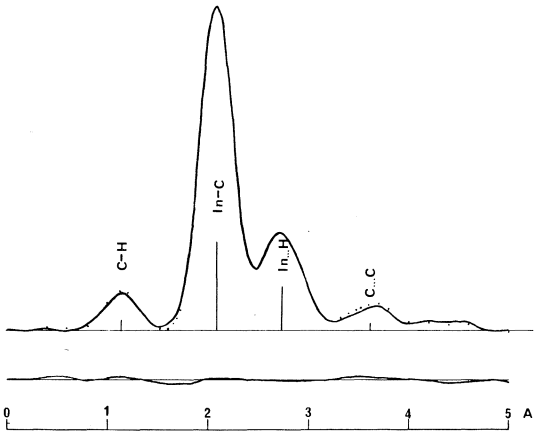

FIG. 2. The radial distribution. Experimental, dots; theoretical, solid curve. The lower curve is the difference (experimental − theoretical).

carried out for the InC_3 skeleton. The unobserved out-of-plane bending frequency was assumed to be 200 cm^{-1}. Mean square amplitudes and perpendicular correction coefficients, calculated by the method of Stølevik *et al.* (16) are also presented in Table 2. The calculated l_{InC}, 5.6 pm, was smaller than the experimental value, 8.6 pm. The origin of this disagreement was probably the inaccuracy of the In phase factor, $\eta(s)$ used in eq. 1. The effect of phase factors on the molecular intensity is illustrated by the calculated $sI_m(s)$ curves, *C* and *D*, presented in Fig. 1. Inclusion of phase factors in curve *C* resulted in the damping out of intensity as seen by comparison to *D* which was calculated without phase factors.

The experimental curve, *A*, damped out more rapidly than curve *C*, which was calculated with l_{InC} = 5.6 pm. It appears that the experimental l_{InC} refined to a larger value in order to compensate for inaccuracy of the term cos $[\eta_{In}(s) - \eta_c(s)]$ in eq. 2 which was kept constant in the analysis.

Inaccuracy of l_{InC} has a small effect on the $r_g(0)$ distances since they are calculated from the thermal average, r_a, by the relationship $r_a = r_g(0) - l^2/r$. Assuming the calculated l_{InC} = 5.6 pm was more accurate than the 8.6 pm value would give r(InC) = 209.1 pm instead of 209.3 pm.

Results

The apparent small deviation of the model from planarity was attributed to a shrinkage (17) of 0.4 pm in $r(C \cdots C)$ which is comparable with the calculated perpendicular correction, 0.3 pm. Hence, the planar structure is confirmed by the present result. Effects due to internal rotation of the methyl groups could not be examined because the affected H · · · H distances did not contribute an observable component to the total intensity.

The indium–carbon length is significantly shorter than that reported by Pauling and Laubengayer (2), but this is not surprising in view of the difficulties inherent in the "visual" method of analysis used by these workers. In general In—C distances in crystalline indium–alkyl systems are longer: Me_3In(crystal), 216(4), 224(6), 225(6) pm (6); $Me_2In(OAc)$, 211(1) pm (19); $Et_2In(OAc)$, 229 pm (20); $Et_2In(CH_3{\cdot}COS)$, 214 pm (21). Other reported In—C bond lengths refer to crystalline triphenyl- and tris-(cyclopentadienyl)indium. In both of these substances, the situation is complicated by intermolecular interactions: the "short" In—C bond lengths are 211.1 (1.4) and 215.5 (1.4) pm in $InPh_3$ (22) and 223.7, 237.4, 244.3 and 246.6 pm (all ±0.9 pm) in $InCp_3$ (23).

It is clear that the In—C bond length in gaseous $InMe_3$ is somewhat less than in indium–alkyl and

Can. J. Chem. Downloaded from www.nrcresearchpress.com by 210.87.254.40 on 09/05/12
For personal use only.

indium–aryl crystalline systems, and that there are other variations in this distance which await further explanation.

This work was supported in part by Operating and Equipment Grants from the National Research Council of Canada.

1. A. W. LAUBENGAYER and W. J. GILLIAM. J. Am. Chem. Soc. **63**, 477 (1941).
2. L. PAULING and A. W. LAUBENGAYER. J. Am. Chem. Soc. **63**, 480 (1941).
3. F. GLOCKING and R. G. STAFFORD. J. Chem. Soc. A, 1761 (1971).
4. G. P. VAN DER KELEN and M. A. HERMAN. Bull. Soc. Chim. Belg. **65**, 362 (1956).
5. J. R. HALL, L. A. WOODWARD, and E. A. EBSWORTH. Spectrochim. Acta, **20**, 1249 (1964).
6. (*a*) R. G. VRANKA and E. L. AMMA. J. Am. Chem. Soc. **89**, 3121 (1967); (*b*) E. L. AMMA and R. E. RUNDLE. J. Am. Chem. Soc. **80**, 4141 (1958).
7. L. S. BARTELL. Physical methods in chemistry. 4th ed. Vol. 1. *Edited by* A. Weissberger and B. W. Rossiter. Interscience, New York. 1971.
8. L. M. DENNIS, R. W. WORK, and E. G. ROCHOW. J. Am. Chem. Soc. **56**, 1047 (1934).
9. K. KUCHITSU and L. S. BARTELL. J. Chem. Phys. **35**, 1945 (1961); L. S. BARTELL. J. Chem. Phys. **23**, 1219 (1955).
10. L. SCHÄFER, A. C. YATES, and R. A. BONHAM. J. Chem. Phys. **55**, 3055 (1971).
11. C. TAVARD, D. NICHOLAS, and M. ROUAULT. J. Chim. Phys. **64**, 540 (1967).
12. W. C. HAMILTON. Statistics in physical science. Ronald Press, New York. 1964. Chapt 4; W. HARSHBARGER, G. LEE, R. F. PORTER, and S. H. BAUER. Inorg. Chem. **8**, 1683 (1969).
13. L. S. BARTELL and M. G. ANASHKIN. J. Mol. Struct. **17**, 193 (1973).
14. K. KUCHITSU. Molecular vibrations and structure studies. *Edited by* S. J. Cyvin. Elsevier, Amsterdam. 1972. Chapt. 10.
15. S. SHIBATA, L. S. BARTELL, and R. M. GAVIN, Jr. J. Chem. Phys. **41**, 717 (1964).
16. R. STØLEVIK, H. M. SEIP, and S. J. CYVIN. Chem. Phys. Lett. **15**, 263 (1972).
17. S. J. CYVIN. Molecular vibrations and mean square amplitudes. Elsevier, Amsterdam. 1968. Chapt. 15.
18. H. FUJII and M. KIMURA. Bull. Chem. Soc. Jap. **44**, 2643 (1971).
19. F. W. B. EINSTEIN, M. M. GILBERT, and D. G. TUCK. J. Chem. Soc. Dalton, 248 (1973).
20. H. D. HANSEN. Z. Naturforsch. B**27**, 82 (1973).
21. H. D. HANSEN. J. Organometal. Chem. **39**, C37 (1973).
22. J. F. MALONE and W. S. MCDONALD. J. Chem. Soc. A, 3362 (1970).
23. F. W. B. EINSTEIN, M. M. GILBERT, and D. G. TUCK. Inorg. Chem. **11**, 2832 (1972).

Can. J. Chem. Downloaded from www.nrcresearchpress.com by 210.87.254.40 on 09/05/12
For personal use only.

Sur le spectre électronique de l'ion ozonide, 0_3^-

PAUL A. GIGUÈRE ET KAZIMIERA HERMAN
Département de Chimie, Faculté des Sciences, Université Laval, Québec, Québec G1K 7P4

Reçu le 12 août 1974

PAUL A. GIGUÈRE et KAZIMIERA HERMAN. Can. J. Chem. **52**, 3941 (1974).

L'ozonide de potassium dissous dans l'ammoniac liquide absorbe assez fortement en u.v. à partir de 300 nm en plus de la forte absorption dans le bleu–violet. Les résultats contradictoires rapportés précédemment s'expliquent par la présence d'autres espèces comme O_3, O_2^- et HO_2 qui absorbent aussi dans cette région. La progression irrégulière des fréquences dans le système visible suggère l'activité d'un second mode de vibration de l'état excité.

PAUL A. GIGUÈRE and KAZIMIERA HERMAN. Can. J. Chem. **52**, 3941 (1974).

Potassium ozonide dissolved in liquid ammonia absorbs fairly strongly in the u.v. from 300 nm, in addition to the strong band in the violet–blue. Previous conflicting results were due to interference of other species, such as O_3, O_2^-, and HO_2, which also absorb in that region. The irregular spacing of the maxima in the visible band points to some interference of a second vibrational mode of the upper state.

Les données actuelles sur l'absorption en u.v. de l'ion ozonide sont sujettes à caution. Czapski (1), qui a fait une revue de la question, en a conclu que les variations d'absorption rapportées par divers auteurs (2–4) sont dues non pas à l'ozonide lui-même, mais plutôt à quelque produit de décomposition, comme par exemple, le superoxyde O_2^-. La difficulté vient de ce que les systèmes étudiés jusqu'ici sont susceptibles de produire en même temps d'autres espèces qui absorbent plus ou moins fortement dans l'u.v. Ainsi la photolyse éclair par l'u.v. à vide de solutions aqueuses alcalines produit aussi de l'ozone, tandis que celle du peroxyde d'hydrogène (5) donne, entre autres, le radical HO_2. En marge d'une étude sur le spectre Raman des ozonides alcalins en solution dans l'ammoniac, qui a éventuellement révélé la photolyse facile de ces systèmes (6), nous avons été amenés à mesurer le spectre visible et u.v. du radical-ion O_3^-.

Méthode expérimentale

L'ozonide de potassium a été préparé à partir de KOH (Baker Analyzed) débarrassé de carbonate, puis soigneusement desséché avant l'ozonisation. Cette précaution est essentielle pour un bon rendement. Le produit de départ était d'abord finement broyé en atmosphère sèche, puis chauffé à 300 °C pendant 5 h dans un courant d'azote sec. La masse fondue, devenue très dure après refroidissement, était concassée puis pulvérisée dans un mortier d'agate. Toutes ces opérations devaient être faites à l'abri de l'humidité dans une boîte à gants. L'ozonisation se faisait à environ −70 °C dans un courant d'oxygène ozonisé à quelque 5%. Selon la concentration recherchée la durée de la réaction variait de 15 min (pour les spectres u.v.) à 2 h (pour les spectres Raman). L'extraction par l'ammoniac liquide suivait aussitôt, d'après la technique de Whaley et Kleinberg (7). Le potassium a été dosé par absorption atomique dans le produit hydrolysé après évaporation sous vide de l'ammoniac.

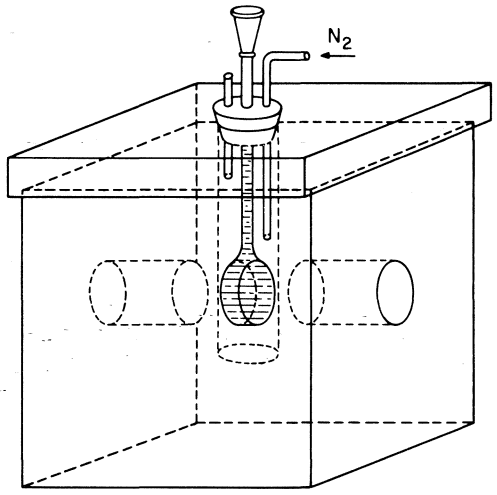

FIG. 1. Cuve à absorption réfrigérée pour les spectres u.v. en solution ammoniacale.

Les spectres ont été mesurés avec un spectromètre de Cary, N° 15, au moyen d'une cuve à absorption réfrigérée de construction speciale (fig. 1). La cuve en quartz, de 1 cm d'épaisseur, était munie d'un long tube de remplissage. Elle était montée au centre d'un bloc de Styrofoam muni de deux tubes latéraux fermés par des fenêtres de quartz, et évacués, pour le passage du faisceau lumineux. Une circulation d'azote sec refroidi permettait de maintenir la température à quelque −65 °C dans la cavité centrale. Le bloc de Styrofoam s'adaptait exactement au compartiment porte-échantillon du spectromètre. Il était

Can. J. Chem. Downloaded from www.nrcresearchpress.com by 210.87.254.6 on 09/05/12
For personal use only.

Can. J. Chem. Downloaded from www.nrcresearchpress.com by 210.87.254.6 on 09/05/12
For personal use only.

muni d'un couvercle étanche pour empêcher l'accès de la lumière extérieure. Le faisceau de référence traversait des plaques de quartz pour compenser l'absorption des six fenêtres.

Discussion des résultats

Comme le montre la fig. 2 la solution de KO_3 commence à absorber dans l'u.v. à partir de 300 nm. A noter que cette courbe de log I_0/I de l'ozonide a été corrigée pour l'absorption par l'ammoniac. Comme cette dernière croît brusquement vers 230 nm, l'étude du spectre de l'ozonide n'a pu être poussée très loin. On voit cependant que vers 240 nm l'absorption a déjà atteint le dixième de celle au maximum de la bande visible, et qu'elle continue à croître régulièrement vers les hautes fréquences. Incidemment, nous avons trouvé pour le coefficient molaire d'extinction au maximum dans le visible une valeur, $\varepsilon_{457} = 2050\ M^{-1}\ cm^{-1}$, assez voisine de celle mesurée par Dorfman *et coll.* (8) en solutions aqueuses, $\varepsilon_{430} = 1900 \pm 120\ M^{-1}\ cm^{-1}$.

Il ne fait pas de doute que l'absorption dans l'u.v. est due à l'ion ozonide. Les réactions de photolyse ou de radiolyse étudiées jusqu'ici en système aqueux (1) donnent, outre les ozonides, de l'ozone ou des superoxydes en concentrations difficiles à évaluer. La présence de ces autres espèces est exclue dans notre méthode de préparation. De plus, les superoxydes (dont HO_2) ont un maximum d'absorption assez marqué vers 230 nm (9), tandis que celui de l'ozone se situe vers 260 nm (10). Il n'y a aucune indication de tel maximum dans nos spectres. D'ailleurs, le superoxyde de potassium est à peine soluble dans l'ammoniac, contrairement à la conclusion de Thompson et Kleinberg (11). On sait maintenant (12) que la bande à 380 nm rapportée par ces auteurs provient en fait du nitrite, sous-produit de la synthèse de KO_2 dans l'ammoniac. Ajoutons que diverses préparations de l'ozonide nous ont toujours donné le même rapport d'absorption dans le visible et l'u.v.

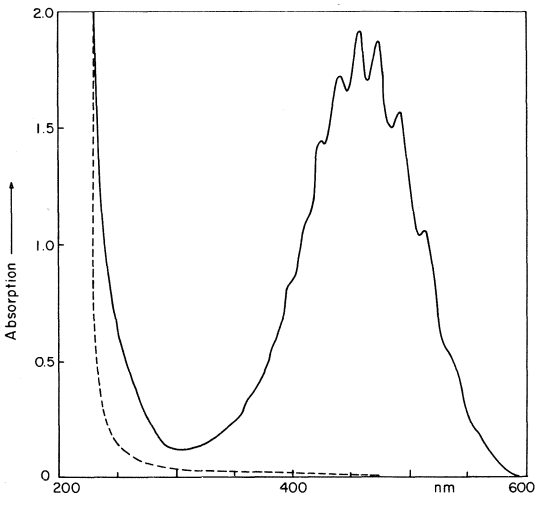

FIG. 2. Spectre d'absorption dans le visible et l'u.v. de l'ozonide de potassium en solution ammoniacale. La ligne brisée correspond à l'ammoniac liquide.

Enfin, une nouvelle preuve de l'origine commune de ces deux systèmes nous est venue d'une autre source. En cherchant à obtenir le spectre Raman de l'ion ozonide en solution ammoniacale nous avons découvert que la photolyse par le laser à Ar^+ ne conduit pas au superoxyde, comme dans le cas du solide (6, 13, 14) mais plutôt à l'oxydation du solvant, avec formation d'un intermédiaire métastable non encore identifié. Or, au cours de la photolyse en lumière bleue, région où les superoxydes n'absorbent pas, l'absorption décroît au même taux dans le visible et l'u.v. en autant qu'on peut en juger par la pente des courbes à 540 et 260 nm.

Par la même occasion nous avons pu mesurer la structure de la bande dans le bleu–violet avec une meilleure résolution que précédemment (fig. 2). Les présentes fréquences (tableau 1) montrent un décalage moyen de 8 nm avec celles de Solomon *et al.* (15). Quant à celles de Jacox et Milligan (16), elles se rapportent à l'ion en matrice inerte. Nos fréquences sont plus ou moins décalées vers le rouge par les interactions moléculaires en solution ammoniacale. Dans le cas du radical HO_2 le décalage est de l'ordre de 20 nm entre l'état gazeux (17) et la solution aqueuse (9).

Le contour assez irrégulier des divers pics, et leur espacement inégal portent à croire qu'il s'agit d'un second mode de vibration de l'état excité. D'après la théorie de Walsh (18) la bande correspondant à la transition $^2A_2 \rightarrow {}^2B_1$ devrait montrer les progressions des deux modes symétriques ν_1' et ν_2'. Jacox et Milligan ont identifié la progression observée avec ν_1', le mode de valence symétrique. Il est probable, cependant, que le mode de déformation ν_2' contribue également à la structure. En effet, dans les autres molécules à 18 ou 19 électrons de valence comme SO_2 et ClO_2, la fréquence de déformation de l'état excité est nettement inférieure à celle de l'état fondamental (19). Comme cette

TABLEAU 1. Longueur d'onde et espacement des maxima dans la bande visible de l'ion ozonide

λ (nm)		Ce travail	
Solomon *et al.* (15)	Jacox et Milligan (16)	λ (nm)	Δν (cm^{-1})
		~565	
			~957
		~536	
			837
	515	513	
			790
503	—	493	
			858
485	481	473	
			740
466	463.5	457*	
			794
449*	446.2	441	
			799
433	430	426	
			739
418	415	413	
			912
	—	398	
			849
	389.5	~385	
			~835
	377	~373	

*Maximum.

dernière est d'environ 600 cm^{-1} d'après les résultats les plus récents (20) on peut prévoir une valeur de l'ordre de 400 cm^{-1} pour ν_2'; d'où possibilité d'interférence avec ν_1'.

De même l'espacement moyen de 820 cm^{-1} pour ν_1' représente une forte diminution par rapport à la fréquence de l'état fondamental (14, 20), 1010 cm^{-1}, et par le fait même, un allongement appréciable de la liaison dans l'état excité. On peut évaluer celle-ci à environ 1.48 Å par comparaison avec la liaison O—O dans les peroxydes covalents, dont la fréquence caractéristique est de l'ordre de 850 cm^{-1}. On arrive à une valeur semblable d'après la règle de Badger à partir de l'estimation de 1.38 ± 0.04 Å pour la distance interatomique dans l'ion à l'état fondamental (20). Cette conclusion est en accord avec la théorie de Walsh (18) qui prévoit également une ouverture de l'angle au sommet dans le niveau excité.

Notons enfin que nos résultats jusqu'à 800 nm ne montrent aucune indication d'un autre système dans le proche infrarouge, identifiable à la transition $^2A_1 \rightarrow {}^2B_1$ observée dans les molécules analogues SO_2 et ClO_2 (19). Quant au continuum correspondant à la transition à une orbitale antiliante, cause de la photodissociation, il doit être assez faible à en juger par nos résultats, tant à 300 qu'à 600 nm.

Les auteurs sont redevables au Ministère de l'Education du Québec pour une subvention de recherches, et au Professeur Claude Barbeau pour les analyses par absorption atomique.

1. G. CZAPSKI. Annual review of physical chemistry, Vol. 22. Annual Reviews Inc., Palo Alto, California. 1971. p. 171.
2. G. E. ADAMS, J. W. BOAG et B. D. MICHAEL. Proc. R. Soc. A**281**, 321 (1966).
3. E. HAYON et J. J. MCGARVEY. J. Phys. Chem. **71**, 1472 (1967).
4. L. DOGLIOTTI et E. HAYON. J. Phys. Chem. **71**, 2511 (1967).
5. V. R. LANDI et L. J. HEIDT. J. Phys. Chem. **73**, 2361 (1969).
6. K. HERMAN. Résultats inédits.
7. T. P. WHALEY et J. KLEINBERG. J. Am. Chem. Soc. **73**, 79 (1951).
8. W. D. FELIX, B. L. GALL et L. M. DORFMAN. J. Phys. Chem. **71**, 384 (1967).
9. G. CZAPSKI et L. M. DORFMAN. J. Phys. Chem. **68**, 1169 (1964).
10. H. TAUBE. Trans. Faraday Soc. **53**, 656 (1957).
11. J. K. THOMPSON et J. KLEINBERG. J. Am. Chem. Soc. **73**, 1243 (1951).
12. G. CZAPSKI et B. HALPERIN. Israel J. Chem. **5**, 185 (1967).
13. J. B. BATES, M. H. BROOKER et G. E. BOYD. Chem. Phys. Lett. **16**, 391 (1972).
14. A. I. KARELIN, V. Y. ROSOLOVSKII, S. A. TOKAREVA et J. I. VOL'NOV. Dokl. **206**, 641 (1972).
15. I. J. SOLOMON, A. J. KACKMAREK, J. M. MCDONOUGH et K. HATTORI. J. Am. Chem. Soc. **82**, 5640 (1960).
16. M. E. JACOX et D. E. MILLIGAN. J. Mol. Spectrosc. **43**, 148 (1972).
17. T. T. PAUKERT et H. S. JOHNSTON. J. Chem. Phys. **56**, 2834 (1972).
18. A. D. WALSH. J. Chem. Soc. 2266 (1953).
19. G. HERZBERG. Electronic spectra and structure of polyatomic molecules. Van Nostrand, Princeton, N.J. 1966. pp. 604–607.
20. L. ANDREWS et R. C. SPIKER, JR. J. Chem. Phys. **59**, 1863 (1973).

Can. J. Chem. Downloaded from www.nrcresearchpress.com by 210.87.254.6 on 09/05/12
For personal use only.

Coordination Compounds of Indium. Part XXVI. Ligand Exchange Studies with Trifluoromethyl-β-diketonato(dimethyl)indium(III) compounds

H. L. CHUNG AND D. G. TUCK

Department of Chemistry, University of Windsor, Windsor, Ontario N9B 3P4

Received June 14, 1974

H. L. CHUNG and D. G. TUCK. Can. J. Chem. **52**, 3944 (1974).

The ligand exchange between Me_2InL and HL (L = $CF_3.CO.CH.CO.R^-$ anion; R = methyl or *t*-butyl) has been studied by ^{19}F n.m.r. spectroscopy, using benzene and di-isobutylketone as solvents. The exchange is first order in both Me_2InL and HL. Activation free energies were derived from measurements of the coalescence temperature. The results are compared with those of earlier studies. The rate-controlling process in the exchange is identified as the rotation of one monodentate diketonate ligand about a partial double bond prior to intramolecular proton transfer to a second monodentate ligand.

H. L. CHUNG et D. G. TUCK. Can. J. Chem. **52**, 3944 (1974).

On étudie par spectroscopie r.m.n. du ^{19}F l'échange de coordinats entre Me_2InL et HL (L = l'anion $CF_3.CO.CH.CO.R^-$; R = méthyle ou *t*-butyle) en se servant du benzène et de la di-isobutylcétone comme solvants. L'échange est du premier ordre pour Me_2InL et pour HL. Des mesures de température de coalescence on déduit les énergies libres d'activation. On compare ces résultats avec ceux d'études antérieures. On identifie le mécanisme qui contrôle la vitesse de l'échange comme étant la rotation du groupe dicétonate monodentate autour d'une liaison double partielle précédant le transfert intramoléculaire de protons à un second coordinat monodentate. [Traduit par le journal]

Introduction

The study of the kinetics of ligand exchange plays an important role in establishing an understanding of the behavior of the complexes of a metallic element. For indium, quantitative data in this field are sparse, despite the fact that rearrangement reactions occur easily with the complexes of this element and have important consequences in preparative work (2). In an earlier investigation (3), the exchange between InL_3 and trifluoromethyl-β-diketones HL (L = $CF_3.CO.CH.CO.R^-$; R = methyl, *i*-butyl, phenyl, 2-naphthyl, and 2-thienyl) was studied in a variety of solvents. The exchange is fast and ^{19}F n.m.r. methods proved to be a convenient way of obtaining kinetic data. The exchange was found to be first order in InL_3 concentration, but zero order in free ligand concentration, and the rate controlling process was identified as the rotation of a monodentate ligand about a partial double bond prior to intramolecular proton transfer.

We have now extended these studies to the organo-indium species Me_2InL, where L is again a trifluoromethyl-β-diketonate; the parent acetylacetonato(dimethyl)indium(III) was first reported by Coates and Whitcombe (4). The experimental methods used in the present work again involved ^{19}F n.m.r. and the results are different from, but in general agreement with, those reported earlier (3). We may note that Glass and Tobias (5) have reported similar studies of, *inter alia*, $Me_2Ga(acac)$ and $Me_2Tl(acac)$ with free Hacac (acac = acetylacetonate anion) using proton n.m.r. methods, and identified metal–oxygen bond cleavage as the rate-controlling process.

Some preparative work has also been carried out in the course of this study, and adducts of $Me_2In(tfac)$ (tfac = $CF_3.CO.CH.CO.CH_3^-$ anion) with some bidentate donors are described. The existence of such adducts bears upon the mechanism proposed for the ligand exchange process.

Experimental

Preparative

Reagents and solvents were generally reagent grade materials; solvents were distilled over drying agents.

Indium trichloride, prepared by passing chlorine gas over indium metal heated to about 150 °C, was obtained as a white powder. Trimethylindium was prepared (*a*) by the reaction of methyl lithium in ether (4.16 ml, 2.09 *M*) with indium trichloride (0.64 g, 2.90 mmol) in 15 ml of

[1]For Part XXV, see ref. 1.

Can. J. Chem. Downloaded from www.nrcresearchpress.com by 210.87.254.5 on 09/05/12
For personal use only.

TABLE 1. Analytical results and melting points for $Me_2In(CF_3.CO.CH.CO.R)$ and adducts

Compound	Melting point (°C)	Observed (%)			Calculated (%)		
		C	H	In	C	H	In
R = CH_3	93	28.3	3.3	38.3	28.2	3.4	38.6
R = t-C_4H_9	46	—	—	33.2	—	—	33.8
R = C_6H_5	—	—	—	31.0	—	—	31.9
$Me_2In(tfac)(bipy)$*	140	44.8	3.9	26.5	44.9	4.0	25.4
$Me_2In(tfac)(phen)$	110	47.7	3.8	23.2	47.7	3.8	24.0
$Me_2In(tfac)(diphos)$†	66	57.0	4.9	‡	56.9	4.9	‡

*N: observed, 6.0%; calcd., 6.2%.
†P: observed, 9.1%; calcd., 8.9%.
‡See text.

TABLE 2. Nuclear magnetic resonance spectra of $CF_3.CO.CH_2.CO.R$, $Me_2In(CF_3.CO.CH.CO.R)$, and adducts of $Me_2In(tfac)$ in $CDCl_3$ at 35°

		^1H Chemical shifts (Hz)[a]			^{19}F Chemical shifts (Hz)[b]
		R	γ-proton	CH_3—In	
HL	R=CH_3	150	370	—	102
	t-C_4H_9	88	370	—	120
	C_6H_5	467[c]	404	—	120
Me_2InL	R=CH_3	146	353	24	151
	t-C_4H_9	88	365	25	155
	C_6H_5	467[c]	398	26	165
Adducts:	bipy[d]	140	355	12,24	149
	phen[e]	146	357	12,29	214
	diphos[f]	133	348	9,14	168

[a]Relative to external TMS; spectrometer frequency 60 MHz.
[b]Relative to external $CF_3.COOD$; spectrometer frequency 56.4 MHz.
[c]Center peak of multiplet.
[d]Multiplet centered at 486 for free bipy appears at 501 Hz in complex.
[e]Multiplet centered at 480 for free phen appears at 497 Hz in complex.
[f]Diphos CH_2 triplet unchanged in complex at 137 Hz.

ether, followed by distillation *in vacuo* (6) or (*b*) by heating a mixture of dimethylmercury (12 g) and indium metal (7.6 g) at 135° for 1 week (7).

The three trifluoromethyl-β-diketonato(dimethyl)indium(III) compounds ($Me_2In(CF_3.CO.CH.CO.R)$; R = methyl, *t*-butyl, or phenyl) were prepared by mixing Me_3In and the appropriate parent diketone in a 1:1 molar ratio in ether. The white solids obtained after evaporation of the solvent were dried *in vacuo*. The R = phenyl compound was not used in the kinetic studies, since the substance is extremely hygroscopic and some difficulty was experienced in obtaining good crystalline material. Although the indium analysis of the freshly prepared material was satisfactory, it was not possible to obtain reliable carbon and hydrogen values because of the deliquescence.

Adducts of $Me_2In(CF_3.CO.CH.CO.CH_3)$ with the bidentate ligands 2,2′-bipyridyl (bipy), 1,10-phenanthroline (phen), and 1,2-bis(diphenylphosphino)ethane (diphos) were prepared by mixing chloroform solutions of the compounds concerned. The 1:1 adducts were recrystallized from chloroform – petroleum ether and dried *in vacuo*. Analytical results for all the compounds concerned are presented in Table 1. Melting points are uncorrected. Indium analysis was not possible for Me_2InL-(diphos), since treatment with concentrated nitric acid gave turbid solutions which were not suitable for atomic absorption work, but satisfactory analyses were reported for C, H, and P.

Nuclear Magnetic Resonance Spectroscopy

^1H and ^{19}F n.m.r. spectra were obtained with a Jeolco JNM-C-60 HL high resolution nuclear magnetic resonance spectrometer operating at oscillator frequencies of 60 or 56.4 MHz. Resonance frequencies were measured with reference to external standards of TMS and CF_3-COOD, respectively. A large scale expansion and slow sweep time were employed in order to ensure accurate values in measurement of line-widths and coalescence temperatures. The temperature variation experiments employed a variable temperature controller, previously calibrated against a thermometer inserted in the n.m.r. sample chamber.

Kinetic Studies

As in the earlier work (3), the ^{19}F chemical shifts are much larger than those for the proton resonance (see Table 2), and the kinetic studies are therefore based entirely on ^{19}F measurements. Two series of experiments

Can. J. Chem. Downloaded from www.nrcresearchpress.com by 210.87.254.5 on 09/05/12
For personal use only.

Can. J. Chem. Downloaded from www.nrcresearchpress.com by 210.87.254.5 on 09/05/12
For personal use only.

were carried out. In the first of these, the order of the reaction was determined by measuring the line-width, and hence the ^{19}F n.m.r. lifetime, as a function of the concentration of complex and free ligand respectively. In the second series, the free energies of activation for the exchange in differing solvents were obtained from measurements of the coalescence temperature of solutions containing equimolar amounts of complex and ligand. The differences in the ^{19}F chemical shifts of the two reactants ($\Delta\nu$ in Table 4) were taken from measurements of the spectra of separate solutions of the individual species in the solvent in question at 35° (*c.f.* ref. 3).

Molecular Weight Studies

The molecular weights of $Me_2In(CF_3.CO.CH.CO.CH_3)$ and its diphos adduct were measured in benzene in order to establish the degree of association, using a Hewlett–Packard 302B vapor pressure osmometer. Results were obtained at four different concentrations; benzil was used as a standard for calibration.

Results and Discussion

The background theory to this work has been discussed in the previous paper (3) and need not be repeated here.

^{19}F Nuclear Magnetic Resonance Lifetime Measurements

The order of the exchange reaction can be established by following the lifetimes of the individual species as a function of reactant concentration, measuring the n.m.r. linewidths below the coalescence temperature. The system $Me_2In(CF_3.CO.CH.CO.CH_3)/CF_3.CO.CH_2.CO.CH_3$ (=$Me_2In(tfac)$/Htfac) in di-isobutylketone was chosen for this purpose, since the ^{19}F resonances are well-resolved ($\Delta\nu$ = 49 Hz at −20 °C) below the coalescence temperature (16 °C). An additional convenience is that the indium complex is air stable. The results are summarized in Table 3. The changes in the volume of the solution due to addition of complex (or ligand) were sufficiently small that they could be neglected, so that concentrations were taken to be proportional to the quantities added.

Table 3*a* establishes that the half-width of the ^{19}F resonance due to $Me_2In(tfac)$ is constant (average value 2.5 ± 0.2 Hz) under the experimental conditions, whereas the corresponding quantity for free Htfac is a linear function of the concentration of that substance. Similarly, the results in Table 3*b* show a constant half-width for Htfac (average 3.9 ± 0.1 Hz), and values for $Me_2In(tfac)$ which are linearly dependent on the complex concentration. The rate-law for the exchange between $Me_2In(tfac)$ and Htfac in di-isobutylketone at −20 °C is therefore of the form

TABLE 3. ^{19}F n.m.r. line-widths at half-height as a function of concentration in the system $Me_2In(tfac)$/Htfac/di-isobutylketone at −20 °C

(*a*) Varying $Me_2In(tfac)$, constant Htfac (0.094 mmol)

$Me_2In(tfac)$ added (mmol)	Line-width (Hz)*	
	Htfac	$Me_2In(tfac)$
0	1.6	—
0.071	2.2	2.8
0.085	2.8	2.8
0.097	2.8	2.4
0.118	2.9	2.2
0.158	3.5	2.4
0.192	3.6	2.5
0.222	4.1	2.4
0.257	4.1	2.2
0.308	5.0	2.4

(*b*) Varying Htfac, constant $Me_2In(tfac)$ (0.158 mmol)

Htfac added (mmol)	Line-width (Hz)*	
	Htfac	$Me_2In(tfac)$
0	—	1.2
0.085	4.2	2.7
0.122	3.8	3.4
0.170	3.9	4.6
0.200	3.8	4.8
0.220	3.9	5.9
0.249	3.9	6.1
0.294	3.9	6.9

*Estimated accuracy on individual values ±0.2 Hz.

$$[1] \qquad R = k[Me_2In(tfac)]^1\,[Htfac]^1$$

This expression is in marked contrast to that reported for the exchange between the tris-chelate complex $In(tfac)_3$ and the free ligand, for which situation the rate-law was found (3) to be

$$[2] \qquad R = k[In(tfac)_3]^1\,[Htfac]^0$$

We return to this difference below.

Experimental Free Energies of Activation

The studies by Glass and Tobias (5) on ligand exchange with the gallium and thallium analogs of $Me_2In(acac)$ gave values for E_A, whereas the studies of $In(tfac)_3$ and similar compounds lead to $\Delta G^{\ddagger}$. For reasons discussed earlier (3), we have restricted the present series of measurements to those systems in which coalescence of the two resonances could be observed, so that $\Delta G^{\ddagger}$ values are again obtained. At coalescence one has

TABLE 4. Free energies of activation for ligand exchange in $Me_2In(CF_3.CO.CH.CO.R)/CF_3.CO.CH_2.CO.R$ systems

	Benzene				Di-isobutylketone			
R	$\Delta\nu(^{19}F)$ (Hz)	T_c (°C)	Concentration (M)	$\Delta G^{\ddagger}$ (kcal mol^{-1})	$\Delta\nu(^{19}F)$ (Hz)	T_c (°C)	Concentration (M)	$\Delta G^{\ddagger}$ (kcal mol^{-1})
CH_3	53	32	0.34	13.4	58	16	0.46	12.8
t-C_4H_9	38	40	0.33	14.0	45	32	0.23	13.3

[3] $$1/\tau_A = \sqrt{2}\pi\Delta\nu$$

where τ_A is the average lifetime of one reactant molecule A, and $\Delta\nu$ is the chemical shift difference between the species A and B (8, 9). For a second-order process, as established in eq. 2 above,

[4] $$\tau_A = 1/k_c[A]$$

and $\Delta G^{\ddagger}$ can then be obtained by substitution into the Eyring rate equation

[5] $$-\Delta G^{\ddagger} = RT_c \ln \frac{hk_c}{\kappa \boldsymbol{k} T_c}$$

in which k_c is the rate constant at the coalescence temperature T_c, $\boldsymbol{k}$ is the Boltzmann constant, and κ is the transmission coefficient, to which a value of 0.5 is assigned. The values of $\Delta G^{\ddagger}$ obtained by this procedure are given in Table 4.

Reaction Mechanism

Rapid ligand exchange occurs in each of the systems studied. We may also report here that accurate measurements could not be made in dimethylsulfoxide solution because the coalescence temperature lies below the accessible temperature range (freezing point of dmso +18.5 °C), in each case, so that the values of $\Delta G^{\ddagger}$ must lie below 12.5 kcal mol^{-1} ($\Delta\nu$ = 125 Hz). Similarly, experiments with acetonitrile did not lead to detectable splitting of the single peak down to −38° in the case of R = t-butyl ($\Delta\nu$ = 28 Hz; $\Delta G^{\ddagger} < 10.4$ kcal mol^{-1}).

The primary step in the ligand exchange mechanism for the six-coordinate InL_3 complexes was assumed to be the opening of one chelate ring to give a five-coordinate species with one monodentate ligand,

[6] 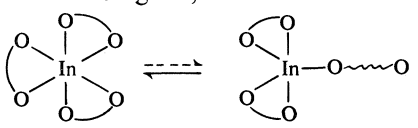

This process was shown to be in keeping with the known coordination chemistry of indium(III) (3), and with the mechanism proposed for other similar exchange systems (10). The steady-state concentration of these five-coordinate indium(III) complexes is undetectably small (3, 11).

Although such a process is readily invoked for tris-chelate complexes, it seems an unlikely first step in the case of the four-coordinate Me_2InL complexes. Three-coordination is relatively rare in indium(III) chemistry, and those species which are formally InX_3 are strong electron pair acceptors, readily increasing the coordination number of the metal atom to four, five, or six by the coordination of neutral or anionic ligands (12). It therefore seems most unlikely that the process

[7]

can lead to any significant formation of three coordinate species in solution. Glass and Tobias (5) suggest that this process occurs with the gallium analog, but this step is not in fact crucial to their argument for gallium, although it is a likely process in such six-coordinate species as $Me_2Sn(acac)_2$, which they also discuss in their paper.

In establishing the mechanism, we first note that $Me_2In(tfac)$ in benzene is a monomer (mol. wt. found 289; calcd. 298), and it seems reasonable to assume that the same holds for the t-butyl compound. Since benzene is a poor donor towards indium(III), the formation of dimeric or higher species in donor solvents is unlikely, and the dimethyl complexes are therefore taken to be monomeric under the conditions of the present experiments. A second important point is that $Me_2In(tfac)$ is an acceptor which forms adducts with donor ligands (see below). In the light of these experimental observations the proposed mechanism is

Can. J. Chem. Downloaded from www.nrcresearchpress.com by 210.87.254.5 on 09/05/12
For personal use only.

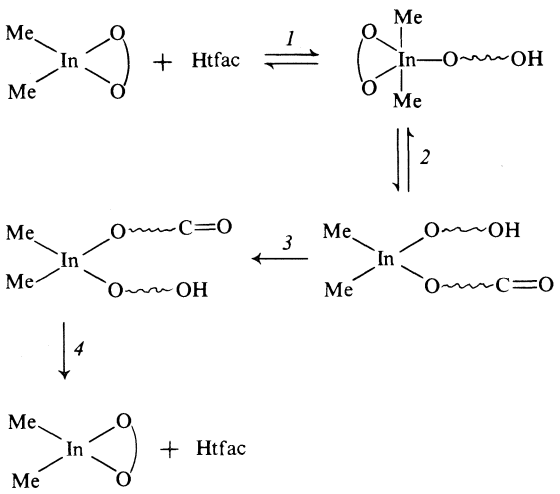

The concentration of the proposed neutral five-coordinate intermediate $[Me_2In(tfac)(Htfac)]$ is clearly given by the concentration product $K_1[Me_2In(tfac)][Htfac]$, and the experimentally determined kinetic order could be taken as identifying the formation of this species as the rate controlling step. There is, however, some information on the analogous $4 \leftrightarrow 5$-coordination change in anionic indium(III) and thallium(III) chloride complexes, and it seems that the equilibrium

[8] $$InCl_5^{2-} \rightleftharpoons InCl_4^- + Cl^-$$

has a small equilibrium constant ($K = 4.5$ for Tl(III)) (13). Similarly, it has been argued that preparative evidence points to small energy differences between $InCl_5^{2-}$ and $InCl_4^-$, and between InX_3L and InX_3L_2 adducts (12, 14, 15). While these statements apply to equilibrium studies, there is equally no evidence for a high activation energy barrier in such processes; indeed such evidence as exists implies that change of coordination number requires little activation energy in indium(III) systems. A more obviously relevant system is the $6 \rightarrow 5$-coordination change in the isomerization of $In(tfac)_3$, where the activation free energy is less than 11.0 kcal mol^{-1} (11), which is lower than the activation free energy for ligand exchange in either $In(tfac)_3$ or $Me_2In(tfac)$. We therefore assume that the formation of the intermediate $[Me_2In(tfac)(Htfac)]$ is *not* the rate-controlling process in the present system, that the forward reaction (step *1*) is fast, and the equilibrium constant for the formation of the intermediate is small.

This leaves either the ring-opening process (step *2*) or the intramolecular proton transfer (step *3*) as possible rate-controlling processes. Without repeating the arguments presented in ref. 3, it seems that the more likely process is step 3, in which the partial double-bond character of the monodentate ligand system hinders the rotation which must precede proton transfer from one monodentate diketonate ligand to the other. The rate is given by:

$$R = k_3[Me_2In(tfac)(Htfac)]$$
$$= K_1K_2k_3[Me_2In(tfac)][Htfac]$$

in agreement with the experimental result (eq. 1).

The experimentally determined activation free energies displayed in Table 4 are some 3–6 kcal mol^{-1} lower than those reported previously for exchange in InL_3/HL systems. This seems not unreasonable, since the ligand rotation process in the InL_3 case is occurring within the constraints of a six-coordinate species, whereas in the present work the transition state is in the more open four-coordinate complex. The order of activation free energies with respect to R and solvent is similar to that found in the earlier work; in particular, basic solvents enhance the rate of exchange, presumably by acting as a bridge in the intramolecular proton transfer process. In general, the kinetic evidence on exchange in InL_3/HL and Me_2InL/HL systems supports a simple mechanism which applies to both systems.

Preparative Evidence

A large number of adducts of neutral and anionic indium(III) halides, pseudohalides, dithiolates, etc., has been described in the literature (12), and, as noted above, the existence of such adducts supports the formation of the species $[Me_2In(tfac)(Htfac)]$ in step *1* of the reaction mechanism. It seemed worthwhile to confirm the acceptor properties of $Me_2In(tfac)$ by the preparation of addition compounds with 2,2′-bipyridyl, 1,10-phenanthroline, and 1,2-bis-(diphenylphosphino)ethane. The 1:1 adducts are air-stable crystalline materials, white (diphos) or pale yellow (bipy, phen) in color, and soluble in chloroform. The 1,10-phenanthroline com-

Can. J. Chem. Downloaded from www.nrcresearchpress.com by 210.87.254.5 on 09/05/12
For personal use only.

plex is a monomer in benzene solution (mol. wt. found 522, calculated 478). The compound $Me_2In(tfac)(bipy)$ is the methyl analog of $Cl_2In(acac)(bipy)$, whose preparation was reported elsewhere (1), and whose structure (16) has been shown by X-ray methods to be that of the *cis*-isomer of a six-coordinate $InO_2N_2Cl_2$ species, so that it seems safe to conclude that the adducts of $Me_2In(tfac)$ are also six-coordinate indium(III) complexes.

The ^1H and ^{19}F n.m.r. spectra of these addition compounds are summarized in Table 2. In freshly prepared solutions, all three compounds show two resonances due to the methyl groups attached to indium, confirming the *cis*-stereochemistry proposed above, since only one resonance would be observed for a *trans*-octahedral species. There are a number of interesting stereochemical problems with these $InO_2N_2Me_2$ compounds, but these problems are more suitably discussed in terms of the five- and six-coordinate adducts of dimethyl(acetato)indium(III), since the crystal structure of this compound is known (17); these matters will be discussed in a future publication (18). In general, the preparative work described here, and that on the derivatives of $Me_2In(OAc)$ confirms the reality of the equilibrium *1* in the proposed reaction mechanism.

This work was supported in part by Operating Grants from the National Research Council of Canada.

1. J. G. Contreras and D. G. Tuck. J. Chem. Soc. Dalton. 1249 (1974).
2. D. G. Tuck. Proceedings of C.N.R.S. Conference No. 191, Editions du C.N.R.S. 1970. p. 159.
3. G. M. Tanner, D. G. Tuck, and E. J. Wells. Can. J. Chem. **50**, 3950 (1972).
4. G. E. Coates and R. A. Whitcombe. J. Chem. Soc. 3351 (1956).
5. G. E. Glass and R. S. Tobias. J. Organometal. Chem. **15**, 481 (1968).
6. H. C. Clark and A. L. Pickard. J. Organometal. Chem. **13**, 61 (1968).
7. L. M. Dennis, R. W. Work, and E. G. Rochow. J. Am. Chem. Soc. **56**, 1047 (1934).
8. J. A. Pople, W. G. Schneider, and H. J. Bernstein. High resolution nuclear magnetic resonance. McGraw-Hill, New York. 1959. p.223.
9. H. S. Gutowsky and C. H. Holm. J. Chem. Phys. **25**, 1228 (1956).
10. A. C. Adams and E. M. Larsen. Inorg. Chem. **5**, 814 (1966).
11. R. C. Fay and T. S. Piper. Inorg. Chem. **3**, 348 (1964).
12. A. J. Carty and D. G. Tuck. Prog. Inorg. Chem. In press.
13. D. F. Shriver and I. Wharf. Inorg. Chem. **8**, 2167 (1969).
14. A. J. Carty and D. G. Tuck. J. Chem. Soc. A, 1081 (1966).
15. J. Gislason, M. H. Lloyd, and D. G. Tuck. Inorg. Chem. **10**, 1907 (1971).
16. J. G. Contreras, F. W. B. Einstein, and D. G. Tuck. Unpublished results.
17. F. W. B. Einstein, M. M. Gilbert, and D. G. Tuck. J. Chem. Soc. Dalton, 248 (1973).
18. J. J. Habeeb and D. G. Tuck. Can. J. Chem. This issue.

Can. J. Chem. Downloaded from www.nrcresearchpress.com by 210.87.254.5 on 09/05/12
For personal use only.

Coordination Compounds of Indium. Part XXVII.[1] Addition Compounds of Acetato(dimethyl)indium(III)

J. J. HABEEB AND D. G. TUCK

Department of Chemistry, University of Windsor, Windsor, Ontario N9B 3P4

Received June 14, 1974

J. J. HABEEB and D. G. TUCK. Can. J. Chem. **52**, 3950 (1974).

The compound $Me_2In(OAc)$, which is polymeric in the crystalline state, reacts with neutral donor ligands in organic solvents to yield three series of adducts. With monodentate donors, the product is $Me_2In(OAc)L$ (L = dimethylsulfoxide or pyridine), which is formulated as a five-coordinate monomer in solution. With bidentate donors, the product is either the monomeric six-coordinate $Me_2In(OAc)L^{II}$ (L^{II} = ethylenediamine or 1,2-bis(diphenylphosphino)-ethane), or the complex $[Me_2In(OAc)]_2L^{II}$ (L^{II} = 2,2′-bipyridyl or 1,10-phenanthroline). The n.m.r. and vibrational spectra of these compounds are discussed.

J. J. HABEEB et D. G. TUCK. Can. J. Chem. **52**, 3950 (1974).

Le composé $Me_2In(OAc)$, polymère à l'état cristallin, réagit dans des solvants organiques avec des ligands donneurs neutres pour donner trois séries de produits d'addition. Avec des donneurs monodentates, le produit est $Me_2In(OAc)L$ (L = diméthylsulfoxyde ou pyridine), qui est considéré en solution, comme un monomère pentacoordonné. Avec des donneurs bidentates, le produit est soit le monomère hexacoordonné $Me_2In(OAc)L^{II}$ (L^{II} = éthylène-diamine ou bis(diphénylphosphino)-1,2 éthane), soit le complexe $[Me_2In(OAc)]_2L^{II}$ (L^{II} = bipyridyl-2,2′ ou phénanthroline-1,10). On discute les spectres r.m.n. et vibrationnels de ces produits. [Traduit par le journal]

Introduction

In the course of earlier work on the chemistry of organoindium compounds, the crystal structure of acetato(dimethyl)indium(III), $Me_2In(OAc)$, was determined by X-ray methods (1). The crystal structure of this substance, which was first prepared by Clark and Pickard (2), is based on a six-coordinate indium atom, bonding to two approximately *trans*-methyl groups and a bidentate acetate group, with two weaker In–O contacts from different adjacent acetate groups. The overall effect is to give a polymeric crystal structure involving Me_2InO_4 coordination. The analogous $Et_2In(OAc)$ has a very similar structure (3), while thioacetato(diethyl)indium(III) differs in that only the oxygen atom of the bidentate thioacetate group takes part in bridge formation (4). Such structures are all in keeping with the tendency of indium(III) to be five- or six-coordinate when bonded to small electronegative ligand atoms (5).

The mass spectrum of $Me_2In(OAc)$ at 90 °C showed the presence of derivatives of monomeric species, including the molecular ion, in the gas phase, but in addition ions such as $[Me_2In_2(OAc)_2]^+$ and $[Me_2In_2(OAc)]^+$ were detected (6), implying that thermal decomposition may lead to the formation of both monomeric and dimeric residues by the break-down of the crystalline polymer. We have now investigated another process which involves depolymerization, namely the formation of adducts of $Me_2In(OAc)$ with typical mono- and bidentate neutral donor molecules. In this work too, derivatives of both $Me_2In(OAc)$ and $[Me_2In(OAc)]_2$ have been obtained; spectroscopic methods have been used in elucidating the structures of these compounds.

[1]For Part XXVI, see ref. 8.

Experimental

General

Spectroscopic and analytical techniques were as in earlier work. Acetato(dimethyl)indium(III) was prepared by the reaction of trimethylindium and acetic acid (2), and purified by sublimation.

Preparative

Addition compounds of $Me_2In(OAc)$ with 1,10-phenanthroline (phen) and 1,2-bis(diphenylphosphino)ethane (diphos) were prepared by mixing solutions of the reactants in ethanol, followed by the addition of dry ether to precipitate the adduct. With 2,2′-bipyridyl (bipy), the reaction was carried out in 1:1 ethanol:chloroform. In the case of dimethylsulfoxide (dmso) and ethylenediamine (en), $Me_2In(OAc)$ was dissolved in excess ligand, which was subsequently pumped off *in vacuo*. The white solids obtained by these various routes were washed several times with dry ether and dried *in vacuo*. The analytical results are given in Table 1.

Can. J. Chem. Downloaded from www.nrcresearchpress.com by 210.87.254.5 on 09/05/12
For personal use only.

TABLE 1. Analytical results on adducts of Me_2InOAc

Compound	Found (%)				Calculated (%)			
	C	H	N	In	C	H	N	In
$Me_2In(OAc).dmso$	25.4	5.3	—	40.8	25.5	5.3	—	40 8
$Me_2In(OAc).py$*	—	—	—	40.0	38.1	4.9	4.9	40.5
$[Me_2In(OAc)]_2.bipy$	37.9	4.6	4.9	40.0	38.3	4.6	5.0	40.8
$[Me_2In(OAc)]_2.phen$	40.0	4.3	4.7	39.4	40.7	4.6	4.7	39.1
$Me_2In(OAc).en$	27.1	6.5	10.8	43.2	27.2	6.5	10.6	43.5
$Me_2In(OAc).diphos$	59.6	5.3	—	19.3	59.8	5.5	—	19.1

*Acetate: calcd., 20.9; found, 20.6.

The pyridine adduct is the most unstable of the compounds prepared in this study. Acetato(dimethyl)indium(III) dissolves in dry pyridine; the addition of ether produced no precipitate, but removal of the excess by pumping left a residue of hard yellow solid. Analysis of this material immediately after washing with heptane showed it to be the 1:1 adduct (see Table 1), which loses pyridine on standing. A typical C, H, and N analysis was done some four days after the original preparation (*cf.* Table 1).

Anal. Calcd. for $(CH_3)_2InO_2C_2H_3 \cdot 0.17C_5H_5N$: C, 26.7; H, 4.6; N, 1.1. Found: C, 26.0; H, 4.4; N, 1.1.

The pyridine adducts of indium(III) triacetate and triformate also lose pyridine on standing at room temperature (6).

Results and Discussion

The analytical results show that three series of adducts of $Me_2In(OAc)$ can be prepared, namely $Me_2In(OAc)L$ (L = monodentate neutral donor), $Me_2In(OAc)L^{II}$ (L^{II} = bidentate neutral donor), and $[Me_2In(OAc)]_2L^{II}$. It will be convenient to discuss the spectroscopic and structural information on these three groups separately.

$Me_2In(OAc)L$ Compounds

Acetato(dimethyl)indium(III) dissolves readily in dimethylsulfoxide at room temperature, and molecular weight determinations showed that the solute species is a monomer (Mol. wt. for $Me_2In(OAc)$ requires $M = 204$; found 198, 210), presumably solvated by dimethylsulfoxide. The n.m.r. ^1H spectrum at 60 MHz shows only one sharp resonance for the methyl group bonded to indium (at 0.52 p.p.m. from external TMS in $CDCl_3$, and at 0.05 p.p.m. from TMS in dmso-d_6), and one for the acetato methyl group (at 2.48 p.p.m. in $CDCl_3$, 2.15 p.p.m. in dmso-d_6). The vibrational spectrum of solid $Me_2In(OAc).dmso$ has two bands in the In—CH_3 stretching region (R, 499 vs, 551 w; i.r., 496 m, 553 s cm^{-1}), corresponding to ν_{sym} and ν_{as} of the Me_2In group in the adduct (*cf.* frequencies of 496 and 551 cm^{-1} in $Me_2In(OAc)$ (2, 6)). The Raman band at 499 cm^{-1} is also seen in the spectrum of a solution of $Me_2In(OAc)$ in dimethylsulfoxide. The In—CH_3 rocking mode is at 736 m cm^{-1} in the solid, and the main acetate group vibrations are at 1565, 1468, and 958 cm^{-1}, which represent only slight changes from the spectrum of the parent compound (*cf.* ref. 6), but serve to show that the acetate group remains bonded in a bidentate manner to the metal atom. A band at 1020 cm^{-1} is assigned to ν(S—O) of oxygen-bonded dimethylsulfoxide.

The structural conclusion to be drawn from these results is that a monomeric $Me_2In(OAc).dmso$ species is present in solution, and in keeping with other InX_3L_2 species (5), the molecule is assigned the *trans* trigonal bipyramidal structure shown. A distorted form of this monomer

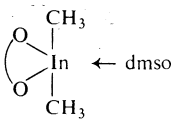

may also be present in the solid state, although it is more likely that intermolecular bridging via the acetato oxygen atoms produces a polymeric structure (*cf.* the discussion of the bipy complex below). The frequencies of the In—CH_3 and acetate vibrations are not sufficiently sensitive to be used diagnostically with any certainty in this context (2, 6).

A similar situation applies in the pyridine case. The ^1H n.m.r. spectrum in pyridine-d_5 has singlets at 2.18 (OAc) and 0.05 p.p.m. (CH_3—In) from external TMS, and the vibrational spectrum of the solid in the ν(In—CH_3) region (R, 492 s, 548 vw; i.r., 498 w, 555 s cm^{-1}) resembles that of the dmso adduct. The spectrum of a freshly prepared sample shows the typical bands of coordinated pyridine, but these disappear as pyridine is lost on standing, (*cf.* Preparative above),

Can. J. Chem. Downloaded from www.nrcresearchpress.com by 210.87.254.5 on 09/05/12
For personal use only.

leaving the spectrum of the parent $Me_2In(OAc)$. Here again then, the evidence points to a trigonal pyramidal structure for $Me_2In(OAc).py$ in solution with *trans*-methyl groups, but a probable polymeric lattice in the solid state.

$Me_2In(OAc)L^{II}$ Compounds

A complete analysis of the vibrational spectrum of $Me_2In(OAc)$diphos is not possible because of the rich spectrum of the ligand itself. In particular, three strong bands at 442, 476, and 511 cm^{-1} in the infrared obscure part of the $\nu(In—CH_3)$ region, allowing only the absorption at 554 m cm^{-1} to be assigned to this vibration (presumably ν_{as} by analogy with other compounds). A Raman band at 498 s cm^{-1} is assigned to ν_{sym} of $In—CH_3$.

The n.m.r. spectrum of diphos itself in CD_2Cl_2 consists of the phenyl group resonances at 7.15 p.p.m., and a 1:2:1 triplet centered at 2.05 p.p.m., with a coupling constant of 7.0 Hz, clearly therefore due to the ethylene bridge protons. In the $Me_2In(OAc)$ adduct, this triplet is centered at 2.06 p.p.m., where it is almost coincident with the acetate methyl group resonance at 2.00 p.p.m. Two resonances of equal intensity are observed for the $CH_3—In$ groups in freshly prepared solutions in both CD_2Cl_2 and $CDCl_3$ (at +0.05 and −0.02 p.p.m.). As with the phenanthroline case discussed below, the $CH_3—In$ resonances decrease in intensity with time due to reaction with chlorinated hydrocarbon solvents. In perdeuterotoluene, the low solubility of the compound gives rise to a weak spectrum, but two equal intensity $CH_3—In$ bands are observed at +0.20 and −0.47 p.p.m. from external TMS. The presence of a sharp triplet for the C_2H_4 group shows that the compound is relatively rigid, in that the H—H coupling is not averaged out by any intramolecule motion. Similarly, the detection of two $CH_3—In$ resonances is to be expected for a kinetically stable monomeric species with a *cis*-$(CH_3)_2InO_2P_2$ kernel. This stereochemistry is identical to that established by X-ray methods (7) for the compound $Cl_2In(acac)(bipy)$, while recent preparative work in this laboratory (8) has also yielded compounds such as $Me_2In(tfac)$(diphos) (tfac = $CF_3.CO.CH.CO.CH_3^-$ anion), for which *cis*-dimethyl groups were postulated on the basis of n.m.r. spectroscopy. There is an increasing accumulation of evidence that such compounds are predominantly in the *cis* form, and the reasons for this have been discussed elsewhere (5).

The ethylenediamine adduct gave a more complicated set of spectra. Vibrational spectroscopy again showed two $In—CH_3$ stretching modes (R, 521 w, 490 vs; i.r., 524 m, 492 w cm^{-1}), and confirmed the coordination of ethylenediamine to the metal. The ^1H n.m.r. spectrum of $Me_2In(OAc).en$ in $CDCl_3$ is strongly temperature dependent as far as the ligand protons are concerned. The dimethylindium group gives rise to a singlet at 0.47 p.p.m. upfield from external TMS over the range of temperatures investigated (0 to 60 °C; precipitation of solute prevented work below 0 °C), and while this singlet broadens slightly with increasing temperature, it does not show any significant change in frequency. The acetate methyl is likewise a sharp singlet at 2.47 p.p.m., and also appears to be temperature independent. Ethylenediamine in $CDCl_3$ shows two proton resonance at 1.50 (NH_2) and 3.07 (CH_2) p.p.m., but for the complex in the same solvent we find a sharp and a broad singlet at 3.38 (CH_2) and 2.90 (NH_2) p.p.m. respectively. The lower field resonance does not change on raising the temperature, but the NH_2 proton absorption broadens and moves to lower field, until at 55 °C it is essentially coincident with the signal due to the acetate methyl group. This behavior is reversible on lowering the temperature and is therefore not the result of reaction with the solvent. We believe that these n.m.r. spectra establish that in solution the six-coordinate complex is in rapid equilibrium with a five-coordinate species in which the ethylenediamine acts as a monodentate ligand.

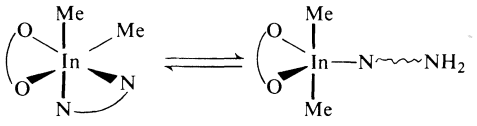

Such behavior has not been previously reported for nitrogen donor complexes of indium(III), but the related $In(tfac)_3$ (9) and $Me_2In(tfac)$ (8) systems have both been held to undergo ligand exchange via intermediates in which monodentate diketonate ligands are involved. Rapid isomerization of indium(III) tris(β-diketonate) complexes has also been explained in similar

Can. J. Chem. Downloaded from www.nrcresearchpress.com by 210.87.254.5 on 09/05/12
For personal use only.

terms (10). The proposed equilibrium explains both the shift of the NH_2 proton resonance and the presence of a single CH_3—In resonance. Conductivity measurements showed that Me_2In-(OAc).en is a nonconductor in nitromethane, so that one can rule out any equilibrium processes involving ionic dissociation of the acetate ligand.

$[Me_2In(OAc)]_2L^{II}$ Compounds

In the case of both 2,2′-bipyridyl and 1,10-phenanthroline, the analytical results on the addition compound require two molecules of $Me_2In(OAc)$ for each bidentate ligand. The molecular weight of the phenanthroline adduct in dimethylsulfoxide at 43.4 °C is 595 (calcd. 588), confirming that the compound is stable as a derivative of dimeric $Me_2In(OAc)$ under these conditions. At higher temperatures the measured molecular weight decreases, and above 75° values as low as 210 (*cf.* the molecular weight of $Me_2In(OAc)$) were recorded, showing that irreversible decomposition to $Me_2In(OAc)$ and ligand can occur under such relatively severe treatment. The actual experimental value depends both on temperature and on length of time of heating.

The spectral features of the 1,10-phenanthroline and 2,2′-bipyridyl compounds are quite similar. Both show two ν(In—CH_3) modes (phen: i.r., 530 s, 478 w, R, 480 s; bipy: i.r., 507 w, R, 503 s, 533 w cm^{-1}). The ^1H n.m.r. spectra of freshly prepared solutions have two CH_3—In resonances (phen: 0.72 and 0.42; bipy: 0.72 and 0.65 p.p.m. from TMS) and one acetate resonance (phen: 2.46; bipy: 2.42 p.p.m.). Rapid changes occur in the CH_3—In region on standing at room temperature over approximately 5–15 min, with an overall drop in intensity, and a change in the relative intensities of the two peaks, with the high field peak decreasing the more quickly. This behavior is apparently the result of a reaction between the methyl groups and chloroform; similar reactions have been observed in a number of other methylindium systems, and will be discussed more fully elsewhere.

Two possible structures can be constructed to explain these results. The first could invoke acetate bridging of the type seen in copper(II) acetate, with additional bridging by the bipyridyl molecule (structure **1**).

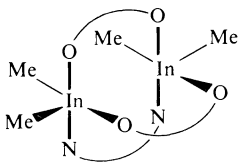

1

but this requires either five-coordinate indium, or an indium–indium bridge, both of which are unlikely in the compounds of this nature. A more likely model is that based on $Me_2In(OAc)$ itself

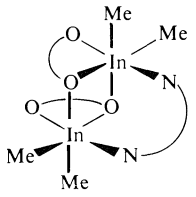

2

which possesses all the features required by the spectral results and is the structure preferred on the basis of present information.

General

Attention has been drawn on a number of occasions to the ease with which indium(III) complexes change coordination number and stereochemistry. Slight alterations in preparative conditions frequently produce significant changes in the nature of the products obtained from reactions in solution. The present work is an extreme example of such behavior, in that three different classes of compound have been identified with three different nitrogen (and other) donors. Clearly, the basicity of the ligand is one of the parameters involved in deciding on the relative stability of $Me_2In(OAc)L$, Me_2In-$(OAc)L^{II}$, and $[Me_2In(OAc)]_2L^{II}$. Strong monodentate bases can cause complete break up of the lattice. In the case of the bidentate ligands, the higher basicity of ethylenediamine relative to (say) 2,2′-bipyridyl must be one factor contributing to the formation of a derivative of monomeric, rather than dimeric, $Me_2In(OAc)$. Steric factors may also be important, since the examination of models suggests that the NH_2 protons of ethylenediamine (and, *a fortiori*, the phenyl groups of diphos) might interfere sterically with the other ligands (CH_3, acetate) in structure **2**, thus favoring the complete breakdown to the

Can. J. Chem. Downloaded from www.nrcresearchpress.com by 210.87.254.5 on 09/05/12
For personal use only.

monomeric $Me_2In(OAc).en$ (or diphos). As in other indium(III) complexes then, easy rearrangement processes, and in the case of the ethylenediamine adduct, fluxional behavior, give rise to a related series of complexes of differing stereochemistry and coordination number.

This work was supported in part by Operating Grants from the National Research Council of Canada.

1. F. W. B. Einstein, M. M. Gilbert, and D. G. Tuck. J. Chem. Soc. Dalton, 248 (1973).
2. H. C. Clark and A. L. Pickard. J. Organometal. Chem. **8**, 427 (1967).
3. H. D. Hausen. J. Organometal. Chem. **39**, C37 (1972).
4. H. D. Hausen. Z. Naturforsch. **B27**, 82 (1972).
5. A. J. Carty and D. G. Tuck. Prog. Inorg. Chem. In press.
6. J. J. Habeeb and D. G. Tuck. J. Chem. Soc. Dalton, 242 (1973).
7. J. G. Contreras, F. W. B. Einstein, and D. G. Tuck. Unpublished results.
8. H. L. Chung and D. G. Tuck. Can. J. Chem. This issue.
9. G. M. Tanner, D. G. Tuck, and E. J. Wells. Can. J. Chem. **50**, 3950 (1972).
10. R. C. Fay and T. S. Piper. Inorg. Chem. **3**, 348 (1964).

Can. J. Chem. Downloaded from www.nrcresearchpress.com by 210.87.254.5 on 09/05/12
For personal use only.

Rearrangement Studies with ^{14}C. XL. The Acetolysis of 2-Phenylethyl-1-^{14}C Triflate

CHOI CHUCK LEE AND DON UNGER

Department of Chemistry and Chemical Engineering, University of Saskatchewan, Saskatoon, Saskatchewan S7N 0W0

Received May 23, 1974

CHOI CHUCK LEE and DON UNGER. Can. J. Chem, **52**, 3955 (1974).

2-Phenylethyl-1-^{14}C triflate (**1**-OTf-1-^{14}C) was synthesized by the inverse addition of equivalent amounts of **1**-OH-1-^{14}C and pyridine to trifluoromethanesulfonic acid anhydride. Solvolysis of **1**-OTf-1-^{14}C in unbuffered HOAc resulted in about 32% rearrangement of the ^{14}C-label from C-1 to C-2, a value that is almost the same as that observed for the analogous acetolysis of **1**-OTs-1-^{14}C. Partial reaction of **1**-OTf-2-d_2 in HOAc-d_4 showed that unreacted **1**-OTf-d_2 was isotopically scrambled, indicating the occurrence of ion-pair returns. Acetolysis of **1**-OTf-1-^{14}C in the presence of added NaN_3 or NaN_3 and NaOAc, however, gave results indicating differences in behaviors between **1**-OTf and **1**-OTs and it is concluded that the acetolysis of **1**-OTf and **1**-OTs are mechanistically similar but not identical.

CHOI CHUCK LEE et DON UNGER. Can. J. Chem. **52**, 3955 (1974).

On a synthétisé le triflate de phényl-2 éthyle- ^{14}C-1 (OTf-**1**-^{14}C-1) par une addition inverse de quantités équivalentes de OH-**1**-^{14}C-1 et de pyridine à l'anhydride trifluorométhanesulfonique. La solvolyse du OTf-**1**-^{14}C-1 dans AcOH non tamponné résulte, en un réarrangement de C-1 à C-2 d'environ 32% du ^{14}C marqué, une valeur qui est à peu près la même que celle observée pour une acétolyse analogue du OTs-**1**-^{14}C-1. La réaction partielle de OTf-**1**-d_2-2 dans AcOH-d_4 montre que le OTf-1-d_2 non réagi était un mélange isotopique, indiquant l'existence d'un retour d'ions-pairs. L'acétolyse de OTf-**1**-^{14}C-1 en présence de NaN_3 ajouté ou NaN_3 et NaOAc, donne des résultats indiquant des différences dans les comportements entre OTf-**1** et OTs-**1** et on en déduit que l'acétolyse de OTf-**1** et de OTs-**1** se fait par un mécanisme comparable, mais non identique. [Traduit par le journal]

In an earlier attempt in this laboratory to synthesize 2-phenylethyl-1-^{14}C triflate (**1**-OTf-1-^{14}C) from the reaction of 2-phenylethyl-1-^{14}C iodide (**1**-I-1-^{14}C) with AgOTf, it was found that the ^{14}C-label in the product was completely scrambled between the C-1 and C-2 positions (1). A number of alternate methods of synthesis was also tried but they failed to give the desired **1**-OTf. The possibility of preparing the triflate ester from reaction of the alcohol with trifluoromethanesulfonic acid anhydride in pyridine (2) was not attempted because **1**-OTf was found to react readily with pyridine to give 2-phenylethylpyridinium triflate. Indeed this pyridinium salt may serve as a good solid derivative for **1**-OTf. In the present work, **1**-OTf-1-^{14}C was successfully synthesized by a modification of the preparation in the presence of pyridine. Instead of using pyridine as solvent, an inverse dropwise addition of equimolar amounts of **1**-OH-1-^{14}C and pyridine in CCl_4 to trifluoromethanesulfonic acid anhydride in CCl_4 gave the desired **1**-OTf-1-^{14}C, which on oxidation yielded nonradioactive PhCOOH.

In the earlier work (1), it was pointed out that since a great deal of data is available on isotopic scramblings accompanying solvolyses of 2-phenylethyl-1-^{14}C tosylate (**1**-OTs-1-^{14}C), it would be of interest to have a comparison of the behavior of the triflate and tosylate by studying similar solvolyses of **1**-OTf-1-^{14}C. When duplicate acetolyses of **1**-OTf-1-^{14}C (0.5 *M* in glacial HOAc) were effected at 50° for 2 h, **1**-OAc-^{14}C was obtained in high yields and oxidation of this product to PhCOOH indicated nearly 32% rearrangement of the ^{14}C-label from C-1 to C-2, the data being summarized in Table 1. This extent of ^{14}C scrambling is almost the same as that observed previously by Coke and co-workers (3) and by Lee *et al.* (4) for the analogous solvolysis of the tosylate ester, **1**-OTs-1-^{14}C, in unbuffered glacial HOAc (Table 1).

Internal returns during acetolysis of **1**-OTs-1-^{14}C gave rise to extensive scrambling of the label in the tosylate ester recovered at different stages of completion of the reaction (3). In our previous work (1), the rate of acetolysis of **1**-OTf at 30° was found to be 9.44×10^{-5} s^{-1},

Can. J. Chem. Downloaded from www.nrcresearchpress.com by 210.87.254.105 on 09/05/12
For personal use only.

Can. J. Chem. Downloaded from www.nrcresearchpress.com by 210.87.254.105 on 09/05/12
For personal use only.

TABLE 1. Data from solvolyses of 0.5 *M* 2-phenylethyl-1-^{14}C triflate (**1**-OTf-1-^{14}C) in HOAc with or without added salt

Added salt	Product yield (%)*		Specific activity (d.p.m./mmol)				Rearrangement from C-1 to C-2 (%)		Rearrangement in reaction with **1**-OTs-1-^{14}C (%)	
	1-OAc	**1**-N_3	**1**-OAc	PhCOOH	**1**-N_3	PhCOOH	**1**-OAc	**1**-N_3	**1**-OAc	**1**-N_3
None	95.8		274 000	86 900			31.7		32.6†	
None	97.6		345 000	110 000			31.9		31.4‡	
0.7 *M* NaN_3	85.2	5.4	289 000	54 500	33 300	8350	18.9	25.1	8.1‡	5.8‡
0.7 *M* NaN_3	88.9	5.5	304 000	53 700	33 300	8000	17.7	24.0		
0.7 *M* NaN_3 + 0.7 *M* NaOAc	85.1	6.5	292 300	31 600	59 800	5550	10.8	9.3		
0.7 *M* NaN_3 + 0.7 *M* NaOAc	88.6	5.9	279 000	30 200	45 900	4260	10.8	9.3		

*Obtained from isotope dilution calculations.
†From ref. 3.
‡Mean value of duplicate runs from ref. 4.

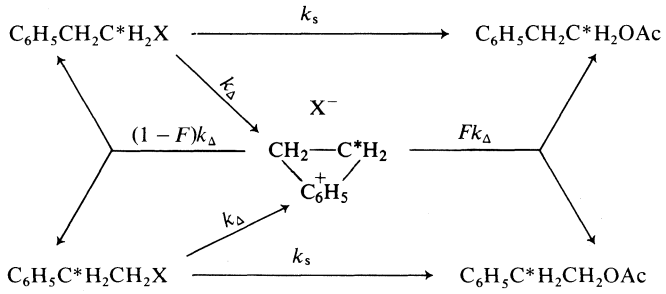

(X = OTs or OTf)

SCHEME 1

which was faster than the corresponding rate for **1**-OTs by a factor of about $10^{4.9}$. Thus with the more reactive **1**-OTf-1-^{14}C as substrate, while it should be possible to stop the reaction before completion, reisolation of the triflate ester for studies of scrambling arising from internal returns likely would be difficult to carry out in practice. In the present work, internal returns were investigated by treating 2-phenylethyl-2,2-d_2 triflate (**1**-OTf-2-d_2) in HOAc-d_4 in an n.m.r. tube and monitoring the D-distributions by n.m.r. At 30° after reaction times of 3.25 and 5.0 h, it was noted that the rearrangement of the D-label from C-2 to C-1 in the **1**-OAc-d_2 product was 34 and 35%. For the unreacted **1**-OTf-d_2 present in the same reaction mixture, the analogous extents of D-scrambling were 24 and 33%, respectively, at 3.25 and 5.0 h. These results thus demonstrate that similar to **1**-OTs, extensive return processes also occur during the acetolysis of **1**-OTf. Such behavior together with the nearly identical ^{14}C-scrambling in the reaction products from **1**-OTf-1-^{14}C and **1**-OTs-1-^{14}C suggests that acetolyses of **1**-OTf and **1**-OTs are mechanistically similar, thus lending further support to the conclusion of Streitwieser and co-workers (5, 6), arrived at for the ethyl and propyl systems, that solvolysis of triflates is no more limiting than that of tosylates.

As shown in Scheme 1, the overall extent of ^{14}C scrambling in the **1**-OAc-^{14}C from the acetolysis of either **1**-OTf-1-^{14}C or **1**-OTs-1-^{14}C would be the composite result of product formation from the ethylenebenzenium ion (the k_Δ process) and from direct displacement (the k_s process) which may involve rearranged starting material that resulted from ion-pair returns (3, 4). While about 32% rearrangement was observed in the acetolysis of either **1**-OTf-1-^{14}C or **1**-OTs-1-^{14}C, it is likely, however, that various competing processes did not contribute in identical ways to the net rearrangement in the reactions with the two sulfonate esters.

The azide ion is a strong nucleophile and it has been utilized as a mechanistic probe for the k_s process in the acetolysis of **1**-OTs-1-^{14}C (4). When **1**-OTf-1-^{14}C was acetolyzed in the presence of added NaN_3 or NaN_3 and NaOAc, the results, also summarized in Table 1, show that there are differences in behavior between **1**-OTf-1-^{14}C and **1**-OTs-1-^{14}C. The presence of 0.7 *M* NaN_3 in the acetolysis of 0.5 *M* **1**-OTs-1-^{14}C decreased the extent of ^{14}C scrambling in the resulting **1**-OAc-^{14}C to about 8%, and furthermore, the **1**-N_3-^{14}C obtained from the same reaction was rearranged to a lesser extent than the acetate (4). On the other hand, the analogous acetolysis of **1**-OTf-1-^{14}C in the presence of NaN_3 (Table 1) gave a **1**-OAc-^{14}C product with about 18% rearrangement, whereas the **1**-N_3-^{14}C obtained was rearranged to a greater extent than the acetate.

In discussing the results from **1**-OTs-1-^{14}C (4), it was suggested that a factor that might have played a part in decreasing the rearrangement could be that in the presence of added NaN_3, the reaction rate was enhanced (7, 8). In fact, the acetolysis of 0.5 *M* **1**-OTs in the presence of 0.7 *M* NaN_3 has been found to be about 13 times faster than the analogous reaction without any added NaN_3 (9). With a faster reaction in the presence of NaN_3, there would be less opportunity for the occurrence of many cycles of ion-pair formation and ion-pair returns, thus resulting in a lower amount of rearrangement in the reaction product. Similar explanations could be applied to the results obtained in the acetolysis of **1**-OTf-1-^{14}C in the presence of NaN_3; how-

Can. J. Chem. Downloaded from www.nrcresearchpress.com by 210.87.254.105 on 09/05/12
For personal use only.

Can. J. Chem. Downloaded from www.nrcresearchpress.com by 210.87.254.105 on 09/05/12
For personal use only.

ever, the differences observed in the actual magnitudes of rearrangement in the **1**-OAc-^{14}C and **1**-N_3-^{14}C products from **1**-OTf-1-^{14}C and **1**-OTs-1-^{14}C could be regarded as indications that there are differences in the relative contributions of the k_s, k_Δ, and ion-pair return processes in the acetolysis of the two esters, **1**-OTf and **1**-OTs.

From the acetolysis of **1**-OTf-1-^{14}C in the presence of added NaN_3, the findings of more isotopic scrambling in the **1**-N_3-^{14}C than the **1**-OAc-^{14}C is unexpected. While the reason for this observation is not completely clear, a possible explanation may lie in the fact that different sulfonic acids are liberated during the solvolysis of **1**-OTs-1-^{14}C and **1**-OTf-1-^{14}C. Coke and coworkers (3) have noted that the presence of HOTs during acetolysis of **1**-OTs-1-^{14}C has a slight effect on the extent of rearrangement, tending to increase it. The stronger sulfonic acid, HOTf, liberated during the acetolysis of **1**-OTf-1-^{14}C, may exert a greater influence on the isotopic rearrangement, and this effect may be different for the formation of **1**-OAc-^{14}C and **1**-N_3-^{14}C. Thus while the acetolysis of **1**-OTs-1-^{14}C with added NaN_3 (4) gave **1**-OAc-^{14}C and **1**-N_3-^{14}C with rearrangements of about 8 and 6%, respectively, the analogous reaction with **1**-OTf-1-^{14}C gave **1**-OAc-^{14}C and **1**-N_3-^{14}C, respectively, with about 18 and 25% rearrangement (Table 1). When the acetolysis of **1**-OTf-1-^{14}C was carried out in the presence of NaN_3 and NaOAc, the liberated HOTf would be neutralized. The presence of both acetate and azide ions would enhance the k_s processes, and the overall rearrangements in both **1**-OAc-^{14}C and **1**-N_3-^{14}C were lowered to about 11 and 9%, respectively (Table 1), with less rearrangement in the **1**-N_3-^{14}C since the azide ion is a stronger nucleophile. Thus considering all the results from the present work, it may be concluded that the acetolyses of **1**-OTf and **1**-OTs are mechanistically similar but not identical.

Experimental

2-Phenylethyl-1-^{14}C Triflate (1-OTf-1-^{14}C)

A solution of 4.88 g (40 mmol) of **1**-OH-1-^{14}C and 3.16 g (40 mmol) of pyridine in 20 ml of CCl_4 was added dropwise to 11.28 g (40 mmol) of trifluoromethanesulfonic acid anhydride dissolved in 10 ml of CCl_4 and maintained at ice bath temperature. The reaction mixture immediately turned yellow and the pyridinium triflate salt that was formed precipitated and was removed by filtration through Celite. The filtrate was decolorized several times with activated charcoal and the solvent was distilled off leaving 8.1 g (82%) of **1**-OTf-1-^{14}C. After purification by distillation at 65–70° and 1 Torr, the n.m.r. and mass spectra of the product were identical to those reported earlier for **1**-OTf (1). Oxidation of the product by alkaline $KMnO_4$ gave nonradioactive PhCOOH.

2-Phenylethylpyridinium Triflate

To a solution of 1.58 g (20 mmol) of pyridine in 10 ml of CCl_4 was added dropwise 2.54 g (10 mmol) of **1**-OTf. A colorless oil immediately separated out and solidified upon standing. The 2-phenylethylpyridinium triflate was collected by filtration and recrystallized from ethanol to give 3.0 g (90%) of the salt, m.p. 101–104°; n.m.r. (acetone-d_6) δ 9.07, 8.67, 8.12 (m, pyridine H's, 5) 7.25 (m, Ar H's, 5) 5.05 (t, C-1 H's, 2) 3.45 (t, C-2 H's, 2).

Anal. Calcd. for $C_{14}H_{14}O_3NSF_3$: C, 50.50; H, 4.20; N, 4.20. Found: C, 50.33; H, 4.37; N, 4.17.

Acetolysis Reactions

The reactions were carried out at 50° for 2 h with 0.5 *M* solutions of **1**-OTf-1-^{14}C in glacial HOAc with or without the presence of 0.7 *M* NaN_3 or 0.7 *M* NaN_3 and 0.7 *M* NaOAc. Inactive carriers, **1**-OAc or **1**-OAc and **1**-N_3, were added prior to product isolation so that yields could be calculated by isotope dilution. A typical run is described below.

A solution of 3.18 g (12.5 mmol) of **1**-OTf-1-^{14}C in 25 ml of glacial HOAc was heated at 50° for 2 h. The resulting material was poured into 100 ml of ice water and an appropriate amount of ordinary **1**-OAc was added as carrier. The mixture was then extracted several times with pentane and the combined extract was washed with H_2O, dried over $MgSO_4$, and fractionated to give **1**-OAc-^{14}C. Knowing the weights of carrier added and the specific activities of the **1**-OTf-1-^{14}C and the recovered **1**-OAc-^{14}C, isotope dilution calculations gave the yield of acetate product.

The reaction products, **1**-OAc-^{14}C or **1**-OAc-^{14}C and **1**-N_3-^{14}C, were converted to solid derivatives for ^{14}C assays as previously described (4). Oxidation of the products with alkaline $KMnO_4$ yielded PhCOOH whose activity gave the extent of rearrangement of the ^{14}C-label from C-1 to C-2.

Studies on Ion-pair Returns

$PhCD_2COOH$, obtained from several cycles of exchange and reisolation by prolonged refluxing of $PhCH_2COONa$ in D_2O, was reduced with $LiAlH_4$ to give **1**-OH-2-d_2 which in turn was converted to **1**-OTf-2-d_2 in the same way as in the analogous conversion of **1**-OH-1-^{14}C to **1**-OTf-1-^{14}C. While the n.m.r. spectrum of **1**-OTf showed triplets at δ 4.60 and 3.08 for the C-1 and C-2 protons, in the spectrum of **1**-OTf-2-d_2, the triplet at δ 3.08 has disappeared and the triplet at δ 4.60 became a broad singlet. A 10% solution of **1**-OTf-2-d_2 in HOAc-d_4 was placed in an n.m.r. tube and maintained at 30° in a water bath. The n.m.r. spectrum was taken after 3.25 and 5.0 h. Besides the signals at δ 4.6 and 3.0 for the C-1 and C-2 protons of the triflate substrate, the C-1 and C-2 protons of the acetate product appeared at δ 4.2 and 2.8. From the integrated areas of these peaks, deuterium scramblings in the unreacted **1**-OTf-d_2 and the **1**-OAc-d_2 product were determined.

The financial support given by the National Research Council of Canada is gratefully acknowledged.

1. C. C. Lee and D. Unger. Can. J. Chem. **51**, 1494 (1973).
2. T. M. Su, M. F. Sliwinski, and P. v. R. Schleyer. J. Am. Chem. Soc. **91**, 5386 (1969).
3. J. L. Coke, F. E. McFarlane, M. C. Mourning, and M. G. Jones. J. Am. Chem. Soc. **91**, 1154 (1969).
4. C. C. Lee, D. Unger, and S. Vassie. Can. J. Chem. **50**, 1371 (1972).
5. A. Streitwieser, Jr., C. L. Wilkens, and E. Kiehlmann. J. Am. Chem. Soc. **90**, 1598 (1968).
6. G. A. Dafforn and A. Streitwieser, Jr. Tetrahedron Lett. 3159 (1970).
7. D. J. Raber, J. M. Harris, R. E. Hall, and P. v. R. Schleyer. J. Am. Chem. Soc. **93**, 4821 (1971).
8. D. J. Raber, J. M. Harris, and P. v. R. Schleyer. J. Am. Chem. Soc. **93**, 4829 (1971).
9. D. Unger. Ph.D. Thesis, University of Saskatchewan, Saskatoon, Saskatchewan, 1973.

Can. J. Chem. Downloaded from www.nrcresearchpress.com by 210.87.254.105 on 09/05/12
For personal use only.

Formation of Adducts in the Nitration of *p*-Xylene. Exchange and Rearomatization Reactions of *p*-Xylene Adducts

ALFRED FISCHER AND JOHN NEILSON RAMSAY

Department of Chemistry, University of Victoria, Victoria, British Columbia V8W 2Y2

Received May 13, 1974

ALFRED FISCHER and JOHN NEILSON RAMSAY. Can. J. Chem. **52**, 3960 (1974).

Nitration of *p*-xylene in acetic anhydride gives as the major product *cis* and *trans* isomers of the adduct 1,4-dimethyl-4-nitro-1,4-dihydrophenyl acetate (**1**) as well as 2-nitro-*p*-xylene. The acetoxynitro adducts **1***a* and **1***b* are stereospecifically cleaved to the hydroxynitro adducts **2***a* and **2***b*, respectively, by sodium methoxide. Acid-catalyzed exchange of OAc in **1** for OCH_3, OCHO, $OCH_2C_6H_4CH_3$-*p* occurs and is nonstereospecific. Rearomatization of **1** gives 2-nitro-*p*-xylene, side-chain (benzylic) derivatives, and 2,5-xylyl acetate. The relevance of these reactions to side-chain substitution of arenes under electrophilic conditions is discussed.

ALFRED FISCHER et JOHN NEILSON RAMSAY. Can. J. Chem. **52**, 3960 (1974).

La nitration du *p*-xylène dans l'anhydride acétique conduit comme produits majeurs aux isomères *cis* et *trans* de l'adduit acétate de diméthyl-1,4 nitro-4 dihydro-1,4 phényle (**1**), de même qu'au nitro-2 *p*-xylène. Le méthylate de sodium coupe les adduits acétoxynitro **1***a* et **1***b* d'une manière stéréospécifique et conduit aux adduits hydroxynitro **2***a* et **2***b*. L'échange, catalysé par les acides, du groupe OAc dans **1** pour OCH_3, OCHO, $OCH_2C_6H_4CH_3$-*p* se produit d'une manière non-stéréospécifique. La réaromatisation de **1** conduit au nitro-2 *p*-xylène, à des dérivés benzylique et à l'acétate de xylyl-2,5. On discute du rapport qui existe entre ces réactions et les réactions de substitution sur la chaine latérale qui se produisent sur des arènes dans des conditions électrophiles. [Traduit par le journal]

Introduction

Electrophilic attack at a substituted position (*ipso* attack (1)) is well established. *Ipso* nitration of methylbenzenes in acetic anhydride affords nitronium acetate (acetyl nitrate) adducts which contain the 4-nitro-1,4-dihydro-*p*-tolyl acetate moiety (2). The diastereoisomeric adducts[1] **1** were among the first examples of such compounds to be isolated (2*b*). The present paper reports the conversion of the acetoxydienes **1** to the corresponding hydroxy **2**, methoxy **3**, and formyloxy **4** compounds, and delineates the rearomatization reactions of tertiary acetate adducts. It is because of the concomitant gain in resonance energy that the adducts readily undergo such rearomatization reactions. Indeed, the challenge in working with these compounds is to prevent inadvertent rearomatization. Secondary acetate adducts afford aryl acetates by elimination of nitrous acid (2*a–c*, 3) and nitroarenes by elimination of acetic acid accompanied by the migration of the nitro group. Both 1,2- and 1,3-shifts of nitro groups have been observed (4, 5, 3*b*, *c*). Tertiary acetate adducts, in which the simple 1,4-elimination of nitrous acid cannot occur, exhibit a greater variety of rearomatization reactions. One of these reactions is the

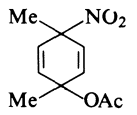

1*a*

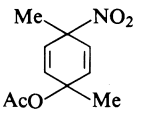

1*b*

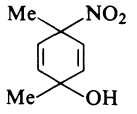

2*a*

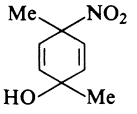

2*b*

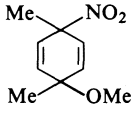

3*a*

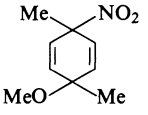

3*b*

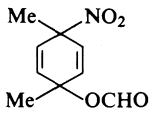

4

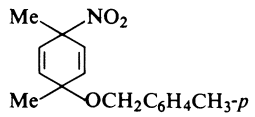

5

[1]Individual members of a pair of diastereoisomeric adducts are designated as *a* and *b*.

Can. J. Chem. Downloaded from www.nrcresearchpress.com by 210.87.254.6 on 09/05/12
For personal use only.

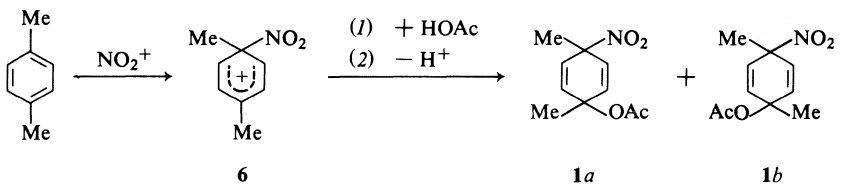

6 1*a* 1*b*

SCHEME 1

formation of side-chain (benzylic) derivatives (2*d*, 6). Side-chain substitution of arenes under electrophilic conditions is a well-established reaction and has been actively investigated by Baciocchi and co-workers (7) and by Suzuki and co-workers (8). Both groups have proposed a number of speculative mechanisms for side-chain substitution but no structural evidence which demonstrates the existence of any proposed intermediate has been adduced. However they have established through reactivity studies that the initial step in side-chain substitution is similar to that for nuclear substitution *viz.* attack by the electrophile at an aromatic ring position (9, 10). The present work on the *p*-xylene adducts and the preliminary report on the pseudocumene adducts (2*d*) establish that such adducts, or the *ipso* cyclohexadienyl cations from which the adducts are formed reversibly and which are obtained by *ipso* attack of nitronium ion on the arene (Scheme 1), are key intermediates in the formation of the side-chain derivatives. Furthermore, our work establishes the orientation of the side-chain substitution with respect to the initial step of *ipso* attack and delineates a common mechanistic pathway for the formation of a variety of side-chain products. Finally, we are able to relate the side-chain reactions to other rearomatization reactions leading to nitroarene and to aryl acetate.

Results and Discussion

Formation and Interconversion (Exchange) Reactions of Adducts

Reaction of *p*-xylene with nitric acid in acetic anhydride gave a mixture consisting of 80% diene adducts and 2-nitro-*p*-xylene. The acetoxynitrodienes **1***a* and **1***b* and the hydroxynitrodienes **2***a* and **2***b* were isolated from the crude product by low temperature chromatography. A small amount of an adduct identified as the *p*-methylbenzyloxynitrodiene **5** was also obtained. The acetoxynitrodienes are formed by attack of nitronium ion at an *ipso* position of *p*-xylene to form the cyclohexadienyl cation **6** which subsequently adds acetate (as acetic acid or acetic anhydride followed by deprotonation or deacetylation, respectively) to generate the pair of diastereoisomeric adducts[2] (Scheme 1). The *ipso* position in *p*-xylene is more activated than the unsubstituted position (12). The origin of the hydroxynitrodienes was not established. Cation **6** could be trapped by other nucleophiles as well as acetate, such as water. It is unlikely that water would be present in the acetic anhydride solution but it is known that nitronium nitrate (**6***a*) or nitrite[3] adducts can be formed in these reaction mixtures and it is likely that the hydroxynitrodiene is formed by solvolysis of one or the other of these on work-up. A similar origin is proposed for the *p*-methylbenzyloxynitrodiene **5**. *p*-Methylbenzyl derivatives are formed as rearomatization products of the adducts. Reaction of cation **6** with such a derivative, or its solvolytic product *p*-methylbenzyl alcohol, assumed to be formed during work-up, would give **5**. The identity of **5** was confirmed through its synthesis by reaction of the acetoxydiene **1** with *p*-methylbenzyl alcohol in chloroform containing catalytic sulfuric acid. Presumably this reaction involves the intermediate formation of cation **6** which reacts with the *p*-methylbenzyl alcohol to give **5** after deprotonation (see below).

Reaction of acetoxydiene **1***a* with sodium methoxide in methanol resulted in stereospecific conversion into **2***a*; similarly **1***b* gave **2***b* stereospecifically. The methoxide must have cleaved the ester by attack at the acyl rather than the alkyl group, otherwise methoxydiene **3** would have been formed. It follows that the stereo-

[2]Only 1,4-adducts have been obtained in all of the addition reactions studied. Two reasons can be advanced for the absence of 1,2-adducts. First, the *para* position in the cyclohexadienyl cation has a greater positive charge than the *ortho* position (11) and therefore should be more reactive towards nucleophiles. Second, there would be severe eclipsing interactions in the 1,2-adduct between the nitro or methyl group and adjacent acetate group.

[3]Unpublished work with D. R. A. Leonard.

Can. J. Chem. Downloaded from www.nrcresearchpress.com by 210.87.254.6 on 09/05/12
For personal use only.

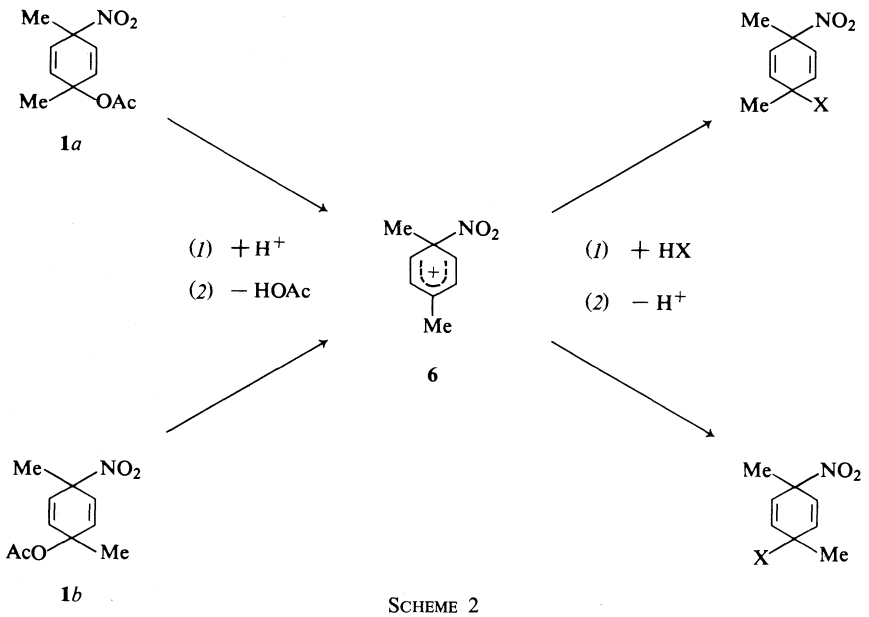

SCHEME 2

chemistry of **1***a* and **2***a* must be the same and likewise **1***b* and **2***b* must have the same stereochemistry. Base-catalyzed cleavage of a tertiary alkyl ester should conform to the $B_{AC}2$ mechanism (13) which is consistent with the above results. In contrast the acid-catalyzed methanolysis of **1***a* gave a mixture of the diastereoisomeric methoxynitrodienes **3** and likewise acid-catalyzed methanolysis of **1***b* gave the same mixture of diastereoisomers. Thus, acid-catalyzed methanolysis must involve alkyl–oxygen fission; formation of the diastereoisomeric mixture is consistent with the operation of the $A_{AL}1$ mechanism involving the intermediate cyclohexadienyl cation **6** (Scheme 2; X = OMe). The $A_{AL}1$ mechanism would be expected for the acid catalyzed solvolysis of a tertiary acetate (13) and it is especially favored here since the intermediate cation is not merely tertiary but is also stabilized by the cyclohexadienyl resonance. Even in chloroform containing only 1% methanol the exchange proceeded readily. The other exchange reactions such as the formation of the formyloxy adduct **4** on treatment of **1** with formic acid and, as mentioned above, the formation of the benzoyloxy compound **5**, and the epimerization of both **1***a* and **1***b* to form the diastereoisomeric mixture in anhydrous acetic acid, all follow the same pathway (Scheme 2: X = OCHO, $OCH_2C_6H_4CH_3$-*p*, OAc, respectively). It is likely that in solvents of low dielectric content (such as anhydrous acetic acid) the ionic species are associated. Such association, if it occurs, is without apparent effect on the reaction products and it is unnecessary to take formal account of it in the mechanism. The exchange reactions were complicated by competing or subsequent rearomatization reactions which are discussed next.

Rearomatization Reactions of Adducts

Three types of rearomatization product were obtained: (*i*) 2-nitro-*p*-xylene; (*ii*) side-chain (benzylic) derivatives; (*iii*) 2,5-xylyl acetate. The reactions leading to these products will be discussed in turn.

(i) Formation of Nitroarene

The first reported formation of a nitroarene from an acetyl nitrate adduct was that of 3-nitro-*o*-xylene from the *o*-xylene adduct on treatment with 70% sulfuric acid (4). Subsequently there have been other examples reported of the formation of aromatic nitro compounds from adducts (2*d*, 3*b*, *c*, 5). Myhre's (4) mechanism, applied to the *p*-xylene adduct **1** is shown in Scheme 3. A 1,2-nitro shift in the *ipso* cyclohexadienyl cation **6** converts it into the cyclohexadienyl cation intermediate for substitution **7**. Such a nitro shift in the cyclohexadienyl cation from hexamethylbenzene has been shown to occur readily by Olah and co-workers (14). In the case of the *p*-xylene adduct it is not possible to distinguish between a 1,2- and a 1,3-

Can. J. Chem. Downloaded from www.nrcresearchpress.com by 210.87.254.6 on 09/05/12
For personal use only.

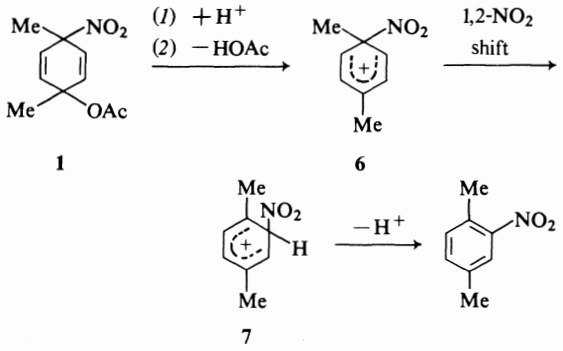

SCHEME 3

nitro shift, since both lead to 2-nitro-*p*-xylene. As mentioned in the introduction, 1,3-nitro shifts have been observed, but in those cases the 1,2-shift would give a substantially less stable cyclohexadienyl cation than either the *ipso* cation or that obtained by a 1,3-shift. Since, in the case of **6**, the cations resulting from 1,2- and 1,3-shifts are the same we suggest that the 1,2-shift is more likely. 2-Nitro-*p*-xylene was obtained when adduct **1***a* was treated with trifluoroacetic acid. It was also obtained as a significant product when adducts **1***a* and **1***b* were treated with a catalytic amount of sulfuric acid in deuteriochloroform (40–50% yield) and again when **1***a* was treated with nitric acid in chloroform (23% yield); in each case the other products were side-chain derivatives. It is to be noted that the 2-nitro-*p*-xylene is formed under conditions involving the presence of strong acid (which would catalyze the unimolecular loss of acetic acid to generate cation **6**) and the absence of nucleophiles and basic species more reactive than the acetic acid liberated in the reaction. Thus the shift of the nitro group in cation **6** is able to compete with deprotonation of **6**, a key step in the formation of the benzylic products (see below), and also with the combination of **6** with a nucleophile to form exchanged adduct (Scheme 2).

(ii) Formation of Side-chain Derivatives

Side-chain substitution products, *p*-$CH_3C_6H_4CH_2Y$, were formed in significant amounts in several reactions. Thus, *p*-methylbenzyl nitrate (77%) was obtained from reaction of **1***a* with nitric acid in chloroform, as well as 2-nitro-*p*-xylene. *p*-Methylphenylnitromethane (35%), *p*-methylbenzyl acetate (15%), and *p*-tolualdehyde (5%) were obtained from treatment of both **1***a* and **1***b* with a catalytic amount of sulfuric acid in deuteriochloroform, and again 2-nitro-*p*-xylene was the other product. *p*-Methylbenzyl acetate (29%) and *p*-methylphenylnitromethane (17%) were formed in the rearomatization accompanying the epimerization of both **1***a* and **1***b* in anhydrous acetic acid containing acetic anhydride, and 2,5-xylyl acetate was the other aromatic product. Methyl *p*-methylbenzyl ether (15%) was formed when the methoxynitrodiene **3***a* was heated under reflux in methanol containing sulfuric acid and methyl 2,5-xylyl ether was the nuclear substituted aromatic product. Finally *p*-methylbenzyl acetate, *p*-tolualdehyde, and (probably) *p*-methylphenylnitromethane were formed on pyrolysis of **1***a*, in addition to several other products. These results suggest that in the side-chain substitution product *p*-$CH_3C_6H_4CH_2Y$ the group Y originates from the nucleophilic species HY. Furthermore, these side-chain derivatives are formed in competition with the 2-nitro-*p*-xylene with larger amounts of 2-nitro-*p*-xylene being formed when only weak nucleophiles are present (*e.g.* sulfuric acid and nitric acid) and little or none being formed in the presence of substantial amounts of stronger nucleophiles (*e.g.* acetic acid and methanol). These conclusions are supported by similar results obtained with the pseudocumene adducts. We account for these results in terms of competitive processes occurring in the cyclohexadienyl cation **6**, a key intermediate in the formation of the 2-nitro-*p*-xylene. The 1,2-nitro shift in **6**, a unimolecular process, is in competition with a bimolecular process involving the abstraction of a proton from the *para*-methyl group in **6** to give the methylenecyclohexadiene intermediate **8** leading to side-chain product (Scheme 4). Clearly, the outcome of this competition will be determined by the bases present: the stronger the base and the higher its concentration the more likely that

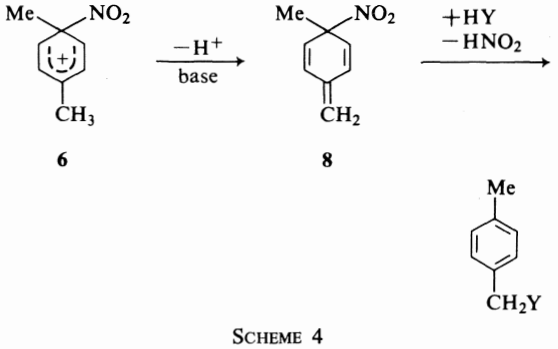

SCHEME 4

Can. J. Chem. Downloaded from www.nrcresearchpress.com by 210.87.254.6 on 09/05/12
For personal use only.

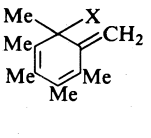

9

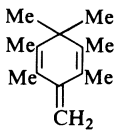

10

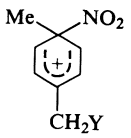

11

deprotonation of **6** will occur before rearrangement to **7**. Thus in the presence of sulfuric acid, or nitric acid, where the liberated acetic and nitrous acids present in only small amount are the most basic species available, the 1,2-nitro shift is an important reaction and substantial amounts of 2-nitro-*p*-xylene are formed. In contrast, in methanol as solvent, the more basic species methanol present at high concentration is able to deprotonate **6** before the nitro shift occurs and no 2-nitro-*p*-xylene is formed. Good nucleophiles present at high concentration reduce the concentration of **6** because they combine with **6** to form adducts (Scheme 2). However the effect of this should be to reduce the rate of the rearrangement and deprotonation reactions to the same extent and thus not to affect the competition between them.

Methylenecyclohexadienes have been proposed as intermediates in the formation of side-chain derivatives from arenes on treatment with electrophilic reagents by Baciocchi *et al.* (9, 15) for side-chain bromination and chlorination of hexamethylbenzene, by Andrews and Keefer (16) for side-chain chlorination of hexamethylbenzene with iodine monochloride, by Suzuki *et al.* (17) for side-chain nitrate formation from pentamethylbenzene, by Robinson (18) for side-chain nitration of 1,4-dimethylnaphthalene, and in subsequent papers by these and other authors for other side-chain substitution reactions. The earlier proposals were for a methylene-1,3-cyclohexadiene intermediate such as **9**. More recently it has been recognized that a 1,4-diene intermediate, with the methylene group and the tetrahedral carbon atom in a 1,4 relationship, is possible (10, 19) and in fact probable (7). Work with Wright and co-workers on side-chain substitution of methylbenzenes accompanying nitration (20) and our studies on the rearomatization of diene adducts (2, 3) conclusively establish that only the cross-conjugated triene such as **8** and not the conjugated triene such as **9** can be an intermediate in the formation of side-chain products. Specifically: (*i*) only those methylbenzenes which have methyl groups *para* to each other form side-chain derivatives, thus *p*-xylene does but *o*-xylene does not, pseudocumene (1,2,4-trimethylbenzene) does but hemimellitene (1,2,3-trimethylbenzene) and mesitylene do not, all of the tetramethylbenzenes do as does pentamethylbenzene (20) and hexamethylbenzene (19); (*ii*) the side-chain derivatives formed are those in which the methyl group substituted is that *para* to the most activated *ipso* position (20); (*iii*) only those adducts which have a methyl group *ipso* to the acetate give side-chain products on rearomatization, the adducts which are secondary acetates do not; (*iv*) the methyl group substituted is that *ipso* to the acetate and *para* to site of attack by the nitronium ion, not that which is *ortho* or *ipso* to the site of initial electrophilic attack. The isolation (21) of the cross-conjugated triene **10** from the methylation of hexamethylbenzene gives credence to the proposed intermediate **8**. Baciocchi *et al.* (9) and Nakamura (10) have also suggested the possibility of the simultaneous deprotonation and introduction of the group Y, thus obviating the formation of the discrete triene intermediate. These mechanisms were proposed at the time that both groups thought that the methyl group substituted was that *ortho* to the site of electrophilic attack and were associated with a cyclic intramolecular transfer of the electrophile from ring to side-chain. It is unlikely that concerted removal of the proton and shift of the electrophile to the methyl group in the *para* position could occur as has been explicitly recognised by Astolfi *et al.* (19). We therefore favor the mechanism outlined in Scheme 4 which proposes the cross conjugated triene as a discrete intermediate.

Two different general mechanisms for the conversion of the triene intermediate **8** into side-chain product can be envisaged: (*i*) electrophilic attack at the methylene group with prior, simultaneous, or subsequent loss of the nitro group as a nitronium ion, eq. 1, and (*ii*) nucleophilic attack at the methylene group with prior (S_N1'), simultaneous (S_N2'), or (unlikely) subsequent (acid-catalyzed) loss of the nitro group as nitrite, eq. 2. Reaction by pathway *i* has been proposed by Astolfi *et al.* (19) for the side-chain nitration of hexamethylbenzene and by Illuminati *et al.* (7) for the side-chain chlorination of isodurene. Robinson (18) and Suzuki and Nakamura

Can. J. Chem. Downloaded from www.nrcresearchpress.com by 210.87.254.6 on 09/05/12
For personal use only.

Can. J. Chem. Downloaded from www.nrcresearchpress.com by 210.87.254.6 on 09/05/12
For personal use only.

[1] 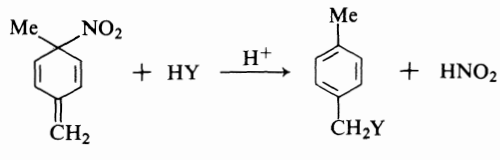

8

[2]

8

(22) have both proposed an addition–elimination sequence which is a variant of *i* for the side-chain nitration of 1,4-dimethylnaphthalene. It is evident that while the formation of side-chain nitro and halo derivatives could conceivably occur via *i*, involving the nitronium and (incipient) halonium ions as the active electrophiles, the side-chain ester compounds could not be formed directly by this pathway. Reaction by pathway *ii* has been suggested (7) to account for the formation of side-chain chloride in the chlorination of isodurene in acetic acid and a special variant of the S_N1' mechanism involving a cage rearrangement via an ion-pair intermediate has been proposed (10) to account for the formation of side-chain nitrate via nitrite, eq. 3. A similar ion-pair mechanism has been recognised as a possible mechanism for side-chain chlorination (7).

We suggest that *all* of the side-chain products are formed via pathway *ii*, eq. 2, and thus the derivatives p-$CH_3C_6H_4CH_2Y$: Y = NO_2, OAc, ONO_2, OMe are obtained by nucleophilic attack of HONO (nucleophilic nitrogen), HOAc, $HONO_2$ (nucleophilic oxygen), HOMe, respectively on **8**. Nitrous acid and acetic acid are liberated from the adducts in the course of the rearomatization reaction and thus these are available to compete as nucleophiles with introduced nucleophiles (if any). Thus when a catalytic amount of sulfuric acid in chloroform is used only the acetate and the nitromethane are formed but when nitric acid or methanol is present these are able to compete effectively and the nitrate and methyl ether are obtained, respectively. We reject pathway *i* for formation of the side-chain nitro derivative on two counts. First, pathway *i* requires the nitronium ion to be a leaving group from carbon. The nitronium ion would be most disposed to act as a leaving group if it were leaving from a positively charged species, *i.e.* if the electrophile Y^+ was added prior to the departure of NO_2^+ so that the intermediate cyclohexadienyl cation **11** was formed. Loss of NO_2^+ from a cyclohexadienyl cation has been observed but only in the case where the cation contains the strongly electron-withdrawing cyano substituent attached to the ring (3*c*). Such loss has not been observed in other cations which contain less strongly electron-withdrawing substituents and would not be expected in the case of **11** (2, 3). Attempts to detect the release of nitronium ion from the cyclohexadienyl cation formed from hexamethylbenzene, by intercepting it with benzene and mesitylene, were unsuccessful (14). Second, the side-chain nitro derivative is often formed in competition with side-chain esters which can only be formed directly by pathway *ii* (eq. 2). It seems unlikely that these products would be formed at comparable rates under quite different conditions, as observed, if they were formed by entirely different mechanisms.

Our results which support pathway *ii*, eq. 2, for the conversion of the triene **8** to side-chain derivatives do not distinguish between the unimolecular (S_N1') and bimolecular (S_N2') variations of this pathway. A variant of the S_N1' pathway is that involving formation of a benzyl cation nitrite anion ion-pair with recombination in the solvent cage to form *p*-methylbenzyl nitrite (10) and (we would suggest) *p*-tolylnitromethane. Suzuki and Nakamura have suggested that the benzylnitrite formed in this way is subsequently converted into the nitrate and acetate. Formation of the acetate in this indirect manner is unlikely since the conversion of benzyl nitrate to benzyl acetate is slow, even in refluxing acetic acid (23), and nitrate would be expected to be

[3] 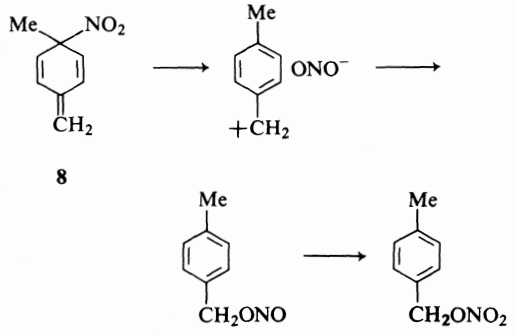

more readily displaced than nitrite. It seems similarly unlikely that nucleophilic displacement of nitrite by nitrate could be sufficiently fast to account for the formation of the benzyl nitrate. Pentamethylbenzyl acetate accompanies the pentamethylbenzyl chloride formed by chlorination of hexamethylbenzene in acetic acid. It has been shown that the side-chain chloride is not solvolyzed under the reaction conditions and thus the side-chain acetate cannot be formed via the pentamethylbenzyl chloride (9).

p-Tolualdehyde often accompanied the formation of other side-chain products. Benzyl nitrite gives benzaldehyde on autodecomposition (24) and benzyl nitrate undergoes acid-catalyzed oxidative cleavage to benzaldehyde (23, 25). Thus the *p*-tolualdehyde could have been formed via *p*-methylbenzyl nitrite or nitrate.

(iii) Formation of Aryl Acetate

2,5-Xylyl acetate formed by elimination of nitrous acid with rearrangement of the acetate was obtained in several reactions, most notably on treatment of adduct **1** with wet acetic acid and with aqueous acidic tetrahydrofuran. The rearrangement is intramolecular. Propionate was not incorporated when the decomposition was carried out in propionic acid (2*b*), in acetic acid-d_4 only minor incorporation of the deuterated acetate was observed, and in aqueous tetrahydrofuran the acetate rather than the phenol was the major product. It is likely that the acetate shift is 1,2, as in the case of the pseudocumene adducts (2*d*) rather than 1,3. Water has a striking catalytic effect on the reaction. In anhydrous acetic acid adduct **1** was epimerized. Decomposition to the xylyl acetate occurred to the extent of 35% over 18 h and 20% of the *p*-methylbenzyl acetate and 13% of 2-nitro-*p*-xylene were also formed. However in wet acetic acid adduct **1** decomposed completely in less than 30 min to the xylyl acetate, the only product. We suggest that there is concerted acid-catalyzed loss of the nitro group (to form nitrous acid) accompanied by migration of the acetate (Scheme 5). A possible reason for the dramatic catalytic effect of the water is that it acts as base accepting the proton in a fully concerted transition state **12**. It is plausible that when the more weakly basic acetic acid has to accept the proton then the energy of the transition state is raised sufficiently for reactions via the cyclohexadienyl cation (epimerization, formation of 2-nitro-*p*-xylene and side-chain derivative) to be able to compete.

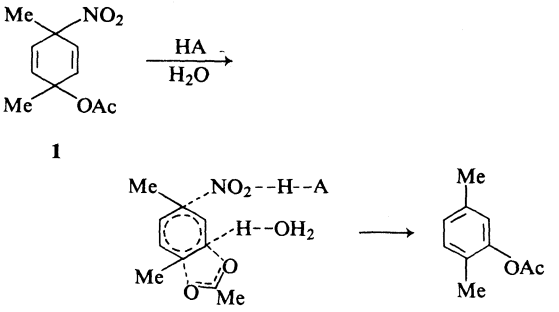

SCHEME 5

Rearomatization of the methoxynitro adduct **3** gave methyl 2,5-xylyl ether as the major product and some methyl *p*-methylbenzyl ether. Formation of the side-chain derivative presumably occurs via the cyclohexadienyl cation **6** and the triene **8**. Insufficient information is available to delineate the mechanism of formation of the nuclear substitution product.

Attempted Assignment of the Stereochemistry of Diastereoisomeric Adducts

Two methods were used to assign the stereochemistry of the acetoxynitrodienes **1***a* and *b* and hydroxynitrodienes **2***a* and *b*. Addition of the shift reagent *tris*-(1,1,1,2,2,3,3-heptafluoro-7,7-[$^2H_6$]dimethyl-4,6-[$^2H_3$]octanedionato)europium(III) {Eu([$^2H_9$]fod)$_3$} which complexes at the acetate and hydroxyl functions respectively of **1** and **2** should shift the 4-methyl protons of the *trans* isomers, with europium *cis* to 4-methyl, more rapidly downfield than in the *cis* isomers (2*c*). The relative gradients of the slopes of plots of the chemical shift against amount of reagent added, normalized to a gradient of the 1-CH_3 protons = 1.0, are shown in Table 1. The normalized gradients for corresponding protons of the members of each diastereoisomeric pair are the same, even in the case of the 4-methyl protons. Thus this method of assignment failed.

The second method of stereochemical assignment used dipole moment measurements. For the acetoxynitrodienes **1** the *cis* isomer is calculated to have a lower dipole moment than the *trans* (6*a*). Similar calculations for the hydroxynitrodienes **2**, using 1.60 D and 63° as values for the group moment of the OH group and its angle to the C—O bond, respectively (26), indi-

Can. J. Chem. Downloaded from www.nrcresearchpress.com by 210.87.254.6 on 09/05/12
For personal use only.

TABLE 1. Relative gradients (gradient 1-CH_3 = 1.00) of proton chemical shifts for diene adducts resulting from the addition of Eu([$^2H_9$]fod)$_3$

Compound	2-H	3-H	4-CH_3	1-OCH_3	1-$OCOCH_3$
1*a*	1.24	0.36	0.25	—	1.53
1*b*	1.21	0.40	0.24	—	1.45
2*a*	1.05	0.39	0.24	—	—
2*b*	1.06	0.43	0.26	—	—
3*a*	0.82	0.68	0.39	1.06	—
3*b*	0.74	0.62	0.48	1.00	—

cate that the *trans* isomer of **2** should have the lower dipole moment (*cis* = 3.68 D, *trans* = 2.77 D). Thus **1***a* should be the *cis* isomer and **1***b* the *trans* and likewise **2***a* the *trans* isomer and **2***b* the *cis*, although it should be noted that the measured dipole moments of **2***a* and *b* differ by less than 0.2 D. This assignment of stereochemistry is in conflict with the established stereochemical relationship between **1***a* and **2***a* and between **1***b* and **2***b* (see above) and thus the dipole moment method of assignment failed.

The effect of Eu([$^2H_9$]fod)$_3$ on the methoxynitrodienes **3***a* and *b* was also investigated and the normalized gradients are also shown in Table 1. In this case the normalized gradient of the 4-CH_3 protons of adduct **3***b* is 23% larger that that of the corresponding protons of **3***a*, whereas for all of the other protons the normalized gradients in **3***b* are slightly less than in **3***a*. These results suggest that **3***b* is the *trans* adduct with OCH_3 *cis* to 4-CH_3. However since the method failed in the cases of the acetoxynitro- and hydroxynitrodienes, which are each more sensitive to the addition of the shift reagent than the methoxynitrodienes, this conclusion must be regarded as tentative.

Experimental

Ultraviolet spectra were determined on Cary 17 or Unicam SP 700 spectrometers. Infrared spectra were determined on a Perkin–Elmer 337 spectrometer calibrated with polystyrene. Nuclear magnetic resonance spectra at 60 MHz were obtained on Perkin–Elmer R12A and Varian HA-60-IL spectrometers and, at 220 MHz, on the Varian HR 200 spectrometer at the Ontario Research Foundation, Sheridan Park, Ontario. Tetramethylsilane was used as an internal standard. Mass spectra were obtained on an Hitachi Perkin–Elmer RMU-7 spectrometer. Molecular weights were determined in methylene dibromide using an Hitachi Perkin–Elmer Model 115 molecular weight apparatus (vapor pressure osmometer). Dipole moments (**p**) were derived by use of Higasi's equation (27) from dielectric constant measurements (3*a*) of benzene solutions of the adducts. The dielectric constants were measured with a Sargent Chemical Oscillometer Model V with inductive cell compensator. Microanalyses were by Dr. D. McGillivray. Gas–liquid chromatography analyses were performed on a Micro Tek MT 220 gas chromatograph using as stationary phases QF1 (5%), PEGA (2½%), and DEGS (10%) on Chromosorb G acid-washed and silanized. Nitric acid was purified by distilling the fuming acid (300 cm^3) at 100 Pa from urea (10 g) and sulfuric acid (500 cm^3). Alumina was deactivated with 4% of 10% acetic acid. Ether and pentane were dried by distillation from sodium and phosphorus pentoxide, respectively. *p*-Methylbenzyl alcohol (Aldrich), *p*-xylene (Eastman), 2,5-dimethylphenol (Aldrich), and *p*-tolualdehyde (Baker) were commercial products. 2,5-Dimethylphenyl acetate (i.r. (CCl_4) 1775 and 1230 cm^{-1} ($OCOCH_3$), n.m.r. (CCl_4) τ 3.15 (m, Ar*H*), 7.70 (s, 5-CH_3), 7.80 (s, $OCOCH_3$), and 7.91 (s, 2-CH_3)) was obtained by acetylation of 2,5-dimethylphenol with acetic anhydride (28*a*). Methyl 2,5-xylenyl ether (n.m.r. (CCl_4) τ 3.4 (m, Ar*H*), 6.30 (s, OCH_3), 7.72 and 7.90 (ArCH_3)) was prepared from 2,5-dimethylphenol (2,5-xylenol) by heating under reflux with sodium and methyl iodide (28*b*). *p*-Methylbenzyl acetate (i.r. (CCl_4) 1750 and 1230 cm^{-1} ($OCOCH_3$); n.m.r. (CCl_4) τ 2.96 (m, Ar*H*), 5.12 (s, CH_2), 7.75 (s, ArCH_3), and 8.10 (s, $OCOCH_3$)) was obtained by acetylation (28*c*) of *p*-methylbenzyl alcohol. *p*-Methylbenzyl bromide (n.m.r. (CCl_4) τ 2.82 (m, Ar*H*), 5.60 (s, CH_2), 7.65 (s, CH_3)) was formed by reaction of the alcohol with phosphorus tribromide (29). *p*-Methylbenzyl nitrate (i.r. 1650 and 1270 cm^{-1} (ONO_2); n.m.r. (CCl_4) τ 2.90 (Ar*H*), 4.75 (CH_2), 7.70 (CH_3)) was prepared from the bromide by heating under reflux with silver nitrate in acetonitrile (30). Methyl *p*-methylbenzyl ether (n.m.r. (CCl_4) τ 3.00 (Ar*H*), 5.75 (CH_2), 6.80 (OCH_3), 7.72 (CH_3)) was obtained by heating the bromide under reflux with sodium methoxide in methanol (31). The appropriate parent ion and fragment peaks were observed in the mass spectra of the compounds described.

Nitration of p-Xylene in Acetic Anhydride

A cold solution of nitric acid (94 g, 1.5 mol) in acetic anhydride (250 cm^3) was added slowly with stirring to *p*-xylene (106 g, 1 mol) in acetic anhydride (250 cm^3) at −45° and the mixture was stirred for 30 min. The solution was then cooled to −70° in solid carbon dioxide–methanol, ether (2 dm^3) added, and ammonia condensed into the stirred solution. Excess ammonia was removed with an aspirator, more ether added, and the mixture poured onto ice-water. The combined ethereal layer and ether extract of the aqueous layer was washed and dried ($MgSO_4$) and the ether evaporated at 14°. Integration of

Can. J. Chem. Downloaded from www.nrcresearchpress.com by 210.87.254.6 on 09/05/12
For personal use only.

Can. J. Chem. Downloaded from www.nrcresearchpress.com by 210.87.254.6 on 09/05/12
For personal use only.

the n.m.r. spectrum of the crude reaction mixture revealed that diene adducts constituted 80% of the reaction mixture.

Chromatography at −45° on 4% deactivated alumina and elution first with pentane yielded 2-nitro-*p*-xylene; i.r. 1540 and 1350 cm^{-1} (NO_2); n.m.r. (CCl_4) τ 2.35 (s, 3-*H*), 2.88 (s, 5- and 6-*H*), 7.53 (s, 1-CH_3), 7.65 (s, 4-CH_3). Further elution with ether–pentane mixtures yielded in the 10% ether fraction 2,5-dinitro-*p*-xylene, m.p. 150° (lit. (32) 142°); i.r. (CCl_4) 1550 and 1350 cm^{-1} (NO_2); n.m.r. ($CDCl_3$) τ 2.10 (s, 2, 3-*H* and 6-*H*), 7.40 (s, 6, 1-CH_3 and 4-CH_3); mass spectrum (70 eV) *m/e* (relative intensity) 196 (15, M), 179 (35, M − OH), 133(25), 123(20), 105(35), 91(55), 77(100).

Also isolated from the 10% ether fraction, after removal of the dinitroxylene was 1,4-dimethyl-4-nitro-1,4-dihydrophenyl *p*-methylbenzyl ether (**5**); i.r. (CCl_4) 1550 and 1345 cm^{-1} (NO_2); n.m.r. (CCl_4) τ 3.00 (s, Ar*H*), 4.00 (m, 2-, 3-, 5-, and 6-*H*), 5.85 (s, ArCH_2), 5.95 (s, ArCH_2), 7.70 (s, ArCH_3), 8.27 (s, 4-CH_3), 8.35 (s, 4-CH_3), 8.65 (s, 1-CH_3), 8.72 (s, 1-CH_3). The n.m.r. spectrum indicates that both diastereomers were present with the aromatic, diene, and aromatic methyl peaks of the two isomers overlapping.

The 20% ether fraction afforded one diastereoisomer of 1,4-dimethyl-4-nitro-1,4-dihydrophenyl acetate (**1***a*) as a white solid, m.p. 47–49 °C; u.v. (CH_3OH) 198 nm (ε 840 m^2 mol^{-1}); i.r. (CCl_4) 1755 and 1240 ($OCOCH_3$), 1555 cm^{-1} (NO_2); n.m.r. (220 MHz, C_6D_6) τ 4.26 (s, 4, 2-, 3-, 5- and 6-*H*), 8.42 (s, 3, $OCOCH_3$), 8.50 (s, 3, 4-CH_3), 8.80 (s, 3, 1-CH_3); n.m.r. (220 MHz $CDCl_3$) τ 3.93 (s, 4), 8.01 (s, 3, $OCOCH_3$), 8.21 (s, 3, 4-CH_3), 8.54 (s, 3, 1-CH_3); mass spectrum (70 eV) *m/e* (relative intensity) 164 (3, M − HNO_2), 123(100), 106(50), 91(75), 43(25); μ 3.75 D (12.5 × 10^{-30} C m).

Mol. Wt. Calcd. for $C_{10}H_{13}NO_4$: 211. Found: 211.

The 40% ether fraction contained a 1:1 mixture of dienes **1***a* and *b* which on rechromatography yielded in the 15% ether fraction a second diastereoisomer of 1,4-dimethyl-4-nitro-1,4-dihydrophenyl acetate (**1***b*) as a white solid, m.p. 58–59 °C; u.v. (CH_3OH) 196 nm (ε 1400 m^2 mol^{-1}); i.r. (CCl_4) 1745 and 1230 ($OCOCH_3$), 1550 cm^{-1} (NO_2); n.m.r. (220 MHz, C_6D_6) τ 4.00 (m, 2, 3-*H* and 5-*H*), 4.10 (m, 2, 2-*H* and 6-*H*), (J_{23} 10.25, J_{26} 2.30, J_{35} 2.34 Hz), 8.40 (s, 3 $OCOCH_3$), 8.75 (s, 6, 4-CH_3 and 1-CH_3); n.m.r. (220 MHz $CDCl_3$) 3.81 (s, 4), 8.03 (s, 3, $OCOCH_3$), 8.29 (s, 3, 4-CH_3), 8.51 (s, 3, 1-CH_3); mass spectrum (70 eV) *m/e* (relative intensity) 164 (10, M − HNO_2), 123(100), 106(55), 91(62), 43(25); μ 4.18 D (13.9 × 10^{-30} C m).

Mol. Wt. Calcd. for $C_{10}H_{13}NO_4$: 211. Found: 212.

The 70% ether fraction of the original reaction mixture was subjected to rechromatography and gave in the 50–60% ether fraction one diastereoisomer of 1,4-dimethyl-4-nitro-1,4-dihydrophenol (**2***b*), recrystallized from ether–pentane to give colorless crystals, m p. 52°; u.v. (CH_3OH) 194 nm (ε 900 m^2 mol^{-1}); i.r. (CCl_4) 3610 (OH) 1555 cm^{-1} (NO_2); n.m.r. (220 MHz, $CDCl_3$) τ 3.88 (m, 2, 3-*H* and 5-*H*), 3.96 (m, 2, 2-*H* and 6-*H*), (J_{23} 9.97, J_{25} −0.08, J_{26} 2.32, J_{35} 2.32 Hz), 8.30 (s, 3, 4-CH_3), 8.67 (s, 3, 1-CH_3); mass spectrum (70 eV) *m/e* relative intensity) 123 (95, M − NO_2), 108(85), 91(100); μ 3.13 D (10.4 × 10^{-30} C m).

Anal Calcd. for $C_8H_{11}NO_3$: C, 56.80; H, 6.55; N, 8.30. Found: C, 56.41; H, 6.44; N, 8.40.

Elution with 100% ether gave the second diastereoisomer of 1,4-dimethyl-4-nitro-1,4-dihydrophenol (**2***a*), recrystallized to give colorless crystals, m.p. 114°; u.v. (CH_3OH) 196 nm (ε 1065 m^2 mol^{-1}); i.r. ($CDCl_3$) 3610 (OH), 1550 cm^{-1} (NO_2); n.m.r. (220 MHz, $CDCl_3$) τ 3.86 (m, 2, 3-*H* and 5-*H*), 3.99 (m, 2, 2-*H* and 6-*H*), (J_{23} 9.94, J_{25} −0.10, J_{26} 2.33, J_{35} 2.30 Hz), 8.25 (s, 3, 4-CH_3), 8.63 (s, 3, 1-CH_3); mass spectrum (70 eV) *m/e* (relative intensity) 123 (100, M − NO_2), 108(70), 91(85); μ 2.97 D (9.9 × 10^{-30} C m).

Anal. Calcd. for $C_8H_{11}NO_3$: C, 56.80; H, 6.55; N, 8.30. Found: C, 56.70; H, 6.71; N, 7.85.

Base-catalyzed Methanolysis of the Acetate Adducts **1**

Diene **1***a* (50 mg 0.24 mmol) was dissolved in methanol (10 cm^3) containing sodium hydroxide (50 μmol) at ambient temperature and stirred for 18 h. The solution was then extracted with ether, washed, dried ($MgSO_4$) and the solvent evaporated. Integration of the n.m.r. spectrum revealed that partial methanolysis (30%) of the acetate had taken place and that no other (rearomatization) products had been formed. The presence of the hydroxy diene **2***a* (τ 4.0, 8.25, 8.63) was confirmed by addition of an authentic sample which enhanced the characteristic n.m.r. peaks.

In a similar experiment with **1***b* the acetate function was cleaved to the extent of 40% to form the hydroxy diene **2***b*, n.m.r. τ 4.0, 8.30, and 8.67, whose presence was confirmed by peak enhancement on addition of authentic **2***b*.

In neither experiment were the remaining acetate adducts, the predominant constituent of each product mixture, epimerized.

Reaction of Adducts **1***a and* **1***b with Acidified Methanol*

The *p*-xylene adduct **1***a* (50 mg, 0.24 mmol) was dissolved in deuteriochloroform containing methanol (1%) and sulfuric acid (10 μmol). The n.m.r. spectrum, two superimposed quartets in the region τ 3.7–4.2 (4, vinyl *H*) and methyl signals at 7.0 and 7.1 (s, OCH_3), 8.2 and 8.3 (s, 4-CH_3), and 8.70 and 8.78 p.p.m. (s, 1-CH_3), showed that exchange of the methoxyl for the acetoxy group had taken place and that the diastereoisomers of methyl 1,4-dimethyl-4-nitro-1,4-dihydrophenyl ether (**3**) had been formed in a 1:1 ratio.

The same product mixture was obtained when the reaction was repeated using the adduct **1***b*. The reaction was also carried out in neat [$^2H_4$]methanol (0.4 cm^3) containing sulfuric acid (10 μmol). The exchange was complete in 15 min and both **1***a* and *b* gave the same 1:1 mixture of the diastereoisomeric [$^2H_3$]methyl 1,4-dimethyl-4-nitro-1,4-dihydrophenyl ethers with n.m.r. identical to that of **3** above apart from the absence of the methoxyl proton singlets at τ 7.0 and 7.1.

On a preparative scale adduct **1***a* (5 g, 0.024mol) was dissolved in methanol (200 cm^3) containing sulfuric acid (1 mmol) and stirred for 8 h at 20°. After work-up the n.m.r. spectrum of the crude reaction mixture revealed complete conversion of the acetoxynitrodiene to the methoxynitrodiene (absence of the acetoxy signal at τ 8.1) and that the *cis* and *trans* methoxynitro isomers were present in a 1:1 ratio. Chromatography at −45° on 3% deactivated alumina, and elution with pentane and ether–pentane mixtures afforded in the 4% ether fraction one

Can. J. Chem. Downloaded from www.nrcresearchpress.com by 210.87.254.6 on 09/05/12
For personal use only.

diastereoisomer of 1,4-dimethyl-4-nitro-1,4-dihydrophenyl methyl ether (**3***a*) as an oil; n.m.r. (CCl_4) 1555 and 1345 cm^{-1} (NO_2); τ (60 MHz, CCl_4), 3.87 (m, 2, 3-*H* and 5-*H*), 4.24 (m, 2, 2-*H* and 6-*H*), (J_{23} 9.98, J_{25} −0.14, J_{26} 2.27, J_{35} 2.27 Hz), 6.95 (s, 3, OCH_3), 8.32 (s, 3, 4-CH_3), 8.78 (s, 3, 1-CH_3); mass spectrum (70 eV) *m/e* (relative intensity) 137.095 (55, M − NO_2, $^{12}C_9{}^1H_{13}{}^{16}O_1$ requires 137.097), 122(80), 106(75), 91(100). Elution with 12½% ether yielded the other diastereoisomer of 1,4-dimethyl-4-nitro-1,4-dihydrophenyl methyl ether (**3***b*) as an oil; i.r. (CCl_4) 1555 and 1345 cm^{-1} (NO_2); τ (60 MHz, CCl_4) 3.90 (m, 2, 3-*H* and 5-*H*), 4.17 (m, 2, 2-*H* and 6-*H*), (J_{23} 10.1, J_{25} −0.13, J_{26} 2.5, J_{35} 2.5 Hz), 7.03 (s, 3, OCH_3), 8.26 (s, 3, 4-CH_3), 8.71 (s, 3, 1-CH_3); mass spectrum (70 eV) *m/e* (relative intensity) 137.092 (78, M − NO_2, $^{12}C_9{}^1H_{13}{}^{16}O_1$ requires 137.097), 122(78), 106(60), 91(100).

Reaction of Adduct **1***a with Benzyl Alcohol*

Diene **1***a* was reacted with benzyl alcohol in chloroform containing a catalytic amount of sulfuric acid. The product exhibited i.r. and n.m.r. absorptions of the expected 1,4-dimethyl-4-nitro-1,4-dihydrophenyl *p*-methylbenzyl ether (see above) as well as those of rearomatization products.

Reaction of Adducts **1***a and* **1***b with Acetic Acid*

Diene **1***a* (50 mg, 0.24 mmol) was added to [$^2H_4$]acetic acid (0.4 cm^3) and the reaction was followed by n.m.r. The reaction was complete after 30 min. The major product was 2,5-dimethylphenyl acetate; i.r. 1775 and 1230 cm^{-1}; n.m.r. τ 3.15, 7.70, 7.80, and 7.91 p.p.m., addition of the shift reagent Eu([$^2H_9$]fod)$_3$ to a solution of the isolated product moved the acetate peak downfield from the aromatic methyl peaks and integration of the resulting spectrum revealed that the ratio of these was 0.75:2 and thus not more than 25% of the acetate had exchanged with the [$^2H_3$]acetate from the solvent. The retention time of the product was identical with that of an authentic sample of 2-acetoxy-*p*-xylene on coinjection into the gas chromatograph. When one reaction was worked up after 15 min a small amount of the diastereoisomeric hydroxy dienes **2** was detected; i.r. 3400 (OH); n.m.r. τ 8.64 and 8.68 (1-CH_3 of each isomer).

The same results were obtained with diene **1***b* except that even less of the acetate exchanged with the solvent.

The experiment was repeated using acetic anhydride made anhydrous by heating under reflux with 10% acetic anhydride for 18 h. The solution of adduct **1***a* was allowed to stand at 20 °C for 18 h and then worked up and examined by n.m.r. The product consisted of 24% **1***a*, 8% **1***b*, 35% 2,5-dimethylphenyl acetate, 20% *p*-methylbenzyl acetate, and 13% *p*-methylphenylnitromethane (n.m.r. τ 4.70). The i.r. confirmed the presence of both aryl acetate (1780 cm^{-1}) and alkyl acetate (1750 cm^{-1}). From **1***b* there was obtained 30% **1***a*, 20% **1***b*, 28% 2,5-dimethylphenyl acetate, 14% *p*-methylbenzyl acetate, and 7% *p*-methylphenylnitromethane.

When water was added to a solution of **1***a* in anhydrous acetic acid decomposition proceeded rapidly (< 30 min) and only 2,5-dimethylphenyl acetate was obtained.

Reaction of Adduct **1** *with Formic Acid*

The diene **1***a* (50 mg, 0.24 mmol) was added with stirring to formic acid at 8° until the first appearance of color (30 s). The mixture was immediately cooled to −70 °C, ether was added and the resulting solution poured onto ice-water and worked up. Rearomatization had occurred to the extent of 25% but the predominant product was 1,4-dimethyl-4-nitro-1,4-dihydrophenyl formate; i.r. 1745 (OCOH) and 1550 cm^{-1} (NO_2); n.m.r. τ 2.2 (s, 1, OCO*H*), 4.0 (m, 4, vinyl *H*), 8.2 (s, 3, CH_3), 8.3 (s, 3, CH_3).

Pyrolysis of Adduct **1***a*

A solution of diene **1***a* in carbon tetrachloride was injected into the inlet of a gas chromatograph, at 225 °C. Decomposition proceeded smoothly giving rise to sharp, well-resolved peaks. Seven products were observed, six of which were identified by coinjection of authentic samples and comparison of their retention times with those in the decomposed mixture. The compounds were in order of decreasing peak area: *p*-xylene, 2-nitro-*p*-xylene, 2,5-dimethylphenyl acetate, unidentified compound, *p*-methylbenzyl acetate, tolualdehyde, and 2,5-dimethylphenol. It is likely that the unidentified compound was *p*-methylphenylnitromethane.

Reaction of Adduct **1***a in Acidified Aqueous Tetrahydrofuran*

Diene **1***a* (50 mg, 0.24 mmol) was dissolved in 50% aqueous tetrahydrofuran (10 cm^3) containing sulfuric acid (10 μmol). The reaction mixture was stirred for 18 h after which time the solution was worked up in the usual manner. Infrared and n.m.r. spectra revealed the presence of 2,5-dimethylphenyl acetate (86%), and 2,5-dimethylphenol (14%; i.r. 3400 cm^{-1} (OH); τ 3.55 (ArH)). The identities of the nuclear acetate and the phenol were confirmed by the correspondence of retention times with those of authentic samples on gas chromatography (PEGA). A second reaction was worked up after 15 min and the n.m.r. spectrum revealed the presence of small amounts of hydroxy dienes **2** (i.r. 3620 cm^{-1} (OH); τ 8.64 and 8.68 (1-CH_3)).

Reaction to Adduct **1***a with Nitric Acid in Chloroform*

Diene **1***a* (50 mg, 0.24 mmol) was dissolved in chloroform (3 cm^3), cooled to −60°, and nitric acid (70 μmol) added. The solution was then warmed to 0°, quenched immediately in water, and worked up. Infrared and n.m.r. established that the products were *p*-methylbenzyl nitrate (77%; i.r. 1650 and 1280 cm^{-1} (ONO_2); τ 2.90, 4.75, and 7.70 p.p.m.; and 2-nitro-*p*-xylene (23%; i.r. 1545 cm^{-1} (NO_2); τ 2.35, 2.90, 7.50 and 7.70 p.p.m.).

Reaction of Adducts **1***a and* **1***b with Sulfuric Acid in Deuteriochloroform*

Diene **1***a* (50 mg, 0.24 mmol) was dissolved in deuteriochloroform (0.4 cm^3) containing sulfuric acid (10 μmol) and the reaction followed by n.m.r. The four products observed were *p*-tolylnitromethane (40%; i.r. 1560 cm^{-1} (NO_2); τ 2.80, 4.80, and 7.75 p.p.m.), 2-nitro-*p*-xylene (40%; i.r. 1535 cm^{-1} ($ArNO_2$); τ 2.35, 2.90, 7.50, 7.70 p.p.m.), *p*-methylbenzyl acetate (15%; i.r. 1750 cm^{-1} ($OCOCH_3$); τ 2.95, 5.05, 7.75 p.p.m.), and tolualdehyde (5%; i.r. 1700 cm^{-1} (CHO); τ 0.15). The presence of 2-nitro-*p*-xylene, *p*-methylbenzyl acetate and tolualdehyde was confirmed by the identity of retention times with those of authentic samples on g.l.c.

Similar results were obtained when the reaction was carried out on **1***b*.

Reaction of 1a with Trifluoroacetic Acid

Diene **1***a* (50 mg, 0.24 mmol) was added to trifluoroacetic acid (5 cm^3) at $-60°$. The solution was allowed to warm to $-30°$ then quenched in ice-water and worked up. Infrared and n.m.r. spectra revealed one major product, 2-nitro-*p*-xylene (i.r. 1545 cm^{-1} (NO_2); τ 2.35, 2.90, 7.50, and 7.65), confirmed by g.l.c.

Rearomatization of the Methoxynitro Diene 3a

Diene **3***a* (50 mg) was refluxed in methanol (10 cm^3) containing sulfuric acid (200 μmol) for 18 h. After work-up the n.m.r. spectrum revealed the presence of methyl 2,5-xylenyl ether (85%; τ 3.35, 6.30, 7.70, and 7.90 p.p.m.), and methyl-*p*-methylbenzyl ether (15%; τ 3.00, 5.75, 6.80, and 7.70 p.p.m.), which could not be separated on g.l.c.

We thank the National Research Council of Canada and the University of Victoria for financial support.

1. C. L. Perrin and G. A. Skinner. J. Am. Chem. Soc. **93**, 3899 (1971).
2. (*a*) D. J. Blackstock, A. Fischer, K. E. Richards, J. Vaughan, and G. J. Wright. Chem. Commun. 641 (1970); (*b*) D. J. Blackstock, J. Cretney, A. Fischer, M. P. Hartshorn, K. E. Richards, J. Vaughan, and G. J. Wright. Tetrahedron Lett. 2793 (1970); (*c*) A. Fischer and J. N. Ramsay. J. Chem. Soc. Perkin II, 237 (1973); (*d*) A. Fischer and J. N. Ramsay. J. Am. Chem. Soc. **96**, 1614 (1974).
3. (*a*) A. Fischer, C. C. Greig, A. L. Wilkinson, and D. R. A. Leonard. Can. J. Chem. **50**, 2211 (1972); (*b*) A. Fischer and C. C. Greig. J. Chem. Soc. Chem. Commun. 50 (1974); (*c*) A. Fischer and C. C. Greig. Can. J. Chem. **52**, 1231 (1974); J. Chem. Soc. Chem. Commun. 396 (1973).
4. P. C. Myhre. J. Am. Chem. Soc. **94**, 7921 (1972).
5. R. C. Hahn and M. B. Groen. J. Am. Chem. Soc. **95**, 6128 (1973).
6. (*a*) A. Fischer and A. L. Wilkinson. Can. J. Chem. **50**, 3988 (1972); (*b*) A. Fischer and D. R. A. Leonard. Can. J. Chem. **50**, 3367 (1972).
7. G. Illuminati, L. Mandolini, A. Patara, and E. Baciocchi, Tetrahedron Lett. 4161 (1972).
8. H. Suzuki. Bull. Inst. Chem. Res. Kyoto Univ. **50**, 407 (1972) and references cited therein.
9. E. Baciocchi, A. Ciana, G. Illuminati, and C. Pasini. J. Am. Chem. Soc. **87**, 3953 (1965).
10. K. Nakamura. Bull. Chem. Soc. Jap. **44**, 133 (1971).
11. C. MacLean and E. L. Mackor. Mol. Phys. **4**, 241 (1961).
12. A. Fischer and G. J. Wright. Aust. J. Chem. **27**, 217 (1974).
13. C. K. Ingold. Structure and mechanism in organic chemistry. 2nd ed. Cornell University Press, Ithaca, N.Y. 1969. Chapt. 15.
14. G. A. Olah, H. C. Lim, and Y. K. Mo. J. Am. Chem. Soc. **94**, 3667 (1972).
15. E. Baciocchi and G. Illuminati. Ricerca Sci. Rend. **7**, 462 (1964).
16. L. J. Andrews and R. M. Keefer. J. Am. Chem. Soc. **86**, 4158 (1964).
17. H. Suzuki, K. Nakamura, and K. Maruyama. Bull. Chem. Soc. Jap. **41**, 1487 (1968).
18. R. Robinson. J. Chem. Soc. B, 1289 (1970).
19. R. Astolfi, E. Baciocchi, and G. Illuminati. Chem. Ind. (Milan), **53**, 1153 (1971).
20. D. J. Blackstock, A. Fischer, K. E. Richards, and G. J. Wright. Aust. J. Chem. **26**, 775 (1973).
21. W. von E. Doering, M. Saunders, H. G. Boyton, H. W. Earhart, E. F. Wadley, W. R. Edwards, and G. Laber. Tetrahedron, **4**, 178 (1958).
22. H. Suzuki and K. Nakamura. Bull. Chem. Soc. Jap. **44**, 303 (1971).
23. S. D. Ross, E. R. Coburn, and M. Finklestein. J. Org. Chem. **33**, 585 (1968).
24. R. G. Gillis. J. Org. Chem. **21**, 805 (1956).
25. H. Suzuki and K. Nakamura. Synthesis, 606 (1972).
26. D. D. Tanner and T. S. Gilman. J. Am. Chem. Soc. **85**, 2892 (1963).
27. K. Higasi. Bull. Inst. Phys. Chem. Res. (Tokyo), **22**, 805 (1943). B. Krishna and K. K. Srivastava. J. Chem. Phys. **32**, 663 (1960).
28. A. I. Vogel. Practical organic chemistry. Longmans, London. 1956 (*a*) p. 669; (*b*) p. 671; (*c*) p. 783.
29. E. D. Bergmann and J. Szmyuszkovicz. Bull. Soc. Chim. Fr. 566 (1953).
30. H. Suzuki and K. Nakamura. Bull. Chem. Soc. Jap. **43**, 473 (1970).
31. A. I. Vogel. J. Chem. Soc. 616 (1948).
32. C. Blankman. Chem. Zentr. 1495 (1910).

Can. J. Chem. Downloaded from www.nrcresearchpress.com by 210.87.254.6 on 09/05/12
For personal use only.

Electrochemical Reduction of Pyrazines into Dihydropyrazines. Preparation of Dihydropyrazines

JOSEPH ARMAND, KHALED CHEKIR, AND JEAN PINSON

Laboratoire de Chimie IV, Université de Paris VI, 8, rue Cuvier 75005 Paris, France

Received June 10, 1974

JOSEPH ARMAND, KHALED CHEKIR, and JEAN PINSON. Can. J. Chem. **52**, 3971 (1974).

The electrochemical reduction of several pyrazines in an alkaline hydroorganic medium leads to 1,4-dihydropyrazines too easily oxidizable to be isolated. These derivatives isomerize into 1,2- or 1,6-dihydropyrazines, the rate of this reaction depending among other things on the p*H* and on the cosolvent. The different chemical and electrochemical preparations of dihydropyrazines are discussed. It is shown that 3,6-dihydro-2,5-diphenylpyrazine and 1,6-dihydro-2,5-diphenylpyrazine are in thermodynamic equilibrium.

JOSEPH ARMAND, KHALED CHEKIR et JEAN PINSON. Can. J. Chem. **52**, 3971 (1974).

La réduction électrochimique de diverses pyrazines en milieu hydroorganique alcalin fournit des dihydro-1,4 pyrazines, trop oxydables pour pouvoir être isolées. Ces dérivés s'isomérisent en dihydro-1,2 ou dihydro-1,6 pyrazines avec une vitesse dépendant en particulier du p*H* et de la nature du cosolvant. Les différents modes d'obtention, chimiques et électrochimiques des dihydropyrazines sont discutés. Il est montré que la dihydro-3,6 diphényl-2,5 pyrazine forme un équilibre thermodynamique avec la dihydro-1,6 diphényl-2,5 pyrazine.

Can. J. Chem. Downloaded from www.nrcresearchpress.com by 210.87.254.5 on 09/05/12
For personal use only.

The reduction of pyrazines, by the usual chemical reagents, generally leads to hexahydro derivatives, *i.e.* to piperazines. Few semihydrogenated derivatives, dihydro- and tetrahydropyrazines, are known.

The electrochemical reduction of pyrazines in an alkaline hydroorganic medium was investigated to determine the intermediates involved in the reduction of pyrazines into piperazines and to find out whether the electrochemical reduction could be of interest for the preparation of dihydro- and tetrahydropyrazines.

Besides, a large number of organic compounds of biological or pharmaceutical interest possess the pyrazine ring. Oxido reduction reactions seemingly involving the pyrazine ring often take place in these compounds (1). Therefore there is an additional interest of a detailed knowledge of the electrochemical behavior of pyrazines.

This investigation is divided into two parts. This first paper deals with the reduction of pyrazines into dihydropyrazines and with the preparation of dihydropyrazines.

A. Electrochemical Reduction of Pyrazines into Dihydropyrazines

The pyrazines have been studied by polarography in hydroorganic mediums (2, 3) but with the exception of pyrazine itself in acidic medium, no preparative electrolysis has been carried out. As the dihydropyrazines are unstable in acidic medium, this investigation was carried out in alkaline medium. The following pyrazines were investigated: 2,5-diphenylpyrazine (**1**); 2,3-diphenylpyrazine (**2**); tetramethylpyrazine (**3**); 2,5-di-2′-pyridylpyrazine (**4**); 2,3-di-2′-pyridylpyrazine (**5**); tetra-2′-pyridylpyrazine (6).

1. 2,5-Diphenylpyrazine (1)

Between p*H* 1 and 13, **1** exhibits a single 2e cathodic wave, its $E_{1/2}$ depends on the p*H*: $E_{1/2} = -0.38 - 0.079pH$ (50% DMF).

During the electrolysis of a dilute solution of **1** in a water–DMF medium (0.5 *N* NaOH; $c = 2 \times 10^{-3}$ *M*; $E = -1.45$ V) an anodic wave appears with an $E_{1/2}$ very close to that of the cathodic wave of **1** (Fig. 1). Then this anodic wave decreases at the expense of another anodic wave, at a less negative potential, and of a cathodic wave, at a potential slightly more negative than that of **1**.

In a water–methanol medium (80% CH_3OH; 0.2 *N* NaOH; $c = 5 \times 10^{-4}$ *M*; $E = -1.35$ V) the same phenomenon is observed but the rate of disappearance of the first anodic wave is much faster at a given p*H* (Fig. 2).

The solubility of **1** is too low to carry out a preparative electrolysis.

The polarograms at different p*H* and the u.v. spectrum of the final reduction product are

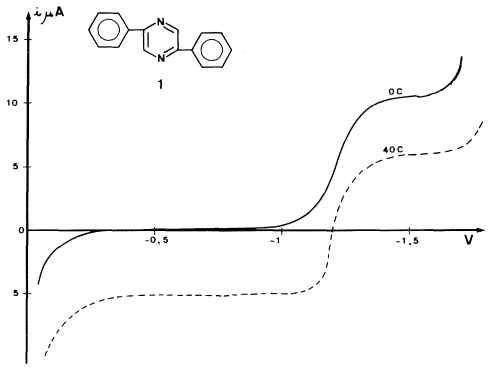

FIG. 1. Electrolysis of **1** in dilute solution; 0.5 *N* NaOH; $c = 2 \times 10^{-3}$ *M*; $V = 200$ ml; 50% DMF; $E = -1.45$ V. Polarograms before (0 °C) and during electrolysis (40 °C).

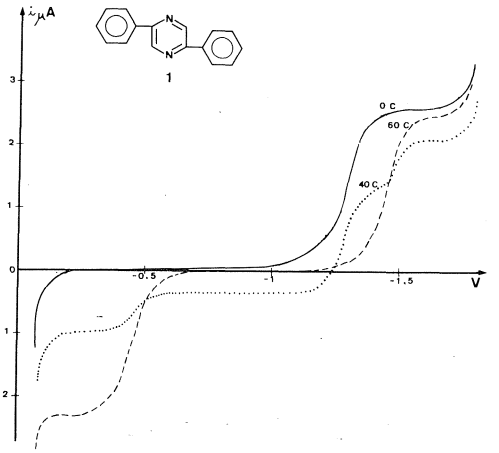

FIG. 2. Electrolysis of **1** in dilute solution; 0.2 *N* NaOH; $c = 5 \times 10^{-4}$ *M*; $V = 200$ ml; 80% CH_3OH; $E = -1.35$ V. Polarograms before (0 °C) and during electrolysis (40 °C, 60 °C).

identical with those of 1,6-dihydro-2,5-diphenylpyrazine (**7**)[1] which is prepared from 3,6-dihydro-2,5-diphenylpyrazine (**10**) (see B.4). Besides, it is generally assumed (2, 3) that the primary reduction product of pyrazines is a 1,4-dihydro derivative although no 1,4-dihydropyrazine has ever been isolated. This hypothesis has been confirmed recently: 1,4-dihydro-2,3-diphenylquinoxaline (**11**) has been prepared by electrochemical reduction of 2,3-diphenylquinolaxine (**12**) (4) (see Scheme 1). These results allow us to propose the reduction path outlined in Scheme 2.

[1]In a previous communication (16) a misinterpretation of the n.m.r. spectrum led us to assign the 1,2-dihydro-2,5-diphenylpyrazine structure to **7**.

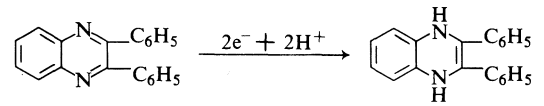

12 **11**

SCHEME 1

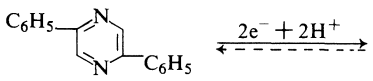

1

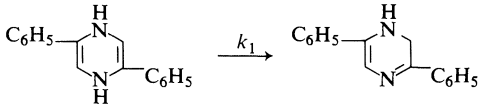

13 **7**

SCHEME 2

The value of k_1 depends on the p*H* and the nature and the amount of the cosolvent.

2. 2,3-Diphenylpyrazine (2)

Between p*H* 7 and 14, **2** displays a single 2e wave (perturbed by adsorption phenomena between p*H* 7 and 9.5) and its $E_{1/2}$ depends linearly on the p*H* according to $E_{1/2} = -0.38 - 0.07pH$ ($c = 10^{-3}$ *M*; 50% CH_3OH).

The results of the electrolysis in dilute solutions are similar to those observed with **1**; thus at p*H* 12 ($c = 2 \times 10^{-3}$ *M*; 50% CH_3OH; $E = -1.45$ V) an anodic wave appears with an $E_{1/2}$ close to that of the cathodic wave of **2** (Fig. 3). The u.v. spectrum of 1,4-dihydro-2,3-diphenylpyrazine (**14**) exhibits a shoulder at 340 nm (ε 4500) and a maximum at 257 nm (ε 8200). At p*H* 13.2 (50% CH_3OH; $c = 2 \times 10^{-3}$ *M*; $E = -1.45$ V) the same phenomena are observed as in the case of **1**: the anodic wave of the 1,4-dihydro derivative decreases with time and a cathodic and an anodic wave appear simultaneously (Fig. 4).

A large preparative electrolysis is carried out at p*H* 13.4 in order to isolate the rearranged product of the 1,4-dihydro derivative **14**. It is possible in a glove box under nitrogen to isolate a solid. The n.m.r. spectrum allows us to conclude that this compound is 1,2-dihydro-2,3-diphenylpyrazine (**8**). The proposed reduction is shown in Scheme 3.

3. Tetramethylpyrazine (3)

The polarograms at p*H* from 7 to 14 show that tetramethyl pyrazine presents a 2e cathodic

Can. J. Chem. Downloaded from www.nrcresearchpress.com by 210.87.254.5 on 09/05/12
For personal use only.

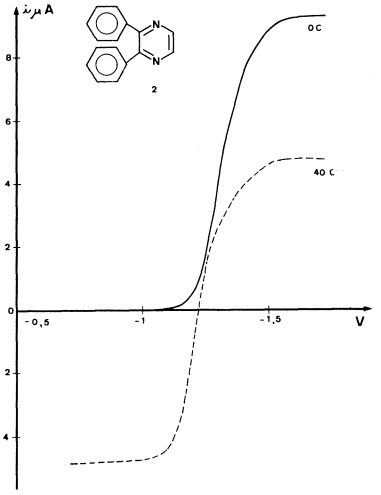

FIG. 3. Electrolysis of **2** in dilute solution; pH = 12.2; $c = 2 \times 10^{-3}$ M; $V = 200$ ml; 50% CH_3OH; $E = -1.45$ V. Polarograms before (0 °C) and during electrolysis (40 °C).

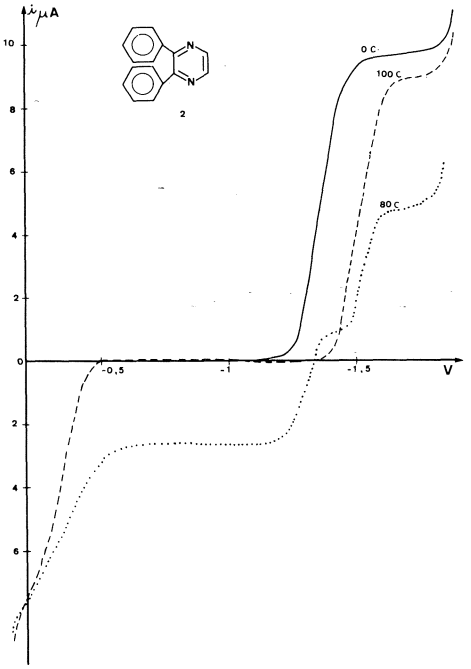

FIG. 4. Electrolysis of **3** in dilute solution; pH = 13.22; $c = 2 \times 10^{-3}$ M; $V = 200$ ml; 50% CH_3OH; $E = -1.45$ V. Polarograms before (0 °C) and during electrolysis (80 °C, 100 °C).

wave the $E_{1/2}$ of which varies with the pH (2). At a pH higher than 11, adsorption phenomena are observed which decrease the wave height. At a pH higher than 13 this wave becomes

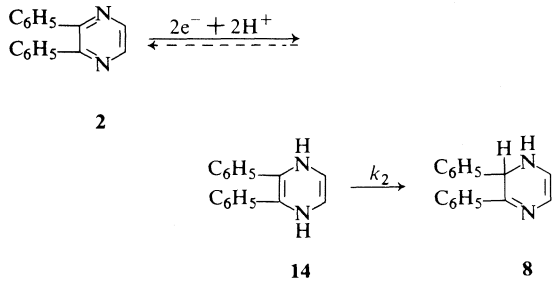

SCHEME 3

nearly nonexistent. Therefore, it is impossible to carry out an electrolysis in this pH range, the current intensity being too low.

Two waves appear during an electrolysis in dilute solution at pH 10.2 ($E = -1.4$ V; $c = 2 \times 10^{-3}$ M; 20% CH_3OH): an anodic wave, the half-wave potential of which is close to that of the cathodic wave of **3**; its height remains small and it disappears at the end of the electrolysis; a cathodic wave appears ($E_{1/2} = -1.45$ V) the height of which at the end of the electrolysis is about twice that of **3** before electrolysis. These waves are assigned respectively to 1,4-dihydrotetramethylpyrazine (**15**) and 1,2-dihydrotetramethylpyrazine (**16**) (Fig. 5). The number of coulombs corresponds to 2 electrons per molecule.

Preparative electrolyses were performed in an attempt to isolate the 1,2-dihydro derivative **16**; they were unsuccessful because of the large

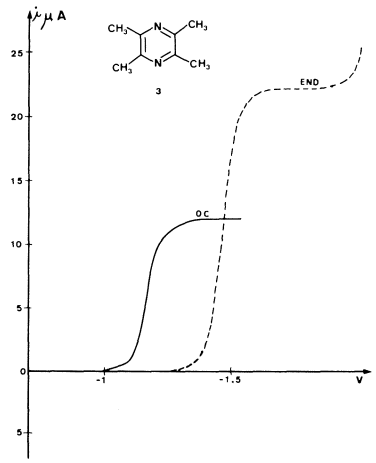

FIG. 5. Electrolysis of **3** in dilute solution; pH = 10.24; $c = 2 \times 10^{-3}$ M; $V = 200$ ml; 20% CH_3OH; $E = -1.40$ V. Polarograms before (0 °C) and after electrolysis.

Can. J. Chem. Downloaded from www.nrcresearchpress.com by 210.87.254.5 on 09/05/12
For personal use only.

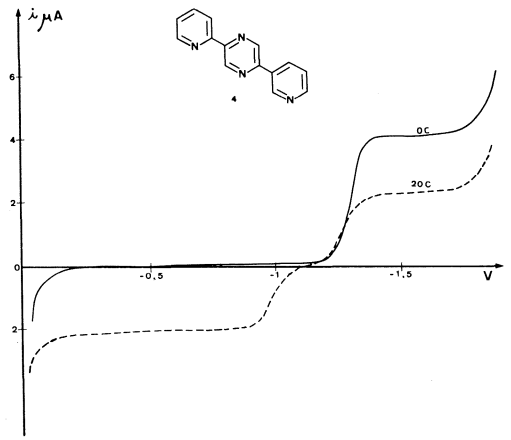

FIG. 6. Electrolysis of **4** in dilute solution; 0.1 *N* NaOH; $c = 10^{-3}$ *M*; $V = 200$ ml; 75% DMF; $E = -1.40$ V. Polarograms before (0 °C) and during electrolysis (20 °C).

solubility in water, the volatility, and the easy oxidizability of the electrolysis product.

4. 2,5-Di-2′-pyridylpyrazine (4)

The reduction of this compound was undertaken to isolate 1,4-dihydro derivative **17** for which a reduced oxidability could be expected as the result of hydrogen bonds formation.

As a matter of fact, 1,2-stilbenediol (**18**) is easily oxidized ($E_{1/2} = -0.7$ V at p*H* 10 (5)) but pyridoïn (**19**) is more stable ($E_{1/2} = -0.2$ V at p*H* 10 (6)) because of hydrogen bonding with the pyridine nitrogen.

Electrolysis of **4** in dilute solution gives a compound whose anodic wave is very close to the cathodic wave of **4** (Fig. 6). The $E_{1/2}$ for the 1,4-dihydro derivative **17** is, under the electrolysis conditions (75% DMF; 0.1 *N* NaOH; $c = 10^{-3}$ *M*), close to −1.0 V, that is to say, much too negative and reoxidation cannot be avoided in the course of preparative electrolysis.

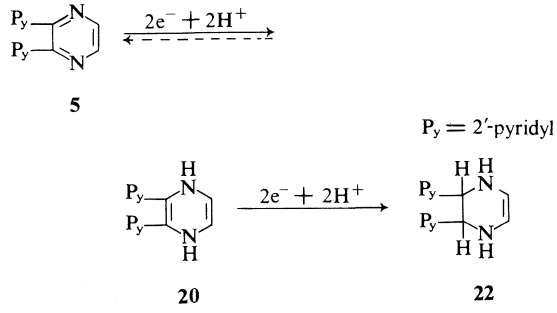

SCHEME 4

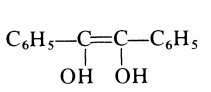

18

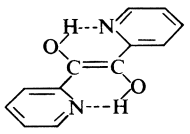

19

5. 2,3-Di-2′-pyridylpyrazine (5) and Tetra-2′-pyridylpyrazine (6)

Compounds **5** and **6** present a 2e wave the $E_{1/2}$ of which varies linearly with the p*H* according to $E_{1/2} = -0.37 - 0.066pH$ (50% CH_3OH; $c = 10^{-3}$ *M*) for **5** and $E_{1/2} = -0.27 - 0.076pH$ (50% DMF; $c = 10^{-3}$ *M*) for **6**.

In the case of **5** this wave is followed by a second wave, the height of which decreases from 4e to 2e when the p*H* changes from 7 to 14; it is due to the 1,4-dihydro derivative **20**.

In a water–DMF medium, electrolysis in dilute solution on the plateau of the second wave at p*H* 13 (50% DMF; $c = 2 \times 10^{-3}$ *M*; $E = -1.8$ V) consumes 4 electrons per molecule. The solution exhibits a 2e anodic wave ($E_{1/2} = -0.48$ V) and no cathodic wave; in addition its u.v. spectrum is different from that of 1,4,5,6-tetrahydro-2,3-di-2′-pyridylpyrazine (**21**). Thus, the anodic wave is assigned to the 1,2,3,4-tetrahydro-2,3-di-2′-pyridylpyrazine (**22**). The reduction is shown in Scheme 4.

A coulometry in 0.1 *N* NaOH on the plateau of the first wave (50% DMF; $c = 2 \times 10^{-3}$ *M*; $E = -1.4$ V) consumes 4 electrons per molecule. The polarograms recorded during this

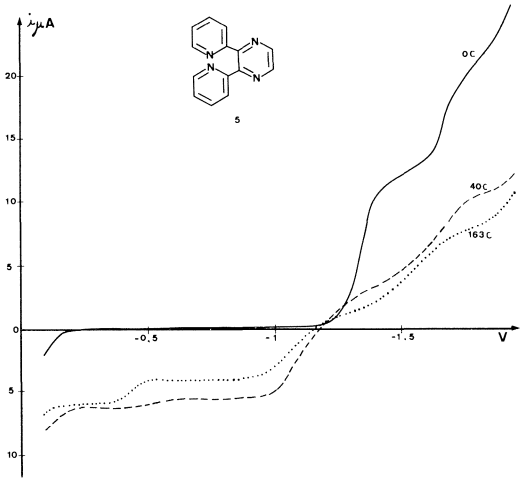

FIG. 7. Electrolysis of **5** in dilute solution; 0.1 *N* NaOH; $c = 2 \times 10^{-3}$ *M*; $V = 200$ ml; 50% DMF; $E = -1.40$ V. Polarograms before (0 °C) and during electrolysis (40 °C, 163 °C).

Can. J. Chem. Downloaded from www.nrcresearchpress.com by 210.87.254.5 on 09/05/12
For personal use only.

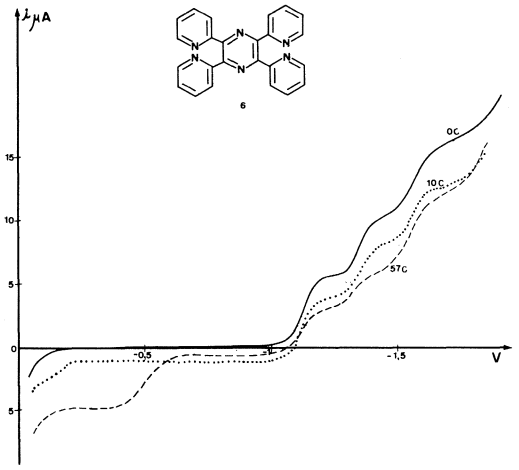

FIG. 8. Electrolysis of **6** in dilute solution; 0.1 *N* NaOH; $c = 10^{-3}$ *M*; *V* = 200 ml; 50% DMF; *E* = −1.25 V. Polarograms before (0 °C) and during electrolysis (10 °C, 57 °C).

electrolysis (Fig. 7) show that the 1,4-dihydropyrazine **20** is formed and rearranges into another 1,2- or 1,6-dihydropyrazine. This last compound, being as reducible as **5**, is reduced in its turn into 1,2,3,4-tetrahydro-2,3-di-2′- pyridylpyrazine (**22**)

The behavior of **6** is analogous to that of **5** (Fig. 8).

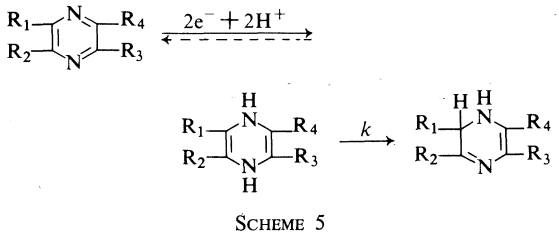

SCHEME 5

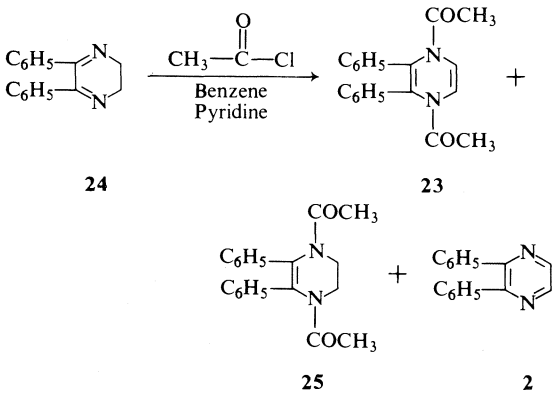

SCHEME 6

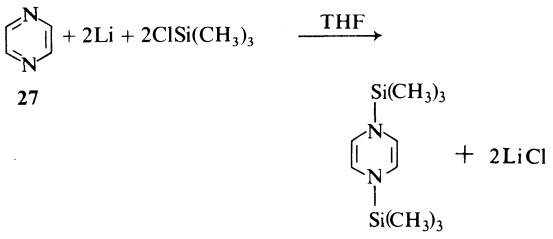

SCHEME 7

6. Conclusion

These results show that pyrazines are reduced to highly oxidizable 1,4-dihydro derivatives which cannot be isolated. These 1,4-dihydropyrazines isomerize in solution to 1,2- or 1,6-dihydropyrazines. The rate of this isomerization depends on the pyrazine, on the p*H*, and on the co-solvent (nature and amount of the co-solvent). The reaction shown in Scheme 5 thus seems general.

It should be noted that the isomerization of this 1,4-dihydro derivative seems univocal: the 2,3-diphenylpyrazine (**2**) only gives the 1,2-dihydro-2,3-diphenylpyrazine (**8**) and the 2,5-diphenylpyrazine (**1**) only gives the 1,6-dihydro-2,5-diphenylpyrazine (**7**).

B. Preparation of Dihydropyrazines

1. 1,4-Dihydropyrazines

Several authors have assigned the 1,4-dihydropyrazine structure to compounds which correspond to different formulae (7). To the best of our knowledge, no 1,4-dihydropyrazine has ever been prepared chemically or electrochemically. However, a diacetyl derivative **23** has been obtained recently by reaction of acetyl chloride with 2,3-diphenyl-5,6-dihydropyrazine (**24**) (7) (Scheme 6).

At about the same time, a silylated derivative (**26**) has been obtained by reduction of pyrazine (**27**) by lithium in the presence of $ClSi(CH_3)_3$ (8) (Scheme 7).

The interest of these compounds lies in the fact that they are antiaromatic molecules with 8 π electrons, thus analogous to cyclooctotetraene and to 1*H*-azepine the chemistry of which is the subject of a large number of papers.

The preparation of diacetyl derivatives was attempted until now without success, by electrochemical reduction of pyrazines in aprotic medium in the presence of an electrophile such as acetyl chloride or acetic anhydride.

Can. J. Chem. Downloaded from www.nrcresearchpress.com by 210.87.254.5 on 09/05/12
For personal use only.

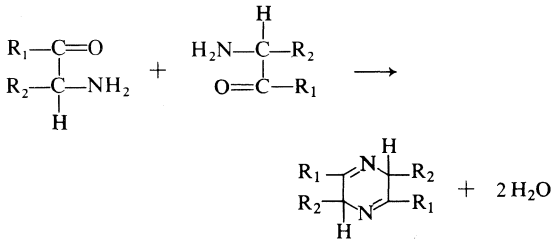

SCHEME 8

2. 2,3- (or 5,6-) Dihydropyrazines

These compounds are the most stable dihydropyrazines and they are synthesized by condensation of α-diketones with 1,2-diamines. A good number of 2,3-dihydropyrazines have been prepared and their chemical and physicochemical properties have been studied (9, 10).

In order to investigate the behavior of *cis*-2,3-dihydro-2,3-diphenylpyrazine (**28**) its preparation was attempted (11). The n.m.r. spectrum of the compound obtained shows that it does not have the expected formula but most probably that of an imidazoline (see Experimental).

3. 2,5- (or 3,6-) Dihydropyrazines

It is well known that the condensation of 2 molecules of α-aminoketone in alkaline medium in the absence of oxygen yields a 2,5- (or 3,6-) dihydropyrazine (10, 12).

The 2,5-dihydro-2,5-dimethyl-3,6-diphenylpyrazine is prepared by condensation of 2-amino-2-methylacetophenone according to ref. 13. The n.m.r. spectrum (in $CDCl_3$) of the solid confirms the proposed formula. The methyl groups are split into two doublets which are assigned to the *cis* and *trans* isomers (see Experimental).

The condensation of 2-aminoacetophenone yields a solid (14), whose n.m.r. spectrum indicates a mixture of 3,6-dihydro-2,5-diphenylpyrazine (**10**) and 1,6-dihydro-2,5-diphenylpyrazine (**7**).

Thus, the only general preparation of these compounds is the condensation of 2 molecules of α-aminoketone; this only leads to 2,5- (or 3,6-) dihydropyrazines with the same substituent in the 3,6- and 2,5-positions (Scheme 8).

These compounds easily undergo a rearrangement into 1,2- or 1,6-dihydro derivatives as will be seen now.

4. 1,2- (or 1,6-) Dihydropyrazines

4.1 Isomerization of 2,5- (or 3,6-) Dihydropyrazines

The preparation of 2,5-diphenylpyrazine is described by Nomine *et al.* (14, 15). 2-Aminoacetophenone is first condensed in an ammonia solution, then the solid obtained is heated in alcohol under nitrogen. According to the authors, this leads to the 1,6-dihydro-2,5-diphenylpyrazine (**7**). This 1,6-dihydro compound can be oxidized by heating in benzene in the presence of air to give the pyrazine. After some i.r. and u.v. studies these authors proposed the following reaction (Scheme 9).

As the arguments given by these authors seemed unreliable we prepared the 1,6-dihydro derivative according to their experimental method; the 1,6-dihydro derivative **7** is obtained as shown by the n.m.r. spectrum but mixed with about 20% of pyrazine **1**. As for the solid ob-

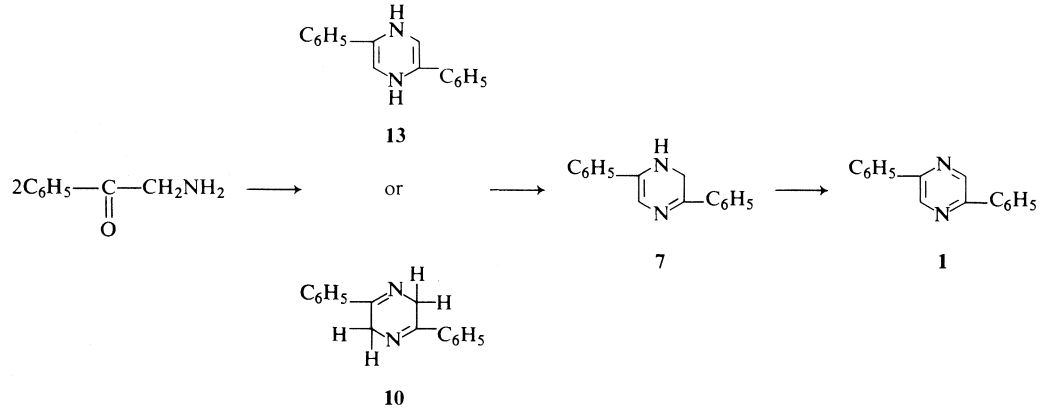

SCHEME 9

Can. J. Chem. Downloaded from www.nrcresearchpress.com by 210.87.254.5 on 09/05/12
For personal use only.

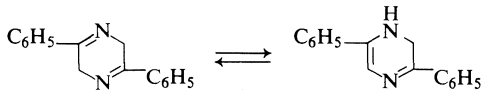

10 7

SCHEME 10

tained by condensation of 2-aminoacetophenone the u.v. spectrum in methanol and the n.m.r. spectrum show that it is a mixture of 3,6-dihydro-2,5-diphenylpyrazine (**10**) and of 1,6-dihydro-2,5-diphenylpyrazine (**7**).

The 1,6-dihydro derivative **7** can be prepared free of pyrazine. When the isomerization is carried out in acetone at 25 °C under argon in the dark the 1,6-dihydropyrazine **7** is obtained pure in 90% yield.

The n.m.r. spectrum of a solution of this 1,6-dihydropyrazine in $CDCl_3$ is that of a mixture of 3,6- and 1,6-dihydro derivatives **10** and **7** in the ratio of 30:70. The same spectrum is obtained from the product of condensation of 2-aminoacetophenone. This result (Scheme 10) shows that there is a thermodynamic equilibrium between these two isomers.

When deuterated acetone is added to the chloroformic solution, the equilibrium is displaced towards the 1,6-dihydro derivative **7**.

Thus, the preparation of 1,6-dihydro derivatives by isomerization of the 3,6-dihydro derivatives necessitates a careful experimental preparation: the solvent must be chosen so that equilibrium (Scheme 10) is completely displaced to the right, causing the oxidation to pyrazine to be difficult and the recovery of the easily oxidized final product easy.

It should be noted that the isomerization of the 3,6-dihydro compounds should only lead to 1,6-dihydro derivatives because the 1,2-dihydro derivative is less stable than the 1,6-dihydro derivative **7**. In the 1,6-dihydro derivative **7** the two phenyl groups are conjugated through the dienic system (extended conjugation) whereas in the 1,2-dihydro derivative only one phenyl group is linked to the dienic system in a cross-conjugated way.

4.2. Electrochemical Reduction of Pyrazines

The preparation of 1,2-dihydro-2,3-diphenylpyrazine (**8**) shows that the electrochemical reduction can be a valuable route to some 1,2- (or 1,6-) dihydro derivatives. There are, however, some limitations to this method: the reduction cannot be stopped always at the 2 electron stage as in the case of 2,3-di-2′-pyridylpyrazine (**5**) and of tetra-2′-pyridylpyrazine (**6**) where the dihydro derivatives obtained by isomerization of the 1,4-dihydropyrazines are as reducible as the starting pyrazine; and the high oxidizability of the 1,2- (or 3,6-) dihydro derivatives does not always permit their isolation especially if the procedure involves an evaporation of the solution as in the case of tetramethylpyrazine (**3**).

4.3. Chemical Reductions

Simultaneously with the publication of our preliminary communication (16) describing the electrochemical preparation of 1,2-dihydro-2,3-diphenylpyrazine (**8**), Williams *et al.* (17) showed that the reduction of pyrazines substituted by carboalkoxy groups by sodium dithionite in alkaline medium or by catalytic hydrogenation could lead to 1,2- (or 1,6-) dihydropyrazines. We applied their experimental procedure to the catalytic hydrogenation of all the pyrazines studied in part A. In the case of tetramethylpyrazine (**3**) and of 2,3-diphenylpyrazine (**2**) there is no absorption of hydrogen. The 2,5-diphenylpyrazine (**1**) gives the 2,5-diphenylpiperazine (**29**). The 2′-pyridylpyrazines **5** and **6** give a mixture of piperazines, dihydro- and tetrahydropyrazines (all the attempted separations resulted in the reoxidation into the starting compound).

As a conclusion, the different methods describing the preparation of 1,2- (or 1,6-) dihydro pyrazines are complementary, none of them being general.

Experimental

1. Techniques

The different techniques used in this study have already been described (4, 18). All the potentials are given by reference to the saturated calomel electrode. The p*H*'s are measured with a Radiometer model 4 p*H* meter equipped with a combined glass–aqueous calomel electrode model GK2302 B. The microanalyses were performed in the microanalysis laboratory of the Université Paris VI by M. E. Dorme. All the compounds for which the name analysis is followed by a molecular formula gave analytical results in agreement by 0.2% at most.

2. Part A

2.1. Preparation of pyrazines

2,5-Diphenylpyrazine (1)

The experimental procedure of ref. 14 was followed: the 2-aminoacetophenone hydrochloride in ammonia solution gives the 3,6-dihydro-2,5-diphenylpyrazine (**10**); the oxidation by air in boiling benzene of the 1,6-dihydro-2,5-diphenylpyrazine (**7**) (obtained by isomerization of the

Can. J. Chem. Downloaded from www.nrcresearchpress.com by 210.87.254.5 on 09/05/12
For personal use only.

3,6-dihydro compound) gives **1** (85% yield). Analysis: $C_{16}H_{12}N_2$; m.p. 197 °C (lit. (14) m.p. 195.5 °C);

n.m.r. ($CDCl_3$): 10 protons, 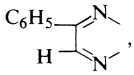 ,

multiplet centered at 7.8 p.p.m.;

and 2 protons, 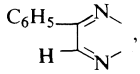 , singlet at 9.06 p.p.m.;

u.v. (CH_3OH): λ_{max} 324 (ε 17 200), 297 (ε 15 000), 269 nm (ε 15 800).

2,3-Diphenylpyrazine (2)

This was obtained by oxidation of the 5,6-dihydro-2,3-diphenylpyrazine (**24**) (19) prepared by condensation of benzile with ethylenediamine (20) (70% yield): Anal. $C_{16}H_{12}N_2$; m.p. 121 °C (lit. (19), m.p. 118–119 °C); n.m.r. ($CDCl_3$): 10 protons, 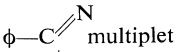 multiplet centered at 7.4 p.p.m.; and 2 protons, 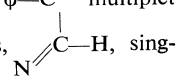 , singlet at 8.71 p.p.m.; u.v. (CH_3OH): λ_{max} 310 (ε 7300), 285 (ε 9600), 266 nm (ε 10 100).

Tetramethylpyrazine (3)

This was obtained from diacetylmonoxime (21) (60% yield). Analysis: $C_8H_{12}N_2$; m.p. 86 °C (lit. (21), m.p. 85–86 °C); n.m.r. ($CDCl_3$): 12 protons, 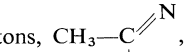 , singlet at 2.41 p.p.m.

2,5-Di-2′-Pyridylpyrazine (4)

The procedure of ref. 22 was used with some modifications: 4 g of 2-(ω-aminoacetyl)pyridine hydrochloride was dissolved in 40 ml of deoxygenated water; under a nitrogen atmosphere, 5 ml of 22% ammonia was added dropwise. The product which precipitated after 3 h of stirring was filtered, washed with water, and dried under vacuum on P_2O_5. The 3,6-dihydro 2,5-di-2′-pyridylpyrazine was dissolved in the minimum amount of acetonitrile (about 200 ml for 100 mg) and left in contact with air for 24 h. Compound **4** precipitated, was filtered, and washed with acetonitrile and ether (80% yield). Analysis: $C_{14}H_{10}N_4$; m.p. 227 °C (lit. (22), m.p. 226–227 °C);

n.m.r. ($CDCl_3$): 8 protons, ,

2 multiplets centered at 7.5 and 8.7 p.p.m.;

and 2 protons, 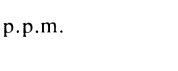 , singlet at 9.96 p.p.m.

The 2-(ω-aminoacetyl)pyridine was prepared according to ref. 23.

2,3-Di-2′-Pyridylpyrazine (5)

This was prepared (24) by refluxing a solution of 2 g of 5,6-dihydro-2,3-dipyridylpyrazine in 25 ml of mesitylene in the presence of 0.2 g of 10% Pd–C for 20 h (70% yield). Analysis: $C_{14}H_{10}N_4$, m.p. 168 °C (lit. (24), m.p. 167 °C);

n.m.r. ($CDCl_3$): 8 protons, 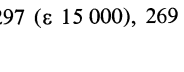 ,

3 multiplets centered at 7.33, 7.9, and 8.5 p.p.m.;

and 2 protons, 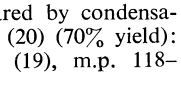 , at 8.7 p.p.m.

Tetra-2′-Pyridylpyrazine (6)

This was prepared (24) by heating for 2 h at 180 °C a mixture of 20 g of pyridoïn and 90 g of ammonium acetate (70% yield). Analysis: $C_{24}H_{16}N_6$; m.p. 284 °C (lit. (24) m.p. 284 °C);

n.m.r. ($CDCl_3$): 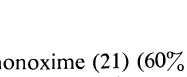 ,

3 multiplets centered at 7.33, 7.91, and 8.45 p.p.m.

2.2. Electrochemical Reduction of Pyrazines into Dihydropyrazines

2.2.1. Electrolysis in Dilute Solutions

Generally 200 ml of solution was used with pyrazine concentrations ranging from 5×10^{-4} to 2×10^{-3} *M*. When the 1,4-dihydro derivative isomerized slowly the number of Faradays measured was always between 2 and 3. Although the electrolyses were performed under argon a partial reoxidation could not be prevented.

2.2.2. Preparative Electrolysis of 2,3-Diphenylpyrazine (2)

Preparation of ***8***. The electrolysis was carried out on 200 ml of 0.5 *N* sodium hydroxide solution (p*H* 13.4) containing 50% CH_3OH and 1 g of **2** at $E = -1.4$ V. The current intensity was 200 mA at the beginning of the electrolysis and fell to 10 mA after 7 h and 890 C (830 C for 2 F). The electrolysis was stopped and the solution was processed in a glove box under nitrogen: the solution was filtered and the solid washed with deoxygenated water and CCl_4 to yield 300 mg of yellow crystals; m.p. 125 °C

---

n.m.r. (DMSO + D_2O): 10 protons, 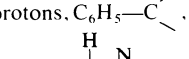 , multiplet centered at 7.5 p.p.m.;

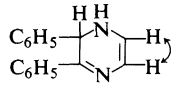

$J = 5$ Hz

8

1 proton, 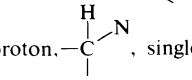 , singlet at 5.77 p.p.m. (doublet before addition of D_2O, $J = 4$ Hz;

1 proton, 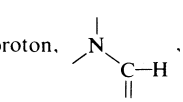 , doublet at 6.15 p.p.m. (triplet before addition of D_2O);

1 proton, 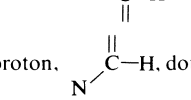 -H, doublet at 6.31 p.p.m.; u.v. (CH_3OH): λ_{max} 384 nm (ε 7000).

Can. J. Chem. Downloaded from www.nrcresearchpress.com by 210.87.254.5 on 09/05/12
For personal use only.

Can. J. Chem. Downloaded from www.nrcresearchpress.com by 210.87.254.5 on 09/05/12
For personal use only.

By comparison of the polarograms of **7** and **8** (assuming that the compounds have similar diffusion coefficients), the purity of **8** was estimated to be higher than 90%.

Preparative Electrolysis of Tetramethylpyrazine (3). Electrolysis was carried out on 50 ml of aqueous solution containing 1 g of **3** (p*H* 10.2; $E = -1.4$ V). The current intensity which was 350 mA at the beginning fell to 10 mA after consumption of about 2 electrons per molecule (1420 C).

All the attempted isolations of the product were unsuccessful: on one hand the compound was highly soluble in water and an extraction with ether was unoperative; on the other hand the product was volatile and distilled along with water if one tried to concentrate the solution. In addition, a partial reoxidation occurred in the course of this distillation.

3. Part B

3.1. Condensation of 2-aminoacetophenone

*Preparation of **10**.* The procedure of refs. 14 and 15 was used: 5 ml of 22% ammonia are added dropwise into a solution of 4.25 g of 2-aminoacetophenone hydrochloride in 40 ml of water under nitrogen and a yellow orange product precipitated. The solution was stirred for 3 h, cooled, and the solid was filtered, washed with water, and dried under vacuum over P_2O_5 (66% yield); m.p. 164 °C (lit. (14, 15), m.p. 165 °C). This solid, in solution in methanol, under nitrogen, exhibited a u.v. spectrum with a band at λ_{max} of 406 nm which increased with time to reach a maximum after 4 h corresponding to ε 11 000 for a molecular weight of M 234 (that of the starting compound **10**). Some pyrazine was also formed and could be detected by its characteristic u.v. spectrum.

An n.m.r. spectrum in $CDCl_3$ presented a multiplet centered at 7.6 p.p.m., assigned to the protons of the four phenyl groups of **10** and **7**, a singlet at 6.96 p.p.m. assigned to the 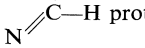 proton of **7**, a singlet at 4.4 p.p.m. due to the two protons of the $-CH_2-N=$ group of **10**, a doublet at 4.16 p.p.m. due to the two protons of the 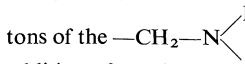 group of **7** (it gives a singlet by addition of D_2O), and a broad signal at 3.4 p.p.m. which disappeared on addition of D_2O and was assigned to the proton of **7**. The relative intensities showed that the mixture contained 30% of 3,6-dihydro-2,5-diphenylpyrazine (**10**) and 70% of 1,6-dihydro-2,5-diphenylpyrazine (**7**).

When the chloroformic solution was diluted in deoxygenated methanol and the u.v. spectrum recorded, the band at 406 nm increased and reached the same absorption coefficient as above.

When the n.m.r. spectrum was recorded in a $CDCl_3$–acetone-d_6 mixture, the percentage of 1,6-dihydro derivative was higher than in pure $CDCl_3$. When this solution was diluted in methanol the band at 406 nm increased to reach the same intensity as above.

This band at λ_{max} 406 nm is due only to the 1,6-dihydro 2,5-diphenyl pyrazine (**7**) (see below); the 3,6-dihydro derivative (**10**) does not absorb in this region. The relative amounts of 1,6- and 3,6-dihydro derivatives calculated from the n.m.r. spectrum in $CDCl_3$ or in $CDCl_3$–acetone-d_6 were identical to those calculated from the u.v. spectrum in methanol taking an absorption coefficient of ε 12 300 at λ_{max} 406 nm (see below).

3.2. Preparation of the 1,6-Dihydro-2,5-diphenylpyrazine (7)

A solvent must be selected where the isomerization is fast but where the oxidation into pyrazine is slow. The transformation into pyrazine takes place even under argon (disproportionation or reaction with the solvent) and the light acts as a catalyst. The best results are obtained in an inactinic flask in acetone at 25 °C: in a 500 ml inactinic flask, 1 g of the solid obtained by condensation of 2-aminoacetophenone was dissolved in 250 ml of deoxygenated acetone. The temperature was maintained at 25 °C (in a thermostatic bath) for 5 h, and the solution was then poured into 750 ml of deoxygenated water; the solid which precipitated was filtered under nitrogen and dried under vacuum over P_2O_5 in the dark (90% yield). Analysis: $C_{16}H_{14}N_2$; m.p. 169 °C; u.v. (CH_3OH): λ_{max} 406 (ε 12 300), 245 nm (ε 15 600). This spectrum does not change with time.

From the preceding results, this compound was the pure 1,6-dihydro-2,5-diphenylpyrazine (**7**). The n.m.r. spectrum of **7** in $CDCl_3$ was identical to that of the mixture of 1,6- and 3,6-dihydro derivatives. This shows that these two compounds are in equilibrium and that both isomerization rates are high. The addition of acetone displaced the equilibrium towards the 1,6-dihydro compound as seen in 3.1.

3.3. Tentative Preparation of the 2,3-Dihydro-2,3-diphenylpyrazine (28)

According to ref. 11 the condensation of *meso*-stilbenediamine (prepared as in ref. (25)) with glyoxal yielded the 2,3-dihydro-2,3-diphenylpyrazine (**28**).

The experimental procedure of ref. 11 gave a solid with m.p. 163.4 °C (*cf.* ref. 11) but the analysis corresponded to the formula $C_{16}H_{16}N_2O$. This could be in agreement with the expected compound containing 1 mol of water but this is excluded by the n.m.r. spectrum; n.m.r. ($CDCl_3$): 1 proton (NH), broad signal at 2.0 p.p.m. which disappeared by addition of D_2O; 2 protons, singlet at 3.73 p.p.m.; 1 proton H_1, doublet at 4.40 p.p.m.; 1 proton H_2, multiplet centered at 4.6 p.p.m., gave a doublet on addition of D_2O, $J_{H_1-H_2} = 4$ Hz; 10 protons C_6H_5, 2 multiplets between 6.6 and 7.4 p.p.m. This spectrum and the analysis are in agreement with the formula of the following imidazoline:

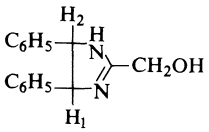

As a matter of fact, it is known that this type of compound is obtained by reaction of α-diamines with acids or their derivatives and that glyoxal gives glycolic acid in alkaline medium.

3.4. Preparation of the 2,5-Dihydro-2,5-dimethyl-3,6-diphenylpyrazine

3.4.1. Preparation of 2-Amino-2-methyl-acetophenone

By reduction of 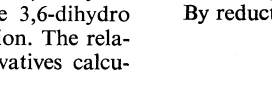 (26): 16.5 g of

oxime was added to a solution of 45 g $SnCl_2$ in 65 ml of concentrated hydrochloric acid. The reduction product precipitated as a stannic double salt $(C_9H_{11}NO_2)_2H_2SnCl_6$ (88% yield), m.p. 224 °C. To recover the aminoketone hydrochloride, the salt was dissolved in water and H_2S was bubbled through the solution. When the precipitation of tin sulfide was over, the solution was filtered and the filtrate evaporated to dryness. The 2-amino-2-methylacetophenone hydrochloride obtained was purified by dissolution in alcohol and reprecipitation by ether (75% yield); m.p. 184 °C (lit. (26), m.p. 183–184 °C); n.m.r. (DMSO-d_6): 3 protons, $-CH_3$, doublet at 1.51 p.p.m.; 1 proton, C—CH, quadruplet centered at 5.2 p.p.m.; 5 protons, C_6H_5, multiplet at 8 p.p.m.; 2 protons, NH_2, broad signal at 8.7 p.p.m. (disappeared by addition of D_2O).

Condensation of 2-Amino-2-methylacetophenone. This was condensed under the same conditions as 2-aminoacetophenone (see 3.1). The solid obtained was dried under vacuum over P_2O_5. Analysis: $C_{18}H_{18}N_2$. n.m.r.: this spectrum showed that the 2,5-dihydro-2,5-dimethyl-3,6-diphenylpyrazine (**30**) was obtained alone as a mixture of the *cis* and *trans* isomers: a multiplet between 7.0 and 8.0 p.p.m. (10 protons) assigned to the aromatic protons; a multiplet centered at 4.55 p.p.m. (2 protons attributed to the CH_3—C—H protons and two doublets at 1.30–1.40 and 1.37–1.50 p.p.m. (6 protons) $J = 6$ and 7.8 Hz assigned to the two methyl groups of the two isomers. The isomeric ratio is approximately 70:30.

3.5. Catalytic Hydrogenations

The pyrazines (500 mg) were dissolved in 100 ml of 95% ethanol or methanol with 100 mg of 10% Pd–C (Merck Product) and hydrogenated under pressure at room temperature.

In the case of tetramethylpyrazine (**3**) and of 2,3-diphenylpyrazine (**2**), no hydrogen was absorbed; the 2′-pyridylpyrazines **5** and **6** gave mixtures of piperazines, di- and tetrahydrogenated products, as can be seen from the polarograms and u.v. spectra of the solids obtained by filtration and evaporation of the alcoholic solutions. The attempted separations only resulted in the reoxidation of the di- and tetrahydro derivatives into the starting pyrazines.

The 2,5-diphenylpyrazine (**1**) gave the 2,5-diphenylpiperazine (**28**), (80% yield), m.p. 195 °C (lit. (14) m.p. 195–196 °C); n.m.r. spectrum of **28**: a multiplet centered at 7.5 p.p.m. (10 protons) assigned to the aromatic protons; a doublet of doublets centered at 4.01 p.p.m. (2 protons) due to the C*H*—N$\diagdown\!\!\diagup$ protons; a multiplet (eight peaks) between 2.7 and 3.4 p.p.m. (4 protons) assigned to the diastereotopic $\diagdown\!\!\diagup CH_2$ protons (ABX spectrum); and a singlet at 2.1 p.p.m. (2 protons) due to the two $\diagdown\!\!\diagup$N—H (this signal disappeared by addition of D_2O).

The coupling constants were calculated for the only possible combination of the eight peaks which constitute the AB part of the spectrum: $J_{AX} = 2.6$ Hz, $J_{BX} = 10.6$ Hz; and $J_{AB} = 11.4$ Hz.

These results along with the known values of the J_{aa}, J_{ae}, and J_{ee} coupling constants between axial and equatorial protons of cyclohexane derivatives show that the 2,5-diphenylpiperazine (**28**) is the pure *trans* isomer. Analysis: $C_{16}H_{18}N_2$.

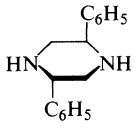

28

1. H. I. X. Mager and W. Berends. Rec. Trav. Chim. **78**, 109 (1959).
2. J. Volke, D. Dumanovic, and V. Volkova. Coll. Czech. Chem. Commun. **30** (1), 246 (1965).
3. L. N. Klatt and R. L. Rouseff. J. Am. Chem. Soc. **94**, 7295 (1972).
4. J. Pinson and J. Armand. Coll. Czech. Chem. Commun. **36**, 585 (1971).
5. R. H. Philip, Jr., R. L. Flurry, and R. A. Day, Jr. J. Electrochem. Soc. **111**, 328 (1964).
6. J. Holubek and J. Volke. Coll. Czech. Chem. Commun. **25**, 3292 (1960).
7. S-J. Chen and F. W. Fowler. J. Org. Chem. **36**, 4025 (1971).
8. R. A. Sulzbach. Angew. Chem. Int. Ed. **10**, 127 (1971).
9. Y. T. Pratt. *In* Heterocyclic compounds vol. 6. *Edited by* R. C. Elderfield. J. Wiley and Sons, N.Y. 1957. p. 408.
10. G. W. H. Cheeseman and E. S. G. Werstink. *In* Advances in heterocyclic chemistry. Vol. 14. *Edited by* A. R. Katritzky and A. J. Boulton. Academic Press, N.Y. 1972. p. 99.
11. T. Hayashi. Sc. Pap. I.P.C.R. **38**, 455 (1941).
12. S. H. Wilen. J. Chem. Soc. **25**, (1970).
13. S. Gabriel. Ber. **41**, 1127 (1908); **44**, 57 (1911).
14. G. Nomine, L. Penasse, and V. Delaroff. Ann. Pharm. Fr. **16**, 436 (1958).
15. G. Nomine, J. Mathieu, R. Jequier, and P. Bellet. Ann. Pharm. Fr. **16**, 125 (1958).
16. J. Armand, P. Bassinet, K. Chekir, J. Pinson, and P. Souchay. C. R. Acad. Sc. (C). **275**, 279 (1972).
17. J. R. Williams, J. J. Cossey, and M. Adler. J. Org. Chem. **37**, 2963 (1972).
18. J. Pinson and J. Armand. Can. J. Chem. **50**, 1581 (1972).
19. Mason and Dryfoos. J. Chem. Soc. **63**, 1297 (1893).
20. Q. Brewster. J. Chem. Ed. **16**, 566 (1939).
21. F. B. Kipping. J. Chem. Soc. 2891 (1929).
22. F. H. Case and E. Koft. J. Am. Chem. Soc. **81**, 905 (1959).
23. G. R. Clemo, T. Holmes, and G. Leitch. J. Chem. Soc. 753 (1938).
24. H. A. Goodwin and F. Lions. J. Am. Chem. Soc. **81**, 6415 (1959).
25. M. N. H. Irving. J. Inorg. Chem. **27**, 270 (1965).
26. L. Behr-Bregowski. Ber. **30**, 1521 (1897).

Can. J. Chem. Downloaded from www.nrcresearchpress.com by 210.87.254.5 on 09/05/12
For personal use only.

Syntheses of Some Phosphino- and Phosphinatoazoles

SVEN FISCHER AND LOUIS K. PETERSON
Department of Chemistry, Simon Fraser University, Burnaby, British Columbia V5A 1S6
AND
JOHN F. NIXON
School of Molecular Sciences, University of Sussex, Brighton BN1 9QJ, Great Britain

Received July 23, 1974

Can. J. Chem. Downloaded from www.nrcresearchpress.com by 210.87.254.5 on 09/05/12
For personal use only.

SVEN FISCHER, LOUIS K. PETERSON, and JOHN F. NIXON. Can. J. Chem. **52**, 3981 (1974).

The following *N*-substituted azoles have been prepared: (*a*) diphenylphosphine derivatives of pyrazole (**1***a*), 3,5,-dimethylpyrazole (**1***b*), 3(5)-methylpyrazole (isomers **2***a* and **2***b*), pyrrole (**7**), imidazole (**8**), and 1,2,4-triazole (**9**); (*b*) diphenylphosphinatopyrazole (**4***b*); (*c*) dichlorophosphinopyrazole (**5***a*) and dichlorophosphino-3,5-dimethylpyrazole (**5***b*); (*c*) 1,1-phenylphosphinobis(pyrazole) (**3**); (*d*) tris(pyrazolyl)phosphine (**6***a*) and tris(3,5-dimethylpyrazolyl) phosphine (**6***b*). Synthetic methods involved reactions (*i–iv*): (*i*) azole with chlorophosphine (**1–3**, **8**, **9**) or ϕ_2P(O)Cl (**4***a*) in ethereal solution with triethylamine as hydrogen halide acceptor; (*ii*) trimethylsilylazole with phosphorus trichloride (**5**, **6**); (*iii*) potassium pyrrolide with diphenylchlorophosphine (**8**); (*iv*) sulfur oxidation of **1***a* (**4***b*). Nuclear magnetic resonance spectral assignments are discussed.

SVEN FISCHER, LOUIS K. PETERSON et JOHN F. NIXON. Can. J. Chem. **52**, 3981 (1974).

On a préparé les azoles *N*-substitués suivants: (*a*) les dérivés diphénylphosphine du pyrazole (**1***a*), diméthyl-3,5 pyrazole (**1***b*), méthyl-3(5) pyrazole (isomères **2***a* et **2***b*), pyrrole (**7**), imidazole (**8**) et le triazole-1,2,4 (**9**); (*b*) diphénylphosphinatopyrazole (**4***b*); (*c*) dichlorophosphinopyrazole (**5***a*) et le dichlorophosphinodiméthyl-3,5 pyrazole (**5***b*); (*d*) phényl-1 phosphino-1 bis(pyrazole) (**3**); (*e*) tris(pyrazolyl)phosphine (**6***a*) et le tris(diméthyl-3,5 pyrazolyl)phosphine (**6***b*). Les méthodes de synthèse font appel aux réactions (*i–iv*): (*i*) l'azole avec la chlorophosphine (pour **1–3**, **8**, **9**) ou ϕ_2P(O)Cl (**4***a*) dans une solution éthérée avec la triéthylamine comme accepteur d'acide halogène-hydrique; (*ii*) la triméthylsilylazole avec le trichlorure de phosphore (**5**, **6**); (*iii*) le pyrrolidure de potassium avec la diphénylchlorophosphine (**8**); (*iv*) l'oxydation du soufre de **1***a* (**4***b*). Les attributions spectrales déduites de l'étude r.m.n. sont discutées.

[Traduit par le journal]

Introduction

There is current interest in the chemistry of azoles and their organometallic derivatives (1–15). Organo derivatives of Group III (1–4) and Group IV (5–15) metal azoles have been studied in some detail and Group V (**1***c*) derivatives have been mentioned. The trialkylsily- and trialkygermylpyrazoles, imidazoles, and triazoles have been shown to exhibit metallotropic exchange between two nitrogen sites (12, 13, 15) and there is an extensive chemistry of pyrazolylborate anions as ligands (1*c*, 16–21).

Results and Discussion

In this paper we report syntheses of a series of phosphino- and phosphinatoazole compounds (**1–9**) (Fig. 1) which are of interest as potential ligands in coordination chemistry. Synthetic routes are summarized in eqs. 1 (for compounds **1**, **2**, **3**, **8**, and **9**), 2 (for **7**), and 3 (for **5** and **6**).

Compound **4***a* was obtained essentially according to eq. 1, with ϕ_2P(O)Cl in place of the chloro-

$$[1]\quad \mathrm{AzH} + \gtrless\mathrm{P{-}Cl} \xrightarrow[(-\mathrm{HCl})]{\mathrm{Et_3N{-}Et_2O}} \gtrless\mathrm{P{-}Az}$$

(AzH = azole)

$$[2]\quad \mathrm{K^+Az^-} + \gtrless\mathrm{P{-}Cl} \xrightarrow[(-\mathrm{KCl})]{\text{hexane}} \gtrless\mathrm{P{-}Az}$$

$$[3]\quad x\mathrm{Me_3Si{-}Az} + \mathrm{PCl_3} \longrightarrow x\mathrm{Me_3SiCl} + \mathrm{Cl_{3-}}_x\mathrm{P(Az)}_x$$

phosphine, but it could not be obtained by an attempted O_2 oxidation of **1***a* in solution in hexane. However, **1***a* was oxidized by sulfur in refluxing benzene, to form **4***b*. The compounds **5***b*, **6***a*, and **6***b* were obtained by the reaction of appropriate proportions of PCl_3 and azole, in ethereal solution but yields were low and side

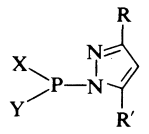

1*a* R, R′ = H; X, Y = ϕ
1*b* R, R′ = Me; X, Y = ϕ
2*a* R = Me; R′ = H; X, Y = ϕ
2*b* R = H; R′ = Me; X, Y = ϕ
3 R, R′ = H; X = ϕ; Y = pyraxolyl
5*a* R, R′ = H; X, Y = Cl
5*b* R, R′ = Me; X, Y = Cl
6*a* R, R′ = H; X, Y = pyrazolyl
6*b* R, R′ = Me; X, Y = 3,5-dimethylpyrazolyl

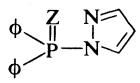

4

a Z = O
b Z = S

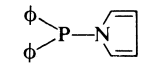

7

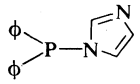

8

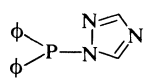

9

FIG. 1

reactions gave dark colored residues. The alternative routes (eq. 3) involving the elimination of Me_3SiCl from trimethylsilylazoles were quantitative, being analogous to the PCl_3 cleavage of trialkylsilylamines (22). There was no reaction between pyrrole and ϕ_2PCl in ethereal solution, even in the presence of triethylamine. The pyrrolide anion, however, reacts readily with ϕ_2PCl (eq. 2), giving **7**, as a thermally unstable yellow oil. The products **1**–**9** were characterized by mass and n.m.r. spectroscopy, and/or elemental analysis and the reaction stoichiometry. All compounds were moisture sensitive, the dichlorophosphinopyrazoles **5***a* and **5***b* being particularly reactive. The compounds **1**–**9** except for **7**, are thermally stable, and can be sublimed or distilled in the 100–150 °C temperature range at low pressure. They are liquids or low melting solids and they dissolve readily in a variety of nonhydroxylic organic solvents. Only parent ions for monomeric species were observed in the mass spectra, together with readily identifiable fragmentation patterns. By contrast, the analogous Group III derivatives of pyrazole (1–4, 23) are known to be dimeric or polymeric both in the solid state and in solution, whereas the Group IV derivatives show varying tendencies for intermolecular association in solution (14, 15).

In theory, *N*-substitution reactions (24) of 3(5)-methylpyrazole could lead to a mixture of 3-methyl- and 5-methyl-1-substituted pyrazoles. Indeed, the reaction of ϕ_2PCl with methylpyrazole was found to yield a mixture of the isomers **2***a* and *b*, in a 6:1 molar ratio, as evidenced by the ^1H n.m.r. spectrum of the reaction products. In a similar fashion, isomeric mixtures resulted from the reaction of 3(5)-methylpyrazole with trimethylchlorosilane (25) or with Me_3E (E = B, Al, Ga) (3). In contrast, only one isomer was formed in the reaction of sodium 3(5)-methylpyrazolide with phosgene (26), and when 3-phenylpyrazole reacts with bis(tri-*n*-butyltin) oxide (14). Mechanistically, the pyrazole moiety would be expected to maintain its π-stabilized, aromatic character in its substitution reactions by utilizing its pyridine type (2 *N*) site, rather than its sp^2 hybridized (1 *N*) site in the reaction step preceding elimination of HX (eqs. 4*a* and 4*b*) (24*d*). Clearly, there is some steric preference for eq. 4*a* and ready isomerization can provide the appropriate pyrazole tautomer for major reaction via this route. The large 3-phenyl substituent would be even more specifically directional in its effect than the smaller 3-methyl group.

[4*a*] 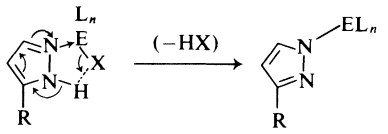

[4*b*] 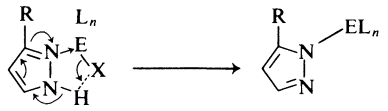

(E = metalloid; L_n = other ligands;

X = alkyl or halogen, or $OSnBu_3$)

Following synthetic routes known for the dialkylaminodifluorophosphines, R_2NPF_2, (27) various attempts were made to prepare the analogous difluorophosphinopyrazoles. The former types of compound have been obtained via: (*a*) the action of PF_3 upon R_2NH (28) or R_2NSnMe_3 (22); (*b*) the reaction between

Can. J. Chem. Downloaded from www.nrcresearchpress.com by 210.87.254.5 on 09/05/12
For personal use only.

TABLE 1. Proton n.m.r. data* for 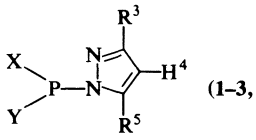 (**1–3, 5, 6**) and 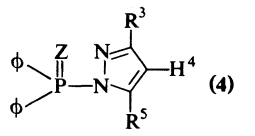 (**4**)

	Compound	τ R³	τ H⁴	τ R⁵	$J_{R^3H^4}$	$J_{H^4R^5}$	J_{PR^3}	J_{PH^4}	J_{PR^5}
1*a*	X, Y = ϕ; R³, R⁵ = H	†	3.76	†	0.3	1.7	†	1.7	†
1*b*	X, Y = ϕ; R³, R⁵ = Me	7.88(s)	4.25	7.56	—	0.75	—	3.0	0.75
2*a*	X, Y = ϕ; R³ = Me; R⁵ = H	7.75(s)	3.99	†	0.3	—	—	2.2	†
2*b*	X, Y = ϕ; R³ = H; R⁵ = Me	—	—	7.49	—	—	—	—	—
3	X = ϕ; Y = pyrazole; R³, R⁵ = H	2.32	3.74	2.12	0.4	2.4	1.5	1.6	2.1
4*a*‡	Z = O; R³, R⁵ = H	†	3.52	1.77	1.6	2.6	†	1.6	1.1
4*b*‡	Z = S; R³, R⁵ = H	†	3.75	1.72	1.6	2.7	†	1.6	2.4
5*a*	X, Y = Cl; R³, R⁵ = H	2.15	3.41	1.81	—	2.0	—	—	—
5*b*	X, Y = Cl; R³, R⁵ = Me	7.68	4.08	7.45	—	—	—	—	—
6*a*	X, Y = pyrazolyl; R³, R⁵ = H	1.97	3.40	1.83	—	1.5	1.5	2.5	2.0
6*b*	X, Y = 3,5-dimethylpyrazole; R³, R⁵ = Me	7.75(s)	4.00	7.70(s)	—	—	—	—	—

*In solutions in CCl_4 (**1***a*, **1***b*, **2***a*, **2***b*, **3**) or in $CDCl_3$ (**4***a*, **5***a*, **5***b*, **6***a*, **6***b*).
†Obscured by phenyl resonances.
‡In compounds **4***a* and *b*, couplings of 0 5 and 0.6 Hz, respectively, were assigned to $J_{H^3H^5}$.

R_2NH and CCl_3PF_2 (29); and (*c*) the fluorination of R_2NPCl_2, using SbF_3 (29–31), ZnF_2 (30, 32), or NaF (31, 33). In contrast, analogous reactions involving pyrazole or 3,5-dimethylpyrazole in place of R_2NH, or trimethylstannylpyrazole in place of the stannylamine, or dichlorophosphinopyrazole (**5***a*) in place of R_2NPCl_2, all failed to yield the expected difluorophosphinopyrazole product. Thus, PF_3 failed to react with pyrazole or trimethylsilylpyrazole, whereas reaction with trimethylstannylpyrazole appears to proceed as in eq. 5, giving $P(Az)_3$ in good yield.

[5] $3Me_3SnAz + PF_3 \rightarrow P(Az)_3 + 3Me_3SnF$

(Az = pyrazolyl or 3,5-dimethylpyrazolyl)

The reaction of pyrazole with CCl_3PF_2 only occurs slowly, over a period of several weeks, in solution in benzene, as monitored by proton n.m.r. spectroscopy. Although $CHCl_3$ was a readily detected product, there was no ^{19}F n.m.r. evidence for any $AzPF_2$ species. On separating the products, a considerable amount of PF_3 was observed, presumably arising from the disproportionation of $AzPF_2$. Attempted fluorination reactions of $AzPCl_2$ with SbF_3 and AsF_3 also gave some PF_3, together with inseparable, involatile residues.

The ^1H n.m.r. spectra of compounds **1–9** in solution in CCl_4 or $CDCl_3$ show characteristic bands for the phenyl groups, and for the substituents at the 3, 4, and 5 positions of the pyrazole ring. In some cases the H^3 and/or H^5 band is overlapped by, and contributes to the intensity of the phenyl resonance envelope (see Table 1). The resonances, at ambient temperatures, indicate the nonequivalence of the 3 and 5 positions, which establishes that the compounds are monomeric and stereochemically rigid in these solvents. In solution in toluene, bromobenzene, or carbon disulfide, however, the 3 and 5 positions of several of the phosphinopyrazoles are equivalent at room temperature and only give separate resonances at low temperatures. Similar observations on related systems have been interpreted as intermolecular metallotropic exchange (15). The assignments for the 3 and the 5 positions were based upon the following criteria: (*a*) couplings $J_{H^4R^5}$ are consistently greater than corresponding couplings $J_{R^3H^4}$ (R^3, R^5 = H or Me), in view of the greater double bond contributions in the former; (*b*) couplings J_{PR^5} are larger than J_{PR^3} (R = H or Me); (*c*) the R^5 resonance is consistently downfield, relative to R^3. Similar arguments have been applied in the structure assignments of related pyrazole derivatives (4, 26, 34) and decoupling studies facilitated the interpretation of coupling data. Where two or more couplings were present, the bands appeared as a sequence of doublets or as sets of overlapping triplets resulting from the fortuitous overlapping of doublets (*e.g.*, the H^4 resonances for **4***a* and *b*). Methylation of the pyrazole ring at the 3 and 5 positions increases J_{PH^4}, while oxidation of the P^{III} phosphine substituent to

Can. J. Chem. Downloaded from www.nrcresearchpress.com by 210.87.254.5 on 09/05/12
For personal use only.

Can. J. Chem. Downloaded from www.nrcresearchpress.com by 210.87.254.5 on 09/05/12
For personal use only.

P^V (as in **4***a* and *b*) has little influence upon this coupling. The J_{PH^5} couplings, however, show greater variations (1.1 Hz in **4***a*, 2.4 Hz in **4***b*, and 2.1 Hz in **1***a*).

The coordination chemistry of some of the above ligands will be reported later.

Experimental

All materials were handled under anhydrous conditions, using a high vacuum system or a dry, inert atmosphere system. The solvents ether, benzene, and hexane were refluxed over $LiAlH_4$, distilled, and stored over sodium wire. Tetrahydrofuran (THF) was refluxed over $LiAlH_4$ and distilled before use. The azoles pyrazole, 3(5)-methylpyrazole, 3,5-dimethylpyrazole, pyrrole, imidazole, and triazole (Koch-Light, Aldrich) were sublimed or distilled; phosphorus trichloride (May and Baker) was distilled but diphenylchlorophosphine and phenyldichlorophosphine (K and K) were used without further purification. Triethylamine (Hopkins and Williams) was dried over sodium wire.

Elemental analyses were performed by the departmental analysts (at Simon Fraser University and University of Sussex) or by Alfred Bernhardt, West Germany.[1] Nuclear magnetic resonance spectra were obtained using Varian T-60, A56/60, XL 100, HA-100, and Jeol JNM-PS-100 spectrometers, and the Perkin Elmer 457 was used for i.r. measurements. Mass spectra were determined with the double focussing Hitachi Perkin Elmer RMU-6E and the AEI MS9 instruments. 1-Trimethylsilylpyrazoles (12, 15) were prepared by the reaction of Me_3SiCl with the appropriate pyrazole in the presence of triethylamine, whereas 1-trimethylstannylpyrazoles were prepared from Me_3SnCl and the appropriate potassium pyrazolide (25). $\phi_2P(O)Cl$ was prepared from $\phi_2P(O)OH$ following published procedures (35). The syntheses described below were carried out on a 5 millimolar scale.

*Preparation of 1-Diphenylphosphinopyrazole (**1a**), 1-Diphenylphosphino-3,5-dimethylpyrazole (**1b**), 1-Diphenylphosphino-3-methylpyrazole (**2a**), 1-Diphenylphosphino-5-methylpyrazole (**2b**), 1-Diphenylphosphinoimidazole (**8**), 1-Diphenylphosphino-1,2,4-triazole (**4**)*

To a stirred ethereal solution of the azole and triethylamine (1:1.05 molar ratio) an equivalent amount of diphenylchlorophosphine, in ether, was added slowly. A white precipitate of triethylamine hydrochloride formed immediately. After stirring for 3 h, the precipitate was filtered off and washed twice with ether. The filtrates were combined, the solvent was distilled off, and the residue was purified by distillation or sublimation under reduced pressure. Yields, 95–100%.

1*a*: m.p. 37 °C; mass spectrum (*m*/*e*), M_{obs}^+ 252, M_{calcd} 252.26.

Anal. Calcd. for $C_{15}H_{13}N_2P$: C, 71.42; H, 5.19; N, 11.11. Found: C, 71.7; H, 5.20; N, 11.7.

1*b*: m.p. 40–42 °C; mass spectrum (*m*/*e*), M_{obs}^+ 280, M_{calcd} 280.31.

Anal. Calcd. for $C_{17}H_{17}N_2P$: C, 72.86; H, 6.09; N, 10.00. Found: C, 73.0; H, 6.01; N, 10.4.

2*a*, **2***b*: the mixed isomers melted in the range 65–73 °C; they were not separated; mass spectrum, M_{obs}^+ 266, M_{calcd} 266.11.

Anal. Calcd. for $C_{16}H_{15}N_2P$: C, 72.15; H, 5.68; N, 10.53. Found: C, 72.4; H, 5.84; N, 12.0.

8: m.p. 95–97 °C; mass spectrum, M_{obs}^+ 252, M_{calcd} 252.26; n.m.r. spectrum ($CDCl_3$ solution), τ 2.30 (d of d's, $J_{PH} = J_{H^2H^5} = 0.95$ Hz); 2.8 (center of the H^5 multiplet); 2.9 (center of the H^4 multiplet); 2.5–2.75 (phenyl resonances).

Anal. Calcd. for $C_{15}H_{13}N_2P$: C, 71.42, H, 5.19, N, 11.10. Found: C, 71.5; H, 5.15; N, 11.9.

9: m.p. 64–66 °C; mass spectrum, M_{obs}^+ 253, M_{calcd} 253.26; n.m.r. spectrum ($CDCl_3$ solution), τ 1.63 (d, 1H, H^5; J_{PH}, 1.2 Hz); 1.85 (s, 1H, H^3); 2.54–2.62 (multiplet, phenyl resonances, 10H).

Anal. Calcd. for $C_{14}H_{12}N_3P$: C, 66.39; H, 4.77; N, 16.59. Found: C, 66.7; H, 4.79; N, 16.8.

*Preparation of 1,1′-Bis(pyrazolyl)phenylphosphine (**3**)*

Phenyldichlorophosphine, in ether, was added slowly, with stirring, to an ethereal solution containing 2 equiv. of pyrazole and triethylamine (5% excess). The subsequent procedure followed the pattern described above. Yield, 98–99%; m.p. 48–50 °C; mass spectrum, M_{obs}^+ 242, M_{calcd} 242.22.

Anal. Calcd. for $C_{12}H_{11}N_4P$: C, 59.50; H, 4.58; N, 23.13. Found: C, 59.1; H, 4.61; N, 23.7.

*Preparation of 1-Diphenylphosphinatopyrazole (**4a**)*

Appropriate proportions of $\phi_2P(O)Cl$, pyrazole, and triethylamine were mixed, in solution in ether, as described above. The precipitate (Et_3NHCl) was filtered off and washed several times with ether. Upon removing part of the solvent from the filtrate, **4***a* was precipitated. It was filtered off and sublimed at 160 °C/0.05 Torr. Yield, 67%; m.p. 112–114 °C; mass spectrum, M_{obs}^+ 268, M_{calcd} 268.26.

Anal. Calcd. for $C_{15}H_{13}N_2OP$: C, 67.16; H, 4.88; N, 10.44. Found: C, 68.8; H, 5.05; N, 11.6.

*Preparation of 1-Diphenylthiophosphinatopyrazole (**4b**)*

A solution of compound **1***a* in benzene was heated under reflux with an equivalent amount of sulfur for 8 h, giving a colorless solution. The solvent was distilled off, leaving an oil which crystallized, after 2 days, into colorless prisms. Yield, 100%; m.p. 105–106 °C; mass spectrum, M_{obs}^+ 284, M_{calcd} 284.32.

Anal. Calcd. for $C_{15}H_{13}N_2PS$: C, 63.37; H, 4.61; N, 9.85. Found: C, 63.5; H, 4.68; N, 10.0.

*Preparation of 1-Dichlorophosphinopyrazole (**5a**) and 1-(Dichlorophosphine)-3,5-dimethylpyrazole (**5b**)*

Phosphorus trichloride and the appropriate 1-trimethylsilylpyrazole (1.1:1 molar ratio) were sealed together in a glass ampoule for 24 h. The products were separated by vacuum fractionation. The reaction stoichiometry was

$$PCl_3 + Me_3Si\text{-}Az \rightarrow Me_3SiCl + Cl_2P\text{-}Az$$

(Az = pyrazolyl or 3,5-dimethylpyrazolyl)

5*a* yield, 98%; m.p. 107–108 °C; mass spectrum, M_{obs}^+ 168, M_{calcd} for $C_3H_3Cl_2N_2P$, 168.91.

[1]Alfred Bernhardt, Mikroanalytisches Laboratorium, 5251 Elbach über Engelskirchen, Fritz-Pregl-Strasse 14–16, West Germany.

5*b*: yield, 98%; mass spectrum, M_{obs}^+ 196, M_{calcd} for $C_5H_7Cl_2N_2P$, 196.93.

Preparation of Tris(1-pyrazolyl)phosphine (6a) and Tris-1(3,5-dimethylpyrazolyl)phosphine (6b)

Phosphorus trichloride and the appropriate 1-trimethylsilylpyrazole (1:4.5 molar ratio) were allowed to react in a sealed ampoule for 24 h. The volatile products were separated by vacuum fractionation, and the residue was purified by sublimation or distillation under reduced pressure. The reaction stoichiometry was

$$PCl_3 + 3Me_3Si—Az \rightarrow 3Me_3SiCl + P(Az)_3$$

6*a*: yield, 98–100%; m.p. 104 °C; mass spectrum, M_{obs}^+ 232, M_{calcd} 232.09.

Anal. Calcd. for $C_9H_9N_6P$: C, 46.55; H, 3.88; N, 36.20. Found: C, 44.7; H, 4.05; N, 35.0.

6*b*: yield, 98–100%; m.p. 101 °C; mass spectrum, M_{obs}^+ 316, M_{calcd} 316.15.

Preparation of 1-Diphenylphosphinopyrrole (7)

An ice-cooled suspension of potassium pyrrolide in hexane, prepared according to literature methods (36), was treated with an equivalent amount of diphenylchlorophosphine in hexane. The stirred mixture was allowed to warm to room temperature over a period of 3 h. The solution was filtered, the solvent was removed, and the product was distilled under reduced pressure to yield a yellow oil. Yield, 67%; mass spectrum, M_{obs}^+ 251, M_{calcd} 251.27; n.m.r. spectrum, τ 2.8–2.9 (phenyl resonances, 10H); 3.30 (d of t's, 2H; H^2, H^5; J_{HH}, 2.2 Hz; J_{PH}, 4.0 Hz); 3.82 (d of t's, 2H; H^3, H^4; J_{HH}, 2.2 Hz; J_{PH}, 0.4 Hz).

Anal. Calcd. for $C_{16}H_{14}NP$: C, 76.48; H, 5.62; N, 5.57 Found: C, 77.3; H, 5.45; N, 4.8.

We thank the National Research Council of Canada for financial support of this research. One of us (L.K.P.) is most grateful to the University of Sussex for the use of research facilities within the School of Molecular Sciences during 1974.

1. S. Trofimenko. J. Am. Chem. Soc. (*a*) **88**, 1852 (1966); (*b*) **89**, 3165, 3170, 4948 (1967); (*c*) Chem. Rev. **72**, 497 (1972).
2. A. Arduini and A. Storr. J. Chem. Soc. (Dalton), 503 (1974).
3. L. K. Peterson and K. I. Thé. Unpublished work.
4. A. D. Garnovskii, O. Yu. Okhlobystin, O. A. Osipov, K. M. Yunusov, Yu. V. Kolodyazhnyi, L. M. Golubinskaya, and V. I. Svergun. J. Gen. Chem. USSR, **42**, 910 (1972).
5. L. Birkofer, P. Richter, and A. Ritter. Ber. **93**, 2804 (1960).
6. L. Birkofer, W. Gilenberg, and A. Ritter. Angew. Chem. **73**, 143 (1961).
7. G. J. M. van der Kerk, J. G. A. Luijten, and M. J. Janssen. Chimia, **16**, 10 (1962).
8. J. G. A. Luijten, M. J. Janssen, and G. J. M. van der Kerk. Rec. Trav. Chim. **81**, 202 (1962).
9. J. G. A. Luijten and G. J. M. van der Kerk. Rec. Trav. Chim. **82**, 1181 (1963).
10. J. G. A. Luijten, F. Rijkens, and G. J. M. van der Kerk. Adv. Organomet. Chem. **3**, 397 (1965).
11. L. Birkofer and P. Werner. Ber. **99**, 2512 (1966).
12. D. H. O'Brien and C.-P. Hrung. J. Organomet. Chem. **27**, 185 (1971).
13. F. A. Cotton and D. J. Ciappenelli. Syn. Inorg. Metal-org. Chem. **2**, 197 (1972).
14. S. Kozima, T. Itano, N. Mihara, K. Sisido, and T. Isida. J. Organomet. Chem. **44**, 117 (1972).
15. V. N. Torochesnikov, N. M. Sergeyev, N. A. Viktorov, G. S. Goldin, V. G. Poddubny, and A. N. Kultsova. J. Organomet. Chem. **70**, 347 (1974).
16. S. Trofimenko. (*a*) J. Am. Chem. Soc. **91**, 3183 (1969); (*b*) Acc. Chem. Res. **4**, 17 (1971).
17. P. Meakin, S. Trofimenko, and J. P. Jesson. J. Am. Chem. Soc. **94**, 5677 (1972).
18. F. A. Cotton, J. L. Calderon, M. Jeremic, and A. Shaver. J. Chem. Soc. Chem. Commun. 777 (1972).
19. R. B. King and A. Bond. J. Am. Chem. Soc. 96, 1334, 1338, 1343 (1974).
20. N. F. Borkett and M. I. Bruce. J. Organomet. Chem. **65**, C51 (1974).
21. D. J. O'Sullivan and F. J. Lalor. J. Organomet. Chem. **65**, C47 (1974).
22. R. Jefferson, J. F. Nixon, T. M. Painter, R. Keat, and L. Stobbs. J. Chem. Soc. (Dalton), 1414 (1973).
23. D. F. Rendle, A. Storr, and J. Trotter. J. Chem. Soc. Chem. Commun. 189 (1973).
24. (*a*) T. L. Jacobs. Pyrazoles and related compounds. *In* Heterocyclic compounds. Vol. 5. *Edited by* R. C. Elderfield. J. Wiley and Sons, New York. 1957. p. 45; (*b*) A. N. Kost and I. Grandberg. *In* Advances in heterocyclic chemistry. Vol. 6. *Edited by* A. R. Katritzky and A. J. Boulton. Academic Press, New York. 1966. p. 347; (*c*) R. Fuxo. *In* The chemistry of heterocyclic compounds. *Edited by* A. Weissberger. Interscience Publishers, New York. 1967; (*d*) A. R. Katritzky and J. M. Lagowski. *In* The principles of heterocyclic chemistry. Methuen and Co., London. 1967. p. 146.
25. J. F. Nixon, L. K. Peterson, and F. Zarkesh. Unpublished work.
26. L. K. Peterson, E. Kiehlmann, A. R. Sanger, and K. I. Thé. Can. J. Chem. **52**, 2367 (1974).
27. J. F. Nixon. Adv. Inorg. Chem. Radiochem. **13**, 363 (1970).
28. R. G. Cavell. J. Chem. Soc. (A), 1992 (1964).
29. C. G. Barlow and J. F. Nixon. J. Chem. Soc. (A), 228 (1966).
30. Zh. M. Ivanova. Zh. Obshch. Khim. **35**, 164 (1965).
31. R. Schmutzler. Inorg. Chem. **3**, 415 (1964).
32. H. Nöth. Chem. Ber. **96**, 1109, 1298 (1963).
33. J. G. Morse, K. Cohn, R. W. Rudolph, and R. W. Parry. Inorg. Synth. **10**, 147 (1967).
34. (*a*) K. I. Thé and L. K. Peterson. Can. J. Chem. **51**, 422 (1973); (*b*) K. I. Thé, L. K. Peterson, and E. Kiehlmann. Can. J. Chem. **51**, 2448 (1973).
35. W. A. Higgins, P. W. Vogel, and W. G. Craig. J. Am. Chem. Soc. **77**, 1864 (1955).
36. G. R. Clemo and G. R. Ramage. J. Chem. Soc. 49 (1931).

Can. J. Chem. Downloaded from www.nrcresearchpress.com by 210.87.254.5 on 09/05/12
For personal use only.

Proton Magnetic Resonance Study of Conformational Equilibria of the Pyridinealdehydes in Solution. Comparison with Other Methods

WERNER DANCHURA, TED SCHAEFER, J. BRIAN ROWBOTHAM,[1] AND DONALD J. WOOD

Department of Chemistry, University of Manitoba, Winnipeg, Manitoba R3T 2N2

Received June 17, 1974

WERNER DANCHURA, TED SCHAEFER, J. BRIAN ROWBOTHAM, and DONALD J. WOOD. Can. J. Chem. **52**, 3986 (1974).

A p.m.r. study of the pyridinealdehydes shows that accurate spectral analysis yields long-range spin–spin coupling constants which are a precise measure of the conformational equilibria in solution. Thus, in CS_2 solution the ON-*trans* form of 2-pyridinealdehyde is more stable than the ON-*cis* form by at least 2.3 kcal/mol, while in acetone solution it is 1.6 kcal/mol more stable than the *cis* form. Classical solvation theory allows the conclusion that in the gas phase the *trans* form is more stable than the *cis* form by about 7 kcal/mol, in contradiction to the predictions of approximate MO theory at the INDO level. The *trans* form of 3-pyridinealdehyde is also more stable than the *cis* form in polar and in nonpolar solvents. The results are compared with those of other experiments on these equilibria.

WERNER DANCHURA, TED SCHAEFER, J. BRIAN ROWBOTHAM et DONALD J. WOOD. Can. J. Chem. **52**, 3986 (1974).

Une étude de la résonance magnétique de protons des pyridinealdéhydes montre qu'une analyse spectrale exacte conduit à des constantes de couplage spin–spin à longue distance qui sont une mesure précise de l'équilibre conformationnel en solution. Ainsi en solution dans le CS_2 la forme ON-*trans* de la pyridine-2 aldéhyde est plus stable que la forme ON-*cis* d'au moins 2.3 kcal/mol alors qu'en solution dans l'acétone elle est plus stable que la forme *cis* de 1.6 kcal/mol. La théorie de solvatation classique permet de conclure qu'en phase gazeuse la forme *trans* est plus stable que la forme *cis* de 7 kcal/mol, en contradiction avec les prévisions de la théorie approchée des OM (INDO). La forme *trans* de la pyridine-3 aldéhyde est aussi plus stable que la forme *cis* dans les solvants polaires et non-polaires. On compare les résultats avec ceux d'autres expériences faites sur ces équilibres. [Traduit par le journal]

Introduction

The conformational preference of the aldehyde group in benzaldehyde derivatives can be deduced from the long-range spin–spin coupling constants between the aldehydic proton and the ring protons (1, 2). The coupling over five bonds, $^5J_m^{H,CHO}$, is highly stereospecific, relatively insensitive to intrinsic ring-substituent and solvent effects, and if accurate values are extracted by careful analytical procedures can yield energy differences between conformers with an accuracy of from 100 to 400 cal/mol, depending on the proportions of the conformers.

A model in which the nitrogen atom polarizes the σ electron system but does not strongly alter the π electron contribution to the coupling constants, accounts for a variety of long-range couplings between methyl protons and ring protons or fluorine nuclei in fluorinated methyl derivatives of pyridine (3). Now, $^5J_m^{H,CHO}$ is dominated by a σ electron mechanism (2, 4) and therefore an investigation of the conformational preferences of the aldehyde group in the pyridinealdehydes must consider the intrinsic effect of the nitrogen atom on $J^{H,CHO}$ before conformational deductions can be made.

This paper reports on the relative stabilities of **1***a* and *b* and of **2***a* and *b* in solution. Solvation energies are estimated from a classical theory. The present results are compared with previous

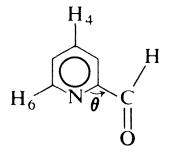

1*a*, ON-*cis*

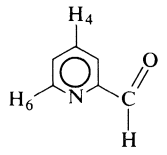

1*b*, ON-*trans*

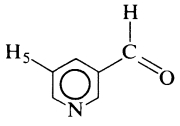

2*a*, ON-*cis*

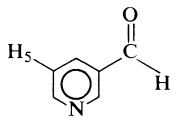

2*b*, ON-*trans*

[1]Research associate, 1973–1974.

Can. J. Chem. Downloaded from www.nrcresearchpress.com by 210.87.254.5 on 09/05/12
For personal use only.

Can. J. Chem. Downloaded from www.nrcresearchpress.com by 210.87.254.5 on 09/05/12
For personal use only.

TABLE 1. Proton chemical shifts* and spin–spin coupling constants† of the pyridine aldehydes as 10 mol% solutions at 32 °C

	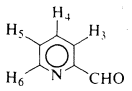			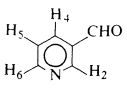			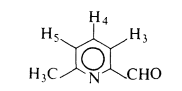
Parameter	CS_2	C_6D_6	$(CH_3)_2C{=}O$	CS_2	C_6D_6	CS_2	CS_2‖
ν_{CHO}	995.496 (3)‡	1009.882 (2)	1002.586 (4)	1004.804 (3)	951.379 (3)	1001.563 (3)	988.395 (5)
ν_2	—	—	—	894.0	874.5	877.5	—
ν_3	782.509 (7)	763.840 (2)	793.992 (6)	—	—	759.073 (3)	760.784 (17)
ν_4	779.921 (6)	701.105 (3)	802.824 (6)	805.820 (3)	757.566 (2)	—	764.485 (19)
ν_5	744.274 (3)	668.883 (2)	767.054 (5)	739.462 (3)	666.541 (2)	759.073 (3)	727.082 (4)
ν_6	870.0	838.5	886.5	873.0	844.5	877.5	257.521 (5)
$^3J_o^{H,H}$	7.789 (4) 3, 4§	7.771 (4)	7.777 (6)	7.838 (4)	7.863 (3)	4.944 (6)	7.673 (7) 3, 4
	7.530 (18) 4, 5	7.582 (4)	7.567 (9)	4.802 (5)	4.815 (4)	—	7.762 (25) 4, 5
	4.732 (5) 5, 6	4.779 (5)	4.772 (10)	—	—	—	—
$^4J_m^{H,H}$	1.293 (18) 3, 5	1.271 (4)	1.294 (9)	2.182 (5) 2, 4	2.180 (5)	1.795 (8) 3, 5	1.049 (26)
	1.704 (9) 4.6	1.706 (6)	1.677 (9)	1.814 (5) 4, 6	1.807 (5)	−0.240 2, 6	—
	—	—		−0.180 2, 6	−0.210	—	—
$^5J_p^{H,H}$	0.968 (9)	0.966 (5)	0.984 (10)	0.914 (5)	0.907 (4)	0.921 (6)	—
$^4J_o^{H,CHO}$	−0.064 (7)	−0.002 (3)	−0.066 (7)	−0.230 (5) 2, 3	−0.229 (6)	−0.097 (4)	−0.068 (9)
	—	—	—	−0.118 (4) 3, 4	−0.148 (4)	—	—
$^5J_m^{H,CHO}$	0.897 (7) 2, 4	0.877 (4)	0.828 (7)	0.572 (4) 3, 5	0.595 (3)	0.397 (5)	0.897 (9)
	0.00 2, 6	0.00	0.00	—	—	—	—
$^6J_p^{H,CHO}$	−0.017 (4)	−0.012 (3)	−0.010 (7)	−0.001 (5)	−0.001 (5)	—	−0.021 (6)
Root mean square error†	0.0104	0.0084	0.0122	0.0091	0.0072	0.0118	0.0232

*In Hz to low field of internal tetramethylsilane.
†In Hz.
‡The number in parentheses is the standard deviation in the last place, *i.e.*, in mHz.
§The numbers separated by commas give the ring positions.
‖$^4J_o^{H,CH_3} = -0.470$ (3), $^5J_m^{H,CH_3} = 0.294$ (6), $^6J_m^{HCO,CH_3} = 0.001$ (4), $^6J^{H,CHO} = -0.579$ (5) Hz.

work on the relative proportions of the presumably planar conformational isomers.

Experimental

Pyridine derivatives from Aldrich were prepared as degassed, 10 mol% solutions containing a small amount of internal tetramethylsilane (TMS). ^{1}H n.m.r. spectra were calibrated on an HA100 spectrometer in the frequency sweep mode by reading differences between manual and sweep oscillator frequencies at intervals of a few Hertz. Line widths at half-height were often as little as 0.10 Hz, except for the protons *ortho* to the nitrogen atom where incompletely relaxed coupling to the nitrogen quadrupole caused considerable broadening.

Variable temperature measurements were made in a manner previously described (*5a*) and double resonance experiments (*5b*) yielded the relative signs of the coupling constants.

Molecular orbital calculations at the CNDO/2 and INDO-MO-FPT levels of approximation (6, 7) gave theoretical values of spin–spin coupling constants involving the aldehyde proton, dipole moments, and energies of the various planar conformers. The calculations were performed as described in detail for other molecules (2, 8). The geometry of the pyridine ring was taken from microwave data (9) and a standard geometry (10) was assumed for the aldehyde group. The C—C bond between ring and aldehyde carbon atoms made 120° bond angles and convergence to 10^{-3} Hz was demanded in the computed coupling constants.

Other computations are described below.

Results and Discussion

Spectral Analyses

These were performed with the computer program LAME (11) and the results are given in Table 1. The r.m.s. deviations between calculated and observed transitions are given there, as are the probable errors in the spectral parameters which were normally considerably less than 0.01 Hz. An attempt was made to obtain $^5J_m^{H,CHO}$ to an accuracy of 0.02 Hz, *i.e.*, with a probable error of 0.004 Hz. This was not possible in all cases but repeated analyses on very similar spectra, calibrated on different days, suggested that 0.02 Hz is a reasonable error estimate for $^5J_m^{H,CHO}$ in most of the solutions.

An example of the spectral quality attainable for these compounds is given in Fig. 1, where a splitting of 0.12 Hz is clearly resolved.

$^5J_m^{H,CHO}$ as a Measure of Conformational Populations

4-Pyridinealdehyde, 3

In **3** the observed value of $^5J_m^{H,CHO}$ in CS_2 solution (Table 1) is 0.40 Hz, an average of the couplings to H_2 and H_6. For benzaldehyde in CCl_4 solution the coupling is 0.38 Hz, suggesting

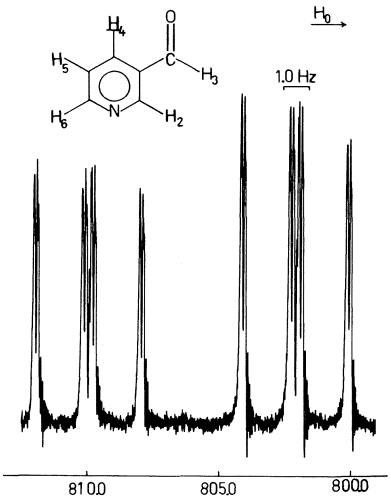

FIG. 1. The p.m.r. spectrum at 100 MHz of H_4 of 3-pyridinealdehyde as a 10 mol % solution in CS_2. The smallest splittings giving rise to the many doublets are 0.12 Hz in magnitude. The chemical shift scale is in Hz to low field of internal TMS.

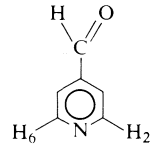

3

a negligible change in $^5J_m^{H,CHO}$ induced by the electronegative nitrogen atom. Furthermore, the available experimental evidence (2, 12) on many benzaldehyde derivatives indicates that $^5J_c^{H,CHO}$, *e.g.* $^5J_m^{H_6,CHO}$ in **3**, is negligibly small, as does the theoretical evidence (see CNDO/2 results in Table 2).

A 10 mol% solution of **3** in acetone gave $^5J_m^{H,CHO}$ as 0.40 Hz, as expected if solvent effects on this coupling are to be disregarded in subsequent arguments.

2-Pyridinealdehyde, 1

Here $^5J_m^{H_4,CHO}$ is 0.90 Hz in CS_2, 0.88 Hz in C_6D_6, 0.83 Hz in acetone, and 0.80 Hz in DMSO solution.[2] Furthermore, the spectra implied no coupling from H_6 to the aldehyde proton, *i.e.*, $^5J_m^{H_6,CHO} = 0$. The absence of this coupling is confirmed by the results for 6-methyl-2-pyridinealdehyde were $^5J_m^{H_4,CHO}$ in CS_2 solution is

[2]Because of the relatively small chemical shift between H_3 and H_4 in CS_2, acetone, and DMSO, the line spacings in the aldehyde proton region are *not* a measure of $^5J_m^{H,CHO}$.

Can. J. Chem. Downloaded from www.nrcresearchpress.com by 210.87.254.5 on 09/05/12
For personal use only.

Can. J. Chem. Downloaded from www.nrcresearchpress.com by 210.87.254.5 on 09/05/12
For personal use only.

TABLE 2. Calculated aldehyde proton-proton coupling constants* (Hz) in the planar conformations of the pyridine aldehydes

	^4J_c		^4J_t		^5J_c		^5J_t		^6J	
	INDO	CNDO	INDO	CNDO	INDO	CNDO	INDO	CNDO	INDO	CNDO
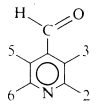	0.20	0.57	−0.54	0.23	0.26	0.03	1.77	0.97	—	—
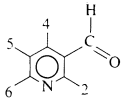	0.37	0.62	−0.46	0.12	0.19	0.03	—	—	−0.17	0.05
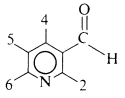	0.19	0.56	−0.48	0.21	—	—	1.63	0.92	−0.28	0.00
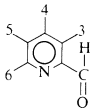	−0.55	0.11	—	—	0.32	0.03	1.76	0.97	−0.34	0.02
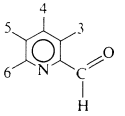	—	—	−0.41	0.37	0.23	0.05	1.92	1.06	−0.34	0.01

*The subscript *c* or *t* designates the bond arrangement in which the C—H bond of the aldehyde lies *cis* or *trans* to the ring C—H bond containing the coupled proton.

identical to that in **1** and the line widths of the aldehyde proton resonance were the same as in **1**.

The polar solvents favor the more polar ON-*cis* form, **1***a*, and the implication is therefore that the ON-*trans* form **1***b* is much more stable than **1***a* in CS_2 and C_6D_6 solutions and, by comparison with the magnitude of $^5J_m^{H,CHO}$ in **3** and in benzaldehyde, that the nitrogen atom increases $^5J_t^{H,CHO}$ by only about 10% when the aldehyde group is bonded to C-2 in pyridine.

In toluene-d_8 the proton resonance spectrum of **1** approaches the first-order perturbation theory, so that spectral analysis is relatively easy. Between −50 and 90 °C there occurs no change in $^5J_m^{H,CHO}$ to within the experimental error of 0.02 Hz. It follows that $\Delta G^0 = G_{1b}^0 - G_{1a}^0 = \Delta G_{tc}^0$ is at least −2.3 kcal/mol over this temperature range.[3] Therefore at 25 °C more than 99% of the molecules exist in the *trans* form **1***b* in CS_2 and C_6D_6 solutions. This result is compared below with other estimates of the populations of **1***a* and *b*.

In acetone solution one has $n_t = 0.83/0.89 = 0.93 \pm 0.03$ (n_t is the fractional population of the *trans* form) and ΔG_{tc}^0 is -1.6 ± 0.3 kcal/mol.[4] In DMSO solution, $n_t = 0.90 \pm 0.03$ and ΔG_{tc}^0 is -1.3 ± 0.3 kcal/mol. These results are discussed further in the section on solvation energies.

3-Pyridinealdehyde, 2

Because $^5J_m^{H,CHO}$ is invariant to electronic perturbation by the nitrogen atom in **3** and changes by only 10% in **1**, where the polar centers are in close proximity, it is a reasonable assumption that $^5J_m^{H,CHO}$ is independent[5] of the nitrogen atom in **2**. No coupling to nitrogen from the aldehyde proton will be observable even if **2** exists in the *cis* form, **2***a*. Equal populations of **2***a* and *b* therefore imply $^5J_m^{H,CHO} = 0.39$ Hz, where the average of 0.40 Hz in **3** and 0.38 Hz in benzaldehyde is taken.

In CS_2 solution, $^5J_m^{H,CHO}$ is 0.57 Hz at 32 °C, implying $n_t = 0.73 \pm 0.03$ and $\Delta G_{tc}^0 = 0.6 \pm 0.1$ kcal/mol. Then ΔG_{tc}^0 is -0.7 ± 0.1 kcal/mol C_6D_6. In toluene-d_8 the coupling is 0.59 Hz at 32 °C, equal to that in C_6D_6. At 90 °C, $^5J_m^{H,CHO}$ is 0.55 Hz, giving ΔG_{tc}° as 0.6 ± 0.1 kcal/mol; at −30 °C in toluene-d_8 $^5J_m^{H,CHO}$ becomes 0.65 Hz and ΔG_{tc}^0 is -0.8 ± 0.1 kcal/mol.

In acetone at 32 °C one has $^5J_m^{H,CHO}$ as 0.51 Hz and ΔG_{tc}° as -0.4 ± 0.1 kcal/mol. In all these solutions the ON-*trans* form **2***b* is more stable than the ON-*cis* form **2***a* but the more polar ON-*cis* form increases in relative stability in the solvent of higher dielectric constant.

Comparisons with Other Estimates of Conformational Populations

(a) Spin–spin Coupling Constants

On the basis of observed line spacings, Karabatsos and Vane (1) estimated that **1** exists 70–85% in the *trans* form, **1***b*, in DMSO and CCl_4 and that **2** is 70% *trans*, **2***b*, in DMSO. Bramwell and Randall (14) found $^5J_m^{H,CHO}$ to be 0.80 ± 0.05 Hz for a 20% solution of **1** in C_6D_6, 0.50 ± 0.05 Hz for a 30% solution of **2** in $CDCl_3$, and probably less than 0.3 Hz for a 30% solution of **3** in $CDCl_3$; all at 35 °C. No conformational estimates were made.

(b) Computed Coupling Constants

Five-bond couplings, $^5J_m^{H,CHO}$. As discussed above, the deduction of conformational equilibria depends on reliable values of $^5J_{cis}^{H,CHO}$ and $^5J_{trans}^{H,CHO}$. Galasso (15) calculates $^5J_m^{H,CHO}$ by the INDO-MO-FPT method. However, it is known (2) that such calculations for benzaldehydes overestimate the magnitude of $^5J_m^{H,CHO}$ and that CNDO/2 computations yield more reliable estimates of the conformational dependence of this coupling, although overestimates of 10 to 15% do still occur.

In Table 2 our computed values of the aldehydic proton couplings are given for the planar forms of the pyridinealdehydes (see Experimental for computational details). The CNDO/2 values are somewhat high. For example, the predicted value is (0.03 + 0.97)/2 or 0.50 Hz in **3**, whereas the measure value is 0.40 Hz. Note that the computed $^5J_t^{H,CHO}$ is not altered by the presence of a nitrogen atom in the coupling path for **1***a*. The presence of 10% of the *cis* form, **1***a*, as found above for the DMSO solution should therefore entail a coupling of 0.08 Hz for $^5J_m^{H_6,CHO}$. Such a coupling was not observed and we prefer to conclude that the theory is inadequate on this point. Calculations in which the angle θ in **1***a* was increased from 120° to as much

[3]The entropy difference of the two conformers is presumably very small.

[4]Where 0.89 Hz is the mean of the values in CS_2 and C_6D_6.

[5]One may note that $^4J_m^{H_3,H_5}$ in pyridine is equal to $^4J_m^{H,H}$ in benzene (12, 13).

Can. J. Chem. Downloaded from www.nrcresearchpress.com by 210.87.254.5 on 09/05/12
For personal use only.

Can. J. Chem. Downloaded from www.nrcresearchpress.com by 210.87.254.5 on 09/05/12
For personal use only.

as 128° changed the calculated dipole moment by 0.7% and decreased the CNDO/2 value of $^5J_m^{H_6,CHO}$ from 0.97 to 0.91 Hz, so that bond angle changes are hardly the cause of the discrepancy between theory and observation.

Six-bond couplings, $^6J_p^{H,CHO}$. Benzaldehyde is planar (16) and the observed value of $^6J_p^{H,CHO}$ is not significantly different from zero, in agreement with the CNDO/2 calculation. In the pyridinealdehydes no six-bond coupling is observed (Table 1), also in agreement with CNDO/2. Nonzero $^6J_p^{H,CHO}$ values occur in nonplanar benzaldehyde derivatives (17), so that the pyridinealdehydes are probably planar molecules. Of course, torsional oscillations of the aldehyde moiety about the planar minimum will occur (18) but the barriers to rotation are all over 4 kcal/mol and therefore (19) the contributions of nonplanar conformations to the observed coupling constants are negligible.

Four-bond couplings, $^4J_o^{H,CHO}$. In benzaldehyde derivatives the INDO values are in much better agreement with experiment than are the CNDO/2 numbers. Thus, for benzaldehyde INDO predicts $^4J_t^{H,CHO}$ as −0.41 Hz and $^4J_c^{H,CHO}$ as 0.21 Hz, the average being equal to the observed −0.10 Hz (20); CNDO/2 finds 0.40 Hz (2). For **3** the mean INDO number is −0.17 Hz whereas the observed $^4J_o^{H,CHO}$ is still −0.10 Hz.

For **1***a* INDO finds −0.41 Hz while the observed value is very near zero. For **2**, where the observed ratio of **2***b* to **2***a* is 3:1, the calculated INDO values predict $^4J_o^{H_2,CHO}$ as +0.03 Hz and $^4J_o^{H_4,CHO}$ as −0.27 Hz, compared to the measured −0.23 and −0.12 Hz, respectively. Accordingly, the INDO predictions are quantitatively incorrect but also qualitatively wrong, in that the changes in $^4J_c^{H,CHO}$ and $^4J_t^{H,CHO}$ caused by the nitrogen atom are opposite to the observed ones.

It appears that $^4J_o^{H,CHO}$ is an unsuitable parameter in the study of these conformational equilibria.

(c) Chemical Shifts

The large magnetic anisotropy (21) of the carbonyl bond should be reflected in an excess low-field shift of the H_3 resonance of 2-pyridinealdehyde if it exists as the *trans* form, **1***b*. If the shifts of the ring protons in pyridine in CCl_4 solution (13) and of 4-pyridinealdehyde in CS_2 solution (Table 1) are taken as reference numbers, then an additivity scheme predicts the observed ring proton shifts in **1** and **2** in CS_2 solution to within an average deviation of 0.045 p.p.m.; except for H_3 in **1**, where the observed shift is 0.23 p.p.m. to low field of the predicted value. This is strong qualitative evidence for the predominance of the *trans* isomer but does not, of course, give a quantitative value for the equilibrium constant. Compound **2** exists 3:1 as **2***b* to **2***a* and H_4 is observed to be 0.08 p.p.m. to low field of the predicted value, a somewhat weaker indication of the predominance of the *trans* form, **2***b* (the deviation of 0.08 p.p.m. was included in the quoted average).

Other chemical shift evidence for the preponderance of the *trans* form of **1** comes from the ASIS (22) value of −0.14 p.p.m. (shift in CS_2 minus shift in benzene) for the aldehyde proton. The ASIS is 0.55 p.p.m. in **2** and has similar values in other aromatic aldehydes (23), as expected if the benzene solvent molecules tend to avoid the electron rich regions (22, 24) of the solute molecule. In **1** the *trans* form places the aldehyde proton between the nitrogen and oxygen atoms. The benzene molecules avoid this region of **1***b* more than they avoid the TMS reference molecules and a negative ASIS arises. Note that H_4 and H_5 in **1***b* are most distant from the oxygen and nitrogen atoms and that their ASIS are the largest at 0.79 and 0.75 p.p.m., respectively. Again, a reliable quantitative deduction of the equilibrium constant between **1***a* and *b* is not possible on this basis.

(d) Dipole Moments and Molecular Polarizabilities

In benzene solution at 25 °C the observed dipole moments, μ, are 3.35, 2.37, and 1.74 D for **1**, **2**, and **3**, respectively (25). Barassin *et al.* (25) estimated μ_c and μ_t for **1** as 4.8 and 3.40, respectively. From the expression $\mu_{obs}^2 = n_t\mu_t^2 + n_c\mu_c^2$ the fraction of the *trans* form, n_t, is then 1.03. On the other hand, the INDO calculations yield μ_c = 4.65 D and μ_t = 2.92 D, giving n_t = 0.79. The computations assume a bond angle θ in **1***a* of 120°. If the bond angle is changed by 3°, the C—H bond of the aldehyde group moving towards the nitrogen atom, μ_t increases to 3.02 D. If errors of 0.1 D are assumed in measured and calculated dipole moments, n_t may rise to 0.89, still rather less than the 0.99 deduced from $^5J_m^{H,CHO}$.

For **2**, INDO computes 1.09 and 3.18 D for

TABLE 3. Molecular constants and calculated parameters for 2- and 3-pyridine aldehyde*

Parameter		2-Pyridine aldehyde		3-Pyridine aldehyde	
		Cis (**1***a*)	*Trans* (**1***b*)	*Cis* (**2***a*)	*Trans* (**2***b*)
μ (INDO)	A	4.65 (4.65)†	2.92 (2.93)	3.81 (3.87)	1.09 (1.03)
k‡ (kcal/mol)	A	8.20	3.26	5.80	0.41
h§ (c.m.)	A	11.93	6.27	2.00	17.51
h (c.v.)	A	18.11	8.00	2.97	18.15
μ‖ (vector)	B	4.80 (4.85)	3.35 (3.34)	3.81 (3.85)	1.38 (1.31)
k (kcal/mol)	B	8.93	4.25	5.73	0.67
h (c.v.)	B	21.26	11.39	3.77	19.98
$E_c - E_t$ (INDO)		0.85 kcal/mol		0.11 kcal/mol	

*For the 2- and 3-pyridinealdehyde, respectively, the refractive index, u_D, is 1.5353 and 1.5496; the molecular radius is 3.36 and 3.34 Å, calculated from the molar volume; the dipole moment, μ, in benzene solution is 3.35 and 2.37 D (25).
†The dipole moments in brackets are values obtained by vectorial summation of two C—N and one C=O dipole(s), these being used in the calculation of the quadrupolar components and of their energy of interaction with the surrounding dielectric (30).
‡The dipolar parameter in the theory of Abraham (30).
§The quadrupolar parameter, calculated with the origin at the center of mass (c.m.) or center of volume (c.v.), in kcal/mol.
‖The dipole moment as estimated in ref. 25.

trans and *cis* forms, respectively, yielding $n_t = 0.66_5$ and errors of 0.1 D in the various moments also allow an n_t of 0.73 in benzene solution, close to the value obtained from ${}^5J_m^{H,CHO}$. The estimated dipole moments of Barassin are $\mu_c = 1.38$ and $\mu_t = 3.81$, giving $n_t = 0.71$.

The observed (INDO) dipole moments of pyridine (26), **3**, and benzaldehyde (27) are 2.20 (2.09), 1.74 (1.79), and 2.99 (2.75) D, respectively, and differences of up to 0.2 D between CNDO/2 and INDO moments were found for the conformational isomers of these aldehydes. It appears that estimates of conformational populations based on ${}^5J_m^{H,CHO}$ may be somewhat more accurate than those based on MO dipole calculations. Estimates of conformational moments based on vector additivity may also be inaccurate, marred by mesomerism, for example (28), although agreement to within 3% with conformational population deductions based on ${}^5J_{in}^{H,CHO}$ are found here for **1** and **2** in benzene solution.

Similar criticisms apply to Kerr constant data (29), from which 75% *trans* form was deduced for **1** in benzene solution at 25 °C.

(e) Torsional Frequencies in the Far Infrared

No evidence for two conformers in the gas or liquid phases of **1** and **2** was found from the far i.r. spectra (18), in agreement with our conclusions about **1**. The clear disagreement on **2** remains unexplained. Perhaps the aldehydic torsion bands coincide for the two forms. In this connection we note that the torsion bands occur at the same frequency in solution (near 130 cm^{-1}) for all three pyridinealdehydes.

(f) Medium Effects on the Conformational Equilibrium

A classical theory, which considers the interaction of the electric dipole and quadrupole fields of the solute molecule with a uniform dielectric medium (30–32), has had considerable success in accounting for the conformational equilibria in solution of haloethanes, halocyclohexanes, and of 2-furanaldehyde (33). The assumptions and calculational details underlying the theory have been adumbrated (30) and are not repeated here.

In Tables 3 and 4 the molecular parameters, calculated solvation energies and predicted conformational populations in CS_2, acetone, and DMSO are reproduced. The quadrupole moments were calculated from the net INDO dipole moments (bracket A in the tables) and from those estimated by Barassin (bracket B), vectorially resolved in C=O and C—N dipoles. The origin for the quadrupole moments evaluations was taken as the center of mass (34) and also, as recommended and described by Abraham (30), as the center of volume of the solute molecule.

2-Pyridinealdehyde, *1*. The solvation energy strongly favors the *cis* form (Table 4), although the INDO calculation, an approximation to the gas phase, favors the *trans* form by 0.85 kcal/mol. An INDO calculation by Galasso (15) uses a slightly different geometry and integral parameterization to favor the *trans* form by 1.55 kcal/mol.

In view of the success of the theory in predicting *cis–trans* equilibria of 2-furanaldehyde

Can. J. Chem. Downloaded from www.nrcresearchpress.com by 210.87.254.5 on 09/05/12
For personal use only.

Can. J. Chem. Downloaded from www.nrcresearchpress.com by 210.87.254.5 on 09/05/12
For personal use only.

TABLE 4. Solvation energies* and calculated populations for 2- and 3-pyridine aldehyde

		2-Pyridinealdehyde						3-Pyridinealdehyde			
		CS_2†		Acetone†		DMSO†		CS_2		Acetone	
Parameter		*Cis*	*Trans*	*Cis*	*Trans*	*Cis*	*Trans*	*Cis*	*Trans*	*Cis*	*Trans*
$-E_{dip}$ (k)	A‡	2.56	1.02	5.33	2.12	5.68	2.26	1.82	0.13	3.80	0.27
$-E_{quad}$ h (c.m.)	A‡	1.97	1.04	3.65	1.92	—	—	0.33	2.89	0.61	5.35
h (c.v.)	A‡	2.99	1.32	5.54	2.45	5.82	2.56	0.49	3.00	0.91	5.55
$-E_{dip}$ (k)	B	2.78	1.32	5.80	2.75	—	—	1.80	0.21	3.76	0.44
$-E_{quad}$ h (c.v.)	B	3.52	1.88	6.50	3.48	—	—	0.62	2.97	1.15	5.50
$E_c - E_t$ $A_{c.m.}$		−2.47		−4.94		—		0.87		1.21	
$A_{c.v.}$		−3.21		−6.30		−6.68		0.82		1.11	
$B_{c.v.}$		−3.10		−6.07		—		0.76		1.03	
INDO		0.85		0.85		0.85		0.11		0.11	
populations§ $A_{c.m.}$		0.947	0.063	0.999	0.001	—	—	0.164	0.836	0.102	0.898
$A_{c.v.}$		0.090	0.020	1.000	0.000	1.000	0.000	0.177	0.823	0.118	0.882
$B_{c.v.}$		0.975	0.025	1.000	0.000	—	—	0.192	0.808	0.134	0.866

*All energies in kcal/mol.
†The dielectric constants were CS_2, 2.64; acetone, 19.5; DMSO, 45.0.
‡A and B refer to different assumptions about the dipole moments of the *cis* and *trans* isomers, see Table 3.
§These include the INDO energy differences as approximations to gas phase values, see text, and calculated at 32 °C.

Can. J. Chem. Downloaded from www.nrcresearchpress.com by 210.87.254.5 on 09/05/12
For personal use only.

in various media and of the relatively small errors in its predictions for **2** (see below), the gas phase energy difference between the conformers of **1** is probably substantially wrong, as given by INDO. One may reason as follows. $^5J_m^{H,CHO}$ implies ΔG_{tc}^0 as -1.6 ± 0.3 and -1.3 ± 0.3 kcal/mol in acetone and DMSO, respectively, whereas solvation theory predicts the change in ΔG_{tc}° as 380 cal/mol, in qualitative agreement with the indicated 0.3 kcal/mol. On the assumption that the theory gives ΔG_{tc}^0 in a given solvent as well as its change in going from solvent to solvent, it follows that ΔG_{tc}° (vapor) is -7.3 ± 1.0 kcal/mol, where the average of the different solvation energies in acetone solution in Table 4 is used and the error of 1 kcal/mol is perhaps overestimated. Similarly, ΔG_{tc}^0 in CS_2 solution is then calculated as $-7.3 + 2.9 = -4.4$ kcal/mol. Hence it is not surprising that $^5J_m^{H,CHO}$ did not change between -50 and 90 °C in a toluene-d_8 solution of **1**.

The large value of ΔG_{tc}^0 in the vapor phase may possibly arise from electrostatic repulsion between the negatively charged nitrogen and oxygen atoms in the *cis* form. Following Lehn and Ourisson (35) one can calculate the dipole–dipole energies in the *cis* form. Using a C=O dipole of 3.75 D and a C—N dipole of 1.05 D (in the ring) one has a repulsion energy of 7.7 kcal/mol in the *cis* form and 4.8 kcal/mol in the *trans* form. Of course, the dipoles are in rather close proximity and the proper dielectric constant of the intervening medium is unknown (unity was used here) so that the 2.9 kcal/mol by which the *trans* form is favored in this estimate may be considered as semiquantitative evidence for the argument based on electrostatic effects.

The semiempirical INDO-MO approximation eliminates many multicenter, two-electron integrals and therefore favors more highly connected structures, as is particularly well illustrated by its incorrect predictions about the conformations of carbonium ions (36). *Ab initio* calculations on 2-pyridinealdehyde are needed to check our conclusions about ΔG_{tc}^0 (vapor).

3-Pyridenealdehyde, **2**. Solvation theory predicts (Table 4) an increase of about 300 cal/mol in the relative stability of the *trans* form when the solvent changes from CS_2 to acetone, the quadrupolar term outweighing the dipolar term as the dielectric constant of the medium increases. $^5J_m^{H,CHO}$ shows that the *trans* form is still favored in acetone solution but that its relative stability has decreased by about 200 cal/mol. The dipolar term overestimates this increase in the stability of the *cis* form by 1500 cal/mol. Clearly, the quadrupolar term is essential but its contribution has been overestimated, perhaps because of a faulty resolution of the net dipole moment of **2** into its components, approximated here by three components only.[6]

Nevertheless, ΔG_{tc}^0 is given as -600 cal/mol by $^5J_m^{H,CHO}$ whereas the solvation theory finds -800 cal/mol (Table 4). If the INDO value were $+110$ cal/mol instead of the calculated -110 cal/mol, and taken as the vapor energy difference, the agreement with experiment would be exact.

In any event, the predictions of the relative energies of **2***a* and **2***b* based on solvation and MO theories are in error by 500 cal/mol at most, so that the conclusions reached about the vapor phase stabilities of the *cis* and *trans* forms of 2-pyridinealdehyde, **1**, may well be correct to within 1 kcal/mol.

To summarize, the coupling over five bonds between aldehyde and ring protons in the pyridinealdehydes is increased by 10% from its value in benzaldehyde when the aldehyde group is situated *ortho* to the nitrogen but is changed very little in the 3- and 4-pyridinealdehydes. This coupling is used to show that the ON-*trans* form of 2-pyridinealdehyde is more stable than the ON-*cis* form by at least 2.3 kcal/mol in CS_2 and C_6D_6 solutions. In acetone and DMSO the *trans* form is favored by 1.6 and 1.3 kcal/mol, respectively, at 32 °C. Solvation theory then shows that the *trans* form is favored by about 7 kcal/mol in the vapor phase, presumably because of strong repulsive dipole–dipole forces in the *cis* form.

For 3-pyridinealdehyde the *trans* form is favored by 0.6 kcal/mol in CS_2, 0.7 kcal/mol in C_6D_6, and 0.4 kcal/mol in acetone solutions, all at 32 °C. The *trans* form has a lower dipole moment than the *cis* form, 1.4 compared to 3.8 D, but it predominates in solution because the

[6]Such ambiguity is perhaps unavoidable in a theory of this kind. A modification in which the assumption of a continuum is relaxed (30) is not applied here because, in our opinion, the Onsager theory is then no longer the fundamental model.

quadrupolar interactions with the dielectric continuum favoring the *trans* form overcome the dipolar interactions favoring the *cis* form.

The use of $^5J_m^{H,CHO}$ in finding conformational preferences is compared favorably to other methods, such as dipole moment, Kerr constant, chemical shifts, far i.r. measurements, and also to semiempirical MO calculations. Accurate spectral analyses are imperative, however.

We are grateful to the National Research Council of Canada for financial support.

1. G. J. KARABATSOS and F. M. VANE. J. Am. Chem. Soc. **85**, 3886 (1963).
2. R. WASYLISHEN and T. SCHAEFER. Can. J. Chem. **49**, 3216 (1971).
3. J. B. ROWBOTHAM and T. SCHAEFER. Can. J. Chem. **50**, 2344 (1972).
4. S. FORSÉN, B. ÅKERMARK, and T. ALM. Acta Chem. Scand. **18**, 2313 (1964).
5. (*a*) J. PEELING, T. SCHAEFER, and C. M. WONG. Can. J. Chem. **48**, 2839 (1970); (*b*) R. FREEMAN and W. A. ANDERSON. J. Chem. Phys. **37**, 2053 (1962).
6. J. A. POPLE, J. W. MCIVER, JR., and N. S. OSTLUND. J. Chem. Phys. **49**, 2960, 2965 (1968).
7. P. A. DOBOSH. Program Number 141, Quantum Chemistry Program Exchange, University of Indiana, Bloomington, Indiana.
8. R. WASYLISHEN and T. SCHAEFER. Can. J. Chem. **50**, 2989 (1972).
9. B. BAK, L. HANSEN, and J. RASTRUP-ANDERSON. J. Chem. Phys. **22**, 2013 (1954).
10. J. A. POPLE and M. GORDON. J. Am. Chem. Soc. **89**, 4253 (1967).
11. C. W. HAIGH and J. M. WILLIAMS. J. Mol. Spectrosc. **32**, 398 (1969).
12. D. G. DEKOWALEWSKI and S. CASTELLANO. Mol. Phys. **16**, 567 (1969).
13. S. CASTELLANO, C. SUN, and R. KOSTELNIK. J. Chem. Phys. **46**, 327 (1967).
14. M. R. BRAMWELL and E. W. RANDALL. Spectrochim. Acta, **26A**, 1877 (1970).
15. V GALASSO Mol. Phys. **26**, 81 (1973).
16. S. FORSÉN and P. N. SKANCKE. *In* Selected topics in structure chemistry. *Edited by* P. Andersen, O. Bastiansen, and S. Furberg. Universitetsforlaget, Oslo, Norway. 1967.
17. C. L. BELL, S. S. DANYLUK, and T. SCHAEFER. Can. J. Chem. **47**, 3529 (1969).
18. F. A. MILLER, W. G. FATELEY, and R. E. WITKOWSKI. Spectrochim. Acta, **23A**, 891 (1967).
19. J. B. ROWBOTHAM, A. F. JANZEN, J. PEELING, and T. SCHAEFER. Can. J. Chem. **52**, 481 (1974).
20. R. J. KOSTELNIK, M. P. WILLIAMSON, D. E. WISNOSKY, and S. M. CASTELLANO. Can. J. Chem. **47**, 3313 (1969).
21. J. W. APSIMON, H. BIERBECK, D. K. TODD, P. V. DEMARCO, and W. G. CRAIG. Can. J. Chem. **49**, 1335 (1971).
22. P. LASZLO. Prog. N.M.R. Spectrosc. **3**, 231 (1967).
23. G. KOTOWYCZ and T. SCHAEFER. Can. J. Chem. **46**, 3110 (1968).
24. T. SCHAEFER. Can. J. Chem. **39**, 1864 (1961).
25. J. BARASSIN, G. QUEGUINER, and H. LUMBROSO. Bull. Chem. Soc. France, 4707 (1967).
26. J. BARASSIN and H. LUMBROSO. Bull. Chem. Soc. Fr. 1947 (1959).
27. H. LUMBROSO, D. M. BERTIN, M. ROBBA, and B. ROQUES. C. R. Acad. Sci. **262C**, 36 (1966).
28. A. R. KATRITZKY, E. W. RANDALL, and L. E. SUTTON. J. Chem. Soc. 1769 (1957).
29. R. J. W. LE FÈVRE and P. J. STILES. J. Chem. Soc. (B), 420 (1966).
30. R. J. ABRAHAM and E. BRETSCHNEIDER. *In* Internal rotation in molecules. *Edited by* W. J. Orville-Thomas. J. Wiley and Sons, New York. 1974. Chapt. 13.
31. L. ONSAGER. J. Am. Chem. Soc. **58**, 1486 (1936).
32. R. J. ABRAHAM and M. A. COOPER. J. Chem. Soc. (B), 202 (1967).
33. (*a*) B. R. LARSEN, F. NICOLAISEN, and J. T. NIELSEN. Acta Chem. Scand. **26**, 1736 (1972); (*b*) R. J. ABRAHAM and T. M. SIVERNS. Tetrahedron, **28**, 3015 (1972).
34. J. O. HIRSCHFELDER, C. F. CURTISS, and R. B. BIRD. Molecular theory of gases and liquids. J. Wiley and Sons, New York. 1954. p. 1032.
35. J-M. Lehn and G. OURISSON. Bull. Chem. Soc. Fr. 1113 (1963).
36. V. BUSS, P. V. R. SCHLEYER, and L. C. ALLEN. Top. Stereochem. **7**, 253 (1973).

Can. J. Chem. Downloaded from www.nrcresearchpress.com by 210.87.254.5 on 09/05/12
For personal use only.

Can. J. Chem. Downloaded from www.nrcresearchpress.com by 210.87.254.40 on 09/05/12
For personal use only.

Sulfur-free Penicillin Derivatives. VI. Synthesis of the 1-Oxacephem Ring System

SAUL WOLFE, JEAN-BERNARD DUCEP, KAM-CHUNG TIN, AND SHUI-LUNG LEE

Department of Chemistry, Queen's University, Kingston, Ontario K7L 3N6

Received September 20, 1974

SAUL WOLFE, JEAN-BERNARD DUCEP, KAM-CHUNG TIN, and SHUI-LUNG LEE. Can. J. Chem. **52**, 3996 (1974).

The title compound has been synthesized by ring closure of an alkyl 2-(2′-chloro-3′-*S*-phthalimido-4′-oxo)azetidinyl-3-methyl-4-hydroxy-*trans*-2-butenoate using S_N1 experimental conditions. The required *E*-allylic alcohols were obtained in two ways starting with an alkyl 2-(2′-chloro-3′-*S*-phthalimido-4′-oxo)azetidinyl-3-methyl-2-butenoate. The first involves allylic bromination with 1 molar equiv. of *N*-bromosuccinimide, conversion of the mixed *Z*- and *E*-allylic bromides into the mixed *Z*- and *E*-allylic formates, and deformylation to a mixture of *E*-alcohol and lactone. The alcohol was separated from the lactone via its tetrahydropyranyl derivative, and then regenerated. In the second route, allylic bromination was performed with 2 molar equiv. of *N*-bromosuccinimide and the resulting dibromo compound was converted into the β,γ-unsaturated olefin with zinc in acetic acid. Epoxidation with peroxytrifluoroacetic acid followed by exposure to triethylamine again afforded a mixture of *E*-alcohol and lactone. The u.v. spectrum of a 1-oxacephem shows a maximum at 266 nm.

SAUL WOLFE, JEAN-BERNARD DUCEP, KAM-CHUNG TIN et SHUI-LUNG LEE. Can. J. Chem. **52**, 3996 (1974).

Le composé désiré a été préparé par cyclisation d'un (chloro-2′ *S*-phtalimido-3′ oxo-4′) azétidinyl-2 méthyl-3 hydroxy-4 butène-2 oate d'alkyle *trans* utilisant des conditions expérimentales S_N1. Les alcools allyliques-*E* nécessaires ont été obtenus de deux façons en partant d'un (chloro-2′ *S*-phtalimido-3′ oxo-4′) azétidinyl-2 méthyl-3 butène-2 oate d'alkyle. La première façon implique une bromuration allylique avec un équivalent molaire de *N*-bromosuccinimide, la transformation du mélange des bromures allyliques-*E* et -*Z* en un mélange de formiates allyliques -*E* et -*Z* et la déformylation pour donner un mélange d'alcool -*E* et de lactone. L'alcool est séparé de la lactone par l'intermédiaire de son dérivé tétrahydropyrannyle et est ensuite regénéré. Dans la deuxième route, la bromuration allylique est effectuée avec deux équivalents de *N*-bromosuccinimide et le composé dibromé qui en résulte est transformé en oléfine β,γ non-saturé à l'aide du zinc dans l'acide acétique. L'époxydation de cet oléfine par l'acide peroxytrifluoroacétique suivie par un contact avec de la triéthylamine conduit à nouveau à un mélange d'alcool-*E* et de lactone. Le spectre u.v. de l'oxa-1 céphem montre un maximum à 266 nm. [Traduit par le journal]

We wish to report the transformation of the thiazolidine ring of the penicillin nucleus into a dihydrooxazine ring, to form the oxygen analog (**1***a*) of a Δ^3-cephem (**1***b*).

The starting materials were the (2R)-*cis*- and (2*S*)-*trans*-chloroazetidinones **2***a–c* (Ft = phthalimido), which are obtained (1) from anhydro-6-phthalimidopenicillin (2) by chlorinolysis, hydrolysis of the derived acid chloride, and esterification with diazomethane or diphenyldiazomethane. Each of these azetidinones was monobrominated (NBS) (3, 4) to give approximately 1:1 mixtures of **3***a* + *b*, **3***c* + *d*, and **3***e* + *f*. The functionality present in the *E*-isomers **3***b*, **3***d*, and **3***f* allows two approaches to be considered for the generation of the six-membered ring, which differ in the timing of attachment of the C—O bond to the β-lactam. In the route described here, this bond has been formed in the final step of the synthesis, by cyclization of the *E*-allylic alcohols **4***a–c*.

The conversion of the allylic bromides into the required allylic alcohols was achieved in two ways. In the first, the mixtures **3***a* + *b*, **3***c* + *d*, and **3***e* + *f* were treated, in chloroform or methylene chloride at room temperature, with excess tetramethylguanidinium formate to form mixtures of the formate esters **5***a* + *b* (64%),

5*c* + *d* (57%), and **5***e* + *f* (52%). The esters were obtained in each case as approximately 2:1 *Z*:*E* mixtures; **5***a–d* have been described previously (3). The n.m.r. spectrum of **5***e* + *f* showed peaks at 8.22 (0.33H, s), 8.10 (0.67H, s), 7.83 (4H, d), 7.37 (10H), 7.03 (1H, s), 6.13 (1H, d, 4.0), 5.68 (1H, d, 4.0), 5.37 (2H, br s), 2.37 (2.0H, s), 2.32 (1.0H, s). Removal of the formyl groups (HCl, MeOH–CH_2Cl_2, 0°, 1.5 h) gave the *E*-alcohols **4***a–c*, admixed with the lactones **6***a* or **6***b*. The tetrahydropyranyl ethers **7***a–c* were separated from the lactones by chromatography on silica gel to yield, from **5***a* + *b*: **6***a* (59%) and **7***a* (36%), m.p. 115–116.5°; from **5***c* + *d*: **6***b* (62%) and **7***b* (31%); from **5***e* + *f*: **6***a* (63%) and **7***c* (29%). Removal of the tetrahydropyranyl protecting groups (HCl, MeOH–CH_2Cl_2, 0°, 4 h) afforded. Compound **4***a* (93%), m.p. 134.5–135.5°; anal. found: C, 54.09; H, 4.20; N, 7.44; n.m.r.: 7.79 (4H, d), 6.17 (1H, d, 4.0), 5.71 (1H, d, 4.0), 4.75 (1H, d, 12.5), 4.25 (1H, d, 12.5), 3.82 (3H, s), 2.78 (1H, s, exchanges with D_2O), 2.38 (3H, s); **4***b* (98%), n.m.r.: 7.75 (4H, d), 6.18 (1H, d, 1.5), 5.55 (1H, d, 1.5), 4.30 (1H, d, 13), 4.27 (1H, d, 13), 3.85 (3H, s), 3.17 (1H, br s), 2.35 (3H); **4***c* (95%), n.m.r.: 7.83 (4H, d), 7.25

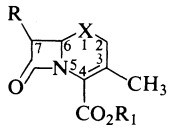

1

a X = O
b X = S

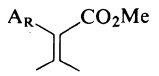

2*a*

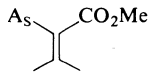

2*b*

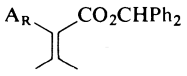

2*c*

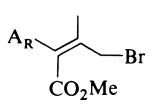

3*a*

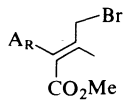

3*b*

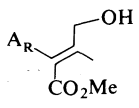

4*a*

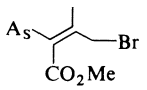

3*c*

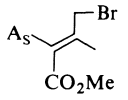

3*d*

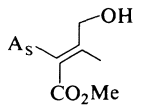

4*b*

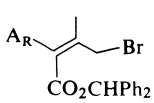

3*e*

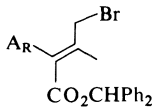

3*f*

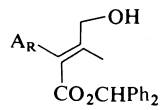

4*c*

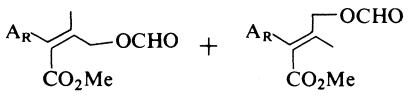

5*a*

5*b*

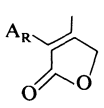

6*a*

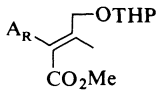

7*a*

Can. J. Chem. Downloaded from www.nrcresearchpress.com by 210.87.254.40 on 09/05/12
For personal use only.

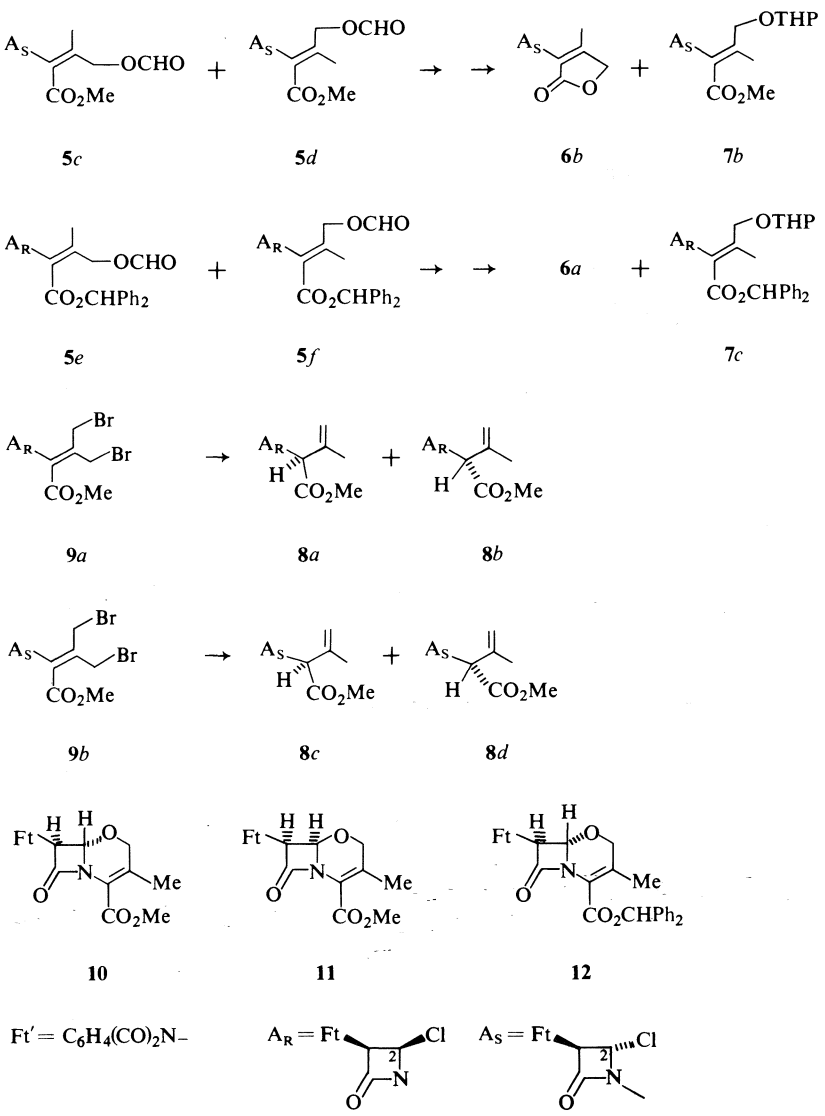

(10H), 7.00 (1H, s), 6.08 (1H, d, 4), 5.80 (1H, d, 4), 4.32 (1H, d, 14), 4.08 (1H, d, 14), 2.80 (1H, br s), 2.38 (3H, s).

A second synthesis of the alcohols **4***a* and **4***b* proceeded via the β,γ-unsaturated olefins **8***a–d*. These were prepared by zinc dust debromination (2 equiv. zinc/mol, HOAc, 0°, 4 min) of the monobromo compounds **3***a* + *b* and **3***c* + *d* or, better, by debromination of the dibromo compounds **9***a* and **9***b* (4.4 equiv. zinc/mol, HOAc, 0°, 4 min). The β,γ-isomers were obtained as 1:1 mixtures of epimers in each case; n.m.r. of **8***a* + *b* (78% from **9***a*): 7.92 (4H, d), 6.43 (0.5H, d, 4.0), 6.05 (0.5H, d, 4.0), 5.76 (0.5H, d, 4.0), 5.74 (0.5H, d, 4.0), 5.27 (2H, br s), 5.14 (0.5H, s), 4.76 (0.5H, s), 3.85 (3H, s), 2.05 (3H, br s); n.m.r. of **8***c* + *d* (90% from **9***b*): 7.77 (4H), 5.95 (0.5H, d, 2), 5.88 (0.5H, d, 2), 5.57 (0.5H, d, 2), 5.47 (0.5H, d, 2), 5.25 (1H, br s), 5.15 (1H, br s), 4.83 (0.5H, s), 4.22 (0.5H, s), 3.83 (1.5H, s), 3.80 (1.5H, s), 2.00 (3H, br s). Each of the β,γ-isomers rearranged rapidly to the α,β-isomer upon exposure to triethylamine (5). Oxidation of the mixture **8***a* + *b* (CF_3CO_3H, CH_2Cl_2, 20°, 1.5 h), afforded a mixture of four epoxides which, without purification, was rearranged (triethylamine–methanol) to a 3:1 mixture of **6***a* and **4***a*. These were separated as described above. The

Can. J. Chem. Downloaded from www.nrcresearchpress.com by 210.87.254.40 on 09/05/12
For personal use only.

mixture **8***c* + *d* similarly afforded a 2:1 mixture of the lactone **6***b* and the *E*-allylic alcohol **4***b*.

Depending on the experimental conditions (4, 6), substitution at C-2 of these azetidinones may proceed by S_N1 or S_N2 pathways. When S_N2 conditions are employed, the rate of the reaction depends upon the nature of the C-3 substituent in the order H_2N > acylamino > phthalimido (1). The alcohols **4***a–c* contain a phthalimido substituent at C-3 and did not cyclize under a variety of S_N2 conditions (Et_3N, NaH, LiH). Unimolecular conditions were therefore necessary, with the result that the oxacephems **1***a* were obtained as epimeric mixtures at C-6, upon treatment of **4***a–c* with stannous chloride in dimethoxyethane or tetrahydrofuran or, in the case of the crystalline alcohol **4***a*, upon heating to the melting point.

Cyclization proceeded smoothly to give oxacephems in yields of 80–92% and, under identical conditions, the same mixture of epimers was formed from **4***a* and *b*, indicative of a common intermediate (4, 6). Some variation in the proportions of these epimers could be achieved by systematic variation of the experimental conditions. Thus, treatment of **4***a* (229 mg) at room temperature with 1.38 molar equiv. of $SnCl_2$ in dimethoxyethane (15 ml) yielded 176 mg (86% after recrystallization from chloroform–hexane) of **10**, m.p. 170–171°, $[\alpha]_D$ −16.9 (*c* 0.3, $CHCl_3$).

Anal. Calcd. for $C_{17}H_{14}N_2O_6$: C, 59.65; H, 4.12; N, 8.18. Found: C, 59.78; H, 3.94; N, 8.42.

The i.r. (KBr): 5.61, 5.65, 5.79μ; n.m.r.: 7.80 (4H, d), 5.33 (1H, d, 1.8), 5.27 (1H, d, 1.8), 4.37 (2H, s), 3.90 (3H, s), 2.03 (3H, s). The u.v. spectrum of 10 shows λ_{max} (EtOH) 266 (12 500), 226 (40 000). The presence of a maximum at 266 nm supports conclusions (7, 8) that the Δ^3-cephem chromophore near 260 nm is not associated with the presence of sulfur. Repetition of the above experiment with 1.67 molar equiv. of $SnCl_2$ in dimethoxyethane (30 ml) afforded, in 90% yield, a 1:1 mixture of **10** and **11**, which possesses the natural configuration at C-6; $[\alpha]_D$ 52.5 (*c* 0.3, $CHCl_3$); M^+, 342; n.m.r.: 7.80 (4H, d), 5.56 (1H, d, 3.8), 5.10 (1H, d, 3.8), 4.30 (2H), 3.90 (3H, s), 2.03 (3H, s). The n.m.r. spectrum of the oxacephem **12** showed peaks at 7.68 (4H, d), 7.23 (10H), 6.83 (1H), 5.20 (1H, d, 1.5), 5.13 (1H, d, 1.5), 4.26 (2H), 1.97 (3H).

We thank the National Research Council of Canada for financial support of this work.

1. S. Wolfe, W. S. Lee, G. Kannengiesser, and J. B. Ducep. Can. J. Chem. **50**, 2894 (1972).
2. S. Wolfe, J. D. Godfrey, C. T. Holdrege, and Y. G. Perron. Can. J. Chem. **46**, 2549 (1968).
3. S. Wolfe, W. S. Lee, J. B. Ducep, and G. Kannengiesser. Can. J. Chem. **50**, 2898 (1972).
4. S. Wolfe, S. L. Lee, J. B. Ducep, G. Kannengiesser, and W. S. Lee. Can. J. Chem. submitted for publication.
5. R. D. G. Cooper and F. L. José. J. Am. Chem. Soc. **92**, 2575 (1970).
6. S. Wolfe and M. P. Goeldner. Tetrahedron Lett. 5131 (1973).
7. P. V. Demarco and R. Nagarajan. *In* Cephalosporins and penicillins. Chemistry and biology. *Edited by* E. H. Flynn. Academic Press, New York, 1972. Chapt. 8.
8. D. B. Boyd. J. Am. Chem. Soc. **94**, 6513 (1972).

Can. J. Chem. Downloaded from www.nrcresearchpress.com by 210.87.254.40 on 09/05/12
For personal use only.

Can. J. Chem. Downloaded from www.nrcresearchpress.com by 210.87.254.105 on 09/05/12
For personal use only.

Canadian Journal of Chemistry

Published by
THE NATIONAL RESEARCH COUNCIL OF CANADA

Journal canadien de chimie

Publié par
LE CONSEIL NATIONAL DE RECHERCHES DU CANADA

Volume 52 Number 24 December 15, 1974

Volume 52 numéro 24 15 décembre 1974

The Fluoridation of Nonstoichiometric Calcium Hydroxyapatite. An Infrared Study

C. H. AMBERG, H. C. LUK,[1] AND K. P. WAGSTAFF[2]

Department of Chemistry, Carleton University, Ottawa, Canada K1S 5B6

Received May 21, 1974

C. H. AMBERG, H. C. LUK, and K. P. WAGSTAFF. Can. J. Chem. **52**, 4001 (1974.

Calcium deficient hydroxyapatites were impregnated to varying degrees with fluoride in very dilute solutions of NaF at room temperature. Ca/P ratios were determined before and after fluoridation. Phosphate loss upon fluoridation was consistent with an initial mechanism of OH^- vacancy filling by F^-, with equivalent amounts of PO_4^{3-} ions escaping to restore charge balance. Infrared measurements confirmed previous evidence of OH/F exchange and the formation of OH···F hydrogen bonds, which increased with progressive thermal activation, considerable exchange having occurred already at 120 °C and possibly below. The first signs of lattice collapse occurred near 600 °C, with the fluorided sample exhibiting somewhat better stability.

C. H. AMBERG, H. C. LUK et K. P. WAGSTAFF. Can. J. Chem. **52**, 4001 (1974).

On imprègne en fluorure, à la température ambiante et à des degrés variables, les hydroxyapatites déficientes en calcium par des solutions très diluées de NaF. On détermine les rapports Ca/P avant et après la fluoruration. Une perte de phosphate par fluoruration est compatible avec un mécanisme initial de lacunes OH^- remplies par F^-, avec un départ de quantités équivalentes d'ions PO_4^{3-} pour rétablir l'équilibre des charges. Des mesures infrarouges confirment une indication antérieure de l'échange OH/F et la formation des ponts hydrogène OH---F qui augmente avec une activation thermique progressive, un échange considérable s'étant déjà produit à 120 °C et probablement au dessous. Les premiers signes de destruction de la maille apparaissent près de 600 °C, l'échantillon fluoruré présentant une meilleure stabilité.

[Traduit par le journal]

Introduction

Although there is a wealth of publications on the structure and properties of nonstoichiometric calcium hydroxyapatite, a material occurring naturally in bones and teeth, uncertainty still exists regarding the manner in which calcium-to-phosphorus ratios depart from the stoichiometric value of 1.667, representative of the formula $Ca_{10}(PO_4)_6(OH)_2$ (1, 2). Of the major conflicting views, two models involving ionic defects have been proposed without recourse to the presence of octacalcium phosphate, a phosphate of low calcium content (3–5). In support of these models, which may be represented by the formulae **1**, $Ca_{10-x}(HPO_4)_x(PO_4)_{6-x}(OH)_{2-x}$ and **2**, $Ca_{10-x}(HPO_4)_x(PO_4)_{6-x}(OH)_{2-x}(H_2O)_x$ where $x < 1$, are the following observations in our laboratory for precipitated hydroxyapatites (6): (*i*) X-ray and i.r. spectra have shown the absence of octacalcium phosphate, (*ii*) deuterium exchange with the proton of HPO_4^{2-} groups is exceedingly difficult, whereas for octacalcium

[1]In partial fulfillment of the requirements for the degree of M.Sc.

[2]Present address: Physical Chemistry Division, A.E.C.L., Chalk River, Ontario.

TABLE 1. Analytical data for fluorided calcium-deficient hydroxyapatites

No.	Ca/P	Surface area ($m^2\ g^{-1}$)	Initial F^- added (mol × 10^4)	F^- in 3 g FHA (mol × 10^4)	Mol % OHF	Calculated PO_4^{3-} lost from 3 g FHA (mol × 10^4)
1	1.57	80	0.504	0.452	1.51	4.59
2	1.55	78	2.02	1.86	6.18	2.09
3	1.56	79	6.05	5.77	19.3	3.35
4	1.58	75	15.1	12.4	41.5	5.58
5	1.59	72	6.00	5.60	18.9	3.51
6	1.61	70	15.0	10.7	35.9	5.47
7	1.61	72	25.0	13.5	45.3	5.47
8	1.62	73	35.0	13.7	46.1	6.44

phosphate it is relatively easy (7), (*iii*) the constancy of the integrated intensity of the i.r. librational hydroxyl band with increasing nonstoichiometry can only be explained by the replacement of OH^- groups by water molecules. Such a band is absent in pure octacalcium phosphate.

With regard to partial fluoridation of such nonstoichiometric hydroxyapatites, it is well known that fluoride ions exchange quite readily with both surface and bulk hydroxyl groups (8); the reaction is one of biological significance, since fluoridation is widely recognized as a preventive measure against dental caries. Whereas lattice hydroxyl groups in the apatite crystal lie a short distance above the centers of the calcium triangles (9), which are arranged in columns parallel to the *c*-axis, the fluoride ions that replace them are finally located in the plane of and at the centers of these triangles (10), as in pure fluorapatite (8). In such a position, hydrogen-bonding between a fluoride ion and an adjacent hydroxyl group in a column is possible and in fact gives rise to a second hydroxyl stretching band shifted to a frequency lower than that of the O—H ··· OPO_3 species (11–15).

In an earlier investigation, consideration of the relative intensities of the two hydroxyl stretching bands for a series of progressively fluorided hydroxyapatites led to the proposal that the hydroxyl/fluoride exchange proceeded by a substitution and hydroxyl rearrangement mechanism along the *c*-axis of the crystallites (12, 15). The results of further i.r. studies on the same system are reported here in an effort to shed new light on the mode of fluoride incorporation into hydroxyapatites. Attempts to follow up earlier catalytic experiments on different calcium and strontium hydroxyapatites (6) with similar experiments on fluorided samples have not been successful so far. The test reaction, the dehydration of 1-butanol, led to polymerization and coking so that it became impossible to stabilize catalytic activity. However, estimates of initial activity led to values similar to those reported earlier on nonfluorided materials.

Experimental

Materials

Samples of pure, and partially fluorided, calcium deficient hydroxyapatite of differing Ca/P ratio and fluoride concentration were prepared and analyzed by the methods described previously (6), the fluoridation again being carried out by stirring 3 g of hydroxyapatite into 200 cc of solution containing the required amount of NaF. No heat treatments beyond drying at 110–120° were applied before analysis.

Methods

Specimens of the original and fluoride impregnated material were evacuated overnight at temperatures in the range 100–700 °C prior to the preparation of KBr pellets (1.5 mg in 200 mg KBr) for use in the investigation of the librational hydroxyl band region (800–450 cm^{-1}). The hydroxyl stretching region (3700–3400 cm^{-1}) was studied using pressed wafer samples (12, 15) previously evacuated at temperatures in the range 300–700 °C. The lower temperature limit in this case was determined by the necessity of removing adsorbed water that gives rise to a very broad band centered around 3000 cm^{-1}. Infrared spectra in both regions were recorded at room temperature on a Perkin–Elmer 225 grating spectrophotometer.

Results and Discussion

Analysis

In Table 1 are summarized the analytical data for two series of fluorided hydroxyapatites together with their specific surface areas, determined by the B.E.T. method using nitrogen adsorption at 77 °K. Samples 1–4 were prepared from a nonstoichiometric hydroxyapatite having a Ca/P ratio of 1.53 and a surface area of 84

Can. J. Chem. Downloaded from www.nrcresearchpress.com by 210.87.254.105 on 09/05/12
For personal use only.

Can. J. Chem. Downloaded from www.nrcresearchpress.com by 210.87.254.105 on 09/05/12
For personal use only.

$m^2\ g^{-1}$, whereas the starting material for samples 5–8 possessed a Ca/P ratio of 1.56 and a surface area of 92 $m^2\ g^{-1}$.

In both series it can be seen that fluoridation resulted in a loss of surface area and an increase in Ca/P ratio, the latter being necessarily associated with an overall loss of phosphate during the impregnation process. Although the causes of these phenomena are beyond the scope of the present work, it is pertinent to discuss several aspects of the analytical results in the light of similar observations reported in the literature (16–18). It is generally held that fluoride ions exchange easily with hydroxyl groups at, or near, the hydroxyapatite surface and that further exchange occurs quite readily with bulk hydroxyl ions. However, it is difficult to explain the maintenance of electroneutrality during an increase in Ca/P ratio without invoking an additional mode of fluoride incorporation. This, of course, presupposes that fluoride ions are the main source of negative charge available for the balancing process. According to the models outlined earlier, occupation of hydroxyl vacancies or substitution of water molecules at hydroxyl sites by fluoride ions are distinct possibilities. Increased Ca/P ratios may also arise when high concentrations of fluoride ($>3 \times 10^{-2}\ M$) are used in the impregnating solution (18). In such cases, mixed phases of calcium fluoride and hydroxyapatite are formed according to the equation

$$Ca_{10}(PO_4)_6(OH)_2 + 20F^- \rightarrow 10CaF_2 + 6PO_4^{3-} + 2OH^-$$

The maximum fluoride concentration used in the present impregnating solutions was always $<1.8 \times 10^{-2}\ M$. A plot of mol% OHF (based on the formula $Ca_{10}(PO_4)_6OHF$ representing 100% nominal exchange) in the fluorided hydroxyapatite (FHA) against the initial fluoride content in solution is shown in Fig. 1. It is evident that the amount of fluoride incorporated increases proportionally to the initial fluoride solution content up to $\sim 1.5 \times 10^{-3}$ mol F^-, after which it appears to level off at ~46 mol% OHF, the fluoride in solution at this stage approaching 4×10^{-3} mol. A similar exchange dependence on fluoride solution concentration has been reported for the formation of fluorapatite (17), and hence these results together with the fact that no peaks due to CaF_2 were found in the X-ray spectra of the impregnated

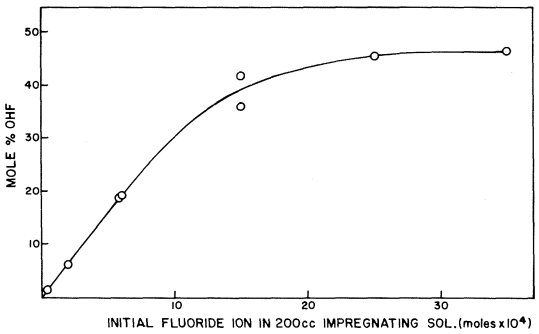

FIG. 1. Effect of fluoride content in the original impregnating solution on the extent of fluoridation.

materials are taken as evidence for successful partial fluoridation of the apatite lattice.

With the assumption that the change in Ca/P ratio can be correlated with the extent of fluoridation, a least-squares treatment was applied to the data given in Table 1 and the results are plotted in Fig. 2 as the calculated phosphate loss against the fluoride content in the impregnated material. The best-fitting straight line was calculated for samples 2–8 in both series. Sample 1, which corresponded to low fluoridation and apparently abnormally high phosphate loss, was not included in the statistical analysis; this seems reasonable to us, since a similar pattern for phosphate loss from fluorided hydroxyapatites at low fluoride concentrations has been reported (16). Furthermore, it follows from the Ca/P ratios that in the two starting materials, 40 and

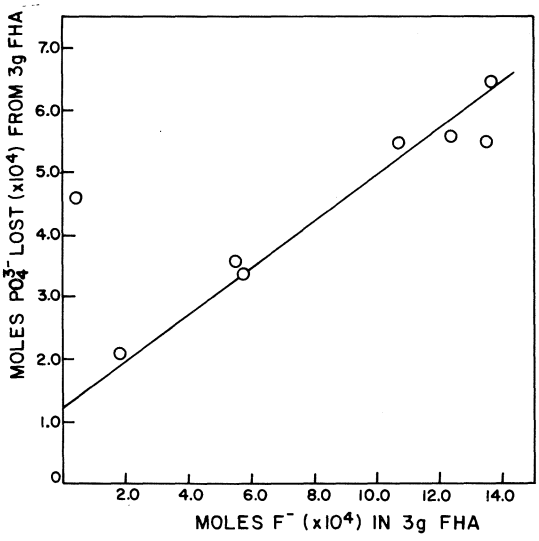

FIG. 2. Least-squares plot of phosphate loss against fluoride uptake in calcium-deficient hydroxyapatite.

30% respectively of the hydroxyl groups are missing according to model **1** or are replaced by water molecules according to model **2**. Comparison of the quantity of fluoride theoretically required to form $Ca_{10}(PO_4)_6OHF$ with the maximum quantities of fluoride incorporated in the two hydroxyapatites then shows that in either case all the fluoride could be accommodated at these defect sites. The equivalent loss of PO_4^{3-} groups to maintain electroneutrality is indicated by the close approach of the slope of the best-fitting line in Fig. 2 to a value of 1/3. The apparent positive intercept on the ordinate would then suggest some more complex ion exchange process during the initial stage of the impregnation. It must be noted, however, that although these results show a similarity in behavior for the two starting materials and serve to account to some extent for the overall phosphate loss, they are not intended to represent a detailed analytical study of the fluoridation process, but rather to characterize the samples for the infrared spectral study.

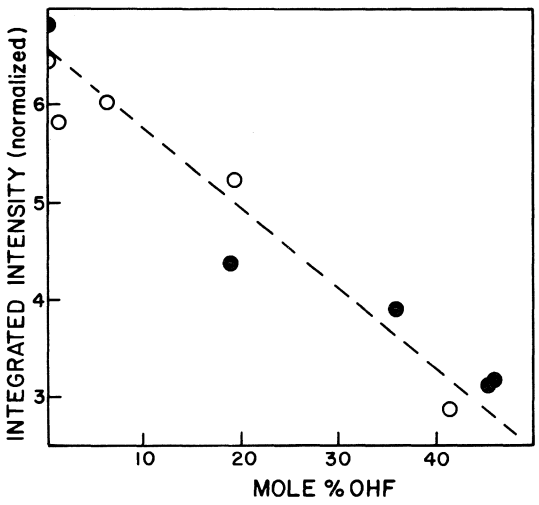

FIG. 3. Effect of fluoridation on the integrated intensity of the ν_L(OH) band of calcium-deficient hydroxyapatite having original Ca/P ratios of 1.53 (○) and 1.56 (●).

Librational Hydroxyl Band Region

For both the original and fluoride-treated hydroxyapatites, the true intensities of the librational hydroxyl band at 635 cm^{-1}, which overlaps with the incompletely split $\nu_4(f_2)$P—O mode at 603 and 568 cm^{-1}, were determined using the method described previously (6). These values were then normalized to the integrated intensity of the 603 cm^{-1} band (intensity multiplied by half-band width), which was thus used as an internal standard, and are plotted against the mol% OHF in the fluorided material in Fig. 3. It is seen that the integrated intensity of the ν_L(OH) band generally decreases as the extent of fluoridation increases in both series, an effect consistent with the contention that fluoride exchanges to a considerable extent with either lattice hydroxyl groups or water molecules in hydroxyl sites at the lowest temperature (~120 °C) required for sample preparation, conceivably even at room temperature.

In an earlier study, a series of progressively fluorided hydroxyapatites was evacuated at 500 °C prior to infrared measurements to ensure the complete diffusion of fluoride ions into the lattice (12, 15). To observe any structural changes brought about by heating a freshly impregnated hydroxyapatite, a sample of fluorided material, sample 4, was evacuated at various temperatures up to 700 °C prior to pellet preparation, following which the librational hydroxyl band intensity was measured in each case. The results are shown in Fig. 4 together with those obtained for the corresponding material without fluoride. It is clearly seen that evacuation up to ~500 °C has little effect on the librational band intensities, a small, gradual decrease being evident for the fluorided case. When both materials are subjected to outgassing temperatures above 500 °C, the librational band intensity rapidly decreases until final disappearance of the band above 600 °C. The band of the fluorided hydroxyapatite disappears at a slightly higher temperature, probably reflecting the increased stability brought about by fluoridation. It is not clear why the librational band disappears at a temperature well below 780 °C, the point of complete lattice collapse established by Bett *et al.* (5) for calcium deficient hydroxyapatites. Our own data for the OH stretching mode, in agreement with the latter authors, also indicate considerable retention of OH species beyond 600 °C (Fig. 5), even though the intensity decrease with temperature becomes steep in that region. In the absence of more discriminating information one can only conclude that an early onset of structural changes brings about a loss of librational freedom; or else that of the two or more unresolved species contributing to the OH stretching band near

Can. J. Chem. Downloaded from www.nrcresearchpress.com by 210.87.254.105 on 09/05/12
For personal use only.

Can. J. Chem. Downloaded from www.nrcresearchpress.com by 210.87.254.105 on 09/05/12
For personal use only.

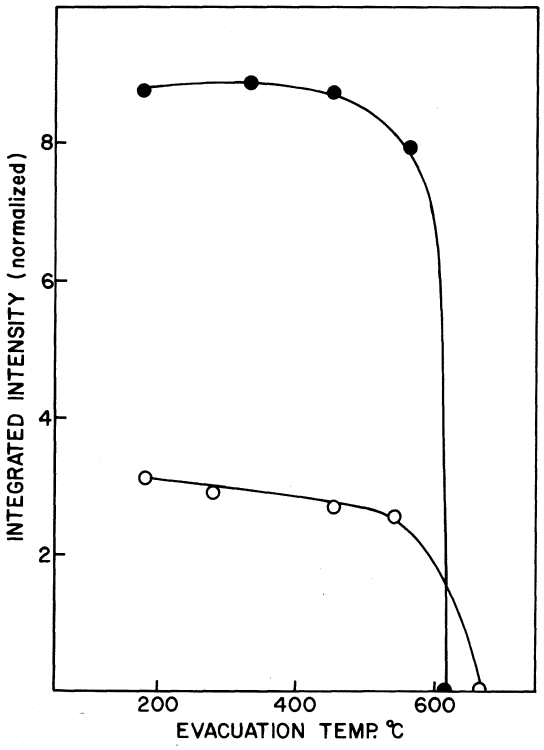

FIG. 4. Effect of evacuation temperature on the integrated intensities of the ν_L(OH) bands for sample 4 (○) and the corresponding unfluorided hydroxyapatite (●).

3570 cm^{-1} only one exhibits a librational mode at 635 cm^{-1}, and that this is the one that vanishes at the lower temperature.

Stretching Hydroxyl Band Region

Figure 5 shows the infrared spectrum in the hydroxyl stretching frequency region for sample 4 and is typical of a fluorided hydroxyapatite. The salient features of the spectrum are the two strong, overlapping bands centered at 3572 and 3540 cm^{-1} and two relatively weak and ill-defined bands at approximately 3670 and 3650 cm^{-1}. Although there is some doubt as to the assignment of the latter bands, it is well established that the band at 3572 cm^{-1} arises from an O—H···O hydrogen bond (6, 14) and the band at 3540 cm^{-1} from an O—H···F hydrogen bond (11–15). The existence of side bands reported by Menzel and Amberg (15) at 3565 and 3549 cm^{-1} was not confirmed in the present work, though this may be due to the differences in sample preparation and fluoride impregnation. Bands similar to the weak bands in the 3660 cm^{-1}

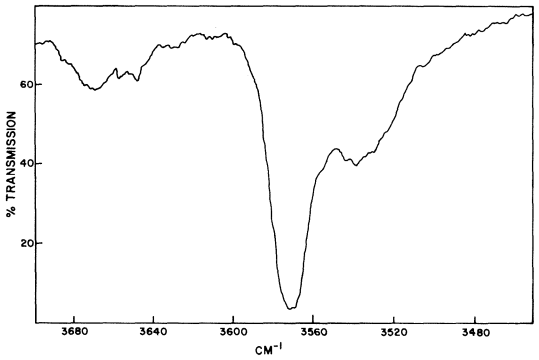

FIG. 5. Infrared spectrum in the hydroxyl stretching frequency region for sample 4.

region have been observed for nonfluorided hydroxyapatites and have been variously assigned to a stretching vibration of a surface hydroxyl species (14) and tentatively to the stretching mode of the non-hydrogen-bonded part of water molecules in hydroxyl group sites (6).

The effect of evacuation temperature on the integrated intensities of the 3572 and 3540 cm^{-1} bands for sample 4 was also studied, the two bands being resolved graphically. The results are shown in Fig. 6, where it is seen that the integrated intensity of the O—H···O stretching band shows a similar dependence on evacuation temperature as that of the librational hydroxyl band in that a significant decrease occurs at high temperatures upon collapse of the lattice. In contrast, the integrated intensity of the O—H···F stretching band increases rapidly with evacuation temperature up to ~550 °C, an effect that can only be associated with the formation of new O—H···F hydrogen bonds. If, as is commonly assumed, the diffusion path of the fluoride ions is along the *c*-axis through the centers of the calcium triangles in a column, then it would appear likely that this bond formation occurs by thermal activation of hydroxyl groups adjacent to such fluoride ions. On the other hand, one cannot exclude alternative diffusion paths, especially in view of the fact that X-ray spectra of our apatites exhibit some broadening and that one must therefore assume the existence of regions of low degree of crystallinity or of very small crystallite size. The resulting defect or grain boundary regions could equally well facilitate the transfer of fluoride ions. In either case, the slight decreases with pretreatment temperature seen for the integrated intensities of the libra-

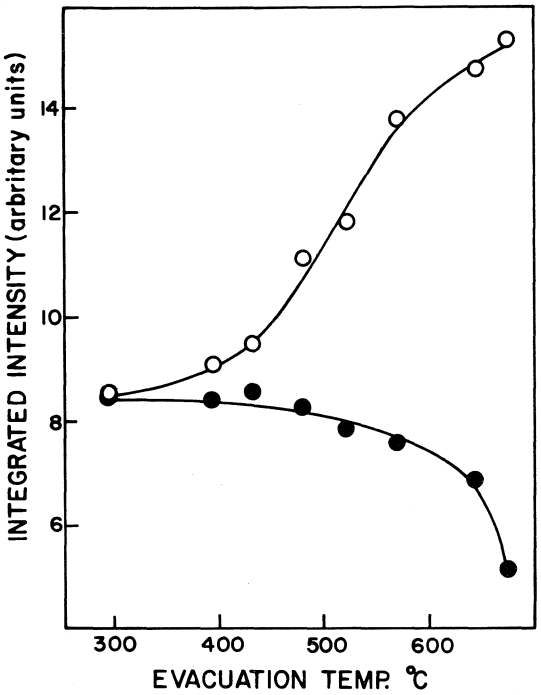

FIG. 6. Effect of evacuation temperature on the integrated intensities of the hydroxyl stretching bands associated with O—H···F (○) and O—H···O (●) hydrogen bonds in sample 4.

tional and stretching O—H···O bands of fluorided hydroxyapatites are consistent with these mechanisms. For the series of progressively fluorided samples subjected to a 500 °C outgassing pretreatment, the integrated intensity of the O—H···F stretching band was found to be ~1.8 times that of the O—H···O band (15). Consideration of the fluoridation mechanism as involving a hydroxyl substitution and a subsequent adjacent hydroxyl rearrangement then led to an integrated intensity ratio per hydrogen-bond of 3.6. Although the results shown in Fig. 6 are not strictly comparable with those of Menzel and Amberg (15), the differences in rates of increase and decrease of the integrated intensities of the O—H···F and O—H···O bands respectively with pretreatment temperature are thought to be due to some disparity between the numbers of O—H···O bonds broken and O—H···F bonds formed. Indeed, there is evidence from ^{19}F n.m.r. studies of mineral hydroxyapatite containing small quantities of fluoride to suggest that configurations of the type O—H···F···H—O occur along the *c*-axis of the crystal (13, 19). In this case, three O—H···O bonds would be broken and one of their hydroxyl groups inverted by partial fluoridation of an otherwise ordered column in the apatite lattice. Such localized structures have been suggested as giving rise to enhanced stability of the apatite lattice and may explain the resistance of the O—H···F bond to cleavage at higher temperatures.

We thank the National Research Council of Canada for financial support.

1. W. E. BROWN. International symposium on structural properties of hydroxyapatites and related compounds. Gaithersburg, Md., 1968. W. A. Benjamin, New York, N.Y.
2. J. C. ELLIOT. Calcif. Tissue Res. **3**, 293 (1969).
3. L. WINAND and G. DUYCKAERTS. Bull. Soc. Chim. Belg. **71**, 142 (1962).
4. E. E. BERRY. J. Inorg. Nucl. Chem. **29**, 317 (1967); **29**, 1585 (1967).
5. J. A. S. BETT, L. G. CHRISTNER, and W. K. HALL. J. Am. Chem. Soc. **89**, 5535 (1967).
6. S. J. JORIS and C. H. AMBERG. J. Phys. Chem. **75**, 3167 (1971); **75**, 3172 (1971).
7. E. E. BERRY and C. B. BADDIEL. Spectrochim. Acta, A, **23**, 1781 (1967).
8. R. A. YOUNG and J. C. ELLIOT. Arch. Oral Biol. **11**, 699 (1966).
9. M. I. KAY, R. A. YOUNG, and A. S. POSNER. Nature, **204**, 1050 (1964).
10. K. SUNDARSANAN and R. A. YOUNG. Acta Cryst. B, **25**, 1534 (1969).
11. J. C. ELLIOT. Ph.D. Thesis, University of London, London, England. 1964.
12. C. H. AMBERG, R. A. BEEBE, and B. MENZEL. Second Canadian symposium on catalysis. Hamilton, Ontario. June, 1967.
13. R. A. YOUNG, W. VAN DER LUGT, and J. C. ELLIOT. Nature, **223**, 729 (1969).
14. N. W. CANT, J. A. S. BETT, G. R. WILSON, and W. K. HALL. Spectrochim. Acta, A, **27**, 425 (1971).
15. B. MENZEL and C. H. AMBERG. J. Colloid Interface Sci. **38**, 256 (1972).
16. H. G. MCCANN. J. Biol. Chem. **201**, 247 (1953).
17. H. G. MCCANN and F. A. BULLOCK. J. Dent. Res. **34**, 59 (1955).
18. D. O. DESHAZER and C. J. SWARTZ. Arch. Oral Biol. **12**, 1071 (1967).
19. W. VAN DER LUGT, D. I. M. KNOTTNERUS, and W. G. PERDOK. Acta Cryst. B, **27**, 1509 (1971).

Can. J. Chem. Downloaded from www.nrcresearchpress.com by 210.87.254.105 on 09/05/12
For personal use only.

Production de $O_2(b^1\Sigma_g^+)$, $v' = 0$, 1 et 2 par la reaction $O(2^1D_2) + O_2(X^3\Sigma_g^-)$

MICHEL J. E. GAUTHIER[1] ET DAVID R. SNELLING[2]

Centre de recherches pour la défense, Valcartier et Centre de recherches sur les atomes et les molécules, C.P. 880, Courcelette, Québec G0A 1R0

Reçu le 23 mai 1974

MICHEL J. E. GAUTHIER et DAVID R. SNELLING. Can. J. Chem. **52**, 4007 (1974).

On a observé les émissions des bandes 0–0 et 1–1 de la transition $O_2(b^1\Sigma_g^+ \rightarrow X^3\Sigma_g^-)$ à 762 et 771 nm respectivement dans la photolyse de mélanges $O_3/O_2/Ar$ à 253.7 nm. On a observé aussi les variations de ces émissions, à différentes concentrations d'ozone, en fonction de la concentration d'oxygène, et on peut en tirer les conclusions suivantes: entre le quart et la moitié des molécules $O_2(b^1\Sigma_g^+)$ formées par la réaction d'échange d'énergie $O(2^1D_2) + O_2(X^3\Sigma_g^-)$ sont à l'état vibrationnel $v' = 1$, les autres sont formées à l'état $v' = 0$. De plus, on montre que O_3 désexcite $O(2^1D_2)$ huit fois plus efficacement que O_2 et on obtient des valeurs approximatives de 0.6 et 1.0 pour les vitesses relatives des réactions de $O_2(b^1\Sigma_g^+)$, $v' = 1$ avec O_2 et O_3 par rapport à la vitesse de la réaction de $O_2(b^1\Sigma_g^+)$, $v' = 0$ avec O_3.

MICHEL J. E. GAUTHIER and DAVID R. SNELLING. Can. J. Chem. **52**, 4007 (1974).

The emissions of the 0–0 and 1–1 bands of the $O_2(b^1\Sigma_g^+ \rightarrow X^3\Sigma_g^-)$ transition have been observed at 762 and 771 nm respectively in the photolysis of $O_3/O_2/Ar$ mixtures at 253.7 nm. From the dependence of these emissions on the concentration of oxygen for various ozone concentrations the following conclusions can be drawn: one-quarter to one-half of the $O_2(b^1\Sigma_g^+)$ molecules formed in the energy transfer from $O(2^1D_2)$ to $O_2(X^3\Sigma_g^-)$ are in the vibrational state $v' = 1$, the remainder being in the $v' = 0$ state. Furthermore, it is shown that O_3 deactivates $O(2^1D_2)$ eight times more effectively than O_2. The relative rates of the reactions of $O_2(b^1\Sigma_g^+)$, $v' = 1$ with O_2 and O_3 are also discussed and approximate values of 0.6 and 1.0 are determined relative to the rate of the reaction of $O_2(b^1\Sigma_g^+)$, $v' = 0$ with O_3.

Introduction

Le travail décrit ici faisait partie d'un programme de recherches sur la chimie de l'atmosphère pour comprendre les mécanismes de la photolyse de l'ozone à des altitudes où cette réaction photochimique déclenche une série de réactions qui impliquent plusieurs états excités. On a donc cherché à identifier les produits de la réaction primaire de la photolyse de l'ozone à 253.7 nm et à déterminer le rôle de ces produits dans l'équilibre photochimique de l'atmosphère.

Le produit le plus important est sans contredit l'atome d'oxygène à l'état excité 2^1D_2 qui réagit ensuite très rapidement dans l'atmosphère avec les constituants mineurs H_2O, CH_4 et H_2 ou avec une molécule d'oxygène ou d'azote. Nous étudierons ici la réaction de $O(2^1D_2)$ avec O_2. On sait déjà (1–3) que cette réaction physique d'échange d'énergie excite la molécule d'oxygène à l'état $b^1\Sigma_g^+$ dans au moins 75% des collisions qui désexcitent $O(2^1D_2)$. Pour simplifier l'écriture dans ce qui suit, les termes O, $O(^1D)$, O_2, $O_2(^1\Delta)$ et $O_2(^1\Sigma)$ couramment employés seront utilisés pour désigner respectivement $O(2^3P_J)$, $O(2^1D_2)$, $O_2(X^3\Sigma_g^-)$, $O_2(a^1\Delta_g)$ et $O_2(b^1\Sigma_g^+)$. Quant à la production de $O_2(^1\Sigma)$ dans la photolyse de l'ozone, nous avons établi les limites suivantes sur la contribution possible de la réaction photochimique primaire et de la réaction $O(^1D) + O_3$: pas plus de 5% de la photolyse produit $O_2(^1\Sigma)$ et moins de 5% du O_2 formé par la deuxième réaction peut l'être à l'état $^1\Sigma$. De plus, on a montré que O_3 désexcite $O(^1D)$ (9.7 ± 1.5) fois plus efficacement que O_2 (2).

L'énergie disponible dans la réaction $O(^1D) + O_2$ pourrait exciter en plus les deux premiers niveaux vibrationnels de l'état électronique $^1\Sigma$ comme l'ont remarqué plusieurs auteurs depuis 20 ans (4, 5). Nous étudierons la réaction en mesurant l'émission de la transition $^1\Sigma \rightarrow {}^3\Sigma$ de O_2 et nous tenterons de démontrer que $O_2(^1\Sigma)$ existe dans notre système avec une excitation vibrationnelle. Nous observerons les bandes 0–0 à 762 nm et 1–1 à 771 nm mais nous ne pourrons pas détecter d'émission à 780 nm qui correspondrait à la bande 2–2.

[1]Adresse actuelle: Centre de recherches en sciences de l'environnement, Université du Québec à Montréal, C.P. 8888, Montréal 101, Québec H3C 3P8.

[2]Auteur à qui on doit adresser toute correspondance.

Can. J. Chem. Downloaded from www.nrcresearchpress.com by 210.87.254.6 on 09/05/12
For personal use only.

Can. J. Chem. Downloaded from www.nrcresearchpress.com by 210.87.254.6 on 09/05/12
For personal use only.

Matériel et méthodes

Le montage expérimental utilisé pour ce travail a déjà servi pour l'étude du mécanisme de formation des singulets de l'oxygène dans la photolyse de l'ozone (2, 6) et pour la mesure de l'efficacité de formation de $O_2(^1\Sigma)$ dans la réaction $O(^1D) + O_2$ (1). Les détails du montage ont déjà été décrits (6, 7).

On effectue la photolyse de mélanges d'ozone et d'autres gaz dans un système dynamique qui utilise la radiation de résonance du mercure à 253.7 nm. Les réactions se produisent dans une cellule cylindrique en quartz de 6.5 cm de diamètre et de 60 cm de longueur. Neuf lampes en U à basse pression de mercure irradient la cellule sur une longueur de 15 cm. On mesure la concentration d'ozone au moyen de l'absorption de la radiation d'une lampe Pen-Ray à 253.7 nm. Les molécules séjournent dans la cellule en moyenne de 0.5 à 2 s. Nous avons utilisé des pressions d'ozone de 1 à 22 mTorr (1 Torr = 133.3 N m^{-2}) et des pressions de O_2, Ar et SF_6 qui pouvaient s'élever respectivement jusqu'à 0.9, 0.8 et 1.0 Torr. La fraction de O_3 décomposé se situait toujours entre 0.13 et 0.30 et le débit total à travers la cellule était de 2.0 1 s^{-1}.

La cellule est couplée axialement à un spectromètre Czerny–Turner, *f*/8, muni de fentes de 32 mm de hauteur et dont la largeur a été ajustée à 2 mm pour ce travail, ce qui donne une largeur de fente spectrale de 2.4 nm. La fente d'entrée se situe à 20 cm de la zone illuminée et, avec cet arrangement optique, le cône de visée du spectromètre est entièrement contenu dans la cellule. Un photomultiplicateur EMI 9659AM refroidi à 253 K sert à détecter les radiations infrarouges de l'oxygène.

On utilise de l'oxygène et de l'argon Gold Label de Matheson. Pour obtenir le mélange O_3/Ar on procède comme suit: on utilise l'Ozonator de Welsbach pour fabriquer l'ozone à partir d'oxygène Gold Label. A la sortie de l'ozoniseur, le mélange ozoné à 5% passe à travers un piège qui contient environ un litre de gel de silice et qui est refroidi à l'aide d'un mélange de méthanol et de glace sèche à 193 K. On adsorbe l'ozone jusqu'à obtenir une couleur bleue prononcée puis on pompe lentement le piège pour enlever l'oxygène. En conservant toujours le piège à basse température, on fait ensuite passer l'argon qui entraîne une quantité relativement constante d'ozone. On peut ajuster la quantité d'ozone désorbé en variant le débit linéaire d'argon à travers le piège. On obtient ainsi un mélange pratiquement exempt d'oxygène. On a utilisé aussi un mélange O_3/SF_6 qui a été préparé comme précédemment (2).

Résultats et analyse

Mécanisme de production de $O_2(^1\Sigma)$

Nous avons observé l'émission de $O_2(^1\Sigma)$ illustrée à la fig. 1 dans la photolyse de l'oxygène ozonisé. L'émission à 762 nm montre, avec une résolution moyenne, les branches P et R de la bande 0–0. Le continuum en pointillé provient de la fluorescence de la cellule de quartz et est enregistré avec la cellule sous vide. On obtient l'intensité de la bande en mesurant la surface sous la courbe au-dessus du continuum. On

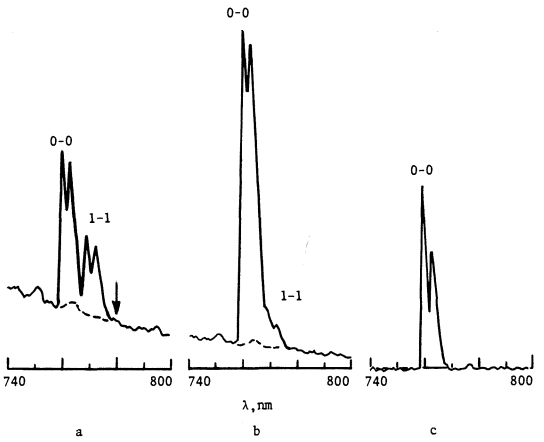

FIG. 1. Spectres d'émission de la transition $^1\Sigma \rightarrow {}^3\Sigma$ de O_2. (*a*) et (*b*), photolyse d'un mélange O_3/O_2/Ar pour $P(O_3) = 0.012$ Torr et $P(Ar) = 0.41$ Torr; (*a*), $P(O_2) = 0.032$ Torr; (*b*), $P(O_2) = 0.17$ Torr; le continuum en pointillé est produit par la fluorescence du quartz; la flèche indique la position où devrait apparaître l'origine de la bande 2–2; (*c*), émission observée dans une décharge micro-onde dans l'oxygène.

confirme l'identité de l'émission en la comparant au spectre obtenu avec une décharge micro-onde dans l'oxygène. Tel qu'on l'avait déjà démontré (2), on peut voir à la fig. 2 (courbe *A*) que l'intensité de $O_2(^1\Sigma)$ à 762 nm augmente avec l'addition de O_2 à un mélange O_3/Ar. Il y a toujours un peu de O_2 présent dans la cellule qui vient de l'ozone photolysé et aussi de la décomposition de l'ozone qui peut survenir avant l'entrée du mélange dans la cellule (cette décomposition était inférieure à 10%). On tient toujours compte de ces deux sources de O_2 lorsqu'on trace les graphiques. L'argon a été choisi comme diluant parce qu'il ne désexcite pas $O(^1D)$.

Le mécanisme de réactions est donné au tableau 1. La constante de la réaction de $O_2(^1\Sigma)$ avec l'ozone est $k_5 = (2.3 \pm 0.5) \times 10^{-11}$ (3, 8) tandis que la constante de désexcitation de $O_2(^1\Sigma)$ par O_2 est 2.5×10^{-16} (8–10). (Les constantes de vitesses des réactions sont données en cm^3 $molécule^{-1}$ s^{-1}.) On a déjà montré (2) pour notre système que la réaction qui prédomine pour limiter la concentration de $O_2(^1\Sigma)$ est la réaction avec O_3 et que la désexcitation de $O_2(^1\Sigma)$ sur les parois ainsi que la désexcitation par collision avec O_2 sont négligeables.

Excitation vibrationnelle de $O_2(^1\Sigma)$ et bande 1–1 de la transition $^1\Sigma \rightarrow {}^3\Sigma$.

On sait que l'échange d'énergie entre $O(^1D)$

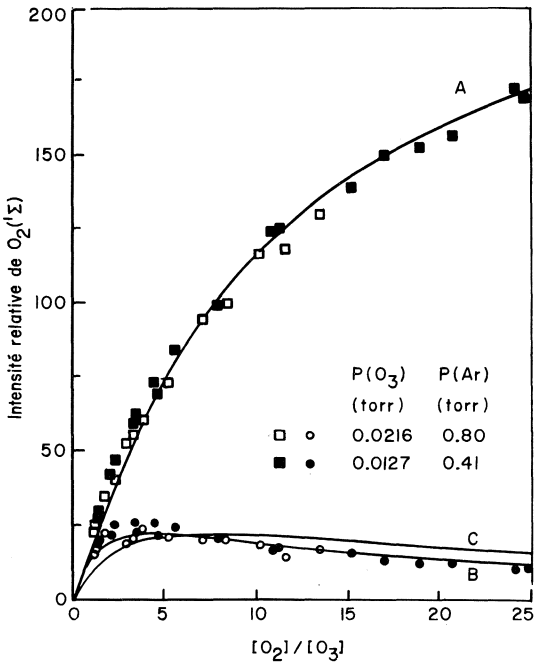

FIG. 2. Variation de l'intensité de $O_2(^1\Sigma)$ *vs.* $[O_2]/[O_3]$. Courbe *A*, émission de $O_2(^1\Sigma)$, $v' = 0$ à 762 nm; courbe *B*, émission de $O_2(^1\Sigma)$, $v' = 1$ à 771 nm; courbe *C*, voir le texte.

et O_2 peut produire $O_2(^1\Sigma)$ avec jusqu'à deux quanta de vibration.

$$O(^1D) + O_2 \rightarrow O + O_2(^1\Sigma)^{v' \leq 2}$$

L'émission de $O_2(^1\Sigma)$, $v' = 1$ ou 2 n'est pas observée en général à cause de la présence de grandes quantités de désactivants vibrationnels incluant l'oxygène. De plus, dans nos expériences précédentes (2), nous n'avions pas une résolution suffisante. D'ailleurs, l'émission de $O_2(^1\Sigma)$, $v' = 0$, 1 ou 2 est toujours très faible parce que la transition est strictement interdite pour l'émission normale de dipôle électrique. Les probabilités de transitions spontanées existent bien que très faibles pour des transitions dipolaires magnétiques.

Néanmoins, nous avons observé la bande d'émission 1–1, dont l'origine (11) se situe à 771.07 nm. Elle est illustrée à la fig. 1*a* pour les conditions où elle était maximale par rapport à la bande 0–0 (origine à 762.15 nm). La bande 2–2 dont l'origine se situe à 780.44 nm n'est pas observée.

Les intensités observées à la fig. 1*a* de l'émission des états $v' = 0$, 1 et 2 de $O_2(^1\Sigma)$ sont dans le rapport $1/0.45/<0.02$. Ces intensités doivent être corrigées pour tenir compte des facteurs de Franck–Condon qui sont différents pour les bandes 0–0, 1–1 et 2–2 ainsi que de la sensibilité différente du système de détection aux trois longueurs d'ondes 762, 771 et 780 nm. Les intensités corrigées sont dans le rapport $1/0.56/<0.025$. La correction sera explicitée ci-dessous.

TABLEAU 1. Mécanisme de réactions

[1]*	$O_3 + h\nu \rightarrow O(^1D) + O_2(^1\Delta)$
[2*a*]†	$O(^1D) + O_3 \rightarrow 2O + O_2^v$ $(v \leq 4)$
[2*b*]†	$\rightarrow O_2^v + O_2^v$ $(v \leq 18)$
[3]‡	$O(^1D) + M \rightarrow O + M$
[4*a*]	$O(^1D) + O_2 \rightarrow O + O_2$
[4*b*]	$\rightarrow O + O_2(^1\Delta)$
[4*c*]†	$\rightarrow O + O_2(^1\Sigma)^0$
[4*d*]†	$\rightarrow O + O_2(^1\Sigma)^1$
[5]†	$O_2(^1\Sigma)^0 + O_3 \rightarrow 2O_2 + O$
[6]†	$O_2(^1\Sigma)^1 + O_3 \rightarrow 2O_2 + O$
[7]†	$O_2(^1\Sigma)^1 + O_2 \rightarrow O_2(^1\Sigma)^0 + O_2^1$
[8]	$O + O_3 \rightarrow 2O_2$

*Il est maintenant reconnu que la photolyse de l'ozone à 253.7 nm produit les molécules d'oxygène à l'état $^1\Delta$ et non à l'état $^3\Sigma$ ou $^1\Sigma$.

†O_2^v, $O_2(^1\Sigma)^0$ et $O_2(^1\Sigma)^1$ veulent dire respectivement $O_2(^3\Sigma)$, $v'' = v$, $O_2(^1\Sigma)$, $v' = 0$ et $O_2(^1\Sigma)$, $v' = 1$. Dans la réaction 2*b*, on suppose que l'énergie se répartit également entre les deux molécules O_2.

‡M représente une molécule, autre que O_3 ou O_2, comme Ar, par exemple, qui peut désexciter $O(^1D)$.

Ces intensités corrigées sont proportionnelles aux concentrations à l'état stationnaire de chaque état de vibration de $O_2(^1\Sigma)$. Si on suppose que les temps de vie des états $O_2(^1\Sigma)$, $v' = 1$ et 2 ne sont pas plus grands que celui de $O_2(^1\Sigma)$, $v' = 0$, les vitesses de production de $v' = 1$ et 2 sont de 0.56 et <0.025 relativement à une production unitaire de $v' = 0$. La dernière hypothèse est valable puisque $O_2(^1\Sigma)$ est contrôlé par la réaction avec O_3 et que la réaction ne serait probablement pas plus lente si $O_2(^1\Sigma)$ avait une excitation vibrationnelle.

Donc, même si la réaction est presque résonante pour produire l'état $v' = 2$, il semble que $v' = 0$ soit produit plus efficacement que l'état $v' = 1$ et beaucoup plus que l'état $v' = 2$. Il faut remarquer que la vitesse relative de production de $v' = 1$ de 0.56 est un minimum si on suppose que la vitesse de désexcitation de $O_2(^1\Sigma)$, $v' = 1$ est au moins aussi grande que pour $v' = 0$.

Production de $O_2(^1\Sigma)$, $v' = 1$

Pour faire l'analyse quantitative du comportement des deux bandes en fonction des

Can. J. Chem. Downloaded from www.nrcresearchpress.com by 210.87.254.6 on 09/05/12
For personal use only.

pressions de O_3 et O_2, nous devrons tenir compte du mécanisme de réactions présenté au tableau 1 et nous tenterons d'estimer les vitesses relatives de formation de $O_2(^1\Sigma)$ dans les états $v' = 1$ et $v' = 0$.

Bien que l'échange d'énergie entre $O(^1D)$ et O_2, la réaction 4*d*, soit le processus logique pour produire $O_2(^1\Sigma)$, $v' > 0$ dans notre système, on ne peut pas exclure à priori le pompage d'energie vibrationnelle par une molécule O_2^v, produite éventuellement par $O(^1D) + O_3$ ou par $O + O_3$, à une molécule $O_2(^1\Sigma)$.

[9] $$O_2^v + O_2(^1\Sigma)^0 \rightarrow O_2^{v-1} + O_2(^1\Sigma)^1$$

Ce processus devrait être efficace puisque la constante vibrationnelle est pratiquement la même aux deux niveaux électroniques et que la réaction est même exothermique. D'après Herzberg (11), $\omega_e' = 1432.7\ cm^{-1}$ pour $O_2(^1\Sigma)$ tandis que $\omega_e'' = 1580.4\ cm^{-1}$ pour $O_2(^3\Sigma)$. Pour $O_2(^1\Delta)$, la constante $\omega_e' = 1509.3\ cm^{-1}$ est encore plus rapprochée de ω_e'' et la transition serait encore plus probable.

La molécule O_2^v serait produite efficacement par $O(^1D) + O_3$ et aussi par $O + O_3$, les réactions 2 et 8. Cette dernière réaction est exothermique de 94 kcal mol^{-1} et, si on suppose l'équipartition de l'énergie, les deux molécules O_2 peuvent être produites avec chacune $v \leqslant 11$. La réaction 2*b* est exothermique de 139 kcal mol^{-1}, et Fitzsimmons et Bair (12) ont observé des bandes d'absorption dans le système Schumann–Runge $^3\Sigma_u^- \leftarrow {}^3\Sigma_g^-$ à partir de niveaux aussi élevés que $v'' = 23$. Baiamonte *et al.* (13) ont observé les états jusqu'à $v'' = 30$ et ont montré que O_2^v était produit par la réaction 2*b* aussi bien que par la réaction 8, mais que la réaction 2*a* était au moins dix fois plus efficace que la réaction 2*b*. Il y aura une concentration à l'état stationnaire non nulle de O_2^v aussi bien que de $O_2(^1\Sigma)$ et $O_2(^1\Delta)$ dans la cellule. On peut s'attendre à ce que toute excitation vibrationnelle causée par cet échange d'énergie entre O_2^v et $O_2(^1\Sigma)$ soit équilibrée rapidement entre tous les états de O_2 (13). Ce qui ne se produirait pas pour une excitation vibrationnelle de $O_2(^1\Sigma)$ produit par $O(^1D) + O_2$, réaction 4*d*.

De plus, si $O_2(^1\Sigma)$, $v' = 1$ et 2 étaient produits par échange d'énergie vibrationnelle, la molécule O_2^v produite par les réactions $O + O_3$ ou $O(^1D) + O_3$ viendrait à l'équilibre très rapidement par des processus vibrationnels–vibrationnels (V–V) avant d'être désexcitée par échange V–V avec O_3 ou par une désexcitation vibrationnelle–translationnelle avec une autre molécule. On aurait donc une concentration à l'état stationnaire de O_2^v et, puisque l'excitation vibrationnelle s'équilibre rapidement, $O_2(^1\Delta)$ et $O_2(^1\Sigma)$ auraient aussi la même excitation vibrationnelle et on devrait observer les émissions des états $v' > 0$ de $O_2(^1\Sigma)$ et de $O_2(^1\Delta)$.

Pour évaluer la possibilité de ce pompage vibrationnel, on étudie la réaction analogue pour le pompage de $O_2(^1\Delta)^v$ dans la photolyse d'un mélange O_3/Ar. L'écart entre les deux constantes vibrationnelles est encore plus faible, donc le processus serait plus probable que pour $O_2(^1\Sigma)$. La réaction $O(^1D) + O_3$ est très rapide ($k_2 = (5.3 \pm 2.6) \times 10^{-10}$) (14, 15), de sorte qu'on aurait une vitesse de production pratiquement égale de O_2^v et de $O_2(^1\Delta)^0$ si on suppose un rendement quantique unitaire de $O(^1D)$ et de $O_2(^1\Delta)^0$ dans la photolyse.

Nous reproduisons un spectre de l'émission de $O_2(^1\Delta)$ à la fig. 3. La bande 1–1 est absente, le pompage vibrationnel est donc éliminé et le mécanisme de production de $O_2(^1\Sigma)^1$ demeure exclusivement l'échange d'énergie entre $O(^1D)$ et O_2.

Désexcitation de $O(^1D)$ et de $O_2(^1\Sigma)$, $v' = 1$ par O_3 et O_2

Si on suppose que $O_2(^1\Sigma)$, $v' = 0$ et 1 sont

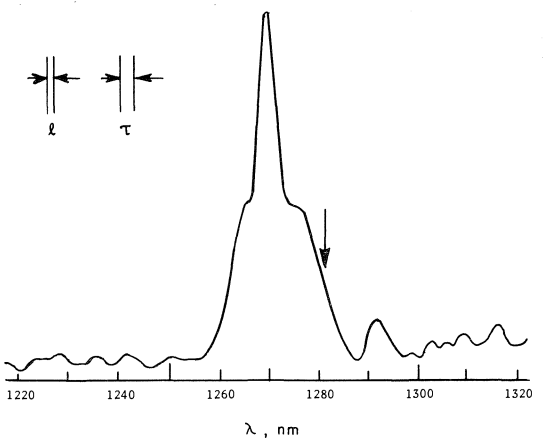

FIG. 3. Spectre d'émission de la bande 0–0 de la transition $^1\Delta \rightarrow {}^3\Sigma$ de O_2. La flèche indique la position où devrait apparaître l'origine de la bande 1–1 à 1280.5 nm; origine de bande 0–0: 1268.6 nm. $P(O_3) = 0.025$ Torr; $P(O_2) = 0.37$ Torr; $P(Ar) = 0.42$ Torr; *l*, largeur de fente spectrale; τ, constante de temps du système de détection; température, 298 K; fraction de O_3 décomposé, 0.25.

Can. J. Chem. Downloaded from www.nrcresearchpress.com by 210.87.254.6 on 09/05/12
For personal use only.

Can. J. Chem. Downloaded from www.nrcresearchpress.com by 210.87.254.6 on 09/05/12
For personal use only.

désexcités par les réactions 5, 6 et 7, on peut résoudre les équations de vitesses pour obtenir les expressions des concentrations à l'état stationnaire des espèces excitées. On tentera ensuite d'analyser le comportement observé à la fig. 2 des bandes 0–0 et 1–1 de $O_2(^1\Sigma)$ en fonction des pressions de O_3 et de O_2. Finalement on étudiera l'éventualité d'un autre mécanisme de désexcitation de $O_2(^1\Sigma)$, $v' = 1$.

Donc, suivant le mécanisme proposé, les concentrations à l'état stationnaire des espèces excitées sont, pour un mélange $O_3/O_2/Ar$:

$$[10]\quad [O_2(^1\Sigma)^0] = (\phi_0 F J_1/k_5) \times (1 + (k_2[O_3]/k_4[O_2]))^{-1}$$

$$[11]\quad F = 1 + ((\phi_1/\phi_0)/(1 + (k_6[O_3]/k_7[O_2])))$$

$$[12]\quad [O_2(^1\Sigma)^1] = \phi_1 J_1 [O_3](k_6[O_3] + k_7[O_2])^{-1}(1 + (k_2[O_3]/k_4[O_2]))^{-1}$$

où $[O_2(^1\Sigma)^0]$ et $[O_2(^1\Sigma)^1]$ sont les concentrations à l'état stationnaire des états excités $O_2(^1\Sigma)^0$ et $O_2(^1\Sigma)^1$ respectivement et seront proportionnelles aux intensités d'émission mesurées de la bande 0–0 à 762 nm pour $O_2(^1\Sigma)^0$ et de la bande 1–1 à 771 nm pour $O_2(^1\Sigma)^1$; $\phi_1(=k_{4d}/k_4)$ et $\phi_0(=k_{4c}/k_4)$ sont les fractions des molécules O_2 produites aux états $O_2(^1\Sigma)^1$ et $O_2(^1\Sigma)^0$ respectivement dans la réaction $O(^1D) + O_2$; $J_1[O_3]$ est la vitesse de la photolyse et $k_2(=k_{2a} + k_{2b})$ et $k_4(=k_{4a} + k_{4b} + k_{4c} + k_{4d})$ sont respectivement les constantes totales de désexcitation de $O(^1D)$ par O_3 et par O_2.

J_1 est approximativement constant pour les pressions d'ozone utilisées puisque l'absorption de radiation est faible. En effet, de la loi de Beer–Lambert, $I = I_0 \exp(-\varepsilon l\,[O_3])$, on peut calculer que $\Delta I/I_0 = 1 - \exp(-\varepsilon l\,[O_3])$. Dans nos conditions expérimentales, $\varepsilon l\,[O_3] \ll 1$ et on peut faire l'approximation $\Delta I = I_0\,\varepsilon l\,[O_3]$. L'intensité absorbée est donc proportionnelle à la pression d'ozone. Pour ces expériences, la pression de O_3 est maintenue constante à 10% près et, pour cette marge de pressions, l'approximation d'absorption linéaire sera excellente.

On peut transformer les expressions ci-dessus pour obtenir:

$$[13]\quad [O_2(^1\Sigma)^0]/[O_2(^1\Sigma)^1] = (k_6\phi_0/k_5\phi_1) \times (1 + (k_7[O_2]/k_6[O_3])(1 + (\phi_1/\phi_0)))$$

$$[14]\quad F[O_2(^1\Sigma)^0]^{-1} = (k_5/\phi_0 J_1) \times (1 + (k_2[O_3]/k_4[O_2]))$$

Si on définit

$$[15]\quad [O_2(^1\Sigma)^1]_c = [O_2(^1\Sigma)^1] \times (1 + (k_2[O_3]/k_4[O_2]))$$

on obtient

$$[16]\quad [O_2(^1\Sigma)^1]_c^{-1} = (k_6/\phi_1 J_1)(1 + (k_7[O_2]/k_6[O_3]))$$

A partir de ces expressions, nous pouvons utiliser nos données de la fig. 2 pour tracer trois graphiques que nous reproduisons aux figs. 4, 5 et 6. Figure 4, $[O_2(^1\Sigma)^0]/[O_2(^1\Sigma)^1]$ *vs.* $[O_2]/[O_3]$. Le rapport pente sur ordonnée à l'origine doit donner $(k_7/k_6)(1 + (\phi_1/\phi_0))$. Figure 5, $F[O_2(^1\Sigma)^0]^{-1}$ *vs.* $[O_3]/[O_2]$. Le rapport pente sur ordonnée à l'origine doit donner k_2/k_4. Figure 6, $[O_2(^1\Sigma)^1]_c^{-1}$ *vs.* $[O_2]/[O_3]$. Le rapport pente sur ordonnée à l'origine doit donner k_7/k_6.

Pour les figs. 5 et 6, le rapport pente sur ordonnée à l'origine est indépendant de l'échelle utilisée en ordonnée. Il n'est donc pas nécessaire de corriger les intensités afin de compenser pour le changement de sensibilité du système de détection. Pour la fig. 4, non seulement on ne

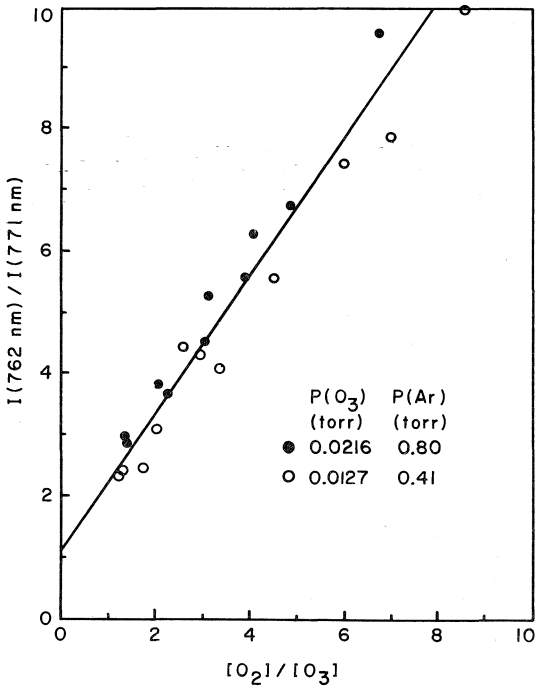

FIG. 4. Graphique de $I(762\text{ nm})/I(771\text{ nm})$ *vs.* $[O_2]/[O_3]$ pour deux expériences avec un mélange $O_3/O_2/Ar$ où $I(762\text{ nm})$ et $I(771\text{ nm})$ sont directement proportionnels aux concentrations de $O_2(^1\Sigma)^0$ et de $O_2(^1\Sigma)^1$ respectivement. Pente/ordonnée à l'origine, 1.0 ± 0.25.

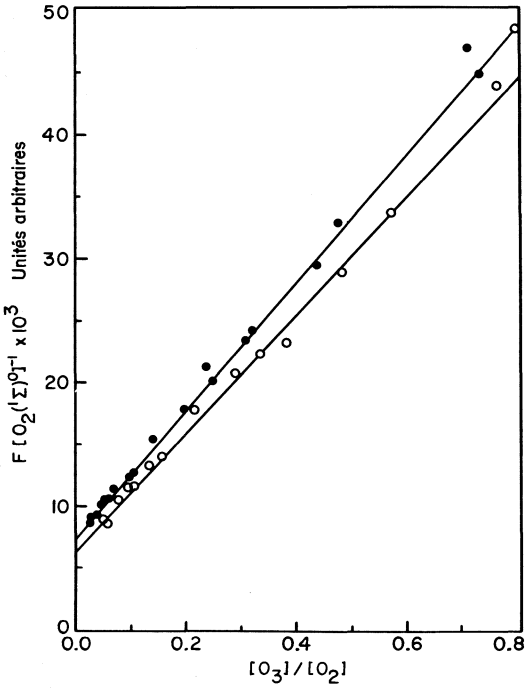

FIG. 5. Constante relative ozone–oxygène. Variation de $F[O_2(^1\Sigma)^0]^{-1}$ *vs.* $[O_3]/[O_2]$ pour deux expériences avec un mélange $O_3/O_2/Ar$. Pente/ordonnée à l'origine, 8.0 ± 0.5. Conditions expérimentales, voir fig. 4.

corrige pas les intensités mais les deux expériences sont assimilées en une seule pour obtenir la pente et l'ordonnée à l'origine parce que d'après le mécanisme proposé, $[O_2(^1\Sigma)^0]/[O_2(^1\Sigma)^1]$ ne dépend que de $[O_2]/[O_3]$.

On a obtenu la pente et l'ordonnée à l'origine des droites par la méthode des moindres carrés où on a tenu compte des incertitudes comme suit. D'abord, on suppose qu'il n'y a pas d'erreur en abscisse mais seulement en ordonnée. Ensuite, si on a un ensemble d'observations de x avec des incertitudes σ_x, la règle générale est de donner à chaque observation un poids proportionnel à $(\sigma_x)^{-2}$ (16). Par exemple, si on calcule une moyenne $(\sum wx)/(\sum w)$, on prendra $w = (\sigma_x)^{-2}$. Dans notre cas, nous portons en ordonnée l'inverse d'une intensité et le poids attaché à chaque point dépendra de l'incertitude sur la mesure de l'intensité. Cette dernière peut se situer entre les deux cas suivants: (*a*) l'incertitude relative est constante et (*b*) l'incertitude absolue est constante.

Le premier cas se présenterait si l'intensité était assez grande et si on avait un bon rapport signal à bruit pour tous les points. Le deuxième cas se retrouve pour la mesure de l'émission de la bande 1–1 de $O_2(^1\Sigma)^1$ qui est très faible et qui est partiellement masquée par la queue de la branche R de la bande 0–0. Pour ces deux cas, on devra utiliser des poids selon le tableau suivant:

Cas	σ_I	σ_I^{-1}	Poids
a	$\propto I$	$\propto I^{-1}$	$\propto I^2$
b	constant	$\propto I^{-2}$	$\propto I^4$

Pour les figs. 4 et 6, nous utilisons des poids en I^4 et pour la fig. 5, un poids en I^3. C'est pourquoi les points très dispersés aux grandes valeurs d'ordonnée sur ces graphiques n'ont pas grande influence sur la valeur de la pente.

Si on tient compte de l'incertitude expérimentale, tous les points de la fig. 4 sont bel et bien sur la même droite, ce qui confirme la dépendance linéaire pour deux expériences avec $O_3/O_2/Ar$ et le rapport pente sur ordonnée à l'origine donne

$$(k_7/k_6)(1 + (\phi_1/\phi_0)) = 1.0 \pm 0.25$$

L'incertitude sur ce résultat, et sur ceux des figs. 5 et 6 est donnée par le double de l'écart-type auquel on ajoute un autre 10% pour tenir compte de la possibilité d'erreur systématique dans la mesure des débits et des concentrations de O_3.

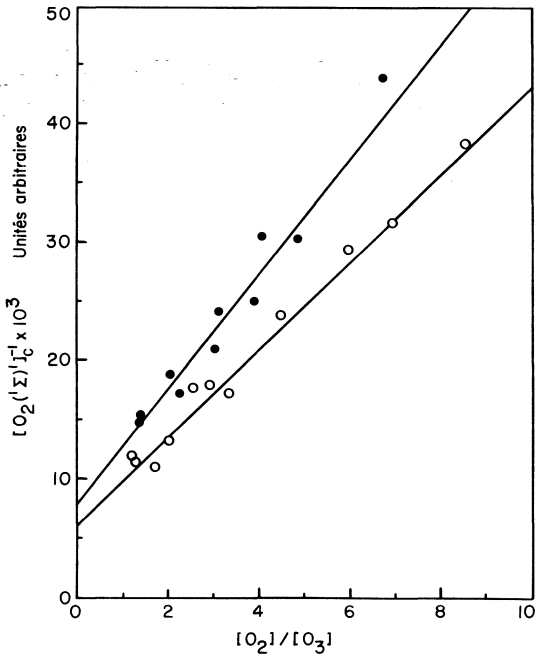

FIG. 6. Variation de $[O_2(^1\Sigma)^1]_c^{-1}$ *vs.* $[O_2]/[O_3]$ pour deux expériences avec un mélange $O_3/O_2/Ar$. Pente/ordonnée à l'origine, 0.60 ± 0.06. Conditions expérimentales, voir fig. 4.

Can. J. Chem. Downloaded from www.nrcresearchpress.com by 210.87.254.6 on 09/05/12
For personal use only.

Can. J. Chem. Downloaded from www.nrcresearchpress.com by 210.87.254.6 on 09/05/12
For personal use only.

Pour tracer la fig. 5 qui doit donner k_2/k_4, on a besoin des valeurs de ϕ_1/ϕ_0 et de k_7/k_6 car F est une fonction de ces deux quantités. De plus, pour tracer la fig. 6 qui doit donner k_7/k_6, on a besoin de la valeur de k_2/k_4 pour calculer l'ordonnée, $[O_2(^1\Sigma)^1]_c^{-1}$. On peut résoudre le problème par un procédé itératif. On fait d'abord la fig. 5 en prenant $F = 1$. On obtient une valeur de k_2/k_4 que l'on utilise ensuite pour tracer la fig. 6. On obtient alors k_7/k_6 puis on calcule ϕ_1/ϕ_0 avec le résultat de la fig. 4. On réitère jusqu'à la convergence, c'est-à-dire qu'on refait les figs. 5 et 6 jusqu'à ce que les valeurs de k_2/k_4, k_7/k_6 et ϕ_1/ϕ_0 ne varient plus. Les deux derniers graphiques sont présentés aux figs. 5 et 6 et les valeurs obtenues dans l'itération sont données ci-dessous. Remarquons ici que les pentes et les ordonnées à l'origine changent d'une expérience à l'autre pour les figs. 5 et 6, mais que le rapport pente sur ordonnée à l'origine est le même à

Itération pour deux expériences avec Ar

k_2/k_4	k_7/k_6	ϕ_1/ϕ_0
10.8	0.73	0.37
9.1	0.66	0.52
8.44	0.626	0.60
8.16	0.612	0.63
8.05	0.606	0.65
7.99	0.603	0.66

5% près. Donc $k_2/k_4 = 8.0 \pm 2.0$; $k_7/k_6 = 0.60 \pm 0.20$; $\phi_1/\phi_0 = 0.66 \pm 0.30$; $\phi_1/(\phi_0 + \phi_1) = 0.40 + 0.09$ où $0.40 - 0.14$. Même si on ne peut pas obtenir k_7/k_6 et ϕ_1/ϕ_0 avec une bonne précision, k_2/k_4 converge rapidement et ne change que de 25% du début à la fin du procédé itératif. Donc O_3 désexcite $O(^1D)$ 8 fois plus efficacement que O_2; la constante de désexcitation de $O_2(^1\Sigma)^1$ par O_2 égale 0.60 fois celle de O_3; finalement, entre le quart et la moitié des molécules $O_2(^1\Sigma)$ formées par $O(^1D) + O_2$ le sont à l'état $v' = 1$, le reste est formé à l'état $v' = 0$.

L'ordonnée à l'origine de la fig. 4 est de 1.15 ± 0.20 et devrait égaler $k_6\phi_0/k_5\phi_1$ d'après l'expression 13. Cependant, nous n'avons pas mis en ordonnée le rapport des concentrations de $O_2(^1\Sigma)^0$ et de $O_2(^1\Sigma)^1$ mais bien le rapport des intensités observées de $O_2(^1\Sigma)^0$ et de $O_2(^1\Sigma)^1$ qui n'a pas été corrigé pour tenir compte des facteurs de Franck–Condon qui sont différents pour chaque bande ainsi que du changement de sensibilité du système de détection à 762 et 771 nm. La correction est appliquée comme suit: on calcule la concentration relative $[O_2(^1\Sigma)^0]/[O_2(^1\Sigma)^1]$, à partir des intensités relatives mesurées, à l'aide de la relation suivante

$$[17] \quad I(v'v'') \propto N(v')\nu^3(v'v'')R_e^2 q(v'v'')$$

où $I(v'v'')$ est l'intensité en photons par seconde, $N(v')$ est le nombre de molécules excitées à l'état v', $\nu(v'v'')$ est le nombre d'onde de la bande et $q(v'v'')$ est le facteur de Franck–Condon. Alors, si on suppose que le moment de la transition électronique R_e est essentiellement le même pour les deux transitions, on obtient le rapport suivant

$$[18] \quad \frac{[O_2(^1\Sigma)^0]}{[O_2(^1\Sigma)^1]} = \frac{(762.15)^3 q(1,1) Q(771) I(762)}{(771.07)^3 q(0,0) Q(762) I(771)} = 0.78 \frac{I(762)}{I(771)}$$

où $q(1, 1) = 0.802$ et $q(0, 0) = 0.933$ sont les probabilités de transition de Fraser *et al.* (17) et $Q(\lambda)$ est le rendement quantique du photomultiplicateur à la longueur d'onde λ. Après correction, $k_6\phi_0/k_5\phi_1$ devient donc 0.90 ± 0.16.

Les courbes *A* et *B* de la fig. 2 ont été calculées avec le mécanisme que nous venons de décrire et avec une valeur ajustée de J_1 pour obtenir l'intensité relative observée. La courbe *C* a été calculée avec les mêmes paramètres et le même mécanisme plus une réaction de désexcitation de $O_2(^1\Sigma)^1$ par Ar qui aurait une constante vingt fois plus faible que k_6. Cette réaction supplémentaire a été clairement surestimée et elle a probablement une constante plusieurs ordres de grandeur plus faible que k_6.

En plus des deux expériences avec $O_3/O_2/Ar$ discutées jusqu'ici, nous avons effectué deux autres expériences avec $O_3/O_2/SF_6$. Si on utilise les quatre expériences, les valeurs de k_2/k_4, k_7/k_6 et ϕ_1/ϕ_0 obtenues par un procédé itératif semblable sont respectivement 9.6, 0.72 et 0.30, ce qui est en accord avec les résultats ci-dessus. Par contre, nou avons remarqué que le SF_6 pouvait contenir un bon pourcentage d'impuretés, c'est pourquoi nous n'avons retenu que les résultats obtenus avec l'argon.

Discussions

Dans son étude sur la photolyse de O_2 dans le continuum Schumann–Runge, Noxon (18) n'a observé que l'émission de la bande 0–0 de $O_2(^1\Sigma)$. Il a utilisé un filtre d'interférence de largeur de bande de 4.0 nm pour faire un balayage de 780 à 755 nm ce qui courve les

Can. J. Chem. Downloaded from www.nrcresearchpress.com by 210.87.254.6 on 09/05/12
For personal use only.

positions des bandes 1–1 et 2–2. En tenant compte de la transmission du filtre, il n'a pu que donner des limites supérieures assez conservatrices de 10% et de 5% pour l'émission des bandes 1–1 et 2–2 respectivement.

Gilpin *et al.* (8) ont fait quelques observations de l'émission de la bande 1–1 avec un filtre d'interférence à 770.2 nm d'une largeur de bande 1.0 nm et ont déduit qualitativement que l'état $O_2(^1\Sigma)^1$ était produit par $O(^1D) + O_2$. Néanmoins, notre travail est le seul où la bande 1–1 a été clairement identifiée par un spectre d'émission.

Filseth *et al.* (19) n'ont pu observé d'émission des bandes 1–1 et 2–2 et en ont déduit que pour les conditions employées, $O_2(^1\Sigma)$, $v' > 0$ est ou bien formé initialement par $O(^1D) + O_2$ dans des proportions relativement faibles ou bien que $O_2(^1\Sigma)$, $v' > 0$ est désexcité par O_2 en moins de 10^3 collisions. Nos observations nous permettent de confirmer la deuxième hypothèse. En effet, avec nos valeurs de ϕ_1/ϕ_0 (0.66 ± 0.30) et de $k_6\phi_0/k_5\phi_1$ (0.90 ± 0.16), on peut calculer que $0.27 \leqslant k_6/k_5 \leqslant 1.02$. Il est physiquement peu probable que k_6 soit inférieur à k_5. Autrement dit, on peut supposer que la constante de la réaction entre $O_2(^1\Sigma)^1$ et O_3 est au moins aussi élevée que la constante de $O_2(^1\Sigma)^0 + O_3$. Donc $k_6 \simeq k_5 = 2.3 \times 10^{-11}$ (3). Puisque $k_7/k_6 = 0.60 \pm 0.20$, on peut déduire que $k_7 \simeq 1.5 \times 10^{-11}$, c'est-à-dire que $O_2(^1\Sigma)^1$ est certainement désexcité par O_2 en moins de 25 collisions[3]. Filseth *et al.* (19) ne pouvaient donc pas observer les bandes 1–1 et 2–2 dans leurs conditions expérimentales.

D'un autre côté, notre valeur de $k_6\phi_0/k_5\phi_1$ indique aussi que ϕ_1 se rapproche de la limite supérieure d'une demie obtenue ci-dessus. En effet, pour obtenir une valeur de k_6/k_5 d'au moins un, il faudrait que ϕ_1/ϕ_0 soit plus grand que 0.94, c'est-à-dire que $\phi_1/(\phi_0 + \phi_1)$ soit supérieur à 0.48, ce qui est en accord avec la plus grande valeur de ϕ_1. Il semble donc très probable que près de la moitié des molécules $O_2(^1\Sigma)$ soient formées à l'état $v' = 1$ par la réaction $O(^1D) + O_2$. Il est assez intéressant de remarquer aussi que si $k_7 \simeq 1.5 \times 10^{-11}$, et si on se rappelle que la constante de désexcitation de $O_2(^1\Sigma)^0$ par O_2 est de 1.5×10^{-16} (18), on peut conclure que $O_2(^1\Sigma)^1$ est désexcité par O_2 10^5 fois plus efficacement que $O_2(^1\Sigma)^0$. Ce qui se conçoit bien puisque la première réaction n'enlève que l'excitation vibrationnelle de $O_2(^1\Sigma)^1$ tandis que la deuxième enlève l'excitation électronique de $O_2(^1\Sigma)^0$. Dans l'atmosphère, l'état $O_2(^1\Sigma)^1$ n'a donc aucune chance de produire une émission qui soit comparable à celle de $O_2(^1\Sigma)^0$.

Bates (20) a proposé que la désexcitation vibrationnelle de l'état $O_2(^1\Sigma)^1$ pourrait procéder rapidement par un échange d'énergie *électronique* entre une molécule excitée et une autre à l'état fondamental selon la réaction suivante:

$$[19] \qquad O_2(^1\Sigma)^1 + O_2{}^0 \rightarrow O_2{}^1 + O_2(^1\Sigma)^0$$

Ce mécanisme serait probablement facilité par la distance internucléaire à l'équilibre r_e et le quantum vibrationnel ω_e presque égaux dans les deux états. Remarquez bien que cette réaction est différente de la réaction 7. Jones et Bayes (21) ont observé l'échange d'énergie électronique entre $^{32}O_2(^1\Delta)$ et $^{36}O_2(^3\Sigma)$ et obtiennent une constante supérieure à 1.7×10^{-11}. Ces auteurs suggèrent aussi que la réaction se fait par l'échange d'un électron et il n'est pas impossible que dans ce processus, la molécule qui serait au niveau $O_2(^1\Delta)^1$ garde son excitation vibrationnelle, ce qui reviendrait au même qu'un simple échange d'excitation vibrationnelle qui se ferait à une vitesse de 1.7×10^{-11}. Dans notre cas, avec $O_2(^1\Sigma)^1$, nous obtenons aussi une constante de vitesse très grande de 1.5×10^{-11} pour le processus qui enlève le quantum de vibration de $O_2(^1\Sigma)^1$. Bien que nous ayons supposé qu'il s'agissait d'un échange d'énergie vibrationnelle par la réaction 7, nous ne pouvons pas déterminer si la désexcitation de $O_2(^1\Sigma)^1$ se produit selon la réaction 7 ou la réaction 19.

Dans le mécanisme proposé, O_3 réagit avec $O_2(^1\Sigma)^1$ pour donner $2O_2 + O$ par la réaction 6. Il se pourrait que O_3 désexcite plutôt $O_2(^1\Sigma)^1$ à $O_2(^1\Sigma)^0$ pour réagir ensuite avec ce dernier par la réaction 5 ou même que ces deux processus de désexcitation de $O_2(^1\Sigma)^1$ soient efficaces. Pourtant, nous avons établi que la constante de la réaction 6 était comparable à celle de la réaction 5, et donc environ 1/10 de la fréquence de collision de la théorie cinétique des gaz. Il est peu probable qu'un échange d'énergie vibrationnelle entre $O_2(^1\Sigma)^1$ et O_3 soit assez rapide pour concurrencer la réaction 6. De plus, nous avons montré que l'échange d'énergie vibrationnelle entre $O_2(^1\Sigma)^1$ et O_2, un processus presque résonant, procède avec une constante d'environ 1.5×10^{-11}, et il est peu probable que la réac-

[3]Pour que tout soit bien clair, précisions ici que c'est l'excitation vibrationnelle de $O_2(^1\Sigma)^1$ qui est enlevée par O_2 en moins de 25 collisions.

Can. J. Chem. Downloaded from www.nrcresearchpress.com by 210.87.254.6 on 09/05/12
For personal use only.

tion analogue avec O_3 soit aussi rapide. Cette dernière supposition est confirmée jusqu'à un certain point par l'observation expérimentale que de grandes quantités de SF_6 ne désexcitent pas $O_2(^1\Sigma)^1$. En résumé, on peut dire que O_2 enlève efficacement le quantum de vibration de $O_2(^1\Sigma)^1$ en moins de 25 collisions tandis que O_3 réagit directement pour donner $2O_2 + O$ en moins de 15 collisions.

Nous avons déjà mesuré le rendement quantique $f(= \phi_0 + \phi_1)$ en $O_2(^1\Sigma)$ dans la réaction $O(^1D) + O_2$ et nous avons comparé nos résultats à ceux des autres chercheurs (1). Nous avions montré que si on suppose que la photolyse de O_3 produit $O_2(^1\Delta)$ avec une efficacité unitaire, le rendement quantique est de 0.89 ± 0.33. Au début de cette année, Snelling publiait dans ce journal (3) les résultats de ses travaux sur la photolyse éclair de l'ozone qui lui ont permis de mesurer entre autres le rendement quantique f de même que les constantes de vitesse des réactions $O_2(^1\Sigma) + O_3$ et $O + O_2 + O_2$. Snelling a fait aussi une évaluation critique très détaillée des différentes publications qui traitent de f et a conclu que $f \geqslant 0.75$. Nous référons le lecteur à ces discussions et en particulier à celles qui portent sur le travail de McGrath *et coll.* (22, 23) qui ont étudié l'excitation vibrationnelle de O_2 dans la photolyse éclair de l'ozone. Maintenant, si on suppose que $\phi_1/(\phi_0 + \phi_1) = 0.40$ et que $f \geqslant 0.75$, le rendement quantique en $O_2(^1\Sigma)$, $v' = 1$ de la réaction $O(^1D) + O_2$ devient $\geqslant 0.30$. On peut donc affirmer qu'au moins 30% des collisions réactives entre $O(^1D)$ et O_2 produisent $O_2(^1\Sigma)$ avec un niveau d'excitation vibrationnelle $v' = 1$.

Quand à la constante relative k_2/k_4, nous avions déjà obtenu 9.7 ± 1.5 (2) ce qui est en parfait accord avec la nouvelle valeur de 8.0 ± 2.0. Le National bureau of standards (14, 15, 25) recommande l'adoption des valeurs suivantes pour les deux constantes absolues: $k_2 = (5.3 \pm 2.6) \times 10^{-10}$ et $k_4 = (7.4 \pm 1.5) \times 10^{-11}$, ce qui fait une constante relative de $k_2/k_4 = 7.2 \pm 4.8$. A notre connaissance, il n'y a pas eu d'autres mesures directes de la constante relative k_2/k_4. Le travail récent le plus important est celui de Husain *et al.* à Cambridge (24) qui ont mesuré les constantes absolues de désexcitation de $O(^1D)$ en utilisant la spectroscopie par absorption atomique dans l'ultraviolet sous vide ($\lambda = 115.2$ nm, $O(3^1D_2{}^0 \leftarrow 2^1D_2)$). Ils obtiennent respectivement pour k_2 et k_4, $(2.7 \pm 0.2) \times 10^{-10}$ et $(7.0 \pm 0.5) \times 10^{-11}$ ce qui donne une constante relative k_2/k_4 de 3.9, un facteur de deux plus bas que notre résultat. Bien que leur méthode soit indiscutable et qu'ils citent des écarts-types très faibles, leur valeur de k_2 semble trop basse d'un facteur de deux si on se fie à la revue du National bureau of standards.

1. D. R. SNELLING et M. GAUTHIER. Chem. Phys. Lett. **9**, 254 (1971).
2. M. GAUTHIER et D. R. SNELLING. J. Chem. Phys. **54**, 4317 (1971).
3. D. R. SNELLING. Can. J. Chem. **52**, 257 (1974).
4. D. R. BATES et A. DALGARNO. J. Atmos. Terr. Phys. **4**, 112 (1953).
5. J. W. CHAMBERLAIN. Physics of the aurora and airglow. Academic Press, New York. 1961.
6. M. GAUTHIER et D. R. SNELLING. Chem. Phys. Lett. **5**, 93 (1970).
7. M. GAUTHIER. Thèse de doctorat, Université Laval, Québec, Québec. 1973.
8. R. GILPIN, H. I. SCHIFF et K. H. WELGE. J. Chem. Phys. **55**, 1087 (1971).
9. K. H. BECKER, W. GROTH et U. SCHURATH. Chem. Phys. Lett. **8**, 259 (1971).
10. I. D. CLARK et J. F. NOXON. J. Chem. Phys. **57**, 1033 (1972).
11. G. HERZBERG. Spectra of diatomic molecules. D. Van Nostrand, Princeton, N.J. 1950.
12. R. V. FITZSIMMONS et E. J. BAIR. J. Chem. Phys. **40**, 451 (1964).
13. V. D. BAIAMONTE, L. G. HARTSHORN et E. J. BAIR. J. Chem. Phys. **55**, 3617 (1971).
14. D. GARVIN. (*Rédecteur*). Chemical kinetics data survey V. Sixty-six contributed rate and photochemical data evaluations on ninety-four reactions. NBSIR 73-206, 1973.
15. D. GARVIN et R. F. HAMPSON, (*Rédecteurs.*) Chemical kinetics data survey VII. Tables of rate and photochemical data for modelling of the stratosphere. NBSIR 74-430, 1974.
16. A. G. WORTHING et J. GEFFNER. Treatment of experimental data. Wiley, New York. 1943.
17. P. A. FRASER, W. R. JARMAIN et R. W. NICHOLLS. Astrophys. J. **119**, 286 (1954).
18. J. F. NOXON. J. Chem. Phys. **52**, 1852 (1970).
19. S. V. FILSETH, A. ZIA et K. H. WELGE. J. Chem. Phys. **52**, 5502 (1970).
20. D. R. BATES. The physics of the upper atmosphere. *Dans* The earth as a planet. *Rédigé par* G. P. Kuiper. Univ. Chicago Press, Chicago. 1954. Chapt. XII.
21. I. T. N. JONES et K. D. BAYES. J. Chem. Phys. **57**, 1003 (1972).
22. K. F. LANGLEY et W. D. MCGRATH. Planet. Space Sci. **19**, 416 (1971).
23. D. W. MCCULLOUGH et W. D. MCGRATH. Chem. Phys. Lett. **12**, 98 (1971).
24. R. F. HEIDNER III, D. HUSAIN et J. R. WIESENFELD. J. Chem. Soc. Faraday Trans. II. **69**, 927 (1973).
25. R. J. CVETANOVIC. Can. J. Chem. **52**, 1452 (1974).

A Study of the Effect of Solvent and Temperature on the Electron Paramagnetic Resonance Parameters and Linewidths of Copper(II) bis(Diethyldithiocarbamate)

F. Geoffrey Herring and Robert L. Tapping

Department of Chemistry, University of British Columbia, 2075 Wesbrook Place, Vancouver, British Columbia V6T 1W5

Received June 24, 1974

F. Geoffrey Herring and Robert L. Tapping. Can. J. Chem. **52**, 4016 (1974).

The effect of varying solvent and temperature on the e.s.r. parameters and linewidths of copper(II) bis(diethyldithiocarbamate) has been studied. The temperature and solvent dependences of the isotropic hyperfine coupling constant (a_0) have been interpreted in terms of vibronic and axial ligation effects. The rotational correlation time, τ_R, of $Cu(DEDC)_2$ has been measured in the solvents employed. The values of τ_R measured at 300 K have been used to obtain the anisotropic interaction parameter, κ, which is found to correlate roughly with the dipole moment and molar refractivity of the solvent.

F. Geoffrey Herring et Robert L. Tapping. Can. J. Chem. **52**, 4016 (1974).

On étudie l'influence de la variation des solvants et de la température sur les paramètres de r.p.e. et les largeurs des bandes du bis(diéthyldithiocarbamate) cuivre(II). On interprète les effets de la température et de solvant sur la constante de couplage hyperfine isotrope (a_0) en termes d'effets vibronique et de fixation axiale. On mesure, dans les solvants utilisés, le temps de corrélation rotationnel τ_R de $Cu(DEDC)_2$. On utilise les valeurs de τ_R mesurées à 300 K pour obtenir le paramètre d'interaction anisotrope κ qui correspond approximativement au moment dipolaire et à la réfractivité moléculaire du solvant. [Traduit par le journal]

Introduction

The variation of the electron paramagnetic resonance (e.p.r.) spin Hamiltonian parameters (g- and A-) with changes in the nature of the ligand (substituent changes) in square planar copper(II) complexes (CuL_2) has been well studied and can be said to be fairly well understood (1–7). The dependence of the g-tensor and hyperfine coupling tensor (A) on the rigid matrix in which the square planar complex is situated has also been the subject of extensive study. The results can be readily interpreted in terms of changes in the admixture of the metal and ligand orbitals together with concomitant changes in the d–d excitation energies which determine the magnitude of the g- and A-tensors (8, 9). In particular, large variations in the g- and A-tensors are to be expected if specific interactions such as ligand addition or solvation occur at the vacant coordination site of the square planar complex (9–12). The variations in g and A due to substituent effects are most reliably interpreted using the anisotropic components of the g- and A-tensors (9, 13) rather than the isotropic components (g_0 and a_0), although g_0 has been shown to be reliable (9) in this regard. The discussion of Zink and Drago (14) points out possible pitfalls in the interpretation of e.p.r. parameters.

The corresponding studies of the dependence of the e.p.r. parameters of square planar copper(II) complexes measured in the liquid phase upon temperature and solvent variation are quite limited by comparison to the studies in the solid state. Falle and Luckhurst (15), for example observed a strong temperature dependence of the isotropic component of the hyperfine coupling tensor (a_0) of copper(II) acetylacetonate as did Wilson and Kivelson (18). The decrease of a_0 with temperature was interpreted in terms of a vibrational effect involving the motions of the copper and four oxygen atoms. The effect of solvent on the isotropic e.p.r. parameters of square planar copper(II) complexes has only been investigated in a few cases (12, 16, 17), although some attempt has been made to use the variation of a_0 and g_0 as indicators of specific solvent effects (16).

The variation of the linewidths of the e.p.r. spectra of copper(II) square planar complexes has been the subject of some study (18, 19). Two types of linewidth modulation are conveniently classifiable: (*a*) modulation due to reorientational effects (18) (*b*) lifetime broaden-

Can. J. Chem. Downloaded from www.nrcresearchpress.com by 210.87.254.5 on 09/05/12
For personal use only.

Can. J. Chem. Downloaded from www.nrcresearchpress.com by 210.87.254.5 on 09/05/12
For personal use only.

ing in addition to (*a*) by a rapid Lewis acid–base equilibrium (19*f*, 20, 21). In the first case the assumption is made that in solvents considered to be weakly interacting (*i.e.* nonspecific interactions or noncoordinating) it is the incomplete motional averaging of the anisotropy of g and A that is the dominant contribution to the m_I-dependent linewidth ($\Delta H(m_I)$). Thus the measurement of the parameters, α, β, γ, and δ, in

$$[1] \quad \Delta H(m_I) = \alpha + \beta m_I + \gamma m_I^2 + \delta m_I^3$$

can lead to information as to the nature of the intermolecular potential in which the spin probe moves (22, 23). This is accomplished by determining the rotational correlation time (τ_R) of the spin probe from either β or γ (18, 19*f*, 22, 24–26) in eq. 1. Hence the parameter κ can be obtained (22, 23), which indicates the magnitude of the anisotropy of the intermolecular potential in which the molecule moves (22).

In the presence of coordinating solvents, however, it is possible that a rapid Lewis acid–base reaction of the type

$$CuL_2 + B \rightleftharpoons CuL_2B$$

can, and does (19*f*, 20, 21), lead to lifetime broadening under the appropriate conditions. If the primary interest is to measure the parameters in eq. 1 and hence obtain the reorientational correlation times for CuL_2 and/or CuL_2B, this reaction presents a complication but can be accounted for from a knowledge of the equilibrium constant and the lifetime of the adduct (19*d*). One can, in fact, by careful analysis and choice of conditions obtain the parameters in eq. 1 for both CuL_2 and CuL_2B but this, optimally, would require studies in mixed solvents which can only serve to complicate the interpretation of the results. Consequently it is usual to obtain parameters for CuL_2B in pure B and correct for, or neglect, the contribution to the linewidth from the small amount of CuL_2 present. It is no doubt for this reason that the study of the solvent and temperature dependences of the e.p.r. linewidths of CuL_2 (19) and similar complexes (22–26) has largely been confined to those solvents that can be considered as noncoordinating.

In the light of the foregoing it would seem that a complete study of the solvent and temperature variation of a_0, g_0, and τ_R could lead to valuable insight into the liquid state, as has a study of the adduct lifetime (τ_B) (27). With this in mind we have studied the solvent and temperature dependence of $\Delta H(m_I)$, a_0, and g_0 for copper(II) bis(diethyldithiocarbamate) ($Cu(DEDC)_2$) in both noncoordinating and coordinating solvents. The probe $Cu(DEDC)_2$ was chosen because of its inherently narrow e.p.r. lines so that eq. 1 can be readily employed and because a substantial amount is known about its behavior in the presence of Lewis bases (19–21, 27, 28).

Experimental Procedures

Physical Measurements and Materials

Spectra were recorded on a Varian E-4 spectrometer, equipped with a Varian (V6040) variable temperature accessory. Field calibration was made with a proton resonance magnetometer. The microwave frequency was monitored with a Hewlett–Packard 5425L counter equipped with an X-band plug-in unit. Absolute field position measurements were accurate to ± 0.2 G and the frequency reproducible to ± 20 kHz in 9 GHz. The *g*-value measurements are reliable to ± 0.0002 and hyperfine splittings to ± 0.05 G. Calibration of the thermocouple used in the temperature measurement indicated that the maximum absolute error in the thermocouple was less than 0.02 °C. The error in actual sample temperature as compared to the thermocouple reading was usually ≤ 0.5 °C.

The $^{63}Cu(DEDC)_2$ was prepared from 99.5% copper-63 metal, as described previously (21), and was dissolved in the appropriate solvent immediately prior to e.p.r. measurement. All solutions were thoroughly degassed before measurement, and care was taken to keep all samples and solvents in an inert atmosphere at all times. Solvents used were of Spectroscopic Grade and used without further purification.

Determination of τ_R

The determination of τ_R from the linewidth parameters in eq. 1 has been discussed by Kivelson and co-workers (22), Luckhurst and Ockwell (24), Angerman and Jordan (25), and Chasteen and Hanna (26). The consensus is that τ_R is most reliably determined from the parameter γ. Previous measurements of γ have been carried out on vanadyl systems in which $I = \frac{7}{2}$ so that eight e.p.r. lines are observed and consequently a least squares method can reasonably be applied. In the present case only four e.p.r. lines are observed so that the determination of γ requires the straightforward solution of four simultaneous equations; in fact the unique solution is

$$\gamma = \tfrac{1}{4}[\Delta H(\tfrac{3}{2}) + \Delta H(-\tfrac{3}{2}) - \Delta H(\tfrac{1}{2}) - \Delta H(-\tfrac{1}{2})]$$

Thus the accuracy of γ simply relies on the uncertainty in the measurement of $\Delta H(m_I)$ and in order to reduce this uncertainty a number of repetitions is required. The values of γ obtained in this work are the result of at least three or four repetitions per temperature and solvent.

The suggestion that τ_R is most reliably obtained from γ

Can. J. Chem. Downloaded from www.nrcresearchpress.com by 210.87.254.5 on 09/05/12
For personal use only.

rests on the observation that a plot of γ *vs.* η/T (η = viscosity) is linear over a reasonable temperature range as required by the theory of Kivelson and co-workers (18, 22). The data obtained in the present work for the noncoordinating solvents, where viscosity data is available, show that in the case of $Cu(DEDC)_2$ γ is linear with respect to η/T except for chloroform where some curvature is apparent. Once it is established that γ for the molecule under consideration behaves according to theory the value of τ_R can be obtained from (18, 22)

$$[2]\quad \frac{\sqrt{3}}{2}\cdot\frac{\gamma}{\tau_R}=\frac{1}{9}\left[\frac{1}{2}(\Delta a)^2-\frac{7}{5}\Delta a\Delta\bar{g}\frac{a_0}{\omega_0}\right]-\frac{u}{90}\left\{(\Delta a)^2+\frac{a_0}{\omega_0}[10\Delta a\Delta\bar{g}+24\Delta a\Delta\bar{g}f-5(\Delta a)^2f]\right\}$$

where $\Delta a = A_{zz} - \frac{1}{2}(A_{xx} + A_{yy})$, $\Delta\bar{g} = g(\omega_0/g_0)$, $\Delta g = g_{zz} - \frac{1}{2}(g_{xx} + g_{yy})$, $u = (1 + \omega_0^2\tau_R^2)^{-1}$, $f = \omega_0^2\tau_R^2u$, and ω_0 is the microwave Larmor angular frequency. The value of τ_R is obtained by an iterative cycle using eq. 2; an approximate value of τ_R is obtained from the secular and pseudosecular terms independent of u and then the nonsecular terms (dependent on u) are included until a self-consistent value of τ_R is obtained. The determination of τ_R requires a knowledge of a_0, g_0, Δa, and Δg at the temperature of interest. The usual practice is to assume that these parameters are temperature independent but we have included the temperature dependence of a_0 and g_0, a small correction, but not that of Δa and Δg. The temperature variation of Δa and Δg is not known so that the values obtained by Weeks and Fackler (6) at room temperature have been employed over the temperature range studied here.

Once the value of τ_R has been obtained the value of β can be calculated and compared to the experimentally determined value as a test of the theory. Generally it is found that the two values agree to within 10 to 20% indicating fair agreement with theory (22, 25, 26). The expression for β is readily obtainable from the literature (22, 26) and is not repeated here. It is also possible to compute values of α' and α'' ($\alpha = \alpha' + \alpha''$) from a knowledge of τ_R (22), generally the agreement with theory and experiment is not as good as that for β (22, 26) especially for the spin-rotational (α'') term in the case of copper (18). In the present study we restrict ourselves to the determination of τ_R from γ and a comparison of calculated and observed β-values. The other aspects mentioned will be the subject of further study.

Results

Isotropic hyperfine splittings (a_0) and g-values (g_0) of $Cu(DEDC)_2$ were measured in a number of solvents over the temperature range 200 to 300 K. The following trends were observed: (*a*) in noncoordinating solvents a_0 is linear with respect to temperature and the slope $(d|a_0|/dT) > 0$, (*b*) in coordinating solvents a_0 is again linear with respect to temperature but $d|a_0|/dT < 0$; (*c*) the g-factor of $Cu(DEDC)_2$ appears to be fairly insensitive to temperature in both coordinating and noncoordinating solvents, the former having a slightly greater temperature dependence ($dg_0/dT \sim 6 \times 10^{-5}\ K^{-1}$ for coordinating and $\sim 1.5 \times 10^{-5}\ K^{-1}$ for noncoordinating). The temperature variation a_0 for $Cu(DEDC)_2$ in benzene and pyridine is illustrated in Fig. 1; the results for other solvents are similar. The aforementioned temperature dependences are in accord with those observed for copper(II) acetylacetonate (15, 18).

At a given temperature the value of $|a_0|$ in coordinating solvents is less than that observed in noncoordinating solvents, similar results have been obtained previously for square planar copper(II) complexes (12, 17, 19–21). Table 1 shows typical results for a_0 and g_0 at 300 K for the solvents used in this work. It may also be noted that a linear relationship exists between a_0 and g_0 as has been reported previously (3, 31).

The rotational correlation time can be related to the macroscopic viscosity by

$$[3]\quad \tau_R = \frac{V\eta}{kT}$$

where k is the Boltzman constant, T the absolute temperature, and V the effective volume of the solute usually equated to $4\pi r_0^3/3$ where r_0 is an effective radius of the solute. Kivelson and co-workers (22, 29, 30) have introduced the

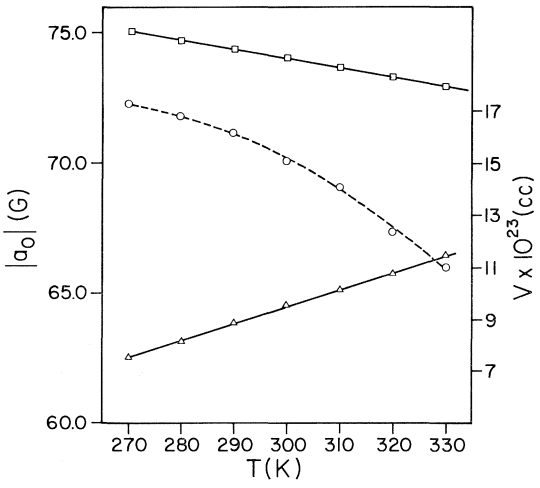

FIG. 1. Temperature variation of a_0 in benzene (solid line and squares), a_0 in pyridine (solid line and triangles), and effective volume V in benzene (dashed line).

TABLE 1. Physical constants of various solvents* and $Cu(DEDC)_2$ in these solvents

Solvent†	g_0	$\lvert a_0\rvert$ (G)	η (cp)	τ_R ($\times 10^{11}$ s)	V ($\times 10^{23}$ cm^3)	κ	μ (D)	R (cc/mol)
Benzene	2.0455	74.02	0.588	1.9	15.1	0.51	—	24.65
Toluene	2.0453	74.30	0.570	3.1	24.0	0.81	0.37	29.4
Chloroform	2.0467	74.70	0.525	2.5	22.1	0.74	1.20	20.75
Carbon tetrachloride	2.0421	78.18	0.88	3.4	17.0	0.57	—	26.8
Cyclohexane	2.0422	78.13	0.91	2.5	12.8	0.43	—	27.9
2,6-Lutidine	2.0422	77.72	—	—	—	~0.6	1.66	33.9
Pyridine	2.0551	64.55	0.845	4.7	22.9	0.77	2.33	24.1
2-Picoline	2.0467	73.02	0.840	4.1	20.4	0.69	1.93	28.8
3-Picoline	2.0557	63.92	0.937	5.8	25.4	0.86	2.54	28.8
4-Picoline	2.0577	62.58	1.05	6.3	24.9	0.84	2.75	29.9
3,4-Lutidine	2.0558	62.82	—	—	—	—	1.87	34.5

*η is the viscosity, τ_R the rotational correlation time, V the apparent molecular volume of $Cu(DEDC)_2$ in the solvent, μ the dipole moment, and R the molar refractivity.
†T = 300 K; solvent data from Chemical Rubber Handbook and/or International Critical Tables.

anisotropic interaction parameter, κ, which lies between zero and unity such that $V = 4\pi r_0^3\kappa/3$. Thus the further κ is from unity the more anisotropic is the potential in which the solute moves *i.e.* the further away from hard sphere interactions. It has been found that κ is independent of pressure, temperature, and density for the vanadyl acetonylacetonate system (22). The determination of the value of κ depends on a choice of r_0 so that the interpretation of relative values of κ is more important when discussing differences in solvent behavior.

In the present work we have adopted a procedure equivalent, but not identical, to that of Kivelson and co-workers (22). Initially we evaluate an effective volume V ($=\tau_R kT/\eta$) and then use a value of the molecular volume (V_m) from the crystallographic data (31) to obtain κ from V/V_m. As pointed out by Kivelson and co-workers (22), perhaps a better estimate of r_0 is obtained from translational diffusion coefficients; however, in the absence of these V_m is the next best thing. Kivelson and co-workers (22) obtain κ by least squares fitting eq. 2 together with $\tau_R = \frac{4}{3}(\pi r_0^3/k)(\eta/T)\kappa$ thus, apparently, constraining κ to be temperature independent. An alternative approach is to evaluate the effective volume (V) at each temperature in order to ascertain any possible temperature dependence, this was done in the present work.

As mentioned earlier Fig. 2 illustrates the linearity of γ with respect to η/T; in addition Fig. 2 also shows the correspondence between β_{obs} and β_{calc} for $Cu(DEDC)_2$ in toluene. The temperature dependence of V for $Cu(DEDC)_2$

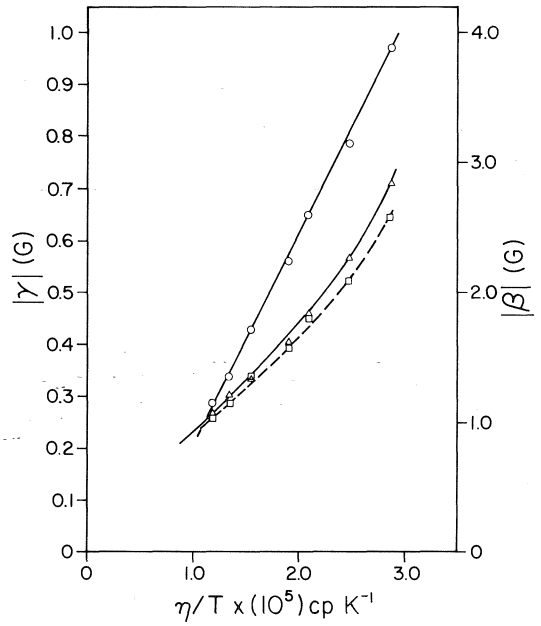

FIG. 2. The dependence of γ_{obs} (solid line and circles), β_{obs} (solid line and triangles), and β_{calc} (dashed line and squares) in toluene with η/T.

in benzene is shown in Fig. 1 (dashed line). In the case shown V decreased with increasing temperature, but in other solvents (*e.g.* chloroform, carbon tetrachloride) V increases, the percentage changes being roughly comparable. The most likely causes are; (*a*) the unknown temperature dependence of Δa and Δg which may be expected to be quite large (18); (*b*) changes in the solvation of the complex. The former uncertainty precludes any reliable interpretation of the temperature variation of V

Can. J. Chem. Downloaded from www.nrcresearchpress.com by 210.87.254.5 on 09/05/12
For personal use only.

Can. J. Chem. Downloaded from www.nrcresearchpress.com by 210.87.254.5 on 09/05/12
For personal use only.

in terms of the second cause noted above. The values of V (and hence κ) at 300 K may be regarded as reliable since Δa and Δg were obtained from the spin Hamiltonian parameters measured at room temperature by Weeks and Fackler (6) for $Cu(DEDC)_2$. The values of Δa and Δg for the adduct were obtained from spin Hamiltonian parameters deduced from a computer simulation of an e.p.r. spectrum of $^{63}Cu(DEDC)_2$ in pyridine at 77 K. The value of τ_R is then obtained from γ measured at 300 K. The correlation times for the various bases were used to obtain a value of V and hence κ (using the value of V_m for $Cu(DEDC)_2$). The linewidths measured in the coordinating solvents were also corrected for lifetime broadening due to the free complex CuL_2. The formation of CuL_2B is about 80% in neat base. Thus the κ values for CuL_2B in 3-, 4-picoline, and 3,4-lutidine should not be compared with the values for the other solvents and, in fact, the κ values should only be used to indicate relative changes for these coordinating solvents. The exception to this being 2-picoline where complexation is so small corrections were made for CuL_2B so that the results correspond to CuL_2 in 2-picoline. No complex formation is detectable in 2,6-lutidine (27). The results of these measurements and calculations are included in Table 1.

Discussion

The temperature dependence of e.p.r. spin Hamiltonian parameters has been observed on many occasions previously (15, 18, 24, 32). In the present work we have shown that a_0 increases with temperature in coordinating solvents and in noncoordinating solvents decreases with temperature. The trend observed for the latter solvents is similar to the temperature effects reported previously; *i.e.* a decrease in a_0 with increasing temperature (15, 18, 32). This variation has generally been ascribed, in the case of transition metal complexes, to vibronic effects leading to a reduced a_0 due to the population of higher vibronic states which possess smaller Fermi contact terms.

A quantitative description of the temperature induced changes in the isotropic hyperfine coupling of copper(II) bis(acetylacetonate) [$Cu(acac)_2$] was attempted by Falle and Luckhurst using the Boltzman average

$$[4] \qquad a_0 = \frac{a^0 + \sum_i a^i \exp(-\Delta E^i/kT)}{1 + \sum_i \exp(-\Delta E^i/kT)}$$

where a^0 is the splitting in the vibrational ground state, a^i that in the ith vibrational state, and ΔE^i is the energy difference between the ground and the ith state. Equation 4 predicts, for a small temperature range, a linear dependence of a_0 on temperature for low values of i. Falle and Luckhurst terminated the power series to one term and fitted the data for $Cu(acac)_2$ using $\Delta E^1 = 350\ cm^{-1}$ and $a^0 = 261$ Mc/s and $a^1 = 75$ Mc/s. Although the agreement between the experimental points and the theoretical curve was good Falle and Luckhurst felt that the large difference between a^0 and a^1 belied this simple interpretation *i.e.* the small nuclear displacements should induce only small changes in a^i with respect to a_0. The series should obviously include more terms.

The temperature dependence of a_0 can be explained in an alternative way using the work of McGarvey (13). In this interpretation, we make the assumption that as the temperature is increased the average Cu—S (or O) bond length in $Cu(DEDC)_2$ (or $Cu(acac)_2$) increases and we discuss the variation of a_0 in these terms. This is obviously equivalent to the ideas of Falle and Luckhurst but now focuses attention on the reason for the difference between a^0 and a^i.

The isotropic hyperfine coupling constant is given by

$$[5a] \qquad a_0 = -K + \Delta g_0 P$$

where

$$\Delta g_0 = g_0 - g_e$$

$$P = g_e g_N \beta_e \beta_N \langle r^{-3} \rangle = 388 \times 10^{-4}\ cm^{-1} \text{ for } ^{63}Cu$$

and

$$[5b] \qquad -K = \frac{2}{3}\left(\frac{g_e g_N \beta_e \beta_N}{hca_0^3}\right)\chi$$

where

$$\chi = \frac{4\pi}{3}\langle \Psi | \sum_i \delta(r_i)\hat{S}_{zi} | \Psi \rangle$$

The spin density χ can be expressed in terms of core polarization of the inner s orbitals (ns; $n = 1$, 2, or 3) of the Cu^{2+} ion by the outer d positive hole by configuration mixing of the outer s orbitals (ms; m = 5, 6, ... , ∞) as follows

$$[6]\quad \chi = 8\pi\alpha^2\Big\{\delta^2 \sum_{n=1}^{3} [ns(0)4s(0)]J(4s3d3d4s)/(E_{\psi^*} - E_{\psi}) + \sum_{n=1}^{3}\sum_{m=5}^{\infty} [ns(0)ms(0)]J(ms3d3dns)/(E_m - E_n) + (\gamma')^2 \sum_{m=5}^{\infty} [4s(0)ms(0)]J(ms3d3d4s)/(E_m - E_{\psi})\Big\} + 8\pi[4s(0)4s(0)]\{(\gamma')^2\delta^2\alpha^2 J(4s3d3d4s) - \tfrac{1}{4}\gamma\gamma'\delta\delta'(\alpha')^2 J(p_x p_x p_x p_x)\}/(E_{\psi^*} - E_{\psi})$$

where we have employed the m.o.'s

$$\sigma = \alpha d_{x^2-y^2} - \alpha'\phi_L(x^2 - y^2)$$
$$\pi = \beta d_{xy} - \beta'\phi_L(xy)$$
$$\pi_1 = \varepsilon d_{xz,yz} - \varepsilon'\phi_L(xz,yz)$$
$$\psi = \gamma' 4s + \gamma\phi_L(s)$$
$$\psi^* = \delta 4s - \delta'\phi_L(s)$$

where ϕ_L denotes a symmetry adapted linear combination of ligand p orbitals, thus for example $\phi_L(s) = \frac{1}{2}(-p_x{}^1 - p_y{}^2 + p_x{}^3 + p_y{}^4)$, for a square planar complex with the x and y directions along the Cu—S directions. It will be noted that in this formulation allowance has been made for the participation of the copper 4s orbital in the bonding of the complex.

In order to discuss the temperature dependence of a_0 we first note that Δg_0 for $Cu(DEDC)_2$ in the solvents studied here is largely insensitive to temperature variation and we shall assume that the same is true for P, *i.e.* the temperature dependence of a_0 is due only (or mainly) to variations in K. We turn now to a description of the terms in χ. The first two terms in eq. 6 represent the polarization of the inner s orbitals by the positive hole by mixing in of the outer s orbitals, the effective mixing of the 4s orbital being reduced by δ^2 due to participation in bonding. The overall effect of this polarization is to produce a negative term, in fact the negative 2s contribution dominates the positive 3s contribution (13, 33). The third term is the polarization of the inner σ orbital involving the copper 4s orbital (4) and this term will likely be small and positive for free copper (33, 34). The final term represents the polarization of the orbital ψ by configuration interaction with ψ^*. As pointed out by McGarvey (13) this term can be quite important since $E_{\psi^*} - E_{\psi}$ can be quite small and $J(p_x p_x p_x p_x) > J(4s3d3d4s)$ so that an additional negative contribution to χ can occur if, for example, covalency effects were to increase.

If we make the assumption that an increase in temperature increases the Cu—S bond lengths then we would expect the m.o. coefficients of the metal orbitals to approach unity, *i.e.* covalency decreases. A consideration of eq. 6 shows that such an effect would cause a decrease in χ. The main reason for this being the rapid decrease of the term involving $J(p_x p_x p_x p_x)$ because of its dependence on $(\alpha')^2$ which should rapidly approach zero as $\alpha \to 1$. The first two terms in eq. 6 are likely to remain essentially constant whereas the third and fourth terms are small. The reduction of χ by increased in-plane bond lengths is exactly analogous to the decrease in χ due to ligand addition along the z-axis (13).

The increase of a_0 for $Cu(DEDC)_2$ in coordinating solvents as the temperature is increased is due to two effects: (*a*) the reduction of the equilibrium constant (K) for the exothermic fast Lewis acid–base equilibrium mentioned earlier (19–21, 28). The average isotropic hyperfine coupling being given by

$$[7]\quad \langle a_0\rangle = \frac{1}{1 + T_B K} a_0{}^{CuL_2} + \frac{KT_B}{1 + T_B K} a_0{}^{CuL_2B}$$

where T_B is the concentration of base and the hyperfine coupling of the free complex ($a_0{}^{CuL_2}$) is greater than that of the adduct ($a_0{}^{CuL_2B}$) for the reason mentioned earlier; (*b*) the effect of minimized axial interactions due to the larger copper–base bond length at higher temperatures. The latter effect would lead to a gradual increase in the absolute value of χ and hence $a_0{}^{CuL_2B}$. Such an effect has been observed (21) for the values of $a_0{}^{CuL_2B}$ obtained from a least-squares fit of eq. 7. The lengthy extrapolation to $T_B \geqslant 100\,M$ from the experimentally-attained $T_B \approx 10$–$12\,M$ renders these results somewhat tenuous but the effect is readily discernible.

Can. J. Chem. Downloaded from www.nrcresearchpress.com by 210.87.254.5 on 09/05/12
For personal use only.

Can. J. Chem. Downloaded from www.nrcresearchpress.com by 210.87.254.5 on 09/05/12
For personal use only.

In conclusion then we may say that in non-coordinating solvents the decrease in a_0 is due to vibronic effects in the copper complex itself and not to axial coordination effects, whereas in coordinating solvents the temperature dependence is due to axial ligation effects. Thus the temperature variation of a_0 is of minimal use in divining solvent effects. That there is a linear relationship between a_0 and g_0 for $Cu(DEDC)_2$ in all the solvents studied here was pointed out previously. The existence of such a relationship we feel is evidence in support of the above formulation of χ (eq. 6). The variation of Δg_0 depends upon, in the main, the excitations $E_{xy} \rightarrow E_{x^2-y^2}$ and $E_{xz,yz} \rightarrow E_{x^2-y^2}$ and the variation of χ upon $E_\psi \rightarrow E_{\psi^*}$ if the above model is to be believed. It is not unreasonable that $E_\psi \rightarrow E_{\psi^*}$ will mimic the variation of $E_{xy} \rightarrow E_{x^2-y^2}$ and $E_{xz,yz} \rightarrow E_{x^2-y^2}$ so that a linear dependence between a_0 and Δg_0 can be expected (35).

We turn now to the variation of a_0 and g_0 from solvent to solvent. Previously we have noted that it is possible to obtain what may be called "solvent interaction free" (s.i.f.) isotropic hyperfine coupling constants from the measurement of a_0 of $Cu(DEDC)_2$ in, for example, a benzene/pyridine mixture. This is achieved by extrapolating the plot of a_0 *vs.* T_B to zero base strength. We have found that the a_0 obtained is independent of the coordinating or non-coordinating solvent and is truly solvent independent to within experimental error. Furthermore, the value of the isotropic hyperfine coupling constant for $Cu(DEDC)_2$ diluted in the corresponding Ni(II) complex is -82.8 ± 1.5 G whereas the s.i.f. value is -78.7 ± 0.15 G so that it is felt that these parameters truly represent the isotropic hyperfine coupling constant in the absence of specific solvent interactions. The fact that the s.i.f. parameter is less than that observed in the Ni(II) complex presumably reflects the fact that the s.i.f. parameter is only approximately representative of true solvent inertness.

The a_0 values for $Cu(DEDC)_2$ measured in benzene, toluene, and chloroform, shown in Table 1, indicate that these three solvents interact with the complex in a roughly comparable way. The reduction of a_0 in these solvents relative to the s.i.f. value is indicative of axial interactions (at the vacant coordination site) (11) which, as indicated previously (13), can lead to reduction in the absolute value of a_0. These interactions may be of the type described by Antosik *et al.* (11) but it is difficult to provide any well-defined interpretation. The above considerations suggest that carbon tetrachloride, cyclohexane, and 2,6-lutidine are relatively inert solvents as far as axial interactions are concerned.

An alternative explanation of the variation is to suggest that the solvation sphere around the complex decreases, leading to increased values of a_0 because of reduced interactions. Some evidence for this suggestion can be found in the correlation of a_0 with R, the molar refractivity. The molar refraction is a measure of molecular volume. Thus, as R increases we may expect a_0 to increase and this is seen to be generally true. An exception is toluene, in which a direct axial interaction due to the presence of a dipole moment could lead to a reduced a_0. The large reduction in a_0 for the pyridines again demonstrates the sensitivity of the hyperfine coupling tensor to strong axial interactions. The results in Table 1 show that the g-value of $Cu(DEDC)_2$ increases as a_0 decreases which reflects the general reduction of the d_{xy} to $d_{x^2-y^2}$ and d_{xz}, d_{yz} excitations as axial interactions increase.

The above solvent dependence of a_0 and g_0 is in accord with the results of other workers (11–17). In general, it may be stated that the variation of a_0 from solvent to solvent is a fairly insensitive measure of solute–solvent interactions and at best only leads to qualitative conclusions as to whether or not specific axial interactions are important in a particular solvent. The main reason for this is the difficulty in interpreting the Fermi contact contribution to the hyperfine coupling. The anisotropic hyperfine and g-tensors are no doubt more sensitive (9, 16).

A convenient indicator of solute–solvent interactions is the rotational correlation time of a molecule in a given solvent. As indicated earlier, e.p.r. provides a method for measuring such rotational correlation times. The rotational correlation times shown in Table 1 demonstrate that the addition of a pyridine molecule to form the adduct CuL_2B leads to somewhat slower rotational correlation times. In order to proceed further with the interpretation of the τ_R values it is necessary to adopt a model of the liquid state.

Can. J. Chem. Downloaded from www.nrcresearchpress.com by 210.87.254.5 on 09/05/12
For personal use only.

The simplest model is that embodied in eq. 3, where the solvent is assumed to provide a continuous medium for the rotation of a molecule of volume V. The apparent volume V can then be interpreted in terms of solvation effects. The results in Table 1 show that for these molecules in which we expect for low solvation, *i.e.* solvents with no dipole moment, V is small (*i.e.* benzene, carbon tetrachloride, and cyclohexane), whereas for those solvents possessing dipole moments V is large. Thus at first sight this interpretation is qualitatively reasonable. However, if the apparent volumes are compared with any reasonable estimate of the solute volume, V_m, we find that invariably $V < V_m$. This result is not in accord with the simple idea of solvation since it might well be expected that $V > V_m$ in this case. As mentioned previously, Kivelson and co-workers (22, 23) have introduced the so-called anisotropic interaction parameter, κ, to account for $V_m > V$; *i.e.* $V = \kappa V_m$. Kivelson and co-workers (29, 30) have devised a theory which shows that κ can be expressed as the ratio of the mean square torques to the mean square forces experienced by the spin-probe:

$$\kappa \sim (\tfrac{3}{4}r_0^2)\langle \text{Torques}^2\rangle/\langle \text{Forces}^2\rangle$$

The value of κ is interpreted as follows: $\kappa \to 0$ for hard spheres (where intermolecular torques are expected to vanish) and $\kappa \to 1$ for very anisotropic intermolecular potentials.

The results shown in Table 1 indicate that those solvents possessing a dipole moment provide highly anisotropic intermolecular potentials and torques for $Cu(DEDC)_2$, whereas those solvents with no dipole moment produce small values of κ. This result is in accord with the findings of Kivelson and co-workers (22) for $VO(acac)_2$. The other correlation apparent from Table 1 is that as the molar refraction (R) decreases, κ increases; *i.e.* as the volume in the solvent increases the intermolecular potential becomes more isotropic (22). The major exception to this trend is again the result for toluene where, even though R is large, κ is 0.81. This result, as indicated earlier in regard to the variation of a_0, indicates that toluene must be interacting in a rather specific way with $Cu(DEDC)_2$. The reduction of κ as R increases is also in rough correlation with the variation of a_0 with R, although the precise significance of the dual correlation is not clear. It is also important to note that the present κ values agree qualitatively with the theory of Wirtz and co-workers (36) in which

$$[8] \qquad \kappa = [6(r_s/r_0) + (1 + r_s/r_0)^{-3}]^{-1}$$

where r_0 is the solute and r_s the solvent molecular radius. If r_0 is set equal to $(3V_m/4)^{1/3}$ and $r_s = (3R/4)^{1/3}$, where R is the molar refraction, eq. 8 yields κ-values that are too small but decrease as do the experimental values when R increases. A similar conclusion was reached by Kivelson and co-workers (22).

The following conclusions can be reached: (*a*) the present study has shown that the temperature and solvent variation of a_0 and g_0 are at best qualitative indicators of solute–solvent interactions; (*b*) studies of rotational correlation times in coordinating solvents can be complicated by the presence of fast Lewis acid–base reactions and a lack of knowledge of the anisotropies of the spin Hamiltonian parameters; and (*c*) in noncoordinating solvents the results for κ obtained for $Cu(DEDC)_2$ are comparable to those obtained for $VO(acac)_2$, but the present work must be extended to establish the validity of this conclusion.

The National Research Council of Canada is thanked for its financial support of this work.

1. A. H. Maki and B. R. McGarvey. J. Chem. Phys. **29**, 31 (1958).
2. A. H. Maki and B. R. McGarvey. J. Chem. Phys. **29**, 35 (1958).
3. H. A. Kuska and M. T. Rogers. J. Chem. Phys. **43**, 1744 (1965).
4. H. A. Kuska, M. T. Rogers, and R. E. Drullinger. J. Phys. Chem. **71**, 109 (1967).
5. A. D. Toy, S. H. H. Chasteen, J. R. Pilbrow, and T. D. Smith. Inorg. Chem. **10**, 2219 (1971).
6. M. J Weeks and J. P. Fackler. Inorg. Chem. **7**, 2548 (1968).
7. E. Buluggia and A. Vera. J. Chem. Phys. **59**, 2886 (1973).
8. T. Chiang. J. Chem. Phys. **48**, 1814 (1968).
9. J. Ammeter, G. Rist, and Hs. H. Günthard. J. Chem. Phys. **57**, 3852 (1972).
10. K. Falk, E. Ivanora, B. Roos, and T. Vanngard. Inorg. Chem. **9**, 556 (1969).
11. S. Antosik, N. M. D. Brown, A. A. McConnell, and A. L. Parte. J. Chem. Soc. A, 545 (1969).
12. B. R. Libutti, B. B. Wayland, and A. F. Garito. Inorg. Chem. **8**, 1510 (1969).
13. B. R. McGarvey. J. Phys. Chem. **71**, 51 (1967).
14. J. I. Zink and R. S. Drago. J. Am. Chem. Soc. **94**, 4550 (1972).
15. H. R. Falle and G. R. Luckhurst. Mol. Phys. **10**, 597 (1966).

16. I. ADATO and I. ELIEZER. J. Chem Phys. **54**, 1472 (1971).
17. A. E. LUTSKII, N. M. KOLEKVSKII, O. A. OSIPOV, and Z. I. ZUMAREV. Theor. Exp. Chem. **4**, 463 (1968).
18. R. WILSON and D. KIVELSON. J. Chem. Phys. **44**, 4445 (1966).
19. (*a*) V. F. ANUFRIENKO and A. A. SHKLYAEV. Dokl. Akad. Nauk. SSSR, **191**, 107 (1970); (*b*) V. F. ANUFRIENKO and A. A. SHKLYAEV. Dokl. Akad. Nauk. SSSR, **196**, 884 (1971); (*c*) E. I. BERUS, V. F. ANUFRIENKO, Y. N. MOLIN, and A. A. SHKLYAEV. Dokl. Akad. Nauk. SSSR, **200**, 1129 (1971); (*d*) A. A. SHKLYAEV and V. F. ANUFRIENKO. Dokl. Akad. Nauk. SSSR, **201**, 1154 (1971); (*e*) A. A. SHKLYAEV, V. F. ANUFRIENKO, E. I. BERUS, and Y. N. MOLIN. Dokl. Akad. Nauk. SSSR, **207**, 138 (1972); (*f*) A. A. SHKLYAEV and V. F. ANUFRIENKO. Zhur. Strukt. Khim. **12**, 601 (1971); (*g*) A. A. SHKLYAEV, F. M. GUMEROV, and V. F. ANUFRIENKO. Zhur. Strukt. Khim. **13**, 406 (1972).
20. B. J. CORDEN and P. H. RIEGER. Inorg. Chem. **10**, 263 (1971).
21. J. B. FARMER, F. G. HERRING, and R. L. TAPPING. Can. J. Chem. **50**, 2079 (1972).
22. J. HWANG, D. KIVELSON, and W. PLACHY. J. Chem. Phys. **58**, 1753 (1973) and references therein.
23. R. HUANG and D. KIVELSON. Pure Appl. Chem. **32**, 207 (1972).
24. G. R. LUCKHURST and J. N. OCKWELL. Mol. Phys. **16**, 165 (1969).
25. N. S. ANGERMAN and R. B. JORDAN. J. Chem. Phys. **54**, 837 (1971).
26. N. D. CHASTEEN and M. W. HANNA. J. Phys. Chem. **76**, 3951 (1972).
27. F. G. HERRING and R. L. TAPPING. J. Phys. Chem. **78**, 316 (1974).
28. J. B. FARMER, F. G. HERRING, and R. L. TAPPING. Can. J. Chem. **51**, 1530 (1973).
29. R. MCCLUNG and D. KIVELSON. J. Chem. Phys. **49**, 3380 (1968).
30. D. KIVELSON, M. G. KIVELSON, and I. OPPENHEIM. J. Chem. Phys. **52**, 1810 (1970).
31. C. M. GUZY, J. B. RAYNOR, and M. C. R. SYMONS. J. Chem. Soc. A, 2791 (1969).
32. (*a*) J. S. VAN WIERINGEN and J. G. RENSEN. Phillips Res. Rep. **20**, 659 (1965); (*b*) F. HOLUJ, S. M. QUICK, and M. ROSEN. Phys. Rev. B**6**, 3169 (1972); (*c*) A. H. REDDOCH, C. L. DODSON, and D. H. PASKOVICH. J. Chem. Phys. **52**, 2318 (1970); (*d*) R. E. MOSS. Mol. Phys. **10**, 339 (1966).
33. A. J. FREEMAN and R. E. WATSON. Phys. Rev. **123**, 2027 (1961).
34. A. J. FREEMAN and R. E. WATSON. *In* Hyperfine interactions. *Edited by* A. J. Freeman and R. B. Frankel. Academic Press, 1967. p. 53.
35. L. J. BOUCHER, E. C. TYNAN, and T. F. YEN. *In* Electron spin resonance of metal complexes. *Edited by* T. F. Yen. Plenum, 1969.
36. A. SPERNOL and K. WIRTZ. Z. Naturforsch. **8**a, 522 (1953); T. GIERER and K. WIRTZ. Z. Naturforsch. **8**a, 532 (1953).

Can. J. Chem. Downloaded from www.nrcresearchpress.com by 210.87.254.5 on 09/05/12
For personal use only.

Thermolysis of Some 4-Alkylidene-1-pyrazolines

ROBERT J. CRAWFORD, DOUGLAS M. CAMERON, AND HIROKAZU TOKUNAGA

Department of Chemistry, University of Alberta, Edmonton, Alberta T6G 2G2

Received May 27, 1974

ROBERT J. CRAWFORD, DOUGLAS M. CAMERON, and HIROKAZU TOKUNAGA. Can. J. Chem. **52**, 4025 (1974).

The thermolysis of 4-methylene-1-pyrazoline and the kinetic isotope effects of 3,3-d_2, 3,3,6,6-d_4, and 3,3,5,5,6,6-d_6 compounds were examined. Data suggest a simultaneous cleavage of both carbon–nitrogen bonds with the formation of an intermediate which by ^{13}C labelling is shown to be other than the triplet planar trimethylenemethane. Product studies on 3,3-dimethyl-4-methylene-1-pyrazoline and 4-isopropylidene-1-pyrazoline are best rationalized in terms of the Chesick type intermediate.

ROBERT J. CRAWFORD, DOUGLAS M. CAMERON et HIROKAZU TOKUNAGA. Can. J. Chem. **52**, 4025 (1974).

La thermolyse de la méthylene-4-pyrazoline-1 et les effets isotopiques des composés 3,3-d_2, 3,3,6,6-d_4 et 3,3,5,5,6,6-d_6 ont été examinés. Les résultats suggerent une rupture simultanée des deux liaisons carbone–azote avec formation d'un intermédiaire qui, par marquage au ^{13}C, s'averé être différent du triméthyleneméthane plan à l'état triplet. Les produits de la diméthyl-3,3-méthylene-4-pyrazoline-1 et de l'isopropylidene-4-pyrazoline sont interprétés au mieux avec un intermédiaire du type Chesick.

Introduction

The thermolysis of azoalkanes is a convenient and frequently used method of generating radicals. Can the thermolysis of 4-methylene-1-pyrazoline (1) be used to generate trimethylenemethane? In this, and the succeeding paper, we have undertaken a kinetic and product study in an attempt to define the nature of the initial thermolysis step and the existence of any intermediates in this reaction.

Dowd (2) has by electron spin resonance spectroscopy demonstrated that the photolysis of **1** generates a triplet of geometry **2**. An alternative geometry for trimethylenemethane is that of **3** which Chesick (3) has suggested as an intermediate in the interconversion of 2-methylmethylenecyclopropane and ethylidenecyclopropane. This same Chesick type of intermediate has been invoked in the majority of mechanistic studies of methylenecyclopropane (4) and is a possibility in the thermolysis of **1**.

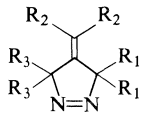

1

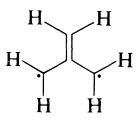

2

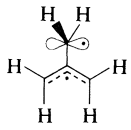

3

1*a* $R_1 = R_2 = R_3 = H$
1-d_2 $R_1 = D; R_2 = R_3 = H$
1-d_4 $R_1 = R_2 = D; R_3 = H$
1-d_6 $R_1 = R_2 = R_3 = D$

Results and Discussion

Table 1 lists the kinetic data for the thermolysis of 4-methylene-1-pyrazoline (**1***a*). The activation energy, 32.6 ± 0.3 kcal mol^{-1}, may be compared with that of 1-pyrazoline (5), 42.4 ± 0.3 kcal mol^{-1}, and 3-vinyl-1-pyrazoline (6) of 32.2 ± 0.4 kcal mol^{-1}. The latter represents the stabilization of the diradical-like transition state[1] by the allylic resonance energy and clearly the thermolysis of **1**, reacting at a rate 140 times greater than that of 1-pyrazoline, is being accelerated by a comparable stabilization.

In order to establish the relationship of the carbon–nitrogen bond ruptures we have examined the deuterated substrates **1**-d_2, **1**-d_4, and **1**-d_6. The rate constants for the thermolysis of **1***a* used in Table 2 were interpolated from a graphical plot of $\log k$ *vs.* $1/T$ of the data from Table 1. The corrections for incomplete deuteration are given in Table 2 and represent analyses obtained by multiple determination of n.m.r. integrations on neat samples of the deuterated compounds. A control run of a sample of **1**-d_4 carried to 50% completion then reisolated indicated that there was no observable increase of protons at the vinylic position. We estimate that

[1]The definitions of diradicals, putative diradicals, etc. are extensive; however, we refer the reader to an excellent discussion of these concepts by G. Jones II in ref. 29, and will use the term diradical in the sense described therein.

Can. J. Chem. Downloaded from www.nrcresearchpress.com by 210.87.254.105 on 09/05/12
For personal use only.

TABLE 1. Kinetics for the thermolysis of 4-methylene-1-pyrazoline (**1***a*)

Experiment No.	Temperature (°C)	10^4k (s^{-1})	Activation parameters
1	165.3	9.84±0.09	$E_a = 32.6 \pm 0.3$ kcal mol^{-1}
2	170.3	15.0 ±0.1	$\log A = 13.24 \pm 0.15$
3	176.5	25.0 ±0.2	
			$\Delta S^{\ddagger} = -1.1 \pm 0.5$e.u.
4	184.9	49.4 ±0.5	
5	187.9	61.7 ±0.6	

TABLE 2. Secondary deuterium kinetic isotope effects for the thermolysis of deuterated 4-methylene-1-pyrazolines

Temperature (°C)	Compound	$10^4 k_{obs}$ (s^{-1})	$10^4 k_{corr}$[a] (s^{-1})	k_H/k_D
167.75	**1**-d_2	9.9 ± 0.2	9.7 ± 0.2	1.26 ± 0.03
	1*a*	12.2 ± 0.1[b]		
169.0	**1**-d_4	10.6 ± 0.2	10.5 ± 0.2	1.30 ± 0.03
	1*a*	13.6 ± 0.1[b]		
172.9	**1**-d_6	11.9 ± 0.2	11.7 ± 0.2	1.60 ± 0.04
	1*a*	18.7 ± 0.2[b]		

[a]Corrected for incomplete deuteration $k_D = (k_{obs} - k_H f_H)/f_D$ where f_D is the fraction deuterated (n.m.r.).
[b]Obtained by extrapolation from data in Table 1.

2% rearrangement would have been detected and thus we can rule out the formation of any pretransition state intermediate such as the allylic azo intermediate **4**. Seltzer *et al.* (7) have

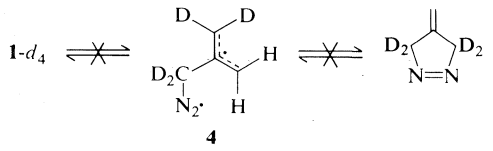

4

demonstrated that the substitution of a deuterium, α to the azo nitrogen that is undergoing valence change in the rate determining transition state, leads to an increase in activation free energy, $\delta\Delta G^{\ddagger}$, of 90–120 cal mol^{-1} per deuterium. For **1**-d_2 we see that $\delta\Delta G^{\ddagger}$ per α deuterium is 101 ± 6 cal mol^{-1} and if **1**-d_4 represents the effect of the α-deuterium plus two γ-deuteriums then the two γ-deuteriums contributed an increase of 27 cal mol^{-1}. Using this correction we can then calculate the effect of the four α-deuteriums in **1**-d_6 as being 97 ± 3 cal mol^{-1} per deuterium. These results are in accord with a transition state wherein both carbon–nitrogen bonds have undergone considerable bond breaking (8). When the methylenecyclopropane generated from the thermolysis of **1**-d_2 is analyzed by n.m.r. it is found that the product consists of a 60:40 mixture of **5***a*:**5***b*. Thus while no

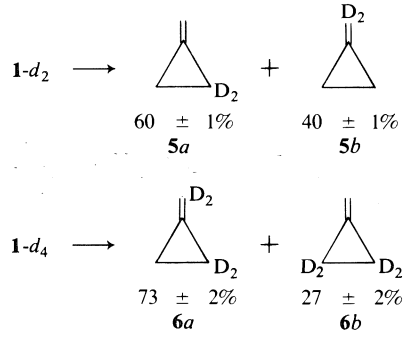

deuterium is scrambled prior to the breaking of the carbon–nitrogen bonds it is obvious that the *exo* and ring methylenes are scrambled, and to an extent that approaches the statistical 2:1 expected for **5***a*:**5***b*. If from **1**-d_2 an intermediate, or a set of intermediates, of composition equivalent to $(CH_2)_2CCD_2$ is produced then there are two possible modes by which **5***a* can be produced, $2k_H$, where k_H represents the rate constant for the conversion of the protiomethylene group to the *exo*-methylene as in **5***a*, and one by which the deuteriomethylene group may be transformed, k_D. Thus k_H/k_D in the product determining step is 0.75 ± 0.03 suggesting a preference on the part of the protium for the ring methylene position of methylenecyclopropane. It follows, by analogy, that for

Can. J. Chem. Downloaded from www.nrcresearchpress.com by 210.87.254.105 on 09/05/12
For personal use only.

TABLE 3. The proton n.m.r. integration of the ^{13}C side bonds of **8***a* and **8***b* from the thermolysis of **7** (1 h at 165°)

Pressure (Torr)	R_{obs}	%**8***a*	%**8***b*
450	1.76 ± 0.04[a]	63.7 ± 0.5	36.3 ± 0.5
250	1.75 ± 0.04	63.6 ± 0.5	36.4 ± 0.5
250	1.82 ± 0.04	64.5 ± 0.6	35.5 ± 0.5

[a]Standard deviation of eight or more analyses of each sample.

1-d_4 we could expect an intermediate, or set of intermediates, of composition $CH_2C(CD_2)_2$ to be produced and that the ratio **6***a*:**6***b* can be represented by $2k_D/k_H$ from which a value[2] of $k_H/k_D = 0.74 \pm 0.07$ is obtained. The similarity of these results, besides the possibility of their being fortuitous, suggests that there is an isotope effect in the product determining step and implies that the three methylene groups have either become equivalent as in **2** or have become radomized in a set of intermediates equivalent to **3**. An alternative explanation is that **1**-d_2 and **1**-d_4 give rise to **5***a* and **6***a* in a concerted process and that in the gas phase the methylenecyclopropanes produced are "hot" and undergo subsequent isomerizations; such a possibility is diminished by observation that the same product ratios are obtained in solution as in the gas phase. Equilibration of a sample of **5***a* prepared by the copper-catalyzed decomposition of diazomethane-d_2 in the presence of allene was unchanged after 3 h at 180° and upon heating for 2 h at 250° the n.m.r. spectrum indicated an equilibrium mixture of 67.6 ± 1.1% of **5***a* and 32.4 ± 1.1% **5***b*. This further complicates the "hot species" argument in that if **5***a* were the initially generated species the system would appear to have gone past the equilibrium mixture. A further possibility is that the methylene groups were equivalent by interconversion of intermediates, such as **3**, and that it is a "ponderal effect"[3] which determines just which groups rotate to form the ring methylenes; in this case the deuterium, being of greater mass, is slower to move out of the plane than is protium. Labelling the carbon atom, thus changing the mass on the rotational axis, should remove any "ponderal effect", thus we prepared a sample of **7** from 67% enriched ^{13}C-diazomethane. The ratio, *R*, of **8***a* to **8***b* was determined by integrating the proton n.m.r. of the ^{13}C—H side bands at δ 0.5 and 2.1 ($J_{^{13}C-H}$ = 161 Hz) located on both sides of the ^{12}CH ring methylene protons at δ 1.3 and dividing by the ^{13}C—H side bands at δ 4.8 and 6.4 ($J_{^{13}C-H}$ = 162 Hz) on both sides of the ^{12}C—H vinylic protons at δ 5.6. The data in Table 3, assuming for complete randomization of the natural abundance ^{13}C in the allene, were obtained under conditions that did not give rise to any proton saturation as evidenced by a control sample of methylenecyclopropane which gave a value of $R = 2.01 \pm 0.03$. At the 95% confidence limit, applying the *t*-test, we can conclude that the data is different from that expected on a statistically random basis of 2.00 for *R*.

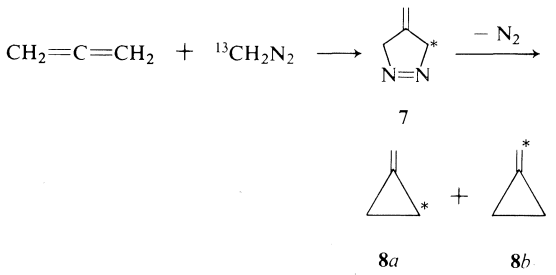

It is of interest to note that the ^{13}C—H coupling constant of both the ring methylene and the vinylic methylene group correspond to sp^2 hybridization (12).

The results for **1**-d_2, **1**-d_4, and **7** imply that the original position of the methylene group may in fact impart a bias as to where that group ends up in methylenecyclopropane and since these results cannot be readily reconciled with a mechanism producing intermediates such as **2** or **3** we decided to examine products derived from the isomeric pair of pyrazolines **9** and **10**. A synthesis of 3,3-dimethyl-4-methylene-1-pyrazoline (**9**) was achieved by the 1,3-dipolar cyclo-

[2]If k_H and k_D are defined as the rate constant for forming the ring methylene then the values are 1.33 and 1.35 for **1**-d_2 and **1**-d_4 (1).

[3]A ponderal entropy effect upon a rotor has been predicted (9) and qualitative agreement with intramolecular cyclizations *vs.* rotations in 1,3- and 1,4-diradicals have been observed (10, 11).

Can. J. Chem. Downloaded from www.nrcresearchpress.com by 210.87.254.105 on 09/05/12
For personal use only.

TABLE 4. Thermolysis products of **9** and **10** at various temperatures (P_0 = 400 Torr)

Temperature (°C)	Compound	%**13**[a]	%**14**
160.1 ± 0.1	**9**	82.1 ± 0.3	17.9 ± 0.3
	10	63.2 ± 0.2	36.8 ± 0.2
190.8 ± 0.1	**9**	81.2 ± 0.3	18.8 ± 0.3
	10	62.2 ± 0.3	37.8 ± 0.3
200.4 ± 0.1	**9**	81.0 ± 0.5	19.0 ± 0.5
	10	62.6 ± 0.4	37.4 ± 0.4

[a]Product proportions quoted are those obtained by extrapolating to zero conversion since **13** and **14** are slowly interconverting at the higher temperatures.

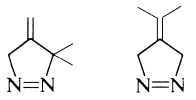

9 **10**

addition of 2-diazopropane to allene. An isomeric cycloaddition product (**11**) was produced and separation of **9** from this impurity and acetone azine (**12**) was difficult. It proved to be more convenient to use the product mixture of **9**, **11**, and **12**. Since **12** was demonstrated to be

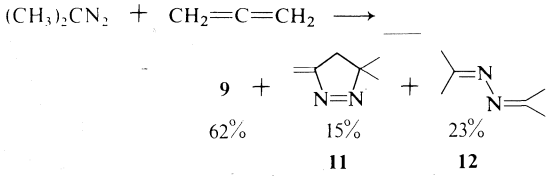

62% 15% 23%

11 **12**

stable under the thermolysis conditions it was used as an internal reference in the gas chromatographic (g.c.) analysis. The ratio of **11**:**12** remained constant throughout all of the thermolysis studies below 210°. Upon heating the mixture for 2 h at 200° **11** and **12** were chromatographically separated from **13** and **14**. The structure **11** was assigned on the basis of its exact mass, its n.m.r. spectrum (see Experimental), and upon its conversion to **13** and **14** when degassed samples of **11** and **12** were heated for 2 h at 250°.

During the thermolysis studies of **9** the ratio of 2,2-dimethylmethylenecyclopropane (**13**) and isopropylidenecyclopropane (**14**) varied slightly over the course of the reaction, since **13** and **14** are slowly equilibrating under the reaction conditions (13). The values obtained by extrapolation to zero time are given in Table 4. The product distribution appears to be essentially independent of temperature. Extrapolation from equilibrium data at higher temperatures (13) suggests that at 190.8° the thermodynamic proportions are 20.1% **13** and 79.9% **14**.

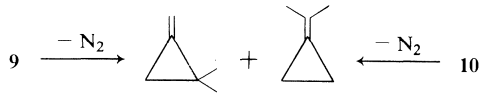

13 **14**

Attempts to synthesize 4-isopropylidene-1-pyrazoline (**10**) by the cycloaddition of diazomethane to 3-methyl-1,2-butadiene resulted primarily in the production of an isomeric compound whose spectral and analytical properties

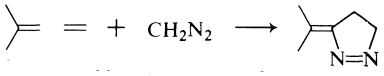

corresponded with those expected for 3-isopropylidene-1-pyrazoline. A synthesis of **10** was achieved via the dibromide **15**. The product

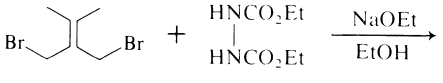

15

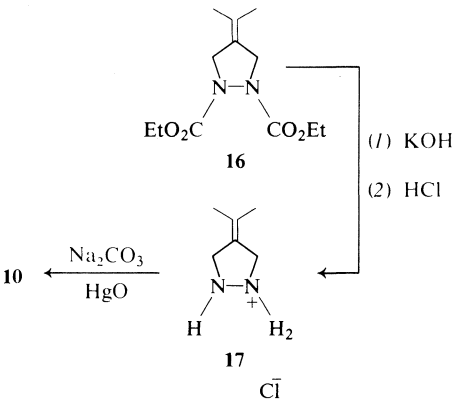

16 **17**

Can. J. Chem. Downloaded from www.nrcresearchpress.com by 210.87.254.105 on 09/05/12
For personal use only.

Can. J. Chem. Downloaded from www.nrcresearchpress.com by 210.87.254.105 on 09/05/12
For personal use only.

proved to be far more sensitive to tautomerism than any of the previously mentioned 4-alkylidene-1-pyrazolines and had to be handled with extreme care. A control run with **9** and **10** demonstrated that they were not interconverting under the reaction conditions. The low conversion yields of **13** and **14** from **10** are also given in Table 4. It is obvious from these results that the thermolysis data for **9** and **10** cannot be explained by a common intermediate and thus a planar trimethylenemethane intermediate analogous to **2** can be ruled out, and that the point of origin of a group is important. Attractive possibilities are the singlet intermediates **18** and **19**. Least

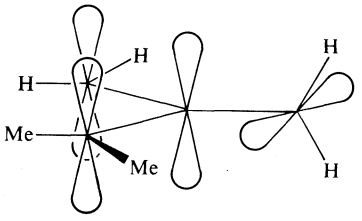

18

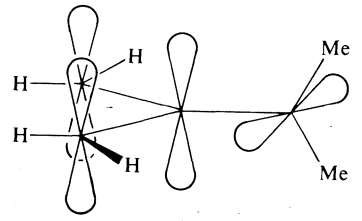

19

motion principles (14) would suggest that **18** is the intermediate produced upon thermolysis of **10**. Rotation of the isopropylidene group of **18** produces **13** whereas rotation about the allylic methylene group gives rise to **14**. Thermolysis of **9** would be expected to give rise to **19** as well as **18**. Rotation of either allylic methylene group in **19** would give rise exclusively to **13**. The product proportions can be rationalized if the rotation of the isopropylidene group of **18** is favored 63:37 over that of the methylene group.[4] Thus **19** leads exclusively to **13**, and **14** is only produced from **18**. Scheme 1 illustrates this pattern and if such is the case then the product proportions from **9**

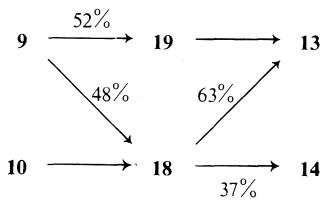

SCHEME 1

require that **18** and **19** be produced in the proportions 48:52.

We were unable to measure accurately the rates of thermolysis of **9** and **10** but found that at 160.07° that samples had undergone 53 and 55% conversion, implying a rate constant of $2.1 \times 10^{-4}\ s^{-1}$ and $2.3 \times 10^{-4}\ s^{-1}$, respectively. This places the methylated pyrazolines **9** and **10** at about one-third the rate of **1***a*, a rather unexpected observation and we are currently examining systems wherein tautomerism cannot interfere.

The application of Scheme 1 in an analogous manner to the pyrazoline **1**-d_4 suggests a 75:25 mixture of **6***a*:**6***b* if isotope effects in each of the ring closing steps are minimal, and this agrees well with the results. Applying this same mechanism to **1**-d_2 suggests a 75:25 ratio of **5***a*:**5***b*, and for **7** the ratio of **8***a*:**8***b* is similarly expected to be 75:25, both compounds give results considerably different from that predicted. Triplet trimethylenemethane dimerizes (15) to produce 1,4-dimethylenecyclohexane, a species which we have been unable to observe in any of our reactions. We have attempted to trap any diradical intermediate by carrying out the thermolysis of **1***a* in neat cyclohexene and neat diethylfumarate. The latter would be expected to be reasonably diylophilic (16). Careful programmed temperature g.c. failed to reveal any materials of molecular weight greater than that of the reactant. It seems doubtful that any triplet **2** was produced.

We have been unable to resolve the detailed mechanism of thermolysis of **1** in terms of a single pathway and it may be that a combination of more than one mechanism is required to explain all of the data derived from the parent system. It is also possible that this is a case similar to the bicyclo[2.1.0]pent-2-ene isomerization described by Flowers and Frey (17) wherein the initially produced intermediate has sufficient excess energy that the observed product distribution is not representative of the mechanism, even

[4]Several factors, *e.g.* the relief of strain, or the greater stability of tertiary radicals, could explain the preference of the isopropylidene group in rotation over that of the methylene. Since **14** is thermodynamically more stable than **13** it is not the stability of the products that controls the preference.

Can. J. Chem. Downloaded from www.nrcresearchpress.com by 210.87.254.105 on 09/05/12
For personal use only.

at higher pressures. New thermodynamic data (18) allow us to estimate the heat of formation of **1** at 64 kcal mol^{-1}. This places the heat of formation of the transition state for the thermolysis of **1** at 96 kcal mol^{-1} which is 12 kcal mol^{-1} above the estimated heat of formation of the transition state for the Chesick rearrangement of methylenecyclopropane. The question of chemical activation of this rearrangement depends upon how much of the 42 kcal mol^{-1} of excess energy resides in the C_4H_6 species *vs.* how much is in the nitrogen produced. At the present time we are unable to predict how this energy is partitioned.

The recent calculations of Hehre *et al.* (19) place the heat of formation of the high symmetry (D_{3h}) singlet **2** at 132 kcal mol^{-1} (88 kcal mol^{-1} above the heat of formation of methylenecyclopropanes value of 44 kcal mol^{-1} (20) thus excluding the possibility of this species. However Yarkony and Schaefer (21) find a 47 kcal mol^{-1} energy change on relaxation of **2** to C_{2v} symmetry, thus placing the planar singlet at 84 kcal mol^{-1} within 4 kcal mol^{-1} of the heat of formation of singlet **3** (19). Theoretically then both of these latter two species are thermally plausible. Our data for **9** and **10** suggest that intermediates **18** and **19** are capable of explaining the product distributions. If, however, **1** should prove to be unique, as regards mechanism, then we can question whether the product determining step involves a nitrogen containing intermediate. Discussion of this point is deferred to the accompanying paper.

Experimental

The n.m.r. spectra were recorded on Varian A-60 and A-100 analytical spectrometers. The analytical gas chromatography was carried out using a Perkin–Elmer 900 GC equipped with capillary columns and a Hewlett Packard 3370A Electronic Integrator. Mass spectra were determined on an AEI MS-9 double focusing high resolution spectrometer.

*4-Methylene-1-Pyrazoline (**1**)*

Allene (30 ml) was condensed into a pressure bottle at Dry Ice – acetone temperatures and a solution of diazomethane (6 g, 0.14 mol) in ether (50 ml) was added before the bottle was sealed and allowed to warm to room temperature. After 15–20 h the yellow color had disappeared, the flask was recooled, opened, and allowed to warm to room temperature. The ether and excess allene were evaporated under reduced pressure and the residue distilled as quickly as possible, b.p. 49–50° (33 Torr); 8 g (69% yield); n_D^{25} 1.4714 (lit. (22) n_D^{25} 1.473); u.v. λ_{max} 322 nm (ε 490, ethanol). The i.r. spectrum ν_{max} 1670 cm^{-1} (—HC=CH_2) and 1540 cm^{-1} (—N=N—). The n.m.r. spectrum TMS ($CDCl_3$) δ 5.13 (quintet, J = 2.6 Hz, 2H) and δ 4.88 (triplet, J = 2.6 Hz, 4H).

*4-Methylene-1-pyrazoline-3,3-d_2 (**1**-d_2)*

The method of synthesis was analogous to that described for **1** using diazomethane-d_2, which was prepared via the method Leitch *et al.* (23) with additional D_2O exchanges at 0°. The n.m.r. spectrum of the **1**-d_2 produced indicated 93 ± 2% isotopic purity.

*4-Methylene-1-pyrazoline-3,3,6,6-d_4 (**1**-d_4)*

A solution of diazomethane (5 g, 0.12 mol) in ether 60 ml was added at −60° to allene-d_4 (6 g, 0.14 mol) (24). The mixture was allowed to warm to room temperature and after 24 h worked up as described above. Yield of **1**-d_4, 4 g (40%) (22). The n.m.r. spectrum indicated that the 3- and 6-positions were >95% deuterium.

*4-Methylene-1-pyrazoline-3,3,5,5,6,6-d_6 (**1**-d_6)*

Using allene-d_4 (6 g, 0.14 mol) and diazomethane-d_2 (3 g, 0.07 mol) in a procedure analogous to that outlined for **1**-d_4 a sample of 2 g (33%) of **1**-d_4 was obtained. An n.m.r. spectrum of **1**-d_6 using benzene as an integration reference indicated that the sample was 95 ± 3% perdeuterio.

*4-Methylene-1-pyrazoline-3-^{13}C (**7**)*

Commercially available 67% ^{13}C-methyliodide was converted to ^{13}C-diazomethane by using the ^{14}C-diazomethane techniques of Stoll *et al.* (25). The ^{13}C-diazomethane was then added to allene by the procedure described above for **1**-d_2.

*3,3-Dimethyl-4-methylene-1-pyrazoline (**9**)*

A solution of 2-diazopropane (26) (14 g, 0.21 mol) in ether was added at −78° to allene (30 ml) and then allowed to warm to 0 °C in a pressure bottle. After 3 h the solution became colorless. Removal of the excess allene and ether followed by distillation of the residual material gave 8 g of a mixture, b.p. 55°/27 Torr. The mixture proved to be (n.m.r.) 62% **9**, 15% **11**, and 23% **12**. Careful column chromatography on Fluorosil gave a pure sample of **9**, n.m.r. spectrum δ 4.95 (multiplet, 4H) δ 1.35 (singlet, 6H). Exact mass calcd. for $C_7H_{10}N_2$: 122.0844; found: 122.0845. The ketazine (**11**) was identified from its g.c. retention time, its n.m.r. doublet at δ 1.83 and 2.00, and by comparison with an authentic sample. The isomeric impurity was tentatively assigned the structure **11** on the basis of its n.m.r. spectrum in deuteriochloroform δ 6.05 (triplet $J \simeq$ 3 Hz, 1H), δ 5.5 (triplet $J \simeq$ 2 Hz, 1H), δ 2.10 (doublet of doublets $J \simeq$ 3 Hz, $J \simeq$ 2 Hz, 2H), and δ 1.15 (singlet, 6H) and from its exact mass in a sample wherein all of **9** had reacted. Calcd. for $C_7H_{10}N_2$: 122.0844; found: 122.0843. Samples of **11** and **12** were obtained by thermolysis of a 200 mg sample of the 62:23:15 mixture at 200° for 2 h followed by separation from **13** and **14** by preparative g.c. Subsequent heating of this mixture of **11** and **12** at 250° for 2 h gave only **12**, **13**, and **14**.

*Preparation of 1,2-Dicarbethoxy-4-isopropylidenepyrazolidine (**16**)*

A solution of *sym*-dicarbethoxyhydrazine (8.91 g, 50 mmol) in 1,2-dimethoxyethane (DME) (200 ml) was placed in a 500 ml three-necked flask fitted with a magnetic stirrer, reflux condenser, and a gas inlet tube. After flushing with nitrogen a dispersion of sodium hydride

Can. J. Chem. Downloaded from www.nrcresearchpress.com by 210.87.254.105 on 09/05/12
For personal use only.

(57% dispersion, 2.22 g, 53 mmol) was added and the solution stirred for 30 min. This was followed by the dropwise addition of a solution of 2-isopropylidene-1,3-dibromopropane (27) (11.3 g, 46.7 mmol) in DME (40 ml) and continued stirring (overnight). A solution of sodium ethoxide (56 mmol, from 1.3 g sodium metal) in ethanol (40 ml) was then added over the period of 1 h and the reaction mixture stirred for an additional 24 h at room temperature. The volume of the solution was then reduced to 50 ml at the water aspirator and the reaction mixture was poured into 800 ml ice water. After extracting with ether (3 × 100 ml) the organic layers were combined and dried over anhydrous sodium sulfate. Upon removing the solvent the residual layer was distilled 114–118°/0.1 Torr, 8.54 g (72%).

Anal. Calcd. for $C_{12}H_{20}N_2O_4$ (mol. wt. 256.1418): C, 56.23; H, 7.87; N, 10.93. Found (256.1421, mass spectrum): C, 56.33; H, 8.11; N, 11.07.

The n.m.r. spectrum δ TMS ($CDCl_3$) 1.27 (triplet, $J = 7$ Hz, CH_3^- of ester 6H); 1.65 (slight multiplet, allylic CH_3, 6H); 4.20 (complex multiplet, ring methylene + ester CH_2, 8H).

*Preparation of 4-Isopropylidenepyrazolidine Hydrochloride (**17**)*

Ethylene glycol (500 ml), water (120 ml), and potassium hydroxide (118 g, 2.1 mol) were added to a 1-*l* three-necked flask fitted with a reflux condenser, gas inlet tube, and stirrer. After flushing with nitrogen, **16** (80 g, 0.31 mol) was added and the solution was stirred and heated on a steam bath for 8 h. The reaction mixture was then distilled at approximately 95°/0.1 Torr. The distillate was trapped in a Dry Ice – acetone bath and at 0 °C hydrochloric acid (29 ml, 0.35 mol) was added. The solvent was then removed at a rotary evaporator and the chilled residue solidified. After washing with dry ether on porous plate the solid was allowed to stand over P_2O_5 under reduced pressure, m.p. 118–120°, 33.5 g (73%).

Anal. Calcd. for $C_6H_{13}N_2Cl$: C, 48.58; H, 9.05; N, 18.67; Cl, 24.30. Found: C, 48.48; H, 8.81; N, 18.85; Cl, 23.86.

The n.m.r. spectrum, δ external TMS (D_2O) 1.65 (multiplet, 6H) 3.80 (multiplet, 4H).

*Preparation of 4-Isopropylidene-1-pyrazoline (**10**)*

The hydrochloride **17** (7.4 g, 50 mmol) was slowly added to a well-stirred slurry of red mercuric oxide (65 g) anhydrous sodium sulfate (65 g) and sodium carbonate (5.3 g, 50 mmol) in ether (100 ml). The reaction mixture was stirred for an additional 3 h before filtration. The ether solution was then evaporated and the product distilled, 37°/0.1 Torr, to produce 2.33 g (42%). Exact mass calcd. for $C_6H_{10}N_2$: 110.0844; found: 110.0844.

The n.m.r. spectrum of a neat sample, δ external TMS, 1.67 (quintet, $J = 2.5$ Hz, 6H), 4.90 (septet, $J = 2.5$ Hz, 4H). In $CDCl_3$ the sample tautomerized to 3-isopropylidene-2-pyrazoline as evidenced by the n.m.r. spectrum δ TMS ($CDCl_3$) 1.69 (triplet, $J = 3$ Hz, 3H), 1.85 (triplet, $J = 3$ Hz, 3H), 4.02 (septet, $J = 3$ Hz, 2H), 5.46 (disappeared with D_2O exchange, 1H) 7.27 (singlet, 1H).

*Product Studies on the Thermolysis of **9** and **10***

A sample of 30–60 μl of **9** was transferred, on a vacuum line, to a 25 ml break-seal, degassed, sealed, and heated for the appropriate period in a thermostated oil bath. The product was then transferred to a sampling tube and 30–60 μl of chloroform was added. Three such tubes were examined at each time duration at each temperature and all analyses were carried out in triplicate on each sample.

*Preparation and Isomerization of Dideuteriomethylene-2,2-dideuteriocyclopropane (**6a**)*

Allene-d_4 (5 g, 110 mmol) (24) was condensed into a 200-ml three-necked flask, containing cuprous chloride (0.5 g, 5 mmol), equipped with a Dry Ice condenser, a dropping funnel, and a magnetic stirrer. Diazomethane (3 g, 70 mmol) in ether (40 ml) was added dropwise and the stirring continued until all signs of nitrogen evolution ceased. The product was separated from ether and allene-d_4 by preparative g.c. using a 3/8 in. × 20 ft column of Ucon 15M on Chromosorb W; 0.56 g (15%). The n.m.r. spectrum corresponded to a 90:10 mixture of **6***a*:**6***b*. This did not change when the n.m.r. tube was maintained at 180° for 1 h. After 16 h at 180° the spectrum corresponded to an 87:13 mixture. On heating a sample at 212° for 2 h a 78:22 mixture resulted. After 1 h at 251° the mixture was that of the equilibrium value of 67% **6***a* and 33% **6***b*; further heating did not change the spectrum.

Controls

*Noninterconversion of **9** and **10***

A sample of **10** (60 μl was heated at 160.1° for 60 min. The product was transferred on the vacuum line to an n.m.r. tube and $CDCl_3$ was added. The spectrum indicated the presence of 55% thermolysis products (35.8% **13** and 19.3% **14**) and 31.5% of **10** along with 13.5% of its tautomer 4-isopropylidene-2-pyrazoline; no trace of **9**, or its tautomer could be detected.

A sample of the mixture of **9**, **11** and **12** upon heating at 160.1° for 1 h, and analyzed by n.m.r. as described for **10**, showed only the presence of 53% thermolysis products along with **9**, **11**, and **12** but not **10** or its tautomer.

*Isomerization of **1**-d_4*

A sample of **1**-d_4 was heated in a sealed tube for 12 min at 166° (1 half-life) and the remaining 4-methylene-1-pyrazoline was transferred to an n.m.r. tube. The tube was warmed to 0° and the methylenecyclopropane-d_4 was pumped off. The n.m.r. spectrum was identical to the initial starting material.

Attempts to Trap Trimethylenemethane

Cyclohexane (3 g, 37 mmol) and **1***a* (0.5 g, 6 mmol) were heated in a 10 ml autoclave for 30 min at 190°. A temperature programmed g.c. analysis of the resulting mixture indicated only methylenecyclopropane and cyclohexene. The C_{10} region, as judged by the retention times of *cis*- and *trans*-decalin, was completely free of peaks. Under the conditions of analysis a 0.1% yield of an adduct could have readily been observed.

In a similar experiment diethyl fumarate was used in place of the cyclohexene and no adduct was observed.

*Thermolysis of **1**-d_4 in Decalin Solution*

Decalin (20 ml) was heated to reflux (185°) in a 50-ml three-necked flask fitted with a reflux condenser and rubber septum. A gas burette was connected to the top of the condenser. A sample of **1**-d_4 (100 μl) was then injected into the liquid. When the gas evolution ceased, a slow stream of nitrogen was passed through the entire system forcing all of the gases to pass through a trap

cooled in liquid nitrogen. The methylenecyclopropane-d_4 in the trap was distilled into an n.m.r. tube containing CCl_4 and TMS. The integration ratio of ring to vinyl protons was 2.62 ± 0.10 which corresponds to 72.4 ± 0.8% **6***a* and 27.6 ± 0.8% **6***b*.

Kinetic Measurements

The kinetic results were obtained by following the increase of pressure with time during the thermolysis of the 1-pyrazolines. A transducer converted the pressure reading to e.m.f., which was indicated on a recorder. It is known that in the pressure range used (50–700 Torr) that the transducer e.m.f. (E) is directly proportional to the pressure. A plot of ln $(E_\infty - E_t)$ *vs.* t gives k. All reactions followed first-order kinetics to greater than 85% completion. The stainless steel cell system was essentially that described by Smith and Bagley (28), wherein temperature control was obtained by an insulated large aluminum block. The temperature did not change ±0.1° over the duration of the reaction, but there was a slow drift from day to day. Least squares analysis on the kinetic data using 20 points gave rate constants wherein the probable error was less than 1%.

We wish to acknowledge the financial support of the National Research Council of Canada, and some early exploratory work carried out by Dr. Manfred Schneider.

1. R. J. Crawford and D. M. Cameron. J. Am. Chem. Soc. **88**, 2589 (1966).
2. P. Dowd. J. Am. Chem. Soc. **88**, 2587 (1966); P. Dowd and K. Sachdev. J. Am. Chem. Soc. **89**, 715 (1967); P. Dowd, A. Gold, and K. Sachdev. J. Am. Chem. Soc. **90**, 2715 (1968); P. Dowd, G. Senqupta, and K. Sachdev. J. Am. Chem. Soc. **92**, 5726 (1970).
3. J. P. Chesick. J. Am. Chem. Soc. **85**, 2720 (1963).
4. J. J. Gajewski. J. Am. Chem. Soc. **93**, 4450 (1971); W. von E. Doering and H. D. Roth. Tetrahedron, **26**, 2825 (1970); M. Jones, Jr., M. E. Hendrick, J. C. Gilbert, and J. R. Butler. Tetrahedron Lett. 845 (1970).
5. R. J. Crawford and A. Mishra. J. Am. Chem. Soc. **88**, 3963 (1966); B. H. Al-Sader and R. J. Crawford. Can. J. Chem. **46**, 3302 (1968).
6. R. J. Crawford and D. M. Cameron. Can. J. Chem. **45**, 691 (1967).
7. S. Seltzer. J. Am. Chem. Soc. **83**, 2625 (1961); S. Seltzer and F. T. Dunne. J. Am. Chem. Soc. **87**, 2628 (1965). For a complete summary see E. A. Halevi *in* Progress in physical organic chemistry. Vol. 1. Interscience Publishers, Inc., New York, N.Y. 1963. p. 109.
8. R. J. Crawford and M. Ohno. Can. J. Chem. **52**, 3134 (1974).
9. H. E. O'Neal and S. W. Benson. J. Phys. Chem. **72**, 1866 (1968).
10. R. G. Bergman and W. L. Carter. J. Am. Chem. Soc. **91**, 7411 (1969).
11. J. A. Berson, D. C. Tompkins, and G. Jones, II. J. Am. Chem. Soc. **92**, 5799 (1970); W. R. Dolbier Jr. and J. H. Alonso. J. Am. Chem. Soc. **95**, 4421 (1973).
12. J. B. Stothers. Carbon-13 NMR spectroscopy. Academic Press, New York. 1973. pp. 321–330.
13. R. J. Crawford and H. Tokunaga. Can. J. Chem. This issue.
14. O. S. Tee. J. Am. Chem. Soc. **91**, 7144 (1969); S. I. Miller. Advan. Phys. Org. Chem. **6**, 185 (1968), and references cited therein.
15. P. Dowd. Accts. Chem. Res. **5**, 242 (1972).
16. J. A. Berson, D. M. McDaniel, and L. R. Corwin. J. Am. Chem. Soc. **94**, 5509 (1972).
17. M. C. Flowers and H. M. Frey. J. Am. Chem. Soc. **94**, 8636 (1972).
18. P. S. Engel, J. L. Wood, J. A. Sweet, and J. L. Margrave. J. Am. Chem. Soc. **96**, 2381 (1974).
19. W. J. Hehre, L. Salem, and M. R. Willcott. J. Am. Chem. Soc. **96**, 4428 (1974).
20. K. B. Wiberg and R. A. Fenoglio. J. Am. Chem. Soc. **90**, 3395 (1968).
21. D. R. Yarkony and H. E. Schaefer III. J. Am. Chem. Soc. **96**, 3754 (1974).
22. I. A. D'yakonov. J. Gen. Chem. (U.S.S.R.), **15**, 473 (1945); Chem. Abstr. **40**, 4718 (1946).
23. L. C. Leitch, P. E. Gagnon, and A. Cambron. Can. J. Res. **288**, 256 (1950).
24. A. T. Morse and L. C. Leitch. J. Org. Chem. **23**, 990 (1958).
25. A. Stoll, J. Rutschmann, A. von Wartburg, and J. Renz. Helv. Chim. Acta, **39**, 993 (1956).
26. S. M. Andrews, A. C. Day, P. Raymond, and M. Whiting. Org. Syn. **50**, 27 (1970).
27. J. A. Marshall and T. M. Warne, Jr. J. Org. Chem. **36**, 178 (1971).
28. G. G. Smith and F. D. Bagley. Rev. Sci. Instr. **32**, 703 (1961).
29. G. Jones II. J. Chem. Educ. **52**, 175 (1974).

Can. J. Chem. Downloaded from www.nrcresearchpress.com by 210.87.254.105 on 09/05/12
For personal use only.

Thermolysis of 3,3,5,5-Tetramethyl-4-methylene-1-pyrazoline and the Thermal Isomerization of Some Alkylidenecyclopropanes

ROBERT J. CRAWFORD AND HIROKAZU TOKUNAGA

Department of Chemistry, University of Alberta, Edmonton, Alberta T6G 2G2

Received May 27, 1974

ROBERT J. CRAWFORD and HIROKAZU TOKUNAGA. Can. J. Chem. **52**, 4033 (1974).

The thermolysis of 3,3,5,5-tetramethyl-4-methylene-1-pyrazoline (**1**) proceeds at 1/63 the rate of 4-methylene-1-pyrazoline. The activation parameters, $\log(k/s^{-1}) = (15.53 \pm 0.3) - (40.7 \pm 0.4)/\theta$ where $\theta = 2.303\,RT$ in kcal mol^{-1}, suggest that **1** is undergoing thermolysis by a mechanism different from that for 4-methylene-1-pyrazoline. The 2,2,3,3-tetramethylmethylenecyclopropane (**5**) produced rapidly isomerizes under the reaction conditions to 2,2-dimethylisopropylidenecyclopropane (**4**). The four opposed methyl groups of **5** have created sufficient ground state destabilization as to cause its isomerization to be 147 times faster than the conversion of 2,2-dimethylmethylenecyclopropane to isopropylidenecyclopropane.

The products are considered in terms of two possible intermediates, one wherein an allylic diazenyl diradical is considered and the second wherein a Chesick type of intermediate is invoked. For the latter it is demonstrated that substituents on the orthogonal radical center can affect the rotational propensities of methylene *vs.* isopropylidene of the allylic system.

ROBERT J. CRAWFORD et HIROKAZU TOKUNAGA. Can. J. Chem. **52**, 4033 (1974).

La thermolyse de la tétraméthyl-3,3,5,5-méthylène-4-pyrazoline-1 (**1**) s'effectue avec une vitesse égale à 1/63 de la vitesse de décomposition de la méthylène-4-pyrazoline-1. Les paramètres d'activation, $\log(k/s^{-1}) = (15.53 \pm 0.3) - (40.7 \pm 0.4)/\theta$ ou $\theta = 2.303\,RT$ en kcal mol^{-1}, suggèrent que **1** subit la thermolyse selon un mécanisme différent de celui de la méthylène-4-pyrazoline-1. Le tétraméthyl-2,2,3,3-méthylènecyclopropane (**5**) produit, s'isomérise rapidement, dans les conditions de la réaction, pour donner le diméthyl-2,2-isopropylidènecyclopropane (**4**). Les quatre groupes méthyle opposés de (**5**) créent une déstabilisation de l'état fondamental suffisante pour que son isomérisation soit 147 fois plus rapide que la conversion du diméthyl-2,2-méthylènecyclopropane en isopropylidènecyclopropane.

On considère les produits en faisant intervenir deux intermédiaires possibles, l'un dans lequel un diradical allylique–diazényl est considéré et le second dans lequel un intermédiaire du type Chesick est invoqué. Pour ce dernier, il est démontré que les substituents sur le centre radicalaire orthogonal peuvent affecter la tendance à la rotation du groupe méthylène par rapport au groupe isopropylidène du système allylique.

Introduction

As a consequence of our work on the thermolysis of 4-alkylidene-1-pyrazolines (1) we have carried out an investigation of the gas phase thermolysis of 3,3,5,5-tetramethyl-4-methylene-1-pyrazoline (**1**). This structure has the advantage that the tautomerism, which plagued our previous studies, is no longer possible. Our principal objectives in studying **1** were to compare the competition between the isopropylidene group and the methylene group, of the presumed intermediate **2***a*, with the same competition observed in **2***b*, the implied intermediate in the thermolysis of 4-isopropylidene-1-pyrazoline (1), and to examine the thermolysis kinetics of a substituted 4-alkylidene-1-pyrazoline.

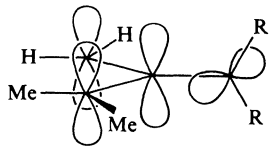

2

a R = Me

b R = H

The synthesis of **1** has been reported and we followed Mock's (2) procedure for the transformation of **3** to **1**. We prepared **3** by the oxidation of the corresponding tetramethyl-4-pyrazolidone which was readily prepared by the reaction of hydrazine and α,α′-dibromodiisopropylketone.

Can. J. Chem. Downloaded from www.nrcresearchpress.com by 210.87.254.5 on 09/05/12
For personal use only.

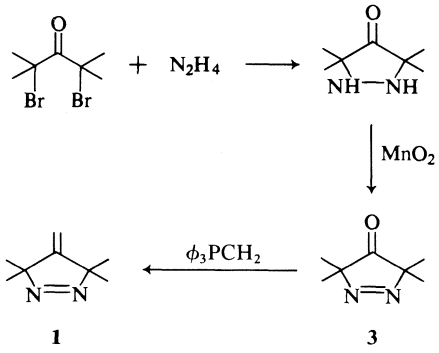

Much to our surprise we found the thermolysis of **1** to be somewhat slower than 4-methylene-1-pyrazoline and our initial investigation suggested that only one product, 2,2-dimethylisopropylidenecyclopropane (**4**) was produced. However, careful examination of the gas chromatograph of the products on low conversion revealed that 2,2,3,3-tetramethylmethylenecyclopropane (**5**) was present and that it was rapidly isomerizing under the reaction conditions. It became necessary to study the interconversion and thermodynamic stability of **4** and **5** and thus we report herein on the mechanism of the thermolysis of **1** and the isomerization of **4** and **5**.

Results

The thermolysis of **1** at 400 Torr was carried out in sealed ampoules. After heating in a constant temperature bath the ampoules were reattached to the vacuum line and the product was transferred to a sample tube, toluene added, and the concentrations of **1**, **4**, and **5** measured by analytical gas chromatography (g.c.). Table 1

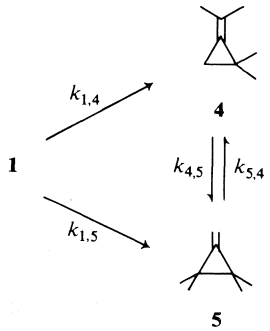

gives a sample rate at 165.2° along with the proportions of **4** and **5** present. The rate constants and activation parameters for the thermolysis of **1** are given in Table 2.

TABLE 1. Thermolysis of **1** in the gas phase at 180.17 ± 0.02°

Time (min)	**1** (%)	**5**:**4**	$10^5 k$ (s^{-1})
15.0	94.0±0.5[a]	0.7018±0.0011[a]	
30.0	87.7±0.3	0.4910±0.0010	
45.0	82.0±0.6	0.3616±0.0009	7.97 ± 0.08
60.0	75.9±0.7	0.2773±0.0009	
90.0	66.6±0.8	0.1803±0.0007	
120.0	57.6±0.7	0.1244±0.0009	
150.0	49.7±0.6	0.0921±0.0007	
180.0	42.4±0.3	0.0700±0.0005	

[a]The error listed is the standard deviation of nine analyses, triplicate analyses on three tubes at each time.

A pure sample of **5** was obtained by the preparative g.c. separation of a 57:43 mixture of **5**:**4**. This mixture was obtained from the direct photolysis, at 0°, of **1** in pentane using Pyrex-filtered radiation from a 450 W Hanovia high pressure lamp. No attempt was made to carry out a photochemical study but the length of time required for 98% conversion, 72 h, and the constancy of the 57:43 ratio throughout the reaction was ascertained from following the reaction by g.c. analysis.

At temperatures high enough so that equilibrium could be attained in a reasonable time, either **4** or **5** gave the same equilibrium mixture of starting material and product. The amount

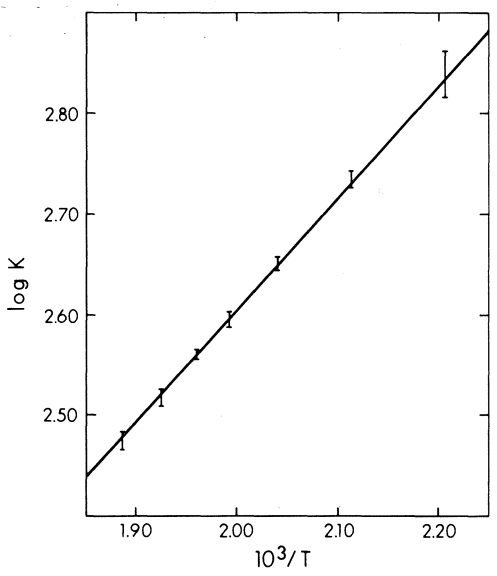

FIG. 1. Temperature dependence of the 2,2,3,3-tetramethylmethylenecyclopropane and 2,2-dimethylisopropylidenecyclopropane equilibrium constant with the best fit line from a least-squares calculation.

Can. J. Chem. Downloaded from www.nrcresearchpress.com by 210.87.254.5 on 09/05/12
For personal use only.

TABLE 2. Rate constants and activation parameters for the thermolysis of **1**

Temperature (°C)	$10^5 k_s$ (s^{-1})	Activation parameters
165.15±0.02	1.64±0.04	E_a = 40.7 ± 0.4 kcal mol^{-1}
		log A = 15.53
180.17±0.02	7.97±0.08	
		$\Delta H^{\ddagger}$ = 39.8 ± 0.4 kcal mol^{-1}
200.11±0.03	52.1±0.3	$\Delta S_{150}{}^{\ddagger}$ = +9.8 ± 0.9 e.u.

TABLE 3. Equilibrium data for **4** ⇄ **5** at various temperatures (K = [**4**]/[**5**])

Temperature (°C)	Reaction time (h)	%**5** at equilibrium	K^a
180.15	144	0.16±0.02	653±33[b]
200.11	24	0.20±0.01	512±10
217.10	16	0.24±0.01	421±8
228.85	10	0.27±0.01	371±7
237.30	10	0.29±0.01	343±4
246.35	6	0.32±0.01	311±8
258.60	6	0.35±0.01	281±6

[a]Calculated directly from integration data using a Perkin-Elmer 900 g.c. equipped with a Hewlett Packard 3370A Electronic Integrator. The relative sensitivities of 5 and 4 to the flame ionization detector was 1.00 ± 0.01.
[b]Error listed is the standard deviation of nine analyses, triplicate analyses on each of three samples.

TABLE 4. First-order rate constants for the rearrangement of **5** to **4** ($k_{5,4}$)

Temperature (°C)	10^5 ($k_{5,4}+k_{4,5}$) (s^{-1})	Activation parameters
145.28±0.03	1.80±0.02	E_a = 36.4 ± 0.03 kcal mol^{-1}
		log A = 14.27
155.22±0.02	4.91±0.05	
		$\Delta H^{\ddagger}$ = 35.6 ± 0.3 kcal mol^{-1}
165.28±0.02	13.3±0.1	$\Delta S_{150}{}^{\ddagger}$ = +4.0 ± 0.9 e.u.

of **5** at equilibrium was so small that the samples had to be handled with care to prevent any preferential loss of the more volatile **5**. A break-seal containing a 10 μl sample of **4**, or **5**, was carefully degassed on a vacuum line, heated in an oil bath for the required period, then reattached to the vacuum line, and the contents transferred to a small sampling tube to which was added 20 μl of toluene; upon thorough mixing triplicate g.c. analyses of each tube were carried out using a 0.01 in. i.d. × 150 ft capillary column coated with β,β′-oxydipropionitrile. The ratio of toluene to **4** and **5** was essentially constant, whether the toluene was added before or after the heating, indicating that the vacuum transfers were essentially quantitative. Table 3 gives the equilibrium data obtained and Fig. 1 shows a plot of the log K *vs.* $1/T$. A least-squares calculation gives $\Delta H = -5.18 \pm 0.15$ kcal mol^{-1} and $\Delta S = +1.44 \pm 0.21$ e.u. for the conversion of **5** to **4**.

Kinetic data for the conversion of **5** → **4** are given in Table 4 along with the activation parameters for this isomerization. At 165.15° the equilibrium constant, $K = k_{5,4}/k_{4,5}$, extrapolated from the data in Table 3, has a value of 793, thus the process measured is essentially that of $k_{5,4}$ since $k_{4,5}$ is $0.0012k_{5,4}$. For comparison purposes we have examined the equilibrium between 2,2-dimethylmethylenecyclopropane (**6**) and isopropylidenecyclopropane (**7**),

Can. J. Chem. Downloaded from www.nrcresearchpress.com by 210.87.254.5 on 09/05/12
For personal use only.

TABLE 5. Equilibrium data for **6** ⇄ **7** at various temperatures (K = [**7**]/[**6**])

Temperature (°C)	Reaction time (h)	%**6** at equilibrium	K
220.30±0.02	72	21.34±0.04[a]	3.68±0.01
236.25±0.03	36	22.02±0.06	3.54±0.01
253.21±0.04	12	22.64±0.10	3.41±0.02
272.33±0.08	12	23.32±0.15	3.29±0.03
285.32±0.08	8	23.77±0.09	3.21±0.02

[a]Error listed in the standard deviation of nine analyses, triplicate determinations on each of three samples.

materials available to us from an accompanying study (1). Table 5 gives the equilibrium data obtained. A least squares calculation gives $\Delta H = -1.17 \pm 0.07$ kcal mol^{-1} and $\Delta S = 0.22 \pm 0.10$ e.u. for the isomerization of **6** to **7**. Measurement of the specific reaction rate constants, between **6** and **7**, in the gas phase (300 Torr) gave $k_{6,7} = (8.38 \pm 0.12) \times 10^{-6}$ s^{-1} and $k_{7,6} = (2.11 \pm 0.03) \times 10^{-6}$ s^{-1} at 190.10 ± 0.02°.

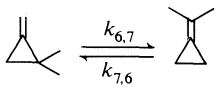

6 **7**

Experimental

The n.m.r. spectra were recorded on Varian A-60 and A-100 analytical spectrometers. The analytical gas chromatography was carried out using a Perkin-Elmer 900GC equipped with capillary columns and a Hewlett Packard 3370A Electronic Integrator. Mass spectra were determined on an AEI MS-9 double focusing high resolution spectrometer.

3,3,5,5-Tetramethyl-4-pyrazolidone

A solution of 2,4-dibromo-2,4-dimethyl-3-pentanone (135 g, 0.5 mol) (3) in ethanol (100 ml) was added slowly to a stirred solution of 64% hydrazine hydrate (105 ml, 1.3 mol N_2H_4) in ethanol (500 ml) along with 0.2 g of EDTA. Upon completion of addition the flask was warmed, with occasional swirling of the contents, on the steam bath for 1 h. The hydrazine hydrobromide, which precipitated upon cooling, was removed by suction filtration and the filtrate reduced to approximately one third its original volume. On cooling, the solution produced 19.5 g (27%) of white crystals, m.p. 115–117° (dec.), an additional 5 g was obtained by concentration of the mother liquor. The yield from this preparation varied from 20 to 50%.

A good microanalysis of this compound was not obtained. The percentage hydrogen was always lower than expected as the sample was always contaminated with some of the oxidation product **3**.

The n.m.r. spectrum, δ TMS ($CDCl_3$) 1.15 (sharp singlet, 12 H) and 3.61 (broad signal, NH, 2H). Traces of **3** were present as evidenced by a singlet at δ 1.33 (see the following preparation).

3,3,5,5-Tetramethyl-1-pyrazolin-4-one (3)

A mixture of 3,3,5,5-tetramethyl-4-pyrazolidone (5 g, 35 mmol) and active manganese dioxide (6.2 g, 71 mmol) (4) in pentane (400 ml) was shaken in pressure bottles for 24 h. After filtration the solution was concentrated to 25 ml and refrigerated. The product consisted of 2.7 g (55%) of white crystals which on sublimation gave m.p. 83.5–85°.

Anal. Calcd. for $C_7H_{12}N_2O$: C, 59.97; H, 8.63; N, 19.98. Found: C, 59.60; H, 8.56; N, 19.78.

The n.m.r. spectrum, δ TMS (CCl_4) displayed a single peak at 1.33; u.v. (ethanol) λ_{max} 356 nm (log ε 2.18); i.r. (CCl_4) cm^{-1}, strongest peaks at 2990, 2940, 1760, 1468.

3,3,5,5-Tetramethyl-4-methylene-1-pyrazoline(1)

Sodium hydride (167 mmol; 7.1 g as a 57% dispersion in mineral oil) was added to a 500-ml three-necked flask fitted with a reflux condenser, gas inlet tube, and magnetic stirrer. The mineral oil was removed by washing with dry *n*-pentane (3 × 200 ml). The last of the *n*-pentane was removed by evacuating the flask and then dimethyl sulfoxide (150 ml) was added and warmed to 80° for 1 h. Upon cooling triphenylphosphonium bromide (59.5 g, 0.167 mol) was added to the resulting solution of the methyl sulfinyl carbanion. Upon completion of addition the solution was warmed to 60° for 1 h. A sample of **2** (15.0 g, 107 mmol) was added and the solution stirred at 55° overnight. The reaction mixture was then poured into water (4 l) and the triphenylphosphine oxide removed by filtration. The precipitate was washed, and the filtrate extracted, with pentane (3 × 1 l). The combined extracts were dried over anhydrous sodium sulfate and concentrated to 50 ml and the residual crystals sublimed at one atmos. and 50° to give 11.2 g (76%) of crystals m.p. 35.0–36.2° (lit. (2) 34.5–35.5°). The n.m.r. spectrum, δ TMS ($CDCl_3$) 5.00 (singlet, 2H) and 1.42 (singlet, 12H); u.v. (CH_3OH) λ_{max} 328 nm (log ε 2.24).

Preparation of 4 and 5 by the Photolysis of 1

A *n*-pentane (150 ml) solution of **1** (6.5 g, 47 mmol) was photolyzed at 0 °C using Pyrex-filtered light from a 450 W Hanovia high pressure mercury lamp. The reaction was followed by g.c. (SE 30 column, 0.25 in. i.d. × 5 ft) and required 72 h for 98% conversion. During the photolysis the ratio of **5**:**4** stayed constant at 57:43. Upon completion the reaction mixture was concentrated to 30 ml using a spinning band column and the residue was subjected to preparative g.c. using a 10 ft × 0.25 in. column of UCW 98 (flow rate 40 ml/min, room temperature).

Can. J. Chem. Downloaded from www.nrcresearchpress.com by 210.87.254.5 on 09/05/12
For personal use only.

Can. J. Chem. Downloaded from www.nrcresearchpress.com by 210.87.254.5 on 09/05/12
For personal use only.

The n.m.r. spectrum of **4**, δ TMS ($CDCl_3$) 1.74 (broad singlet, 6H) 1.14 (singlet, 6H) 0.79 (singlet 2H). Exact mass calcd. for C_8H_{14}: 110.1096; found: 110.1096.

The n.m.r. spectrum of **5** δ TMS ($CDCl_3$) 5.14 (singlet, 2H) 1.12 (singlet, 12H). Exact mass calcd. for C_8H_{14}: 110.1096; found: 110.1096.

Kinetic Measurements

Thermolysis of 1

Pyrex break-seals (18 mm diameter and 70 mm long) were attached to a vacuum line and were evacuated and flamed before filling. A sample of **1** (25–30 mg), such as to give 300 Torr at 200°, was transferred to each break-seal and the sample removed from the vacuum line. Kinetic runs were made by immersing the break-seals in a well-stirred, thermostatted, silicone oil bath for the appropriate length of time and then quickly quenching the samples in ice water. The break-seals were then reattached to the vacuum line and the contents vacuum transferred to a sample vial (5 mm diameter, total length 45 mm) attached to the vacuum line by a carefully ground 5/20 joint. Each sample was analyzed in triplicate using a 150 ft × 0.01 in. diameter capillary column at 50°. Transfers were shown to be quantitative by the addition of toluene as an internal reference at the initial filling and at the sampling stage. An example of the analytical data is given in Table 1.

Rate of Isomerization of 4 and 5

Samples of **5** (10 μl, 99.87 ± 0.01% pure) were transferred to break-seals which were attached to the vacuum line, degassed, and sealed. After heating for the appropriate period in a well stirred, thermostatted, silicone oil bath the break-seals were reattached to the vacuum line and the product handled in the same manner as described for the kinetics of the thermolysis of **1**. The reaction was demonstrated to be first order by a set of tubes wherein 2, 10, and 30 μl of sample were used in tubes of the same volume, and no difference in the ratio of **4**:**5** could be detected when they were heated for an identical period of time.

Equilibration of 6 and 7

Samples of pure **6** and pure **7** were obtained by the thermolysis of 3,3-dimethyl-4-methylene-1-pyrazoline (1) followed by preparative g.c. separation using a 20 ft × 0.25 in. i.d. column of β,β′-oxydipropionitrile at 25°. The equilibration studies were carried out in a manner analogous to that described for **4** except that chloroform was used as an internal reference and the g.c. analyses were carried out using a 150 ft × 0.01 in. capillary column coated with β,β-oxydipropionitrile. Triplicate analyses were carried out on each tube and three tubes were examined at each temperature.

Discussion

It is apparent from Table 1 that the product proportions, as represented by the ratio **5**:**4**, decrease throughout the reaction. From Tables 2 and 4, at 165°, it can be seen that **5** is isomerizing to **4** at least eight times faster than it is being produced from **1**. This prevents the direct observation of our principal objective, which is the initial ratio of **5**:**4** and thus we have attempted to assess this ratio on the basis of kinetic data.

The concentration of **1**, C_1, at any time, t, during the reaction is given by the equation:

$$[1] \qquad C_1 = C_1{}^0 C^{-k_s t}$$

where $k_s = k_{1,4} + k_{1,5}$, and the concentration of **5** is given by eq. 2.

$$[2] \quad dC_5/dt = k_{1,5}C_1 + k_{4,5}C_4 - k_{5,4}C_5$$

From Table 3 we see that $k_{4,5}$ is small and that the rate, $k_{4,5}C_4$, is such that we can treat the system as an irreversible process. Rearranging eq. 2 and substituting for C_1 from eq. 1 we get:

$$[3] \qquad dC_5/dt + k_{5,4}C_5 = k_{1,5}C_1{}^0 e^{-k_s t}$$

Equation 3 is a linear differential equation with constant coefficients. Its solution is:

$$[4] \qquad C_5 = \frac{k_{1,5}C_1{}^0}{(k_{5,4} - k_s)}(e^{-k_s t} - e^{-k_{5,4}t})$$

A plot of the concentration of **5** at time t *vs.* $(e^{-k_s t} - e^{-k_{5,4}t})$ gives a straight line of slope $(k_{1,5}C_1{}^0)/(k_{5,4} - k_s)$ from which we can calculate the value of $k_{1,5}$. Using the data in Table 1 and a least-squares fit for eq. 4 we obtain $(3.92 \pm 0.26) \times 10^{-5}\ s^{-1}$ for $k_{1,5}$. The percentage of **1** that is converted directly to **5** is 49 ± 3%. Similar calculations at 165.15 and 200.11° give 50.5 ± 0.7 and 51.3 ± 1.0%. The amount of **5** present, upon the thermolysis of a sample of **1**, for 15 min at 165.17°, was 49.4 ± 0.2% of the C_8H_{14} product. Correction to zero conversion suggests that the ratio $k_{1,5}/k_s$ is 0.524 ± 0.003.

Table 6 lists the activation parameters for those 4-alkylidene-1-pyrazolines which have been studied in the gas phase. While the span of relative rates is not large the surprising factor is that the replacement of hydrogen by methyl slows down the rate. This is not what is normally expected, and it can be seen from Table 6 that **1** is one third the rate of 3,3,5,5-tetramethyl-1-pyrazoline (**12**), thus there appears to be no acceleration from the allylic nature of the incipient radical. We can only surmise that the bulkier methyl groups have prevented any manifestation of the allylic nature and suggest that the cleavage of the carbon–nitrogen bond(s) in **1** is occurring in the plane of the ring. Professor Paul Engel has informed us of similar kinetic parameters observed for the thermolysis of 3,3,5,5-tetra-

TABLE 6. The relative rates, at 160.17°, and activation parameters for the gas phase thermolysis of some 4-alkylidene-1-pyrazolines and for 3,3,5,5-tetramethyl-1-pyrazoline

Compound	E_a (kcal mol^{-1})	log A	$\Delta S_{200}^{\neq}$ (e.u.)	Relative rate	Reference No.
8	32.6 ± 0.3	13.24	−1.1	62.8	1
1	40.7 ± 0.4	15.53	+9.8	1.0	This work
9	39.8 ± 0.6	13.6	+0.7	0.031	[a]
10	—	—	—	21	1
11	—	—	—	24	1
12	37.7 ± 0.4	14.49	4.6	3.0	5

[a]Private communication from Prof. P. Engel, Department of Chemistry, Rice University, Houston, Texas.

methyl-4-isopropylidene-1-pyrazoline (**9**). This suggests that neither **1** nor **9** can fold to an envelope conformation analogous to cyclopentene and other 1-pyrazolines (6). It is apparent however that **1** and **9**, have sufficiently different activation parameters from those observed for **8** that the transfer of mechanistic constraints, based on kinetics, must be severely restricted.

Although we cannot readily characterize the transition state for the thermolysis of **1** relative to 4-methylene-1-pyrazoline we can compare the product distributions from **1**, **10**, and **11**. If the initial step consists of breaking a carbon–nitrogen bond then the allylic diazenyl[1] species **13** will be produced. The products can then arise via a displacement of nitrogen by either of the allylic termini in a mechanism analogous to that suggested by Roth and Martin (7) for bicyclic azo compounds. This may be controlled by the rotational conformations of **13**, which vary as we go from R = H to R = CH_3, thus rationalizing

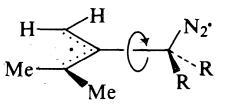

13

a R = Me

b R = H

why the ratio of **6**:**7** (63:37) from **11** is different from that of observed for **5**:**4** (52:48) from **1**.

If the nitrogen is lost from the hydrocarbon residue either in the rate determining step, or in a rapid subsequent step, then the Chesick (8) intermediate **2** is produced, and we must ask why is the isopropylidene group only slightly faster (1.10 times at 165°) than the methylene group, whereas for **2***b* it is 1.70 times faster in rotating out of the allylic plane. If **2***a* and *b* are intermediates in the thermolysis of **1** and **11** then the rotational propensities exhibited are altered by the nature of the orthogonal radical center. These rotational propensities are different from the rotational preferences (R_A) observed by Doering and Sachdev (9) from

[1]While this bypasses some of the mechanistic constraints implied by **8** (1) it is not in serious conflict with the small increase in rate on going from **10** to **1**.

Can. J. Chem. Downloaded from www.nrcresearchpress.com by 210.87.254.5 on 09/05/12
For personal use only.

studies on the isomerization of cyclopropanes. The nature of the incipient π bond and the relative stability of the rotating radical center can affect the propensities shown herein and raise complications from which Doering's R_A values are free. An estimate of the geometry of the transition state for an intermediate such as **2***a* going to a product may be obtained by examining the alkylidenecyclopropane rearrangement of **5** ⇄ **4**. Assuming that the transition state is best represented by the extension of the cyclopropyl bond we have Scheme 1. The near equivalence of products

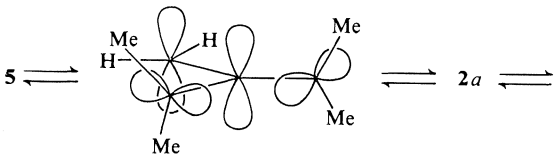

TS_1

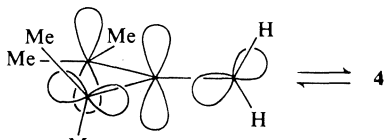

TS_2

$\delta\Delta G(TS_1 - TS_2) = -0.09$ kcal/mol^{-1}

SCHEME 1

5 and **4** from **1** then suggests that $\delta\Delta G^{\ddagger}$ for TS_1 and TS_2 is essentially zero.

The isomerization **6** ⇄ **7** and their production from **11** via **2***b* give Scheme 2 wherein a free energy difference ($\delta\Delta G^{\ddagger}$) of 0.49 kcal mol^{-1} is observed for $TS_3 - TS_4$. The similarity of the free energy ($\Delta G^{\ddagger}$) changes on going from **4** → TS_2 (40.1 kcal mol^{-1} at 190°) and from **7** to TS_4 (39.5 kcal mol^{-1} at 190°) suggests that these two processes are very similar, whereas the free energy change on going from **5** to TS_1 (34.1 kcal mol^{-1} at 190°) and that on going from **6** to TS_3 (37.8 kcal mol^{-1} at 190°) are quite different.[2] This suggests that the

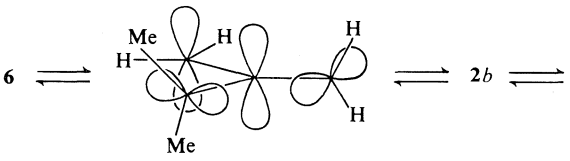

TS_3

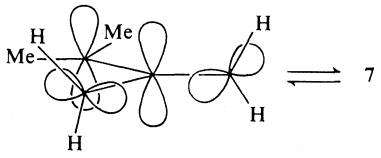

TS_4

$\delta\Delta G(TS_3 - TS_4) = -0.46$ kcal/mol^{-1}

SCHEME 2

lower rotational propensity of the isopropylidene group in **2***a* relative to that in **2***b* comes from the steric factors in TS_1, and that even though the cyclopropane bond is stretched to near-breaking the steric factors which destabilize **5** are still manifested, although significantly attenuated.

Only by examining additional 4-alkylidene-1-pyrazolines can we decide whether the thermolysis of **8** is misleading and the intermediates such as **2** or **13** are involved. The decision between the intermediates **2** or **13** must also await further experimentation but the use of chiral 4-alkylidene-1-pyrazolines can resolve this question. We are continuing to explore the thermolysis of these systems.

We wish to acknowledge the financial support of the National Research Council of Canada and to thank Prof. P. Engel and L. Shen for the communication of their data.

1. R. J. CRAWFORD, D. M. CAMERON, and H. TOKUNAGA. Can. J. Chem. This issue.
2. W. L. MOCK. Ph.D. Thesis, Harvard University, Cambridge, Mass. 1964.
3. A. FAVORSKII. J. Russ. Phys. Chem. Soc. **44**, 1339 (1913). Chem. Abstr. **7**, 984 (1913).
4. J. ATTENBURROW *et al.* J. Chem. Soc. 1094 (1952).
5. R. J. CRAWFORD and A. MISHRA. J. Am. Chem. Soc. **88**, 3963 (1966).
6. J. R. DURIG and W. C. HARRIS. J. Chem. Phys. **52**, 6096 (1970); D. E. MCGREER and J. W. MCKINLEY. Can. J. Chem. **49**, 105 (1971).
7. W. R. ROTH and M. MARTIN. Ann. **702**, 1 (1967).
8. J. P. CHESICK. J. Am. Chem. Soc. **85**, 2720 (1963).
9. W. VON E. DOERING and K. SACHDEV. J. Am. Chem. Soc. **96**, 1168 (1974).

[2]An alternative way of stating this is to point out that at 190° the rate at which the ring methylene of **4** becomes the *exo*-methylene of **5** is 2.14×10^{-6} s^{-1} at 190°, and for a ring methylene of **7** to become the *exo*-methylene of **6** is 1.11×10^{-6} s^{-1}, both very comparable. The rate at which the *gem*-dimethyl of **7** becomes the isopropylidene of **6** is 8.38×10^{-6} s^{-1} at 190°, and for a *gem*-dimethyl of **5** to become the isopropylidene of **4** is 6.15×10^{-4} s^{-1}. The free energy changes above are then corrected for by the $\delta\Delta G^{\ddagger}$ values of Schemes 1 and 2.

Can. J. Chem. Downloaded from www.nrcresearchpress.com by 210.87.254.5 on 09/05/12
For personal use only.

Photochemical and Thermal Decomposition of 1-Pyrazolines

PAUL S. ENGEL AND LAN SHEN

Department of Chemistry, Rice University, Houston, Texas 77001

Received July 3, 1974

PAUL S. ENGEL and LAN SHEN. Can. J. Chem. **52**, 4040 (1974).

Quantum yields for photochemical nitrogen extrusion from seven 1-pyrazolines were found to range from 0.12 to 0.88 but 4-oxo-3,3,5,5-tetramethyl-1-pyrazoline (**8**) proved to be photochemically and thermally remarkably stable. 4-Isopropylidene-3,3,5,5-tetramethyl-1-pyrazoline (**7**) decomposed thermally with E_a = 39.8 kcal mol^{-1} and $\Delta S^{\ddagger}$ = 0.7 e.u. The high stability of this compound contrasts with 4-methylene-1-pyrazoline (**17**).

PAUL S. ENGEL et LAN SHEN. Can. J. Chem. **52**, 4040 (1974).

Les rendements quantiques de la formation d'azote par décomposition photochimique de sept pyrazolines-1 s'échelonnent de 0.12 à 0.88 mais l'oxo-4 tétraméthyl-3,3,5,5 pyrazoline-1 (**8**) est remarquablement stable du point de vue photochimique et thermique. Pour la décomposition thermique de l'isopropylidène-4 tétraméthyl-3,3,5,5 pyrazoline-1 (**7**), on a E_a = 39.8 kcal mol^{-1} et $\Delta S^{\ddagger}$ = 0.7 e.u. La grande stabilité de ce composé est en contraste par rapport à celle du méthylène-4 pyrazoline-1 (**17**). [Traduit par le journal]

Can. J. Chem. Downloaded from www.nrcresearchpress.com by 210.87.254.5 on 09/05/12
For personal use only.

1-Pyrazolines have been studied intensively during the past several years with particular emphasis on the mechanism of their thermolysis (1) and photolysis (2), and on the fate of the resulting 1,3-biradical (3). These compounds

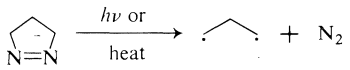

are useful in the synthesis of cyclopropanes (4) whereas the closely related 4-alkylidene-1-pyrazolines (5) are important precursors to trimethylenemethane biradicals (6).

Since it is known that the photostability of azoalkanes varies widely (7), a study of the effect of structure on the efficiency of pyrazoline decomposition was considered to be of interest. We have found that direct photolysis of 1-pyrazolines in solution generally proceeds with high quantum yield. Additionally, remarkably high thermal stability has been noted for a 4-alkylidene-1-pyrazoline.

Most of the compounds employed in this study were prepared by standard synthetic methods; thus, **2** and **6** were made by cycloaddition (3*a*) of a diazoalkane (4*c*,*e*) to an olefinic ester, **3** and **4** by oxidative addition to 3,5,5-trimethyl-2-pyrazoline (8, 9), and **8** by oxidative cyclization of the diaminoketone (10). Compound **5** was obtained from **2** by lithium aluminum hydride reduction (11) whereas **7** was made from **8** by treatment with isopropyllithium followed by dehydration (10).

The quantum yields for nitrogen evolution shown in Table 1 were obtained using the photolysis of 2,3-diazabicyclo[2.2.1]heptene-2 (DBH) as an actinometer. The data show that photolysis of 1-pyrazolines is an efficient process, approaching in some cases the unit quantum yield of DBH. This may be taken as a good omen for the general success of cyclopropane synthesis from 1-pyrazolines, in contrast to the less cooperative 2,3-diazabicyclo[2.2.2]octene-2 systems **10**–**13** (refs. 13, 14, 7, and 15, respectively). The only exceptions in Table 1 are 3-chloropyrazoline **4** and the 4-ketopyrazoline **8**.

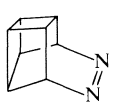

10

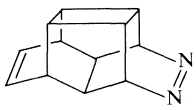

11

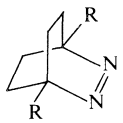

12

R = H, CH_3

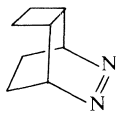

13

Compound **4** resembles the acyclic azoalkane **14**, which we have found to produce nitrogen

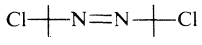

14

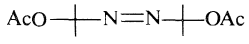

15

Can. J. Chem. Downloaded from www.nrcresearchpress.com by 210.87.254.5 on 09/05/12
For personal use only.

TABLE 1. Nitrogen quantum yields for 1-pyrazolines irradiated in benzene at 313 nm

Compound	Φ
1	0.88
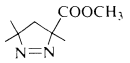 2	0.86
3	0.44
4	0.12
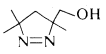 5	0.50
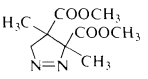 6	0.52*
7	0.45
8	0.012
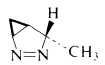 9	0.86†

*Reference 16.
†Reference 12.

with a quantum yield of only 0.01 (16). Levi and Malament (17) have recently discovered that this apparent inertness is due to facile, reversible conversion of such compounds to an unstable intermediate in which the α-carbon has lost its stereochemistry (probably an *N*-chlorohydrazone). This reaction may account for the lower nitrogen quantum yield in **4**. Diacetoxy azoalkane **15** undergoes reversible photodissociation into an acetate anion and an α-azo carbonium ion (17) at the expense of nitrogen extrusion ($\Phi_{N_2} = 0.005$) (16) but the related pyrazoline **3** still produces nitrogen with good efficiency. We tentatively suggest that the photoepimerization reactions have geometric requirements which are not entirely met in pyrazolines. An alternate but unsatisfactory explanation recognizes that the primary photochemical act in most acyclic azoalkanes is isomerization to the labile *cis* form rather than nitrogen extrusion. The quantum yield data are therefore consistent with the following order of reaction rates: pyrazoline nitrogen extrusion > photoepimerization > *trans–cis* isomerization. The problem here is that the first reaction is not faster than the third, as evidenced by the observation of fluorescence in pyrazolines but not in acyclic azoalkanes, even *cis* ones.

Pyrazoline **8**, which possesses a 4-keto group, decomposes very inefficiently. Interestingly, the reluctance of this material to lose nitrogen was responsible for the failure of Mock's otherwise elegant synthesis of tetramethylcyclopropanone (10). Although reversible photoionization is not an attractive explanation in this case, the actual reason for the photostability of **8** is still unknown. An interaction between the two functional groups is seen in the photoelectron spectrum (18) of **8** but it is not apparent how this leads to rapid radiationless decay. Looking into the photochemistry of **8** a bit further, we found that the gas produced consisted of a 3:1 ratio of carbon monoxide and nitrogen.

During the course of this study, an attempt was made to effect thermal decomposition of **7** and **8**. To our surprise, both compounds were very stable. Thus, heating **8** for 4.5 h at 205° gave only about 35% decomposition. A more detailed study of **7** gave the activation parameters shown in Table 2, along with those for three other pyrazolines. Since the activation energy for thermolysis of **17** is about 10 kcal mol^{-1} lower than that for **16**, one might expect the same trend in **1** *vs.* **7**. Instead, the addition of an isopropylidene group to **1** raises the activation energy by 2 kcal mol^{-1}. The resonance stabilization inherent in the trimethylenemethane moiety must be manifested in the transition state for thermolysis of **17** but not of **7**. This would be the case if loss of nitrogen required considerable bending of the C—N bonds into the plane of the olefin π bond. Whereas such a motion encounters little hin-

TABLE 2. Activation parameters for thermolysis of 1-pyrazolines

Compound	E_a (kcal mol^{-1})	$\Delta S_{200}^{\ddagger}$ (e.u.)	k_{rel} (200°)	Reference
16	42.4±0.3	11.5±0.6	1.0	1*a*
17	32.6±0.3	−0.9±0.5	68.4	5*d*, 20
1	37.7±0.4	4.9±0.8	5.4	1*a*
7	39.8±0.6	0.7±1.1	0.069	This work

drance in **17**, this process in **7** forces the *cis* 3 and 5 methyl groups into close proximity. The activation energy difference between **1** and **7** could be due to a difference in ground state ring strain, with **7** being more stable. Crawford *et al.* have made a more complete study of systems like **7** and have reached similar conclusions (19, 20).

Experimental

General

Ultraviolet spectra were run in hexane on a Cary 17 spectrophotometer. Nuclear magnetic resonance spectra were taken on a Varian A 56-60 in CCl_4 unless otherwise specified.

Synthesis

The published synthesis (21) of **1** was only minimally successful in our hands. The compound was purified by recrystallization from pentane at −78° followed by vacuum distillation, b.p. 74–75°/63 mm; u.v. λ_{max} 327 nm, ε 204. Pyrazoline **2** (11) was prepared in 63% yield from 2-diazopropane (4*c*) and methyl methacrylate, b.p. 69–71°/0.5 mm; u.v. λ_{max} 327 nm, ε 165. Lead tetraacetate oxidation (8) of 3,5,5-trimethyl-2-pyrazoline afforded compound **3** in moderate yield, b.p. 42.5°/0.1 mm; u.v. λ_{max} 330 nm, ε 214. Pyrazoline **4** was synthesized by an extension of the method used on phenylhydrazones (9). 3,5,5-Trimethyl-2-pyrazoline (4.6 g) (21) in 50 cc methylene chloride was cooled to −50° and chlorine gas was bubbled in. The initially cloudy solution became a clear, deep yellow within 15 min. After the solution had warmed to ambient temperature, the solvent was removed by rotary evaporation and the residue was distilled, b.p. 56°/10 mm; yield 4.2 g; u.v. λ_{max} 332 nm, ε 105; n.m.r. (deuteriobenzene): δ 1.10, 1.18, 1.67 (methyls), AB quartet centered at 1.44, J = 14 Hz (CH_2). Lithium aluminum hydride reduction of pyrazoline **2** followed by mercuric oxide oxidation gave **5** (11) in 47% overall yield, b.p. 74–75°/0.5 mm; u.v. λ_{max} 328 nm, ε 185; n.m.r. δ 1.26, 1.34, 1.40 (methyls), AB quartet centered at 1.37, J = 12.5 Hz (ring CH_2), AB quartet centered at 3.68, J = 11.9 Hz (CH_2). Compound **6** (λ_{max} 330 nm, ε 242) was a gift from S. R. Wilson while **7** (λ_{max} 324 nm, ε 162) and **8** (λ_{max} 356 nm, ε 164) were made without difficulty according to Mock's procedure (10).

Quantum Yields

0.05 *M* solutions of the pyrazolines were irradiated in a photochemical merry-go-round with 313 nm light isolated by an aqueous potassium chromate filter. Nitrogen yields were measured with a Töpler pump and gas buret and were compared with the gas yield from identical solutions of 2,3-diazacyclo[2.2.1]heptene-2.

Kinetic Studies

Approximately 0.01 *M* solutions of pyrazoline **7** in hexadecane were degassed and sealed into 1 cm Pyrex u.v. cells. These were heated six at a time in a high temperature silicone oil bath. Tubes were removed periodically and their absorbance determined on the Cary 17. The rate constants, which were computed using a least squares treatment, were as follows: (temperature °C, $k \times 10^4$ s^{-1}) 218.88, 0.772; 227.98, 1.641; 234.75, 2.750. The activation parameters are shown in Table 2.

The authors thank the Robert A. Welch Foundation and the National Science Foundation for financial support.

1. (*a*) R. J. CRAWFORD and A. MISHRA. J. Am. Chem. Soc. **88**, 3963 (1966); (*b*) J. W. TIMBERLAKE and B. K. BANDLISH. Tetrahedron Lett. 1393 (1971).
2. (*a*) R. MOORE, A. MISHRA, and R. J. CRAWFORD. Can. J. Chem. **46**, 3305, (1968); (*b*) G. L. LOPER and F. H. DORER. J. Am. Chem. Soc. **95**, 20 (1973).
3. (*a*) D. MCGREER, N. W. K. CHIU, M. G. VINJE, and K. C. K. WONG. Can. J. Chem. **43**, 1407 (1965); (*b*) C. G. OVERBERGER, N. WEINSHENKER, and J. P. ANSELME. J. Am. Chem. Soc. **86**, 5364 (1964); (*c*) M. SCHNEIDER and R. J. CRAWFORD. Can. J.

Can. J. Chem. Downloaded from www.nrcresearchpress.com by 210.87.254.5 on 09/05/12
For personal use only.

Chem. **48**, 628 (1970); D. H. WHITE, P. B. CONDIT, and R. G. BERGMAN. J. Am. Chem. Soc. **94**, 7931 (1972).
4. (*a*) D. C. PITTMER and R. GLASSMAN. J. Org. Chem. **35**, 999 (1970); (*b*) E. L. ALLRED and J. C. HINSHAW. J. Am. Chem. Soc. **90**, 6885 (1968); (*c*) S. D. ANDREWS, A. C. DAY, P. RAYMOND, and M. C. WHITING. Org. Synth. **50**, 27 (1970); (*d*) C. BERGER, M. FRANCK-NEUMANN, and G. OURISSON. Tetrahedron Lett. 3451 (1968); (*e*) G. W. COWELL and A. LEDWITH. Q. Rev. **24**, 119 (1970).
5. (*a*) P. DOWD. J. Am. Chem. Soc. **88**, 2587 (1966); (*b*) H. KATO. Chem. Commun. 496 (1968); (*c*) S. D. ANDREWS and A. C. DAY. J. Chem. Soc. **B**, 1271 (1968); (*d*) R. J. CRAWFORD and D. M. CAMERON. J. Am. Chem. Soc. **88**, 2589 (1966); (*e*) J. J. GAJEWSKI, A. YESHURUN, and E. S. BAIR. J. Am. Chem. Soc. **94**, 2138 (1972).
6. P. DOWD. Acc. Chem. Res. **5**, 242 (1972).
7. P. S. ENGEL and C. STEEL. Acc. Chem. Res. **6**, 275 (1973).
8. J. P. FREEMAN. J. Org. Chem. **28**, 885 (1963).
9. M. W. MOON. J. Org. Chem. **37**, 383 (1972).
10. W. L. MOCK. Ph.D. Thesis, Harvard University, Cambridge, Mass. 1964.
11. E. L. ALLRED and C. R. FLYNN. J. Am. Chem. Soc. **94**, 5891 (1972).
12. D. F. EATON. Ph.D. Thesis, California Institute of Technology, Pasadena, California. 1972.
13. J. P. SNYDER. Ph.D. Thesis, Cornell University, Ithaca, N.Y. 1965. Diss. Abstr. **26**, 5728 (1966); D. W. MCNEIL, M. E. KENT, E. HEDAYA, P. F. D'ANGELO, and P. O. SCHISSEL. J. Am. Chem. Soc. **93**, 3817 (1971).
14. J. A. BERSON and R. F. DAVIS. J. Am. Chem. Soc. **94**, 3658 (1972).
15. H. TANIDA, S. TERATAKE, Y. HATA, and M. WATANABE. Tetrahedron Lett. 5341 (1969).
16. P. S. ENGEL and D. J. BISHOP. Unpublished results.
17. N. LEVI and D. S. MALAMENT. Israel. J. Chem. In press.
18. K. N. HOUK, Y. M. CHANG, and P. S. ENGEL. J. Am. Chem. Soc. Submitted.
19. R. J. CRAWFORD and H. TOKUNAGA. Can. J. Chem. This issue.
20. R. J. CRAWFORD, D. M. CAMERON, and T. TOKUNAGA. Can. J. Chem. This issue.
21. R. J. CRAWFORD, A. MISHRA, and R. J. DUMMEL. J. Am. Chem. Soc. **88**, 3959 (1966).

Can. J. Chem. Downloaded from www.nrcresearchpress.com by 210.87.254.5 on 09/05/12
For personal use only.

Adsorption and Desorption of Hydrogen, Carbon Monoxide, and Their Reaction Products on a Catalyst for the Synthesis of Methanol

C. AHARONI AND H. STARER

Faculty of Chemical Engineering, Technion, Israel Institute of Technology, Haifa, Israel

Received January 29, 1974

C. AHARONI and H. STARER. Can. J. Chem. **52**, 4044 (1974).

Mixtures of hydrogen and carbon monoxide were adsorbed on a catalyst for the methanol synthesis and desorbed at increasing temperatures. The fraction of CO converted into methane increases when the ratio CO adsorbed to hydrogen adsorbed decreases, and when the temperatures of adsorption and desorption increase. Methanol is obtained in small amounts at high temperature, low pressure, and low $CO:H_2$ ratio. It is assumed that the surface is heterogeneous and that hydrogen and CO form an intermediate adsorbed compound converted into methane or methanol by reaction with adsorbed hydrogen.

C. AHARONI et H. STARER. Can. J. Chem. **52**, 4044 (1974).

On fait adsorbé des mélanges d'hydrogène et de monoxyde de carbone sur un catalyseur servant à la synthèse du méthanol et on effectue des désorptions en augmentant la température. La fraction de CO qui est transformée en méthane augmente quand le rapport de CO adsorbé/hydrogène adsorbé diminue; les mêmes effets sont obtenus lorsque les températures d'adsorption et de désorption augmentent. On obtient du méthanol en petite quantité à haute température, à basse pression et à des rapports $CO:H_2$ qui sont bas. On fait l'hypothèse que la surface est hétérogène et que l'hydrogène et le CO forme un composé intermédiaire adsorbé qui se transforme en méthane ou en méthanol par réaction avec l'hydrogène adsorbé.

[Traduit par le journal]

Can. J. Chem. Downloaded from www.nrcresearchpress.com by 210.87.254.40 on 09/05/12
For personal use only.

The mechanism of the methanol synthesis has been the subject of many investigations. A common approach consists of: (*a*) postulating a particular mechanism for each stage of the reaction: adsorption, surface reaction, and desorption, (*b*) combining the rate or equilibrium-state equations for the stages into an overall equation, (*c*) testing the overall equation for applicability to the experimental data. This approach has often led to useful analytical expressions for the measured kinetic data but it did not prove to be suitable for selecting without ambiguity the correct mechanism from a series of postulated ones. The overall equations inevitably contain too many arbitrary parameters, and the experimental data could be fit by equations derived from widely different models: Langmuir–Hinshelwood, Temkin–Pyzhev, and others. Each of the following reaction stages has been postulated, and assumed to be rate determining: adsorption of CO or H_2 (1), trimolecular reaction between adsorbed CO and adsorbed H_2 (2), reaction between the adsorbed surface compound CH_3O and an adsorbed hydrogen atom (3), Eley–Rideal reaction between a surface compound and gaseous H_2 (3, 4), two-step hydrogenation of adsorbed CO by adsorbed hydrogen (5), desorption of methanol (6).

An alternative approach consists of attempting to determine the appropriate equation for each stage from direct observation of its occurrence. This requires devising suitable experimental and theoretical procedures which allow the stage under consideration to be isolated or distinguished from the others. The main achievement of the investigations of this type has been the recognition of a relatively rapid interaction between adsorbed hydrogen and adsorbed CO leading to the formation of a surface compound poorer in hydrogen than methanol, which is presumably the precursor. Nagarjunan *et al.* (7), working with pure zinc oxide, noted that the adsorption of each of the reactants is enhanced by the presence of the other, and the composition of the adsorbed phase is independent of the partial pressures. Tsuchiya and Shiba (4) noted a similar effect at 250 °C with a commercial catalyst, $Zn:Cr:Cu = 1:0.49:0.16$ and took the average composition of the adsorbate (1.5 H_2 to 1 CO) as the stoichiometric composition of the surface compound. Aharoni and Tompkins (8) compared the kinetics of the mixed adsorption with that of the pure gases on pure ZnO at room temperature. The rates decrease exponentially with the amounts adsorbed in all cases, but the exponential factors change abruptly during

Can. J. Chem. Downloaded from www.nrcresearchpress.com by 210.87.254.40 on 09/05/12
For personal use only.

mixed adsorption; similar to those for the pure gases at the beginning they become smaller later on. The point at which this change occurs was taken as the point at which the rate of formation of the surface compound becomes equal to the rate of adsorption of the component. The ratio of the rates of adsorption after that point (1 H_2 to 1 CO) was taken as the stoichiometric ratio in the surface compound.

In an attempt to find out what happens to the surface compound after its formation, we performed a series of experiments in which CO and H_2 were adsorbed at 30 or 200 °C and the reaction products desorbed and analyzed at various temperatures (30, 200, and 400 °C, or 200 and 400 °C). At low temperature the adsorption of pure CO is largely reversible but adsorption of the CO–H_2 compound is not (8). We can assume therefore that the carbon-containing gases evolved at high temperature, after adsorption and desorption at 30 °C, are products of reactions involving the surface compound, via reduction, oxidation, or decomposition. At 200 °C complex formation also takes place, simultaneously with other reactions.

Experimental

The catalyst used was the commercial material, ICI, 25-1, containing zinc oxide and 12% chromia, in the form of pellets 5 × 5 mm. A sample weighing 72.33 g after evacuation at 400 °C was used for all the experiments.

The pretreatment consisted of (*a*) evacuating at 400 °C for ½ h, (*b*) reducing with hydrogen at the same temperature for 3 h (the pressure of hydrogen usually dropped from 100 to 1 Torr during that stage), (*c*) evacuating at 400 °C for 15 h to pressures of the order of 10^{-5} Torr. The pretreatment was performed before each adsorption run, but the pretreatment for the first runs (1 and 2) did not include reduction. In runs 3 and 8 to 11 the pretreatment was followed by presorption of hydrogen at 350 °C before adsorption of the CO–hydrogen mixture and with this procedure very large amounts of hydrogen were introduced into the adsorbed phase.

A conventional volumetric apparatus was used. Gas mixtures of known composition were prepared in two interconnected tubular vessels of known volume, and admitted into a cell containing the catalyst. The system was connected to a U-tube manometer and to the sample valve of a gas chromatograph, and changes in pressure and composition resulting from adsorption or desorption could thus be observed.

Desorption was induced by allowing the gas in the adsorption cell to expand into an evacuated vessel of the same size, for 10 to 15 min, and the process was repeated 7 to 12 times, until pressures of the order of 0.5 Torr were reached. The system was left for a few hours at these conditions and the change was finally less than 0.1 Torr per hour. The cell was subsequently heated to the higher temperature, 200 or 400 °C, and this produced desorption followed by readsorption (see Fig. 1). When no more changes could be observed, expansions were performed again and pressures of the order of 0.1 to 0.2 Torr were obtained. At the highest working temperature, 400 °C, expansions were followed by cooling for 2 h by means of a trap filled with liquid air, and the condensable gases evolved at this temperature (H_2O, CO_2, CH_3OH) could be desorbed at very low pressures.

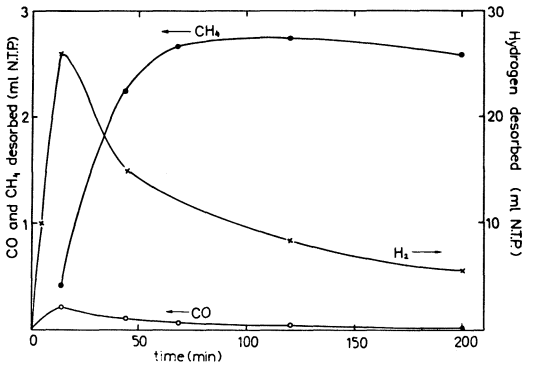

FIG. 1. Gases desorbed when the catalyst is heated to 400 °C, after adsorption and evacuation at 200 °C (run no. 11). The temperature of 400 °C is reached in about 20 min. The desorption was performed at constant volume, and therefore the partial pressure of each component is proportional to the amount desorbed, the maximum (at 14 min) corresponds to a total pressure of 92.9 Torr.

The gas chromatograph apparatus was a Packard 7622 equipped with a thermal conductivity detector. Two columns, both at 90 °C were used alternately. A 6 ft long column of Linde Molecular Sieve 5A (14 to 16 mesh) was used for the separation of hydrogen, methane, and carbon monoxide and a carbowax 1500 M column of the same length was used for the separation of water, methanol, and carbon dioxide. The limit of detection, for each product was around 0.01 ml at normal temperature and pressure.

Results and Discussion

The results are summarized in Tables 1 to 3. In the runs with adsorption at 200 °C (Table 1) the gas phase contains at the end of the adsorption stage, hydrogen and a small amount of methane; carbon monoxide is totally absent. Decrease of the pressure by repeated expansions results in the desorption of more hydrogen, but not methane or other carbon compounds. When the temperature is subsequently raised to 400 °C, the pressure increases as a result of desorption and the desorbed gases are H_2, CO, and CH_4. The desorption of methane increases steadily with the time, but hydrogen and carbon monoxide are readsorbed and

TABLE 1. Experimental results: adsorption at 200 °C, desorption at 200 and 400 °C

	Run number			
	7	8	9	11
At end of adsorption stage				
CO adsorbed (ml N.T.P.)	54.9	36.2	9.9	7.4
H_2 adsorbed (ml N.T.P.) (including H_2 presorbed)	109.9	101.3	78.7	64.8
H_2 presorbed (ml N.T.P.)	0†	62.8	38.4	25.0
Ratio CO adsorbed to H_2 adsorbed	0.500	0.358	0.126	0.114
CH_4 partial pressure (mm Hg)	0.4	0.4	0.5	0.5
CO and other C compounds partial pressure	0	0	0	0
H_2 partial pressure (mm Hg)	32.3	44.2	74.6	75.3
Time of adsorption (min)	3155	1100	1200	1450
Products in gas phase at end of desorption stages*				
1st stage 200 °C CH_4	0.027	0.022	0.080	0.100
CH_3OH, CO_2, CO	0	0	0	0
2nd stage 400 °C CH_4	0.075	0.13	—	0.84
CH_3OH	0	0	—	0.023
CO_2	0.63	0.14	—	0.13
CO, H_2	0	0	—	0
H_2O	0.02	0.09	—	0.12
CO undesorbed in any form	0.32	0.75	—	0.11

*The data refer to the total amount desorbed at the end of the desorption stage, *i.e.* after maintaining the system at the given temperature and at reduced pressure during a time sufficiently long so that no further change occurs, and including the amounts desorbed during the preceding stages. For the compounds containing carbon the data are given as ratios to the amount of adsorbed CO at the end of the adsorption stage and for hydrogen and water as ratios to the amount of adsorbed hydrogen.

†0, signifies "undetectable" with the analytical procedure used (see Experimental section).

neither remain finally in the gas phase (Fig. 1). Lowering of the pressure to 10^{-1} mm (by cooling the trap with liquid air) induces the desorption of substantial amounts of CO_2 and water. Methanol is detected only in one of the runs (run 11) at 400 °C and low pressure.

In the adsorption runs at 30 °C, (Table 2) the gas phase at the end of the adsorption stage contains hydrogen and CO or only CO and when the pressure is reduced more of the same gases are desorbed. Methane is desorbed when the temperature is raised to 200 °C. Reduction of the pressure does not induce further desorption, but heating to 400 °C does. Water and CO_2 appear at 400 °C and low pressures. Methanol is detected at the same conditions but only in runs 3 and 10. Hydrogen and CO are desorbed and readsorbed completely during heating to 200 and to 400 °C. With unreduced catalyst (Table 3), CO and hydrogen do not react and the only carbon-containing gases obtained are CO and CO_2. Carbon dioxide is formed more easily than on reduced catalyst and it is evolved in larger amounts at lower temperatures and higher pressures.

Methane formation depends both on the desorption conditions and on the conditions at the surface prior to desorption. In order to determine separately the effect of each of these factors on the yield we have plotted the ratio $CH_4(g):CO(a)$ against the ratio $CO(a):H_2(a)$, (Fig. 2); where $CH_4(g)$ is the total amount of methane desorbed at the end of any of the desorption stages, and CO(a) and $H_2(a)$ the

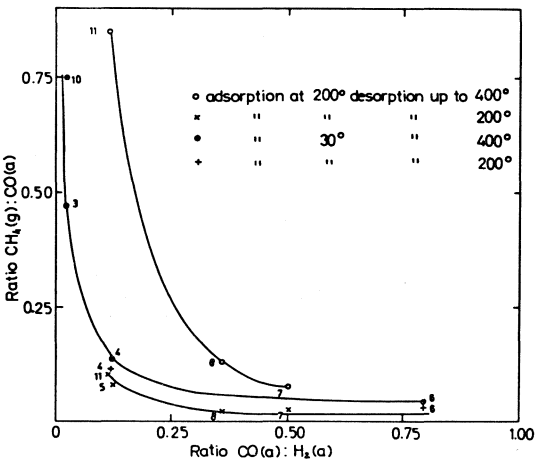

FIG. 2. Ratio $CH_4(g):CO(a)$ against ratio $CO(a):H_2(a)$. The figures near the points indicate the corresponding run.

Can. J. Chem. Downloaded from www.nrcresearchpress.com by 210.87.254.40 on 09/05/12
For personal use only.

TABLE 2. Adsorption at 30 °C desorption at 30, 200, and 400 °C*

	Run number				
	3	4	5	6	10
At end of adsorption stage					
CO adsorbed (ml N.T.P.)	1.4	1.5	10.3	7.9	1.4
H_2 adsorbed (ml N.T.P.) (including H_2 presorbed)	67.9	12.6	0	10.0	55.0
H_2 presorbed (ml N.T.P.)	64.7	0	0	0	39.7
Ratio CO adsorbed to hydrogen adsorbed	0.021	0.119	∞	0.79	0.025
CO partial pressure (mm Hg)	0.4	0.3	11.9	6.2	0.7
Other C compounds partial pressure	0	0	0	0	0
H_2 partial pressure (mm Hg)	35.1	16.4	0	0	3.3
Time of adsorption (min)	2610	1485	1365	2992	2995
Products in the gas phase at end of desorption stages					
1st stage 30 °C CO	0.5	0.6	—	0.14	0
Other C compounds	0	0	—	0	0
2nd stage 200 °C CH_4	—	0.107	0	0.041	—
CO, CH_3OH, H_2, H_2O	—	0	0	0	—
CO_2	—	0	0	Traces	—
3rd stage 400 °C CH_4	0.47	0.134	0	0.041	0.75
CH_3OH	0.022	0	0	0	0.021
CO_2	0.036	0.41	0.128	0.009	0.081
CO, H_2	0	0	0	0	0
H_2O	0.07	0.63	0	0.18	0.05
CO undesorbed in any form	0	0	—	0.81	0.15

*See Table 1 footnotes.

TABLE 3. Adsorption at 30 °C on unreduced catalyst

	Run 1	Run 2
Ratio H_2:CO before adsorption	pure CO	1:1
At end of adsorption stage		
Amount adsorbed (ml N.T.P.)	21.1	14.1
Final pressure (mm Hg)	78.1	16.7
Time of adsorption (min)	95	2489
At end of desorption stages		
CO_2 desorbed at 100 °C (ml N.T.P.)	0	1.1
at 200 °C (ml N.T.P.)	1.9	1.5
at 400 °C (ml N.T.P.)	4.3	1.6

amounts of CO and hydrogen on the surface at the end of the adsorption stage. The points in each plot refer to results at the same desorption temperature, with the pressure reduced in the same fashion to a low value, and with a sufficiently long desorption time until no further change was observed. The consistency of the plots obtained indicate that the fractional yield of methane depends on the conditions prior to desorption.

The following effects are noted (*1*) the yield $CH_4(g)$:CO(a) increases when the ratio CO(a):H_2(a) decreases, and the graphs are approximately hyperbolic (replotting against the ratio H_2(a):CO(a) gives fairly good straight lines); (*2*) the yield is low except when hydrogen is in very large excess. At favorable adsorption and desorption temperatures, and stoichiometric ratio (CO:H_2 = 1:2), less than 8% of the adsorbed CO gives methane, and in order to obtain a 80% yield a ratio CO:H_2 of 1 to 10 is required; (*3*) the yield depends on the temperature at which adsorption has taken place. For desorption between 200 and 400 °C and a

Can. J. Chem. Downloaded from www.nrcresearchpress.com by 210.87.254.40 on 09/05/12
For personal use only.

ratio $CO(a):H_2(a) = 0.11$, the yield is 13% if the reactants were adsorbed at 30 °C and 84% if they were adsorbed at 200 °C. However, the fraction of methane desorbed at 200 °C does not depend noticeably on whether the adsorption was performed at 30 or at 200 °C.

The dependence of the yield on the temperature of adsorption indicates heterogeneity of the surface. The low energy sites that subsequently give methane at 200 °C are occupied by the reactants at 30 as well as 200 °C. The higher energy sites that give methane at higher temperature are not easily occupied and consequently methane formation on them depends on the temperature of adsorption. For a homogeneous surface, evolution of an additional amount of methane above 200 °C after formation at that temperature has stopped could occur because of a change of the factors $\exp(-E/RT)$ or $\exp(\Delta H/RT)$ (where E is the energy of activation of formation and ΔH the heat of desorption); but the ratio between the amounts evolved above and below that temperature would not depend on the temperature at which adsorption has taken place. Another indication of the heterogeneity of the surface is the fact that hydrogen and CO are desorbed and readsorbed during heating. Presumably they leave the low energy sites and are adsorbed by the high energy ones.

The formation of methane is unaffected by changes of pressure; lowering of the pressure from a few cm of mercury to 10^{-1} mm does not induce further desorption. We conclude that all the methane formed is completely and irreversibly desorbed. The temperature at which this product evolves from a given reaction site is determined by the energy of activation for formation and desorption at that site but not by the enthalpy of adsorption. The fact that methane does not show any marked tendency to be readsorbed after its desorption when the temperature is increased (Fig. 1) is consistent with these assumptions.

The conditions under which methanol is obtained are different; high temperature (400 °C) and low pressure (10^{-1} mm Hg) are required. Obviously the last stage of its formation, the desorption, is a reversible process and the high temperature and low pressure are both required in order to favorably shift the equilibrium. This observation is not in contradiction with the well-known fact that pressure favors the formation of methanol in the conventional isothermal process. In our experiments the pressure refers to the partial pressures of the methanol and the other reaction products, whereas in the conventional process it refers to the partial pressures of the reactants as well as the products. The yield of methanol, in our experiments, is in relation to a given amount of adsorbed CO that depends on the partial pressure of that component during adsorption. The extremely low pressures required for the desorption of methanol are due to the fact that only the sites with the highest enthalpy of adsorption are used in the process. The catalyst containing adsorbed CO is submitted to evacuation at increasing temperatures, before it is submitted to the reaction temperature, and the CO adsorbed on sites of lesser energy has ample opportunity to desorb or to undergo other reactions beforehand.

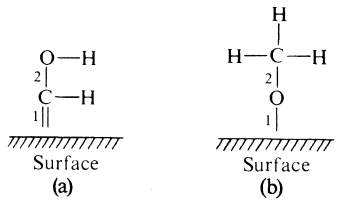

FIG. 3. Possible structures of the intermediate compound. (*a*) $H_2:CO = 1$, (*b*) $H_2:CO = 1.5$, both can give either methane or methanol.

Tables 1 and 2 show also that methanol is formed only when the ratio $CO(a):H_2(a)$ is sufficiently low (0.1 for adsorption at 200 °C and 0.02 for adsorption at 30 °C). This indicates that adsorbed hydrogen is involved in its formation as in the case of methane. It also indicates that methane is not produced as a result of further hydrogenation of methanol, otherwise the yield of methanol would have been decreased by a large excess of hydrogen. Probably both products derive from the same intermediate compound, the hydrogen–CO surface compound postulated in other works (4, 7, 8) in order to explain the results of mixed adsorption. We may assume either of the structures (*a*) or (*b*) of Fig. 3 (In (*a*) the ratio $H_2:CO = 1$ as postulated in ref. 8 and in (*b*) it is equal to 1.5 as postulated in refs. 4 and 9). Methanol is formed if bond *1* (carbon-to-surface, or oxygen-to-surface) is ruptured and hydrogenated. Methane is formed if bond *2* (carbon-to-oxygen) is ruptured and hydrogenated before bond *1*. Water is a product of

Can. J. Chem. Downloaded from www.nrcresearchpress.com by 210.87.254.40 on 09/05/12
For personal use only.

this reaction, and its presence has been noted in all the runs. If these reactions are assumed to be reversible, selectivity is determined by the readiness with which the products undergo the next step, *i.e.* desorption. In all the runs the catalyst containing the adsorbed species was kept for long periods of time at conditions at which only methane could be desorbed and therefore its formation was strongly favored.

The $CO–H_2$ intermediate compound does not necessarily undergo further hydrogenation to methane and methanol, the evolution of CO and hydrogen that takes place when the catalyst is heated (Fig. 1) points to some decomposition. When these gases are adsorbed separately at this temperature range they are not desorbed as such but as CO_2 and H_2O. The H_2 and CO evolved are therefore the products of some reaction, presumably the decomposition of the intermediate compound. Irreversible adsorption of hydrogen and carbon monoxide is also noticeable; they leave the surface as CO_2 and H_2O or remain adsorbed.

In conclusion, this work gives some indications about the characteristics of the surface hydrogenation of carbon monoxide. The reaction takes place in two stages. The first ending with the formation of an intermediate product takes place fairly rapidly and at a wide range of temperatures and adsorbate compositions. In the second stage two competing parallel reactions take place leading to the formation of methane and methanol. Both reactions occur with greater difficulty than the first stage reaction. They require higher temperatures and give smaller yields. The selectivity is determined by the desorption conditions, methane can be desorbed irreversibly at conditions where equilibrium does not favor the desorption of methanol. The second hydrogenation stage must also compete with the redecomposition of the product formed in the first stage and ending with the oxidation of CO and hydrogen without interaction. The heterogeneity of the surface adds further complexity to the system, the energies of activation of the intermediate reactions and the enthalpies of adsorption of reactants, products, and intermediates, depend on the adsorption sites involved and would vary with the temperature of the process. At isothermal conditions different reactions could take place on sites with different energies. At increasing temperature transfer of adsorbate from low energy sites to high energy sites takes place.

The gift of catalyst samples from I.C.I. Ltd., is gratefully acknowledged.

1. V. M. Cherednichenko and M. I. Temkin. Zhur. Fiz. Khim. **31**, 1072 (1957).
2. G. Natta, P. Pino, G. Mazzanti, and I. Pasquon. La chimica e l'industria, **35**, 705 (1953).
3. T. Saida and A. Ozaki. Bull. Chem. Soc. Jap. **37**, 1817 (1964).
4. S. Tsuchiya and T. Shiba. J. Catal. **4**, 116 (1965); Bull. Chem. Soc. Jap. **38**, 1726 (1965).
5. I. Pasquon. Chim. e industria, **42**, 352 (1960).
6. H. Uchida and Y. Ogino. Bull. Chem. Soc. Jap. **31**, 45 (1958).
7. T. S. Nagarjunan, M. V. C. Sastri, and T. Kuriacose. J. Catal. **2**, 223 (1963).
8. C. Aharoni and F. C. Tompkins. Trans. Faraday Soc. **66**, 434 (1970).
9. J. L. Borowitz. J. Catal. **13**, 106 (1969).

Can. J. Chem. Downloaded from www.nrcresearchpress.com by 210.87.254.40 on 09/05/12
For personal use only.

The Alkylation of Ambident Anions. IV. The Alkali Metal and Silver Salts of Formanilides[1,2]

ALLAN R. STEIN[3] AND SEE-HUA TAN

Department of Chemistry, Memorial University of Newfoundland, St. John's, Newfoundland A1C 5S7

Received June 27, 1974

ALLAN R. STEIN and SEE-HUA TAN. Can. J. Chem. **52**, 4050 (1974).

Systematic studies of the alkylation of a number of ambident or ambifunctional anions have been reported. For the vast majority of the anions examined reaction involved competition between carbon and a heteroatom and few competition between two heteroatoms. A study of the factors influencing the site of alkylation of the ambident anion of mono-*N*-substituted amides, where competition is between oxygen and nitrogen, has been undertaken. With the alkali metal and tetraalkylammonium salts of formanilide anions, the alkylation product is invariably the corresponding *N*-alkylformanilide. No detectable *O*-alkylation is observed as the solvent is varied from nonpolar through polar aprotic solvents, the alkylating agent through the various benzyl halides and *para*-substituted benzyl halides and the *para*-substituent on the formanilide from strongly electron donating ($-OCH_3$) through strongly electron withdrawing ($-NO_2$) groups. In contrast, with the silver formanilide salts, *O*-alkylation predominates but here the *O*:*N* alkylation ratio varies with the parameters examined. A rationale based on thermodynamic *vs.* kinetic control and reaction of dissociated *vs.* undissociated anion is presented to predict the site of reaction in these and other ambident systems.

ALLAN R. STEIN et SEE-HUA TAN. Can. J. Chem. **52**, 4050 (1974).

On rapporte les études faites sur l'alkylation de certains anions ambidentates ou ambifonctionnels. Pour la plupart des anions étudiés, la réaction fait intervenir une concurrence entre le carbone et un hétéroatome et peu de concurrence entre deux hétéroatomes. On étudie les facteurs qui influencent le site d'alkylation de l'anion ambidentate des amides *N*-monosubstitués où la concurrence se fait entre l'oxygène et l'azote. Avec les sels de métaux alcalins où les sels de tétraalkylammonium des anions formanilides, le produit de l'alkylation est invariablement le *N*-alkylformanilide correspondant. On n'observe pas de *O*-alkylation alors qu'on fait varier le solvant de nonpolaire à polaire aprotique, et qu'une variété d'halogénures de benzyle et d'halogénures de benzyle *para*-substitués servent à l'alkylation et que pour les substituants en *para* du formanilide on utilise une variété de groupes allant de groupes fortement donneurs d'électrons ($-OCH_3$) à des groupes fortement accepteurs d'électrons ($-NO_2$). Par contre, avec les sels d'argent du formanilide, la *O*-alkylation prédomine, mais ici le rapport d'alkylation *O*:*N* varie avec les paramètres examinés. On présente une explication logique pour prévoir le site de la réaction pour les systèmes ambidentates et aussi pour d'autres systèmes. Cette explication est basée sur une comparaison entre la thermodynamique et le contrôle cinétique d'une part et entre une réaction à anions dissociés et une réaction à anions non-dissociés d'autre part. [Traduit par le journal]

The term "ambident anion" was introduced by Kornblum *et al.* in 1955 (1) for anion systems containing two centers susceptible to electrophilic attack but in which only one of the centers takes part in the transition state of the electrophilic attack. Ambident or ambifunctional anions were, of course, known much earlier. For example the alkylation of polyhydroxylic benzene salts was first examined in the 1880's with carbon and oxygen alkylation being observed (2) and as early as the 1860's it was recognized that the reaction of silver cyanide with alkyl halides gave an isomer of the product obtained with potassium or sodium cyanide (3). Such ambifunctional nucleophilic species are far more commonly encountered than most practicing chemists realize. Gompper has, for example, listed some three dozen classes of compounds and anions exhibiting such behavior (4*a*). It is only in the past two decades however, that systematic studies of the factors involved in the competition between the nucleo-

[1]While not sequentially numbered, refs. 20, 21, and 6*a* are considered to be parts I, II, and III of this series.

[2]Taken in part from the M.Sc. Thesis of S.-H. Tan (1971), available on interlibrary loan from Memorial University of Newfoundland Library, St. John's.

[3]To whom correspondence should be addressed.

Can. J. Chem. Downloaded from www.nrcresearchpress.com by 210.87.254.42 on 09/05/12
For personal use only.

Can. J. Chem. Downloaded from www.nrcresearchpress.com by 210.87.254.42 on 09/05/12
For personal use only.

TABLE 1. A summary of the effect of some variables on the site of alkylation of phenol and pyrrole anions

Variable and change made	Effect of change on ambifunctional anion alkylation			
	Phenol anions	Reference	Pyrrole anions	Reference
Temperature; increasing	Increased *ortho*-carbon alkylation	22	Small increase in 2-alkylation	11
Counter ion; $R_4N^+ \rightarrow K^+ \rightarrow Na^+ \rightarrow Li^+(MgX^+)$	Increased *ortho*-carbon alkylation, slower reaction	22, 24	Greatly increased 2-alkylation	11, 23
Solvent; increasing polarity, aprotic	Increased oxygen alkylation	22, 24, 25	Increased *N*-alkylation	11
Solvent; aprotic to polar protic	Much *para*-carbon alkylation	26, 27	—	
Alkyl halide; saturated to allylic halide	Much increased *ortho*-carbon alkylation	22	—	
Substituents on anion electron donors	*meta*, increased *ortho*-carbon, *para*, increased oxygen alkylation	22, 20	—	
Physical state; homogeneous to heterogeneous reaction media	Increased *ortho*-carbon alkylation	22, 28, 6*a*	Increased 2-alkylation	11

Can. J. Chem. Downloaded from www.nrcresearchpress.com by 210.87.254.42 on 09/05/12
For personal use only.

philic centers of ambident anions for reaction with electrophiles have been undertaken (4). These studies have greatly increased the appreciation of the importance of solvent character and composition, of ion pairs, of counter ion and related factors in such systems and in fact in any chemical reaction.

In Table 1 are summarized the effects of some of the variables examined upon the competition between the nucleophilic sites for reaction with alkyl halides in two of the most extensively studied systems, the ambifunctional anions of phenols and pyrroles. Obviously the variables listed are not all independent. Changing the solvent, for example, from a nonpolar one like toluene to a better cation solvating one like dimethylformamide (DMF) also changes the degree of heterogeneity of the reaction mixture and the degree of S_N1–S_N2 character of the transition state for alkylation. The heterogeneity of the reaction is also affected by the counter ion and by temperature. Attempts to explain the empirical observations on the basis of the S_N1 *vs.* S_N2 character of the alkylation (1) or the homogeneity *vs.* heterogeneity of the reaction media (5) have met with dubious success (4*c*, 6).

The most extensively studied ambifunctional anions are the enolate (4, 7) and the phenolate or phenoxide anions (4, 6*a*, 8) for which the competition for alkylation is between carbon and oxygen (reaction 1).

[1] 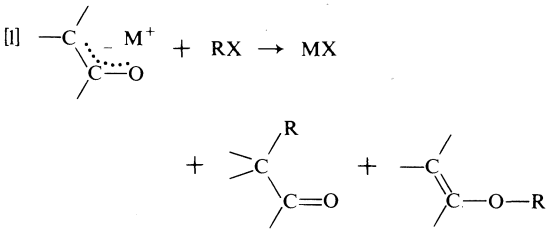

Other species studied to a greater or lesser extent include the cyanide (1, 18) and pyrryl anions (11), and the anions of the various esters, nitriles, etc. (4*a*) where the competition for alkylation is between carbon and heteroatom, usually oxygen, nitrogen, sulfur, or phosphorus. Relatively few systematic studies of anions in which there is competition between different heteroatoms have been reported. For example, the only ambifunctional anions in which alkylation competition between oxygen and nitrogen has been examined in any detail are the nitrite (1), 4-hydroxy-pyrimidine (9), pyridone (10), and oxime anions (4*c*). Consequently a systematic study of the factors influencing the oxygen–nitrogen alkylation competition on the salts of mono-*N*-substituted amides was undertaken.

[2] 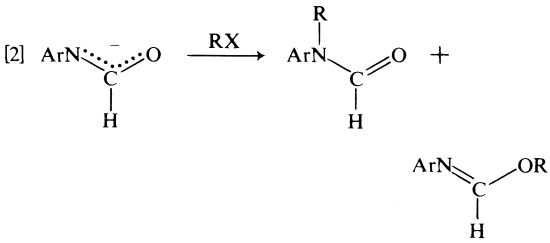

Nitrogen alkylation of the ambifunctional anion (reaction 2) would lead to the amide, *N*-alkylformanilide, while oxygen alkylation would lead to that class of product variously called imidate (ester of an imidic acid), imidoester, iminoether, etc. In this article the imidate nomenclature will be used so that for R = benzyl and Ar = C_6H_5, the oxygen alkylation product is benzyl *N*-phenylformimidate.

The anion of formanilide was chosen for the initial studies because the various formanilides are easily prepared, *para*-substituents on the aromatic ring can be readily varied from strongly electron donating to strongly electron withdrawing substituents with little or no steric effect at the reaction center, the substituent effect would be far more pronounced at one of the ambident centers (nitrogen) than at the other and, finally, there are no acidic carbon hydrogens as there would be with, for example, acetanilides which could lead to complications. The study of *N*-aryl or alkyl benzamides was contemplated but initial examination showed the benzimidate products from alkylation of benzanilide anions were not sufficiently thermally stable for gas chromatographic analysis.

Results

The system examined is summarized in Table 2. Tabulations of results appear in the Experimental Section and some generalizations follow.

The Alkali Metal and Tetramethyl Ammonium Salts

Typical results appear in Table 3.

Reaction Product

The exclusive detectable alkylation product was the *N*-alkylated amide, that is the corre-

TABLE 2. Alkylation of salts of formamides: the cases examined*

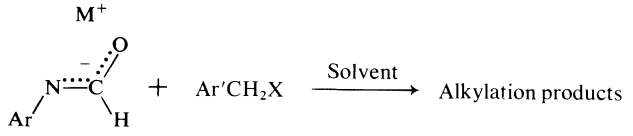

Ar	M^+	Ar′	X	Solvent
C_6H_5—	$[(CH_3)_4N^+]$	C_6H_5—	Cl	Hexane, hex
(*p*-$CH_3C_6H_4$—)	K^+	*p*-$CH_3OC_6H_4$—	Br	(Benzene)
p-$CH_3OC_6H_4$—	(Na^+)	*p*-BrC_6H_4—	I	Toluene, tol
p-BrC_6H_4—	Li^+	(*p*-$NO_2C_6H_4$—)		Dimethoxyethane, DME Dimethylformamide, DMF
(*p*-$NO_2C_6H_4$—)	Ag^+			(Dimethyl sulfoxide, DMSO)†

*Not all combinations and permutations were run but except for those cases enclosed within parentheses where relatively few reactions were run, a large number for each variable were done.
†DMSO was partially reduced to the sulfide and the imidates were unstable in basic DMSO. It was used for few reactions.

sponding *N*-benzylformanilide product in all cases.

Reaction Rate

Since the majority of the reaction mixtures were visibly heterogeneous, meaningful kinetic studies were not possible. Any rate constants obtained could represent some combination of the alkylation rates for the dissociated, the associated or ion-paired, and the solid salt or possibly the rates for dissociation or solution of the salt. Some generalizations can be reported though.

(*i*) Solvent effects: the more ionizing, better solvating solvents give a faster, more nearly complete reaction. For example, with the potassium salt of *p*-bromoformanilide with benzyl bromide at 22° for 40 h the alkylation yields in hexane, toluene, DME, and DMF were 46, 63, 95, and 96% respectively.

(*ii*) Cation effects: in all cases the lithium salt reacted more slowly with progressively smaller rate increases through the series Li^+, Na^+, K^+, $(CH_3)_4N^+$. For example the lithium salts in the less solvating solvents, hexane, toluene, and often even DME, required heating to give appreciable conversion. In hexane even prolonged heating normally gave 5% or lower yields. By contrast the potassium and tetramethylammonium salts react readily at room temperature even in hexane.

(*iii*) Alkyl halide structural effects: benzyl iodide reacted readily at room temperature almost invariably while in the less ionizing solvents, especially hexane and toluene, with the lithium salts benzyl bromide alkylations required a reflux period. Benzyl chloride itself would not react with the lithium salts in any of the solvents. Substituents on the benzyl halides had the anticipated effects; *para*-electron withdrawing substituents retarded, donors accelerated the reactions.

(*iv*) Formanilide substituent effects: formanilide substituents with the lithium salts in particular have the opposite effect to that one might predict. Thus with benzyl iodide in DME, lithium *p*-methoxyformanilide was only 64% alkylated after 3 h at reflux while the *p*-hydrogen analog was 87% converted, and at room temperature the latter was essentially stable but the *p*-bromoanalog was nearly 90% alkylated in 4 days.

The Silver Salts

Reaction Product

In marked contrast to the alkali metal salts, where the product was exclusively that of *N*-alkylation, with the silver salts the major product was almost invariably that of oxygen benzylation, the corresponding imidate. Here however both *O*- and *N*-alkylation products resulted and the *O*/*N* product ratio varied with the parameters examined. Some typical results appear in Table 4.

Reproducibility in the *O*/*N* ratios was very difficult to achieve. While the amide is quite inert, the imidate is very susceptible to hydrolysis (14). Removal of the products, especially the imidate, from the solid, unreacted silver formanilide and the silver halide co-product was difficult and especially so in the less polar hydrocarbon solvents. Consequently, the specific *O*/*N* ratios should be considered minimum

Can. J. Chem. Downloaded from www.nrcresearchpress.com by 210.87.254.42 on 09/05/12
For personal use only.

TABLE 3. Some reactions of alkali metal and tetraethylammonium formanilides

M^+	Formanilide	Benzyl	Halide	Solvent	Conditions*	Yield†
Li^+	*p*-H	*p*-H	I	DME	24 h	negl.
				DME	1 h, reflux	87%
				DMF	24 h	81.2
		p-H	Br	hex	3.5 h, reflux	4.8
				tol	3.5 h, reflux	2.1
				DME	2 h, reflux	95
				DMF	20 h	77
		p-Br	Br	DME	7 d	88
				DMF	7 d	98
		p-NO_2	Br	DME	6 d	88
		p-CH_3O	Br	DMF	3 d	94
		p-H	Cl	DME	36 h, reflux	negl.
		p-CH_3O	Cl	DMF	3 d	97
K^+	*p*-H	*p*-H	I	DME	1 d	95
				DMF	1 d	93.5
		p-H	Br	hex	20 h	85.5
				tol	20 h	95
				DME	20 h	93.5
				DMF	20 h	96
		p-Br	Br	DME	7 d	98
				DMF	7 d	98
		p-NO_2	Br	DME	6 d	74
		p-CH_3O	Br	DME	3 d	99
				DMF	3 d	91.5
		p-H	Cl	DME	2 d	<2
				DMF	2 d	98
		p-CH_3O	Cl	DME	3 d	88
				DMF	3 d	90.5
Et_4N^+	*p*-H	*p*-H	Br	DMF	3 h, 20 °C	82%
Li^+	*p*-CH_3O	*p*-H	I	DME	3 h, reflux	64
				DMF	3 d	83
		p-H	Br	hex	24 h	negl.
				hex	16 h, reflux	5
				tol	24 h	negl.
				tol	16 h, reflux	6
				DME	45 min, reflux	73
				DMF	48 h	74
K^+	*p*-CH_3O	*p*-H	I	DME	3 d	88
				DMF	3 d	79
		p-H	Br	hex	20 h	77
				tol	20 h	78
				DME	20 h	67
				DMF	20 h	66
Li^+	*p*-CH_3O	*p*-H	I	DME	4 d	89
				DMF	4 d	98
Li^+	*p*-Br	*p*-H	Br	hex	19 h, reflux	4.3
				tol	19 h, reflux	82
				DME	6 h	negl.
				DME	20 min, reflux	92
				DMF	48 h	86
K^+	*p*-Br	*p*-H	I	DME	4 d	92
		p-H	Br	hex	40 h	46
				tol	40 h	63
				DME	40 h	95
				DMF	40 h	96
Li^+	*p*-NO_2	*p*-H	I	DME	4 d	36
K^+	*p*-NO_2	*p*-H	I	DME	4 d	93

*Reactions were run at room temperature, 22 ± 1 °C unless otherwise stated.
†Yields are based upon weight of formanilide salt. No detectable formanilide was found in any reactions.

Can. J. Chem. Downloaded from www.nrcresearchpress.com by 210.87.254.42 on 09/05/12
For personal use only.

TABLE 4. Some reactions of silver formanilides

Formanilide	Benzyl	Halide	Solvent	*O*/*N* product ratio	Yield* (%)
p-H	*p*-H	I	hex	0.1–0.2	60–80
			tol	0.6–0.7	80–83
			DME	14–21	>85
			DMF	1.3	70
p-H	*p*-H	Br	hex	8	58–74
			tol	8.5	80–92
			DME	17	80–98
			DMF	1.4	72.5
p-H	*p*-H	Cl	All solvents, negl. reaction in 20 days at 22°		
p-H	*p*-Br	Br	hex	4.8	69
			tol	7.0	79
			DME	13.2	83
			DMF	2.0	97
p-H	*p*-CH_3	Br	hex	10.7	79
			DME	12.6	79
			DMF	1.6	78
p-CH_3O	*p*-H	I	hex	0.4	71
			tol	0.6	93
			DME	4.2	95
			DMF	0.8	80
p-CH_3O	*p*-H	Br	hex	3.7	78
			tol	12.2	67
			DME	8.8	58
			DMF	1.0	61.5
p-Br	*p*-H	I	hex	0.04	93
			tol	0.3	93
			DME	9.4	85
			DMF	0.9	76
p-Br	*p*-H	Br	hex	1.3	82
			tol	6.0	77
			DME	10	88
			DMF	0.5	77

*Reactions were run 2 or 3 days at 22° with continuous shaking and yields are based upon the weight of starting silver salt and analysis of the product solution.

values, at best approximations, and interpreted with care. Some generalizations can, however, be made about the product distribution.

(*i*) Solvent effects: *O*/*N* ratio increases in going from hexane to aromatic hydrocarbons to DME where it normally maximizes and then decreases markedly in DMF.

(*ii*) Halide structural effects: in DMF, the *O*/*N* ratio is comparatively independent of the choice of benzyl halide and is about one. In the nonpolar hydrocarbon solvents benzyl iodide gives a markedly lower *O*/*N* ratio than benzyl bromide while in DME the ratios maximize and are about equal for the two halides. With benzyl bromide *para*-electron withdrawing substituents apparently decrease, donors increase the ratio in the less polar solvents.

(*iii*) Formanilide substituent effects: both electron donors and electron withdrawing *para* substituents lead to reduced *O*/*N*-benzylation ratios.

Reaction Rates

All reactions tabulated were run for 2 or 3 days at room temperature with continuous shaking and the variation in degree of completion in duplicate reactions using different salt preparations was often of the same order as that with different solvents, alkylating agents, and formanilides. No conclusions concerning rates can be reached.

Can. J. Chem. Downloaded from www.nrcresearchpress.com by 210.87.254.42 on 09/05/12
For personal use only.

Can. J. Chem. Downloaded from www.nrcresearchpress.com by 210.87.254.42 on 09/05/12
For personal use only.

Discussion

Since a difference in activation energy of only a few kcal/mol would result in a 100:1 product ratio, the activation energies must be nearly equal to get similar amounts of the two products in ambident anion alkylations. Imidates thermally rearrange to the corresponding *N*-substituted amide, a reaction known as the Chapman rearrangement (13). Under conditions where the amide is comparatively stable, imidates rapidly hydrolyze (14). Calorimetric studies have not been done but bond strength or bond dissociation energy values can be used to estimate the difference in stability between the imidate and amide. Unfortunately, values for bonds in appropriate systems are not readily available but by assuming that the only difference between the two products is that in the imidate, two C—O bonds and a C=N bond replace the appropriate C—N bonds and the C=O bond of the amide, the imidate can be estimated to be at least 3 kcal/mol higher in energy.

Imidates then are clearly thermodynamically less stable than the isomeric amide so that via the Hammond Postulate, the transition state for *N*-alkylation should lie lower than that for *O*-alkylation. The difference in activation energy for *N*- or *O*-alkylation would presumably be lower than the difference in product stability but should be an appreciable fraction of it.

Under what conditions would *O*-alkylation or *N*-alkylation of the formanilide anion be expected? Obviously when the alkylation proceeds by a mechanism which approximates thermodynamic control, the more stable *N*-alkylated formanilide will be the almost exclusive product. Only under reaction conditions where kinetic rather than thermodynamic product control occurs could *O*-alkylation be significant. In the alkylation of solvated or free anion the reaction would be expected to approach thermodynamic control since there should be no factors other than the energetic requirements favoring one product over the other. In the case of the alkylation of ion paired, aggregated, or crystalline salt, however, kinetic product determination is possible. If the counter ion is associated principally with one site of the ambifunctional species, that atom should be sterically and electronically less favorable for attack by the alkylating agent. The prediction then is that with the free or solvated formanilide anion, only *N*-alkylation would be observed while for associated material, when the counter ion is associated with nitrogen, oxygen alkylation should be favored. When the counter ion is associated with oxygen, nitrogen alkylation should again predominate. The predictions should apply whether the transition states are analogous to those proposed for phenolate alkylations (5) with linear, "classical" S_N2 displacement of the leaving group of the alkylating agent (here the negative charge would be developing on a leaving group far removed from the counteracting charge of the cation) or if bent, six center transition states occur.

In other systems, the rate of alkylation of dissociated material is invariably much higher than that of associated material (4*c*, 15). Thus in the more ionizing, better solvating solvents where appreciable concentrations of dissociated formanilide are present and equilibrium between associated and dissociated material should be maintained throughout the reaction, the thermodynamically favored *N*-alkylated product forms. Even if the reaction mixture is visibly heterogeneous, the reaction could occur almost exclusively on the dissociated anion especially with the tetraethylammonium and potassium salts (where the cation requires less solvation than for example the smaller lithium cation) in DMF and progressively less so in DME, the aromatic and saturated hydrocarbon solvents. At the other extreme, the concentration of the dissociated species would be extremely low for lithium formanilides in the nonionizing solvents like hexane so that the usually slower reaction of associated material, the heterogeneous reaction, would be the dominant one. Here kinetic control of the reaction still leads to the thermodynamically more stable product, that of *N*-alkylation.

The observation that especially with the lithium salts, electron withdrawing substituents in the *para*-position of the formanilide leads to a rate acceleration in DME, for example, rather than the retardation expected on electronic grounds is understandable in light of the above explanations. The electron withdrawing substituent further distributes the negative charge of the formanilide anion reducing the solvation necessary for dissociation, the concentration of the free anion is increased, and the faster reaction of the dissociated anion makes a larger contribution to the overall reaction rate.

In the cases reported here, both the homo-

Can. J. Chem. Downloaded from www.nrcresearchpress.com by 210.87.254.42 on 09/05/12
For personal use only.

geneous and the heterogeneous reactions of the alkali and tetramethylammonium cations lead to *N*-alkylation. These cations, if the proposed heterogeneous mechanisms are correct, must be associated with oxygen of the ambident formanilide anion. This is predicted by the theory of hard and soft acids and bases (16). While the lithium cation is "softer" than the potassium cation, all the alkali metal cations are considered to be "hard". Oxygen carrying a negative charge is "harder" than nitrogen. Since "hard" cations would associate with the "harder" oxygen center of the ambifunctional anion, *N*-alkylation occurs. With "soft" cations association would be at the "softer" nitrogen and oxygen alkylation should become important. The silver cation is "soft" and a standard route to the imidates is the alkylation of the silver salt of the corresponding mono- *N*-substituted amide (17).

Even with the silver counter ion, there would still be a competition between alkylation of dissociated and associated anion. Reaction of the dissociated species should be analogous to the alkylation of dissociated formanilide in the presence of any other cations and would be expected to lead to the thermodynamically more stable *N*-alkylated formanilide. Undissociated silver formanilide with the "soft" silver counter ion associated with the "softer" nitrogen would be expected to give principally *O*-alkylation through the kinetically controlled reaction. Thus in DMF where the degree of dissociation should be greatest among the solvents employed, the thermodynamically more favored amide product is more important than in DME where the degree of dissociation is lower.

It is perhaps initially surprising that the amount of *O*-alkylation falls off again in the least ionizing solvents employed, the hydrocarbons. There must be a change in mechanism. In these solvents with very low dielectric constant, even moderate separation of the ionic centers would be energetically undesirable so that a four-center reaction involving silver, halide, formanilide, nitrogen, and the halide carbon is a likely competitive transition state. Such a transition state would be more favorable for the iodide than bromide alkylating agent because the "soft" silver cation would form a more stable system with the "softer", larger iodide (16). With benzyl bromide, electron donors in the *para*-position would be expected to favor, withdrawers to disfavor this four center ion pair exchange mechanism.

Similar rationalizations and predictions of the sites of reaction for other ambifunctional anions with alkylating agents can be made. Given information as to which product's formation is thermodynamically favored, which center of the anion is "harder" or "softer", and assuming that reaction of dissociated material approaches thermodynamic product control while reaction of associated material is principally at the site not occupied by the counter ion, the empirical observations in the following illustrative examples are those that would be predicted.

The anion of pyridone is an ambident species somewhat analogous to the formanilide anion. Both oxygen and nitrogen alkylation can occur and while the products are more nearly equal in stability, *N*-alkylation is thermodynamically preferred at least for the less sterically demanding alkyl halides (10*b*). Again oxygen is the "harder" site. As expected on alkylation with benzyl bromide, the sodium salt in nonpolar or polar aprotic solvents gives predominantly *N*-benzylated product. The silver salt in nonpolar solvents (pentane or benzene) gives exclusively *O*-benzylation but in DMF the *O*/*N* ratio is nearly 1 (10).

Another anion in which there is competition between oxygen and nitrogen and in which the nitrogen is the "softer" center and leads to the more stable product, is the nitrite ion. Silver nitrite gives far more of the nitrite ester and less of the nitroalkane than does the sodium salt and solvent effects are logical (1). The cyanide ion has long been known to give alkyl cyanides or the considerably less stable isocyanides (17) depending upon the cation (1). Here nitrogen is the "hard" center and alkali metal cyanides give alkyl cyanides regardless of whether the solvent used is polar, nonpolar, protic, or aprotic (18). With "softer" cations like Ag^+, Cu^+, Hg^+, Zn^{2+} which associate at the "soft" carbon, alkylation occurs predominantly on the more available nitrogen, but in the more ionizing solvents more alkyl cyanide is found (18).

Experimental Section

Solvents

All solvents were reagent grade, thoroughly dried, and distilled in oven-dried glassware under a nitrogen atmosphere immediately before use. Hexane, benzene, toluene, and dimethoxyethane (DME) were dried by

Can. J. Chem. Downloaded from www.nrcresearchpress.com by 210.87.254.42 on 09/05/12
For personal use only.

refluxing over sodium wire for some hours before distillation while dimethylformamide (DMF) was heated at 50° over calcium hydride for at least 24 h before vacuum distillation.

Formanilides

Formanilide obtained from Eastman Organic Chemicals was twice recrystallized from aqueous ethanol and dried as below. Substituted formanilides were prepared from the corresponding *para*-substituted anilines available from Eastman or Aldrich Chemical Co. The anilines were refluxed with a three- to five-fold excess of formic acid for 2–4 h, the excess formic acid and water were distilled, and the residue treated with a fresh portion of formic acid if necessary to increase conversion. The residue was cooled, allowed to crystallize, the solid broken into small pieces and then repeatedly washed with ice water until the washings were no longer acidic. Sharp melting, analytically pure colorless (except for the yellow *para*-nitro analog) crystals were obtained after several recrystallizations from aqueous ethanol and drying in a vacuum desiccator over phosphorus pentoxide.

Benzyl Halides

Benzyl chloride, bromide, and iodide were obtained from Aldrich and purified by vacuum fractionation. The purity of the *p*-methoxybenzyl chloride, *p*-methyl-, and *p*-nitrobenzyl bromide from Eastman and the *p*-bromobenzyl bromide from Aldrich was checked by gas chromatography and all were used without purification. *p*-Methoxybenzyl bromide was prepared according to Kornblum *et al.* (1) and used immediately.

Formanilide Salt Preparation and Alkylation

All glassware was oven dried, all manipulations were performed in a nitrogen filled drybox, and all reactions were conducted under a slight positive pressure for dry nitrogen.

Lithium Formanilides

Into a 500 ml flask containing 0.105 mol of formanilide, 200 ml of DME was distilled and after the formanilide was completely dissolved, 0.794 g (0.100 mol) of lithium hydride was added. The flask, equipped with a condenser topped by a dry nitrogen source and bubbler was slowly heated to reflux in an oil bath while being stirred magnetically. Hydrogen evolution commenced at about 50° and the white lithium formanilide salt gradually deposited at gentle reflux. Hydrogen evolution usually ceased after about 5 h but reflux was continued several additional hours. The flask was cooled, transferred to the drybox, and the white salt collected by suction filtration through a sintered glass funnel. After several washings with cold DME, the salt was sucked dry, transferred to a tarred 250 ml flask, heated at 50–60°, and pumped overnight to remove the last traces of solvent. Yields normally exceeded 90%.

Potassium and Sodium Formanilides

The procedure used was analogous to that for the lithium salt except that 0.100 mol of freshly cut and trimmed alkali metal was used and benzene replaced the DME. (Benzene was used as the solvent because, especially the potassium salts, were moderately soluble in DME.) With potassium, the reaction proceeded rapidly when the metal began to fuse. Sodium was coated with a layer of salt, reaction was slow and completion difficult to achieve. Yields exceeded 90% for the potassium salts.

Purity of the Alkali Metal Formanilides

Titrimetric determination of the neutralization equivalents by titrating an aqueous solution to the phenolphthalein end-point with standard hydrochloric acid showed the salts to almost invariably have an excess alkalinity of about 2%. In the case of the lithium salts this was mainly due to LiOH impurity in the hydride used. With potassium and especially the sodium salts which were little used for that reason, there were occasionally minute, salt encrusted globules of unreacted metal present. While some hydroxide would also invariably be present there was no apparent difference in the alkylation results when no or when considerable excess alkalinity was shown, only salt with 98% or greater titrimetric purity was used.

Tetraethylammonium Formanilides

The silver formanilides were prepared according to Comstock and Kleeberg (19) and about 0.025 mol was stirred in the dark for 3 days with a molar equivalent of tetraethylammonium chloride (Aldrich) in 60 ml of dry DME. The quantitatively precipitated silver chloride was removed by suction filtration in the drybox, the DME removed at 28–30° under vacuum, and the residual salt used without further purification.

Silver Formanilides

Silver formanilides and the substituted formanilides were prepared, collected, and purified by a process analogous to that of Comstock and Kleeberg (19) and dried over P_2O_5 in a vacuum desiccator for several days. The salts were protected from light throughout by subdued lighting and by wrapping flasks, etc. in aluminum foil. Yields of dry, finely ground powder were over 90%. Purity was checked by igniting a sample of 0.5–0.7 g of the silver salt in a porcelain crucible. The residual silver metal was taken up in 3 *N* nitric acid, any carbon and other residues removed by filtration, and the silver determined as silver chloride. Typical silver contents, determined and theoretical values respectively, are: silver formanilide 46.0%, 47.32%; silver *p*-methoxyformanilide 41.8%, 40.9%; silver *p*-bromoformanilide 35.1%, 34.6%. Because the silver formanilide salts smoked extensively on ashing, a very fine, powdery ash formed initially and even prolonged heating over a burner did not oxidize the last of the carbon, duplicate and triplicate runs normally agreed only to within about 2%.

General Alkylation Procedure

All manipulations were done in a nitrogen filled drybox and the silver salts were protected from light throughout. About 40–50 ml of the solvent chosen was distilled into a 100 ml flask containing 0.01–0.02 mol of finely ground formanilide salt. A 5% excess of the appropriate benzyl halide (neat if it was a liquid, in a small amount of the solvent if solid) was dropped in with stirring or swirling. The flask was stoppered and allowed to stand with either occasional stirring or shaking in the drybox or

TABLE 5. Melting points and elemental analyses of *O*- and *N*-alkylated products

		N-Alkylated product		*O*-Alkylated product		
R_1*	R_2*	M.p. (°C)	Found	M.p. (°C)	Found	Calculated
H	H	48 (lit. 48)		13–14	C: 79.59 H: 6.15 N: 6.56	C: 79.60 H: 6.20 N: 6.62
H	CH_3	45	C: 79.88 H: 6.68 N: 6.19	69	C: 80.11 H: 6.80 N: 6.25	C: 80.00 H: 6.66 N: 6.22
H	CH_3O	69	C: 74.43 H: 6.06 N: 6.00	†	†	C: 74.69 H: 6.22 N: 5.81
H	Br	77	C: 57.83 H: 4.15 N: 4.64 Br: 27.57	79–80	C: 57.89 H: 4.33 N: 4.87 Br: 27.34	C: 57.93 H: 4.13 N: 4.83 Br: 27.58
CH_3O	H	48.5–49	C: 74.59 H: 6.11 N: 5.86	80.5	C: 74.55 H: 6.39 N: 5.91	C: 74.69 H: 6.22 N: 5.81
Br	H	61.5	C: 57.72 H: 4.33 N: 4.63 Br: 27.35	71.5–72	C: 57.75 H: 4.20 N: 4.73 Br: 27.53	C: 57.93 H: 4.13 N: 4.83 Br: 27.58
NO_2	H	100				
H	NO_2	100.5–101				

*R_1 and R_2 are, respectively, the *para*-substituent on the formanilide and on the benzyl halide used to prepare the particular alkylated formanilide.
†Thermal rearrangement of the *O*- to *N*-alkylated product upon distillation prevented isolation of analytical samples.

with continuous shaking with a mechanical shaker for 4 h to 4 days at room temperature except for the lithium salts which were usually refluxed in hexane and DME to shorten the reaction time. No change in the alkylation product composition was observed with reaction time and *N*-alkylated or *O*-alkylated formanilide added to the reaction was recovered quantitatively in the products. The reaction mixture was suction filtered and the solid, a mixture of unreacted formanilide salt and of metal halide, was washed with several small fractions of fresh solvent. The filtrate volume was noted and it was subjected to quantitative gas chromatographic analysis. The column packing was 1.5% OV-17 on 60–80 mesh Chromosorb G in a 10-ft, 1/8 in. o.d. stainless steel column except for the analysis of products with *p*-bromo- or *p*-nitro- substituents where a 6 ft column was used. The thermal conductivity detector was calibrated for each formanilide and corresponding *N*- and *O*-alkylation product. With a 45 ml/min helium flow rate at 227° for the unsubstituted and 255° for the mono-substituted cases, the formanilides had a retention time of 0.5–1.2 min, the formimidates about 2.5 min, and the *N*-benzyl formanilide about 3.5 min. Unreacted benzyl halide eluted immediately after the solvent.

Detection limits for the unreacted and alkylated formanilides ranged from less than 0.3% yields for recovered unsubstituted formanilide and the corresponding formimidate to about 0.75% yields of the disubstituted *N*-benzylformanilides. No measurable formimidate was found in any of the alkylations of alkali metal or tetramethylammonium formanilide salts. Usually 95% or more of the starting formanilide was accounted for by products and/or recoverable from unreacted salt. Alkylation product yields and, for the silver salts, *O*/*N* product ratios are reported in the accompanying tables.

Preparation and Purification of the N-Alkylation Products

The *N*-alkylation products could be isolated in fair to good yields from the appropriate lithium or potassium formanilides after reaction with the benzyl halide usually in DME. A 1:1 molar ratio of reactant and halide in DME was refluxed for 3–4 h, the solvent was stripped off, and the residue taken up in ether and water. The ethereal extracts were dried over $MgSO_4$ and concentrated. After 2–3 recrystallizations from ether analytically pure *N*-benzyl formanilides were obtained in overall yields of about 50%. Melting points and analyses are reported in Table 5 while some spectral data appears in Table 6.

Preparation and Purification of the O-Alkylation Products

The crude formimidates were obtained from the benzylation of the appropriate silver formanilide in DME. Separation from the *N*-alkylation product was achieved by collection from the gas chromatograph using an 8 ft, 1/4 in. o.d. stainless steel column packed with the same material as the analytical column run under similar conditions. Liquid materials were purified

Can. J. Chem. Downloaded from www.nrcresearchpress.com by 210.87.254.42 on 09/05/12
For personal use only.

TABLE 6. Spectral data of *N*-alkylated formanilides

R_1	R_2	Infrared C=O (cm^{-1})	Nuclear magnetic resonance (τ)* H—C=O	—CH_2—	CH_3—	Ultraviolet (mμ)† λ_{max}(log ε)	Mass spectra (mass unit) Base peak	Parent peak (%)
H	H	1666	1.40	4.97		233(3.91)	91	211(47.75)
H	CH_3	1666	1.54	5.00	7.68	222(4.01)	105	225(22.80)
H	Br	1669	1.42	5.05		225(4.20)	169	289(39.47)
							171(96.49)	291(38.60)
H	CH_3O	1669	1.44	5.03	6.26	227(3.98)		
						285(sh)		
Br	H	1666	1.42	5.00		243(4.23)	91	289(12.75)
								291(12.75)
CH_3O	H	1675	1.75	5.06	6.31	230(4.02)	91	241(60.75)
						280(sh)		
NO_2	H	1670	1.07	4.85				
H	NO_2	1666	1.32	4.85				

*All show singlet absorption, the aromatic protons are multiplet and are not reported.
†Determined in methanol, measured from 220 mμ.

TABLE 7. Spectral data of *O*-alkylated formanilides

R_1	R_2	Infrared (cm^{-1}) C=N	C—O—C	Nuclear magnetic resonance (τ)* H—C=N	—OCH_2—	CH_3—	u.v.(mμ)† λ_{max}(log ε)	Mass spectra (mass unit) Base peak	Parent peak (%)
H	H	1644	1160–1200	2.29	4.73		248(4.17)	91	211(16.57)
H	CH_3	1636	1150–1200	2.23	4.73	7.66	248(4.14)	105	225(13.10)
H	Br	1639	1150–1200	2.20	4.73		220(4.35)	169	289(18.80)
							250(sh)	171(98.50)	291(18.80)
Br	H	1647	1150–1205	2.20	4.69		252(4.03)	91	289(5.55)
									291(5.55)
CH_3O	H	1647	1170–1210	2.10	4.67	6.22	250(4.01)	91	241(71.92)
							290		
							295		

*All show singlet absorption, the aromatic protons are multiplet and are not reported.
†Determined in hexane, measured from 220 mμ.

by distillation at 65° or lower under the appropriate pressure (about 0.05 mm Hg), solids by repeated sublimation at similar pressures and temperatures 5° below their melting points. Samples were deemed pure when they were sharp melting if solids, gave only formimidate peaks on the gas chromatograph, and no carbonyl absorption was present even at high concentration in the infrared. Melting points and analytical results appear in Table 5 while in Table 7 some spectral data are presented.

Calibration of the Gas Chromatograph

Various concentrations in the appropriate range of the parent formanilide and the *N*- and *O*-alkylation products were prepared in the solvents employed for this study and constant volumes (5 μl) injected into the gas chromatograph. Calibration curves based upon the disc integrator area values were linear and were used to calculate the concentrations and yields of products for the individual alkylations.

Control Studies

Tests for the Rearrangement of Benzyl N-Phenylformimidate

To each of two flasks containing 5.70 g (0.025 mol) of silver formanilide, 50 ml of freshly distilled dry DMF was added. To one of the flasks 1.70 g of benzyl *N*-phenylformimidate was added and 4.20 g (0.025 mol) of benzyl bromide was added slowly to each flask. After 3 days at room temperature with continuous stirring the usual product work-up and analysis showed the control to contain 2.40 g of the formimidate and 0.66 g of *N*-benzyl formanilide while the reaction with 1.70 g of the formimidate added contained 4.10 g of formimidate and 0.65 g of the *N*-benzyl formanilide. The conversion was 58% in both cases. Similarly, all added formimidate appeared in the product of a 7-day reaction and in reactions in DME and hexane with benzyl bromide and iodide after 18 h of reflux with either silver or potassium salts. No rearrangement was taking place under the reaction conditions.

Test for Moisture Sensitivity

Since the formimidates are known to be much more sensitive to hydrolysis than are the *N*-alkylation products (14) controls with added water were performed. A series of four reactions were done in each of DMF and DME. In each solvent, 4.50 g (0.02 mol) of silver formanilide was dissolved in 50 ml of the solvent, 2.40 g (0.02 mol)

Can. J. Chem. Downloaded from www.nrcresearchpress.com by 210.87.254.42 on 09/05/12
For personal use only.

of benzyl bromide was added. To the solvent in two reactions, no water was added, the other two had 0.45 g (0.025 mol) and 0.90 g (0.050 mol) of water added. For the four reactions in DMF the quantities of formimidate were in the ratio 1, 1, 0, 0; *N*-benzyl formanilide 1, 1.2, 2, 2, and formanilide (*i.e.*, formanilide in solution in DMF, not total unreacted material) 1, 1, 2, 2. Also more than five times as much benzyl alcohol was detected in the reactions with added water but at most trace amounts of aniline were present in the aqueous runs. The lack of *O*-alkylation product was clearly not due to hydrolysis of that product but due to little or no product being formed.

In contrast to the results in DMF, in DME the *O*/*N* alkylation ratio was not consistently affected but the alkylation yield was reduced with the bulk of the water accounted for in benzyl alcohol and free formanilide in the solution.

The authors gratefully acknowledge the financial support of Memorial University of Newfoundland without which this study could not have been undertaken.

1. N. KORNBLUM, R. A. SMILEY, R. K. BLACKWOOD, and D. C. IFFLAND. J. Am. Chem. Soc. **77**, 6269 (1955).
2. J. HERZIG and S. ZEISEL. Monatsch. **9**, 217, 882 (1882); **11**, 291, 311 (1890); W. WILL. Chem. Ber. **21**, 602 (1888).
3. W. LIEKE. Ann. **112**, 316 (1859); A. GAUTIER. Ann. Chim. Paris, [4] **17**, 103, 203, 218 (1869); Ann. **142**, 289 (1867); **146**, 119, 124 (1868); **149**, 29, 155 (1869); **151**, 239 (1869).
4. (*a*) R. GOMPPER. Angew. Chem. Int. Ed. **3**, 560 (1964); (*b*) W. J. LENOBLE. Synthesis, **2**, 1 (1970); (*c*) S. G. SMITH and M. P. HANSON. J. Org. Chem. **36**, 1931 (1971); (*d*) S. A. SHEVELEV. Usp. Khim. **39**, 1773 (1970); Russ. Chem. Rev. **39**, 844 (1970).
5. N. KORNBLUM and A. P. LURIE. J. Am. Chem. Soc. **81**, 2705 (1959).
6. (*a*) D. Y. CURTIN and A. R. STEIN. Can. J. Chem. **47**, 3637 (1969); (*b*) A. L. KURTS and I. P. BELETSKAYA. Izv. Akad. Nauk. S.S.R. Ser. Khim. 831 (1970).
7. (*a*) M. SUAMA, T. SUGITO, and K. DCHIKAWA. Bull. Chem. Soc. Jap. **46**, 1999 (1971); (*b*) G. BRAM, F. GUIBÉ, and M. F. MOLLET. Tetrahedron Lett., 2951 (1970).
8. B. MILLER and K. H. LAI. Chem. Commun. **7**, 334 (1971).
9. J. P. JONAK, G. C. HOPKINS, H. J. MINNEMEYER, and H. TIECKELMANN. J. Org. Chem. **35**, 2512 (1970); **31**, 3969 (1966).
10. (*a*) N. M. CHUNG and H. TIECKELMANN. J. Org. Chem. **35**, 2517 (1970); (*b*) G. C. HOPKINS, J. P. JONAK, H. J. MINNEMEYER, and H. TIECKELMANN. J. Org. Chem. **32**, 4040 (1967).
11. C. F. HOBBS, C. K. MCMILLIN, E. P. PAPADOPOULOS, and C. A. VANDERWERF. J. Am. Chem. Soc. **84**, 43 (1962).
12. J. W. JANUS. J. Chem. Soc. 3551 (1955).
13. J. W. SCHULENBERG and S. ARCHER. Org. React. **14**, 1 (1965).
14. R. H. DEWOLFE. J. Org. Chem. **36**, 162 (1971).
15. (*a*) G. H. BARLOW and H. E. ZAUGG. J. Org. Chem. **37**, 2246 (1972) and refs. therein; (*b*) J. SMID. Angew. Chem. Int. Ed. **11**, 112 (1972) and refs. therein.
16. (*a*) R. G. PEARSON. J. Am. Chem. Soc. **85**, 3533 (1963); (*b*) R. G. PEARSON and J. SONGSTAD. J. Am. Chem. Soc. **89**, 1827 (1967) and refs. therein; (*c*) B. SAVILLE. Angew. Chem. Int. Ed. **6**, 928 (1967).
17. D. SHAW, B. K. DUNNING, and H. O. PRITCHARD. Can. J. Chem. **47**, 669 (1969).
18. A. R. STEIN. Unpublished results.
19. W. J. COMSTOCK and F. KLEEBERG. J. Am. Chem. Soc. **12**, 499 (1890).
20. A. R. STEIN. Can. J. Chem. **43**, 1493 (1965).
21. A. R. STEIN. Can. J. Chem. **43**, 1508 (1965).
22. D. Y. CURTIN, R. J. CRAWFORD, and M. WILHELM. J. Am. Chem. Soc. **80**, 1391 (1958).
23. P. A. CANTOR and C. A. VANDERWERF. J. Am. Chem. Soc. **80**, 970 (1958).
24. D. Y. CURTIN and D. H. DYBVIG. J. Am. Chem. Soc. **84**, 225 (1962).
25. N. KORNBLUM, P. J. BERRIGAN, and W. J. LENOBLE. J. Am. Chem. Soc. **85**, 1141 (1963).
26. N. KORNBLUM, R. SELTZER, and P. HABERFIELD. J. Am. Chem. Soc. **85**, 1148 (1963).
27. R. BARNER and H. SCHMID. Helv. Chim. Acta, **43**, 1393 (1960).
28. N. KORNBLUM and A. P. LURIE. J. Am. Chem. Soc. **81**, 2705 (1959).

Can. J. Chem. Downloaded from www.nrcresearchpress.com by 210.87.254.42 on 09/05/12
For personal use only.

Conformational Studies on 1,3-Dioxepanes. Part IV.[1] Applications of Geminal Coupling Constants to Conformational Analysis of 1,3-Dioxepanes

T. Bruce Grindley[2] and Walter A. Szarek[3]

Department of Chemistry, Queen's University, Kingston, Ontario K7L 3N6

Received April 1, 1974

T. Bruce Grindley and Walter A. Szarek. Can. J. Chem. **52**, 4062 (1974).

The magnitude of —OCH_2O— group geminal H,H coupling contants, the size of the vicinal coupling constants, and the tenets of conformational analysis were used to establish that in solution the conformation of the 1,3-dioxepane rings in derivatives of 1,3:2,5-di-*O*-methylenemannitol and 2,5-*O*-methylenemannitol is predominantly the twist-chair in which the C_2 axis passes through the acetal carbon.

T. Bruce Grindley et Walter A. Szarek. Can. J. Chem. **52**, 4062 (1974).

On a fait appel à l'amplitude des constantes du couplage géminé H,H du groupe —OCH_2O—, de même qu'à la grandeur des constantes du couplage vicinal et aux fondements de l'analyse conformationnelle pour établir que la conformation, en solution, des cycles dioxépane-1,3 des dérivés du di-*O*-méthylène-1,3:2,5 mannitol et du *O*-méthylène-2,5 mannitol est principalement sous la forme chaise croisée dans laquelle un axe C_2 passe par le carbone de l'acétal.

[Traduit par le journal]

Introduction

Classical strain minimization calculations (2, 3) have shown that four cycloheptane conformations exist which may be divided into two pseudorotation[4] families separated by an inversion barrier of approximately 8.1 kcal/mol (2). In the chair family, the C_s symmetric chair (C) conformation is the maximum of the pseudorotation itinerary and the C_2 symmetric twist-chair (TC) is the minimum, whereas in the boat family, the boat (B) and twist-boat (TB) conformations are of approximately equal energy.[5] As for the chair conformation of cyclohexane, conformations of cycloheptane having substituents in axial orientation are significantly higher in energy than those having substituents in equatorial orientation. In contrast to cyclohexane, however, the presence of substituents at different axial positions in cycloheptane gives rise to conformations of different energies. Figure 1 shows chair (C) and twist-chair (TC) conformations. In the C_2 symmetric TC (and TB) conformation the two positions (isoclinal positions) at the carbon through which the axis of symmetry passes are equivalent and are energetically similar to equatorial positions.

Some evidence is available on the shapes of seven-membered rings in the solid state from X-ray crystallography (5–7), although the 1,3-dioxepane system has not been investigated. All of the conformations in the compounds examined have been intermediate between the chair and twist-chair conformations.

In the case of 1,3-dioxepanes, an estimate of

[1]For Part III, see ref. 1.

[2]Present address: Department of Chemistry, Dalhousie University, Halifax, Nova Scotia B3H 3J5.

[3]Author to whom inquiries should be addressed.

[4]The term pseudorotation has been described by Hendrickson (2) as "the passage of a ring with a plane of symmetry through an atom to one with an axis of symmetry bisecting the bond adjacent to that atom, and *vice versa*;" however, there are other views of this term (see ref. 4).

[5]Although the two calculations (2, 3) agree closely on the geometry and relative energies of the twist-chair (6.0 (2) or 5.8 (3) kcal/mol), boat (8.7 (2) or 8.2 (3) kcal/mol), and twist-boat (8.4 (2) or 8.5 (3) kcal/mol) conformations, they do disagree on the geometry and relative energies of the chair (7.4 (2) or 6.5 (3) kcal/mol). These energies are relative to chair cyclohexane. Relative to TC cycloheptane, the values are C (1.4 (2) or 0.7 (3) kcal/mol), TB (2.4 (2) or 2.6 (3) kcal/mol), and B (2.7 (2) or 2.4 (3) kcal/mol). Hendrickson (2) has defined the term chair, as applied to seven-membered rings, as the plane symmetric pseudorotation partner of the twist-chair, and has shown that it is only a transient state in the pseudorotation process. Since the chair represents a maximum on the process, the fact that Bixon and Lifson (3), by employing the method of steepest descent for determining conformations of minimum energy, obtained a conformation of different energy and asymmetric geometry is not surprising. For the present publication, the geometry of the chair conformation obtained by Hendrickson (2) has been used.

Can. J. Chem. Downloaded from www.nrcresearchpress.com by 210.87.254.42 on 09/05/12
For personal use only.

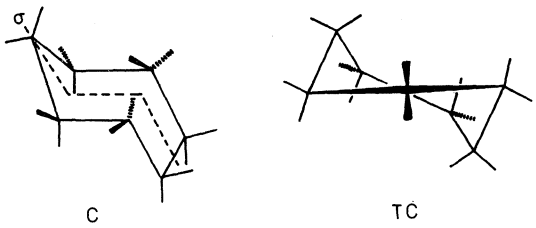

FIG. 1. The chair (C) and twist-chair (TC) conformations of cycloheptane.

the type of distortion from the ideal cycloheptane conformations that might be expected can be obtained from 1,3-dioxane conformational analysis (8). Thus, for example, the shorter C—O bond distances should make the large transannular H–H repulsive interactions, that are present in cycloheptanes, more severe in 1,3-dioxepanes, if a hydrogen on the acetal carbon (C-2) is in an axial orientation; the magnitudes of these interactions can, of course, be reduced if the 1,3-dioxepane ring is in a conformation having the symmetry axis through C-2.

In the present publication, all of the 1,3-dioxepanes have been derived from sugar alcohols (alditols). The conformations are specified by an appropriate letter and the number, as a subscript, of the atom through which the axis or plane of symmetry would pass if the ring were viewed as an unsubstituted cycloheptane. The numbering system is that of the parent alditol; the acetal carbon of the seven-membered ring is indicated by the symbol C-a.

Results and Discussion

1,3-Dioxepane Ring Trans-fused to One 1,3-Dioxane Ring

In an earlier study (9), it was shown that the 1,3-dioxepane ring in 2,5-*O*-isopropylidene-1,3:4,6-di-*O*-methylene-D-mannitol (**1**, R=Me) and in 1,3:2,5:4,6-tri-*O*-methylene-D-mannitol (**1**, R=H) exists in the twist-chair conformation ($TC_{C\text{-}a}$). In the present work, the n.m.r. spectrum of **1** (R = Me) has been recorded at 220 MHz in chloroform-*d* for comparison with the spectra of less restricted 1,3-dioxepane derivatives (see below). The signals for H-2, H-5, H-3, and H-4 form an AA′XX′ pattern, respectively, in which H-2 and H-5 are further coupled in a first-order fashion to H-1 and H-6. Since AA′XX′ patterns are symmetrical (10), the vicinal coupling constants $J_{2,3}$, $J_{3,4}$, and $J_{4,5}$ could be obtained from the XX′ part (see Table 1). In compound **1**, the pseudorotation itinerary of the seven-membered ring is restricted by the two *trans*-fused 1,3-dioxane rings to those conformations in which these rings are fused equatorially to the 1,3-dioxepane ring (see Fig. 2). Of these conformations, $TC_{C\text{-}2}$, $TC_{O\text{-}2}$, $C_{C\text{-}4}$, $C_{C\text{-}3}$, $TC_{O\text{-}5}$, $TC_{C\text{-}5}$, and $TB_{C\text{-}a}$ require excessive torsional strain[6] in at least one of the 1,3-dioxane rings. Removal of one of the *trans*-fused 1,3-dioxane rings in compound **1** (R = H), as in compounds **2**–**7**, removes the excessive torsional strain from the $TC_{C\text{-}5}$, $C_{C\text{-}3}$, and $TC_{O\text{-}5}$ conformations, thus enabling an examination of their stabilities relative to that of the $TC_{C\text{-}a}$.

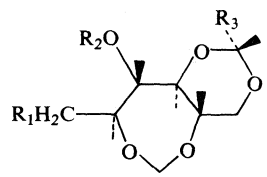

2 and **3** (D-series), **4**–**7** (L-series)
(Structure shown is for the L-series)
2 R_1 = OH; R_2 = H; R_3 = Ph
3 R_1 = OAc; R_2 = Ac; R_3 = Ph
4 $R_1 = R_2 = R_3$ = H
5 $R_1 = R_3$ = H; R_2 = Ac
6 $R_1 = R_3$ = H; R_2 = COPh
7 $R_1 = R_3$ = H; R_2 = Ts

1,3 - *O* - Benzylidene - 2,5 - *O* - methylene - D - mannitol (**2**) was synthesized by partial hydrogenation of 1,3:4,6-di-*O*-benzylidene-2,5-*O*-methylene-D-mannitol (9) in glacial acetic acid. Acetylation of **2** gave 4,6-di-*O*-acetyl-1,3-*O*-benzylidene-2,5-*O*-methylene-D-mannitol (**3**). Compounds **4**–**7** were prepared by known methods (see Experimental).

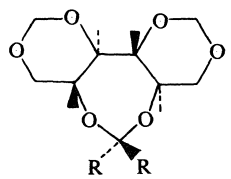

1

[6]Torsional strain was evaluated by a consideration of the dihedral angle (O-1—C-6—C-5—C-4) which would be expected in the 1,3-dioxane rings if the 1,3-dioxepane ring possessed the conformation calculated by Hendrickson (2) for cycloheptane. Conformations in which a dihedral angle in a 1,3-dioxane ring was outside the limits 35–37° were considered to have excessive torsional strain. The corresponding angle in 2-(*p*-chlorophenyl)-1,3-dioxane was found to be 55° (11).

Can. J. Chem. Downloaded from www.nrcresearchpress.com by 210.87.254.42 on 05/05/12
For personal use only.

Can. J. Chem. Downloaded from www.nrcresearchpress.com by 210.87.254.42 on 09/05/12
For personal use only.

TABLE 1. Proton magnetic resonance spectral data[a]

Compound	Solvent	2,5 —OCH_2O— group			Chemical shift (τ)				Vicinal coupling constants (Hz)		
		Chemical shift (τ)	J_{gem} (Hz)	Δν (Hz)	H-2	H-3	H-4	H-5	$J_{2,3}$	$J_{3,4}$	$J_{4,5}$
1[b]	$CDCl_3$	—	—	—	6.24	6.53	6.53	6.24	9.3	8.5	9.3
2	D_2O	5.18	−4.5	2.5	[c]	[c]	[c]	[c]	[c]	[c]	[c]
3	$CDCl_3$	5.19	−4.3	3.4	[c]	[c]	4.82	[c]	[c]	7.4	9.6
4	$CDCl_3$	5.26	−4.5	2.5	[c]	[c]	[c]	[c]	[c]	[c]	[c]
5	$CDCl_3$	5.25	−4.6	2.5	[c]	[c]	5.08	[c]	[c]	8.4	9.7
5[b]	$CDCl_3$	5.21	−4.5	8.0	6.28	6.64	5.12	6.20	9.5	8.7	9.8
6	$CDCl_3$	5.20	−4.4	2.5	[c]	[c]	4.86	[c]	[c]	8.5	10.0
7	$CDCl_3$	5.28	−4.5	2.5	[c]	[c]	[c]	[c]	[c]	[c]	[c]
8	$CDCl_3$	5.21	−5.1	2.8	[c]	[c]	[c]	[c]	[c]	[c]	[c]
9[d]	$CDCl_3$	5.12	[e]	[e]	5.96	4.89	4.89	5.96	10.1	8.7	10.1
10	$CDCl_3$	5.12	[e]	[e]	6.03	4.92	4.92	6.03	10.1	8.2	10.1
11	D_2O	5.28	−4.5	5.2	[c]	[c]	[c]	[c]	[c]	[c]	[c]
12	$CDCl_3$	5.24	−4.9	2.5	[c]	[c]	5.27	[c]	[c]	7.7	9.8
13	$(CD_3)_2CO$	5.22	−4.7	2.5	[c]	[c]	[c]	[c]	[c]	[c]	[c]
14	D_2O	5.11	−4.8	4.8	[c]	[c]	[c]	[c]	[c]	[c]	[c]
15[b]	$CDCl_3$	5.20	[f]	[f]	[c]	[c]	[c]	[c]	[c]	[c]	[c]
16[b]	$CDCl_3$	5.06	−4.5	7.7	5.91	4.84	4.96	6.06	9.7	8.7	10.0
16[b]	C_6D_6	5.46	−4.5	1.5	6.29	4.55	4.69	6.29	9.7	8.5	9.9
17	$CDCl_3$	5.08	−4.5	2.0	5.69	4.81	6.09	5.91	9.6	7.8	9.6

[a]Recorded at 60 MHz unless otherwise noted.
[b]Recorded at 220 MHz.
[c]Not obtained because of signal overlap.
[d]Data obtained from ref. 1.
[e]Unobservable because of equivalence due to C_2 symmetry of the compound.
[f]Not observed because of accidental equivalence of chemical shifts.

Can. J. Chem. Downloaded from www.nrcresearchpress.com by 210.87.254.42 on 09/05/12
For personal use only.

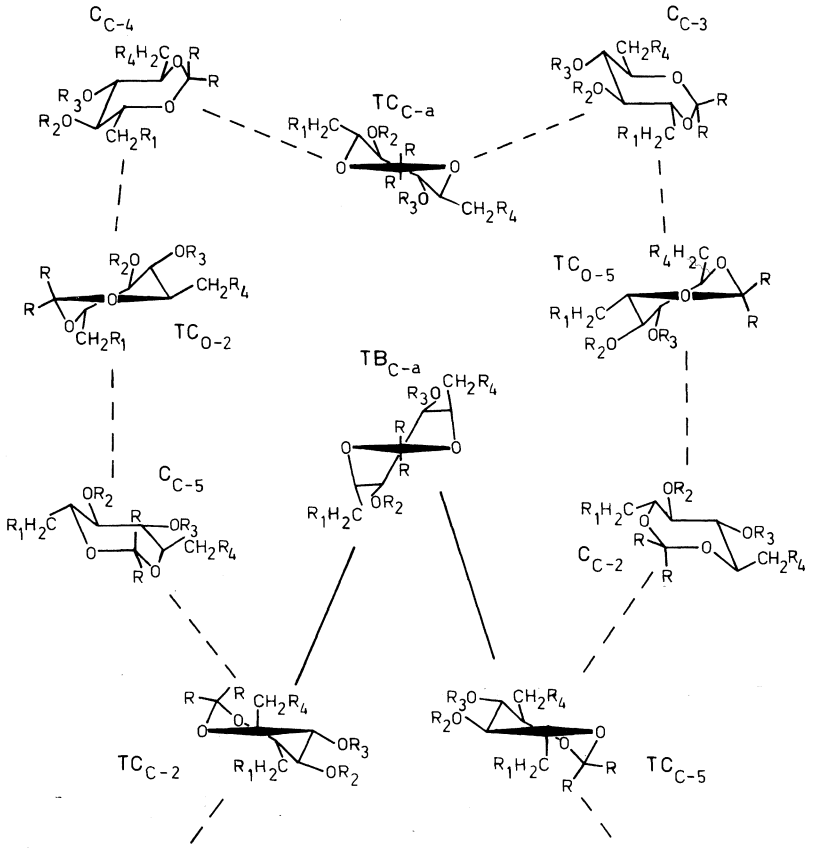

FIG. 2. The conformational itinerary of 2,5-*O*-isopropylidene(R = Me)- and 2,5-*O*-methylene(R = H)-D-mannitol derivatives considered in this publication. R_1, R_2, R_3, and R_4 are defined elsewhere; dashed lines indicate interconversion by pseudorotation; solid lines indicate inversion. The pseudorotations indicated at the bottom of the figure lead to conformations with axial substituents.

By a first-order analysis of the 220 MHz n.m.r. spectrum (see Fig. 3) of 4-*O*-acetyl-1,3:2,5-di-*O*-methylene-L-rhamnitol (**5**) in chloroform-*d* (all $\Delta\nu > 6J$), all of the vicinal coupling constants could be obtained unequivocably. In the 60 MHz spectra of compounds **5** and **6**, the alditol protons H-lax, H-2, H-leq, H-3, H-4, H-5, and H-6,6′,6″ give rise to ABCMXYZ$_3$ patterns; the H-4 signal in these spectra (and in that of **3**) was observed as a doublet of doublets at lowest field of all of the alditol signals. Assignments of couplings involving H-4 (see Table 1) were made by spin decoupling in the case of **5** and **6** and, in the case of **3**, by comparison with the spectra of **5** and **6**; although this first-order analysis of the H-4 signal in the 60 MHz spectra of **5** and **6** may be valid because of the availability of the 220 MHz spectrum of **5** for comparison, it may not, perhaps, be justified in the case of **3** because of possible overlap of the H-6,6′ and H-5 signals. The similarity of the coupling constants $J_{2,3}$, $J_{3,4}$, and $J_{4,5}$ in compounds **3**, **5**, and **6** to those in compound **1** (R = Me) suggests that all of these compounds exist predominantly in the $TC_{C\text{-}a}$ conformation, although, since all of the conformations under consideration (see Fig. 2) have the substituents on the seven-membered

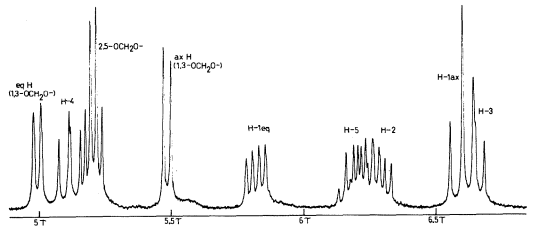

FIG. 3. Partial n.m.r. spectrum at 220 MHz of 4-*O*-acetyl-1,3:2,5-di-*O*-methylene-L-rhamnitol (**5**) in chloroform-*d*.

Can. J. Chem. Downloaded from www.nrcresearchpress.com by 210.87.254.42 on 09/05/12
For personal use only.

TABLE 2. Calculated geminal coupling constants in —OCH_2O— groups in 1,3-dioxepane conformations

Compound	Conformation	H—C—O—R dihedral angles (°)[a]		Corresponding J_{gem} (Hz)[b]			Calibrated J_{gem} (Hz)[c]	J_{gem} (Hz) calculated from $\sin^2 \tau_i$ relationship[d]
		C-a → O-2	C-a → O-5	C-2 → O-2	C-a → O-5	Average		
1,3-Dioxane	Chair	297	177	−2.5	−2.5	−2.5	−6.2[e]	−6.9
1,3-Dioxepanes	$TC_{C\text{-}a}$	201	201	−1.4	−1.4	−1.4	−4.2	−3.9
	$C_{C\text{-}3}$	174	240	−2.7	−0.2	−1.5	−4.3	−4.1
	$TC_{O\text{-}5}$	152	279	−3.2	−1.3	−2.3	−6.3	−7.2
	$C_{C\text{-}2}$ or $C_{C\text{-}5}$	157	306	−3.2	−2.7	−2.9	−7.9	−9.6
	$TC_{C\text{-}5}$	168	328	−2.8	−3.3	−3.1	−8.2	−10.5

[a]Obtained from the known geometry of 1,3-dioxane (11), and from the calculated geometries of cycloheptane conformations (2) for the 1,3-dioxepanes.
[b]Obtained from the curve of Maciel *et al.* (13) using the appropriate dihedral angle.
[c]Calibrated J_{gem} for 1,3-dioxepanes = (J_{gem} (average) × (6.2/2.5)) − 0.8.
[d]Calculated using the relationship in footnote 7, $J_{gem} = -16.01 + 5.49 \sum_{i=1}^{4} \sin^2 \tau_i$; the values of τ_i employed for the 1,3-dioxepane conformations were those obtained from the corresponding calculated cycloheptane conformations.
[e]Experimentally determined (19) value used to calibrate J_{gem} values for the 1,3-dioxepanes.

Can. J. Chem. Downloaded from www.nrcresearchpress.com by 210.87.254.42 on 09/05/12
For personal use only.

ring equatorially oriented, it might be expected that the various conformations would give rise to similar vicinal coupling constants.

The absence in compounds **2–7** of the C_2 symmetry of **1** makes the 2,5—OCH_2O— protons nonequivalent by symmetry and anisochronous in their n.m.r. spectra, and provides a more effective criterion for conformational analysis, namely, the magnitude of the geminal H,H coupling constant (J_{gem}) in the —OCH_2O— group. A heteroatom, with lone electron pairs, adjacent to a methylene group can cause an algebraic increase in J_{gem} in two ways (12): withdrawal of electrons from orbitals symmetric between hydrogen atoms (generally inductive effects) increases J_{gem} in a manner independent of geometry (as a first approximation), while back-donation from heteroatom lone pairs into orbitals antisymmetric between hydrogen atoms increases J_{gem} in a manner dependent on geometry. In addition, J_{gem} is affected by the size of the H—C—H angle, diminishing with decreasing H—C—H angle (and hence increasing O—C—O angle) (13). The combination of these effects has resulted in a range of values for J_{gem} in —OCH_2-O— groups from ~1 Hz in 1,3-dioxolanes (14) to −8.4 Hz in a 1,3,6,8-tetraoxecane (15).

The dependence of the magnitude of J_{gem} on the geometry about the —OCH_2O— group has been treated in a variety of ways (3, 16–18). The geometrical relationship developed by Maciel *et al.* (13), who, from an INDO calculation, related the H—C—O—H dihedral angle in methanol to the magnitude of J_{gem}, has been adopted in this publication rather than a $\sin^2 \phi$ relationship[7] (18), because it predicts a lower maximum at a H—C—O—H dihedral angle of 60° than at one of 240°. An example of the validity of this approach was provided by the observation (15) of an algebraically smaller value of J_{gem} (−6.2 Hz) in the —OCH_2O— groups in the BCB2 conformation of *trans-syn-trans*-4,5:9,10-biscyclohexano-1,3,6,8-tetraoxecane, which has one H—C—O—R angle ~60°, than would have been predicted by a $\sin^2 \phi$ relationship. In the present work, the curve relating J_{gem} to the H—C—O—H dihedral angle (13) has been applied to the 1,3-dioxepanes on the assumptions that the replacement of O—H by O—R has no effect on the shape of the curve and that the effects of the two heteroatoms are independent. An additional assumption is that the introduction of the —OCH_2O— group into a cycloheptane ring does not cause severe distortions of most of the conformations (2). The magnitude of J_{gem} in the 1,3-dioxepane was calibrated with respect to the value of J_{gem} in 1,3-dioxane of known geometry (11) in the following manner. The average of the two values of J_{gem} obtained from the two H—C—O—R angles by using the curve of Maciel *et al.* (13) was multiplied by the factor (see Table 2, footnote *c*) required to convert the corresponding value of J_{gem} in 1,3-dioxane to its experimentally determined (19) value, namely, −6.2 Hz. From the value of J_{gem} so obtained, 0.8 Hz was subtracted for the 1,3-dioxepanes, since the O—C—O angle is undoubtedly larger in these rings (compare refs. 2, 5–7) than in 1,3-dioxanes (11, 20); the value 0.8 Hz was obtained from a plot (13) of J_{gem} *vs.* H—C—H angle in methane, and was the difference in values of J_{gem} for H—C—H angles of 108 and 105°.[8] The results are given in Table 2. Comparison of these results with the experimental values of J_{gem} obtained from the n.m.r. spectra of compounds **2–7** (−4.3 to −4.6 Hz, see Table 1) suggests that either conformations $TC_{C\text{-}a}$ or $C_{C\text{-}3}$, or both, must be important for the 1,3-dioxepane rings.

In the $TC_{C\text{-}a}$ conformation, the two geminal —OCH_2O— protons in compounds **2–7** might be expected to be nearly isochronous in the n.m.r. spectra, because the structural features responsible for the deviation from C_2 symmetry are relatively distant from these protons. In contrast, however, in the $C_{C\text{-}3}$ conformation, the

[7]Anteunis *et al.* (18) have given the relationship $J_{gem} = -6.54 + 4.86 \sum_{i=1}^{4} \sin^2 \tau_i$; however, treatment by us of the data presented in Table 2 of that publication by a least-squares method yielded the relationship $J_{gem} = -16.01 + 5.49 \sum_{i=1}^{4} \sin^2 \tau_i$, where τ_i is defined as the angle between the bisector of the CH_2 moiety and a lone-pair orbital of oxygen in the —OCH_2O— grouping. In the present work, the use of the latter relationship gives results similar to those derived from the approach of Maciel *et al.* (13) (see Table 2).

NOTE ADDED IN PROOF: In a private communication, Professor Anteunis has informed us that the relationship given in ref. 18 is erroneous and should read $J_{gem} = -14.57 + 4.86 \sum_{i=1}^{4} \sin^2 \tau_i$.

[8]The H—C—H angles of 108 and 105° correspond to O—C—O angles of 111° (for 1,3-dioxanes) and 115° (for seven-membered rings) (compare ref. 2).

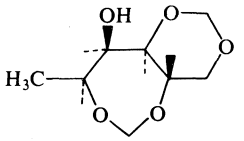

8

two —OCH_2O— protons might be expected to be in different environments, because they are axially and equatorially oriented. Thus, the observed small chemical-shift differences are probably more consistent with the $TC_{C\text{-}a}$ conformation (see Table 1); on the basis of calculations (2) on cycloheptane, the twist-chair conformation would be expected to be more stable than a chair.

6-Deoxy-1,3:2,5-di-*O*-methylene-L-talitol (**8**) has also been investigated. In this case, J_{gem} for the 2,5-OCH_2O— protons was found to be slightly larger (−5.1 Hz) than the values obtained in the case of compounds **2**–**7** (~ −4.5 Hz), suggesting that the 1,3-dioxepane ring in **8** exists to a slightly smaller extent in the $TC_{C\text{-}a}$ conformation.

Monocyclic 1,3-Dioxepane Ring Systems

Removal of the second *trans*-fused 1,3-dioxane ring, as in compounds **9**–**17**, removes the excessive torsional strain from all the conformations shown in Fig. 2. As has been discussed previously (1), other conformations need not be considered, because they would have at least one axial substituent. Since compounds **9** and **10** have C_2 symmetry, their pseudorotation itineraries will be symmetric about the $TC_{C\text{-}a}$ conformation and hence the pairs of conformations $TC_{C\text{-}2}$ and $TC_{C\text{-}5}$, $C_{C\text{-}2}$ and $C_{C\text{-}5}$, $TC_{O\text{-}2}$ and $TC_{O\text{-}5}$, and $C_{C\text{-}3}$ and $C_{C\text{-}4}$ are degenerate;

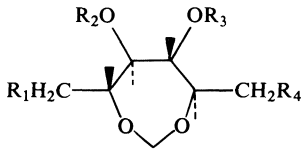

9, **10**, and **13**–**17** (D-series), **11** and **12** (L-series) (Structure shown is for the D-series)

9 $R_1 = R_4 = OAc$; $R_2 = R_3 = Ac$
10 $R_1 = R_4 = OCH_2Ph$; $R_2 = R_3 = Ac$
11 $R_1 = R_2 = R_3 = H$; $R_4 = OH$
12 $R_1 = H$; $R_2 = Ac$; $R_3 = CH_2OAc$; $R_4 = OAc$
13 $R_1 = OH$; $R_2 = R_3 = H$; $R_4 = OCOPh$
14 $R_1 = OH$; $R_2 = R_3 = H$; $R_4 = OTs$
15 $R_1 = OH$; $R_2 = R_3 = H$; $R_4 = OCPh_3$
16 $R_1 = OAc$; $R_2 = R_3 = Ac$; $R_4 = OCPh_3$
17 $R_1 = R_4 = OCOPh$; $R_3 = COPh$; $R_2 = H$

in the case of compounds **11**–**17**, however, there is a slight deviation from C_2 symmetry. In view of the finding in the previous section, namely, that the conformations in one-half of the pseudorotation itinerary are higher in energy than the $TC_{C\text{-}a}$ conformation, then the $TC_{C\text{-}a}$ conformation of the 1,3-dioxepane ring should also be the predominant one in the case of compounds **11**–**17**. The $TB_{C\text{-}a}$ conformation can be considered to be less favored than the $TC_{C\text{-}a}$ on the basis of the calculation (2) of the TB conformation of cycloheptane being 2.4 kcal/mol higher in energy than the TC.

Compounds **9**, **11**, **12**, and **14** were prepared by known methods (see Experimental); compound **10** was obtained by acetylation of 1,6-di-*O*-benzyl-2,5-*O*-methylene-D-mannitol (21). Selective monobenzoylation and monotritylation of 2,5-*O*-methylene-D-mannitol (22) afforded compounds **13** and **15**, respectively. Acetylation of **15** gave the triacetate **16**, and benzoylation of 2,5-*O*-methylene-D-mannitol yielded the tribenzoate **17**.

The parameter most sensitive to conformational change in the 1,3-dioxepane-ring systems discussed in this paper, namely, J_{gem} in the —OCH_2O— group,[9] is only slightly larger in the case of the n.m.r. spectra of compounds **11**–**17** (average value −4.7 Hz) than had been observed for **2**–**7** (average value −4.5 Hz); this observation suggests that the $TC_{C\text{-}a}$ conformation of the 1,3-dioxepane ring is still the preferred one for compounds **11**–**17**.

In the case of 3,4-di-*O*-acetyl-1,6-di-*O*-benzyl-2,5-*O*-methylene-D-mannitol (**10**), the vicinal coupling constants $J_{2,3}$, $J_{3,4}$ and $J_{4,5}$ were obtained by analyzing the H-3 and H-4 signals in the 60 MHz n.m.r. spectrum as the AA′ part of an AA′BB′ pattern (10). The doublet of doublets attributable to H-4 in the spectrum of compound **12** was analyzed on a first-order basis, and the

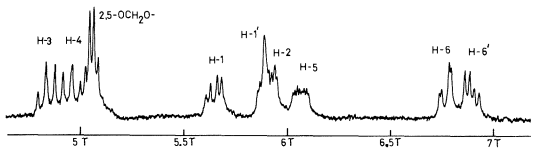

FIG. 4. Partial n.m.r. spectrum at 220 MHz of 1,3,4-tri-*O*-acetyl-2,5-*O*-methylene-6-*O*-trityl-D-mannitol (**16**) in chloroform-*d*.

[9]An illustration of this sensitivity is given in Part V of this Series.

Can. J. Chem. Downloaded from www.nrcresearchpress.com by 210.87.254.42 on 09/05/12
For personal use only.

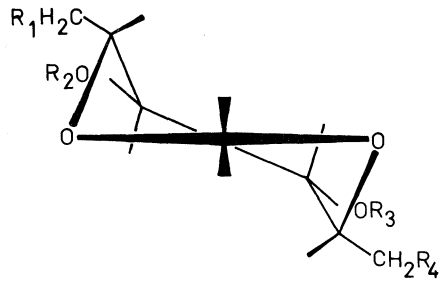

FIG. 5. The favored $TC_{C\text{-}a}$ conformation of the 1,3-dioxepane ring in compounds **9**–**17**. The structure shown is for the D-series.

assignment of $J_{3,4}$ and $J_{4,5}$ (see Table 1) was confirmed by spin decoupling. No vicinal coupling constants could be ascertained for compounds **11** and **13**–**15** because of overlap of signals. Nuclear magnetic resonance spectra of compounds **16** and **17** were measured at 220 MHz; the spectrum of 1,3,4-tri-*O*-acetyl-2,5-*O*-methylene-6-*O*-trityl-D-mannitol (**16**) in chloroform-*d* is shown in Fig. 4. Where necessary, a second-order analysis of the spectra of **16** and **17** was performed by standard methods (10). The coupling constants $J_{2,3}$, $J_{3,4}$, and $J_{4,5}$ observed for compounds **9**, **10**, **12**, **16**, and **17** (see Table 1) were very similar to those for compounds **1**, **3**, **5**, and **6**, indicating that the $TC_{C\text{-}a}$ conformation was again predominant in solution. It is interesting to note that, when a relatively larger group is present at C-3 and C-4, as in compounds **12** or **17**, then $J_{3,4}$ decreases slightly. Figure 5 shows the preferred $TC_{C\text{-}a}$ conformation of the 1,3-dioxepane ring in compounds **9**–**17**.

Experimental

Melting points were determined on a Fisher-Johns apparatus and are uncorrected. Optical rotations were measured with a Perkin-Elmer Model 141 automatic polarimeter at 23 ± 2°. The term "petroleum ether" indicates the fraction of b.p. 60–80°. Thin-layer chromatography was carried out on glass microplates coated with silica gel (Camag) and with ethyl acetate – petroleum ether (1:1, v/v) (*A*) or ethyl acetate (*B*) as the developing solvent. The developed plates were air dried, sprayed with 5% ethanolic sulfuric acid, and heated at 150°. Infrared spectra were recorded on a Beckman IR5A spectrophotometer. Nuclear magnetic resonance spectra at 60 MHz were measured with a Varian T-60 or Bruker HX-60 spectrometer using tetramethylsilane as an internal lock signal or on a Varian A-60A using tetramethylsilane as an internal standard for non-polar solvents. In deuterium oxide, the internal standard was sodium 4,4-dimethyl-4-silapentane-1-sulfonate (τ 10.00). Nuclear magnetic resonance spectra at 220 MHz were measured on a Varian HR-220 spectrometer at the Canadian 220 MHz NMR center. The coupling constants were measured at sweep widths of 250 Hz or 100 Hz; vicinal coupling constants obtained on a first-order basis and geminal coupling constants are considered precise to within ±0.2 Hz at 60 MHz or ±0.1 Hz at 220 MHz. Mass spectra were determined with a JEOL JMS-OISC double-focusing spectrometer.

Physical constants of known compounds are recorded in Table 3.

*1,3-O-Benzylidene-2,5-O-methylene-*D*-mannitol (2)*

1,3:4,6-Di-*O*-benzylidene-2,5-*O*-methylene-D-mannitol (9) (m.p. 255–257°, $[\alpha]_D$ −134.9° (*c*, 1.7 in chloroform)) (1.5 g) was subjected to a hydrogen pressure of 1 atm in the presence of a palladium-on-carbon catalyst (1.39 g) at room temperature until 0.625 l (2.5 equiv.) had been consumed (10 h). The solution was filtered and the filtrate was concentrated; t.l.c. in solvent *A* showed that three components were present. Column chromatography on silica gel using ether as eluent gave compound **2** (320 mg, 27%) which was recrystallized from chloroform – petroleum ether and then from ethanol – petroleum ether to give white needles, m.p. 157–158°; $[\alpha]_D$ −69.5° (*c*, 1.00 in chloroform); λ_{max} (Nujol) 2.9 (OH), 13.4, 14.5 μm (Ph); n.m.r. data ($CDCl_3$): τ 2.44–2.74 (5-H, multiplet, Ph), 4.53 (1-H, singlet, benzylidene-methine H).

*4,6-Di-O-acetyl-1,3-O-benzylidene-2,5-O-methylene-*D*-mannitol (3)*

Compound **2** (35 mg) was acetylated with pyridine

TABLE 3. Physical constants of 1,3-dioxepane derivatives prepared by literature methods

Compound	Melting point (°C)		$[\alpha]_D$[a] (deg)		Reference No.
	This work	Literature	This work	Literature	
1	208–212	208–212	−88.7	−88.7	9
4	137–138	136–137	+90.8	+93.0	23
5	139–140	140–141	+40.4	+44.4	23
6	136–137.5	135–136	+37.3	+37.4	23
8	123–124	122	+81.6	+78.0	24
11	124–125.5	124–125	+60.2	+62.1	23
12	87.5–88.5	87.8	−12.2	−10.4	23
14	124–126	124–125	−28.9	−32.6	23

[a]The same solvents were employed in this work as in the literature.

Can. J. Chem. Downloaded from www.nrcresearchpress.com by 210.87.254.42 on 09/05/12
For personal use only.

Can. J. Chem. Downloaded from www.nrcresearchpress.com by 210.87.254.42 on 09/05/12
For personal use only.

(2 ml) and acetic anhydride (1.5 ml) in the usual manner. Fine white needles (40 mg, 80%) were isolated and after two recrystallizations from ethanol had m.p. 154–155°; $[\alpha]_D$ −81.8° (*c*, 1.07 in chloroform); λ_{max} (Nujol) 5.7 (OAc), 13.1, 14.2 μm (Ph), no absorption attributable to OH; n.m.r. data ($CDCl_3$): τ 2.51–2.85 (5-H, multiplet, Ph), τ 4.58 (1-H, singlet, benzylidene–methine H), τ 8.11 (6-H, singlet, OAc).

Anal. Calcd. for $C_{18}H_{22}O_8$: C, 59.0; H, 6.0. Found: C, 58.9; H, 6.1.

*1,3:2,5-Di-O-methylene-4-O-p-tolylsulfonyl-*L*-rhamnitol (7)*

1,3:2,5-Di-*O*-methylene-L-rhamnitol (***4***) (23) was treated with *p*-toluenesulfonyl chloride in dry pyridine in the usual manner to give compound **7** which, after recrystallization from ethanol, had m.p. 117–118°; $[\alpha]_D$ +49.3° (*c*, 1.2 in chloroform).

Anal. Calcd. for $C_{15}H_{20}O_7S$: C, 52.3; H, 5.8; S, 9.3. Found: C, 52.7; H, 6.0; S, 9.6.

*3,4-Di-O-acetyl-1,6-di-O-benzyl-2,5-O-methylene-*D*-mannitol (10)*

A solution of 1,6-di-*O*-benzyl-2,5-*O*-methylene-D-mannitol (21) (m.p. 85–88°, $[\alpha]_D$ −51.5° (*c*, 1.54 in chloroform)) (0.3 g) in pyridine (1.5 ml) and acetic anhydride (1 ml) was kept at room temperature for 12 h and then poured into ice water. The resultant product was obtained by filtration and recrystallized twice from ethanol–water to give **10** as white needles (0.31 g, 83%), m.p. 74.5–75.5°; $[\alpha]_D$ +36.4° (*c*, 1.10 in chloroform); n.m.r. data ($CDCl_3$): τ 2.70 (10-H, singlet, Ph), τ 5.49 (4-H, AB quartet, $J_{AB} = -12.6$ Hz, $\Delta\nu_{AB} = 1.4$ Hz, benzyl H's), τ 8.12 (6-H, singlet, OAc).

Anal. Calcd. for $C_{25}H_{30}O_8$: C, 65.5; H, 6.6. Found: C, 65.7; H, 6.7.

*1-O-Benzoyl-2,5-O-methylene-*D*-mannitol (13)*

To a magnetically stirred solution of 2,5-*O*-methylene-D-mannitol (22) (m.p. 173–174°, $[\alpha]_D$ −47.4° (*c*, 1.2 in water)) (2.7 g) in dry pyridine at 0° was added benzoyl chloride (2.0 ml, 1.1 equiv.). The solution was stirred at 0° for 1 h and at room temperature for 12 h, and then concentrated several times from toluene. Thin-layer chromatography (solvent *B*) indicated that the syrup contained the starting material and two other components. The syrup was dissolved in water (50 ml) and the solution was partitioned with chloroform (50 ml); the aqueous layer was separated and extracted several times with chloroform. The chloroform extracts were dried ($MgSO_4$) and concentrated to a crystalline mass (0.45 g, 10%). The residue was recrystallized twice from chloroform – petroleum ether and once from water to give **13** as white needles, m.p. 156–158°; $[\alpha]_D$ −31.2° (*c*, 0.996 in methanol); n.m.r. data [$(CD_3)_2CO$]: τ 1.87–2.54 (5-H, multiplet, OCOPh), τ 5.44 (2-H, AB part of ABX pattern, $J_{1,1'} = 11.5$ Hz, $J_{1,2} = 0.7$ Hz, $J_{1',2} = 6.6$ Hz, $\Delta\nu_{AB} = 12.0$ Hz, H-1,1'). The mass spectrum (inlet termperature 162°) showed major peaks having *m/e* 255, 237, 225, 207, 195, 165, 123, and 105.

Anal. Calcd. for $C_{14}H_{18}O_7$: C, 56.4; H, 6.1. Found: C, 56.5; H, 6.1.

*2,5-O-Methylene-1-O-trityl-*D*-mannitol (15)*

2,5-*O*-Methylene-D-mannitol (22) (2 g) and trityl chloride (3.2 g, 1.2 equiv.) (recrystallized from petroleum ether containing acetyl chloride) were kept in dry pyridine at room temperature for 2 days and at 37° for 3 days; the mixture was then poured into ice water. The water was decanted and the gummy white residue was dissolved in chloroform; the solution was dried ($MgSO_4$) and concentrated. Thin-layer chromatography (solvent *B*) indicated that triphenylcarbinol and two other compounds were present. The mixture was chromatographed on a silica gel column using an elution gradient which was changed from petroleum ether – ethyl acetate (1:1, v/v) to ethyl acetate to afford **15** (1.1 g, 24%). Recrystallization from ethanol–water gave wavy white fronds, m.p. 143.5°; $[\alpha]_D$ +41.6° (*c*, 2.42 in methanol); n.m.r. data ($CDCl_3$) at 220 MHz: τ 2.63–2.86 (15-H, multiplet, Ph); λ_{max} (Nujol): 3.0 (OH), 13.3, 14.3 μm (Ph).

Anal. Calcd. for $C_{26}H_{28}O_6$: C, 71.5; H, 6.5. Found: C, 71.0; H, 6.9.

*3,4,6-Tri-O-acetyl-2,5-O-methylene-1-O-trityl-*D*-mannitol (16)*

Compound **15** (0.5 g) was acetylated with pyridine (8 ml) and acetic anhydride (5 ml) in the usual manner to yield the syrupy compound **16** (0.59 g, 91%). Distillation gave a light yellow glass, b.p. 230–235°/20 Torr; $[\alpha]_D$ +22.5° (*c*, 3.25 in chloroform); λ_{max} (chloroform): 5.7–5.8 (OAc), 13.6, 14.3 μm (Ph); n.m.r. data (C_6D_6) at 220 MHz: τ 2.38–3.02 (15-H, multiplet, Ph), τ 8.23, 8.25, 8.48 (9-H, 3 singlets, OAc); n.m.r. data ($CDCl_3$): τ 2.54–2.81 (15-H, multiplet, Ph), τ 7.92, 8.01, 8.39 (9-H, 3 singlets, OAc). The major mass-spectral peaks (inlet temperature 154–155°) occurred at the following *m/e*: 563, 562 (M^+), 485, 319, 303, 289, 259, and 243.

*1,3,6-Tri-O-benzoyl-2,5-O-methylene-*D*-mannitol (17)*

Benzoyl chloride (2.32 ml, 3.5 equiv.) was added dropwise to a magnetically stirred solution of 2,5-*O*-methylene-D-mannitol (1.2 g) in dry pyridine (40 ml) at 0°. After the solution had been stirred at 0° for 1 h and at room temperature for 3 days, water was added (1 ml), and the mixture was stirred for 15 min and then poured into ice water (100 ml). The aqueous solution was extracted with chloroform (3 × 75 ml); the chloroform extracts were washed successively with cold 2 N sulfuric acid (2 × 100 ml), sodium hydrogen carbonate solution (2 × 100 ml), and water (2 × 100 ml). The chloroform solution was dried ($MgSO_4$) and concentrated. Thin-layer chromatography (solvent *A*) showed the presence of two components (R_F 0.3 and 0.6) in approximately equal proportions. The mixture was separated on a column of silica gel with an eluent which changed in composition from ethyl acetate – petroleum ether (4:1, v/v) to (1:1, v/v). The faster-moving component (0.85 g, 27%) was recrystallized from ethanol and then twice from chloroform – petroleum ether to give pure **17**, m.p. 126–127°; $[\alpha]_D$ +39.6° (*c*, 1.51 in chloroform); n.m.r. data ($CDCl_3$) at 220 MHz: τ 1.58–1.68 and 2.08–2.34 (15-H, multiplet, OCOPh), τ 6.48 (1-H doublet, $J = 4.47$ Hz, disappeared by deuteriation, OH). The major mass-spectral lines (inlet temperature 171°) occurred at *m/e* 475, 384, 354, 121, and 105.

Anal. Calcd. for $C_{28}H_{26}O_9$: C, 66.4; H, 5.2. Found: C, 66.3; H, 5.1.

The authors are grateful to the National Research Council of Canada for their generous financial support of this work. The counsel of Dr. J. F. Stoddart in the preparation of compounds **2** and **3** is also acknowledged.

1. J. F. STODDART and W. A. SZAREK. J. Chem. Soc. (B), 437 (1971).
2. J. B. HENDRICKSON. J. Am. Chem. Soc. **89**, 7036, 7043, 7047 (1967).
3. M. BIXON and S. LIFSON. Tetrahedron, **23**, 769 (1967).
4. J. DALE. Acta Chem. Scand. **27**, 1130 (1973).
5. P. GROTH. Acta Chem. Scand. **21**, 2631 (1967).
6. J. JACOBS and M. SUNDARALINGAM. Chem. Commun. 157 (1970).
7. J. P. BEALE, N. C. STEPHENSON, and J. D. STEVENS. Chem. Commun. 487 (1970).
8. F. G. RIDDELL and M. J. T. ROBINSON. Tetrahedron, **23**, 3417 (1967); E. L. ELIEL and M. C. KNOEBER. J. Am. Chem. Soc. **90**, 3444 (1968); E. L. ELIEL. Acc. Chem. Res. **3**, 1 (1970).
9. T. B. GRINDLEY, J. F. STODDART, and W. A. SZAREK. J. Chem. Soc. (B), 172 (1969).
10. E. W. GARBISCH, JR. J. Chem. Ed. **45**, 480 (1968).
11. A. J. DE KOK and C. ROMERS. Rec. Trav. Chim. Pays-Bas, **89**, 313 (1970).
12. J. A. POPLE and A. A. BOTHNER-BY. J. Chem. Phys. **42**, 1339 (1965).
13. G. E. MACIEL, J. W. MCIVER, JR., N. S. OSTLUND, and J. A. POPLE. J. Am. Chem. Soc. **92**, 4151 (1970).
14. M. ANTEUNIS, F. ANTEUNIS-DE KETELAERE, and F. BORREMANS. Bull. Soc. Chim. Belges, **80**, 701 (1971).
15. T. B. GRINDLEY and W. A. SZAREK. Can. J. Chem. **52**, 2566 (1974).
16. R. CAHILL, R. C. COOKSON, and T. A. CRABB. Tetrahedron, **25**, 4681, 4711 (1969).
17. A. A. BOTHNER-BY. Advan. Magn. Res. **1**, 195 (1965).
18. M. ANTEUNIS, G. SWAELENS, and J. GELAN. Tetrahedron, **27**, 1917 (1971).
19. G. SWAELENS, M. ANTEUNIS, and D. TAVENIER. Bull. Soc. Chim. Belges, **79**, 441 (1970).
20. H. R. BUYS. Rec. Trav. Chim. Pays-Bas, **88**, 1003 (1969); J. GELAN, G. SWAELENS, and M. ANTEUNIS. Bull. Soc. Chim. Belges, **79**, 321 (1970).
21. J. GIGG and R. GIGG. J. Chem. Soc. (C), 1865 (1967).
22. A. T. NESS, R. M. HANN, and C. S. HUDSON. J. Am. Chem. Soc. **65**, 2215 (1943).
23. W. T. HASKINS, R. M. HANN, and C. S. HUDSON. J. Am. Chem. Soc. **67**, 1800 (1945).
24. J. W. BIRD and J. K. N. JONES. Can. J. Chem. **41**, 1877 (1963).

Can. J. Chem. Downloaded from www.nrcresearchpress.com by 210.87.254.42 on 09/05/12
For personal use only.

Conformational Studies on 1,3-Dioxepanes. Part V.[1] The Effect of Introduction of an sp^2-hybridized Carbon Atom

T. Bruce Grindley[2] and Walter A. Szarek[3]

Department of Chemistry, Queen's University, Kingston, Ontario K7L 3N6

Received May 13, 1974

T. Bruce Grindley and Walter A. Szarek. Can. J. Chem. **52**, 4072 (1974).

It has been demonstrated, by a consideration of geminal and long-range coupling constants, that the introduction of an sp^2-hybridized carbon atom into a 1,3-dioxepane ring markedly affects the conformational equilibrium.

T. Bruce Grindley et Walter A. Szarek. Can. J. Chem. **52**, 4072 (1974).

On démontre, à l'aide des constantes des couplages géminé et à longue distance, que l'introduction d'un carbone sp^2 dans un cycle dioxepane-1,3 affecte l'équilibre conformationnel d'une façon importante. [Traduit par le journal]

Can. J. Chem. Downloaded from www.nrcresearchpress.com by 210.87.254.42 on 09/05/12
For personal use only.

Introduction

Previous work in this laboratory indicated (1–3) that the conformations of 1,3-dioxepane derivatives can be related to those of cycloheptane. Strain minimization calculations (4, 5) have shown that there are two families of cycloheptane conformations, the chair and the boat, separated by an inversion barrier of approximately 8.1 kcal/mol (4). Within each conformational family there is pseudorotation of the C_2 symmetric forms (the twist-chair (TC) or twist-boat (TB))[4] over the C_s symmetric barriers (the chair (C) or boat (B)).[4] Figure 1 shows chair (C) and twist-chair (TC) conformations. Since cycloheptane conformations have relatively large bond angles (112–118°)(4–6), introduction of an sp^2-hybridized carbon atom should cause only small distortions in the conformations. Some evidence of the similarity of cycloheptanone and cycloheptane conformations was obtained from conformational calculations (7), carbon-13 magnetic resonance spectroscopy (8), and X-ray crystallography (9). Allinger *et al.* (7) have calculated that there are small differences in energy between the four possible TC conformations of cycloheptanone (see Fig. 2). A number of conformational studies of substituted cycloheptanones have been described (8, 10, n.m.r.; 11, i.r.; 12, c.d. and o.r.d.), and in most of these it has been safely assumed that the effects on the conformations of the introduction of an sp^2-hybridized carbon atom are small.

In previous investigations (1–3) it was shown that 1,3-dioxepane derivatives having *trans* sub-

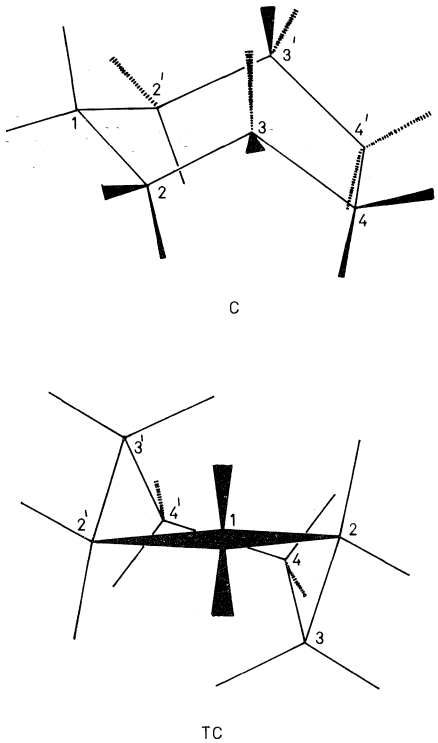

FIG. 1. The chair (C) and twist-chair (TC) conformations of cycloheptane.

[1]For Part IV, see ref. 1.

[2]Present address: Department of Chemistry, Dalhousie University, Halifax, Nova Scotia B3H 3J5.

[3]Author to whom inquiries should be addressed.

[4]The energies, relative to the chair conformation of cyclohexane, are 6.0 (4) or 5.8 (5), 8.4 (4) or 8.5 (5), 7.4 (4) or 6.5 (5), and 8.7 (4) or 8.2 (5) kcal/mol for the TC, TB, C, and B forms, respectively.

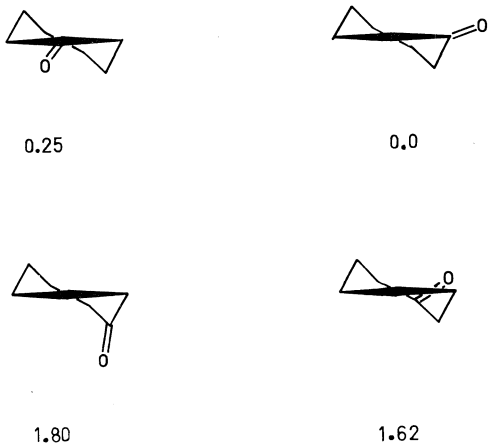

FIG. 2. The four possible TC conformations of cycloheptanone; the numbers are the calculated (7), relative energies (kcal/mol).

stituents at positions 4, 5, 6, and 7 prefer the TC conformation in which the C_2 axis passes through the acetal carbon and in which the substituents are equatorial (see Fig. 3 for 2,5-*O*-methylene-D-mannitol). The present publication is concerned with derivatives having an sp^2 carbon atom in the 1,3-dioxepane ring. As in the previous work (1), all of the 1,3-dioxepanes have been derived from sugar alcohols (alditols). The conformations are specified by an appropriate letter and the number, as a subscript, of the atom through which the axis or plane of symmetry would pass if the ring were viewed as an unsubstituted cycloheptane. The numbering system is that of the parent alditol; the acetal carbon of the seven-membered ring is indicated by the symbol C-a.

Results and Discussion

The compounds studied in the present work are 1-deoxy-2,5:4,6-di-*O*-methylene-L-*arabino*-hex-3-ulose (**1**) and its (2,5-dichlorophenyl)-hydrazone (**2**), and 1,6-di-*O*-benzyl-2,5-*O*-methylene-D-*arabino*-hex-3-ulose (**3**) and its (2,4-dinitrophenyl)hydrazone (**4**). Compound **1** was originally prepared (13) by oxidation of 1,3:2,5-di-*O*-methylene-L-rhamnitol with chromium trioxide in glacial acetic acid – benzene; in the present work the oxidation was achieved using methyl sulfoxide – acetic anhydride (14) or ruthenium tetroxide (15). Compound **3** was obtained by the selective oxidation of 1,6-di-*O*-benzyl-2,5-*O*-methylene-D-mannitol with methyl sulfoxide – acetic anhydride as described by Grindley *et al.* (16).

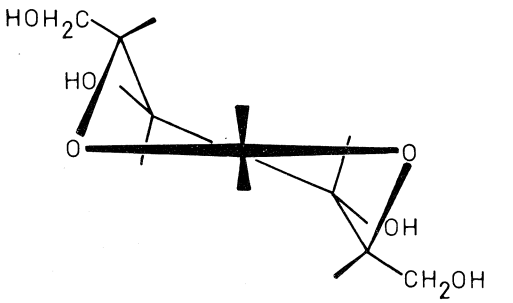

FIG. 3. The favored TC conformation of the 1,3-dioxepane ring in 2,5-*O*-methylene-D-mannitol.

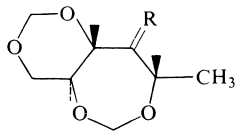

1 R = O

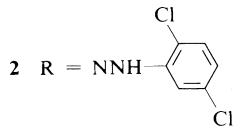

2 R = NNH–

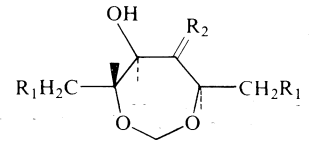

3 R_1 = OCH_2Ph; R_2 = O

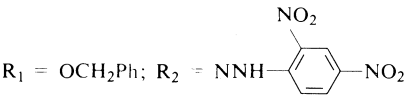

4 R_1 = OCH_2Ph; R_2 = NNH–

On the basis of the earlier study (1) the conformational itinerary of the seven-membered rings in compounds **1**–**4** is restricted to the forms shown in Fig. 4 (illustrated with compound **3**). In Table 1 are listed p.m.r. data for these compounds; calculated geminal coupling constants in the 2,5-OCH_2O— groups in 1,3-dioxepane conformations considered in the earlier work (1) are given in Table 2. The 220 MHz n.m.r. spectrum of compound **1** in chloroform-*d* is shown in Fig. 5. Significantly, the magnitudes of the geminal coupling constants (J_{gem}) in the 2,5-OCH_2O— groups of the 1,3-dioxepanone **1** (−6.8 to −7.1 Hz) and its (2,5-dichlorophenyl)-hydrazone **2** (−7.7 Hz) were markedly different from the values observed (1) in the spectra of the

Can. J. Chem. Downloaded from www.nrcresearchpress.com by 210.87.254.42 on 09/05/12
For personal use only.

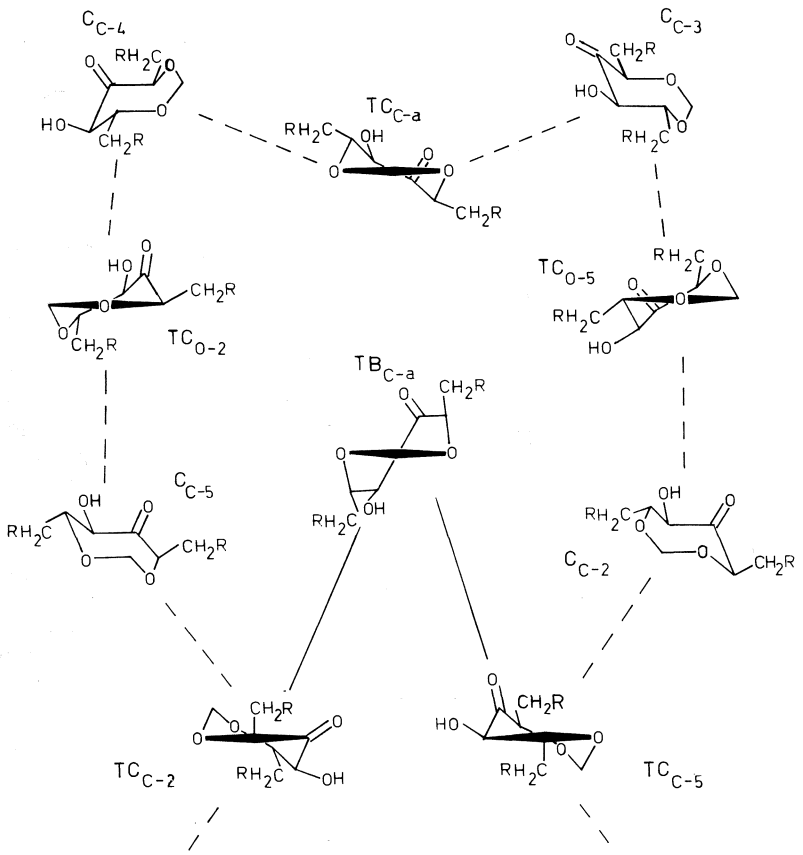

FIG. 4. The conformational itinerary of 1,6-di-*O*-benzyl-2,5-*O*-methylene-D-*arabino*-hex-3-ulose (R = OCH_2Ph, **3**); dashed lines indicate interconversion by pseudorotation, solid lines indicate inversion. The pseudorotations indicated at the bottom of the figure lead to conformations with axial substituents.

related 1,3-dioxepanes (−4.3 to −4.6 Hz) indicating a large change in the conformational equilibrium. In compounds **1** and **2**, it is reasonable to expect that transannular effects of the carbonyl group on the electron distribution about the 2,5-OCH_2O— group and hence on the magnitude of J_{gem} would be small, since the distances from the carbonyl group to the

TABLE 1. Proton magnetic resonance spectral data[a]

		2,5-OCH_2O— group		
Compound	Solvent	Chemical shift (τ)[b]	J_{gem} (Hz)	Δν (Hz)
1	$CDCl_3$	5.13	−7.1	16.5
1[c,d]	$CDCl_3$	5.11	−7.0	61.6[e]
1	$CDCl_3$–C_6D_6 (1:1)	5.51	−6.8	21.3
2	$CDCl_3$	5.24	−7.7	13.0
3	$CDCl_3$	4.97	−6.3	2.3
3	C_6D_6	5.22	−5.8	2.7
4	$CDCl_3$	5.08	−5.4	2.3

[a]Recorded at 60 MHz unless otherwise noted.
[b]The chemical shift quoted is the center of gravity of the AB system.
[c]Recorded at 220 MHz.
[d]The chemical shifts observed for H-4 and H-5 were τ 5.64 and 6.38, respectively, and $J_{4,5}$ = 9.1 Hz; in the other cases listed in this table, these parameters were not obtained because of signal overlap.
[e]This value at 220 MHz corresponds to 16.8 Hz at 60 MHz.

Can. J. Chem. Downloaded from www.nrcresearchpress.com by 210.87.254.42 on 09/05/12
For personal use only.

TABLE 2. Calculated (1) geminal coupling constants in 2,5-OCH_2O— groups in 1,3-dioxepane conformations

Conformation	Calculated J_{gem} (Hz)[a]
TC_{C-a}	−4.2
C_{C-3} or C_{C-4}	−4.3
TC_{O-5} or TC_{O-2}	−6.3
C_{C-2} or C_{C-5}	−7.9
TC_{C-5} or TC_{C-2}	−8.2

[a]The approximate nature of these calculated values is indicated in ref. 1.

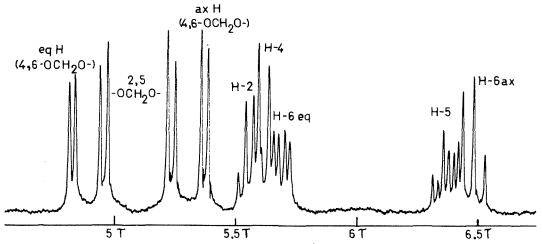

FIG. 5. Partial n.m.r. spectrum at 220 MHz of 1-deoxy-2,5 : 4,6-di-*O*-methylene-L-*arabino*-hex-3-ulose (**1**) in chloroform-*d*.

methylene carbon are much larger in the conformations under consideration than in α-keto methylene systems in which such effects are known (17) to be important. For compounds **1** and **2**, which have a 1,3-dioxepane ring *trans*-fused to one 1,3-dioxane ring, the conformations C_{C-3}, TC_{O-5}, TC_{C-5}, and TB_{C-a} require excessive torsional strain. A comparison of the observed values of J_{gem} (Table 1) with the calculated values (Table 2) suggests that the conformations TC_{O-2}, C_{C-5}, TC_{C-2}, and C_{C-2} are important; in contrast, the preferred conformation of the seven-membered ring in the saturated precursor of compound **1**, namely, 1,3:2,5-di-*O*-methylene-L-rhamnitol, has been shown (1) to be the TC_{C-a} conformation. Additional evidence against any significant contribution of the TC_{C-a} form to the conformational equilibrium of compound **1** was obtained by the observation of a long-range coupling (0.4 Hz) between H-2 and the higher-field 2,5-OCH_2O— proton in the 60 MHz n.m.r. spectrum of **1** in chloroform-*d* or chloroform-*d*–benzene-*d* (1:1). The assignment of the long-range coupling was confirmed by spin decoupling. The TC_{C-a} conformation, in which both of the 2,5-OCH_2O— protons have nearly equivalent relationships to H-2 or H-5, would be inconsistent with the observation of this particular long-range coupling. The change in conformational preference can be accounted for by a consideration of two factors. Firstly, replacement of a hydroxyl-bearing carbon by an sp^2-hybridized carbon atom produces a change in the steric and electrostatic interactions between the substituents at C-3 and C-4. If the 1,3-dioxepane rings of compounds **1** and **2** assume cycloheptane conformational geometries (4), and if the C=X bond (X = O or N) occupies the position which would have been the bisector of the original H—C—O angle, then the dihedral angles between the substituents at C-3 and C-4 are 5.7, 12.3, 23.5, 28.1, and 23.5° in the TC_{C-a}, TC_{O-2}, C_{C-5}, TC_{C-2}, and C_{C-2} conformations, respectively. Clearly, this first factor least disfavors the last three conformations.

The second factor is concerned with the changes in transannular H—H interactions. The twist-chair conformation of cycloheptane (see Fig. 1) has two such repulsive interactions, namely, between H-2ax and H-3′ax and between H-3ax and H-2′ax. These interactions are absent in the TC_{C-a} conformation in the case of compounds **1** and **2**, since there are oxygens at the 2 and 2′ positions. In each of the TC_{O-2} and TC_{C-2} conformations of 1,3:2,5-di-*O*-methylene-L-rhamnitol there is one H–H repulsive interaction, and, since one of the axial hydrogens is at the acetal carbon, the effect is more severe than in cycloheptane. The two major H–H interactions in the TC conformation of cycloheptane account for most of the nonbonded H–H strain (2.12 kcal/mol (4)); the single, but more severe, interaction in each of the TC_{O-2} and TC_{C-2} conformations of 1,3:2,5-di-*O*-methylene-L-rhamnitol can thus be estimated to be 1–2 kcal/mol. The introduction of an sp^2-hybridized carbon atom relieves this interaction in each of these conformations. The chair conformation of cycloheptane (see Fig. 1) has one very important transannular interaction, namely, between H-3ax and H-3′ax. In the C_{C-2} conformation of compounds **1** and **2** this interaction is also present, but is larger because of the shorter C—O bond lengths; however, in the C_{C-5} conformation the interaction is absent, although it did exist in this conformation of the saturated precursor (1,3:2,5-di-*O*-methylene-L-rhamnitol). The interaction between H-3ax and H-3′ax in the chair conformation of cycloheptane accounts for much of the nonbonded H–H strain (2.21 kcal/mol (4)); thus, the corresponding interaction in the C_{C-2} conformation of compounds **1** and **2** can be estimated to be 2–4 kcal/mol. The absence of an

Can. J. Chem. Downloaded from www.nrcresearchpress.com by 210.87.254.42 on 09/05/12
For personal use only.

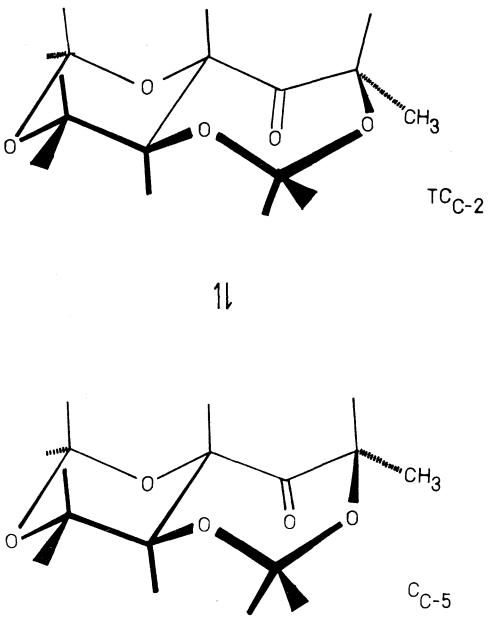

FIG. 6. The favored C_{C-5} and TC_{C-2} conformations of the 1,3-dioxepane ring in 1-deoxy-2,5:4,6-di-*O*-methylene-L-*arabino*-hex-3-ulose (**1**) and its (2,5-dichlorophenyl)hydrazone (**2**).

interaction of this magnitude in the C_{C-5} conformation of **1** and **2**, compared to a relief of only 1–2 kcal/mol in the TC_{O-2} or TC_{C-2} conformation, together with the fact that, in the case of cycloheptane, the TC conformation has been calculated (4) to be only 1.4 kcal/mol more stable than the C conformation, suggests that the C_{C-5} conformation of **1** and **2** may be of comparable energy to that of the TC_{O-2} or TC_{C-2}. Since the TC_{O-2} conformation has already been shown to be disfavored on the basis of the steric and electrostatic interactions between the substituents at C-3 and C-4, then the preferred conformations appear to be C_{C-5} and TC_{C-2} (see Fig. 6).

The key features of the n.m.r. spectral data of 1,6-di-*O*-benzyl-2,5-*O*-methylene-D-*arabino*-hex-3-ulose (**3**) and its (2,4-dinitrophenyl)hydrazone (**4**) (see Table 1) are the slightly more positive values of J_{gem} and the significantly lower values of $\Delta\nu$ for the 2,5-OCH_2O— group than in the case of compounds **1** and **2**; moreover, the magnitude of J_{gem} for **3** was observed to be solvent dependent. These results indicate that there is a considerable reduction in the conformational preference for the C_{C-5} and TC_{C-2} forms for compounds **3** and **4**. In an earlier study (1) it was found that, in the case of a saturated analog of **3**, namely, 1-*O*-benzoyl-2,5-*O*-methylene-D-mannitol, $J_{gem} = -4.7$ Hz, and it was concluded that this compound adopted the TC_{C-a} conformation. It is suggested, therefore, that the conformational equilibrium of **3** or **4** is more complex than that of either **1** or **2**; the difference, presumably, reflects the greater flexibility of the former two compounds.

The work described in this paper clearly indicates that, at least in the case of the present compounds, the introduction of an sp^2-hybridized carbon atom into a seven-membered ring can significantly change the conformational situation (compare ref. 12*a*). The results obtained are consistent with the calculations by Allinger *et al.* (7) which showed that those TC conformations of cycloheptanone having the carbonyl group adjacent to the atom through which the C_2 axis passes are favored.

Experimental

Melting points were determined on a Fisher-Johns apparatus and are uncorrected. Optical rotations were measured with a Perkin-Elmer Model 141 automatic polarimeter at 23 ± 2°. Nuclear magnetic resonance spectra at 60 MHz were measured with a Varian T-60 or Bruker HX-60 spectrometer using tetramethylsilane as an internal lock signal; n.m.r. spectra at 220 MHz were measured on a Varian HR-220 spectrometer at the Canadian 220 MHz NMR Centre. The coupling constants were measured at sweep widths of 250 or 100 Hz and are considered precise to within ±0.2 Hz at 60 MHz or ±0.1 Hz at 220 MHz. Geminal coupling constants were assumed to be negative by analogy with other work (17).

Compounds **2** (13), **3** (16), and **4** (16) were authentic samples prepared earlier in this laboratory.

*1-Deoxy-2,5:4,6-di-O-methylene-*L*-arabino-hex-3-ulose (**1**)*

(*A*) 1,3:2,5-Di-*O*-methylene-L-rhamnitol (18) (0.74 g) was kept for 6.5 h in dry methyl sulfoxide (15 ml) and acetic anhydride (11 ml). The solution was poured into ice water (60 ml) and the mixture was stirred for 20 min and then extracted with chloroform (2 × 40 ml). The extracts were dried (magnesium sulfate) and concentrated to a small volume (~5 ml); ethanol (15 ml) was then added. The resultant precipitate was recrystallized from chloroform – petroleum ether (b.p. 60–80°) to give **1** as white crystals (0.61 g, 82%), m.p. 152–153°; $[\alpha]_D$ +1.9° (*c*, 1.2 in chloroform) (lit. (13) m.p. 151–152°; $[\alpha]_D$ +3.3° (chloroform)).

(*B*) A mixture of 1,3:2,5-di-*O*-methylene-L-rhamnitol (350 mg), potassium metaperiodate (105 mg), potassium carbonate (12 mg), and ruthenium dioxide (15) (35 mg) in ethanol-free chloroform (6 ml) and water (10 ml) was stirred vigorously for 12 h; isopropanol (1 ml) was then added and the mixture was stirred for a short time. The chloroform layer was separated and the water layer was

Can. J. Chem. Downloaded from www.nrcresearchpress.com by 210.87.254.42 on 09/05/12
For personal use only.

washed with chloroform; the chloroform solution and washings were filtered through Celite. The filtrate was dried (magnesium sulfate) and evaporated. The residue (320 mg, 91%) was recrystallized from acetone – petroleum ether (b.p. 60–80°) to give **1** as long, white needles, m.p. 152–153°.

The authors are grateful to Professor J. K. N. Jones, F.R.S., for his interest and encouragement, and to the National Research Council of Canada for its generous financial support of this work.

1. T. B. GRINDLEY and W. A. SZAREK. Can. J. Chem. This issue, preceding paper.
2. J. F. STODDART and W. A. SZAREK. J. Chem. Soc. (B), 437 (1971).
3. T. B. GRINDLEY, J. F. STODDART, and W. A. SZAREK. J. Chem. Soc. (B), 172, 623 (1969).
4. J. B. HENDRICKSON. J. Am. Chem. Soc. **89**, 7036, 7043, 7047 (1967).
5. M. BIXON and S. LIFSON. Tetrahedron, **23**, 769 (1967).
6. P. GROTH. Acta Chem. Scand. **21**, 2631 (1967).
7. N. L. ALLINGER, M. T. TRIBBLE, and M. A. MILLER. Tetrahedron, **28**, 1173 (1972).
8. M. CHRISTL and J. D. ROBERTS. J. Org. Chem. **37**, 3443 (1972).
9. T. SATO, H. MINATO, M. SHIRO, and H. KOYAMA. Chem. Commun. 363 (1966).
10. G. D. BORGEN and J. DALE. Acta Chem. Scand. **26**, 3593 (1972); A. ZSCHUNKE, E. J. STRUBER, and R. BORSDORF. J. Prakt. Chem. **311**, 296 (1969).
11. R. BORSDORF, W. FLAMME, H. KUMPFERT, and M. MUHLSTÄDT. Tetrahedron, **24**, 65 (1968).
12. (*a*) J. B. HENDRICKSON. Tetrahedron, **19**, 1387 (1963); (*b*) J. B. JONES, J. M. ZANDER, and P. PRICE. J. Am. Chem. Soc. **89**, 94 (1967); (*c*) K. KURIYAMA, T. IWATA, M. MORIYAMA, M. ISHIKAWA, H. MINATO, and K. TAKEDA. J. Chem. Soc. (C), 420 (1967); (*d*) J. B. JONES and J. M. ZANDER. Can. J. Chem. **47**, 3501 (1969).
13. J. W. BIRD and J. K. N. JONES. Can. J. Chem. **41**, 1877 (1963).
14. J. D. ALBRIGHT and L. GOLDMAN. J. Am. Chem. Soc. **89**, 2416 (1967).
15. B. T. LAWTON, W. A. SZAREK, and J. K. N. JONES. Carbohydr. Res. **10**, 456 (1969).
16. T. B. GRINDLEY, J. W. BIRD, W. A. SZAREK, and J. K. N. JONES. Carbohydr. Res. **24**, 212 (1972).
17. A. A. BOTHNER-BY. Adv. Magn. Res. **1**, 195 (1965); R. CAHILL, R. C. COOKSON, and T. A. CRABB. Tetrahedron, **25**, 4681, 4711 (1969); G. E. MACIEL, J. W. MCIVER, JR., N. S. OSTLUND, and J. A. POPLE. J. Am. Chem. Soc. **92**, 4151 (1970).
18. W. T. HASKINS, R. M. HANN, and C. S. HUDSON. J. Am. Soc. Chem. **67**, 1800 (1945).

Can. J. Chem. Downloaded from www.nrcresearchpress.com by 210.87.254.42 on 09/05/12
For personal use only.

The Preparation of Protio and Deuterio Derivatives of the Tetracyanoquinodimethane–Tetrathiofulvalene Complex

D. DOLPHIN[1]

Department of Chemistry, The University of British Columbia, Vancouver, British Columbia V6T 1W5

AND

W. PEGG AND P. WIRZ

Department of Chemistry, Harvard University, Cambridge, Massachusetts 02138

Received July 18, 1974

D. DOLPHIN, W. PEGG, and P. WIRZ. Can. J. Chem. **52**, 4078 (1974).

The preparation and purification of the protio and deuterio derivatives of tetracyanoquinodimethane and tetrathiofulvalene, and of the anisotropic organic conductors prepared from these compounds, are reported.

D. DOLPHIN, W. PEGG et P. WIRZ. Can. J. Chem. **52**, 4078 (1974).

Nous décrivons la préparation et la purification des dérivés protio et deutério du tétracyanoquinodimethane et du tétrathiofulvalène ainsi que des conducteurs organiques anisotropics préparés à partir de ces composés.

Can. J. Chem. Downloaded from www.nrcresearchpress.com by 210.87.254.6 on 09/05/12
For personal use only.

The recent reports by Heeger and co-worker (1) on the anomalous conductivity of the tetracyanoquinodimethane–tetrathiofulvalene complex (TCNQ–TTF) **1** prompts us to report the synthesis and purification[2] of both the protio and deuterio complexes of **1** and of the intermediates in their preparation.

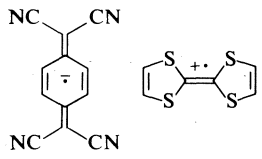

1

Tetrathiofulvalene (TTF), 2

Tetrathiofulvalene (TTF) (**2**) has been prepared by both Coffen *et al.* (2) and Wudl *et al.* (3) from 1,3-dithiolium hydrogen sulfate (**8**) via deprotonation in analogy to the synthesis of substituted tetrathiofulvalenes (4, 5). Olofson *et al.* (6) have also employed a similar method for

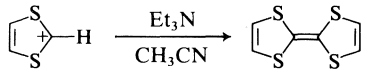

2

[1]Author to whom correspondence should be addressed.

[2]Professor Heeger informed us that materials of the highest purity are necessary in order to observe the anomalous conductivity.

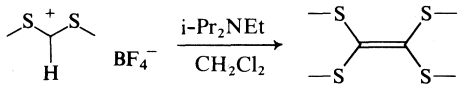

the synthesis of tetrathiomethoxyethylene from dithiomethoxymethyl fluoroborate.

The reaction sequence we have employed for the synthesis of TTF and its tetradeuterio derivative is shown in Scheme 1.

The preparation of 1,3-dithiolium hydrogen sulfate was based upon the method of Klingsberg (7). We have found, however, that extension of the reaction time and the use of pure thiophosgene increased the reported 66% yield of unrecrystallized material to an 83% yield of recrystallized 4,5-dicyano-1,3-dithiole-2-thione (**4**). Moreover the diacid (**5**) was previously prepared via the biscarboxamide, which was in turn hydrolyzed to the impure diacid. But in our hands hydrolysis of the dinitrile in refluxing hydrochloric acid gives the diacid, which on purification with charcoal yields the pure product directly.

The remaining steps from the diacid to TTF follow those previously reported (2, 3, 7). However we find that each intermediate can be purified to give purer products than previously reported. The resulting TTF was purified by precipitation from methanol with water followed by vacuum sublimation to give crystalline material. This material is both light (3) and air sensitive (8) and does not keep well for long

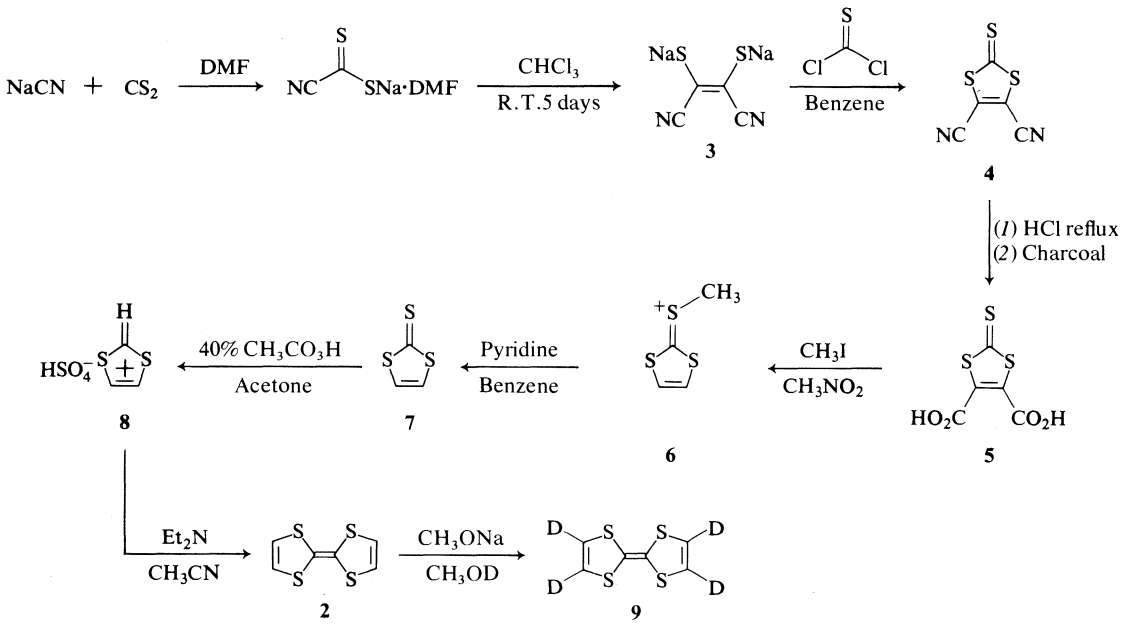

SCHEME 1

periods of time at room temperature, even under argon. We find that it is best to store the 1,3-dithiolium hydrogensulfate which keeps well for extended periods of time and to prepare the TTF as it is needed and use it immediately.

TTF-d_4 has not previously been reported but we find that under basic conditions at room temperature TTF undergoes exchange (9) in the presence of CH_3O^-/CH_3OD to give a high recovery (after sublimation) of product containing 95.4% deuterium.

7,7,8,8-Tetracyano-p-quinodimethane (TCNQ)

While TCNQ is commercially available, we find that a purer product is obtained if the synthetic procedure of Acker and Hertler (10) is followed, with purification of the intermediates at each step. The synthesis involves the condensation of 1,4-cyclohexanedione with malononitrile and oxidation of the resultant adduct, with bromine in pyridine–acetonitrile, to afford TCNQ. When the reaction is carried out on a large scale no problems are encountered. On a small scale, especially when working with deuteriated samples, care had to be exercised in the oxidation step (see below).

Lunelli and Pecile (11) have previously reported the synthesis of deuterated TCNQ from deuterated 1,4-cyclohexanedione. They report that the deuterium content of the TCNQ is essentially unchanged from that of the 1,4-cyclohexanedione even when using undeuterated malononitrile, although they fail to measure the deuterium content of the intermediate bismethylenecyclohexane. In our hands the reported procedure of Acker and Hertler as used by Lunelli and Pecile gives a measurable deuterium content increase in the final product of TCNQ-d_4. For example cyclohexanedione of 93.0% deuterium content gives TCNQ of 97.4% deuterium content (measured by mass spectrum) via an intermediate produced from protiomalononitrile. The mass spectrum of the intermediate is too complex (strong $P^+ - H$ peaks) to estimate whether deuterium is lost in the condensation step. However, the use of cyclohexanedione (97.6% deuterated) and 80% deuterated malononitrile gave an intermediate whose mass spectrum was interpreted to include 97.6% deuterium content (*i.e.*, unchanged). The subsequent oxidation of this intermediate gave TCNQ which was 99.5% deuterated. These results show that there is an isotope effect in the stepwise elimination of HBr and DBr.

The oxidation step quite often gave TCNQ (crude) whose physical appearance varied. In one reaction where bromine was deficient (due to strong argon flow over the condenser) an olive green product was obtained. The mother liquors from this reaction were blue and contained

Can. J. Chem. Downloaded from www.nrcresearchpress.com by 210.87.254.6 on 09/05/12
For personal use only.

Can. J. Chem. Downloaded from www.nrcresearchpress.com by 210.87.254.6 on 09/05/12
For personal use only.

$TCNQ^{-\cdot}$ (formally incomplete oxidation). The use of bromine in amounts greater than the slight excess reported by Acker and Hertler (10) gave chocolate brown products, sometimes of a sticky nature.

Melting points of 'crude' TCNQ could only be estimated since the decomposition which accompanied melting gave products which were so dark that complete melting could not be observed. Multiple recrystallizations of deuterated TCNQ did finally produce a substance with m.p. 289.5–290.5 (no decomposition) in a capillary sealed under argon.

Such melting without decomposition can be taken as a sign of high purity and samples of TCNQ which melt with decomposition are not pure.

Experimental

*4,5-Dicyano-1,3-dithiole-2-thione (7, 12), **4***

A solution of (36 g, 0.194 mol) disodium dimercaptomaleonitrile (**3**) in benzene (300 ml) was chilled in an ice bath as thiophosgene (15 ml, 0.194 mol) (Aldrich) was added dropwise, with stirring, over a 30 min period. The ice bath was removed and the mixture was allowed to come to room temperature with stirring for an additional 2 h. The solvent was removed at reduced pressure and the residue was recrystallized from CCl_4 to afford 29.6 g (83%) of beautiful, yellow-brown needles, m.p. 122–123°.

Klingsberg (7) reports only a 66% yield *prior* to recrystallization. He reports a 90–95% recovery of golden-yellow needles from methylcyclohexane. This compound is also reported by Mayer and Gebhardt (12) in 80% yield (red-brown from CCl_4). They report that sublimation (120°/12 Torr) yields light yellow needles, m.p. 124°.

*1,3-Dithiole-2-thione-4,5-dicarboxylic Acid (7), **5***

A mixture of the 4,5-dinitrile (**4**) (29 g, 157 mmol), concentrated HCl (1970 ml), and water (136 ml) was refluxed for 6.5 h. Upon standing overnight in the refrigerator a crystalline product was obtained. The precipitate was filtered and pressed dry for 20 min in the Büchner funnel. The filter cake was dissolved in warm ether (500 ml), the solution was treated with charcoal (5 g) and some anhydrous magnesium sulfate for 5 min. Filtration through Celite and evaporation of solvent under reduced pressure gave 29.3 g (84%) of the yellow diacid, m.p. 165° (lit. (7) m.p. 160° (dec.) (from chlorobenzene); 151–153° (dec.) (from toluene)).

*2-Methylthio-1,3-dithiolium Iodide (7), **6***

A mixture of 1,3-dithiole-2-thione-4,5-dicarboxylic acid (**5**) (29 g, 0.131 mol), nitromethane (157 ml), and methyl iodide (130 ml) was placed in a 1-l flask and refluxed in an 85° oil bath for 30 h, at which time CO_2 evolution had ceased. The cooled reaction mixture was stirred an additional 48 h at room temperature before the product was filtered and washed with ethyl ether (40 ml). The precipitate was dried under vacuum at 50°. The product, 33.1 g (92%), was a yellow-brown solid, m.p. 123–124°. The mother liquors yielded another 0.5 g, m.p. 118–120, upon refrigeration for 2 days (lit. (7) m.p. 116–121°).

*1,3-Dithiole-2-thione (7), **7***

A mixture of 2-methylthio-1,3-dithiolium iodide (5) (17 g, 61.5 mmol), benzene (250 ml), and pyridine (12 ml) was refluxed, with stirring, for 6 h. The cooled reaction mixture was chilled in ice and a mixture of unreacted starting material and *N*-methylpyridinium iodide was filtered off. The filtrate and washings were evaporated under reduced pressure to afford 6.0 g solid. The filter cake was suspended in benzene (200 ml) and pyridine (12 ml) and refluxed a further 3 h. After work-up as above another 1.5 g solid was obtained. The combined 7.5 g solid was dissolved in a small volume of methylene chloride and placed on a column of 50 g silica gel (Activity II). Elution with methylene chloride and evaporation of the solvent gave 7.2 g (87%) of thione, m.p. 49–50° (lit. (7) m.p. 50–51° (petroleum ether Soxhlet extraction)).

*1,3-Dithiolium Hydrogen Sulfate, **8***

Following the method of Klingsberg (7), 4.2 g (86%) of the product was obtained from 5.6 g of the thione. The salt can be recrystallized by adding methylene chloride to a hot solution of the salt in trifluoroacetic acid.

*Tetrathiofulvalene (2, 3), **2***

Acetonitrile used in this procedure was stirred overnight over basic alumina (Woelm grade I) and filtered directly into the dropping funnel under argon. Triethylamine was refluxed over and distilled from 2-naphthylisocyanate.

1,3-Dithiolium hydrogen sulfate (**8**) (5.0 g, 25 mmol) was suspended in acetonitrile (25 ml). The slurry was chilled in an ice bath as a solution of triethylamine (10 ml) in acetonitrile (25 ml) was added dropwise over a 15 min period. The ice bath was removed and the reaction mixture was stirred for a further 1.5 h. The reaction mixture was then poured into a mixture of 1 *N* sodium hydrogen sulfite (100 ml) and CH_2Cl_2 (100 ml). The mixture was shaken and the methylene chloride drawn off and washed with water, dried over anhydrous magnesium sulfate, and concentrated to dryness under vacuum. This residue was extracted three times with 150-ml portions of boiling hexane which were combined and evaporated to afford 950 mg of product. The undissolved residue from above was dissolved in CH_2Cl_2, adsorbed onto 3 g silica gel (activity II) and chromatographed on 40 g silica gel with CH_2Cl_2 as eluent (column prepared with CCl_4). Material isolated in this chromatography was extracted with hexane as above to afford another 200 mg of product. The combined 1.15 g of crude TTF (**2**) was filtered off (coarse filter) and dried *in vacuo* over P_2O_5. The isolated TTF weighed 1.03 g (20%) and had m.p. 119–120°. As gradient sublimation was reported (13) to give a pure product, a 400 mg sample was sublimed 90–105°/10^{-3} Torr and 380 mg was recovered, m.p. 119–120° (lit. (3) m.p. 118.5–119 (obtained by vacuum sublimation); (2) 98–102° (obtained directly via column chromatography on alumina with $CHCl_3$ as eluent)).

*Tetrathiofulvalene-d_4, **9***

A 1.13 *M* solution of sodium methoxide in methanol-d_1 was prepared by dissolving clean sodium metal (520 mg) in methanol-d_1 (20 ml, 99 atom % d_1) under argon in an oven-dried flask. To this solution was added tetrathiofulvalene (101 mg). After 76 h at room temperature the methoxide solution was partially acidified with 38% DCl in D_2O (1.7 ml). The reaction mixture was diluted with

Can. J. Chem. Downloaded from www.nrcresearchpress.com by 210.87.254.6 on 09/05/12
For personal use only.

methylene dichloride (100 ml) and washed with two small portions of D_2O. The methylene chloride solution was dried over anhydrous sodium sulfate, filtered, and concentrated on a rotary evaporator to afford 100 mg of brown-yellow solid, m.p. 118–120 (sealed capillary, under argon).

This solid was sublimed at 85–95°/0.01 Torr to provide 86.9 mg orange solid (84.3%); m.p. 118.0–119.5°, remelting at 119.5–120.0 (sealed capillary under argon). Mass spectral analysis (see below) indicates a deuterium content of 95.4%.

Mass Spectral Analysis of TTF (Deuterated)

The normal P + 1 and P + 2 abundance due to ^{13}C and ^{34}S in d_0 samples are 9 and 18%, respectively. The 'corrected' value below has had P + 1 and P + 2 contributions removed to reflect only deuterium isotope contributions.

	Relative abundance (%)	
Ion (m/e)	Observed	Corrected
206	1.0	1.0 (d_2)
207	20.5	20.5 (d_3)
208	100.0	98.2 (d_4)
(209)	(13.0)	(9.3)
(210)	(17.5)	(17.5)

Values for *m/e* 209 and 210 are included to show internal consistency; these ions are the expected P + 1 and P + 2 ions for the d_4 ion alone.

Cyclohexanedione-d_8

Modification of the procedure of Lunelli and Pecile (11). A three-necked 100-ml flask equipped with spinbar and condenser with an argon supply was heated as D_2O (5 ml) was added. After 1 h of simmering throughout the apparatus, the D_2O was drawn off and discarded. The flask was dried under a flow of argon. The flask was cooled and charged with D_2O (50 ml, 99.8 mol%) and phosphorus oxychloride (2.5 ml). After 30 min of stirring, 1,4-cyclohexanedione (5.00 g, 44.6 mmol) (Baker Chemical Co.) was added. After 40 h at room temperature sodium carbonate (5 g) was added and the mixture was extracted with methylene chloride (3 × 50 ml). The extracts were combined, dried over sodium sulfate, filtered, and concentrated to a solid. The procedure was repeated using the residue to afford 4.25 g of an orange solid. This solid was sublimed at atmospheric pressure under argon (80–110°) to provide 3.42 g (63.9%) white needles of deuterated cyclohexanedione. The deuterium content was found to be 97.6%-*d* by mass spectral analysis.

1,4-Bis(dicyanomethylene)cyclohexane-d_4 (10, 11)

Malononitrile was deuterated as follows. Malononitrile (2 g) was dissolved in D_2O (20 ml). After 3.5 h the D_2O was extracted with methylene dichloride (3 × 20 ml). These were combined, dried over anhydrous sodium sulfate, filtered, and concentrated to afford 1.9 g of deuterated malononitrile, estimated to be 76.8% deuterated by mass spectroscopy.

The malononitrile was melted with deuterated cyclohexanedione (1.68 g, 14.0 mmol) and a solution of β-alanine (16.5 mg) in D_2O (4.0 ml) was added and stirred. Within seconds the product appeared as white needles. When cool the mixture was filtered, and the precipitate was washed well with D_2O. The product was dried over Drierite in a vacuum dessicator. The weight of the product was 2.98 g, m.p. 217.5–221.5° (dec.) (sealed capillary).

The crude reaction product was recrystallized from ethyl acetate to provide three crops of crystalline material: (*i*) 1.63 g, m.p. 221–224 slight decomposition; (*ii*) 0.76 g, m.p. 220–224 decomposition; (*iii*) 0.14 g, m.p. 217.5–221.5 decomposition; total 2.53 g (83.8%).

TCNQ-d_4 (10, 11)

Bis(dicyanomethylene)cyclohexane (1.20 g, 5.55 mmol) was suspended in freshly distilled acetonitrile (21.5 ml, from P_2O_5 under argon). To this solution was added bromine (1.85 g, 11.55 mmol). The mixture was chilled in ice and the internal temperature was maintained below 5° as a solution of pyridine (1.84 ml, 1.80 g, 22.8 mmol) in acetonitrile (2.9 g) was added dropwise over a 15 min period. The mixture was stirred in an ice bath for an additional 30 min and allowed to come to room temperature for 1 h. To this mixture was added H_2O (50 ml). After stirring for 15 min the crude TCNQ-d_4 was filtered off and dried over Drierite *in vacuo* (20 mm) for 72 h. The product was an orange-brown powder and weighed 1.05 g (91.0%). The partially molten material was too opaque to accurately observe the melting point. A sample recrystallized three times from acetonitrile had m.p. 289.5–290.5° (sealed capillary under argon). Multiply recrystallized TCNQ-d_4 was used in all complexation reactions. It is important in recrystallization of TCNQ that the minimum volume of acetonitrile is used; the rate of solution is low and may require refluxing for some time before total dissolution occurs. As an example 980 mg TCNQ-d_4 was recrystallized from 40 ml acetonitrile and 850 mg was recovered.

Preparation of TCNQ–TTF Complexes

All four possible combinations using both deuterated and undeuterated TCNQ and TTF were prepared in the same fashion.

Example

In refluxing acetonitrile (3 ml) under argon was dissolved TCNQ-d_4 (39.4 mg, 0.189 mmol). To the refluxing solution was added TTF-d_0 (38.3 mg, 0.188 mmol) in acetonitrile (3 ml). The reaction mixture at once precipitated a mass of black needles which were digested for 15 min before cooling. The product was filtered off and dried. This procedure afforded 72.6 mg (93.9%) of the TCNQ-d_4–TTF-d_0 complex.

Similarly a 95.3% yield of TCNQ-d_0 and 96.1% yield of TCNQ–TTF-d_8 were obtained.

The work was supported by the National Science Foundation (Grant GH-33576) and the National Research Council of Canada.

1. A. F. Garito and A. J. Heeger. Acc. Chem. Res. **7**, 232 (1974).
2. D. L. Coffen. Tetrahedron Lett. 2633 (1970); D. L. Coffen, J. Q. Chambers, D. R. Williams, P. E. Garrett, and N. D. Canfield. J. Am. Chem. Soc. **93**, 2258 (1971).

3. F. WUDL, G. M. SMITH, and E. S. HUFNAGEL. Chem. Commun. 1453 (1970).
4. H. PRINZBACH, H. BERGER, and A. LÜTTRINGHAUS. Angew. Chem. Int. Ed. **4**, 435 (1965).
5. A. TAKAMIZAWA and K. HIRAI. Chem. Pharm. Bull. (Jap.), **17**, 1931 (1969).
6. R. A. OLOFSON, S. W. WALINSKY, J. P. MARINO, and J. L. JERNOW. J. Am. Chem. Soc. **90**, 6554 (1968).
7. E. KLINGSBERG. J. Am. Chem. Soc. **86**, 5290 (1964).
8. W. F. COOPER, N. C. KENNY, J. W. EDMONDS, A. NAGEL, F. WUDL, and P. COPPENS. Chem. Commun. 889 (1971).
9. D. J. CHADWICK, J. CHAMBERS, G. D. MEAKINS, and R. L. SNOWDEN. J. Chem. Soc. 201 (1973).
10. D. S. ACKER and W. R. HERTLER. J. Am. Chem. Soc. **84**, 3370 (1962).
11. B. LUNELLI and C. PECILE. Gazz. Chim. Ital. **99**, 496 (1969).
12. R. MAYER and B. GEBHARDT. Chem. Ber. **97**, 1298 (1964).
13. A. R. MCGHIE, A. F. GARITO, and A. J. HEEGER. J. Cryst. Growth. **22**, 295 (1974).

Can. J. Chem. Downloaded from www.nrcresearchpress.com by 210.87.254.6 on 09/05/12
For personal use only.

Cyclizations of Azidoformates to Tetrahydro-1,3-oxazin-2-ones and Oxazolidin-2-ones

PAUL FRANCIS ALEWOOD, MICHAEL BENN, AND ROLF REINFRIED
Department of Chemistry, The University of Calgary, Calgary, Alberta T2N 1N4

Received July 23, 1974

PAUL FRANCIS ALEWOOD, MICHAEL BENN, and ROLF REINFRIED. Can. J. Chem. **52**, 4083 (1974).

Thermolysis of azidoformates in polychloromethane solvents was found to be superior to photolysis as a method for preparing perhydro-1,3-oxazin-2-ones and oxazolidin-2-ones. For some substrates preparatively useful yields of the oxazinones could be obtained but more usually oxazolidone formation competed effectively and often was predominant.

PAUL FRANCIS ALEWOOD, MICHAEL BENN et ROLF REINFRIED. Can. J. Chem. **52**, 4083 (1974).

On a démontré que la thermolyse des azidoformates dans des solvants du type polychlorométhane est supérieure à la photolyse comme méthode de préparation des perhydrooxazin-1,3 ones-2 et oxazolidinones-2. Pour quelques substrats les rendements en oxazinone sont assez élevés et la réaction peut servir à la préparation de ces composés. Ordinairement la formation d'oxazolidone entre en compétition et souvent prédomine. [Traduit par le journal]

Can. J. Chem. Downloaded from www.nrcresearchpress.com by 210.87.254.42 on 09/05/12
For personal use only.

Recently we have been confronted with a problem which required a specific attack on a chemically unactivated C—H bond at a carbon atom β-related to a carbinol center: a system like **1**.

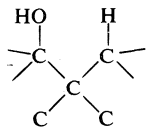

1

A possible solution seemed to be provided by observations that thermolysis, or photolysis, of azidoformates (**2**) generates alkoxycarbonyl nitrenes (**3**) which can undergo a variety of reactions (see Scheme 1) including intramolecular cyclizations: usually reported to yield oxazolidin-2-ones (**4**) but occasionally as also giving tetrahydro-1,3-oxazin-2-ones (**5**) (1).

Specifically, when we commenced our work, the gas-phase thermolysis of **2** (R = H) was said (2) to yield **4** (R = H) (63%) and **5** (R = H) (8%), whereas hexahydrobenzyl azidoformate similarly gave **9** and **10** in 3:1 ratio (2); the thermolysis of **2** (R = n-$C_{15}H_{31}$) in cyclohexane was suspected (1*b*) (a suspicion now known to be correct (3)) to give **5** (R = n-$C_{15}H_{31}$) (8%) as well as **4** (R = n-$C_{15}H_{31}$) (5%).

We decided to reinvestigate the thermal and photochemical decomposition of some simple alkyl azidoformates in the hope that we could establish conditions which would provide a preparatively useful route to tetrahydro-1,3-oxazin-2-ones and thus a convenient solution to our problem.

In order to achieve good yields of **5**, a number of competing reactions of the nitrene **3** have to be minimized: (*a*) the cyclization to oxazolidinone **4**; (*b*) and (*c*) reactions with solvent to give carbamates (**7** and **8**); (*d*) dimerization; and (*e*) elimination to carbonyl compounds.

Although it appeared most unlikely that we would be able to totally prevent the competing cyclization (*a*) to oxazolidinone where this was a possibility, for our initial experiments we selected neopentyl azidoformate (**11**), a substrate in which this reaction is prevented.

The reactions *b* and *c* (Scheme 1) of nitrenes with solvent are thought (1*a*, *b*) to produce **7** by way of a double hydrogen abstraction by triplet nitrene, whereas **8** normally arises as a result of singlet nitrene inserting into C—H bonds (in special cases involving 'activated' C—H bonds, it seems that **8** can also be formed by radical combination after a triplet nitrene species has abstracted a single hydrogen atom from the solvent (1*a*)). In order to minimize these reactions it appeared best to generate the nitrene in an 'inert' solvent[1] and to avoid singlet–triplet conversion.

[1]Gas-phase thermolyses, or photolyses, would clearly exclude reactions *b* and *c* but we were interested in establishing conditions which could be used with azidoformates of low volatility, such as of steroids and triterpenes.

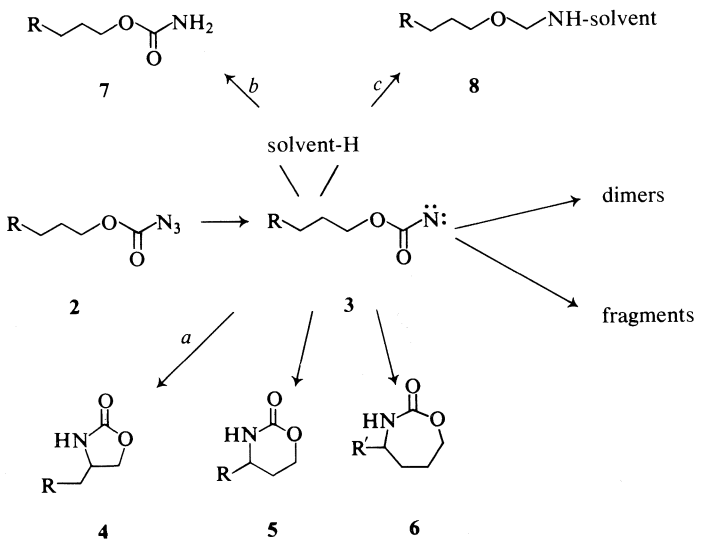

SCHEME 1

Dimerization reactions might be reduced by using dilute solutions; although *d* (Scheme 1), like *e*, is anyway usually relatively unimportant in terms of consuming **3**.

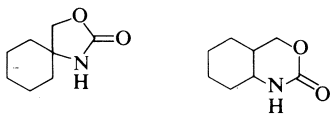

9 **10**

TABLE 1. Thermolyses[a] (and photolyses[b]) of neopentyl azidoformate

Solvent	Products (% by g.l.c. analysis[c,d]) 12	14	Other
Cyclohexane	11	—	85
Benzene[c]	—	—	100
Acetonitrile[c]	—	15	82
Perfluorokerosene-L	—	40	60
Perfluoromethylcyclohexane	5	40	52
	(—)	(—)	(95)
1,1,2-Trichlorotrifluoroethane	10	55	35
Carbon tetrachloride	17	74	—
Chloroform[c]	20	80	—
	(75)	(10)	(15)
Bromoform	70	—	30
Methylene chloride	10	90	—
	(21)	(79)	—
Tetrachloroethylene	39	61	—
	(50)	(—)	(50)

[a]1% (w/v) solutions, at 130°, for 24 h, under N_2 (sealed bottle).
[b]1% (w/v) solutions, under N_2, at 254 nm, for 24 h.
[c]See Experimental.
[d]Relative peak areas (±2%).

We carried out thermal and photochemical decompositions of **11** in a variety of solvents, monitoring the reactions by g.l.c. analyses. (The synthesis of **11**, as well as of authentic samples of carbamates **12** and **13**, and 5,5-dimethyltetrahydro-1,3-oxazin-2-one (**14**) are indicated in Scheme 2). Where the reactions appeared to be clean, the products were isolated. The results of these experiments are summarized in Table 1.

The results indicated that for thermolysis

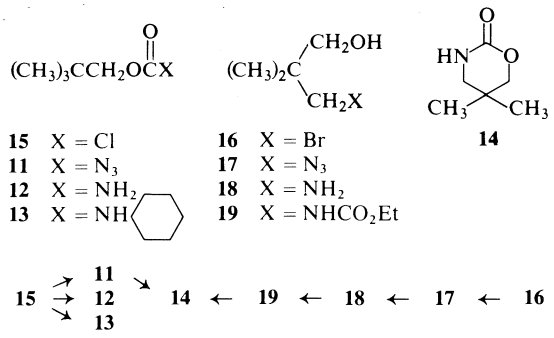

SCHEME 2

saturated chlorinated solvents were best, giving high yields of **12**, with little side-product formation. This was not unexpected: no insertions into C–halogen bonds have been reported for nitrenes; if attack occurs it would probably be on halogen to yield an ylide, unstable with respect to the reactants, *cf.* the behavior (4) of nitrogen ylides.

Thermolysis of **11** in bromoform gave no

Can. J. Chem. Downloaded from www.nrcresearchpress.com by 210.87.254.42 on 09/05/12
For personal use only.

Can. J. Chem. Downloaded from www.nrcresearchpress.com by 210.87.254.42 on 09/05/12
For personal use only.

detectable yield of **14**, but did give a high yield of the abstraction product **12**, a result consistent with this solvent exerting a heavy-atom effect, converting a singlet nitrene into the triplet state.

Fair yields of **14**, together with rather complex mixtures of other (unidentified) products, were obtained using the fluorinated hydrocarbon solvents.

Thermolysis in benzene, acetonitrile, and cyclohexane gave predominately products arising from attack on solvent: **20**, **21**; and **12** plus **13**, respectively.

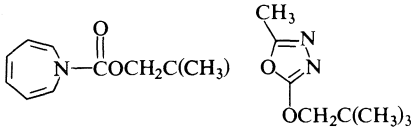

20 **21**

It was anticipated that solvents which were poor for the thermal cyclization of **11** would also be poor in photolytic decompositions. Consequently we confined our investigation to one fluorinated and three chlorinated hydrocarbon solvents. Of these, only methylene chloride showed correspondence to its behavior for the thermolysis of **11**, in giving good yields of **14**; the others gave very complex mixtures in which, in the case of the chloroform and carbon tetrachloride, **12** was a major component.

Photolysis of chloroform and carbon tetrachloride is known to be easy (5) and presumably the multiplicity of products observed is a consequence of this. Methylene chloride is more resistant to photolysis and has been reported to have a singlet stabilizing effect on carbonyl nitrenes (6).

As our primary objective was to establish conditions for good conversion of azidoformates to tetrahydro-1,3-oxazin-3-ones we decided to concentrate upon the preparatively convenient thermolysis in chloroform solution.

Under these conditions, propyl azidoformate (**2**, R = H) gave **4**, **5**, **7** (all R = H) in the ratio of 26:2.8:1.0. Thus the ratio of oxazolidin-2-one to tetrahydro-1,3-oxazinone is only slightly higher than that reported for the vapor-phase thermolysis.

We surmised that the low yield of **5** relative to **4** might be due in part to an inherent preference (1*a*, *b*) for nitrene insertion into methylene rather than methyl C—H bonds and indeed found that thermolysis of **2** (R = CH_3) gave **4**, **5**, and **7** (all R = CH_3) in the ratio 3.5:4.8:1.0, with no trace of **6** (R′ = H). This result is in accord with the behavior of octadecyl azidoformate, and suggests that in fully flexible systems alkoxycarbonyl nitrenes insert into equivalent C—H bonds with a slight (*ca.* 1.3:1.0) preference for formation of the six-membered ring (**5**) rather than five-membered ring product (**4**). Presumably there is a corresponding preference for the geometry shown in **22**, over that in **23**, for the transition state for the insertion reaction. (For some recent computations which support the three centered transition state commonly drawn for these nitrene insertions see ref. 7.)

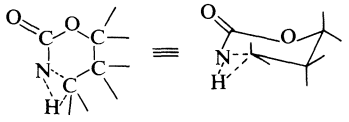

22

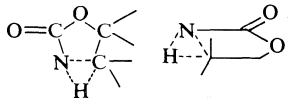

23

As Edwards has pointed out (1*b*) this behavior is in marked contrast to the intramolecular attack on C—H bonds by simple radicals: where the process which leads to **24** is greatly preferred to that which gives **25** (8).

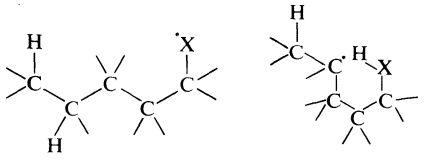

24

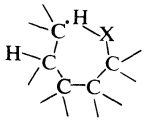

25

Although the thermolysis of alkyl azidoformates may provide a workable synthesis of 5-alkyl-tetrahydro-1,3-oxazin-2-ones some restrictions should be noted: (*i*) as already mentioned alkoxycarbonyl nitrenes discriminate between primary, secondary, and tertiary 'unactivated' C—H bonds, the insertion factors having been estimated (1*b*) as 1:10:30; and (*ii*) in constrained systems, the population of conformers which

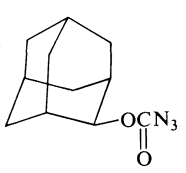

26

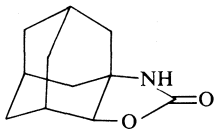

27

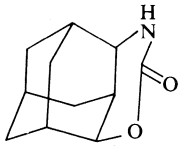

28

lead to **22** may be low compared to those which give **23**.

Thus thermolysis of 2-adamantyl azidoformate (**26**) gave us a high yield of **27**, with no discernible **28**; while Edwards and Paryzek (9) found that a similar thermolysis of **29** gave **30** (52%) and **31** (9%), whereas the isomer **32** gave **33** (52%), **34** (26%), and **35** (7%).

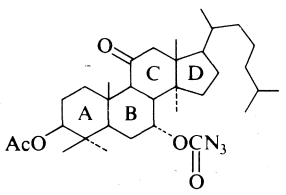

29

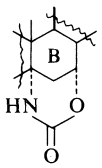

31

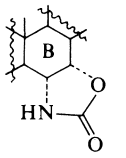

30

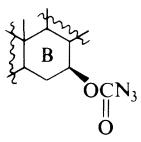

32

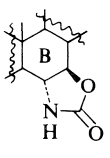

33

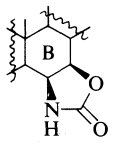

34

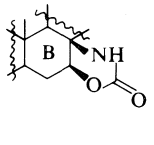

35

We conclude that for the preparation of oxazolidin-2-ones and perhydro-1,3-oxazin-2-ones from azidoformates (*i*) thermolysis in polychloromethane solvents is to be preferred to photolysis (the commonly employed photolysis in cyclohexane being much poorer[2]) and (*ii*) under special circumstances preparatively useful yields of the oxazinones can be obtained but more commonly formation of the oxazolidinones competes effectively and often predominates.

Experimental

Melting and boiling points are uncorrected. Infrared spectra were measured on a Perkin-Elmer model 337 spectrometer and significant absorptions are reported ± 5 cm^{-1} units. Proton magnetic resonance spectra were measured with Varian A60 and HA100 spectrometers. The mass spectra were recorded on a Varian M18-CH5 spectrometer with direct inlet, at 70 eV; significant ions are recorded in a.m.u. Gas–liquid chromatographic analyses were run on a Bendix 2500 unit, using 6 ft glass columns and nitrogen carrier gas flow of *ca.* 40 ml min^{-1}.

Azidoformates

The azidoformates were prepared from the corresponding chloroformates by the procedure of Breslow *et al.* (12).

*Neopentyl Azidoformate (**11**)*

This compound was obtained as a colorless liquid, b.p. 46–48°/10 mm; ν_{max}(film) 2200, 2150, 1735, 1250, and 750 cm^{-1}; τ ($CDCl_3$) 9.05 (s, 9H) and 6.08 (s, 2H); *m/e* 142 (M − 15), 129, 102, 71, 70, 57 (base peak).

Anal. Calcd. for $C_6H_{11}N_3O_2$: C, 45.85; H, 7.05. Found: C, 46.30; H, 6.63.

*Propyl Azidoformate (**2**, R=H)*

This compound was obtained as a colorless liquid, b.p. 31°/10 mm (lit. (13) b.p. 35°/14 mm); ν_{max} (film) 2200, 2150, 1730, 1230, and 750 cm^{-1}; τ ($CDCl_3$) 9.05 (t, $J = 7$ Hz, 3H), 8.30 (m, 2H), and 5.83 (t, $J = 6.5$ Hz, 2H); *m/e* 101 (M − 28), 70, 58 and 43 (base peak).

*Butyl Azidoformate (**2**, R=CH_3)*

This compound was obtained as a colorless liquid, b.p. 49°/10 mm; ν_{max}(film) 2200, 2150, 1735, 1230, and 750 cm^{-1}; τ ($CDCl_3$) 9.0 (t, $J = 6.5$ Hz, 3H), 8.0–8.8 (m, 4H), and 5.76 (t, $J = 6.5$ Hz, 2H); *m/e* 115 (M − 28), 100, 86, 70, 56 (base peak), and 43.

*2-Adamantyl Azidoformate (**26**)*

This compound was obtained as a colorless solid, m.p. 55° (lit. (10) m.p. 52–54°), after distillation, b.p. 108–109°/1 mm; ν_{max}(film) 2170, 2120, 1705, and 1230 cm^{-1}; τ 7.9–8.5 (broad, 16H) and 5.08 (t, $J = 4$ Hz, 1H); *m/e* 221 ($M^{+\cdot}$, very weak), 193, 150, 135 (base peak), and 134 a.m.u.

Anal. Calcd. for $C_{11}H_{15}N_3O_2$: C, 59.71; H, 6.83. Found: C, 59.48; H, 6.80.

[2]For example, it has recently been reported (10) that the photolysis of **26** in cyclohexane was unsatisfactory for the preparation of **27**, giving only 15% of that compound together with 41% of 2-adamantyl *N*-cyclohexylcarbamate, *cf.* our 80% conversion of **26** to **27**. Earlier, a similar photolysis of 1-adamantyl azidoformate had been found to give a 45% yield of adamanto-[2,1-*d*]oxazolidin-2-one (11). In our hand, thermolysis of 1-adamantyl azidoformate in chloroform gave an 86% yield of the oxazolidinone (see Experimental).

Can. J. Chem. Downloaded from www.nrcresearchpress.com by 210.87.254.42 on 09/05/12
For personal use only.

Can. J. Chem. Downloaded from www.nrcresearchpress.com by 210.87.254.42 on 09/05/12
For personal use only.

Carbamates

The carbamates were prepared by the procedure of Breslow *et al.* (12) and obtained in nearly quantitative yields.

*Neopentyl Carbamate (**12**)*

This compound was recrystallized from hexane to give colorless crystals, m.p. 82° (lit. (14) m.p. 82.0–82.5°).

*Propyl Carbamate (**8**, R=H)*

This compound was obtained as colorless crystals from hexane, m.p. 59° (lit. (15) m.p. 60°).

*Butyl Carbamate (**8**, R=CH_3)*

This compound was also obtained as colorless crystals from hexane, m.p. 50–52° (lit. (16) m.p. 54°).

*2-Adamantyl Carbamate (**36**)*

This compound was obtained as colorless crystals, from ethanol, m.p. 136–137°; ν_{max}(Nujol) 3450, 1680, and 1660 cm^{-1}; τ ($CDCl_3$) 8.7–7.7 (broad, 16H), 5.2 (t, J = 4 Hz, 1H), and 5.1–4.5 (broad, 2H, exchanged with D_2O); *m/e* 195 ($M^{+\cdot}$), 134 (base peak) and 92 a.m.u.

Anal. Calcd. for $C_{11}H_{17}NO_2$: C, 67.75; H, 8.77; N, 7.18. Found: C, 68.20; H, 8.67; N, 7.24.

*Neopentyl N-Cyclohexyl Carbamate (**13**)*

This compound was obtained as a liquid, b.p. 95–97°/1 mm, which crystallized on standing, m.p. 85–86°; ν_{max}(film) 3300, 1705, 1680, 1540, and 1150 cm^{-1}; τ ($CDCl_3$) 9.04 (s, 9H), 8.9–7.9 (broad, 10H), 6.7–6.4 (broad, 1H) 6.22 (s, 2H), and 3.0 (broad, 1H); *m/e* 213 ($M^{+\cdot}$), 198, 170, 141, 125, and 100 a.m.u.

Aminoalcohols

*2,2-Dimethyl-3-aminopropanol (**18**)*

To a stirred mixture of sodium azide (50 g, 770 mmol) in methyl carbitol (150 ml) and water (70 ml) was added, in one portion, 2,2-dimethyl-3-bromo-1-propanol (17).

On continued stirring the reactants dissolved completely and the homogeneous solution was heated to 95° and kept at this temperature for 3 days, after which time g.l.c. analysis (5% Versamid 900, 175°) revealed that the bromoalcohol had been consumed. The cold reaction mixture was extracted with ether, and the ether extracts were then repeatedly washed with water to remove the carbitol. Removal of solvent from the dried ($MgSO_4$) ether extracts gave (**17**) as a colorless liquid, b.p. 69–70°/10 mm 6.0 g (51%); ν_{max}(film) 3400, 2100, and 1040 cm^{-1}; τ ($CDCl_3$) 9.08 (s, 6H), 7.12 (s, 1H), 6.80 (s, 2H), and 6.66 (s, 2H).

This total product was dissolved in ethanol (50 ml) containing suspended 5% Pt–C catalyst and hydrogenated for 24 h at 60 p.s.i. After removal of catalyst and solvent, **18** was obtained as a light yellow oil, 4.4 g (92%), which crystallized and recrystallized from petroleum ether (40–60°) as a colorless solid, m.p. 78–80° (lit. (18) m.p. 98–100°); ν_{max}(film) 3380, 3300, 3200, 1400, 1370, and 1040 cm^{-1}; τ ($CDCl_3$) 9.08 (s, 6H), 7.0–6.0 (broad, m, 4H); *m/e* 104 (M + 1) (strong), 103, 85, 72, 70, 57 (base peak), 30, and 31 a.m.u.

4-Aminobutanol

By a procedure analogous to that described above, 4-bromobutanol was converted to 4-azidobutanol (46%), b.p. 76–78°/10 mm; ν_{max}(film) 3350, 2100, 1250, and 1050 cm^{-1}; τ ($CDCl_3$) 8.35 (m, 4H), 6.8 (m, 2H), and 6.3 (m, 2H). The azidoalcohol was then reduced over 5% Pt–C to yield 4-aminobutanol (61%), b.p. 104–107°/10 mm; n_D^{23} 1.4585 (lit. (19) b.p. 100°/10 mm; n_D 1.4610).

3-Aminobutanol

This aminoalcohol was prepared according to the literature procedure and obtained (31%) as a colorless liquid, b.p. 75–77°/10 mm; n_D^{23} 1.4530 (lit. (20) b.p. 81–82°/19 mm; n_D^{20} 1.4534).

Preparation of Cyclic Carbamates

All the cyclic carbamates were prepared from aminoalcohols by the methods of Dreschell (21) and Homeyer (22): a mixture of the aminoalcohol (1.0 mol), diethyl carbonate (1.1 mol), and a catalytic amount of sodium methoxide (*ca.* 10 mg) was heated in an oil bath until the calculated amount of ethanol had distilled out. (Oxazolidone formation usually required about 4 h at 100–150° and the tetrahydrooxazinones required 150–170° and up to 24 h.) The residue was then taken up in chloroform and the solution washed with water and then dried ($MgSO_4$). Removal of solvent, followed by distillation then gave the cyclic carbamates.

*5,5-Dimethyltetrahydro-1,3-oxazin-2-one (**14**)*

This compound was obtained as a colorless liquid, b.p. 120–125°/0.1 mm, which crystallized on standing. Recrystallization from acetone gave a colorless solid, m.p. 112–113°; ν_{max}(KBr) 3300, 1700, 1660, and 1100 cm^{-1}; τ ($CDCl_3$) 8.95 (s, 6H) 6.95 (broad, s, 2H), 6.10 (s, 2H), and 3.18 (broad, s, 1H); *m/e* 129 ($M^{+\cdot}$), 114, 98, 70, and 56 a.m.u.

Anal. Calcd. for $C_6H_{11}NO_2$: C, 55.80; H, 8.59; N, 10.85. Found: C, 56.12; H, 8.63; N, 10.66.

*Tetrahydro-1,3-oxazin-2-one (**5**, R=H)*

This compound was obtained as a colorless liquid, b.p. 144–146°/0.1 mm; m.p. 76–79° (lit. (23) m.p. 77°).

*4-Methyltetrahydro-1,3-oxazine-2-one (**5**, R=CH_3)*

This was obtained as a colorless liquid, b.p. 120–135°/0.1 mm, which crystallized from acetone, m.p. 55–56° (lit. (12) m.p. 98.5–99.5°); ν_{max}(neat: 3250 (N—H), 1700 (C=O), 1290, 1095 cm^{-1}; *m/e*: 115 ($M^{+\cdot}$), 100, 70, 56, 42; τ ($CDCl_3$): 8.75 (3H, doublet, J = 6 Hz), 7.85–8.6 (2H, complex multiplet), 6.25–6.60 (1 H, multiplet), 5.60–6.0 (2H, multiplet), 2.85 (1H, broad).

Anal. Calcd. for $C_5H_9NO_2$: N, 12.15. Found: N, 11.71.

Double irradiation was carried out on the Varian HA100 spectrometer on a sample containing D_2O: irradiation at 5.60–6.0 (H-6) simplified the complex multiplet at 7.85–8.60 (H-5) giving two sets of doublets, J_1 = 14 Hz, J_2 = 8 Hz, J_3 = 4 Hz; irradiation at 6.25–6.60 (H-4) collapsed the doublet at 8.75 (CH_3 to a singlet, and reduced the number of lines of the complex multiplet at 7.85–8.6; irradiation at 7.85–8.60 simplified the multiplet at 5.60–6.0 to an AB doublet of doublets J = 11 Hz; irradiation at 8.75 simplified the multiplet at 6.25–6.60. to an approximate triplet J = 6 Hz with finer splitting.

*4-Methyloxazolidin-2-one (**4**, R=H)*

This compound was obtained as a colorless liquid, b.p. 122–124°/1 mm (lit. (24) b.p. 123–124°/4 mm, which crystallized on standing, m.p. 56–57°; τ ($CDCl_3$) 8.70 (d, J = 6 Hz, 3H) 6.2–5.2 (m, 3H), 3.25 (broad, s, 1H); *m/e* 101 ($M^{+\cdot}$) 86, 70, 56, 42.

Anal. Calcd. for $C_4H_7NO_2$: C, 47.53; H, 6.98; N, 13.86. Found: C, 47.46; H, 6.74; N, 13.53.

*4-Ethyloxazolidin-2-one (**4**, R=CH_3)*

This compound was also obtained as a colorless liquid, b.p. 135°/1.0 mm; n_D^{23} 1.4635 (lit. (12) b.p. 129–131°/0.5 mm; n_D^{20} 1.4637) which crystallized on cooling, m.p. 16°; ν_{max}(film) 3300, 1750, 1230, 1050, 930, and 770 cm^{-1}; τ ($CDCl_3$) 9.01 (t, J = 6.5 Hz, 3H), 8.40 (q, J = 6.5 Hz, 2H) 6.40–5.30 (m, 3H), and 3.1 (broad s, 1H).

Thermolyses of Azidoformates

Typical thermolysis conditions consisted of heating a 1% (w/v) solution of azidoformate, under an atmosphere of nitrogen at 120° in a sealed bottle, overnight. The products obtained after removing the solvent were characterized as described for the individual cases below.

Neopentyl Azidoformate

(a) In benzene. Thermolysis of **11** (1.0 g) in benzene yielded a single product (t.l.c., benzene–chloroform 2:1 (v/v), R_f 0.5) isolated by p.l.c. as a yellow liquid (550 mg) which upon distillation gave a colorless liquid, b.p. 91.2°/0.1 mm which rapidly darkened on standing; ν_{max}(neat): absence of N—H, 3050, 1700, 1650, 1620, 750 cm^{-1}; τ ($CDCl_3$): 8.98 (5, 9H), 5.3–6.2 (m, 6H), 3.88 (s, 2H); u.v., λ_{max}(hexane): 320 nm; *m/e*: 120 (P-87, 118, 87, 85, 83). The above spectral data are consistent with the structure **20**.

(b) In acetonitrile. Thermolysis of **11** (520 mg) yielded a brown liquid (420 mg), the g.l.c. analysis (Versamid 900, 5%, programming 130–190°) of which indicated two main products in *ca.* 82 and 15% yield. The minor product, of longer retention time, corresponded to 5,5-dimethyltetrahydro-2*H*-1,3-oxazine-2-one. To isolate the major product the mixture was rapidly distilled *in vacuo* to give a colorless liquid, 200 mg (36%), b.p. 75°/10 mm; ν_{max}(neat): 1640, 1580, 1235, 730, and 620 cm^{-1}; τ ($CDCl_3$): 8.95 (s, 9H), 7.57 (s, 3H), 5.82 (s, 2H); *m/e*: 155 (M − 15), 141, 114, 101 (base), 83. This was consistent with structure **21**.

(c) In chloroform. Thermolysis of **11** (500 mg) in chloroform (50 ml) gave a clear colorless liquid product, which crystallized on standing; g.l.c. analysis (Versamid 900, 5%, 130–190°) revealed only two compounds, **14** (*ca.* ≥ 80%) and 12 (*ca.* ≤ 20%). Separation of a portion (328 mg) of this product by p.l.c. (Merck Silica Gel PF_{254}, chloroform–methanol 19:1) resulted in the isolation of **14** (224 mg) (68%).

Propyl Azidoformate

Thermolysis of **2** (R=H) (900 mg) in chloroform gave a light-brown oil (700 mg); g.l.c. analysis (Versamid 900, 5%, 180–200°) revealed three compounds **7**, **5**, and **4** (all R=H) in an approximate ratio of 1:25.7:2.78, totalling *ca.* 97% of the product.

Butyl Azidoformate

Thermolysis of **2** (R=CH_3) (850 mg) in chloroform also gave a light-brown oil (605 mg) and g.l.c. analysis (Versamid 900, 5%, 130–180°) revealed the presence of three compounds, **7**, **5**, and **4** (all R=CH_3), in approximate ratio 1:3.5:4.8, totalling 93% of the products.

2-Adamantyl Azidoformate

Thermolysis of **26** (1.16 g) in chloroform gave a white solid, g.l.c. analysis (OV-1, 3%, 120–250°) of which revealed only two components in approximate ratio 95:5. Chromatography on silica gel (Merck G), eluting with benzene and chloroform gave two compounds. The first (900 mg) was recrystallized from petroleum ether – ethyl acetate as a colorless solid, m.p. 145–146° (lit. (10) m.p. 133–134°); ν_{max}(Nujol) 3300, 1750, and 1730 cm^{-1}; τ ($CDCl_3$) 8.6–7.4 (m, 13H), 5.88 (d, J = 4 Hz, 1H), and 2.90 (b, 1H); *m/e* 193, 192 (M − 1, base peak) 149 and 136 a.m.u.

Anal. Calcd. for $C_{11}H_{15}NO_2$: N, 7.30. Found: N, 7.27.

These data are consistent with structure **27**. The second compound (60 mg) had m.p. 135° undepressed on admixture with 2-adamantyl carbamate and also had the same retention time and R_f upon g.l.c. and t.l.c. comparison with **36**.

Thermolysis of 1-Adamantyl Azidoformate

Thermolysis of this (11) (1.15 g) in chloroform (containing 0.75% ethanol) yielded a white solid; t.l.c. (silica gel, chloroform–methanol 9:1) revealed only two components (R_f 0.75 and 0.80), as did g.l.c. (Versamid 900, 5%, 180°) in an approximate ratio of 9:1. Chromatography on silica gel (Merck G) eluting successively with chloroform and chloroform – ethyl acetate (10:1) resulted in the isolation of these individual products. The first (73 mg, 6%) was recrystallized from ethyl acetate to give colorless crystals, m.p. 112–114°; ν_{max}(KBr) 3250, 1685, and 1050 cm^{-1}; τ ($CDCl_3$) 8.75 (t, J = 6 Hz, 3H), 8.39 (d, J = 2 Hz, 6H), 8.20 (d, J = 2 Hz, 6H), 7.84 (b, 3H), 5.82 (q, J = 6 Hz, 2H), and 3.05 (bs, 1H); *m/e* 207, 152, and 135 (base peak) a.m.u. These data are consistent with this product being 1-adamantyl *N*-ethoxy carbamate (formed by attack on the ethanol in the thermolysis solvent).

The second compound (900 mg, 86%) recrystallized from ethyl acetate as colorless crystals, m.p. 139° (lit. (11) m.p. 130–133°). The i.r. and p.m.r. spectra of this product were identical with those reported for adamanto[2,1-*d*]-oxazolidin-2-one.

We wish to thank Dr. O. E. Edwards of the Biochemistry Laboratory, National Research Council, Ottawa, for his most useful comments. Thanks are also due to the National Research Council for financial support of this work.

1. (*a*) W. Lwowski. *In* Nitrenes. *Edited by* W. Lwowski. Interscience, New York. 1970. p. 185. (*b*) O. E. Edwards. *In* Nitrenes. *Edited by* W. Lwowski. Interscience, New York. 1970. p. 225.
2. D. Kuhling. Dr.-Ing. Thesis. Technischen Hochschule. Darmstadt, 1965.
3. D. S. Breslow and G. A. Ward. J. Org. Chem. **38**, 4205 (1973).
4. V. Franzen and G. Wittig. Angew. Chem. **72**, 417 (1960).
5. J. Calvert and J. Pitts. Photochemistry. John Wiley & Sons, New York. 1966.
6. G. R. Felt, S. Linke, and W. Lwowski. Tetrahedron Lett. 2037 (1972).
7. P. F. Alewood, P. M. Kazmaier, and A. Rauk. J. Am. Chem. Soc. **95**, 5466 (1973).
8. W. Carruthers. Some modern methods of organic synthesis. Cambridge University Press, London. 1971. p. 172.

Can. J. Chem. Downloaded from www.nrcresearchpress.com by 210.87.254.42 on 09/05/12
For personal use only.

9. O. E. EDWARDS and Z. PARYZEK. Can. J. Chem. **51**, 3866 (1973).
10. J. W. GREIDANUS. Can. J. Chem. **52**, 1062 (1974).
11. W. V. CURRAN and R. B. ANGIER. J. Chem. Soc. Chem. Commun. 563 (1967); J. Org. Chem. **34**, 3668 (1969).
12. D. S. BRESLOW, T. J. PROSSER, A. F. MARCANTONIO, and C. A. GENGE. J. Am. Chem. Soc. **89**, 2384 (1967).
13. R. HUISGEN and H. BLASCHKE. Chem. Ber. **98**, 2985 (1965).
14. R. FESSENDEN and M. COAN. J. Med. Chem. **8**, 604 (1965).
15. P. CARRE and H. PASSEDOUET. C. R. **204**, 347 (1936).
16. F. D. CHATTAWAY and E. SAERENS. J. Chem. Soc. **117**, 708 (1920).
17. S. SEARLES, JR., R. G. NICKERSON, and W. K. WITSIEPE. J. Org. Chem. **24**, 1839 (1959).
18. J. CALDWELL. U.S.P. 2, 618, 658 (1952); Chem. Abstr. **47**, P9997 (1953).
19. A. MARSAK-FLEURY and J. LAROCHE. Bull. soc. Chim. Fr. 1270 (1963).
20. V. RODIANAS and N. KISSELEVA. Izvest. Akad. Nauk. SSSR. Ser. Khim. 575 (1956); E. E. VAN TAMELEN and J. E. BRENNER. J. Am. Chem. Soc. **79**, 3839 (1957).
21. E. DRESCHEL. U.S.P., 2, 701, 246; Chem. Abstr. **50**, P2686 (1956).
22. J. HOMEYER. U.S.P. 2, 399, 118; Chem. Abstr. **40**, P4184 (1946).
23. R. DELABY and R. DAMIENS. C. R. **239**, 674 (1954).
24. H. NAJER, P. CHABRIER, and R. GIUDECELLI. Bull. Soc. Chim. Fr. 1611 (1959).

Can. J. Chem. Downloaded from www.nrcresearchpress.com by 210.87.254.42 on 09/05/12
For personal use only.

Unusual Reactions of Peroxides. II. Decomposition of Diphenylmethyl Peroxides[1]

R. HIATT, D. J. LEBLANC, AND C. THANKACHAN

Department of Chemistry, Brock University, St. Catharines, Ontario

Received July 11, 1974

R. HIATT, D. J. LEBLANC, and C. THANKACHAN. Can. J. Chem. **52**, 4090 (1974).

Thermal decomposition of bisdiphenylmethyl peroxide at 110–130 °C in solution yields approximately 90% H_2 + $2Ph_2CO$ by a nonradical mechanism. In C_2Cl_4, toluene, or nitrobenzene $\log k\ (s^{-1}) = 11.0 \pm 0.5 - (27\,000 \pm 1000)/2.303RT$. Photolytic decomposition of this peroxide in toluene yielded no H_2.

t-Butyl diphenylmethyl peroxide decomposed in toluene with $\log k\ (s^{-1}) = 16.7 - 38\,600/2.303RT$, giving free radical products and no H_2. There is some evidence for facile disproportionation of the initial alkoxy radicals in the solvent cage.

R. HIATT, D. J. LEBLANC et C. THANKACHAN. Can. J. Chem. **52**, 4090 (1974).

La décomposition thermique, en solution et à 110–130 °C, du peroxyde de bisdiphénylméthyle conduit avec un rendement approximatif de 90% à de l'hydrogène + $2Ph_2CO$; le mécanisme de la réaction n'est pas radicalaire. Dans le C_2Cl_4, le toluène ou le nitrobenzène, $\log k\ (s^{-1}) = 11.0 \pm 0.5 - (27\,000 \pm 1000)/2.303RT$. La décomposition photolytique de ce peroxyde dans le toluène ne fournit pas d'hydrogène.

Le peroxyde double de *t*-butyle et de diphénylméthyle se décompose dans le toluène avec un $\log k\ (s^{-1}) = 16.07 - 38\,600/2.303RT$; la réaction donne des produits provenant d'une réaction radicalaire et ne fournit pas d'hydrogène. Il y a quelques données indiquant qu'il y a une disproportionnation facile, dans une cage de solvent, des radicaux alkoxy formés initialement.

[Traduit par le journal]

Introduction

The production of H_2 from suitably constituted peroxides (**1**) has been the subject of sporadic investigation over the past 75 years (1–3),

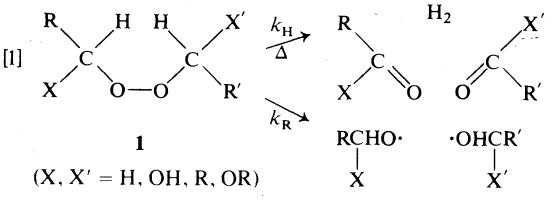

but remains a reaction that is not well characterized. Our discovery (4) that a simple alkyl peroxide (**1**, R = R′ = Et; X = X′ = Me) could yield substantial amounts of H_2 in competition with the more normal homolysis when thermally decomposed in solution was particularly surprising since pyrolysis of this peroxide or similar ones in the vapor phase yields little or no H_2 (3).

This effect of phase is not easily explained since the competition between k_H and k_R (eq. 1) in solution is not affected by the polarity or the viscosity of the solvent (4). Unexplained as well is the effect that the character of groups R, R′, X, and X′ have on the k_H/k_R ratio.

Since part of the difficulty of explanation has lain in the scarcity of good data we have undertaken the study of several other primary and secondary alkyl peroxides. These, unlike the tertiary alkyl peroxides, have been rarely decomposed in solution and should yield other useful information, specifically on the fate of the alkoxy radicals generated by the k_R route (4).

Bisdiphenylmethyl peroxide seemed a particularly good candidate since it had been reported to yield benzophenone quantitatively when pyrolyzed in nitrobenzene (5). Thus a generous H_2 yield could be confidently predicted.

The unsymmetrical *t*-butyl diphenylmethyl peroxide, which should not yield H_2, was also decomposed to provide a comparison.

Experimental

Bisdiphenylmethyl peroxide was prepared by the method of Cadogan *et al.* (5), reacting benzhydrol with diphenylmethyl hydroperoxide in the presence of a catalytic amount of *p*-toluenesulfonic acid. Using a 3:1 excess of benzhydrol (5) consistently gave product

[1]Taken in part from the M.Sc. Thesis of C. Thankachan, Brock University, 1972, and the B.Sc. Thesis of D. J. LeBlanc, Brock University, 1973.

Can. J. Chem. Downloaded from www.nrcresearchpress.com by 210.87.254.42 on 09/05/12
For personal use only.

Can. J. Chem. Downloaded from www.nrcresearchpress.com by 210.87.254.42 on 09/05/12
For personal use only.

contaminated with bisdiphenylmethyl ether in varying amounts ranging from 100 to 7%, as determined by n.m.r. analysis. A 1:1 mixture of hydroperoxide and benzhydrol, however, was found to yield peroxide apparently pure.

Comparisons of samples differing in purity showed that the presence of ether affected neither rates nor products of the thermal reaction. For the photolytic work only samples of pure peroxide were used.

Nuclear magnetic resonance analysis (Varian A-60, $DCCl_3$ solvent), showed a carbinyl proton singlet for the peroxide at 6.1 p.p.m. downfield from TMS, while the corresponding ether singlet appeared at 5.45 p.p.m.

t-Butyl diphenylmethyl peroxide was prepared similarly from *t*-BuO_2H and benzhydrol. Nuclear magnetic resonance analysis showed the carbinyl proton at 6.0 p.p.m. and the methyl proton singlet at 1.25 p.p.m. No extraneous peaks were evident.

Solvents were reagent grade, used without further purification.

Rate Measurements

Samples were degassed, sealed under vacuum, and immersed in a constant temperature bath. Analysis for residual peroxide depended on the solvent. In tetrachloroethene solvent the disappearance of peroxides was directly related to the appearance of benzophenone, the latter monitored by its absorption at 287 nm. In toluene and nitrobenzene, peroxide concentration was measured by n.m.r., using in toluene its methyl proton absorption, and in nitrobenzene added TMS, as internal standards. None of the standard iodometric methods nor any of the modifications we tried gave reliable results.

Products

Nongaseous products were analysed by g.l.c. Gaseous products were determined volumetrically since for $(Ph_2CHO)_2$ and Ph_2CHO_2t-Bu, respectively, mass spectrometric analysis showed H_2 and CH_4 to be the only noncondensible products.

Photolyses were carried out using a mercury lamp (G.E. H-85M3) fixed in the center of a cage designed to rotate samples around the light source, the whole being immersed in a water bath for temperature control.

Results and Discussion

Thermal Decomposition of Bisdiphenylmethyl Peroxide

The first-order rate constants for decomposition in three solvents are shown in Table 1. Variations in the initial concentration of peroxide (P_0) gave no change in rate constant; whereas P_0 variations in any given solvent were relatively small, no more than a factor of 2–3, the difference between P_0's in C_2Cl_4 and in toluene or nitrobenzene is more than 1000-fold, again with no significant change in rate constant. Thus, the decomposition is almost certainly first order.

While this in itself does not eliminate radical-induced decomposition as a factor, the very low yields of benzhydrol (Table 2) do rule out this possibility.[2] The major products, H_2 and Ph_2CO indicate a predominantly nonradical pathway, as do the Arrhenius parameters (Table 1). Unlike *s*-Bu_2O_2 which yielded only 25–30% H_2 (4), the measured E_a is 10 kcal less than expected for O—O homolysis (6) and is comparable to the activation energy for decompositions of peroxyhemiacetals which give similarly high H_2 yields (2).

Evidently O—O homolysis does compete, to the extent of 5–10%, as shown by the presence in the products (Table 2) of some benzhydrol and, in toluene, of bibenzyl. The 20° temperature range, however, is not sufficient to show the trend towards more homolysis at higher temperatures which the difference in activation energy for k_H and k_R would predict.

Thermal Decomposition of t-Butyl Diphenylmethyl Peroxide

Rates and products for the pyrolysis of this unsymmetrical peroxide in toluene are given in Tables 3 and 4, respectively. Despite the high initial concentrations of peroxide, the decompositions were first order and produced a linear log k *vs.* $1/T$ plot with E_a = 38 kcal/mol. Methane was the only gaseous product and the reaction would appear to be one of simple O—O homolysis,

$$[5]\quad Ph_2CHO_2t\text{-}Bu \xrightarrow{\Delta} Ph_2CHO\cdot + t\text{-}BuO\cdot \rightarrow \text{products}$$

except for the relatively low, P_0 dependent yield of bibenzyl, and the high *t*-BuOH/AcMe ratio, also P_0 dependent.

The results do settle two points: (*i*) For an alkyl peroxide to generate H_2, both alkyl groups must be *non*tertiary. (The contrary is claimed for some peroxyhemiacetals (7).) Benzhydryloxy radical does not cleave off H·. (*ii*) A benzhydryloxy as one half of an alkyl peroxide does not in itself lead to an abnormally low E_a for homolysis.

Additional conclusions from the data are more tenuous. Comparisons of the products (Table 4)

[2] A hydrogen atom chain is conceivable:

$$[2]\quad Ph_2CHO\cdot \rightarrow Ph_2CO + H\cdot$$

$$[3]\quad H\cdot + (Ph_2CHO)_2 \rightarrow H_2 + Ph_2\dot{C}O_2CHPh_2$$

$$[4]\quad Ph_2\dot{C}O_2CHPh_2 \rightarrow Ph_2CO + PhCHO\cdot$$

But even if H· were generated in this manner (which it is not, see below), its probable addition to solvents such as C_2Cl_4 or $PhNO_2$ makes a clean chain of this type exceedingly unlikely.

Can. J. Chem. Downloaded from www.nrcresearchpress.com by 210.87.254.42 on 09/05/12
For personal use only.

TABLE 1. Rate constants for the thermal decomposition of bisdiphenylmethyl peroxide

Temperature (°C)	P_0[a] (mol/l)	10^5 k[b] (s^{-1})	E_a (kcal/mol)	log A (A in s^{-1})
		In tetrachloroethylene		
111.0	0.0003–0.001	3.4		
120.0	0.0005–0.00075	8.60	26.6	10.6
130.0	0.00045–0.00092	18.7		
		In toluene		
111.0	0.26–0.49	3.40		
120.0	0.72	9.20	28.0	11.6
130.0	0.25–0.30	19.3		
		In nitrobenzene		
111.0	0.54	4.35		
120.0	0.46–0.55	10.65	27.0	11.0
130.0	0.31–0.47	23.4		

[a]Initial concentration of peroxide.
[b]Average of several runs.

TABLE 2. Products from thermal decomposition of bisdiphenylmethyl peroxide

Temperature (°C)	P_0[a] (mol/l)	Products in mol/l (%)[b]				Total[b] Ph_2C
		Ph_2CO	Ph_2CHOH	H_2	$(PhCH_2)_2$	
		In tetrachloroethylene				
111.0	0.130	0.24(92)	0.015(6)	0.120(92)		98
120.0	0.117	0.22(94)	0.014(6)	0.103(88)		100
130.0	0.111	0.195(88)	0.016(7)	0.100(90)		95
		In toluene				
111.0	0.115	0.21(91)	0.050(22)	0.110(95)	0.010(9)	113
130.0	0.111	0.19(85)	0.030(14)	0.100(90)	0.008(7)	99
		In nitrobenzene				
120.0	0.306	0.575(94)	[c]	[c]		—
130.0	0.295	0.55(93)	[c]	[c]		—
		In fluorocarbon oil				
125.0	0.148	[c]	[c]	0.122(83)		—

[a]Initial concentration of peroxide.
[b]Percentage based on 1 mol of peroxide yields 2 mol of Ph_2CO + Ph_2CHOH and 1 mol of H_2 (or bibenzyl in toluene).
[c]Present but not analyzed quantitatively.

TABLE 3. Rate constants for the decomposition of *t*-butyl diphenylmethyl peroxide in toluene

Temperature (°C)	P_0[a] (mol/l)	10^5 k[b] (s^{-1})	E_a (kcal/mol)	Log A (A in s^{-1})
125.0	1.99	3.15		
135.5	1.85	11.77	38.6	16.7
135.5	1.99	10.03		
144.0	1.98	29.9		
144.0	2.90	28.1		

[a]Initial concentration.
[b]Average of several runs.

TABLE 4. Products from the thermal decomposition of *t*-butyl diphenylmethyl peroxide at 125 °C in toluene

P_0[a] (mol/l)	Products in (mol/l) (%)						Balance (%)	
	AcMe	*t*-BuOH	Ph_2CO	Ph_2CHOH	$(PhCH_2)_2$	CH_4	Me_2C	Ph_2C
0.85	0.095(11)	0.76(89)	0.73(86)	0.12(14)	0.12(14)		100	100
0.377	0.060(16)	0.315(83)	0.305(81)	0.060(16)	0.070(18.5)	0.042(11)	97	99

[a]Initial concentration of peroxide.
[b]Percentage based 1 mol of peroxide yields 1 mol of acetone + *t*-BuOH and 1 mol of Ph_2CO + Ph_2CHOH.

with those from *t*-Bu_2O_2 homolysis in toluene at 125 °C, 90–100% bibenzyl (8) and a *t*-BuOH/acetone ratio of only 2.9 (9), suggest that much of the *t*-BuO_2CHPh_2 is decomposing by a *t*-BuO· induced chain.

[6] *t*-BuO· + *t*-BuO_2CHPh_2 → *t*-BuOH + *t*-$BuO_2\dot{C}Ph_2$

[7] *t*-$BuO_2\dot{C}Ph_2$ → *t*-BuO· + Ph_2CO

However, the activation energy for decomposition, measured using initial peroxide concentrations actually 2–5 times greater than those for the product studies (Tables 3 and 4) does not support this hypothesis. Peroxide decompositions having a substantial radical-induced component normally exhibit apparent activation energies 8–12 kcal lower than the value for O—O homolysis (10, 11).

The alternative explanation for the high *t*-BuOH/acetone ratios and the low yields of bibenzyl and benzhydrol requires fairly efficient Ph_2CHO·—*t*-BuO· disproportionation inside and perhaps outside the solvent cage, coupled with some PhCHO·—$PhCH_2$· disproportionation. Some simple arithmetic can be applied to, say, the second entry in Table 4. The 16% yield of acetone requires that 64% of the *t*-BuO·'s escape the solvent cage and abstract from toluene or undergo β-scission in a 3 to 1 ratio. Starting with 100 caged pairs:

[8] $[Ph_2CHO\cdot \cdot O\text{-}t\text{-}Bu]$ (100) → Ph_2CO + *t*-BuOH (36) (36); $Ph_2CHO\cdot$ + *t*-BuO· (64) (64)

[9] *t*-BuO· + $PhCH_3$ → *t*-BuOH + $PhCH_2$· (64) (48) (48); *t*-BuO· → Me_2CO + Me· (16) (16); Me· + $PhCH_3$ → MeH + $PhCH_2$· (16) (16)

[10] $Ph_2CHO\cdot$ + $PhCH_3$ → Ph_2CHOH + $PhCH_2$· (64) (16) (16); $PhCH_2$· → Ph_2CO + $PhCH_3$ (48) (48)

[11] $PhCH_2\cdot$ → $(Ph\cdot CH_2)_2$ (38) (19)

As a check this scheme produces total *t*-BuOH, 84 as compared to experimental 83%; total PH_2CO, 84 as compared to 81%; and 80 $PhCH_2$·'s produced compared to 86 consumed. The agreement is as good as could be expected considering the simplicity of the treatment. A more sophisticated analysis including some contribution from radical induced decomposition and other feasible radical reactions is not warranted in the absence of much more extensive data.

The postulated 36% of cage disproportionation seems not unreasonable. Requiring 75% of the free Ph_2CHO·'s to react with $PhCH_2$· may appear so, but a similar conclusion, based on deuterium isotope labelling experiments, was reached earlier (4) for *s*-BuO· and $PhCH_2$·, as advanced to account for the alkoxy radical products from *s*-Bu_2O_2 decompositions in toluene, there buttressed by isotopic labelling experiments. While for 2*s*-BuO·, cage disproportionation appeared negligible and higher yields of bibenzyl were obtained, it seems very likely that Ph_2CHO· would disproportionate more readily than *s*-BuO·.

Photolysis of Bisdiphenylmethyl Peroxide

Photolytic decompositions were carried out on the off-chance that some H_2 would be produced, even though similar decompositions of *s*-Bu_2O_2 had given none. The more complex molecule with its four phenyl groups offers quite different possibilities for electronically excited states as well as the possibility for benzophenone-sensitized decomposition as the reaction proceeded and products built up. In fact, photolyses using a

Can. J. Chem. Downloaded from www.nrcresearchpress.com by 210.87.254.42 on 09/05/12
For personal use only.

TABLE 5. Products from the photolysis of 0.44 *M* bisdiphenylmethyl peroxide in toluene at 20 °C

Time (min)	% peroxide decomposed	Products (mol/mol of peroxide decomposed)			
		Ph_2CHOH	Ph_2CO	$(PhCH_2)_2$	$HOCPh_2CH_2Ph$
15	51	1.23	0.53	0.12	—
120	76	1.18	0.56	0.24	0.33

NOTE: Ph_2CH balance 88% (15 min) and 103% (120 min); H balance +0.46 atoms/mol (15 min); + 0.14 (120 min).

low pressure Hg lamp at 20, 50, and 80° produced no H_2, nor any gaseous products whatsoever. Typical products are shown in Table 5. It is evident that as Ph_2CO builds up, its photoreduction becomes the main process, the decomposition of peroxide slows considerably, and the fate of $Ph_2CO\cdot$ radicals is totally obscured.

To conclude, the demonstration that a simple alkyl peroxide can be as efficient a hydrogen generator as any alkylidine peroxide suggests that the strength of the C—H bond is a more important factor than any supposed polar influences. Again the absence of solvent effects is observed, and the failure of Ph_2CHO_2t-Bu to produce H_2 conclusively eliminates an H atom mechanism. The clues to behavior of nontertiary alkoxy radicals in soluion provided by Ph_2CHO_2t-Bu suggest that further, more detailed study of this and similarly constituted peroxides would be well worthwhile.

The authors thank the National Research Council of Canada for financial support of this work.

1. O. BLANK and H. FINKENBEINER. Ber. **31**, 2979 (1898).
2. L. J. DURHAM and H. S. MOSHER. J. Am. Chem. Soc. **82**, 4537 (1962); **84**, 2811 (1964).
3. R. HIATT. Organic peroxides. Vol. III. *Edited by* D. Swern. Wiley, New York. 1971. Chapt. 1.
4. R. HIATT and S. SZILAGYI. Can. J. Chem. **48**, 615 (1970).
5. J. I. G. CADOGAN, D. H. HEY, and W. A. SANDERSON. J. Chem. Soc. 4498 (1958).
6. S. W. BENSON and R. SHAW. Organic peroxides. Vol. I. *Edited by* D. Swern. Wiley, New York. 1970. Chapt. 2.
7. U.S. Patent No. 2,400,041 (1946).
8. R. HIATT, T. MILL, K. C. IRWIN, and J. K. CASTLEMAN. J. Org. Chem. **33**, 1421 (1968).
9. J. H. T. BROOKS. Trans. Faraday Soc. **53**, 327 (1957).
10. R. HIATT and K. C. IRWIN. J. Org. Chem. **33**, 1436 (1968).
11. S. W. BENSON. J. Chem. Phys. **40**, 1007 (1964).

Can. J. Chem. Downloaded from www.nrcresearchpress.com by 210.87.254.42 on 09/05/12
For personal use only.

Conformations of Sugars: Proton Dihedral Angles from *Gauche* Coupling Constants

T. P. FORREST

Chemistry Department, Dalhousie University, Halifax, Nova Scotia B3H 3J5

Received July 2, 1974

T. P. FORREST. Can. J. Chem. **52**, 4095 (1974).

Proton coupling constants have been used in calculating dihedral angles of vicinal *gauche* protons in variety of pyranose derivatives of glucose, mannose, arabinose, xylose, altrose, and galactose. The calculations involve the use of a formula which was derived from a correlation of the coupling constants of ethane derivatives with the electronegativities of substituents and their orientation relative to the coupled protons.

The results indicate that the formula has general applicability and gives more reasonable values than a Karplus equation in which the constants have been adjusted to fit some compounds of the series. The calculated dihedral angles indicate that an equatorial substituent generally causes little distortion of dihedral angles, whereas an axial substituent generally causes the equatorial proton on the same carbon to have a smaller than normal dihedral angle with the adjacent axial proton and a larger than normal dihedral angle with the adjacent equatorial proton.

T. P. FORREST. Can. J. Chem. **52**, 4095 (1974).

Les constantes de couplage du proton ont été utilisées dans le calcul des angles dièdres des protons *gauches* vicinaux dans une variété de dérivés pyranosiques du glucose, mannose, arabinose, xylose, altrose et galactose. Les calculs font appel à l'utilisation d'un formule déduite d'une corrélation des constantes de couplage des dérivés de l'éthane avec les électronégativités des substituants et leurs orientations relatives aux protons couplés. Les résultats indiquent que la formule a une possibilité d'application générale et donne des valeurs plus cohérentes que l'équation de Karplus dans laquelle les constantes ont été ajustées pour correspondre à quelques composés de la série. Le calcul des angles dièdres montre qu'un substituant en position équatoriale cause généralement une faible distorsion des angles dièdres, alors qu'un substituant en position axiale fait que le proton équatorial sur le même carbone forme avec le proton axial adjacent un angle dièdre plus petit que normal et un angle dièdre plus grand que normal avec le proton équatorial adjacent. [Traduit par le journal]

The application of n.m.r. spectroscopy to the field of sugar stereochemistry was pioneered by Lemieux *et al.* (1) and led to the formulation of rules relating stereochemistry to both coupling constants and chemical shifts (2). One of the most promising developments in the field was the proposal by Karplus (3) of a specific relationship between vicinal coupling constants and dihedral angles. This relationship was widely used to calculate dihedral angles but unfortunately several other factors, such as substituent electronegativities, bond lengths, and bond angles which also influence the size of the coupling constant were unaccounted for, leading to serious errors in the values of angles calculated from the Karplus equation (4). The problem of compensating for other factors can be alleviated to some extent by determining constants for the Karplus equation from a set of model compounds and limiting the use of that equation to compounds in which these other factors do not change within the series of model compounds and those subject to analysis. This method can be severely restrictive, as it is very difficult to obtain a series in which the dihedral angle only and no other factor affecting the coupling constant changes. Consequently, quite unreasonable values of dihedral angles have been calculated leading to a lack of confidence in this method of determining dihedral angles (5).

One of the major reasons for these unreliable results lies in the failure to compensate for changes in the electronegativity of the substituents attached to the atoms bearing the coupled protons. As well as the number and electronegativities of substituents, the orientation of the substituents relative to the coupled protons is extremely important, the substituent having maximum effect when antiperiplanar to a coupled proton (6, 7). Recently we have developed a method of calculating the values of coupling constants for *gauche* protons from the electro-

Can. J. Chem. Downloaded from www.nrcresearchpress.com by 210.87.254.42 on 09/05/12
For personal use only.

Can. J. Chem. Downloaded from www.nrcresearchpress.com by 210.87.254.42 on 09/05/12
For personal use only.

negativities of substituents and their orientation relative to the coupled protons (8). The method consists of the modification of a base value of the coupling constant by two correction factors, one of which is angle independent and for substituents with electronegativities greater than hydrogen, increases the size of the constant, and another which is angle dependent and decreases the size of the coupling constant, as indicated in eq. 1,

$$[1]\quad J = (4.1 + 0.63\sum\Delta X)(1 - 0.462\Delta X_1) \times (1 - 0.462\Delta X_2)$$

where, $\sum\Delta X$ represents the sum of the electronegativity differences between the substituent and hydrogen for all substituents regardless of their orientation and ΔX_1 and ΔX_2 are those of the substituents which are antiperiplanar to a coupled proton. If we assume a relation between coupling constant and dihedral angle such as shown in eq.2 (9), this equation may be used in conjunction with eq. 1 to calculate a value for the dihedral angle of the coupled protons (eq. 3).

$$[2]\quad J = A\cos^2\phi$$

$$[3]\quad \cos^2\phi = \frac{0.25J_{obs}}{(4.1 + 0.63\sum\Delta X)(1 - 0.462\Delta X_1)(1 - 0.462\Delta X_2)}$$

Although the equation was derived primarily from data on acyclic compounds, we have used eq. 3 to calculate dihedral angles of protons in *gauche* orientations in several derivatives of pyranose sugars (**1–7**) without attempting to modify the constants to make the results fit any pyranose models. A modified Karplus equation (eq. 4) has been formulated for pyranoses, which also introduces a factor dependent upon the electronegativities of substituents and their orientation relative to the coupled protons (10).

$$[4]\quad J = (6.6 - 1.0\cos\phi + 5.6\cos 2\phi) \times \left(1 - \sum_{i=1}^{4} f_i\Delta X_i\right)$$

The constants in this equation were obtained from the best fit of experimental data for a series of trimethylsilyl derivatives of mono- and disaccharides. This equation was also used to calculate values for the *gauche* dihedral angles in compounds **1–7** and the results are given in Table 1 as well as those obtained from eq. 3.

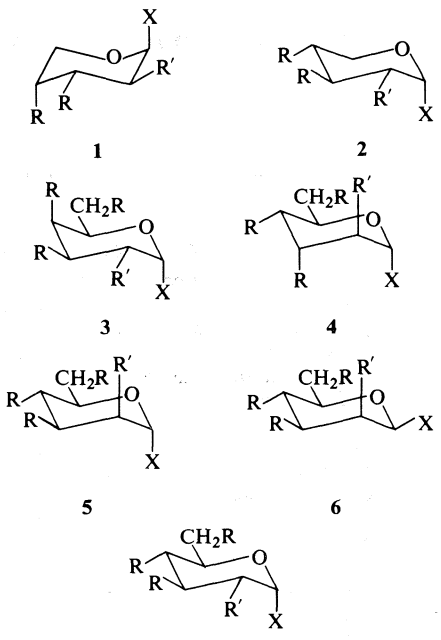

a R = R′ = OAc, X = Br
b R = R′ = OAc, X = Cl
c R = R′ = OAc, X = OCH_3
d R = R′ = X = OBz
e R = R′ = X = OTMS
f R = R′ = X = OAc
g R = OAc, R′ = X = Cl
h R = OAc, R′ = Cl, X = OCH_3
i R = OAc, R′ = I, X = OBz
j R = OAc, R′ = X = H
k R = OAc, R′ = H, X = OAc
l R = R′ = X = OCD_3
m R = X = OAc, R′ = Cl

The values of dihedral angles calculated from eq. 3 are in many cases very close to the normal *gauche* dihedral angle, but in other cases a substantial deviation from normal is indicated. Some illustrative examples are discussed below in terms of the effect of substituents on the proton dihedral angles, and a comparison is made of the results obtained from eq. 3 and 4. The values calculated from the two equations are in many cases very similar; however, there are some examples in which quite different values are obtained. In one case, **1***a*, an X-ray analysis (see footnote *b*, Table 1) of the compound has been carried out and proton dihedral angles are reported (11). Although proton positions are not obtained very accurately by X-ray diffraction, and the measurement was made in the crystal-

TABLE 1. Coupling constants and calculated dihedral angles of pyranose derivatives

Compound	Protons	J_{obs}	J_{calc}[a] (60°)	ϕ_{calc} eq. 3	ϕ_{calc} eq. 4	Reference No.
Tri-*O*-acetyl-β-D-arabinopyranosyl bromide, **1***a*	1,2	3.8[e]	3.44	58	47[b]	13
	3,4	3.4[e]	1.83	47	48[b]	
	4,5	0.7[f]	2.18	74	84[b]	
	4,5′[c]	1.8[f]	0.94	46	62[b]	
Tri-*O*-acetyl-β-D-arabinopyranosyl chloride, **1***b*	1,2	3.2[e]	3.01	59	51	13
	3,4	3.0[e]	1.83	50	52	
	4,5	0.6[f]	2.18	75	—[d]	
	4,5′	1.7[f]	0.94	48	63	
Methyl 2,3,4-tri-*O*-acetyl-β-D-arabinopyranoside, **1***c*	1,2	3.2[e]	2.45	55	49	14
	3,4	3.3[e]	1.83	48	49	
	4,5	1.3[f]	2.18	67	71	
	4,5′	1.8[f]	0.94	46	62	
Methyl 2,3,4-tri-*O*-benzoyl-β-D-arabinopyranoside, **1***d*	1,2	3.3[e]	1.98	50	47	14
	3,4	3.3[e]	1.83	48	49	
	4,5	1.1[f]	2.18	69	74	
	4,5′	2.0[f]	0.94	43	59	
Tri-*O*-acetyl-α-D-xylopyranosyl bromide, **2***a*	1,2	4.0[e]	3.44	57	46	13
	4,5	5.8[f]	4.88	57	38	
Tri-*O*-acetyl-α-D-xylopyranosyl chloride, **2***b*	1,2	3.9[e]	3.14	55	45	13
Methyl 2,3,4-tri-*O*-acetyl-α-D-xylopyranoside, **2***c*	1,2	3.5[e]	2.45	53	47	14
	4,5	5.7[f]	4.88	57	39	
Methyl 2,3,4-tri-*O*-benzoyl-1,2-α-D-xylopyranoside, **2***d*	1,2	3.4[e]	1.98	49	46	14
	4,5	5.8[f]	4.88	57	38	
Tetra-*O*-acetyl-α-D-galactopyranosyl bromide, **3***a*	1,2	3.5	3.44	60	50	15
	3,4	3.1	1.83	49	51	
Pentakis-*O*-trimethylsilyl-α-D-galactopyranose, **3***e*	1,2	3.1[g]	2.20	54	50	10
	3,4	2.6[g]	2.03	56	56	
Penta-*O*-acetyl-α-D-altropyranose, **4***f*	1,2	1.4[e]	2.50	68	67	16
	2,3	3.5[e]	4.23	63	51	
Penta-*O*-acetyl-α-D-mannopyranose, **5***f*	1,2	1.8[e]	2.50	65	63	17
Methyl 2,3,4,6-tetra-*O*-acetyl-α-D-mannopyranoside, **5***c*	1,2	1.6[e]	2.45	66	65	17
Tetra-*O*-acetyl-α-D-mannopyranosyl bromide, **5***a*	1,2	1.6	2.35	66	66	15
Pentakis-*O*-trimethylsilyl-α-D-mannopyranose, **5***e*	1,2	2.2[g]	2.45	62	59	10
	2,3	2.5[g]	2.03	56	57	
3,4,6-Tri-*O*-acetyl-2-deoxy-2-chloro-α-D-mannopyranosyl chloride, **5***g*	1,2	1.4	2.29	67	69	18
Methyl 3,4,6-tri-*O*-acetyl-2-deoxy-2-chloro-α-D-mannopyranoside, **5***h*	1,2	1.1	2.35	70	73	19
Tetra-*O*-acetyl-2-deoxy-2-chloro-α-D-mannopyranose, **5***m*	1,2	1.8[e]	2.39	64	63	17
	2,3	3.6[f]	2.78	55	49	

Can. J. Chem. Downloaded from www.nrcresearchpress.com by 210.87.254.42 on 09/05/12
For personal use only.

TABLE 1. (*Concluded*)

Compound	Protons	J_{obs}	J_{calc}[a] (60°)	ϕ_{calc} eq. 3	ϕ_{calc} eq. 4	Reference No.
3,4,6-Tri-*O*-acetyl-1-*O*-benzoyl-2-deoxy-2-iodo-α-D-mannopyranose, **5*i***	1,2	1.6[e]	2.28	65	66	20
Tri-*O*-acetyl-1,2-dideoxy-D-*arabino*-hexopyranose, **5*j***	1′,2	3.6[e]	2.28	51	53	
	1,2	2.0[e]	1.86	59	65	17
	1,2′	3.6[e]	4.16	62	55	
Tetra-*O*-acetyl-2-deoxy-α-D-*arabino*-hexopyranose, **5*k***	1,2	1.5	2.18	65	68	21
	1,2′	3.6	1.72	44	48	
	2,3	5.0	4.47	58	38	
Penta-*O*-acetyl-β-D-mannopyranose, **6*f***	1,2	1.4[e]	1.08	55	64	17
	2,3	3.2[f]	1.82	48	60	
Methyl 2,3,4,6-tetra-*O*-acetyl-β-D-mannopyranoside, **6*c***	1,2	1.2[e]	1.06	58	67	17
	2,3	3.4[f]	2.03	47	48	
Tetra-*O*-acetyl-2-deoxy-β-D-*arabino*-hexopyranose, **6*k***	1,2	2.4	2.67	62	60	21
	2,3	5.0	4.47	58	58	
3,4,6-Tri-*O*-acetyl-2-deoxy-2-chloro-β-D-mannopyranosyl chloride, **6*g***	1,2	1.2	1.58	64	70	18
	2,3	3.5	2.75	56	50	
Pentakis-*O*-trimethylsilyl-β-D-mannopyranose, **6*e***	1,2	0.9[g]	1.20	64	73	10
	2,3	2.7[g]	2.03	55	55	
Penta-*O*-acetyl-α-D-glucopyranose, **7*f***	1,2	3.6[e]	1.98	48	44	17
Methyl 2,3,4,6-tetra-*O*-acetyl-α-D-glucopyranoside, **7*c***	1,2	3.7[e]	2.45	52	45	17
Tetra-*O*-acetyl-α-D-glucopyranosyl bromide, **7*a***	1,2	3.9	3.44	58	47	15
Pentakis-*O*-trimethylsilyl-α-D-glucopyranose, **7*e***	1,2	3.0[g]	2.20	54	51	10
3,4,6-Tri-*O*-acetyl-2-deoxy-2-chloro-α-D-glucopyranosyl chloride, **7*g***	1,2	3.5	3.01	57	50	18
Methyl 3,4,6-tri-*O*-acetyl-2-deoxy-2-chloro-α-D-glucopyranoside, **7*h***	1,2	3.8	2.45	51	45	19
Tetra-*O*-acetyl-2-deoxy-2-chloro-α-D-glucopyranose, **7*m***	1,2	3.6[e]	1.99	48	46	17
Methyl-d_3 2,3,4,6-tetra-*O*-methyl-d_3-α-D-glucopyranoside, **7*i***	1,2	3.5[g]	2.40	53	47	22

[a]Electronegativity (23) Δ values: C = 0.4, OR = 1.2, OTMS = 1.3, OCOR = 1.4, Br = 0.75, Cl = 0.95, I = 0.45.
[b]Angles from X-ray structure: $\phi_{1,2} = 64 \pm 7$, $\phi_{3,4} = 41 \pm 4$, $\phi_{4,5} = 86 \pm 5$, $\phi_{4,5'} = 44 \pm 5$.
[c]Prime mark designates the axial proton. The H-5 signal at higher field in the β-D-*arabino* derivatives (**1*a–d*)** is assigned to the axial proton, based on comparison of chemical shifts with those of the H-5 protons in similarily substituted α-D-*xylo* and α-D-*lyxo* derivatives. This is the reverse of previous assignments (2, 5, 11, and 13) in which the higher field signal had been assigned to the equatorial proton.
[d]Imaginary number obtained.
[e]First order (100 MHz).
[f]X approximation.
[g]Iterative analysis.

Can. J. Chem. Downloaded from www.nrcresearchpress.com by 210.87.254.42 on 09/05/12
For personal use only.

Can. J. Chem. Downloaded from www.nrcresearchpress.com by 210.87.254.42 on 09/05/12
For personal use only.

line state, the values may be used as a guide for comparison with the results obtained from n.m.r. measurements. The values of $\phi_{3,4}$ and $\phi_{4,5}$ obtained from both equations agree with the results from the X-ray analysis, in that $\phi_{3,4}$ has decreased from the normal value of a *gauche* dihedral angle and that $\phi_{4,5}$ has increased from normal. This is also in agreement with the results of valence-force minimization calculations (12) which indicate that an axial substituent on a six-membered ring causes the equatorial proton on the same carbon to assume a smaller dihedral angle with the adjacent axial proton and a greater dihedral angle with the adjacent equatorial proton. The X-ray data indicate that $\phi_{1,2}$ in **1***a* is near normal, in agreement with the result from eq. 3 and contrary to that from eq. 4. The X-ray value for $\phi_{4,5'}$ is less than 60° as would be expected from the results of the valence-force minimization calculations and is compatible with the result from eq. 3 but not eq. 4.

In those cases in which there is no axial substituent on the carbons bearing the coupled protons, the dihedral angles ($\phi_{1,2}$ in **5***j* and **6***k*; $\phi_{1,2'}$ in **5***j*; $\phi_{2,3}$ in **5***k* and **6***k*; $\phi_{4,5}$ in **2***a*, **2***c*, and **2***d*) are all found from eq. 3 to be near normal (57–62°). These results are consistent with the finding (12) that an equatorial substituent has very little effect on the dihedral angles of the protons on a six-membered ring. Only one exception to this was found, that of $\phi_{1',2}$ in **5***j*, which was calculated from eq. 3 to be 51°. Equation 4 yielded values ranging from 38 to 65° with an average of 49°.

For those cases in which there is an axial substituent on a carbon, the dihedral angle formed by the equatorial proton on that carbon with the adjacent equatorial proton ($\phi_{1,2}$ in **4***f*, **5***f*, *c*, *a*, *e*, *g*, *h*, *m*, *i*, and *k*; $\phi_{2,3}$ in **4***f*; $\phi_{4,5}$ in **1***a*, *b*, *c*, and *d*) is found from eq. 3 to be greater than 60° (15 values, range 74–62°, average 67°). Calculation of the values of these angles from eq. 4 gave results ranging from 51 to 84° with an average value of 67°. The dihedral angle formed by the equatorial proton on a carbon bearing an axial substituent and the adjacent axial proton is expected to be smaller than normal. Of the 39 examples of this type of dihedral angle ($\phi_{1,2}$ in **1**, **2**, **3**, **6***c*, *e*, *f*, *g*, and **7**; $\phi_{3,4}$ in **1** and **3**; $\phi_{4,5'}$ in **1**; $\phi_{2,3}$ in **5***e*, and *m*, **6***c*, *e*, *f*, and *g*; $\phi_{1,2'}$ in **5***k*) all but two, $\phi_{1,2}$ in **6***e* and *g*, are less than 60°. When the axial substituent is a halogen or trimethylsilyl group and is situated on carbon 1, the size of the dihedral angle is only slightly less than normal.

In conclusion, it would appear that this method of calculating dihedral angles (in the range of about 45–75°) in sugars based upon the relationship established with substituted ethanes gives reasonable values and may be applied generally, whereas a Karplus equation that is modified to fit a specific set of data may be quite unreliable for use with other very similar compounds. It would be unwise, however to draw conclusions based on small differences in the angles calculated by this method, particularly when large deviations from 60° are indicated, since other coupling altering factors such as bond lengths and bond angles are assumed to be constant and the constants in eq. 3 have been obtained from a relatively small set of data and may be adjusted with the accumulation of further data.

The financial assistance of the National Research Council of Canada and the hospitality of the University of Guelph where the work was carried out are acknowledged.

1. R. U. Lemieux, R. K. Kulling, H. J. Bernstein, and W. G. Schneider. J. Am. Chem. Soc. **80**, 6098 (1958).
2. R. U. Lemieux and J. D. Stevens. Can. J. Chem. **43**, 2059 (1965).
3. M. Karplus. J. Chem. Phys. **30**, 11 (1959).
4. M. Karplus. J. Am. Chem. Soc. **85**, 2870 (1963).
5. P. L. Durette and D. Horton. Org. Magn. Res. **3**, 417 (1971).
6. D. H. Williams and N. S. Bhacca. J. Am. Chem. Soc. **86**, 2742 (1964).
7. H. Booth. Tetrahedron Lett. 411 (1965).
8. T. P. Forrest. Org. Magn. Res. **6**, 355 (1974).
9. H. Booth. Progr. Nucl. Magn. Res. Spectrosc. **5**, 149 (1969).
10. D. G. Streefkerk, M. J. A. de Bie, and J. F. G. Vliegenthart. Tetrahedron, **29**, 833 (1973).
11. P. W. R. Corfield, J. D. Mokren, P. L. Durette, and D. Horton. Carbohydr. Res. **23**, 158 (1972).
12. C. Altona and M. Sundaralingam. Tetrahedron, **26**, 925 (1970).
13. P. L. Durette and D. Horton. Carbohydr. Res. **18**, 57 (1971).
14. P. L. Durette and D. Horton. Carbohydr. Res. **18**, 403 (1971).
15. D. Horton and W. N. Turner. J. Org. Chem. **30**, 3387 (1965).
16. B. Coxon. Carbohydr. Res. **1**, 357 (1966).
17. G. Descotes, F. Chizat, and J. C. Martin. Bull. Soc. Chim. Fr. 2304 (1970).

18. K. IGARASKI, T. HOWA, and T. IMAGAMA. Tetrahedron Lett. 755 (1968).
19. R. U. LEMIEUX and B. FRASER-REID. Can. J. Chem. **42**, 532 (1964).
20. L. D. HALL and J. F. MANVILLE. Carbohydr. Res. **8**, 295 (1968).
21. L. D. HALL. *In* Deoxy sugars. *Edited by* S. Hanessian. Advances in Chemistry. Series 74. American Chemical Society, Washington. 1968. p. 755.
22. J. HAVERKAMP, J. P. C. M. VAN DONGEN, and J. F. G. VLEIGENTHART. Tetrahedron, **29**, 3431 (1973).
23. M. L. HUGGINS. J. Am. Chem. Soc. **75**, 4123 (1953).

Can. J. Chem. Downloaded from www.nrcresearchpress.com by 210.87.254.42 on 09/05/12
For personal use only.

Complex Fluoroanions in Solution. VI. Complexes of Methyl and Ethyl Fluorides with Group VB Pentafluorides[1]

S. BROWNSTEIN

Division of Chemistry, National Research Council of Canada, Ottawa, Canada K1A 0R9

Received June 26, 1974

S. BROWNSTEIN. Can. J. Chem. **52**, 4101 (1974).

Methyl and ethyl fluorides form two unique complexes with tantalum and niobium pentafluorides. These complexes have been identified by their proton and fluorine resonance spectra and some evidence obtained for their structures.

S. BROWNSTEIN. Can. J. Chem. **52**, 4101 (1974).

Les fluorures de méthyle et d'éthyle forment deux complexes uniques avec les pentafluorures de tantale et de niobium. On a identifié ces complexes à l'aide de leurs spectres de résonance magnétique nucléaire du proton et du fluor; on a aussi obtenu quelques indications sur leur structures. [Traduit par le journal]

Can. J. Chem. Downloaded from www.nrcresearchpress.com by 210.87.254.40 on 09/05/12
For personal use only.

Introduction

Complexes of simple alkyl fluorides with boron trifluoride have been prepared, but were only characterized by their melting or decomposition points (1). The infrared spectrum of the methyl fluoride – boron trifluoride complex has been obtained at low temperature and found to differ only slightly from the sum of those of the individual components (2). From the results the complex was characterized as being very weak. Recently complexes of methyl and ethyl fluorides with antimony penta-fluoride have been reported. On the basis of their proton and carbon magnetic resonance spectra, especially the absence of observable proton–fluorine spin coupling, structure **1** was initially proposed for these complexes (3). This conclusion was later modified by the same authors who suggested that the complex has structure **2**, but undergoes rapid intramolecular fluorine exchange, perhaps via structure **1**, which would be present in very low concentration (4).

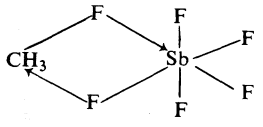

1

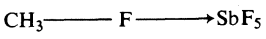

2

A second research group disputes these conclusions and claims that 1 : 1, 1 : 2, and in SO_2ClF also 1 : 3, complexes of alkyl fluoride with antimony fluoride are present (5). They assign structure **3** to the 1 : 2 complex and also invoke rapid intramolecular exchange of the alkyl group to explain the absence of proton–fluorine spin coupling and various features of the fluorine resonance spectra for all the complexes.

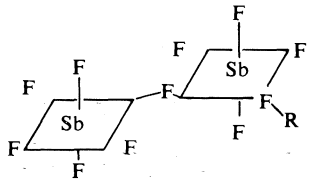

3

Complexes of RX with antimony pentafluoride have also been observed where X is chlorine, bromine, or iodine (6). In these cases the complex is formulated as a dialkyl halonium ion with a structure represented by R_2X^+. Such a structure was also proposed, but rejected, for the complex formed between ethyl fluoride and antimony pentafluoride (5). Because of the controversy concerning these complexes and in view of their great importance in carbonium ion mechanisms and Friedel–Crafts reactions it would be desirable to investigate similar complexes with other binary fluorides to obtain further information on such complex species.

It has been shown that under appropriate conditions complexes may be formed between MF_5 and NF_6^- where M and N are from among the elements phosphorus (7), arsenic (8), antimony (8), vanadium (9), niobium (8), tantalum (8), tungsten (10), and molybdenum (11). It has also

[1]NRCC No. 14298.

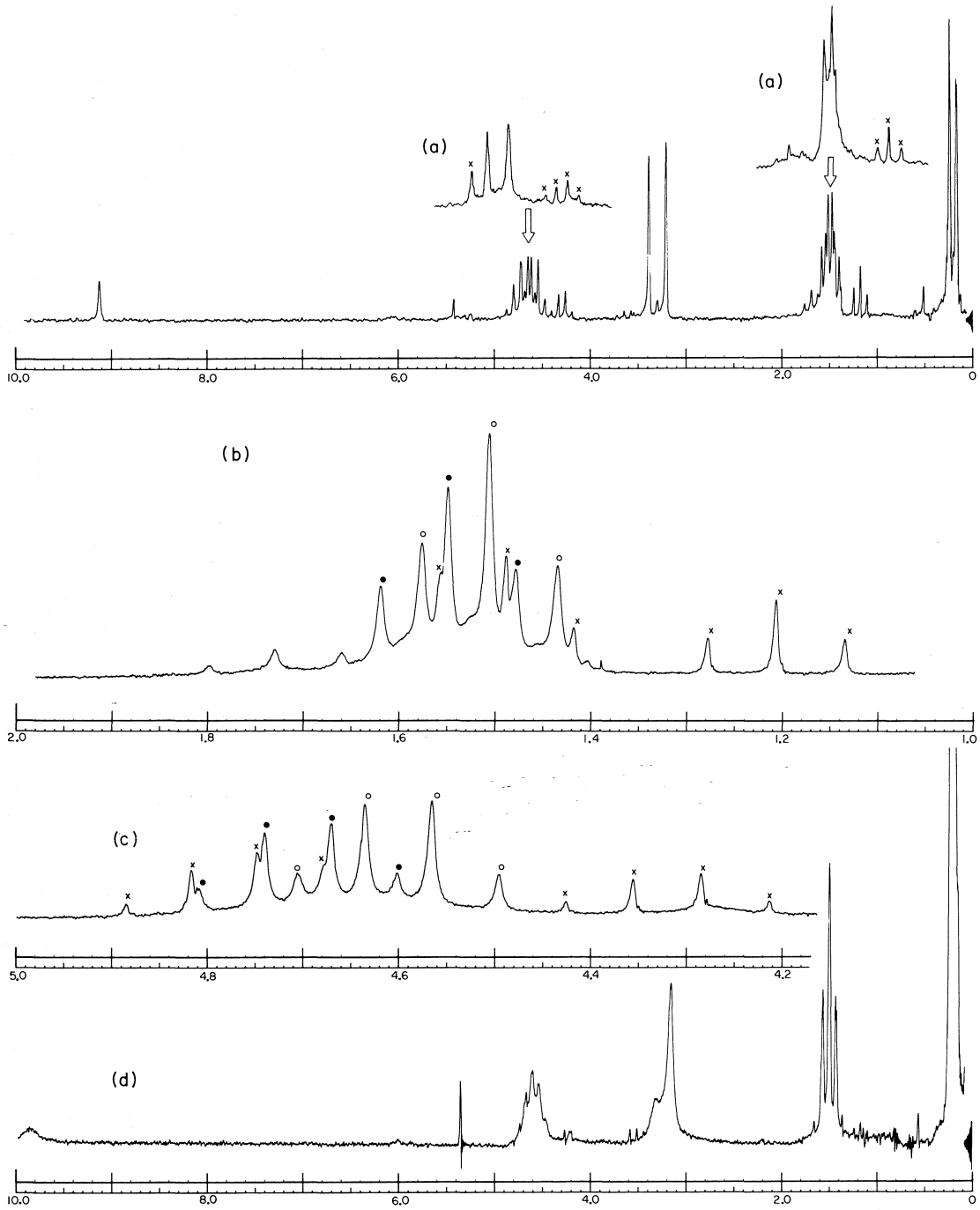

FIG. 1. The proton resonance spectrum of an equimolar sulfur dioxide solution of ethyl fluoride and tantalum pentafluoride. All lines marked with × arise from unreacted ethyl fluoride. (*a*) Proton spin decoupling of the methyl and methylene proton regions, and a twofold scale expansion. (*b*) Tenfold scale expansion of the methyl proton region. The two sets of methyl group lines are marked with ○ and ●. (*c*) Tenfold scale expansion of the methylene proton region. (*d*) At 25 °C.

Can. J. Chem. Downloaded from www.nrcresearchpress.com by 210.87.254.40 on 09/05/12
For personal use only.

Can. J. Chem. Downloaded from www.nrcresearchpress.com by 210.87.254.40 on 09/05/12
For personal use only.

been shown that arsenic pentafluoride will react with *t*-butylchloride to give the *t*-butyl cation in a similar manner to the reaction with antimony pentafluoride (12). Therefore it seems reasonable that some of the above mentioned binary fluorides should form reasonably stable complexes with methyl and ethyl fluorides. The proton and fluorine magnetic resonance spectra show no indication of complex formation between arsenic pentafluoride and ethyl fluoride at −80 °C in sulfur dioxide as solvent, nor is there evidence of complex formation with molybdenum pentafluoride or vanadium pentafluoride.

Under similar conditions complexes are formed with tantalum and niobium pentafluorides and these results are described in detail.

Experimental

Proton resonance spectra were obtained at 100.0 and 25.1 MHz and fluorine resonance spectra at 94.1 MHz on a slightly modified Varian Associates HA-100 spectrometer. All sample preparation and reagent manipulation was done with standard vacuum line techniques or using a vacuum dry box. Sulfur dioxide and methyl and ethyl fluorides were dried in contact with phosphorus pentoxide before being transferred to storage bulbs on the vacuum line. Methylene chloride was purified and stored as previously described (13). Tantalum and niobium pentafluorides (Ozark–Mahoning) were used as received. Any samples containing insoluble material, perhaps oxyfluorides, were rejected. Chemical shifts are reported in p.p.m. from internal $CFCl_3$ and tetramethylsilane.

Results and Discussion

The proton resonance spectrum at 100 MHz and −83 °C of a 1 : 1 solution of ethyl fluoride and tantalum pentafluoride in SO_2 is shown in Fig. 1. The sample was prepared at liquid nitrogen temperature, then thawed, mixed, and maintained at all times at Dry Ice temperature. It can be clearly seen that in addition to unreacted ethyl fluoride, whose spectral lines are marked with a cross, there are two nonequivalent ethyl groups. The one with chemical shifts of 1.506 and 4.600 is 1.28 times more intense than the one with chemical shifts of 1.549 and 4.705. The spin coupling constant between the methyl and methylene protons is 7.0 Hz for each ethyl group. In order to insure that there are indeed two unique ethyl groups, rather than one ethyl group with methyl and methylene protons spin coupled to a fluorine nucleus, a proton resonance spectrum was also obtained at 25.1 MHz. If the separation of the two triplets and two quartets was due to spin coupling this separation should remain unchanged at 25.1 MHz. It was found that the separations decreased by a factor of four, in complete agreement with theoretical predictions for nonequivalent ethyl groups whose methyl and methylene resonances, respectively, are slightly chemically shifted. Other lines in this spectrum are at 9.14, presumably a proton associated with some fluoranion, 3.40, and 3.23. These lines may arise from decomposition of the ethyl fluoride – tantalum pentafluoride complexes. In addition there is a doublet at 0.12 (J = 6 Hz) from trimethylsilylfluoride produced by a reaction with the tetramethylsilane employed as reference.

In order to elucidate the structure of the two ethyl containing species a fluorine resonance spectrum of a similar sample, not containing tetramethylsilane, was obtained at −80 °C. It is remarkably devoid of information, containing only one very broad line (half width of 1.5 KHz) at −76.4 °C, the region where fluorine bonded to tantalum is normally found (8), and a weak broad and featureless line at 184 p.p.m. attributed to fluorine on carbon. Therefore there is rapid exchange on the n.m.r. time scale between the fluorines bonded to tantalum in the two ethyl fluoride – tantalum pentafluoride complex species. There is also rapid exchange between the fluorines attached to carbon, but not averaging of these fluorines with those bonded to tantalum.

A change in solvent composition or a change in temperature causes a change in separation of the two methyl and methylene groups. Increasing the concentration of fluorotrichloromethane in the solvent increases the separation of the groups. Increasing the temperature decreases the separation between the groups. At room temperature there is no chemical shift between the two methyl groups and only a small shift between the two methylene groups, as shown in Fig. 1*d*. There is still no appreciable averaging of the two nonequivalent groups. When the sample is cooled the low temperature spectrum is again obtained.

With a sulfur dioxide solution containing two equivalents of tantalum pentafluoride for each ethyl fluoride only the lower field ethyl group is observed in the proton resonance spectrum. The fluorine resonance spectrum is uninformative due to rapid exchange averaging. It is possible that the species giving rise to the lower field ethyl group is associated with two tantalum pentafluoride units and the higher field ethyl group with only one, but this cannot be proven

Can. J. Chem. Downloaded from www.nrcresearchpress.com by 210.87.254.40 on 09/05/12
For personal use only.

in the absence of resolved fluorine resonance spectra. Methylene chloride and fluorotrichloromethane were unsatisfactory as solvents for lower temperature studies. However, it was found possible to keep the reactants in solution at −100 °C with a solvent of approximately equal parts of SO_2 and SO_2ClF. Under these conditions an analysis of the proton resonance spectrum indicated that only the 1 : 1 complex was present in a sample prepared with equivalent quantities of TaF_5 and ethyl fluoride. The fluorine resonance spectrum had a broad doublet (J = 160 Hz) at −120.2 p.p.m. and broad single lines at −73.2 and 79.5 p.p.m. from the 1 : 1 complex. By comparison with other complexes of TaF_5 it is possible to assign the line at −120.2 to fluorine 1 in structure **4** (8, 14). The line at

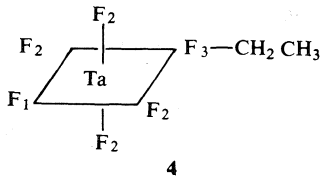

4

−73.2 is assigned to fluorine 2 and that at 79.5 to fluorine 3. The spin coupling (J_{1-3}) of 160 Hz observed for the line attributed to fluorine 1 was somewhat inconclusively collapsed by simultaneous irradiation of fluorine 3. The combination of proton and fluorine resonance results suggest structure **4** for the 1 : 1 complex with a somewhat weakened carbon–fluorine bond, since no proton–fluorine spin coupling is observed. With the binary solvent pair it was not possible to resolve separate fluorine lines for a sample prepared with two equivalents of TaF_5 for each ethyl fluoride.

The proton resonance spectrum of a 1 : 1 solution of methyl fluoride and tantalum pentafluoride in sulfur dioxide at −80 °C has a peak at 5.40 p.p.m. in addition to those of unreacted methyl fluoride. This agrees well with the values of 5.33 (3) and 5.56 (5) previously found for the methyl fluoride – antimony pentafluoride complex. The spectrum does not change when there is a two-fold excess of tantalum pentafluoride. The fluorine resonance spectrum of the 1 : 1 solution at −80 °C has only a very broad peak (half-width 1300 Hz) at −76.4 p.p.m. and the quartet from unreacted methyl fluoride. Upon warming to room temperature there is irreversible decomposition of the sample. It would seem that only a single complex is formed between methyl fluoride and tantalum pentafluoride, in contrast with the results for ethyl fluoride.

The proton resonance spectrum at 100 MHz and −75 °C of a 1 : 1 solution of ethyl fluoride and niobium pentafluoride in sulfur dioxide is shown in Fig. 2. The spectrum is almost identical with that for the corresponding solution with tantalum pentafluoride. Two sets of lines are present from ethyl groups, in addition to those from unreacted ethyl fluoride. From proton resonance spectra obtained at 25.1 MHz, one may exclude the possibility of the ethyl doubling arising from proton–fluorine spin coupling. One of the ethyl groupings has chemical shifts of 1.485 and 4.574 p.p.m. for the methyl and methylene groups respectively. The other ethyl group has chemical shifts of 1.539 and 4.700. Thus the ethyl groups are at slightly higher field than in the corresponding tantalum system. Similar results may be obtained when there is no tetramethylsilane in the system. The fluorine resonance spectrum of such samples has only a single very broad line at −159 p.p.m., the region where fluorine bonded to niobium is found, and a weak doublet (J = 420 Hz) at 184 p.p.m. attributed to the fluorine of the complexed ethyl fluoride.

When a 2:1 ratio of niobium pentafluoride to ethyl fluoride is used the results are similar to those with the 1 : 1 ratio except that the low field ethyl signals are more intense relative to those of the high field ethyl group, than for a 1 : 1 ratio. This is similar to, but less pronounced than, the same result in the tantalum pentafluoride – ethyl fluoride system. Only a single very broad line was observed in the fluorine resonance spectrum.

The reaction between niobium pentafluoride and methyl fluoride appears to be quite slow and reaches an equilibrium in which unreacted methyl fluoride and two complexed methyl fluoride species are simultaneously present. This mixture appears stable at room temperature towards decomposition into miscellaneous products, in contrast with the results for tantalum pentafluoride. A freshly prepared solution of niobium pentafluoride and methyl fluoride in sulfur dioxide has a proton resonance spectrum at −70 °C which is primarily that of the unreacted methyl fluoride doublet. In addition there are weak lines of approximately equal intensity at 3.35 and 4.36 p.p.m. From spectra at 25.1 MHz it was demonstrated that these lines arise

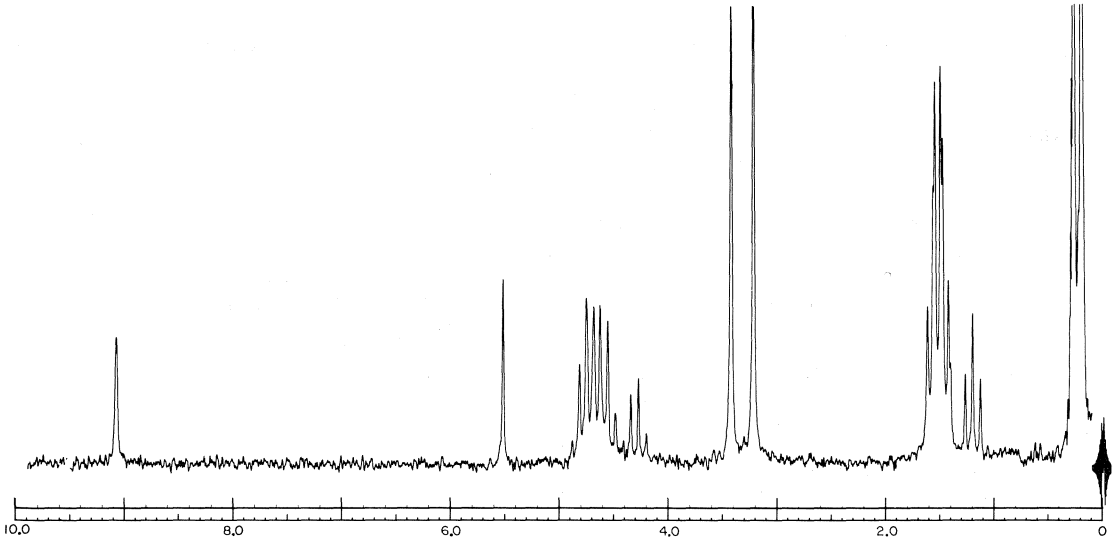

FIG. 2. The proton resonance spectrum of an equimolar sulfur dioxide solution of ethyl fluoride and niobium pentafluoride.

from chemically shifted species and are not due to proton–fluorine spin coupling. All the lines remain sharp in spectra taken at room temperature indicating negligible exchange, on the n.m.r. time scale, between the various species. The lines from the product gradually increase in intensity, at the expense of those from methyl fluoride, and reach an equilibrium value of 1.36 times more intense after about 1 h at room temperature. The fact that both product lines appear and grow maintaining equal intensity suggests that only one product is produced containing two nonequivalent methyl groups. The fluorine resonance spectra indicated extensive fluorine averaging and did not give further information on the structure of the complex. Similar results are obtained with a 2 : 1 ratio of niobium pentafluoride to methyl fluoride.

The complexing of methyl and ethyl fluorides with group V pentahalides does not seem to be restricted to antimony pentafluoride. Unfortunately rapid fluorine exchange prevents elucidation of the structures of these complexes.

1. G. A. OLAH, S. KUHN, and J. OLAH. J. Chem. Soc. 2174 (1957).
2. R. NAKANE and T. OYAMA. J. Phys. Chem. **70**, 1146 (1966).
3. G. A. OLAH, J. R. DEMEMBER, and R. H. SCHLOSBERG, J. Am. Chem. Soc. **91**, 2112 (1969).
4. G. A. OLAH, J. R. DEMEMBER, R. H. SCHLOSBERG, and Y. HALPERN. J. Am. Chem. Soc. **94**, 156 (1972).
5. J. BACON and R. GILLESPIE. J. Am. Chem. Soc. **93**, 6914 (1971).
6. G. A. OLAH and J. R. DEMEMBER. J. Am. Chem. Soc. **91**, 2113 (1969).
7. S. BROWNSTEIN. J. Inorg. Nucl. Chem. **35**, 3567 (1973).
8. S. BROWNSTEIN. Inorg. Chem. **12**, 584 (1973).
9. S. BROWNSTEIN and G. LATREMOUILLE. Can. J. Chem. In press.
10. S. BROWNSTEIN. Can. J. Chem. **51**, 3575 (1973).
11. S. BROWNSTEIN. Can. J. Chem. **51**, 2530 (1973).
12. S. BROWNSTEIN and J. BORNAIS. Can. J. Chem. **49**, 7 (1971).
13. S. BROWNSTEIN. Can. J. Chem. **47**, 605 (1969).
14. S. BROWNSTEIN and MARJORIE JEAN FARRALL. Can. J. Chem. **52**, 2236 (1974).

Can. J. Chem. Downloaded from www.nrcresearchpress.com by 210.87.254.40 on 09/05/12
For personal use only.

Kinetics of the Cu(II) – Nitrilotriacetic Acid Reaction

JAMES MAGUIRE

Water Science Section, Inland Waters Directorate, Department of the Environment, Ottawa, Canada K1A 0E7

Received April 30, 1974

JAMES MAGUIRE. Can. J. Chem. **52**, 4106 (1974).

The kinetics of the reaction between Cu(II) and nitrilotriacetic acid (NTA) to form the 1:1 complex have been studied by the stopped-flow technique over the p*H* range 2–6. The reaction is kinetically first order in both [Cu(II)] and $[NTA]_{total}$; the rate constant has a minimum value of 1.1×10^5 l mol^{-1} s^{-1} in the p*H* range 3.5–5 and increases with either increasing or decreasing p*H*. An explanation for the observed kinetic behavior may be that in the case of the monoprotonated species $HNTA^{2-}$ there is a rate-limiting transfer of a proton from nitrogen before complex formation takes place, and that this transfer is facilitated with increasing acidity.

JAMES MAGUIRE. Can. J. Chem. **52**, 4106 (1974).

On a étudié la cinétique de la réaction entre le Cu(II) et l'acide nitrilotriacétique (NTA) conduisant à un complexe 1:1; cette étude a été effectuée à l'aide de la technique du flux stoppé dans la zone de p*H* 2–6. La réaction est cinétiquement du premier ordre en [Cu(II)] et en $[NTA]_{total}$; la constante de vitesse a une valeur minimum de 1.1×10^5 l mol^{-1} s^{-1} dans la zone de p*H* de 3.5–5 et augmente ensuite soit par augmentation ou diminution du p*H*. Une explication pour l'évolution cinétique observée peut-être que dans le cas de l'espèce monoprotoné $HNTA^{2-}$ il y a un transfert, limitant la vitesse, du proton de l'azote avant que la formation du complexe puisse avoir lieu et que ce transfert est facilité avec une augmentation de l'acidité.

[Traduit par le journal]

Can. J. Chem. Downloaded from www.nrcresearchpress.com by 210.87.254.42 on 09/05/12
For personal use only.

Introduction

For environmental reasons it is important to study complexation of heavy metal ions by such agents as polyaminocarboxylic acids. Nitrilotriacetic acid (NTA) has received a good deal of attention because it is used in detergent formulations. Equilibrium studies of Cu(II)–NTA complex formation have been made (1–5), and Whitlow (6) has determined the crystal and molecular structure of sodium nitrilotriacetatocopper(II) monohydrate by single-crystal X-ray analysis. Rabenstein and co-workers (7, 8) have studied by nuclear magnetic resonance the ligand-exchange kinetics and solution equilibria of cadmium, zinc, and lead nitrilotriacetic acid complexes with special attention to the state of protonation of the ligand; in the case of copper it was of interest to examine the kinetics of the Cu(II)–NTA reaction.

Experimental Section

The disodium salt of nitrilotriacetic acid was obtained from Eastman Chemical Co., and cupric chloride from J. T. Baker Chemical Co. Routine absorbance measurements were made with a Cary 14 spectrophotometer, and the 1:1 stoichiometry of the complex was established. Kinetic measurements were made spectrophotometrically at 25° with a Durrum stopped-flow apparatus. The reaction was followed at 240 nm, where there is a maximum in the difference spectrum between the Cu(II)–NTA complex and either copper or NTA. The value of $[NTA]_{total}$ in one of the driving syringes (typically 10^{-4} *M*) was always kept at least ten times the concentration of copper in the other driving syringe so that upon mixing pseudo first-order kinetics were observed (*i.e.*, the rate of the reaction is given by $v = k_{obs}$[Cu(II)], where $k_{obs} = k[NTA]_{total}$. Because the dissociation constant of the Cu(II)–NTA complex is so small (9) the rate constant for dissociation can be ignored). Photographs were taken of these curves, and the values of k_{obs} were obtained by computer analysis. Plots of k_{obs} *vs.* $[NTA]_{total}$ yielded values for the second-order formation rate constant k. Each value of k is an average of at least three determinations, except in the p*H* range 2–3, where twenty determinations were made at each p*H* value. Experiments were performed at an ionic strength of 0.05 *M*, using KNO_3. The p*H* (measured with an Orion 801 p*H* meter and Fisher combination electrode calibrated with standard buffers) was adjusted using concentrated KOH or HNO_3. At p*H* values lower than 2 and higher than 6 the rate of the reaction was too fast to follow with the stopped-flow apparatus.

Results and Discussion

Figure 1 shows the effect of p*H* on the rate constant for reaction between copper(II) and nitrilotriacetic acid. The variation of the second-order rate constant k with p*H* can be explained by different reactivities of the different species of reactants. In the formal mathematical analysis of the curve in Fig. 1 use is made of the Critchlow–Dunford method (10, 11) involving the concept of transition-state acid dissociation constants. In

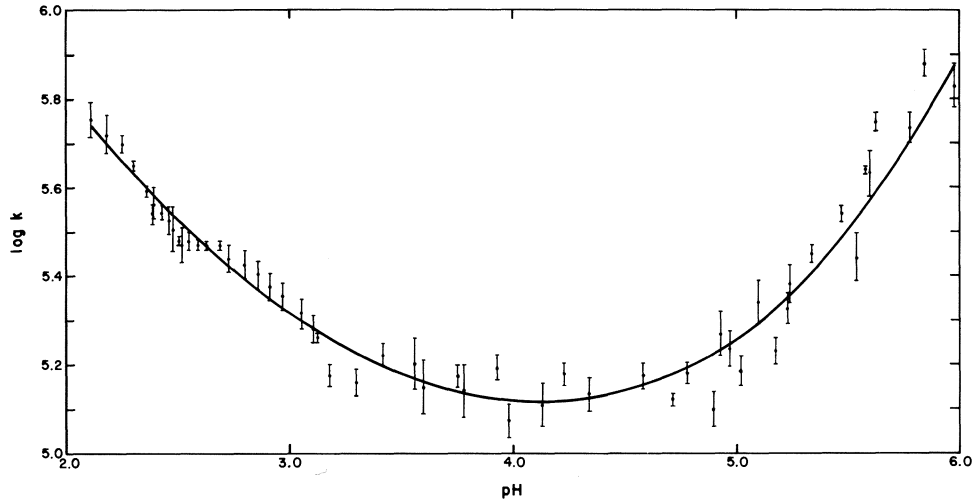

FIG. 1. A plot of the logarithm of the second-order rate constant k *vs.* pH for the reaction between Cu(II) and NTA at 25° and ionic strength 0.05 M. The error bars represent standard deviations. Each value of k is an average of at least three determinations, except in the pH range 2–3 where twenty determinations were made at each pH value.

this treatment, an acid dissociation in the transition state gives rise to an increase in slope with increasing pH in a plot of log k *vs.* pH, whereas an acid dissociation in the ground state causes a decrease in slope. The number and approximate pK values of such ionizations may therefore be read off the plot by an extension of Dixon's rules (12) in the same way as the (ground state) pK values of an enzyme or enzyme-substrate complex. The use and validity of the concept of transition-state acid dissociation constants as an aid in interpreting pH-rate profiles has been discussed in detail elsewhere (10, 11, 13, 14). The application of this style of treatment yields the same results as classical techniques for analysis of log k *vs.* pH curves, but the simplicity of this method more readily lends itself to an understanding of the chemical reaction involved; this is of great advantage in complicated systems in which both reactants are present in more than one state of ionization.

In the numerical analysis of the results an attempt was made to describe the system in terms of an inverted bell-shaped curve; this resulted in a poor fit of the calculated curve to the experimental data in the pH range 2.5–3. A more satisfactory model involves a ground state dissociation and a transition state dissociation at about pH 2.8 and 2.4, respectively, superimposed on the large-scale effect of the inverted bell-shaped curve. The solid line in Fig. 1 is a result of the fit of the data to the equation

$$[1]\quad k = k' \frac{\left(1 + \frac{K_z^\dagger}{[H^+]} + \frac{[H^+]}{K_y^\dagger} + \frac{[H^+]^2}{K_x^\dagger K_y^\dagger}\right)}{\left(1 + \frac{[H^+]}{K_a}\right)}$$

in which k' is the pH-independent rate constant in the pH range 3.5–5, K_a is the acid dissociation constant associated with the dissociation responsible for the decrease in slope (with increasing pH) at pH 2.8, and $K_x^\dagger$, $K_y^\dagger$, and $K_z^\dagger$ are the transition-state acid dissociation constants associated with the dissociations responsible for the increases in slope at pH values of 2.4, 3.5, and 5 respectively. The best fit values of these parameters are shown in Table 1. The rate constant k' in the pH region 3.5–5 of Fig. 1 can be taken as referring to the process $Cu^{2+} + HNTA^{2-}$ because this is the pH region in which $HNTA^{2-}$ is the predominant protonated species of nitrilotriacetic acid. Values for pK_2 of nitrilotriacetic acid ($H_2NTA^- \rightleftarrows HNTA^{2-} + H^+$) reported in the literature range from 2.49 (5, 15, 16) to 2.95

TABLE 1. Least-squares values of the parameters of eq. 1

Parameter	Value
k'	$(1.12 \pm 0.05) \times 10^5$ l mol^{-1}s^{-1}
pK_a	2.80 ± 0.10
p$K_x^\dagger$	2.11 ± 0.12
p$K_y^\dagger$	3.25 ± 0.05
p$K_z^\dagger$	5.24 ± 0.04

Can. J. Chem. Downloaded from www.nrcresearchpress.com by 210.87.254.42 on 09/05/12
For personal use only.

(2). It seems likely that the calculated pK_a value of 2.8 represents the dissociation of H_2NTA^- to $HNTA^{2-}$ (pK_2), and that the difference of 0.3 pH units between 2.8 and commonly accepted values of 2.5 is due to experimental error in the data of Fig. 1.

The infrared spectroscopic data of Chapman *et al.* (17) indicate that in the monoprotonated species $HNTA^{2-}$ in aqueous solution the proton resides on the nitrogen atom. From the fact that only one carboxylate antisymmetric stretching band was observed, it was deduced that all the available carboxylate groups interact in an equivalent manner with the single proton, probably through hydrogen bonding. Similarly, the diprotonated species H_2NTA^- has two carboxylate groups interacting with the proton on nitrogen, and H_3NTA, a zwitterion in solution, has one carboxylate group interacting with the proton on nitrogen. It appears that intramolecular ring formation of the protonated forms of NTA must be broken before coordination can occur. To account for the fact that $HNTA^{2-}$ reacts with copper at a slower rate than NTA^{3-}, it may be that a rate-limiting proton transfer from nitrogen in $HNTA^{2-}$ must occur before complex formation takes place. This suggestion has been made in studies of similar metal–polyaminocarboxylic acid complexes (7, 8, 18, 19). The decreased extent of intramolecular ring formation noted above for the species H_2NTA^- and H_3NTA compared to $HNTA^{2-}$ is probably responsible for the increased rate of reaction below pH 4.

1. G. SCHWARZENBACH and E. FREITAG. Helv. Chim. Acta, **34**, 1492 (1951).
2. S. RAMAMOORTHY, C. GUARNASCHELLI, and D. FECCHIO. J. Inorg. Nucl. Chem. **34**, 1651 (1972).
3. S. RAMAMOORTHY, P. G. MANNING, and C. GUARNASCHELLI. J. Inorg. Nucl. Chem. **34**, 3443 (1972).
4. W. A. E. MCBRYDE and V. CHEAM. Inorg. Nucl. Chem. Lett. **9**, 95 (1973).
5. W. A. E. MCBRYDE, J. L. MCCOURT, and V. CHEAM. J. Inorg. Nucl. Chem. **35**, 4193 (1973).
6. S. H. WHITLOW. Inorg. Chem. **12**, 2286 (1973).
7. D. L. RABENSTEIN and R. J. KULA. J. Am. Chem. Soc. **91**, 2492 (1969).
8. D. L. RABENSTEIN. J. Am. Chem. Soc. **93**, 2869 (1971).
9. L. G. SILLEN and A. E. MARTELL. The stability constants of metal–ion complexes. The Chemical Society, London. 1964.
10. J. E. CRITCHLOW and H. B. DUNFORD. J. Theor. Biol. **37**, 307 (1972).
11. J. E. CRITCHLOW and H. B. DUNFORD. J. Biol. Chem. **247**, 3703 (1972).
12. M. DIXON and E. C. WEBB. Enzymes. Longmans, Green, London. 1964. pp. 116–145.
13. H. B. DUNFORD, J. E. CRITCHLOW, R. J. MAGUIRE, and R. ROMAN. J. Theor. Biol. In press.
14. R. J. MAGUIRE. Ph.D. dissertation. University of Alberta, Edmonton, Alberta. 1972.
15. H. M. IRVING, M. G. MILES, and L. D. PETTIT. Anal. Chim. Acta, **38**, 475 (1967).
16. G. SCHWARZENBACH, H. ACKERMANN, and P. RUCKSTUHL. Helv. Chim. Acta, **32**, 1175 (1949).
17. D. CHAPMAN, D. R. LLOYD, and R. PRINCE. J. Chem. Soc. 3645 (1963).
18. J. C. CASSATT and R. G. WILKINS. J. Am. Chem. Soc. **90**, 6045 (1968).
19. D. B. RORABACHER, T. S. TURAN, J. A. DEFEVER, and W. G. NICKELS. Inorg. Chem. **8**, 1498 (1969).

Can. J. Chem. Downloaded from www.nrcresearchpress.com by 210.87.254.42 on 09/05/12
For personal use only.

C_6F_5X Bond Dissociation Energies: Determination from Appearance Potential Measurements and Correlation with Thermochemical Data

STANLEY JAMES W. PRICE[1] AND HENRY J. SAPIANO

Department of Chemistry, University of Windsor, Windsor, Ontario N9B 3P4

Received July 15, 1974

STANLEY JAMES W. PRICE and HENRY J. SAPIANO. Can. J. Chem. **52**, 4109 (1974).

Appearance potentials for $C_6F_5^+$ from C_6F_5X (X = F, Cl, Br, I) have been determined relative to argon (15.76 eV) by the extrapolated voltage difference method. The respective appearance potential values are 16.86, 15.85, 14.93, and 13.21 eV with an estimated precision of ± 0.05 eV. Combining differences in these values with the kinetic values of $D[C_6F_5—I]$ = 66.2 kcal mol^{-1} leads to $D[C_6F_5—F]$ = 150.4 $\pm$ 2.0 kcal mol^{-1}, $D[C_6F_5—Cl]$ = 127.1 $\pm$ 2.0 kcal mol^{-1}, and $D[C_6F_5—Br]$ = 105.9 $\pm$ 2.0 kcal mol^{-1}.

Comparison with $D[C_6F_5—X]$ (X = F, Cl, I) from thermochemistry (1) indicates that the combined excitation energies, kinetic energies, and chemical shifts for the process $C_6F_5X \rightarrow C_6F_5^+ + X$ are constant within experimental error.

STANLEY JAMES W. PRICE et HENRY J. SAPIANO. Can. J. Chem. **52**, 4109 (1974).

Les potentiels d'apparition de l'ion $C_6F_5^+$ dérivé du C_6F_5X (X = F, Cl, Br, I) ont été déterminés par rapport à l'argon (15.76 eV), par la méthode de différence de voltage extrapolé. Les valeurs respectives des potentiels d'apparition sont 16.86, 15.85, 14.93 et 13.21 eV avec une précision qui est estimée à ± 0.05 eV. En combinant les différences entre ces valeurs avec les valeurs cinétiques de $D[C_6F_5—I]$ = 66.2 kcal mol^{-1}, on obtient des valeurs de $D[C_6F_5—F]$ = 150.4 $\pm$ 2.0 kcal mol^{-1}, $D[C_6F_5—Cl]$ = 127.1 $\pm$ 2.0 kcal mol^{-1} et $D[C_6F_5—Br]$ = 105.9 kcal mol^{-1} $\pm$ 2.0 kcal mol^{-1}.

La comparaison de ces valeurs avec les valeurs équivalentes dérivées de la thermochimie (1) indique que les énergies d'excitations combinées, les énergies cinétiques et les déplacements chimiques pour le processus $C_6F_5X \rightarrow C_6F_5^+ + X$ sont constants aux erreurs expérimentales près.

[Traduit par le journal]

Introduction

In a recent publication (1) data on the heat of formation of iodopentafluorobenzene was combined with $D[C_6F_5—I]$ = 66.2 kcal mol^{-1} (2) to obtain $\Delta H_{f298}^0[C_6F_5,g]$ = −92.6 kcal mol^{-1}. Using this value and the appropriate values of $\Delta H_{f298}^0[C_6F_5X,g]$ (X = OH, H, F, Cl, I, CH_3, CF_3) (3–5) the corresponding $D[C_6F_5—X]$ bond dissociation energies were evaluated. With the exception of $D[C_6F_5—I]$ all of these bond dissociation energies must be assigned error limits of at least ± 3.0 kcal mol^{-1} largely because of the uncertainty in $\Delta H_{f298}^0[C_6F_5I,g]$ (1). It should be noted that *differences* between the various $D[C_6F_5—X]$ (X ≠ I) are not affected and are probably accurate to about ± 1.0 kcal mol^{-1}.

In an attempt to provide a value for $D[C_6F_5—Br]$ appearance potentials of $C_6F_5^+$ from C_6F_5X (X = F, Cl, Br, I) have been measured by standard electron impact procedures. It must be understood, particularly in the case of aromatic systems, that unknown excitation energies, kinetic energies, and chemical shifts make absolute determination (of the energy required for bond rupture and adiabatic ionization) by simple electron impact methods impossible. However, for $C_6F_5X \rightarrow C_6F_5^+ + X$, since in each case the same ion has been studied ($C_6F_5^+$) and the neutral fragment is an atom, it seems reasonable to assume that *differences* in appearance potentials should correspond closely to differences in $D[C_6F_5—X]$ bond dissociation energies. Comparison with thermochemical data has shown that this is the case.

Experimental

Materials

C_6F_6, C_6F_5Cl, C_6F_5Br, and C_6F_5I were obtained from Imperial Smelting Corporation. Each compound was subjected to fractional distillation with head and tail fractions being discarded. Analysis by gas chromatography (6 ft × 1/8 in. o.d. silicon oil DC 710 on 80–100 mesh Chromosorb W, N_2 carrier, 60 cc/min, isothermal at 105 °C, electron capture, and flame ionization detec-

[1]To whom correspondence should be addressed.

Can. J. Chem. Downloaded from www.nrcresearchpress.com by 210.87.254.6 on 09/05/12
For personal use only.

Can. J. Chem. Downloaded from www.nrcresearchpress.com by 210.87.254.6 on 09/05/12
For personal use only.

tion) showed no detectable impurities. C_6H_5Br (Eastman Organic) was similarly treated. Argon (Liquid Carbonic) was used without further purification.

Apparatus and Procedure

Appearance potentials of $C_6F_5^+$ were measured using an MS10 C2 mass spectrometer. The extrapolated voltage difference method (6, 7) was used with argon as the reference gas. The appearance potential of $C_6F_5^+$ from C_6F_5I was also determined relative to $C_6H_5^+$ from C_6H_5Br. In all cases measurements were made over a range of 4 to 5 eV above the potential at which the ion beam was first detected. The total pressure in the ion source was kept at less than 1×10^{-5} Torr in all cases. Peaks were tuned in manually. Measurements were made at intervals of 0.5 eV or less and the height of each peak in a given run was checked at least six times, three times each during descending and ascending eV measurements. A low trap current (10 μA) produced sufficiently intense spectra so that it was possible to operate the filament under very favorable conditions.

Results and Discussion

Experimental results are given in Table 1. In the extrapolated voltage difference procedure the linear portions of the appearance potential (a.p.) curves for the reference gas and the substance of interest are first made parallel by multiplying the readings for one of the gases by the appropriate factor. The curved portions are then used to obtain a plot of the separation of the curves (in eV) *vs.* peak height which when extrapolated to zero peak height gives the difference in appearance potentials. In all cases a.p. Ar = 15.76 eV was used as the reference. For $C_6F_5^+$ from C_6F_5X (X = F, Cl, Br) the total convergence between $C_6F_5^+$ and Ar^+ (from the start of the curved a.p. tail to zero ion current) was 0.1 eV or less making the linear extrapolation to zero peak height very straightforward. When X = I the lower portion of the $C_6F_5^+$ a.p. plot showed significantly greater curvature.

TABLE 1. Appearance potentials for $C_6F_5^+$ from C_6F_5X

	Appearance potential (eV)*	
X	This work	Literature values (8)
F	16.86	16.9±0.1
Cl	15.85	15.9±0.1
Br	14.93	15.2±0.1
I	13.21	—

*All present values were determined by the extrapolated voltage difference method (6, 7). Literature values (8) were determined by the semilogarithmic method. All values contain undetermined excitation energies.

TABLE 2. Comparison of $D[C_6F_5—X]$ values determined from thermochemistry with values derived from appearance potential studies

	$D[C_6F_5—X]$ (kcal mol^{-1})	
X	From thermochemistry*	From appearance potentials†
OH	145.5±3.0	
H	152.1±3.0	
F	153.6±3.0	150.4±2.0
Cl	130.0±3.0	127.1±2.0
Br	—	105.9±2.0
I	66.2±1.0‡	66.2±1.0‡
CH_3	142.2±3.0	
CF_3	96.6±3.0	

*All values in this column are based on $\Delta H_{f298}^0[C_6F_5,g] = -92.6$ kcal mol^{-1} determined from the kinetic value of $D[C_6F_5—I]$ and $\Delta H_{f298}^0[C_6F_5I,g] = -133.3 \pm 3.0$ kcal mol^{-1} (1).
†Based on the kinetic value of $D[C_6F_5—I]$ and differences in a.p. values.
‡Kinetic value (2).

The extrapolated a.p. difference (2.55 eV leading to a.p. $C_6F_5^+$ from C_6F_5I = 13.21 eV) was therefore felt to be less reliable than for the other C_6F_5X compounds studied.

In order to check the precision of the a.p. determination of $C_6F_5^+$ from C_6F_5I the a.p. of $C_6H_5^+$ from C_6H_5Br was first determined relative to argon. The a.p. of $C_6F_5^+$ from C_6F_5I was then determined relative to that for $C_6H_5^+$ from C_6H_5Br. The value obtained for the a.p. for $C_6F_5^+$ from C_6F_5I determined in this way is also 13.21 eV. It should be noted that these procedures provide only an internal check on the precision of the e.v.d. determinations.

In Table 2 a comparison is made between $D[C_6F_5X]$ values based on thermochemical methods and a.p. differences. Both sets of data use the kinetic value of $D[C_6F_5—I]$ = 66.2 kcal mol^{-1} as a base. The apparent difference of approximately 3 kcal mol^{-1} indicated by the results for X = F, Cl, and I is within the combined limits of experimental error. It would therefore appear that the contributions to the observed appearance potentials from excitation energies, kinetic energies, and chemical shifts are in fact constant within experimental error for the process $e + C_6F_5X \rightarrow C_6F_5^+ + X + 2e$ (X = F, Cl, or I and presumably then also for X = Br). The value of $D[C_6F_5—Br]$ obtained from the a.p. differences should then be a reasonable measure of this bond dissociation energy.

This work has been supported by an operating grant from the National Research Council of Canada.

1. M. J. KRECH, S. J. W. PRICE, and W. F. YARED. Can. J. Chem. **52**, 2673 (1974).
2. M. J. KRECH, S. J. W. PRICE, and W. F. YARED. Int. J. Chem. Kinet. **6**, 257 (1974).
3. J. D. COX, H. A. GUNDRY, D. HARRUP, and A. J. HEAD. J. Chem. Thermodyn. **1**, 77 (1969).
4. M. J. KRECH, S. J. W. PRICE, and W. F. YARED. Can. J. Chem. **50**, 2935 (1972).
5. M. J. KRECH, S. J. W. PRICE, and W. F. YARED. Can. J. Chem. **51**, 3662 (1973).
6. R. W. KISER. Introduction to mass spectrometry and its applications. Prentice–Hall, Englewood, N.J. 1965. p. 169.
7. J. W. WARREN. Nature, **165**, 810 (1950).
8. J. L. FRANKLIN, J. G. DILLARD, H. M. ROSENSTOCK, J. T. HERRON, K. DRAXL, and F. H. FIELD. Ionization potentials, appearance potentials and heats of formation of gaseous positive ions. NSRDS–NBS 26. 1969.

Can. J. Chem. Downloaded from www.nrcresearchpress.com by 210.87.254.6 on 09/05/12
For personal use only.

Erratum: Concertedness in the Thermolysis of Some 1-Pyrazolines

ROBERT J. CRAWFORD AND MASATOMI OHNO
Department of Chemistry, University of Alberta, Edmonton, Alberta T6G 2G2
Received October 11, 1974
(Ref. Can. J. Chem. **52**, 3134 (1974)

Table 4 on page 3138 should read as follows:

TABLE 4. Activation enthalpies (kcal mol^{-1}), entropies, and relative rates of thermolysis, at 50°, for several azo compounds[a]

	$\Delta H^{\ddagger}$	log A	$\Delta S^{\ddagger}$	Relative rate
n-C_3H_7—N=N—*n*-C_3H_7	45.1±0.5(15)	14.6	+6±2	1.0
n-C_3H_7—N=N—Allyl	35.0±0.3(7)	14.8	+7±1	10^7
Allyl—N=N—Allyl	33.5±0.5(16)	14.5	+6±2	5.6×10^7
	39.7±0.3(2)	15.4	10.6±0.5	1.0
5-*cis*	30.7±0.3	14.3	+4.7±2	10^5
1	22.2±0.4	12.3	−4.4±2.0	5.2×10^8
	39.6±0.3	15.7	11.0±0.5	1
5-*trans*	30.7±0.2	14.3	+4.7±2	10^5
2	25.1±0.2	13.9	+2.9±1.0	10^8

[a]Compounds 1, 2, and 5 were measured in diphenyl ether solution, all others in the gas phase.

Erratum: Studies on Theoretical Psychotogens. Synthesis of *O*-Methylated Neurotransmitters and Metabolic Precursors

J. R. BUTTERICK AND A. M. UNRAU
Department of Chemistry, Simon Fraser University, Burnaby, British Columbia V5A 1S6
(Ref.: Can. J. Chem. **52**, 2873 (1974))

Abstract lines 2 and 3 refer to "*erythro, threo*;" these are incorrect and should be deleted.

Can. J. Chem. Downloaded from www.nrcresearchpress.com by 210.87.254.105 on 09/05/12
For personal use only.

Marine Organic Chemistry. II. Synthesis of 3β,6α-Dihydroxy-5α-pregn-9(11)-en-20-one, the major Sapogenin of the Starfish *Asterias forbesi*

JOHN W. APSIMON AND JOHAN A. EENKHOORN

Department of Chemistry, Carleton University, Ottawa, Canada K1S 5B6

Received July 12, 1974

JOHN W. APSIMON and JOHAN A. EENKHOORN. Can. J. Chem. **52**, 4113 (1974).

A seven-step synthesis of 3β,6α-dihydroxy-5α-pregn-9(11)-en-20-one (**7**), starting from 11-oxoprogesterone, is presented.

JOHN W. APSIMON et JOHAN A. EENKHOORN. Can. J. Chem. **52**, 4113 (1974).

On présente la synthèse en sept étapes de la dihydroxy-3β,6α preg-5α ène-9 (11) one-20 (**7**), à partir de la oxo-11 progestérone. [Traduit par le journal]

Can. J. Chem. Downloaded from www.nrcresearchpress.com by 210.87.254.40 on 09/05/12
For personal use only.

Asterone, 3β,6α-dihydroxy-5α-pregn-9(11)-en-20-one (**7**), the major sapogenin isolated from the glycosides found in several starfish (1), can be considered as a potential source of corticosteroids. In order to study the conversion of asterone (**7**) to these steroids, a synthetic sequence, summarized in Scheme 1, was developed to obtain compound **7** in reasonable amounts. This route is described in this article. The 3β,6α-dihydroxy system found in asterone (**7**) can be derived from a steroidal 3-keto-4-ene by a deconjugation–reduction process, affording a 3β-hydroxy-5-ene system which in turn, after "hydroboration-oxidation," could provide the two equatorial hydroxyl groups characteristic of compound **7**. Ketalization of a 3-keto-4-ene steroid can provide the deconjugated, 5-unsaturated-ethylene ketal (2). However, the α-branch of the ketal blocks the α-side of the molecule (3) leading to hydroboration from the β-face, so that after oxidation of the organoborane, a 6β-hydroxy-5β-*H* derivative would result. Hence, we decided to proceed via a 3-acetoxy-3,5-diene, since sodium borohydride reduction of this system is known to give a 3β-hydroxy-5-ene species (4), and hydroboration–oxidation of this system is known to give a 5α-*H*,6α-hydroxy species (5). The 9(11)-double bond can be introduced by dehydration of an 11-axial hydroxyl group, which in turn can be obtained by metal hydride reduction of an 11-keto derivative (6). The preferential dehydration of the 11-axial hydroxyl group of triol **5** constitutes the major advantage of our approach over that recently reported by Turner and Smith (7). Starting from 11α-hydroxyprogesterone, they obtained a 3β,6α,11α-trihydroxypregnane derivative via an analogous series of reactions but were forced to protect two of the equatorial hydroxyl groups before being able to eliminate the third equatorial 11-hydroxyl group as the tosylate. Djerassi and co-workers (8) synthesized asterone (**7**) via a different sequence of reactions, from 3β,6α-diacetoxy-20-ethylenedioxy-5α-pregnane by reaction with iodobenzene dichloride, followed by hydroxylis in less than 11% yield.

Following the above strategy, we were able to obtain asterone (**7**) in 18% overall yield in a seven-step synthesis from 11-oxoprogesterone. Thus, treatment of 11-oxoprogesterone with acetic anhydride and perchloric acid in ethyl acetate at room temperature (9) gave the enol acetate **1** in 84% yield which was ketalized to yield the ketal **2** in 82% yield. Longer reaction times were observed to cause deacetylation, followed by ketalization resulting in formation of increasing amounts of 3,20-diketal. Cleavage and reduction of the dienol acetate **2** with sodium borohydride in ethanol afforded the 3β-hydroxy-5-ene compound **3**, which without purification was reduced with lithium aluminum hydride in diethyl ether to give the enediol **4** in 58% yield. Comparison of calculated (10) chemical shift values for the angular methyl groups with those observed, confirmed the structures assigned to compounds **4** and **5**. (See Table 1.) Hydroboration of compound **4** provided the desired triol **5** in 57% yield which on treatment with glacial acetic acid – perchloric acid at 100° underwent acetylation of the equatorial 3β- and 6α-hydroxyl groups, deblocking of the 20-keto function and dehydration of the axial 11β-hydroxyl group to

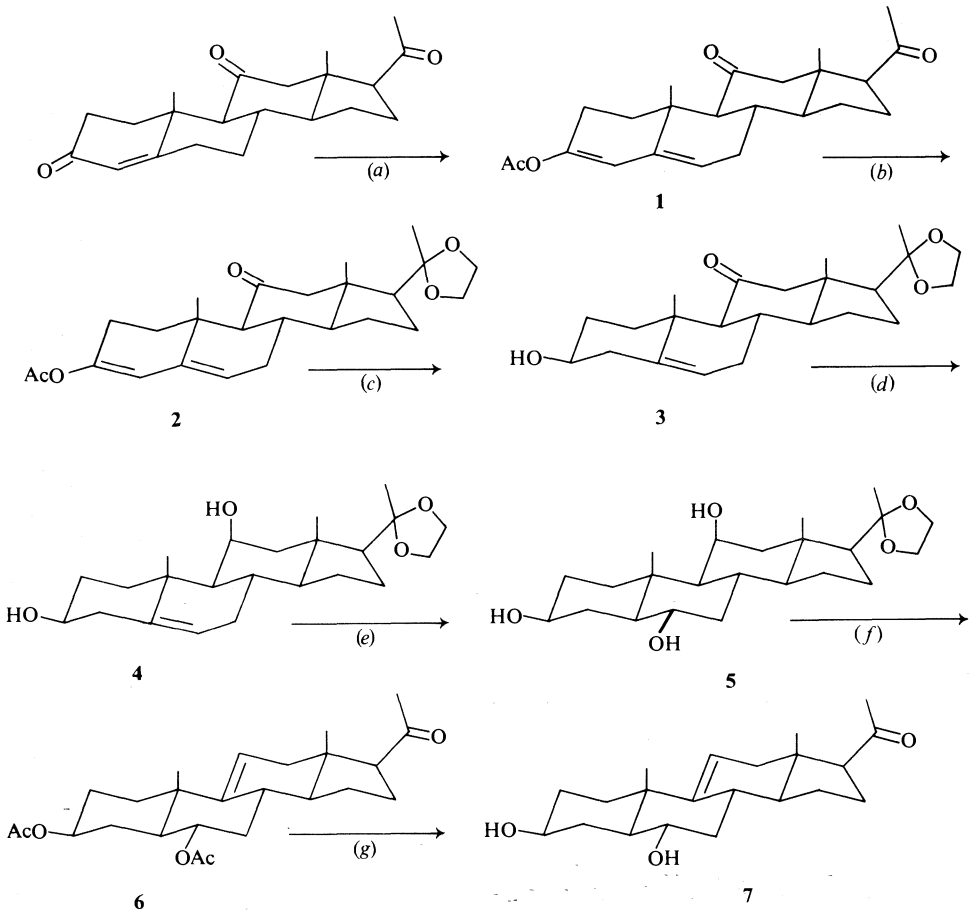

a EtOAc, Ac_2O, $HClO_4$
b Benzene, $HOCH_2CH_2OH$, TsOH, reflux
c $NaBH_4$, EtOH
d LAH, ether
e (*1*) B_2H_6, THF
(*2*) H_2O_2, NaOH
f AcOH, $HClO_4$, Δ
g MeOH, KOH, reflux

SCHEME 1

yield the crude diacetate **6** which was hydrolyzed with methanolic potassium hydroxide to afford asterone (**7**) (79% yield from compound **5**).

Experimental

Melting points were determined on a Fisher–Johns melting point apparatus and are uncorrected. The n.m.r. spectra were obtained on a Varian T-60 or Varian XL-100 spectrometer with tetramethylsilane as internal standard and deuterio-chloroform as solvent. Chemical shifts are expressed in the δ scale and the following abbreviations apply: s, singlet; d, doublet; t, triplet; m, multiplet. Infrared spectra were determined on a Perkin–Elmer 257 i.r. spectrophotometer and run in methylene chloride unless stated otherwise. Ultraviolet spectra were obtained on a Perkin–Elmer 202 u.v.–visible spectrophotometer and were run in 95% ethanol.

11-Oxoprogesterone

Material obtained from Upjohn Co. was recrystallized from methanol, m.p. 178–179 °C; u.v.: λ_{max} 238 (14 900) n.m.; i.r.: $\bar{\nu}$ 1701 (CO), 1667 (α,β-unsaturated CO) cm^{-1}; n.m.r. 0.65 (s, 3, CH_3-18H), 1.42 (s, 3, CH_3-19H), 2.12 (s, 3, CH_3CO), 5.72 (s, 1, vinyl H).

*3-Acetoxypregna-3,5-diene-11,20-dione (**1**)*

To a solution of 11-oxoprogesterone (10.0 g, 30.5 mmol), dissolved in ethyl acetate (200 ml) was added a mixture of acetic anhydride (39 ml) and ethyl acetate (120 ml), followed by a solution of perchloric acid (0.04 ml) in ethyl acetate (40 ml). The resulting yellow solution was stirred for 15 min at room temperature. The reaction was stopped by addition of saturated sodium bicarbonate solution (100 ml). The mixture was added to a slurry of sodium bicarbonate (100 g) in water (200 ml) and was stirred till carbon dioxide evolution had

Can. J. Chem. Downloaded from www.nrcresearchpress.com by 210.87.254.40 on 09/05/12
For personal use only.

Can. J. Chem. Downloaded from www.nrcresearchpress.com by 210.87.254.40 on 09/05/12
For personal use only.

TABLE 1. Observed and calculated (10) chemical shifts of the 18- and 19-methyl group protons in the proton n.m.r. spectra of selected steroids

	Found		Calculated	
	19-H	18-H	19-H	18-H
11-Oxoprogesterone	1.42	0.65	1.418	0.651
dienol acetate **1**	1.20	0.64	1.251	0.642
dienol acetate ketal **2**	1.21	0.78	1.251	0.775
hydroxyenone **3**	1.21	0.75	1.242	0.751
enediol **4** (11β-OH compound)	1.28	1.00	1.283	1.026
(11α-OH compound)			1.142	0.809
triol **5** (6α-OH, 5α-H)	1.06	1.00	1.067	1.000
(6β-OH, 5β-H)			1.400	1.034
Asterone diacetate (**6**)	1.02	0.57	1.018	0.588
Asterone (**7**)	0.95	0.55	0.951	0.588

ceased. The organic layer was separated and the aqueous layer was extracted with ethyl acetate. The combined organic layers were washed with saturated sodium bicarbonate solution and with water till neutral and were dried (Na_2SO_4). The solvent was removed *in vacuo* and 11.3 g of a white solid was obtained. Recrystallization from methanol containing some pyridine afforded 9.5 g of white crystalline product, m.p. 145–147° (lit. (11) m.p. 143–145°), *i.e.* *84%* yield; u.v.: λ_{max} 233 (19 100) nm; i.r.: $\bar{\nu}$ 1751 (acetate CO), 1708 and 1701 (CO) cm^{-1}; n.m.r.: 0.64 (s, 3, CH_3-18H), 1.20 (s, 3, CH_3-19H), 2.12 (s, 3, CH_3CO), 2.14 (s, 3, CH_3COO), 5.35 (b, 1, vinyl H-6), 5.67 (s, 1, vinyl H-4).

3-Acetoxy-20-ethylenedioxypregna-3,5-dien-11-one (2)

A mixture of enolacetate **1** (10.0 g, 27.0 mmol) dissolved in benzene (500 ml), ethylene glycol (50 ml), and *p*-toluenesulfonic acid (0.5 g) was stirred at reflux temperature for 3 h. During this time water was removed using a Dean-Stark apparatus. To the cooled solution were added 200 ml of saturated sodium bicarbonate solution. The benzene layer was separated and the aqueous layer was extracted with benzene. The combined organic layers were washed with water till neutral and were dried (Na_2SO_4). The solvent was removed *in vacuo* and the resulting solid residue was recrystallized from methanol containing some pyridine to afford 9.2 g of white crystalline product, m.p. 116–118° (82% yield). Repeated recrystallization from methanol (pyridine) gave an analytical sample, m.p. 117–119°; u.v.: λ_{max} 232 (18 300) nm; i.r.: $\bar{\nu}$ 3033 (ketal C—H stretch), 1751 (acetate CO), 1701 (CO) cm^{-1}; n.m.r.: 0.78 (s, 3, CH_3-18H), 1.21 (s, 3, CH_3-19H), 1.28 (s, 3, CH_3-21H), 2.14 (s, 3, CH_3COO), 3.94 (m, 4, OCH_2CH_2O), 5.35 (b, 1, vinyl H-6), 5.66 (s, 1, vinyl H-4).

Anal. Calcd. for $C_{25}H_{34}O_5$: 72.43; 8.27 H. Found: 72.40 C; 8.18 H.

3β-Hydroxy-20-ethylenedioxypregn-5-en-11-one (3)

To a solution of enol acetate ketal **2** (5.5 g, 13.3 mmol), dissolved in 95% ethanol (550 ml), was added sodium borohydride (1.1 g). The colorless solution was stirred at room temperature for 23 h. After addition of 100 ml of water, the reaction mixture was stirred for 1 h more. The solvent was removed *in vacuo* and the residue was treated with a mixture of water and ether. The ether layer was separated and the aqueous layer was extracted with ether. The combined organic layers were washed with saturated sodium chloride solution and were dried (Na_2SO_4). Evaporation *in vacuo* of the solvent afforded 5.0 g of white solid (100% yield), which was used without purification in the next step; i.r.: $\bar{\nu}$ 3590 (OH), 1700 (CO) cm^{-1}; n.m.r.: 0.75 (s, 3, CH_3-18H), 1.21 (s, 3, CH_3-19H), 1.28 (s, 3, CH_3-21H), 3.94 (m, 4, OCH_2CH_2O), 3.6 (m, 1, *H*COH), 5.35 (b, 1, vinyl H).

20-Ethylenedioxypregn-5-ene-3β,11β-diol (4)

To a solution of 3β-hydroxy-20-ethylenedioxypregn-5-en-11-one (**3**) (5.0 g, 13.3 mmol) dissolved in anhydrous ether (500 ml) 2.5 g of lithium aluminum hydride was added. The reaction mixture was stirred at room temperature for 23 h, was then cooled to 0°, and was treated with 250 ml of saturated potassium sodium tartrate solution. The ether layer was separated and the aqueous layer was extracted with ether. The combined organic layers were washed with saturated sodium chloride solution, were dried (Na_2SO_4) and concentrated *in vacuo*. The white solid residue (5.0 g) was recrystallized from acetone to give 2.7 g (7.2 mmol) of crystalline product, m.p. 208–212° (lit. (12) m.p. 210–215.5°).

From the mother liquor an additional 0.2 g of product was obtained, m.p. 207–210°. Total yield amounted to *58%*; i.r.: $\bar{\nu}$ 3590 (OH) cm^{-1}, no absorption in CO region; n.m.r.: 1.00 (s, 3, CH_3-18H), 1.28 (s, 3, CH_3-19H), 1.28 (s, 3, CH_3-21H), 3.94 (m, 4, OCH_2CH_2O), 3.6 (m, 1, HCOH-3), 4.3 (b, 1, *H*COH-11), 5.23 (b, 1, vinyl H).

20-Ethylenedioxy-5α-pregnane-3β,6α,11β-triol (5)

To a solution of enediol **4** (3.0 g, 8.0 mmol) dissolved in 100 ml of dry tetrahydrofurane at 0 °C was added dropwise a solution of 0.1 *M* diborane in tetrahydrofurane (75 ml). The reaction was allowed to proceed for 2 h at 0 °C. A 3 *N* aqueous sodium hydroxide solution (75 ml) was added dropwise to the reaction mixture, followed by 40% aqueous hydrogen peroxide solution (75 ml). The reaction mixture was stirred for 1 h at room temperature. The tetrahydrofurane layer was separated and washed several times with saturated sodium chloride solution, was dried (Na_2SO_4) and was concentrated *in vacuo* to give 2.9 g (7.4 mmol, *92%* yield) of a white solid. Recrystallization from acetone afforded 1.8 g (4.6 mmol, *57%* yield) of crystalline product, m.p. 235–237°. Repeated recrystallization from acetone gave an analytical sample, m.p. 238–241°; i.r. (nujol): $\bar{\nu}$ 3530, 3478, 3406 (OH) cm^{-1}; n.m.r. (dilute solution of crude material for solubility reasons): δ 1.00 (s, 3, CH_3-18H), 1.06 (s, 3, CH_3-19H), 1.31 (s, 3, CH_3-21H), 3.93 (m, 4, OCH_2-CH_2O), 3.6 (m, 2, *H*COH), 4.3 (b, 1, *H*COH-3).

Anal. Calcd. for $C_{23}H_{38}O_5$: 70.01 C; 9.71 H. Found: 70.13 C; 9.80 H.

3β,6α-Diacetoxy-5α-pregn-9(11)-en-20-one (6)

A solution of triol **5** (0.90 g, 2.3 mmol) dissolved in 45 ml of glacial acetic acid, containing 0.45 ml of perchloric acid, was heated on a steam bath for 1 h. The reaction mixture was poured into 450 ml of water. The product was extracted into ether. The organic extracts

were washed with saturated sodium bicarbonate solution and with saturated sodium chloride solution till neutral. The dried solution (Na_2SO_4) was concentrated *in vacuo* and afforded 1.0 g (100%) of light brown resin; i.r.: $\bar{\nu}$ 3018 (=C—H), 1730 (acetate CO), 1700 (CO) cm^{-1}; n.m.r. 0.57 (s, 3, CH_3-18H), 1.02 (s, 3, CH_3-19H), 2.13 (s, 3, CH_3CO), 2.03 (s, 6, CH_3COO), 4.8 (m, 2, HCOAc), 5.40 (b, 1, vinyl H).

3β,6α-Dihydroxy-5α-pregn-9(11)-en-20-one (7)

To a solution of diacetate **6** (1.0 g, 2.3 mmol) in 33 ml of methanol was added a solution of 1.7 g of potassium hydroxide in 5 ml of water and 12 ml of methanol. The resulting solution was refluxed for 2 h. The solvent was removed *in vacuo* and the residue was taken up in methylene chloride and water. The organic layer was washed with water, was dried (Na_2SO_4), and concentrated *in vacuo* to give 0.7 g (92%) of a yellow solid. Recrystallization from benzene afforded 0.60 g (79%) of white crystalline product, m.p. 166–168°; recrystallization from acetone afforded a sample with m.p. 196–198° (lit. (1*c*) m.p. 193–196°; i.r.: $\bar{\nu}$ 3590, 3380 (OH), 3015 (=C—H), 1697 (CO) cm^{-1}; n.m.r.: 0.55 (s, 3, CH_3-18H), 0.95 (s, 3, CH_3-19H), 2.13 (s, 3, CH_3CO), 3.56 (m, 2, *H*COH), 5.35 (b, 1, vinyl H), 2.5–3.5 (s, 2, OH, concentration dependent).

We wish to thank the National Research Council of Canada for generous financial assistance.

1. (*a*) S. Ikegami, Y. Kamiya, and S. Tamura. Agr. Biol. Chem. (Tokyo), **36**, 1777 (1972); Tetrahedron Lett. 1601 (1972); (*b*) Y. M. Sheikh, B. M. Tursch, and C. Djerassi. J. Am. Chem. Soc. **94**, 3278 (1972); (*c*) Y. Shimizu. J. Am. Chem. Soc. **94**, 4051 (1972); (*d*) J. W. ApSimon, J. A. Buccini, and S. Badripersaud. Can. J. Chem. **51**, 850 (1973).
2. B. J. Magerlein and R. H. Levin. J. Am. Chem. Soc. **75**, 3654 (1953).
3. S. Berstein, W. S. Allen, C. E. Linden, and J. Clemente. J. Am. Chem. Soc. **77**, 6612 (1955); S. Bernstein and R. Littell. J. Org. Chem. **26**, 3610 (1961).
4. B. Belleau and T. F. Gallagher. J. Am. Chem. Soc. **73**, 4458 (1951); W. G. Dauben and J. F. Eastham. J. Am. Chem. Soc. **73**, 4463 (1951).
5. S. Wolfe, M. Nussim, Y. Mazur, and F. Sondheimer. J. Org. Chem. **24**, 1034 (1959).
6. L. H. Sarett, M. Feurer, and K. Folkers. J. Am. Chem. Soc. **73**, 1777 (1951); S. Bernstein, R. H. Lenhard, and J. W. Williams. J. Org. Chem. **18**, 1166 (1953).
7. D. S. H. Smith and A. B. Turner. Tetrahedron Lett. 5263 (1972).
8. J. E. Gurst, Y. M. Sheikh, and C. Djerassi. J. Am. Chem. Soc. **95**, 628 (1973).
9. B. E. Edwards and P. N. Ras. J. Org. Chem. **31**, 324 (1966).
10. R. F. Zürcher. Helv. Chim. Acta, **44**, 1380 (1961); Helv. Chim. Acta, **46**, 2054 (1963).
11. J. J. Schneider. Tetrahedron, **28**, 2717 (1972).
12. W. J. Wechter and H. C. Murray. J. Org. Chem. **28**, 755 (1963).

Can. J. Chem. Downloaded from www.nrcresearchpress.com by 210.87.254.40 on 09/05/12
For personal use only.

The Mass Spectra of Derivatives of Polyporic Acid[1]

R. D. GRIGSBY,[2] W. D. JAMIESON, A. G. MCINNES, W. S. G. MAASS, AND A. TAYLOR

Atlantic Regional Laboratory, National Research Council of Canada, Halifax, Nova Scotia B3H 3Z1

Received July 2, 1974

R. D. GRIGSBY, W. D. JAMIESON, A. G. MCINNES, W. S. G. MAASS, and A. TAYLOR. Can. J. Chem. **52**, 4117 (1974).

The diacetate and di-*O*-methyl derivative of polyporic acid have anomalous mass spectra. Ions are observed at *m/e* values equal to the molecular weight but ions 2 mass units larger than these, often of greater intensity, are also observed. The abundance of such ions depends on the temperature of the sample, the pressure in the source, and the partial pressure of water in the instrument. In addition, ions *m/e* 420 and 462 are found in the spectrum of the diacetate which are parents of the M + 2 ion(s). Similarly, M + 17 and M + 32 ions are observed in the spectrum of the dimethoxy compound. When deuterium oxide and the ester or the perdeuterioacetyl derivative were introduced into the source M + 4 ions were seen in the mass spectra. These unusual reactions should permit diagnosis of the 2,5-dihydroxy-1,4-benzoquinone moiety in newly isolated natural products.

R. D. GRIGSBY, W. D. JAMIESON, A. G. MCINNES, W. S. G. MAASS et A. TAYLOR. Can. J. Chem. **52**, 4117 (1974).

On observe des spectres de masse anormaux pour les dérivés diacétate et di-*O*-méthylés de l'acide polyporique. On observe des ions aux valeurs *m/e* égales au poids moléculaire, ainsi que des ions ayant deux unités de masse de plus que les premiers, et d'intensité souvent plus élevée. L'abondance de tels ions dépend de la température de l'échantillon, de la pression dans la source et de la pression partielle de l'eau dans l'instrument. De plus, on trouve dans le spectre du diacétate des ions *m/e* 420 et *m/e* 462 qui sont parents des ions M + 2. De la même façon, on observe dans le spectre du dérivé diméthoxy des ions M + 17 et M + 32. Quand on introduit dans la source l'oxyde de deutérium et l'ester ou le dérivé acétylé perdeutérié, on observe des ions M + 4 sur les spectres de masse. Ces réactions extraordinaires devraient permettre la diagnose du fragment dihydroxy-2,5 benzoquinone-1,4 dans les produits naturels nouvellement isolés.

[Traduit par le journal]

Introduction

It has been known for some years (1–3) that benzoquinones have anomalous mass spectra. Reports of M + 2 ions of greater abundance than expected for the presence of naturally occurring isotopes are common, and estimates of their intensity, with respect to the molecular ions, have varied in the range 2–28%. It has been recognized (4, 5) that these anomalous ions occur more abundantly when the source of the mass spectrometer contains small quantities of water, presumably absorbed on metallic surfaces. During the course of studies of the chemistry of cochliodinol (6) we were led to the conclusion that the apparent molecular ions observed for cochliodinol and several of its derivatives were 2 units greater than the molecular weight; with one exception ions corresponding to the molecular weight were not found. A full examination of these results is deferred but they did suggest a mass spectroscopic study of more stable and more volatile model compounds. Polyporic acid (**1**, R = H) was chosen for this work and the results are reported.

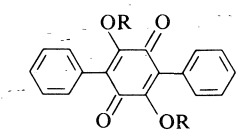

1

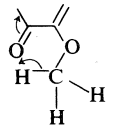

2

Experimental

All spectra were recorded using an electron beam energy of *ca.* 82 eV on a Dupont/CEC 21-491 double focussing, low resolution mass spectrometer. The ion source temperature was varied from 200 to 220°. Approximately 25 μg samples dissolved in tetrahydrofuran (3 ml) were loaded into an all-glass probe having a temperature measurement error of ±3° and a temperature control error of ±1°. Heating was controlled by a variable transformer and temperature was measured with a digital thermometer (available from Mass Spectrometer Accessories, P.O. Box 9314, College Station, Texas 77840, U.S.A.).

[1]NRCC No. 14282.

[2]Visiting Research Officer 1973–1974. Present address: Department of Biochemistry and Biophysics, Texas A & M University, College Station, Texas 77801.

Can. J. Chem. Downloaded from www.nrcresearchpress.com by 210.87.254.105 on 09/05/12
For personal use only.

Can. J. Chem. Downloaded from www.nrcresearchpress.com by 210.87.254.105 on 09/05/12
For personal use only.

Spectra were recorded over the temperature range 90–135°. To test for the effect of increasing pressure on fragmentation, spectra were taken with the ion-source pumping valve either open or almost completely closed. The influence of water and deuterium oxide on the ion reactions was tested by running 3 μl loads of these compounds in the expansion volume inlet (≃150°), while introducing the polyporic acid derivatives through the direct inlet probe. Ion reactions were determined using a CEC 21-110B instrument by the method of Beynon *et al.* (7). Precise mass measurements were made with the same instrument by the peak matching method using an appropriate ion in the spectrum of perfluorokerosene as a standard.

Polyporyl Di(trideuterioacetate)

Polyporic acid (**1**, R = H, 220 mg) purified by hydrolysis of its diacetate, was dissolved in hexadeuterioacetic anhydride (>99.9 atom% [^{2}H], Merck, Sharpe and Dohme; 2 ml), the solution was kept 0.5 h at 4°, diluted with ice and water (100 ml), and the yellow crystalline precipitate was collected. This product was chromatographed on silica gel and the yellow chloroform eluate collected. *Polyporyl di(trideuterioacetate)* (**1**, R = $COC[^2H]_3$) separated from ether as yellow prisms, m.p. 215°.

Anal. Calcd. for $C_{22}[^2H]_6H_{10}O_6$: C, 69.1; O, 25.1. Found: C, 68.8; O, 25.1.

Results

At constant temperature, *e.g.* 120° (Fig. 1), sequential scans of the mass spectrum of polyporyl diacetate (1, R = Ac) showed that during about 40 min the relative abundances of pairs or ions at *m/e* 378, 376; 336, 334 changed. After this time the measured spectra were relatively constant until the sample was almost exhausted (after about 60 min). The curve in Fig. 1 for the ratio I_{378}/I_{376} indicates that there is a volatile *m/e* 376 species that is distilled before precursors of *m/e* 376 of higher molecular weight, *e.g.* *m/e* 418. The curves in Fig. 1 are least mean squares fits of the data to empirical equations of the second degree. The indices of fit were approximately 0.9 in each case but similar results and calculations for the pair of ions at *m/e* 292, 294 indicated that no significant change with time was observed for these ions.

The mass spectra of polyporyl diacetate at 100, 110, and 130° between *m/e* values of 263 and 421 are given in Table 1. The values in Table 1 are calculations of the % total ionization after the contribution of *m/e* 18 has been subtracted. Ions which were less than 0.01% of the total ionization are not included in the table. Throughout the mass range, there are clear differences in the abundance of ions in the three spectra; indeed only the ions *m/e* 274, 276, and

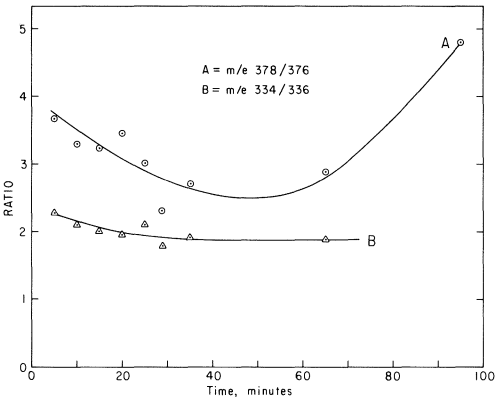

FIG. 1. Changes in the ratios of ions of *m/e* 378, 376, and 334, 336 in the mass spectrum of polyporyl diacetate at 120°.

277 have about the same abundance at each temperature. However, the most striking differences are to be found in the pairs of ions at *m/e* 378, 376; 336, 334; 294, 292. The change in abundance of the latter pair of ions is shown in Fig. 2 where the units of the ordinates are calculated from the expression $(100 \times n/2)(I_i/\sum I_n)$. In this expression $\sum I_n$ is the sum of the abundances of *n* selected ions (in this case *m/e* 264, 292, 294, 334, 336, 376, and 378) and I_i is the intensity of the *m/e* 292 (or 294) ion. Thus the ion *m/e* 292 increases in intensity from 49 to 211 units as the

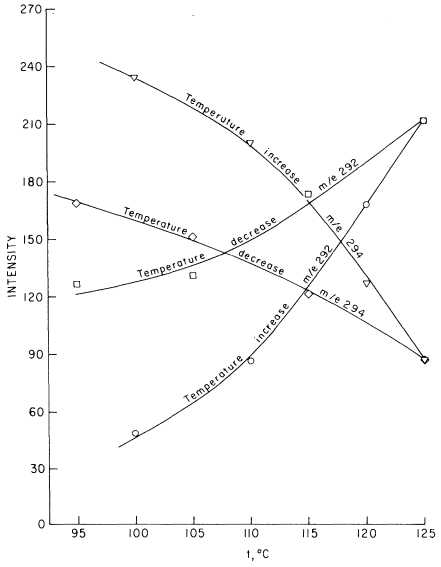

FIG. 2. Changes in intensities of ions of *m/e* 292 and *m/e* 294 in the mass spectrum of polyporyl diacetate with increase and decrease of sample temperature.

TABLE 1. Mass spectra of polyporyl diacetate (m/e > 263)

	% total ionization			
m/e	100°	130°	110°	110° (Valve closed)*
264	0.51	3.01	1.36	0.89
265	0.18	0.56	0.31	0.20
266		0.08	0.07	
273		0.14	0.09	0.07
274	0.11	0.18	0.13	0.13
275	1.23	0.52	1.07	1.43
276	0.51	0.41	0.51	0.49
277	0.24	0.11	0.18	0.15
278	2.36	0.27	0.87	1.13
279	0.50	0.07	0.16	0.25
280				0.05
290		0.14		0.05
291		0.19	0.11	0.05
292	5.02	29.33	12.92	7.42
293	1.43	6.23	3.01	2.19
294	12.63	7.03	12.58	15.18
295	2.89	1.41	2.56	3.21
296	0.39	0.19	0.40	0.44
297		0.04	0.07	0.05
305	0.09			
306		0.24	0.11	0.05
307		0.05		
317			0.09	0.07
318	0.11		0.07	0.05
319	0.10	0.05	0.07	
320	0.14	0.05	0.11	0.10
334	0.33	2.55	1.40	0.79
335	0.09	0.56	0.40	0.24
336	2.48	1.13	2.45	2.78
337	0.67	0.29	0.56	0.69
338	0.12	0.06	0.11	0.12
376		0.12	0.09	0.05
377		0.03		
378	0.56	0.45	1.02	1.05
379	0.22	0.12	0.29	0.27
380		0.02	0.07	0.05
420		0.05	0.13	0.10
421		0.02	0.07	0.05
18	14.4	0.76	2.06	7.46

*Ion source almost completely closed (see text).

temperature is increased from 100 to 125° but decreases to 127 units as the sample is cooled to 100°. The behavior of the ion m/e 294 is almost exactly the inverse. Similarly, the behavior of the ion m/e 336 is almost exactly the inverse of that of m/e 334. However, a much greater discrepancy was observed in the least mean squares fit of the data for the m/e 336 ion on decreasing the temperature of the sample as compared to the curve obtained on temperature increase. Thus the phenomena are not exactly reversible, possibly due to difficulties of measuring the abundances at different temperatures in the equilibrium phase shown in Fig. 1. When the spectra were measured at only two temperatures, *e.g.* the data given in Table 2 for the di-*O*-methyl derivative (**1**, R = OMe), when time was available for equilibrium to be established at both temperatures, almost complete reversibility of the spectra was observed. A similar reversibility is evident from the data given in Table 3. Here it is shown that an ion of low abundance at m/e 420 decomposes to an ion m/e 378 with loss of a neutral fragment of mass 42. Only 0.04% of the ions

Can. J. Chem. Downloaded from www.nrcresearchpress.com by 210.87.254.105 on 09/05/12
For personal use only.

TABLE 2. Effect of sample temperature and the presence of water or deuterium oxide on the mass spectrum of di-*O*-methylpolyporic acid*

Temperature (°C)	*m/e*		Relative intensity ratio				
	18	20	320/322	322/324	305/307	307/309	287/289
106	69		1.57		2.34		2.34
110	45		2.00		3.17		2.71
137	15		5.67		11.25		3.83
109	20		2.17		3.09		3.09
110	515		0.96		2.05		1.64
110	37		2.00		3.17		2.56
110	800	3600	4.44	0.63	4.75	0.98	3.41
110	19	5	2.86	10.87	3.76	12.5	3.26

*The rows of data are in chronological order.

TABLE 3. Ion reactions in the mass spectrometer for polyporyl diacetate

Time of measurement (min)	Probe temperature (°C)	Daughter ion		Parent ions	
		m/e	Relative intensity (*m/v*)	*m/e*	Relative intensity (*m/v*)
0	105	378	1.13	420	0.0005
20	131	378	4.81	420	0.0084
35	105	378	1.25	420	0.0013

of *m/e* 378 are daughters of the species *m/e* 420 at 105° but at 131° the percentage increases to 0.18% and then decreases to 0.1% when the sample temperature is lowered to 105°.

Although the abundance of each ion of each pair varies with temperature as shown, *e.g.* in Fig. 2, the sum of the values for % ionization for each of the pairs is nearly independent of temperature (as it should be for any two ions in a mass spectrum). Hence the sums of the abundances for each of the three pairs of ions also remain in proportion to each other at all temperatures at which the spectra were measured. Evidence was obtained (Table 3) for two sequences of fragmentation reactions (Table 4) *viz.* 420 → 378 → 336 → 294 and 418 → 376 → 334 → 292. These degradative reactions, like other ion reactions that occur in the mass spectrometer, are presumably temperature independent. It is the reactions producing the species that generate these two fragmentation processes that are dependent on the temperature of the sample.

The effects of increasing the partial pressure of water in the mass spectrometer are shown in Table 5 for polyporyl diacetate and similar, though more scanty data, are given in Table 2 for di-*O*-methylpolyporic acid. Again, the main changes that occur in the spectrum of the ester lie in the relative abundances of the pairs of ions at *m/e* 378, 376; 336, 334; 294, 292. The value of the change in ratio of the heavier ion to the lighter one was about 6 in the case of the 378/376 pair and about 2 in the other cases. Thus the abundance of *m/e* 378 compared to *m/e* 376 increased by a factor of at least 6 as the intensity of *m/e* 18 increased 34 times. When the ion-source pumping valve was closed, causing the intensity of the *m/e* 18 ion to increase by about 4 times, the I_{378}/I_{376} ratio increased by a factor of about 2 as seen in Table 1. In the presence of deuterium oxide the spectrum of the ester was much more complex because of the

TABLE 4. Precursor ions in the spectrum of polyporyl diacetate

Daughter ion (*m/e*)	Parent ions	
	m/e	*m/e*
376	418	
336	378	349
334	376	346
294	336	305
292	334	304

Can. J. Chem. Downloaded from www.nrcresearchpress.com by 210.87.254.105 on 09/05/12
For personal use only.

TABLE 5. Mass spectra of polyporyl diacetate and polyporyl di(trideuterioacetate) in the absence and presence of water or deuterium oxide

	% total ionization					
	Polyporyl diacetate			Polyporyl di(trideuterioacetate)		
m/e	Normal	Water	Deuterium oxide	Normal	Water	Deuterium oxide
264	1.36	1.22	0.93	0.15	0.19	0.13
265	0.31	0.27	0.27	0.25	0.23	0.19
266	0.07	0.05	0.09	2.05	1.22	1.35
267			0.04	0.47	0.23	0.41
268				0.10	0.07	0.13
269						0.09
273	0.09	0.11	0.07			
274	0.13	0.16	0.11	0.10	0.07	
275	1.07	1.49	0.54	0.17	0.28	0.13
276	0.51	0.67	0.99	0.45	0.96	0.28
277	0.18	0.20	0.62	0.45	0.73	0.66
278	0.87	1.29	0.26	0.17	0.23	0.75
279	0.16	0.31	0.37	0.27	0.78	0.28
280		0.05	0.56	0.17	0.42	0.16
281			0.34	0.07	0.12	0.27
282			0.10			0.60
283			0.04			0.19
290		0.13	0.04	0.17	0.07	
291	0.11	0.07	0.07	0.10		
292	12.92	7.80	7.47	0.12	0.45	
293	3.01	2.45	1.91	0.95	1.55	0.44
294	12.58	14.07	2.28	12.62	7.05	8.64
295	2.56	2.81	8.09	2.60	2.33	1.98
296	0.40	0.45	10.68	4.75	11.51	1.04
297	0.07	0.05	1.91	3.37	5.17	3.49
298			0.30	1.47	1.22	13.03
299			0.04	0.30	0.23	2.95
300				0.07		0.38
306	0.11	0.09	0.07			
310				0.17	0.14	0.16
334	1.40	0.73	0.79			
335	0.40	0.18	0.20			
336	2.45	2.27	0.37			
337	0.56	0.64	1.46	0.07	0.07	
338	0.11	0.09	1.85	1.77	0.99	1.00
339			0.42	0.35	0.33	0.22
340			0.07	0.97	2.56	0.16
341				0.72	1.13	0.69
342				0.40	0.31	2.54
343				0.10	0.07	0.69
344						0.13
376	0.09		0.06			
378	1.02	0.69	0.14			
379	0.29	0.18	0.43			
380	0.07		0.49			
382			0.04	0.17	0.09	0.13
383				0.07	0.07	
384				0.25	0.75	
385				0.42	0.49	0.22
386				0.22	0.23	0.82
387				0.07	0.05	0.25

Can. J. Chem. Downloaded from www.nrcresearchpress.com by 210.87.254.105 on 09/05/12
For personal use only.

Can. J. Chem. Downloaded from www.nrcresearchpress.com by 210.87.254.105 on 09/05/12
For personal use only.

presence of HDO; in this spectrum (Table 5) groups of three ions at *m/e* 380, 379, 376; 338, 337, 334; and 296, 295, 292 were found. The analogous spectra of polyporyl di(trideuterioacetate) were very similar (Table 5), 2 units of mass 44 were lost from ions of *m/e* 382, 384, and 386, respectively, in the absence, and presence of water or deuterium oxide. The reactions, therefore, that generate the parents of *m/e* 378 do not involve exchange of the hydrogen atoms of the acetate groups with water (or D_2O) because they are lost, or undoubtedly retained in the fragmentation sequence given. The fragmentation of the di-*O*-methyl compound is even more remarkable, as in this case the principle ion reactions are loss of a methyl group and then loss of water. In the latter reaction, in the presence of deuterium oxide we have: $309^+ \rightarrow 291^+ + 18$ ($m^* \simeq 274$) and the deuterium atoms introduced into the *m/e* 309 species are clearly not involved in the elimination of the elements of water. If these protons eliminated as water are originally located as substituents of the carbon atoms of a methoxyl group and their loss is achieved by a series of rearrangements, *i.e.* **2**, then these shifts, which generate groups having potentially exchangeable protons, appear to occur faster than any exchange reaction. Hence, in this case too, ions are generated in the mass spectrometer that are of higher, though unknown, mass than the molecular weight of the sample.

These results clearly implicate water as a reagent involved in the formation of ions of greater molecular weight than the sample but its presence is not mandatory, as may be seen by an inspection of the mass spectrum of polyporyl di(trideuterioacetate) (Table 5). Here the ions *m/e* 386, 385, and 384 were of greater abundance that the ion *m/e* 382 even though ions of *m/e* 19 and 20 were not detected in the spectrum. Though the resolution of our instrument will not allow a decision to be made between, *e.g.* $C_{22}[^2H]_6H_{12}O_6$ (Found: 384.1473; required 384.14799) and $C_{22}[^2H]_7H_{10}O_6$ (required 384.14645), it seems likely that the *m/e* 384 ion consists of the latter species, at least in part. This additional deuterium atom is thus acquired from another perdeuteriated ester molecule, possibly (see above) as part of a perdeuteriated acetyl group.

Discussion

The results indicate that species are generated which have molecular weights greater than the sample, when polyporic acid and its derivatives are introduced into the electron impact source of a mass spectrometer. In view of the prevailing low pressure of such a source it seems unlikely that the reactions observed are bimolecular. The participation of water in the reaction suggests that it occurs on the metallic surfaces of the source, where water is known to be absorbed. The transfer of acetyl groups may occur at the same sites but may also be the result of a solid-state reaction in the sample or even reaction in the gas phase if these molecules vaporize as quinhydrone-like dimers. At present a decision cannot be made between such possibilities but any explanation of the phenomena requires the reduction of a benzoquinone moiety for the formation of tri- and tetraacetates. Aplin and Pike (4) have noted that these reactions appear to be dependent on the redox potential of the quinone but insufficient data are available at the moment to establish such a relationship.

The results should be of use to natural product chemists who wish to establish the presence of 2,5-dihydroxy-1,4-benzoquinones in plant extracts. Thus, if the mass spectrum of the metabolite contains an ion two mass units greater in the presence of deuterium oxide than in its absence (when exchangeable groups are accounted for) the presence of this quinone moiety may be suspected. Confirmation may then be sought by an examination of the spectrum of the perdeuterioacetyl derivative which should contain ions 8 mass units greater than the acetate ester.

1. J. H. Bowie, D. W. Cameron, R. G. F. Giles, and D. H. Williams. J. Chem. Soc. (B), 335 (1966).
2. M. C. Gaylord and L. R. Brady. J. Pharm. Sci. **60**, 1503 (1971).
3. M. Lounasmaa and A. Karjalainen. Acta Chem. Scand. **27**, 3427 (1973).
4. R. T. Aplin and W. T. Pike. Chem. Ind. 2009 (1966).
5. J. W. Cornforth, G. Ryback, P. M. Robinson, and D. Park. J. Chem. Soc. (C), 2786 (1971).
6. D. Brewer, W. A. Jerram, and A. Taylor. Can. J. Microbiol. **14**, 861 (1968).
7. J. H. Beynon, R. A. Saunders, and A. E. Williams. The mass spectra of organic molecules. Elsevier, Amsterdam. 1968. p. 55.

The Chemistry of High Molecular Weight Fulvic Acid Fractions[1]

JEAN A. NEYROUD[2] AND MORRIS SCHNITZER
Soil Research Institute, Agriculture Canada, Ottawa, Canada K1A 0C6

Received August 12, 1974

Can. J. Chem. Downloaded from www.nrcresearchpress.com by 210.87.254.42 on 09/05/12
For personal use only.

JEAN A. NEYROUD and MORRIS SCHNITZER. Can. J. Chem. **52**, 4123 (1974).

Fulvic acid (FA) was methylated, dissolved in benzene, and fractionated over Al_2O_3 with the aid of organic solvents of increasing polarities. This paper is concerned with fractions eluted with ethyl acetate (III), ethyl acetate — methanol (1:1) (IV), and methanol (V), which were quantitatively the most abundant ones and which we consider as being most representative of the original FA. Each fraction was characterized by chemical and spectroscopic methods and by degradation with alkaline permanganate. Fractions IV and V were also degraded by NaOH hydrolysis and by alkaline CuO-oxidation. The degradation products were identified with the aid of a gas chromatograph — mass spectrometer — computer system.

The number-average molecular weights of the three fractions were: III, 821; IV, 945; and V, 1,397. Infrared, proton n.m.r., and carbon-13 n.m.r. spectra provided, except for functional groups, little detailed information on the chemical structures of the fractions. The major degradation products were benzenecarboxylic and phenolic acids in addition to smaller amounts of aliphatic (mainly *n*-fatty) acids. Evidence is presented that may be interpreted to indicate: (*a*) esterification of some of the fatty acids to OH groups of phenolic acids; (*b*) the existence in the fractions of ether (C—O) linkages; and (*c*) rupture of C—C bonds during degradation. While in both the lower and the higher molecular weight FA fractions benzenecarboxylic and phenolic acids were the basic "building blocks", the latter appeared to be more complex and more stable in the higher-molecular weight fractions, possibly because chemical bonding as well as hydrogen bonding, van der Waal's forces, and π-bonding were involved simultaneously.

JEAN A. NEYROUD et MORRIS SCHNITZER. Can. J. Chem. **52**, 4123 (1974).

L'acide fulvique (AF) a été méthylé, dissout dans le benzène et fractionné sur Al_2O_3 à l'aide de solvants organiques de polarités croissantes. Cet article concerne les fractions éluées par l'acétate d'éthyle (III), l'acétate d'éthyle – méthanol (1:1) (IV) et le méthanol (V), lesquelles étaient les plus abondantes et que nous considérons les plus représentatives de l'acide fulvique original. On a caractérisé chaque fraction par des méthodes chimiques et spectroscopiques et par dégradation par le permanganate en milieu basique. Les fractions IV et V ont aussi été dégradées par l'hydrolyse avec NaOH et par l'oxydation alkaline avec CuO. On a identifié les produits dégradés à l'aide d'un chromatographe associé à un spectromètre de masse et d'un ordinateur.

Les poids moléculaires approximatifs des trois fractions sont: III, 821; IV, 945; et V, 1,397. L'infrarouge et la r.m.n. du proton et du carbone-13, apportent peu d'information détaillée sur la structure chimique des fractions, sauf, en ce qui concerne les groupes fonctionnels. Les produits majeurs de la dégradation sont des acides benzènecarboxyliques et phénoliques en plus de petites quantités d'acides aliphatiques (principalement les acides gras). Une évidence est présentée qui peut être interprété pour indiquer; (*a*) une estérification de quelques acides gras au groupe OH des acides phénoliques; (*b*) l'existence dans les fractions de liaisons éther (C—O); et (*c*) rupture des liaisons C—C pendant la dégradation. Dans les fractions AF ayant de bas et de hauts poids moléculaires, les acides benzènecarboxyliques et phénoliques sont des "éléments d'édification de base", ces derniers apparaissant plus complexes et plus stables dans les fractions à haut poids moléculaire, peut être parce que les liens chimiques aussi bien que les ponts-hydrogène, les forces de Van der Waal et les liaisons-π sont impliqués simultanément.

[Traduit par le journal]

Introduction

Previous reports from this laboratory (1) have described the development of a nondegradative approach to unravelling the chemical structure of fulvic acid (FA), a water-soluble, relatively low molecular weight humic material, widely occurring in soils and waters. The FA was first exhaustively methylated so as to make it soluble in benzene. The benzene-soluble methyl esters and ethers were then separated over Al_2O_3 with the aid of solvents of increasing polarities into fractions that differed in molecular weights, oxygen-containing functional groups and spectroscopic properties. Further separation

[1]Contribution No. 516, Soil Research Institute.

[2]Visiting scientist from the Federal Agricultural Research Station at Lausanne, Switzerland.

Can. J. Chem. Downloaded from www.nrcresearchpress.com by 210.87.254.42 on 09/05/12
For personal use only.

of a number of low molecular weight fractions by t.l.c. and preparative gas chromatography resulted in the identification of over 21 different phenolic and benzenecarboxylic acids, n-C_{14} to n-C_{36} fatty acids and alkanes, and a number of dialkyl phthalates (1). From fractions that were prepared by the use of more polar solvents, that is those of increasing molecular complexity, we were less and less able to isolate relatively simple compounds. These more complex and higher molecular weight fractions were quantitatively the major ones and, judging from their analytical characteristics, more representative of the initial FA than the lower molecular weight fractions. It is for these reasons that we decided to prepare some of these fractions and to investigate them by a number of spectroscopic and chemical methods that included degradation into simpler compounds that we could identify and whose chemical structures would hopefully provide information on that of the initial materials. The results of this investigation are reported herein.

Experimental

Origin and Separation of FA

The FA originated from the Bh horizon of the Armadale soil, a poorly-drained Podzol in Prince Edward Island. Methods of extraction, purification, and methylation of the FA were the same as those described previously (1). The separation of the methylated material over Al_2O_3 was simplified in the following manner: 50.0 g of benzene-soluble, methylated FA (originating from 100.0 g of unmethylated FA) was chromatographed over neutral Al_2O_3 (2500 g) with the aid of 3 l of each of the following solvents: benzene (fraction I, 0.2 g); benzene – ethyl acetate (3:1) (fraction II, 1.5 g), ethyl acetate (fraction III, 2.5 g); ethyl acetate – methanol (9:1) (fraction IV, 6.0 g), and methanol (fraction V, 4.0 g). This paper deals exclusively with the characterization of fractions III, IV, and V.

NaOH Hydrolysis

One gram of each fraction, dissolved in 100 ml of 2 *N* NaOH solution, was transferred to a 300 ml stainless steel autoclave equipped with a magnetic stirrer and a heating mantle. The air in the autoclave was displaced by N_2. The system was heated to 170 °C with constant stirring over a period of 1 h and then maintained at that temperature for 2 h. Following cooling to room temperature, the alkaline solution was acidified to p*H* 2 with 6 *N* H_2SO_4 and extracted in a liquid–liquid extractor for 24 h with 500 ml of ethyl acetate. The organic extract was then taken to dryness on a rotary evaporator, dissolved in a small volume of CH_3OH, and methylated with an ether solution of diazomethane, generated from Diazald. Since preliminary analysis on the gas chromatograph showed that the extract was still too complex, it was further separated by t.l.c. on SiO_2 with toluene – ethyl acetate (1:1) as solvent system. After the t.l.c. separation, the plate was inspected under a u.v. lamp and six fractions were marked out, scraped off the plate, and extracted with ethyl acetate. Each yield listed in Table 2 is the sum of the yields for the particular compound that we obtained from the six fractions.

CuO–NaOH Oxidation

To 1 g of each fraction, dissolved in 100 ml of 2 *N* NaOH solution in a 300 ml stainless steel autoclave, 5 g of CuO was added. After displacing the air in the autoclave by N_2, the system was heated to 170 °C and then maintained at that temperature for 2 h. Following cooling to room temperature, suspended CuO was removed by centrifugation and washed with distilled water. The supernatant solution plus washings were acidified to p*H* 2 and extracted with ethyl acetate. The rest of the procedure was the same as that described above under NaOH hydrolysis.

Alkaline $KMnO_4$ Oxidation

The method used was identical with that described previously (1).

Separation and Identification of Degradation Products

Each methylated fraction was dissolved in benzene and examined as a 2.5% (w/v) solution by analytical gas chromatography (Hewlett-Packard, model 5700 A, flame ionization detector, 1500 × 6 mm coiled glass column packed with 3% OV 17 on Chromosorb W HMDS, 80 to 100 mesh, programmed from 90–310 °C at a rate of 8 °C/min and a N_2 flow rate of 30 ml/min). Compounds represented by well-defined peaks were isolated by preparative gas chromatography under the same conditions as those outlined above except that aliquots from 10% (w/v) solutions in benzene were injected into the gas chromatograph. Materials eluting from the gas chromatograph were collected in capillary tubes. Each fraction was also analyzed on a gas chromatographic – mass spectrometric (g.c.–m.s.) – computer system. The instrument used was a Finigan 3100D GC-MS, interfaced with a model 6000 data system. The g.c.–m.s. conditions were as follows: g.c. column: 1500 × 6 mm, 3% OV 17 on Chromosorb W, HMDS, glass column; injector temperature: 250 °C; oven programmed from 90–270 °C at 10 °C/min and a He flow rate of 30 ml/min. The separator temperature was 250 °C, m.s. pressure: 1×10^{-5} Torr, m.s. resolution: 1:500; electron energy: 70 eV and mass range 40–500.

Preliminary identification of gas chromatographic peaks was first made by recording "mass chromatograms" for fragments characteristic of specific compounds or groups of compounds expected to occur in the mixture by searching through the stored spectral data for specific m/e ratios (2). The identity of the compound in each peak was then confirmed by: (*i*) running its mass spectrum; (*ii*) eluting it from the gas chromatograph and recording its micro-i.r. spectrum; (*iii*) matching its mass and i.r. spectrum with the known compound to which it corresponded; and (*iv*) co-chromatographing (on the gas chromatograph) of known and unknown.

Spectroscopic Methods

Infrared spectra were recorded on KBr pellets on a Beckman IR-12 i.r. spectrophotometer. Proton n.m.r. spectra of each fraction dissolved in $CDCl_3$ (50 mg/0.4

TABLE 1. Analytical characteristics of untreated and methylated FA and of methylated FA fractions

Element or group	% dry ash-free				
	Untreated FA	Methylated FA	Fraction III	Fraction IV	Fraction V
C	50.90	56.68	53.92	55.21	54.62
H	3.35	5.00	4.97	4.50	4.76
N	0.75	0.45	0.49	1.25	0.98
S	0.25	0.30	0	0.01	0.41
O	44.75	37.57	40.62	38.99	39.23
OCH_3	0.30	28.18	31.11	28.65	25.99
$\overline{Mn}$	951	1080	821	945	1397
Yield (%)	100.0	75.0 50.0*	2.5	6.0	4.5

*Methylated FA soluble in benzene.

ml) were run on a Varian model T-60 n.m.r. spectrometer, with TMS as internal standard. A carbon-13 n.m.r. spectrum of fraction III was recorded by Dr. G. W. Buchanan of Carleton University, Ottawa, Ontario. The spectrum was run on a 20% (w/v) solution of the sample in acetone-d_6 on a Varian XL-100 spectrometer, operated at 25.2 MHz by the Fourier-Transform technique; 5960 scans were accumulated.

Analytical Methods

Carbon and hydrogen were determined by dry combustion, nitrogen by the automated Dumas method, sulfur by oxygen-flask combustion, and oxygen by difference; OCH_3 was measured by the Zeisel method. Number-average mol. wt. ($\overline{Mn}$) of the FA fractions were measured in chloroform by vapor pressure osmometry on a Hewlett-Packard model 302 VP osmometer at 37 °C.

All solvents were purified by distillation through high-efficiency columns.

Results and Discussion

Analytical Characteristics of Fractions

The data in Table 1 show that the fractions contained less C but more O than did the unfractionated methylated FA. While fraction III was somewhat enriched in OCH_3, fraction V contained most of the S. Variations in $\overline{Mn}$ indicate that the fractionation procedure was based not solely on the increasing polarities of the eluants but also on differences in number-average molecular weights of the materials that were separated. The three fractions accounted for 13% of the weight of the untreated FA but for 26% of that of the methylated FA that was soluble in benzene.

Spectroscopic Analyses

Infrared spectra of the methylated FA and of the three fractions derived from it are shown in Fig. 1, curves *a* to *d*. The four spectra resembled each other, showing often broad bands due to the overlapping of individual absorptions. The main bands were in the region of 3400 (hydrogen-bonded OH), at 3000 (aromatic C—H), near 2960 and 2840 (aliphatic C—H), 1740 (C=O) of CO_2CH_3), near 1620 (probably aromatic

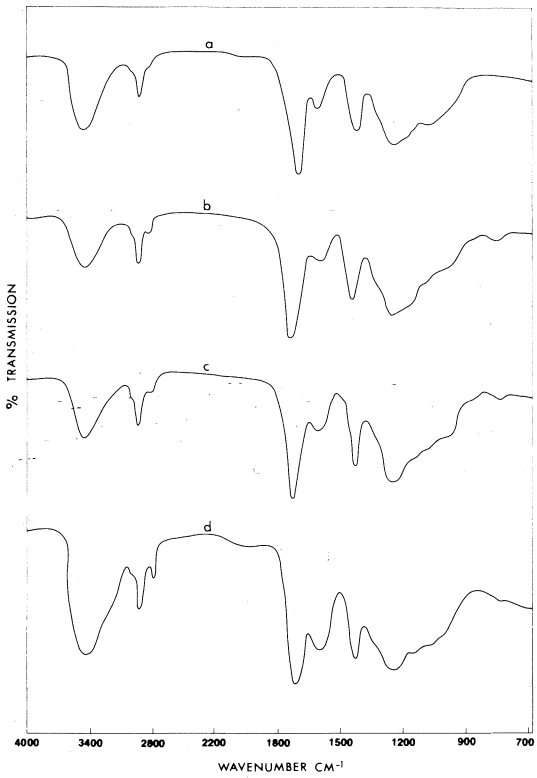

FIG. 1. Infrared spectrum of (*a*) methylated, unfractionated FA; (*b*) fraction III; (*c*) fraction IV; (*d*) fraction V.

Can. J. Chem. Downloaded from www.nrcresearchpress.com by 210.87.254.42 on 09/05/12
For personal use only.

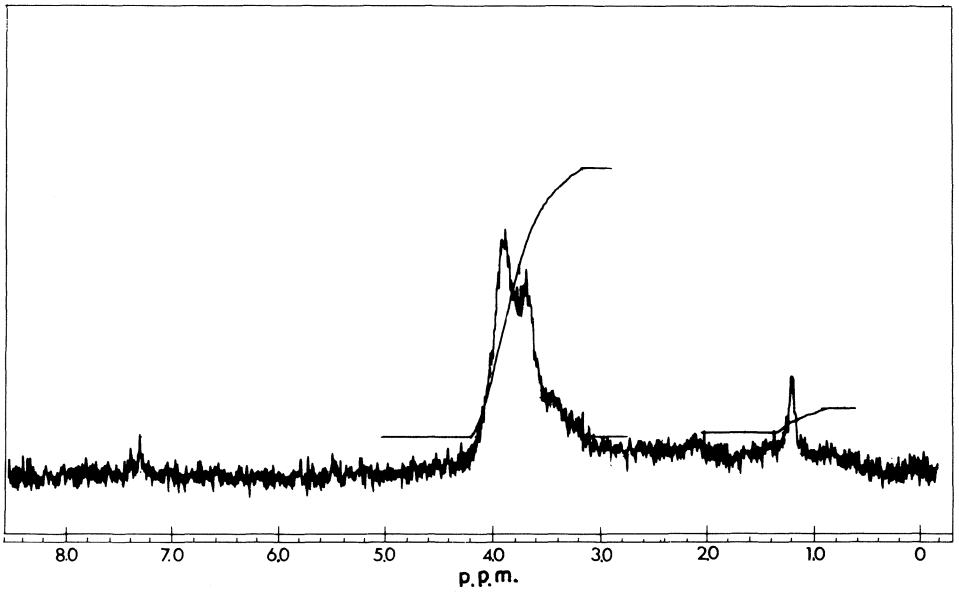

FIG. 2. Proton n.m.r. spectrum of fraction III.

C=C conjugated with C=O), 1440 (aliphatic C—H), and near 1250 cm^{-1} (due probably to the C—O—C stretch of ethers formed by the methylation of phenolic OH groups). It is likely that the C—H stretch of added CH_2 in OCH_3 groups contributed significantly to the absorbances at 2960, 2840, and 1440 cm^{-1}. The relatively high absorbances near 3400 cm^{-1} suggest that either some OH groups could not be methylated or that the FA materials retained water so strongly that it could not be removed even by thorough drying in a vacuum desiccator over P_2O_5 (at 10 mm Hg) at 50 °C. Curves *b* to *d* show additional but weak bands near 1180 (C—O—C), 1120 (aliphatic ether), and 780 cm^{-1} (C—H out-of-plane deformation of benzene derivatives?).

Analyses by Nuclear Magnetic Resonance

Figure 2 is the proton n.m.r. spectrum of fraction III. Since the n.m.r. spectra of the other two fractions were very similar to that of fraction III, we shall confine our discussion to the spectrum of the latter. The spectrum showed bands at about 1.2 p.p.m. (highly shielded aliphatic CH_2), a shoulder near 2.1 p.p.m., another but broader and more extended shoulder between 3.1 and 3.5 p.p.m. (possibly due to aliphatic side chains attached to an aromatic ring), and prominent peaks near 3.7 and 3.9 p.p.m., due to OCH_3 and CO_2CH_3, respectively. The small peak at 7.3 p.p.m. originated from the solvent. Especially noteworthy was the absence of olefinic and aromatic protons in the spectrum. This may mean that the aromatic rings in the FA fraction were either fully or almost fully substituted by atoms other than hydrogen or that relaxing effects of the spins of unpaired electrons (free radicals) that occur in humic substances (4) interfered with n.m.r. measurements.

The ^{13}C n.m.r. spectrum of fraction III (Fig. 3) was practically a straight line with a small but extended peak near 53.5 p.p.m. (most likely due to ^{13}C in different types of OCH_3 groups (3)) and a hump near 166.0 p.p.m. (due to aromatic ^{13}C bonded to a OCH_3 group (3)). The sharp peaks between 27.9 and 32.5 p.p.m. originated from deuteroacetone which was used as solvent. Compared to ^{13}C n.m.r. spectra for beech and spruce lignins (3), which consist of large numbers of well-defined peaks, the spectrum for FA fraction III was most disappointing. A possible reason for our failure to obtain a more informative ^{13}C n.m.r. spectrum is the presence in the FA fraction of too many different types of ^{13}C atoms occurring in too many different environments, so that there is not sufficient concentration of one ^{13}C type to produce a distinct n.m.r. peak.

Chemical Degradation of Fractions

Of the degradative methods that we used, NaOH hydrolysis was probably the mildest and $KMnO_4$ oxidation the most drastic one. Since

Can. J. Chem. Downloaded from www.nrcresearchpress.com by 210.87.254.42 on 09/05/12
For personal use only.

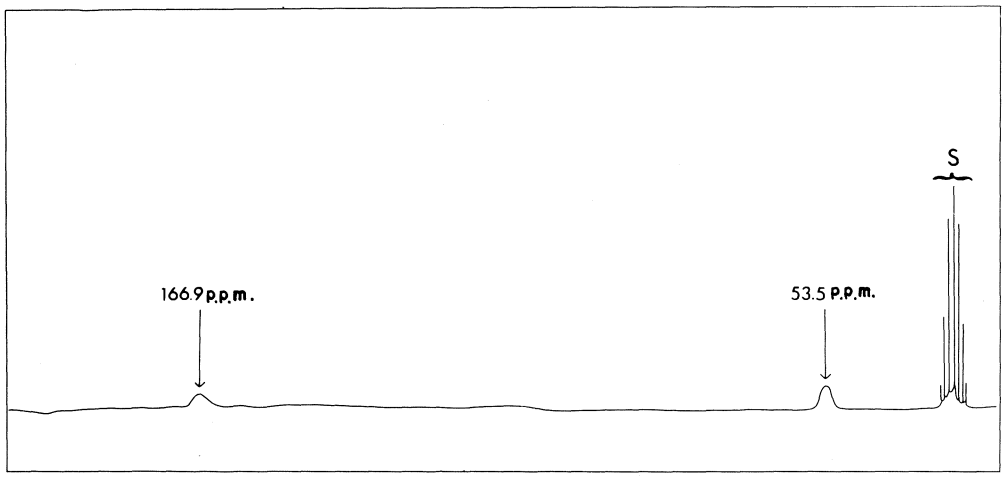

FIG. 3. Carbon-13 n.m.r. spectrum of fraction III; S = solvent (acetone-d_6).

we did not have sufficient material of fraction III for all three degradation procedures, we decided to confine our efforts in this instance to $KMnO_4$ oxidation only. We shall refer, in the context of this discussion, to the degradation products as benzenecarboxylic, phenolic and aliphatic acids rather than as esters and ethers. The reasons for doing so are the following: (*a*) the OCH_3 content of the initial FA and of the unmethylated fractions was $<0.5\%$; (*b*) the FA was methylated prior to the chromatographic separation into fractions; and (*c*) following degradation, each fraction was methylated again so as to make it sufficiently volatile for gas chromatographic separations and mass spectrometric analysis. As shown in Table 2 and Fig. 4 the major compounds produced from all three fractions by $KMnO_4$ oxidation were benzenepolycarboxylic acid methyl esters **31**, **29**, **23**, and **24**, that is, the hexa-, penta-, and tetra-forms. The only phenolic acid compounds formed in appreciable amounts were **27**, **30**, and **28**. It is noteworthy that the $KMnO_4$ oxidation of fraction III yielded larger amounts of complex phenolic acids than did that of fractions IV and V.

The NaOH hydrolysis of fractions IV and V released appreciable amounts of phenolic acids, especially **7**, **13**, **15**, and **22**. In addition, small amounts of benzenedicarboxylic and somewhat larger amounts of benzenetricarboxylic and benzenetetracarboxylic acids were produced but no benzenepenta- and benzenehexacarboxylic acids.

The largest amounts of phenolic acids per unit weight of initial material were released by CuO–NaOH oxidation. Note the relatively high yields of **7**, **8**, **13**, **15**, **21**, **22**, and **27**. As was the case with NaOH hydrolysis, no benzenecarboxylic acids higher than the tetra were produced. Amounts of "typical" lignin degradation products formed were small, although some of the more complex phenolic acids could have originated from condensed lignins.

In addition to the benzenecarboxylic and phenolic acids, small amounts of dialkyl phthalates (which consisted of bis(2-ethylhexyl) phthalate, dioctyl phthalate, and an unknown dialkyl phthalate) were found amongst degradation products from all three fractions. The NaOH hydrolysis and CuO–NaOH oxidation of fraction V yielded an appreciable amount of dioctyl adipate (**26**), possibly an impurity, whereas the CuO–NaOH oxidation of fraction IV produced a small amount of fumaric acid. Also the milder degradation methods released from fractions IV and V varying amounts of *n*-fatty acids, ranging from *n*-C_{14} to *n*-C_{18}, with the *n*-C_{16} and *n*-C_{18} fatty acids being the most prominent ones.

Major Types of Degradation Products

Yields of major types of compounds produced by the degradation of 1.0 g of each of the three fractions are summarized in Table 3. Normal fatty acids accounted for most of the alpihatic compounds released from fraction IV and for a substantial portion of aliphatic compounds originating from fraction V. It is especially noteworthy that the products resulting from the

Can. J. Chem. Downloaded from www.nrcresearchpress.com by 210.87.254.42 on 09/05/12
For personal use only.

Can. J. Chem. Downloaded from www.nrcresearchpress.com by 210.87.254.42 on 09/05/12
For personal use only.

TABLE 2. Compounds (mg) produced by the chemical degradation of 1.0 g of each FA fraction

Compound No.	Compound	Fraction No. III	Fraction No. IV			Fraction No. V		
		$KMnO_4$	NaOH hydrolysis	CuO–NaOH oxidation	$KMnO_4$ oxidation	NaOH hydrolysis	CuO–NaOH oxidation	$KMnO_4$ oxidation
1	4-Methoxybenzoic acid methyl ester	0	1.08	4.36	0	0.32	0.36	0
2	1,2-Benzenedicarboxylic acid dimethyl ester	1.96	0.96	0.32	0.76	0.52	0.40	1.32
3	1,3-Benzenedicarboxylic acid dimethyl ester	0	0.32	0.16	0	0.08	0.36	0
4	1,4-Benzenedicarboxylic acid dimethyl ester	0	0.80	0.48	0	0.12	0.16	0
5	3,5-Dimethoxybenzoic acid methyl ester	0	0.32	0.16	0	0.08	0.32	0
6	*n*-C_{14}-Fatty acid methyl ester	0	2.44	3.04	0	0.60	1.88	0
7	3,4-Dimethoxybenzoic acid methyl ester	0	7.20	8.00	0	1.80	4.80	0
8	2,3-Dimethoxybenzoic acid methyl ester	0	2.32	16.52	0	6.08	3.84	0
9	2-Carbomethoxyphenylacetic acid methyl ester	0	1.48	1.44	0	0.32	0.72	0
10	*n*-C_{15}-Fatty acid methyl ester	0	1.84	1.28	0	0	0.64	0
11	Dimethyl fumarate	0	0	3.78	0	0	0	0
12	3-Carbomethoxyphenylacetic acid methyl ester	0	5.44	1.40	0	1.48	2.40	0
13	4-Methoxy-1,3-benzenedicarboxylic acid dimethyl ester	1.96	12.00	25.20	0.76	6.96	10.80	1.72
14	*n*-C_{16}-Fatty acid methyl ester	0	3.88	8.40	0	2.40	3.80	0
15	4-Methoxy-2-carbomethoxyphenylacetic acid methyl ester	1.96	9.40	8.56	1.12	5.56	7.12	0.44
16	1,2,3-Benzenetricarboxylic acid trimethyl ester	5.89	8.60	15.20	1.71	3.16	5.80	5.84
17	1,2,4-Benzenetricarboxylic acid trimethyl ester	0	2.80	1.04	0	2.88	2.40	0
18	1,3,5-Benzenetricarboxylic acid trimethyl ester	3.60	6.32	5.20	0.28	4.76	2.44	3.92
19	*n*-C_{18}-Fatty acid methyl ester	0	4.00	4.44	0	2.36	2.24	0
20	3,4-Dicarbomethoxyphenylacetic acid methyl ester	8.84	3.08	1.00	2.28	3.80	2.44	3.92
21	3-Methoxy-1,2,4-benzenetricarboxylic acid trimethyl ester	1.31	4.44	6.76	1.12	1.20	1.52	0.56
22	2-Methoxy-1,3,5-benzenetricarboxylic acid trimethyl ester	2.62	5.84	3.96	3.80	7.00	11.60	2.60
23	1,2,3,4-Benzenetetracarboxylic acid tetramethyl ester	11.78	3.92	10.48	17.08	5.28	8.92	16.72
24	1,2,4,5-Benzenetetracarboxylic acid tetramethyl ester	10.80	1.36	5.68	10.64	3.84	3.92	10.40
25	1,2,3,5-Benzenetetracarboxylic acid tetramethyl ester	0	2.52	3.64	0	1.80	2.44	0
26	Dioctyl adipate	0	0	0	0	12.80	4.52	0
27	5-Methoxy-1,2,3,4-benzenetetracarboxylic acid tetramethyl ester	16.04	1.20	5.60	6.80	0	2.40	6.96
28	2-Methoxy-1,3,4,5-benzenetetracarboxylic acid tetramethyl ester	5.24	0	0	6.32	0	0	3.92
29	Benzenepentacarboxylic acid pentamethyl ester	24.55	0	0	30.36	0	0	19.08
	Dialkyl phthalates	4.25	6.48	12.20	4.92	7.80	14.40	6.52
30	Methoxybenzenepentacarboxylic acid pentamethyl ester	9.82	0	0	6.08	0	0	6.08
31	Benzenehexacarboxylic acid hexamethyl ester	35.35	0	0	37.80	0	0	27.36
32	Pentacarbomethoxyphenylacetic acid methyl ester	15.71	0	0	7.60	0	0	3.92
Total identified (mg)		161.68	100.04	158.30	139.43	83.00	102.64	121.28
Weight of methylated fractions after t.l.c. separation (mg)		216.00	554.00	336.00	191.00	358.00	358.00	161.00
% identified		75	18	47	73	22	29	75

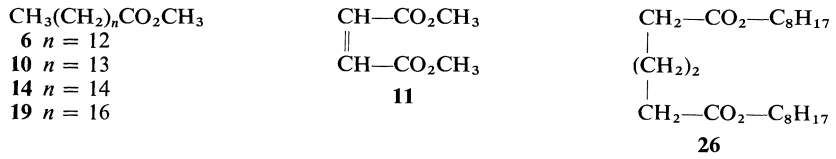

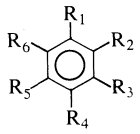

1 $R_1 = CO_2CH_3$; $R_4 = OCH_3$; $R_2 = R_3 = R_5 = R_6 = H$
2 $R_1 = R_2 = CO_2CH_3$; $R_3 = R_4 = R_5 = R_6 = H$
3 $R_1 = R_3 = CO_2CH_3$; $R_2 = R_4 = R_5 = R_6 = H$
4 $R_1 = R_4 = CO_2CH_3$; $R_2 = R_3 = R_5 = R_6 = H$
5 $R_1 = CO_2CH_3$; $R_3 = R_5 = OCH_3$; $R_2 = R_4 = R_6 = H$
7 $R_1 = CO_2CH_3$; $R_3 = R_4 = OCH_3$; $R_2 = R_5 = R_6 = H$
8 $R_1 = CO_2CH_3$; $R_2 = R_3 = OCH_3$; $R_4 = R_5 = R_6 = H$
9 $R_1 = CH_2COCH_3$; $R_2 = CO_2CH_3$; $R_3 = R_4 = R_5 = R_6 = H$
12 $R_1 = CH_2CO_2CH_3$; $R_3 = CO_2CH_3$; $R_2 = R_4 = R_5 = R_6 = H$
13 $R_1 = R_3 = CO_2CH_3$; $R_4 = OCH_3$; $R_2 = R_5 = R_6 = H$
15 $R_1 = CH_2CO_2CH_3$; $R_2 = CO_2CH_3$; $R_4 = OCH_3$; $R_3 = R_5 = R_6 = H$
16 $R_1 = R_2 = R_3 = CO_2CH_3$; $R_4 = R_5 = R_6 = H$
17 $R_1 = R_2 = R_4 = CO_2CH_3$; $R_3 = R_5 = R_6 = H$
18 $R_1 = R_3 = R_5 = CO_2CH_3$; $R_2 = R_4 = R_6 = H$
20 $R_1 = CH_2CO_2CH_3$; $R_3 = R_4 = CO_2CH_3$; $R_2 = R_5 = R_6 = H$
21 $R_1 = R_2 = R_4 = CO_2CH_3$; $R_3 = OCH_3$; $R_5 = R_6 = H$
22 $R_1 = R_3 = R_5 = CO_2CH_3$; $R_2 = OCH_3$; $R_4 = R_6 = H$
23 $R_1 = R_2 = R_3 = R_4 = CO_2CH_3$; $R_5 = R_6 = H$
24 $R_1 = R_2 = R_4 = R_5 = CO_2CH_3$; $R_3 = R_6 = H$
25 $R_1 = R_2 = R_3 = R_5 = CO_2CH_3$; $R_4 = R_6 = H$
27 $R_1 = R_2 = R_3 = R_4 = CO_2CH_3$; $R_5 = OCH_3$; $R_6 = H$
28 $R_1 = R_3 = R_4 = R_5 = CO_2CH_3$; $R_2 = OCH_3$; $R_6 = H$
29 $R_1 = R_2 = R_3 = R_4 = R_5 = CO_2CH_3$; $R_6 = H$
30 $R_1 = R_2 = R_3 = R_4 = R_5 = CO_2CH_3$; $R_6 = OCH_3$
31 $R_1 = R_2 = R_3 = R_4 = R_5 = R_6 = CO_2CH_3$
32 $R_1 = CH_2CO_2CH_3$; $R_2 = R_3 = R_4 = R_5 = R_6 = CO_2CH_3$

FIG. 4. Chemical structures of compounds identified.

permanganate oxidation of fractions III, IV, and V contained almost identical proportions of benzenecarboxylic acids, that is, 73, 78, and 76%, whereas the percentages of phenolic compounds in the oxidation mixtures were 24, 19, and 18%, also very similar. These data indicate great structural similarities between the three fractions.

Structural similarities, especially between fractions IV and V, are also indicated by the almost identical benzenecarboxylic to phenolic weight ratios amongst degradation products formed by each of the three procedures (see Table 3). The percentages of dialkyl phthalates, which were either impurities or, more likely, adsorbed on the fulvic materials, were 3, 3, and 6%. Our findings that $KMnO_4$ oxidation, in contrast to the other two procedures, did not produce any aliphatic compounds, suggests that the latter types of compounds were destroyed during the rather drastic $KMnO_4$ oxidation procedure. The most efficient method for producing phenolic compounds was CuO–NaOH oxidation, whereas $KMnO_4$ oxidation afforded the highest yields of benzenecarboxylic acids.

NaOH Hydrolysis vs. CuO–NaOH Oxidation

The data in Tables 2 and 3 show that compared to CuO–NaOH oxidation, the NaOH hydrolysis of 1.0 g of fractions IV and V produced similar types and amounts of aliphatic and benzenecarboxylic acids although somewhat smaller amounts of phenolic compounds. The results convey the impression that heating with 2 *N* NaOH for 3 h at 170 °C in an autoclave brings about solvolysis of the FA fractions with

Can. J. Chem. Downloaded from www.nrcresearchpress.com by 210.87.254.42 on 09/05/12
For personal use only.

Can. J. Chem. Downloaded from www.nrcresearchpress.com by 210.87.254.42 on 09/05/12
For personal use only.

TABLE 3. Types of compounds (mg) produced by the chemical degradation of 1.0 g of each FA fraction

	Fraction No.					
	III	IV			V	
Type of compound	$KMnO_4$ oxidation	NaOH hydrolysis	Cu(O)–NaOH oxidation	$KMnO_4$ oxidation	NaOH hydrolysis	Cu(O)–NaOH oxidation	$KMnO_4$ oxidation
Aliphatic	0	12.16(12)	20.94(13)	0	18.16(21)	13.08(22)	0
Phenolic	38.95(24)*	43.80(44)	79.12(50)	26.00(19)	29.00(35)	42.76(42)	22.28(18)
Benzenecarboxylic	118.48(73)	37.60(38)	46.04(29)	108.51(78)	28.04(34)	32.40(32)	92.48(76)
Dialkyl phthalates	4.25(3)	6.48(6)	12.20(8)	4.92(3)	7.80(10)	14.40(14)	6.52(6)
Total	161.68	100.04	158.30	139.43	83.00	102.64	121.28
Weight ratio of *benzenecarboxylic*/phenolic	3.0	0.9	0.6	4.2	1.0	0.8	4.2

*Percentage of compounds identified.

Can. J. Chem. Downloaded from www.nrcresearchpress.com by 210.87.254.42 on 09/05/12
For personal use only.

the concomitant cleavage of C—O bonds and that this reaction occurs in the presence as well as in the absence of CuO. In other words, the main reaction governing the CuO–NaOH oxidation of the fulvic materials appears to be alkaline hydrolysis. In the case of lignin, dissolution by alkali at elevated temperatures is thought to result from the solvolytic cleavage of ether linkages between phenylpropane units, with the simultaneous formation of phenolic hydroxyl groups (5). More specifically, the reactions that occur during alkali hydrolysis of lignin are: (*a*) α-ether cleavage, involving the rupture of benzyl ether linkages if there is a free phenolic OH group in the position *para* to the propyl side chain; (*b*) β-ether cleavage, that is, cleavage of β-aryl ether linkages of compounds without free phenolic OH groups if there is an adjacent OH or C=O group in the α or γ positions on the propyl side chain; (*c*) diaryl ether cleavage; and (*d*) cleavage of methoxyls of strongly acidic phenols such as vanillin (5). Our failure to find aromatic aldehydes and ketones among CuO–NaOH oxidation products resulting from the fulvic acid fractions lends further support to our contention that the main reaction governing the CuO–NaOH oxidation of the fulvic fractions was base hydrolysis rather than oxidation. In addition to C—O cleavage, rupture of C—C bonds may also occur. These reactions may involve β—γ as well as α—β cleavages of C atoms on the propyl side chain. The cleavage of C—C bonds is often followed by secondary condensation reactions (5). Thus, C—O as well C—C bonds in lignin or lignin-like materials that may also include the FA fractions may be ruptured during alkaline hydrolysis at elevated temperatures. Since only relatively small amounts of benzenecarboxylic acids were produced by the two alkaline treatments, it appears that C—O cleavage was more important than C—C rupture.

Possible Interaction Between Phenolic and Fatty Acids

Sodium hydroxide hydrolysis as well as alkaline CuO oxidation, both done in 2 *N* NaOH solution, released in addition to phenolic and benzenecarboxylic acids also *n*-fatty acids, ranging from *n*-C_{14} to *n*-C_{18} (see Tables 2 and 3). Attempts to extract *n*-fatty acids from the three fractions without any pretreatment were unsuccessful. Thus, the fatty acids were so tightly held by the fulvic fractions that strong base at elevated temperature was required to free them. A consideration of possible retention mechanisms may therefore be in order. We see two possibilities: (*a*) the fatty acids are firmly adsorbed (with the aid of hydrogen bonding and van der Waal's forces) on external surfaces and in internal voids of the fulvic materials; and (*b*) the fatty acids are esterified to OH groups of phenolic acids which are released simultaneously. The data show the following phenolic to fatty acids molar ratios: 4.3 (fraction IV, NaOH hydrolysis), 5.5 (fraction IV, CuO–NaOH oxidation), 6.3 (fraction V, NaOH hydrolysis), and 5.4 (fraction V, CuO–NaOH oxidation). There is in each instance an excess of phenolic over fatty acids. It is possible that some of the phenolic acids react with fatty acids to form esters of the following type:

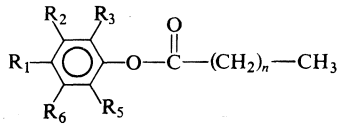

1

where R_1 (see Table 2) = CO_2H or OH; R_2 = H or OH or CO_2H; R_3 = H or OH or OCH_3 or CO_2H; R_4 = OH; R_5 = H or OH or CO_2H; R_6 = H or CO_2H and *n* ranges from 12 to 16. Structure **1** is similar to the polyhydric phenolic esters described by Markley (6), which include resorcinol dipalmitate, hydroquinone dipalmitate, etc. Esters could form via any free OH group on the aromatic ring **1**, that is, at positions R_1, R_2, R_3, and R_5 in addition to R_4, so that the occurrence in the fulvic fractions of a considerable variety of phenol fatty acid esters is a distinct possibility.

The data presented herein suggest that in addition to being adsorbed physically, fatty acids can also interact chemically with phenolic fulvic "building blocks." By this reaction mechanism fulvic substances could fix, stabilize and preserve relatively large amounts of hydrophobic organic compounds provided that they have at least one CO_2H group.

Chemistry of Fractions

From the results of this and our earlier investigations (1) we propose the following: The lower molecular weight FA fractions consist of molecular associations of benzenecarboxylic and

phenolic acids (the "building blocks") which are held together by relatively weak linkages such as hydrogen bonds, van der Waal's forces, π-bonding, etc. In the higher molecular weight fractions, by contrast, the "building blocks," although made up of the same types of benzenecarboxylic and phenolic acids, are more complex and more stable. The increased stability of each "building block" may arise either from more energetic linkages of the types discussed above or from additional chemical bonding via C—O and C—C bonds. We are presenting evidence in this paper that may be interpreted to indicate: (*a*) esterification of some of the fatty acids to OH groups of phenolic acids; (*b*) the existence of ether (C—O) linkages between oxygens of phenolic OH groups and carbon on aliphatic side chains of aromatic rings; this possibility is based on the behavior of lignin under experimental conditions that were similar to the ones that we employed; and (*c*) rupture of C—C bonds during degradation. Thus, whereas the "building blocks" in the higher molecular weight fractions may be chemically more complex than those in the lower molecular weight ones, we believe that the molecular forces holding the "building blocks" together are similar, consisting mainly of hydrogen bonds, van der Waal's forces, and π-bonding.

The failure of spectrophotometric and spectrometric methods (u.v., i.r., n.m.r., e.s.r., X-ray) to provide worthwhile information (except possibly for functional groups) on the chemical structure of humic and fulvic materials does not facilitate the task of chemists working in this field in developing meaningful concepts of the chemical structure of humic materials. Although the advent of the gas chromatographic – mass spectrometry – computer system has provided us with a powerful tool for the qualitative and quantitative analysis of very complex humic and fulvic acid degradation mixtures, we are still searching for methods that will tell us how the "building blocks" fit together and what type(s) of structures are produced. Thus, the chemistry of humic and fulvic acids continues to challenge the ingenuity of chemists.

We thank S. I. M. Skinner for g.c.–m.s.–computer analyses and G. W. Buchanan of Carleton University for the recording of the Carbon-13 n.m.r. spectrum.

1. (*a*) G. Ogner and M. Schnitzer. Can. J. Chem. **49**, 1053 (1971); (*b*) S. U. Khan and M. Schnitzer. Can. J. Chem. **49**, 2302 (1971).
2. R. A. Hites and K. Biemann. Anal. Chem. **42**, 855 (1970).
3. H. D. Ludemann and H. Nimz. Biochem. Biophys. Res. Commun. **52**, 1162 (1973).
4. M. Schnitzer and S. U. Khan. Humic substances in the environment. Marcel Dekker, New York. (1972). pp. 86–90.
5. A. F. A. Wallis. *In* Lignins. *Edited by* K. V. Sarkanen and C. H. Ludwig. Wiley Interscience, New York. 1971. pp. 361–369.
6. K. S. Markley. *In* Fatty acids. Part II. *Edited by* K. S. Markley. Interscience, New York. 1961. pp. 928–930.

Can. J. Chem. Downloaded from www.nrcresearchpress.com by 210.87.254.42 on 09/05/12
For personal use only.

Influence des groupes *tert*-butyle, triméthylsilyle et triméthylgermyle sur la stéréochimie de réactions d'addition en série cyclohexénique. I. Synthèse des alcènes et hydroboration

CHRISTIAN FREPPEL, MARC-ANDRÉ POIRIER[1] ET JEAN-CLAUDE RICHER
Département de Chimie, Université de Montréal, B.P. 6210, Montréal, Québec H3C 3V1

ET

YVETTE MARONI
Equipe de recherche du CNRS No 13, Laboratoire de synthèse & physicochimie organique, Université Paul Sabatier, 118 Route de Narbonne, 31077 Toulouse Cedex, France

ET

GEORGES MANUEL
Laboratoire des Organométalliques, Université Paul Sabatier, 118 Route de Narbonne, 31077 Toulouse Cedex, France

Reçu le 19 août, 1974

CHRISTIAN FREPPEL, MARC-ANDRÉ POIRIER, JEAN-CLAUDE RICHER, YVETTE MARONI et GEORGES MANUEL. Can. J. Chem. **52**, 4133 (1974).

On décrit la synthèse des *tert*-butyl-1 (**1***a*), triméthylsilyl-1 (**1***b*) et triméthylgermyl-1 (**1***c*) diméthyl-4,4 cyclohexènes ainsi que celle des *tert*-butyl-6 (**2***a*), triméthylsilyl-6 (**2***b*) et triméthylgermyl-6 (**2***c*) diméthyl-3,3 cyclohexènes. On examine la stéréochimie de la réaction d'hydroboration de ces alcènes; on note que celle-ci est gouvernée d'une part par l'influence stérique des divers substituants et d'autre part par les effets stériques et électroniques des groupes triméthylsilyle et triméthylgermyle.

CHRISTIAN FREPPEL, MARC-ANDRÉ POIRIER, JEAN-CLAUDE RICHER, YVETTE MARONI, and GEORGES MANUEL. Can. J. Chem. **52**, 4133 (1974).

Syntheses of 1-*tert*-butyl-(**1***a*), 1-trimethylsilyl-(**1***b*) and 1-trimethylgermanyl-4,4-dimethylcyclohexene (**1***c*) are described as are those of 6-*tert*-butyl- (**2***a*), 6-trimethylsilyl- (**2***b*) and 6-trimethylgermanyl-3,3-dimethylcyclohexene (**2***c*). The stereochemistry of the hydroboration of these alkenes is examined. The stereochemistry is governed, on the one hand, by the steric influence of the various substituents and on the other by the steric and electronic effects of the trimethylsilyl and trimethylgermanyl groups. [Journal translation]

Introduction

Dans un travail antérieur (1), on a mis en évidence l'influence stérique prépondérante du groupe *tert*-butyle sur la stéréochimie des réactions d'addition sur le *tert*-butyl-3 cyclohexène (**2***d*). Afin de pouvoir comparer l'influence des groupes *tert*-butyle, triméthylsilyle et triméthylgermyle sur la stéréochimie de réactions d'addi-

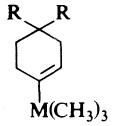

1

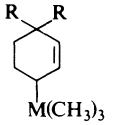

2

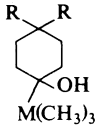

5

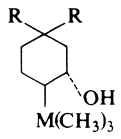

18

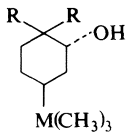

19

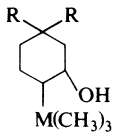

20

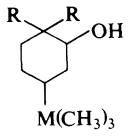

21

Série
a M = C; R = CH_3
b M = Si; R = CH_3
c M = Ge; R = CH_3
d M = C; R = H
e M = Si; R = H

[1]Les résultats rapportés dans cette publication sont tirés en partie du mémoire soumis par M. Marc-André Poirier en vue de l'obtention du grade de M.Sc. (août 1972).

Can. J. Chem. Downloaded from www.nrcresearchpress.com by 210.87.254.105 on 09/05/12
For personal use only.

tion en série cyclohexénique, nous avons effectué la synthèse de nouveaux cyclohexènes *gem*-diméthylés des types **1** et **2** et nous avons examiné la stéréochimie de leur réaction d'hydroboration (2). Ce sont les résultats obtenus au cours de cette étude qui font l'objet de la présente communication.

Résultats et discussion

Synthèse des alcènes

Les alcènes du type **1** ont tous été préparés à partir de la diméthyl-4,4 cyclohexanone (**4**) suivant le schéma réactionnel 1. Les alcènes **2***b*

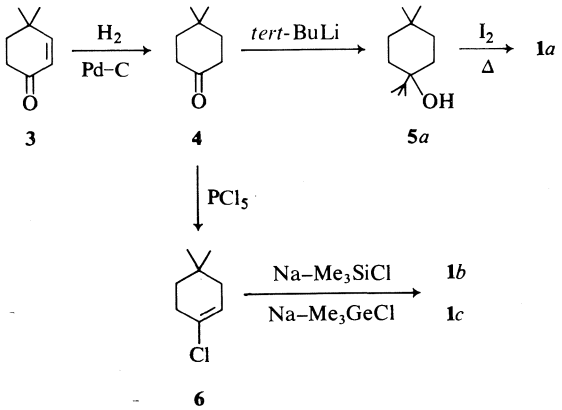

SCHÉMA 1

et **2***c* ont été synthétisés à partir du diméthyl-4,4 cyclohexène-2 ol (**7**) suivant le schéma réactionnel 2. On a obtenu l'alcène **2***a* à partir de la *tert*-butyl-5 diméthyl-2,2 cyclohexanone (**15**) à laquelle on peut arriver soit selon la voie *A* à partir de la *tert*-butyl-4 cyclohexanone (**10**) soit selon la voie *B* à partir de la diméthyl-2,2

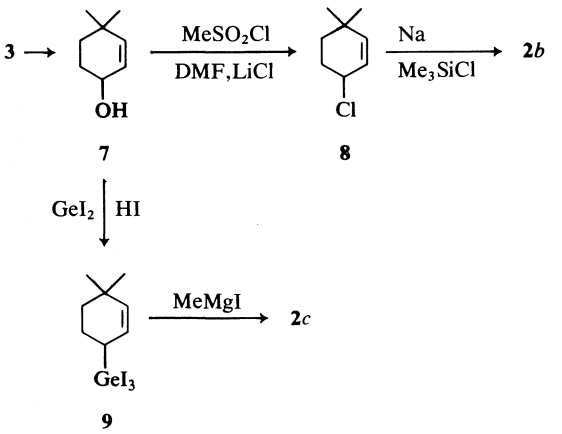

SCHÉMA 2

cyclohexanone (**16**); le tout d'après les réactions décrites au schéma 3. Depuis que ce travail a été complété, House et Umen (3) ont rapporté la synthèse de **15** à partir de **10** suivant la voie *A*.

Hydroboration des alcènes

Les résultats obtenus lors de l'hydroboration (2) des alcènes du type **1** et du type **2** suivie d'une oxydation de l'organoborane par H_2O_2 en milieu alcalin sont rapportés respectivement dans les tableaux 1 et 2. Il ressort d'une manière évidente de l'examen du tableau 1 que la régiosélectivité de l'hydroboration des alcènes **1** est fortement influencée par la nature des substituants présents sur la double liaison. La régiospécificité de la réaction d'hydroboration de l'alcène **1***a* peut être rationnalisée en faisant appel aux effets combinés de l'influence stérique du groupe *tert*-butyle de même qu'à la forme de résonance **I**-1 favorisée dans ce cas. La forte proportion d'alcool tertiaire obtenu lors de l'hydroboration des alcènes **1***b* et **1***c* est à rapprocher des résultats obtenus par Musker et Larson (4) lors de l'hydroboration du triméthylsilyl-1 cyclohexène (**1***e*); ces résultats indiquent à quel point la présence du silicium et du germanium dans ces alcènes favorise par effet pπ–dπ (5, 6) la forme de résonance **I**-2 qui contrebalance l'effet stérique des groupes triméthylsilyle et triméthylgermyle (schéma 4).

TABLEAU 1. Pourcentages relatifs des alcools obtenus par hydroboration des alcènes du type **1**

	% alcool	
Alcène	**18**	**5**
1*a*	100	0
1*b*	33	67
1*c*	34	66
1*e*	10	90

TABLEAU 2. Pourcentages relatifs des isomères obtenus par hydroboration des alcènes du type **2**

	% alcool			
Alcène	**18**	**19**	**20**	**21**
2*a*	62	38	0	0
2*b*	27	54	8	11
2*c*	30	50	4	16
2*d*	43	54	1	2

Can. J. Chem. Downloaded from www.nrcresearchpress.com by 210.87.254.105 on 09/05/12
For personal use only.

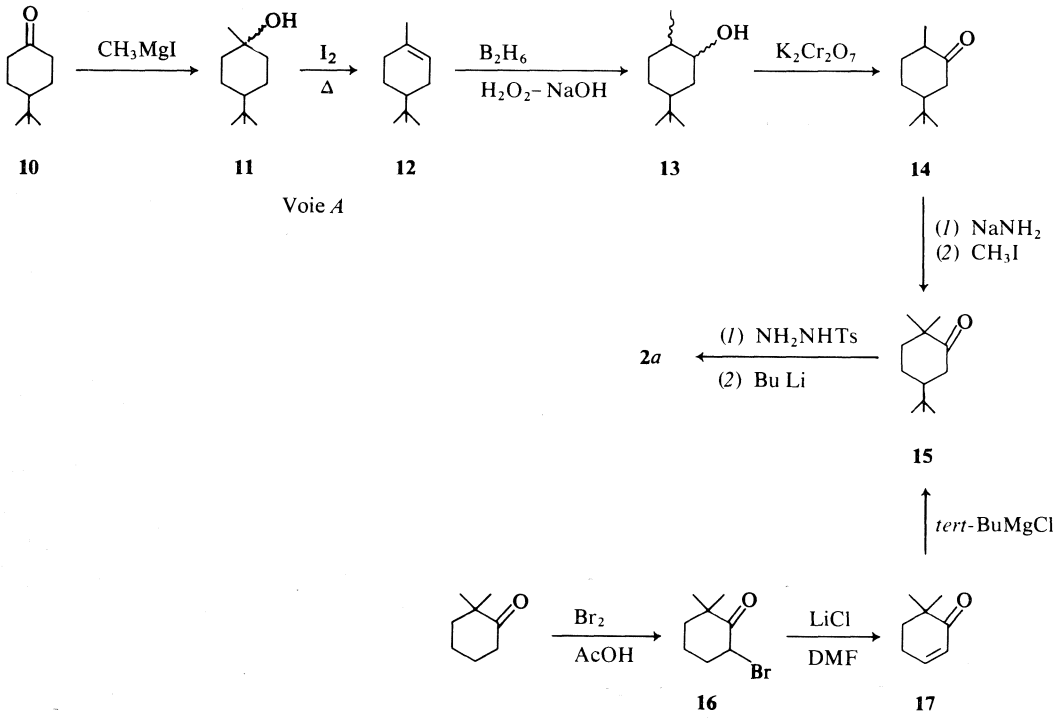

SCHÉMA 3

Pour ce qui est de la stéréochimie des alcools du type **18** obtenus lors de ces réactions d'hydroboration, elle résulte du fait bien connu que l'addition du borane sur la double liaison se fait d'une façon *cis* et que l'oxydation du borane se produit avec retention de configuration (6).

En ce qui concerne la stéréochimie et la régiospécificité de la réaction d'hydroboration des alcènes du type **2**, l'examen du tableau 2 nous amène à faire les constatations suivantes: (*a*) on a déjà noté précédemment (1) que les réactions d'addition sur le *tert*-butyl-3 cyclohexène (**2***d*) se produisent principalement par la face opposée à celle occupée par le groupe *tert*-butyle (voir schéma 5) pour conduire aux produits **18***d* et **19***d*; l'influence du groupe *tert*-butyle se fait sentir même sur cette face et provoque la formation d'une quantité prépondérante de **19***d* par rapport à **18***d*; (*b*) l'examen des résultats obtenus avec l'alcène **2***a* met en évidence d'une part l'influence du groupe CH_3 pseudo-axial (R_a) qui combiné avec la présence du groupe *tert*-butyle sur la même face de la molécule provoque une attaque exclusive sur la face opposée avec la seule formation des alcools **18***a* et **19***a*. L'influence stérique du groupe CH_3 pseudo-axial sur la régiosélectivité des réactions d'hydroboration a récemment été notée (7) en comparant des résultats obtenus lors de l'hydroboration du *tert*-

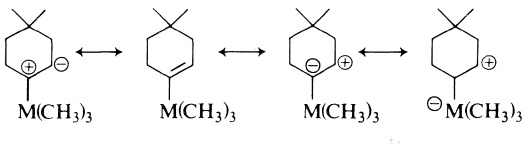

SCHÉMA 4

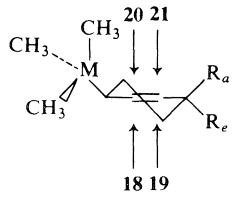

SCHÉMA 5

Can. J. Chem. Downloaded from www.nrcresearchpress.com by 210.87.254.105 on 09/05/12
For personal use only.

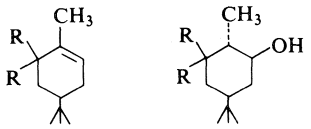

22 **23**

Série
a R = H
b R = CH_3

butyl-4 méthyl-1 cyclohexène (**22***a*) et du *tert*-butyl-4 triméthyl-1,6,6 cyclohexène (**22***b*); la quantité d'alcool **23** passe de 62.2% dans le premier cas (*a*) à 83.0% dans le deuxième cas (*b*). D'autre part on note que la présence du groupe CH_3 pseudo-équatorial (R_e) inhibe l'attaque menant à l'alcool **19***a*; il en résulte une formation prépondérante de l'alcool **18***a*. (*c*) La comparaison des résultats obtenus lors de l'hydroboration de l'alcène **2***a* par opposition avec ceux obtenus lors de celle des oléfines **2***b* et **2***c* indique clairement que l'influence stérique du groupement $(CH_3)_3M$ est atténuée dans les oléfines **2***b* et **2***c* dans lesquelles la longueur du lien C–M est accrue. Il en résulte que la réaction d'hydroboration se fait (environ 20% du total) par la face portant les groupes $(CH_3)_3M$. Il est à remarquer que la proportion d'alcools des types **18** et **20** [α du groupement $(CH_3)_3M$] par rapport aux alcools des types **19** et **21** [β des groupes $(CH_3)_3M$] diminue lorsque l'on passe de la série carbonée (alcène **2***a*) aux séries sililée et germaylée (séries **2***b* et **2***c*). Cette inversion ne peut être reliée à l'encombrement stérique des groupes $(CH_3)_3M$ puisque l'on peut faire l'hypothèse pour les cas des alcènes **2***b* et **2***c* dans lesquels les liens C—M deviennent de plus en plus longs que l'effet stérique du groupe $(CH_3)_3M$ devrait diminuer et favoriser la formation des alcools en position α par rapport au groupe $(CH_3)_3M$ (alcools des types **18** et **20**). Afin de rendre compte de ces anomalies on doit faire intervenir l'effet inductif très puissant (8) du groupe $(CH_3)_3M—CH(R)—$ (lorsque M = Si, Ge) qui amène la création d'une charge négative sur le carbone en γ du silicium. Cette délocalisation entraîne la formation des alcools des types **19** et **21** qui sont stériquement les moins favorisés.

Des résultats obtenus au cours de ce travail, on peut donc conclure que le groupe *tert*-butyle affecte le cours des réactions d'addition sur les alcènes du type **1***a* et **2***a* par son encombrement stérique. Par ailleurs, lors des réactions d'addition sur les oléfines du type **1***b* ou **1***c*, ces facteurs stériques sont presque complètement contrebalancés par l'effet pπ–dπ. Finalement dans les réactions d'addition sur les oléfines du type **2***b* et **2***c*, les effets stériques sont atténués par l'élongation du lien C—M et par l'effet inductif très puissant du groupe $(CH_3)M—CH—R$ (lorsque M = Si, Ge) qui provoque la formation de dérivés stériquement défavorisés.

Partie expérimentale

Les points de fusion ont été pris sur un appareil Cole-Parmer de la compagnie Instrument & Equipment.

Les spectres i.r. ont été pris sur un spectrophotomètre Beckman modèle IR-8 à double faisceau et sauf indication contraire, tous les spectres ont été pris entre deux plaques de NaCl.

Les spectres de résonance magnétique ont été déterminés sur un spectromètre modèle C-60-H de la compagnie Jeol. Le solvant choisi est le chloroforme deutérié pour les séries carbonées et le tétrachlorure de carbone pour les séries silylées et germylées. Les déplacements chimiques sont exprimés en p.p.m. et se réfèrent au tétraméthylsilane utilisé comme référence interne pour les séries carbonées; le chloroforme est utilisé comme référence interne pour les séries silylées et germylées.

Les indices de réfraction ont été déterminés à l'aide d'un réfractomètre du type Abbe. La pureté de tous les nouveaux produits décrits dans ce travail a été déterminée par chromatographie en phase gazeuse et leur identité confirmée par spectrométrie de masse à l'aide d'un spectromètre Hitachi Perkin-Elmer modèle RMU6-D opérant avec une énergie de faisceau d'électrons ionisant de 70 eV.

Synthèse des alcènes

*tert-Butyl-1 diméthyl-4,4 cyclohexène (**1a**)*

*Synthèse du tert-butyl-1 diméthyl-4,4 cyclohexanol (**5a**).* Dans un ballon de 500 ml à trois tubulures, muni d'un réfrigérant et d'une ampoule à brome, on introduit 12.6 g (0.1 mol) de diméthyl-4,4 cyclohexanone (**4**) (préparée d'après la méthode d'Eliel et Lukach (9)) dans 80 ml d'éther anhydre sous atmosphère d'azote. On porte le mélange à reflux et on ajoute goutte à goutte 60 ml de *tert*-butyllithium (2.1 *M* dans le pentane). On maintient 4 h sous agitation au reflux du solvant puis on traite avec de l'eau glacée. La phase éthérée lavée à l'eau, séchée sur Na_2SO_4 et évaporée fournit 12.0 g de l'alcool **5***a* (65% du rendement théorique) dont les caractéristiques sont les suivantes: p.e. 54°/0.65 mm Hg; p.f. 37–39°; i.r. 3520 cm^{-1} (OH); r.m.n. (CCl_4) pic à 0.90 p.p.m. (*gem*-diméthyle et *tert*-butyle), (DMSO-d_6) pic à 3.47 p.p.m. (C—OH, s).

*Synthèse du tert-butyl-1 diméthyl-4,4 cyclohexène (**1a**).* Dans un ballon de 50 ml, on introduit 4.2 g (0.023 mol) de *tert*-butyl-1 diméthyl-4,4 cyclohexanol (**5***a*) et 0.1 g d'iode. Le contenu du ballon est chauffé à 150 °C pendant 3 h, puis extrait à l'éther. La phase organique lavée avec une solution à 10% de thiosulfate de sodium et à l'eau est ensuite séchée sur Na_2SO_4, filtrée et concentrée sous vide. L'alcène est chromatographié sur une colonne de gel de silice en utilisant de l'éther de pétrole 30–60° comme éluant et fournit ainsi 2.5 g de produit **1***a* à l'état pur (65% du rendement théorique) présentant les caractéris-

Can. J. Chem. Downloaded from www.nrcresearchpress.com by 210.87.254.105 on 09/05/12
For personal use only.

Can. J. Chem. Downloaded from www.nrcresearchpress.com by 210.87.254.105 on 09/05/12
For personal use only.

tiques suivantes: p.e. 78°/33 mm Hg; n_D^{23} 1.4461; i.r. 3045 (C—H) 1385 et 1365 cm^{-1} (*tert*-Bu); r.m.n. (CCl_4) pics à 0.88 (singulet intégrant pour 6 protons et correspondant au *gem*-diméthyle), 1.02 (9 protons du groupe *tert*-butyle) et 5.27 p.p.m. (proton vinylique).

Triméthylsilyl-1 et triméthylgermyl-1 diméthyl-4,4 cyclohexène

*Chloro-1 diméthyl-4,4 cyclohexène (**6**).* Dans un ballon de 1 l, muni d'un réfrigérant et d'une ampoule à brome, on place, suivant la méthode de Mousseron et Jacquier (10), 21.2 g (0.1 mol) de PCl_5 et 20 ml d'éther anhydre. La diméthyl-4,4 cyclohexanone ((**4**), 12.6 g soit 0.1 mol) est ajoutée par petites fractions sous agitation magnétique à la température ambiante. On porte le mélange réactionnel au reflux de l'éther jusqu'à disparition totale du pentachlorure de phosphore. Après refroidissement, le liquide ainsi obtenu est versé lentement en agitant sur de la glace pilée. La couche éthérée traitée à la manière habituelle conduit par distillation à 10.2 g (70% du rendement théorique) du chloro-1 diméthyl-4,4 cyclohexène (**6**) possédant les caractéristiques suivantes: p.e. 52°/8 mm Hg; n_D^{23} 1.4667; i.r. 1660 (C—H), 1365, 1370 (CH_3—C—CH_3), 765 cm^{-1} (C—Cl); r.m.n. (CCl_4) pics à 0.97 (6 protons du *gem*-diméthyle), et 5.60 p.p.m. (proton vinylique).

*Diméthyl-4,4 triméthylsilyl-1 cyclohexène (**1***b*).* Utilisant la technique de Mironov *et al.* (11), on ajoute à 1 g (0.043 at.-g) de sodium fondu dans 4 ml de toluène au reflux, une quantité de triméthylchlorosilane (2.4 g soit 0.022 mol) suffisante pour abaisser le point d'ébullition du mélange à 100 °C. On introduit goutte à goutte 3.0 g (0.02 mol) de chloro-1 diméthyl-4,4 cyclohexène (**6**) de façon à entretenir le reflux. On maintient le mélange réactionnel à 130 °C pendant 1 h, puis filtre sur terre de diatomée. La distillation conduit à 1.7 g (47% du rendement théorique) d'alcène **1***b* présentant les caractéristiques suivantes: p.e. 36°/0.55 mm Hg; n_D^{23} 1.4546; i.r. 3020, 1620 (C=CH), 1360, 1380 (CH_3—C—CH_3), 1240 cm^{-1} du ($SiMe_3$); r.m.n. (CCl_4) pics à 0.04 (9 protons du $SiMe_3$), 0.89 (6 protons correspondants au *gem*-diméthyle) et 5.84 p.p.m. (proton vinylique).

*Diméthyl-4,4 triméthylgermyl-1 cyclohexène (**1***c*).* Suivant la technique de Mironov et Kranchenko (12) on disperse, dans un ballon de 100 ml, 0.8 g de sodium dans 7 ml de toluène sec au reflux. On ajoute 2.8 g de triméthylchlorogermane et 2.5 g de chloro-1 diméthyl-4,4 cyclohexène (**6**) et porte à 130 °C pendant 1 h. On filtre ensuite sur terre de diatomée et distille 1.0 g (30% du rendement théorique) d'alcène **1***c* à l'état pur possédant les caractéristiques suivantes: p.e. 74°/7 mm Hg; n_D^{18} 1.4759; i.r. 3000 (C—H), 1620 (C=C) 1360, 1375 (CH_3—C—CH_3), 820 cm^{-1} ($GeMe_3$); r.m.n. (CCl_4) pics à 0.10 (singulet pour les 9 protons du ($GeMe_3$)), 0.86 (singulet intégrant pour les 6 protons du *gem*-diméthyle) et 5.68 p.p.m. (proton vinylique).

*Diméthyl-3,3 triméthylsilyl-6 cyclohexène (**2***b*)*

*Chloro-1 diméthyl-4,4 cyclohexène-2 (**8**).* Dans un ballon de 300 ml à trois tubulures, muni d'un réfrigérant et d'une ampoule à brome et maintenu sous azote, on ajoute 3.4 g (0.08 mol) de chlorure de lithium dissout dans un minimum de DMF sec à une solution de 10.0 g (0.08 mol) de diméthyl-4,4 cyclohexène-2 ol ((**7**) préparé selon les indications de Julia et ses collaborateurs (13)) dans 10.6 g (0.09 mol) de *s*-collidine. On refroidit le contenu du ballon à 0 °C et on introduit lentement 11.0 g (0.1 mol) de chlorure de méthanesulfonyle. Le mélange réactionnel est agité à 25 °C pendant 4 h puis hydrolysé sur de la glace pilée et extrait à l'éther. La phase organique est lavée avec une solution saturée de nitrate cuivrique puis à l'eau, séchée sur Na_2SO_4, filtrée et concentrée sous vide. La distillation conduit à 8.4 g (74% de rendement théorique) du produit **8** présentant les caractéristiques suivantes: p.e. 32°/0.7 mm Hg; i.r. 3010, 775 et 740 cm^{-1}; r.m.n. (CCl_4) pics à 1.00 et 1.07 (2 singulets correspondants au *gem*-diméthyle), 4.40 (CHCl) et 5.55 p.p.m. (2 protons vinyliques sous forme de multiplet).

*Synthèse du diméthyl-3,3 triméthylsilyl-6 cyclohexène (**2***b*).* Appliquant la méthode de silylation décrite à la section 1.22 au chlorure **8**, on obtient l'alcène **2***b* avec un rendement de 47%. Ses caractéristiques sont: p.e. 43°/0.55 mm Hg; n_D^{23} 1.4585; i.r. 3010 (CH=CH), 1250 cm^{-1} ($SiMe_3$); r.m.n. (CCl_4): pics à 0.06 (9 protons correspondants au $SiMe_3$), 0.84 et 0.89 (6 protons correspondants au *gem*-diméthyle) et 5.34 p.p.m. (2 protons vinyliques sous forme de multiplet).

*Synthèse du diméthyl-3,3 triméthylgermyl-6 cyclohexène (**2***c*).* Dans un ballon de 100 ml, on ajoute successivement 5.0 g (0.04 mol) de diméthyl-4,4 cyclohexène-2 ol (**7**), 13.0 g (0.04 mol) de GeI_2 (préparé selon les indications de Foster (14)) et 10.0 g d'acide iodhydrique à 57% (excès de 20%). La réaction est exothermique et est complétée après chauffage à 60 °C pendant 24 h. On introduit alors goutte à goutte la solution éthérée du dérivé triiodé **9** ainsi obtenu à la solution magnésienne obtenue à partir de 11.5 g (0.5 mol) de magnésium et 71.0 g (0.5 mol) d'iodure de méthyle. On maintient au reflux de l'éther pendant 20 h, hydrolyse, lave la phase organique à l'eau, sèche sur K_2CO_3, filtre et évapore. La distillation conduit à 5.0 g (rendement global de 50%) de l'alcène **2***c* présentant les caractéristiques suivantes: p.e. 71°/1 mm Hg; n_D^{23} 1.4723; i.r. 3000 (C—H), 1630 (C=C) et 830 cm^{-1} ($GeMe_3$); r.m.n. (CCl_4) pics à 0.13 (9 protons du $GeMe_3$), 0.96 et 0.99 (6 protons correspondants au *gem*-diméthyle) et 5.39 p.p.m. (2 protons vinyliques apparaissant sous forme de multiplet).

*Synthèse du tert-butyl-5 diméthyl-3,3 cyclohexène (**2***a*)*

*tert-Butyl-5 diméthyl-2,2 cyclohexanone (**15**).* Dans un ballon de 500 ml à trois tubulures, muni d'un réfrigérant surmonté d'un tube à chlorure de calcium anhydre, on introduit 8.2 g de magnésium et de l'éther anhydre. Par une ampoule à brome, on ajoute 120 ml d'éther anhydre contenant 15.7 g (0.17 mol) de chloro-2 méthyl-2 propane. Une fois l'addition terminée, le mélange réactionnel est porté au reflux pendant 1 h puis refroidi; on y ajoute alors 1.6 g de chlorure cuivreux puis par l'ampoule à brome, 10.6 g (0.085 mol) de diméthyl-6,6 cyclohexène-2 one (**17**, préparée à partir de la bromo-2 diméthyl-6,6 cyclohexanone **16** en suivant la méthode decrite par Holysz (15)) diluée dans 100 ml d'éther anhydre. Le mélange réactionnel est porté à reflux pendant 1 h puis hydrolysé par une solution de chlorure d'ammonium à 10%; la phase éthérée est séchée sur du sulfate de sodium anhydre filtrée puis concentrée sous vide et le produit purifié par distillation conduit à 9 g (58% du rendement théorique) de *tert*-butyl-5 diméthyl-2,2 cyclohexanone (**15**) possédant les caractéristiques suivantes: p.e. 111°/13 mm Hg (litt. (3) 107–108/11 mm Hg); p.f. 35–36°; i.r. 1700, 1370, 1350 cm^{-1}; r.m.n. ($CDCl_3$) pics à 0.92 (9

Can. J. Chem. Downloaded from www.nrcresearchpress.com by 210.87.254.105 on 09/05/12
For personal use only.

protons du *tert*-butyle), 1.5 (3 protons du méthyle axial) et 1.15 p.p.m. (3 protons du méthyle équatorial).

*Tosylhydrazone de la tert-butyl-5 diméthyl-2,2 cyclohexanone (**15**).* La tosylhydrazone est obtenue en mélangeant 13.5 g (0.74 mol) de cétone **15** avec 13.6 g (0.73 mol) de *p*-toluènesulfonylhydrazine. Un vide de 10–20 mm de Hg est créé à l'aide d'un système adapté directement au ballon. Le ballon est plongé dans un bain d'huile à 80–90 °C sous agitation manuelle pendant 15–20 min. De l'éther est alors ajouté au mélange et la tosylhydrazone précipite. Après recristallisation dans l'éthanol 95%, 20 g (77% du rendement théorique) de tosylhydrazone sont obtenus et possèdent les caractéristiques suivantes: p.f. 149–150 °C; i.r. 3230, 1600, 1340 et 1170 cm^{-1}; r.m.n. ($CDCl_3$) pics à 0.85 (9 protons du *tert*-butyle), 0.90 et 1.02 (2 singulets intégrant chacun pour 3 protons et correspondant aux groupements méthyles axial et équatorial), 2.40 (3 protons du groupe méthyle attaché au noyau aromatique) et 7.20 p.p.m. (proton sur l'azote).

*tert-Butyl-6 diméthyl-3,3 cyclohexène (**2a**).* Dans un ballon à trois tubulures de 1 l muni d'un réfrigérant et d'une ampoule à addition et le tout maintenu sous atmosphère d'azote, on ajoute 136 ml d'éther anhydre à 20 g (0.059 mol) de tosylhydrazone de la cétone **15**. Plus de deux équiv. d'une solution à 15% de butyl-lithium dans l'hexane sont ensuite ajoutés à cette suspension suivant les indications de Shapiro et Heath (16). Pendant toute l'addition du réactif à 25 °C, le milieu est soumis à une agitation magnétique. Une fois l'addition terminée, le mélange réactionnel est maintenu à reflux pendant 3 h puis hydrolysé lentement à froid par 100 ml d'eau. La phase organique est extraite par de l'éther, séchée sur du sulfate de sodium anhydre, concentrée sous vide et conduit ainsi à 9.7 g (99% du rendement théorique) de l'alcène **2***a* qui est purifié par chromatographie sur une colonne de gel de silice et qui possède les caractéristiques suivantes: p.e. 74–75 °C/10 mm Hg; n_D^{25} 1.4500; i.r. 3030, 740 cm^{-1}; r.m.n. ($CDCl_3$) 0.90 (9 protons du *tert*-butyle), 1.00 (6 protons du *gem*-diméthyle) et 5.5 p.p.m. (2 protons oléfiniques sous forme de massif).

Hydroboration des oléfines et analyse des alcools obtenus

Hydroboration

L'hydroboration des oléfines du type **1** ou du type **2** a été réalisée sur des échantillons de 0.01 mol d'oléfines en solution dans 20 ml de tétrahydrofuranne en suivant la procédure expérimentale décrite par Brown et Zweifel (2). On a constaté que l'hydolyse des boranes intermédiaires s'effectue plus facilement en présence de soude aqueuse 10 *N* plutôt que 3 *N*. Les rendements moyens en alcool sont de 90%.

Analyse des produits

Les mélanges d'alcools provenant des réactions d'hydroboration des alcènes **1** et **2** ont été analysés par chromatographie en phase gazeuse à l'aide d'un chromatographe à ionisation de flamme Research Chromatograph 700 de la compagnie F et M muni d'une colonne de 6 pd × 1/8 de po remplie de Diatoport 5750 (80–100) supportant 6% de son poids de LAC 728. Les temps de retention (en min) des alcools dans ces conditions sont résumés au tableau 3. L'identification des pics a été réalisée par superposition avec des échantillons authentiques dont la préparation sera décrite dans une publication ultérieure.

TABLEAU 3. Temps de retention (en min) des alcools

Alcool	Série *a**	Série *b*†	Série *c*†
5	3.7	3.2	5.3
20	5.5	4.3	6.4
18	7.3	5.1	7.2
19	8.3	6.3	9.2
21	10.1	7.4	10.8

*Température de la colonne, 115 °C; débit d'hélium, 37 ml/min.
†Température de la colonne, 120 °C; débit d'hélium, 26 ml/min.

Les auteurs remercient vivement le Conseil national de recherches, le CNRS français, et les autorités chargées d'administrer les accords Franco–Québécois pour l'aide financière apportée sous forme d'octroi de recherches, de bourse d'études et de frais de mission. Les auteurs tiennent à remercier le Dr. Pierre Maroni pour l'accueil chaleureux réservé à M. Marc-André Poirier durant son stage à Toulouse. Les auteurs tiennent aussi à exprimer leur reconnaissance aux Dr. Mazerolles et Lesbre pour leur compréhension et leurs discussions utiles.

1. J. C. RICHER et C. FREPPEL. Can. J. Chem. **46**, 3709 (1968).
2. H. C. BROWN et Z. ZWEIFEL. J. Am. Chem. Soc. **83**, 2544 (1961).
3. H. O. HOUSE et M. J. UMEN. J. Org. Chem. **38**, 1000 (1973).
4. W. K. MUSKER et G. L. LARSON. Tetrahedron Lett. 3481 (1968).
5. J. J. EISCH et J. T. TRAINOR. J. Org. Chem. **28**, 487 (1963).
6. A. N. EGOROCHKIN, N. S. VYAZANKIN et S. Y. KHORSHEV. Russ. Chem. Rev. **41**, 425 (1972).
7. J. C. RICHER et C. LAMARRE. Sous presse.
8. A. W. P. JARVIE. Organometal. Chem. Rev. A, **6**, 153 (1970).
9. E. L. ELIEL et N. J. LUKACH. J. Am. Chem. Soc. **79**, 5986 (1957).
10. M. MOUSSERON et R. JACQUIER. Bull. Soc. Chim. Fr. 648 (1950).
11. V. F. MIRONOV, N. G. MAKSIMOVA et V. V. NEPOMNINA. Bull. Acad. Sc. U.S.S.R. 313 (1967).
12. V. F. MIRONOV et A. L. KRANCHENKO. Bull. Acad. Sc. U.S.S.R. 988 (1965).
13. S. JULIA, M. JULIA, H. LIMARES et J. C. BLONDEL. Bull. Soc. Chim. Fr. 1952 (1962).
14. L. S. FOSTER. Inorg. Synth. **3**, 63 (1950).
15. R. P. HOLYSZ. J. Am. Chem. Soc. **75**, 4432 (1953). (1964).
16. R. H. SHAPIRO et M. J. HEATH. J. Am. Chem. Soc. **89**, 5734 (1967).

Can. J. Chem. Downloaded from www.nrcresearchpress.com by 210.87.254.40 on 09/05/12
For personal use only.

COMMUNICATIONS

Synthesis of 3β,14β,19-Oxygenated Cardenolides

G. KRUGER

Bio-Research Laboratories, Ltd., Pointe Claire, Quebec H9R 1G6

Received November 30, 1973[1]

G. KRUGER. Can. J. Chem. **52**, 4139 (1974).

The synthesis of 3β,14β,19-oxygenated and of 3β,19-oxygenated-14-dehydro cardenolides from the bulk steroid pregnenolone acetate **1***a* is reported. The 19-oxygenated cardenolides which have been prepared include coroglaucigenin esters **4***e* and **4***f* and corotoxigenin acetate **4***g*. Coroglaucigenin and corotoxigenin occur in nature as glycosides in a number of plant species. In the synthetic scheme developed, successive transformations of the 3β-acetoxy-10β-methyl-5-ene moiety of **1***a* afford 19-hydroxy- or acyloxy-14-enes via 19-hydroxy-8(14)-enes and 8,19-oxido-14-enes.

G. KRUGER. Can. J. Chem. **52**, 4139 (1974).

On rapporte la synthèse, à partir de l'acétate de prègnénolone, de déhydro-14 cardénolides oxygénés en 3β,19 et 3β,14β,19. Les cardénolides oxygénés en 19 qui ont été préparés incluent les esters **4***e* et **4***f* de la coroglaucigénine et l'acétate **4***g* de la corotoxygénine. La coriglaucigénine et la corotoxygénine se retrouvent à l'état naturel sous forme de glycosides dans un certain nombre d'espèces de plantes. Dans le schéma de synthèse qui a été développé, des transformations de la partie acétoxy-3β méthyl-10β ène-5 de la molécule **1***a* conduisent aux hydroxy-19 ou acyloxy-19 ènes-14 par l'intermédiaire des hydroxy-19 ène-8(14) et des oxydo-8,19 ènes-14.

[Traduit par le journal]

Most of the presently known heart-active steroids are 3β,14β-oxygenated cardenolides or bufadienolides. A characteristic structural feature of some of the most potent members of these groups is the presence of an oxygen atom in position 19 (1).

Though several syntheses of 3β,14β-oxygenated cardenolides and bufadienolides of the 10β-methyl series from bulk steroids have recently been reported (2), no conversions of the latter to 19-oxygenated cardenolides appear to have been published so far. This publication reports the synthesis of 3β,14β,19-oxygenated and of 3β,19-oxygenated-14-dehydro cardenolides from the bulk steroid pregnenolone acetate **1***a*. The 19-oxygenated cardenolides which have been prepared include coroglaucigenin esters **4***e* and **4***f* and corotoxigenin acetate **4***g*. Coroglaucigenin and corotoxigenin occur in nature as glycosides in a number of plant species (3). The preparation of coroglaucigenin from 3,19-dioxo-14-hydroxy-14β-carda-4,20(22)-dienolide (4*a*), which can be obtained from the aglycone strophanthidin and hence from several naturally occurring 14β-hydroxy cardenolides, by a novel reduction employing lithium borohydride and pyridine (4) has recently been reported.

In the synthetic scheme developed successive transformations of the 3β-acetoxy-10β-methyl-5-ene moiety of **1***a* afford 19-hydroxy- or acyloxy-14-enes via 19-hydroxy-8(14)-enes and 8,19-oxido-14-enes. For some of the transformations 19-oxygen functions are required instead of being an encumbrance. In the previously reported partial syntheses introduction of a 14(15)-double bond has been effected either by microbiological 14α- or 15-hydroxylation and subsequent dehydration, dehydrogenation of 16-en-20-ones to 14,16-dien-20-ones (2, 5) or by enolization of 15-en-17-ones to 14,16-dien-17-ols (6). The synthetic scheme thus differs in essential respects from the previous syntheses. It may, by suitable variations, be employed for the preparation of analogs possessing novel structural features.

In the initial steps of the synthesis pregnenolone acetate **1***a* was converted to 20β-pivaloxy analog **1***c* via 20β-alcohol **1***b* and hence to 19-hydroxy-4,6-dien-3-one **2***a*, employing methods similar to those reported for the preparation of

[1]Revision received October 17, 1974.

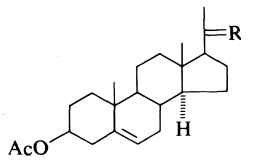

1

a R = O
b R = β-OH
c R = β-OPiv

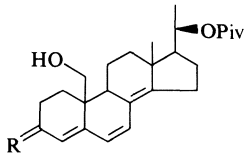

2

a 4,6-diene, R = O
b 4,6,8(14)-triene, R = O
c 4,6,8(14)-triene, R = β-OH
d 8(14)-ene,5α-H, R = β-OH

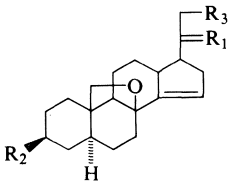

3

a R_1 = β-OPiv; R_2 = OH; R_3 = H
b R_1 = O; R_2 = OAc; R_3 = H
c R_1 = O; R_2 = R_3 = OAc
d R_1 = O; R_2 = OAc; R_3 = OH
e R_1 = O; R_2 = OAc, R_3 = OCO—CH_2—P(O)$(OEt)_2$
f R_2 = OAc; R_3, R_1 = 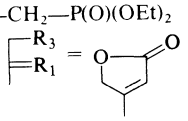

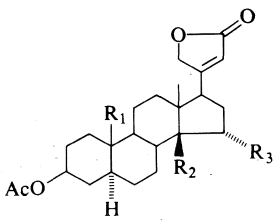

4

a R_1 = CH_2OH; R_2R_3 = 14-ene
b R_1 = CH_2OAc; R_2R_3 = 14-ene
c R_1 = CH_2OFm; R_2R_3 = 14-ene
d R_1 = CH_2OFm; R_2 = OH; R_3 = Br
e R_1 = CH_2OFm; R_2 = OH; R_3 = H
f R_1 = CH_2OH; R_2 = OH; R_3 = H
g R_1 = Fm; R_2 = OH; R_3 = H

Piv = O=C—$C(CH_3)_3$ Ac = O=C—CH_3
Fm = O=C—H

the analogous 19-hydroxy-17β-pivaloxyandrosta-4,6-dien-3-one from androstenolone acetate (7). Treatment of **2***a* with sodium methoxide in dimethyl sulfoxide under nitrogen (8) followed by addition of the mixture to an externally cooled solution of 2,3-dichloro-5,6-dicyano-1,4-benzoquinone in ether – glacial acetic acid, subsequent decolorization of the dark mixture with aqueous sodium bisulfite, and extraction of the organic phase with aqueous base afforded hydroxytrienone **2***b*, m.p. 223–225°, u.v. (MeOH) 346 nm in an estimated yield of 14% from **1***a*.

Reduction of **2***b* with sodium borohydride gave **2***c*, u.v. (MeOH) 285 nm, which was catalytically hydrogenated to **2***d*, u.v. (MeOH) 210 nm. Oxidation of **2***d* with pyridinium hydrobromide perbromide in presence of pyridine gave 8,19-oxide **3***a*, m.p. 132–133°.[2] Conversion of the latter to the corresponding 3-pyranyl ether, liberation of the 20β-hydroxy group by treatment with sodium bis(methoxyethoxy)aluminum hydride in benzene, oxidation with chromium trioxide in pyridine, regeneration of the 3β-hydroxy group from its tetrahydropyranyl ether by treatment with aqueous acetic acid, and subsequent acetylation gave 8,19-oxido-14-en-20-one **3***b*, m.p. 200–204°. Oxidation of **3***b* with lead tetraacetate in presence of methanol and boron trifluoride etherate (9) gave 21-acetate **3***c*, m.p. 152–155°, which on selective hydrolysis with aqueous potassium hydroxide in methanol gave 21-hydroxy-20-one **3***d*, m.p. 199–205° (evacuated sealed tube), in 17% yield from trienone **2***b*.

Esterification of **3***d* in benzene with (diethylphosphono) acetic acid and dicyclohexylcarbodiimide (10) gave phosphonoacetate **3***e*, which was converted to cardenolide **3***f*, m.p. 222–224°, u.v. (MeOH) 218 nm, by treatment with 50% aqueous potassium hydroxide. Hydrogenolysis[3] of **3***f* with zinc in glacial acetic acid (11*a*) at room temperature gave 19-alcohol **4***a*, which after treatment with acetic anhydride, preparative thin-layer chromatography of the product and subsequent recrystallization gave 3β,19-diacetate **4***b*, m.p. 163–165°, $[\alpha]_D^{24}$ −30.8 (*c* 0.91,

[2]20β-Pivaloxy-8,19-oxide **3***a* on treatment with sodium bis(methoxyethoxy)aluminum hydride in benzene and subsequent acetylation of the resulting 3,20-diol gave 3β,20β-diacetoxy-8,19-oxido-5α-pregn-14-ene, m.p. 188–189° (lit. (14) m.p. 189–190°), $[\alpha]_D^{25}$ −9° (*c* 1.035, $CHCl_3$) (lit. (18) $[\alpha]_D^{20}$ −7° (*c* 1.03, $CHCl_3$)), which had previously been obtained, besides other products, from 3β,20β-diacetoxy-19-hydroxy-5α-pregnane during a study on the oxidation of saturated 19-hydroxy steroids by lead tetraacetate (18).

[3]The synthesis of the 19-hydroxy-20β-pivaloxy-5α-pregn-14-ene **4***a* from 19-hydroxy-20β-pivaloxypregna-4,6-dien-3-one **2***a* was preceded by an analogous synthesis of 19-hydroxy-17β-pivaloxy-5α-androst-14-ene from 19-hydroxy-17β-pivaloxyandrosta-4,6-dien-3-one (11*a*). The structure of the 14α,15α-epoxide obtained from the 19-hydroxyandrost-14-ene was determined by X-ray analysis (11).

Can. J. Chem. Downloaded from www.nrcresearchpress.com by 210.87.254.40 on 09/05/12
For personal use only.

Can. J. Chem. Downloaded from www.nrcresearchpress.com by 210.87.254.40 on 09/05/12
For personal use only.

$CHCl_3$) (lit. (3*c*) $[\alpha]_D^{16}$ −32.0 (*c* 0.482, $CHCl_3$)); n.m.r. ($CDCl_3$, δ) 5.91 (1, broadened s or t, $J = 2$; 22-H), 5.30 (1, m or broadened d, $J = 2$; 15-H), 4.76 (2, d, $J = 2$; 21-H), 4.50–4.95 (1, m; 3α-H of 5α-series (12*a* and *d*)), 4.30 (2, s; 19-H), 2.09 (3, s; 19-OAc), 2.01 (3, s; 3-OAc), and 0.82 (3, s; 18-methyl); identical by i.r. (KBr) with "β-anhydrocoroglaucigenin diacetate" (3*c*) (see below); m.p. of mixture with the latter compound 162–164°.

Treatment of **3***f* with zinc and 90% aqueous formic acid at room temperature gave first 19-alcohol **4***a* and then 19-formate **4***c*, m.p. 120–122° (change of crystalline to turbid, viscous mesophase), 171–173° (change of mesophase to isotropic phase); n.m.r. ($CDCl_3$, δ) 8.16 (1, broadened s; 19-OCHO), 5.92 (1, broadened s or t, $J = 2$; 22-H), 5.10-5.45 (1, m; 15-H), 4.76 (2, d, $J = 2$; 21-H), 4.6–4.95 (1, m; 3α-H), 4.43 (2, s; 19-H), 2.01 (3, s; 3-OAc), and 0.81 (3, s; 18-methyl). Oxidation of 14-ene **4***c* with *N*-bromoacetamide in acetone between 0 to 5° followed by reduction of the resulting bromohydrin **4***d* with Raney nickel by procedures similar to previously reported ones (5, 13) and recrystalization of the crude product from ether–hexane gave a product consisting of 14β-hydroxy cardenolide **4***e*, m.p. 234–239°, u.v. max 218 nm, and a small amount of the analogous epoxide, *i.e.*, 3β-acetoxy-19-formyloxy-14,15β-oxido-5α,14β-card-20(22)-enolide as indicated by t.l.c. Subsequent preparative t.l.c. followed by recrystallization from ether–hexane gave the purified 14β-alcohol **4***e*, m.p. 247–251°; i.r. (KBr) 3660, 3420 (sh), 3100 (weak), 1770, 1735, 1719, 1710, 1381, 1365, 1265, 1255, 1175, 1145, 1030, 1002, 960, 910, 889, and 869 cm^{-1}; n.m.r. ($CDCl_3$, δ) 8.13 (1, broadened s; 19-OCHO), 5.89 (1, broadened s; 22-H), 4.91 (2, broadened s or incompletely resolved dd; 21-H), 4.8–5.0 (1, m; 3α-H of 5α-series (12*a* and *d*)), 4.39 (2, s; 19-H), 2.80-2.95 (m; 17α-H (14)), 2.01 (3, s; 3-OAc), and 0.88 (3, s; 18-methyl of 14β-ol[4]), in 14% yield from 21-hydroxy-20-one **3***d*. The analytical sample of **4***e*, which was similarly purified by chromatography and subsequent recrystallization, had m.p. 248–254°; *m/e* 460 (molecular ion) 458, 442, 440, 400 (strong), 382 (strong), 354 (strong).

Anal. Calcd. for $C_{26}H_{36}O_7$: C, 67.80; H, 7.87. Found: C, 67.75; H, 7.66.

After optimization of the individual steps of the synthesis of 3β,14β,19-oxygenated cardenolide **4***e* from bulk steroid **1***a* it was possible to purify all intermediate reaction products by simple precipitation or recrystallization procedures so that it became unnecessary to resort to their chromatographic purification.

Selective hydrolysis of **4***e* with aqueous potassium hydroxide in methanol gave 19-ol **4***f*, m.p. 229–236°. Oxidation of **4***f* with *t*-butyl chromate (15) gave aldehyde **4***g*, m.p. 221–229°, identical by i.r. (KBr) with corotoxigenin 3-acetate (see below).

Treatment of authentic[5] β-anhydrocoroglaucigenin, which previously had been tentatively considered (3*c*) as 14(15)-anhydrocoroglaucigenin, and of authentic[5] corotoxigenin with acetic anhydride and pyridine, followed by preparative t.l.c. and subsequent recrystallization from hexanemethylene chrloride, gave the reference cardenolides β-anhydrocoroglaucigenin diacetate, m.p. 161–163° (lit. (3*c*) m.p. 161–163°) and corotoxigenin 3-acetate, m.p. 214–216°, m.p. (evacuated sealed tube) 240–250° (lit. (3*c*) m.p. 220–230° and 227–234°, lit. (3*a*) m.p. 256°, respectively).[6]

Preliminary biological tests showed that the synthetic 14β,19-oxygenated cardenolides **4***e* and **4***f* inhibit ATP-ase (16) almost as much as

[4]It has previously been noted (19*a*) that 14β-oxygenation of 14-enes leads to a downfield, while 14α-oxygenation leads to an upfield, shift of δ(18-methyl); *cf.* also the n.m.r. data cited for xysmalogenin (5-dehydrodigitoxigenin) 3-acetate, for its 14-ene analog (19*b*) and for the 3-oxo-14-ene analog of digitoxigenin (5); for the effect of the double bond in position 5, and the 3-oxo and 3β-acetoxy group on δ(18-methyl) see ref. 12*b*. Support for the structure of 14β-ol **4***e* is further given by a direct comparison of its n.m.r. spectrum with that of digitoxigenin 3-acetate, which was found to have ($CDCl_3$, δ) 5.90 (1, broadened s; 22-H), 5.11 (1, m; 3α-H of 5β-series (12*a*)), 4.92 (2, m or incompletely resolved dd; 21-H), 2.82–2.98 (m; 17α-H (14)), 2.02 (3, s; 3-AOc), 0.95 (3, s; 19-methyl), and 0.87 (s, 3; 18-methyl), and with that of strophanthidin 3-acetate which has also been dipicted in (12*c*).

[5]The author is indebted to Professor T. Reichstein, University of Basle, Switzerland, for a generous gift of samples of β-anhydrocoroglaucigenin, corotoxigenin, and coroglaucigenin.

[6]The melting points of compounds **4***b*, *e*, *f*, and *g* as well as those of the two reference cardenolides are corrected. With the exception of the second melting point cited for corotoxigenin 3-acetate they have been determined on a micro hot stage.

strophanthidin 3-acetate and also possess a substantial inotropic effect[7] (17).

The author is indebted to Mrs. S. Dahr, Mrs. K. Kirchhof, Mrs. G. Teodosiu, Mr. J. M. Thiemann, and Mrs. N. Y. Wang for their capable and persevering assistance and to Dr. C. Chappel, President of Bio-Research Laboratories, Ltd. for his continued interest in this work and for providing the means for it.

1. K. K. Chen. J. Med. Chem. **13**, 1029 (1970).
2. (*a*) F. Sondheimer. Chem. Brit. **1**, 454 (1965); (*b*) R. Wiechert. Agnew. Chem. Intern. Edit. **9**, 321 (1970); (*c*) P. J. May. Specialist Periodical Reports, Terpenoids and Steroids, The Chemical Society, London, 1971. Vol. 1, p. 404.
3. (*a*) A. Stoll, A. Pereira, and J. Renz. Helv. Chim. Acta, **32**, 293 (1949); (*b*) O. Schindler and T. Reichstein. Helv. Chim. Acta, **35**, 730 (1952); (*c*) A. Hunger and T. Reichstein. Helv. Chim. Acta, **35**, 1073 (1952); (*d*) K. D. Roberts, Ek. Weiss, and T. Reichstein. Helv. Chim. Acta, **46**, 2886 (1963); K. D. Roberts, Ek. Weiss, and T. Reichstein. Helv. Chim. Acta, **49**, 316 (1966); (*f*) R. Tschesche, D. Forstmann, and V. K. M. Rao. Chem. Ber. **91**, 1204 (1958).
4. (*a*) U. Stache, W. Haede, K. Radscheit, and W. Fritsch. Ger. Offen. 2,033,599, Jan. 20, 1972; (*b*) U. Stache, W. Haede, K. Radscheit, and W. Fritsch. Chem. Abstr. **76**, 438, 86021m (1972); (*c*) Y. Kamano and G. R. Pettit. J. Org. Chem. **39**, 2319 (1974).
5. W. Fritsch, U. Stache, W. Haede, K. Radscheit, and H. Ruschig. Justus Liebigs' Ann. Chem. **721**, 168 (1969).
6. (*a*) A. Afonso. U.S. Patent 3,595,883, July 27, 1971; (*b*) A. Afonso. Chem. Abstr. **75**, 332, 98733n (1971); (*c*) A. Afonso. Can. J. Chem. **47**, 3693 (1969).
7. G. Kruger. J. Org. Chem. **36**, 2129 (1971).
8. G. Kruger. J. Org. Chem. **33**, 1750 (1968).
9. G. R. Pettit, C. L. Herald, and J. P. Yardley. J. Org. Chem. **35**, 1389 (1970).
10. W. Eberlein, J. Nickl, J. Heider, G. Dahms, and H. H. Machleidt. Chem. Ber. **105**, 3686 (1972).
11. (*a*) G. Kruger and G. I. Birnbaum. Tetrahedron Lett. 1501 (1973); (*b*) G. I. Birnbaum. Acta Cryst. B**29**, 1426 (1973).
12. (*a*) N. S. Bhacca and D. H. Williams. Applications of NMR spectroscopy in organic chemistry. Holden-Day, San Francisco. 1966. pp. 78–81; (*b*) N. S. Bhacca and D. H. Williams. Applications of NMR spectroscopy in organic chemistry. Holden-Day, San Francisco. 1966. p. 20; (*c*) N. S. Bhacca and D. H. Williams. Applications of NMR spectroscopy in organic chemistry. Holden-Day, San Francisco. 1966. p. 45; (*d*) J. E. Bridgeman, P. C. Cherry, A. S. Clegg, J. M. Evans, Sir Ewart R. H. Jones, A. Kasal, V. Kumar, G. D. Meakins, Y. Morisawa, E. E. Richards, and P. D. Woodgate. J. Chem. Soc. (C), 250 (1970).
13. Y. Kamaro and G. R. Pettit. J. Org. Chem. **38**, 2202 (1973).
14. K. Tori and K. Aono. Annual Report of Shionogi Research Laboratory. No. 15, 130 (1965).
15. A. Katz. Helv. Chim. Acta, **40**, 487 (1957).
16. S. M. Kupchan, M. Mokotoff, R. S. Sandhu, and L. E. Hokin. J. Med. Chem. **10**, 1025 (1967).
17. R. H. Thorp and L. B. Cobbin. Cardiac stimulant substances. Academic Press, New York. 1967. pp. 28–33.
18. D. Hauser, K. Heusler, J. Kalvoda, K. Schaffner and O. Jeger. Helv. Chim. Acta, **47**, 1961 (1964).
19. (*a*) F. W. Villaescusa and G. R. Pettit. J. Org. Chem. **37**, 569 (1972); (*b*) E. Yoshii and K. Ozaki. Chem. Pharm. Bull. **20**, 1585 (1972).

[7]ATP-ase was obtained from the brain of guinea pigs. These animals also furnished the atrial preparations used in the determination of the inotropic effects. The tests were carried out in these laboratories by Dr. P. Dussault and Dr. J. Chiz, respectively. Detailed biological results, which will include novel compounds obtained by variants of the synthesis developed, will be published at a later date.

Can. J. Chem. Downloaded from www.nrcresearchpress.com by 210.87.254.40 on 09/05/12
For personal use only.

Bicyclooctanone Rearrangement, [3.2.1] → [3.3.0], via β-Enolization. Evidence for γ-Enolization in Bicyclo[3.3.0]octan-2-one[1]

A. L. JOHNSON,[2] N. O. PETERSEN,[3] M. B. RAMPERSAD, AND J. B. STOTHERS
Department of Chemistry, University of Western Ontario, London, Ontario N6A 3K7

Received September 9, 1974

A. L. JOHNSON, N. O. PETERSEN, M. B. RAMPERSAD, and J. B. STOTHERS. Can. J. Chem. **52**, 4143 (1974).

Under homoenolization (β-enolization) conditions (*t*-BuO⁻–*t*-BuOH, 185°) 3,3-dimethylbicyclo[3.2.1]octan-2-one rearranges to 3,3-dimethylbicyclo[3.3.0]octan-2-one in good yield. From reactions in *t*-butyl alcohol-O-*d*, the progress of deuterium incorporation was determined by ^{2}H n.m.r. to compare the reactivity toward β-enolate formation for the various potential sites in **1**. Similar experiments with **2** gave evidence for competitive γ proton abstraction (γ-enolization); the first example of this process in a relatively flexible carbon skeleton.

A. L. JOHNSON, N. O. PETERSEN, M. B. RAMPERSAD et J. B. STOTHERS. Can. J. Chem. **52**, 4143 (1974).

Dans des conditions (*t*-BuO⁻–*t*-BuOH, 185°) d'homoénolisation (β-énolisation), la diméthyl-3,3 bicyclo[3.2.1]octanone-2 se réarrange, avec de bons rendements, en diméthyl-3,3 bicyclo[3.3.0]octanone-2. En se basant sur les résultats obtenus lorsque la réaction a été effectuée en présence de *t*-butanol-O-*d*, le taux d'incorporation du deutérium a pu être déterminé par la résonance magnétique nucléaire du ^{2}H et l'on a pu ainsi comparer la réactivité, vis à vis de la formation du β-énolate, en diverses positions de **1** susceptibles d'énolisation. Des expériences similaires avec **2** ont permis de mettre en évidence la présence d'une réaction d'abstraction du proton en position γ (γ énolisation); ce résultat est le premier exemple d'un tel processus dans une molécule avec un squelette carboné relativement flexible.

[Traduit par le journal]

The reversible formation of 'enolates' from ketones by remote proton abstraction with strong base has received relatively little attention since the discovery and detailed characterization of β-enolization (homoenolization)[4] of camphenilone by Nickon and Lambert (1). Nevertheless the process has synthetic utility (2) and warrants further investigation to define its scope more precisely in terms of suitable molecular geometries and the stereochemistry of ketonization. At present these features are established only for the bicyclo[2.2.1]heptan-2-one skeleton (1,3) and adamantanone (4) but several other polycyclic systems should be suitable substrates. One of these, 3,3-dimethylbicyclo[3.2.1]octan-2-one (**1**), has three different skeletal carbons at which β-enolization could occur, as well as the methyl carbons, and a comparison of the relative reactivities of these centers could be instructive as to the structural requirements for facile β-enolate formation. This information as well as the stereochemistry of the ring opening may be determined directly by ^{2}H n.m.r. to monitor the progress of deuterium incorporation for reactions in *t*-butyl alcohol-O-*d*, as we have demonstrated (*3b*, 4). Furthermore, ^{2}H spectra permit detection of lightly labelled centers which could arise by slower exchange of more remote protons. Although, in principle, γ-enolization can occur, the available examples have the γ carbon rigidly constrained close to the carbonyl group (5). We wish to report the first observation of γ-enolization in a relatively flexible system, 3,3-dimethylbicyclo[3.3.0]octan-2-one (**2**), which is itself generated readily by β-enolization of **1**. The smooth conversion of **1** → **2** constitutes a synthetically useful approach to the bicyclo-[3.3.0]octanone skeleton.

Ketone **1**[5] prepared by methylation ($NaNH_2$–

[1]Part XXVIII in the series NMR Studies. For Part XXVII see ref. *3b*.

[2]Present address: College of Southern Idaho, Twin Falls, Idaho.

[3]Present address: California Institute of Technology, Pasadena, California.

[4]While homoenolization neatly describes the process at β carbons, more remote proton abstraction can occur. We suggest, therefore, a more general term to specify the reaction site. For example, β-enolization and γ-enolization refer to proton removal from β and γ carbons, respectively. For the latter bishomoenolization could be used but seems unnecessarily confusing.

[5]This ketone (ν_{max} ($CDCl_3$) 1700 cm^{-1}) is a liquid whose 2,4-dinitrophenylhydrazone melted at 157.5–158.0°.

Anal. Calcd. for $C_{10}H_{16}O$: C, 78.89; H, 10.59. Found: C, 79.11; H, 10.41.

Can. J. Chem. Downloaded from www.nrcresearchpress.com by 210.87.254.105 on 09/05/12
For personal use only.

TABLE 1. Deuterium incorporation in **1** and **2**

Substrate	Time (h)	Compound	Atoms D/ molecule[a]	% exchange/hydrogen by ^{2}H n.m.r. (±2%)[b] H-1	H-6 *Exo*	H-6 *Endo*	H-7 *Exo*	H-7 *Endo*	H-8 *Exo*	H-8 *Endo*	Methyl *Exo*	Methyl *Endo*
1	48	**1**	3.15	75			75	68			19	13
		2	4.55	81			62	39	84	82	30	5
	148	**1**	3.37	59			59	81			28	18
		2	4.74	59			65	50	75	74	39	11
	334	**1**	3.43	50			52	80			29	25
		2	4.79	49			69	47	76	69	42	14
2	125	**2**	2.89	56	[c]	6	15[d]	3	15	15	56	4
	342	**2**	3.31	42	[c]	12	24[d]	5	26	19	59	9

[a]Using a Varian M66 spectrometer at 30 eV ionization voltage.
[b]Spectra obtained by FT operation of a Varian XL-100-15 at 15.4 MHz with noise decoupling at 100 MHz and integrated by line-shape fitting (3*b*, 4). Samples were examined as 10% solutions in $CHCl_3$–C_6F_6 (4:1) containing $Pr(fod)_3$.
[c]Not resolved, 8 included in *exo*-7 signal.
[d]Includes *exo*-6 absorption.

CH_3I) of the commercially available parent ketone, was dissolved in *t*-BuO^-–*t*-BuOH (0.7 *M*) to furnish a solution 0.2 *M* in ketone. Aliquots were sealed in glass tubes under nitrogen and heated at 185° for various times. Gas–liquid chromatographic analysis of the product (pentane extraction, 80–90% yields) revealed a new compound, besides **1**, isolable by preparative g.l.c. The new liquid ketone (1740 cm^{-1}) had two methyl singlets (0.95, 1.00, CCl_4; 0.90, 0.98 p.p.m. C_6D_6) and a multiplet (2H) near 2.5 p.p.m. in its ^{1}H spectrum. Its ^{13}C spectrum contained 10 signals for 5 carbon types: methyl (2), methylene (4), methine (2), quaternary (1), and 1 carbonyl signal. Mol. Wt. Calcd. for $C_{10}H_{16}O$: 152.1200. Found (*m/e*): 152.1205. Structure **2** was confirmed by methylation to a trimethyl ketone,[6] identical (i.r., ^{1}H and ^{13}C n.m.r., g.l.c.) to that obtained by methylation of *cis*-bicyclo[3.3.0]octan-2-one (6). The conversion, **1** → **2**, had a half-life of *ca.* 60 h; thus good yields are obtainable in 100–200 h.

Compound **1** can β-enolize at the methyls and at C-4, -7, and -8, the latter leading to **2** via **A**. To compare reactivities at these sites, reactions were run in *t*-butyl alcohol-O-*d* using ^{2}H n.m.r. to follow ^{2}H incorporation and the results for recovered **1**-d_x and **2**-d_x are listed in Table 1. Exchange occurred at five sites in **1**: C-1, *exo*- and *endo*-7, and both methyls.[7] Bridgehead exchange was rapid, >90% in 1 h, and *exo*-deuteration was faster than *endo* at C-7 and at the methyls. Thus, β-enolization primarily involved C-7 (**B**), C-8 (**A**), and the methyl carbons. Since ^{2}H was not observed at C-8 after 334 h, cleavage of **A** was exclusively to **2**. Further, since methyl exchange was preferentially *exo*, this process occurred at a faster rate than β-enolization at C-7 because the latter generates **B** which renders the methyls equivalent. A sample of **1**-d_x isolated after 734 h was found to contain 2–3% ^{2}H at C-6 and C-8 (*anti* only) presumably arising from **2** (see below). From these runs, spectra of **2** had seven ^{2}H signals[8]: C-1, -7, -8, and the methyls (Table 1), a labelling pattern entirely consistent with its formation via **A** with subsequent rapid bridgehead exchange.

Incorporation of ^{2}H in **2** results from exchange in **1** before conversion to **2** *and* from exchange after its formation. To examine the latter processes separately, samples of **2** were treated with *t*-BuO^-–*t*-BuOD at 185°. The ^{2}H spectra of the recovered **2**-d_x samples (Table 1) differed significantly from those for **2**-d_x generated from **1**, described above. *Eight* ^{2}H signals were resolved

[6]The trimethyl ketone (ν_{max} ($CDCl_3$) 1735 cm^{-1}) had three methyl singlets (1.03, 1.06, 1.13 p.p.m. CCl_4) in its ^{1}H spectrum while its ^{13}C spectrum contained signals for a carbonyl, two quaternary, one methine, four methylene, and three methyl carbons.

Anal. Calcd. for $C_{11}H_{18}O$: C, 79.45; H, 10.92. Found: C, 79.37; H, 10.70.

[7]The ^{2}H assignments were confirmed by ^{13}C n.m.r. and by comparison of ^{1}H and ^{2}H spectra of solutions containing $Pr(fod)_3$; with 0.25 equiv. of $Pr(fod)_3$ all 12 ^{1}H shifts could be determined using spin-decoupling tc establish individual assignments.

[8]The ^{2}H assignments for **2** also followed from a shift reagent study ($Pr(fod)_3$) with the difference that the *exo*-6 and *exo*-7 multiplets were not resolved.

Can. J. Chem. Downloaded from www.nrcresearchpress.com by 210.87.254.105 on 09/05/12
For personal use only.

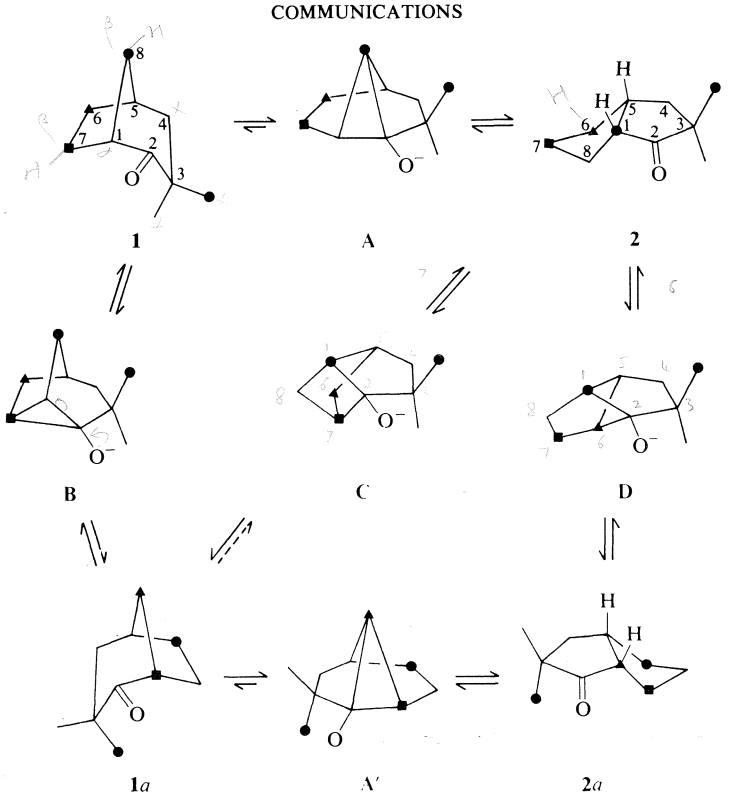

SCHEME 1

revealing exchange of H-1, H-6, H-7, H-8, and the methyls. The presence of ^2H at C-6 and C-7 clearly implies that γ-enolates **C** and **D** are intermediates. Also, **C** must open primarily to **2**, rather than **1***a*, otherwise in the experiments with **1**, C-6 (**1***a*) would be significantly labelled because this carbon is the bridgehead carbon in **2** (the fates of individual carbons are indicated by ●, ▲, and ■ in Scheme 1). Nevertheless, **C** does provide a path for ^2H incorporation at C-6 and C-8 in **1** (**1***a*) at which small amounts of ^2H were detected after a very long reaction time (734 h), as noted above. The formation of **1** (**1***a*) via **A** (**A′**) must be a very minor process otherwise *both* 8 hydrogens would be exchanged because C-8 in **1** (**1***a*) is the bridgehead carbon in **2** (**2***a*) which undergoes rapid exchange but only *anti*-8 exchange (~2%) was detected after 734 h.

From these results we conclude that the abstraction of β and γ protons from **2** are competitive processes. Thus, γ-enolization occurs in moderately flexible systems. Work directed at a quantitative comparison of the stereoselectivity of β-enolization and γ-enolization in this system as well as measurement of the rate of racemization of **1** and **2** is in progress and will be described in due course.

We wish to thank the National Research Council of Canada for financial support of this study and Ināra Grikis for technical assistance.

1. A. NICKON and J. L. LAMBERT. J. Am. Chem. Soc. **84**, 4604 (1962); **88**, 1995 (1966); A. NICKON, J. L. LAMBERT, and J. E. OLIVER. J. Am. Chem. Soc. **88**, 2787 (1966).
2. A. NICKON, H. KWASNIK, T. SWARTZ, R. O. WILLIAMS, and J. B. DIGIORGIO. J. Am. Chem. Soc. **87**, 1615 (1965); R. M. COATES and J. P. CHAM. Chem. Commun. 1481 (1970); D. M. HUDYMA, J. B. STOTHERS, and C. T. TAN. Org. Magn. Res. In Press.
3. (*a*) D. H. HUNTER, A. L. JOHNSON, J. B. STOTHERS, A. NICKON, J. L. LAMBERT, and D. F. COVEY. J. Am. Chem. Soc. **94**, 8582 (1972); (*b*) A. L. JOHNSON, J. B. STOTHERS, and C. T. TAN. Can. J. Chem. In press.
4. J. B. STOTHERS and C. T. TAN. J. Chem. Soc. Chem. Commun. 738 (1974).
5. J. L. LAMBERT. Ph.D. Thesis. Johns-Hopkins University (1963); R. Howe and S. WINSTEIN. J. Am. Chem. Soc. **87**, 915 (1965); T. FUKUNAGA. J. Am. Chem. Soc. **87**, 916 (1965).
6. A. C. COPE, H. H. LEE, and H. E. PETREE. J. Am. Chem. Soc. **80**, 2849 (1958); A. C. COPE, M. BROWN, and H. E. PETREE. J. Am. Chem. Soc. **80**, 2852 (1958).

Can. J. Chem. Downloaded from www.nrcresearchpress.com by 210.87.254.105 on 09/05/12
For personal use only.